ELSEVIER

Talanta 44 (1997) 1–13

Talanta

Review

Microcells for voltammetry and stripping voltammetry

Ya. I. Tur'yan

National Physical Laboratory of Israel, Danciger "A" Bldg., The Hebrew University, Givat Ram, Jerusalem 91904, Israel

Received 12 February 1996; revised 19 June 1996; accepted 24 June 1996

Abstract

The designs and applications of "non-flow" microcells in voltammetry and stripping voltammetry for samples with volumes from sub-microliters to 5 ml are reviewed. The analysis of microcell designs was carried out on the basis of their classification: (i) microcells with a static sample, including thin-layer microcells with a static sample; (ii) microcells with forced convection of the sample; and (iii) microcells for batch injection of samples. Two working electrode types (the usual state and inverted state) are discussed. The use of working micro- and mercury-film electrodes and of the accelerated removal of dissolved oxygen are also considered in detail.

Keywords: Microcells; Review; Sample batch injection; Stripping voltammetry; Voltammetry.

1. Introduction

Electrochemical methods of anlysis, including voltammetry and stripping voltammetry, are widely used [1–3] in microanalysis with small volumes of samples. Voltammetry and stripping voltammetry can be used for the analysis of small volumes of samples after their preconcentraion by different methods [4], for the automation of anlaysis [5–10] and for the anlaysis of the limited volume materials in biology, medicine and the environment, such as biological fluids [11,12], brain slices [13], products of enzymatic reactions [9], catecholamines [14] and human cerebrospinal fluid [15].

The possibilities of voltammetric and stripping voltammetric microanalysis essentially depend on the design of the microcell where the measuring process takes place. We define the "microcell" as the complex of following elements: the working, auxillary and reference electrodes, the electrode compartments and electrolytic diaphragms and the devices for sample inlet and outlet, for removal of dissolved oxygen and for sample forced convection.

The term "micro" is not related to the cell size but to the sample volume, which we conditionally accepted up to 5 ml: 0.5–5 ml [16–23], 20–300 μl [5–13,24–27] and $\leqslant$10 μl [10,14,15,25,28–53].

There are flow-through and "non-flow" microcells. In flow-through microcells, sample is introduced in to the cell with a continuously moving carrier solution and leaves the cell together with it. In "non-flow" microcells, sample is introduced to the cell directly and discretely with a pipette or some mechanical closer. After analysis it is re-

PII S0039-9140(96)02040-1

moved from the cell or from the measuring zone with the same device or by the rotation of the mixer or working electrode or by displacement by the next sample of the electrolyte.

Flow-through microcells are intended mainly for detection in liquid chromatography and flow injection analysis. These cells have been considered in detail in reviews by Kissinger [54], Gunasingham and Fleet [55], Berisci et al. [1] and for stripping voltammetry by Lunque de Castro and Izquierdo [56]. Therefore, the novel aspects of this review are the analysis of designs and application of "non-flow" microcells in which a sample is introduced directly and discretely with a pipette. These microcells are widely used in voltammetry and stripping volammetry. Some microcells that were developed for other electrochemical methods of analysis are also included in this review since they are suitable in principle for the voltammetry and stripping voltammetry.

Designs of "non-flow" microcells can be classfied depending on the sample state in the cell:

(i) microcells with a static (motionless) sample;

(ii) microcells with forced convection of the sample;

(iii) microcells for bath injection of samples. These cells are designed for the analysis of groups of samples during a relatively short time. In such a microcell a sample during analysis can be in either the static state or in the forced-convection state. Therefore, such a cell can be classified as (iii) and (i) or (ii) types simultaneously.

2. Designs of microcells and their applications

2.1. Types of electrodes

We consider here only working electrodes and among them such important kinds as micro-, mercury-film and modified electrodes. Others electrodes will be considered in the analysis of cell design.

2.1.1. Working microelectrodes

Wightman and co-workers [57–59] pioneering work was the basis for the use of working micro- and submicroelectrodes in microcells [45–53]. The surface area of these microelectrodes is ~ 0.1 mm^2 but often it is 10^{-4}–10^{-3} mm^2. Microelectrodes have been fabricated from carbon paste [35, 60], carbon fiber of diameter 8–10 μm [45–47, 52], cylindrical graphite fiber of diameter 8 μm [50], Pt wire of diameter 10 μm [47], Au film of surface area 0.12–5.7 mm^2 [48], Pt film of surface area 4×10^{-3} mm^2 [53] and 0.1 mm^2 [49] and Cu, Ag and Pt wire of diameter of 25 μm [51]. Working solid microelectrodes can be plated with a mercury film (see below).

Advantages of the working microelectrodes are following [45–53]: (1) possiblility of the use of the extremely small sample volumes, down to the sub-microliter level; (2) decrease in the current capacity and the possibility of potential rapid scanning; (3) rapid reaching of the steady-state current; (4) high current density compared with that of the usual rotating disk electrode, which together with the better reproducibility and the simpler design of the microcell, allow the same or a shorter preconcentration time to be achieved in stripping voltammetric analysis as with a rotating disk electrode; (5) insignficant iR distortion allows the use of non-aqueous solvents and low concentrations of the supporting electrolyte, and as a consequence the effect of contamination is decreased, which is of particular importance in the stripping voltammetry; and (6) there is a possibility of combining the functions of auxiliary and reference electrodes in one electrode and electrolytic diaphragms can be excluded.

The drawback of working microelectrodes is the necessity to amplify a very small current. Therefore, the ratio of the analytical signal to noise is decreased and the detection limit is increased correspondingly. In order to decrease or to eliminate this drawback completely, the application of a microelectrode array is reasonable. The microelectrode array increases the analytical signal proportionally to the number of microelectrodes (with a sufficient distance between them). Although we do not know of the use of such kinds of microelectrodes in microcells, the recent development [61] of an iridium-based ultramicroelectrode array (without or plated with mercury) by microlithography is very promising for microcells.

2.1.2. *Working mercury-film electrodes*

There are two directions in the development of these electrodes: (1) the development of mercury-film electrodes for voltammetry that are ecologically sounder than the classical dropping mercury electrode (DME), while the advantages of the DME such as a high hydrogen overpotential and excellent reproductibilty have been retained and (2) the development of mercury-film electrodes for stripping voltammetry.

Mercury films that have been used in voltammetry (first direction) have a greater thickness. It has been shown that only in mercury films with thickness $\geqslant 10-25\ \mu m$ do the electrochemical properties of the film correspond to those of metallic mercury [62,63]. A mercury-film has been electrochemicaly plated and dissolved on a Pt microelectrode in the automatic regime imitating the DME [63].

In stripping voltammerty (second direction), very thin mercury films with a thickness of $\leqslant 1\ \mu m$ have been used. The films for stripping voltammetry are obtained either by preliminary electrochemical plating or in situ [64]. In stripping voltammetry on mercury-film electrodes including microcells [8,28,30,36,37,43,47,51], a lower detection limit and better reproducibility are achieved. In microcells, mercury-film working macroelectrodes have been prepared by the electrochemical plating of mercury on glassy carbon [8,28,30,43] and impregnated graphite [26,27,36,37] and for microelectrodes on carbon fiber [47], Cu, Au and Pt [51].

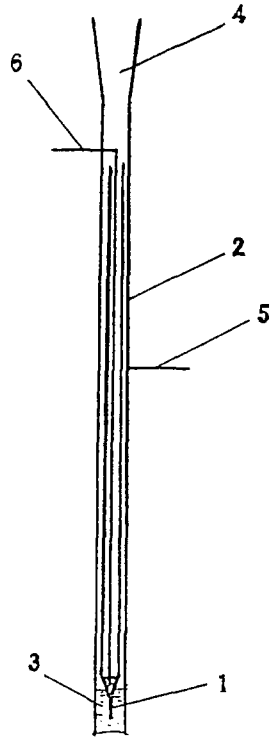

Fig. 1. Capillary microcell.

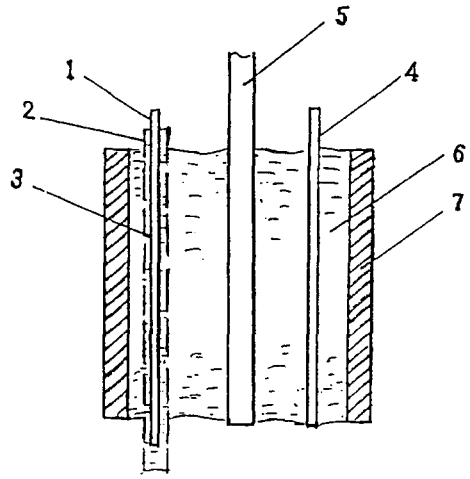

Fig. 2. Microcell with Nafion membrane.

Methods of preparation of mercury films have been considered in detail in many publications [2, 3, 65], so here newer work in this field is considered. The problem of the mercury-film regeneration to obtain a film in situ has been considered in connection with the formation of Hg_2Cl_2 [66]. To resolve this problem, the use of a supporting electrolyte containing a high concentration of NaSCN has been proposed [67]. The other technique for improving the regeneration of a mercury film in situ was developed by Lovrić and co-workers [68,69]. They first used a mercury film in situ, then the analysis was continued in situ but in a solution with an Hg^{2+} concentration ~ 100 times smaller. Frenzel [70] has shown that better adhesion of the mercury film takes place on the rough surface of a carbon electrode. Brainina et al. [71] proposed to add to the supporting electrolyte Zn^{2+} ions, which form adatoms on the electrode surface that improve the adhesion of the mercury film on the carbon

electrode. Ping Wu [72] showed that rapid scanning of the potential at the anodic stripping stage worsens the mercury-film structure.

2.1.3. Working modified electrodes

Modification of the working electrode surface can accelerate the electrode process and make it more selective. Application of physical, physicochemical and chemical activation of the working electrode surface has often been used in macrocells [73,74]. For microcells only a few examples of modification of the working electrode, by enzyme glutamate dehydrogenase [9], 7,7,8,8-tetracyanoquiodimethane [33], poly(vinylferrocene) [49,52] and poly(vinylpyridine) [52], are known.

2.2. Removal of dissolved oxygen

This aspect concerns all microcell types ((i–iii); see Introduction). In many cases, especially when using voltammetry with mercury and mercury-film working electrodes, the dissolved oxygen inferferes with the analysis. To accelerate the removal of the dissovled oxygen in voltammetry, Yarnitzky [75] sprayed the sample into the nitrogen compartment. In another study [22] a thin sample film was poured down the wall of a capillary tube in which nitrogen flows at the center. Baranski and co-workers [45,51] proposed to put the microcell in a special chamber through which an inert gas, saturated by the vapor of the corresponding solvent, passes. The time of the oxygen removal is ~5 min.

In anodic stripping voltammetry, the problem connected with dissolved oxygen is simplified since the dissolved oxygen does not influence the stage of metal preconcentration although it influences the anodic stripping stage [76,77]. For exclusion of this influence, an increase in the scanning rate during the anodic stripping stage was proposed by Wojciechowscki and Balcerzak [77]. The expedience of this approach is confirmed by the results of stripping voltammetric analysis in microcells [8,36,37,47,50]. At the same time, for greater accuracy, Baranski [47] took into account the background current in the presence of oxygen.

2.3. Microcells with static sample

The advantages of the use of a static sample are the possibility of decreasing the sample volume and applying a relatively simple design of microcell. The higher limit of detection [78] in comparision with that reached with microcells with forced convection of the sample [36,37] is a drawback to the static sample approach.

Two different working electrodes (in the usual and inverted states) are used in these cells.

2.3.1. Working electrode in the usual state

The working electrode in the usual state, that is, set from top to bottom, has been used in a number of microcells, e.g. Fig. 1 [50]. As the working electrodes, hanging mercury drop [16,17,22,31] and solid macro [15,18,19,30,44] and micro [35,50,60] electrodes have been applied.

The microcell [50] (Fig. 1) is sufficiently simple and is based on a two-electrode system. In Fig. 1, (1) is the cylindrical graphite fiber working microelectrode, (2) is the reference/auxiliary stainless-steel needle, (3) is the sample, (4) is the hole

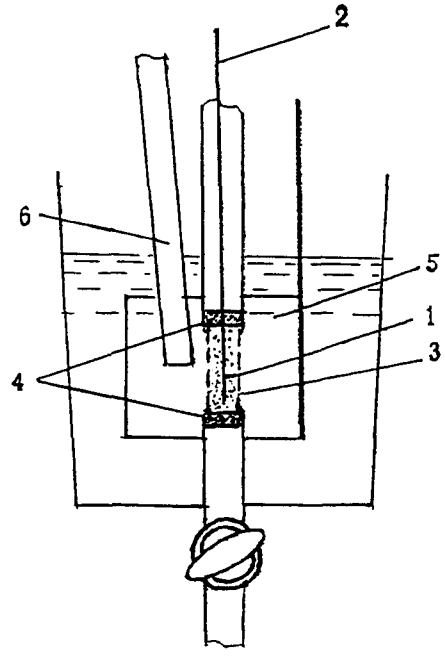

Fig. 3. Microcell with the packed graphite working electrode.

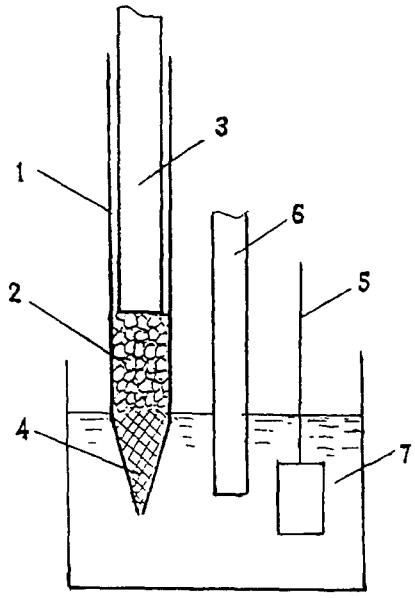

Fig. 4. Microcell with capillary packed-bed working electrode.

for the micropipette for aspirating/dislodging a sample, (5) is the reference/auxiliary electrode contact and (6) is the working electrode contact. In the case of the anodic stripping voltammetry, it has been recommended [50] to preplate the reference/auxiliary stainless-steel needle (2), with mercury. A two-electrode system of the catheter type has also been used in a microcell [60] but the electrodes were immersed in a supporting electrolyte in the outer compartment and this caused the undesirable dilution of a sample.

The possibility of using a very small sample volume ($\leqslant 1$ μl) in a microcell [44] (Fig. 2) has been

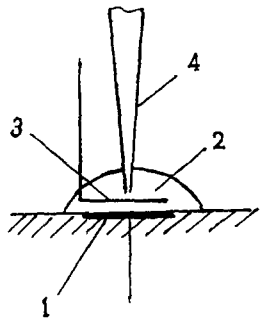

Fig. 5. Microcell with inverted working electrode.

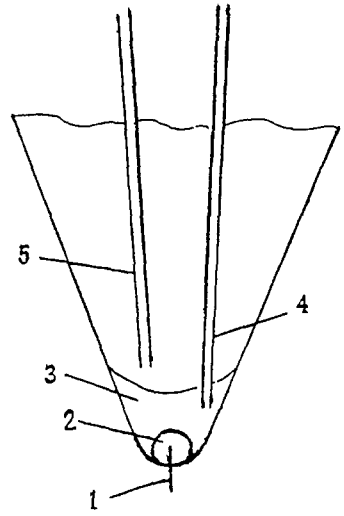

Fig. 6. Microcell with working mercury-drop electrode.

reported with the working microelectrode placed in a Nafion membrane tube. In Fig. 2 (1) is the working microelectrode (Au wire), (2) is the Nafion membrane tube, (3) is the sample, (4) is the auxiliary electrode (Au wire), (5) is the reference electrode, (6) is the supporting electrolyte and (7) is a Teflon tube. Sample (4) and supporting electrolyte (6) enter the microcell by the capillary action. Since cations diffuse through the Nafion membrane, only anions can be determined in the sample.

Microcells with the working solid electrode in the form of a packed bed [15, 18, 19] have been developed. In the cell (Fig. 3) [19], (1) is the packed-bed electrode in the form of powdered graphite, (2) is pencil lead for contact, (3) is a Vycor porous glass tube, (4) are cotton plugs, (5) is the platinum auxiliary electrode and (6) is the reference electrode. The sample and solvent for washing of

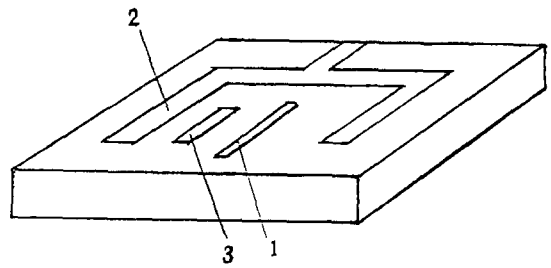

Fig. 7. Microcell with inverted microlithographicallly fabricated microelectrodes.

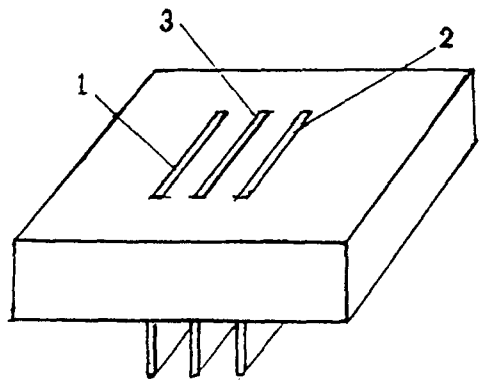

Fig. 8. Microcell with inverted metal foil microelectrodes in a multi-decker sandwich heat-sealing film.

tube (3) are removed by an aspirator. It is more efficient to use a microcell [15] with a packed-bed working electrode also but having a simpler design (Fig. 4). In Fig. 4, (1) is a glass capillary tube for the sample (10–40 μl), (2) is granular glassy carbon, (3) is pencil lead for contact, (4) is glass wool, (5) is the platinum auxiliary electrode, (6) is the reference electrode and (7) is the supporting electrolyte. The filling of the microcell with a sample was carried out by immersion of the tip in a sample solution. For emptying, the tip is touched to a tissue.

2.3.2. Working electrode in inverted state

This kind of solid working electrode, which is set from bottom to top, is illustrated in Fig. 5 [24]. The analogous state of the mercury working electrode is shown in Fig. 6 [42]. Working electrodes in the inverted state have been used in microcells more often than working electrodes in the usual state because of the possibility of applying a sample of smaller volume. Both macro [12,13,24,29,34,43] and micro [45–49,51,53] working electrodes in the inverted state have been used in microcells.

The first development of the working electrode in the inverted state by Iwamoto et al. [24] was based on the use of a Pt plate (Fig. 5). On the surface of the Pt plate (1), the sample drop (50 μl) (2) is placed. The Pt wire auxiliary electrode is in the form of a ring (3) and the tip (4) of the electrolytic bridge of the reference electrode is immersed in the sample drop. In the microcell (Fig. 5), a capillary with mercury as the working electrode that is directed upwards has also been used [24].

The cone form of the microcell with the mercury drop working electrode on the bottom of the cell is shown in Fig. 6 [42]. In Fig. 6, (1) is the Pt contact, (2) is the mercury drop of 5 μl volume, (3) is the sample of 10 μl volume, (4) is the capillary of the electrolytic bridge of the auxiliary and simultaneously of the reference electrode and (5) is the capillary for the inlet of nitrogen. In the microcell (Fig. 6), deaeration of the sample is carried out simultaneously with the pre-electrolysis (stripping voltammetry), but nitrogen is admitted higher than the sample level.

In microcells [48, 49, 53], all three electrodes (working, auxiliary and reference) have been inverted, which allowed a decrease in sample volume, e.g. down to sub-microliter levels [53]. In the microcells shown in (Fig. 7) [48, 49], the three-electrode system was fabricated by microlithography. In Fig. 7, (1) is the working microelectrode (Au [48], Pt [49]), (2) is the auxiliary microelectrode (Au [48], Pt [49]) and (3) is the reference microelectrode (Au [48], Ag/AgCl [49]). The sample volume is ~ 2 μl [48,49].

The microcell shown in (Fig. 8) [53] consists of three strips of metal foil in a multi-decker sandwich heat-sealing film. In Fig. 8, (1) is the working microelectrode (4 μm Pt foil) and (2) is the auxiliary microelectrode (100 μm Ag foil). This micro

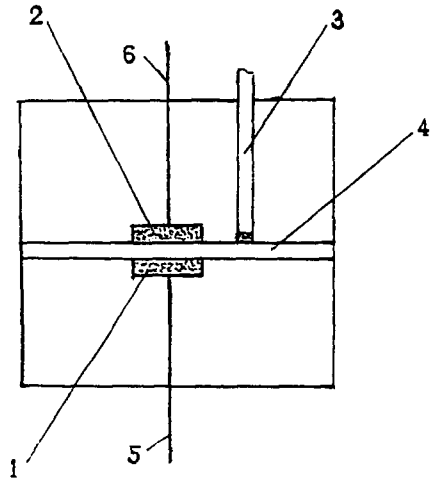

Fig. 9. Kissinger-type microcell for a static sample.

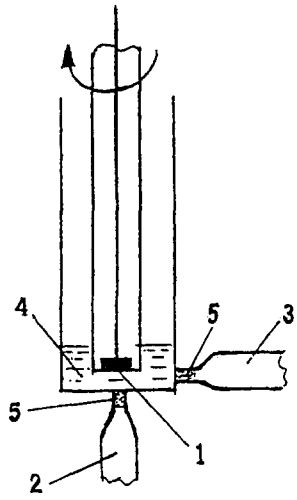

Fig. 10. Microcell with a working rotating disk electrode.

cell has a sample volume of 0.05–1.0 μl.

The use of a very small current in the microcells shown in Fig. 7 and 8 obviated the need to separate the electrode compartments by diaphragms.

2.3.3. Thin-layer microcells

In thin-layer electrochemical cells [79,80] which will be discussed below, both types of working electrodes (usual and inverted states) have been applied. In such microcells the sample is usually in the form of a very thin layer between the working and auxiliary electrodes. Although thin-layer microcells are applied for flow-through systems more often [54,55], there are also some thin-layer microcells [11,14,26,27,32,38,40,41] for a static sample that are of interest. There are thin-layer microcells [11,32] that are suitable for both flow and static samples which is advantgeous. A microcell similar to the Kissinger type [54] has been used [32] for static samples (Fig. 9). In Fig. 9, (1) is the carbon paste working electrode, (2) is the carbon paste auxiliary electrode, (3) is the electrolytic capillary of the reference electrode (Ag/AgCl), (4) is the sample layer (2–5 μl, but a 100 μl volume was used to wash and fill the microcell), (5) is the working electrode contact and (6) is the auxiliary electrode contact.

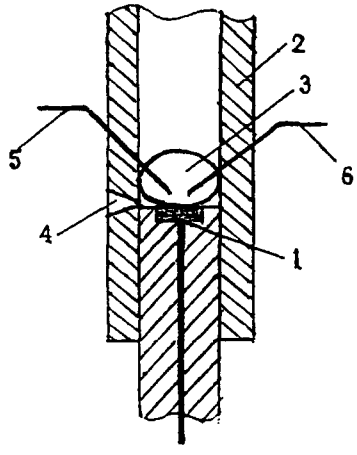

Fig. 11. Capillary microcell for the batch injection analysis.

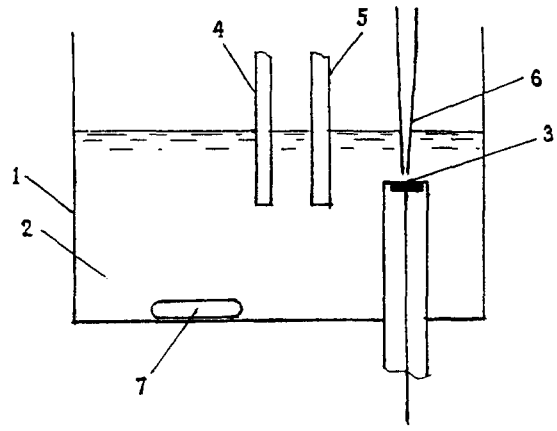

Fig. 12. Microcell with static working disk electrode for batch injection analysis

2.4. Microcells with forced convection of sample

In comparison with the static sample, in the case of forced-convection of the sample the diffusion of the analyte to the working electrode surface is accelerated and hence the analytical signal is increased and the detection limit decreased by about an order of magnitude [36,37]. In stripping voltammetry under the same conditions, the use of forced convection of a sample decreases the times of pre-electrolysis and of analysis.

Usually in non-flow microcells, forced convection was carried out in one of the following ways: rotation of the working electrode [5,20,21,28,36,

37], stirring of the sample by a magnetic stirrer [23], vibration pump [81] or rotation of the cell [82, 83]. In the case of the vibration pump [81], the fall of the mercury drop used as the working static merucry electrode was eliminated.

As the rotating working electrode, a disk electrode is usually used [84]. The rotating disk in microcells has been made from the one of following materials: glassy carbon without [5] and with a mercury film [28], Au [20], Pt [20,21] and impregnated graphite with a mercury film [36,37]. The sample volume is 0.5–4.0 ml [20,21,23] but the sample volume can be also decreased to 200 μl [28,36,37].

A microcell with a rotating disk working electrode is shown in Fig. 10 [28]: (1) is the rotating disk working electrode, (2) is the auxiliary electrode, (3) is the reference electrode and (4) is the sample. The auxiliary and reference electrodes are separated by electrolytic plugs (5) of porous ceramics.

It should be noted that forced convection has been successfully combined with hydrodynamic modulation [85–93]. Although this effect was applied in macrocells, it can also be used in microcells to decrease the influence of the current which is not connected with the diffusion of the analyte

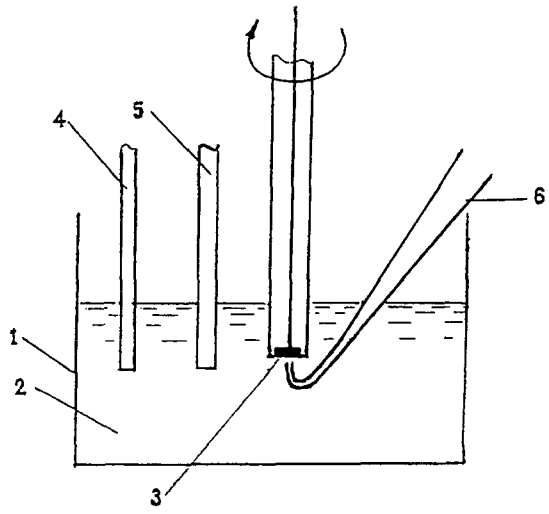

Fig. 13. Microcell with working rotating disk electrode for batch injection analysis.

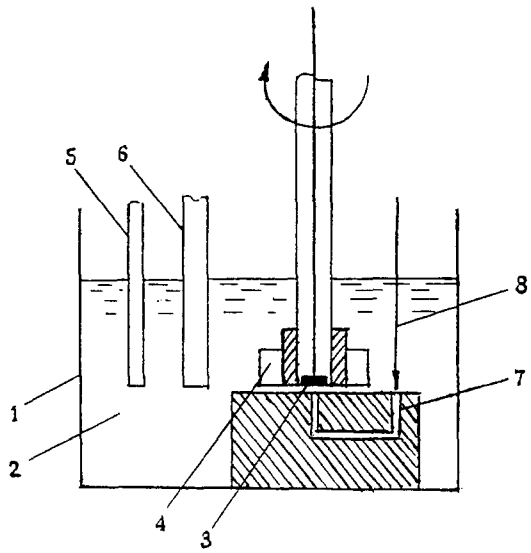

Fig. 14. Microcell with working rotating disk electrode with impeller for batch injection analysis.

to the working electrode surface. Hence it allows the detection limit to be decreased.

2.5. Microcells for batch injection of sample

In these microcells the working electrode can be in the usual state [5, 36, 37], but more often it is in the inverted state [6–10, 25, 94, 95].

The first microcell for voltammetric batch-injected analysis was proposed by Karolczak et al. [25]. This cell (Fig. 11) is distinguished by its exceptional simplicity. In Fig. 11, the working carbon paste electrode (1) in a Teflon sheath is put in a Teflon capillary (2). The sample (3) does not wet the Teflon and the carbon paste. The injection port (4) serves as an inlet for the sample (1–300 μl) by a micropipette and for sample removal by an aspirator without washing. The residuals are negligible (< 1%). The auxiliary electrode (5) is a platinum wire and (6) is the reference electrode in the form of a silver wire.

A different approach to batch injection analyses was developed by Wang and co-workers [5–8], Amine et al. [9] and Brett and co-workers [10,94,95]. The principle of the flow large-volume wall-jet cell developed by Gunasingham and co-workers [96–98] for liquid chromatography and

flow injection analysis has been used in microcells [5–10, 94, 95] for batch injection analysis. An example of such a microcell is shown in Fig. 12: (1) is a large compartment, (2) is a large volume of supporting electrolyte, (3) is the static working electrode (glassy carbon [8, 95], carbon paste [6] and modified carbon paste [9], Pt disk [9, 10, 94] and ion-selective electrodes [6, 7] have been used), (4) is the auxiliary electrode, (5) is the reference electrode, (6) is the micropipette tip for the inlet of a sample (10–100 μl) (for maximum sensitivity, the minimum sample volume of 14 μl is required at a fixed distance of the tip from the center of the working electrode (2–3 mm) [94]) and (7) is a magnetic stirring bar. The important advantage of this design and of the design with rotating working electrodes (see below) is the possibility of automatic removal of the sample. The latter, after contact with the surface of the working electrode, is washed by the large-volume of supporting electrolyte in compartment (1). Since considerable dilution of the sample takes place in this case, a large number of analyses can be carried out without replacing the supporting electrolyte in compartment (1). In the case of anodic stripping voltammetry [8], the magnetic stirring is switched off before the inlet of a sample and carrying out the pre-electrolysis and stripping stage. After the stripping stage the magnetic stirring is switched on again for cleaning of the working electrode.

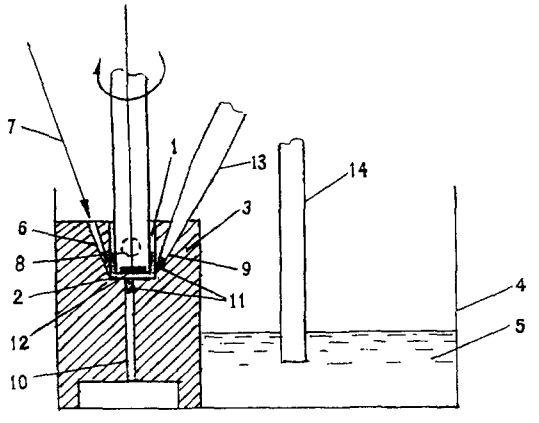

Fig. 15. Microcell with working rotating disk electrode for batch injection analysis.

A microcell with a rotating working electrode [5] has been used for batch injection voltammetric analysis. In this cell (Fig. 13), (1) is a large compartment, (2) is the large-volume supporting electrolyte, (3) is the rotating disk working electrode (glassy carbon), (4) is the auxiliary electrode, (5) is the reference electrode and (6) is the plastic tip for sample injection by micropipette.

A cell [99] with a rotating disk working electrode (Fig. 14) was used for macrosamples but it can also be applied for batch injection voltammetric microanalysis. In Fig. 14, (1) is the compartment, (2) is the supporting electrolyte, (3) is the rotating disk working electrode (glassy carbon), (4) is the impeller fixed to the shaft of the rotating electrode and rotating together with it, (5) is the auxiliary electrode, (6) is the reference electrode, (7) is the channel for internal circulation of electrolyte, and (8) is the micropipette for inserting the sample in channel (7). In the case of a working rotating disk electrode with an impeller, additional internal circulation of electrolyte occurs. The inlet sample is first moved down in channel (7) and then up to the working electrode surface. On contact of the sample with the electrode surface the analytical signal is generated. Such a system is analogous to the usual system for detection in flow injection analysis. However, the system [99] is different from the others in its simplicity and compactness. In comparison with the microcell in Fig. 13, in the microcell in Fig. 14 steadier movement of the sample to the working electrode surface and a more intensive hydrodynamic effect have been achieved [99].

We have seen that the microcell with a static working electrode (Fig. 12) was used for batch injection in anodic stripping voltammetry and this design did not allow the use of a rotating working electrode for stripping voltammetric analysis. At the same time, the design in Fig. 15 [36, 37] with the rotating disk working electrode in the microcell for batch injection in anodic stripping voltammetry decreased the detection limit by approximately an order of magnitude. In Fig. 15, (1) is the inner microcompartment, (2) is the sample (200–300 μl), (3) is the body of the microcompartment, (4) is the outer large compartment, (5) is the supporting electrolyte, (6) is the channel

Table 1
Use of microcells in analysis

Analyte	Sample volume, (μl)	Method	Ref.
Microcells with static sample and working electrode in the usual state			
Dopamine	10–40	Voltammetry	[15]
p-Nitrophenol, hydroquinone, *p*-phenylenediamine	2000	Chronopotentiometry	[19]
Acetaminophen, chlorpromazine, ascorbic acid	50	Voltammetry	[60]
Catecholamine epinephrine	10	Voltammetry	[50]
Pb(II), Cd(II)	10	Stripping voltammetry	[50]
Pb(II)	50–100	Stripping voltammetry	[31]
$Fe(CN)_6^{3+}$	0.25–1	Voltammetry	[44]
Microcells with static sample and working electrode in the inverted state			
Brain ascorbate	100	Chronoamperometry	[13]
Dopmaine, chlorpromazine, ferrocynaide	50	Voltammetry	[29]
Methyl viologen, thionine	250	Voltammetry	[34]
Ascorbic acid	25	Voltammetry	[49]
Ferrocene, *p*-nitrotoluene, anthraquione, ferri/ferrocynaide	0.05–1	Voltammetry	[53]
I, Zn(II)	50	Chronopotentiomentry	[24]
Hg(II), Pb(II)	5	Stripping voltammetry	[43]
Cu(II), Pb(II), Cd(II)	5	Stripping voltammetry	[45]
Pb(II), Cd(II)	5	Stripping voltammetry and potentiometry	[46, 47]
Br^-, S^{2-}, cysteineanion	10	Stripping voltammetry	[51]
Thin-layer microcells with static sample			
Chlorpromazine	23	Voltammetry	[11]
Adrenaline, noradrenaline, dopamine, dopa	1	Voltammetry	[14]
10-(3-Dimethylaminopropyl)-2-chlorphenothiazine hydrochloride	2–5	Voltammetry	[32]
Cu(II), Pb(II), Cd(II), Zn(II)	50–70	Stripping voltammetry	[26, 27]
Microcells with sample forced-convection			
Fe(III)	500–1000	Voltammetry	[20]
Pb(II), Cd(II)	200	Stripping voltammetry	[28]
Pb(II), Cd(II), Zn(II)	200	Stripping voltammetry	[36, 37]
Pb(II)	120	Stripping potentiometry	[82]
Cu(II), Pb(II)	400	Stripping potentiometry	[83]

Table 1 continued

Analyte	Sample volume, (μl)	Method	Ref.
Microcells for the batch injection of samples			
Caffeic acid, ferrocyanide	50–100	Chronoamperometry	[5]
Glucose, hydroquinone, ferrocyanide, Cl^-	20–50	Chronoamperometry, potentiometry	[6]
Products of enzymic reactions	30	Chronoamperometry	[9]
Ascorbic acid, ferrocyanide	10–100	Amperometry, voltammetry	[10]
Phenolic compounds	1–300	Voltammetry	[25]
Cl^-, F^-, pH	20	Potentiometry	[7]
Pb(II), Cd(II), Zn(II)	100–300	Stripping voltammetry	[8, 36, 37]
Cu(II), Pb(II), Cd(II), Zn(II)	10–100	Stripping voltammetry	[95]

for inlet of the sample, (7) is the micropipette for the injection of the sample, (8) is a channel for displacement of the sample and washing solution into the outer large compartment, (9) is a channel for the auxiliary electrode, (10) is a channel for electrolytic contact with the reference electrode, (11) are electrolyte plugs made of hardened ashless filter-paper or porous ceramic, (12) is the rotating disk working electrode, (13) is the auxiliary electrode and (14) is the reference electrode. The inner microcompartment is replaced with another that enables one to work with different volumes of samples and working electrode sizes.

Recently, Brett et al. [95] have shown that the detection limit in anodic stripping voltammetry using microcells with batch injection analysis can be significantly decreased with employment of a static working electrode also. The microcell of the type in Fig. 12 was used but instead of a manual micropipette a programmable motorized electronic micropipette was applied [95] (see also [94]). The choice of the optimal sample dispensing rate allowed the maximum hydrodynamic well-jet effect to be obtained [94,95,100] and hence a significant increase in the analytical signal. This also ensured the complete displacement of the analyte sample with a new sample without the use of a mixer (Fig. 12).

The application of all the microcells considered above is surveyed in Table 1. Microcells have been used for the analysis of both organic and inorganic substances. Microcells with a static sample and the working electrode in the inverted state have a number advantages in the simplicity of design and the very low sample volume. In this respect, such microcells with microeletrodes fabricated by microlithography are especially promising. Microcells for batch injection analysis accelerate the analysis (to 30–60 and more samples per hour) and facilitate complete automation. These microcells with forced-convection of the sample (rotating working electrode [36,37] or wall-jet effect [95]) have permitted the batch injection stripping voltammetric anaysis of metal traces with nanomolar detection limits.

Acknowledgement

The author expresses his gratitude to Dr. I. Kuselman for valuable discussions.

References

[1] J.N Berisci, P.J. Riley and G.G. Wallace, in M.R. Smyth and J.G. Vos (Eds.), Wilson and Wilson's Comprehensive Analytical Chemistry, Vol 27, Analytical Voltammetry, Elsevier, Amsterdam, 1992, pp. 71–113.
[2] J. Wang, Stripping Analysis, VCH, Deerfield Beach, FL, 1985.
[3] Kh. Z. Brainina, E. Ya. Neiman and V.V. Slepushkin, Inversion Electroanalitical Methods, Khimiya, Moscow, 1988.
[4] H.A. Laitinen and W.E. Harris, Chemical Analysis, Khimiya, Moscow, 2nd edn., 1979, pp. 282–308, 444–462.
[5] L. Chen, J. Wang and L. Angnes, Electroanalysis, 3 (1991) 773.
[6] J. Wang and Z. Taha, Anal. Chem., 63 (1991) 1053.
[7] J. Wang and Z. Taha, Anal. Chim. Acta, 252 (1991) 215.
[8] J. Wang, J. Lu and L. Chen, Anal. Chim. Acta, 259 (1992) 123.
[9] A. Amine, J.-M. Kauffmann and G. Palleshi, Anal. Chim. Acta, 273 (1993) 213.
[10] C.M.A. Brett, A.M.O. Brett and L.C. Mitoseriu, Anal. Chem., 66 (1994) 3145.
[11] T.B. Jarbawi, W.R. Heineman and G.J. Patriarche, Anal. Chim. Acta, 126 (1981) 57.
[12] C. Banissi-Sabourdy, B. Planques, J.-P. David, C. Jeannin, M. Potel, A. Bizien, C. Di Menza, J. Brugere-Picoux, H. Brugere, J. Chatelain and R. Buvet, Bioelectrochem. Bioenerg., 28 (1992) 127.
[13] J.O. Schenk, E. Miller and R.N. Adams, Anal. Chem., 54 (1982) 1452.
[14] R.R. Fike and D.J. Curran, Anal. Chem., 49, (1977), 1205.
[15] J.L. Messner and R.C. Engstrom, Anal. Chem., 53 (1981) 128.
[16] L. Ješovsky, Chem. Tech. (Leipzig), 13 (1961) 519.
[17] W.L. Underkofler and I. Shain, Anal. Chem., 33 (1961) 1966.
[18] J.H. Strohl and T.A. Polutanovich, Anal. Lett., 2 (1969) 423.
[19] R.L. Bamberger and J.H Strohl, Anal. Chem., 41 (1969) 1450.
[20] B. Miller and S. Bruckenstein, Anal. Chem., 46 (1974) 2033.
[21] P.N. Bartlett and R.G. Whitaker, Anal. Chem., 61 (1989) 2803.
[22] C.N. Yarnitzky, Electroanalysis, 2, (1990), 581.
[23] Electrochemical Accessories, Catalog, Princton Applied Research, Princeton, N.J., 1991, p. E2.
[24] R.T. Iwamoto, R.N. Adams and H. Lott, Anal. Chim. Acta, 20 (1959) 84.
[25] M. Karolczak, R. Dreiling, R.N. Adams, L.J. Felice and P.T. Kissinger, Anal. Lett., 9 (1976) 783.
[26] T.P. De Angelis and W.R. Heineman, Anal. Chem., 48 (1976) 2262.
[27] T.P. De Angelis, R.E. Bond, E.E. Brooks and W.R. Heineman, Anal. Chem., 49 (1977) 1792.
[28] R. Eggli, Anal. Chim. Acta, 91 (1977) 129.
[29] J. Wang and B.A. Frelha, Anal. Chem., 54 (1982) 334.
[30] T. Miwa, Y. Nishimura and A. Mizuike, Anal. Chim. Acta, 140 (1982) 59.
[31] X. Yu and L. Yang, Fenxi Huaxue, 15, (1987) 756; Chem. Abstr., 108 (1988) 123616m.
[32] G. Farsang and T. Dankhazi, Anal. Lett., 22, (1989), 1305.
[33] J. Kulys and E.J. D'Costa, Anal. Chim. Acta, 243 (1991) 173.
[34] E.T. Smith and M.W.W. Adams, Anal. Biochem., 207 (1992) 94.
[35] Electochemical Products and Services, Catlog, Bioanalytical Systems, West Lafayette, IN, 1993, p.22.
[36] Ya. I. Tur'yan, E.M. Strochkova, I. Kuselman and A. Shenhar, Isr. Pat. Appl. No. 112018 (1994).
[37] Ya. I. Tur'yan, E.M. Strochkova, I. Kuselman and A. Shenhar, Fresenius' J. Anal. Chem., 354 (1996) 410.
[38] D.M. Oglesby, S.H. Omang and C.N. Reilley, Anal. Chem., 37 (1965) 1312.
[39] D.M. Oglesby. L.B. Anderson, B. McDuffie and C.N. Reilley, Anal. Chem., 37 (1965) 1317.
[40] A.T. Hubbard and F.C. Anson, Anal. Chem., 40 (1968) 615.
[41] A. Yildiz, P.T. Kissinger and C.N. Reilley, Anal. Chem., 40 (1968) 1018.
[42] L. Huderová and K. Štulik, Talanta, 19 (1972) 1285.
[43] K. Štulik and M. Štulikova, Anal. Lett., 6 (1973) 441.
[44] J. Čaja, A. Czerwinski and H.B. Mark, Jr., Anal. Chem., 51 (1979) 1328.
[45] A.S. Baranski and H. Quon, Anal. Chem., 58, (1986), 407.
[46] W. Frenzel, Anal. Chim. Acta, 196, (1987), 141.
[47] A.S. Baranski, Anal. Chem., 59, (1987), 662.
[48] M. Morita, M.L. Longmire and R.W. Murray, Anal. Chem., 60 (1988) 2770.
[49] M. Koudelka and C.G. Francis, Anal. Chim. Acta, 219 (1989) 45.
[50] M. Wojciechowski and J. Balcerzak, Anal. Chim. Acta, 237 (1990) 127.
[51] A.R. Harman and A.S. Baranski, Anal. Chim. Acta, 239 (1990) 35.
[52] C.-L. Wang, K.E. Creasy and B.R. Shaw, J. Electroanal. Chem., 300 (1991) 365.
[53] W.J. Bowyer, M.E. Clark and J.L. Ingram, Anal. Chem., 64 (1992) 459.

[54] P.T. Kissinger, in P.T. Kissinger and W.R. Heineman (Eds.), Laboratory Techniques in electroanalytical Chemistry, Marcel Dekker, New York, 1984, pp. 611–635.
[55] H. Gunasingham and B. Fleet, in A.J. Bard (Ed.) Electroanalytical Chemistry, Vol. 16, Marcel Dekker, New York, 1989, pp. 89–180.
[56] M.D. Luque de Castro and A. Izquierdo, Electroanalysis, 3 (1991) 457.
[57] M.A. Dayton, J.C. Brown, K.J. Stutts and R.M. Wightman, Anal. Chem., 52 (1980) 946.
[58] R.M. Wightman, Anal. Chem., 53 (1981) 1125A.
[59] M.A. Dayton, A.G. Ewing and R.M. Wightman, J. Electroanal. Chem., 146 (1983) 189.
[60] J. Wang, L.D. Hutchins, S. Selim and L.B. Cumming, Talanta, 30 (1983) 121.
[61] S.P. Kounaves, W. Deng, P.R. Hallock, G.T.A. Kovacs and C.W. Storment, Anal. Chem., 66 (1994) 418.
[62] Z. Yashida, Bull. Chem. Soc. Jpn. 54 (1981) 562.
[63] D.A. Khosroeva, Ya. I. Tur'yan and H.K. Strizov, Zh. Anal. Khim., 47 (1992) 1289.
[64] T.M. Florence, J. Electroanal. Chem., 27 (1970) 273.
[65] T.M. Florence, Analyst, 111 (1986) 489.
[66] B.K. Filanovski, M.A. Sokolov and L.A. Butirskaya, Zh. Anal. Khim., 42 (1987) 1820.
[67] T.G. Zupko, Ya. I. Tur'yan, Z.A. Temerdashev, I. Ya. Tur'yan and L.M. Maluka, Zh. Anal. Khim., 48 (1993) 1947.
[68] M. Mlaker and M. Lovrić, Analyst, 115 (1990) 45.
[69] D. Omanovic, Z. Pebarec, T. Magjer, M. Lovrić and M. Branica, Electroanalysis, 6 (1994) 1029.
[70] W. Frenzel, Anal. Chim. Acta, 273 (1993) 123.
[71] Kh. Z. Brainina, E.A. Vilchinskaya and R.M. Khanina, Analyst, 115 (1990) 1301.
[72] H. Ping Wu, Anal. Chem., 66 (1994) 3151.
[73] K. Štulik, Electroanalysis, 4 (1992) 829.
[74] J. Wang, in D. Littlejohn and D.T. Burns (Eds.), Reviews on Analytical Chemistry–Euroanalysis VIII, Royal Society of Chemistry, Cambridge, 1994, pp. 291–297.
[75] C.N. Yarnitzky, Anal. Chem., 57 (1985) 2011.
[76] A.R. Fernando and J.A. Plambeck, Anal. Chem., 61 (1989) 2609.
[77] M. Wojciechowski and J. Balcerzak, Anal. Chem., 62 (1990) 1325.
[78] I. Kuselman and A. Shenhar, Anal. Chim. Acta, 306 (1995) 301.
[79] C.N. Reilley, Rev. Pure Appl. Chem., 18 (1968) 137.
[80] A.T. Hubbard and D.G. Peters, Crit. Rev. Anal. Chem., No. 3 (1973) 201.
[81] C.N. Yarnitzky, Electroanalysis, 1 (1989) 327.
[82] D. Jagner, L. Renman and Y. Wang, Electroanalysis, 5 (1993) 283.
[83] D. Jagner, E. Shalin, B. Axelsson and R. Ratanda-Ohpas, Anal. Chim. Acta, 278 (1993) 237.
[84] F. Opekar and P. Beran, J. Electroanal. Chem., 69 (1976) 1.
[85] B. Miller, M.I. Bellavance and S. Bruckenstein, Anal. Chem., 44 (1972) 1983.
[86] B. Miller and S. Bruckenstein, Anal. Chem., 46 (1974) 2026.
[87] W.J. Blaedel and R.C. Engstrom, Anal. Chem., 50 (1978) 476.
[88] J.M. Rosamilia and B. Miller, Anal. Chem., 55 (1983) 1142.
[89] B. Miller and J.M. Rosamilia, Anal. Chem., 55 (1983) 1261.
[90] D.S. Austin, D.C. Johnson, T.G. Hines and E.T. Berti, Anal. Chem., 55 (1983) 2222.
[91] J.M. Rosamilia and B. Miller, Anal. Chem., 56 (1984) 2410.
[92] S.A. Schuette and R.L. McCreery, Anal. Chem., 58 (1986) 1778.
[93] S.A. Schuette and R.L. McCreery, Anal. Chem., 59 (1987) 2692.
[94] C.M.A. Brett, A.M.O. Brett and L.C. Mitoseriu, Electroanalysis, 7 (1995) 225.
[95] C.M.A. Brett, A.M.O. Brett and L. Tugula, Anal. Chim. Acta, 322 (1996) 151.
[96] H. Gunasingham, Anal. Chim. Acta, 159 (1984) 139.
[97] H. Gunasingham, B.T. Tay, K.P. Ang and L.L. Koh, J. Chromatogr. 285 (1984) 103.
[98] H. Gunasingham, B.T. Tay and K.P. Ang, Anal. Chem., 56 (1984) 2422.
[99] Ya. I. Tur'yan, E.M. Strochkova, L.I. Kuselman and A. Shenhar, J. Electroanal. Chem., in press.
[100] J. Yamada and H. Matsuda, J. Electroanal. Chem., 44 (1973) 189.

ELSEVIER

Talanta 44 (1997) 15–22

Talanta

Silica-immobilized formylsalicylic acid as a selective phase for the extraction of iron(III)

Mohamed E. Mahmoud[a], Ezzat M. Soliman[b]

[a]*Chemistry Department, Faculty of Science, Alexandria University, P.O. Box 426, Ibrahimia, Alexandria 21321, Egypt*
[b]*Chemistry Department, Faculty of Science, El-Minia University, El-Minia, Eqypt*

Received 8 January 1996; revised 9 April 1996; accepted 10 April 1996

Abstract

The immobilization of formylsalicylic acid compounds on the surface of amino group-containing silica gel phases is described. The resulting phases were tested for the extraction of iron(III) and showed an exchange capacity of 0.95–0.96 mmol g^{-1}. The other metal ions tested showed lower metal capacity values than iron(III). The selectivity of the phases tested for the extraction of iron(III) from a mixture containing several other metal ions was evaluated using atomic absorption spectrometry. A method for the recycling of immobilized silica gel after metal extraction is described for practical applications.

Keywords: Iron(III) extraction; Silica-immobilized formylsalicylic acid

1. Introduction

Immobilization and cross-linking of organic compounds with certain functional groups on the surface of silica gel has gained importance in different research and industrial fields [1–13]. However, irreversible binding of the metal ions and lack of selectivity are the main disadvantages of some of the silica gel-bound ligands reported [9,14]. The development of highly selective and high-affinity chelating phases is based on the selection of donor atoms employed in selective metal ion binding. Examples of such immobilized phases are the use of crown ether derivatives for the selective extraction and preconcentration of some cations such as alkali and alkaline earth metal ions [15,16]. Another example is the selection and immobilization of thioaniline derivatives on the surface of silica gel for application as a selective sorbent for the separation and preconcentration of Pd(II) from large quantities of Rh(II) and Ir(II) [17]. Iron is an essential metal and is used for the treatment of anaemia, but excessive intake or overdosing requires a selective analytical method or medication for metal treatment. Deferrioxamine B is a naturally occurring trihydroxamic acid which shows a high affinity and selectivity for iron(III), leading to its use in the treatment of iron overload in Couley's anaemia [18,19].

PII S0039-9140(96)01960-1

Formylsalicylic acid derivatives have been reported to form stable metal complexes with different metal ions in the solid state [20,21]. Moreover, the iron(III)–salicylic acid complex formed in solution showed higher sensitivity than other iron(III) complexes with phenolic compounds [22]. The immobilization of formylsalicylic acid has not been reported previously, and in this work we immobilized 3- and 5-formylsalicylic acid ($C_8H_6O_4$) on the surface of silica gel by a direct chemical reaction of the amino group-containing silica gel phase and the aldehyde group of formylsalicylic acid, in order to evaluate their performance in the extraction of different metal ions, and with the anticipation of such a phase being selective for the extraction and preconcentration of iron(III).

2. Experimental

2.1. Materials and solvents

The silica gel used was of TLC grade with a 70–230 mesh size and 60 Å pore diameter, purchased from Woelm Pharma (Eschwege, Germany). 3-Aminopropyltrimethoxysilane, 3-chloropropyltrimethoxysilane and ethylenediamine were purchased from Aldrich (Milwaukee, WI, USA). Organic solvents were dried according to literature methods. 3-Formylsalicylic acid and 5-formylsalicylic acid were synthesized according to the literature [23,24].

2.2. Synthesis of silica gel-bound amines

For the synthesis of silica gel-bound amines, the silica gel particles were first activated by refluxing with concentrated hydrochloric acid for 4 h, filtered off and washed with doubly distilled water several times until acid-free and dried in an oven for 6 h. A 20 g amount of the dry silica gel was transferred into a round-bottomed flask, then 150 ml of dry toluene were added followed by 20 ml of 3-aminopropyltrimethoxysilane (or 3-chloropropyltrimethoxysilane) and refluxed overnight. The silica gel-bound amino or chloro derivative was filtered off, washed with toluene, ethanol and diethyl ether and dried at 60°C for 6 h. The product was silica gel-bound 3-aminopropyl phase (SGBAP) or 3-chloropropyl phase (SGBCP). A 20 g amount of SGBCP was suspended in 100 ml of dry toluene and 20 ml of ethylenediamine were added to the suspension and refluxed for 12 h. The amine derivative was filtered off, washed with toluene, ethanol and diethyl ether and dried in an oven at 60°C for 6 h. The product was silica gel-bound ethylenediamine (SGBEDA).

2.3. Synthesis of silica gel-bound formylsalicylic acid (SGBFSA)

For the synthesis of silica gel-bound formylsalicylic acid, 1.8 g of 3- or 5-formylsalicylic acid was dissolved by heating in 150 ml of dry toluene, then 10 g of SGBAP or SGBEDA were added to the solution. The mixture was reflexed for 2 h, left to cool, filtered, washed with toluene, ethanol and diethyl ether and dried under vacuum at 80°C for 5 h. The synthetic route to the silica gel-immobilized formylsalicylic acid phases is illustrated in Scheme 1.

2.4. Metal capacity of bonded phases

The capacity of the modified phases for the extraction of different metal ions from aqueous solution was determined in triplicate by the batch equilibrium technique. Typically, 100 mg of the silica gel phase were equilibrated with 1.0 ml of 0.1 M metal ion solution and 9 ml of acetate buffer solution in a 50 ml volumetric flask and automatically shaken for 30 min at room temperature. After equilibration, the mixture was filtered and washed with 50 ml of doubly distilled water and the unextracted metal ion was determined by EDTA titration using the buffer and indicator appropriate for each ion.

2.5. Iron selectivity measurement

To 100 mg of the immobilized silica gel phases, 10 ml of bufferd mixture (pH 5.5) containing eight metal ions, viz. Fe(III), Mg(II), Mn(II), Co(II), Ni(II), Cu(II), Zn(II) and Cd(II), approximately 500 ppm each, were added and automati-

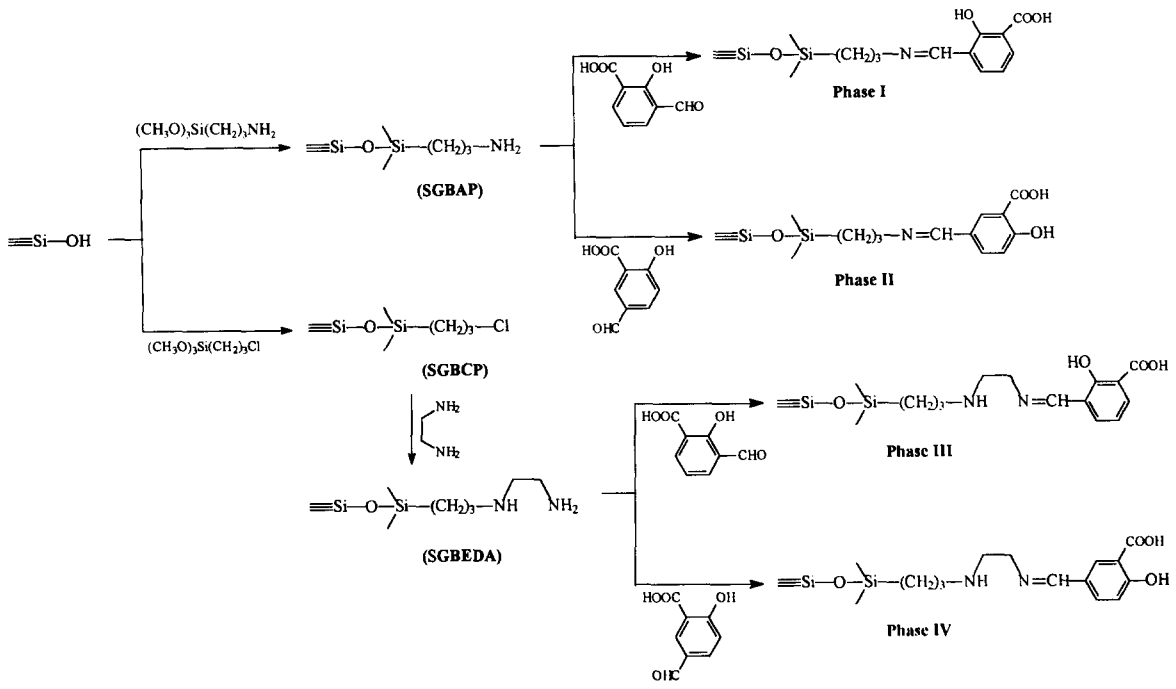

Scheme 1. Synthetic routes to phases I–IV.

cally shaken for 30 min. After equilibration, the extracted metal ions on the surface of silica gel were filtered off and washed with 20 ml of doubly distilled water. The filtrate and washings were quantitatively transferred into a 50 ml volumetric flask and diluted to volume with doubly distilled water. A standard solution containing the same metal ions were also prepared for quantitative evaluation. The sample mixtures and the standard solution were subjected to atomic absorption spectrometry at the wavelength appropriate for the metal ion under investigation.

2.6. Recycling procedure

Recycling of the immobilized phases after first use for metal extraction was carried out by treatment of the phase–Fe(III) complex with an excess (100 ml) of 0.1 M EDTA solution [25]. The mixture was automatically shaken for 30 min, filtered, washed with 25 ml of 0.1 M EDTA and 100 ml of doubly distilled water and dried in an oven at 80°C and used for a second metal ion extraction.

2.7. Apparatus

IR spectra of the immobilized phases were obtained from KBr pellets by using a Perkin-Elmer Model 1430 ratio-recording spectrometer. pH measurements were carried out by using a Schott Geräte pH meter, which was calibrated against two standard buffer solutions of pH 4.0 and 9.2. Atomic absorption spectrometry was performed with a Perkin-Elmer Model 2380 atomic absorption spectrometer at the appropriate wavelength for each metal ion tested.

3. Results and discussion

3.1. Characterization of the bonded phases

The immobilization of formylsalicylic acid on the surface of silica gel modified with two amine derivatives was confirmed by IR analysis. Comparison of the band assignments listed in Table 1 indicates that formylsalicylic acid is covalently

bonded to the silica gel amino group through Schiff base bond formation, characterized by the presence of a new band at 1530–1580 cm^{-1} corresponding to $\nu_{C=N}$ of all the phases studied. In addition, the ν_{NH_2} band present in silica gel-modified amine derivatives is absent in the IR spectra of phases I–IV owing to the participation of the amino group in the Schiff base formation. The characteristic $\nu_{C=O}$ band at 1600–1700 cm^{-1} in the four phases I–IV is further evidence of the presence of a carbonyl group in the structure of the immobilized phases I–IV, which is direct evidence for the presence of a carboxylic moiety. The total amount of formylsalicylic acid immobilized on the silica surface was determined according to the iron(III) probe method [26,27] and found to be 0.95 ± 0.01 mmol g^{-1} of the synthesized phases I–IV.

Table 1
Infrared spectral data for the immobilized phases

Bonded phase	IR band (cm^{-1})	Band assignment
SGBAP	3410, 3390	$\nu(NH_2)$
	2890	ν(C–H) aliphatic
	<1400	ν(Si–O)
SGBEDA	3455	ν(N–H)
	3415, 3385	$\nu(NH_2)$
	2890	ν(C–H) aliphatic
	<1400	ν(Si–O)
I	3650	ν(O–H)
	1653	ν(C=O)
	1560	ν(C=N)
	<1400	ν(Si–O)
II	3655	ν(O–H)
	1652	ν(C=O)
	1577	ν(C=N)
	<1400	ν(Si–O)
III	3660	ν(O–H)
	3453	ν(N–H)
	1645	ν(C=O)
	1534	ν(C=N)
	<1400	ν(Si–O)
IV	3667	ν(O–H)
	3431	ν(N–H)
	1645	ν(C=O)
	1534	ν(C=N)
	<1400	ν(Si–O)

3.2. Metal capacity in different buffer solutions

The metal capacity values, expressed in mmol g^{-1} of phases I–IV and determined in different buffer solutions, are given in Table 2. These values are the averages of three measurements and the relative standard deviations were found to be in the range 0.00–0.05% for $n = 3$. The Mg(II) metal capacity values are low at lower pH solutions, but slightly increase with increase in the pH of the metal ion solution. The maximum Mg(II) metal capacity value was found to be in the range 0.10–0.22 mmol g^{-1} in buffer solutions of pH 5–6. Zn(II) was found to behave similarly, the maximum capacity for Zn(II) being in the same range as for Mg(II) under the same buffering conditions. One can conclude from the metal capacity values of both Mg(II) and Zn(II) that phases I–IV have little affinity for these metal ions.

Cd(II) and Pb(II) were also found to show little tendency towards extraction and binding by immobilized phases I–IV. The metal capacity values for these ions lie in the range 0.12–0.20 mmol g^{-1}, determined in higher pH solution. In the same manner, Co(II) and Ni(II) showed metal capacity values in the range 0.12–0.29 mmol g^{-1}. The difference between Co(II) and Ni(II) is that the higher metal capacity value for Co(II) is determined in low pH solutions (pH 3–4), whereas that of Ni(II) is determined in higher pH solution (pH 5–6).

There is no or little contribution of the ethylenediamine moiety in phases III and IV, which may be attributed to the position of the active chelating sites on the surface (OH and COOH) if compared with the position of the ethylenediamine moiety away from the surface.

The maximum metal capacity value of Cu(II) showed a dramatic increase from 0.45 mmol g^{-1} for phase II to a maximum of 0.78 mmol g^{-1} for phase I (Table 2). The basic difference between these two phases is the position of the nitrogen atom, which is in the *ortho* position in the case of phase I and in the *para* position in the case of phase II. This situation may assist the chelation of Cu(II) by the nitrogen atom [21] in phase I, leading to an increase in the metal capacity. The

Table 2
Metal capacity in mmol g^{-1} of phases I–IV in different buffer solutions[a]

Metal ion	pH	Metal capacity (mmol g^{-1})			
		Phase I	Phase II	Phase III	Phase IV
Mg(II)	2.0	0.04	0.04	0.12	0.04
	3.1	0.05	0.06	0.16	0.08
	4.0	0.06	0.08	0.18	0.21
	5.0	0.08	0.10[b]	0.19[b]	0.22[b]
	6.0	0.12[b]	0.08	0.12	0.08
Fe(III)	1.6	0.10	0.04	0.02	0.10
	2.6	0.12	0.06	0.08	0.20
	3.7	0.14	0.12	0.12	0.34
	4.5	0.50	0.45	0.38	0.70
	5.5	0.96[b]	0.95[b]	0.95[b]	0.96[b]
Co(II)	2.0	0.18	0.12	0.02	0.10
	3.1	0.22	0.20[b]	0.08	0.16
	4.0	0.25[b]	0.18	0.22[b]	0.29[b]
	5.0	0.10	0.16	0.20	0.16
	6.0	0.16	0.10	0.12	0.14
Ni(II)	2.0	0.02	0.08	0.14	0.10
	3.1	0.04	0.04	0.12	0.09
	4.0	0.06	0.14	0.10	0.08
	5.0	0.08	0.16[b]	0.14	0.23[b]
	6.0	0.12[b]	0.06	0.22[b]	0.12
Cu(II)	2.0	0.04	0.02	0.02	0.04
	3.1	0.10	0.03	0.16	0.06
	4.0	0.25	0.06	0.24	0.09
	5.0	0.70	0.45[b]	0.36	0.12
	6.0	0.78[b]	0.30	0.44[b]	0.25[b]
Cd(II)	2.0	0.12	0.10	0.02	0.01
	3.1	0.13	0.06	0.06	0.04
	4.0	0.14	0.08	0.10	0.10
	5.0	0.15[b]	0.12[b]	0.16[b]	0.12[b]
	6.0	0.12	0.04	0.08	0.08
Pb(II)	2.0	0.04	0.04	0.04	0.02
	3.1	0.10	0.07	0.06	0.07
	4.0	0.11	0.14	0.11	0.09
	5.0	0.12	0.18[b]	0.16	0.16[b]
	6.0	0.15[b]	0.06	0.20[b]	0.12

[a] The relative standard deviations are in the range 0.00–0.05% for $n = 3$.
[b] Maximum metal capacity values.

same trend is also evident when comparing phases III and IV. This assumption of nitrogen participation in Cu(II) binding may help in designing new selective phases for Cu(II) extraction and preconcentration.

Finally, Fe(III) was found to be the only metal ion highly extracted by all four immobilized phases I–IV. The metal capacity values of Fe(III) are all above 0.95 mmol g^{-1}, which is indicative of the higher selectivity of these phases towards Fe(III). The reason for such high selectivity is mainly based on the presence of two chelating oxygen atoms, one of which is a carboxylic [22] in all phases tesed. Comparison of the metal capac-

Table 3
Metal capacity (mmol g^{-1}) with different shaking times (min) and at selected optimum buffer conditions

Metal ion	pH	Shaking time (min)	Metal capacity (mmol g^{-1})[a]			
			Phase I	Phase II	Phase III	Phase IV
Fe(III)	5.5 for I–IV	30	0.96	0.95	0.95	0.96
		20	0.92 (96.0)	0.75 (79.0)	0.80 (84.0)	0.90 (94.0)
		10	0.90 (94.0)	0.72 (76.0)	0.70 (74.0)	0.84 (88.0)
		5	0.86 (90.0)	0.65 (68.0)	0.64 (67.0)	0.72 (73.0)
		2	0.70 (73.0)	0.62 (65.0)	0.63 (66.0)	0.64 (67.0)
Co(II)	3.1 for II, 4.0 for I, III and IV	30	0.25	0.20	0.22	0.29
		20	0.18	0.18	0.18	0.20
		10	0.16	0.15	0.10	0.16
		5	0.12	0.09	0.08	0.10
		2	0.10	0.05	0.03	0.08
Ni(II)	5.0 for II and IV, 6.0 for I and III	30	0.12	0.16	0.22	0.23
		20	0.12	0.15	0.18	0.20
		10	0.12	0.11	0.10	0.12
		5	0.10	0.09	0.08	0.11
		2	0.09	0.08	0.07	0.10
Cu(II)	5.0 for II, 6.0 for I, III and IV	30	0.78	0.45	0.44	0.25
		20	0.75	0.39	0.32	0.20
		10	0.71	0.30	0.26	0.16
		5	0.69	0.20	0.24	0.15
		2	0.68	0.15	0.20	0.14
Cd(II)	5.0 for I–IV	30	0.15	0.12	0.16	0.12
		20	0.15	0.12	0.12	0.10
		10	0.14	0.10	0.09	0.08
		5	0.11	0.08	0.05	0.07
		2	0.09	0.07	0.03	0.06
Pb(II)	5.0 for II and IV, 6.0 for I and III	30	0.15	0.18	0.20	0.16
		20	0.14	0.16	0.16	0.13
		10	0.10	0.13	0.10	0.10
		5	0.07	0.09	0.08	0.08
		2	0.06	0.06	0.07	0.07

[a] Values in parantheses are the percentage extraction relative to the values at 30 min.

ity values of Fe(III) in Table 2 with those found in the literature [6,8,17] reveals a superior selectivity for the extraction of Fe(III) by the immobilized silica gel phases containing 3- or 5-formylsalicylic acid.

3.3. Metal capacity at different shaking times

The shaking time is an important factor in determining the possibility of application of the immobilized phases I–IV for the selective extraction of Fe(III) from a mixture containing several metal ions. Table 3 gives the effect of shaking time on the extraction of each metal ion at the selected optimum pH found in the previous section. The percentage extraction compared with the maximum metal capacity value in the case of Fe(III) is also included in Table 3. It is notable from Table 3 that Fe(III) is rapidly extracted, giving a metal capacity value of 0.62 mmol g^{-1} after only 2 min of shaking, corresponding to about 65% extraction of the Fe(III) present in the solution. This minimum value of the metal capacity determined after shaking for 2 min is higher

Table 4
Atomic absorption data for iron(III) selectivity test

Sample	Fe(III)		Mg(II)		Mn(II)		Co(II)		Ni(II)		Cu(II)		Zn(II)		Cd(II)	
	mmol l^{-1}	Extraction (%)	mmol l^{-1}	Extraction (%)	mmol l^{-1}	Extraction (%)	mmol l^{-1}	Extraction (%)	mmol l^{-1}	Extraction (%)	mmol l^{-1}	Extraction (%)	mmol l^{-1}	Extraction (%)	mmol l^{-1}	Extraction (%)
Phase I	0.072	96.2	3.868	2.1	1.784	2.9	1.799	0.0	1.874	2.6	1.558	6.6	1.667	2.7	1.139	3.0
Phase II	0.107	94.3	3.826	3.1	1.766	3.9	1.782	0.0	1.942	0.0	1.574	5.6	1.682	1.8	1.130	3.7
Phase III	0.054	97.1	3.909	1.0	1.802	2.0	1.748	1.9	1.959	0.0	1.526	8.5	1.698	0.9	1.157	1.4
Phase IV	0.125	93.4	3.868	2.1	1.820	1.0	1.731	2.9	1.857	3.5	1.542	7.6	1.652	3.6	1.139	3.0
Standard	1.880	—	3.950	—	1.838	—	1.782	—	1.925	—	1.668	—	1.713	—	1.174	—

than almost any other metal ion capacity value even after 30 min of shaking, except for one value for Cu(II)–phase I. These trends in the variation of metal capacity values with shaking time are useful in the evaluation of the immobilized phases I–IV as highly selective for Fe(III) extraction.

3.4. Selective extraction of Fe(III)

The results of Fe(III) metal capacity determination as a function of either shaking time or pH prompted us to perform selective extraction studies of Fe(III) by the immobilized phases I–IV from mixtures containing other metal ions. A mixture of metal ions was prepared with similar ppm concentrations of Fe(III), Mg(II), Mn(II), Co(II), Ni(II), Cu(II), Zn(II) and Cd(II). However, Pb(II) precipitated in this mixture of metal ions and was therefore excluded from selectivity investigation. The mixture of metal ions was extracted with the four immobilized phases I–IV under the same experimental conditions of buffer, shaking time and dilution steps. A standard solution containing the same eight metal ions was also prepared for quantitative determination of the percentage extraction of each metal ion. The results of the atomic absorption analysis of the four phases and the standard are given in Table 4. Interpretation of selectivity is always based on the separation factor, α, which is a direct measure of the concentration or distribution ratios of the two solutes between the two phases. However, the data in Table 4 are expressed in mmol l^{-1} and percentage extraction values for simplicity. These values clearly demonstrate that only Fe(III) was isolated by the four phases tested, the values being in the range 93.4–97.1%, which is an excellent match with the metal capacity values previously described. On the other hand, the remaining seven metal ions were found to be less than 4% extracted by the immobilized phases, except for Cu(II), with extraction in the range 5.6–8.5%. Comparison of the percentage extractions obtained for Fe(III) and Cu(II) shows the great affinity of phases I–IV to Fe(III), but with some noticeable interference by Cu(II) ion. The interference of Cu(II) in selective extraction of Fe(III) by phases I–IV is mainly attributed to the high metal

Table 5
Comparison of metal capacities (mmol g^{-1}) of the original and recycled phases

Metal ion	Metal capacity							
	Phase I		Phase II		Phase III		Phase IV	
	Original	Recycled	Original	Recycled	Original	Recycled	Original	Recycled
Fe(III)	0.96	0.90	0.95	0.92	0.95	0.89	0.96	0.90
Cu(II)	0.78	0.70	0.45	0.39	0.44	0.42	0.25	0.20
Pb(II)	0.15	0.16	0.18	0.14	0.20	0.17	0.16	0.16

capacity value expected under the experimental conditions of the selectivity test. Therefore, optimization of the selective extraction of Fe(III) in the presence of Cu(II) can be accomplished by selection of the appropriate experimental conditions, such as the pH of the solution, which favour the elimination of Cu(II) interference.

3.5. Recycling of Fe(III)–phase I–IV complex

Selection of the Fe(III)–phase I–IV complex for recycling was based on the higher affinity of the metal ion to different silica gel phases. EDTA was used as the recycling reagent because of its high capability for back-extraction of metal ions from the complexes formed [25,28] and elution from the surface of immobilized silica gel. The recycled phases were subjected to a second metal ion extraction from a solution containing Fe(III), Cu(II) and Pb(II), and the results of this study are shown in Table 5. The values of the metal capacity of recycled phases (Table 5) indicate the possibility of using EDTA as a good recycling agent based on the similarity of the values of the metal capacity in the second extraction to those of the initial metal extraction given in Table 2.

References

[1] D.C. Locke, J. Chromatogr. Sci., 11 (1973) 120.
[2] D.C. Locke, J. Chromatogr. Sci., 12 (1974) 433.
[3] M. Novotny, S.L. Bektesh and K. Grohmann, J. Chromatogr., 83 (1973) 25.
[4] K. Unger, Porous Silica, Elsevier, Amsterdam, 1979.
[5] N. Becker and K. Unger, Fresenius Z. Anal. Chem., 304 (1980) 374.
[6] M. Lührmann, N. Stelter and A. Kettrup, Fresenius Z. Anal. Chem., 322 (1985) 47.
[7] M.G. Gennaro, E. Mentasti and C. Sarzanini, Polyhedron, 5 (1986) 1013.
[8] T. Seshadri, G. Dietz and H.-J. Haupt, Fresenius Z. Anal. Chem., 319 (1984) 403.
[9] D.E. Leyden and G.H. Luttrel, Anal. Chem., 47 (1975) 1612.
[10] K. Moriya, K. Tanizawa and Y. Kanaoka, Chem. Pharm. Bull., 37 (1989) 2849.
[11] M.E. Mahmoud and G.A. Gobar, Alexandria Eng. J., 33 (1994) D159.
[12] R. Kocjan and M. Garbacka, Talanta, 41 (1994) 131.
[13] N.L. Dias Filho, Y. Gushikem, E. Rodriguez, J.C. Moreira and W.L. Polito, J. Chem. Soc. Dalton Trans., (1994) 1493.
[14] T. Seshadri and A. Kettrup, Fresenius' Z. Anal. Chem., 310 (1982) 1.
[15] J.S. Bradshaw, R.L. Bruening, K.E. Krakowiak, B.J. Tarbet, M.L. Bruening, R.M. Izatt and J.J. Christenen, J. Chem. Soc., Chem. Commun., (1988) 812.
[16] M.L. Bruening, D.M. Mitchell, J.S. Bradshaw, R.M. Izatt and R.L. Bruening, Anal. Chem., 63 (1991) 21.
[17] T. Seshadri and H.-J. Haupt, Anal. Chem., 60 (1988) 47.
[18] J.C. Hsu, H.-C. Huang and C.Y. Liu, Transition Met. Chem., 18 (1993) 453.
[19] R.J. Motekaitis, Y. Sun and E. Martell, Inorg. Chim. Acta, 198 (1992) 421.
[20] M.J. Adam and L.D. Hall, Can. J. Chem., 60 (1982) 2229.
[21] U. Casellato, D. Fregona, S. Sitran, S. Tamburini and P.A. Vigato, Inorg. Chim. Acta, 110 (1985) 161.
[22] P.H. Gore and P.J. Newman, Anal. Chim. Acta, 31 (1964) 111.
[23] J.C. Duff and E.J. Bills, J. Chem. Soc., (1932) 1987.
[24] M. Vidali, U. Casellato, P.A. Vigato, L. Doretti and F. Mada Losso, J. Inorg. Nucl. Chem., 39 (1977) 1985.
[25] M.E. Mahmoud, Anal. Lett., in press.
[26] M.A. Marshall and H.A. Mottola, Anal. Chem., 55 (1983) 2089.
[27] V.I. Fadeeva, T.I. Tikhomirova, I.B. Yuferova and G.V. Kudryavtsev, Anal. Chim. Acta, 219 (1989) 201.
[28] A.I. Vogel, Quantitative Inorganic Analysis, 5th edn., Longman, Harlow, 1989.

ELSEVIER

Talanta 44 (1997) 23–30

Talanta

Determination of nickel by direct automatic potentiometric titration with EDTA and a chemically modified electrode based on a strong acid ion exchanger containing 4-(3,5-dichloro-2-pyridylazo)-1,3-diaminobenzene

P.S. González, C.A. Fontán*, V.A. Cortínez

Departamento de Química Analítica "Dr. Carlos B. Marone", Universidad Nacional de San Luis, Chacabuco y Pedernera, CP 5700, San Luis, Argentina

Received 3 November 1995; revised 8 April 1996; accepted 10 April 1996

Abstract

A chemically modified electrode (CME) was constructed and evaluated for use as an end-point indicator in the automatic titration of Ni(II) with EDTA. The CME consisted of a graphite paste prepared by mixing a strong acid ion exchanger containing 4-(3,5-dichloro-2-pyridylazo)-1,3-diaminobenzene and graphite powder–Nujol paste. This mixture showed high mechanical resistance in strongly acidic and alkaline solutions (6 M HCl–pH 12). The CME did not require any special conditioning prior to use. It could be used over long periods (5–6 months) of continuous work without renewing either the electroactive surface or paste. In buffered solutions (pH 3–4.5), automatic direct potentiometric titrations could be carried out over a wide interval of Ni(II) concentrations, ranging from 3 to 6000 ppm, with satisfactory accuracy and precision. For practical analysis, the electrode was applied to the determination of nickel in two certified composition alloys. Interferent ions were previously separated by applying an ion-exchange procedure.

Keywords: Chemically modified electrode; Graphite paste electrode; Nickel; Potentiometric titrations

1. Introduction

In parallel with the development of new ion-selective electrodes for the direct potentiometric determination of ions or substances in solution, from the analytical viewpoint research on chemically modified electrodes (CME) for end-point detection in automatic potentiometric titrations is also of interest. Generally, for sufficiently high concentrations, potentiometric titrations give good accuracy, they are not strongly dependent on the exact interpretation of small changes in voltage and are not limited by the accuracy of the electrode response to changes in solution concentrations. However, the development of suitable end-point sensors is not very simple. Thus, in addition to the often severe chemical limitations inherent to the titrimetric procedures (e.g. interferences, side-reactions, pH

* Corresponding author.

PII S0039-9140(96)01961-3

effects, suitability of reagents), there are other factors relating to the electrode behaviour, e.g. response times, slope of titration curves and overall voltage changes. In general, fundamentally high rates of potential change (especially at low concentration levels) are needed to ensure that the end-point and equivalence point are as close as possible.

In an earlier paper [1], we reported the construction of a simple electrode of 4-(3,5-dichloro-2-pyridylazo)-1,3-diaminobenzene (3,5-Cl2-PADAB)-modified graphite paste. This electrode was shown to be reliable as an end-point indicator in the automatic potentiometric titration of Zn(II) with EDTA, but owing to the relatively high reactive solubility in acidic solutions (pH < 4), its use was restricted only to neutral or alkaline solutions. We report here the construction and performance of a chemically modified electrode system consisting of a conventional graphite paste mixed with a strong acid ion exchanger which contains absorbed 3,5-Cl2PADAB. Both macroporous resin and ion exchangers modified with selective complexing agents have been widely used for the preconcentration or separation of metal ions [2–16]. This kind of ligand immobilized substances, so-called chelating agents resins, have also been incorporated into a conventional graphite power–Nujol oil pastes for the developement of CMEs. Most of these electrodes were not potentiometric sensors; the modified substance was incorporated in order to preconcentrate the analyte from dilute solution. Then, once the analyte had been extracted into the electrode surface, the analytical measurements were made in some other medium by using voltammetric method [17–26]. The successful developement of carbon paste electrodes should involve, at least, a permanently immobilized and stable species. In addition, such a modifier must be insoluble enough to avoid a continuous flow of the modifier from the electrode to the working solution (from the electrode response viewpoint, the dissolution of any component of the modified substance yields a continuous potential drift and a stable potential is not attained). Initial experiment carried out with the pure 3,5-Cl2PADAB-modified resin showed that it was almost insoluble in water over a wide range of pH. No disolution of 3,5-Cl2PADAB was observed after several days of exposure to these solutions. We also found that the electrode developed in this work possessed high mechanical stability in both strongly acidic and alkaline solutions. Although it proved to be sensitive to changes in Co(II), Zn(II), Cu(II) and Ni(II) concentrations, it was used as an end-point sensor for the automatic potentiometric titration of Ni(II) with EDTA.

2. Experimental

2.1. Apparatus

All potentiometric titrations were made with an Orion Automatic Titrator (Model 960 Autochemistry System, Orion Research, Cambridge, MA, USA), by using ion exchanger modified-graphite paste electrodes in conjunction with a double-junction Ag/AgCl electrode (Orion 90-02). The titrator was programmed to record millivolt readings during the analysis when the electrode response reached a pre-set stability. All titrations were started when the electrode responses became stable (± 1 mV min^{-1}) after immersion in sample solutions. Typically, such stability was attained in not more than 0.5–1 min in stirred solutions. Measured increments of titrant were automatically added from the titrator's burete. During the course of a titration, each new pre-set titrant volume was added after the potential had become stable to ± 1 mV or less. Near the end-point, the electrode response was slower than at the start of the titrations. In general, in these regions $\pm$ mV min^{-1} stability was attained 2–3 min after addition of each titrant volume. When the Ni(II) concentrations were higher than 2000 ppm, pre-dose volumes of titrant were added to reduce the time of titrations. The end-points were taken by applying either the first- or second-derivative technique to the data generated during the titrations.

2.2. Reagents

2.2.1. Standard nickel solution (ca. 0.1 M)

Ni(II) standard solution was prepared by dissolving the required amount of metal (99.95% pure) in 50 ml of 1 + 1 hydrochloric acid. The solution was diluted with distilled water in a 1000 ml volumetric flask.

2.2.2. Standard EDTA solution (ca. 0.1 M)

The disodium salt was dissolved in distilled water and standardised by potentiometric titration with a Zn(II) solution prepared from 99.99% pure metal.

2.2.3. 3,5-Cl2PADAB reagent

The reagent was synthesized and purified in our laboratory as described previously [27].

2.2.4. Formic acid–formate buffers

Several stock buffers were prepared by adjusting 1 M formic acid solutions (500 ml each) to the required pH with concentrated sodium hydroxide solution. All reagents were of analytical grade. All solutions were prepared in doubly distilled water and diluted further as required.

2.3. Electrode preparation

The electrode body was constructed as described previously [1].

2.3.1. Preparation of 3,5-Cl2PADAB-modified resin

Dowex 50W-X12 H^+ form resin (200–400 mesh) was cleaned before being used by boiling for 2 h with methanol. The resin was packed into a glass tube (200 mm × 6 mm i.d.) to give a bed about 2 cm high. The column was first washed with 50 ml 5% (v/v) HCl and then with a large volume of distilled water to remove acid from the column. A 0.05% (w/v) solution of 3,5-Cl2-PADAB in 95% ethanol was passed through the column at a 10 ml min^{-1} flow rate until the effluents became strongly coloured. At this point, to ensure complete resin "saturation", an additional 50 ml of reactive solution was passed through the bed at a 0.5 ml min^{-1} flow rate. Then both the inner tube walls and column were carefully washed with several portions of pure ethanol (100 ml in total). Finally, the modified resin was dried overnight at 90°C and stored in a tightly stoppered 2 ml vial. The final product was not appreciably hygroscopic.

2.3.2. Preparation of modified carbon pastes

The pastes were prepared by mixing a weighed amount of modified resin and the required weight of carbon (spectroscopically pure graphite powder, 400 mesh). Before mixing, the resin was wetted with a few drops of Nujol oil and then thoroughly mixed with a spatula. When necessary, more Nujol was added, drop by drop, until the entire mixture appeared uniformly wetted. The modified pastes were packed firmly into the cavity of the electrode body, then the surfaces of pastes were smoothed off by rubbing the electrode across a flat piece of glass, Finally, the excess paste was scraped off with a glass spatula.

2.4. General procedure for Ni(II) titrations

Pipette a sample volume containing between 0.15 and 300 mg of Ni into a 100 ml beaker. If necessary, dilute to 50 ml with distilled water and neutralize to litmus paper with dilute sodium hydroxide or hydrochloric acid solution. Add 1 ml of pH 3 sodium formate–formic acid buffer (ca. 1 M); connect both the working and reference electrodes, stir the solution continuously with a magnetic stirrer and start the titration when a stable potential (±1 mV) is attained.

2.5. Recommended procedure for Ni(II) separation

2.5.1 Preparation of resin column

Slurry an adequate amount of resin (Dowex 1-X10 type, 200–400 mesh, Cl^- form) with water and pour into 25 ml burette containing a small plug of glass-wool at the bottom, to form a 20 cm bed. Allow the resin to settle and then wash it with hot dilute acetone (1 + 1) until the effluent is colourless. Rinse with 100 ml of dis-

tilled water, then wash the resin with 9 M HCl (50 ml) to displace water, adjusting the burette tap so that the flow rate is ca. 10 ml min^{-1}. Just before use, allow the solution to flow from the burette until the surface is ca. 1 cm below the top of the resin level. After samples have passed through column, to displace iron(III), regenerate the resin by passing 0.1 M HCl solution (about 150 ml) until Fe(III) is not detectable with 5% KSCN solution.

2.5.2. Ni(II) separation

With a clean, dry pipette, pour 5 ml of the solution to be analysed on the top of column and let it flow in slowly until the liquid surface is ca. 1 cm below the top of the resin level, discarding the first few millilitres of effluent. Change the receiver to a 50 ml Pt dish and elute Ni(II) with two portions of 5 ml each of 9 M HCl. Evaporate the solution to near 0.5 ml on a sand-bath and allow it to cool. Dilute the residue with 5 ml of water, and quantitatively transfer the solution into a 100 ml beaker. Wash the dish with three 10 ml portions of water. Add 1 ml of 1 M formic acid–formate buffer (pH 3.5), mix well and titrate with EDTA when the potential is stable (± 1 mV min^{-1}).

2.5.3. Preparation of samples

IPT standard No. 24 samples (about 100 mg) were dissolved in 20 ml of concentrated hydrochloric acid and the solutions were evaporated until almost dry. The residues were taken up in 25 ml of 9 M HCl, quantitatively transferred into a 100 ml volumetric flask and finally diluted to volume with 9 M HCl. Portions of 5 ml of each of these solutions were loaded on to the column.

When the chromium content was low, as in IPT standard No. 45, it was most convenient to dissolve samples (about 3 g) in 50 ml of dilute (1 + 1) HNO_3. The resultant solutions were evaporated carefully just to dryness and allowed to cool. The residues were then dissolved in 10 ml of 9 M HCl and auantitatively transferred into a 100 ml volumetric flask with the aid of several portions of 9 M HCl. Finally, 9 M HCl was added to reach the 100 ml mark. Portions of 5 ml each of these last solutions were loaded on to the column for Ni(II) separation.

Results and discussion

We found that an electrode prepared with plain carbon–Nujol paste, that is, a paste containing neither 3,5-Cl2PADAB nor 3,5-Cl2PADAB-modified strong acid ion-exchange resin, was not sensitive to Ni(II) or another ions in the pH range 0–12. However, when the electrode was filled with a graphite–Nujol paste mixed with 3,5-Cl2PADAB-saturated resin, it showed a well defined response to concentration changes of ions such as Ni(II), Co(II), Cu(II) and Zn(II). In aqueous solution, 3,5-Cl2PADAB reacts with the above ions (pH 2–11) to form coloured complexes which have been used as the basis for development of several spectrophotometric [27–31] and titrimetric [1,32] procedures. The reagent could also be absorbed by a strong acid ion-exchange resin, and once absorbed it maintained the ability to react with these ions. In these cases, apparently the reactions did not occur in solution but in the grains of the ion exchanger. For example, it was clearly observed that when the modified resin was immersed in a solution containing an excess of Cu(II), after a few seconds of contact with liquid, the deep red colour of resin changed to the characteristic red–purple colour of the Cu(II)–Cl2PADAB complex. The complex formed in this way was also strongly retained by the resin and was more stable than the same complex formed in solution. Thus, the red–purple Cu(II)–3,5-Cl2PADAB complex formed in solution at pH 2–5.5 was rapidly destroyed by increasing the acidity of the medium to pH < 2 by addition of HCl. Otherwise, the same complex formed with the reagent retained by the resin was not destroyed even if the HCl concentration was increased to 6 M. The complex was partially desorbed or destroyed by HCl at concentrations higher than 6 M, by (1 + 1) 6 M HCl–ethanol mixtures and by EDTA solution at pH > 2.

The absorption of 3,5-Cl2PADAB and the reactions of the modified resin with the above metallic ions can be understood by considering that (1) 3,5-Cl2PADAB possesses two amino groups located in *ortho* and *para* positions with respect to the azo group, and (2) that in the complexation reactions with metallic ions only the *o*-amino and azo nitrogen atoms participate [28].

Furthermore, if an interaction with the ion exchanger occurs through the *p*-amino group as follows:

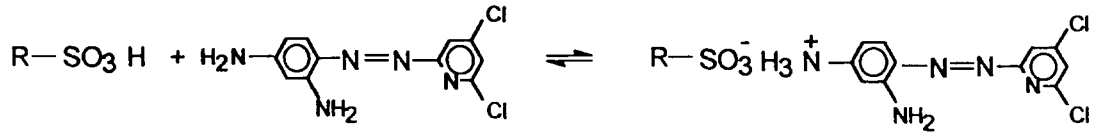

Solid (pale yellow) Solution (red) Solid (dark red)

Form 1

the resultant product will keep both the *o*-amino and azo groups free to react with the metallic ions according to

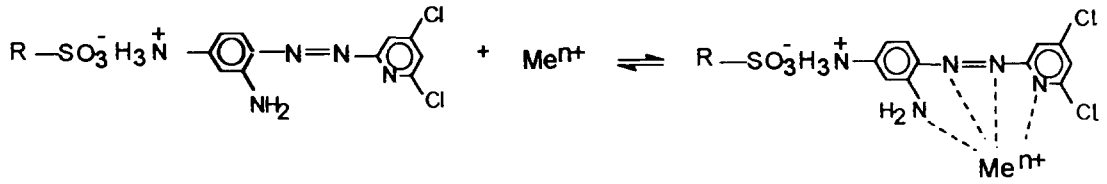

Solid Solution Solid

Form 2

The above assumption is in good agreement with the experimental results.

The calibration of the electrode as a direct potentiometric sensor was attempted at pH 3, 3.5 and 4 with pure Ni(II) solutions for concentrations down to 10^{-3} M and with Ni(II)–EDTA and Ni(II)–CDTA buffer [33,34] solutions for concentrations lower than 10^{-5} M. These solutions covered the pa_{Ni} range from ca. 3 to 12. For the calculations, the Ni(II)–formate complexes were neglected. The ionic strength in all solutions was adjusted to 0.1 by addition of the calculated amount of KNO_3. The results obtained indicated that the electrode response was not linear in either $-\log a_{Ni(II)}$ or $-\log_{[Ni(II)]}$. However, some initial titrations of the metallic ion carried out with EDTA as the titrant showed that the electrode should be suitable as an end-point indicator for these titrations. Therefore, the studies were orientated in that sense.

3.1. Paste composition

The electrode response was strongly affected by the paste composition. Several modified graphite pastes containing different amounts of 3,5-Cl2PADAB (from 1% to 80% (w/w), relative to the weight of graphite powder) were prepared and assayed. Below 40%, the behaviour of the electrode was poor, showing a slow response and smooth potential jump at the end-point, while ion-exchanger contents higher than 60% yielded pastes without mechanical resistance. The ion-exchanger grains of electrodes containing more than 60% were rapidly removed from the paste when they were immersed in solutions. However, with 40–60% pastes, the CME showed the best response and suitable mechanical resistance. Usually, 50% modified pastes were used in subsequent studies.

3.2. Electrode conditioning

The CME did not need any conditioning before use. We found that previous exposure to Ni(II) solutions as a conditioning process was not necessary for the electrode to work. However, the first

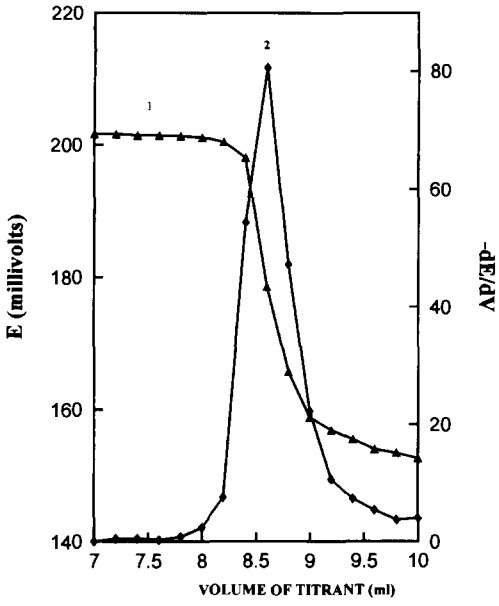

Fig. 1. Typical electrode response in the titration of Ni(II) at pH 3.5. (1) Titration of 50 ml of 244 ppm Ni(II) (7 ml pre-dose volume). (2) Curve obtained by applying the first derivative method to the data for curve 1.

titrations carried out with all recently prepared electrodes gave curves that showed inflection points not coincident with the theoretical end-point. Typically, exact results were obtained after carrying out two or three titrations of standard Ni(II) solutions. Once working, a large number of determinations could be made at various concentration levels, over a period of almost 6 months of continuous work, without the need to renew the electrode surface or paste.

Table 1
Some typical results obtained in EDTA potentiometric titrations of Ni(II) using a graphite paste electrode containing, 3,5-Cl2PADAB absorbed by a strong acid ion exchanger.

Ni(II) taken (ppm)	Ni(II) found (ppm)[a]	Error (%)	Standard deviation (ppm)
3.29	3.31	0.6	0.07
6.53	6.49	0.6	0.07
30.13	30.25	0.39	0.11
66.93	67.05	0.17	0.52
233.17	234.40	0.10	0.55
601.50	604.10	0.42	3
3007.50	3025.00	0.60	7
6001.00	5976.70	0.60	20

[a] Mean of 20 titrations.

3.3. Ni(II) titrations. Influence of pH

The influence of pH on the Ni(II) titrations was studied by carrying out titrations of buffered (formic acid–sodium formate or acetic acid–sodium acetate buffers) 10^{-3} M Ni(II) solutions in the pH range 2–6. In the pH range 3–4.5 the accuracy and repeatability obtained were insensitive to variations of pH. However, with a gradually more acidic or alkaline medium (up to pH 2 and pH 6, respectively), although the potential jump at the end-point became small,

Table 2
Maximum concentrations of foreign ions tolerated in Ni(II) determination by the proposed method.

Ion	Maximum concentration tolerated (ppm)	Ion	Maximum concentration tolerated (ppm)
Fe(III)	23	Thiosulphate	9600
Cu(II)	20	Nitrate	12400
Zn(II)	20	Phosphate	47500
Pb(II)	63	Fluoride	3800
Co(II)	24	Chloride	35500
Ca(II)	20000	Thiocyanate	29000
Mg(II)	12000		
Cr(III)	156		
Mn(II)	55		
Mo(VI)	96		

Table 3
Compositions of certified samples and results obtained for the determination of Ni

Sample Composition (% w/w)		Ni found (% w/w)	Error (%)	Standard deviation (ppm)
IPT No. 45 (nodular)	C (total) 2.95, C (graphitic) 2.66, Si 2.82, Mn 0.425, P 0.017, S 0.011, Cu 0.194, Cr 0.221, Ti 0.004, Mg 0.0031			
	Ni 0.196	0.195	0.51	0.005
IPT No. 24 (AISI 316)	C (total) 0.044, Si 0.528, Mn 1.500, P 0.039, S 0.004, Cu 0.030, Cr 17.81, Mo 2.640, Co 0.045, Fe 67.42			
	Ni 9.930	9.98	0.57	0.04

Ni(II) could be titrated with lower accuracy but with good precision. Therefore, in all subsequent work, a pH value of 3.5 was employed for the titrations. Fig. 1 illustrates a typical titration of Ni(II) at pH 3.5.

3.4. Accuracy and precision. Range of determinable Ni(II) concentrations

At pH 3.5 and with formic acid–formate buffered solutions, direct Ni(II) potentiometric titrations could be carried out in the range from nearly 3 to 6000 ppm with an accuracy of better than 0.5% (relative error) and a repeatibility lower than 0.71 (relative standard deviation). Some typical results obtained are shown in Table 1.

3.5.Interferences

The influence of foreign ions on the Ni(II) determination by the proposed method was studied for several cations, principally those which were expected to be interferents (e.g. Cu(II), Zn(II), Co(II), and Fe(III)). The cations tested were added as their chlorides or nitrates because these anions, as well as perchlorate, sulphate, acetate and formate, did not interfere at concentrations up to 1 M. An ion was considered to interfere when it produced an error greater than 0.6% (relative error) in the nickel determination. Table 2 shows the results obtained.

The greatest limitations were brought by the metallic ions mentioned above, and interference could not be controlled either by masking or by reducing them to another oxidation state. Previous separations proved to be the best way to avoid their interference. For that purpose, and to extend the method's application to samples containing large amounts of iron, cobalt, zinc, chromium and molybdenum, several separation procedures were tried. The ion-exchange method suggested by Kraus [35,36] was the simplest and most convenient manner for nickel separation from samples containing high proportions of other metals.

3.6. Applications

To evaluate the electrode performance in practical analytical work, two alloy samples certified by the Instituto de Pesquisas Tecnológicas (IPT), of San Pablo state, Brazil (IPT Nos. 24 and 45) were analysed for their nickel content. The sample compositions and the results obtained are shown in Table 3. In both cases, six determinations were carried out on three portions of each sample.

4. Conclusions

The method developed in this work showed good accuracy and precision in direct automatic potentiometric titrations of Ni(II) with EDTA. The CME was constructed by using easily available and inexpensive materials. The 3,5-Cl2PADAB-modified ion exchanger and the modified resin–carbon paste were very easily prepared and rapidly incorporated into the electrode body or replaced. They could be stored for long periods without loss or reactivity. For example, no difference in the electrode behaviour was found on comparing the results obtained from a freshly prepared modified paste with those for the same paste after 10 months of storage in a stoppered vessel, protected against direct sunlight. The electrode did not need any special conditioning to work correctly. All electrodes used in this work were ready to use immediately after their preparation. At pH 3–4.5 they gave excellent results for automatic Ni(II) titrations over a wide range of concentration (3–6000 ppm). This was especially attractive because it should allow application of the method to samples with high nickel contents without carrying out extensive dilutions before titrations. Only inexpensive and easily available reagents were required for the titrations. Furthermore, no external standards for instrument calibration were required. The only calibration necessary was standardization of the EDTA solution. In the above pH range, the titration curves were symmetrical, with the inflection points coincident with the theoretical end-points. Typically, overall potential jumps of 80–100 mV were obtained at the end-points.

Although the method showed several interferences, which could only be avoided by applying a simple separation procedure, the above findings suggest the resin–carbon paste electrodes could be advantageously employed for Ni(II) determinations in a wide variety of materials, such as minerals, soils and some industrial effluents.

References

[1] J. Raba, C.A. Fontán and V.A. Cortínez, Talanta, 41 (1994) 273.
[2] K. Brajter, J. Chromatogr., 102 (1974) 385.
[3] K. Brajter, Chem. Anal. (Warsaw), 21 (1976) 1195.
[4] K. Brajter and K. Slonawska, Chem. Anal. (Warsaw), 24 (1979) 273.
[5] K. Brajter, K. Slonawska and Z. Vorbrodt, Chem. Anal. (Warsaw) 24 (1979) 763.
[6] K. Brajter, K. Kleyny and Z. Vorbrodt, Talanta, 27 (1980) 433.
[7] K. Brajter and Y. Miazek, Talanta, 28 (1981) 759.
[8] K. Brajter and I. Miazek, Z. Fresenius', Anal. Chem., 315 (1983) 121.
[9] K. Brajter and K. Kleyny, Talanta, 37 (1985) 521.
[10] K. Brajter, I. Miazek and E. Dabek-Zlotorzynska, Fresenius' Z. Anal. Chem., 321 (1995) 492.
[11] K. Brajter, I. Miazek and E. Dabek-Zlotorzynska, Talanta, 33 (1986) 149.
[12] Y. Sakai and N. Mori, Talanta, 33 (1986) 161.
[13] K. Brajter and K. Slonawska, Mikrochim. Acta, 1 (1989) 137.
[14] K. Pyrzynska and K. Brajter, Anal. Chim. Acta, 255 (1991) 169.
[15] E. Olbryeh-Sleszynska, K. Brajter, W. Matuszewski, M. Trojamowicz and W. Frenzal, Talanta, 39 (1992) 779.
[16] A. Masi and R. Olsina, An. Quím., 89 (1993) 341.
[17] G.T. Cheek and R.F. Nelson, Anal. Lett., 411 (1978) 393.
[18] H.S. White, J. Leddy and A.J. Bard, J. Am. Chem. Soc., 104 (1982) 4811–4817.
[19] K. Kalcher, Fresenius' Z. Anal. Chem., 321 (1985) 666.
[20] M.K. Halbert and R.P. Baldwin, Anal. Chem., 57 (1985) 591.
[21] Y. Sakai and N. Mori, Talanta, 33 (1986) 161.
[22] K. Kalcher, Talanta, 33 (1986) 489.
[23] L.M. Santos and R.P. Baldwin, 58 (1986) 352.
[24] P. Li, Z. Gao, Y. Xu and G. Wang, Anal. Chim. Acta, 229 (1990) 213.
[25] Z. Gao, P. Li, S. Dong and Z. Zhao, Anal. Chim. Acta, 232 (1990) 367.
[26] L.M. Aleixo, B. de Fátima, M. Souza, O.E.S. Godinho, G. de Olivera Neto and Y. Gushikem, Anal. Chim. Acta, 271 (1993) 143.
[27] C.A. Fontán, R.A. Olsina and C.B. Marone, Bull. Chem. Soc. Jpn., 61 (1988) 4113.
[28] E. Kiss, Anal. Chim. Acta, 66 (1973) 385.
[29] F. Kai, Y. Sakanashi, S. Satoh and S. Uchikawa, Anal. Lett., 16 (1983) 1013.
[30] C.A. Fontán, R.A. Olsina and C.B. Marone, Anal. Asoc. Quím. Argent., 71 (1983) 449.
[31] C.A. Fontán, R.A. Olsina and C.B. Marone, Bull. Chem. Soc. Jpn., 61 (1988) 4121.
[32] C.A. Fontán and R.A. Olsina, Talanta, 36 (1989) 945.
[33] J. Ruzicka and E.N. Hansen, Anal. Chim. Acta, 63 (1973) 115.
[34] E.H. Hansen, C.G. Lamm and J. Ruzicka, Anal. Chim. Acta, 59 (1972) 403.
[35] K.A. Kraus and G.E. Moore, J. Am. Chem. Soc., 75 (1953) 1460.
[36] J.A. Welcher, Standard Methods of Chemical Analysis, 6th edn., Vol. II, Part A, Van Nostrand, Princeton, NJ, 1965.

ELSEVIER

Talanta 44 (1997) 31–37

Talanta

Application of SQUAD to the refinement of formal potentials from coulometric steady-state and spectrophotometric measurements

Ma. Teresa Ramírez *, Alberto Rojas-Hernández, Ignacio González

Departmento de Química, Universidad Autónoma Metropolitana-Iztapalapa, Apdo Postal 55-534, C.P. 09340, México, D.F. Mexico

Received 20 November 1995; revised 24 May 1996; accepted 31 May 1996

Abstract

The application of SQUAD to the refinement of formal potentials from potentiometric or coulometric steady-state and spectrophotometric measurements was tested. The formal potential thus obtained for the $Fe(CN)_6^{3-}/Fe(CN)_6^{4-}$ couple in 0.5 M H_2SO_4 agreed with published data. This method was found to be satisfactory for the determination of typical standard potentials and it is suggested that it may be advantageous when dealing with multi-component systems.

Keywords: Coulometry; Formal potentials; Potentiometry; Spectrophotometry; SQUAD

1. Introduction

Several studies have been published using spectrophotometric, potentiometric and coulometric data to determine experimental standard potentials [1,2]. Most of these have used the cell potential (E) and absorbance values in a specific wavelength to determine the standard potential through graphical methods. In this way, it is only possible to determine standard potentials with a 100 mV/n separation in simple systems with few components (two or three). When the system is multi-component, it could be convenient to solve multiple regression with computer programs such as SQUAD [3–8], SCOGS [7,8], LETAGROP-SPEFO [8] and DALSFEK [9]. However, these programs have been designed for systems where oxidation state changes do not exist.

Sillén [10] suggested the use of an equilibrium constant for the redox couple. We evaluate the capability of using the SQUAD program with potentiometric or coulometric measurements and spectrophotometric data to refine these equilibrium constants and their standard potentials. In order to demonstrate the methodology used to achieve this task, we

* Corresponding author. Tel.: (52)(5) 7244670; fax: (52)(5) 7244666; e-mail: mtrs218@xanum.uam.mx

PII S0039-9140(96)02005-X

selected a simple system, the $Fe(CN)_6^{3-}$ / $Fe(CN)_6^{4-}$ couple in 0.5 M H_2SO_4 over a Pt electrode, as a typical example for the redox couple.

2. Theory

SQUAD [3–8] is a program with the capability of refining the stability constant of a general complex, $M_m M'_l H_k L_n L'_q$, where m, l, n, $q \gg 0$ and k is positive (for protons) and negative (hydroxide ions), employing a non-linear least-squares approach.

The data fed to SQUAD are absorption spectra, chemical composition (total concentration of M, M'L, L' and pH) and a chemical model to describe the system. The residual sum (U) is calculated from the following equation [6]:

$$U = \sum_{1}^{I} \sum_{1}^{NW} (A_{i,k}^{\text{calc.}} - A_{i,k}^{\text{obs}})^2 \quad (1)$$

where the absorbance values $A_{i,k}$, for each spectrum, give a total of I for each wavelength and a grand total of NW.

In order to use the SQUAD program to refine standard potentials for several redox couples, we proposed to following the stability constant defined by Sillén [10] for a redox couple:

$$\text{Ox} + ne^- \rightleftharpoons \text{Red} \quad (2)$$

The Nernst law is

$$E = E^\circ + 2.303 \frac{RT}{nF} \log \frac{|\text{Ox}|}{|\text{Red}|} \quad (3)$$

The product of $F/2.303RT$ on both sides of Eq. (2) gives

$$pe = \frac{1}{n} \log K + \frac{1}{n} \log \frac{|\text{Ox}|}{|\text{Red}|} \quad (4)$$

where

$$pe \equiv \frac{F}{2.303RT} E \quad \text{and}$$

$$\frac{1}{n} \log K \equiv \frac{F}{2.303RT} E^\circ \quad (5)$$

Eq. (4) is of the Henderson–Hasselbalch type and demonstrates that [e] and pe can be introduced in the place of [H] or pH in the input data of SQUAD to refine this kind of cumulative constant for the redox couple (and then E°).

The same idea has been used in other approaches in different electrochemical studies [11].

3. Experimental

3.1. Reagents and instrumentation

All the reagents were of analytical grade from Baker and Merck and aqueous solutions were prepared using deionized water (Millipore, 18 $\mu\Omega^{-1}$).

Solutions of Fe(III) and Fe(II) were separately prepared by weighing both salts, $K_3Fe(CN)_6$ and $K_4Fe(CN)_6 \cdot 3H_2O$, and dissolving them in 0.5 M H_2SO_4.

A Radiometer–Tacussel Model LPH4430T potentiometer was used for the potentiometric studies. The reference electrode (saturated calomel electrode (SCE), Tacussel) and the working electrode (platinum electrode) were introduced into the electrochemical cell for potentiometric measurements.

3.2. Procedure

The solutions, 1.095×10^{-3} M $K_3Fe(CN)_6$ and 1.023×10^{-3} M $K_4Fe(CN)_6 \cdot 3H_2O$, were placed in 10 or 25 ml burets as required, different aliquots were transferred to the beaker of the cell and the measurement of the equilibrium potential was taken (e.g. 24 ml of Fe(III) and 1 ml of Fe(II) solution).

For controlled-potential coulometry, a Model 377A PAR coulometry cell system was used. A three-electrode glass cell was used under a nitrogen atmosphere, a platinum-gauze working electrode was used for the oxidation and reduction systems and the reference electrode (SCE) was introduced by means of a Luggin capillary. The counter-electrode was a platinum mesh. The study was performed using a DEA 332 Digital Electorchemical Analyzer with IMT 101 electrochemical interface from Radiometer–Tacussel, with Voltamaster II software.

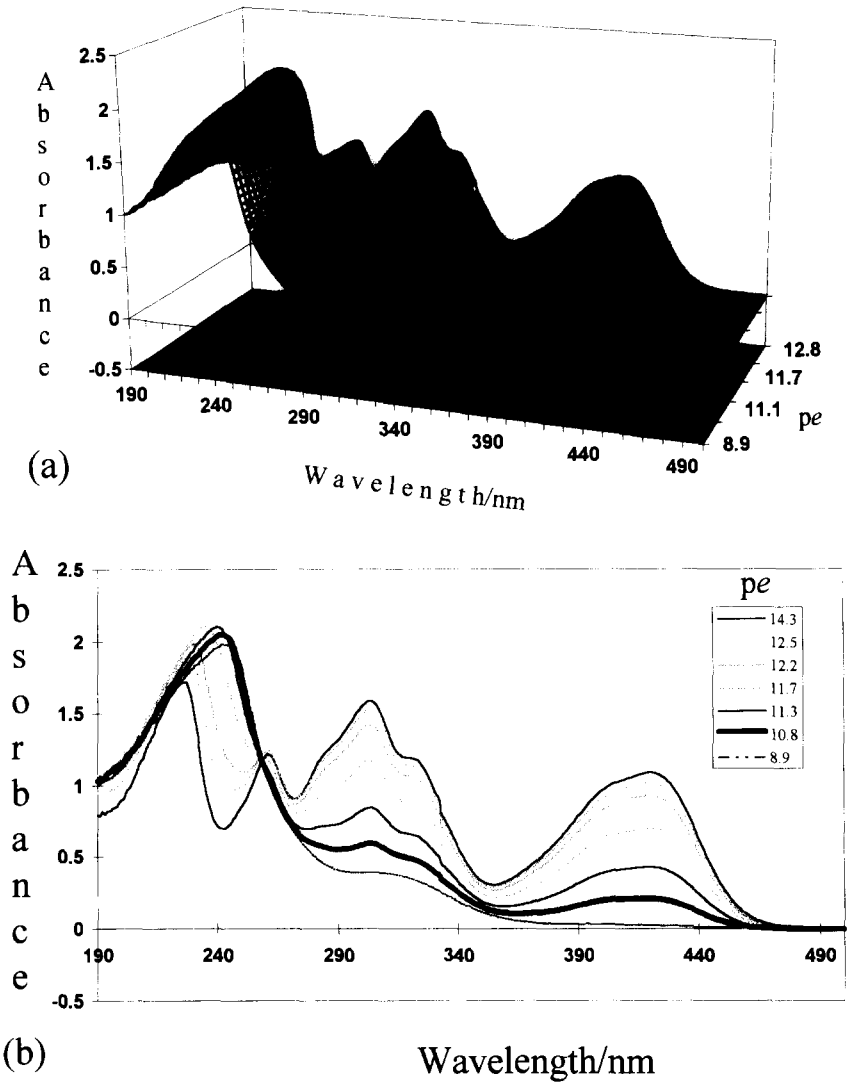

Fig. 1. Absorption spectra for solutions containing different $Fe(CN)_6^{3-}/Fe(CN)_6^{2-}$ ratios in 0.5 M H_2SO_4 volumetrically mixed. (a) Three-dimensional representation. (b) Typical absorption spectra for several *pe* values. In both cases *pe* is calculated following Sillén's suggestion, from potentiometric measurements.

For the spectrophotometric study, a Perkin-Elmer Lambda 17 double-beam UV-visible spectrophotometer with 1 cm quartz cells was utilized.

4. Results and discussion

4.1. Potentiometric study

The experimental E vs. $\log\{[Fe(CN)_6^{3-}]/[Fe(CN)_6^{4-}]\}$ plot is linear following the equation $E\,(mV) = 676.5\ (\pm 0.1)\ mV + 59.8\ (\pm 0.4)\ [mV^{-1}]\log\{[Fe(CN)_6^{3-}]/[Fe(CN)_6^{4-}]\}$ ($r^2 = 0.9999$) in agreement with the Nernst law. A slight blue coloration appeared when $[Fe(CN)_6^{4-}] \gg [Fe(CN)_6^{3-}]$, which was probably due to the formation of Prussian Blue by to the slow degradation of $Fe(CN)_6^{3-}$ in the acidic medium.

Representative absorption spectra obtained for different $Fe(CN)_6^{3-}/Fe(CN)_6^{4-}$ ratios as a function

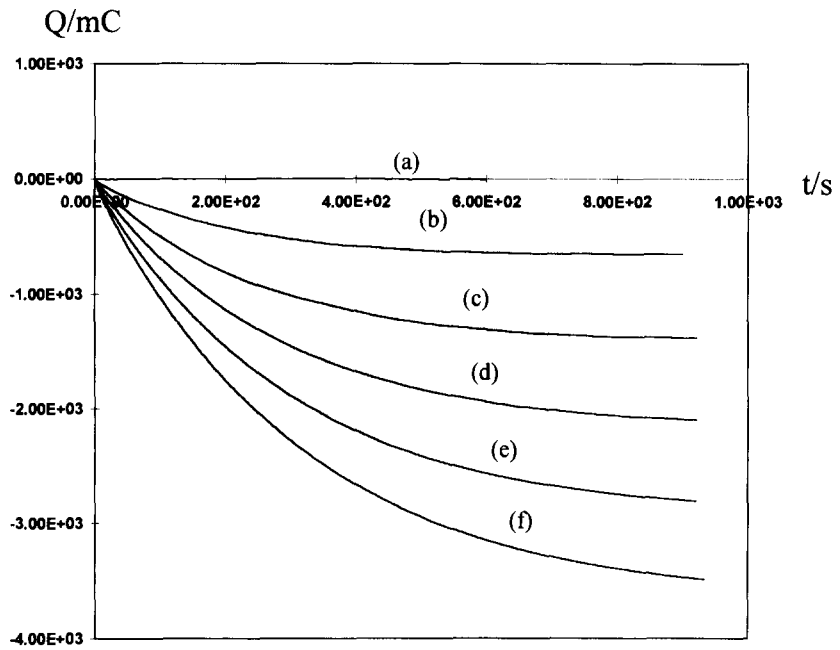

Fig. 2. Time dependence of charge involved in controlled-potential coulometry at 470 mV vs. NHE for different amounts of $K_3Fe(CN)_6$ dissolved in 0.5 M H_2SO_4: (a) 0, (b) 8.13×10^{-3}, (c) 1.63×10^{-2}, (d) 2.44×10^{-2}, (e) 3.25×10^{-2} and (f) 4.06×10^{-2} mmol.

of *pe* are shown in Fig. 1. In this case *pe* was calculated from the potential measurement with a platinum electrode immersed in the solution and using Eqs. (4) and (5).

4.2. Coulometric study

In order to analyze the $K_3Fe(CN)_6$ behavior under the above conditions, a coulometric study was carried out. The charge (Q) vs. time plots obtained in this process are shown in Fig. 2. From these curves and for long times, a Q vs. $[K_3Fe(CN)_6]$ plot was constructed for 470 mV vs. SHE. The charge varied linearly with the number of moles of $K_3Fe(CN)_6$ in solution (correlation coefficient = 0.9999) and the function was Q (mC) = -66 (± 435) mC + 91052 (± 9026) [mC mmol^{-1}] mmol $K_3Fe(CN)_6$. Considering that the slope of this function is equal to the product nF, the number of electrons involved in the reaction is 0.9 ± 0.1. This indicates that the $Fe(CN)_6^{3-}$ has been transformed into $Fe(CN)_6^{4-}$.

Solutions containing 15 ml of 8.17×10^{-4} M $K_3Fe(CN)_6$ were electrolyzed, imposing different potentials in the range 780–520 mV vs. SHE for 800 s. Solutions containing 15 ml of 8.57×10^{-4} M $K_4Fe(CN)_6 \cdot 3H_2O$ were similarly electrolyzed, imposing different potentials in the range 520–850 mV vs. SHE for 800 s.

For a liquid junction between two different electolytes, E_j may be estimated on the basis of the Henderson equation. In this case, $E_j = 14$ mV for $KCl-H_2SO_4$ solutions [12], and the potentials obtained in potentiometric and coulometric methods are corrected taking this E_j value into account.

Fig. 3 shows representative spectra obtained from steady-state solutions in coulometric experiments at several imposed potentials. The spectra are also represented as functions of *pe*. In this case *pe* is calculated from the potential imposed at the working electrode.

4.3. SQUAD results

The spectral behavior of the potentiometric and

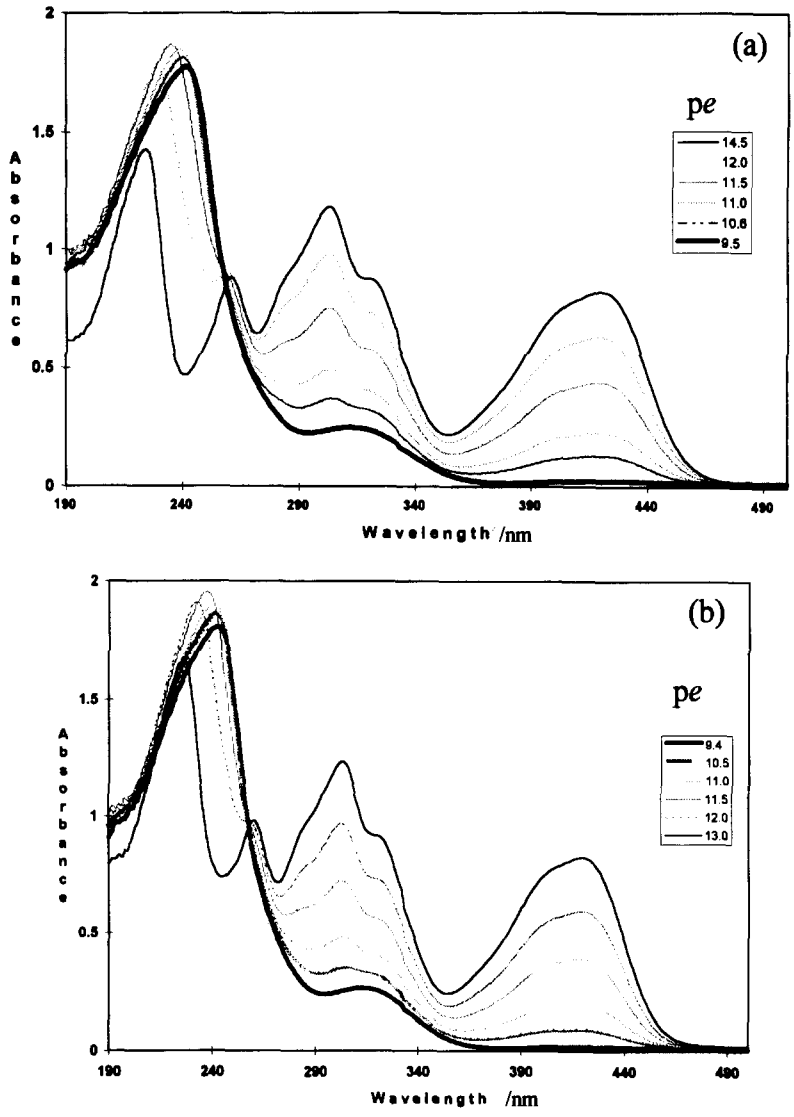

Fig. 3. Typical absorption steady-state spectra for different imposed potentials in coulometric experiments from solutions initially in 0.5 M H_2SO_4 containing (a) 8.17×10^{-4} M $Fe(CN)_6^{3-}$ and (b) 8.57×10^{-4} M $Fe(CN)_6^{4-}$. The imposed potentials are shown as *pe* values.

coulometric methods is similar. Only one isosbestic point is observed in all cases ($\lambda = 258$ nm). This can be associated with the presence of only one redox couple over the potential range considered.

In Table 1, the values of the equilibrium constants (and standard potentials) obtained from refinement achieved with SQUAD by assuming only one redox couple with the exchange of one electron are reported.

The statistical data (Table 1) are within the range of experimental error expected in all cases.

The difference between $E°$ obtained from electrolysis of $Fe(CN)_6^{3-}$ or $Fe(CN)_6^{4-}$ (approximately 10 mV) could indicate a hysteresis of the electron exchange in the redox couple, probably due to kinetic complications (see below). On the other hand, the difference between $E°$ obtained from electrolysis of $Fe(CN)_6^{3-}$ and the potentiometric

Table 1
SQUAD results for the $Fe(CN)_6^{3-}/Fe(CN)_6^{4-}$ formal potential in 0.5 M H_2SO_4 from experimental data

System	Log $K \pm \sigma$	$E°$ (mV vs. SHE)	Standard deviation σ_A [a]	Sum of squares U [b]
Potentiometric	11.6422 ± 0.0137	688.75	4.4464×10^{-2}	1.6943
Coulometric Fe(III) → Fe(II)	11.4601×0.0166	677.98	2.3662×10^{-2}	0.3354
Coulometric Fe(III) → Fe(II)	11.6733×0.0173	690.59	4.5156×10^{-2}	1.4661

[a] σ_A represents a global standard deviation of refinement of absorbance data.
[b] U represents the sum of squares of residuals, Eq. (1).

method could be due to the slight degradation of $Fe(CN)_6^{3-}$ in acidic media in the latter case.

In order to verify the quality of these data, several $E°$ values reported in the literature were compared with those obtained in this study (Table 2). Our results agreed with the published values.

The difference between the formal potentials in H_2SO_4, HCl and $HClO_4$ media and the standard potential may be explained by the protonation of hexacyanoferrate (II) [10]. Fig. 4 shows the Pourbaix-type diagram for the redox couple. For the construction of this diagram it was assumed that $Fe(CN)_6^{3-}$ and $H_iFe(CN)_6^{i-4}$ complexes are kinetically inert [13]. From this diagram it is evident that the protonation of hexacyanoferrate (II) increases the formal potential with respect to the standard potential.

Under the experimental conditions of this study, the redox couple involved was

$$2H^+ + Fe(CN)_6^{3-} + e^- \rightleftharpoons H_2Fe(CN)_6^{2-} \quad (6)$$

The protons included in the coordination sphere in hexacyanoferrate (II) indicate chemical reactions coupled to electron exchange. This could explain the hysteresis observed in the coulometric experiments.

Table 2
Published formal potentials for the $Fe(CN)_6^{3-}/Fe(CN)_6^{4-}$ couple

$E°_{Fe(CN)_6^{3-}/Fe(CN)_6^{4-}}$ (V vs. SHE)	Conditions	Ref.
0.356	Standard	[12,14]
0.48	0.01 M HCl	[14]
0.56	0.1 F HCl	[12,14]
0.689	0.5 M H_2SO_4	This work, potentiometric method.
0.678	0.5 M H_2SO_4	This work, coulometric method, Fe(III) → Fe(II)
0.691	0.5 M H_2SO_4	This work, coulometric method, Fe(II) → Fe(III)
0.690	1 M H_2SO_4	[15]
0.72	1 M H_2SO_4	[14]
0.72	1 M $HClO_4$	[12,14]
0.71	1 M HCl	[12,14]

5. Conclusions

From the above results, it is possible to propose the refinement of formal potentials by the SQUAD program, using the log K proposed by Sillén for redox couples.

The data can be obtained from potentiometric and spectrophotometric measurements. In addition, we showed that refinement of the formal potential from coulometric steady-state and spectrophotometric measurements is also possible. The application of this methodology to redox systems with several couple electron exchanges and chemical reactions will contribute to the understanding of the electrochemical behavior of complex systems. Interpretation of the data must be done carefully, such as in this case for $Fe(CN)_6^{3-}/Fe(CN)_6^{2-}$ in 0.5 M H_2SO_4, since spectrophotometric changes may result from a chemical reaction irrelevant to the

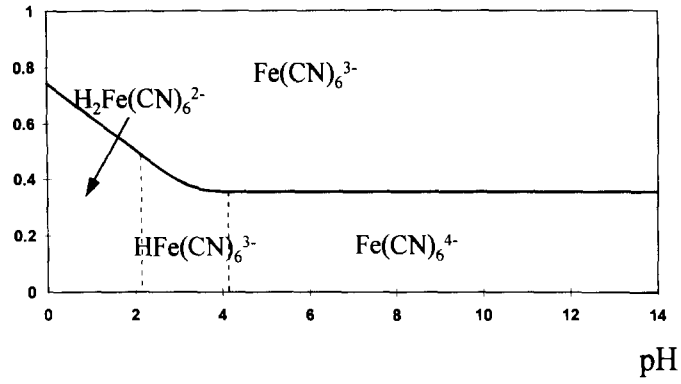

Fig. 4. Pourbaix diagram for the $Fe(CN)_6^{3-}/Fe(CN)_6^{2-}$ couple. Data taken from Sillén [10]. It is assumed that $Fe(CN)_6^{3-}$ and $H_iFe(CN)_6^{i-4}$ are inert complexes [13].

potential being measured. The application of the methodology to complex systems will be demonstrated in future studies.

Acknowledgements

This work was financially supported by CONACYT. The authors thank Professor Josef Havel for helpful comments.

References

[1] F.M. Hawkridge and T. Kuwana, Anal. Chem., 7 (1973) 1021.
[2] L. Mackey, E. Steckhan and T. Kuwana, Ber. Bunsenges. Phys. Chem., 79 (1975) 587.
[3] D.J. Leggett and W.A. McBryde, Anal. Chem., 47 (1975) 1065.
[4] D.J. Leggett, Anal. Chem., 49 (1977) 276.
[5] D.J. Leggett, Anal. Chem., 50 (1978) 718.
[6] D.J. Leggett, S.L. Kelly, L.R. Shiue, Y.T. Wu, D. Chang and K.M. Kadish, Talanta, 30 (1983) 579.
[7] D.J. Leggett, Computational Methods for the Determination of Formation Constants, Plenum Press, New York, 1985.
[8] F.R. Hartley, C. Burgess and R.M. Alcock, Solution Equilibria, Wiley, New York, 1980.
[9] M. Meloun, J. Havel and E. Högfeldt, Computation of Solution Equilibria, Wiley, Chichester, 1988.
[10] G. Sillén, Stability Constants of Metal-Ion Complexes, Special Publication No. 17, Chemical Society, London, 1971.
[11] E. Vieil and F. Miomadre, J. Electroanal. Chem., 395 (1995) 15.
[12] L. Meites, Handbook of Analytical Chemistry, McGraw-Hill, New York, 1963.
[13] A.J. Bard, Chemical Equilibrium, Harper and Row, New York, 1966, p. 94.
[14] R.A. Day and A.L. Underwood, Quantitative Analysis, Prentice Hall, Englewood Cliffs, NJ, 1989.
[15] A.J. Bard and L.R. Faulkner, Électrochimie, Principes, Méthodes et Applications, Masson, Paris, 1983.

ELSEVIER

Talanta 44 (1997) 39–46

Talanta

Direct determination of cadmium in solids using a capacitively coupled microwave plasma atomic emission spectrometer

Andrea M. Pless[1], Andrea Croslyn, Mary Jane Gordon, Benjamin W. Smith, James D. Winefordner*

Department of Chemistry, University of Florida, Gainesville, FL 32611, USA

Received 14 March 1996; revised 23 May 1996; accepted 23 May 1996

Abstract

A capacitively coupled microwave plasma (CMP) operating at 800 W was examined for the direct determination of cadmium in solids. The laboratory-constructed system contained a tungsten cup electrode capable of holding microsample quantities. A low-powered plasma was used to heat the sample, while at higher powers the plasma was used for sample vaporization and excitation. This plasma enabled thermal vaporization (TV) sample introduction to be accomplished in situ as the plasma formed directly around the sample. Thus, the need for sample preparation, procedural steps and sample transport was eliminated. This technique was capable of the direct determination of trace elements in solid samples in less than 5 min. The effects of experimental parameters such as gas flow rate, atomization power and electrode position were investigated. Detection limits obtained for Cd by TV–CMP-AES were in the picogram range with a relative standard deviation of $<20\%$. The accuracy and precision of the method were also evaluated by measuring Cd in several NIST Standard Reference Materials.

Keywords: Atomic emission spectrometry; Cadmium; Capacitively coupled microwave plasma; Solids

1. Introduction

The direct analysis of solids is important for several reasons. Because many samples occur naturally in solid form, pretreatment is usually needed to convert the sample into a liquid for analysis. Dissolution of the solid prior to analysis is often time consuming and requires the use of hazardous chemicals. Contamination from the added reagents can also occur [1]. Dilution errors and sample transfer losses arising from sample handling steps are possible and can lead to poor detection limits [2]. Also, some digestion procedures may result in the loss of some volatile elements [3]. In addition, the resultant solution can contain a high salt content with the potential for clogging nebulizers [4]. The plasma perfor-

* Correspsonding author. Fax: (352) 392-4651; e-mail: jdwin@chem.ufl.edu.

[1] Present address: Air Products and Chemicals, Inc., 7201 Hamilton Blvd., Allentown, PA 18195, USA.

PII S0039-9140(96)02006-1

mance as an excitation and atomization source can be degraded from the introduction of the solvent [5]. These problems can be avoided by the direct analysis of solids, as this would allow the sample to be analyzed in its natural state [2]. However, direct introduction of solids into plasmas does suffer from some disadvantages. Poorer precision is observed than with solution nebulization techniques [6]. Sample heterogeneity becomes more of a concern owing to the small sample sizes required of this method [2]. Furthermore, calibration curves are more difficult to determine as compared with solution analysis, where aqueous standards are used directly [7]. Even so, direct analysis of solids offers a means of rapidly quantifying the elemental content of a sample before it is subjected to extensive pretreatment.

Several methods have been used for the direct introduction of solids into an inductively coupled plasma (ICP). These include direct sample insertion (DSI) [2,8,9], electrothermal vaporization (ETV) [7,10,11], arcs [12], sparks [13], laser ablation [2] and slurry nebulization [14]. However, these techniques have some difficulties, including transport losses of analyte, background shifts, the need for matrix modifiers, the difficulty with availability of standards and tedious sample preparation and/or sample introduction procedures. Some of these problems can be alleviated by performing direct solid introduction into a capacitively coupled microwave plasma (CMP). The CMP allows for the analysis of an analyte in situ as the plasma forms directly around the sample. Thus, the need for sample preparation and procedural steps is eliminated. Also, this method allows for discrete sampling without any resultant sample dilution or losses.

Until recently, no work has been reported on methods of direct solid sampling without employing some means of analyte vapor transport into microwave plasmas. Ali et al. [4] developed a method for the rapid screening of solids using CMP-AES. The solid powder samples were placed in a graphite cup electrode and then the electrode was heated to initiate vaporization and atomization of the analyte. This method was evaluated using samples of tomato leaves (NIST SRM 1573a) and coal fly ash (SRM 1633a). Limits of detection were observed in the nanogram range.

Masamba et al. [5] used this same technique for the direct analysis of steel samples. Metal samples are conducting, easily machined into different shapes, resistant to sputtering and relatively homogeneous. For these reasons, metals are amenable to direct analysis. The steel samples were machined into cylinders which could fit snugly into the top of a hollow graphite holder. Power was supplied to the holder to create a plasma for vaporization and atomization of the analyte. Detection of constituents in steel was possible from less than 1 $\mu g\ g^{-1}$ to the per cent range.

In this work, a CMP with a tungsten cup was used for the determination of cadmium. Samples of graphite powder, to which Cd has been added, and a variety of NIST of Standard Reference Materials (SRMs) were evaluated. A mixture of helium and hydrogen was used as the plasma gas. The effects of experimental parameters were examined. The detection limit for solid Cd was in the picogram range. The results were compared with those previously obtained for Cd in solution [15]. The accuracy and precision of this method of direct analysis were also investigated.

2. Experimental

2.1. Instrumentation

The laboratory-constructed CMP system consisted of a high-voltage power supply which transferred energy to a 2450 MHz magnetron. The actual microwave power output of the magnetron could not be measured, thus the power used represented the amount of power supplied to the magnetron. The energy propagated as a standing wave through a brass waveguide with the plasma forming at the surface of the electrode. The tungsten cup electrode supported by a graphite holder sits in the center tube of a two concentric tube quartz torch and is shown in Fig. 1. The tungsten cup was capable of holding a volume of up to 10 μl. The plasma gas was introduced through the bottom of the torch.

Emission was detected by a 1 m Jobin-Yvon spectrometer which contained a photodiode array (PDA) detector. The design of this CMP system was described in greater detail elsewhere [15].

2.2. Sample preparation

The Cd solid standards used for analysis were prepared from cadmium chloride salt obtained from Fisher Scientific (Fairlawn, NJ, USA). The Cd salt was added to a 10 g quantity of high-purity graphite powder (grade SP2X, lot 721, Union Carbide, New York, USA) and thoroughly mixed in plastic vials using a ball-mill. This solid standard was quantitatively diluted with additional spectroscopic-grade graphite powder to prepare the remaining concentrations. It was necessary to use coarse graphite powder for the standards because fine powder caused atomization difficulties.

The SRMs studied were obtained from the National Institute of Standards and Technology (NIST). These solid samples included coal fly ash (1633a), tomato leaves (1573a), Montana soil (2711), bovine liver (1577b) and oyster tissue (1566a). No pretreatment or dilution steps were performed on these samples prior to analysis.

2.3. Procedure

The solid samples were deposited into the tungsten cup using a micropipettor (Model 225, Drummond Scientific, Broomall, PA, USA) with glass capillary tips, which was originally designed for liquid introduction. The pipettor was set to 1 μl and the end of the capillary was inserted into the solid sample. The pipettor was repeatedly moved back and forth until the tip was filled. Any sample adhering to the outside walls of the capillary was wiped off before deposition into the tungsten cup. The amount of sample dispensed was determined by calibration. The calibration was performed by weighing 20 loads of the graphite standard with a microbalance. It was determined that for a 1 μl load, 0.6 mg of Cd solid in graphite was introduced with about an 8% relative standard deviation (RSD).

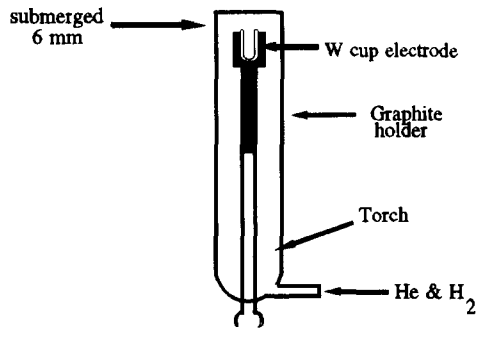

Fig. 1. Exaggerated view of tungsten cup design. The inner diameter is 3 mm, the outer diameter is 4 mm and the depth is 2 mm.

Once deposited in the electrode cup, the sample was subjected to a preatomization step which used a low-powered plasma to heat the sample. Preatomization was performed at a microwave power of 124 W for 3 s. After this step, the gas flow rates were set to the appropriate levels. The power was then rapidly increased to the atomization power, while simultaneously starting the computer for data acquisition. The emission signal was integrated for 1.0 s intervals for a 3 s time period. The electrode was submerged 6 mm below the top of the torch as shown in Fig. 1. The emission signal was observed at 5 mm above the electrode cup. All experimental parameters were optimized for the best signal-to-background ratios.

After each sample had been measured, it was necessary to clean the electrode cup. This was accomplished using a laboratory-constructed "vacuum cleaner". A Pasteur pipet was connected to a side-arm flask with a rubber hose. The top of the flask was attached to a ceiling vent. The pipet was placed inside the tungsten cup and the suction from the vent was used to remove any residue. This method proved satisfactory for sample removal as it was quick and easy to use.

2.4. Detection limits

Peak heights were used in the analysis of the data. The peak height was obtained from the maximum signal over a 3 s time interval to vaporize and excite the analyte. The peak height from this spectrum was corrected for the blank signal. The blank was graphite powder which had also been subjected to mixing with a ball-mill. The

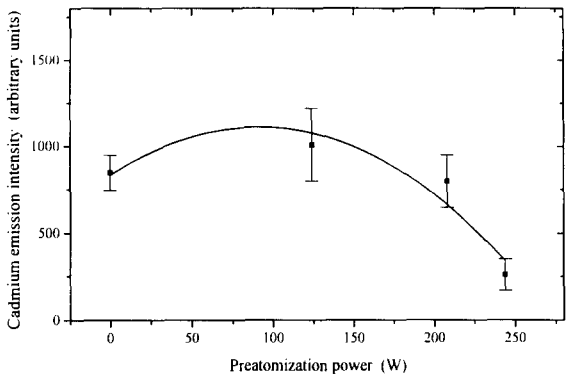

Fig. 2. Effect of preatomization power on solid Cd signal.

signals were background corrected by the computer software. All signals are reported as the mean of the three measurements with error bars representing one standard deviation from the mean. The calibration curve was obtained using the optimal experimental conditions determined from solid Cd. The optimization studies for each parameter were performed individually while all other experimental conditions were held constant. The optimal conditions were defined as those which produced a maximum signal-to-background ratio. The detection limit was determined as three times the standard deviation in the blank. The blank standard deviation was calculated from 10 measurements of the blank signal at a wavelength of 228.802 nm.

3. Results and discussion

3.1. Preatomization stage

The preatomization stage was necessary for the analysis of the solid Cd samples by thermal vaporization introduction into the CMP. It was found that elimination of this step produced an initial instability of the plasma which led to atomization difficulties. Also, the sample would sputter out of the electrode, contributing to irreproducible signals. However, it was found that preatomization at high powers results in signal losses of Cd as shown in Fig. 2. These losses were attributed to the volatile nature of this analyte. Similar results were found by previous researchers [4,16]. It was determined that a preatomization power of 124 W was sufficient for solid Cd measurements.

Optimization of the duration of the preatomization stage was also necessary. The preatomization time is the difference between the time the plasma was ignited and the time when the power was increased for atomization. It was found that the Cd signal was relatively constant with increasing preatomization times up to 60 s.

3.2. Temporal profile

The emission signals obtained were transient, which is an inherent characteristic of the thermal vaporization technique. The temporal profile of 180 pg of Cd in graphite powder is displayed in Fig. 3. For Cd in graphite, the signal lasted approximately 3 s. These results were similar to those observed for aqueous Cd [15].

3.3. Electrode position

The vertical distribution of the Cd emission for Cd in graphite is shown in Fig. 4. The observation height is the position above the electrode in the plasma where the signal is observed. A 0 mm observation height corresponds to the electrode surface being even with the center of the entrance slit of the spectrometer. The maximum signal-to-background ratio, and therefore the optimal emission signal, were observed to occur at 5–6 mm observation height; this low height was attributed to the volatile nature of Cd. Similarly to aqueous Cd [15], the background level also increased at 5–6 mm. In addition, the emission intensity began to decrease at observation heights greater than 7 mm.

The horizontal distribution of the emission of Cd (in graphite) across the plasma was also examined. A cylindrical-shaped plasma was used for the measurements and produced a uniform emission intensity for Cd (in graphite samples) over a width of 1 mm. These results are similar to those obtained for cylindrical plasmas with aqueous analytes [15]. The emission intensity across the plasma was asymmetric.

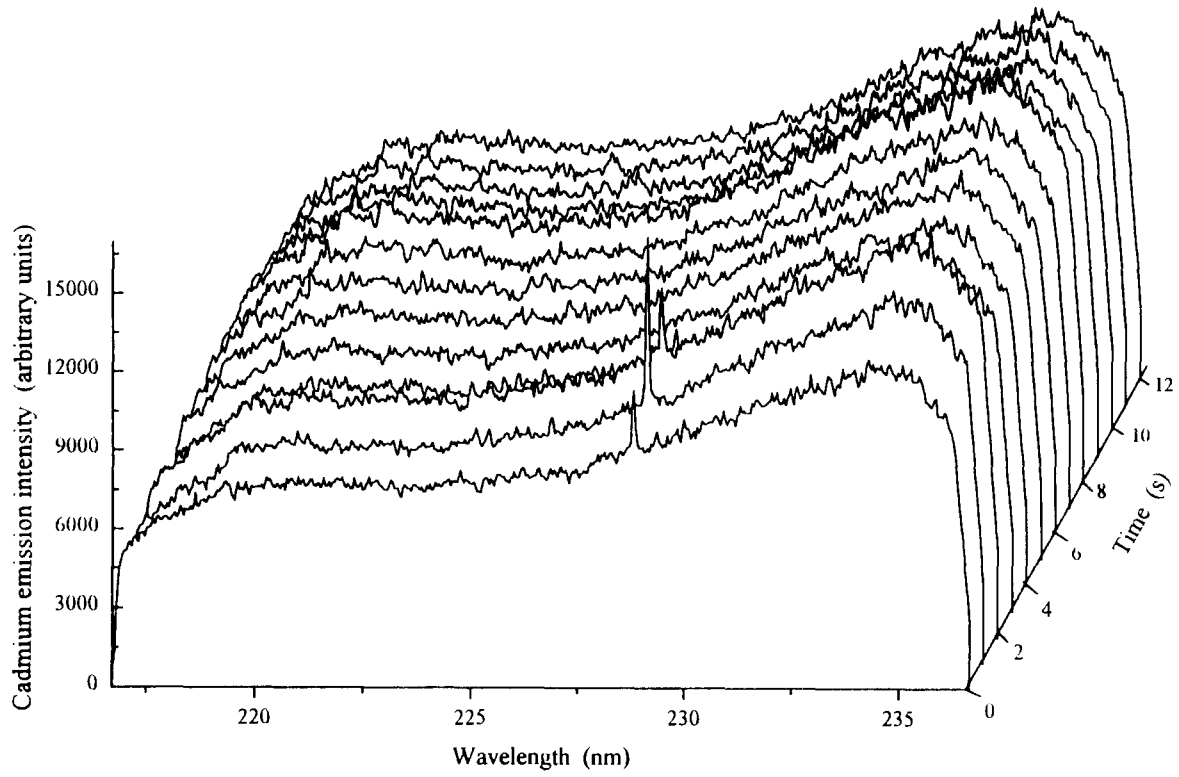

Fig. 3. Temporal profie of 180 pg of the emission signal Cd (in graphite powder) at 228.802 nm.

3.4. Atomization power

It was found that the emission intensity for Cd in graphite increased with increasing atomization power to a maximum; the maximum occurred when 800 W of power was supplied (see Fig. 5). Further increase in the atomization power led to a decrease in the intensity. These observations differ from those reported for Cd in aqueous samples [15]. The higher atomization power required here was probably due to the solid nature of the matrix.

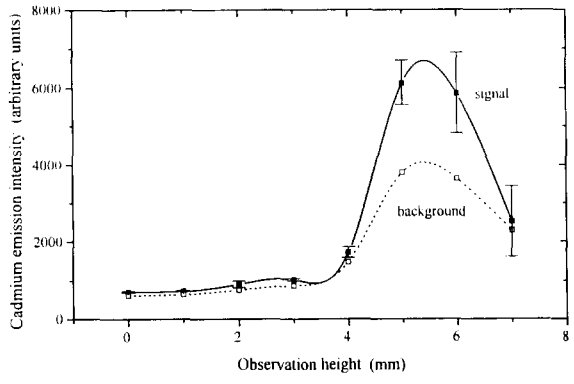

Fig. 4. Vertical distribution of solid Cd signal and background.

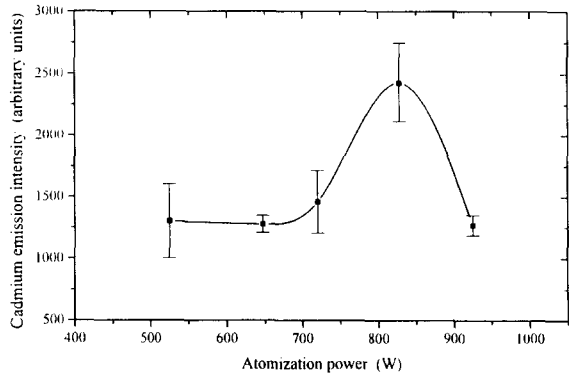

Fig. 5. Effect of atomization power on the emission signal for Cd in graphite.

Table 1
Comparison of optimal conditions selected for solid and aqueous [15] Cd

Parameter	Solid	Aqueous
Wavelength (nm)	228.802	228.802
Observation height (mm)	5	4
Displacement (mm)	0	0
He flow rate (l min^{-1})	7	5
H_2 flow rate (cm^3 min^{-1})	380	460
Preatomization/drying power (W)	124	90
Preatomization/drying time (s)	20	45
Atomization power (W)	828	525–630

3.5. Plasma gas flow rate

The helium flow rate did not have a significant effect on the Cd signal (in graphite). However, the emission intensity did experience a twofold increase at 7 l min^{-1}. The reason for this increase is unknown. Further investigation of solids with a CMP needs to be performed before definite conclusions can be drawn. The plasma was observed to be cylindrical in shape at this flow rate. These findings are similar to those for Cd in aqueous samples [15].

Just as for Cd in pollution samples [15,17–19], a small addition (of ca. 400 cm^3 min^{-1}) results in the maximum. The signal was not detectable unless at least 100 cm^3 min^{-1} of H_2 was introduced. If flow rates higher than 400 cm^3 min^{-1} were used, the emission signal decreased slightly, probably as a result of the decrease in the excitation temperature of the plasma with increase in hydrogen addition. [18].

3.6. Trace Cd determination

The operating conditions used for evaluating the analytical performance of TV–CMP-AES for solid Cd were based upon the optimization studies just described. The optimal conditions were selected as those which produced a maximum signal-to-background ratio while all other parameters were held constant. These conditions are given in Table 1. The conditions for both matrices were similar, with the main difference being the atomization power required for analysis. The higher power necessary for the solid analyses is probably due to the nature of the matrix. The analytical calibration curve for Cd in graphite was linear and had a log–log slope of 1.0 over the region from the detection limit to at least two orders of magnitude higher. The absolute detection limit obtained for Cd in graphite was 40 pg and the concentration detection limit was 70 ng g^{-1}. These absolute and relative detection limits are also compared with those obtained for Cd in solid samples by analogous methods [4,20] in Table 2.

When comparing the results obtained for Cd in both an aqueous and a solid matrix, many similarities are observed (Table 1). As mentioned previously, many of the operating conditions chosen to be optimal for the Cd measurement closely agree. Likewise, the trends observed for most of the experimental parameters agree. However, it was still discovered that the determination of Cd was not independent of the matrix studied. This was demonstrated by the fact that there was a threefold difference in the slopes of the calibration curves obtained for these matrices. This difference was largely a result of the dissimilar trend in the atomization power required for analysis. The solid matrix required a higher power for Cd measurement, and above this power the emission intensity decreased. In an aqueous matrix, the atomization power increased to a maximum and then reached a steady state. Further studies of the behavior of solids in a CMP should be investigated before any more conclusions can be drawn.

Table 2
Comparison of detection limits for Cd

Technique	LOD	
	pg	ng g^{-1}
This work (solid)	40	70
Graphite cup TV–CMP [4]	300	30
DSI–ICP-AES [20][a]	300	1

[a] DSI = direct solid introduction.

Table 3
Determination of Cd in solid SRMs

Sample	SRM	Measured concentration[a] ($\mu g\ g^{-1}$)	Certified concentration ($\mu g\ g^{-1}$)	Bias (%)
Montana soil	2711	38 ± 11	41.70 ± 0.25	−9
Tomato leaves	1573a	1.4 ± 0.4	1.52 ± 0.04	−8
Bovine liver	1577b	0.6 ± 0.3	0.50 ± 0.03	20

[a] The ± values represent confidence intervals for the three measurements at the 95% level.

3.7. Standard reference materials

The accuracy and precision of the method developed for the determination of Cd in solids using CMP-AES were examined. Analyses were performed using a variety of SRMs obtained from NIST without any prior sample preparation. The operating conditions used were those listed in Table 1. The results observed for Cd measurment are displayed in Table 3 compared with the certified concentrations provided by NIST. The listed concentration ranges are within one standard deviation of the mean of three measurements. These values were obtained based upon the calibration of Cd in graphite powder. The observed concentrations closely agree with the certified values for each of the SRMs Montana soil, tomato leaves and bovine liver, showing less than 10% bias for the first two and 20% for the third. The accuracy may possibly be improved by performing the calibration by the method of standard additions, thus eliminating any errors caused by matrix effects. Even so, the precision of the measurments was less than about 20%. The precision was limited by sampling precision and data processing precision (selection of temporal peak). Current work involves the measurement of the peak area, which should minimize the latter.

4. Conclusions

The method developed for the determination of Cd in solid samples using TV–CMP-AES is capable of measurement at trace levels. A detection limit of 40 pg was possible with an RSD of <20%. The experimental conditions were found to agree closely with those obtained for the determination of Cd in aqueous solution. The main difference in the operating conditions between these two matrices was the atomization power, which at present makes the current method matrix dependent. Even so, this technique provided reasonable accuracy when applied to solid standard reference materials and compared favorably with other atomic methods of analysis. In addition, this preliminary investigation demonstrated the promise of TV–CMP for the direct analysis of solid samples.

Acknowledgements

The authors acknowledge the financial support of the Engineering Research Center (ERC) for Particle Science and Technology at the University of Florida, The National Science Foundation (NSF), grant EEC-94-02989, and the Industrial Partners of the ERC.

References

[1] F.J. Langmyhr, Analyst, 104 (1979) 993.
[2] C.W. McLeod, M.W. Routh and M.W. Tikkanen, in A. Montaser and D.W. Golightly (Eds.), Inductively Coupled Plasmas in Analytical Atomic Spectrometry, VCH, New York, 1992, Ch. 16.
[3] M. Abdullah and H. Haraguchi, Anal. Chem., 57 (1985) 2059.

[4] A.H. Ali, K.C. Ng and J.D. Winefordner, J. Anal. At. Spectrom., 6 (1991) 211.
[5] W.R.L. Masamba, B.W. Smith and J.D. Winefordner, Appl. Spectrosc., 46 (1992) 1741.
[6] J.M. Carey and J.A. Caruso, CRC Crit. Rev. Anal. Chem., 23 (1992) 397.
[7] V. Karanassios, J.M. Ren and E.D. Salin, J. Anal. At. Spectrom., 6 (1991) 527.
[8] V. Karanassios and G. Horlick, Spectrochim. Acta Rev., 13 (1990) 89.
[9] W.T. Chan and G. Horlick, Appl. Spectrosc., 44 (1990) 380.
[10] D.R. Hull and G. Horlick, Spectrochim Acta, Part B, 39 (1984) 843.
[11] H. Nickel, Z. Zadgorska and G. Wolff, Spectrochim. Acta, Part B, 48 (1993) 25.
[12] P.B. Farnsworth and G.M. Hieftje, Anal. Chem., 55 (1983) 55 1414.
[13] A. Aziz, J.A.C. Broekaert, K. Laqua and F. Leis, Spectrochim. Acta, Part B, 39 (1984) 1091.
[14] L. Ebdon, M.E. Foulkes and S. Hill, J. Anal. At. Spectrom., 5 (1990) 67.
[15] A.M. Pless, B.W. Smith, M.A. Bolshov, J.D. Winefordner, Spectrochim. Acta, Part B, in press.
[16] B.M.Spencer and J.D. Winefordner, Can. J. Spectrosc., 39 (1994) 43.
[17] W.R.L. Masamba, A.H. Ali and J.D. Winefordner, Spectrochim. Acta, Part B, 47 (1992) 481.
[18] W.R.L. Masamba and J.D. Winefordner, Spectrochim. Acta, Part B, 48 (1993) 521.
[19] B.M. Spencer, B.W. Smith and J.D. Winefordner, Appl. Spectrosc., 48 (1994) 289.
[20] H. Matusiewicz and R.M. Barnes, Anal. Chem., 57 (1985) 406.

ELSEVIER

Talanta 44 (1997) 47–51

Talanta

Line selection and interference correction for the analysis of tungsten alloy by inductively coupled plasma atomic emission spectrometry

Zun Ung Bae[a,*], Sang Hak Lee[a], Sung Ho Lee[b]

[a]*Department of Chemistry, Kyungpook National University, Taegu 702-701, South Korea*
[b]*Central Research Institute, Korea Tungsten Co., Dalsung, Kyungpook 711-860, South Korea*

Received 17 October 1995; revised 20 May 1996; accepted 30 May 1996

Abstract

A method for the analysis of tungsten alloy to determine selected elements using inductively coupled plasma atomic emission spectroscopy is described, with emphasis on line selection and spectral interference. The spectral interference coefficients were calculated for the spectral lines of selected major and trace elements. These values were used to select analytical lines and to calibrate concentrtions of the analytes. The detection limits of the elements for this method were determined and compared with those obtained by flame atomic absorption spectrometry and direct current carbon arc emission spectrometry. The results indicated that the detection limits for all of the elements determined by the proposed method are significantly better than those obtained by other techniques. In this study, the analytical reliability of the proposed method was estimated by comparison of the analytical data for the two types of tungsten alloys produced by the Korean Tungsten Company with those obtained by the matrix matching method and the results indicated that the accuracy of multi-element analysis is satisfactory.

Keywords: Inductively coupled plasma atomic emission spectrometry; Interference correction; Line selection; Tungsten alloy

1. Introduction

Tungsten alloys are of great importance in various branches of industry. They are mainly employed for radiation shields, balance weights and inertial navigation systems [1]. A detailed knowledge of the levels of the major and trace elements in metal alloys is essential since they may have either a deleterious or beneficial effect upon the mechanical and physical properties of alloys [2–5]. Trace element analysis of metal alloys can be a problem owing to the difficulty of dissolution and the instability of the sample solutions. Inductively coupled plasma atomic emission spectroscopy (ICP-AES) is a popular tool in the determination of trace elements [6–22], but a current limitation is the spectral interferences observed with elements that emit line-rich spectra. In order to

* Corresponding author. Fax: (82) 53-950-6330.

PII S0039-9140(96)02007-3

overcome this problem, a number of studies have been carried out to develop methods for isolating elements from complex matrices, including coprecipitation [9–11], complex formation [12,13] hydride conversion [14], adsorption [15], ion exchange [16] and chromatography [17–19]. However, these methods are concomitant with the risk of contamination from the chemicals and tedius time-consuming procedures.

In this study, the interfering spectral lines for nearly all of the elements in tungsten alloy that can be determined by ICP-AES were investigated. Spectral interferences, which arise from the incomplete isolation of the net signal at the analysis line, seriously affect the analytical results, particularly when high concentrations of matrix constituents are present. For the analytical lines of elements of interest we calculated the spectral interference correction coefficient (K_{ij}), which is defined by the ratio of the spurious concentration observed for element i and the actual concentration of interference j to evaluate quantitatively the amount of spectral interference on the individual lines. The corrected concentrations of the elements for the real samples were obtained using the K_{ij} values and the results were compared with those obtained by other analytical methods such as flame atomic absorption spectrometry (FAAS) and direct current carbon arc atomic emission spectrometry (d.c. arc AES). The detection limits for the analytes were also evaluated for the procedure suggested in this paper.

2. Experimental

2.1. Instrumentation

For ICP-AES, a JY 38 Plus ICP system (Jobin-Yvon, Longjumeau, France) was employed. Argon was used to purge the optical path and the monochromator for wavelengths in the range 180–195 nm. Since solutions containing hydrofluoric acid were employed in the present study, a hydrofluoric acid-resistant sample introduction system was used. This system consists of a platinum–iridium concentric nebulizer (Jobin-Yvon; Cat. No. 20925080), a PTFE nozzle, a Scott-type coaxial plastic spray chamber (Jobin-Yvon; Cat. No. 11285268), a plastic sheathing tube and a sapphire sample introduction tube. A force-fed Miniplus II peristaltic pump (Jobin-Yvon; Cat. No. 21357000) was used to deliver sample solution at a rate of 1.5 ml min^{-1}. The other operating conditions for ICP-AES are listed in Table 1. For FAAS a Model 3030B atomic absorption spectrometer (Perkin-Elmer, Norwalk, CT, USA) was used, and for d.c. arc AES a Model 70-000 system (Thermo Jarrell Ash, Franklin, MA, USA) with a 3.4 m focal length monochromator with a ruled grating was employed.

2.2. Samples and reagents

Two types of tungsten alloys (Grades P and T) used for real sample analysis were supplied by the Korea Tungsten Company (Kyungpook, Korea). Water was purified with a Milli-Q system (Millipore, Bedford, MA, USA). Concentrated hydrofluoric acid and nitric acid were of analytical-reagent grade. Metal standard solutions for ICP measurements were prepared by diluting 1000 ppm stock solutions obtained from Spex Industries, (Edison, NJ, USA). Internal standard and buffer materials used for d.c. arc AES were silver chloride (Zeebac; reagent grade) and Specpure graphite powder (Bay Carbon; spectrographic grade), respectively.

2.3. Sample preparation

2.3.1. ICP-AES and AAS

Tungsten and related samples were dissolved in a mixture of high-purity hydrofluoric and nitric

Table 1
Operating conditions for ICP-AES

Sample delivery	1.5 ml min^{-1} using peristaltic pump
Ar gas flows:	
Cooling	13–15 l min^{-1}
Coating	0.2–0.4 l min^{-1}
Nebulizing	0.3–0.5 l min^{-1}
Observation height	15 mm above upper coil
Slit widths	Entrance 20 μm, exit 20 μm
Spectral range	170–800 nm
Generator frequency	40.68 MHz

Table 2
ICP-AES interference correction coefficients (K_{ij}) for tungsten alloy analysis[a]

Analyte line (nm)		K_{ij}				
		Co	Nb	Ta	Ti	W
Al	396.152	0.004	1.247	0.719	0.528	0.018
Co	238.892		0.005	0.083	0.005	0.222
Cr	284.325	0.109	0.204	0.204	0.102	0.020
Fe	238.204	0.076	0.038	0.260	0.003	0.027
Nb	313.079	0.085		0.655	84.16	0.025
Ni	231.604	0.520	0.005	7.652	0.158	0.107
Ta	238.706	0.418	69.46		0.009	0.264
Ti	323.451	0.002	0.074	0.185		0.005
V	290.882	0.066	8.308	0.253	0.004	0.028
W	207.911	0.005	0.006	0.008	0.005	

[a] Only the K_{ij} values for major elements are listed. The analyte wavelengths with the lowest ΣK_{ij} values are listed.

acids, adding 3 ml of each acid slowly to 1 g of sample. The mixture was then heated in a microwave digestion system (CEM; Model MDS-81D) until dissolution was achieved. The system was operated at 90% power (576 W) for 3 min, 0% for 3 min and 50% (320 W) for 3 min in sequence. The resulting solution was diluted with deionized water to give a final volume of 100 ml. In order to determine minor components in samples using the matrix matching method, standard solutions were prepared using aqueous solutions containing the same percentage of major constituents as those in the real samples.

2.3.2. D.c. arc AES

For d.c. arc AES, the sample was mixed with buffer (2 parts sample + 3 parts buffer) with a Wig-L-Bug shaker for 60 s. The composition of buffer used was 1 part silver chloride (Zeebac; reagent grade) and 2 parts Specpure graphite powder (Bay Carbon; spectrographic grade). The mixture of 75 mg was then loaded into graphite cups (Bay Carbon; Model S-12). Trace element analysis was carried out with a current of 10 A and an arcing period of 40 s. The signal at the 244.793 nm line of Ag was used as an internal standard.

3. Results and discussion

3.1. Line selection

Line selection was performed for the major and trace elements using a solution containing 10 g l^{-1} of each of the major components. Spectral interferences of spectral lines of the elements to be determined were studied by scanning the spectra of the interfering elements using the profiling mode of the analysis program. For the simultaneous determination of elements of interest in tungsten alloy, the most sensitive line for each element cannot always be used owing to the possible interferences of spectral lines of major components.

In order to evaluate quantitatively the amount of spectral interferences, the interference ocrrection coefficients (K_{ij}) for all of the lines of the elements were calculated. K_{ij} is defined by Eq. (1) and the values are listed in Table 2 [23–25].

$$K_{ij} = \frac{\text{spurious concentration observed for element } i \text{ (ng ml}^{-1}\text{)}}{\text{actual concentration of interferent } j \text{ (}\mu\text{g ml}^{-1}\text{)}} \quad (1)$$

A K_{ij} value of 0.01 means that a spurious concentration of 100 ppb was observed for the element i

Table 3
Detection limits (ppm) for elemental analysis of tungsten alloy by ICP-AES

Elements	Wavelength (nm)	K_{ij} method	FAAS	D.c. Arc AES
Al	396.152	0.010	0.091	0.07
Co	238.892	0.022	0.080	0.06
Cr	284.325	0.010	0.055	0.05
Fe	238.204	0.015	0.040	0.05
Nb	313.079	0.025		0.52
Ni	231.604	0.050	0.070	0.05
Ta	238.706	0.480		0.53
Ti	323.451	0.005	0.051	0.04
V	290.882	0.013		0.09
W	207.911	0.030	1.0	0.50

in the matrix solution of 1.00% (w/v). Therefore, it is recommended to select the wavelength at which the sum of K_{ij} values of the interferent elements are the lowest. The corrected concentrations using the K_{ij} values were calculated from the equation

$$C_i' = C_i - \sum K_{ij} C_j \quad (2)$$

where C_i', C_i and C_j are the corrected, measured and matrix concentration, respectively. Thus the corrected concentrations should provide more reliable

Table 4
Analytical results for multi-element analysis by ICP-AES using K_{ij} and matrix matching methods

Sample	Element	Wavelength (nm)	Certified value	K_{ij} method[a]	Matrix matching method[a]	Concentration unit
Grade P	Co	238.892	5.0 ± 0.1	5.05 ± 0.10	5.06 ± 0.09	%
	Nb	313.079		< 0.03		%
	Ta	238.706	2.0 ± 0.1	1.90 ± 0.10	1.89 ± 0.15	%
	Ti	323.451	2.0 ± 0.1	2.05 ± 0.08	2.08 ± 0.09	%
	W	207.911	85.0 ± 0.8	85.40 ± 0.61	85.45 ± 0.50	%
	Fe	238.204		95 ± 10	90 ± 10	ppm
	Ni	231.604		140 ± 18	145 ± 20	ppm
	Al	396.152		< 0.01		ppm
	Cr	284.325		< 0.01		ppm
	V	290.882		< 0.02		ppm
Grade T	Co	238.892	10.0 ± 0.5	10.20 ± 0.15	10.15 ± 0.10	%
	Nb	313.079	2.00 ± 0.1	1.95 ± 0.10	1.94 ± 0.09	%
	Ta	238.706	7.0 ± 0.2	7.20 ± 0.12	7.25 ± 0.15	%
	Ti	323.451	8.00 ± 0.2	7.93 ± 0.13	7.90 ± 0.12	%
	W	207.911	60.0 ± 0.8	59.3 ± 0.75	59.8 ± 0.80	%
	Fe	238.204		115 ± 15	120 ± 13	ppm
	Ni	231.604		120 ± 10	115 ± 15	ppm
	Al	396.152		< 0.01		ppm
	Cr	284.325		< 0.02		ppm
	V	290.882		< 0.02		ppm

[a] Errors are standard deviations for five measurements.

data in the determination of trace elements in a tungsten matrix.

3.2. Detection limit

The detection limits for 10 elements are listed in Table 3. These detection limits are the concentrations required to give a signal three times greater than the standard deviation of the background fluctuation. The relative standard deviation of the background was determined for each selected analytical line for 10 replicates measured with a 0.5 s integration time. The average value of the standard deviation was found to be about 1% for the matrix solution. This value does not significantly differ from that found for pure waer. On the other hand, the signal-to-background ratios were substantially decreased in the presence of matrix, which explains the difference between the detection limits measured in water and with matrix. In comparison with the detection limits in aqueous solution, the ICP-AES detection limits in the matrix solution were decreased by factors varying from 1 to 20. The values of the detection limits for the elements determined by the present technique are also compared with those obtained by FAAS and d.c. arc AES in Table 3. The results indicate that the detection limits for all the elements except V, Ta and Ni determined by the proposed method are better than those obtained by the other techniques.

3.3. Analysis of tungsten alloys

Determinations of major and trace elements in two types of tungsten alloys obtained from the Korea Tungsten Company were performed by the K_{ij} correction method. The results are presented in Table 4. The certified values listed in Table 4 were obtained by collaborative trials. The concentrations of major elements obtained by the K_{ij} correction method are in good agreement with the certified values and those obtained by the matrix matching technique. The analytical data for the trace elements were also found to agree with those obtained by the matrix matching method.

References

[1] M.B. Bever, Encyclopedia of Materials and Engineering, MIT Press, Boston, MA, 1986, p. 4159.
[2] H. Yamaguchi, K. Yamada, O. Kujirai and R. Hasegawa, Bunseki Kagaku, 42 (1993) 145.
[3] D.Herbert, A. Bbdolvahab, L. Benno, K. Erich, F. Gernot and G. Manfred, Mikrochim. Acta, 108 (1992) 163.
[4] H. Danninger, W. Pisan and B. Lux, Int.J. Refract. Hard Met., 5 (1986) 144.
[5] E. Kny and H.M. Otner, Int. J. Refract. Hard Met., 4 (1985) 77.
[6] G. Henrion, J. Gelbrecht and H. Lippert, Z. Chem., 20 (1980)108.
[7] F. Mogi, K. Itoh, N. Okamoto, M. Narita and M. Fujine, Denki Seiko, 59 (1988) 263.
[8] X. Xu, F. Zhang and J. Zhang, Youkuangye, 8 (1989) 45.
[9] K.C. Ng and J.A. Caruso, Anal. Chem., 55 (1983) 1513.
[10] O. Kujirai, M. Kohri, K. Yamada and H. Okochi, Anal. Sci., 6 (1990) 379.
[11] O. Kujirai, K. Yamada, M. Kohri and H. Okochi, Fresenius' J. Anal. Chem., 339 (1991) 133.
[12] K.C. Ng, M. Zerezghi and J.A. Caruso, Anal. Chem., 56 (1984) 417.
[13] J.M.E. Almendro, C.B. Ojeda, A.G. de Torres and J.M.C. Pavon, Analyst, 117 (1992) 1749.
[14] E.D. Salin and M.M. Habib, Anal. Chem. 56 (1984) 1186.
[15] Z. Guangyao, S. Zhixing, L. Xingyin and C. Xijun, Anal. Lett., 25 (1992) 561.
[16] L.L.W. Somasiri, A. Birnie and A.C. Edwards, Analyst, 116 (1991) 601.
[17] E.D. Salin and G. Horlick, Anal. Chem., 51 (1979) 2284.
[18] K.A. Forbes, J.F. Vecchiarelli, P.C. Uden and R. Barnes, Anal. Chem., 62 (1990) 2033.
[19] N.S. Safronova, S. Matveeva, Y.I. Favelinsky and V.A. Ryabukhin, Analyst, 120 (1995) 1427.
[20] R. Ullmann and H. Ringer, Fresenius' J. Anal. Chem., 323 (1986) 139.
[21] I.B. Brenner, S. Erlich, G. Vial, J. MacCormack, P. Grosdaillon and Aric L.E. Asher, J. Anal. At. Spectrom., 2 (1987) 637.
[22] M. Carre, O. Diaz de Rodriguez, J.M. Mermet, M. Bridenne and Y. Marot, J. Anal. At. Spectrom., 6 (1991) 49.
[23] P.W.J.M. Boumans, in P.W.J.M. Boumans (Ed.), Inductively Coupled Plasma Emission Spectroscopy, Part 1, Wiley, New York, 1987, p. 421.
[24] R.I. Botto, in R.M. Barnes (Ed.), Developments in Atomic Plasma Spectrochemical Analysis, Heyden, Philadelphia, 1981, p. 141.
[25] R.I. Botto, Anal. Chem., 54 (1982) 1654.

ELSEVIER

Talanta 44 (1997) 53–60

Talanta

Ion-association method for the spectrophotometric determination of the antitussive drug noscapine

Bahruddin Saad[1], Salah M. Sultan, Fakhr Eldin O. Suliman*

Department of Chemistry, King Fahd University of Petroleum and Minerals, P.O. Box 2026, Dhahran 31261, Saudi Arabia

Received 31 October 1995; revised 22 May 1996; accepted 24 May 1996

Abstract

A simple, sensitive and fairly rapid method for the determination of noscapine is described, based on the measurement of the absorbance of the organic soluble ion-association complex formed between the noscapine monocation and a bulky counter anion. Methyl Orange, Bromothymol Blue and Bromocresol Green (BCG) were examined as counter ions. The effect of few solvents, the counter-ion concentration and pH on the extraction were also investigated. The most suitable system was based on BCG (pH 3.0) with chloroform as the extraction solvent. The use of the other counter ions, in conjuction with their respective solvents, was found to be less sensitive. The BCG system exhibits negligible or no interference when used for the determination of 38 ppm of noscapine in the presence of several drug excipients, thus lending itself as a possible procedure for the determination of this alkaloid in pharmaceutical preparations.

Keywords: Bromoscresol Green; Drug formulations; Extraction; Ion association; Noscapine

1. Introduction

Noscapine (**I**) is an important naturally occurring opium alkaloid, and is present in amounts of 6–11% of the raw material depending on season and locality [1,2]. Unlike morphine and codeine, it has no analgesic activity or abuse potential. Its major pharmaceutical action is its anti-tussive activity, which has been reported to be equivalent to that of codeine [1].

Noscapine and its metabolites in plasma have been determined using high-performance liquid chromatography (HPLC) [3–7]. Frequently, the use of a coupled-column arrangement was mandatory for the analytes to be separated first into two fractions on a polar precolumn [6,7]. Each fraction was next transferred to an analytical column for the final separation. HPLC procedures for the determination of noscapine in cough syrups [8] and capsules [9] have also been reported. In the former work, noscapine was oxidized by bromine generated on-line prior to detection.

* Corresponding author. Fax: 966-3-860 4277.

[1]Permanent address: School of Chemical Sciences, Universiti Sains Malaysia, 11800 Penang, Malaysia.

PII S0039-9140(96)02009-7

The British Pharmacopoeia (BP) procedures [10,11] for the determination of noscapine in pharmaceutical preparations include an absorption method, which lacks specificity, and an acid–base titrimetric method in a non-aqueous medium with potentiometric end-point detection. Neither method is suitable for the determination of low levels of the alkaloid.

Simpler alternative methods that use inexpensive instruments are clearly needed for the determination of this pharmaceutically important anti-tussive drug. The use of bulky dyes for the formation of ion-association complexes that form the basis of extractive spectrophotometric methods for the determination of drugs in pharmaceutical preparations has been reported [12,13]. A method for the determination of anti-inflammatory agents using Methylene Violet was reported [12], and some phenotiazines were determined spectrophotmetrically by monitoring their ion-association complexes with Brilliant Blue and Orange-II [13]. In this work, the use of three bulky dyes as anionic counter ions for the formation of noscapine ion-association complexes whose absorbance can be monitored upon extraction was investigated. The systems were further optimized with respect to pH, choice of solvent, counter ion concentration and shaking time. Key analytical characteristics of the complexes were compared. Determinations of noscapine in the presence of common drug excipients were also performed.

2. Experimental

2.1. Apparatus

All absorbance measurements were made on a Perkin-Elmer Lambda 5 UV–visible spectrophotometer with matched quartz cuvettes of 1 cm path length. pH measurements of the aqueous phase were performed using a Corning combination glass electrode (Catalog No. 476530) in conjunction with a Corning Model 21 pH meter.

2.2. Reagents and solutions

All chemicals were of analytical-reagent grade, except noscapine hydrochloride, which was a gift from Dumex (Amsterdam, The Netherlands). Chloroform-stabilized ethanol and toluene were purchased from Fluka, methyl isobutyl ketone from Baker and dichloromethane from Winlab. These solvents were claimed to have purities of at least 99.9%. The counter ions were obtained from the following sources: Bromothylmol Blue (BTB) from Fisher Scientific, Methyl Orange (MO) from BDH and Bromocresol Green (BCG), sodium salt, from Allied Chemical. Demineralized, distilled water was used throughout.

2.2.1. Standard solutions

The masses of reagents used to prepare 10^{-2} M stock standard solutions in 50 ml volumetric flasks were BCG 0.3600 g, MO 0.1637 g and noscapine hydrochloride 0.2067 g. A BTB stock standard solution was prepared by dissolving 0.3232 g of the reagent in 5 ml of ethanol and diluting to the mark with water. Working standard solutions were prepared by dilution of the stock standard solutions as required.

2.2.2. Noscapine tablet solutions

A standard solution was prepared by crushing five tablets (Longatin; Dumex, Copenhagen, Denmark) and dissolving an amount of the powder equivalent to 100 mg of noscapine in 50 ml of water. The mixture was warmed at 70°C in a water-bath for 10 min, agitated by an electrical shaker for 10 min and filtered through an ordinary filter-paper. After washing several times with hot water, the filtrate plus washings were cooled to room temperature and the final volume was made up to 100 ml.

2.2.3. Buffer solutions

Buffer solutions were prepared in 200 ml volumetric flasks, as follows: acetate buffer (pH 3.0), dissolve 0.80 g of anhydrous sodium acetate, add glacial acetic acid to adjust the pH to 3.0 and dilute to the mark; acetate buffer (pH 3.5), dissolve 100.0 g of ammonium acetate, adjust the pH to 3.5 with 7 M hydrochloric acid and dilute to

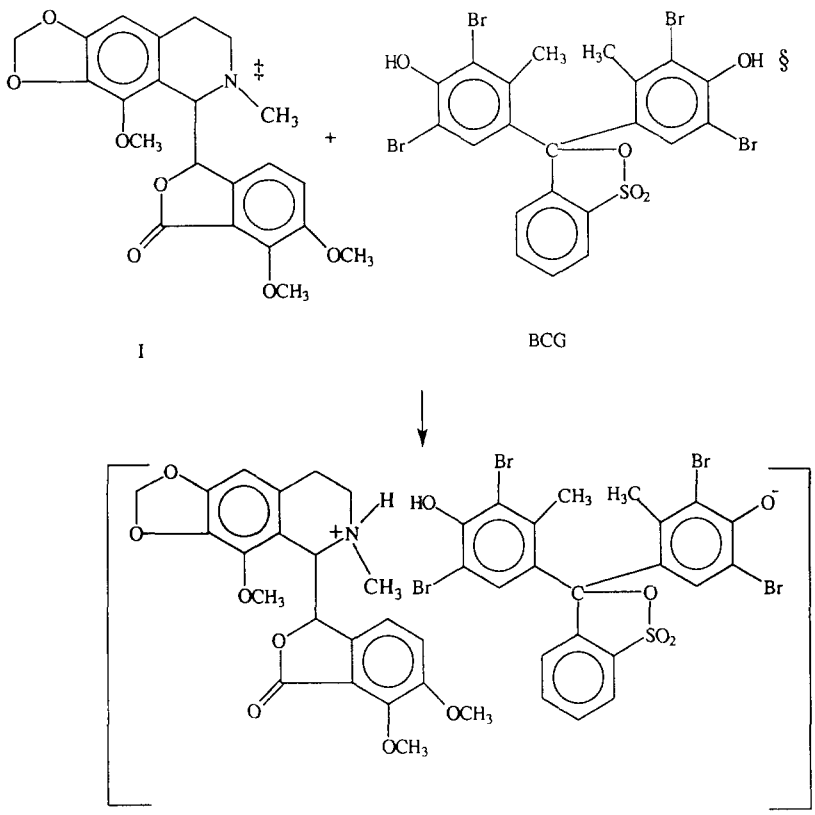

I BCG

Drug-dye complex

‡ $pK_a = 7.8$

§ $pK_a = 4.9$

the mark; phosphate buffer (pH 4.5), dissolve 3.4025 g of potassium dihydrogenorthophosphate, adjust the pH to 4.5 with 0.1 M HCl and dilute to the mark; and phosphate buffers (pH 5.5–8.0), mix 50 ml of 0.2 M potassium dihydrogen-orthophosphate solution, adjust to the required pH by addition of 0.2 M sodium hydroxide and dilute to the mark.

2.3. General procedure for extraction-spectrophotometry

Volumes of 1 ml each of counter ion and buffer solution were transferred into a series of 125 ml separating funnels then, aliquots of 1.0 mM alkaloid solution were added. The total volume of the aqueous phase was adjusted to 5 ml by the addition of distilled water. Finally, 10 ml of extraction solvent were added to each funnel and the contents were shaken vigorously for 60 s and then allowed to stand for a few minutes until the two phases had completely separated. The absorbance of the separated organic layer was measured at the respective λ_{max} against a reagent blank (see Table 2). At least duplicate measurements were made in all cases.

Table 1
Physical properties of background extracts of counter ions in different extraction solvents

Extraction solvent	Counter ion		
	MO	BTB	BCG
Chloroform	Colorless	Intense yellow	Slight yellow
Toluene	Colorless	Slight yellow	Colorless
Methyl isobutyl ketone	Slight yellow	Intense yellow	Intense yellow
Dichloromethane	Colorless	Intense yellow	Colorless

3. Results and discussion

3.1. Background absorption

A preliminary investigation of the background absorption of 1 ml of 10^{-3} M counter ion solution (without noscapine) was conducted. The characteristics of the extracts are shown in Table 1 and reveals that the BTB system has a high background absorption, especially when chloroform, methyl isobutyl ketone or dichloromethane was used as the extracting solvent. For systems that are highly coloured, no further investigations were conducted.

3.2. Choice of organic solvent

Chloroform, methyl isobutyl ketone, toluene and dichloromethane were used as solvents in the extraction. The absorbances for 38 ppm of noscapine, corrected for the corresponding blanks, for the MO and BCG system are shown in Figs. 1 and 2, respectively. It is evident that the most suitable solvent for the MO-based complex is dichloromethane, whereas for the BCG system dichloromethane and chloroform seem to be promising solvents. For BTB, the only suitable solvent that merits further study was toluene. The respective solvents were in further studies.

3.3. Effect of pH

The pH of the aqueous phase is an extremely important factor for ion-pair extractions [13–15]. Here the influence of pH on the extraction was evaluated by measuring the absorbance of the complex when 38 ppm of noscapine was used, and that of the corresponding blanks over the pH range 3–8, by the addition of the appropriate buffers. In general, it was found that negligible or no extraction occurred at pH > 6 for all systems.

For the BTB system, it was found that the optimum pH was 4.0 when toluene was used as the solvent and the most suitable pH for the MO- and BCG-based complexes was 3.0. These pH values were adopted in further studies.

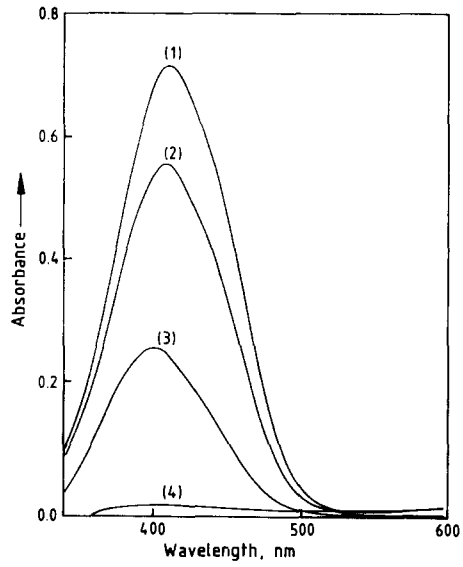

Fig. 1. Typical absorption of noscapine–MO complex n different solvents: (1) dichloromethane; (2) chloroform; (3) methyl isobutyl ketone; and (4) toluene. Conditions: noscapine, 38 ppm; MO, 10^{-3} M; pH, 3.0; reference, blanks in respective solvent.

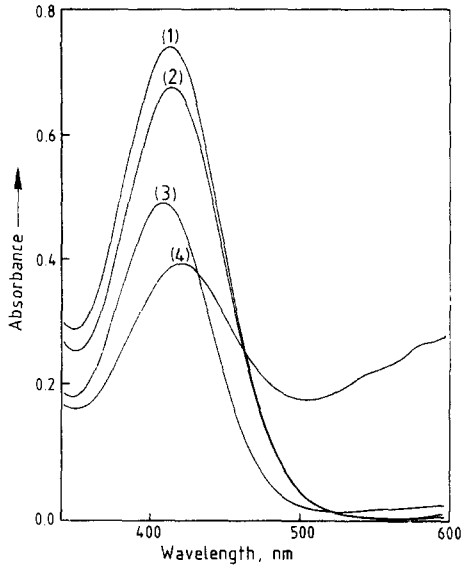

Fig. 2. Typical absorption of noscapine–BCG complex in different solvents: (1) dichloromethane; (2) chloroform; (3) toluene; and (4) methyl isobutyl ketone. Conditions: noscapine, 38 ppm; BCG, 10^{-3} M; pH, 3.0; reference, blanks in respective solvent.

3.4. Counter-ion concentration

The influence of the respective counter-ion concentrations on the absorbance of the extracted ion pair was studied by fixing the alkaloid concentration at 38 ppm and varying the counter-ion concentration from 0.1 to 1.2 mM. The results are plotted in Fig. 3, which shows that the signal remains constant at counter-ion concentrations >0.80 mM for the BCG and BTB systems and >1.0 mM for the MO system. A fixed concentration of 1.0 mM counter-ion was subsequently used for all systems in order to minimize the blank absorbance; also, no further improvement in precision was observed for concentrations of counter ion higher than 1.0 mM.

3.5. Effect of shaking time

The extraction was studied by manual shaking and varying the shaking time from 30 to 300 s for the complexes based on 38 ppm of alkaloid. It was found that the absorbance remained constant over this time period for all complexes. A shaking time of 60 s was adopted for all extractions. It was further observed that the yellow extracts remained stable for at least 2 days.

3.6. Calibration

The most suitable extraction conditions were as follows: MO, extraction solvent dichloromethane, pH 3.0; BTB, extraction solvent toluene, pH 4.0; and BCG, extraction solvent chloroform or dichloromethane, pH 3.0. In all instances, a shaking time of 60 s and counter-ion concentration of 1 mM were adopted.

The calibration graphs were generated by using 8–10 points, each point being repeated at least twice. The day-to-day variation in the calibration graph was found to be within acceptable limits, as well as the repetitive determination of standard solutions carried out over a period of several

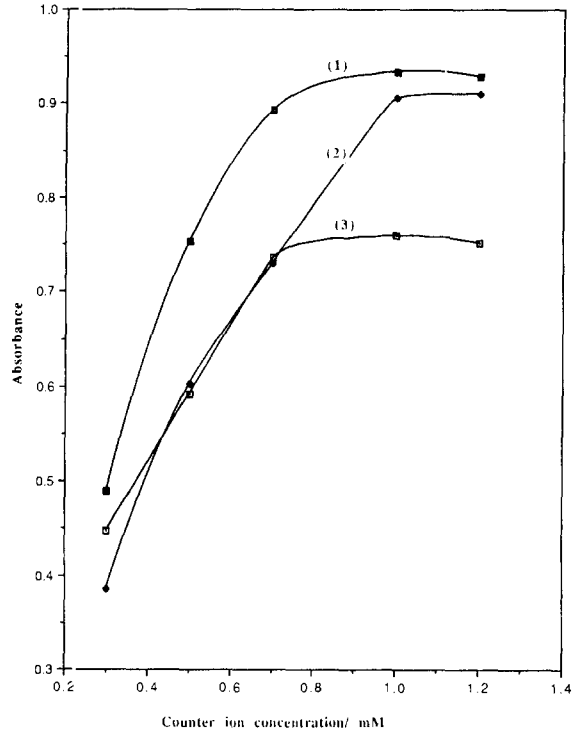

Fig. 3. Effect of counter ion concentration: (1) BCG; (2) MO; (3) BTB. Conditions: noscapine, 38 ppm. For BTB: solvent, toluene; pH, 4.0. For BCG: solvent, chloroform, pH, 3.0. For MO: solvent, dichloromethane; pH, 3.0. Absorbance measured at the respective λ_{max}.

Table 2
Analytical characteristics of noscapine–counter ion complex

Counter ion	Extraction solvent	λ_{max} (nm)	Molar absorptivity ($l\ mol^{-1}\ cm^{-1}$)	Detection limit (ppm)	Dynamic linear range (ppm)	Calibration equation		
						Slope	Intercept	Correlation coefficient, r
BTB	Toluene	403	7800	1.9	6–60	0.0192	0.1214	0.997
MO	Dichloromethane	426	7300	2.0	6–70	0.0179	0.2571	0.998
BCG	Chloroform	413	9100	1.6	5–60	0.0222	0.0765	0.999
BCG	Dichloromethane	412	9300	1.5	4–60	0.0228	0.2217	0.999

days, where a relative standard deviation (RSD) of not more than 1.0% was obtained. The linearity of the calibration graphs was studied under the above conditions for the respective counter ions. The analytical characteristics of the extraction are summarized in Table 2. The detection limit was calculated as described earlier [16] using the equation $3s/S$, where s is the standard deviation of the blank and S is the corresponding slope of the calibration graph. The upper and lower limits of the dynamic linear range of concentration were estimated from the calibration graph, noting when the points started to deviate from the straight line. The molar absorptivity of the ion-association systems obtained are comparable to those based on phenothiazine derivatives [12] and anti-inflammatory drugs [12] described earlier. Table 2 reveals that the most sensitive counter ion is BCG. The use of chloroform or dichloromethane yields almost comparable characteristics. However, chloroform was chosen as the extraction solvent owing to its lower volatility for application studies. The BCG-based ion-association complex is not only the most sensitive but also exhibits the lowest detection limit and the widest dynamic linear concentration range (Table 2).

The choice of counter ions was based on the guidelines suggested by Toei [17], where it is desirable for ion-association reagents to be univalent and bulky and for the charge to be distributed over the whole ion. It was further suggested [17] tha the use of plane-type cationic or anionic ion-association reagents will yield sensitive spectrophotometric systems. The interaction of aromatic surfaces is also believed to play a significant role in ion association and is termed aromatic stacking. Although the forces that drive aromatic–aromatic interactions are not yet clear, it has been suggested that both dispersion forces and interactions between partial charges within adjacent rings are responsible for these attractions; another component that is believed to add to these interactions was thought to arise from the hydrophobic nature of hydrocarbon aromatics [18]. The fact that the BCG and the BTB systems are more sensitive than the MO systems is probably due to their bulkiness. The ability of BCG to form ion-association complexes with alkaloids has been reported earlier [19].

3.7. Determination of noscapine in drug formulation

Interferences from some common drug excipients were examined and the results are given in Table 3. It was found that these compounds exhibit minimum interference, even when present at 50 times the level of noscapine. Determination of 38 ppm of noscapine in a mixture containing 380 ppm each of ascorbic acid, citric acid, glucose, magnesium sulfate and starch are also satisfactory, with an RSD of 0.6% and a recovery of 96%. The RSD of five determinations of 38 ppm noscapine standard solution was 0.50%.

The method was successfully applied to the determination of the drug in proprietary Longatin tablets (Dumex), claimed to contain 25 mg noscapine, and a recovery of 00.9% was obtained with an RSD of not more than 0.8%, indicating that the method is suitable for the determination of noscapine in drug formulations without interferences from excipients such as starch and glu-

Table 3
Effect of foreign compounds on the determination of 38.0 ppm noscapine

Foreign compound	Concentration (ppm)	Noscapine recovered (%)[a]
Ascorbic acid	380	96
	1900	105
Citric acid	380	101
	1900	102
Glucose	380	98
	1900	103
Magnesium sulfate	380	104
	1900	103
Starch	380	104
	1900	105
Mixture[b]		96
		RSD 0.6% ($n = 5$)

[a] Mean, $n = 2$.
[b] 380 ppm each of the compounds in the first column.

cose. The same batches were analyzed by the BP[10] method and the results obtained were compared statistically utilizing Student's t-test. The present method showed almost the same degree of accuracy as the BP method, as was inferred from the value of t at the 95% confidence level ($t_{\text{experimental}} = 1.6$ and $t_{\text{theoretical}} = 2.78$, $n = 5$). Noscapine is a controlled drug in Saudi Arabia and the only proprietary drug obtained was Longatin. The proposed method has the advantage of being virtually free from interferences (see Table 2) as well as having moderately low detection limits, and it may therefore be suitable for the determination of this drug in biological fluids. A few metabolites of noscapine have been identified in urine and rat liver microsomes [6], e.g. narcotoline and cotarnine. Also, it has been reported that *N*-demethylated noscapine and *N*-demethylated narcotoline or cotarnine are other possible metabolites of noscapine [6]. Both narcotoline and cotarnine preserve the isoquinoline part of the parent compound and are therefore able to form ionpairs with the BCG counter ion and could pose a major interference to the determination of noscapine in biological fluids by this method. Related drugs such as codeine are of the same nature as noscapine and are considered determinable by the same procedure and could be thoroughly studied in future work.

4. Conclusion

An extractive spectrophotometric procedure for the determination of noscapine was developed based on BCG with chloroform as the extraction solvent. The proposed procedure is fairly rapid, simple, sensitive and accurate and promises good prospects for the determination of noscapine in pharmaceutical preparations. Additionally, the method uses cheaper instrumentation than HPLC.

Acknowledgements

B. Saad is indebted to KFUPM for a postdoctoral fellowship and also to the Universiti Sains Malaysia, Penang, for leave of absence. The authors thank Dumex (Copenhagen, Denmark) for the gift of a noscapine sample.

References

[1] M.C. Gerald, Pharmacology, an Introduction to Drugs, Prentice-Hall, Englewood Cliffs, NJ, 1974, p. 241.
[2] The Merck Index, Merck, Rahway, NJ, 10th edn., 1983, p. 6559.
[3] M. Johansson, S. Eksborg and A. Arbin, J. Chromatogr., 275 (1983) 355.
[4] K.M. Jensen, J. Chromatogr., 274 (1983) 381.
[5] V. Haikala, J. Chromatogr., 337 (1985) 429.

[6] M. Johansson and D. Westerlund, J. Chromatogr., 452 (1988) 241.
[7] M. Johansson and D. Westerlund, J. Chromatogr., 459 (1988) 301.
[8] W.T. Kok, U.A. Th. Brinkman and R.W. Frei, Chim. Acta, 162 (1984) 19.
[9] V. Haikala, J. Chromatogr., 389 (1987) 299.
[10] British Pharmacopoeia, Vol. 1, HMSO, London, 1980, p. 311.
[11] British Pharmacopoeia, Vol. 1, HMSO, London, 1993, p. 458.
[12] C.S.P. Sastry, A.S.R. Tiperneni and M.V. Suryanarayama, Analyst, 114 (1989) 513.
[13] S.L. Bhongade and A.V. Kasture, Talanta, 40 (1993) 1525.
[14] M. Oue, K. Kimura and T. Shono, Analyst, 113 (1988) 551.
[15] S. Motomizu, M. Onada, M. Oshima and T. Iwachido, Analyst, 113 (1988) 743.
[16] C.M. Legua, P.C. Falco and A.S. Cabeza, Anal. Chim. Acta, 283 (1993) 635.
[17] K. Toei, Anal. Sci. 3 (1987) 479.
[18] L.F. Newcomb and S.H. Gellman, J. Am. Chem. Soc., 116 (1994) 4993.
[19] E. Bishop, Indicators, Pergamon Press, Oxford, 1972, p. 106.

ELSEVIER

Talanta 44 (1997) 61–68

Talanta

Selective spectrophotometric determination of *p*-aminophenol and acetaminophen

Fardous A. Mohamed [a,*], Mohamed A. AbdAllah[b], Soad M. Shammat[b]

[a]*Department of Pharmaceutical Analytical Chemistry, Faculty of Pharmacy, Assiut University, Assiut, Egypt*
[b]*Department of Chemistry, Faculty of Science, King Saud University, Riyadh, Saudi Arabia*

Received 15 January 1996; revised 24 May 1996; accepted 6 June 1996

Abstract

A specific spectrophotometric method was developed for the determination of *p*-aminophenol and acetaminophen. The method is based on the reaction of *p*-aminophenol at ambient temperature with sodium sulphide in presence of an oxidant to produce a methylene blue-like dye. Different oxidizing agents were tried, e.g. Ce(IV) and Fe(III). The colour developed within 10 min and remained stable for at least 3 h. The method was applied successfully to the determination of *p*-aminophenol in the presence of acetaminophen without prior separation. The method was also applied to the analysis of various commercially available acetaminophen dosage forms and excellent recoveries were obtained comparable to those obtained by official procedures. The reaction product was isolated and a possible reaction mechanism was suggested.

Keywords: Acetaminophen; *p*-Aminophenol, Pharmaceutical analysis; Spectrophotometry

Introduction

Acetaminophen (*N*-acetyl-*p*-aminophenol or paracetamol) is an effective analgesic and antipyretic agent. *p*-Aminophenol is the hydrolytic product of acetaminophen and is reported to have significant nephrotoxicity and teratogenic effects and has been detected in acetaminophen as an impurity or synthetic intermediate [1].

Numerous methods have been reported for the determination of *p*-aminophenol and acetaminophen in pure form, pharmaceutical preparations and biological fluids, including gravimetric [1], titrimetric [2–4], UV[5], derivative [6–8] and differential [9] spectroscopic methods. Spectrophotometric [10–14], fluorimetric [15–17], chromatographic [18–23] and electrochemical procedures [24] have also been reported. Many of these procedures suffer from interferences from other active ingredients or additives especially those carrying phenolic or amine functional groups, and chromatographic separation is usually required.

* Corresponding author.

PII S0039-9140(96)02013-9

Aromatic diamines have been used before for the determination of sulphide and sulphide-producing compounds in the presence of Fe(III) through the formation of methylene blue dye [25]. In this work, the applicability of the principle of this reaction for the determination of acetaminophen and *p*-aminophenol was investigated using sodium sulphide and Fe(III) or Ce(IV) as reagents. As a result of this investigation, a rapid, sensitive and selective spectrophotometric method for the determination of acetaminophen and *p*-aminophenol was developed. Advantages are that the reaction occurs at room temperature and using distilled water as a solvent.

2. Experimental

2.1. Apparatus

A Varian Model DMS100 UV–visible spectophotometer connected to a Varian Model DS15 data station and a Hewlet–Packard Model 82905B printer was used.

A Model 1500 Fourier transform IR spectrophotometer, equipped with a data station, Model PPI printer–plotter and 1502 central processing unit was obtained from Perkin-Elmer.

Elemental microanalyses were performed with Perkin-Elmer Model 2400, CHNO Elemental Analyser.

2.2. Materials and reagents

Pharmaceutical-grade acetaminophen (Riedel-de Haën, Seelze-Hannover, Germany) and *p*-aminophenol (BDH, Poole, UK) were used as working standards without further treatment. Various commercially available dosage forms were purchased from the local market. All other chemicals and solvents were of analytical grade. Distilled water was used throughout.

2.3. Reagent solutions

Sodium sulphide was used as a 0.025% aqueous solution.

Fe(III) solution was prepared as 0.5% ammonium iron (III) sulphate in 0.03 M sulphuric acid and Ce(IV) solution as 0.08% cerium(IV) sulphate in 0.03 M sulphuric acid.

2.4. Preparation of standard solution

p-Aminophenol: prepare accurately a 50 μg ml^{-1} *p*-aminophenol aqueous solution.

Intact acetaminophen: prepare accurately a 1 mg ml^{-1} acetaminophen aqueous solution.

Hydrolysed acetaminophen: transfer accurately 0.1 g of acetaminophen into a 100 ml volumetric flask, add 20 ml of 5 M H_2SO_4, Heat in a boiling water-bath for 30 mins, cool and dilute to volume. Dilute quantitatively in order to obtain a concentration of 50 μg ml^{-1}.

2.5. Preparation of samples

2.5.1. Tablets

Weigh and finely powder 20 tablets. Transfer an accurately weighed amount of powder equivalent to 100 mg of acetaminophen into a 100 ml volumetric flask, add 20 ml of 5 M H_2SO_4, mix well and place in a boiling water-bath for 30 min, then cool and dilute to volume with distilled water. Filter through a Whatman 41 filter-paper. Discard the first portion of the filtrate. Use the clear solution as a stock solution.

2.5.2. Liquid preparations (Syrups, suspension and drops)

Measure accurately a volume of either syrup, suspension or drop samples equivalent to 100 mg of acetaminophen and transfer it to a 100 ml calibrated flask. Add 20 ml of 5 M H_2SO_4 and proceed as for tablets for suspensions and omitting the filtration step for syrups and drops.

2.6. General assay procedure

Transfer 10 ml of either *p*-aminophenol or hydrolysed acetaminophen standard or sample solution into a 50 ml volumetric flask. Add 5 ml of sodium sulphide reagent followed by 5 ml of Fe(III) or Ce(IV) solution. Stopper the flask and

Table 1
Microanalysis data

Systematic names	Molecular formula	Mol. wt.	C(%)		H(%)		N(%)	
			Calc.	Found	Calc.	Found	Calc.	Found
3,7-Bis(dihydroxy) phenothiazine picrate	$C_{18}H_{10}N_4O_9S$	458.0	47.16	48.08	2.18	2.26	12.22	12.63
3,7-Bis(dihydroxy) phenothiazine perchlorate	$C_{12}H_8ClNO_6S$	329.5	43.70	42.27	2.42	2.16	4.25	4.93

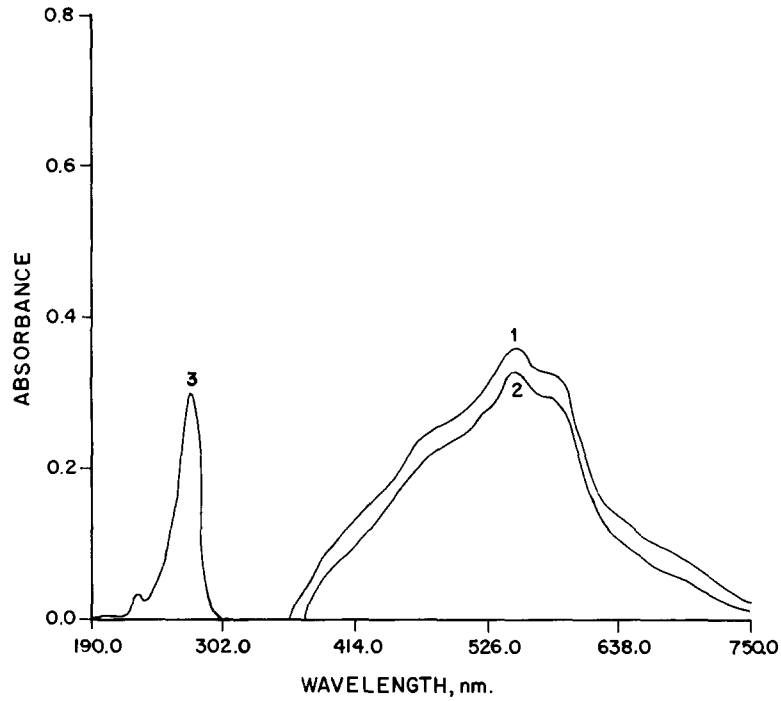

Fig. 1. Absorption spectra for the reaction product of 10 μg ml^{-1} *p*-aminophenol with (1) Fe(III) and (2) Ce(IV) and Na_2S reagents and (3) for the pure compound.

shake for about 30 s, then allow it to stand for 15 min in the case of Fe(III) and 10 min in the case of Ce(IV). Dilute to volume with distilled water, allow to stand for a further 10 min, then measure the absorbance at 550 nm against the corresponding reagent blank.

2.7. Preparation and identification of chromogen

Prepare about 500 ml of the coloured product of *p*-aminophenol with sodium sulphide and Fe(III). To this solution add portionwise a saturated aqueous solution of picric or perchloric acid and stir the mixture vigorously. Keep the mixture in a refrigerator for 24 h. Filter the precipitate picrate salt and wash with water several times. Recrystallize from aqueous ethanol. Dry in vacuum desiccator over calcium chloride and subject to microanalysis and IR identification.

2.8. Microanalysis data

The microanalysis data for the compounds studied are given in Table 1.

3. Results and discussion

3.1. Absorption spectra

p-aminophenol was allowed to react with sodium sulphide in the presence of an oxidant to produce a bluish violet colour ($\lambda_{max} = 550$ nm). The absorption spectra of the reaction product using Fe(III) or Ce(IV) as oxidants are shown in Fig. 1. Colourless reagent blanks were obtained for both oxidants. *N*-Bromosuccinimide was tried as an oxidant but low absorption intensities were obtained.

3.2. Effect of sodium sulphide concentration

The effect of changing the sulphide concentration on the absorbances of solutions containing 10 μg ml^{-1} *p*-aminophenol was studied. From Fig. 2, it is evident that the absorbance increase with increase in sulphide concentration reached a maximum on using 0.025% (w/v) sodium sulphide for both oxidants. Therefore, 0.025% (w/v) sodium sulphide was used in all subsequent work.

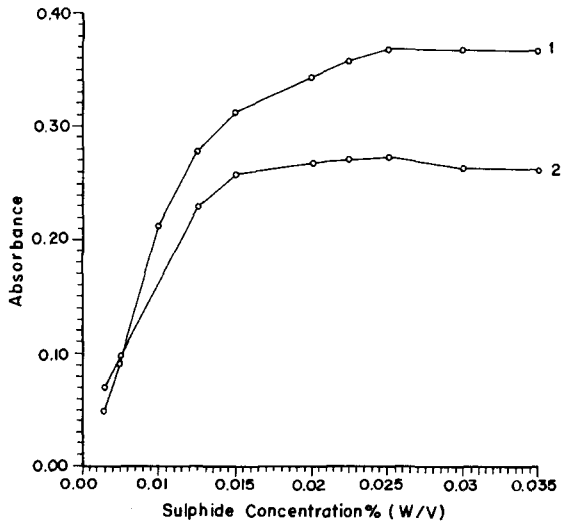

Fig. 2. Effect of variation of sodium sulphide concentration on the absorption intensitiy of the reaction products of 10 μg ml^{-1} *p*aminophenol with (1) Fe(III) and (2) Ce(IV) and Na_2S reagents.

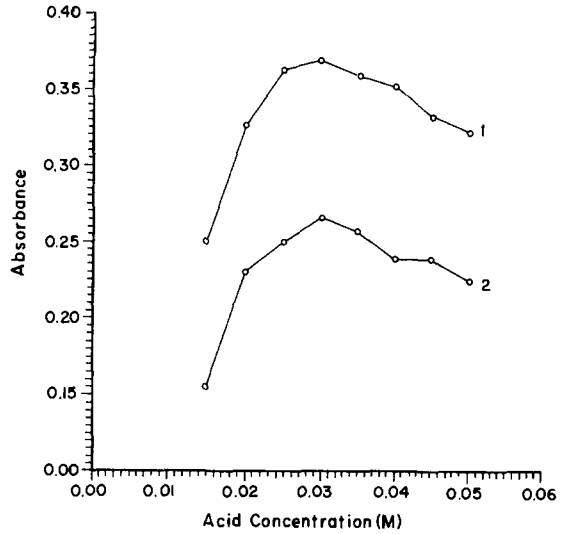

Fig. 3. Effect of variation of sulphuric acid concentration on the absorption intensity of the reaction product of 10 μg ml^{-1} *p*-aminophenol with (1) Fe(III) and (2) Ce(IV) and Na_2S reagents.

3.3. Effect of sulphuric acid concentration

Various concentrations of sulphuric acid, ranging from 0.01 to 0.05 M, were tried to dissolve the oxidant. Fig. 3 indicates that 0.03 M is necessary for maximum colour intensity for both oxidants.

3.4. Effect of oxidant concentration

In order to study the influence of oxidant concentration, the reaction was carried out in a series of 50 ml calibrated flasks containing 10 μg ml^{-1} *p*-aminophenol solution and 5 ml of 0.025% sodium sulphide solution. This was followed by 5 ml of different oxidant concentrations ranging from 0.1 to 0.8% (w/v) in the case of Fe(III) or from 0.03 to 0.15% in the case of Ce(IV) solution. Figs. 4 and 5 indicate that the highest intensities and most reproducible results are obtained on using 5 ml of 0.5% Fe(III) or 5 ml of 0.08% Ce(IV) dissolved in 0.03 M sulphuric acid.

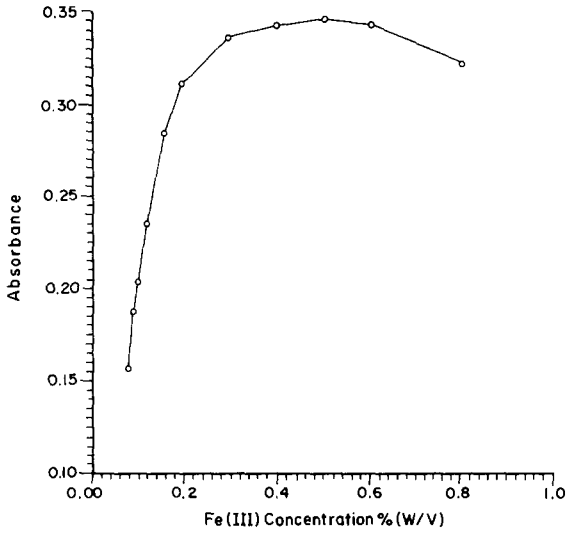

Fig. 4. Effect of variation of Fe(III) concentration on the absorption intensity of the reaction product of 10 μg ml^{-1} *p*-aminophenol with Fe(III) and Na_2S reagents.

3.5. Order of reagent addition

The order of reagent addition was very important as the sulphide solution has to be added to the sample and finally the oxidant. Changing the order produced low results.

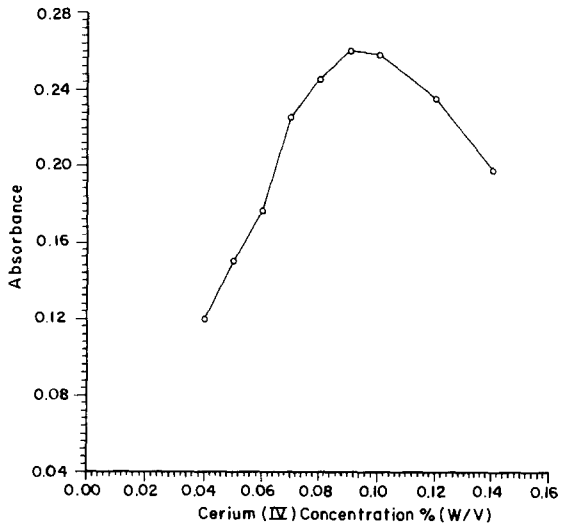

Fig. 5. Effect of variation of Ce(IV) concentration on the absorption intensity of the reaction product of 10 μg ml^{-1} *p*-aminophenol with Ce(IV) and Na_2S reagents.

Table 2
Effect of dilution solvents on the absorption intensity for the interaction product of 10 μg ml^{-1} *p*-aminophenol with sodium sulphide and Fe(III) or cerium (IV) reagents

Solvent	Fe(III)		Ce(IV)	
	λ_{max} (nm)	A^a	λ_{max} (nm)	A^a
Distilled water	550.0	0.300	550.0	0.285
Ethanol	550.0	0.323	551.3	0.245
Methanol	548.0	0.286	546.0	0.239
Dimethyl sulphoxide	553.3	0.257	553.9	0.265
Propan-2-ol	549.3	0.295	550.0	0.267
Acetone	548.6	0.287	548.3	0.290
Dioxane	550.3.	0.294	548.6	0.305

3.6. Effect of temperature and reaction time

The reaction time was determined by following the colour development at room temperature and in a thermostatically controlled water-bath at different temperatures. The flasks were removed after different periods ranging from 5 to 50 min. The absorbance was measured at 5 min intervals against a reagent blank treated similarly. It was observed that at higher temperatures, absorption was maximum after few seconds then decreased rapidly with increasing heating time, probably due to loss of H_2S at higher temperatures. At room temperature the absorbance increased gradually and reached a maximum after 15 and 10 min using Fe(III) and Ce(IV) respectively. Hence these reaction times at room temperatures were chosen for colour development.

3.7. Effect of solvent variation

Dilution of the coloured reaction product with different solvents showed no effect on λ_{max} whereas the absorption intensity was influenced slightly (Table 2). However, distilled water was used as solvent throughout this study.

3.8. Colour stability

After dilution of the coloured solutions with distilled water, a gradual increase in absorption

Table 3
Comparative summary of some statistical data for *p*-aminophenol determined using sodium sulphide and Fe(III) or cerium (IV) reagents

Oxidant	Concentration range ($\mu g\ ml^{-1}$)	Slope	Intercept (r)	Correlation coefficient
Ammonium iron(III) sulphate	1–12	0.033	−0.002	0.9998
Cerium(IV) sulphate	2–18	0.034	−0.001	0.9990

Table 4
Results of determination of acetaminophen in pharmaceutical preparations compared with the official BP method [5]

Drug propietary name	Recovery ± S.D.%[a]		
	Proposed method[b]		Official BP method
	A[c]	B[d]	
Adoltablets (500 mg)	100.8 ± 0.7 $t = 1.88$ $F = 2.35$	100.0 ± 0.6 $t = 1.04$ $F = 1.55$	100.3 ± 0.5
Revanin tablets	100.9 ± 0.8 $t = 0.53$ $F = 1.55$	100.9 ± 0.7 $t = 0.65$ $F = 1.28$	100.7 ± 0.6(500 mg)
Noflu tablets (400 mg)	101.9 ± 0.9 $t = 0.77$ $F = 1.54$	10 ± 1 $t = 0.67$ $F = 2.94$	101.6 ± 0.7
Distalgesic tablets (32.5 mg)	105.8 ± 0.9 $t = 1.85$ $F = 2.15$	10 ± 0.9 $t = 1.56$ $F = 2.20$	105.1 ± 0.7
Dolomol syrup	101.1 ± 0.8 $t = 2.26$ $F = 3.31$	101.4 ± 0.9 $t = 1.27$ $F = 4.18$	101.9 ± 0.4(120 mg/5 ml)
Tempra drops (80 mg/0.8 ml)	100.7 ± 0.6 $t = 2.17$ $F = 2.02$	99.7 ± 0.7 $t = 1.30$ $F = 2.35$	100.7 ± 0.5
Calpol suspension	98.5 ± 0.8 $t = 1.06$ $F = 2.00$	98.1 ± 0.9 $t = 1.90$ $F = 2.52$	98.9 ± 0.6(120 mg/5 ml)

[b] F: Tabulated = 6.39 at the 95% confidence level.
t: Tabulated = 2.78 at the 95% confidence level.
[a] Average of five determinations expressed as a percentage of the label claim.
[c] Recovery using Fe(III).
[d] Recovery using Ce(IV).

intensity was observed throughout the first 10 – min and it then remained constant for more than 3 h. Therefore, absorption measurements were carried out 10 min after dilution with distilled water.

3.9. Quantification

Under the proposed experimental conditions, a linear response between the absorbance and concentration was observed over the concentration

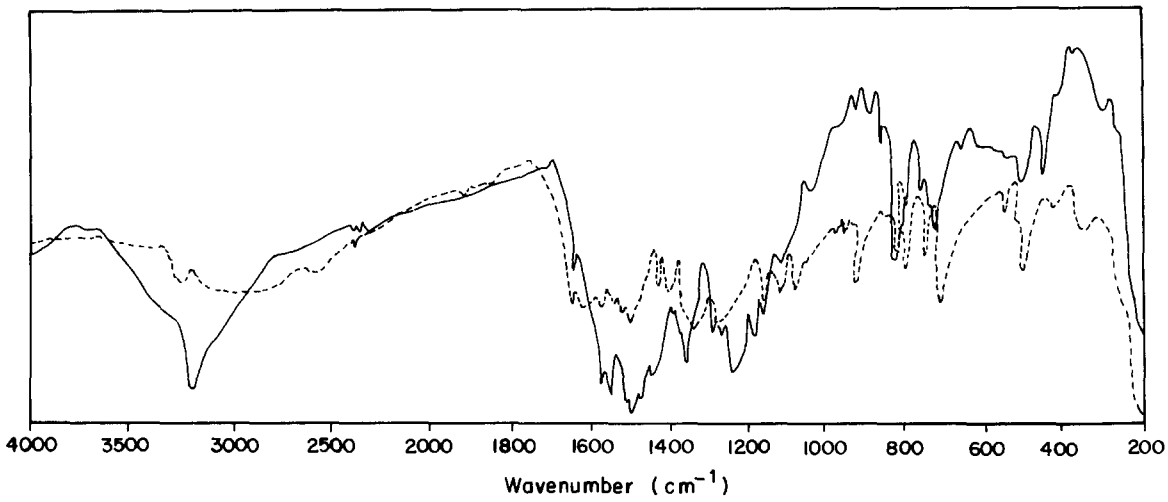

Fig. 6. IR spectra for (–) perchlorate and (---) picrate salts of the dye resulting from the reaction of *p*-aminophenol with Na_2S and Fe(III) reagents.

ranges given in Table 3. Correlation coefficients, intercepts and calibration data are listed in the table.

3.10. Applications

3.10.1. Determination of acetaminophen

Under the proposed experimental conditions, no colour was observed with the intact acetaminophen solution. Only the hydrolysed acetaminophen solution gave an intense colour. Hence the proposed method was applied to the determination of acetaminophen in pure form and in pharmaceutical formulations after its hydrolysis to *p*-aminophenol. Several commercially available acetaminophen formulations, including tablets, drops, syrups and suspension, were analysed for their content of acetaminophen without further treatment. The same samples were analysed using the official method [5]. The official BP procedure depends on UV measurements for paracetamol tablets whereas for solutions and suspensions a liquid chromatographic method is used.

On applying the proposed procedures, good recoveries were obtained with tablets, capsules, solutions, syrups and suspensions without interference from frequently encountered excipients and additives. Moreover, compounds which are usually dispensed with paracetamol, such as acetylsalicylic acid, codeine, caffeine, chlorpheniramine and ascorbic acid, did not interfere. As shown in Table 4, the results are in good agreement with those given by the offical BP method.

3.10.2. Determination of p-aminophenol in the presence of acetaminophen

p-Aminophenol, which is reported to have significant toxicity such as teratogenic effects and nephrotoxicity, has been detected in acetaminophen as an impurity which can either be a synthetic intermediate or a degradation product [1]. The proposed method was applied to the determination of *p*-aminophenol in pure form and in the presence of acetaminophen. The method allowed the determination of *p*-aminophenol in the presence of acetaminophen without prior separation. The results obtained are accurate and precise. Average recoveries of 100.4 ± 0.8 and 100 ± 1 were obtained using Fe(III) and Ce (IV) as oxidants, respectively.

3.11. Investigation of reaction mechanism

The reaction product could be isolated as picrate and perchlorate salts and subjected to microanalysis, UV–Vis and IR identification tests.

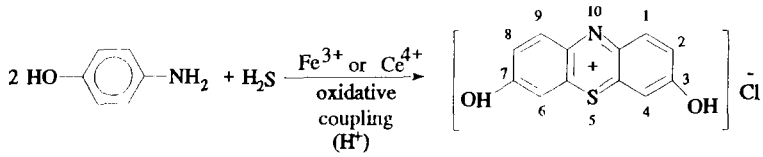

Scheme. 1. Suggested mechanism for the reaction *p*-aminophenol with Na_2S and Fe(III) to form a methylene blue-like dye.

A λ_{max} of 550 nm was obtained. On the other hand, the IR spectrum of both picrate and perchlorate salts of the isolated reaction product of *p*-aminophenol with sodium sulphide (Fig. 6) shows a significant difference from that of the pure compound in region of 3500–3100 cm^{-1}. The disappearance of the doublet peaks that are characteristic of a primary amino group indicates that the nitrogen is the possible reaction site. In addition, analogous structures have been reported before for methylene blue [25] and methylene blue–like structure [26]. From the microanalysis data and IR spectra, a mechanism for the reaction could be suggested (Scheme 1).

4. Conclusion

The proposed method offers several advantages over previously reported procedures. With the proposed method any UV-absorbing material, e.g. caffeine, pheniramine and acetylsalicylic acid, should not interfere when present in the quantities encountered in pharmaceutical preparations. The proposed method could be used in the detection of *p*-aminophenol in the presence of acetaminophen. In addition, it could be used for determination of acetaminophen in biological fluids, which will be our target in the future.

References

[1] A. Yesilada, H. Erdogen and M. Ertan, Anal. Lett., 24 (1991) 129.
[2] A.G. Fogg, P.J. Sausins and J.R. Smithson, Anal. Chim. Acta 49 (1970) 342.
[3] M.K. Srivastava, S. Ahmad, D. Singh and I.C. Shukla, Analyst 110 (1985) 735.
[4] P. Parimco, R.R. Sethuraman, A. Amalraj and N. Seshadari, Indian Drugs, 26 (1989) 704.
[5] British Pharmacopoeia 1993, H.M. Stationery Office, London, 1993.
[6] D.Y. Tobias, J. Assoc. Off. Anal. Chem 66 (1983) 1450.
[7] M.A. Kornay, M. Dedair, H. Mahgoub and M.A. Elsayed, J. Assoc. off. Anal. Chem., 69 (1986) 608.
[8] M.K. Sharaf El-Din, M.A. Abuijeie and M.H. Abdel Hay, Anal. Lett. 24 (1991) 2187.
[9] A.A. El-Kheir, S. Belal and El-Shanawani, Pharmazie, 40 (1985) 62.
[10] S.M. Hassan, M.I Walash, S.M. El-Sayed and A. M. Abou Ouf, J. Assoc. Off. Anal. Chem. 64 (1981) 1442.
[11] J.M. Calatayud and S.S. Vives, J. Pharm. Biomed. Anal., 7 (1989) 1165.
[12] S.M. Sultan, I.Z. Alzamil, A.M. Aiz Alrahman, S.A. Altamrah and Y. Asha, Analyst, 111 (1986) 919.
[13] P.B. Issopoutos, Anal. Lett. 23 (1990) 1057.
[14] A.A. El Kheir, S. Belal, M. El Sadek and A. El-Shanwani, Analyst, 111 (1986) 319
[15] A. Oztunc, Analyst 107 (1982) 585.
[16] J.M. Calatay and C.G. Benito, Anal. Chim. Acta 231 (1990) 259.
[17] I.I. Koukli, A.C. Calokerinos and T.P. Hadjiioannou, Analyst, 114 (1989) 711.
[18] D.J. Krieger, J. Assoc. Off. Anal Chem., 67 (1984) 339.
[19] R. Thomis, E. Roets and J. Hoogmartens, J. Pharm. Sci., 73 (1984) 1830.
[20] B. Schultz, J. Chromatogr., 299 (1984) 484.
[21] T.L. Ascah and B.T. Hunter, J. Chromatogr., 455 (1988) 279.
[22] H.L. Rau, A.R. Aroor and P.G. Rao, Indian Drugs, 28 (1991) 285.
[23] M.A. Abmigeie, M.E. Abdel Hamid and E.A. Ebrahim, Anal. Lett. 22 (1989) 365
[24] O. Lau, S. Luk and Y. Cheung, Analyst 114 (1989) 1047.
[25] M.A. Abdalla, A.S. Fogg and C. Burgess, Analyst, 107 (1982) 213.
[26] S.R. El-Shabouri, A.F. Youssef, F.A. Mohamed and A.M.I. Rageh, J. Assoc. Off. Anal. Chem. 69 (1986) 821.

ELSEVIER

Talanta 44 (1997) 69–74

Talanta

Lability of heavy metal species in aquatic humic substances characterized by ion exchange with cellulose phosphate

J.C. Rocha[a,*], I.A.S. Toscano[a], P. Burba[b]

[a] *Analytical Chemistry Department, Institute of Chemistry of Araraquara, UNESP 14800-900, CP 355, Araraquara, SP, Brazil*
[b] *Institute for Spectrochemistry and Applied Spectroscopy (ISAS), 44139 Dortmund, Germany*

Received 21 February 1996; revised 4 June 1996; accepted 12 June 1996

Abstract

Labile metal species in aquatic humic substances (HSs) were characterized by ion exchange on cellulose phosphate (CellPhos) by applying an optimized batch procedure. The HSs investigated were pre-extracted from humic-rich waters by ultrafiltration and a resin XAD 8 procedure. The HS–metal species studied were formed by complexation with Cd(II), Ni(II), Cu(II), Mn(II) and Pb(II) as a function of time and the ratio ions to HSs. The kinetics and reaction order of this exchange process were studied. At the beginning (<3 min), the labile metal fractions are separated relatively quickly. After 3 min, the separation of the metal ions proceeds with uniform half-lives of about 12–14 min, revealing rather slow first-order kinetics. The metal exchange between HSs and CellPhos exhibited the following order of metal lability with the studied HSs: Cu > Pb > Mn > Ni > Cd. The required metal determinations were carried out by atomic absorption spectrometry.

Keywords: Aquatic humic substances; Cellulose phosphate; Heavy metal species; Ion exchange; Lability

1. Introduction

The main mass of organic carbon distributed in natural aquatic environments and soils is concentrated in humic substances (HSs). In general, HSs, final products of microbial degradation processes of plant remnants in soils and waters, are complex mixtures of organic macromolecules of varying molecular-weight distributions, substructures and functionalities [1]. They can be transported into natural waters by the leaching process or formed directly in aquatic environments by the decomposition of plants and aquatic organisms. Despite their great variety and heterogeneity, HSs mostly exhibit comparable functional groups of phenolic and carboxylic types and are characterized by their exceptional complexation capabilities towards metal ions, as studied during the last decade [2–6].

* Corresponding author Fax: (+55) 162-22-7932.

PII S0039-9140(96)02017-6

Due to their complexation properties HSs are important natural buffers in the environment, binding strongly both inorganic and organic pollutants. The thermodynamic and kinetic stability of the HS–pollutant species formed influences directly their transport, accumulation and bioavailability in the biosphere [7,8]. In aquatic systems, the concentrations of dissolved metal ions and HSs and their ratio can vary considerably and hence might influence the formation of HS–metal species as well as their distribution between liquid and solid phases (e.g. suspended matter, sediment). Therefore, investigations of exchange processes between HSs and metal ion are of great interest when studying the hydrogeochemical turnover of metal in soil and natural waters [9], especially under the influence of acid rain caused by the increasing pollution of the atmosphere by man-made nitrogen and sulfur oxides [10].

From this point of view, analytical information on the lability of HS–metal species and their possible transformation into species of either higher or lower stability is of increasing relevance. For this purpose, a variety of methods have been proposed, such as electrochemical and chromatography techniques, in order to study the complexing capacity of HSs, the HS–metal equilibrium and the dynamics of complexes [11,12]. The advantageous application of immobilized chelators for the differentiation of labile and inert metal species in HSs by ligand exchange has been described in other reports [13–15]. In the previous papers, both the kinetics and the degree of metal exchange have been used for the operational characterization of metal labilities in aquatic HSs. In the present study, the lability of metal fractions complexed with dissolved HS was characterized by ion exchange on cellulose phosphate (CellPhos), which has been shown recently to be a collector of high efficiency and with fast kinetics for traces of heavy metals dissolved in aqueous salt solutions [16]. Applying an optimized batch procedure based on the usage of CellPhos, a number of important parameters (such as pH, HS concentration, complexation time) which influence the lability of environmentally relevant metal ions (e.g., Cd, Ni, Mn, Cu and Pb) in HSs were evaluated [17].

2. Experimental

2.1. Sampling of aquatic HSs

Humic-rich water was sampled (100 l) from a reservation bog lake (Venner Moor (VM 4); 8 mg l^{-1} dissolved oxygen content (DOC), pH 3.7) located in Münster, Germany and recently described elsewhere [18,19]. After filtration through a 0.45 μm membrane, 50 l of the sample was concentrated by ultrafiltration (UF) to 0.5 l (maintaining the original pH of 4.5) using a Millipore Pellicon system in tangential flow mode (0.42 m^2 membrane area, nominal molecular weight cut-off 1000 Da, 30 ml min^{-1} penetration rate). The UF concentrate (VM 4-UF with 90% recovery of HSs) contained 3.5 mg ml^{-1} DOC, exhibiting a complexing capacity of 3.3 mmol Cu(II) g^{-1} DOC (referred to DOC of HS), which was determined by a Cu(II)-selective electrode.

2.2. CellPhos and cellulose HYPHAN sorbents

The cellulose sorbent CellPhos used in this study for the separation of labile metal fractions in HSs was functionalized according to Ref. [20]. It is comparable to the commercial Chelex P (Bio-Rad, USA). This collector has a surface area of 1.94 ± 0.06 m^2 g^{-1} and 1.3 ± 0.09 mol g^{-1} of immobilized phosphate groups.

Cellulose HYPHAN (functional group: 1-(2-hydroxyphenylazo)-2-naphthol, supplied by Riedel-de Haën AG, Hannover, Germany) used for the removal of heavy metals from HS concentrates was applied according to recommendations given in Ref. [14].

2.3. Preparation of standardized HS solutions

In order to remove the metals naturally contained in the HS concentrate (50 ml VM 4-UF) it was magnetically stirred for 72 h with 1 g of cellulose HYPHAN. The pH value was maintained at 8.0. After filtering and adjusting the pH to 4–5 the purified HS solution was stored in polyethylene bottles for defined periods of time in a refrigerator at 4°C.

Stardardized HSs loaded with heavy metal ions under defined conditions were prepared in the following way. First, the HS concentrate was diluted to the desired HS concentration (e.g. 10 mg ml^{-1} HS, 10 ml sample) by adding high-purity water (Milli-Q system, Millipore) and then spiked with a multimetal standard solution (e.g. 0.5 μg ml^{-1} Cd, 2.0 μg ml^{-1} Cu, 1.0 μg ml^{-1} Mn, 2.0 μg ml^{-1} Ni, 2.0 μg ml^{-1} Pb), adjusting the pH to the desired values with dilute solutions of NaOH and HCl. After defined periods of time (complexation time) these standardized HS samples were used in subsequent batch experiments.

2.4. Batch procedure

Distribution coefficients, K_d, of metal ions between the chosen adsorbent (CellPhos) and dissolved HS were evaluated by a batch procedure. 10.0 ml of standardized HS, preloaded with metal ions for a complexation time of 24 h, and 80.0 mg of CellPhos were stirred for 24 h. The collector was filtered through a filter paper (2 cm diameter) previously precleaned with 1.0 M HCl p.a. Then the resin, together with the filter paper, was eluted with 3.0 ml of 2.0 M HCl suprapur. After centrifugation of the eluate the metals contained were determined by flame atomic absorption spectrometry (AAS).

2.5. Metal determinations by AAS

Trace metals concentrated in the eluate were determined according to the operating instructions of the manufacturer (Spectrometer Varian-Intralab-AA 1475). Synthetic metal standards having the same acid concentration (2.0 M HCl) as the experimental samples were used for calibration.

3. Results and discussion

Efficient multielement preconcentration by an ion-exchange batch process requires collectors with high distribution coefficients, K_d, preferably $>10^4$, as calculated by the following equation:

$$K_d = C_{col}/C_{sol}(ml\ g^{-1})$$

where C_{col} is the concentration of metals in the collector (mg g^{-1}) and C_{sol} is the concentration of metals in solution (mg ml^{-1}). When using the ion exchanger CellPhos as collector for the labile metal fraction in the HS solution, K_d values of 10^2–10^3 (ml g^{-1}) were obtained in the pH range 3.0–11.0. As shown in Fig. 1, all metals exhibit curves with a maximum in neutral solutions and a small reduction in slightly acidic and alkaline solutions. Therefore, metal ions complexed by HSs are easily exchanged by the phosphate groups of the collector. At pH < 3 metal ions are increasingly remobilized from both HS molecules and phosphate groups of the collector.

Chelating ion exchangers based on cellulose often exhibit high distribution coefficients of the order of 10^4 for metal ions such as Cu, Ni, Co, Pb, Mn and Zn in salt solutions [13,14,21]. Moreover, the separation of the metal ions from aqueous solutions by cellulose collectors (but in the absence of HS) can be characterized by a relatively short half-life, $t_{1/2}$, in the range of 8–20

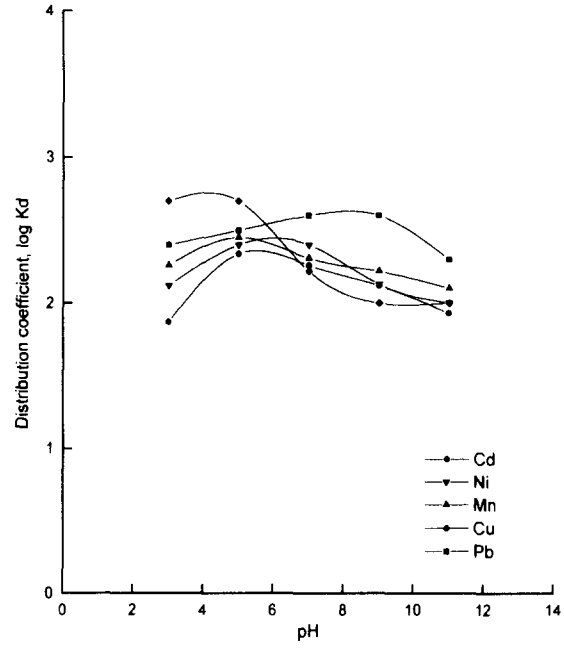

Fig. 1. Metal distribution coefficient K_d on CellPhos in the presence of HSs as a function of pH (1.0 mg ml^{-1} HS VM-4 UF, 24 h equilibrium, 10 ml sample, 80.0 mg CellPhos).

s as recently shown in Ref. [14]. The equilibrium between collector and solution phase is established within a matter of minutes. In a recent paper [13] it was shown, however, that the separation kinetics of metal ions complexed by HSs can be delayed by orders of magnitude. Both effects, the delayed kinetics and the reduced recovery rates of HS-bound metal fractions, have been utilized for the operation characterization of their lability. The following order was reported: Mn > Zn > Cu > Ni > Fe [14].

The collector HYPHAN applied for the evaluation of this lability order [14], however, suffered from the drawback of a relatively high working pH (8.0) necessary for quantitative metal separation by a batch operation, in contrast to the CellPhos usage proposed in the present study. Similar labilities of aquatic HS–metal species could be shown as well by means of an analogous flow procedure based on a strongly chelating collector of EDTA-type [21].

The separation of metal ions complexed to HS (1.0 mg ml^{-1}, VM 4-UF, 0.1 μmol ml^{-1} sum of Cd, Cu, Mn, Ni and Pb) by means of CellPhos is shown in Fig. 2a as a function of the contact time. Accordingly, a contact time of >60 min is required to attain the exchange equilibria as shown in reaction (1) and to obtain a final recovery of 65–75% metal by CellPhos, depending on the element.

The kinetics and reaction order of this ion-exchange process can be derived from Fig. 2b, which exhibits the separation of the exchange-labile Cu, Mn and Pb (concentration C_L) logarithmically plotted as a function of the contact time. At the very beginning (3), merely 50% of the HS-bound Cu(II) and about 20% of the Mn and Pb are separated relatively quickly. After 3 min, the separation of the HS-bound metal ions proceeds with uniform $t_{1/2}$ values of about 12–14 min, revealing rather slow first order kinetics compared to metal exchange by CellPhos from aqueous salt solutions ($t_{1/2}$ in the range 10–25 s [17]). These first-order kinetics indicate that either slow dissociation of the HS–metal complexes may occur or else delayed transport of the macromolecular HS–metal complexes within the narrow pore system of the cellulose collector may take place.

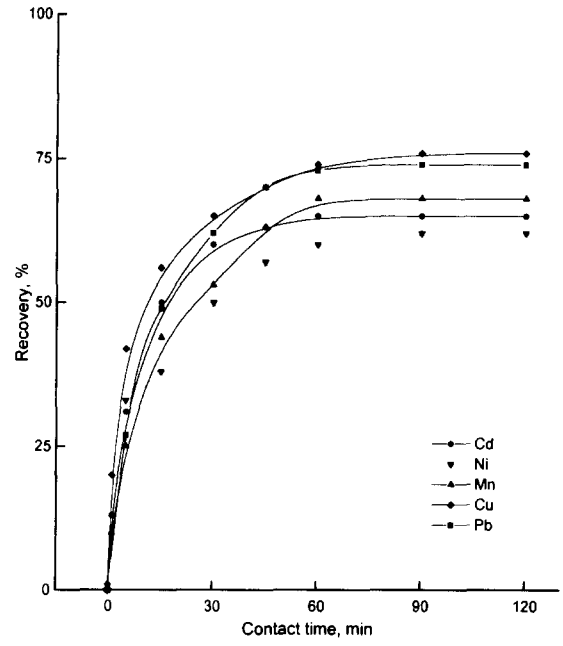

(a)

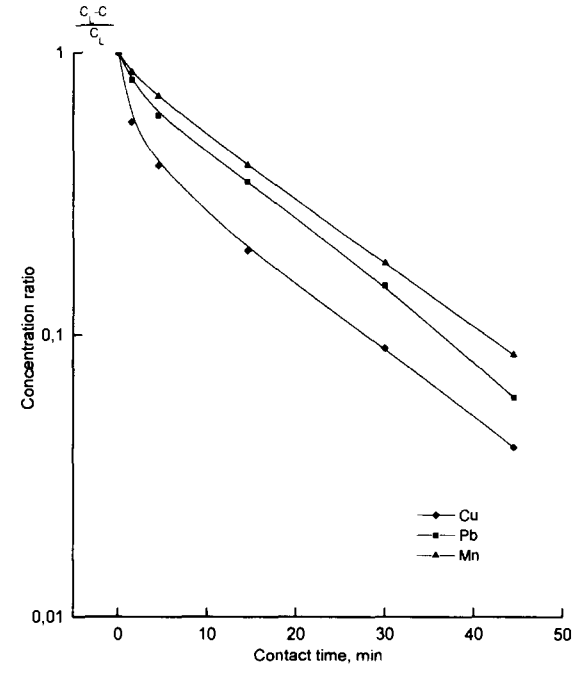

(b)

Fig. 2. (a) Batch separation of HS-bound metal ions as a function of the contact time (1.0 mg ml^{-1} HS VM-4 UF, 2.0 μg ml^{-1} of each trace metal, pH 5.0, 24 h equilibrium, 80.0 mg CellPhos). (b) Separation of exchange-labile metal fractions (concentration C_L) from HSs as a function of the contact time (for conditions, see Fig. 2a).

In principle, the exchange of metal ions between resins and labile macromolecular metal complexes such as HS–M can be described by the following equilibrium:

$$\underset{\text{solution}}{\text{HS–M}} \overset{K_{HS}}{\rightleftharpoons} \text{HS} + \text{M} + \text{EX} \overset{K_{Ex}}{\rightleftharpoons} \underset{\text{exchanger}}{\text{M–Ex}} \quad (1)$$

where HS–M indicates species formed between metal and HSs, Ex indicates ion exchanger, solid phase, and M–Ex indicates species formed between metal and collector. Thus, the concentrations of species HS–M and M–Ex, governed by the equilibrium constants K_{HS} and K_{Ex}, are shifted towards HS–M as the concentration of HSs increases. The influence of increasing HS concentration on the metal distribution on the collector CellPhos is shown in Fig. 3. An eightfold increase in the HS concentration (e.g 4.0 mg ml^{-1} HS) lowers the metal distribution coefficients K_d by about a factor of five to about 10^2 ml g^{-1}. Consequently, in the case of very high HS concentrations only a multistage flow procedure using CellPhos-filled columns can be used for quantitative separation of labile metals fractions in HSs.

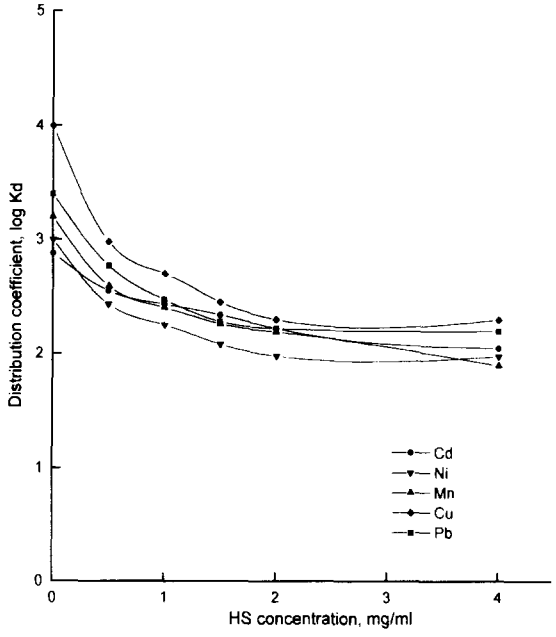

Fig. 3. Metal distribution coefficients K_d as a function of the HS concentration (HS VM-4 UF, 2.0 μg ml^{-1} of each trace metal, pH 5.0, 24 h equilibrium, 80.0 mg CellPhos).

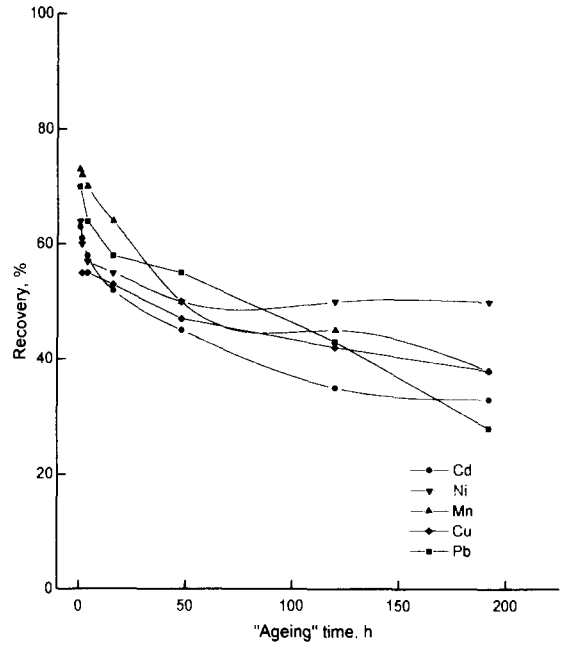

Fig. 4. Lability of heavy metals in HSs as a function of "ageing" (batch procedure, 1 mg ml^{-1}) HS VM-4 UF complexed with 2.0 μg ml^{-1} of each trace metal, pH 5.0, 80.0 mg CellPhos).

Another important parameter strongly influencing the lability of metals bound in HSs is the time of complexation ("ageing") of the HS–M species formed, as has recently been shown in a paper dealing with the exchange process between HS–metal species and chelating collectors [14]. A similar transformation effect (as shown in Fig. 4) may be observed in the case of metal exchange between dissolved HSs and CellPhos. For instance, after a complexation period of 8 days the Cu(II) recovery is reduced form $\approx$55% to $\approx$20%. A similar decrease in metal lability in HSs can be observed for several other metal ions.

4. Conclusions

The thermodynamic and kinetic stabilities of HS–metal species depends on a variety of environmental parameters, in particular the pH values, the metal and HS concentrations and their ratio, the complexation capability of the HSs and

potential transformation processes which are still poorly characterized. Thus, the stability of HS–metal species in aquatic environments cannot be described solely by conventional thermodynamic stability functions measured for HS–metal complexes freshly formed "in vitro". There is a special demand for analytical methods applicable for the evaluation of the lability of HS–metal species and their changes due to potential ageing processes.

Our investigations using the collector CellPhos for the characterization of labile metal fractions in aquatic HSs are an additional confirmation of the utility of the ion-exchange method. Both the kinetics and the degree of separation can be used for the operational evaluation of the metal lability in HSs as a function of different parameters (e.g. pH, ratio of metal: HS, complexation time). In particular, the influence of the complexation time of HS–metal species on their lability shows that the " reactivity" of such species depends not only on their thermodynamic stability but also on typical transformation processes. The operational character of such ion-exchange procedures, however, only allows the description of a relative order of metals labilities in dissolved HSs under standardized conditions.

References

[1] G.R. Aiken, D.M. McKnight, R. Wershaw and P. MacCarthy, Humic Substances in Soil, Sediment and Water, John Wiley and Sons, New York, 1985, pp. 1–9.
[2] I.H. Suffet and P. MacCarthy, Aquatic Humic Substances: Influence on Fate and Treatment of Pollutants, American Chemical Society, Washington, 1989.
[3] G. Weber, in F.H. Frimmel and R.f. Christman (Eds), Humic Substances and Their Role in the Environment, John Wiley and Sons, New York, 1988, pp. 165–179.
[4] R. Becker and H. Klamberg, in G. Matthess, F.H. Frimmel, P. Hirsch, H.D. Schulz and E. Usdowski (Eds.), Progress in Hydrogeochemistry, Spinger-Verlag, Berlin, 1992, pp. 71–77.
[5] J. Buffle, Complexation Reactions in Aquatic Systems—An Analytical Approach, Horwood, Chichester, UK, 1990, p. 862.
[6] B. Allard, H. Boren and A. Grimvall, Humic Substances in the Aquatic and Terrestrial Environment, Springer-Verlag, Berlin, 1991, pp. 263–368.
[7] M. Zhang and T.M. Florence, Anal. Chim. Acta, 197 (1987) 137.
[8] R.A. Saar and J.H. Weber, Environ. Sci. Technol., 16 (1982) 510.
[9] F.H. Frimmel, in G. Matthess, F.H. Frimmel, P. Hirsch, H.D. Sculz and E. Usdowski (Eds.), Progress in Hydrogeochemistry, Springer-Verlag, Berlin, 1992, pp. 61–64.
[10] P. Warneck, Chemistry of the Natural Atmosphere, Int. Geophys. Ser. 41, Academic Press, New York, 1988.
[11] T.M. Florence and G.E. Batley, Crit. Rev. Anal. Chem., 9 (1980) 219.
[12] J. Buffle, Complexation Reactions in Aquatic Systems: An Analytical Approach, Horwood, Chichester, UK, 1990, pp. 427–610.
[13] P. Burba and P.G. Willmer, Fresenius, J. Anal. Chem., 342 (1992) 167.
[14] P. Burba, Fresenius, J. Anal. Chem., 348 (1994) 301.
[15] Y. Lu, C.L. Chakrabarti, M.H. Back, D.C. Gregoire and W.H. Schoeder, Environ. Anal. Chem., 60 (1995) 313.
[16] A. Naghmush, K. Pyrzynska and M. Trojanowicz, Talanta, 42 (1995) 851.
[17] P.M. Padilha, J.T.S. Campos, J.C. Moreira and C.C. Federici, Quim. Nova, 18 (1995) 529.
[18] P. Burba, V. Shkrinev and B. Spivakov, Fresenius, J. Anal. Chem., 351 (1995) 74.
[19] B. Aster, P. Burba and J.A.C. Broekart, Fresenius, J. Anal. Chem., 354 (1996) 722.
[20] F.M. Ford and Wm. P. Hall, U.S. Pat. 2,482,755, 1949.
[21] P. Burba, J.C. Rocha and D. Klockow, Fresenius, J. Anal. Chem., 349 (1994) 800.

ELSEVIER

Talanta 44 (1997) 75–83

Talanta

Spectrophotometric determination of lithium with Quinizarin in drugs and serum

Laura Gámiz Gracia, Luis Cuadros Rodríguez*, Manuel Román Ceba

Department of Analytical Chemistry, Faculty of Sciences, University of Granada, c/ Fuentenueva s.n., E-18071 Granada, Spain

Received 4 October 1995; revised 15 May 1996; accepted 17 June 1996

Abstract

A very sensitive analytical method is proposed for the determination of lithium based on the reaction of Li^+ ion wiht 1,4-dihydroxyanthraquinone (Quinizarin). In dimethylsulfoxide medium (90%) and in the presence of sodium hydroxide and sodium carbonate, a bluish-violet color ($\lambda_{max} = 601$ nm) develops and is stable over a period of 30 min to 2.5 h. The NaOH and Quinizarin concentrations were optimized simultaneously using the response surface methodology from sequential experimental Doehlert designs. Beer's law is obeyed in the concentration range 14–250 ppb Li^+ in aqueous and serum matrices, and the errors (RSD) in the determination of 100 ppb Li^+ are 4.0% and 3.9% respectively. The proposed procedure was satisfactorily applied to the determination of lithium in drugs and human serum (no deproteinization is required).

Keywords: Doehlert experimental design; Lithium; Quinizarin; Visible-spectrophotometry

1. Introduction

Lithium, like other alkali metals, shows relatively poor chemical coordination. However, its high charge density provides greater affinity to ligands with donor oxygen atoms than the rest of the alkali metals and therefore lithium forms stable chelates in solution more easily [1,2]. Therefore, few organic reagents which form colored chelates with alkali metals are known.

Several chromogenic organic reagents with two aromatic rings linked by an azo group (–N=N–) with ortho substituents –OH in one ring and –COOH, $-PO(OH)_2$ or $-AsO(OH)_2$ in the second ring have been used as complexing agents of Li^+ (Thoron, Quinazolinazo, Nitroantranylazo, Phosphonazo R, Arsenazo III) in photometric determinations [3]. Among these, Thoron (*o*-(2-hydroxy-3,6-disulfo-1-naphthylazo)benzenearsonic acid) has been the most used. Proposed by Kuznetsov [4], it gives, together with Li^+ ion, an orange color in a strong basic medium. The spectrophotometric method using this reagent, developed by Thomason [5], has been used for the determination of lithium in high-purity beryllium and beryllium oxide [6], sea water [7], mollusc shells [8] and blood serum [9].

* Corresponding author. Fax: (+34) 58-27-42-58.

PII S0039-9140(96)02018-8

Multidentate ligands derived from 3-fenilformazano ($NH{=}N{-}C(Ph){=}N{-}NH_2$) have also been suggested as spectrophotometric reagents for Li^+ [10–14].

Recently, with the development of macrocyclic ligands such as crown and aza-crown ethers, cryptands and spherands, new spectrophotometric methods for the determination of lithium in drugs, serum and urine samples have been proposed. These methods show good selectivity against other alkali metals but due to the low solubility of this type of ligand anhydrous media [15], extraction processes [16,17] or the use of a water–micellar medium is required for solubilization [18].

Quinizarin (1,4-dihydroxyanthraquinone) is a chromogenic and fluorogenic agent of metallic ions that shows high selectivity in its reactions since the O-donors are blocked by two strong intramolecular hydrogen bondings [19]; therefore, few spectrophotometric methods using this reagent are known. This reagent has been applied for the determination of Mg^{2+} [20] and UO_2^{2+} [21] and for the simultaneous determination of Lu^{3+} and Pr^{3+} [22] and Tm and Nd [23]. Other similar reagents have also been used occasionally such as Quinizarin-sulfonic acid (1,4-dihydroxy-anthra quinone-2-sulfonic acid) for Be^{2+} [24] and Al^+ [25]; Leucoquinizarin(1,4,9,10-tetrahydroxyanthracene) for Mg^{2+} [26] and Be^{2+} [27], and naphthazarin (*5,8-dihydroxy-1,4-naphthoquinone*) for Th^{4+} [28], and Th^{4+} and UO_2^{2+} simultaneously [29].

Response surface methodology (RSM) [30] is a group of mathematical and statistical techniques used for analyzing and modeling a problem where a particular response is a function of several variables, and where the aim is to optimize this response. RSM obtains an appropriate estimate of the real functional relationship between the instrumental response and the experimental factors under study. A quadratic function is the best solution as it is a simple model which can describe a great variety of surfaces [31], allows the prediction of the existence of curvature in the system and permits the computation of the maximum coordinates. In addition, this type of function can be simply obtained with a three-level experimental design.

In this paper, a sensitive method for the spectrophotometric determination of lithium in dimethylsulfoxide: water medium in the range 14–250 ppb lithium is proposed. The method is suitable for the clinical assay of lithium.

2. Experimental

2.1. Instrument

A Perkin-Elmer Lambda 5 UV–Vis spectrophotometer with two matched 1 cm quartz cells, thermostatically controlled at 25.0 ± 0.5°C with a water-bath circulator (Frigiterm S-382, J.P. Selecta), and a Corning 410 Flame Photometer were used.

A Casio FX-850 P pocket micro-computer with scientific library was used to calculate *P* values os statistic tests. All the calculations for optimization were carried out using the STATGRAPHICS data analysis package [32].

2.2. Reagents and materials

All materials, solvents and reagents were of analytical grade and were used without further purification. Doubly-distilled water was used throughout.

2.2.1. Lithium solution

A stock solution of Li^+ (500 ppm) was prepared by dissolving 1.24 g of lithium nitrate (Merck) in 250 ml of water. Working solutions were prepared by appropriate dilution of the stock solution.

2.2.2. Quinizarin solution

A 10^{-3} M solution was prepared by dissolving 60 mg of 1,4-dihydroxyanthaquinone (Merck) in 250 ml of dimethylsulfoxide.

2.2.3. Sodium hydroxide solution

A 1 M stock solution was prepared by dissolving 10 g of NaOH (Merck) in water. Working solutions were prepared daily by appropriate dilution of the stock solution.

2.2.4. Sodium carbonate solution

A 2.5 M stock solution was prepared by dissolving 66.237 g of sodium carbonate (Merck) in 250 ml of water. Working solutions were prepared by appropriate dilution.

2.3. Drug and serum

In order to verify the applicability of the proposed analytical method, the determination of lithium in the following real samples was validated

2.3.1. Otogén (Rimafar Laboratory S.A., Madrid, Spain)

Tablet containing lithium carbonate, potassium bromide, potassium iodide, thiamine and excipient. Mean weight of tablet: 319 mg.

2.3.2. Plenun (Lasa Laboratory, Barcelona, Spain)

Tablet containing lithium carbonate and exicipient. Mean weight of tablet: 516 mg.

2.3.3. Glucosor-Litio (Soria Natural, S.A., Soira, Spain)

Solution containing lithium gluconate, glucose and distilled water.

2.3.4. Serum

Blood serum from healthy individuals who had not been treated with lithium salts was centrifuged for 5 min at 4000 rev min^{-1} [33] and the supernatant liquid was separated and kept frozen at −15°C until the analysis. Once thawed, analyis must be done within 7 days [34]. Serum samples required no deproteinization.

2.4. General procedure for drugs

Using a micropipet, the indicated amount of standard or sample preparation was added to a test tube, followed by 50 μl of 0.1 M NaOH, 40 μl of 0.25 M Na_2CO_3 and water to make up to 1 ml. 250 μl of this solution was pipeted into another test tube, followed by 2.15 ml of dimethylsulfoxide and 100 μl of 10^{-3} M Quinizarin. The tubes were kept at 25°C in a thermostatic bath for 30 min. The absorbance of the solution was measured at 601 nm against a reagent blank prepared similarly. The calibration was made under identical conditions.

2.4.1. Otogen

Exactly 319 mg, obtained from 10 tablets previously powdered, was placed in a 100 ml glass beaker. 10 ml of 1 M hydrochloric acid was added and the solution was digested close to dryness. The residue was extracted with 10 ml of hot water, filtered, washed, transferred to a 100 ml volumetric flask and made up to volume with water. 40 μl of this solution was used for the analysis of lithium as described in section 2.4.

2.4.2. Plenur

The same procedure was followed, starting with 516 mg of the sample, transferring the final filtrate into a 250 ml volumetric flask and making up to volume with water. This solution was diluted 1:10 with water taking 50 μl for the subsequent analysis as described in section 2.4.

2.4.3. Glucosor-Litio

1 ml of sample was pipeted into a 10 ml volumetric flask and made up to volume with water. 100 μl of this solution was used, as described in section 2.4.

2.5. Procedure for serum

Accurately pipeted amounts (40, 50 and 70 μl) of standard lithium solution (50 ppm) were added to 500 μl of centrifuged serum and these solutions were diluted with water to make up to 1 ml. 100 μl portions of each of these spiked serum soltutions were pipeted into a test tube, followed by 100 μl of 0.1 M NaOH, 10 μl of 0.25 M Na_2CO_3, 40 μl of water, 2.15 ml of dimethylsulfoxide and 100 μl of 10^{-3} M Quinizarin. The procedure was completed as described in section 2.4. The calibration was made with lithium standards of increasing concentration, containing 100 μl of centrifuged pooled serum (obtained by mixing serum of 10 individuals) diluted 1:1 with water, and operating under the conditions described above.

3. Results and discussion

All the abosorbance measurements for optimization, calibration and interference experiments were performed against a corresponding solvent blank prepared under identical conditions.

3.1. Effect of dimethylsulfoxide: water ratio

The maximum absorption wavelengths and the absorbance difference between chelate and reagent are strongly dependent on the solvent. All the described spectrophotometric methods require a polar, water-miscible solvent and so water, methanol, ethanol, ethyline glycol, 2-propanol, acetone, acetonitrile, *N,N*-dimethylformamide, hexamethylphosphotriamide, dimethylsulfoxide, 1,4-dioxan and pyridine were tested in order to find the maximum absorbance difference. The results of this experiment are shown in Table 1. Dimethylsulfoxide was selected because it showed the maximum difference and the maximum hipsochromic displacement between the two spectra.

Table 1
Experimental values of wavelengths and absorbance for the system lithium–Quinizarin in different solvent/water mixtures (9/1, v/v) (Experimental conditions: $[Li^+] = 1.2 \times 10^{-4}$ M; $[NaOH] = 5 \times 10^{-3}$ M; $[Quinizarin] = 4.8 \times 10^{-5}$ M)

Solvent	λ_b[a]	λ_b[c]	$\Delta\lambda$[c]	$A^d{}_{max}(\lambda_d)$[e]
Water	550	550	0	0.023
Methanol	552	548	4	0.040
Ethanol	548	548	0	0.014
Ethylene glycol	547	547	0	0.040
2-Propanol	596	596	0	0.150
Acetone	600	595	5	0.294
Acetonitrile	595	590	5	0.186
DMF[f]	612	602	10	0.278
HMPT[g]	569	566	3	0.032
DMS[h]	616	604	12	0.294
1,4-Dioxan	604	596	8	0.286
Pyridine	570	565	5	0.232

[a] Maximum wavelength of the blank (nm).
[b] Maximum wavelenth of the chelate (nm).
[c] Difference betweeen [a] and [b] (nm).
[d] Maximum absorbance difference between chelate and reagent.
[e] Wavelength corresponding to maximum of [d] (nm).
[f] *N,N*-Dimethylformamide.
[g] Hexamethylphosphotriamide.
[g] Dimethylsulfoxide.

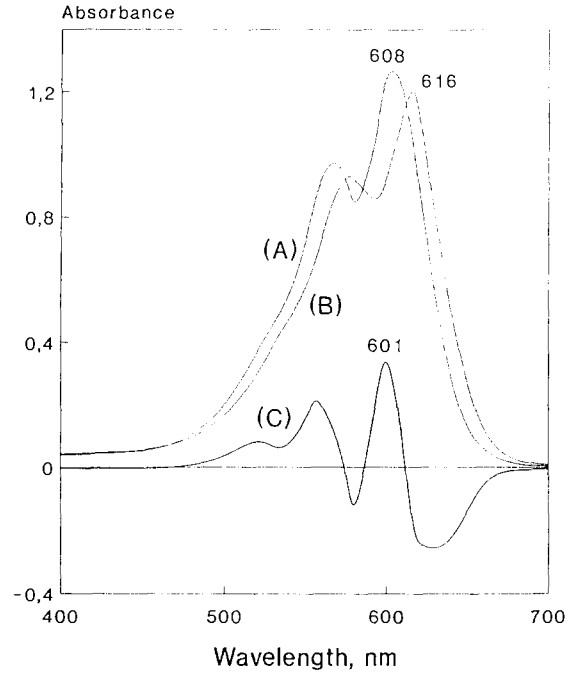

Fig. 1. Absorption spectra in 90% dimethylsulfoxide: (A) chelate; (B) ligand blank; (C) difference. ($[Li^+] = 1.2 \times 10^{-3}$ M, $[Quinizarin] = 4.8 \times 10^{-4}$ M, $[NaOH] = 5 \times 10^{-3}$ M)

As the proportion of water was increased, the absorbance of the chelate, measured against a reagent blank, decreased. Thus a proportion of 10% of water was selected as this provided sufficient aqueous phase for the preparation of the samples.

3.2. Absorption spectra

Fig. 1 shows absorption spectra of chelate and ligand blank against the solvent in 90% dimethylsulfoxide. Both curves show a maximum difference at 601 nm.

3.3. Effects of the Quinizarin and sodium hydroxide concentrations

Sodium hydroxide was selected (instead of KaOH or an organic base) in order to give an homogeneous background for the serum analysis. Molecular spectroscopic methods for the determination of lithium show a great interfering effect

from the other ions in solution, of which Na^+ is the principal one in a serum matrix, so in order to prevent possible interference from Na^+, NaOH was selected.

The NaOH and Quinizarin concentrations were optimized using the RSM from sequential experimental Doehlert designs [35] (Fig. 2), proposed by Bosque Sendra et al. [36,37], in order to obtain the maximum absorbance while simultaneously varying these two parameters for a constant lithium concentration of 1.2×10^{-4} M. These designs have never been used in optimization of experimental variables in analytical methods by molecular absorption spectrophotometry in solution.

As the central point, the values $-\log[\text{NaOH}] = 2.0$ and $10^5 \times [\text{Quinizarin}] = 2.0$ M were chosen for the first experimental design. Table 2 (Design I) shows the proposed Doehlert design and the experimental results obtained for the chelate absorbance measured against a reagent blank. Since

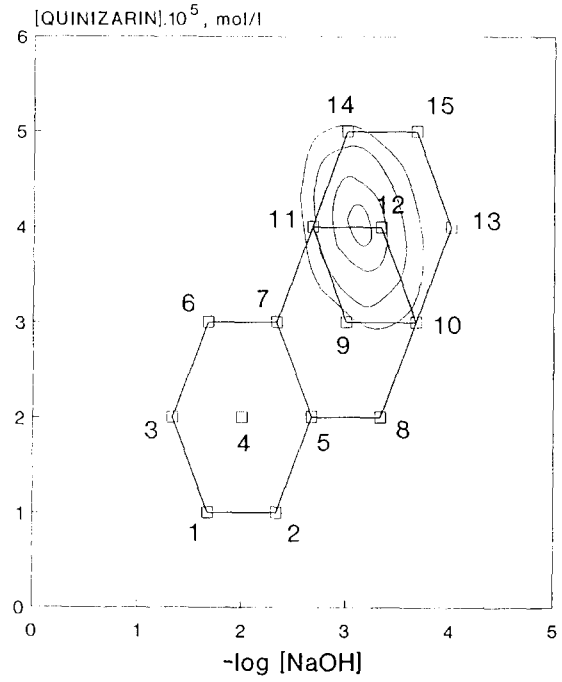

Fig. 2. Representation of the Doehlert designs I, II and III used for the simultaneous optimization of the Quinizarin and NaOH concentrations. Contour diagram of the response surface obtained from design III (the curves indicate 0.4, 0.5, 0.6 and 0.64 units of absorbance).

one of the factors is at five levels and the other at three levels, it is preferable to choose the variable with the stronger effect as the first factor. In this case, the five-level factors was chosen for $-\log[\text{NaOH}]$. The experimental data obtained fitted the function

$$A = 544.86 - 277.33Y - 372.38X + 115.15XY + 33.13Y^2 + 76.85X^2$$

where A = absorbance, $X = -\log[\text{NaOH}]$ and $Y = 10^5 \times [\text{Quinizarin}]$ (concentrations in moles per liter). The application of Lagrange's criterion ($\partial^2 A/\partial X^2 = 153.8, \partial^2 A/\partial Y^2 = 66.2, H(X, Y) = -3089.5$) indicated the presence of a saddle point. As no maximum was found, the absorbance maximum variation directions at points 5 and 7 (Fig. 2) were calculated, since this appeared to be the direction of increase in the response. The maximum variation directions of response found for each point were 29.77° and 31.2°. Because the two directions are almost parallel, a new experimental design is carried out in the referred direction (Fig. 2).

The proposed Doehlert design II was centred on the point $X = 3.0$, $Y = 3.0$, and the new experimental results obtained are shown in Table 2 (Design II). The equation which fits the new experimental values is

$$A = -1049.59 - 283.82Y + 11.4076X + 25.76XY + 49.59Y^2 - 198.25X^2$$

The application of Lagrange's criterion indicated the presence of a saddle point ($\partial A^2/\partial X^2 = -396.5$, $\partial A^2/\partial Y^2 = 99.2$, $H(X, Y) = 39\,991.9$). The absorbance maximum variation directions at the (11) and (12) points were calculated (Fig. 2). The maximum variation directions of responses found for each point were 44.47° and −68.91°. The lines drawn from the points, with the calulated directions, intersected at a coordinate point $X = 3.15$ and $Y = 4.47$.

Table 2 (Design III) shows the proposed Doehlert design III, centred on $X = 3.33$ and $Y = 4.00$, and the experimental results obtained. The contour diagram of the response surface is shown in Fig. 2. The new equation fitted to the experimental values is

Table 2
Experimental values used in the simultaneous optimization of Quinizarin and NaOH concentrations (mol l^{-1}), from Doehlert designs I, II and III ($[Li^+] = 1.2 \times 10^{-3}$ M)

Doehlert design	Experiment	$10^5 \times$ [Quinizarin]	−log[NaOH]	Absorbance
(I)	1	1.0	1.67	0.075
	2	1.0	2.33	0.129
	3	2.0	1.33	0.80
	4	2.0	2.00	01.46
	5	2.0	2.67	0.281
	6	3.0	1.67	0.170
	7	3.0	2.33	0.376
(II)	8	2.0	3.33	0.423
	9	3.0	3.00	0.415
	10	3.0	3.67	0.276
	11	4.0	2.67	0.446
	12	4.0	3.33	0.622
(III)	13	4.0	4.00	0.179
	14	5.0	3.00	0.490
	15	5.0	3.67	0.031

$$A = -13\,029.40 + 2669.22Y + 5318.84X - 238.81XY - 239.41Y^2 - 696.71X^2$$

The application of Lagrange's criterion indicated the presence of a maximum ($\partial A^2/\partial X^2 = -1393.4$, $\partial A^2/\partial Y^2 = -478.8$, $H(X, Y) = 610\,172.6$), which is the required optimum and corresponded to 4.0×10^{-5} M Quinizarin and 7.4×10^{-4} M NaOH.

The pK_1 and pK_2 values of Quinizarin in water are 9.35 and 11.78 respectively [38] while in 9:1 dimethylsulfoxide:water they should be slightly higher due to the lower value of the dielectric constant (46.5) of this proton-donor solvent with respect to that of water (78.3) [39]. The optimum working value of apparent pH found ($\approx$10.9) shows that only the first acid disociation occurs and the corresponding mono-anion is the reactive species.

3.4. Effect of concentrations of salts

The effect of increasing concentrations (10^{-4}–0.1 M) of different salts (Na_2CO_3, NaCl, KCl) on the abosorbance of the chelate, measured at 601 nm against a reagent blank, was studied. A maximum absorbance was obtained for a 10^{-3} M concentration of Na_2CO_3.

3.5. Effect of temperature

When the solution was thermostated between 10 and 50°C the absorbance of the chelate showed a linear decrease (temperature coefficient = -8.1×10^{-3} absorbance units $°C^{-1}$), while the absorbance of the reagent blank appeared to be constant. A working temperature of 25°C was chosen.

3.6. Other variables

The effect of the order of addition was studied, and found to be insignificant. Measurements were stable 30 min to 2.5 h after the preparation.

2.5. Calibration curve (Beer's law)

Experiments indicated that the Beer's law was obeyed for lithium concentrations up to 250 ppb, while higher concentrations yielded a non-linear response. New factorial designs (2^2) were performed in order to check the optimized NaOH

Table 3
Statistics and performance characteristics of the analytical methods from the calibration data set in aqueous and serum matrices

Parameter	Matrix	
	Water	Serum
Statistics		
Residual standard deviation (a.u.)[a]	3.909	2.883
Intercept (a.u.)	-2.51×10^{-3}	1.55×10^{-3}
Slope (a.u. per ppb Li)	0.63×10^{-3}	0.36×10^{-3}
% Lack-of-fit P value	39.9	62.4
Performance[b]		
Linearity (%)	98.3	98.3
Analytical sensitivity (ppb Li)	6.2	8.0
Detection limit (ppb Li)	13.2	13.3
Determination limit (ppb Li)	44.1	44.3
Precision (relative standard deviation, %):		
50 ppb Li	9.0	7.4
100 ppb Li	4.0	3.9
150 ppb Li	2.6	2.6
200 ppb Li	2.0	2.0
250 ppb Li	1.8	1.8

[a] a.u.: absorbance units.
[b] Calculated as indicated in Ref. [41].

and Quinizarin concentrations given above for a lithium concentration of 250 ppb. The result indicated that both values were suitable for calibration.

The calibration linearity was tested by "lack-of-fit" statistical F-test [40]. Three replicates for the aqueous matrix and five for serum of 0, 50, 100, 150, 200 and 250 ppb lithium standard solution were taken in order to set up the calibrations.

3.8. Analtyical performance characteristics

The main statistical and performance characteristics, calculated from the calibration data set [41], are shown in Table 3. The IUPAC detection limits [42], calculated from 10 replicates of the reagent blank, were 17.6 ppb and 14.5 ppb for aqueous medium and serum respectively.

The ruggedness [43] of the new analytical method for the determination of 100 ppb Li^+, for variations of $\pm 10\%$ in procedure temperature and concentrations of Quinizarin, NaOH and Na_2CO_3 and for a variation of $\pm 5\%$ in the proportion of water, was studied using a 2^{7-4} saturated factorial design with two dummies. The method was rugged for every variable and no interactions between tested variables were found.

3.9. Effect of diverse ions

The effect of various ions on the determination of 50 ppb Li^+ in aqueous medium was studied, setting the tolerance limit at an error of $\pm ts_R$ [44] over the predicted value for the absorbance of the chelate measured against a reagent blank (t = one-tail Student t value for n-2 degrees of freedom and an α value of 0.05; S_R, standard deviation of the analytical response, predicted for the tested analyte concentration, obtained from the calibration data set). The tolerance limits of various ions are shown in Table 4. Note that the tolerance limits of some ions are low. Thus, in the case of a complex matrix, and as blood serum, a new calibration is required.

Table 4
Tolerance concentrations of several ions in the determination of 50 ppb Li^+

Anion[a]	Tolerance (ppb)	Cation[b]	Tolerance (ppb)
Cl^-	>50 000	K^+	500
I^-	10 000	Mg^{2+}	50
SO_4^{2-}	5000	Zn^{2+}	5
Br^-, NO_3^-	1000	Fe^{3+}	2.5
SiO_3^{2-}	500	Cu^{2+}, Ca^{2+}, Pb^{2+}	1
F^-, PO_4^{3-}	100		
$C_2O_4^{2-}$	10		

[a] All the test solutions were prepared from the sodium salts. (The tolerance concentration of Na^+ ion, calculated from the tolerance concentration of the Cl^- ion, is >32 000 ppb.)
[b] All the test solutions were prepared from the corresponding nitrates.

3.10. Application of the proposed method to real samples

3.10.1. Drugs

The basic method, as described, was applied for the determination of lithium in various pharmaceutical preparations, using flame photometry as the reference method. Results in Table 5 show the values found from both methods and the *P* value of the corresponding Welch *t*-test [45].

3.10.2. Blood serum

An accurate volume of standard was added to three different samples of serum, so that the final concentration of Li^+ was of the order of the therapeutic levels (approximately 4–8 ppm). Table 6 shows the recovery of the added lithium. The pooled recovery was 96.7%.

Table 6
Recovery of added Li^+ in different serum samples

Serum	Added (ppm)	Found (ppm)	% Recovery
1	4.00	3.24	81.0
	4.00	3.24	81.0
	4.00	2.69	67.3
	4.00	3.93	98.3
	4.00	3.79	94.8
2	5.00	5.32	106.3
	5.00	5.45	109.1
	5.00	5.59	111.8
	5.00	5.18	103.5
	5.00	5.45	109.1
3	7.00	8.21	117.4
	7.00	7.52	107.5
	7.00	6.70	95.7
	7.00	7.52	107.4
	7.00	7.38	105.4

A *t*-test, which compares the mean value against a reference value, was carried out in order to check if this value was significantly different from 100%. The statistic used, $t = (\bar{\Re} - 100)\sqrt{n}/s_{\Re}$ ($\bar{\Re}$, pooled recovery; $s_{\Re}$, recovery standard deviation), was obtained from the statistic for the comparison of the means of paired samples [46]. The following data were obtained: $\bar{\Re} = 99.4$; $s_{\Re} =$

Table 5
Determination of lithium in various drugs using flame photometry as the reference method and the proposed spectrophotometric method

Drug	Flame photometry		Proposed method		% *P* value[b]
	$c \pm s_c$[a]	n[b]	$c \pm s_c$[a]	n[a]	
Otogén (mg Li_2CO_3 per tablet)	18.0 ± 0.1	9	18.4 ± 0.3	9	1.1
Plenur (mg Li_2CO_3 per tablet)	335 ± 4	9	340 ± 7	8	8.7
Glucosor-Litio (mg Li gluconate per ml)	3.28 ± 0.02	3	3.2 ± 0.1	3	31.1

[a] Mean and standard deviation of *n* determinations.
[b] *P* value for Welch's *t*-test.

15.783; $t = 1.605$; d.o.f. = 14, P value = 93.1. The high P value shows that the difference between the pooled recovery and 100 is solely due to random error, and therefore the method does not show systematic error.

References

[1] N.S. Poonia and A.V. Bajaj, Chem. Rev., 79 (1979) 389.
[2] U. Olsher, R.M. Izatt, J.S. Bradshaw and N.K. Dalley, Chem. Rev., 91 (1991) 137.
[3] Z. Marczenko, Separation and Spectrophotometric Determinations of Elements, Ellis Horwood, Chichester, UK, 1986, p. 124.
[4] V.I. Kunetsov, Zh. Anal. Khim., 3 (1953) 295.
[5] P.F. Thomason, Anal. Chem., 28 (1956) 1527.
[6] R.F. Apple and J.C. White, Talanta, 13 (1966) 43.
[7] K. Uesugi and T. Murakami, Analyst, 15 (1966) 482.
[8] D.A. Román, An. Quin., 84 (1988) 236.
[9] J.K. Trautman, V.P.Y. Gadzekpo and G.D. Christian, Talanta, 30 (1983) 587.
[10] S.L. Zelichenok, V.M. Ostrovskaya, L.O. Agzibekova and V.M. Dziomko, Zh. Anal. Chem., 30 (1975) 2311.
[11] R.V. Sitnijova, A.N. Krilova, S.L. Zelichenok, V.M. Dziomko, V.M. Ostrovskaya, T.E. Zhukova and E.I. Tolmacheva, Zh. Anal. Khim., 37 (1988) 611.
[12] A.S. Atiyat, Y.A. Ibrahim and G.D. Christian, Microchem. J., 37 (1988) 114.
[13] M.S. Kravchenco, V.M. Ostrovskaya and M.Sh. Fumarova, Vysokochist. Veshchestva, 6 (1990) 152.
[14] R.H. Engebrecht, M. Delton and J. Schaeffer, Clin. Chem., 36 (1990) 1044.
[15] K. Nakashima, S. Nakatsuji, S. Akiyama, T. Kaneda and S. Mishumi, Chem. Lett., (1982) 1781.
[16] Y.P. Wu and G.A. Pacey, Anal. Chim. Acta, 162 (1984) 285.
[17] K. Sasaki and G. Pacey, Anal. Chim. Acta, 172 (1985) 141.
[18] E. Chapoteau, B.P. Czech, W. Zazulac and A. Kumar, Clin. Chem., 38 (1992) 1654.
[19] M.R. Reta, R. Cottana, J.D. Anunciata and J.J. Silver, Spectochim. Acta, 49 (1993) 903.
[20] T. Pal and N.R. Jana, Talanta, 41 (1994) 1291.
[21] N.K. Agnihotri, V.K. Singh and H.B. Singh, Analyst, 120 (1995) 1809.
[22] F. García Sánchez, M. Hernández López and J.C. Márquez Gómez, Talanta, 34 (1987) 693.
[23] F. García Sánchez, M. Hernández, J.C. Márquez, A.L. Ramos, C. Cruces and C. Carnero, Inorg. Chim. Acta, 140 (1987) 249.
[24] M.W. Cucci, W.F. Newman and B.J. Mulryan, Anal. Chem., 21 (1949) 1358.
[25] E.G. Owens and J.H. Yoe, Anal. Chem., 31 (1959) 384.
[26] M.A. Bello López, M. Castejón Mochón, J.L. Gómez Ariza and A. Guiraum Pérez, Analyst, 111 (1986) 429.
[27] M.A. Bello López, M. Castejón Mochón, J.L. Gómez Ariza and A. Guiraum Pérez, Analyst, 111 (1986) 1293.
[28] T. Moeller and M. Tecotzky, Anal. Chem., 27 (1955) 1056.
[29] N.K. Agnihotri, V.K. Singh and H.B. Singh, Talanta, 40 (1993) 1851.
[30] G.E.P. Box, W.G. Hunter and J.S. Hunter, Statistics for Experimenters. An Introduction to Design, Data Analysis and Model Building, John Wiley/Reverté, Barcelona, 1989, p. 525 (Spanish translation).
[31] J. Lawson, J. Erjavec and J.M. Madrigal, Estrategias Experimentales para el Mejoramiento de la Calidad en la Industria, Grupo Editorial Iberoamérica, México, 1932, p. 181.
[32] STATGRAPHICS 6.0, Statistical Graphics Corporation, Rockville, MD, 1993.
[33] E. Buurret, I. Mpynier, L. Bardet and M. Fussellier, Anal. Chim. Acta, 172 (1985) 157.
[34] P. Rostran, Clin. Chem., 36 (1990) 582.
[35] D.H. Doehlert, Appl. Stat. 19 (1970) 231.
[36] J.M. Bosque Sendra, M. Nechar, L. Cuadros Rodríguez and M.F. Molina Molina, Anal. Proc., 32 (1995) 375.
[37] M. Nechar, M.F. Molina Molina, L. Cuadros Rodríguez and J.M. Bosque Sendra, Anal. Chem. Acta, 316 (1995) 185.
[38] J. Barbosa, E. Bosch and R. Carrera, Talanta, 32 (1985) 1077.
[39] A. Navas Días, Talanta, 38 (1991) 571.
[40] Analytical Methods Committee, Analyst, 119 (1994) 2363.
[41] L. Cuadros Rodríguez, A.M. García Campaña, C. Jiménez Linares and M. Román Ceba, Anal. Lett., 26 (1993) 1243.
[42] IUPAC Analytical Chemistry Division, Pure Appl. Chem., 55 (1983) 553.
[43] M. Mulholland, Trends Anal. Chem., 7 (1988) 383.
[44] A.M. García Campaña, L. Cuadros Rodríguez, C. Jiménez Linares, F. Alés Barrero and M. Román Ceba, Anal. Lett., 28 (1995) 369.
[45] A. Martín Andrés and J.D. Luna del Castillo, Bioestadística para les Ciencias de la Salud, 3rd edn., Norma, Madrid, 1990, p. 243.
[46] J.C. Miller and J.N. Miller, Statistics for Analytical Chemistry, 2nd edn., Ellis Horwood, Chichester, UK, 1988, p. 58.

ELSEVIER

Talanta 44 (1997) 85–96

Talanta

Complexing influence of cobalt and nickel ions on the electrochemical reduction of pterin and related compounds at a mercury drop

Urszula Kucharska

Institute of General Food Chemistry, Technical University of Lodz, Stefanowskiego 4/10, 90-924 Lodz, Poland

Received 22 November 1995; revised 20 May 1996; accepted 17 June 1996

Abstract

The effect of Co^{2+} and Ni^{2+} ions on the electrochemical reduction of pterin and its derivatives, pteroic and pteroylmonoglutamic acids, has been studied. The measurements were carried out in aqueous solutions at fixed pH (7.5 ± 0.2), temperature (298 ± 0.2 K) and ionic strength ($\mu = 1.00$; $NaClO_4$) using polarographic techniques. By employing cyclic voltammetry and differential pulse polarography displacements were determined of the half-wave potentials $E_{1/2}$ of ligands of the reducible organic compounds at a dropping mercury electrode. The recorded polarograms and inherent potential differences were then utilized to calculate conditional stability constants of the complexes. The Casassas–Eek method was employed for the interpretation of the potential differences of the free and complexed ligands. The log β_1 values of the stability constants revealed moderate stability of the complexes. The donor atoms of the ligands in the coordination compounds have also been identified.

Keywords: Complexes; Cobalt; Nickel; Pterin derivatives; Stability constants

1. Introduction

The polarographic behaviour of pterin (Pte) as a function of pH has been studied by Komenda and co-workers [1,2]. Similar studies have also been reported by Kretzschmar and Jaenicke [3] with pteroylmonoglutamic acid, which is also known by the trivial names folic acid or vitamin $B_9(B_c)$. Earlier studies [4–9] revealed the formation of coordination compounds between folic acid and metal ions. The present work has focused on transformations taking place in aqueous solutions during electrochemical reduction of Pte and pteroic (PteAc) and pteroylmonoglutamic (PteGlu) acids (Scheme 1) in the presence Co^{2+} and Ni^{2+} ions.During these investigations, carried out with model solutions at fixed pH, temperature and ionic strength, variations of the half-wave potentials of reduction of the ligands (R_1, R_2, R_3; Scheme 1) with varying concentrations of either metal (M) or ligand (L) were expected. The variation of the half-wave potential of an organic

PII S0039-9140(96)02019-X

compound in the presence of a metal ion may be due to a chemical reaction (e.g. complexation) occurring in the solution. The magnitude of the half-wave potential of the free and complexed ligand has a direct bearing on the form being complexed. A chemical reaction occuring in solution results in a variation in the concentrations of the oxidized and reduced forms of the depolarizer, thus shifting the equilibrium potential according to the Nernst equation. When the oxidized form is involved in the reaction, its concentration drops and the equilibrium potential is displaced towards negative values, whereas involvement of the reduced form shifts the potential towards positive values [10].

Previous electrochemical studies of the complexes were restricted by certain limitations, such as the reversibility of the electrode reaction of the metal ion and the formation of a single complex in solution at large ligand excess [11–13]. The restrictions of the De Ford–Hume method have been highlighted by some authors [14,15] in particular in relation to the accuracy required for measuring the half-wave potential. A comprehensive analysis of errors in the determination of the stability constants from polarographic measurements has been presented by Klatt and Rouseff [14]. They also accounted for the conditions for detection of consecutive complexes occurring in solutions analyzed by polarography. Slopes of the current–voltage curves at large ligand excess have already been analyzed by many authors [16–19].

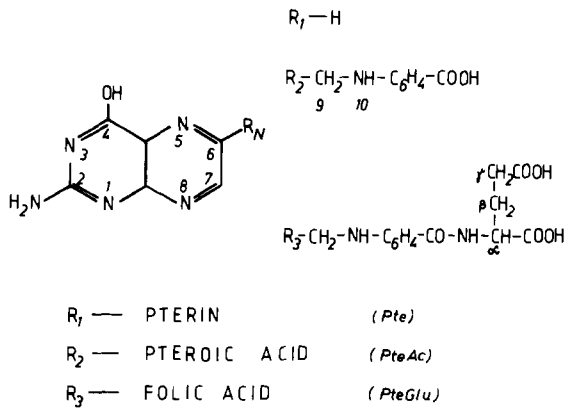

Scheme 1. Chemical formulae of Pte, PteAc and PteGlu.

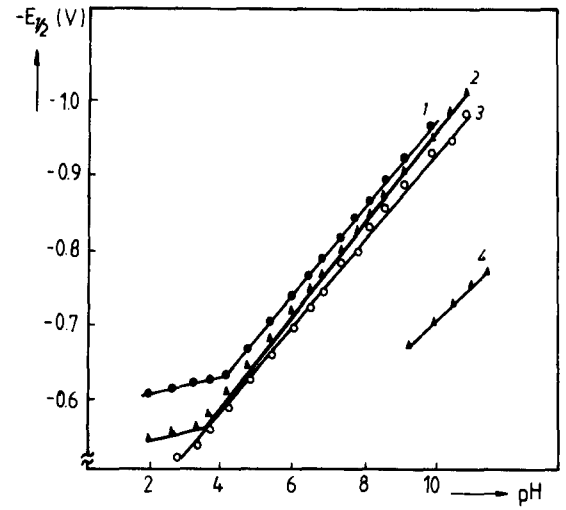

Fig. 1. Variations of the half-wave potential of the ligand, $E_{1/2}$, with pH for solutions of Pte (3), PteAc (1) and PteGlu (2) and (4) in Britton–Robinson buffer solutions at 298 K.

Casassas and Eek [20], as well as Naideker [21], have modified the De Ford–Hume method and adapted it to systems containing electroreducible organic compounds as complexons. Using an excess of the metal ion has been suggested for these systems, in order to create conditions for competition for each ligand molecule. These conditions enabled full identification of complexes with the lowest stability constant, i.e. of the M:L = 1:1 type. Also, the consecutive complexes could be analyzed in this way. In some cases, however, the stability constants of these species were determined with large errors. The errors were analyzed by Casassas and co-workers [22–24] in many systems. The main feature of the Casassas–Eek method is the inclusion and analysis of the hydrogen ion concentration which plays a crucial role in the reduction processes of organic compounds. In the De Ford–Hume method, only the reduction of hydrated metal ions has been studied over certain concentration and potential ranges. Furthermore, De Ford and Hume [13] assumed that the ligand is an electrochemically inert species, making the method inapplicable in some instances.

Complexation reactions of the 3d″ metal ions by folic acid were previously studied using poten-

tiometric and spectrophotometric methods [9,25]. Relevant stability constants have now been verified by the polarographic method, although the primary objective of this study was investigation of the influence of the Co^{2+} and Ni^{2+} ions in the electrochemical reduction of folic acid. Furthermore, it was also interesting to examine the interaction of some fragments of pteroylmonoglutamic acid with the ions. Results of the previous papers [9,25] suggested unambiguously that the Casassas–Eek method should be applied in as much as the solutions metal its restictions. The ligands are reversibly reducible at the dropping mercury electrode (DME) at potentials more positive than those of uncomplexed ions. The reduction of a ligand at the mercury electrode can be described by the following general equation:

$$L + nH^+ + ze^- \rightleftarrows H_nL \quad (1)$$

and the redox potential of the electrode is given by

$$E = E_o - \frac{RT}{zF} \ln \frac{(c^\circ)_{HnL}(v^\circ)_{HnL}}{(c_L)(c_H^\circ)^n(v_L)(v_H)^n} \quad (2)$$

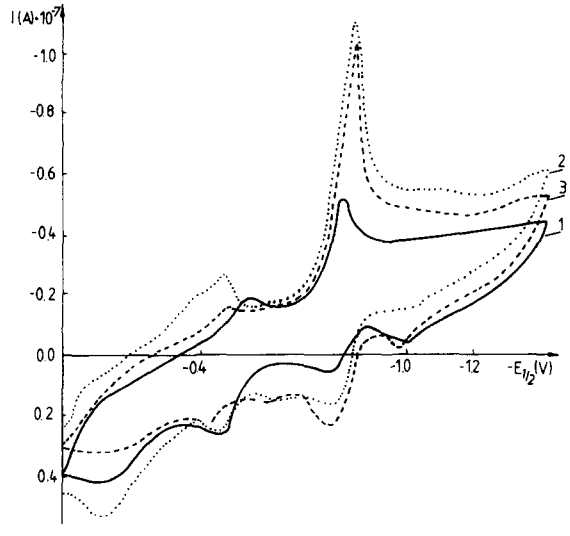

Fig. 2. Cyclic voltammograms of the ligands: (1) 1.03×10^{-5} M folic acid; (2) 1.04×10^{-5} M PteAc; (3) 1.04×10^{-5} M Pte in the system DME–SCE–Pt electrode. Potential scan rate 20 m V s^{-1}; pH 7.5; $T = 298$ K.

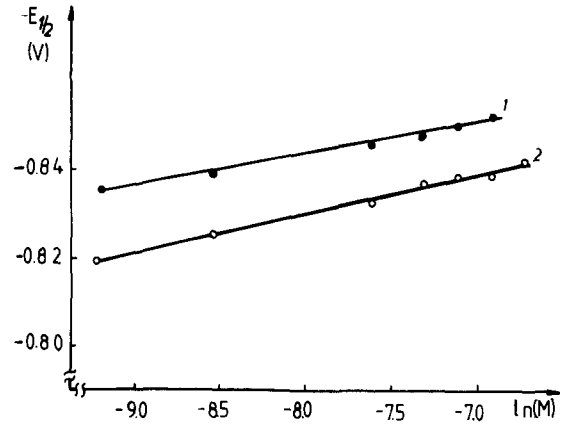

Fig. 3. Variations of the half-wave potential, $E_{1/2}$, of 5×10^{-5} M aqueous solutions of PteGlu in the presence of (1) Ni^{2+} and (2) Co^{2+} ions with the natural logarithm of the metal ion concentration. pH 7.5; $T = 298$ K; $\mu = 1.0$ ($NaClO_4$).

where E_o is the standard potential of the L–H_nL couple, c is the concentration, v is the activity coefficient of the oxidized (c_L, v_L, L) and reduced (c_{HnL}, v_{HnL}, H_nL) forms, c_H is the hydrated ion concentration, and v_H is its activity coefficient. The complexation process can thus be given by

$$L + pM^{n+} \rightleftarrows L(M^{n+})_p \quad (3)$$

where $p = 1, 1/2, 1/3, \ldots, 1/N$. Bearing in mind all the considerations described in Refs [20,21] we can obtain Eq. (4), which links the half-wave potential differences of the free and complexed ligand, $(E_{1/2})_c$, with the calculated stability constants:

$$F_o[M] = \exp\left[\frac{zF}{RT}\right]\Delta E_{1/2} + \ln\frac{I_L}{I_{exp}} = v_L \sum_1^P (\beta_p c_M^{1/p} v_{LM_p}) \quad (4)$$

At a large excess of the metal ion, favouring the formation of a 1:1 complex, only one type of complex predominates in the solution at 298 K and Eq. (4) can be simplified to yield:

$$\Delta E_{1/2} = 0.059/z(1 + \beta_1[M^{n+}]) \quad (5)$$

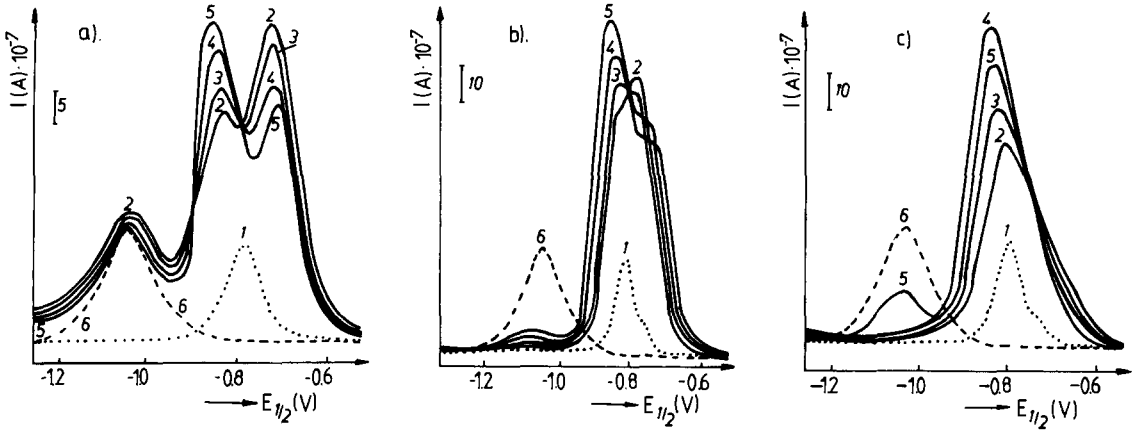

Fig. 4. Experimental DPP curves of the ligands: (a) Pte ($c = 1 \times 10^{-5}$ M); (b) PteAc ($c = 1.5 \times 10^{-5}$ M); (c) PteGlu ($c = 5 \times 10^{-5}$ M) in the presence of Ni^{2+} ions (1) in the absence of metal ions; (2) 5×10^{-4}; (3) 8×10^{-4}; (4) 1.0×10^{-3}; (5) 5.0×10^{-3}; (6) 8.0×10^{-3} M $Ni(ClO_4)_2$ solution without ligand. Potential scan rate 20 mV s^{-1}; pH 7.5; $T = 298$ K; $\mu = 1.0$ ($NaClO_4$).

Biernat and Korita [26] introduced a correction adequate for entirely irreversible processes by which Eq. (4) assumes the shape

$$F_o[M] = \exp\left[\frac{\alpha z F}{RT}\right]\Delta E_{1/2} + \ln\frac{I_L}{I_{exp}} = \nu_L \sum_1^P (\beta_p c_M^{1/p} \nu_{LM_p}) \quad (6)$$

where α is the so-called transfer coefficient of the electrode reaction which accounts for the deviation from the reversibility of the process.

2. Experimental

2.1. Chemicals

Water used for the preparation of solutions was demineralized by ion exchange and then distilled over $KMnO_4$. Pte, PteGlu and PteAc solutions from 1×10^{-3} to 1×10^{-6} M were prepared from analytical-grade reagents (Sigma). The solutions were freshly prepared and protected from light. During measurements the samples were kept in light-protected cells. Stock solutions of $Co(ClO_4)_2$ and $Ni(ClO_4)_2$ were prepared by the procedure of Ulmgren and Wahlberg [27]. The metal concentrations in the solutions were determined complexometrically [28] and spectrophotometrically [29,30]. The ionic strength of the solutions was maintained by aqueous $NaClO_4$ solutions prepared from analytical-grade $NaClO_4 \cdot H_2O$ crystals (Reachim). The pH was adjusted by standardized $HClO_4$ (p.a., VEB Jenapharm) and NaOH (p.a., POCh, Gliwice, Poland) solutions [31]. The pH-meters were calibrated against standard solutions (Radelkis) and Britton–Robinson buffers were used for adjusting the pH over the range 2.0–11.0 [32].

2.2. Equipment

The pH measurements were run on an automatic titrimeter OP-506 (Radelkis) equipped with a combination electrode (OP-0808P) and an automatic MEKB 6.25075 flask-burette. The temperature was held constant by means of a U-10 thermostat. Absorption spectra were taken on Specord UV–Vis and Specol-20 (Carl Zeiss, Jena, Germany) spectrophotometers. The differential pulse polarograms were recorded on a PA-4 (Lab. Praha) precision polarographic analyzer fitted with a static mercury drop electrode (SMDE) and a XY 4106 recorder. A DME served as the cathode and a platinum plate (surface area 1.5 cm^2) was the counter electrode. A saturated calomel electrode (SCE) served as a reference electrode and was mounted close to the working

electrode over a Luggin capillary filled with a NH_4NO_3 solution. All polarographic measurements were carried out in a 25 ml light-protected glass vessel equipped with a double jacket enabling the access of argon and mounting of the electrode system.

2.3. Procedure

Before running each series of polarographic measurements, the performance of the measuring system was thoroughly checked by taking polarograms with a 5.0×10^{-4} M $CdCl_2$ solution in 0.1 M KCl. The half-wave potential of this system was $-0.640(\pm 0.002)$ V. Analyzed solutions were prepared in 25 ml flasks and 10 ml aliquots were transferred from them to the polarographic cell. The solutions were purged with oxygen-free argon for 15 min and then a polarogram was recorded. Throughout the measurement process the rate of potential variation of 20 mV s^{-1}, the amplitude of 50 mV and the drop lifetime of 2 s were held constant. In the series of measurements aimed at recording potential variations of the reduction of the ligands (R_1, R_2, R_3) as a function of pH, Britton–Robinson buffers of pH 2.5–11.0 were used. The measurements were run in Pte, PteAc and PteGlu solutions of concentrations ranging from 1×10^{-7} M–10×10^{-4} M. In another series of measurements, variations in the positions of polarographic waves of the reduced ligands due to complexation were measured. In these solutions the ligand concentration was held constant and the metal ion concentration was raised from a 10-fold to a 20-fold excess at constant pH (7.5 ± 0.2), temperature (298 ± 0.2 K) and ionic strength ($\mu = 1.00$; $NaClO_4$). Differential pulse polarograms were recorded repeatedly in these solutions.

3. Results and discussion

The differential pulse polarograms of 5×10^{-5} M Pte, PteAc and PteGlu solutions at various pHs exhibited three peaks due to free folic acid (PteGlu). A similar pattern was observed in systems containing Pte and PteAc without the metal ions [1–3]. In the presence of metal ions the peak at $E_{1/2} = -0.808$ V at pH 7.5 is shifted due to reduction at the N(5) and N(8) nitrogen atoms of the rigid Pte framework. The remaining peaks are unaffected. The $E_{1/2} = -0.808$ V peak is due to a reversible two-electron transformation accompanied by the transfer of two electrons onto the pyrazine ring [33]. A plot of the potential vs. pH is shown in Fig 1. Using the cyclic voltammetry technique it was possible to prove the reversibility of electroreduction processes at the DME based on the separation of the cathodic $(E_{1/2})_c$ and anodic $(E_{1/2})_a$ peaks. Support for this statement is provided by the separation of the cathodic and anodic peaks as illustrated in Fig. 2. These results show that $E_{1/2}$ satisfies quite well the relation $(E_{1/2})_a - (E_{1/2})_c = 0.059/n$ V. The two remaining conditions for the reversibility of the process, namely $I_{pc} = I_{pa}$ and $E_{1/2} = 1/2\ (E_{pc} - E_{pa})$, have also been roughly satisfied [33]. The reversibility of the system has previously been reported by Dryhurst [33] and by Dillard and Hanck [35] by calculation of the half-wave potential on the basis of differential pulse polarography (DPP). Further, it was shown that the limiting current d.c. polarography increased linearly with the square root of the height of mercury, thus revealing the process to be diffusion-controlled. Inspection of potential variations of the PteGlu peaks in the presence of Co^{2+} and Ni^{2+} reveals that a chemical reaction proceeds in these systems. A plot of the metal concentration vs. peak potential is a rising curve (Fig. 3). It can thus be concluded that complexation takes place in these solutions under the adopted experimental conditions. Variations in the peak potential of the reduction of PteGlu due to this process displace the equilibrium potential towards negative values, revealing complexation of the oxidized form of PteGlu by the metal ions. The complexation of PteAc and Pte by the ions takes a different course as illustrated by the polarograms shown in Fig. 4. With Pte, the peak for the reduction of this molecule is displaced towards both positive and negative values, indicating complexation of both the oxidized and reduced forms. In the Co^{2+} and Ni^{2+} concentration range from 8×10^{-4}–3.5×10^{-3} M, peaks of higher currents at more positive potentials and those of lower currents at more negative poten-

Table 1
Results of polarographic investigation of the system with fixed parameters pH 7.5 (± 0.2), $T = 298.0$ (± 0.2) K, $\mu = 1.00$ M ($NaClO_4$). Composition of the system: $L-Ni(ClO_4)_2-HClO_4-H_2O$; L = Pte, PteAc, PteGlu

Ligand (c_L)	Metal conc. c_M	Potential of peak 1 $-E_{1/2}$(V)	Potential difference $\Delta E_{1/2}$(V)	Potential of peak 2 $E_{1/2}$(V)	Potential difference $\Delta E_{1/2}$	$F_o([Ni^{2+}])$ peak 1	$F_o([Ni^{2+}])$ peak 2	log β_1 from peak 1	log β_1 from peak 2
Pte	0.0000	0.807		0.807					
(1×10^{-5})	8.0×10^{-4}	0.836	0.029	0.736	0.034	10.546	14.226	4.12 ($\pm$0.02)	4.25 ($\pm$0.03)
	8.4×10^{-4}	0.838	0.031	0.762	0.035	11.331	14.598	4.13 ($\pm$0.04)	4.24 ($\pm$0.02)
	1.0×10^{-3}	0.840	0.033	0.760	0.037	13.183	18.197	4.12 ($\pm$0.03)	4.26 ($\pm$0.03)
	1.2×10^{-3}	0.842	0.035	0.757	0.039	15.459	19.854	4.11 ($\pm$0.03)	4.24 ($\pm$0.03)
	1.5×10^{-3}	0.849	0.042	–	–	19.324	–	4.11 ($\pm$0.04)	–
	2.0×10^{-3}	0.851	0.044	–	–	26.365	–	4.12 ($\pm$0.02)	–
	2.4×10^{-3}	0.855	0.048	–	–	30.918	–	4.11 ($\pm$0.03)	–
	3.6×10^{-3}	0.855	0.048	–	–	46.377	–	4.12 ($\pm$0.04)	–
PteAc	0.0000	0.811		0.811					
(1×10^{-5}	5.0×10^{-4}	0.835	0.024	0.783	0.028	6.441	8.891	4.11 ($\pm$0.02)	4.25 ($\pm$0.03)
	7.1×10^{-4}	0.839	0.028	0.779	0.032	9.146	12.338	4.12 ($\pm$0.03)	4.24 ($\pm$0.02)
	1.0×10^{-3}	0.843	0.032	0.775	0.036	12.313	17.783	4.12 ($\pm$0.04)	4.26 ($\pm$0.03)
	1.3×10^{-3}	0.847	0.036	0.772	0.039	15.629	22.591	4.11 ($\pm$0.02)	4.24 ($\pm$0.02)
	2.3×10^{-3}	0.854	0.043	–	–	30.320	–	4.08 ($\pm$0.03)	–
	2.6×10^{-3}	0.856	0.045	–	–	32.732	–	4.12 ($\pm$0.02)	–
	3.5×10^{-3}	0.858	0.047	–	–	43.059	–	4.10 ($\pm$0.03)	–
	3.9×10^{-3}	0.858	0.047	–	–	59.873	–	4.09 ($\pm$0.04)	–
	5.2×10^{-3}	0.859	0.048	–	–	63.353	–	4.11 ($\pm$0.03)	–
	8.0×10^{-3}	0.859	0.048	–	–	78.584	–	4.11 ($\pm$0.03)	–
PteGlu	0.00000	0.808							
(1×10^{-5}	9.0×10^{-5}	0.833	0.025	–	–	6.827	–	4.25 ($\pm$0.03)	–
	1.0×10^{-4}	0.836	0.028	–	–	7.413	–	4.26 ($\pm$0.02)	–
	2.0×10^{-4}	0.839	0.031	–	–	13.896	–	4.25 ($\pm$0.03)	–
	5.0×10^{-4}	0.845	0.037	–	–	33.804	–	4.25 ($\pm$0.04)	–
	6.4×10^{-4}	0.848	0.040	–	–	44.277	–	4.26 ($\pm$0.03)	–
	8.0×10^{-4}	0.850	0.042	–	–	52.855	–	4.24 ($\pm$0.04)	–
	9.0×10^{-4}	0.859	0.051	–	–	58.109	–	4.26 ($\pm$0.02)	–
	1.1×10^{-3}	0.863	0.055	–	–	72.676	–	4.25 ($\pm$0.04)	–
	2.5×10^{-3}	0.874	0.066	–	–	165.17	–	4.24 ($\pm$0.02)	–
	5.2×10^{-3}	0.885	0.066	–	–	166.46	–	4.24 ($\pm$0.02)	–

Table 2
Results of polarographic investigation of the system with fixed parameters pH 7.5 (±0.2), $T = 298.0$ (±0.2) K, $\mu = 1.00$ M ($NaClO_4$). Composition of the system: $L-Co(ClO_4)_2-HClO_4-H_2O$; L = Pte, PteAc, PteGlu

Ligand (C_L)	Metal conc. c_M	Potential of peak 1 $-E_{1/2}$(V)	Potential difference $\Delta E_{1/2}$(V)	Potential of peak 2 $-E_{1/2}$(V)	Potential difference $\Delta E_{1/2}$	$F_0([Co^{2+}])$ peak 1	F_o ($[Co^{2+}]$) peak2	log β_1 from peak 1	log β_1 from peak 2
Pte	0.0000	0.807		0.807					
(1×10^{-5})	8.0×10^{-4}	0.839	0.032	0.757	0.050	12.971	54.020	4.24 (±0.03)	4.83 (±0.02)
	8.4×10^{-4}	0.843	0.036	0.755	0.051	14.262	54.231	4.25 (±0.02)	4.81 (±0.03)
	1.0×10^{-3}	0.845	0.038	0.754	0.055	16.983	66.073	4.24 (±0.03)	4.82 (±0.02)
	1.2×10^{-3}	0.849	0.042	0.751	0.056	20.851	79.283	4.27 (±0.03)	4.82 (±0.01)
	1.5×10^{-3}	0.851	0.044	0.749	0.062	24.322	96.848	4.26 (±0.02)	4.81 (±0.03)
	2.0×10^{-3}	0.855	0.048	0.745	0.064	33.194	135.222	4.25 (±0.03)	4.83 (±0.02)
	2.4×10^{-3}	0.856	0.049	0.743	0.066	39.817	154.962	4.24 (±0.02)	4.81 (±0.02)
	3.6×10^{-3}	0.859	0.052	0.737	0.070	62.503	237.854	4.24 (±0.03)	4.82 (±0.02)
PteAc	0.0000	0.811		0.811					
(1×10^{-5})	7.0×10^{-5}	0.839	0.028	0.788	0.023	1.2165	6.4565	4.24 (±0.02)	4.81 (±0.03)
	9.0×10^{-5}	0.844	0.033	0.778	0.033	1.7378	13.2140	4.24 (±0.03)	4.82 (±0.03)
	1.0×10^{-4}	0.847	0.036	0.771	0.040	3.4756	33.8041	4.23 (±0.03)	4.83 (±0.03)
	2.0×10^{-4}	0.850	0.039	0.765	0.046	8.4912	51.6523	4.24 (±0.02)	4.81 (±0.04)
	5.0×10^{-4}	0.854	0.043	–	–	13.5860	–	4.23 (±0.03)	–
	8.0×10^{-4}	0.864	0.055	–	–	15.6401	–	4.22 (±0.04)	–
	9.0×10^{-4}	0.870	0.059	–	–	17.7832	–	4.23 (±0.03)	–
	1.0×10^{-3}	0.872	0.061	–	–	18.9832	–	4.25 (±0.03)	–
	1.2×10^{-3}	0.873	0.062	–	–	21.2342	–	4.24 (±0.02)	–
	1.5×10^{-3}	0.873	0.062	–	–	24.7564	–	4.23 (±0.03)	–
PteGlu	0.0000	0.808							
(1×10^{-5})	1.5×10^{-4}	0.819	0.011	–	–	11.6437	–	4.89 (±0.03)	–
	3.0×10^{-4}	0.825	0.017	–	–	21.7330	–	4.86 (±0.02)	–
	4.5×10^{-4}	0.828	0.020	–	–	31.1324	–	4.84 (±0.02)	–
	6.0×10^{-4}	0.833	0.025	–	–	39.6416	–	4.84 (±0.02)	–
	9.0×10^{-4}	0.839	0.031	–	–	68.2719	–	4.84 (±0.02)	–
	1.2×10^{-3}	0.843	0.035	–	–	88.9572	–	4.88 (±0.03)	–
	1.5×10^{-3}	0.853	0.045	–	–	99.9667	–	4.87 (±0.02)	–
	1.8×10^{-3}	0.863	0.046	–	–	103.774	–	4.86 (±0.01)	–

tials than the peak of Pte itself are recorded. Further, an increase in the peak currents at more negative potentials is noted upon raising the metal ion concentration. At the same time, the peak currents decreases at more positive potentials than the peak of Pte reduction. These results show that the contribution of complexed oxidized Pte species increases with increasing Ni^{2+} and Co^{2+} ion concentrations. A similar picture is seen with PteAc, although the contribution of the reduced forms to the complexatin process is much smaller than that of the reduced forms of Pte at equal metal ion concentrations. This is supported by the peak heights of PteAc at more negative potentials (strong currents) and by the PteAc peaks at more positive potentials (weak currents) than the reduction peak of the free ligand. The differences can be attributed to the presence and the structure of the R_N substituent at C(6) in the Pte molecule.

The presence of R_2 or R_3 at C(6) facilitates the complexation of the Co^{2+} and Ni^{2+} ions. At the same time, the unsubstituted Pte molecule undergoes more readily reduction at the DME and more readily binds the Co^{2+} and Ni^{2+} ions than do its reduced forms (PteAc and PteGlu). This is evidenced by missing peaks at more positive potentials in systems containing PteGlu and by a smaller number of peaks of weak currents at more positive potentials in the PteAc systems as compared with those containing Pte (Fig. 4). Based on the potential variations of the peak obtained by DPP, stability constants of the complexes were calculated by the Casassas–Eek method [20]. The values of peak currents and potential differences related to the free and complexed ligands were substituted into Eq. (4). The obtained F_o values were plotted against metal concentration, [M] (Fig. 5). From this relation, both the form and composition of the complexes were calculated.

The results of polarographic investigation of the systems comprising Pte, PteAc and the Co^{2+} and Ni^{2+} ions are summarized in Tables 1 and 2. The variations of the polarographic peak currents of Pte, PteAc and PteGlu vs. natural logarithms of the Ni^{2+} ion concentration are shown in Fig. 6 and plots of the potential variations of the complexed PteAc and Pte vs. natural logarithms of the Ni^{2+} ion concentration are presented in Fig. 7.

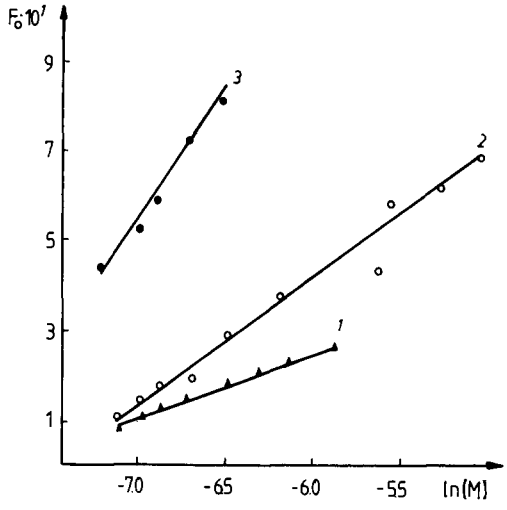

Fig. 5. Graphical presentation of the calculated F_o values as a function of the natural logarithm of the Ni^{2+} ion concentration: (1) Pte; (2) PteAc; (3) PteGlu.

The data of Tables 1 and 2 indicate that the complexation reaction practically ceases to proceed over the higher concentration range because there is no displacement of ligand reduction peaks upon raising the metal ion concentration. In po-

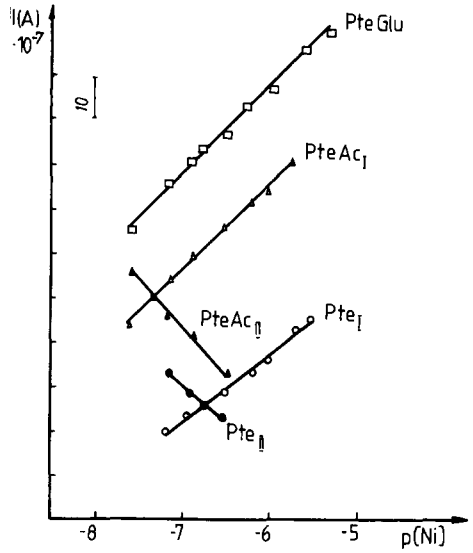

Fig. 6. Variations of peak currents for Pte, PteAc and PteGlu as a function of the decimal logarithm of the Ni^{2+} ion concentration. pH 7.5; $T = 298$ K; $\mu = 1.0$ ($NaClO_4$).

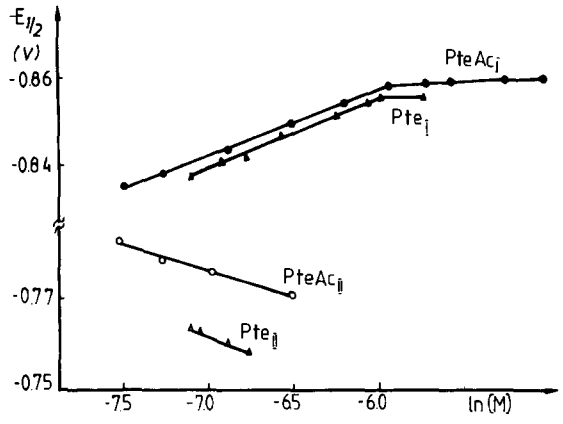

Fig. 7. Variations of the half-wave potential, $E_{1/2}$, for Pte and PteAc as a function of the natural logarithm of the Ni^{2+} ion concentration pH 7.5; $T = 298$ K; $\mu = 1.0$ ($NaClO_4$).

larograms recorded at higher Co^{2+} ion concentrations, a new peak appears at $E_{1/2} = -1.080$ V, while in Ni^{2+} solutions the peak appears at $E_{1/2} = -1.100$ V (Fig. 4). According to the instructions of Galus [36] the peaks can be assigned to hydrated ions, $[Ni(H_2O)_p]^{2+}$ and $[Co(H_2O)_p]^{2+}$, occurring in excess of ions in the solutions. Generally, electrochemical reduction of the hydrated ions can be described by the following equation:

$$[Ni(H_2O)_p]^{2+} + 2e^- \rightarrow Ni^0(Hg) + pH_2O \qquad (7)$$

This particular case of electrochemical reduction is attributed to variations in the water activity in solution [36]. The calculated stability constants of the complexes are summarized in Table 3 together with those determined by other methods under the same conditions [9,25,37].

The properties of the Co^{2+} and Ni^{2+} complexes with Pte, PteAc and PteGlu were investigated in order to identify the complexed species under identical experimental conditions. Another purpose was to identify the coordination sites of the ligand molecules. It can be hypothesized that when the same donor atoms are involved in the coordination of the metal ions, the stability constants determined under identical conditions should be comparable.

Bearing in mind the results reported by Pullman and Pullman [38], dealing with the reactivity of particular atoms in the folic acid molecule and related compounds (Pte, PteAc), an assumption has been made that the N(5) and N(10) atoms are the most readily coordinated. According to Pullman and Pullman just these atoms exhibit the highest free valency, which is a measure of the atomic polarizability under the influence of metal ions. Consequently, these centres carry the largest partial charges and the activation energy required for electrophilic or radical addition is relatively low. Indeed, the determined stability constants of the Co^{2+} and Ni^{2+} complexes with Pte, PteAc and PteGlu are very close to one another (Table 3). Small differences between these stability constants can be attributed to the presence of various subtituents at the C(6) atom of the Pte framework. The theoretically predicted reactivities of the atoms in the ligand molecules and coordination sites at N(5) and N(10), on the basis of the literature evidence, seem to be confirmed by the results of the present study. The good agreement between the stability constants suggests that the lone pair of electrons of the atoms acts as an electron donor in the coordination bonds. Somewhat higher values of log β_1 for the folate complexes, as compared to those for the pteroate and pterate complexes, show that the chain length of the substituent R_N and the presence of the glutamate residue in this molecule stabilize the compound.

A computer-assisted (POTECOM program) inspection of various ionic and neutral forms reveals complexation through the deprotonated form [9,25]. The established composition of the folate complexes (M:L = 1:1) also reveals the possibility of coordination through the oxygen atom of the C_γ carbonyl group of glutamic acid. The preferred geometry of the Co^{2+} and Ni^{2+} complexes is an octahedral or square-planar one where the central atom is surrounded by six or four donor atoms respectively [39]. The Co^{2+} and Ni^{2+} complexes obtained from the deprotonated anion of the trinuclear ligand, PteGlu (H_2L^-), are likely to have octahedral or pseudo-tetrahedral symmetry about the central ion respectively [40].

It should also be assumed that the PteAc and Pte molecules from octahedral species with the Co(II) and Ni(II) ions. The coordination bond is

Table 3
Stability constants of the Co(II) and Ni(II) complexes with PteGlu, PteAc and Pte determined by three independent methods under identical conditions; pH 7.5 (±0.2), $T = 298$ K, $\mu = 1.00$ ($NaClO_4$)

Ligand	Metal ion	log β_1 values determined by			Ref.
		Potentiometry	Spectrophotometry	Polarography	
PteGlu	Co(II)	4.60 (±0.06)	5.20 (±0.10)	4.88 (±0.03)	[9], [25p.w.],[a]
	Ni(II)	4.1 (±0.1)	4.80 (±0.06)	4.26 (±0.03)	[9], [25p.w.],
	Cu(II)	6.53 (±0.05)	6.75 (±0.08)	6.64 (±0.04)	[9], [37p.w.],
	Zn(II)	5.30 (±0.08)	5.93 (±0.07)	5.91 (±0.02)	[9], [25p.w.].
PteAc	Co(II)	Missing	4.22 (±0.05)	4.23 (±0.04)	[25],p.w.
	Ni(II)	Missing	4.05 (±0.04)	4.10 (±0.03)	[25],p.w.
Pte	Co(II)	Missing	4.23 (±0.03)	4.25 (±0.06)	[25],p.w.
	Ni(II)	Missing	4.10 (±0.04)	4.13 (±0.04)	[25],p.w.

[a]p.w. = present work.

likely to have a certain contribution to the ionic bond due to the difference in electronegativites of the cation and the donor atom of the ligand. Since the N(5) atom is incorporated in the ring with conjugate double bonds, its lone pair of electrons participates in delocalization of π electrons of the pyrazine ring of the Pte framework. Owing to this displacement, the nitrogen atom loses part of its electrons, thus lowering the effective charge. Houghton's [41] concept of the σ-donor strength of a ligand is a quantitative measure of the capacity of various ligands to impart covalent character to the σ-bond formed in a complex. The σ-donor strength depicts the tendency of a ligand to lower the positive charge on the central atom by increasing the electron density on this atom. A change in the nature and sequence of substituents R_N or an increase in the length of the glutamate chain (the tendency observed with PteGlu in natural systems [42,43]) can affect the σ-donor strength of the ligands. The chemical nature of these substituents leads to a change in electron density on the coordinating nitrogen and oxygen atoms of the ligand through the influence of the mesomeric and inductive effects.

An octahedral structure of the Ni(II) and Co(II) complexes with organic compounds containing the ethylenediamine moiety has been established by magnetic susceptibility measurements [39,41]. The oxygen–Ni(II) (or –Co(II)) bonds in these complexes have been found to be ionic, whereas for the nitrogen–Ni(II)(or –Co(II)) bonds a partial positive charge on the nitrogen atom was detected. By analogy, it can be assumed that the ligands studied here can coordinate the Co^{2+} and Ni^{2+} ions through the N(5) atom of the rigid Pte framework and through the oxygen atom at C(4). With PteAc and PteGlu, the R_2 and R_3 substituents respectively at C(6) introduce a highly reactive N(10) atom. Consequently, the neighbouring atoms N(5), C(6), C(9) and N(10) in PteAc and PteGlu jointly form an ethylenediamine framework. The capacity for the formation of coordination bonds with the Co^{2+} and Ni^{2+} ions by this framework has already been widely discussed in the literature [33,39–41]. Also in this case such complexation appears to be highly probable. The presence of glutamate in PteGlu enables the participation of the oxygen atom of the C_γ carbonyl group in bonding to the central ion. Less probable, however, is coordination through the carboxyl group at C_α, owing to the large distance from the assumed coordination centre. Obviously, the presence of the water molecules in the coordination sphere of the complex cannot be ruled out.

It seems quite likely that the nature and distribution of functional groups in the molecules of the Co(II) and Ni(II) complexes of Pte, PteAc and PteGlu markedly affect their physical and chemical properties [37,44–47]. The electronic spectra of the PteGlu complexes with these ions reported earlier [9,25] seem to be supported by the results of the present study. The bands at 280 and 300

nm for Ni(II) and Co(II) respectively also indicate the complexation within the Pte framework. The observed bathochromic shifts of these maxima are probably due to the effect accompanying bond formation of weakening of the ligand field strength [48] due to the change of conformation and the formation of a chelate. The electronic spectrum of folic acid exhibits three bands (at 255, 282 and 365 nm) in the UV region. The 255 and 365 nm bands are assigned to electron transitions in the Pte fragment of the molecule, whereas the 282 nm band is assigned to a transition in the *p*-aminobenzoate fragment [49–51]. In the spectra of folic acid solutions containing Co^{2+} and Ni^{2+} ions the 255 nm band is missing and the 365 mn band is displaced [9,25]. Further, a distinct increase in the intensity of the 280 nm band is noted on raising the Ni^{2+} ion concentration (the 300 nm band also increases on intensity with the addition of Co^{2+} ions). This finding supports the assumption of the ion binding to the rigid Pte framework. It seems highly probable that the nondisplaceable 282 nm band or the slightly shifted 280 nm band in systems with the Ni^{2+} ions (300 nm with Co^{2+}) is responsible for the variations in steric accommodation of the *p*-aminobenzoic acid residue. These variations are probably due to the formation of new bonds with the metal ions. The electronic spectra of the Co^{2+} and Ni^{2+} complexes of PteGlu, PteAc and Pte display some other bands assignable to metal–ligand electron transitions and to those within the molecule of the coordinated ligand [9,25,37].

The results of this work are complementary with the earlier ones and both sets of results strengthen the suggestion made as to the mode of binding of the metal ions with the ligands.

Bearing in mind the total effort devoted to the study of the complexing effect of the Co^{2+} and Ni^{2+} ions on the electrochemical reduction of the ligands should be emphasized. The first distinctsign of the influence is the variation of the reduction potential of the pterins on variation of the Co^{2+} and Ni^{2+} concentrations in solution. Further, distinct differences have been noted in the variations of the peak currents of reduction of the ligands as the metal ion concentrations were varied. Thus, complexation has a distinct influence on the rate of formation of the reduced forms of the compounds.

This study enables the identification of those forms of Pte, PteAc and PteGlu which complex the Co^{2+} and Ni^{2+} ions in aqueous solutions. Good agreement should also be emphasized between the stability constants determined by three independent methods [9,25,37].

The results of this study reveal the important role played by the Co^{2+} and Ni^{2+} ions in formation of unique conformations of the ligands which are likely to control their bioactivity in living organisms.

References

[1] J. Komenda, L. Kisova and J. Kondelka, Collect. Czech. Chem. Commun., 25 (1960) 1020.
[2] J. Komenda and D. Laskafeld, Collect. Czech. Chem. Commun., 27 (1962) 199.
[3] K. Kretzschmar and W. Jaenicke, Z. Naturforsch., Teil B, 26 (1971) 225, 999.
[4] A. Albert, Biochem. J., 54 (1953) 646.
[5] R. Nayan and A.K. Dey, Z. Naturforsch., Teil B, 25 (1970) 1453.
[6] Y.D. Fridman and M.G. Levina, Koord. Khim., 1 (1975) 1667; 11 (1985) 61.
[7] M.M. El-Dessouky, B.M. Abd-Elwahab and B.M. Turk, J. Radioanal. Nucl. Chem., 125 (1988) 255.
[8] N.A. El-Maali, M.A. Ghanodour, J-C. Vire and G.J. Patriarche, Electroanalysis, 1 (1989) 87.
[9] J. Maslowska and U. Kucharska, Pol. J. Chem., 67 (1993) 587.
[10] Z. Galus, Chem. Anal (Warsaw), 10 (1965) 803.
[11] M. Von Stackelberg and H. Von Freyhold, Z. Electrochem., 46 (1940) 120.
[12] J.J. Lingane, Chem. Rev., 29 (1941) 1.
[13] D.D. De Ford and D.N. Hume, J Am. Chem. Soc., 73 (1951) 5321.
[14] L.N. Klatt and R.L. Rouseff, Anal. Chem., 42 (1970) 1234.
[15] H. Irving, Adv. Polarogr., 1 (1960) 42.
[16] J. Koryta, Prog. Polarogr., 1 (1962) 295.
[17] P.R. Buck, J. Electroanal Chem., 5 (1963) 295.
[18] C.G. Butler and C.R. Kaye, J. Electroanal. Chem., 8 (1964) 463.
[19] M.E. Macovschi, J. Electroanal. Chem., 16 (1968) 457.
[20] E. Casassas and L. Eek, J. Chim. Phys., Phys.-Chim. Biol, 64 (1967) 971, 978.
[21] E. Naideker, Ph.D. Thesis, University of Warsaw, 1968.
[22] E. Casassas and M. Esteban, J. Electroanal. Chem., 194 (1985) 11.

[23] E. Casassas and M. Esteban, Electrochim. Acta, 32 (1986) 327.
[24] M. Esteban, E. Casassas and L. Fernandez, J. Electroanal. Chem., 241 (1988) 113.
[25] U. Kucharska, Ph.D. Thesis, Technical University of Lodz, 1993.
[26] J. Biernat and J. Korita, Collect. Czech. Chem. Commun., 25 (1960) 38.
[27] P. Ulmgren and O. Wahlbreg, Acta Chem. Scand., 28 (1974) 631.
[28] H. Flaschka, EDTA Titrations, Pergamon Press, Oxford, 1964.
[29] J. Fries and H. Getrost, Organische Reagenzin fur die Spuren Analyse, E. Merck, Darmstadt, Germany 1977, p. 2.
[30] Z Marczenko, Spectrophotometric Determination of Elements, Ellis Horwood, Chichester U. K 1979.
[31] G. Schwarzenbach and W. Biederman, Helv Chim. Acta 31 (1948) 331.
[32] J. Heyrowski and J. Kuta, Principles of Polarography, Academic Press, New York, 1966.
[33] G. Dryhurst, Electrochemistry of Biological Molecules, Academic Press New York, 1977, p 335.
[34] D. R. Crow, J. Electroanal. Chem., 16 (1968) 137.
[35] J. M. Dilliard and K. W. Hanck, Anal. Chem., 48 (1976) 218.
[36] Z. Galus, Electrochimia, 4 (1968) 553.
[37] J. Maslowska and U. Kucharska, Pol. J. Chem., 61 (1995) 1463.
[38] A. Pullman and B. Pullman, Biochim. Biophys. Acta, 44 (1960) 251.
[39] N.N. Greenwood and A. Earnshaw, Chemie der Elmente VCH, Weinheim, Germany, 1988, p.1480.
[40] F. Basolo and R.C. Johnson, Coordination Chemistry. The Chemistry of Metal Complexes, W.A. Benjamin, New York 1964.
[41] R.P. Houghton, Metal Compounds in Organic Chemistry, Cambridge University Press, Cambridge 1979.
[42] W. Friedrich (Ed.), Vitamins, Walter de Gruyter, Berlin, 1988.
[43] T. Brody and E.L.R. Stokstad, Methods Enzymol. 122 (1986) 367.
[44] D.P. Graddon, Coord, Chem. Rev. 4 (1969) 1 .
[45] E. Sinn and C. M. Harris, Coord. Chem. Rev., 4 (1969) 391.
[46] L. Randaccio and N. Bresciani-Pahor, Chem. Soc. Rev., 18 (1989) 225.
[47] K.Ueno and A E. Martell, J. Phys. Chem., 61 (1957) 257.
[48] L.E. Orgel, An Introduction to Transition-Metal Chemistry. Ligand-Field Theory, John Wiley and Sons, New York, 1960.
[49] R.G. Kallen and W.P. Jencks, J. Biol. Chem., 241 (1966) 5845.
[50] J.S. Erickson and Ch.K. Mathews, J. Biol. Chem., 247 (1972) 5661.
[51] M. Poe, J. Biol. Chem., 248 (1973) 7025, 252 (1977) 3724.

ELSEVIER

Talanta 44 (1997) 97–103

Talanta

Mixed-ligand chelate extraction of trivalent lanthanides with 4,4,4-trifluoro-1-phenyl-1,3-butanedione and neutral oxo-donors

M.L.P. Reddy*, S. Sujatha, R. Luxmi Varma, T.R. Ramamohan, T.P. Rao, C.S.P. Iyer, A.D. Damodaran

Regional Research Laboratory (CSIR) Trivandrum-695 019, India

Received 21 September 1995; revised 24 June 1996; accepted 26 June 1996

Abstract

Mixed-ligand chelate extraction of trivalent lanthanides such as Nd(III), Eu(III) and Lu(III) into benzene with mixtures of 4,4,4-trifluoro-1-phenyl-1,3-butanedione (HBFA) and bis-2-ethylhexyl sulphoxide (B2EHSO) or triphenylphosphine oxide (TPhPO) from thiocyanate solutions was investigated. The results demonsrate that these metal ions are extracted as $Ln(BFA)_3$ with HBFA alone and in the presence of a neutral oxo-donor, B2EHSO or TPhPO(S), as $Ln(BFA)_3 \cdot S$ and $Ln(BFA)_3 \cdot 2S$. The equilibrium constants of the above species increase monotonically with decreasing ionic radii of these metals ions. The addition of a neutral donor to the metal chelate system not only enhances the extraction efficiency but also improves the selectivity among these trivalent lanthanides. Hence this mixed-ligand system may be useful for the extraction and separation of individual lanthanides and also for the separation of lanthanides as a group from other metal ions.

Keywords: Mixed-ligand chelate extraction; Trivalent lanthanides

1. Introduction

Mixed-ligand chelate extraction of trivalent lanthanides by mixtures of a chelating agent and a neutral oxo-donor has been studied extensively by several workers and the relevant data are covered in reviews on synergistic extraction [1,2]. Several models have been proposed to explain the synergism observed in these systems. However, the role of each of the factors involved in such models is not fully understood. To clarify the roles of dehydration and of expansion of metal ion coordination number, calorimetric studies were conducted on the reaction between thenoyltrifluoroacetone (HTTA) complexes of UO_2^{2+}, Th^{4+} and Nd^{3+} cations with tributyl phosphate (TBP) and tri-*n*-octylphosphine oxide (TOPO) neutral adducts [3]. These studies were conducted in organic solvents and it was confirmed that the major role of the neutral adduct is to increase the organophilicity of the complex when the adduct displaces some or

* Corresponding author. Fax: (91) 471-490186; e-mail: rrlt@sirnetm.ernet.in.

PII S0039-9140(96)02024-3

all of the hydration of the binary β-diketonate complexes.

Many studies have been carried out on the synergistic extraction of trivalent lanthanides using a mixture of HTTA and a neutral organophosphorus reagent such as TBP or TOPO or *n*-octyl(phenyl)-*N*,*N*-diisobutylcarbamoylmethylphosphine oxide (CMPO) [4–6]. Compared with these, the systematic study of synergistic extraction systems involving 4,4,4-trifluoro-1-phenyl-1,3-butanedione (HBFA) and a neutral oxodonor is sparse [7]. Shigematsu et al. [7] studied the extraction of selected lanthanides with mixtures of HBFA and TBP or TOPO. HBFA has been found to extract metal ions from more acidic solutions than HTTA ($pK_a = 6.25$) owing to its lower pK_a value (6.03). However, no studies relevant to the extraction of trivalent lanthanides with HBFA in the presence of bis-2-ethylhexyl sulphoxide (B2EHSO) as a neutral donor have been reported. B2EHSO, a sterically hindered branched-chain extractant, has recently been explored in our laboratory as a synergist in the extraction of trivalent lanthanides and actinides with various β-diketones such as HTTA and 4-acylpyrazolones [8–10]. A very high synergistic enhancement of the order of 10^3 has been observed in the above mixed-ligand systems. Further, a few systems have also shown improved selectivites either among the trivalent lanthanides or between the trivalent lanthanides and actinides. This prompted us to initiate a systematic study on the extraction of trivalent lanthanides using B2EHSO as a synergist in the presence of HBFA as a chelating agent, with a view to elucidating the nature of the complexes extracted into the organic phase and also to investigate the selectivity of this mixed-ligand system. For comparison, studies were also carried out with HBFA in the presence of triphenylphosphine oxide as a neutral oxodonor.

2. Experimental

HBFA and TPhPO were purchased from Aldrich Chemical (USA). B2EHSO was obtained from Fairfield Chemical (USA) and purified by the method reported in the literature [11]. Tracer solutions of ^{147}Nd, $^{152,154}Eu$ and ^{177}Lu were supplied by the Board of Radiation and Isotope Technology (BRIT), (India). All other chemicals were of reagent grade.

The solvent extraction procedure and the experimental details were as described previously [8,9]. All the computer programs were written in FORTRAN 77 and executed on a 32 bit mini-computer (HCL Horizon III).

3. Results and discussion

3.1. Theoretical

Lanthanide ions in the aqueous phase adopt a variety of complex forms in the presence of thiocyanate ions, but under the present experimental conditions it is sufficient to consider only the first two complexes as defined by

$$Ln^{3+} + i SCN^- \overset{\beta_i}{\rightleftharpoons} Ln(SCN)_i^{(3-i)+} \quad (1)$$

where Ln = Nd(III) or Eu(III) or Lu(III) and $i = 1$ and 2. Then the total concentration of Ln(III) in the aqueous phase $[Ln_t]$ is given by

$$[Ln_t] = [Ln^{3+}]\,(1 + \beta_1[SCN^-] + \beta_2[SCN^-]^2) \quad (2)$$

The values of the stability constants β_1 and β_2 were obtained from the literature [12] (β_1, Nd = 6.47; β_2, Nd = 1.30; β_1, Eu = 5.05; β_2, Eu = 1.35; β_1, Lu = 2.82).

The extaction of a trivalent lanthanide ion, Ln^{3+}, with a chelating extractant, HA, can be expressed as follows:

$$Ln_{aq}^{3+} + 3HA_{org} \overset{K_{ex}}{\rightleftharpoons} LnA_{3org} + 3H_{aq}^{+} \quad (3)$$

where k_{ex} is the extraction constant. The distribution ratio of the metal, D_0, can be written as

$$D_0 = \frac{[LnA_3]}{Ln^{3+} + \Sigma[LnA_n^{3-n}] + \Sigma[Ln(SCN)_i^{3-i}]} = \left(\frac{P_{HA}}{K_{HA}}\right)^3 K_{ex}\left(\frac{[A^-]^3}{1 + \Sigma\beta_i[SCN^-]^i + \Sigma\alpha_n[A^-]^n}\right) \quad (4)$$

where P_{HA} and K_{HA} are the partition and acid dissociation constant of HA, respectively, α_n is the stability constant of MA_n^{3-n} in the aqueous

phase and A^- is the chelating anion in the aqueous phase. In the lower concentration region of A; $\alpha_n[A^-]^n$ is negligibly small; hence $D_0(1+\beta_1[SCN]+\beta_2[SCN]_2)$ depends on the third power of $[A^-]$.

The mechanism of extraction of trivalent lanthanide, Ln^{3+}, with a chelating agent in the presence of neutral oxo-donor (S) may be expressed as follows:

$$Ln_{aq}^{3+} + 3HA_{org} + mS_{org} \xrightleftharpoons{K_{syn,m}} LnA_3 \cdot mS_{org} + 3H^+_{aq} \quad (5)$$

where $m = 0$, 1 and 2. The the distribution ratio, D can be written as

$$D = \frac{[HA]^3}{[H^+]^3}\left(K_{ex} + \sum_{m=1}^{2} K_{syn,m}[S]^m \times \frac{1}{1+\alpha_n[A^-]^n+\beta_i[SCN]^i}\right) \quad (6)$$

As is well known, chelating agents are weak acids and the neutral donors are bases; the chelating agent and the neutral oxo-donor will interact in the organic phase, leading to reduced concentrations of the free chelating agent and neutral donor. This reaction can be written as

$$HA_{org} + S_{org} \xrightleftharpoons{K_I} HA{\cdot}S_{org} \quad (7)$$

The constants $K_{syn,m}$ and K_I are deduced by non-linear regression analysis using the following procedure.

(1) Assume values of $K_{syn,m}$ and K_I.

(2) The equilibrium concentration of the species occuring in Eq. (6) were determined with the knowledge of the initial concentrations [HA] and [S], P_{HA}, K_{HA} and the assumed values of K_I by solving a quadratic equation and a linear equation.

(3) The values of the assumed equilibrium constants which lead to the minimum root mean square fractional error, y, where

$$y = \sqrt{\frac{1}{N}\sum_{j=1}^{N}\left(\frac{D_{calc.i} - D_{expt.i}}{D_{expt.i}}\right)^2}$$

for all the experimental data were taken to be equilibrium constants for the system under consideration.

The adduct formation reaction in the organic phase and the stability constants, β_m, are given by

$$LnA_{3org} + mS_{org} \xrightleftharpoons{\beta_m} LnA_3{\cdot}mS_{org} \quad (8)$$

$$\beta_m = K_{syn,m}/K_{ex}$$

where $m = 1$ or 2.

3.2. Extraction of trivalent lanthanides with HBFA alone

The extraction of Nd(III), Eu(III) and Lu(III) from 0.1 mol dm^{-3} ammonium thiocyanate solution of pH 3.0 with HBFA (0.1–0.6 mol dm^{-3}) in benzene was studied. The plots of $\log\{D(1+\beta_1[SCN]+\beta_2[SCN]^2)\}$ against the logarithim of the equilibrium concentration of the BFA- anion in the aqueous phase are shown in Fig. 1. The equilibrium concentration of BFA^- in the aqueous phase was calculated from its partition and dissociation constants, using the equation

$$[BFA^-] = \frac{C_{HA}}{(P_{HA}+1)[H^+]/K_{HA}+1}$$

where C_{HA} denotes the initial concentration of HBFA. The literature values of $pK_{HA} = 6.03$ and $\log P_{HA} = 2.61$ were used [13]. The slope of the

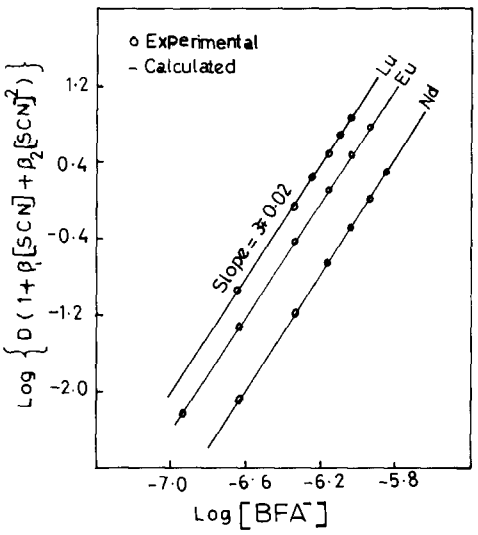

Fig. 1. Effect of HBFA concentration on the extraction of Nd(III), Eu(III) and Lu(III). Aqueous phase 0. 1 mol dm^{-3} thiocyanate pH 3 $[Ln]^{3+} = 1.0 \times 10^{-6}$.

Table 1
Two-phase equilibrium constants of trivalent Nd, Eu and Lu–HBFA–neutral oxo-donor–benzene systems

Complex	Log (equilibrium constant)		
	Nd(III)	Eu(III)	Lu(III)
$Ln(BFA)_3$	-8.09 ± 0.01	-7.33 ± 0.01	-6.97 ± 0.02
$Ln(BFA)_3 \cdot B2EHSO$	-5.62 ± 0.01	-3.21 ± 00.01	-2.65 ± 0.02
$Ln(BFA)_3 \cdot 2B2HSO$	-3.30 ± 0.01	-1.15 ± 0.01	–
$Ln(BFA)_3 \cdot TPhPO$	–	-1.71 ± 0.01	-1.02 ± 0.01
$Ln(BFA)_3 \cdot 2TPhPO$	-0.53 ± 0.01	1.98 ± 0.02	–
HBFA·B2EhSO	1.07 ± 0.01	$1.07. \pm 0.01$	1.07 ± 0.01
HBFA·TPhPO	1.27 ± 0.02	1.27 ± 0.02	1.27 ± 0.02

plot (Fig. 1) is 3 ± 0.02, indicating the extraction of simple metal chelates, $Ln(BFA)_3$, for all the metal ions studied here. This was further confirmed by analysing the data in Fig. 1 using Eq. (4). The best fit between the experimental and calculated D values was obtained only when the formation of simple metal chelate species, $Ln(BFA)_3$, was assumed. The extraction constants (K_{BFA}) for the above species were determined by non-linear regression analysis and are shown in Table 1. It is clear that the K_{BFA} value increases with decreasing ionic radius of the ln^{3+} ion. A similar type of behaviour has also been observed for the K_{TTA} values for the extraction of trivalent lanthanides with HTTA from thiocyanate solutions [9].

3.3. Extraction with a mixture of HBFA and B2EHSO or TPhPO

The extraction of Nd(III), Eu(III) and Lu(III) from 0.1 mol dm^{-3} ammonium thiocyanate solution (pH 3.0) with mixtures of HBFA (0.1–0.5 mol dm^{-3}) + B2EHSO (0.0002–0.07 mol dm^{-3}) in benzene was studied and the results are shown in Figs. 2 and 3. It was found that these metal ions are not extracted in practice by B2EHSO alone into xylene from thiocyanate solutions. However, with mixtures of HBFA + B2EHSO, about 5–20-fold enhancement in the extraction of Nd(III) and 20–200-fold enhancement in the extraction of Eu(III) and Lu(III) were observed.

It can be seen from Fig. 2 of the plot of log $\{D[H+]^3(1+\beta_1[SCN^-]+\beta_2[SCN^-]^2)/1+[B2EHSO](K_{syn.1}/K_{BFA}+K_{syn.2}/K_{BFA})[B2EHSO])\}$ vs. log [HBFA] at constant B2EHSO that only three HBFA moieties are attached to the synergistic species for all the metal ions studied here. The plots of $\log\{D[H^+]^3(1+\beta_1[SCN^-]+\beta_2[SCN^-]^2)/([HBFA]^3-K_{BFA})\}$ vs. log [B2EHSO] at constant HBFA concentration yields a slope of 1 ± 0.01 in the case of Lu(III) and non-integral values in the case of Nd(III) and Eu(III),

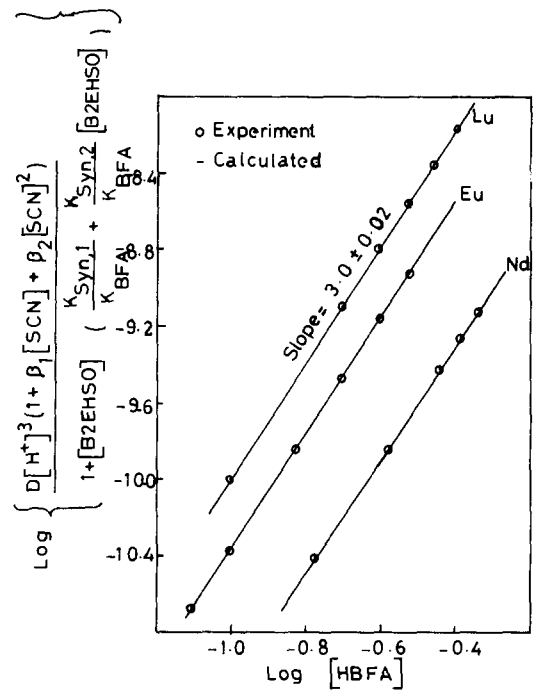

Fig. 2. Effect of HBFA concentration on the extraction of Nd(III), Eu(III) and Lu(III) at fixed B2EHSO concentration. Aqueous phase, 0.1 mol dm^{-3} thiocyanate (pH 3); $Ln^{3+} = 1 \times 10^{-6}$ mol dm^{-3}.

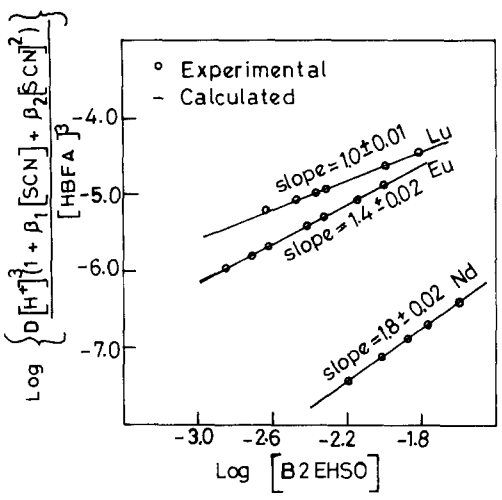

Fig. 3. Effect of B2EHSO concentration on the extraction of trivalent Nd(III), Eu(III) and Lu(III) at fixed HBFA concentration. Aqueous phase, 0.1 mol dm^{-3} thiocyanate (pH 3); $[Ln^{3+}] = 1 \times 10^{-6}$ mol dm^{-3}.

indicating the extraction of the species $Ln(BFA)_3 \cdot m$B2EHSO, where $m = 1$ or 2 for Nd(III) and Eu(III) and $m = 1$ for Lu(III). This was further confirmed by analysing the equilibrium data presented in Figs. 2 and 3 using Eq. (6). The best fit between the experimental and calculated D values was obtained only when the formation of the species $Nd(BFA)_3 \cdot$B2EHSO/2B2EHSO, $Eu(BFA)_3 \cdot$B2EHSO/2B2EHSO and $Lu(BFA)_3 \cdot$B2EHSO was assumed. The synergistic extraction constants for the above species and interaction constant (K_1) were deduced by non-linear regression analysis and are given in Table 1.

The extraction of Nd(III), Eu(III) and Lu(III) from 0.1 mol dm^{-3} ammonium thiocyanate solution (pH 3.0) with HBFA (0.1–0.6 mol dm^{-3}) in the presence of TPhPO (0.0001–0.007 mol dm^{-3}) in benzene was also investigated and the results are shown in Figs 4 and 5. It was found that the extraction of these metal ions is negligible with TPhPO alone under the present experimental conditions. However, with mixtures of HBFA + TPhPO about 5–80-fold enhancement in the extraction of Nd(III) and 10–140-fold synergistic enhancement in the extraction of Eu(III) and Lu(III) were observed. The plots (Fig. 4) of $\log \{D[H^+]^3(1 + \beta_1[SCN^-] + \beta_2[SCN^-]^2)/(1 + [TPhPO](K_{syn,1}/K_{BFA}) + (K_{syn,2}/K_{BFA})[TPhPO])\}$ at constant concentration of TPhPO are linear with slopes of 3 ± 0.02 for all the metal ions, indicating that three molecules of HBFA are involved in the respective extractable complexes. It can be seen from Fig. 5 that the slope of the plot $\log\{(D[H^+]^3(1 + \beta_1[SCN] + \beta_2[SCN]^2)/[HBFA]^3 - K_{BFA}\}$ vs. log [TPhPO]) is equal to 2 ± 0.02 for Nd(III) and 1.0 ± 0.02 for Lu(III) and is a non-integral value (1.3 ± 0.02) for Eu(III), indicating the extraction of the species $Nd(BFA)_3 \cdot 2TPhPO$, $Eu(BFA)_3 \cdot TPhPO/2TPhPO$ and $Lu(BFA)_3 \cdot TPhPO$. This was further confirmed by analysing the data using Eq. (6). The synergistic extraction constants and interaction constants were obtained by non-linear regression analysis and are given in Table 1.

It can be clearly seen from Table 1 that the synergistic extraction constants for both systems studied here with increase with decreasing ionic radii of these trivalent metal ions. Further, the values of $K_{syn,1}$, $K_{syn,2}$ and K_1 for the TPhPO

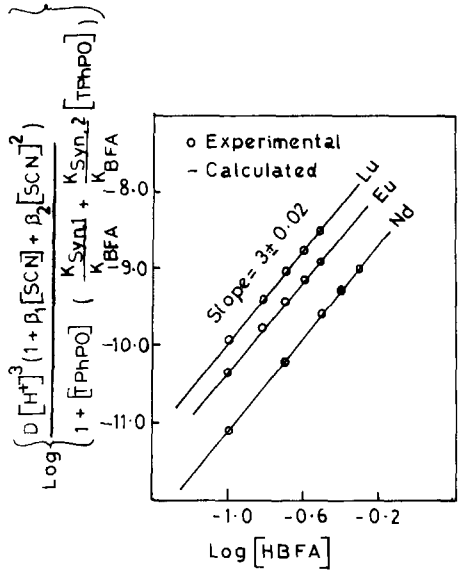

Fig. 4. Effect of HBFA concentration on the extraction of Nd(III), Eu(III) and Lu(III) at fixed TPhPO concentration. Aqueous phase, 0.1 mol dm^{-3} thiocyanate (pH 3); $[Ln^{3+}] = 1 \times 10^{-6}$ mol dm^{-3}.

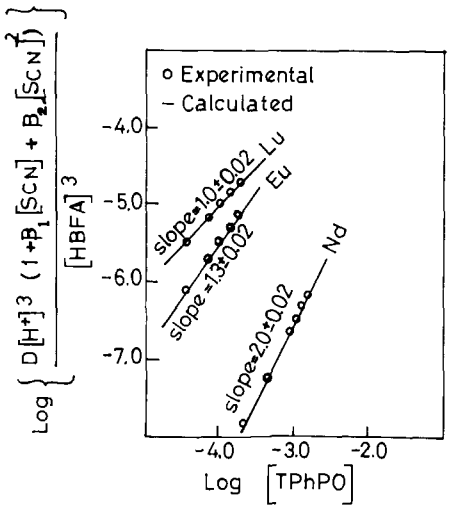

Fig. 5. Effect of TPhPO concentration on the extraction of Nd(III), Eu(III) and Lu(III) at fixed HBFA concentration. Aqueous phase, 0.1 mol dm^{-3} thiocyanate (pH 3); $[Ln^{3+}] = 1 \times 10^{-6}$ mol dm^{-3}.

system are higher than those for B2EHSO system, which is in the order of basicity of these neutral oxo-donors.

The stability constants (β_1 and β_2) for the organic phase synergistic reaction of the trivalent lanthanide–HBFA chelate with neutral oxo-donors were calculated according to Eq. (8) and are given in Table 2. These stability constants for both systems increase with decreasing ionic radii of the trivalent lanthanides. Comparing the log β_1 and β_2 values of Eu–HBFA–S (where S = B2EHSO, TBP, TPhPO and TOPO) of various oxo-donors given in Table 3, it can be concluded that the stability of these adducts follow the order B2EHSO < TBP < TPhPO < TOPO, which is also

Table 2
Equilibrium constants for the organic phase synergistic reactions of trivalent Nd, Eu and Lu–HBFA chelates with B2EHSO or TPhPO in benzene

Ln(III)	Mixture	Log β_1	Log β_2
Nd	HBFA + B2EHSO	2.47 ± 0.01	4.79 ± 0.01
Eu		4.12 ± 0.02	6.19 ± 0.02
Lu		4.32 ± 0.01	–
Nd	HBFA + TPhPO	–	7.56 ± 0.01
Eu		5.62 ± 0.02	9.31 ± 0.01
Lu		5.95 ± 0.01	–

Table 3
Log β_1 and log β_2 values for the formation of $Eu(BFA)_3 \cdot S$ and $Eu(BFA)_3 \cdot 2S$ adducts

S	Log β_1	Log β_2	Ref.
B2EHSO	4.12	6.19	This work
TBP	4.60	7.80	[7]
TPhPO	5.62	9.31	This work
TOPO	6.93	11.86	[7]

the order of basicity of these neutral oxo-donors [8,14].

It can be concluded from the above study that in the extraction of Nd(III) with HBFA in the presence of B2EHSO or TPhPO, the predominant species extracted into the organic phase is $Nd(BFA)_3 \cdot 2B2EHSO$ or $Nd(BFA)_3 \cdot 2TPhPO$. In the cases of Eu(111), two types of species, $Eu(BFA)_3 \cdot B2EHSO/2B2EHSO$ or $Eu(BFA)_3 \cdot TPhPO/2TPhPO$, are extracted into the organic phase. However, in the case of Lu(III), the only species extracted into the organic phase is $Lu(BFA)_3 \cdot B2EHSO$ or $Lu(BFA)_3 \cdot TPhPO$. This is possibly because of the smaller ionic radius of Lu compared with Nd and Eu, causing steric hindrance during the attachment of the second molecule of the neutral oxo-donor.

Table 4 gives the separation factors between these trivalent lanthanides, defined as the ratio of the respective distribution ratios with HBFA (0.3 mol dm^{-3}), (0.3 mol dm^{-3} HBFA + 0.005 mol dm^{-3} B2EHSO) and (0.3 mol dm^{-3} HBFA + 0.0001 mol dm^{-3}) TPhPO systems. It is interesting to note that the addition of B2EHSO or TPhPO to the metal chelate system significantly improves separation factors between these trivalent metal ions.

Table 4
Separation factors for Nd(III), Eu(III) and Lu(III) with HBFA and HBFA + B2EHSO or TPhPO systems

Extractant	Separation factor	
	Eu/Nd	Lu/Eu
HBFA (0.3 mol dm^{-3})	6.2	2.8
HBFA (0.3 mol dm^{-3}) + B2EHSO (0.005 mol dm^{-3})	52.8	3.8
HBFA (0.3 mol dm^{-3}) + TPhPO/ (0.0001 mol dm^{-3})	48.9	5.0

4. Conclusion

The extraction equilibria of trivalent lanthanides with HBFA and also with mixtures of HBFA + B2EHSO or TPhPO has been investigated. The mechanism of extraction can be explained by a simple chemically based model presented in this paper. The results demonstrated that not only enhanced extraction but also better selectivities can be achieved with these mixed-ligand systems. Hence such a system would be of practical values in the extraction and separation of individual lanthanides and also for their separation as a group from other metal ions.

References

[1] J.N Mathur, Solvent Extr. Ion Exch., 1 (1983) 349.
[2] G. Duyckaerts and J.F. Desreux, Int. Solvent Extr. Conf., Toronto, 1977, p 73.
[3] M.S. Caceci, G.R. Choppin and Q. Liu, Solvent Extr. Ion Exch., 3 (1985) 605.
[4] D.J. Pruett, M.C. Clark and D.D. Ensor, Sep. Sci Technol., 25 (1990) 1777.
[5] T.V. Healy, J. Inorg. Nucl. Chem., 19 (1961) 314.
[6] T. Sekine and D. Dyrssen, J. Inorg. Nucl. Chem., 29 (1967) 1475.
[7] T. Shigematsu, M. Tabushi, M. Matsui and T. Honjyuo, Bull. Chem. Soc. Jpn., 40 (1967) 2807.
[8] P.B. Santhi, M.L.P. Reddy, T.R. Ramamohan and A.D. Damodaran, Talanta, 41 (1994) 9.
[9] P.B. Santhi, M.L.P. Reddy, T.R. Ramamohan and A.D. Damodaran, Radiochim. Acta, 64 (1994) 205.
[10] P.B. Santhi, M.L.P. Reddy, T.R. Ramamohan, A.D. Damodaran, J.N. Mathur, M.S. Murali and R.H. Iyer, Solvent Extr. Ion Exch., 12 (1994) 633.
[11] B.A. Moyer, C.E. Caley and C.F. Baes, Solvent Extr. Ion Exch., 6 (1988) 785.
[12] R.M. Smith and A.E. Martell, Critical Stability Constants, Vol. 4, Inorganic Complexes, Plenum Press New York, 1976.
[13] T. Sekine, T. Saitou and H. Iga, Bull. Chem. Soc. Jpn., 56 (1983) 700.
[14] R. Shanker and K.S. Venkateswarlu, J. Inorg. Nucl. Chem., 32 (1970) 229.

ELSEVIER

Talanta 44 (1997) 105–109

Talanta

Simultaneous determination of Amaranth and Sunset Yellow by ratio derivative voltammetry

Yongnian Ni*, Jieling Bai

Department of Chemistry, Nanchang University, Nanchang 330047, China

Received 28 December 1995; revised 18 June 1996; accepted 26 June 1996

Abstract

A ratio derivative voltammetric method for resolving overlapping voltammograms without a pre-separation is described. The method is based on the use of the first derivative of ratios of the voltammograms of binary mixtures. The voltammogram of the mixture is obtained and the amplitudes of the current at appropriate potentials are divided by the corresponding amplitudes in the voltammogram of a standard solution of one of the components, and the first derivative of the ratio voltammogram is obtained. The concentration of the other component is then determined from a calibration graph. The method has been successfully applied for resolving binary mixtures of Amaranth and Sunset Yellow, which have overlapped adsorptive voltammograms in pH 6.0 McIlvane buffers.

Keywords: Amaranth; Dyes; Ratio derivative voltammetry; Sunset yellow

1. Introduction

The electrochemical behaviour of a variety of azo compounds has been investigated over the years, and the mechanism of the polarographic reduction of azo compounds has been known for some time [1,2]. Fogg and co-workers [3–12] studied a series of applications of the use of polarography and voltammetry in the determination of these colouring matters. The addition of tetraphenylphosphonium chloride (TPPC) was found to be advantageous in some instances in improving the selectivity as the reduction potentials of some colouring matters, such as Tartrazine, were shifted to more negative potentials, and procedures were given for the determination of Tartrazine–Sunset Yellow, Tartrazine–Green S, Amaranth-Green S and Chocolate Brown–Tartrazine–Green S in soft drinks by differential-pulse polarography (DPP) without prior separation of the colouring matters from the samples [3–5]. Dominguez et al. [13] reported a polarographic method for the determination of Sunset Yellow and Tartrazine in the presence of polyvinyl-pyrrolidone. With this method, it was possible to determine Sunset Yellow in the presence of up to 10 times as much Tartrazine at pH 10.0. However, the determination of Tartrazine in the presence of Sunset Yellow was only possible

* Corresponding author.

PII S0039-9140(96)02028-0

when the Sunset Yellow interferent/Tartrazine ratio was less than 1, and also a different medium of pH 1.6 should be used.

In this paper, a mathematical method which is based on the use of the first derivative of the ratio voltammogram, for the voltammetric analysis of binary mixtures of colouring matters with overlapping voltammetric waves is proposed.

2. Theory

Salinas et al. [14] developed a new spectrophotometric method, named the "ratio derivative spectrum" for resolving binary mixtures. This method has been widely used to solve spectrophotometric problems [15–20]. In this paper, this method is extended to resolve voltammetric problems.

For a binary mixture containing components A and B, the voltammogram of the mixture can be defined by the equation

$$I_i = a_{A,i}C_A + a_{B,i}C_B + I_{i0} \quad (1)$$

where I_i is the voltammetric curent of the mixture at potential E_i, C_A and C_B are the concentrations of A and B, $a_{A,i}$ and $a_{B,i}$ are the proportional coefficients of A and B at potential E_i and I_{i0} is the residual current at E_i, which can be simply denoted as $I_{i0} = k_0 + kE_i$ (k_0 and k are constants here) in a limited potential region.

If Eq. (1) is divided by the proportional coefficient of one of the components (e.g. $a_{A,i}$), the following equation can be obtained:

$$I_i/a_{A,i} = C_A + C_B(a_{B,i}/a_{A,i}) + (k_0 + kE_i)/a_{A,i} \quad (2)$$

By using the first-derivative approach, the following equation can be written:

$$d(I_i/a_{A,i})/dE = C_B d(a_{B,i}/a_{A,i})/dE + k/a_{A,i} \quad (3)$$

where $k/a_{A,i}$ is a constant. Eq. (3) indicates that the amplitude of the "ratio derivative voltammogram" of the mixture at any given potential is dependent only on the value of C_B and is independent on the value of C_A in the mixtures.

A calibration graph is obtained by recording and storing the voltammograms of solutions of pure B at different concentrations. The amplitudes for B are then divided, potential by potential, by the corresponding amplitudes of unit concentration for A. The "ratio voltammograms" thus obtained are then differentiated with respect to potential and the derivative values for a given potential are plotted against C_B to give a calibration graph. Application of the method to a sample containing both A and B, and use of the calibration graph, will then give the value of C_B in the mixture. Component A can be determined by an analogous procedure if it is also overlapped by B.

3. Experimental

3.1. Apparatus

The voltammograms were obtained with a BAS 100A electroanalyser equipped with an electrolytic cell stand (PARC 303A, EG&G). A three-electrode cell containing a mecury drop electrode (the function of a hanging mercury drop electrode (HMDE) was used in this work) as the working electrode, an Ag–AgCl (3 M KCl) electrode as the reference electrode and a Platinum wire as the counter electrode was used. The pH of the solution was measured with a pH meter (Orion SA720). All experiments were performed at 20 °C.

3.2. Reagents

Stock solutions of 10 μg ml^{-1} of Amaranth and Sunset Yellow were prepared by dissolving the crystalline dyes in deionized water. McIlvane buffers (pH 6.0; $I = 0.5$ mol l^{-1}) were prepared from potassium phosphate, citric acid and potassium chloride [21]. All reagents were of analytical-reagent grade.

3.3. Procedure

A suitable amount of Amaranth or Sunset Yellow or their binary mixtures, together with 5.0 ml of buffer solution, was placed in a cell and made up to 10.0 ml with deionized water. The solution was purged with purified nitrogen for 300 s and then electrolysed for 240 s at an HMDE with an accumulative potential of -100 mV. After a 10 s

quiet time, the potential was scanned from −100 to −1100 mV versus the Ag–AgCl reference electrode at a scan rate of 100 mV s^{-1}. The voltammograms were recorded by using a DMP-40 plotter (Houston Instruments) and stored in an IBM 386 computer with an interval of 2 mV. Fig. 1 shows the voltammetric waves of Amaranth and Sunset Yellow.

For the determination of Amaranth, the stored voltammograms of the mixtures were divided by a standard voltammogram (divisor) of Sunset Yellow. The ratio voltammograms thus obtained were smoothed through the use of seven experimental points and the first derivatives were calculated with $\Delta E = 4$ mV [22]. The concentration of the Amaranth was proportional to the amplitude of the minimum at −465 mV (see Fig. 3).

Generally, both components with seriously overlapped voltammograms in binary mixture can be evaluated by the proposed ratio derivative voltammetric method. In this work, however, Sunset Yellow can be determined directly at its peak potential, −500 mV, because there is no influence from Amaranth at this potential (see Fig. 1).

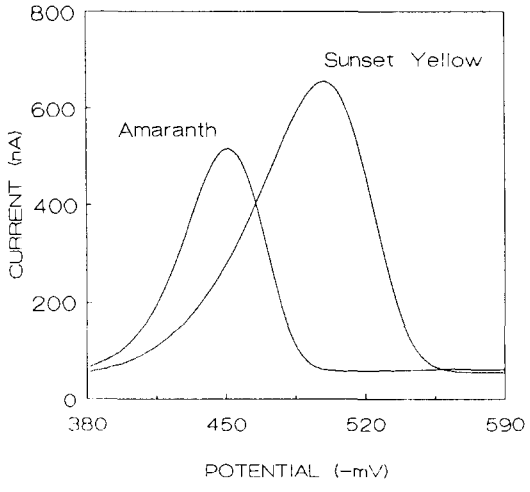

Fig. 1. Voltammetric waves of Amaranth (0.15 μg ml^{-1}) and Sunset Yellow (0.15 μg ml^{-1}).

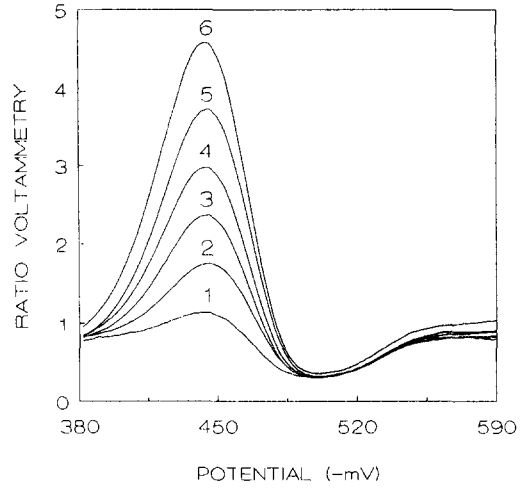

Fig. 2. Ratio voltammograms for different concentrations of Amaranth (0.03 μg ml^{-1} Sunset Yellow as divisor): (1) 0.03; (2) 0.06; (3) 0.09; (4) 0.12; (5) 0.15; (6) 0.18 μg ml^{-1}.

4. Results and discussion

4.1. Selection of the standard solution for divisor

In this work, if the voltammogram of component A with known concentration C_A^0 is used to replace the proportional coefficient (i.e. the voltammogram of unit concentration) as divisor. Eq. (3) will then become

$$d(I_i/a_{A,i}C_A^0)/dE = (C_B/C_A^0)d(a_{B,i}/a_{A,i})/dE + k/(a_{A,i}C_A^0) \quad (4)$$

This is valid for the determination of B. Hence in pratical experiments, a solution with suitable concentration was chosen as a standard factor (divisor). In this work, 0.03 μg mg^{-1} Sunset Yellow was used as a standard factor for the determination of Amaranth. The term $k/(a_{A,i}C_A^0)$ represents the effect of the residual current, and in most cases it can be eliminated.

4.2. Determination of Amaranth and Sunset Yellow in synthetic mixtures

Figs 2 and 3 are the ratio voltammograms and their ratio derivative voltammograms of Amaranth with different concentrations (the voltam-

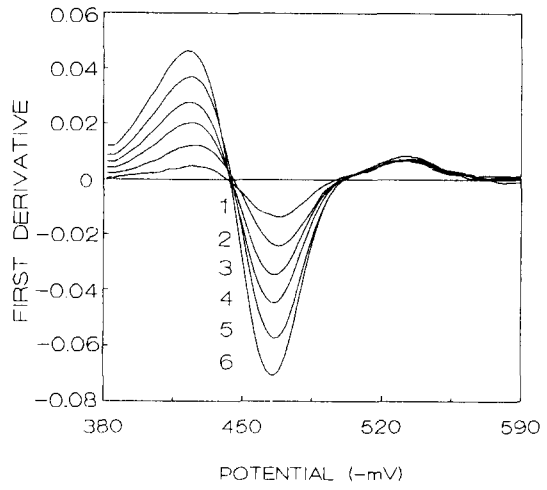

Fig. 3. First derivatives of ratio voltammograms for different concentrations of Amaranth (0.03 μg ml^{-1} Sunset Yellow as divisor); (1) 0.03; (2) 0.06; (3) 0.09; (4) 0.12; (5) 0.15; (6) 0.18 μg ml^{-1}.

mogram of 0.03 μg ml^{-1} Sunset Yellow as divisor). The amplitudes of the derivative voltammogram at the peak potential, −465 mV, were selected as the measurement potential. The calibration graph for Amaranth is represented by $D_1 = -9.53 \times 10^{-4} - 0.379\ C$ ($r = 0.9985$).

The calibration graph at −500 mV for the determination of Sunset Yellow can easily be obtained as $I = 18.4 + 3.88 \times 10^3\ C$ ($r = 0.9997$).

Table 2
Determination of Amaranth and Sunset Yellow in drinks

Samples	Found (μg ml^{-1})[a]	
	Amaranth	Sunset Yellow
Orange juice	1.1 (0.1)	32.4 (0.8)
Fruit juice	4.1 (0.4)	8.9 (0.5)
Merida orangeade	2.1 (0.4)	49.9 (1.5)

[a]Values in parentheses are standard deviations ($n = 3$).

In this work, ten synthetic mixtures of Amaranth and Sunset Yellow were analysed by the proposed method. The results are given in Table 1.

4.3. Determination of Armaranth and Sunset Yellow in drink

The proposed method was also applied to the determination of these two colouring matters in several soft drinks produced in China. The samples were dissolved in a certain volume of deionized water, gently warmed to dissolve completely and filtered. Measurements were carried out directly as described above using an HMDE. The results are given in Table 2 and are in agreement with the manufacturer's specifications.

Table 1
Resolution of Amaranth and Sunset Yellow mixtures by the proposed method

Sample No.	Added (μg ml^{-1})		Found (μg ml^{-1})		Recovery (%)	
	Amaranth	Sunset Yellow	Amaranth	Sunset Yellow	Amaranth	Sunset Yellow
1	0.030	0.160	0.025	0.171	83.3	106.9
2	0.030	0.100	0.024	0.110	80.0	110.0
3	0.030	0.040	0.032	0.040	106.7	100.0
4	0.160	0.160	0.138	0.140	86.3	87.5
5	0.160	0.100	0.150	0.096	93.8	96.0
6	0.160	0.040	0.169	0.042	105.6	105.0
7	0.100	0.160	0.084	0.147	84.0	91.9
8	0.100	0.100	0.097	0.108	97.0	108.0
9	0.100	0.040	0.101	0.043	101.0	107.5
10	0.080	0.080	0.074	0.076	92.5	95.0

5. Conclusion

The results show that the proposed method is effective for resolving binary mixtures and suitable for the simultaneous voltammetric determination of Amaranth and Sunset Yellow in the concentration range 0.03–0.16 $\mu g\ ml^{-1}$, which is much more sensitive than spectrophotometric approaches [19]. This work indicates that some voltammetric problems can benefit from the mathematical methods often used in spectrophotometry.

Acknowledgments

The financial support for this project was provided by the Jiangxi Province Natural Science Foundation and the National Natural Science Foundation of China (No. 29365011).

REFERENCES

[1] J.P. Hart and W.F. Smyth, Analyst, 105 (1980) 929.
[2] T.M. Florence, J. Electroanal. Chem., 52 (1974) 115.
[3] A.G. Fogg and K.S. Yoo, Analyst, 104 (1979) 723.
[4] A.G. Fogg and K.S. Yoo, Analyst, 104 (1979) 1087.
[5] A.G. Fogg and D. Bhanot, Analyst, 105 (1980) 234.
[6] A.G. Fogg and D. Bhanot, Analyst, 105 (1980) 868.
[7] A.G. Fogg and D. Bhanot, Analyst, 106 (1981) 883.
[8] A.G. Fogg and A.M. Summan, Analyst, 109 (1984) 743.
[9] A.G. Fogg and A.M. Summan, Analyst, 109 (1984) 1029.
[10] A.G. Fogg, A.A. Barros and J.O. Cabral, Analyst, 111 (1986) 831.
[11] A.G. Fogg and D. Bhanot, Analyst, 112 (1987) 1319.
[12] A.A. Barros, J.O. Cabral and A.G. Fogg, Analyst, 113 (1988) 853.
[13] F.B. Dominiguez, F.G. Diego and J.H. Mendez, Talanta, 37 (1990) 655.
[14] F. Salinas, J.J. Berzas Nevado and A. Espinosa Mansilla, Talanta, 37 (1990) 347.
[15] J.J. Berzas Nevado, C. Guiberteau Cabanillas and F. Salinas, Anal. Lett., 23 (1990) 2077.
[16] J.J. Berzas Nevado, C. Guiberteau Cabanillas and F. Salinas, Talanta, 39 (1992) 547.
[17] B. Morelli, Anal. Lett. 27 (1994) 2751.
[18] B. Morelli, Talanta, 41 (1994) 673.
[19] J.J. Berzas Nevado, J. Rodriguez Flores and M.J. Villasenor Llerena, Talanta, 40 (1993) 1391.
[20] J.J. Berzas Nevado, C. Guiberteau Cabanillas and A.M. Centento Salcedo, Talanta, 42 (1995) 2043.
[21] P.J. Elving J.M. Markowitz and I. Rosenthal, Anal. Chem., 28 (1956) 1179.
[22] P.A. Gorry, Anal. Chem., 62 (1990) 570.

ELSEVIER

Talanta 44 (1997) 111–117

Talanta

Control samples for the determination of pH in low ionic strength waters: consensus values from interlaboratory tests

M.J. Gardner[a,*], J.E. Ravenscroft[a], C. Ackers[b]

[a] *WRC, Henley Road Medmenham, Marlow SL7 2HD, UK*
[b] *Central Regional Council, St. Ninians Road, Stirling FK8 2HB, UK*

Received 19 February 1996; revised 17 April 1996; accepted 4 July 1996

Abstract

The results of a series of interlaboratory tests using low ionic strength buffer solutions are reported. The test data and other background information are presented as the basis for more realistic quality control materials for pH determination in low ionic strength waters. The effect of atmospheric carbon dioxide on the pH of low ionic strength reference samples is discussed. Several control samples are recommended for routine use.

Keywords: pH determination; Quality control; Waters

1. Introduction

In an earlier paper [1], we identified four desirable characteristics for an analytical quality control (AQC) sample for pH determination in low ionic strength waters: (a) it should be of known pH value, to allow systematic error to be assessed; (b) it should have a similar susceptibility to the main sources of measurement error as real samples; (c) it should be adequately stable to allow its use in an extended series of batches of analysis; and (d) it should be a similar pH (and ionic strength; see (b)) to unknown samples. Subsequently, Peck and Metcalf [2] identified the need to make separate checks on sample handling and on the measurement stage of analysis. In their view, this necessitated two types of control sample. The first would be adequately stable (not susceptible to change by exchange of carbon dioxide (CO_2)), of well characterized pH and appropriate ionic strength. This sample would be used to validate the measurement process. The second sample would be subject to the sources of potential sample instability, as a check on sample handling. In a well argued paper, they went on to use computer modelling of chemical equilibria to compare calculated pH values with the results of careful measurement and interlaboratory tests. They recommended two solutions/test samples which would be used as more realistic AQC solu-

* Corresponding author. FAX: 01491-579094.

PII S0039-9140(96)02042-5

tions (than high ionic strength buffers) for the determination of the pH value of environmental samples.

The most common practice for the day to day determination of pH, in environmental and water laboratories, is to use a buffer solution as an AQC sample. Such solutions are of relatively high ionic strength in comparison with the natural waters that are examined routinely. The use of a high ionic strength buffer solution satisfies few (none apart from (a)) of the key quality control criteria above.

This paper is intended to extend the process of defining a range of more relevant (i.e. than high ionic strength buffers) control samples for pH determination. The two solutions recommended by Peck and Metcalf [2] are of very low ionic strength (ca. 10^{-4} M). These are appropriate to monitoring of very soft upland waters, those which are most susceptible to acidification. The samples discussed here are more applicable to determinations of pH in a wider range of surface and potable waters (ionic strength ca. 10^{-3} M). The aim of this paper is to present the results of a series of interlaboratory tests for pH determination in water samples. The test samples used and the measured values for pH are presented as an illustration of the types of solution which might be employed as more realistic, routine quality control test samples. The group of laboratories carried out a rigorous programme of internal performance testing. This helps to provide consensus estimates of pH which can be regarded as reliable reference values for future use. The role of atmospheric CO_2 in determining the reference pH value of low ionic strength check samples is also discussed.

2. Interlaboratory tests

SADWSS (the Scottish Association of Directors of Water and Sewerage Services) coordinates AQC activity between Scottish Regional Council laboratories in order to achieve and to demonstrate adequate standards of accuracy in chemical analysis. Principal areas of activity for the SADWSS AQC Group are drinking water quality monitoring and the control of effluents discharged to rivers and estuaries. Laboratories of the Department of the Environment (Northern Ireland) Water Executive are also involved in the AQC programme. WRc has acted on behalf of SADWSS to design within- and between-laboratory AQC test programmes and to conduct and interpret a series of within-laboratory and interlaboratory tests for a wide range of determinands. This work has been carried out over a period of 6 years, beginning in 1990.

The accuracy of chemical analysis can often fall short of that required for its intended purpose. A stepwise approach to testing different components of the analytical system has been devised [3] and applied in water analysis in the UK for a number of years. Applications have included the determination of pH [4,5]. This approach was used by the laboratories involved in SADWSS programme.

For pH determination, the work programme involved: (a) adoption of a best practice approach to pH determination as recommended by Covington et al. [6]; (b) within-laboratory tests of precision; and (c) confirmation that adequate accuracy has been achieved by means of an interlaboratory test. The within-laboratory tests can be summarized as follows. In each of 11 batches of analysis, each laboratory made duplicate determinations on the solutions, including a NIST postassium hydrogenphthalate (0.05 M) buffer, a 1×10^{-4} M solution of hydrochloric acid, a 1×10^{-5} M solution of hydrochloric acid and two samples of drinking water. The results of these tests were subjected to an analysis of variance and the overall (total) standard deviation [7] of results was estimated for each laboratory–sample combination. The maximum acceptable value for total standard deviation was set at 0.05 pH units. Laboratories which failed to achieved this standard of precision took action to improve and repeated the tests as a demonstration of satisfactory control over random error.

3. Experimental

Each test involved the distribution of 1 l portions of five test solutions. Samples were prepared

in 50 l portions which were homogenized and distributed by overnight carrier in fully filled low-density polyethylene bottles. Participants were advised that pH determinations should be carried out within 3 days of sample receipt. Test samples were chosen to be of pH value relevant to participants' routine work. Interest centred on the pH region of 5–6 for the control of aluminium flocculation in water treatment processes and of higher pH values, in the range 7–9, for potable waters supplied to the water distribution system. Participants were asked to carry out four pH determinations on each sample, in two separate batches of analysis. The pH values of the samples were determined at WRc before distribution and 3 and 6 days afterwards. Samples were found not to change by more than 0.05 pH units (except hydrogencarbonate buffers, see below). The target for comparability of pH measurement was that laboratories' mean results should not differ from the reference value by more than 0.1 pH unit. Reference values were established by the coordinating laboratory (WRc) by measurement using two pH systems, each incorporating free flowing junctions (Orion "Ross" pH electrode and separate reference calomel (or "Ross" reference) electrodes).

An essential confirmatory check on the reference pH values and on sample stability for the interlaboratory tests was provided by comparison between the consensus mean pH (after rejection of data from laboratories which showed a consistent bias of greater than 0.1 pH units for several solutions in a given test) and the WRc value. Since the laboratories operated a rigorous programme of within-laboratory quality control, the incidence of rejection was low, not more than two rejections per test.

4. Results

Data from the interlaboratory tests reported here were obtained over a period of 4 years. Table 1 shows the results of the series of interlaboratory test for pH determination. Each test involved analysis of five solutions. Of these, several were intended as candidates for routine quality control samples. The compositions of these solutions and the relevant results are shown, together with the consensus mean values and WRc reference values. In each case the range of participants' results is shown. The number of laboratories taking part in each test (and hence contributing to the consensus value) was 11 at the start of the series of tests (1990). The results of these laboratories have been reported in Table 1 for the whole series of tests.

5. Discussion

The 'true pH value' is the key to be addressed for all check samples/buffers. pH values may be assigned in a number of ways. Primary reference values and pH scales are set for standard buffers with respect to a number of conventions (see, for example, Ref. [8]). The observed pH of most measurements is relative to the pH of these primary buffer values. The question here, in relation to the routine quality control (QC) check solutions used in these interlaboratory tests, is one of deciding on an accepted value for routine QC use, rather than assigning a primary reference value. The values given in Table 1 are those observed in a series of interlaboratory tests. We propose that these values can act as a guide to the reference value, against which bias can be evaluated, for routine control purposes.

For the dilute acid samples and the succinate buffers, the difference between the WRc values and the consensus mean values is 0.04 units pH or less. Nevertheless, the laboratory mean value is often negatively biased with respect to the WRc value. A principal source of error for pH determination in lower ionic strength sample is negative bias caused by liquid junction potential effects. This probably accounts for much of the observed bias. The tendency towards negative bias is clearer (although not necessarily larger) in the case of the phosphate buffers, particularly for the lower ionic strength samples. The largest difference is −0.04 pH units, for the lowest ionic strength samples (a test carried out at the start of the series of tests (12/90) was excluded; after this test, many laboratories took steps to minimize liquid junction errors by ensuring a more freely flowing junction, either by applying pressure to the reference cell or

Table 1
Results of interlaboratory tests of pH check sample solutions

Solution composition	Date of test	Ionic strength (M) (no CO_2)	Interlaboratory test consensus mean pH value (range of values)	WRC measured pH value	Calculated pH value (no CO_2)	Calculated pH value (with CO_2[a])	Reported value
Phosphate buffer solutions:							
2.5×10^{-2} M $KH_2PO_4 + 2.5 \times 10^{-2}$ M Na_2HPO_4	12/90	1×10^{-1}	6.88 (6.85–6.98)	6.88			6.88 (NIST assigned)
8.7×10^{-3} M $KH_2PO_4 + 0.03$ M Na_2HPO_4	4/92	1×10^{-1}	7.42 (7.38–7.85)	7.44	7.414	7.403	7.44
8.7×10^{-4} M $KH_2PO_4 + 3.0 \times 10^{-3}$ M Na_2HPO_4	4/92	1×10^{-2}	7.53 (7.46–7.60)	7.64	7.620	7.540	
2.5×10^{-3} M $KH_2PO_4 + 2.5 \times 10^{-3}$ M Na_2HPO_4	9/95	1×10^{-2}	7.05 (7.00–7.10)	7.07	7.081	7.050	7.08
1×10^{-3} M $KH_2PO_4 + 1.08 \times 10^{-3}$ M Na_2HPO_4	9/95	4×10^{-3}	7.13 (7.08–7.17)	7.17	7.167	7.108	
5×10^{-4} M $KH_2PO_4 + 5 \times 10^{-4}$ M Na_2HPO_4	12/90	2×10^{-3}	7.03 (6.93–7.15)	7.14	7.154	7.050	
	6/93		7.11 (6.98–7.14)	7.14			
	3/95		7.10 (7.00–7.15)	7.14			
1.25×10^{-4} M $KH_2PO_4 + 1.25 \times 10^{-4}$ M Na_2HPO_4		5×10^{-4}		7.17	7.186	6.892	6.89
Hydrogencarbonate buffer solutions:							
0.05 M $NaHCO_3$	4/92	5×10^{-2}	8.88 (8.82–9.05)	8.92	8.119	9.627	
2.5×10^{-3} M $NaHCO_3$	9/95	2.5×10^{-3}	8.38 (8.30–8.55)	8.50	8.288	8.644	
1×10^{-3} M $NaHCO_3$	12/90	1×10^{-3}	8.03 (7.80–8.17)	8.06	8.290	8.267	
0.01 M borax	7/91	3×10^{-2}	9.25 (9.19–9.40)	9.24	9.241	8.675	9.24 (NIST assigned)
	6/93		9.22 (9.19–9.26)	9.23			
Succinate buffer solutions:					No effect of CO_2	Atmospheric	
2.5×10^{-2} M NaH succinate + 2.5×10^{-2} M Na_2 succinate	6/93	1×10^{-1}		5.41 (5.52–5.61)		5.40	5.41
0.6×10^{-3} M NaH succinate + 1.8×10^{-3} M Na_2 succinate	9/95	6×10^{-3}		5.57 (5.54–5.62)		5.58	
Dilute acid samples:					No effect of CO_2	Atmospheric	
2.5×10^{-5} M HCl	12/90	2.5×10^{-5}	4.60 (4.34–4.70)	4.62			
2.6×10^{-5} M HCl	6/93	2.69×10^{-5}	4.55 (4.49–4.67)	4.57			
5×10^{-5} M HCl	9/94	5×10^{-5}	4.32 (4.29–4.39)	4.30			
1×10^{-5} M HCl		1×10^{-5}		5.01			

Measurements were made at 20 ± 1°C; calculated values are for 20°C.
[a] With CO_2 refers to full equilibration with atmospheric CO_2; loss or gain can occur.

by using a newer electrode (with a less blocked junction)). Given this and acknowledging that it is not possible to justify either value as completely unbiased, we propose that analysts using the solutions as control samples should expect to obtain long-term mean pH values which are in the range limited by the WRc value and the laboratory mean. Measured mean pH values less than the lower limit of this range might be considered as evidence of negative bias (i.e. sources such as calibration or liquid junction errors should be investigated). Values higher than the upper limit of the range might be taken to be evidence of positive bias (perhaps arising from calibration errors or lack of electrode equilibration). The results for hydrogencarbonate buffers (see Ref. [2]) are not reliable for reasons discussed below.

The results of these tests can be compared with those from the interlaboratory tests carried out by Koch and Marinenko [9]. They obtained a very small between-laboratory range of results (less than 0.1 pH unit) for a dilute acid standard solution. This study illustrates a wider range of 0.1–0.36 pH unit for similar samples. The relatively high precision demonstrated by Koch and Marinenko related to closely defined procedures used in relatively specialist laboratories whose main interest was surface water acidification. The wider range shown relates to routine measurements in water utility laboratories. The standard of accuracy achieved in this study met the requirements defined for drinking water quality monitoring by the UK Water Supply Regulations (Department of the Environment, 1990) in most cases.

5.1. Effect of CO_2 on pH for low ionic strength buffers

The measured pH values in Table 1 are compared with two values calculated using the MINTEQ chemical equilibrium model [10]. The first is arrived at on the assumption that atmospheric CO_2 does not interact with the sample; the second assumes equilibration with a partial pressure of 315 ppm with respect to the volume of CO_2. The former assumption is the one usually made for standard buffers. This is consistent with the practical approach of establishing the pH of these solutions in the absence of CO_2 and the fact the effect of exposure to atmospheric CO_2 has relatively little effect on the pH of solutions of high buffer capacity (and high ionic strength). However, as the molarity of buffer solutions is decreased, it becomes increasingly difficult to justify the assumption the CO_2 has no effect under normal measurement conditions. We have to ask the question, "how much does CO_2 change the pH of a buffer of ionic strength nearer to that of real samples?" Samples of pH <6 are unlikely to be affected by CO_2. For the solutions of higher pH, it cannot be immediately assumed that the sample in question achieves full equilibration with the atmosphere.

Covington et al. [11] have undertaken primary reference pH determination for a diluted version of the standard NIST phosphate buffer. They chose a 10-fold dilution. Their value was based on use of a platinum-hydrogen electrode system with exclusion of atmospheric CO_2 (the normal convention for reference buffers). Peck and Metcalf [2] established an empirical value for a 200-fold dilution of the same standard NIST buffer; this was backed up by model calculations (assuming equilibration with atmospheric CO_2). Our results for a 50-fold dilution of the same standard buffer and other samples are given in Table 1.

The results suggest that caution is required in using equilibrium computer modelling to calculate the reference pH value for low ionic strength buffers, which may be sensitive to atmospheric CO_2. In such models, it is sensible, at first sight, to include the influence of a normal partial pressure of CO_2. It is also tempting to assume that the modelled value is the pH when the buffer is in equilibrium with a normal laboratory atmosphere. However, this is not the case. The modelled value is a true equilibrium value. True equilibrium may only be achieved after a considerable time and may involve the exchange (absorption or loss) of a substantial quantity of CO_2, more than might be available in practice. The data in Table 1 suggest that full equilibrium may not be achieved under the normal conditions of measurement, either for the buffer samples or for real waters. Even for samples such as the 50-fold dilution of

Table 2
Recommended AQC samples

Buffer composition	Ionic strength (M)	Nominal pH value
5×10^{-4} M $KH_2PO_4 + 5 \times 10^{-4}$ M Na_2HPO_4	2×10^{-3}	7.14 (7.11–7.15)
0.01 M borax	3×10^{-2}	9.23 (9.22–9.25)
0.6×10^{-3} M NaH succinate + 1.8×10^{-3} M Na_2 succinate	6×10^{-3}	5.58 (5.57–5.59)
2.5×10^{-5} M HCl	2.5×10^{-5}	4.61 (4.60–4.62)

the NIST phosphate buffer, which are not very sensitive to CO_2, it appears that the modelled value which does not take account of atmospheric CO_2 is a closer estimate of the consensus/reference value than a fully equilibrated value.

In the case of the hydrogencarbonate sample, the stability of the sample is so poor that neither the "no CO_2" nor the "full CO_2" value is appropriate. These samples are probably only suitable to be used as check samples if special precautions are taken to ensure adequate equilibration. The modelled equilibrium values for hydrogencarbonate buffers involve a substanial loss of CO_2. This appears not to reach completion under normal laboratory measurement conditions.

6. Conclusions and recommendations

The determination of pH is often regarded as "trivial", something which may be entrusted to non-analysts or even to poorly trained personnel. pH remains the most fundamental measure of water quality, one which controls the fate and behaviour of a wide range of key quality parameters. Accurate pH determination is far from straightforward; the production of useful pH data requires an awareness of potential sources of error and validation by the application and documentation of soundly based AQC procedures.

The determination of pH in natural waters can be subject to at least three critical sources of error which are not addressed by checks using buffer samples: ionic strength-based, liquid junction potential errors, bias due to lack of glass electrode equilibration and CO_2 exchange effects. Although the principles of analytical quality control are now appreciated and at least partially implemented in the majority of water laboratories, routine AQC practice can still fail to provide a reliable check on accuracy. There is a need for more relevant control analyses, measurements which are subject to the same potential sources of error as those which can affect routine analyses. The use of more sophisticated control materials is an important step in the development of improved approaches to routine AQC for the determination of pH and a wide range of other determinands.

The samples summarised in Table 2 are recommended as routine AQC samples, which might be used for pH determination in natural waters.

The use of such QC buffers provides a more realistic assessment of measurement error for pH. The effect of poor sample handling remains a challenge; reliable techniques for the evaluation of the effect of CO_2 exchange still need to be developed.

Acknowledgement

The authors acknowledge the permission of the SADWSS AQC Group to publish this work.

References

[1] M.J. Gardner, R. Gill and J.E. Ravenscroft, Analyst, 115 (1990) 371.
[2] D.V. Peck and R.C. Metcalf, Analyst, 116 (1991) 221.
[3] A.L. Wilson, Analyst, 104 (1979) 273.

[4] W. Davison and M.J. Gardner, Anal. Chim. Acta, 182 (1986) 17.
[5] Analytical Quality Control (Harmonised Monitoring) Committee, Analyst, 109 (1984) 431.
[6] A.K. Covington, P.D. Whalley and W. Davison, Pure Appl. Chem., 57 (1985) 877.
[7] R.V. Cheeseman, M.J. Gardner and A.L. Wilson, A Manual of Analytical Quality Control for the Water Industry, WRc Publication NS30, WRc, Marlow, 1989, pp. 1–156.
[8] R.G. Bates, Determination of pH: Theory and Practice, Wiley, New York, 2nd edn., 1973.
[9] W.F. Koch and G. Marinenko, J. Res. Natl. Bur. Stand. US, 91(1), (1986) 23.
[10] A.R. Felmy, D.C. Girvin and E.A. Jenne, MINTEQ—A Computer Program for Calculating Geochemical Equilibria, EPA 600/3-84/032, US Environmental Protection Agency, Athens, GA, 1984, pp. 1–15.
[11] A.K. Covington, P.D. Whalley and W. Davison, Analyst, 108 (1983) 1528.

ELSEVIER

Talanta 44 (1997) 119–123

Talanta

Short communication

Spectrophotometric determination of total procyanidins in wine vinegars

M. Carmen García-Parrilla[a], Francisco J. Heredia [a], Ana M. Troncoso[a], A. Gustavo González[b,*]

[a]*Department of Food Science and Nutrition, Faculty of Pharmacy, University of Seville, 41012 Seville, Spain*
[b]*Department of Analytical Chemistry, Faculty of Chemistry, University of Seville, 41012 Seville, Spain*

Received 30 October 1995; revised 10 May 1996; accepted 6 June 1996

Abstract

A widely-used method for the spectrophotometric determination of procyanidins in wines has been adapted to wine vinegar samples. Reagent concentrations have been established and the analytical method tested for possible matrix effects. The recovery of catechin was approximately 98% and the limit of reliable measurement was 0.48 mg l^{-1}. The within-day and between-day precisions were evaluated and according to the two-tailed *F*-test the precisions were statistically equivalent. Application to wine vinegars obtained by traditional and quick acetification methods showed differences in concentration between the two groups.

Keywords: Procyanidins; Spectrophotometry; Wine vinegars

1. Introduction

Phenols encompass heterogeneous groups naturally occurring in plant products. Their occurrence in grapes and wines [1] has been exhaustively reviewed. Among the wine and vinegar constituents, flavanoids represent an important kind of phenol [2]. Grape anthocyanins are particularly interesting as they are responsible for wine colour development. During the maturation of wines, anthocyanins slowly undergo numerous chemical processes involving colourless flavanoids that were originally present in the grape to produce procyanidins, whose presence in wines is an indicator of the extent of contact of musts (unfermented grape juices) with grape seeds and, to a lesser extent, with grape skins. Accordingly, analytical procedures for determination of procyanidins in wines and vinegars were developed. Today, HPLC methods are well suited for these purposes as well as for pattern recognition [3–8], but they are also expensive and time-consuming. Here we are interested in procedures for the rapid estimation of the global procyanidin content using simple instrumentation.

*Corresponding author. Fax: (+34) 5–45571.

PII S0039-9140(96)02012-7

Procyanidins containing the phloroglucinol group can be spectrophotometrically quantitated by reaction with vanillin (or other similar aldehydes) to yield a quinoid product whose colour can vary from a pale to a deep pink. The product has an absorption maximum at 500 nm. This procedure was proposed in 1959 by Swain and Hillis [9] for the "catechins assay in wines" and has remained, practically unchanged. However, when the method is applied to vinegars, excessively scattered results are obtained [10]. The aim of the present paper is a deeper study of the variables that influence the reaction development and their corresponding optimization for wine vinegars, as well as the improvement of the procedure in terms of sensitivity and reliability.

2. Experimental

2.1. Reagents

D-catechin (Fluka), vanillin, concentrated hydrochloric acid, methanol and ethanol (Merck) were used as received. Glass-distilled water was used throughout. Vanillin solutions can be kept for longer than 4 months if stored in an amber bottle in a refrigerator. D-catechin stock solution and alcoholic hydrochloric acid solutions should be prepared daily.

2.2. Apparatus

Absorbance measurements were carried out using a Milton Roy Spectronic 3000 photodiode array spectrophotometer fitted with matched silica cuvettes of 10 mm pathlength.

2.3. Samples

20 commercial wine vinegars were studied: 10 of them were obtained from quick acetification processes and the other 10 were obtained by the dynamic solera system (slow acetification of sherry vinegars).

3. Results and discussion

3.1. Study of influencing variables

In order to attain optimal conditions for reaction development, a preliminary study of the influence of the variables or factors substantially involved in the chemical process was done. The starting point was the reaction scheme of Broadhurst and Jones [11], who established the optimum addition order. Thus, we have taken from these authors the following procedure. To a 25 ml volumetric flask containing 2.5ml of catechin solution (or a sample containing catechin), add 7.5 ml of vanillin reagent and then, add hydrochloric acid solution to the mark. Mix well and allow to stand for about 25 min. Measure the absorbance at 500 nm. Note that protection from direct light is needed. The solvent used for preparing the vanillin reagent (alcohol) is the same solvent used for the hydrochloric acid solution. Accordingly, we have chosen to vary the following factors: the nature of the alcoholic solvent, the concentration of hydrochloric acid and the vanillin concentration. The catechin probe was a solution of 100 mg l^{-1}. The original reagents used were 8 M HCl in ethanol and 1% vanillin in ethanol.

3.1.1. Effect of the nature of alcohol

Methanol and ethanol were used as solvents in order to compare their influence on the measured absorbance. The effect of substituting ethanol for methanol (all other conditions were fixed with the original reagents and a catechin concentration of 100 mg l^{-1}), is in all cases, an enhancement of the absorbance. This indicates that methanol is the better choice for the development of the reaction. This effect can be explained according to the high polarity of methanol which may cause a hyperchromic effect on the $n-\pi^*$ transition responsible for the colour intensity.

3.1.2. Effect of the concentration of hydrochloric acid

Different methanolic hydrochloric acid solutions ranging from 2 to 10 M in HCl were prepared by taking the required volume of

concentrated hydrochloric acid in a volumetric flask and then adding methanol to the mark. The development of the reaction was monitored at fixed concentrations of 1% vanillin in methanol and 100 mg l^{-1} catechin. As can be observed in Fig. 1, the measured absorbance increases with the concentration of hydrochloric acid. However, for HCl concentrations greater than 7.2 M, vanillin-containing blanks seem to undergo some condensation process leading to green-yellowish products. So, in order to avoid this undesirable behavior of the blanks, a fixed concentration of 7.2 M HCl was selected for further experiments. The corresponding absorbance vs. hydrochloric acid concentration plot for blanks is also presented in Fig. 1.

3.1.3. *Effect of the vanillin concentration*

The reaction was performed using several vanillin solutions whose concentrations ranged from 1% to 16% in methanol. The fixed conditions were 100 mg l^{-1} catechin and 7.2 M HCl in methanol. The more the vanillin concetration increases, the more the reaction displays its sensitivity. Saturation was attained at about 12% of

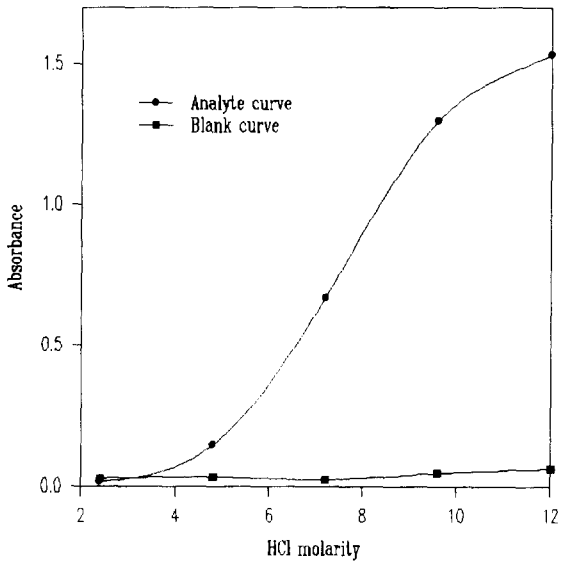

Fig. 1. Effect of the concentration of hydrocloric acid on the colour development of the vanillin reaction for a catechin probe and for a blank as indicated in the text.

vanillin. Accordingly, the analytical optimized procedure for catechin determination is as follows. To a 25 ml volumetric flask add 2.5 ml of vinegar sample containing not more than 100 mg l^{-1} catechin, 7.5 ml of 12% vanillin reagent and 7.2 M HCl in methanol to the mark. Mix well and measure the absorbance at 500 nm after 25 min. Readings are stable for at least 10 min.

3.2. *Evaluation of the analytical procedure*

3.2.1. *Accuracy: Constant and proportional bias*

For preventing possible matrix effects of vinegar samples, the Method of Standard Additions (MOSA) was applied in conjunction with the conventional external calibration (EC) [12] using catechin aqueous standards. Assuming the non-existence of direct matrix effects, the determination of the Total Youden Blank (TYB) is a prior step in the application of MOSA. Cardone [13] had pinpointed the difference between the typical analytical blank and the TYB, namely that the analytical blank cannot be subtracted from the analytical signal, because it comes from a treated solution of free-matrix sample analyte. The Youden plot [14] consists of plotting the analytical signal against increasing amounts of test portion (TP). The value obtained from extrapolation to TP = 0 is the TYB, directly involved in the occurrence of constant bias in calibration. Accordingly, in order to remove possible constant bias in our case, a Youden plot was performed for all vinegar samples by taking different sample volumes of vinegar (six points) and then measuring the absorbance after the application of the proposed analytical assay. For all vinegars TYBs are within the range 0.0098–0.0091. According to the Student t-test (at a 5% confidence level), these intercepts have no statistical significance [15] and consequently there is no constant bias in all the studied vinegar samples.

MOSA and EC were then carried out for the study of possible proportional bias in calibration. MOSA slopes for all vinegar samples were averaged to the value $b_{MOSA} = 0.044 \pm 0.002$, whereas the EC slope was taken as $b_{EC} = 0.045 \pm 0.003$. The difference between these slopes is statistically

Table 1
Total procyanidines, expressed as catechin (mg l^{-1}) of different vinegar samples

Vinegars from quick acetification methods (sample number)	Catechin concentration (mg l^{-1})[a]	Vinegars from sherry (sample number)	Catechin concentration (mg l^{-1})
1	154.0	1	10.5
2	217.0	2	4.1
3	92.2	3	6.1
4	61.8	4	20.6
5	59.9	5	9.8
6	217.3	6	18.1
7	364.2	7	32.7
8	106.0	8	14.1
9	408.2	9	13.6
10	414.4	10	14.2

[a]Data are means of triplicate determinations.

non-significant and, therefore, the neglection of proportional bias is acceptable. This ensures that conventional EC may be used for the quantization of catechin in vinegars. The recoveries calculated from the quotient b_{MOSA}/b_{EC} were about 98%, indicating the suitability and reliability of the assay. Accordingly, the linear dynamic range for the EC straight line was 0–10 mg l^{-1} catechin. By taking the sensitivity as the slope of the EC curve, the proposed procedure is somewhat more sensitive than the conventional one according to the optimization performed as described above. The limit of reliable measurements (LRM) is calculated from EC data following the method proposed by the AOAC [16]. The averaged value from the LRMs obtained from 11 between-days calibration graphs is 0.48 mg l^{-1} catechin. For validation purposes, a further assesment for accuracy was performed with spiked vinegar samples by calculating the recovery as the mean value of the recoveries found at each fortification level. In all cases recoveries were close to 100% and, accordingly, the method is suitably validated.

3.2.2. Precision

For the study of precision, target samples of 40 mg l^{-1} catechin were analyzed according to the proposed procedure. The within-day precision or repeatability expressed as the percent RSD is 2.7% (10 replicates). The between-days precision or reproducibility is 5.6% (six randomized determinations over 1 month using the same materials, appartatus and stock reagent solutions). The two-tailed F-test indicated that within the frame of our experiments both precision measurements are statistically equivalent.

3.2.3. Application to vinegar samples

The proposed procedure was applied to the determination of total procyanidins expressed as catechin in 20 vinegar samples as indicated above. Vinegars containing more than 100 mg l^{-1} procyanidins were suitably diluted with water. Results obtained from EC graphs (mean of triplicate determinations) are presented in Table 1. As can be observed, the procyanidin contents of quick acetification vinegars range from 414.4–59.9 mg l^{-1} whereas procyanidin concentrations of sherry vinegars are 4.1–32.7 mg l^{-1}, noticeably lower. This is statistically proved using the non-parametric Tuckey quick test [17]. From these results, the total procyanidin content can be considered as a good descriptor for pattern recognition of different wine vinegars. Moreover, the determination of total procyanidins in wine vinegars may be of interest in order to elucidate the quality of the substrate employed for the acetification. If the substrate wine is of overpressure basis (where the musts are processed at high pressure) the procyanidin content may presumably be higher than with a quality wine substrate.

In order to compare the results obtained from the proposed procedure with those obtained from the "traditional" method of Swain and Hillis [9], this latter was applied to the same vinegar samples presented in Table 1. However, in all cases, the catechin content cannot be reliably calculated because of the dramatic fading of the absorbance measurement, which leads to data so strongly dispersed as to make comparison impossible. This behaviour is in agreement with the results reported by Gil and Gómez-Cordovés [10] and indicates that the Swain and Hillis method for determination of procyanidins in wines cannot be applied to vinegars without adaptation.

4. Conclusions

The traditional method for spectrophotometric determination of total procyanidins by reaction with vanillin has been optimized. EC graphs suffice for reliable determinations of catechins in vinegar samples. Quick acetification vinegars exhibit greater procyanidin contents than sherry vinegars.

References

[1] V.L. Singleton and P. Essau, Phenolic Substances in Grapes and Wines and their Significance, Academic Press, New York, 1969, Chapter 2.

[2] M. Bourzeix, Compuestos Fenólicos de Uva y Vino. Enología. Temas Actuales, Fondo Editorial Anque, Madrid, 1982, pp. 177–217.

[3] J. Rigaud, M.T. Escribano, C. Prieur, J.M. Souquet and W. Cheynier, J. Chromatogr. A, 654 (1993) 255–260.

[4] J.M.R. Da Silva, J. Rigaud, V. Cheynier, A. Cheminat and M. Moutounet, Phytochemistry, 30 (1991) 1259–1264.

[5] C. Prieur, J. Rigaud, V. Cheynier and M. Moutounet, Phytochemistry, 36 (1994) 781–784.

[6] P. Etievant, P. Schlich, A. Bertrand, P. Symonds and J.C. Bouvier, J. Sci. Food Agric., 42 (1988) 39–54.

[7] P. Archier, S. Coen and J.P. Roggero, Sci. Aliment., 12 (1992) 453–466.

[8] C. Santos, E.M. Francia and M.T. Escribano. Food Chem, 53 (1995) 197–201.

[9] T. Swain and W.E. Hillis, J. Sci. Food Agric., 10 (1959) 63–68.

[10] C. Bill and C. Gómez-Cordovés, Anal., Bromatol., 37 (1985) 153–159.

[11] R.B. Broadhurst and W.T. Jones, J. Sci. Food Agric., 29 (1978) 788–794.

[12] L.C. Rodríguez, A.M. García Campaña, F.A. Barrero, C.J. Linares and M. Román Ceba, J. Assoc. Off. Anal. Chem. 78 (1995) 471–476.

[13] M.J. Cardone, J. Assoc. Off. Anal. Chem., 66 (1983) 1283–1294.

[14] W.J. Youden, Anal. Chem., 19 (1947) 946–950.

[15] J.C. Miller and J.N. Miller, Statistics for Analytical Chemistry, Ellis Horwood Limited, Chichester, UK, 1988, pp. 115–17.

[16] G.T. Wernimont, Use of Statistics to Develop and Evaluate Analytical Methods, Association of Official Analytical Chemists, Arlington, VA, 1987, p. 76.

[17] J.C. Miller and J.N. Miller, Analyst, 113 (1988) 1351–1356.

ELSEVIER

Talanta 44 (1997) 125–129

Talanta

Short communication

Cathodic stripping voltammetry of copper-complexed reactive dyes at a hanging mercury drop electrode: Reactive Violet 5

Arnold G. Fogg[a,*], A. Rahim, H.M. Yusoff,[a] Rahmalan Ahmad[b]

[a]*Chemistry Department, Loughborough University of Technology, Loughborough, Leicestershire, LE11 3TU, UK*
[b]*Chemistry Department, Universiti Teknologi Malaysia, 80990 Johor Bahru, Malaysia*

Received 28 February 1996; revised 10 June 1996; accepted 10 June 1996

Abstract

Reactive Violet 5 and its hydrolysis product, which is produced as a side product in the dyeing process, can be determined in an admixture at sub-ppb levels by cathodic stripping voltammetry because the potentials of their azo reduction peaks are separated sufficiently. For both dyes, at intermediate pH values the azo peak is preceded by a complexed -copper reduction peak at a less negative potential, which aids the identification of the dyes. The use of pH 6 EDTA buffer removes the complexed-copper peak, as does the use of an acidic buffer (pH < 3). This unusual use of EDTA as a pH buffer facilitates the determination of mixtures of the dye and its hydrolysis product.

Keywords: EDTA; Hydrolysis product; Reactive Violet 5; Stripping voltammetry

1. Introduction

There is a need for methods of determining dyes, and particularly reactive dyes which form a major part of the dye market, at concentration levels below those which can be determined by visible and UV spectroscopy. In the case of the most efficient reactive dyes about 80% of the dye becomes covalently bonded to cotton [1]. Much of the rest of the dye becomes hydrolysed and has to be washed out of the fabric. This residual dye has to be removed from the effluent before discharge. Visible observation of the effluent is used to indicate satisfactory removal of the colour. However, it would be useful to be able to determine the exact concentration of dye, below that which can be observed visibly, in the discharge. Such low-concentration determinations would be useful in developing methods of removing dyes from effluent, e.g. in assessing the effectiveness of zeolites for this purpose. Further, for health reasons there is a need to monitor any unhydrolysed reactive dyes that are discharged as their half-lives in near neutral solution are long and they will react with proteins, etc. in the ecosystem. Finally, in the development of new reactive dyes there is a need for methods capable of monitoring the dyes

* Corresponding author.

PII S0039-9140(96)02014-0

and their products in dyeing and dyeing simulation (e.g. by reaction with methanol) reactions.

In addition to visible observation, HPLC with UV–Visible detection is used to monitor reactive dyes and their reaction products, but there are difficulties in distinguishing (i.e. in obtaining sufficiently different retention times) between the dyes and their products and, in some situations, the detection limit is not adequate [2,3]. Electrolytes in effluent are a further problem in applying HPLC [3].

In previous publications from this laboratory the ability to determine reactive dyes down to sub-ppb levels by cathodic stripping voltammetry (CSV) has been demonstrated [4–7]. Chromophores, such as azo and anthraquinone groups, are reducible at the hanging mercury drop electrode (HMDE), although the differential pulse signal of the anthraquinone group has been shown to be absent in the case of very fast reduction processes owing to the nature of the differential pulse technique [4]. The chloro- and dichloro-triazine groups are also reducible. The hydrolysis and methanolysis reactions of Procion Blue MX-R and Cibacron Blue 3GA were followed by differential pulse CSV by observing the loss of the chlorotriazine peak or the appearance of the anthraquinone peak: the latter peak is present in the case of the hydrolysed dyes [4]. The differential pulse CSV peaks of these reactive dyes are also present for solutions of the dyes in borate buffer, owing to the complexation of the aminoanthraquinone group by boron, which apparently slows the rate of reduction [4]. The hydrolysis of several azo reactive dyes having the same basic structure but different potential leaving groups has been followed by observing the loss of the peak due to the leaving group [7].

In this present study the CSV of Reactive Violet 5 (**I**)

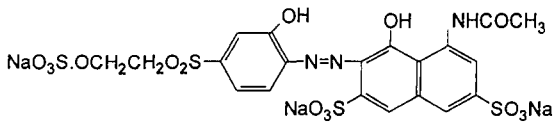

(I)

and its hydrolysis product are reported. This is the first report of the CSV of a copper-complexed reactive dye and further illustrates the dual use of EDTA as a pH buffer and as a complexant.

2. Experimental

2.1. Apparatus and reagents

CSV was carried out with a Metrohm 646/647 VA Processor, using a multi-mode electrode in the HMDE mode. The three-electrode system was completed by means of a glassy carbon auxiliary electrode and an Ag/AgCl (3 M KCl) reference electrode. All potentials are quoted relative to this reference electrode. Differential pulse voltammetry was carried out with a pulse amplitude of 50 mV, a scan rate of 10 mV s^{-1} and a pulse interval of 1 s.

A sample of Reactive Violet 5 was kindly provided by Zeneca Specialities. Standard solutions were made by dissolving weighed amounts of the dye in water before making up to volume.

Britton–Robinson buffer, 0.02 M in acetic, *o*-phosphoric and boric acids, was adjusted to the required pH with dilute sodium hydroxide solution. The pH 6 EDTA buffer was 0.04 M in EDTA.

The general procedure used to obtain cathodic stripping voltammograms was as follows. A 20 ml aliquot of buffer solution was placed in a voltammetric cell and the required volumes of dye and copper(II) solutions were added using a micropipette. The stirrer was switched on and the solution was purged with nitrogen gas for 5 min. After forming a new HMDE, accumulation was effected for the required time at the appropriate potential whilst stirring the solution. A medium drop size ($\approx$0.40 mm^2) was used. At the end of the accumulation time the stirrer was switched off, and after 10 s had elapsed to allow the solution to become quiescent, the negative-going potential scan was initiated. When further volumes of dye or copper(II) solution were added to the cell, the solution was deoxygenated with nitrogen gas for 1 min before carrying out further voltammetry.

Standard solutions of hydrolysed Reactive Violet 5 were prepared by dissolving weighed

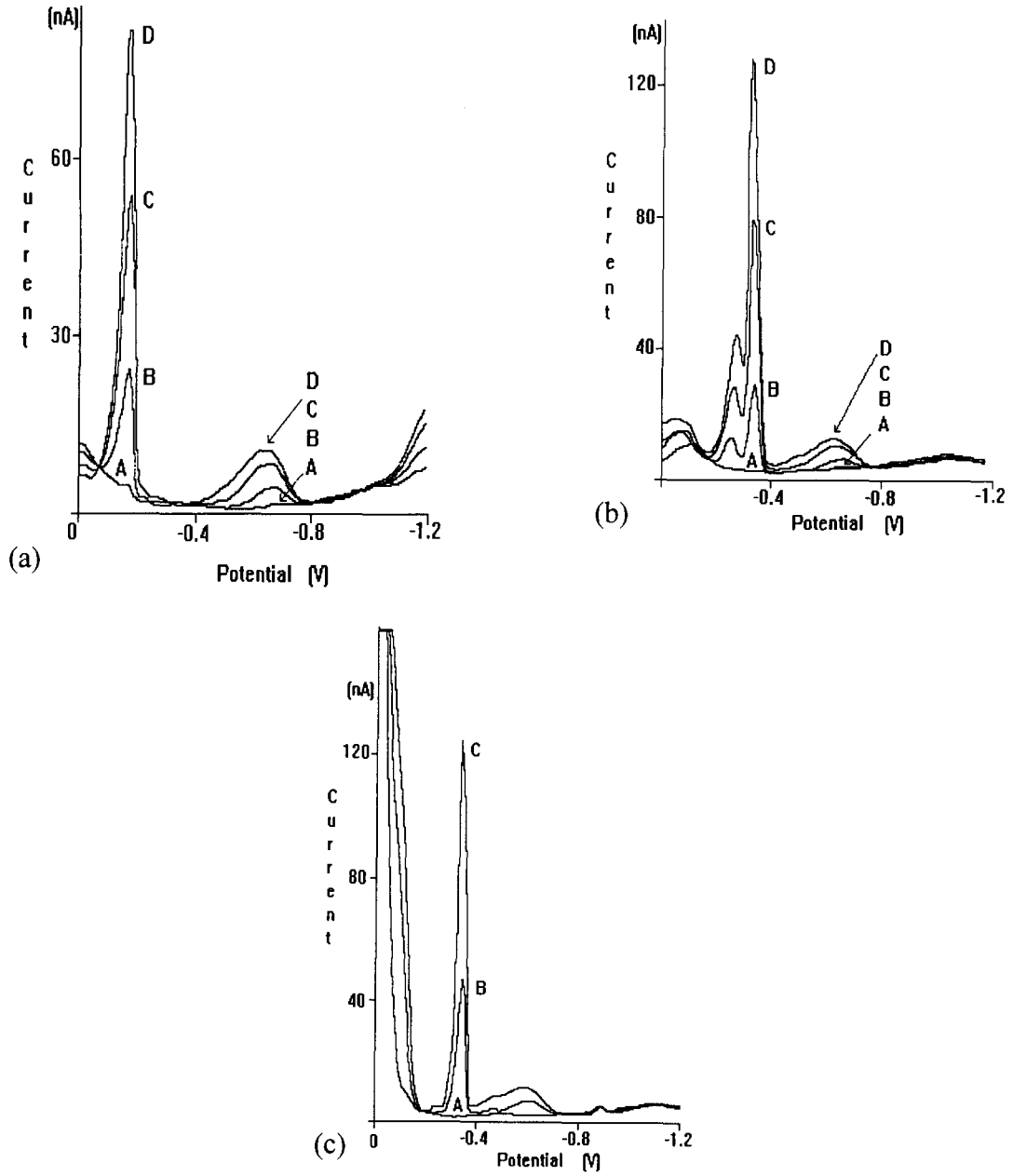

Fig. 1. Cathodic stripping voltammograms of Reactive Violet 5 in various buffers: (a) Britton–Robinson buffer pH 3; (b) Britton–Robinson buffer pH 6; (c) EDTA buffer pH 6. Reactive Violet 5 concentration: (a,b) A,0; B,1; C,3; D,5 $\times 10^{-7}$ M; (c) A,0; B,2; C,5 $\times 10^{-7}$ M.

amounts of Reactive Violet 5 in 5 ml of 0.1 M sodium hydroxide solution, heating for 4 h, cooling, neutralising with 0.1 M hydrochloric acid solution, and diluting with water to the required volume.

3. Results

Typical cathodic stripping voltammograms of Reactive Violet 5 at the 1×10^{-7}–5×10^{-7} level in Britton–Robinson and EDTA buffers are

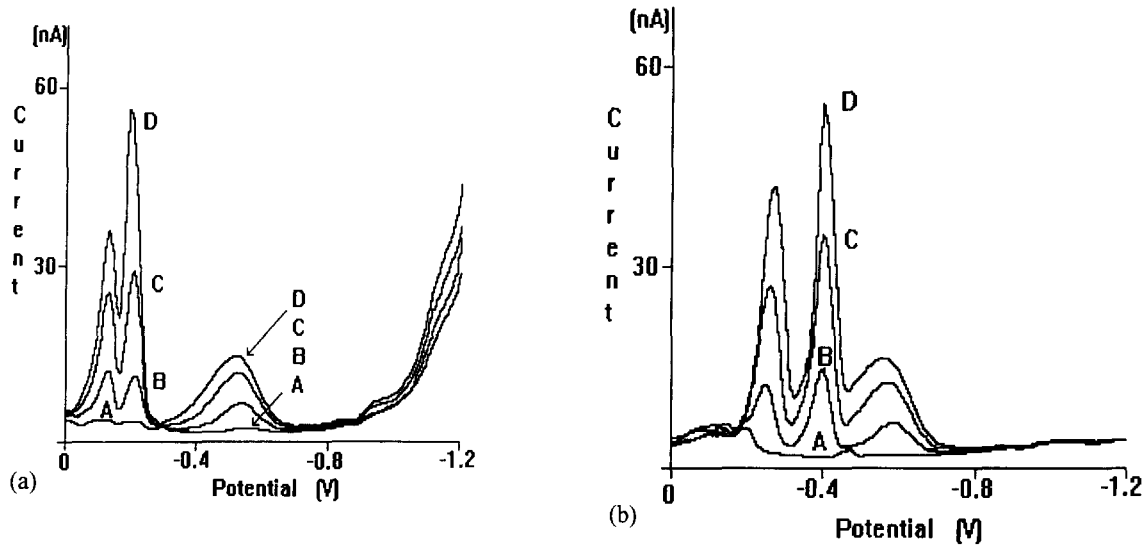

Fig. 2. Cathodic stripping voltammograms of hydrolysed Reactive Violet 5 in various buffers: (a) Britton–Robinson buffer pH 3; (b) Britton–Robinson buffer pH 6. Hydrolysed Reactive Violet 5 concentration: A,0; B,1; C,3; D,5 × 10^{-7} M.

shown in Fig. 1. In pH 3 Britton–Robinson buffer (Fig. 1a) the azo peak is clearly seen at −0.17 V without the complexed-copper peak, but in pH 6 Britton Robinson buffer (Fig. 1b) the complexed-copper peak is clearly seen at −0.29 V and is incompletely resolved from the azo peak at −0.36 V. In pH 6 EDTA buffer (Fig. 1c) the complexed-copper peak is absent. With accumulation at 0 V the slope of a large peak at a less negative potential due to reduction of the mercury EDTA complex is apparent, but the azo peak is completely resolved from this at −0.36 V.

In the case of hydrolysed Reactive Violet 5 the azo peak appears at −0.23 V in pH 3 Britton–Robinson buffer and the complexed-copper peak is also present at −0.17 V (Fig. 2a), in contrast to the situation with the reactive dye. The complexed-copper peak at −0.31 V is better resolved from the azo peak at −0.45 V in pH 6 Britton–Robinson buffer (Fig. 2b). As with the reactive dye the complexed-copper peak is absent in pH 6 EDTA buffer (not shown).

In pH 6 EDTA buffer the azo peaks of Reactive Violet 5 and its hydrolysis product are resolved. Typical cathodic stripping voltammograms showing this are given in Fig. 3: here accumulation is effected at −0.20 V which avoids the appearance of the mercury EDTA peak. Preliminary experiments have been carried out showing that the hydrolysis of Reactive Violet 5 down to concentrations of about 1 × 10^{-9} M can be followed very conveniently in this buffer.

4. Discussion

EDTA, a tetrabasic acid with pK_a values of 2.0, 2.67, 6.16 and 10.26, is used extensively as a complexing agent. Indeed it is the best known complexant in general use. Its complexing properties seem to have overshadowed its acid–base characteristics, except as a means of making its reactions with metals more selective as indicated in numerous texts on classical analytical chemistry. Its use solely as a pH buffer seems to have been largely neglected, although its use as a complexing agent in other pH buffers over a wide range of pH values is clearly well established. In previous publications concerned with the determination of sulfonamides we have shown that interferences in CSV due to copper(II), and in

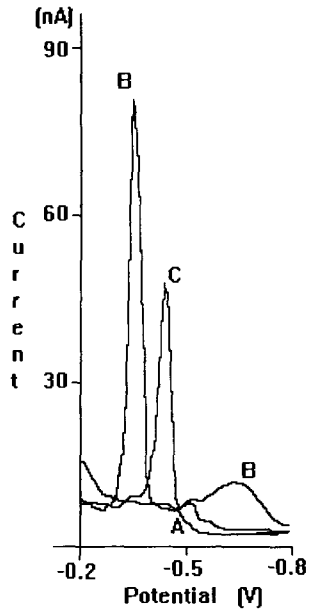

Fig. 3. Cathodic stripping voltammograms showing that Reactive Violet 5 and hydrolysed Reactive Violet 5 can be determined in an admixture in EDTA buffer pH 6. A, buffer only; B, Reactive Violet 5 concentration = 3×10^{-7} M; C, hydrolysed Reactive Violet 5 concentration = 3×10^{-7} M.

particular due to unwanted accumulation of copper(I) salts leading to the appearance of unwanted copper (I) reduction peaks, can be avoided by the use of EDTA buffers [8,9].

In the present case of Reactive Violet 5 the appearance of the complexed-copper peak serves to help identify the dye, but the use of the EDTA pH buffer makes its determination easier. Indeed, because the azo peaks of Reactive Violet 5 and its hydrolysis product are sufficiently well separated, the use of the EDTA pH buffer allows the hydrolysis of the reactive dye to be monitored effectively.

Further work is in progress to study the CSV of reactive dyes with various reactive groups, and on the use of CSV in dye pollution studies.

Acknowledgements

The authors thank Drs. J.A. Taylor and A.H.M. Renfrew of Zeneca Specialities for the provision of dyes and information, and for their interest in this work. A.R.H.M.Y. thanks the Technical University of Malaysia (UTM) for financial support and leave of absence.

References

[1] Kirk-Othmer Encyclopedia of Chemical Technology, 4th edn., Vol. 8, John Wiley & Son, New York, 1994, pp. 542, 809.
[2] D.A. Oxspring, E. O'Kane, R. Marchand and W.F. Smyth, Anal. Methods Instrum. 1 (1993) 196.
[3] J.A. Taylor, personal communication, 1996.
[4] A.G. Fogg and M.V.B. Zanoni, Anal. Proc., 31 (1994) 173.
[5] M.V.B. Zanoni and A.G. Fogg, Anal. Proc., 31 (1994) 217.
[6] M.V.B. Zanoni, A.G. Fogg, J. Barek and J. Zima, Anal. Chim. Acta, 315 (1995) 41.
[7] J. Barek, A.G. Fogg, J.C. Moreira, M.V.B. Zanoni and J. Zima, Anal. Chim. Acta, 320 (1996) 31.
[8] A.G. Fogg, A.R.H.M. Yusoff and R. Ahmad, Anal. Proc., 32 (1995) 189.
[9] A.G. Fogg, A.R.H.M. Yusoff and R. Ahmad, Anal. Proc., 32 (1995) 337.

ELSEVIER

Talanta 44 (1997) 131–134

Talanta

Short communication

Determination of L-phenylalanine in serum by flow-injection analysis using immobilized phenylalanine dehydrogenase and fluorimetric detection

Nobutoshi Kiba*, Akiko Itagaki, Motohisa Furusawa

Department of Applied Chemistry and Biotechnology, Faculty of Engineering, Yamanashi University, Kofu 400, Japan

Received 25 March 1996; revised 7 June 1996; accepted 12 June 1996

Abstract

A flow-injection system with an immobilized enzyme reactor is proposed for the determination of L-phenylalanine. Phenylalanine dehydrogenase from *Rhodoccus* sp. M4 was immobilized on tresylated poly (vinyl alcohol) beads (13 μm) and packed into a stainless-steel column (5 cm × 4 mm i.d.). Serum sample was deproteinized with tungstic acid and filtered through an ultrafiltration membrane. The sample solution (30 μl) was injected into the carrier stream (water). The NADH formed was detected at 465 nm (excitation at 340 nm). The calibration graph was linear for 0.9–600 μm L-phenylalanine; the detection limit was 0.3 μm. The sample throughout was 25 h^{-1} without carryover. The half-life period of the immobilized enzyme was 23 days.

Keywords: Flow-injection analysis; Fluorescence detection; Immobilized enzyme reactor; L-phenylalanine; Serum

1. Introduction

The measurement of L-phenylalanine (Phe) is of clinical importance in the diagnosis and therapy of phenylketonuria. Enzymatic methods have been developed for the selective determination of Phe based on the conversion of Phe in to phenylpyruvate with concomitant reduction of nicotineamide adenine dinucleotide (NAD^+) to reduced nicotineamide adenine dinucleotide (NADH) with phenylalanine dehydrogenase (EC 1.4.1.–., PheDH) [1–8]. PheDH has been immobilized on a nylon coil and applied in a bioluminescence continuous-flow system for the determination of Phe in serum [9]. The PheDHs used were purified from *Thermoactinomyces* sp. [1], *Brevibacterium* sp. [2], *Rhodococcus* sp. [3–8] and *Bacillus badius* [9]. Among them, the enzymes from *Rhodococcus* sp. are more specific for Phe and are stable in the presence of glycerol [10,11]. The PheDH from *Rhodococcus* sp. M4 has been immobilized on aminopropyl-substituted controlled-pore glass (CPG) and used as a reactor in

* Corresponding author. Fax: (81)552-208568.

PII S0039-9140(96)02016-4

the fluorimetric flow-injection system for the determination of Phe in serum [12,13]. The method is not very sensitive because the reactor was used in the neutral buffer (pH 7.1) to prolong the lifetime of the reactor; the optimum pH for the PheDH is 10.0 [10,11] and CPG is unstable in alkaline solution [14].

This paper describes a flow-injection system for the enzymatic determination of Phe with PheDH immobilized on poly(vinyl alcohol) beads contained in a packed-bed reactor. The enzyme from *Rhodococcus* sp. M4 was used. The enzymatic reaction was performed in a basic buffer (pH 10.0). The NADH produced in the reactor was monitored fluorimetrically. The flow-injection method was applied to the determination of Phe in serum.

2. Experimental

2.1. Materials and reagents

PheDH from *Rhodococcus* sp. M4 was obtained from Calbiochem (San Diego, CA, USA) with an activity of 12 U ml^{-1}. The activity was measured with Phe as substrate at pH 10.0 at 30°C. NAD^+ (free acid, 96%) and NADH (disodium salt, 99.5%) were purchased from Kohjin (Tokyo, Japan) and Boehringer Mannheim (Mannheim, Germany), respectively. L-Amino acids were purchased from Sigma (St. Louis, MO, USA). Poly(vinyl alcohol) beads (GS-520, 13 μm diameter) were obtained from Showa Denko (Tokyo, Japan). All other chemicals, which were purchased from Nacalai Tesque (Tokyo, Japan), were of analytical-reagent grade.

A glycine buffer (pH 10.0) consisting of 0.2 M glycine–0.2 M sodium chloride–0.2 M sodium hydroxide–2% (v/v) glycerol was used. NAD^+ solution (8 mM NAD^+ in water) was prepared fresh daily. The carrier solution was water.

2.2. Preparation of the immobilized enzyme reactor

PheDH was immobilized on the poly(vinyl alcohol) beads. The beads (1 g) were washed with dry acetone (20 ml). The beads were suspended in 20 ml of a mixture of dry acetone and pyridine (1:1 v/v). With vigorous magnetic stirring, 1 ml of 2,2,2-trifluoroethanesulphonyl chloride (tresyl chloride) was added dropwise to the suspension during 5 min. The reaction was continued for 5 min. The beads were washed with acetone (10 ml) and 1 mM HCl (20 ml). The beads were packed into a stainless-steel column (5 cm × 4mm i.d.) by the slurry-packing method. Enzyme solution (PheDH 26 U in 10 ml of 2% (v/v) glycerol in 10 mM phosphate buffer) was circulated through the column at 0.2 ml min^{-1} for 6 h at 10°C. During the process the enzyme solution was kept at 2–5°C. The reactor was washed with 10% glycerol in 0.1 M phosphate buffer (pH 7.0) and stored in a refrigerator when not in use. The coupling yield was evaluated by measuring the decrease in the activity of PheDH in the enzyme solution after the process. The PheDH was immobilized with a 95% yield. Also, epoxy-activated beads (epoxy-beads) and glutaraldehyde-activated beads (glutar-beads) were used for the coupling of PheDH; the preparation methods for the activated beads were similar to those described previously [15] and coupling conditions were identical with those described above. The yields for epoxy-beads and glutar-beads were 5% and 24%, respectively.

2.3. Flow system and procedure

A schematic diagram of the flow system is shown in Fig. 1. The system consisted of three piston

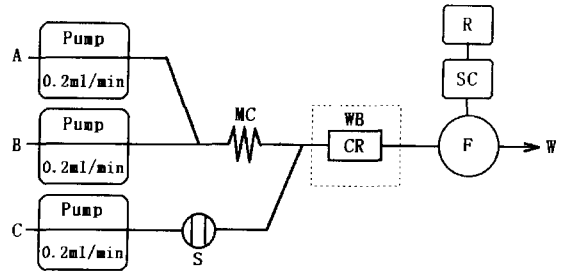

Fig. 1. Schematic diagram of the flow-injection system for the determination of L-phenylalanine with an immobilized phenylalanine dehydrogenase reactor. A, 8 mM NAD^+ solution; B, 2% (v/v) glycerol in 0.2 M glycine buffer; C, carrier solution (water); S, injector with a 30 μl loop; MC, mixing coil (100 cm × 0.5 mm i.d.); WB, water-bath thermostated at 20°C; CR, enzyme column reactor (5 cm × 4 mm i.d.); F, spectrofluorimeter with a flow-through cell (15 μl); SC, signal cleaner; R, recorder; W, waste. All connecting tubing (0.5 mm i.d.) was made of PTFE.

pumps (Hitachi L-6000), an injection valve (Sanuki SVI-6M2) equipped with a 30 μl loop, a reactor, a spectrofluorimeter (Jasco FP-210) with a flow-through cell (15 μl) connected to a signal cleaner (SIC SC77) and a recorder (TOA FBR-251A). The reactor was maintained at 20°C.

Serum (50 μl) was deproteinized by adding 10% (w/v) sodium tungstate solution (100 μl) and 0.06 M sulphuric acid (100 μl). The mixture was filtered through an ultrafiltration membrane (Advantec Q0100, nominal molecular weight cut-off 10 000) and the filtrate (30 μl) was injected into the carrier stream (water). The time taken to prepare the sample solution was about 3 min.

The present method was compared with liquid chromatography (amino acid analyser, Kyowa Seimitsu K-201; column, TSKgel SCX, 150 × 6.0 mm i.d.; mobile phase, citrate buffer; solvent gradient, post-column derivatization with ninhydrin).

3. Results and discussion

3.1. Reactor performance

The effect of pH on the activity of the reactor was studied in the pH range 9.0–11.0 using glycine buffer. The optimum pH was about 10.0. The peak height in the glycine buffer was about 1.2 times that in carbonate buffer at the same pH. Borate buffer consisting of 0.2 M borax–0.1 M NaOH (pH 9.5–11.0) inhibited the enzymatic reaction completely. The temperature dependence of the reactor was investigated over the range 15–30°C. The reactor exhibited maximum activity at 20°C.

The effect of NAD^+ concentration on the activity was studied over the range 1–12 mM at the 600 μM Phe level. The response increased with increasing concentration, first rapidly and then gradually. Above 6 mM, the response was almost constant. A concentration of 8 mM NAD^+ was chosen to prevent interference of phenylpyruvate and ammonium ions, which are products of the enzymatic reaction; at this concentration, the NAD^+ concentration in the reactor is 2.7 mM.

The peak height was measured by changing the flow-rates of the glycine buffer, the NAD^+ solution and the carrier solution (water), keeping the flow-rate ratio of these solutions at 1:1:1. The peak height decreased linearly as the total flow-rate increased from 0.3 to 0.9 ml min^{-1}. The peak height at 0.3 ml min^{-1} was about 2.4 times that at 0.9 ml min^{-1}. A total flow-rate of 0.6 ml min^{-1} was selected as a compromise between sensitivity and sample throughput; at this flow-rate, the sample throughput was 25 h^{-1}.

Under the conditions of 8 mM NAD^+ at pH 10.0 and 20°C, the conversion efficiency of the reactor was 90% immediately after the preparation of the reactor. The efficiency was measured by using NADH. Under the same conditions, the response for Phe (10 μM) was not affected by the presence of 30 μM phenylpyruvate and 100μM ammonium ion. Also, no interferences was recorded with 1 mM L-ascorbic acid, 2 mM uric acid and 50 mM glucose.

Amino acids normally found in proteins, other than Phe, did not give any response.

The operational stability of the reactor was evaluated over 4 weeks. The reactor was used for analyses of 50 samples (20 μM Phe) for 2 h per day and then washed with 10% (v/v) glycerol in 0.1 M phosphate buffer (pH 10.0) and stored 4°C when not in used. The decrease in activity obeyed first-order kinetics. The kinetic constant was 2.9×10^{-2} day^{-1}; the half-life period of the reactor was 23 days.

3.2. Calibration

The calibration graph of peak height against Phe concentration was linear over the range 0.9–600 μM with a correlation coefficient of 0.999 (12 data points) under the same conditions as described in section 2.3; since the serum sample was diluted five fold, this method can be applied to the assay of samples containing 5 μM–3 mM Phe. Below a concentration of 0.9 μM a concave graph was obtained and above a concentration of 600 μM the graph was convex. The relative standard deviation (RSD) for seven replicate injections of 10.0 μM Phe was 0.65% with a reactor having a conversion efficiency of 88%. By the use of a reactor having a conversion efficiency of 50%, the RSD for the same runs was 1.3%. To obtain precise results, the reactor must be used within a

Table 1
Recovery of phenylalanine added to pooled serum[a]

Added (μM)	Recovered (μM)[b]	Recovery (%)
5.00	4.87	97
10.0	10.3	103
50.0	49.0	98
100	101	101
500	500	100
1000	998	100
2500	2520	101

[a] Values corrected for Phe (63.6 μM) already present in serum.
[b] All values are means ($n = 5$).

coversion efficiency of 50%. The limit of detection (signal-to-noise ratio = 3) with a reactor having a conversion efficiency of 80% was 0.3 μM (2 ng in a 30 μl injection) with RSD 5.6%.

3.3. Application

This method was applied to the determination of Phe in serum.

Pooled human serum was repeatedly analysed for 30 day with the reactor. The reactor was used for analyses of 50 samples in a day and standards were measured at 25-sample intervals, in order to correct the variation of the conversion efficiency. The reactor was renewed every 10 days (about 500 injections) because more precise results were obtained. The method gave satisfactorily precise and reproducible results; for serum containing 62.7 μM Phe, the within-day RSD was 0.88% and the day-to-day RSD was 1.2%.

Serum of known Phe concentration was supplemented with Phe to give final concentrations of 0.073–2.50 mM. The recoveries were in the range range 97–103%, as shown in Table 1.

The results ($n = 21$, from 51 to 849 μM) were compared with those obtained by liquid chromatrography. The calculated linear regression and correlation coefficient were $y = 0.997x + 1.58$ and $r = 0.998$, respecively.

4. Conclusion

The flow-injection system with immobilized PheDH reactor and fluorescence detection is useful for the sensitive and reliable measurement of Phe and can easily be used for the analysis of serum. The PheDH immobilized on polymer beads is stable enough to permit the measurement of more than 500 samples.

References

[1] T. Ohshima, H. Sugimoto and K. Soda, Anal. Lett., 21 (1988) 2205.
[2] W. Hummel, H. Schutte and M.-R. Kula, Anal. Biochem., 170 (1988) 397.
[3] U. Wendel, W. Hummel and U. Langenbeck, Anal. Biochem., 180 (1989) 91.
[4] U. Wendel, M. Koppelkamm, W. Hummel, J. Sander and U. Langenbeck, Clin. Chim. Acta, 192 (1990) 165.
[5] H. Naruse, Y.Y. Ohshi, A. Tsuji, M. Maeda, K. Nakamura, T. Fujii, A. Yamaguchi, M. Matsumoto and M. Shibata, Screening, 1 (1992) 63.
[6] K.C. Dooley, Clin. Biochem., 25 (1992) 271.
[7] M.A. Vilaseca, C. Farre and F. Ramon, Clin. Chem., 39 (1993) 129.
[8] R. Taylar, I.C. Smith, S.J. Standing, Clin, Chim. Acta, 218 (1993) 207.
[9] S. Girotti, E. Ferri, S. Ghini, R. Budini, G. Carrea, R. Bovara, S. Piazzi, R. Merighi and A. Roda, Talanta, 40 (1993) 425.
[10] W. Hummel, H. Schutte, E. Schmidt, C. Wandrey and M.-R. Kula, Appl. Microbiol. Biotechnol., 26 (1987) 409.
[11] H. Misono, J. Yonezawa, S. Nagata and S. Nagasaki, J. Bacteriol. 171 (1989) 30.
[12] W. Hummel, S. Tauschensky, U. Spohn, U. Wendel and U. Langenbeck, in R.D. Schmid and F. Scheller (Eds.), Biosensors: Application in Medicine, Environmental Protection and Process Control, GBF Monographs, Vol. 13. VCH, Weinheim, 1989, p. 313.
[13] W. Hummel and U. Wendel, in R.D. Schmid (Ed.), Flow Injection Analysis (FIA) Based on Enzymes or Antibodies, GBF Monographs, Vol. 14, VCH, Weinheim, 1991, p. 135.
[14] E.P. Plueddemann, Silane Coupling Agents, Plenum Press, New York, 1982, p. 225.
[15] N. Kiba, A. Kato and M. Furusawa, Anal. Chim. Acta, 311 (1995) 71.

ELSEVIER

Talanta 44 (1997) 135

Talanta

Announcement

Fifth International Symposium on Pharmaceutical Sciences Ankara, Turkey 24–27 June 1997

Contact: Maksut Coşkun, Ankara University, Faculty of Pharmacy, 06100 Tandoğan, Ankara, Turkey
Fax: 90.312.2131081
E-mail: coskun@pharmacy.ankara.edu.tr
URL:http://www.pharmacy.ankara.edu.tr

ELSEVIER

Talanta 44 (1997) 137–150

Talanta

Review

Solubility of chelating agents and metal-containing compounds in supercritical fluid carbon dioxide

Neil G. Smart[a,b,*], Thomas Carleson[c], Timothy Kast[c], Anthony A. Clifford[d], Mark D. Burford[d], Chien M. Wai[b]

[a]*Company Research Laboratory, BNFL, Springfields Site, Preston, PR4 0XJ, UK*
[b]*Department of Chemistry, University of Idaho, Moscow, ID 83843, USA*
[c]*Department of Chemical Engineering, University of Idaho, Moscow, ID 83843, USA*
[d]*School of Chemistry, University of Leeds, Leeds, LS2 9JT, UK*

Received 16 April 1996; revised 29 May 1996; accepted 30 May 1996

Abstract

The solubility of 49 metal-containing compounds and 15 "free" ligands in supercritical fluid carbon dioxide is reviewed. Solubilities were found to range over eight orders of magnitude, with the highest value of solubility being 56 g l^{-1}. Metals complexed with fluorine substituted ligands were found to be the most soluble, and metals complexed with phenyl-substituted ligands the least soluble. A general trend for increasing solubility with increasing oxidation state is observed and this is correlated with the increased number of coordinating ligands protecting the metal center from interaction with the supercritical fluid and also due to the increased number of solvation interactions with the increased number of ligand groups.

Keywords: Carbon dioxide; Chelating agents; Metal-containing compounds; Solubility; Supercritical fluids

1. Introduction

Interest in supercritical fluids (SFs), particularly carbon dioxide as a solvent for use in extraction processes, has been driven by increased environmental legislation restricting the use of conventional solvents [1]. This has resulted in the development of both analytical and large-scale techniques for organic waste extraction from contaminated matrices [2]. Extensive data are available for the solubility of organic compounds in SF CO_2 and means of solubility prediction have been proposed [3,4]. Solubility is one key aspect to achieving quantitative extractions in a reasonable time using the minimum of extraction fluid and an extraction system which can be constructed on a practical scale.

Recently, the use of SFs modified by the addition of complexing agents has been utilized in the

* Corresponding author. Fax: (208)-885-6173.

PII S0039-9140(96)02008-5

extraction of metal ions from various solid and liquid matrices [5,6]. This was first demonstrated by Laintz et al. [7], with the extraction of Cu^{2+} via in situ chelation and extraction into SF CO_2. This has opened up a whole new area of research into the use of SFs in environmentally acceptable technology, as an analytical preconcentration technique and as an extractive system for large-scale metallurgical purification [8]. Initially, metal extraction using SFs has been considered not to be feasible owing to the charge neutralization requirements. By addition of a complexing agent to the SF phase, the charge on the metal ion can be neturalized and lipophilic groups introduced to the metal–complex system. Solubilization of the metal complexes into the SF is then possible [9]. Wide ranges of solubilities have been observed for metal complexes, the solvation of which is influenced by several parameters, including pressure and temperature of SFs, modifier effect in SF, ligand used, the identity of the metal, the oxidation state of metal and the complexant functional group [10].

In this paper, solubility data relevant to metal extraction are reviewed with a view to assessment of present data and identification of the most promising areas for future work. The major aim of this review is to ensure that currently available data in this rapidly expanding area are compiled and assessed, to allow focusing of future research efforts such that the technique can be developed to its full potential.

The data presented are split into three areas: ligand solubility, metal complex solubility and organometallic solubility. Where sufficient data are available, correlation with a solubility model is made [11]. The relevance of the available literature to the area of metal extraction using SFs is discussed. Abbreviations used for the ligand and metal complex names are given in Section 7.

2. Data correlation model

This review is correlated using a model based on the relationship between ln(solubility) and ln(density) [11]. Although limited in scope, this model does not require additional physical parameters of the solutes such as critical constants for equation of state approaches or molar volumes and solid activities as in the Hildebrand solubility parameter approach [12].

This model relates the solubility of a solute to solvent density and absolute temperature:

$$\ln S = k \ln D + C \quad (1)$$

where S = solubility of the solute (g l^{-1}), D is the density of the SF (g l^{-1}), k is a constant for the solute–solvent system and is an indication of the solvation of the solute in the SF and C is a constant which varies with temperature, is independent of density and is related to the volatility of the solute. The solvation process is therefore closely related to the vapor pressure of the solute and the intermolecular interactions between the solute and solvent. The vapor pressure of a given solute depends mainly on temperature, whereas the solvent strength of a supercritical fluid depends on the density of the fluid. Other properties such as viscosity, diffusivity and polarity can also change with temperature and pressure and may affect solubility. Therefore, a knowledge of k and C for the temperatures studied will allow the solubilities to be determined over an extended range of densities. Eq. (1) predicts a linear relationship between $\ln S$ and $\ln D$ with a slope proportional to k and intercept C.

All data presented in this review are represented as a function of g l^{-1} for both the solute concentration and SF concentration (density) unless stated otherwise.

3. Solubility of 'Free' Ligands in SF CO_2

The ligands that have been investigated in SF CO_2, β-diketones, dithiocarbamates and organophosphate systems [13–16]. The relevance of ligand solubility to metal extraction capability is obvious, in that a reasonable quantity of ligand must be solubilized to be able to access the metal ions in the various matrices.

Table 1
Solubility of triazolocrown ethers in SF CO_2 [13]

Compound	MW	P(atm)	T	D	Fluid	S
Crown 1	418.5	200	60	733	CO_2	5.43×10^{-3}
Crown 2	406.5	200	60	733	CO_2	4.06×10^{-3}
Crown 3	518.0	200	60	733	CO_2	0.223
Crown 1	418.0	200	60	772	CO_2 + 5% MeOH	0.0878
Crown 2	406.0	200	60	772	CO_2 + 5% MeOH	0.0812
Crown 3	518.0	200	60	772	CO_2 + 5% MeOH	0.673

3.1. Macrocyclic ligands

The only ligands from the macrocyclic class that have been investigated for the extraction of metals are the crown ethers [13]. The crown ethers are a class of selective ligands which form stable complexes with metal ions based primarily on the ionic radius–cavity size compatibility concept. Modification of crown structure by attaching negatively charged functional groups to the host can eliminate the need for counter ions, which are conventionally required for the transport of charged complexes into an organic phase.

Solubility data available for triazolocrown ether systems are given in Table 1. The triazolocrown systems are a group of macrocyclic compounds containing two triazolo subcyclic units, which are suitable for complexation with divalent metal ions [17]. The solubility significantly increases on modifying the CO_2 with 5% MeOH [13]. The increase in solubility for each crown ether system is one order of magnitude on going from pure CO_2 to 5% MeOH-modified CO_2. This correlated with the extraction data for Hg^{2+} and Au^{3+} from both solid (cellulose-based) and aqueous materials, where the extractions in the MeOH-modified solutions are greatly enhanced compared with pure CO_2.

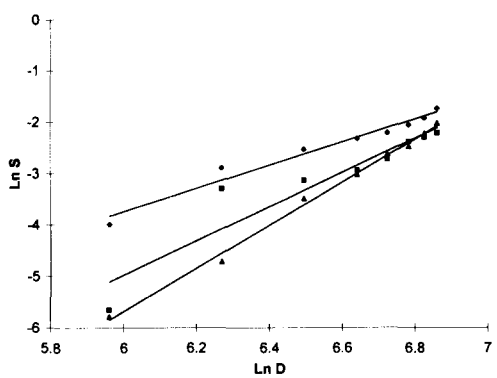

Fig. 1. Ln(solubility) of (◆) F6 crown, (■) F2 crown and (▲) H crown in SF CO_2 at 50°C as a function of ln(density).

Elsewhere the solubility of carboxylic acid substituted crown ether systems have been presented [18]. This data are illustrated in Fig. 1 and the correlation parameters obtained are shown in Table 2. At all densities, the solubility of the fluorine-substituted ligands is greater than that of the non-fluorinated ligand. Increasing the amount of fluorine substitution also increases solubility. At higher densities of CO_2, the difference between the fluorinated and non-fluorinated systems decreases.

3.2. β-Diketones

No solubility data are available for β-diketone systems in SF CO_2. The most commonly studied systems are acetylacetone (acac), trifluoroacetylacetone (tfa), hexafluoroacetylacetone (hfa) and thenoyltrifluoroacetylacetone (tta) [5,10,14,15]. Of these ligands, only tta is a solid, the others being liquids at room temperature. Under supercritical fluid extraction (SFE) conditions, all these ligands show high miscibility with CO_2. For example, substituting two CF_3 groups into the acac molecule significantly increases the acidity of the ligand by four orders of magnitude (e.g. acac $pK_a = 8.67$, hfa $pK_a = 4.46$), and this enables hfa to extract metals from much more acidic media [19]. This reduction in the basic strength of the

Table 2
Correlation parameters of ligands in SF CO_2

Compound	Fluid	T(°C)	k	C	Ref.
F6 crown	CO_2	50	2.26	−17.27	[18]
F2 crown	CO_2	50	3.34	−25.02	[18]
H crown	CO_2	50	4.20	−30.91	[18]
TOPO	CO_2	37	11.44	−72.81	[30]
TOPO	CO_2	47	8.45	−52.68	[30]
TPP	CO_2	37	6.62	−41.91	[30]
TPP	CO_2	47	7.15	−45.17	[30]
TPA	CO_2	47	9.47	−62.20	[30]
DnDA	CO_2	37	5.97	−39.93	[30]
DnDA	CO_2	47	5.59	−36.93	[30]
THA	CO_2	47	7.42	−43.90	[30]
TOA	CO_2	47	6.61	−40.54	[30]

fluorinated ligand can be advantageous as water (which is generally required in the SF process to obtain extractions) in contact with SF CO_2 is strongly acidic [13].

The β-diketone ligands are used almost exclusively in protonated forms. The β-diketones are rendered acidic by the tautomeric equilibrium established between the enol and keto forms:

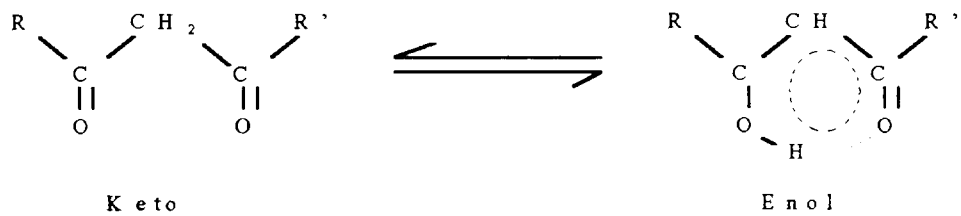

Form 1.

The fluorinated ligands have been found to be almost exclusively in the enol form under the high pressures and temperatures relevant to SFE [20]. The non-fluorinated ligand (acac) is found to be partly in each form in the SF phase [21]. The acidity of the ligand originates from the enol form and the deprotonated β-diketone involved in the metal complexation process. Elsewhere it has been shown that the presence of electron-withdrawing fluorine substituents can significantly increase ligand acidity [22].

3.3. Dithiocarbamates

The dithiocarbamates studied in SFE work are commonly used as salts (Na^+ and NH_4^+) of the ligand rather than in the acidic form [6,7]. The first work on metal extraction in SF CO_2 was demonstrated using the fluorinated ligand sodium bis(trifluoroethyl)dithiocarbamate (NaFDDC). This ligand was found to have greatly enhanced solubility compared with the non-fluorinated analogue (Table 3) in SF CO_2. For non-fluorinated dithiocarbamates, the alkylammonium salts serve as a suitable means for solubilization of the ligands for analytical extractions (Table 3) [23]. Increasing the alkyl chain length of the alkylammonium salts by two carbon units increased the solubility of the ligand by an order of magnitude.

Elsewhere, these ligands have been assessed for the extraction of toxic heavy metals using liquid CO_2 as the extraction fluid [24]. No data are available regarding ligand solubility in this medium.

3.4. Organophosphorus reagents

Organophosphorus reagents such as tributyl

Table 3
Solubility of metal dithiocarbamate complexes in SF CO_2

Compound	MW	P (atm)	T (°C)	D (g L^{-1})	Fluid	S	Ref.
$Zn[SCSN(C_4H_9)_2]_2$	474.0	237.4	55	802.4	CO_2	0.248	[23]
$Zn[SCSN(C_2H_5)_2]_2$	361.8	237.4	55	802.4	CO_2	0.0119	[23]
$Zn[SCSN(C_4H_5)]_2$	357.9	237.4	55	802.4	CO_2	0.018	[23]
NaFDDC	279.2	100	50	409.4	CO_2	0.131	[5]
NaDDC	171.1	100	50	409.4	CO_2	0.0257	[5]
$Cu(FDDC)_2$	576.0	100	50	409.4	CO_2	0.524	[5]
$Cu(DDC)_2$	360.2	100	50	409.4	CO_2	3.96×10^{-4}	[5]
$Ni(FDDC)_2$	571.2	100	50	409.4	CO_2	0.411	[5]
$Ni(DDC)_2$	355.2	100	50	409.4	CO_2	3.02×10^{-4}	[5]
$Co(FDDC)_2$	571.4	100	50	409.4	CO_2	0.503	[5]
$Co(DDC)_2$	355.5	100	50	409.4	CO_2	8.53×10^{-4}	[5]
$Bi(FDDC)_2$	721.4	150	50	705.5	CO_2	0.527	[5]
$Bi(DDC)_2$	505.5	150	50	705.5	CO_2	4.55×10^{-3}	[5]
$Hg(FDDC)_2$	713.0	150	50	705.5	CO_2	3.57	[5]
$Hg(DDC)_2$	497.1	150	50	705.5	CO_2	4.08×10^{-3}	[5]
$Hg(FDDC)_2$	713.1	150	50	770	CO_2 + 5% MeOH	8.56	[5]
$Hg(DDC)_2$	497.1	150	50	770	CO_2 + 5% MeOH	0.0149	[5]
$(C_4H_9)_4N[SCSN(C_4H_9)_2$	446.8	169.6	45	785.1	CO_2	0.0232	[23]
$(C_4H_9)_4N[SCSN(C_2H_5)_2$	390.7	169.6	45	785.1	CO_2	0.00291	[23]
$Na[SCSN(C_2H_5)_2]$	171.2	169.6	45	785.1	CO_2	0.00109	[23]
$H_4N[SCSNC_4H_8]$	164.3	169.6	45	785.1	CO_2	6.00×10^{-4}	[23]

phosphate (TBP) and phosphine oxides such as tributylphosphine oxide (TBPO), tri-*n*-octylphosphine oxide (TOPO) and triphenylphosphine oxide (TPPO) have long been established for use as extractive ligands for actinide elements [25]. Recently, these compounds have been used in an SF environment for the extraction of U and Th from solid and liquid matrices [26]. Such reagents have found great technological importance within the nuclear industry; in particular, TBP is extensively used in the extraction and separation of U and Pu in the Purex process [27].

TBP is a viscous liquid at room temperature. The phase behavior of TBP in SF CO_2 has been described in detail by Page et al. [28] and this is shown in Table 4. Elsewhere 2% TBP-modified CO_2 has been shown to have a large influence on organic compound solubilities in the SF phase, as reported by Lemert and Johnson et al. [29].

The solubility of triphenyl phosphate (TPP) has been measured by Schmitt et al. [30]. These data are illustrated in Fig. 2, using the correlation method described earlier, and the constants k and C generated are given in Table 2. Temperature had no significant effect on the solubility of TPP at constant density between 37 and 47°C. The solubilities of different phosphine oxides have been measured by both Schmitt and Reid [30] and Lin et al. [26]. The TOPO ligand shows solubilities approximately one order of magntiude higher than those of the TPP ligand. High solubilities have been observed for TOPO and TBPO as shown in Table 5. A much lower solubility is observed for the phenyl-substituted phosphine oxide TPPO. This correlates with the qualitative observation that aromatic substituent groups such as phenyl have a negative effect on the SF solubility of organic compounds [31].

3.5. Amines

Although no SFE data are available for the extraction of metals using amines as extractants,

Table 4
P–T–χ surface for vapor–liquid separation of TBP–CO_2 [28]

2.3 mol %		3.8 mol %		5.6 mol %		11.0 mol %		15.5 mol %	
T(°C)	P (atm)	T(°C)	P (atm)	T(°C)	P (atm)	T(°C)	P (atm)	T(°C)	P (atm)
40.2	84.6	25.5	65.1	39.2	84.2	44.1	85.6	49.0	93.3
42.2	86.7	36.3	83.8	50.0	112.7	59.8	118.1	61.7	116.3
47.1	98.4	47.0	110.5	63.7	141.4	75.4	156.4	75.4	145.4
60.7	128.6	51.0	117.4	74.4	171.2	86.2	177.6	84.2	159.1
70.5	145.3	54.9	133.9	87.2	193.6	105.7	209.7	102.8	190.3
86.2	173.1	55.8	135.9	88.1	196.0	126.3	240.4	114.5	210.9
102.8	197.7	71.5	168.0	103.8	216.1	135.1	252.2	128.2	234.4
116.5	213.7	72.5	169.9	115.5	234.2	153.7	275.1	150.7	262.8
128.2	224.2	73.5	171.8	125.3	249.8				
129.2	224.8	87.2	196.9	136.1	260.5				
143.9	231.0	103.8	222.6	137.0	262.8				
144.9	232.2	127.3	256.1	146.8	269.6				
		142.9	258.6						
		162.4	270.1						

they are known to extract metals under conventional solvent extraction conditions [32]. Limited solubility data are available for amines from the work of Schmitt and Reid [30] and this is shown in Fig. 2. The amines investigated in this study included triphenylamine (TPA), di-*n*-dodecylamine (DnDA), trihexylamine (THA) and trioctylamine (TOA). The correlation coefficients k and C are given on Table 2. Trihexylamine is the most suitable, forming a completely miscible phase with CO_2 at approximately 150 bar. Similarly to the case of the phosphine oxides, the phenyl-subsituted ligands show the lowest SF solubility from the amine range of compounds, for which data are available.

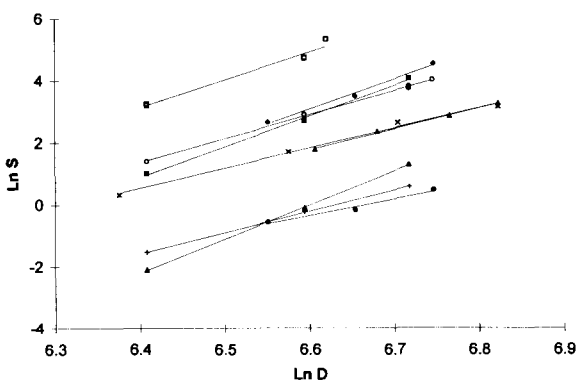

Fig. 2. Ln (solubility) of organic ligands in SF CO_2 as a function of ln(density): (◆) TOPO, 37°C; (■) TOPO, 47°C; (▲) TPP, 37°C; (×) TPP, 47°C; (△) TPA, 47°C; (●) DnDA, 37°C; (+) DnDA, 47°C; (□) THA, 47°C; (○) TOA, 47°C.

3.6. Other extractive reagents

Yazdi and Beckman [33] have measured the solubilities of a range of fluorinated polymeric ethers with picolylamine, bis(picolylamine), dithiol and dithiocarbamate functionalities. The molecular weights of these compounds were between 2500 and 7500. Although very high solubilities of the ligands are observed in weight per cent terms (ca. 5%), the solubilities in terms of molar concentration are very low.

3.7. Prediction techniques for ligand solubilities

Harrington et al. [34] have recently shown that the solubility of many organic compounds

Table 5
Solubilities of phosphates and phosphine oxides in SF CO_2 (26)

Compound	MW*P*	*T* (atm)	Density (°C)	*S* (g l^{-1})	(g l^{-1})
TBPO	218	200	60	0.7318	184.9
TOPO	387	150	40	0.7878	20.18
TOPO	387	200	45	0.8211	25.35
TPPO	278	200	60	0.7318	2.127

can be estimated to within 30% accuracy using an equation of state approach. Critical to this approach is the determination of the van de Waals interaction parameter k_{12}. This parameter describes the forces involved in the interaction between solute and solvent. The k_{12} parameter is usually determined by correlation of experimentally determined solubility values with the Peng–Robinson equation of state. Once the k_{12} value is known, then solubilities at a range of conditions can be estimated. Harrington et al. [34] demonstrated that the k_{12} parameter can be predicted via a group contribution approach. Here the various contributions of individual functional groups to the k_{12} parameter are assumed to be additive. The functional groups for which sufficient data are available to make reaslistic predictions are given in Table 6. This approach gives a fast method to assess the likely solubility of ligands for which no experimental solubility data are available.

Table 6
Functional groups for which group contribution methods can be applied for solubility prediction in SFs using the method presented by Harrington et al. [34]

Functional group	Ring or arm
CH =	Ring
$-CH_2-$	Ring
= C <	Ring
CH_3	Arm
–CH<	Arm
–OH	Arm
COOH	Arm
>CO	Ring
>C<	Arm
$-CH_2$	Arm
=N	Ring
–NH–	Arm
NH_2	Arm
N<	Arm
S	Arm
Cl	Arm

4. Solubility of metal complexes in SF CO_2

The metal complexes that have been studied in terms of solubility in SF CO_2 cover a range of systems including most of the ligand types given above. Unfortunately few systematic investigations have been carried out, thus limiting the ability to model such data. The correlation procedures discussed above are utilized where possible.

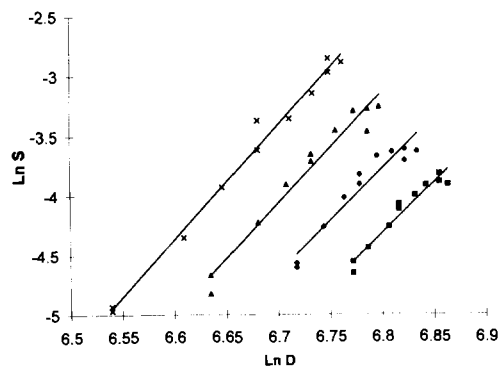

Fig. 3. Ln (solubility) of [({5,7,12,14-tetramethyl}-2,3:9,10-dibenzo[*b,i*]tetraazocyclotetradecine)nickel(II)] in SF CO_2 + 10% (v/v) methanol as a function of ln(density): (■) 40°C; (◆) 50°C; (▲) 60°C; (×) 70°C.

Table 7
Correlation parameters for metal complexes in SF CO_2

Compound	Fluid	T (°C)	k	C	Ref.
Ni cyclam	CO_2 + 10% MeOH	40	8.49	−62.06	[35]
Ni cyclam	CO_2 + 10% MeOH	50	8.67	−62.72	[35]
Ni cyclam	CO_2 + 10% MeOH	60	9.27	−66.16	[35]
Ni cyclam	CO_2 + 10% MeOH	70	9.59	−67.68	[35]
Ferrocene	CO_2	40	4.42	−27.63	[35]
Ferrocene	CO_2	50	3.87	−23.63	[35]
Ferrocene	CO_2	60	3.81	−22.96	[35]
Ferrocene	CO_2	70	3.82	−22.67	[35]
$Cu(acac)_2$	CO_2	150	4.53	−28.33	[38]
$Cu(acac)_2$	CO_2	170	3.71	−22.55	[38]
$Y(acac)_3$	CO_2	150	1.96	−13.91	[38]
$Y(acac)_3$	CO_2	170	3.53	−23.08	[38]
$Y(hfa)_3$	CO_2	150	1.35	−6.25	[38]
$Y(hfa)_3$	CO_2	170	2.34	−12.20	[38]
$Ba(hfa)_2$	CO_2	150	2.61	−15.16	[38]
$Ba(hfa)_2$	CO_2	170	4.71	−27.55	[38]
$Cu(acac)_2$	CO_2	40	4.15	−30.40	[40]
$Cu(bzac)_2$	CO_2	40	6.03	−43.67	[40]
$Cu(tfbzm)_2$	CO_2	40	9.77	−67.54	[40]
$Cu(dmhd)_2$	CO_2	40	11.44	−77.07	[40]
$Cu(dibm)_2$	CO_2	40	7.23	−47.45	[40]
$Cu(thd)_2$	CO_2	40	7.80	−51.20	[40]
$Cu(tod)_2$	CO_2	40	7.59	−48.85	[40]
$Cu(hfa)_2 \cdot H_2O$	CO_2	40	3.59	−21.02	[40]
$Cu(hfa)_2$	CO_2	40	3.56	−20.36	[40]
$Cu(tfa)_2$	CO_2	40	3.15	−20.06	[40]
Li(acac)	CO_2	60	0.82	−16.47	[39]
$Co(acac)_2\ H_2O$	CO_2	60	2.50	−25.74	[39]
$Cu(acac)_2$	CO_2	60	2.65	−26.50	[39]
$Mn(acac)_2\ 2H_2O$	CO_2	60	1.20	−16.31	[39]
$Co(acac)_3$	CO_2	60	2.18	−22.03	[39]
$Mn(acac)_3$	CO_2	60	2.27	−22.23	[39]
$Zn(acac)_2$	CO_2	60	2.58	−23.77	[39]
$In(acac)_3$	CO_2	60	3.83	−31.82	[39]
$Ga(acac)_2$	CO_2	60	3.81	−31.08	[39]
$Cr(acac)_3$	CO_2	40	7.55	−51.24	[40]
$Cr(acacBr)_3$	CO_2	40	4.72	−33.76	[40]
$Cr(thd)_3$	CO_2	40	2.24	−11.05	[40]
trans–$Cr(tfa)_3$	CO_2	40	2.78	−15.67	[40]
cis–$Cr(tfa)_3$	CO_2	40	3.93	−23.92	[40]
$Cu(FDDC)_2$	CO_2	50	1.36	−8.76	[7]

4.1. Macrocyclic systems

The solubilities of metal crown ether systems have not yet been investigated, probably owing to the nature of the complexes that are formed, usually ion pairs which are difficult to obtain in a purified crystal form.

Cowey et al. [35] have reported the solubility of a nickel cyclam complex, [({5,7,12,14-tetra-methyl} -2,3:9, 10-dibenzo[*b,i*]tetraazocyclotetradecine)-nickel (II)] (referred to subsequently as Ni cylam in this paper), in SF CO_2 modified with 10% (N/N) methanol. Ni cyclam had very poor solubility in pure CO_2 such that it could not be

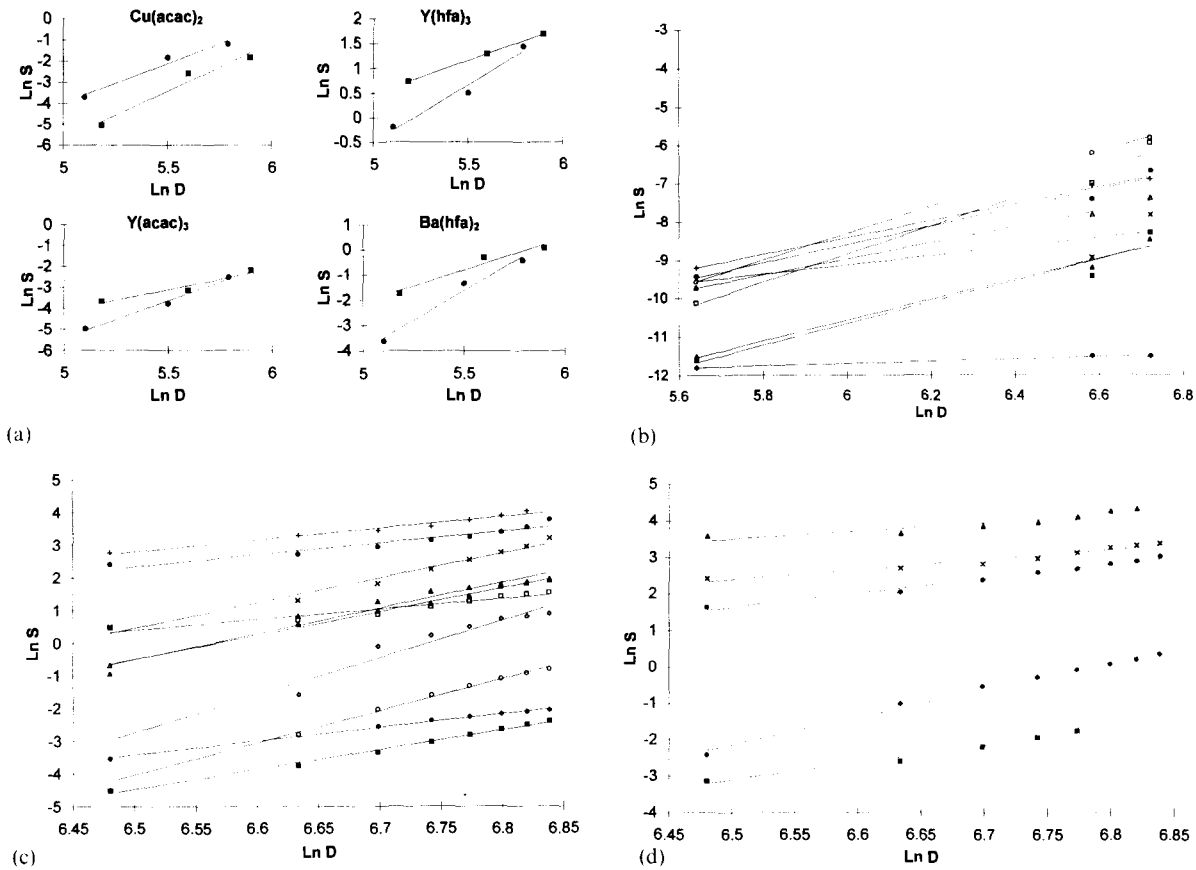

Fig. 4. Ln(solubility) of metal β-diketone complexes in SF CO_2 as a function of ln(density). (a) (i) $Cu(acac)_2$, (■) 150°C, (●) 170°C; (ii) $Y(hfa)_3$, (■) 150°C, (●) 170°C; (iii) $Y(acac)_3$, (■) 150°C, (●) 170°C; (iv) $Ba(hfa)_2$, (■) 150°C, (●) 170°C.
(b) All 60°C: (○) $Ga(acac)_2$; (□) $In(acac)_2$; (+) $Zn(acac)_2$; (●) $Mn(acac)_3$; (△) $Co(acac)_3$; (×) $Mn(acac)_2{\cdot}2H_2O$; (▲) $Cu(acac)_2$; (■) $Co(acac)_2{\cdot}2H_2O$; (◆) Li(acac).
(c) All 40°C: (◆) $Cu(acac)_2$; (■) $Cu(bzac)_2$; (▲) $Cu(thd)_2$; (×) $Cu(tod)_2$; (□) $Cu(tfa)_2$; (●) $Cu(hfa)_2 \cdot H_2O$; (+) $Cu(hfa)_2$; (○) $Cu(dmhd)_2$; (△) $Cu(dibm)_2$; (◌) $Cu(tfbzm)_2$.
(d) All 40°C: (◆) $Cr(acac)_3$; (■) $Cr(acacBr)_3$; (▲) $Cr(thd)_3$; (×) *trans* $Cr(tfa)_3$; (●) *cis* $Cr(tfa)_3$.

quantified by the technique used by these workers. The Ni cyclam complex is a nearly planar system and the effect of adding methanol as a modifier was interpreted as involving the formation of an octahedral MXL_2 system with the methanol solvating the two *trans* sites of the complex and reducing the polarity. The actual solubility of the nickel cyclam complex is still low, however, as shown in Fig. 3. For a given density of SF, it was observed that the solubility increased significantly with increase in temperature. The correlation constants are shown in Table 7. In the case of Ni cyclam, a range of data at differing temperatures and densities are available. The highest solubilities were observed at the highest temperatures and pressures studied, which indicates that the solubility of the Ni cyclam complex is significantly influenced by the complex volatility, even at temperatures as low as 70°C. It is observed that the effect of increasing density on the solubility of the Ni cyclam complex is almost independent of the temperature, i.e. as the temperature increases, the relative changes in solubility are equivalent for a given SF density change.

Brauer et al. [36] have studied the solubility of a range of fluorinated metal porphyrin complexes. The solubility of these complexes is low, but they do show measurable solubility in pure CO_2. Al-

though the above systems are of interest for extraction, the main interest in SF solubility has been the possibility of using these as catalytic systems [37]. Hence, in such cases, low solubility may not be critical as in the area of extraction.

4.2. Metal β-diketone systems

Three major systematic studies of the solubility of metal β-diketone complexes in SF CO_2, have been carried out [38–40]. The metal β-diketone systems are by far the most extensively studied system for solubility in SF CO_2. The various correlation parameters for the β-diketone complexes are given in Table 7.

Hamdi et al. [38] have studied the solubilities of a range of different metal acetylacetone and metal hexafluoroacetylacetone complexes in SF CO_2. The data obtained are shown in Fig. 4(a). The solubilities of the acetylacetone were determined at high temperatures (150–170°C) in this study. At such temperatures, the density of CO_2 is low (e.g. 160–360 g l^{-1}) and the major contributing factor to the solubility is likely to be the metal complex volatility. It is therefore surprising that for the hexafluoroacetylacetone complexes it is observed that solubility decreases with increasing temperature, indicating a decrease in solvating effects even at temperatures as high as 150–170°C. The effect of fluorination of the complex on solubility can be observed from the data presented for the yttrium system. With fluorination of the methyl groups of the acetylacetone ligand, increases in solubility of between three and four orders of magnitude are observed.

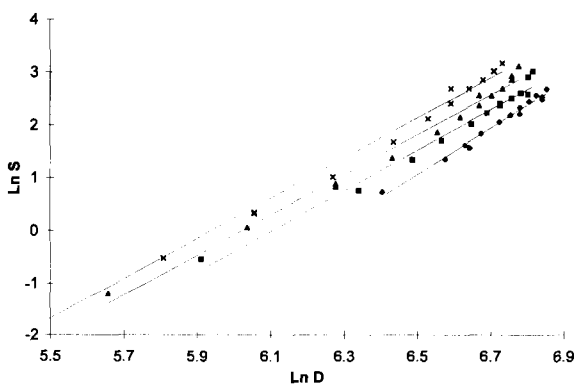

Fig. 5. Ln(solubility) of ferrocene in SF CO_2 as a function of ln(density): (◆) 40°C; (■) 50°C; (▲) 60°C; (×) 70°C.

Saito et al. [39] have studied acetylacetone complexes of different metals at temperatures lower than those of Hamdi et al. [38] (60°C compared with 150°C) and these data are shown in Fig. 4(b). At these milder temperatures, the solubility of the metal complexes is much lower than those observed at >150°C. The poorest solubility was observed for the Li complex, which can be interpreted in terms of the inability of the single acac ligand to shield the ionic Li center from the SF CO_2. The highest solubility was observed for In and Ga, which can be correlated with their behavior, lying between metallic and non-metallic systems. For elements which exist in the oxidation states 2+ and 3+ (Mn and Co), it was observed that the higher oxidation state complex shows an enhanced solubility. This can be correlated with a more complete shielding of the 3+ metal ion center with a greater number of ligands so that the solvation of the resulting complex is enhanced owing to the increase in solute–solvent interactions between the SF CO_2 and the complex.

Lagalante et al. [40] have studied the solubility of copper and chromium β-diketone systems, with nine different ligand types being studied. The data obtained are illustrated in Fig. 4(c) and (d). In this work, a direct correlation was observed between the metal complex solubility and the Hildebrand solubility parameter of the uncomplex ligand. This illustrates that for a given metal system, the nature of the ligand side-chains influences the solubility of the metal complex in accordance with 'regular' solution theory. Lagalante et al. [40] observed that the fluorinated ligand systems showed the highest solubility, with the hexafluoroacetylacetone complexes having the highest values. The lowest solubility was observed for the benzyl-substituted β-diketone sysem, correlating with the general observation for organic compounds where aromatic substituted systems showed the lowest solubilities. Similar trends were observed for the Cr β-diketone complexes to those for the Cu β-diketone complexes in terms of the effects of different ligand substituents on the

solubility. The high solubility of $Cu(hfa)_2$ complexes correlates with vapor pressure data for the Cu β-diketone complexes, where the $Cu(hfa)_2$ has a vapor pressure an order of magnitude greater than that of the non-fluorinated $Cu(acac)_2$ complex [41].

However, in all cases where the same ligand was used for Cu and Cr, the Cr complexes showed higher solubilities [40]. This may be due to the greater protection of the metal ion center from the SF CO_2 and to the enhanced solvation effects for the 'extra' ligand, as discussed previously. Molecular weight does not seem to influence the solubility of the metal complexes, since although that of Cr (52.0) is slightly lower than Cu (63.6), the requirement of Cr for three ligands to satisfy valency requirements, compared with two ligands for Cu, means that the overall complex molecular weight is always higher for the Cr system.

One interesting complex is hexafluoroacetylacetonecopper(I)trimethylphosphine ($hfaCuPme_3$), which shows SF CO_2 solubilities of the order of 0.1 M [42]. This complex is of interest in metal deposition technology, forming copper films upon spraying from an SF on to a hot surface via a disproportional reaction of the Cu(I) complex [43].

4.3. Metal dithiocarbamates

A range of metal dithiocarbamate metal complex solubilities have been investigated. Laintz et al. [7] showed that fluorination of the end methyl groups of diethyldithiocarbamate ligands resulted in greatly enhanced solubilities of the metal complexed systems in SF CO_2. This is illustrated in Table 3. Solubility enhancement in the range of 300-fold were observed for the fluorinated complexes. The lowest enhancements in solubility were observed for the sodium complexes, indicating that in this system, it is the interaction between the sodium ion and the SF that strongly influences the solubility value. The effect of methanol modification of the SF is illustrated for the Hg–dithiocarbamate complexes, where modification with 5% methanol increases the observed solubility by nearly one order of magnitude [16]. Laintz et al. [7] have studied the solubility of $Cu(FDDC)_2$ complexes in SF CO_2 at various densities. The correlation parameters are shown in Table 7. The solubility is observed to increase significantly with increase in density.

Wang and Marshall [23] studied dithiocarbamate complexes with various hydrocarbon tail groups, observing the highest solubility for butyl-substituted ligands. The solubilities of the butyl-substituted dithiocarbamates approach those of the fluorinated systems, but are still slightly lower.

4.4. Organophosphorus reagents

No data have been reported for the solubility of metal organophosphorus complexes in CO_2. Similarly to the crown ethers, metal organophosphorus complexes involve ion-pair extraction via a coordination complex. Such systems are difficult to obtain as purified crystal systems.

5. Organometallic systems

5.1. Ferrocene

Only one organometallic compound, ferrocene, has been extensively studied with regard to solubility in SF CO_2 [34]. Ferrocene shows high solubility, as illustrated in Fig. 5. The effect of increasing density on solubility is almost independent of temperature. The high solubility of ferrocene was interpreted as being due to the nature of the bonding in the ferrocene compound. Ferrocene is a system in which the metal 3d, p and s orbitals are filled such that no free coordination sites are available for interaction with the solvating CO_2, resulting in ferrocene having properties resembling those of an aromatic compound.

5.2. Other organometallics

The catalytically active compound $RuCl_2[P(CH_3)_3]$ has been shown to be soluble in SF CO_2, but only qualitative measurements have been carried out [44]. A number of studies of the behavior of organometallic systems in SF CO_2 have been carried out, with particular reference to reactivity

and catalysis [45,46]. These studies indicate that a wide range of organometallic systems show high SF solubility, although rarely is a direct measurement of this parameter made.

A wide range of toxic environmental contaminants have been shown to be soluble in SF CO_2, as evidenced by determination by SF chromatography or by extraction using SF CO_2 [5,8,13,16].

6. Relevance to metal extraction

From the data presented above, it can be seen that, in general, many ligands show relatively high SF CO_2 solubilities or are completely miscible [30]. Even ligands containing fairly polar functional groups, such as amines, show high SF solubilities, such that their potential as an extractive reagent is not likely to be limited by solubility. In general, it appears that the most favorable configuration for high SF solubility is a fluorine-substituted ligand system [5,7,15]. For analytical applications, the fluoroine-substituted systems are clearly the most suitable. However, the high costs of fluorine-substituted ligands will probably limit their use to the analytical scale. For hydrocarbon-based ligands, aliphatic substituted systems show high solubilities approaching those of the fluorine-substituted systems and these may have potential for larger scale application [23]. Phenyl-substituted ligands showed the lowest solubilities and are not likely to find many SF applications [26,30].

In parallel with the 'free' ligands, metal complexed systems show the highest solubility for fluorine-substituted systems, then aliphatic substituted systems and the lowest for phenyl-substituted systems [40].

The maximum metal complex solubilities observed in an SF CO_2 system are in the range 30–60 g l^{-1} for both non-fluorinated and fluorinated systems [35,40]. This is equivalent to dissolution of between 5 and 10 g l^{-1} of metal into the SF system. For analytical purposes, it is unlikely that this level of metal ion loading of the SF would be required; however, for larger scale applications this may limit some processes.

The fluorinated complexes show the highest solubilities [40]. In general, increasing ligand hydrocarbon tail lengths increase the solubility [40]. Also, a general trend exists for trivalent complexes to be more soluble than divalent complexes, which in turn are more soluble than monovalent complexes [39].

The use of both β-diketones and dithiocarbamates as extractive reagents is of great interest, since for natural aqueous samples these ligands are effective in the pH range 2–5 [32]. SF CO_2 has recently been shown to establish a pH in aqueous systems of approximately 2.9, via the formation of a carbonic acid solution [47]. Hence the pH of unbuffered aqueous systems will approach closely that favored for efficient extraction.

The organophosphorus reagents have been found to be effective for extractions from acidic media such as concentrated nitric acid solution [26]. This is particularly relevant to the nuclear industry, where these reagents are used in the purification of actinide elements. Unfortunately, no data are available for the solubility of these metal complex systems in SF CO_2, since reasonable solvent loading of the SF phase will be essential to achieving industrial-scale extractions. Experimental data in this area would thus be of great interest.

From Tables 2 and 7 it is observed that, in many cases, the values of k are lower for the fluorinated than aliphatic substituted systems. This indicates that the solvation effects are lower for the fluorinated systems. Consequently, at higher SF pressures, the enhanced solubility of fluorine-substituted systems may not be significant.

7. Abbreviations used

Crown 1	dicyclohexane bis(triazolo)-crown ether
Crown 2	dibenzo bis(triazolo)-crown ether
Crown 3	bis(*t*-butylbenzo)bis(triazolo)-crown ether
F6 crown	*sym*-bis(3-fluorobenzo)-16-crown-5-oxyacetic acid

F2 crown	*sym*-[3,5-bis(trifluoromethyl)phenyl] dibenzo-16-crown-5-oxyacetic acid
H crown	*sym* dibenzo-16-crown-5-oxyacetic acid
acac	pentane-2, 4-dione
tfa	1,1,1-trifluoropentane-2, 4-dione
hfa	1,1,1,6,6,6-hexafluoropentane-2, 4-dione
tta	1-thienyl-4,4,4-trifluoropentane-1, 3-dione
FDDC	bis(trifluoro)diethyldithiocarbamate
TBP	tributyl phosphate
TBPO	tributyl phosphine oxide
TOPO	tri-*n*-octylphosphine oxide
TPPO	triphenylphosphine oxide
TPP	triphenyl phosphate
TPA	triphenyl amine
DnDA	di-*n*-dodecylamine
THA	trihexylamine
TOA	trioctylamine
Ni cylam	[({5,7,12,14-tetra methyl}-2,3:9,10-dibenzo[*i*,*i*]tetraazocycloetetradecine)
bzac	1-phenylpentane-1, 3-dione
thd	2,2,6,6,-tetramethylheptane-3, 5-dione
tod	2,2,7-trimethyloctane-3, 5-dione
dmhd	1,1-dimethylhexane-3,5-dione
dibm	2,6-dimethylheptane-3,5-dione
tfbzm	1,1,1-trifluoro-4-phenylbutane-2,4-dione
acacBr	3-bromopentane-2,4-dione
PMe_3	trimethylphosphine
DDC	bis(diethyl)dithiocarbamate

Acknowledgements

The authors gratefully acknowledge the financial support of BNFL, EPSRC, NATO travel grant and the INEL University Research Consortium.

References

[1] C. Phelps, N.G. Smart and C.M. Wai, J. Chem. Educ., in press.
[2] K.M. Dooley, C.C. Koa, R.P. Gambrell and F.C. Knopf, Ind. Eng. Chem. Res., 26 (1987) 2058; S.J. MacNaughton and N.R. Foster, Ind. Eng. Chem. Res., 33 (1994) 2757; B.O. Brady, C.C. Koa, K.M. Dooley, F.C. Knopf and R.P. Gambrell, 26 (1987) 261.
[3] K.D. Bartle, A.A. Clifford, S.A. Jafar and G.F. Shilstone, J. Phys. Chem. Ref. Data, 20 (1991) 713.
[4] K.P. Johnston, D.G. Peck and S. Kim, Ind. Eng. Chem. Res., 28 (1989) 1115.
[5] Y. Lin, N.G. Smart and C.M. Wai, Trends Anal. Chem., 14 (1995) 123.
[6] K.E. Laintz, J.J. Yu and C.M. Wai, Anal. Chem., 64 (1992) 311.
[7] K.E. Laintz, C.M. Wai, C.R. Yonker and R.D. Smith, Anal. Chem., 64 (1992) 2875.
[8] F. Dehghani, F.P. Lucien, N.J. Cotton, T. Wells and N.R. Foster, Proc. 3rd Int. Symp. on Supercritical Fluids, 17–19 October 1994, Strasbourg, Vol. 2, p. 35; K.E. Laintz and E. Tachikawa, Anal. Chem., 66 (1994) 2190; J. Wang and W.D. Marshall, Anal. Chem., 66 (1994) 3900; Y. Liu, V. Lopez-Avila, M. Alcaraz and W.F. Beckert, J. High. Resolut. Chromatogr., 17 (1994) 527; J.W. Oudsema and C.F. Poole, J. High Resolut. Chromatogr., 16 (1993) 198; B.N. Hansen, B.M. Hybertson, R.M. Barkley and R.E. Sievers, Chem. Mater., 4 (1992) 749; M. Johansson, T. Berglof, D.C. Baxter and W. French, Analyst, 120 (1995) 755; Y. Liu, V. Lopez-Avila, M. Alcaraz and W.F. Beckert, J. High. Resolut. Chromatogr., 16 (1993) 106; J. Wang and W.D. Marshall, Analyst, 120 (1995) 623.
[9] K.E. Laintz, C.M. Wai, C.R. Yonker and R.D. Smith, J. Supercrit. Fluids, 4 (1991) 194.
[10] N.G. Smart, Y. Lin and C.M. Wai, Environ. Lab. Chem., February (1996) 26.
[11] Y.V. Tsekhanskaya, M.B. Iomtev and E.V. Mushkina, Zh. Fiz. Khim., 38 (1964) 2166; J. Chrastil, J. Phys. Chem., 86 (1982) 3016.
[12] J.F. Brennecke and C.A. Eckert, AIChE J., 35 (1989) 1409.
[13] S. Wang, S. Elshani and C.M. Wai, Anal. Chem., 67 (1995) 919.
[14] Y. Lin, R.D. Brauer, K.E. Laintz and C.M. Wai, Anal. Chem., 65 (1993) 2549.
[15] Y. Lin, C.M. Wai, F.M. Jean and R.D. Brauer, Environ. Sci. Technol., 28 (1994) 1190.
[16] C.M. Wai, Y. Lin, R.D. Brauer, S. Wang and W.F. Beckert, Talanta, 40 (1993) 1325.
[17] S. Elshani, P.M. Apgan, S.F. Wang and C.M. Wai, J. Heterocycl. Chem., 31 (1994) 1271.
[18] K. Laintz and C.M. Wai, US Pat. 5 356 538, (1994).
[19] J. Noro and T. Sekine, Bull. Chem. Soc. Jpn., 66 (1993) 1647.
[20] C. Phelps, C.M. Wai, C.R. Yonker and S.P. Wallen, J. Phys. Chem., submitted for publication.
[21] Y. Yagi, S. Saito and H. Inomata, J. Chem. Eng. Jpn., 26 (1993) 116.
[22] R.N. Haszeldine, W.K.R. Musgrave, F. Smith and L.M. Turton, J. Chem. Soc., (1951) 609.
[23] J. Wang and W.D. Marshalol, Anal. Chem., 66 (1994) 1658.

[24] A. Lakhani, M. Landrigan and A. Schultheis, US Pat. Appl. 5 087 370, (1992).
[25] S. Ahrland, in J.J. Katz, G.T. Seaborg and L.R. Moss (Eds.), The Chemistry of the Actinide Elements, Vol. 2, Chapman and Hall, London, 1986, p 1521.
[26] Y. Lin, N.G. Smart and C.M. Wai, Environ. Sci. Technol. 29 (1995) 2706.
[27] K. Alcock, G.F. Best, E. Hesford and H.A.C. McKay, J. Inorg. Nucl. Chem., 6 (1958) 328.; J.R. Ferraro, J. Inorg. Nucl. Chem., 10 (1959) 319; R.A. Zingaro and J.C. White, J. Inorg. Nucl. Chem., 12 (1960) 315; A. Aln, M. Miloud, A.E. Hossadi and M. Khaliguzzaman, J. Radioanal. Nucl. Chem., 116 (1987) 271.
[28] S.H. Page, S.R. Sumpter, S.R. Goats and M.L. Lee, J. Supercrit. Fluids, 6 (1993) 95.
[29] R.M. Lemert and K.P. Johnston, Ind. Eng. Chem. Res., 30 (1991) 1222.
[30] W.J. Schmitt and R.C. Reid, Chem. Eng. Commun., 64 (1988) 155.
[31] M.D. Luque de Castro, M. Valcarcel and M.T. Tena, in Analytical Supercritical Fluid Extraction, Springer, New York, 1994, p. 101.
[32] S. Ahrland, J.O. Liljenzin and J. Rydberg, in J.C. Bailar, H.J. Emeleus, R. Nyholm and A.F. Trotman-Dickenson (Eds.) Comprehensive Inorganic Chemistry, Vol. 5, Pergamon Press, Oxford, 1973 p. 547.
[33] A. Yazdi and E.J. Beckman, Proc. 3rd Int. Symp. on Supercritical Fluids, 17–19 October 1994, Strasbourg, Vol. 2, p. 283.
[34] J.D. Harrington, H. Jiang, T.E. Carlson and C.M. Wai, J. Supercrit. Fluids, submitted for publication.
[35] C.M. Cowey, K.D. Bartle, M.D. Busford, A.A. Clifford, S. Zhu, N.G. Smart and N.D. Tinker, J. Chem. Eng. Data, 40 (1995) 1217.
[36] R. Brauer, S. Elshani and C.M. Wai, unpublished results, 1996.
[37] T.G. Traylor, K.W. Hill, W. Fann, S. Tsuchiya and B.E. Dunlap, J. Am. Chem. Soc., 114 (1992) 1308; T.G. Traylor, S. Tsuchrya, Y. Byun and C. Kim, J. Am. Chem. Soc., 115 (1993) 2775.
[38] R.M. Hamdi, J.F. Bocquet, K. Chhor and C. Pommier, J. Supercrit. Fluids, 4 (1991) 55.
[39] N. Saito, Y. Ikushima and T. Goto, Bull. Chem. Soc. Jpn., 63 (1990) 1532.
[40] A.F. Lagalante, B.N. Hansen, T.J. Bruno and R.E. Sievers, Inorg. Chem., 34 (1995) 5781.
[41] E.W. Berg and H.W. Dowling, J. Chem. Eng. Data, 6 (1961) 556.
[42] R.D. Brauer and C.M. Wai, unpublished results, 1996.
[43] H.K. Shin, M.J. Hampden-Smith, E.N. Duesler and T.T. Kodas, Polyhedron, 10 (1991) 645.
[44] P.G. Jessop, Y. Hsiao and T. Ikariya, J. Am. Chem. Soc., 116 (1994) 118.
[45] M. Poliakoff, S.M. Howdle and S.G. Kazarian, Angew. Chem., Int. Ed. Engl., 34 (1995) 1275, and references cited therein..
[46] P.G. Jessop, T. Kariya and R. Noyori, Science, 269 (1995) 1065, and references cited therein..
[47] K. Toews, R. Scholl, C.M. Wai and N.G. Smart, Anal. Chem., 67 (1995) 4040.

ELSEVIER

Talanta 44 (1997) 151–157

Talanta

Spectrophotometric determination of a nanomolar amount of ascorbic acid using its catalytic effect on copper(II) porphyrin formation[1]

Masaaki Tabata*, Hirofumi Morita

Department of Chemistry, Faculty of Science and Engineering, Saga University, 1 Honjo-machi, Saga 840, Japan

Received 1 May 1996; revised 6 June 1996; accepted 7 June 1996

Abstract

A simple, fast and sensitive flow-injection method is proposed for the determination of nanomolar amounts of ascorbic acid in tea, urine and blood. The procedure is based on the accelerating effect of a nanomolar level of ascorbic acid on the reaction of cooper(II) with 5,10,15,20-tetrakis(1-methylpyridinium-4-yl)porphyrin, H_2tmpyp^{4+}. Ascorbic acid reduces Cu(II) to Cu(I) which catalyzes the incorporation of Cu(II) into H_2tmpyp^{4+} to form $Cu^{II}(tmpyp)^{4+}$. In this method two solutions, one containing ascorbic acid and H_2tmpyp^{4+} and the other containing copper(II) and acetate buffer (pH 5.0), were injected into two flowing streams of water through two sample injectors of 120 μl sample volume. The mixture was allowed to react in a 2 m reaction coil and the colored solution of $Cu^{II}(tmpyp)^{4+}$ was monitored at 550 nm ($\varepsilon = 2.01 \times 10^4$ M^{-1} cm^{-1}). The present method was applied to the determination of ascorbic acid in tea, urea and blood. Reducing agents such as sugars and vitamins B_1, B_2, B_6 and B_{12} did not give serious errors at a concentration of 10^{-6} M for the determination of 1.0×10^{-8} M ascorbic acid. The relative standard deviation of the present method was 2.8% for the determination of 1.0×10^{-8} M ascorbic acid. The reaction mechanism was clarified from the kinetic results of the formation of $Cu^{II}(tmpyp)^{4+}$ in the presence of various concentrations of ascorbic acid, copper(II) and hydrogen ion.

Keywords: Ascorbic acid; Blood; Catalytic determination; Cu(II) porphyrin; Tea; Urine

1. Introduction

Ascorbic acid is an essential vitamin and participates in many different biological processes. It occurs naturally in most fruit juices and vegetables. Often, it is added during the manufacture of juices or soft drinks to improve their nutritional value, to attract consumers or to prevent the autoxidation of commerical products. Owing to the wide use of ascorbic acid in canned fruits,

* Corresponding author. Tel.: (+81) 952-28-8560; Fax. (+81) 952-28-8548; e-mail: tabatam@cc.saga-u.ac.jp

[1] Presented at the 1995 International Chemical Congress of Pacific Basin Societies (PACIFICHEM'95) in the Symposium on kinetic and Mechanistic Aspects of Analytical Chemistry, Honolulu, HI, USA, December 17–22, 1995.

PII S0039-9140(96)02010-3

Table 1
Effect of foreign ions on the determination of 1.0×10^{-8} M ascorbic acid

Foreign ion	C(M)	Recovery(%)	Foreign ion	C(M)	Recovery(%)
Ca^{2+}	10^{-4}	104	SO_4^{2-}	10^{-4}	108
Mg^{2+}	10^{-4}	99	SCN^-	10^{-5}	103
Mn^{2+}	10^{-6}	101	SO_3^{2-}	10^{-5}	97
Fe^{3+}	10^{-6}	103	$S_2O_3^{2-}$	10^{-6}	70
Co^{2+}	10^{-5}	103	Vitamin B_1	10^{-6}	97
Ni^{2+}	10^{-6}	99	Vitamin B_2	10^{-6}	103
Al^{3+}	10^{-5}	98	Vitamin B_6	10^{-6}	101
Pb^{2+}	10^{-5}	95	Vitamin B_{12}	10^{-6}	107
Cl^-	10^{-4}	101	Sucrose	10^{-6}	98
Br^-	10^{-4}	99	Fructose	10^{-6}	99
I^-	10^{-4}	101	Glucose	10^{-6}	98

vegetables and drugs, and because of its importance in human physiology, numerous methods have been reported for the determination of ascorbic acid, including titrimetric [1,2] spectrophotometric [3–6], fluorometric [7], chemiluminescence [8] and kinetic [9] methods. A highly sensitive and rapid analytical method is required for the analysis of a sample, such as blood, which contains a low concentration of ascorbic acid in a small volume of sample. In addition, the method must take into account the instability of ascorbic acid in air.

A catalytic method is a suitable method for sensitive analysis. Since catalytic measurements require both reproducibility of the mixing of the analyte with reagents and a definite reaction time, a flow-injection (FI) method is considered to be very appropriate for the catalytic method of analysis, as it has been used in routine analysis, [10,11].

This paper describes an FI spectrophotometric method based on the accelerating effect of ascorbic acid on the formation rate of 5, 10,15,20-tetrakis(1-methylpyridine-4-yl)porphyrinatocopper(II), $Cu^{II}(tmpyp)^{4+}$, and the increase in absorbance of the Cu(II) porphyrin. The procedure is simple, precise, sensitive and selective for the accurate determination of ascorbic acid in tea, urine and blood even at nanomolar level of ascorbic acid. Other compounds normally present along with ascorbic acid, such as metal ion, anions, vitamins and sugars, did not interfere with the determination of ascorbic acid at a 100-fold excess.

2. Experimental

2.1. Reagents

H_2tmpyp^{4+} tosylate, (Fig. 1) was purchased from Dojindo Chemical Institute (Kumamoto, Japan). The concentration of the porphyrin solution was determined spectrophotometrically using copper(II). A copper(II) solution was prepared by dissovling copper(II) nitrate in water and its concentration was determined by ethylenediaminetetraacetic acid (EDTA) titration using 4-(2-thi-azolylazo)resorcinol as an indicator. Sodium nitrate was recrystallized from distilled water. Ascorbic acid was used without further purification and its solution was prepared freshly before measurement. A small amount of a complexing agent such as *trans*-1,2-diaminocyclohexane-*N*,*N*,*N*′,*N*′-tetraacetric acid (DCTA) or EDTA was added to the sample solution to prevent the catalytic decomposition of ascorbic acid by contamination with metal ions such as iron(III). Buffer solutions were prepared by mixing acetic acid and sodium acetate solutions.

2.2. Apparatus and measurements for kinetic study

All kinetic experiments were carried out under anaerobic conditions and the temperature was controlled to within ±0.1°C. Most measurements were performed at 25°C. The ionic strength was maintained at 0.10 M with sodium nitrate. Absorption spectra were recorded on a Shimadzu UV-2100 spectrophotometer. The spectral changes during the course of the reaction were the disappearance of the characteristic absorption bands of H_2tmpyp^{4+} (*Q* bands at 520, 558 and 647 nm) and the growth of the characteristic band of $Cu^{II}(tmpyp)^{4+}$ (*Q* band at 550 nm). The isosbestic points were observed at 490, 534 and 577 nm. The change in absorbance at 550 nm was monitored with a thermostated 10 mm cell as a function of time at a given temperature by a Neslab small refrigerated thermostat, type RTE-100. The reaction was stated by mixing two solutions, i.e. one containing sodium nitrate (0.1 M), copper(II) nitrate and buffer, and the other containing sodium nitrate (0.1 M), H_2tmpyp^{4+}, ascorbic acid and buffer. The mixing was carried out with a sample-mixing device (Type MX7, Ohtsuka Denshi) under a nitrogen atmosphere. The pH was measured by a Radiometer 85 ion analyzer with a combined electrode (GK2401C). A 1.000×10^{-2} M nitric acid solution containing 0.09 M sodium nitrate was employed as the standard hydrogen ion concentration ($-\log [H^+] = 2.000$; $I = 0.1$.

Table 2
Determination of ascorbic acid in tea, urine and blood using the present method

Sample	Volume taken[a]	Ascorbic acid found (M)
Tea	2 ml[b]	$(1.94 \pm 0.06) \times 10^{-7}$ [b]
Human urine	10 μl	$(6.9 \pm 1.7) \times 10^{-5}$
Human blood	100 μl	$(1.31 \pm 0.29) \times 10^{-6}$

[a] The sample was taken in a 25 ml volumetric flask.
[b] The sample was diluted 12 500 times and the known concentration of ascorbic acid in the sample is 2.04×10^{-7} M.

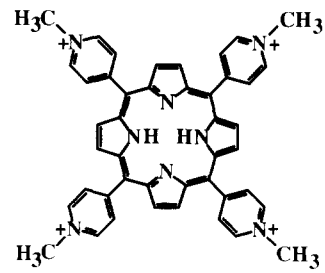

Fig. 1. 5,10,15,20-Tetrakis(1-methylpyridinium-4-yl)porphyrin (H_2tmpyp^{4+}).

2.3. FI manifolds and experimental conditions

A schematic diagram of the FI manifold is shown in Fig. 2. The system consists of a two-channel manifold with two plunger pumps (Jasco RP-4F, FIU high pressure reciprocal pumps) operating at a flow rate of 1.9 ml min^{-1} and two six-way valve injectors of 120 μl sample volume were placed in each line. Two solutions were injected into each stream. One solution contained copper(II) nitrate (4.000×10^{-4} M), acetate buffer (pH 5.0, 10^{-2} M), DCTA (1.0×10^{-4} M), and sodium nitrate (0.1 M), and the other contained ascorbic acid (10^{-9}–10^{-7} M), H_2tmpyp^{4-} (2.5×10^{-5} M), acetate buffer (pH 5.0; 10^{-2} M), DCTA (1.0×10^{-4} M), and sodium nitrate (0.1 M). The two solutions were mixed in a reaction coil. The absorbance at 550 nm was measured by a Jussco UVIDEC-100 VI spectrophotometer with an 8 μl flow cell and recorded on a Graphtec Servocorder SR 6211, and the peak heights were measured. The FI experiment was thermostated at room temperature (25 ± 0.5°C).

3. Results and discussion

3.1. Kinetics and mechanism of formation of $Cu^{II}(tmpyp)^{4+}$ in the presence of ascorbic acid

The rate of metalloporphyrin formation is 10^{-6}–10^{-8} times slower than that of complex formation with open-chain ligands [12,13]. Several methods have been proposed for the enhancement of the incorporation of metal ion into porphyrin [14]. The slow reaction rate is a result of difficulty

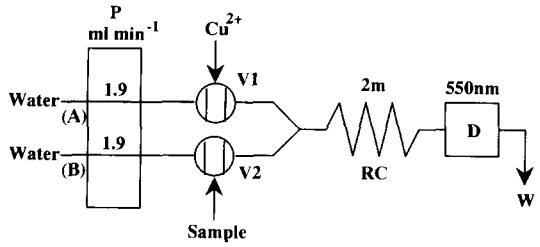

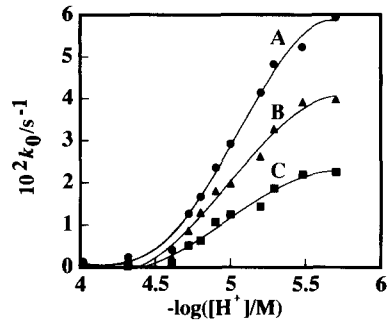

Fig. 2. Manifold used for determination of ascorbic acid: A and B, water streams; P, plunger pump; V1 and V2, six-way loop injector valves of 120 μl sample volume; RC, reaction coil (5 mm i.d.); D, spectrophotometer; W, waste. All flow lines were made from Teflon tubing (0.5 mm i.d.).

in deforming the porphyrin ring. Interestingly, large metal ions such as mercury(II), cadmium(II) and lead(II), which cannot be incorporated into the porphyrin core and just sit on the top of the porphyrin plane due to their large ionic radii, deform the porphyrin core and accelerate the incorporation of other medium-sized metal ions such as copper(II) [13,14]. Copper(I) has an ionic radius comparable to that of cadmium(II). Therefore, it is expected that copper(I) will accelerate metalloporphyrin formation in a similar way to cadmium(II) [15].

The present FI method is based on ascorbic acid reducing copper(II) ion to copper(I), which catalyzes the formation of $Cu^{II}(tmpyp)^{4+}$, and measuring the increase in absorbance of the Cu(II) porphyrin at a definite time after the start of the reaction. This reaction gave a straight line in a first-order kinetic plot. Hence, the kinetic equation for the reaction is described by Eq. (1), where k_0 is the conditional rate constant involving concentrations of ascorbic acid, hydrogen ion and copper(II):

$$-d[H_2tmpyp^{4+}]/dt = d[Cu^{II}(tmpyp)^{4+}]/dt = k_0[H_2tmpyp^{4+}] \quad (1)$$

3.2 Effect of hydrogen ion

The reaction of copper (II) with H_2tmpyp^{4+} was investigated in the presence of ascorbic acid at pH 4–5.6. Fig. 3 shows the effect of hydrogen ion in the presence and absence of ascorbic acid. The rate of formation of $Cu^{II}(tmpyp)^{4+}$ increased with pH. The rapid increase in the rate constant above pH 4.5 can be ascribed to the deprotonation of acetic acid and acsorbic acid ($pK_a = 4.56$ (acetic acid), 4.25 (ascorbic acid) [16]) and to the release of proton from H_2tmpyp^{4+} followed by the formation of $Cu^{I}(tmpyp)^{5+}$ (*vide infra*).

3.3 Effect of ascorbic acid and copper (II)

The formation of $Cu^{II}(tmpyp)^{4+}$ was dramatically accelerated in the presence of ascorbic acid even at nanomolar levels. The observed rate constant was linearly correlated with the total concentration of ascorbic acid (Fig. 4a) and increased significantly with copper(II) concentration, reaching a plateau at the highest concentration of Cu(II) at each temperature (Fig. 4b). The reduction of Cu(II) to Cu(I) was completed within 1 min

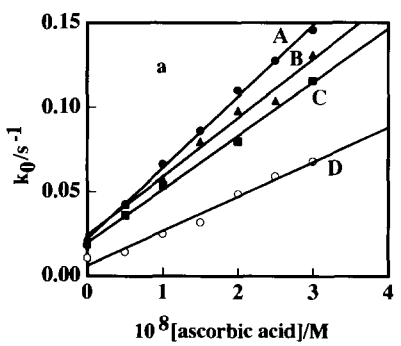

Fig. 3. Effect of pH on the reaction of H_2tmpyp^{4+} with copper(II) in the presence and absence of ascorbic acid: (A) 1.00×10^{-8}; (B) 5.00×10^{-9}; (C) 0 M $[Cu^{2+}] = 1.02 \times 10^{-4}$, $[H_2tmpyp^{4+}] = 1.54 \times 10^{-5}$ and $[DCTA] = 7.5 \times 10^{-6}$ M.

under the present experimental conditions ($[Cu^{2+}] = 1.0 \times 10^{-4}$ M, pH 5.0, $I = 0.1$ $NaNO_3$) [17,18]. The copper(I) formed catalyzes the rate of incorporation of copper(II) into the porphyrin core by deforming the porphyrin plane favorably for the attack of copper(II) from underneath. The mechanism is similar to the effect of large metal ions such as mercury(II), cadmium(II) and lead(II) [14,15,19]. Thus, the reaction mechanism for the accelerating effect of ascorbic acid is expressed by the following reaction scheme:

$$Cu^{2+} + HA^- \xrightarrow{\text{fast}} Cu^+ + HA^{\bullet}; \quad Cu^{2+} + A^{\bullet -} \xrightarrow{\text{fast}} Cu^+ + A$$

$$Cu^+ + H_2tmpyp^{4+} \underset{k_{-1}}{\overset{k_1}{\rightleftharpoons}} Cu^{I}(tmpyp)^{5+} + 2H^+ \quad (2)$$

$$Cu^{I}(tmpyp)^{5+} + Cu^{2+} \xrightarrow{k_2} Cu^{II}(tmpyp)^{4+} + Cu^+ \quad (3)$$

The Cu^+ formed in reaction (3) contributes repeatedly to reaction (2) i.e., Cu^+ plays a role as a catalyst for the formation of $Cu^{II}(tmpyp)^{4+}$. Applying the steady state-approximation for $Cu^{I}(tmpyp)^{5+}$, the observed rate constant for the catalytic reaction is given by

$$k_0 = \frac{k_1 k_2 [Cu^+][Cu^{2+}]}{(k_{-1}[H^+]^2 + k_2[Cu^{2+}])} \quad (4)$$

From this equation, it can be deduced that the catalytic effect of Cu^+ becomes independent of $[Cu^{2+}]$ at high concentration ($k_{-2}[H^+]^2 \ll [Cu^{2+}]$). Thus, Eq. (4) is reduced to $k_0 = k_2[Cu^+]$ at high concentrations of copper(II) as shown in Fig. 4b.

3.4. Optimization of FI method

Ascorbic acid was found to enhance the formation of $Cu(tmpyp)^{4+}$, and the reaction was adapted in order to develop an FI method for the determination of ascorbic acid. A schematic diagram of the FI manifold is shown in Fig. 2. The absorbance of $Cu(tmpyp)^{4+}$ was measured at 550 nm (λ_{max} of $Cu(tmpyp)^{4+}$) and the peak height was also measured. The presence of ascorbic acid caused an increase in the peak height proportional to the ascorbic acid concentration. Flow rate, coil length, temperature and other chemical variables were optimized for the proposed FI method. This study was carried out by altering each variable in turn while keeping the others constant. The effect of the reactor coil length on the peak height was studied in the range 0.3–5 m (0.5 mm i.d.) in the presence of various concentrations of ascorbic acid. The absorbance increased with reactor coil length, reached a maximum at around 2 m, and then gradually decreased above 2 m (Fig. 5). Thus, a 2 m reactor coil was selected.

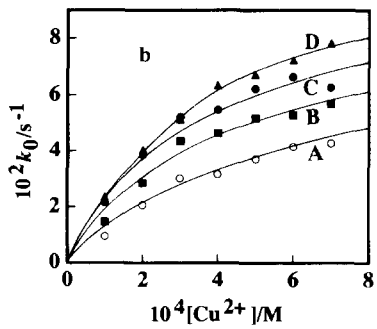

Fig. 4. Effect of ascorbic acid (a) and copper(II) (b) on the formation of $Cu(tmpyp)^{4+}$. (a) $[Cu^{2+}] = 1.02 \times 10^{-4}$; $[H_2tmpyp^{4+}] = 1.54 \times 10^{-5}$; $[DCTA] = 7.5 \times 10^{-6}$ M; pH 5.70 (A); 5.50 (B); 5.29 (C); 5.10 (D). (b) $[H_2tmpyp^{4+}] = 1.52 \times 10^{-5}$; $[DCTA] = 1.00 \times 10^{-5}$; [ascorbic acid] $= 5.00 \times 10^{-9}$ M; pH 4.80; T (°C) = 16.2 (A); 20.7 (B); 25.0 (C); 29.9 (D).

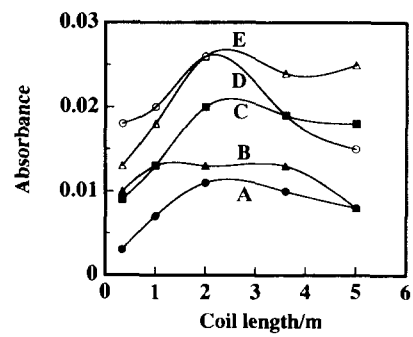

Fig. 5. Effect of reaction coil length on the determination of ascorbic acid using the present FI method. [Ascorbic acid] (10^{-8} M) = 2.00 (A); 4.00 (B); 6.00 (C); 8.00 (D); 10.00 (E).

3.5. Determination of ascorbic acid

With the manifold described above and under the selected experimental conditions, namely pump rate = 1.9 ml min^{-1}, sample volume = 120 μl, reactor coil length = 2.0 m, two solutions were injected simultaneously using two sample injectors with a six-way valve. One solution contained 0.1 M $NaNO_3$, acetate buffer (pH 5.0, $[CH_3COOH] + [CH_3COONa] = 0.01$ M), 1.0×10^{-4} M DCTA and 4×10^{-4} M Cu^{2+} in a 25 ml volumetric flask and the other contained 0.1 M $NaNO_3$, acetate buffer (pH 5.0, $[CH_3COOH] + [CH_3COONa] = 0.01$ M), DCTA = 1.0×10^{-4} M, sample solution (ascorbic acid = 10^{-9}–10^{-7} M) and H_2tmpyp^{4+} (1.80×10^{-5} M). A linear calibration graph was obtained by plotting the peak height (or absorbance) vs. the concentration of ascorbic acid in the range $5.0 \times 10^{-7} - 1.2 \times 10^{-7}$ M ascorbic acid. The regression equation was: absorbance = 4.94×10^5 [ascorbic acid] + 0.0283, with a correlation factor (r) of 0.9949. The relative standard deviation was 2.8% for the determination of 1.0×10^{-8} M ascorbic acid.

3.6. Interference studies

The effect of foreign ions on the present FI method was studied for frequently encountered reducing agents and inorganic ions, in addition to the effect of other vitamins that are likely to be present along with ascorbic acid in foods. The results are summarized in Table 1. Since ascorbic acid is easily decomposed in the presence of trace amounts of iron(III), DCTA was added to the sample solution to mask iron(III). EDTA also showed the same masking effect for the foreign ions as DCTA. Since the stability constant of Fe(DCTA) is larger than that of Fe(EDTA), and the difference between the Fe(III) and Cu(II) stability constants of DCTA is higher than that of EDTA [20], DCTA was used in this method. The present method is based on the ability of ascorbic acid to reduce Cu(II) to Cu(I). Hence, chemical species that can bring about reduction would be expected to interfere with the determination of ascorbic acid. Among the agents listed in Table 1, thiosulfate interfered significantly, but the effects of other reducing agents of sugars were negligible at the 10^{-6} M level. Vitamins B1, B2, B6 and B12 did not produce serious errors in the determination of 10^{-8} M ascorbic acid.

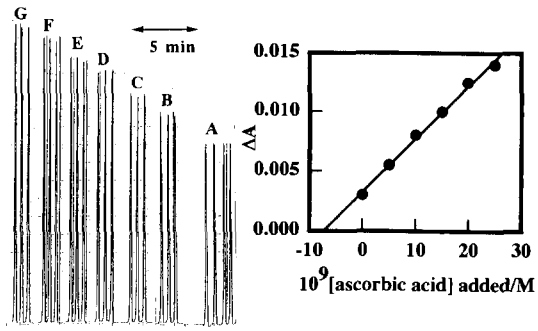

Fig. 6. Typical recorder signals for the determination of ascorbic acid in diluted tea samples after addition of a given concentration of ascorbic acid: (A) blank; (B) 0; (C) 5.0×10^{-9}; (D) 1.00×10^{-8}; (E) 1.50×10^{-8}; (F) 2.0×10^{-8}; (G) 2.5×10^{-8} M.

3.7. Application

In order to check the applicability of the present method to real samples, it was used for the determination of ascorbic acid in samples of tea, human urine and blood. Since the concentrations of ascorbic acid in these samples were too high for the present method, the samples were diluted 312 500, 5000, and 100 times for tea, urine and blood respectively. Typical FI signals and a calibration graph using the standard addition method are shown in Fig. 6 for the determination of ascorbic acid in a diluted tea sample. The blood sample was centrifuged for 5 min at 5000 rev min^{-1} and a 500 μl sample was taken into a 25 ml volumetric flask and diluted with water. It was anticipated that many materials in urine and blood would interfere with the determination of ascorbic acid. However, the interference of these species was greatly reduced due to the marked dilution of the sample before the determination of ascorbic acid. The analytical results for tea, urine and blood are summarized in Table 2. The accuracy and precision of the present method were tested by comparison of the results for the diluted (12 500 times) tea sample with the known concen-

tration of ascorbic acid in the tea sample and by a standard addition method respectively. Satisfactory results were obtained.

4. Conclusion

The proposed method for the determination of ascorbic acid is highly sensitive, selective, simple and precise. The method can be easily adapted for handling large numbers of samples by an FI method and has the potential for automatic routine clinical analysis. The high sensitivity of the proposed method provides rapid analysis of a nanomolar level of ascorbic acid in urine and blood without serious errors from sugars and vitamins.

Acknowledgements

The authors are grateful for financial support from a Grant-in Aid for Scientific Research from the Ministry of Education, Science and Culture of Japan (07640812).

References

[1] D.F. Evered, Analyst, 85 (1960) 515.
[2] H. Vallant, Mikrochim. Acta, (1969) 436.
[3] M.I. Albero, M.S. Garcia, C. Sanchez-Pedreno and J. Rodriguez, Analyst, 117 (1992) 1635.
[4] S.M. Sultan, A.M. Abdennabi and F.E.O. Suliman, Talanta, 41 (1994) 125.
[5] O.H. Abdelmageed, P.Y. Khashaba, H.F. Askal, G.A. Saleh and I.H. Refaat, Talanta, 42 (1995) 573.
[6] A. Jain, A. Chaurasia and K.K. Verma, Talanta 42 (1995) 779.
[7] T. Tevata, S. Hara, M. Yamagauchi, M. Nakamura and Y. Ohkura, Chem. Pharm. Bull., 33 (1985) 3499.
[8] A.A. Alwarthan, Analyst, 118 (1993) 639.
[9] A. Safavi and L. Fotouhi, Talanta, 41 (1994) 1225.
[10] D. Perez-Bendito and M. Silva, Kinetic Methods in Analytical Chemistry, John Wiley & sons, New York, 1988.
[11] H.A. Mottola, Kinetic Aspects of Analytical Chemistry, John Wiley & Sons, New York, 1988.
[12] D.W. Margerum and G.R. Cayley, in A.E. Martell (Ed.), Coordination Chemistry, American Chemical Society, Washington, DC, 1978, pp. 1-194.
[13] D.K. Lavallee, Coord. Chem. Rev., 61 (1985) 55.
[14] M. Tabata and M. Tanaka, Trends Anal. Chem., 10 (1991) 126.
[15] M. Tabata and M. Tanaka, J. Chem. Soc., Dalton Trans., (1983) 1955.
[16] R.M. Smith and A.E. Martell, Critical Stability Constants, Vol. 3, Plenum Press, New York, 1977.
[17] K. Hayakawa, S. Minami and S. Nakamura, Bull. Chem. Soc. Jpn., 46 (1973) 2788.
[18] J. Xu and R.B. Jordan, Inorg. Chem., 29, (1990) 2933.
[19] M. Tabata, W. Miyata and N. Nahar, Inorg. Chem., 34 (1995) 6492.
[20] R.M. Smith and A.E. Martell, Critical Stability Constants, Vol. 1, Plenum Press, New York, 1974.

ELSEVIER

Talanta 44 (1997) 159–164

Talanta

Second-derivative UV spectrophotometric assay for determining the degradation kinetics of 3-bromo-*N*-bromo-*N*-(3,4-dimethyl-5-isoxazolyl-4-amine)-1,2-naphthoquinone

Viviana G. Dabbene, Margarita C. Briñón*, María M. de Bertorello

Departamento de Farmacia, Facultad de Ciencias Químicas, Universidad Nacional de Córdoba, Suc. 16 C.C. 61, 5016 Córdoba, Argentina

Received 4 December 1995; revised 18 June 1996; accepted 26 June 1996

Abstract

The application of the second-derivative UV spectrophotometry for determining the stability of 3-bromo-*N*-bromo-*N*-(3,4-dimethyl-5-isoxazolyl-4-amine)-1,2-naphthoquinone in ethanolic solutions is described. The validity of this method was evaluated using synthetic mixtures of the intact drug and its degradation products and by statistical analysis of the calibration data. In order to verify the usefulness of this method for stability studies, recovery experiments by the standard addition method were also carried out.

Keywords: 3-bromo-*N*-bromo-*N*-(3,4-dimethyl-5-isoxzxolyl-4-amine)-1,2-naphthoquinone; Degradation kinetics; Second-derivative UV spectrophotometry

1. Introduction

The stability of halogenated isoxazolylnaphthoquinones in ethanolic solutions is affected by factors such as temperature and daylight [1–3]. Previously, we have demonstrated that 3-bromo-*N* - bromo - *N* - (3,4 - dimethyl-5-isoxazolyl-4-amine)-1,2-naphthoquinone (**1**) [4], a potential tripanocidal agent [5], decomposes in ethanolic solutions, at 35–50°C under daylight and dark conditions giving two main degradation products: 3 - bromo - 2 - hydroxy - *N* - (3,4 - dimethyl - 5 - isoxazolyl) -1, 4 - naphtho-quinon-4-imine (**2**) and 3-bromo - *N* - bromo - 4 - ethoxy - *N* - (3,4 - dimethyl - 5 - isoxazolyl - 4 - amine) - 1,2 -

* Corresponding author. Fax: (54)-51-334174.

PII S0039-9140(96)02025-5

naphthoquinone (**3**) [2], which require specific methods of analysis.

1

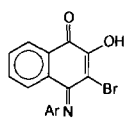

2

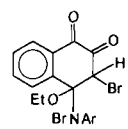

3

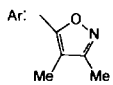

Derivative UV spectrophotometry has proved to be particularly useful in assays of single components in the presence of excipients or degradation products with very similar structures [1,3,6–9]. This paper describes the applicability of second-derivative spectrophotometry for determining the disappearance kinetics of **1** in the presence of its degradation products. The method was validated using synthetic mixtures of **1** with its degradation products and by statistical analysis of the calibration data. In order to verify its usefulness in stability studies of **1**, recovery experiments were performed by the standard addition method [10].

2. Experimental

2.1. Apparatus

UV spectrophotometric studies were carried out on a Shimadzu UV-260 spectrophotometer using 1 cm quartz cuvettes. A Chromatotron Model 7924 T was used for preparative radial chromatography (PRC). The coating rotors were prepared with silica gel 60 PF-254 (Merck). For kinetic measurements, the constant-temperature bath was regulated by a Haake D8 thermostat with ± 0.1°C precision.

2.2. Materials

All chemicals and reagents were of analytical grade. Ethanol was treated with sulfanilic acid and potassium hydroxide/Zn [11]. Compounds **1**–**3** were obtained as reported previously [2,4]. Compounds **1** and **3** are freely soluble in dichloromethane and sparingly soluble in ethanol, therefore dichloromethane was used as the solvent to prepare their stock solutions.

2.3. Second-derivative UV spectrophotometric analysis

Zero-order and second-derivative absorption spectra of standard and sample solutions were recorded at 220–350 nm against ethanol as a blank. Suitable settings were a slit width 1 nm and a fast scan speed. The recorder scale expansion was also optimized to facilitate reading on the recorder tracing. The peak-to-baseline measurements h (mm) were performed at 258.0 nm in duplicate scans of the same solution and normalized (H) [1,3,6]. All transfers and dilutions were carried out in the dark.

2.4. Calibration graph

Five solutions of **1** were prepared in duplicate by diluting aliquots taken from two stock solutions (1.37×10^{-3} M in dichloromethane) with ethanol to obtain final concentrations in the range $(1.37–4.11) \times 10^{-5}$ M. The peak heights h (mm) at 258.0 nm were measured and normalized [1,3,6]. The system obeys Beer's law in the range examined.

2.5. Recovery assays

Dichloromethane stock solutions of **1** (1.47×10^{-3} M) and **3** (1.22×10^{-3} M) were prepared. A stock solution of **2** was prepared in ethanol (1.20×10^{-3} M). Aliquots were transferred into 25 ml volumetric flasks and diluted to volume with ethanol to obtain final concentrations in the ranges $(3.56–1.01) \times 10^{-5}$ M for **1**, $(0.49–2.40) \times 10^{-5}$ M for **2** and $(0.49–2.44) \times 10^{-5}$ M for **3**. The second-derivative spectra for different mixtures of **1** with **2** and **3** were recorded in duplicate and the h values at 258.0 nm were measured, normalized and compared with the corresponding calibration graph run (Table 1).

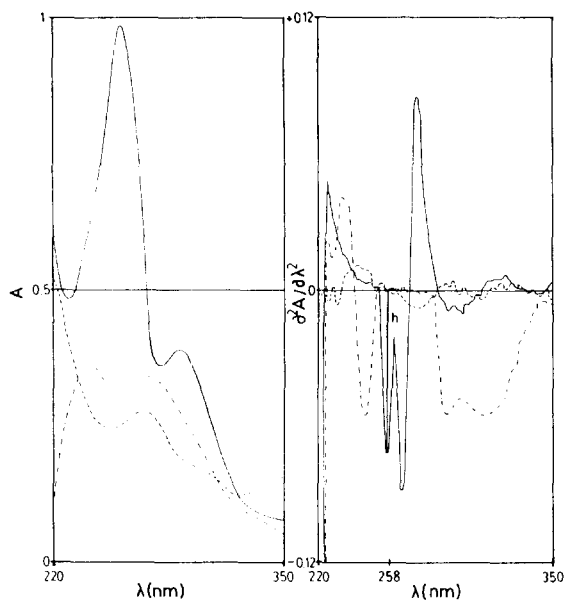

Fig. 1. Zero-order absorption spectra (left) and second-derivate spectra (right) for 3.50×10^{-5} M of **1**, **2** and **3** in 95% ethanol; *h* is the peak-to-baseline distance in mm. (—) **1**; (– · – · –) **2**; (– – –)**3**.

2.5.1. Standard addition method

A stock solution of **1** was prepared in dichloromethane (1.47×10^{-3} M). An aliquot of 6.0 ml was transferred into a 250 ml volumetric flask and diluted to volume with ethanol to obtain a final concentration of 3.53×10^{-5} M. The flask was sealed and then stored at 50°C in a constant-temperature bath for 26 min under daylight. It was then withdrawn and immediately cooled in an ice-bath. Aliquots (15 ml) of this degraded solution were taken and transferred into 25 ml volumetric flasks. Aliquots (0.10–0.60 ml) from the stock solution of **1** were added and then diluted to volume with ethanol. The second-derivative spectra of these solutions were recorded in duplicate. The *h* (mm) values at 258.0 nm were measured, normalized and compound **1** was quantified by the ratio of the intercept on the ordinate and the slope of the calibration line (Table 2) [10]. This assay was performed in quintuplicate.

2.6. Repeatability assay

A solution of 3.53×10^{-5} M of **1** was measured by replicate analysis ($n = 10$) on the same day.

2.7. Kinetic studies

Aliquots were taken from a dichloromethane stock solution of **1** (1.37×10^{-3} M) and diluted with 95% ethanol to produce a final concentration of 3.53×10^{-5} M. The sample solutions were transferred into 5 ml glass ampoules and 5 ml amber-glass ampoules, flame sealed and then stored at the appropriate temperature in a constant-temperature bath. The "zero time" samples were immediately maintained at −20°C. Ampoules were withdrawn at suitable time intervals, immediately cooled in an ice-bath and stored at −20°C in a freezer. Upon removal of the last samples, the stored solutions were allowed to warm to room temperature and then all samples were analysed. These kinetic studies were carried out in duplicate.

3. Results and discussion

The structural similarities between **1** and its degradation products **2** and **3** make it necessary to choose a specific method of analysis. Second-derivative spectrophotometry was found to be

Table 1
Recovery of **1** in the presence of its degradation products **2** and **3** using the second-derivate method

[1] (mg l^{-1})	[2] (mg l^{-1})	[3] (mg l^{-1})	Recovery[a] (%)
15.1	–	–	100.7
12.7	1.7	2.3	101.6
10.0	3.3	4.6	99.8
7.6	5.0	6.9	101.3
5.1	8.3	11.5	101.2
		Mean ± SD:	100.9 ± 0.7

[a] Mean of five determinations.

the best method for determining the residual concentration of **1** under the experimental conditions of this study owing to the lack of interference from the signals of **2** and **3**.

3.1. Spectrophotometric measurements

Fig. 1 (left) shows the zero-order absorption spectra of **1** and its degradation products **2** and **3** in the range 220–350 nm. Owing to the extensive spectral overlap of the absorption bands of these compounds, their second-derivative spectra were recorded, revealing a good selectivity for determining **1** in mixtures of **2** and **3**, as shown in Fig. 1 (right).

The peak-to-base line distance (h) at 258.0 nm for the determination of the remaining concentration of **1** was selected, since at this working wavelength no interference from **2** and **3** was observed.

3.2. Calibration graphs and statistical analysis

The ordinate values of the regression line (H) were calculated from the h (mm) measurements and were proportional to the concentration of pure **1** in the range $(1.37–4.11) \times 10^{-5}$ M. The linear regression equation for **1** [$H = (8.21 \pm 15.1) \times 10^{-4} + (2.24 \pm 0.05) \times 10^{3}c$ (M)], the correlation coefficient ($r = 0.9992$), the standard deviation (1.13×10^{-3}), the limit of detection (LOD: 1.51×10^{-6} M) and the limit of quantitation (LOQ: 5.03×10^{-6} M) were estimated from the calibration data at the $p = 0.05$ level of significance for $n = 5$ standard specimens [10,12].

The good sensitivity of the method is indicated by the slope of the calibration graph. The linearity of the regression line and the negligible scatter of the experimental points are clearly evidenced by the correlation coefficient and the standard deviation. A test of significance for the intercept of the regression line was performed as described previously [1,3,6] to verify whether the intercept a is significantly different from zero. The calculated value of $t = 0.54$ was compared with tabulated data for the t distribution ($t = 3.18$; $n = 5$), and as it does not exceed the 95% criterion, the calculated intercept is not significantly different from zero.

Table 2
Assay results of **1** in degraded samples using the standard addition method

Analyte added (mg l^{-1})	Found (mg l^{-1})	Recovery (%)
–	5.25 ($\pm$0.02)[a]	–
2.5	7.78	101.6
3.8	9.01	99.2
6.2	11.43	99.8
7.5	12.83	101.2
10	15.33	100.9
15	20.35	100.7
	Mean $\pm$ SD: 100.6 $\pm$ 0.9	

[a] Value obtained by standard addition method $\pm$SD ($n = 5$).

The absolute error (S_c) in the determination of a given concentration of **1** was calculated by statistical analysis of the regression equation [6,10]. As the errors are minimal in the range $(2.06–3.50) \times 10^{-5}$ M, the last concentration was chosen for degradation studies.

The validity of the second-derivative spectrophotometric method was tested by successive determinations of **1** in synthetic mixtures with **2** and **3**. The concentrations of the intact drug in these mixtures were in the range $(3.56–1.20) \times 10^{-5}$ M, in the presence of various concentrations of **2** [$(0.49–2.40) \times 10^{-5}$ M] and **3** [$(0.49–2.44) \times 10^{-5}$ M], to reproduce the stability studies conditions. The results are presented in Table 1 and indicate that the recoveries of **1** are in good agreement with the theoretical amounts of the compound.

Even though the recovery experiments demonstrated the applicability of the method, they are not sufficient to prove its specifity owing to intermediates and minor products that may be formed during the degradation reactions. Therefore, a recovery assay was performed using degraded samples of **1** by the standard addition method [10]. It can be seen from Table 2 that the results obtained do not differ significantly from 100%, confirming the accuracy of the method for measuring the kinetic disappearance of **1**.

The precision of the results was determined by using a standard solution (3.53×10^{-5} M; $n = 10$).

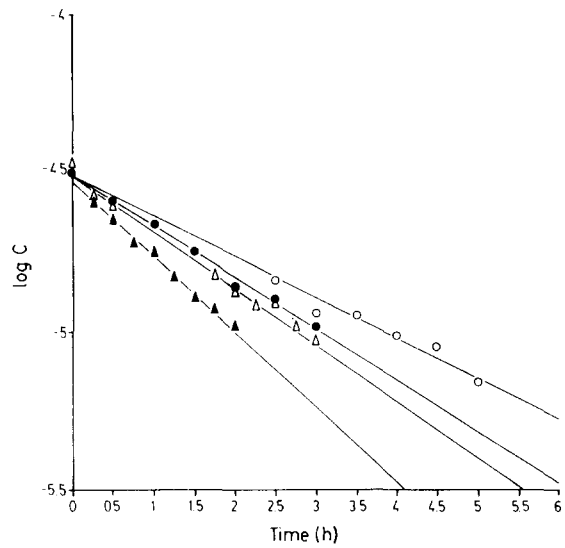

Fig. 2. Effect of temperature on the pseudo-first order rate constants for the degradation of **1** in 95% ethanol in daylight. (○) 35°C, $k_{obs} = 0.293\ h^{-1}$; (●) 40°C, $k_{obs} = 0.368\ h^{-1}$; (△) 45°C, $k_{obs} = 0.442\ h^{-1}$; (▲) 50°C, $k_{obs} = 0.546\ h^{-1}$.

The value obtained of $100.2 \pm 0.10\%$ (found $\pm$ SD) shows that the method has a satisfactory precision.

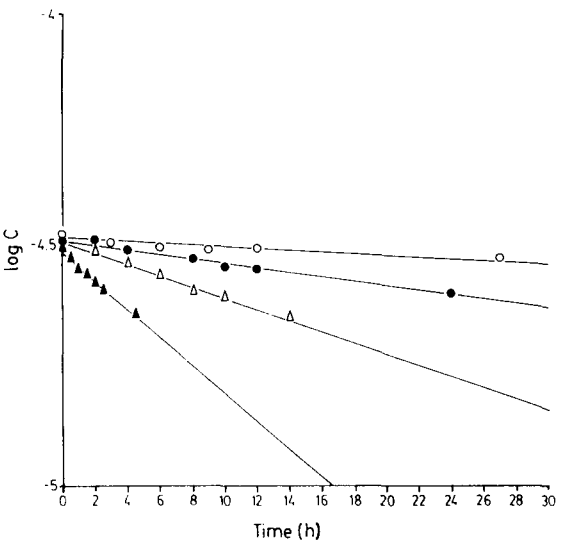

Fig. 3. Effect of temperature on the pseudo-first-order rate consants for the degradation of **1** in 95% ethanol in the dark. (○) 35°C, $k_{obs} = 0.00412\ h^{-1}$; (●) 40°C, $k_{obs} = 0.0105\ h^{-1}$; (△) 45°C, $k_{obs} = 0.0268\ h^{-1}$; (▲) 50°C, $k_{obs} = 0.0682\ h^{-1}$.

3.3. Kinetic studies

Figs. 2 and 3 show the residual concentration of **1** vs. time at different temperatures, exhibiting good linearity ($r > 0.99$). From these plots, the pseudo-first-order degradation rate constants of **1** were calculated [2] and it can be seen that the rate constants under daylight conditions are faster than those in the dark.

4. Conclusions

The advantages of second-derivative UV spectrophotometry, such as simplicity, lack of sample pretreatment and expensive solvents and reagents and the good selectivity, accuracy and precision achieved in the assays make it suitable for stability evaluation of ethanolic solutions of **1** under different experimental conditions.

Acknowledgements

The authors gratefully acknowledge the Consejo Nacional de Investigaciones Científicas y Técnicas (CONICET), the Consejo de Investigaciones Científicas y Tecnológicas de la Provincia de Córdoba (CONICOR) and the Secretaria de Ciencia y Técnica de la Universidad Nacional de Córdoba (SECYT) of Argentina for financial support. V.G.D. thanks CONICET for a fellowship.

References

[1] V.G. Dabbene, M.C. Briñón and M.M. de Bertorello, J. Pharm. Sci., 83 (1994) 1617.
[2] V.G. Dabbene, M.C. Briñón and M.M. de Bertorello, J. Chem. Res., 12 (1995) 508.
[3] V.G. Dabbene, M.C. Briñón and M.M. de Bertorello, Anal. Chim. Acta, 318 (1996) 221.
[4] V.G. Dabbene, M.C. Briñón and M.M. de Bertorello, Org. Prep. Proced. Int., 27 (1995) 75.
[5] M.N. Schwarz de Tarlovsky, S.G. Goijman and A.O.M. Stoppani, Rev. Argent. Microbiol., 20 (1988) 183; M.N. Schwarz de Tarlovsky, S.G. Goijman, M.P. Molina Portela and A.O.M. Stoppani, Experientia, 46 (1990) 502; P. Amuchástegui, E.R.A. Moretti, B. Baso, N.R.

Sperandeo and M.M. de Bertorello, Rev. Argent. Microbiol., 22 (1990) 199.
[6] B. Morelli, Analyst, 113 (1988) 1077; J. Pharm. Sci, 77 (1988) 1042.
[7] A. Parra, M.D. González, V. Ródenas, J. García Villanova and M. L. López, J. Pharm. Biomed. Anal., 10 (1992) 525.
[8] A.M. Elwalily, M.A. Korany, F.M. El-Anwar and S.M. Zamel, Anal. Lett. 25 (1992) 81; H. Abdellatef, M. Elbalkiny and A. Aboulkheir, J. Pharm. Biomed. Anal., 7 (1989) 571.
[9] M.R. Longhi, M.M. de Bertorello and M.C. Briñón, J. Pharm. Sci., 80 (1991) 573.
[10] J.N. Miller, Analyst, 116 (1991) 3.
[11] D.D. Perrin, W. Armanego and D.R. Perrin, Purification of Laboratory Chemicals, Pergamon Press, Oxford, 2nd edn., 1980.
[12] ACS Committee on Environmental Improvement, Anal. Chem., 52 (1980) 2242.

ELSEVIER

Talanta 44 (1997) 165–168

Talanta

Spectrophotometric and inductively coupled plasma atomic emission spectrometric determination of titanium in ilmenites after rapid dissolution with phosphoric acid

Jailson B. de Andrade*, Genebaldo S. Nunes, Merilio P. Veiga, A.C. Spinola Costa, Sergio L.C. Ferreira, Adelaide M.M. Amorim, Selma T. Reis

Instituto de Química, UFBA, Campus Universitário de Ondina, 40.170.290, Salvador, BA, Brazil

Received 14 December 1995; revised 18 June 1996; accepted 22 June 1996

Abstract

The use of 85% phosphoric acid in borosilicate conical flasks for the dissolution of ilmenites at $230 \pm 10°C$ is reported. The samples were quantitatively dissolved in less than 13 min. Titanium was determined by both spectrophotometry and inductively coupled plasma atomic emission spectrometry ICP-AES. Vanadium and iron were determined by ICP-AES. In several samples of ilmenites analyzed, the TiO_2 concentration was in the range 10.6–57.5% and those of FeO and V_2O_5 were in the ranges 31.6–51.4% and 0.39–1.32%, respectively. In the spectrophotometric method, vanadium interference occurs only when the Ti/V concentration ratio is <4. In all samples analyzed this ratio was around 12, resulting in no interferences due to vanadium. Hence the ilmenite dissolution procedure using phosphoric acid was compatible with titanium quantification by both spectrophotometry and ICP-AES.

Keywords: Inductively coupled plasma atomic emission spectrometry; Ilmenites; Phosphoric acid dissolution; Spectrophotometry; Titanium

1. Introduction

Titanium occurs in nature as the minerals rutile, brookite and anatase, and also occurs as titanates, ilmenite and perovskite. Industrially, ilmenite is of greatest importance. The decomposition of ilmenites is a very time-consuming operation, and involves fusion with pyrosulfate and/or the use of several mineral acids. Besides the time-consuming dissolution, the acids are usually volatilized into the atmosphere with consequent contamination problems. It is desirable to develop decomposition methods for solid samples that would allow a rapid and clean analysis [1–3].

* Corresponding author.

PII S0039-9140(96)02026-7

Phosphoric acid has been used successfully to decompose solid samples. Therefore, usually special glassware apparatus [4–11] or platinum crucibles have been required [12,13]. The use of phosphoric acid in determinations which involve atomic absorption spectrometric measurements [12] has been limited owing to nebulizer clogging as a result of solutions with high viscosity. Additionally, the determination of titanium in ilmenites by spectrophotometry using hydrogen peroxide [14] has limitations due to the interferences caused by the high iron concentrations and by vanadium, even at lower concentrations.

In the present work, the use of phosphoric acid in borosilicate conical flasks in the decomposition of ilmenites followed by titanium quantification by spectrophotometry using hydrogen peroxide and inductively coupled plasma atomic emission spectrometry ICP-AES was investigated. Iron and vanadium were quantified by ICP-AES.

2. Experimental

2.1. Reagents

All reagents were of ACS reagent grade. Deionized water (18.0 MΩ cm) was used throughout.

2.2. Apparatus

The absorbance measurements were made in a Varian DMS 80 spectrophotometer using 1.0 cm pathlength silica cells at 404 nm. The ICP-AES determinations were made using an ARL Fisons Model 3410 instrument. The working parameters were incident power 650 W, reflected power <10 W, slit width 20 μm, Meinhard concentric nebulizer and quartz mini-torch. The wavelengths used were Fe 259.9, Ti 334.9 and V 292.4 nm. The gas flow-rates were cooling 7.5 l min^{-1}, intermediate 0.8 l min^{-1}, aerosol carrier 0.8 l min^{-1} and peristaltic pump 2.3 ml min^{-1}.

2.3. Sample preparation

After drying (120°C), ca. 0.1000 g of the sample was placed in conical flasks and 2–3 ml of deionized water were added to disperse it. Then 17 ml of 85% phosphoric acid were added and the system was heated at ca. 230°C to promote the sample dissolution (on average 12 min). The hotplate was thermostatically controlled and it was previously calibrated with a glass thermometer (0–600 ± 1°C). The dissolved sample was placed in a 100 ml volumetric flask and diluted to volume with deionized water.

2.4. Spectrophotometric procedure

Aliquots of 10 ml were transferred into 50 ml volumetric flasks to which were added 4.5 ml of H_2SO_4 (1:1) and 5 ml of 30% H_2O_2 [14] and the volume was completed with deionized water.

2.5. ICP-AES procedure

The determinations were performed after sample dissolution (17 ml of 85% phosphoric acid) and dilution to 100 ml with deionized water, which resulted in a solution containing 15% of phosphoric acid. The standards were also adjusted to contain 15% of phosphoric acid in order for the sample and standard solutions to have the same viscosity. Phosphoric acid concentrations $>30\%$ must be avoided because they can result in nebulizer clogging.

3. Results and discussion

On heating, phosphoric acid undergoes a series of condensation reactions, giving mainly pyrophosphoric acid ($H_4P_2O_7$) and metaphosphoric acid [$(HPO_3)_n$] [1,2]. Fig. 1 shows the temperature profile when 30 ml of phosphoric acid are heated continuously with 0.25 g of ilmenite. The first transition, at ca. 160°C, corresponds to the formation of pyrophosphoric acid. The second, at 280°C, corresponds to the formation of metaphosphoric acid. The formation and decomposition of the $H_4P_2O_7$ were observed by qualitative tests [15]. Hence, as the complete dissolution of the ilmenite occurs in less than 15 min, we can consider that the species responsible for the ore decomposition are pyrophosphoric acid at the beginning and later metaphosphoric acid.

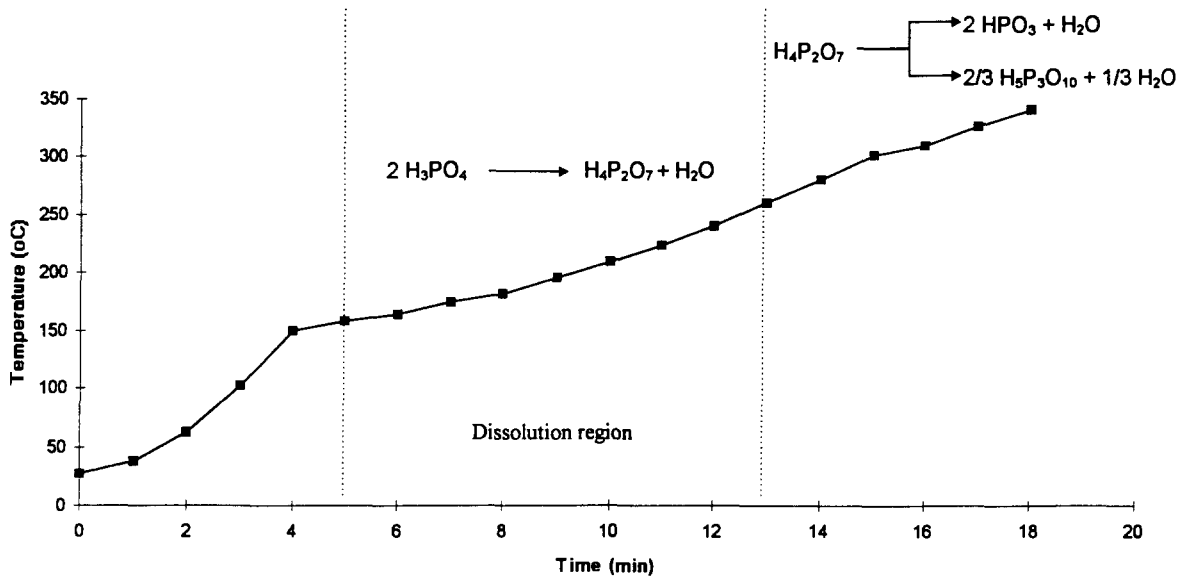

Fig. 1. Temperature profile when 30 ml of phosphoric acid are heated continuously with 0.25 g of ilmenite.

In spectrophotometric titanium determinations, iron in the presence of phosphoric acid forms a strong complex which does not absorb at 404 nm [14]. Therefore, our results demonstrate that the vanadium interference depends on the Ti/V ratio. Table 1 gives the absorbance values measured for seven different solutions containing hydrogen peroxide, 4.8 μg ml^{-1} of titanium and vanadium concentrations in the range 0–4.34 μg ml^{-1}. Vanadium interference, increasing the absorbance value by 6.3% (Table 1), occurred only when its concentration was at least 1.45 μg ml^{-1}, corresponding to a Ti/V concentration ratio of <4. For all samples analyzed this ratio was around 12, resulting in no interference due to vanadium.

Table 1
Absorbance measured in solutions containing titanium at 4.8 μg ml^{-1} and various vanadium concentrations

Ti (μg ml^{-1})	V (μg ml^{-1})	Absorbance	Ti/V
4.80	0	0.16	–
4.80	0.14	0.16	34.3
4.80	0.36	0.16	13.3
4.80	0.72	0.16	6.67
4.80	1.45	0.17	3.3
4.80	2.17	0.17	2.2
4.80	4.34	0.19	1.11

The data for the calibration curves (five points) for TiO_2 concentration in the range 0–160 μg ml^{-1} are given in Table 2.

Method validation was performed with six different aliquots of one sample analyzed both at CEPED (Research and Development Center, Bahia State) using their routine procedures [16] and by the present methodology in which the ore was decomposed with phosphoric acid and titanium was determined by both spectrophotometry and ICP-AES. The results are shown in Table 3.

The application of the $t_{95\%}$ test to the results obtained at CEPED and in this work (Table 3) did not show significant differences. In the sample

Table 2
Calibration curves for UV spectrophotometric and ICP-AES determination of titanium ($A = aC + b$) [a]

Method	a	b	r^2
UV	0.0092	−0.0066	0.9996
ICP-AES	0.0489	−0.0483	0.9994

[a] A = absorbance; C = concentration (g/l^{-1}); a = slope; b = intercept; r = correlation coefficient.

Table 3
Concentrations (%) of TiO_2 in an ilmenite sample determined at CEPED and using the procedures described in this paper

This work [a]		CEPED[b]
UV	ICP-AES	
12.27 (±0.009)	12.14 (±0.096)	12.30

[a] Mean of six different determinations in six independent samples; the ilmenite sample contained 38.2% FeO and 1.0% V_2O_5. Numbers in parentheses are mean relative standard deviations.
[b] CEPED (Research and Development Center, Bahia State) is a State reference bureau. They used a routine analytical procedure [16].

analyzed the concentrations of FeO and V_2O_5 were 38.2% and 1.0%, respectively. Owing to the high complexant activity of the phosphate ion, interferences of iron and vanadium in the spectrophotometric determinations were avoided.

The titanium concentrations determined by spectrophotometry and by ICP-AES were in good agreement when phosphoric acid was used to decompose several samples of ilmenites in which the TiO_2 concentrations were in the range 10.6–57.5% and those of FeO and V_2O_5 were, in the ranges 31.6–51.4% and 0.39–1.32%, respectively.

In conclusion, the ilmenite dissolution procedure using phosphoric acid was compatible with titanium quantification by both spectrophotometry and ICP-AES. One chemist, in a working day of 8 h, can determine titanium spectrophotometrically in at least 20 samples of ilmenite. The method is rapid, inexpensive and clean because it does not emit gases (e.g. SO_2 and/or NO_x) into the atmosphere.

Acknowledgements

This work was supported by the National Research Council of Brazil (CNPq). Helpful discussions with Professor Dr. Jose Oscar Nogueira Reis are acknowledged. G.S.N. and S.T.R. acknowledge CNPq for Graduate Fellowships. M.P.V. is also a faculty member at the Universidade do Estado da Bahia (UNEB).

References

[1] J.B. de Andrade and A.C.S. Costa, Quím. Nova, 7 (1985) 117.
[2] M.P. Veiga, S.D. Cunha, A.C.S. Costa and J.B. de Andrade, Anal. Lett., 27 (1994) 229.
[3] O.P. Bhargava, Analyst, 101 (1976) 125.
[4] T. Kiba, T. Takagi, Y. Yoshimura and I. Kishi, Bull. Chem. Soc. Jpn., 28 (1955) 641.
[5] T. Kiba, I. Akasa and N. Sugishita, Bull. Chem. Soc. Jpn., 30 (1957) 972.
[6] K. Terada, S. Hirakawa and T. Kiba, Bull. Chem. Soc. Jpn., 50 (1977) 396.
[7] K. Terada, T. Ooba and T. Kiba, Talanta, 22 (1975) 41.
[8] T. Mizoguchi and H. Ishii, Talanta, 25 (1978) 311.
[9] T. Mizoguchi and H. Ishii, Talanta, 26 (1979) 33.
[10] T. Mizoguchi, H. Iwahori and H. Ishii, Talanta, 27 (1980) 519.
[11] T. Mizoguchi and H. Ishii, Talanta, 27 (1980) 525.
[12] R. P. Lucas and B. C. Ruprecht, Anal. Chem., 43 (1971) 1013.
[13] P. Hannaker and H. Qing-Lee, Talanta, 31 (1984) 1153.
[14] A.I. Vogel, Textbook of Quantitative Inorganic Analysis, Longman, London, 4th edn, 1968.
[15] T. Moeller, Quantitative Analysis: an Introduction to Equilibrium and Solution Chemistry, McGraw-Hill, New York, 1961.
[16] J. A. Rahm, Anal. Chem., 24 (1952) 1832.

ELSEVIER

Talanta 44 (1997) 169–176

Talanta

Determination of trace impurities in uranium, thorium and plutonium matrices by solvent extraction and inductively coupled plasma atomic emission spectrometry

Mary Gopalkrishnan[a], K. Radhakrishnan[a], P.S. Dhami[a], V.T. Kulkarni[a], M.V. Joshi[a], A.B. Patwardhan[a], A. Ramanujam[a,*], J.N. Mathur[b]

[a] *Fuel Reprocessing Division, Bhabha Atomic Research Centre, Trombay, Bombay-400 085, India*
[b] *Radiochemistry Division, Bhabha Atomic Research Centre, Trombay, Bombay-400 085, India*

Received 19 January 1996; revised 18 June 1996; accepted 25 June 1996

Abstract

Studies on the determination of trace metallic impurities in nuclear materials such as uranium, thorium and plutonium are described. The bulk of the matrix is separated by batch extraction from their nitric acid solutions using 2-ethylhexyl hydrogen 2-ethylhexyl phosphonate (KSM-17, equivalent to PC88-A). The final aqueous phase containing the metallic impurities is fed to a high-temperature source inductively coupled plasma and the analysis is carried out employing a computer-controlled multichannel direct-reading spectrometer. The studies also included the recovery of impurities at various acidities and spectral interferences of the above matrices over the analyte elements. Based on the above studies, methods were standardized for the determination of 19 elements, viz. Al, B, Be, Ca, Cd, Cr, Cu, Fe, Mg, Mn, Ni, Pb, Si, Zn, Ce, Dy, Eu, Gd and Sm, in U/Th/Pu solutions. The relative standard deviation for various elements is in the range 1–5%.

Keywords: Impurities; Inductively coupled plasma atomic emission spectrometry; Plutonium; Thorium; Uranium

1. Introduction

Uranium and plutonium find application as fuels in different types of nuclear reactors. Thorium is an important fertile material whose irradiation in a reactor yields ^{233}U. These materials are required to meet stringent specifications before use in the nuclear fuel cycle [1,2]. The performance of these nuclear materials depends on several factors, of which purity is particularly important. The presence of impurities beyond specified limits will affect the neutron economy and metallurgical characteristics of the fuel and hence it is necessary to characterize them.

Several techniques have been employed for the determination of trace metals, among which spectrochemical methods are the most common since many elements can be estimated simultaneously in a short time using small quantities of samples.

* Corresponding author.

PII S0039-9140(96)02027-9

The great improvements in excitation sources such as inductively coupled plasma (ICP) and detection with photomultiplier tubes have considerably improved the range, precision and sensitivity of spectrochemical methods.

Direct analysis of these nuclear materials for trace metals is not possible since uranium, thorium and plutonium have very complex spectra with thousands of lines spread over the entire range of 200–500 nm. These lines severely interfere with the analytical lines of the elements of interest. Hence it is desirable either to separate the major matrix or to suppress its excitation. Although the d.c. arc–carrier distillation technique [3] is normally employed, this method is mainly applicable to volatile impurities and has poor reproducibility. Solvent extraction employing various extractants or alternatively the ion-exchange techniques [4–8] have been utilized, wherein the major matrix is first separated from the impurity elements and the aqueous fraction thus obtained is analysed by ICP atomic emission spectrometry (ICP-AES). 2-Ethylhexyl hydrogen 2-ethylhexyl phosphonate (KSM-17, equivalent to PC-88A) has been utilized for the extraction of several metal ions [9]. This extractant has also been used in extraction studies of uranium and plutonium at trace concentrations [10]. This paper describes studies on the extraction and separation of U, Th and Pu from impurity elements using 20% KSM-17 in dodecane or xylene. The aqueous portions are analysed for trace metals using a computer-controlled direct-reading spectrometer.

2. Experimental

2.1. Apparatus

The spectrometer system, consisting of a 48-channel polychromator and computer-controlled scanning monochromator, was aligned with an inductively coupled argon plasma located in a glove-box [11]. With added electronics, the polychromator could be used in the $n+1$ mode along with a scanning monochromator facilitating simultaneous measurements. The instrumental parameters and operating conditions are listed in Table 1.

2.2. Reagents

All acids and water used were quartz distilled. Specpure chemicals were obtained from Johnson Matthey (Royston, UK). The extractant KSM-17, of solvent extraction grade, was supplied by Uranium and Rare Earth Extraction Division of Bhabha Atomic Research Centre. Dodecane was obtained from Transware Chemica (Hamburg, Germany). Xylene was supplied by Merck (India).

2.3. Preparation of standards

Individual elements in metal or compound form (Specpure) were used to prepare stock solutions of 1 g l^{-1} concentration in HNO_3–HCl medium. Taking appropriate aliquots, a composite standard containing 21 elements (Table 2) at different concentration levels ranging between 5 and 25 μg ml^{-1} was prepared and designated the High stan-

Table 1
Instruments and operating conditions

Spectrometers	Jobin Yvon (JY-48) 1 m simultaneous spectrometer having a grating with 2550 grooves mm^{-1} Jobin Yvon (JY-38) 1 m sequential spectrometer having a grating with 3600 grooves mm^{-1}
RF generator	Model JY-2300
Frequency	40.68 MHz
Forward power	1.25 kw
Reflected power	0.05 kw
Nebulizer	Pneumatic concentric type with stainless-steel needle and PTFE nozzle
Plasma torch	Demountable assembly with Mermet configuration with three coaxial concentric tubes; central injector alumina and other tubes of silica glass
Argon gas	
Coolant	18.00 l min^{-1}
Sheathing	0.45 l min^{-1}
Aerosol carrier	0.40 l min^{-1}
Integration	Three periods of 10 s each

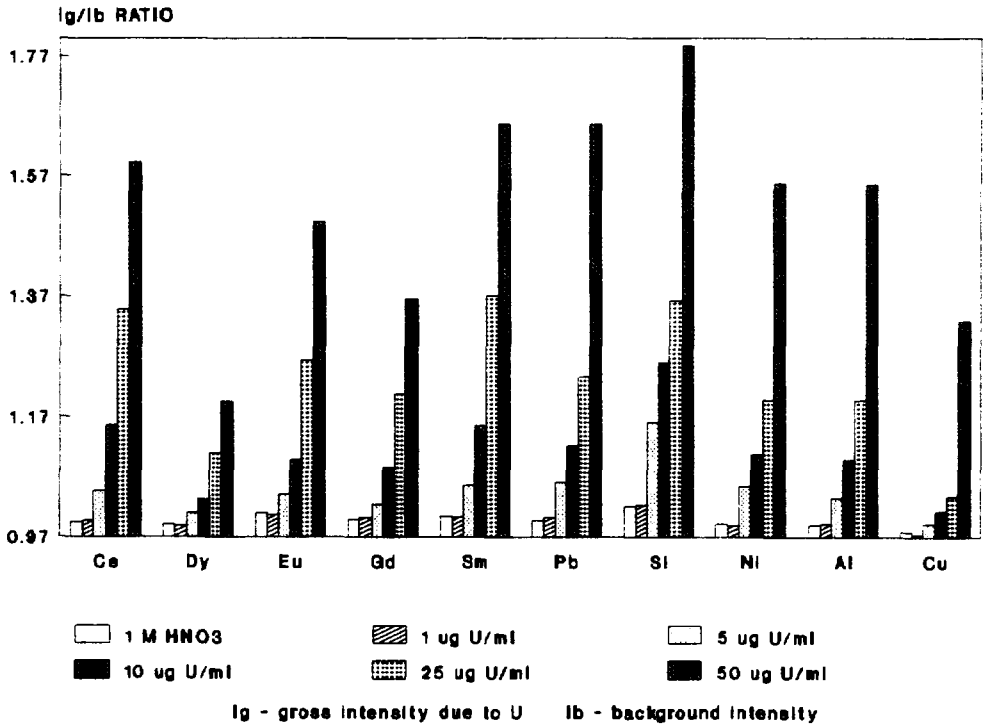

Fig. 1. Effect of uranium on emission intensities of various analytical lines.

dard. Doubly quartz distilled water was used as the low standard. A composite test standard of 1 μg ml^{-1} of each element was used as a check standard for the calculation of precision.

Specpure uranium and thorium oxides were used to prepare stock solutions with metal concentrations of 100 g l^{-1} in HNO_3. Ion-exchange purified and coulometrically certified plutomium nitrate solution was used to prepare the Pu stock solution of 5 g l^{-1}. These solutions were used with appropriate dilutions and acidity adjustments in various studies.

2.4. Preparation of blank

A 10 ml volume of 1 M HNO_3 was contacted three times with 10 ml of 20% KSM-17 in dodecane. The equilibration in this and all other experiments was carried out for 5 min. The aqueous fraction collected at the end of third contact was used as the blank during the analysis of both uranium and plutonium samples. In all the experiments using thorium, xylene was used instead of dodecane as the diluent to avoid third-phase formation problems during extraction. The blank solution for thorium was prepared in the same manner as above.

2.5. Preparation of samples

Uranium oxide or metal samples (1 g of uranium) were dissolved in concentrated. HNO_3 and made up to 10 ml after adjusting the acidity to 1 M HNO_3. A thorium oxide sample, amounting 1 g of Th, was dissolved in a platinum dish using concentrated HNO_3 and HF as described in Ref. [8]. The solution was made up to 10 ml using 1 M HNO_3. The same procedure was adopted for the dissolution of a PuO_2 sample amounting to 50 mg of Pu and the acidity was adjusted to 1 M HNO_3.

Table 2
Elements, wavelengths and detection limits

Element	Wavelengths (nm)	Detection limits by ICP-AES ($\mu g\ g^{-1}$) of	
		U or Th	Pu
Al	308.2	0.05	1.0
B	249.7	0.20	4.0
Be	234.8	0.05	1.0
Ca	396.8	0.10	2.0
Cd	228.8	0.10	2.0
Cr	205.5	0.10	2.0
Cu	324.7	0.05	1.0
Fe	259.9	0.04	0.8
Mg	280.2	0.04	0.8
Mn	257.6	0.05	1.0
Mo	202.0	–	–
Ni	305.0	0.05	1.0
Pb	283.3	0.10	2.0
Si	288.1	0.20	4.0
Zn	213.8	0.20	4.0
Zr	349.6	–	–
Ce	394.3	0.25	5.0
Dy	353.1	0.10	2.0
Eu	393.0	0.10	2.0
Gd	335.0	0.15	3.0
Sm	332.1	0.25	5.0

2.6. Interference studies

Spectral interferences due to uranium for analyte elements were studied using uranium solutions of different concentrations such as 1, 5, 10, 25 and 50 $\mu g\ ml^{-1}$. These solutions were fed into the ICP system without separating uranium and the resultant concentrations due to uranium in different analytical channels were recorded. Similar interference studies were carried out using thorium and plutonium solutions of different concentrations.

2.7. Recovery of impurities

A composite solution containing 21 impurity elements at different concentration levels was prepared. An appropriate aliquot of this composite solution was added to pure uranium solution and made up to 10 ml after adjusting the acidity to 0.5 M HNO_3. This synthetic mixture, containing a total of 1 g of uranium and trace level impurities, was given three contacts with 20% KSM-17 in dodecane. The aqueous fraction was then fed to the ICP system and the analysis was carried out using direct-reading spectrometer. The same extration procedure was followed for pure uranium solution (1 g in 10 ml) and the aqueous fraction collected was used as the blank during these experiments.

Recovery experiments with Th and Pu matrices were conducted in a similar manner, except that in the case of Pu solution, 10 ml contained 50 mg of Pu along with all the impurities.

The recovery studies were also repeated by preparing synthetic mixtures containing impurities in a U/Th/Pu matrix at different acidities such as 1, 2 and 4 M HNO_3.

2.8. Analysis

The aqueous phase obtained after extraction of U/Th/Pu in KSM-17 was analysed using a two-point calibration procedure with a composite standard as the high and doubly distilled water as the low standard. An analytical program incorporating "blank subtraction" mode was written utilizing the source program JY-70 Plasma V-2.3 (Pascal) supplied by Jobin Yvon (France). As mentioned earlier, the ICP source is optically

Table 3
Percentage extraction at 1 M feed acidity

Matrix	Feed concentration ($g\ l^{-1}$)	Extraction (%)			
		1st	2nd	3rd	Total
U	100	85.26	99.72	99.5	~100
Th	100	69.66	99.64	99.27	~100
Pu	5	98.15	98.91	–	~100

Table 4
Recovery of impurities from uranium

Element	Added concentration (μg ml^{-1})	Recovery (%) at acidity			
		0.5 M	1 M	2 M	4 M
Al	5.0	101.2	101.2	101.6	99.8
B	2.0	100.0	100.0	105.0	100.0
Be	2.0	95.0	95.0	110.0	90.0
Ca	5.0	105.5	106.6	107.9	105.8
Cd	2.0	100.0	104.0	90.0	92.0
Cr	5.0	98.4	94.2	93.7	95.9
Cu	5.0	101.2	98.8	102.6	95.8
Fe	5.0	97.9	96.6	82.9	76.0
Mg	5.0	102.0	99.3	99.9	103.8
Mn	5.0	98.2	101.1	100.1	97.3
Mo	5.0	9.4	7.8	4.5	0.5
Ni	5.0	100.3	96.0	98.1	90.3
Pb	5.0	98.9	95.9	103.7	96.4
Si	5.0	101.0	98.0	99.9	100.2
Zn	5.0	100.2	111.1	110.7	107.3
Zr	5.0	3.5	3.4	3.1	2.3
Ce	5.0	96.1	100.6	102.2	104.0
Dy	5.0	64.3	99.0	103.0	101.8
Eu	5.0	100.8	101.2	102.8	97.6
Gd	2.0	95.0	95.0	95.0	95.0
Sm	5.0	99.0	98.9	99.6	101.5

aligned with both spectrometers and this arrangement, combined with suitable software, allowed the simultaneous operation of both spectrometers. Uranium was monitored simultaneously on the sequential spectrometer using the spectral line at 385.9 nm. Similarly, when analysing the aqueous fractions of Th and Pu samples, the spectral lines at 401.9 and 453.6 nm were used for measuring the concentrations of Th and Pu, respectively.

3. Results and discussion

Table 2 lists the wavelengths and detection limits for the various elements as found by ICP-AES utilizing a multichannel direct-reading spectrometer. The limits given were obtained after processing 1 g uranium or thorium or 50 mg plutonium samples. It may be noted that the direction limits achieved in the present method meet the required specification limits for all the elements except boron and a few rare earths. The detection limits for these elements can be improved by increasing the quantity of sample taken for extraction.

It is well know that prior separation of the major matrices helps in achieving lower detection limits. The present extraction studies showed nearly complete removal of the major matrix, thus leaving an aqueous fraction containing U/Th/Pu only at trace levels (<1 μg ml^{-1}) after three contacts with KSM-17. The extent of extraction of the major matrix from 1 M HNO_3 by KSM-17 is given in Table 3. Also, the kinetics of KSM-17 extraction are fast and therefore the time required for separation is considerably reduced. In order to establish the magnitude of spectral interferences, the gross peak intensities (I_g) for 1 M HNO_3 and Specpure uranium solutions (1–50 μg ml^{-1}) were measured at various elemental channels. Similarly, intensities due to doubly distilled water (I_b) were also measured at the peak positions

Table 5
Comparison of the present method with other methods

Ref.	Method of separation	Matrix	Quantity processed	No. of elements determined
This work	Three-stage liquid–liquid extraction of 5 min duration each using 20% KSM-17 in dodecane	U/Th/Pu	1 g/1 g/ 50 mg	19
[4]	Column extraction chromatography using tri(2-ethyl-hexyl) phosphate (TEHP) and di-*n*-hexyl *N*,*N*-diethylcarbamyl methylene phosphonate (DHDECMP)	U	0.2–0.4 g	36
[5]	AGMP-1 anion-exchange resin (50–100 mesh) in HCl	Pu	0.3–0.8 g	32
[6]	Two-step liquid–liquid extraction using 30% TBP in CCl_4 (three contacts) and 0.2 M TOPO–CCl_4 (one contact)	U	10 g	8
[8]	Liquid–liquid extraction using TOPO–xylene and HDEHP–xylene in HNO_3 and HCl with 8–10 contacts	Th	1 g	13

and the ratio I_g/I_b was evaluated; this represents graphically the magnitude of interferences due to uranium for different elements. Since there was a large variation in the magnitude of interferences for different elements, the ratio mode was adopted to show the interferences for the analyte elements simultaneously. Fig. 1 shows a typical graphical representation of the magnitude of spectral interferences at different concentration levels of uranium for those elements whose spectral lines are within a distance of about ± 0.035 nm from the interfering uranium lines [12]. It can be clearly seen that I_g/I_b is practically the same for both 1 M HNO_3 and 1 μg U ml^{-1}, indicating the absence of uranium spectral interference at 1 μg U ml^{-1} and below for the elements shown. For other elements which are not included in Fig. 1, the interference effect is not noticeable even up to 50 μg U ml^{-1} in the aqueous fraction. This suggests that there is no direct spectral interference for these analyte elements at the trace levels of uranium studied. Similarly, no spectral interferences were observed with Th and Pu matrices at levels of 1 μg ml^{-1} and below for the analyte elements studied.

The data obtained during the recovery experiments for 21 elements in the case of U are summarized in Table 4. It can be seen that the recoveries for all the elements at all the acidities studied are in the range 90–110%, except for Dy, Mo, Zr and Fe at all the acidities studied. The recovery improves for Dy at 1 M acidity and above and is almost quantitative; for Mo and Zr it decreases as the acidity increases. For Fe, the recovery is between 98 and 97% at acidities of 0.5–1 M and decreases sharply at 2 and 4 M HNO_3. For the best results, it was decided to maintain an acidity of 1 M for analysis of the samples. Since the recoveries for Mo and Zr are very poor, these elements cannot be determined using the present method.

Table 6
Comparison of detection limits of various methods (all values in $\mu g\ g^{-1}$ of matrix)

Element	Uranium		Thorium			Plutonium	
	[4]	This work	[13]	[8]	This work	[5]	This work
Al	0.081	0.05	25.00	–	0.05	3.80	1.0
B	–	0.20	0.10	–	0.20	2.80	4.0
Be	0.006	0.05	0.10	–	0.05	0.16	1.0
Ca	0.375	0.10	–	–	0.10	0.08	2.0
Cd	0.125	0.10	–	–	0.10	0.56	2.0
Cr	0.125	0.10	10.00	–	0.10	0.74	2.0
Cu	0.125	0.05	10.00	–	0.05	0.22	1.0
Fe	0.125	0.04	10.00	–	0.04	1.02	0.8
Mg	0.006	0.04	–	–	0.04	0.08	0.8
Mn	0.031	0.05	5.00	–	0.05	0.16	1.0
Ni	0.250	0.05	2.00	–	0.05	2.20	1.0
Pb	1.375	0.10	5.00	–	0.10	8.20	2.0
Si	–	0.20	15.00	–	0.20	–	4.0
Zn	0.125	0.20	10.00	–	0.20	0.98	4.0
Ce	–	0.25	–	0.10	0.25	9.20	5.0
Dy	0.125	0.10	–	0.05	0.10	–	2.0
Eu	0.065	0.10	–	0.05	0.10	0.72	2.0
Gd	–	0.15	–	0.01	0.15	–	3.0
Sm	0.313	0.25	–	0.10	0.25	1.99	5.0

The above-mentioned recovery studies were repeated with Th and Pu and the results were similar to those obtained with uranium.

Stripping of Th and Pu from the organic phase could be achieved using 0.3 M oxalic acid containing 0.05 M HNO_3. However, in the case of uranium, back-extraction was possible only with 8 M HCl, where several contacts were necessary for nearly complete recovery.

Huff [4,5] employed column extraction chromatography and anion-exchange separation techniques followed by ICP-AES for the characterization of uranium and plutonium fuels, respectively. Biswas et al. [6] separated uranium by two-step liquid–liquid extraction and determined the rare earths by ICP-AES. Characterization of thorium oxide fuel was carried out by Porwal et al. [13] using a carrier distillation and direct reader technique for common elements, whereas the Bangia et al. [8] determined rare earths in thorium oxide by solvent extraction followed by d.c. arc/photographic detection. A comparison of the salient features of the present procedure along with those cited in the literature is given in Table 5. The greatest advantage of the present method is that a single extractant can be used for the nearly complete separation of all three matrices (U/Th/Pu), thereby permitting the determination of a number of elements simultaneously, including the rare earths.

The detection limits in the present method are compared with those of other methods in Table 6. It can be seen that for uranium and plutonium the detection limits are comparable to those reported in Refs. [4] and [5], respectively, for most of the elements. For thorium, the detection limits for rare earths are comparable to those reported in Ref. [8], whereas those obtained for all the other elements except boron are lower than the values given in Ref. [13]. Hence the present procedure for the extraction of the major matrix and determination of metallic impurities is superior than those used earlier.

4. Conclusion

The separation of major matrices such as ura-

nium, thorium and plutonium from trace metals using KSM-17 and subsequent analysis of the aqueous fraction for trace impurities by ICP-AES has several advantages. Since the kinetics of KSM-17 extraction are fast, the time required for separation is considerably reduced. Analysis by computer-controlled ICP-AES not only yields highly reproducible results but also increases the analytical throughput manyfold. The acidity adjustment is not critical for most of the impurity elements. Uranium, thorium and plutonium can easily be extracted in KSM-17 over a wide range of HNO_3 concentrations. The methods standarized here can be effectively employed for the routine determination of the trace metal constituents in these nuclear materials.

Acknowlegements

The authors are grateful to Shri. N. Venkataraman, Head, Fuel Reprocessing Division, for his keen interest and encouragement during the course of this work.

References

[1] A.G. Page, DAE Symp. on Nuclear and Radiochemistry, Visakhapatnam, IT-7, December 21–24, 1992, pp. 45–53.
[2] A.R. Kaufmann, Nuclear Reactor Fuel Elements (Metallurgy and Fabrication), Interscience, New York, 1962.
[3] B.F. Scribner and M.R. Mullin, J. Res. Natl.Bur. Stand., 37 (1946) 379.
[4] Ed.A. Huff, Spectrochim. Acta, Part B, 42 (1987) 275.
[5] Ed.A. Huff and D.L. Bowers, Appl. Spectrosc., 43 (1989) 223.
[6] S.S. Biswas, P.S. Murthy, A. Sethumadhavan, R. Kaimal and A.V. Sankaran, Anal. Lett., 24 (1991) 887.
[7] A.B. Patwardhan, M.V. Joshi, V.T. Kulkarni, K. Radhakrishnan, S. Sumathi and M. Jacob, Bhabha Atomic Research Centre, Bombay, India, Report No. BARC/E-027, 1993.
[8] T.R. Bangia, V.C. Adya, B.A. Dhawale, B. Rajeswari, M.D. Sastry and P.R. Natarajan, Anal. Lett., 23 (1990) 147.
[9] PC-88A, A Reagent for Metal Extraction, Technical Bulletin 3-83-02, Daihachi Chemical Industry, Japan, 1983.
[10] K.S. Rao, G.A. Inamdar and A. Ramanujam, National Symp. on Organic Reagents—Synthesis and Use in Extraction Metallurgy, BARC, PP-18, February 9–11, 1994, p. 44.
[11] R.K. Dhumwad, A.B. Patwardhan, V.T. Kulkarni and K. Radhakrishnan, 6th ISAS National Symp., RSIC, Shillong, November 15–17, 1988, p. 33.
[12] G.R. Harrison, Wavelength Tables, MIT Press, Cambridge MA, 1939.
[13] N.K. Porwal, A.A. Argekar, P.J. Purohit, A.G. Page and M.D. Shastry, Fresenius' J. Anal. Chem., 338 (1990) 255.

ELSEVIER

Talanta 44 (1997) 177–183

Talanta

Spectrophotometric determination of iron(III) dimethyldithiocarbamate (ferbam)

Ashok Kumar Malik[a], A.L.J. Rao[b,*]

[a]*Department of Chemistry, D.A.V. College, Jalandhar-144008, India*
[b]*Department of Chemistry, Punjabi University, Patiala-147002, India*

Received 15 October 1996; revised 24 June 1996; accepted 26 June 1996

Abstract

A spectrophotometric method was developed for the determination of ferbam (iron(III) dimethyldithiocarbamate) by converting it into an iron–phenanthroline complex, which was then absorbed on microcystalline naphthalene in the presence of tetraphenylborate, and the absorbance was measured at 515 nm against a reagent blank. The molar absorptivity of the complex was 1.2×10^4 l mol^{-1} cm^{-1}. Ten replicate analyses of a sample solution containing 150 μg of ferbam gave a relative standard deviation of 0.84%. Beer's law was obeyed over the concentration range 22.4–372.9 μg of ferbam. The effects of various factors such as reagent concentration and naphthalene, shaking time and diverse ions were studied in detail. The method is sensitive and selective and can be applied to the direct determination of ferbam in commercial samples and in mixtures containing various other dithiocarbamates (e.g. ziram, zineb and maneb) in foodstuffs.

Keywords: Ferbam determination; Iron(III) dimethyldithiocarbamate; Spectrophotometry

1. Introduction

Ferbam (iron(III) dimethyldithiocarbamate) is widely used as a protective fungicide in agriculture. Most of the methods for the determination of ferbam, like other dithiocarbamates, is based on its decomposition by hot mineral acid to the amine and carbon disulphide [1,2]. Dithiocarbamates have also been determined in vegetable foodstuffs using high-performance liquid chromatography [3], extraction voltammetry [4] and titrimetry [5]. Ferbam is determined by converting it into molybdenum [6] and copper [7] complexes in an acidic medium and into a selenium [8] complex by extraction into chloroform. The extraction of the molybdenum complex is slow and requires about 5 min of shaking. Ferbam can also be determined by its decomposition and extraction of the diphenylcarbazone complex [9] of iron into isobutyl methyl ketone. Dithiocarbamate fungicides have also been determined by headspace gas chromatography [10] of the CS_2 evolved under controlled conditions from foodstuffs, atomic absorption spectrometry [11] and

* Corresponding author.

PII S0039-9140(96)02029-2

similar methods as given by the Analytical Methods Committee [12]. Here we present a relatively simple, rapid, sensitive and selective method by converting ferbam into iron–1,10-phenanthroline and adsorption on microcrystalline naphthalene in the presence of tetraphenylborate.

2. Experimental

2.1. Reagents

2.1.1. Ferbam solution

All reagents were of analytical-reagent grade. Ferbam was prepared by the reported method [13] and its purity was checked by elemental analysis. The iron content was checked by decomposing it with concentrated nitric acid and determining the iron by EDTA titration using Variamine Blue B as indicator [14]. A stock solution of ferbam (0.1%) was prepared by dissolving 100 mg in 100 ml of acetonitrile.

2.1.2. 1,10-Phenanthroline (phen) solution (1.0%)

Prepared by dissolving 1.0 g of phen in 100 ml of distilled water with warming.

2.1.3. Hydroxylamine hydrochloride (5%)

Prepared by dissolving 5 g in 100 ml of distilled water.

2.1.4. Sodium tetraphenylborate solution

A 2% solution in water was prepared.

2.1.5. Naphthalene solution

A 20% solution in acetone was prepared.

2.1.6. Buffer solution

Acetate buffer was prepared by dissolving 68 g of sodium acetate trihydrate in 400 ml of distilled water, adjusting the pH to 4.25 by adding 25–30 ml of glacial acetic acid and diluting to 500 ml.

2.1.7. Stock solutions for the study of interferences

Stock solutions of different salts were prepared by dissolving them in water. Disodium ethylenebis(dithiocarbamate) (nabam), zinc dimethyldithiocarbamate (ziram), zinc ethylenebis(dithiocarbamate) (zineb), managanese ethylenebis(dithiocarbamate) (maneb) and tetramethylthiuram disulphide (thiram) were obtained from Wilson Laboratories (Bombay, India). Sodium monomethyldithiocarbamate (vapam), sodium dimethyldithicarbamate (dibam), sodium *N*-methylanilinecarbodithioate and potassium morpholinecarbodithoate [15] and xanthates [16] (ethyl, isopropyl and butyl) used in the interference study were prepared in the laboratory by reacting amine/alcohol, carbon disulphide and sodium/potassium hydroxide at a low temperature (below 4°C) using an ice-salt mixture. The solids (except dibam, which is a liquid) were separated by filtration, washed with diethyl ether and recrystallized. Solutions of dithiocarbamates were prepared by dissolution in distilled water or, for the more insoluble preparations, in organic solvents: ziram and thiram in acetonitrile (Merck Pure) and zineb and maneb in dimethyl sulphoxide. Synthetic samples were prepared by mixing the solutions of the constituents to give the required composition.

2.2. Equipment

The spectral measurements were made on a Bausch and Lomb Spectronic 20 spectrophotometer and an Elico pH meter was used for the pH measurements.

2.3. General procedure for determination of ferbam

To a known volume of solution ($\leqslant 3$ ml) containing 22.4–372.9 μg of ferbam taken in a 100 ml Erlenmeyer flask were added 1.0 ml of phen, 1.5 ml of hydroxylamine hydrochloride, 1.5 ml of acetate buffer (pH 4.25) and 1.0 ml of sodium tetraphenylborate, and the volume was made up to 40 ml with distilled water. This solution was mixed and allowed to stand for 5 min, following which 1.0 ml of naphthalene solution was added and shaken vigorously for 1 min. The naphthalene containing the complex was separated by filtration, air dried in the folds of the filter-paper, dissolved in dimethylformamide (DMF) and diluted to 10 ml with DMF. A preliminary study

Table 1
Determination of ferbam in some commercial samples

Sample	Ferbam present (μg)	Ferbam found (μg)			
		Proposed method	RSD (%)	Method of Ref. [7]	RSD (%)
Fermacarb	15	14.8	1.3	14.7	1.5
	30	29.8	1.5	29.7	1.8
	50	49.6	1.7	49.5	1.9
	100	98.9	2.1	98.8	2.0
	150	149.1	2.2	149.0	2.4
Ferbam (75 WP)	15	14.9	1.5	14.6	1.6
	30	29.7	1.7	29.6	1.7
	50	49.8	1.8	49.7	1.9
	100	99.2	2.0	98.7	2.1
	150	148.8	2.2	148.6	2.3
Ferbam (85% WP)	15	14.4	1.8	14.2	1.9
	30	39.4	1.8	38.9	2.1
	50	49.1	2.2	48.9	2.3
	100	98.6	2.3	98.5	2.3
	150	148.6	2.4	140.0	2.4

[a] Average of ten experiments.

confirmed that the adsorption was complete in one step. Therefore, the absorbance of the DMF solution was measured at 515 nm against a reagent blank prepared under similar conditions.

2.4. Formulation analysis

The method was applied to the determination of ferbam in different commerical samples: Fermacarb containing 75% ferbam, Ferbam 75% WP and Ferbam 85% WP. The formulated products were dissolved directly in acetonitrile, filtered and analysed by the general procedure. Table 1 shows the results of the determinations. The results obtained by the present method were compared with those obtained by the method of Rangaswamy et al. [7].

2.5. Determination of ferbam in crops

A known amount of ferbam in acetonitrile was mixed with 5 g of grain (rice or wheat) and shaken mechanically with 10 ml of chloroform for 5 min. The mixtures were filtered and the residue in the funnels were washed with three 5 ml portions of chloroform. The extracts were evaporated to 2.0 ml on a water-bath and the remaining solvent was removed by blowing a current of dry air at room temperature. The residues were dissolved in acetonitrile and the ferbam content was determined by the general procedure. Untreated samples were taken as a reference. The results of the determinations are given in Table 2.

2.6. Determination of ferbam in synthetic samples

Ferbam was deterimined by the general procedure in synthetic samples prepared by mixing solutions of the constituents. The results are given in Table 3.

3. Results and discussion

The absorption spectra of the iron–phen–TPB complex collected on microcrystalline naphthalene was recorded against the reagent blank prepared under similar conditions. The complex shows maximum absorbance at 515 nm. The absorbances of the reagent and reagent blank were

Table 2
Determination of ferbam in fortified samples

Grain[a]	Ferbam added (μg)	Ferbam found (μg)[b]			
		Proposed method	RSD (%)	Method of Ref. [7]	RSD (%)
Rice	15	14.6	1.8	14.5	1.9
	30	28.5	2.9	28.4	1.9
	50	48.6	1.9	48.5	2.0
	100	98.8	2.0	98.3	2.1
	150	148.2	2.3	148.2	2.2
Wheat	15	14.4	2.1	14.3	2.1
	30	28.9	2.4	28.8	2.3
	50	48.7	2.5	48.5	2.6
	100	98.9	2.4	98.7	2.4
	150	148.6	2.6	147.8	2.5

[a] Amount of grain = 5 g.
[b] Average of three experiments.

Table 3
Determination of ferbam in synthetic samples

No.	Component	Content (%)	Amount of ferbam (μg)[a]		
			Taken	Found	RSD (%)
1	Ferbam	50	60.0	59.9	2.3
	Thiram	50			
2	Ferbam	50	85.0	84.3	1.9
	Zineb	50			
3	Ferbam	80	60.0	60.3	1.7
	Maneb	20			
4	Ferbam	50	40.0	39.8	2.5
	Ziram	50			
5	Ferbam	50	70.0	69.1	1.8
	Thiram	15			
	Ziram	15			
	Zineb	10			
	Maneb	10			
6	Ferbam	11.76	80.0	80.3	1.9
	Maneb	76.48			
	Zineb	11.76			

[a] Average of ten experiments.

negligible at this wavelength. The reaction conditions were examined for 150 μg of ferbam. The optimum pH for the determination of ferbam (Fig. 1) was 2.0–6.5, and pH 4.25 was selected. It was observed that 1.0 ml of 1,10-phenanthroline, 1.5 ml of hydroxylamine hydrochloride and 1.0 ml of sodium tetraphenylborate were sufficient for the determination of ferbam. Adsorption on naphthalene was quantitative when 0.5 ml of 20% naphthalene solution was used with shaking for 30 s. However, for better results, 1.0 ml of naphthalene solution was used and the solution was

shaken vigorously for 1 min. The effect of the aqueous phase on the absorbance was studied by varying the aqueous phase volume between 40 and 2500 ml and applying the general procedure. It was observed that the absorbance remained constant up to 2000 ml but then decreased with increase in the aqueous phase volume. Hence 40 ml of the aqueous phase was maintained.

The method was repeated for the determination for ferbam in the filtrate and negligible absorbance was observed, indicating complete adsorption in the first step.

3.1. Beer's law and sensitivity

The calibration graph for ferbam under the optimum conditions was linear over the concentration range 22.4–372.9 μg of ferbam in dimethylformamide. Ten replicate determinations on sample solutions containing 150 μg of ferbam gave a relative standard deviation of 0.84%. The molar absorptivity was calculated to be 1.2×10^4 l mol^{-1} cm^{-1} at 515 nm.

3.2. Composition of the complex

The Job, mole ratio and logarithmic methods indicated the adsorption of a 1:3:2 (Fe:phen:TPB) complex under these conditions (Fig. 2).

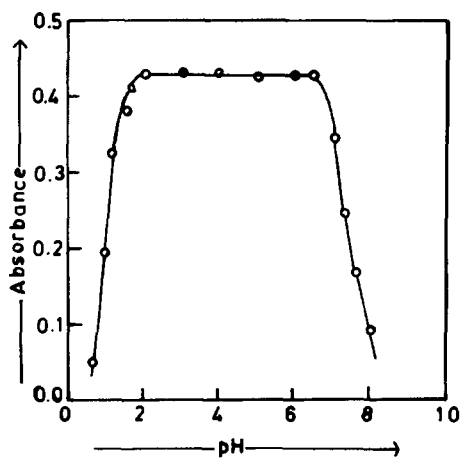

Fig. 1. Effect of pH. Ferbam, 150 μg; wavelength, 515 nm; 1% 1,10-phenanthroline, 1.0 ml; 2% sodium tetraphenylborate, 1.0 ml; 20% naphthalene, 1.0 ml; shaking time, 1 min; reference, reagent blank.

3.3. Interferences

The procedure was applied to the determination of 150 μg of ferbam in the presence of diverse ions. The following foreign ions (mol l^{-1}) did not interfere in the determination of ferbam: bromide

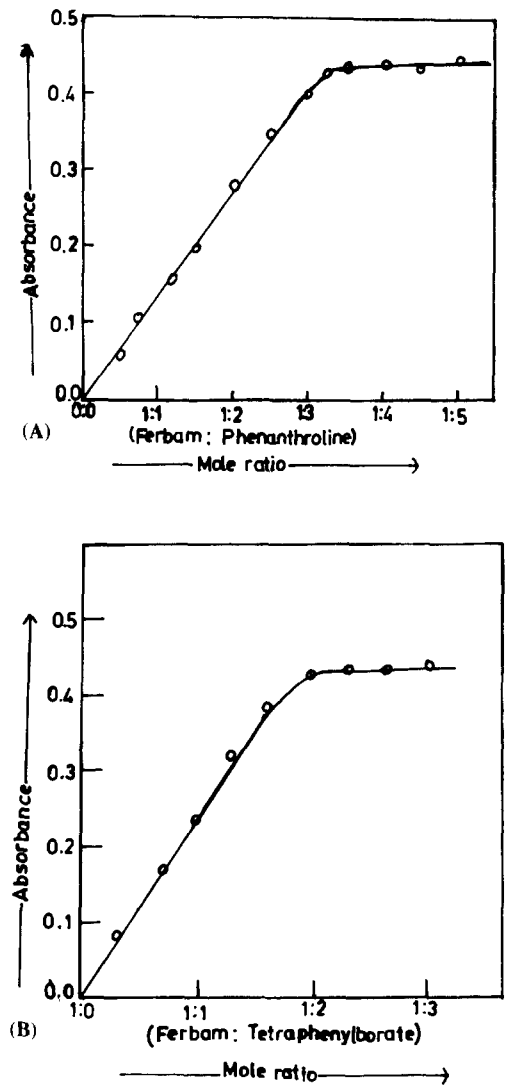

Fig. 2(a). Mole ratio method (comparison with respect to 1,10-phenanththroline). Ferbam, 0.36×10^{-4} M; tetraphenylborate, 0.72×10^{-4} M pH, 4.25; other conditions as in Fig. 1. (b) Mole ratio method (composition with respect to tetraphenylborate). Ferbam 0.36×10^{-4} M; 1,10-phenanthroline, 1.08×10^{-4} M; pH, 4.25; other conditions as in Fig. 1.

Table 4
Comparison of molar absorptivity with other methods

Molar absorptivity (l mol^{-1} cm^{-1})	Method	Comment	Reference
1.33×10^4	Molybdenum	Requires acidic medium (4 N H_2SO_4) and a shaking time of 5 min	[6]
1.46×10^4	Selenite	Not selective for ferbam	[8]
5.3×10^4	Diphenylcarbazone	Interference due to maneb, ziram, zineb, etc., can only be avoided by using masking agents	[9]
1.2×10^4	1,10-Phenanthroline	Highly selective for ferbam	This work

(0.31), chloride (0.71), sulphate (0.26), perchlorate (0.25), acetate (0.42), iodide (0.20), nitrate (0.40), oxalate (0.42) orthophosphate (0.13), citrate (0.13×10^{-2}) and EDTA (0.2×10^{-3}). Of the metal ions examined, Pb^{II} (0.36×10^{-4}) Zn^{II} (0.15×10^{-4}) Cu^{II} (0.57×10^{-4}) Bi^{III} (0.53×10^{-4}) and Cd^{II} (0.49×10^{-4} mol l^{-1}) could be tolerated. Fe^{II} and Fe^{III}, if present along with ferbam, interfere, but this interference can be avoided by pre-extraction of ferbam into chloroform, where Fe^{II} and Fe^{III} remain in the aqueous phase and ferbam can be determined by the general procedure after evaporation of the chloroform to dryness. Of the dithiocarbamates and xanthates examined vapam (0.39×10^{-3}), dibam (0.34×10^{-3}), thiram (0.2×10^{-3}), nabam (0.18×10^{-3}), zineb (0.18×10^{-3}), maneb (0.19×10^{-3}), potassium morpholinecarbodithioate (0.25×10^{-3}), sodium *N*-methylanilinecarbodithioate (0.24×10^{-3}), butyl xanthate (0.35×10^{-3}), isopropyl xanthate (0.32×10^{-3}) and butyl xanthate (0.3×10^{-3}), each tested upto the concentration given in the parentheses (mol l^{-1}), did not interfere in the determination of 150 μg of ferbam in 10 ml of final solution, because they do not undergo complex formation with 1,10-phenanthroline under these conditions.

4. Conclusion

Ferbam, if present with nabam, ziram, zineb, maneb, vapam, sodium dimethyldithiocarbamate, sodium diethyldithiocarbamate and potassium morpholinecarbodithioate, can be determined safely and without any interference by the proposed method. This is not possible with other published methods. The present method is more sensitive than the CS_2 evolution methods, as described by Cullen [17], Chmiel [18] and others, where a minimum 20 μg of CS_2 evolved equivalent to 36.46 μg of ferbam can be determined. It is more sensitive than the direct methods reported by Rangaswamy et al. [7] (0.8 μg ml^{-1}), Verma et al [19] (0.6 μg ml^{-1}), Rao and co-workers (1.0 μg ml^{-1} [8] and 0.8 μg ml^{-1} [9]). With the present method it is possible to determine 0.56 μg ml^{-1} of ferbam, equivalent to 0.31 μg ml^{-1} of evolved CS_2. A comparison of molar absorptivity with some earlier methods is given in Table 4. The wide applicability, simplicity and selectivity of this method makes is preferable to others.

References

[1] D.G. Clarke, H. Baum, E.L. Stanley and W.E. Hester, Anal.Chem., 23, (1951) 1842.
[2] B.W. Simpson, Pestic Sci., 2, (1971) 127.
[3] K.H. Gustafsson and C.H. Falhgren J. Agric. Food Chem. 31, (1983) 461.
[4] N.A. Vlaknovich, E.D. Medyantseva, V.F. Frolova and O.N. Romanova, Zh. Anal. Khim., 38, (1983) 1963.
[5] B.C. Verma, H.S. Sidhu and R.K. Sood, Talanta 29, (1982) 703.
[6] A.L.J. Rao and N. Verma, J. Indian Aca. Forensic Sci. 24, (1985) 1.

[7] J.R. Rangaswamy, P. Poomima and S.K. Majumdar, J. Assoc. Off. Anal. Chem., 53, (1970) 1043.
[8] A. Kumar, A.L.J. Rao and B.K. Puri, Int. J. Environ. Anal. Chem., 44, (1991) 159.
[9] A.K. Malik and A.L.J. Rao, Talanta 38, (1991) 941.
[10] H.A. McLeod and K.A. McCulley, J. Assoc. Off. Anal. Chem., 52, (1969) 1226.
[11] M. Uno, T. Okada, M. Nozawa and K. Tonigawa, Shokuhin Eisengaten Zasshi, 23 (1982) 474, Anal. Abstr. 46 (1984) 3G18
[12] Analytical Methods Committee, Analyst 106, (1981) 782.
[13] Monsanto Chemical, Br. Pat. 692, (1953) 063.
[14] A.I. Vogel, A Text Book of Quantitative Inorganic Analysis, Longman, London, 3rd edn., 1969, p. 444.
[15] G. Marcotrigiano, G.C. Pallacani, C. Pretti and G. Tosi, Bull. Chem. Soc. Jpn., 48, (1975) 1018.
[16] C.C. Dewitt and E.E. Roper, J. Am. Chem. Soc., 54, (1932) 444.
[17] T.E. Cullen, Anal. Chem. 36, (1964) 221.
[18] Z. Chmiel, Chem. Anal. (Warsaw), 24, (1979) 505.
[19] B.C. Verma, R.K. Sood, A. Sood S, Chauhan and D.K. Shorma, Proc. Indian Nalt. Sci. Acad. A, 52, (1986) 662.

ELSEVIER

Talanta 44 (1997) 185–188

Talanta

Simultaneous determination of trace amounts of zinc, lead and copper in rum by anodic stripping voltammetry

Paulo J.S. Barbeira[a], Nelson R. Stradiotto[b]

[a]*Instituto de Quìmica de São Carlos, USP, Caixa Postal 780, 13560-970 São Carlos, SP, Brazil*
[b]*Departamento de Quìmica, FFCLRP, USP, Avc. Bandeirantes 3900, 14040-901 Ribeirão Preto, SP, Brazil*

Received 13 December 1995; revised 24 June 1996; accepted 26 June 1996

Abstract

The determination of traces of Zn, Pb and Cu in rum samples by anodic stripping voltammetry without previous treatment or addition of a supporting electrolyte, using a hanging mercury drop electrode, is described. The choice of an appropriate stripping voltammetric method and deposition potential minimizes the influence of the organic content and ensures good reproductibility of the measurements. The reliability of the method was tested by comparing the results with those given by absorption spectrometry, the differences being about 10%. The method allows heavy metal ions to be determined in the $\mu g\ l^{-1}$ concentration range.

Keywords: Anodic stripping voltammetry; Copper; Lead; Rum; Zinc

1. Introduction

Rum is an alcoholic distillate from fermented sugar cane molasses, having an alcoholic content of about 40% (v/v) and can be consumed pure or matured. It is a widely consumed alcoholic beverage and the control of its heavy metal content is fundamental both from a toxicological point of view and with regard to its acceptance as an alcoholic beverage.

The application of voltammetric techniques, such as polarography and stripping analysis, for heavy metal determinaiton in distilled beverages has only occasionally been reported [1–7], despite their high precision and sensitivity. The procedures requires a previous treatment of the sample for the elimination of organic species, which can be adsorbed on the working electrode surface and suppress the reduction waves. Despite these phenomena, it has been demonstrated that the direct determination of heavy metals in alcoholic beverages, such as Brazilian sugar cane spirits [8], tar and ginger cognacs [9], is possible.

This paper reports the determination of traces of heavy metals in rum samples, pure and oak cask matured, by anodic stripping voltammetry (ASV) with a hanging mercury drop electrode without previous treatment and in the absence of

PII S0039-9140(96)02030-9

a supporting electrolyte. The results were compared with those obtained by atomic absorption spectrometry (AAS).

2. Experimental

2.1. Apparatus and reagents

The instrument used for the ASV analysis was an IBM-PC interfaced instrument consisting of a BASIC program [10], a converter interface and a Metrohm Model E506 polarograph coupled with Metrohm Model 663VA stand. The polarographic cell contained a working electrode (Metrohm Model 6.1246.020 multi-mode electrode), a carbon rod (Metrohm model 6.123.345) as auxiliary electrode and an $Ag/AgCl/KCl_{sat}$ reference electrode.

The AAS measurements were carried out in an atomic absorption/flame emission spectrophotometer (Shimadzu Model AA-680), equipped with an air–acetylene burner of 10 cm slot burner head and metal cathode-hollow lamps (Zn, Pb and Cu). The optimum instrumental conditions for each elements were fixed automatically by the equipment [11].

Triply distilled mercury and stock standard solutions (500 mg L^{-1} each for Zn, Pb and Cu) were prepared by dissolving the metal in nitric acid and diluting as required. The water used was distilled and deionized.

2.2. Analytical procedure

Each mixture and series of standard solutions was analysed by ASV and the peak current was plotted as a function of the metal content. Three measurements were carried out for each sample and the statistical treatment of the data was performed according to Miller and Miller [12,13].

The AAS measurements were carried out by introducing the samples directly into the flame and the absorbances were obtained after a prespray time of 3 s and an integration time of 5 s. The absorbance values were plotted as a function of the standard concentration added. Triplicate measurements were carried out and the data were treated as earlier.

3. Results and discussion

The ASV analysis is subject to the influence of surface-active agents, such as organic species, which can adsorb strongly on the electrode surface, affecting either the metal depostion or the stripping process [14]. This problem is generally circumvented by subjecting the sample to a previous treatment to eliminate the organic species, which can result in losses of analytes and contamination. However, depending on the conductivity of the sample, the analysis can be carried out without such treatment, even in the presence of organic substances, where a suitable deposition potential allows the metallic ions to be deposited on the electrode surface, avoiding the adsorption–desorption phenomena caused by the surface-active species present in the sample [15].

Despite the complex composition of rum, owing to the different organic compounds present in the raw materials (e.g. organic acids, phenolic compounds, esters and higher alcohols), a deposition potential of about −1.3 V vs. Ag/AgCl, allows the metallic ions to be deposited on the electrode surface, minimizing the adsorption of the surface-active species present in the samples.

In order to elucidate the influence of the organic content on the stripping response, different anodic stripping methods were tested, viz. linear-sweep, differential-pulse and square-wave modes. Fig. 1 shows that the voltammograms obtained with the linear-sweep mode gave better resolution of the Zn, Pb and Cu waves than the square-wave and differential-pulse modes, in agreement with results for Brazilian sugar cane spirits [8]. Despite their high sensitivity, high-frequency voltammetric techniques, such as differential-pulse and square-wave methods, are more sensitive to small changes in the rate of the electrode reaction and give rise to organic adsorption–desorption peaks, obscuring or not permitting a good resolution of the metal stripping peaks [15]. On the other hand, the lower sensitivity of linear-sweep voltammetry permitted a good resolution of the metal stripping waves, mainly for Cu. As the Zn, Pb and Cu contents are of the same order of magnitude, the determinations of these ions were performed simultaneously, which was not possible for the

Brazilian sugar cane spirits because its higher copper content (approximately 1 mg l^{-1}) and lower lead content (approximately 10 μg l^{-1}).

The best operating conditions obtained for the determination of traces of Zn, Pb and Cu in rum samples by linear-sweep ASV were Hg drop size 0.52 mm^2, deposition potential −1.3 V vs. $Ag/AgCl_{sat}$, deposition time 600 s, conditioning time 20 s and anodic scan rate 50 mV s^{-1}.

In contrast to Brazilian sugar cane spirits, in rum determinations faster scan rates (50 instead of 5 mV s^{-1}) and larger drop sizes (0.52 instead of 0.25 mm^2) can be used to obtain well defined stripping waves. This difference is due to the presence of different organic species in the beverages that adsorb on the electrode surface, causing distinct interferences on the stripping waves.

Fig. 2 shows the resulting voltammograms obtained after the successive standard additions. The sucessive addition of 25 μL of standard did not cause any significant potential peak shifts or any other alterations to the voltammograms, except for an increase in peak current.

In order to verify the behaviour of different organic matrices, the method was tested with four rum samples of two different types: pure (R1 and R2) and oak-cask matured (R3 and R4). Fig. 3 shows typical linear-sweep stripping voltammograms obtained for the determination of heavy metal ions directly in different samples of rum.

The metal ion contents obtained by ASV and AAS are given in Table 1. As can be seen, the

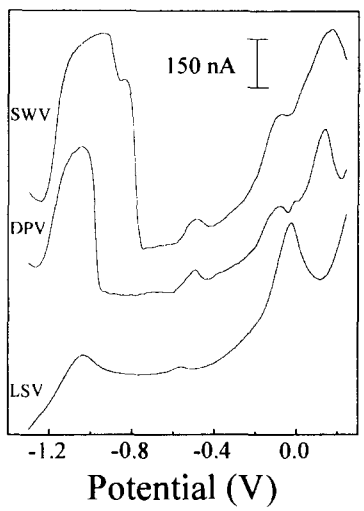

Fig. 1. Voltammograms obtained for rum sample R2 with different anodic stripping techniques: SWV square-wave; DPV, differential-pulse LSV, linear-sweep voltammetry. Operating conditions: SWV, frequency 50 Hz and pulse amplitude +50 mV; DPV, scan rate 10 mV s^{-1} and pulse amplitude +50 mV; LSV, scan rate 50 mV s^{-1}.

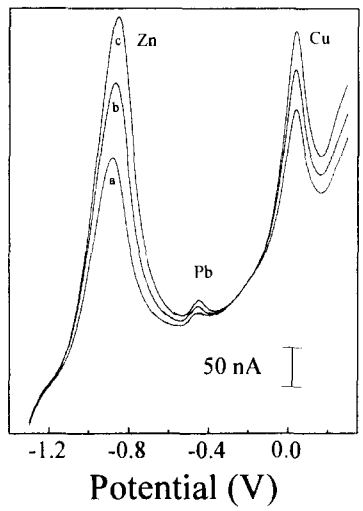

Fig. 2. Linear-sweep anodic stripping voltammograms after successive standard additions for a 5 ml rum sample (R2): (a) 0; (b) 25 and (c) 50 μl. Standard concentrations: Zn, 20; Pb, 20; Cu, 10 mg l^{-1}.

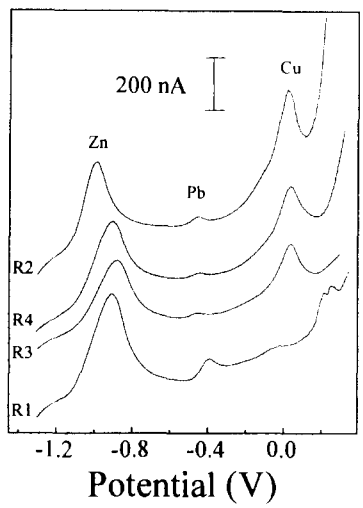

Fig. 3. Linear-sweep anodic stripping voltammograms for different samples of rum (R1 and R2, pure; R3 and R4, oak-cask matured).

Table 1
Concentrations ($\mu g\ l^{-1}$) of Zn, Pb and Cu ions in rum samples

Sample	Element	ASV	AAS
R1	Zn	64 ± 4	70 ± 15
	Pb	65 ± 4	Not detected
	Cu	3 ± 1	Not detected
R2	Zn	44 ± 3	48 ± 11
	Pb	32 ± 3	Not detected
	Cu	14 ± 2	Not detected
R3	Zn	69 ± 3	62 ± 14
	Pb	52 ± 2	Not detected
	Cu	45 ± 3	Not detected
R4	Zn	59 ± 6	68 ± 17
	Pb	23 ± 6	Not detected
	Cu	20 ± 2	Not detected

results obtained by ASV are in agreement with the AAS results with discrepancies of about 10%. The relative errors of the stripping measurements were similar to those for AAS (4%).

The stripping method has the important advantage over AAS of a lower detection limit. For AAS the detection limits are 0.02, 0.2 and 0.09 mg l^{-1} for Zn, Pb and Cu respectively [11], which explains the inability to measure Pb and Cu in all samples. For ASV, these limits can be improved, if necessary, by increasing the deposition times. A further advantage is the simultaneous determination of the three ions, provided that they are present at similar concentrations, and the method is suitable for application in routine analysis.

Acknowledgements

The authors acknowledge the support of this research by CAPES and CNPq.

References

[1] Y. Yamazaki, Bunseki Kagaku, 31 (1982) 309.
[2] Y. Chen, D. Cao, S. Wei, R. Wang and G. Ding, Shipin Yu Fajiao Gongye, 1 (1984) 11.
[3] M. Ma, Zhonghua Yugangyixue Zazhi, 19 (1985) 168.
[4] S. Mannino, Riv. Soc. Ital. Sci. Aliment., 1–2 (1986) 11.
[5] S. Wang and Z. Ni, Yingyong Huaxue, 3 (1986) 81.
[6] S. Liang and X. Li, Lihua Jianyan, Huaxe Fence, 28 (1992) 357.
[7] J. Pisch, J. Shäfer and D. Frahne, GTI Fachz. Lab., 37 (1993) 500.
[8] P.J.S. Barbeira, L.H.Mazo and N.R. Stradiotto, Analyst 120 (1995) 1647.
[9] P.J.S. Barbeira and N.R. Stradiotto, J. Braz. Chem. Soc., in press.
[10] S.A.S. Machado, L. H. Mazo and L.A. Avaca, J. Braz. Chem. Soc., 3 (1992) 89.
[11] Instruction Manual: Atomic Absorption/Flame Emission Spectrophotometer, Shimadzu, Kyoto, 1991.
[12] J.C. Miller and J.N. Miller, Analyst, 113 (1988) 1351.
[13] J.N. Miller, Analyst, 116 (1991) 3.
[14] J. Wang, Stripping Analysis: Principles, Instrumentation and Applications, VCH, Deerfield Beach, FL, 1985.
[15] T.M. Florence, Anal. Chim. Acta, 119 (1980) 217.

ELSEVIER

Talanta 44 (1997) 189–196

Talanta

Development of reference materials for the analysis of acid-extractable metals in sludge

Stuart J. Nagourney, Nicholas J. Tummillo, Jr., John Birri, Kenneth Peist, Jean S. Kane

State of New Jersey Department of Environmental Protection, Laboratories and Quality Assurance, CN 411, Trenton, NJ 08625-0411, USA

Received 3 April 1996; revised 24 June 1996; accepted 25 June 1996

Abstract

The development of reference materials to verify the determination of metals in sludge is described. Effluents from domestic and industrial treatment facilities were dried, size-reduced and homogenized. Multiple aliquots of each material were analyzed in two different government laboratories to determine reference values for the acid-extractable concentrations of more than 15 metals. These acid-extractable concentrations are distinct from total metal values. Different sample preparation and instrumental methods, along with internal quality assurance protocols, were used to confirm the results. The data show good agreement for most metals in the domestic material. Reference values for the leachable concentrations of several toxic metals and major constituents will become part of the Certificate of Analysis for Standard Reference Material (SRM) 2781 issued by the National Institute of Standards and Technology (NIST). Data for the candidate industrial sludge reference material are also presented and discussed.

Keywords: Acid-extractable metals; Atomic absorption spectrometry; Inductively coupled plasma atomic emission spectrometry; Microwave digestion; Reference materials; Sludge

1. Introduction

New Jersey Department of Environmental Protection (NJDEP) regulations require sewage treatment plants to limit the levels of toxic substances in their sludge effluents. Once maximum contaminant levels are established, they become part of the facility's operating permit. When chemical analyses indicate that these permit levels are being exceeded, the NJDEP has statutory authority to assess significant monetary penalties.

Treatment plants process influents from a variety of domestic and industrial sources, resulting in sludges of widely varying physical and chemical composition. Pre- and post-treatment residual management practices also generate sludges of widely varying compositions from liquids containing less than 0.5% suspended solids, through multi-phase samples with several organic and inorganic components, to cakes with solids contents

* Corresponding author. Tel: (609) 530-4100; fax: (609) 530-5387.

PII S0039-9140(96)02031-0

exceeding 50%. Metal levels in sludge can vary from near the limit of detection of the analytical method for some analytes to concentrations of more than 25% (m/v) for other analytes. The NJDEP's permit limits for metals are based on the amount of material that leaches during mineral acid digestion. Decisions such as whether permit conditions are being met, how the material is to be disposed of or whether the sludge can be beneficially used all require accurate analytical data. In as much as sludge is a complex and variable matrix, concurrent analyses of reference materials that approximate the sludge matrix and have defined metal levels with defined uncertainties are essential to insuring the quality of the data being generated.

The NJDEP has authorized the use of a specific analytical method, NJDEP 100 [1] for the determination of a limited number of metals in sludge. The method was developed in the early 1980s by a task force comprised of professional from government, acadame and the private sectors. NJDEP 100 treats sludges with less than 10% total residue as wastewaters [2] and sludges with greater than 10% total residue as solid wastes [3]. This dichotomy is consistent with other analytical protocols developed by the United States Environmental Protection Agency (USEPA) for the determination of metals in various types of water by inductively coupled optical plasma emission spectrometry (ICPOES) [4]. While there are reference materials, performance evaluation samples and laboratory certification programs for wastewaters, no quality assurance materials or certification programs are available from the US government for materials such as sludge with higher than 10% solids content. Sludges from domestic sources typically have lower metals and higher nutrient and organic contents than sludges where industrial sources are a significant component of the influent stream. It is therefore desirable to have separate solid sludge reference materials for these two sources.

NIST certifies the chemical composition of a wide variety of Standard Reference Materials (SRMs) to insure the quality of physical and chemical measurements. SRM certified concentrations are generally provided only for total constituent values [5]. Environmental professionals, including soil scientists and geochemists, often require information about labile or extractable concentrations of metals to address issues such as ionic mobility and vegetative uptake. To provide such information, NIST has begun to provide data on the acid-extractable levels of metals in selected new solid sample environmental SRMs [6].

This paper describes a collaborative project among the NJDEP, USEPA, Region II Technical Support Branch and NISTs Standard Reference Materials Program (SRMP) to develop sludge reference materials from domestic and industrial sources having reference values for their acid-extractable metals content as determined by NJDEP Method 100 and USEPA Method 3050, in addition to certified total concentrations.

2. Experimental

2.1. Reference samples

The candiate domestic sludge reference material SRM 2781 was prepared from more than 100 kg of source product from a Denver, CO, publicly owned treatment work (POTW). The source product was shipped to NIST. Contractors freezedried, radiation sterilized and homogenized the material using crushing, blending and sieving procedures similar to those used for preparing United States Geological Survey and NIST geological reference materials [7]. The candidate industrial sludge reference material SRM 2782, based on a similar amount of electroplating waste supplied by AT&T Bell Laboratories, Murray Hill, NJ, was prepared similarly by contractors for NIST.

Samples were placed in 125 ml polyethylene bottles and supplied to the NJDEP Bureau of Radiation and Inorganic Analytical Services and USEPA, Region II, Technical Support Branch laboratories for chemical analysis.

2.2. Experimental reagents

The NJDEP and USEPA loboratories used Class A glassware and calibrated microliter pipettes to perform all volumetric dilutions. ACS reagent grade chemical, doubly distilled water and redistilled acids were employed for sample preparation and digestions. Individual NIST aqueous SRMs were used for spike recovery studies.

2.3. Sample preparation

The NJDEP used open-vessel hot-plate digestion (NJDEP Method 100) for all of their acid digestions. The USEPA used open-vessel hot-plate digestion (USEPA Method 3050) for the industrial product and Method 3050 and closed-vessel microwave digestion techniques (USEPA Method 3051) to prepare the domestic product for measurement. The digestion conditions for the various preparation methods are shown in Table 1.

The USEPA and NJDEP independently analyzed three aliquots from each of five bottles of the industrial material (SRM 2782) and six bottles of the domestic material (SRM 2781) supplied to each laboratory.

Table 1
Sample preparation methods for sludge reference materials

	EPA Method 3050	EPA Method 3051	DEP Method 100
Sample amount	1 g	1 g	1.0 g
Acid(s)	5 ml HNO_3	10 ml HNO_3 2.5 ml 1:1 HCl	5 ml 1:1 HNO_3 6 ml HNO_3
H_2O_2	3 ml at first; up to 10 ml total	None	2 ml at first; up to 11 ml total
Heating time	15 min at Reflux	100% power 70 psi 20 min	Gentle Reflux
Evaporation	To 5 ml	Not Applicable	To 3 ml

2.4. Instrumentation

The NJDEP used a Perkin-Elmer (PE) Model 5000 atomic absorption spectrometer (AAS) for its flame atomic absorption (FAAS) metal measurements. A similar unit, equipped with a PE Model 500 furnace and a PE AS-50 autosampler, was used for the graphite furnace atomic absorption (GFAAS) measurements. The NJDEP also employed a Thermo-Jarrell Ash Model 25 sequential inductively coupled plasma emission spectrometer (ICPOES) for some of its metal determinations. The USEPA used a CEM Model 81D microwave digestion system for some sample preparations and a Thermo Jarrell-Ash Model 61 Simultaneous ICPOES and a PE 5100 GFAAs, equipped with a Model AS-600 furnace and AS-60 autosampler for its metal determinations. The USEPA performed the metals measurements by either simultaneous ICPOES or GFAAS, using one technique per metal. The NJDEP used FAAS, sequential ICPOES and GFAAS and, where possible, employed more than one technique to measure most of the metals.

Calibration standards were prepared by serial dilution from commercial concentrates; working level concentrations were prepared daily. A minimum correlation coefficient of 0.999 for the linear calibration curve was required. Continuing calibration check samples were analyzed at a frequency of one every 10 determinations. Aqueous quality assurance samples, with known analyte values and from sources other than those used for the calibration solutions, were analyzed at a frequency of one every 10 determinations. Blank solutions, consisting of the reagents used in the sample digestion procedure(s), were prepared and analyzed at a frequency of one every 10 samples. All values were corrected for any blank concentration. The instrumental conditions were identical with the manufacturer's nominal values.

3. Results and discussion

The process of providing values for certification places greater demands on the precision and accuracy of the results than do data ob-

tained for such purposes as environmental surveillance or ambient monitoring. The goal of certification or other reference analyses is to obtain the best estimate of the "true value", which is the actual amount of analyte present in the sample. The overall uncertainty of a certified value includes both random error of measurement and any systematic bias which migh be inherent in the method(s) employed to estimate the true value. Issues such as the method of measurement, the complexity and composition of the sample matrix and the concentration and heterogeneity of the analytes all contribute to the overall uncertainty. For example, isotope dilution, when properly applied, is a method believed to be free from systematic errors and capable of achieving random errors of less than 0.2% relative. When uncertainties at the 95% confidence interval of 1–2% are needed, isotope dilution is often the method of choice for certification measurements. Only if the concentration being measured is at or very near regulatory limits are these narrow uncertainty limits necessary for routine measurements as well as for the certified values used to assure their validity. While wider uncertainties are expected when commonly applied analytical methods such as FAAS, GFAAS and IPCOES are used, reference values based on these methods are useful to confirm results of environmental monitoring such as sludge effluents from treatment plants.

It is difficult to select, homogenize, prepare, analyze and certify the chemical composition of natural non-aqueous environmental samples. NIST has historically focused on the certifying of the total metals content in non-aqueous environmental samples, while the USEPA has required the environmental testing community to use analytical methods that report only the amount of metal leachable by acid digestion test protocols. The amount of metal liberated from a non-aqueous environmental sample varies with the matrix and metal; for some elements in some samples, nearly 100% of the total metal content is released by an extraction such as USEPA Method 3050. For other metals in other sample types, the amount found in an acid leach may only be 30–40% of the total content. The significance of developing reference values for leachable metals content in a non-aqueous environmental sample is that these values can be used to quality assure the results submitted for regulatory purposes such as those required by NJDEP and USEPA.

The experience of NIST, NJDEP and USEPA analysts and NIST SRMP program managers is that ranges of 20–30% are typical for the determination of metals in environmental samples when conducted in separate laboratories. These between-laboratory discrepancies indicate the presence of bias but, at concentrations far removed from regulatory thresholds, have little pratical significance. Similarly, quality control sections of many analytical methods require that recoveries of between 80% and 120% for spike additions be demonstrated. This is viewed as indicative of the absence of significant bias caused by matrix interferences in the routine measurement process.

However, when relative between-method or between-laboratory differences exceed the pooled relative standard deviations, analysis of variance (ANOVA) show that these differences are statistically significant. Spike recovery data can then be used to evaluate method bias.

3.1. Domestic sludge reference material SRM 2781

The precision of replicate analyses of domestic sludge material SRM 2781 was calculated from 18 independent measurements (three aliquots from each of the six bottles) performed at both the NJDEP and USEPA laboratories (Table 2). The difference between the NJDEP results obtained by FAAS and ICPOES is less than 10% relative for 9 of 17 elements. When comparing the means of data obtained by the NJDEP and the USEPA laboratories the between-method differences of the means are greater than 10% only for Ba, Be, Ca, K and Pb. Similarly, the differences between the means of leach results for Methods 3050 and 3051 performed at USEPA are less than 10% relative with the single exception of Al, and less than 5% relative for nine elements. There are insufficient collaborative data to make any statements about Mo, P, Si and Ti.

Table 3 compares the mean values of spike recoveries from the two laboratories for the

Table 2
Acid-leachable concentrations ($\mu g\ g^{-1}$) in domestic sludge reference material SRM 2781: means and SDS for FAAS and ICPOES by NJDEP 100 and USEPA 3050 and 305 methods

Metal	DEP values		EPA values	
	DEP 100 AAS	DEP 100 ICP	3050 ICP	3051 ICP
Ag	86.6 ± 1.1	85.7 ± 1.6	87.5 ± 1.1	85.1 ± 4.7
Al	7680 ± 571	8173 ± 476	7543 ± 97	8849 ± 149
Ba	574 ± 29	532 ± 9	536 ± 11	581 ± 12
Be	1.0 ± 0.1	0.6 ± 0.1	< 0.3	< 0.3
Ca	37427 ± 938	35017 ± 801	35980 ± 434	37260 ± 745
Cd	12.9 ± 0.1	10.4 ± 0.4	10.1 ± 0.1	10.7 ± 0.2
Co	11.7 ± 0.4	12.9 ± 0.5	5.7 ± 0.2	5.8 ± 0.2
Cr	153 ± 4	135 ± 5	136 ± 1	146 ± 3
Cu	599 ± 8	610 ± 9	587 ± 7	604 ± 13
Fe	25250 ± 486	24967 ± 377	24200 ± 255	26200 ± 496
K	2243 ± 65	2591 ± 587	2090 ± 20	2300 ± 39
Mg	4707 ± 98	4729 ± 97	4920 ± 171	5060 ± 83
Mn	746 ± 6	722 ± 7	737 ± 9	771 ± 15
Mo	–	34.2 ± 2.5	–	–
Na	1109 ± 41	1170 ± 64	970 ± 13	921 ± 17
Ni	74.4 ± 10	76.7 ± 1.1	68.3 ± 0.6	69.3 ± 4
P	–	21761 ± 753	–	–
Pb	197 ± 3	176 ± 4	178 ± 3	180 ± 3
Sn	–	66.3 ± 2.7	–	–
Ti	–	102 ± 19	–	–
V	84.0 ± 3.3	80.7 ± 1.5	79.3 ± 1.0	84.0 ± 1.8
Zn	1147 ± 7	1124 ± 24	1096 ± 15	1113 ± 20

domestic material SRM 2781. The NJDEP's mean spike recovery by FAAs is 97.3%; by sequential ICPOES the mean is also 97.3%. The USEPA's mean spike recovery using plate digestion and simultaneous ICPOES is 102.8%; using microwave digestion the mean value is 105.3%. Where the spiking level was less than twice the actual leachable concentration, the results were not reported. These data show acceptable agreement between the added and recovered spike values, and provide evidence of minimal bias or matrix interferences in the measurements of the acid-extractable metals in sludge.

ANOVA can be used to evaluate whether two means from different sets of data are statistically significant [8]. F is the ratio of variance between two sets of data to the variance of data within a set of data. By comparing the calculated value of F with statistical tables for known degrees of freedom, the statistical significance of the means can be assessed. P is a measure of the probability that the actual sample data fall within hypothetical frequencies for infinitely large data populations. The ANOVA analysis for the domestic sludge material (Table 4) illustrates the impact of within-method uncertainties on the significance of laboratory bias despite the routine acceptability of the data. For example, as listed in Table 2, the copper data obtained by the NJDEP differ by only 2% between FAAS and ICPOES, whereas the vanadium data differ by 4%. The vanadium method differences are not statistically significant, since the within-method relative standard deviation (RSD) is 4.7% for each of the two methods. However, the smaller copper method differences are significant, based on the 1.3% and 1.4% RSDs. The USEPA Methods 3050 and 3051 difference of 3% for cobalt is not significant be-

Table 3
Recovery (%) of spike additions to domestic sludge reference material SRM 2781

Metal	DEP spike recoveries		USEPA spike recoveries	
	FAAS	ICPOES	Hot-plate	Microwave
Ag	93.0	[a]	135.0	94.6
Al	–	–	80.0	89.4
Ba	–	95.0	–	120.0
Be	88.7	96.3	101.3	109.3
Ca	–	–	95.1	97.5
Cd	96.7	108.7	94.7	100.2
Co	96.3	102.3	103.0	105.0
Cr	108.0	95.7	107.0	117.0
Cu	98.0	102.0	100.0	102.0
Fe	–	–	104.0	113.0
K	100.0	–	–	–
Mg	–	80.0	107.0	110.0
Mn	–	90.3	102.0	105.0
Mo	–	97.3	–	–
Na	98.7	108.7	–	–
Ni	97.3	95.7	103.0	105.0
P	–	–	–	–
Pb	99.7	95.7	97.5	99.2
Sn	–	102.3	–	–
Ti	–	–	–	–
V	98.7	98.7	105.0	107.0
Zn	92.7	91.3	108.0	110.0
mean	97.3	97.3	102.8	105.3

[a]Dashes indicate spike amounts less than twice the actual analyte concentration.

cause the within-method RSDs are larger, at 3.7% and 3.4%.

Having considered between-method differences for each laboratory, the data can next be compared between laboratories. For example, no significant differences for leachable Ag, Cu, Fe and V are found between the NJDEP and USEPA when laboratory, rather than method, is used as the classification variable. For Ag and Cu, the uncertainty of the interlaboratory means, based upon all data and expressed as the 95% confidence interval, are less than 4% relative. For Fe and V, the uncertainties are slightly larger, but less than 6%. This overall uncertainty level compares very favorable with many certifications for total concentrations of inorganic environmental SRMs whose certificates are based primarily on NIST laboratory analyses. While significant between-laboratory differences are found for leachable Ca, Mg, Mn and Zn, there is less than a 6% range in the 95% confidence interval of the interlaboratory means.

Reference values for these seven elements in the domestic sludge SRM 2781 have been derived. At less than 6%, the confidence intervals of the interlaboratory means are 4–5 times less than the between-laboratory differences of 20–30% experienced in most laboratories. The levels are also well above regulatory criteria. Reference values are also proposed for the following six other elements measured in this study where the interlaboratory means is greater than 6% but less than 10%: Al, Ba, Cr, Mg, Ni and Pb. Only Ca, Cd and Na have 95% confidence intervals that exceed 10%. These values will be included in an addendum to the SRM certificate. Further work is under way to narrow the range and to work on other elements of environmental interest such as

As, Be, Hg, Mo, P, Se and Ti in order to provide reference values for these elements also.

3.2. Industrial sludge reference material SRM 2782

For the industrial sludge SRM 2782, the situation is different. The complex composition of this material presented a considerable challenge to the preparation and measurement steps of the analytical process. The iron content of the sludge is very high, greater than 25% mass fraction as the element. Factors such as the difficulty of small amounts of mineral acid to dissociate large amounts of Fe-containing inorganic and organo-metallic complexes could affect the extent and reproducibility of extraction of less abundant elements. The high amount of Fe also makes it difficult to select interference-free analytical lines for plasma spectrometry for most analytes. These factors are reflected in the data obtained thus far for the leachable content of the industrial sludge material SRM 2782. As shown in Table 5, 12 of the 18 elements where between-laboratory comparisons are made show differences of greater than 10%, with eight elements exceeding 20%. The differences were less than 5% only for Pb. Because data were available from just two of the three leach protocols, the extensive comparisons applied to the domestic material were not possible. Further study and additional measurements are under way that it is hoped will enable NIST to generate reference values for metals in the industrial sludge. The available data presented here are intended to provide some guidance for laboratories in the quality assurance of their industrial sludge measurements until better defined reference values are established.

Table 4
ANOVA analysis for domestic sludge candidate reference material SRM 2781

Metal	DEP Method 100		USEPA	
	FAAS	ICP	3050 ICP	3051 ICP
	F	*P*	*F*	*P*
Ag	3.62	0.084	1.75	0.213
Al	14.65	0.004	277.86	0.000
Ba	1095.42	0.000	50.21	0.000
Be	245.00	0.000	–	–
Ca	30.58	0.000	13.91	0.004
Cd	825.13	0.000	25.98	0.000
Co	23.66	0.000	1.96	0.000
Cr	100.21	0.000	54.91	0.000
Cu	12.72	0.005	9.60	0.011
Fe	0.03	0.839	83.68	0.000
K	473.4	0.000	149.96	0.000
Mg	0.15	0.703	4.54	0.057
Mn	61.59	0.000	23.76	0.000
Na	5.82	0.035	29.99	0.000
Ni	100.11	0.000	3.11	0.106
V	4.09	0.068	37.05	0.000
Zn	32.88	0.000	4.24	0.064

Table 5
Acid-Leachable concentrations (μsg^{-1}) in industrial sludge reference material SRM 2781:means and SDs for FAAs and ICPOES by NJDEP 100 and USEPA 3050 and 3051 methods

Metal	DEP values		USEPA values
	DEP 100 AAS	DEP 100 ICP	3050 ICP
Ag	36.0 ± 0.2	–	27.9 ± 0.8
Al	1532 4	1471 9	1380 50
As	161 ± 1	–	140 ± 12
Ba	149 ± 1	151 ± 1	132 ± 4
Be	–	5.7 ± 0.2	< 0.5
Ca	4354 ± 26	5019 ± 22	4320 ± 141
Cd	4.0 ± 0.1	–	15.4 ± 0.8
Co	74.1 ± 0.2	65.8 ± 0.6	54.4 ± 2.0
Cr	79.8 ± 0.4	96.4 ± 4.8	55.3 ± 1.9
Cu	2381 ± 3	2588 ± 11	2270 ± 53
Fe	242707	267333	232000 ± 5560
K	116 ± 1	–	58.9 ± 5.8
Mg	534 ± 2	482 ± 3	441 ± 17
Mn	265 ± 1	283 ± 2	224 ± 7
Mo	–	< 1	–
Na	2418 ± 15	2443 ± 23	1997 ± 123
Ni	122 ± 1	128 ± 1	90.8 ± 2.0
P	–	4507 ± 10	–
Pb	568 ± 2	593 ± 3	551 ± 30
Sn	–	169 ± 1	< 6.0
Ti	–	70.4 ± 0.5	–
V	23.2 ± 0.2	45.9 ± 0.3	20.6 ± 0.6
Zn	1244 ± 5	1288 ± 10	1170 ± 21

4. Conclusions and recommendations

Even with a complex sample matrix such as sludge, reference values can be derived for the leachable concentration of many metals. Both open-vessel hot-plate acid digestion (NJDEP Method 1000 or USEPA Method 3050) or microwave digestion (USEPA Method 3051) are appropriate methods for sample preparation of these materials and may be measured by either FAAS or sequential or simultaneous ICPOES. Matrix interferences, both physical and chemical, must be addressed for the analysis of sludges containing high levels of dissolved matrix components.

Sludge Standard Reference Materials, with reference values for their acid-extractable metals content, can now support the quality assurance of sludge metal measurements. In the future, quality assurance analyses of the domestic sludge SRM should be required of POTW's compliance data submitted to regulatory agencies such as the USEPA and NJDEP. It is also recommended that these materials become part of any future laboratory certification program for sludge effluents.

Acknowledgements

The authors thank the NJDEP's Bureau of Pretreatment and Residuals for providing the funding for this study and Mary Jo Aiello and Tony Pilawski of that Bureau for many helpful discussions. Thomas LaFisca and Gail Suozzo are NJDEP chemist who conducted some of the chemical analyses. Robert Markow of AT&T Bell Laboratories supplied the industrial sludge source material.

References

[1] New Jersey Administrative Code, NJAC 7:14–4 (1994)
[2] American Public Health Association, Standard Method for the Examination of Water and Wastewaters, APHA, Washington, DC, 1992.
[3] United States Environmental Protection Agency, Test Methods for Evaluating Solid Waste, Volume 1C, Physical/Chemical Methods, SW846, 3rd edn., USEPA, Washington, DC, 1986.
[4] United States Environmental Protection Agency, Office of Water Regulations and Standards, Office of Water, Method 1620, USEPA, Washington, DC, 1989.
[5] J.S. Kane, S.A. Wilson, J. Lipinski, and L. Butler, Am. Environ. Lab., 6 (1988) 14.
[6] S. Rasberry, Am. Environ. Lab., 2 (1993) 34.
[7] J.F. Flanagan, F.J. Us Geol. Surv. Bull., No. 1582, (1986).
[8] L.L. Havlicek and R.D. Crain, Practical Statistics for the Physical Sciences, American Chemical Society, Washington, DC., 1988.

ELSEVIER

Talanta 44 (1997) 197–202

Talanta

Spectrofluorimetric determination of trace amounts of aluminium with 5-bromo-salicylaldehyde salicyloylhydrazone

Chongqiu Jiang*, Bo Tang, Rongying Wang, Jianchong Yen

Department of Chemistry, Shandong Normal University, Jinan, 250014, Shandong, Peiople's Republic of China

Received 8 November 1995; revised 7 June 1996; accepted 25 June 1996

Abstract

The fluorescent reagent 5-bromo-salicylaldehyde salicyloylhydrazone (5-Br-SASH) was synthesized and its ionization constants were established spectrophotometrically. The fluorescent reaction of this reagent with aluminium was studied. Based on this chelation reaction, a spectrofluorimetric method was developed for the determination of aluminium in acetic acid–ammonium acetate buffer solution of pH 5.4. Under these conditions, the Al–5-Br-SASH complex has excitation and emission maxima at 370 and 460 nm, respectively. The linear range of the method is from 0 to 120 ppb and the detection limit is 1.1 ppb of aluminium. The molar ratio of aluminium to the reagent is 1:3. Interferences of other ions were studied. The method was successfully applied to the determination of aluminium in glucose injection and common beverages.

Keywords: Aluminium determination; 5-Bromo-salicylaldehyde salicylolhydrazone; Spectrofluorimetry

1. Introduction

Hydrazones have been widely used in the spectrophotometric determination of metal ions [1] but only in recent years have they found application as fluorescent reagents in this field [2]. Aluminium is a harmful element for humans [3], when it is taken in excess. For this reason, several methods have been developed for the determination of aluminium including the use of hydrazones [4–10].

In this work, 5-bromo-salicylaldehyde salicylolhydrazone (5-Br-SASH) was synthesized and its complex with aluminium was studied. The fluorescence intensity of the complex was increased by the coplanar effect owing to the presence of aromatic rings at both ends of the reagent's structure. Based on this complexation, a spectrofluorimetric method with high sensitivity was developed for the determination of aluminium, without any organic solvents or surfactants. The detection limit is 1.1 ppb of aluminium. The procedure is easily performed and affords good precision and accuracy. This method has been successfully applied to the determination of aluminium in glucose injec-

PII S0039-9140(96)02033-4

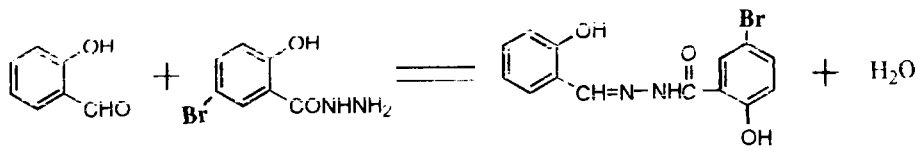

Scheme 1. Synthesis of 5-Br-salicylaldehyde salicyloylhydrazone (5-Br-SASH).

tion and common drinks by the standard additions method.

2. Experimental

2.1. Apparatus

All fluorescent measurements were carried out on an RF-540 recording spectrofluorimeter (Shimadzu, Kyoto, Japan), equipped with a xenon lamp source and 1.0 cm quartz cells. A UV-265 recording spectrophotometer (Shimadzu) equipped with 1.0 cm quartz cells was used for UV scanning. All pH measurements were made with a pHS-3C digital pH meter (Shanghai Leici Device Works, Shanghai, China) with a combined glass–calomel electrode.

2.2. Solutions

All chemicals used were of analytical or higher grades. Deionized water was used for the preparation of all solutions. A stock standard solution of

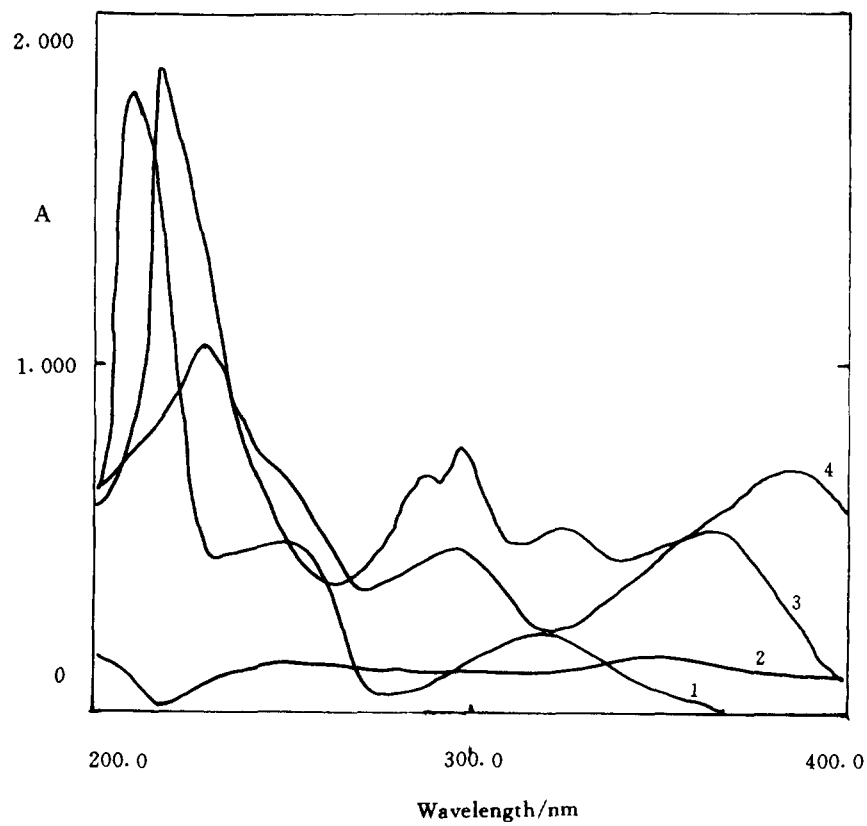

Fig. 1. UV absorption spectra of 5-Br-SASH reagent (4.5×10^{-4} mol dm^{-3}). pH: 1, 0.0; 2, 3.05; 3, 7.60; 4, 12.40.

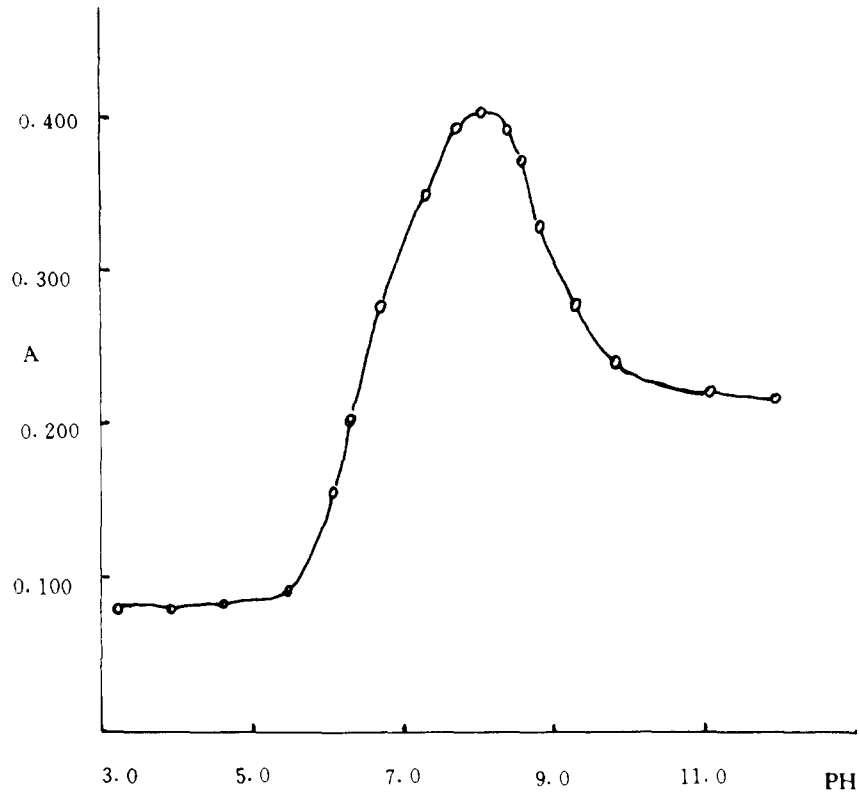

Fig. 2. Effect of pH on UV absorbance of 5-Br-SASH reagent (4.5×10^{-4} mol dm^{-3} at 296.8 nm)

aluminium (100 ppm) was prepared from aluminium metal and working standard solutions were prepared by dilution. An acetic acid–ammonium acetate buffer solution (0.4 mol dm^{-1}, pH 5.4) was used.

5-Br-SASH solution (4.5×10^{-4} mol dm^{-3}) was prepared by dissolving 0.1503 g of the reagent in 1000 ml of absolute ethanol.

2.3. Synthesis and properties of 5-Br-SASH reagent

A 2.3 g amount (about 0.01 mol) of 5- bromo salicylic hydrazide (synthesized by ourselves) was dissolved in 20 ml of 95% ethanol then, a mixed solution of 1.10 ml of salicylaldehyde and 10 ml of 50% ethanol was added slowly and the mixture was refluxed at 85 °C for 2 h. The reaction is shown in Scheme 1. The mixture was then cooled to room temperature, filtered and recrystallized from ethanol. A yellowish white powder was obtained (yield 65%).

The melting point of 5-Br-SASH is 212 °C. Element analysis gave a composition of C 50.60, H 3.31, N 8.34%, which is in good agreement with the theoretical composition of 5-Br-SASH, C 50.17 H 3.26, N 8.36%.

The infrared spectrum of 5-Br-SASH (KBr discs) was obtained and the bands were assigned as follows: OH (3254.9 cm^{-1}), C–OH (1201.4 cm^{-1}), C=O (1639.6 cm^{-1}), C=N (1287.3 cm^{-1}), C–H (3063.7 cm^{-1}) and C=C (1454.2 cm^{-1}) of the aromatic ring.

5-Br-SASH is slightly soluble in water but soluble in ethanol. The ultraviolet spectra of an aqueous solution of the reagent in various pH media show different absorbance maxima (Fig. 1) 5-Br-SASH behaves as a dibasic substance. The

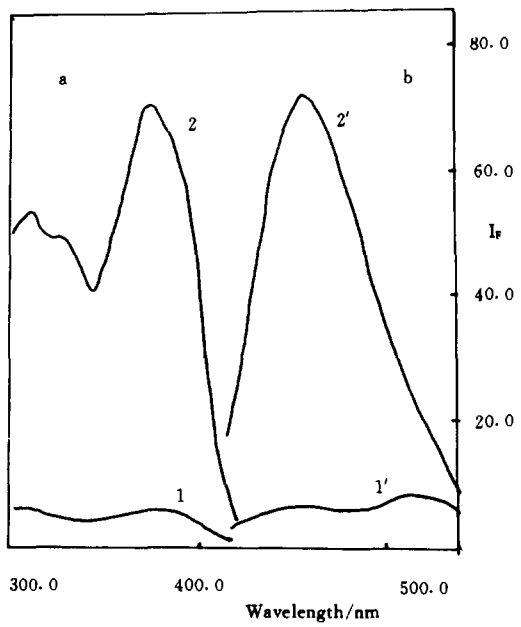

Fig. 3. (a) Excitation and (b) emission spectra of Al–5-Br-SASH complex. 1 and 1′, reagent blank (2.25×10^{-5} mol dm^{-3} 5-Br-SASH, pH 5.4); 2 and 2′, Al–5-Br-SASH complex (100 ppb Al^{3+}, 2.25×10^{-5} mol dm^{-3} 5-Br-SASH, pH 5.4).

ionization constants, determined by a spectrophotometric method [11], are $pK_{a1} = 6.58 \pm 0.06$ and $pK_{a2} = 8.92 \pm 0.08$ (at 0.1 mol dm^{-3} KCl, 25 ± 1 °C) (see Fig 2).

2.4. Fluorimetric determination of aluminium

In a 10 ml colour comparison tube were placed 1.0 ml of 0.5 μg ml^{-1} aluminium solution, 2.0 ml of acetate buffer (pH 5.4) and 0.5 ml of 4.5×10^{-4} mol dm^{-3} 5-Br-SASH and water was then added to the mark. The solution was mixed and equilibrated at room temperature for 30 min, then the fluorescent intensity was measured at 460 nm with excitation at 370 nm againt a reagent blank. A calibration graph was prepared under the same conditions for the determination of aluminium. A suitable amount of masking agent can be added if there are interfering metal ions present in the sample. The standard additions method was used in the determination of aluminium in glucose injection and common drinks.

3. Results and discussion

3.1. Excitation and emission spectra

In order to determine the optimum working wavelength, the spectral characteristics of the Al(III)–5-Br-SASH complex were studied at various pH values. The corrected excitation and emission spectra (Fig. 3) show that the wavelengths of maximum excitation and emission of the Al(III)–5-Br-SASH complex are 370 and 460 nm, respectively. The fluorescence intensity of reagent blank is very low.

3.2. Effect of pH

The pH of the medium had a great effect on the fluorescence intensity of the Al(III)–5-Br-SASH complex. The experimental results show that the optimum pH range for complex formation is between 5.2 and 5.6. Therefore, a pH of 5.4 was fixed with the use of acetate buffer. As the volume of the buffer (from 1.5 to 2.5 ml) had little effect on the fluorescence intensity, 2.0 ml was adopted in subsequent experiments.

3.3. Effect of temperature and time

Heating can be used to speed up the attainment of the maximum fluorescence intensity, but temperature has little effect on the fluorescence intensity of the Al(III)–5-Br-SASH complex. The experimental results show that room temperature can be selected, so the experimental procedure is simple. At room temperature, the fluorescence intensity of the complex reached a maximum after 25 min and remained constant for at least 4 h.

3.4. Effect of amount of 5-Br-SASH

The influence of the amount of 5-Br-SASH on the fluorescence intensities of solution containing 50 ppb of aluminium was studied under the conditions established above. The fluorescence intensity increased with increase in the amount of 5-Br-SASH up to 0.4 ml (4.5×10^{-4} mol dm^{-3}), remained constant between 0.4 and 0.6 ml and decreased slowly thereafter. Thus, 0.5 ml was se-

Table 1
Effect of foerign ions on the fluorimetric determination of aluminium (100 ppb) (tolerable error ± 5%)

Tolerance ratio (m/m)	Foreign ions
1000	K^+, N_a^+, SO_4^{2-}, ClO_4^-, NO_3^-, NO_2^-, HCO_3^-, Br^-, I^-, SO_3^{2-}, Cl^-, $B_4O_7^{2-}$
100	Mg^{2+}, Ca^{2+}, Sr^{2+}, Ba^{2+}, Tl(I), W(VI)
10	Cr^{3+}, Zn^{2+}, Cd^{2+}, Pb^{2+}, Au^{3+}, Co^{2+}, Cu^{2+}, Cr^{3+}, Hg^{2+}, Mn^{2+}, In^{3+}, Ni^{2+}, Se^{4+}
2	Ga^{3+}, Be^{2+}, $H_2PO_4^-$, F^-, Fe^{3+}

Table 2
Determination of aluminium in glucose injection and common drinks ($P = 0.95$)

Sample	5-Br-SASH method[a]		AAS: Al found (ppm)
	Al found (ppm)	RSD (%)	
Glucose injection (5%)	0.081 ± 0.005	2.48	0.0774
Glucose injection (50%)	0.045 ± 0.004	3.58	0.0473
Orange and honey drink	0.59 ± 0.04	2.73	0.56
Mango juice drink	0.418 ± 0.04	3.85	0.39
Average of three determinations			

lected to ensure a sufficient excess of the reagent throughout the experimental work.

3.5. Effect of foreign ions

A systematic study of the interferences of foreign ions in the determination of Al^{3+} (100 ppb) was carried out. For this study, different ions were first added to give a 2000-fold of (m/m) excess over aluminium. If interference occurred, the ratio was gradually reduced until the interference ceased. The criterion for interference was fixed as a ± 5.0% variation of the average fluorescence intensity calculated for the established level of aluminium. The results are shown in Table 1.

3.6. Stoichiometry of the complex

The stoichiometry of the complex was studied under the established experimental conditions by the molar ratio and continuous variation method. [12] The two methods showed that the composition of the complex is 1:3.

3.7. Analytical characteristics

Under the experimental conditions, there is a linear relationship between fluorescence intensity and Al^{3+} concentration in the range 0–120 ppb with a correlation coefficient (r) of 0.9957. The regression equation is $\Delta I_F = 63.69C$ (μg/10 ml) + 5.01. The detection limit as defined by IUPAC [13], was determined to be 1.1 ng ml^{-1} when the K value was taken as 3 and the standard deviation was 0.23 ng ml^{-1} obtained from a series of 11 blank solutions. The relative standard deviation was 1.45% obtained from a series of 11 standards each containing 100 ppb of aluminium.

3.8. Determination of aluminium in glucose injection and common beverages

The developed method was applied to the determination of aluminium in samples of glucose injection and common drinks. The standard additions method [14] was used in all analyses. The results are shown in Table 2 and compared

Table 3
Chatacteristics of fluorimetric methods for aluminium

Reagent	$\lambda_{ex/em}$ (nm)	Solvent	Linear range (ppb)	Detection limit (ppb)	Major interferences	Ref.
8-Hydroxyquinoline	360/415	Chloroform		20	Ga^{3+}, In^{3+}, Cu^{2+}, Fe^{3+}, Co^{2+}, Ni^{2+}, Bi^{3+}	[4]
Morin	440/525	Ethanol–water		50	Cu^{2+}, Cr^{3+}, Fe^{3+}, F^-, PO_4^{3-}	[5]
OBSH	390/475	DMF–water	0–200	5	Ga^{3+}, In^{3+}, Zr(IV) Pd^{2+}, $C_2O_4^{2-}$, F^-, EDTA	[6]
SHPA	383/440	Ethanol–water	4–80	4	In^{3+}, Be^{2+}, As(V), Zn^{2+}, F^-, EDTA	[7]
OSH	387/474	DMF–water	0–160	5	Ga^{3+}, In^{3+}, Sb(Π), Zr(IV), Be^{2+}, F^-, As(V), $P_2O_7^{2-}$	[8]
SABH	375/450	Water	0–140	1.4	Be^{2+}, Ba^{2+}, Fe^{3+}, Ni^{2+}, Sc^{3+}, Ga^{3+}, $C_2O_4^{2-}$, EDTA	[9]
SAPH	384/468	DMF–water	1–50	0.42	Ag^+, Au(Π), Cd^{2+}, Hg^{2+}, Zr(IV), $C_2O_4^{2-}$, citrate	[10]
5-Br-SASH	370/460	Water	0–120	1.1	Ga^{3+}, Be^{2+}, Fe^{3+}, F^-, $H_2PO_4^-$	

[a]OBSH = N,N'-oxalylbis(salicylaldehyde hydrazone); SHPA = salicyloylhydrazone of pyridine 2-aldehyde; OSH = N-oxalylamine(salicylaldehyde hydrazone); SABH = salicylaldehyde benzoylhydrazone; SAPH = salicylaldehyde picolinoylhydrazone

with those obtained by atomic absoption spectometry (AAS) with a graphite furnace.

To 1.0 ml of sample solution of glucose injection, various amounts of aluminium were added, which were then determined fluormetrically by the procedure established above.

For the assay of aluminium in drinks, 10.0 ml of the drink sample was transferred into a crucible and heated to dryness on an electric furnace and then in a muffle furnace for 30 min at 500–550 °C. The residue was dissolved in 1 mol dm^{-3} NaOH. The solution was filtered and washed with 0.1 mol dm^{-3} NaOH. The solution was then transferred into a 50 ml volumetric flask, adjusted to pH 5.0 with dilute H_2SO_4 and diluted to the mark with water. To 1.0 ml of this sample solution, various amounts of standard aluminium were added, which were then determined fluorimetrically by the method developed above.

The proposed method was compared with other common fluorimetric procedures (Table 3).

References

[1] M. Katyse and Y. Dutt, Talanta, 22 (1975), 51.
[2] R.B. Singh, P. Jain and R.P. Singh, Talanta, 29 (1982) 77.
[3] K. Wang, Trace Elements in Life Science, Beijing Chinese Measure Press, Beijing, 1991, p. 84.
[4] W.T. Ress, Analyst, 87, (1962), 202.
[5] F. Will, Anal. Chem., 33, (1961), 1360.
[6] J.L. Gomez Ariza, M.L. Marques, and M.T. Montana, Analyst, 109, (1984), 885.
[7] M. Gallego, M. Valcarcel and M. Garcia-Vargas, Analyst, 108, (1983), 92.
[8] F. de Pablos, J.L. Gomez Ariza and F. Pino, Analyst, 111, (1986), 1159.
[9] W.-C. Cui, B. Tang and H.M. Shi, Fenxi Huaxue, 20(1), (1992), 11.
[10] M.P. Manuel-Vez and M. Garcia-Vargas, Talanta, 41, (1994), 1553.
[11] N.U. Persic-Janjic, A.A. Muk and V.D. Canic, Anal. Chem., 45, (1973), 798.
[12] Wuhan University, Analytical Chemistry, High Education Press, Beijing, 1993, p. 499.
[13] H.M.H.N. Irving, H. Freiser and T.S. West (Eds.), IUPAC, Compendium of Analytical Nomenclature, Definitive Rules, Pergamon Press, Oxford, 1978.
[14] M. Bader, J. Chem. Educ., 57, (1980), 703.

ELSEVIER

Talanta 44 (1997) 203–211

Talanta

Quantitative structure–property relationships for colour reagents and their colour reactions with cerium using computational neural networks

Hua Li[1], Lu Xu*, Ming Guo, Qiang Su

Changchun Institute of Applied Chemistry, Chinese Academy of Sciences, Changchun 130022, People's Republic of China

Received 11 December 1995; revised 18 June 1996; accepted 24 June 1996

Abstract

Quantitative structure–activity/property relationships (QSAR/QSPR) studies have been exploited extensively in the designs of drugs and pesticides, but few such studies have been applied to the design of colour reagents. In this work, the topological indices A_{x1}–A_{x3} suggested in this laboratory were applied to multivariate analysis in structure–property studies. The topological indices of 43 phosphone bisazo derivatives of chromotropic acid were calculated. The structure–property relationships between colour reagents and their colour reactions with cerium were studied using A_{x1} A_{x3} indices with satisfactory results. The purpose of this work was to establish whether QSAR can be used to predict the contrasts of colour reactions and in the longer term to be a helpful tool in colour reagent design.

Keywords: Cerium; Colour reagents; Quantitative structure–property relationships; Neural networks

1. Introduction

Rare earth elements are used widely in the metallurgical and ceramics industries and in the processing of electronic and luminescent materials because they possess special physico-chemical properties. For these reasons, studies of the rare earth elements have become important in recent years. Many methods have been developed for the determination of rare earth elements, the most important being spectrophotometric methods [1–4]. A key step in a spectrophotometric method is the selection of a sensitive, highly selective colour reagent and suitable analytical conditions. Spectorphotometric methods provides sensitive, precise and accurate measurements and they can offer practical and economical advantages over other methods. Many colour reagents, such as asymmetrical phosphone biaszo derivatives of chromotropic acid, owing to their high sensitivity and selectivity, have been synthesized and used for the determination of the rare earth elements in China.

Correlations between the structures of colour reagents and their reactivities and physico-chemical properties are important because they can be used to guide the design of colour reagents.

* Corresponding author. Fax: (86) 431-685653.

PII S0039-9140(96)02034-6

The method of topological indexing of molecular structures has also been used widely in recent years in connection with quantitative structure–activity/property relationships (QSAR/QSPR) studies. The topological index is a numerical quantity that is mathematically derived from the structure graph of a molecule. Many topological indices, such as the Wiener index, W [5], Randic index, ID [6], Hosoya index, Z [7], Balaban index, J [8], and the general a_N index [9], have been proposed to convert chemical structures into numerical values. In recent years, topological indices have gained substantial attention in explaining the biological activities and physical and chemical properties of organic compounds. The topological indices A_{x1}–A_{x3} based on the augmented distance matrices, devised recently in our laboratory, have been successfully employed in studies on structure–activity relationships for compounds such as alkanes, alcohols and barbiturates [10]. In this study, we further applied these indices to the structure–property relationships between colour reagent and their colour reactions with cerium.

2. Neural network algorithms

Computational neural networks are mathematical algorithms, inspired by the current understanding of neurophysiology, that try to model the human brain and its ability to learn. A neural network can be considered as a group of interconnected nodes (neurons) forming a net, where every node receives a weighted input signal, through its inputs (synapses), from everynode connected to it. The efficiency of signal transmission depends on the weights, which correspond to the strength of the synapses joining dendrites. The summation of all the input signals to the node (neuron body) excites it and up to a threshold makes the nodes (neurons) produce an output signal through its output (axon). There are three types of neurons contained in a network: input neurons which accept the input data characterizing each observation, output neurons which provide the predicted value, and hidden neurons which neither receive inputs directly nor provide output values directly. The input signals are weighed as they are transmitted to the nodes of the second layer, the hidden layer. The hidden layer neurons process the data and send a signal to the neurons of the output layer. The output layer provides the predicted value, i.e. the contrasts of the colour reactions in this work. A neural network is trained to relate certain inputs (descriptor values) to target outputs (contrasts). To accomplish this, a variety of neural-network learning algorithms can be used. In this study, back-propagation (BP) and quasi-Newton methods were used. We found that the quasi-Newton method required fewer training cycles than did the back-propagaion algorithm.

2.1. The back-propagation training algorithm

A neuron in the hidden or output layer computes the weighted sum of inputs, net $_j$, given by

$$\text{net}_j = \sum w_{ij} X_i + \theta_j \quad (1)$$

where w_{ij} denotes the connection weight between node i in the previous layer and node j in the current layer, X_i is the ith output from the previous layer node i and θ_j is the bias for node j. The output of node j is calculated using a sigmoidal function:

$$\theta_j = 1/(1 + e^{-\text{net}_j}) \quad (2)$$

For training, the BP algorithm computes the sum-squared error between the network output and the target values:

$$E = \sum (t_p - o_p)^2 \quad (3)$$

where p is an index for training observations. The target value for pattern p is t_p and the computed value is o_p.

The connection weights and biases in the network are adjusted sequentially to reduce the error. This adjustment is made from the output layer to the hidden layer using a gradient descent method. In this method, the partial derivative of the error function is used to determine each weight adjustment, ΔW_{ij}. If the neuron of interest is contained in the output layer, then the error is calculated from the difference between the output value and the target value multiplied by the derivative of the

output value. The error terms for the hidden-layer neurons are more complicated because the target values do not exist and must be calculated recursively from neurons already modified. To improve the training time of the BP algorithm and avoid the hazards of oscillating or becoming trapped in local minima, a momentum term is added to the weight adjustment equation. The full details of BP training have been published previously [11,12].

2.2. Quasi-Newton (BFGS) training algorithm

The BFGS (Broyden–Fletcher–Goldfarb–Shanno [13–18]) quasi-Newton optimization method is an alternative way to minimize the sum-squared error of Eq. (3). The advantages of using the BFGS method over the BP method are that specifying progresses much more rapidly.

The basis of all quasi-Newton methods is that in cycle $K+1$ of the optimization, the error E and gradient $\mathbf{g}_{K+1}$ are assumed to be expressible as truncated Taylor series in the parameters $\mathbf{X}$:

$$E(\mathbf{X}_{K+1}) \approx E(\mathbf{X}_K) + \mathbf{g}_K{}^T\Delta\mathbf{X}_K + 1/2\Delta\mathbf{X}_K{}^T\mathbf{H}_K\Delta\mathbf{X}_K \quad (4)$$

$$\mathbf{g}_{K+1} \approx \mathbf{g}_K + \mathbf{H}_K\Delta\mathbf{X}_K \quad (5)$$

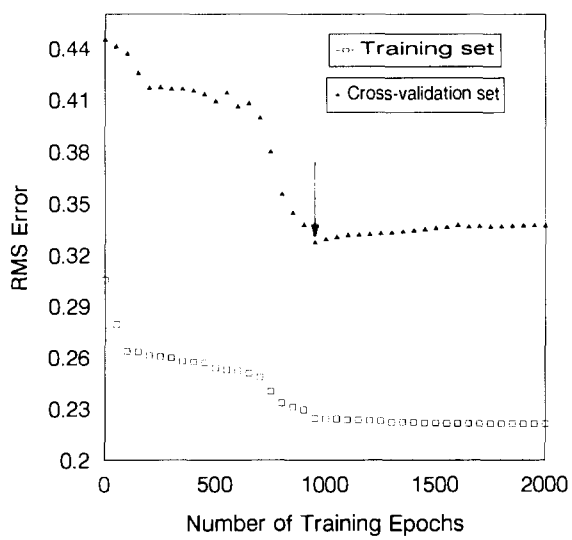

Fig. 1. Plot of RMS error vs. training cycles for quasi-Newton neural network.

where $\Delta\mathbf{X}_K = \mathbf{X}_{K+1} - \mathbf{X}_K$ is the change in the parameters from cycle K to cycle $K+1$ and $\mathbf{H}_K$ is the Hessian matrix of cycle K. The Hessian is defined as the matrix of the second derivatives of the error function with respect to the parameters. For a neural network, the parameters are just the weights and biases.

If $\mathbf{X}_{K+1}$ is to correspond to a minimum of the error functional, then $\mathbf{g}_{K+1} = 0$. This leads to the "Newton" step equation

$$\Delta\mathbf{X}_K = -\mathbf{H}_K{}^{-1}\mathbf{g}_K \quad (6)$$

In the quasi-Newton method, the inverse Hessian matrix $\mathbf{H}_K{}^{-1}$ is never computed directly. Instead, it is iteratively estimated and updated as the optimization proceeds. The initial estimate of the inverse Hesssian matrix $\mathbf{G}$ is obtained from the gradient for two different sets of weights and biases. After computing $\mathbf{g}$ for one set of weights and biases, each weight and bias is changed by a small amount and the gradient is computed a second time. The corresponding change in $\mathbf{g}$ is used to estimate the diagonal elements of $\mathbf{G}$:

$$\mathbf{G}_{ii} \approx \Delta\mathbf{W}_{ij}/\Delta\mathbf{g}_i \quad (7)$$

With an estimate $\mathbf{G}_K$ of the inverse Hessian matrix, the steps in a BFGS cycle are as follows:

(1) Choose search direction d_K according to $\mathbf{d}_K = -\mathbf{G}_k\mathbf{g}_k$.
(2) Determine the scaler α_K to minimize $E(\mathbf{X}_K + \alpha\,\mathbf{d}_K)$.
(3) Let $\mathbf{X}_{K+1} = \mathbf{X}_K + \alpha\,\mathbf{d}_K$.
(4) Compute the gradient $\mathbf{g}_{K+1}$ corresponding to the parameters $\mathbf{X}_{K+1}$.
(5) Update the inverse Hessian matrix $\mathbf{G}$ by the BFGS method.
(6) Iterate.

The line minimization parameter α_K can be estimated using a parabolic fit of the error along $\mathbf{d}_K$:

$$E(\mathbf{X}_K + \alpha\,\mathbf{d}_K) \approx E(\mathbf{X}_K) + \mathbf{a}\alpha + \mathbf{b}\alpha^2 \quad (8)$$

Two pieces of data are needed to find the constants a and b. Satisfactory results are obtained by using (a) the slope, $\partial E/\partial\alpha$ at $\mathbf{X}_K$, which is given by $\mathbf{d}_K{}^T\mathbf{g}_K$, and (b) the error $E(\mathbf{X}_K + \mathbf{S}\mathbf{d}_K)$, where s is an appropriately chosen step size. The minimum of this curve occurs when $\alpha = -a/(2b)$.

When using any iterative training procedure, a criterion must be available for deciding when to stop the iterations. Three approaches were used in this study: (a) the weights were adjusted for each observation until the sum-squared-error reached an acceptable value for the entire training set; (b) the number of training cycles was limited, and training was stopped after a fixed number of training cycles had been reached; and (c) training was stopped when the minimum cross-validation set error was achieved.

3. Topological indices

On the basis of distance matrix indices, A_{x1}–A_{x3} were derived in our laboratory. To facilitate understanding of A_{X1}–A_{x3}, the method is briefly introduced here. The three topological indices are generated from path matrices A, B and C, respectively. These three matrices are defined as follows:

$$A=(a_{ij}),\ a_{ij}=\begin{cases}1 & \text{path}=1\\ 0 & \text{others}\end{cases}\quad (i,j=1,2,\ldots,n)$$

$$B=(b_{ij}),\ b_{ij}=\begin{cases}2 & \text{path}=2\\ 0 & \text{others}\end{cases}\quad (i,j=1,2,\ldots,n)$$

$$C=(c_{ij}),\ c_{ij}=\begin{cases}3 & \text{path}=3\\ 0 & \text{others}\end{cases}\quad (i,j=1,2,\ldots,n)$$

Augmented path matrices G_1–G_3 are obtained by adding two columns into matrices A, B and C, respectively. The elements in the first column of matrices G_1–G_3 are square roots of vertex degrees, and the elements in the second column represent the square roots of the van der Waals radii atoms. From matrices G_1–G_3, we can obtain matrices Z_1–Z_3.

$$Z_1=G_1\cdot G_1';\ Z_2=G_2\cdot G_2';\ Z_3=G_3\cdot G_3'$$

where G_1'–G_3' are the transpose matrices of G_1–G_3. The three new topological indices are defined as

$$A_1=\lambda_{\max 1}2;\quad A_{x2}=\lambda_{\max 2}/2;\quad A_{x3}=\lambda_{\max 3}/3$$

where $\lambda_{\max}$–$\lambda_{\max 3}$ are the largest eigenvalues of matrices Z_1–Z_3.

4. Experimental

The neural network software included two modules: BP and quasi-Newton neural networks, which were written in FORTRAN 77 and installed on a micro VAX II. All computations were performed using multivariate statistic analysis programs (MSAP), which consists of multiple regression analysis, pattern recognition and calculations of topological indices, etc.

The structures of asymmetric phosphone bisazo derivatives of chromotropic acid are shown.

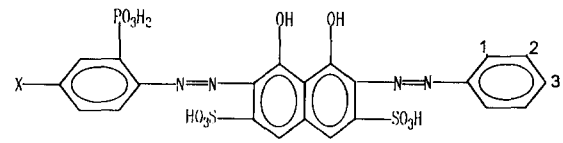

The experimental conditions employed and colour reactions with cerium are listed in Table 1.

5. Results and discussion

5.1. Calculation of descriptors

The topological indices A_{x1}–A_{x3} of 43 asymmetric phosphate bisazo derivatives of chromotropic acid were calculated acid were calculated. A total of three topological indices were generated for each colour reagent.

5.2. Structure-selective factors

From the colour reaction experiment, we know that the different positions of the auxochrome in asymmetric phosphone bisazo derivatives of chromotropic acid play important roles in analytical reactivities. In order to reflect the influences of auxochrome positions on colour reactions, structure-selective factors were introduced:

$$K\begin{cases}0.1\ (ortho)\\ 0.8\ (meta)\\ 0.7\ (para)\end{cases}$$

Table 1
Structures of colour reagents and their colour reactions with cerium

No	Substituent				pH	System (nm)	λ_{max} (nm)	$\Delta\lambda_{max}^{MR}$
	X	1	2	3				
1	Cl			NO_2	1	KCl–HCl	680	130
2	Cl		NO_2		1	KCl–HCl	660	115
3	Cl		$COCH_3$		1	KCl–HCl	660	120
4	Cl			$COCH_3$	1	KCl–HCl	670	120
5	Cl		Br		1	KCl–HCl	663	108
6	Cl			Br	1	KCl–HCl	670	120
7	Cl		SO_3H		0.8–1.8	HCl	650	100
8	Cl			SO_3H	0.8–1.5	HCl	650	100
9	Cl		COOH		0.5–1.2	H_2SO_4/HNO_3	660	113
10[a]	Cl			COOH	0.4–1.5	H_2SO_4/HNO_3	655	115
11[a]	Cl		COOH	COOH	0.4–1.5	H_2SO_4/HNO_3	665	115
12	Cl			PO_3H_2	0.2–1.5	HCl	660	100
13	Cl		Cl	NO_2	2	KCl–HCl	665	125
14	Cl	CH_3		NO_2	2	KCl–HCl	660	105
16[a]	Br			CHO	1.2	HCl	680	120
15[b]	Cl		NO_2		2	KCl–HCl	655	125
17[b]	Cl	NO_2			2	KCl–HCl	655	125
18	Cl	Cl			1	KCl–HCl	660	90
19	Cl		Cl		1	KCl–HCl	660	110
20[a]	Cl			Cl	1	KCl–HCl	668	123
21	Cl	Br			3	KCl–HCl	670	100
22	Cl	COOH			2	KCl–HCl	672	112
23	Cl		COOH		1	KCl–HCl	665	115
24	Cl		OCH_3		1	KCl–HCl	665	115
25[a]	Cl			OCH_3	2	KCl–HCl	678	128
26	Cl		OH		2	KCl–HCl	670	130
27	Cl			OH	2	KCl–HCl	670	135
28	Cl		CH_3		2	KCl–HCl	660	110
29	Cl			CH_3	2	KCl–HCl	670	120
30[a]	Cl				2	KCl–HCl	660	110
31	Br		$COCH_3$		0.8	HCl	670	120
32	Br			$COCH_3$	1	HCl	674	121
33	Br			NO_2	1.2	HCl	678	123
34	Br		NO_2		1.0	HCl	670	122

Table 1 continued

No	Substituent				pH	System (nm)	λ_{max} (nm)	$\Delta\lambda_{max}^{MR}$
	X	1	2	3				
35[a]	Br		Br		1	HCl	674	124
36	Br			Br	1.5	HCl	680	126
37	Br			SO_3H	0.8	HCl	672	120
38	Br		COOH		1.1	HCl	677	122
39	Br			COOH	1.2	HCl	673	123
40[a]	Br		CH_3		0.8	HCl	679	125
41	Br			CH_3	1.2	HCl	685	127
42	Br		SO_2NH_2		1	HCl	674	110
43	Cl	NO_2		NO_2	1	KCl–HCl	685	140

[a] Member of cross-validation set.
[b] 4-Subsituents of colour reagents 16 and 17 are NO_2 and Cl, respectively.

5.3. Objective feature selection

In order to determine which set of descriptors was important in computed topological indices, multiple stepwise regression analysis was necessary to refine the topological indices in order to reduce the possibility of chance correlations andto weed out the less useful topological indices. A model possessing a high multiple correlation value, a small standard deviation of regression and as few topological indices as possible was considered. Thus, ${}^{1/2}A_{x2}$, ${}^{1/2}A_{x3}$, ${}^{1/2}A_{x3}$ and K were selected and taken as the variables in the subsequent sections.

5.4. Results with neural network

To obtain the best network performance, the optimal network architecture must be chosen. Studies of the network structure include the selection of the number of layers and the number of neurons in each layer. The architecture of the neural network in this paper is as follows.

The number of layers is three, i.e. layer input, hidden and output. The number of input neurons is three (one for each descriptor), and there is one output neuron. The number of neurons used in the hidden layer was determined by trial and error.

The input neurons are ${}^{1/2}A_{x2}$, ${}^{1/2}A_{x3}$ and K. Usually, the value of each neuron is defined between 0 and 1, thus the input data should be scaled within the defined region. Note that if the value of a neuron in input layer is zero, the connections from this neuron are always zero, i.e. the information form that neuron cannot be propagated to the following layers. To avoid this situation, the values were set between 0.05 to 0.95 in this work.

The major difference betweeen BFGS and BP learning algorithms is how the weights are adjusted. In BP, the weight adjustments depend on a predetermined learning rate. BFGS networks, on the other hand, utilize variable-step size when individual weights are being adjusted.

The weights are the adjustable parameters altered by training. During the learning procedure,

Table 2
Topological indices A_{x1}–A_{x3} of colour reagents and calculated contrasts using regression and neural network techniques

No.	A_{x1}	$A \times 2$	A_{x3}	K	$\Delta\lambda_{1/2}$ (nm)	$\Delta\lambda_{1/2}$ (neural) (nm)
1	85.5552	108.2253	162.2882	0.7	11.4018	11.0783
2	85.5557	108.3011	162.0922	0.8	10.7238	10.8559
3	85.8838	108.5897	162.2974	0.8	10.9545	10.7498
4	85.8833	108.5116	162.4995	0.7	10.9545	10.8536
5	81.9759	104.8989	159.1555	0.8	10.3923	10.8001
6	81.9755	104.8416	159.1480	0.7	10.9545	11.2343
7	87.3824	110.5111	163.7988	0.8	10.0000	9.9936
8	87.4111	110.4577	164.1430	0.7	10.0000	10.2371
9	85.7204	108.4451	162.1913	0.8	10.6302	10.7991
10[a]	85.7199	108.3669	162.3889	0.7	10.7238	10.9547
11[a]	90.9644	113.8829	168.0342	0.7	10.7238	11.2062
12	87.4401	110.4822	164.1606	0.7	10.0000	10.2111
13	87.4022	110.3158	164.6195	0.7	11.1803	11.3504
14	87.4018	110.2881	164.9061	0.1	10.2470	11.1817
15[a]	83.6956	106.3595	160.5804	0.7	10.9545	11.1426
16	90.6297	113.4767	116.9583	0.8	11.1803	11.1092
17	87.4027	110.4399	165.2505	0.1	11.1803	11.3205
18	82.3288	105.2538	160.1674	0.1	9.4868	9.6955
19	82.3237	105.2149	159.3734	0.8	10.4881	10.6549
20[a]	82.3233	105.1503	159.3708	0.7	11.0905	11.1030
21	81.9806	104.9379	159.8989	0.1	10.0000	9.8419
22	85.7262	108.6144	163.4135	0.1	10.5830	10.5899
23	85.7204	108.4451	162.1913	0.8	10.7238	10.7991
24	84.0101	106.7155	160.7108	0.8	10.7238	10.8213
25[a]	84.0097	106.6450	160.8020	0.7	11.3137	10.9817
26	82.1605	105.0672	159.2718	0.8	11.4017	10.7286
27	82.1600	105.0059	159.2670	0.7	11.6190	11.1654
28	82.3238	105.2150	159.3734	0.8	10.4881	10.6550
29	82.3233	105.1503	159.3708	0.7	10.9545	11.1030
30[a]	80.4816	103.3013	157.8467	0.8	10.4881	10.9060
31	85.3727	108.1232	161.9486	0.8	10.9545	10.8771
32	85.5350	108.1889	162.2565	0.7	11.0000	11.0850
33	85.2081	107.9037	162.0461	0.7	11.0905	11.2700
34	85.2086	107.9797	161.8498	0.8	11.0454	10.9221
35[a]	81.6293	104.5799	158.9175	0.8	11.1355	10.8750
36	81.6289	104.5224	158.9102	0.7	11.2250	11.3553
37	87.0345	110.1114	163.8814	0.7	10.9545	10.5221
38	85.3727	108.1232	161.9486	0.8	11.0454	10.8771
39	85.3722	108.0448	162.1465	0.7	11.0905	11.1699
40[a]	81.9759	104.8947	159.1345	0.8	11.1803	10.7543
41	81.9754	104.8298	159.1319	0.7	11.2694	11.2290
42	86.9776	110.0509	163.8357	0.7	10.4881	10.5712
43	90.6347	113.5647	168.4859	0.1	11.8322	11.6692

[a] Member of cross-validation set.

a series of input patterns with their corresponding expected output values are presented to the network in an iterative adaption of weights when a given input expects a certain output. To obtain the best model, the set of random starting weights needs to be determined. This is a very time-consuming procedure and requires training the network several times using different sets of starting

weights and biases.

The number of output neuron is one. There are two ways to express the output neurons. Typically, single output neuron networks are usually used to predict continuous values. In this manner, the neural network is shown to be analogous to nonlinear regression analysis. Therefore, single output neural networks were used.

The total number of weights including biases should be as few as possible. Finding a compromise between the performance and the training time of the work, the optimum number of neurons in the hidden layer for this application was found to be three. Therefore, a hidden layer with three neurons was used in all the studies, yielding an overall network architecture of 3:3:1.

By stopping the training before the neural network reaches equilibrium one can prevent it from fitting the details of the training data set (to model random noise specific to the calibration data) and to exploit the full potential of all its weights. Another way to avoid overfitting is through the choice of a lean network topology with only a minimum of element. This reduces the number of weights to be trained accordingly. In this experiment, we chose the cross-validation set as a monitor to control the training processing. As long as the cross-validation set results improve, training continues. However, when the cross-validation set ceases to improve, the training must also cease in spite of the continued improvement in the training set results.

Fig. 1 shows a plot of the mean root square error as a function of the number of training epochs for both the training and cross-validation set. The results at epoch 951 is highlighted with an arrow in Fig. 1. The model corresponding to epoch 951 was chosen because the minimum cross-validation set error can be obtained.

The 43 colour reagents were randomly divided into two groups: a training set containing 35 colour reagents and a cross-validation set containing eight (colour reagents labelled footnote a in Table 2). The calculated results by the best model obtained using the network are listed in Table 2, last column. The RMS values for the training set and cross-validation set are 0.2243 and 0.3271, respectively.

6. Conclusion

The topological indices $A_{x1}-A_{x3}$ have been successfully used to model the structure–property relationships between colour reagents and their colour reactions with cerium. The experiments with computational neural networks reveal that the network architecture, initial conditions and the data organization are all important factors affecting the prediction. The performance of the network was enhanced by using the cross-validation set to monitor the training process. After the neural network had been fully trained, it was capable of forming reliable generalizations to predict the contrasts of colour reactions. The study demonstrates convincingly that $A_{x1}-A_{x3}$ are useful topological indices.

Acknowledgments

We thank Professor P.C. Jurs (Department of Chemistry, Pennsylvannia State University, USA) for providing us with the neural network program. The financial support of the National Natural Science Foundation of China is gratefully acknowledged.

References

[1] S.B. Savvin, T.V. Petrova and P.N. Romanov, Talanta, 19 (1972) 1737.
[2] T. Taketatsu, M. Kaneko and N. Kono, Talanta, 21 (1974) 87.
[3] N.U. Perisic-Janjic, A.A. Canic and V.D. Canic, Anal. Chem., 45 (1973) 789.
[4] C.G. Hsu, C.S. Hu, X.P. Ja and J.M. Pan, Anal. Chim. Acta, 124 (1981) 177.
[5] H. Wiener, J. Am. Chem. Soc., 69 (1947) 17.

[6] H. Hosoya, Bull. Chem. Soc. Jpn., 44 (1971) 2332.
[7] M. Randic, J. Am. Chem. Soc., 97 (1975) 6609.
[8] A.T. Balaban, Pure Appl. Chem., 55 (1983) 199.
[9] L. Xu, H.Y. Wang, and Q. Su, Comput. Chem., 16 (1992) 187.
[10] Y.Y. Yao, L. Xu, Y.Q. Yang and X.S. Yuan, J. Chem. Inf. Comput. Sci., 33 (1993) 590.
[11] D.E. Rumelhart, G.E. Hinton and K.J. Williams, in D.E. Rumelhart and J.L. McClelland (Eds.), Microstructures of Cognition, Vol 1, MIT Press, Cambridge, MA, 1986, pp. 318–362.
[12] P.A. Janson, Anal. Chem., 63 (1991) 357A.
[13] C.G. Broyden, J. Inst. Math. Appl., 6 (1970) 76.
[14] R. Fletcher, Comput. J., 13 (1970) 317.
[15] D. Goldfarb, Math. Comput., 24 (1970) 23.
[16] D.F. Shanno, Math. Comput., 24 (1970) 647.
[17] R. Fletcher, Practical Methods of Optimization, Vol. I, Wiley, New York, 1980.
[18] P.C. Jurs and J.W. Ball, Anal. Chem., 65 (1993) 3651.

ELSEVIER

Talanta 44 (1997) 213–220

Talanta

Surface-enhanced Raman spectrometry of triamterene on a silver substrate prepared by the nitric acid etching method

A. Rupérez[a], J.J. Laserna[b,*]

[a]*Department of Physical Chemistry, Faculty of Sciences, University of Málaga, E-29071 Málaga, Spain*
[b]*Department of Analytical Chemistry, Faculty of Sciences, University of Málaga, E-29071, Málaga, Spain*

Received 25 October 1995; revised 21 June 1996; accepted 24 June 1996

Abstract

Surface-enhanced Raman scattering (SERS) spectrometry of the diuretic drug triamterene is discussed. The SERS-active substrate used is a silver foil etched with nitric acid. The influence of solvent and sample doping method on sensivity, intercept and shape of the calibration graphs is discussed.

Keywords: Diuretic drugs; Human urine; Laser spectroscopy; Organic analysis; Raman spectrometry; Surface-enhanced Raman spectrometry; Triamterene

1. Introduction

The surface-enhanced Raman scattering (SERS) effect has been tested on various forms of metal surfaces. The enhancement depends critically on the creation of surface roughness [1]. One of the earlier types of substrate is the metal electrode [2–4], for which the required surface roughness is achieved by repeated oxidation–reduction cycles. Other procedures are available to produce the required roughness in the substrate, some of them involving elaborate laboratory practices [5,6]. For chemical characterization, colloidal silver [7–10] seems to be the most amenable substrate in terms of production, storage and sample handling, although difficulties with the reproducibility of SERS intensities have been reported [11]. Other procedures producing suitable rough surfaces include matrix-isolated metal clusters [12], iodine-roughened silver in an ultra-high vacuum [13], tunnel junction structures [14], metal-capped polymer posts [15], holographic gratings [16], vacuum depositing calcium fluoride on a glass slide and subsequently evaporating metal on to the surface [17,18], metal-coated filter-paper [19,20] and acid-etched metal foils [21–26].

In most previous work involving SERS-active solid substrates the sample was spotted on the substrate, allowed to dry and then subjected to measurement. The development of easily fabri-

* Corresponding author.

PII S0039-9140(96)02036-X

cated SERS-active optical sensors that can be used in solution is important for the application of SERS to in situ analysis. Acid-etched silver foils [26], silver island films [27] and TiO_2-based substrates [28] have been used for this purpose. Simplicity, low cost, speed and availability are outstanding features of these sensing devices.

In the present paper, the use of a silver sensor for surface-enhanced Raman detection of triamterene is discussed. The sensor is used either by applying a sample and drying before Raman examination or by dipping the substrate into the solution where the Raman analysis is performed. The analytical figures of merit, including sensitivity, shape of calibration graphs and limit of detection, are discussed.

2. Experimental

2.1. Instrumentation

The excitation source consisted of an argon ion laser (Coherent Innova 70) tuned at 488 nm, releasing about 40 mW at the sample, and focused with a biconvex glass lens (30 cm focal length). Silver-foil rectangles of 0.8×1 cm^2 were used as the substrate for SERS. Raman scattering was collected at right-angles dispersed with a double spectrometer (Spex Model 1680B) and detected with a thermoelectrically cooled photomultiplier tube (Hamamatsu Model R928) and a photon-counting system (Stanford Research Model SR400). Operation of the photon counter was controlled by an AT personal computer with Stanford Research SR465 software. The acquisition time per spectral element was 1 s and each spectrum consisted of 300 data points. All spectra reported represent single scans and are provided without spectral smoothing (except Figs. 4 and 5, with spectral smoothing of five points (Savitzky–Golay algorithm). The spectrometer resolution was generally set to 14 cm^{-1}. Frequencies were accurate to within 3 cm^{-1} for the bands studied. Spectral data were generated in binary code and converted in ASCII for processing in standard graphics software.

2.2. Chemicals and procedure

All chemicals were of analytical-reagent grade or equivalent and were used without further purification. Chromatography-grade methanol was used throughout. A 0.025 mm thick silver foil was immersed in vigorously stirred nitric acid (diluted 8:20 with water) at room temperature. Stirring was continued for about 2–3 min until the foil showed a milky surface. After etching, the silver foils were thoroughly rinsed with distilled water and dried in air.

2.3. The SERS sensor

The SERS sensor designed and constructed in our laboratory has been described in a previous paper [26]. It basically consisted in a 4 cm long and 2.5 cm wide metallic body with a folding portion in the bottom for holding the substrate. The silver substrate was place in this fold and kept in place with a turning plate to permit easy insertion.

2.4. Sample doping method

The dry-state method appeared to provide good SERS spectra for absorbates that could be dissolved in volatile solvents. In this method, coating of the substrate with the molecules of interest was accomplished by one of two techniques: (1) dipping the silver roughened with HNO_3 in the absorbate solution approximately 30 s, or (2) placing several drops of bulk solution on substrate. As reported earlier [29], the first technique results in a fairly uniform coverage of the absorbate, controlled by the concentration of the absorbate solution. In both cases the substrate was allowed to dry and was then subjected to Raman measurement. In the in situ method, the sensor was immersed in the analyte solution filling a standard 1 cm path glass cuvette for Raman examination.

3. Results and discussion

3.1. Sample doping dependence

The SERS spectrum of a substance results from adsorption of molecular species on a suitably

roughened substrate. For multi-component samples, selective molecular adsorption on substrate surfaces has been demonstrated [30]. The situation may be of relevance when an organic solvent is used. In this case, the organic solvent may behave as a competing adsorbate for the silver surface [31], resulting in large variations in the ability of the analyte to produce a well defined SERS spectrum (SERS activity). This is clearly shown in Fig. 1. Two spectra using the dry-state method corresponding to a triamterene–methanol solution (top) and to methanol (bottom) are plotted. The top spectrum shows the characteristic vibrational modes of triamterene at 1170, 1284, 1349 and 1526 cm^{-1}, superimposed on non-lasing plasma lines of the argon ion laser at 1131, 1168, 1323 and 1506 cm^{-1}; only these bands are observed in the spectrum of methanol. The effect of the substrate in SERS was also studied. For this purpose, the triamterene–methanol spectrum was compared with its equivalent when using colloidal silver as a substrate. Some differences have been observed mainly due to the dynamic behavior of colloids with time. As is known, several bands can change its shape or even appear and disappear, depending on the aggregation state of the colloid. Following the evolution with time of the color change of the colloidal dispersion is a very simple and effective method. Very good long-term stability of the vibrational structure and intensity of the SERS spectrum of triamterene has been observed when an etched silver foil was used.

Fig. 2 shows the SERS spectrum of triamterene in methanol (top) and the SERS and Raman spectra of methanol (center), with the use of in situ method. The conventional Raman spectrum (bottom) shows a broad band centered at 1480 cm^{-1}; this band also appears in the SERS spectrum of methanol when an etched silver foil is inserted directly in solution, superimposed on the scattering spectrum of the substrate (peaks at 1131, 1169 and 1323 cm^{-1}). In the SERS spectrum of triamterene dissolved in methanol (top), the following features can be observed: the peaks corresponding to non-lasing plasma lines of the argon ion laser, the strong band of methanol at 1480 cm^{-1} and the characteristic band of triamterene at 1349 cm^{-1}. It is thus apparent that the solvent plays a major role in the SERS activity of triamterene. The observed effect will depend on the volume of solvent and on the adsorbate concentration.

3.2. Spectral analysis of mixtures

For clinical application, triamterene is used in association with other diuretics. It is known [32] that the relative intensities of SERS features arising from several components in a mixture depend not only on their solution concentration, but also on their relative adsorptivities on the substrate.

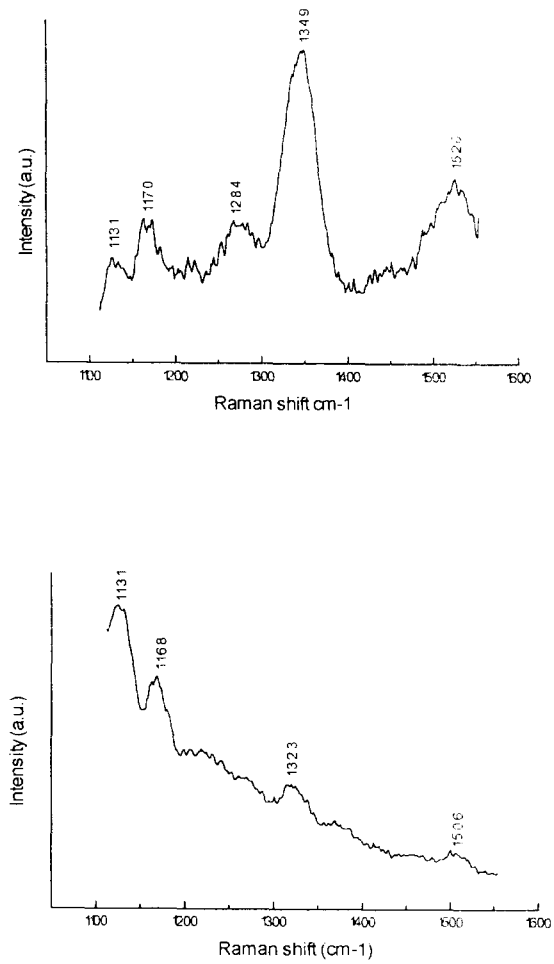

Fig. 1. SERS spectrum of triamterene in methanol (1 μg ml^{-1}) (top) and SERS spectrum of methanol (bottom). Sample volume, 5 μl.

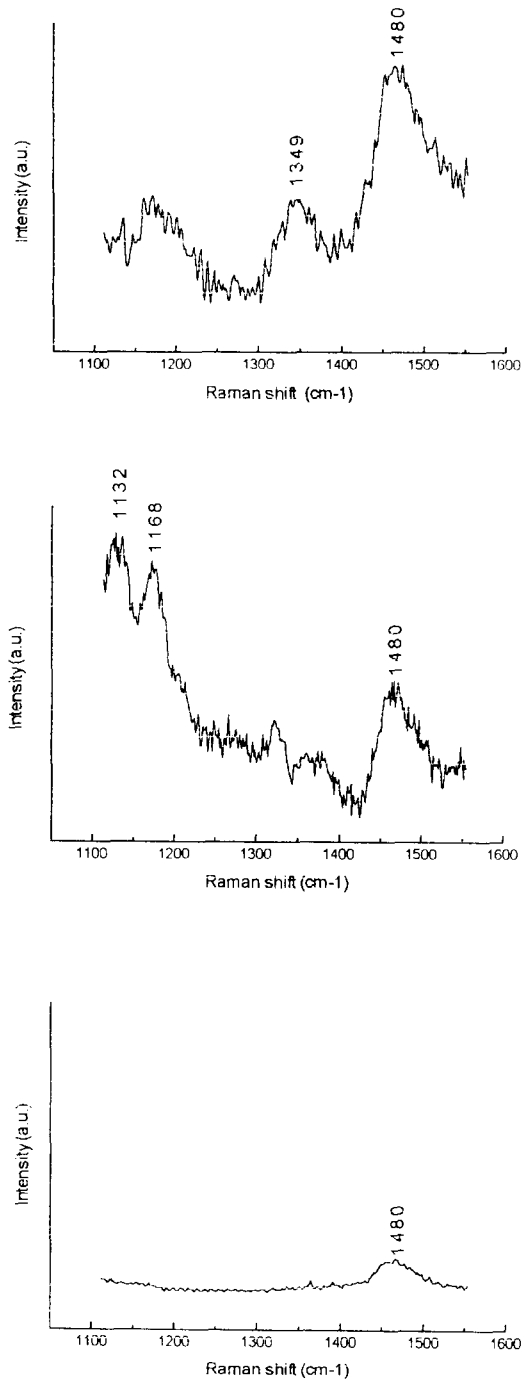

Fig. 2. SERS spectra of a solution of triamterene in methanol (top) and solvent blank (bottom). Drug concentration, 1 μg ml^{-1}. The Raman spectrum of methanol is shown as the lower trace.

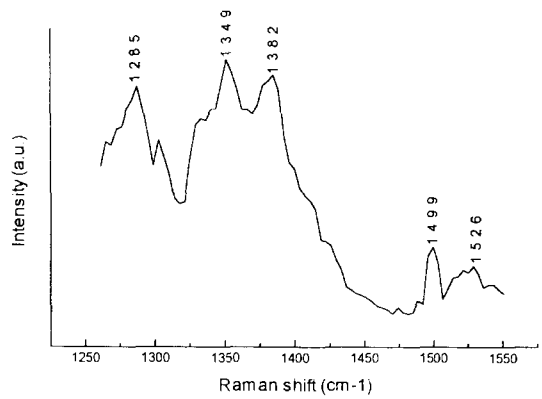

Fig. 3. SERS spectrum of a mixture of triamterene and amiloride in methanol. Triamterene:amiloride concentration ratio, 1:10; drug concentration, 10^{-4} M; sample volume, 5 μl.

When similar concentrations of compounds are used, the extent of the aggregation process depends on the chemical structure of the adsorbed compound [33]. The intensity in the spectrum of a mixture is modulated by the intensity distribution of the species that is most readily adsorbed [34]. For similar adsorptivities, the spectral features of various compounds can be additive and the spectrum of one component can be subtracted from the spectrum of the mixture with the features of the others left intact [34].

In general, diuretics show only moderate SERS activity. Of 10 diuretics investigated on colloidal silver [10], acetazolamide, bendroflumethiazide, ethacrynic acid and xipamide provide no surface-enhanced spectra; pre-aggregation of colloidal dispersions by external agents is required for the large Raman signals of spironolactone, furosemide, bumetamide and chlorthalidone. Amiloride and triamterene show well defined spectra. Amiloride has been extensively studied [35] on colloidal silver using water as solvent and analyzed directly in human urine samples. On colloidal silver, the SERS signal of triamterene show poor reproducibility, probably owing to changes occurring in the colloidal dispersion, easily followed by simple visual observation during data acquisition. Fig. 3 shows the SERS spectrum of a mixture of triamterene and amiloride on a silver substrate prepared by the nitric acid etching method. Triamterene is readily adsorbed, causing displacement of amiloride from the surface when a mixture

Table 1
Analytical figures of merit for SERS detection of triamterene

Matrix	Substrate	Slope[a] (μg^{-1} ml)	Intercept (arbitrary units)	LOD (μg ml^{-1})	Correlation coefficient
Urine	Silver foil[b]	4100	14 800	0.006	0.996
Methanol	Silver foil[b]	3490	7100	0.007	0.998
Methanol	Silver foil[c]	580	6700	0.010	0.994
Methanol	Silver colloid	570	271	0.080	0.865

[a] $n = 6$.
[b] Dry method.
[c] In situ method.

of two compounds is examined. The SERS spectrum of triamterene is dominant even at triamterene:amiloride concentration ratios of 1:10, with no noticeable changes in spectral features. Triamterene is recognized by the characteristic band at 1349 cm^{-1} and peaks centered at 1285 and 1527 cm^{-1}, whereas amiloride is recognized by reproducible bands at 1382 and 1499 cm^{-1} [10].

3.3. Effect of solvent

To evaluate possible matrix effects on the SERS response of the analyte, the analytical figures of merit of the SERS method were evaluated using methanol and urine as solvents for the drug. The spectrum recorded by the in situ method is characterized by a strong signal background which may be due to elastic scattering from suspended material or to luminescent components. No characteristic bands are detected. Fig. 4 shows the spectra of filtered urine under several experimental conditions when 10 μl where spotted on an etched silver foil. Fig. 4(a) corresponds to the spectrum obtained with a freshly prepared sample. Non-lasing emission lines of the argon ion laser were present superimposed on the background, but no characteristic vibrational modes of urine with observed. Fig. 4(b) shows the SERS spectrum after 30 min of continuous irradiation with the laser beam. The baseline increases and the spectrum is flat. The SERS spectrum of urine obtained 10 min after sample preparation is shown in Fig. 4(c). Two medium bands at 1236 and 1253 cm^{-1} can be attributed to urine [7]. Fig. 4(d) shows the same sample after exposure for 15 min to laser radiation; the vibrational structure is partially lost, but the band at 1236 cm^{-1} is observed.

Fig. 5 shows the SERS spectrum of urine sample spiked with 5 µl of triamterene on a freshly prepared sensor substrate (bottom) and after 5 min of continuous irradiation (top). The characteristic peaks of the drug at 1349 and 1526 cm^{-1} are clearly distinguishable, while the band at 1284 cm^{-1} is not observed, presumably owing to the strong background of the solvent in this zone. After 15 min, some of the absorbate activity is changed, as manifested by an increase in the ratio of the triamterene activity at 1349 and 1526 cm^{-1}.

The SERS spectrum of urine sample from a patient receiving combined triamterene–furosemide medication (triamterene:furosemide concentration ratio 25:77) is presented in Fig. 6. Triamterene, used clinically to treat hypertension, is normally excreted in urine as 15–25% of the administered dose in the native form [36]. The spectrum was recorded after filtering the urine sample through a 0.45 μm membrane filter. As shown, triamterene can be recognized by the band at 1349 cm^{-1} and the weak peaks at 1283 and 1526 cm^{-1}. The peak at 1466 cm^{-1} may be due to furosemide [10]. The peak at 1254 cm^{-1} corresponds to urine. Although these data have not been compared with those from another analytical technique, they indicate that the detection of triamterene in human urine by SERS on a silver substrate prepared by the nitric acid etching method is feasible.

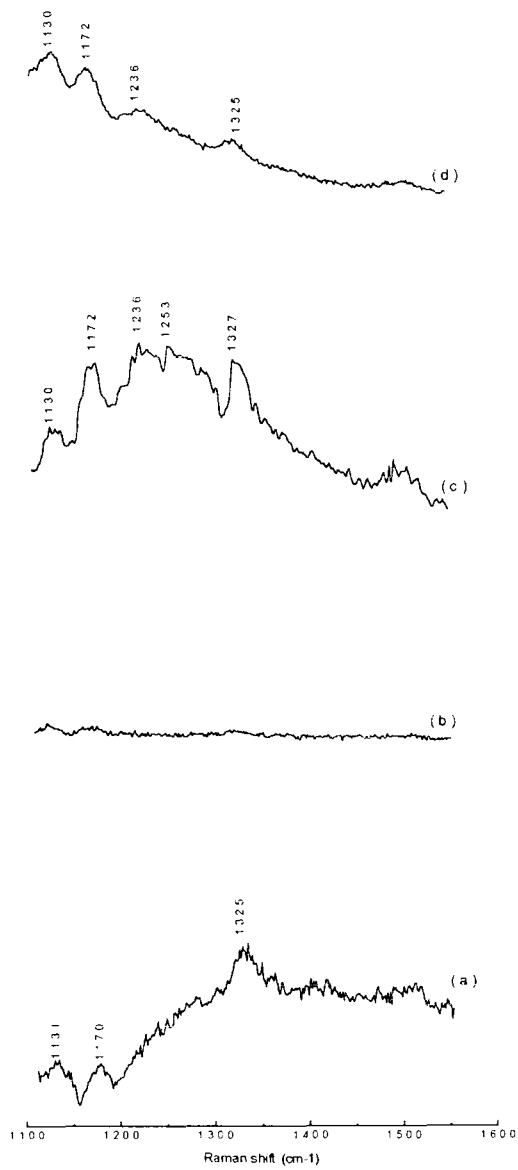

Fig. 4. (a) SERS spectrum of human urine in a freshly prepared substrate; (b) SERS spectrum after 30 min of continuous irradiation; (c) SERS spectrum of urine blank obtained 15 min after spotting; (d) SERS spectrum of the same sample after 15 min of continuous irradiation. Sample volume, 10 μl.

3.4. Quantitative study

The spectral capability of the etched silver foil for the quantitative analysis of human urine spiked with triamterene was evaluated by comparing the results obtained with the silver sensor and colloidal silver. Calculation of the limits of detection (LODs) was described in a previous paper [25]. Table 1 summarizes the analytical figures of merit. Etched silver foils and urine cause a strong signal background [7,27], which results in a higher intercept on the calibration graph. The LODs observed with colloidal silver were worse than those obtained with etched silver foil using the dry method. Large differences between the two methods in the slope of the calibration graph were observed. The slope for the in situ method was similar to that in col-

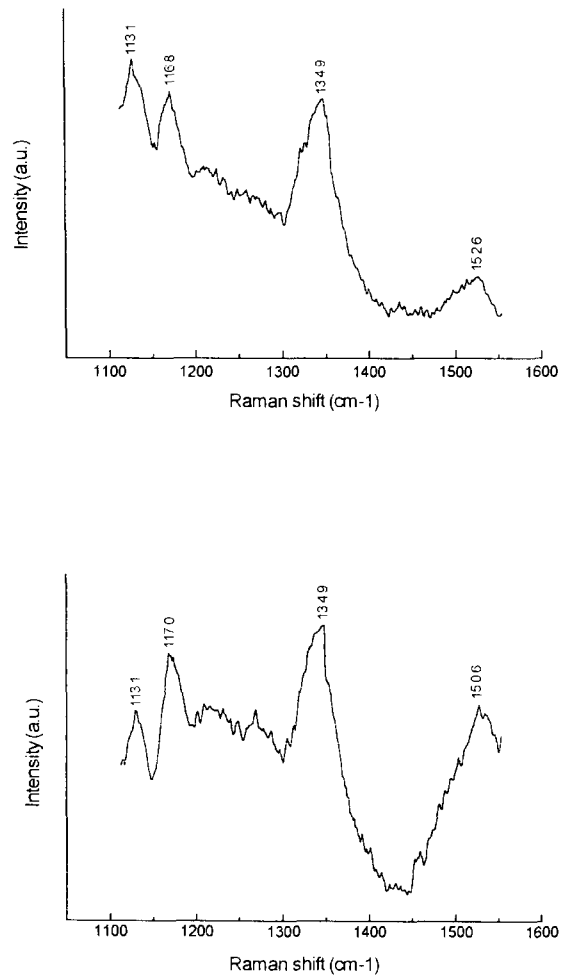

Fig. 5. SERS spectra of triamterene in human urine obtained at 0 min (bottom) and after 15 min of continuous irradiation of the sample (top). Drug concentration, 5 μg ml^{-1}; sample volume, 5 μl.

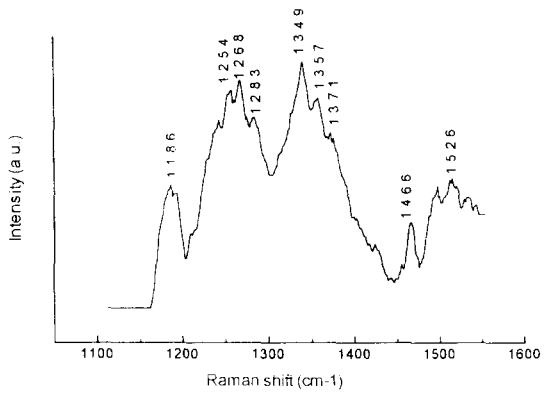

Fig. 6. SERS spectrum of a urine sample from a patient receiving continuous triamterene–furosemide medication (triamterene:furosemide concentration ratio, 25:77).

loidal silver. The correlation coefficients on silver foils are better than 0.99, and the upper limits of the linear part of the calibration graph estimated by polynomial interpolation, are 3.6 and 3.9 μg ml^{-1} for the dry method on a methanol and urine matrix respectively, 7.4 μg ml^{-1} for the in situ method and 14.7 μg ml^{-1} using colloidal silver as substrate. The larger (better) correlation coefficient provided by the etched silver foils may be due to the improved stability under laser irradiation and upon aging of triamterene in this substrate.

4. Conclusions

Strongly enhanced Raman spectra for triamterene can be obtained from acid-roughened silver foils using a simple and inexpensive sensor. The spontaneous adsorption of the analyte from solution directly on the substrate is an advantage of the sensor. The results reported here demonstrate that the detection of triamterene in human urine by SERS on etched silver foils is feasible. Good stability under laser irradiation and upon aging was observed. The main drawback is related to the large background signal observed when urine is used as solvent. The results reported here are important steps in the direction of bringing SERS under experimental control for analytical applications.

Acknowledgements

The research was supported by the Dirección General de Universidades e Investigación (Ministerio de Educación y Ciencia, Madrid, project PB90-0814) and by the Dirección General de Universidades e Investigación (Consejería de Educación y Ciencia (Junta de Andalucía, Sevilla), Spain.

References

[1] A. Rupérez and J.J. Laserna, in J.J. Laserna (Ed.), Modern Techniques in Raman Spectrometry, Wiley, Chichester, 1996, p. 227.
[2] N.S. Lee, Y.Z. Hsieh, R.F. Paisley and M.D. Morris, Anal. Chem., 60 (1988) 442.
[3] H. Feichenfeld and M.J. Weaver, J. Phys. Chem., 93 (1989) 4276.
[4] W.J. Barretto, P.S. Santos and J.C. Rubim, Vib. Spectrosc. 6 (1993) 87.
[5] D.B. Parry and A.L. Dendramis, Appl. Spectrosc., 40 (1986) 656.
[6] R.D. Shelton, J.W. Hass, III, and E.A. Wachter, Appl. Spectrosc., 48 (1994) 1007.
[7] A. Rupérez, R. Montes and J.J. Laserna, Vib. Spectrosc., 2 (1991) 145.
[8] R. Aroca and M. Scraba, Spectrochim. Acta, Part A, 47 (1991) 263.
[9] J.J. Laserna, L.M. Cabalín and R. Montes, Anal. Chem., 64 (1992) 2006.
[10] A. Rupérez, L.M. Cabalín and J.J. Laserna, Trends Appl. Spectrosc., 1 (1993) 188.
[11] J. Neddersen, G. Chumanov and T. Cotton, Appl. Spectrosc., 47 (1993) 1959.
[12] W. Krasser, U. Kettel and P.S. Bechthol, Chem. Phys. Lett., 7 (1982) 223.
[13] P.N. Sanda, J.M. Warlaumont, J.E. Demeth, J.C. Tsang K. Christmann and J.A. Bradley, Phys. Rev. Lett., 45 (1980) 1519.
[14] J.C. Tsang, J.R. Kirtley and J.A. Bradley, Phys. Rev. Lett., 43 (1979) 772.
[15] R.M. Hart, J.G. Bergman and A. Wokaun, Opt. Lett., 7 (1982) 105.
[16] A. Guirlando, M.R. Philpott, D. Heitmann, J.D. Swalen and R. Santo, J. Chem. Phys., 72 (1980) 5187.
[17] C. Murray and D. Allara, J. Chem. Phys., 76 (1982) 1290.
[18] J.M. Bello, D.L. Stokes and T. Vo-Dinh, Appl. Spectrosc., 43 (1989) 1325.
[19] A. Berthod, J.J. Laserna and J.D. Winefordner, J. Pharm. Biomed. Anal., 6 (1988) 599.
[20] J.J. Laserna, W.S. Sutherland and J.D. Winefordner, Anal. Chim. Acta, 237 (1990) 439.

[21] K. Suzan, M. Baiker, A. Baiker, M. Meier and A. Wokaun, J. Chem. Soc., Faraday Trans. 1, 80 (1984) 1305.
[22] G. Xue and J. Dong, Anal. Chem., 36 (1991) 239.
[23] G. Xue, M. Ma, Ming, Z. Junfeng, Y. Lu and K.T. Carron, J. Colloid Interface Sci., 150 (1992) 1.
[24] H. Matsuta and K. Hirokawa, Appl. Spectrosc., 43 (1989) 239.
[25] A. Rupérez and J.J. Laserna, Anal. Chim. Acta, 291 (1994) 147.
[26] A. Rupérez and J.J. Laserna, Analusis, 23 (1995) 91.
[27] K. Sokolov, P. Khodorchenko, A. Petukhov, I. Naviev, G. Chumanov and T.M. Cotton, Appl. Spectrosc., 47 (1993) 515.
[28] J.M. Bello, D.L. Stokes and T. Vo-Dinh, Anal. Chem., 61 (1989) 1779.
[29] S. Garoff, R. Stephens, C.D. Hanson and G.K. Sorenson, Opt. Commun., 41 (1982) 257.
[30] W.S. Sutherland, J.J. Laserna, M.J. Angebranndt and J.D. Winefordner, Anal. Chem., 62 (1990) 689.
[31] A. Rupérez and J.J. Laserna, Appl. Spectrosc., 48 (1994) 219.
[32] J.J. Laserna, A.D. Campiglia and J.D. Winefordner, Anal. Chem., 61 (1989) 1697.
[33] M. Moskovits and D.P. Dilella, in R.K. Chang andT.E. Furtak (Eds.), Surface Enhanced Raman Scattering, Plenum Press, New York, 1982, p. 243.
[34] J. Thornton and R.K. Forcé, Appl. Spectrosc., 45 (1991) 1522.
[35] N. Calvo, R. Montes and J.J. Laserna, Anal. Chim. Acta, 280 (1993) 263.
[36] J.E.F. Reynolds (Ed.), Martindale: The Extra Pharmacopoeia, 29th edn., Pharmaceutical Press, London, 1989.

ELSEVIER

Talanta 44 (1997) 221–230

Talanta

Investigation of HfO^+ interference in the determination of platinum in a catalytic converter (cordierite) by inductively coupled plasma mass spectrometry

M. Parent*, H. Vanhoe, L. Moens, R. Dams

Laboratory of Analytical Chemistry, Institute for Nuclear Sciences, Ghent University, Proeftuinstraat 86, B-9000 Ghent, Belgium

Received 1 February 1996; revised 24 May 1996; accepted 24 June 1996

Abstract

The determination of Pt in cordierite is subject to strong interference by spectral overlap from HfO^+ ions with all Pt isotopes. Two mathematical correction methods based on the HfO^+/Hf^+ ratio and a method for the chemical separation of Hf based on adsorption chromatography and isotope dilution were investigated to correct for this interference. Flow infection was used to prevent clogging of the cone orifice. To enhance the sensitivity and thus lower the detection limit, thermospray nebulization was used for sample introduction and the method was compared with pneumatic nebulization. In addition, the memory effects were evaulated for both systems. Analysis of artificial solutions (1 ng Pt ml^{-1}) yielded results within 3% of the true value. The Pt content (ca. 50 ng g^{-1}) of a cordierite sample, previously exposed to exhaust gases, could be determined with precisions of about 10–25% and the results agreed with earlier determinations by other workers.

Keywords: Cordierite; Inductively coupled plasma mass spectrometry; Isotope dilution; Platinum

1. Introduction

Awareness of the importance of Pt determination for environmental purposes began to develop with the introduction of catalytic converters in motorized vehicles. The possible enhancement of Pt levels in the environment, due to automotive emission of Pt, has motivated the development of analytical methods to determine Pt in environmental samples [1–5]. The Pt concentrations in, e.g., street dust, soil and grass near motorways are, however, still extremely low. Owing to its very low detection limits (ca. 10 ng l^{-1}), inductively coupled plasma mass spectrometry (ICP-MS) is a powerful technique for determining Pt at low levels. With more efficient sample introduction systems, the detection limit can be further improved. In many cases, separation and/or preconcentration methods also allow limits of detection to be improved [6,7]. However, ICP-MS suffers from problems of non-spectral and spectral interferences, which have been reviewed by

* Corresponding author. Fax: (+) 32 9 264 66 99.

PII S0039-9140(96)02037-1

Evans and Giglio [8]. Many problems arise when solutions containing high concentrations of dissolved solids have to be analyzed. The latter may cause clogging of the nebulizer and the sampling orifices and salt deposition on the torch or even a salt build-up on the ion lens stack. Some of these effects can be corrected for by the use of an internal standard [9,10]. Hutton and Eaton [11] found that when analyzing a matrix containing refractory compounds such as alumina, plugging of the interface occurred, leading to a signal reduction of about 85% over a period of 1 h.

In this work, Pt was determined in cordierite (Mg–Fe–Al silicate), used as a catalyst body. Since cordierite contains Al, Zr and Ce as some of its major components, analogous problems can be expected. Associated with the Zr, some Hf is also present. It was found that the sample contains about 8 $\mu g\ g^{-1}$ Hf, which can interfere with the determination of Pt owing to spectral overlap from HfO^+ ions with Pt [5]. Although the contribution of the oxide species can to some extent be minimized by instrumental settings [12], addition of N_2 to the plasma [13], or the use of an efficient desolvation system [13–15], it is not possible to reduce the interference sufficiently. Another method consists in using sample introduction techniques with preliminary evaporation of the solvent, such as electrothermal vaporization [16]. Thirdly, mathematical correction can be applied to separate the signal of the analyte from that of the overlapping oxide [17,18].

Besides HfO^+ interference, memory effects and insufficiently low detection limits also hamper analyses for Pt. In previous experiments [19,20], it was shown that the application of thermospray nebulization (TN) for sample introduction in ICP-MS leads to an increase in the sensitivity by a factor of 10 compared with pneumatic nebulization (PN), while the oxide levels are reduced by a factor of 2.5, even for the elements with the highest MO bond strengths [20].

This paper deals with the optimization of the ICP-MS procedure for determining Pt in cordierite. This was achieved by investigating two methods of interference correction for HfO^+, using the HfO^+/Hf^+ ratio experimentally determined either in a separate experiment or deduced from standard addition of Hf to the sample. A third method applied consisted in the complete removal of Hf by chemical separation and included the application of isotope dilution as a calibration method. Furthermore, the use of thermospray nebulization and flow injection to enhance the performance of the sample introduction system is discussed. All three correction procedures were applied with both PN and TN, in combination with and without flow injection. The memory effects were evaluated for PN and TN. The accuracy and precision of the correction and separation procedures were demonstrated by the analysis of cordierite that had been exposed to the exhaust gases of an engine equipped with a catalyst [21].

2. Experimental

2.1 ICP-MS instrumentation

The instrument used for all the experiments was a VG PlasmaQuad PQI ICP mass spectrometer (VG Fisons, Loughborough UK). The interface in the standard configuration was replaced with a "high-performance interface" supplied by VG Fisons. The operating conditions are summarized in Table 1.

2.2. Pneumatic nebulization system

The instrument is equipped with a Meinhard-type (Tr-30-A3) concentric glass nebulizer and a double-pass Scott-type spray chamber with surrounding liquid jacket, the temperature of which was controlled to within 1 °C with a recirculating refrigeration-heating system.

2.3. Thermospray nebulization system

A laboratory-made thermospray system (TN), consisting of an LC pump and a stainless-steel capillary (i.d. 180 μm), was used in combination with a desolvating unit consisting of a conical flask followed by a heated tube and a modified Friedrichs condenser. More details of the system are given elsewhere [20].

Table 1
VG PlasmaQuad operating conditions

Plasma	R.f. power	Forward: 1350 W Reflected: <5 W
Ion sampling	Sampling cone Skimmer cone	Nickel, 1.0 mm orifice Nickel, 0.75 mm orifice
Vacuum	Expansion stage Intermediate stage Analyzer stage	1.8 mbar 1×10^{-4} mbar 3×10^{-6} mbar
Sample introduction	Ar flow rate	Plasma: 13.5 l min^{-1} Auxillary: 1 l min^{-1} Nebulizer: 0.7 l min^{-1}
Pneumatic nebulization	Sample uptake rate	0.9 ml min^{-1} 1.5 ml min^{-1} (flow injection)
	Spray chamber	Scott-type double bypass, water cooled
	Nebulizer	Meinhard concentric type
Thermospray nebulization	Temperature of aerosol Temperature of cooling water Carrier gas flow rate Sample uptake rate	120 °C 1 °C 830 ml min^{-1} 1.33 ml min^{-1}

A flow injection valve (six-port) with a 200 μl sample loop made of PTFE was connected to the sample introduction system. Semi-continuous measurements were performed using a large sample loop of 5 ml.

2.4. Reagents

Working standard solutions were obtained by successive dilution of 1 g l^{-1} commercial AAS standard solutions (Alfa Products, Germany and Janssen Chimica, Belgium) with 0.14 M HNO_3. The standard solution for isotope dilution was obtained by dissolving 1 mg of isotopically enriched (^{194}Pt: 97.41%) Pt sponge (Campro Scientific, The Netherlands) in aqua regia and subsequent dilution to the required concentration. The glassware used for the enriched isotope solution was kept apart from the rest in order to avoid any cross-contamination. HNO_3(14 M), HCl (10 M) (both purified by sub-boiling distillation of reagent-grade acid from quartz apparatus) and Millipore Milli-Q water were used.

The polystyrene–divinylbenzene resin used was Amberlite XAD-4 with 0.3–0.9 mm particle size (Merck, Germany). The resin was purified by Soxhlet extraction with methanol for 8 h, then dried, ground and sieved [7]. The procedure described by Plantz et al. [6] for synthesizing the bis(carboxymethyl) dithiocarbamate (CMDTC) was applied. $SnCl_2$ solution was prepared by dissolving 0.3 g of $SnCl_2$ (Merck) in 0.5 ml of HCl and subsequently diluting to 1 ml with water.

All other reagents were of analytical grade.

2.5. Sample preparation

Two digestion methods for cordierite were applied: open acid digestion and digestion with a high-pressure asher (HPA), (Kürner, Germany). The open acid digestion was performed because it allows larger sample amounts (several grams) to be handled. In this way, the same solution could be used for Pt determination with PN and TN. For HPA the amount of sample is restricted to ca. 100 mg when glassy carbon vessels of 20 ml are used. The open digestion was applied in experi-

ments in which a mathematical correction for the HfO^+ interference was tested. HPA digestion was applied in combination with the elimination of Hf by chemical separation.

2.5.1. Open acid digestion

Approximately 400 mg of cordierite were weighed into a PTFE beaker and heated with 10 ml of HNO_3 at about 70 °C for ca. 3 h then 5 ml of $HClO_4$ were added, the temperature was raised to 120 °C and the solution was heated overnight. Subsequently, 10 ml of HNO_3, 5 ml of HF and 5 ml of HCl were added, followed by heating for 24 h at 70 °C and evaporation to near dryness. The residue was dissolved by adding 5 ml of HNO_3, 5 ml of HCl and 5 ml of HF, followed by heating at 70 °C for 24 h. Finally, the solution was evaporated to near dryness several times to remove HF and HCl (redissolution with HNO_3). HCl was removed because it attacks the capillary material of the thermospray system. A clear solution was obtained. The contents of the vessels were transferred quantitatively into a volumetric flask and diluted to 10 ml with 0.14 M HNO_3. Next, the solutions were divided in two equal portions and further diluted until the concentration was 20 g l^{-1} for PN and 10 g l^{-1} for TN.

2.5.2. HPA digestion

About 100 mg of cordierte were weighted into a glassy carbon vessel. After adding 1 ml of HF, 1 ml of HCl and 200 μl of ^{194}Pt-enriched spike (for isotope dilution), the samples were decomposed in the HPA at the following temperatures and with a maximum pressure of 130 bar: step 1 temperature ramp from 25 to 120 °C (15 min); step 2, 120 min at 220 °C. After cooling, dilute aqua regia was added and the samples were heated to ensure that all Pt was in the quadrivalent state and to remove HF. Further heating and addition of HCl completely removed the excess of HNO_3, which otherwise would disturb the subsequent adsorption chromatography. The contents of the vessels were transferred quantitatively into a glass vessel and 10 M HCl was added to obtain a concentration of 1 M HCl.

2.6. Adsorption chromatorgraphy

Pt was preconcentrated as the bis(carboxymethyl)dithiocarbamate chelate on a microcolumn packed with XAD-4 [7], and eluted in a small volume of EtOH. Adsorption occurred from strong HCl medium after reduction with $SnCl_2$. The EtOH was evaporated and the residue was dissolved in 0.14 M HNO_3, to avoid problems with the determination of Pt in organic solutions by ICP-MS. Accurate measurement of Pt in samples after isolation through enrichment via adsorption chromatography is only possible by isotope dilution mass spectrometry, as this method allows a correction for the variable yields. The Pt spike was added to the sample before digestion. The Pt concentration was calculated using the $^{194}Pt/^{195}Pt$ ratio.

3. Results and discussion

3.1. Spectral interferences due to HfO^+

Since Hf is present in cordierite, the level of oxides formed by Hf was investigated with both Pn and Tn. HfO^+ species interfere with all Pt isotopes (Table 2) and it is therefore necessary to assess the importance of this interference. Hence an Hf standard solution (50 μg l^{-1}) was introduced via both PN and TN. For PN the level of oxides varied between 0.3% and 0.7%, which is in agreement with the results obtained by Vanhaecke et al. [12]. After careful optimization of the measurement of Hf with TN (see below), the level of oxides was reduced to 0.2–0.3%, owing to the better desolvation system used with TN. It was found that when measuring ^{194}Pt, the apparent Pt concentration due to 50 μg l^{-1} Hf can amount to 450 ng l^{-1} with PN and 250 ng l^{-1} with TN (see Table 3). Table 3 also shows that the formation of oxides and hence the apparent Pt concentration vary from day to day, because the operating conditions change [17]. The other isotopes are also to a large extent interfered with by HfO^+ ions.

3.2. *Study of memory effects*

Memory effects, as encountered for Hg [22,23] and Au [24], are insidious in isotope dilution,

Table 2
Abundance of Hf and Pt nuclides and possible interferences on Pt

Hf and other isotopes	Abundance (%)	Possible interference	Pt isotopes	Abundance (%)
^{174}Hf	0.18	$^{174}Hf^{16}O$	^{190}Pt	0.013
^{176}Hf	5.20	$^{176}Hf^{16}O$	^{192}Pt	0.78
^{177}Hf	18.5			
^{178}Hf	27.2	$^{178}Hf^{16}O$ $^{177}Hf^{16}O^{1}H$	^{194}Pt	32.9
^{179}Hf	13.8	$^{179}Hf^{16}O$ $^{178}Hf^{16}O^{1}H$	^{198}Pt	33.8
^{180}Hf	35.1	$^{180}Hf^{16}O$ $^{179}Hf^{16}O^{1}H$	^{196}Pt	25.3
^{180}W	0.13	$^{180}W^{16}O$		
^{196}Hf	0.15	^{196}Hg		
^{182}W	26.3	$^{182}W^{16}O$	^{198}Pt	7.23
^{181}Ta	99.9	$^{181}Ta^{16}O^{1}H$		
^{198}Hg	10.2	^{198}Hg		

where the isotope ratios in subsequently measured solutions may be very different. A flow injection system with a sample loop of 5 ml was used in this study. In Fig. 1(a) the ^{195}Pt signal observed before, during and after the injection of 10 $\mu g\ l^{-1}$ is plotted. PN was used for sample introduction and 0.14 M HNO_3 as the rinsing solution. It can be seen that the background level is not reached even after 5 min of rinsing. Rinsing with H_2O, 1.4 M HNO_3, 0.1 M HCl and 1% aqua regia was also not successful. Rinsing with 0.1 M HCl seemed to lead to an acceptable level of the background signal, but this was only the result of a suppression of the Pt signal. Only rinsing with 0.1% and 1% Triton X-100 for 2–3 min resulted in nearly complete removal of the Pt signal. Apparently Triton effectively wets the walls of the delivery tubing and the spray chamber, thus facilitating the washing out of Pt. Additional experiments showed that all parts of the sample introduction system contribute to the memory effect, as was mentioned by other workers [25–27].

The memory effects for TN, situated in the capillary and especially in the desolvation unit, were larger than for PN, as can be seen in Fig. 1(b). Also in this case rinsing with Triton X-100 decreased the memory effect significantly. When using flow injection (200 μl loop), the Pt signal also drops quickly to the background level [19].

Table 3
Apparent concentration of Pt due to spectral overlap with HfO^+ (50 $\mu g\ l^{-1}$ Hf) with pneumatic (PN) and thermospray (TN) nebulization

Pt isotope	Interfering polyatomic ion	Apparent Pt concentration ($ng\ l^{-1}$)	
		PN	TN
^{194}Pt	^{178}-$Hf^{16}O$ $^{177}Hf^{16}O^{1}H$	260–450	80–250
^{195}Pt	$^{179}Hf^{16}O$ $^{178}Hf^{16}O^{1}H$	150–250	50–120

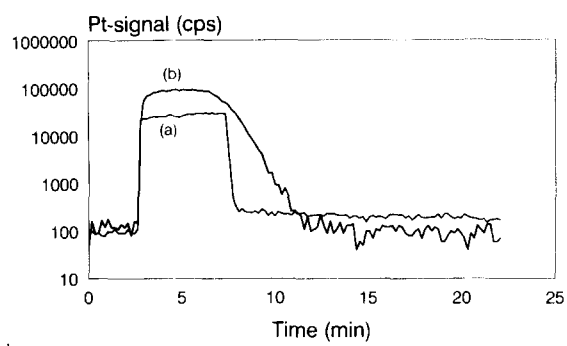

Fig. 1. Memory effect after introduction of 10 $\mu g\ l^{-1}$ Pt with (a) pneumatic nebulization and (b) thermospray nebulization.

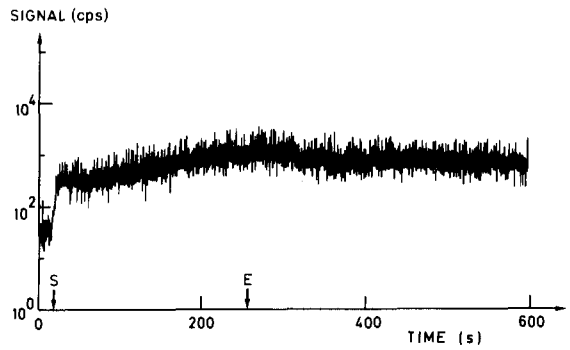

Fig. 2. Memory effect observed for 10 μg l^{-1} Hf with thermospray nebulization.

Persistent memory effects occur on introducing a 10 μg l^{-1} Hf solution in TN (Fig. 2). These are caused by the deposition of HfO_2 near the end of the heated capillary [28]. The Hf oxide precipitation probably occurs because the traces of HF present in the Hf solution evaporate in the heated capillary. The oxide is then only slowly removed by the carrier solution (0.14 M HNO_3). Decreasing the power applied to the capillary or adding HF decreased and prevented, respectively, Hf oxide precipitation (see Fig. 3(a)and (b)). In order to confirm this experiment, solutions of other elements requiring HF for the stability of their solutions (e.g. Zr, Nb, Ta and W) were injected and were found to cause a similar memory effect to Hf.

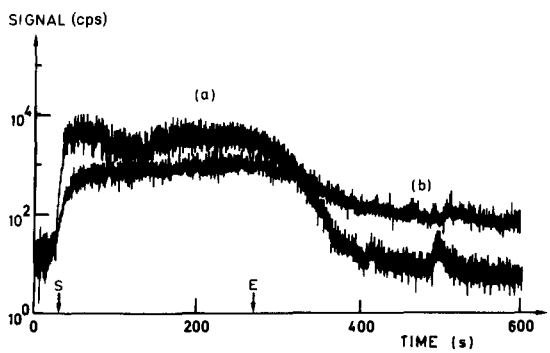

Fig. 3. Memory effect observed for 10 μg l^{-1} Hf with thermospray nebulization (a) in 0.1% HF and (b) with decreased power applied to the capillary.

3.3. *Analysis of artificial solutions*

Fig. 4 shows that with the present instrumental set-up, the maximum ion signal intensities for Hf^+, Pt^+ and HfO^+ were found at the same nebulizer gas flow rate, so that optimisation of the gas flow rate, as applied successfully by Vanhaecke et al. [12] cannot be used to reduce the interference. Therefore, two mathematical correction methods, using the HfO^+/Hf^+ ratio from a standard solution or from standard addition of the interferent Hf to the sample, were applied to correct for the HfO^+ interference. Addition of the interferent has already been applied by Munro et al. [29] for correction for ClO^+ interference and originally suggested by Henshaw et al. [30]. Both mathematical correction methods require a linear dependence of the HfO^+ signal on the Hf concentration. In Fig. 5 the measured HfO^+ signal is plotted versus the Hf concentration. A linear dependence over two orders of magnitude can be observed (correlation coefficient of 0.998). The same conclusions are valid for thermospray nebulization. In all cases the $^{195}Pt^+$ isotope was used for calculations, because the interference is less severe, as can be seen in Table 3. The signals, represented by I, were normalized with the internal standard (TI signal) and were blank subtracted.

3.3.1. *Correction for the HfO^+ interference via the HfO^+/Hf^+ ratio*

The HfO^+/Hf^+ signal ratio was determined in a standard solution containing 50 μg l^{-1} Hf and used to correct for the HfO^+ interference observed in the sample solution. The following equation was used:

$$I_{Pt} = I_{Pt,s} - (I_{Hf,s} R_{HfO}) \quad (1)$$

where I_{Pt} = the corrected Pt signal, $I_{Pt,s}$ = the Pt signal measured for the sample solution, $I_{Hf,s}$ = the signal for Hf in the sample solution and R_{HfO} = the previously determined HfO^+/Hf^+ signal ratio.

3.3.2. *Correction for the HfO^+ interference via standard addition of Hf*

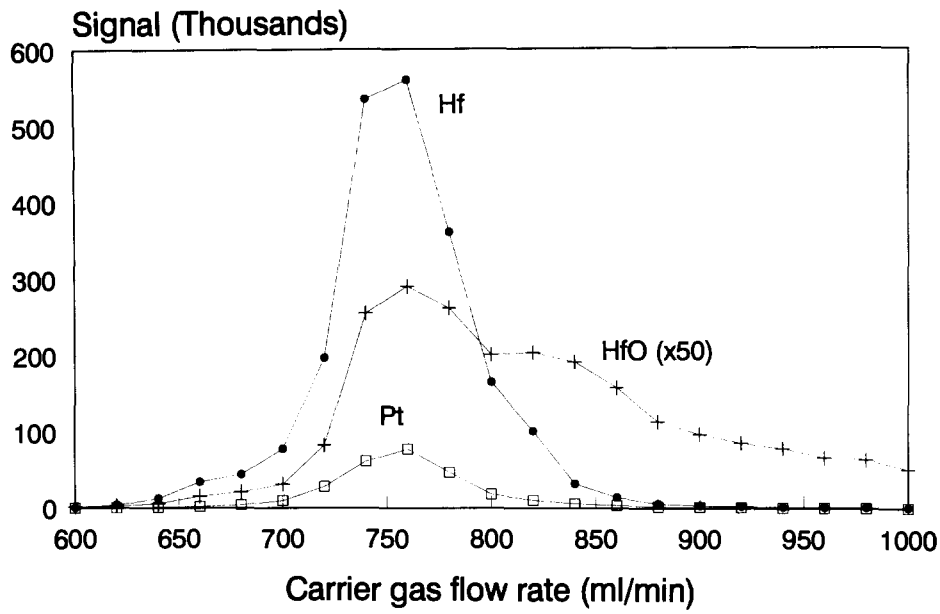

Fig. 4. Dependence of the signal intensity for Pt^+, Hf^+ and HfO^+ on the nebulizer gas flow rate.

A known amount of the Hf interferent was added to the sample solution. From the difference between the intensities of the Pt signals measured in the Hf spiked and unspiked sample solutions, the interference originating from the added amount of Hf can be calculated. After determination of the concentration of Hf in the sample, the contribution of HfO^+ can be subtracted according to the following equation:

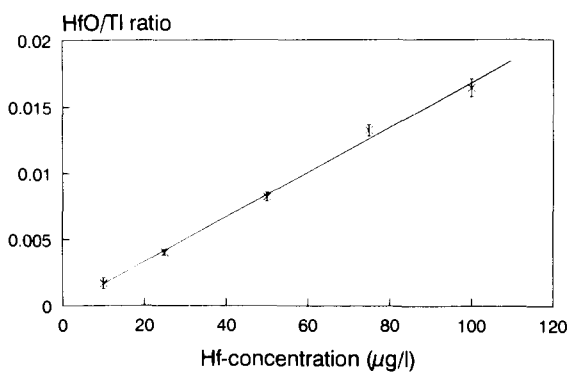

Fig. 5. Dependence of the HfO^+ signal on the Hf concentration.

$$I_{Pt} = I_{Pt,s} - \frac{C_{Hf,s}(I_{Pt+Hf,s} - I_{Pt,s})}{C_{Hf,a}} \quad (2)$$

where $I_{Pt+Hf,s}$ = the signal intensity for Pt in the sample solution to which Hf was added, $C_{Hf,s}$ = the concentration of Hf in the sample solution and $C_{Hf,a}$ = the Hf concentration corresponding to the amount of Hf added to the sample solution.

3.3.3. *Removal of Hf by chemical separation and application of isotope dilution*

Another method consists in separating Hf from the sample solution. Therefore, the adsorption chromatographic procedure proposed by Lee et al. [7] for the enrichment of Pt was applied. Under the conditions described in previous work [31], most of the matrix elements encountered are not strongly retained on the microcolumn used and can thus be separated from Pt. Because the Pt recovery is not quantitative and not reproducible, isotope dilution was used in this work. Isotope dilution requires that the measured isotope ratios reflect the isotopic composition of the sample, mixture or spike and that they are not influenced by interferences. By analyzing a standard solu-

Table 4
Determination of Pt in a solution containing 1 $\mu g\ l^{-1}$ Pt and 50 $\mu g\ l^{-1}$ Hf: comparison of results obtained with pneumatic (PN) and thermospray (TN) nebulization and using differen methods to correct for the HfO^+ interference on Pt^+

Correction method	Pt found ($\mu g\ l^{-1}$)[a]	
	PN	TN
Via the HfO^+/Hf^+ ratio	1.00 ± 0.02	0.99 ± 0.04
Via standard addition of Hf	1.00 ± 0.03	1.03 ± 0.05
Separation of Hf	0.99 ± 0.05	1.01 ± 0.05

[a]With 95% confidence interval.

tion, containing 50 $\mu g\ l^{-1}$ Hf, it could be demonstrated that Hf is separated with 99.9% efficiency.

To check the accuracy of the proposed method, an artificial solution, containing 50 $\mu g\ l^{-1}$ and 1 $\mu g\ l^{-1}$ Pt was analyzed and the results are shown in Table 4. The concentrations of Pt obtained with both sample introduction systems, after correction for HfO^+ or separation of Hf, are in good agreement with the expected concentration. The deviations are smaller than 3% and within the confidence limits.

3.4. Analysis of cordierite

The same correction procedures as used for the artificial solutions were applied. However, the signal intensity ratios for oxide species and their parent atomic ions are known to change with variations in matrix [29,32] composition (e.g. the acids used for destruction), operating conditions [17] and even aging of the interface [29,33]. Corrections based on this ratio can be improved by the use of the oxide ratio of a reference element to correct for possible changes in the HfO^+/Hf^+ ratio [33]. In this work, therefore, an oxide-forming element, with approximately the same MO bond strength as HfO^+, was used [34]; Zr (MO bond strength 182 kcal mol^{-1} [35]), present in cordierite, was chosen. The ZrO^+/Zr^+ ratio measured for the sample solution versus this ratio in the standard solution was used to correct for the matric dependence of the HfO^+/Hf^+ ratio. The scanning region was set from 92 to 207 u. $^{94}Zr^+$ and $^{94}Zr^{16}O^+$ were measured and $^{115}In^+$ was used as an internal standard.

The mathematical correction procedure using the HfO^+/Hf^+ ratio was therefore slightly modified and Eq. (1) was adapted to become

$$I_{Pt} = I_{Pt,s} - \left(I_{Hf,s} R_{HfO} \frac{R_{ZrO,s}}{R_{ZrO}} \right) \quad (3)$$

where $R_{ZrO,s}$ = the ZrO^+/Zr^+ ratio for the sample solution and R_{ZrO} = the ZrO^+/Zr^+ ratio for the standard solution.

The results obtained after correction are summarized in Table 5. It was observed that the MO^+/M^+ oxide ratio varied from sample to sample and was very different from that obtained with a standard solution (a factor of up to 2.5 was observed), as was predicted by other workers [17,29,32,33]. This effect could be readily corrected for by the use of Zr. TN was not used for sample introduction because too severe matrix effects, including obstruction of the interface, occurred.

To alleviate the effects of clogging of the sampling device [36,37], flow injection (FI) was also applied. Because a large mass region (92–207 u)

Table 5
Comparison of results for the determination of Pt in codierite, obtained with pneumatic (PN) and thermospray (TN) nebulization using continuous nebulization (CN) or flow injection (FI), and correction for the HfO^+ interference on $^{195}Pt^+$ with different methods

Correction method	Pt found ($ng\ g^{-1}$)	
	PN	TN
via the HfO^+/Hf^+ ratio:		
CN	32 ± 21	–
FI	47 ± 17	–
Via standard addition of Hf:		
CN	36 ± 20	–
FI	34 ± 9	38 ± 14
Separation of Hf:		
CN	37 ± 3	38 ± 4
FI	37 ± 8	36 ± 3

The values ($\pm$ 95% confidence intervals) are the means for five samples (three in the case of separation of Hf), each measured five times (CN), or four injections (FI). Indicative value: 50 (SD30) ng g^{-1} [21].

had to be scanned when Zr was measured simultaneously with Hf and Pt, the mass region between 120 and 174 u was skipped. Applying FI, no clogging of the cone and skimmer occurred, and the sample could also be measured with TN.

Finally, the Hf was separated by adsorption chromatography and both PN and TN were used in combination with continuous nebulization (CN) and with FI. The results are summarized in Table 5. Most obvious is the much better precision obtained after Hf separation than with mathematical correction procedures. In fact, repeatabilties of about 10% can be achieved. When comparing the two mathematical correction methods, preference should be given to the standard addition of Hf to correct for the interference by HfO^+. FI seems generally to yield slightly more precise results than CN. Our results obtained with different correction and sample introduction methods are in good agreement with each other and suggest a value of 34–38 ng g^{-1}. To evaluate the accuracy, comparison with the indicative value derived by Wegscheider and Zischka [21] from the results of a round robin study on the same sample gives some indication. The large uncertainty, 50 (SD 30)ng g^{-1}, in this indicative value reflects the difficulty of the determination. An alternative comparison can be made with values reported by Alt and Tölg [38] as obtained by ICP-MS (42.0 ng g^{-1}) and by GFAAS (46.1 ng g^{-1}) for the same cordierite sample.

4. Conclusions

The optimization study of the procedure and the determination of Pt in cordierite has shown the superiority of a chemical separation of Hf to avoid the interference of HfO^+. Adsorption chromatography yields a nearly quantitative separation of Hf and Pt losses during the procedure can be corrected for by applying isotope dilution. Mathematical correction yields less precise but for Hf/Pt ratios up to 50 also accurate results, especially when the interference is calculated from an addition of Hf interferent to the sample.

Without chemical separation, flow injection is to be preferred in order to avoid severe matrix effects including clogging of the sampling device and the interface, especially when thermospray nebulization is applied.

Care has to be taken to avoid problems associated with memory effects of Pt and precipitation of Hf oxide. These effects can be avoided by rinsing between solutions with 0.1% Triton X-100 by addition of 0.1% HF to the sample solution.

Acknowledgements

This research was supported by a specialization grant from the Flemish Institute for the Promotion of Scientific and Technological Research in Industry (IWT). Professor, Dr. W. Wegscheider (Austria) kindly provided the cordierite sample.

References

[1] C. Wei and G.M. Morrison, Sci. Total Environm., 146/147 (1994) 169.
[2] J. Messerschmidt, F. Alt and G. Tölg, Anal. Chim. Acta 291 (1994) 161.
[3] D. Wildhagen and V. Krivan, Anal. Chim. Acta, 274 (1993) 257.
[4] F. Alt, A. Bambauer, K. Hoppstock. B. Mergler and G. Tölg, Fresenius, J. Anal. Chem., 346 (1993) 693.
[5] H. Mukai, Y. Ambe and M. Morita, J. Anal. At. Spectrom., 5 (1990) 75.
[6] M.R. Plantz, J.S. Fritz, F.G. Smith and R.S. Houk, Anal, Chem., 61 (1989) 149.
[7] M.L. Lee, G. Tölg, E. Beinrohr and P. Tschöpel. Anal. Chim. Acta, 272 (1993) 193.
[8] E.H. Evans and J.J. Giglio, J. Anal. At. Spectrom., 8 (1993) 1.
[9] C. Vandecasteele, M. Nagels, H. Vanhoe and R. Dams, Anal. Chim. Acta, 211 (1988) 91.
[10] F. Vanhaecke, H. Vanhoe, R. Dams and C. Vandecasteele, Talanta, 39 (1992) 737.
[11] R.C. Hutton and A.N. Eaton, J. Anal. At. Spectrom., 3 (1988) 547.
[12] F. Vanhaecke, C. Vandecasteele, H. Vanhoe and R. Dams, Mikrochim. Acta, 108 (1992) 41.
[13] J.W. Lam and J.W. McLaren, J. Anal. At. Spectrom., 5 (1990) 419.
[14] L.C. Alves, L.A. Allen and R.S. Houk, Anal.Chem., 65 (1993) 2468.

[15] N. Jakubowski, I. Feldmann and D. Stuewer, Spectrochim, Acta, Part B 47B (1992) 107.
[16] R. Tsukahara and M. Kubota, Spectrochim. Acta Part B 45B (1990) 779.
[17] M.A. Vaughan and D.M. Templeton. Appl. Spectrosc., 44 (1990) 1685.
[18] M.A. Vaughan and G. Horlick, Appl. Spectrosc., 44 (1990) 587.
[19] M. Parent, H. Vanhoe, L. Moens and R. Dams, Anal. Chim. Acta, 320 (1996) 1.
[20] H. Vanhoe, L. Moens and R. Dams, J. Anal. At. Spectrom., 9 (1994) 815.
[21] W. Wegscheider and M. Zischka, Fresenius, Z. Anal. Chem., 346 (1993) 525.
[22] D. Beauchemin, Analyst, 118 (1993) 815.
[23] P.S. Ridout, H.R. Jones and J.G. Williams, Analyst, 113 (1988) 1383.
[24] K.K. Falkner and J.M. Edmond, Anal. Chem., 62 (1990) 1477.
[25] D.W. Boomer and M.J. Powell, Anal. Chem., 59 (1987) 2810.
[26] H.P. Longerich, B.J. Fryer and D.F. Strong, Spectrochim. Acta, Part B, 42B (1987) 101.
[27] H. Vanhoe, R. Dams, C. Vandecasteele and J. Versieck, Anal. Chim. Acta, 281 (1993) 401.
[28] J.A. Koropchak and M.Weber, Crit. Rev. Anal. Chem., 23(3) (1992) 113.
[29] S. Munro, L. Ebdon and D.J. McWeeny, J. Anal. At. Spectrom., 1 (1986) 211.
[30] J.M. Henshaw, E.M. Heithmar and T.A. Hinners, Anal. Chem., 61 (1989) 335.
[31] M. Parent, R. Cornelis, F.Alt, K. Strijckmans and R. Dams, Biol. Trace. Elem. Res., 43–45 (1994) 109.
[32] G.E.M. Hall, J.C. Pelchat and J. Loop, J. Anal. At. Spectrom., 5 (1990) 339.
[33] F.E. Lichte, A.L. Meier and J.G. Crock, Anal. Chem., 59 (1987) 1150.
[34] F. Vanhaecke, C. Vandecasteele, H. Vanhoe and R. Dams, poster presented at the 3rd Surrey Conference on Plasma Source Mass Spectrometry, Guildford, Surrey, 1989.
[35] R.C. Weast (Ed.), CRC Handbook of Chemistry and Physics, 51st edn., Chemical Rubber Co., Cleveland, Oh, USA, 1970–71.
[36] Z. Peng, H. Klinkenberg, T. Beeren and W. Van Borm, Spectrochim, Acta Part B, 46B (1991) 1051.
[37] A. Stroh, U. Völlkopf and E. Denoyer, J. Anal. At. Spectrom., 7 (1992) 1201.
[38] F. Alt and G. Tölg, Schlussbericht zum Forschungsvorhaben "Beitrag zur Verbesserung der extremen Spurenanalyse der Platinmetalle in biotischen und umweltrelevanten Materialen, Forschungsverbund "Edelmetallemissionen" des Bundesminister für Forschung und Technologie, 07 VPT 01A, ISAS, Dortmund, 1990–92.

ELSEVIER

Talanta 44 (1997) 231–237

Talanta

Collection of trace heavy metals complexed with ammonium pyrrolidinedithiocarbamate on surfactant-coated alumina sorbents

Masataka Hiraide*, Junichi Iwasawa, Hiroshi Kawaguchi

Department of Materials Science and Engineering, Nagoya University Chikusa-ku, Nagoya 464, Japan

Received 7 March 1996; revised 26 June 1996; accepted 27 June 1996

Abstract

Surfactant aggregates were formed on alumina surfaces by mixing 100 mg of sodium dodecyl sulfate (SDS) and 1.5 g of γ-alumina in 50 ml of water. The SDS-coated alumina incorporated water-insoluble metal–ammonium pyrrolidinedithiocarbamate complexes over the pH range 2–8 with a recovery of >97%. The metals were quantitatively desorbed from the alumina with 4 mol l^{-1} nitric acid, leaving >99% of SDS on the solid phase. They were determined by inductively coupled plasma mass spectrometry or graphite furnace atomic absorption spectrometry. The proposed method was successfully applied to the determination of traces of iron, cobalt, nickel, copper, cadmium and lead in high-purity alumina.

Keywords: Alumina analysis; Inductively coupled plasma mass spectrometry; Sorption; Surfactant micelles

1. Introduction

Ionic or nonionic surfactant molecules form self-aggregate structures called "micelles" in aqueous solutions above the critical micelle concentration. The hydrocarbon cores of the micelles give them the ability to solubilize hydrophobic organic compounds. Similar surfactant aggregates can be formed on solid surfaces such as alumina [1,2] and hydrated iron(III) oxide [3]. They are called "hemi-micelles" or "ad-micelles", whose interior tends to incorporate sparingly soluble organic substances (e.g. pentachlorophenol, toluene, *p*-xylene and trichloroethylene).

Previously, we studied the potential and utility of hemi- and ad-micelles in inorganic trace analysis [4,5]. Hydrophobic chelating agents were introduced into the micelles for the separation and preconcentration of trace elements. For example, dithizone was immobilized on alumina by mixing alumina with an ammoniacal dithizone solution (containing sodium dodecyl sulfate (SDS)) and acidifying the mixture. During the acidification, the SDS was sorbed on the alumina to form surfactant aggregates, into which water-insoluble

* Corresponding author. Tel.: 052-789-3579; fax: 052-789-3241; e-mail: hiraide@emerald.numse.nagoya-u.ac.jp

PII S0039-9140(96)02038-3

dithizone was incorporated. The color of the alumina changed from white to gray–blue. The dithizone-coated alumina was useful for the collection of many trace metals from water [6]. One of the problems is the blank value for copper. In the preparation of the sorbent, copper impurities in SDS were complexed with dithizone and introduced into the alumina. Incomplete desorption (e.g. for cobalt) was another problem.

In the present work, surfactant aggregates were first formed on alumina surfaces by coulombic attraction. Then water-insoluble metal–ammonium pyrrolidinedithiocarbamate (APDC) complexes were trapped in the aggregates. This procedure was simple and effective in eliminating the copper blank. Complete desorption of heavy metals was achieved with dilute nitric acid. The SDS-coated alumina functioned well even in solutions containing large amounts of aluminum ions. Compared with conventional liquid–liquid extraction with APDC, the proposed sorption method can directly be combined with inductively coupled plasma mass spectrometry (ICP-MS) or atomic emission spectrometry (ICP-AES), where the organic extractants can cause plasma instability. Sorption and desorption and also the preparation of the sorbent do not require any toxic organic solvents, which is an advantage from the viewpoint of discharge of solvents to the environment. The proposed method was applied to the determination of metals impurities at the sub-μg g^{-1} level in high-purity alumina.

2. Experimental

2.1. Apparatus

A Seiko SPQ-6500 ICP-mass spectrometer was used for the determination of $^{59}Co^{+}$, $^{58}Ni^{+}$, $^{63}Cu^{+}$, $^{114}Cd^{+}$ and $^{208}Pb^{+}$ under the following plasma conditions: r.f. power 1.2 kW; and argon flow rates 16 l min^{-1} for outer, 0.7 l min^{-1} for intermediate and 1.0 l min^{-1} for carrier.

A Seiko I&E SAS-760 atomic absorption spectrometer equipped with an SAS-715 graphite furnace atomizer was employed for the determination of iron. The graphite tube was heated for 20 s to 150°C, held for 15 s and then heated for 5 s to 900°C and held for 10 s; the tube was further heated at a final atomization temperature of 2400°C for 2 s; the clean-up stage was carried out at 2500°C for 3 s. The wavelength and hollow-cathode lamp current were 248.3 nm and 10 mA, respectively.

A Tokyo Rikakikai AU-60C ultrasonic cleaning bath (28 kHz, 210 W) was used for the purification of alumina particles. A Tokyo Rika NTS-1300S shaker was employed for mixing alumina with SDS at a shaking rate of 160 min^{-1}.

All separation procedures were carried out in a Hitachi ECV-843 BY clean bench.

2.2. Reagents

γ-alumina (10–50 μm particles, chromatographic grade, Katayama Chemicals) was ultrasonically washed in 5 mol l^{-1} nitric acid for 3 min and rinsed thoroughly with water three times.

SDS (special grade for water analysis, Nacalai Tesque) was used without further purification.

An APDC solution (0.1%, w/v) was prepared by dissolving APDC (special grade for AAS, Nacalai Tesque) in water.

Metal standard solutions (1 μg ml^{-1} in 0.1 mol l^{-1} nitric acid) were prepared from commercial standard solutions and diluted to appropriate concentrations with 0.1 mol l^{-1} nitric acid immediately before use.

An aluminum solution (10 mg ml^{-1}) was prepared by dissolving aluminum sulfate in 0.1 mol l^{-1} hydrochloric acid and purifying by extraction with APDC and chloroform [7,8]. The aluminum solution was used for the preparation of synthetic samples, which were employed to study the separation of trace metals from large amounts of aluminum ions.

All reagents were of analytical grade (Nacalai Tesque) unless stated otherwise. Water was purified by distillation and ion exchange and then passed through a Millipore Milli-Q purification system.

Table 1
Effect of quantity of SDS on a flow rate of 50 ml of water

SDS sorbed on alumina	(mg)	1	10	25	50	75	100
Flow rate[a]	(ml min^{-1})	7.5	7.9	8.4	9.2	10.0	12.9

[a] Average of three experiments.

2.3. Preparation of SDS-coated alumina column

Purified alumina particles (1.5 g) were suspended in 50 ml of water and mixed with 100 mg of SDS. The suspension was acidified to pH 2 with 4 mol l^{-1} nitric acid and mixed for 15 min with a mechanical shaker. After discarding the supernatant solution, the SDS-coated alumina was transferred to a Millipore filter holder (column size: 15 mm in diameter × 7 mm height). A 0.4 μm Nuclepore polycarbonate membrane filter (25 mm in diameter) was placed on the sintered-glass disk to prevent the disk from clogging with alumina.

2.4. Recommended procedure for the analysis of high-purity alumina

Place a 700 mg alumina sample in a 30 ml Teflon pressure decomposition vessel and add 20 ml of 4 mol l^{-1} sulfuric acid. Heat the vessel at 220°C for 18 h to decompose the sample completely. After cooling the solution to room temperature, dilute it to 100 ml with water. Transfer a one-fifth aliquot into a 30 ml beaker and adjust the pH to 2.5–3 with 15 and 5 mol l^{-1} aqueous ammonia. After adding 1 ml of APDC solution and mixing for 30 s, pass the solution through the SDS-coated alumina column to collect the metal–APDC complexes. Wash the column with 20 ml of 0.005 mol l^{-1} nitric acid. Desorb the desired trace metals with 1 ml of 4 mol l^{-1} nitric acid and collect in a 10 ml volumetric flask. Repeat the desorption twice more with 1 ml each of 4 mol l^{-1} nitric acid and finally wash the column with 5 ml of water. Adjust the combined solution to 10 ml with water and, after dilution (if necessary), determine the desired metals by ICP-MS (for Co, Ni, Cu, Cd and Pb) and GFAAS (for Fe).

Construct the calibration graphs by taking nanogram quantities of heavy metals and 3 ml of 4 mol l^{-1} nitric acid in a 10 ml volumetric flask and diluting to the mark with water.

3. Results and discussion

3.1. Preparation of SDS-coated alumina

The anionic surfactant SDS is effectively sorbed on the positively charged alumina surfaces to form SDS aggregates [1,2,4]. A clear difference in the sorption was observed on two types of alumina particles [6]. γ-Alumina sorbed the surfactant completely over a wide pH range (1–6), whereas α-alumina sorbed very little SDS because of the chemically inert surface. Therefore, γ-alumina is essential for the preparation of surfactant-coated sorbents.

By shaking 1.5 g of γ-alumina and 100 mg of SDS in a slightly acidic solution, tiny alumina particles were coagulated to form bulky flocs. All SDS was sorbed on the alumina, which was confirmed by the toluidine blue titration method [6,9]. After packing the SDS-coated alumina into a column, 50 ml of water were passed to examine the effect of SDS on the flow rate. As shown in Table 1, the flow rate increased with increase in the amount of SDS. The SDS aggregates did not clog the alumina column but improved in the flow rate of samples. This is favorable for practical use.

3.2. Sorption of metal–APDC complexes on SDS-coated alumina

Previously, we prepared SDS-coated alumina sorbents containing dithizone [4,6] and 1-nitroso-2-naphthol [5]. The dithizone–alumina, however, often caused 30–50 ng copper blanks (originating

from 100 mg of SDS). Incomplete desorption (e.g. 40–50% for cobalt) was another problem. The 1-nitroso-2-naphthol-immobilized alumina cannot be used for multi-element separation.

In the present work, SDS aggregates were formed on alumina in the absence of chelating agents, into which water-insoluble metal complexes were incorporated. By this procedure, the blank value of copper was reduced to less than 1 ng. APDC [7,8,10] was selected as the chelating agent because it reacts with many elements to give sparingly soluble complexes in water. Further, it is more stable than sodium diethyldithiocarbamate (DDTC) in acidic solutions.

Incorporation of APDC complexes in SDS aggregates is illustrated in Fig. 1. The formation of hemi- and ad-micelles may depend on the concentration of SDS. The collection of APDC complexes was first examined in a batch experiment. Copper was complexed with APDC and stirred with the SDS-coated alumina for 15 min. By analyzing the supernatant solution, it was found that nearly complete recovery was obtained for the copper.

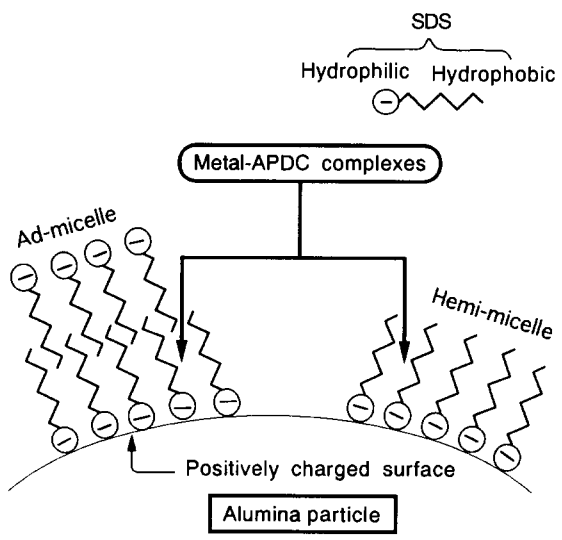

Fig. 1. Incorporation of metal–APDC complexes in surfactant aggregates formed on alumina.

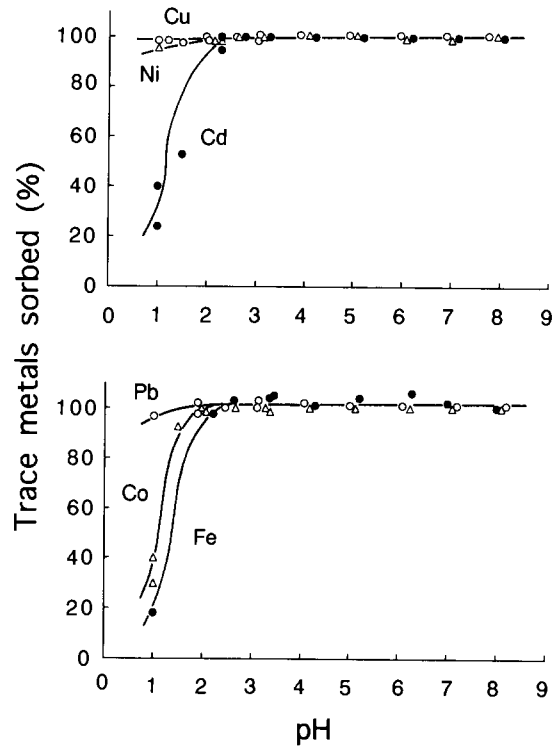

Fig. 2. Sorption of Fe(III), Co(II), Ni(II), Cu(II), Cd(II) and Pb(II) on SDS-coated alumina.

Next, freshly prepared SDS-coated alumina was packed into a column and sorption recoveries were measured for different trace metals. Aqueous sample solutions (20 ml, pH 1) containing trace metals (30 ng ml^{-1} each of Fe, Co, Ni, Cu, Cd

Table 2
Desorption of trace heavy metals from the SDS-coated alumina

Trace metal	Amount desorbed with 4 mol l^{-1} HNO_3 (%)		
	1.0 ml × 3	1.5 ml × 2	3.0 ml × 1
Fe(III)	98, 99	89	82
Co(II)	93, 100	78	80
Ni(II)	98, 101	85	83
Cu(II)	94, 102	86	88
Cd(II)	95, 100	89	86
Pb(II)	94, 112	83	107

Table 3
Effect of aluminum on the recovery of trace heavy metals

Aluminum added (mg)	Trace metal recovered (%)				
	Co(II)	Ni(II)	Cu(II)	Cd(II)	Pb(II)
50	101	105	100	105	109
100	97, 98	94, 97	96, 98	98, 100	97, 111
150	100	97	102	99	98

and Pb) were adjusted to different pH values with 1 and 0.1 mol l^{-1} aqueous ammonia. After adding 1 ml of APDC solution and stirring for 30 s, the solution was passed through the SDS-coated alumina column to sorb the APDC complexes. The effluent from the column was acidified to pH 1 and analyzed by ICP-MS to obtain the sorption recovery. However, the ICP-MS determination of iron at the ng ml^{-1} level was difficult because of an overlap of two spectra ($^{56}Fe^{+}$ and $^{40}Ar^{16}O^{+}$). Therefore, iron was determined by GFAAS.

Fig. 2 shows the percentage of trace metals sorbed as a function of the pH of the solution. All trace metals were recovered in >97% yields over a wide pH range (2–8). At basic pH, some metals (e.g. Fe and Cu) may exist as hydroxide colloids, but these species can also be collected on the column.

3.3. Desorption of trace metals from SDS-coated alumina

Trace heavy metals at the 30 ng ml^{-1} level in 20 ml of water were sorbed on the SDS-coated alumina column at pH 2.5–3 and then desorbed with 3 ml of 4 mol l^{-1} nitric acid. As shown in Table 2, more than 93% of the metals were recovered when three portions of 1 ml of nitric acid were used for the desorption. When 3 ml of nitric acid were added at a time, part of the metals still remained on the column.

Compared with conventional liquid–liquid extraction with APDC and chloroform [7,8,10], the proposed sorption method was directly combined with ICP-MS, because the final nitric acid solution was suitable for the plasma.

3.4. Separation of trace metals from aluminum matrix

Because APDC does not react with aluminum ions [7,8,10], the sorption method was applied to the analysis of high-purity alumina. The recovery of trace heavy metals was studied by using synthetic aluminum solutions. Because commercial aluminum sulfate contained appreciable amounts of metal impurities (nominally <30 $\mu g\ g^{-1}$), the reagent was purified by extraction with APDC and chloroform. When APDC solution was added to the aluminum solution, the solution immediately turned brown. Extraction with chloroform was therefore repeated three times.

Aluminum ions precipitated as hydroxide above ca. pH 4, hence the sorption was carried out at pH 2.5–3. Trace metals at the 30 ng ml^{-1} level in 20 ml of aluminum solution (containing 50–150 mg of aluminum) were sorbed, desorbed and determined by the recommended procedure. Table 3 shows that the SDS-coated alumina is useful for quantitative separation from the aluminum matrix. The amount of aluminum accompanying the desired trace metals was 2–3 mg when a sample containing 100 mg of aluminum was treated by the recommended procedure.

Further, a large volume of aluminum solution (200 ml; containing 1.0 g of aluminum and trace metals at the 30 ng ml^{-1} level) was introduced on to the SDS-coated alumina column and desorption and determination were carried out. Nearly complete recoveries were obtained for the trace metals examined.

Because 100 mg of SDS was used for the preparation of the alumina sorbent, the behavior of SDS in the desorption should be checked. The

Table 4
Determination of heavy metal impurities in high-purity alumina

Sample No.[a]	Amount weighed (mg)	Aliquot taken	Concentration in sample ($\mu g\ g^{-1}$)					
			Fe	Co	Ni	Cu	Cd	Pb
1	700	1/5	2.64	0.053	0.431	1.01	ND[b]	0.579
		1/5	2.79	0.055	0.397	1.03	ND	0.624
		1/5	2.60	0.064	0.424	1.16	ND	0.743
		Av.	2.68	0.057	0.417	1.07	ND	0.649
2	700	1/5	2.43	0.336	0.636	1.57	0.629	2.71
		1/5	2.36	0.329	0.607	1.79	0.529	2.57
		1/5	2.50	0.350	0.664	1.86	0.707	3.00
		1/5	2.21	0.343	0.629	1.79	0.714	3.07
		Av.	2.38	0.340	0.634	1.75	0.645	2.84

[a] Purity: 99.9% (No. 1) and 99.995% (No. 2).
[b] Not detected.

SDS in the final solution was determined by the toluidine blue method [6,9] and found to be 0.4–0.9 mg. In other words, more than 99% of SDS was still strongly sorbed on the alumina. Therefore, no interference occurred in the determination by ICP-MS and GFAAS.

3.5. Analysis of high-purity alumina

Generally, it is difficult or impossible to determine impurities at sub-$\mu g\ g^{-1}$ levels in alumina. For example, direct analysis by ICP-AES after sample decomposition [11,12] caused a decrease in the signal intensity and an increase in the background. Fusion followed by coprecipitation with zirconium hydroxide [13] resulted in high blanks and an increase in the background in ICP-AES. Extraction with dithizone and APDC [14] required large amounts of ammonium tartrate to mask the hydrolysis of aluminum, which can cause appreciable contamination. Analysis of an alumina suspension by AAS [15] needed accurate background correction and tedious preparation of a standard alumina suspension.

Although ICP-MS offers a highly sensitive multi-element determination technique, the mass analyzer is seriously contaminated if large amounts of matrix element are introduced. Therefore, trace elements should be separated from the aluminum prior to the determination. Table 4 shows the analytical results for two samples of high-purity alumina obtained by the recommended procedure. Trace metals at low $\mu g\ g^{-1}$–$ng\ g^{-1}$ levels were determined with relative standard deviations of $<10\%$. It is interesting that the contents of metals sought in sample No. 1 (99.9%, α-alumina) were almost same as or lower than those in sample No. 2 (99.995%, corundum). For accurate evaluation of the purity of alumina, the determination of other elements (especially boron, sodium, silicon and calcium) may be required. Unfortunately, these elements cannot be determined because they do not react with APDC. However, considering the well established APDC chemistry, we hope that the SDS-coated alumina could easily be employed for the separation and preconcentration of trace heavy metals in a wide range of applications.

References

[1] K.T. Valsaraj, Sep. Sci. Technol., 24 (1989) 1191.
[2] K.T. Valsaraj, Sep. Sci. Technol., 27 (1992) 1633.
[3] T.M. Holsen, E.R. Taylor, Y.C. Seo and P.R. Anderson, Environ. Sci. Technol., 25 (1991) 1585.
[4] M. Hiraide, M.H. Sorouradine and H. Kawaguchi, Anal. Sci., 10 (1994) 125.
[5] M. Hiraide, Y. Ohta and H. Kawaguchi, Fresenius' J. Anal. Chem., 350 (1994) 648.

[6] M. Hiraide, J. Iwasawa, S. Hiramatsu and H. Kawaguchi, Anal. Sci., 11 (1995) 611.
[7] O.G. Koch and G.A. Koch-Dedic, Handbuch der Spurenanalyse, Teil 1, Springer, Berlin, 1974, p. 308.
[8] E.B. Sandell and H. Onishi, Photometric Determination of Traces of Metals: General Aspects, Wiley, New York, 1978, p. 529.
[9] M. Hiraide, T. Shima and H. Kawaguchi, Anal. Sci., 10 (1994) 505.
[10] A. Mizuike, Enrichment Techniques for Inorganic Trace Analysis, Springer, Berlin, 1983, p. 30.
[11] T. Ishizuka, Y. Uwamino, A. Tsuge and T. Kamiyanagi, Anal. Chim. Acta, 161 (1984) 285.
[12] H. Morikawa, Y. Iida, T. Ishizuka and F. Yokota, Bunseki Kagaku, 35 (1986) 636.
[13] Y. Harada and N. Kurata, Bunseki Kagaku, 35 (1986) 641.
[14] O.G. Koch, Mikrochim. Acta, I (1958) 92.
[15] Z. Slovak and B. Docekal, Anal. Chim. Acta. 129 (1981) 263.

ELSEVIER

Talanta 44 (1997) 239–248

Talanta

Amperometric detection of amines using cobalt electrodes after separation by ion-moderated partition chromatography

A. Hidayat[a], D.B. Hibbert[a,*], P.W. Alexander[b]

[a]*Department of Analytical Chemistry, University of New South Wales, Sydney, NSW 2052 Australia*
[b]*Department of Physical Science, University of Tasmania, P.O. Box 1214, Launceston, Tasmania 7001, Australia*

Received 21 February 1996; revised 25 June 1996; accepted 26 June 1996

Abstract

A simple and low-cost amperometric sensor for amines has been developed using a cobalt wire electrode working in alkaline solution. The sensor may be used as a detector for high-performance liquid chromatography (HPLC) that avoids the need for derivatization or post-column reaction. Experimental conditions for flow injection analysis (FIA) and HPLC separation, including the applied potential, pH and concentrations of organic modifier and carrier solution, were optimized. A cobalt wire electrode, in the constant potential amperometric mode, gives an excellent response toward amines in ion-exclusion chromatography in unbuffered solution. The sensitivities of the detection and separation of amines on the column are affected by flow rate, the concentration of the mobile phase and the concentration of organic solvent in the mobile phase, whereas the applied potential only affects the sensitivity of the detector. A cobalt electrode is more sensitive than a copper electrode, and comparable in sensitivity to a UV detector for most amines tested. The detection sensitivity is comparable to that obtained with GC methods, but the procedures are far simpler. The detection limits of the order of nanomoles obtained under the chromatographic conditions used offer an alternative for the determination of amines in a variety of matrices, such as in environmental, biomedical and pharmaceutical samples.

Keywords: Amines; Amperometric detection; Cobalt electrodes; Ion-moderated partition chromatography

1. Introduction

The determination of amines by gas chromatography, when effective, is a sensitive technique [1], but derivatization is required for non-volatile amines and the polar nature of amines may cause severe tailing of peaks [2]. In the last decade, several electrochemical approaches have been explored to detect amines after separation by high-performance liquid chromatography (HPLC). HPLC methods for the separation of biogenic amines tend to use reversed-phase sorbents with pre-or post-column derivatization and UV detection. However, this

* Corresponding author.Fax: (61)2-9385-6141.

PII S0039-9140(96)02039-5

procedure adds complexity and may lead to problems associated with side-reactions of the derivatizing compound. HPLC on ion-moderated partition columns with sodium hydroxide as eluent has been reported to separate up to 10 volatile and non-volatile amines [3]. Electrochemical detection has employed polarography, square-wave voltammetry, pulsed amperometry and biosensors. The last method used avocado, mushroom and potato tissue on a Clarke oxygen electrode [4]. However, the most favourable electrochemical detectors for these compounds are limited to carbon-based electrodes [5–7]. Drawbacks of electrochemical detectors are a high overpotential for the oxidation of amines, which leads to poor selectivity, and the use of derivatization procedures or post-column reactions, which also complicates the method [5–7].

Metal or oxidized metal electrodes are preferred to carbon-based electrodes in many respects. They are simpler in construction, robust and have lower oxidation potentials for many redox compounds, and therefore have greater sensitivity and selectivity. As a consequence, there has been extensive exploration of metal/metal oxide electrodes for the constant-potential amperometric detection of organic compunds, including Pt, Au, Cu, Ni, Ag, Pd, Rh, Ir, Fe and W [8–15].

Cobalt, as the phthalocyanine, has also been used as a material for the construction of chemically modified carbon-paste electrodes for many compounds, including amines [16–18]. However, there has been no report on the use of cobalt wire for the constant-potential amperometric detection of these compounds. As metallic wire electrodes respond to complexing agents only in alkaline solution ($pH \gtrsim 6$) [12,19,20,21], our attempts were focused on the use of an alkaline solution as carrier. We report here the performance of cobalt wire as a simple and low-cost amperometric detector for the determination of amines after HPLC separation using an ion-exchange column (Aminex HPX-72-O) with sodium hydroxide as eluent. Its action is compared with that of a copper electrode.

2. Experimental

2.1. Apparatus

The cyclic voltammetric study was performed with a BAS-100B potentiostat equipped with Ag/AgCl (3 M NaCl) reference and platinum wire auxiliary electrodes. An EG&G Princeton Applied Research Polarograph, type 174, was used for constant-potential amperometric detection with a single-line flow injection analysis (FIA) manifold and HPLC systems. The output was recorded and processed by a Macintosh II VX microcomputer.

The flow cell used in both FIA and HPLC detection was made from a Perspex block (5 × 3 × 1 cm) with a 1.2 mm channel allowing the analyte first to contact the working electrode (1 mm diameter wire) along a 1 cm length and then flow away past auxiliary and reference electrodes [22]. The Ag/AgCl reference electrode, prepared by electrolysis at a silver wire electrode in 1.0 M KCl, was coated with 1.0 M KCl in 4% agar gel and was located out of the flowing stream. Each electrode was polished with emery paper and rinsed with deionized water before use. After pretreatment (see below), the potential was kept fixed at the optimum level. Only after a stable baseline current had been obtained in the supporting electrolyte were analytes added and their peak currents determined.

The separation of amines was performed using a Model 510 HPLC pump, U6K injection valve, and Model 484 tunable absorbance detector, all from Waters (Milford, MA, USA) with a resin-based, modified partition column (Aminex HPX-72-0,300 mm × 7.8 mm i.d. × 11 mm o.d.) purchased from Bio-Rad Laboratories (Sydney, Australia).

2.2. Chemicals and solutions

All chemicals were of analytical grade and were used without further purification. Methylamine (me), *n*-propylamine (pro), *n*-butylamine (but), trimethylamine (tma), cysteamine hydrochloride (cys) and benzylamine (ben) were purchased from Sigma Chemical (St. Louis, MO, USA). Stock solutions of the amines 10 mM were prepared in

Milli-Q water and diluted to the required concentrations before use. The solutions were filtered through a Millipore 0.45 μm membrane filter and degassed in an ultrasonic bath prior to use. All water was distilled and passed through a Milli-Q water purification system.

2.3. Procedure

Cyclic voltammetric studies (10 cycles) were performed with a potential scan rate of 50 mV s^{-1}. In the flow injection system, the carrier solution was continuously pumped through the detector cell at a constant flow rate until a stable baseline current was obtained. All experiments were performed at room temperature with sodium hydroxide solution as a carrier. The hydrodynamic voltammograms were obtained in the flow-through cell, point-by-point, allowing for stabilization of the current.

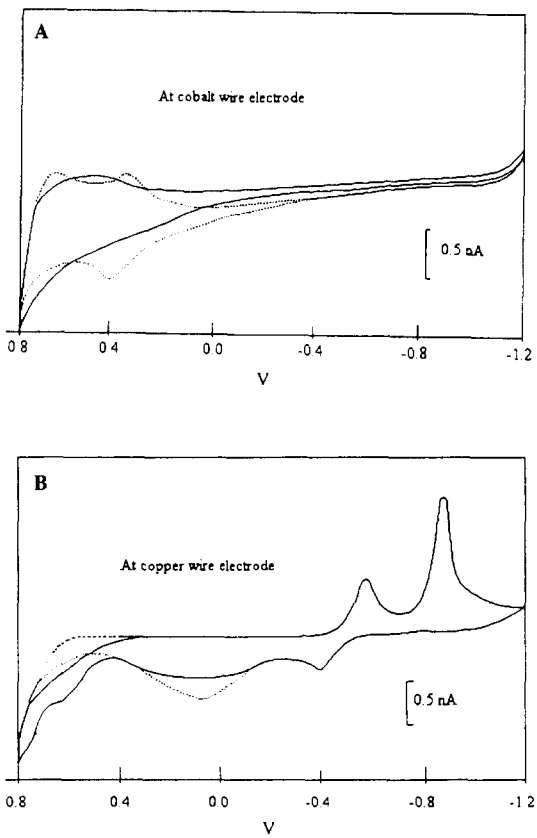

Fig. 1. Cyclic voltammograms at (A) cobalt and (B) copper wire electrodes in 0.1 M NaOH (dotted line) and after addition of 1 mM methylamine (solid line). Sweep rate, 50 mV s^{-1}.

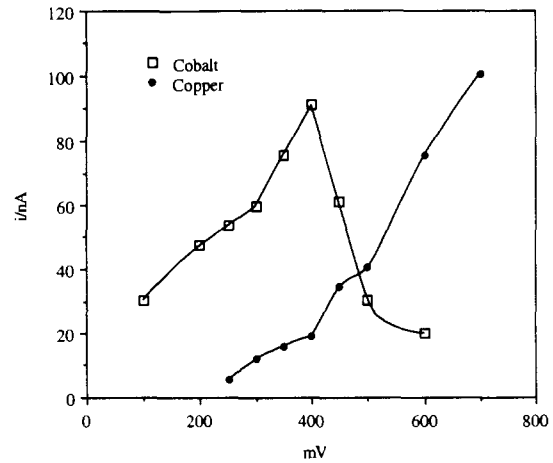

Fig. 2. FIA peak height of 25 nmol (cobalt electrode) and 20 nmol (copper electrode) of methylamine as function of applied potential. Carrier solution, 0.1 M NaOH; flow rate, 0.75 ml min^{-1}.

In HPLC, the effects of eluent concentration, electrode pretreatment, addition of organic solvent and flow rate on the electrode response were investigated by applying each parameter at various levels. The electrochemical detector performance of a cobalt electrode was compared with that of a copper electrode and UV detection. The wavelength used for UV detection recommended by Bio-Rad (210 nm) [23] was chosen with a

Table 1
Effect of pretreatment on the slope of the FIA of methylamine standards at cobalt and copper wire electrodes.

Treatment	Slope (nA $nmol^{-1}$)	
	Cobalt	Copper
None[b]	4.50*	4.07*
Cycled 10 times	4.48*	4.06*
+2 V for 2 min	4.27**	3.89**
+2 V for 10 min	1.41***	3.71***

[a] *,** and *** are statistically significant (95%) groupings by analysis of variance (ANOVA) and least significant difference.
[b] Apply potential at optimum level directly after rinsing with water.

Table 2
Effect of mobile phase concentration on the resolution of the most overlapping peaks (methylamine and propylamine)

NaOH (mM)	Resolution[a]
25	0.68
50	0.69
75	0.73
100	1.35

Flow rate, 0.75 ml min^{-1}; sensor, cobalt at +0.40 V vs. Ag/AgCl.
[a] Average of three replicates.

sensitivity setting of 0.1 a.u.f.s. (absorbance units full-scale). All experiments were performed at room temperature with 0.075 M sodium hydroxide solution as the mobile phase. The injection volume was 20 μl.

3. Results and discussion

3.1. Principles of electrode response

The effect of amines on the electrochemistry at a cobalt surface is twofold. At more positive potentials at which Co^{III} is formed (> 0.5 V vs. Ag/AgCl, 0.075 M NaOH), a so-called catalytic oxidation may occur, in which the amine is oxidized by Co^{III}, which is regenerated electrochemically [8–11,14–17]. Schematically the reactions are

$$Co^{III} + \text{amine} \rightarrow Co^{II} + \text{amine oxidation products} \quad (1)$$

$$Co^{II} \rightarrow Co^{III} + e \quad (2)$$

The species present at the surface include oxides and hydroxy compounds such as CoO, $Co(OH)_2$ and CoO(OH) [24,25]. Nickel has been shown recently to participate in these types of reaction [9]. The cyclic voltammograms in Fig. 1 demonstrate this effect for both cobalt and copper in the presence of methylamine, above +0.5 V.

In constrast to the above mechanism, amines may absorb at potentials below that at which they are oxidized, blocking the surface and leading to a reduction in the oxidation current of the metal. As an example of this behaviour, Luo et al. [11] reported that the addition of glucose and lactic acid reduced the oxidation current of copper wire electrodes. Hui and Huber [26] also reported that the oxidation current of a nickel electrode was reduced by 100 nA after addition of 1.0 mM glycine at an optimum potential of 0.55 V. Similarly to the published cyclic voltammograms of glucose, lactic acid and glycine at copper electrodes [11,26], our results show that the oxidation currents of cobalt and copper wire in 0.1 M NaOH (dotted lines, Fig. 1), were diminished at low potentials (< +0.5 V) with the addition of 1 mM of methylamine (solid lines, Fig. 1). The broad oxidation peak of cobalt at +0.4 V was significantly reduced when 1.0 mM of methylamine was added. A similar trend was observed at a copper electrode with significant depression at the maximum in the oxidation current (+0.05 V).

There is a difference between the dynamic nature of cyclic voltammetry and constant-potential amperometry. However, a similar trend was obtained at a constant potential, with a decrease in the current as the amines were introduced into the system at a cobalt wire held at +0.4 V, and an increase in current at a copper wire held at +0.7 V. The behaviour is consistent, and we note that for cobalt at +0.4 V the baseline was maintained constant over many hours of operation.

3.2. Selection of working potential

Flow-injection studies were carried out to determine whether cobalt and copper electrodes could be used with ion-exclusion chromatography. Methylamine standards were injected into a single-line FIA system using NaOH as the carrier solution and the FIA conditions were optimized for high sensitivity with acceptable precision. First the current was recorded as a function of the applied potential to determine the working potential giving the highest response. Amounts of 25 nmol (cobalt electrode) and 20 nmol (copper electrode) of methylamine were injected into the flow system at applied potentials between 0.0 and +0.7 V.

The results (Fig. 2) show consistency between FIA and cyclic voltammetry, but the changes in current were greater in the flow system. The greatest reduction in current due to injection of methylamine at a cobalt wire occured at +0.40 V. At a copper electrode the FIA peaks steadily increased with increase in applied potential. They were poorly reproducible and the baseline noise was high, giving poor precision when used to calibrate for amines. Subsequent work was therefore concentrated on the use of a cobalt electrode for practical analysis of amines.

3.3. Electrode pretreatment and position

Stitz and Buchberger [9] reported that the sensitivity of a nickel electrode for the detection of carbohydrates and related compounds is strongly influenced by the pretreatment of the electrode surface. Procedures affecting the amount of oxide on the electrode are likely to affect the sensitivity. In this experiment, after polishing with emery paper and rinsing with dionized water, the electrodes were pretreated with four different procedures as follows: (1) the potential was kept fixed at the optimum working level: (2) the electrodes were cycled initially in the blank solution over the desired potential range (−0.4 to 1.1 V), for 10 cycles; (3) a potential of +2 V was applied for 2 min; (4) a potential of +2 V was applied for 10 min.

Table 1 shows that the highest sensitivity was achieved by applying the optimum potential directly after polishing with emery paper and rinsing with deionized water. The same sensitivity was shown when the electrode was cycled 10 times.

Table 3
Effect of organic modifier (methanol) on the peak height and the resolution of the most overlapping peaks (methylamine and propylamine)

Methanol concentration (%)	Peak height (nA)		Resolution
	Methylamine	Propylamine	
0	15	3.4	0.73
0.25	7.4	2.0	1.07
0.5	4.6	1.3	1.08

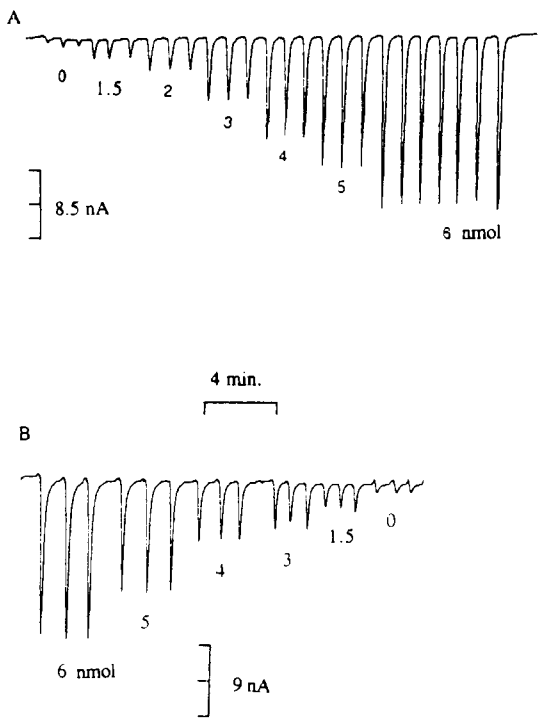

Fig. 3. Typical FIA peaks of the methylamine standards detected at (A) cobalt and (B) copper electrodes. Carrier solution, 0.075 M NaOH; flow rate, 0.75 ml min^{-1}; potential, 0.4 V (cobalt) and 0.5 V (copper).

The sensitivity was reduced significantly when the electrode was pretreated by oxidation at 2 V. The longer the oxidation at a cobalt electrode, the lower was the sensitivity. Completing a thick layer of oxide by this treatment would leave little to be affected by an absorbed amine.

3.4. Concentration of NaOH in the mobile phase

The effect of the concentration of the mobile phase on the detection response was examined to obtain a compromise between maximum sensitivity and solute retention on the chromatographic column. Since only two amines were overlapped (methylamine and propylamine), we focused on the separation of these two compounds.

Table 2 shows the effect of the concentration of NaOH in the range 0.025–0.100 M on the resolution of selected amines. The retention times of

compounds increased slightly as the concentration of sodium hydroxide increased, which improved the resolution. The best overall resolution of six compounds was achieved by using 0.075 M sodium hydroxide as the mobile phase. The resolution of methylamine and propylamine increased from 0.68 to 1.35 on increasing the NaOH concentration 0.025 to 0.10 M (Table 2). Similar observations have been reported where the concentration of ion-interaction reagent in the mobile phase increased, leading to a corresponding increase in solute retention [3,13].

An optimum concentration of alkaline medium is essential to develop the oxide film on the surface of the electrodes to respond sensitively to amines. Detailed studies by UV–visible reflectance spectroscopy and FTIR spectrometry at a nickel electrode surface showed that the main requirement for sensitive detection consists in the formation of a nickel(III) oxide–hydroxide layer in alkaline medium [9]. The same conditions may also be expected to apply to cobalt and copper electrodes. At low alkaline concentration, the oxidation process may not fully develop, and the oxide film is not sufficient to respond to the addition of amines. At high alkaline concentration, however, an unfavourable response occurs because of increasing participation of the equilibrium involving hydroxide ions. We found that the lowest detection limit was achieved at the optimum NaOH concentration of 0.075 M. Stulik et al. [13] also reported that copper electrodes respond to complexing agents only in a solution of pH > 6.0, and that the sensitivity increases with increasing pH and decreasing ionic strength.

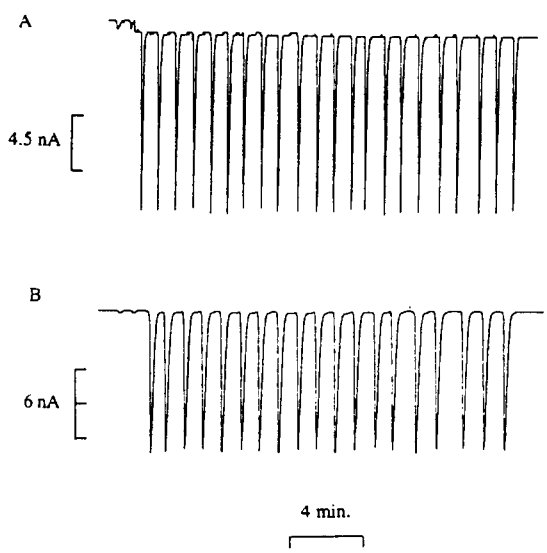

Fig. 4. FIA peaks showing the precision for 12 mmol methylamine detected at (A) cobalt and (B) copper electrodes. Carrier solution, 0.075 M NaOH, flow rate, 0.75 ml min^{-1}; potential, 0.4 V (cobalt) and 0.5 V (copper).

3.5. Flow rate

Decreasing the flow rate improves the resolution of the overlapping peaks, and the best compromise between resolution and retention time was achieved at a flow rate of 0.75 ml min^{-1}. At higher flow rates, propylamine moves in and masks the methylamine peak. These results support the previous report [22] that the optimum flow rate was achieved at 0.6 ml min^{-1}. Mass transfer in Aminex columns is slow, requiring a commensurately low flow rate to avoid band broadening.

3.6. Concentration of organic solvent

As the sensor is used in conjuction with the HPLC system, the effect of added organic solvent was studied. The addition of solutions of methanol between 0.1% and 2% to the carrier solution decreased the response of the cobalt wire electrodes to amines. The result is in agreement with those described in previous studies [13]. According to Stulik et al. [13], the presence of organic solvent suppresses the solubility of the passivating film and the interaction of the test substances with the passivating film. This in turn decreases the relative permittivity in the carrier, which generally causes a decrease in the rate constants for complex reactions. In contrast to the above, we found a positive response at a copper wire electrode when amine was injected into a carrier solution containing methanol. This result is also consistent with several reports on the amperometric detection of organic compounds by a copper wire electrode in an alkaline medium [9,11,13], in which direct oxidation yielding positive currents occurs.

Table 4
Comparison of stability of cobalt and copper electrodes

Injection number or time	Relative response (%)	
	Cobalt	Copper
10	100.0	100.0
20	99.5	99.0
50	102.4	74.4
After 3 h	99.2	55.0
After 6 h	100.8	42.5
After 9 h	99.4	–
RSD (%) ($n = 10$) [a]	1.3	1.9

Electrode potential (vs. Ag/AgCl), Co +0.94 V and Cu +0.5 V; sample, 12 nmol methylamine.
[a] (For the first 10 injections).

Although the FIA experiments at cobalt suggested that the addition of methanol significantly reduced the peak height, we invesitgated whether the addition of a low methanol concentration could improve the resolution of the amine peaks. An organic modifier penetrates and swells the organic backbone of the resin, so that decreased osmotic pressure decreases the intra-particle water volume. This to some extent may affect the resolution of the peaks.

The results in Table 3 show that the improvement in resolution of ovelapping peaks was not significant when methanol was added to the mobile phase. On the other hand, the peak heights were significantly reduced and the baseline was drifting. Therefore, the addition of organic modifier is not recommended with this method.

The effect of atmospheric oxygen in the solutions was studied, since the dissolution of copper in complex-forming media often depends on the presence of oxidants. However, no change occurred when oxygen was removed by passage of nitrogen for 30 min. Therefore, we conclude, in agreement with Stulik et al. [13], that the presence of atmospheric oxygen does not affect the detection.

Fig. 3 shows typical peaks obtained in the FIA system when responding to methylamine using both metallic cobalt and a copper wire electrode as detectors. Various structural types of amines were also investigated. Aliphatic primary, secondary and tertiary and aromatic amines can be

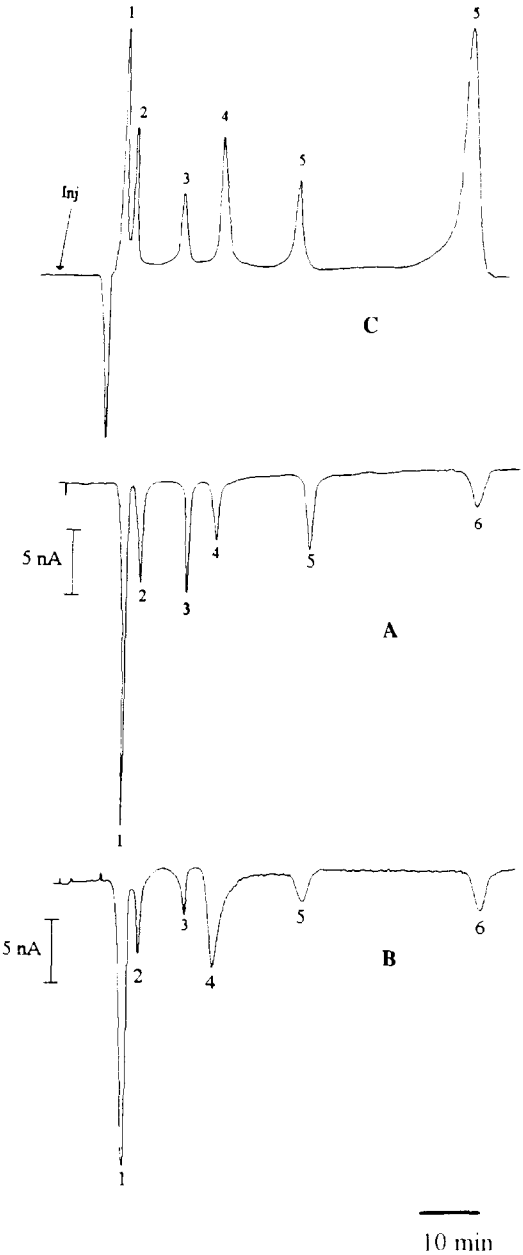

Fig. 5. Chromatograms of a mixture of aliphatic amines separated by ion-moderated partition chromatography and detected by (A) cobalt electrode, (B) copper electrode and (C) UV detector: Peaks 1 = methylamine; 2 = propylamine; 3 = butylamine; 4 = cysteamine hydrochloride; 5 = trimethylamine; 6 = benzylamine.

Table 5
HPLC calibration data for selected amines with amperometric detection at a cobalt electrode at +0.4 V (vs. Ag/AgCl)

Analyte	Linear concentration range (nmol)	Slope (nA nmol^{-1})	r^{2a}	LOD (nmol)[b]
Methylamine	2.6–130.0	1.65	0.989	0.46
n-Propylamine	3.4–101.0	0.77	0.984	0.98
n-Butylamine	5.4–135.0	0.65	0.987	1.15
Trimethylamine	4.2– 91.0	0.79	0.989	1.92
Benzylamine	9.2–166.2	0.12	0.999	6.30

Mobile phase 0.1 M NaOH; flow rate 0.75 ml min^{-1}
[a] Coefficient of determination (the fraction of variance accounted for by the linear model).
[b] LOD (limit of detection) = concentration that yields a current of three times the standard deviation of the background noise.

detected by this method. The sensitivity decreased with increasing chain length and with increasing number of substituents on the nitrogen atom.

3.7. Precision and stability

The precision of the electrode response was examined by injecting a sequence of 10 replicate samples of 12 nmol methylamine under the optimum conditions, using both cobalt and copper electrodes (Fig. 4). The mean values of the peak heights recorded were 23.0 and 14.3 nA with relative standard deviations (RSDs) of 1.3 and 1.9% for the cobalt and copper electrodes, respectively.

The stability of the electrode was tested by injection of 10, 25 and 50 replicate samples after 3,6 and 9 h without resurfacing the electrodes. The results in Table 4 indicate that good stability is obtained particularly with the cobalt electrode. The response eventually begins to decrease after 3–4 days of use but the former sensitivity was easily restored by cycling 10 times between −0.40 and +2.6 V. The long-term stability of the reference electrode must also be monitered. Redox processes at each of the electrodes may lead to poisoning and loss of performance.

The great stability offered by these systems may be due partly to the principle of detection, i.e. oxidation at a reversible layer consisting of high-valent metal oxide and metal hydroxide. The response thus results from the interaction of the analyte with higher valent metallic ions contained in the outer layer. This layer can be converted very rapidly to and from a layer of lower valence metal oxide, electrochemically or chemically thus renewing itself.

The detector cell design, which eliminates possible reactions with the Ag/AgCl reference electrode, may also contribute to the good stability of these sensors.

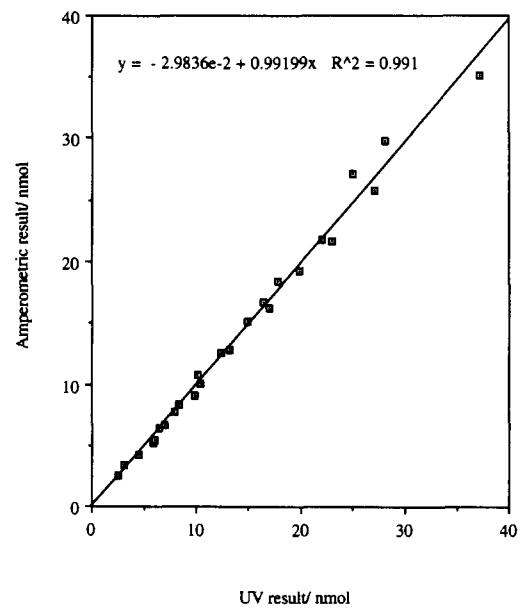

Fig. 6. Amperometric sensor with cobalt wire compared with UV spectrophotometric detection for amines. UV wavelength, 275 nm, carrier solution, 0.1 M NaOH; flow rate, 0.75 ml min^{-1}.

3.8. Analytical performance of the electrodes in the HPLC system

Typical chromatograms of six amines under the optimum chromatographic conditions, using an amperometric detector with cobalt and copper electrodes and a UV detector for comparison, are shown in Fig. 5. The amines separated in order of elution were methylamine, propylamine, butylamine, cysteamine hydrochloride, trimethylamine and benzylamine, with retention times of 10.1, 12.2, 19.8, 24.3, 39.0 and 67.9 min, respectively. All peaks were resolved sufficiently to allow the HPLC system to be of practical use for determining the six amines.

A good separation of the six amines was achieved in this system using only a 0.075 M NaOH carrier, without pre- or post-column derivatization. The retention times of isopropylamine and isobutylamine are identical with those of *n*-propylamine and *n*-butylamine, which suggests that the isomeric amines cannot be separated with this method.

The order of elution suggests that the less polar compounds (benzylamine) are retained more strongly than more polar compunds (methylamine), which shows that a reversed-phase partition is involved in this separation.

The detectors used, amperometric with cobalt and copper wire electrodes and a UV detector, gave similar chromatograms, with reasonable baseline separations of the amines tested. The RSDs of the retention times are $< 2.5\%$, which is good for an HPLC method.

3.9. Linearity, sensitivity and limit of detection

The calibration data for selected amines with amperometric detection at cobalt are shown in Table 5. The calibration graphs exhibit good linearity (correlation coefficients ranging from 0.984 for *n*-propylamine to 0.999 for benzylamine). The linear range of the voltammetric detector was between 30 (for benzylamine) and 300 (methylamine) times the limit of detection.

There was also a difference between the sensitivities of the various compounds shown by the amperometric sensors: the simpler the amines, the higher was the sensitivity. Their detection limits were consistent with their sensitivity which follows their degree of structural complexity. Methylamine could be detected at levels as low as 0.5 nmol whereas benzylamine could not be detected until about 6.3 nmol was present. The cobalt electrode exhibited higher sensitivities than the copper electrode for all amines tested. Compared with the electrode resonse in FIA, the amperometric response toward separated amines with a metallic electrode is lower. This discrepancy is probably due to the higher dispersion in the HPLC system and the difference in dynamic conditions between the two experiments.

Satisfactory precision (the RSD of the peak height was $< 2\%$) was obtained with five replicates, even at the lowest measured concentrations. Compared with a chemically modified electrode (CME) and mercury/gold amalgam electrodes, a cobalt electrode is more stable. A newly resurfaced gold amalgam electrode may operate efficiently for only a few minutes or hours. Using a CME, after some time the response is reduced. Some of the decrease in the electrode response is due to the gradual leaching of the modified chemicals from the CME surface. In fact, some decrease in response has been observed previously even for conventional carbon paste electrodes in electrochemical detection in liquid chromatography upon long-term exposure to a binary mobile phase containing a small fraction of organic components.

The design of the Ag/AgCl reference electrode may also contribute to the stability of this sensor. In this cell design, the silver wire which has been electrolysed with KCl solution was covered with solid agar gel containing 1.0 M KCl. The function of the solid agar gel containing 1.0 M KCl is similar to that of the Ag/AgCl reference electrode with a double junction.

The retention times are comparable to those achieved by Stamler and Loscalzo [27] using capillary zone electrophoresis for separation. As derivatization is not necessary, our method is simpler and cheaper. To our knowledge, this represents the first report on the use of cobalt and copper electrodes for constant-potential amperometric detection in conjunction with ion-moderated partition HPLC for the determination of amines.

3.10. Comparison with UV spectrophotometric detection

The performance in amine determination of a cobalt electrode was compared with that of a copper electrode and UV detection using the wavelength suggested by the instrument manufacturer [23]. Fig. 6 demonstrates the close agreement between amperometric detection with a cobalt electrode and UV detection.

Fig. 5 shows that compared with a UV detector, the cobalt electrode is more sensitive for the detection of methylamine and butylamine but less sensitive for propylamine, trimethylamine and benzylamine. Benzylamine absorbed UV radiation more strongly than other amines which are not aromatic. The UV detector placed prior to the amperometric detector also caused more dispersion. The constraints of working at UV wavelengths is that severe interference by organic compounds other than amines may occur.

References

[1] X.H. Yang, C. Lee and M.I. Scranton, Anal. Chem., 65 (1993) 572.
[2] H.B. Hucker and S.C. Stauffer, J. Chromatogr., 138 (1977) 437.
[3] R.B.H. Wills, J. Silalahi and M. Wootton., J. Liq. Chromatogr., 10 (1987) 3183.
[4] F. Mazzei, F. Botre, M. Lanzi, G. Lorenti, F. Porcelli and C. Botre, Sens. Acutuators, 7 (1992) 427.
[5] K. Shimada, T. Oe, M. Tanaka, and T. Nambara, J. Chromatogr., 487 (1989) 247.
[6] J.B. Barek, F. Pacakova, K. Stulik and J. Zima, Talanta, 32 (1985) 279.
[7] R.M. Smith and A.A. Ghani, Electroanalysis, 2 (1990) 167.
[8] T. Ueda, R. Mitchell and F. Kitamura., J Chromatogr., 592 (1992) 229.
[9] A. Stitz and W. Buchberger., Electroanalysis, 6 (1994) 251.
[10] A. Stitz and W. Buchberger, Fresenius' J. Anal. Chem., 339 (1991) 55.
[11] P. Luo, F. Zhang and R.P. Baldwin, Anal Chim. Acta., 244 (1991) 169.
[12] P. Luo, F. Zhang and R.P. Baldwin, Anal. Chem., 63 (1991) 1702.
[13] K. Stulik, V. Pacakova, K. Le and B. Hennissen, Talanta, 35 (1988) 455.
[14] R.E. Reim and R.M. Van Effen, Anal. Chem., 58 (1986) 3203.
[15] P.W. Alexander, A. Hidayat and D.B. Hibbert, Electroanalysis, 7 (1995) 290.
[16] E.G. Cookeas and C.E. Efstathiou, Analyst, 119 (1994) 1607.
[17] K. Korfhage, M.K. Ravichandran and R.P. Baldwin, Anal. Chem., 56 (1984) 1514.
[18] X. Qi, and R.P. Balwin, Electroanalysis 6 (1994) 353.
[19] W.Th. Kok, H.B. Hanekamp, P. Bos and R.W. Frei, Anal. Chim. Acta, 142 (1982) 31.
[20] K. Stulik, V. Pacanova, M. Weingart and M. Podolak, J. Chromatogr., 367 (1984) 311.
[21] T.A. Gill and J.W. Thompson., J. Food Sci., 49 (1984) 603.
[22] P.W. Alexander, P.R. Haddad and M. Trojanowicz, Anal Chim. Acta, 171 (1985) 151.
[23] Guide to Aminex HPLC Columns for Food and Beverage Analysis, Bio-Rad Richmond, CA, 1993.
[24] R.D. Cowling and A.C. Riddiford, Electrochim. Acta, 5 (1969) 627.
[25] N.A. Hampson, Electrochemistry, 2 (1972) 138.
[26] B.S. Hui and C.O. Huber, Anal. Chim. Acta, 134 (1982) 211.
[27] J.S. Stamler and J. Loscalzo, Anal. Chem., 64 (1992) 779.

ELSEVIER

Talanta 44 (1997) 249–255

Talanta

Spectrophotometric determination of vitamin E (α-tocopherol) using copper(II)–neocuproine reagent

Esma Tütem*, Reşat Apak, Esma Günaydı, Kevser Sözgen

Department of Chemistry, Faculty of Engineering, Istanbul University, Avcılar 34850, Istanbul, Turkey

Received 23 November 1995; revised 22 May 1996; accepted 4 July 1996

Abstract

The possibility of the utilization of the copper(II)–neocuproine spectrophotometric method, which has previously been shown to permit the determination of various reducing agents, to the determination of vitamin E was investigated. The molar absorptivity for vitamin E was found to be $(2.1 \pm 0.1) \times 10^4$ l mol^{-1} cm^{-1} and Beer's law was obeyed between 2.4×10^{-6} and 9.0×10^{-5} M concentrations of α-tocopherol. The relative standard deviation of the slope of the absorbance vs. concentration plot was 2.1%. The results obtained by the copper(II)–neocuproine method were compared with those achieved by both the standard HPLC and the widely used iron(III)–bathophenanthroline method by means of a *t*-test which showed that the precision of the developed method was not essentially different from those of the others. The developed method was successfully applied to three commercial samples, two in dragée and one in ampoule form. The α-tocopheryl acetate contained in the samples, which did not respond directly to the Cu(II)–neocuproine reagent, was subjected to alkaline hydrolysis prior to the analysis of the hydrolysis product, i.e., α-tocopherol. The molar absorptivity due to Cu(I)–neocuproine at 450 nm against a reagent blank indicated a two-electron oxidation of vitamin E by Cu(II)–neocuproine, which may be slightly enhanced by solvent effects. Copper(II)–neocuproine is an oxidant of strength comparable to that of Fe(III)–bathophenanthroline. The developed method, although less sensitive, is easy to use in conventional laboratories, unlike the Fe(III)–bathophenanthroline method, which requires specially prepared reagents and solvents. The method is free from interferences from such common reductants as ascorbic acid and Fe(II) salts, found in pharmaceutical formulations, after washing the formulation with water and collecting vitamin E in the ether extract for subsequent analysis.

Keywords: Copper(II)–neocuproine reagent; Spectrophotometry; α-Tocopherol; Vitamin E

1. Introduction

Vitamin E, also known as α-tocopherol, is an important vitamin found largely in plant materials, e.g. wheat germ, corn, sunflower seed, rapeseed, soybean oils, alfalfa and lettuce. Its complex biological functions may include antisterility, an antioxidant role, i.e. prevention of peroxide attack on unsaturated fatty acids in membrane lipids, and a cofactor between cytochrome *b* and *c* in the respiratory chain. The beneficial role of vitamin E

* Corresponding author. FAX: 90-212-591 1997.

PII S0039-9140(96)02041-3

in preventing degenerative physiological processes and ageing is still being investigated.

Although vitamin E intake in normal diets usually meets the daily requirement of children and adults, there is a constant commercial demand for this vitamin especially by elderly customers. Thus, the development of simple and sensitive methods other than the more expensive HPLC [1–3] and voltammetric [4] techniques for the determination of this vitamin in pharmaceutical preparations has always been a matter of concern.

The existing spectrophotometric methods for vitamin E determination make use of the oxidizability of the 6-hydroxychroman ring of α-tocopherol to the corresponding quinone, i.e., α-tocopherylquinone, by oxidizing agents finally giving coloured products. The official method utilizes the Fe(III)–bipyridyl [5] or bathophenanthroline [6] complex reagent as the oxidizing agent. The Fe(III) in these reagents is reduced by vitamin E to the corresponding Fe(II) complex, the absorbance of which is measured at 520 and 534 nm. Derivative spectrophotometric methods [7], which are not as specific as direct methods, have also been introduced.

In recent years, copper(II)–neocuproine reagent has been developed for determining a number of reducing agents in ammonium acetate-buffered solution [8], and biologically important reductants such as hydrogen peroxide, ascorbic acid and cysteine [9] have been assayed by the use of this reagent. This work was undertaken in order to establish the copper(II)–neocuproine spectrophotometric procedure as a standard method for analysing vitamin E solutions and pharmaceutical preparations.

α-Tocopheryl acetate, which is practically unaffected by the oxidizing influence of air, daylight and UV radiation, is more stable than the parent vitamin, α-tocopherol [10]. Since the acetate derivative is preferentially used in the formulation of pharmaceutical preparations, the conditions for the hydrolysis of this compound to α-tocopherol also need to be investigated for establishing a thorough assay method for vitamin E.

2. Experimental

2.1. Chemicals and reagents

α-Tocopheryl acetate was supplied by Roche (Turkey). Absolute ethanol and light petroleum (b.p. 60–71°C) were prepared from 95% technical alcohol and technical light petroleum (b.p. 60–80°C), respectively [11]. Bathophenanthroline was obtained from Sigma, technical alcohol from Turkish Monopolies, light petroleum from Delta Chemicals (Turkey) and nitrogen gas (bomb) from Habaş (Turkey). All remaining chemicals were supplied by Merck and were of analytical reagent grade. Rovigon and Supradyn dragées and Ephynal ampoules (Roche), the active ingredient of which is α-tocopheryl acetate, were freely purchased in the Turkish market.

2.2. Instrumentation

The molecular absorption spectra and absorbances at selected wavelengths were recorded with a Hitachi 220 A UV–visible spectrophotometer equipped with quartz cells of 1 cm light path. The pH of solutions was measured with a Metrohm E-512 pH meter using a glass electrode. The chromatograph was from Cecil Instruments (Cambridge, UK), and consisted of a pump (CE 1100 HPLC pump), a 20 μl injection valve (Model 7125, Rheodyne, Cotati, CA, USA), an analytical stainless-steel column packed with Spherisorb S5ODS1 (25 cm × 4.6 mm i.d.) from Hichrom (Berkshire, UK) and a variable-wavelength UV detector (CE 1220). Detection was effected at 292 nm for α-tocopherol. Chromatograms were obtained using an integrator (HP 3395 from Hewlett-Packard). Injections were made with a 25 μl syringe from Hamilton (Reno, NV, USA).

2.3. Solutions

α-Tocopherol solution was prepared at 2.46×10^{-4} M concentration in diethyl ether and absolute ethanol and diluted as necessary.

Neocuproine (2,9-dimethyl-1,10-phenanthroline) and bathophenanthroline (4,7-diphenyl-1,10-

phenanthroline) were prepared separately in ethanol and absolute ethanol, respectively, at a concentration of 3.0×10^{-3} M.

The pH 7.0 buffer was a 1.0 M solution of ammonium acetate in water. Solutions of 1.0×10^{-2} M $CuCl_2 \cdot 2H_2O$ and concentrated KOH (160 g per 100 ml) were also prepared separately in water. The Iron(III) chloride solution of concentration 2.0×10^{-3} M was prepared from $FeCl_3 \cdot 6H_2O$ in absolute ethanol. Phosphoric acid solution contained 0.172 M H_3PO_4 in absolute ethanol.

A light petroleum–absolute ethanol mixture was prepared by diluting 600 ml of light petroleum (b.p. 60–71°C) to 1.0 l with absolute ethanol.

The mobile phase for HPLC analysis was acetonitrile–chloroform–2-propanol–water (73:15:3.5:8.5, v/v).

2.4. Procedures

2.4.1. Hydrolysis of α-tocopheryl acetate to α-tocopherol [6]

A 1.10 g amount of α-tocopheryl acetate was dissolved in 4.5 ml of absolute ethanol and 0.33 g of ascorbic acid was added. The mixture was brought to boiling under a nitrogen atmosphere in a round-bottomed flask (equipped with a reflux condenser) immersed in a water-bath. A 1.1 ml volume of concentrated KOH solution was added and the mixture was refluxed for 15 min.

The flask was rapidly cooled, 25 ml of water were added and the mixture was extracted with three successive portions of 30 ml of diethyl ether. The ether phase was successively washed with water until the aqueous phase was neutral to phenolphthalein, dried with anhydrous sodium sulfate, filtered, concentrated to 5 ml under a nitrogen atmosphere by gentle heating and finally diluted to 10 ml with diethyl ether.

The purity and hydrolysis efficiency of the product were determined by comparison of the UV spectra of the hydrolysate and standard mixtures of α-tocopherol and α-tocopheryl acetate prepared in various proportions until the A_{292} of the hydrolysate matched that of a standard mixture. The hydrolysate was further subjected to HPLC analysis by the method of Kaplan et al. [1].

The hydrolysis conditions described above were optimized by changing one of the hydrolytic parameters while keeping the remaining three parameters constant, i.e. initial amount of α-tocopheryl acetate, volumes of absolute ethanol and concentrated KOH solution and amount of ascorbic acid. Since any remaining ascorbic acid from the hydrolysis procedure would interfere with the analysis of the reaction product (α-tocopherol) using the copper(II)–neocuproine reagent [8], the hyrolysis was repeated with a reagent blank not containing α-tocopheryl acetate.

2.4.2. Determination of α-tocopherol by the Fe(III)–bathophenanthroline method [6]

An aliquot of x ml ($0.2 \leqslant x \leqslant 0.4$ ml) of α-tocopherol in diethyl ether or preferentially in absolute ethanol was placed in a test-tube and $4.0 - x$ ml of light petroleum–ethanol and 1.0 ml of bathophenanthroline solution were added. The mixture was agitated, 0.5 ml of $FeCl_3$ solution was added dropwise and the solution was reagitated. After 15 s, 0.5 ml of H_3PO_4 solution was added. The absorbance of the solution at 534 nm against a reagent blank was measured after 3 min, and the colour was stable for 90 min. The procedure was repeated for α-tocopherol hydrolysed from the acetate derivative, and applied to the analysis of Rovigon and Supradyn dragées and Ephynal ampoules.

2.4.3. Determination of α-tocopherol by the Cu(II)–neocuproine method

In a test-tube were placed 1.0 ml of $CuCl_2$ solution, 2.5 ml of neocuproine solution, $3.0 - x$ ml of ethanol, 1.0 ml of ammonium acetate buffer and x ml ($0.3 \leqslant x \leqslant 0.6$ ml) of α-tocopherol solution (in diethyl ether or preferentially in absolute ethanol), in that order. The mixture was agitated and its absorbance was measured after 30 min at 450 nm against a reagent blank containing Cu(II)–neocuproine, solvent and buffer (the colour was stable for at least 90 more min). It is recommended to run three standards along with the sample for each determination. The procedure was applied to the analysis of the hydrolysis product, Rovigon and Supradyn dragées and Ephynal ampoules.

2.4.4. Preparation of pharmaceutical preparations for analysis

Eleven Rovigon dragées were finely ground in an agate mortar and five samples each containing approximately 110 mg of α-tocopheryl acetate were taken. Each of the samples was extracted with four successive portions of absolute ethanol and hydrolysed using the standard procedure.

The contents of eight Ephynal ampoules were thoroughly mixed and five samples each containing approximately 110 mg of α-tocopheryl acetate were taken and subsequently hydrolysed.

Three Supradyn dragées, each having a declared content of 10 mg of vitamin E equivalent, were finely ground, washed with 60 ml of distilled water and dried in an oven at 50°C. The residue was extracted with 30 ml of diethyl ether, evaporated and the residue dissolved in 10 ml of absolute ethanol. The ethanol solution was analysed by HPLC and hydrolysed using the standard hydrolysis procedure except for the amounts of ascorbic acid and KOH solution, which were chosen as 0.033 g and 0.03 ml, respectively, owing to the low vitamin E content. The ether solution of the hydrolysis product was diluted to 10 ml and diluted 20-fold with absolute ethanol such that the final solution contained 5% (v/v) of ether.

The spectra of the hydrolysis products (except Supradyn) were compared with that of standard α-tocopherol. The hydrolysis products were analysed by both spectrophotometric procedures and HPLC for α-tocopherol, and the original α-tocopheryl acetate contents of the pharmaceutical preparations were calculated by taking the efficiency factor of hydrolysis into consideration.

3. Results and discussion

The colour (i.e. A_{450} against the reagent blank) of the Cu(I)–neocuproine complex formed as a result of vitamin E oxidation stabilized after 30 min and remained the same for at least a further 90 min following complex formation.

The UV spectra of α-tocopherol and α-tocopheryl acetate (both 2.46×10^{-4} M) in ethanol is shown in Fig. 1. Since Beer's law was obeyed for both compounds at 292 nm within the concentration range of interest, the hydrolysis efficiency of the corresponding α-tocopheryl acetate solutions was estimated by comparing the absorbances at 292 nm of the hydrolysate and binary standard mixtures at this wavelength. This efficiency was found to be 93%, confirmed by HPLC, and was exploited in the analysis of pharmaceutical preparations of α-tocopheryl acetate.

In the hydrolysis procedure, half to twice as much α-tocopheryl acetate was not affected by an excess of KOH; e.g. 1.1 ml of concentrated KOH solution was sufficient to hydrolyse efficiently 2.20 g of α-tocopheryl acetate. KOH at levels up to 10 times the usual amount did not have a negative effect on hydrolysis.

It was also confirmed that ascorbic acid, introduced for the protection of α-tocopherol from oxidation during the hydrolysis of tocopheryl acetate, could be completely removed from the reaction product by thoroughly washing the organic (ether) phase with successive portions of water. Analysis of the hydrolysed α-tocopherol using the Cu(II)–neocuproine reagent revealed that not even a detectable amount of the ascorbic acid, which would normally show a positive interference in the method [8], accompanied the analyte.

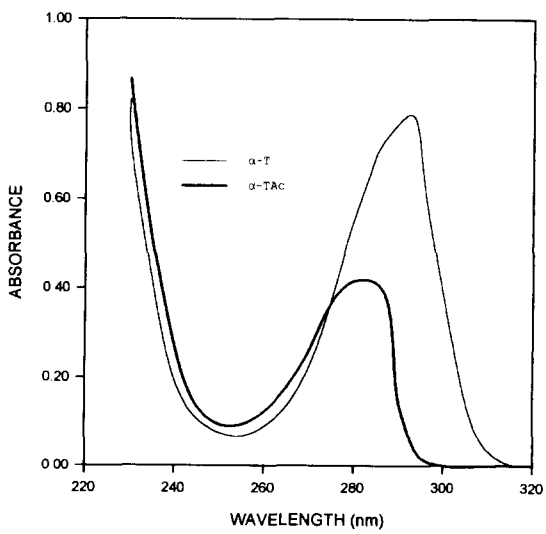

Fig. 1. UV spectrum of 2.46×10^{-4} M α-tocopherol and α-tocopheryl acetate in absolute ethanol.

The molar absorptivity, the concentration range for the validity of Beer's law and the precision of the developed method were found by the aid of absorbance measurements (at 450 nm) of standard α-tocopherol solutions. The spectrophotometric measurements were made on six-analyte sampling groups (whose absorbances (A_{450}) varied between 0.2 and 0.8) on three different occasions selected with 1 week time intervals. The within - and between-run precisions, also known as repeatability and reproducibility [12], respectively, were found by regression analysis of A_{450} vs. concentration curves, and expressed as the relative standard deviation (RSD, %) of the slope [13], i.e. of the molar absorptivity, of the absorbance vs. concentration regression lines.

The mean molar absorptivity was $\bar{\varepsilon} = 2.1 \times 10^4$ l mol^{-1} cm^{-1} with the RSD on each occasion being 2.3, 4.2 and 5.3% (repeatability). The overall linear equation relating the absorbance (A) and concentration (C in mol l^{-1}) of eighteen values at the 95% confidence level was

$$A = (2.1 \pm 0.1) \times 10^4 C + (0.68 \pm 1.7) \times 10^{-2}$$

with an RSD of the slope of 2.1% and a correlation coefficient of the linear plot $r = 0.996$ (reproducibility). Beer's law was obeyed between 2.4×10^{-6} and 9.0×10^{-5} M concentrations of α-tocopherol. The corresponding linear equation for calibration of the Fe(III)–bathophenanthroline method was found to be

$$A = (4.1 \pm 0.4) \times 10^4 C + (1.4 \pm 4.4) \times 10^{-2}$$

at the 95% confidence level with an RSD of 3.8% and $r = 0.996$. The latter method was slightly less reproducible and definitely more laborious (with respect to the preparation of reagents and solvents) than the developed method.

When the precisions of the developed Cu(II)–neocuproine and the standard HPLC method [1] using a slightly polarized mobile phase were compared (95% confidence level, 20 degrees of freedom), a pooled estimate of the standard deviation, s, may be calculated from the two individual standard deviations, s_1 and s_2, of the developed and reference methods (see Table 1):

$$s^2 = [(n_1 - 1)s_1^2 + (n_2 - 1)s_2^2]/(n_1 + n_2 - 2) \quad (1)$$

Table 1
Comparison of the developed and reference methods for α-tocopherol determination

Sample number (n)	Amount of α-tocopherol found (μg)[a]	
	Cu(II)–neocuproine	HPLC
1	54.5	54.9
2	53.0	50.0
3	53.2	52.4
4	53.2	50.6
5	53.4	51.9
6	52.6	51.7
7	51.9	50.4
8	51.3	52.4
9	51.1	54.7
10	49.8	52.8
11	56.2	52.8
Standard deviation	$s_1 = 1.74$	$s_2 = 1.59$
Mean	$\bar{x}_1 = 52.7$	$\bar{x}_2 = 52.2$
Degrees of freedom	$n_1 + n_2 - 2 = 20$	
Critical t-value (95% confidence level)	2.09 [14]	

[a]Amount of α-tocopherol present = 53 μg.

$$t = (\bar{x}_1 + \bar{x}_2)/[s(1/n_1 + 1/n_2)^{1/2}] \quad (2)$$

where t has $n_1 + n_2 - 2 = 20$ degrees of freedom [14]. By applying Eqs. (1) and (2) to the data in Table 1, s was calculated as 1.67 and t was 0.70. Since this t value is smaller than the critical value, $t_{0.95}$, i.e. $0.70 < 2.09$, there is no significant difference between the developed and reference methods at the 95% confidence level, and the null hypothesis [14] is accepted.

Following the hydrolysis of α-tocopheryl acetate in commercial Rovigon and Supradyn dragées and Ephynal ampoules, inspection of the hydrolysates by UV and HPLC (only the latter applicable for Supradyn) confirmed that the hydrolysis product was essentially α-tocopherol. The analyses of these commercial preparations by HPLC and the two spectrophotometric methods are depicted in Table 2. Five samples of each preparation were analysed. The results confirm that the developed method is not inferior in precision to the literature spectrophotometric and HPLC methods, even in a complex multivitamin

Table 2
Comparison of analysis results of commercial formulations of vitamin E (after hydrolysis)

Sample[a]	Form	α-tocopheryl acetate declared (mg)	Amount of vitamin E found (mg)		
			HPLC	Cu(II)–neocuproine	Fe(III) –bathophenanthroline
Rovigon	Dragée	70	65 ± 2	66 ± 2	66 ± 3
Ephynal	Ampoule	100	102 ± 3	103 ± 3	103 ± 4
Supradyn	Dragée	30[b]	21 ± 1	23 ± 2	20 ± 2

[a] All from Roche.
[b] Amount of α-tocopheryl acetate before alkaline hydrolysis was found to be 22 ± 1 mg by HPLC.

and mineral combination such as Supradyn (containing 11 essential vitamins, five minerals comprising the reducing $FeSO_4$ and three oligo-elements of Cu(II), Zn(II) and Mo(VI)).

Since the observed molar absorptivity of the Fe(III)–bathophenanthroline method for vitamin E is approximately twice that of the literature value for this complex reagent [6,15], it may be deduced that vitamin E undergoes a two-electron oxidation with this reagent, possibly to α-tocopherylquinone [16]. In the original paper introducing the copper(II)–neocuproin reagent [8], the authors showed that a two-electron oxidation of a reducing analyte would normally be expected to exhibit a mean molar absorptivity of 1.6×10^4, although higher values were encountered such as those of glutathione ($\varepsilon = 8.5 \times 10^3$, le oxidation) and hydroxylamine ($\varepsilon = 1.8 \times 10^4$, 2e oxidation), depending on the nature of the analyte [8], and solvent effects may also cause some enhancement [17] owing to the affinity of the $[Cu\text{-neocuproine})_2]^+$ cation, i.e. the reduction product of Cu(II)–neocuproine, to add a solvent molecule as ligand in the charge-transfer excited state, thereby increasing the molar absorptivity to a certain extent. When the standard reduction potentials of the two complex reagents are considered, the $[Cu(neocuproine)_2]^{2+,1+}$ couple has been reported to exhibit a potential of $E_c^\circ = 0.603$ V [17–19], while the oxidizing power of Fe(III)–bathophenanthroline is considerably weaker than that of Fe(III)–phenanthroline ($E_c^\circ = 1.2$ V), which is reflected in the observation that Fe(III)–bathophenanthroline is not as easily reduced as the Fe(III)–phenanthroline analogue [20]. The Fe(III)–bathophenanthroline reagent should be an even less potent oxidant in the presence of phosphoric acid (as described in Section 2.4), because it is known that the 0.77 V standard potential of the uncomplexed $Fe^{3+,2+}$ redox couple is reduced to 0.44 V in 0.3 M H_3PO_4 medium [21]. Thus, both the Cu(II)–neocuproine and Fe(III)–bathophenanthroline reagents are oxidizing agents of comparable strength under the experimental conditions employed, and it is reasonable to assume that both reagents lead to 2e oxidation of α-tocopherol as accomplished with other oxidizing reagents such as tris(2,2′-bipyridyl)iron(III), $FeCl_3$ and $Fe(CN)_6^{3-}$ [16].

Although the molar absorptivity of the Fe(III)–bathophenanthroline method is greater than that of the developed method, allowing the achievement of greater sensitivity with the former, the Cu(II)–neocuproine method is less laborious and shows the potential to work better in complex formulations. Moreover, the introduced reagent performs its action in a neutral medium, i.e. ammonium acetate-buffered solution of pH 7.0, where some common potential interferents such as glucose (and reducing sugars with the —$(CHOH)_n$—CHO group) and oxalate would not be oxidized [8], unlike in acidic media where most oxidants should function, thereby adding some selectivity to the proposed method. As vitamin E is not soluble in water, pharmaceutically common interferents which are reducing agents, e.g. ascorbic acid and iron(II) sulfate, would also not interfer after a preliminary aqueous extraction stage. The method is capable of differentiating α-tocopherol from the pharmaceutically desired ana-

logue, α-tocopheryl acetate, where the latter may respond to the method only after hydrolysis.

Both the developed and alternative spectrophotometric methods have the advantage of working in the visible range, permitting the use of simple colorimeters where required instead of the more expensive spectrophotometers. The developed method has a slight superiority in that all solutions of this method except neocuproine are prepared in water while the Fe(III)–bathophenanthroline method requires the preparation of absolute EtOH and a certain boiling range fraction of light petroleum. Both methods have similar precision and, in addition, the Cu(II)–neocuproine reagent in a routine analytical laboratory, lacking more expensive HPLC and GC instruments, handling other reducing substances [8,9] would be more versatile.

References

[1] L.A. Kaplan, J.A. Miller, E.A. Stein and M.J. Stampfer, Methods Enzymol., 189 (1990) 155.
[2] W.A. McCrehan, Methods Enzymol., 189 (1990) 172.
[3] T. Shiozuka, Y. Takizawa and S. Fujioka, Jpn. Kokai Tokkyo Koho JP 63, 158, 455, Chem. Abstr., 111 (1989) 160410x.
[4] S.S. Atuma, J. Sci. Food Agric., 26 (1975) 393.
[5] L. Meites (Ed.), Handbook of Analytical Chemistry, McGraw-Hill, New York, 1982, pp. 13–205.
[6] K. Helrich (Ed.), Official Methods of Analysis of the Association of Official Analytical Chemists, Vol. II, Association of Official Analytical Chemists, Washington, DC, 15th edn., 1990, pp. 1070–1079.
[7] G.J. Bukovits and A. Lezerovich, J. Am. Oil Chem. Soc., 64 (1987) 517.
[8] E. Tütem, R. Apak and F. Baykut, Analyst, 116 (1991) 89.
[9] E. Tütem and R. Apak, Anal. Chim. Acta, 255 (1991) 121.
[10] S. Budavari (Ed.), The Merck Index, Merck, Rahway, NJ, 11th edn., 1989, p. 1579.
[11] B.S. Furniss, A.J. Hannaford, P.W.G. Smith and A.R. Tatchell (Eds.), Vogel's Textbook of Practical Organic Chemistry, Longman, Harlow, 5th edn., 1989, pp. 397, 401.
[12] J.C. Miller and J.N. Miller (Eds.), Statistics for Analytical Chemists, Ellis Horwood, Chichester, 3rd edn., 1994, pp. 18–20.
[13] J.C. Miller and J.N. Miller (Eds.), Statistics for Analytical Chemists, Ellis Horwood, Chichester, 3rd edn., 1994, pp. 110–112.
[14] J.C. Miller and J.N. Miller (Eds.), Statistics for Analytical Chemists, Ellis Horwood, Chichester, 3rd edn., 1994, pp. 55–57.
[15] R.E. Peterson, Anal. Chem., 25 (1953) 1337.
[16] D.C. Herting, in A. Standen (Ed.), Kirk-Othmer Encyclopedia of Chemical Technology, Vol. 21, Wiley, New York, 2nd edn., 1970, pp. 574–585.
[17] R. Tamilarasan, D.R. McMillin and F. Liu, in T.D. Tullius (Ed.), Metal–DNA Chemistry, American Chemical Society, Washington, DC, 1989, pp. 48–58.
[18] C.J. Hawkins and D.D. Perrin, J. Chem. Soc., (1962) 1351.
[18] C.J. Hawkins and D.D. Perrin, J. Chem. Soc., (1963) 2996.
[20] G.S.R. Krishnamurti and P.M. Huang, Talanta, 37 (1990) 745.
[21] J.A. Dean, Langes's Handbook of Chemistry, McGraw-Hill, New York, 12th edn., 1979, pp. 6–11.

ELSEVIER

Talanta 44 (1997) 257–267

Talanta

Effects of cetylpyridinium bromide micelles on the spectrofluorimetric characteristics of polycyclic aromatic hydrocarbons

Juan H. Ayala, Ana M. Afonso, Venerando González*

Department of Analytical Chemistry, Nutrition and Food Science, University of La Laguna, E-38204 La Laguna, Spain

Received 15 January 1996; revised 8 July 1996; accepted 8 July 1996

Abstract

The presence of a micellar medium of cetylpyridinium bromide (CPB) causes, in relation to the aqueous medium, important bathochromic shifts in the excitation spectra of a considerable number of polycyclic aromatic hydrocarbons (PAHs). Furthermore, the CPB acts as a quencher, provoking inhibitions of the fluorescence intensity emitted by PAHs. The micellar inhibition factors show that, generally, the quenching affects alternant hydrocarbons to a greater extent. Some interesting relationships between the hydrocarbon structure and both the characteristic wavelengths of fluorescence spectra and the values of $\Delta\lambda$ are established.

Keywords: Cetylpyridinium bromide; Fluorescence quenching; Micelles; Polycyclic aromatic hydrocarbons

1. Introduction

Polycyclic aromatic hydrocarbons (PAHs) form a family of compounds widely found in the environment as common pollutants of the atmosphere, earth and water. The PAHs most studied, for their mutagenic or carcinogenic characteristics, are those which possess between three and six rings. Among those which contain a greater number of rings, only some show carcinogenic activity. Although it has not been demonstrated, such activity can be related to their low solubility. Consequently, it is frequently necessary to determine PAHs at low concentration in a wide variety of sample matrices. The techniques most used in the analysis of PAHs can be split into two large groups: chromatographic and spectroscopic. Usually, the hydrocarbons are analysed by gas chromatography [1–3], high-performance liquid chromatography [4–7] and supercritical fluid chromatography [8,9]. However, spectroscopic methods have shown strong development in this field owing to their sensitivity, selectivity, rapidity, low cost and possibility of automation. Among these, conventional and synchronous spectrofluorimetry stand out [10–19].

Mixtures of environmental importance rarely contain a single component. The majority of mix-

* Corresponding author.

PII S0039-9140(96)02043-7

tures commonly encountered contain several isomeric pairs or structurally similar PAHs, which emit in approximately the same spectral regions. Use of selective fluorescence quenching agents simplifies observed emission spectra by eliminating signals from undesired chemical interferences having only slightly different molecular structures, so providing a greater selectivity to the analytical methods based on the measurement of fluorescence emission.

Micellar systems form microenvironments that can produce significant changes in the excitation and emission spectra of many molecules, as well as in the emitted fluorescence intensity. There are different factors that may explain these changes [20,21]. Among others, the following can be cited: the greater protection of the singlet state against collisional deactivation, the increase in the viscosity of the medium, the protection against quencher agents and the capacity of micelles to reorder reagents at molecular level and to enhance the interaction between analytes and reactives, quenchers and substrates.

Studies of quenching in micellar medium have been directed preferentially to show that solutes incorporated to a micellar phase are protected against the action of certain quenchers of fluorescence. Thus, it has been demonstrated in systems such as: anthracene–sodium dodecyl sulphate–iodide [22], naphthalene-sodium dodecyl sulphate–bromide [23] and anthracene–cetyltrimethylammonium bromide–pyridinium chloride [22]. On the other hand, Lissi et al. [24] have shown that the quenching of pyrene and 1-methylpyrene by iodide is enhanced by the incorporation of hydrocarbons in cetyltrimethylammonium chloride micelles.

Thus far, very few reports [25] have discussed analytical applications based on the fluorescence inhibition of PAHs in which the quencher is, furthermore, a substance capable of forming micellar aggregates in solution. With the use of a quencher/surfactant such as cetylpyridinium bromide (CPB), in the present work the conventional and synchronous spectrofluorimetric characteristics of an important number of PAHs in a micellar medium of CPB were established, the magnitude of the fluorescence inhibition was quantified and predictions of analytical interest were made. Likewise, and with the purpose of attempting to establish generalized behaviours, the conventional and synchronous signals are related to the structure of PAHs.

2. Experimental

2.1. Apparatus

Fluorescence measurements were made with a Perkin-Elmer LS-50 luminescence spectrometer equipped with a xenon discharge lamp and connected via an RS232C interface to an Epson PCAX2e computer. The control of the spectrometer was accomplished using Fluorescence Data Manager software. The fluorescenc measurements were made in standard 1×1 cm quartz cells, thermostated at 25 ± 0.1°C with a Selecta Frigitherm S 382 ultrathermostat.

2.2. Reagents

The PAHs used (naphthalene, anthracene, 9-methylanthracene, phenanthrene, 2-methylphenanthrene, pyrene, benz[*a*]anthracene, perylene, dibenz [*a*,*h*]anthracene, benzo[*a*]pyrene, fluorene, acenaphthene, acenaphthylene, fluoranthene and benzo[*b*]fluoranthene) were supplied by Aldrich Chemical. Stock solutions (5×10^{-4} M) of each PAH were prepared in ethanol (Merck). Stock solutions (5×10^{-2} M) of CPB (Sigma Chemical) were prepared in deionized water. All chemicals used were of analytical reagent grade.

2.3. Procedures

The conventional and synchronous fluorescence spectra of the PAHs in an aqueous medium were made with solutions incorporating 0.5% (v/v) ethanol. The representatives of the micellar medium corresponded to solutions containing CPB at a concentration of 2.6×10^{-3} M (0.1%, w/v), above its critical micellar concentration (cmc) (7.32×10^{-4} M). This value was determined conductimetrically under experimental conditions

Table 1
Spectrofluorimetric characteristic of PAHs in micellar medium of CPB

Compound	λ_{ex} (nm)[a]	λ_{em} (nm)[a]	D_{ex}	D_{em}
Alternant PAHs:				
Naphthalene	*286*, 301	321, *334*	67	0
Anthracene	326, *337*, 358	*378*, 400, 422	87	−1
9-Methylanthracene	335, 348, *365*	390, *413*, 435	111	−1
Phenanthrene	284, *293*, 323	346, *363*, 383	43	0
2-Methylphenanthrene	*295*, 326	357, *366*, 384	42	0
Pyrene	318, *332*	*372*, 382, 392	92	1
Benz[*a*]anthracene	*287*, 341	*386*, 409	1	0
Perylene	391, *412*	*443*, (469–472)	160	3
Dibenz[*a*,*h*]anthracene	*301*, 350	*396*, *403*, 422	45	−1
Benzo[*a*]pyrene	296, 364, *384*	*405*, 428	88	0
Non-alternant PAHs:				
Fluorene	*298*	*311*	89	9
Acenaphthene	*292*	*321*, 335, 352	67	0
Acenaphthylene	*292*, 303	*336*, 320, 345, 352	68	1
Fluoranthene	*289*, 323, 342, 360	*456*	77	1
Benzo[*b*]fluoranthene	295, *303*, 353	*431*	59	−11

[a] The values in italics correspond to the excitation and emission maxima.

similar to those used in fluorescence measurements.

To calculate the micellar inhibition factor (MIF), straight-line calibration graphs for each of the PAHs were obtained by measuring the fluorescence intensity at the maximum excitation and emission wavelengths, in both aqueous and micellar media. The solutions used were prepared with the quantities of PAH and ethanol necessary to reach the desired concentration of PAH and 0.5% (v/v) of the organic solvent, to which was added the volume of CPB solution required so that the final solutions were 0 or 2.6×10^{-3} M in the surfactant, according to whether it was aqueous or micellar, respectively, and diluted with deionized water.

To study the influence of surfactant concentration on the fluorescence intensity of PAHs, measurements of fluorescence intensity were made at the maximum excitation and emission wavelengths corresponding to the aqueous medium, in solutions prepared in 25 ml calibrated flasks with volumes of 10^{-2} M CPB solution and containing a final concentration of 2×10^{-7} M PAH and 0.5% (v/v) of ethanol.

Three-dimensional spectra were obtained by the elaboration of a Basic program within the OBEY application of the Fluorescence Data Manager software. This program allows successive scanning of several emission or synchronous spectra with different excitation wavelengths or $\Delta\lambda$, respectively, and transforms them into a matrix of experimental data. The file containing this matrix is used as input in the commercial program SURFER to obtain three-dimensional projections and contour maps.

3. Results and discussion

3.1. Conventional fluorescence

Excitation and emission spectra of 15 PAHs in aqeuous and micellar medium of CPB were obtained. Table 1 summarizes some characteristics of the conventional fluorescence spectra of PAHs in the micellar medium and the shifts experienced by the wavelengths of the maxima of the excitation (D_{ex}) and emission (D_{em}) spectra on passing from an aqueous to a micellar medium. Upon

comparing the results, it is observed that in the micellar medium:

(1) The wavelengths of the emission maxima are similar to those which are obtained in aqueous medium, except for fluorene and benzo[*b*]fluoranthene.
(2) The excitation maxima of all PAHs present wavelength values higher than those of aqueous medium. These observed differences can be attributed to the disappearance, provoked by the micellar medium of CPB, of the signals corresponding to the lower wavelength zones in the excitation spectra, the region in which the maxima of aqueous medium tend to be found.

With regard to the relationship between the fluorescence spectral characteristics in the micellar medium and the structures of polycyclic aromatic hydrocarbons, some general trends were found, among which the following are notable:

(1) For a given number of aromatic rings, the linear systems fluoresce, generally, at longer wavelengths than non-linear systems. That is to say, a deviation at smaller wavelengths is produced when the aromatic system is branched.
(2) The methylation of an aromatic system tends to produce deviations to longer wavelengths.
(3) As the degree of conjugation increases, a shift to wavelengths longer than the emission maxima is observed. This phenomenon is sometimes associated with an increase in the emitted fluorescence intensity.
(4) For an aromatic system formed by a series of rings fused in a straight linear chain, the excitation and emission bands exhibit increasing wavelenths as the number of rings and conjugated double bonds increase.
(5) The excitation and emission spectra of the hydrocarbons formed by benzenic rings joined by a five-membered ring are similar to those shown by systems that only contain benzenic rings.

Irrespective of the process of quenching, these relationships between spectrofluorimetric and structural characteristics of the PAHs were similar to those reported by others for various PAHs in hexane [26].

From emission spectra, in aqueous and micellar media of CPB, the values of fluorescence intensity between the 0–0 band and the b_{1g} vibrational band (which is frequently known as the I_1/I_3 or I/III relation [27,28]) were established for all those hydrocarbons that present in the micellar medium a sufficient resolution in their emission spectra. The smallest values correspond to the micellar medium, which confirms the lower polarity of that medium compared with the aqueous medium. This fact and the hydrophobic nature of PAHs explain, generally, the increase in their water solubility in the presence of micelles.

3.1.1. Influence of surfactant concentration

The variation of the fluorescence intensity emitted by hydrocarbons as a function of CPB concentration is illustrated in Figs. 1 and 2. Generally, at concentrations below the cmc, the fluorescence of PAHs decreases suddenly on increasing the surfactant concentration, whereas at concentrations above the cmc, the fluorescence does not vary significantly. In these figures, the effect of a non-micelle-forming pyridinium derivative on the fluorescence inhibition is also compared with that with CPB. These experiments show the important effect of the micellar system and the formation of premicellar clusters on the fluorescence inhibition of PAHs in the presence of CPB. These exponential decreases in the fluores-

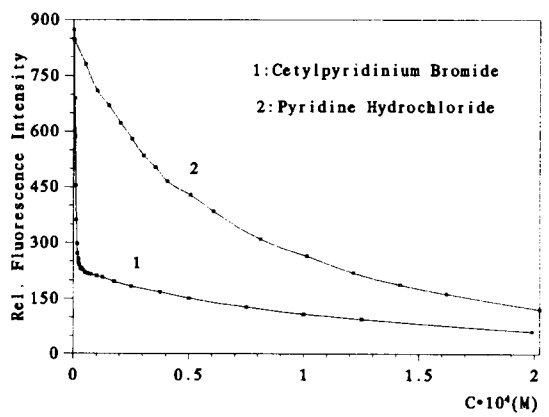

Fig. 1. Influence of the pyridinium salt concentration on the fluorescence intensity of 2×10^{-7} M 9-methylanthracene solutions and 0.5% (v/v) EtOH. Slits: 5 nm.

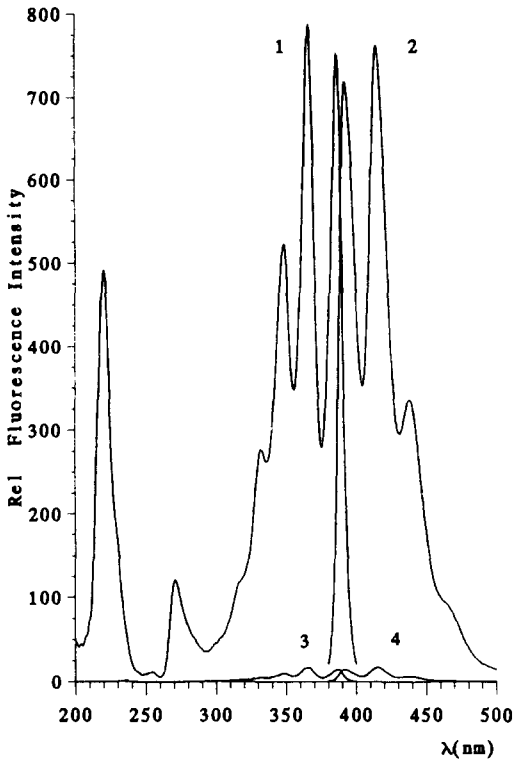

Fig. 2. Excitation (1,3) and emission (2,4) spectra of 2×10^{-6} M 9-methylanthracene solutions and 0.5% (v/v) EtOH. (1,2) Aqueous medium: 2.6×10^{-3} M pyridine hydrochloride. (3,4) Micellar medium: 2.6×10^{-3} M CPB. (1,3) $\lambda_{em} = 413$ nm; (2,4) $\lambda_{ex} = 365$ nm. Slits: 3 nm.

cence, whose intensity varies in a regular way with the quencher concentration, can be considered typical of quenching processes.

The intersection point of lines tangential to the initial and final zones of the curves of fluorescence intensity versus CPB concentration could be considered representative of the phenomenon of micellization and, consequently, it would have to represent the cmc of CPB. However, the values obtained, which oscillate between 2.0×10^{-6} and 3.77×10^{-4} M, are always below the cmc of CPB. It has been described [29] that the coexistence of hydrocarbon molecules and surfactants can induce the formation of micelles and, in this way, a decrease in the cmc of the surfactant is produced. However, the great differences lead us to think that fluorescence inhibitions of the PAHs studied in this work are produced, to a large extent, by the intervention of premicellar clusters.

3.1.2. *Quantification of fluorescence inhibition*

In order to quantify the fluorescence inhibition that PAHs experience in the micellar medium, we used the term micellar inhibition factor (MIF), which relates the behaviour of PAHs in both media. Instead of measurements of fluorescence intensity, we have preferred to employ analytical sensitivities to calculate this factor. Thus we defined this factor as

$$\mathrm{MIF} = B_a/B_m$$

where B_m and B_a represent the slopes of the calibration graphs obtained in the presence and absence, respectively, of 2.6×10^{-3} M CPB. The values of B_m and B_a were obtained using the wavelengths of the optimum excitation and emission maxima in each medium. The values of the MIF found for each one of the PAHs considered in this study are shown in Table 2.

It must be indicated that even though for some PAHs, such as benz[*a*]anthracene and 2-methylphenanthrene, the high values of MIF are associated with the smallest values of analytical sensitivity in the micellar medium, for other derivatives, such as 9-methylanthracene and benzo[*a*]pyrene, the high values of MIF are a consequence of the high sensitivity that these hydrocarbons present in an aqueous medium.

Considering PAHs as a whole, we can conclude that alternant hydrocarbons experience, generally, greater inhibitions that non-alternant hydrocarbons. Although the inhibition processes are complex, this fact could be related to the reduction potentials of PAHs [30], which for non-alternant derivatives are about 0.4 V more positive than for alternant hydrocarbons. Consequently, the latter are better electron donors [31].

The efficiency of a quenching process is a measure of the inhibition that the fluorescence intensity emitted by a fluorophore experiences in the presence of a given quencher concentration or, on the contrary, it can represent the concentration of quencher that produces a fixed decrease in the fluorescence of a fluorophore. Consequently, the efficiency of the quenching (E_Q), in relative terms, can be defined by the equation [32]

Table 2
Quantification of the inhibition of the fluorescence of PAHs in micellar medium of CPB

Compound	Calibration graphs			MIF	$(C_{CPB})_{90}$ ($M \times 10^4$)
	Linear range ($M \times 10^6$)	$b \times 10^{-6}$	r		
Alternant PAHs:					
Naphthalene	0–10	5.61	0.992	97.5	5.0
Anthracene	0–4	2.21	0.999	800.0	4.0
9-Methylanthracene	0–4	3.95	0.999	1234.6	1.3
Phenanthrene	0–10	1.41	0.945	406.5	4.9
2-Methylphenanthrene	0–40	0.35	0.997	1098.9	4.3
Pyrene	0–2	3.80	0.998	584.8	7.0
Benz[*a*]anthracene	0–10	0.59	0.976	1190.5	8.0
Dibenz[*a*,*h*]anthracene	0–2	3.63	0.987	2.5	9.8
Benzo[*a*]pyrene	0–10	0.96	0.987	1612.9	12.2
Non-alternant PAHs:					
Fluorene	0–4	18.90	0.999	66.7	5.0
Acenaphthene	0–2	14.80	0.999	148.6	8.6
Acenaphthylene	0–40	0.36	0.999	123.2	13.0
Fluoranthene	0–2	13.50	0.999	6.1	6.2
Benzo[*b*]fluoranthene	0–2	25.40	0.997	7.9	8.6

$$E_Q = 1 - F/F_0$$

where F and F_0 represent the fluorescence intensities of each of the hydrocarbons in the presence and absence of the quencher, respectively. We express this efficiency as the cetylpyridinium bromide concentration necessary to produce an inhibition of 90% ($E_Q = 0.90$) in the fluorescence emitted by PAHs.

Table 2 shows that the CPB concentrations necessary to reach inhibitions of 90% are, generally, lower or close to the cmc of the surfactant, except in the case of the hydrocarbons dibenz[*a*,*h*]anthracene, benzo[*a*]pyrene and acenaphthylene.

For the CPB concentration used (2.6×10^{-3} M), generally, virtually total inhibition of the fluorescence emitted by naphthalene, anthracene, 9-methylanthracene, phenanthrene, 2-methylphenanthrene and pyrene was obtained, whereas for the remaining PAHs the fluorescence decreased in relation to that observed in the absence of CPB, which exceeded 90% in all cases.

3.1.3. *Considerations of analytical interest*

From the study of the influence of the micellar medium of CPB on the spectrofluorimetric characteristics of PAHs, some predictions of analytical interest can be made. Thus, the important shifts observed in the excitation spectra of PAHs can favour the development of a selective method for their determination. In the same way, the great differences existing in the MIF values could show the potential usefulness of the micellar medium to eliminate interferences in the determination of those PAHs whose fluorescence is less affected by the presence of CPB. This would be the case for non-alternant PAHs that, except for acenaphthylene, possess higher analytical sensitivity and lower MIF than the alternant. The contour map in Fig. 3 shows the possibility of obtaining differentiated signals for complex mixtures of PAHs in the micellar medium of CPB.

Also, it is possible to predict the selective determination of some PAHs by conventional spectrofluorimetry. Thus:

(1) Benzo[*b*]fluoranthene and fluoranthene present characteristic emission spectra between 400 and 540 nm, formed by several bands. Their excitation at short wavelengths and the measurement of fluorescence intensities at emission wavelengths longer than 430 nm could allow one to obtain differentiated sig-

nals from those corresponding to the rest of the PAHs.

(2) The use of excitation wavelengths between 270 and 300 nm and emission wavelengths between 300 and 320 nm could lead to representative spectra of fluorene, which is slightly affected by the presence of other PAHs, with the exception of acenaphthene and naphthalene.

(3) The maximum emission wavelength of perylene is only comparable to those of fluoranthene and benzo[*b*]fluoranthene. On the other hand, the micellar medium causes a shift in the maximum excitation wavelength of perylene, being located more than 100 nm above that corresponding to the other two derivatives. The selective determination of perylene by conventional spectrofluorimetry can be thought of in this way.

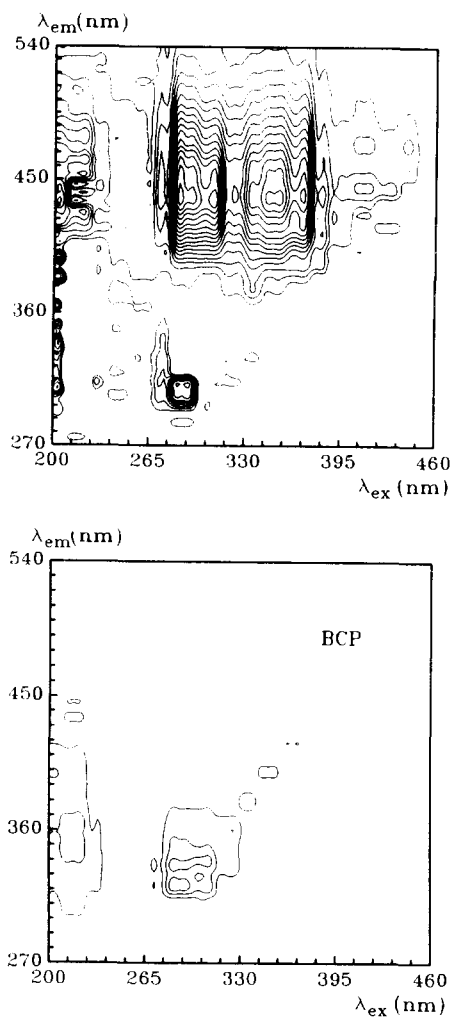

Fig. 3. Contour maps of a 2.6×10^{-3} M CPB solution and of an equimolar mixture of 15 PAHs in 2.6×10^{-3} M CPB corrected to subtract the blank.

3.2. *Synchronous fluorescence*

Synchronous spectra of the PAHs under study were obtained under the conditions indicated in the experimental section. Table 3 shows their main characteristics. Comparison of the micellar medium with the aqueous medium shows that the presence of CPB micelles does not produce important modifications in the Stokes shifts, except for naphthalene, anthracene, dibenz[*a*,*h*]anthracene and benzo[*b*]fluoranthene. The general trend observed could indicate that the micellar medium does not lead to important changes in the energetic distribution of the PAH molecules or that its effect is to stabilize the excited singlet states of the hydrocarbons.

Synchronous spectra must bear a certain relationship to conventional fluorescence spectra. For the purpose of comparison, the values of $\Delta\lambda$ representing the differences between the wavelengths of the emission and excitation maxima of conventional spectra, and also the corresponding values of the wavelength of excitation maxima and the Stokes shifts, can be obtained from Table 1. It can be observed that the values of $\Delta\lambda$ that produce the maximum intensity peaks of the synchronous spectra are near the $\Delta\lambda$ value obtained from conventional spectra. Furthermore, these $\Delta\lambda$ values almost coincide with the Stokes shift established for the hydrocarbons pyrene, perylene, benzo[*a*]pyrene, acenaphthene, acenaphthylene and fluorene. Likewise, it is observed that the wavelengths of the synchronous bands with the greatest intensity for each PAH are almost coincident with the wavelengths of the excitation maxima in conventional spectra for most of the PAHs. Only anthracene, with a difference of 19 nm, deviates from the general behaviour.

Table 3
Synchronous spectrofluorimetric characteristics of PAHs in a micellar medium of CPB

Compound	$\delta\lambda_{s,a}$ (nm)[a]	$\Delta\lambda$ ($\lambda^0_{s,ex}$) (nm)[b]
Alternant PAHs:		
Naphthalene	45	*50* (285), 70 (279), ~100 (227)
Anthracene	2	20 (360), *50* (356), 70 (335), *160* (241)
9-Methylanthracene	24	25 (367), *50* (366), 70 (347), 175 (240)
Phenanthrene	22	50 (295), *60* (294)
2-Methylphenanthrene	31	50 (298), *60* (296)
Pyrene	37	*40* (334), 60 (334)
Benz[*a*]anthracene	44	*100* (289)
Perylene	33	*30* (414), 50 (416), 60 (412)
Dibenz[*a*,*h*]anthracene	109	50 (353), *100* (303), ~125 (~300)
Benzo[*a*]pyrene	21	*20* (386), 50 (357), 130 (299)
Non-alternant PAHs:		
Fluorene	13	*7* (299), 50 (297)
Acenaphthene	31	*30* (292), 40 (295), 50 (288)
Acenaphthylene	34	*30* (292), 50 (288)
Fluoranthene	97	50 (365), ~93 (362), ~110 (345), ~*168* (289)
Benzo[*b*]fluoranthene	102	50 (372), 85 (351), *130* (304), 145 (294)

[a] Stokes shift in the absence of CPB.
[b] The values in italics correspond to the maximum fluorescence intensity.

The changes observed in the behaviour of the PAHs, together with the characteristics of the synchronous spectra, with regard to spectral simplification, small bandwidth and narrow spectral ranges, can provide satisfactory conditions for obtaining important selectivities in the individual determination of PAHs or in the resolution of their mixtures.

To select the optimum values of $\Delta\lambda$, synchronous contour maps were used instead of three-dimensional spectra. These maps were obtained by plotting fluorescence intensity as a function of the excitation wavelengths (horizontal axis) and of the difference ($\Delta\lambda$) between the emission and excitation wavelengths (vertical axis). Thus a set of contour lines that connect points of equal fluorescence intensity was obtained. Although the optimum values of $\Delta\lambda$ can also be selected through contour maps obtained from conventional spectra, the synchronous contour maps [19,33] can supply more selective information.

3.2.1. Consideration of analytical interest

From the synchronous contour maps (Fig. 4), we were able to make some predictions of analytical interest. The most interesting and numerous applications would be obtained at $\Delta\lambda < 50$ nm. Among these, the possible selective determination of perylene at $\Delta\lambda < 37$ nm, with $\lambda^0_{s,ex}$ around 430 nm, or fluorene at $\Delta\lambda \leqslant 10$ nm, with $\lambda^0_{s,ex} = 290$–300 nm, may be mentioned. With regard to the possible resolution of mixtures, Fig. 5 is a representative example of the potential that the combination of synchronous spectrofluorimetry and the micellar medium of CPB has for the analysis of complex mixtures of PAHs.

3.2.2. Relationship between synchronous signals and structure of PAHs in the micellar medium of CPB

As the synchronous signals of each PAH are confined to a limited number of bands within a definite spectral range, one can construct graphical representations which supply useful information about the relationship existing between characteristics of the synchronous spectrum of a PAH and its structure. Thus, Fig. 6 shows the wavelength value of the excitation (λ^0_{ex}) and emission (λ^0_{em}) peaks of PAHs, which present the

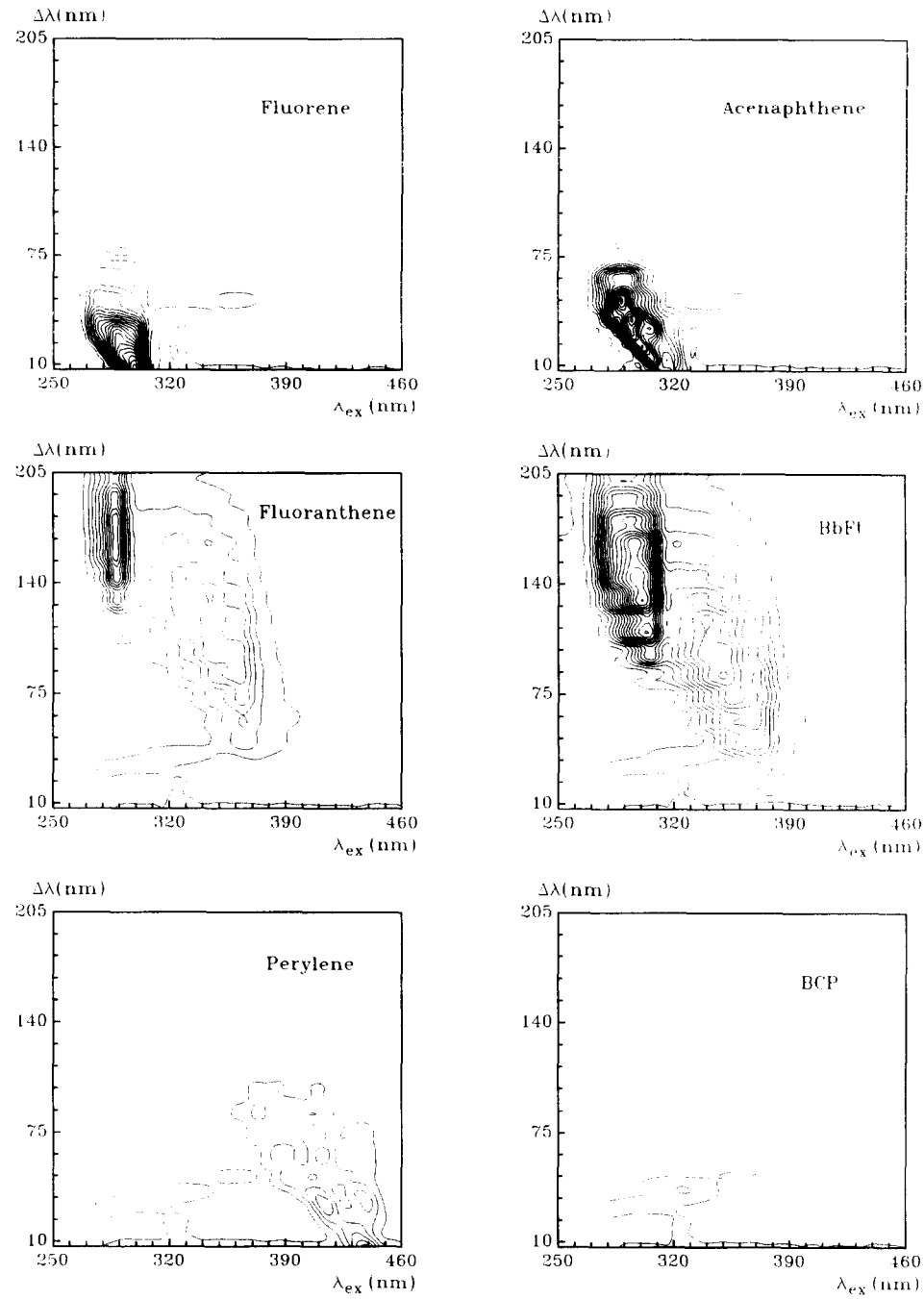

Fig. 4. Synchronous contour maps of a 2.6×10^{-3} M solution of CPB and of 2×10^{-6} M solutions of PAHs in a micellar medium of CPB. **BbFt**: benzo[*b*]fluoranthene.

highest and lowest values, respectively. As is known, both wavelengths limit the synchronous signal of each compound. From Fig. 6 we establish some interesting generalizations. Thus:

(1) Each PAH is identified by a point and significant differences are observed among most of them. The broken lines, representative of different values of $\Delta\lambda$, show that it is possible to obtain synchronous spectra of solutions containing complex mixtures of PAHs which would present characteristic bands for some hydrocarbons or groups of them.

(2) The signal of the 0–0 band of a hydrocarbon increases with increase in the number of rings of the PAH.

(3) Between the wavelengths λ^0_{ex} and λ^0_{em} for all the hydrocarbons considered, a good correlation ($r = 0.870$) exists, which improves considerably when the alternant PAHs are grouped (A) and when, the non-alternant PAHs are grouped (B). The correlation coefficients are 0.950 and 0.991, respectively. Also, the slopes of these lines can be considered as distinguishing parameters of both groups of PAHs.

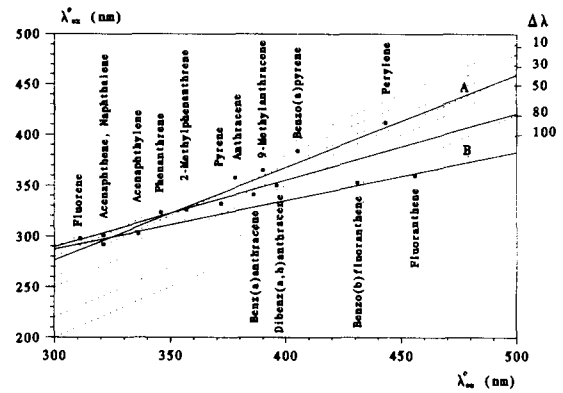

Fig. 6. Correlation between the structure of PAHs and synchronous signal. (A) Alternant PAHs; (B) non-alternant PAHs.

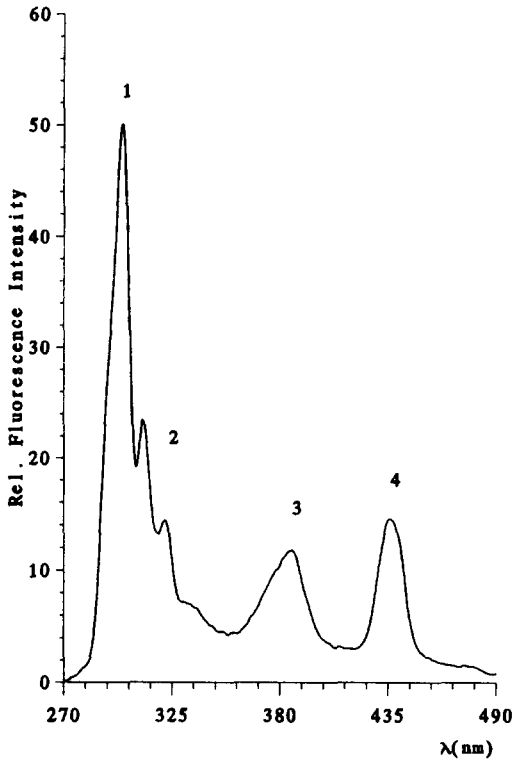

Fig. 5. Synchronous spectrum at $\Delta\lambda = 10$ nm of a mixture of 15 PAHs in a micellar medium of CPB. $C_{PAH} = 55.6$ ng ml^{-1}; $C_{CPB} = 2.6 \times 10^{-3}$ M. Slits: 5–6 nm. (1) Fluorene; (2) acenaphthene and naphthalene; (3) anthracene and 9-methylanthracene; (4) perylene.

It has already been mentioned [7] that there are certain relationships between the wavelengths in conventional fluorescence spectra and the structure of the respective PAHs. The data obtained from synchronous spectra show that also in this case, for a given $\Delta\lambda$ value, certain relationships are found which allow one to correlate values of $\lambda^0_{s,ex}$ with hydrocarbon aromaticity. For comparative purposes, Table 3 shows the wavelengths of the synchronous emission maxima ($\lambda^0_{s,ex}$) at different $\Delta\lambda$, corresponding to the different PAHs studied in a micellar medium of CPB.

From the experimental conditions used, some conclusions can be drawn, among which we would emphasize the following:

(1) Alternant PAHs:

Among these PAHs, which have only benzene rings, we can distinguish between:

(a) PAHs with a linear chain. Among the components of this subgroup, which have no substituents, an important bathochromic effect is observed when the number of aromatic rings

in the molecule increases. This was observed for naphthalene and anthracene.

The substitution of a methyl group in these PAHs leads to a slight bathochromic shift. This happens with 9-methylanthracene.

(b) PAHS with a non-linear chain. For an equal number of aromatic rings, the non-linear hydrocarbon shows a smaller wavelength of the synchronous maximum that the linear hydrocarbon. This is the case for anthracene and phenanthrene.

Also, among non-linear PAHs with an equal number of aromatic rings, a bathochromic shift is produced when the degree of condensation increases. This was observed for dibenz[*a*,*h*]anthracene, benzo[*a*]-pyrene and perylene.

With respect to the influence of the substituent, in the case studied, the introduction of a methyl group in phenanthrene does not lead to a considerable shift in the synchronous band of 2-methylphenanthrene.

(2) Non-alternant PAHs:

The substitution of an aromatic ring by another with a cyclic nature induces a hypsochromic shift. This was observed with anthracene and fluorene.

The introduction of a five-membered ring between two aromatic rings induces a low hypsochromic shift. This is the case for naphthalene and fluorene.

The introduction of a five-membered ring at the α, α'-position of naphthalene hardly induces any shift in the value of $\lambda^0_{s,ex}$.

The addition of one or two aromatic rings to a non-alternant PAH leads to bathochromic shifts. This occurs for acenaphthene, fluorene, fluoranthene and benzo[*b*] fluoranthene.

References

[1] W.J. Simonsick and R.A. Hites, Anal. Chem., 56 (1984) 2749.

[2] W.J. Simonsick and R.A. Hites, Anal. Chem., 58 (1986) 2114.

[3] R.M. Campbell and M.L. Lee, Anal. Chem., 58 (1986) 2247.

[4] J.C. Fetzer, W.R. Biggs and K. Jinno, Chromatographia, 21 (1986) 439.

[5] T. Neilsen, Anal. Chem., 55 (1983) 286.

[6] T.W. Allen, R.J. Hurtubise and H.F. Silver, Anal. Chim. Acta, 141 (1982) 411.

[7] T.W. Allen, R.J. Hurtubise and H.F. Silver, Anal. Chem., 57 (1985) 666.

[8] S.T. Sie and G.W.A. Rijnders, Anal. Chim. Acta, 38 (1967) 31.

[9] R.E. Jentoft and T.H. Gouw, Anal. Chem., 48 (1976) 2195.

[10] T. Vo-Dinh and P.R. Martínez, Anal. Chim. Acta, 125 (1981) 13.

[11] D.J. Futoma, S.R. Smith and J. Tanaka, Crit. Rev. Anal. Chem., 13 (1982) 117.

[12] A.M. Mohan Rao, R. Raja Gopalan and K.G. Vohra, Talanta, 28 (1981) 607.

[13] R.J. Hurtubise, J.F. Schabron, J.D. Feaster, D.H. Therkildsen and R.E. Poulson, Anal. Chim. Acta, 89 (1977) 377.

[14] R.J. Hurtubise, G.T. Skar and R.E. Poulson, Anal. Chim. Acta, 97 (1978) 13.

[15] R.J. Hurtubise, J.D. Phillip and G.T. Skar, Anal. Chim. Acta, 101 (1978) 333.

[16] P. John and I. Soutar, Anal. Chem., 48 (1976) 520.

[17] T. Vo-Dinh, R.B. Gammage and P.R. Martínez, Anal. Chem., 53 (1981) 253.

[18] T. Vo-Dinh, R.B. Gammage and P.R. Martinez, Anal. Chem., 50 (1978) 2054.

[19] J.B.F. Lloyd, Analyst, 105 (1980) 97.

[20] J. Georges, Spectrochim. Acta Rev., 13 (1990) 27.

[21] R. von Wandruszka, Crit. Rev. Anal. Chem., 23 (1992) 187.

[22] H.J. Pownall and L.C. Smith, Biochemistry, 13 (1974) 2594.

[23] R.R. Hautala, N.E. Schore and N.J. Turro, J. Am. Chem. Soc., 95 (1973) 5508.

[24] E.A. Lissi, S. Gallardo and P. Sepulveda, J. Colloid Interface Sci., 152 (1992) 104.

[25] D.W. Armstrong, L.A. Spino, T. Vo-Dinh and A. Alak, Spectroscopy, 2 (1987) 54.

[26] G.G. Guilbault, Practical Fluorescence. Theory, Methods and Techniques, Marcel Dekker, New York, 1973 p. 279.

[27] J.W. Carr and J.M. Harris, Anal. Chem., 59 (1987) 2546.

[28] J.A. Warren, J.M. Hayes and G.J. Small, J. Chem. Phys., 102 (1986) 323.

[29] A. Nakayima, Bull. Chem. Soc. Jpn., 50 (1977) 2473.

[30] I. Bergman, Trans. Faraday Soc., 50 (1954) 829.

[31] U. Breymann, H. Dreeskamp, E. Koch and M. Zander, Chem. Phys. Lett., 59 (1978) 68.

[32] Y. Kusumoto, M. Shizuka and I. Satake, Chem. Lett., (1986) 529.

[33] M.T. Oms, R. Forteza, V. Cerda, F. García and A.L. Ramos, Int. J. Environ. Anal. Chem., 42 (1990) 1.

ELSEVIER

Talanta 44 (1997) 269–274

Talanta

Flame atomic absorption spectrometric determination of copper, zinc, calcium, magnesium and iron in fresh eggs using microvolume injection

Sufen Shang* and Wang Hong

Department of Chemistry, He Bei University, 071002, Baoding, People's Republic of China

Received 12 April 1996; revised 2 July 1996; accepted 5 July 1996

Abstract

The flame atomic absorption spectrometric determination of copper, zinc, calcium, magnesium and iron in fresh eggs using a microvolume injection technique is described. The capillary tube and glass impact bead were removed from the nebulizer and a polypropylene tube was installed in the inlet of the capillary tube of the nebulizer as the interface for microvolume injection. The injection volume was 10 μl and calibration was carried out using aqueous standards. Beer's law was obeyed in the concentration ranges of 0.1–1.5, 0.1–3.0, 0.2–4.0, 0.5–4.0 and 1.0–6.0 mg l^{-1} for Cu, Zn, Ca, Mg and Fe, respectively, and the detection limits were 0.016, 0.016, 0.035, 0.010 and 0.10 mg l^{-1}, respectively. The reliability of the measurements was confirmed by analyzing a certified reference material, GBW 08551 Pork Liver. The precision was 2.6, 2.9, 3.0, 1.3 and 2.5% for Cu, Zn, Ca, Mg and Fe, respectively. The recovery with the standard additions method was good, ranging from 96.2 to 100.0%.

Keywords: Flame atomic absorption spectrometry; Fresh eggs; Metals; Microvolume injection

1. Introduction

Cu, Zn, Ca, Mg and Fe are essential elements in the human body and occur naturally in most fresh vegetables, meats, grains and eggs. The study of essential elements in foodstuffs is of great importance since they play a definitive role in the intrinsic mechanisms regulating vital biological processes [1–3]. Fresh eggs are among the most important and nutritious foods in the daily diet. Many methods have been developed for the determination of essential elements in eggs, such as spectrophotometry and atomic absorption spectrometry [4–6]. These methods usually include several tedious steps including preseparation and preconcentration. Additionally, the amount or volume of sample must be large owing to the low sensitivity of determination. Hence, they are time consuming, complicated and costly in application.

* Corresponding author.

PII S0039-9140(96)02044-9

The purpose of the present investigation was to develop a simple and sensitive method for the determination of these essential elements in fresh eggs by flame atomic absorption spectometry (FAAS) with microvolume injection. The proposed method is based on the use of a polypropylene tube installed in the inlet of the capillary tube of the nebulizer as the interface for microvolume injection. The volume injected was 10 μl. The accuracy of this method was tested by the analysis of a certified reference material. The method is accurate, rapid and economical. The contents of these essential elements in fresh eggs from different districts of China are reported.

2. Experimental

2.1. Instrumentation

A Model WFX-1 F2 (Beijing, China) atomic absorption spectometer was used throughout. A metal-free Eppendorf adjustable-volume digital pipette was applied for microvolume injection. A polypropylene tube was coupled to the inlet of the capillary tube of the nebulizer (the capillary tube had already been removed) as the interface for microvolume injection.

The equipment used, polypropylene vessels, polytetrafluoroethylene (PTFE) calibrated flasks, pipettes and micropipette tips were throughly cleaned by soaking for 24 h in freshly prepared 15% HNO_3, rinsed with doubly distilled, deionized water and dried at 40°C in a dust-free environment.

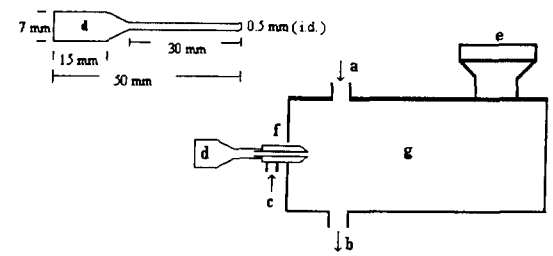

Fig. 1. Microvolume injection installation. a, Acetylene; b, drain; c, air; d, polypropylene tube; e, burner, f, nebulizer; g, spray chamber.

2.1. Reagents and materials

The certified reference material used was GBW 08551 (Pork Liver) from the National Bureau of Environment Protection (Beijing, China) with certified values of 17.2 ± 0.75, 172 ± 8.5, 197 ± 9.0, 747 ± 20 and 1050 ± 35 μg g^{-1} for Cu, Zn, Ca, Mg and Fe, respectively. All reagents were of analytical-reagent grade or better. Aqueous solutions were prepared with doubly distilled, deionized water. High-purity metal salts were used to prepare 1000 mg l^{-1} of stock standard solutions, which were stored in precleaned polypropylene bottles. Working standard solutions were freshly prepared by successive dilution of the stock standard solution to the desired concentration using 0.2% HNO_3.

2.3. Installation of microvolume injection

Some improvements to the instrument were made for the determination of elements with microvolume injection. The capillary tube and

Table 1
Optimum analytical parameters

Parameter	Cu	Zn	Ca	Mg	Fe
Wavelength (nm)	324.7	213.9	422.7	285.2	248.3
Slit width (nm)	0.2	0.2	0.2	0.2	0.2
Lamp current (mA)	2.0	2.0	2.0	1.0	2.0
Integration time (s)	1.5	1.5	1.5	1.5	1.5
Flame gases:					
Air (l min^{-1})	6.8	6.8	6.5	6.5	6.5
Acetylene (l min^{-1})	1.0	1.0	1.0	1.0	1.0

Table 2
Linear regression equation and sensitivity of the calibration graphs

Parameter	Cu	Zn	Ca	Mg	Fe
Analytical range (mg l^{-1})	0.1–0.5	0.5–1.5	1.0–4.0	1.0–4.0	1.0–4.0
Linear regression equation [a]	$A = 0.04\ C$	$A = 2.49 + 0.092\ C$	$A = 0.5 + 8.64\ C$	$A = 2.0 + 0.13\ C$	$A = 2.0 + 7.5\ C$
Correlation coefficient	1.0000	0.9998	0.9999	0.9993	1.0000
Sensitivity (mg l^{-1})	0.073	0.071	0.22	0.024	0.49

[a] Absorbance: C (mg l^{-1}) = concentration of element in standard solution.

glass impact bead were removed from the nebulizer. A polypropylene tube was installed in the inlet of the capillary tube of the nebulizer as the interface for microvolume injection (as shown in Fig. 1). The metal-free Eppendorf adjustable-volume digital pipette was used to draw the standard solution or sample solution and inject it into the polypropylene tube.

The nebulizer was rinsed with doubly distilled, deionized water and the pipette tips were replaced after each injection. The injection volume was 10 μl for standard solutions and sample solutions. The concentrations of Cu, Zn, Ca, Mg and Fe in the sample solutions were obtained from their respective calibration graphs. After the blank correction, the levels of Cu, Zn, Ca, Mg and Fe present in the sample were calculated.

2.4. Analytical conditions and calibration

The optimum analytical parameters used for the determination of the elements studied by FAAS with an air–acetylene flame are given in Table 1.

The light sources were single-element hollow-cathode lamps whose operating parameters were those recommended by the manufacturer.

Calibration against standard solutions was performed for all elements and the calibration graphs were linear in the ranges 0.1–1.5, 0.1–3.0, 0.2–4.0, 0.5–4.0 and 1.0–6.0 mg l^{-1} for Cu, Zn, Ca, Mg and Fe, respectively. The correlation coefficients were >0.999 for all calibration graphs. By considering the level of the elements in fresh egg samples and the convenience of determination, we chose narrower linear ranges for the determination of elements in fresh egg samples and the linear regression equations along with the sensitivity of the calibration graphs are listed in Table 2.

The limits of detection were calculated as twice the standard deviation of the mean blank value. Blank absorbance values were monitored throughout the period of the experiment and were subtracted from the readings before the results were calculated.

2.5. Digestion and measurement

The certified reference material was treated as follows: 1 g of sample was weighed accurately and placed in a PTFE bomb with 3 ml of HNO_3 and 1 ml of H_2O_2. The PTFE bomb was then placed in a microwave oven and irradiated for 10 min at 300 W. After cooling to ambient temperature, the

Table 3
Levels of Cu, Zn, Ca, Mg and Fe found in certified reference material of GBW 08551 (Pork Liver)

Parameter	Cu	Zn	Ca	Mg	Fe
Certified value [a] (μg g^{-1})	17.2 ± 0.8	172 ± 9	197 ± 10	747 ± 19	1050 ± 35
Found [b] (μg g^{-1}) ($n = 7$)	16.7 ± 0.5	167 ± 5	191 ± 6	738 ± 10	1080 ± 30
Precision (RSD, %) ($n = 15$)	2.6	2.8	3.0	1.3	2.5

[a] With 95% confidence limit.
[b] Mean value ± standard deviation.

Table 4
Recovery of Cu, Zn, Ca, Mg and Fe added to an egg sample (each result is the mean of seven measurements)

Parameter	Cu	Zn	Ca	Mg	Fe
Diluent sample ($\mu g\ l^{-1}$)	0.17	1.67	1.26	0.24	5.28
Amount added ($\mu g\ l^{-1}$)	0.15	1.42	2.26	0.28	2.57
Amound found ($\mu g\ l^{-1}$)	0.31	3.01	3.52	0.50	7.84
Recovery (%)	96.9	97.4	100.0	96.2	99.9

digest was diluted to 10 ml with doubly distilled, deionized water in a calibrated PTFE flask.

The egg samples were treated as follows: seven eggs were taken at random, broken and mixed in a homogenizer for a few seconds, then 1 g of sample was weighed accurately in a 50 ml glass beaker containing 3 ml of HNO_3 and 1 ml of H_2O_2. The beaker was placed on an electric heating plate and heated at 180–190°C. The dried digest was dissolved in doubly distilled, deionized water and transferred into a 5.00 ml PTFE calibrated flask and diluted to the mark for the determination of Cu, Fe, Ca and Mg. Another 0.25 g of sample was weighed accurately and placed in a PTFE bomb with 3 ml of HNO_3 and 1 ml of H_2O_2. The PTFE bomb was then placed in a microwave and irradiated for 7 min at 300 W. After cooling to ambient temperature, the digested was diluted to 2 ml with doubly distilled, deionized water in a calibrated PTFE flask for the determination of Zn.

The metal-free Eppendorf adjustable-volume digital pipette was used to draw the standard and sample solutions, which were then injected into the polypropylene tube (Fig. 1) and immediately aspirated from the polypropylene tube into the nebulizer by suction (venturi action) caused by the rapid flow of support gas (air) past the capillary tip. The nebulizer was rinsed with doubly distilled, deionized water and the pipette tip was replaced after each injection. The injection volume was 10 μl for standard and sample solutions. The concentrations of Cu, Zn, Ca, Mg and Fe in the sample solution were obtained from their respective calibration graphs. After the blank correction, the levels of Cu, Zn, Ca, Mg and Fe present in the sample were calculated.

2.6. Analytical quality validation

In order to validate the accuracy of the proposed method, the procedure was applied to a certified reference material (GBW 08551 Pork Liver). The results are shown in Table 3. The standard additions method was used for recovery studies of the elements determined and the results are listed in Table 4.

3. Results and discussion

3.1. Effect of integration time

It took 1.5 s for a 10 μl sample to reach a steady-state signal in the flame and it was also

Table 5
Determination of essential elements in fresh eggs from four districts in China (each result ($\mu g\ g^{-1}$) is the mean of seven measurments).

District	Cu	Zn	Ca	Mg	Fe	Cu/Zn	Ca/Mg
Baoding	0.61	11.38	563.03	194.76	20.99	0.054	2.89
Beijing	0.67	10.96	497.52	210.34	23.21	0.061	2.36
Tianjing	0.56	12.33	627.42	190.07	26.78	0.045	3.30
Nei Monggol	0.64	11.91	580.45	201.63	24.56	0.054	2.88
RSD[a] (%)	3.7	0.9	3.4	1.6	2.7	–	–

[a] The mean of RSD for all four districts.

Table 6
Comparison of analytical results obtained in the normal nebulization mode with those obtained by the microvolume injection technique ($n = 7$)

Parameter [a]	Cu	Zn	Ca	Mg	Fe
N	0.62 ± 0.02	11.45 ± 0.07	559.46 ± 15.7	195.02 ± 2.1	20.51 ± 0.4
M	0.61 ± 0.03	11.38 ± 0.08	563.03 ± 16.9	194.76 ± 2.8	20.99 ± 0.5
t_t [b]	2.45	2.45	2.45	2.45	2.45
t_c [b]	0.94	1.87	0.43	0.23	2.24
F_t [b]	4.28	4.28	4.28	4.28	4.28
F_c [b]	2.25	1.13	1.16	1.78	1.56

[a] Mean ± SD ($\mu g\ g^{-1}$). N, normal nebulization mode; M, microvolume injection technique; t_t = value from the statistical analysis table; F_t = value from statistical analysis table; $t_c = t_c = |\overline{x_N} - \overline{x_M}|/s\sqrt{n_N n_M/n_N + n_M}$; $F_c = s^2_{max}/s^2_{min}$; x = mean of measurements; s = standard deviation.
[b] 95% of confidence level.

found that the largest signal was obtained when the integration time was chosen as 1.5 s. Considering the sensitivity of the determination, the integration time was set as 1.5 s.

3.2. Effect of injection volume

The influence of the injection volume was studied. The same results for the relationship between the integrated absorbance value and the injection volume were obtained for all five elements. For the five elements tested it was found that the integrated absorbance value increased with increases in the injection volume in the range 5–75 μl. If the injection volume was over 75 μl, the integrated absorbance value decreased because the amount of element exceeded the linear range of Beer's law. Moreover, the injection of large volumes produced serious contamination of the nebulizer and caused high background signals. Since an injection volume of 10 μl was sufficient for the determination of the elements studied, 10 μl was chosen as the injection volume for the analysis of standard and sample solutions.

3.3. Effect of temperature of spray chamber

The temperature of the spray chamber had no influence on the analytical results and it was found that if the temperature of the spray chamber was increased contamination of the spray chamber became very serious, especially for the determination of Mg and Fe. Hence the spray chamber was not heated.

3.4. Effect of glass impact bead

In the normal nebulization mode the sample uptake rate is usually 3–8 ml min^{-1} and a glass impact bead is used to improve the dispersion of liquid droplets to produce fine aerosol particles in conventional FAAS. Since the volume of sampling is just 10 μl, the fine aerosol particles were formed without using the glass impact bead. We also attempted to use the glass impact bead to obtain finer aerosol particles, but it was found that this decreased the sensitivity of the microvolume injection method and produced scattered analytical results. This is due to the contamination of elements determined on the surface of the glass impact bead, which became more serious for a 10 μl sampling volume corresponding to the general volume of sampling (i.e. ml level) in the normal nebulization mode. Therefore, the glass impact bead was removed to increase the sensitivity and repeatability of analysis.

The accuracy was verified by analyzing the certified standard reference material, as shown in Table 3. For all elements, the precision (R.S.D.) was better than 3.0%. The reliability of the analytical method was further assessed through recovery studies, by performing seven replicate spectrometric determinations of the elements under consideration in real samples with the standard additions

method. The average recoveries were better than 96% for all elements, as shown in Table 4.

3.5. Applications of the method

The proposed method was applied to the determination of Cu, Zn, Ca, Mg and Fe in fresh egg samples from four districts in China. The number of determinations for each element was seven and the analytical data treated statistically ($P = 0.05$). No significant skin-color difference was found and the Cu/Zn ratios also did not show significant differences for the eggs from the four districts, but the Ca/Mg ratios showed obvious differences due to the different sources of feed. The results are listed in Table 5.

The comparison of analytical results obtained in the normal nebulization mode with those obtained by the microvolume injection method are listed in Table 6. The fresh egg samples were from the city of Baoding. The results of comparison using statistical analysis ($P = 0.05$) showed that there were no significant differences for the standard deviations ($F_c < F_t$) and the mean values ($t_c < t_t$) of the two methods.

In conclusion, the FAAS microvolume injection technique described is a economical, simple and rapid means for the determination of trace elements in fresh eggs. The injection volume was just 10 μl for the determination of the elements studied. It is suitable for the routine determination of elements in foodstuffs. The method could be of interest in poultry and nutriology research and can be recommeded for routine analyses. The proposed method can also be applied to the determination of elements in other types of matrices.

References

[1] R.A. Romero, J.A. Navarro, B. Rodriguez, Iturbe, R. Garcia, O.E. Parra and V.A. Granadillo, Trace Elem. Med., 7 (1990) 176.
[2] J. Shen, S. Chen and C. Zhang, Shanghai Yixue, 14 (1991) 603.
[3] P.A. Walravens, Clin. Chem., 26 (1980) 185.
[4] B. Li and Y. Liu, Fenxi Huaxue, 4 (1983) 266.
[5] Y. Shun, Shi Pin Yu Fa Xiao Gong Ye, 4 (1987) 7.
[6] L. Wang and F. Tang, Hangzhou Daxue Xuebao, Ziran Kexueban, 21 (1994) 311.

ELSEVIER

Talanta 44 (1997) 275–282

Talanta

Thermodynamic study of complex formation between 18-crown-6 and potassium ion in some binary non-aqueous solvents using a conductometric method

Gholamhossein Rounaghi[a,*], Zarrin Eshaghi[b], Ebrahim Ghiamati[b]

[a]*Chemistry Department, Ferdowsi University of Mashhad, Mashhad, Iran*
[b]*Chemistry Department, Birjand University, Birjand, Iran*

Received 23 January 1996; revised 1996; accepted 9 July 1996

Abstract

The complexation reaction between a macrocyclic polyether, 18-crown-6 (18C6), and potassium ion was studied in methanol (MeOH)–acetonitrile (AN), dimethylformamide (DMF)–AN and propylecarbonate (PC)–DMF binary solvent systems at different temperatures using a conductometric method. It was found that the stability of the 1:1 complex formed between K^+ ion and this ligand increases with decreasing temperature. Standard enthalpies and standard entropies of the complex formation were obtained from the temperature dependence of the stability constant. In all cases negative ΔH_c° and ΔS_c° values characterize the formation of 18C6–K^+ complex. The results obtained show that the stability of the complex is governed by the solvent medium and the thermodynamic parameters ΔH_c°, $\Delta S^\circ{}_c$ and $\Delta G^\circ{}_c$ are sensitive to the composition of the mixed solvents. In addition, it was found that the stability constant of the resulting 1:1 complex among various neat solvents used varies in the order PC > MeOH > AN > DMF.

Keywords: Conductometry; 18-Crown-6; Mixed nonaqueous solvents; Potassium ion; Thermodynamic parameters

1. Introduction

Crown ethers have been demonstrated to be highly selective complexing agents for many metal ions and can potentially be applied in thier separation [1–4] and determination. Thermodynamic studies of macrocyclic complexation reactions with metal ions not only result in important information on the thermodynamics of complexation reaction, but also lead to a better understanding of the high selectivity of these ligands towards different metal cations.

While macrocyclic complexes of alkali metal cations have been extensively investigated in aqueous solutions and in a wide variety of neat non-aqueous solvents [5–7], the complexation reactions of these complexes in mixed solvent systems have been investigated only to a very limited extent [7–10]. It is well known that the stability and selectivity of complexations strongly depend

* Corresponding author.

PII S0039-9140(96)02045-0

on the solvating ability of the solvent. It was of interest to us, therefore, to investigate the dependence of the stability constant and thermodynamic parameters of the 18-crown-6 (18C6)-K^+ complex on the composition of several binary solvent mixtures in order to see how the thermodynamics of complexation are affected by the solvent composition.

A large number of physico-chemical techniques such as NMR spectrometry [11–18], calorimetry [19–22], polarography [23,24], spectrophotometry [25–27], conductometry [28–35] and potentiometry [36–39] have been used to study the complex formation between macrocyclic polyethers and alkali metal cations in solutions. Among these various methods, the conductometric technique is a sensitive and inexpensive method with a simple experimental arrangement for such investigations.

In the present study, the formation constant of the 18C6–K^+ complex in acetonitrile (AN)–methanol—(MeOH), AN–dimethylformamide (DMF) and propylene carbonate (PC)–DMF binary solvent systems was determined at different temperatures by the conductometric method.

2. Experimental

2.1. Reagents and solvents

All compounds were obtained from Merck. 18-crown-6 was recrystallized from acetonitrile and dried under vacuum for 72 h at room temperature [40]. Potassium perchlorate was recrystallized from deionized, distilled water three times, dried at 150°C and then kept in a vacuum desicinator over P_2O_5 for 48 h. The solvents were refluxed for 2 days over P_2O_5 dehydration agent, and then fractionally distilled. The middle 70% of the distillate was used. The conductivity of the final product was 2×10^{-7} Ω^{-1} cm^{-1} at 25°C.

The experimental procedure to obtain the formation constant of the 18C6–K^+ complex was as follows. A solution of potassium perchlorate (5×10^{-4} M, 200 cm^3) was placed in a titration cell, thermostated at a given temperature, and the conductance of the solution was measured. A step-by-step increase in the crown ether concentration was effected by a rapid transfer from crown ether solution prepared in the same solvent (2.5×10^{-3}–1.5×10^{-3} M) to the titration cell using a microburet, until the total concentration of the crown ether was approximately five times higher than that of potassium perchlorate. The conductance of the solution was measured after each transfer.

2.2. Apparatus

The conductance measurements were performed on a Metrohm (Herisau, Switzerland) Model 9100, conductometer in a water-bath ultrathermostat with a constant temperature maintained within ±0.05°C. The electrolytic conductance was measured using cells consisting of two platinum electrodes to which an alternating potential was applied. Two cells with cell constants of 0.64998 and 0.71699 cm^{-1} were used throughout.

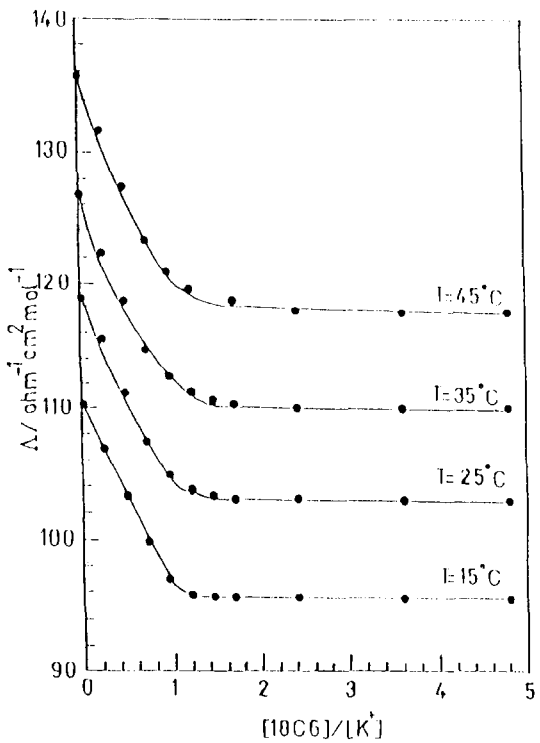

Fig. 1. Molar conductance–mole ratio plots for 18C6–K^+ complex in MeOH–AN (75:25) at different temperatures. Concentration of $KClO_4 = 5 \times 10^{-4}$ M.

Table 1
Formation constants of 18C6–K^+ complex in AN, DMF, MeOH, PC and their binary mixtures at different temperatures

Medium	Log $K_f^\circ \pm$ SD[a]			
	15°C	25°C	35°C	45°C
Pure AN	6.22 ± 0.08	5.90 ± 0.08	5.6 ± 0.1	5.26 ± 0.09
75% AN–25% DMF	5.80 ± 0.07	5.50 ± 0.06	5.18 ± 0.07	4.88 ± 0.09
50% AN–50% DMF	5.39 ± 0.08	5.10 ± 0.05	4.80 ± 0.08	4.49 ± 0.06
35% AN–65% DMF	5.19 ± 0.05	4.90 ± 0.08	4.61 ± 0.09	4.30 ± 0.09
25% AN–75% DMF	5.0 ± 0.1	4.71 ± 0.07	4.42 ± 0.05	4.13 ± 0.07
15% AN–85% DMF	4.83 ± 0.07	4.52 ± 0.07	4.23 ± 0.09	3.95 ± 0.08
Pure DMF	4.59 ± 0.08	4.30 ± 0.07	4.03 ± 0.09	3.74 ± 0.08
Pure MeOH	6.39 ± 0.04	6.07 ± 0.03	5.76 ± 0.05	5.44 ± 0.06
75% MeOH–25% An	6.36 ± 0.08	6.04 ± 0.06	5.72 ± 0.06	5.41 ± 0.07
50% MeOH–50% AN	6.31 ± 0.06	5.99 ± 0.07	5.7 ± 0.1	5.36 ± 0.08
25% MeOH–75% AN	6.3 ± 0.1	5.95 ± 0.05	5.63 ± 0.08	5.32 ± 0.09
Pure PC	6.43 ± 0.07	6.17 ± 0.06	5.85 ± 0.05	5.55 ± 0.05
75% PC–25% DMF	6.00 ± 0.06	5.70 ± 0.08	5.39 ± 0.06	5.09 ± 0.06
50% PC–50% DMF	5.45 ± 0.09	5.2 ± 0.1	4.94 ± 0.08	4.64 ± 0.09
25% PC–75% DMF	5.06 ± 0.08	4.77 ± 0.06	4.5 ± 0.1	4.18 ± 0.07

[a] SD = standard deviation.

3. Results

The variation of molar conductance versus the [18C6]/[K^+] mole ratio for the 18C6–K^+ crown ether complex in AN–DMF, MeOH–AN and PC–DMF binary mixtures were studied at different temperatures. As a typical example, the molar conductance–mole ratio plots for the 18C6–K^+ complex in MeOH–AN (75:25) is shown in Fig. 1. Similar behavior was observed with the other systems.

Since the 18C6 concentration was kept low ($\leq 2.5 \times 10^{-3}$ M) during these experiments, corrections for viscosity changes were neglected. It was also assumed that the association between the potassium ion and perchlorate ion in An, PC, DMF, MeOH and their binary mixtures is negligible under these highly dilute experimental conditions and that 18C6 forms a 1:1 complex with potassium ion in these non-aqueous solvents systems.

A conductometric method for the determination of the stability constants of complexes of crown ethers with metal ions has been used by several investigators [29–35]. The 1:1 binding of an alkali metal cation (M^+) with the crown ethers can be represented by the following equilibrium equation:

$$M^+ + L \rightleftharpoons ML^+ \quad (1)$$

$$\alpha[M]_t[L]_t - (1-\alpha)[M]_t(1-\alpha)[M]_t$$

where M^+, L, ML^+ and α are the alkali metal ion, the crown ether, the complex and the fraction of the free alkali metal ion, respectively. The complex formation constant in terms of the molar concentration can be expressed as

$$k_{ML^+} = \frac{[ML^+]}{[M^+][L]} = \frac{1-\alpha}{\alpha[L]} \quad (2)$$

The observed conductivity, k, at each point in the titration can be written as [35]

$$k = K_{MC10_4} + K_{MLC10_4} \quad (3)$$

where K_{MC10_4} and K_{MLC10_4} are the conductivities of the alkali metal perchlorate and alkali metal crown ether perchlorate, respecitvely. The molar conductivities are given by

$$\Omega_{MC10_4} = \frac{K_{MC10_4}}{[M^+]} = \frac{K_{MC10_4}}{\alpha[M]_t} \quad (4)$$

$$\Omega_{MLClO_4} = \frac{K_{MLClO_4}}{[ML^+]} = \frac{K_{MLClO_4}}{(1-\alpha)M_t} \quad (5)$$

where Ω_{MClO_4} and Ω_{MLClO_4} are the molar conductivities of the alkali metal perchlorate and alkali metal crown ether perchlorate, respectively. As a consequence of Eqs. (4) and (5), Eq. (3) can be transformed into

$$\Omega = \frac{K}{[M]_t} = \alpha\Omega_{MClO_4} + (1-\alpha)\Omega_{MLClO_4} \quad (6)$$

Substituting from Eq. (6) into Eq. (2) gives the following equation:

$$K_{ML^+} = \frac{\Omega_{MClO_4} - \Omega}{(\Omega - \Omega_{MClO_4})[L]} \quad (7)$$

where

$$[L] = [L]_t - \frac{[M]_t(\Omega_{MClO_4} - \Omega)}{\Omega_{MClO_4} - \Omega_{MLClO_4}}$$

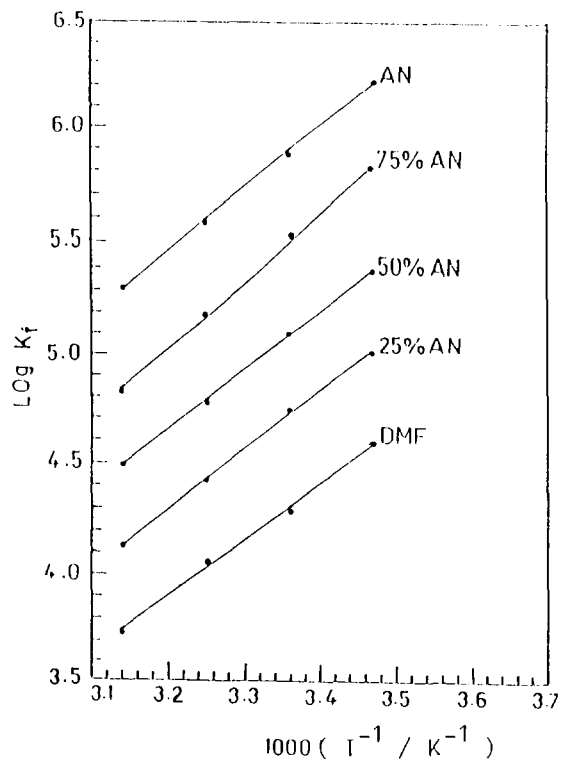

Fig. 2. Van't Hoff plots for 18C6–K^+ complex in AN and DMF and their binary mixtures.

The procedure for obtaining the K_{ML^+} value is as follows. The value of Ω_{MLClO_4} is estimated from the Ω values at points of large $[L]_t$ to $[M]_t$ ratios. The molar conductance data obtained from complexation studies were fitted non-linearly to the Eq. (7), using the Genplot package from Computer Graphic Service [41]. The K_{ML^+} and the estimated Ω_{MLClO_4} at large $[L]_t$ ratios were used as variables until best convergence was obtained.

All calculated normal stability constants K_f° for the 1:1 18C6–K^+ complex in various solvent systems are listed in Table 1. Assuming that the activity coefficients of potassium and 18C6 ions have the same value, K_f° is a thermodynamic equilibrium constant on the molar concentration scale, related to the Gibbs standard energy of the complexation reaction, ΔG°, on the same scale.

Van't Hoff plots of log K_f vs. 1/I for all the systems investigated were constructed. A typical example of these plots is shown in Fig. 2. The changes in the standard enthalpy (ΔH_c°) for the complexation reaction were obtained from the slopes of the van't Hoff plots and the changes in standard entropy ($\Delta_{S_c}^\circ$) were calculated from the relationship $\Delta G_{c,298}^\circ = \Delta H_c^\circ - 298.15\Delta S_c^\circ$. The results are summarized in Table 2.

4. Discussion

Macrocyclic ligands such as crown ethers have been used successfully for diverse processes such as ion transport across artificial and biological membranes, ionic separation and extraction, design of ion-selective electrodes and in the understanding of some natural processes through mimicry of metalloenzymes [42–45]. Their selectivity for specific ions suggests that they may be of utility in the treatment of metallurgical waste streams. Most applications of crown ethers are based on their selective binding with certain cations in solutions.

The stabilities and selectivities on complexation are mainly governed by the solvent medium and the relative sizes of the cation and crown ether cavity. During the complexation step, the ligand should be able to replace as completely as possible the solvent molecules in the first solvation shell of

Table 2
Thermodynamic parameters for 18C6–K^+ complex in AN, DMF, MeOH, PC and their binary mixtures

Medium	Log $K_f^\circ \pm$ SD[a](25°C)	$-\Delta G_c^\circ \pm$ SD[a](25°C) (kJ mol^{-1})	$+\Delta H_c^\circ \pm$ SD[a] (kJ mol^{-1})	$-\Delta S_c^\circ \pm$ SD[a] (J mol^{-1} K^{-1})
Pure AN	5.90 ± 0.08	33.7 ± 0.1	55.7 ± 0.1	73.9 ± 0.5
75% An–25% DMF	5.50 ± 0.06	31.40 ± 0.07	53.6 ± 0.2	74.5 ± 0.6
50% AN–50% DMF	5.10 ± 0.05	29.11 ± 0.06	52.3 ± 0.2	77.7 ± 0.8
35% AN–65% DMF	4.90 ± 0.08	27.85 ± 0.09	51.5 ± 0.4	79.00 ± 1.00
25% AN–75% DMF	4.71 ± 0.07	26.89 ± 0.09	50.9 ± 0.4	81.00 ± 1.00
15% AN–85% DMF	4.52 ± 0.07	25.70 ± 0.09	50.9 ± 0.2	84.6 ± 0.8
Pure DMF	4.30 ± 0.07	24.6 ± 0.1	49.0 ± 0.4	82.00 ± 1.00
Pure MeOH	6.07 ± 0.03	34.71 ± 0.09	55.3 ± 0.3	69.1 ± 0.9
75% MeOH–25% AN	6.04 ± 0.06	34.48 ± 0.08	55.3 ± 0.3	70.00 ± 1.00
50% MeOH–50% AN	5.99 ± 0.07	34.2 ± 0.1	55.2 ± 0.3	70.00 ± 1.00
25% MeOH–75% AN	5.95 ± 0.05	33.97 ± 0.09	55.1 ± 0.3	71.00 ± 1.00
Pure PC	6.17 ± 0.06	35.22 ± 0.05	54.0 ± 0.2	63.0 ± 0.8
75% PC–25% DMF	5.70 ± 0.08	32.54 ± 0.09	52.9 ± 0.1	68.1 ± 0.6
50% PC–50% DMF	5.2 ± 0.1	29.91 ± 0.06	52.3 ± 0.2	75.0 ± 0.6
25% PC–75% DMF	4.77 ± 0.06	27.23 ± 0.06	51.3 ± 0.2	80.8 ± 0.8

[a] SD = standard deviation.

the cation. As a result, variations in the nature of the solvent produce significant changes in the binding properties of the macrocyclic ligand, so that the stability and selectivity for a certain cation over others may be greatly altered according to the nature of the solvent.

Valuable chemical information could be obtained from thermodynamic studies of the interactions between macrocyclic crown ethers and ions in solutions. It was of interest to us to investigate the dependence of complex stabilities and thermodynamic parameters on the composition of several binary solvent mixtures in order to see how variations of the solvent composition affect the stability of complexation. For our initial studies we selected the K^+ ion as the probe cation and used conductometric measurements to determine the stability constant of the potassium complex with 18C6 at different temperatures.

It is obvious from Fig. 1 that addition of the ligand to K^+ ion in solution causes a continuous decrease in the molar conductance, which begins to level off at mole ratios >1. The slope of the corresponding mole ratio plots changes sharply at the point where the ligand to cation mole ratio is 1, indicating the formation of a relatively stable 1:1 complex.

However, in the case of pure DMF (Fig. 3), a gradual decrease in the molar conductance of K^+ ion on addition of the ligand is observed which does not exhibit any considerable change in curvature at a mole ratio of ca. 1, indicating that a weaker 1:1 complex is formed.

The solvation of the ligand and metal cation is influenced by the donor ability and dielectric constant of the solvent and by the shape and size of the solvent molecules. Generally, we expect that in solvents with a high donor ability and dielectric constant, the stability constant of the complex should decrease owing to the competition between the ligand and the solvent molecules for the metal ion. However, it has been shown that the donor ability of the solvent plays the most important role in the behaviour of alkali metal–crown ether complexes in non-aqueous solvents [46]. The results obtained in this work fit this generality with the exception indicated above.

As an example, the variation of the stability constant with the composition of the MeOH–AN binary system is shown in Fig. 4. Similar behavior was observed in the other sytems, i.e. as the mole fraction of MeOH, AN and PC increases in AN–MeOH, AN–DMF and PC–DMF binary mixtures, the stability constant of the 18C6–K^+ complex increases linearly at all temperatures.

As is obvious from Table 1, the stability constant of the 18C6–K^+ complex among various neat solvents decreases in the order PC > MeOH > AN > DMF. This behavior reflects the much stronger cation solvation by DMF, compared with the other solvents, with which the polyether has to complete. DMF (Donor Number = 26.6 K·cal mol^{-1}) with a high donor ability can solvate the K^+ ion strongly and, therefore, compete with the ligand for the potassium ion. Therefore, in this solvent the formation of the 18C6–K^+ complex is weakened.

In strong solvating sovents, such as DMF, the complex formation is poor, whereas in solvents with medium donicites, such as PC and AN, a more stable complex is formed. It is interesting that although DMF and AN have comparable dielectric constants, the formation constant of the complex in AN, a poor donor solvent, is much higher than that in DMF, which has a larger donor number. This indicates that the dielectric constant of the solvent is not a dominant factor in this complexation reaction.

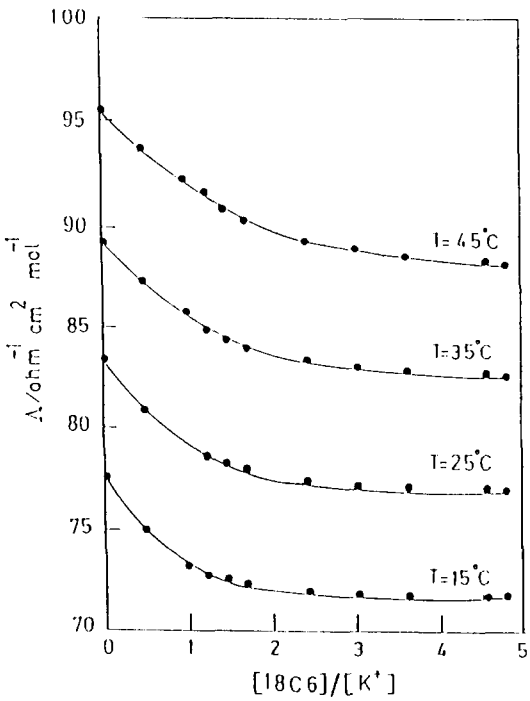

Fig. 3. Molar conductance–mole ratio plots for 18C6–K^+ complex in DMF at different temperatures. Concentration of $KClO_4 = 5 \times 10^{-4}$ M.

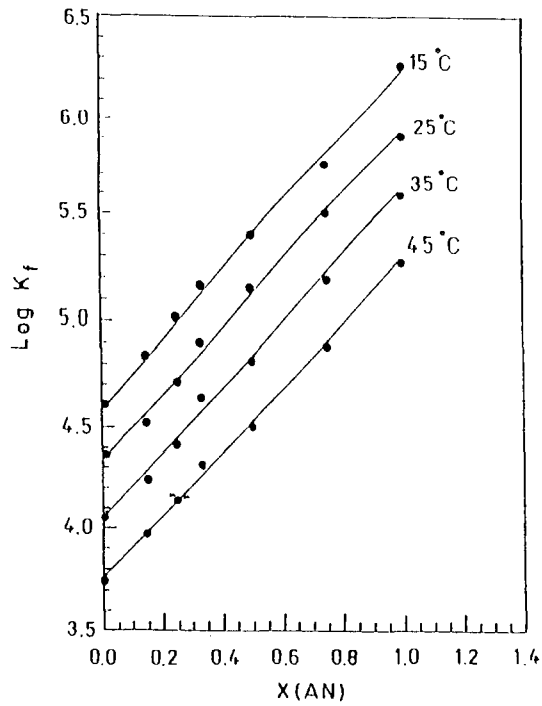

Fig. 4. Variations of stability constant of 18C6–K^+ complex with the composition of the AN–DMF binary system at different temperatures.

Although the donor ability of MeOH is greater than that of AN, the stability constant of the crown ether–K^+ complex in AN is lower than that in MEOH. This behaviour may be due to the fact that the AN molecules form a molecular complex with 18C6 [24].

The normal stability constant (K_f°) of the complex is related to the net changes of standard free energy, ΔG_c°, standard enthalpy, ΔH_c°, and standard entropy, ΔS_c°, of complexation. From these functions, important conclusions may be drawn about the various factors governing complex formation, such as solvation effects, the character of the coordinating bond and the changes in the structure that often take place during complex formation.

The thermodynamic parameters for complex formation are given in Table 2. As expected, the values of ΔH_c° and ΔS_c° depend strongly on the

nature of the medium used. The value and the sign of the standard entropy changes are expected to vary with different parameter, such as changes in flexibility of the macrocyclic ligands during the complexation processes and the extent of cation–solvent, crown ether–solvent and complex–solvent interactions.

Experimental values of ΔH_c° and ΔS_c° for the 18C6–K^+ system in AN–DMF, AN–MeOH and PC–DMF show that in all cases the complexes are enthalpy stabilized but entropy destabilized. On the other hand, the thermodynamic parameters (ΔG_c°, ΔH_c° and ΔS_c°) are sensitive to the composition of the mixed solvents.

It seems reasonable to assume that the decrease in entropy on complexation is related to a change in the conformational entropy of the ligand. It is known that macrocyclic ligands are fairly flexible in free state, and therefore the negative entropy changes may be attributed to the increased ligand rigidity on coordination. It should be stressed, however, that the conformational change of the ligand is not the only factor governing the change in entropy of complexation. The complexation reaction involves not only a change in the solvation of the cation, but also that of the ligand. The relative enthalpy and entropy changes can be understood if ligand solvation is taken into consideration. Information on the interaction of macrocyclic ligand with the solvent molecules is sparse, and addtional studies on the ligand–solvent interaction are necessary before the thermodynamic behavior of macrocyclic complexes in non-aqueous solvents can be better understood.

The data in Table 2 show that in DMF–AN and DMF–PC binary mixtures, lowering the concentration of DMF results in a decrease in ΔG_c° and ΔH_c° but an increase in ΔS_c°. In a strong solvating solvent such as DMF the solvation of the metal ion (and probably that of the ligand) will be stronger than in solvents of lower solvating ability such as AN and PC. Therefore, less energy is necessary for desolvation step of the cation (and probably of the ligand) in the case of AN and PC than DMF solutions.

Acknowledgement

We gratefully acknowledge the support of this work by Birjand University.

References

[1] H.K. Frensdorff, J. Am. Chem. Soc., 93 (1971) 4684.
[2] E. Blasius, K.P. Janzen, H. Luxenburger, V.B. Nguyen, H. Klotz and J. Stockenmer, J. Chromatogr., 167 (1978) 307.
[3] I. Kopolow and J. Smid, Macromolecules, 6 (1973) 135.
[4] L.A. Fernando, M.L. Miles and L.H. Bowen, Anal. Chem., 52 (1980) 1115.
[5] A.I. Popov and J.M. Lehn, in G.A. Melson (Ed.), Coordination Chemistry of Macrocyclic Compounds, Plenum press, New York, 1985, Chapter 9.
[6] M. Hiraoka, Crown Compounds, Elsevier, New York, 1985.
[7] R.M. Izatt, K. Pawak and J.S. Bradshaw, Chem. Rev., 91 (1991) 1721.
[8] J.D. Lamb, R.M. Izatt and J.J. Christensen, in G.A. Melson (Ed), Coordination Chemistry of Macrocyclic Compounds, Plenum Press, New York, 1979, Chapter 3.
[9] P.A. Mosier-Boss and A.I. Popov, J. Am. Chem. Soc., 107 (1985) 6168.
[10] R.M. Izatt, J.S. Bradshaw, S.A. Nielsen, J.D. Lamb and J.J. Christensen, Chem. Rev., 85 (1985) 271.
[11] E. Mei, J.L. Dye and A.I. Popov, J. Am. Chem. Soc., 99 (1977) 5308.
[12] M. Shamsipur, G. Rounaghi and A.I. Popov, J. Solution Chem., 9 (1980) 701.
[13] J.D. Lin and A.I. Popov, J. Am. Chem. Soc., 103 (1981) 3773.
[14] G. Rounaghi and A.I. Popov, J. Inorg. Nucl. Chem., 43 (1981) 911.
[15] S. Khazaelli, J.L. Dye and A.I. Popov, J. Phys. Chem., 86 (1982) 5018.
[16] G. Rounaghi and A.I. Popov, Polyhedron, 5 (1986) 1329.
[17] G. Rounaghi and A.I. Popov, Inorg. Chim. Acta, 114 (1986) 145.
[18] G. Rounaghi and A.I. Popov, Polyhedron, 5 (1986) 1935.
[19] R.M. Izatt, R.E. Terry, D.P. Nelson, Y. Chan, D.J. Eatough, J.S. Bradshaw, L.D. Hansen and J.J. Christensen, J. Am. Chem. Soc., 98 (1976) 7626.
[20] J.D. Lamb, R.M. Izatt, S.W. Swain and J.J. Christensen, J. Am. Chem. Soc., 102 (1980) 475.
[21] B.L. Haymore, J.D. Lamb, R.M. Izatt and J.J. Christensen, Inorg. Chem., 21 (1982) 1598.
[22] G. Michaux and J. Reisse, J. Am. Chem. Soc., 104 (1982) 6895.
[23] A. Agostino, M. Caselli and M. Della Monica, J. Electronal. Chem., 74 (1976) 95.
[24] A. Hofmanova, J. Koryta, M. Brezina and M.L. Mittal, Inorg. Chim. Acta, 28 (1978) 73.

[25] E. Shchori and J. Jagur-Grodzinski, J. Am. Chem. Soc., 94 (1972) 7957.
[26] E. Shchori, N. Nae and J. Jagur-Grodzinski, J. Chem, Soc., Dalton Trans., (1975) 2381.
[27] R. Sinta, P.S. Rose and J. Smid, J. Am. Chem. Soc., 105 (1983) 4337.
[28] N. Matsuura, K. Umemoto, Y. Takeda and A. Sasaki, Bull. Chem. Soc. Jpn., 49 (1976) 1246.
[29] R. Ungaro, B. Elhaj and J. Smid., J. Am. Chem. Soc., 98 (1976) 1598.
[30] N. Nae and J. Jagur-Grodzinski, J. Am. Chem. Soc., 99 (1977) 489; J. Chem. Soc., Faraday Trans. I, 73 (1977) 1951.
[31] Y. Takeda and H. Yano, Bull. Che. Soc., Jpn., 53 (1980) 1720.
[32] Y. Takeda, Bull. Chem. Soc. Jpn, 56 (1983) 866.
[33] Y. Takeda, Bull. Chem. Soc. Jpn, 56 (1983) 3600.
[34] Y. Takeda, Y. Kudo, and S. Fujiware, Bull, Chem. Soc. Jpn., 58 (1985) 1315.
[35] Y. Takeda, H. Yano, M. Ishirashi and H. Isozumi, Bull. Chem. Soc. Jpn., 53 (1980) 72.
[36] D.E. Fenton, D. Perkin and R.F. Newton, J. Chem. Soc, Perkin Trans. 1 (1981) 449.
[37] J. Massaux and J.F. Deseaz, J. Am. Chem. Soc., 104 (1982) 2967.
[38] J. Nakamura, Y. Yumoto and K. Izutsu, Bull. Chem. Soc. Jpn., 55 (1982) 1850.
[39] I.M. Kolthoff, W.J. Wang and M.K. Chantooni, Anal. Chem., 55 (1983) 1202.
[40] F. Ratkovics and A. Laszlo, Magy. Kem. Foly., 83 (1977) 25.
[41] Genplot, Computer Graphic Service, USA, 1989.
[42] I.M. Kolthoff, Anal. Chem., 51 (1979) 1R.
[43] D.A. Laidler and J.F. Stoddart, in S. Patai (Ed.) The Chemistry of Ethers, Crown Ethers, Hydroxyl Groups and Their Sulfur Analogues, Part 1, Wiley, Chichester, 1980, Chapter 1.
[44] F. Vogtle and E. Weber, in S. Patai (Ed.), The Chemistry of Ethers, Crown Ethers, Hydroxyl Groups and Their Sulfur Analogues, Part 1, Wiley, Chichester, 1980, Chapter 2.
[45] F. Vogtle, Topics in Current Chemistry, Springer, New York, 1982.
[46] A.I. Popov, Pure Appl. Chem., 51 (1979) 101.

ELSEVIER

Talanta 44 (1997) 283–295

Talanta

Spectrophotometric determination of uranium in process streams of a uranium extraction plant

B. Narasimha Murty*, Y.V.S. Jagannath, R.B. Yadav, C.K. Ramamurty, S. Syamsundar

Control Laboratory, Nuclear Fuel Complex, Hyderabad-500 062, India

Received 22 January 1996; revised 8 July 1996; accepted 12 July 1996

Abstract

This paper deals with the development and standardization of procedures for the determination of uranium on a routine basis in various process streams of a uranium extraction plant, covering a wide range of concentrations from 350 g l^{-1} down to 5 mg l^{-1} using only a spectrophotometric technique. The self-absorption of uranyl ion in dilute phosphoric acid and the violet–blue colour of the UO_2^{2+}–Arsenazo III complex in 4 M HCl were exploited for high and low concentrations of uranium, respectively. The methods described were applied to samples of varying nature such as aqueous, organics and solids, involve minimal sample preparation and do not require prior separation of uranium from impurities. The interfering impurities in different process streams were also studied. Large quantities of silica as undissolved material poses a serious interference in the case of UNS and UNF. Considerable quantities of iron in UNS, UNF, UNR and UNRC cause interference. Possible remedies in these cases are suggested. Problems with the direct spectrophotometric measurement of organic samples is discussed. The effect of the presence of large quantities of ammonium nitrate and sodium nitrate in WD samples on the determination of uranium is also discussed. The results are compared with those obtained by volumetry and X-ray fluorescence spectrometry for higher concentrations of uranium and by extraction–spectrophotometry (ethyl acetate–thiocyanate method) for lower concentrations. Relative standard deviation of 1% and 5% for high and low concentrations, respectively, were obtained, which are adequate as far as process stream samples are concerned. The compared results are in fair agreement. The problems associated with the determination of uranium in these process streams are discussed. Experimental results for 10 different process streams normally encountered in a uranium extraction plant are tabulated.

Keywords: Process streams; Spectrophotometry; Uranium

1. Introduction

Uranium dioxide powder is a starting material for the manufacture of fuel pellets which are widely used in nuclear power reactors. Its produc-

* Corresponding author. Fax: (91) 40-621-305; e-mail: jvm@nfc.hcu.emet.in.

PII S0039-9140(96)02046-2

tion involves various steps: leaching of uranium from the ore with sulphuric acid [1], purification using anion exchange [2], precipitation of uranium as magnesium diuranate (MDU), purification through solvent extraction [3], precipitation of uranium as ammonium diuranate (ADU) [4], drying, calcination and reduction to uranium dioxide. In our uranium extraction plant, MDU is dissolved in nitric acid and uranium is extracted with tri-*n*-butyl phosphate (TBP) in kerosene and after stripping is precipitated as ADU. In this process, one encounters various process streams such as uranyl nitrate slurry (UNS), uranyl nitrate feed (UNF), uranyl nitrate pure solution (UNPS), uranyl nitrate pure solution evaporated (UNPE), uranyl nitrate extract (UNE), uranyl nitrate lean solvent (UNLS), uranyl nitrate raffinate (UNR), uranyl nitrate raffinate cake (UNRC) and waste disposals (WD1 and WD2). The monitoring of the concentration of uranium in these process streams is essential, each for a different purpose. For example, the knowledge of concentration of uranium in UNR is important for evaluating the efficiency of extraction, in UNE for effective utilization of the extractant and in UNLS for the efficiency of stripping. Some of these process streams, such as UNS, UNF, UNR and UNRC, contain a host of impurities which originate from the eluate in the anion-exchange purification stage as it contains some of the impurities present in the ore and those picked up due to the addition of calcined dolamite to precipitate uranium as MDU. Thus, the determination of uranium in these process streams on a routine basis, covering a wide range of concentrations and without its separation from the impurities, by a single technique having the advantages of simplicity, rapidity, sensitivity, adequate accuracy and precision and cost effectiveness is highly desirable.

There are various techniques, such as gravimetry [5], volumetry [6a], fluorimetry [7], potentiometry [8] polarography [9], coulometry [10], X-ray fluorescence spectrometry (XRF) [11] and spectrophotometry [12,13], for the determination of uranium, spanning very high to very low concentrations. Gravimetric methods require, in general, the absence of or prior separation of interfering elements. Also, they are used for high concentrations of uranium and are time consuming. Volumetric methods involve a number of steps and the use of many chemicals. Fluorimetry, being a sensitive technique, is applicable to low levels of uranium. Electroanalytical techniques, in general, are not preferred on a routine basis. XRF, especially the wavelength-dispersive method, is not sensitive for estimations at low levels and is not cost effective.

Spectrophotometry is increasingly employed in process control owing to its simplicity and adaptability for automation [14,15]. Hence it was decided to exploit this technique for the present purpose. A study of the available information revealed that most of the spectrophotometric methods for low levels of uranium involve prior separation of uranium from impurities by solvent extraction and reduction of Fe(III) to Fe(II) to avoid its interference, followed by the addition of chromophoric reagents such as thiocyanate [16], hydrogen peroxide [17] or hexacyanoferrate(II) [18] to the organic phase. The methods for the determination of macro amounts of uranium in various mineral acids such as HCl [19] and HNO_3 [20] and the determination of uranium directly in TBP are applied mainly to pure solutions and to the extracts obtained with analytical reagent grade TBP [21a], respectively. Also, the information is scattered in various publications and does not emphasize the applicability of the methods to industrial solutions such as the process streams mentioned above. Hence a systematic study was undertaken to develop and standardize procedures for the determination of uranium, on a routine basis, in industrial solutions, where the concentration spans the range from 350 g l^{-1} to as low as 5 mg l^{-1}, using only a spectrophotometric technique.

For this purpose, the low molar absorptivity of the self-absorption of uranyl ion and the selectivity of Arsenazo III (3,6-bis[(arsenophenyl)azo]-4,5-dihydroxy-2,7-naphthalenedisulphonic acid) towards uranyl ion in 2–4 M HCl and the high molar extinction coefficient of the UO_2^{2+}–Arsenazo III complex were exploited for high and low concentrations of uranium, respectively.

2. Experimental

2.1. Reagents

All the reagents used were of analytical grade. Demineralized (DM) water was used for dilution wherever it is not specified. Phosphoric acid (1:1) was taken as a dilute acid.

To prepare 0.1% Arsenazo III solution, 0.1 g of Arsenazo III and 0.5 g of sodium acetate were dissolved in 100 ml of water. The solution was stored in an amber-glass bottle.

A standard solution of uranium was prepared as follows. Nuclear grade uranium metal turnings were degreased with carbon tetrachloride, pickled with 1:1 nitric acid and washed with 1:3 hydrochloric acid followed by DM water and finally with acetone. A weighed quantity (ca. 500 mg) of the cleaned uranium metal turnings were dissolved in nitric acid and evaporated to dryness. The residue was dissolved in water and diluted to 100 ml. This solution was used as a stock standard solution and the requisite working standard solutions were obtained by appropriate dilution.

2.2. Instrumentation

Absorption measurements were carried out on a Shimadzu UV-240 Graphicord UV–visible recording spectrophotometer. Matched glass cells of 1 cm path length were used. The baseline and digital absorbance readings were adjusted to 0.000 for a reagent blank before each set of measurements.

2.3. Procedures

The procedures for the various process stream samples is described under the respective headings. In all cases, the concentration of uranium in the sample was calculated by the method of standard additions against a reagent blank.

In the following samples, the absorbance of the final solution was measured at 420 nm for samples 1, 2 and 3(a) and at both 422 and 500 nm for samples 3(b) and 4.

(1) UNS/UNF. A 10 ml volume of the sample was pipetted into a 250 ml volumetric flask and diluted to volume. A portion of solution was centrifuged and to 20 ml of this solution 5 ml of dilute phosphoric acid were added and made up to 50 ml.

(2) UNPS/UNPE. To 5 ml of sample, 5 ml of dilute phosphoric acid were added and made up to 50 ml.

(3) UNE. Two different methods were followed in this case.

(a) Method 1. To 1 ml of sample, 5 ml of concentrated nitric acid and 2 ml of perchloric acid were added. The organic matter was destroyed completely by heating the mixture on a hot-plate, capable of achieving temperatures of about 200–250°C and provided with heat control, for about 30 min. The clear yellow solution, after cooling to room temperature, was transferred quantitatively into a 50 ml volumetric flask. To this solution, 5 ml of dilute phosphoric acid were added and made up to volume.

(b) Method 2. A 5 ml volume of sample was stripped with 50 ml of 1 M phosphoric acid and the aqueous phase was centrifuged for about 10 min on a REMI centrifuge (220/230 V a.c., 50 Hz) at 3500 rpm. The centrifuged solution was used for absorbance measurements.

(4) UNLS. A 10 ml volume of the sample was stripped with 20 ml of 1 M phosphoric acid and the aqueous phase was centrifuged for ca. 10 min and used for absorbance measurements.

In the following samples, the absorbance of the final solution was measured at 655 nm against a reagent blank. In the case of WD samples the reagent blank was prepared by taking 10 ml of the respective nitrate solution (100 g l^{-1} ammonium nitrate in the case of WD1, 250 g l^{-1} sodium nitrate in the case of WD2 samples) and 1 ml of sulphamic acid was added. After a few minutes about 5 ml of 4 M HCl followed by 2 ml of 0.1% Arsenazo III solution were added and diluted to 25 ml with 4 M HCl.

(5) UNR. To a 1 ml aliquot of the filtered sample in a 25 ml volumetric flask, 1 ml of sulphamic acid was added and after a few minutes about 5 ml of 4 M HCl followed by 2 ml of 0.1% Arsenazo 1II reagent were added and made up to volume with 4 M HCl.

(6) UNRC. The sample (as received) was accurately weighed and digested with 20 ml of concentrated nitric acid on a hot-plate (ca. 15 min). The digested slurry was transferred quantitatively into a 100 ml volumetric flask and diluted to volume and filtered. Taking 2 ml of filtrate, the procedure described for UNR was followed.

(7) Waste disposal (WD1 and WD2). The procedure followed was the same as that for UNR, but with a sample aliquot of 10 ml from a filtered solution of the sample.

An outline of the experimental procedure(s) for the outer methods follows for comparison of results.

2.3.1. Volumetric method [6b]

U(VI) in the sample was reduced to U(IV) in phosphoric acid medium using Fe(II). The excess of Fe(II) present in the solution was destroyed with a mixture of sulphamic acid and nitric acid in the presence of a Mo(VI) as catalyst. U(IV) was oxidized back to U(VI) in sulphuric acid medium. Uranium was determined by titrating the Fe(II) generated (which is quantitatively equivalent to uranium) with standard potassium dichromate solution using barium diphenylamine sulphonate as indicator.

2.3.2. X-ray fluorescence method [21b]

A PW 1404 wavelength-dispersive X-ray spectrometer (Philips, Eindhoven, The Netherlands) with X44 software was used for the determination of uranium concentration. In this method, the primary X-rays were generated from a rhodium target and an LiF_{220} crystal was used for the diffraction at a 2θ angle of 37.235°. Measurements were carried out by exposing standards and samples in a liquid sample cell with a Mylar film. The concentration of uranium in the sample was calculated using a calibration graph of concentration of uranium versus count rate. The necessary normalization was performed to avoid matrix interferences and the required dilutions were made to keep the uranium concentration within the linear dynamic range of the present system (uranium concentrations up to 30 g l^{-1}).

2.3.3. Extractive spectrophotometric method

In this method, the uranium present in the sample aliquot was extracted with ethyl acetate in the presence of aluminium nitrate as a salting-out agent followed by colour development with ammonium thiocyanate in ethanol–ethyl acetate medium. The interference from iron was avoided by reducing it to Fe(II) using tin(II) chloride.

3. Results and discussion

A typical chemical analysis of MDU is given in Table 1. It is clear that MDU contains a host of impurities. These impurities are present in some of the process streams such as UNS, UNF, UNR and UNRC, and silica and iron become problematic or cause serious interference during the determination of uranium in these samples. Silica present as suspended particles in solution and iron present as coloured complexes lead to positive errors.

The flow sheet for the extraction process of uranium with the sampling points for the various process streams is shown in Fig. 1. The typical ranges of concentration of uranium and free nitric acid in these streams are given in Table 2. The high concentrations of uranium in UNS, UNF, UNPS, UNPE, UNE require dilution. Although it appears to involve a dilution error, especially in the case of UNS/UNF samples, calculations revealed that the error is within the precision. It may be of relevance to note that the same degree

Table 1
Typical analysis of magnesium diuranate

Compound/ element	Concentration (%, w/w)	Compound/ element	Concentration (%, w/w)
U_3O_6	68.6	P_2O_5	0.06
Cl^-	0.09	CuO	0.004
F^-	0.02	Na	2.6
SO_4^{2-}	1.2	V_2O_5	0.03
CO_3^{2-}	1.6	MoO_3	<0.01
Fe_2O_3	0.44	As	<0.01
SiO_2	4.1	ThO_2	0.005
CaO	0.90	Acid insolubles	4.6
MgO	10.3	Moisture	5.4

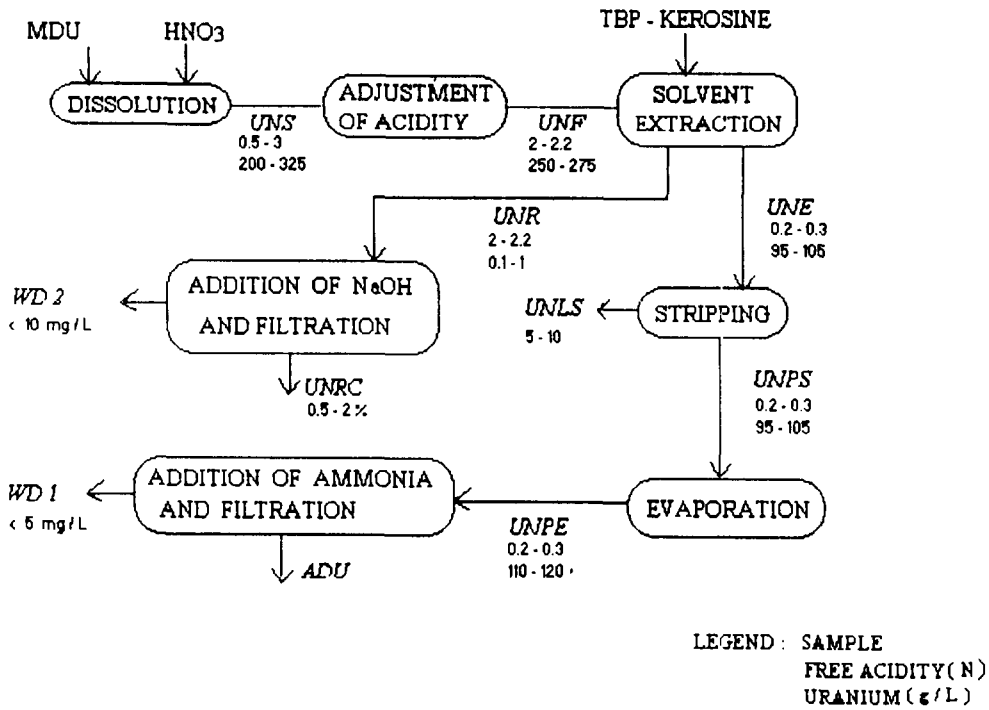

Fig. 1. Flow sheet of uranium extraction process.

of dilution is involved in the other alternative techniques such as XRF and volumetry.

The self-absorption of uranium is used for its determination after removing the interferences due to nitrate ions and other impurities such as iron and silica if they are present in the sample (Table 3). Nitrate ions do not interfere at 420 nm, as they absorb below 350 nm. While uranyl ions are known to form a series of nitrate complexes depending on the nitric acid concentration, each having a different characteristic absorption spectrum [22], it appears that the variations in the free nitric acid concentration in a sample affect the absorbance of uranium. However, the nitric acid concentration decreases to less than 0.1 M on dilution of the sample and the absorbance remains unaffected. This is confirmed by the invariance of absorbance of uranium at this wavelength in its standard solutions in different concentrations of nitric acid up to 0.5 M.

Table 2
Typical range of concentrations of uranium and free acidities in various process streams

Process	Concentration stream ($g\ l^{-1}$)	Free nitric of uraniumacid (M)
UNS	350–375	0.5–3.0
UNF	240–300	2.0–2.5
UNPS	90–110	0.2–0.3
UNPE	115–145	0.3–0.5
UNE	110–120	–
UNLS	6–12	–
UNR	0.1–1.5	2–3
UNRC	0.1–1.5	–
WD1	0.01–0.04	–
WD2	0.005–0.01	–

The concentrations of iron in UNS and UNF samples are 2.5–3 and 1.6–2 $g\ l^{-1}$, respectively. Even after dilution, its interference is significant and causes a positive bias of as high as 10% in terms of the concentration of uranium. However, in the presence of phosphoric acid, Fe(III) is effectively masked by phosphate, thus eliminating its interference. Although UNPS and UNPE do not contain iron, phosphoric acid is added even to

Table 3
Typical concentrations of various interfering impurities in different process streams

Process stream	Concentration of impurity (g l^{-1})				
	Fe	SiO_2	Ca	Mg	Th
UNS	3	25	37	4	0.03
UNF	2	19	28	3	0.02
UNPS	0.01	0.003	0.025	0.01	0.003
UNPE	0.01	0.003	0.025	0.025	0.003
UNR	3	Traces	9	22	0.001
UNRC soln.	0.5	Traces	2	5	0.0002
WD1	Ammonium nitrate:			100–120	
WD2	Sodium nitrate:			250–300	

Calcium and magnesium do not interfere in a spectrophotometric determination as they do not possess any colour and do not form coloured complexes with the reagents used. However, it puts a restriction on the method that the colour development should not be in the (sensitive) pH region. In the case of UNE and UNLS samples, the colour imparted due to the repetitive use of 35% TBP (in kerosine) in a counter-current extraction system causes interference in the determination of uranium.

these samples in order to maintain a uniform procedure for the determination of uranium on a routine basis.

The presence of undissolved silica in UNS and UNF samples is removed by filtration through Whatman filter-paper (No. 540, pore diameter 1.6 μm). This can even be achieved by centrifugation. The form of silica in these samples is such that its presence in the solution as undissolved material can easily be identified by simple visual inspection of the solution after filtration/centrifugation. Therefore, no chemical estimation is necessary for its identification. The concentration of dissolved silica in these samples was observed to be about 0.5 g l^{-1}. This was estimated by a gravimetric method involving dehydration of silica followed by hydrofluorination. However, for the determination of uranium by the present spectrophotometric method, the presence of dissolved silica does not cause any interference and need not be determined. Comparison of the results obtained by the present method with those obtained by volumetry and XRF for UNS, UNF, UNPS and UNPE show excellent agreement (Tables 4–7).

Table 4
Comparison of results obtained for UNS samples (values in g l^{-1})

Sample code	Present method	Volumetry	XRF
UNS-11B	341	342	341
UNS-11C	326	326	324
UNS-952	249	249	249
UNS-971	326	326	325
UNS-11D	318	315	315
UNS-522	254	255	255
UNS-955	374	374	373
UNS-954	356	356	357
UNS-951	319	319	320

Measurement of the absorbance of uranium directly in organic streams such as UNE/UNLS is not possible because of the serious interference from the coloration in these samples due to the prolonged use of TBP–kerosene in nitric acid. Therefore, pre-separation of uranium by stripping or destruction of organic matter becomes necessary. Normally, the estimation is done by redox titrimetry after multi-stage stripping of uranium with a solution of sodium carbonate [23]. This method is tedious and undesirable on routine basis. Alternatively, in one case, the organic matter is completely destroyed by non-hazardous wet chemical oxidation of organic matter using perchloric acid in combination with nitric acid [24]. At about 86°C, nitric acid boils, forming a black solution. On further heating (at about

Table 5
Comparison of results obtained for UNF (values in g l^{-1})

Sample code	Present method	XRF	Volumetry
UNF-510	296	295	296
UNF-952	249	249	249
UNF-520	271	272	270
UNF-535	258	261	260
UNF-512	178	178	179
UNF-513	246	248	247
UNF-516	281	282	283
UNF-518	287	287	288
UNF-521	251	253	251
UNF-599	253	253	254

Table 6
Comparison of results obtained for UNPS (values in g l^{-1})

Sample code	Present method	%RF	Volumetry
UNPS-77	125	128	126
UNPS-98	115	115	114
UNPS-105	93	91	92
UNPS-117	90	83	90
UNPS-134	85	89	86
UNPS-135	89	90	89
UNPS-157	92	94	93
UNPS-158	94	95	94
UNPS-164	96	96	95
UNPS-165	101	101	100

204°C), the boiling perchloric acid oxidizes carbon and the solution becomes clear yellow. The clear solution is taken for absorption measurements. The results obtained for the UNE samples by the present method are in good agreement with those obtained by volumetry (Table 8). However, in UNLS samples, the low concentration of uranium (6–12 g l^{-1}) demands a large sample aliquot (ca. 10 ml) and this procedure therefore becomes cumbersome. In the second case, the sample is stripped with 1 M phosphoric acid and the absorbance of the centrifuged aqueous phase is measured at the wavelength of interest.

Single stripping of the organic phase with 1 M phosphoric acid has been observed to yield about 99% of uranium in the aqueous phase. It has been observed that the efficiency of stripping is independent of the concentration of uranium in the range of concentrations of interest. This was verified by taking different synthetic standards in 35% TBP (in kerosene) having uranium concentrations between 100–130 g l^{-1} and 5–15 g l^{-1} and stripping with a suitable volume of 1 M phosphoric acid, keeping the organic to aqueous ratios at 1:10 and 1:2, respectively, as is the case with UNE and UNLS. In both these cases excellent linearity was obtained. Therefore, once the calibration is established, the amount of uranium that has been actually stripped into the aqueous phase becomes irrelevant as far as the determination of uranium is concerned.

Table 7
Comparison of results obtained for UNPE (values in g l^{-1})

Sample code	Present method	Volumetry
UNPE-407	115	116
UNPE-406	115	116
UNPE-403	123	124
UNPE-402	132	132
UNPE-401	114	113
UNPE-400	130	131
UNPE-399	143	143
UNPE-P1	125	125
UNPE-P2	131	130
UNPE-P3	112	112

Table 8
Comparison of results obtained for UNE with those by non-hazardous wet chemical oxidation method (values in g l^{-1})

Sample code	Present method	Volumetry
EXT-411	110	112
EXT-409	112	112
EXT-408	113	115
EXT-407	115	113
EXT-406	117	119
EXT-405	119	120
EXT-403	111	113
EXT-402	114	114
EXT-400	124	125
EXT-399	116	115

The baseline in the absorption spectrum of the aqueous phase obtained by stripping a UNLS sample with 1 M phosphoric acid has been shifted considerably. This shift was thought to be due to the uniform dispersion of traces of organic matter in the aqueous phase. Interestingly, however, such a baseline shift was not observed in the absorption spectrum of an aqueous phase obtained by stripping a synthetic UNLS sample (prepared using fresh 35% TBP (in kerosene)) with 1 M phosphoric acid. It is observed that the prolonged use of 35% TBP in a counter-current extraction system of a uranium extraction plant imparts a characteristic colour due to nitration, and when the sample is stripped with phosphoric acid this colour is slightly carried away into the aqueous phase, which is responsible for the considerable absorbance over a wide range of wavelength re-

gion and hence for the baseline shift. Also, careful visual observation of the aqueous phase reveals slight haziness in the solution which also must be contributing towards the baseline shift. It was thought that centrifugation of the aqueous phase might help in the removal of the haziness and eliminate the baseline shift. Centrifugation of the aqueous phase did make the solution clear and the magnitude of the baseline shift also decreased significantly (ca. 70%). However, the baseline shift did not disappear completely even after prolonged centrifugation; rather, it remained constant at a particular value irrespective of the centrifugation time. This led us to conclude that the shift is due more to physical reasons.

Visual inspection of the spectrum of the uncentrifuged aqueous phase revealed that in the wavelength region 325–500 nm, the whole spectrum is shifted above the baseline and within this wavelength region at no wavelength is the absorbance less than than at 500 nm. Under these circumstances, it was thought that it is justified to subtract the absorbance at 500 nm from that at 422 nm in order to correct it for the additional absorbance due to the baseline shift and to obtain the actual absorbance of uranium.

The absorption spectra of the uncentrifuged and centrifuged aqueous phase obtained by stripping a UNLS sample with 1 M phosphoric acid are shown in Fig. 2. The molar absorptivity ($\varepsilon_{422\ nm}$) of uranyl ion in 1 M phosphoric acid under the experimental conditions is 16.4 l mol^{-1} cm^{-1}. The concentrations of uranium calculated based on the corrected absorbances agree well with those obtained by volumetry (Tables 9 and 10).

The concentration of uranium in UNR, UNRC and WD samples is very low (Table 2) and hence its self-absorption cannot serve the purpose for its determination. Also, the presence of the main interfering impurity iron, both in UNR and in the solution obtained from UNRC, in high concentrations (2–3 g l^{-1}) and large amounts of ammonium nitrate (100–120 g l^{-1}) in WD1 and sodium nitrate (250–300 g l^{-1}) in WD2 samples lead to further complications. Therefore, the use of a suitable chromophoric agent becomes mandatory.

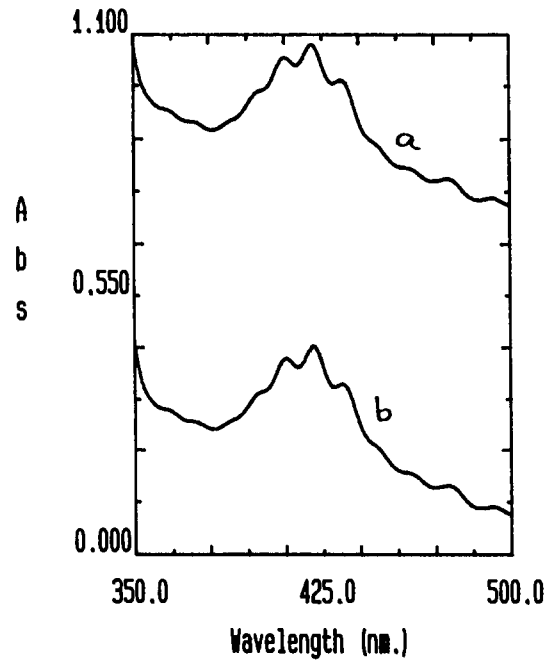

Fig. 2. Absorption spectrum of (a) uncentrifuged and (b) centrifuged aqueous phase. Extraction carried out with 1 M phosphoric acid; [UO_2^{2+}] = 10 g l^{-1}.

The yellow H_2O_2–UO_2^{2+} complex has been used [25] for the determination of uranium without a prior separation, where the interference from iron is avoided by formation of a violet Fe^{3+}–H_2O_2–EDTA complex in an alkaline medium [26]. However, when this procedure was attempted for UNR and UNRC samples, the authors encountered violent decomposition of hydrogen peroxide, presumably due to impurities.

Table 9
Comparison of results obtained for UNE estimated by stripping method (values in g l^{-1})

Sample code	Present method	Volumetry
EXT-701	116	115
EXT-702	113	109
EXT-678	112	114
EXT-679	114	115
EXT-733	112	111
EXT-741	111	113
EXT-747	113	112

Table 10
Comparison of results obtained for UNLS (values in g l^{-1})

Sample code	Present method	Volumetry
UNLS-50	10.6	10.7
UNLS	10.4	10.0
UNLS-71	11.1	11.1
UNLS-111	11.0	11.1
UNLS-112	10.5	10.7
UNLS-140	10.8	10.7
UNLS-159	10.5	10.4
UNLS-196	9.9	9.8
UNLS-219	10.2	10.7

It has been reported that Arsenazo III is the most sensitive reagent [27] for the determination of uranyl ions and quantitative work is best carried out at pH 7–8, but serious interferences are caused by Th^{4+}, Zr^{4+}, Fe^{3+}, rare earths, etc. [28–30]. Hence the determination of uranium under these conditions is not possible for samples of UNR and UNRC. Photometric determinations in strong acid media are preferable for these samples because (i) difficulties caused by partial hydrolysis of ions are eliminated, (ii) careful maintenance of pH is not required and (iii) the selectivity can be increased. It is also known that in HCl medium Arsenazo III reacts selectively with uranyl ions even in the presence of iron and rare earths [31]. Moreover, the interference from Th^{4+}, Zr^{4+}, etc., is insignificant in these samples owing to their very low concentrations compared with uranium. The concentrations of thorium in UNR and UNRC samples are observed to be in the range 1–2 mg l^{-1} and 0.001–0.005% (w/w), respectively, and zirconium was found only in traces. Since the reaction of uranyl ions with Arsenazo III in acid solutions gives rise to the formation of two complexes of the type ML, their proportions being dependent upon acidity [32], the determination is carried out in 4 M HCl using Arsenazo III without any prior separation of uranium.

The absorption spectra of free Arsenazo III and UO_2^{2+}–Arsenazo III in 4 M HCl are given in Fig. 3. The overcompensation due to the absorption of free Arsenazo III at the wavelength of interest (655 nm) is negligibly small.

The violet–blue colour of the UO_2^{2+}–Arsenazo III complex fades rapidly when developed with a WD sample directly. This cannot be attributed to the presence of large quantities of nitrate in these samples because the same complex in 5–6 M HNO_3 has been used for the determination of uranium [33]. As the presence of nitrite in these samples was detected in our studies on the determination of uranium in WD samples by polarography, the fading of the colour of the complex is attributed to nitrite. These WD samples, along with UNR and UNRC, contain nitrite picked up from the commercial nitric acid used in the process. Therefore, removal of nitrite becomes an essential step in the analysis of these samples.

It is known [34] that nitrite can be quantitatively reduced to nitrogen with sulphamic acid and the reduction is completed in 2–3 min at room temperature. The reaction can be written as

$$NO_2^- + HSO_3NH_2 \rightarrow N_2 + HSO_4^- + H_2O$$

Under these conditions, nitrates do not react. Nitrite is destroyed by the addition of a small

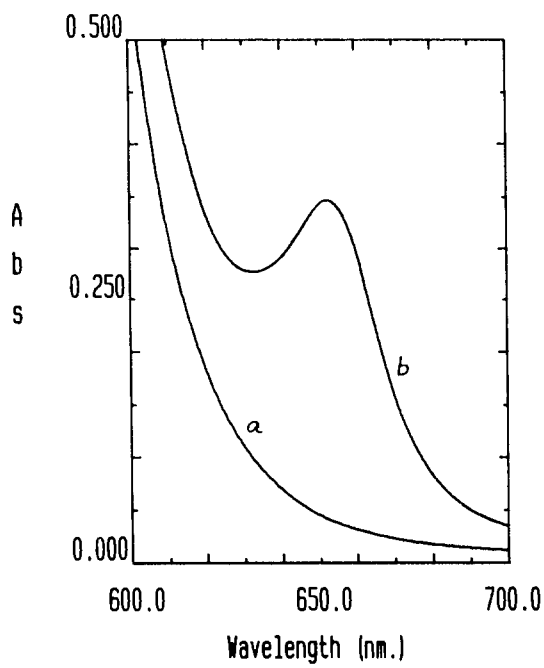

Fig. 3. Absorption spectra in 4 M HCl: (a) free Arsenazo III (against 4 M HCl); (b) U(VI) with Arsenazo III (against reagent blank). $[UO_2^{2+}] = 1.681 \times 10^{-5}$ mol l^{-1}.

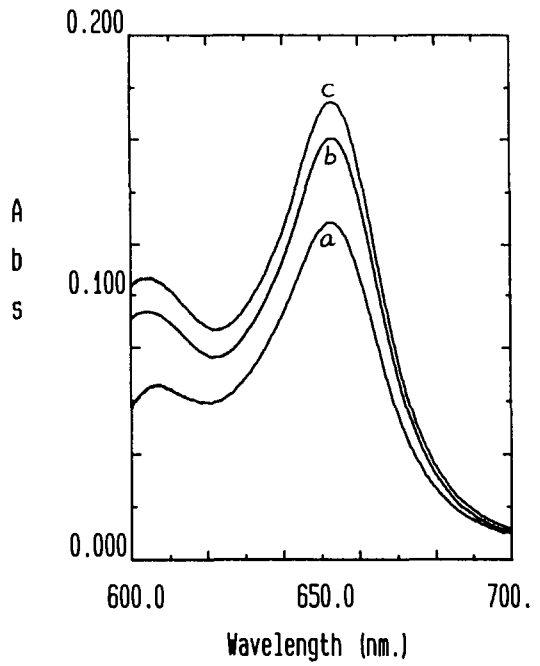

Fig. 4. Absorption spectra in 2 M HCl: U(VI) with Arsenazo III (against reagent blank), (a) without nitrate and (b) and (c) in the presence of 100 g l^{-1} of ammonium nitrate and sodium nitrate, respectively.

quantity of sulphamic acid prior to the addition of Arsenazo III. As it was observed that the action of sulphamic acid is better at lower acidity, it is preferable to add it directly to the sample before addition of 4 M HCl. Considerable variations in the concentration of sulphamic acid did not affect the absorbance of the complex significantly at the wavelength of interest.

It was observed that the presence of large quantities of nitrate enhance the absorbance of the complex (Fig. 4). This could be attributed to the replacement of H_2O in the primary coordination sphere of UO_2^{2+} by nitrate, leading to a slight change in the chemical environment in the resulting complexes, which have considerable differences in their molar absorptivities. The enhancement was quantified by measuring the absorbance of the UO_2^{2+}–Arsenazo III complex in the presence of various amounts of nitrate. Interestingly, the absorbance of the complex increases linearly with increase in the content of nitrate for a particular concentration of uranium. Also, the percentage of enhancement for the same concentration of nitrate ion is greater with sodium nitrate than with ammonium nitrate. The variation of the absorbance of the complex with variation in the amounts of nitrate (NH_4NO_3 and $NaNO_3$) is shown in Fig. 5. The considerable difference in the extent of enhancement can be well understood in terms of the availability of more free nitrate ion for complexation in the former, which is a salt of a strong acid (HNO_3) and a strong base (NaOH), than in the case of the latter, which is a salt of a strong acid (HNO_3) and a weak base (NH_4OH). As more nitrate ion is available, the amount of a particular complex containing nitrate ion in the primary coordination sphere may be increasing and may be responsible for the linear rise in the observed absorbance value with increasing nitrate concentration. This situation may be better explained by the following simple equation:

$$[UO_2(H_2O)_6]^{2+} + R + nNO_3^- \rightarrow [UO_2(H_2O)_{6-n}(NO_3)_n]R + nH_2O$$

where R is Arsenazo III. The observed absorbance depends on the amount of the complex $[UO_2(H_2O)_{6-n}(NO_3)_n]R$ formed in the solution, which in turn depends on the quantity of nitrate available in the solution. The fact that the pres-

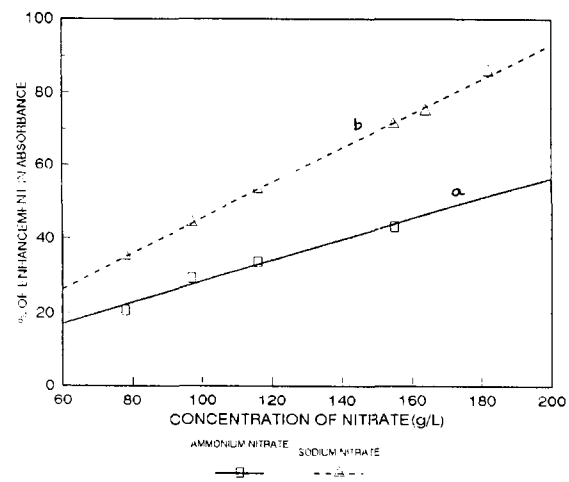

Fig. 5. Variation of absorbance of UO_2^{2+}–arsenazo III complex with varying amounts of (a) ammonium nitrate and (b) sodium nitrate.

Table 11
Comparison of results obtained for UNR (values in g l^{-1})

Sample code	Present method	Ethyl acetate–thiocyanate method
UNR-500	0.47	0.46
UNR-544	2.34	2.41
UNR-545	1.59	1.66
UNR-549	0.38	0.43
UNR-573	0.84	0.85
UNR-574	0.65	0.60
UNR-627	0.72	0.83
UNR-628	0.25	0.35
UNR-645	0.82	0.93
UNR-646	1.25	1.34

ence of nitrate enhances the absorbance of the UO_2^{2+}–Arsenazo III complex can be exploited for the estimation of the content of nitrate (ammonium or sodium salt) in waste disposal samples, which is also a required parameter to be analysed on a routine basis [34].

The results obtained for UNR/UNRC samples by the present method and those obtained by extraction–spectrophotometry are in fair agreement (Tables 11 and 12). Also, the estimated and added quantities of uranium in the case of the two types of waste disposal samples compare well (Tables 13 and 14). The overall analytical scheme for the determination of uranium in the entire range of process stream samples is shown in Fig. 6.

Table 12
Comparison of results obtained for UNRC (values in %)

Sample code	Present method	Ethyl acetate–thiocyanate method
UNRC-14	0.64	0.60
UNRC-15	0.32	0.27
UNRC-16	0.72	0.68
UNRC-17	0.43	0.39
UNRC-28	1.17	1.09
UNRC-161	0.43	0.38
UNRC-162	0.99	0.95
UNRC-170	0.24	0.20
UNRC-186	0.17	0.16
UNRC-193	0.54	0.50
UNRC-222	1.04	1.01

Table 13
Recovery of uranium in waste disposal samples containing ammonium nitrate

Sample No.	Quantity of uranium (mg l^{-1})	
	Added	Found
1	0	1.9
2	1	3.2
3	2	4.1
4	3	5
5	4	5.9
6	5	7.2
7	6	8.1
8	7	8.8

Tables 13 and 14 show the concentration of uranium determined in the waste disposal samples. These were generated to observe the applicability of the present method to different ranges of concentration of uranium containing the sample matrix (especially either large amounts of ammonium nitrate or sodium nitrate). These samples were prepared by taking known amounts of uranium in a beaker followed by evaporation to near dryness and finally making the volume up to 500 ml with a waste disposal sample solution.

The Arsenazo III method for low levels of uranium has the advantage of direct determination of uranium in the presence of impurities, especially iron. It does not involve steps such as solvent extraction and reduction, unlike the well established ethyl acetate–thiocyanate method, which is usually employed for low levels of uranium. Also, the present method is relatively much more sensitive.

Table 14
Recovery of uranium in waste disposal samples containing sodium nitrate

Sample No.	Quantity of uranium (mg l^{-1})	
	Added	Found
1	0	3.4
2	1	4.6
3	2	5.5
4	3	6.5
5	4	7.6
6	5	8.6
7	6	9.5
8	7	10.3

See footnote to Table 13.

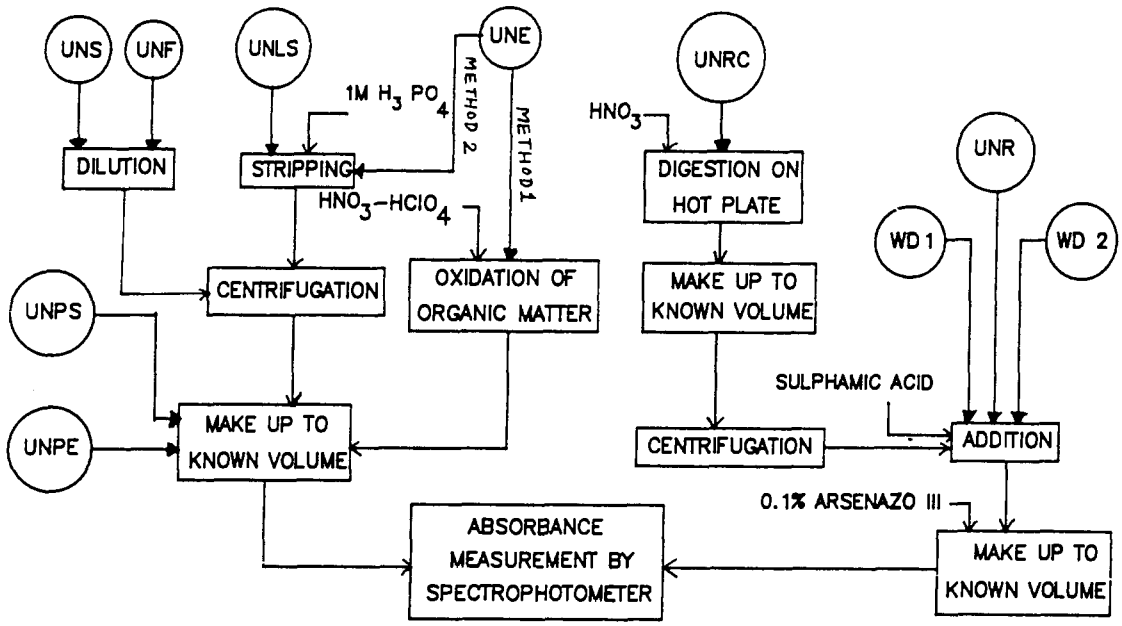

Fig. 6. Analytical scheme for determination of uranium.

Acknowledgement

The authors are grateful to Shri N. Saratchandran, DCE(QA), for his encouragement in the present study.

References

[1] G. Boutonnet, Nucl. Eng. Int., 20 (1975) 100.
[2] R.C. Merritt, The Extractive Metallurgy of Uranium, Colorado School of Mines Research Institute, USAEC, Golden, CO, 1971.
[3] H.A.C. McKay, Proc. Int. Conf. Peaceful Uses of Atomic Energy, Geneva, 7 (1956) 314.
[4] W.T. Bourns and L.C. Watson, Report CRCE-716, Part I, Atomic Energy of Canada, Chalk River, Ontario, 1958.
[5] P.L. Lopez-de-Alba, S. Gonzalez and J. Gomez Lara, J. Radioanal. Nucl. Chem., 136 (1989) 203.
[6a] A.S. Al Ammar and H.M. Basheer, J. Radioanal. Nucl. Chem., 173 (1993) 435.
[6b] W. Davies and W. Gray, Talanta, 11, (1964) 1203.
[7] K.B. Hong, K.W. Jung and K.H. Jung, Talanta, 36 (1989) 1095.
[8] M. Anwar and D. Mohammad, J. Radioanal. Nucl. Chem., 134 (1989) 45.
[9] M. Mlakar and M. Branica, Anal. Chim. Acta, 221 (1989) 279.
[10] G.L. Booman, W.B. Holbrook and J.E. Rein, Anal. Chem., 29 (1957) 219.
[11] A.W. McMahon, Sci. Total Environ., 130 (1993) 285.
[12] J.L. Perez Pavon, B. Moreno Cordero, E. Rodriguez Garcia and J. Hernandez Mendez, Anal. Chim. Acta, 230 (1990) 217.
[13] W. Jianhua and H. Ronghuan, Chem. Anal. (Warsaw), 38 (1993) 497.
[14] W.F. Maddams, UV Spectrom. Group. Bull., 10 (1982) 85.
[15] D.D. Jackson, D.J. Hodgkins, R.M. Hollen and J.E. Rein, Report LA-6091, Los Alamos Scientific Laboratory, Los Alamos, 1976.
[16] S.P. Bag, A.B. Chatterjee, A.K. Chakrabarti and P.R. Chakraborty, Talanta, 29 (1982) 526.
[17] W.B. Smith and J. Drewry, Analyst, 86 (1961) 178.
[18] S. Abe and H. Weisz, Mikrochim. Acta, (1970) 550.
[19] C.M. Callahan, Anal. Chem., 33 (1961) 1660.
[20] Cf. Nikitina, J. Radioanal. Chem., 80 (1983) 183.
[21a] J.A. Perez Bustamante and F. Polomares Delgado, Analyst, 96 (1971) 407.
[21b] R. Narayana Swamy, B. Gopalan, H.R. Ravindra and G. Radhakrishna, National Workshop on X-Ray Emission Spectrometry held at IGCAR, Kalpakkam, India, Report No. 108C, 1989.
[22] W.J. Maeck, G.L. Booman, M.C. Elliott and J.E. Rein, Anal. Chem., 31 (1959) 1130.
[23] K. Bril and S. Holzer, Anal. Chem., 33 (1961) 55.
[24] L. Silverman, The Determination of Impurities in Nuclear Grade Sodium Metal, Pergamon Press, Oxford, 1971, p. 32.

[25] C.J. Rodden and J.C. Warf, in C.J. Rodden (Ed.), Analytical Chemistry of the Manhattan Project, National Nuclear Energy Series, Div. VIII, Vol. 1, McGraw-Hill, New York, 1950, pp. 37 and 72.
[26] K.L. Cheng and P. Lott, Anal. Chem., 28 (1956) 462.
[27] V.F. Luk'yanov, E.P. Duderova, T.E. Barabanova, E.F. Novak, I.A. Stepanova and N.F. Shcherbakova, Zh. Anal. Khim., 44 (1989) 2269.
[28] R. Keil, Fresenius' Z. Anal. Chem., 297 (1979) 384.
[29] C. Liu, Yankuang Ceshu, 7 (1988) 192.
[30] F. Bosch Reig, J. Martinez Calatayud, M.C. Garcia Alvareg Coque and M.C. Pascual Marti, Analyst, 108 (1983) 99.
[31] F.W.E. Strelow and T.N. van der Walt, Talanta, 26 (1979) 537.
[32] J. Borak, Z. Solvak and J. Fisher, Talanta, 17 (1970) 215.
[33] P.R.V. Rao and S.K. Patil, J. Radioanal. Chem., 42 (1978) 399.
[34] S.S.M. Hassan, Anal. Chim. Acta, 58 (1972) 480.

ELSEVIER

Talanta 44 (1997) 297–303

Talanta

Short communication

A selective catalytic voltammetric determination of vitamin C in pharmaceutical preparations and complex matrices of fresh fruit juices

M.H. Pournaghi-Azar*, R. Ojani

Electroanalytical Chemistry Laboratory, Faculty of Chemistry, University of Tabriz, Tabriz, Iran

Received 8 November 1995; revised 4 April 1996; re-revised 20 May 1996; accepted 20 May 1996

Abstract

A simple, selective and precise voltammetric method for the determination of ascorbic acid in pharmaceutical preparations and fresh fruit juices—complex matrices containing various reducing compounds—is described. The method is based on the electrocatalytic oxidation of ascorbic acid in homogeneous solution using electrogenerated ferriciniumcarboxylic acid as mediator. The pH and mediator concentration affecting the performance of the electrocatalytic oxidation of the analyte were optimized. The method was applied to determine vitamin C in deeply coloured, viscous and turbid fruit juice samples with ascorbic acid contents ranging from 15–45 mg per 100 ml, without further dilution, concentration or other pre-treatment of the samples. The amount of mediator used varied depending on the ascorbic acid concentration in the samples. The method was also used for pharmaceutical analysis using a calibration graph. For fruit juice samples the standard addition technique was adopted to prevent the matrix affecting the accuracy of the determination. The relative standard deviation for the analysis of vitamin C in fruit juices ranged from 1.5–5%. The reliability of the method was established by parallel determination against the official methods.

Keywords: Ascorbic acid; Catalytic voltammetry; Fruit juices; Pharmaceutical analysis; Vitamin C

1. Introduction

Ascorbic acid occurs naturally in fruits and vegetables. All current methods for the determination of ascorbic acid take advantage of its redox properties: it can be easily oxidized to dehydroascorbic acid. Some oxidimetric titration methods for the determination of ascorbic acid involve titration with an oxidizing agent such as iodine [1], 2,6-dichlorophenolindophenol [2] or *N*-bromosuccinimide [3]. However, the ascorbic acid concentration can be overestimated if a background determination is not carried out to ac-

* Corresponding author.

PII S0039-9140(96)02003-6

count for interfering compounds. Coloured fruit juices are hard to work with. Some voltammetric methods using conventional electrodes [4–6], a microdisc electrode [7] and a microband electrode [8] have been reported. These methods suffer from interference, loss of response with repeated use because of electrode fouling by oxidation products or a lack of generality. Ascorbic acid often has to be quantified in complicated matrices where the exploitation of heterogeneous as well as homogeneous electrocatalytic oxidation might be advantageous. This provides selectivity and prevents the fouling of the electrode surface. Some research works have been reported in this context [9–16]. A method using a flow-injection system with square-wave voltammetric detection was also reported [17].

Recently we [18] have demonstrated that a polypyrrole/hexacyanoferrate(II)-modified glassy carbon electrode can be used for the catalytic determination of ascorbic acid in buffered solution at pH 4. The method was used for pharmaceutical analysis but was not suitable for the determination of vitamin C in fruit juices. In addition we [19] have reported that ascorbic acid can be oxidized catalytically in homogeneous solution by some electrogenerated ferricinium derivatives in buffered solution at pH 4. The method was used successfully for the simultaneous determination of ascorbic acid and dopamine in the same sample.

The purpose of this communication is to report the results of the voltammetric determination of vitamin C in pharmaceutical preparations and fruit juices exploiting the catalytic oxidation of ascorbic acid in homogeneous solution by electrogenerated ferriciniumcarboxylic acid.

2. Experimental

2.1. Reagents and chemicals

The solvent used for electrochemical studies was doubly-distilled water. Lithium or sodium perchlorate from Fluka was used as supporting electrolyte. The ferrocenecarboxylic acid was from Janssen and was used without further purification. The following solutions were used: ascorbic acid (Sigma): a stock solution was prepared in 0.5% citric acid to give a final concentration of 0.01 M and stored in a refrigerator; 3% m/v methaphosphoric acid–8% v/v acetic acid solution (HPO_3–HOAc); 2,6-dichlorophenolindophenol solution: 0.25 g l^{-1} 2,6-dichlorphenolindophenol (sodium salt) and 0.25 g l^{-1} sodium hydrogen carbonate; iodine solution, 0.05 M; starch solution, 1% m/m; thiosulphate solution, 0.01 M. All other reagents were of analytical grade. The solutions were bubbled with N_2 gas (99.999%) and kept under a nitrogen atmosphere during the electrochemical experiments.

2.2. Pharmaceutical preparations

The following commercial ascorbic acid formulations available from local sources were subjected to the described analytical procedure:

(1) tablets containing ascorbic acid as a single component (chewable tablets);

(2) tablets containing sodium carbonate combined with ascorbic acid (effervescent tablets);

(3) powdered vitamin C;

(4) ampoules containing ascorbic acid as the single component;

(5) multivitamin capsules containing vitamins A, B complex, D_2 and E, nicotinamide, calcium pantothenate, and folic acid together with minerals (Fe^{2+}, Ca^{2+}, Mg^{2+}, Mn^{2+}, Cu^{2+}, Zn^{2+} and Mo^{2+});

(6) multivitamin tablets containing vitamins A, B complex, D_2 and E, nicotinamide, calcium panthothenate, folic acid.

2.3. Instrumentation

The electrochemical experiments were carried out using an EG&G potentiostat/galvanostat model 273 coupled with an IBM personal computer connected to an Epson model FX-850 printer. A conventional three-electrode cell thermostatted at 25 ± 0.1°C with calomel electrode as reference electrode, a platinum wire as auxiliary electrode and a glassy carbon disk as working electrode ($A = 0.126$ cm^2 from EG&G) was used. A pH-meter model 654 (Metrohm) was used. The

working electrode was polished with alumina powder (0.05 μm) and then washed with water and acetone in turn before each voltammetric measurement.

2.4. Procedures

2.4.1. For pharmaceutical preparations

2.4.1.1. Vitamin C tablets, capsules or powders.

An accurately weighed portion of finely powdered sample equivalent to about 100 mg of ascorbic acid was transferred to a 10 ml assay tube and ascorbic acid was extracted with two 5 ml portions of 0.5% citric acid in bidistilled water. The extracts were combined in a 50 ml flask and diluted to volume. A 1 ml portion of extract was diluted with 10 ml of glycine buffer pH 4, containing 0.1 M $LiClO_4$ and 0.1 mM ferrocenecarboxylic acid, in a voltammetric cell and a cyclic voltammogram was recorded using a well polished glassy carbon (GC) electrode. The amount of ascorbic acid was determined by means of a calibration graph.

2.4.1.2. Injection.

An accurate ampoule volume equivalent to about 100 mg of ascorbic acid was transferred to a 50 ml flask and diluted to volume with 0.5% citric acid solution. A 1 ml portion of the solution was diluted in a voltammetric cell to 10 ml as described for tablets and the cyclic voltammogram was recorded using the GC electrode.

2.4.2. For fruit juices

Fresh juice—orange, sweet lemon, lime and grapefruit—was obtained by squeezing the fruit between two glass beakers to avoid contamination from metal ions which could interfere in the determinations. Tomato, strawberry and kiwi juices were obtained using a hand squeezer (polymer material). The juices obtained were filtered into a beaker, a 10 ml portion of the filtrate was transferred into an electrochemical cell, the required amount of $LiClO_4$ (0.1 M) was added as supporting electrolyte, the solution was buffered by direct dissolution of glycine (0.5 M) and the pH was adjusted with a concentrated solution of sodium hydroxide. The concentration of ferrocenecarboxylic acid was optimized for each sample solution in order to record a full catalytic voltammogram (see Section 3). For the determination of ascorbic acid in the sample the standard addition technique was used.

2.4.3. Iodine titration method

A 0.05 M iodine solution was standardized in the usual way with a primary standard of As_2O_3 or titrisol thiosulphate solution. For pharmaceutical analysis an iodimetric procedure described in the US Pharmacopeia (USP) was used [20].

2.4.4. 2,6-Dichlorophenolindophenol (DCPIP) titration method [2]

The indophenol solution was standardized by titration with 2.0 ml of standard ascorbic acid solution and 5 ml of HPO_3–HOAc solution to the end-point (a persistent rosy-pink colour). The consumption of the blank was determined by titrating indophenol solution with 7 ml of HPO_3–HOAc solution plus a given amount of water equivalent to the volume of indophenol solution used in the previous standardization titration.

For sample titration, 100 ml of juice was mixed with an equal volume of HPO_3–HOAc solution before filtering. A volume of the filtrate equivalent to about 250 mg of ascorbic acid was then titrated with indophenol solution using the same procedure as described above, including the titration of the blank.

3. Results and discussion

3.1. Primary investigations

We [19] have reported previously that some electrogenerated ferricinium derivatives are able to catalyse the electrochemical oxidation of ascorbic acid in buffered aqueous solutions at pH 4–5 via a homogeneous process when the ferrocene derivatives are present in dissolved forms (see Scheme 1).

$$\mathrm{FC\ (ferrocene)} \rightleftharpoons \mathrm{FC^{+}\ (ferricinium)} + \mathrm{e}$$

$$\mathrm{2FC^{+} + H_2A\ (ascorbic\ acid)} \rightarrow \mathrm{2FC + A\ (dehydro\text{-}ascorbic\ acid) + 2H^{+}}$$

Scheme 1.

The catalytic peak current is linearly dependent on the ascorbic acid concentration and the range of linearity depends on the amount of mediator in the solution. The analysis of chemically-coupled reactions between the electrogenerated ferricinium derivatives and ascorbic acid reveals that the largest second-order rate constant (k^0) belongs to ferriciniumcarboxylic acid. Therefore in this work we have used ferrocenecarboxylic acid as the most suitable mediator for the mediated oxidation of ascorbic acid (Fig. 1).

3.2. Calibration graph and precision

In the presence of 0.1 mM ferrocenecarboxylic acid in buffered solution with glycine at pH 4 the anodic peak current for cyclic voltammograms with a scan rate of 10 mV s^{-1} was proportional to the ascorbic acid concentration within the range 5×10^{-5}–1×10^{-3} M with only a small intercept. The regression equation was: $i(\mathrm{mA}) = -1.28 + 9757C(\mathrm{M})$; $r = 0.999$, $n = 6$. The mean of three replicate analyses of a solution of ascorbic acid at

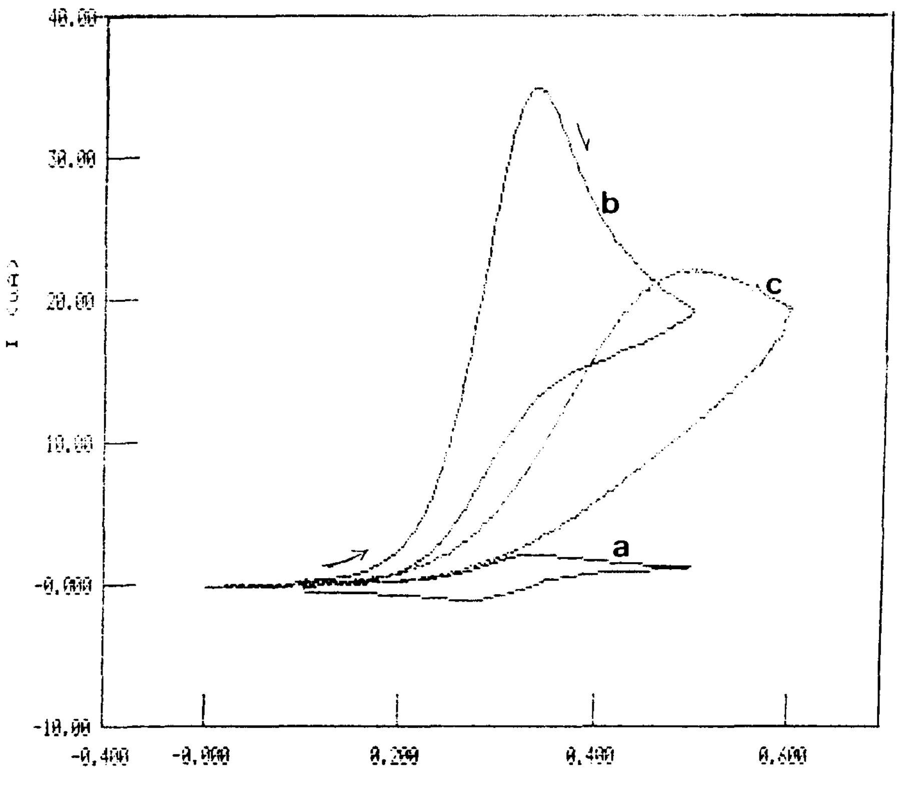

Fig. 1. Cyclic voltammograms of (a) 2 mM ferrocenecarboxylic acid in 0.5 M glycine buffer +0.1 M $LiClO_4$ at pH 4, (b) as for (a) but with addition of 5 mM ascorbic acid, (c) 5 mM ascorbic acid in buffer solution pH 4. Scan rate: 5 mV s^{-1}.

Table 1
Determination of ascorbic acid in dosage forms. Theoretical values for $t = 2.78$ and $F = 39$ ($P = 0.05$)

Pharmaceutical preparation	Claimed (mg)	Found [a] (mg)		F	t
		Proposed method (%RSD)	Iodine method (%RSD)		
Tablet	250 per tablet	260 (1)	255 (1)	2	2.3
Effervescent	1000 per tablet	1055 (2)	1012 (1)	5	2.6
Powder	500 per bag	522 (1)	530 (2)	4	1.3
Ampoule	500 per ml	537 (1)	530 (1)	4	2.2
Multivitamin	60 per tablet	62.1 (1)	63.2 (1)	2	1.1
Multivitamin	150 per capsule	159 (2)	158 (1)	5	1.3

[a] Results based on three replicate determinations per sample.

a concentration of 5×10^{-4} M assayed at its prepared value gave a relative standard deviation of 2.5%. This level of precision is adequate for the quality control analysis of pharmaceutical preparations and natural products.

3.3. Analysis of pharmaceutical preparations

The proposed method was applied to the analysis of several pharmaceutical dosage forms containing ascorbic acid—tablets, powder, ampoules or capsules—purchased from local sources without interference from excipients and other drugs encountered. The evaluation of the ascorbic acid concentration was found to be more suitable with the aid of a calibration graph. The results for the analysis of these preparations with the voltammetric method compared favourably with those obtained by the USP standard method (Table 1).

3.4. Analysis of fresh fruit juices

3.4.1. Optimization of the mediator concentration

The normal concentration range of ascorbic acid was reported [21] for various fruit juices to range from 10–40 mg per 100 ml. Preliminary experiments showed that in order to obtain a full catalytic cyclic voltammogram "increasing the anodic current of the mediator redox couple and substantial elimination of the corresponding cathodic peak on the reverse voltage scan, in the presence of ascorbic acid" for each fruit juice sample (see Fig. 1, curve b), an optimum concentration of the mediator which depends on the vitamin C content of the samples is desirable. Therefore the optimal amount of ferrocenecarboxylic acid that should be added to the test solution was obtained by adding the mediator in increasing amounts until the original oxidation peak of ascorbic acid found at more positive potential disappeared and a full catalytic cyclic voltammogram was obtained. This procedure may be performed quickly and easily by pre-estimation of the ascorbic acid content of the sample with the aid of the non-catalytic signal of ascorbic acid and then adding the mediator into the voltammetric cell at two different times.

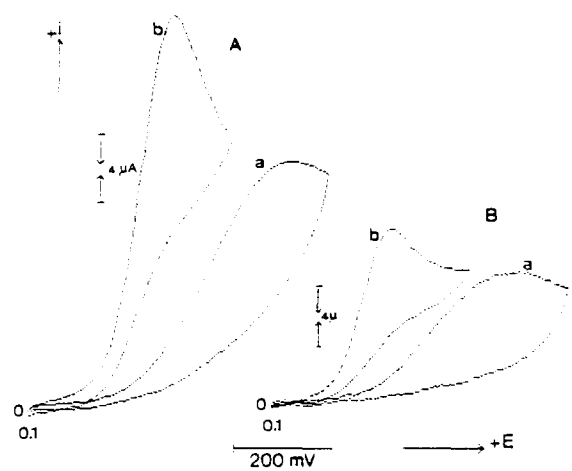

Fig. 2. Cyclic voltammograms recorded in fresh juices: (A) orange; (B) strawberry. A (a) and B (a): pH 4 (glycine buffer), 0.1 M $LiClO_4$. A (b): A (a) + 0.5 mM ferrocenecarboxylic acid. B (b): B (a) + 0.25 mM ferrocenecarboxylic acid. Scan rate: 10 mv s^{-1}.

Table 2
Determination of ascorbic acid in some fresh fruit juices and vegetables. Theoretical values of F and t are 39 and 2.78 ($p = 0.05$) respectively

Juice	Ascorbic acid [a] (mg/100 ml)		F	t
	Proposed method (%RSD)	DCPIP method (%RSD)		
Grapefruit	27.2 (1.7)	27.0 (1.1)	2.5	0.64
Orange	53.3 (1.2)	53.9 (0.7)	3	1.47
Sweet lemon	35.2 (1.3)	34.5 (1.0)	1.7	2.14
Lime	21.1 (2.2)	21.4 (2.4)	1.2	0.76
Kiwi	39.9 (2.3)	40.7 (0.8)	8.3	1.42
Strawberry	20.2 (5.0)	20.9 (3.4)	2.0	1.00
Tomato	7.8 (2.6)	8.1 (3.3)	1.8	1.53

[a] Results based on three replicate determinations per sample.

Fig. 2 shows typical cyclic voltammograms recorded for the mediated oxidation of ascorbic acid in 10 ml of fresh orange juice with very low viscosity and strawberry juice with very high viscosity in the presence of a optimal amount of ferrocenecarboxylic acid in buffered solution at pH 4 as described above. As seen in Fig. 2 the anodic peak currents could be easily evaluated and were found at potentials corresponding to ferrocenecarboxylic acid oxidation without any discernible cathodic peak on the reverse scan (full catalytic voltammograms). The voltammograms were reproducible and variation of the anodic peak current for cyclic voltammograms vs. ascorbic acid concentration added directly to the sample solution was linear with a correlation coefficient better than 0.999. The slopes of the regression equation for graphs obtained from the standard addition technique were quite different from that obtained from the calibration graph in pure buffered solution. Therefore the standard addition technique was adopted for the determination of ascorbic acid in fruit juice samples. Table 2 gives the vitamin C content of some fresh fruit juices determined by the proposed voltammetric method and with a DCPIP titration method (recognized official method of determination of vitamin C [2]). The results of statistical calculation shown in Table 2 indicate a good precision and good agreement between the repeatability of the proposed and DCPIP methods (F-test), and the mean values obtained (t-test).

3.4.2. Interference study

The signals obtained for vitamin C added to the fruit juices were calculated to be 75–85% of the signal in buffered solution depending on the fruit juice sample. This suggests that interference from concomitant reducing agents in the sample is unlikely. This reduced response may be attributed to the high vicosity of the juice matrices, which affects the diffusion coefficient of ascorbic acid, or the matrix effect for electrode fouling.

Fresh fruit juices contain a number of organic acids and sugars such as citric acid, tartaric acid, malic acid, lactic acid, and glucose, fructose and sucrose. These components were added in increasing amounts to 1 mM ascorbic acid in buffered solution and no serious effect was observed even in great excess (up to 50 mM). Some reducing ions, such as Fe(II), Cu(I), Sn(II) and sulphite, may be present in fresh fruit juices. The experimental investigation showed that these ions did not interfere in buffered solution up to 50, 20, 100 and 100 mM respectively. However, in the presence of some organic acids which are naturally occurring in fruit juices, mentioned above, Fe(II) began to interfere as the reducing agent, when its concentration in the solution exceeded 3 mM, due to the modification of the Fe(III)/Fe(II) standard potential in the presence of the complexing acids. Furthermore, the results of the analysis of some pharmaceutical preparations using the proposed method compared favourably with those obtained by the USP method (see Table 1), confirming that

no interference was observed from concomitant mineral ions, other vitamins, glucose, sucrose, nicotinamide and tablet excipients.

4. Conclusion

The proposed voltammetric method is rapid (time spent on manipulations and measurement is less than 15 min), simple, precise, suitable for routine control and can be carried out directly without any pre-treatment for a large number of fruit juice samples. The present method has a high degree of specification for determination of ascorbic acid in fruit juices due to the selective electrocatalytic oxidation of ascorbic acid with ferrocenecarboxylic acid and could be used as a quality control and stability indicating assay for vitamin C. The method has a clear advantage over the spectrophotometric methods for the analysis of samples containing fine particles or of deep colour and high viscosity.

References

[1] M.B. Jacobs, Chemical Analysis of Food and Food Products, 2nd edn., Van Nostrand, New York, 1951, p. 727.
[2] W. Horwitz (Ed.), Official Methods of Analysis of the Association of Official Analytical Chemists, 16th edn., AOAC, Washington, DC, 1995 Chapter 5, p. 16.
[3] S. Numa, Vitamins, 45 (1972) 327.
[4] P.M. Korash, A.G. Eving, R.L. Wilson and R.M. Wightman, J. Neurosci. Methods, 10 (1984) 215.
[5] A.G. Fogg and A.M. Summan, Analyst, 108 (1983) 691.
[6] S. Kozar, A. Bujak, J. Eder-Trifunovic and G. Kniewald, Fresenius' Z. Anal. Chem., 329 (1988) 760.
[7] D.H. Carston, C.P. Jones and D.E. Williams, Talanta, 38 (1991) 17.
[8] M. Farrington, N. Jagota and J.M. Stater, Analyst, 119 (1994) 233.
[9] N. Winograd, H.N. Blount and T. Kuwana, J. Phys. Chem., 73 (1969) 3456.
[10] J.F. Evans, M.T. Henne and G.P. Royer, J. Electroanal. Chem., 80 (1977) 406.
[11] M.F. Dautartas and J.F. Evans, J. Electroanal. Chem., 109 (1980) 301.
[12] K.N. Kuo and R.W. Murray, J. Electroanal. Chem., 131 (1982) 37.
[13] J. Facci and R.W. Murray, Anal. Chem., 54 (1982) 772.
[14] S.A. Wring and J.P. Hart, Anal. Chim. Acta, 229 (1990) 63.
[15] J. Kulys and A. Drungiliene, Electroanalysis, 3 (1991) 209.
[16] M. Petersson, Anal. Chim. Acta, 187 (1986) 333.
[17] F. Ying Sing and M. Song Ying, Anal. Chim. Acta, 261 (1992) 375.
[18] M.H. Pournaghi-Azar and R. Ojani, Iran. J. Sci. Technol., in press.
[19] M.H. Pournaghi-Azar and R. Ojani, Talanta, 42 (1995) 1839.
[20] U.S. Pharmacopeia XX, Mack Co., Easton, PA, 1980.
[21] B.K. Watt, A.L. Merrill, R.K. Pecot, C.F. Adams, M.L. Orr and D.F. Miller, Composition of Food, in Agriculture Handbook No. 8, USDA, Washington, DC, 1963.

ELSEVIER

Talanta 44 (1997) 305–310

Talanta

Cathodic stripping voltammetry of the anticancer agent 5-fluorouracil and determination in urine

Mahmoud Khodari[a,*], Mahmoud Ghandour[b], Ashraf M. Taha[a]

[a]*Chemistry Department, Faculty of Science, South Valley University, Qena, Egypt*
[b]*Faculty of Science, Assiut University, Assiut, Egypt*

Received 9 August 1995; revised 27 March 1996; accepted 5 April 1996

Abstract

Cathodic stripping voltammetry was used to determine 5-fluorouracil (5-FU) in the presence of traces of Cu(II). It was found that the addition of 5×10^{-9} mol dm^{-3} Cu(II) to the measurement cell greatly enhanced the peak current of the adsorbed molecule. Different parameters were tested to optimize the conditions for the determination of 5-FU. The adsorbed form is reduced irreversibly. It was observed that by controlling the deposition potential, the technique could be directed to the determination of Cu(II) or the drug. The linear range was from 5×10^{-9} to 6×10^{-8} mol dm^{-3} for 5-FU and from 6×10^{-9} to 5×10^{-8} mol dm^{-3} for Cu(II). Detection limits of 4.6×10^{-10} and 5×10^{-10} mol dm^{-3} were obtained for 5-FU and Cu(II), respectively. The method was applied to urine and molecules or ions which may interfere were studied. © 1997 Elsevier Science B.V.

Keywords: 5-Fluorouracil; Interferences; Stripping voltammetry

1. Introduction

5-Fluorouracil (5-FU) is an antineoplastic agent used for the treatment of solid tumors of the breast and rectum [1]. The polarographic behavior of 5-FU has been examined and it was shown that it undergoes reduction at pH 1.8–11 with the best defined wave at pH 6–8 [2]. Guerrieri et al. [3] studied the formation of an insoluble mercury compound in the presence of 5-FU using different electrochemical techniques.

Different methods have been reported for the determination of 5-FU, including cathodic stripping voltammetry [4–6]. This technique is based on the interfacial accumulation of the analyte on the working electrode prior to voltammetric measurements of the surface-bound compound. Liquid chromatography with anodic amperometric detection has also been used for the determination of 5-FU and a detection limit of 15 ng/ml can be achieved [7].

The present work is a continuation of our studies in the field of drug analysis using mercury and modified carbon paste electrodes [8–10]. The

* Corresponding author.

PII S0039-9140(96)01957-1

aim was to investigate the adsorptive voltammetric behavior of 5-FU in the presence of traces of Cu(II). Also, 5-FU was used as a ligand to determine Cu(II) at low levels by stripping voltammetry following chelation.

2. Experimental

2.1. Instrumentation

For the voltammetric measurements, an EG&G PAR Model 263 polarographic analyzer with 250/270 research electorchemistry software version 4.0 was used with a PAR 303 static mercury drop electrode (SMDE). Silver/silver chloride (saturated KCl) was used as a reference electrode and a platinum wire as an auxiliary electrode.

All the pH meaurements were made with an Orion Model 601 A digital ionalyzer.

2.2. Chemicals

A stock solution of 1×10^{-3} mol dm^{-3} 5-FU was prepared daily by dissolution of the appropriate amount in doubly distilled water. Borax solution was prepared and adjusted to pH 10 with sodium hydroxide. All other reagent were of analytical grade.

2.3. Procedure

After deaeration with nitrogen for 8 min, a hanging mercury drop electrode (medium size) was formed and the selected deposition potential was applied with stirring for a given time interval while accumulation of the analyte at the electrode proceeded. After a selected deposition time and a rest period of 15 s, the potential was scanned from positive to negative.

3. Results and discussion

Fig. 1(A) shows the reduction peak of the mercury(II) salt of 5-FU [3] and Fig. 1(B) illustrates the same peak in the presence of Cu(II). It can be seen that the addition of Cu(II) enhances the peak

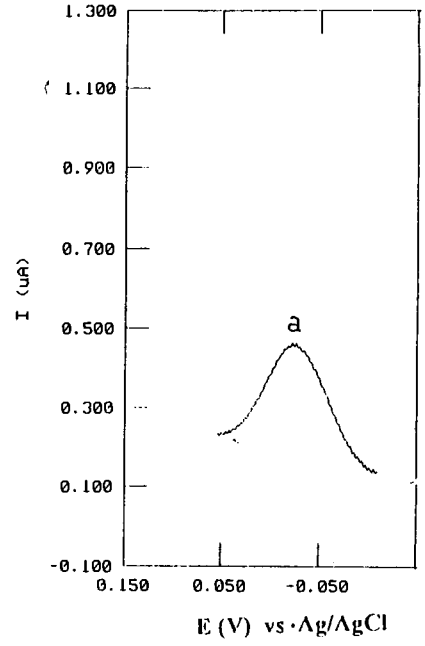

(a)

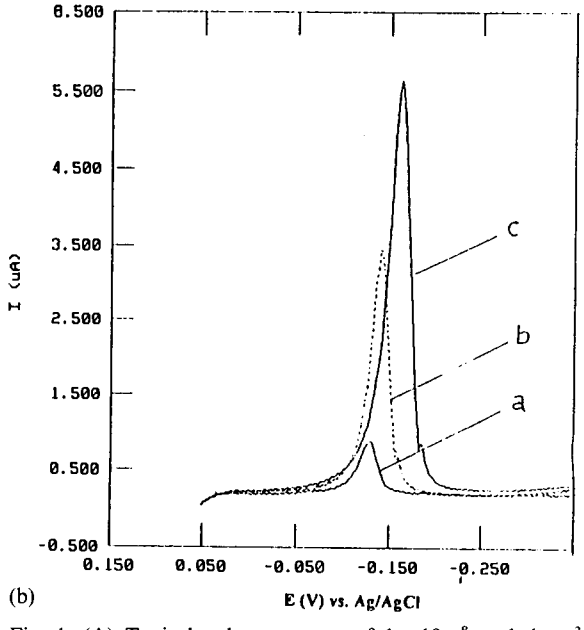

(b)

Fig. 1. (A) Typical voltammogram of 1×10^{-8} mol dm^{-3} 5-FU in the absence of Cu(II) ions. Borax, pH 10, scan rate, 150 mV s^{-1}; deposition potential, +0.05 V; preconcentration time, 180 s. (B) Typical voltammograms of (a) 1×10^{-8}, (b) 6×10^{-8} and (c) 1×10^{-7} mol dm^{-3} 5-FU in the presence of 5×10^{-9} mol dm^{-3} Cu(II) ions. Borax, pH 10; $t_{acc} = 30$ s; scan rate, 150 mV s^{-1}.

current greatly. Also, Fig. 1(B) indicates that the peak potential shifts to the more negative side with increase in 5-FU concentration.

The mechanism of the effect of Cu^{2+} on the peak current has not yet been established. The reduction process of the adsorbed form, investigated by cyclic voltammetry, shows that the phenomenon is totally irreversible. The resulting peak current was characterized with respect to the media, pH and other variables.

3.1. Cyclic voltammetric measurements

Repetitive cyclic voltammograms suggest rapid desorption of the adsorbed form; the peak current decreases in the second and third cycles. Hence linear sweep voltammetry with a fast scan rate (150 mV s^{-1}) is preferable in such cases.

3.2. Effect of supporting electrolyte and pH

A series of supporting electrolytes were tested (sodium acetate, disodium hydrogenphosphate, potassium nitrate, borax). Both the peak height and the peak shape were taken into consideration when choosing the supporting electolyte. The results showed that borax gave the best response. The solution conditions such as the pH and the concentration of 5-FU, affect the peak potential and peak current significantly. The supporting electrolyte concentration has no observable effect on the peak current. The effect of pH was investigated. A small current was observed at pH < 5, which increases gradually up to pH 9 and then increased sharply with a maximum at pH 10. At higher pH, the mercury dissolution current obscured the required peak.

3.3. Effect of accumulation potential and scan rate

The effect of the accumulation potential on the stripping peak current was examined over the range +0.15 to −0.05 V. Fig. 2(a) illustrates the peak current obtained as a function of deposition potential. The graph indicates that on going in the positive direction from −0.05 to 0.15 V, the peak height increases with a maximum at +0.05 V.

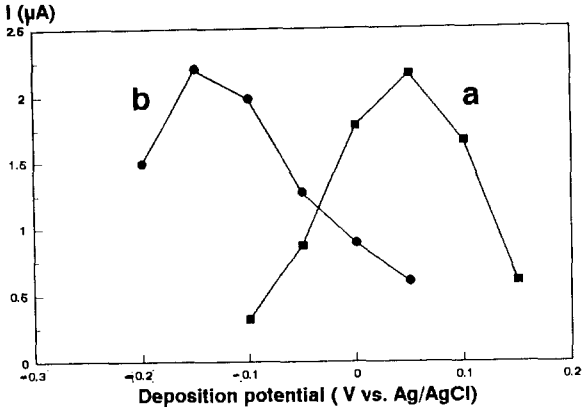

Fig. 2. Effect of accumulation potential on the peak current of (a) 5×10^{-9} mol dm^{-3} 5-FU in the presence of 5×10^{-9} mol dm^{-3} Cu(II) and (b) 1×10^{-8} mol dm^{-3} Cu(II) ions in the presence of 1×10^{-6} mol dm^{-3} 5-FU. t_{acc} = 240 s; borax, pH 10.

The effect of scan rate was studied by varying it from 20 to 500 mV s^{-1}. It was found that the peak current increases and the peak potential shifts to more negative values with increasing scan rate. The peak becomes broader at scan rates higher than 200 mV s^{-1}. For subsequent work, 150 mV s^{-1} was selected. The plot of I vs. V gave a straight line with a slope of 1.08. A slope of 1.0 is expected for ideal reaction of surface species [5]. The shape of curve b in Fig. 2 corresponds to copper behavior and will be explained further below.

3.4. Effect of preconcentration time, interferences and reproducibility

Fig. 3 shows the effect of preconcentration time in the presence of different concentrations of 5-FU. The peak current increased linearly with preconcentration time up to 180 s for 1×10^{-8} mol dm^{-3} 5-FU. A deviation from the linearity was observed at accumulation times longer than 60 and 45 s for 6×10^{-8} and 1×10^{-7} mol dm^{-3} 5-FU, respectively. Table 1 illustrates the data collected. On plotting the peak current against the square root of time, a straight line was obtained with a correlation coefficient of 0.998 and a slope of 0.96. This behavior is expected for mass transport controlled by adsorption [11].

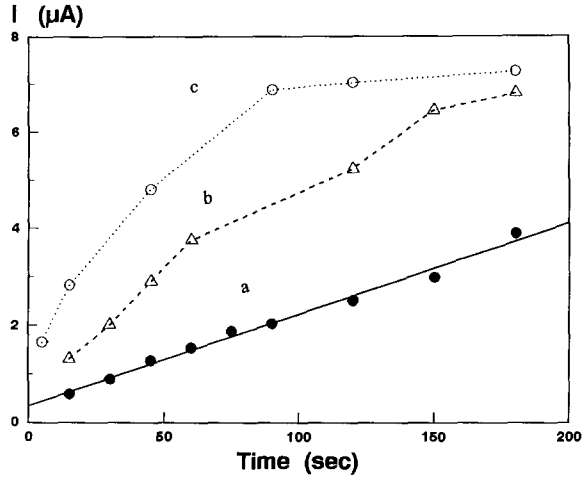

Fig. 3. Effect of accumulation time on the linear sweep voltammetric response of (a) 1×10^{-8}, (b) 6×10^{-8} and (c) 1×10^{-7} mol dm^{-3} 5-FU. Other conditions as in Fig. 1.

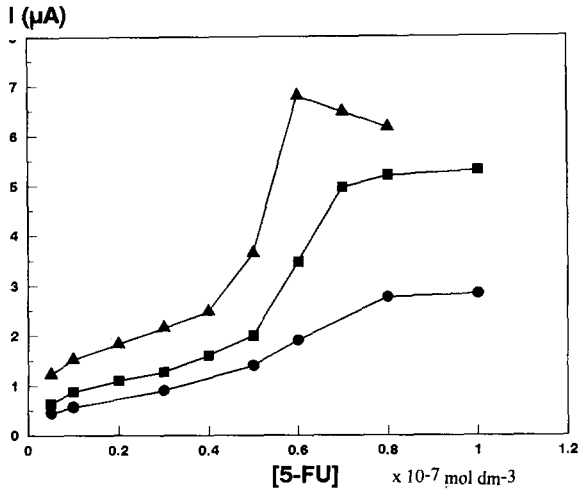

Fig. 4. Current–concentration graphs after preconcentration times of (a) 15, (b) 30 and (c) 90 s for 5-FU in the presence of 5×10^{-9} mol dm^{-3} Cu(II) ions.

The effect of Cu(II) concentration over the range 1×10^{-9}–5×10^{-9} mol dm^{-3} on the stripping peak current of 1×10^{-8} mol dm^{-3} 5-FU was examined. No significant effect on the peak current height was observed and 5×10^{-9} mol dm^{-3} Cu(II) was adopted in subsequent work.

The reproducibility of the results can be attributed to the reproducible area and self-cleaning control provided by the instrument used. The relative standard deviation was calculated for eight successive measurements of 1×10^{-8} mol dm^{-3} 5-FU and was found to be 2.6%.

3.5. Calibration plot

A well defined stripping peak was observed over the concentration range. 1×10^{-8}–1×10^{-7} mol dm^{-3} after 15, 30 and 60 s with stirring at +0.05 V. The resulting calibration plots for these concentrations are shown in Fig. 4. The graphs show positive deviations from linearity at concentrations higher than 6×10^{-8}, 5×10^{-8} and 4×10^{-8} mol dm^{-3} 5-FU, respectively. This phenomenon and the change in the slope of the response might be attributable to surface effects of the investigated molecule [3]. The data obtained from the least-squares analysis are given in Table 2.

Table 1
Characteristics of current–time curves established using different 5-FU concentrations with borax (pH 10)

[5-FU] (mol dm^{-3})	Linearity range (s)	Correlation coefficient	Slope (μA s^{-1})	Intercept (μA)
1×10^{-8}	0–180	0.9896	0.0187	0.348
6×10^{-8}	0–60	0.9974	0.0530	0.425
1×10^{-7}	0–45	0.9813	0.0757	1.43

Table 2
Characteristics of the calibration curves established using different deposition times

Deposition time (s)	Linearity range (mol dm^{-3})	Correlation coefficient	Slope (μA per 10^{-8} mol dm^{-3})	Intercept (μA)
15	5×10^{-9} 6×10^{-8}	0.9784	0.2817	0.1774
30	5×10^{-9} 5×10^{-8}	0.9717	0.2746	0.548
60	5×10^{-9} 4×10^{-8}	0.9997	0.3211	1.196

3.6. Detection limit

The detection limit was calculated from three times the noise using the measurements of 1×10^{-8} mol dm^{-3} and was found to be 4.6×10^{-10} mol dm^{-3} based on a signal-to-noise ratio of 3. This is a significant improvement over the literature data [5,7].

3.7. Interferences and application to biological samples

The influence of ascorbic acid, which is potent interfering compound present in biological samples, was investigated. It was found that an equimolar concentration of ascorbic acid had no effect on the peak response of 5-FU. However, at a higher molar excess (100:1) of ascorbic acid, a depression of the peak response by about 25% was observed.

The method was applied to the determination of 5-FU in spiked urine. The sample was treated with concentrated sulfuric acid to destroy the organic matter, then the pH was raised to 10 by addition of borax and sodium hydroxide. The voltammograms were recorded in the presence of 5×10^{-9} mol dm^{-3} Cu(II). A linear dependence on the 5-FU concentration was observed between 1×10^{-7} and 1×10^{-6} mol dm^{-3} ($r = 0.9985$).

The reproducibility of the results was tested and the relative standard deviation was found to be 3.4% ($n = 8$).

3.8. Determination of Cu(II) in the presence of 5-FU

Cathodic linear sweep voltammetry was used to determine Cu(II) using 5-FU as a complexing agent. The literature showed that Cu(II) forms a complex with this ligand [12]. In the present work we tried to take advantage of the accumulation of the complex by adsorption to determine Cu(II) electroanalytically. It was found that the peak current of 1×10^{-8} mol dm^{-3} Cu(II) increased by a factor of 16 on adding 1×10^{-6} mol dm^{-3} 5-FU. The peak current response was

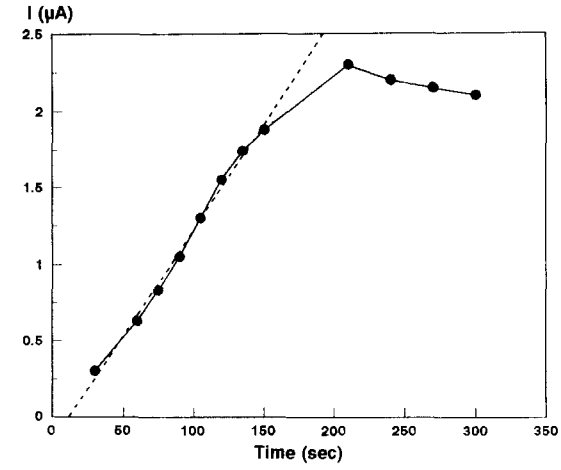

Fig. 5. Peak current of Cu(II)–5-FU complex as a function of deposition time in a borax electrolyte (pH 10) with a deposition potential of -0.15 V.

characterized with respect to the supporting electrolyte, pH, deposition potential and other parameters.

The deposition potential, as can be seen in Fig. 2(b), greatly affects the peak current of Cu(II) and this factor is taken into account to direct the technique toward the determination of 5-FU or Cu(II). After selecting a suitable supporting electrolyte (borate buffer, 0.1 mol dm^{-3}), a concentration of 1×10^{-8} mol dm^{-3} Cu(II) was studied in the presence of 1×10^{-6} mol dm^{-3} 5-FU using linear scan voltammetry at different deposition potentials. It was found that accumulation at an applied potential of -0.15 V gave the best response. The concentration of the drug was investigated as an effective parameter in complexation, i.e. the quantity adsorbed. The ligand concentration was increased from 1×10^{-7} to 1×10^{-5} mol dm^{-3} in the presence of a constant concentration of Cu(II). It was observed that the peak response increases on increasing the ligand concentration up to 1×10^{-6} mol dm^{-3}, then a depression of the peak response occurs, probably owing to surface saturation.

The results obtained on the effect of deposition time on the peak response indicated that on increasing the preconcentration period, the peak current shows a linear relationship with Cu(II)

concentration, y (μA) = 0.0138x (s) − 0.165, until a leveling off is observed corresponding to a maximum degree of surface coverage at $t_{acc} > 180$ s (Fig. 5). An adsorption isotherm is produced which can be described by the Langmuir equation. At the current maximum the electrode is covered by a monolayer of complex ion [13].

A detection limit of 5×10^{-10} mol dm^{-3} Cu(II) was calculated from 5×10^{-9} mol dm^{-3} Cu(II) based on a signal-to-noise ratio of 3. The relative standard deviation was calculated for seven experiments and was found to be 2.9%.

4. Conclusion

The addition of traces of Cu(II) to the preconcentration cell of 5-FU improved significantly the sensitivity of the cathodic stripping voltammetric determination of 5-FU. A detection limit of 4.6×10^{-10} mol dm^{-3} (0.52 ng per 10 ml) was obtained, compared with reported values of 3×10^{-9} mol dm^{-3} [5] and 15 ng per 10 ml [7]. The method was applied to biological samples (urine). A linear dependence of the peak current on 5-FU concentration was observed over the range 1×10^{-7}–1×10^{-6} mol dm^{-3} with a correlation coefficient of 0.9985.

References

[1] C. Heidlberg and F.J. Ansfield, Cancer Res., 23 (1963) 1266.
[2] Y.A. Gawargious, K. Brodersen and N.B. Tadros, Acta Pharm. Fenn., 95 (1986) 27.
[3] A. Guerrieri, T. Cataldi, F. Palmisano and G. Zambonin, Electroanal. Chem. Interfacial Electrochem., 314 (1991) 117.
[4] J. Yan, C. Zhu and C. Pu, Bioelectrochem. Bioenerg., 29 (1993) 347.
[5] J. Wang, M. Lin and V. Villa., Analyst, 112 (1987) 247.
[6] A. Ordieres, M. Gutierrez, A. Garcia, P. Blanco and W.F. Smyth, Analyst, 112 (1987) 247.
[7] A. Guerrieri, T. Cataldi, F. Palmisano and P. Zambonin, Anal. Chim. Acta, 207 (1988) 183.
[8] M. Khodari, Electroanalysis, 5 (1993) 321.
[9] N. Abo el Maali, M.A. Ghandour and M. Khodari, 40 (1993) 1838.
[10] A. Ali, K. Emara and M. Khodari, Analyst, 119 (1994) 1071.
[11] R. Delhay and C. Fike, J. Am. Chem. Soc., 80 (1958) 2628.
[12] G.D. Christian and W.C. Purdy, Biochim. Biophys. Acta, 54 (1961) 587.
[13] C. Vanden Berg, Anal. Chim. Acta, 164 (1984) 195.

ELSEVIER

Talanta 44 (1997) 311–317

Talanta

A rapid, selective and sensitive spectrophotometric method for the determination of Ce(III) using some bisazophenyl-β-diketone derivatives

A.S. Amin[a,*], M.M. Moustafa[a], R.M. Issa[b]

[a]*Chemistry Department, Faculty of Science, Benha University, Benha, Egypt*
[b]*Faculty of Science, Tanta University, Tanta, Egypt*

Received 28 September 1995; revised 7 June 1996; accepted 7 June 1996

Abstract

A rapid, simple, selective and sensitive spectrophotometric method for the determination of cerium(III) using the title azo dyes [1,3-phenylenediamine bisazoacetylacetone ($\mathbf{I}_a$);1,3-phenylenediamine bisazobenzoylacetone ($\mathbf{I}_b$);1,4-phenylenediamine bisazoacetylacetone ($\mathbf{I}_c$); and 1,4-phenylenediamine bisazobenzoylacetone ($\mathbf{I}_d$)] has been developed in neutral and slightly alkaline (pH 7.00, 7.50, 8.00 and 7.00) media. The 1:1 and 2:1 (M:L) complexes formed exhibit their highest absorbances in 30% (v/v) dioxane solutions, having formation constants (log K) of 4.44, 4.95. 5.63 and 5.22 and 8.51, 8.76, 9.73 and 9.37 respectively. Beer's law is obeyed over the concentration ranges 0.10–2.50, 0.05–3.00, 0.05–3.75 and 0.10–3.50 μg ml^{-1} of cerium(III). More accurately, Ringbom optimum concentration ranges are 0.2–2.25, 0.2–2.6, 0.2–3.5 and 0.2–3.3 μg ml^{-1} for the complexes of reagents $\mathbf{I}_a$,$\mathbf{I}_b$,$\mathbf{I}_c$ and $\mathbf{I}_d$ respectively. The molar absorptivities, Sandell sensitivities and relative standard deviations were also calculated. The interferences of 50 foreign ions on the determination of cerium(III) were studied. The method allows the determination of cerium(IV) after prior reduction to the trivalent state. The proposed method was used for cerium determination in two different monazite samples and the results were compared with certified values obtained using atomic absorption spectrometry, indicating that the procedure provided accurate and precise results. © 1997 Published by Elsevier Science B.V.

Keywords: Bisazo dyes, Cerium determination; Monazite analysis; Spectrophotometry.

1. Introduction

The spectrophotometric analysis of cerium(III) is usually carried out with dyestuffs. Of those commonly used, only carboxyarsenazo [1] give both sensitive and selective determination. The reactions of cerium(III) with orthanilic K [2] and 4-(2-pyridylazo) resorcinol [3] lack both sensitivity and selectivity, whereas those with Methylthymol Blue [4], sulpharsazen [5] and Alizarin Red S [6] have low sensitivities. The

* Corresponding author.

PII S0039-9140(96)02011-5

complex formed with Bromopyrogallol Red [7] is formed only on heating the reactant for 10 min at 80–90°C, whereas that formed with Chrome Azurol S [8] is stable for less than 50 min. Although carboxynitrazo [9] and thiazolylazo dyes [10,11] are the most sensitive reagents reported so far for the determination of Ce(III), the maximum development of the coloured complex requires at least 30 min.

In the present study, a method is developed for the rapid, accurate and sensitive determination of Ce(III) using some bisazophenyl-β-diketones as chromogenic reagents due to their selectivity in the reaction with Ce(III). The most favourable conditions are established, and the composition, conditional and real stability constants of the complexes, the molar absorptivity (ε_{MAX}) and the Sandell sensitivity are determined.

2. Experimental

2.1. Apparatus

An Orion Research Model 601 A/Digital Ionalyzer pH-meter with a combined saturated calomel–glass electrode was used for pH measurements. A Perkin-Elmer λ3B recording spectrophotometer equipped with 10 mm matched silica cells was used. The atomic absorption measurements for the determination of cerium ion were carried out using an Hitachi atomic absorption Z-6100 polarized Zeeman spectrometer. All experiments and measurements were carried out at ambient temperature.

2.2. Reagents

All chemicals were of analytical-reagent grade, unless otherwise stated.

The bisazo dyes used in the present investigation were prepared according to the procedure described previously [12]. The four reagents used have the following structures.

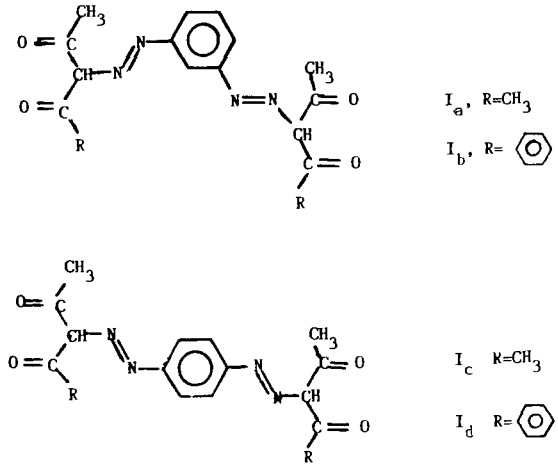

A stock solution of Cerium(III) was prepared by dissolving 0.5556 g of Cerium(III) sulphate octahydrate (Fluka) in 250 ml of bidistilled water containing 1.0% sulphuric acid. The solution was standardised complexometrically [13] and was found to contain 1 mg ml^{-1} cerium. Working solutions were prepared by appropriate dilution of the stock solution.

1×10^{-3}M solutions of reagents $\mathbf{I}_a$–$\mathbf{I}_d$ were prepared by dissolving an accurately weighted amount of the purified solid reagent in 100 ml of dioxane.

Sodium tetraborate, $Na_2B_4O_7$, buffer solutions (0.05 M) of the required pH were prepared [14].

2.3. General procedure

For each of the systems investigated, an aliquot of slightly acidic solution containing < 100 μg of Cerium(III) was mixed with 12.5 ml of borate buffer of pH 7.0, 7.5, 8.5 or 7.0, and then mixed with 2.5 ml of 1×10^{-3}M $\mathbf{I}_a$,$\mathbf{I}_b$,$\mathbf{I}_c$ or $\mathbf{I}_d$ respectively, to form the complexes. A further 5 ml of dioxane was added to dissolve any complex precipitated. The contents were then diluted to 25 ml with bidstilled water in a volumetric flask. The absorbance was measured at 573, 533, 511 and 638 nm for Cerium(III) complexes of ligands $\mathbf{I}_a$, $\mathbf{I}_b$, $\mathbf{I}_c$ and $\mathbf{I}_d$ respectively, against appropriate reagent blanks prepared under identical conditions.

Table 1
Effect of foreign ions (concentration of Ce(III) = 2 μg ml^{-1})

Foreign ions	Tolerance limit (μg)			
	I_a	I_b	I_c	I_d
Cl^-, Br^-, I^-, $B_4O_7^{2-}$	8000	75000	10000	9000
Acetate, oxalate, tartrate, malonate	5000	4000	6000	5000
Ascorbate, succinate, phosphate	4000	3500	4500	4500
So_4^{2-}, $S_2o_3^{2-}$, SCN^-	3000	3000	4000	3500
Cn^-, NH_2OH, HCl	2500	2500	3500	3000
Urea, thirourea, citrate	2000	2000	3000	3000
Mg^{2+}, Ca^{2+}, Ba^{2+}, Sr^{2+}	6000	6000	8000	1000
Al^{3+}, Mo^{6+}, W^{6+}, Cr^{6+}	4000	3500	5000	4500
Ag^{+} [a], Au^{3+}	750	600	800	700
Zr^{4+} [b], Cr^{3+} [c], In^{3+} [c]	300	250	300	250
Hf^{4+} [b], V^{5+} [b], Ti^{4+} [d]	100	80	100	75
Pt^{2+} [b], Pd^{2+} [b]	50	40	50	30
Th^{4+} [e], U^{6+} [f]	20	15	20	10
Co^{2+} [b]	10	5	10	5
Cu^{2+} [b], Ni^{2+} [b], Mn^{2+} [b]	3	1	1	5
Fe^{3+} [b], Hg^{2+} [b]	3	–	–	–

[a–f]Masking agents: [a]$S_2o_3^{2-}$; [b]CN^-; [c]$C_2O_4^{2-}$; [d]tartrate; [e]CH_3COO^-; [f]malonate.

2.4. Procedure for the determination of cerium in monazite samples

To 1.0 g of the sample, 20 ml of 8.0 M sulphuric acid was added and heat was applied to decompose the sample. After cooling to room temperature the residue was dissolved in water. The solution was transferred to a 50 ml separating funnel containing 20 ml of tri-*n*-butylphosphate to extract Ce(IV) and Th(IV). By adding 5 ml of 1.0 M sodium nitrite, the Ce(IV) was reduced to Cerium(III) which returned to the aqueous phase and was then separated. The resulting aqueous solution was placed in a 25 ml calibrated flask and made up to the mark with water. An appropriate volume was taken and the above procedure for cerium determination was followed.

3. Results and discussion

Cerium(III) was found to react instantaneously with ligands I_a–I_d in neutral and slightly basic media to form slightly soluble orange–red complexes. Investigations were carried out to establish the most favourable conditions to achieve maximum colour development in the quantitative determination of Cerium(III). The influence of each of the following variables on the reaction was tested.

3.1. Effect of pH

The protonation constants of the reagents under consideration were calculated [15] and found to be 10.97, 7.57, 11.43 and 8.11 for reagents I_a, I_b, I_c and I_d respectively. The protonation reaction [15] can be represented as

m-Bis-azobenzene-di(β-diketone) :

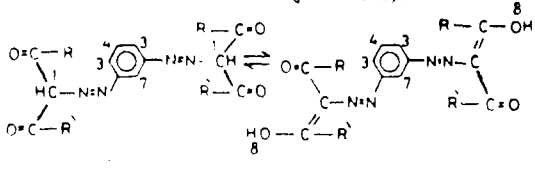

p-Bis-azobenzene-di(βdiketone) :

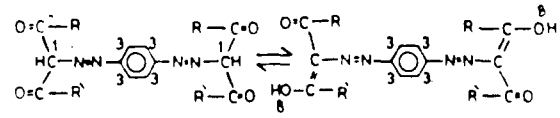

Table 2
Comparison of the selectives, times required and sensitivities of different methods for the spectrophotometric determination of cerium

Reagent	λ_{MAX}	$10^4 \times \varepsilon$	Comment	Ref.
Chiorophosphomazo III	675	5.9	Highly susceptible to interference	[19]
Arsenazo III	665	4.7	Highly susceptible to interference	[20]
Arsenazo M	640	8.3	Highly susceptible to interference	[21]
p-Acetylchlorophosphonazo	675	11.6	5 min standing time	[22]
4-(2-Thiazolylazo) resorcinol	550	4.09	Colour stable for 1.5 h	[11]
1-(2-Thiazolylazo)-2-naphthol	620	5.14	Colour stable for 2.0 h	[11]
p-Acetylarsenazo	670	–	10 min required for complete colour development	[23]
o-Iodobenzyoyl-*o*-tolylhydroxylamine	450	0.57	5 min after extraction with chloroform	[24]
1,3-Phenylenediamine bisazoacetylacetone	573	2.58	Rapid, selective, without heating or extraction	This work
I,3-Phenylenediamine bisazobenzoylacetone	533	2.43	Rapid, selective, without heating or extraction	This work
1,4-Phenylenediamine bisazoacetylacetone	511	2.39	Rapid, selective, without heating or extraction	This work
1,4-Phenylenediamine bisazobenzolyacetone	638	2.28	Rapid, selective, without heating or extraction	This work

On varying the pH of the reaction mixture from 5.0 to 10.5, complexes with the four ligands gave maximum absorbance values in the pH ranges 6.5–7.5, 7.0–8.0, 7.5–9.5 and 6.0–8.0 for $\mathbf{I}_a$, $\mathbf{I}_b$, $\mathbf{I}_c$ and $\mathbf{I}_d$ complexes resprctively (Fig. 1). The absorbance–pH curves are parabolic relations, indicating the increased formation of the complexes with increasing pH due to the decreased acidity of the medium and enhanced ionisation of the active protons on the ligands. The decrease in absorbance on the alkaline pH side is due to either the hydrolysis of the complexes or the formation of other types of hydroxoazo complexes having lower absorbance. This behaviour is quite common for complexes formed by proton displacement from the ligand through the metal ion [16]. Hence, the pH values of 7.0, 7.5, 8.5 and 7.0 were chosen for all further studies with $\mathbf{I}_a$, $\mathbf{I}_b$, $\mathbf{I}_c$ and $\mathbf{I}_d$ respectively. It was also observed that the absorbance remained constant with the addition of >10 ml of borate buffer in each case. Accordingly, 12.5 ml of buffer solution of appropriate pH value was used for all further studies.

3.2. Effect of reagent concentration

When the volume of the reagent added to an aliquot of solution containing 50 μg of Cerium(III), was varied from 0.5 to 5.0 ml, the maximum absorbance was observed with the addition of 1.5 ml for Cerium(III)–$\mathbf{I}_a$ and Cerium(III)–$\mathbf{I}_c$ complexes whereas 2 ml was required for Cerium(III)–$\mathbf{I}_b$ and Cerium(III)–$\mathbf{I}_d$ complexes. Hence, 2.5 ml of 10^{-3} M reagent solution was employed for all further studies.

3.3. Effect of solvent ratio

Dioxane was found to be the best solvent to dissolve the slightly soluble Cerium(III) $\mathbf{I}_a$–$\mathbf{I}_d$ complexes and the maximum absorbance was observed in the presence of 25–35% (v/v) dioxane. At least 6.3 ml of dioxane was required for the dissolution of the complex and the absorbance decreased with the addition of >10 ml. All measuremetns were therefore made in the presence of 7.5 ml (30% v/v) of dioxane.

Table 3
Results for the determination of Cerium(III) in two different monazite samples

Sample No.[a]	Reagent	Reference value (%)[b]	Found (%)[c]	Recovery (%) (±SD)	% RSD	t-test[d]	F value[e]
Monazite I		54.85					
	$\mathbf{I}_a$		54.40	99.18 (0.61)	1.95	1.14	2.19
	$\mathbf{I}_b$		54.25	98.91 (0.83)	1.60	1.33	2.47
	$\mathbf{I}_c$		55.10	100.46 (0.52)	2.17	0.99	1.81
	$\mathbf{I}_d$		54.55	99.45 (0.47)	1.44	1.78	2.69
Monazite II		66.20					
	$\mathbf{I}_a$		66.75	100.68 (0.58)	1.82	1.05	2.11
	$\mathbf{I}_b$		67.00	101.21 (0.64)	2.26	1.57	2.36
	$\mathbf{I}_c$		65.75	99.32 (0.49)	1.53	1.24	2.28
	$\mathbf{I}_d$		66.80	100.91 (0.76)	1.72	1.82	2.66

[a]The samples were provided by the Geology Department, Faculty of Science, Benha University, Egypt.
[b]Obtained by atomic absorption spectrometry.
[c]Average of six determinations.
[d]Theoretical value for t-test is 2.57.
[e]Theoretical value for F value is 5.05.

3.4. Spectral characteristics

Absorption spectra of the Cerium(III) complexes with ligands $\mathbf{I}_a$–$\mathbf{I}_d$ were recorded (Fig. 2) at the recommended pH values. As the complexes exhibited maximum absorbances at 573, 533, 511 and 638 nm and their exhibited maximum absorbances at 407, 363, 404 and 410 nm respectively, all measurements were made at corresponding λ_{MAX} values for each complex.

3.5. Composition of the complex

Under the optimum conditions of pH, reagent concentration and solvent ratio described above, the metal: ligand ratios were found to be 1:1 and 2:1, using Job's continuous variation and molar ratio methods. The conditional formation constants (log K), calculated using the Harvey–Manning equation [17], were found to be 4.44, 4.95, 5.63 and 5.22 for the (1:1) complexes, whereas the real constants were 4.75, 5.20, 6.00, and 5.50 respectively. For (2:1) complexes, the conditional formation constants (log K) amount to 8.51, 8.96, 9.73 and 9.37 for $\mathbf{I}_a$, $\mathbf{I}_b$, $\mathbf{I}_c$ and $\mathbf{I}_d$ respectively, while the true constants were 8.88, 9.20, 10.05 and 9.50 respectively. The values indicate that the stability of the complexes increases in the order $\mathbf{I}_a < \mathbf{I}_b < \mathbf{I}_d < \mathbf{I}_c$.

3.6. Beer's law, sensitivity and stability

The absorbance values of the Cerium(III)–$\mathbf{I}_a$–$\mathbf{I}_d$ complexes followed Beer's law over the concentra-

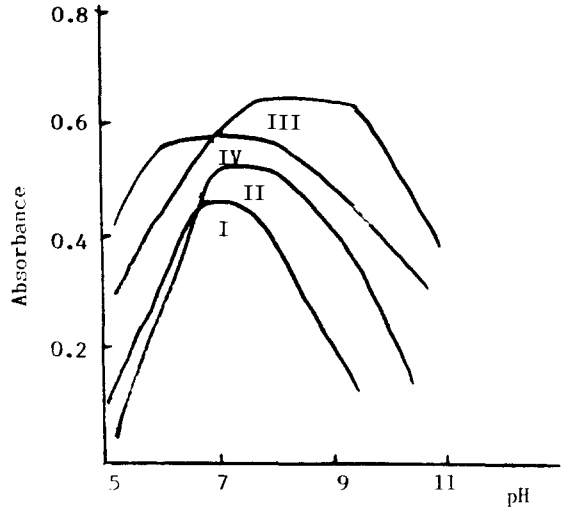

Fig. 1. Effect of pH on the absorbance of I-Ce(III)-I_a complex, II-Ce(III)-I_b complex, III-Ce(III)-complex and IV-Ce(III)-I_d complex.

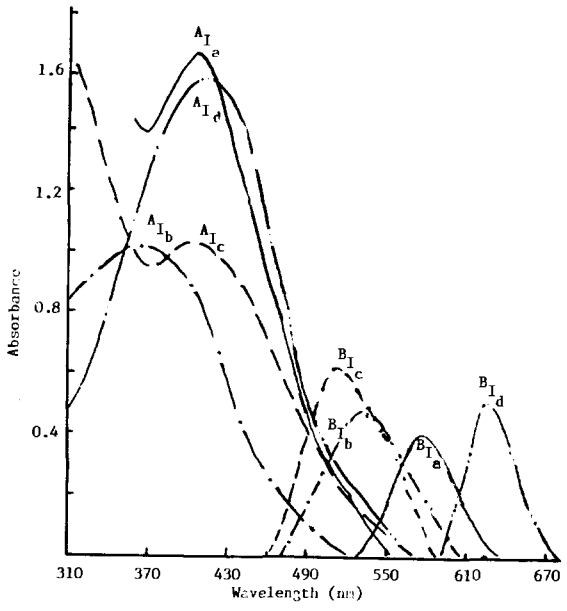

Fig. 2. Absorption spectra of: (A) 1×10^{-4} M ligands I_{a-d} at pH 7.0, 7.5, 8.5 and 7.0 against buffer of the same pH value. (B) 1×10^{-4} M ligands $I_{a-d} + 1 \times 10^{-4}$M Ce(III) at pH 7.0, 7.5, 8.5 and 7.0 against 1×10^{-4} M ligands (I_{a-d}) at the same pH value.

tion ranges 0.10–2.50, 0.05–3.00, 0.05–3.75 and 0.10–3.50 μg ml^{-1} respectively in the measured solutions. They have molar absorptivities of 2.58, 2.43, 2.39 and 2.28 $\times 10^4$ l mol^{-1} cm^{-1} and Sandell sensitivities of 5.4, 5.8, 5.9 and 6.1 ng cm^{-2} respectively. For more accurate results Ringbom optimum concentration ranges were established and were found to be 0.2–2.25, 0.2–2.60, 0.2–3.50 and 0.2–3.30 μg ml^{-1} using $\mathbf{I_a}$, $\mathbf{I_b}$, $\mathbf{I_c}$ and $\mathbf{I_d}$ respectively.

Although the proposed method offers a sensitivity equal to that of Gaokar and Eshawar [11], the proposed method showed longer stabilities of the complexes formed: 3.0, 4.5, 6.0 and 5.0 h using $\mathbf{I_a}$, $\mathbf{I_b}$, $\mathbf{I_c}$ and $\mathbf{I_d}$ respectively compared to stabilities of 1.5 and 2.0 h using 4-(2-thiazolylazo) resorcinol and 1-(2-thiazolylazo)-2-naphthal respectively [11].

3.7. Effect of foreign ions

The interference of various ions in the determination of cerium(III) was studied. The tolerance limit was set as that which causes an error of $\pm 2.0\%$ in the determination of 2.0 μg of Cerium(III) per millimeter. EDTA caused a negative interference due to its complexing action on Ce(III), hence decreasing the effective concentration of the Ce(III)–bisazo-β-diketone complexes. Mn(II), Ni(II), Cu(II), Co(II), Hg(II), Fe(III), Sc(III), Y(III) and La(III) caused positive interferences based on their ability to form complexes with the bisazo-β-diketone which absorbed in the same spectral region as the Ce(III) complexes. The tolerance limits of the various ions are given in Table 1.

Comparison of the proposed method with others (Table 2) shows that the proposed method is simple, rapid, sensitive and selective. It does not require heating, standing time or extraction with organic solvents.

3.8. Precision and accuracy

The relative standard deviation and relative mean error, calculated from 10 replicate determinations with 2.0 μg of Ce(III) per millilitre were found to be $\pm 0.88\%$ and $\pm 0.65\%$ for the Ce(III)–$\mathbf{I_a}$ system, $\pm 0.51\%$ and $\pm 0.33\%$ for the Ce(III)–$\mathbf{I_b}$ system, $\pm 0.67\%$ and $\pm 0.42\%$ for the Ce(III)–$\mathbf{I_c}$ system and $\pm 0.75\%$ and $\pm 0.65\%$ for the Ce(III)–$\mathbf{I_d}$ system.

3.9. Analytical applications

3.9.1. Determination of cerium (IV)

It was found to be possible to use the described method for the determination of Cerium(IV) after prior reduction to Cerium(III) with a reducing agent. Hence 2 ml of solution containing 50 μg of Cerium(IV) in a 25 ml measuring flask was reduced with 300 μg of hydroxylammonium chloride and the resulting cerium(III) solution was analysed with reagent $\mathbf{I_a}$, $\mathbf{I_b}$, $\mathbf{I_c}$ or $\mathbf{I_d}$, as described in Section 2.3 indicating the same sensitivity and limits of determination as in the case of Ce(III).

3.9.2. Determination of cerium in monazite samples

In order to confirm the usefulness of the proposed method, it has been applied to the determina-

tion of Cerium(III) as Ce_2O_3 in two monazite samples. The results observed are compared with those obtained using the atomic absorption technique (Table 3) and indicate that the method is reliable and accurate.

The results obtained by the proposed method were compared with those of the AAS method using the t-test for accuracy and the F-value for the assessment of precision [18] for five degrees of freedom and a 95% confidence level. The calculated values did not exceed the corresponding theoretical values, indicating insignificant differences between the results (Table 3).

4. Conclusion

The data obtained above indicate that the proposed method described for the spectrophotometric determination of Ce(III) ions is quite rapid, precise and sensitive. Thus the chromogenic reagents utilised in the described method above can safely be used under the proper conditions for the satisfactory analysis of Ce(III) ion in solution. The proposed method was successfully applied to the determination of cerium in two different monazite samples. The method also allows the determination of Ce(IV) after prior reduction to Ce(III).

References

[1] S.S. Shukurov, F.M. Shenyakin and N.N. Basargin, Dokl. Akad. Nauk Tadzh. SSR, 13 (1970) 36 (Anal. Abst., 20 (1971) 2363).
[2] A.I. Kirillov, L.P. Shaulina and N.A. Vlasov, izv. Vyssh. Uchebn. Zaved., Khim, Khim. Tekhnol., 18 (1975) 551 (Anal. Abstr., 31 (1976) 1870).
[3] K.N. Munshi and A.K. Dey, Anal. Chem., 36 (1964) 2003.
[4] L.S. Serdyuk and V.S. Smirnaya, Zh. Anal. Khim., 20 (1965) 191.
[5] E.A. Bashirov, Azerb. Khim. Zh., 3 (1969) 97 (Anal. Abstr., 20 (1971) 1583)
[6] E. Hlner, Z. Chem. Lpz., 5 (1965) 389 (Anal. Abstr., 14 (1967) 615).
[7] J. Herrington and K.C. Steed, Anal. Chim. Acta, 22 (1960) 180.
[8] H. Yoshizo and N. Hiroshi, Bunseki Kagaku, 17 (1968) 824.
[9] S.B. Savvin, T.V. Petrova and P.N. Romanov, izv. Akad. Nauk SSSR, Ser. Khim., 6 (1972) 1257 (Anal. Abstr., 24 (1973) 2115).
[10 R.H. Hovind, Analyst, 100 (1975) 769.
[11] U.G. Gaokar and M.C. Eshwar, Analyst, 111 (1986) 1393.
[12] H.A. Dessouki, R.M. Issa and M.M. Moustafa, Acta Chim. Hung., 126 (1989) 653.
[13] F.J. Welcher, Analytical Uses of Ethylendiaminetetraacetic Acid, Van Nostrand Reinhold, New York, 1958, p. 176
[14] H.T.S. Britton, Hydrogen Ions, 4th edn. Chapman and Hall, London, 1952.
[15] R.M. Issa, A.K. Ghomeim, E.M. Deifallah and M.M. Moustafa, J. Indian Chem. Soc., 71 (1994) 377.
[16] R.M. Issa, F.A. Aly, M. Gaber and M.I. Ayad, Egypt. J. Chem., 29 (1986) 49.
[17] A.E. Harvey and D.L. Manning, J. Am. Chem. Soc., 71 (1950) 4488.
[18] J.C. Miller and J.N. Miller, Statistics in Analytical Chemistry, 2nd edn., Ellis Horwood, Chichester, UK, 1988.
[19] J.M. Pan, Yuanzineng Kexue Jishu (At. Energy Sci. Technol.), 6 (1983) 722.
[20] S.B. Savvin, Zh. Anal. Khim., 17 (1962) 785.
[21] S.B. Savvin, R.F. Propistsova and R.V. Strel'nikova, Zh. Anal. Khim., 24 (1969) 31.
[22] C.-G. Hsu, H. Li and J.M. Pan, Talanta, 41 (1994) 1357.
[23] Q.-Z. Zhai, Talanta, 41 (1994) 703.
[24] B.K. Pal., B.K. Mitra and S.P.D. Thakur, J. Indian Chem. Soc., 65 (1988) 862.

ELSEVIER

Talanta 44 (1997) 319–326

Talanta

Determination of nanogram levels of zirconium by chelating ion exchange and on-line preconcentration in flow injection UV–visible spectrophotometry

Rajesh Purohit[1], Surekha Devi*

Department of Chemistry, Faculty of Science, M.S. University of Baroda, Baroda-390 002, India

Received 21 February 1996; revised 11 June 1996; accepted 25 June 1996

Abstract

Trace quantities of zirconium were preconcentrated on a series of chelating resins. The experimental conditions for preconcentration such as pH, time and metal ion concentration were optimized for the batch processes. Continuous flow manifolds were developed for the on-line preconcentration of zirconium using microcolumns containing chelating resins. Calibration plots were obtained with correlation coefficients of 0.9990 ± 0.0008. The determination of zirconium was performed using Xylenol Orange at 535 nm. Binary and ternary mixtures of zirconium, thorium and titanium did not show any cross-contamination during column chromatographic separation. © 1997 Published by Elsevier Science B.V.

Keywords: Chromatographic separation; Flow injection; Preconcentration; Zirconium

1. Introduction

The determination of trace amounts of metal ions by on-line preconcentration through liquid–liquid extraction or ion exchange and flow injection analysis has been reported for most metal ions. However, there are few reports on the determination of zirconium using flow injection analysis. Zirconium, being transparent to thermal neutrons, is widely used in nuclear reactors. It is highly active metal but, like aluminium, has a tendency to form a stable cohesive protective oxide film. Hence nanogram level determinations of zirconium are critically important. Various types of supports such as alumina [1], Chelex-100 [2], resin 122 [3] and 8-hydroxyquinoline (oxine)-based resins [4] have been reported for the preconcentration of metal ions before determination. The reported chelating resins containing oxine groups [5–7] exhibited low metal exchange capacities and slow exchange rates. Attempts were made to improve these properties but these resins required moist storage and were unstable at $\geqslant 2$

* Corresponding author.

[1] Present address: Gujarat Jalseva Training Institute, Gandhinagarz-382015, India.

PII S0039-9140(96)02032-2

Table 1
Physico-chemical properties of the resins [a]

Property	8HOQFR	8HOQFHQ	8HOQFuR	8HOQFuHQ	8HOQBR
Moisture content (g g^{-1})	0.03	0.03	0.64	1.98	1.51
True density (g cm^{-3})	1.40	1.50	1.25	1.16	1.18
Void volume (cm^3 g^{-1})	0.78	0.66	0.53	0.49	0.63
Sodium exchange capacity (mmol g^{-1})	4.60	5.00	2.80	3.30	2.60
$t_{1/2}$ for sodium exchange (min)	7.0	4.0	10.0	12.0	24.0
Zr(IV) exchange capacity (m mol g^{-1})	0.42	0.46	0.42	0.46	0.46
$t_{1/2}$ for 0.1 M Zr(IV) exchange (min)	17.0	23.0	23.0	24.0	14.0
K_d (distribution coefficient for 0.1 M Zr(IV) at pH 4–5)	51.0	60.0	51.0	60.0	60.0

[a] Abbreviations represent resins synthesized using 8HOQ = 8-hydroxyquinoline, F = formaldehyde, Fu = furfuraldehyde, B = benzaldehyde, R = resorcinol and HQ = hydroquinone.

M acid conditions. Oxine-based chelating resins synthesized by a modified route have been reported [8] which are stable above 2 M acid conditions and do not require moist storage. They have been used successfully for the preconcentration and separation of copper [8], nickel [9], zinc [10] lead [11] and cadmium [10].

Preconcentration of zirconium was carried out by Blasius and Kynst [12] using catechol *O,O*-diacetic acid derivatives. Dowex 50W X4 was used by Fritz and Palmer [13] whereas Vernon [14] and Phillips [15] reported poly(hydroxamic acid) resins for the preconcentration of zirconium. We report here the use of oxine-based resins for the preconcentration of zirconium at the batch level and an on-line continuous flow method.

2. Experimental

2.1. Reagents

AR-grade zirconium oxychloride and high-purity deionized water were used to prepare a standard solution of zirconium. The zirconium solution was standardized using a colorimetric method [16].

Acetate buffers of different pH were prepared from 0.2 M sodium acetate and acetic acid. Xylenol Orange concentration of 0.5% (w/v) was prepared freshly.

2.2. Synthesis of resins

Resins based on 8 hydroxyquinoline (8HOQ), resorcinol (R) or hydroquinone (HQ) and formaldehyde (F), furfuraldehyde (Fu) or benzaldehyde (B) cross-linking agents were synthesized as described earlier [8]. the relevant physico-chemical properties of the resins are given in Table 1. The series of resins were used for batch and column chromatographic studies of zirconium exchange. The optimum pH for the exchange of zirconium and $t_{1/2}$(time required for 50% exchange of metal ions) in batch processes were determined according to literature methods [17]. Zirconium was determined colorimetrically [16] in the supernatant solution and also on elution from the resin.

The kinetics of the zirconium exchange and the mode of diffusion of zirconium towards the resin were determined through an interruption test [17, 18] and were also confirmed by the method reported by Nativ et al. [19]. During the interruption test, resin beads were interrupted by removing them from the solution for 10 min and then reimmersing them in the solution, and metal exchange was further studied. From the nature of the plot of percentage exchange against time, the mode of diffusion of the metal was determined [15]. The efficiency of elution of zirconium from the resin was tested by using various eluents of different strength.

Table 2
Column characteristics[a]

Property	8HOQFR	8HOQFHQ	8HOQFuR	8HOQFuHQ	8HOQBR
Column length (cm)	17.5	17.5	9.0	10.5	9.3
Interstitial volume (V_0, cm^3)	9.2	9.8	4.8	5.2	4.6
Breakthrough capacity (mequiv g^{-1})	0.043	0.048	0.082	0.055	0.039
Total capacity (mequiv g^{-1})	0.24	0.32	0.31	0.30	0.23
Degree of utilization [b]	0.18	0.15	0.27	0.18	0.17

[a] Metal concentration 1 mg cm^{-3}; flow rate 1 cm^3 min^{-1}.
[b] Breakthrough capacity/total capacity.

2.3. Chromatographic separations

Chromatographic columns of 10–18 cm length and 7 mm i.d. were prepared using synthesized resins: 8HOQFR, 8HOQFHQ, 8HOQFuR, 8HOQFuHQ and 8HOQBR. Breakthrough and column capacities and interstitial volumes were determined according to the reported methods [20] and results are given in Table 2. Binary and ternary mixtures of zirconium, titanium and thorium containing 400 μg cm^{-3} metal in ratios of 1:1 and 1:1:1 were passed through the column at the pre-established pH and a flow rate of 1 cm^3 min^{-1}. The columns were thoroughly washed with deionized water. Separation of metals was achieved by following the selective desorption technique. Cross-contamination in the separation was studied by estimating each component individually in all fractions of the column effluent.

2.4. On-line preconcentration of zirconium

A continuous flow manifold for the preconcentration of zirconium at the nanogram was constructed as shown in Fig. 1. A Gilson Minipuls peristaltic pump was used along with a Rheodyne RH 5020 rotary injection valve. Microcolumns of 40 mm length and 2 mm i.d. containing the resins under study were connected to the manifold using 0.5 mm i.d. Teflon tubing. A UV–visible spectrophotometer with a 20 μl flow cell was used as a detector. The absorbance vs. time response was recorded on an x–t chart recorder at 535 nm. Experimental conditions influencing the extent of preconcentration, such as pH, microcolumn length, flow rate and metal concentration, were optimized. The chelated zirconium(IV) was eluted from the microcolumns by injecting 20 μl of 2 M hydrochloric acid followed by the appropriate acetate buffer to avoid carryover of the samples. A three-way valve was used to control the flow of zirconium solution and buffer.

3. Results and discussion

The relevant physico-chemical properties of the resins are given in Table 1. These resins were further used to study the exchange of zirconium(IV) ions. The nature of the cross-linking agent and the type of monomer play important roles in the sodium exchange process and resins containing hydroquinone always showed a higher exchange capacity than the corresponding resorcinol-containing resins. Variations in the cross-linking agent affected the exchange capacity considerably. However, for the exchange of zirconium such variations in the nature of resins had little effect on the chelating properties or on the $t_{1/2}$ values.

The effect of pH on zirconium exchange is illustrated in Fig. 2. The maximum exchange was observed at pH 4, suggesting potential use of resins in acidic effluent treatment. The zirconium selectivity order of the resins based on the distribution coefficient K_d and the exchange capacity was observed to be 8HOQFHQ = 8HOQFuHQ = 8HOQBR > 8HOQFR = 8HOQFuR. The study of the effect of the zirconium ion concentration on the exchange capacity indicated the exchange process is concentration dependent and all the resins, irrespective of their structure, show saturation at a 0.1 M zirconium concentration.

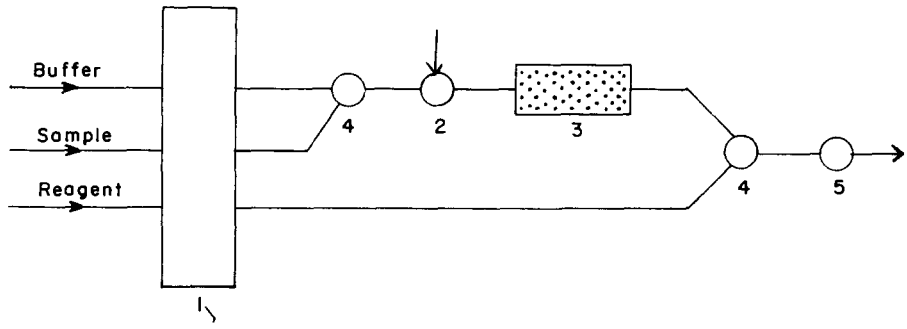

Fig. 1. Flow injection manifold for on-line preconcentration and determination of Zr(IV) using Xylenol Orange as reagent. 1, Peristaltic pump; 2, injection valve; 3, resin column; 4, three-way valve; 5, detector.

From the kinetics of the zirconium exchange, it was observed that complete exchange takes place in less than 4 h and the $t_{1/2}$ values for 8HOQFR, 8HOQFHQ, 8HOQFuR, 8HOQFuHQ and 8HOQBR are 17, 23, 30, 24 and 14 min, respectiviely. The exchange process was observed to be diffusion controlled through the interruption test. As discussed earlier in the interruption test, the interruption pause gives time for the concentration gradient in the beads to level off, hence resulting in an increased exchange rate after reimmersion of the resin particles in the particle diffusion controlled process. In film diffusion, no such concentration gradient exists in the beads and the exchange rate depends on the concentration differences across the film. In this case, interruption does not affect the concentration across the film and hence has no effect on the exchange rate. From the nature of the plots, it is observed that zirconium exchange is a particle diffusion and not a film diffusion process. Particle diffusion was also confirmed with the mathematical model proposed by Nativ et al. [19]. A plot of time vs. $[1-3(1-x)^{2/3}+2(1-x)]$ was constructed, where x is the fractional conversion of the resin, which is the ratio between the measured and maximum exchange capacities. According to this model, film diffusion gives a straight line passing through the origin. The plots with straight line giving an intercept on the abscissa indicate that the diffusion is not a film diffusion but is a particle diffusion process (Fig. 3) in zirconium exhange.

The simple Langmuir isotherm equation [21] for the adsorption of a single adsorbate on a single site surface is still frequently applied in ion-exchange reactions with specific assumptions. The first assumption is that the selectivity coefficient or separation factor remains unchanged or hardly changed during the exchange involved, and the second is that for homovalent and heterovalent exchange, the concentration of one of the ions or of the adsorbed solution is constant. Based on these assumptions, Misak [22] derived certain equations for the study of ion exchange through the Langmuir isotherm for single site heterovalent exchange.

$$\frac{C_A}{q_A}=\frac{C_A}{Q}\left(1-\frac{m}{\alpha n}\right)+\frac{C_0}{\alpha n Q}$$

where C_A = equilibrium concentration of exchanging ion A in solution (mol cm^{-3}), q_A = amount of metal A sorbed (mequiv. g^{-1}), Q = maximum sorption capacity (mequiv g^{-1}), α = separation factor and C_0 = initial concentration of ion A in the solution.

This equation was applied to the data obtained from the kinetic study of zirconium exchange at 0.1 M concentration. From the plot of C_A/q_A against C_A the exchange capacity Q was calculated from the slope, taking $m=4$ and $n=1$ for zirconium ion and resin. The value of Q calculated graphically using the equation based on the Langmuir isotherm for ion exchange agrees well with the experimental value. Hence the proposed

mathematical equation for ion exchange is assumed to be valid with the above-mentioned assumption. From the results for Q and α selectivity coefficient K was calculated by using the equation

$$K = \alpha^{n} \left(\frac{q_A/Q}{C_A} \right)^{n-m}$$

and was found to be 0.04986. It was observed that the selectivity coefficient for the resins under study remains almost unchanged, indicating the similar behaviour of the resins towards zirconium exhange.

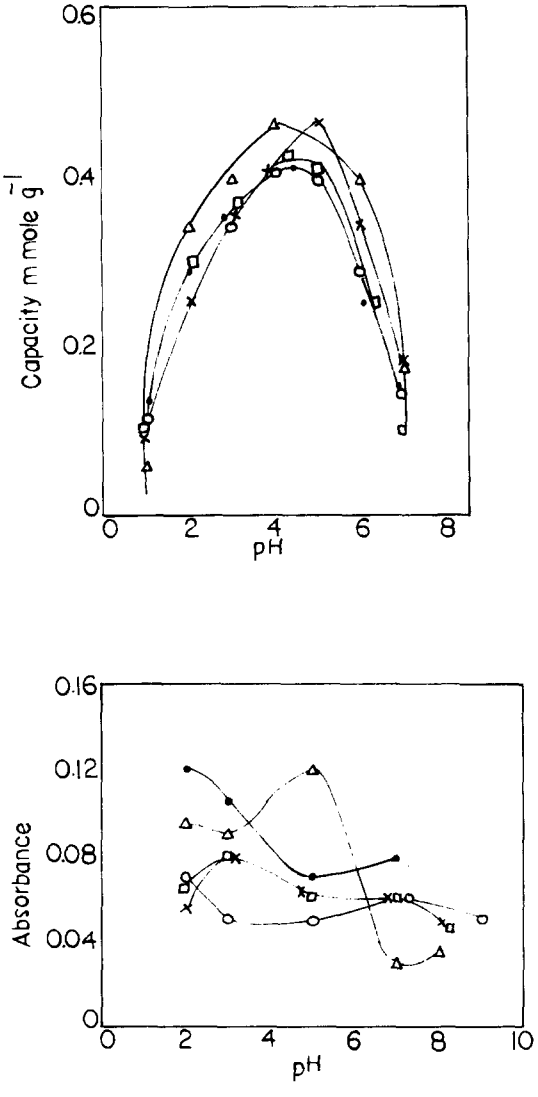

Fig. 2. Effect of pH on zirconium exchange. ●, 8HOQFR; ×, 8HOQFHQ; O, 8HOQFuR; Δ, 8HOQFuHQ; □, 8HOQBR.

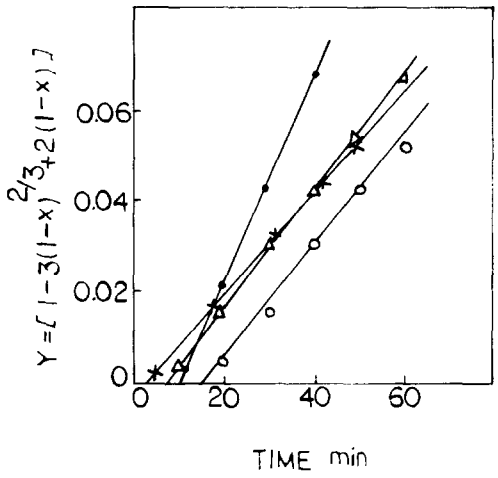

Fig. 3. Interruption test for exchange process. Symbols as in Fig. 2

3.1. Elution of zirconium from resins

Various eluents of different strengths were used for the elution of zirconium from the resins. It was observed that zirconium can be quantitatively eluted with 0.2–1.0 M hydrochloric acid, sulphuric acid, nitric acid, sodium citrate, sodium tartrate and potassium thiocyanate, whereas phosphoric acid, perchloric acid, sodium chloride and thiourea were not able to elute zirconium from the resins.

3.2. Binary and ternary separations

Volumes of 25 cm^3 of mixtures of zirconium and titanium or zirconium and thorium solutions each containing the metal ions in a 1:1 ratio were passed through the columns with characteristic properties as given in Table 2 at pH 5 and a flow rate of 1 cm^3 min^{-1}. The column effluent did not show any metal, confirming quantitative uptake of the metal ions. The element systems were selected in such a way that no cross-contamination was observed. Each aliquot was analysed for the metals in the mixture. Zirconium and titanium

Table 3
Efficiency of recovery of zirconium, titanium and thorium from binary and ternary mixtures.

Mixture	Resin	Zirconium			Titanium			Thorium		
		Taken (mg)	Recovered (mg)	Recovery (%)	Taken (mg)	Recovered (mg)	Recovery (%)	Taken (mg)	Recovered (mg)	Recovery (%)
Binary	8HOQFR	10	10.11	101.1	10	10.28	102.8			
	8HOQFHQ	10	10.07	100.7	10	10.36	103.6			
	HOQFur	10	10.12	101.2	10	9.92	99.2			
	8HOQFuHQ	10	09.86	98.6	10	10.37	103.7			
	8HOQBR	10	10.22	102.2	10	9.98	99.8			
	8HOQFR	10	10.28	102.8				10	10.11	101.1
	8HOQFHQ	10	10.36	103.6				10	10.70	100.7
	8HOQFur	10	9.92	99.2				10	10.12	101.3
	HOQFuHQ	10	10.22	102.22				10	9.86	98.7
	HOQBR	10	9.89	99.8				10	10.37	103.7
Ternary	8HOQFR	10	10.28	102.8	10	10.80	100.8	10	10.11	101.1
	8HOQFHQ	10	10.04	100.4	10	10.20	102.0	10	10.07	100.1
	HOQFuR	10	10.24	102.4	10	9.88	98.8	10	10.12	101.1
	HOQFuHQ	10	10.08	100.8	10	10.29	102.9	10	9.86	98.6
	8HOQF	10	9.98	99.80	10	10.16	101.6	10	10.37	103.7

Values given are the means of five measurements (standard deviations 0.158–0.246).

[16] were determined colorimetrically using Xylenol Orange and chromotropic acid, respectively, and thorium titrimetrically using EDTA. Zirconium was masked with potassium oxalate wherever necessary. The results are given in Table 3 and in Fig. 4. The results of triplicate determinations showed 99.2–102.8% recoveries. The separation of ternary mixtures of zirconium, titanium and thorium at pH 5 was achieved without any cross-contamination using specific eluents as shown in Fig. 4. The observed recoveries for triplicate sets were 98.8–102.8%, as shown in Table 3.

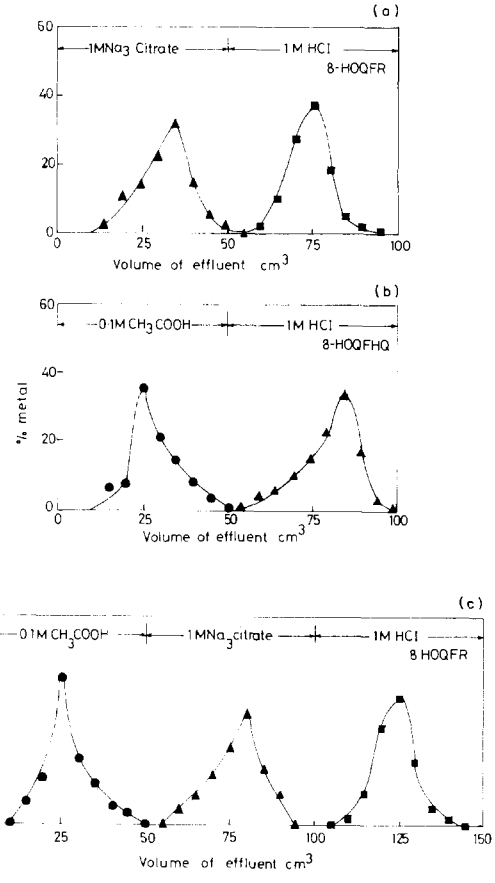

Fig. 4. Separation of (▲) zirconium, (■) titanium and (●) thorium from mixtures (a) Zirconium–titanium; (b) thorium–zirconium; (c) thorium–zirconium–titanium. Volume of solution, 25 cm^3; flow rate, 1 cm^3 min^{-1} amounts of metal 10 mg each.

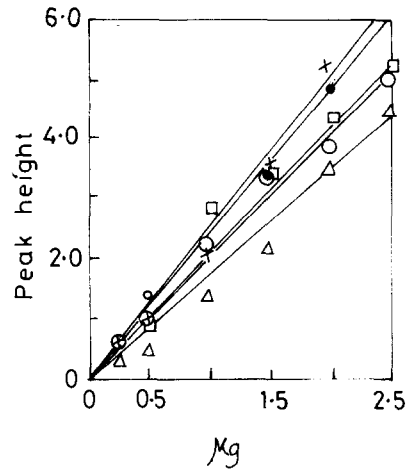

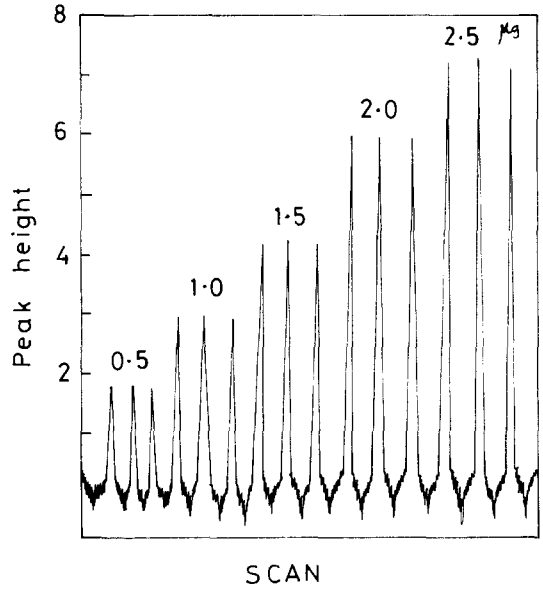

Fig. 5. Calibration of zirconium(IV). Amounts of Zr(IV) 25, 50, 75, 100, 125 and 150 ng; pH, 3; Xylenol Orange concentration 0.01% (w/v); eluent 20 μl of 2 M HCl. Symbols as in Fig 2.

3.3. Flow injection system

The determination of zirconium at nanogram levels was carried out after on-line preconcentra-

tion on microcolumns containing 8HOQFR, 8HOQFHQ, 8HOQFuR, 8HOQFuHQ and 8HOQBR resins in a continuous flow system as shown in Fig. 1. Solutions containing 50 ng cm^{-3} (1×10^{-7} M) zirconium were passed through the systems at a flow rate of 3 cm^3 min^{-1}. Continuous monitoring of the column effluents showed a quantitative uptake of the zirconium by all the resin columns. From the study of the effect of pH on the on-line preconcentration in the flow system than in a batch system (Fig. 2). However, 20 μl of 2 M hydrochloric acid could elute zirconium quantitatively from all the resin columns. The dispersion of the system under study was calculated by using 5 μg cm^{-3} of zirconium solution in the sample channel (Fig. 1) and also injecting 20 μl of 5 μg cm^{-3} of zirconium solution through the manifold with an empty microcolumn and also without a microcolumn. Introduction of the microcolumn did not influence the dispersion coefficient to a significant extent. The dispersion coefficient was calculated to be 2.2. The sharp elution peaks obtained showed faster kinetics during exchange processes.

From the study involving different column lengths for the preconcentration, it was observed that 4 cm long columns of 2 mm i.d. are sufficient for the preconcentration and longer (>6 cm) columns increase the dispersion. Similarly, a 2 cm^3 min^{-1} flow rate was observed to be optimum whereas at lower and higher flow rates either the peaks were not sharp or greater dispersion was observed.

A calibration plot for the preconcentration of 5 cm^3 of zirconium solution in the conentration range 0.5–2.5 μg cm^{-3} was obtained for each resin after elution of zirconium with 20 μl of 2 M hydrochloric acid. The results were recorded in triplicate as shown in Fig. 5. The regression coefficients were 0.9982, 0.9996, 0.9986, 0.9992 and 0.9976 for the resins 8HOQFR, 8HOQFHQ, 8HOQFuR, 8HOQFuHQ and 8HQOBR, respectively. The lowest detection limit was found to be 10 ng cm^{-3}, which was based on twice the standard deviation of the blank signals. The RSD values were in the range 0.8–2.65%.

From this study, it is concluded that the synthesized resins are effective for the preconcentration of zirconium at the nanogram level using a flow injection manifold. The colorimetric method established using Xylenol Orange reagent was successful for the determination of zirconium in the presence of Cu(II), Ni(II), Pb(II), Zn(II), Cd(II), Fe(II), Mn(II), Al(III), Cr(VI), Mo(VI), Th(IV), V(V), Ce(IV), UO_2^{2+} and Ti(IV) under optimized conditions. The efficient separation of zirconium from titanium and thorium was achieved by column chromatography. Continuous recording gave no signal during preconcentration, indicating the high efficiency of the resins for the removal of zirconium from the solution.

References

[1] Y. Zhang, P. Riby, A.G. Cox, C.W. McLeod, A.R. Date and Y.Y. Cheung, Analyst, 133 (1988) 125.
[2] S. Olsen, L.C.B. Pessenda, J. Ruzicka and E.H. Hansen, Analyst, 108 (1983) 908.
[3] Z. Fang, S. Xu and S. Zhang, Anal. Chim. Acta, 164 (1984) 41.
[4] F. Vernon and K.M. Nyo, Anal. Chim Acta, 93 (1977) 203.
[5] H. Berhard and F. Grass, Mikrochim, Acta, 3 (1966) 426.
[6] V. Sykara and F. Dubsky, Collect. Chem. Commun., 32 (1967) 3342.
[7] J.R. Parrish and R. Stevenson, Anal. Chim. Acta, 63 (1973) 403.
[8] R. Purohit and S. Devi, Talanta, 38 (1991) 753.
[9] R. Purohit and S. Devi, Analyst, 120 (1995) 555.
[10] R. Purohit and S. Devi, Analyst, 116 (1991) 825.
[11] R. Purohit and S. Devi, Anal. Chim. Acta, 259 (1992) 53.
[12] E. Blasius and G.Z. Kynst, Anal. Chem., 203 (1964) 321.
[13] J.S. Fritz and T.A. Palmer, Talanta, 2 (1962) 393.
[14] F. Vernon, Pure. Appl. Chem. 54 (1982) 2151.
[15] R.J. Phillips, U.S. Dept. Energy Rep., IS-T-910, 154 (1980).
[16] A.I. Vogel, Handbook of Quantitative Inorganic Analysis, Longman, London, 1987, p. 483.
[17] F. Helfferich, Ion Exchange, McGraw-Hill, New York, 1962, p. 256.
[18] Y.R.E. Kresmen and J.A. Kitchener, Discuss. Faraday Soc., 7 (1949) 90.
[19] M. Nativ, S. Godstein and G. Schmuckler. J. Inorg. Nucl. Chem, 37 (1975) 1951.
[20] J. Inczedy, Analytical applications of Ion Exchange, Pergamon Press, Oxford, 1966.
[21] I. Langmuir, J. Am. Chem. Soc., 40 (1918) 1170.
[22] N.Z. Misak, React. Polym. 21 (1993) 53.

ELSEVIER

Talanta 44 (1997) 327–337

Talanta

Extraction equilibria of some transition metal ions by bis(2-ethylhexyl)phosphinic acid

Yukio Nagaosa *, Yao Binghua

Faculty of Engineering, Fukui University, Bunkyo, Fukui 910, Japan

Received 18 December 1995; received in revised form 9 July 1996; accepted 12 July 1996

Abstract

Measurements of dimerization constants ($K_{d,HR}$) and distribution constants ($K_{D,HR}$) of bis(2-ethylhexyl)phosphinic acid (PIA-8) in three kinds of organic diluents were carried out by a potentiometric two-phase titration technique at 298 ± 0.1 K. Extraction of iron(III), zinc(II), copper(II), manganese(II), cadmium(II), cobalt(II) and nickel(II) by PIA-8 from 1.0 mol dm^{-3} ammonium sulfate solution into heptane was investigated as a function of pH and extractant concentration. The data have been analyzed both graphically and numerically to determine the stoichiometry of extracted species and their extraction constants. The extracted metal species were found to be $FeR_3 \cdot 2HR$ for iron(III), ZnR_2 and $ZnR_2 \cdot 3HR$ for zinc(II), $CuR_2 \cdot HR$ and $CuR_2 \cdot 5HR$ for copper(II), $MnR_2 \cdot 2HR$ and $MnR_2 \cdot 3HR$ for manganese(II), $CdR_2 \cdot 3HR$ for cadmium(II), $CoR_2 \cdot HR$ and $CoR_2 \cdot 4HR$ for cobalt(II) and $NiR_2 \cdot 3HR$ and $NiR_2 \cdot 6HR$ for nickel(II), respectively. © 1997 Elsevier Science B.V.

Keywords: Bis(2-ethylhexyl)phosphinic acid; Extraction equilibrium; Solvent extraction; Transition metal ions

1. Introduction

Organophosphorus acid extractants have been widely studied for the separation and recovery of several metals in acidic media [1–5]. Particularly, enhanced selectivity has been reported with dialkylphosphinic acids like bis(2,4,4-trimethylpentyl) phosphinic acid (Cyanex 272), e.g. in the separation of cobalt(II) and nickel(II) [6]. Cyanex 272 as an extractant, however, possesses a high selectivity for the separation of cobalt(II)–nickel(II) and an ability to reject calcium(II); two problems concerning the viscosity of the organic phase and the extraction rate have been reported. The polymers are formed in the organic phase as the loaded cobalt increases, and as a result the viscosity of the organic phase increases as reported by Komasawa et al. [7]. Consequently, the loading ability of the organic phase has to be limited to prevent any large increase in viscosity, and a subsequent decrease in mass transfer rates occurs. Dreisinger and Cooper [8] also reported that the extraction rate of metal ions by Cyanex 272 extractant was considerably lower than that with bis(2-ethylhexyl)phosphoric acid (D2EHPA).

Little is known about bis(2-ethylhexyl)phosphinic acid (PIA-8) as an organophos-

* Corresponding author. Fax: +81 776 278747; e-mail: nagaosa@acbio.acbio.fukui-u.ac.jp

PII S0039-9140(96)02047-4

phorus acid extractant for the separation by solvent extraction of transition metal ions to date. Therefore, we first have estimated the dimerization constants and the distribution constants of PIA-8 in some organic diluents by a potentiometric two-phase titration technique. The extraction equilibria of iron(III), zinc(II), copper(II), manganese(II), cadmium(II), cobalt(II) and nickel(II) by PIA-8 from 1.0 mol dm^{-3} ammonium sulfate solution into heptane have then been investigated. The stoichiometry of the extracted metal species and their conditional extraction constants have also been determined by means of numerical and graphical analyses. In this paper, the results of the studies will be discussed.

2. Experimental

2.1. Reagents and apparatus

PIA-8 was delivered from Daihachi Chemical Industry (Osaka, Japan). No further purification was made before use (the purity was 96.6%). Heptane of analytical reagent grade (Wako Pure Chemicals, Osaka, Japan), kerosene (a mixture of aliphatic hydrocarbons C_{11}–C_{13}, which had a density of 790 kg m^{-3} at 295 K, Nacalai Tesque, Kyoto, Japan) and Naphtezol M (a mixture of aromatic hydrocarbons containing 55% naphtens, 35% iso-paraffins and 10% *n*-paraffins, which had a density of 816 kg m^{-3} at 288 K, Nippon Petrochemistry, Tokyo, Japan) were used as organic diluents without purification. The standard stock solutions of iron(III), zinc(II), copper(II), cadmium(II), manganese(II), cobalt(II) and nickel(II) were prepared by dissolving their sulfates in 0.1 mol dm^{-3} sulfuric acid. All inorganic reagents were of analytical reagent grade and used without further purification.

An Iwaki Model 2366 KM Shaker was used to equilibrate the two phases. A Toa Model HM-30S pH meter (TOA Electronic, Tokyo, Japan) was used for pH measurements. Metal ion concentrations were determined by the titration method using ethylenediaminetetraacetic acid (EDTA) or a Seiko Model SPS-7000 Plasma Spectrometer (Seiko Electronic, Tokyo, Japan).

2.2. Procedures

2.2.1. Two-phase potentiometric titration

Equal volumes (35.0 cm^3 each) of distilled water and organic diluent were placed into a 100 cm^3 stoppered conical Erlenmeyer flask in a thermostatted water bath at 298 ± 0.1 K. A potentiometric two-phase titration was carried out while maintaining both the neutralized fraction constant and the phase ratio equal to unity. This was achieved by successively adding 1.0 ml of each of 0.100 mol dm^{-3} PIA-8 in organic diluent and 1.0 cm^3 of 5.00×10^{-2} mol dm^{-3} sodium hydroxide solution. The two phases were stirred for 1800 s and allowed to stand for 900 s. The pH value of the aqueous phase was then measured. Nitrogen was used to prevent the dissolution of carbon dioxide.

2.2.2. Measurement of extraction equilibrium

Equal volumes (15.0 cm^3 each) of organic and aqueous phases were placed in a 50 cm^3 separation funnel, and the two phases were then shaken for 600 s on the mechanical shaker at 298 ± 0.1 K.

Preliminary experiments showed that the extraction equilibria were accomplished for a shaking time of 600 s. The aqueous phase was prepared by diluting the standard stock solution, to which 2.0 mol dm^{-3} ammonium sulfate solution was added in order to maintain the ion strength constant. The initial concentration of metal ions was 2.00×10^{-2} mol dm^{-3}, and the initial concentration of PIA-8 in the organic phase ranged from 0.1–0.48 mol dm^{-3} as the dimeric acid [$(HR)_2$]. After phase separation, the pH value of the aqueous phase was measured by using the pH meter. The concentration of metal ions in the aqueous phase was determined by using the Plasma Spectrometer or by titration with 2.00×10^{-2} mol dm^{-3} EDTA using Cu-PAN (PAN was used for copper(II) and Tiron for iron(II)) as the indicator. The concentration of metal ion in the organic phase was calculated from the concentration of metal ion in the aqueous phase according to the mass balance law. The distribution ratio (D) was calculated in the usual manner.

3. Results and discussion

3.1. Aggregation and distribution of extractant

Organophosphorus acid extractants are known to be present as dimers in such organic diluents as heptane, toluene and carbon tetrachloride [9] and to be as monomers in methyl alcohol and *n*-decyl alcohol [10]. In general, it is important to know the aggregation degree of the extractant in organic solvents and the distribution of the extractant between the aqueous and organic phases in order to clarify the extraction mechanism of the metal ions.

Several equilibrium constants concerning PIA-8 as the extractant can be expressed as the following equations:

$$2(HR)_{org} = (HR)_{2,org}$$

$$K_{d,HR} = [(HR)_2]_{org}/[HR]^2_{org} \quad (1)$$

$$(HR)_{aq} = (HR)_{org}$$

$$K_{D,HR} = [HR]_{org}/[HR]_{aq} \quad (2)$$

$$(HR)_{aq} = H^+_{aq} + R^-_{aq}$$

$$K_a = [H^+]_{aq}[R^-]_{aq}/[HR]_{aq} \quad (3)$$

where $K_{d,HR}$, $K_{D,HR}$ and K_a are the dimerization constant, the distribution constant and the acid dissociation constant, respectively. In the case of the potentiometric two-phase titration, the two-phase dissociation constants of K_{aE} and K_{2aE} can be expressed by using K_a, $K_{D,HR}$ and $K_{d,HR}$ [11]:

$$K_{aE} = [H^+]_{aq}[R^-]_{aq}/([HR]_{aq} + [HR]_{org})$$
$$= K_a/(1 + K_{D,HR}) \quad (4)$$

$$K_{2aE} = [H^+]^2_{aq}[R^-]^2_{aq}/[(HR)_2]_{org} = K^2_{aE}/K_{d,HR} \quad (5)$$

then,

$$\log K_{d,HR} = pK_{2aE} - 2pK_{aE} \quad (6)$$

$$\log K_{D,HR} = pK_{aE} - pK_a \quad (7)$$

According to the mass balance law, the total concentration of extractant can then be written as

$$C_{HR} = [HR]_{org} + [HR]_{aq} + [R^-]_{aq} + 2[(HR)_2]_{org} \quad (8)$$

When Eqs. (4) and (5) are substituted into Eq. (8), the following equation is obtained.

$$\frac{C_{HR} - [R^-]_{aq}}{[H^+]_{aq}[R^-]_{aq}} = \frac{1}{K_{aE}} + \frac{2}{K_{2aE}}[H^+]_{aq}[R^-]_{aq} \quad (9)$$

Here the value of the $[R^-]_{aq}$ can be calculated from the mass balance [12]: $[R^-]_{aq} = ghC_{HR} + 10^{-pH} - 10^{pH-14}$, where g is the neutralization percentage, and h is the correction factor of the aqueous volume. Thus, a plot of $(C_{HR} - [R^-]_{aq})/([H^+]_{aq}[R^-]_{aq})$ against $[H^+]_{aq}[R^-]_{aq}$ should obtain a straight line with a slope of $2/K_{2aE}$ and an intercept of $1/K_{aE}$. As shown in Fig. 1, good linear relationships were obtained for PIA-8 in the diluents. From their intercepts and slopes obtained, further, the $K_{d,HR}$ and $K_{D,HR}$ values were calculated by using Eqs. (6) and (7), as summarized in Table 1 (where $pK_a = 4.48$ was determined in our previous paper [12]). The results indicate that

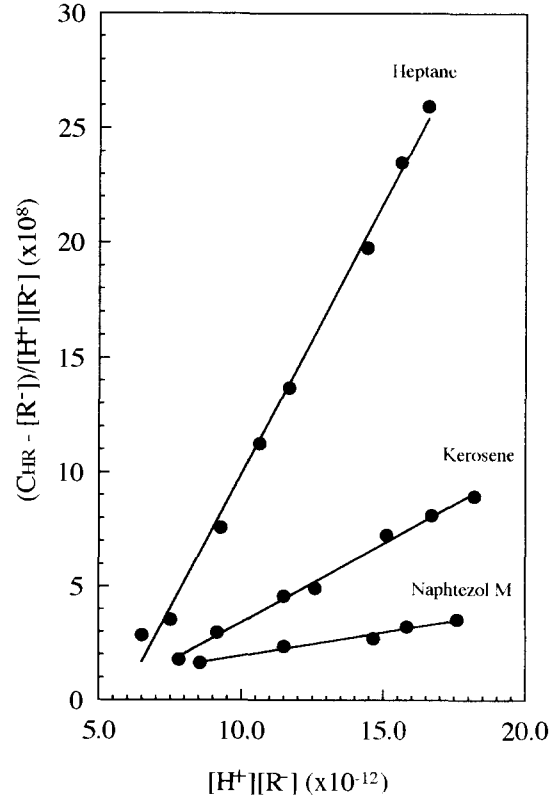

Fig. 1. Regression curves of titration data with PIA-8 solutions in various diluents.

Table 1
Dimerization constants and distribution constants of PIA-8 in various diluents at 298 K

Organic diluent	pK_{aE}	pK_{2aE}	$\log K_{d,HR}$	$\log K_{D,HR}$
Heptane	9.17	20.1	1.75	4.69
Kerosene	8.55	19.5	2.44	4.07
Naphtezol M	7.11	19.0	4.80	2.63

PIA-8 exhibited the largest $\log K_{D,HR}$ value and the smallest $\log K_{d,HR}$ value in the heptane/water system. In order to ascertain the validity of the potentiometric titration method used, the $K_{d,HR}$ and $K_{D,HR}$ values of Cyanex 272 in kerosene/water were also estimated to be $\log K_{d,HR} = 4.56$ and $\log K_{D,HR} = 3.20$, respectively. Both values are close to those already reported ($\log K_{d,HR} = 4.20$, $\log K_{D,HR} = 2.97$ for Cyanex 272 in the kerosene/water system) [13]. Accordingly, it is concluded that the potentiometric two-phase titration technique is acceptable to estimate the dimerization and distribution constants of PIA-8.

3.2. Extraction equilibria of metal ions

It is well known that transition metal ions easily form the corresponding ammine complexes with ammonia in aqueous media.

$$M_{aq}^{n+} + pNH_3 = [M(NH_3)_p]_{aq}^{n+} \tag{10}$$

$$\beta_p = \frac{[M(NH_3)_p^{n+}]_{aq}}{[M^{n+}]_{aq}[NH_3]_{aq}^{p}} \tag{11}$$

where β_p is the stability constant of the complex $[M(NH_3)_p^{n+}]_{aq}$ ($p = 1, 2, \ldots, 6$). For the system investigated, the constants $\beta_1 - \beta_6$ for cobalt(II) and nickel(II), and $\beta_1 - \beta_4$ for zinc(II), copper(II) and cadmium(II) are available except for iron(III) and manganese(II), respectively. Furthermore, the total concentration of the metal ion in ammonium sulfate solution can be expressed as follows:

$$C_{M,aq} = [M^{n+}]_{aq} + \sum [M(NH_3)_p]$$

$$= [M^{n+}]_{aq}(1 + \sum \beta_p [NH_3]^p) \tag{12}$$

The concentration of the free metal ion can therefore be calculated by using the following relationship:

$$[M^{n+}]_{aq} = \frac{C_{M,aq}}{1 + \sum \beta_p [NH_3]^p} \tag{13}$$

Assuming that the metal ion (M^{n+}) is extracted as a form of oligomerized species $(MR_n \cdot mHR)_x$ by the dimer PIA-8 ($(HR)_2$) into an organic diluent from aqueous media. The general extraction reaction can be expressed as follows:

$$xM_{aq}^{n+} + \frac{x(m+n)}{2}(HR)_{2,org}$$

$$= (MR_n \cdot mHR)_{x,org} + xnH_{aq}^{+} \tag{14}$$

The extraction equilibrium constant (K_{ex}) for this reaction is

$$K_{ex} = \frac{[(MR_n \cdot mHR)_x]_{org}[H^+]_{aq}^{xn}}{[M^{n+}]_{aq}^{x}[(HR)_2]_{org}^{x(m+n)/2}} \tag{15}$$

where n, m and x represent the valence of the metal ion, the coordination number of the extractant in the extracted species, and the oligomerization number of the extracted species, respectively. According to the mass balance law, the total concentration of metal ions in the organic phase, $C_{M,org}$, can be written as

$$C_{M,org} = \sum_{x=1} \sum_{m=1} x[(MR_n \cdot mHR)_x]_{org}$$

$$= \sum_{x=1} \sum_{m=1} xK_{ex}[M^{n+}]_{aq}^{x}$$

$$\times [(HR)_2]_{org}^{x(m+n)/2}[H^+]_{aq}^{-xn} \tag{16}$$

If the extracted metal species exists only as $(MR_n \cdot mHR)_x$ (x = a constant) in the organic phase, the following expression can be obtained:

$$C_{M,org} = [M^{n+}]_{aq}^{x}[H^+]_{aq}^{-nx} \sum_{m=1} xK_{ex}$$

$$\times [(HR)_2]_{org}^{x(m+n)/2} \tag{17}$$

or

$$\log C_{M,org} = x(\log[M^{n+}]_{aq} - n \log[H^+]_{aq}) + \log \sum_{m=1} xK_{ex}[(HR)_2]_{org}^{x(m+n)/2} \quad (18)$$

The value of the oligomerization number (x) of the extracted species can thus be obtained from the slope for the plots of $\log C_{M,org}$ against ($\log [M^{n+}]_{aq} - n \log [H^+]_{aq}$) at a constant extractant concentration. Table 2 summarizes the results of the slope analysis for several metal ions at 0.32 mol dm^{-3} extractant concentration [$(HR)_2$]. It can be seen that the regression straight lines with slopes close to unity were obtained at the low concentration of the metal ions investigated. this indicates that the metal ions were extracted as monomers ($MR_n \cdot mHR$), that is, $x = 1$.In the case of $x = 1$, the following expressions can be derived from Eqs. (13) and (17).

$$C_{M,org} = K_{ex}[(HR)_2]_{org}^{(m+n)/2}[M^{n+}]_{aq}[H^+]_{aq}^{-n} \quad (19)$$

$$C_{M,aq} = [M^{n+}]_{aq}(1 + \sum_{p=1} \beta_p[NH_3]_{aq}^p) \quad (20)$$

The distribution ratio D for the metal ion between the aqueous and organic phases becomes

$$\log D = \log K'_{ex} + (m+n)/2 \log [(HR)_2]_{org} + n\text{pH} \quad (21)$$

where $K'_{ex} = K_{ex}/(1 + \Sigma \beta_p[NH_3]^p)$ represents the conditional extraction constant of the metal ions.

Table 2
Results of slope analysis for the determination of x values in the extraction of metal ions by 0.32 mol dm^{-3} PIA-8 in heptane at 298 K[a]

Metal ion	$\log C_{M,org}$ against ($\log [M^{n+}]_{aq} - n \log[H^+]_{aq}$)			
	Intercept	Slope	Point	Coefficient
Fe(III)	−5.15	0.98	8	0.999
Zn(II)	−4.13	1.08	8	0.999
Cu(II)	−8.03	1.05	7	0.994
Mn(II)	−7.54	0.90	8	0.999
Co(II)	−7.91	0.92	8	0.999
Cd(II)	−7.07	0.93	7	0.997
Ni(II)	−13.4	1.12	8	0.995

[a] Aqueous phase: 0.02 mol dm^{-3} metal ion and 1.0 mol dm^{-3} ammonium sulfate solution; organic phase: 0.32 mol dm^{-3} PIA-8 in heptane; phase ratio: O/A = 1:1; shaking time: 600 s.

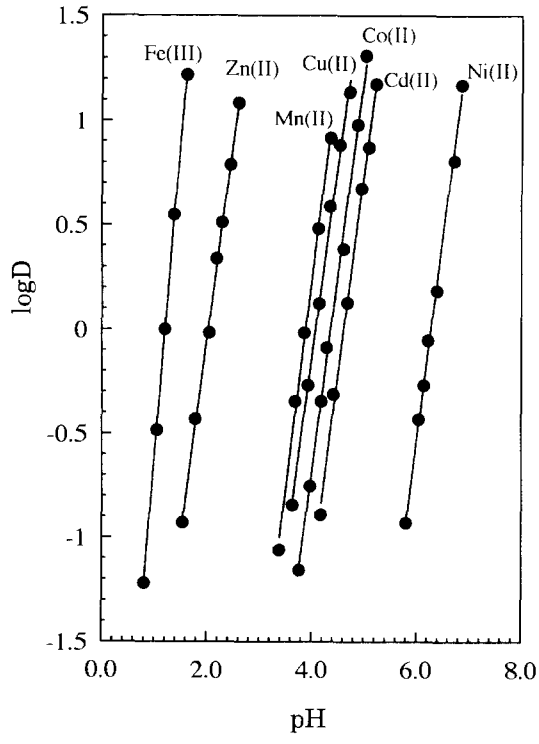

Fig. 2. Plots of log D against pH for the extraction of metal ions by PIA-8 in heptane. Organic phase: 0.32 mol dm^{-3} PIA-8 solutions in heptane; aqueous phase: 0.02 mol dm^{-3} metal ion in 1.0 mol dm^{-3} ammonium sulfate solution; shaking time: 600 s at a phase-volume ratio of 1:1.

Plots of log D against pH at a constant extractant concentration should therefore give a straight line of slope n. As is evident from Fig. 2, good linear relationships were obtained for all metal ions. The slopes were close to two for all divalent metal ions and three for iron(III). The results of $n = 2$ and 3 indicate that the extracted metal species included two and three ligand anions, respectively.

In order to investigate the stoichiometry of the extracted metal species, the plots of ($\log D - xn\text{pH}$) against $\log [(HR)_2]_{org}$ were carried out using the experimental data at a constant pH for each metal ion. Table 3 summarizes the results of the slope analysis. It can be seen that the m values were close to three and two for the extraction of iron(III) and cadmium(II), respectively. This indicates that iron(III) and cadmium(II) are predominantly ex-

Table 3
Results of slope analysis for the determination of m values in the extraction of metal ions by PIA-8 in heptane at 298 K[a]

Metal ion	$(\log D - n\mathrm{pH})$ against $\log[(HR)_2]_{org}$			Experimental value (m)
	pH	Slope	r	
Fe(III)	1.75	2.52	0.999	2.02
Zn(II)	2.02	1.74	0.998	1.58
Cu(II)	3.88	2.14	0.996	2.28
Mn(II)	4.07	2.35	0.998	2.69
Co(II)	4.36	2.09	0.999	2.20
Cd(II)	4.60	2.49	0.999	2.98
Ni(II)	6.28	2.69	0.999	3.38

[a] Aqueous phase: 0.02 mol dm^{-3} metal ion and 1.0 mol dm^{-3} ammonium sulfate solution; organic phase: 0.1–0.48 mol dm^{-3} PIA-8 in heptane; phase ratio: O/A = 1:1; shaking time: 600 s.

tracted as the forms $FeR_3 \cdot 2HR$ and $CdR_2 \cdot 3HR$ into the organic phase, respectively. The extracted species FeR_3 has already been reported for the extraction of iron(III) by mono(n-octyl)phosphinic and di(n-octyl)phosphinic acids [14]. This may be due to the relatively higher HR concentration used in this work. In the extraction of cadmium(II), on the other hand, the species $CdR_2 \cdot 3HR$ described above was found with bis(2-ethylhexyl)phosphoric acid in dodecane [14,15]. The different species $CdR_2 \cdot 2HR$ and $CdR_2 \cdot 3HR$ or $CdR_2 \cdot 4HR$ were also reported for the extraction of cadmium(II) by Cyanex 272 [16,17]. Table 4 gives their conditional extraction constants graphically determined by the slope analysis, together with those numerically calculated by the usual computer program [18]. Both constants were so coincident that the numerical calculation was valuable for the determination of the exact extraction constant for the one species extracted. In Table 3, on the other hand, the fractional values of m were obtained for the extraction of zinc(II), copper(II), manganese(II), cobalt(II) and nickel(II). This indicates that two or more kinds of metal species coexist in the organic phase. In this case, the stoichiometry of the extracted species should be determined by means of numerical analysis, instead of the slope analysis.

Table 4
Extracted species and conditional extraction constants for Fe(III) and Cd(II) with PIA-8 in heptane at 298 K

Metal ion	Extracted species	$-\log K'_{ex}$	
		Numerical[a]	Graphical[b]
Fe(III)	$FeR_3 \cdot 2HR$	3.44 ± 0.06	3.4
Cd(II)	$CdR_2 \cdot 3HR$	7.78 ± 0.07	7.7

[a] The results were obtained from the numerical calculation, and the error given corresponds to $3\sigma(\log K'_{ex})$, in which $\sigma(\log K'_{ex})$ was defined to be $(\Sigma((\log K'_{ex})_i - (\log K'_{ex})_{average})^2/(N_p - 1))^{1/2}$.
[b] The $\log K'_{ex}$ value was averaged from values obtained by plotting $(\log D - n\mathrm{pH})$ against $\log[(HR)_2]_{org}$ and $(\log D - (m+n)/2 \log[(HR)_2]_{org})$ against pH.

Assuming that two kinds of metal species are coextracted into the organic phase, Eq. (19) can be written as

$$C_{M,HR} = [MR_n \cdot iHR]_{org} + [MR_n \cdot jHR]_{org} \quad (22)$$

The distribution ratio D for the metal ion is then expressed as

$$D = \frac{[MR_n \cdot iHR]_{org} + [MR_n \cdot jHR]_{org}}{C_{M,aq}} \quad (23)$$

Substituting Eq. (15) into Eq. (23), the following equation can be obtained

$$\frac{D \cdot [H^+]^n_{aq}}{K'_{ex}(i) \cdot [(HR)_2]^{(i+n)/2}_{org}} = 1 + \frac{K'_{ex}(j)}{K'_{ex}(i)} [(HR)_2]^{(j-i)/2}_{org} \quad (24)$$

where $K'_{ex}(i)$ and $K'_{ex}(j)$ represent the conditional extraction constants of the metal ions extracted as the type $MR_n \cdot iHR$ and $MR_n \cdot jHR$, respectively.

Table 5
Extracted species and conditional extraction constants for Zn(II), Cu(II), Mn(II), Co(II) and Ni(II) with PIA-8 in heptane at 298 K

Metal ion	(i,j)	Extracted species	Q_{min} ($\times 10^2$)	$\sigma(\log D)$ ($\times 10^2$)	$-\log K'_{ex}(i)$	$-\log K'_{ex}(j)$
Zn(II)	(0,3)	ZnR_2, $ZnR_2 \cdot 3HR$	0.042	0.91	3.78 ± 0.03	2.96 ± 0.03
Cu(II)	(1,5)	$CuR_2 \cdot HR$, $CuR_2 \cdot 5HR$	0.278	2.36	6.89 ± 0.07	6.12 ± 0.07
Mn(II)	(2,3)	$MnR_2 \cdot 2HR$, $MnR_2 \cdot 3HR$	0.569	3.38	7.43 ± 0.08	6.79 ± 0.08
Co(II)	(1,4)	$CoR_2 \cdot HR$, $CoR_2 \cdot 4HR$	0.135	1.64	8.07 ± 0.05	7.43 ± 0.05
Ni(II)	(3,6)	$NiR_2 \cdot 3HR$, $NiR_2 \cdot 6HR$	0.019	0.62	10.56 ± 0.0	10.60 ± 0.02

Although the values of i, j and $K'_{ex}(i)$, $K'_{ex}(j)$ can be obtained by some graphical method [19–21], it is more convenient to determine them by means of numerical analysis [18]. Defining two variables, Y and X, and a parameter z as

$$\log Y = \log D - 2\mathrm{pH} - (i+n)/2 \log [(\mathrm{HR})_2]_{org} - \log K'_{ex}(i) \quad (25)$$

$$\log X = \frac{1}{z}(\log K'_{ex}(j) - \log K'_{ex}(i)) + \log[(\mathrm{HR})_2]_{org} \quad (26)$$

$$z = (j-i)/2 \quad (27)$$

and substituting Eqs. (25)–(27) into Eq. (24), the resultant equation is

$$\log Y = \log(1 + X^z) \quad (28)$$

Using Eq. (28), a set of theoretical curves of $\log Y$ against $\log X$ for different z values was constructed by the computer program, which was written for the system of two kinds of extracted species, and then compared with the experimental curves of $(\log D - 2\mathrm{pH} - (i+n)/2 \log [(\mathrm{HR})_2]_{org})$ against $\log [(\mathrm{HR})_2]_{org}$ for different i values. This program orders the computer to search for the best set of conditional extraction constants $K'_{ex}(i)$ and $K'_{ex}(j)$ by minimizing the error squares sum defined by

$$Q = \sum(\log D_{exp} - \log D_{calc})^2 \quad (29)$$

where D_{exp} is the distribution ratio of metal ions determined experimentally and D_{calc} is the value calculated by the computer program. This program also calculated the standard deviation $\sigma(\log D)$, defined by $\sigma(\log D) = (Q/(N_p - 1))^{1/2}$, where N_p is the total number of experimental points. The free reagent concentration $[(\mathrm{HR})_2]_{org}$ used in the plots given by Eq. (30) on a dimeric basis

$$[(\mathrm{HR})_2]_{org} = C_t - (i+j+n)/2C_{M,org} \quad (30)$$

where C_t and $C_{M,org}$ are the total concentration of extractant and the concentration of metal ion in the organic phase, respectively.

By superimposing the experimental curves on the theoretical model function, a position was found where the experimental curves coincide with one of the theoretical curves. In other words, the error squares sum Q is the smallest (expressed as Q_{min}) in this position. As seen from Fig. 3, the best fit was found to be $i = 0$, $z = 1.5$ for zinc(II), $i = 1$, $z = 2$ for copper(II), $i = 2$, $z = 0.5$ for manganese(II), $i = 1$, $z = 1.5$ for cobalt(II) and $i = 3$, $z = 1.5$ for nickel(II), respectively. This indicates that the metal species extracted into the organic phase may be considered to be ZnR_2 and $ZnR_2 \cdot 3HR$ for zinc(II), $CuR_2 \cdot HR$ and $CuR_2 \cdot 5HR$ for copper(II), $MnR_2 \cdot 2HR$ and $MnR_2 \cdot 3HR$ for manganese(II), $CoR_2 \cdot HR$ and $CoR_2 \cdot 4HR$ for cobalt(II), and $NiR_2 \cdot 3HR$ and $NiR_2 \cdot 6HR$ for nickel(II), respectively. The corresponding values of Q_{min} and $\sigma(\log D)$ are summarized in Table 5.

The extracted species described above were compared with the reported for the extraction of divalent metal ions with other organophosphorus acids. For the extraction of copper(II) and zinc(II), the m values of the extracted species are different from those obtained with Cyanex 272 in Isopar-H from 0.1 mol dm^{-3} sodium nitrate solution; the extracted species were determined to be $CuR_2 \cdot 2HR$ for copper(II), and $ZnR_2 \cdot HR$ and

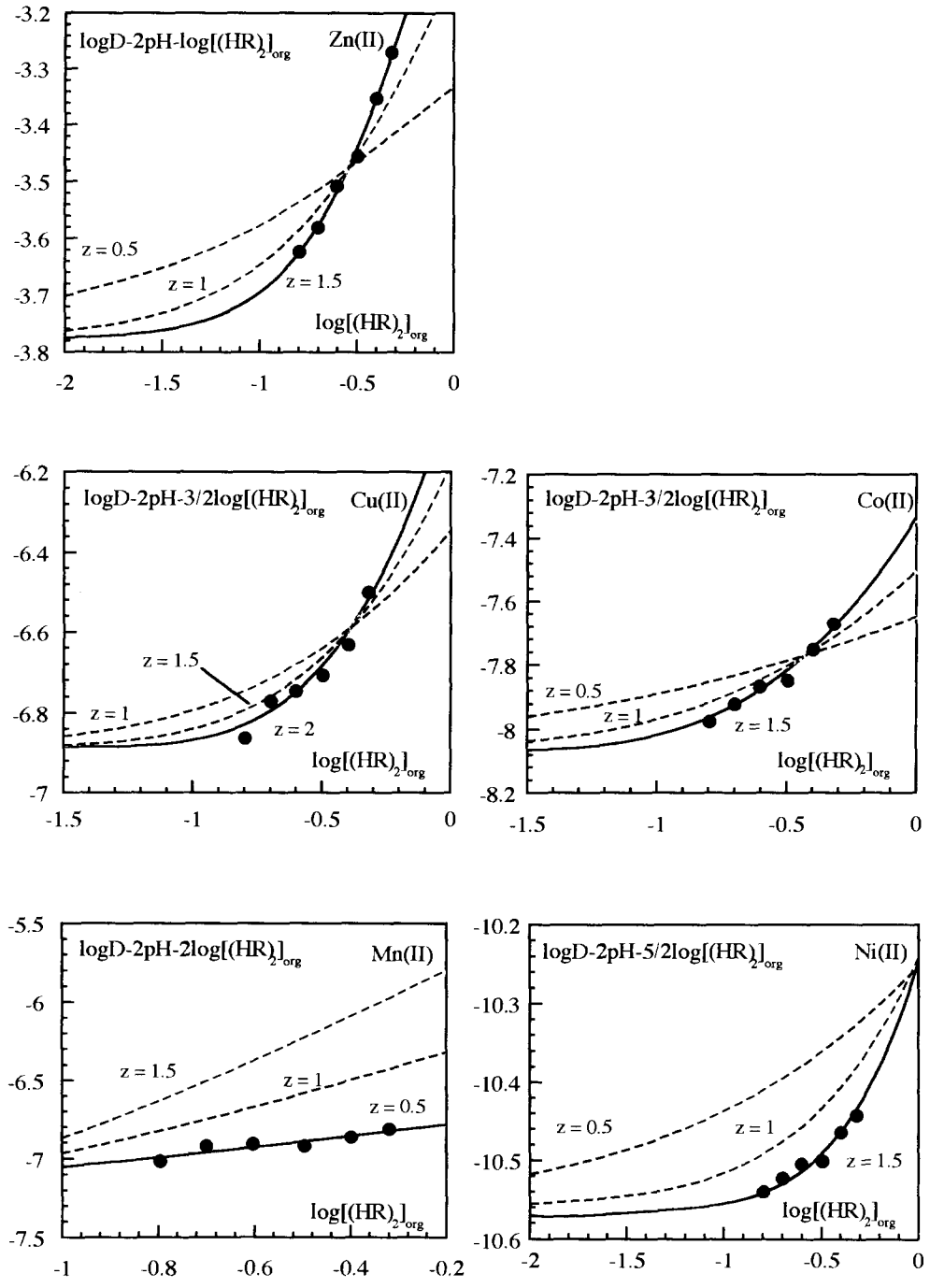

Fig. 3. Plots of $\log D - n\mathrm{pH} - (i+n)/2 \log[(\mathrm{HR})_2]_{org}$ against $\log[(\mathrm{HR})_2]_{org}$ for the extraction of metal ions by PIA-8 in heptane. The curves correspond to the theoretical function $\log(1 + X^z)$ for different z values.

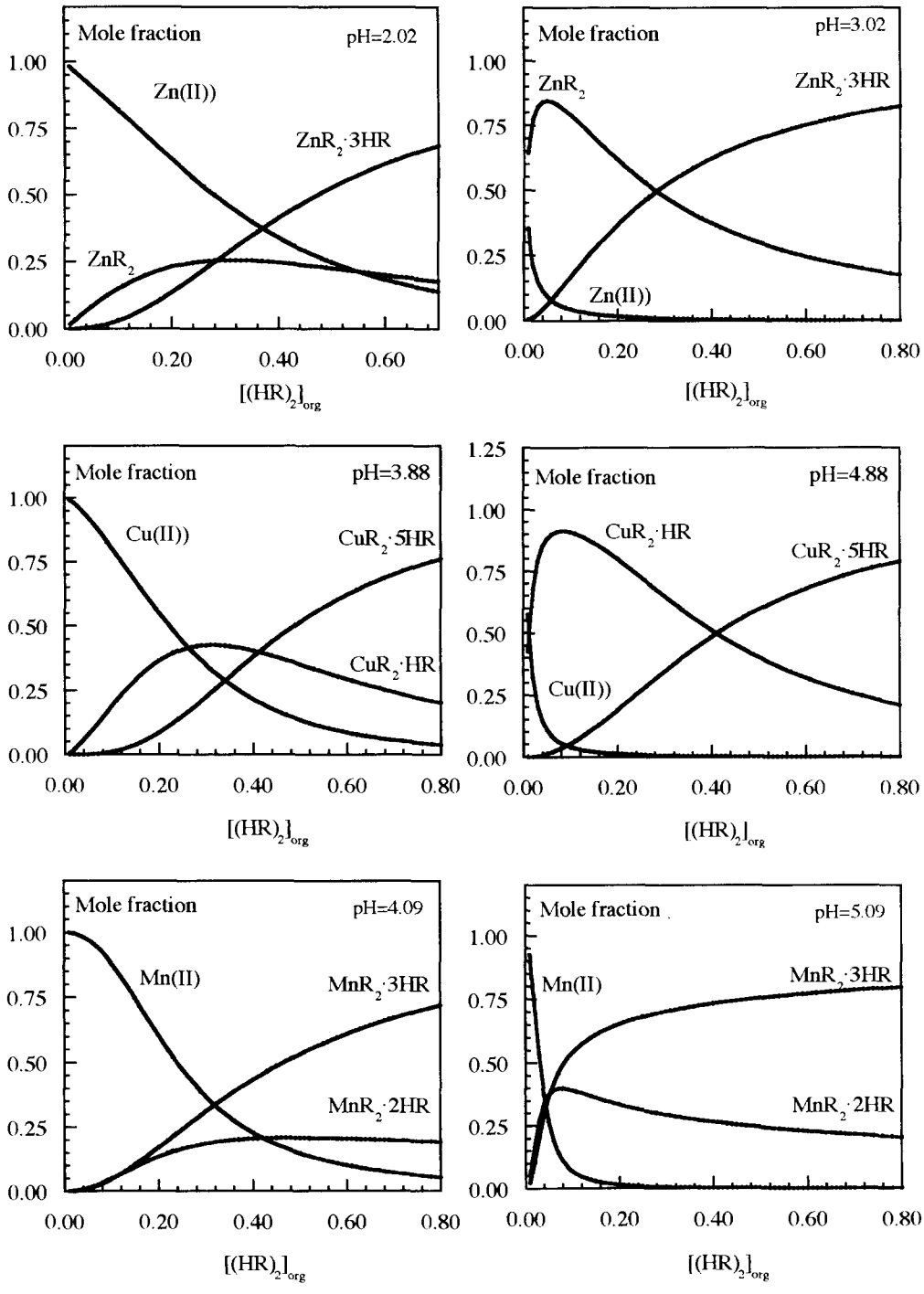
Mole fraction
pH=2.02
Zn(II))
ZnR2·3HR
ZnR2
[(HR)2]org
Mole fraction
pH=3.02
ZnR2
ZnR2·3HR
Zn(II))
[(HR)2]org
Mole fraction
pH=3.88
Cu(II))
CuR2·5HR
CuR2·HR
[(HR)2]org
Mole fraction
pH=4.88
CuR2·HR
CuR2·5HR
Cu(II))
[(HR)2]org
Mole fraction
pH=4.09
Mn(II)
MnR2·3HR
MnR2·2HR
[(HR)2]org
Mole fraction
pH=5.09
Mn(II)
MnR2·3HR
MnR2·2HR
[(HR)2]org

Fig. 4.

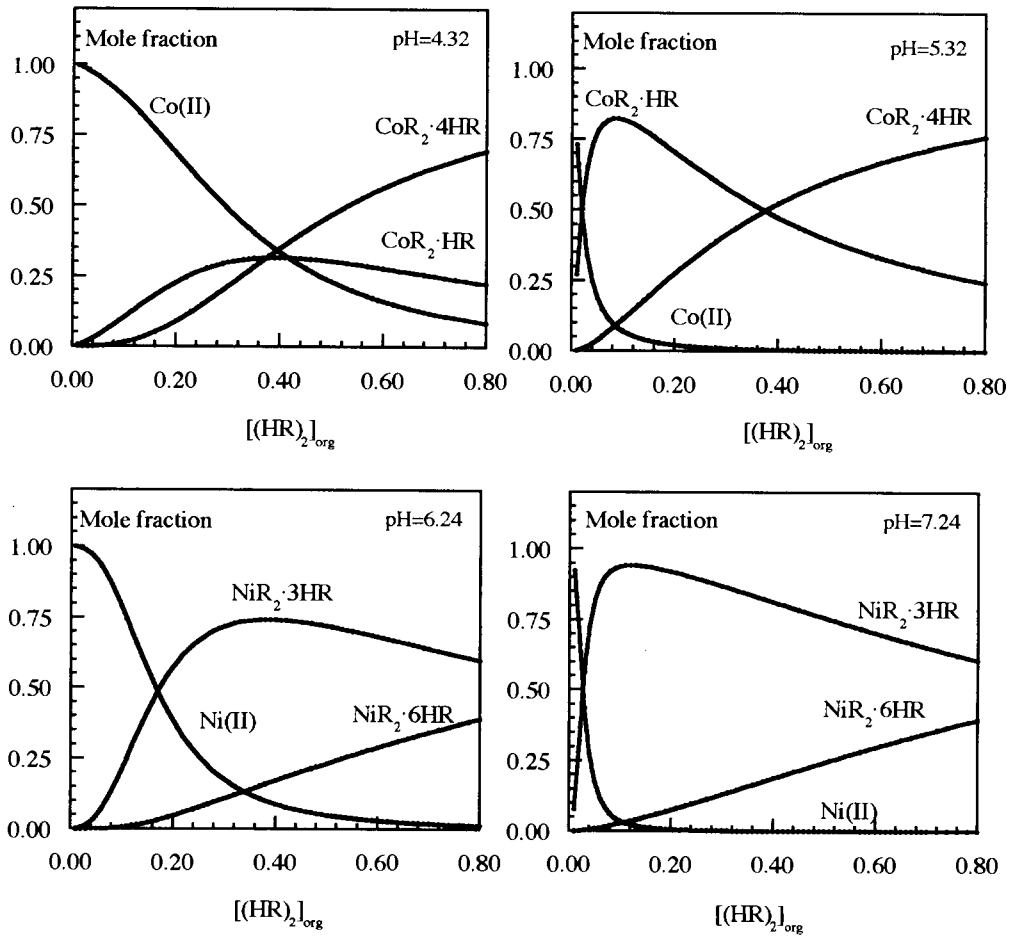

Fig. 4. Distribution diagrams of metal ions as a function of the total HR concentration at two selected pH values.

$ZnR_2 \cdot 2HR$ for zinc(II), respectively [16]. The extracted species $CoR_2 \cdot 2HR$ and $NiR_2 \cdot 4HR$ were reported for the extraction of cobalt(II) and nickel(II) by di(*n*-octyl)phosphinic acid in toluene and bis(2-ethylhexyl)phosphoric acid in dodecane from 1.0 mol dm^{-3} sodium nitrate solution, respectively [14,15]. The differences in the m values may be mainly due to the different concentration ratio of extractant HR to the metal ion investigated. The diluents may also affect the stoichiometry of the extracted species. The general stoichiometry can be written as $MR_n \cdot mHR$, ($n = 2$ or 3, $m = 1, 2, \ldots, 6$) for the present extraction system.

Using the Eqs. (25) and (26), the conditional extraction constants [$K'_{ex}(i)$ and $K'_{ex}(j)$] and the corresponding standard derivations for zinc(II), copper(II), manganese(II), cobalt(II) and nickel(II) were calculated. The results are summarized in Table 5.

In order to investigate the contributions of free metal ion and the extracted metal species in the extraction system, the mole fractions of them as a function of total HR concentration were calculated at two selected pH values. As shown in Fig. 4, the dominant extracted species were found to be ZnR_2 for zinc(II), $CuR_2 \cdot HR$ for copper(II), $CoR_2 \cdot HR$ for cobalt(II) and $NiR_2 \cdot 3HR$ for nickel(II) at relatively higher pH values and lower HR concentrations ($[(HR)_2]_{org} < 0.2$ mol cm^{-3}). How-

ever, the mole fractions of ZnR_2, $CuR_2 \cdot HR$ and $CoR_2 \cdot HR$ decreases sharply and are gradually substituted by $ZnR_2 \cdot 3HR$, $CuR_2 \cdot 5HR$ and $CoR_2 \cdot 4HR$ as the HR concentration increases, respectively. For the extraction of manganese(II), the metal species $MnR_2 \cdot 3HR$ dominates in the whole range of HR concentration, and its mole fraction is always larger than 0.75 ($[(HR)_2]_{org} > 0.3$ mol dm^{-3}). The mole fraction of $MnR_2 \cdot 2HR$, on the other hand, is relatively small and decreases gradually with increasing HR concentrations. For the extraction of nickel(II), it can be seen that the extracted species $NiR_2 \cdot 3HR$ is predominant in the whole range of experimental conditions used, and its mole fraction first sharply increases and then gradually decreases with increasing HR concentrations. At relatively lower HR concentrations ($[(HR)_2]_{org} <$ 0.2 mol dm^{-3}), the mole fraction of the species $NiR_2 \cdot 6HR$ is very small, whereas it increases linearly with increasing HR concentrations ($[HR)_2]_{org} > 0.2$ mol dm^{-3}).

4. Conclusions

The extraction equilibria of some transition metal ions by PIA-8 from 1.0 mol dm^{-3} ammonium sulfate solution into heptane were studied at 298 ± 0.1 K, and the following conclusions were obtained.

(1) The dimerization constant ($K_{d,HR}$) and the distribution constant ($K_{D,HR}$) of PIA-8 in heptane, kerosene and Naphtezol M diluents were determined by the potentiometric two-phase titration technique. The two equilibrium constants are closely related to the characteristic of the organic diluent.

(2) The oligomerization number x of the metal species extracted into heptane was determined to be close to unity for all metal ions investigated at lower metal ion concentrations. Accordingly, the metal ions were extracted as monomers ($MR_n \cdot mHR$) into the organic phase.

(3) The extraction equilibria of some transition metal ions were studied by both the slope analysis and the numerical analysis. The metal species extracted into the organic phase are considered to be $FeR_3 \cdot 2HR$ for iron(III), ZnR_2 and $ZnR_2 \cdot 3HR$ for zinc(II), $CuR_2 \cdot HR$ and $CuR_2 \cdot 5HR$ for copper(II), $MnR_2 \cdot 2HR$ and $MnR_2 \cdot 3HR$ for manganese(II), $CdR_2 \cdot 3HR$ for cadmium(II), $CoR_2 \cdot HR$ and $CoR_2 \cdot 4HR$ for cobalt(II) and $NiR_2 \cdot 3HR$ and $NiR_2 \cdot 6HR$ for nickel(II), respectively. The conditional extraction constants for the metal species are summarized in Tables 4 and 5. In the relatively high pH region, the extracted species ZnR_2 for zinc(II), $CuR_2 \cdot HR$ for copper(II), $CoR_2 \cdot HR$ for cobalt(II) and $NiR_2 \cdot 3HR$ for nickel(II) dominated at lower extractant concentrations ($[(HR)_2]_{org} < 0.2$ mol dm^{-3}), and their mole fractions decreased sharply with increasing extractant concentrations except for $NiR_2 \cdot 3HR$. With respect to the extraction of manganese(II), the species $MnR_2 \cdot 3HR$ dominated in the whole extractant concentration range investigated.

References

[1] J.S. Preston, Hydrometallurgy, 9 (1982) 115.
[2] X. Qingren, S. Dingzhang, J. Yatong and Y. Chengye, Solv. Extr. Ion Exch., 4 (1986) 927.
[3] T. Cecconie and H. Freiser, Solv. Extr. Ion Exch., 7 (1989) 15.
[4] N. Miralles, A.M. Sastre, M. Aguilar and M. Cox, Solv. Extr. Ion Exch., 10 (1992) 51.
[5] T.K. Brian, Hydrometallurgy, 32 (1993) 365.
[6] W.A. Rickelton, D.S. Flett and D.W. West, Solv. Extr. Ion Exch., 2 (1984) 815.
[7] I. Komasawa, T. Otake and Y. Ogawa, J. Chem. Eng. Jpn, 17 (1984) 410.
[8] D.B. Dreisinger and W.C. Cooper, Solv. Extr. Ion Exch., 4 (1986) 317.
[9] Z. Kolarik, Pure. Appl. Chem., 54 (1982) 2593.
[10] G.W. Mason, S. Lewey and D.F. Pepard, J. Inorg. Nucl. Chem., 26 (1964) 2271.
[11] W.Q. Wang and G.X. Xu, He Hua Xue and Fangshe Hua Xue (Chinese), 4 (1980) 248.
[12] B.H. Yao, Y. Nagaosa, M. Satake, A. Nomura and K. Horita, Solv. Extr. Ion Exch., 14 (1996) 849.
[13] F. Xun, H. Zhengshui, L. Yide and J.A. Golding, Solv. Extr. Ion Exch., 8 (1990) 573.
[14] M. Martinez, N. Miralles, A.M. Sastre and C. Herranz, Hydrometallurgy, 33 (1993) 95.
[15] R. Grimmand, Z. Kolarik, J. Inorg. Nucl. Chem., 36 (1974) 189.
[16] A.M. Sastre, N. Miralles and E. Figguerola, Solv. Extr. Ion Exch., 8 (1990) 1166.
[17] B.K. Tait, Talanta, 42 (1995) 137.
[18] D.H. Liem, Acta Chem. Scand., 25 (1971) 1521.
[19] F.J.C. Rossotti and H.S. Rossotti, Acta Chem. Scand., 9 (1955) 1166.
[20] L.G. Sillen, Acta Chem. Scand., 10 (1956) 186.
[21] F.J.C. Rossotti, H.S. Rossotti and L.G. Sillen, Acta Chem. Scand., 10 (1956) 203.

ELSEVIER

Talanta 44 (1997) 339–347

Talanta

Amperometric biosensor for ethanol based on immobilization of alcohol dehydrogenase on a nickel hexacyanoferrate modified microband gold electrode

Chen-Xin Cai *, Kuan-Hong Xue, Yi-Ming Zhou, Hui Yang

Department of Chemistry, Nanjing Normal University, Nanjing 210097, People's Republic of China

Received 5 February 1996; accepted 12 July 1996

Abstract

Alcohol dehydrogenase (ADH) has been immobilized on a nickel hexacyanoferrate modified microband gold electrode surface by a glutaraldehyde/bovine serum albumin (BSA) cross-linking procedure to provide a new amperometric sensor for the assay of ethanol. The resulting enzyme electrode exhibits excellent electrocatalysis for the oxidation of reduced nicotinamide-adenine dinucleotide (NADH). The amperometric determination is based on the electrochemical detection of NADH which is generated in the enzymatic reaction of ethanol with NAD^+ under catalysis of ADH. The influence of various experimental conditions was examined for the determination of the optimum analytical performance. The sensor responds rapidly to ethanol with a detection limit of $(5.0 \pm 0.3) \times 10^{-7}$ mol l^{-1}. The response current increases linearly with ethanol concentration up to 5 mmol l^{-1}. The sensor remains relatively stable for about 1 week. © 1997 Published by Elsevier Science B.V.

Keywords: Alcohol dehydrogenase; Amperometry; Biosensors; Electrocatalytic oxidation; NADH

1. Introduction

Ethanol is an important compound in medicine, biotechnology and the food industry, etc., and it is often monitored for toxicological and psychological effects. In certain industrial fields, such as fermentation and distillation, the ethanol concentration can reach toxic levels, causing inflammation of the nasal mucous membrane and conjunctiva, irritation of the skin and, at high levels, even alcohol poisoning. Hence, several analytical methods have been developed for the determination of ethanol and some other aliphatic alcohols [1–3]. Much work has been performed to enhance the detection of aliphatic alcohol at platinum and gold electrodes using preprogrammed multistep potential waveforms; this was developed by Johnson and co-workers [4,5]. However, the oxidation of aliphatic alcohol exhibits a large overpotential at common electrode surfaces. A mixed-valent ruthenium oxide–ruthenium cyanide (mRuO/RuCN) modified glassy carbon electrode was used to catalyze the oxidation of ethanol by Kulesza and Bandoch [6,7], and Cataldi and co-

* Corresponding author.

PII S0039-9140(96)02049-8

workers [8,9], respectively. In this paper, we report the results of the determination of ethanol based on the electrocatalytic oxidation of reduced nicotinamide-adenine dinucleotide (NADH) at a modified microelectrode.

Although the direct oxidation of coenzyme NADH at the electrode surface, after an enzyme turnover (e.g. a dehydrogenase), is a reasonable approach for substrate determination, it is not very useful analytically. There are several reason for this. The direct oxidation of NADH at a bare electrode surface is irreversible and requires a high overpotential, which is increased further by the presence of the enzyme [10]. It has been reported that the oxidation of NADH at a solid electrode proceeds via two successive one-electron transfer steps involving radical intermediates, which often cause side reactions and lead to electrode fouling [11]. In addition, the process of electrochemical oxidation of NADH is not very reproducible since it has been shown to depend on the history and pretreatment of the electrode surface. The high overpotential and poor reproducibility usually limit its use for the direct electrochemical detection of NADH in enzymatic reaction.

However, these problem can be circumvented when the electrode is modified with mediators. Many compounds were found to enhance the electron transfer rate and reduce the overpotential for the oxidation of NADH. Alkylphenazinium ions [12], *o*– and *p*-quinones [13–17] and methylene blue [18], etc. have been immobilized on the surface of the carbon electrode through covalent binding, direct absorption or through adsorption of a polymer containing the mediating functional group which was used to catalyze the oxidation of NADH. For example, Hajizadeh and co-workers [19] have shown that thionine can modify the surface of a spectroscopic graphite electrode by cross-linking. When such a chemically modified electrode was used in flow injection determination of NADH, a linear range of $7.0 \times 10^{-7} \sim 1.8 \times 10^{-3}$ mol l^{-1} was obtained. Gorton, Johansson and co-workers [20–29] have extensively investigated the electrocatalytic oxidation of NADH by adsorbed aromatic compounds containing catechol functionalities and adsorbed phenoxazines. Albery and Bartlett [30] have reported the oxidation of NADH on electrodes made of a conducting organic salt. Bernadette and Christopher [31] reported the oxidation of NADH at a hexacyanoferrate modified nickel electrode.

Electrocatalytic oxidation of NADH at the conducting polymer (such as poly(3-methylthiophene [32]), poly(metallophthlocyanine) [33], poly(thionine) [34], poly(idole-5-carboxylic acid) [35], poly(-methylene blue) [36], poly(3,4-dihydroxybenzaldehyde) [37] etc.) modified electrode was reported recently. Using cyclic voltammetry and scanning electrochemical microscopy (SECM), Grundig and co-workers [38] studied the NADH oxidation at *N*-methyl phenazine (NMP^+) methosulfate, 1-methoxy-5-methyl phenazine ($M\text{-}NMP^+$) methosulfate and Meldola blue etc., containing composite electrodes.

Other compounds, such as oxometalates [39], ruthenium complexes [40], pyrroloquinoline quinone [41] etc. were also reported to act as a catalyst for the oxidation of NADH.

Recently, Norwell and Kuhr's [42] experimental results indicated that NADH could be directly oxidized at a carbon fibre electrode with a low overpotential after the carbon fibre electrode had been treated electrochemically.

The alcohol dehydrogenase (ADH) has been widely studied and immobilized onto the electrode surface by several methods. For example, Karyakin et al. [43] immobilized ADH onto the surface of poly(neutral red) modified glassy carbon electrode through the Nafion membrane, and investigated the response of the resulting enzyme electrode to reduction of acetaldehyde. Somasundrum and Bannister [35], Bernadette and Christopher [31] immobilized ADH onto a poly(indole-5-carboxylic acid) modified glassy carbon electrode and a hexacyanoferrate modified porous nickel electrode respectively, by a glutaraldehyde/albumin cross-linking procedure and measured the response of the enzyme electrode to ethanol. They also determined the apparent Michaelis–Menten constant for the enzyme. For coimmobilization of the ADH and the cofactor, Mizutan and Yabuki [44] entrapped ADH,

NAD^+ and Medola blue in polypyrrole film. But they found that the sensor lacked stability and sensitivity. Grundig et al. [38] used the following method to immobilize ADH and the cofactor. They deposited ADH and the polyethylene glycol modified NADH containing solution of prepolymer of the polyurethanehydrogel onto a dialysis membrane. Then the dialysis membrane layered with immobilization gel was fixed onto the surface of a mediator modified electrode.

On the other hand, microelectrodes have received considerable attention in some applications due to their many advantages in comparison with conventionally sized electrode. Although, there are many studies on the electrochemical oxidation of NADH and the ADH based enzyme electrode using various types of mediators at conventionally sized electrodes, few have studied the elctrocatalytic oxidation of NADH and the NAD^+/NADH dependent enzymatic reaction at microelectrodes for the development of a microsensor which depends on NADH for in vivo analysis and biotechnology. Recently, we [45] demonstrated that the nickel hexacyanoferrate modified microband gold electrode (NiHCH/Au) exhibited excellent electrocatalytic activity for the oxidation of NADH in phosphate buffer solution. A noticeable reduction of the overpotential for the oxidation of NADH and a remarkably stable voltammetric response at the NiHCF/Au microelectrode were observed. The aim of this study is to immobilize enzyme (ADH) on the NiHCF/Au surface and investigate the resulting enzyme electrode in the determination of ethanol.

2. Experimental

2.1. Chemicals

β-Nicotinamide adenine dinucleotide (NAD^+) and alcohol dehydrogenase (ADH, alcohol: NAD^+ oxidoreductase; EC 1.1.1.1, from baker's yeast, had an activity of 300 U mg^{-1}) were obtained from Sigma Chemical Company and used as received. Glutaraldehyde (25% w/v), obtained from Aldrich Chemical Company, was diluted to 2.5% w/v with distilled water. Bovine serum albumin (BSA) was obtained from Shanghai Industry of Biochemistry, Chinese Academy of Sciences. Absolute ethanol (99.7%) was purchased from the Second Reagent Factory of Shanghai and used as received. Other reagents used were of analytical grade. The phosphate buffer solution was made up with 0.1 mol l^{-1} Na_2HPO_4 and 0.1 mol l^{-1} NaH_2PO_4. All solutions were prepared with doubly distilled, deionized water. The ethanol aqueous solution was prepared with phosphate buffer solution (pH 7.5). The ADH stock solution was prepared with phosphate buffer solution (pH 7.5) and stored at 4°C.

2.2. Instrumentation

Electrochemical experiments were performed with a PAR M270 electrochemical system (EC&G, USA). A type 501 thermostat (Shanghai, China) was used to control the experimental temperature. A three-electrode water-jacketed electrochemical cell, with a platinum wire as the counter electrode, a saturated calomel electrode (SCE) as the reference electrode and a modified microband gold electrode (ca. 0.1 μm × 1.0 cm) as the working electrode, was employed. The electrolytic cell volume is about 5 ml. The fabrication of the microband gold electrode was the same as previously reported [46]. The working electrode was polished with sandpaper and 0.05 μm alumina slurry, and then cleaned ultrasonically in double distilled water. Prior to use, the electrode was pretreated by continuous cyclic scans from 0 to -2.0 V at 50 mV s^{-1} in phosphate buffer solution (pH 7.5) until a constant background was observed.

2.3. Preparation of the NiHCF/Au electrode

The NiHCF film was electrochemically grown on the microband gold electrode in 2×10^{-4} mol l^{-1} $Ni(NO_3)_2$ and 2×10^{-4} mol l^{-1} $K_3Fe(CN)_6$ aqueous solution containing 0.1 mol l^{-1} $NaNO_3$ as the supporting electrolyte by a continuous scan between -0.1 and $+1.0$ V at a scan rate of 50 mV s^{-1}. The film thickness can be controlled by the cyclic scan times. In our experiment, five continuous scan were used, which corresponds to

a surface coverage of NiHCF of about 3.1×10^{-9} mol cm^{-2}. The cyclic voltammetric experiments of the modified electrode were performed in the potential range of $0 \sim +0.8$ V. A couple of well-defined redox peaks occurred with the formed potential of $+0.42$ V, which corresponded to the hexacyanoferrate(II/III) redox couple [45].

2.4. Biosensor preparation

ADH was immobilized on the NiHCF/Au electrode by a glutaraldehyde/BSA cross-linking procedure. The ADH (3 mg) was dissolved in 100 μl of 0.1 mol l^{-1} phosphate buffer solution (pH 7.5) containing 4 mg BSA. Then the glutaraldehyde (2.5% w/v), which is a bifunctional cross-linking agent, was added to the ADH solution up to a final concentration of a 0.9% w/v. In the process, the mixture was stirred thoroughly. The NiHCF/Au microelectrode was dipped into this solution for 2–3 s and then removed. The enzyme electrode was placed in a desiccator for some time to allow the gel formation. This procedure was repeated three or four times. The resulting enzyme electrode (defined as NiHCF/ADH/Au) was incubated in phosphate buffer solution (pH 7.5) at 4°C for at least 5 h before use.

2.5. Amperometric measurements

The amperometric measurements were carried out with the NiHCF/ADH/Au enzyme electrode under constant stirring at a fixed potential of $+0.55$ V in phosphate buffer solution (pH 7.5) containing NAD^+. The background current was first allowed to decay to a constant value, then the ethanol was added. After the solution was stirred for a short while, the steady-state current was measured. All test solutions were deaerated by passing highly pure nitrogen for 30 min before the electrochemical experiments, and a continuous flow of nitrogen was maintained over the sample solution during experiments. The electrochemical experiments were performed inside a Faraday cage at 25 ± 0.1°C.

3. Results and discussion

3.1. Detection of NADH generated by enzymatic reaction

We [45] have shown that the NiHCF modified microband gold electrode can catalyze the oxidation of NADH in solution, with a reduction of overpotential of about 340 mV. The steady-state current increases linearly with NADH concentration in the range 0.5–8.0 mmol l^{-1}. The present experimental results show that the NiHCF/Au microelectrode can also catalyze the oxidation of NADH, which is generated from the reaction of NAD^+ and ethanol catalyzed by ADH.

The electrochemical experiments were performed by the following procedures. Firstly, the cyclic voltammogram of NiHCF/Au in a phosphate buffer solution was recorded, then NAD^+ and ethanol were added to the buffer solution to assess their effects on the electrochemical behavior of the NiHCF/Au electrode and finally the cyclic voltammogram of the NiHCF/ADH/Au electrode in the NAD^+ and ethanol containing solution was recorded to determine whether the anodic current increases. Curve a in Fig. 1 shows

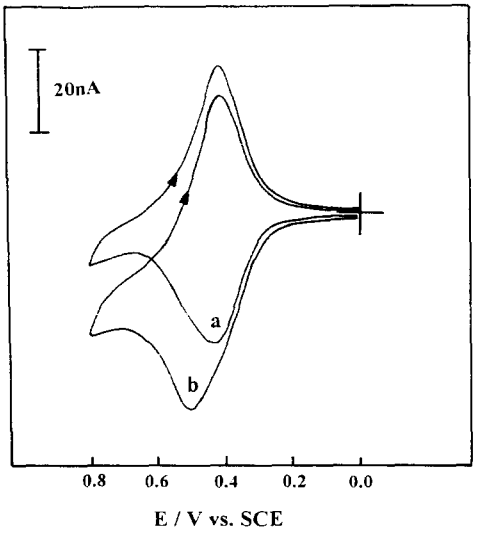

Fig. 1. Cyclic voltammograms of the NiHCF/Au (a) and NiHCF/ADH/Au (b) electrode in 0.1 mol l^{-1} phosphate buffer solution (pH 7.5) containing 1.0 mmol l^{-1} NAD^+ and 1.0 mmol l^{-1} ethanol at a scan rate of 5 mV s^{-1}.

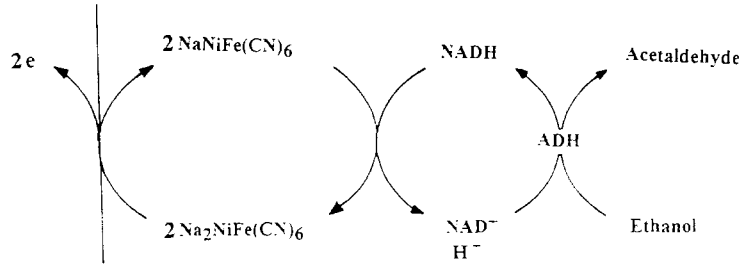

Fig. 2. Scheme of the respective reaction sequences of the electrochemical coupled enzymatic oxidation of ethanol.

the cyclic voltammogram of the NiHCF/Au electrode in a phosphate buffer solution containing NAD^+ and ethanol. This voltammogram is almost the same as that of NiHCF/Au in phosphate buffer without NAD^+ and ethanol (not shown here, Fig. 4a in Ref. [45]). This result indicates that NAD^+ and ethanol had only a minor influence on the electrochemical behaviour of the NiHCF/Au electrode. In Fig. 1, curve b is the cyclic voltammogram of NiHCF/ADH/Au in phosphate buffer in the present NAD^+ and ethanol. It can be seen that there is a great increase in the anodic current, corresponding to the oxidation of hexacyanoferrate(II) to hexacyanoferrate(III), compared to the voltammogram of NiHCF/Au in the same solution (Fig. 1a). ADH catalyzes the oxidation of ethanol with a simultaneous reduction of an equivalent amount of NAD^+ to NADH. The NADH reduces the hexacyanoferrate(III) to hexacyanferrate(II). Thus hexacyanoferrate(II) is regenerated by NADH during the scan, and the anodic peak current increases greatly. The overall reaction process is shown in Fig. 2. The catalytic current is not observed if any component shown in the scheme is absent.

By fixing the concentration of NAD^+ in solution, the increase of the peak current should depend on the concentration of ethanol at the same NiHCF/ADH/Au electrode. This is the basis for the determination of ethanol by detecting NADH amperometrically with the NiHCF/ADH/Au enzyme electrode.

3.2. *Effect of potential*

To find an optimum operating potential for amperometric measurements, the potential dependence of the ethanol response at the NiHCF/ADH/Au electrode is examined. Fig. 3 displays a hydrodynamic voltammogram in the 0.1 to 0.8 V potential range. The amperometric response of ethanol starts at +0.2V. With increasing oxidation potential, the response rises sharply and reaches a limiting value at potentials higher than +0.55 V. Such a potential dependence profile is in agreement with the cyclic voltammogram results (Fig. 1). A quite similar hydrodynamic

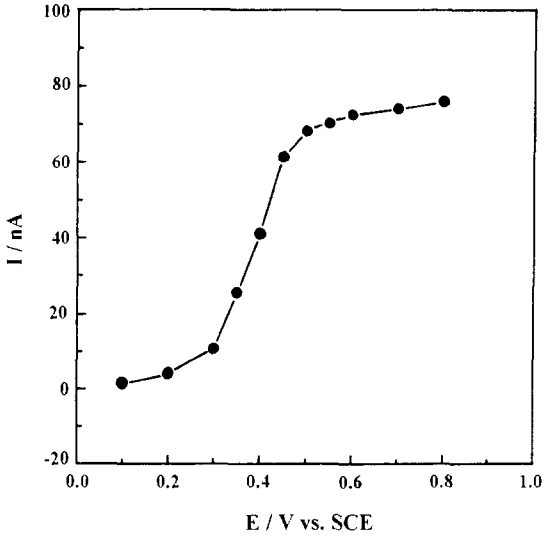

Fig. 3. Hydrodynamic voltammogram obtained at the NiHCF/ADH/Au electrode for 4.0 mmol l^{-1} ethanol in 0.1 mmol l^{-1} phosphate buffer solution (pH 7.5) containing 1.0 mmol l^{-1} NAD^+. Stirring rate: 300 rev min^{-1}.

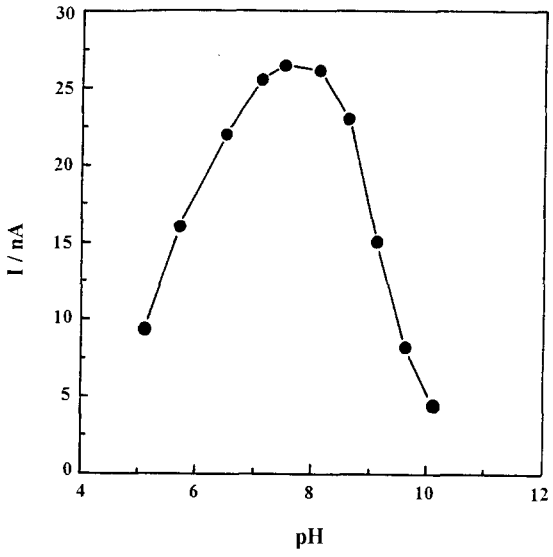

Fig. 4. Effect of solution pH on the response to 1.5 mmol l^{-1} ethanol. The operating potential is +0.55 V vs. SCE. Other conditions are the same as Fig. 3.

voltammogram can be obtained when the NiHCF/Au electrode performed in phosphate buffer solution containing NADH. This result indicates that the response to ethanol is attributed to NADH formation in the process of catalytic oxidation on the NiHCF/ADH/Au electrode.

3.3. Effect of solution pH

The effect of solution pH on the ethanol response at the NiHCF/ADH/Au electrode is shown in Fig. 4. Different volumes of 0.1 mol l^{-1} Na_2HPO_4/NaH_2PO_4 and 0.1 mol l^{-1} $Na_2B_4O_7/Na_2CO_3$ buffers were used to adjust the pH. The amperometric response is enhanced by increasing the solution pH in the range of pH 6.0 to 7.0, and reaches a maximum value between pH 7.0 and 8.0. It decreases markedly with an increase in pH above 8.5. Our previous report has shown that the NiHCF/Au electrode is stable in the pH range of 5.0 to 8.0. Therefore, pH 7.5 is selected by considering both the sensitivity and the stability of the electrode; consequently further studies were carried out at this pH.

3.4. Effect of NAD^+ concentration

NAD^+ is necessary in the reaction catalyzed by ADH. The effect of NAD^+ concentration on the response of the enzyme electrode to ethanol was studied at an ethanol concentration of 4 mmol l^{-1}. A plot of the steady-state current as a function of NAD^+ concentration is presented in Fig. 5. It is evident that the steady-state current increases with increasing concentration of NAD^+ for concentration below 0.6 mmol l^{-1}, whereas the response levels off for NAD^+ concentrations above 0.7 mmol l^{-1}. Based on these results and in order to ensure that the response of the sensor was independent of NAD^+ concentration, a value of 1.0 mmol l^{-1} NAD^+ was employed in the following measurements.

Consequently, the amperometric experiments in the present study are performed in 0.1 mol l^{-1} Na_2HPO_4/NaH_2PO_4 buffer solution (pH 7.5) containing 1.0 mmol l^{-1} NAD^+ at the potential of +0.55 V.

3.5. Response of ethanol at the NiHCF/ADH/Au electrode

Fig. 6 shows the amperometric response of the NiHCF/ADH/Au enzyme electrode to successive

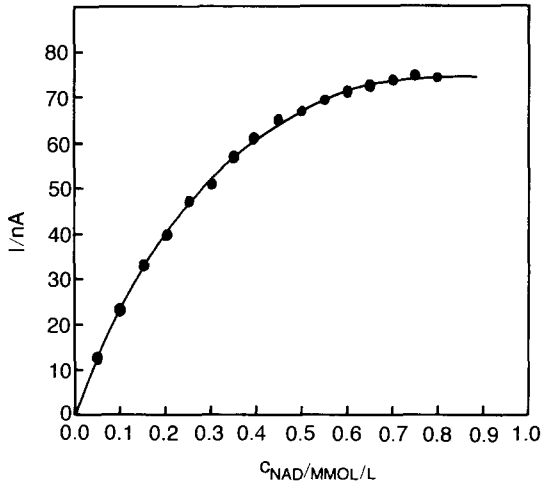

Fig. 5. Plot of response current as a function of NAD^+ concentration at an ethanol concentration of 4.0 mmol l^{-1}. Other conditions are the same as Fig. 4.

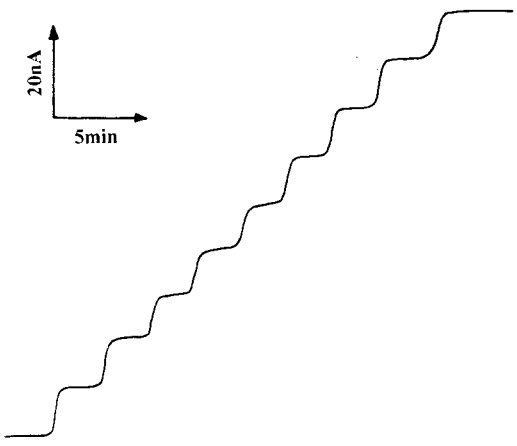

Fig. 6. Amperometric response to successive increments of 0.5 mmol l^{-1} ethanol. Other conditions are the same as Fig. 4.

injections of ethanol. The enzyme electrode rapidly responses to the ethanol concentration changes and reaches a steady state with 50 s. The calibration plot of response current against the concentration of ethanol is presented in Fig. 7. The linear response is observed up to 5 mmol l^{-1}. The lack of linearity in the high range of ethanol concentration might be due to the ADH saturation by ethanol. The detection limit of ethanol, at a signal-to-noise ratio of three, is found to be $(5.0 \pm 0.3) \times 10^{-7}$ mol l^{-1}. The results indicate that the NiHCF/ADH/Au electrode is an excellent detector for ethanol, because a wide linear range and low detection limits can be achieved.

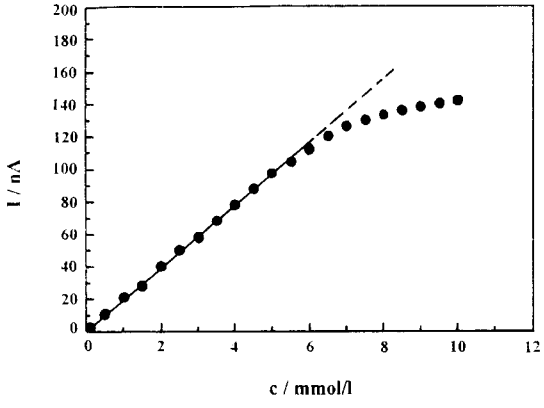

Fig. 7. Calibration curve for ethanol at a NiHCF/ADH/Au electrode.

The average current response of 38.2 nA, with the relative standard deviation of 2.5%, is obtained for ten successive determinations at the ethanol concentration of 2.0 mmol l^{-1}, which shows that the modified electrode can be used to determine ethanol precisely. The stability of the NiHCF/ADH/Au electrode was evaluated by measuring periodically the response to ethanol. The response remained at 90% of the initial value for two days and decayed to half of the initial value after one week, indicating the NiHCF/ADH/Au enzyme electrode display a highly stable response for ethanol. The decrease in the response to ethanol might be mainly due to the loss of ADH enzyme activity, because the NiHCF/Au electrode exhibited excellent stability for NADH oxidation and the NiHCF did not dissolve into solution from the electrode surface for at least one week.

For immobilized enzymes used in amperometric biosensors, the observed electrochemical response may be either mass transport limited or kinetically controlled [47]. Mell and Malloy [47] suggested that for an immobilized enzyme reaction that is kinetically controlled, the steady-state current, i_{SS}, is proportional to the initial rate of the enzymatic process. In this case, a plot of i_{SS} vs. the substrate concentration, c, gives a typical Michaelis–Menten type response. To perform kinetic analysis on the enzyme electrode, we analyze it simply using the Eadie–Hofstee form of the Michaelis–Menten equation. The Eadie–Hofstee plot of ethanol is shown in Fig. 8. The plot of i_{SS} vs. i_{SS}/c for the ethanol is linear with a slope of -42.5 mmol l^{-1}. This implies that the rate-controlling process is the enzymatic reaction. An average value of the apparent Michaelis–Menten constant (K_M^{app}) of 41.7 ± 2.3 mmol l^{-1} for ethanol is obtained.

A survey of the literature shows that K_M^{app} for ethanol in the presence of ADH has been extensively studied by various methods. Ciolkosy and Jordan [48], working at pH 8.8, obtained $K_M^{app} =$ 3.2 mmol l^{-1} using the electrochemical method; Somasundrum and Bannister [35] determined K_M^{app} to be 9.2 mmol l^{-1} using the same method and the same pH as Ref. [48]; Dickinson and Monger [49] obtained $K_M^{app} = 21.7$ mmol l^{-1} at pH 7.05 using a spectrophotometrical method. These val-

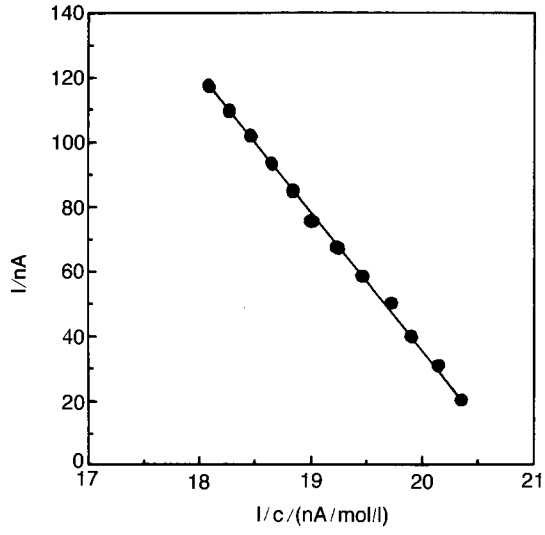

Fig. 8. Electrochemical Eadie–Hofstee plot of ethanol for the enzyme electrode using the data of Fig. 7.

ues and the present experimental result are quite different. The reason for this is that K_M^{app} is not an intrinsic property of the enzyme, but of the system. The microenvironment around the immobilized enzyme might greatly affect the value of K_M^{app}. In addition, the present result was obtained at a microelectrode while the literature's results were obtained using conventionally sized electrodes. The difference between planar and radial diffusion at a conventionally sized and microelectrode might also affect the K_M^{app} value. So the results characterizes the enzyme electrode and not the enzyme.

4. Conclusions

We have prepared and characterized the performance of an ethanol biosensor based on immobilization of ADH on the NiHCF modified microband gold electrode surface by the glutaraldehyde/BSA cross-linking procedure. The analytical signal is based on the electroacatalytic oxidation of enzymatically generated NADH at a NiHCF/Au electrode. We have characterized the response of the biosensor in terms of the effects of operating potential, pH of the solution and the concentration of NAD^+. The sensor exhibits high sensitivity and a limit of detection as well as a rapid response.

References

[1] K. Mitsubayashi, K. Yokoyama, T. Takeuchi and I. Karube, Anal. Chem., 66 (1994) 3297.
[2] G. Marko-Varga, K. Johansson and L. Gorton, J. Chromatogr. A, 660 (1994) 153.
[3] I.G. Casella, T.R.I. Cataldi, A.M. Salvi and E. Desimoni, Anal. Chem., 65 (1993) 3143.
[4] G.G. Neuburger and D.C. Johnson, Anal. Chem., 59 (1987) 204.
[5] W.R. LaCourse, D.C. Johnson, M.A. Rey and R.W. Slingsby, Anal. Chem., 63 (1991) 134.
[6] P.J. Kulesza, J. Electroanal. Chem., 220 (1987) 295.
[7] P.J. Kulesza and M. Bandoch, J. Electroanal. Chem., 323 (1992) 131.
[8] T.R.I. Cataldi, D. Centong, E. Desimoni and V. Forastiero, Anal. Chim. Acta, 310 (1995) 257.
[9] T.R.I. Cataldi, D. Centong, A. Guerrieri, Anal. Chem., 67 (1995) 101.
[10] J. Moiroux and P.J. Elving, J. Am. Chem. Soc., 102 (1980) 6533.
[11] P.J. Elving, W.T. Bresenahan, J. Moiroux and Z. Samec, Bioelectrochem. Bioenerg., 9 (1982) 365.
[12] A. Torstensson and L. Goron, J. Electroanal. Chem., 130 (1981) 199.
[13] C. Ueda, D.C.-S. Tse and T. Kuwana, Anal. Chem., 54 (19982) 850.
[14] H. Huck and H.L. Schmidt, Agnew. Chem., 93 (1981) 421.
[15] K. Ravichandran and R.P. Baldwin, J. Electroanal. Chem., 126 (1981) 293.
[16] M. Fukui, C. Kitani, C. Degrand and L.L. Miller, J. Am. Chem. Soc., 104 (1982) 28.
[17] E. Lorenzo, L. Sanchez, F. Pariente, J. Tirado and H.D. Abruna, Anal. Chim. Acta, 309 (1995) 79.
[18] Q. Chi and S. Dong, Analyst, 119 (1994) 1063.
[19] K. Hajizdeh, H.T. Tang, H.B. Halsall and W.R. Heineman, Anal. Lett., 24 (1991) 1453.
[20] B. Persson and L. Gorton, J. Electroanal. Chem., 292 (1990) 115.
[21] B. Persson, J. Electroanal. Chem., 287 (1990) 61.
[22] L. Gorton, J. Chem. Soc., Faraday Trans. 1, 82 (1986) 1245.
[23] L. Gorton, G. Johansson and A. Torstensson, J. Electroanal. Chem., 196 (1985) 81.
[24] L. Gorton, A. Torstensson, H. Jaegfeldt and G. Johansson, J. Electroanal. Chem., 161 (1984) 103.
[25] H. Jaegeldt, A. Torstensson, L. Gorton and G. Johansson, Anal. Chem., 53 (1981) 1979.
[26] H. Jaegfeldt, T. Kuwana and G. Johansson, J. Am. Chem. Soc., 105 (1983) 1805.

[27] F. Ni, H. Feng, L. Gorton and T.M. Gorton, Langmuir, 6 (1990) 66.
[28] L. Gorton, G. Bremle, E. Csoregi, G. Johnsson-Pettersson and B. Persson, Anal. Chim. Acta, 249 (1991) 43.
[29] J. Kulys, G. Gleixner, W. Schuhmann and H.L. Schmidt, Electroanalysis, 5 (1993) 201.
[30] W.J. Albery and P.N. Bartlett, J. Chem. Soc., Chem. Commun., (1984) 234.
[31] F.Y. Bernadette and R.L. Christopher, Anal. Chem., 59 (1987) 2111.
[32] N.F. Atta, A. Galal, A.E. Karagozler, H. Zimmer, J.F. Rubinson and H.B. Mark Jr., J. Chem. Soc., Chem. Commun., (1990) 1347.
[33] F. Xu, H. Li, S.J. Cross and T.J. Guarr, J. Electroanal. Chem., 368 (1994) 221.
[34] T. Ohsaka, K. Tanaka and K. Tokuda, J. Chem. Soc., Chem., Commun., (1993) 222.
[35] M. Somasundrum and J.V. Bannister, J. Chem. Soc., Chem. Commun., (1993) 1629.
[36] A.A. Karyakin, E.E. Karyakina, W. Schuhmann, H.L. Schmidt and S.D. Varfolomeyev, Electroanalysis, 61 (1994) 821.
[37] F. Pariente, E. Lorenzo and H.D. Abruna, Anal. Chem., 66 (1994) 4337.
[38] B. Grundig, G. Wittstock, U. Rudel and B. Strehlitz, J. Electroanal. Chem., 395 (1995) 143.
[39] K. Essaadi, B. Keita and L. Nadjo, J. Electroanal. Chem., 367 (1994) 275.
[40] M. Somasundrum. J. Hall and J.V. Bannister, Anal. Chim. Acta, 195 (1994) 47.
[41] E. Katz, T. Lotzbeyer, D.D. Schlereth, W. Schumann and H.L. Schmidt, J. Electroanal. Chem., 373 (1994) 189.
[42] W.B. Nowall and W.G. Kuhr, Anal. Chem., 67 (1995) 3583.
[43] A.A. Karyakin, O.A. Bobrova and E.E. Karyakina, J. Electroanal. Chem., 399 (1995) 179.
[44] F. Mizutani and S. Yabuki, Chem. Sens. Technol., 4 (1992) 167.
[45] C.C. Cai, H.X. Ju and H.Y. Chen, Anal. Chim. Acta, 310 (1995) 145.
[46] C.C. Cai. H. X. Ju and H.Y. Chen, Acta Chim. Sin., 53 (1995) 281.
[47] L.D. Mell and J.T. Malloy, Anal. Chem., 47 (1975) 299.
[48] M.K. Ciolkosz and J. Jordan, Anal. Chem., 65 (1993) 164.
[49] F.M. Dickinson and G.P. Monger, Biochem. J., 131 (1973) 261.

ELSEVIER

Talanta 44 (1997) 349–356

Talanta

Evaluation of perchlorate tolerant photo-cured calcium selective electrodes for use in flow injection potentiometry

Lucy Tina Di Benedetto [a,*], Telis Dimitrakopoulos [a,*], John R. Farrell [b], Peter J. Iles [b]

[a] *Department of Physical Sciences, University of Tasmania, P.O. Box 1214, Launceston, Tas., 7250, Australia*
[b] *Department of Applied Chemistry, Royal Melbourne Institute of Technology, Plenty Road, Bundoora, 3038, Vic., Australia*

Received 14 May 1996; received in revised form 17 July 1996; accepted 22 July 1996

Abstract

A photo-cured membrane selective to calcium, based on the calcium bis [4-(1′,1′,3′,3′-tetramethylbutyl)phenyl]phosphate ionophore and incorporating the lipophilic additive, potassium tetraki(4-chlorophenyl)borate, that can tolerate up to 200 nM perchlorate ionic background in the flow injection potentiometry mode has been previously reported (T. Dimitrakopoulos, J.R. Farrell and P.J. Ives, Electroanalysis, 8 (1996) 391). Improvements in the electrode slope and sensitivity of the previously described photo-cured calcium membrane-based electrode were achieved when anhydrous calcium chloride salt was dissolved into the pre-cured membrane composition and then photo-cured. Similar to the previously reported photo-cured calcium ion-selective electrode (ISE), the improved photo-cured calcium ISE can measure calcium in a high perchlorate background in the flow injection potentiometric mode. © 1997 Elsevier Science B.V.

Keywords: Calcium selective electrodes; Flow injection potentiometry; Perchlorate tolerance; Photo-cured membranes

1. Introduction

Poly (vinyl chloride) (PVC) has been universally accepted as the preferred polymer base for liquid membranes, and is employed in numerous commercially available ion-selective electrodes (ISEs). However, the manufacture of PVC membranes poses a disadvantage that arises from the solvent-cast procedure that can take up to 2 days, producing a liquid membrane that is durable and flexible, but exhibits poor adhesion to solid-contact electrodes [1].

An alternative method for the rapid manufacture of liquid polymer membranes that are more robust than the PVC-based membranes has been reported [1–11] and involves a photopolymerisation process. The photopolymerisation process involves the photo-curing of acrylate-based membranes that are cross-linked with an ester and initiated by a benzophenone photoinitiator for up to 40 min using an ultra-violet mercury vapour lamp. Membranes formed with the photo-curing

* Corresponding authors. Fax: + 61 324 3839; e-mail: tdimitra@postoffice.newnham.utas.edu.au or ldibened@postoffice.newham.utas.edu.au

PII S0039-9140(96)02057-7

technique are mechanically stronger and more hydrophobic than PVC membranes, due to the lower amount of plasticiser required in these photo-cured membranes. Other advantages of photo-cured membranes were good sensitivity, fast response and excellent adhesion to solid-contact electrodes. Photo-cured membranes have been developed to date for ammonium [3], calcium [1,2,4,5], lithium [6], nitrate [7], pH [8], potassium [9,10] and sodium [11] ISEs, most of which were applied to flow injection potentiometric (FIP) measurements.

A recent report on a photo-cured calcium ISE which was base on the calcium bis[4-1′,1′,3′,3′-tetramethylbutyl)phenyl]phosphate ionophore and the potassium tetrakis(4-chlorophenyl)borate lipophilic additive exhibited an excellent tolerance to high levels of perchlorate in the FIP mode [2], compared with other reported calcium ISEs [12,13]. The photo-cured calcium ISE was successfully used to determine total calcium levels in nitric/perchloric acid-digested milk samples in the FIP mode. However, this photo-cured membrane-based ISE experienced severe interferences from barium and zinc ions. The observed zinc ion interference for the photo-cured calcium ISE has been observed with other calcium ISEs based on similar phosphate ester-based ionophores [14]. However, the barium ion interference reported was unique and was believed to be due to the introduction of the lipophilic addictive, potassium tetrakis(4-chloropheny)borate, whereby this lipophilic anion exhibited some ion-exchange process between the potassium and the barium ion at the membrane/aqueous interface.

In this study, the introduction of anhydrous calcium chloride salt into the pre-cured membrane and then photo-curing results in a modified photo-cured calcium ISE that exhibits a hyper-Nernstian response, an improved selectivity over divalent ions, including barium and zinc, and a wider pH independent range, compared with a photo-cured membrane of similar membrane composition but without calcium chloride [2]. The modified photo-cured calcium ISE exhibits an excellent tolerance to lipophilic sample anions, such as perchlorate, and was used to determine the total calcium level in nitric/perchloric acid-digestion, cows' milk in the FIP mode.

2. Experimental

2.1. Materials

Metal chloride salts were used in this study and were all of analytical reagent grade. In addition, anhydrous calcium chloride (Mallinckrodt, Aanalytical reagent), nitric acid (Mallinckrodt, Analytical reagent), perchloric acid (BDH, AnalaR), sodium hydroxide (May and Baker Australia Pty Ltd., Analytical reagent), sodium perchlorate anhydrous (Mallinckrodt, Analytical reagent), and distilled water were used throughout this study.

The polymer matrix of the photo-cured membrane prepared in this study consists of Ebcryl 600 (bisphenol A epoxyacrylate) and Uvecryl P36 (copolymerisable benzophenone photoinitiator), both of which were obtained from UCB Chemical Sector (Belgium), and 1,6-hexanediol diacrylate was obtained from Anchor Chemicals Australia Pty. Ltd. The lipophilic additive used was potassium tetrakis(4-chlorophenyl)borate and the ionophore used was calcium bis[4-(1′,1′,3′,3′-tetramethylbutyl)phenyl]phosphate, both obtained from Fluka (AG purum). The plasticiser used was dioctyl phenylphosphonate (DOPP), obtained from Sigma Chemical Co.

2.2. Electrode preparation

The composition of pre-cured membrane mixtures investigated in this study are presented in Table 1. The pre-cured membrane mixtures were each mixed in a centrifuge for 30 min and blended with a thin glass rod until a homogeneous mixture was achieved. Each pre-cured membrane was applied directly onto a 6 mm copper disk embedded in a 12 mm diameter poly(methyl methacrylate) body, and exposed to a high intensity medium pressure (150 W) mercury vapour lamp for 5 min under a nitrogen atmosphere, producing photo-cured membranes approximately 0.2 mm thick. A minimum of three photo-cured membranes was prepared and evaluated form each membrane composition presented in Table 1. The resultant photo-cured calcium ISEs were conditioned in 100 mM calcium chloride for a minimum of 10 min prior to any measurements.

2.3. Flow injection potentiometric measurements

The electrode flow-through cell used in FIP measurements and FIP instrumentation employed in this study have been described elsewhere [2,15]. The carrier and the reference streams used in the flow cell were 100 mM NaCl. Manual injections were carried out using a Rhenodyne 5020 teflon injection valve fitted with a 100 μl sample loop. The background solutions were pumped through the electrode flow cell at a flow rate of 1.5 ml min^{-1} using a four-channel peristaltic pump (Ismatec Sa).

2.4. Steady-state measurements

Steady-state measurements with the calcium ISE were performed with an Orion double junction reference electrode (Ag/AgCl/saturated KCl// 10% KNO_3). The electrode potential was monitored by an Orion 701A meter and a Hitachi (QD 25) pen chart recorder was used to record the response profile of the ISE. The stability criterion used in this arrangement was ± 0.2 mV for 2 min.

The calcium ion activities were calculated using Debye–Hückel equation [16]. Calculation of the electrode slope and standard deviation were determined using a Macintosh application called Macurvefit Ver. 0.7 e written in THINK C by Kevin Raner (CSIRO, Division of Chemical and Polymers, Melbourne, Australia).

Table 1
Pre-cured membrane compositions prepared and investigated in this study

Membrane components	Ca1 membrane (wt.%) [2]	Ca2 membrane (wt.%)
Ebcryl 600	44.8%	44.7%
1,6-hexanediol diacrylate	22.4%	22.3%
Uvecryl P36	5.4%	5.3%
Duictyl phenylphosphonate	20.8%	20.8%
Ca-MBPP ionophore	606%	5.9%
KCITPB	0.5%	0.5%
$CaCl_2$ anhydrous	—	0.5%

Ca-MBPP, calcium bis[4-(1′,1′,3′,3′-methylbutyl)phenyl]phosphate; KCITPB, potasssium tetrakis(4-chlorphenyl)borate.

3. Results and discussion

The pre-cured membrane compositions that were investigated for this study are presented in Table 1. The photo-cured Ca1 membrane-based ISE has been studied and evaluated previously [2]. The pre-cured mixture of the Ca2 membrane was developed by taking a portion of the pre-cured Ca1 membrane mixture and dissolving anhydrous calcium chloride into it. Similar to the Ca1 membrane, the photo-cured Ca2 membrane was hard and transparent.

The anhydrous calcium chloride was dissolved in the Ca2 pre-cured membrane mixture without the aide of any volatile solvents, such as tetrahydrofuran. The solubility of the introduced calcium salt was enhanced by the DOPP plasticiser. It is well known that DOPP is a coordinating plasticiser and can interact with the calcium ion [13,17,18], and this enhanced the solubility of the introduced calcium chloride into the Ca2 membrane mixture.

3.1. Calcium response of the photo-cured Ca2 ISE

The photo-cured Ca2 ISE exhibited a hyper-Nernstian slope of 35.4 ± 0.4 mV change per activity decade, a log–linear rante between 0.01 and 100 mM and a detection limit of 0.001 mM in pure calcium chloride solution in the steady-state mode. Hyper-Nernstian responses are not uncommon in liquid polymer membrane type solid-contact electrodes [2,5]. It is not clearly understood how a given substrate can facilitate an electron exchange process at the membrane/metal interface. However, applying liquid polymer membranes onto metal substrate will result in analytically useful potentiometric devices, and the performance of these solid-contact-based membrane ISEs are determined solely by the liquid polymer membrane [14].

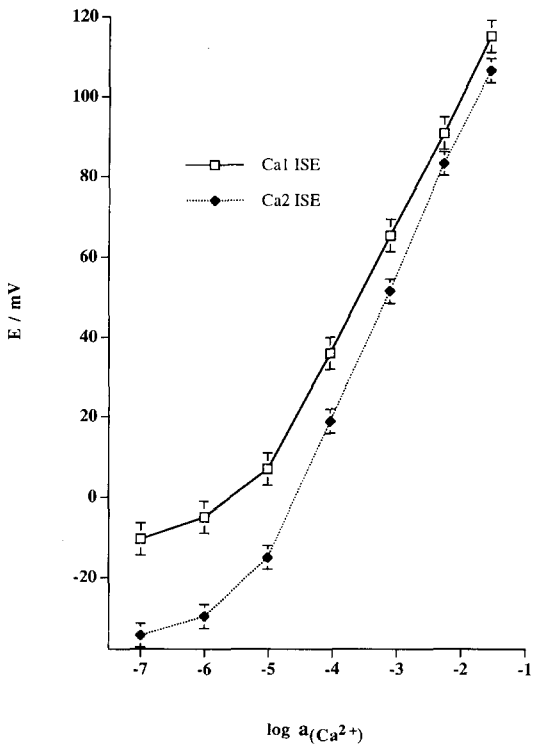

Fig. 1. Comparison of the calibration plots for the photo-curved Ca1 [2] and Ca2 ISEs in pure calcium chloride solution in the steady-state mode.

Comparison of the electrode performance between the photo-cured Ca1 and Ca2 ISEs shows a similar log–linear range and detection limit, however the electrode slope of the Ca2 ISE was higher than that of the Ca1 ISE. Comparative calibration curves for the photo-cured Ca1 and Ca2 ISEs in the study-state mode are given in Fig. 1. The increased hyper-Nernstian response exhibited by the photo-cured Ca2 ISE compared with the Ca1 ISE [2], was unlikely due to the presence of the lipophilic calcium–phosphonyl oxygen complex in the membrane phase.

The membrane resistances determined for the Ca1 and Ca2 ISEs were 6.2×10^9 Ω cm (3.5% relative standard deviation (RSD), $n = 3$) and 9.6×10^8 Ω cm (4.8% RSD, $n = 3$), respectively. A significant reduction in the resistane of the photo-cured Ca2 membrane would facilitate the increase in the electrode slope of this ISE. The photo-cured Ca2 ISE was stored in a 100 mM calcium chloride solution when not in use and was still operational after 3 months with no adverse effect on the observed hyper-Nernstian response and the log–linear range.

Previous studies have looked at the role of the DOPP plasticiser in liquid polymer membranes containing phosphate ester type ionophore [13,17]. Two blank photo-cured membranes (B1 and B2) were prepared without either calcium bis[4-1′,1′,3′,3′-tetramethylbutyl)phenyl]phosphate ionophore or the lipophilic additive potassium tetrakis(4-chlorophenyl)borate; membrane B1 contained the DOPP plasticier only and membrane B2 contained the DOPP plasticiser and the anhydrous calcium chloride. The calcium ion responses observed for the B1 and B2 ISEs are presented in Fig. 2. As demonstrated in previous studies for PVC-based ISEs [17], the photo-cured B1 and B2 membrane-based ISEs both exhibited

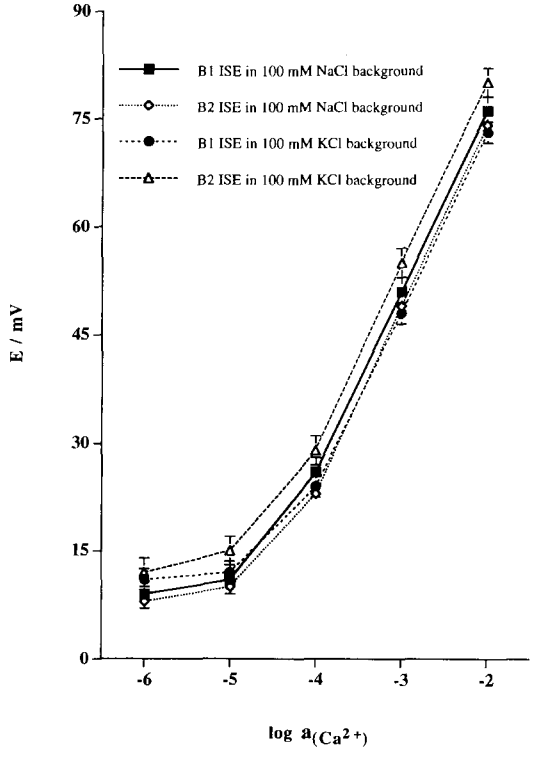

Fig. 2. Comparison of the calibration plots for the photo-cured B1 and B2 ISEs in the steady-state mode with calcium chloride solutions in a 100 mM NaCl and a 100 mM KCl background.

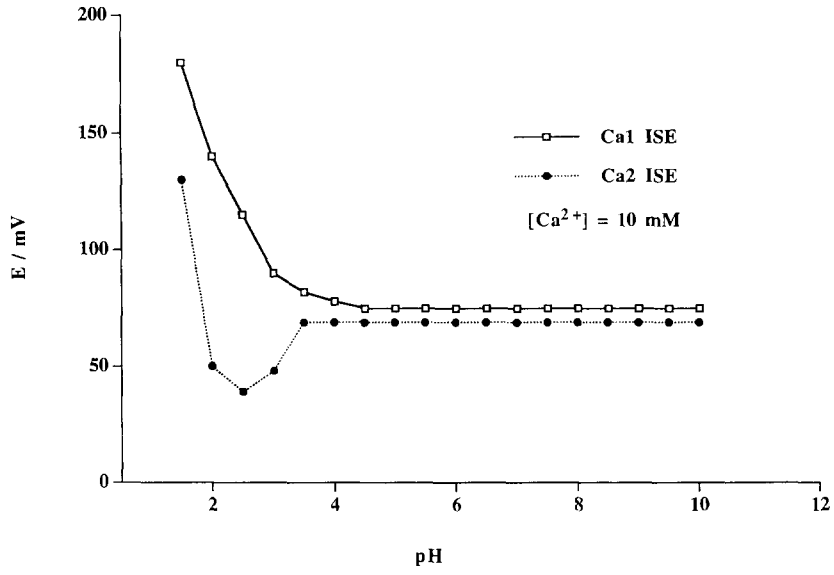

Fig. 3. Comparison of the pH profiles for the photo-cured Ca1 [2] and the Ca2 ISEs.

sub-Nernstian responses of 24.5 ± 0.2 and 26.3 ± 0.6 mV change per activity decade, respectively, and a log–linear range between 0.1 and 10 mM with calcium standards in a 100 mM sodium chloride background. Similar electrode slopes were observed for the B1 and B2 ISEs with calcium standards in 100 mM potassium chloride background as shown in Fig. 2. The B1 and B2 ISEs clearly demonstrated a favourable response to calcium ion, even in the presence of interfering ions, sodium and potassium, and reinforces the known chelating properties of the DOPP plasticiser towards the calcium ion [13,17,18].

These observations strongly suggest that the calcium chloride introduced into the Ca2 pre-cured membrane was complexed with the DOPP plasticiser forming a lipophilic calcium–phosphonyl oxygen in the Ca2 membrane phase [2,13]. The positivity charge calcium phosphonyl oxygen complex would then be counterbalanced by the lipophilic tetrakis(4-chlorophenyl)borate anion in the membrane phase [2], so that it would not compete against the phosphate ester type ionophore for the determinant. It is still not clear what role the calcium–phosphonyl oxygen complex has in the Ca2 membrane phase of the photo-cured electrode, however, some improvements in the electrochemical behaviour were observed when compared with the photo-cured Ca1 ISE.

3.2. Comparing the pH profiles for the photo-cured Ca1 and Ca2 ISEs

Fig. 3 compares the pH profiles for the Ca1 and Ca2 ISEs. The Ca2 ISE showed a wider negligible response to hydrogen ions between $3.5 < pH < 10.0$, compared with the Ca1 ISEs, $4.5 < pH < 10.0$. However, the most striking difference in the pH profiles was the observed 'pH dip' for the Ca2 ISEs, that was not observed for the Ca1 ISE.

The 'pH dip' observed for the photo-cured Ca2 ISE is typical of other reported calcium ISEs that employed similar phosphate ester type ionophores [17,19]. As discussed in previous studies [17], the 'pH dip' is the result of the extraction behaviour of the organophosphates present in liquid polymer membranes and these complexes of different stoichiometries can be extracted depending on the pH. Clearly, the discrepancy in the observed pH profiles of the photo-cured Ca1 and Ca2 ISEs suggests that the presence of the calcium–phosphonyl oxygen complex in the photo-cured Ca2 membrane has influenced the extraction process

of the organophosphates in acidic conditions. The pH dependence of the photo-cured Ca2 ISE has shifted to pH $\leq$ 3.5 compared with the Ca1 ISE at pH $\leq$ 4.5 [2]. However, further research is still required to thoroughly understand the mechanism and explain these observations.

3.3. Selectivities

The selectivity coefficients for the photo-cured Ca1 and Ca2 ISEs were determined by the fixed interference methods and are given in Fig. 4. The selectivities for calcium over interfering monovalent ions were comparable between the photo-cured Ca1 and Ca2 ISEs. However, differences between the photo-cured Ca1 and Ca2 ISEs were observed with selectivity coefficients for calcium over interfering divalent ions as shown in Fig. 4. The photo-cured Ca1 ISE experienced severe interference with measurements conducted in barium and zinc ionic backgrounds, and this has been discussed in detail in a previous study [2].

The selectivity observed for the photo-cured Ca2 ISE over interfering divalent ions was superior and included the observed selectivity over barium and zinc ions compared with the photo-cured Ca1 ISE. The enhanced selectivity observed for the Ca2 ISE over interfering divalent ions compared with the Ca1 ISE can be attributed to the presence of the calcium–phosphonyl oxygen complex in the Ca2 membrane phase and this well be further investigated. Varying the amount of anhydrous calcium chloride in photo-cured membranes similar in composition to the Ca2 membrane, showed no significant difference in selectivity compared with that observed for the Ca2 membrane-based ISE.

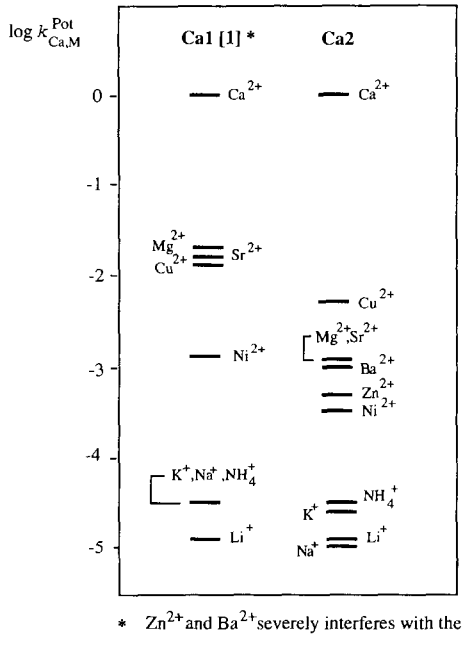

* Zn^{2+} and Ba^{2+} severely interferes with the Ca1 ISE.

Fig. 4. The determined selectivity coefficients for the photo-curved Ca2 ISE compared with the Ca1 ISE [2].

3.4. The photo-cured Ca2 ISEs in FIP mode

The time taken for the photo-cured Ca2 ISE to achieve 90% of complete steady-state was 3 s, making the Ca2 ISE ideally suited for FIP measurements. The photo-cured Ca2 ISE exhibited an electrode slope of 30.3 $\pm$ 0.3 mV change per activity decade and a log–linear range between 0.01 and 10 mM of calcium in a 100 mM sodium chloride background in the FIP mode. Typical flow injection peak heights are presented in Fig. 5. The peak heights in the FIP mode represent 95% of complete steady-state. A sample throughput rate of 150 injections h^{-1} with a high precision was achieved and baseline drifting of 5 mV day^{-1} was observed for the photo-cured Ca2 ISE in the FIP mode. Baseline drifting of the Ca2 ISE was observed at the higher concentration in the FIP mode; however, electrode drifting in flow injection has little effect on calibrations since data processing can account for any drift when calculating peak heights.

Similar to the Ca1 ISE, the Ca2 ISE could tolerate high levels of perchlorate background in the FIP mode, without any pernicious effect on the calcium ion response. The photo-cured Ca2 ISE exhibited a near-Nernstian slope of 28.2 $\pm$ 0.4 and 24.7 $\pm$ 0.3 mV change per activity with calcium standards containing a 10 mM sodium perchlorate and a 100 mM sodium perchlorate background, respectively in the FIP mode. The log–linear range for the Ca2 ISE was between 0.01 and 10 mM in the FIP mode. The calibration plots for the Ca2 ISE in various perchlorate back-

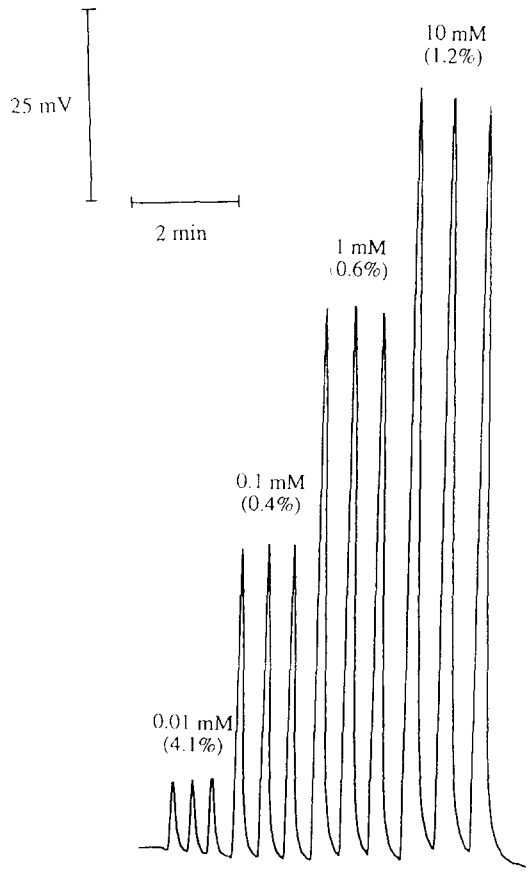

Fig. 5. Typical peak heights observed for the photo-cured Ca2 ISE in the FIP mode; the carrier and the referencev streams were 100 mM NaCl, the total flow rate was 1.5 ml min^{-1} and the sample volume was 100 μl. Relative standard deviations are given in parentheses.

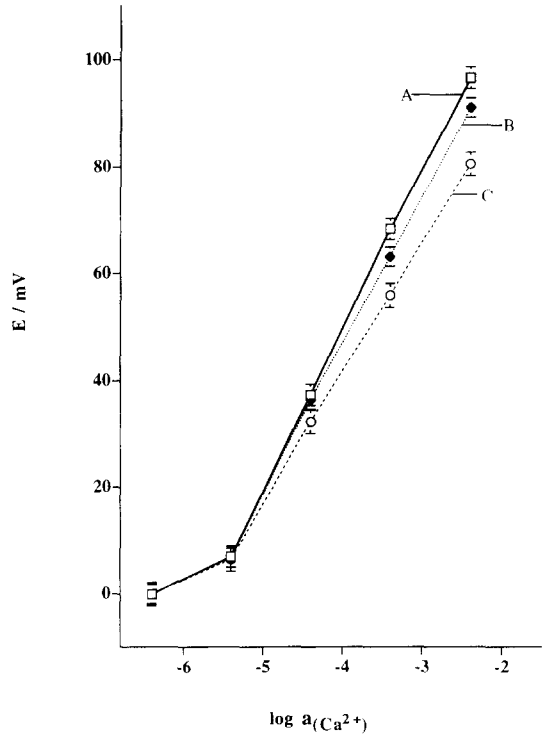

Fig. 6. FIP calibration plots for the photo-cured Ca2 ISE with calcium standards in (A) 100 mM NaCl; (B) 90 mM NaCl/10 mM NaClO 4 (C) 100 mM NaClO 4 backgrounds. Total flow rate was 1.5 ml min^{-1} and the sample volume was 100 μl.

grounds in the FIP mode are presented in Fig. 6. Comparison of the electrode performance between the photo-cured Cal and Ca2 ISEs in the FIP mode are summarised in Table 2. Clearly, the photo-cured, Ca2 ISE exhibits a higher electrode slope than the Cal ISE in the FIP mode.

To determine the reliability of the photo-cured Ca2 ISE, the total calcium level in a full cream milk sample that was digested with a nitric/perchloric acid mixture was measured. The acid digestion of the milk sample was necessary in order to release all the complexed calcium. The nitric/perchloric acid digestion of the milk samples was performed in triplicate and the procedure has been reported elsewhere [2]. The acid-digested samples were diluted 250-fold and the final background was 200 mM sodium perchlorate and 100 mM NaCl. The background of the calcium standards used in this experiment matched the acid-digested milk samples. The calcium levels determined in the acid-digested milk samples by

Table 2
The electrode slope exhibited by the photo-cured Cal and Ca2 ISEs with various backgrounds in the FIP mode

Background	Electrode slope (SD) mV per pCa^{2+}	
	Cal ISE [2]	Ca2 ISE
100 mM NaCl	27.8 (0.7)	30.3 (0.3)
10 mM $NaClO_4$/90 mM NaCl	26.9 (0.8)	28.2 (0.4)
100 mM $NaClO_4$	23.2 (0.1)	24.7 (0.2)

Table 3
Determined total calcium levels in full cream milk

Method of analysis	$[CA^{2+}]^a$ (mg l^{-1})
Ca1 ISE in FIP mode	1087 (2.0%)[b]
Ca2 ISE in FIP mode	1103 (1.1%)[b]
AAS	1132 (3.3%)[b]
Labelled	1100

[a] Mean of the measurement; RSD in parenthess.
[b] Diluted 250 fold.

the photo-cured Ca2 ISE in FIP mode, compared favourably with atomic absorption spectroscopy (AAS) measurements and the results are presented in Table 3.

4. Conclusion

The introduction of anhydrous calcium chloride into the photo-cured membrane of the Ca2 ISE resulted in an improvement in the selectivity over interfering divalent ions, as wider pH independent range, and a greater electrode slope compared with the photo-cured Ca1 ISE [2]. The calcium chloride added to the Ca2 membrane dissolved easily with the aid of the DOPP plasticiser which is known to coordinate with calcium, and a lipophilic calcium–phosphonyl oxygen complex is believed to have formed. The formation of the calcium–phosphonyl oxygen complex in the Ca2 membrane had lowered the membrane resistance compared with the photo-cured membrane of the Ca1 ISE, and this could have prompted the hyper-Nernstian slope and improved selectivity over divalent interfering ions that was observed for the Ca2 ISE. Further research is in progress to explain the improved selectivity observed for the photo-cured Ca2 ISE compared with the Ca1 ISE, including pH, and the role of the calcium–phosphonyl oxygen in these photo-cured membranes. Similar to the photo-cured Ca1 ISE, the reliability and sensitivity of the photo-cured Ca2 ISE in FIP mode was demonstrated, since both ISEs were used to potentiometrically measure 0.1 mM calcium a 200 mM perchlorate background for the digested milk samples.

Acknowledgements

We thank the Australian Research Council and the University of Tasmania for their financial support.

References

[1] G.J. Moody, J.M. Slate and J.D.R. Thomas, Analyst, 113 (1988) 103.
[2] T. Dimitrakopoulos, J.R. Farrell and P.J. Iles, Electroanalysis, 8 (1996) 391.
[3] A. Bratov, N. Abramova, J. Munoz, C. Dominiguez, S. Alegret and J. Bartoli, J. Electrochem. Soc., 141 (1994) L111.
[4] R.W. Cattall, I.C. Hamilton and P.J. Iles, Anal. Chim. Acta, 169 (1985) 403.
[5] T.J. Cardwell, R.W. Cattrall, I.C. Hamilton and P.J. Iles, Anal. Chim. Acta, 177 (1985) 239.
[6] T. Dimitrakopoulos, J.R. Farrell and P.J. Iles, Anal. Chim. Acta, 335 (1996) 111.
[7] C. Dumschat, R. Fromer, H. Rautschek, H. Rautschek, H. Muller and H.J. Timpe, Anal. Chim. Acta, 219 (1989) 179.
[8] F.R. del Mundo, T.J. Cardwell, R.W. Cattrall, P.J. Iles and I.C. Hamilton, Electroanalysis, 1 (1989) 179.
[9] T.J. Cardwell, R.W. Cattall, I.C. Hamilton and P.J. Iles, Anal. Chim. Acta, 204 (1988) 329.
[10] A. Bratov, N. Abramova, J. Munoz, C. Dominguez, S. Alegre and J. Bartioli, Anal. Chim., 67 (1995) 3589.
[11] T. Dimitrakopoulos, J.R. Farrell and P.J. Iles, Anal. Chim. Acta, 334 (1996) 133.
[12] W.E. Morf, The principles of Ion-Selective Electrodes and Membrane Transport, Elsevier, New York, 1981.
[13] A. Halanicki, M. Trojanowicz and A. Augustowska, 3rd Symposium on Ion-Selective Electrodes, Matrafured, Elsevier Science, Amsterdam, 1980, pp. 251–255.
[14] R.W. Cattrall and I.C. Hamilton, Ion-Selective Electrode Rev., 6 (1984) 125.
[15] L.T. Di Benedetto and T. Dimitrakipoulos, Electroanalysis, (1996) in press.
[16] D.A. Skogg and D.M. West, Fundamentals of Analytical Chemistry, 4th edn., CBS Publishings, Japan, 1982, p. 118.
[17] J. Ruzicka, E.H. Hansen and J Chr. Tjell, Anal. Chim. Acta, 67 (1973) 155.
[18] R.W. Cattrall, J. Newlands and M.F. Mackeay, Anal. Chim. Acta, 155 (1983) 235.
[19] G.J. Moody, R.B. Oke and J.D.R. Thomas, Analyst, 95 (1970) 910.

ELSEVIER

Talanta 44 (1997) 357–363

Talanta

Biotin ligands labeled with daunomycin as an electrochemical probe for avidin and biotin interaction

Shunitz Tanaka *, Fumie Yamamoto, Kazuharu Sugarwara[1], Hiroshi Nakumura

Division of Material Science, Graduate School of Environmental Earth Science, Hokkaido University, Sapporo, 060, Japan

Received 2 April 1996; received in revised form 6 August 1996; accepted 9 August 1996

Abstract

Electroactive biotin ligands were prepared by the reaction of daunomycin with biotinylating reagents with a different spacer. These biotin ligands exhibited similar electrochemical properties to those of daunomycin, but the adsorptivity of the ligands on the electrode increased with increasing length of the spacer. The electrode response of these ligands decreased when specifically bound with avidin. This made it possible to detect electroinactive avidin indirectly. Biotin was detected by observing the competitive reaction between biotin and the ligands for the limited binding sites of avidin. The binding strength of the labeled biotins with avidin was compared with that of unlabeled biotin by using an enzyme assay. © 1997 Elsevier Science B.V.

Keywords: Avidin–biotin interaction; Daunomycin-labeled biotin ligands; Electrochemical detection

1. Introduction

Avidin–biotin binding is one of the strongest bindings between proteins and ligands. Therefore, the strong interaction has been applied in various fields and is referred to as avidin–biotin technology [1–5]. An avidin–biotin binding assay is one of the typical avidin–biotin technologies using this strong interaction. In these assays, it is necessary to detect the information about the binding by using various methods. Generally, the avidin–biotin interaction has been investigated by a photometric procedure which uses fluorescent ligands and enzyme conjugates [6,7]. However, these methods usually require the use of a separation procedure such as filtration or centrifugation before measuring in order to separate a free labeled biotin from a bound biotin. Radioisotopic ligands are very useful but the handling and disposal of the ligands is problematic. An avidin–biotin assay using an electrochemical procedure is difficult because both avidin and biotin are electroinactive. If it were possible to evaluate the avidin–biotin interaction electrochemically, a new electrochemical assay without a separation procedure could be developed. Therefore, we attempted to detect avidin–biotin interaction electrochemically by preparing biotins labeled with an electroactive compounds (LBs). When the LB and avidin are

* Corresponding author. Tel.: + 181 11 7062219; fax: + 181 11 7166101.

[1] Present address: Faculty of Engineering, Kigami Institute of Technology, Kitami 090, Japan.

PII S0039-9140(96)02062-0

mixed, the LB becomes electroinactive through binding with avidin. Therefore, the electroinactive avidin can be detected indirectly from the change of the electrode response of the LB. The biotin can also be detected by observing the competitive reaction biotin and the LB for the limited binding sites of avidin. Previously, we prepared a labeled biotin ligand with daunomcyin as an electroactive compound. We then evaluated the interaction between avidin and biotin using the biotin ligand electrochemically [8].

It has also been reported that the affinity for labeled ligand–protein binding depends on the length of the spacer. The role of a spacer is to remove steric hindrance between two functional moieties and to facilitate the specific binding. If the length of the spacer is too short, the binding will be affected by steric hindrance. In this study, we prepared three LBs having spacers of different lengths as electrochemical probes for avidin–biotin binding assay. Subsequently, we observed the electrochemical behaviors of these LBs in the absence and presence of avidin. We also attempted to detect biotin using the competitive reaction of biotin and the LBs. Finally, the binding strength of these LBs with avidin was compared with that of biotin by an enzyme assay using a microtiter plate.

2. Experimental

2.1. Materials

Sulfosuccimidyl D-Biotin (Biotin-Sulfo-Osu), sulfosuccinimidyl *N*-(D-biotinyl)-6-aminohexanoate (Biotin-AC_5-Sulfo-Osu) and sulfosuccinimidyl *N*-[*N'*-D-biotinyl-6-aminohexanoyl]-6'-aminohexamoate (Biotin-$(AC_5)_2$-Sulfo-Osu) were purchased from Pierce Rockford (IL, USA). Daunomycin was supplied by Sigma, St. Louis, (MO, USA) and avidin and biotin by Wako Pure Chemicals (Osaka, Japan). Biotinamidocaproyl bovine serum albumin (Biotin-BSA; ca. 9.6 mol of biotin per mole of BSA), bovine serum albumin fraction V(BSA) and 3',3,5,5'-tetramethylbenzidine (TMB) were supplied by Sigma. Horseradish peroxidase avidin D conjugate (Av-P, 1.5 M peroxidase–1 M avidin) was purchased from Vector Labs Burlingame (CA, USA). Phosphate buffer was prepared with 0.1 MKH_2PO_4 and the pH was adjustable to pH 7 with the addition of 0.1 M NaOH. High quality nitrogen gas was used for deaeration of solutions for electrochemical measurements. All other reagents were of analytical-reagent grade.

2.2. Apparatus

All electrochemical measurements were carried out using a Yanaco P-1100 polarographic analyzer (Yanagimoto Scientific, Kyoto, Japan) with a Rikadenki Electronic Model RY-101AT recorder (Rikadenki Kogyo, Tokyo, Japan). Visible spectra of daunomycin and several biotins modified with daunomycin were measured with a Shimazu UV-2200 UV–VIS recording spectrophotometer (Shimazu Tokyo, Japan).

2.3. Electrode

A glassy carbon electrode (Model No. 11-2012, 3.0 mm diameter; Bioanalytical Systems (BAS, West Lafayette IN, USA)) was used as the working electrode. Before a measurement was carried out, the electrode was polished with 1.0, 0.3 and 0.05 μm alumina (Baikoski International, Charlotte, NC, USA) followed by 10 min of ultrasonication. An Ag/AgCl electrode (Model No. 11-2020; BAS) was used as the reference electrode and a platinum wire as the counter electrode. All potentials were measured against the Ag/AgCl electrode. Strong adsorption of the LBs on the electrode required us to reproduce a new electrode surface for all subsequent attempts of the procedure described above.

2.4. Preparation of LB

LBs were prepared as follows: 2 mM biotinylation reagent in DMF (500 μl) and 1 mM daunomycin in 50 mM phosphate buffer (pH 7.0) (250 μl) were mixed and incubated for 24 h at 4°C. The reaction product was separated from the biotiny-

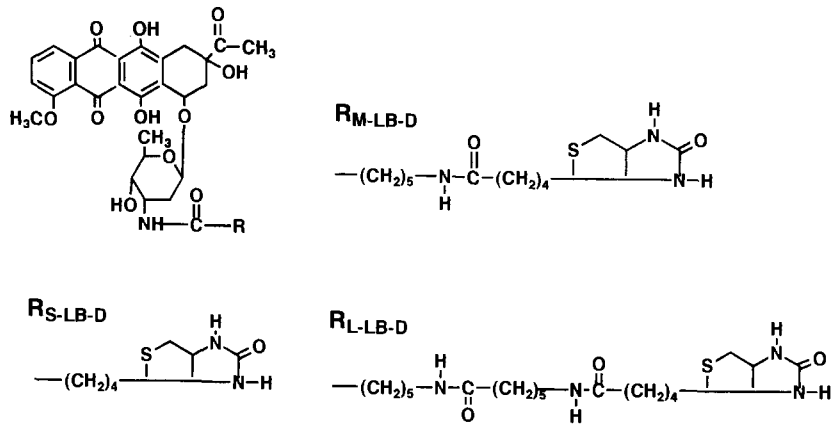

Fig. 1. Structure of labeled biotins prepared in this study.

lation reagent by TLC (Developing solvent chloroform–methanol–formic acid (80:20:2)). The concentration of LBs was determined from the absorbance at 475 nm because the spectra of the LBs were identical with that of daunomycin in visible region. The proposed structures of the LBs as shown in Fig. 1, and were supported by NMR data. The LBs labeled with Biotin-Sulfo-Osu, Biotin-AC_5-Sulfo-Osu and Biotin-$(AC_5)_2$-Sulfo-Osu are abbreviated to S-LB-D, M-LB-D and L-LB-D, respectively.

To examine the stability of the reagent, the spectra of LBs were measured. After 2 months, the spectra were the same as those at the time of preparation. Only one spot was observed on TLC even it was developed 2 months later. Therefore, it was concluded that the LBs were stable for at least 2 months.

2.5. Procedure for electrochemical avidin–biotin assay

Avidin and the LBs were mixed in 10 ml of 0.1 M phosphate buffer solution (pH 7.0) and the solution was incubated for 1 h at room temperature while being stirred. To investigate the competitive reaction between the LBs and biotin, biotin was added to a solution containing LB and the avidin. The solution was incubated under same conditions as described above. After the incubation, the solution (10 ml) was subjected to a voltammetric measurement. Deaeration of the solution was carried out for 15 min under nitrogen, then a polished electrode was immersed in the solution and a potential of -1.00 V was applied to the electrode for 5 min to reduce and accumulate the LB with stirring. After a rest time of 15 s, voltammograms of the LB were recorded by scanning the potential from -1.00 to -0.30 V using differential-pulse polarography (scan rate 5 mV s^{-1}).

2.6. Procedure for enzyme assay

After microtiter plates (Wako Pure Chemicals) had been washed with a detergent solution and water, 0.002% biotin BSA (200 μl) in phosphate buffer solution was added to the wells of the plate, which was left to stand at 4°C for 16 h. The plate was then washed three times with 10 mM phosphate buffer containing 0.1 M sodium chloride (pH 7.4) and 0.1% BSA (PBS-B) solution. Furthermore, 1% BAS solution (200 μl) was added to each well and kept for 1 h at 4°C to eliminate all remaining hydrophobic binding sites. The solution was discarded and the plate rinsed three times with PBS-B and subsequently once with PBS-B before being used.

Sample (100 μl), PBS-B (50 μl) and Av (0.12 nM, 50 μl) were mixed in the wells. The mixture was incubated overnight at 4°C with continuous shaking at 80 oscillations min^{-1} on a Thermo Shaker NTS-1300 (Eyela, Tokyo, Japan). After incubation, the wells of the plate were washed five

times with a 10 mM phosphate buffer containing 0.1 M sodium chloride (pH 7.4) (PBS), then TMB solution (100 μl) was added to each well. The enzyme reaction began with the addition of 0.01% hydrogen peroxide (50 μl). This mixture was shaken for 30 min. The reaction was stopped by adding 0.1 M sulfuric acid (50 μl). The absorbance of this solution was measured at 450 nm. The absorbance of a blank solution was taken as the unit (1.0) and the absorbance with 1×10^{-5} M biotin was taken as zero, and the ratios of the absorbances at various concentrations of biotin and LBs were plotted against concentration.

3. Results and discussion

3.1. Adsorptive behavior of LB on an electrode

Daunomycin has two pairs of redox peaks. The oxidation peak at −0.65 V and the reduction peak at −0.70 V were based on the redox reaction of the quinone part of the reagent molecule. The oxidation peak at +0.5 V and the reduction peak at +0.30 V were due to the redox reaction of the hydroquinone part [9]. The biotins labeled with daunomycin (LBs) also have the same pairs of redox peaks at the same potentials as for daunomycin itself. This suggests that labeling with biotin did not affect the electrochemical behavior of the daunomycin moiety. We investigated the binding behavior by using the oxidation peak at −0.65 V vs. (Ag/AgCl) by differential-pulse voltammetry because this peak was the sharpest among the four peaks.

Fig. 2 shows the relationship between the peak current and the accumulation time for 4×10^{-7} M daunomycin and LBs on the electrode. Daunomycin was adsorbed on the glassy carbon electrode and the peak current increased linearly until 15 min. The peak currents of M-LB-D and S-LB-D increased with increasing accumulation time up to 10 min and L-LB-D up to 5 min. When sufficient accumulation time had elapsed, the peak currents remained constant. These values are probably due to the adsorptive equilibrium of the LBs on the electrode surface. The peak current of M-LB-D is similar to that of L-LB-D, but is larger than those of S-LB-D and daunomycin. It was found that the adsorption of M-LB-D and L-LB-D on the electrode is stronger than that of S-LB-D and daunomycin. This enhancement of the adsorbing properties of the ligands may be attributed to the increase in hydrophobicity with increasing length of the spacer and by converting the ionic amino group of daunomycin into a more hydrophobic biotin moiety.

3.2. Change of the LB electrode response based on the interaction with avidin

The different pulse voltammograms of M-LB-D and daunomycin with and without avidin are shown in Fig. 3. The peak shape of the LB in the solution containing avidin was similar to that without avidin, but the peak current of the LB decreased considerably. When avidin was added to the solution containing daunomycin, the peak current of daunomycin did not decrease even after 2 h. Accordingly, it was concluded that the decrease in the peak current of LB was not due either to hindrance of the electrode reaction by the adsorption of protein on the electrode or to non-specific binding of ligand with protein. Therefore, the change in the peak current of the LB was considered to be due to the specific binding between avidin and biotin.

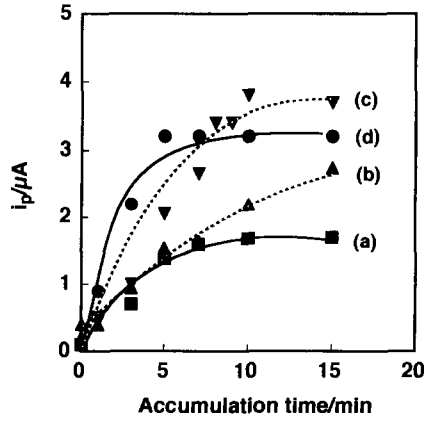

Fig. 2. Dependence of peak current on accumulation time 4×10^{-7} M S-LB-D (a), daunomycin (b), M-LB-D (c) L-LB-D (d). Results obtained by differential-pulse voltammetry (0.01 M phosphate buffer, $E_a = -1.0$ V, $t_a = 5$ min, scan rate = 5 mV s^{-1}).

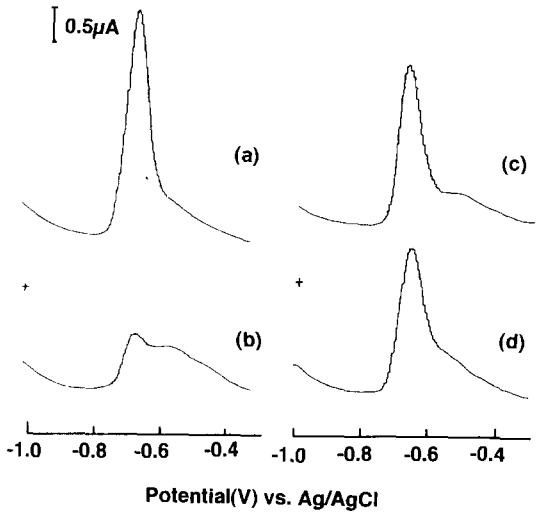

Fig. 3. Voltammograms of daunomycin and M-LB-D with and without avidin. (a) 4×10^{-7} M M-LB-D; as (a) $+ 6 \times 10^{-8}$ M avidin; (c) 4×10^{-7} M daunomycin; (d) as (c) $+ 1.2 \times 10^{-7}$ M avidin.

The dependence of the peak current of the LBs on the concentration of avidin is shown in Fig. 4. The peak current of the LBs decreased with increasing concentration of avidin, which made the detection of the electroinactive avidin possible. The detection limits for avidin calculated from the relative standard deviation (10%) of the peak current without avidin were 5×10^{-9} M using S-LB D, and 2×10^{-9} M using M-LB-D and L-LB-D. When a sufficient amount of avidin was added to bind all of the LBs, the peak current became close to zero. It can be suggested that the LB lost its electroactivity because the electroactive part of the daunomycin was covered with a large volume of avidin. If so, the length of the spacer should affect the electrode response of the LB-avidin conjugates. More detailed observations showed that when a high concentration of avidin was added, the peak current of S-LB-D was almost zero but M-LB-D and L-LB-D showed a small peak current even when a high concentration of avidin was added. This suggests that when avidin binds with M-LB-D and L-LB-D, the electroactive part is not completely covered with avidin because the electroactive part is located far from the binding site of avidin owing to the presence of a longer spacer. Therefore, the electroactivity of the ligands can be maintained but the diffusion constant decreases considerably. In contrast, the electroactive part of S-LB-D is covered completely with avidin because of the short spacer length.

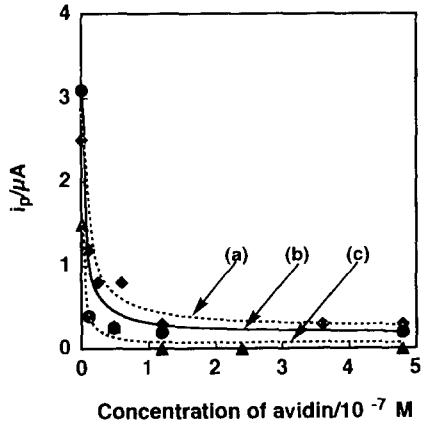

Fig. 4. Effect of avidin on peak current. 4×10^{-7} M L-LB-D (a) M-LB-D (b) and S-LB-D (c).

3.3. Competitive assay for biotin

The competitive reaction of the LB ad biotin for the limited binding sites of avidin makes the assay of biotin possible. When biotin, at various concentrations, was incubated in a solution containing a constant concentration of avidin and the LB, the peak current of the LB increased with increasing the concentration of avidin and the LB, the peak current of the LB increased with increasing the concentration of biotin, as shown in Fig. 5. This is because biotin occupies the binding sites of avidin and, as a result, the amount of free LB increases with increase in biotin content. The response curves of three types of LBs were not as varied. The best response curve was obtained by using L- and M-LB-D, as shown in Fig. 5. The relative standard deviation of the peak current at 1×10^{-7} M was 12% using M-LB-D.

3.4. Enzyme assay using microtiter plate

To investigate the strength of the binding of these ligands with avidin, an enzyme assay [10] was carried out and the results are shown in Fig.

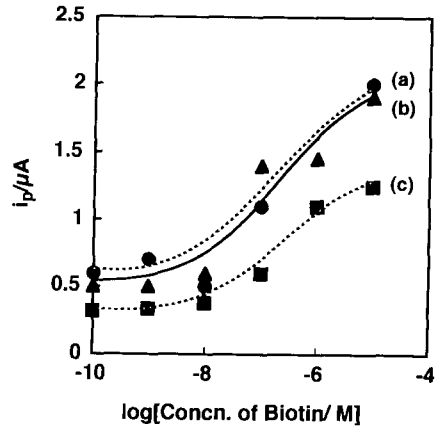

Fig. 5. Competitive binding assay for biotin using LBs by the electrochemical procedure. 4×10^{-7} M L-LB-D (a), M-LB-D (b), S-LB-D (c). Concentration of avidin 1.2×10^{-7} M.

6. The order of the binding strength was M-LB-D > L-LB-D > biotin > S-LB-D. This is due to the difference in the length of spacer between biotin and the daunomycin part. The binding constant of M-LB-D is the largest of the LBs and that of S-LB-D is the smallest. Since the distance between the biotin part and the electroactive compound is short in S-LB-D, it is thought that steric hindrance weakens the binding between the LB and avidin. The distance of the spacer does not affect the binding. The binding strength of M-LB-D and L-LB-D seemed to be slightly larger than that of biotin. If the distance of the spacer is too long, the compounds have high hydrophobicity.

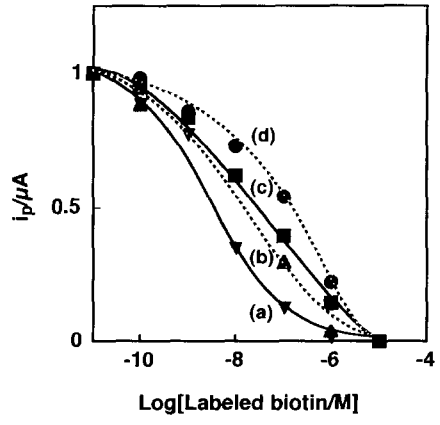

Fig. 6. Enzyme assay using microtiter plate for LBs and biotin (a) M-LB-D; (b) L-LB-D; (c) biotin; (d) S-LB-D.

The increase in the hydrophobicity of the ligand due to labeling caused it to bind non-specifically with avidin, having hydrophobic properties.

4. Conclusion

Three electroactive ligands for avidin-biotin assay were prepared. The binding behaviors of these LBs with avidin were investigated by using electrochemical and enzyme assay methods. These ligands, adsorbed strongly on the electrode, were detected sensitively by accumulation voltammetry. It was found that the adsorption of the ligands becomes stronger as the length of the spacer increases because of an increase in hydrophobicity. The electrode response of these LBs decreased drastically by binding with avidin. Therefore, the detection of 10^{-9} M avidin became possible. Biotin was also detected electrochemically using the competition reaction with these LBs. It is concluded that these LBs represent a new electrochemical probe for the measurement of the avidin–biotin interaction.

Acknowledgements

The authors thank the Ministry of Education, Science and Culture of Japan for support of this work under a Grant-in-Aid for Scientific Research (No. 07640795).

References

[1] E.A. Bayer, M. Safars and M. Wilchek, Anal. Biochem., 161 (1987) 262.
[2] F.R. Harmon, M. Berger, H. Beegen and H.G. Wood, J. Biol. Chem., 255 (1980) 9458.
[3] Y. Germani, H. deRocqunigny and J.L. Guesdon, J. Immunol. Methods, 146 (1992) 25.
[4] M. Wilchek and E. Bayer, Anal. Biochem., 171 (1988) 1.
[5] D.M. Mock, G. Langford, D. Dubois, N. Criscimagna and P. Horowitz, Anal. Biochem., 151 (1985) 178.
[6] K.L. Brillhart and T.T. Ngo, Anal. Lett., 24 (1991) 2157.
[7] S. Daunert and L.G. Bachas, Anal. Chim. Acta, 208 (1988) 43.
[8] K. Sugawara, S. Tanaka and H. Nakamura, Anal. Chem., 67 (1995) 209.

[9] E.N. Chaney and R.P. Baldwin, Anal. Chem., 54 (1982) 2556.

[10] S. Tanaka, T. Takeuchi and G.A. Rechnitz, J. Chromatogr., 597 (1992) 443.

ELSEVIER

Talanta 44 (1997) 365–371

Talanta

Extractive separation of trivalent lanthanide metals with a combination of Di(2-ethylhexyl)phosphoric acid and 1,10-phenanthroline

Md. Hasan Zahir, Yoshitaka Masuda *

Division of Science of Materials, Graduate School of Science and Technology, Kobe University, Rokkodai Nada-ku, Kobe 657, Japan

Received 12 January 1996; received in revised form 14 August 1996; accepted 16 August 1996

Abstract

The equilibrium extraction behavior of a series of trivalent lanthanide ions (Ln^{3+}) using a chloroform–Kerosine solution containing Di(2-ethylhexyl)phosphoric acid, combined with an adductant, 1,10-phenanthroline monohydrate (phen), was studied. The enhancement of the extraction by addition of such a neutral adductant is explained in terms of the extraction of the quaternary complex, $M(HX_2)_3(phen)_2$, in addition to the neutral complex, $M(HX_2)_3$, into the organic phase. The stoichiometry, extraction constants and separation factors of these systems were determined. The extraction constants of these systems partially follow the order of the atomic numbers. The synergistic extraction constants increased in the other Gd > Er > Ho > Eu > Ce > La > Pr and the highest separation factor was observed for Er–Ho (2.09). $pH_{1/2}$ values were also obtained. In this synergistic extraction system, both the extraction equilibrium constants and the separation factors were found to be greater than those of commercial extractants. © 1997 Elsevier Science B.V.

Keywords: Di(2-ethylhexyl)phosphoric acid; Lanthanides; 1,10-Phenanthroline; Solvent extraction

1. Introduction

The separation of trivalent lanthanides by solvent extraction is still an interesting and formidable problem. As a part of a systematic evaluation of the use of chelating extractants in extracting and separating trivalent lanthanides, the equilibrium extraction behavior of a series of representative lanthanide ions with chloroform containing one of several kinds of ligands alone or combined with adduct-forming agents has been studied in detail [1–6]. Many acidic organophosphorus compounds have been studied for the extraction of lanthanide metals [7–10]. One of the most important acidic organophosphorus compounds is Di(2-ethylhexyl)phosphoric acid (HDEHP), whose extraction behavior has been described by Marcus et al. [10]. HDEHP and its analogs, in organic solvents of low polarity, are present as dimers [10,11].

* Corresponding author. Fax: +81 78 8030722.

PII S0039-9140(96)02067-X

In synergistic systems, the extracting power of the mixture exceeds the sum of the extracting powers of its components. This phenomenon greatly enhances extraction or synergism with a mixture of extractants and has attracted considerable attention in recent years. Handley and Dean [12,13] examined Di(2-ethylhexyl)phosphorodithioic acid (HDEHPDT) as a metal extractant. According to their results, americium and europium could be extracted into dodecane fairly well with HDEHPDT. That a 'hard' metal ion such as Eu^{3+} can be extracted with a 'soft' ligand such as DEHPDT was reminiscent of our findings that a nitrogen ligand such as 1,10-phenanthroline (phen) seemed to bond with lanthanide chelates at least as readily as with the hydrated lanthanide ions [3].

Komatsu and Freiser [14] have reported extensive investigations on the solvent extraction of trivalent lanthanide metal ions (Ln^{3+}) with mixed ligands. They described the adduct formation of La(III), Pr(III), Eu(III), Ho(III) and Yb(III) with bis(2,4,4-trimethylpentyl)phosphinic acid (HBTMPP), tri-*N*-octylphosphine oxide (TOPO), octyl(phenyl)

-*N*,*N*-diisobutylcarbamoylmethylphosphine oxide (CMPO) and methylenebis(diphenylphosphine) oxide (MBDPO) in chloroform. The equilibrium extraction behavior of series of representative trivalent lanthanide ions (La, Pr, Eu and Yb) was studied with either chloroform solutions of selected 1-phenyl-3-methyl-4-acyl-5-pyrazolones (acyl = decanoyl, phenacetyl, 3-phenylpropionyl and *p*-*tert*-butylbenzoyl) (HP) alone or these solutions in combination with phen, TOPO or methyltrioctylammonium chloride (R_3R' NCl) [15]. Extraction of La(III) and Y(III) [16] and Eu(III) [17] with HDEHP was carried out by Peppard and co-workers, and the extraction behavior of the metals was clarified.

Nitrogen bases such as 1,10-phenanthroline, which have high proton affinity, are appropriate auxiliary ligands. This paper reports a study of adduct formation reactions between the lanthanides and auxiliary ligands aimed at obtaining a better understanding of the extractive separation of lanthanides. The role of the diluent was also examined for the evaluation of the association constant.

2. Experimental

2.1. Apparatus

Extraction was carried out in a Taiyo M incubator at 25 ± 0.1°C. Ultraviolet and visible absorption spectra were measured with a Shimadzu self-recording spectrophotometer (Model 240-UV–Vis) with 10 mm optical path glass cells. The pH of the aqueous phase was measured with a Hitachi Horiba M-7II pH-meter. A Kokusan H-200 centrifuge was also used for rapid and complete separation of the phases.

2.2. Materials

A 1×10^{-2} standard solution of lanthanide nitrates was prepared by dissolution of a suitable amount of the pure oxide (99.99%) (gadolinium was purchased from Santoku Chemicals, Osaka, Japan, hydrated $Ce(NO_3)_3$ from Wako Pure Chemical Industries, Osaka, Japan, and other rare earths from Nacalai Tesque, Kyoto, Japan) in a small volume of concentrated nitric acid, followed by dilution with distilled water. The solution was then heated in order to remove any excess acid. The solution was diluted to 100 ml with distilled water and the concentration was determined as 1×10^{-3} M. The solution was standardized complexometrically at pH 5.1–5.6 with xylenol orange as metal indicator [18]. The prepared solution was then stored in a polyethylene bottle.

2.3. Preparation of Di(2-ethylhexyl)phosphoric acid stock solution

For the preparation of a stock solution of HDEHP, 348 cm^3 of chemically pure HDEHP (DP-8R, Daihachi Chemicals) were placed in a clean, 1 dm^3 volumetric flask and diluted to volume with chloroform–kerosine so that the solution was 1 mol dm^{-3}. This solution was washed three times with 500 cm^3 of 6 mol dm^{-3} HCl and three times with 500 cm^3 of distilled water, after

Table 1
Percentage extraction of rare earth metal ions by HDEHP in the presence of phen[a]

Solvent	La^{3+}	Ce^{3+}	Pr^{3+}	Sm^{3+}	Eu^{3+}	Gd^{3+}	Tb^{3+}	Dy^{3+}	Ho^{3+}	Er^{3+}	Yb^{3+}	Lu^{3+}	Y^{3+}
$CHCl_3$	91.91	99.92	84.58	99.53	97.20	98.99	91.21	98.28	93.81	98.71	84.50	79.33	93.27
Kerosine	65.02	73.03	57.69	72.64	70.31	72.10	64.32	71.39	66.92	71.82	57.61	52.44	66.38

[a] [Metal nitrate ion] = 1×10^{-4} M; [ligand] = 2×10^{-3} M; [phen] = 2×10^{-3} M; [succinic acid] = 2×10^{-3} M; 25°C.

which the solution was left overnight. Since water is slightly soluble in HDEHP, the final HDEHP contains a small amount (1–2%) of water, which can be removed by using a rotating evaporator at 50°C and 15 mmHg pressure [8]. A 0.01 M phen solution was prepared by dissolving 1.9823 g of 1,10-phenanthroline monohydrate (Nacalai Tesque) in chloroform and diluting it to 100 cm^3 with the same solvent. A 0.001 M Arsenazo III solution was prepared by dissolving 0.0776 g of the reagent (Dojin Chemicals) in 100 cm^3 of distilled water. This solution was freshly prepared each week. Chloroform was used after distillation. All other chemicals were of analytical grade.

2.4. Solvent extraction procedure

The distribution experiments were performed at room temperature. An aliquot (10 cm^3) of the aqueous solution containing the metal ion (1×10^{-4} M) was placed in a stoppered 50 cm^3 glass tube. After the addition of 10 cm^3 of synergistic mixture containing the extractant solution (2×10^{-3} M) and neutral adductant solution (2×10^{-3} M), the mixture was shaken for 10 min at 200 strokes min^{-1} at 25 ± 0°C, which was sufficient for equilibration. The mixture was then centrifuged at 2000 rpm for 5 min and the pH of the aqueous phase was measured. The metal content in the aqueous phase was determined spectrophotometrically by the Arsenazo III method [19], as was the lanthanide concentration in the organic phase following back-extraction into hydrochloric acid. The concentration of metal ion in the organic phase was determined after back-extraction into 6 M hydrochloric acid for 30 min; 5 cm^3 of strip liquor thus obtained were transferred in to a separating funnel and washed once with 5 cm^3 of pure chloroform to remove the free ligand completely, then the strip liquor was allowed to evaporate. The residue was decomposed and diluted, then the pH was adjusted to 2.5. The solution was transferred into a 10 cm^3 volumetric flask, 0.5 cm^3 of the Arsenazo III was added and the mixture was diluted to volume with distilled water. The absorbance was measured at 650 nm. Neither the extractant nor its complexes in chloroform showed appreciable absorption in the visible region, hence Arsenazo III was used in the dual role of a calorimetric reagent and a scavenger for the lanthanides.

3. Results and discussion

3.1. Effect of pH on lanthanide(III) extraction systems containing HDEHP and adductant into chloroform–kerosine

First, we determined the percentage extraction of metal nitrates at pH 3–3.5 into chloroform (shown in Table 1). The effective extraction of lanthanides with HDEHP in the presence of phen occurs at aqueous phase pH values ranging from 3.00 to 3.35 for La^{3+}, 3.10 to 3.45 for Ce^{3+}, 3.15 to 3.40 for Pr^{3+}, 2.89 to 3.20 for Sm^{3+}, 2.99 to 3.25 for Eu^{3+}, 2.77 to 3.00 for Gd^{3+}, 2.85 to 3.20 for Tb^{3-}, 2.76 to 3.25 for Dy^{3+}, 2.88 to 3.10 for Ho^{3+}, 2.90 to 3.10 for Er^{3+}, 2.99 to 3.30 for Yb^{3+}, 2.80 to 3.20 for Lu^{3+} and 2.77 to 3.15 for Y^{3+}. The logarithmic distribution coefficients diminish monotonically with increasing aqueous acidities (at pH > 6.0), implying that the extractions are dominated by an ion-exchange reaction in which hydrogen is liberated. Gaikwad and Damodaran [20] studied the extraction behavior of Ho(III) with (2-ethylhexylphosphoric acid mono-2-ethylhexyl ester) (EHPNA) and they con-

cluded that there is no clear separation of phases at higher pH values. The percentage extraction of Ln^{3+} reaches the maximum in the case of phen adduct formation at pH 2.9–3.50.

3.2. Percentage extraction

The order of extraction with 2-thenoyltrifluoroacetone (1-(2-thienyl)-4,4,4-trifluorobutane-1,3-dione) (HTTA) in the presence of a bidentate heterocyclic amine, phen or 2,9-dimethyl-1,10-phenanthroline (dmp), was scandium(III) > lutetium(III) > europium(III) > neodymium(III) > praseodymium(III) > lanthanum(III), but enhancement of the extraction by tba^+ (tetrabutylammonium cation) was nearly the same with lanthanum(III) to europium(III); enhancement was negligible in the case of scandium(III) delated [21]. The results (shown in Table 1) were compared with the previous data concerning the synergistic enhancement of these metal complexes; the similarity of ternary complex extraction and synergistic extraction was also considered. In the case of Ce^{3+}, Eu^{3+}, Er^{3+} and Gd^{3+} the extraction of $M(HX_2)_3B_2$ is much greater than that of $M(HX_2)_3$, to the point where extraction of $M(ClO_4)(HX_2)_3$ is also negligible. It is concluded that synergistic extraction systems in which adduct formation occurs enhance the separation capability. In a mixed complex system containing 7-dodecenyl-quinolin-8-ol (DDQ), the donating ability of quinolin-8-ol (HQ) is not sufficient to form an adduct [4]. The effect of phenanthroline on the extraction of Eu(III) with DDQ-8 (quinolinol mixtures) was examined and it appeared that the formation with mixed complexes with a mixture of two chelating extractants and adduct formation with mixed complexes further enhance the separation capability in the lanthanide series. On the other hand, in the case of both La^{3+} and Pr^{3+}, the extraction of $Ln(HX_2)_3B_2$ take place in a similar pH region, resulting in the extraction behavior shown in Fig. 1. In Table 1, the enhancement of the extraction of La^{3+} and Pr^{3+} is not very marked, and the slopes for the straight portion are 2.7 for La^{3+} and Pr^{3+}. Obviously, lanthanides are extracted by a different mechanism under these conditions.

3.3. Slope analysis

A traditional and effective means of obtaining both stoichiometric and equilibrium constant information about extraction processes, slope analysis, is based on an examination of the logarithmic variation of the distribution ratio, D, with relevant experimental variables. The log–log plots of the extraction in the form of D vs. a concentration variable indicate the stoichiometry of the formation of the extractable complex and thus leads to the derivation of a suitable equilibrium expression and then to the calculation of equilibrium constants.

Plots of log D vs. variables such as the pH of the aqueous phase and the logarithm of the concentration of $[(HX)_2]$ were constructed [22]. Straight lines with a slope of +3 for lanthanides were obtained with a low extent of metal extracted. Thus the extraction reaction can be written as

$$Ln^{3+} + 3(HX)_{2(o)} \rightarrow Ln(HX_2)_{3(o)} + 3H^+ \quad (1)$$

Examination of Eq. (1) leads to the conclusion that the slope of a log D vs. pH plot should be +3, indicating that three hydrogen ions are released in the extraction of the metal ion (the subscript (o) designates concentration in the organic phase). The extraction constant, K_{ex}, for this reaction

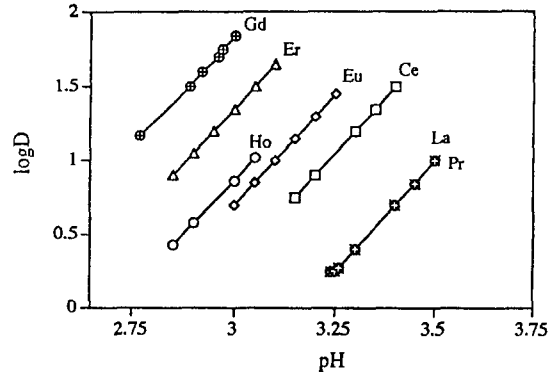

Fig. 1. Distribution constants for lanthanides between chloroform and the aqueous phase as a function of pH in the aqueous phase. Aqueous phase: $[Ln^{3+}] = 1 \times 10^{-4}$ M; succinic acid $= 2 \times 10^{-3}$ M. Organic phase: HDEHP $= 2 \times 10^{-3}$ M; [phen] $= 2 \times 10^{-3}$ M.

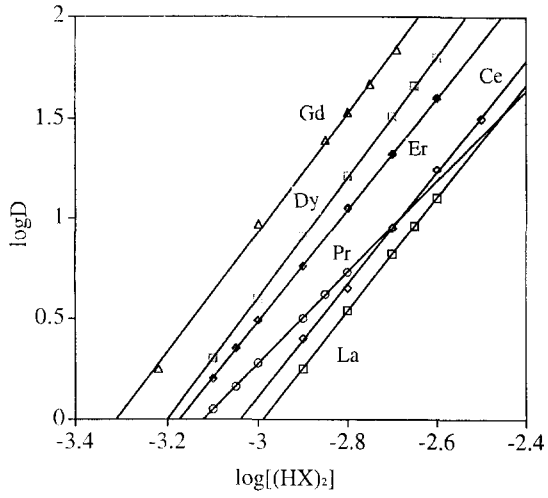

Fig. 2. Distribution constants for lanthanides as a function of HDEHP concentration in the presence of phen in the organic phase. Aqueous phase: $[Ln^{3+}] = 1 \times 10^{-4}$ M; succinic acid = 2×10^{-3} M. Organic phase: [phen] = 2×10^{-3} M; HDEHP = 2×10^{-3} M.

$$K_{ex} = [Ln^{3+}(HX_2)_3]_o[H^+]^3/[Ln^{3+}][(HX)_2]^3 \quad (2)$$

or

$$\log K_{ex} = \log D_o - 3pH - 3\log[(HX)_2] \quad (3)$$

As mentioned above, the adduct formation of tris-DEHPA complexes of Ln^{3+} with the nitrogen-containing chelating agent phen with a representative =N–C–C–N= donor group was studied. It was found that HDEHP complexes showed an exceptionally large tendency to form adducts with the nitrogen-containing the chelating agent phen. The data support the conclusion that the plot of log D vs. $\log[(HX)_2]_o$ exhibits a slope of +3 (Fig. 2), that the plot of $\log D/D_o$ vs. $\log[phen]_o$ is linear with a slope of 2, indicating that two molecules of phen are included in the extracted species [22], where D represents the distribution ratio with time of adduct formation (Fig. 3) and that the plot of log D vs. pH also has a slope of +3 (Fig. 1). Thus,

$$Ln^{3+} + 3(HX)_{2(o)} + 2B_{(o)} \rightarrow Ln(HX_2)_3B_{2(o)} + 3H^+ \quad (4)$$

$$\log D/D_o = \log K_{ex(B)}/K_{ex} + n \log[B]_o \quad (5)$$

where $K_{ex(B)}$ represents the extraction constant with the adduct formation and K_{ex} the extraction constant with HDEHP.

The results of the extraction of lanthanides using a mixture of HDEHP and phen are shown in Table 1, where it is seen from the lower $pH_{1/2}$ (pH of 50% extraction) values that highly enhanced extractions are achieved in the presence of as little as 10^{-3} M auxiliary reagent. According to Eq. (4), the values for log $K_{ex(B)}$ were evaluated as 6.22, 5.81, 5.33, 5.15, 4.90, 3.95 and 3.95 for Gd^{3+}, Er^{3+}, Ho^{3+}, Eu^{3+} Ce^{3+}, La^{3+} and Pr^{3+}, respectively. As seen from the above data, remarkable extraction efficiencies and selectivities were observed. This strongly indicates a new possibility that the separation efficiency can be improved, even in the synergistic solvent extraction system. However, HDEHP in a synergistic extraction system has proved to be an efficient extractant because of its higher separation factors for consecutive elements. Although heavy rare earths were selectively extracted with these extractants, the extraction sequence of yttrium with respect to rare earths was Dy > Y > Lu. (Table 1).

Generally, in the chelate extraction of lanthanides; the extraction constant increases with increasing atomic number [23]. This general tendency was also observed in the present system. The extraction constant increases as the atomic

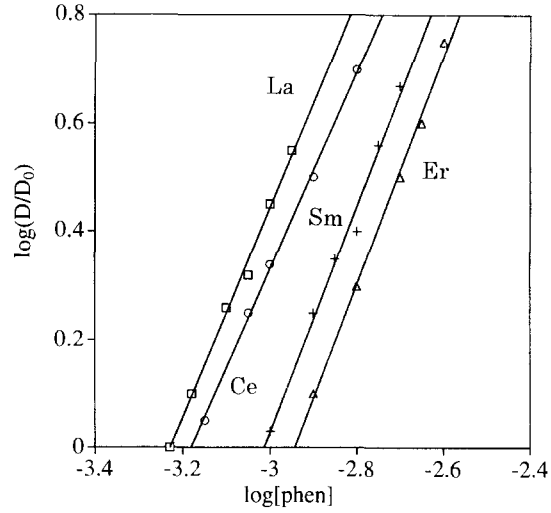

Fig. 3. Plots of $\log D/D_o$ vs. log[phen] at constant HDEHP and pH (3.10). Aqueous phase: $[Ln^{3+}] = 1 \times 10^{-4}$ M; succinic acid = 2×10^{-3} M. Organic phase: HDEHP = 2×10^{-3} M; [phen] = 2×10^{-3} M.

Table 2
Summary of results for extraction of lanthanides with HDEHP and phen as neutral ligand[a]

Element	Slope[b]	$pH^{c}_{1/2}$
La	2.74 ± 0.11[b]	3.15
Ce	3.00 ± 0.09	2.9
Pr	2.80 ± 0.03	3.15
Eu	3.15 ± 0.07	2.76
Gd	3.00 ± 0.31	2.1
Ho	3.05 ± 0.02	2.7
Er	3.22 ± 0.07	2.55

[a] $[HDEHP]_{(o)} = 2 \times 10^{-3}$ M; $[phen]_{(o)} = 2 \times 10^{-3}$ M in chloroform.
[b] Mean ± S.D. ($n = 2$).
[c] $pH_{1/2}$ is the pH value at which $\log D = 0$.

number increases until Gd^{3+}, and then it starts to decrease. It is interesting that the extraction constants $K_{ex(B)}$ of La^{3+} and Pr^{3+} are much smaller than those of the other six trivalent metal complexes with the same ligand and the $K_{ex(B)}$ values of the quaternary compounds from the neutral complex of europium(III), holmium(III) and erbium(III) are similar to each other, although the values for the cerium(III) complexes are slightly smaller than those for the other complexes. It is very interesting that the values of $\log K_{ex(B)}$ with HDEHP are very large compared with those with HDEHP alone in chloroform. This is because the steric hindrance of the synergistic mixture is low. In Table 2, the values of $pH_{1/2}$ show that lanthanide(III) can be extracted at slightly lower pH in the system with HDEHP alone than in the mixed system under the same extraction conditions and may be influenced by the distribution constant of the $Ln(HX_2)_3$ complex. In the present study, chloroform was employed as the solvent. It was observed that the extraction constant $K_{ex(B)}$, given by Eq. (5), is more than one order of magnitude larger in chloroform than in kerosine.

Fig. 4 shows the $\log K_{ex(B)}$ values for the systems studied here as a function of atomic number of the lanthanide metal ions. It is interesting that the relationship is linear up to Gd^{3+} and suggests that the slope might provide a good way of describing the selectivity of extractants used for the Ln^{3+} group.

3.4. Separation factor

The separation factor (SF) is the ratio of the distribution coefficients of two solutes measured under the same conditions. By convention, SF is greater than unity and a synonym for it is the separation coefficient. Mathematically it can be written as $SF = \log D_I / \log D_{II}$, where the subscripts I and II refer to two distinct metal ions.

In the study of metal ion separations, the dependence of the separation factors on metal ion concentrations, aqueous acidities, organic phase extractant concentrations, temperature of extractions and adduct concentration was investigated in order to determine the optimum experimental conditions in order to achieve the greatest separation factors. For evaluation of the selectivity of HDEHP, we compared the separation factors for different pairs of lanthanide(III). The values of $\log (D_I/D_{II})$ show that the separation of lanthanides becomes better only for Er–Ho, Gd–La and not for Gd–Ce. However, there is a very small gain or no gain in the separation of Ce–Ho and Eu–La, as shown by the values of $\log (D_I/D_{II})$ in Table 3.

All experiments were performed in the absence of perchlorate ion. In the absence of the perchlorate ion, the slope of the $\log D$ vs. pH lines was found to be 2.97, but when the perchlorate ion was present the slope was 1.98 [24]. Thus in the

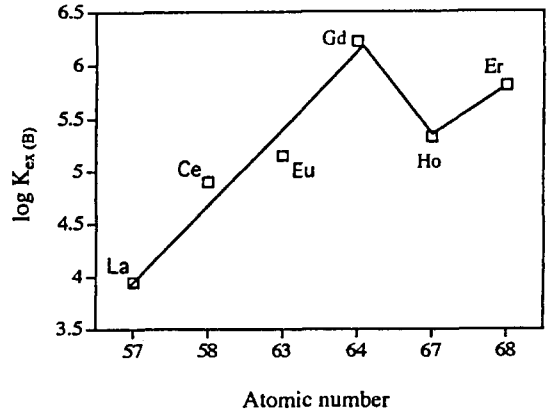

Fig. 4. Relationship between $\log K_{ex(B)}$ and the atomic number of lanthanide ions. Organic phase containing HDEHP with phen, in the absence of sodium perchlorate.

Table 3
Logarithmic separation factors in the extraction of lanthanide(III) with HDEHP and 1,10-phenanthroline

Separation	Log (separation factor)
Er–Ho	2.09
Gd–La	1.84
Ho–La	1.79
Ce–Ho	1.75
Eu–La	1.45
Gd–Ce	1.26

case of lanthanide(III) ion extraction, the following equation can be written:

$$Ln^{3+} + 3(HX)_{2(o)} + 2phen \rightarrow Ln(HX_2)_{3(o)}(phen)_2 + 3H^+ \quad (6)$$

Although all the systems examined exhibit excellent extractability, the selectivities are inferior in case of La(III) and Pr(III). It is notable that addition of phen improves the separation of the heavier lanthanides by virtue of a surprising increase in the extractability of the lighter metal (Ce^{3+}) to a greater extent than those of the heavier metals. Hence such a system would be of practical value in extracting the lanthanides as a group.

Acknowledgements

The present report is part of a project financed by the Ministry of Education, Science and Culture, Government of Japan (No. 06241250) for the development of new preparation methods for rare earth compounds and (No. 05303004) for the evaluation and characterization of organic solvents.

References

[1] T. Hori, M. Kawashima and H. Freiser, Sep. Sci. Technol., 15 (1980) 861.
[2] M. Kawashima and H. Freiser, Anal. Chem., 53 (1981) 284.
[3] O. Tochiyama and H. Freiser, Anal. Chem., 53 (1981) 874.
[4] E. Yamada and H. Freiser, Anal. Chem., 53 (1981) 2115.
[5] O. Tochiyama and H. Freiser, Anal. Chim. Acta, 13 (1981) 233.
[6] S. Inoue, C. Fabara Ordonez and H. Freiser, Solv. Extr. Ion Exch., 3 (1985) 839.
[7] J. Stary, Talanta, 13 (1966) 421.
[8] Z. Kolarik, S. Drazanova and V. Chotivka, J. Inorg. Nucl. Chem., 33 (1971) 1125.
[9] B. Weaver and R. R. Shown, J. Inorg. Nucl. Chem., 33 (1971) 1909.
[10] Y. Marcus, A.S. Kertes and E. Yanir (Eds.), Equilibrium Constants of Liquid–Liquid Distribution Reactions, Introduction and Part 1: Organophosphorus Reactants, Butterworths, London, 1974.
[11] G. Duyckaerts, P. Dreze and A. Simon, J. Inorg. Nucl. Chem., 13 (1960) 332.
[12] T.H. Handley, Nucl. Sci. Eng., 16 (1963) 440.
[13] T.H. Handley and J.A. Dean, Anal. Chem. 34 (1963) 440.
[14] Y. Komatsu and H. Freiser, Anal. Chim. Acta, 227 (1989) 397.
[15] Y. Sasaki and H. Freiser, Inorg. Chem. 22 (1993) 2289.
[16] D.F. Peppard, E.P. Horwitz and G.W. Mason, J. Inorg. Nucl. Chem., 24 (1962) 429.
[17] D.F. Peppard, G.W. Mason, J.L. Maier and W.J. Driscoll, J. Inorg. Nucl. Chem., 4 (1957) 334.
[18] K. Marczenko, Spectrophotometric Determination of Elements, Wiley, New York, 1976, p. 441.
[19] Z. Marczenko, Spectrophotometric Determination of Elements, Wiley, New York, 1976, p. 442.
[20] A.G. Gaikwad and A.D. Damodaran, Sep. Sci. Technol., 28 (1993) 1019.
[21] S. Nakamura and N. Suzuki, Bull. Chem. Soc. Jpn., 66 (1993) 98.
[22] Y. Masuda and Md. H. Zahir, Talanta, 42 (1995) 93.
[23] J.S. Preston, Hydrometallurgy, 14 (1985) 171.
[24] S. Umetani and H. Freiser, Inorg. Chem., 26 (1987) 3179.

ELSEVIER

Talanta 44 (1997) 373–382

Talanta

Comparison of different methods for the determination of volatile organic compounds in water samples

Raimo A. Ketola *, Vesa T. Virkki, Marja Ojala, Veikko Komppa, Tapio Kotiaho

VTT Chemical Technology, P.O. Box 1401, FIN-02044 VTT, Finland

Received 1 April 1996; received in revised form 16 August 1996; accepted 20 August 1996

Abstract

The aim of this work was to compare the characteristics of three methods, membrane inlet mass spectrometry (MIMS), purge-and-trap gas chromatography–mass spectrometry (P&T) and static headspace gas chromatography (HSGC), for the determination of volatile organic compounds in water samples as used in routine analysis. The characteristics examined included linear dynamic ranges, detection limits of selected environmentally hazardous volatile organic compounds (e.g. toluene, benzene and trichloroethene) in water, required analysis time and reproducibility of the analytical methods. The MIMS and P&T methods had the lowest detection limits for all the tested compounds, ranging from 0.1 to 5 $\mu g\ l^{-1}$. Linear dynamic ranges using the MIMS method were about four orders of magnitude and using the P&T method about two orders of magnitude. Detection limits of the HSGC method were 10–100 times higher than those of the other two methods, but the linear dynamic ranges were larger, even up to six orders of magnitude. The analysis time per sample was shortest for the MIMS method, from 5 to 10 min, and ranged around from 35 to 45 min for the HSGC and P&T methods. The reproducibilities of the methods were of the same order of magnitude, in the range of 1–13%. Agreement between the analytical results obtained for spiked samples and for environmental water samples by the three different methods was very good. © 1997 Elsevier Science B.V.

Keywords: Membrane inlet mass spectrometry; Purge-and-trap gas chromatography–mass spectrometry: Static headspace gas chromatography; Volatile organic compounds; Water analysis

1. Introduction

In order to demonstrate the excellent capabilities of membrane inlet mass spectrometry (MIMS) in environmental analysis and to enhance the acceptance of MIMS among analytical chemists, we have compared the MIMS method developed at VTT Chemical Technology with the routine water analysis methods used at VTT Chemical Technology, viz. purge-and-trap gas chromatography–mass spectrometry (P&T) and static headspace gas chromatography (HSGC), in the determination of environmentally significant compounds in water.

* Corresponding author. Fax: +358 9 456 7026; e-mail: raimo.ketola@vtt.fi

PII S0039-9140(96)02072-3

MIMS is an analytical technique based on the separation of organic compounds from water or air by a thin membrane, which is installed between the sample and the ion source of a mass spectrometer [1]. Organic compounds, as well other compounds, dissolve in the membrane, diffuse through it and finally evaporate directly into the ion source of the mass spectrometer. As the flow of water or the major constituents of air (nitrogen and oxygen) through the membrane is smaller than the flow of organic compounds, 10–100-fold enrichment of the organic compounds compared with water or air may be obtained [2]. The main reason for this is the greater solubility of organic compounds in the typically used dimethylsilicone membrane compared with the solubility of water or gases. The first application of a membrane as an interface between a sample and a mass spectrometer was reported by Hoch and Kok in 1963 [3]. They studied the kinetics of photosynthesis by determining in situ the amounts of oxygen and carbon dioxide. Since then, MIMS has frequently been used for monitoring of fermentation and biochemical reactions [1,4–7].

A very rapidly expanding application field of MIMS is environmental monitoring, as evidenced by some recent reviews [1,8–10]. For example, MIMS has been used to monitor hazardous organic compounds, such as halogenated aliphatic compounds, volatile aromatic compounds, chloramines, low molecular weight aldehydes, acrolein and acrylonitrile in water samples. MIMS has recently also been shown to have very good capabilities for the high-precision measurement of dissolved gases in environmental water samples [7] and for the measurement of dissolved gases in sediment samples [11]. An interesting series of MIMS studies was also recently published, demonstrating the on-site analysis capabilities of membrane inlet mass spectrometry during the characterization of a waste dump [8], detection of organic compounds at parts per 10^{15} levels in aqueous solutions [12], direct determination of organic compounds at parts per 10^{9} levels in air [13] and measurement of microbial degradation of halogenated compounds at parts per 10^{12} levels [14]. Various trapping methods combined with conventional membrane inlet mass spectrometric methods have also been designed recently in order to gain more selectivity or to enhance the detection limits of compounds which are difficult to measure using conventional MIMS method [15–17]. One of these studies showed how an affinity membrane can be used to gain more selectivity in the analysis of aldehydes from water samples [16]. Perhaps the most promising method is the trap-MIMS method introduced by Leth and Lauritsen [17] for the determination of semi-volatile organic compounds. A detection limit of 10 ppb was obtained for pentachlorophenol, an improvement of more than 30 times over the conventional MIMS method.

Static or dynamic headspace methods are the primary methods currently used to extract volatile organic compounds from water samples. These headspace methods rely on the establishment of equilibrium partitioning of an analyte between dissolved and gas phases. In the static headspace method (HSGC), a water sample is placed in a headspace vial and an aliquot of the closed airspace above the water phase is sampled directly to a gas chromatographic column with split injection. Owing to the high detection limits of the static headspace method, sample pretreatment is often used, e.g. salting-out with sodium sulfate or chloride and adjustment of pH. In dynamic headspace methods, of which the purge-and-trap method (P&T) is the commonest, the analytes are removed from the water phase by bubbling them with an inert gas such as helium or nitrogen, collecting them in an adsorbent trap, such as Tenax or activated charcoal, and desorbing them from the trap into a gas chromatographic column via a cold trap. The theory and construction of headspace methods have been reviewed by Koester and Clement [18], Crompton [19], Soniassy et al. [20] and Poole and Schuette [21]. These techniques provide a clean sample, free from its matrix, and are best suited for the determination of low molecular weight, slightly water-soluble volatile organic compounds. Theoretical considerations of the P&T method have been studied in detail by Pankow and co-workers [22–24]. Both headspace methods can be automated by commercially available headspace autosamplers. The P&T method has been used in the

determination of vinyl chloride and dichloroethenes in water samples [25] and of volatile halogenated hydrocarbons in rainwater and ambient air [26]. Automation of the P&T method has been studied for the rapid determination of volatile compounds [27] and optimization of the parameters of the P&T [28] and HSGC methods has also been studied [29].

Harland and Nicholson [30] compared the MIMS method with two purge-and-trap methods (GC-FID and GC–MS) in one intercomparison study in which six volatile halogenated hydrocarbons were determined in five environmental samples. The MIMS method was used in the selected-ion monitoring (SIM) mode. The concentration levels of the hydrocarbons in the samples were from < 0.1 to 90 $\mu g\ l^{-1}$, and the analytical results were in good agreement. However, the comparison included only this intercomparison exercise and not a detailed study of the characteristics of the methods.

In the following, the results of a comparison of the MIMS method with the conventional water analysis methods, purge-and-trap gas chromatography–mass spectrometry (P&T) and static headspace gas chromatography (HSGC), are presented. The analytical characteristics compared include detection limits and linear dynamic ranges of a set of environmentally significant organic compounds (e.g. benzene, toluene and trichloroethene), reproducibility of the methods, agreement of the results obtained by the different methods and the required analysis time.

2. Experimental

2.1. Membrane inlet mass spectrometry

Samples were analyzed using a quadrupole mass spectrometer with a mass range of 1–500 u and equipped with an open cross-beam electron impact (70 eV) ion source (QMG 421C, Balzers, Liechtenstein). Either a capillary or a sheet membrane inlet was used for sample introduction. The design of the capillary inlet has been described in detail [8]. The capillary membrane used was a hollow-fibre dimethylsilicone membrane (Silastic, Dow Corning, Midland, MI, USA), length 40 mm, o.d. 0.635 mm and i.d. 0.305 mm. The interface between the ion source of the mass spectrometer and the capillary membrane inlet was constructed on a standard 70 mm Conflat flange. Samples from the capillary inlet were directed to the ion source of the mass spectrometer using 50 cm × 0.22 mm i.d. deactivated silica capillary tubing and a 1 ml min^{-1} flow of helium through the membrane inlet and the interface silica capillary. The sheet membrane inlet was built on the basis of the design of Lauritsen [31]. The material of the sheet membrane was also dimethylsilicone (Specialty Silicone Products, Ballston Spa, NY USA) and had thickness 100 μm and contact area 28 mm^2. The interface and the membrane inlets were electrically heated to 70°C.

During operation of the system, a water stream is continuously supplied to the membrane inlet via a peristaltic pump (IPS4, Ismatec, Switzerland), typically at a flow-rate of 10 ml min^{-1}, and aliquots of sample solution are sampled into this stream as needed. A typical sampling lasts 3 min. The temperature of the flowing water was equilibrated at 70°C with a circulating water-bath (Lauda M3, MGW, Germany). Detection limits (signal-to-noise ratio 3:1) and linear dynamic ranges of the test compounds were measured by SIM. Identification and quantification of the compounds in samples were accomplished by scanning the mass range (45–200 u) of the sample and processing the spectrum obtained with a calculation program designed at VTT Chemical Technology [32]. This calculation program uses a modified algorithm of the general deconvolution method, which assumes that the intensity of any mass-to-charge ratio (m/z) is a linear function of the concentration of the chemical compounds which contribute to that particular m/z. The testing of the calculation program is still in progress, and the results will be published elsewhere.

2.2. Static headspace gas chromatography

Samples were analyzed using a Model 5890 Series II gas chromatograph (Hewlett-Packard, Palo Alto CA, USA) equipped with a Hewlett-

Packard Model 7694 headspace sampler, two flame ionization detectors (FID) and two capillary columns, 30 m × 0.32 mm i.d. SPB-1, film thickness 1.0 μm (Supelco, Bellefonte, PA, USA), and 30 m × 0.32 mm i.d. × OV-1701, film thickness 1.0 μm (J&W Scientific, Folsom, CA, USA). The carrier gas was hydrogen. The temperatures of the sampler oven, the sample loop and the transfer line of the headspace sampler were 80, 120 and 120°C, respectively. The GC cycle time was 43 min, the sample vial equilibrium time 30 min and the injection time 1.0 min. Analyses were carried out using the following temperature program: 45°C, held for 5 min, then increased at 10°C min^{-1} to 210°C, held for 2 min. The temperature of the injector was 220°C and that of the detectors 250°C. Sample volumes were 10 ml in 20 ml headspace bottles. Detection limits of the compounds were calculated from those peaks for which the signal-to-noise ratio was at least 3:1.

2.3. Purge-and-trap gas chromatography–mass spectrometry

Samples were analyzed using a system consisting of an LSC 2000 purge-and-trap sampler (Tekmar, Cincinnati, OH, USA), a Model 5890 Series II gas chromatograph (Hewlett-Packard) equipped with a DB-1 capillary column, 30 m × 0.32 mm i.d., film thickness 1.0 μm (J&W Scientific) and a JMS-AX505WA mass spectrometer with electron impact ionization at 70 eV (Jeol, Tokyo, Japan). The conditions of the purge-and trap sampler were as follows: standby time 30 min, prepurge time 0 min, preheat time 0 min, sample time 20 min, purge time 6 min, dry purge time 2 min, cool down temperature −120°C, desorb preheat temperature 200°C, desorb time 4 min at 225°C, inject time 2 min at 250°C and bake time 8 min at 250°C. The GC temperature program was as follows: 30°C, held for 5 min, then increased at 20°C min^{-1} to 110°C and at 10°C min^{-1} to 300°C, held for 5 min. The carrier gas and purging gas was helium and the sample volume was 5 ml. Identification of compounds in the samples was accomplished by analysing mass spectra obtained over the mass range 29–400 u. Quantification was performed on the basis of the peak areas obtained from the single ion chromatograms extracted from the data measured in the scanning mode. Detection limits of the compounds were calculated from those peaks for which the signal-to-noise ratio was at least 3:1. Better detection limits can be obtained in the SIM mode, but to save analysis time the samples were analysed only in the scanning mode.

Aqueous standard solutions were prepared by volumetrically diluting stock standard solutions (typically 10 g l^{-1} in methanol) of commercial reagents using deionized water. The final concentrations of the standard solutions were in the range 0.1–500 μg l^{-1}. The commercial reagents used were trichloroethene [79-01 – 6] (99.5%), benzene [71-43-2] (99.5%), tetrachloroethene [127-18-4] (99%), carbon tetrachloride [56-23-5] (99.7%), xylenes (mixture of isomers) [95-47-6], [108-38-3], [106-42-3] (99.8%), toluene [108-88-3] (99.5%), chloroform [67-66-3] (99%), benzaldehyde [100-52-7] (99%), butan-2-one [78-93-3] (99.5%) from Merck (Darmstadt, Germany), acetone [67-64-1] (99.5%) from Mallinckrodt, St. Louis, MO, USA) and methyl *tert*-butyl ether [1634-04-4] from Neste Oy (Finland).

Spiked samples were prepared by diluting the stock standard solutions (10 g l^{-1}) with methanol to a concentration of 100 mg l^{-1} and diluting these solutions to the final concentration with deionized water. The content of methanol in the spiked sample was about 1%. All unknown and spiked samples were stored in 100 ml headspace vials and similar headspace vials were also used as sample vials in the MIMS method. The 12 environmental water samples analyzed were obtained from various customers of VTT Chemical Technology. Appropriate dilutions of the samples were made with deionized water when needed for both the MIMS method and the P&T method.

3. Results and discussion

The analytical characteristics of the MIMS, P&T and HSGC methods were studied with nine different volatile test compounds presented in Table 1, including six halogenated organic compounds and three aromatic compounds. Note that

Table 1
Detection limits and linear dynamic ranges (LDR) of selected compounds (in μg l^{-1}) measured by MIMS, P&T and HSGC

Compound	MIMS		P&T		HSGC[a]	
	Detection limit	LDR	Detection limit	LDR	Detection limit	LDR
Toluene	0.1	0.3–1000	0.2	0.2–15	3	3–380 000
Benzene	0.1	0.1–1000	0.2	0.2–20	4	4–100 000
Xylenes	0.1	0.1–5000	0.2	0.2–15	4	4–100 000
1,2-Dichloroethane	0.4	0.4–4000	0.2	0.2–15	12	12–100 000
1,1,1-Trichloroethane	0.6	0.6–5000	0.2	0.2–15	30	30–100 000
Trichloroethene	0.1	0.1–1000	0.2	0.2–20	8	8–100 000
Tetrachloroethene	0.1	0.3–1000	0.2	0.2–20	10	10–100 000
Chloroform	0.3	0.5–5000	0.2	0.2–30	30	30–100 000
Carbon tetrachloride	0.5	0.5–5000	0.2	0.2–20	40	40–100 000

[a] The upper limit of LDR by the HSGC method is partly determined by the solubilities of the tested compounds in water.

the P&T and the HSGC methods are the analytical methods used in routine water analysis at VTT Chemical Technology. All methods were optimized for routine analysis and for this reason the operating conditions used were a compromise between several different factors (e.g. detection limits required by government regulations, speed of analysis and capability to identify unknowns) and therefore the best performance characteristics of these techniques were not necessarily obtained. For example, lower detection limits with all three different methods can be obtained. Typical detection limits using the P&T method range from 0.01 to 0.1 μg l^{-1} [33], but detection limits below 1 ng l^{-1} have been reported [34]. With the MIMS method the typical detection limit range is 0.1–10 μg l^{-1}. However, it has already been demonstrated that under optimum conditions detection limits at parts per 10^{15} (ppq) levels can be achieved, for example a detection limit of 500 ppq was measured for toluene in water [12]. With the HSGC method, detection limits of 0.1–1 μg l^{-1} are often obtained [35,36]. Organic chloro compounds, e.g. trichloroethene and chloroform, can be measured by the HSGC method even at lower levels under optimum conditions, i.e. at 0.05–0.2 μg l^{-1} using an electron-capture detector (ECD) [37].

In this study, the main interest was to measure the detection limits and the linearity of the signals of these compounds with the three different routine analysis techniques. The detection limits (signal-to-noise ratio 3:1) for most of the compounds are comparable for the MIMS method and for the P&T method, being in the range 0.1–1.0 μg l^{-1}. In the case of the HSGC method the detection limits are about 10–100 times higher than those for the other two methods. The reason for this is that in the MIMS and P&T methods, compounds can be concentrated very effectively by the membrane or by the adsorbent trap, respectively. In the HSGC method this kind of concentration step is lacking and the concentrations of the compounds detected are determined by their Henry's laws coefficients at the temperature of measurement. For this reason the total amount of a compound detected is not as large in the HSGC method as in the MIMS and P&T methods.

The linear dynamic ranges of test compounds by the MIMS method are three to four orders of magnitude, which is more than sufficient for the analysis of unknown samples with varying concentrations. For the P&T method the linear dynamic ranges are much narrower, about two orders of magnitude, owing to the limited capacity of the adsorbent trap and the cryofocusing trap. These narrow linear dynamic ranges can cause problems in the analysis of samples containing analytes in a wide concentration range. However, with a different P&T configuration a linear dynamic range up to 5000 μg l^{-1} has been achieved [38]. The best performance in this respect was obtained with the HSGC method, for which linear dynamic ranges up to six orders of magni-

Table 2
Analytical results for a spiked sample measured by the three methods and RSD between calculated and measured concentrations

Compound	Concentration (μg l^{-1})				RSD (%)		
	Spiked	MIMS	HSGC	P&T	MIMS	HSGC	P&T
Toluene	50	51	41	44	1	13	8
Tetrachloroethene	8	12	8	12	35	0	35
1,2-Dichloroethene	98	120	110	90	16	9	6
C2-benzenes	201	240	210	190	14	3	4
Benzene	20	26	19	12	21	4	28
C3-benzenes	52	48	43	40	5	12	16
1,1,1-Trichloroethane	432	370	410	350	10	4	13
1,1-Dichloroethane	49	59	44	—[c]	14	7	—[d]
Dichloromethane	47	59	50	49	18	5	3
1,2-Dichloroethane	108	79	110	200	19	1	60
Trichloroethene	800	760	720	820	4	7	2
Sum[a]	1865	1820	1760	1800	2	4	2
Mean[b]					13	6	16

[a] Sum is the total amount of analytes.
[b] Mean is measured as an average of the RSDs between observed and spiked concentrations.
[c] Not found.
[d] Not measured.

tude were measured, owing to the very wide dynamic range of the flame ionization detector. The linear dynamic ranges of some compounds might be even wider, but for practical reasons the upper limit in the measurements was limited to 100 mg l^{-1} except in the case of toluene. For the HSGC method our results are in good agreement with the literature, e.g. using the HSGC method with a photoionization detector (PID) followed by FID the useful working range was reported to be 1–15 000 μg l^{-1} [35].

The identification and quantitation capabilities of the three methods were compared by analyzing spiked samples. A good example of these results is presented in Table 2. The concentrations of the analytes were calculated for each method using external standards. For the MIMS method the results were calculated using the calculation program developed at VTT [32] and external standards of three different concentration levels (5.0, 20 and 50 μg l^{-1}). Three different external standards (1.0, 5.0 and 10 μg l^{-1}) were also used for the P&T method. For the HSGC method, however, external standards of five different concentration levels were used (10, 50, 100, 500 and 1000 μg l^{-1}). Note that the notation C2-benzenes and C3-benzenes in Table 2 indicates the sum of benzene derivatives substituted by two (dimethylbenzenes and ethylbenzene) or three carbons (trimethylbenzenes, ethylmethylbenzenes, propylbenzene and isopropylbenzene), respectively. These compounds can be quantitated separately using the HSGC and P&T methods due to the chromatographic separation. The sum of these compounds can also be calculated with the MIMS method, but the identification of individual compounds is difficult.

The results presented in Table 2 show that compounds with low concentrations can be quantified reliably by all the three methods, even if the concentration difference between some compounds is as much as two orders of magnitude. The small variations between the observed and spiked concentrations are believed to be due to evaporation of the compounds during the preparation of the spiked sample and standards. The loss of volatile compounds in the sample handling has been experienced before, e.g. by Wise et al. [39]. Note that the high content of methanol in the sample did not seem to affect the analysis, although it can interfere with the chromatographic behavior of low molecular weight com-

Table 3
Results of the analysis of two waste water samples by the three methods

Compound	Concentration (μg l^{-1})					
	Sample A			Sample B		
	MIMS	HSGC	P&T	MIMS	HSGC	P&T
1,2-Dichloroethene	420	490	360	2000[d]	1600	960
Dichloromethane	48	28	—[b]	2000	1200	1300
1,1-Dichloroethane	40	38	—[b]	[b]	[b]	[b]
Chloroform	48	—[a,b]	26	[b]	[b]	[b]
Tetrachloroethene	58	60	55	650	440	310
Trichloroethene	200	160	180	2000	1100	1400
Toluene	—[b]	—[b]	—[b]	3900	2700	2100
Benzene	—[b]	—[b]	—[b]	50	[b]	[b]
C2-benzenes	—[b]	—[b]	—[b]	3000	1800	1300
C3-benzenes	—[b]	—[b]	—[b]	500	310	230
1,1-Dichloroethene	—[b]	—[b]	—[b]	[d]	500[c]	1000
Carbon tetrachloride	—[b]	—[b]	—[b]	50	[b]	[b]
1,1,1-Trichloroethane	—[b]	—[b]	—[b]	4700	4300	2400

[a] Detection limit 50 μg l^{-1}.
[b] Not found.
[c] Quantitated by 1,2-dichloroethene.
[d] Sum of 1,2-dichloroethene and 1,1-dichloroethene.

pounds. The smallest mean difference between observed and spiked concentrations was obtained with the HSGC method (6%) and the largest with the P&T method (16%). The largest differences between observed and spiked concentrations with the MIMS and the P&T methods were observed in the case of tetrachloroethene, probably owing to its low concentration. In the case of the P&T method, relatively large errors were also observed in the determination of 1,2-dichloroethane and benzene. The former error was probably due to inadequate chromatographic separation of 1,2-dichloroethane from 1,1,1-trichloroethane when a dimethylpolysiloxane column was used. The latter error was due to the leakage of benzene from the Tenax adsorbent trap, which was observed in the analysis of blank samples. The leakage of benzene and alkylbenzenes from the adsorbent is due to decomposition of the Tenax trap material [40]. From Table 2, it can also be seen that the MIMS method gives the closest result for the total amount of volatile organic compounds in the sample.

A number of unknown environmental water samples were also analyzed during this study in order to compare the capabilities of these three methods in the analysis of typical water samples delivered to VTT by customers of the laboratory. The analytical results for two of these samples are presented in Table 3. The samples were waste water samples containing hazardous organic compounds in various concentrations. The results show that all three methods produced same results, i.e. the same compounds are identified and the concentrations of the compounds are about the same. They also show that in some cases the MIMS method overestimate the concentrations of some of the analytes. This is due to the fact that in the MIMS method all the compounds are analyzed at the same time on the basis of a multicomponent mass spectrum and therefore unidentified minor compounds can cause overestimation of the concentration of the identified compounds if the minor compounds produce the same fragment ions as the identified major compounds. However, it should be noted that in all cases presented the errors are small and that the same

Table 4
Agreement of analytical results obtained by three methods (MIMS, HSGC and P&T) by calculating the RSD for the analytical results of unknown or spiked samples (the total number of samples was ten)

Compound	No. of analytes	Concentration range (μg l^{-1})	RSD range (%)	Mean RSD (%)
Halogenated compounds	31	0.2–4700	2–71	26
Aromatics	26	0.2–27000	4–52	25

compounds were identified with the MIMS method as with the other two methods.

On the basis of the results presented above, the analysis time per sample for the three different methods can also be discussed. The analysis time is shortest for the MIMS method, the cycle time from sampling of one sample to sampling of the next being 5–10 min. The cycle time can easily be changed by varying the sampling time; especially for high-concentration samples, very short sampling times (1 min or less) can be used. At low compound concentrations very short cycle times, less than 5 min, can be obtained, since the signals of the monitored ions return from their maximum to the ground level very rapidly. In the HSGC and P&T methods the analysis time depends on the GC run time and the headspace parameters. In our experiments the analysis time was 43 min for the HSGC method and 40 min for the P&T method. In both cases the analysis time can be shortened by a few minutes, at the expense of accuracy and reproducibility. This comparison clearly shows that a much larger sample throughput can be obtained with the MIMS method than with the other two methods.

Table 5
Characteristics of the three analytical methods

Characteristic	MIMS	P&T	HSGC
Detection limit (μg l^{-1})	<1	<1	1–10
Linear dynamic range	10^4	10^2	10^6
Repeatability (%)	1–11	2–13	1–8
Analysis time (min)	5–10	35–45	35–45
On-line monitoring capability[a]	+++	+	+
Identification capability[a]	++	+++	++[b]
Simplicity of instrumentation[a]	++	+	+++

[a] +++, Very good; ++, good; +, fair.
[b] Flame ionization detector used.

The repeatability of the analysis method was measured from three successive injections of the same sample and calculating the relative standard deviation (RSD) of the repeated injections from the measured concentrations of compounds in the sample. The repeatability obtained from ten individual measurements with each method ranged between 1 and 11% (mean 8%) for the MIMS method, 1 and 8% (mean 6%) for the HSGC method and 2 and 13% (mean 8%) for the P&T method. The results obtained are very close to those reported earlier by Ho [33] (1–10% with the P&T method) and Roe et al. [36] (2–8% with the HSGC method). As can be seen from these results, the repeatabilities of all three methods were good, demonstrating that minor changes in the measurement conditions do not affect the analytical results.

The agreement of the analytical results obtained by the three different methods was estimated by calculation of the RSD of the analytical results measured for unknown or spiked samples (Table 4). The total number of compounds measured was 57 (31 halogenated compounds and 26 aromatic compounds) from ten unknown samples. The RSDs were usually good, ranging from 2 to 40%, demonstrating that all three methods gave comparable results in the determination of volatile organic compounds in water. Larger RSD values (40–71%) were normally obtained for samples containing low concentrations of analytes, i.e. at concentration levels close to detection limits, whereas very good agreement (RSD < 10%) was obtained in the concentration range from 10 to 1000 μg l^{-1}. The mean RSDs of both compound classes (halogenated and aromatic compounds) were almost the same, indicating that equally

good data can be obtained for these classes of compounds.

4. Conclusions

The analytical characteristics of the three methods are summarized in Table 5. As can be seen, in the determination of volatile organic compounds MIMS is very comparable to the conventional P&T and HSGC methods. The main advantages of the MIMS method are low detection limits and short analysis times. The MIMS method is also the only method of these three which can be used for continuous on-line monitoring [41–44]. The major difficulty with the MIMS method is the lack of chromatographic resolution of components, especially with heavily contaminated samples, but the recently developed deconvolution program for multicomponent mass spectra resolves this problem in many cases. The major advantages of the P&T method are low detection limits and the capability to analyze very complex mixtures owing to the gas chromatographic separation. In addition, identification of unknowns is relatively easy since commercial reference libraries of electron impact mass spectra can be used to assist the identification. The best qualities of the HSGC method are the wide dynamic range, separation of compounds by GC and simpler instrumentation than for the other two methods. The major disadvantages of the HSGC method are poor detection limits compared with the other two methods and poor identification capability when a flame ionization detector is used. The measured results also showed that the reproducibilities of the methods are of the same order of magnitude and that agreement between the analytical results obtained by the three different methods is very good.

The main conclusion of this study is that in many cases MIMS can produce much faster analytical results of the same quality as the conventional P&T and HSGC methods for water analysis, and therefore it should be the preferred method especially when high throughput is required.

Acknowledgements

The assistance of Kaija Luomanperä and Harri Sorsa is gratefully acknowledged. Financial support of the Technology Development Center (TEKES) is also gratefully acknowledged.

References

[1] T. Kotiaho, F.R. Lauritsen, T.K. Choudhory, R.G. Cooks and G.T. Tsao, Anal. Chem., 63 (1991) 875A.
[2] M.A. LaPack, J.C. Tou, V.L. McGuffin and C.G. Enke, J. Membr. Sci., 86 (1994) 263.
[3] G. Hoch and B. Kok, Arch. Biochem. Biophys., 101 (1963) 160.
[4] H. Degn, J. Microbiol. Methods, 15 (1992) 185.
[5] F.R. Lauritsen and D. Lloyd, in: C. Fenselau (Ed.), Mass Spectrometry for the Characterization of Microorganisms, ACS Symposium Series 541, American Chemical Society: Washington, DC, 1994, pp. 91–106.
[6] F.R. Lauritsen, in Proceedings of the COMETT II Course 'Advanced Instrumentation, Data Interpretation, and Control of Biotechnological Processes', October 24–27, 1994, Gent, Belgium, Kluwer, Dordrecht, 1995.
[7] T.M. Kana, C. Darkangelo, M.D. Hunt, J.B. Oldham, G.E. Bennett and J.C. Cornwall, Anal. Chem., 66 (1994) 4166.
[8] V. Virkki, R.A. Ketola, M. Ojala, T. Kotiaho, V. Komppa, A. Grove and S. Facchetti, Anal. Chem., 67 (1995) 1421.
[9] P.S.H. Wong, R.G. Cooks, M.E. Cisper and P.H. Hemberger, Environ. Sci. Technol., 29 (1995) 215A.
[10] S. Bauer, Trends Anal. Chem., 14 (1995) 202.
[11] K.L. Thomas and D. Lloyd, FEMS Microbiol. Ecol., 16 (1995) 103.
[12] M. Soni, S. Bauer, J.W. Amy, P. Wong and R.G. Cooks, Anal. Chem., 67 (1995) 1409.
[13] M.E. Cisper, C.G. Gill, L.E. Townsend and P.H. Hemberger, Anal. Chem., 67 (1995) 1413.
[14] F.R. Lauritsen and S. Gylling, Anal. Chem., 67 (1995) 1418.
[15] A.A. Rivlin, Rapid Commun. Mass Spectrom., 9 (1995) 397.
[16] C. Xu, J.S. Patrick and R.G. Cooks, Anal. Chem., 67 (1995) 724.
[17] M. Leth and F.R. Lauritsen, Rapid Commun. Mass Spectrom., 9 (1995) 591.
[18] C.J. Koester and R.E. Clement, Crit. Rev. Anal. Chem., 24 (1993) 263.
[19] T.R. Crompton, in The Analysis of Natural Waters, Vol. 2 Direct Preconcentration Techniques, Oxford University Press, Oxford, 1993.
[20] R. Soniassy, P. Sandra and C. Schlett, in HP Publication 5962–6216E: Water Analysis, Organic Micropollutants,

Hewlett-Packard, Avondale, PA, 1994, Chapters 1 and 2, pp. 11–72.
[21] C.F. Poole and S.A. Schuette, J. High Resolut. Chromatogr. Chromatogr. Commun., 6 (1983) 526.
[22] J.F. Pankow, M.P. Ligocki, M.E. Rosen, L.M. Isabelle and K.M. Hart, Anal. Chem., 60 (1988) 40.
[23] J.F. Pankow and M.E. Rosen, Environ. Sci. Technol., 22 (1988) 398.
[24] J.F. Pankow, Environ. Sci. Technol., 25 (1991) 123.
[25] J. Wittsiepe, D. Wallschlager, F. Selenka and E. Jackwerth, Fresenius J. Anal. Chem. 346 (1993) 1028.
[26] M. Fujita, W.T. Jung, H. Tatematu, D.H. Sohn and T. Maeda, J. High. Resolut. Chromatogr., 14 (1991) 83.
[27] H.T. Badlings, C. de Jong and R.P.M. Dooper, J. High Resolut. Chromatogr. Chromatogr. Commun., 8 (1985) 755.
[28] R. Kostiainen, Chromatographia, 38 (1994) 709.
[29] Z. Penton, J. High Resolut. Chromatogr., 15 (1992) 834.
[30] B.J. Harland and P.J. Nicholson, Sci. Total Environ., 135 (1993) 37.
[31] F.R. Lauritsen, Int. J. Mass Spectrom. Ion Processes, 95 (1990) 259.
[32] V. Virkki, R. Ketola, J. Juujärvi, E. Oja, H. Sorsa and T. Kotiaho, presented at the XXIX Annual Conference of the Finnish Physical Society, Jyvaskyla, Finland, March 1995.
[33] J.S.-Y. Ho, J. Chromatogr. Sci., 27 (1989) 91.
[34] F. Caron and J.R. Kramer, Anal. Chem., 61 (1989) 114.
[35] B.G. Oliver, in: B.K. Afghan and A.S.Y. Chau (Eds.), Analysis of Trace Organics in the Aquatic Environment, CRC Press, Boca Raton, FL, 1989, pp. 2–29.
[36] V.D. Roe, M.J. Lacy, J.D. Stuart and G.A. Robbins, Anal. Chem., 61 (1989) 2584.
[37] D. Herzfeld, K.-D. van der Gun and R. Louw, Chemosphere, 18 (1989) 1425.
[38] A.P. Bianchi, M.S. Varney and J. Phillips, J. Chromatogr., 557 (1992) 429.
[39] M.B. Wise, C.V. Thompson, M.V. Buchanan, R. Merriweather and M.R. Guerin, Spectroscopy, 8 (1993) 14.
[40] Laboratory Services Branch Draft Method, Determination of Volatile Organics in Drinking Water and Aqueous Samples by Purge and Trap GC/MS, Ontario Ministry of the Environment, 1992.
[41] K.F. Hansen, F.R. Lauritsen and H. Degn, Biotechnol. Bioeng., 44 (1994) 347.
[42] M.J. Hayward, T. Kotiaho, A.K. Lister, R.G. Cooks, G.D. Austin, R. Narayan and G.T. Tsao, Anal. Chem., 62 (1991) 1798.
[43] M.A. LaPack, J.C. Tou and C.G. Enke, Anal. Chem., 63 (1991) 1631.
[44] R. Ketola, T. Honkanen, T. Mansikka, R. Kostiainen, T. Kotiaho, V. Komppa, K. Wickström and H. Vahervuori, presented at the 44th ASMS Conference on Mass Spectrometry and Allied Topics, Portland, OR, 1996.

ELSEVIER

Talanta 44 (1997) 383–399

Talanta

Miniaturized protein microsequencer with PTH amino acid identification by capillary electrophoresis I. An argon pressurized delivery system for adsorptive and covalent sequencing

Karen C. Waldron[1], Xing-Fang Li, Min Chen[2], Ian Ireland, Darren Lewis, Michael Carpenter, Norman J. Dovichi *

Department of Chemistry, University of Alberta, Edmonton, Alta., T6G 2G2, Canada

Received 6 June 1996; received in revised form 26 August 1996; accepted 26 August 1996

Abstract

The design of a simple, highly miniaturized instrument for manual microsequence analysis of proteins and peptides is described. The reaction chamber is made of fused silica capillary tubing with all reagents and solvents necessary for coupling and cleavage delivered via two valves and a syringe-based dispenser. Only two pressure regulators are required. A section of the flow-through reaction chamber is heated by thermoelectric modules to control the sequencing reaction temperature. Conversion of the extracted amino acid product to the more stable phenylthiohydantoin (PTH) form is performed off-line so that it may be dissolved in 1 μl buffer for identification. Approximately 0.1% of this PTH product is analyzed by micellar electrokinetic capillary chromatography (MECC) with thermo-optical absorbance detection (TOAD), providing femtomole detection of the phenylthiohydantoin amino acids. Preliminary results at the 50 pmol level for both adsorptive and covalent sequencing methods are presented. © 1997 Elsevier Science B.V.

Keywords: Amino acid sequence; Capillary electrophoresis; Edman degradation; Insulin chain B; Micellar electrokinetic capillary chromatography; Microchemistry; Microsequencer; Miniaturization; Myoglobin; Peptides; Proteins; Phenylthiohydantoin

1. Introduction

The determination of the primary amino acid sequence of minute amounts of proteins remains important in biology. Current technology relies on the repetitive application of the Edman degradation reaction [1]. In this reaction, the N-terminal amino group of the polypeptide reacts with

* Corresponding author. Tel.: +1 403 4922845; fax: +1 403 4928231.

[1] Present address: Department of Chemistry, University of Montreal, Montreal, Quebec H3C 3J7 Canada.

[2] Present address: Environmental and Occupational Toxicology Division, Health Protection Branch, Health Canada, Tunney's Pasture, Ottawa, Ontario K1A 0L2 Canada.

PII S0039-9140(96)02077-2

phenylisothiocyanate (PITC) under basic conditions (the coupling reaction) to form the phenylthiocarbamyl (PTC) derivative. After excess reagent is extracted, the PTC peptide is treated with anhydrous acid (the cleavage reaction) to release the cyclic anilinothiazolinone (ATZ) amino acid. In the process, the peptide is truncated by one amino acid residue. Last, the ATZ product is extracted from the truncated peptide and treated with aqueous acid (the conversion reaction) to produce the more stable phenylthiohydantoin (PTH) amino acid. There are also two common side products produced in the sequencing reaction, diphenylthiourea (DPTU) and dimethylphenylthiourea (DMPTU). Cysteine does not survive the Edman degradation reaction. As a result, there are 19 possible PTH amino acid products for unmodified amino acids, plus the two main interfering products. Chromatographic analysis of the PTH product obtained from each degradation cycle is compared with a standard chromatogram of the 21 possible products for positive amino acid identification.

Introduction of the gas–liquid–solid phase (adsorptive sequencing) instrument in 1981 revolutionized microsequencing by providing sequence information on as little as 5 pmol of protein [2]. In the last 15 years most reports on improving the sensitivity of Edman degradation have not progressed significantly beyond the picomole barrier [3–9]. Kent et al. [10] have pointed out that rare proteins are only present at the 30–300 fmol level on 2D-polyacrylamide gels and that sequencing improvements ranging from better immobilization of the sample to better data analysis of the products was necessary to achieve a significant increase in sequencing sensitivity over methods that were currently being used. This task remains important as protein analysis progresses [11].

In response to this challenge, improvements in sequencing sensitivity have come from many sides. Miniaturization and modification of sequencer components, from separation column to reaction cartridge, are typical. Reduction of HPLC column inner diameter from 4 to 2 mm resulted in a four-fold improvement in sensitivity. The continuous flow reactor described by Shively's group consisted of concentric Teflon tubes in which Polybrene-coated silica beads [3] or polyvinylidene difluoride (PVDF) membrane [7] were used for adsorptive immobilization of polypeptide sample. While high sensitivity sequence analysis on PVDF-bound protein at the 5 pmol level was reported, the authors suggested that at least 10 pmol protein sample be loaded for accurate sequencing results. Similarly, the Hewlett–Packard biphasic reaction column sequencer relies on adsorption for sample immobilization. The hydrophobic packing doubles as a clean-up column for removal of salts, urea and sodium dodecyl sulfate that may be present after protein purification. The biphasic column system can sequence less than 5 pmol protein [12], but routine use at this level is difficult. Regardless of configuration, miniaturizing the reaction cartridge volume permits the use of less reagent and thereby reduces the level of non-specific reactions that give rise to background noise in the chromatographic identification of sequencing products.

From another perspective, advances in the Edman degradation chemistry for amino-terminal sequencing have focused on PITC analogs to provide enhanced sensitivity of the amino acid derivatives through a variety of detection methods. For example, detection limits were 300 amol for ethylenetrimethylamino phenylthiohydantoins (P(ETAP)THs) [13] by HPLC-electrospray mass spectrometry (ESI-MS), 100 amol for dimethylaminoazobenzene thiohydantoins (DABTHs) [14] by micellar electrokinetic capillary chromatography-thermo-optical absorbance detection (MECC-TOAD), and 2 zmol for fluorescein thiohydantoins (FTHs) [15] by capillary electrophoresis (CE) with laser induced fluorescence detection. Unfortunately, these reagents have not found use in routine sequencing because of their poor coupling chemistry. Only recently, the PITC analog 4-(3-pyridinylmethylaminocarboxypropyl) phenylisothiocyanate [16] was used successfully to sequence 500 fmol of synthetic peptide in a commercial sequencer with modified adsorptive sequencing chemistry and HPLC-ESI-MS analysis of thiohydantoins [17]. Alternatively, postcleavage reaction of the ATZ derivatives with 4-aminofluorescein demonstrated sequence analysis on 500 fmol protein using HPLC with fluores-

cence detection [18]. For non-chemical degradation, tandem mass spectrometry has demonstrated rapid and sensitive primary sequence determination [19], but is typically limited to peptides smaller than 10 residues; large peptides generate very complex spectra that are difficult to interpret. However, ESI-MS coupled to capillary electrophoresis has been successfully used for protein identification by peptide mass mapping of 38 fmol of a tryptic digest from bovine serum albumin [20].

Given the reliance of routine microsequencing on PITC degradation chemistry, further improvements in sequencing sensitivity have focused on the UV-absorbing PTH amino acid derivatives. Increasing yields and reducing non-specific reactions with PITC to improve signal/noise have typically been achieved by modification of sequencing protocols and sample loading techniques [8]. Efforts to improve chromatographic identification include injecting a larger proportion of the conversion product [21], improving the resolution of PTH peaks from degradation by-products peaks [22], and reducing sequencing times to improve throughput. However, further miniaturization of sequencer components has not progressed much because of the large amounts of PTH product required for detection in HPLC. It remains that detection of PTHs at very low levels, amongst a high background of UV-absorbing by-products, is the limiting factor to improving polypeptide sequencing sensitivity. As Calaycay et al. [7] pointed out, "The sequencing levels depend heavily on the performance of the narrow-bore HPLC system. It is clear that further improvements in the detection of all the PTH amino acids are in order before femtomole level sequencing can be achieved". It is our feeling that advances in detection techniques have not been fully investigated as a means of improving sequencing sensitivity.

We reported subfemtomole detection of PTH amino acids in 1992 [23] using a MECC-TOAD technique. While it is trivial to apply MECC-TOAD determination of the PTHs to manual sequencing studies [24], it has been difficult to efficiently transfer this analysis method to automated sequencers. The bottleneck comes from interfacing the large volumes of product formed in commercial sequencers ($> 100\ \mu l$) to the small volumes injected into the CE (< 10 nl). In order to address this 10 000 fold volume differential, we have investigated additional miniaturization of the sequencer first described by Hewick et al. in 1981. This work describes two configurations of a protein microsequencer and presents some preliminary sequencing results.

2. Experimental

2.1. Materials

Sequencing grade ethyl acetate, *n*-heptane, 12.5% trimethylamine (TMA) in water, polytetrafluoroethylene (PTFE) membrane (Zitex™) and PTH amino acid standard were purchased from Applied Biosystems (Foster City, CA). Sequencing grade PITC, anhydrous trifluoroacetic acid (TFA), Polybrene, oxidized insulin chain B, oxidized insulin chain A, β-lactoglobulin-A and Tyr-bradykinin were from Sigma Chemical (St. Louis, MO). Glass fibre filter disks (GFF) pre-cycled with Polybrene were received as a gift from R. Aebersold. Porton sequencing disks were received as samples from Beckman Instruments. Sodium dodecyl sulfate (SDS), sodium dihydrogen orthophosphate and HPLC-grade acetonitrile were obtained from BDH, (Toronto, ON). Sodium tetraborate and 1-chlorobutane were supplied by Fisher Scientific (Fair Lawn, NJ). Covalent sequencing reagents (NMM: 5% *N*-methylmorpholine in 70% methanol, 50/50 heptane/ethyl acetate, methanol), Immobilon-CD membrane, PVDF, Sequelon-AA (aryl amine) reagent kit and Sequelon-DITC (diisothiocyanate) myoglobin standard were purchased from Millipore Canada (Nepean, ON). Porasil T silica beads were donated by F. Cantwell. Pre-purified argon (Union Carbide Canada, Edmonton, AB) was passed through an OT-3-2 oxygen trap from Chromatographic Specialties (Brockville, ON). Distilled water was purified with a NANOpure ultrapure water system (Barnstead Corp., Dubuque, IA) for buffer preparation. Teflon tubing, large-bore fused silica tubing, and Hamilton

glass syringes were obtained from Chromatographic Specialties (Brockville, ON). Narrow-bore fused silica tubing and Innerlok™ connectors were purchased from Polymicro Technologies (Phoenix, AZ).

2.2. Identification of PTH amino acids

Separation and detection of PTH amino acids was performed using the MECC-TOAD instrument described in detail elsewhere [23,24]. A 40 cm long fused silica capillary (50 μm i.d., 190 μm OD) was used for the separations. The column length from injection (anode) to detection was 35 cm. Separation buffer of 10.7 mM sodium phosphate, 1.8 mM sodium tetraborate and 25 mM SDS, pH 6.7, was filtered through a Millex-GS 0.22 μm syringe filter unit (Millipore, MA) before use. Sequencing produce was dissolved in 1 μl 10% acetonitrile/90% running buffer spiked with internal standard (5×10^{-5} M PTH-tyrosine or PTH-alanine). The dry PTH amino acid standard was dissolved in acetonitrile (5×10^{-5} M) and stored at −20°C. A 5 μl aliquot of standard was dried and re-dissolved in the same volume of 10% acetonitrile/separation buffer for injection into the CE system. Samples and standard were injected hydrodynamically (injection volume 1 nl) and separated at 10 kV. The current was 8 μA.

2.3. Instrument design

A schematic of the instrument is shown in Fig. 1A. Purified argon was directed to two stainless steel manifolds (M1, M2) each equipped with a pressure regulator (M1 at 3.5 psig, M2 at 8.0 psig), pressure relief valve, and twelve 1/16 in. fittings (Swagelok). Reagents and solvents were delivered to the Valco 16-position multiport valve V1 (machined from Hastalloy C, Chromatographic Specialties) through capillary tubing feed lines from delivery vessels pressurized via 1/16 in. Teflon tubing from manifold M1. The delivery vessels were adapted from amber 5 ml Reactivials (Chromatographic Specialties) and Teflon 1/16 in. male-run tees (Cole-Parmer) that were screwed into inserts (threaded inside with 1/8 in. NPT, machined in-house from Teflon) that fit through the holes in the Reactivial caps. The top arm of each tee was connected to 360 μm OD fused silica capillary tubing adapted with a 2 cm long Teflon sleeve to provide a gas-tight fitting against the ferrule. The tubing from manifold M1 to the TMA and TFA vials was adapted with 0.3 psi check-valves (Swagelok) to prevent back flow of solvent vapours into M1.

The capillary tubing feed lines, connected to valve V1 using fused silica tubing adapters (Valco), had inner diameters of either 75, 100 or 250 μm and lengths from 30 to 60 cm depending on desired flow rate. The V1 outlet was connected to the reaction chamber RC via 250 μm i.d. capillary tubing (12 cm) and an Innerlok compression fitting, IL. The tapered inner diameter of the IL provided an excellent compression seal with the polyimide-coated capillary and allowed rapid connection to the reaction chamber. The outlet of the reaction chamber was left open for manual collection of waste or anilinothiazolinone (ATZ) amino acid derivative. Electronic switching of valve V1 provided sequential access to the sixteen ports for timed deliveries of solvents, reagents and argon. Manipulation of argon pressure, capillary length, and capillary i.d. were used to control flow rates of reagents and solvents to the reaction chamber. Wetted pH paper held at the reaction chamber outlet was used to monitor the pH during coupling and cleavage. Sequencing reagents were delivered according to the protocol in Table 1.

The coupling reaction was carried out at 55°C and the cleavage at 48°C. The extracted ATZ product was collected directly into a 600 μl microcentrifuge vial containing 10 μl 25% TFA for off-line conversion. The mixture was vortexed and rapidly dried by vacuum centrifuge. The dried ATZ amino acid was converted to the PTH form by adding 20 μl 25% TFA, flushing with argon, and heating 10 min at 60°C in a dry block. The converted PTH amino acid derivative was dried and stored at −20°C or reconstituted in 1 μl acetonitrile/running buffer from which 1 nl (0.1%) was injected for identification by MECC-TOAD.

The single-valve instrument was later modified by adding a Hamilton Microlab-500 dual-syringe dispenser, ML, (Chromatographic Specialties) for

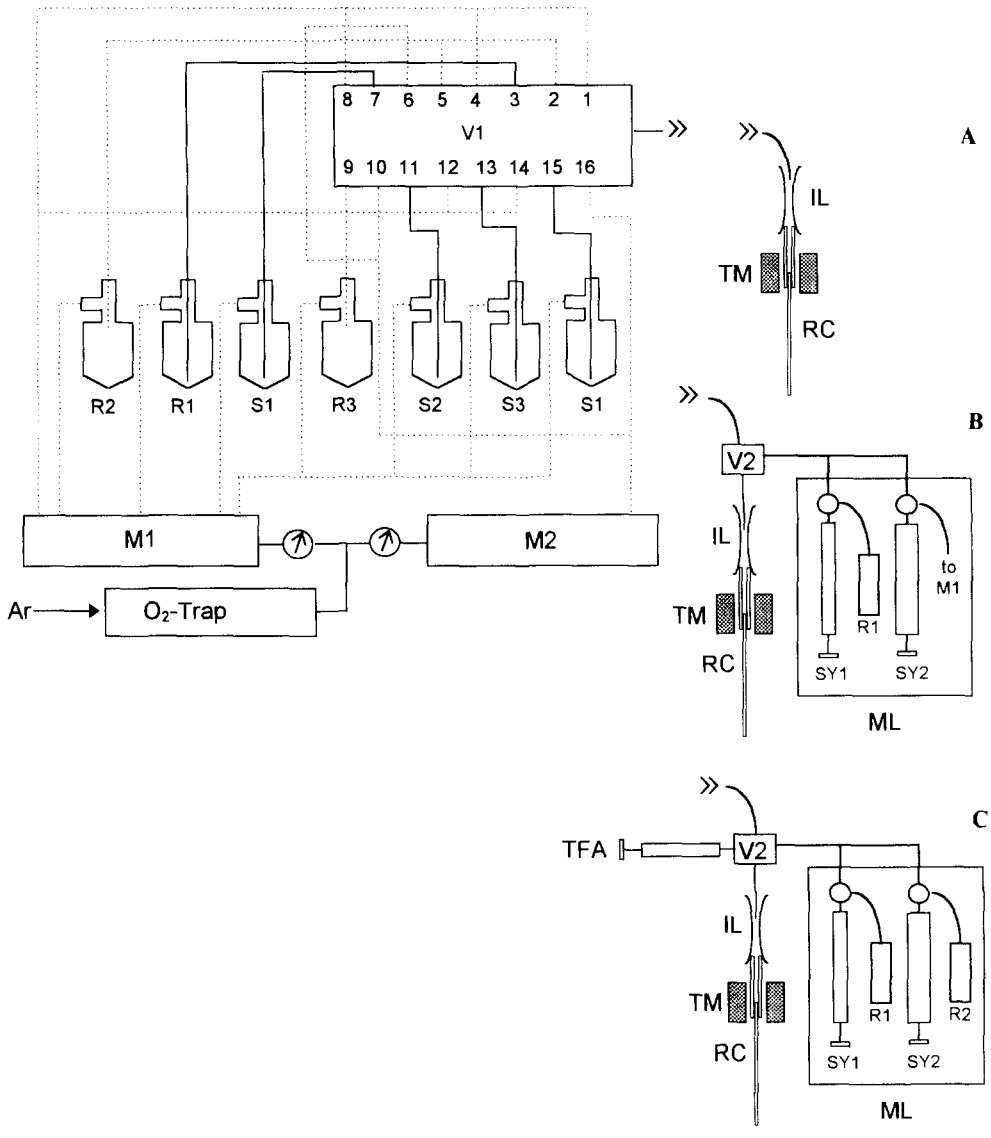

Fig. 1. Schematic of a miniaturized instrument for adsorptive (A, B) and covalent (C) sequencing. Components are described in detail in the text. In figures A, B and C: V1, valco multiposition distribution valve; M1, M2, argon manifold; IL, Innerlok compression fitting; RC, reaction chamber; TM, thermoelectric module; R1–R3, reagents; S1–S3, solvents. In figures B and C: V2, PTFE multiport distribution valve; ML, Microlab-500 dual-syringe dispenser; SY1, SY2, syringes. In figure C: TFA, syringe containing liquid TFA.

accurate PITC delivery, and a 5-way PTFE micro-tubing distribution valve, V2, (Cole-Parmer) as shown in Fig. 1B. Valve V1 was coupled to position 1 of valve V2 through 5 cm of 250 μm i.d., 1/16 in. OD Teflon tubing. The ML syringe dispenser was equipped with one 25 μl syringe (SY1) and one 250 μl syringe (SY2) whereby each could be programmed to deliver a specific volume at a given speed. SY1 was used to deliver R1 (PITC in solvent). SY2 was connected to argon manifold M1. A low-volume tee (machined in-house from Teflon) was used to connect the

Table 1
Sequencer protocol for adsorptive sequencing chemistry: coupling and cleavage reactions[a]

Step	V1 position	Reagent/solvent[b]	Flow rate/amount delivered	Time (s)
1. Dry	1	Argon	3.5 psig	120
2. Coupling	2	R2	1.6 μl/s	60
3. Coupling	3	R1	3.5–8 μl	1
4. Coupling	4	Argon	3.5 psig	60
5. Coupling	5	R2	1.6 μl s^{-1}	720
6. Dry	6	Argon	8 psig	120
7. Wash	7	S1	13 μl	10
8. Dry	8	Argon	3.5 psig	120
9. Cleavage	9	R3	6.5 μl/s	300
10. Dry	10	Argon	8 psig	120
11. Extraction	11	S2	10 μl	15
12. Extraction	12	Argon	3.5 psig	210
13. Wash	13	S3	14 μl	60
14. Dry	14	Argon	3.5 psig	240
15. Wash	15	S1	18 μl	60
16. Dry	16	Argon	8 psig	120

[a] Conversion reaction was carried out off-line.
[b] R1, 5% PITC in heptane; R2, 12.5% TMA in water (vapour); R3, anhydrous TFA (vapour); S1, ethyl acetate; S2, benzene; S3, 1-chlorobutane.

Teflon tubing outlets of the ML dispenser to position two of valve V2 through 5 cm of 250 μm i.d. Teflon tubing. A combination of electronic switching of valve V1, activation of the ML dispenser and manual switching of valve V2 were used to time the delivery of solvents and reagents to the reaction chamber for coupling and cleavage, following the protocol in Table 2. Coupling temperature, cleavage temperature, and conversion conditions were the same as for the initial instrument design.

The modified instrument was adapted for covalent sequencing by replacing reagents and solvents with those suitable for covalently bound polypeptide (Table 3). A glass syringe containing anhydrous TFA for both cleavage and ATZ product extraction was connected to position three of valve V2, as shown in Fig. 1C. Concurrent delivery of PITC (via syringe SY1) and *N*-methylmorpholine (NMM) coupling buffer (via syringe SY2) was necessary as the Microlab-500 (ML) could only activate the syringes simultaneously. Position four and nine of valve V1 were unused (plugged). The argon manifolds M1 and M2 were maintained at 3 and 30 psig, respectively. Delivery of reagents and solvents for covalent coupling and cleavage reactions followed the protocol in Table 3. The reaction chamber was held at 56°C for all eighteen steps. The extracted ATZ product was collected into a 200 μl polypropylene microvial containing 10 μl 25% TFA, and was dried with a stream of argon for 2 min. The ATZ amino acid was converted to the PTH form as described above, except heating was at 67°C.

2.4. Reaction chamber

The flow-through reaction chamber, analogous to the reaction cartridge described by Hewick in 1981 [2], was constructed from two lengths of polyimide-coated fused silica capillary tubing and a mat of porous PTFE membrane as shown in Fig. 2. The upper 4 cm length of 400 μm i.d., 525 μm OD capillary was easily cut to very flat ends using a fused silica cutting stone (Chromatographic Specialties). By gently pushing and turning the capillary tube end against a piece of PTFE, a tiny mat exactly the size of the tube's inner diameter could be cut. The mat was pushed into place using the lower 8 cm length of 100 μm i.d., 360 μm OD capillary. The reaction chamber was secured by gluing the two capillaries together with 5 min epoxy.

Table 2
Sequencer protocol for adsorptive sequencing chemistry with ML: coupling and cleavage reactions[a]

Step	V1	V2[b]	Reagent/solvent[c]	Flow rate/amount delivered	Time (s)
1. Dry	1	1	Argon	3.5 psig	120
2. Coupling	2	1	R2	1.6 μl s^{-1}	60
3. Coupling	3	2	R1, argon (SY2)	3, 18 μl	10
4. Coupling	3	1	R2	1.6 μl s^{-1}	300
5. Coupling	4	2	R1, argon (SY2)	3, 18 μl	10
6. Coupling	4	1	R2	1.6 μl s^{-1}	300
7. Coupling	5	2	R1, argon (SY2)	3, 18 μl	10
8. Coupling	5	1	R2	1.6 μl s^{-1}	300
9. Dry	6	1	Argon	8 psig	120
10. Wash	7	1	S1	13 μl	10
11. Dry	8	1	Argon	3.5 psig	120
12. Cleavage	9	1	R3	6.5 μl s^{-1}	300
13. Dry	10	1	Argon	8 psig	120
14. Extraction	11	1	S2	10 μl	15
15. Extraction	12	1	Argon	3.5 psig	210
16. Wash	13	1	S3	14 μl	60
17. Dry	14	1	Argon	3.5 psig	240
18. Wash	15	1	S1	18 μl	60
19. Dry	16	1	Argon	8 psig	120

[a] Conversion reaction was carried out off-line.
[b] Positions 3 and 4 of V2 were unused (plugged).
[c] See Table 1.

The elevated temperature required for coupling and cleavage was generated with thermoelectric modules, made in-house from copper blocks and solid-state thermoelectric devices (Melcor, Trenton, NJ), as shown in Fig. 3. Temperature control was achieved by adjusting the voltage applied to the thermoelectrics with a 10 volt/10 ampere power supply (Kepco, Flushing, NY). The copper heat sinks (10 × 20 × 2 mm) and grooved copper plates (6 × 15 × 1 mm) were attached to the thermoelectrics with heat conducting glue made from silver paint and epoxy. These thermoelectric modules, TM, were mounted on a Hoffman open-side tubing clamp (Fisher Scientific) which could be easily opened to insert the reaction chamber along the groove in a few seconds. To calibrate the applied voltage versus temperature, the reaction chamber was filled with water and a thermocouple (Digi-Sens, Cole-Parmer) was inserted to the level of the PTFE mat. The voltage versus temperature curve was linear from 25 to 70°C, with the desired temperature being reached in 50 s. During degradation, the thermocouple was coated with a thermal compound (Dow Corning) and inserted into a small hole (0.5 mm i.d.) drilled in one copper plate to monitor the temperature, which stayed within ± 2°C of the set point.

A variety of sample immobilization techniques were tried for adsorptive sequencing in the reaction chamber. A mat from either a glass fibre disk (GFF precycled with Polybrene) or a Porton disk was cut and inserted into the reaction chamber in the same manner as the PTFE mat. For some experiments, porous silica beads (Porasil T) precoated with Polybrene solution (100 mg ml^{-1} in 50% methanol) and dried in a vacuum desiccator were poured into the reaction chamber using a pipette tip as a funnel. A loosely packed bed of beads was obtained by gently tapping the tube as the particles were poured.

2.5. Sample loading

Samples consisted of aqueous solutions of polypeptide, approximately 0.1 mM in 0.3% TFA. A sample volume of 0.2 μl or less was drawn

Table 3
Sequencing protocol for covalent sequencing chemistry: coupling and cleavage reactions[a]

Step	V1[b]	V2[c]	Reagent/solvent[d]	Amount delivered	Time (s)
1. Dry	1	1	Argon	3 psig	30
2. Coupling	2	1	R2	5 μl	5
3. Coupling	3	1	Argon	3 psig	45
4. Coupling	4	2	R1, R2	4, 42 μl	300
5. Coupling	4	2	R1, R2	4, 42 μl	300
6. Coupling	4	2	R1, R2	4, 42 μl	300
7. Wash	5	1	S1	125 μl	25
8. Wash	6	1	S2	75 μl	15
9. Dry	7	1	Argon	3 psig	20
10. Dry	8	1	Argon	30 psig	120
11. Cleavage	9	3	R3	45 μl	300
12. Extraction	10	1	Argon	3 psig	60
13. Wash	11	1	S1	125 μl	25
14. Dry	12	1	Argon	3 psig	35
15. Wash	13	1	S2	100 μl	20
16. Dry	14	1	Argon	3 psig	40
17. Wash	15	1	S1	150 μl	30
18. Dry	16	1	Argon	30 psig	180

[a] Conversion reaction was carried out off-line.
[b] Positions 4 and 9 of V1 were unused (plugged).
[c] Position 4 of V2 was unused.
[d] R1, 10% PITC in acetonitrile; R2, 5% NMM in 70/30 methanol:water (liquid); R3, anhydrous TFA (liquid); S1, methanol; S2, 50/50 heptane/ethyl acetate.

through either the upper or lower half of the reaction chamber, to the adsorptive support, via an Innerlok attached to a 1 μl glass syringe. The difference in weight of the reaction chamber before and after protein loading (at a known concentration) was used to estimate the amount of loaded sample. The loaded sample was dried with a stream of argon.

For non-Polybrene immobilization, small pieces (1 × 5 mm) of PVDF or Immobilon-CD membrane were pre-wet with methanol and 1 μl of polypeptide sample applied. The pieces were further cut into 0.3 mm strips using a razor blade and inserted into the reaction chamber using tweezers. Similarly, Sequelon disks with covalently bound polypeptide were cut and inserted into the reaction chamber for covalent sequencing. A larger diameter reaction chamber was used (4 mm of 530 μm i.d., 700 μm OD) to simplify insertion of the membrane strips. Insulin chain B was bound to Sequelon-AA following the manufacturer's directions, and stored at −20°C. The weight of membrane inserted into the reaction chamber versus total weight of disk (with known amount of bound polypeptide) was used to calculate the amount of sample loaded into the reaction chamber.

3. Results

3.1. Identification of PTH amino acids

Optimization of the MECC separation of 19 PTH amino acids and two degradation by-products has been described elsewhere [24]. For this work, PTH product from each cycle was dissolved in 10% acetonitrile: 90% separation buffer compared with 100% separation buffer described previously. The addition of 10% acetonitrile improved PTH product solubility without significantly altering the MECC elution profile. An internal standard of either PTH-tyrosine (PTH-Y) or PTH-alanine (PTH-A) was also added to permit quantification of the PTH product.

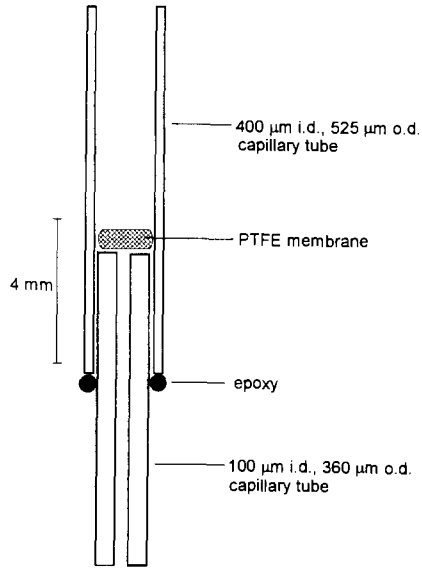

Fig. 2. Schematic of fused silica capillary-based reaction chamber.

3.2. Instrument design

The primary objective in the design of the sequencer was to miniaturize the reaction volume to improve compatibility with the nl injection volumes required for capillary electrophoresis. A second objective was to simplify the plumbing in comparison to commercial sequencers, which typically have four or more pressure regulators and six or more valves. A third objective was to design a system made mostly from commercially available parts so that it could be constructed and used in any laboratory. The initial instrument design shown in Fig. 1A required only two pressure regulators and one valve for the coupling, cleavage and extraction steps.

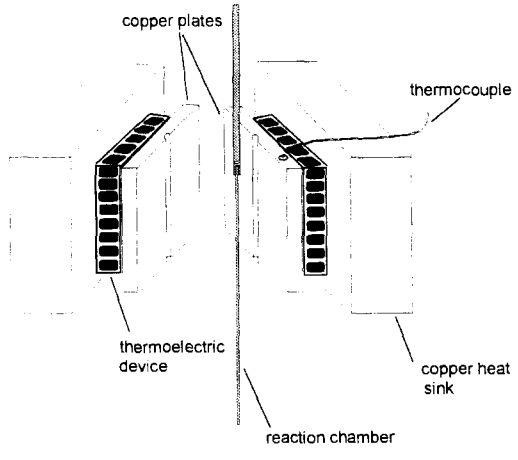

Fig. 3. Schematic of thermoelectric modules for temperature control during coupling and cleavage reactions.

Polyimide-coated fused silica capillary tubing was used for delivery of solvents and reagents to the Valco multiposition valve (V1) because it was impermeable to oxygen, flexible, inert, simple to connect and costs about the same as Teflon tubing when bought in bulk. Several different inner diameters of capillary tubing were investigated for delivery. Either 75 or 100 μm i.d. tubing proved best for delivery of argon and gas phase reagents (TMA vapours and TFA vapours) whereas 250 μm i.d. tubing was required for delivery of solvents to keep working pressures below 30 psig.

The use of valve V1, originally designed for capillary GC and LC, simplified the sequencer plumbing compared with commercial designs. However, the sequential nature of activation of valve V1 limited the sequencer to 16 steps for reagent and solvent delivery and drying (Table 1). This constraint required that extracted ATZ amino acid product be converted to the PTH form off-line. Additional drawbacks of valve V1 were its relatively large internal volume (~ 8 μl) and internal flow path (circular), neither of which were well matched to the reaction chamber volume (0.3 μl). A small volume (1–2 μl) of reagent R1 (PITC in heptane) delivered from the pressurized vessel was trapped inside valve V1 when argon was applied in the ensuing step. Essentially, a widening of the flow path from 250 μm i.d. (delivery line to V1) to 760 μm i.d. (the port diameter of V1) caused the reagent plug to become meniscus-like and rupture upon application of argon pressure. The result was that reagent R1 adhered to the valve's inner surface, never reaching the reaction chamber, until it was washed through with solvent. Consequently, R1 delivery was inconsistent, ranging from 3.5 to 8 μl.

Delivering an excess volume of R1 (PITC in heptane) in order to overcome the V1 valve design was also problematic. The sample support was

unable to absorb the excess liquid. Drying with argon left an insufficient amount of PITC for coupling. When some R1 was purposely allowed to remain in the reaction chamber, residual heptane impeded coupling. The best yields achieved for sequencing either insulin chain B or β-lactoglobulin-A were 15% in cycle one, and 0% in cycle two. Increasing the PITC concentration to 10% in heptane did not significantly improve yields because this mixture did not leave sufficient PITC on the sequencing support. The higher concentration of PITC led to DPTU contamination of valve V1. Extraction of the ATZ amino acid was initially done with 1-chlorobutane and later benzene, which reduced the background peaks in the MECC analysis.

The Microlab-500 syringe dispenser, ML, was added to the sequencer both for accurate delivery of R1 to the reaction chamber and to compensate for lack of random access (via valve V1) to reagents, solvents and argon for gas-phase coupling. Unfortunately, the PTFE valve V2 that was used to interface the ML dispenser and valve V1 to the reaction chamber had a fairly large internal volume and delivery of less than 2 μl was problematic. Nevertheless, reproducible delivery of PITC in heptane, R1, was made possible by programming syringe SY1 for 3 μl of R1 at maximum syringe speed and syringe SY2 for 18 μl of argon at slower syringe speed as a means to transfer R1 to the reaction chamber. Three deliveries of R1/argon were made during coupling to increase the amount of PITC available for reaction. Long argon drying steps after each R1 delivery made no difference in sequencing yields and were eliminated as indicated in Table 2. This sequencer protocol was used for all subsequent adsorptive sequencing studies.

The miniaturized instrument was adapted for covalent sequencing by changing the reagents and solvents and adding a source of liquid TFA for cleavage and product extraction (Fig. 1C). Simultaneous delivery of R1 (PITC in acetonitrile) and liquid phase R2 (coupling buffer), which are fully miscible, circumvented the need for R1 solvent removal. A large amount of R2 (42 μl, equal to the dead volume from valve V2 to reaction chamber RC) was used for coupling (Table 3) to ensure that the sample support stayed wet with reagent after each delivery from the ML dispenser. Ideally, another syringe to accurately deliver and hold a smaller R1/R2 liquid plug would have been preferable; a syringe-based sequencer that addresses this is described in Li et al. [25], the following paper in this series. The third port of valve V2 was used for TFA (liq), which could not be delivered through V1 as it adsorbed strongly to the inner surfaces of valve V1, requiring several rinses with ethyl acetate. A 45 μl aliquot of TFA was delivered such that the leading edge of the plug just wet the sample support. Ideally, a 5 μl plug of TFA would be sufficient if a deliver-hold-transfer mechanism were used. When the cleavage reaction was complete, the remainder of the TFA plug was passed slowly through the reaction chamber by argon pressure to extract ATZ product for off-line conversion to PTH amino acid.

3.3. Reaction chamber and sample loading

The reaction chamber (Fig. 3) was analogous to the Hewick et al. adsorptive sequencing reaction cartridge [2], except with 1000 times smaller volume to better match that needed for capillary electrophoresis analysis. The aim was also to develop a simple method for making the reaction chamber. Construction of the reaction chamber from fused silica tubing was based on several considerations. First, tubing with a variety of inner diameters is commercially available. Second, fused silica has good thermal conductivity for temperature control during coupling and cleavage. Third, the polyimide coating keeps the tubing flexible yet is transparent so reagent flow can be visually monitored. Last, it is compatible with performing electrophoretic separations for future on-line CE injection of sequencing products.

Approximately 15 min were required to build five reaction chambers at a cost of about $2 each. Over 100 mats could be made from each piece of PTFE, which was used primarily because the glass fibre mat had very little structural integrity when wet and tended to collapse into the lumen of the lower capillary. Several methods of loading sample for adsorptive degradation were tried. The

Table 4
Initial yields for adsorptive sequencing

β-Lactoglobulin A		Insulin chain B		Insulin chain A		Y-Bradykinin	
Sample (pmol)	% Yield (PTH-leu)	Sample (pmol)	% Yield (PTH-phe)	Sample (pmol)	% Yield (PTH-gly)	Sample (pmol)	% Yield (PTH-tyr)
52	17	40	75	95	61	66	26
60	8	150	71				
200	20	180	36				
220	14	190	11				
1000	6	250	13				
		260	36				
		890	10				

simplest and quickest method was to draw protein solution up through the lower half of the reaction chamber using a 1 μl syringe and Innerlok. For example, a 10 mm long plug of solution in 100 μm i.d. tubing equals 0.08 μl, which could easily be seen in the tube. Ideally, one wants to just wet the support and evaporate the solvent leaving a residue of polypeptide, similar to the requirement for R1 delivery. Unfortunately, as little as 0.05 μl of solution would more than soak a glass fibre mat since its surface area was only 0.12 mm^2. Very long drying times at 8 psig argon were required to remove solvent and frequently some of the sample solution was lost from the end of the reaction chamber.

In general, poor sequencing results were obtained using mats made from either the glass fibre or Porton disks. A sample of 240 pmol insulin chain B loaded into a reaction chamber containing one PTFE and two glass fibre mats gave less than 10% yield of PTH-phenylalanine (PTH-F) in cycle 1 and no PTH-valine (PTH-V) in cycle 2. A sample of 120 pmol insulin chain B loaded into a reaction chamber containing one Porton mat with PTFE yielded about 28% PTH-F in cycle 1 but no PTH-V in cycle 2. Unfortunately, both cycles performed using the Porton support showed a large amount of peptide in the extract, indicating that sample washout had occurred. Haniu and Shively [26] attributed similar results to the low mass of the supporting material. Sample loading onto PVDF or Immobilon-CD membrane suffered from the same problems as glass fibre mats. Very poor adsorptive sequencing results were obtained with both these membrane supports: less than 5% yields in cycle 1 and 0% yield in cycle 2, for both insulin chain B and β-lactoglobulin-A samples.

In order to increase absorption of solution into the sample support and facilitate protein adsorption, a bed of porous silica beads analogous to Shively's continuous flow reactor [3] was used. Porasil T (25–37 μm, pore size = 15 nm, surface area = 300 $m^2\ g^{-1}$) was coated with Polybrene and packed into the reaction chamber as described in the methods section. The bed depth was kept less than 5 mm Porasil T to minimize backpressure during sequencing. Coatings from 5 to 50% (w/w) Polybrene to Porasil T were investigated for sample loadings ranging from 25 to 250 pmol insulin chain B. Poor yields (< 5%) in the first cycle were seen when less than 10% Polybrene was used and no correlation between yield and percent Polybrene was found for 20–50% coating. Precycling of Polybrene-coated Porasil T had little effect on sequencing yields but did decrease the number of background peaks in the electropherograms of cycles 1 and 2. Unfortunately, any traces of Polybrene in the extracted ATZ product adversely affected the CE analyses by altering the electroosmotic flow. Therefore, a loading of 20% Polybrene to Porasil T was used for further work. Table 4 presents a summary of initial yields for various polypeptide sample sizes sequenced following the protocol of Table 2 after immobilization on 20% Polybrene to Porasil T. It is

Table 5
Demonstration of lag observed with adsorptive sequencing. All samples were immobilized on 20% Polybrene:Porasil T.

Insulin Chain B								β-Lactoglobulin-A							
Cycle	190 pmol		250 pmol		890 pmol			Cycle	200 pmol		1000 pmol				
	Yield[a]	Lag[a]	Yield	Lag	Yield	Lag			Yield	Lag	Yield	Lag			
1.	Phe	21	33		92			1.	Leu	39	56				
2.	Val	20	15 (F)	11	2 (F)	82	55 (F)		2.	Ile	42	16 (L)	103	110 (L)	
3.	Asn	—[b]	—	13	6 (F) 7 (V)	32	26 (F) 49 (V)		3.	Val	27	0 (I)	154	36 (L), 80 (I)	
4.	Gln	9	16 (F), 0 (V)			29	43 (V) 45 (N)		4.	Thr			57	59 (I), 35 (V)	
5.	His	—	5 (N), 10 (Q)												
6.	Leu	10	2 (Q)												

[a] pmol.
[b] Not quantified due to noise in electropherogram.

important to note also that the proportion of protein to total Polybrene (w/w) in the reaction chamber was typically 10 times less than in commercial systems yet no sample wash-out was observed in the electropherograms.

Occasionally, incomplete coupling or cleavage in a given degradation cycle can lead to lag, the phenomenon in which amino acid product from cycle $n-1$ is detected in cycle n. Lag was often observed in both the second and third degradation cycles and was particularly severe for large samples such as 1 nmol of β-lactoglobulin-A. Table 5 demonstrates lag from samples sequenced by adsorption on Porasil T coated with 20% Polybrene following the protocol in Table 2. Although the volume of R1 delivered contained a large molar excess of PITC, it is conceivable that much less remained on the sample support because of overwetting. Coupling times of 40 min, additional R1 deliveries to the reaction chamber and cleavage times of 15 min made little difference in either the sequencing yields or the appearance of lag. These results suggest that insufficient PITC was present rather than an incomplete coupling reaction. Shively et al. [3] indicated that overloading (overwetting) a glass fibre disk may result in loss of the sample, or in our case loss of reagent.

Improved yields were observed with covalent sequencing. Using the protocol in Table 3, seven cycles of 55 pmol myoglobin covalently bound to

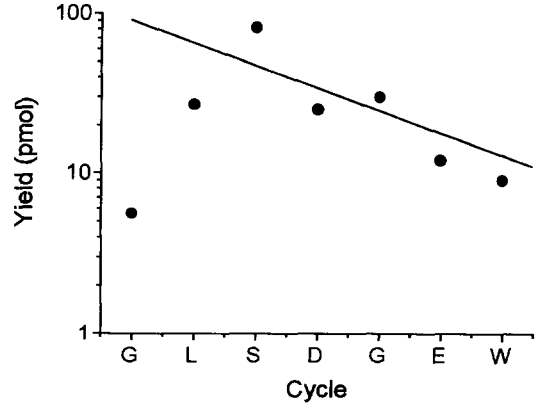

Fig. 4. Cycle yields for the covalent sequencing of 55 pmol horse heart myoglobin covalently attached to Sequelon-DITC membrane.

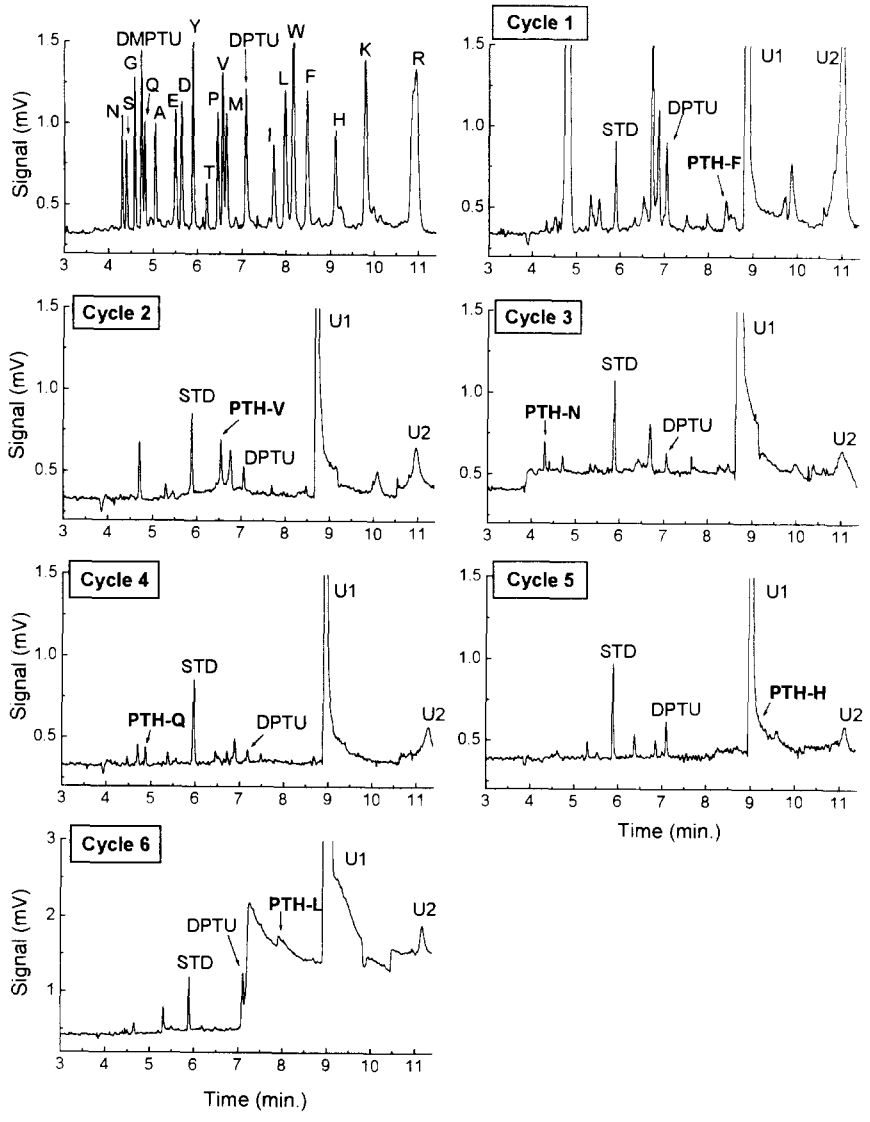

Fig. 5. Electropherograms showing covalent sequencing results for 53 pmol insulin chain B covalently attached to Sequelon-AA membrane. Top left panel: injection of 50 fmol standard PTH mixture, labelled with the one-letter amino acid abbreviations. Remaining panels: cycles 1–6 results, in which 0.1% of PTH amino acid product from sequencing was injected. U1, U2: unconfirmed by-product peaks.

Sequelon-DITC were sequenced with a repetitive yield of 73%. The repetitive yield was calculated from the slope of a plot of log [yield] versus cycle number 2–7 as shown in Fig. 4. The cycle 1 result was not included in the calculation because it is the N-terminal amino acid covalently bound to the membrane. The first seven amino acid residues in myoglobin are: G_1 (glycine), L_2 (leucine), S_3 (serine), D_4 (aspartic acid), G_5, E_6 (glutamic acid), W_7 (tryptophan). The covalent sequencing protocol (Table 3) was later modified to increase the ratio of R1 to R2 (from 4:42 μl to 3:9 μl) and to reduce the total volume of reagents delivered to the reaction chamber. Valve V1 was kept at posi-

tion 3 (argon) for steps 4–6 and valve V2 was opened briefly after each delivery of R1:R2 to facilitate reagent transfer to the reaction chamber.

Sequencing results for 53 pmol insulin chain B covalently bound to Sequelon-AA using the modified coupling reaction volumes are presented in Fig. 5. The first six amino acid residues in insulin chain B are: F_1 (phenylalanine), V_2 (valine), N_3 (asparagine), Q_4 (glutamine), H_5 (histidine), L_6 (leucine). For each cycle, an internal standard (STD) of 5×10^{-5} M PTH-tyrosine was added. A standard mixture of 19 PTH amino acids and two by-products is shown in the first panel. The first degradation cycle showed several large background peaks resulting from contamination acquired during sample storage. The polypeptide sample had been covalently coupled to the membrane and stored at -20°C for approximately 1 month before being sequenced. The unidentified peaks labelled U1 and U2 were seen in all degradation cycles. U1 was presumed to be diphenylurea (DPU) which typically migrates between PTH-F and PTH-H in standard solutions (data not shown). The unlabelled by-product peaks seen in cycle 1 gradually diminished over the course of the six degradation cycles, emphasizing the importance of the wash steps in the sequencing protocol. In cycle 5, PTH-histidine (PTH-H) was obscured by the unidentified by-product peak U1 and could not be detected, as discussed further in the next section. The baseline in cycle 6 rose sharply after DPTU eluted, caused by a contamination in the separation capillary, however PTH-leucine (PTH-L) was quantified by its peak height minus the increased baseline relative to the internal standard peak height (STD = 5×10^{-5} M PTH-Y). The repetitive yield for cycles 1–6 was 89%. The negative peak (acetonitrile) seen at 3.93 min in cycles 1–6 indicates the electroosmotic flow.

4. Discussion

Capillary electrophoresis has steadily grown as a separation method for biomolecules since its resurgence in 1981 [27]. CE has demonstrated improved efficiency, resolution, and speed compared with HPLC for the separation of the PTH amino acids. In addition, the low cost of capillary tubing and the minute solvent consumption in CE reduce the overall operating cost compared to HPLC. On the other hand, difficulties associated with manipulating the small volumes of CE are many. These difficulties dominate the design of our miniaturized sequencer.

The difficulties we found with absorbing liquid samples onto the tiny glass fibre supports were multiplied when delivering liquid reagents during sequencing, particularly reagent R1, the PITC in solvent. The conditions necessary for efficient coupling are that PITC be in large molar excess of polypeptide and that the reaction take place under aqueous, alkaline conditions. For adsorptive sequencing, it is essential that R1 solvent (e.g., heptane) be evaporated if it is not miscible with the coupling buffer. Ideally, a film of PITC is deposited on the support and comes in contact with the sample for coupling. Whereas the 12 mm disks used in many sequencing instruments may have regions that are not totally wet by reagents, our problem was overwetting. For example, a single glass fibre mat was fully wet with only 0.05 μl liquid, a strip of PVDF with 0.2 μl and a bed of Porasil T with 1 μl, all of which were volumes too small to deliver through V1. The smallest volume of reagent R1 that could be delivered (3.5 μl) contained 850 nmol PITC, which remained dissolved in heptane leaving an insufficient amount deposited on the support for quantitative coupling. This phenomenon was blamed for the low sequencing yields ($< 10\%$) using the protocol in Table 1.

Purposely allowing R1 to remain in the reaction chamber, after delivering coupling buffer which deprotonates the N-terminus, also gave poor results. The presence of heptane created an organic–aqueous interface, which retarded phase transfer across the interface. Aqueous conditions are necessary for the polypeptide-PITC reaction, not only to establish an alkaline environment but also because water may act as a catalyst in the coupling reaction [28]. Whether the coupling base acts as a buffer [29], a catalyst [30,31], or simply a means to guarantee deprotonation of the N-terminus is not clear.

To ensure that sufficient PITC was available for coupling, three deliveries of R1 followed by 300 s coupling buffer (R2) were used. Although the cycle yields presented in Table 4 are less than half of those reported for the continuous flow reactor (CFR) sequencer packed with Porasil B [3], or for the CFR with PVDF membrane [7], they are promising. Our reaction chamber had about 15 times smaller volume than the CFR, e.g., a 15-fold lower capacity to absorb liquid. Precise deliveries of reagent R1 and solvent S2 are crucial to sequencer performance, hence the limiting factor for our adsorptive sequencing system.

The importance of reaction volume on sequencing efficiency is evident from the advancements in polypeptide degradation since 1951. The Edman reaction [1] was initially carried out in 2 ml solution, the first automated sequencer [32] required 0.4 ml each of sample and PITC to create a thin film in a spinning cup and the current commercial sequencing instruments are based on ca. 100 μl sized reaction cartridges [12]. Microscale chemical reactors such as the automated micro batch analyzer developed by Sweileh and Dasgupta [33] typically have 100–1000 μl volumes, requiring ng amounts of sample and μl volumes of reagent. Although such reactor designs are ideal for complex, multi-step chemical reactions and direct measurement, miniaturization to accommodate pg samples and nl volumes is challenging. On the other hand, successful peptide mapping analysis of 3 nl β-lactoglobulin by enzymatic digestion in a capillary tube was accomplished by injecting 37 nl of enzyme followed by the protein sample [34]. Unfortunately, the step-wise nature of the Edman degradation and its complicated chemistry prevent the use of such a simple analysis technique. To overcome the dilemma of sub-μl liquid deliveries to our reaction chamber—the amounts needed to achieve effective PITC solvent evaporation—covalent sequencing was pursued.

Covalent sequencing, whereby polypeptide is covalently bound to a solid support, is typically used when there is a danger of sample wash-out from solvents and reagents. Our goal was to take advantage of the miscibility of acetonitrile (R1 solvent) and *N*-methylmorpholine (R2) (Table 3) to make PITC and polypeptide soluble in the same phase for chemical reaction. Repetitive yields for covalent sequencing were increased over those for adsorptive sequencing, presumably because coupling efficiency and product extraction were improved. The low initial yield (6 pmol, Fig. 4) for degradation of 55 pmol myoglobin (on Sequelon-DITC) was expected because of the covalently bound N-terminal amino acid. The high yield for PTH-serine (PTH-S) in cycle 3 (80 pmol) was attributed to the quantification method and age of the PTH standard (14–21 days). Peak height comparison is ideally made with a freshly prepared standard, otherwise PTH-S is partially converted to PTH-dehydroalanine and an erroneous signal response is obtained.

Repetitive yield was improved for the degradation of 53 pmol insulin chain B on Sequelon-AA (Fig. 5) by reducing the total volume of coupling reagent and increasing the proportion of PITC. Unfortunately, the by-product U1 (possibly diphenylurea, DPU) was frequently seen accompanied by relatively low amounts of DPTU. The presence of DPU suggests desulfurization of DPTU or PITC by atmospheric oxygen. When U1 was present in nmol amounts it did not interfere with sequence assignment. However, at the μmol level seen in cycle 5 of Fig. 5, U1 co-migrated with PTH-histidine. On-line conversion (currently under design) will provide an oxygen-free atmosphere during conversion and should eliminate peak overlap by U1. The unidentified peak U2 eluting at the same time as PTH-arginine (PTH-R) was seen in both adsorptive and covalent sequencing results. This peak was persistent regardless of extraction solvent (chlorobutane, benzene or TFA) and its migration time implied either a cationic species (like PTH-R) or, more likely, a hydrophobic species well retained in the micellar separation phase. We are working to identify and reduce this by-product. Despite the numerous unidentified peaks, relatively few overlapped exactly with analyte peaks in cycles 2–6. Nevertheless, reducing the background of by-product and contamination peaks is imperative to the identification of PTH amino acids in an unknown sample.

5. Conclusions

A major difficulty with miniaturization of the protein microsequencer was that of accurately delivering very small reagent volumes. These constraints made adsorptive sequencing in the capillary-based reaction chamber difficult. For the same reason, methods of sample loading were limited. The reaction chamber would not be useful, for example, with peptides purified by HPLC or by other large volume techniques. However, emerging methods of preparative micro-LC and CE would be compatible with the nanosequencer, given the development of a device for automated transfer. It should be possible to achieve compatibility with electroblotted samples if the delivery of sub-ml volumes can be achieved. Adsorptive sequencing with liquid TFA cleavage and extraction, which is used in newer commercial instruments, would also be possible with nl volume manipulation. Liquid TFA would permit a smaller extraction volume to be used and conversion to the PTH without drying may be possible, a necessary step for a capillary-based conversion chamber.

The ability to identify femtomole quantities of PTH amino acids drives our effort to sequence femtomole quantities of polypeptides. To realize this goal, a larger proportion of converted extract must be injected onto the CE column. Unfortunately, injection of more than 5 nl in CE separations leads to severe peak broadening and loss of resolution. Therefore, development of automated on-line injection will be necessary whereby the PTH amino acid derivative is formed in a minute volume and electrophoretically directed into the separation capillary.

The results reported represent preliminary results in the development of a fully automated nanosequencer using capillary electrophoretic analysis of the degradation products. The next paper in this series demonstrates that many of the difficulties encountered with this instrument can be eliminated through the use of syringe-driven reagent delivery and the elimination of the reagent valves [25].

Acknowledgements

This work was supported by an operating grant from the Natural Sciences and Engineering Research Council. Additional support from SCIEX is acknowledged. KCW and XFL acknowledge NSERC Industrial Postdoctoral fellowships, sponsored by SCIEX. II acknowledges a predoctoral fellowship from the Alberta Heritage Foundation for Medical Research. NJD acknowledges a McCalla Professorship from the University of Alberta.

References

[1] P. Edman, Acta Chem., Scand. 4 (1950) 283.
[2] R.M. Hewick, M.W. Hunkapiller, L.E. Hood and W.J. Dreyer, J. Biol. Chem., 256 (1981) 7990.
[3] J.E. Shively, P. Miller and M. Ronk, Anal. Biochem., 163 (1987) 517.
[4] P. Tempst and L. Riviere, Anal. Biochem., 183 (1989) 290.
[5] R. Aebersold, G.D. Pipes, R.E. Wettenhall, H. Nika and L.E. Hood, Anal. Biochem., 187 (1990) 56.
[6] M. Baumann, Anal. Biochem., 190 (1990) 198.
[7] J. Calaycay, M. Rusnak and J.E. Shively, Anal. Biochem., 192 (1991) 23.
[8] N.F. Totty, M.D. Waterfield and J.J. Hsuan, Protein Sci., 1 (1992) 1215.
[9] D.F. Reim and D.W. Speicher, Anal. Biochem., 207 (1992) 19.
[10] S. Kent, L. Hood, R. Aebersold, D. Teplow, L. Smith, V. Farnsworth, P. Cartier, W. Hines, P. Hughes and C. Dodd, BioTechniques, 5 (1987) 314.
[11] J.E. Shively, Methods: A Companion to Methods in Enzymology, 6 (1994) 207.
[12] K. Granlund-Moyer, C.G. Miller and J.A. Sahakian, 10th Int. Conf. Methods Protein Structure Analysis, Snowbird, Utah, Sept. 8–13, 1994, Abstract LA3.
[13] R. Aebersold, E.J. Bures, M. Namchuck, M.H. Goghari, B. Shushan and T.C. Covey, Protein Sci., 1 (1992) 494.
[14] K.C. Waldron, S. Wu, C.W. Earle, H.R. Harke and N.J. Dovichi, Electrophoresis, 11 (1990) 777.
[15] S. Wu and N.J. Dovichi, Talanta, 39 (1992) 173.
[16] E.J. Bures, H. Nika, D.T. Chow, H.D. Morrison, D. Hess and R. Aebersold, Anal. Biochem., 224 (1995) 364.
[17] E.J. Bures, H. Nika, D.T. Chow, D. Hess, H.D. Morrison, M. Bartlet-Jones, D.J.C. Pappin and R. Aebersold, in M.Z. Atassi and E. Appella (Eds.), Methods in Protein Structure Analysis: Proc. 10th Int. Conf., Snowbird, Utah, September 8–13, 1994, Plenum Press, New York 1995, pp. 57.
[18] V. Farnsworth and K. Steinberg, Anal. Biochem., 215 (1993) 190.

[19] H.A. Scoble, J.E. Vath, W. Yu and S.A. Martin, in P. Matsudaira (Ed.), A Practical Guide to Protein and Peptide Purification for Microsequencing, Academic Press, San Diego, 1993, pp. 125.
[20] D. Figeys, I. van Oostveen, A Ducret and R. Aebersold, Anal. Chem., 68 (1996) 1822.
[21] G.S. Begg and R.J. Simpson, in B. Wittmann-Liebold (Ed.), Methods in Protein Sequence Analysis, Proc. 7th Int. Conf., Berlin, July 3 8, 1988, Springer-Verlag, Berlin, 1988, pp. 108.
[22] D.F. Reim and D.W. Speicher, Anal. Chem., 216 (1994) 213.
[23] K.C. Waldron and N.J. Dovichi, Anal. Chem., 64 (1992) 1396.
[24] M. Chen, K.C. Waldron, Y. Zhao and N.J. Dovichi, Electrophoresis, 15 (1994) 1290.
[25] X.-F. Li, K.C. Waldron, J. Black, D. Lewis, I. Ireland and N.J. Dovichi, Talanta, succeeding paper in this journal.
[26] M. Haniu and J.E. Shively, Anal. Biochem., 173 (1988) 296.
[27] J.W. Jorgenson and K.D. Lukacs, Anal. Chem., 53 (1981) 1298.
[28] M.J. Little and P.R. Banks, Frederick Conf. Capillary Electrophoresis, Frederick, MD Oct. 23–25, 1995.
[29] P. Edman and A. Henschen, in S.B. Needleman (Ed.), Protein Sequence Determination, Springer-Verlag, New York, 1975, pp. 232.
[30] D.P.N. Satchell and R.S. Satchell, Chem. Soc. Rev., 4 (1975) 244.
[31] S. Ege, Organic Chemistry, 3rd Edn., D.C. Heath and Co., Lexington, 1994, pp. 1355.
[32] P. Edman and G. Begg, Eur. J. Biochem., 1 (1967) 80–91.
[33] J.A. Sweileh and P.K. Dasgupta, Anal. Chim. Acta, 214 (1988) 107–120.
[34] H-T. Chang and E.S. Yeung, Anal. Chem., 65 (1993) 2947.

ELSEVIER

Talanta 44 (1997) 401–411

Talanta

Miniaturized protein microsequencer with PTH amino acid identification by capillary electrophoresis II. A syringe-pump-based system for covalent sequencing

Xing-Fang Li, Karen C. Waldron[1], James Black, Darren Lewis, Ian Ireland, Norman J. Dovichi *

Department of Chemistry, University of Alberta, Edmonton, Alta., T6G 2G2, Canada

Received 6 June 1996; received in revised form 26 August 1996; accepted 26 August 1996

Abstract

A miniaturized protein and peptide microsequencer consisting of a fused silica capillary reaction chamber is described. Extremely small volumes of reagents, 2 μl or less, were delivered directly to the reaction chamber through individual fused silica capillary lines using low pressure syringe pumps. Other than an argon gas controller, no valves were used in the delivery system. The short flow path and very low dead volume were achieved by directly connecting the narrow-bore capillaries to the reaction chamber. This configuration minimized side reactions. The elimination of valves, as well as the use of capillaries for the reaction chamber and delivery lines, greatly simplified the construction of the sequencer. The performance of the sequencer was evaluated by sequencing 8–33 picomoles of myoglobin and insulin chain B that were covalently attached to Sequelon-DITC and Sequelon-AA membranes. © 1997 Elsevier Science B.V.

Keywords: Amino acid sequence; Capillary electrophoresis; Edman degradation; Insulin chain B; Micellar electrokinetic capillary chromatography; Microsequencing; Miniaturization; Myoglobin; Peptides; Phenylthiohydantoin; Proteins

1. Introduction

Since Edman first automated the isothiocyanate degradation chemistry for peptide sequencing in 1967 [1], this technology has been improved drastically [2] through the immobilization of proteins and peptides [3–5], improvements in degradation chemistry [6–9], miniaturization and automation of the sequencers [10–15], and the incorporation of HPLC separation and UV detection of phenylthiohydantoin (PTH) amino acids [16,17]. Edman degradation chemistry is still the most useful method for determining the primary structures of proteins and peptides [18]. However, the performance of the Edman chemistry depends heavily on the design of the sequencer [5,13,19].

* Corresponding author. Tel.: +1 403 4922845; fax: +1 403 4928231.

[1] Present address: Department of Chemistry, University of Montreal, Montreal, QC Canada.

PII S0039-9140(96)02076-0

Commercial sequencers can routinely determine sequence of 20 residues from 10–100 picomoles of peptides [5,19,20]. Still, there is a continuous demand for higher sensitivity in the overall sequencing process [19].

The sensitivity of commercially available sequencers is limited by the UV detection of phenylthiohydantoin (PTH)—amino acids [18]. Our group has developed a sensitive CE-based system for PTH-amino acid determination: micellar electrokinetic capillary chromatography with thermooptical absorbance detection (MECC-TOAD) [21]. The mass detection limits of this system for determination of PTH-amino acids are less than 1 femtomole [22]. However, the CE system can not be coupled directly to commercially available protein sequencers because of incompatibility of volume. Less than 10 nl of the sample solution is typically injected into the CE to preserve the high efficiency of separation, whereas more than 100 μl of solution is collected from existing commercial sequencers. Thus, miniaturization of the sequencer is essential in order to overcome this volume mismatch and to take advantage of the sensitive, fast and efficient determination of PTHs by MECC-TOAD.

We described the design of a miniaturized sequencer consisting of a capillary-sized reaction chamber and a multiport valve delivery system to address the problem of volume compatibility with CE [23]. However, that sequencer could not reproducibly deliver sub-μl volumes of reagent because of μl dead volumes in the multiport valves. The gas-liquid phase Edman degradation of picomole levels of proteins adsorbed on Polybrene-coated silica beads or polyvinylidene difluoride (PVDF) membranes was not successful. Adequate sequencing results were only obtained when proteins were covalently bound to solid supports, but the background peaks were large. By reducing the amounts of reagent used for Edman degradation, we observed a trend of reduced background peaks, as others have already pointed out [13,15]. Unfortunately, the multiport valve and argon pressurized delivery system described by Waldron et al. [23] precluded the use of less than 4 μl of reagent or solvent. Therefore, in order to further reduce the reagent volumes, we redesigned the miniaturized microsequencer to eliminate the valves and the argon pressurized delivery system. In this paper, we describe the design of a miniaturized sequencer where syringe pumps are directly coupled via capillary tubing to the reaction chamber to deliver reagents and solvents for covalent polypeptide sequencing. This system is able to deliver less than 2 μl of each reagent. As a result, the background peaks are significantly reduced. Preliminary results for this microsequencer are presented.

2. Experimental

2.1. Materials

All the reagents and solvents used for Edman degradation were sequencing grade. Coupling buffer (NMM, 5% *N*-methylmorpholine in 70/30 methanol:water with 0.1% cyclohexylamine), wash solvent 1 (WSH1, 0.1% cyclohexylamine in methanol), wash solvent 2 (WSH2, 1:1 heptane/ethylacetate with 0.1% cyclohexylamine), Sequelon-DITC (diisothiocyanate) Performance Evaluation Standard (Sequelon-DITC-myoglobin, horse heart), and the solid phase covalent attachment kits including Sequelon-DITC and Sequelon-AA (aryl amine) were purchased from Millipore Canada (Mississauga, ON). A mixture of 19 PTH-amino acids, diphenylthiourea (DPTU) and dimethylphenylthiourea (DMPTU) standard, and 5% phenylisothiocyanate (PITC) in heptane were bought from Applied Biosystems (Foster City, CA). Anhydrous trifluoroacetic acid (TFA) was obtained from Sigma Chemical (St. Louis, MO). Fused silica capillary was purchased from Polymicro Technologies (Phoenix, AZ).

2.2. Design of the miniaturized microsequencer

A schematic of the microsequencer is shown in Fig. 1. The plumbing system for delivery of reagents and solvents consisted of five syringe pumps (Model sp210iw, World Precision Inst., Sarasota, FL) equipped with Hamilton gas-tight syringes (250 or 500 μl, Chromatographic Specialties, Brockville, ON) and six 10 cm long fused

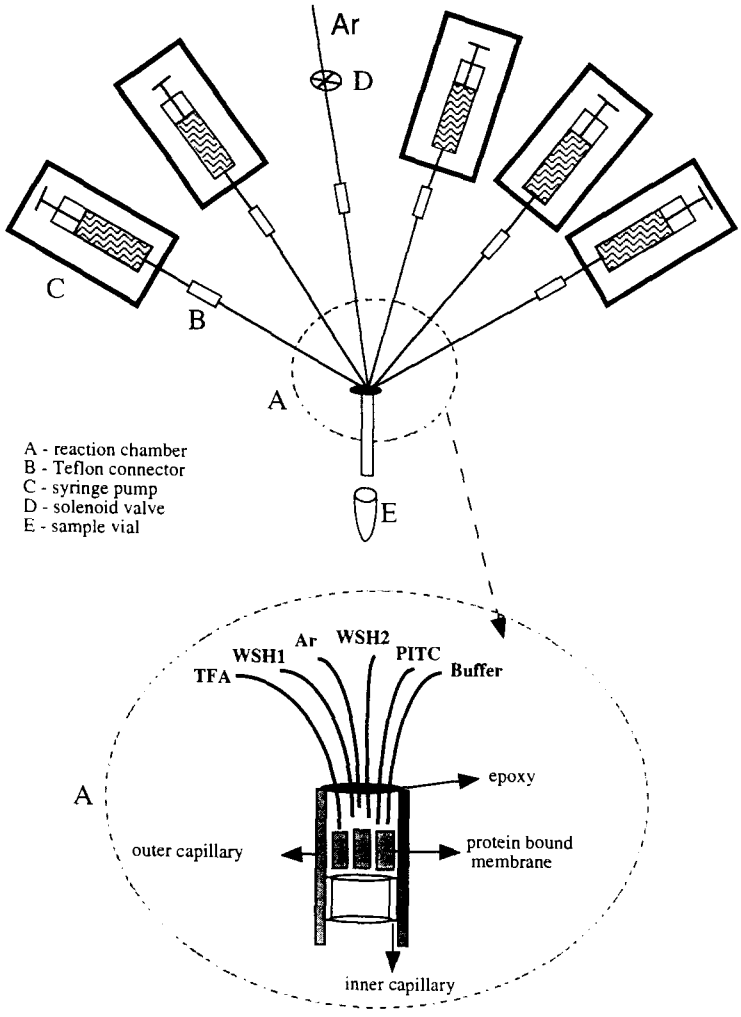

Fig. 1. Schematic of the syringe-pump-based microsequencer. Insert A describes the details of the reaction chamber assembly, showing the positions of the reagent/solvent inlet capillaries relative to the protein-bound membrane. A, reaction chamber; B, Teflon connector; C, syringe pump; D, solenoid valve; and E, sample vial.

silica capillary tubes (100 μm i.d., 200 μm o.d.). The reagents and solvents required to perform Edman degradation cycles were delivered individually by the syringe pumps each connected via the capillaries to the reaction chamber. Connection between each capillary and syringe was simply made with a 1 cm long piece of Teflon tubing (0.2 mm i.d.) from LC Packings International (San Francisco, CA). Argon gas (5 psig) was used for all drying steps and to facilitate collection of the extract from each Edman degradation cycle. The flow of argon was controlled electronically using an on/off solenoid valve (Lee Company, Westbrook, CT).

A miniature reaction chamber was constructed from a 4 cm long piece of wide-bore fused silica capillary (750 μm i.d., 850 μm o.d.) to which the six inlet capillaries for the delivery of reagents (NMM, PITC, TFA), solvents (WSH1, WSH2) and argon were connected using epoxy (Fig. 1A). The distances between the ends of the inlet capillaries and the membrane were varied: 1 mm for

the capillaries delivering PITC, NMM and TFA, 2 mm for WSH1 and WSH2, and 4 mm for argon. This configuration was used to reduce cross contamination between the reagents and solvents. The specific positions were obtained by aligning the inlet capillaries (cut from stock) on a piece of masking tape before they were inserted into the reaction chamber. The desired arrangement is shown in Fig. 1A. The six inlet capillaries were then inserted into the 4 cm long wide-bore capillary reaction chamber and fixed in place with epoxy (1:2, glue/hardener). The epoxy was allowed to dry completely for at least 30 min. The dry epoxy plug is resistant to the organic solvents used in the experiments. The reaction chamber-inlet capillary assembly was cleaned with methanol by connecting the free end of the wide-bore capillary to a syringe and withdrawing the solvent through the inlet capillaries from a reservoir. The assembly was then dried by argon and weighed on an analytical balance.

2.3. Sample loading

Membrane strips (0.5–0.8 mm wide) containing immobilized polypeptide were cut from an 8 mm disk and loaded into the wide bore capillary reaction chamber using a pair of tweezers. The membrane was gently pushed into place with a free piece of capillary and the reaction chamber assembly was re-weighed. The amount of protein loaded was calculated based on the weight of the membrane used to that of the 8 mm disk containing 120 pmol of myoglobin or insulin chain B. Finally, the loaded reaction chamber assembly was connected to the syringes, which had been preloaded with the degradation reagents and solvents and positioned on the syringe pumps. The sequencer was ready to perform Edman degradation cycles.

2.4. Edman degradation cycles

The reaction chamber was held and preheated by the thermoelectric modules described previously [23]. A temperature of 51°C was used for both coupling and cleavage. A typical sequencing program describing the amounts of reagents and solvents, order of delivery, and timing of the coupling and cleavage reactions is given in Table 1. The flow rate (8 μl min^{-1}) and the desired amount of each reagent or solvent was manually programmed with the syringe pump microprocessors. During the method development, a microscope (model STEMI 1000, Carl Zeiss Canada, Don Mills, ON) was used to determine whether sufficient reagent was delivered to wet the membrane completely. This procedure helped to minimize the consumption of reagents and solvents.

Conversion of the ATZ-amino acids (extracted with TFA) to the PTH form was carried out off-line. The extract from each Edman degradation cycle after cleavage was collected into a 200 μl vial, to which 25 μl of 25% aqueous TFA solution was added and mixed. The solution was heated at 67°C for 10 min and then dried on a vacuum centrifuge. The residue in the vial was dissolved in 1 μl of internal standard (5.8×10^{-5} M PTH-tyrosine (PTH-Y) in 10% acetonitrile/90% water) and then analyzed by MECC-TOAD for identification of the PTH-amino acid.

Table 1
General sequencing protocol

Step No.	Reagent/solvent delivered[a]	Time, s
1	NMM, 2 μl	
2	PITC, 2 μl	
3	Coupling reaction	300
4	Ar, 5 psi	10
5	PITC, 2 μl	
6	NMM, 2 μl	
7	Coupling reaction	300
8	Ar	30
9	WSH1, 8 μl × 3	
10	Ar	30
11	WSH2, 8 μl × 4	
12	Ar	180
13	TFA, 3 μl[b]	
14	Cleavage reaction	300
15	TFA, 4 μl × 3[b]	Collect extract
16	Repeat solvent wash steps 9–12	

Temperature of reaction chamber: 51°C.
[a] The rate of syringe pumps was kept at 8 μl min^{-1}.
[b] The TFA was collected for conversion.

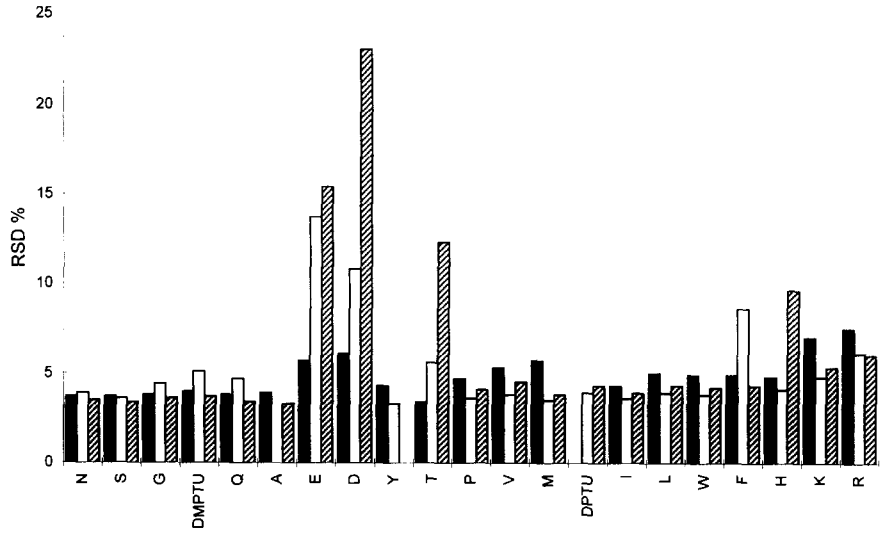

Fig. 2. Comparison of relative standard deviation (RSD) values of migration times of PTH-amino acids relative to (■) DPTU, (□) PTH-A, and (▨) PTH-Y.

2.5. Separation and identification of PTH-amino acids

The MECC-TOAD instrument and the details of the separation conditions used for the determination of PTH-amino acids have been described elsewhere [21,22]. Briefly, separation of the PTH residues from Edman degradation cycles was achieved by using a preconditioned 40 cm long fused silica capillary (50 μm i.d., 185 μm o.d.) and separation buffer containing 10.7 mM sodium phosphate, 1.8 mM sodium tetraborate, and 25 mM SDS at pH 6.7. The sample, dissolved in 1 μl of the internal standard PTH-Y, was injected hydrodynamically ($\Delta h = 4$ cm for 12 s) and the separation was carried out at 9 kV. The migration times were normalized either to the internal standard PTH-Y or to the by-product DPTU. The identification of a PTH residue from Edman degradation was obtained by matching the normalized migration time of the residue with that of the standard mixture of 19 PTHs, DPTU and DMPTU.

3. Results and discussion

3.1. PTH-amino acid identification by MECC-TOAD

We have previously demonstrated that the MECC-TOAD for the separation and detection of PTH-amino acids offers the advantages of fast and complete separation within 10–11 min and mass detection limits of less than 1 fmol [22]. Nine replicates of analyses of the standard mixture (19 PTH-amino acids, DMPTU and DPTU) were conducted over a period of 8 h. The same vial of separation buffer was used for all analyses. The relative migration time of the PTH-amino acids to that of PTH-A, or PTH-Y, or DPTU were calculated from the electropherograms. The RSD values of the relative migration times from the nine replicates are presented in Fig. 2. When the migration times of PTH amino acids were determined relative to PTH-A, the RSD values for most of the components were less than 4% except those of PTH-E, PTH-D and PTH-F, for which the RSDs were 14, 11, and 8%, respectively. Similar results were obtained when PTH-Y was used

to correct for migration time. RSD values of the relative migration times for most of the components were about 4%, but those of PTH-E, PTH-D, PTH-T and PTH-H were higher than 10%. Although PTH-E and PTH-D have larger shifts in migration time compared with other PTHs, their migration order does not change under the given conditions. The migration time of the components relative to DPTU gave the most consistent RSD values for all the PTH amino acids, mostly below 5%. DPTU is a common by-product from Edman degradation and thus, a convenient internal standard for migration time matching. However, this by-product peak is occasionally eliminated when small amounts of coupling reagents are used. Also, the unknown concentration of DPTU excludes its use as a standard for quantitation of the PTH amino acid obtained in each cycle. Therefore, it is necessary to use a second internal standard which gives a double check on the migration time for identification and makes calculation of yields possible. In this study, PTH-Y was used as the internal standard because its stock solution was stable at −20°C for over 1 year.

Normalization of migration times to an internal standard demonstrates that the identification of the PTH-amino acids by CE analysis can be as reliable as that with HPLC. The reproducibility of migration time from CE was generally below 1% when the running buffer was frequently replenished [22], whereas the reproducibility of migration time from HPLC is about 0.5% [24]. The above CE runs gave relatively higher RSD values than routine analysis we did because the above runs were intentionally carried out using the same buffer over 8 h to observe the extreme variation of migration time. In addition, MECC-TOAD determination is about four times faster and mass detection limits are about 1000 times lower than those of HPLC [22,24].

3.2. Design of miniaturized sequencer

We and others [13,15] have observed that reduction of the amount of reagents used in Edman degradation is necessary in order to minimize the background peaks. However, delivery of a few μl of reagent using most adsorptive or covalent sequencing instruments [11–15] is difficult because the requirements of valves to control the delivery of reagents. The use of valves substantially increases dead volume and also complicates the electronics and software for controlling the valves in the sequencer. To overcome these problems and deliver sub μl amounts of reagent, we designed a unique, valveless microsequencer that uses syringe pumps instead of gas pressurization to deliver reagents (Fig. 1). The Teflon tubing sleeves used to connect the inlet capillaries to the syringe pumps did not require ferrules and nuts to secure them. Combined with the elimination of valves in the liquid flow path, this design minimized the overall dead volume of the system. The desired reagents and solvents were accurately and reproducibly delivered to the reaction chamber. In addition to the present sequencer design being very simple, it is also economical.

The amount of PITC required for each Edman degradation cycle was less than 4 μl, as shown in Table 1. Therefore, a 250 μl syringe contained enough PITC for 62 cycles. Commercial sequencers can typically perform about 40 cycles after which the identification of PTH-amino acid residue becomes ambiguous in the HPLC analysis. Thus, there is no need to refill the syringes during repetitive sequencing cycles on the same polypeptide.

Fused silica capillaries were used in the plumbing system, instead of the usual Teflon tubing [12,13,15], because of their facile connection to both the syringes and the reaction chamber. Six narrow-bore capillaries (200 μm o.d.) could easily fit inside the wide-bore capillary reaction chamber, which would not have been possible with Teflon tubing. Fused silica capillaries are also less permeable to oxygen than Teflon. The syringe-pump-based design allowed delivery of reagents and solvents through individual flow paths, directly to the sample membrane. With this configuration, the problem of side reactions taking place along the flow path was eliminated.

We previously reported [23] that a few μl of reagent was easily lost to the walls or vaporized inside the valves and along the Teflon flow path when argon was used to push reagents to the reaction chamber. Unfortunately, excess amount of liquid were used in order to deliver enough reagent to the reaction chamber, which caused

severe side-reactions. By-products were very large and interfered with the MECC separation of the PTH-amino acid residues. This problem was eliminated using the present reaction chamber assembly, as illustrated in Fig. 1A. The distance between the inlet ends of the TFA, NMM and PITC delivery lines and the membrane was about 2 mm. An aliquot of 1 μl reagent gave a 4.5 mm long plug in the 750 μm i.d. reaction chamber. When the plug of reagent reached the membrane, it quickly wet the membrane, indicating that 1 μl of reagent was sufficient for complete wetting. This is essential to obtain high yields in the coupling and cleavage reactions. Therefore, up to 2 μl of reagents delivered to the reaction chamber using syringe pumps would be sufficient for coupling PITC to the polypeptide sample, which is demonstrated in the following section.

3.3. Edman degradation

The performance of the syringe-pump-based microsequencer was evaluated by sequencing myoglobin and insulin chain B, covalently attached to the Sequelon-DITC and Sequelon-AA membranes, respectively. An initial set of sequencing experiments was performed on 33 pmol of Sequelon-DITC-myoglobin (Millipore evaluation standard). Because the protein N terminus and lysyl residues were covalently attached to the DITC-membrane, the first PTH amino acid from Edman degradation was not analyzed. The concentration of the expected amino acid from each cycle was calculated based on the peak height of the product calibrated against that of the internal standard PTH-Y; consequently, the picomoles of the product in 1 μl of solution was obtained. The pseudo-initial yield (cycle 2) was 76% and the repetitive yield was 87% from 33 pmol of myoglobin. No internal standard was used for the analysis of PTH-D from cycle 4, so the yield of cycle 4 was not quantified. The yields of PTH amino acid obtained from 18 cycles of sequencing 22 pmol of Sequelon-DITC-myoglobin were 64% for cycle 2 and 90% for repetitive yield. PTH-W from cycle 7 and PTH-K from cycle 16 were not detected. This may be due to degradation of these products during conversion. We have successfully identified these products in other sequencing experiments when the conversion is carried out in 5% aqueous TFA at 65°C.

Insulin chain B was covalently attached to Sequelon-DITC and Sequelon-AA membranes by following the directions from the Millipore kits. A 26 pmol sample of Sequelon-AA-insulin chain B was subjected to four cycles of sequencing. The yields of cycles 1, 2, 3, and 4 were 33, 32, 26, and 25%, respectively, giving an average repetitive yield of 90%. The sequence analysis of 37 pmol Sequelon-DITC-insulin chain B gave yields of about 17% in each of the first four cycles and over 90% repetitive yield. These results were in agreement with the MilliGen® Sequencer user's manual which states that the initial yield in solid phase sequencing varies from 30 to 60% and the repetitive yield is over 90%.

The electropherograms representing the results of sequencing 11 cycles of 33 pmol Sequelon-DITC-myoglobin are shown in Fig. 3. It is noteworthy that only 1–2 nl of the 1 μl sample (0.1%) was injected for identification by MECC-TOAD. The PTH residues were positively identified by using the migration times normalized to the 19-PTH amino acid standard. Four major by-products, DPTU, U1, U2 and U3, were observed. DPTU, U1 and U3 were completely separated from the PTH amino acids. However, U2 eluted close to PTH-R. Both U2 and U3 had somewhat variable migration times. It was observed that an increased level of background peaks appeared when the reagents were left inside the syringes at room temperature for several days. In Fig. 3, cycles 5–10 were performed on the same day, 3 days after the first four cycles were completed. Cycle 11 was carried out 7 days after the first four cycles. A comparison of the background peaks for degradation cycles done under the same conditions but on different days showed increased background with old reagents. In the 4–5 min. region (Fig. 3), background peaks progressively increased with time after loading the syringes with reagents.

A number of preliminary studies were conducted to reduce the background peaks. One of the important factors investigated was the amount of each reagent used in coupling and cleavage. To

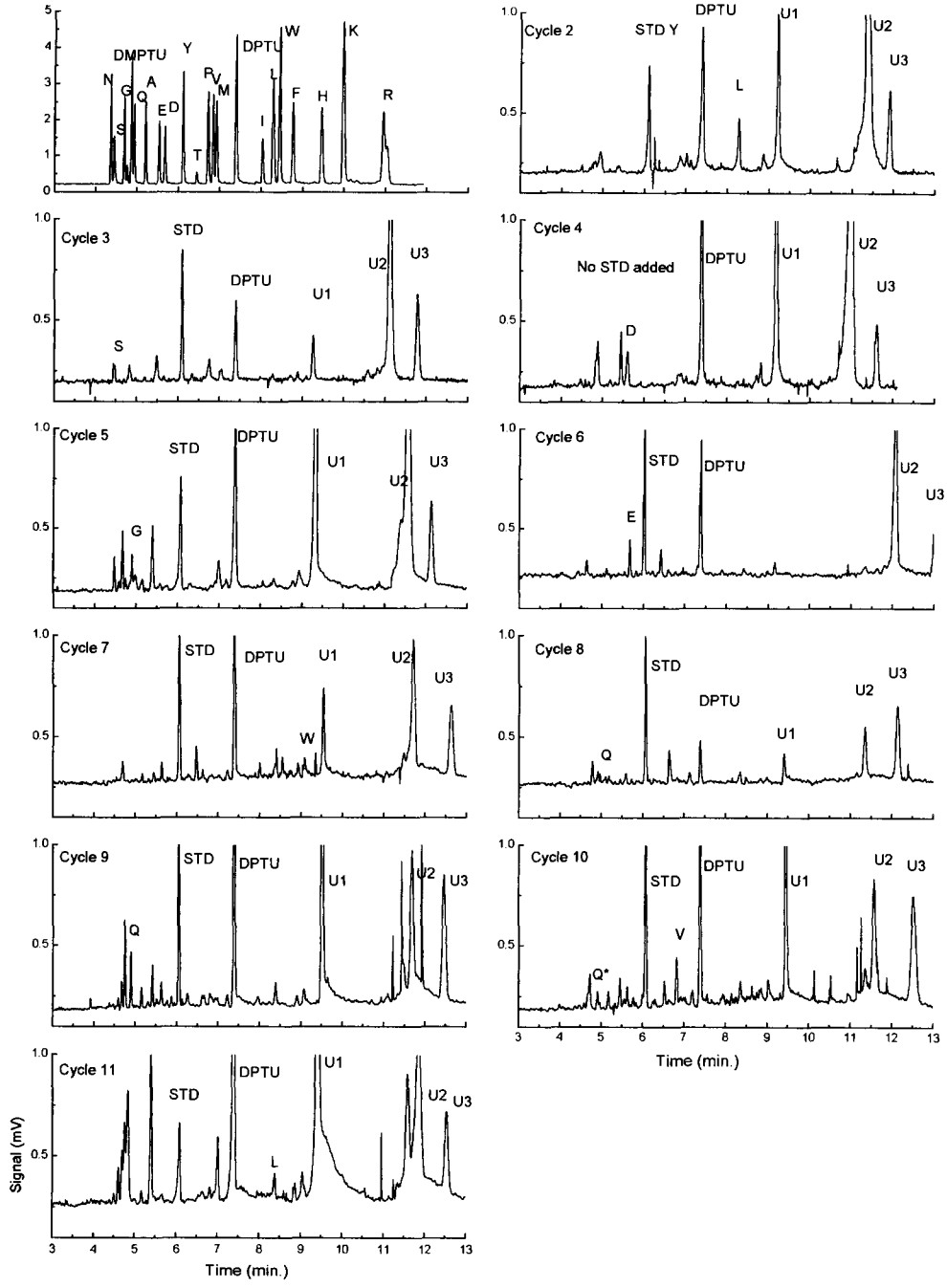

Fig. 3. Original electropherograms showing sequencing results of 33 picomoles of Sequelon-DITC-myoglobin.

minimize the volumes of liquid delivered, a microscope was used to observe how much reagent was necessary to completely wet the membrane. As mentioned in the previous section, as little as 1 μl of PITC or NMM completely wet the membrane (about one fourth of the commercial 8 mm disk). As expected, reduction of the amounts of PITC and NMM used for Edman degradation resulted in lower background peaks. In Fig. 3, the DPTU and U1 peaks in cycles 6–8 were significantly reduced compared with those in other cycles because only 1 μl of PITC and NMM was used for each coupling reaction, compared with 2–4 μl of PITC and NMM that was used in the other cycles.

During the experiments, it was found that more than 8 min of flushing with argon at 5 psig was necessary to completely remove the residual TFA vapor from inside the reaction chamber after ATZ amino acid extraction. However, if 1 μl of NMM is used to neutralize residual TFA followed by 1 min argon, the level of by-products DPTU and U1 are reduced, as demonstrated in cycles 2 and 3 of Fig. 3. In addition, the overall cycle time is reduced. Nevertheless, the pre-flush with NMM did not significantly change the amounts of the other two by-products, U2 and U3.

The amount of TFA used for cleavage and extraction produced different levels of background peaks. Examples from sequencing 22 pmol of Sequelon-DITC-myoglobin are presented in Fig. 4. Cycles 2 and 6 were performed under similar conditions, the only difference being 12 μl (4 μl × 3) of TFA were used for extraction in cycle 6 compared with 6 μl (2 μl × 3) of TFA used in cycle 2. Reduced background peaks were observed when 50% less TFA (cycle 2) was used for extraction. Precise control of the amount of coupling and cleavage reagents can lead to a clean electropherogram. The conditions used for cycle 15 shown in Fig. 4 are summarized in Table 2. Reduced amounts of PITC and NMM were used for coupling, and less TFA was used for cleavage and extraction. In addition, 2 μl of TFA was used to quickly flush the membrane before cleavage (step 14), resulting in a clean electropherogram for cycle 15. However, it is important to note that flushing with TFA before cleavage must be completed within a few seconds, because cleavage takes place almost immediately when the acid reaches the membrane. The idea is to remove by-products that persist after solvent washes but before the cleavage reaction. We found that this step, like all steps in each cycle, must be precisely controlled. As expected, the yield for cycle 15 was lower than those from previous cycles, presumably due to the loss of the product during the flushing and incomplete extraction. This timing precision implies that automation of the sequencer and precise control of the wash and extraction processes and temperature could improve the yield further.

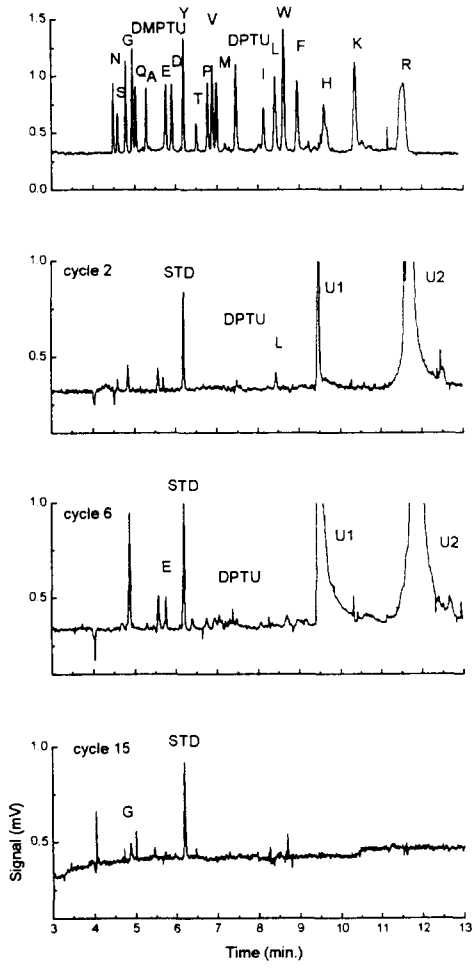

Fig. 4. Comparison of the background peaks from cycles 2, 6, and 15 of 22 picomoles Sequelon-DITC-myoglobin sequenced under different conditions, described in the text.

Table 2
Sequencing protocol for cycle 15

Step No.	Reagent/solvent delivered*	Time, s
0	NMM, 2 μl	
1	Ar, 5 psi	60
2	NMM, 1 μl	
3	PITC, 1 μl	
4	Reaction	300
5	Ar, 5 psi	10
6	PITC, 1 μl	
7	NMM, 1 μl	
8	Reaction	300
9	Ar	60
10	WSH1, 8 μl × 3	
11	Ar	20
12	WSH2, 8 μl × 4	
13	Ar	180
14	TFA, 2 μl	
15	Ar	4
16	TFA, 1 μl[b]	
17	Reaction	300
18	TFA, 2 μl × 2[b]	Collect extract
19	Repeat solvent wash steps	

Temperature of reaction chamber: 51°C.
[a] and [b] same as Table 1.

The potential of the syringe-pump-based microsequencer in sequence analysis of < 10 pmol levels of polypeptides was explored. A standard, 8 pmol Sequelon-DITC-myoglobin, was sequenced using the conditions in Table 2. The residues from cycle 5 and cycle 10 were positively identified, but determination of the residues from other cycles was difficult due to the low percentage of product that could be analyzed. For example, a cycle yield of 65% represents 5 pmol PTH amino acid, but only 5 fmol is injected into the MECC-TOAD system. Further advances in on-line injection of the degradation products are necessary to achieve femtomole sequencing levels.

4. Conclusion

We have developed a miniaturized syringe-pump-based microsequencer. Its performance is demonstrated by sequencing 8–37 pmol of myoglobin and insulin chain B covalently bound to Sequelon membranes. To our knowledge, this is the smallest volume sequencer and the first to be constructed with a reaction chamber made from fused silica capillary and valveless delivery of reagents. The instrument can deliver solvents and reagents directly to the reaction chamber so that side reactions can be minimized. The elimination of background peaks was demonstrated with precise control of the amounts of reagents, the wash and the extraction processes. The advantages of the new design include simplicity and economy in both construction and operation of the sequencer.

The syringe-pump-based sequencer can deliver extremely small amounts of TFA for cleavage and subsequent extraction, resulting in the elimination of the evaporation step between extraction and conversion of the ATZ amino acids. While we currently rely on off-line conversion of the ATZ to PTH derivative, we are developing a system with on-line conversion. The on-line system will generate PTH amino acids in a much smaller volume, which is compatible with direct injection into our CE analysis system.

From our experience, covalent sample attachment is more suitable for ultra-sensitive sequencing of proteins and peptides than adsorptive methods, when Edman degradation is carried out in a capillary-sized reaction chamber. Since many samples for sequencing are presented as electroblots [4,25], it is essential to make the syringe-pump-based sequencer compatible with protein electrotransfer techniques. In combination with on-line conversion and on-line MECC-TOAD analysis, the miniaturized microsequencer should provide a 10–100-fold improvement in polypeptide sequencing sensitivity.

Acknowledgements

This project was supported by an operating grant from the Natural Sciences and Engineering Research Council (NSERC) of Canada. Additional support was provided by SCIEX. XFL and KCW acknowledge NSERC Industrial Postdoctoral fellowships sponsored by SCIEX. NJD acknowledges a McCalla Professorship from the University of Alberta.

References

[1] P. Edman and G. Begg, Eur. J. Biochem., 1 (1967) 80.
[2] J.E. Shively, Methods: A Companion to Methods in Enzymology, 6 (1994) 207.
[3] G.E. Tarr, J.F. Beecher and D.J. McKean, Anal. Biochem., 84 (1978) 622.
[4] D.J.C. Pappin, J. Coull and H. Koester, Anal. Biochem., 187 (1990) 10.
[5] R. Aebersold, Nature, 343 (1990) 291.
[6] P. Edman, Acta Chem. Scand., 4 (1950) 277.
[7] H. Maeda, N. Ishida, H. Kawauchi and K. Tuzimura, J. Biochem., 65 (1969) 777.
[8] J.Y. Chang, E.H. Creaser and K.W. Bentley, Biochem. J., 153 (1976) 607.
[9] R. Aebersold, E.J. Bures, M. Namchuck, M.H. Goghari, B. Shushan and T.C. Covey, Protein Sci., 1 (1992) 494.
[10] B. Wittman-Liebold, H. Grafunder and H. Kohls, Anal. Biochem., 75 (1976) 621.
[11] R.M. Hewick, M.W. Hunkapiller, L.E. Hood and W.J. Dreyer, J. Biol. Chem., 256 (1981) 7990.
[12] R.A. Laursen, Eur. J. Biochem., 20 (1971) 89.
[13] J. Calaycay, M. Rusnak and J.E. Shively, Anal. Biochem., 192 (1991) 23.
[14] B. Wittman-Liebold, L. Matschull, U. Pilling, H.-A. Bradaczek, and J. Graffunder, in H. Jornvall, J.-O. Hoog and A.-M. Gustavsson (Eds.), Methods in Protein Sequence Analysis, Birkhauser Verlag, Basel, 1991, pp. 9–21.
[15] J.E. Walker, I.M. Fearnley and R.A. Blows, Biochem. J., 237 (1986) 73.
[16] C.L. Zimmerman, E. Apella and J.J. Pisano, Anal. Biochem., 77 (1977) 569.
[17] D.H. Hawke, P.-M. Yuan and J.E. Shively, Anal. Biochem., 120 (1982) 302.
[18] P. Tempst, S. Geromanos, C. Elicone, H. Erdjument-Bromage, Methods: A Companion to Methods in Enzymology, 6 (1994) 248.
[19] S. Kent, L. Hood, R. Aebersold, D. Teplow, L. Smith, V. Farnsworth, P. Cartier, W. Hines, P. Hughes and C. Dodd, BioTechniques, 5 (1987) 314.
[20] D.W. Speicher, Methods: A Companion to Methods in Enzymology, 6 (1994) 262.
[21] K.C. Waldron and N.J. Dovichi, Anal. Chem., 64 (1992) 1396.
[22] M. Chen, K.C. Waldron, Y. Zhao and N.J. Dovichi, Electrophoresis, 15 (1994) 1290.
[23] K.C. Waldron, X.-F. Li, M. Chen, I. Ireland, D. Lewis, M. Carpenter and N.J. Dovichi, Talanta, preceeding paper in this Journal.
[24] B.A. Bidlingmeyer, S.A. Cohen and T.L. Tarvin, J. Chromatogr., 336 (1984) 93.
[25] J. Mozdzanowski and D.W. Speicher, Anal. Biochem., 207 (1992) 11.

ELSEVIER

Talanta 44 (1997) 413–421

Talanta

Spectroscopic properties of polycyclic aromatic compounds Part 6. The nitromethane selective quenching rule visited in aqueous micellar zwitterionic surfactant solvent media

Siddharth Pandey [a], William E. Acree [a,*], Bongsup P. Cho [b], John C. Fetzer [c]

[a] *Department of Chemistry, University of North Texas, Denton, Texas 76203-0068, USA*
[b] *Department of Medicinal Chemistry, University of Rhode Island, Kingston, Rhode Island 02881, USA*
[c] *Chevron Research and Technology Center, Richmond, California 94802-0627, USA*

Received 18 June 1996; received in revised form 26 August 1996; accepted 27 August 1996

Abstract

Applicability of the nitromethane selective quenching rule for discriminating between alternant versus nonalternant polycyclic aromatic hydrocarbons (PAHs) is examined for 58 representative PAH solutes dissolved in micellar *N*-hexadecyl-*N*,*N*-dimethyl-3-ammonio-1-propanesulfonate and in micellar *N*-dodecyl-*N*,*N*-dimethyl-3-ammonio-1-propanesulfonate solvent media. Results of measurements show that zwitterionic surfactants can be considered, for the most part, as providing a polar solubilizing media as far as the nitromethane selective quenching rule is concerned. Nonalternant PAHs that contain electron donating methoxy- and hydroxy-functional groups (and methyl-groups to a much lesser extent) are noted exceptions. © 1997 Elsevier Science B.V.

Keywords: Fluorescence quenching; Micellar solvent media; Nitromethane selective quenching rule; Zwitterionic surfactants

1. Introduction

This study continues a systematic examination of the effect that solvent media and substituent functional group has on the ability of nitromethane to selectively quench fluorescence emission of alternant polycyclic aromatic hydrocarbons (PAHs). Emission intensities of nonalternant PAHs are for the most part unaffected by nitromethane addition. Published studies [1–8] involving over 63 PAHs have identified dibenzo[hi,wx]heptacene, benzo[k]fluoranthene and naphtho[2,3b]fluoranthene as among the few exceptions to the so-called nitromethane selective quenching rule in the PAH6 benzenoid, fluorenoid, fluoranthenoid and 'methylene-bridged' cyclopenta-PAH subclasses. More recent measurements [9,10] revealed that nitromethane quenched fluorescence emission of all eighteen acenaphthylene- and acephenanthrylene-derivatives studied thus far which is completely contrary to what would be expected based upon the fact that the solutes are listed as 'textbook' examples

* Corresponding author. Fax: +1 817 5654318; e-mail: acree@cas1.unt.edu

PII S0039-9140(96)02084-X

of nonalternant PAH molecules. The unusual fluorescence quenching behavior of the acenaphthylene- and acephenanthrylene-derivatives results from the molecules' fixed double bond in the five-membered ring. The double bond is alkenic in nature, rather than aromatic as one might believe. This observation is confirmed by independent NMR coupling measurements [11–14].

Breymann et al. [7] attributed nitromethane's selectivity to an electron/charge transfer reaction whereby an electron is transferred from the excited PAH fluorophore to nitromethane, which acts as an electron acceptor. From a strictly thermodynamic point-of-view, it is conceivable that the extent of quenching could be altered simply by changing the electronic nature of the surrounding solvent media in order to either stabilize or destabilize the positive charge (or partial positive charge) that is temporarily formed on the polycyclic aromatic hydrocarbon. Micellar solutions provide a very convenient means to introduce ionic character, and still have a solvent media capable of solubilizing the larger, hydrophobic PAH solutes. Anionic surfactants could perhaps stabilize a positive charge on the PAH ring system, whereas cationic surfactants would tend to inhibit fluorescence emission quenching by nitromethane.

The above ideas were borne out in two preliminary studies [15,16] involving micellar sodium dodecylsulfate (SDS), sodium dodecanoate (SDD, also called sodium laurate), tetradecyltrimethylammonium bromide (TTAB, also called myristyltrimethylammonium bromide) and cetyltrimethylammonium bromide (CTAB) solutions. Nitromethane quenching selectivity was lost in only the anionic SDS and SDD solutions. Except for benzo[k]fluoranthene, dibenzo[b,k]-fluoranthene, dibenz[a,e]acephenanthrylene and naphtho[2,3b]fluoranthene, emission intensities of the eleven nonalternant PAHs studied were for the most part not significantly affected by nitromethane addition in the case of the cationic surfactant solvent media. These four PAHs are known exceptions to the nitromethane selective quenching rule. Earlier studies further documented that the presence of micellar aggregates was a necessary condition for the anionic headgroup charge to affect the quenching mechanism. At SDS and SDD molar concentrations below the cmc, nitromethane quenching selectivity was again observed.

While our earlier studies did suggest that the anionic versus cationic headgroup plays an important role in the observed loss of quenching selectivity, we did not explore what happens when both types of charges are present in the micelle. In this communication we report the fluorescence behavior of 25 alternant and 33 nonalternant polycyclic aromatic hydrocarbons in micellar *N*-hexadecyl-*N*,*N*-dimethyl-3-ammonio-1-propanesulfonate (SB-16, also called palmityl sulfobetaine) and *N*-dodecyl-*N*,*N*-dimethyl-3-ammonio-1-propanesulfonate (SB-12, also called lauryl sulfobetaine) solvent media as a function of added nitromethane concentration. Zwitterionic surfactants are neutral compounds. The two formally charged substituent groups are separated by intervening atoms and are generally not electronically conjugated with each other. The resulting micelle's conformational structure is determined to a large extent by the electrostatic energy of interaction between the charged substituent groups and the internal energy of the ion bridge/tether. For aliphatic ion bridge structures the all-trans conformation must have the lowest internal energy [17], but in this conformation the distance between oppositely charged substituents is large. The distance may be reduced by rotating the bonds within the ion bridge to the less favorable gauche conformation.

2. Experimental

Micellar solutions of *N*-hexadecyl-*N*,*N*-dimethyl-3-ammonio-1-propane-sulfonate (Sigma, circa 5.0×10^{-3} M) and *N*-dodecyl-*N*,*N*-dimethyl-3-ammonio-1-propanesulfonate (Sigma, circa 1.0×10^{-2} M) were prepared by dissolving the surfactant in doubly de-ionized water. Dibenz[e,l]acephenanthrylene, 3-methoxydibenz[e,l]acephenanthrylene and 3-methoxyindeno[1,2,3hi]chrysene (see Fig. 1 for molecular structures) were synthesized and purified by procedures described elsewhere [18]. Synthetic refer-

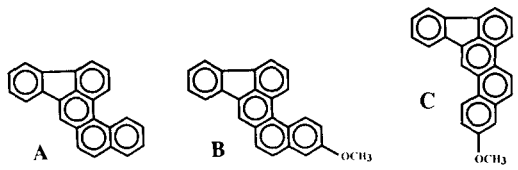

Fig. 1. Molecular structures of dibenz[e,l]acephenanthrylene (A); 3-methoxydibenz[e,l]acephenanthrylene (B); and 3-methoxyindeno-[1,2,3hi]chrysene (C).

ences and/or commercial suppliers for the remaining 55 PAH solutes contained in Tables 1 and 2 are listed in our earlier papers (for a single source listing see Tucker [19]). Stock solutions were prepared by dissolving the solutes in dichloromethane, and were stored in closed amber glass bottles in the dark to retard any photochemical reactions between the PAH solutes and dichloromethane solvent. Carbon tetrachloride and chloroform (to a much lesser extent) are reported to react with polycyclic aromatic hydrocarbons via a hypothesized concerted transannular addition with free radical formation [20–25]. Small aliquots of each stock solutions were transferred into test tubes, allowed to evaporate, and diluted with the micellar solvent media of interest. All solutions were ultrasonicated, vortexed and allowed to equilibrate for a minimum of 24 h before any spectrofluorometric measurements

Table 1
Summary of nitromethane quenching results for alternant polycyclic aromatic hydrocarbons dissolved in micellar SB-12 and micellar SB-16 solvent media

Chemical name	λ_{ex} (nm)	SB-12 (%Red[a,b])	SB-16 (%Red[a,b])
Alternant polycyclic aromatic hydrocarbons (PAH6 benzenoids)			
Pyrene	338	94	95
Perylene	403	37	33
Coronene	334	43	26
Benzo[ghi]perylene	380	83	80
Benzo[e]pyrene	335	81	76
Benzo[a]pyrene	350	78	71
Dibenzo[a,e]pyrene	360	74	69
Anthranthrene	306	27	25
Anthracene	340	38	29
Naphtho[2,3g]chrysene	350	55	50
Chrysene	320	81	77
Methylene-bridged Cyclopenta-polycyclic aromatic hydrocarbons			
11-*H*-Benz[bc]aceanthrylene	350	78	70
13-*H*-Dibenzo[a,g]fluorene	340	72	65
4-*H*-Benzo[b]cyclopenta[mno]chrysene	330	63	52
4-*H*-Cyclopenta[pqr]picene	330	78	72
13-*H*-Dibenz[bc,l]aceanthrylene	330	73	65
13-*H*-Dibenz[bc,k]aceanthrylene	400	40	27
9-*H*-Benz[6,7]indeno[1,2l]phenanthrene	345	69	62
Alternant polycyclic aromatic hydrocarbons (fixed C=C double bond)			
Acenaphthylene	288	85	83
Aceanthrylene	360	52	47
Benz[e]aceanthrylene	360	73	60
3-Methylbenz[j]aceanthrylene	300	73	68
6-Methylbenz[j]aceanthrylene	300	63	58
Benzo[def]cyclopenta[hi]chrysene	300	58	54
Acenaphth[1,2a]acenaphthylene	406	39	33

[a] Unless otherwise indicated, only one small 25 μl drop of 'neat' nitromethane was added to 10 ml of dissolved PAH solution.
[b] % Reduction $= 100 \times (F_{initial} - F_{final})/F_{initial}$; where $F_{initial}$ refers to the corrected PAH emission intensity prior to nitromethane addition and F_{final} is the corrected emission intensity after nitromethane addition.

Table 2
Summary of nitromethane quenching results for nonalternant polycyclic aromatic hydrocarbons dissolved in micellar SB-12 and micellar SB-16 solvent media

Chemical name	λ_{ex} (nm)	SB-12; Red[a,b]		SB-16; Red[a,b]	
		50 μl	100 μl	50 μl	100 μl
Nonalternant fluoranthenoids and fluorenoids					
Benz[def]indeno[1,2,3hi]chrysene	406	4%	9%	4%	7%
Benz[def]indeno[1,2,3qr]chrysene	408	0%	0%	1%	4%
Benzo[k]fluoranthene	306	25%[c]		12%[c]	
Dibenzo[a,e]fluoranthene	390	0%	0%	0%	0%
Benzo[ghi]fluoranthene	340	1%	1%	0%	0%
Naphtho[1,2b]fluoranthene	350	14%	27%	9%	19%
Benzo[a]fluoranthene	406	1%	2%	3%	4%
Naphtho[2,1a]fluoranthene	400	1%	3%	1%	3%
Naphtho[2,3b]fluoranthene	316	18%[c]		9%[c]	
Benzo[b]fluoranthene	346	18%	29%	11%	19%
Naphtho[2,1k]benzo[ghi]fluoranthene	368	1%	5%	2%	5%
Naphtho[1,2k]benzo[ghi]fluoranthene	366	2%	5%	0%	2%
Fluoreno[2,3,4,9defg]chrysene	315	0%[c]		0%[c]	
Indeno[1,2,3cd]pyrene	326	0%[c]		0%[c]	
Benzo[j]fluoranthene	315	0%[c]		0%[c]	
Dibenz[e,l]acephenanthrylene	371	9%	17%	8%	15%
Nonalternant fluoranthenoid and fluorenoid derivatives					
1-Methylfluoranthene	360	9%		6%	
2-Methylfluoranthene	355	8%		5%	
3-Methylfluoranthene	355	10%		6%	
7-Methylfluoranthene	357	7%		4%	
8-Methylfluoranthene	355	8%		5%	
10-Methylbenzo[b]fluoranthene	347	16%		10%	
t-Butyldibenzo[ghi,mno]fluoranthene	300	2%		1%	
10-Methoxybenzo[j]fluoranthene	320	2%		0%	
10-Methoxybenzo[b]fluoranthene	347	33%		30%	
12-Methoxybenzo[b]fluoranthene	347	35%		30%	
3-Methoxybenzo[k]fluoranthene	312	36%		27%	
9-Methoxybenzo[k]fluoranthene	310	41%		36%	
3-Methoxydibenz[e,l]acephenanthrylene	378	25%		20%	
3-Methoxyindeno[1,2,3hi]chrysene	368	32%		24%	
9-Hydroxybenzo[k]fluoranthene	310	2%		0%	
10-Hydroxybenzo[j]fluoranthene	325	0%		0%	
10-Hydroxybenzo[b]fluoranthene	346	33%		30%	

[a] Unless otherwise indicated, only 1 small 50 μl and 100 μl drops of 'neat' nitromethane was added to 10 ml of dissolved PAH solution.

[b] % Reduction $= 100 \times (F_{initial} - F_{final})/F_{initial}$; where $F_{initial}$ refers to the corrected PAH emission intensity prior to nitromethane addition and F_{final} is the corrected emission intensity after nitromethane addition.

[c] Because of the large primary inner-filtering correction only one small 25 μl drop of nitromethane was added to 10 ml of dissolved PAH solution.

were made. Experimental results were unaffected by longer equilibration times.

Absorption spectra were recorded on a Milton Roy Spectronic 1001 Plus and a Hewlett-Packard 8450 A photodiode-array spectrophotometer in the usual manner. The fluorescence spectra were measured on a Shimadzu RF-5000U spectrofluorimeter with the detector set at high sensi-

tivity. Solutions were excited at the wavelengths listed in Tables 1 and 2. Fluorescence data were accumulated in a 1 cm^2 quartz cuvette at 23°C (ambient room temperature) with excitation and emission slit width settings of 15 and 3 nm, respectively. The fluorescence spectra represent a single scan which was then solvent blank corrected and verified by repetitive measurements.

Emission intensities associated with the quenching measurements were corrected for primary inner-filtering artifacts and self-absorption arising from the absorption of excitation radiation by nitromethane and the PAH solute, respectively, according to the following expression [26–28]:

$$f_{prim} = F^{corr}/F^{obs} = 2.303A(y-x)/[10^{-Ax} - 10^{-Ay}] \quad (1)$$

which differs slightly from the approximate form [29]

$$f_{prim} \approx 10^{0.5A} \quad (2)$$

In the above equations F^{corr} and F^{obs} refer to the corrected and observed fluorescence emission signal, respectively, A is the absorbance per cm of pathlength at the excitation wavelength, and x and y denote distances from the boundaries of the interrogation zone to the excitation plane. Several of the PAHs have excitation wavelengths in the 300–320 nm spectral region and a few drops of nitromethane gave solutions having appreciable absorbances. Computational procedures and interrogation zone dimensions are discussed in greater detail elsewhere [3–5,30,31]. Every effort was made to work at solution absorbances of A $cm^{-1} \leq 0.95$ ($f_{prim} \leq 3.0$), where Eqs. (1) and (2) are valid. Secondary inner-filtering corrections were not necessary as nitromethane is 'optically transparent' in most of these PAH emission ranges.

3. Results and discussion

Tables 1 and 2 summarize our fluorescence quenching measurements for 25 alternant and 33 nonalternant polycyclic aromatic hydrocarbons dissolved in micellar SB-12 and micellar SB-16 solvent media. Experimental results are reported in the last columns as the percent reduction in the original fluorescence emission intensity observed after the addition of nitromethane. As indicated in the table footnotes, numerical entries correspond to either 25 μl, 50 μl or 100 μl of neat quenching agent added to circa 10 ml of solution. All emission intensities used in the computations were corrected for primary inner-filtering and solute self-absorption as discussed in the last paragraph of the Experimental section. Estimated nitromethane molar concentrations are as follows: 0.044 M (25 μl), 0.088 M (50 μl) and 0.176 M (100 μl). Molar concentrations are calculated using an average droplet mass of 0.0270 g obtained by weighing 25 individual Eppendorf pipette droplets of nitromethane, which ranged in size from 0.0267–0.0275 g. Uncertainties in the percent reductions are believed to be ± 2% (or better) based upon replicate measurements for select solutes.

Readers should note that acenaphthylene- and aceanthrylene-derivatives are listed in Table 1 as alternant PAHs. Classification of aromatic molecules as alternant versus nonalternant PAHs depends upon the nature of the aromatic ring system. Earlier quenching studies [9,10] labelled aceanthrylene- and acephenanthrylene-derivatives as nonalternant PAHs assuming that the C=C double bond in the cyclopenta-ring was aromatic. NMR coupling measurements [11–14] show that the double bond is alkenic, and should not have been considered as part of the aromatic ring system when the molecules were initially classified as nonalternant PAHs. Placement of these seven acenaphthylene- and aceanthrylene-derivatives in Table 1 as alternant PAHs is consistent with the C=C double bond in the cyclopenta-ring being nonaromatic in nature.

Careful examination of Tables 1 and 2 reveals that nitromethane quenches the fluorescence emission of all 25 alternant PAH6 benzenoids and alkylated derivatives, in accordance with the nitromethane selective quenching rule. Similar behavior is observed for both zwitterionic surfactant solutions. No special significance is given at the present time to the slightly larger percent reductions observed in the SB-12 micelle solution as such differences may result simply from the size of

the added nitromethane droplet and/or differences in the nitromethane partitioning behavior between the micellar phase(s) and the bulk aqueous solution. More interesting quenching behavior is observed in the case of the 35 nonalternant fluoranthenoid and fluorenoid compounds. Five of the parent nonalternant PAHs, benzo[k]fluoranthene, naphtho[2,3b]fluoranthene, naphtho[1,2b]fluoranthene, benzo[b]fluoranthene and dibenz[e,l]acephenanthrylene are quenched by nitromethane in both micellar solvent medias. The first two compounds have been previously noted to be exceptions to the nitromethane selective quenching rule [3,6,32], and their behavior here is not totally unexpected. (Note: naphtho[1,2b]fluoranthene was considered to be 'borderline' case in our initial quenching study [3], and its behavior is also in agreement with earlier findings). What is unexpected, however, is the large number of methyl- and methoxy-nonalternant PAH derivatives that are quenched in zwitterionic solutions.

Rationalization of why nitromethane quenches the fluorescence emission of nonalternant PAHs (particularly the methyl- and methoxy-derivatives) dissolved in the zwitterionic surfactant solutions must take into account the fact that most of the fluorophore molecules reside somewhere within the micellar interior. Polycyclic aromatic hydrocarbons, especially the larger multi-ring ones, are extremely hydrophobic and they have very limited aqueous solubilities. In several earlier solvent polarity probe studies, we noted that it was impossible with our Shimadzu spectrofluorimeter to determine meaningful emission intensity ratios for coronene, methylcoronene, 1,2-dimethylcoronene and other larger PAHs because of extremely weak fluorescence signals [33,34]. We even substituted neat acetonitrile for the recommended aqueous-acetonitrile solvent media (20:80 by volume) in our quenching studies [35] in order to solubilize the larger PAHs. The large increase in emission intensity that is observed in the micellar SB-12 and micellar SB-16 solvents results from the enhanced PAH solubility, combined with inability of oxygen to effectively quench PAH molecules residing inside the micellar pseudophase.

Excited-state lifetimes of PAHs are on the order of nanoseconds, [36,37] and the micelle-to-aqueous pseudophase transfer rate is on the order of μs (micelle residence times being several μs [38,39]). Any hypothesized quenching mechanism must have the PAH molecule residing somewhere within the interior of the micelle during the electron transfer. Exciplex formation and/or a significant change in the basic quenching mechanism is unlikely as we failed to observe new band(s) in any of the recorded emission and absorption spectra.

To gain better insight into actual location of the dissolved PAH inside the micelle and the role that solvent polarity has upon presumed charge transfer quenching mechanism, we examined fluorescence behavior of alternant and nonalternant PAHs dissolved in *n*-heptane and cyclohexane in the presence of nitromethane. These measurements are summarized in Table 3 as the percent reduction in the original fluorescence emission signal observed after the addition of either 25 μl or 50 μl of 'neat' nitromethane to 10 ml of solution. Nitromethane has a limited solubility in hydrocarbon solvents. Even at the 50 μl addition of nitromethane the calculated mole fraction concentration of $X_{\text{nitromethane}} \approx 0.0095$ in cyclohexane is still three times less than the published solubility ($X_{\text{nitromethane}} \approx 0.030$) in cyclohexane at 25°C [40]. Experimental solubility data could not be found for nitromethane in *n*-heptane; however, Marsh [41] reported both excess enthalpies and excess volumes for miscible nitromethane + *n*-hexane mixtures at 25°C up to $X_{\text{nitromethane}} = 0.03526$, which is still 2–3 times larger than the 50 μl quenching study. *n*-Hexane and *n*-heptane are saturated hydrocarbons differing by a single CH_2-group. Nitromethane should have similar solubility in both alkanes. Moreover, we did not see any cloudiness in the solutions after shaking, and the measured absorbances doubled when the aliquot size was increased from 25 μl to 50 μl of nitromethane. These observations also indicate that the solubility limit was not exceeded.

Careful examination of Table 3 reveals that nitromethane no longer selectively quenched fluorescence emission of alternant PAHs. Emis-

Table 3
Summary of nitromethane quenching results for alternant and nonalternant polycyclic aromatic hydrocarbons dissolved in *n*-heptane and cyclohexane solvent media

Chemical name	λ_{ex} (nm)	*n*-Heptane (%Red[a,b])	Cyclohexane (%Red[a,b])
Alternant polycyclic aromatic hydrocarbons (PAH6 benzenoids)			
Pyrene	338	59	76
Perylene	403	0	0
Coronene	334	0	0
Benzo[ghi]perylene	380	0	0
Benzo[e]pyrene	335	37	56
Benzo[a]pyrene	350	6	18
Dibenzo[a,e]pyrene	360	10	25
Anthranthrene	306	2	5
Anthracene	340	65	65
Naphtho[2,3g]chrysene	350	6	13
Nonalternant Fluoranthenoids and Fluorenoids			
Benz[def]indeno[1,2,3hi]chrysene	406	1	2
Benz[def]indeno[1,2,3qr]chrysene	408	0	0
Dibenzo[a,e]fluoranthene	390	3	0
Benzo[ghi]fluoranthene	340	0	0
Naphtho[2,1a]fluoranthene	400	0	0
Benzo[a]fluoranthene	406	0	0
Naphtho[1,2b]fluoranthene	350	0	0
Benzo[b]fluoranthene	346	2	1
Benzo[k]fluoranthene	306	0[c]	0[c]
Naphtho[2,3b]fluoraanthene	316	0[c]	1[c]

[a] Unless otherwise indicated, only one small 25 μl drop of 'neat' nitromethane was added to 10 ml of dissolved alternant PAH solution, and one small 50 μl drop of 'neat' nitromethane was added to 10 ml of dissolved nonalternant PAH solutions.
[b] % Reduction $= 100 \times (F_{initial} - F_{final})/F_{initial}$; where $F_{initial}$ refers to the corrected PAH emission intensity prior to nitromethane addition and F_{final} is the corrected emission intensity after nitromethane addition.
[c] Because of the large primary inner-filtering correction only one small 25 μl drop of nitromethane was added to 10 ml of dissolved PAH solution.

sion signals of perylene, coronene, benzo[ghi]perylene, anthanthrene, benzo[a]pyrene and naphtho[2,3g]chrysene were for all practical purposes unaffected by nitromethane, as were signals of all ten nonalternant PAHs studied. Even in the case of pyrene, benzo[e]pyrene and anthracene where sizeable quenching was observed, the percentage reduction in emission intensity was still significantly less than was observed in our initial study [5] involving the much more polar 'neat' acetonitrile and binary aqueous-acetonitrile (20:80 by volume) solvent mixtures.

Results of these measurements suggest that dissolved PAHs must reside somewhere within a fairly polar region of the zwitterionic micelles, other-wise, one would not observe the large percentage reductions in emission signals that are given in Table 1. Nitromethane and the PAH fluorophore must be situated in fairly close proximity to each other in order for electron transfer to effectively occur. Nitromethane, because of its very limited solubility in saturated hydrocarbons, resides in the polar region(s) of the micelle. The close proximity requirement then places the solubilized PAH solutes in a fairly polar region within the micelle. Experimental I/III band emission intensity ratios for pyrene (I/III $\approx$ 1.06), benzo[ghi]perylene (I/III $\approx$ 1.02) and coronene (I/III $\approx$ 0.55) dissolved in SB-12 and SB-16 also indicate a moderately polar molecular environment around the solubilized PAH probe molecule. Much smaller ratios of I/III $\approx$ 0.58 for pyrene [42], I/III $\approx$ 0.38 for benzo[ghi]perylene [43] and I/III $\approx$ 0.12 for coronene [44] would be expected if

the PAH were solubilized in an entirely hydrocarbon-like micellar region. Similarly, we believe that nonalternant PAHs also reside in a polar molecular environment within the micelle. The above argument seems reasonable as a search of the published chemical literature [45–51] reveals that most authors conclude that the site of solubilization of aromatic probes is close to the micelle surface in the so-called palisade layer.

We rationalize the experimental quenching data in zwitterionic solutions in terms of earlier observations involving anionic and cationic surfactants. Presence of micellar aggregates is a necessary condition for the anionic substituent's negative charge to affect the quenching mechanism [16]. Micelles may either provide a favorable geometry for electron transfer to occur with concurrent stabilization of the developing positive charge on the PAH, and/or increase the local concentration of nitromethane around the solubilized PAH solute molecule. The positively charged tetraalkylammonium substituent is anchored to the anionic substituent by $-CH_2CH_2CH_2-$ tethers. In close proximity to the dissolved PAH and nitromethane molecules, the tetraalkylammonium substituent would be in a position either to 'fix' the nitro-group in a conformation unfavorable for electron transfer or to interact with the PAH's aromatic π-cloud, pulling electron density toward the cation and away from any surrounding nitromethane quencher molecules. Both types of cationic interactions should discourage electron transfer from the excited PAH fluorophore to nitromethane, which acts as the electron acceptor. Almgren et al. [50] invoked weak specific interaction between the solubilized PAH and the cationic head group to explain large differences between the maximum solubilities of pyrene (and other PAHs) in anionic micelles versus micelles of tetraalkylammonium cationic surfactants. Two published papers [50,52] have used the change in the I/III band emission intensity in pyrene's fluorescence spectrum to calculate the equilibrium constant for presumed pyrene-tetraalkylammonium association complexes. Proton and ^{13}C NMR data [53,54] have also been used as experimental evidence to support PAH-tetraalkylammomium group interactions in both homogeneous and heterogeneous solvent media.

In zwitterionic surfactant solutions the solubilized polycyclic aromatic hydrocarbon can conceivably interact with both charged substituent groups. Fluorescence quenching data in Tables 1 and 2 suggest that zwitterionic surfactants can be considered, for the most part, as providing a polar solubilizing media as far as the nitromethane selective quenching rule is concerned. Nonalternant PAH solutes that containing electron donating methoxy- and hydroxy-functional groups (and to a much lesser extent methyl-groups) are noted exceptions. We believe that the increased quenching and loss of nitromethane selectivity results because the surfactant's positively-charged tetraalkylammonium substituent interacts with the lone electron pairs on the oxygen atoms, rather than with the aromatic π-electron cloud. There would then be sufficient electron density for complete/partial electron transfer to nitromethane which acts as the electron acceptor. Depending upon the PAH's molecular structure, the anionic sulfonate group might still be favorably situated so as to stabilize any developing charge on the PAH aromatic ring system that might occur.

Dissimilar fluorescence quenching behavior in micellar anionic, cationic, zwitterionic and nonionic solvent media is important from an analysis standpoint. Cationic and nonionic surfactants would be the solvent medias of choice if one wished to use nitromethane as a selective fluorescence quenching agent to simplify observed emission spectra. A possible application would involve the chromatographic separation of unknown PAH mixtures with fluorescence detection. With trace nitromethane added to the micellar mobile phase one would observe reduced fluorescence emission signals from alternant PAHs which might facilitate resolution or quantification of co-eluting solutes.

Acknowledgements

This work was supported in part by the University of North Texas Research Council. The authors also acknowledge support from the American Cancer Society (# CN-130).

References

[1] G.-P. Blümer and M. Zander, Fresenius Z. Anal. Chem., 296 (1979) 409.
[2] F.K. Ogasawara, Y. Wang and V.L. McGuffin, Appl. Spectrosc., 49 (1995) 1.
[3] S.A. Tucker, W.E. Acree, Jr., B.P. Cho, R.G. Harvey and J.C. Fetzer, Appl. Spectrosc., 45 (1991) 1699.
[4] V.L. Amszi, Y. Cordero, B. Smith, S.A. Tucker, W.E. Acree, Jr., C. Yang, E. Abu-Shaqara and R.G. Harvey, Appl. Spectrosc., 46 (1992) 1156.
[5] S.A. Tucker, H. Darmodjo, W.E. Acree, Jr., J.C. Fetzer and M. Zander, Appl. Spectrosc., 46 (1992) 1260.
[6] H. Dreeskamp, E. Koch and M. Zander, Z. Naturforsch., 30A (1975) 1311.
[7] U. Breymann, H. Dreeskamp, E. Koch and M. Zander, Chem. Phys. Lett., 59 (1978) 68.
[8] S.H. Chen, C.E. Evans and V.L. McGuffin, Anal. Chim. Acta, 246 (1991) 65.
[9] S.A. Tucker, H.C. Bates, V.L. Amszi, W.E. Acree, Jr., H. Lee, P.D. Raddo, R.G. Harvey, J.C. Fetzer and G. Dyker, Anal. Chim. Acta, 278 (1993) 269.
[10] S.A. Tucker, J.M. Griffin, W.E. Acree, Jr., P.P.J. Mulder, J. Lugtenburg and J. Cornelisse, Analyst, 119 (1994) 2129.
[11] P.P.J. Mulder, B.B. Boere, A. Baart, J. Cornelisse and J. Lugtenburg, Recl. Trav. Chim. Pays-Bas, 112 (1993) 22.
[12] R. Sangaiah, A. Gold and G. E. Toney, J. Org. Chem., 48 (1983) 1632.
[13] P.P.J. Mulder, J. Olde Boerrigter, B.B. Boere, H. Zuihof, C. Erkelens, J. Cornelisse and J. Lugtenburg, Recl. Trav. Chim. Pays-Bas, 112 (1993) 287.
[14] A.W.H. Jans, C. Tintel, J. Cornelisse and J. Lugtenburg, Magn. Reson. Chem., 24 (1986) 101.
[15] S. Pandey, W.E. Acree, Jr. and J.C. Fetzer, Anal. Chim. Acta, 324 (1996) 175.
[16] S. Pandey, J.R. Powell, W.E. Acree, Jr., B.P. Cho, J. Kum, C. Yang and R.G. Harvey, Polycyclic Aromat. Compds., in press.
[17] E.L. Eliel, Stereochemistry of Carbon Compounds, MacGraw-Hill, New York, 1962.
[18] B.P. Cho, Tetrahedron Lett., 36 (1995) 2403.
[19] S.A. Tucker, Ph.D. Dissertation, University of North Texas, Denton, Texas, 1994.
[20] N. Selvarajan, N.M. Panicker, S. Vaidyanathan and V. Ramakrishnan, Indian J. Chem., 18A (1979) 23.
[21] M.V. Encinas, M.A. Rubio and E.A. Lissi, Photochem. Photobiol., 37 (1983) 125.
[22] M.V. Encinas, M.A. Rubio and E.A. Lissi, J. Photochem., 18 (1982) 137.
[23] W.M. Wiczk and T. Latowski, Z. Naturforsch., 42A (1987) 1290.
[24] E.J. Bowen and K.K. Rohatgi, Disc. Faraday Soc., 14 (1953) 146.
[25] S.A. Tucker, L.E. Cretella, R. Waris, K.W. Street, Jr., W.E. Acree, Jr. and J.C. Fetzer, Appl. Spectrosc., 44 (1990) 269.
[26] C.A. Parker and W.J. Barnes, Analyst, 82 (1957) 606.
[27] J.F. Holland, R.E. Teets, P.M. Kelly and A. Timnick, A., Anal. Chem., 49 (1977) 706.
[28] M.C. Yappert and J.D. Ingle, Appl. Spectrosc., 43 (1989) 759.
[29] J.R. Lakowicz, Principles of Fluorescence Spectroscopy, Plenum Press, New York, 1983.
[30] S.A. Tucker, W.E. Acree, Jr., J.C. Fetzer and J. Jacob, Polycyclic Aromat. Compds., 3 (1992) 1.
[31] S.A. Tucker, V.L. Amszi and W.E. Acree, Jr., J. Chem. Educ., 69 (1992) A8.
[32] S.A. Tucker, H.C. Bates, W.E. Acree, Jr. and J.C. Fetzer, Appl. Spectrosc., 47 (1993) 1775.
[33] S.A. Tucker, W.E. Acree, Jr., J.C. Fetzer and R.H. Mitchell, Appl. Spectrosc., 47 (1993) 1040.
[34] S.A. Tucker, W.E. Acree, Jr. and J.C. Fetzer, Appl. Spectrosc., 49 (1995) 8.
[35] S.A. Tucker and W.E. Acree, Jr., Appl. Spectrosc., 46 (1992) 1388.
[36] I.B. Berlman, Handbook of Fluorescence Spectra of Aromatic Molecules, Academic Press, New York, 1965.
[37] K. Nakashima and I. Tanaka, Langmuir, 9 (1993) 90.
[38] M. Almgren, F. Greiser and J.K. Thomas, J. Chem. Soc., Faraday Trans. 1, 75 (1979) 1674.
[39] R.J. Hunter, Foundations of Colloid Science, Vol. I, Oxford Science, Oxford, 1989.
[40] H. Stephen and T. Stephen, Solubilities of Inorganic and Organic Compounds: Ternary and Multicomponent Systems, Vol. 2, Part 2, Pergamon Press, Oxford, 1964, p. 1547.
[41] K.N. Marsh, J. Chem. Thermodyn., 17 (1985) 29.
[42] D.C. Dong and M.A. Winnik, Can. J. Chem., 62 (1984) 2560.
[43] R. Waris, M.A. Rembert, D.M. Sellers, W.E. Acree, Jr., K.W. Street, Jr., C.F. Poole, P.H. Shetty and J.C. Fetzer, Appl. Spectrosc., 42 (1988) 1525.
[44] R. Waris, M.A. Rembert, D.M. Sellers, W.E. Acree, Jr., K.W. Street, Jr. and J.C. Fetzer, Analyst, 114 (1989) 195.
[45] J.K. Thomas, Chem. Rev., 80 (1980) 283 and references there-in.
[46] J.K. Thomas, Acc. Chem. Res., 10 (1977) 133 and references there-in.
[47] P. Mukerjee and J.R. Cardinal, J. Phys. Chem., 82 (1978) 1620.
[48] R.A. Pyter, C. Ramachandran and P. Mukerjee, J. Phys. Chem., 86 (1982) 3206.
[49] C. Ramachandran, P. Pyter and P. Mukerjee, J. Phys. Chem., 86 (1982) 3198.
[50] M. Almgren, F. Grieser and J.K. Thomas, J. Am. Chem. Soc., 101 (1979) 279.
[51] P. Lianos, M.-L. Viriot and R. Zana, J. Phys. Chem., 88 (1984) 1098.
[52] M. Almgren, B. Medhage and E. Mukhtar, J. Photochem. Photobiol. A: Chem., 59 (1991) 323.
[53] K. Viaene, A. Verbeeck, E. Gelade and F.C. De Schryver, Langmuir, 2 (1986) 456.
[54] J.H. Fendler, E. Fendler, G.A. Infante, P.-S. Shih and L.K. Patterson, J. Am. Chem. Soc., 97 (1975) 89.

ELSEVIER

Talanta 44 (1997) 423–426

Talanta

Ultratrace determination of europium in high-purity lanthanum, praseodymium and dysprosium oxides by luminescence spectrometry

N. Mahalakshmi Sita, T. Prasada Rao *, C.S.P. Iyer, A.D. Damodaran

Regional Research Laboratory (CSIR), Trivandrum 695 019, India

Received 6 May 1996; received in revised form 26 August 1996; accepted 26 August 1996

Abstract

A luminescence spectrometric method was developed for the determination of ultra trace amounts of europium (down to 1×10^{-13} M) in high purity lanthanum, praseodymium and dysprosium oxides. This is based on the enhanced luminescence of europium-thenoyltrifluoroacetone (TTA)-dibenzo-18-crown-6 (DBC)-Triton X-100 in the presence of terbium. The fluorescence intensity is linear with europium concentration in the range 1×10^{-11}–1×10^{-6} M under the recommended conditions. The optimized procedure is successfully utilized for the determination of ultratrace amounts of europium in lanthanium, praseodymium and dysprosium oxides. © 1997 Elsevier Science B.V.

Keywords: Luminescence spectrometry; Rare earth oxides; Ultra trace quantities

1. Introduction

High purity individual rare earth oxides are increasingly used as major components in refractive index lenses and fibre optics (La_2O_3), lasers (Y_2O_3), phosphor (YVO_3) and magnetic bubble memory films (Gd_2O_3) [1,2]. The electrical and magnetic properties of these materials are influenced by the levels of contaminating foreign trace elements particularly other lanthanides. It is therefore important that such contaminants at trace levels be identified and quantified [3].

Various luminescence methods described for the determination of traces of lanthanides in high purity rare earth oxides are reviewed elsewhere by us [3] but these are not sensitive. Enhanced luminescence was observed during a study of Eu-TTA-1,10-phenanthroline-surfactant system in the presence of terbium and this allows the determination of 10^{-11}–10^{-8} M of europium with a detection limit of 10^{-13} M [4,5]. Unfortunately, 10 fold amounts of La, Ce, Pr, Nd, Ho, Er, Yb, Y and Lu interfere in the determination of 10^{-9} M of Eu [5]. This paper describes similar phenomenon observed during a study of Eu-TTA-dibenzo-18-crown-6 surfactant system in the presence of terbium which enables the determination of 10^{-11}–10^{-6} M of europium with a detection limit of 10^{-13} M. On the other hand, in the present procedure 10^3 fold amounts of lan-

* Corresponding author. Fax: +91 471 490186.

PII S0039-9140(96)02085-1

thanum, praseodymium and dysprosium do not interfere in the determination of 10^{-8} M europium enabling us in the determination of ultra-trace amounts of europium in high purity lanthanum, praseodymium, dysprosium and their mixtures of oxides.

2. Experimental

2.1. Apparatus

A LS-50-B luminescence spectrometer (Perkin Elmer) was used. An ELICO LI-120 digital pH meter was used for pH adjustment.

2.2. Reagents

Standard solutions (1×10^{-3} M) of lanthanides were prepared by dissolving the oxides (99.9%) in dilute hydrochloric acid. Working solutions were prepared by dilution with distilled water. Aqueous 1×10^{-2} M solutions of TTA and dibenzo-18-crown-6 (DBC) in acetonitrile were used. The concentration of non-ionic surfactant, Triton X-100 solution was 1% (w/w). The buffer solution was 0.3 M ammonium acetate. All the reagents used were of analytical grade.

2.3. Procedure

To a 25 ml volumetric flask, solutions were added in the following order. Standard solutions of Eu^{3+} and Tb^{3+}, TTA, Dibenzo-18-crown-6, buffer and surfactant solutions. The mixture was diluted to 25 ml with distilled water and allowed to stand for 10 min. The fluorescence intensity was measured in a 1 cm quartz cell at excitation and emission wavelengths of 371 and 614 nm, respectively.

3. Results and discussion

The emission spectra of the systems investigated are as shown in Fig. 1. The emission spectra of Eu-TTA-DBC-Triton X-100 in the presence and absence of terbium are similar to each other and

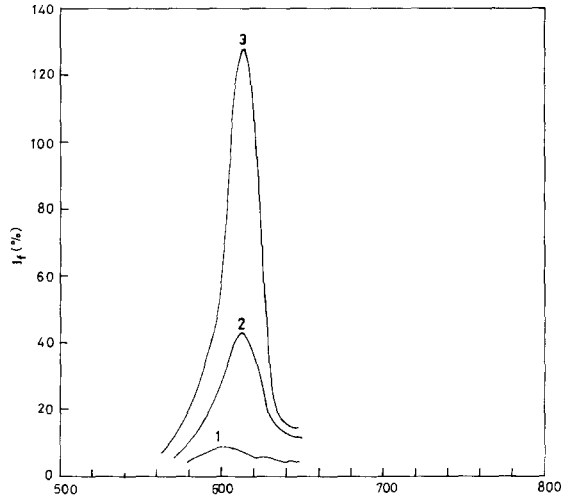

Fig. 1. Emission spectra: (1) Eu-TTA-DBC-Triton X-100; (2) Tb-TTA-DBC-Triton X-100; and (3) Eu-Tb-TTA-DBC-Triton X-100. Conditions: 1.0×10^{-4} M DBC, 3×10^{-2} M ammonium acetate, 5×10^{-2}% Triton X-100.

show the emission spectra of Eu^{3+}. The maximum excitation wavelength (not shown in Fig. 1) is 371 nm and the maximum emission wavelength is 614 nm. However, the intensity of Eu-Tb-TTA-DBC-Triton X-100 is 1–2 orders of magnitude stronger than that of the system without terbium.

The effect of terbium concentration on the fluorescence intensity of the europium system is

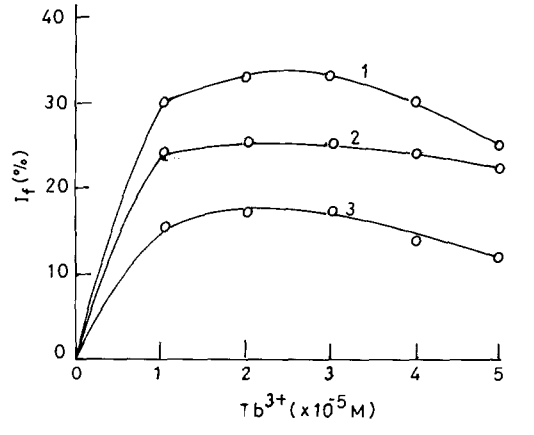

Fig. 2. Effect of terbium concentration. Europium concentration: (1) 1×10^{-8} M; (2) 1×10^{-9} M; and (3) 1.0×10^{-10} M. Conditions: 1.0×10^{-4} M TTA, 1.0×10^{-4} M DBC, 3×10^{-2} M ammonium acetate, 5×10^{-2}% Triton X-100.

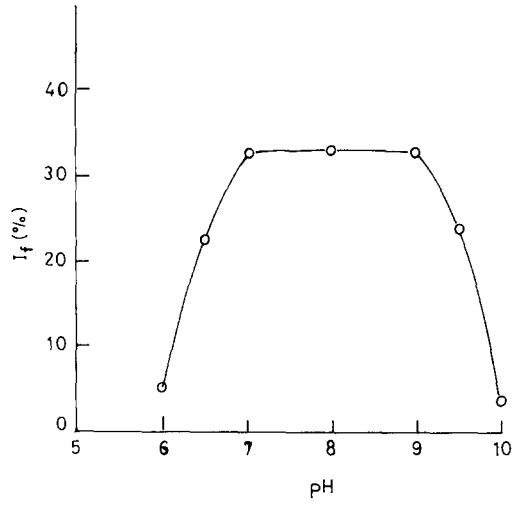

Fig. 3. Effect of pH on Eu-Tb-TTA-DBC-Triton X-100 system. Conditions: 1.0×10^{-8} M Eu^{3+}, 2.0×10^{-5} M Tb^{3+}, 1.0×10^{-4} M TTA, 1×10^{-4} M DBC, 5×10^{-2}% Triton X-100.

shown in Fig. 2. For 1×10^{-9} M Eu^{3+} the fluorescence intensity reaches a maximum at 1.5×10^{-5} M, Tb^{3+}, whereas in the range of 1×10^{-8}–1×10^{-10} M of Eu^{3+} the maximum fluorescence intensity occurs in the range $1.5–2 \times 10^{-5}$ M. Fig. 3 shows the effect of pH on the fluoresence intensity in the presence of terbium. The greatest fluorescence intensity occurs over the pH range 7.0–9.0. The type of buffer also effects the fluorescence intensity. Under the general conditions used for Fig. 3 at pH 7 ammonium acetate and hexamine-HCl buffers gave the same fluorescence intensity but ammonia–ammonium chloride reduced the intensity (by 10%) and citrate and phosphate buffers quenched the fluorescence completely. Thus, ammonium acetate ($> 10^{-3}$ M) was chosen for further use. The effects of TTA, DBC and Triton X-100 on the fluorescence intensity of Eu-Tb system were examined. The concentration ranges that gave greatest intensity were 7×10^{-5}–1.5×10^{-4} M TTA, $> 10^{-5}$ M DBC and 2.0–10.0×10^{-2}% (w/w) Triton X-100.

The nature of crown-ether was found to have strong influence on the fluorescence intensity of Eu-Tb system. DBC gave nine-fold higher fluorescence intensity compared with dicyclohexyl-18-crown-6 though enhanced luminescence for europium was observed in the presence of terbium in latter crown ether also. DBC was used in subsequent studies.

The fluorescence intensity of Eu-Tb system is a linear function of the concentration in the range 1×10^{-11}–1×10^{-6} M under the recommended conditions. The sensitivity is thus, two orders of magnitude better than that of Eu-TTA-DBC-Triton X-100 system. The detection limit (for an SNR value of 3) is 1.5×10^{-13} M, which is about four orders of magnitude less than that of the Eu-TTA-DBC-Triton X-100 system.

The effect of lighter and middle lanthanides on the fluorescence intensity of Eu-Tb system were studied. At 1×10^{-8} M europium, 10^{-5} M amounts of lanthanum, praseodymium and dysprosium oxides do not interfere. However, *Y* and heavy lanthanides were found to interfere at concentrations $> 10^{-7}$ M. Table 1 shows the results of the determination of europium in certain commercial high purity rare earth oxides and their mixtures.

3.1. Enhancement mechanism

Fig. 2 shows that there is no constant mole ratio between Eu^{3+} and Tb^{3+} in the Eu-Tb-TTA-DBC-Triton X-100 system. Fig. 4 shows that the absorption spectrum of this system is similar to that of the system without terbium. These results show that terbium does not form a new compound with the Eu-TTA-DBC-Triton X-100. It should also be noted that the enhancement effect occurs only in aqueous phase in the presence of surfactants and not in organic solvents (e.g., benzene, *n*-butanol, cyclohexane and TBP).

Table 1
Analysis of high purity rare earth oxides and their mixtures

Rare earth oxides (wt%)	Eu_2O_3 found (wt%)[a]
La_2O_3 (99.9%)	0.007 ± 0.002
Pr_6O_{11} (99.9%)	0.008 ± 0.001
Dy_2O_3 (99.9%)	0.0016 ± 0.002
$La_2O_3 + Pr_6O_{11} + Dy_2O_3$	0.0031 ± 0.002

[a]Mean ± S.D. ($n = 5$)

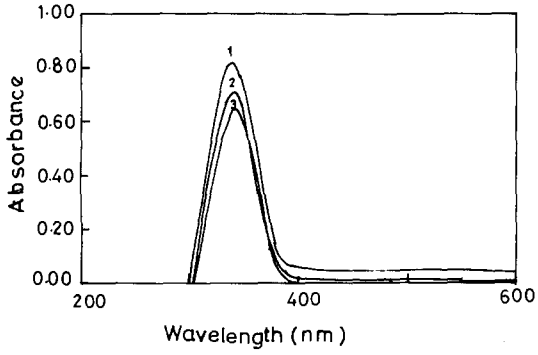

Fig. 4. Absorption spectra: (1) Eu-Tb-TTA-DBC-Triton X-100 system; (2) Tb-TTA-DBC-Triton X-100 system; and (3) Eu-TTA-DBC-Triton X-100 system. Conditions: 1×10^{-7} M, Eu^{3+}, 2.0×10^{-5} M Tb^{3+}, 1.0×10^{-4} M TTA, 1.0×10^{-4} M DBC, 3×10^{-2} M ammonium acetate, 5×10^{-2}% Triton X-100.

The excited singlet states of TTA in these complexes undergo a radiationless transiton to their triplet states. Europium can be excited both by intramolecular energy transfer as suggested by Crosby et al. [6], from the excited triplet state of TTA in the Eu-TTA-1,10-phenanthroline by Tb-benzoic acid due to the wrapping effect [7]. On the other hand, the enhancement in the Eu-TTA-dibenzoylpyridinium ion by yttrium was attributed to the energy transfer from yttrium complex to europium complex [8]. Because the concentration of terbium complex is much greater than that of the europium complex (in the present case) in the Triton X-100 solution, the enhancement effect was a result of two mechanisms, one of which was the wrapping effect of Tb complexes over Eu complexes and the other was intermolecular energy transfer from terbium to europium [9]. Triton X-100 also plays an important role in the dissolution of both complexes and their protection against collision with solvent (water) molecules, which would cause loss of energy.

Acknowledgements

The authors gratefully acknowledge the financial support extended by STED, Government of Kerala.

References

[1] T.K.S. Murthy and C.K. Gupta, Science and Technology of Rare Earth Materials, Academic Press, New York, 1980.
[2] E.L. Dekalb and V.A. Fassel, in K.A. Gschneidner Jr. and L. Eyring (Eds.), Handbook on the Physics and Chemistry of Rare Earths, Vol. 4, Amsterdam, 1979, Ch. 37D.
[3] V. Bhagavathy, T. Prasada Rao and A.D. Damodaran, in K.A. Gschneidner Jr. and L. Eyring (Eds.), Handbook on the Physics and Chemistry of Rare Earths, Vol. 21, Ch. 146, 1995.
[4] Y. Jing-He, Z. Gui-Yun, X. Jing-Hua and Z. Xin-Yong, Proceedings of Second Academic Discussion of Photometry of the Chinese Chemical Society, 3 (1984) 5.
[5] Y. Jing-He, Z. Gui-Yung and W. Bo, Anal. Chim. Acta, 198 (1987) 287.
[6] G.A. Crosby, R.E. Whan and R.M. Alire, J. Chem. Phys., 34 (1961) 744.
[7] W. Li, W. Li, Y. Gui and Q. Wang, J. Alloys Comp., 192 (1993) 34.
[8] L. Gao and B. Chen, Beijing Shifan Daxue Xuebao Ziran Fexuban, 28 (1992) 261.
[9] W. Li, W. Li, G. Yu, Q. Wang and Y. Jui, J. Alloys Comp., 191 (1993) 107.

ELSEVIER

Talanta 44 (1997) 427–441

Talanta

Characterization of associates in ternary mixtures of amines, diprotic acid dyes and quaternary ammonium compounds in dichloromethane and in dichloromethane/water systems

Alberto Hernandez Gainza

Departamento de Quimica-Fisica, Facultad de Farmacia, Universidad de Granada, 18071 Granada, Spain

Received 30 April 1996; received in revised form 27 August 1996; accepted 28 August 1996

Abstract

Ternary mixtures of Bromocresol Green (BCGH), Benzethonium Chloride (BZ^+Cl^-), and Quinine (Q) in dichloromethane (CH_2Cl_2 for ratios $1:\geq 1:\geq 1$ ($BCGH_2$:BZ^+Cl^-:Q) generate species $BCGH^-BZ^+$, BZ^+BCG^--H-Q) and $BCG^{2-}(BZ^+)_2$ in chemical equilibrium; whose thermodynamic parameters are determined. A new method to study ternary mixtures in a non-polar solvent has been given and other amines (A) and quaternary ammonium compounds (QAC) instead of Q and BZ^+Cl^- have also been researched. Species $BCGH^-BZ^+$, and $BCG^{2-}(BZ^+)_2$ are ion associates of 1:1 and 1:2 (dye:BZ^+Cl^-) stoichiometry and species BZ^+BCG^--H-Q presents a hydrogen bond, being of 1:1:1 (dye:BZ^+Cl^-:Q) stoichiometry. The Vis-VU, IR and ^{1}H-NMR spectra of the associates suggest that they are in nature resonance hybrids. A new and fundamental equation which governs extraction of any 1:1:1 associate is deduced and checked experimentally, showing that its extraction depends on the high capacity of the amine to accept hydrogen bonds and the high extractability of the ammonium ion. Extraction of the 1:1:1 associate using different amines and ammonium ions is studied both, experimentally and by the new equation, checking that the 1:1:1 associate containing Q and BZ^+ is selectively extracted due to the fact that Q has a high hydrophobicity and high capacity to form hydrogen bonds and species BZ^+Cl^- has a high ion-associability. Selective extraction of this 1:1:1 associate is useful for quantitative determination in complex mixtures of ammonium ions of high ion associability as BZ^+Cl^-. © 1997 Elsevier Science B.V.

Keywords: Extraction global equation; Ternary associates spectroscopy; Ternary associates theory; Thermodynamic equilibria

1. Introduction

Several methods have been published for the quantitative determination of amines and quaternary ammonium ions, in which acid dyes form colored ion-pairs extractable from the aqueous solution with organic solvents [1–5]. The extract is used spectrophotometrically to determine a trace component in the ion-pair, which is generally of 1:1 stoichiometry (dye:amine or dye:ammonium). A review of this type of analytical methods and of the used ion-association reagents was also published [6]. However, these analysis methods are unspecific. This is a disad-

PII S0039-9140(96)02086-3

vantage and therefore extraction of an 1:1:1 associate (dye:ammonium:quinine) using a diprotic acid dye such as Bromocresol Green ($BCGH_2$) and Quinine (Q) in order to determine quaternary ammonium compounds (QAC) with an enhanced selectivity was proposed [7]. Quinine was only used for enhancing the extractability and selectivity of the 1:1:1 associate, which was identified as the species responsible for the visible absorption band of the extract used for the quantitative determinations; but neither nature of the 1:1:1 species nor the causes for the selective extraction were fully clarified. These problems are now studied for the first time by means of new experimental results and theoretical equations.

At a first stage, ternary mixtures in a single dichloromethane phase of a sulphonphthalein dye, $BCGH_2$, Benzethonium Chloride, BZ^+Cl^-, and Q, in different proportions are investigated for the first time finding new associates of different composition and nature. A new and simple method to study equilibria of three components in a nonpolar solvent from spectrophotometric measurements is now put forward since the known methods were put forward in an aqueous medium [8–10]. Absorption peaks, P, molar absorptivities, ϵ, equilibrium constants, K, and thermodynamic parameters of the complexes obtained in these ternary mixtures are compared with the same data obtained for complexes in $BCGH_2$-Q binary mixtures. Through the comparison between the obtained results in binary and ternary mixtures (P, ϵ, K, etc.), this paper provides new evidences which can be helpful in deciding the controversial points regarding the nature, composition and absorption peaks of the ternary and binary compounds. From this information, it is established why Q can be used for enhancing the selectivity and extractability of some QAC. This paper shows, for the first time, the nature and physicochemical properties of the 1:1:1 associates described in extraction studies using Vis-UV, IR and ^{1}H-NMR data, justifying its importance from an analytical point of view. Resonance of associates is also proposed for the first time to explain some details of the nature of associates obtained in ternary mixtures and their analytical applications.

At a second stage, extraction of associates in ternary mixtures of a sulphonphthalein dye, $BCGH_2$, Benzethonium Chloride, BZ^+Cl^-, and Q, is carried out in dichloromethane/water systems. Extraction of $BCGH_2$-Q and $BCGH_2$-benzethonium binary mixtures is also carried out to compare the associates extracted in the two kinds of mixtures. Then, a new equation, which combines the results of equilibrium among associates in dichloromethane of the first stage and those of extraction of the second one is deduced and checked experimentally using both, data in literature and our own data. This equation demonstrated the importance of studies of formation of ternary associates in the organic phase for extraction studies for the first time from a quantitative point of view and it suggests that extraction of the 1:1:1 ternary associate is a global process of the processes that occur in both phases.

2. Experimental

2.1. Apparatus

All vis-VW spectrophotometric measurements were made on a Perkin–Elmer Lambda 5 spectrophotometer, with a B. Braun AG models Frigomix 1.495 and thermomix 1.441 thermostat with a ± 0.2°C accuracy). Quartz cells of 1 cm with Teflon stoppers were also used. A Radiometer Copenhagen PHM64 Research pH meter was used with a combined electrode for the pH measurements. The electrode was calibrated with standard buffer solutions of pH = 4.00 and pH = 7.03 at 293.16 K unless otherwise stated; the precision of the measurements was of ± 0.01. The ^{1}H-NMR spectra were recorded on a Bruker AM-60 Spectrometer with $CDCl_3$ as solvent. The IR spectra were made on a Perkin-Elmer 298 IR spectrophotometer with potassium bromide pellets. The KBr has been previously dried in an oven at 200°C. All calculations were made with an IBM compatible computer. Some of the substances were dissolved with the help of a Selecta ultrasons ultra sound apparatus.

2.2. Reagents

The reagents used were CH_2Cl_2 (Probus HPLC, with $< 0.02\%$ water content), methanol (Probus HPLC), $BCGH_2$ (Merck), atropine, tropine, homatropine, methylatropine, tetramethylammonium chloride, tetraethylammonium, chloride (Sigma), Q, benzethonium chloride and proton sponge (Fluka-Chemie). All the solid materials were of analytical grade and all amines were used as free bases without further purification after storage in a desiccator with phosphorous pentoxide.

3. Results and discussion

3.1. Absorption spectra, composition and equilibrium constants of associates in dye-quaternary ammonium compound-amine ternary mixtures

This section and the following provide a new method to study the associates obtained in ternary mixtures in a single nonpolar phase. Also an attempt will be made to give an interpretation of the results of the experimental data (as for example the use of the Job's method with three reagents or when a reagent and the product show the same absorption maximum, etc.) and of the calculated constants from these data (as for example molar absorptivities, equilibrium constants and thermodynamic parameters, etc.).

Ternary mixtures of $BCGH_2$, BZ^+Cl^-, and Q, when the concentrations are in the order $[BCGH_2] = [BZ^+Cl^-] \leq [Q]$, that is to say, proportions $1{:}1{:} \geq 1$ ($BCGH_2$:BZ^+Cl^-:Q), present in dichloromethane, CH_2Cl_2, two new absorption bands with maxima at 415 and 630 nm which pass through an isosbestic point as can be seen in Fig. 1A. Also the $BCGH_2$-Q binary mixture shows two absorption bands but with maxima at 415 and 547 nm and an isosbestic point as shown in Fig. 1B. Therefore, the ternary mixture gives an absorption band at 630 nm which does not appear in the binary mixture. Job's method was used to deduce the stoichiometry of the products responsible for the new absorption bands. Job's method for the binary mixture has been carried out by measuring the absorbance at 415 and 547 nm of different proportions of 10^{-4} M solutions of $BCGH_2$ and 10^{-4} M of Q, such that $[BCGH_2] + [Q] = 10^{-4}$ M. The absorbance of these solutions are plotted against the molar fractions of the dye as shown in Fig. 2. The concentrations used in the Job's method for the ternary mixture were identical but differ in that here, the dye has been initially mixed with an equimolar concentration of BZ^-Cl^-. The concentration of this third component has been ignored for the dye molar fraction calculations as could be observed in Fig. 2 where, moreover, it can be seen that curves at 415 nm are identical for both binary and ternary mixtures. The plots in Fig. 2 suggest 2:1 and 1:2 stoichiometries ($BCGH_2$:Q) for the binary mixtures measured at 415 and 547 nm. Accordingly, in the binary mixture the three following processes are assumed as reactions Eqs. (1)–(3); where $BCGH_2$ is the free dye, Q

$$BCGH_2 + Q \rightleftarrows BCGH^-QH^+ \quad (1)$$

$$BCGH^-QH^+ + Q \rightleftarrows QH^+BCG\ \ H-Q \quad (2)$$

$$BCGH^-QH^+ + BCGH_2 \rightleftarrows (BCGH^-)_2QH_2^{2+} \quad (3)$$

quinine base, $(BCGH^-)_2QH_2^{2+}$ and $BCGH^-QH^+$ are the ion associates of 2:1 and 1:1 stoichiometry. The QH^+BCG^--H-Q associate shows a hydrogen bridge and it is of 1:2 stoichiometry (dye:Q). Eqs. (1)–(3) were previously studied from data in binary mixtures [11]. The same stoichiometries of $BCGH_2$ to Q have also been obtained for the ternary mixtures at 415 and 630 nm as can be seen in Fig. 2. The fact that the stoichiometric relation does not vary in the ternary mixture while the absorption maximum does, could be interpreted as follows: in the binary mixture, Eqs. (1) and (2) for absorption at 547 nm and Eqs. (1) and (3) for absorption at 415 nm would justify the observed stoichiometries, and the peaks at 415 and 547 nm would be assigned to the $(BCGH^-)_2QH_2^{2+}$ and QH^+BCG^--H-Q species (Fig. 1B). On the other hand, in the ternary mixture, four processes should be assumed. The first one is given by Eq. (1) and the rest by the following equations:

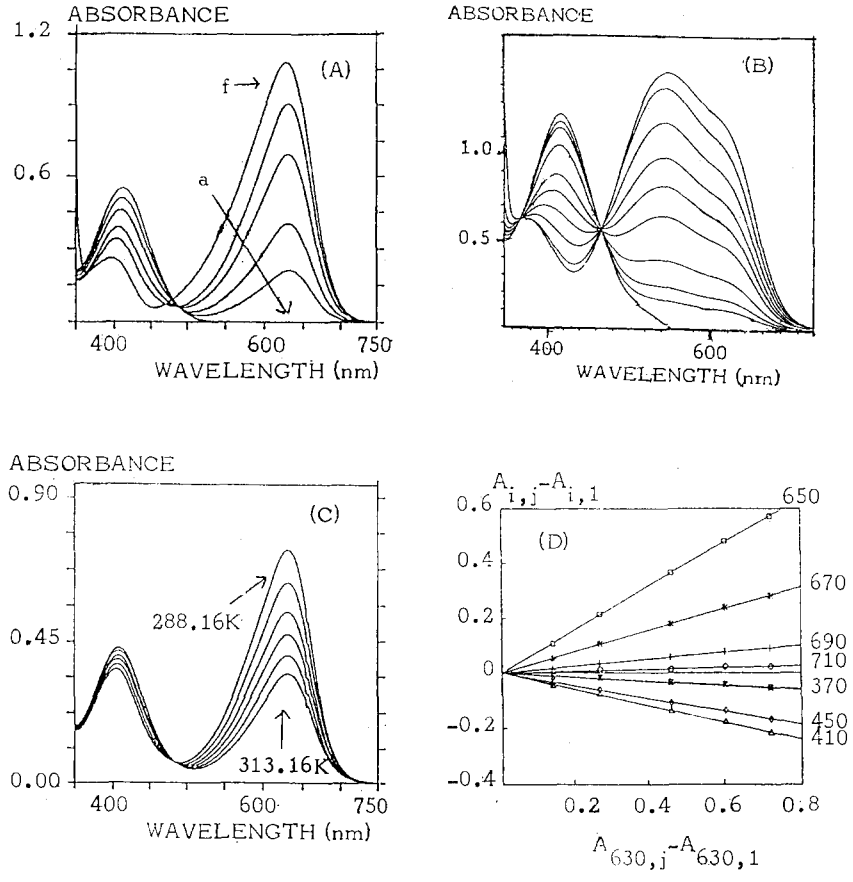

Fig. 1. (A) Visible-ultraviolet spectra of CH_2Cl_2 solutions of Bromocresol Green, $BCGH_2$, 3×10^{-5} M; Benzethonium Chloride, BZ^+Cl^-, 3×10^{-5} M and different concentrations of Quinine, Q, 3 (curve a), 4, 5, 8, 120 and 5000×10^{-5} M (curve f). T = 293.16 K. (B) Visible-ultraviolet spectra of CH_2Cl_2 solutions of $BCGH_2$, 6.6×10^{-5} M and different concentrations of Q, 6.6, 7.7, 8.3, 9.4, 11.8, 14.0, 17.02, 32, 37.9 and 60×10^{-5} M. T = 288.16 K. (C) Visible-ultraviolet spectra of CH_2Cl_2 solutions of $BCGH_2$, 3.4×10^{-5} M; BZ^+Cl^-, 3.4×10^{-5} M and Q, 6.8×10^{-5} M at 288.16, 293.16, 298.16, 303.16, 308.16 and 313.16 K. (D) Coleman's method for two species whose sum of concentrations is constant from the spectral data in Fig. 1A. The numbers correspond to the wavelength, *i*, of the row of the matrix which has been resolved graphically according to Coleman.

$$BCGH^-QH^+ + BZ^+Cl^- \rightleftarrows BCGH^-BZ^+ + Cl^-QH^+ \quad (4)$$

$$BCGH^-BZ^+ + Q \rightleftarrows BZ^+BCG^- - H - Q \quad (5)$$

$$Cl^-QH^+ + BCGH_2 \rightleftarrows BCGH^-Cl^-QH_2^{2+} \quad (6)$$

where Cl^-QH^+ is Q hydrochloride (colourless). Eqs. (1), (4) and (5) justify the 1:2 stoichiometry at 630 nm of the ternary mixture; since the products of Eq. (4) contain dye (species $BCGH^-BZ^+$) and Q (species Cl^-QH^+) in a 1:1 ratio and Eq. (5) consumes one more molecule of Q thereby justifying the 1:2 stoichiometry. As Eqs. (1) and (4) are quantitative [11] (the latter will be shown later), in proportions 1:1: ≥ 1 ($BCG:BZ^+Cl^-:Q$), species $BCGH_2$ and $BCGH^-QH^+$ do not exist in the ternary mixture; therefore, only Eq. (5) will be present in the solution and species $BCGH^-BZ^+$ and BZ^+BCG^--H-Q will justify the absorption maxima at 415 and 630 nm in Fig. 1A. Eqs. (1), (4) and (6) justify the 2:1 stoichiometry at 415 nm in ternary mixtures since the products of Eq. (4) contain dye (species $BCGH^-BZ^+$) and Q (species Cl^-QH^+) in a 1:1 ratio and Eq. (6) con-

sumes one more molecule of dye thereby justifying the 2:1 stoichiometry. The fact that the curve at 415 nm in Fig. 2 is identical for binary and ternary mixtures is justified by identical absorption spectra of $(BCGH^-)_2QH_2^{2+}$, $BCGH^-BZ^+$, $BCGH^-Cl^-QH_2^{2+}$ species (see next paragraph) as well as identical values of equilibrium constants for Eqs. (3) and (6) since in both reactions the same nitrogen of Q and the same proton of the dye are neutralized [11]. Similarly, in ternary mixtures in an excess of dye ($[BCGH_2] > [BZ^+Cl^-] = [Q]$) only Eq. (6) will be present in the solution together with $BCGH^-BZ^+$ species generated by Eq. (4). Eq. (4) is a reaction of ionic exchange, Eq. (5) is the formation of a hydrogen bridge between OH in $BCGH^-BZ^+$ and amino nitrogen in Q, and Eq. (6) is a neutralization reaction whose study was carried out in [11] from dye-Q hydrochloride binary mixtures.

As Eq. (4) is complete, curve 'a' in Fig. 1A, where the three reagents ($BCG:BZ^+Cl^-:Q$) are in a 1:1:1 ratio, is assigned to the $BCGH^-BZ^+$ species generated in Eq. (4). The molar absorptivity of the $BCGH^-BZ^+$ ion pair determined from absorbance value at 415 nm of $BCGH_2$-BZ^+Cl^--Q mixtures in proportions 1:1:1 was $19\,800 \pm 700$ $l \times mol^{-1}\ cm^{-1}$ at 293.16 K. This value is similar

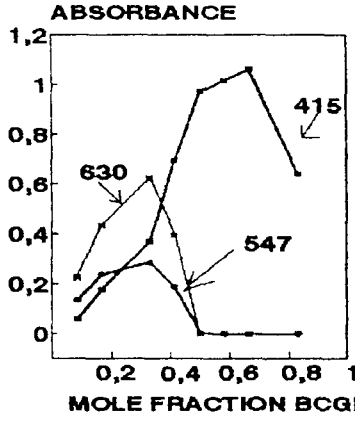

Fig. 2. Continuous variation plots between $BCGH_2$ and Q for the binary mixture ($BCGH_2$-Q: $[BCGH_2] + [Q] = 10^{-4}$ M) at 415 and 547 nm and for the ternary mixture ($BCGH_2$, BZ^+Cl^-, Q: $[BCGH_2] + [Q] = 10^{-4}$ M and $[BCGH_2] = [BZ^+Cl^-]$) at 415 and 630 nm. T = 293.16 K.

to that given before for species $BCGH^-QH^+$ and to those of $BCGH^-$ajmalineH$^+$ and $BCGH^-$homatropineH$^+$ in the same solvent [12] (CH_2Cl_2). Therefore, this value corresponds to the molar absorptivity of the $BCGH^-$ anion in this solvent, ϵ_{BCGH^-} since the cation only acts as the stabilizer of $BCGH^-$ in the nonpolar solvent. Obviously, this value is also similar to that of the molar absorptivity of $BCGH^-Cl^-QH_2^{2+}$ species and it is half the $(BCGH^-)_2QH_2^{2+}$ species determined in [11].

Ternary mixtures corresponding to Fig. 1A, in proportions $1:1:\geq 1$ ($BCGH_2$:BZ^+Cl^-:Q), are cut in an isosbestic point; therefore Eq. (5) is an equilibrium. Fig. 1C shows the displacement of this equilibrium with temperature. Fig. 1D is the Coleman's test [13] from Fig. 1A, which clearly shows two absorbent species whose sum of concentrations is constant in agreement with the already established. An identical result is obtained when the Coleman's test is applied to the spectral curves in Fig. 1C. Eq. (5) satisfies the following prerequisites: (a) is an 1:1 addition reaction; (b) the reagents do not absorb at the maximum absorption of the addition compound; and (c) the addition compound follows Beer's Law. Therefore, the iterative Rosseinsky's method [14], making use of a computer program in TURBOBASIC described previously in [11,12] was used to calculate $K_{BZBCG\text{-}H\text{-}Q}$ ($K_{BZBCG\text{-}H\text{-}Q} = [BZ^+GCG^-\text{-}H\text{-}Q]/[BCGH^-BZ^-][Q]$) of Eq. (5) and the molar absorptivity of BZ^+BCG^--H-Q, $\epsilon_{BZBCG\text{-}H\text{-}Q}$. These constants at several temperatures together with the thermodynamic parameters of Eq. (5) are presented in Table 1. The $\epsilon_{BZBCG\text{-}H\text{-}Q}$ value in Table 1 from equilibrium data is similar to that obtained in curve 'f' on Fig. 1A when a strong excess of Q is added. This suggests that Eq. (4) is highly displaced to the right as indicated before. As Eqs. (1) and (2) also satisfy prerequisites a, b and c; the same method to calculate K_{BCGHQH} (Eq. (1)) and $K_{QHBCG\text{-}H\text{-}Q}$ (Eq. (2)) was used. The K_{BCGHQH} value ($K_{BCGHQH} = [BCGH\ QH^+]/[BCGH_2][Q]$), was $10^{10.82}$ $l \times mol^{-1}$ at 298.16 K. The $K_{QHBCG\text{-}H\text{-}Q}$-value, ($K_{QHBCG\text{-}H\text{-}Q} = [QH^+BCG^-\text{-}H\text{-}Q]/[BCGH^-QH^+][Q]$), molar absorptivity for QH^+BCG^--H-Q, $\epsilon_{QHBCG\text{-}H\text{-}Q}$, and thermodynamic parameters for Eq. (2) are also

Table 1
Physicochemical properties for QH^+BCG^--H-Q, BZ^+BCG^--H-Q, and BCG^{2-} $(BZ^+)_2$ as formed by Eqs. (2), (5) and (7)

Associate	T (K)	K,[a] $l \times mol^{-1}$	ϵ,[a,b]	rmsd,[c]	r^2,[d]
QH^+BCG^--H-Q	287.66	39000 ± 5000	24500 ± 900	0.005	0.998
(Reaction 2)	293.66	26000 ± 3000	24000 ± 1000	0.004	0.999
	298.66	14000 ± 3000	26000 ± 2000	0.007	0.981
	304.66	12000 ± 2000	23000 ± 2000	0.005	0.994
	309.16	9000 ± 2000	23000 ± 2000	0.004	0.992
	313.16	6000 ± 1000	26000 ± 4000	0.005	0.962
$\Delta G° = -23.7 \pm 0.6$[e]; ($\Delta H° = -52 \pm 12$; $\Delta S° = -93 \pm 38$; 0.974)[f]					
BZ^+BCG^--H-Q	293.16	130000 ± 50000	30000 ± 2000	0.004	0.999
(Reaction 5)	298.16	91000 ± 48000	27000 ± 3000	0.004	0.999
	303.16	61000 ± 24000	27000 ± 3000	0.003	0.999
	308.16	49000 ± 32000	25000 ± 4000	0.004	0.998
	313.16	29000 ± 17000	26000 ± 5000	0.003	0.999
$\Delta G° = -28.3 + 2.1$[e]; ($\Delta H° = -56 \pm 11$; $\Delta S° = -92 \pm 36$; 0.996)[f]					
BCG^{2-} $(BZ^+)_2$	288.16	0.21 ± 0.08	24000 ± 1200[g]	0.011	0.999
(Reaction 7)	293.16	0.17 ± 0.05	24000 ± 1100[g]	0.009	0.999
	298.16	0.13 ± 0.02	23500 ± 700[g]	0.005	0.999
	303.16	0.08 ± 0.01	23500 ± 500[g]	0.003	0.999
	308.16	0.06 ± 0.01	24000 ± 900[g]	0.005	0.991
$\Delta G° = -23.8 \pm 0.6$[e]; ($\Delta H° = -52 \pm 12$ $\Delta S° = -93 \pm 38$ 0.974)[f]					

[a] Confidence intervals for a 0.95 level are given.
[b] $L \cdot mol^{-1}$ cm^{-1}.
[c] Root mean squared deviation.
[d] The values of the determination coefficient in a first approximation.
[e] Free energy variations, $\Delta G°$(kJ mol^{-1}), at 298.16 K.
[f] The enthalpy, $\Delta H°$(kJ mol^{-1}), and enthropy, $\Delta S°$ (J K^{-1} mol^{-1}) variations, calculated using the least squares method from van't Hoff plot.
[g] ϵ' Values and confidence intervals for a 0.95 probability.

presented in Table 1. By analogy with Eq. (2) which was studied in [11], Eq. (5) is the formation of a hydrogen bridge and BZ^+BCG^--H-Q species is a 1:1:1 associate because contains dye, Q and ammonium cation in that ratio. Data in Table 1 for QH^+BCG^--H-Q and BZ^+BCG^--H-Q species suggest some interesting points. So, the previous discussion suggests that the two species are Hydrogen Bonded Complexes (HBC) and an ordinary HBC will not show [15–17], a) high K and $\Delta H°$-values (see Table 1); high visible peak (630 nm) and high molar absorptivity (Table 1). Resonance hybrid of the hydrogen-bonded structure in a later section (see Scheme 1) could be responsible for these results which indicate that this type of HBC is very stable.

Reactions of the type (2) and (5) were also carried out using other amines (A) and QAC following the same methods given for Q and benzethonium. The $K_{AHBCG\text{-}H\text{-}A}$-values using different amines together the absorption maximum

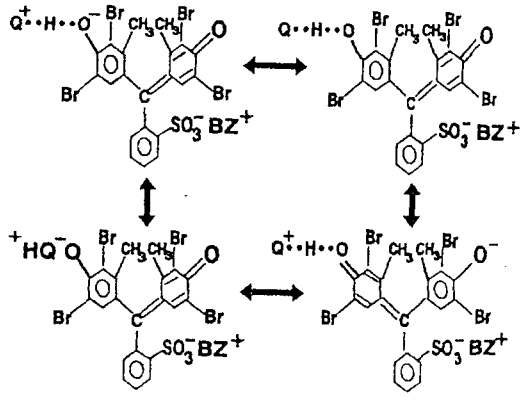

Scheme 1.

Table 2
Association constants, K, and extraction constants, E, of 1:1:1 associates using $BCGH_2$ and different amines and quaternary ammonium compounds by Eq. (14)

Substance	$K^a_{AHBCG\text{-}H\text{-}A}$	λ^b_{max}	$K^a_{BZBCG\text{-}H\text{-}A}$	$k^a_{d(A)}$	$E^a_{BZBCG\text{-}H\text{-}A}$	pK_{AH^+}
Tropine	4.48	585	4.96	−0.27	7.58	10.73
Quinine	4.41	547	5.11	2.04	12.47	8.30
Atropine	3.77	575	4.25	2.69	10.35	10.21
Homatropine	3.60	575	4.07	2.47	10.10	10.10
Proton Sponge	1.28	630	1.28	–	–	12.00
	log $K_{QACBCG\text{-}H\text{-}Q}$		log $E_{BCGHQAC}$		log $E_{QACBCG\text{-}H\text{-}Q}$	
Tetramethylammonium	4.70		1.50		4.60	
Tetraethylammonium	4.81		3.02		6.33	
Methylatropine	4.86		4.69		7.95	
Benzethonium	5.11		8.96		12.47	

$K^{-1}_{BCGH} = 10^{4.66}$; T = 298.16 K.
[a] Logarithm of these constants.
[b] Wavelength in nm of AH^+BCG^--H-A species.

of every one of the AH^+BCG^--H-A associates (λ_{max}) the $K_{BZBCG\text{-}H\text{-}A}$ values corresponding to associates formation of type BZ^+BCG^--H-A (in these cases λ_{max} is always 630 nm) are given in the upper part of Table 2. It can be seen that the 1:1:1 associate (species BZ^+BCG^--H-A) is always more stable than the 1:2 associate (species AH^+BCG^--H-A) and that the increase from $K_{AHBCG\text{-}H\text{-}A}$ to $K_{BZBCG\text{-}H\text{-}A}$ is related to λ_{max}. So, the increase maximum ($K_{BZBCG\text{-}H\text{-}A} = 5K_{AHBCG\text{-}H\text{-}A}$) is obtained with Q of $\lambda_{max} = 547$ nm, the lowest wavelength of all the amines, and with proton sponge of $\lambda_{max} = 630$ nm, the highest one, there is no increase ($K_{AHBCG\text{-}H\text{-}A} = K_{BZBCG\text{-}H\text{-}A}$). In a later section will be shown the double nature Hydrogen Bond Complex (HBC)-Ion Associate of this type of associates and as the character HBC increases when decreases λ_{max}. With proton sponge there is no increase because it can not form hydrogen bonds with the dye due to its particular structure [15,16], so that in this case Eqs. (2) and (5) are two neutralizations, which explains the low values of $K_{AHBCG\text{-}H\text{-}A} = K_{BZBCG\text{-}H\text{-}A} = 19\ 1 \times mol^{-1}$. The increase from $K_{AHBCG\text{-}H\text{-}A}$–$K_{BZBCG\text{-}H\text{-}A}$ in the HBC means that $BCGH^-BZ^+$ shows more ability than $BCGH^-AH^+$ species to form a hydrogen bridge through OH-phenol with the amine. Since the component dye is the same in the two associates (BCG^--H-Q), this must be due to the different nature of the cation (AH^+ or BZ^+). So, the positive charge in molecular structure of benzethonium cation, BZ^+, is buried or sterically hindered which would lead to an increase in the planarity of the dye ring system and to an easier formation of the hydrogen bridge (also this would explain the bathochromic effect when QH^+ is replaced by BZ^+). On the other hand, in AH^+ the positive charge is exposed to the molecular surface of the cation which could decrease the planarity of the dye ring system giving an associate with a lower λ_{max} and would make the formation of the hydrogen bridge more difficult. Moreover, the two protons in $BCGH^-AH^+$ could interchange which would make the formation of a hydrogen bridge with another Q molecule more difficult. This proton interchange is not possible in the $BCGH^-BZ^+$ species.

In Table 2 (upper part), it can be seen that ability to form hydrogen bonds, measured by $K_{AHBCG\text{-}H\text{-}A}$ or $K_{BZBCG\text{-}H\text{-}A}$ value, is related to the amine basicity which, could be measured by its pK_{AH^+} value in water. However, structure is also important since Q is less basic than atropine and homatropine in water and it has a higher capacity to form a hydrogen bridge; and proton sponge is the more basic of all amines and can not form hydrogen bonds. On the other hand, $K_{QACBCG\text{-}H\text{-}Q}$-

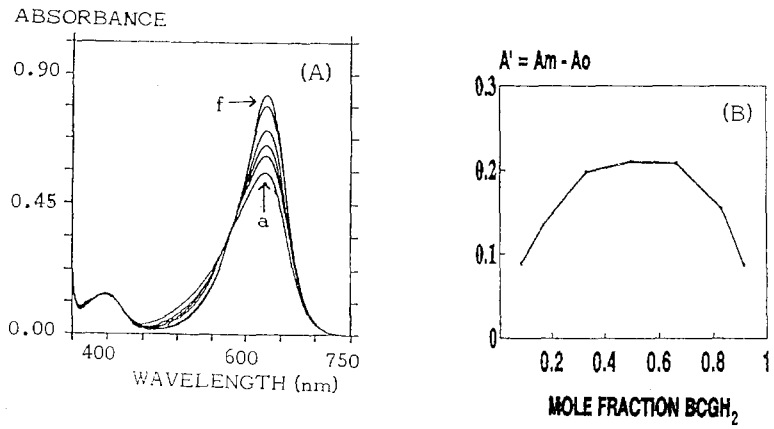

Fig. 3. (A) Visible-ultraviolet spectra of CH_2Cl_2 solutions of $BCGH_2$, 1.5×10^{-5} M; Q 2×10^{-3} M and different concentrations of BZ^+Cl^-, 1.5 (curve a), 4.5 (b), 10.4 (c), 23.7 (d), 79.4 (e), 150.2×10^{-6} M (curve f). T = 288.16 K. (B) Continuous variation plot for the reaction of BZ^+ BCG-H-Q with BZ^+Cl^-, in CH_2Cl_2. T = 288.16 K.

values with various ammonium ions using Q are also given in Table 2 (lower part). It can be seen that the highest increase from $K_{QHBCG\text{-}H\text{-}Q}$ – $K_{QACBCG\text{-}H\text{-}Q}$ is obtained when QAC is benzethonium (five times). This is consistent with the fact that the positive charge in molecular structure of BZ^+ is stronger buried or sterically hindered than in the other ammonium ions.

3.2. Ternary mixtures in an excess of benzethonium chloride

Until now, only one benzethonium cation, BZ^+, has been taking part in the described complexes. This is due to the fact that the anterior experiments have been carried out with an equimolar concentration of $BCGH_2$ and BZ^+Cl^-. In order to obtain and study in solution the $BCG^{2-}(BZ^+)_2$ ion associate, a ternary mixture of ratios $1{:}1{:}\gg 1$ ($[BCGH_2] = [BZ^+Cl^-] \ll [Q]$), at a concentration of Q sufficient to ensure the complete formation of BZ^+BCG^--H-Q species by Eq. (5), was registered (curve 'a' in Fig. 3A). To avoid the side reaction of the solvent due to the excess of Q [18], this solution was freshly prepared every time. Then increasing amounts of BZ^+Cl^- were added to the solution and the spectrum registered each time BZ^+Cl^- is added (b–f in Fig. 3A). These spectra showed an increase in absorbance at 630 nm while the maximum wavelength of absorption remained unvariable. This absorbance increase is attributed to the presence of a new species in the solution, the $BCG^{2-}(BZ^+)_2$ ion associate which, although with the same maximum wavelength as BZ^+BCG^--H-Q, has a higher molar absorptivity, and $\epsilon_{BCG(BZ)_2}$. This new species is formed after the breaking of the hydrogen bridge of the BZ^+BCG^--H-Q species as suggested by Eq. (7).

$$BZ^+BCG^- - H - Q + BZ^+Cl^- \rightleftarrows BCG^{2-}(BZ^+)_2 + Cl^-QH^+ \quad (7)$$

To demonstrate that in proportions $1{:}>1{:}\gg 1$ ($[BCGH_2] < [BZ^+Cl^-] \ll [Q]$), Eq. (7) is present in the solution. Job's method was used, following the guidelines explained in a previous paper [19] which takes into account the complete overlapping of the band of the reagent, BZ^+BCG^--H-Q, and the product, $BCG^{2-}(BZ^+)_2$. In accordance with the instructions given there [19], the Lambert-Beer can be expressed here as $A' = A_m - A_0 = x\ (\epsilon_{BCGBZ_2} - \epsilon_{BZBCG\text{-}H\text{-}Q}) = x\epsilon'$. A_m is the experimental absorbance of the system given by Eq. (7); A_0 is the absorbance due to the BZ^+BCG^--H-Q species this being equal to the total (or initial) dye concentration, $C^0_{BCGH_2}$, in the experiment multiplied by the molar absorptivity of the BZ^+BCG^--H-Q species ($A_0 = \epsilon_{BZBCG\text{-}H\text{-}Q}\ C^0_{BCGH_2}$. A_0 is equally to the absorbance found in a previous identical experiment where the species

BZ^+Cl^- is excluded; 'x' is the concentration of the products of Eq. (7), $\epsilon_{BCG(BZ)_2}$ the molar absorptivity of $BCG^{2-}(BZ^+)_2$ and $\epsilon_{BZBCG\text{-}H\text{-}Q}$ the molar absorptivity of the BZ^+BCG^--H-Q species. The difference between and $\epsilon_{BCG(BZ)_2}$ and $\epsilon_{BZBCG\text{-}H\text{-}Q}$ is the ϵ' value. To determine the stoichiometry of BZ^+BCG^--H-Q to BZ^+Cl^-, solutions of $BCGH_2$-BZ^+Cl^- and excess of Q (being $C^0_{BCGH_2} = C^0_{BZCl} \ll C^0_Q$ the BZ^+BCG^--H-Q species is generated immediately) were mixed with solutions of BZ^+Cl^-, such that $[BZ^+BCG^-\text{-H-Q}] + [BZ^+Cl^-] = 5.6 \times 10^{-5}$ M and their absorbances, A_m, measured at 630 nm. The stoichiometric balance of BZ^+BCG^--H-Q–BZ^+Cl^- was determined by plotting A′ values against the mole fraction of the $BCGH_2$ (equal to mole fraction of BZ^+BCG^--H-Q) as can be seen in Fig. 3B. The stoichiometry was always 1:1, which demonstrates that Eq. (7) is present in the solution.

Isoosbestic point in Fig. 3A and Coleman's test as used before suggest that Eq. (7) is a chemical equilibrium. The equilibrium constant of Eq. (7), $K_{BCG(BZ)_2} = [BCG^{2-}(BZ^+)_2]\,[Cl^-QH^+]/[BZ^+BCG^-\text{-H-Q}]\,[BZ^+Cl^-]$ and the molar absorptivity of the new ion associate could also be determined simultaneously from the values of the corrected absorbance, A′, and the concentrations of the reagents following an iterative method previously given for reactions of type $A + B \rightleftarrows C + D$, where A and C are exclusively absorbent [19]. The $K_{BCG(BZ)_2}$, ϵ' and thermodynamic parameters from the plot of $\ln K_{BCG(BZ)_2}\epsilon'$ against 1/T, the van't Hoff alternative plot [20,21], are given in Table 1 together with statistical indices. From ϵ' values in Table 1, $\epsilon_{BCG(BZ)_2} = 52\,000 \pm 4000$ l mol^{-1} cm at 298.16 K, was calculated being similar to that obtained by displacing Eq. (7) to the right with an strong excess of BZ^+Cl^- (curve 'f' in Fig. 3A). This last spectrum corresponds to the $BCG^{2-}(BZ^+)_2$ species. As the absorption peak and molar absorptivity of this species are similar to those of BCG^{2-}(ammonium$^+$)$_2$ using other ammonium ions, such as tetrabutylammonium or tetrapentylammonium (and to those of the BCG^{2-} anion in water [22]); thus, spectrum of $BCG^{2-}(BZ^+)_2$ species in CH_2Cl_2 is only due to the BCG^{2-} anion and ammonium ion only acts as the stabilizer of BCG^{2-} in the nonpolar solvent. Data on Table 1 suggest that $BCG^{2-}(BZ^+)_2$ species is not very stable and enthalpy and enthropy changes are similar to those usually observed in the ordinary ion-association formation reactions [16,17].

3.3. Resonance, nature and structure of associates

This section attempts to go further into this matter using new spectral data as such as IR and H^1-NMR spectra and also information from literature.

Resonance of associates, in particular that of the QH^+BCG^--H-Q and BZ^+BCG^--H-Q species, must be introduced to explain some of their properties of great analytical importance which were shown in the previous sections. Canonical resonance structures of $BCGH^-$ and BCG^{2-} anions in dichloromethane ($BCGH^-QH^+$, $BCGH^-BZ^+$, $BCGH^-Cl^-QH_2^{2+}$, $(BCGH^-)_2QH_2^{2+}$ and $BCG^{2-}(BZ^+)_2$ species) could be similar to those described in literature for both anions in water [29] because in dichloromethane cations of ion associates only act as the stabilizer of the anions as discussed before. So, visible absorption for $BCGH^-$ ion associates in dichloromethane would be mainly due to an one-sided quinonoid ring system and absorption for $BCGH^{2-}$ ion associates would be due to symmetrical structures with two alternative quinonoid rings as in water. These symmetrical ones are always more stable than the asymmetrical ones which would justify the peak at higher wavelength and the higher molar absorptivity of BCG^{2-} ion associates, (630 nm, $\epsilon_{BCG^{2-}} = 52\,000 \pm 4000$ l × mol^{-1} cm^{-1} at 298.16 K (Section 3.2) in dichloromethane, compared with that of the $BCGH^-$ anion (415 nm and $\epsilon_{BCGH^-} = 19\,500 \pm 500$ l × mol^{-1} cm^{-1} at 298.16 K) in the same solvent. The IR (KBr-disc) and H^1-NMR ($CDCl_3$) peaks of $BCGH^-QH^+$, $BCGH^-BZ^+$, $BCGH^-Cl^-QH_2^{2+}$, $(BCGH^-)_2QH_2^{2+}$ and $BCG^{2-}(BZ^+)_2$ associates are in agreement with the nature before assigned to these species. These associates were obtained at solid state by direct precipitation in water at pH = 1.5 and after recrystallized following a similar method to that

described previously [24] ($BCG^{2-}(BZ^{+})_2$ associate was obtained at pH = 9). So, IR spectra of associates containing Q show an absorption peak at 2580 cm^{-1} being similar to that shown by Q hydrochloride which according to literature [25] is assigned to ^{+}NH (quinuclidine). Therefore, the nitrogen of associates of Q is guaternary and they are ion associates in agreement with that previously discussed. The IR peak at 3480 cm^{-1} assigned to O–H in $BCGH_2$ or to $BCGH^{-}$ associates (KBr-disc) disappears in the $BCG^{2-}(BZ^{+})_2$ spectrum suggesting the presence of BCG^{2-} in the species and, therefore, confirming that it is in nature an ion associate, also in agreement with that previously discussed. Identical confirmation for associates nature containing Q was obtained by the ^{1}H-NMR spectra since these associates presented peaks at 3.20 (quartet), 2.03 (broad singlet) and 1.27 (broad triplet) ppm which are similar to those to the hydrogens of quinuclidine in Q hydrochloride [25]. This also suggests that the nitrogen of these associates is quaternary and that the hydrogen is completely transferred from the dye to Q.

Vis-UV absorption peaks and molar absorptivities in CH_2Cl_2 of ternary associates ($QH^{+}BCG^{-}$-H-Q, $BZ^{+}BCG^{-}$-H-Q and $BCG^{2-}(BZ^{+})_2$) are summarized in Table 3. These data justify the nature assigned to each and every of these species. Species $QH^{+}BCG^{-}$-H-Q, $BZ^{+}BCG^{-}$-H-Q have similar molar absorptivity but lower than that of BCG^{2-} anion (or $BCG^{2-}(BZ^{+})_2$ species), therefore, they do not contain the BCG^{2-} anion; they have a hydrogen bond. Different absorption peaks of $QH^{+}BCG^{-}$-H-Q and $BZ^{+}BCG^{-}$-H-Q associates in Table 2 could be explained by the different nature of the cation (QH^{+} or BZ^{+}). When a more polar solvent is used (acetone or ethanol) absorption peak and molar absorptivity of $QH^{+}BCG^{-}$-H-Q increases until it reaches that of the BCG^{2-} anion, in agreement with that in more polar solvents BCG^{2-} anion should be present. When this last experiment is carried out with $BZ^{+}BCG^{-}$-H-Q only molar absorptivity increases to reach that of the BCG^{2-} anion. Although species $BZ^{+}BCG^{-}$-H-Q (a 1:1:1 associate) is a HBC it has its peak at the same wavelength as the BCG^{2-} anion, so that their canonical resonance structures must contain both, BCG^{2-} anions and hydrogen bonds as shown in Scheme 1. Bottom left structure shows a BCG^{2-} anion and the other three structures show a HBC. This suggests that $BZ^{+}BCG^{-}$-H-Q species is of complex nature. As $\epsilon_{BCG^{2-}}$ is approximately equal to $2\epsilon_{BZBCG\text{-}H\text{-}Q}$ $BZ^{+}BCG^{-}$-H-Q species is mainly a HBC, although in a less proportion than $QH^{+}BCG^{-}$-H-Q species whose absorption peak and $\epsilon_{QHBCG\text{-}H\text{-}Q}$ indicate a purer hydrogen bond. Species $QH^{+}BCG^{-}$-H-Q is also of complex nature since its spectrum shows a shoulder at 630 nm in addition to the peaks at 415 and 547 nm as it can be seen in Fig. 1B, however, it is in a much higher proportion than $BZ^{+}BCG^{-}$-H-Q species a HBC (their canonical resonance structures are similar to those in Scheme 1 but substituting BZ^{+} by QH^{+}). Resonance hybrid of the H-bonded structure of the two ternary associates could justify their particular physicochemical properties as discussed before. An additional and complementary explanation for the batho- and hyperchromicity of associates containing BZ^{+} against to those containing QH^{+} (see Table 3) is that the substitution of BZ^{+} by QH^{+} increases the planarity of the dye ring system as explained in the previous section.

To obtain further information of the bond nature of ternary associates in $QH^{+}BCG^{-}$-H-Q and $BZ^{+}BCG^{-}$-H-Q species their ^{1}H-NMR spectra in $CDCl_3$ were recorded using TMS as an internal reference. Species were obtained in $CDCl_3$ by Eqs. (2) and (5). Peaks of hydrogens of quinuclidine in Q hydrochloride according to literature [25] appear at 3.20 (quartet), 2.03 (broad singlet) and 1.27 (broad triplet) ppm and peaks of Q free base appear at 3.00 (quartet), 1.75 (broad singlet). Peaks of ternary associates, obtained by

Table 3
Visible absorption maxima, λ_{max}, and molar absorptivities, ϵ, of ternary associates in CH_2Cl_2

Associate	λ_{max} (nm)	ϵ(L·mol^{-1} cm^{-1})
$QH^{+}BCG^{-}$-H-Q	547	26000 ± 2000
$BZ^{+}BCG^{-}$-H-Q	630	27000 ± 3000
$BCG^{2-}(BZ^{+})_2$	630	52000 ± 4000

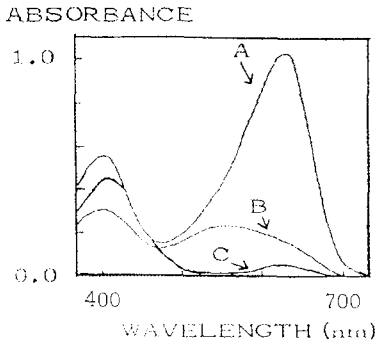

Fig. 4. Visible absorption spectra of dichloromethane phase of after extracting 100 ml of aqueous phase at pH = 8.4 with 10 ml of CH_2Cl_2 (CH_2Cl_2 reference). (A) Aqueous phase: $[BCGH_2] = 1.5 \times 10^{-4}$ M, $[BZ^+Cl^-] = 4 \times 10^{-6}$ M and $[Q] = 1.4 \times 10^{-5}$ M. (B) $[BCGH_2] = 1.5 \times 10^{-4}$ M and $[Q] = 1.4 \times 10^{-5}$ M. (C) $[BCGH_2] = 1.5 - 10^{-4}$ M and $[BZ^+Cl^-] = 4 \times 10^{-6}$ M. T = 293.16 K.

Eqs. (2) and (5) at 283.16 K, to increase the formation of these associates ($\Delta H°$ is negative), are close to those of Q hydrochloride suggesting that the amino nitrogen is almost quaternary so that a strong hydrogen bonding would probably be involved.

3.4. Extraction of associates in dichloromethane/water systems and its relation with the process in each phases

The present theory on extraction of ternary associates [7,26–28] cannot explain the relation between the extraction process and the processes which occur in each phase. In the following discussion an attempt will be made to deduce an equation which combines all the processes and to check it experimentally from our data and by the use of the data from literature.

Absorption spectra of dichloromethane phase after extracting from an aqueous phase containing a binary mixture ($BCGH_2$-Q or $BCGH_2$-BZ^+Cl^-) and a ternary mixture ($BCGH_2$-BZ^+Cl^--Q) at pH = 8.4 (ionic strength = 0.1) are presented on Fig. 4. Curve 'C' on this figure, corresponding to the $BCGH_2$-BZ^-Cl^- binary mixture, shows two peaks with maxima at 415 and 630 nm. If extraction of this mixture is carried out at pH = 4.7 then only absorption at 415 nm would be observed [1]. On the other hand, at pH = 12 only absorption at 630 nm will appear [26]. Spectra of the dichloromethane phase at pH = 4.7 and 12 are similar to those of the $BCGH^-BZ^+$ and $BCG^{2-}(BZ^+)_2$ species obtained in previous sections. Therefore, curve 'C' in Fig. 4 corresponds to a mixture of the two species in the dichloromethane phase. Similarly, curve 'B' corresponds to a mixture of $BCGH^-QH^+$ and QH^+ BCG^--H-QH species. The spectrum corresponding to the ternary mixture on Fig. 4 (curve 'A') is similar to that of the BZ^+BCG^--H-Q species (the 1:1:1 associate) obtained before, which indicates that curve 'A' corresponds to this species. Therefore, species obtained by extraction can also be obtained by reaction in a single dichloromethane phase. This, last method makes it study easier. For example, our work confirms a 1:1:1 stoichiometry for associate extracted from ternary mixture (curve 'A') which was unclear from other extraction studies [7]. Although stoichiometry of associates in binary extraction studies was clear, this one is confirmed again in this paper by study in a single dichloromethane phase. The nature and structure of associates is also described better by this method as shown in the previous sections. Other advantages of studying associates in a single organic phase will be shown later.

The extraction constant for the Q, E_Q, in the partition experiment could be defined by Eq. (8):

$$E_Q = [Q]_{org}[H^+]/[QH^+] = k_{d(Q)}K_{QH^+} \quad (8)$$

being $[Q]_{org}$ the Q concentration in organic phase, $[H^+]$ and $[QH^+]$ are the concentrations of those species in aqueous phase in a partition experiment using only Q. The extraction constant, E_Q, is a true constant since it can also be written as the product $k_{d(Q)}K_{QH^+}$, being K_{QH^+} the second dissociation constant acid in water, w, for Q ($K_{QH^+} = [Q]_w[H^+]/[QH^-]$) and $k_{d(Q)}$ its partition coefficient defined by $k_{d(Q)} = [Q]_{org}/[Q]_w$. Therefore, extraction constant, E_Q, represents a global constant of the two processes. As in literature the product $k_{d(Q)}K_{QH^+}$ (equal to E_Q) is $10^{-6.26}$ mol × l^{-1} in the dichloromethane/water system [2]; experiments of partition with only guinine were not necessary to be carried out.

The extraction constant of the $BCGH^-BZ^+$ ion pair, E_{BCGHBZ}, could be written by Eq.:

$$E_{BCGHBZ} = [BCGH^-QH^+]_{org}/[BCGH^-][BZ^+] \quad (9)$$

where $[BCGH^-BZ^+]_{org}$ is the concentration of the ion pair in organic phase, $[BCGH^-]$ and $[BZ^+]$ are the concentrations of these species in aqueous phase. The E_{BCGHBZ} value was determined by partition experiments in dichloromethane/water systems containing dye and BZ^+Cl^- at various pH from 5 to 7, according to Schill method described for Bromothymol Blue [2]. The value obtained was $10^{8.96}$ $l \times mol^{-1}$.

Extraction constants for ternary associates (QH^+BCG^--H-Q, BZ^+BCG^--H-Q and $BCGZ^{2-}(BZ^+)_2$) into a two phase system would be

$$E_{QHBCG-H-Q} = \frac{[QH^+BCG^- - H - Q]_{org}}{[BCG^{2-}][QH^+]^2} \quad (10)$$

$$E_{BZBCG-H-Q} = \frac{[BZ^+BCG^- - H - Q]_{org}}{[BCG^{2-}][BZ^+][QH^+]} \quad (11)$$

$$E_{BCG(BZ)_2} = \frac{[BGC^{2-}(BZ^+)_2]_{org}}{[BCG^{2-}][BZ^+]^2} \quad (12)$$

where $[]_{org}$ is the concentration of the associate in organic phase and [] is the concentration of the species in aqueous phase. A very useful decomposition for $E_{BZBCG-H-Q}$ is given by the following equation:

$$E_{BZBCG-H-Q} = E_{BCGHBZ}E_Q K_{BZBCG-H-Q}K^{-1}_{BCGH} - \quad (13)$$

where $K^{-1}_{BCGH} - (K^{-1}_{BCGH} - = [BCGH^-]/[BCG^{2-}][H^+])$ is the inverse of the second dissociation acid constant of $BCGH_2$ which is [23] $10^{4.66}$ $mol \times l^{-1}$. Eq. (13) is obviously satisfied since it really corresponds to a decomposition of the extraction constant, which must be considered the global constant of all processes into the two phases. Eq. (13) shows the important and quantitative relation between the extraction process of the 1:1:1 ternary associate and that of association ($K_{BZBCG-H-Q}$) which was studied in a previous section. By this equation $E_{BZBCG-H-QH}$ was $10^{12.47}$ $l \times mol^{-1}$. An approximate calculation for $E_{QHBCG-H-Q}$ and $E_{BCG(BZ)_2}$ from data on Fig. 4 leads to, $10^{10.81}$ and $10^{4.04}$ $l \times mol^{-1}$. Therefore, $E_{BZBCG-H-QH} > E_{HBCG-H-Q} > E_{BCG(BZ)_2}$. Eq. (13) can be generalized for any dye (DH_2), amine (A) and QAC as shown in Eq. (14), which will be discussed in the next section.

$$E_{QACD-H-A} = E_{DHQAC}E_A K_{QACD-H-Q}K^{-1}_{DH} - \quad (14)$$

3.5. Analytical applications. The high extractability and selectivity of 1:1:1 associates containing Q

In the following discussion an attempt will be made to explain different extractabilities of the ternary associates from a qualitative point of view by the use of theories from literature and from a quantitative point of view by the Eq. (14) deduced before.

High extractability of BZ^+BCG^--H-Q species in comparison with the other ones in Fig. 4 for the ternary mixture at pH = 8.4 is the great analytical interest and can be explained by three factors. The first one is the high pH level at which the divalent anion, BCG^{2-}, will be present in the aqueous phase, so that extraction of associates of $BCGH^-$ (yellow associates) must be poor as shown in this figure and discussed in the last section. The second one, the different nature of the ternary associates (QH^+BCG^--H-Q, BZ^+BCG^--H-Q and BCG^{2-} $(BZ^+)_2$ species) which justifies that $E_{BCG(BZ)_2}$ value and therefore extractability of BCG^{2-} $(BZ^+)_2$ species is the lowest of the three ternary associates. So, BCG^{2-} $(BZ^+)_2$ species is in nature an ion associate of a divalent anion, therefore less extractable than QH^+BCG^--H-Q and BZ^+BCG^--H-Q species, in which the dye acts almost as monovalent (BCG^--H-Q) due to the hydrogen bridge with Q. Associates of a divalent anion are less extractable because they attach strongly water molecules by their two charges in the aqueous phase which must be released after neutralization with the two cations. The release of water molecules and extraction of the ion-associate is easier with a monovalent anion since water molecules are more weakly attached in this last case [6]. The third

factor, is the different cation in QH^+BCG^--H-Q and BZ^+BCG^--H-Q species which must justify that $E_{BZBCG\text{-}H\text{-}QH} > E_{QHBCG\text{-}H\text{-}Q}$, since they have the same anion (BCG^--H-Q). So, in benzethonium cation, BZ^+, water molecules can not approach the cationic nitrogen, because the nitrogen atom is surrounded by bulky groups therefore, according to literature this kind of cation will show high ion-associability and its ion associate with univalent anion (BCG^--H-Q) will be easily extracted. On the other hand, in protonated Q, QH^+, the charge is jutting out into water and is slightly hydrated which will hinder the extraction of its ion associate with the anion BCG^--H-Q. This explains that extractability of BZ^+BCG^--H-Q be higher than QH^+BCG^--H-Q and consequently $E_{BZBCG\text{-}H\text{-}Q} > E_{QHBCG\text{-}H\text{-}Q}$. Moreover, at pH = 8.4 (Fig. 4), extraction of QH^+BCG^--H-Q species is difficult because $[QH^+]$ will be low in aqueous phase ($pK_{QH^+} = 8.3$) and, in Eq. (10), $[QH^+BCG^-\text{-H-Q}]$ depends on $[QH^+]^2$.

Eq. (13) or Eq. (14) is the fundamental equation for extraction of any 1:1:1 associate. It shows that if the same dye and amine are used (for example $BCGH_2$ and Q); extraction of 1:1:1 species is mainly based on the high extractability of the ammonium cation (high $E_{BCGHQAC}$-value) and on the strength of the hydrogen bond between the second proton of the dye and amine ($K_{QACBCG\text{-}H\text{-}Q}$ -value in this example) since the product $E_Q K_{BCGH}^{-1}$ in Eq. (14) (A is Q and D is $BCGH_2$) is identical for all the QAC. In the lower part in Table 2 are given $E_{BCGHQAC}$ (obtained in similar way to E_{BCGHBZ}), and $K_{QACBCG\text{-}H\text{-}Q}$ and, from these constants, $E_{QACBCG\text{-}H\text{-}Q}$ values were computed by Eq. (14) using different QAC. The low $E_{QACBCG\text{-}H\text{-}Q}$ values, except when Benzethonium was used, indicated that extraction of ammonium ions of short chains as 1:1:1 associates is negligible. On the other hand, in the upper part in Table 2, extraction constants, $E_{BZBCG\text{-}H\text{-}A}$, for different amines using Benzethonium and $BCGH_2$ were also calculated by Eq. (14) (E_A and $K_{BZBCG\text{-}H\text{-}A}$ determined by the same method given for Q in previous sections). The low values of $E_{BZBCG\text{-}H\text{-}A}$ indicate that extraction of amines as 1:1:1 associates must be negligible except when Q is used. Both, not interference of amines and QAC were experimentally confirmed because spectrum of ternary mixture on Fig. 4 did not change after addition of amines and ammonium ions of Table 2 in the usual concentration ranges of the analytical methods. These results show why using Q high extractability and selectivity of 1:1:1 species containing benzethonium is obtained and they also explain why benzethonium could be quantitative determined using the two phase method without interference of some other amines and QAC [7]. This analytical method for QAC, based on extraction of a 1:1:1 species, is very important because of its enhanced selectivity since this is the main problem of this type of analytical methods in the literature [28–30].

As before mentioned, according to Eq. (14) if $BCGH_2$ is used, high extractability of an 1:1:1 species is based on high values for $K_{QACBCG\text{-}H\text{-}A}$ and $E_A = k_{d(A)}K_{AH^+}$. Q provides the best values for the three constants because Q with low pK_{QH^+} (high K_{QH^+}) has a high capacity to form hydrogen bridges (high $K_{QHBCG\text{-}H\text{-}Q}$ or $K_{BZBCG\text{-}H\text{-}Q}$ values) having, moreover, a high $k_{d(Q)}$ (Table 2). In Table 2, tropine ($pK_{AH^+} = 11.73$) has a higher $K_{AHBCG\text{-}H\text{-}A}$ value than Q but its pK_{AH^+} is much higher and its $k_{d(A)}$ is lower so that, taken into account Eq. (14), its 1:1:1 ternary associate will not be extracted (see in Table 2 its low $E_{BZBCG\text{-}H\text{-}A}$-value). Although in the future other amine with better values of the three constant than Q could be found, extraction of its 1:1:1 associate will not be selective among QAC of similar extractability (as for example Benzalkonium or tetrapentylammonium) because according to Eq. (14), $E_{QACD\text{-}H\text{-}A}$ will be similar with similar ammonium compounds. This limitation is inherent to the procedure of determination of QAC based on extraction of a 1:1:1 associate using any amine and dye. Consequently, although by this method the selectivity is enhanced, it presents the general limitation of the analytical methods based on the extraction of ion associates.

Finally, Eq. (14) also permits to study other dyes, moreover $BCGH_2$. But when K_{DH}^{-1}- increases, $K_{BZD\text{-}H\text{-}A}$ decreases and conversely; so that, according to Eq. (14), other dyes do not improve much the quantitative determination of Benzethonium (or other ions of similar ex-

tractability, such as Benzalkonium or Berberine) with $BCGH_2$. This result has been shown experimentally in extraction studies with other dyes [28].

4. Conclusions

Identical associates of a dye, ammonium salt and guinine can be obtained by association reactions in a single dichloromethane phase as by extraction in a dichloromethane/water two phase system. Nature and physicochemical properties of associates are described better from studies of association reactions in the extraction solvent as a single phase. A new method to study associates in ternary mixtures in a single dichloromethane phase is put forward and it can be used for the dye-amine-ammonium salt system. After mixing in dichloromethane $BCGH_2$, Benzethonium chloride (BZ^+Cl^-) and Q five associates can be generated: $BCGH^-QH^+$, $BCGH^-BZ^+$, $BCG^{2-}(BZ^+)_2$, QH^+BCG^--H-Q and BZ^+BCG^--H-Q (the 1:1:1 associate). The spectrophotometric properties (Vis-UV, IR, ^{1}H-NMR) suggest that the first three associates are ion associates in nature while the two last ones present a hydrogen bridge. All the associates are in nature resonance hybrids which justifies the high values of the equilibrium constants and thermodynamic parameters of associates containing a hydrogen bonding. Extraction in a two phase system must be considered a global process of the processes which occur in each of the phases. A new and fundamental equation can be deduced to govern quantitatively the relation of the global process into the two phase system with the processes in each of the two phases. This equation suggests that extraction of a 1:1:1 associate (for example BZ^+BCG^--H-Q species) is primarily based on the high ion associability of the QAC (measured for its E_{BCGHBZ}-value) and secondarily it is based on the high capacity to form hydrogen bond of the amine (its $K_{QACD\text{-}H\text{-}A}$-value) with a not too high value of its dissociation constant in water ($pK_{QH^+} = 8.3$). As Q and Benzethonium have the best values of those constants, its 1:1:1 associate is selective against the QAC of short hydrophobic chains (low ion associability) and amines in general. However, extraction of this 1:1:1 associate is not selective among QAC of similar hydrophobic chains. This is the classic limitation of the known analytical methods based on extraction of ion associates which the 1:1:1 method will not be able to surpass although in the future other amine with higher capacity to form hydrogen bridges than Q could appear.

References

[1] H.M.N.H. Irwing and J.J. Markham, Anal. Chim. Acta, 39 (1967) 7–12.
[2] G. Schill, Acta Pharm. Suec., 2 (1965) 13–45.
[3] G.N. Thomis and A.Z. Kotionis, Anal. Chim. Acta, 16 (1957) 201–206.
[4] S. Motomizu and K. Tôei, Anal. Chim. Acta, 120 (1980) 267–277.
[5] L.G. Chatten and K.O. Okamura, J. Pharm. Sci., 62 (1973) 1319.
[6] K. Tôei, Anal. Sci., 3 (1987) 479–488.
[7] T. Sakai, Anal. Chim. Acta, 147 (1983) 331–337.
[8] J.I. Watters and E.D. Loughran, J. Am. Chem. Soc., 75 (1953) 4819–4823.
[9] R. DeBitt and J.I. Watters, J. Am. Chem. Soc., 76 (1954) 3810–3814.
[10] R.M. Alcok, F.R. Hartley, and D.E. Rogers, J. Chem. Soc., Dalton, Trans., (1978) 115–123.
[11] A.H. Gainza and M.T. Quintela, J. Chem. Soc., Perhin Trans., 2 (1994) 905–911.
[12] A.H. Gainza, Can. J. Chem., 65 (1987) 1279–1291.
[13] J.S. Coleman, L.P. Varga and S.H. Mastin, Inorg. Chem., 9 (1970) 1015–1018.
[14] D.R. Rosseinsky and H. Kellawi, J. Chem. Soc., (A) (1969) 1207–211.
[15] N. Nishimura, K. Masaki, J. Miyake and T. Sakai, Chem. Lett., (1988) 1239–1242.
[16] N. Nishimura, Y. Osawa, K. Kuramoto and K. Sukemichi, Bull. Chem. Soc. Jpn., 64 (1991) 2438–2443.
[17] R.A. Hudson, R.M. Scott and S.N. Vinogradov, J. Phys. Chem., 76 (1972) 1989–1993.
[18] A.H. Gainza, R.I. Konyaso and R.A. Asenjo, J. Pharm. Sci., 83 (1994) 226–231.
[19] A.H. Gainza and R.I. Konyeaso, Can. J. Chem., 69 (1991) 937–944.
[20] P. Farrel and P. Ngo, J. Phys. Chem., 77 (1973) 2545–2551.
[21] I. Hanazaki, J. Phys. Chem., 76 (1972) 1982–1989.
[22] E. Martinez, A.H. Gainza and J. Thomas, An. Real. Acad. Farm, 51 (1985) 605.
[23] E. Banyai, in E. Bishop (Ed.), Indicator, International Series of Monographs in Analytical Chemistry, Vol. 51, Pergamon Press, Oxford, 1972.
[24] G. Schill, Acta Pharm. Suec., 1 (1964) 169–182.

[25] F.J. Muthadi, M.A. Loutfy and M.M. Hassan, in Klaus Florey, (Ed.), Analytical Profiles of Drug Substances, Vol. 12, Academic Press, 1983, pp. 547.
[26] Y. Kaneda and M. Iwada, Eisei Kagaku, 22 (1976) 370–374.
[27] T. Sakai, N. Ohno, H. Sasaki and T. Kamato, Mikrochim. Acta, 106 (1992) 45–55.
[28] T. Sakai, N. Ohno, H. Sasaki and T. Hyuga. Anal. Sci., 7 (1991) 39–43.
[29] R. Modin and G. Schill, Talanta, 22 (1975) 1017–1021.
[30] F. Matsui and W.N. French, J. Pharm. Sci., 60 (1971) 287–291.

ELSEVIER

Talanta 44 (1997) 443–449

Talanta

Determination of trace amounts of carbaryl in water by solid-phase laser-induced fluorescence

M. del Olmo [a], J. Laserna [b], D. Romero [b], J. Rohand [a], J.L. Vilchez [a,*]

[a] *Department of Analytical Chemistry, University of Granada, E-18071 Granada, Spain*
[b] *Department of Analytical Chemistry, University of Málaga, E-29071 Málaga, Spain*

Received 13 June 1996; received in revised form 13 August 1996; accepted 29 August 1996

Abstract

A quick and very sensitive method is proposed for the determination of the insecticide carbaryl, following transformation in 1-naphthol, using solid-phase fluorescence excited by a pulsed nitrogen laser and detected with a charge-coupled device. Carbaryl is hydrolized in an alkaline medium resulting in 1-naphthol. This hydrolysis product is fixed on QAE Sephadex A-25 gel at pH 11.20. The fluorescence of the gel, packed in a 1 mm silica cell, was measured directly using a solid-surface attachment. The detection limit obtained was 1.8 ng. A recovery study was carried out on several types of water samples to check the efficiency of the method. The results obtained are compared with data published in a previous paper where the LS-50 spectrofluorimeter was used. The detection and quantification limits are improved here by an order of magnitude. © 1997 Elsevier Science B.V.

Keywords: Carbaryl; Solid-phase laser-induced fluorescence; Water analysis

1. Introduction

Carbaryl (1-naphthyl-N-methylcarbamate) is one of the major active ingredients of widely applicable insecticides [1–3]. Along with its relatively short half-life various studies have indicated that both carbaryl and its hydrolysis product 1-naphthol may cause toxic effects by the inhibition of the enzyme cholinesterase and by their teratogenic character [4–6]. Consequently, the determination of carbaryl residues in natural water is clearly important. Various methods have been proposed for its determination in formulations, crops, waters and soils. They usually involve a chromatographic separation, such as TLC [7,8], GC [9,10] or HPLC [11–17], in order to avoid matrix interferences.

Molecular luminescence techniques provide very sensitive methods of analysis and several spectrofluorimetric methods have been proposed for carbaryl determination based on its native fluorescence [18–21].

The use of lasers as sources in molecular luminescence has several potential advantages over traditional non-coherent light sources [22]. Since the radiance of a laser is greater than that of the traditional blackbody sources, laser excitation increases the sensitivity of fluorometric methods,

* Corresponding author.

PII S0039-9140(96)02089-9

and often improves the observed limits of detection [23]. With increasing source intensity, and the onset of saturation, an increased linear dynamic range and freedom from quenching effects can be observed. In addition, the narrow spectral width of the laser source results in slightly narrower fluorescence peaks and, therefore, in higher selectivity. Recent advantages in charge-coupled device (CCD) image detector technology have brought its application to analytical spectroscopy because they offer negligible dark current, high quantum efficiency, low readout noise, wide dynamic range, and the ability to bind photogenerated charge from multiple pixels [24–26]. CCDs are thus, the detectors of choice, in particular if the multiplex advantage can be fully exploited. This results in lower limits of detection, more rapid analysis, the opportunity to use lower power and less expensive lasers.

In this paper, we demonstrate the versatility of the solid-phase fluorescence method [27] by applying a pulsed nitrogen laser as the excitation source and a charge-coupled device camera for the fluorescence detection of carbaryl, via transformation in 1-naphthol, in natural waters. The solid-phase fluorescence combines the direct measurement of solid-surface signal using a small amount of a suitable solid support to preconcentrate the analyte. The results obtained are compared with data reported in our previous paper [28], where a LS-50 spectrofluorimeter was used.

2. Experimental

2.1. Instrumentation

Fig. 1 shows a block diagram of the system setup. A pulsed nitrogen laser (Laser Photonics, model UV-12, wavelength 337.1 nm, pulse duration 10 ns) was used to irradiate the sample at room temperature in air at atmospheric pressure. The laser was focused onto the sample with a quartz planoconvex lens with a focal length of $f = 45$ mm. The laser energy measured on the sample surface by using an energy-meter Gentec was 2 mJ. Fluorescence was collected onto the entrance slit of a triple indexable grating spectrograph (Acton Research Corporation, model SpectraPro 275, Czerny-Tuner; $F/3.8$), fitted with classically ruled gratings of 300, 600 and 1800 grooves/mm. Optical collection was performed with a glass biconvex lens with focal length of 10 cm. The spectrometer entrance slit was 15 mm high by 20 μm wide. The area of the spot of laser radiation illuminating the sample was 900 × 100 μ^2 measured by using a 6X JUNIOR SIZE COMPARATOR magnifying glass equipped with a micrometric scale. A solid-state two-dimensional charge-coupled device (CCD) (EG&G PAR, Thomson CSF, THX-31195A) was used to detect the fluorescence. The CCD consists of 512 × 512 elements each being 19 μm × 19 μm. The active area is 9.7 mm × 9.7 mm. The CCD was cooled to − 60°C by a Peltier system. When cooled to − 60°C, this detector exhibits a dark current of 10 photoelectrons pixel^{-1} s^{-1} and a readout noise of 4–5 electrons per scan. For data acquisition, the CCD system was optically triggered with a beam deflected from the laser and a fast photodiode. Operation of the detector was controlled by a personal computer with Optical Multichannel Analyzer (OMA) Spec 4000 software. The spectrometer is connected to the controlling PC by a conventional IEEE-488 general-purpose interface bus (GPIB).

For comparison to the proposed system, a commercial spectrofluorimeter was also used, the Perkin Elmer Model LS-50 equipped with a Xenon discharge lamp (20 kW), Monk-Gillieson monochromators, a Quantic Rhodamine 101

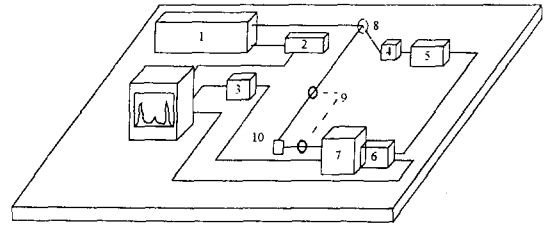

Fig. 1. Schematic diagram of the system setup. (1) Nitrogen laser (wavelength 337.1 nm, pulse duration 10 ns); (2) pulse generator; (3) spectrograph control; (4) photodiode; (5) amplifier; (6) charge coupled device (CCD); (7) triple indexable grating spectrograph with 300, 600 and 1800 grooves mm^{-1} blaced at 600 nm; (8) mirrors; (9) planoconvex lens; and (10) two motorized linear stage.

counter to correct the excitation spectra and a Gated photomultiplier. The luminescence spectrometer was interfaced with a Mitac MPC 3000F-386 microcomputer supplied with FL Data Manager software for spectral acquisition. The excitation and emission slits were both maintained at 2.5 nm. The scan rate of the monochromators was maintained at 240 $nm \cdot min^{-1}$.

A Crison 501 digital pH-meter with saturated calomel and glass electrodes and an Agitaser 2000 rotating agitator were also used.

2.2. Reagents

All reagents were of analytical-reagent grade unless stated otherwise. Stock solutions of Carbaryl (Riedel-de Haën) and 1-Naphthol (Merck) with a concentration of 100 $mg \cdot l^{-1}$ were prepared by exact weighing of the reagent and dissolution in ethanol 96% (v/v) (Panreac). Working solutions were prepared by adequate dilution with deionized water. These solutions were stored in a dark bottle at 4°C remaining stable for at least 6 months.

QAE Sephadex A-25 dextran type anion-exchange gel (Sigma) was used in the chloride form and without pre-treatment in order to avoid contamination.

2.3. Treatment of water samples

Water samples were filtered through a cellulose acetate filter (0.45 μm pore size, Millipore HAWP 04700) and collected in dark glass bottles previously cleaned with hydrochloric acid and washed with deionized water. The samples were stored at 4°C until analysis which was performed with the minimum possible delay [29].

2.4. Basic procedure for analyzing carbaryl

A 500 ml water sample containing between 0.07 and 40.0 $\mu g \cdot l^{-1}$ of carbaryl was transferred into a glass bottle, and 10 ml of 0.1 M NaOH solution and 100 mg of QAE Sephadex A-25 gel were also added. The mixture was shaken mechanically for 10 min after which the gel beads were collected by filtration under suction and packed in a 1 mm silica cell together with a small volume of the filtrate with the aid of a pipette. A blank solution containing all the reagents except carbaryl was prepared and treated in the same way as described above.

For each concentration of analyte, ten scans were taken, and the average of the peak heights was used in the calibration curve.

The measured relative fluorescence intensity (RFI) of the gel beads containing the fluorescent product was the diffuse transmitted fluorescence (DTF) emitted from the gel at the unexcited surface of the cell. The optimum angle formed between the cell plane and the excitation beam was 45° in all instances [27].

2.5. Procedure for water samples

A volume of natural water sample containing an adequate amount of carbaryl was levelled off to 500 ml with deionized water, placed in a glass bottle and 10 ml of 0.1 M NaOH solution and 100 mg of QAE Sephadex A-25 gel were added. The mixture was shaken mechanically for 10 min and then treated as described under Basic Procedure. The standard addition method was used for calibration purposes.

3. Results and discussion

3.1. Spectral characteristics

Fig. 2 compares the emission spectra of the carbaryl hydrolized-gel system taken with (a) the LS-50 spectrofluorimeter and (b) the pulsed nitrogen laser system. The excitation wavelength of 337.1 nm provided by the nitrogen laser is very close to the excitation maximum of the system located at 333 nm when the LS-50 spectrofluorimeter is used.

The differences between the spectra are worth noting. While in the Fig. 2a the emission maximum wavelength is located at 450 nm, the spectrum obtained with laser excitation (Fig. 2b) shows a shoulder at this position, but the maximum emission is now at 485 nm. This spectral shape is very similar to the phosphorescent signal

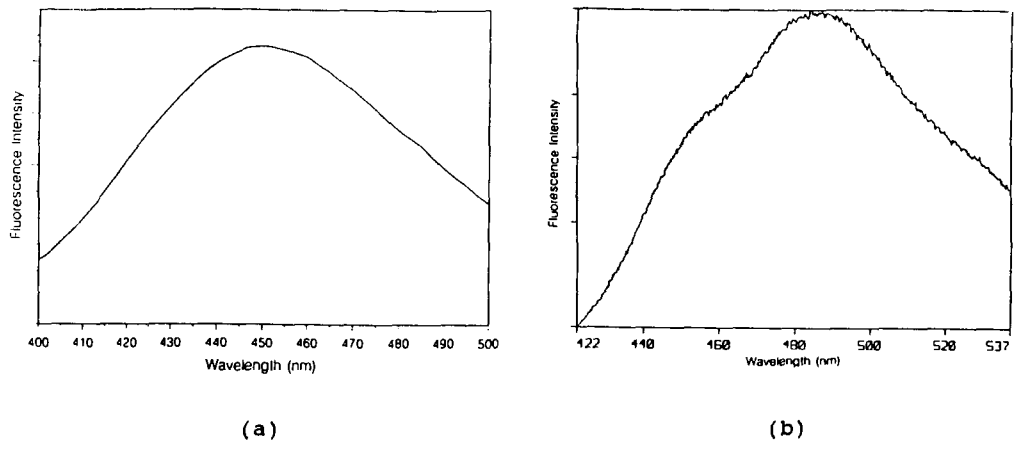

Fig. 2. Emission spectra of carbaryl hydrolized-gel system taken with (a) the LS-50 spectrofluorimeter maintaining an excitation wavelength of 333 nm and (b) the pulsed nitrogen laser system.

emitted by carbaryl and 1-naphthol using Whatman N°1 chromatography paper as the solid support [30]; however, these two compounds, in the absence of a heavy atom, show another maximum phosphorescent emission at room temperature located at 515 nm.

From a study of the half-life of the excited state of the system in the solid phase, it was concluded that the luminescence process was fluorescence because τ is lower than 10 ns, i.e., the pulse duration. Campligia et al. found phosphorescence lifetime values of 1185 ± 121 and 1083 ± 267 ms for carbaryl and 1-naphtol fixed on chromatographic paper in the absence of a heavy atom.

3.2. Experimental variables

As we reported in a previous paper [28], carbaryl shows native fluorescence in neutral and acidic media but, is not fixed on QAE Sephadex A-25 at pH values lower than 8.0. Its hydrolysis product, 1-naphthol, exhibits fluorescence in basic media only, and is quantitatively fixed on QAE-gel at pH higher than 11.0, showing fluorescence with excitation and emission maxima at 333 nm and 450 nm, respectively.

The optimum pH for the simultaneous hydrolysis and fixation of the carbaryl was found to be 11.20 fixed with an adequate volume of NaOH 0.1 M solution.

The fluorescence intensity was shown to be independent of the ionic strength, adjusted with NaOH, NaCl and $NaClO_4$ up to $1.5\ 10^{-4}$ M.

The shaking time necessary for maximum RFI development (with the hydrolysis step and fixation in the gel phase taking place simultaneously) was 10 min, remaining constant thereafter.

The addition order of the reagents did not affect the results obtained. The order used was carbaryl, buffer and gel.

As the use of a large amount of the gel lowered the RFI, only the amount required to fill the cell and facilitate handling the 100 mg was used in all measurements.

With regard to the stability of the QAE-carbaryl hydrolized system, Fig. 3 shows different spectra of the same sample taken at intervals of 10 min. The sample was constantly irradiated. The fluorescence emitted remained constant for at least 1.5 hours regardless of the radiation received.

3.3. Analytical parameters

The calibration graphs for samples treated according to the procedure described above are linear for the concentration range 0.07–40.0 $\mu g \cdot l^{-1}$ for a 500 ml sample volume. To check the linearity of the calibration standard, the lack-of-fit test [31] was applied for ten replicates of each standard.

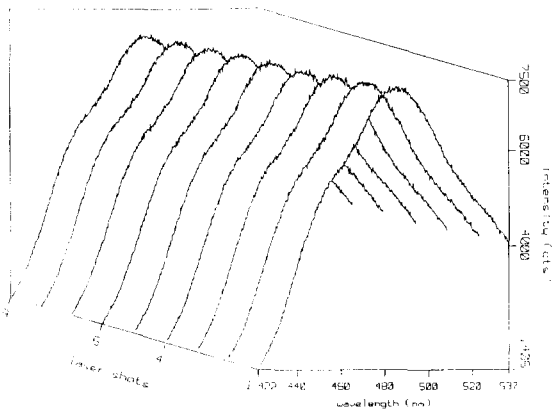

Fig. 3. Spectra of QAE-carbaryl hydrolized system taken at intervals of 10 min.

Table 1 shows the results obtained for the analytical parameters of the proposed method and those obtained previously by using a commercial LS-50 spectrofluorimeter. The precision determined as relative standard deviation (RSD) was measured for a carbaryl concentration of 10 and 30 $\mu g \cdot l^{-1}$, respectively, for each excitation system, by performing ten independent determinations.

The IUPAC detection limit ($K = 3$) and the quantification limit ($K = 10$) were calculated for 500 ml sample volume (Table 1) through 10 individual samples prepared according to the procedure without analyte in both cases. The detection limits are given in bulk concentration and amount of analyte in laser probe volume for the laser system.

It is worthy of note that the detection and quantification limits obtained in this case are one order of magnitude below those found with the LS-50 spectrofluorimeter.

Table 1
Analytical parameters obtained with a commercial spectrofluorimeter (Perkin Elmer LS-50) and the laser system

Parameters	Values found	
	Laser system	LS-50 commercial
Slope ($l \cdot \mu g^{-1}$)	651.97	6.93
Correlation coefficient	0.999	0.998
Lack-of-fit test (P-value)	0.22	—
Linear Dynamic Range ($\mu g \cdot l^{-1}$)	0.07–40.0	0.4–60.0
LOD[a] ($\mu g \cdot l^{-1}$)	0.02	0.1
LOD (ng)	1.8	—
LOQ[b] ($\mu g \cdot l^{-1}$)	0.07	0.4
RSD (%)	2.4	0.9

[a] Limit of detection.
[b] Limit of quantification.

4. Applications to real samples

We tried to find carbaryl in ground water from the Santa María farm located near Granada and tap water from the city's supply but we did not find this insecticide above our DL.

To check the accuracy of the proposed method, a recovery study was carried out on various types of sample waters. The volume of water used was 500 ml in all instances and three determinations were required for each sample tested. Table 2 summarizes the values obtained. In all instances the values found were close to 100%.

Validation of the proposed method for natural water was also carried out, through a standard addition of carbaryl to the different types of water samples. The t-test was applied to check the similarity between the representative values of the slope of standard calibration and standard addition calibration obtained by standard additions of carbaryl to natural water samples. The statistics used [32] is calculated with the following equation:

$$t(b) = \frac{|b_S - b_A|}{s_p \sqrt{\frac{1}{\sum(c_{i,S} - \bar{C}_S)^2} + \frac{1}{\sum(c_{i,A} - \bar{C}_A)^2}}}$$

In this equation, b_A and b_s are the slopes of standard addition calibration (AC) and standard calibration (SC), respectively; s_s represents the regression standard deviation of SC; $c_{i,A}$ and $\bar{C}_A$ the concentration of added standard set used in AC and the average concentration of this set; and $c_{i,S}$ and $\bar{C}_S$ the concentration of standard set used in SC and the average concentration of the same set.

Table 2
Recovery assays of carbaryl in water samples

Water	Added ($\mu g \cdot l^{-1}$)	Found[a] ($\mu g \cdot l^{-1}$)	Recovery (%)	RSD (%)
Tap (Granada City)	1.0	0.95	95.0	2.0
	10.0	10.74	107.4	1.5
	20.0	19.50	97.5	2.8
	40.0	38.91	97.3	0.9
Ground (Santa María Farm)	1.0	1.07	107.0	3.2
	10.0	10.85	108.5	1.4
	20.0	19.16	95.8	2.7
	40.0	41.03	102.6	2.9

[a] Mean of three independent determinations.

The null hypothesis is accepted for a significance level (P value) greater than 10% (the usual value of 5% should not be used because this test is excessively robust). The Student's t and P values calculated were 0.652 and 52.6% for ground water and 0.754 and 46.5% for tap water, respectively. In both cases, $P > 10\%$; thus, we may conclude that there are no matrix effects and the method is accurate.

As already reported in the previous paper and subsequently tested following the proposed method, the usual levels of the different ions present in the waters sampled do not interfere with carbaryl recovery. The usual chlorine level in local tap water (O.6 $ng \cdot ml^{-1}$) did not produce any interference either.

Acknowledgements

This research was partially supported by the Spanish C.I.C.Y.T. (Project AMB-94-0776).

References

[1] Union Carbide Corporation, Technical Information Bulletin, 1974.
[2] R.J. Kuhr and H. Wyman Dorough, 'Carbamate Insecticides: Chemistry, Biochemistry and Toxicology', CRC Press, Cleveland, Ohio, 1976.
[3] C. de Liñan, 'Vademecum de productos fitosanitarios y nutricionales', Ed. Embajadores, 1990.
[4] R. Elespuru, W. Lijinski and J.K. Setlow, Nature, 247 (1974) 386.
[5] M. Uchiyama, Bull. Envirom. Contam. Toxicol., 14 (1975) 589.
[6] J. Seifert and J.E. Cadbla, Biochem. Pharmacol., 27 (1978) 2611.
[7] M. Chiba and H.V. Morley, J. Assoc. Off. Agr. Chem., 47 (1964) 667.
[8] G.F. Ernst, S.J. Roder, G.H. Tjan and J.T.A. Jansen, J. Assoc. Off. Anal. Chem., 58 (1975) 1015.
[9] R.J. Argauer, H. Shimanuki and C.C. Alvarez, J. Agric. Food Chem., 18 (1970) 688.
[10] O. Wueest and W. Meler, Z. Lebensm-Unters Forsch., 177 (1983) 25.
[11] B.J. Duck and M. Wodias, J. Anal. Toxicol., 177 (1985) 9.
[12] M.C. Pietrogrande, G. Blo and C. Bighi, J. Chromatogr., 349 (1985) 63.
[13] T.D. Spittler, R.A. Marafioti, G.W. Helfman and R.A. Morse, J. Chromatogr., 352 (1985) 439.
[14] S. Kawai, Bunseki Kagaku, 36 (1987) 574.
[15] R.T. Krause, J. Assoc. Off. Anal. Chem., 63 (1980) 1114.
[16] R.T. Krause and E.M. August, J. Assoc. Off. Anal. Chem., 66 (1983) 234.
[17] M. de Berardinis Jr. and W.A. Wargin, J. Chromatogr., 246 (1982) 89.
[18] J.J. Aaron and N. Some, Analusis, 10 (1982) 481.
[19] M.J. Larkin and M.J. Day, Anal. Chim. Acta, 108 (1979) 425.
[20] R.J. Argauer and W. Bontoyan, J. Assoc. Off. Anal. Chem., 53 (1970) 1166.
[21] F. García Sanchez and C. Cruces, Talanta, 37 (1990) 573.
[22] T. Vo-Dinh and D. Eastwood, (Eds.), Laser Techniques in Luminescence Spectroscopy, ASTM Publishers, STRI 1066, Philadelphia, PA, 1990.
[23] J.H. Richardson and M.E. Ando, Anal. Chem., 49 (1977) 955.
[24] Y. Talmi (Ed.), Multichannel Image Detectors, ACS Symposium Series 102, American Chemical Society, Washington, DC, 1979.
[25] P.M. Epperson, J.Y. Sweedler, R.B. Bilhorn, R. Gary and M.B. Denton, Anal. Chem., 60 (1988) 327A.

[26] P.M. Epperson and M.B. Denton, Anal. Chem., 61 (1989) 1513.
[27] F. Capitán, E. Alonso, R. Avidad, L.F. Capitán-Vallvey and J.L. Vilchez, Anal. Chem., 65 (1993).
[28] J.L. Vilchez, R. Avidad, A. Navalón, J. Rohand and L.F. Capitán-Vallvey, Int. J. Environ. Anal. Chem., 53 (1993) 139.
[29] American Public Health Authority, in S.A. Díaz de Santos (Ed.), Standard Methods For the Examination of Water and Wastewater, 17 Edn., American Water Works Association and Water Pollution Control Federation, 1992.
[30] A.D. Campiglia and C.G. de Lima, Anal. Chem., 59 (1987) 2822.
[31] Statgraphics version 6.0, Manugistics Inc. and Statistical Graphics Corporation, USA, 1992.
[32] A. Martín Andrés and J.B. Luna del Castillo, Bioestadística para las Ciencias de la Salud, Norma, Madrid, Spain, 1990.

ELSEVIER

Talanta 44 (1997) 451–456

Talanta

Flame atomic absorption spectrometric determination of zinc after colloid precipitate flotation with hydrated iron(III) oxide and iron(III) tetramethylenedithiocarbamate as collectors

Katarina Čundeva, Trajče Stafilov *

Institute of Chemistry, Faculty of Science, St. Cyril and Methodius University, Skopje, Macedonia

Received 1 July 1996; received in revised form 28 August 1996; accepted 4 September 1996

Abstract

Colloid flotation of zinc from fresh water with a combination of two collectors, hydrated iron(III) oxide ($Fe_2O_3 \cdot xH_2O$) and iron(III) tetramethylenedithiocarbamate ($Fe(TMDTC)_3$), permits rapid separation of the precipitate before its atomic absorption spectrometric (AAS) analysis. All important parameters necessary for the successful flotation like optimal mass of collectors, pH of the medium, electrokinetic potential of the collector particle surfaces, type of tenside, induction time etc., were checked. At the optimal pH value of medium (5.5) establishing by recommended procedure, zinc was separated quantitatively (97.4–98.8%) with 5 mg Fe(III) as constitutive element of the two collectors used. The content of zinc was determined by flame atomic absorption spectrometry (FAAS). These results were compared with the results obtained by inductively coupled plasma—atomic emission spectrometry (ICP-AES). The FAAS detection limit for zinc is 9.4 $\mu g\ l^{-1}$. The proposed method is simple, rapid and applicable to the zinc separation at $\mu g\ l^{-1}$ levels from a large volume of water. © 1997 Elsevier Science B.V.

Keywords: Determination; Flame atomic absorption spectrometry; Precipitate flotation; Zinc

1. Introduction

In the recent years there has been an increased interest in the separation of trace heavy metals from large volumes of dilute aqueous solution by flotation techniques [1–10]. These techniques were developed to extend the range of analysis to trace concentration of heavy metals in natural waters by divers instrumental methods which follow the flotation [1–3]. There are reports of zinc separation by colloid precipitate flotation using hydrated metal oxides like $Fe_2O_3 \cdot xH_2O$ or $Al_2O_3 \cdot xH_2O$ as collectors [1–5] or by ion flotation with divers dithiocarbamates [6,8]. This paper is the first attempt for flame atomic absorption spectrometry (FAAS) determination of zinc after its preconcentration by colloid precipitate flotation using a combination of two colloid collectors $Fe_2O_3 \cdot xH_2O$ and $Fe(TMDTC)_3$. The same combination of collectors have been applied [9] for separation of several metals from sea water using neutron activation, but not for zinc. The necessity

* Corresponding author.

PII S0039-9140(96)02095-4

of the first induction time [1,10] for a coprecipitation step of flotation with $Fe_2O_3 \cdot xH_2O$ as first collector was investigated. The improvement of the zinc preconcentration by using $Fe(TMDTC)_3$ as second collector was studied. The method developed is simple, rapid (need about 30 min) and applicable for Zn determination from a large volume of fresh water. This method can be compared with differential pulse anodic stripping voltammeter (DPASV) with hanging mercury electrode or mercury film electrode which achieve detection limits for zinc (1 $\mu g\, l^{-1}$ or less) and need short analysing time (about 15 min) [11–13].

2. Experimental

2.1. Apparatus

Apparatus employed in this work have been previously described [10]. For AAS measurements an air-acetylene flame was applied. The Zn Perkin–Elmer hollow cathode lamp was used as a primary source. Instrumental parameters are shown in Table 1. Inductively coupled plasma-atomic emission spectrometric measurements (ICP-AES) were performed by Varian spectrometer Model Liberty 110. The flotation cell used to carry out the preconcentration was a glass cylinder (4 × 105 cm) with a sintered glass disc (porosity No. 4) at the bottom to generate air bubbling.

2.2. Reagents and standards

All chemicals used for preparation of solutions, were of an analytical-reagent grade except for sodium dodecylsulfate (NaDDS) and sodium oleate (NaOL). The aqueous solutions were prepared in redistilled water.

Table 1
Optimal instrumental parameters for FAAS determination of Zn

Wavelength	213.8 nm
Spectral bandpass	2.0 nm
Lamp current	15.0 mA

Stock solution of Zn was made from $ZnSO_4 \cdot 7H_2O$ as 1 mg ml^{-1} solution. Before each investigation standard solutions were freshly prepared by diluting this stock solution. The stock solution of $FeCl_3$ (30 g l^{-1}) was made in the same way, as previously described [10]. Series of standards with concentrations of Fe ranging from 2.5 to 100 mg ml^{-1} were obtained by dilution this Fe stock solution. The diluted standards of Zn and Fe serve to investigate the optimal conditions for performing the flotation procedure, to obtain data for construction the calibration curve (concentration absorbance) and for the method of standard additions of the natural water analysis. By dissolving an appropriate quantity of ammonium tetramethylenedithiocarbamate (NH_4TMDTC) in water the stock solution was prepared as 0.1 mol l^{-1}. Before each flotation the solution of NH_4TMDTC was filtered. The 0.5% solutions of tensides used were prepared by dissolving appropriate amounts of NaDDS and NaOL in 95% ethanol. The pH of the working solutions was regulated by 0.1 mol l^{-1} solution of HNO_3 and 2.5 and 10% solutions of KOH. Solution of KCl ($c = 3.57$ mol l^{-1}) was used to adjust the ionic strength.

2.3. Flotation procedure

The recommended flotation procedure is for clear and uncontaminated fresh water. The investigated samples were tap water from the city of Skopje and water from the lake of Ohrid. Immediately after the sampling, the lake waters were filtered trough a membrane filter (0.5 mm width of pores) to remove the lake plankton. The tap water was not filtered. To prevent the possible hydrolytic precipitation a few ml of conc. HNO_3 had to be added to 1 l of natural water. The pH had to be ca. 2.8–3.

An acidified water sample (1 l) was placed in 1000 ml beaker. After adding 6 ml of KCl and 1 ml of 5 mg ml^{-1} of the $FeCl_3$ solution, the pH was adjusted to 5.5 with a solution of KOH (2.5 or 10%). The yellow-brown precipitate was stirred 5 min (a first induction time). Then to the solution with precipitate of $Fe_2O_3 \cdot xH_2O$, 2 ml of NH_4TMDTC solution were added. The precipitate changed its colour to black $Fe(TMDTC)_3$. After stirring of 15 min (a second induction time),

0.6 ml of NaDDS and NaOL alcoholic solutions were added and the contents of the beaker were transferred quantitatively into the flotation cell with the small portion of 0.1 mol l^{-1} NH_4NO_3. Air (50 ml min^{-1}) was passed from the perforated bottom of the cell for 2–3 min. Then, the glass pipette-tube was immersed into the cell through the foam layer and the water phase was sucked off. Hot 65% HNO_3 solution (10 ml) was added to the cell to destroy the scum. The solution was sucked off and collected in a volumetric flask of 25 ml. The cell and the pipette-tube were washed with 4 mol l^{-1} HNO_3 solution. The flask was filled up to the mark with the same solution and the sample was ready for FAAS measurements.

To obtain the optimal experimental parameters, like collector mass, medium pH, type of tenside, ionic strength, induction time, for zinc standard solutions of this colligend were treated by the flotation procedure and then they were tested by FAAS.

3. Results and discussion

3.1. Coprecipitation with hydrated iron(III) oxide

In the previous paper [10] two induction time of 15 min were used. The necessity of the first induction time for a coprecipitation of Zn with $Fe_2O_3 \cdot xH_2O$ as the first collector was investigated. The series of flotation were performed by addition of different Fe(III) quantities (2.5–100 mg l^{-1}) to the working solutions at a constant pH (5.5) and ionic strength (0.02 mol l^{-1}) regulated with KCl. The results of these investigations are presented in Table 2. The data show that Zn recoveries at the pH of 5.5 with 5 mg of Fe were poor (22.17–30.44%). The maximal recoveries of this colligend, under these conditions, were obtained with 100 mg Fe(III) (56.95–60.03%), but they were insufficient too. These data show that the role of $Fe_2O_3 \cdot xH_2O$ as collector in the recommended procedure with two collectors at pH 5.5 was not decisive for colligend separation from water matrix as Feng and Ryan asserted [9].

Table 2
The values of the Zn flotation recovery dependence on the iron(III) mass coprecipitating with $Fe_2O_3 \cdot xH_2O$ in the presence of 0.02 mol l^{-1} KCl at pH 5.5

Sample number	γ(Fe) mgl^{-1}	Recovery (%)	
		γ(Zn) = 1 μg ml^{-1}	γ(Zn) = 2 μg ml^{-1}
1	2.5	30.44	22.17
2	5.0	37.49	27.95
3	10	40.29	29.92
4	20	41.00	32.97
5	30	46.00	34.38
6	40	52.53	36.38
7	60	60.44	41.88
8	80	59.80	52.71
9	100	60.03	56.95

3.2. Effect of the Fe(III) tetramethylenedithiocarbamate mass on Zn recoveries

The dependence of Zn recoveries on the mass of $Fe(TMDTC)_3$ was determinated trough the mass of Fe(III), as a constitutive element of this collector. The series of flotation were performed by addition of different Fe(III) amounts (2.5–100 mg l^{-1}) to the working solutions (containing 1 and 2 mg ml^{-1} Zn) at a constant pH (5.5) and ionic strength (0.02 mol l^{-1}). The results

Table 3
The values of the zinc flotation recovery dependence on the iron(III) mass coprecipitating with $Fe(TMDTC)_3$ and 0.02 mol L^{-1} KCl as an ionic strength adjuster at pH 5.5

Sample number	γ(Fe) mg l^{-1}	Recovery (%)	
		γ(Zn) = 1 μg ml^{-1}	γ(Zn) = 2 μg ml^{-1}
1	2.5	92.8	92.3
2	5.0	98.2	97.5
3	10	100.0	98.8
4	20	98.1	98.2
5	30	98.3	98.7
6	40	97.4	98.8
7	60	96.5	98.1
8	80	96.0	98.6
9	100	96.0	98.7

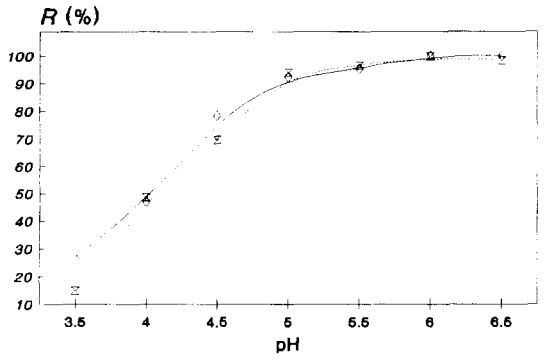

Fig. 1. Dependence of zinc flotation recovery R (%) on medium pH values in the presence of constant mass of iron(III) (5 mg), 2 ml 0.1 mol l^{-1} NH_4TMDTC solution, 0.6 ml 0.5% alcoholic solutions of tensides (NaDDS and NaOL) and KCl (0.02 mol l^{-1}) as an ionic adjuster (——◇—— $\gamma(Zn) = 1$ μg ml^{-1}; - - -x- - - $\gamma(Zn) = 2$ μg ml^{-1}).

in Table 3 and Figure 2 show that the quantitative Zn recoveries obtained after flotation with this collector at pH 5.5 using the minimum of 5 mg Fe(III) were satisfactory (97.5–98.2%). The data in Table 3 show that the leading role in the preconcentration was performed by $Fe(TMDTC)_3$ as the second collector which has better hydrophobility. That means that the first induction time can be reduced. The reducing of the first induction time had shortened the overall time for performing of the method. The different mass of colligend (25 and 50 mg) had no appreciable effect on the flotation efficiency.

3.3. Influence of pH

The influence of pH on the Zn flotability R (%) was studied at different pH values from solutions containing 25 and 50 mg of zinc with a constant mass of Fe(III) (5 mg) at constant ionic strength (0.02 mol l^{-1}). The pH was regulated within the working range of 3.5–6.5. The investigation on the pH values higher than 6.5 were not performed. Namely, at pH higher than 6.5 the collector $Fe(TMDTC)_3$ did not exist due to its hydrolysis. Fig. 1 illustrates a significant effect of pH on the zinc recoveries (95.3–100.0%) within the range of 5.5 to 6.5. The Zn recoveries within the pH range of 3.5–4.5 were poor due to hydrolysis of surfactants NaDDS and NaOL as anionits.

3.4. Choice of tenside

The particles of hydrated Fe(III) oxide had a positive electrokinetic ζ potential of 0.026 V at pH 5.5. The ζ potential of Fe(III) thetramethylenedithiocarbamate, at the same pH, was 0.046 V. According to the signs of the ζ potentials of two collectors used, they need anionits during the step of flotation. The combination of two anionits NaDDS and NaOL was shown successful. NaDDS provides a good foaming in hard water because of its soluble calcium and magnesium salts. The long chain of NaOL increases the aerofility of collector particles. When NaOL is added to the system the air bubbles attached and fixed more easily to the collector particles and the foaming is much better.

3.5. Induction time

The time necessary for incorporation of the colligend Zn in the collector precipitate is termed the induction time τ. The investigation of the relation between Zn recoveries and τ are given in Table 4. From the results, it can be concluded that the separation of colligend was quantitative over a range of 5–20 min. In practice, the first induction time of 5 min and the second induction time of 15 min were used.

3.6. Detection limit

To evaluate the detection limit of the method ten successive blank measurements were made. The FAAS detection limit of Zn is 9.04 μg l^{-1}. It was estimated as three values of the standard deviation (S.D.)($s = 3.013$ μg l^{-1}). The relative S.D. was 9.62%.

Table 4
The influence of the induction time on Zn flotation recoveries

$\gamma(Zn)$ 1 μm ml^{-1}					
τ_1 min^{-1}	5	10	5	15	15
τ_2 min^{-1}	10	10	15	15	20
R (%)	96.5	96.3	100.0	97.9	98.9

Table 5
Results of the FAAS and ICP-AES determination of zinc in natural water with the method of standard additions

Sample of water	AAS				ICP-AES
	Added μg l^{-1} Zn	Estimated μg l^{-1} Zn	Found μg l^{-1} Zn	Recovery (%)	Found μg l^{-1} Zn
Ljubaništa (Oh.[a])	0.00	—	21.00	—	19.7
6.75 DH°[b]	2.50	23.5	23.3	99.2	
pH = 7.30	6.25	27.5	29.00	105.5	
Gradišta (Oh.)	0.00	—	22.01	—	20.5
6.61 DH°	2.50	24.51	24.04	98.1	
pH = 7.43	6.25	28.26	27.59	97.6	
Labino (Oh.)	0.00	—	50.09	—	56.5
3.91 DH°	2.50	52.59	49.62	94.4	
pH = 7.30	6.25	56.34	56.73	100.7	
Daljan (Oh.)	0.00	—	98.01	—	100.9
5.97 DH°	2.50	100.51	98.67	98.2	
pH = 7.68	6.25	104.26	101.6	97.5	
Rašče (Sk.)[c]	0.00	—	83.07	—	90.0
20.26 DH°	2.50	86.2	79.48	92.2	
pH = 7.08	6.25	89.95	90.14	100.2	

[a] Oh., water from the lake of Ohrid.[b] DH (Deutsche Härte), German degree of water hardness.[c] Sk., tap water from the city of Skopje (a source Rašče).

3.7. Analysis of natural water

The possibility of usage of FAAS were studied. The applicability of the proposed procedure has been verified by the method of standard additions. For this purpose known amounts of Zn were added to 1000 ml aliquots of lake and tap water samples. Then these were floated and tested by AAS. The recoveries of 92.2–105.5% (Table 5) show that the preconcentration and separation of this colligend is satisfactory. The results obtained by AAS were compared with the results obtained by ICP-AES determinations; the samples were concentrated by evaporation (from a volume of 1000–25 ml) of tap and lake water (Table 5). A calculation of Student's *t*-test for our results gives the values range from 2.36 for water sample from Daljan to 2.76 for sample from Ljubaništa, whereas the theoretical value (95%) of *t* was 2.78. As calculated *t* values are smaller than theoretical, there is no significative difference between the two methods.

4. Conclusion

The experimental conditions for FAAS determinations of Zn following colloid flotation preconcentration and separation with two collectors have been established. The necessity of the first induction time [1,11] for a coprecipitation step of flotation with hydrated iron(III) oxide ($Fe_2O_3 \cdot xH_2O$) as the first collector was investigated. The adding of $Fe(TMDTC)_3$ as a second additional collector, which ameliorates the flotation separation, was studied. The dithiocarbamate added increases the hydrophobility of the sublate which is the most important criterion for the successful flotation. During the air bubbling step of flotation, the collector precipitate of $Fe(TMDTC)_3$, as a compound with a better hydrophobility than $Fe_2O_3 \cdot xH_2O$, improves and facilitates the separation of the foam layer from the liquid phase processing water sample. The recommended method extends the range of conventional atomic absorption determination for zinc, simplifies the determination procedure and shortens the overall time of the experiment.

References

[1] M. Caballero, R. Cela and J.A. Perez-Bustamante, Talanta, 37 (1990) 275.
[2] A. Mizuike, Flotation, in Enrichment Techniques for Inorganic Trace Analysis, Chp. 10, Springer-Verlag, Heidelberg, 1983, p. 94.
[3] A. Mizuike and M. Hiraide, Pure Appl. Chem., 54 (1982) 1556.
[4] M. Hiraide, Y. Yoshida and A. Mizuike, Anal. Chim. Acta, 81 (1976) 185.
[5] S.-D. Huang, T.-P. Wu, C.-H. Ling, G.-L. Sheu, C.-C. Wu and M.-H. Cheng, J. Colloid Interface Sci., 124 (1988) 666.
[6] G.A. Stalidis, K.A. Matis and N.K. Lazaridis, Sep. Sci. Technol., 24 (1989) 97.
[7] V. Srinivasan and M. Subbaiyan, Sep. Sci. Technol., 24 (1989) 145.
[8] D. Hualing and H. Zhide, Talanta, 36 (1989) 633.
[9] X. Feng and D.E. Ryan, Anal. Chim. Acta, 162 (1984) 47.
[10] K. Čundeva and T. Stafilov, Fresenius' J. Anal. Chem., 352 (1995) 354.
[11] Z. Komy, E. Roekens and R. Van Grieken, Anal. Chim. Acta, 204 (1988) 179.
[12] S. Daniele, M.A. Baldo, P. Ugo and G. Mazzocchin, Anal. Chim. Acta, 219 (1989) 19.
[13] P.L. Buldini, D. Ferri and D. Nobili, Electroanalysis (N.Y.), 3 (1991) 559.

ELSEVIER

Talanta 44 (1997) 457–466

Talanta

The study of complex equilibria of uranium(VI) with selenate

P. Lubal *, J. Havel

Department of Analytical Chemistry, Faculty of Science, Masaryk University, Kotlářská 2, 611 37 Brno, Czech Republic

Received 3 June 1996; received in revised form 13 August 1996; accepted 12 September 1996

Abstract

Uranyl (M)-selenate (L) complex equilibria in solution were investigated by spectrophotometry in visible range and potentiometry by means of uranyl ion selective electrode. The formation ML and ML_2 species was proved and the corresponding stability constants calculated were: $\log \beta_1 = 1.57_6 \pm 0.01_6$, $\log \beta_2 = 2.42_3 \pm 0.01_3$ ($I = 3.0$ mol l^{-1} $Na(ClO_4, SeO_4)$ (spectrophotometry) at 298.2 K. Using potentiometry the values for infinite dilution ($I \rightarrow 0$ mol l^{-1}) were: $\log \beta_1 = 2.64 \pm 0.01$, $\log \beta_2 \leqslant 3.4$ at 298.2 K. Absorption spectra of the complexes were calculated and analysed by deconvolution technique. Derivative spectrophotometry for the chemical model determination has also been successfully applied. © 1997 Elsevier Science B.V.

Keywords: Derivative spectrophotometry; Stability constants; Spectra deconvolution; Uranyl selenate

1. Introduction

Uranyl ion is linear oxocation, which starts to hydrolyse at pH higher than 2.5 for concentrations ≈ 0.1 mol l^{-1} [1,2] if no other complexing agents is present. It can be assigned according Hard and Soft Acids and Basis (HSAB) principle to hard acids therefore it tends to form more stable complexes with harder bases, such as ligands with oxygen donor atom like carbonate, sulphate, oxalate, aromatic hydroxycompounds, etc., and/or with harder halogenide anions (fluoride, chloride) and, of course, with hydroxide under the formation of polynuclear hydroxospecies) [1–3]. The affinity to oxygen is so high that the existence of a ternary polynuclear species, in uranyl-carbonate-hydroxide [4,5] and/or uranyl-sulphate-hydroxide [6] systems has been proved. The highest co-ordination number of uranyl in its compounds in solution is mostly equal to four, in solid state it is equal to six.

The complex equilibria in uranyl-sulphate system have been investigated by means of different methods (potentiometry, spectrophotometry, extraction, solubility, dialysis, ion-exchanger, calorimetry etc.) (reviewed in [2] and [3]). It is evident that in uranyl-sulphate system species ML and ML_2 are formed [3], but there are some doubts about the formation of species ML_3.

Stability constants of uranyl with selenate has not been determined as yet. As selenate is isoelectronic with sulphate, it could be suggested that the same species such as in uranyl-sulphate system will be formed. Detailed study of the interactions

* Corresponding author.

PII S0039-9140(96)02103-0

of uranyl with selenate is the subject of this work. Some results of this work were preliminary reported elsewhere [7].

2. Theory

2.1. Determination of the number of light-absorbing species

Generalised form of Bouger–Lambert–Beer law can be written in matrix notation:

$$\mathbf{A} = \mathbf{EC} \tag{1}$$

where $\mathbf{A}$ is the $n_w \times n_s$ absorbance matrix, $\mathbf{E}$ is the $n_w \times n_c$ matrix of molar absorptivities, $\mathbf{C}$ is the $n_c \times n_s$ concentration matrix. Here n_w denotes the number of wavelengths, n_s means the number of solutions whose spectra have been recorded, and n_c is the number of components which absorb in chosen spectral range. The rank of the matrix, rank(**A**) (RM) is obtained from the equation

$$\text{rank}(\mathbf{A}) = \min(\text{rank}(\mathbf{E}), \text{rank}(\mathbf{C})) \leqslant \min(n_w, n_c, n_s) \tag{2}$$

Since the rank(**A**) is equal to the rank of **E** or **C**, whichever is the smaller, and since rank(**E**) $\leqslant n_c$ and rank(**C**) $\leqslant n_c$, then provided n_w and n_s equal to or greater than n_c, it will only be necessary to determine the rank of **A** and find the number of absorbing species. Also we assume that the rank(**A**) is equal to the number of linearly independent columns of **A** expressed as number of nonzero eigenvectors (it means that the concentration of one or more species can not be expressed as a linear combination of the other species in all experiments).

For calculation of RM the Simmonds–Wernimont–Kankare method [8] was applied. The second moment matrix given by formula

$$\mathbf{M} = \frac{1}{n_s}\mathbf{A}\mathbf{A}^T \tag{3}$$

is symmetric (square) matrix of order n_s and of rank n_c, rank(**M**) $\leqslant n_c$. Each element of the absorbance matrix **A** is a subject to experimental error and because of that fact, the number of nonzero eigenvalues is $\min(n_w, n_s)$. Let the eigenvalues of **M** be EV_i, matrix trace of **M**, tr(**M**), summation of the eigenvalues, and suppose that there are k independent components in the system. Then the residual standard deviation of absorbance is given by

$$s_k(A) = \frac{\text{tr}(\mathbf{M}) - \sum_{i=1}^{k} EV_i}{\sqrt{n_w - k}} \tag{4}$$

Relative variance

$$RV(\%) = \frac{EV_i}{\text{tr}(\mathbf{M})} \times 100 \tag{5}$$

Cumulative relative variance

$$CRV(\%) = \frac{\sum_{i=1}^{k} EV_i}{\text{tr}(\mathbf{M})} \times 100 \tag{6}$$

and Malinowski's indicator function IND_k by Malinowski [9]

$$IND_k = \frac{s_k(\mathbf{A})}{(n_w - k)^2} \tag{7}$$

Let the precision of the absorbance measurement be given by the S.D. of absorbance of spectrophotometer used, $s_{inst}(\mathbf{A})$. Then we may say that if $s_k < s_{inst}(\mathbf{A})$, it is probable that $n_c < k$ and Malinowski's indicator function number shows minimum value [9].

3. Experimental

3.1. Reagents

Uranyl perchlorate was prepared from solid uranyl nitrate (Lachema Brno, Czech Republic) adding slight excess of concentrated 70% (w/w) perchloric acid and evaporating almost to dryness until negative reaction for nitrate was obtained. The product was two times recrystallised from diluted perchloric acid solution. The prepared substance was dissolved in water adding slight amount of perchloric acid, which concentration was then determined by Gran transformation [10] of the alkalimetric titration. The uranyl content was determined gravimetricaly as U_3O_8 (precipitation by H_2O_2) and by 8-hydroxyquinoline [11].

Uranyl nitrate (Lachema Brno, Czech Republic) for potentiometric measurements was dissolved in acidic solution of nitric acid and the stock solution was standardised as described above.

Sodium perchlorate p.a. (Lachema Brno, Czech Republic) was purified removing traces of heavy metal ions precipitation with sodium hydroxide and the product was several times recrystallised [12].

Sodium selenate was prepared by Dr Černík from Department of Inorganic Chemistry of Masaryk University. The sample was found to be free of any selenite traces [13]. Also sodium selenate (Fluka, Switzerland) was used.

3.2. Apparatus

UV-VIS measurements were done on a one beam diode array spectrophotometer HP 8452A (Hewlett Packard, USA). The derivative spectra were computed using HP 8452A standard software.

The proton concentration of solutions was checked using combined RADELKIS OP-8080 glass electrode (MOM, Hungary), in which inner saturated potassium chloride solution was removed from the reference part of the electrode and substituted with 2.99 mol l^{-1} sodium perchlorate solution and 0.01 mol l^{-1} sodium chloride, saturated with silver chloride. The reliability of the electrode was tested measuring time stability of the potential. The electrode parameters were determined by calibrating the corresponding electrode cell titrating known amount of perchloric acid by standardised sodium hydroxide solution at given ionic strength medium. The recalculation of $-\log[H^+]$ values from measured potential was done by means of equation

$$E = E^0 + g(-\log[H^+]) + E_j \quad (8)$$

where E^0 is potential of cell at $-\log[H^+] = 0$, g is Nerstian slope given by the term 2.30259 RT/F and E_j is a junction potential. For the potentiometric measurements a digital pH-meter RADELKIS OP-208 (MOM, Hungary) was used. The uranyl concentration was measured using uranyl electrode described elsewhere [14]. As reference electrode saturated calomel electrode was used. The potentiometric titrations were carried out by an automatic titrator TTT 81 with microprocessor connected to automatic burette ABU 80 and digital pH-meter PHM 84, (all Radiometer Copenhagen, Denmark).

All experiments were carried out at ionic strength $I = 3.00$ mol l^{-1} $Na(ClO_4 + SeO_4)$ (spectrophotometry, $-\log[H^+]$ values in solutions were from 2.26 (0.0 mol l^{-1} selenate concentration) to 2.86 (0.6 mol l^{-1} selenate concentration) and sodium selenate concentration up to 0–0.03 mol l^{-1} (potentiometry, $-\log[H^+]$ adjusted to the value equal to 3.5 when hydrolysis of uranyl under the presence of selenate is negligible) and at the temperature equal to 298.2 ± 0.5 K. Hydrolysis of uranyl for concentrations used is negligible at this $-\log[H^+]$ value [2]. So, it was not necessary to take into consideration the formation of mixed hydroxo-selenate species.

3.3. Computation

For the calculations SQUAD [15], SUPERQUAD [16], SIBYLA [17] and HALTAFALL [18] programs were used running on a PC AT 386.

4. Results and discussion

4.1. The spectrophotometric study

First, kinetic stability of uranyl-selenate mixtures was tested. The absorbance of the solutions were checked during 24 h period. The change in absorbance values for the whole spectra never exceeded 0.01 absorbance unit. Thus, it was concluded, that the equilibrium is reached very fast. The solutions were stable for at least 24 h.

The absorption spectra recorded are given in Fig. 1. Experimental conditions are given therein. It is possible to observe that increasing selenate concentration absorption maxima of uranyl are shifted towards the longer wavelengths.

Rank of the absorbance matrix enables to predict the number of light-absorbing species in solution. The number of complexes formed was estimated from the first step of factor analysis of

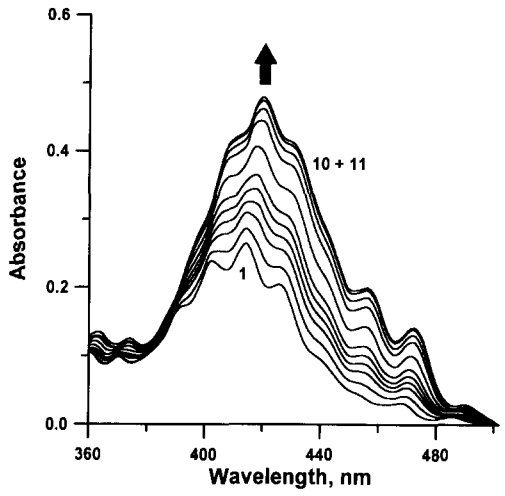

Fig. 1. Absorption spectra of uranyl at various selenate concentrations. Total concentration of uranyl $c_M = 0.0331$ mol l^{-1}. Total selenate concentration in mol l^{-1}: 1, 0.00; 2, 0.012; 3, 0.024; 4, 0.036; 5, 0.048; 6, 0.060; 7, 0.118; 8, 0.236; 9, 0.354; 10, 0.470; 11, 0.590.

absorption matrix (Principal Component Analysis) (Table 1). It follows from this analysis that there are 2–3 absorbing species formed, which is indicated by relative variance, cumulative relative variance and residual standard deviation values. Malinowski's indicator function IND_k [9] gives unreliably high number of the components. This criterion should be considered unreliable [19] in most of the cases. From low contribution of relative variance to the trace of second moment absorbance matrix we can conclude that there are three species in the solutions with different spectral properties.

Independently the formation of protonated species in $-\log[H^+]$ region 1.4–3.0 was also checked. The evidence for no formation of protonated species was found.

Therefore it was assumed, that the following equilibria take place in solution:

$$UO_2^{2+} + rSeO_4^{2-} \rightleftarrows UO_2(SeO_4)_r^{(2r-2)-} \quad (A)$$

with stability constant values

$$\beta_r = [UO_2(SeO_4)_r^{(2r-2)-}][UO_2^{2+}]^{-1}[SeO_4^{2-}]^{-r} \quad (9)$$

4.1.1. The search of the chemical model

The stoichiometry of species does not exceed 1:2 (stoichiometric ratio $r = 2$, Fig. 2). From above described facts it has been deduced, that there are only three absorbing species, i.e., stoichiometry M, ML and ML_2 in solution can be suggested.

Table 1
The results of factor analysis of spectrophotometric data for the system uranyl-selenate calculated by SIBYLA program for (a) normal and (b) first derivative spectra

k	Eigen value × 100	Variance (%)	Cumulative variance (%)	$S_k(A) \times 1000$	$IND_k \times 10^6$
(a)					
1	395.40	98.69	98.69	32.727	13.60
2	5.19	1.30	99.99	3.415	1.48
3	0.05	0.01	100.00	1.084	0.49
4	0.02	0.00	100.00	0.320	0.15
5	0.01	0.00	100.00	0.179	0.09
RM		2–3	2–3	3	5
tr(**M**) = 4.0064					
(b)					
1	0.019	94.16	94.16	1.545	0.644
2	0.01	5.55	99.71	0.349	0.151
3	0.00	0.29	100.00	0.037	0.016
4	0.00	0.00	100.00	0.022	0.011
RM		3	3		4
tr(**M**) = 2.0047×10^{-3}					

Experimental data: set of 21 solutions × 50 wavelengths, uranyl concentration: c_M 0.0331 mol l^{-1}, selenate concentration: c_L 0–0.6 mol l^{-1}.

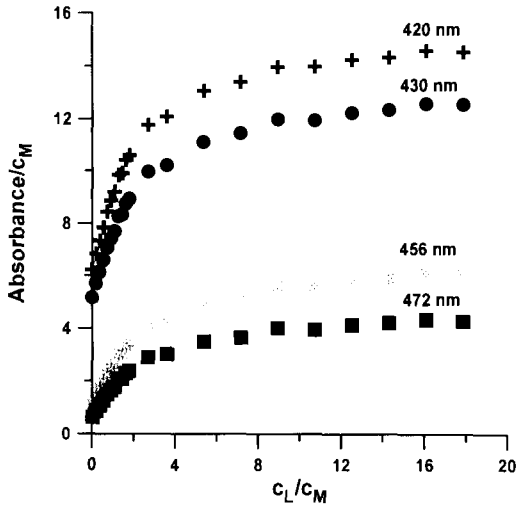

Fig. 2. Plots of absorbance vs. selenate concentration at selected wavelengths. Uranyl concentration $c_M = 0.0331$ mol l^{-1}.

Chemical model, i.e., the composition of the complexes and corresponding stability constants was searched for by the classical approach using 'trial and error' method [19].

A certain chemical model was suggested and then applying least-squares procedure of SQUAD program, minimising the sum of squares of residuals, U,

$$U = \sum_{i=1}^{n_w \times n_s} (\mathbf{A}_{exp,i} - \mathbf{A}_{calc,i})^2 = \min \quad (10)$$

where $\mathbf{A}_{exp}$ are experimental and $\mathbf{A}_{calc}$ calculated values of absorbances and the summation is done over all experimental points, number of solutions (n_s) times number of wavelengths (n_w). The program also calculates the S.D. of absorbance defined as

$$\sigma(\mathbf{A}) = \sqrt{\frac{U}{(n_s \times n_w - n)}} \quad (11)$$

where n is the number of parameters estimated. The 'best' one is that one for which is the lowest values of U and $\sigma(\mathbf{A})$ are obtained.

Several chemical models were tried. The most probable seems to be the model which consists of species M, ML and ML_2 (Table 2). The calculated molar absorptivities are given in Fig. 3.

As stability constants values show higher S.D. values computed from nonderivative spectroscopy, while lower values were found for the first up to the fourth derivative spectra Table 1 (Table 2). It is caused by similarity of spectra (Table 3), therefore the calculation of stability constants values has also been tried using derivative spectra with lower S.D. were observed for derivative spectra (Table 2). Also the choice of the wavelength values has influence on the correct stability constants values of the chemical model (Table 2).

Derivative spectra are very good alternative for the calculation of chemical model parameters (Table 2). Comparing calculated stability constants from both methods it is possible to see that results from derivative spectra have lower S.D's. The explanation is in this fact that peaks are

Table 2
Results of the equilibrium data analysis of the system uranyl-selenate from spectrophotometric data by SQUAD program

Spectrum order	log β (ML)	log β (ML_2)	$\sigma(A)$
0 derivative[a]	1.067 ± 0.005	not calculated	6.32×10^{-3}
0 derivative[a]	not calculated	2.58 ± 0.02	14.44×10^{-3}
0 derivative[a]	1.69 ± 0.04	2.37 ± 0.05	3.23×10^{-3}
0 derivative[b]	1.74 ± 0.05	2.49 ± 0.09	2.83×10^{-3}
1st derivative[b]	1.597 ± 0.008	2.41 ± 0.01	8.01×10^{-5}
2nd derivative[b]	1.565 ± 0.007	2.42 ± 0.01	2.78×10^{-5}
3rd derivative[b]	1.579 ± 0.008	2.43 ± 0.01	1.27×10^{-5}
4th derivative[b]	1.563 ± 0.008	2.43 ± 0.01	0.53×10^{-5}

Experimental data: set of 21 solutions × 50 wavelengths. Uranyl concentration c_M 0.0331 mol l^{-1}, selenate concentration c_L 0–0.6 mol l^{-1}.

[a] 50 chosen wavelengths in region 350–500 nm, e.g., 350, 354, 358, 362, 366, 370, 374, 378, 382, 386, 390, 392, 394, 398, 400, 402, 404, 408, 410, 414, 418, 420, 422, 424, 426, 428, 430, 432, 434, 436, 438, 440, 442, 444, 446, 448, 450, 454, 456, 458, 462, 466, 468, 470, 472, 474, 482, 486, 490 and 494 nm.

[b] 50 chosen wavelengths in region 360–500 nm, e.g., 360, 362, 364, 366, 370, 374, 378, 382, 386, 390, 392, 394, 398, 400, 402, 404, 408, 410, 414, 418, 420, 422, 424, 426, 428, 430, 432, 434, 436, 438, 440, 442, 444, 446, 448, 450, 454, 456, 458, 462, 466, 468, 470, 472, 474, 478, 482, 486, 490 and 494 nm.

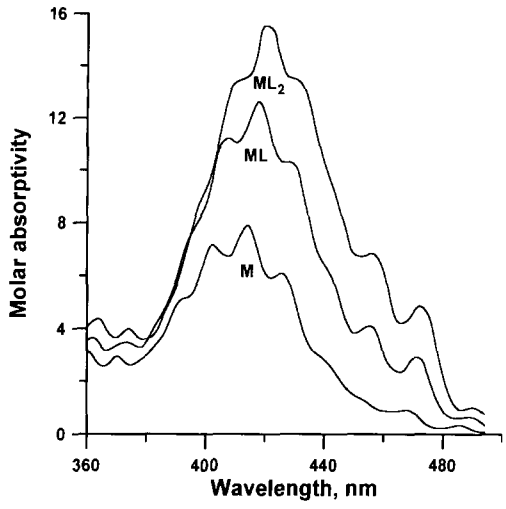

Fig. 3. Calculated spectra of individual species.

separated better to each other. On the other hand, the values of stability constants calculated by both methods are reliable because they are in region of 99.74% probability of each other confidence interval (three times S.D.) [20].

This improvement has several reasons. We can write combining mass balance equation and stability constant relationship with Bouger–Lambert–Beer law, respectively:

$$\mathbf{A}_{i,j} = \sum_{k=1}^{n} \varepsilon_{i,k}\beta_k[\mathrm{M}][\mathrm{L}]^k \tag{12}$$

for $i = 1, \ldots, n_w$ (number of chosen wavelength in measured spectra), $j = 1, \ldots, n_s$ (c_M, c_L, or pH is changed), $k = 1, \ldots, n$ (the number of complexes), $M, ML, \ldots, ML_n$.

If we differentiate over wavelength values n times, we obtain

$$\frac{\partial^n \mathbf{A}_{i,j}}{\partial\lambda^n} = \sum_{k=1}^{n} \frac{\partial^n \varepsilon}{\partial\lambda^n}\beta_k[\mathrm{M}][\mathrm{L}]^k \tag{13}$$

Choosing wavelength values in region where the position of wavelength under condition $\partial^n A_{i,j}/\partial\lambda^n = 0$ changing ligand or metal concentration, we get overdetermined system in which we can efficiently eliminate 'background'. This determination of the chemical model is more certain. At the same time respective contribution of individual species to total signal is higher for values obtained from derivative spectrophotometry than from normal spectrophotometry. This fact is already known in works concerning analytical determination of several components in mixture [21]. Second, the data are contemporaneously smoothed as it has been shown somewhere [22]. Above discussed facts all together play very important role in derivative spectra evaluation.

The distribution diagram calculated using the stability constants values as calculated (Table 2) is shown in Fig. 4.

4.1.2. Deconvolution of the spectra

The calculated spectra for each species were deconvoluted into one broad and two narrow bands of gaussian profile [23]:

$$\varepsilon_i = \varepsilon_{\max,i} \mathrm{e}^{-5.545(\lambda - \lambda_{\max,i})^2/2\sigma_i^2} \tag{14}$$

where ε_i is the calculated molar absorptivity, ε_{max} is the molar absorptivity at wavelength of the maximum molar absorptivity peak, λ is the wavelength, λ_{max} is the wavelength of the maximum absorptivity peak, and σ-half is the width of the absorption band, i.e., its width in half height of the band.

The area of spectral band is given by relationship [24,25] for so called oscillator strength

$$f_i = 1000 \ln(10)\frac{mc^2}{\pi e^2 N_A}\int_{\nu_1}^{\nu_2} \varepsilon \, \mathrm{d}\nu$$
$$= 4.315 \times 10^{-9} \int \varepsilon \, \mathrm{d}\nu \tag{15}$$

where m and e is charge and mass of electron, c is velocity of the light in vacuum, N_A is Avogadro number. We get after a simplification [24,25]

$$f_i \approx 4.60 \times 10^{-9} \varepsilon_{\max,i} \nu_{1/2} \tag{16}$$

if the band has gaussian shape with half-width $\nu_{1/2}$. After rearrangement for wavelength values in nanometers the relation Eq. (16) is equivalent to Eq. (17):

$$f_i \approx 4.60 \times 10^{-2} \varepsilon_{\max,i} \left(\frac{1}{\lambda_{\max,i} - \sigma_i} - \frac{1}{\lambda_{\max,i} + \sigma_i}\right) \tag{17}$$

This parameter is proportional probability of light absorption as quadrate of so called transition moment defined by relationships [24]

Table 3
Deconvolution of calculated molar absorptivities into three bands of Gaussian profile

Species	Band parameters	Band number			Statistical parameters	
		1	2	3	R^2	s
M	ε_{max}	2.4 ± 0.2	7.3 ± 0.1	0.6 ± 0.1		
	λ_{max} (nm)	360 (fix)	410.4 ± 0.4	467 ± 4	0.988	0.2555
	σ (nm)	34 ± 3	50 ± 2	26 ± 8		
	f_i	4.8×10^{-5}	2.0×10^{-4}	6.6×10^{-6}		
ML	ε_{max}	3.0 ± 0.2	12.0 ± 0.1	2.2 ± 0.2		
	λ_{max} (nm)	362 (fix)	416.0 ± 0.3	467 ± 2	0.991	0.3362
	σ (nm)	26 ± 4	50 ± 1	28 ± 4		
	f_i	5.5×10^{-5}	3.2×10^{-4}	2.6×10^{-5}		
ML_2	ε_{max}	3.8 ± 0.2	15.0 ± 0.1	3.6 ± 0.2		
	λ_{max} (nm)	364 (fix)	420.7 ± 0.4	467 ± 4	0.992	0.3953
	σ (nm)	24 ± 3	51 ± 1	26 ± 8		
	f_i	6.4×10^{-5}	4.0×10^{-4}	4.0×10^{-5}		

Remark: fixed values were obtained from logaritmic analysis of spectra [23].

$$P = \langle \psi_a | M | \psi_b \rangle = e\sqrt{D} \quad (18)$$

where D is so called dipole strength of electron transition between states defined wave functions Ψ_a and Ψ_b treated by means of dipole moment operator M. Those relationships connect experimental chemistry with theoretical quantum chemistry.

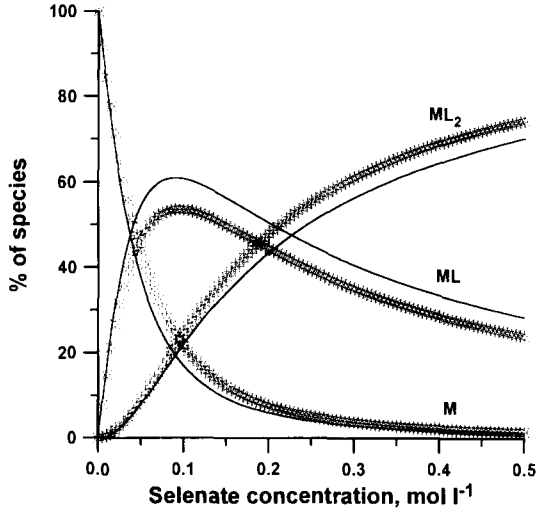

Fig. 4. Distribution diagram for uranyl-selenate complexes. Total uranyl concentration $c_M = 0.0331$ mol l^{-1}. Full drawn lines calculated for stability constants values log $\beta_1 = 1.742$ and log $\beta_2 = 2.488$. Dashed drawn lines calculated for stability constants values log $\beta_1 = 1.576$ and log $\beta_2 = 2.423$.

Also the deconvolution into the bands of studentian or lorentzian profile [23] was done, but using gaussian profile gave the best fit (Table 3). The parameters of gaussian profile show for complexes very low shift of wavelength of maximal molar absorptivity peak and higher maximal molar absorptivity value at wavelength of maximum molar absorptivity. The results are comparable with [24] where authors deconvoluted 24 (14 in VIS region and 10 in UV region) gaussian profile bands for the uranyl spectra. They represent three main bands in VIS region and also enable to calculate basic energy levels [24]. The oscillator strength values for uranyl were estimated for those three bands (Table 3) and they have been compared with literature data [1,26,27]. These values are in agreement with data found in the literature. Also increasing oscillator strength values in order M, ML and ML_2 species which can be assigned decreasing energy electron levels and therefore higher probability of electron transitions between levels.

The structures and intensities of the bands in spectrum are influenced mainly by geometry of the ligands co-ordinated to the uranyl moiety [27]. The electron transitions in the complexes are from point of view of the molar absorptivities spin allowed and Laporte forbidden [28] (for uranyl

cation it probably indicates octahedral aqua-complex $UO_2(H_2O)_6^{2+}$ in slight acid solution, of course, for complexes we suppose also deformed octaedrical structure, where two water molecules at octaeder corners are bonded less weakly than selenate or water in the square plane.

It was observed, that increasing pH up to four ($c_M = 0.0331$ mol l^{-1}, $c_L = 0.59$ mol l^{-1}), faint precipitate is formed in solution. The formed species is probably $[(UO_2)_2(SeO_4)_2(OH)_2]^{2-}$ while its charge is compensated by two sodium ions from the ionic medium (the product composition is the most probable). Uranyl ion has the most probably co-ordination number six in this compound. This hypothesis is supported by the fact that species of similar composition were proved for sulphate [6] and their formation was deduced from hydrolysis data in sodium sulphate medium [3,29]. Furthermore, products of similar composition were synthesised [30].

4.2. The potentiometric study

The equilibria in uranyl-selenate system were also investigated potentiometricaly by means of an uranyl electrode which enables to determine directly the concentration of free metal ion.

As it was already shown for uranyl electrode in [14], this one has no response in presence 0.01 mol l^{-1} sodium perchlorate as ionic medium. For 3 mol l^{-1} sodium perchlorate only constant response of uranyl electrode was observed which can be caused by the preferred formation of associate ion carrier with perchlorate than for associate with $UO_2(OH)^+$. Hence, all experiments were done without any adjustment of ionic strength in uranyl concentration region 0.1–0.5 mmol l^{-1} at $-\log[H^+]$ about 3.5 where protonation of selenate and the formation of uranyl hydrolytic polynuclear species are negligible [31]. The slope of the electrode was lower than the theoretical one given by Nerstian equation. The function of uranyl electrode is not still completely clear, there is only a hypothesis that species responsible as active carrier one of the electrode [14] is complex $UO_2(OH)^+$. The following equation was derived [14]:

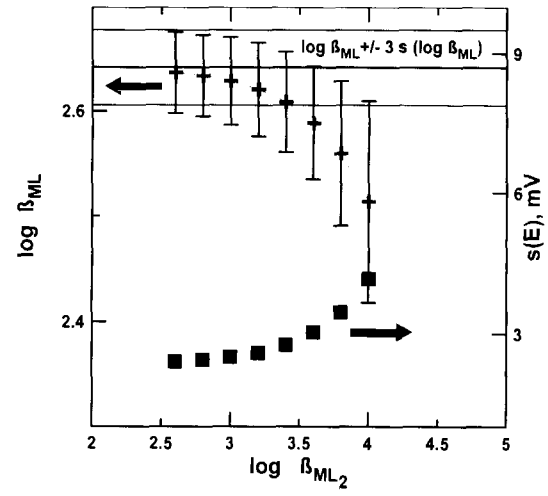

Fig. 5. The search of the chemical model from potentiometric data.

$$E = \text{const} + \frac{RT}{F} \ln a_{UO_2^{2+}} + \frac{RT}{F} \ln a_{OH^-} \qquad (19)$$

That is why the measurements were carried out at constant pH value. At lower uranyl concentration we can also assume that $a_{UO_2^{2+}} \approx c_{UO_2^{2+}}$.

It is clear from spectrophotometric results that species ML and ML_2 are formed, but it was possible to calculate from potentiometric data only stability constant for ML species ($\log \beta_1 = 2.64$). The explanation is that complexes formed are rather weak and thus even at very high ligand excess (several hundreds times over uranyl concentration) solutions are diluted and complex ML_2 is formed at low amount (maximum amount is 20% rel at very high ligand excess) in course of the ML species formation. This is detectable from calculations. Therefore the model with fixed stability constant values for species ML_2 was also tested (Fig. 5). It can be estimated from Fig. 5 and also from experimental points at very high ligand excess that stability constant value of species ML_2 does not exceed 3.4 ($\log K_2$ lower than 0.8). Both values for species ML and ML_2 are lower than for the complexes in the uranyl-sulphate system, respectively [3] (weighted average of $\log \beta(ML) = 3.1 \pm 0.1$, $\log \beta(ML_2) = 3.9 \pm 0.2$ and thus $\log K_2 = 0.8$) and this is in agreement with their protonation constants values (selenate is a weaker base than sulphate and so it should

form a little weaker complexes with the same metal ions as sulphate) and polarizability (HSAB principle).

If we consider $\log \beta_1^*$ as stability constant value at zero ionic strength (in our case 2.64) and $\log \beta_1$ (for 3 mol l^{-1} sodium perchlorate from derivative spectrophotometry measurements 1.58 ± 0.01) as stability constant value at ionic strength I_m given in molality scale (3 mol l^{-1} sodium perchlorate solution has molality 3.502 mol kg^{-1}), we can write according [3,32] the equation:

$$\log \beta_1 + 8D = \log \beta_1^* - \Delta\varepsilon I_m \quad (20)$$

where $D = A\sqrt{I_m}/(1 + 1.5\sqrt{I_m})$ is the derived Debye-Hückel term, and $\Delta\varepsilon = -\varepsilon(SeO_4^{2-}, Na^+) - \varepsilon(UO_2^{2+}, ClO_4^-)$ is obtained from interaction coefficients representing solute interactions in solution. After substitution of all known terms and value $\varepsilon(UO_2^{2+}, ClO_4^- = 0.26$ from [3] we obtain for $\varepsilon(SeO_4^{2-}, Na^+ = -0.009$. Then, from all known and calculated values the relationship Eq. (21) can be derived. This equation is suitable for the estimation of the activity coefficient in sodium selenate solution

$$\log \gamma_{\pm} = \frac{-0.51052\sqrt{3c_m}}{1 + 1.5\sqrt{3c_m}} + 2\varepsilon(SeO_4^{2-}, Na^+) \times c_m \quad (21)$$

where c_m is molal concentration of sodium selenate and additional term describes deviation from an ideal solution behaviour for 2:1 electrolyte. Comparing $\varepsilon(SO_4^{2-} = -0.12 \pm 0.06$ from [3] the solutions of sodium selenate have more ideal behaviour as electrolyte 2:1 than sodium sulphate. The relationship Eq. (21) can be used for the calculation of stability constants of the selenate with different metal ions under presence of sodium ions as supporting electrolyte.

Acknowledgements

We thank Ing. Jaroslav Šenkýř, PhD for the preparation of the uranyl ion selective electrode and also to RNDr Lubomír Knesel, Hewlett-Packard company (Prague, Czech Republic) for lending us HP 8452A demo equipment.

References

[1] E. Rabinovitch and R.L. Belford, Spectroscopy and Photochemistry of Uranyl Compounds, Pergamon Press, New York, 1964.
[2] J. Havel, and L. Sommer, Chromogenic Reactions of Uranium, Folia Fac. Sci. Nat. Univ. Purk. Brun., Brno, 1973.
[3] I. Grenthe, J. Fuger, R.J.M. Konings, R.M. Lemire, A.B. Muller, C. Nguyen Trung and H. Wanner, Chemical Thermodynamics of Uranium, NEA-TDB, OECD, North-Holland, Amsterdam 1992, and References therein.
[4] I. Grenthe and B. Lagerman, Acta Chem. Scand., 45 (1991) 122.
[5] G. Bidoglio, P. Cavalli and I. Grenthe, Talanta, 38 (1991) 433.
[6] I. Grenthe and B. Lagerman, Radiochim. Acta, 61 (1993) 169.
[7] P. Lubal and J. Havel, XX Annual Congress IV Spanish-Italian Congress on Thermodynamics of Metal Complexes, 8–11 June 1993, Rome, Italy; Chemometrics III, 11–15 July 1993, Brno, Czech Republic.
[8] J.J. Kankare, Anal. Chem., 43 (1970) 1322.
[9] E. Malinowski, Factor Analysis in Chemistry, Wiley-Interscience, New York, 1991.
[10] G. Gran, Anal. Chim. Acta., 206 (1988) 111.
[11] D.I. Rjabčikov and M.M. Senjavin (Eds.), Analitičeskaja Chimija Urana (Analytical Chemistry of Uranium), Akad. Nauk, Moscow, 1962.
[12] Some Laboratory Methods, KTH Stockholm, 1981.
[13] A. Okáč, Qualitative Analytical Chemistry, Academia, Prague, 1966.
[14] J. Šenkýř, D. Ammann, P.C. Meier, W.E. Morf, E. Pretsch and W. Simon, Anal. Chem., 51 (1979) 786.
[15] D.J. Leggett (Ed.), Computational Methods for the Determination of Formation Constants, Plenum Press, New York, 1985; J. Havel, unpublished results.
[16] P. Gans, A. Sabatini and A. Vacca, J. Chem. Soc., (D) (1985) 1195.
[17] J. Havel and L. Jančář, Scripta Fac. Sci. Nat. Univ. Purk. Brun., 28 (1990) 295.
[18] N. Ingri, W. Kakolowicz, L.G. Sillén and B. Warnquist, Talanta, 14 (1967) 1261.
[19] J. Havel, Scripta Fac. Sci. Nat. Univ. Purk. Brun., 17 (1987) 305.
[20] D.C. Harris, Quantitative Chemical Analysis, W.H. Freeman and Company, New York, 1991.
[21] C. Bosch Ojeda, F. Sanchez Rojas and J.M. Cano Pavon, Talanta, 42 (1995) 1195.
[22] T.C. O'Haver and T. Bergley, Anal. Chem., 53 (1981) 1876.
[23] P. Pelikán, M. Čeppan and M. Liška, Applications of Numerical Methods in Molecular Spectroscopy, CRC Press, Boca Raton, 1994.
[24] A.B.P. Lever, Inorganic Electronic Spectroscopy, Elsevier, Amsterdam, 1986.

[25] C.K. Jorgensen, Acta Chem. Scand., 9 (1954) 405; C.J. Ballhausen, Acta Chem. Scand., 8 (1954) 821.
[26] J.T. Bell and R.E. Biggers, J. Mol. Spec., 18 (1965) 247; J.T. Bell and R.E. Biggers, J. Mol. Spec., 18 (1968) 312.
[27] Gmelin Handbook of Inorganic and Organometalic Chemistry, Vol A5 (Spectra), Gmelin Institute for Inorganic Chemistry Frankfurt am Main, 1982.
[28] J.E. Huhey, E.A. Keiter and R.L. Keiter, Inorganic Chemistry—Principles of Structure and Reactivity, Harper Collins College Publishers, 1993.
[29] A. Peterson, Acta Chem. Scand., 15 (1960) 101; I. Grenthe and J. Havel, unpublished results.
[30] I.I. Čerňjajev, Kompleksnyje Sojedinenija Urana (Complex Compunds of Uranium), Nauka, Moscow, 1964.
[31] L. Šůcha and S. Kotrlý, Handbook of Chemical Equilibria in Analytical Chemistry, SNTL, Prague 1988, p. 78.
[32] G. Anderegg and S. Kholeif, Talanta, 41 (1994) 1507; G. Anderegg and S. Kholeif, Talanta, 42 (1995) 1067.

ELSEVIER

Talanta 44 (1997) 467–474

Talanta

Square wave adsorptive voltammetric determination of sunset yellow

J.J. Berzas Nevado *, J. Rodríguez Flores, M.J. Villaseñor LLerena

Department of Analytical Chemistry and Foods Technology, University of Castilla La Mancha, 13071 Ciudad Real, Spain

Received 11 April 1996; received in revised form 12 September 1996; accepted 17 September 1996

Abstract

Square wave adsorptive stripping voltammetry was used for determining trace amounts of dye Sunset Yellow (E-110) for the first time. Its adsorptive voltammetric behaviour followed by a square wave mode step was investigated at different pH media. Sunset Yellow in 0.5 M NH_4Cl/NH_3 buffer solution gave an adsorptive stripping voltammetric peak at the hanging mercury drop electrode at -0.60 V using an accumulation potential of -0.40 V. The effect of experimental parameters that affected this determination are discussed. The calibration graph to determine Sunset Yellow was linear in the range 5–90 $\mu g\ l^{-1}$, obtaining a relative standard deviation of 2.2% for a solution of 30 $\mu g\ l^{-1}$ ($n = 10$) in the same day. The determination limit was 5 $\mu g\ l^{-1}$ after 15 s of accumulation at -0.40 V. The proposed method was applied to determine this dye in several commercial refreshing drinks, which contained small amounts of this compound. Measurements were made directly over diluted solutions of commercial samples. Similar results were obtained between adsorptive stripping square-wave voltammetric values and the obtained by application of a HPLC method with spectrophotometric detection. © 1997 Elsevier Science B.V.

Keywords: Adsorptive stripping voltammetry; Chromatography; Dyes; Sunset Yellow

1. Introduction

Food colorants may often be considered simply cosmetic in nature, but the role they play in our food supply is actually very significant. Colour is the first sensory quality by which foods are judged and food quality and flavour are closely associated with colour. Consumers are conditioned to expect foods of certain colours and to reject any deviation from expectations. The psychological basis for the need for food colours is well established [1].

Colorants also play a significant role in enhancing the aesthetic appeal of food. They are very important ingredients in many convenience foods such as confectionery products, gelatin desserts, snacks and beverages, since many of these would be colourless and would thus appear undesirable without the inclusion of colorants.

The term colour additive can be applied to any dye, pigment or other substance made (artificial colorant) or obtained from a vegetable, animal, mineral or another natural source, that are capable of coloring foods, drugs or cosmetics [2].

* Corresponding author.

PII S0039-9140(96)02105-4

Sunset Yellow, subject of this work, is a synthetic dye available as yellow powder that can be present in common foods (drinks, yoghurts, ice cream, sweets, etc., ...). The presence and content of this dye must be controlled because it is not totally inoccuo. Development of regulations for use of foods colorants was reviewed by Haveland-Smith [3].

Recently, we have developed spectrophotometric methods in order to determine this dye in two different binary mixtures and a ternary mixture with other two yellow colorants [4–6]. These methods were applied to several commercial products.

On the other hand, chromatographic methods have been previously used for colorant analysis in foods [7–10].

Fogg et al. have reported sensitive methods to determine several dyes (Quinoline Yellow, Tartrazine, Carmoisine, etc., ...) by means of the use of paste carbon electrode in static systems or in continuous flow systems [11–13].

Fogg et al. have also realized a theoretical and general study about the voltammetric behaviour of several synthetic colorants (reduction peak potentials and intensities) by means of DPS and DPP techniques [14,15]. Sunset Yellow was not determined in any commercial product in both cases, since the study made was almost brief and theoretical. The sensitivities reached by Fogg et al. in the analysis of some dyes in commercial samples (cosmetic and tablets coatings) were smaller than the obtained by us in soft drinks.

The polarographic reduction mechanism of azo-compounds has been known for some time [16,17]. The electrode process must be consistent with the mechanism that postulates a step-wise breakage of the molecule, similar to that occurring in the metabolic processes of these dyes.

$$R-N=N-R_1+4H^++4e^- \rightarrow R-NH_2+R_1-NH_2$$

where RNH_2 is sulfanilic acid and R_1NH_2 is 1-amino-2-hydroxy-6-naphthalenesulphonic acid [18].

In this work, a study of the electrochemical behaviour of Sunset Yellow (whose formula is given) has been achieved taking into account the possible adsorption of the molecule on the mercury and following the study by square wave voltammetry with a previous stripping period. The method proposed by us permits to reach a similar sensitivity than the obtained by the already mentioned DPP method and it reduces at least ten times the length of real time of analysis (27 s).

Sunset Yellow

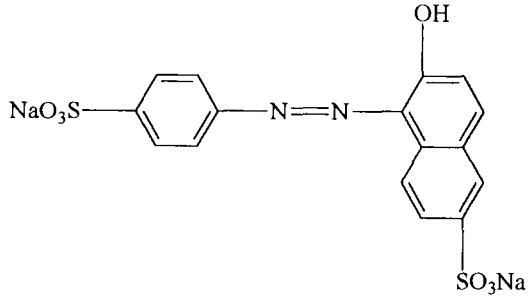

The sensitivity of adsorptive stripping methods is obviously their greatest advantage. In the other hand, a serious drawback is the interference from other surface-active substances that may be present in the solution. In this case, competitive adsorption usually occurs and produces a decrease in the measured current or in concentrations of surface-active substances and, consequently, significant suppressions of the signal are observed. In such conditions, it is necessary to employ a suitable separation of interfering compounds. If the sample contains interfering compounds that are electrochemically active but are not adsorbed on the electrode surface, classical separation procedures will be not necessary then.

Another advantage of stripping analysis is the possibility of working with very diluted samples that produces a logical decrease of interferences in foods techniques.

The simultaneous use of adsorptive stripping techniques and square wave measurements provides a very sensitive, selective and rapid approach. The method here proposed has yielded good results in the determination of Sunset Yellow in three different commercial products: Tof

lemon and Gatorade orange (both contain E-104 (Quinoline Yellow) and E-110 (Sunset Yellow) as dyes) and in other third refreshing drink flavour orange (Product 3), which also contains two dyes: E-102 (Tartrazine) and E-110 (Sunset Yellow).

2. Experimental

2.1. Reagents

All solvents and reagents were of analytical grade unless indicated otherwise. Solutions of voltammetric study were made with deionized water (Milli-Q quality). Sunset Yellow (E-110) solution was reached from Sancolor S.A enterprise. Stock solutions had a concentration of 10 mg l^{-1}. In order to achieve all voltammetric studies following solutions were also prepared: a 0.1 M HCl solution, an $HOAc/OAc^-$ buffer solution (0.1 M and pH = 4.8), a NaH_2PO_4/Na_2HPO_4 buffer solution (0.1 M and pH = 7.7) and a NH_4Cl/NH_3 buffer solution (0.1 M and pH = 10.0). All these were prepared from suprapure reagents. Methanol (HPLC quality) was used in chromatographic analysis

Three commercial products containing Sunset Yellow were studied. These are the followings:

Refreshing drink Tof, flavour lemon: with carbonated water, sugars, lemon juice, citric acid, lemon flavoring, emulsifiers E-915 (glycerol esters) and E-414 (arabic gum), sweetenings, preservative E-211 (sodium benzoate) and dyes: E-104 (Quinoline Yellow) and E-110.

Gatorade, flavour orange: with water, glucose, saccharose, citric acid, mineral salts, natural flavorings and dyes: E-104 and E-110.

Product 3, (refreshing drink flavour orange): with carbonated water, sugars, orange juice, citric acid, orange essences, sodium benzoate, dyes E-102 (Tartrazine) and E-110 and ascorbic acid.

Ingredients above summarized are in the three cases in order decreasing of concentration.

The trade name of third product has not been given because its manufacturing enterprise want to remain anonymous.

2.2. Apparatus

Square-wave voltammograms were obtained with a Princenton Applied Research (PAR) Model 384B polarographic analyzer combined with a stand PAR Model 303 A static mercury drop electrode (SMDE), using an Ag/AgCl reference electrode, a PAR Model 305 magnetic stirrer, a TANDOM computer using 384 B software and a EPSON FX 850 printer.

The HPLC equipment used was: a SHIMADZU model SPD-M10A, with a double pump system, that permit us to work in gradient mode, and as stationary phase a chromatographic column Apex C_{18} (25 cm of length and 5 μm as particle diameter).

2.3. Procedure

The general procedure for adsorptive stripping voltammetric method was as follows: in order to achieve all voltammetric assays, 10 ml of 0.5 M NH_4Cl/NH_3 buffer solution were placed in the polarographic cell, using in all assays an accumulation potential of −0.40 V, an accumulation time of 15 s and a rest period of ten seconds, being after that scans run in the negative direction between −0.4 and −0.9 V in these conditions. Experimental and instrumental parameters that affected the process were optimized and the obtained results are the followings: NH_4Cl/NH_3 concentration = 0.5 M, t_{ac} (accumulation time) = 15 s, E_{ac} (accumulation potential) = −0.40 V, ΔE (pulse amplitude) = 50 mV, Δs (scan increment) = 4 mV, frequency = 70 Hz and electrode area = 2.5 mm^2.

All results shown in this paper were obtained at room temperature (25 ± 1°C).

The determination of Sunset Yellow in these three commercial products was also verified by HPLC using a diode-array detector with measurements at 420, 440 and 480 nm (wavelengths where the Sunset Yellow absorbance was maximum) and the stationary phase already mentioned in Section 2.2. As mobile phase we have employed a mixture of methanol and 0.1 M buffer solution NaH_2PO_4/Na_2HPO_4 (pH = 7.0) following the next gradient of concentrations.

Time (min)	Concentrations
0–2	20% methanol constant
2–5	20–100% methanol in linear gradient
5–7	100% methanol constant

The flow rate was 1.5 ml min^{-1}. In such conditions the retention time of this dye was 4.6 min.

3. Results and discussion

Firstly, a preliminary study about the adsorptive voltammetric behaviour of Sunset Yellow at different pH values (1.3, 4.7, 7.7 and 10.0) was realized for 0 and 30 s of accumulation time. In the first case (pH:1.3) there was not shown any reduction process in the checked potential range for the studied dye, whereas in the other three pH tested an only reduction peak was obtained, whose potential peak was shifted to potential more negative when the pH increased, which involves that E_p was pH dependent, (as expected for a reaction in which hydrogen ions take part in the electrochemical process), and whose intensity rose with the use of accumulation times. It was selected a value of pH 10 (NH_4Cl/NH_3 buffer) as optimum medium because the reduction peak obtained showed the highest sensitivity and the best definition.

We have chosen SWAdSV with regard DPAdSV by means of a brief investigation, in which square-wave voltammetry response was found to be very sensitive to the adsorption of Sunset Yellow on the mercury drop surface. In this study, a sample was treated in the same experimental conditions and with the most similar instrumental parameters by both techniques.

Later experiments were carried out in order to find optima chemical and instrumental conditions to determine Sunset Yellow by the technique chosen.

The selection of the optimum concentration of NH_4Cl/NH_3 buffer solution was made in order to reach the best signal over the background, subsequently, concentration of NH_4Cl/NH_3 buffer solution was varied between 0.01 and 0.50 M for a 200 μg l^{-1} Sunset Yellow solution. In Fig. 1 it is shown this experience and as it can be seen when the concentration buffer was increased between 0.01 and 0.25 M the peak response also increased, reaching a plateau between 0.25 and 0.50 M. This last concentration was chosen as optimum because it yielded the maximum peak response into the constant intensity area. The potential peak (E_p) stayed constant in all this experience.

In conditions above mentioned, the stability for a 30 μg l^{-1} solution of Sunset Yellow was tested, so, this solution seemed to be stable for two hours, which was enough to recorder all scans of an experience by SWAdSV technique, whereas for higher periods than 2 h, a decrease of the peak current associated with this reduction process was observed.

With regard to the advantageous use of nitrogen atmosphere maintained over the solution surface, parallel experiences were realized in presence and absence of N_2 showing similar results in both cases; for this reason, faster analysis could be even achieved satisfactorily by using non deoxygenated samples.

After that, it was achieved the optimization of instrumental parameters that affected the response to the adsorption phenomenon and to the

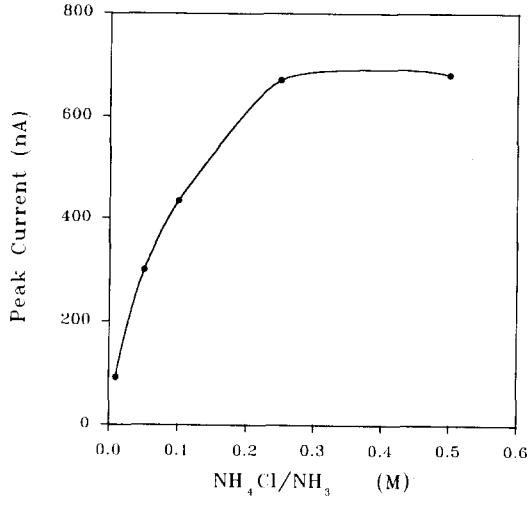

Fig. 1. Influence of NH_4Cl/NH_3 concentration over SWAdSV signal for a 200 μg l^{-1} Sunset Yellow solution. Experimental conditions: $\Delta E = 50$ mV, $\Delta s = 2$ mV, frequency = 50 Hz, electrode area = 2.5 mm^2.

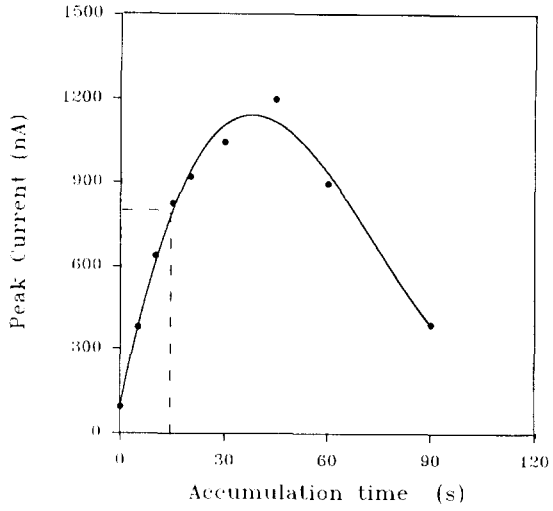

Fig. 2. Influence of accumulation time over the SWAdSV signal for a 30 μg l^{-1} Sunset Yellow solution. Experimental conditions: $[NH_4Cl/NH_3] = 0.5$ M, $E_{acc} = -0.4$ V, $\Delta E = 50$ mV, $\Delta s = 2$ mV, frequency = 50 Hz, electrode area = 2.5 mm^2.

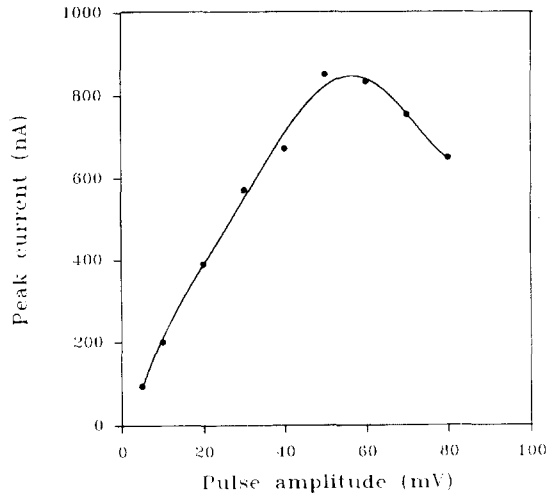

Fig. 3. Effect of pulse amplitude over the SWAdSV signal for a 30 μg l^{-1} Sunset Yellow solution. Experimental conditions: $[NH_4Cl/NH_3] = 0.5$ M, $E_{acc} = -0.4$ V $t_{acc} = 15$ s, $\Delta s = 2$ mV, frequency = 50 Hz, electrode area = 2.5 mm^2.

own technique. In all these assays a concentration of 30 μg l^{-1} of Sunset Yellow was used as suitable in order to prevent a rapid saturation of the mercury drop. Results obtained are the followings:

As optimum accumulation time (t_{acc}) it was chosen a value of 15 s because provided the largest peak current in the linearity range, whereas for accumulation times between 15 and 45 s the signal showed a not linear increase and even decreased the peak intensity for larger accumulation times as it is shown in Fig. 2. The potential of the reduction peak stayed constant for all this experience, however light shifts in E_p values to positive potentials were observed when very high accumulation times were tested. The linear relation found between I_p and t_{acc} in the range 0–15 s was the following:

$I_p(nA) = 98.33 + 54.28 t_{acc} \quad r = 0.9997 \quad n = 5$

In order to select the most suitable accumulation potential (E_{acc}) several values were tested (−0.30, −0.35, −0.40 and −0.45 V). The I_p value was independent of E_{acc} from −0.30 to −0.40 V and decreased for −0.45 V. An $E_{acc} =$ −0.40 V was selected as optimum. The variation of accumulation potential did not produce shifts in E_p values.

The influence of the pulse amplitude (ΔE) over the peak intensity was studied between 5 and 80 mV and a not linear relationship was observed in this range, being selected as optimum a value of 50 mV, because gave the largest peak intensity, decreasing the obtained signal for higher values of this parameter. In the other hand, an increase in ΔE values produced a shift in E_p to positive potentials. The effect of pulse amplitude over the peak intensity is shown in Fig. 3.

When the scan increment (Δs) was tested, the increase of this parameter (2, 4, 6, 8 and 10 mV) produced an increase in the peak intensity (Table

Table 1
Variation of I_p and E_p with Δs for the reduction process of 30 μg l^{-1} Sunset Yellow solution

Δs (mV)	E_p(V)	I_p(nA)
2	−0.57	820.3
4	−0.59	1090.4
6	−0.61	1115.1
8	−0.62	1190.5
10	−0.64	1234.3

Experimental conditions: $[NH_4Cl/NH_3] = 0.5$ M, $t_{acc} = 15$ s, $E_{acc} = -0.4$ V, $\Delta E = 50$ mV, frequency = 50 Hz, electrode area = 2.5 mm^2.

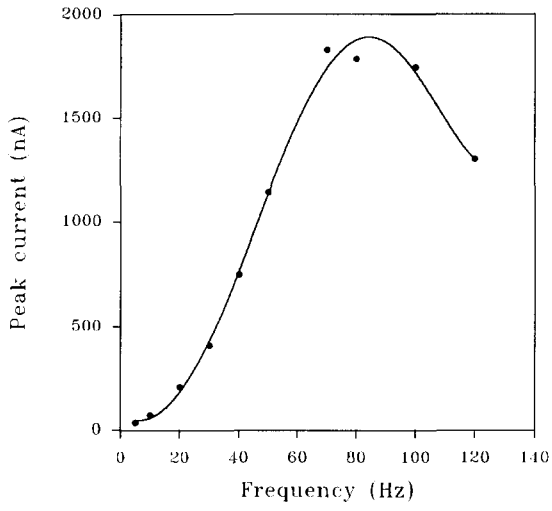

Fig. 4. Influence of frequency over the SWAdSV signal for a 30 μg l^{-1} Sunset Yellow solution. Experimental conditions = $[NH_4Cl/NH_3] = 0.5$ M, $t_{acc} = 15$ s, $E_{acc} = -0.4$ V, $\Delta E = 50$ mV, $\Delta s = 4$ mV, electrode area = 2.5 mm^2.

1), but also a distortion in this signal was observed, resulting a poorer resolution. It was concluded that an intermediate value of 4 mV was the most appropriate.

With regard to the frequency, the influence of this parameter was studied between 5 and 120 Hz, and a not linear response was obtained in this range, being selected as optimum a value of 70 Hz, because provided the largest peak current, decreasing this signal for higher values of this parameter as it is shown in Fig. 4. When frequency values were increased, E_p values showed a shift to negative potentials.

In these conditions, a very reasonable scan rate of 280 mV/s ($\Delta s \times$ frequency) was reached in this determination.

It was also tested the influence of the electrode area (1.0, 1.6 and 2.5 mm^2) over the peak current. In this experience, the increase of the size of area yielded, as expected, an increase in the peak response and did not affect the value of E_p. The size 'large' (2.5 mm^2) was considered as suitable in this experience because provided the largest intensity.

In conditions previously optimized, the repeatability of the signal was checked in the same day by measurements of a 30 μg l^{-1} Sunset Yellow solution and a relative standard deviation of 2.2% was obtained in such conditions ($n = 10$)

Once established the most suitable chemical and instrumental conditions, voltammograms at different concentrations of Sunset Yellow were recorded in such conditions in order to check the linearity range, showing an only peak at -0.60 V (Fig. 5). A calibration graph was established between 5.0 and 90.0 μg l^{-1} against their respective peak intensities, being the obtained equation:

$$I_p(nA) = 163.9 + 59.87C_s(\mu g\, l^{-1}) \quad r = 0.9994$$

$$n = 7$$

The determination limit (minimum signal measurable over the background voltammogram) reached in these conditions was 5.0 μg l^{-1}.

In Table 2 optima conditions selected by the studied technique have been summarized and also the variation range tested for each parameter.

4. Applications

The procedure for the preparation of the samples was the same in all cases: a known volume of

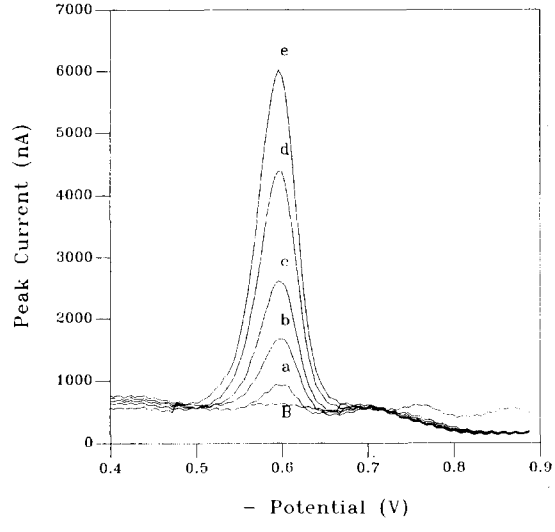

Fig. 5. Background (B) and square wave adsorptive stripping voltammograms at different concentrations of Sunset Yellow: (a) 5.0, (b) 15.0, (c) 30.0, (d) 60.0 and (e) 90.0 μg l^{-1}. Experimental conditions: $[NH_4Cl/NH_3] = 0.5$ M, $t_{acc} = 15$ s, $E_{acc} = -0.4$ V, $\Delta E = 50$ mV, $\Delta s = 4$ mV, frequency = 70 Hz, electrode area = 2.5 mm^2.

Table 2
Optima conditions to determine Sunset Yellow by SWAdSV

Parameter	Variation range	Optimum value
NH_4Cl/NH_3 concentration	0.01–0.5 M	0.5 M
Accumulation time	0–90 s	15 s
Accumulation potential	−0.30–0.45 V	−0.40 V
Pulse amplitude	5–80 mV	50 mV
Scan increment	2–10 mV	4 mV
Frequency	5–120 Hz	70 Hz
Electrode area	1.0–2.5 mm^2	2.5 mm^2
Linearity range	5.0–430.6 $\mu g\ l^{-1}$	5.0–90.0 $\mu g\ l^{-1}$

the commercial product (200, 20 and 100 μl of Tof lemmon, Gatorade lemmon and the third refreshing drink, respectively) was added in a 10 ml NH_4Cl/NH_3 0.5 M solution, which was placed in the voltammetric cell.

Standard addition method was used for determining contents of studied dye in order to avoid matrix effects. In Table 3 have been summarized the mean and standard deviations (estimated from five determinations) of results obtained in these analysis by standard additions method in each product. In Fig. 6 are shown voltammograms obtained when additions of Sunset Yellow of 10.0, 20.0 and 40.0 $\mu g\ l^{-1}$ were made over a diluted solution of commercial product Gatorade in 0.5 M NH_4Cl/NH_3.

In conditions already described in experimental section for HPLC study, three linear calibration graphs were established between 0.2 and 12.0 mg l^{-1} with slopes of 14.98, 17.43 and 31.70 arbitrary units of peak area $\times 1\ mg^{-1}$ at 420, 440 and 480 nm, respectively ($r = 0.9996$, 0.9994 and 0.9997).

Table 3
Contents ($\mu g\ l^{-1}$) of Sunset Yellow in commercial products

Refreshing drinks	SWAdSV	HPLC
Tof (lemon)	192 ± 4[a]	200 ± 5
Gatorade (lemon)	5790 ± 116	—
Refreshing drink (orange)	2142 ± 42	1960 ± 39

— Already explained in Section 4.
n (number of determinations) = 5.
[a] Mean ± S.D.

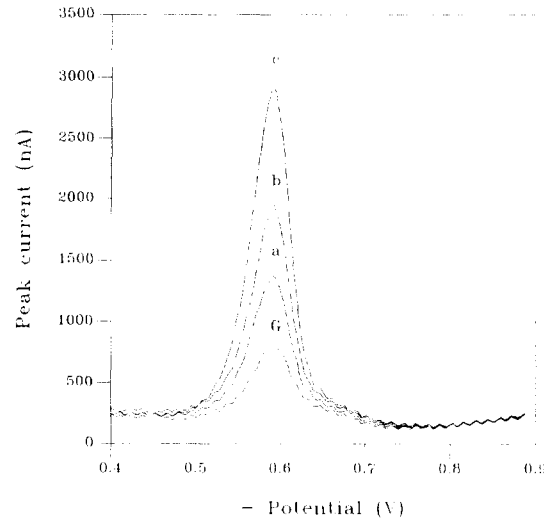

Fig. 6. Square-wave voltammograms of Gatorade (G) and standard additions of Sunset Yellow of (a) 10.0, (b) 20.0 and (c) 40.0 μg^{-1}. Experimental conditions: $[NH_4Cl/NH_3] = 0.5$ M, $t_{acc} = 15$ s, $E_{acc} = -0.4$ V, $\Delta E = 50$ mV, $\Delta s = 4$ mV, frequency = 70 Hz, electrode area = 2.5 mm^2.

Chromatographic results are also summarized in Table 3 and as it can be seen these results are in accordance with the obtained by voltammetric method. Sunset Yellow was not determined in Gatorade product by HPLC because voltammetric and chromatographic studies were achieved in different time periods, so when we realized chromatographic analysis this product had varied its composition and Sunset Yellow had been replaced by β-Carotene (E-160 a)

In the other hand, the presence of dye Quinoline Yellow in the composition of commercial products Tof and Gatorade did not involve interferences in the voltammetric determination of Sunset Yellow because in chemical conditions established Quinoline Yellow did not give reduction peaks at potentials where Sunset Yellow was reduced.

With regard to Tartrazine (Product 3), this colorant produced small interferences in the determination of studied dye, because gave a current peak at potentials (−0.61 V) very nearly to the Sunset Yellow (−0.60 V), which produced small differences between chromatographic and voltammetric results, (as it is shown in Table 3), that

could be due to the possible contribution of Tartrazine over voltammetric signal of Sunset Yellow, nevertheless, for similar concentrations, Sunset Yellow had a higher tendency than Tartrazine to be absorbed in the surface drop electrode in the accumulation step and consequently higher possibilities to be reduced in the cathodic run, showing higher peak currents. The presence of small amounts of Sunset Yellow restrain the Tartrazine signal corresponding to higher concentrations. In order to quantify this behaviour seven samples of different concentration ratios (Sunset Yellow: Tartrazine) were tested from ratios 4:1 to 1:10. It was observed a great contribution of Tartrazine over the analytical signal of Sunset Yellow (25–250%) from ratios 1:1 to 1:10, whereas in the other tested ratios there was not this interference.

5. Conclusions

Adsorptive stripping square-wave voltammetry is an useful technique to determine Sunset Yellow in commercial refreshing drinks. The sensitivity and accuracy of the method allowed in the determination of Sunset Yellow, and the relatively short accumulation times and inexpensive instrumentation are some of advantages provided by this technique.

We advise the proposed method using standard addition method measurements (in order to prevent matrix effect), taking into account good results obtained, the speed of the determination in analysis (very short length of real time analysis: 27 s), the simplicity of treatment of the sample (measurements have been made directly over a diluted solution of commercial product) and higher sensitivities reached in commercial applications with regards to other techniques [18] in the determination of contents of the studied dye in complex matrix as foods.

Satisfactory results and small values of standard deviations obtained in the determination of the dye in these three commercial products are an indication of the applicability of this method in other beverages and foods that contain this dye.

Acknowledgements

The authors thank the DGICYT of the Ministerio de Educación y Ciencia (Spain) for supporting this study (Project PB 94-0743)

References

[1] M.A. Amerind, R.M Pangborn and E.B. Roessler, Principles of Sensory Evaluation of Food, Ed. Academic Press, New York, 1965.
[2] R.L. Newsome, in A.L. Branen, P.M. Davidson and S. Salminen (Eds.), Food Additives, New York, 1989.
[3] R.D. Combes and R.B. Haveland-Smith, Mutat. Res., 98 (1982) 101.
[4] J.J. Berzas Nevado, J. Rodríguez Flores and M.J. Villaseñor LLerena, Analusis, 21 (1993) 395.
[5] J.J. Berzas Nevado, J. Rodríguez Flores and M.J. Villaseñor LLerena, Anal. Lett., 27 (1994) 1009.
[6] J.J. Berzas Nevado, J. Rodríguez Flores and M.J. Villaseñor LLerena, Bull. Soc. Chim. Belg., 102 (1993) 527.
[7] M.L. Puttemans, L. Dryon and D.L. Massart, J. Assoc. Off. Anal. Chem., 65 (1982) 737.
[8] M.L. Puttemans, L. Dryon and D.L. Massart, J. Assoc. Off. Anal. Chem., 66 (1983) 1039.
[9] M.L. Puttemans, L. Dryon and D.L. Massart, J. Assoc. Off. Anal. Chem., 67 (1984) 880.
[10] M.L. Puttemans, M. de Voogt, L. Dryon and D.L. Massart, Anal. Chim. Acta, 178 (1985) 189.
[11] A. Fogg and D. Bhanot, Analyst, 105 (1980) 868.
[12] A. Fogg and D. Bhanot, Analyst, 106 (1981) 883.
[13] A. Fogg and D. Bhanot, Analyst, 109 (1984) 1029.
[14] A. Fogg, A. Barros and J. Cabral, Analyst, 111 (1986) 831.
[15] A. Araujo, J. Cabral and A. Fogg, Analyst, 113 (1988) 853.
[16] J.P. Hart and W.F. Smyth, Analyst, 105 (1980) 929.
[17] T.M. Florence, J. Electroanal. Chem., 52 (1974) 115.
[18] F. Becerro, F. González and J. Hernández, Talanta, 37 (1990) 655.

ELSEVIER

Talanta 44 (1997) 475–481

Talanta

Inhibition of the enzyme phosphoenolpyruvate-carboxylase (PEPC) by different pollutants

Kathrin Stein *, Gerd Ohlenbusch

Institute of Inorganic and Analytical Chemistry, Technical University of Clausthal, Paul-Ernst-Str. 4, 38678 Clausthal-Zellerfeld, Germany

Received 1 April 1996; received in revised form 10 September 1996; accepted 17 September 1996

Abstract

The inhibitory effect of different pollutants on the enzyme phosphoenolpyruvate-carboxylase was investigated. For this enzyme, different procedures are described for determining the activity of the enzyme. Determination of the presence of the enzymatically-formed oxaloacetate was found to be more suitable for this purpose because of the higher sensitivity compared with that of the enzymatically-formed phosphate. In order to detect possible inhibitors of this enzyme, inhibition tests were carried out with different pesticides and metal ions. The enzyme activity was decreased by ziram, ferbam and pentachlorophenol. Of the tested metal ions, the enzyme reacts very sensitively to mercury ions, however cobalt, lead, zinc and copper also showed an inhibition effect. © 1997 Elsevier Science B.V.

Keywords: Heavy metal ions; Inhibitors; Pesticides; Phosphoenolpyruvate-carboxylase (PEPC)

1. Introduction

In routine analysis of drinking water, sewage and soil, a larger part of the samples proved to be non-polluted. Using traditional instrumental analysis methods for this is very expensive. Thus, biochemical analysis procedures have received more and more attention in the last few years. Enzymes may be used as powerful instruments to detect hazardous substances in food and even in environmental substances. Enzyme inhibition tests are part of this methodology. Screening tests can be carried out with these kinds of samples. The polluted ones can be separated from the non-polluted ones, so that only the actual polluted samples must be examined with the more exact, but also more expensive, instrumental methods. This can significantly cut costs and save time. The enzyme inhibition test is especially well suited as a screening test. Here, the fact that the activity of enzymes is selectively inhibited by certain pollutants is explored. The intensity of the inhibition correlates with the concentration of the pollutant. It is necessary to be able to use a variety of inhibition tests to screen different pollutants. With respect to the enormous multiplicity of enzymatic reactions it seems possible to design enzymatic screening tests for nearly each substance of interest [1]. Therefore it is very important to find enzyme-inhibitor-systems with environmental rele-

* Corresponding author.

PII S0039-9140(96)02107-8

vance. The interest on such screening tests for pesticides is very high. A well examined example is the acetylcholinesterase inhibition test, which has been available on the market for a longer time. Organophosphorous acid esters and *N*-methyl carbamates can be detected in water samples. Another example is the inhibition of the enzyme aldehyde dehydrogenase, dithiocarbamates used as fungicides inhibit this enzyme [2]. By using microtiterplates, the time needed to carry out enzyme inhibition tests is reduced tremendously, since up to 96 tests can be carried out simultaneously. Thus, sample preparation is the most time consuming step. Another pollutant of great interest is the herbicide atrazine, which is given as a possible inhibitor of the enzyme phosphoenolpyruvate carboxylase by Wiegand-Rosinus et al. [3]. Therefore the inhibition behaviour of phosphoenolpyruvate carboxylase is experimentally examined. We could not measure an inhibition of this enzyme by atrazine. To determine other inhibitors of the enzyme, the inhibition test is carried out with the pesticides ferbam, ziram, aldrin, heptachlor, aldicarb, carbofuran, parathionethyl and pentachlorophenol, which are choosen as examples of different chemical structures (normally the inhibition depends on the chemical structure), and the metal ions mercury, thallium, aluminium, nickel, chromate, cobalt, lead, zinc and copper (the activity of a lot of enzymes is inhibited by heavy metal ions).

The activity of enzymes can be determined by measuring the products formed after the enzymatic reaction. The enzyme phosphoenolpyruvate carboxylase acts as catalyst in the following reaction:

$$PEP + HCO_3^- \xrightarrow{PEPC} OAA + P_i$$

PEP, phosphoenolpyruvate; PEPC, phosphoenolpyruvate carboxylase; OAA, oxaloacetate; P_i, inorganic phosphate.

Some authors described the determination of CO_2 or bicarbonate with the use of phosphoenolpyryvate decarboxylase in buffer solutions, food or animal tissues, plasma or serum. All these applications malate dehydrogenase was used to measure the formed oxaloacetate [4–7]. Instead of a coupled enzymatic reaction the formed products could be measured photometrically. This is more suitable for an inhibition test, because of the possible influence of the investigated inhibitors on the second enzymatic reaction. For the photometric determination of inorganic orthophosphate, a large number of different procedures are described [8–14]. In this work, the phosphate reacts with molybdate-vanadate solution, and the formed molybdato-vanadato-phosphate complex is measured at a wavelength of 405 nm [8,11]. Oxaloacetate can be measured photometrically as well. The diazonium salt, fast violet B, forms a red complex with oxaloacetate, which could be measured photometrically at 490 nm [15].

2. Experimental

2.1. Apparatus

Microtiterstrip reader (Behring EL 301), MaxiSorp-microtiterstrips (Nunc Ltd.), pH-meter E 603 (Metrohm).

2.2. Reagents

For all solutions bi-distilled water was used.

2.2.1. Activity measurement by determining the enzymatically formed phosphate

$KHCO_3$ (MicroSelect, Fluka); solution: 50 mg are dissolved in 25 ml water. $MgCl_2 \cdot 6H_2O$ (p.a., Merck); solution: 51 mg are dissolved in 25 ml water. HCl (p.a., Riedel-de Haën); 37%. Tris–(hydroxymethyl)–aminomethane (TRIS) (p.a., Merck); solution: 6 mg TRIS are dissolved in water, the pH is adjusted to 8.6 with HCl (1 mol l^{-1}) and filled to 50 ml. Cofactor solution: 4 ml $KHCO_3$ solution, 2 ml $MgCl_2 \cdot 6H_2O$ solution and 1 ml TRIS solution are mixed. Nitric acid, Baker; 70–71%. Ammoniumvanadate (p.a., Riedel-de Haën); solution: 25 mg ammoniumvanadate are dissolved in hot water, 0.2 ml concentrated nitric acid are added and the mixture is filled to 10 ml with water. Sulphuric acid (p.a., Merck); 95–97%. Ammoniummolybdate-tetrahydrate (p.a., Merck); solution: 1 g ammoniummolybdate is dissolved in approximately 50°C warm water, 1 ml concen-

trated H_2SO_4 is added and the mixture is filled with water to 10 ml. Reagent solution: 3 ml each of freshly made ammoniummolybdate and ammoniumvanadate solution are mixed.

Phosphoenolpyruvate-carboxylase (E.C. 4.1.1.31) (suspension of the enzyme from corn in 2.4 mol l^{-1} ammonium sulphate solution, 10 mmol l^{-1} phosphate buffer (pH 7), 1 mmol l^{-1} biotin, 5 mmol l^{-1} dithiothreitol and 1 mmol l^{-1} phenylmethylsulfonylfluoride; 8.1 mg protein ml^{-1}; 2.4 U mg^{-1} protein),(Sigma); solution (750 U l^{-1}): 38.6 µl enzyme suspension was diluted with 961.4 µl water.

Phosphoenolpyruvate tricyclohexylaminsalt (PEP) >98%, (Fluka); stock solution: 93.1 mg PEP are dissolved in 2 ml water. For getting the substrate curve solutions in the concentration range from 1×10^{-1} to 1.34×10^{-3} mol l^{-1} the stock solution is diluted adequately. For the following inhibition test 46.6 mg PEP was dissolved in 2.5 ml water. Acetonitril (p.a., Riedel-de Haën).

2.2.2. Activity measurement by determining the enzymatically formed oxaloacetate

TRIS; solution (1 mol l^{-1}): 1.2114 g TRIS are dissolved in 10 ml water. $MgCl_2 \cdot 6H_2O$ (p.a., Merck); solution (0.2 mol l^{-1}): 40.6 mg are dissolved in 10 ml water. $KHCO_3$ (MicroSelect, Fluka); solution (0.4 mol l^{-1}): 40.1 mg are dissolved in 10 ml water. Triton X-100 (alkylphenylpolyethylenglycol) (SERVA); solution (1%): 1 ml is dissolved in 100 ml water. Fast violet B (FVB) standard (Fluka); solution (6 g l^{-1}): 30 mg FVB are dissolved in 5 ml Triton X-100-solution. The solution must be prepared freshly every day. Oxaloacetic acid 99%ig (Fluka); solution (2.5 mmol l^{-1}): 330 mg oxaloacetic acid are dissolved in 100 ml water. TRIS buffer: 0.5 ml TRIS solution and 0.5 ml $MgCl_2$ solution are mixed and filled with water to 7 ml. Subsequently the pH is adjusted to 8 with HCl (1 mol l^{-1}) and filled with water to 10 ml. Enzyme solution: 10.3 µl enzyme suspension are diluted with 989.7 µl water. Phosphoenolpyruvate tricylcohexylaminsalt (PEP) (Fluka); solution: 20 mg PEP are dissolved in 200 µl $MgCl_2$ solution (0.2 mol l^{-1}), 200 µl TRIS buffer (1 mol l^{-1}) and 100 µl $KHCO_3$ solution (0.4 mol l^{-1}). Subsequently, the pH is adjusted to 9 with HCl (1 mol l^{-1}) and filled with water to 2 ml.

2.2.3. Inhibitors

Pentachlorophenol (PCP), (AccuStandard Ehrenstorfer, Augsburg); stock solution (1 g l^{-1}): 10 mg PCP are dissolved in 10 ml methanol. Sample solutions are prepared by adequately diluting with water in the concentration range from 2 mg l^{-1} to 100 mg l^{-1}. Ferbam (Ehrenstorfer, Augsburg); 84% stock solution (0.84 l^{-1}): 10 mg Ferbam are dissolved in 10 ml acetonitril. Sample solutions are prepared by diluting adequately with water in the concentration range from 1.05 mg l^{-1} to 84 mg l^{-1}. $HgNO_3$ (p.a., Fluka); standard solution (1 g l^{-1} Hg^{2+}): 161.8 mg $HgNO_3$ are dissolved in 100 ml nitric acid. All other used pesticides, Ehrenstorfer, Augsburg, all other tested heavy metal stock solution 1 g l^{-1}, Merck.

3. Procedure

3.1. Activity measurement by determining the enzymatically formed phosphate

For determining the substrate curve, 70 µl cofactor solution, 40 µl PEP solution and 40 µl enzyme solution are poured in the wells of the microtiter strip. After 13 min enzymatic reaction time, 30 µl reagent solution are added. Photometric measurements are carried out after another 2 min at 405 nm against the reagent blank containing water instead of PEP solution.

3.2. Determination of the inhibition using photometric phosphate determination

For inhibition tests, 70 µl cofactor solution, 80 µl standard solution (inhibitor) and 40 µl enzyme solution (750 U l^{-1}) are poured in the wells of the microtiter plate. After an incubation period of 30 min, in which the inhibition reaction takes place, 40 µl PEP solution are added, and after another 30 min of reaction time, 30 µl reagent solution are added. After 2 min, photometric measurements are carried out at 405 nm against reagent blank. 100% activity is determined using water instead of the inhibitor solutions. The inhibition was calculated as follows:

$$I[\%] = \frac{A_0 - A_i}{A_0} 100\%$$

A_0, absorption of the non-inhibited reaction; A_I, absorption of the inhibited reaction; I, inhibition.

3.3. Activity measurement by determining the enzymatically formed oxaloacetate

For determining the complex formation rate between FVB and enzymatically formed oxaloacetate, the following volumes of solutions are poured into the wells: 60 μl buffer, 40 μl oxaloacetic acid, 60 μl water and 90 μl FVB solution. After the addition of the FVB solution, the absorption is determined photometrically at intervals of 1 min at 490 nm against reagent blank, containing water instead of oxaloacetate.

3.4. Determination of the inhibition using photometric oxaloacetate determination

For inhibition tests, 100 μl inhibitor solution and 30 μl enzyme solution are poured in the wells of the microtiter plate. After 30 min incubation period, 30 μl PEP solution are added and after another 30 min reaction time, 30 μl FVB solution are added. The absorption is measured 15 min later at 490 nm against reagent blank, containing water instead of PEP solution. 100% activity is determined using water instead of inhibitor solution.

4. Results and discussion

4.1. Determining the enzymatic activity by means of photometric phosphate determination

In the acidic pH range, which is necessary for photometric phosphate determination, the enzyme denatures immediately and forms very fine flakes, but in the concentration range from 0.5 to 5 μmol l^{-1} phosphate a linear relationship between absorption and concentration (regression coefficient: $r = 0.996$) is observed at this acidic pH.

For the development of the inhibition tests, the optimal substrate concentration has to be determined. For this, a substrate curve is measured by determining the absorbance at different substrate concentrations (Fig. 1). Normally, the substrate concentration at the beginning of the steady state range should be chosen for the inhibition test [16]. Here, a small fluctuation in the substrate concentration (e.g., due to pipetting deviation) does not lead to larger deviations of the absorption. In this case, with a substrate concentration of 6 mmol l^{-1}, a compromise was chosen. This concentration is not in the steep increase section of the substrate curve. A sufficiently high signal is observed, and the costs for the expensive substrate phosphoenolpyruvate are not yet too high. From the Lineweaver–Burk plot, the Michaelis constant is determined to be $K_M = 4.1$ mmol. This value matches well with the value given in the literature (approximately 1 mmol) [17].

By using atrazine no inhibition effect could be observed at concentrations up to 100 mg l^{-1}. Since the possible inhibition mechanism is not known, a series of other pesticides are tested regarding their inhibition to this enzyme. An inhibition effect on the enzyme is observed for the fungicides ziram, ferbam and pentachlorophenol.

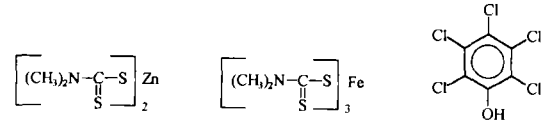

ziram ferbam pentachlorophenol

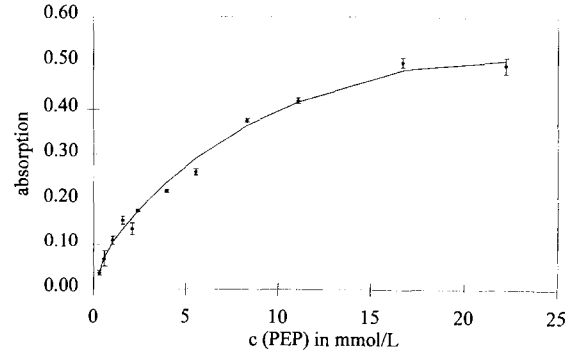

Fig. 1. Substrate curve for phosphoenolpyruvate (PEP) (mean values from $n = 5$ measurements).

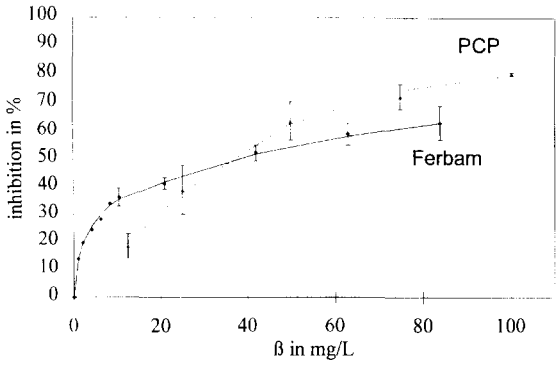

Fig. 2. Inhibition caused by pentachlorophenol (mean values from $n = 3$ measurements) and by ferbam (for $c > 20$ mg/l: mean values from $n = 3$ measurements) (photometric phosphate determination).

For the other investigated pesticides (aldrin, aldicarb, atrazine, azinphosethyl, carbofuran, heptachlor and parathionethyl), no inhibition effect could be measured up to concentration of 100 mg l^{-1}.

The inhibition curve was determined for ferbam and PCP (Fig. 2). Often the 10% inhibition value is given as a detection limit. Under this not optimised condition 10% inhibition was observed at 7.5 mg l^{-1} PCP and below 1 mg l^{-1} ferbam. Since the inhibitors are dissolved in organic solvents the influence of the solvent was investigated. 10% of methanol leads to a decrease in activity of 25%, but 10% of DMSO leads to an inhibition of the enzyme of 20%. In contrast to this, the solvent acetonitrile leads only to a little increase in enzyme activity. The weak amounts of solvents in the sample, which influence likewise the activity of the enzyme, were mathematically considered at the evaluation by measuring the influence of the solvent and substracted rsp added this inhibition rsp activation caused by the solvent from the measured total inhibition rsp the measured activation was taken into account determining the not inhibited activity. Since it is well known, that enzymes can be inhibited by heavy metal ions, the suspicion is obvious, that the inhibition caused by ferbam is developed by the iron ion of the molecule. Therefore, an inhibition test with $FeCl_3 \cdot 6H_2O$ solution is carried out. The concentration of the iron ions is the same as the iron concentration in the solution of 100 mg l^{-1} ferbam. With this iron solution, however, no inhibition of the enzyme could be observed. Therefore, the observed inhibition of the ferbam solution is caused by the ferbam molecule itself, and not by the iron ion.

4.2. Determination the enzymatic activity by means of oxaloacetate detection

Years ago Norris et al. described a method using FVB for the oxaloacetate determination formed by phosphoenolpyruvate carboxylase [15]. In determining the enzyme activity by means of the oxaloacetate concentration after 15 min the oxaloacetate is almost completely transformed with the Fast Violet B (FVB). For the following measurements, the absorption is measured 15 min after addition of the FVB solution (Fig. 3). Because of the inhibition effect of FVB itself [15], it must be added at the end of the enzymatic reaction. The absorption in the investigated concentration range from 10 to 500 µmol l^{-1} oxaloacetate showed a very good linearity (regression coefficient: $r = 0.9999$). Because of the higher sensitivity of the photometric oxaloacetate determination compared with the phosphate determination weaker enzyme concentrations can be used. This way, the detection limit of the inhibitor is improved. As shown in the inhibition curve of Fig. 4, 20 mg l^{-1} PCP cause almost 100% inhibition of the enzyme, while at determination of the enzymatic activity by means of measuring the

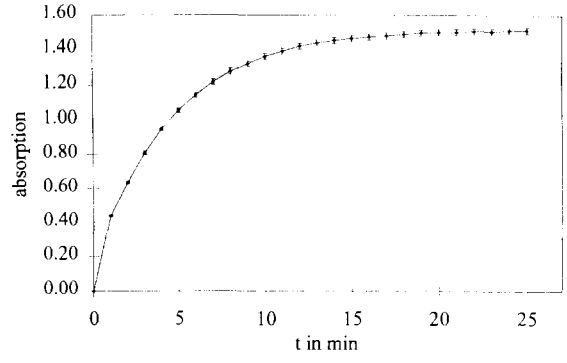

Fig. 3. Formation rate of the diazonium colour complex (mean values from $n = 3$ measurements).

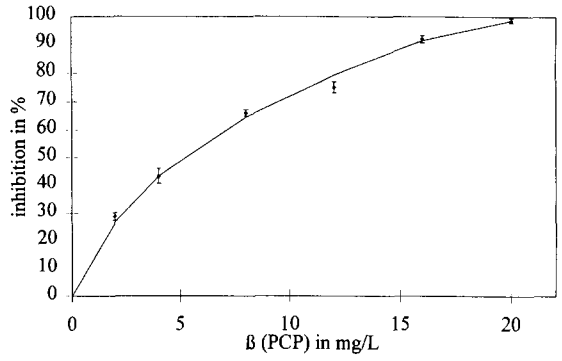

Fig. 4. Inhibition caused by pentachlorophenol (mean values from $n = 2$ measurements) (photometric oxaloacetate determination).

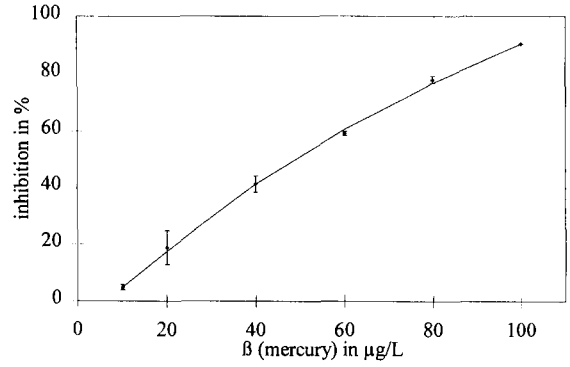

Fig. 5. Inhibition caused by mercury(II)-ions (mean values from $n = 2$ measurements) (photometric oxaloacetate determination).

enzymatically formed phosphate with 100 mg l^{-1} PCP, an inhibition of only 80% is observed (compare Fig. 2).

The mercury(II) ion is a very strong inhibitor for phosphoenolpyruvate carboxylase, as it is for a lot of other enzymes. As shown by the inhibition curve in Fig. 5, Hg(II) could be detected in the µg l^{-1} concentration range (10% inhibition for 15 µg l^{-1} Hg(II)). Analogously, the inhibition effect of other heavy metal ions were investigated. At concentrations of 1 mg l^{-1} thallium, aluminium, nickel and chromate, no inhibition was observed. However, cobalt (< 10% inhibition at 1 mg l^{-1}), lead (< 10%), zinc (27%) and copper (54%) are also inhibitors of this enzyme.

5. Prospect

In this work the determination of the enzymatic formed oxaloacetate was found to be more suitable for a phosphoenolpyruvate inhibition test, because of its higher sensitivity, which results in a higher sensitivity to the inhibitors examined. The described investigations are basic points for the optimisation of the inhibition test under the view of the further application, e.g., determination of PCP in extracts of leather, wood or cotton, determination of Hg^{2+} ions in natural waters, extracts from soil or food and so on, which will be done at the time. Such inhibitions test are a tool in the field of the analysis with the respect to the effect of pollutants on the environment.

References

[1] A. Prell-Swaid and G. Schwedt, Acta Hydrochim. Hydrobiol., 22 (1994) 70–75.
[2] M. Wiegand-Rosinus, K. Haberer, U. Obst and A. Wild, Z., Wasser-Abwasser-Forsch., 23 (1990) 98–101.
[3] M. Wiegand-Rosinus, U. Obst, K. Haberer and A. Wild, Environ. Tox. Water Qual., 7 (1992) 313–321.
[4] V.L. Crow and F.G. Marty, J. Diary Res., 58 (1991) 521–525.
[5] G.P. Dobson, R.L. Veech, U. Hoeger and J.V. Passonneau, Anal. Biochem., 195 (1991) 232–237.
[6] R.R. Punzalan, G.F. Johnson, B.A. Cunningham and R.D. Feld, Clin. Chem., 36 (1990) 2057–2062.
[7] N.P. Hall, M.J. Cornelius and A.J. Keys, Anal. Biochem., 132 (1983) 152–157.
[8] B. Lange and Z.J. Vejdelek, Photometrische Analyse, Verlag Chemie, Weinheim Deerfield Beach Basel, 1980.
[9] J.J. Pauer, H.R. van Vliet and F. van Staden, Water, SA 14 (1988) 125–130.
[10] N. Lacy, G.D. Christian and J. Ruzicka, Quimica Acta, 8 (1989) 201–209.
[11] W. Reichard and B. Eckert, Nahrung, 37 (1993) 79–81.
[12] S. Motomizu, T. Wakimoto and K. Toei, Talanta, 30 (1983) 333–338.
[13] H.J. Altmann, A. Fürstenau, A. Gielewski and L. Scholz, Z. Anal. Chem., 256 (1971) 274–276.
[14] M. Hoenig, R.J. Lee and D.C. Ferguson, J. Biochem. Biophys., Meth., 19 (1989) 249–252.
[15] K.A. Norris, A.R. Atkinson and W.G. Smith, Clin. Chem., 21 (1975) 1093–1101.

[16] K. Stein and G. Schwedt, Vom Wasser, 79 (1992) 211–224.

[17] M.H. O'Leary, Ann. Rev. Plant Physiol., 33 (1982) 297–315.

ELSEVIER

Talanta 44 (1997) 483–489

Talanta

Short communication

Detection and semiquantitative determination of bismuth(III) in water on immobilized and plasticized polyurethane foams with some chromogenic reagents

M.S. El-Shahawi*[1], R.S. Al-Mehrezi

Department of Chemistry, Faculty of Science, UAE University, P.O. Box 17551, Al-Ain, United Arab Emirates

Received 7 November 1995; revised 16 April 1996; re-revised 17 May 1996; accepted 22 May 1996

Abstract

Polyurethane foams immobilizing 1,2-di-(2-fluorophenyl)-3-mercaptoformazan (F_2H_2Dz) and dithizone (H_2Dz) have been used for the detection of bismuth(III) in water via batch, dynamic and pulsated column modes of extraction. The detection limits of bismuth(III) with the F_2H_2Dz- and H_2Dz-immobilized foams were found to be 0.01 and 0.02 $\mu g\ ml^{-1}$ respectively. Lower concentrations ($\leqslant 1$ ppb) of bismuth(III) were also detected by employing dynamic and pulsated columns packed with plasticized tri-*n*-butylphosphate and F_2H_2Dz-immobilized reagent foams. The electronic spectra and partition coefficients of the reagents H_2Dz and F_2H_2Dz and their bismuth(III) chelates in chloroform and in polyurethane foams have been determined. Bismuth (V) was also detected by the proposed procedure after prior reduction to bismuth(III) with sulphur dioxide at pH < 1. The effect of diverse ions on the detection of 1 μg of bismuth(III) was critically investigated using F_2H_2Dz-immobilized foam. © 1997 Elsevier Science B.V.

Keywords: Bismuth(III); Chromogenic reagents; Polyurethane foams

1. Introduction

Various reagents have been used for the detection, extraction and spectrophotometric determination of bismuth(III) [1]. Most of these reagents suffer from limitations, e.g. long extraction period, low stability of the compounds formed, low tolerance limit, critical pH and interferences [1,2].

Open cell polyurethane foams have been successfully used for the extraction and collection of various species in aqueous media [3]. Foams loaded with dithizone and other chromogenic reagents (chromofoams) have been reported for the sensitive detection and semiquantitative determination of some metal ions, including bismuth(III), employing batch and column extraction modes [4–9].

There has been no study of the use of 1,5-di(2-fluorophenyl)-3-mercaptoformazan agent in the detection and proconcentration of bismuth(III)

* Corresponding author. Fax: (+971) 3-671-291.

PII S0039-9140(96)02004-8

Table 1
Characteristic absorption (cm^{-1}) in KBr discs[a] and electronic (nm) spectral data for the reagents F_2H_2Dz and H_2Dz and their bismuth(III) chelates in chloroform and in polyurethane foams (values in parentheses)

Compound	Wave number (cm^{-1})				λ_{max} (nm)	$\varepsilon(10^{-3}$ l mol^{-1} $cm^{-1})$	log k_{ex} l
	ν(N–H)	ν(N=H)	δ(N–H)+(C=N)	ν(N–C–S)			
F_2H_2Dz	3320 (br)	2380 (w)	1510 (s)	1485 (s)	632 (614.5)	25.3	
		1598 (s)		1450 (s)	545 (460.5)	23.7	
H_2Dz	3340 (br)	2365 (w)	1515 (s)	1505 (s)	615 (614)	35.8	
				1465 (s)	448 (480)	17.9	
$Bi(F_2HDz)_3$	3440 (m)	1615 (s)	1535 (s)	1485 (s)	490 (487)	91.4	9.75
	3245 (m)	1595 (m)		1460 (s)	(605)		
	3090 (br)			1440 (m)			
$Bi(HDz)_3$	3420 (m)	1610 (s)					
	3190 (m)	1590 (m)	1530 (s)	1490 (s)	489 (478)	80	11.49
	3060 (m)			1480 (sh)	(616)		

[a] s = strong, m = medium, w = weak, sh = shoulder, br = broad.

and other metal ions in aqueous solution employing polyurethane foams. Thus, the present paper describes the use of the immobilized and plasticized 1,5-di-(2-fluorophenyl)-3-mercaptoformazan (F_2H_2Dz) and dithizone (H_2Dz) polyurethane foams for the sensitive and selective detection and the semiquantitative determination of traces of bismuth(III) in aqueous media.

2. Experimental

2.1. Reagents and materials

All the reagents used were of analytical-reagent-grade unless otherwise specified. An open cell polyether type polyurethane foams (bulk density 30 kg m^{-3}) was supplied by Greiner K.G. Schaumstoffwerk (Kremsmunster, Austria). The foam material (cubes with 0.5 cm sides) was washed and dried as previously described [10]. A stock solution containing 1 mg ml^{-1} of bismuth(III) was prepared by dissolving the appropriate amount of bismuth(III) nitrate pentahydrate in deionized water acidified with a few drops of 0.5 M nitric acid and standardized by EDTA titration. A bismuth(III) solution (100 μg ml^{-1}) was also prepared by dissolving 0.123 g of bismuthic acid in 100 ml of 0.5 M KOH [11]. Tri-*N*-butylphosphate (TBP; BDH) was used without further purification. A series of standard bismuth(III) and (V) solutions was prepared by dilution with water acidified with a few drops of nitric acid.

The reagent F_2H_2Dz was prepared by the nitroformazyl method [12,13]. This reagent and the H_2Dz (Merck) solutions were prepared by dissolving 10 mg of each reagent separately in 50 ml of chloroform. The F_2H_2Dz- and H_2Dz-loaded foams were prepared by mixing the dried foam cubes with F_2H_2Dz and H_2D-2 solutions (10 ml g^{-1} dry foam) respectively and stirring for 10 min. The reagent-loaded foam cubes were then squeezed and dried as reported [10]. Plasticized F_2H_2Dz and H_2Dz foams were prepared by mixing the dried foam cubes with F_2H_2Dz and H_2Dz (0.1% w/v) in TBP respectively, stirring for 15 min and then drying [10].

2.2. Apparatus

A Shimadzu UV 2101 PC UV–visible scanning spectrophotometer and a Shimadzu FTIR-8101 Fourier transform infrared spectrophotometer were used for recording the IR and electronic spectra of the reagents and their bismuth(III) complexes in chloroform and in parallelepiped polyurethane foam. An Orion pH-meter, glass

Table 2
Comparative sensitivity of batch and dynamic modes of extraction for the detection of bismuth(III) ions (ppb) using F_2H_2Dz and H_2Dz immobilized or plasticized TBP foams

Method	Amount of bismuth(III) detected (ppb)			
	F_2H_2Dz		H_2Dz	
	Batch	Dynamic	Batch	Dynamic
Unloaded foam	100	–	100	–
Immobilized reagent foam	10	5	20[a]	10[a]
Plasticized TBP reagent foam	5	1	20	10

[a] Data were obtained from Ref. [4].

columns (16 cm height × 5 mm i.d.) and medical syringes (100 ml capacity) as pulsating columns were used.

2.3. General procedures

2.3.1. Batch experiment

One of the immobilized reagent or plasticized TBP–reagent foam cubes was shaken with 3–5 ml of the bismuth(III) aqueous solution (pH < 4) for 2 min. The colour of the reagent foam changed from green to orange–brown and to orange with H_2Dz and F_2H_2Dz respectively. The colour that developed on the foam cube was taken as evidence for the detection of bismuth(III).

2.3.2. Column experiments

1 g of the F_2H_2Dz or H_2Dz-loaded or plasticized reagent–TBP foams was packed in a glass column by the vacuum method of foam column packing [14]. 250 ml of the bismuth(III) solution of optimum pH was allowed to pass through the foam column at a flow rate of 2–3 ml min^{-1}. The coloured foam bed produced was used for the detection of bismuth(III) ions.

2.3.3. Pulsating column experiments

50 ml of the bismuth(III) solution of suitable pH was transferred to a 100 ml medical syringe. The solution was then compressed and released with one cube of F_2H_2Dz-immobilized or plasticized F_2H_2Dz–TBP foam. An orange colour on the foam cube was then observed after 25 successive pulses.

3. Results and discussion

Table 1 summarizes the IR data for the regions of interest in the spectra of the solid reagents H_2Dz and F_2H_2Dz and their solid complexes of bismuth(III) in a potassium bromide disc. The reagents F_2H_2Dz and H_2Dz and their bismuth(III) complexes were characterized by IR spectral [15–17] (Table 1) and elemental analysis. The electronic spectra of the reagents and bismuth(III) complexes in chloroform and in parallelepiped polyurethane foams are also given in Table 1 and Fig. 1. The electronic spectra of the bismuth(III) complexes in chloroform (Fig. 1A) and in polyurethane foams (Fig. 1B) have well-defined bands at 489–490 and 478–487 nm respectively and a broad shoulder of low intensity at 270–360 nm. The introduction of fluorine atoms at the C-2 position of the phenyl radicals of H_2Dz leads to small bathochromic shifts of both of its bands (632 and 454 nm → 615 and 448 nm respectively) for H_2Dz. The position of λ_{max} for the bismuth(III) complex of F_2H_2Dz in chloroform underwent similar shifts (Table 1) as compared with the bismuth(III) complex of H_2Dz. The relative molar absorptivities in chloroform of the two absorption bands of F_2H_2Dz and its bismuth(III) complex were similarly affected by the introduction of fluorine atoms compared with H_2Dz and its bismuth(III) complex (Table 1).

3.1. Detection and semiquantitative determination of bismuth(III) with F_2H_2Dz

Bismuth(III) forms orange–red and orange–

Table 3
Detection of 1 μg of bismuth(III) with F_2H_2Dz-immobilized polyurethane foams in the presence of some interfering ions

Foreign ions	Compound added	Tolerance limit	Note
Cd^{2+}	$CdBr_2$	$1:1 \times 10^4$	Add a few crystals of sodium sulphite
Fe^{2+}	$FeSO_4$	$1:1 \times 10^4$	Add 1 ml of NaF (1 M)
Fe^{2+}	$FeCl_3$	$1:1 \times 10^4$	Add 1 ml of NaF (1 M)
Ni^{2+}	$NiCl_2 \cdot 4H_2O$	$1:1 \times 10^3$	Add a few drops of KCN (1 M)
Au^{3+}	$AuCl_3$	$1:1 \times 10^3$	Add a few crystals of sodium sulphite and adjust pH to $\simeq 1$
MnO_4^-	$KMnO_4$	$1:1 \times 10^3$	Add one crystal of sodium azide
Mn^{2+}	$MnSO_4$	$1:1 \times 10^4$	Add bromine water and boil the solution
Hg^{2+}	$HgCl_2$	$1:1 \times 10^4$	Add one crystal of ascorbic acid
Pd^{2+}	$Pd(NO_3)_2$	$1:1 \times 10^3$	Add one crystal of NaF or thiourea
Cr^{3+}	$CrCl_3 \cdot 6H_2O$	$1:1 \times 10^3$	Add H_2O_2 and boil the solution
Ag^+	$AgNO_3$	$1:1 \times 10^3$	Add a few crystals of KCNS
Zn^{2+}	$ZnSO_4$	$1:1 \times 10^3$	Adjust the pH of the aqueous solution to <2 with HNO_3 (1 M)
Oxalate	$H_2C_2O_4 \cdot 2H_2O$	$1:1 \times 10^3$	Add bromine water and boil the solution
VO_3^-	NH_4VO_3	$1:1 \times 10^3$	Add 1 ml of NaF (1 M)

brown complexes [12, 18] with F_2H_2Dz and H_2Dz in acidic aqueous solution ($pH < 5.2$) respectively. These reactions were tried with foam immobilized with F_2H_2Dz and H_2Dz and plasticized reagent–TBP foam for the detection and semiquantitative determination of bismuth(III) in aqueous solution.

On shaking one cube of the unloaded foam with the mixed test solution of $Bi(F_2HDz)_3$ in a test tube at $pH < 4$ for 2–3 min as little as 0.10 ppm bismuth(III) was easily detected. The sensitivity of the test was significantly improved by immobilizing or plasticizing the foam cubes with the reagent F_2H_2Dz. On shaking one cube of the immobilized F_2H_2Dz foam and one cube of the plasticized F_2H_2Dz–TBP with 2–3 ml of the test aqueous solution of bismuth(III) concentrations as low as 0.01 and 0.005 ppm were easily detected respectively. The relatively high available surface area of the foam cube acts as an efficient collector for the bismuth(III) ions present in the aqueous solution at low concentration. In addition, it is easy to observe the characteristic red colour of the reaction product on/in the thin membranes of the foam material. The TBP plays a dual purpose [5] as it acts as an efficient non-volatile solvent for the reagent F_2H_2Dz and as a plasticizer for the plastic foam itself. This enhances the permeability of the foam material and the rate of sorption of bismuth(III) ions from the aqueous solution on the plasticized reagent foam. A comparison between these results (Table 2), those reported with the usual spot test [19] and those of Hamza et al. [4] employing H_2Dz-loaded foam shows that the F_2H_2Dz-immobilized foam and platicized F_2H_2Dz-TBP foam methods are much more sensitive for the detection of bismuth(III) than H_2Dz and other chelating agents [4, 19].

The colour density on the foam cubes was found to depend on the concentration of the bismuth(III) ions. Thus, semiquantitative determination of bismuth(III) was achieved by comparison of the colour of the plasticized F_2H_2Dz-TBP foam cube with a standard colour scale prepared from 0.01, 0.05, 0.1, 0.5, 1 and 10 ppm bismuth(III) solutions under the same experimental conditions.

The proposed F_2H_2Dz-loaded and plasticized F_2H_2Dz–TBP foams were easily packed in the column mode producing a foam bed suitable for the detection of bismuth(III) present in an extremely dilute aqueous solution. Concentrations

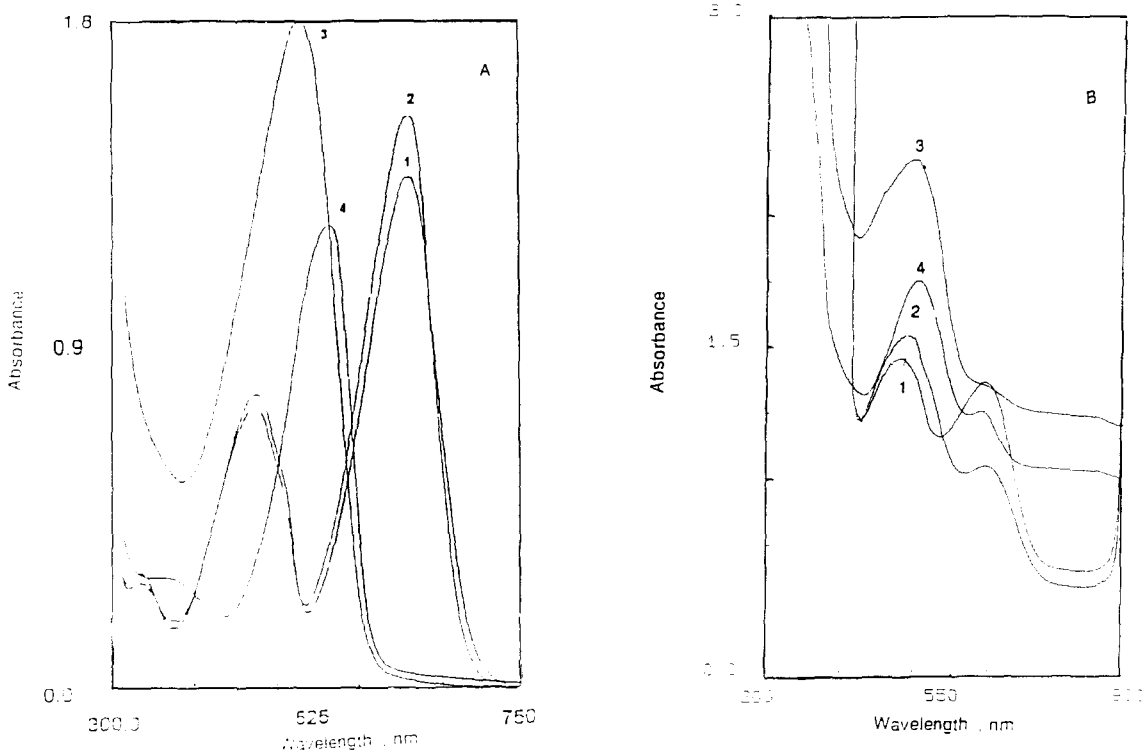

Fig. 1. Electronic spectra of (1) F_2H_2Dz, (2) H_2Dz, (3) $Bi(F_2HDz)_3$ and (4) $Bi(HDz)_3$ in chloroform (A) and in polyurethane foam (B).

as low as 5 and 1 ppb of bismuth(III) in aqueous solution were easily detected with F_2H_2Dz-loaded and plasticized F_2H_2Dz–TBP foams respecively. The length of the coloured zone was found to be proportional to the bismuth(III) concentration in the aqueous phase (Fig. 2). Thus, semiquantitative determination of bismuth(III) in extremely dilute solutions was found to be possible using a standard colour covering the range 5–80 ppb and employing F_2H_2Dz-loaded foam.

The proposed F_2H_2Dz-loaded and plasticized F_2H_2Dz–TBP foam cubes were used in a medical syringe for the detection of bismuth(III). As little as 5 ppb of bismuth(III) was easily detected after 25 successive pulses with F_2H_2Dz-loaded and plasticized F_2H_2Dz–TBP foams. Semiquantitative determination was also found to be possible with standards of 5, 10, 15, 20 and 25 ppb bismuth(III) solution by comparison of the colour of the foam cubes at a constant number of pulses $\geqslant 25$.

3.2. Determination and semiquantitative determination of bismuth(III) with H_2Dz foam

The use of H_2Dz allows the detection of as little as 0.02 ppm bismuth(III) in aqueous solution by shaking one cube of H_2Dz-loaded foam or plasticized H_2Dz–TBP foam with the test solution. These data are in good agreement with the data reported by Hamza et al. [4]. As little as 5 ppb of bismuth(III) was easily detected in aqueous solution by H_2Dz-loaded and plasticized H_2Dz–TBP foam columns at a flow rate of 2–3 ml min^{-1}. The semiquantitative determination of bismuth(III) with immobilized foams was found to be possible in the concentration range 1–30 ng ml^{-1} (Fig. 2).

The results obtained with F_2H_2Dz were much better thatn those obtained with H_2Dz. The higher acidity of F_2H_2Dz ($pK_a = 4.05$) and the higher extraction constant of its bismuth(III) complex ($\log K_{ex} = 11.41$) compared to the values

for H_2Dz ($pK_a = 4.7$) [20] and its $Bi(HDz)_3$ complex ($\log K_{ex} = 9.8$) may partially account for this behaviour. The distribution ratios of $Bi(F_2HDz)_3$, ($\log D = 4.1$) and $Bi(HDz)_3$ ($\log D = 3.8$) in the thin membrane of the polyurethane foam may also play significant roles in the preconcentration. Similarly, the fluorine atom at the ortho position of the phenyl moiety of H_2Dz was found to increase the partition coefficient of F_2H_2Dz between CCl_4 and H_2O to 2.1×10^4 compared to 1.1×10^4 for H_2Dz [21,22] in the same two-phase system. The partition coefficient of $Cu(F_2HDz)_2$ between CCl_4 and H_2O was found to be 1.53×10^5 [21], compared to 7.3×10^4 for $Cu(HDz)_3$ (calculated from the stability constants data of Ref. [23]).

Bismuth (V) was also detected by the proposed method after prior reduction to bismuth(III).

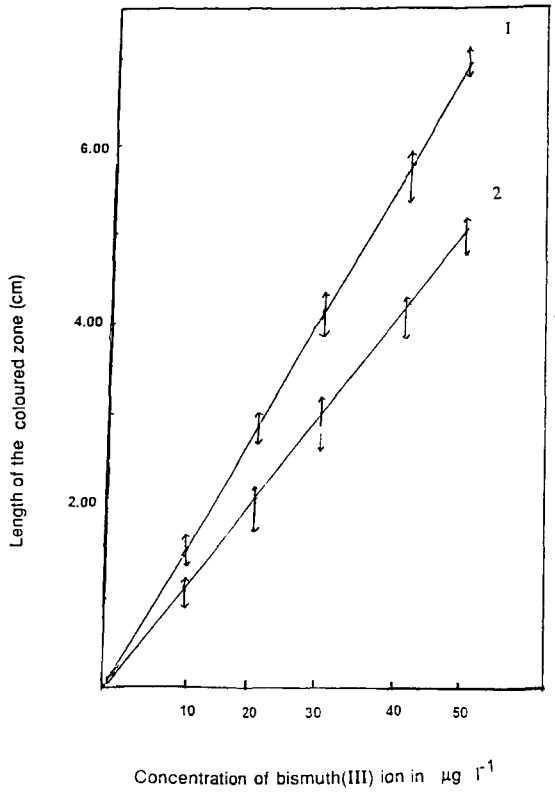

Fig. 2. Relationship between the length of the coloured zone (cm) on the immobilized (1) F_2H_2Dz, (2) H_2Dz, foam columns and the concentration of bismuth(III) in ppb.

Sodium sulphite (1%) in acid media was found to be the most convenient reducing agent, where the unreacted sulphur dioxide was easily removed by boiling. As little as 0.02 ppm of bismuth (V) was easily detected in batch mode after reduction to bismuth(III) followed by shaking this solution with plasticized F_2H_2Dz–TBP foams.

3.3. Interference study

Elimination of interferences in the detection of bismuth(III) in water employing the F_2H_2Dz-loaded foam was considered to be a prime importance. Thus, the selectivity of the proposed batch F_2H_2Dz-loaded foam method for the detection of bismuth(III) in the presence of diverse ions was critically investigted. It was possible to detect 1 μg of bismuth(III) in the presence of up to 1 mg of the following ions: Li^+, Ca^{2+}, Ba^{2+}, Mg^{2+}, Sr^{2+}, Al^{3+}, NH_4^+, Mn^{2+}, Zn^{2+}, SO_4^{2-}, NO_3^-, Br^-, Cl^-, VO_3^-, WO_4^{2-}, SO_3^{2-}, BrO_3^-, NO_2^-, NO_3^-, ClO_4^-, SeO_3^{2-}, SeO_4^{2-}, SbO_2^-, AsO_2^-, acetate, citrate, tartrate, ascorbate, phosphate and chromate. In the presence of some other ions ($\leqslant 0.01$ mg) which interfered seriously with the proposed method, simple modifications were made to the aqueous sample solution to eliminate their interferences, affording unambiguous and sensitive detection of bismuth(III) as given in Table 3.

3.4. Application of the proposed method

The feasibility of the method for the detection of bismuth in sea and waste water samples was also examined. A water sample (0.2 l) acidified with 0.1 mol l^{-1} nitric acid was allowed to pass through a 0.45 μm Millipore filter, and then 10 ml of 1×10^{-3} mol l^{-1} disodium salt of EDTA and 10 ml of 1×10^{-3} mol l^{-1} NaF were added. The reaction mixture was allowed to stand for 15 min and then 1 ml of sodium sulphite solution and 5 ml of concentrated HCl were added. The solution was boiled to dryness, diluted with 20 ml of distilled water and the pH was then adjusted to 9–10 with ammonia follwed by the addition of 10 ml of 2% (w/v) sodium diethyldithiocarbamate (NaDDC). The $Bi(DDC)_3$ complex produced was

then extracted by shaking with 10 ml of xylene [24]. Back extraction of bismuth(III) was achieved with 5 ml of concentrated HNO_3 and finally the pH of the solution was adjusted to 3–5. Negative results for the detection of bismuth in sea and waste water with batch immobilized-F_2H_2Dz foam were obtained while with a column packed with F_2H_2Dz foam it was possible to detect bismuth(III) in the concentration range 10–20 ppb in seawater. This concentration range was detected by flameless atomic absorption spectrometry to be 12 ± 2 ppb bismuth.

An attempt was made to demonstrate the utility of the method for the quantitative collection of bismuth(III) at $3 < pH < 5$ with a column packed with F_2H_2Dz foam. 100 ml of a 10 μg ml^{-1} aqueous solution of bismuth(III) was precolated through a foam column (12 cm height × 1.5 i.d.) packed with F_2H_2Dz foam at 1–2 ml min^{-1}. Analysis of the effluent solution by atomic absorption spectrometry showed quantitative collection (95–98%) of bismuth(III) on the foam column with a standard deviation σ of 1.30.

4. Conclusion

This article has demonstrated the possible use of plasticized or immobilized polyurethane foams for the sensitive and selective detection and quantitative collection of bismuth(III) in water at extremely low concentrations. Elimination of the interference of diverse ions in the detection of bismuth in water by the proposed procedure is of prime importance. Much work still remains to be done on improving the selectivity and utility of the method for the direct determination of bismuth(III), or bismuth (V) after prior reduction, either by direct solid phase spectrometry on parallelpiped polyurethane foams or by elution of the $Bi(F_2HDz)_3$ chelate from the packed foam column with a selective eluting agent.

Acknowledgements

The authors thank Professor A.M. Kiwan for valuable discussions and for the loan of the reagent F_2H_2Dz.

References

[1] A.P. Argekar and A.K. Shetty, Analyst, 120 (1995) 1819 (and references cited therein).
[2] M.S. El-Shakawi and S.M. Al-Dhaheri, Fresenius' J. Anal. Chem., 320 (1995) 279.
[3] M.S. El-Shawawi, A.M. Kiwan, S.M. Al-Dhaheri and M.H. Saleh, Talanta, 42 (1995) 1471.
[4] A.G. Hamza, A.B. Farag, T.A. Amireh, Z.E. El-Bassyouni and F.M. Al-Nowaiser, Anal. Sci., 6 (1990) 889.
[5] T. Braun, J.D. Navartil and A.B. Farag, Polyurethane Foam Sorbents in Separation Science, CRC Press, Boca Raton, FL, 1985.
[6] A.B. Farag, A.M.A. Helmy, M.S. El-Shahawi and S. Farrag, Analusis, 17 (1989) 478.
[7] A.G. Hamza, A.B. Farag and A. Al-Herthani, Microchem. J., 32 (1985) 13.
[8] A.B. Farag, A.M. El-Wakil, M.E.M. Hassouna and M.H. Abdel-Rahman, Anal. Sci., 3 (1987) 541.
[9] A.B. Farag, A. El-Waseef and M.H. Abdel-Rahman, Acta. Chim. Hung., 122 (1986) 273.
[10] M.S. El-Shahawi, Talanta, 41 (1994) 1481.
[11] D.R. Lide, Handbook of Chemistry and Physics, 2nd edn., CRC Press, Boca Raton, FL, 1991.
[12] A.M. Kiwan and A. Y. Kassim, Anal. Chim Acta, 88 (1977) 177 (and references cited therein).
[13] D.M. Hubbard and E.W. Scott, J. Am. Chem. Soc., 65 (1943) 2390.
[14] T. Braun and A.B. Farag, Anal. Chim. Acta, 73 (1974) 301.
[15] S. Taki and T. Kato, Tech. Rep. Tohoku Univ., 21 (1957) 319, 26 (1962) 35.
[16] L.G. Bellamy, Advances in Infrared Group Frequencies, Methuen, London 1968, p. 357.
[17] A. Mawby and H.M. N.H. Irving, Anal. Chim. Acta, 55 (1971) 269.
[18] Z. Marczenko, Separation and Spectrophotometric Determination of Elements, Ellis Horwood, New York, 1986, p. 169.
[19] F. Feigl and V. Anger, Spot Tests in Inorganic Analysis, 6th edn., Elsevier, Amsterdam, 1972.
[20] H. Irving and C.F. Bell, J. Chem. Soc., (1952) 1716; (1953) 3538.
[21] A.Y. Kassim, Ph.D. Thesis, University of Kuwait, Kuwait, 1975.
[22] I.M. Kolthoff, E.B. Sandell, E.J. Meehan and S. Bruckenstein, Quantitative Chemical Analysis, Macmillan, London, 1969, p. 352.
[23] G. Iwantscheff, Das Dithizone and Seine Anwendung in der Mikro-und Spurenanalyse, 2nd edn., Verlag Chemie, Weinheim, Germany, 1972.
[24] Y. Shijo, M. Mitsuhashi, T. Shimizu and S. Sakurai, Analyst, 117 (1992) 1929.

ELSEVIER

Talanta 44 (1997) 491–495

Talanta

Short communication

Cathodic stripping voltammetric determination of 2-mercaptobenzothiazole using the catalytic cobalt peak

Arnold G. Fogg [a,*], Razali Ismail [a], Rahmalan Ahmad [b], Florin G. Banica[a, 1]

[a] *Chemistry Department, Loughborough University, Loughborough, Leicestershire LE11, UK*
[b] *Chemistry Department, Technical University of Malaysia, Johor Bahru, Malaysia*

Received 24 May 1996; received in revised form 24 July 1996; accepted 31 July 1996

Abstract

Previously, thiols have been determined indirectly by cathodic stripping voltammetry (CSV) after accumulation as their mercury and copper(I) salts. Following a previous report of the first use of the catalytic nickel peak (for the determination of cysteine), this paper reports the first use of the catalytic cobalt peak in CSV (for the determination of 2-mercaptobenzothiazole (MBT)): only a very ill-defined catalytic cobalt peak had been observed previously with cysteine, and was unreported. MBT is accumulated at pH 4 (Britton–Robinson buffer) as its cobalt(II) complex at -0.1 V, and is then determined indirectly by observing the reduction of the cobalt(II) in the complex at -0.95 V, i.e., with a much lowered overpotential: hydrated cobalt(II) is reduced at -1.2 V. The peak is catalytic because the thiol released on reduction of the complex complexes further cobalt ions and causes their reduction. The detection limit for the determination of MBT was calculated to be 2.5×10^{-9} M (3σ) using an accumulation time of 1 min. The sensitivity is about three times that obtained with the corresponding catalytic nickel peak. © 1997 Elsevier Science B.V.

Keywords: Catalytic cobalt peak; 2-Mercaptobenzothiazole; Thiols

1. Introduction

Mercury is oxidized more readily, i.e., at a less positive potential, in the presence of complexants or precipitants for mercury(I) or -(II). In this way, thiols can be accumulated as their mercury salts and can be determined by monitoring the reduction of the complexed mercury ions during a cathodic potential sweep. An accumulation potential in the region of $+0.2$–0 V is usual [1]. In the presence of copper(II), many thiols can be accumulated as their copper(I) complexes, and can be determined by monitoring the reduction of the copper(I) in the complex during a cathodic sweep. An accumulation potential in the region of -0.1

* Corresponding author.
[1] Present address: Norwegian University of Science and Technology, Department of Chemistry, N-7055 Dragvoll-Trondheim, Norway.

PII S0039-9140(96)02060-7

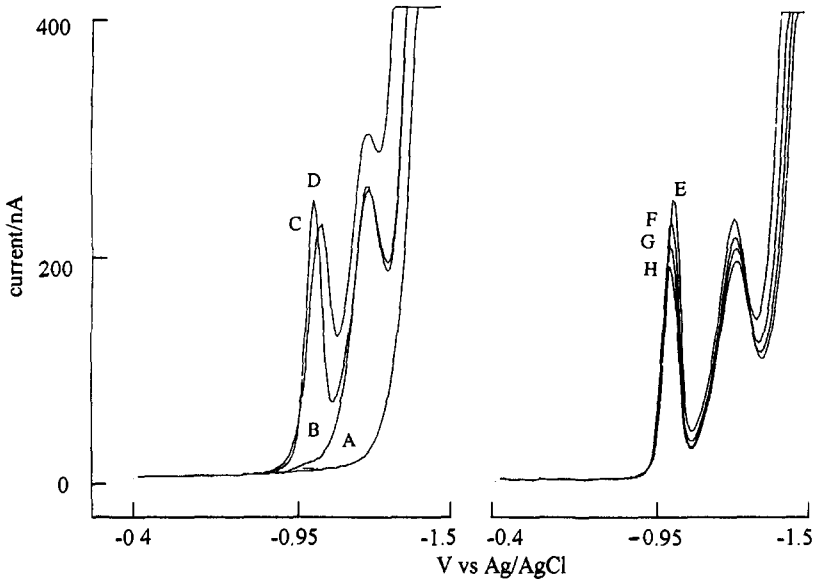

Fig. 1. Effect of pH on the CSV of MBT in the presence of cobalt(II) in Britton–Robinson buffer. Accumulation potential = −0.40 V; accumulation time = 60 s; MBT concentration = 1.2×10^{-7} M; cobalt(II) concentration = 3.4×10^{-4} M. (a) pH 3.1 buffer only; (b) pH 3.1 buffer plus cobalt only; (c)–(h) buffer plus cobalt(II) plus MBT. pH: (c) 3.1; (d) 3.6; (e) 4.0; (f) 4.3; (g) 4.5; (h) 4.7.

V is necessary [1]. Recently, we reported the first use of the catalytic nickel peak in cathodic stripping voltammetry (CSV) [2–6]. Hydrated nickel(II) is reduced at about −1.0 V, but nickel(II) in complexes of thiols such as cysteine [2], penicillamine [5] and glutathione [3] is reduced at about −0.6 V owing to the reduced overpotential. This latter peak is catalytic because the thiol released on reducing the complexed nickel(II) is free to complex further nickel(II) ions and to cause their reduction. In the case of cysteine, penicillamine and glutathione, however, the peak is relatively small. More recently, 2-mercaptobenzothiazole (MBT) was shown to give a much larger catalytic nickel peak when determined by CSV in this way [7].

The catalytic cobalt wave has been studied mechanistically in polarography [8], including studies of cobalt complexes of thiols and selenium analogues [9–13]. More interest has been shown polarographically in the catalytic hydrogen evolution process, which occurs in the presence of cobalt, and which gives a peak at a more negative potential than the catalytic cobalt peak [13]. We observed the catalytic cobalt peak in the CSV of cysteine at pH 7 in a brief excursion from our main study with nickel [2], but the peak was very ill-defined and was not reported. Here we report the first recorded use of the catalytic cobalt peak in CSV, in the determination of MBT.

Derivatives of MBT are used extensively as accelerators in the vulcanization of rubber [14]. MBT is also used as a corrosion inhibitor in antifreezes based on ethylene glycol. Because of its widespread use, MBT has been detected in many environmental samples, including waste waters. Liquid–liquid extraction and HPLC have been used to determine MBT and its derivatives [15], as have polarography and voltammetry [13,16]. Goyal and Kumar [16] studied the oxidation of MBT at a pyrolytic carbon electrode: a platinum ring-disc electrode was used to determine MBT in ethylene glycol samples at 3×10^{-4} – 6×10^{-2} M levels. Calusaru [13] showed that by forming the cobalt(II)–MBT complex, MBT could be determined polarographically at 1×10^{-6} – 1×10^{-5} M levels using the catalytic hydrogen peak produced by the complex. The method described here would need to be tested for its suitability for application to any of these sample types.

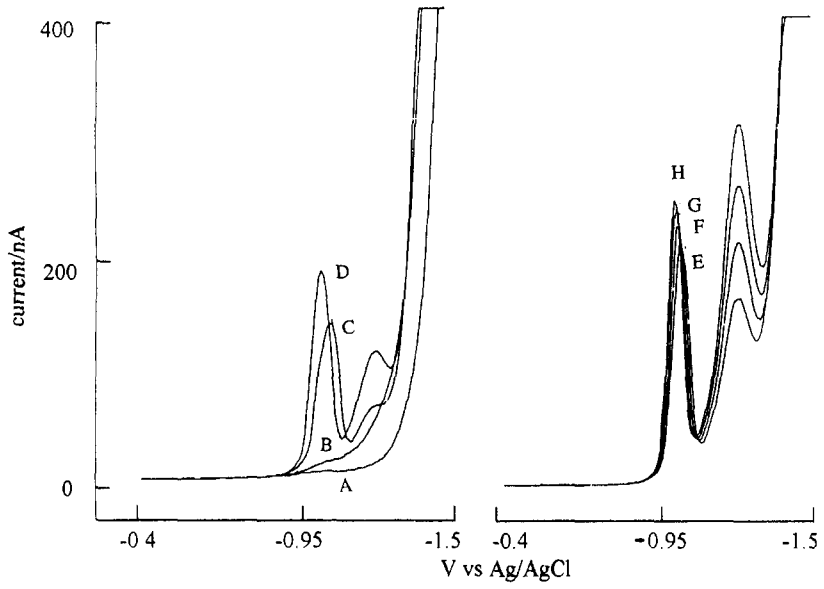

Fig. 2. Effect of cobalt(II) concentration on the CSV of MBT in the presence of cobalt(II) in pH 4 Britton–Robinson buffer. Accumulation potential = −0.40 V; accumulation time = 60 s; MBT concentration = 1.2×10^{-7} M. (a) Buffer only; (b) buffer plus MBT only; (c)–(h) buffer plus MBT plus cobalt(II). Cobalt(II) concentration: (c) 0.85; (d) 1.7; (e) 2.55; (f) 3.40; (g) 4.24; (h) 5.1×10^{-4} M.

2. Experimental

Cathodic stripping voltammetry was carried out with a Metrohm 646/647 VA processor, using a multi-mode electrode in the hanging mercury drop electrode (HMDE) mode. The three-electrode system was completed by means of a glassy carbon auxiliary electrode and an Ag/AgCl (3 M KCl) reference electrode. All potentials are quoted relative to this reference electrode. Differential-pulse voltammetry was carried out with a pulse amplitude of 50 mV, a scan rate of 10 mV s^{-1} and a pulse interval of 1 s.

Stock solutions of MBT (Aldrich) in methanol (3×10^{-3} M) were prepared fresh every 3 days. More dilute solutions were prepared daily by diluting these solutions with methanol. Standard cobalt(II) solutions were prepared daily by diluting standard solutions (Spectrosol, BDH). Britton–Robinson buffer was prepared by dissolving boric acid (2.47 g), orthophosphoric acid (2.7 ml) and glacial acetic acid (2.3 ml) in water and diluting to 1 l. Appropriate volumes of this solution were adjusted to the required pH with sodium hydroxide solution (3 M).

The general procedure used to obtain cathodic stripping voltammograms was as follows: a 20 ml aliquot of buffer was placed in the voltammetric cell and the solution was purged with nitrogen for 6 min with the stirrer on. After an initial blank run, the required volumes of MBT and cobalt solutions were added by means of a micropipette. After forming a new mercury drop, accumulation was effected for the required time at the predetermined accumulation potential whilst the solution was stirred. The small mercury drop size was used on the Metrohm 647 VA stand. At the end of the accumulation period, the stirrer was switched off and after 10 s had elapsed to allow the solution to become quiescent a negative-going potential scan was initiated. When further volumes of MBT solution or reagents were added, the solution was deoxygenated for a further 20 s before producing further voltammograms.

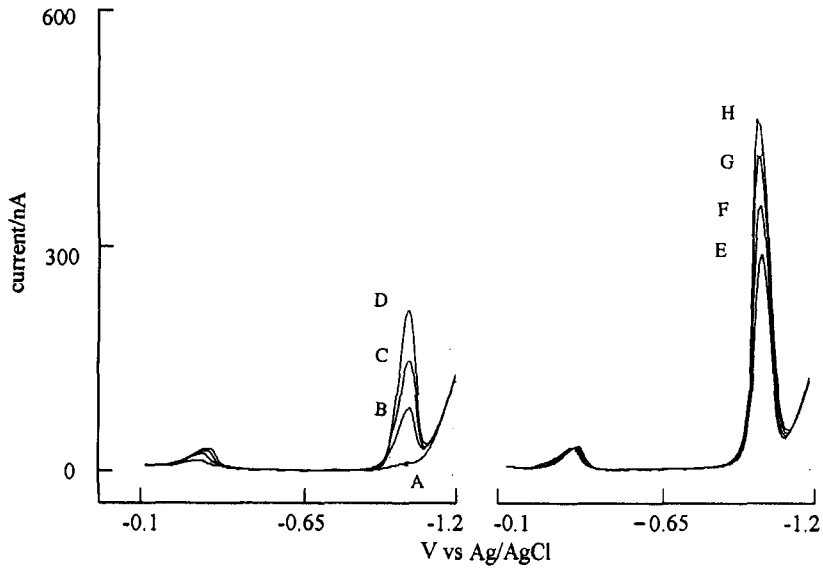

Fig. 3. Cathodic stripping voltammograms obtained for producing a calibration graph for the determination of MBT in pH 4.0 Britton–Robinson buffer. Accumulation potential = −0.10 V; accumulation time = 60 s; cobalt(II) concentration = 2.55×10^{-4} M; MBT concentration = (a) 0; (b) 0.3; (c) 0.6; (d) 0.9; (e) 1.2; (f) 1.5; (g) 1.8; (h) 2.1×10^{-7} M.

3. Results and discussion

Typical cathodic stripping voltammograms for MBT based on accumulation of the cobalt(II) complex are shown in Figs. 1–3. The effect of pH on the catalytic cobalt peak is shown in Fig. 1. pH 4.0 is optimum, giving a well defined peak of maximum height with good separation from the diffusion-controlled hydrated cobalt(II) peak. Cathodic stripping voltammograms showing the effect of cobalt(II) concentration are shown in Fig. 2. The catalytic peak is clearly seen to be well formed and approaching its maximum height at cobalt(II) concentrations of about 2.55×10^{-4} M, and this concentration of cobalt was usually used subsequently in determining MBT; above this concentration of cobalt the peak continues to increase slightly. The hydrated cobalt(II) diffusion peak, which is much smaller than the catalytic peak at relatively low cobalt(II) concentrations, increases in size when excess of cobalt(II) is added. Cathodic stripping voltammograms obtained for producing a calibration graph are shown in Fig. 3 for 2.55×10^{-4} M cobalt(II); the sensitivity would be increased slightly if a slightly higher concentration of cobalt(II) were used. Calibration graphs obtained with 1 min accumulation, including that using the voltammograms shown in Fig. 3, were rectilinear from 3×10^{-8} to 2.7×10^{-7} M MBT. The standard deviation of the signal at 3×10^{-8} M was 2.8% ($n = 8$). From this, the detection limit was calculated to be 2.5×10^{-9} M (3σ, $n = 8$): the sensitivity (2.4 nA for 1 nmol l^{-1}) is about three times that obtained with the corresponding catalytic nickel peak. With longer accumulation times, well defined peaks could be obtained with more dilute MBT solutions, a 7×10^{-9} M MBT solution producing a peak current of 75 nA for a 5 min accumulation. An accumulation time of 60 s, however, was normally used. The effect of accumulation time on peak height at higher concentrations (1.2×10^{-7} M MBT and 2.55×10^{-4} M cobalt(II)) had been studied. The peak height increased regularly (but sub-linearly) with increasing accumulation time up to about 6 min, when the unit increase with time became small. Peak currents for accumulation times of 0, 60, 120, 180, 360, and 480 s were 60, 206, 324, 420, 588, and 644 nA, respectively.

This work was carried out as part of a larger study of indirect CSV methods for determining thiols and other compounds, and is the first reported use of the catalytic cobalt peak in CSV. The appropriate choice of methods involving the accumulation of thiols as mercury, copper(I), nickel and cobalt salts and complexes seems to depend on the particular thiol that is being determined. Thus, MBT is poorly determined as its mercury salt, and is better determined as its copper(I), nickel or cobalt salts or complexes. Cysteine can be determined voltammetrically as its nickel complex but has not been determined successfully as its cobalt complex so far. Trimercapto-*s*-triazine (TMT), which is used to remove heavy metals from effluents, gives excellent mercury(II), nickel and cobalt peaks, but gives no peak with copper(II), presumably owing to formation of colloidal copper(II) TMT (to be published elsewhere). Studies on the CSV of a range of thiols, and other compounds that can be determined indirectly this way, are continuing, in order to establish what factors govern whether complexes and salts are accumulated from solution or not. The possibility is also being considered of the use of accumulation of such complexes and salts at screen-printed electrodes for use in sensor devices.

Acknowledgements

R.I. thanks the Technical University of Malaysia (UTM) for financial support and leave of absence.

References

[1] A.G. Fogg, Anal. Proc., 31 (1994) 313.
[2] F.G. Banica, J.C. Moreira and A.G. Fogg, Analyst, 119 (1994) 309.
[3] F.G. Banica, A.G. Fogg and J.C. Moreira, Analyst, 119 (1994) 2343.
[4] F.G. Banica, A.G. Fogg and J.C. Moreira, Talanta, 42 (1995) 227.
[5] A. Ion, F.G. Banica, A.G. Fogg and H. Kozlowski, Electroanalysis, 8 (1996) 40.
[6] F.G. Banica, A.G. Fogg, A. Ion and J.C. Moreira, Anal. Lett., 29 (1996) 1415.
[7] A.G. Fogg, R. Ismail, R. Ahmad and F.G. Banica, Analyst, 121 (1996) 1877.
[8] A. Calusaru, J. Electroanal. Chem., 15 (1967) 269.
[9] M. Zielinski and J. Kuta, Collect. Czech. Chem. Commun., 34 (1969) 2523.
[10] A. Calusaru and V. Voicu, J. Electroanal. Chem., 20 (1969) 463.
[11] I.M. Kolthoff, P. Mader and S.E. Khalafalla, J. Electroanal. Chem., 18 (1968) 315.
[12] J.M.L. Fonseca, P.S. Pedrero and C.G. Posa, J. Chim. Phys. Biol., 77 (1980) 9.
[13] A. Calusaru, Analyst, 115 (1990) 1223.
[14] Kirk-Othmer Encyclopedia of Chemical Technology, Vol. 22, Wiley, New York, 3rd edn., p. 960.
[15] O. Fiehn, T. Reemtsma and M. Jekel, Anal. Chim. Acta, 295 (1994) 297.
[16] R.N. Goyal and A. Kumar, Indian J. Chem. Sect. A, 31 (1992) 237.

ELSEVIER

Talanta 44 (1997) 497–500

Talanta

Short communication

Cathodic stripping voltammetric determination at a hanging mercury drop electrode of the environmental heavy metal precipitant trimercapto-*s*-triazine (TMT)

Arnold G. Fogg [a,*], Razali Ismail [a], A. Rahim H.M. Yusoff [a], Rahmalan Ahmad [b], Florin G. Banica [a,1]

[a] *Chemistry Department, Loughborough University, Loughborough, Leicestershire LE11 3TU, UK*
[b] *Chemistry Department, Technical University of Malaysia, Johor Bahru, Malaysia*

Received 24 May 1996; received in revised form 20 August 1996; accepted 27 August 1996

Abstract

Trimercapto-*s*-triazine (TMT) is available commercially for precipitating heavy metals in effluents prior to discharge and for recovering silver and copper. The TMT content of an effluent for discharge is normally monitored down to about 2 ppm by means of its UV absorption at 285 nm. Indirect cathodic-stripping voltammetric methods of determining TMT at sub-ppb levels in standard solutions are reported here. These methods might prove suitable for the determination of TMT in effluent at levels lower than is currently possible. TMT can be accumulated and determined indirectly at pH 9.0 as its mercury salt down to sub-ppb levels. Accumulation is made at 0 V and the mercury TMT reduction peak is at −0.47 V. Alternatively, by adding nickel(II), TMT can be determined optimally at pH 7.8, using the catalytic nickel peak at −0.73 V and accumulating between −0.10 and −0.60 V: at this pH the HgTMT peak at −0.47 V is small. At slightly higher pH (pH 8.6) the nickel TMT complex can be accumulated directly at −0.40 V, but at this pH, however, a slightly increased sensitivity can be achieved by accumulating TMT as its mercury salt, at −0.1 V in the presence of nickel(II), the nickel TMT complex being formed during the potential sweep on the release of the TMT when the mercury salt is reduced. Unlike many other thiols TMT is not accumulated as its copper(I) salt on addition of copper(II) to the solution. © 1997 Elsevier Science B.V.

Keywords: Cathodic stripping voltammetry; Trimercapto-*s*-triazine; TMT; Catalytic nickel peak

1. Introduction

Trisodium trimercapto-*s*-triazine (TMT) is available commercially as a 15% solution (TMT15; Degussa, Hanau, Germany) for the pre-

* Corresponding author.
[1] Present address: Norwegian University of Science and Technology, Department of Chemistry, N-7055 Dragvoll, Trondheim, Norway.

PII S0039-9140(96)02073-5

cipitation of divalent heavy metals and silver from aqueous solutions. It is used in the treatment of effluent before discharge and in the recovery of metals, e.g. copper and silver, from electroplating and photographic baths and from electrical components (see Degussa literature).

A few years ago we were pleased to provide initial information on the voltammetric determination of heavy metals in samples provided by chemists at Powergen who were assessing the suitability of the technique for analysis of effluent from the Flue Gas Desulphurisation plant being installed at Ratcliffe on Soar Power Station. This plant, now in operation, removes sulfur dioxide from the flue gases. This is done by means of a limestone slurry, which is converted first into calcium sulfite, and then, through the injection of air, to calcium sulfate (gypsum), which is sold for plasterboard production and other purposes. Small concentrations of heavy metals enter the system from the limestone or the coal, via the flue gases: these are removed from the effluent initially with lime and then with TMT15.

Trade literature from Degussa gives methods for the determination of TMT. At higher levels (e.g. in TMT15), TMT can be determined acidimetrically by potentiometric titration with hydrochloric acid. At lower levels, e.g. in treated effluent, it can be determined by means of its UV absorption at 285 nm. Typical dosage levels of TMT15 are reported to be 50–100 ml per cubic meter of effluent (ie. 7.5–15 ppm TMT). Calibration graphs are constructed from 1–10 ppm TMT using standard TMT solutions prepared in water having a similar salt composition to the effluent as high salt levels are reported to cause a reduction in the absorbance at 285 nm.

General studies are being made in our laboratories of the indirect determination of thiols by cathodic stripping voltammetry [1–7]. In particular the first use of nickel and cobalt catalytic reduction peaks in CSV have been reported [1,7]. Comparisons are being made of the use of accumulation and determination of the mercury, copper(I), nickel and cobalt salts of thiols. In this communication we report on the cathodic stripping voltammetry of TMT in standard solutions using these methods, and give some indication of possible interference from heavy metals, including copper and nickel, in the determinations.

2. Experimental

Cathodic stripping voltammetry was carried out with a Metrohm 646/647 VA Processor, using a multi-mode electrode in the HMDE mode. The three-electrode system was completed by means of a glassy carbon auxiliary electrode and an Ag/AgCl (3M KCl) reference electrode. All potentials are quoted relative to this reference electrode. Differential-pulse voltammetry was carried out with a pulse amplitude of 50 mV, a scan rate of 10 mV s^{-1} and a pulse interval of 1 s.

Samples of TMT15 were kindly provided by Powergen. Stock solutions of TMT (1.2×10^{-2} M) were prepared fresh every week: more dilute solutions were prepared daily by diluting these solutions. Standard copper(II), nickel(II) and other heavy metal solutions were prepared daily by diluting standard atomic absorption solutions from various manufacturers. Britton Robinson buffer (BRB) was prepared by dissolving boric acid (2.47 g), orthophosphoric acid (2.7 ml) and glacial acetic acid (2.3 ml) in water and diluting to 1 l. Appropriate volumes of this solution were adjusted to the required pH with sodium hydroxide solution (3 M).

The general procedure used to obtain cathodic stripping voltammograms was as follows: a 20 ml aliquot of buffer was placed in the voltammetric cell and the solution was purged with nitrogen for 6 min with the stirrer on. After an initial blank run, the required volumes of TMT and metal solutions were added by means of a micropipette. After forming a new mercury drop, accumulation was effected for the required time at the predetermined accumulation potential whilst the solution was stirred. The small mercury drop size was used on the Metrohm 647 VA stand. At the end of the accumulation period the stirrer was switched off and after 10 s had elapsed to allow the solution to become quiescent a negative-going potential scan was initiated. When further volumes of TMT solution or reagents were added the solution was deoxygenated for a further 20 s before producing further voltammograms.

3. Results

Typical cathodic stripping voltammograms of TMT at pH 2–9.4 are shown in Fig. 1. At the lower pH values (pH < about 7.5) two peaks are observed, which may be attributed to the reduction of mercury(II)-TMT. The smaller second peak is absent at higher pH values. There is a shift in the potential of the main peak from −0.1 to −0.47 V over this pH range, and the peak height reaches a maximum value at about pH 9.0. This pH was used subsequently. Calibration graphs were very reproducible, but were rectilinear up to 7×10^{-7} M when a disproportionate increase of peak current was obtained, followed by a levelling off of the current. At this time we have no explanation for the disproportionate increase in current, although it may be associated with the accumulation of different layers of HgTMT. The final levelling off of the current is normally owing to saturation of the surface of the drop. The limit of detection (three standard deviations) was calculated to be 5×10^{-9} M.

The addition of copper(II) removed the mercury TMT peak: a 7-fold excess of copper(II) eliminated the peak completely. No peak indicating the accumulation of copper(I) TMT was observed (see Fig. 2). Addition of cadmium also removed the mercury TMT peak, and small peaks

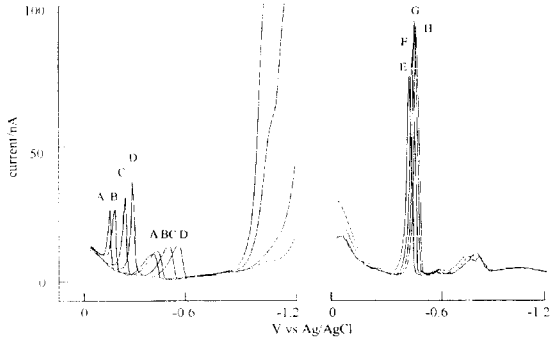

Fig. 1. The effect of pH on cathodic stripping voltammograms of TMT at a hanging mercury drop electrode. Accumulation potential, 0.0 V; accumulation time, 60 s; TMT concentration, 2.4×10^{-7} M. pH = A, 2.15; B, 2.50; C, 3.59; D, 4.44; E, 8.15; F, 8.69; G, 9.06; H, 9.41.

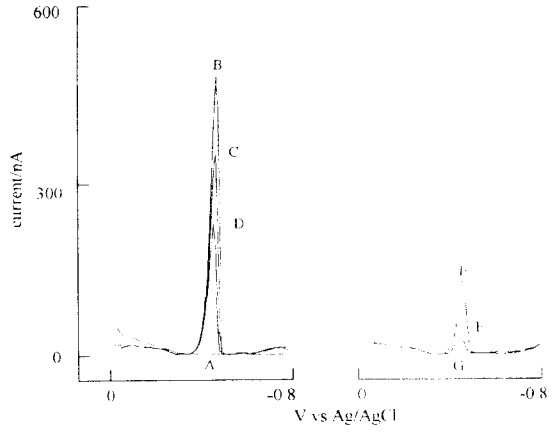

Fig. 2. Interference of copper(II) in the determination of TMT. Accumulation potential, 0.0 V; accumulation time, 60 s; TMT concentration, 2.4×10^{-7} M. pH = 9.0. Copper(II) concentration: A, 0 (buffer only); B, 0 (buffer + TMT only); C, 3.14; D, 6.28; E, 9.44; F, 12.6; G, 15.7×10^{-7} M.

became evident between −0.6– −0.8 V indicating some small accumulation of a cadmium TMT species (not shown). Lead, cobalt and zinc did not interfere at this pH: there was no sign of a catalytic cobalt peak but the possibility of its appearing at lower pH values needs to be investigated.

On the addition of a high concentration (e.g. 5×10^{-4} M) of nickel(II) the catalytic nickel peak of NiTMT appeared at −0.73 V in addition to the HgTMT peak at −0.47 V, when accumulation was effected at −0.1 V at pH 8.6. This indicates that TMT is accumulated still as HgTMT at −0.1 V, but is converted to NiTMT when the TMT is released when the HgTMT is reduced at −0.47 V during the potential scan. TMT can be accumulated directly at −0.4 V, but with a slightly reduced sensitivity. The optimum pH for the production of the catalytic nickel peak is slightly lower (pH 7.8) than for the production of the peak of the mercury salt: at this pH the mercury peak is very small, even when accumulation is effected at −0.20 V. Typical cathodic stripping voltammograms obtained for producing a calibration graph for the determination of TMT as its nickel complex with an accumulation time of 60 s are shown in Fig. 3.

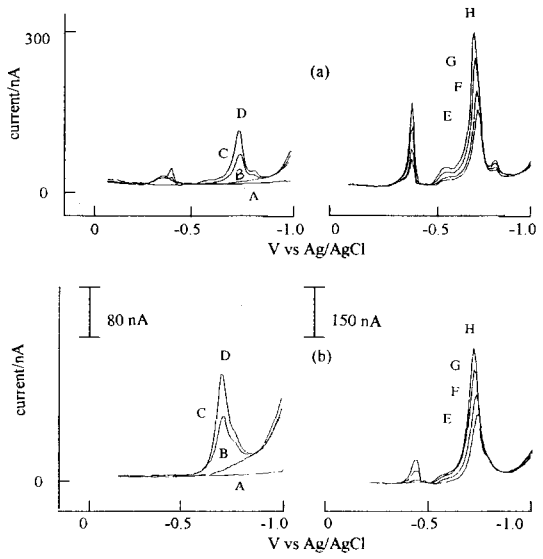

Fig. 3. Cathodic stripping voltammograms obtained for producing a calibration graph for the determination of TMT as its nickel complex (a) at pH 8.6 and (b) at pH 7.8. Accumulation potential, (a) -0.1 V and (b) -0.2 V; accumulation time, 60 s. Nickel(II) concentration: 5.1×10^{-4} M. TMT concentration: A, 0 (buffer only); B, 0 (buffer + Ni only); C, 0.3; D, 0.6; E, 0.9; F, 1.2; G, 1.8; H, 2.4×10^{-7} M.

4. Discussion

The values of the solubility products for M_3TMT_2 are quoted in the Degussa literature as being 1.0×10^{-18} (nickel) and 1.3×10^{-31} (copper(II)). This explains why the nickel CSV method can be applied but not the copper(I) method. The nickel salt/complex is sufficiently soluble for the nickel method to be applied, whereas addition of copper(II) to a TMT solution of about 1×10^{-7} M causes precipitation, or initially a colloidal solution of the copper(II) salt, which does not allow accumulation of the copper(I) salt at the electrode surface.

Determinations of the trace metals remaining after TMT treatment of effluent are made by well-established stripping voltammetric methods after UV irradiation to destroy TMT remaining in the effluent (J.A. Lees, Private communication and [8]). The trace metals remaining in the effluent could be present as dissolved or colloidal TMT complexes. The CSV methods described in this communication will determine free TMT and soluble TMT complexes that can be accumulated as Hg_3TMT_2 (solubility product $= 1.4 \times 10^{-47}$), but apparently not colloidal TMT complexes.

Acknowledgements

The authors are grateful to Dr Jill Lees of Powergen for her interest in this project. R.I. and A.R.H.M.Y. thank the Technical University of Malaysia (UTM) for financial support and leave of absence.

References

[1] F.G. Banica, J.C. Moreira and A.G. Fogg, Analyst, 119 (1994) 309.
[2] F.G. Banica, A.G. Fogg and J.C. Moreira, Analyst, 119 (1994) 2343.
[3] F.G. Banica, A.G. Fogg and J.C. Moreira, Talanta, 42 (1995) 227.
[4] A. Ion, F.G. Banica, A.G. Fogg and H. Kozlowski, Electroanalysis, 8 (1996) 40.
[5] F.G. Banica, A.G. Fogg, A. Ion and J.C. Moreira, Anal. Lett., 29 (1996) 1415.
[6] A.G. Fogg, R. Ismail, R. Ahmad and F.G. Banica, Analyst, 121 (1996) 1877.
[7] A.G. Fogg, R. Ismail, R. Ahmad and F.G. Banica, Talanta, 44 (1997).
[8] 'The Determination of Twelve Trace Metals in Marine and other Waters by Voltammetry or AAS', H.M. Stationery Office, London, 1988.

ELSEVIER

Talanta 44 (1997) 501–503

Talanta

Book reviews

Handbook of Sensors and Actuators, Volume 2, Solid State Magnetic Sensors, by C.S. Roumenin, Elsevier, Amsterdam, 1994, xiii + 417 pp., US$148.50. ISBN 0-444-89401-2.

One of a series of handbooks on sensors and actuators, this book is intended to be of use to scientists and engineers interested in using miniature sensing elements to detect and measure magnetic fields. The author's aim is to present the overall progress made in the field of magnetotransducers, to summarise the scientific achievements, and to provide a handbook for researchers and engineers interested in solid-state magnetosensors.

After introducing the principles and technologies used to measure magnetic fields, the background theory of the Hall effect, magnetoresistance, magnetodiode and related effects, and coherent phenomena associated with superconductivity in condensed matter—including the principles of operation of the incredibly sensitive SQUIDs (Superconducting Quantum Interference Devices)—are dealt with in detail. The characteristics of solid-state magnetic field sensors and methods for their determination are summarised.

About half the book is devoted to an extensive review of developments associated with the various classes of miniature magnetosensor: Hall sensors (first developed about 100 years ago) and magnetoresistors; magnetodiode sensors; bipolar magnetotransistors (whose characteristics have greatly improved, although the theory of their action is incomplete) and related sensors; SQUID sensors (both DC and RF). Factors such as the choice of materials and geometry are considered, and the implications for fabricating and packaging the sensors in single-chip form are made clear.

The functional approach to the construction of magnetosensors, which has lead to the invention of multisensors, gradiometers and vector magnetometers, is described. The incorporation into the circuit environment of solid-state sensors as electronic devices is considered, including biasing and signal processing circuitry, flip-flop based sensors, interfacing with digital systems, and a discussion of improvements that may be made to solid-state magnetosensors are surveyed. In addition to accurate measurement of d.c. and a.c. magnetic fields, electrical quantities and a variety of non-electrical and non-magnetic quantities may be measured. Useful appendices on magnetic terms and units, and important quantities and constants used in this area, are included.

C. Aust

Physical Properties of Polymers Handbook, edited by J.E. Mark, American Institute of Physics, New York, 1996, xv + 723 pp., £95.00. Also available from Oxford University Press. ISBN 1-56396-295-0.

This is the third volume from the AIP series in Polymers and Complex Materials. The books in the series are designed to help those who concentrate on one type of complex material to gain an insight from systematic expositions of other mate-

ELSEVIER

Talanta 44 (1997) 501–503

Talanta

Book reviews

Handbook of Sensors and Actuators, Volume 2, Solid State Magnetic Sensors, by C.S. Roumenin, Elsevier, Amsterdam, 1994, xiii + 417 pp., US$148.50. ISBN 0-444-89401-2.

One of a series of handbooks on sensors and actuators, this book is intended to be of use to scientists and engineers interested in using miniature sensing elements to detect and measure magnetic fields. The author's aim is to present the overall progress made in the field of magnetotransducers, to summarise the scientific achievements, and to provide a handbook for researchers and engineers interested in solid-state magnetosensors.

After introducing the principles and technologies used to measure magnetic fields, the background theory of the Hall effect, magnetoresistance, magnetodiode and related effects, and coherent phenomena associated with superconductivity in condensed matter—including the principles of operation of the incredibly sensitive SQUIDs (Superconducting Quantum Interference Devices)—are dealt with in detail. The characteristics of solid-state magnetic field sensors and methods for their determination are summarised.

About half the book is devoted to an extensive review of developments associated with the various classes of miniature magnetosensor: Hall sensors (first developed about 100 years ago) and magnetoresistors; magnetodiode sensors; bipolar magnetotransistors (whose characteristics have greatly improved, although the theory of their action is incomplete) and related sensors; SQUID sensors (both DC and RF). Factors such as the choice of materials and geometry are considered, and the implications for fabricating and packaging the sensors in single-chip form are made clear.

The functional approach to the construction of magnetosensors, which has lead to the invention of multisensors, gradiometers and vector magnetometers, is described. The incorporation into the circuit environment of solid-state sensors as electronic devices is considered, including biasing and signal processing circuitry, flip-flop based sensors, interfacing with digital systems, and a discussion of improvements that may be made to solid-state magnetosensors are surveyed. In addition to accurate measurement of d.c. and a.c. magnetic fields, electrical quantities and a variety of non-electrical and non-magnetic quantities may be measured. Useful appendices on magnetic terms and units, and important quantities and constants used in this area, are included.

C. Aust

Physical Properties of Polymers Handbook, edited by J.E. Mark, American Institute of Physics, New York, 1996, xv + 723 pp., £95.00. Also available from Oxford University Press. ISBN 1-56396-295-0.

This is the third volume from the AIP series in Polymers and Complex Materials. The books in the series are designed to help those who concentrate on one type of complex material to gain an insight from systematic expositions of other mate-

rials with analogous microstructural complexities, and to keep up with experimental and theoretical advances occurring in disciplines other than their own. The first two volumes were *Statistical Physics of Macromolecules* and, *Biomimetics: Design and Processing of Materials.*

The large multi-authored text is divided into 10 parts and contains 52 chapters. Properties emphasised are those that are most relevant to physical chemistry and chemical physics, so that the more synthetic-organic topics such as the polymerization process and the chemical modification of polymers are not included. The first part of the book concentrates on Structure and is followed by a Theory section containing topics such as scaling and fractal dimension, computational parameters and rotational isomeric state models. Part 3, the largest in the book, deals with Thermodynamic properties such as heat capacities, thermal conductivities, glass temperatures, solubility parameters and many others. The small (29 pages) Spectroscopy section contains information on NMR, IR and, Neutron and X-ray scattering. Part 5 covers Mechanical Properties such as impact behaviour and viscoelasticity and includes chapters on adhesives and gels. Part 6 deals with Crystallinity and morphology and contains, for example, chapters on densities, unit cell information and crystallization kinetics. The 6 chapters of Part 7 concentrate on Electro-Optical and Magnetic Properties such as electrical conductivity, electroluminescence and the refractive index. Part 8 contains details of Responses to Radiation, Heat and Chemical Agents such as flammability, degradation and pyrolysability. The chapter on synthetic biodegradable polymers for medical applications is an overview of general interest, with many useful references for further reading. Part 9 of the book deals with surface and interfacial properties, acoustic properties and permeability of polymers to gases and vapors. Finally, part 10 lists a number of definitions, units and conversion factors.

The many figures, tables and equations are of high quality, numerous references are included and the extensive indexing enables information to be located easily. Overall, this handbook succeeds in collating useful information on polymer properties and deserves a place in science libraries as well as in the numerous laboratories involved with polymer activities.

P.J. Cox

Practical Surface Analysis, Volume 2—Ion and Neutral Spectroscopy, edited by D. Briggs and M.P. Seah, Second edition, Wiley, Chichester, 1992, xvi + 738 pp., £50.00. ISBN 0-471-96498-0.

My favourable opinion of the hard-back version of this book, reviewed in Talanta, 1993, 40, 1995, remains unchanged even though the book is no longer up-to-date. The paper-back version will be welcomed by under- and post-graduate students because it is a relatively cheap, highly valuable book. Research supervisors will also welcome this version, for their highly-prized, hardback version need no longer be 'borrowed' by their students.

J.B. Craig

Mass Spectrometry in the Biological Sciences, edited by A.L. Burlingame and S.A. Carr, Humana, Totowa, New Jersey, 1996, xii + 570 pp., $145.00. ISBN 0-89603-340-6.

This book contains 26 chapters written by leading practitioners in 'biological mass spectrometry' and is based on the 3rd International Symposium for Mass Spectrometry in the Health and Life Sciences; held in San Francisco in 1994.

I place Biological Mass Spectrometry in inverted commas because this is a book that has been largely written by mass spectrometerists and concentrates (mostly) on the changes offered by biopolymers in their quest to work at ever higher mass and with increasingly involatile and intractable molecules. I do not mean to be overly critical on this point, but there are a lot of other areas in the biosciences that are benefitting from the application of mass spectrometry. Some of these rely on new application of 'old' technology, but others are a direct result of recent develop-

rials with analogous microstructural complexities, and to keep up with experimental and theoretical advances occurring in disciplines other than their own. The first two volumes were *Statistical Physics of Macromolecules* and, *Biomimetics: Design and Processing of Materials.*

The large multi-authored text is divided into 10 parts and contains 52 chapters. Properties emphasised are those that are most relevant to physical chemistry and chemical physics, so that the more synthetic-organic topics such as the polymerization process and the chemical modification of polymers are not included. The first part of the book concentrates on Structure and is followed by a Theory section containing topics such as scaling and fractal dimension, computational parameters and rotational isomeric state models. Part 3, the largest in the book, deals with Thermodynamic properties such as heat capacities, thermal conductivities, glass temperatures, solubility parameters and many others. The small (29 pages) Spectroscopy section contains information on NMR, IR and, Neutron and X-ray scattering. Part 5 covers Mechanical Properties such as impact behaviour and viscoelasticity and includes chapters on adhesives and gels. Part 6 deals with Crystallinity and morphology and contains, for example, chapters on densities, unit cell information and crystallization kinetics. The 6 chapters of Part 7 concentrate on Electro-Optical and Magnetic Properties such as electrical conductivity, electroluminescence and the refractive index. Part 8 contains details of Responses to Radiation, Heat and Chemical Agents such as flammability, degradation and pyrolysability. The chapter on synthetic biodegradable polymers for medical applications is an overview of general interest, with many useful references for further reading. Part 9 of the book deals with surface and interfacial properties, acoustic properties and permeability of polymers to gases and vapors. Finally, part 10 lists a number of definitions, units and conversion factors.

The many figures, tables and equations are of high quality, numerous references are included and the extensive indexing enables information to be located easily. Overall, this handbook succeeds in collating useful information on polymer properties and deserves a place in science libraries as well as in the numerous laboratories involved with polymer activities.

P.J. Cox

Practical Surface Analysis, Volume 2—Ion and Neutral Spectroscopy, edited by D. Briggs and M.P. Seah, Second edition, Wiley, Chichester, 1992, xvi + 738 pp., £50.00. ISBN 0-471-96498-0.

My favourable opinion of the hard-back version of this book, reviewed in Talanta, 1993, 40, 1995, remains unchanged even though the book is no longer up-to-date. The paper-back version will be welcomed by under- and post-graduate students because it is a relatively cheap, highly valuable book. Research supervisors will also welcome this version, for their highly-prized, hardback version need no longer be 'borrowed' by their students.

J.B. Craig

Mass Spectrometry in the Biological Sciences, edited by A.L. Burlingame and S.A. Carr, Humana, Totowa, New Jersey, 1996, xii + 570 pp., $145.00. ISBN 0-89603-340-6.

This book contains 26 chapters written by leading practitioners in 'biological mass spectrometry' and is based on the 3rd International Symposium for Mass Spectrometry in the Health and Life Sciences; held in San Francisco in 1994.

I place Biological Mass Spectrometry in inverted commas because this is a book that has been largely written by mass spectrometerists and concentrates (mostly) on the changes offered by biopolymers in their quest to work at ever higher mass and with increasingly involatile and intractable molecules. I do not mean to be overly critical on this point, but there are a lot of other areas in the biosciences that are benefitting from the application of mass spectrometry. Some of these rely on new application of 'old' technology, but others are a direct result of recent develop-

rials with analogous microstructural complexities, and to keep up with experimental and theoretical advances occurring in disciplines other than their own. The first two volumes were *Statistical Physics of Macromolecules* and, *Biomimetics: Design and Processing of Materials.*

The large multi-authored text is divided into 10 parts and contains 52 chapters. Properties emphasised are those that are most relevant to physical chemistry and chemical physics, so that the more synthetic-organic topics such as the polymerization process and the chemical modification of polymers are not included. The first part of the book concentrates on Structure and is followed by a Theory section containing topics such as scaling and fractal dimension, computational parameters and rotational isomeric state models. Part 3, the largest in the book, deals with Thermodynamic properties such as heat capacities, thermal conductivities, glass temperatures, solubility parameters and many others. The small (29 pages) Spectroscopy section contains information on NMR, IR and, Neutron and X-ray scattering. Part 5 covers Mechanical Properties such as impact behaviour and viscoelasticity and includes chapters on adhesives and gels. Part 6 deals with Crystallinity and morphology and contains, for example, chapters on densities, unit cell information and crystallization kinetics. The 6 chapters of Part 7 concentrate on Electro-Optical and Magnetic Properties such as electrical conductivity, electroluminescence and the refractive index. Part 8 contains details of Responses to Radiation, Heat and Chemical Agents such as flammability, degradation and pyrolysability. The chapter on synthetic biodegradable polymers for medical applications is an overview of general interest, with many useful references for further reading. Part 9 of the book deals with surface and interfacial properties, acoustic properties and permeability of polymers to gases and vapors. Finally, part 10 lists a number of definitions, units and conversion factors.

The many figures, tables and equations are of high quality, numerous references are included and the extensive indexing enables information to be located easily. Overall, this handbook succeeds in collating useful information on polymer properties and deserves a place in science libraries as well as in the numerous laboratories involved with polymer activities.

P.J. Cox

Practical Surface Analysis, Volume 2—Ion and Neutral Spectroscopy, edited by D. Briggs and M.P. Seah, Second edition, Wiley, Chichester, 1992, xvi + 738 pp., £50.00. ISBN 0-471-96498-0.

My favourable opinion of the hard-back version of this book, reviewed in Talanta, 1993, 40, 1995, remains unchanged even though the book is no longer up-to-date. The paper-back version will be welcomed by under- and post-graduate students because it is a relatively cheap, highly valuable book. Research supervisors will also welcome this version, for their highly-prized, hardback version need no longer be 'borrowed' by their students.

J.B. Craig

Mass Spectrometry in the Biological Sciences, edited by A.L. Burlingame and S.A. Carr, Humana, Totowa, New Jersey, 1996, xii + 570 pp., $145.00. ISBN 0-89603-340-6.

This book contains 26 chapters written by leading practitioners in 'biological mass spectrometry' and is based on the 3rd International Symposium for Mass Spectrometry in the Health and Life Sciences; held in San Francisco in 1994.

I place Biological Mass Spectrometry in inverted commas because this is a book that has been largely written by mass spectrometerists and concentrates (mostly) on the changes offered by biopolymers in their quest to work at ever higher mass and with increasingly involatile and intractable molecules. I do not mean to be overly critical on this point, but there are a lot of other areas in the biosciences that are benefitting from the application of mass spectrometry. Some of these rely on new application of 'old' technology, but others are a direct result of recent develop-

ments in mass spectrometry. As an inorganic mass spectrometerist I feel duty bound to mention that a section on inductively coupled plasma mass spectrometry and more on the measurement and application of stable isotope tracers (organic and inorganic) would have been useful additions.

Space does not permit an in-depth review of every chapter and it is hard to single out individual contributions from the text that is of such consistently high quality. However, to give a flavour of the contents I have selected a handful for special mention: Designing TOF/MS for the Future (R. Cotter et al), The Role of Fourier Transform Ion Cyclotron Resonance MS in Biological Research—New Developments and Applications (R.D. Smith et al), MALDI-TOF MS in the Quest for Novel Antibiotics (P. Tempst et al), Approaches to the Practical Use of Recognition Studies (A.M. Lawson et al) and Applications of Accelerator MS in Tocicology: A Highly Sensitive Tool for Low-Level Isotope Measurement (K.W. Turtletaub and J.S. Vogel). In addition to these there were chapters on DNA Sequencing, IR-MALDI MS of Proteins, Capillary LC/Electrospray MS and Tandem LC/MS in Drug Biotransformations.

This book is a must for all MS laboratories with an interest in biological applications. No one can fail to be impressed by the massive strides that have been made in the development and application of MS over the past decade. Equally no one can be in any doubt that we are only at the beginning of a most exciting phase of collaboration with our bioscience colleagues.

B.A. McGaw

Thin-Layer Chromatography: Reagents and Detection Methods, Volume 1b by H. Jork, W. Fuk, W. Fischer and H. Zimmer, VCH, Weinheim, 1994, xvi + 496 pp., £81.00. DM 198.00. ISBN 3-527-28205-X.

This volume is part of a series. Volume 1, which covers Physical and Chemical Detection Methods, is to be published in three Volumes (Volumes 1a, 1b and 1c). Volume 2 will be concerned with Biochemical and Biological Detection Methods. The particular volume under review deals with Activation Reactions, Reagent Sequences and Reagents.

Volume 1a is divided into three parts. Part 1 covers, in 137 pages, Specific Detection Methods and involves (i) Activation Reactions, (ii) Reagents for the Recognition of Functional Groups and (iii) Reagent sequences. Activation Reactions are subdivided into Photochemical, Thermochemical and Electrochemical Activation Reactions. Each method is briefly described with listings of examples where the methods have been successfully used. In addition a number of more detailed procedures, e.g. for the detection of testosterone, are provided. The section on Reagents for the Recognition of Functional Groups is a short section (11 pages) and essentially provides a list of reagents for the detection of specific functional groups, e.g. aldehydes, amines etc. The third section of Part 1 (*ca* 80 pages) covers Reagents Sequences, which involve the use of combinations of such reactions as electrophilic substitutions, oxidations and reductions, azo couplings, metal complexations etc. for the detection of specific compounds or families of compounds. An example of a reaction sequence involves the sequential addition of (i) cerium(IV) sulphate/sodium arsenite/sulphuric acid, (ii) methylene blue and (iii) ammonia vapour for the detection of iodide ions and organoiodine compounds. For each quoted recipe, the preparation of all the necessary reagents, the method of application and, where known, the underlying chemistry are detailed.

The major part (Part II, with over 300 pages) of this Volume is an alphabetical listing of reagents and their uses for the detection of specific types of compounds. For each reagent listed, the formula, the preparation of reagent solutions, the method of application, the chemical reactions undergone, the compounds detected and examples of tested procedures are all generally given.

The excellent index at the end of this Volume covers not only Volume 1a but also Volume 1b. The book is truly a mine of useful information. It clearly has a place in all chemistry libraries and is highly recommended by this reviewer.

J.L. Wardell

ments in mass spectrometry. As an inorganic mass spectrometerist I feel duty bound to mention that a section on inductively coupled plasma mass spectrometry and more on the measurement and application of stable isotope tracers (organic and inorganic) would have been useful additions.

Space does not permit an in-depth review of every chapter and it is hard to single out individual contributions from the text that is of such consistently high quality. However, to give a flavour of the contents I have selected a handful for special mention: Designing TOF/MS for the Future (R. Cotter et al), The Role of Fourier Transform Ion Cyclotron Resonance MS in Biological Research—New Developments and Applications (R.D. Smith et al), MALDI-TOF MS in the Quest for Novel Antibiotics (P. Tempst et al), Approaches to the Practical Use of Recognition Studies (A.M. Lawson et al) and Applications of Accelerator MS in Tocicology: A Highly Sensitive Tool for Low-Level Isotope Measurement (K.W. Turtletaub and J.S. Vogel). In addition to these there were chapters on DNA Sequencing, IR-MALDI MS of Proteins, Capillary LC/Electrospray MS and Tandem LC/MS in Drug Biotransformations.

This book is a must for all MS laboratories with an interest in biological applications. No one can fail to be impressed by the massive strides that have been made in the development and application of MS over the past decade. Equally no one can be in any doubt that we are only at the beginning of a most exciting phase of collaboration with our bioscience colleagues.

B.A. McGaw

Thin-Layer Chromatography: Reagents and Detection Methods, Volume 1b by H. Jork, W. Fuk, W. Fischer and H. Zimmer, VCH, Weinheim, 1994, xvi + 496 pp., £81.00. DM 198.00. ISBN 3-527-28205-X.

This volume is part of a series. Volume 1, which covers Physical and Chemical Detection Methods, is to be published in three Volumes (Volumes 1a, 1b and 1c). Volume 2 will be concerned with Biochemical and Biological Detection Methods. The particular volume under review deals with Activation Reactions, Reagent Sequences and Reagents.

Volume 1a is divided into three parts. Part 1 covers, in 137 pages, Specific Detection Methods and involves (i) Activation Reactions, (ii) Reagents for the Recognition of Functional Groups and (iii) Reagent sequences. Activation Reactions are subdivided into Photochemical, Thermochemical and Electrochemical Activation Reactions. Each method is briefly described with listings of examples where the methods have been successfully used. In addition a number of more detailed procedures, e.g. for the detection of testosterone, are provided. The section on Reagents for the Recognition of Functional Groups is a short section (11 pages) and essentially provides a list of reagents for the detection of specific functional groups, e.g. aldehydes, amines etc. The third section of Part 1 (*ca* 80 pages) covers Reagents Sequences, which involve the use of combinations of such reactions as electrophilic substitutions, oxidations and reductions, azo couplings, metal complexations etc. for the detection of specific compounds or families of compounds. An example of a reaction sequence involves the sequential addition of (i) cerium(IV) sulphate/sodium arsenite/sulphuric acid, (ii) methylene blue and (iii) ammonia vapour for the detection of iodide ions and organoiodine compounds. For each quoted recipe, the preparation of all the necessary reagents, the method of application and, where known, the underlying chemistry are detailed.

The major part (Part II, with over 300 pages) of this Volume is an alphabetical listing of reagents and their uses for the detection of specific types of compounds. For each reagent listed, the formula, the preparation of reagent solutions, the method of application, the chemical reactions undergone, the compounds detected and examples of tested procedures are all generally given.

The excellent index at the end of this Volume covers not only Volume 1a but also Volume 1b. The book is truly a mine of useful information. It clearly has a place in all chemistry libraries and is highly recommended by this reviewer.

J.L. Wardell

ELSEVIER

Talanta 44 (1997) 505–510

Talanta

Announcements

NATO Advanced Research Workshop on Biosensors for Direct Monitoring of Environmental Pollutants in Field

Smolenice (Slovakia)
4–8 May 1997

Scientific Programme
Trends of analytical methodology for determination of indoor and outdoor pollutants. DNA, biological recognition and receptor based sensors, biosensors for in field uses, ground water analysis and remote sensing, biosensors for environmental pollutants based on non-aqueous systems, micromachining, industrialization and market aspects of biosensors for environmental pollutants.

Organizing Committee
D.P. Nikolelis (Greece), M. Trojanowicz (Poland), G.G. Guilbault (Ireland), U.J. Krull (Canada), J. Wang (USA), M. Mascini (Italy).
Local Organizing Committee
V. Tvarozek, T. Hianik, D. Donoval, I. Novotny, M. Snejdarkova.

Applications for participation should be sent to:
Dr. D.P. Nikolelis (Director NATO ARW), Laboratory of Analytical Chemistry, Chemistry Department, Athens University, Panepistimiopolis-Kouponia, 15771 Athens, Greece. Fax: +301 723 1608.

Chemistry, Energy and the Environment 3

Hotel Palácio, Estoril, Portugal 25–28 May 1997

The workshop will cover modern trends in the development of chemistry for energy storage and energy conservation processes, its contribution to environmental protection, alternative options on the central roles to be played by chemistry in the energy industry and their relevance to society, and several aspects on Energy and New Technologies, as well as Energy and The Environment. The aim is to promote the exchange of information and ideas between scientists in industry, academia and government and to provide a forum for people dealing with these problems from around the world.

Workshop topics will include:

- Chemistry—friend or foe of the environment?
- Catalysis in the service of the environment.
- The challenge of the environmentally-friendly production of energy.
- Hydrogen as an energy source.
- Nuclear waste.
- Renewable energy water production processes.
- Energy sources for 2000 and beyond.
- Electrochemical decontamination.

Call for papers:

Authors are invited to submit titles of papers covering any of the above topics, and/or related topics. These titles should reach CAC Sequeira, Instituto Superior Técnico, Av. Rovisco Pais, 1096 Lisboa Codex, Portugal.

Further information write to:

César Sequeira, Institute Superior Técnico, 1096 Lisboa Codex, Portugal. Tel./fax: +351 1 7783594
or
John Moffat, University of Waterloo, Ontario N2L 3G1, Canada. Tel.: +1 519 8884567; fax: +1 519 7460435.

First Symposium 'In Vino Analytica Scientia' Applications of Analytical Chemistry to Wines, Alcohols and Spirits

University of Bordeaux-2: 12–14 June 1997

Under the Patronage of: Federation of European Chemical Societies (Analytical Chemistry Division and Food Chemistry Division), Société Française de chimie (Division de Chimie Analytique) and Office International de la Vigne et du Vin.
Ecole Européenne de Chimie Analytique (EECA) will organise the *1st Symposium 'In Vino Analytica Scientia'* (Applications of Analytical Chemistry to Wines, Alcohols and Spirits) at the University of Bordeaux-2, the 12, 13, 14 June 1997, with the Vinexpo Exhibition.The official languages will be English and French with simultaneous translation.

This international meeting of researchers, oenologists and professionals will take stock of the latest benefits of Analytical Chemistry in the improvement of both products and processes.

Scientific Programme:
- Constituents of grapes, wines and spirits
- Chemical and biochemical reactions
- Contaminants and traces
- Flavours and sensory analysis
- Chemical and biochemical sensors
- Quality and authenticity of products

Invited Speakers:
V. Cheynier (F), M. Forina (I), G. Friedbacher (A), A. Mosandl (D), P. Schreier (D), G.R. Scollary (AUS), J.R. da Silva (P), H.K. Sivertsen (N), M. de la Torre Borona (E), J. Vercauteren (F), J.C. Villetaz (CH), J. Wang (USA)

Presidium:
Honorary President: P. Ribéreau-Gayon
Presidents: R. Kellner, W. Pfannhauser

Scientific Committee:
Chairman: C.J. Ducauze
F. Bandion (A), Al. Bertrand (F), M. Comtat (F), J. Empis (P), M. Karayannis (GR), R. Lobinski (F), G.J. Martin (F), M.-H. Merle (F), B. te Nijenhuis (NL), A.C. Noble (USA), A. Rapp (D), D.N. Rutledge (F), J.C. Sapis (F), G.R. Scollary (AUS), M. Valcarcel (E), H.H. Widmer (CH), P.G. Zambonin (I)

Organising Committee:
Chairman: Y. Glories
O.F.X. Donard, L.J. Eveleigh, Ph. Garrigues, C. Gonzalez, J. Vercauteren, N. Vivas

For further information please contact:
D.N. Rutledge, Tel.: + 33 144 081648; fax: + 33 144 081653

Organisation:
Congress Rive Droite, 28, rue Baudricourt, 33100 Bordeaux, France. Tel.: + 33 556 328229; fax: + 33 556 327953

Tenth International Conference on Partitioning in Aqueous Two-phase Systems, Advances in the Principles and Applications of Separation Science in Biotechnology, Cell Biology and Environmental Recovery
Reading, UK
10–15 August 1997

This will be the 10th International Conference on Partitioning of Proteins, Metal Ions and Biological Particles in Aqueous Two-phase Systems. Theoretical, predictive, applied and engineering aspects of this emerging technology, which has found important applications, will be presented and discussed.

The conference will provide a focus for presentation and debate on developments and major issues in the principles and applications of separation science in biotechnology, cell biology and environmental ion recovery. It is expected that the meeting will be a forum for interdisciplinary debate with active participation of academics and industrial colleagues.

Abstracts of papers and posters for presentation at the conference are invited. Original contributions on any aspect of the following themes will be welcome:

- physicochemical properties of proteins important in bioseparations; interactions between liquid phase components and proteins
- modelling partitioning; thermodynamics
- prediction of partitioning of macromolecules and metal ions
- applications of partitioning; separation of enzymes and recombinant proteins
- studies of phase separation and development of new polymers
- biomedical applications; partitioning of cells, organelles and plasma membranes
- novel and complementary techniques

Authors intending to submit papers should send a title and 200–300 word abstract to the SCI Conference Secretariat to arrive no later than Friday, 1 February 1997.

For further details contact:

SCI, Society of Chemical Industry, 14/15 Belgrave Square, London SW1X 8PS; Tel.: +44 171 2353681; fax: +44 171 2357743; e-mail: conferences@chemind.demon.co.uk

Twenty-Eighth Annual International Symposium On Environmental Analytical Chemistry

Geneva, Switzerland 2–5 March 1988

The aim of this 28th Symposium is to actively encourage progress in methods, instrumentation, applications and to facilitate the transfer of know-how in different fields. It is targeted at scientists, analysts, manufacturers, end-users and post-graduate students.

Tentative main topics of the Symposium:
- Analyzing trace polar products in the environment
- New extraction, separation and instrumental techniques
- Chiral separations in environmental analysis
- Micro-Total analysis Systems (TAS)
- In situ measurements and speciation
- Quality assurance issues for environmental analysis for harmonization within EC and non-EEC countries
- Environmental and Education
- Other topics

All topics will be introduced in plenary lectures and invited research lectures followed by brief research presentations and posters. An exhibition of scientific equipment will also be organised. A short course on Sample Handling and Analysis of Organic Pollutants will be organised in Archamps, France, 27–28 February 1988.

For further details contact:
Mrs. M. Frei-Husler, IAEAC Secretariat, Postfach 46, CH-4123 Allschwil 2, Switzerland. Tel.: +41 61 4812789; fax: +41 61 4820805.

ELSEVIER

Talanta 44 (1997) 511–515

Talanta

Properties and analytical application of room temperature phosphorescence of 1-bromonaphthalene induced by *p*-octylpolyethylene glycol phenylether in aqueous *β*-cyclodextrin solution

Xinzhen Du *, Yong Zhan, Yunbao Jiang, Xianzhi Huang, Guozhen Chen

The Research Laboratory of SEDC of Analytical Science for Material and Life Chemistry, Department of Chemistry, Xiamen University, Xiamen 361005, People's Republic of China

Received 28 March 1996; received in revised form 8 July 1996; accepted 12 July 1996

Abstract

Intense room temperature phosphorescence of 1-bromonaphthalene (1-BrN) induced by *p*-octylpolyethylene glycol phenylether was studied in aqueous *β*-cyclodextrin solution. The mode of inclusion complex formation was approached. The optimal conditions were obtained. Interferences of foreign substances with phosphorescence were examined. The phosphorescence intensity is proportional to the concentration of 1-BrN in the range $0 \sim 5.18$ μg ml^{-1}. The recovery is 90–102% and the relative standard deviation is less than 4.5%. The proposed method is simple and convenient. © 1997 Elsevier Science B.V.

Keywords: 1-Bromonaphthalene; *β*-Cyclodextrin; *p*-Octylpolyethylene glycol phenylether; Phosphorescence

1. Introduction

Micelle-stabilized room temperature phosphorescence (MS-RTP) and cyclodextrin-induced room temperature phosphorescence (CD-RTP) have been proposed for analytical purposes in the eighties [1–5]. Good spectral selectivity was obtained because a majority of organic species do not show phosphorescence at room temperature and the substrates have little or lower background emission in the proximity of the phosphorescence wavelength. For MS-RTP, deoxygenation is needed for the attainment of RTP. However, oxygen removal from micellar solutions by the nitrogen-purging technique results in plentiful bubbles. It has an effect on the precision of analysis. For CD-RTP of polycyclic aromatic hydrocarbons (PAHs) without an internal heavy atom, a bromonated alkane or alcohol was required as an external heavy-atom perturber, sometimes combined with deoxygenation by nitrogen [6–9]. Although no bubbles appear, a phosphoroscope was required for phosphorescence measurements because serious emulsification of the solutions causes strong scattering lights.

* Corresponding author.

PII S0039-9140(96)02048-6

Bromonated naphthalenes are a series of interesting compounds which normally exhibit weaker fluorescence than their parent naphthalene due to their internal heavy atom effect [10,11]. In the presence of acetonitrile or an alcohol, the intense RTP of 1-bromonaphthalene (1-BrN) has been observed from aqueous cyclodextrin solutions without deoxygenation on a conventional spectrofluorimeter [12–15]. Since the microcrystals of the inclusion complex containing an alcohol absorb onto the inner walls of glassware, the phosphorescence intensity is usually unstable at a fixed concentration of phosphors. In this work, *p*-octylpolyethylene glycol phenylether (OP), a detergent, was employed for the attainment of stable phosphorescence. It can induce intense RTP of 1-BrN in aqueous β-cyclodextrin (β-CD) solution like an alcohol and enables the complex precipitate to disperse in solution due to the complex with the polar head group of OP. As a result, the accuracy and the precision were improved. Furthermore, the interaction of OP with β-CD and 1-BrN and the potential application were also discussed.

2. Experimental

2.1. Reagents

1-BrN, purchased from Shanghai Reagent Co., was distilled under reduced pressure. A solution of 200.7 μg ml^{-1} 1-BrN was prepared by dissolving it in 2.33×10^{-2} mol l^{-1} OP solution in an ultrasonic bath. β-CD, purchased from Suzhou Gourment Factory, was dissolved in distilled water and recrystallized three times. OP was purchased from Shanghai Reagent Co. and was used as received. Twice demineralized water was distilled.

2.2. Apparatus

All steady-state luminescence spectra were performed on a Hitachi 650-10S fluorescence spectrophotometer equipped with a 150 W xenon lamp as the excitation light source. Excitation and emission slits of 3 nm were employed. The scan speed of the monochormators was maintained at 240 nm min^{-1}. The quartz cell was washed with ethanol to guarantee the thorough cleaning of organic species that absorb onto the inner walls of the glassware. It was carefully washed with distilled water prior to use.

2.3. General procedures

An aliquot of 2.33×10^{-2} mol l^{-1} OP solution containing 1-BrN was transferred into a 10 ml volumetric flask and an appropriate amount of β-CD was added. After dilution to the mark with water, the samples were allowed to stand for at least 45 min. The samples were introduced into the cell, which was later capped with a Teflon stopper. The RTP signal was monitored at 492 nm when the samples were excited at 290 nm.

3. Results and discussion

3.1. RTP spectra of a ternary inclusion complex

In aqueous solution, 1-BrN exhibits weak fluorescence with an excitation wavelength of 277 nm and emission wavelength of 337 nm. Upon addition of β-CD to the solution, the fluorescence intensity slightly increases due to the formation of the β-CD:1-BrN inclusion complex but no RTP appears. In the presence of both β-CD and OP, 1-BrN gives rise to intense phosphorescence emission at 492 nm and 525 nm at room temperature in aerated aqueous solution, accompanied by the emulsification of the solution. The excitation wavelength redshifts to 290 nm (see Fig. 1). These phenomena suggest that OP has a significant effect on the microenvironment surrounding 1-BrN because phosphorescence is highly sensitive to the properties of environment. A favorable microenvironment is provided in the apolar cavity of β-CD upon addition of OP. It is reasonable to attribute the appearance of RTP to the formation of a ternary complex among β-CD, 1-BrN and OP.

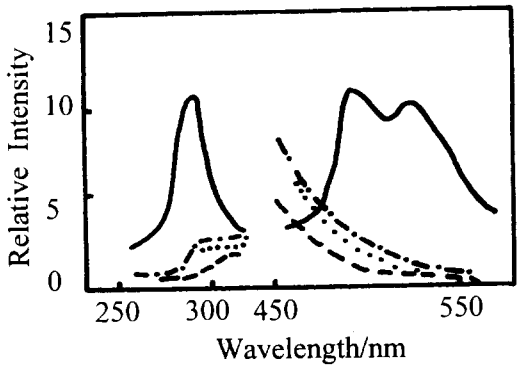

Fig. 1. RTP spectra of inclusion complexes. OP (•-•), β-CD + OP(•••), 1-BrN + OP(– – –) and β-CD + 1-BrN + OP(——). 1-BrN: 20.70 μg ml^{-1}; β-CD: 8.0×10^{-3} mol l^{-1}; OP: 2.33×10^{-3} mol^{-1} l^{-1}. Photomultiplier, gain: 1.0. Slit width: 3 × 3 mμ.

3.2. Effect of β-CD on RTP

The influence of β-CD on the RTP of 1-BrN was examined at a fixed concentration of 1-BrN and OP. As shown in Fig. 2, the phosphorescence is too weak to be observed at a β-CD concentration below 1.0×10^{-3} mol l^{-1} in the presence of 2.33×10^{-3} mol l^{-1} OP. Subsequently, the phosphorescence intensity rapidly increases with the increasing concentration of β-CD. Although the higher β-CD concentration results in more intense RTP, β-CD of 8.0×10^{-3} mol l^{-1} was used in the experiment due to the limit of its solubility in water.

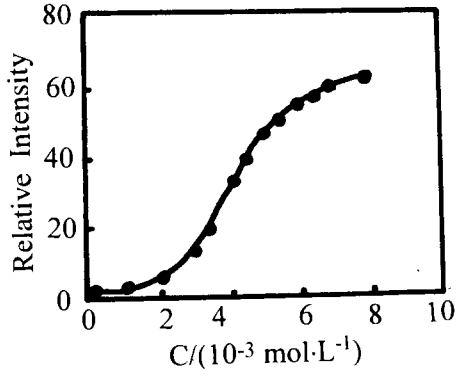

Fig. 2. Dependence of RTP on β-CD concentration. 1-BrN: 20.70 μg ml^{-1}; OP: 2.33×10^{-3} mol l^{-1}.

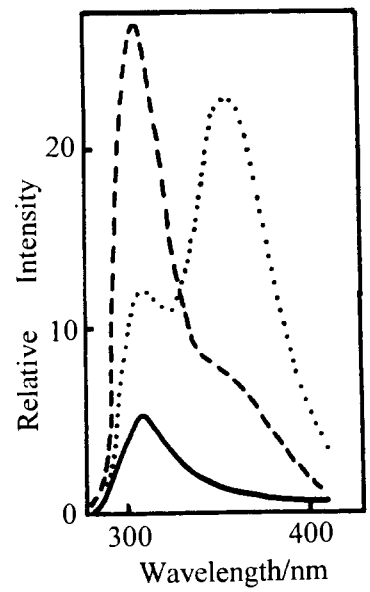

Fig. 3. Fluorescence spectra of OP. OP(•••); β-CD + OP(– – –) and β-CD + 1-BrN + OP(——). 1-BrN: 20.70 μg ml^{-1}; β-CD: 8.0×10^{-3} mol l^{-1}; OP: 2.33×10^{-3} mol l^{-1}.

3.3. Effect of OP on RTP

OP is a nonionic detergent with a *tert*-octyl group as its hydrophobic part and a polyethylene glycol group as its hydrophilic one. It contains ether groups, a phenyl group and a hydroxyl group. Surface tension measurements suggest that the micelles are not present in aqueous solution containing excess β-CD since the β-CD molecule includes an OP molecule. Fig. 3 shows the fluorescence spectra from a micellar solution of OP in the absence and presence of excess β-CD. The fluorescence at 307 nm ($\lambda_{ex} = 287$ nm) and 360 nm ($\lambda_{ex} = 297$ nm) can be attributed to the OP monomer and OP aggregates, respectively.

Upon addition of OP to the solution containing 1-BrN and 8×10^{-3} mol l^{-1} β-CD, RTP can be observed at 1.54×10^{-4} mol l^{-1} OP. This is accompanied by the slight emulsification of the solution, in which the micelles are not present in aqueous solution due to the inclusion of β-CD with OP. As shown in Fig. 4, the addition of more OP to the solution leads to more intense RTP. In the presence of 2.33×10^{-3} mol l^{-1} OP, the phosphorescence maximum is obtained. Since OP

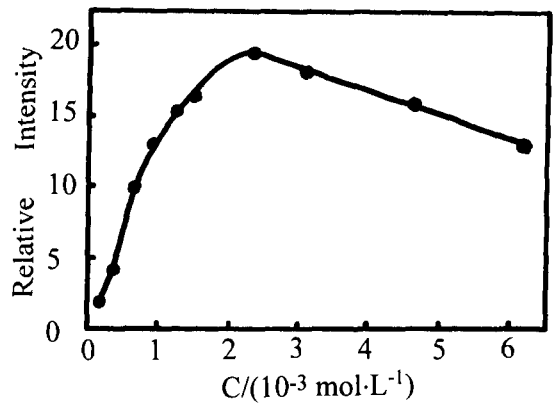

Fig. 4. Dependence of RTP on OP concentration. 1-BrN: 20.70 μg ml^{-1}; β-CD: 8.0×10^{-3} mol l^{-1}.

is an amphiphilic molecule, the complex precipitate homogeneously disperses in aqueous solution. Consequently, the phosphorescence intensity appears stable and good precision was achieved. After the highest phosphorescence intensity, a further increase in OP concentration results in a decrease in the phosphorescence intensity. RTP completely disappears and the solutions become transparent in the presence of more than 1.24×10^{-2} mol l^{-1} OP (more than 8.0×10^{-3} mol l^{-1}). The spectral changes indicate that the complex has completely dissociated. In terms of the surface tension of the solutions, the micelles occurs in the presence of excess OP. Since the spectral properties of 1-BrN in the solutions are similar to those of 1-BrN in the micellar solution of OP, it is possible that the 1-BrN molecule transfers from the β-CD cavity to the micellar core.

The phosphorescence enhancement upon addition of OP indicates that OP is also a micorenvironment regulator in the apolar cavity of β-CD like an alcohol. The hydrocarbon part of OP is incorporated into the apolar cavity of β-CD through the hydrophobic interaction. This result is analogous to those reported by Park and Song [16] and Li and Purdy [17]. By the Benesi–Hildebrand method [18], the stoichiometry of the 1:1:1/β-CD:1-BrN:OP complex was obtained with phosphorescence measurements. The apparent inclusion constant was estimated as 1.80×10^{-5} mol^{-2} l^2, which is much greater than the value of 720 mol^{-1} l of the β-CD:1-BrN complex. On the other hand, it is seen from Fig. 3 that the ternary complex formation results in a greatly decreased fluorescence of OP at 307 nm. One plausible explanation is that 1-BrN and the phenyl ring of OP locate close to each other in the cavity and 1-BrN seriously quenches the fluorescence of OP due to its external heavy-atom effect. For this reason, most of water molecules in the cavity are replaced by the 1-BrN molecule and the hydrocarbon part of the OP molecule. The rotation of the 1-BrN molecule in the cavity is restricted and the

Table 1
Analytical results of the synthetic samples

Components (μg ml^{-1})	Added (μg ml^{-1})	Found (μg ml^{-1})	Recovery (%)	RSD (%)
1-BrN	1.24	1.26	102	1.4
1-BrN	1.66	1.68	101	1.8
1-BrN	3.31	3.35	101	4.1
naphthalene: 5.13; anthracene: 7.13; biphenyl: 6.16	4.14	3.76	91	4.2
naphthalene: 1.28; acenaphene: 1.54; biphenyl: 1.54; 1-naphthol: 1.44	4.14	3.89	93	1.9
naphthalene: 1.28; anthacene: 1.78; phenanthrene: 1.78; acenaphthenel: 1.54; fluorene: 1.66; biphenyll: 1.54; 1-Naphthol: 1.44; chrysene: 2.28	4.14	3.86	93	1.9
naphthalene: 2.56; anthacene: 3.56; Phenanthrene: 3.56; acenaphthene: 3.08; fluorene: 3.32; biphenyl: 3.08; 1-naphthol: 2.88; chrysene: 4.56	4.14	3.71	90	1.6

RSD relative standard deviation.

rigidity of the 1-BrN molecule is promoted. Furthermore, the longer phosphorescence lifetime of 1-BrN (3.62 ms) also indicates that the excited triplet state of the 1-BrN molecule in the β-CD cavity is shielded from efficient triplet state quencher oxygen molecules in the solution to some extent. As a result, the probability of a radiationless transition greatly decreases and the phosphorescence intensity dramatically increases.

3.4. Interferences of foreign species

Interferences of other PAHs with the RTP of 1-BrN were studied. Under our experimental conditions, the PAHs examined do not phosphoresce but show strong fluorescence at room temperature. For the determination of 4.14 μg ml^{-1} 1-BrN, 9-fold amounts of anthracene and an equivalent amount of chrysene do not interfere, and 3.7-fold amounts of biphenyl and an equivalent amount of fluorene result in a decrease by 10% in the phosphorescence intensity. Equivalent amounts of phenanthrene and acenaphthene reduce the phosphorescence intensity by 15%. Three-fold amounts of naphthalene and an equivalent amount of 1-naphthol reduce the phosphorescence intensity by 25%.

3.5. Analysis of synthetic samples

A linear relationship between the phosphorescence intensity and 1-BrN concentration was examined. In the range $0 \sim 5.18$ μg ml^{-1}, the phosphorescence intensity is proportional to the concentration of 1-BrN. The straight line has a regression equation of $I_p = 3.355C + 5.703$ and a regression coefficient of 0.9994. Based on a signal-to-noise ratio of three, the limit of detection was estimated as 4.04 ng ml^{-1}. The analytical results of synthetic samples are listed in Table 1. The recovery is 90–102% and the precision is good ($n = 11$). It is suitable for the determination of 1-BrN in a mixture of PAHs.

References

[1] L.J. Cline Love, M. Skrilec and J.G. Habarta, Anal. Chem., 52 (1980) 754.
[2] M. Skrilec and L.J. Cline Love, Anal. Chem., 52 (1980) 1559.
[3] M.E. Rolie, C.N. Ho and I.M. Warner, Anal. Chem., 54 (1983) 2445.
[4] S. Scypinski and L.J. Cline Love, Anal. Chem., 56 (1984) 322.
[5] M.E. Diaz Garcia and M. Scanz-Medel, Anal. Chem., 56 (1986) 1436.
[6] L.J. Cline Love and R. Weinberger, Spectrochim. Acta, 38B (1983) 1421.
[7] H. Kim and S.R. Crouch, Anal. Chem., 61 (1989) 2475.
[8] A.M. Dela La Pena, F. Salinas, M.J. Gomez, M. Sanchez-Pena and I. Duran-Meras, Talanta, 40 (1993) 1657.
[9] S. Hamai, J. Chem. Soc., Chem. Commun., (1994) 2243.
[10] R.J. Hutubise, Anal. Chem., 55 (1983) 669A.
[11] J.J. Donkerbroek, J.J. Elzas, R.W. Frei and N.H. Velthorst, Talanta, 28 (1981) 717.
[12] N.J. Turro, J.D. Bolt, Y. Kuroda and I. Tabushi, Photochem. Photobiol., 35 (1982) 69.
[13] N.J. Turro, G.S. Cox and X. Li, Photochem. Photobiol., 37 (1983) 149.
[14] A. Ponce, P.A. Wong, J.J. Way and D.G. Nocera, J. Phys. Chem., 97 (1993) 11137.
[15] Y. Zhang, X.Z. Huang, J.G. Xu and G.Z. Chen, Chem. J. Chinese Univ., 15 (1994) 181.
[16] J.W. Park and H.Y. Song, J. Phys. Chem., 93 (1989) 6454.
[17] S. Li and W.C. Purdy, Chem. Rev., 92 (1992) 1457.
[18] H.A. Benesi and H. Hildebrand, J. Am. Chem. Soc., 71 (1949) 2703.

ELSEVIER

Talanta 44 (1997) 517–526

Talanta

Assay of cisapride in pharmaceutical formulations by extraction spectrophotometry

C.S.P. Sastry [a,*], Y. Srinivas [a], P.V. Subba Rao [b]

[a] *Department of Organic Chemistry, Foods, Drugs and Water, Andhra University, Visakhapatnam-530 003, India*
[b] *Department of Physical Chemistry, Andhra University, Visakhapatnam-530 003, India*

Received 21 March 1996; received in revised form 16 July 1996; accepted 22 July 1996

Abstract

Four simple and sensitive spectrophotometric methods (A–D) for the assay of cisapride in pure and dosage forms based on the formation of chloroform soluble ion-associates under specified experimental conditions are described. Four acidic dyes, namely, Suprachen Violet 3B (SV 3B, method A), Erioglaucine A (EG-A, method B), Naphthalene Blue 12 BR (NB-12BR, method C) and Tropaeolin 000 (TP 000, method D) are utilized. The extracts of the ion-associates exhibit absorption maxima at 595, 640, 620 and 500 nm for methods A, B, C and D, respectively. Beer's law and the precision and accuracy of the methods are checked by the UV reference method. The results are reproducible with an accuracy of ± 1.0%. The methods are found to be suitable for the determination of cisapride in the presence of the other ingredients that are usually present in dosage forms. © 1997 Elsevier Science B.V.

Keywords: Cisapride; Ion-associates; Spectrophotometry

1. Introduction

Cisapride (CPD) is a gastrointestinal stimulant agent, effective in the relief of gastrointestinal or esophagus disorders and in the promotion of gastric emptying of a gastrointestinal motility [1]. It is a prokinetic agent believed to facilitate acetylcholine release from the myenteric plexus of the gut [2]. It is chemically known as (±) *cis*-4-amino-5-chloro-*N*-[1-[3-fluorophenoxy)propyl]-3-methoxy-4-piperidyl]-2-methoxy benzamide. The drug is official in the British Pharmacopoeia [3]. Literature mentions only a few methods such as fluorimetry [4], high performance liquid chromatography [5,6], thin layer chromatography [7] and a fluorescent polarization immunoassay method [8] for its determination in biological fluids and dosage forms. Although spectrophotometric methods are the instrumental methods of choice commonly used in industrial laboratories, no colorimetric method has been reported so far for the determination of cisapride. Therefore, the need for a fast, low cost and selective method is obvious, especially for routine quality control analysis of pharmaceutical products containing cisapride.

* Corresponding author. Tel.: +91 54873, ext. 236/348.

PII S0039-9140(96)02050-4

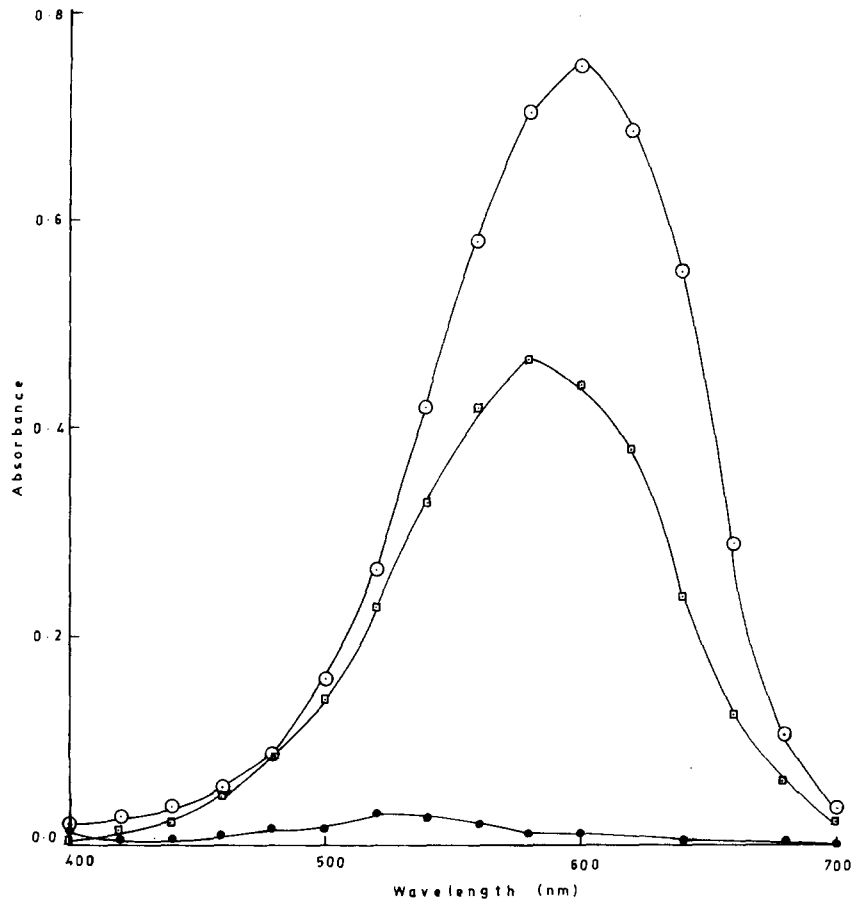

Fig. 1. Absorption spectra of the CPD-SV3B system (⊙——⊙) (concentration of CPD: 6.43×10^{-5} M; SV3B: 9.26×10^{-4} M), aqueous SV3B (□——□) (aqueous SV3B: 2.77×10^{-4} M), and reagent blank vs. chloroform (●——●).

As the extraction spectrophotometric procedures are popular for their sensitivity and selectivity in the assay of drugs [9,10], the technique was therefore utilized in the present work for the estimation of cisapride. A thorough literature survey of the extraction spectrophotometric determination of drugs reveals that many acid dyes belonging to azo [11–19], amino anthroquinone [20–22], indigoid [14,15], triphenylmethane [14,15,23] and sulphopthalein [14,24] are studied in the determination of compounds exhibiting basic properties (e.g. amines, quaternary ammonium compounds, heterocyclic compounds). In continuation of these studies, the present paper describes four simple and sensitive extraction spectrophotometric methods for the determination of cisapride, based on its tendency to form chloroform extractable ion-association complexes with acidic dyes belonging to different chemical classes, namely, Suprachen Violet 3B, SV 3B (amino anthroquinone; method A), Erioglaucine A, EG-A (triphenyl methane; method B), Naphthalene Blue 12BR, NB-12BR (diazo; method C) or Tropaeolin 000, TP 000 (monoazo; method D) under specified experimental conditions by exploiting the basic nature of the drug molecule.

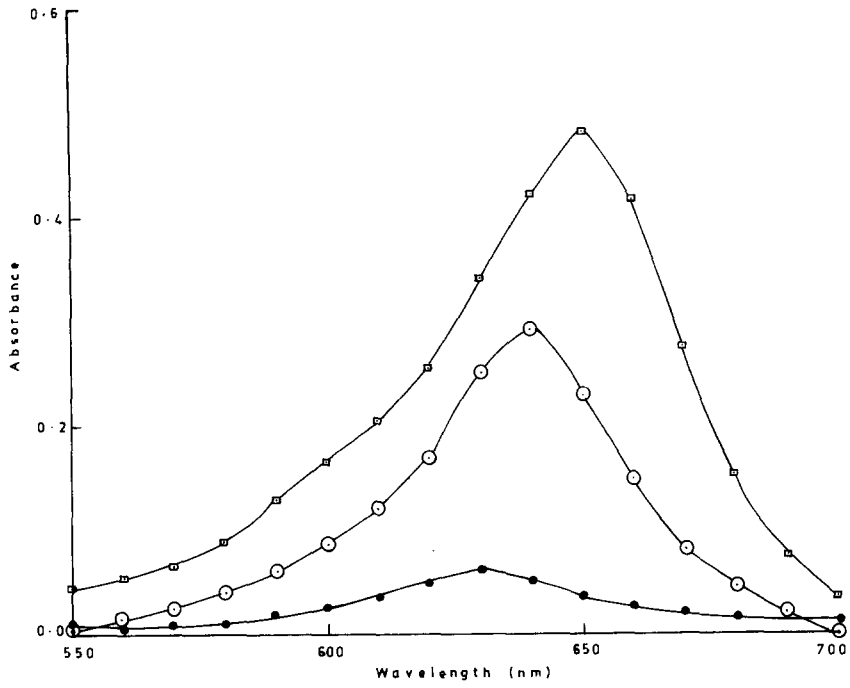

Fig. 2. Absorption spectra of the CPD-EG A system (⊙——⊙) (concentration of CPD: 6.43×10^{-6} M; EG A: 1.69×10^{-3} M), aqueous EG A (□——□) (aqueous EG A: 6.09×10^{-5} M), and reagent blank vs. chloroform (●——●).

2. Experimental

2.1. Instruments

A Milton Roy Spectronic 1201 UV-visible spectrophotometer and a Systronic 106 digital spectrophotometer with 1 cm matched quartz cells were used for all the absorbance measurements. An Elico LI 120 digital pH meter was used for pH measurements.

2.2. Reagents

All reagents and chemicals used were of analytical or pharmacopoeial grade purity and doubly distilled water was used throughout.

2.2.1. Dye solutions

Aqueous solutions of SV 3B (0.2% W/V, Chroma, Stuttgart, Germany), EG-A (0.4% W/V, Gurr, High Wycombe, Bucks, UK), NB-12BR (0.2% W/V, BDH, Poole, UK) and TP 000 (0.2% W/V, Fluka, Switzerland) were prepared by dissolving the required amount in doubly distilled water. The solutions were washed with chloroform to remove the chloroform-soluble impurities and the residual solvent was removed by bubbling with nitrogen.

2.2.2. Buffer solutions

The glycine–HCl buffer solutions (pH 1.3 for methods A, B and pH 1.5 for method C) were prepared [25].

2.3. Preparation of standard drug solution

A 1 mg ml^{-1} stock solution of cisapride was prepared by dissolving 100 mg of the drug in 100 ml of chloroform. Working standard solutions were obtained by appropriate dilution of the stock solution with the same solvent (50 μg ml^{-1}, for methods A, C, D and 10 μg ml^{-1}, for method B).

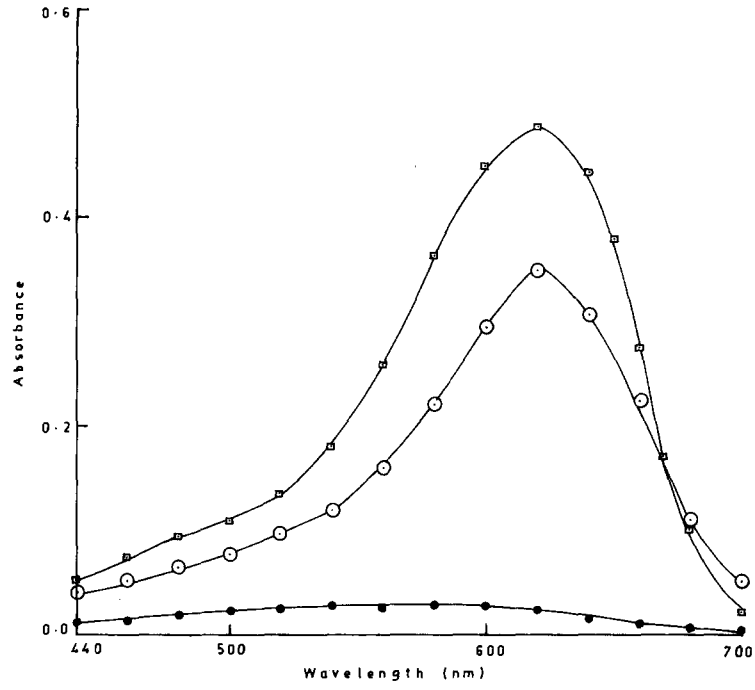

Fig. 3. Absorption spectra of the CPD-NB 12BR system (⊙——⊙) (concentration of CPD: 2.14×10^{-5} M; NB-12BR: 2.11×10^{-4} M), aqueous NB-12BR (□——□) (aqueous NB-12BR: 1.90×10^{-5} M), and reagent blank vs. chloroform (●——●).

2.4. Recommended procedures

2.4.1. Methods A and B

Aliquots of standard CPD solution (0.5–8.0 ml; 50 μg ml^{-1}, method A or 0.5–6.0 ml; 10 μg ml^{-1}, method B) were placed in a series of 125 ml separating funnels. A volume of pH 1.3 buffer solution (6.0 ml for method A or 10.0 ml for method B) and 2.0 ml of SV 3B solution (method A) or 5.0 ml of EG-A solution (method B) were added. The total volume of the aqueous phase in each separating funnel was adjusted to 10.0 ml and 15.0 ml with distilled water for methods A and B, respectively. A requisite volume of chloroform was added to each funnel to make the organic layer up to 10.0 ml and contents were shaken for 2 min. The two phases were allowed to separate, the separated chloroform layer was dried over sodium sulphate and the absorbance was measured at appropriate λ_{max} (595 nm, method A or 640 nm, method B) against the corresponding reagent blank within the stability period (1 min–3 h, method A or 1–30 min, method B). The amount of CPD was computed from the respective calibration curves.

2.4.2. Methods C and D

Aliquots of standard CPD solution (0.5–4.0 ml; 50 μg ml^{-1}, method C or 1.0–5.0 ml; 50 μg ml^{-1}, method D) were placed in a series of 125 ml separating funnels. Then 5.0 ml of pH 1.5 buffer and 1.0 ml of NB-12BR solutions (for method C) or 6.0 ml of 0.1 M HCl and 2.0 ml of TP 000 solutions (for method D) were added to each separating funnel. The total volume of the aqueous phase was adjusted to 15.0 ml and 10.0 ml with distilled water for methods C and D, respectively. A requisite volume of chloroform was added to each funnel to make the organic layer 10.0 ml and the contents were shaken for 2 min. The two phases were allowed to separate, the separated chloroform layer was dried over sodium sulphate and the absorbance was measured at appropriate λ_{max} (620 nm, method C or 500 nm,

method D) against the corresponding reagent blank within the stability period (1–30 min; method C or 1 min–2 h; method D). The amount of CPD was computed from the respective calibration curves.

2.5. Analysis of pharmaceutical formulations

A portion of pharmaceutical preparation (tablets, chewable tablets and suspension) equivalent to 100 mg of active ingredient was extracted with chloroform (3 × 20 ml) and filtered if any insoluble portion was left. The combined chloroform extract was made up to 100 ml with the same solvent to obtain a solution of 1 mg ml^{-1}. The stock solution was further diluted to provide the working standard solutions and these were analyzed as described under the procedure for bulk samples.

3. Results and discussion

Conditions under which the reaction of CPD with each dye fulfils the essential analytical requirements were investigated. All the experimental conditions studied were optimized at room temperature (25 ± 3°C) and were established by varying one parameter at a time [26] and observing its effect on the absorbance of the coloured species.

In the preliminary experiments, in view of developing methods of analysis suitable for assaying small quantities of CPD, several acidic dyes such as Alizarin Red S, Suprachen Violet 3B, Fast Green FCF, Erioglaucine A, Orange II, Tropaeolin 000, Alizarin Violet 3B, Naphthalene Blue 12 BR, Bromocresol Green and Bromopyragallol Red were tested at various pH ranges as the colour producing agents by a dye salt partition technique. Different organic solvents such as benzene, chloroform, carbontetrachloride, ethyl acetate, dichloromethane and methyl isobutyl ketone were tested for the extraction of the ion-association complex formed between the CPD and each dye. The criterion for the best dye was the highest absorbance value of the complex in the organic phase at the wavelength of maximum absorbance [10]. The above studies reveal that four dyes namely SV 3B (Cl No. 60730), EG-A (Cl No. 42090), NB-12 BR (Cl No. 20500) and TP 000 (Cl No. 14600) gave better results than the other dyes. These dyes also gave low absorbance for the reagent blank. Chloroform was suggested as the solvent of choice for the extraction of the coloured complex with respect to maximum stability.

Figs. 1–4 shows the absorption spectra of the ion-association complexes of CPD with the four dyes, extracted into chloroform and of the reagent blank, obtained as described in the procedure. The spectra are very similar in shape to the absorption spectrum of an aqueous solution of the respective dye, indicating that these ion-association complex spectra show the characteristics λ_{max} (595 nm, method A; 640 nm, method B; 620 nm

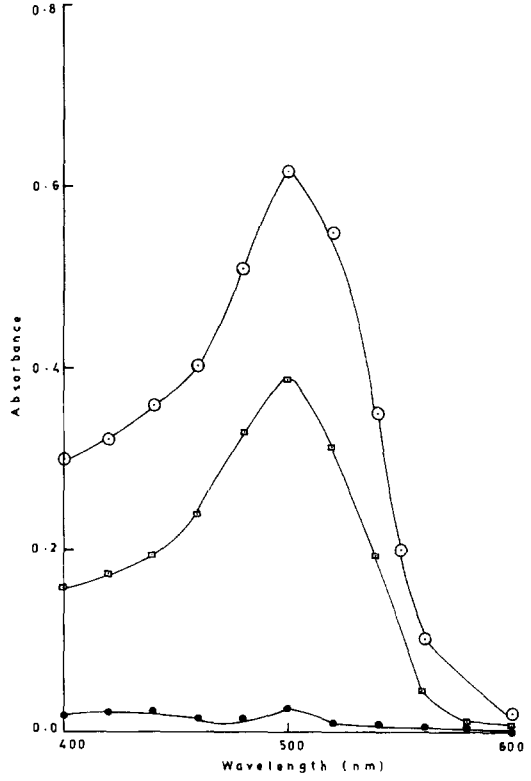

Fig. 4. Absorption spectra of the CPD-TP 000 system (⊙——⊙) (concentration of CPD: 3.21×10^{-5} M; TP 000: 1.14×10^{-3} M and HCl: 6.0×10^{-2} M), aqueous TP 000 (□——□) (aqueous TP 000: 2.28×10^{-5} M; HCl: 2.4×10^{-2} M) and reagent blank vs. chloroform (●——●).

Table 1
Optical and regression characteristics, precision and accuracy of the proposed methods

Parameters	Methods			
	A	B	C	D
λ_{max} (nm)	595	640	620	500
Beer's Law limits (μg ml^{-1})	2.5–40.0	0.5–5.0	2.5–17.5	2.5–25.0
Detection limits (μg ml^{-1})	0.956	0.257	0.166	0.289
Molar absorptivity (1 mol^{-1} cm^{-1})	1.21×10^{4}	4.56×10^{4}	1.69×10^{4}	1.98×10^{4}
Sandell's sensitivity (μg Cm^{-2} per 0.001 absorbance unit)	0.040	0.011	0.029	0.024
Regression equation (Y)[a]				
Slope (b)	2.51×10^{-2}	9.32×10^{-2}	3.61×10^{-2}	4.14×10^{-2}
Standard deviation on slope (s_b)	0.16×10^{-3}	0.46×10^{-3}	0.45×10^{-3}	0.004×10^{-3}
Intercept (a)	-0.23×10^{-2}	0.54×10^{-2}	-0.84×10^{-2}	-0.19×10^{-2}
Standard deviation on intercept(s_a)	3.99×10^{-3}	1.35×10^{-3}	5.06×10^{-3}	0.07×10^{-3}
Standard error of estimation (s_e)	6.31×10^{-3}	1.93×10^{-3}	6.00×10^{-3}	1.98×10^{-3}
Correlation coefficient	0.9998	0.9999	0.9996	0.9999
Relative standard deviation (%)[b]	0.28	0.77	0.56	0.45
Range of errorb (95% confidence limit)	0.30	0.81	0.59	0.48

[a] $Y=a+bC$ where C is the concentration in μg ml^{-1} and Y is absorbance units.
[b] Six replicate samples (concentrations of 30, 3, 10 and 15 μg ml^{-1} of pure drug for methods A, B, C and D, respectively.

method C; and 500 nm, method D) values of the respective dye itself.

In order to establish the optimum pH range (for methods A, B and C) or acid strength (for method D), the CPD was allowed to react with the respective dye in aqueous solution buffered between pH 1.0–10.0 (methods A, B and C) or in dilute HCl ranging from 0.05–1.5 M (method D) and the complex formed was extracted into chloroform for absorbance measurement. The results show that a quantitative extraction was produced between pH 1.1–1.5 (methods A and B), 1.4–1.8 (method C) or with an acid strength of 0.08–0.12 M HCl (method D). All subsequent studied were carried out at pH 1.3 (for methods A and B) and pH 1.5 (for method C) or 0.1 M HCl (for method D). The pH was adjusted using a glycine–HCl buffer solution (this buffer was chosen on account of its elevated complexing ability, which could be of use in overcoming interferences). The volume of this buffer added (4–10 ml) had no effect in methods A, B and C, respectively. A 6.0 ml portion of 0.1 M HCl solution was found to be optimal in method D. The minimum shaking time was determined by varying the shaking time from 1–10 min; although 1 min was sufficient, prolonged shaking had no adverse effect on the extraction and 2 min was selected for this study. A ratio of 1:1 (for methods A and D) or 2:3 (for methods B and C) of organic to aqueous phases was required for efficient extraction of the coloured species and lower reagent blank reading. It was found that better reproducibility and a lower reagent blank were achieved if the dye was purified by extraction with chloroform initially.

3.1. Analytical data

The optical characteristics such as the Beer's law limits, molar absorption coefficient, Sandell's sensitivity, regression equation and correlation coefficient obtained by linear least squares treatment [27] of the results for the systems involving cisapride with the mentioned dyes are presented in Table 1. The precision of each method was tested by estimating six replicates of CPD within Beer's law limits. The percent standard deviation and the percent range of error at 95% confidence limit are given in Table 1.

In order to confirm the utility of the proposed methods, they were applied to the estimation of CPD in various pharmaceutical formulations and

Table 2
Assay and recovery of cisapride in dosage forms

Pharmaceutical preparation	Labelled amount (mg)	Amount found[a] (mg)				Found by reference method[b]	Recovery by proposed methods[c] (%)			
		Proposed methods								
		A	B	C	D		A	B	C	D
Tablets I	10	10.27 ± 0.062	9.86 ± 0.046	10.15 ± 0.129	9.88 ± 0.056	9.97 ± 0.088	100.5 ± 0.98	99.2 ± 0.16	100.2 ± 1.06	99.3 ± 0.36
Tablets II	10	9.96 ± 0.103	10.12 ± 0.112	9.89 ± 0.071	9.92 ± 0.095	10.21 ± 0.092	99.5 ± 0.54	100.7 ± 0.73	99.1 ± 0.13	99.2 ± 0.19
Chewable tablets I	10	9.97 ± 0.091	9.98 ± 0.099	10.13 ± 0.121	9.99 ± 0.115	9.95 ± 0.134	99.8 ± 1.05	99.8 ± 0.34	100.4 ± 0.74	100.2 ± 0.97
Chewable tablets II	10	10.24 ± 0.065	9.97 ± 0.066	9.95 ± 0.043	9.92 ± 0.053	9.93 ± 0.072	100.9 ± 0.69	99.3 ± 0.34	99.2 ± 0.17	99.7 ± 0.43
Suspension I	60	59.60 ± 0.991	59.91 ± 1.16	60.15 ± 1.15	59.47 ± 0.93	59.90 ± 1.02	99.3 ± 0.45	99.8 ± 0.84	100.2 ± 0.91	99.1 ± 0.37
Suspension II	30	30.12 ± 1.03	29.85 ± 0.99	30.05 ± 1.13	29.80 ± 0.47	30.12 ± 0.972	100.4 ± 0.37	99.5 ± 0.82	100.2 ± 0.68	99.3 ± 0.72

I and II Formulations that are manufactured by two different pharmaceutical companies.
[a] Average ± standard deviation of six determinations.
[b] UV reference method, developed in our laboratory.
[c] Percent recovery of 10 mg added to the dosage forms.

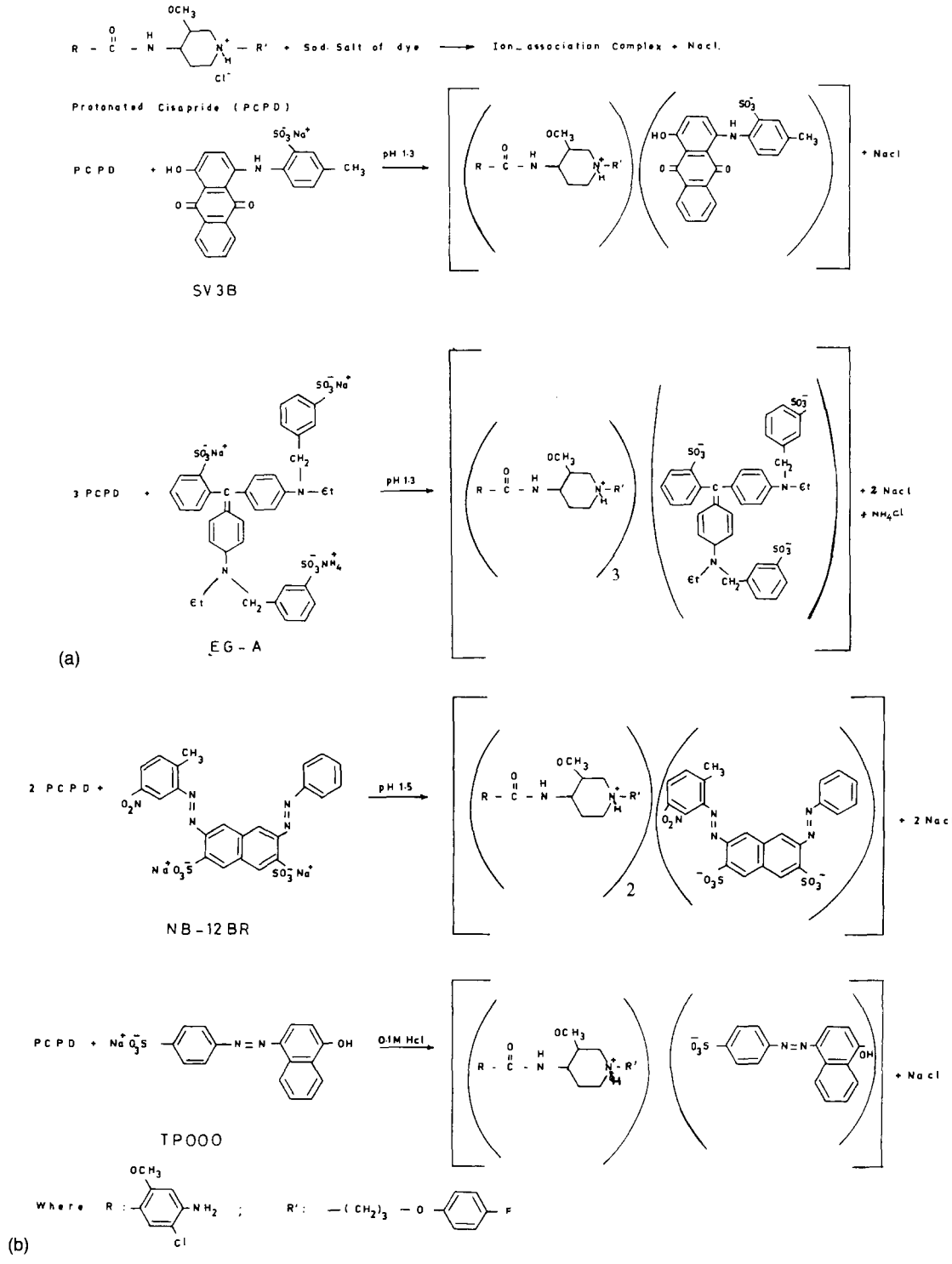

Scheme 1. Structures of SV 3B, EG A, NB-12BR, TP 000 and their respective complexes with cisapride.

the results are presented in Table 2. The results obtained by the proposed and UV reference (which is developed in our laboratory, showing characteristic λ_{max} at 308 nm in methanol medium) methods for the dosage forms were compared statistically by means of F- and t-tests and were found not to differ significantly. As an additional check of accuracy of the proposed methods, recovery experiments were performed by adding a fixed amount of the CPD to the preanalysed formulation and the results are also summarized in Table 2.

3.2. Chemistry of the ion-association complex

Cisapride being basic in nature forms an ion-association complex with the acidic dye which is extractable into chloroform. The stoichiometric ratio of the dye to drug was determined by the slope ratio method [28] and found to be 1:1 (for methods A and D), 1:3 (for method B) or 1:2 (for method C). The quantitative measure of the effect of complexation on acid–base equilibrium is most likely to be interpretable in terms of electronic, steric and other effects of complexing. The possible structure of the ion-association complex in each instance was established based on the analogy reports for similar types of molecules with acidic dyes and was further confirmed by slope-ratio studies. The protonated nitrogen (positive charge) of the drug molecule in acid medium is expected to attract the oppositely charged part (negative charge) of the dye and behave as a single unit being held together by electrostatic attraction as given in Scheme 1.

4. Conclusion

A significant advantage of an extraction spectrophotometric determination is that it can be applied to the determination of individual compounds in a multicomponent mixture. This aspect of spectrophotometric analysis is of major interest in analytical pharmacy since it offers distinct possibilities in the assay of a particular component in a complex dosage formulation. In the present study, cisapride was determined successfully as a pure compound as well as a component in representative dosage formulations. The ingredients usually present in the dosage forms of cisapride did not interfere in the proposed methods. Thus, the proposed methods are simple, rapid with reasonable precision and accuracy when compared with many of the reported methods and offer advantage in that only a small amount of drug or dosage formulation (even 0.5 μg ml^{-1}) is enough for analysis.

Acknowledgements

The authors are thankful to Sun Pharmaceutical Industries (Bombay, India) for their generous gift sample of cisapride and the authorities of Andhra University for providing research facilities.

References

[1] J. Robert Sims and W. Slivka, PCT Int. Appl. WO 9501, 803 (cl. A 61K37/54), 19 January 1995, US Appl. 87, 590, 06 July 1993, 21 pp.
[2] F. Onat, B. Yegen, K. Berkman and S. Oktay, Gen. Pharmacol., 26 (1994) 1253.
[3] British Pharmacopoeia, Vol. I, HMSO, London, 1995, p. 1746.
[4] M.I. Gonzalez Martin, C. Gonzalez Perez and M.A. Blanco Lopez, Anal. Lett., 27 (1994) 1713.
[5] R. Woestenborghs, W. Lorreyne, F. Van Rompaey and J. Heykants, J. Chromatogr., 424 (1988) 195.
[6] E.K. Iyer and H.P. Tipnis, Indian Drugs, 31 (1994) 519.
[7] I. Ojanpera, P. Lillsunde, J. Vartiovaara and E. Vuori, J. Planar Chromatogr. Mod. TLC, 4 (1991) 373.
[8] Y. Chen, Z. Zhang, P. Liu, X. Xu and Q. Chen, Zhongguo Yiyuan Yaoxue Zazhi., 14 (1994) 442.
[9] R. Foster, J. Phys. Chem., 84 (1980) 2135.
[10] V. Das Gupta, Ind. J. Pharm., 35 (1973) 77.
[11] R.T. Sane, U.M. Vaidya, V.G. Nayak, A.Y. Dhamankar, S.K. Joshi, V.J. Doshi, S.V. Sawant, V.B. Malkar, U.R. Pandit, A.Y. Sathe, Swati Jukar and A.D. Nadkarni, Indian Drugs, 19 (1982) 398.
[12] R.T. Sane, M.L. Kabul, V.G. Nayak and A.D. Nadkarni, Ind. J. Pharm. Sci., 46 (1984) 151.
[13] R.T. Sane, V.B. Malkar, V.G. Nayak and A.D. Nadkarni, Indian Drugs, 20 (1982) 78.
[14] R.T. Sane, M.L. Kabul, V.G. Nayak, V.B. Malkar and V.J. Banawalikar, Indian Drugs, 21 (1984) 25.
[15] R.T. Sane, M.L. Kabul, V.G. Nayak, V.B. Malkar and R.S. Samant, Ind. J. Pharm. Sci., 46 (1984) 151.

[16] F. Klaus (Ed.), Anally. Profiles of Drug Substances, Academic Press, New York, Vol. 3, 1977, p. 129.
[17] B. Pitarch, J. Manes and F. Basch, An. R. Acd. Farm., 652 (1986) 279.
[18] R.T. Sane, V.G. Nayak, N.R. Naik and D.D. Gupta, Indian Drugs, 20 (1983) 334.
[19] H. Shingu, O. Koshitani, H. Fujiwara and T. Nadai, Iyakuhin Kenkyu, 10 (1979) 336.
[20] C.S.P. Sastry, T. Tirupathi Rao, A. Sailaja and T.A.S.R. Prasad, Ind. J. Pharm. Sci., 54 (1992) 125.
[21] C.S.P. Sastry, A. Sailaja, T. Tirupathi Rao and D. Murali Krishna, Indian Drugs, 29 (1992) 473.
[22] B.S. Sastry, J. Venkateswara Rao, C.S.P. Sastry and T. Tirupathi Rao, Indian Drugs, 29 (1992) 277.
[23] M.M. Popelkova Molaz, Cesk. Farm, 34 (1985) 422.
[24] D. Rodulovic, M.S. Jovanovic and L. Zivanovic, Pharmazi, 41 (1986) 434; C.A., 105, 158936f.
[25] Ju Lurie, Hand Book of Analytical Chemistry, Mir Publishers, Moscow, 1975, p. 253.
[26] D.L. Massart, B.G.M. Vandeginite, S.N. Deming, Y. Michotte and L. Kaufman, Chemometrics, A Text Book, Elsevier, Amsterdam, 1988, p. 293.
[27] M.D. Pattergill and D.E. Sands, J. Chem. Educ., 58 (1979) 244.
[28] H. Irwing, F.T.C. Rossotti and R.J.P. Williams, J. Chem. Soc., II (1958) 1906.

ELSEVIER

Talanta 44 (1997) 527–534

Talanta

Formation and dissociation kinetics of triaza-crown-alkanoic acid complexes of transition metal(II) and lanthanide (III)

Ki-Young Choi [a,*], Dong Won Kim [b], Chang Suk Kim [b], Choon Pyo Hong [c], Haiil Ryu [c], Yong-Ill Lee [d]

[a] *Department of Chemistry, Mokwon University, Taejeon 301-729, South Korea*
[b] *Department of Chemistry and Chemical Education, Chungbuk National University, Cheongju 360–763, South Korea*
[c] *Department of Chemical Education, Kongju National University, Kongju 314–701, South Korea*
[d] *Department of Chemistry, Konyang University, Nonsan 320-800, South Korea*

Received 29 April 1996; received in revised form 12 July 1996; accepted 22 July 1996

Abstract

The formation and dissociation rates of some transition metal(II) and lanthanide(III) complexes of the 1,7,13-triaza-4,10,16-trioxacyclooctadecane *N',N'',N'''*-triacetic acid (**1**) and 1,7,13-triaza-4,10,16-trioxacyclooctadecane-*N',N'',N'''*-trimethylacetic acid (**2**) have been measured by the use of stopped-flow and conventional spectrophotometry. Experimental observations were made at 25.0 ± 0.1°C and at an ionic strength of 0.10 M KCl. The complexation of Zn^{2+} and Cu^{2+} ions with **1** and **2** proceeds through the formation of an intermediate complex (MH_3L^{+*}) in which the metal ion is incompletely coordinated. This may then lead to a final product in the rate-determining step. Between pH 4.68 and 5.55, the diprotonated (H_2L^-) form is revealed to be a kinetically active species despite its low concentration. The stability constants (log $K_{MH_3L^{+*}}$) and specific base-catalyzed rate constants (k_{OH}) of intermediate complexes have been determined from the kinetic data. The dissociation reactions of **1** and **2** complexes of Co^{2+}, Ni^{2+}, Zn^{2+}, Ce^{3+}, Eu^{3+} and Yb^{3+} were investigated with Cu^{2+} ions as a scavenger in acetate buffer. All complexes exhibit acid-independent and acid-catalyzed contributions. The buffer and Cu^{2+} concentration dependence on the dissociation rate has also been investigated. The metal and ligand effects on the dissociation rate of some transition metal(II) and lanthanide(III) complexes are discussed in terms of the ionic radius of the metal ions, the side-pendant arms and the rigidity of the ligands. © 1997 Elsevier Science B.V.

Keywords: Alkanoic acid complexes; Lanthanide; Transition metal

1. Introduction

In recent years there has been a growing interest in the development of macrocyclic polyaza-polycarboxylate ligands which can be used as contrast agents for magnetic resonance imaging (MRI) [1,2] and as NMR shift probes for biological systems [3] by forming metal chelates of high thermodynamic and kinetic stability [4]. The kinetic behavior of the Ln^{3+} ions with DOTA (1,4,7,10-tetraazacyclododecane-*N,N',N'',N'''*-te-

* Corresponding author. Fax: +82 42 2219717.

PII S0039-9140(96)02052-8

traacetic acid) and TETA (1,4,8,11-tetraazacyclotetradecane-*N*,*N*′,*N*″,*N*‴-tetraaceticacid) differs considerably from that of the first-row transition metal ions, since the DOTA and TETA complexes of Ni^{2+} and Cu^{2+} formed relatively quickly as demonstrated by Kasprzyk and Wilkins [5]. Macrocyclic polyazapolycarboxylate ligands have some additional features including cavity size, steric factors, conformation and preorganization which affect the rates of formation and dissociation for their complexes. Formation kinetics on the lanthanide complexes of NOTA (1,4,7-triazacyclononane-*N*,*N*′,*N*″-triacetic acid) and DOTA have been investigated and the formation of intermediates ($LnHNOTA^{+*}$ and LnH_2DOTA^{+*}) was proposed, followed by reorganization in the rate-determining step to the final product [6,7]. The size effect of Ln^{3+} ions on the formation rate of Ln^{3+} complexes was not pronounced as observed for the dissociation reactions of these chelates [6,7]. Additional studies on the dissociation kinetics of lanthanide complexes of macrocyclic polyazapolycarboxylate, triaza-crown-alkanonate and DTPA-bis(amide) ligands were also reported [8–13]. In these studies, the dissociation of the complexes occurred via both acid-independent and acid-assisted pathways and the dissociation rates varied with the size of metal ions and the ligand topology.

The main objective of this research is to determine the formation and dissociation rates of some divalent and trivalent metal complexes with various macrocyclic triazatrioxa ligands with acetate and methylacetate groups as *N*-pendant arms (Fig. 1). We intend to investigate the effect of the cavity size and rigidity of the macrocycle as well as pendant arms effects on the kinetic properties of these complexes.

2. Experimental

2.1. Chemicals and reagents

1,7,13-Triaza-4,10,16-trioxacyclooctadecane trihydrobromide was prepared by the previous procedure [14]. Ligands 1,7,13-triaza-4,10,16-trioxacyclooctadecane-*N*,*N*′,*N*″-triacetic acid (**1**) and 1,7,13-triaza-4,10,16-trioxacyclooctadecane-*N*,*N*′,*N*″-trimethylacetic acid (**2**) were synthesized according to the method of Martell et al. [15]. The ligands were characterized by ^1H NMR, mass spectrometry and elemental analysis (1: found: C, 39.76; H, 6.06; N, 7.63%; $C_{18}H_{33}N_3O_9 \cdot 3HCl$ requires C, 39.68; H, 6.11; N, 7.71%. 2: found: C, 42.85; H, 6.78; N, 7.06 %; $C_{21}H_{39}N_3O_9 \cdot 3HCl$ requires C, 42.97; H, 6.70; N, 7.16%). The stock solutions of $CoCl_2$, $NiCl_2$, $CuCl_2$, $ZnCl_2$, $CeCl_3$, $EuCl_3$ and $YbCl_3$ were prepared from solid samples (Aldrich, 99.9%). The concentrations of the sample solutions were determined by EDTA titration using Murexide or xylenol orange as indicators. The concentrations of **1** and **2** stock solutions were determined by titration against a standardized $CuCl_2$ solution using Murexide as an indicator. Potassium chloride was used to control the ionic strength in all kinetic studies. All solutions were made in deionized water. All other chemicals were reagent grade and were used without further purification.

2.2. Measurements

The pH values of the sample solutions were measured with a Beckman combination electrode and Beckman Model ϕ 71 pH meter. The H^+ ion concentrations were calculated from the measured pH values in acetate buffer solution of 0.10 M (KCl) ionic strength by the procedures reported previously [16]. Kinetic measurements were car-

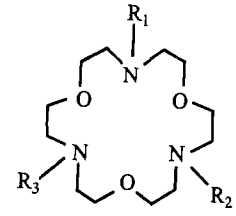

1. $R_1 = R_2 = R_3 = CH_2COOH$

2. $R_1 = R_2 = R_3 = CHCOOH$ (with CH_3)

Fig. 1. Structure of the triaza-crown-alkanoic acids.

ried out on a Hi-Tech stopped-flow spectrophotometer interfaced with a scientific data acquisition system and a UVIDEC-610 spectrophotometer at 25.0 ± 0.1°C with the use of a Lauda RM6 circulatory water bath.

The formation reactions of Zn^{2+} complexes were studied in slightly buffered solutions (0.01 M acetic acid/sodium acetate) by monitoring the pH decrease (0.05–0.17 pH unit) with bromocresol green ($4.6 < pH < 5.2$, observation wavelength 615 nm) as an indicator [5]. The reaction of Cu^{2+} with **2** was studied by monitoring the formation of complex directly at 260 nm. The data agreed well with some runs using the indicator method [5]. The concentration of the indicator was 2.0×10^{-5} M, while that of the acetate buffer varied between 5.0×10^{-3} and 2.0×10^{-2} M, independent of the reaction rate. The concentration of the ligands was 2.0×10^{-4} M, while that of the Cu^{2+} and Zn^{2+} ions was varied between 4.0×10^{-4} and 4.0×10^{-3} M.

The dissociation reactions of the complexes were studied in acidic solutions in the presence of excess Cu^{2+} ions. Under these conditions, a dissociation reaction takes place and the progress of the exchange may be monitored by the formation of copper complexes at 270 nm. The Cu^{2+} ion was used as a scavenger of free ligands. The complex concentration in the reaction mixtures was 5.0×10^{-5} M, while that of the Cu^{2+} ion was varied between 2.0×10^{-4} and 1.0×10^{-3} M. The buffer solutions were made by using a constant acetate ion concentration and varying the concentration of acetic acid necessary for attainment of the desired pH.

3. Results and discussion

3.1. Formation kinetics

The formation rate of Zn(**1**), Cu(**2**) and Zn(**2**) complexes in the presence of excess metal ion can be given as

$$d[ML^+]\,dt^{-1} = k_{obs}[L]_T \quad (1)$$

where $[L]_T$ is the total concentration of the free ligand and k_{obs} is a pseudo-first-order rate constant. At a given pH 4.64–5.55, the values of k_{obs} increased with increasing $[M^{2+}]$ and the plot of the k_{obs} values against $[M^{2+}]$ gave a saturation curve, as found for the formation of Ln(NOTA) [6] and Ln(DOTA)$^-$ [7]. The relationship between k_{obs} values and $[M^{2+}]$ can be described [17] by

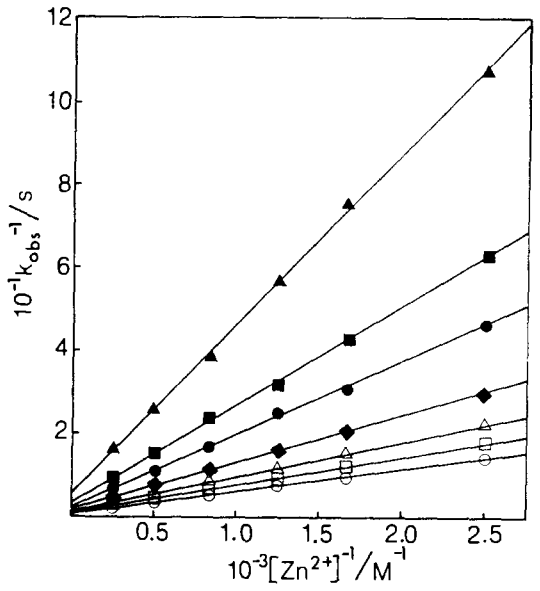

Fig. 2. Plots of k_{obs}^{-1} vs $[Zn^{2+}]^{-1}$ for the formation kinetics of Zn(**2**) at different pH values. [**2**] = 2.0×10^{-4}M; [OAc^-] = 0.01 M; $T = 25.0 \pm 0.1$°C; $I = 0.10$ M (KCl); pH = 4.68(○), 4.89(□), 5.04(△), 5.26(◆), 5.37(●), 5.45(■), 5.55(▲).

$$k_{obs} = \frac{k_1 K[M^{2+}]}{1 + K[M^{2+}]} \quad (2)$$

where K is the equilibrium constant characterizing the formation of the intermediate and $k_1$is the rate constant of the intermediate to product in the rate-determining step. Plots of $1/k_{obs}$ against $1/[M^{2+}]$ lead to straight line as show in Fig. 2. The values of k_1, K and the second-order rate constant $k_2 = k_1 K$ were deduced from Eq. (2) and are summarized in Table 1. The present work shows no significant variation in the values of K with various pH. The protonated forms of **1** and **2** could contribute to the complexation kinetics of M^{2+} ions between pH 4.64 and 5.55. The concentrations of protonated ligands were computed with the use of ligand protonation constants. (Protonation constants (log K_i) in 0.10 M KCl and 25.0 ± -

Table 1
Rate data for the metal complex formation with **1** and **2** at 25.0 ± 0.1°C, $I = 0.10$ M (KCl) and $[OAc^-] = 1.0 \times 10^{-2}$ M

Metal ions	pH	$k_1(s^{-1})$	$K(M^{-1})$	$k_2(M^{-1}\ s^{-1})$
1				
Zn^{2+}	4.68	2.65×10^1	2.13×10^2	5.64×10^3
	4.81	2.95×10^1	2.06×10^2	6.07×10^3
	4.95	3.34×10^1	2.03×10^2	6.79×10^3
	5.09	4.10×10^1	2.14×10^2	8.76×10^3
	5.16	4.57×10^1	2.11×10^2	9.64×10^3
	5.29	5.48×10^1	2.21×10^2	12.1×10^3
	5.41	6.62×10^1	2.15×10^2	14.3×10^3
2				
Zn^{2+}	4.68	2.09×10^{-1}	1.16×10^2	2.42×10^1
	4.89	3.42×10^{-1}	1.23×10^2	4.20×10^1
	5.04	4.61×10^{-1}	1.23×10^2	5.67×10^1
	5.26	7.63×10^{-1}	1.13×10^2	8.62×10^1
	5.37	9.81×10^{-1}	1.22×10^2	12.0×10^1
	5.45	11.7×10^{-1}	1.26×10^2	14.7×10^1
	5.55	14.6×10^{-1}	1.27×10^2	18.5×10^1
Cu^{2+}	4.64	2.24×10^1	5.89×10^2	1.32×10^4
	4.85	2.50×10^1	6.94×10^2	1.73×10^4
	4.97	2.84×10^1	7.24×10^2	2.06×10^4
	5.15	3.42×10^1	7.79×10^2	2.66×10^4
	5.24	3.84×10^1	7.90×10^2	3.03×10^4
	5.33	4.23×10^1	8.01×10^2	3.39×10^4
	5.43	4.92×10^1	8.27×10^2	4.07×10^4

0.1°C are 9.57, 8.15, 7.67, 2.05 and 1.07 for **1** [15] and 9.70, 9.18, 7.27, 3.86 and 2.94 for **2**, which were calculated by fitting the potentiometric data to the PKAS program [18]). In this pH range, the species H_3L is at a high concentration (81.99–99.62%) while H_2L^- is at a low concentration (0.07–1.42%).

The stability constant of the intermediate $(MH_3L^+)^*$ can be calculated from the value of K at a given pH, using known protonation constants of the ligands by Eq. (3)

$$K_{(MH_3L^+)^*} = K(1 + (K_3[H^+])^{-1} \quad (3)$$

The calculated stability constants of three intermediate complexes $(MH_3L^+)^*$, summarized in Table 2 along with the literature value [19], are relatively pH-independent over most of the pH range examined. The stability constants of the intermediate here are about one order of magnitude higher than those for the corresponding monoacetate and monomethylacetate complexes [20]. This suggests that the M^{2+} ion is coordinated with more than one carboxylate oxygen in the intermediate formation. A similar result is also observed for the formation of $Ln(N_3O_2Ac)$

(1,4,10-traiza-7,13-dioxacyclopentadecane-*N*,*N*′,*N*″-triacetic acid) [12]. The intermediate of the Cu(**2**) complex has a larger stability constant than that of the Zn(**2**) complex. This fact may be attributed to the thermodynamic stability ($\log \beta_{Cu(2)} = 13.45$ vs. $\log \beta_{Zn(2)} = 13.00$). (The stability constant was obtained from the experimental data with the aid of the BEST program [18]. Values were obtained in 0.10 M (KCl) at 25.0 ± 0.1°C). The stability constants for intermediates of Zn(**1**) and Zn(**2**) are not significantly different, and are about one order of magnitude lower than the value of $K_{ZnH_2L^{+*}}$ found previously for $Zn(N_3O_2Ac)$ [19].From the kinetic data, the second-order rate constant k_{H_nL} also represents $(k_1K)_{H_nL}$. If one species is markedly more reactive than all others, the second-order rate constant could be obtained from the following expression [5]

$$k_2 = k_{H_nL}(1 + (K_{H_{(n+1)}L})^{-1}[H^+])^{-1} \quad (4)$$

Table 2
Stability constants ($\log K_{MH_3L^{+*}}$), second-order rate constants (k_{H_nL}) and base-catalyzed rate constants (k_{OH}) of the intermediate complexes at 25.0 ± 0.1°C and $I = 0.10$ M (KCl)

Complexes	$\log K_{MH_3L^{+*}}$	$k_{H_2L^-}(M^{-1}\ s^{-1})$	$k_{H_3L^-}(M^{-1}\ s^{-1})$	$k_{OH}(M^{-1}\ s^{-1})$
Zn(**1**)	2.33 ± 0.11	(7.97 ± 0.26) × 10^6	(2.67 ± 0.11) × 10^6	(1.51 ± 0.04) × 10^{10}
Zn(**2**)	2.15 ± 0.15	(1.99 ± 0.05) × 10^6	(2.90 ± 0.07) × 10^4	(3.18 ± 0.09) × 10^8
Cu(**2**)	2.94 ± 0.11	(4.37 ± 0.45) × 10^8	(6.63 ± 0.18) × 10^6	(9.33 ± 0.16) × 10^9
$Zn(N_3O_2Ac)$[a]	2.91 ± 0.07			(1.42 ± 0.04) × 10^{10}

[a] Ref. [19].

where $K_{H_{(n+1)}L}$ is the protonation constants of **1** and **2**. From the plots of k_2 against $(1+(K_{H_{(n+1)}L})^{-1}[H^+])^{-1}$, the second-order rate constants for the H_2L^- and H_3L species are collected in Table 2. Despite their very low concentration in the pH range observed, the H_2L^- species appears to be kinetically much more reactive than the H_3L species (except for the Zn(**1**) reaction), even though the latter is the major component in solution [21]. These experimental results show differences from those reported by Kumar and Tweedle [4], where H_3L and H_2L^- are the predominant species due to the difference in the basicities of ligands. The low reactivity of the H_3L form may be assigned to the formation of trizwitterionic forms of **1** and **2**. The three $N-H^+$ groups in the 18-membered cycle of H_3L probably hinder the rearrangement of the intermediate complex into the final chelate product due to the electrostatic repulsion with the incoming metal ion.

The value of k_1, the rate of rearrangement of the intermediate, was increased with increasing pH as shown in Table 1. This implies that the rearrangement of the intermediate complex into the final chelate product is catalyzed by the OH^- ion. This observation is consistent with the previously reported works [4,12,19]. Fig. 3 shows that the plot of k_1 as a function of $[H^+]^{-1}$ gives a linear line. An expression consistent with this functional dependence is given by Eq. (5) [4]

$$k_1 = k_{H_2O} + k_{OH}K_W[H^+]^{-1} \quad (5)$$

where k_{H_2O} and k_{OH} are the water and hydroxide-catalyzed rate constants of the rearrangement of the intermediate. The k_{OH} values calculated form the slope of the straight line in Fig. 3 and Eq. (5) ($\log K_W = 13.78$) are listed in Table 2. The values of second-order rate constants for proton transfer (k_{OH}) are diffusion controlled. This may be attributed to the low basicity of nitrogen express as macrocyclic ligands [4]. A significant contribution from the base form of the buffer is not expected, since the concentration of buffer used in the present work is low. The k_{OH} value of Zn(**2**) is about two orders of magnitude smaller than that of Zn(**1**). This indicates that the substitution of three methyl groups on the acetate pendant arms of **1** makes the ligand more rigid [22,23]. On the other hand, the hydroxide-catalyzed dissociation rate of Cu(**2**) is about 30 times faster than that of Zn(**2**). Probably the cavity size (18-membered cycle) of **2**, which is too large for the Cu^{2+} ion, plays a major role in the metal complex formation reaction. Similar results reported that the formation rates of alkaline earth complexes of DOTA were increased with decreasing ionic size [5].

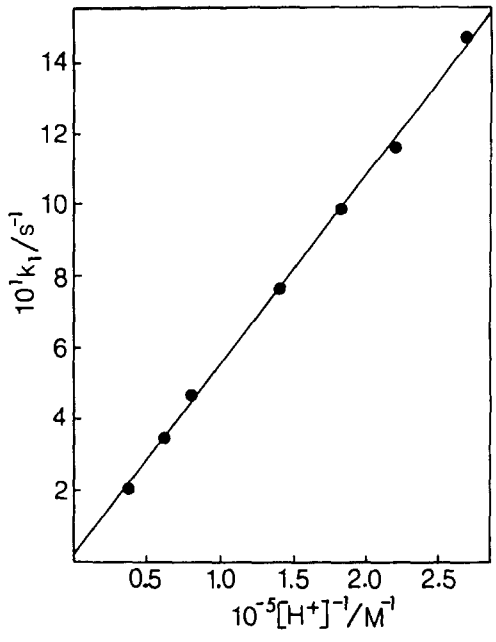

Fig. 3. Plots of k_1 vs. $[H^+]^{-1}$ for the formation kinetics of Zn(**2**) at 25.0 ± 0.1°C and $I = 0.10$ M (KCl).

3.2. Dissociation kinetics

The rates of the dissociation reactions for some transition and lanthanide complexes of **1** and **2** have been measured between pH 4.07 and 5.18. In the presence of excess Cu^{2+} ions, the rate of exchange may be expressed as

$$-d[ML]\,dt^{-1} = k_{obs}[ML] \quad (6)$$

where k_{obs} is a pseudo-first-order rate constant. The values of k_{obs} for **1** and **2** complexes were found to be independent of $[OAc^-]$ but dependent on $[Cu^{2+}]$. The dependence of k_{obs} on $[Cu^{2+}]$ is illustrated in Fig. 4 at different pH values. The data in Fig. 4 indicate that the dissociation rate of complex is proportional to $[Cu^{2+}]$. The small

positive intercepts along the ordinate of these data plots indicate that $[Cu^{2+}]$-independent dissociation also occurs. Thus, the data can be described by

$$k_{obs} = k_d + k_{Cu}[Cu^{2+}] \quad (7)$$

where k_d and k_{Cu} are the functions of acidity, $[H^+]$. Fig. 5 shows that k_d is proportional to $[H^+]$, while k_{Cu} is proportional to $[H^+]^{-1}$. On the basis of these results, the overall rate of dissociation reaction can be expressed as

$$-d[ML]\,dt^{-1} = k_d[ML] + k_H[ML][H^+] + k_{Cu}[ML][Cu^{2+}] + k_{CuH-1}[ML][Cu^{2+}][H^+]^{-1} \quad (8)$$

The rate constants (k_d, k_H, k_{Cu} and k_{CuH-1}) calculated from the experimental data are presented in Table 3. As can be seen, the first and second terms in Eq. (8) are responsible for the dissociative pathway of the Cu^{2+}-independent mode. The

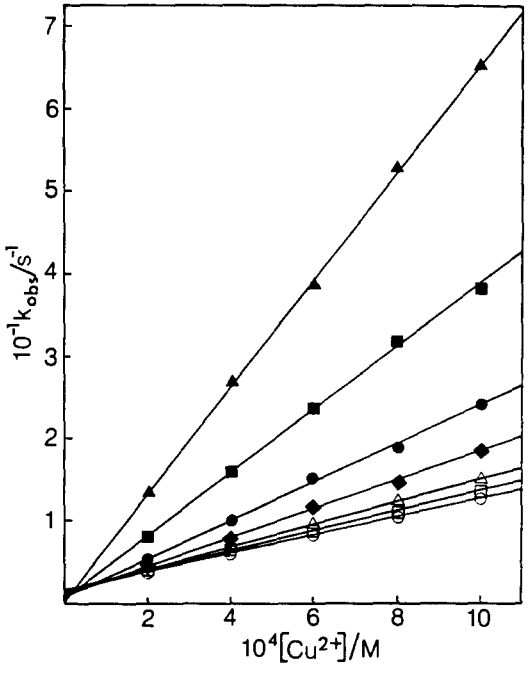

Fig. 4. Plots of k_{obs} vs. $[Cu^{2+}]$ for the dissociation kinetics of Eu(**1**) at different pH values. [Eu(**1**)] = 5.0×10^{-5} M; $[OAc^-]$ = 0.01 M; $T = 25.0 \pm 0.1$°C; $I = 0.10$ M (KCl); pH = 4.08(○). 4.17(□), 4.27(△), 4.40(◆), 4.64(•), 4.91(■), 5.18(▲).

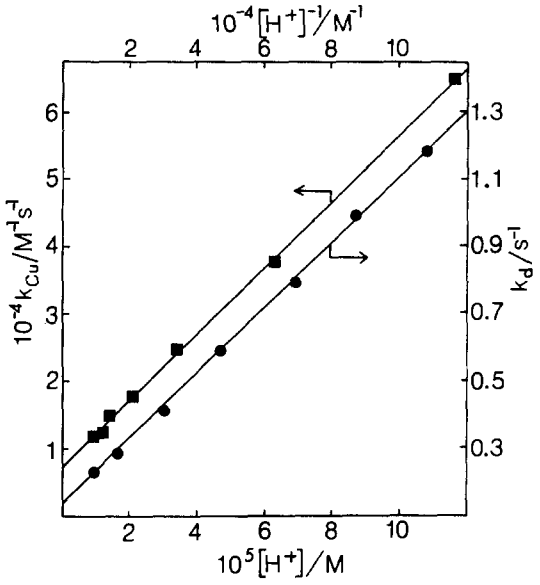

Fig. 5. Plots of k_d vs. $[H^+]$ and k_{Cu} vs $[H^+]^{-1}$ for the dissociation kinetics of Eu(**1**). [Eu(**1**)] = 5.0×10^{-5} M; $[OAc^-]$ = 0.01 M; $T = 25.0 \pm 0.1$°C; $I = 0.10$ M (KCl).

rate-determining step involves the loss of metal ion from the complexes and the rapid reaction of the released ligand with Cu^{2+} ion. Eq. (8) also represents the associative pathway of the Cu^{2+}-dependent mode, which is composed of the direct attack of the Cu^{2+} ion on partially dissociated M–L and the $[H^+]^{-1}$ dependence. $[H^+]^{-1}$ behavior can be interpreted by the existence of the attack of hydrolyzed copper species ($CuOH^+$) on M–L, even though the investigated pH is not higher. k_{CuOH^+} is therefore obtained by the expression.

$$k_{CuH-1} = k_{CuOH^+}\beta_{CuOH^+} \quad (9)$$

where β_{CuOH^+} ($= k_{CuOH^+}K_W$) is a stability constant (i.e. 2.0×10^{-8}) [9].

Table 3 gives a summary of the rate constants for dissociation of various metal complexes of **1** and **2**. A comparison of the rate constants k_d and k_H of the transition metal and lanthanide complexes of **1** and **2** demonstrates the order $Co^{2+} > Ni^{2+} > Zn^{2+}$ and $Ce^{3+} > Eu^{3+} > Yb^{3+}$, respectively. Both rate constants are significantly affected by metal ionic size. An increase in the cation radius from Co^{2+} to Zn^{2+} leads to an

Table 3
Rate constants for the dissociation reactions of metal complexes of macrocyclic ligands at 25.0 ± 0.1°C and $I = 0.10$ M (KCl)

Complexes	$k_d(s^{-1})$	$k_H(M^{-1}s^{-1})$	$k_{Cu}(M^{-1}s^{-1})$	$k_{CuOH}(M^{-1}s^{-1})$
Co(**1**)$^-$	$(3.01 \pm 0.08) \times 10^{-1}$	$(7.97 \pm 0.17) \times 10^3$	$(9.01 \pm 0.10) \times 10^3$	$(3.15 \pm 0.08) \times 10^7$
Ni(**1**)$^-$	$(2.17 \pm 0.06) \times 10^{-1}$	$(6.04 \pm 0.14) \times 10^3$	$(8.61 \pm 0.08) \times 10^3$	$(2.99 \pm 0.06) \times 10^7$
Zn(**1**)$^-$	$(2.69 \pm 0.09) \times 10^{-3}$	$(1.96 \pm 0.05) \times 10^1$	1.67 ± 0.04	$(8.95 \pm 0.17) \times 10^3$
Ce(**1**)	$(1.60 \pm 0.05) \times 10^{-1}$	$(1.12 \pm 0.04) \times 10^4$	$(7.43 \pm 0.11) \times 10^3$	$(2.71 \pm 0.05) \times 10^7$
Eu(**1**)	$(1.32 \pm 0.04) \times 10^{-1}$	$(9.76 \pm 0.12) \times 10^3$	$(6.81 \pm 0.10) \times 10^3$	$(2.49 \pm 0.06) \times 10^7$
Yb(**1**)	$(8.60 \pm 0.11) \times 10^{-2}$	$(6.31 \pm 0.09) \times 10^3$	$(6.12 \pm 0.06) \times 10^3$	$(2.12 \pm 0.03) \times 10^7$
Co(**2**)$^-$	$(1.87 \pm 0.04) \times 10^{-1}$	$(7.05 \pm 0.08) \times 10^3$	$(1.25 \pm 0.03) \times 10^3$	$(9.53 \pm 0.14) \times 10^6$
Ni(**2**)$^-$	$(1.41 \pm 0.03) \times 10^{-1}$	$(6.01 \pm 0.06) \times 10^3$	$(1.01 \pm 0.04) \times 10^3$	$(7.85 \pm 0.15) \times 10^6$
Zn(**2**)$^-$	$(7.91 \pm 0.12) \times 10^{-4}$	5.47 ± 0.10	$(4.61 \pm 0.07) \times 10^{-1}$	$(2.63 \pm 0.05) \times 10^3$
Ce(**2**)	$(6.86 \pm 0.11) \times 10^{-2}$	$(5.06 \pm 0.08) \times 10^3$	$(4.04 \pm 0.06) \times 10^3$	$(1.08 \pm 0.04) \times 10^7$
Eu(**2**)	$(6.54 \pm 0.05) \times 10^{-2}$	$(4.52 \pm 0.04) \times 10^3$	$(3.87 \pm 0.03) \times 10^3$	$(1.00 \pm 0.02) \times 10^7$
Yb(**2**)	$(5.28 \pm 0.14) \times 10^{-2}$	$(3.71 \pm 0.06) \times 10^3$	$(3.56 \pm 0.06) \times 10^3$	$(8.58 \pm 0.13) \times 10^6$
En(N_3O_2Ac)[b]	$(1.62 \pm 0.03) \times 10^{-5}$	1.38 ± 0.06	[a]	[a]

[a] Not observed.
[b] Ref. [12].

increase in kinetic stability probably because the Zn^{2+} ion fits into a ligand somewhat better than the Co^{2+} and Ni^{2+} ions. However, the consistent decrease in the dissociation rates of **1** and **2** complexes from Ce^{3+} to Yb^{3+} parallels the thermodynamic stability of these complexes with decreasing ionic size or increasing charge density of Ln^{3+} ions. The dissociation rates of **1** complexes were found to be faster than those of **2** complexes. This indicates that the substitution of three methyl groups on the acetate pendant arms of **1** increases the rigidity of the macrocycle, yielding a complex with even greater kinetic stability. A methyl substitution in other polyazapolycarboxylate ligands has also been observed to increase the inertness of their resulting complexes [22–24]. An acid-catalyzed dissociation rate of Eu(**1**) is about four orders of magnitude faster than that of Eu(N_3O_2Ac), even though **1** has the increased ring size (18-membered cycle) compared with N_3O_2Ac (15-membered cycle). This may be attributed to the decrease of macrocycle rigidity by the flexibility of **1** and the mismatch caused by the large cavity size.

Acknowledgements

The present studies were supported by the Basic Science Research Institute Program, Ministry of Education of Korea, 1995, Project No. BSRI-95-3435.

References

[1] R.B. Lauffer, Chem. Rev., 87 (1987) 901.
[2] K. Kumar and M.F. Tweedle, Pure Appl. Chem., 65 (1992) 515.
[3] A.D. Sherry and C.F.G.C. Geraldes, in J.-C. Bunzli and G.R. Choppin (Eds.), Lanthanide Probes in Life, Medical and Environmental Science, Theory and Practice, Elsevier, Amsterdam, 1989.
[4] K. Kumar and M.F. Tweedle, Inorg. Chem., 32 (1993) 4193.
[5] S.P. Kasprzyk and R.G. Wilkins, Inorg. Chem., 21 (1982) 3349.
[6] E. Brucher and A.D. Sherry, Inorg. Chem., 29 (1990) 1555.
[7] E. Brucher, I. Lazar and I. Toth, Inorg. Chem., 33 (1994) 4070.
[8] K. Kumar, C.A. Chang and M.F. Tweedle, Inorg. Chem., 32 (1993) 587.
[9] K.Y. Choi, J.C. Kim and D.W. Kim, J. Coord. Chem., 30 (1993) 1.
[10] K.Y. Choi, K.S. Kim and J.C. Kim, Bull. Chem. Soc. Japan, 67 (1994) 267.
[11] K.Y. Choi, K.S. Kim and J.C. Kim, Polyhedron, 13 (1994) 567.
[12] K.Y. Choi, D.W. Kim and C.P. Hong, Polyhedron, 14 (1995) 1299.

[13] K.Y. Choi, J.J. Oh and Y.I. Lee, Microchem. J., in press.
[14] Y. Sun, M.J. Welch and A.E. Martell, Tetrahedron, 47 (1991) 8863.
[15] R. Delgado, Y. Sun, R.J. Motekaitis and A.E. Martell, Inorg. Chem., 32 (1993) 3320.
[16] H.M. Irving, M.C. Miles and L.D. Petit, Chim. Acta, 38 (1967) 475.
[17] R.G. Wilkins, Kinetics and Mechanisms of Reactions of Transition Metal Complexes, Allyn and Bacon, Boston, MA, 1974, p. 26.
[18] A.E. Martell and R.J. Motekaitis, The Determination and Use of Stability Constants, VCH, New York, 1988.
[19] K.Y. Choi, S.H. Kang, D.W. Kim, Y.S. Chung, C.S. Kim, J.J. Oh, C.P. Hong and Y.I. Lee, Supuramol. Chem., 7 (1996) 27.
[20] A.E. Martell and R. M. Smith, Critical Stability Constant, Vol. 6, Plenum, New York, 1989.
[21] S.P. Kasprzyk and R.G. Wilkins, Inorg. Chem., 27 (1988) 1834.
[22] E. Brucher, S. Cortes, F. Chavez and A.D. Sherry, Inorg. Chem., 30 (1991) 2092.
[23] S.I. Kang, R.S. Ranganathan, J.E. Emswiler, K. Kumar, J.Z. Gougoutos, M. Malley and M.F. Tweedle, Inorg. Chem., 32 (1993) 2912.
[24] K.Y. Choi, K.S. Kim and C.P. Hong, Bull. Korean Chem. Soc., 15 (1994) 782.

ELSEVIER

Talanta 44 (1997) 535–544

Talanta

Determination of halides by microwave induced plasma and stabilized capacitive plasma atomic emission spectrometry after on-line continuous halogen generation

J.F. Camuña [a], M. Montes [a], R. Pereiro [a], A. Sanz-Medel [a,*], C. Katschthaler [b], R. Gross [b], G. Knapp [b]

[a] *Department of Physical and Analytical Chemistry, Faculty of Chemistry, University of Oviedo, Oviedo, Spain*
[b] *Institute for Analytical Chemistry, Micro- and Radiochemistry, Graz University of Technology, Graz, Austria*

Received 6 May 1996; received in revised form 19 July 1996; accepted 22 July 1996

Abstract

This paper describes a comparative study of the microwave induced plasma (MIP) and the stabilized capacitive plasma (SCP) for halide determinations. The MIP is generated in a Beenakker cavity TM_{010} using a tangential flow torch and the SCP consists of a 27.12 MHz discharge sustained in a liquid-cooled, fused silica tube surrounded by two annular electrodes. Both discharges are operated in helium at atmospheric pressure and detection was carried out by Atomic Emission Spectrometry (AES). The halides (I^-, Br^-, Cl^-) are converted to volatile halogens by continuous flow generation based on chemical oxidation and on-line separation from the aqueous phase, via a gas–liquid separator, to be finally introduced into the plasma. The different factors affecting the emission intensity of the volatile halogens generated are compared for both discharges and the analytical performance characteristics are also evaluated. Detection limits of 17 ng ml^{-1}, 24 ng ml^{-1} and 55 ng ml^{-1} are obtained for the determination of Cl^-, Br^-, and I^-, respectively, in the ultraviolet-visible (UV-VIS) region using the MIP-AES and 45 ng ml^{-1}, 135 ng ml^{-1} and 400 ng ml^{-1} for Cl^-, Br^-, and I^- with the SCP-AES. Lines in the near infrared (NIR) region were also evaluated for the SCP-AES detection; improvements in detection limits higher than 30 times were observed in the NIR region as compared with the UV-VIS with detection limits in the NIR of 1.4 ng ml^{-1} for Cl^-, 3 ng ml^{-1} for Br^- and 13 ng ml^{-1} for I^-. © 1997 Elsevier Science B.V.

Keywords: Continuous halogen; Generation; Halides; Microwave induced plasma; Stabilized capacitive plasma

1. Introduction

Different plasma sources, using He as the discharge gas, have been proposed as sensitive means for halogen detection by Atomic Emission Spectrometry (AES) such as inductively coupled plasmas [1], glow discharges [2], furnace atomic non-thermal excitation spectrometry [3], etc. Among those, the microwave induced plasmas MIPs, owing to their high electronic temperature, offer particularly good analytical sensitivity for

* Corresponding author. Tel./fax: + 34 8 5103474; e-mail: ASM@dwarf1.quimica.uniovi.es

PII S0039-9140(96)02055-3

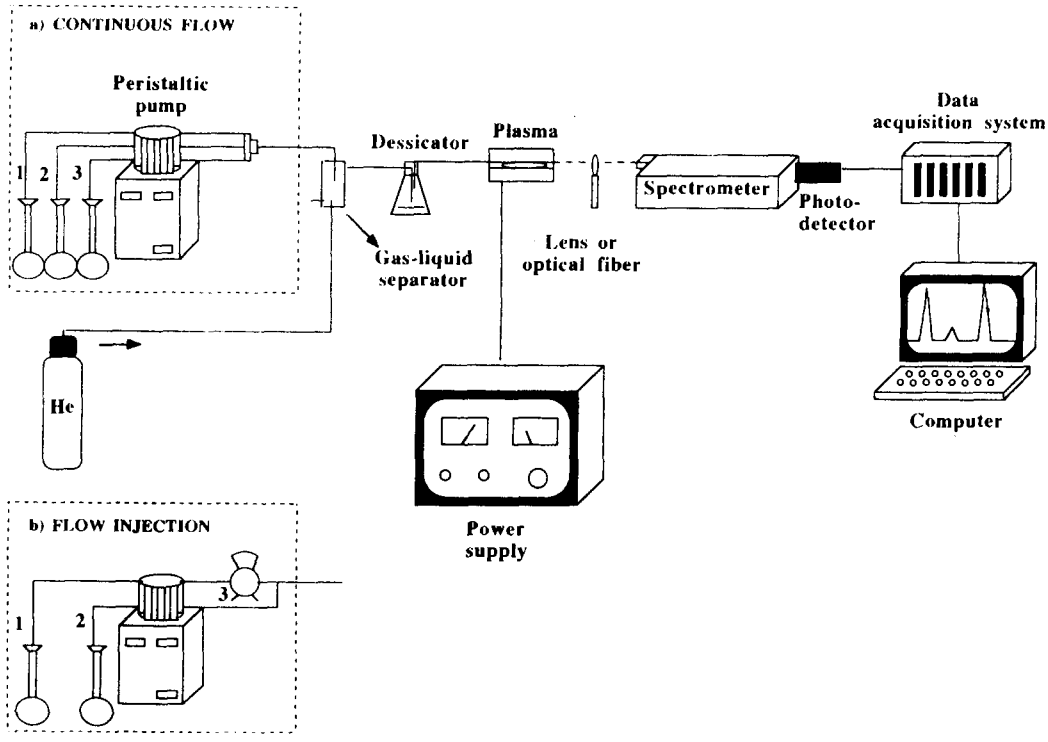

Fig. 1. Schematic diagram of the continuous halogen introduction system and the plasma-AES set-up. 1. Oxidant; 2. Sample; 3. M H_2SO_4 (channel 3 was used only for iodide analysis).

the analysis of non-metals such as the halogens [4–6]. However, the limited thermal energy available in the *commonly used low-power* MIPs (< *150 W*) leads to difficulties with sample desolvation, restricting the real-life use of these discharges to gas phase sample introduction, as in gas chromatography where MIP-AES has become a popular detector [7–9].

More recently, the stabilized capacitive plasma (SCP) has attracted special attention and interest for non-metal excitation using He as plasma gas [10–12]. This plasma has also been evaluated as a gas chromatographic detector [12] and good results (in terms of sensitivity, chemical and spectral interferences) were observed for non-metals in this particular application of SCP-AES.

Alternative means of gas phase sample introduction to MIPs and SCPs for total halogens analysis include chemical [13–17] or electrothermal [11–18] volatilization of halides.

Using chemical volatilization, by on-line chemical oxidation to the corresponding halogen with an adequate oxidant ($KMnO_4$ or H_2O_2) in acid media, we have investigated the comparative analytical performances of both low power plasma for halide analysis: the MIP-AES generated in a Beenakker cavity and the SCP-AES device. Analytical figures of merit and discussion on excitation characteristics observed with both plasma systems are given. Finally, the application of both detection systems to the *determination* of chloride in real water samples is described.

2. Experimental

A block diagram of the experimental set-up used is shown in Fig. 1. Details of the sample introduction system, the plasma components and the spectrometric equipment are described below.

Table 1
Optimum sample and oxidant flow rates

Halogen	Oxidant flow (ml min^{-1})	Sample flow (ml min^{-1})	H_2SO_4 (ml min^{-1})
Chlorine	0.12	4.5	—
Bromide	0.12	4.5	—
Iodine	2.1	2.1	2.1

2.1. Sample introduction system and procedure

Sample solutions were prepared in 7.5 M H_2SO_4 when analyzing bromide or chloride. In order to prevent any chemical oxidation of iodide to volatile iodine by sulfuric acid, the iodide samples were prepared in aqueous medium. For on-line oxidation of samples containing chloride or bromide a solution of 0.05 M $KMnO_4$ in concentrated H_2SO_4 was pumped to the sample stream. For iodide the dissolved samples were mixed on-line with two solutions: one of 3 M H_2SO_4 and the second one containing 3 M H_2O_2. Flow rates of samples and reagents selected in the continuous system are given in Table 1. The generated volatile halogen passed through a gas–liquid separator consisting of a glass tube (2 cm i.d. and 6.5 cm long) where the gas–liquid sample mixture interacted with a smooth flow of He which passes through a glass-frit membrane (Fig. 2). The liberated halogen vapour was stripped off continuously by the carrier-gas stream of He, while residual moisture was removed by bubbling through a desiccator flask filled with concentrated H_2SO_4. The dried gaseous mixture is then introduced directly into the plasma discharge (see Fig. 1) for atomization and excitation.

2.2. Plasma–AES equipment

The components of the two plasma systems used are listed in Table 2 and have been described in detail elsewhere [10,19]. The Beenakker cavity of the MIP was mounted on a translation stage (Oriel Corp.) over an optical bench so that the vertical and horizontal positions could be adjusted within a reproducibility of better than 0.02 mm. A Tangential Flow Torch (TFT) was used as the discharge tube [19–21]. It consists of two coaxial alumina ceramic capillaries (2.5 mm i.d., 4 mm o.d., 30 mm long, and 1 mm i.d., 2 mm o.d., 60 mm long, respectively) positioned in a fitting holder for the addition of a tangential gas flow. Reflected power was kept all time at values lower than 3 W. The plasma was viewed axially and imaged 1:1 on the entrance slit of the monochromator using a fused silica lens.

The SCP is a 27.12 MHz discharge in helium at atmospheric pressure [10,12]. The discharge is sustained in a water-cooled, fused silica tube surrounded by two annular electrodes. The outer surface of the tube is efficiently cooled to a temperature below 100°C by a thin film of fast flowing water. The light emitting region is a disused filament in the centre of the tube at a length of about 20 mm symmetrical to the electrodes. The emitted light from the SCP is collected "end-on" but, in contrast to the MIP detection, an optical fibre, directly mounted on the torch in order to direct the spectral emission to the slit of the spectrometer, was used for the SCP.

Helium (99.999%) was chosen as plasma gas because of its high excitation energy. In the case of the SCP a dopant gas addition of 0.03% O_2 was used.

2.3. Reagents

All the reagents used in this study were of analytical reagent grade and high-purity water (Milli-Q Water) was used throughout.

Stock solutions of iodide, bromide and chloride (1000 μg ml^{-1}) were prepared by dissolving the corresponding potassium halides (dried previously at 110°C) in Milli-Q water. Calibration standard solutions were prepared by serial dilution of the stock solutions in Milli-Q water for I^- and in 7.5 M H_2SO_4 for Br^- and Cl^-.

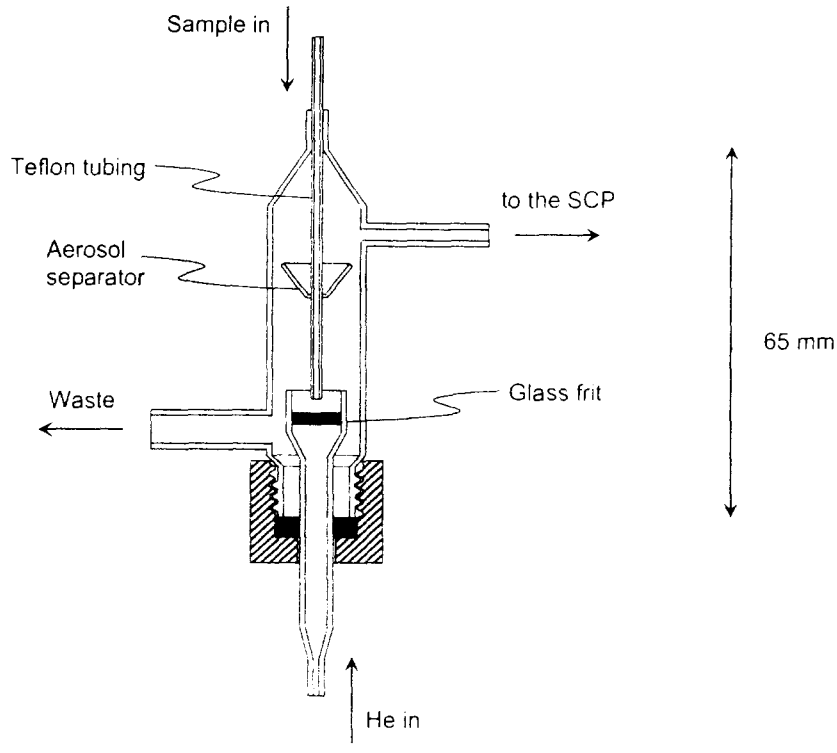

Fig. 2. Diagram of the gas–liquid separator.

2.4. Real sample analysis

To check the applicability of the technique, the chloride content of some commercial mineral waters, tap water, and groundwaters was analyzed. Samples were prepared using sulfuric acid at a final concentration of 7.5 M H_2SO_4. The calibration was carried out using synthetic standard solutions prepared in 7.5 M H_2SO_4.

For method validation, the determination of chloride in the same real water samples was also carried out by ion chromatography using an ion chromatograph (Dionex Corporation) with suppressed conductivity detection.

3. Results and discussion

In order to obtain maximum analyte emission, both chemical generation and plasma excitation parameters were examined and individually optimized for each halide. These parameters included plasma variables (flow rates of the gases forming the plasma and microwave power) and also the conditions for continuous chemical halogen generation and halogen stripping from the liquid phase; flow rates of the liquid samples and of the individual oxidation reagents, type of gas–liquid separator, etc.

The optimization studies were carried out following a univariant search and using the ratio I_N/I_B (where I_N is the background-corrected net analyte emission intensity and I_B the background emission intensity) as the analytical parameter to be maximized.

3.1. Wavelength selection

There are several emission lines lying in the UV-VIS and NIR regions which have been recommended for halogen determined by Plasma-AES at atmospheric pressure [13–18,22]. The emission lines selected offering the best signal to background ratios with our detection systems are

Table 2
MIP-AES and SCP-AES components

Components	Description and specifications
MIP system	
Microwave generator with reflected power meter	Microwave Generator AF, GMW 24-301 DR. Frequency 2450 MHz. Maximal forward power 300 W. Power output with modulation input with coaxial cable KNW 243 N, 50 Ω
Beenakker resonator	Water-cooled microwave resonant cavity from AF. Model HMW 25-471 NM TM_{010} silver-plated.
Monochromator	1-m Jobin–Yvon HR-1000 M Czerny–Turner mount with a grating of 2400 grooves mm^{-1}. Slit width 0.1 mm.
Photmultiplier	R-212 Hamamatsu.
Read-out system	Jobin–Yvon Spectralink system controlled by a computer.
SCP system	
Plasma generatator and supply	Anton Paar KG, ESD Engineering samples.
Monochromator	Jobin–Yvon HR-640. Grating 1200 (IR) and 2400 (UV-VIS) grooves mm^{-1} Slit width 0.1 mm.
Fiber optic	Polymicro Technologies (Phoenix, AZ).
Photodiodes (IR measurements)	S2387, Hamamatsu Photonics.
Photomultiplier (UV measurements)	R-212 Hamamatsu.
Data acquisition	Chromstar Hard-Land Software, Bruker Franzen Analytik.

collected in Table 3 for both SCP and MIP detectors (in this latter case only UV-VIS detection was available).

3.2. Effect of plasma parameters

The effect of microwave forward power in the Beenakker cavity was studied for each continuously generated halogen as explained in the Section 2, in the range 75–100 W. The results obtained have been plotted in Fig. 3. As can be seen, the plots are very similar for the three analytes under study; consequently the observed effect of microwave forward power does not seem to be dependent on the energy of the high lying state of the excited analyte (29 eV for the Cl 479.45 nm ionic line, 26.11 eV for the Br 470.48 nm ionic line, and 6.95 eV for the I 206.16 nm atomic line) or the spectral region (UV for iodine and VIS for bromine and chlorine) for the power values investigated.

Table 3
NIR and UV-VIS wavelengths (nm) investigated

Halogen	SCP		MIP
	UV-VIS	NIR	UV-VIS
Cl	479.45	837.59	479.45
Br	470.48	827.24	470.48
I	206.16	973.17	206.16

The commercial SCP-AES instrument used here works at a fixed value of 140 W, hence, it was not possible to evaluate the effect of the radiofrequency power in our experiments.

The observed influence of plasma carrier flow rate on analytical signals (I_N/I_B) of halogens in

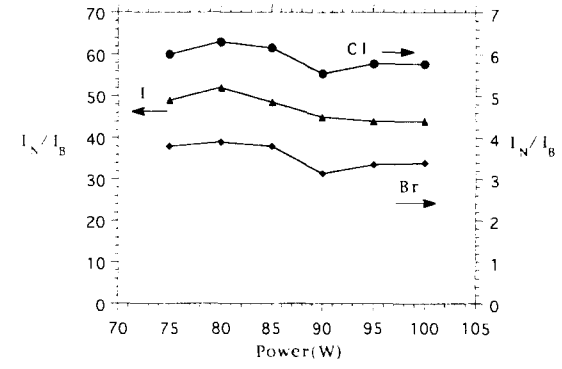

Fig. 3. Effect of the microwave forward power on the determination of chloride by MIP-AES.

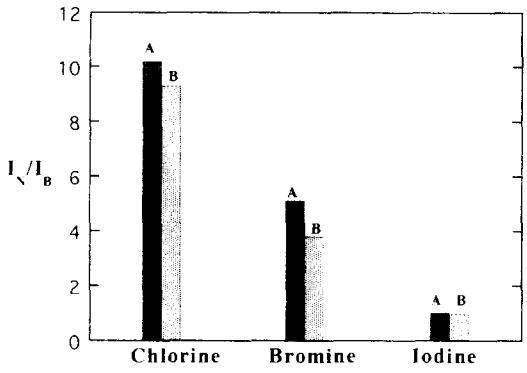

Fig. 4. Influence of sample He flow rates for the two plasmas on the observed analytical signal (net signal over background, I_N/I_B):(a) SCP; (b) MIP.

the SCP and the MIP is plotted in Fig. 4(a) and 4(b) for each of the three halogens. Over the range of flow rates evaluated, no noticeable changes in the background emission were observed. Interestingly, different behavior was noticed in the two plasmas studied; in the SCP (Fig. 4(a)) it can be observed that the optimum plasma gas flow rate is quite dependant upon the type of analyte: for chlorine optimum flow rates were in the region of 20–40 ml min^{-1}, for bromine in the region 40–70 ml min^{-1} and for iodine the optimum was in the range 120–150 ml min^{-1}. These results could be rationalized in terms of volatility: Cl_2 is lighter, and so more volatile than bromine and iodine; being easier to transport by the carrier gas, the use of higher flow rates will just dilute the volatilized analyte and decrease its residence time in the plasma. The heavier iodine needs higher flows of carrier gas for its transport [14] while bromine would show an intermediate transport behavior (see Fig. 4(a)). The optimization results of carrier gas flows using the MIP-AES system (Fig. 4(b)) indicated a much smaller effect of residence time of analytes in this plasma. It seems that the TFT used for MIP generation requires a minimum carrier gas flow for efficient transport (e.g. around 60–70 ml min^{-1}) but it is much less sensitive to the use of higher flow rates (210 ml min^{-1} was the maximum flow rate tested). In any case, the volatility effect is still noticeable as iodine needs higher flows for optimum transport/atomization/excitation than the other halogens. The effect of the tangential gas flow in the torch, at the flow rates under study (70–230 ml min^{-1}) was not critical for chlorine or bromine excitation; however, for iodine a gradual improvement in sensitivity was observed by increasing the tangential flow rate from 70 to 180 ml min^{-1}.

Table 4 collects the finally selected conditions for the plasma operating parameters in the SCP and the MIP for the analysis of the three halides.

3.3. Halogen generation conditions

In order to establish optimum conditions for on-line generation of chlorine, the $KMnO_4$ concentration and flow rates of $KMnO_4/H_2SO_4$ and of the sample were varied and the corresponding plasma emission signals from a 10 μg ml^{-1} solution of chloride were recorded following the general procedure. Selected optimum conditions are collected in Table 1 and in the Section 2.

The continuous on-line bromine generation has been carried out previously in our laboratory using ClO^- as oxidant [17]. However, 0.05 M $KMnO_4$ plus concentrated H_2SO_4 was selected here, thus allowing the possibility of performing a simultaneous determination of both chloride and bromide (for iodine analysis $KMnO_4$ cannot be

Table 4
Selected plasma operating parameters

Parameter	Cl		Br		I	
	SCP	MIP	SCP	MIP	SCP	MIP
Power (W)	140	80	140	80	140	80
Outer He flow (ml min^{-1})	—	150	—	150	—	175
Sample He flow (ml min^{-1})	40	100	70	100	130	140

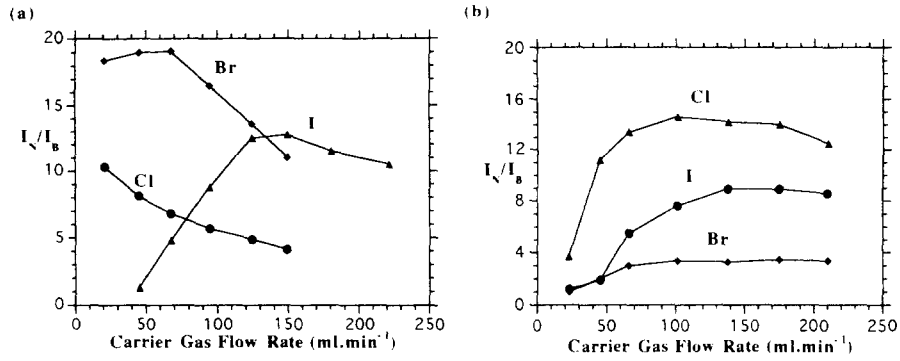

Fig. 5. Comparison of two gas–liquid separator designs using the SCP-AES detection system for the determination of halides. A: GLS depicted in Fig. 2 (experimental conditions as stated in Table 3); B: GLS described in [16] (He flow-rate 70 ml min^{-1} for Cl^- analysis; 70 ml min^{-1} for Br^- analysis; 150 ml min^{-1} for I^- analysis).

used because it transforms iodide into non-volatile IO_3^-).

The influence of the gas–liquid separator (GLS) device was also studied in the SCP-AES detector by comparing the design shown in Fig. 2 and a GLS described previously in the literature [16,23]. As can be seen in Fig. 5 significantly higher analytical signals were obtained for the three halogens using the GLS of Fig. 2 which was then selected for further experiments.

3.4. Comparative analytical performance characteristics

Analytical performance characteristics were evaluated for chloride, bromide and iodide determinations with the MIP (UV-VIS emission lines) and SCP (UV-VIS and NIR emission lines) detectors using the optimum experimental conditions. The linear ranges, the detection limits (calculated as the concentration of analyte producing a net signal equal to three times the standard deviation of the background emission intensity), and the precisions (expressed as relative standard deviation for ten replicators) observed for the three elements in both discharges are summarized in Table 5. While in the UV-VIS region the delectability of halogens is clearly better using the MIP-AES, using the NIR atomic emission lines in the SCP provided the best detection limits observed, demonstrating the usefulness of this spectral region for halogen determinations. The comparatively poor precision obtained for iodine at 206.16 nm in the SCP has already been reported [24].

3.5. Interference studies

The chemical generation and separation of volatile molecular halogen avoids most of the possible interferences which could affect plasma detection. However, matrix interferences may occur in the halogen chemical generation process itself.

The effect of different salts on the generation of chlorine using the MIP-AES detector was studied in this work. The results have been compiled in Table 6 which shows that no effect was observed from ions such as F^-, NO_3^-, PO_4^{3-}, CrO_4^{2-} even at ratios of 500:1 (maximum level tested). However, anions consuming oxidant (such as I^-, SCN^- or $C_2O_4^{2-}$) interfere, but increasing the flow of oxidant or the oxidant concentration used would improve significantly the tolerance ratio to those potential interferences.

A study of interferences in the analysis of iodide by MIP-AES has been carried out elsewhere [25], using a "surfatron" as the MIP cavity. The effect of some common salts that might accompany iodide in real samples was tested and the results showed that this determination was very selective.

No spectral interference was observed at any of the emission lines under study in both plasmas. It has been reported that the atomic line I(I) at 973.17 nm could be overlapped by phosphorus

Table 5
Analytical performance characteristics

Wavelength	Characteristic	SCP-AEA			MIP-AES		
		Cl	Br	I	Cl	Br	I
NIR	DLl (ng ml^{-1})	1.4	3	13			
	Precision (RSD)	3.2%	3.8%	2.2%			
	Linear range	≈3 orders of magnitude	≈3 orders of magnitude	≈3 orders of magnitude	—[a]	—[a]	—[a]
UV-VIS	DL (ng ml^{-1})	45	135	400	17	24	55
	Precision (RSD)	1.5%	2.7%	7.5%	3%	1.4%	4%
	Linear range	≈2 orders of magnitude	≈2 orders of magnitude	≈2 orders of magnitude	≈3 orders of magnitude	≈3 orders of magnitude	*3 orders of magnitude

DL, detection limit; RSD, relative standard deviation.
[a] Not determined.

Table 6
Selectivity studies for the determination of 2 μg ml^{-1} of chloride at 479.45 nm with the MIP-AES

Foreign ion	Tolerance ratio
F^-	500:1
I^-	50:1
$C_2O_4^{2-}$	20:1
NO_3	500:1
SCN^-	10:1
PO_4^{3-}	500:1
CrO_4^{2-}	500:1

emission [24]. However, phosphorus is not a source of spectral interference in our method since no volatile phosphorus species are formed with the proposed system.

3.6. Real sample analyses

The optimized method was tested in real analysis for the determination of chloride in mineral waters using MIP-AES. The real sample measurements for SCP-AES (tap water, groundwaters) were carried out using a flow injection (FIA) mode for halogen generation [26]. The results observed with both detectors are collected in Tables 7 and 8. As can be seen, good agreement was observed with results for the same samples obtained by ion chromatography, which validates the proposed methodologies.

4. Conclusions

This comparative study of two different inexpensive plasmas as excitation sources confirms the feasibility of highly sensitive halide determinations by resorting to continuous halogen generation as the sample introduction approach. For the case of the emission lines evaluated in the UV-VIS region, better detection limits were obtained with the MIP than with the SCP, however, it has also to be noted that different light collection systems were used for both detectors and that could give rise to slight modifications in the detection limits. The NIR region offers particular advantages as shown by SCP results. This calls for further exper-

Table 7
Results of the determination of chloride in mineral waters by MIP-AES

Sample	MIP (mg l^{-1}) ± S.D.	IC (mg l^{-1}) ± S.D.[a]
I	2.20 ± 0.02	2.8 ± 0.2
II	5.10 ± 0.01	5.4 ± 0.1
III	16.3 ± 0.7	16.0 ± 0.3

[a]Results from ion chromatography (IC), as alternative technique, for the same samples.

iments using the MIP as excitation source and NIR lines for detection.

It is worth noting that the determination of chloride was the most sensitive of the three halogens assayed with both detectors. Finally, the use of the same oxidant mixture for Cl^- and Br^- analysis provides the possibility for simultaneous determination of both elements with a multichannel detector.

Acknowledgements

The authors wish to thank Dr Bernhard Platzer from Graz University of Technology for valuable comments. Financial support is gratefully acknowledged from DGICYT (Spain) through project PB 94-1331 and from the Fonds zur Förderung der Wissenschaftlichen Forschung, Austria, under Grant No. P09236-CHE. The authors also express their gratitude to the Acciones Integradas Hispano-Austriacas (project 8.B) for providing travel funds for this collaborative program.

Table 8
Results of the determination of chloride in waters by SCP-AES

Sample	SCP (mg l^{-1}) ± S.D.	IC (mg l^{-1}) ± S.D.[a]
Polluted groundwater	175 ± 3	172 ± 1
Groundwater	17 ± 1	17.3 ± 0.1
Tap water	2.3 ± 0.1	2.1 ± 0.1

[a]Results from ion chromatography (IC), as alternative technique, for the same samples.

References

[1] S. Chan and A. Montaser, Spectrochim. Acta Part B, 42 (1987) 591.
[2] R. Pereiro, T.K. Starn and G.M. Hieftje, Appl. Spectrosc., 49 (1995) 616.
[3] K. Dittrich, 1990 Winter Conference Plasma Spectrochemistry, Conference Abstracts, St. Petersburg, FL, Paper WP 17.
[4] E. Bulska, J. Anal. At. Spectrom., 7 (1992) 201.
[5] A.T. Zander and G.M. Hieftje, Appl. Spectrosc., 35 (1981) 357.
[6] J.F. Camuña-Aguilar, R. Pereiro-García, J.E. Sánchez-Uria and A. Sanz-Medal, Spectrochim. Acta Part B, 49 (1994) 545.
[7] A.J. McCormack, S.C. Tong and W.D. Cooke, Anal. Chem., 37 (1965) 1470.
[8] B.D. Quimby, P.C. Uden and R.M. Barnes, Anal. Chem., 50 (1978) 2112.
[9] G.L. Long, G.R. Ducatte and E.D. Lancaster, Spectrochim. Acta Part B, 49 (1994) 75.
[10] B. Platzer, R. Gross, E. Leitner, A. Schalk, H. Sinabell, H. Zach and G. Knapp, An element-specific detector for gas chromatography based on a novel capacitively coupled plasma, in P.C. Uden (Ed.), Element-Specific Chromatographic Detection by Atomic Emission Spectroscopy, ACS Symp. Ser. 479, American Chemical Society, Washington, DC, 1992, Chapter 9.
[11] C. Katschthaler, X. Quan, H. Krizová, R. Gross and G. Knapp, Spectrochim. Acta Part B, 50 (1995) 453.
[12] R. Gross, B. Platzer, E. Leitner, A. Schalk, H. Sinabell, H. Zach and G. Knapp, Spectrochim. Acta Part B, 47 (1992) 95.
[13] N.W. Barnett, J. Anal. At. Spectrom., 3 (1988) 969.
[14] M.D. Calzada, M.C. Quintero, A. Gamero, J. Cotrino, J.E. Sánchez Uría and A. Sanz-Medel, Talanta, 39 (1992) 341.
[15] M.D. Calzada, M.C. Quintero, A. Gamero and M. Gallego, Anal. Chem., 64 (1992) 1374.
[16] T. Nakahara, S. Morimoto and T. Wasa, J. Anal. At. Spectrom., 7 (1992) 211.
[17] F. Camuña, J.E. Sánchez Uría and A. Sanz-Medel, Spectrochim. Acta Part B, 48 (1993) 1115.
[18] M. Wu and J.W. Carnahan, Appl. Spectrosc., 44 (1990) 673.
[19] J.F. Camuña-Aguilar, R. Pereiro-García, J.E. Sánchez-Uría and Sanz-Medel, Spectrochim, Acta Part B, 49 (1994) 475.
[20] A. Bollo-Kamara and E.G. Codding, Spectrochim. Acta Part B, 36 (1981) 973.
[21] H. Feuerbacher and M. Oppermann, Improvements of the He-MIP by discharge tubes of selected ceramics, Paper presented at the Winter Conf. Plasma Spectrochemistry, Conference Abstracts, San Diego, CA, 1988.
[22] J.E. Freeman and G.M. Hieftje, Spectrochim. Acta Part B, 40 (1985) 653.
[23] T. Nakahara, S. Yamada and T. Wasa, Appl. Spectrosc., 44 (1990) 1673.

[24] B. Platzer and G. Knapp, Comprehensive nonmetal emission spectra of the stabilized capacitive plasma (SCP) discharge in helium at atmospheric pressure, Spectrochim. Acta, Part B, in the press.

[25] M.C. Quintero, J. Cotrino, M. Saez, A. Menéndez, J.E. Sánchez Uría and A. Sanz-Medel, Spectrochim. Acta Part B, 47 (1992) 79.

[26] C. Katschthaler, Dissertation, Graz University of Technology, 1996.

ELSEVIER

Talanta 44 (1997) 545–551

Talanta

Flow injection spectrophotometric determination of cyanide by the phenolphthalin method

Amin T. Haj-Hussein *

Chemistry Department, Yarmouk University, Irbid, Jordan

Received 11 June 1996; received in revised form 29 July 1996; accepted 30 July 1996

Abstract

The phenolphthalin method for the determination of cyanide has been modified and adapted to a continuous flow system based on the flow injection principle. Aqueous cyanide samples are injected into a carrier stream (0.001 M NaOH), which is then merged with the combined reagent stream of phenolphthalin and carbonate buffer (pH 10.3), and the mixture is passed through an on-line cupric sulfide packed column. The resulting phenolphthalein (the oxidized form of phenolphthalin) is measured in a flow-through spectrophotometer at 552 nm, to determine the cyanide content. The chemical factors and flow injection analysis (FIA) variables influencing the system are discussed. The calibration graph is linear from 0.6 to 4.3 ppm cyanide. At a sampling rate of about 70 samples h^{-1} with 50 μl sample injections, precision was about 1% relative S.D. © 1997 Elsevier Science B.V.

Keywords: Flow injection; Phenolphthalin; Spectrophotometry; Cyanide

1. Introduction

The phanolphthalin method [1–4], is based on the oxidation of phenolphthalin to phenolphthalein by cyanide in the presence of copper. This method was once very widely used in cyanide analysis but has yielded to the generally superior methods based on the Konig reaction [2,5]. Robbie [4] studied the method extensively and found that the color intensity produced is significantly dependent on the amount of alkali, and the color fades if more alkali is added. He reported also that the color formed increases due to the slow spontaneous conversion of excess phenolphthalin reagent as the solution stands. Thus, the conventional phenolphthalin method requires an immediate measurement of the color produced [4], or addition of a stabilizing reagent after color development [6]. Even experienced analysts very often fail to obtain reproducible results manually. The adaptation of such a method to a continuous system seems therefore justified. Flow injection analysis (FIA) [7] is now a well established technique for carrying out automatic wet chemical analysis in a rapid and efficient way. In this paper the adaptation of the phenolphthalin method for the determination of cyanide to the FIA system is described. Since the residence time is short and can be kept constant, the color instability problem was solved and reproducible results were ob-

* Corresponding author. Fax: +962 2 274725.

PII S0039-9140(96)02056-5

tained. Also the intensity of the color produced, which is significantly dependent on the pH of the medium, was controlled by using a carbonate buffer continuously pumped into the FIA system. Furthermore, the copper required in this FIA method was produced in situ using an on-line cupric sulfide packed column. So, the inconvenience of using the phenolphthalin-$CuSO_4$ reagent (prepared fresh daily in the conventional method) was eliminated. The proposed FIA method has the advantages of stability of reagents, reproducibility, sensitivity and rapidity of determination, and is a quantitative technique.

2. Experimental

2.1. Reagents

All chemicals used were of analytical reagent grade, unless otherwise specified; all solutions were prepared with deionized water.

2.1.1. Cupric sulfide

This was prepared by adding a solution of 0.01 M sodium sulfide to a solution of 0.01 M cupric sulfate up to nearly the equivalent point, leaving a slight excess of the latter. The precipitate, CuS, was filtered, washed with water and dried.

2.1.2. Phenolphthalin solutions

These were phenolphthalin in 3 vol.% ethanol prepared by dissolving the calculated amount of phenolphthalin (Sigma, 95%) in 3.0 ml absolute ethanol, and diluting to 100 ml with water. Phenolphthalin solutions of concentrations 0.5×10^{-4}, 1.0×10^{-4}, 2×10^{-4}, 3.0×10^{-4} and 4.0×10^{-4} M, were prepared. All solutions are stable for 2 weeks or more without precipitation occurring, except for the 4.0×10^{-4} M solution which is stable only for a day at room temperature.

2.1.3. Buffer solutions

The carbonate, phosphate and ammonia buffer solutions were prepared as previously described [8]. Carbonate buffer solutions of 0.025, 0.050, 0.10 and 0.30 M $NaHCO_3/NaCO_3$ at pH 10.3 and 0.2 M at pH 9.5, 10.0, 10.3, 10.6, 11.0, and 11.3 were prepared. The phosphate buffer solutions were 0.20 M Na_2HPO_4/Na_3PO_4 at pH 9.5, 10.0, 10.5, 11.0, and 11.3. The ammonia buffer solutions were 0.20 M NH_4Cl/NH_3 at pH 9.5, 10.0, 10.3, 10.6 and 11.0. The pH of these buffers were adjusted to the required value with NaOH or HCl. All pH measurements were made using a Metrohm Herisau (Type E 520) pH meter equipped with a combined Metrohm AG 9100 electrode.

2.1.4. Sodium hydroxide dilution solution, 1.0×10^{-3} M NaOH

This was prepared by dissolving 0.04 g NaOH in 1 l of water.

2.1.5. Standard cyanide solutions

Stock cyanide solution was prepared by dissolving the calculated amount of potassium cyanide (BDH, 96%) in sodium hydroxide dilution solution, and the solution was standardized using the Liebig method [9]. A stock standard solution of 0.03846 M (1000 ppm) was prepared. Working standards in the range 3.8×10^{-6}–3.8×10^{-4} M (0.1–10 ppm) cyanide were prepared by successive dilution of the stock solution with sodium hydroxide dilution solution. Because cyanide solutions are very reactive and unstable, these solutions were stored in closed, dark bottles in a cool place.

2.1.6. Interfering ions/solutions

Solutions of diverse ions were prepared from the sodium or potassium salts of the anions and chlorides of the cations. In each case the appropriate amount of foreign ion and standard cyanide solution was introduced into a 25 ml volumetric flask and made up to 25 ml with sodium hydroxide dilution solution.

2.2. Apparatus

The schematic of the manifold for this study is shown in Fig. 1. The carrier and reagent solutions were delivered by a four-channel RAININ (Rabbit) peristaltic pump operated with Tygon tubing. Sample solutions were injected manually into the carrier stream using a Rheodyne six-bore injector

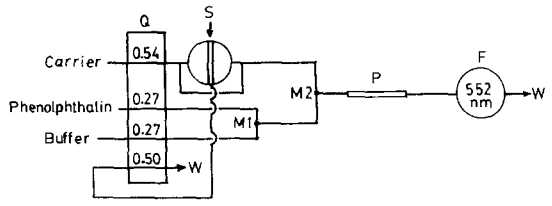

Fig. 1. Manifold for FIA spectrophotometric determination of cyanide. The internal diameter of the microline tubing was 0.51 mm. The abbreviations represent the following: S, point of injection; Q, flow rate (ml min^{-1}); M1 and M2, confluence points; P, packed column; F, flow-through cell; W, waste.

(Type 50). A Varian DMS 100 UV-visible spectrophotometer equipped with a 10 mm Hellma-type flow cell (Model QS 178.012) was used as detector and was connected to a linear 1200 chart recorder. Tubing, made of Microline (0.51 mm i.d.) was used throughout. The confluence points were KEL-F polymer tees. Press-to-fit connections made of silicone rubber tubing were used for the entire manifold.

2.3. Microcolumn construction

The body of the on-line column (Fig. 2) was a 6.0 cm long glass tube (1.4 mm i.d. and 4.0 mm o.d.). An on-line filter (polyethylene porous bed, 4.0 mm in diameter, 2.0 mm thickness) was fixed by 3.0 mm i.d. Tygon tubing at both ends of the column. The column was packed with 80 mg of crushed cupric sulfide particles of appropriate grain size (about 0.8–1.2 mm). A thick-walled silicone rubber tube of 0.51 mm i.d. was inserted at both ends of the Tygon tubing to minimize the dead volume.

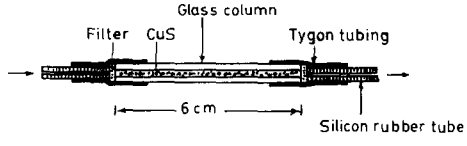

Fig. 2. Design of the microcolumn for the on-line FIA/spectrophotometric system.

2.4. FIA

The flow system illustrated in Fig. 1 was used. The reagent stream contains phenolphthalin and carbonate buffer. Since a mixture of these two components is not stable, because alkali tends to cause the phenolphthalin to convert to the phenolphthalein form [4], they are mixed in the FIA system at point M1. Different volumes in the range 25–100 μl of cyanide sample solutions were continuously pumped through the sample loop, and then injected in the carrier stream (0.001 M NaOH solution). The carrier stream, containing the sample zone, was merged with the premixed reagent stream of phenolphthalin and carbonate buffer at confluence point M2. The combined stream was passed through the CuS packed column (the distance between M2 and the packed column was reduced to about 3 cm to avoid excessive dispersion of the sample solution) in which the phenolphthalin is oxidized to phenolphthalein, and directed to the flow-through cell of the spectrophotometer (the distance between the packed column and the flow cell was reduced as much as possible, to about 25 cm, in order to secure limited dispersion of the color produced). The absorbance of phenolphthalein was monitored at 552 nm. The output of the spectrophotometer was registered on the chart recorder. When the baseline was reached, another slug of sample could be injected.

3. Results and discussion

Determination of cyanide by this FIA/spectrophotometric method is based on the measurement of the absorbance of the red color of the phenolphthalein produced in an alkaline solution. Absorbance measurements were performed using the manifold shown in Fig. 1. The absorption spectrum for phenolphthalein at pH 10.3 (carbonate buffer) obtained by injecting a standard cyanide solution (1.5×10^{-4} M) is shown in Fig. 3. The curve exhibits a band with maximum absorption at 552 nm which was used as the optimum wavelength for studying the chemical factors and the FIA variables influencing the system.

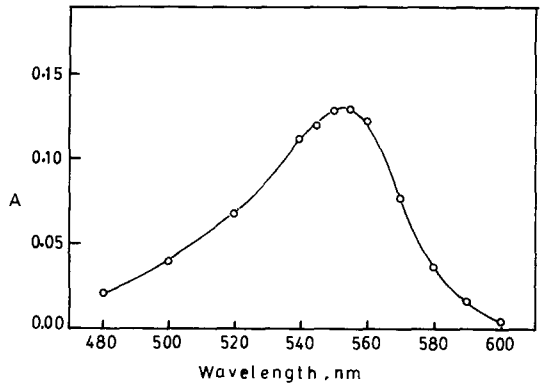

Fig. 3. Absorption spectrum of phenolphthalein at pH 10.3 with the manifold shown in Fig. 1. Carrier, 1.0×10^{-3} M NaOH; phenolphthalin concentration, 3.0×10^{-4} M; carbonate buffer concentration, 0.20 M; cyanide concentration, 1.5×10^{-4} M; injection volume, 50 μl.

3.1. Optimization of chemical factors

Cyanide solutions readily dissolve CuS forming the colorless tetracyanocuprate(I) ions [10]. Thus, in the presence of cyanide, copper acquires powerful oxidizing characteristics owing to the formation of extremely stable cuprocyanide complexes. Under these conditions phenolphthalin is oxidized to phenolphthalein (red in alkaline medium). Accordingly, the heterogeneous chemical reaction in this FIA system can be represented by the following redox equation:

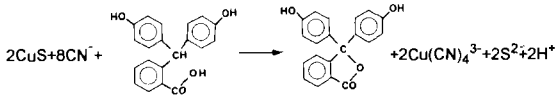

Considering this redox reaction, several chemical factors had to be optimized to achieve reproducible results. These include pH of the reaction medium, buffer concentration and phenolphthalin concentration.

3.1.1. pH

In this FIA system, two consecutive processes are affected by variation in the pH of the reaction medium. The first process is the oxidation of phenolphthalin to phenolphthalein. The second one is the color change of the phenolphthalein (indicator) formed, which is believed to be due to structural change, including the production of quinonoid and resonance forms [9]. By increasing the pH of the medium, the tendency to form phenolphthalein in the redox process is enhanced and subsequently the intensity of the red color is increased. But if the reaction is carried out in highly alkaline solution, the red color first produced disappears owing to a further structural change [9]. Therefore, the pH of the reaction medium should be carefully controlled to achieve reproducible results. To determine the optimum pH value, three different alkaline buffer solutions were examined. The results are shown in Fig. 4. Ammonia buffer was not suitable because it formed an intense blue color of mixed amine complexes of copper(II), which absorbs at the peak of the absorption band of phenolphthalein. Phosphate buffer was not satisfactory owing to the low absorbance values obtained, which decreases the sensitivity of the method. The most suitable buffer was carbonate, which had the advantage in that it's maximum absorbance value at

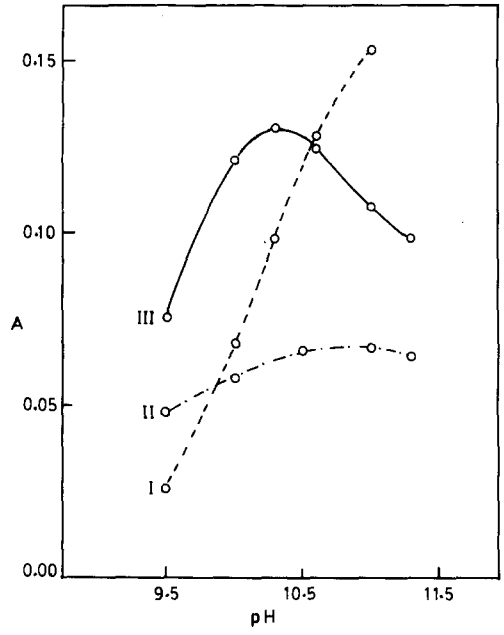

Fig. 4. Effect of buffer pH on the determination of cyanide with the manifold shown in Fig. 1. The buffer solutions used were 0.20 M ammonia buffer (I), 0.20 M phosphate buffer (II), and 0.20 M carbonate buffer (III). Wavelength, 552 nm; other conditions as given in Fig. 3.

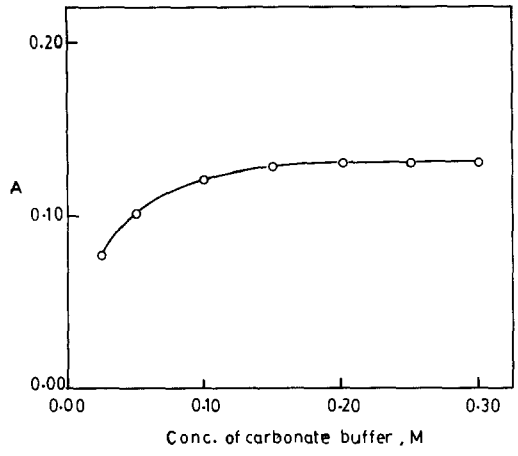

Fig. 5. Effect of carbonate buffer (pH 10.3) concentration. Wavelength, 552 nm; other conditions as given in Fig. 3.

pH 10.3 decreases the opportunity for interferences from some cations in water samples that may form hydroxide precipitates at higher pH values. Furthermore, the solubility of CuS varies with the pH of the medium. In a previous work [11], it was found that the solubility of CuS was negligible at pH > 9.2. Consequently, carbonate buffer of pH 10.3 was selected for use.

3.1.2. Carbonate buffer concentration

The effect of carbonate concentration (pH 10.3) was determined using a standard cyanide solution (1.5×10^{-4} M) and phenolphthalin solution (3.0×10^{-4} M). The absorbance values at 552 nm were measured in the concentration range 0.025–0.30 M carbonate buffer solution. Fig. 5 shows that the absorbance of phenolphthalein formed is dependent on the carbonate buffer solution, and a concentration of 0.20 M is necessary for the development of maximum absorbance.

3.1.3. Phenolphthalin concentration

The effect of phenolphthalin concentration was determined using a concentration of 1.5×10^{-4} M cyanide and 0.20 M carbonate buffer (pH 10.3). The absorbance values at 552 nm were measured in the concentration range 0.5×10^{-4}–4.0×10^{-4} M phenophthalin solutions. Fig. 6 shows that the absorbance of phenolphthalein formed is dependent on the phenolphthalin concentration. The concentration of 3.0×10^{-4} M was chosen because it is much more stable than a 4.0×10^{-4} M solution, and this quantity of phenolphthalin is enough to allow a complete cyanide reaction.

3.2. Optimization of FIA variables

3.2.1. Sample volume injection

The injection volume has a significant effect on peak height, sensitivity, range of linearity and sampling rate [7]. The peak height was found to increase with the injected sample volume (Fig. 7). The range of linearity of cyanide concentrations was found to decrease as the sample volume increased (Fig. 7), and tailing became larger, thus lowering the sampling rate. At a flow rate of 1.08 ml min^{-1}, it was found that the sampling rate decreased from 80 to 40 samples h^{-1} as the injection volume increased from 25 to 100 μl. A 50 μl sample loop was selected.

3.2.2. Flow rate

The signal increased about 9% when the flow rate was changed from 1.08 to 1.6 ml min^{-1}. The higher the flow rate, the higher the peak, but the reproducibility was poor when the flow rate exceeded 1.08 ml min^{-1}. Moreover the flow rate has a significant effect on the residence time and dispersion [7]. Thus, to reduce dispersion, the

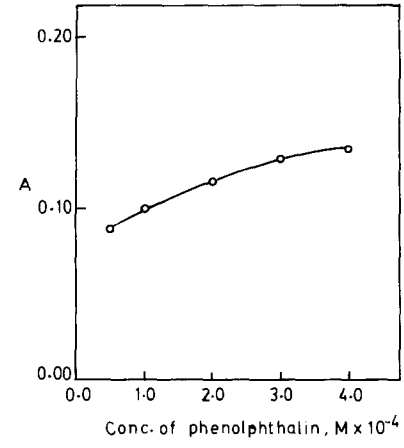

Fig. 6. Effect of phenolphthalin concentration. Wavelength, 552 nm; other conditions as given in Fig. 3.

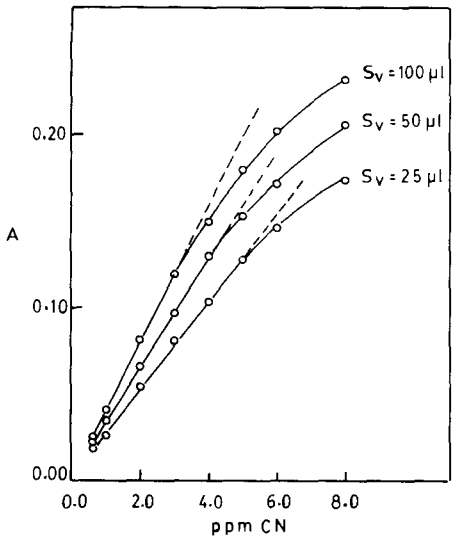

Fig. 7. Effect of injection volume on the determination of cyanide with the manifold shown in Fig. 1. Wavelength, 552 nm; other conditions as given in Fig. 3.

pumping rate should be decreased which results in an increase in the residence time. In this system, a high reproducibility of measurements with a reasonable sampling rate were achieved at a flow rate of 1.08 ml min^{-1}. At this flow rate, the average sampling rate with 50 µl sample injections was around 70 samples h^{-1}.

3.2.3. System characterization

The flow system in Fig. 1 was used for preparing the calibration graph. Standard cyanide solutions were injected from a sample loop of 50 µl. At a flow rate of 1.08 ml min^{-1}, with 50 µl sample injections, the calibration graph (Fig. 7) is linear in the range 0.6–4.3 ppm cyanide. The resulting linear calibration graph has a regression coefficient of 0.999. The detection limit of cyanide, defined as the concentration that gives a signal three times the S.D. of the background signal, was 0.1 ppm. For successive injections of standard cyanide solution (3.9 ppm) the precision of the method was found to $< 1\%$ relative S.D.

3.3. Interference study

In order to apply the proposed FIA determination of free cyanide to natural waters, the effect of foreign substances was examined. In each case, the solution was made to contain 0–200 ppm foreign ion and 4 ppm CN and the recommended procedure followed thereafter. A 2% relative error in the determination of cyanide was considered permissible. The following ions showed no interferences at concentrations of 200 ppm: Ca^{2+}, Mg^{2+}, Cl^-, $HClO_3$-, SO_4^{2-}, NO_2^-, NO_3^-, and F^-. This indicates that the major constituents, in amounts larger than those normally found in natural waters, have no effect on the determination of cyanide by the proposed method.

However, it is known that the phenolphthalin method is sensitive to foreign oxidizing materials. Childs and ball [12] reported that ferricyanides and aqueous solutions of halogens give similar color, because of direct oxidation of phenolphthalin. Moreover, it is reported [13] that oxidizing agents, such as chlorine, decompose most cyanides, also oxidized products of sulfide convert CN^- to SCN^--rapidly, and aldehydes convert cyanide to cyanohydrin. Therefore, in order to apply the proposed FIA method for the determination of total cyanide in waters and waste waters, all known interferences should be eliminated. Oxidizing agents and sulfides can be removed by special procedures, and most other interfering substances removed by distillation [13].

3.4. Application of method

The method was evaluated by recovery studies using cyanide-free natural water samples, obtained from a drilled well (Al-Husn, Jordan) more than 300 m deep. The samples were only filtered to remove possible interference from suspended

Table 1
Recovery results from cyanide determination in spiked water samples

Set Number	Amount of CN (ppm)		Recovery (%)
	Added	Found[a]	
1	2.00	2.03	101.5
2	3.00	2.98	99.3
3	4.00	3.95	98.7

[a] Each value represents the mean of five determinations.

particles. Various amounts of cyanide stock solution were introduced into 25 ml volumetric flasks along with 5 ml water samples. The volume in each flask was made up to 25 ml with sodium hydroxide dilution solution, and the recommended procedure followed thereafter. Five samples and three standards were determined at each cyanide concentration chosen for the study. Average values for the absorbances of standards were used in constructing a calibration curve from which sample absorbances were converted into ppm cyanide found. The results are summarized in Table 1. The recoveries varied from 98.7 to 101.5% (mean 99.8%).

4. Conclusion

A sensitive and reasonably fast FIA/phenolphthalin procedure for the determination of cyanide is developed. The incorporation of a cupric sulfide packed column provides a simple means of producing the copper required in the FIA system. Also, the use of carbonate buffer (pH 10.3) offers the advantage of controlling the intensity of the color produced and decreases the interfering effects of some cations in water samples. The calibration graph is linear in the range 0.6–4.3 ppm of cyanide when using a sample volume of 50 μl. The detection limit is found to be 0.1 ppm cyanide.

Although some FIA spectrophotometric methods [14–16] for the determination of cyanide based on the Konig reaction reported lower limits of detection, the detection limit obtained by the proposed method is considered to be within the sensitivity range of the best colorimetric methods known for cyanide determination [17]. Moreover, the proposed method is quite economical in comparison. However, the most important features of this FIA system are its simplicity, ease of automation, stability of reagents and high precision and sampling frequency.

References

[1] F. Weehuizen, Pharm. Weekblad., 42 (1905) 95.
[2] I.M. Kolthoff, Z. Anal. Chem., 57 (1918) 11.
[3] R.I. Nicholson, Analyst, 66 (1941) 189.
[4] W.A. Robbie, Arch. Biochem., 5 (1944) 49.
[5] D.F. Boltz and J.A. Howell, Colorimetric Determination of Nonmetals, Wiley, 1978, p. 74.
[6] R.L. Maute and M.L. Owens, Jr., Anal. Chem., 26 (1954) 1723.
[7] J. Ruzicka and E. H. Hansen, Flow Injection Analysis, 2nd edn., Wiley, New York, 1988, pp. 27, 30.
[8] G.D. Christian, Analytical Chemistry, 5th edn., Wiley, New York, 1994.
[9] A.I. Vogel, A text-book of Quantitative Inorganic Analysis, 3rd edn., Longman, London, 1961, pp. 52, 271.
[10] Vogel's Text-book of Macro and Semimicro Qualitative Inorganic Analysis, 5th edn., Longman, London, 1979, p. 315.
[11] A.T. Haj-Hussein, G.D. Christian and J. Ruzicka, Anal. Chem., 58 (1986) 38.
[12] A.E. Childs and W.C. Ball, Analyst, 60 (1935) 294.
[13] Standard Methods for the Examination of Water and Wastewater, 16th edn., American Public Health Association, Washington, DC, 1985, pp. 327–346.
[14] J.A. Sweileh, Anal. Chim. Acta, 220 (1989) 65.
[15] A. Tanaka, K. Mashiba and T. Deguchi, Anal. Chim. Acta, 214 (1985) 259.
[16] A. Rios, M.D. Luque de Castro and M. Valcarcel, Talanta, 31 (1984) 673.
[17] L.S. Bark and H.G. Higson, Analyst, 88 (1963) 751.

ELSEVIER

Talanta 44 (1997) 553–562

Talanta

Preconcentration and atomic absorption determination of iron by sequential injection analysis

E. Rubí [a], M.S. Jiménez [b], F. Bauzá de Mirabó [c], R. Forteza [c], V. Cerdà [c,*]

[a] *Department of Analytical Chemistry, University of Santiago de Compostela, Av. de las Ciencias s/n, 15706, Santiago de Compostela, Spain*

[b] *Analytical Spectroscopy and Sensors Group (GEAS), Department of Analytical Chemistry, Faculty of Sciences, University of Zaragoza, 50009, Zaragoza, Spain*

[c] *Department of Chemistry, University of the Balearic Islands, E-07071 Palma de Mallorca, Spain*

Received 12 February 1996; received in revised form 26 April 1996; accepted 8 August 1996

Abstract

A sequential injection analysis (SIA) assembly for the atomic absorption determination of Fe(III) in natural waters is proposed. Iron is preconcentrated on a microcolumn packed with a chelating resin (Chelex 100) that is inserted in the manifold. The sample is passed through the column and the iron retained by the resin is subsequently eluted with 2 M HNO_3. The proposed SIA system affords automatic preconcentration, elution, detection of Fe(III), data acquisition and treatment. When 9 ml of iron solution containing 0.4 or 1 mg l^{-1} was passed through the resin, the retention efficiency was 93.1 ± 0.6 and 7.4 ± 3.0% respectively, and when 27 ml of iron solution of 0.2 mg l^{-1} was preconcentrated, the retention was 8.4 ± 2.9%. The detection limits thus achieved is 12 μg l^{-1} when 9 ml of sample are preconcentrated and 6 μg l^{-1} for 27 ml. © 1997 Elsevier Science B.V.

Keywords: Atomic absorption spectrophotometry; Automation; Chelex 100; Iron(III) preconcentration; Sequential injection analysis; Water

1. Introduction

Sequential injection analysis (SIA) was developed by Růžička and co-workers in 1990 and has been studied by several groups with regards to its theoretical foundation and potential applications [1–6]. Whereas in flow injection analysis (FIA) the samples are injected into a continuous flow, in SIA the sample and reagent zones are first sequentially aspirated and stacked into a channel and then the flow is reversed in order to transport them into the detector. For this purpose, a multiposition selector valve has been used as distributor and either a sinusoidal flow pump [3,6], specially designed for SIA, or a peristaltic pump [5] as liquid drives.

SIA methodology has important advantages over conventional FIA. Thus, the instrumental set-up is much more flexible (a given assembly can be used to implement various determinations with little alteration); the experimental components un-

* Corresponding author. E-mail: vcerda@p01.uib.es

PII S0039-9140(96)02059-0

dergo little wear; hydrodynamic variables can be controlled by straightforward means; the manifold does not have to be changed if flow parameters or injection volumes are modified; the analyte/reagent ratio can readily be optimized in order to ensure sensitive responses with substantially decreased reagent consumption; and reaction times can be prolonged with no detriment to the dispersion.

The aim of the present work was to study the feasibility of combining SIA methodology and on-line preconcentration of metals using a column packed with a chelating resin (Bio-Rad Chelex 100) and its subsequent determination by atomic absorption spectrophotometry. For this purpose, we chose the determination of Fe(III) in natural waters.

In preconcentration by sorbent extraction with a flow injection system, a chelating agent is added to the sample solution. The metal chelates thus formed are preconcentrated in an appropriate column and subsequently eluted with an organic solvent. By making the correct selection of a suitable chelating agent and eluent, numerous advantages can be achieved. On-line preconcentration techniques in flow injection, when combined with atomic absorption spectrometry, have provided a sensitive and rapid method for the analysis of trace elements [7–23].

Olsen et al. [7] developed an FIA system including a Chelex 100 column for the determination of Cd, Pb, Cu and Zn in sea water. They employed two different procedures for this purpose. One uses two injection valves that are serially arranged with the resin column. One valve is employed to inject 1 ml of sample, which is later preconcentrated, and the other to inject 180 μl of 2 M HNO_3 to elute the metals. Such a simple assembly does not allow the pH of samples acidified with HNO_3 for preservation to be adjusted. The second procedure involves injecting the sample into a water stream that is subsequently merged with ammonium acetate and passed through a coil and then through the resin column. The ensuing method allows Pb concentrations down to 10 ng ml^{-1} and cadmium and zinc down to 1 ng ml^{-1} to be determined at a rate of 30–60 samples h^{-1}.

Hirata et al. [8] reported a procedure for the determination of seven heavy metals including Fe(III) by use of an automated on-line column preconcentration system for flow injection atomic absorption spectrometry. The resin used, Muromac A-1, is similar to Chelex 100 and contains an iminodiacetic group.

Di and Davey [9] proposed a flow injection on-line preconcentration system, combined with graphite furnace atomic absorption spectrometry, for the determination of gold in ores samples. An α-aminopyridine resin was used. The reported detection limit was 0.065 μg l^{-1} of gold.

Hartenstein et al. [24] used a Chelex 100 column in an FIA manifold for the multielement ICP-AES determination of barium, beryllium, cadmium, cobalt, copper, manganese, nickel and lead. The sensitivity is increased by a factor of 20 relative to conventional aspiration of samples.

2. Experimental

2.1. Reagents

All reagents used were analytical-grade chemicals. A stock standard solution containing 1000 mg l^{-1} Fe(III) was prepared by dissolving the required amount of metallic iron in HNO_3 and diluting to volume with distilled water. Working-strength solutions containing 0.012–20 mg l^{-1} Fe(III) were made from the stock solution by dilution and adding 1:1000 HNO_3 to pH 3–3.5, where retention on the column and solution stability were maximal.

The column eluent, 2 M HNO_3 was of analytical grade and purchased from Merck.

The chelating resin (Chelex 100, 50–100 mesh) was obtained from Sigma.

Finally, 0.2 M acetic–acid acetate buffers of pH 3, 4, 5 and 6 and 0.2 M formic–acid formate buffers of pH 2, 3, 4 and 5 were prepared using NaOH for pH adjustment.

2.2. Apparatus

Fig. 1 depicts the automated assembly used for the proposed SIA determination. It consisted of

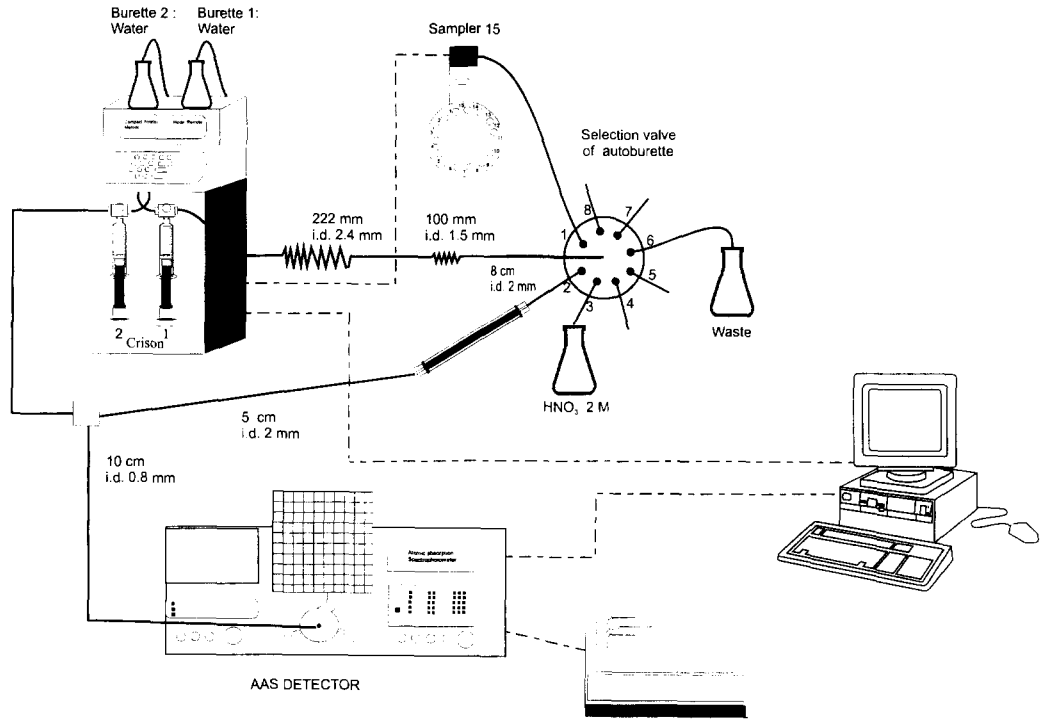

Fig. 1. Instrumental set-up used for the SIA preconcentration and determination of Fe(III).

the following elements: (1) an automated Compact Titrator from Crison (Alella, Barcelona, Spain) that was controlled via a PC and equipped with an autosampler; the titrator includes two 10 ml burettes that can be used simultaneously and an eight-way switching valve; (2) an IBM Personal System 2 computer that was used for instrumental control and data acquisition and processing; (3) a Crison 15 autosampler holding up to 15 samples of 100 ml each; (4) a Perkin-Elmer Model 703 atomic absorption spectrophotometer equipped with a standard air-acetylene burner and an iron hollow-cathode lamp (Table 1); (5) a Perkin-Elmer Plasma 2000 ICP spectrophotometer; and (6) a model 939 atomic absorption spectrometer furnished with a Model 90 graphite furnace and an FS 90 autosampler, all from Unicam.

The software package GFLOW[1], developed by the authors' group, was used to control the instrumentation and acquire and process data. The software allows one to select the desired operating sequence, viz. aspirating or propelling a preset reagent volume by means of either burette, con-

Table 1
Instrumental parameters for AAS measurements

Parameter	Value
Wavelength	248.3 nm
Slit width	0.2 nm
Lamp current	30 mA
Air flow-rate	17.5 l min^{-1}
Acetylene flow-rate	2.8 l min^{-1}
Height of light path above burner	2 cm
Aspiration rate	6.5 ml min^{-1}

[1] The software used can be obtained on request from SCI-WARE Bank of Programs, Associations of Environmental Sciences and Techniques (AEST), Department of Chemistry, Universitat de les Illes Balears, E-07071 Palma de Mallorca, Spain.

trolling the pumping rate in order to adjust the flow-rate, switching between the channels, using any of the samples on the autosampler, etc. This endows the process with high flexibility in the mixing of reagents or samples and controlling their flow through different components.

2.3. Preparation of the microcolumn

The column consisted of a 55 mm × 2.5 mm i.d. × 10 mm o.d. methacrylate cylinder on the ends of which two small circles of filter-paper were attached.

After one of the microcolumn ends had been stoppered, the resin was loaded with the aid of a syringe, up to 45 mm of the column length. Because Chelex 100 contracts and expands with changes in pH, the resin should be in contracted form (viz. in an acidic medium such as 2 M HNO_3) prior to filling. Also it should be kept in de-ionized water when not in use.

The same column was used in all the experimental work without any significant alteration.

2.4. Procedure

As can be seen in Fig. 1, burette 1 was connected via an in-out valve to a bottle containing distilled water or to the eight-way switching valve by which reagents or samples were aspirated or propelled. The burette was connected to the switching valve via two Teflon coils. The coil lying closer to the burette, with a volume of about 10 ml, prevented samples and reagents from reaching the burette. That lying closer to the switching valve, with a 5 ml volume, was used to intercalate the different reagents or samples for delivery to the manifold.

Burette 2 also was loaded with distilled water that was then propelled to a T-piece where it merged with channel 2 from the switching valve, which was used to elute the sample retained on the Chelex 100 column. The simultaneous use of the two burettes allowed one to be employed to aspirate the different solutions (sample, eluent) and the other to propel water to the nebulizer, thereby achieving a virtually continuous solution supply, as required by an air-acetylene atomic absorption spectrophotometer. This would have been impossible with a single burette.

The flow-rate of the stream fed to the nebulizer was set at 6.5 ml min^{-1}, which was appropriate for a flame atomic absorption application, taking into account that the sample was aspirated into the flame via a conventional pneumatic nebulizer.

Channel 1 of the switching valve was used to aspirate samples and channel 3 to aspirate nitric acid, which was propelled to channel 2 in order to elute the retained Fe. Channel 6 led to waste and channels 4, 5, 7 and 8 were not used.

Before the process was started, the two burettes and channels were loaded with the required reagents. For this purpose, an appropriate volume of each reagent was aspirated and then propelled to waste.

The operating conditions employed are summarized in Table 2. Briefly, a clean-up step (a–c) was used where the sample was aspirated and sent to waste in order to fill the length of tubing between the sampler and channel 1 with sample. In step c, burette 2 was filled with 2 ml of water, which left a free capacity of 10 ml for the operations involved in the subsequent steps. Because burette 1 was simultaneously used to sweep the sample to waste, no solution reached the nebulizer during this step. However, the effect on the flame was minimal since the step duration was considerably decreased by the high pumping rates used. These steps (a–c) were only implemented with each sample changeover.

Then, 9 ml of sample were aspirated through channel 1 (step d) and a volume of 9.8 ml was propelled to channel 2 (i.e. to the preconcentration column, step e). This was followed by a burette equilibration step (f). Nitric acid (2 M) was aspirated through channel 3 (step g) and on to the detector in order to elute the sample retained on the column (step h). Note that burette 2 was always on and that while burette 1 aspirated the solution, burette 2 propelled water to the detector in order to feed the nebulizer with a continuous flow.

At the end of step h, the two burettes were in the same position as at the start of step d. From there, the operating sequence was continued in order to perform new injections of the same sam-

Table 2
Procedure using the preconcentration column

Step	Burette 1				Burette 2		
	Channel	q (ml min^{-1})	Action[a]	V (ml)	q (ml min^{-1})	Action[a]	V (ml)
a	2	6.5	P. Ch. 2	3			
b	1	6.5	A. Ch.1	2	6.5	P.T.	2
c	6	50	P. Ch. 6	8	50	A.E.B.	2
d	1	6.5	A. Ch. 1	9	6.5	P.T.	9
e	2	6.5	P. Ch. 2	9.8	6.5	A.E.B.	9
f	3	6.5	A.E.B.	5.8	6.5	P.T.	6
g	3	6.5	A. Ch. 3	1	6.5	P.T.	1
h	2	6.5	P. Ch. 2	6	6.5	A.E.B.	7

[a] P. Ch. = propulsion towards the stated channel; P.T. = propulsion towards the T-piece; A. Ch. = aspiration from the stated channel; A.E.B. = aspiration from the external bottle.

ple. At each sample changeover, the programme was restarted from step a.

In order to compare the sample concentration efficiency of the Chelex 100 column, the column was removed and experiments were repeated. For this purpose, the method summarized in Table 3 was used. Essentially, it involved cleaning and filling of the sample channel (steps a–c), followed by switching of the valve to position 1 and aspiration of 1 ml of sample (step d), and back to position 2 to propel 3 ml of sample to the detector (step e). Finally, the burette was equilibrated (step f) in order to restart the cycle (injection of the sample) from step d. Each new sample was processed from step a.

It should be noted that, because the solutions containing Fe(III) were only transported to the detector, thus undergoing little dispersion, their injection resulted in very slow baseline restoration unless the propelling flow-rate was markedly increased. This was the solution adopted for the system including no column. Also, because this experiment was carried out for comparison with the method using the pre-column, the manifold was simplified by suppressing the water stream from the second burette.

Table 3
Procedure using no preconcentration column

Step	Burette 1			
	Channel	q (ml min)$^{-1}$	Action[a]	V (ml)
a	2	6.5	P. Ch. 2	3
b	1	6.5	A. Ch. 1	2
c	6	50	P. Ch. 6	4
d	1	6.5	A. Ch. 1	1
e	2	50	P. Ch. 2	3
f	2	6.5	A. E. B.	2

[a] See Table 2.

2.5. Sample conditioning

When natural waters were sampled, 10 ml of concentrated hydrochloric acid (Merck, Suprapur) per litre of sample solution were immediately added. The samples were filtered if necessary. For the digestion, 25 ml of nitric acid (Merck, Suprapur) were added to 250 ml of sample and boiled until the volume was ca. 50 ml. Finally an appropriate volume of NH_3 (Merck, Suprapur) was added to obtain pH 3–3.5. The final volume was adjusted to 100 ml with distilled water.

3. Results and discussion

3.1. Optimization of experimental variables

3.1.1. Influence of flow-rate

Variable flow-rates of sample through the column were tried in order to investigate their effect on Fe(III) retention. No change was observed below a flow-rate of 6.5 ml min^{-1}. Experi-

ments were carried out by using 9 ml of a 0.2 mg l^{-1} standard solution at 6.5, 3.0, 2.0, 1.8 and 1.4 ml min^{-1}. The highest flow-rate tried 6.5 ml min^{-1}, was adopted for subsequent experiments.

3.1.2. Influence of the inner diameter of the preconcentration column

Experiments were conducted with 9 ml of a 0.2 ppm standard and columns of 1.5, 2, 2.5, 3 and 3.5 mm i.d. The peak absorbances varied very little with the column inner diameter. In any case, the 2.5 mm i.d. column provided better reproducibility (the RSD was 5.8, 6.0, 2.8, 5.3 and 3.2% for the 1.5, 2, 2.5, 3 and 3.5 mm i.d. columns respectively), which it is probably due to poorer resin packing in the columns of smaller inner diameter.

3.1.3. Influence of nitric acid concentration

Most reported applications of Chelex 100 use 2 M HNO_3 as the eluent for metal preconcentration and in all our preliminary experiments were conducted with this eluent. This section deals with the effect of changing the nitric acid concentration of Fe(III) elution and hence on the absorbance signal. For this purpose, we used 1 ml of 0.5, 1.0, 1.5, 2.0, 3.0 and 4.0 M HNO_3 and 9 ml of 0.4 mg l^{-1} Fe(III) standard, each experiment being repeated five times.

The absorbance increased with increasing HNO_3 concentration up to 2 M, above which it remained constant. We therefore adopted a 2 M HNO_3 concentration as it ensured adequate analytical signals and complete elution of Fe(III).

3.1.4. Influence of pH

The amount of metal absorbed by the Chelex 100 resin is a function of pH. As a rule, absorption below pH 2 is very low but increases sharply between pH 2 and 4, and usually peaks at pH 4. The recommended pH for Fe(III) retention varies among samples; thus sea water is adjusted to pH < 8 [24], pH 5–5.5 [25] or even pH 1.6 [26], depending on the accompanying metals in the sample.

We performed tests at various pH values using Fe(III) standards in order to check whether iron retention by the resin changed with pH. The standards were supplied with a known, constant amount of buffer. The pH values were adjusted with either a formic acid–formate buffer of pH 2, 3, 4 or 5, or an acid–acetic acetate buffer of pH 3, 4, 5 or 6. Tests were conducted with 9 ml of a 0.2 mg l^{-1} standard. The results showed that higher signals were obtained at pH 3–3.5 and dropped at pH 6. Therefore, pH 3.5 was chosen for both standards and samples. Finally, the use of a few ml of 1:1000 HNO_3 was found to result in no appreciable alteration of the signal, so this solution was subsequently employed for pH adjustment as it was easier to prepare and ensured greater stability of standards and samples.

3.1.5. Regeneration of the column

Quigley and Vernon [27] recommended periodic recycling of Chelex 100 resin to its NH_4^+ form. Kingston et al. [25] flushed the resin previously in order to convert it into the NH_4^+ form and then with water to remove excess ammonia. Olsen et al. [7] used a similar procedure, except that they employed ammonium acetate as carrier in an FIA system.

We studied the effect of using the column in the NH_4^+ rather that the H^+ ion form on Fe(III) retention. For this purpose, 2 ml of 0.05 M ammonium acetate was passed at the end of the cycle, followed by 2 ml of water, in order to remove completely excess ammonium ions, otherwise iron(III) hydroxide would have precipitated and the absorbance signal would have been diminished as a result. The results obtained showed that the signal was not altered by this regeneration operation; in fact, the signal obtained at a given Fe(III) concentration was the same whether the resin was used in the H^+ or the NH_4^+ form.

3.2. Calibration graph and reproducibility

The linear range and reproducibility for the proposed method were determined under the above described optimal conditions. To this end, Fe(III) solutions with concentrations in the range 0.01–1.2 mg l^{-1} were used in triplicate injections of 9 ml each. The calibration graph was linear between 0.05 and 1.2 mg l^{-1} Fe(III), and conformed to the equation absorbance = 0.319 [Fe(III) (mg l^{-1})] + 0.007, with $r = 0.999$. The

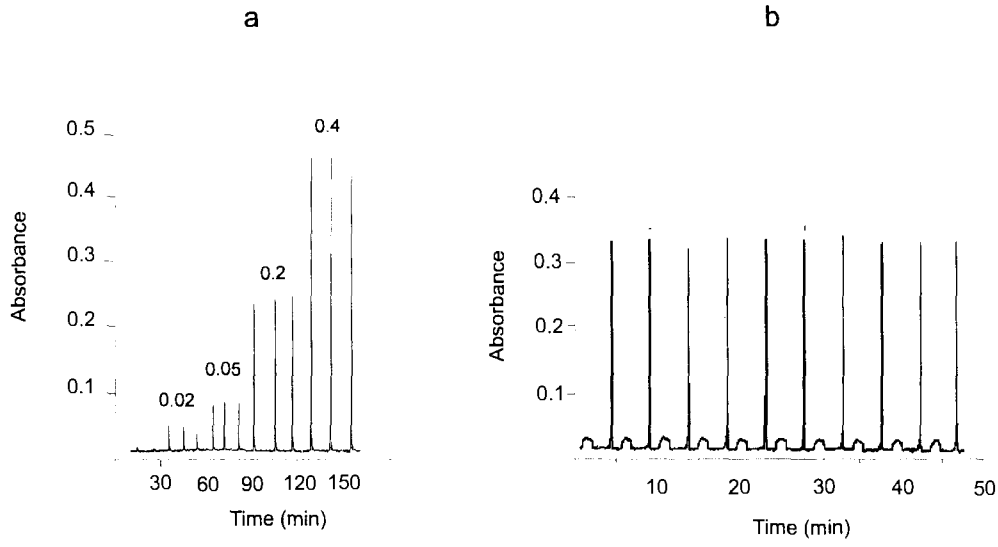

Fig. 2. (a) Calibration performed with 27 ml of standards containing 0.02, 0.05, 0.2 and 0.4 mg l^{-1} Fe(III), following preconcentration on Chelex 100. $[HNO_3] = 2$ M. (b) Study of the reproducibility of the preconcentration column by use of 9 ml of a 1 mg l^{-1} standard. $[HNO_3] = 2$ M.

detection limit, 0.012 mg l^{-1}, was calculated as $3\sigma_b/S$, where σ_b is the standard deviation for 10 measurements of the blank and S is the sensitivity of the method, calculated as the slope of the calibration graph. The RSD obtained for 10 cycles using 9 ml injections of a 1 mg l^{-1} concentration was 4% (Fig. 2(b)). In this figure, the small secondary peaks are due to the unretained Fe(III).

Since increasing the sample volume passed through the column could theoretically improve the detection limit, we used a volume of 27 ml (3×9 ml owing to the volume constraint of the burette, 10 ml). A new calibration graph was constructed using standards of 0.02–0.4 mg l^{-1} (Fig. 2(a)), the linear portion of which conformed to the equation absorbance = 1.153 [Fe(III (mg l^{-1})) + 0.013 with $r = 0.999$. The detection limit was 0.006 mg l^{-1} and the reproducibility 4.8% (RSD).

In order to compare the proposed system with another excluding the Chelex 100 column (i.e. with no preconcentration) a new calibration graph was constructed from 1 ml injections of Fe(III) concentrations of 1, 5, 10, 15 and 20 mg l^{-1}. The calibration curve conformed to the equation absorbance = 0.0112 [Fe(III) (mg l^{-1}) + 0.022, with $r = 0.980$ (Fig. 3(a)). The reproducibility, calculated from 10 cycles replicates using 1 ml of a 10 mg l^{-1} standard, was 2% (RSD) (Fig. 3(b)). The detection limit was calculated as in the previous experiments and was 0.08 mg l^{-1}.

A comparison of the different calibration curves reveals that the methods which concentrate 9 and 27 ml of sample give a slope 28 and 103 times higher than that with no preconcentration, respectively. Such high slopes testify to the efficiency of the concentration procedure.

3.3. Efficiency of the column

The efficiency of the microcolumn was estimated by first calculating the theoretical amount of Fe (in μg) that it should be able to retain based on its dimensions (4.5 × 2.5 mm i.d.) and retention capacity (0.4 mequiv M^{2+} ml^{-1} resin). Therefore, the theoretical amount of Fe that the resin should retain was 21 000 μg, so there should be no saturation problems.

We then calculated the retention efficiency of the column packed with Chelex 100 (5.5 cm × 2.5 mm i.d.) from the following equation:

$$E\ (\%) = \frac{C_s - C_w}{C_s} \times 100$$

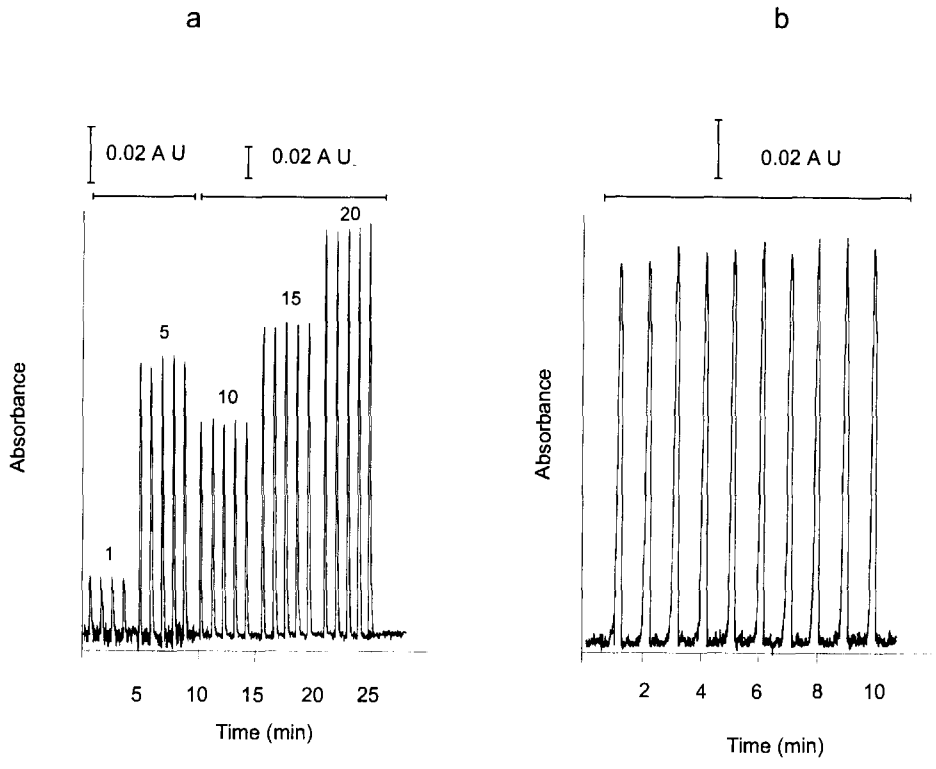

Fig. 3. (a) Calibration performed with 1 ml of standards containing 1, 5, 10, 15 and 20 mg l^{-1} Fe(III), with no preconcentration. (b) Study of the reproducibility by use of 1 ml of a 10 mg l^{-1} Fe(III) standard, with no preconcentration.

where C_s is the analyte concentration in the sample prior to passage through the column and C_w the concentration of unretained analyte. Both were referred to the same volume.

In order to calculate the efficiency, several preconcentration cycles were performed as described above. A 9 ml volume of iron solution containing 0.4 or 1 mg l^{-1} of iron was passed through the resin. The eluted fraction (9.8 ml) was acidified with HNO_3 and made up to 10 ml. Then 2 M HNO_3 was passed through the column to collect a new fraction (5 ml) that was made up to 10 ml with distilled water. The iron concentrations in the two fractions, C_w and C_s, were determined by ICP-AES. As can be seen from the results (Table 4), the retention efficiency was $93.1 \pm 0.6\%$ for the 0.4 mg l^{-1} solution and $7.4 \pm 3.0\%$ for the 1.0 mg l^{-1} solution, i.e. the resin was more effective with low iron concentrations, which was an advantage in view of the intended application.

We calculated the column efficiency for the method in concentrating 27 ml of sample, using the same procedure as above. The results obtained are given in Table 4. The sample was a standard solution containing 0.2 mg l^{-1} of iron; a volume of 27 ml was passed through the column, so an amount of 5.4 μg was loaded, which led to a theoretical concentration of 0.54 mg l^{-1} after elution with 2 M HNO_3 and dilution to a final volume of 10 ml. The retention efficiency thus obtained was $78.4 \pm 2.9\%$.

We also calculated the retention efficiency for Fe(II) ion, concentrating 27 ml of standard solution of 0.2 mg Fe(II) l^{-1}. The column efficiency turned out to be $71.7 \pm 3.7\%$, similar to that for Fe(III).

3.4. Application to real samples

The proposed method was applied to the determination of iron in various water samples using

Table 4
Study of the retention efficiency of the column

Sample	Sample No.	Concentration (mg l^{-1})		Mean	Efficiency (%)
		Theoretical (C_s)	Found (C_s-C_w)		
9 ml of 0.4 mg l^{-1} Fe(III)	1	0.360	0.337		93.6
	2	0.360	0.335		93.1
	3	0.360	0.333		92.5
				0.335 ± 0.002	93.1 ± 0.6
	4	0.900	0.659		73.2
	5	0.900	0.716		79.6
	6	0.900	0.695		77.2
	7	0.900	0.716		79.6
				0.697 ± 0.027	77.4 ± 3.0
27 ml of 0.2 mg l^{-1} Fe(III)	1	0.540	0.412		76.3
	2	0.540	0.430		79.6
	3	0.540	0.442		81.9
	4	0.540	0.408		75.6
				0.423 ± 0.016	78.4 ± 2.9
27 ml of 0.2 mg l^{-1} Fe(II)	1	0.540	0.389		72.0
	2	0.540	0.360		66.7
	3	0.540	0.392		72.6
	4	0.540	0.408		75.6
				0.387 ± 0.020	71.7 ± 3.7

SIA with atomic absorption spectrophotometry after concentration of 27 ml of the sample using the Chelex 100 resin. The sample was treated with nitric acid as described above to convert all types of Fe into soluble Fe(III).

Three public supply waters of different origins and one water from a well were studied. The results thus obtained were compared with those provided by electrothermal atomic absorption spectrometry (ETAAS). Table 5 indicates that the results obtained by SIA were satisfactory.

Table 5
Determination of Fe(III) in real samples

Sample No.	Concentration (mg l^{-1})	
	ETAAS	Proposed method
1[a]	0.018	0.020
2[a]	0.056	0.066
3[a]	0.032	0.025
4[b]	0.114	0.105

[a] Public supply water.
[b] Well water.

4. Conclusions

This paper has demonstrated that SIA is useful for the preconcentration of metal ions by use of Chelex 100 resin. The proposed iron determination features good reproducibility and sensitivity. The ensuring method is suitable for the fully automatic determination of Fe(III) in drinking water.

Among other advantages, the same assembly can be used for other determinations with minimal reagent consumption. Also, the SIA assembly is highly robust; its components undergo very little wear, so they can be used for months without replacement.

Finally, Table 6 summarizes the analytical figures of merit for the three methods tested (without a column, with a column and 9 ml of sample and with a column and 27 ml of sample). As can be seen, the detection limit obtained with the resin and 27 ml of sample was roughly 15 times lower and the slope (sensitivity) was 100 times higher than when no preconcentration was applied. On the other hand, the reproducibility was lower,

Table 6
Analytical parameters of methods with and without preconcentration using a Chelex 100 column

Parameter	Without concentration	Concentration of 9 ml sample	Concentration of 27 ml sample
Detection limit (mg l^{-1})	0.088	0.012	0.006
Reproductibility (RSD) (%)	2.0	4.0	4.8
Sensitivity, slope of calibration graph (AU l mg^{-1})	0.011	0.319	1.153
Linear range (mg l^{-1})	1–20	0.05–1.2	0.02–0.4

[a] AU = absorbance units.

probably owing to the increased number of steps or operations involved.

Acknowledgements

The authors are grateful to CICyT (Spanish Council for Research in Science and Technology) for financial support of this work as part of the Projects AMB94-1033 and AMB94-0534.

References

[1] J. Růžička and G.D. Marshall, Anal. Chim. Acta, 237 (1990) 329.
[2] J. Růžička and T. Gübeli, Anal. Chem. 63 (1991) 1680.
[3] T. Gübeli, G.D. Christian and J. Růžička, Anal. Chem. 63 (1991) 2407.
[4] J. Růžička, Anal. Chim. Acta, 261 (1992) 3.
[5] A. Ivaska and J. Růžička, Analyst, 118 (1993) 885.
[6] M. Guzmán, C. Pollema, J. Růžička and G.D. Christian, Talanta, 40 (1993) 81.
[7] S. Olsen, L.C.R. Pessenda, J. Růžička and E.H. Hansen, Analyst, 108 (1983) 905.
[8] S. Hirata, K. Honda and T. Kumamaru, Anal. Chim. Acta, 221 (1989) 65.
[9] P. Di and D.E. Davey, Talanta, 42 (1995) 1081.
[10] P. Di and D.E. Davey, Talanta, 41 (1994) 565.
[11] J. Růžička and A. Arndal, Anal. Chim. Acta, 216 (1989) 243.
[12] F. Malamas, M. Begtsson and G. Johansson, Anal. Chim. Acta, 160 (1984) 1.
[13] Z. Fang, J. Růžička and E.H. Hansen, Anal. Chim. Acta, 164 (1984) 23.
[14] Z. Fang, S. Xu and S. Zhang, Anal. Chim. Acta, 164 (1984) 41.
[15] Z. Fang, S. Xu and S. Zhang, Anal. Chim. Acta, 169 (1985) 321.
[16] Z. Fang and B. Welz, J. Anal. At. Spectrom., 4 (1989) 543.
[17] M.J.C. Taylor, D.E. Barnes and G.D. Marshall, Anal. Chim. Acta, 265 (1992) 71.
[18] W. Qi, X. Wu, C. Zhou, H. Wu and Y. Gao, Anal. Chim. Acta, 270 (1992) 205.
[19] H. Koizumi, T. Hadeishi and R. McLaughlin, Anal. Chem. 50 (1978) 387.
[20] F.E. Brinckman, W.R. Blair, K.L. Jewett and W.P. Iverson, J. Chromatogr. Sci., 15 (1977) 493.
[21] K. Backstrom and L.G. Danielsson, Anal. Chem., 60 (1988) 1354.
[22] S. Nakashima, R.E. Sturgeon, S.N. Willie and S.S. Berman, Fresenius'Z. Anal. Chem., 330 (1988) 592.
[23] A. Cantarero, M. Gómez, M.A. Palacios and C. Cámara, Anal. Chim. Acta, 296 (1994) 205.
[24] S. Hartenstein, J. Růžička and G.D. Christian, Anal. Chem., 57 (1985) 21.
[25] H.M. Kingston, I.L. Barnes, T.J. Brady, T.C. Rains and M.A. Champ, Anal. Chem., 50 (1978) 2064.
[26] R.E. Sturgeon, S.S. Berman, J.A.H. Desaulniers, A.P. Mykytiuk, J.W. McLaren and D.S. Russell, Anal. Chem., 52 (1980) 1585.
[27] M.N. Quigley and F. Vernon, Anal. Proc., 28 (1991) 175.

ELSEVIER

Talanta 44 (1997) 563–570

Talanta

Solvent extraction separation of iron(III) and aluminium(III) from other elements with Cyanex 302

H.S. Ajgaonkar, P.M. Dhadke *

Inorganic Chemistry Laboratory, Department of Chemical Technology, University of Bombay, Matunga, Bombay 400 019, India

Received 5 February 1996; received in revised form 29 July 1996; accepted 8 August 1996

Abstract

A rapid method was developed for the solvent extraction separation of iron(III) and aluminium(III) from other elements with Cyanex 302 in chloroform as the diluent. Iron(III) was quantitatively extracted at pH 2.0–2.5 with 5×10^{-3} M Cyanex 302 in chloroform whereas the extraction of aluminium(III) was quantitative in the pH range 3.0–4.0 with 10×10^{-3} M Cyanex 302 in chloroform. Iron(III) was stripped from the organic phase with 1.0 M and aluminium(III) with 2.0 M hydrochloric acid. Both metals were separated from multicomponent mixtures. The method was applied to the separation of iron and aluminium from real samples. © 1997 Elsevier Science B.V.

Keywords: Cyanex 302; Aluminium(III); Iron(III); Solvent extraction

1. Introduction

Organophosphorus acids and their esters and oxides have been widely used for the purification and separation of various metals such as Cu(II), Co(II), Ni(II), Zn(II), Cd(II) and lanthanides [1,2]. The quantitative extraction of iron(III) from 0.5 M nitric acid was possible with 0.1 M mono(2-ethylhexyl)phosphoric acid in hexane [3]. The extraction of iron(III) with di-*n*-butylthiophosphoric acid was incomplete from 0.2 M hydrochloric or sulphuric acid solutions [4]. However, the extraction of aluminium(III) with di-*n*-butyldithiophosphoric acid and di(2-ethylhexyl)dithiophosphoric acid has been reported [5]. Numerous studies have been carried out on the extraction of iron(III) from hydrochloric and sulphuric acid media with di(2-ethylhexyl)phosphoric acid (HDEHP) with kerosene as a diluent [6,7]. Extraction of aluminium from a weakly acidic medium with concentrated solution of HDEHP in kerosene was carried out [8]. The extraction of aluminium(III) was possible from sulphuric acid solution using HDEHP [9]. The mechanism of extraction of Ti(IV) and Al(III) by HDEHP in kerosene was also investigated [10]. The same group also studies the extraction of Al(III) from formic acid solution with the same reagent [11]. The extraction of Fe(III) from KSCN with tri-*n*-butylphosphate (TBP) and Al(III) from HCl with TBP (100%) has been reported [12,13]. The extraction of iron(III) and aluminium(III) involving tri-*n*-butylphosphine

* Corresponding author.

PII S0039-9140(96)02063-2

sulphide was not quantitative from HCl solutions [14].

Organothiophosphinic acids were recently introduced as extractants [15]. The most important among them is bis(2,4,4-trimethylpentyl)monothiophosphinic acid (Cyanex 302). It was first used for the extraction of zinc from sulphate solution containing calcium [16]. Several applications of this reagent to the extraction of various metals such as Cu(II), Cd(II), Ag(I), Ni(II), Zr(IV), Th(IV), Sc(III) and Pd(II) have been reported [17–20]. However, systematic investigations on the solvent extraction of iron(III) and aluminium(III) with Cyanex 302 are lacking. This paper presents an account of such investigations.

2. Experimental

2.1. Apparatus and reagents

A Systronics MK VI combined electrode digital pH meter and a GBC model 911 A UV–visible spectrophotometer with 10 mm Corex quartz cuvettes were used.

Cyanex 302 (Cytec Industries, USA) was used as received. A stock solution of iron(III) was prepared by dissolving 8.634 g of $(NH_4)Fe(SO_4)_2 \cdot 12H_2O$ in 1 l of distilled water containing 5.0 ml of sulphuric acid and a stock solution of aluminium(III) by dissolving 2.920 g of $Al_2(SO_4)_3 \cdot 16H_2O$ in 250 ml of distilled water containing a few drops of sulphuric acid. The solutions were standardized volumetrically (Fe(III)) and gravimetrically (Al(III)) [21] and contained 1496.6 μg ml^{-1} of Fe(III) and 1000 μg ml^{-1} of Al(III). Working standard solutions containing 40 μg ml^{-1} of Fe(III) and 10 μg ml^{-1} of Al(III) were prepared by appropriate dilution of the stock solutions.

2.2. Procedure

Aliquots of solutions containing iron(III) and aluminium(III) were taken and the pH was adjusted to 2.0 for iron(III) and 4.0 for aluminium(III) with dilute sulphuric acid and ammonia solution. The total volume was made up to 10 ml. The solutions were then transferred into separating funnel, 10 ml of Cyanex 302 solution in chloroform of appropriate concentrations were added and the solutions were shaken for about 8 min. The two phases were allowed to settle and separate. The metals were stripped from the organic phase with 1.0 M hydrochloric acid (iron(III)) and 2.0 M hydrochloric acid (aluminium(III)). The metals in the aqueous phase were determined spectrophotometrically at 480 nm as the complex with potassium thiocyanate for iron(III) [21] and at 520 nm with aluminon for aluminium(III) [22]. The concentrations of metals were calculated from the calibration graphs.

3. Results and discussion

3.1. Effect of pH

The effect of pH on the percentage extraction of iron(III) and aluminium(III) by Cyanex 302 in chloroform was studied in the range 0–5.0. As shown in Fig. 1, the extraction of iron(III) was quantitative in the pH range 2.0–2.5 and that of aluminium(III) in the pH range 3.0–4.0. Since most of the time pH was adjusted with acetate

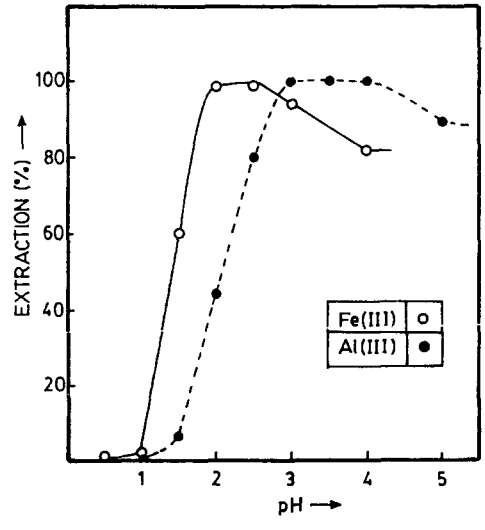

Fig. 1. Effect of pH on the extraction of iron(III) and aluminium(III). Fe(III), 50 μg; Al(III), 15 μg.

Table 1
Effect of Cyanex 302 concentration

Cyanex 302 concentration(10^{-3} M)	Iron(III)		Aluminium(III)	
	D	Extraction (%)	*D*	Extraction (%)
0.1	0.046	4.4	0.138	12.1
0.25	0.097	8.8	—	—
0.5	0.238	19.2	0.239	19.3
0.75	0.42	29.6	0.383	27.7
0.85	—	—	0.478	32.3
1.0	0.516	34.0	0.724	42.0
1.4	0.849	45.9	—	—
1.6	1.045	51.1	—	—
1.8	1.871	65.1	—	—
2.0	—	—	1.124	52.9
2.2	2.749	73.3	—	—
2.5	5.134	83.7	—	—
3.0	—	—	1.558	60.9
4.0	—	—	2.498	71.4
5.0	399	99.7	4.40	81.5
8.0	—	—	25.38	96.2
10.0	399	99.7	999	99.9
30.0	399	99.7	–	–
50.0	399	99.7	999	99.9
100.0	—	—	999	99.9

buffer, neither metal was hydrolysed. No perceptible precipitation of aluminium(III) or iron(III) was observed at pH > 2.5 and pH > 4.0, respectively. This was because ammonium acetate–acetic acid buffer was used, which prevents the hydrolysis of both ions. Hence all subsequent extractions of iron(III) were carried out at pH 2.0 and those of aluminium(III) at pH 4.0. The mechanism of extraction is as follows:

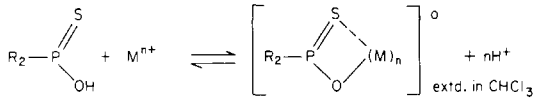

where M = Fe or Al, $n = 3$ and R = 2,4,4-trimethylpentyl.

3.2. Effect of Cyanex 302 concentration

Iron(III) and aluminium(III) were extracted with various concentration of Cyanex 302 ((0.1–100) × 10^{-3} M) (Table 1). The extraction of iron(III) was quantitative with 5×10^{-3} M Cyanex 302 and that of aluminium(III) with 10×10^{-3} M Cyanex 302. A decrease in the concentration of Cyanex 302 gave lower *D* values for both iron(III) and aluminium(III).

3.3. Effect of diluents

Various polar and non-polar solvents were tested as diluents for the extraction of iron(III) and aluminium(III) with 5×10^{-3} and 10×10^{-3} M Cyanex 302, respectively. The extraction of iron(III) was quantitative with chloroform, toluene, xylene, carbon tetrachloride and hexane as diluents but benzene and cyclohexane proved to be poor diluents. The extraction of aluminium(III) was quantitative with chloroform, carbon tetrachloride, hexane, cyclohexane and benzene but xylene and toluene proved to be poor diluents. Owing to clear phase separations, chloroform was preferred as the diluent for both metal ions (Table 2).

Table 2
Effect of various diluents

Diluent	Dielectric constant	Iron(III)		Aluminium(III)	
		D	Extraction (%)	*D*	Extraction (%)
Chloroform	4.80	399	99.7	999	99.9
Carbon tetrachloride	2.00	399	99.7	999	99.9
Hexane	1.90	39	97.5	999	99.9
Cyclohexane	2.02	9.0	90.0	999	99.9
Benzene	2.20	19.0	95.0	999	99.9
Xylene	2.28	65.6	98.5	9.16	90.1
Toluene	2.23	399	99.7	8.46	89.4

3.4. Effect of stripping agents

The organic phases were extracted with various mineral acids of different concentrations to strip both metals into the aqueous phase (Table 3). All mineral acids were effective for the quantitative stripping of iron(III) and aluminium(III). For practical purposes we preferred 1.0 M hydrochloric acid for iron(III) and 2.0 M hydrochloric acid for aluminium(III) because they facilitate the direct spectrophotometric determination of both metal ions.

3.5. Effect of metal ion concentration

Iron(III) and aluminium(III) were extracted with concentrations ranging from 5–60 μg ml^{-1} for Fe(III) and from 0.5–3.5 μg ml^{-1} for Al(III). The system adhered to beer's law in the ranges 5–50 μg ml^{-1} for Fe(III) and 0.5–3.0 μg ml^{-1} for Al(III). Higher concentrations of the metals can be extracted with high concentrations of the reagent.

3.6. Effect of period of equilibration

The solutions were shaken for periods ranging from 2–20 min. the extraction of iron(III) was quantitative with an 8 min period of equilibration and that of aluminium(III) with 6 min. Therefore, equilibrium periods of 8 min for iron(III) and 6 min for aluminium(III) were adopted.

3.7. Nature of the extracted species

The composition of the extracted species was ascertained for both metals by plotting log *D* against log Cyanex 302 concentration at a fixed pH. For iron(III) the slope was 3.0 (Fig. 2) and for aluminium(III) the slope was 1.1 (Fig. 3). This shows that the probable compositions of the extracted species are [Fe(Cyanex 302)$_3$ SO_4] and [Al(Cyanex 302)HSO_4^-].

3.8. Separation of iron(III) and aluminium(III) from diverse ions

The effect diverse ions on extraction of iron(III) and aluminium(III) was studied. The tolerance limit was set as an error of ±2% in absorbance measurements. In the extraction of iron(III) the alkali and alkaline earth metals showed no interference up to 50 μg ml^{-1}. Metals such as Ni(II), Cr(III), Tl(III), Pb(II), Cd(II), As(III) and Zn(II) did not interfere in the range 5–100 μg ml^{-1}, but ions such as V(V), Ru(III), Os(VIII), Al(III), Mo(VI) and Hg(I) interfered to a large extent. Noble metals such as Pt(IV) and Au(III) showed no interference up to 25 μg ml^{-1}. The interference of Cu(II) was removed by extracting Cu(II) with 8×10^{-2} M Cyanex 302 at pH 1.0 prior to the extraction of iron(III). Iron(III) was also separated from Co(II) and Mn(II) by first extracting iron(III) followed by the extraction of both metals.

During the extraction of aluminium(III), alkali and alkaline earth metals were tolerated up to 75

Table 3
Effect of various stripping agents

Stripping agent	Recovery (%)									
	0.5 M acid		1.0 M acid		1.5 M acid		2.0 M acid		3.0 M acid	
	Fe(III)	Al(III)	Fe(III)	Al(III)	Fe(III)	Al(III)	Fe(III)	Al(III)	Fe(III)	Al(III)
HCL	91.8	58.1	99.7	74.1	99.7	86.0	99.7	99.9	99.7	99.9
H_2SO_4	77.7	99.9	85.0	99.8	—	99.8	98.4	99.9	—	99.7
HNO_3	87.0	89.9	99.7	99.9	—	100	99.8	99.8	99.5	99.9
$HClO_4$	99.8	99.7	99.8	100	—	100	99.8	99.8	—	—

μg ml^{-1}. Transition metals such as Co(II) and Ni(II) did not interfere up to 37.5 μg ml^{-1} and Mn(II) and Cr(III) showed no interference up to 35 μg ml^{-1}. Metals such as Zn(II), V(V), Ru(III), Os(VIII), Fe(III), Be(II), Pd(II) and Mo(VI) showed strong interference even at low concentrations. The interference of Cu(II) was removed by extracting Cu(II) prior to the extraction of aluminium(III). In both cases the cations used were invariably in the form of chloride or nitrate, which are water soluble.

Anions such as chloride, bromide, iodide, sulphate, sulphite, nitrate, nitrite, thiocyanate, phosphate and thiourea were tolerated up to 20 and 30 μg ml^{-1} for iron(III) and aluminium(III), respectively. At such low concentrations iron(III) and aluminium(III) were not precipitated as iodide or phosphate, respectively. Oxalate and EDTA interfere strongly in both metal extractions. In the case of anions generally the sodium salts were used whereas in the case of oxy anions such as molybdate the corresponding ammonium salts were used.

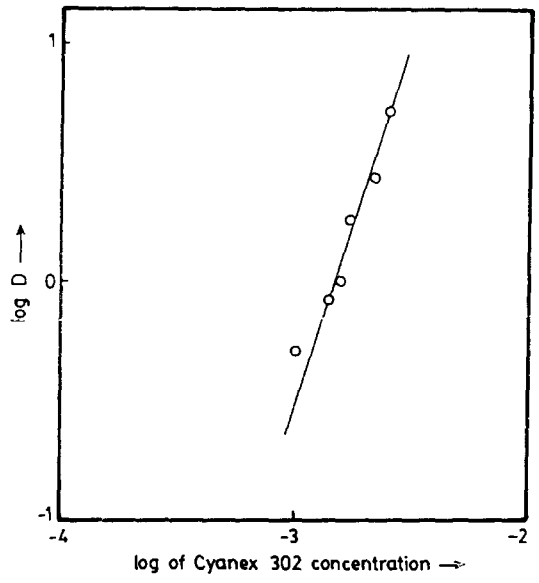

Fig. 2. Log–log plot for iron(III) for the determination of the composition of the complex.

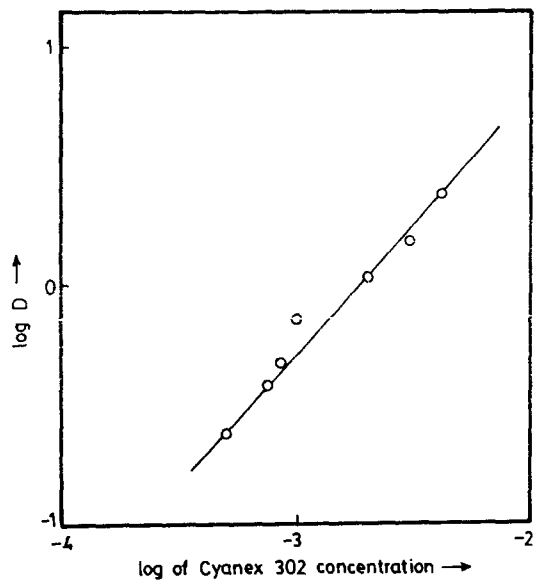

Fig. 3. Log–log plot for aluminium(III) for the determination of the composition of the complex.

Table 4
Separation of iron(III) from multicomponent mixtures

Sample no.	Mixture	Amount taken (μg ml^{-1})	pH	Cyanex 302 extractant concentration (M)	Diluent	Recovery (%)
1	Cu(II)	5	1.0	0.08	Xylene	99.1
	Fe(III)	5	2.0	0.005	Chloroform	98.5
	Co(II)[a]	2.5	7.5	0.0075	Toluene	98.6
2	Cr(VI)	2	1.0	0.05	Toluene	99.8
	Fe(III)	10	2.0	0.005	Chloroform	98.9
	Mn(II)[a]	10	9.0	0.005	Toluene	98.7
3	Fe(III)	5	2.0	0.05	Chloroform	99.2
	Co(II)[a]	2	7.5	0.0075	Toluene	98.5
	Mg(II)	2.5	7.5	Unextracted	–	99.9
4	Cu(II)	10	1.0	0.08	Xylene	98.9
	Fe(III)	5	2.0	0.005	Chloroform	99.5
	Mn(II)[a]	15	9.0	0.005	Toluene	99.0
5	Cu(II)	15	1.0	0.08	Xylene	99.1
	Fe(III)	10	2.0	0.005	Chloroform	99.8
	Ni(II)	10	2.0	Unextracted	–	99.9

[a] Extraction was carried out in the presence of ammonium sulphate as a salting-out agent.

3.9. Separation of iron(III) and aluminium(III) from multicomponent mixtures

Various metals showed different extents of extraction at different pH values and concentrations of Cyanex 302. Such differences were fully exploited to devise a different separation by resorting to a technique selective for extraction at different pH values with varying concentration of Cyanex 302. Copper and chromium were separated from iron(III) and aluminium(III) by first extracting these elements, followed by the extraction of iron(III) and aluminium(III), whereas cobalt(II) and manganese(II) were separated by first extracting iron(III) and aluminium(III) followed by the extraction of other elements. Magnesium and nickel were not extracted under these conditions. The details of separation are presented in Tables 4 and 5.

3.10. Application to analysis of real samples

The utility of the proposed approach was tested by analysing ores, alloys (ilmenite, monel metal, steel) and pharmaceutical samples such as Impheron injection and Fecontin F tablets for iron(III) and Digene and Siloxogene tablets for aluminium(III) (Table 6). A known weight of sample of ore or alloy was treated with acids and evaporated to dryness. The samples were again disintegrated with perchloric acid and evaporated to dryness, then the residue was dissolved in water and diluted to a known volume. The reaction with acids was invariably carried out in hood to prevent spillage and explosion. Heating was carried out slowly on a sand-bath with appropriate precautions.

Iron(III) was extracted from the diluted sample solution using the proposed method. In the case of monel metal, Cu(II) was removed by first extracting the sample with Cyanex 302 followed by extraction of iron(III), whereas with EN 36A (steel) and ilmenite ore iron(III) was extracted using the proposed method. Metals such as titanium, nickel and manganese were not extracted under these conditions.

Aluminium(III) was extracted from the pharmaceutical samples such as Digene and Siloxogene tablets using the proposed method. The experimental results 99.2 mg for Digene tablets and 99.4 mg for Siloxogene tablets showed good agreement with the certified values of 100 mg for both samples.

Table 5
Separation of aluminium(III) from multicomponent mixtures

Sample no.	Mixture	Amount taken (μg ml^{-1})	pH	Cyanex 302 extractant concentration (M)	Diluent	Recovery (%)
1	Cu(II)	5	1.0	0.08	Xylene	99.1
	Al(III)	1.5	4.0	0.01	Chloroform	99.8
	Co(II)[a]	2.5	7.5	0.0075	Toluene	98.9
2	Cu(II)	5	1.0	0.08	Xylene	98.7
	Al(III)	2.5	4.0	0.01	Chloroform	99.9
	Mn(II)[a]	10	9.0	0.0075	Toluene	99.0
3	Cr(VI)	1	1.0	0.05	Toluene	99.0
	Al(III)[a]	2	4.0	0.01	Chloroform	99.4
	Ni(II)	5	4.0	Unextracted	–	99.9
4	Cr(VI)	2	1.0	0.05	Toluene	98.8
	Al(III)	2	4.0	0.01	Chloroform	99.7
	Co(II)[a]	2	7.5	0.0075	Toluene	98.9
5	Al(III)	2.5	4.0	0.01	Chloroform	99.7
	Co(II)	2.5	7.5	0.0075	Toluene	99.1
	Mg(II)	2.5	7.5	Unextracted	–	99.9

[a] Extraction was carried out in the presence of ammonium sulphate as a salting-out agent.

4. Conclusion

The proposed separation methods are simple, rapid and selective and compare favourably with existing methods. The extraction of Fe(III) and Al(III) was possible with very low concentrations of the reagent compared with other methods. Large amounts of diverse ions were tolerated and the various elements were separated at microgram concentrations. The overall time required for extraction and determination is less than 20 min and the concentration of stripping agent required is very low.

Acknowledgements

The authors thank Professor S.M. Khopkar, Professor Emeritus, IIT Bombay, and Emeritus scientist, CSIR, Department of Chemical Technology, University of Bombay, for his untiring and helpful guidance in persuing this research work and Cytec Industries for the gift of Cyanex 302.

Table 6
Application to analysis of real samples

Sample	Iron(III)		Recovery (%)
	Present	Found	
Ilmenite ore	36.8%	36.5%	99.1
Monel metal	2.0%	1.97%	98.5
EN 36A (steel)	94.85%	94.00%	99.1
Impheron injection (Rallis)	50 μg ml^{-1}	49.8 μg ml^{-1}	99.6
Fecontin F tablets	2 mg ml^{-1}	1.98 mg ml^{-1}	99.0

References

[1] M.N. Gandhi, N.V. Deorkar and S.M. Khopkar, Talanta, 40 (1993) 1535.
[2] K. Kando, K. Momoto and P. Nakashio, Solvent Extr. Ion Exch., 7 (1989) 1027.
[3] S.K. Yadav, O.V. Singh and S.K. Tandon, Ind. J. Chem., 30A (1991) 982.
[4] T.H. Handley, Anal. Chem., 35 (1963). 991.
[5] I. Toth, E. Brucher and Z. Szabo, Talanta, 37 (1990) 1175.
[6] S.Q. Yu and J.-Y. Chen, Hydrometallurgy, 22 (1989) 267.
[7] T. Sato and T. Nakamura, Hydrometallurgy, 15 (1985) 209.
[8] R.W. Cattrawl, Aust. J. Chem., 14 (1961) 163.
[9] C.A. Blake, Jr., C.F. Baes, K.B. Brown, C.F. Coleman and J.C. White, in Proceeding of 2nd International Conference on Peaceful Uses of Atomic Energy, UN, Geneva, 1958, Vol. 28, p. 289.
[10] T. Sato and T. Nakamura, Anal. Chim. Acta, 76 (1975) 401.
[11] T. Sato, T. Yashino, T. Nakamura and T. Kudo, J. Inorg. Nucl. Chem., 43 (1981) 1361.
[12] L.M. Melnick, H. Freiser and H.F. Beeghly, Anal. Chem., 25 (1953) 856.
[13] T. Ishimori, K. Watanabe and E. Nakamura, Bull. Chem. Soc. Jpn., 33 (1960) 636.
[14] R.B. Hitchcock, J.A. Dean and T.H. Handley, Anal. Chem., 35 (1963) 254.
[15] Cyanex 302, Technical Brochures, American Cyanamid, NJ, 1990.
[16] W.A. Rickelton and R.J. Boyle, Solvent Extr. Ion Exch., 8 (1990) 783.
[17] K.C. Sole and J.B. Hiskey, Hydrometal., 37 (1995) 129.
[18] C. Wang and Li. Deqian, Solvent Extr. Ion Exch., 13 (1995) 503.
[19] A. Almela and M.P. Elizalde, Hydrometallurgy, 37 (1995) 47.
[20] K.C. Sole T.L. Ferguson and J.B. Hiskey, Solvent Extr., Ion Exch., 12 (1994) 1033.
[21] A.I. Vogel, Text Book of Quantitative Inorganic Analysis, 3rd edn., Longman, London, 1961.
[22] E.B. Sandell, Colorimetric Determination of Traces of Metals, Interscience, NY, 1944, Vol. 3, 153.

ELSEVIER

Talanta 44 (1997) 571–576

Talanta

Simultaneous determination of platinum(II) and palladium(II) by reversed phase high-performance liquid chromatography with spectrophotometric detection after collection on and elution from resin coated with dimethylglyoxal bis(4-phenyl-3-thisomicarbazone)

Suwaru Hoshi [a,*], Koki Higashihara [a], Mamiko Suzuki [a], Yasutoshi Sakurada [a], Kazuharu Sugawara [a], Masayuki Uto [b], Kunihiko Akatsuka [a]

[a] *Department of Applied and Environmental Chemistry, Kitami Institute of Technology, Kitami 090, Japan*
[b] *Department of Functional Materials, Kitami Institute of Technology, Kitami 090, Japan*

Received 20 May 1996; received in revised form 30 July 1996; accepted 8 August 1996

Abstract

Amberlite XAD-7 resin coated with dimethylglyoxal bis(4-phenyl-3-thiosemicarbazone) (DMBS) was prepared and applied to the preconcentration of platinum(II) and palladium(II) from aqueous solution. Platinum(II) and palladium(II) were collected quantitatively on resin coated with the reagent (DMBS-XAD-7) from acidic solution in the presence of iodide ion by a bach method. The metal ions were then easily eluted from DMBS-XAD-7 as their DMBS chelates with a small volume of *N,N*-dimethylformamide. This collection and elution method was applied to the simultaneous determination of platinum(II) and palladium(II) by reversed-phase high-performance liquid chromatography with spectrophotometric detection using an ODS column and acetone–water as the mobile phase. The proposed method was applied to the determination of the metals in commercially available samples. © 1997 Elsevier Science B.V.

Keywords: Dimethylglyoxal bis(4-phenyl-3-thiosemicarbazone)-coated XAD-7 resin; Palladium(II); Platinum(II); Reversed-phase high-performance liquid chromatography

1. Introduction

High-performance liquid chromatographic (HPLC) methods for the separation and determination of metal ions as their chelate compounds have been widely developed in recent years [1–12]. Dithiosemicarbazone compounds have also been applied to the separation of metal chelates by HPLC because of the formation of kinetically inert metal chelates [13–15]. The dithiosemicarbazones, however, have the disadvantage of low solubility in common solvents except *N,N*-

* Corresponding author. Fax: +81 157 247719.

PII S0039-9140(96)02064-4

dimethylformamide and dimethyl sulfoxide. Therefore, it is difficult to use these compounds in preconcentration methods such as solvent extraction.

In trace metals, preconcentration or separation of the analytes from a matrix is frequently a necessity. The use of supports loaded with chelating reagents is particularly convenient because it is easy to prepare such resins. Therefore, preconcentration and separation methods for trace metal ions have been developed by using various supports coated with a large number of cheating reagents [16–23]. We have also prepared Amberlite XAD resins loaded with dithiosemicarbazone compounds and applied them to the collection of metal ions from aqueous solution [24]. In this process, the metal ions collected on the resin were readily eluted as their dithiosemicarbazone chelates with a small volume of *N,N*-dimethylformamide. Based on the results, the determination of trace mercury by reversed-phase HPLC with spectrophotometric detection after collection on and elution from Amberlite XAD-7 coated with dimethylglyozal bis(4-phenyl-3-thiosemicarbazone) (DMBS) has been developed [25].

In this work, we found that the collection of platinum(II) on Amberlite XAD-7 coated with DMBS (DMBS–XAD-7) was accelerated dramatically in the presence of iodide ion. Based on this result, we tried to develop a method for the simultaneous determination of platinum(II) and palladium(II) by reversed phase HPLC with spectrophotometric detection after collection on and elution from DMBS-XAD-7.

2. Experimental

2.1. Reagents and apparatus

Dimethylglyoxal bis(4-phenyl-3-thiosemicarbazone) (DMBS) was synthesized as reported in the literature [26] and the reagent solution was prepared by dissolving it in *N,N*-dimethylformamide (DMF).

Amberlite XAD-7 resin (acrylic ester type, bead size 250–850 μm), purchased from Rohm and Haas, was washed successively with 5 mol dm^{-3} hydrochloric acid, distilled water and methanol and then dried at 40°C for 24 h in a vacuum drying oven.

Standard palladium(II) and platinum(II) solutions (1 mg cm^{-3}) were prepared by dissolving 0.1667 g of palladium(II) chloride (Wako Pure Chemicals, Osaka, Japan) and 0.2128 g of potassium tetrachloroplatinate(II) (Wako Pure Chemicals) in 10 cm^3 of 5 mol dm^{-3} nitric acid diluting to volume in a 100 cm^3 volumetric flask. The palladium(II) solution was standardized by titration with EDTA and the platinum(II) solution by spectrophotometry with tin(II) chloride, and were further diluted as required. Other chemicals used were of analytical or HPLC grade.

All absorbance measurements were made with a Hitachi U-2000 spectrophotometer. A Hitachi–Horiba Model $F\text{-}7_{AD}$ pH meter was used for all pH measurements. HPLC was performed at room temperature with a Hitachi Model L-6200 system, L-4200 UV–visible detector and D-2500 chromato-integrator. The column used was an ERC-ODS 1282 (250 × 6 mm i.d.) (ERC, Japan).

2.2. Preparation of the resin loaded with DMBS

Amberlite XAD-7 resin (25 g) was mixed with 50 cm^3 of 0.01 mol dm^{-3} DMBS in solution DMF and the mixture was stirred at room temperature for 2 h. The resin loaded with DMBS was filtered off, washed with water and dried at room temperature for 48 h at 50°C in a vacuum drying oven.

2.3. Standard procedure

To a solution containing up to 1 μg of palladium(II) and 2 μg of platinum(II) in a 50 cm^3 screw-capped glass bottle, 0.2 cm^3 of 1 mol dm^{-3} potassium iodide solution and 0.2 cm^3 of 1 mol dm^{-3} nitric acid solution were added to make a 0.01 mol dm^{-3} (pH 2), then the volume was made up to 20 cm^3 with water. An amount of DMBS-XAD-7 was added and the mixture was shaken for 30 min. The solution was filtered through a polyethylene column (65 × 9 mm i.d.) fitted with a porous polyethylene disk of 20 μm pore size, and then platinum and palladium were eluted from the

resin as their DMBS chelates with 1 cm^3 of DMF. A 10 mm^3 volume of the solution was injected into the HPLC system.

2.4. Analysis of real samples

To 0.01 g of each sample in a Teflon beaker a mixture of 2.5 cm^3 of hydrochloric acid and 2.5 cm^3 of nitric acid was added and the beaker was heated at 150°C on a hot-plate until the solution evaporated to dryness. This procedure was repeated several times until decomposition occurred. After cooling, the residue was dissolved in 50 cm^3 of 0.5 mol dm^{-3} nitric acid. The platinum and palladium in each sample was determined by the proposed method.

3. Results and discussion

3.1. Complexation and spectrophotometric properties

Chelate formation of platinum(II) and palladium(II) with DMBS was examined in 80:20 (v/v) DMF-water because of the low solubilities of DMBS and its metal chelates in aqueous solution. Platinum(II) and palladium(II) formed 1:1 chelates with DMBS. The absorbtion spectra of Pt(II) and Pd(II)-DMS chelates are shown in Fig. 1. The absorption maxima and molar absorption coefficients (ε, dm^{-3} mol^{-1} cm^{-1}) of their metal chelates were 442 nm for planinum ($\varepsilon = 25\,000$) and 430 nm for palladium ($\varepsilon = 24\,000$). Palladium(II) reacted quantitatively with DMBS at room temperature, but it was necessary to heat for quantitative chelate formation of platinum(II) with DMBS for 20 min at 80°C.

3.2. Collection and elution behavior of platinum(II) and palladium(II) on the reagent-loaded resin

The total amount of DMBS loaded on the reagent-loaded resin was 22.9 μmol g^{-1} and the capacity of copper(II) for the DMBS-loaded resin was 21.0 μmol g^{-1} [24]. These results indicated that DMBS formed a 1:1 chelate with copper(II)

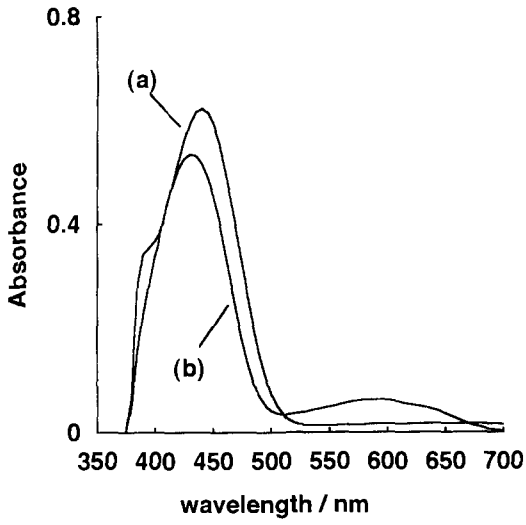

Fig. 1. Absorption spectra of (a) Pt– and (b) Pd–DMBS chelates in 80:20 (v/v)DMF-water. $[Pt^{2+}] = 2.4 \times 10^{-5}$ mol dm^{-3}; $[DMBS] = 2.0 \times 10^{-4}$ mol dm^{-3}; reference, reagent blank.

[26]. Platinum(II) was not collected quantitatively on the reagent-loaded resin within a shaking time of 60 min (Fig. 2, no other ligands) owing to the slow chelate formation with DMBS as described in the previous section. In order to accelerate the

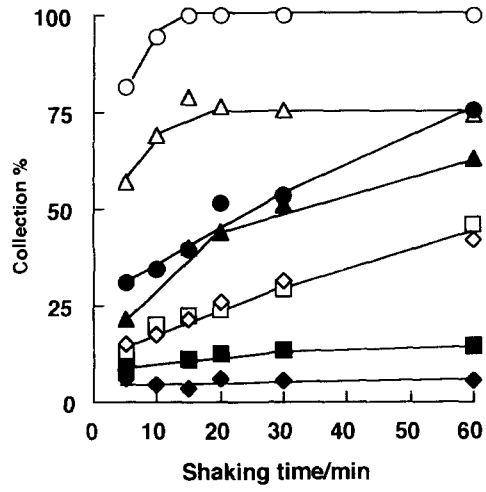

Fig. 2. Effect of shaking time on the collection of planinum(II) in the presence of some ligands. [Pt] = 2 μg/20 cm^{-3}; $[HNO_3] = 0.01$ mol dm^{-3}; [ligand] = 0.01 mol dm^{-3}; DMBS–XAD-7 = 0.1 g. (○) I^-; (△) SCN^-; (▲) Br^-; (□) Cl^-; (■) NO_2^-; (◇) hydroxylammonium chloride; (◆) thiourea; (●) no other ligands.

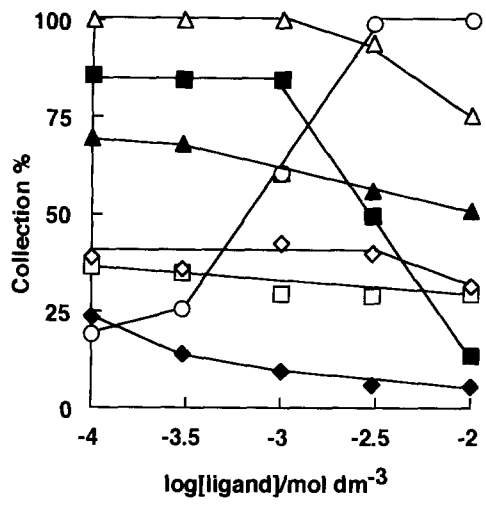

Fig. 3. Effect of ligand concentration on the collected of platinum(II) [Pt] = 2 μg/20 cm^{-3}; [HNO_3] = 0.01 mol dm^{-3}; DMBS–XAD-7 = 0.1 g; shaking time = 30 min. (○) I^-; (△) SCN^-; (▲) Br^-; (□) Cl^-; (■) NO_2^-; (◇) hydroxylammonium chloride; (◆) thiourea.

reaction between the DMBS on the resin and platinum(II) in solution, the effects of the shaking time and of the ligand concentrations on the collection were examined in the presence of various ligands. As shown in Fig. 2, iodide ion accelerates the collection of platinum(II) on the resin decreased with increasing ligand concentration for all ligand systems except iodide ion, as shown in Fig. 3. Quantitative collection takes place at higher concentrations in the presence of iodide ion, at lower concentrations in the presence of thiocyanate ion. In the case of chloride and bromide ions, the predominant species in solution can be estimated to be $Pt(II)L_n^{m-}$ ($L = Cl^-$ or Br^-, $n = 3$ or 4 and $m = -1$ or -2) at 1×10^{-2} mol dm^{-3} of the ligands from their known stability constants [27]. It may be suggested that higher order complexes of platinum(II) form with increasing ligand concentration and the percentage collection on the resin is low for the ligand systems except iodide ion, although the stability constants of platinum(II) with thiocyanate, nitrite, hydroxlammonium chloride and thiourea are unknown. The accelerated process with iodide ion cannot be explained in detail. A further study using other ligands is required to clarify the accelerated process.

The collection of palladium(II) on the resin was not particularly by iodine ion affected in the concentration range above 5×10^{-3} mol dm^{-3}. The concentration of iodide ion for the collection of both metal ions was adjusted to 0.01 mol dm^{-3}. The optimum pH conditions were determined in the presence of iodide ion. Platinum(II) and palladium(II) were found to be optimally collected from aqueous solution in the pH range 0–4 (Fig. 4). Quantitative collection of the metal ions was could not be achieved owing to hydrolysis at higher pH values. In this study, the optimum pH of the solution for collection was adjusted to 2 by adding 5 mol dm^{-3} nitric acid to make a 0.01 × mol dm^{-3} solution. A 100-fold concentration of platinum and palladium simultaneously could be achieved under these conditions.

3.3. Chromatographic conditions

We have investigated on the separation behavior of some platinum(II) and palladium(II) dithiosemicarbazone chelates by reversed-phase HPLC with an ODS column [15]. The elution peaks of the metal dithiosemicarbazone chelates on the chromatogram were not successfully separated by using methanol–water or acetonitrile–water mobile phases. The resolved separation of

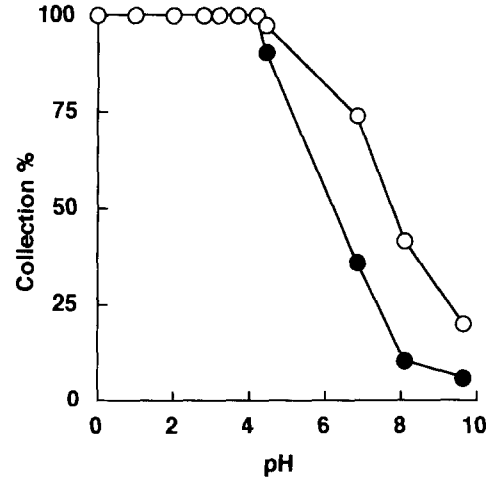

Fig. 4. Effect of pH on the collection. (○) [Pt] = 2 μg/20 cm^{-3}; (●) [Pd] = 1 μg/20 cm^3; [KI] = 0.01 mol dm^{-3}; DMBS–XAD-7 = 0.1 g; shaking time = 30 min.

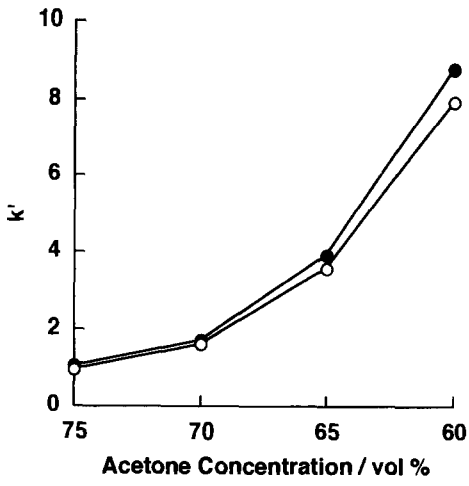

Fig. 5. Relationship between capacity factor (k') of (○) Pt- and (●) Pd–DMBS, and acetone concentration in the mobile phase. Each mobile phase contained 1×10^{-3} mol dm^{-3} CH_3COONa and 1×10^{-4} mol dm^{-3} EDTA.

platinum(II) and palladium(II) chelates was achieved by using acetone–water as the mobile phase. The effect of the acetone content in the mobile phase on the retention behavior of platinum(II) and palladium(II)–DMBS chelates was studied, and the results are shown in Fig. 5. The retention increased as the aqueous component in the mobile phase increased. The optimum composition of the mobile phase was 65:35 (v/v) acetone–water, and sodium acetate was added at 1×10^{-3} mol dm^{-3} because this addition led to reproducibility of the elution peaks and stability of the baseline on the chromatogram. To avoid contamination with metal ions through contact between the eluent and metal parts of the HPLC apparatus, EDTA was also added at 1×10^{-4} mol dm^{-3}. A typical chromatogram is shown in Fig. 6. Their elution peaks were identified with 80:20 (v/v) DMF–water containing DMBS or the DMBS chelates. The most suitable detection wavelength was 425 nm.

3.4. Calibration

Calibration graphs were constructed by the standard procedure. The calibration graphs were linear over the range 0–2 μg for platinum and 0–1 μg for palladium. $C_{Pt}(\mu g) = [H(\mu V) + 27.04]/966.60$ and $C_{Pd}(\mu g) = [H(\mu V) - 18.80]/1640.80$, where H is the peak height at 425 nm on the chromato-integrator. The detection limits as signal-to-noise ratio of 3:1 were 65 ng for platinum and 10 ng for palladium.

3.5. Effect of diverse ions

The effect of Cu and Hg, which were also collected on the resin in acidic medium, and some precious metal ions was on the determination of both metal ions was examined. The tolerance limit was taken as being the amount causing an error of ±3% in the peak heights for platinum and palladium alone on the chromatogram. For the determination of 1 μg of platinum and 0.5 μg of palladium, Cu and Hg were tolerated at levels up to 20 μg and Au, Ag, Rh, Ru and Ir up to 40 μg. The recovery of platinum decreased more with the above amounts of Cu, Hg and Ag owing to competitive reactions with DMBS on the resin, Ni, Zn, Cd and Pb, which were collected on the resin in alkaline medium, did not interfere at levels up to 500 μg. Common anions such as chloride and sulfate ions did not interfere at levels up to 1000 μg.

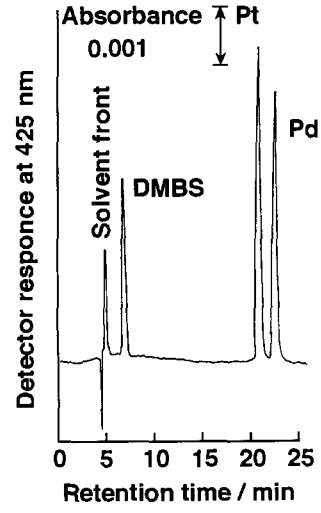

Fig. 6. Chromatogram of Pt- and Pd-chelates Pt = 2 μg; Pd = 1 μg; mobile phase = 65:35 (v/v) acetone–water containing 1×10^{-3} mol dm^{-3} CH_3COONa and 1×10^{-4} mol dm^{-3} EDTA; flow-rate 1 cm^3 min^{-1}; sample size = 10 mm^3.

Table 1
Determination of platimum and palladium in real samples

Sample	Experimental results		Indicated value	
	Pt (wt.%)	Pd (wt.%)	Pt (wt.%)	Pd (wt.%)
Dental alloy (Ortop Type 4)[a]	4.0, 3.9, 4.2, 4.1, 4.3 Av. 4.1 ± 0.16, RSD 3.9%	4.3, 4.2, 4.3, 4.4, 4.1 Av. 4.3 ± 0.11, RSD 2.8%	4.0	4.0
Platium–palladium wire[b]	87.7, 88.0, 86.0, 88.0, 90.1 Av. 88.0 ± 1.46, RSD 1.7%	10.5, 10.1, 10.4, 10.1, 10.3 Av. 10.3 ± 0.18, RSD 1.7%	90	10

[a] Purchased from Sankin Kogyou, Japan (Other components: Au 69%; Ag 8%; Cu 12%; others 3%).
[b] Purchased from Nilaco, Japan.

4. Application

The proposed method was applied to the determination of platinum and palladium in commercially available dental alow and platinum–palladium wire and the results are given in Table 1. The results obtained with the proposed method were in good agreement with the indicated value for each sample.

The proposed method can be applied to the determination of platinum and palladium in the samples with other components such as dental alloy and with different concentrations of metal ions such as platinum–palladium wire.

References

[1] H. Hoshino, K. Nakano and T. Yotsuyanagi, Analyst, 115 (1990) 133.
[2] J. Miura, Anal. Chem., 62, (1990) 1424.
[3] M.V. Main and J.S. Fritz, Talanta, 38 (1991) 253.
[4] E. Kaneko, H. Hoshino and T. Yotsuyanagi, Anal. Chem., 63 (1991) 219.
[5] X. Xu, H. Zhang and J. Cheng, Anal. Sci., 63 (1991) 2532.
[6] E. Kaneko, H. Hoshino and T. Yotsuyanagi, Chem. Lett., (1992) 955.
[7] Q. Liu, Y. Wang, J. Liu and J. Cheng, Anal. Sci., 9 (1993) 523.
[8] N. Uehara, A. Katamine and Y. Shijo, Analyst, 119 (1994) 1333.
[9] H. Zhang, W. Mou and J. Cheng, Talanta, 41 (1994) 1459.
[10] L.Y. Li, M.-D. Gui and Y.-Q. Zhao, Talanta, 42 (1995) 89.
[11] T. Okutani, T. Yamaji and A. Sakuragawa, Anal. Sci., 11 (1995) 765.
[12] S. Oszwaldowski, Analyst, 120 (1995) 1751.
[13] P. Heizmann and K. Ballshmiter, J. Chromatogr., 137 (1977) 153.
[14] S. Hoshi, N. Takahashi, S. Inoue and M. Matsubara, Bunseki Kagaku, 35 (1986) 819.
[15] S. Hoshi, S. Katoh, M. Nara and M. Matsubara, Bunseki Kagaku, 40 (1991) 429.
[16] K. Isshiki, F. Tsuji, T. Kuwamoto and E. Nakayama, Anal. Chem., 59 (1987) 2491.
[17] J.L. Lundgren and A.A. Schilt, Anal. Chem., 49 (1977) 974.
[18] K. Terada and K. Nakamura, Talanta, 28 (1981) 123.
[19] K. Terada, K. Matsumoto and T. Inaba, Anal. Chim. Acta, 158 (1984) 207.
[20] K.S. Lee, W. Lee and D.W. Lee, Anal. Chem., 50 (1978) 255.
[21] H. Akaiwa, H. Kawamoto and K. Ogura, Talanta, 28 (1981) 337.
[22] T. Braun and A.B. Farag, Anal. Chim. Acta, 76 (1975) 107.
[23] A. Chow and D. Buksak, Can. J. Chem., 53 (1975) 1373.
[24] S. Hoshi, H. Fujisawa, K. Nakamura, S. Nakata, M. Uto and K. Akatsuka, Talanta, 41 (1994) 503.
[25] S. Hoshi, H. Fujisawa, and M. Uto, Bunseki Kagaku, 43 (1994) 603.
[26] A.G. Asuero and J.M. Cano, Analyst, 103 (1978) 140.
[27] E. Hogfeldt, Stability Constants of Metal-Ion Complexes. Part A: Inorganic Ligands, IUPAC Chemical Data Series, No. 21, Pergamon Press, Oxford, 1979.

ELSEVIER

Talanta 44 (1997) 577–583

Talanta

Determination of thiosulfate at the 10^{-6} M level by its oxidation with iodine in an organic phase and spectrophometric measurement of triiodide

Tomozo Koh *, Tatsuo Sugimoto, Masahiro Matsui, Yasuyuki Miura

Department of Chemistry, Faculty of Science, Tokai University, Hiratsuka 259-12, Japan

Received 4 March 1996; received in revised form 6 August 1996; accepted 9 August 1996

Abstract

A highly sensitive method is proposed for the determination of thiosulfate based on the oxidation of aqueous thiosulfate (100 or 200 ml) by iodide in 4 ml of carbon tetrachloride. The excess of iodine was extracted into 8 ml of aqueous iodide solution as triiodide to be measured spectrophotometrically; the thiosulfate could therefore be indirectly highly concentrated and determined selectively. The side-reaction of thiosulfate in a large volume of solution with the hypoiodite formed from the iodine in carbon tetrachloride could be compensated for by adding a certain amount of extra thiosulfate. A linear calibration graph with a negative slope was obtained over the concentration ranges 1.1×10^{-7}–1×10^{-5} M (12 ppb–1.12 ppm) for 100 ml of thiosulfate solution and 6×10^{-8}–5×10^{-6} M (6.7 ppb–0.56 ppm) for 200 ml of thiosulfate solution. The proposed method was successfully applied to the determination of various amounts of thiosulfate in hot-spring and lake-water samples. © 1997 Elsevier Science B.V.

Keywords: Iodine oxidation; Spectrophotometry; Thiosulfate; Water

1. Introduction

A mixed solution of standard iodate and an excess amount of iodide has proved to be an excellent primary standard solution for iodine [1], because the mixture is extremely stable and a standard iodine solution can be readily prepared by the addition of acid, in which the following reaction proceeds to stoichiometric completion:

$$IO_3^- + 8I^- + 6H^+ \rightarrow 3I_3^- + 3H_2O \quad (1)$$

Ozawa [2] has proposed a method for the determination of thiosulfate based on its oxidation with the iodine produced from the mixture of standard iodate and iodide:

$$2S_2O_3^{2-} + I_2 \rightarrow S_4O_6^{2-} + 2I^- \quad (2)$$

followed by spectrophotometric measurement of the excess amount of triiodide. This method has been extensively used for the determination of polythionates and further for the determination of polythionates in mixtures, where the thiosulfate formed from the polythionates by their cyanolysis

* Corresponding author. Fax: +81 463 589543.

PII S0039-9140(96)02065-6

[3] and sulfitolysis [4–7] was measured. However, iron(III) interfered considerably in the determination of thiosulfate, even when present at a concentration as low as 1 ppm, because of its oxidation of the iodide in the triiodide. Therefore, for the determination of thiosulfate in real samples, the iron(III) present has to be removed by separation of a cation-exchange column [8,9]. Further, the method [2] using aqueous triiodide is limited by its sensitivity. Recently, a new reaction of thiosulfate [10] in the presence of a large amount of formaldehyde with iodine in an organic phase was studied in detail and used for the determination of thiosulfate, this method has advantages over the former method in terms of sensitivity and selectivity, but polythionates interfere in the determination of thiosulfate.

In this study, we developed a selective and sensitive method for the determination of thiosulfate, in which aqueous thiosulfate in 100 or 200 ml of solution reacts with iodine in 4 ml of carbon tetrachloride. The excess of iodine is then extracted into an aqueous iodide solution as triiodide and the triiodide formed is measured spectrophotometrically at 350 nm. The proposed method is free from interferences from iron(III) and other sulfur species, including polythionates and is at least 10- or 20-fold more sensitive than a conventional method using aqueous triiodide. This method was applied successfully to the determination of thiosulfate in the presence of large amounts of iron(III), sulfide and sulfite in hot-spring and lake-water samples.

2. Experimental

2.1. Reagents and apparatus

All of the reagents used were of analytical-reagent grade and were used as received. Doubly distilled water was used throughout. An approximately 0.1 M thiosulfate solution was prepared by dissolving sodium thiosulfate pentahydrate in oxygen-free water containing a small amount of sodium carbonate (0.01%, w/v) as a stabilizer. This solution was standardized by iodimetry 1 week after preparation. Working standard thiosulfate solutions (in 0.01%, w/v, Na_2CO_3) were prepared by appropriate dilution with oxygen-free water. An approximately 0.05 M iodine solution was prepared by dissolving a known amount of iodine in carbon tetrachloride. A 10 ml volume of this solution was pipetted into a 200 ml conical beaker containing 10 ml of water and then standardized against a standard thiosulfate solution by iodimetry; the beaker was shaken during the titration and the disappearance of the purple color due to iodine in the organic phase was taken as the end-point of the titration. Working standard solutions were prepared by suitable dilution with carbon tetrachloride. Standard solutions of 5×10^{-2} and 1.5×10^{-5} M iodine in carbon tetrachloride were stable for up to 2 and 1 week, respectively, after preparation.

A Shimadzu Model UV-160A recording spectrophotometer with 10 mm quartz cells was used for all absorbance measurements. An Iwaki Model KM shaker was used to promote both the reaction of iodine with thiosulfate in the two different phases and the extraction of the iodine in carbon tetrachloride into the aqueous phase as triiodide.

2.2. Recommended procedure

Place 100 ml of solution containing up to 1×10^{-5} M thiosulfate and 2 ml of 10 M sulfuric acid in a 300 ml separating funnel. For samples containing sulfide and sulfite, bubble nitrogen through the solution at a flow-rate of 400 ml min^{-1} for 20 min [10] in order to remove completely the sulfide and sulfite. Allow the mixture to stand for at least 10 min after bubbling, then add 1.5 ml of 1×10^{-4} M thiosulfate and 4 ml of 1.5×10^{-4} M iodine in carbon tetrachloride and shake the funnel for 2 min to allow the iodine to react with the thiosulfate in the aqueous phase. Transfer an exactly given volume of the organic phase into another 50 ml separating funnel and add 5 ml of 1 M potassium iodide (in 0.04%, w/v, Na_2CO_3). After introducing nitrogen into the funnel at a flow-rate of 250 ml min^{-1} for 2 min to displace the air, add 3 ml of 1.2 M acetic acid and shake the funnel for 1 min to extract the excess iodine into the aqueous phase as triiodide [10].

Measure the absorbance of the aqueous phase at 350 nm using 10 mm quartz cells. An iodine-free reagent blank was subtracted from all the absorbances measured in the procedure.

3. Results and discussion

3.1. Calibration

A series of standard solutions (100 ml) of thiosulfate were treated as described in Section 2.2. After the reaction of thiosulfate with the iodine in carbon tetrachloride, the excess iodine was extracted into an aqueous iodide solution as triiodide, and the triiodide formed was measured spectrophotometrically. Hence the absorbance for the triiodide should decrease with increase in the concentration of thiosulfate. As can be seen in Fig. 1, the calibration graph obtained for thiosulfate coincided exactly with that obtained for

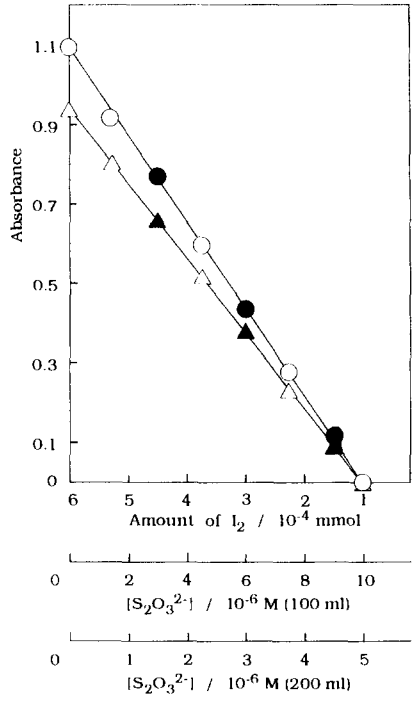

Fig. 1. Calibration graphs for thiosulfate and iodine. ○, $S_2O_3^{2-}$ in 100 ml of solution; ●, I_2 (expected) by using 100 ml of water; △, $S_2O_3^{2-}$ in 200 ml of solution; ▲, I_2 (expected) by using 200 ml of water.

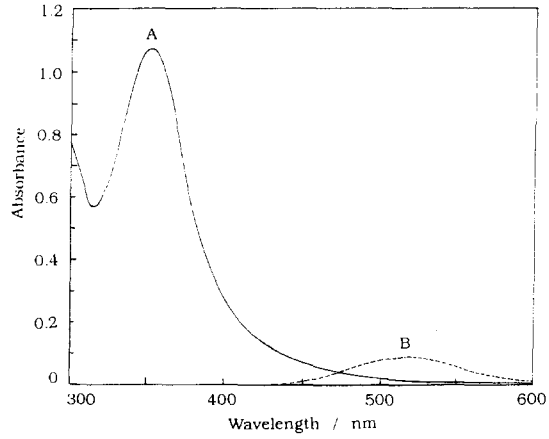

Fig. 2. Absorption spectra of the reagent blank and the iodine in carbon tetrachloride. A 4 ml volume of 1.5×10^{-4} M iodine solution in carbon tetrachloride was used. A, reagent blank measured as triiodide in 8 ml of solution; B, iodine in 4 ml of carbon tetrachloride.

iodine (expected graph) by using a series of standard solutions (4 ml of carbon tetrachloride solutions) of iodine and 100 ml water (in place of 100 ml of thiosulfate solution) in the procedure. In this instance, the amount scale for iodine is drawn in the opposite direction to scale for the thiosulfate concentration; the absorbance for 1×10^{-4} mmol of iodine reached zero in the procedure, because some iodine was consumed by the thiosulfate added. Even when 200 ml of thiosulfate solution were used to which 4 ml of 10 M sulfuric acid were placed, the calibration graph obtained for thiosulfate agreed well with that for iodine, demonstrating that the reaction of thiosulfate with iodine in carbon tetrachloride proceeded to stoichiometric completion according to Eq. (2). The difference between the calibration graph for 100 ml of thiosufate solution and that for 200 ml of thiosulfate solution is due to the difference in the amount of the iodine dissolved in water. The proposed method could be applied to the determination of thiosulfate in the concentration ranges 1.1×10^{-7}–1×10^{-5} M (12 ppb–1.12 ppm) for 100 ml of thiosulfate solution and 6×10^{-8}–5×10^{-6} M (6.7 ppb–0.56 ppm) for 200 ml of thiosulfate solution. The precision was determined from 11 replicate results obtained for a 100 ml aliquot of a 6.0×10^{-6} M standard thiosulfate

solution; the mean concentration of thiosulfate was found to be 6.0×10^{-6} M, with a standard deviation of 3.4×10^{-8} M (3.9 ppb) of $S_2O_3^{2-}$ and a relative standard deviation of 0.58%.

3.2. Absorption spectra

Fig. 2 shows the absorption spectra of the reagent blank (A) obtained in the procedure and of a solution of 1.5×10^{-4} M iodine in carbon tetrachloride (B). The reagent blank was obtained as follows. A 4 ml volume of 1.5×10^{-4} M iodine solution in carbon tetrachloride was shaken with a solution containing 100 ml of water, 2 ml of 2 M sulfuric acid and 1.5 ml of 1×10^{-4} M thiosulfate, then the iodine in carbon tetrachloride (its absorption spectrum shown in Fig. 2 (B)) was extracted into 8 ml of an aqueous solution of iodide as triiodide. The absorption spectrum (A) of the reagent blank has a much higher maximum absorption at 350 nm than that (B) of a solution of 1.5×10^{-4} M iodine in carbon tetrachloride which has its maximum absorption at 520 nm. Therefore, the excess iodine for the reaction with thiosulfate was measured as triiodide [10] at 350 nm in the procedure.

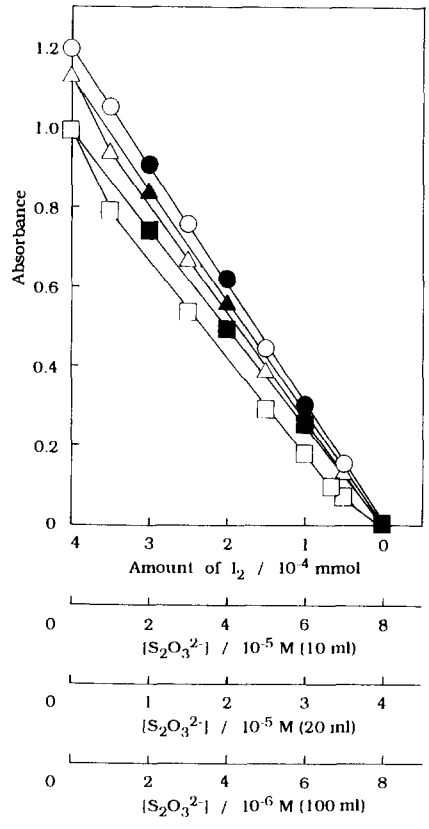

Fig. 3. Calibration graphs obtained for thiosulfate by using 10, 20 and 100 ml of thiosulfate solution. A 4 ml volume of 1×10^{-4} M iodine solution in carbon tetrachloride was used. ○, $S_2O_3^{2-}$ in 10 ml of solution; ●, I_2 (expected) by using 10 ml of water; △, $S_2O_3^{2-}$ in 20 ml of solution; ▲, I_2 (expected) by using 20 ml of water; □, $S_2O_3^{2-}$ in 100 ml of solution; ■, I_2 (expected) by using 100 ml of water.

3.3. Reaction of thiosulfate with iodine in carbon tetrachloride

Before 4 ml of iodine solution in carbon tetrachloride were added to an aqueous thiosulfate solution in the procedure, a strong acid (sulfuric acid) had to be added in order to prevent the iodine from transferring into the aqueous phase; an oxonium ion concentration range 0.3–1.3 M proved sufficient. Hence, 1 ml of 2 M H_2SO_4, 2 ml of 2 M H_2SO_4 and 2 ml of 10 M H_2SO_4 were used, for 10, 20 and 100 ml volumes of thiosulfate solution, respectively. Each 10 ml of solution of a series of amounts of standard thiosulfate was allowed to react with 4 ml of 1×10^{-4} M iodine in carbon tetrachloride by shaking the separating funnel, and the excess iodine was measured spectrophotometrically as triiodide according to the procedure. The resulting graph is shown in Fig. 3.

The calibration graph for thiosulfate was in good agreement with that obtained for iodine (expected graph) by using a series of standard solutions (4 ml) of iodine in carbon tetrachloride and 10 ml of water. However, when the volume of thiosulfate solution was increased to 20 and 100 ml, the calibration graph obtained for thiosulfate deviated negatively from the expected graph; the larger the volume of thiosulfate solution, the greater the calibration graph deviated, as shown in Fig. 3. This deviation can be attributed to partial oxidation of thiosulfate to oxidation states higher than that of tetrathionate ion (see Eq. (2)), by the hypoiodite ion formed as a result of the hydrolysis of the iodine transferred even into a strongly acidic medium. In order to eliminate the

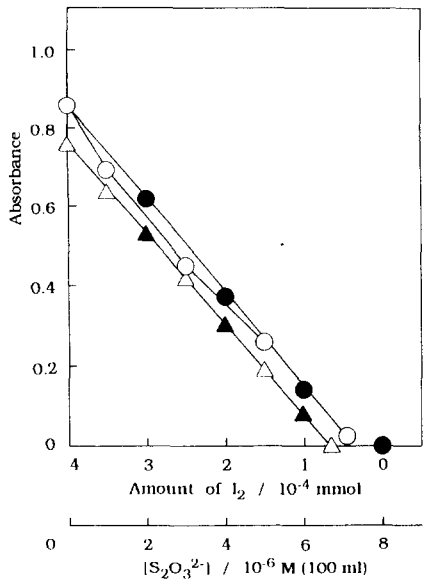

Fig. 4. Compensation for the side-reaction of thiouslfate in 100 ml of iodine solution in carbon tetrachloride. A 4 ml volume of 1×10^{-4} M iodine solution in carbon tetrachloride was used. ○, $S_2O_3^{2-}$ in 100 ml of solution plus 0.5 ml of 1×10^{-4} M $S_2O_3^{2-}$; ●, I_2 (expected) by using 100 ml of water plus 0.5 ml of 1×10^{-4} M $S_2O_3^{2-}$; △, $S_2O_3^{2-}$ in 100 ml of solution plus 1 ml of 1×10^{-4} M $S_2O_3^{2-}$; ▲, I_2 (expected) by using 100 ml of water plus 1 ml of 1×10^{-4} M $S_2O_3^{2-}$.

effect of this side-reaction from the determination of thiosulfate, an attempt was made to add thiosulfate for reaction with the hypoiodite. When 0.5 ml of 1×10^{-4} M thiosulfate solution was added to a solution containing 100 ml of up to 7.1×10^{-6} M thiosulfate solution and 2 ml of 10 M sulfuric acid, the calibration graph for thiosulfate approached the expected graph more closely (Fig. 4). Fig. 4 also shows that the calibration graph agreed completely with the expected graph when 1 ml of 1×10^{-4} M thiosulfate solution was used additionally. In the procedure, 1.5 ml of 1×10^{-4} M thiosulfate solution and accordingly 4 ml of a carbon tetrachloride solution of 1.5×10^{-4} M iodine, higher than 1×10^{-4} M, were used to compensate for the side-reaction between the iodine in carbon tetrachloride and the thiosulfate in samples. The iodide ion in the aqueous phase proved not to bring about any measurable change in either the reagent blank or the absorbance of thiosulfate in amounts up to 3000 μg. This means that the amount of iodide ion (19 μg) transferred into the aqueous phase as a result of the reaction of iodine with the thiosulfate added to compen-

Table 1
Effect of foreign ions on the determination of 67.3 μg of thiosulfate in 100 ml of solution[a]

Ion	Amount added (μg)	Thiosulfate found (μg)	Error (%)
None	—	67.3	—
Na^+	10000	67.0	−0.4
K^+	10000	67.1	−0.3
NH^{4+}	10000	67.9	0.9
Mg^{2+}	10000	67.3	0
Ca^{2+}	100001	67.2	−0.1
Ba^{2+}	10000	66.5	−1.2
Zn^{2+}	10000	67.2	−0.1
Cd^{2+}	10000	66.5	−1.2
Pb^{2+}	1000	52.0	−22.7
	10000[b]	66.2	−1.5
Mn^{2+}	10000	66.6	−1.0
Fe^{2+}	10000	67.4	0.1
Cu^{2+}	10000	66.5	−1.2
Al^{3+}	10000	68.0	1.0
Fe^{3+}	10000	59.8	−11.1
	1000	67.1	0.3
	10000[b]	67.0	−0.5
F^-	10000	67.1	−0.3
Cl^-	10000	66.7	0.6
Br^-	10000	68.8	2.2
I^-	3000	67.6	0.4
NO_3^-	10000	68.0	1.0
NO_2^-	10000	23.2	−63.5
	1000	67.1	−0.3
	10000[c]	67.1	−0.3
HCO_3^-	10000	67.4	0.1
HSO_3^-	100	82.6	22.7
	5000[d]	67.8	0.7
SO_4^{2-}	10000	67.5	0.3
S_2^-	5000[d]	67.5	0.3
$S_3O_6^{2-}$	10000	67.0	0.1
$S_4O_6^{2-}$	10000	67.5	0.3
$S_5O_6^{2-}$	10000	67.6	0.4
$S_6O_6^{2-}$	10000	67.4	0.1
HPO_4^{2-}	10000	67.0	−0.4
$HAsO_4^{2-}$	100	65.4	−2.8
EDTA	150000	67.2	−0.1

[a] A change in the volume of the sample solutions (97–103 ml) did not have any effect on the determination of thiosulfate.
[b] 2 ml of 0.2 M EDTA solution were added.
[c] 2 ml of 0.5 M amidosulfuric acid solution were added.
[d] Nitrogen was bubbled through the solution according to the procedure.

Table 2
Determination of thiosulfate in hot-spring and lake-water samples

Sample	Dilution (-fold)	Thiosulfate content (ppm)			Recovery (%)
		Added	Found[a]	Found in sample	
Hot-spring A	5	—	0.195 ± 0.003	0.975	—
	5	0.224	0.4195 ± 0.002	—	100.0
	5	0.448	0.644 ± 0.002	—	99.7
	10	—	0.097 ± 0.002	0.970	—
	10	0.224	0.322 ± 0.003	—	100.8
	10	0.448	0.542 ± 0.003	—	99.3
Hot-spring B	5	—	0.210 ± 0.003	1.05	—
	5	0.224	0.435 ± 0.001	—	100.4
	5	0.448	0.435 ± 0.001	—	99.9
	10	—	0.107 ± 0.002	1.07	—
	10	0.224	0.329 ± 0.003	—	99.4
	10	0.448	0.554 ± 0.002	—	99.2
Hot-spring C	5	—	0.209 ± 0.004	1.05	—
	5	0.224	0.434 ± 0.001	—	100.7
	5	0.448	0.657 ± 0.001	—	100.0
	10	—	0.104 ± 0.004	1.04	—
	10	0.224	0.328 ± 0.002	—	100.2
	10	0.448	0.553 ± 0.002	—	100.3
Lake-water	5	—	0.584 ± 0.003	2.92	—
	5	0.224	0.809 ± 0.003	—	100.4
	5	0.448	1.03 ± 0.001	—	99.6
	10	—	0.292 ± 0.002	2.92	—
	10	0.224	0.517 ± 0.003	—	100.4
	10	0.448	0.740 ± 0.002	—	106.0

[a] Corrected for four determinations.

sate for the side-reaction is too small to form triiodide; the equilibrium constant [11] for the following reaction:

$$I^-(aq) + I_2(org) \rightleftharpoons I_3^-(aq) \quad (3)$$

is not high, but is $10^{0.99}$ at 20°C when the organic solvent is carbon tetrachloride.

When sulfide and sulfite were removed from thiosulfate by bubbling nitrogen through the sample solution, a considerably higher absorbance was unexpectedly obtained, this higher absorbance was thought to be caused by the fact that the following hydrolysis reaction of iodine:

$$I_2 + H_2O \rightleftharpoons HIO + H^+ + I^- \quad (4)$$

is substantially depressed in an oxygen-free medium. The oxygen dissolved in water was also removed together with the sulfide and sulfite when the sample solution was purged with nitrogen. However, the higher absorbance continued to decrease gradually with time and eventually reached a normal value in 10 min. Hence the mixed solution purged with nitrogen had to be allowed to stand for at least 10 min as in the procedure.

3.4. Effects of foreign ions

A 100 ml volume of solution containing 67.3 μg of thiosulfate (6×10^{-6} M) and various amounts of foreign ions was treated as described in the procedure. The results are given in Table 1. In a previous method based on the oxidation of thiosulfate with aqueous triiodide [2], copper(II), iron(III), nitrite and iron(II), which oxidize iodide and reduce iodine, interfered in the determination of thiosulfate when present in amounts similar to

that of thiosulfate. In the proposed method, copper(II) and iron(II) were tolerated in amounts of up to 10 000 μg and both of iron(III) and nitrite up to 1000 μg. Iron(III) and lead(II) were tolerated in amounts of up to 10 000 μg when masked by the addition of 2 ml of 0.2 M EDTA solution and nitrite up to 10 000 μg when decomposed by the addition of 2 ml of 0.5 M amidosulfuric acid solution. All polythionates of tri-, tetra-, penta- and hexathionate were tolerated in amounts of up to 10 000 μg. Further, both sulfite and sulfide could be completely removed in amounts of up to 5000 μg from thiosulfate by bubbling nitrogen through the solution according to the procedure. Iodide did not interfere with the determination of thiosulfate in amounts of up to 3000 μg and arsenate up to 100 μg. The other ions listed in Table 1 were tolerated in amounts as high as 10 000 μg with an error of less than 2%.

3.5. Application to real samples

In order to remove the sulfite and sulfide in real samples, nitrogen was bubbled, according to the procedure, through 150 ml of solution containing 120 or 60 ml of the samples, a known amount of thiosulfate and 3 ml of 10 M sulfuric acid. A 25 ml aliquot of the solution from which the sulfite and sulfide had been removed was transferred into a 300 ml separating funnel and the volume was adjusted to 100 ml; in this instance the original samples were to be diluted to 5- or 10-fold, respectively. A 100 ml of mixed solution was treated according to the procedure, in which 2 ml of 0.2 M EDTA solution were added for both hot-spring C and lake-water samples, containing large amounts of iron(III). The thiosulfate content was determined using the standard additions method. The results are summarized in Table 2. The results obtained for the samples diluted to 5- and 10-fold the original volume were in good agreement with each other.

Potential matrix interferences from unknown species in real samples were investigated by adding known amounts of thiosulfate to the sample solutions. The recoveries ranged from 99.2 to 100.8% with an average of 100.4%, which is adequate for the analysis of environmental samples.

References

[1] T. Koh, Anal. Sci., 6 (1990) 3.
[2] T. Ozawa, Nippon Kagaku Zasshi, 87 (1966) 576.
[3] T. Koh and K. Taniguchi, Anal. Chem., 45 (1973) 2018.
[4] T. Koh and K. Taniguchi, Anal. Chem., 46 (1974) 1679.
[5] T. Koh, K. Taniguchi and I Iwasaki, Bull. Chem. Soc. Jpn., 51 (1978) 164.
[6] T. Koh, Y. Miura, M. Ishimori and N. Yamauro, Anal. Sci., 5 (1989) 79.
[7] T. Koh and K. Okabe, Analyst, 119 (1994) 2457.
[8] T. Koh and K. Okabe, Anal. Sci., 8 (1992) 285.
[9] T. Koh, K. Okabe and Y. Miura, Analyst, 118 (1993) 669.
[10] T. Koh, H. Wakabayashi and Y. Yonemura, Bull. Chem. Soc. Jpn., 67 (1994) 119.
[11] L.G. Sillén and A. E. Martell, Stability Constants of Metal-ion Complexes, Supplement No. 1, Special Publication No. 25, Chemical Society, London 1971, p. 222.

ELSEVIER

Talanta 44 (1997) 585–591

Talanta

Second-order data by flow injection analysis with spectrophotometric diode-array detection and incorporated gel-filtration chromatographic column

Iben Ellegaard Bechmann

Department of Chemistry, Technical University of Denmark, DK-2800 Lyngby, Denmark

Received 24 April 1996; received in revised form 29 July 1996; accepted 29 July 1996

Abstract

A flow injection analysis (FIA) system furnished with a gel-filtration chromatographic column and with photodiode-array detection was used for the generation of second-order data. The system presented is a model system in which the analytes are blue dextran, potassium hexacyanoferrate(III) and heparin. It is shown that the rank of the involved sample data matrices corresponds to the number of chemical components present in the sample. The PARAFAC (parallel factor analysis) algorithm combined with multiple linear regression and the tri-PLS (tri-linear partial least-squares regression), which allows unknown substances to be present in the sample, are implemented for FIA systems and it is illustrated how these three-way algorithms can handle spectral interferents. The prediction ability of the two methods for pure two-component samples and also the predictions ability in the presence of unknown interferents are satisfactory. However, the predictions obtained by tri-PLS are slightly better than those obtained using PARAFAC regression algorithm. © 1997 Elsevier Science B.V.

Keywords: Multivariate calibration; PARAFAC; Spectral interferents; Tri-PLS

1. Introduction

Data structures produced by analytical chemical systems in general and by flow injection analysis (FIA) systems in particular can be divided into classes reflecting the complexity of the data, ranging from scalars, vectors and matrices to higher order data structures. More than 90% of the papers published in analytical chemical journals are based on zeroth-order data structures [1]. This simple data structure arises when only one measurement per sample is recorded. A set of calibration samples thus gives a vector. The measurement can be a variety of signals, e.g. potential, current, absorbance or, as often used in FIA, the height (or area) of the sample peak. The use of zeroth-order data requires that the measured signal is absolutely selective and additionally that the signal is a known function (e.g. linear) of the concentration of the analyte. If the selectivity assumption is not fulfilled for all samples, an improvement can be achieved by using first-order data structures [1], which gives the possibility of detecting outlying samples. First-or-

PII S0039-9140(96)02066-8

der data, where each sample gives rise to a vector and a set of calibration samples hence yields a matrix, can be obtained in two ways in FIA: (1) by recording the actual measurement (e.g. the absorbance at a given wavelength) as a function of time; and (2) by recording multiple measurements at a given time (e.g. the UV/VIS spectrum at the peak maximum). The condition for employing first-order data is that the responses are linear and additive for all analytes.

The number of FIA papers published on first-order data using two-way data analytical methods for instance partial least-squares (PLS) regression is increasing [2–5]. From a multivariate chemometric point of view, second-order data structures [1], where each sample gives rise to a matrix and a set of calibration samples to a cube, are, however, much more interesting because these data make it possible not only to detect outlying samples but also to determine correct analyte concentrations even though the analytical signal is not selective. This has been called the second-order advantage [1]. Second-order data can be achieved, for instance, by scanning multiple wavelengths at multiple times. The majority of papers published concerning second-order data in FIA rely on spectrophotometric diode-array detection [6,7]. The condition for optimal use of second-order data is that the data structure is bilinear, which means that the responses are linear and additive for all analytes and that no co-elution of analytes is allowed. This bilinear data structure is found in chemical systems obeying the Lambert–Beers law and where the analytes are separated in time by a column, e.g. in chromatographic systems combined with a photodiode-array detector.

In this work, a flow injection system with an incorporated gel-filtration chromatographic column and a UV/VIS photodiode-array detector was used for the generation of second-order data. In an earlier paper [8], the application of a gel-filtration chromatographic column in a FIA system for enzymatic determination of formaldehyde in aqueous fish extracts was reported. In that work, the purpose of providing the FIA system with a gel-filtration chromatographic column was on-line removal of the protein fraction of the extract prior to the enzymatic analysis. The purpose of this work was partly to improve the possibilities of the application of gel-filtration chromatographic columns in FIA and partly to illustrate the general advantages of using second-order FIA data, especially in cases where unknown spectral interferents are present. In that context, attention is drawn to an early paper [9] where the resemblance of flow injection analysis with chromatographic systems in general is discussed further. The system presented here is a model system where the analytes blue dextran, potassium hexacynoferrate(III) and heparin were chosen to illustrate the benefit of the methodology used. The data structure produced by the FIA system is a bilinear data structure, where each sample produces a 76 (times) × 188 (wavelength) matrix. Among the most common methods used for second-order calibration are unfolding methods, where the calibration cube is unfolded to an ordinary matrix which is then treated by standard two-way methods (e.g. PLS). In the case of response matrices where each chemical component gives rise to a matrix of rank one, the rank annihilation factor analysis (RAFA) method [10] or the general rank annihilation method (GRAM) can be used [10,11] for the prediction of correct analyte concentration in presence of spectral interferents.

In this paper, the tri-linear parallel factor analysis (PARAFAC) algorithm [12–14] and the newly developed tri-linear partial least-squares regression (tri-PLS) [15] are implemented for FIA systems. PARAFAC is a generalization of PCA to higher order data arrays, but there are some important differences between the two methods. Tri-PLS is a generalization of the ordinary two-way PLS methods. A short description of the two methods is given in Section 3. Compared with the unfolding methods, the multi-linear models are much simpler because they use fewer parameters.

2. Experimental

2.1. Apparatus

2.1.1. FIA system

The FIA system used in the experiments was a simple one-line FIA system. All tubing employed

was PTFE (0.5 mm i.d.) and the carrier stream was propelled by an Ismatec MS-4 Reglo peristaltic pump. The sample (50 μl) was aspirated into the valve by the same pump. The carrier stream was pumped through a gel-filtration chromatographic column (HiTrap Desalting; Pharmacia, Uppsala, Sweden). The detector was a TIDAS (Zeiss J and M Analytische Mess- und Regeltechnik, Germany) photodiode array spectrophotometer furnished with a 8 μl flow cell. A 12-port injection valve (made in this laboratory) was used for injection of the sample. The photodiode array starts scanning 20 s after injection and continues for a further 75 s at 1.0 s intervals. The wavelength range recorded in each scan is 220–594 nm (every 2 nm). Injection of one sample thus, generates a data matrix containing 76 × 188 absorbances. An example of the data structure produced by injection of 50 μl sample is depicted in Fig. 1.

2.1.2. Gel-filtration column

The column used in this work was a HiTrap desalting column (Pharmacia) of dimensions 25 × 16 mm i.d. The column is filled with Sephadex G-25 Superfine and has a fractionation range between 1000 and 5000 Da. This column shows a significantly better separation of low and high molecular weight substances than the Sephadex G-25 column used in the previous work [8], which was packed in this laboratory and consisted of a piece of PVC into with was machined a tubular cavity of 52 × 3.3 mm i.d. When not in use, the column reactor was stored filled with a 20% (v/v) ethanol solution in a refrigerator at 5°C to prevent microbiological growth.

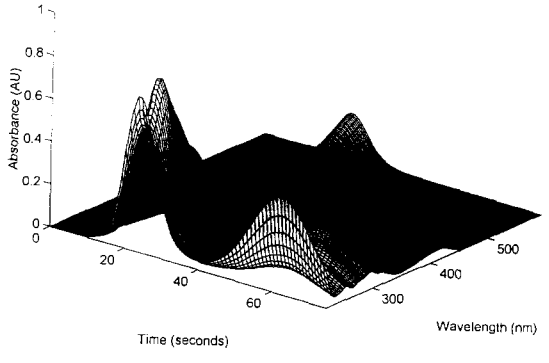

Fig. 1. Three-dimensional plot of the data matrix corresponding to injection of a mixture of blue dextran and $K_3Fe(CN)_6$.

Table 1
Concentrations of blue dextran and $K_3Fe(CN)_6$ for nine calibration samples

Sample	Blue dextran (mg ml^{-1})	$K_3Fe(CN)_6$ (mg ml^{-1})
C1	0.00	0.00
C2	2.65	0.00
C3	5.30	0.00
C4	0.00	0.80
C5	2.65	0.80
C6	5.30	0.80
C7	0.00	1.60
C8	2.65	1.60
C9	5.30	1.60

2.2. Reagents

The samples use in the model system were made from stock solutions of a high molecular weight substance (Blue dextran, Mw $\approx 10^6$ g mol^{-1}; Sigma) and a low molecular weight substance (potassium hexacyanoferate(III), Mw = 329.2 g mol^{-1}; Merck) in degassed, distilled Millipore-filtered water containing 0.9% NaCl. The stock solutions, which contained 26.5 g l^{-1} blue of dextran and 1.62 g l^{-1} of potassium hexacyanoferrate(III), were diluted with 0.9% NaCl solution for the preparation of samples. A solution of heparin (Tinzaparine, MW $\approx$ 4000 g mol^{-1}) containing 10 g l^{-1} was used in some of the test samples as an interfering component.

2.3. Programs

Data collection and control of the pump and valve were performed by a software package from J&M Analytische Mess- und Regeltechnik (Germany). All calculations were preformed in Matlab ver. 4.0 for Windows (Math Works), partly by use of PARAFAC and multi-linear PLS algorithms available from the Internet at http://newton.foodsci.kvl.dk/foodtech.html (R. Bro and C.A. Andersson).

3. Theory

3.1. Data structure

The data structure produced by the FIA system is a bilinear data structure, where each sample produces a J (times) $\times$ K (wavelength) matrix. If all responses are linear and no noise is present, the rank of the measured response matrix will be equal to the number of chemical substances present in the sample. However, the true rank of the sample matrix is often not determinable because of real data contain non-linearities and noise. For this reason, it is necessary to determine a pseudo-rank instead. In the present work, principal component analysis (PCA) [10] is used for this purpose. In this context the rank equals the number of principal components which is necessary to explain 99% of the variance in the response matrix. The dimension of the three-way calibration data array, $\mathbf{X}$, is $I \times J \times K$, where I is the number of samples in the calibration set. The pre-processing of this kind of raw data is more complicated than in the two-way case. In this work no centering and no scaling were used in the PARAFAC models. The data arrays used for tri-PLS are centered by unfolding the data array to a $I \times JK$ matrix and then mean center the unfolded matrix. No scaling was used.

3.2. PARAFAC

PARAFAC performs a tri-linear decomposition of the data array, $\mathbf{X}$, and can be regarded as a generalization of the bilinear PCA. In PARAFAC the tri-linear model of $\mathbf{X}$ is found to minimize the sum of squares

$$\left(\sum e_{ijk}^2\right)$$

in the model

$$x_{ijk} = \sum_{f=1}^{F} a_{if} b_{jf} c_{kf} + e_{ijk}$$

where x_{ijk} is an element in $\mathbf{X}$ ($i = 1, ..., I$, $j = 1, ..., J$, and $k = 1, ..., K$), a are the scores, b and c are loadings in the model and F is the number of factors. In contrast to PCA, the number of factors to be included in the PARAFAC model must be determined before the modelling.

A very obvious advantage of PARAFAC over PCA is the uniqueness of the solution. The loadings in a spectral bilinear PCA model reflect the pure spectra of the analytes measured, but it is not possible without external information actually to find the pure spectra. In the data used for the PARAFAC model represent a second-order data structure, the true analyte spectra can often be found directly, if only the concentrations vary independently pairwise and no spectra are linearly dependent on any of the others. In this work, PARAFAC is used for prediction purposes by

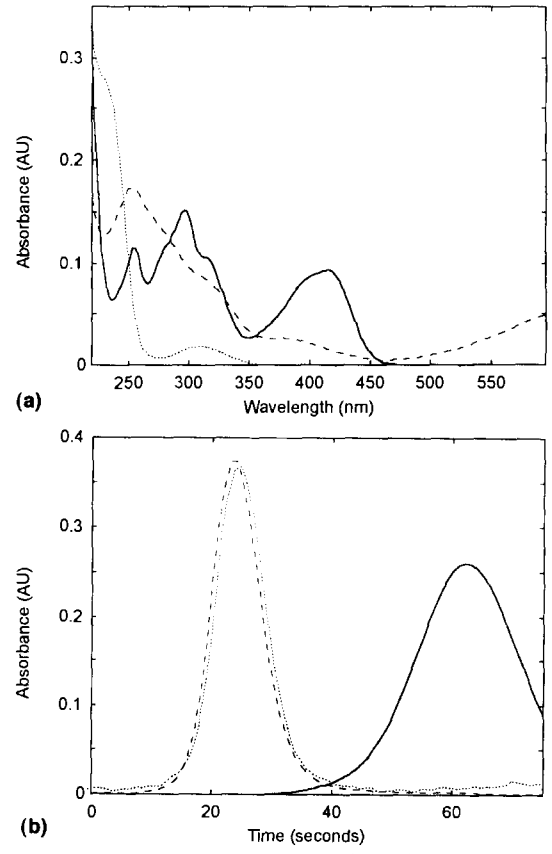

Fig. 2. (a) Normalized pure spectra of the three components. Dash line, blue dextan; solid line, $K_3Fe(CN)_6$; Dotted line, heparin. (b) Normalized concentration profiles calculated by alternating regression on each of the pure sample matrices. Lines as in (a).

following the strategy of principal component regression (PCR) [10]. The scores from the PARAFAC model are used for the predictions using multiple linear regression.

3.3. Tri-PLS

The tri-linear PLS is a natural extension of the ordinary bi-linear PLS method. By the tri-linear decomposition in tri-PLS the calibration cube **X** is decomposed into a set of rank-one cubes describing **X** in some optimal sense. This does not mean, however, that the part of **X** relevant for describing the dependent variables (the analyte concentrations) has to be of rank one. One advantage of tri-PLS over PARAFAC is the incorporation of the dependent variables (the analyte concentrations) in the decomposition of the measured calibration cube, which might stabilize the predictive model. The theory of multi-linear PLS can be found elsewhere [15].

4. Results and discussion

The samples used for calibration consisted of mixtures of the two analytes, blue dextran and potassium hexacyanoferrate(III). The samples were prepared as a two-factor, three-level factorial design, i.e. the calibration set consisted of nine samples. The compositions of the calibration samples are given in Table 1.

An independent test set of 12 different test samples was prepared. To illustrate how the PARAFAC and the tri-PLS algorithms handle spectral interferents, some of the test samples in addition contained heparin.

The pure spectra and the concentration profiles of blue dextran, potassium hexacyanoferrate(III) and heparin are shown in Fig. 2(a) and (b), respectively.

The spectra and time profiles are found by resolution of each of the three data matrices measured on pure standards using the alternating least squares (ALS) algorithm [10]. From Fig. 2(b), it is seen that the time profiles of the dextran and the $K_3Fe(CN)_6$ differ owing to different resolution times on the gel-filtration column. The resolution times of heparin and dextran are almost the same owing to their molecular weights of close to 4000 Da and higher than 5000 Da, respectively. In the current application, the exclusion limit of the column is apparently about 4000 Da and not 5000 Da as specified by Pharmacia. The spectral characteristics of the three components, however, are different. The data structure obtained by injection of a pure mixture of blue dextran and $K_3Fe(CN)_6$ is thus, expected to be a bilinear second-order data structure.

A PARAFAC model with two components should give the right solution since there are two

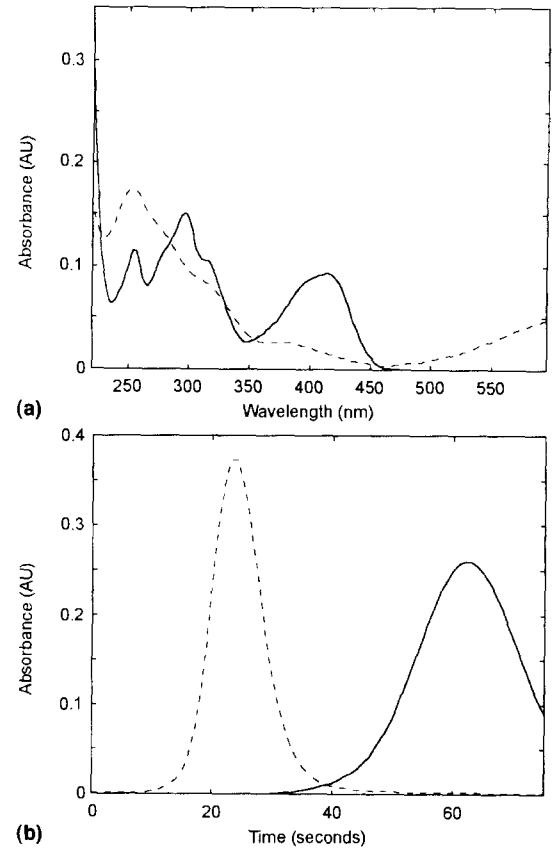

Fig. 3. (a) Spectra found by the PARAFAC algorithm (normalized loading vectors of second mode) for the analytes used for calibration. Dashed line blue dextran; Solid line $K_3Fe(CN)_6$. (b) Time profiles found by the PARAFAC algorithm (normalized loading vectors of third mode) for the analytes used for calibration. Lines as in (a).

Table 2
True and predicted concentrations (in mg ml^{-1}) obtained by the PARAFAC algorithm and tri-PLS algorithm for the 12 test samples

Sample	True			Predicted by PARAFAC		Predicted by tri-PLS		Rank[a]
	Dextran	$K_3Fe(CN)_6$	Heparin	Dextran	$K_3Fe(CN)_6$	Dextran	$K_3Fe(CN)_6$	
T1	0.00	0.00	0.00	0.00	0.00	0.00	0.00	—
T2	2.25	0.00	0.00	2.26	0.00	2.25	0.00	1
T3	4.50	0.00	0.00	4.51	0.00	4.50	0.00	1
T4	0.00	0.68	0.00	0.01	0.68	0.00	0.68	1
T5	2.25	0.68	0.00	2.26	0.68	2.25	0.68	2
T6	4.50	0.68	0.00	4.51	0.68	4.50	0.68	2
T7	0.00	1.36	0.00	0.00	1.36	0.00	1.36	1
T8	2.25	1.36	0.00	2.26	1.36	2.25	1.36	2
T9	4.50	1.36	0.00	4.51	1.36	4.50	1.36	2
T10	3.15	0.00	2.00	3.20	0.00	3.18	0.00	2
T11	0.00	0.80	2.00	0.00	0.80	0.00	0.80	2
T12	3.15	0.80	2.00	3.26	0.82	3.24	0.81	3

[a] The 'Rank' column indicate the pseudo-rank of the sample matrix determined by PCA.

analytes in the calibration set. The spectral loadings of a two-component PARAFAC model are shown in Fig. 3(a) and the corresponding time loadings are shown in Fig. 3(b). From comparison with Fig. 2(a) and (b), it is seen that the model estimates precisely both the pure spectra and the time profiles of the two analytes.

The PARAFAC model was validated by test set validation with the nine samples in a calibration set and 12 other samples in a test set. For the predictions of analyte concentrations in the test samples, a regression model was made from the scores of the two-component PARAFAC model. For comparison, the results of using a tri-PLS model with two PLS components were also calculated. The true concentrations and the concentrations predicted by PARAFAC for the 12 test samples are given in Table 2 together with the concentrations predicted by tri-PLS. The pseudo-rank determined by PCA of the measured data matrices for the 12 test samples is also given in Table 2.

The rank of a sample matrix containing only one substance equals one and the rank of a sample matrix containing two substances equals two, and analogously with three substances. This indicates that an FIA system furnished with a gel-filtration column acts as expected of a chromatographic system.

It appears that the prediction of $K_3Fe(CN)_6$ concentrations in the presence of heparin in general is better than the predictions for dextran in the presence of heparin. This can be explained by the almost identical resolution profiles of the two high molecular weight substances used. Comparing the predicted and actual concentrations obtained by applying the two methods on the 12 test samples, the root mean square error of prediction (RMSEP) can be calculated. The RMSEP for the prediction of dextran is 0.03 mg ml^{-1} and that for $K_3Fe(CN)_6$ is below 0.01 mg ml^{-1}. The predictions obtained by tri-PLS are slightly better than those obtained by PARAFAC, but both the PARAFAC and the tri-PLS algorithms give satisfactory predictions in the presence of unknown chemical interferents. However, tri-PLS does not possess the uniqueness properties of PARAFAC and it is therefore not possible without external information actually to find the pure spectra of the analytes. If the investigated samples contain specific chemical components of interest, the PARAFAC algorithm might therefore be preferable.

Acknowledgements

The author thanks Professor Elo H. Hansen for valuable comments and suggestions. Rasmus Bro is thanked for helpful comments and for placing the Matlab m-files for PARAFAC and tri-PLS on the Internet. The Danish Ministry of Agriculture and Fisheries is acknowledged for financial support. This work was performed in collaboration with the Danish Institute for Fisheries Research, Department of Seafood Research.

References

[1] K.S. Booksh and B.R. Kowalski, Anal. Chem., 66 (1994) 782A.
[2] P. MacLaurin, P.J. Worsfold, P. Norman and M. Crane, Analyst, 118 (1993) 617.
[3] O. Hernandez, A.I. Jimenez, F. Jimenez and J.J. Arias, Anal. Chim. Acta, 310 (1995) 53.
[4] O. Hernandez, F. Jiminez, A.I. Jimenez and J.J. Arias, Analyst, 121 (1996) 169.
[5] C. Ridder and L. Nørgaard, Chemom. Intell. Lab. Syst., 14 (1992) 297.
[6] L. Nørgaard and C. Ridder, Talanta, 41 (1994) 59.
[7] L. Nørgaard and C. Ridder, Chemom. Intell. Lab. Syst., 23 (1994) 107.
[8] I.E. Bechmann, Anal. Chim. Acta, 320 (1996) 155.
[9] J. Ruzicka and G. D. Christian, Analyst, 115 (1990) 475.
[10] E.R. Malinowski, Factor Analysis in Chemistry, 2nd edn, Wiley, New York, 1991.
[11] E. Sanchez and B.R. Kowalski, Anal. Chem. 58 (1986) 496.
[12] A.K. Smilde, P.H. van der Graaf and D.A. Doornbos, Anal. Chim. Acta, 235 (1990) 41.
[13] A.K. Smilde, Chemom. Intell. Lab. Syst., 15 (1992) 143.
[14] A.K. Smilde, Y.-D. Wang and B.R. Kowalski, J. Chemom., 8 (1994) 21.
[15] R. Bro, J. Chemom., 10 (1996) 47.

ELSEVIER

Talanta 44 (1997) 593–604

Talanta

Porphyrins as ligands for trace metal analysis by high-performance liquid chromatography

Zhihong Shi, Chengguang Fu *

Research Centre of Physical and Chemical Analysis, Hebei University Baoding, 071002, People's Republic of China

Received 16 April 1996; received in revised form 5 August 1996; accepted 15 August 1996

Abstract

The role of porphyrins in the determination of metal ions by high-performance liquid chromatography (HPLC) is examined. In assessing the current status of the area, recent advances and developments are discussed and future potential is pointed out. © 1997 Elsevier Science B.V.

Keywords: High-performance liquid chromatography; Porphyrin ligands; Trace metal analysis

1. Introduction

High-performance liquid chromatography (HPLC) has been mainly used as a technique for the separation of organic solutes and its leading position in this role remains unchallenged. Although as early as 1972 Huber et al. [1] had accomplished the separation and determination of metal ions by HPLC, related research work in this field did not provoke interest until the 1980s. Rapid improvements in HPLC methodology and the application of superior metal chelate systems have significantly enhanced the potential usefulness of HPLC for the separation and determination of metal ions. Many reagents have been successfully used as ligands to form metal chelates pre-column, in situ or post-column, such as pyridylazo [2–4], thiazolylazo [5], 8-hydroxyquinoline [6], complexones [7], diethyldithiocarbamate [8] and β-diketones [9].

Several reviews have been published on the determination of metal ions with organic chelating reagents by HPLC [10–14]. The present paper stresses applications of porphyrins as ligands to the separation and determination of metal ions by HPLC.

It is well known that a porphyrin is a kind of highly sensitive chromogenic reagent. Porphyrins and their metal chelates generally exhibit characteristically sharp and intense absorption in the visible region. The band at about 400–500 nm, which is called the Soret band, shows the most intense absorption. Molar absorptivities of the order of 10^5 are often recorded.

The Soret band is regarded as the band of choice for the spectrophotometric determination of metalloporphyrins. If a porphyrin reacts easily and quantitatively with a metal ion, the porphyrin

* Corresponding author.

PII S0039-9140(96)02068-1

must be useful as a sensitive spectrophotometric reagent for the determination of metal ions. Many porphyrins, including lipophilic and water-soluble types, have been synthesized and used for the spectrophotometric determination of metals [15–20].

However, there is a major problem in utilizing a porphyrin for the spectrophotometric determination of metals: the Soret bands of porphyrins and their metal chelates overlap so closely that the determination of a certain metal ion often suffers serious interference from other metals. When the method is applied to practical samples, a complicated separation procedure is often needed. Therefore, the simultaneous determination of different metals is rarely effective.

To solve the above problems, HPLC is the best choice. Considering the remarkably high stability of metal porphyrin chelates and the similarity of the chelates' absorbance, a porphyrin is an ideal chelating reagent for the determination of metal ions by HPLC. In addition, the intense color of the chelates should permit selective detection in the visible region of the spectrum.

The authors have attempted here to include all the work reported on the application of porphyrins to the HPLC determination of metal ions. Related high-performance thin-layer chromatographic (HPTLC) studies are also covered. It is hoped only that this review will introduce readers not familiar with this area to its potential usefulness.

2. Application of porphyrins in the determination of metal ions by HPLC

In general, there are two types of HPLC separation of metalloporphyrins: the separation of different porphyrin complexes of a certain metal ion and the separation of metalloporphyrins with respect to their central metal ions. The HPLC separations of the naturally occurring porphyrins and metalloporphyrins are examples of the former type of separation [21–23] and the determination of trace metals as their porphyrin chelates by HPLC belongs to the latter type. The latter type of HPLC separation is more difficult because each metal ion is surrounded by a bulky macrocyclic porphyrin structure to which various organic functional groups are further bonded. The difficulty in the separation of metalloporphyrins increases with increase in the chemical similarity of the central metal ions.

From the literature, it seems that the porphyrins which have been employed as ligands for the separation and determination of trace metals by HPLC can be classified into the following three groups: (i) porphyrins with no substituents; (ii) porphyrins with substituents at positions 5, 10, 15 and 20 (see Fig. 2 and Table 1); and (iii) porphyrins with substituents on the pyrrole rings.

2.1. Porphyrins with no substituents

21*H*,23*H*-porphine (H_2P) is the simplest synthetic porphyrin (Fig. 1). H_2P and its metal chelates are not soluble in water.

Wakui et al. [24] reported the HPTLC and HPLC behavior of several metal complexes of H_2P. The chromatographic mobility of H_2P and its Ni(II), Cu(II), Zn(II) and Pd(II) complexes were investigated by HPTLC on an octadecyl-bonded silica gel plate with various polar organic solvents. The mobility generally decreased according to the central metal ion of the complex in the order $Zn(II) > H_2P > Ni(II) > Pd(II) > Cu(II)$. According to the R_f data obtained for H_2P and its metal complexes from the HPTLC study, methanol is a good choice of eluent for the separation of these metal porphyrin complexes. The HPLC separation of H_2P and its four metal complexes was achieved on a LiChrosorb RP-18 column using methanol or acetonitrile as mobile phase and the eluates were detected at 390 nm. With acetonitrile, the retention time of every compound was shorter than that observed with

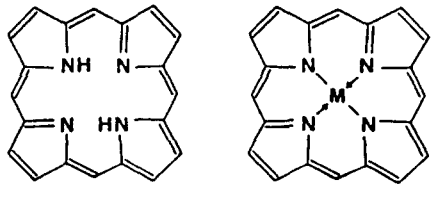

Fig. 1. H_2P (left) and complex with divalent metal M (right).

Table 1
Porphyrins with substituents at positions 5, 10, 15 and 20

Name	Abbreviation	Substituents	Solubility in water
meso-Tetraphenylporphine	TPP		Insoluble
meso-Tetrakis(*p*-tolyl)porphine	TTP	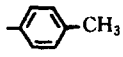	Insoluble
meso-Tetrakis(3-bromophenyl)porphine	*m*-BrTPP		Insoluble
meso-Tetrakis(4-hydroxyphenyl)porphine	THPP	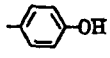	Slightly soluble
meso-Tetrakis(*N*-methyl-4-pyridyl)porphine	T(4-MPy)P	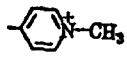	Slightly soluble
meso-Tetra(4-carboxyphenyl)porphine	TCPP	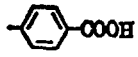	Soluble
meso-Tetra(*p*-sulfophenyl)porphine	$TPPS_4$	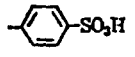	Soluble
meso-Tetrakis(3-bromo-4-sulfophenyl)porphine	*m*-$BrTPPS_4$	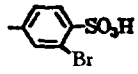	Soluble
meso-Tetrakis(4-methoxyl-3-sulfophenyl)porphine	$T(4\text{-}MOP)PS_4$	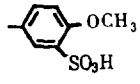	Soluble

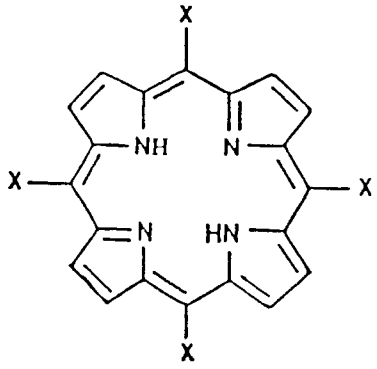

Fig. 2. The general structure of porphyrins. Substituents at the positions marked X are numbered 5, 10, 15 and 20.

methanol. However, the resolution between NiP, PdP and CuP was insufficient. It was shown that the metal complexes left the column without undesirable changes. It is unfortunate that the authors did not apply their work to the quantitative determination of metal ions.

2.2. Porphyrins with substituents at positions 5, 10, 15 and 20

The general structure of these porphyrins is shown in Fig. 2 and substituents are listed in Table 1.

In Fig. 2, substituents at the positions marked *X* are numbered 5, 10, 15 and 20. For example, the porphyrin where all four *X*s are phenyl groups is 5, 10 15, 20-tetraphenylporphine; this compound also has the trivial names meso-tetraphenylporphine and $\alpha,\beta,\gamma,\delta$-tetraphenylporphine.

2.2.1. TPP

TPP is one of the typical synthetic water-insoluble porphyrins. In 1975, Hui et al. [25] reported on the TLC behavior of the TPP chelates of manganese, iron, cobalt, nickel, copper, zinc, rhodium, cadmium, mercury and lead on silica gel and alumina. Good separations can be deduced from the published R_f data. Saitoh et al. [26] studied the HPTLC behavior of TPP and its chelates of Mg(II), Ni(II), Cu(II), Zn(II), Cd(II), Mn(III) and Fe(III). Cellulose and silica gel were chosen for normal-phase distribution and two kinds of alkylated silicas were chosen for reversed-phase distribution. These HPTLC studies clarified that the reversed-phase separation mode on an octadecyl-bonded silica gel coupled with a non-aqueous mobile phase is a good choice for the separation of complexes of divalent metals with TPP. Since metal TPP chelates are relatively insoluble in water and methanol, conventional reversed-phase systems using an aqueous mobile phase would not be effective in this case.

In a later paper, Saitoh et al. [27] described the HPLC behavior of TPP and its nine metal chelates on a C_{18}-bonded stationary phase. The retention of the chelate depends on its central metal ion, increasing in the order Zn(II) < V(IV) < Fe(III) < Mg(II) ≈ Cd(II) ≈ (H_2TPP) < Ni(II) = Pd(II) < Cu(II) < Mn(III).

A common mobile phase used in reversed-phase HPLC is methanol–water, whereas from the retention data for the TPP compounds obtained by Saitoh et al. we can see that methanol is not suitable for their rapid HPLC separation because of the considerable retention. It can be predicted that much larger retention volumes will be observed with methanol–water than with methanol alone. Acetonitrile is not useful for similar reasons, if it is used alone. Ethanol, acetone and *N*,*N*-dimethylformamide give relatively small retention volumes for the TPP compounds. Taking account of the solubility of the TPP compounds, the viscosity and the cost, acetone is considered to be the most convenient eluent.

The chelates of Mg(II), V(IV), Ni(II), Cu(II), Zn(II) and Pd(II) were separated in about 8 min using a LiChrosorb RP-18 column (250 × 4 mm i.d. 7 μm), with acetone–acetonitrile (40:60, v/v) as mobile phase at a flow-rate of 1 ml min^{-1}; the eluates were detected at 420 nm.

In order to extend the applicability of HPLC to the porphyrin complexes of trivalent metals, Suzuki et al. [28] studied the specific retention behavior of metal(III) TPP chelates in non-aqueous reversed-phase HPLC. The authors attributed the exceptionally large retention observed for MnTPPCl and CoTPPCl to the dissociation of the complexes in the mobile phase and the adsorption of the cationic metal TPP complexes on

the unmodified surface silanol sites on the reversed-phase column packing material. Any undesirable large retention could be suppressed by the addition of NH_4Cl to the mobile phase. It is interesting that the retention of MnTPPCl and CoTPPCl decreases dramatically with an increase in the concentration of NH_4Cl added to the mobile phase: a linear relationship between log k′ and log [NH_4Cl], with the slope of about -1, was observed for these two metal (III) complexes in the concentration range of NH_4Cl from 2.5×10^{-4} to 1.3×10^{-2} mol l^{-1}. The retention of the trivalent Mn, Fe and Co complexes of MTPPCl type can be controlled by regulating the NH_4Cl concentration in the ethanolic mobile phase. The successful separation of Mn(III), V(IV), Fe(III) and Ni(II) complexes of TPP has been accomplished by the use of ethanol containing 2.57×10^{-3} mol l^{-1} NH_4Cl as mobile phase.

It is known that the complexes of TPP with rare earths (REs) are considerably less stable than those of other metals, e.g. Fe(II), Fe(III), Ni(II) and Cu(II), owing to the large ionic radii of the RE(III) ions (> 100 pm at coordination number > 6) compared with the best fit (64 pm) for the hole in N-4 moiety of porphyrin [29]. The suppression of undesirable decomposition of the complexes in the chromatographic process is the prime requisite for the successful HPLC separation of RE-porphyrins.

Suzuki et al. [30] successfully developed RE–TPP complexes on an octadecyl-bonded silica TLC plate with a developing solvent containing both acetylacetone and diethylamine. The complexes showed high stability during the separation process.

In a later study Saitoh et al. [31] examined the feasibility of reversed-phase HPLC for the separation of the complexes of TPP with 12 rare earths, viz. Y(III), Nd(III), Sm(III), Eu(III), Gd(III), Tb(III), Dy(III), Ho(III), Er(III), Tm(III), Yb(III) and Lu(III), which have very similar chemical properties. All these RE–TPP complexes can be chromatographed with high stability in their migration process along the column with a methanol–water mixture containing a small amount of acetylacetone and an amine as mobile phase. The elution sequence for the RE complexes depends on the amine added to the mobile phase. The amine functions as a base which promotes the dissociation of Hacac to $acac^-$ ion, and accordingly the mixed ligand complex RE(TPP)(acac) is stabilized. Amines, particularly the mixed ligand complex RE(TPP)(acac) is stabilized. Amines, particularly di-*n*-alkylamines, also function as hydrophobic neutral ligands with which an RE–TPP can form an adduct complex, and accordingly the retention is enhanced. The effect of the latter function depends on the amine used, which is explained in terms of a steric effect of the alkyl moiety in the amine molecule. The Nd, Gd, Tb, Dy, Ho, Er and Lu complexes are successfully separated in 15 min, as shown in Fig. 3.

It appears that Saitoh et al.'s study will be useful in porphyrin chemistry where the separation or purification of RE–TPP complexes is required. However, when the method is applied to the determination of RE(III) ions by HPLC in aqueous samples, the development of a successful procedure for the quantitative formation of RE–TPP complexes is still urgently needed.

Little work has been done on the quantitative determination of trace metals. The scheme for the determination of metals has two essential points: quantitative chelation of the metal–TPP complexes at the microgram level and separation and measurement of the metal chelates within a short time. Reversed-phase HPLC is known to be a

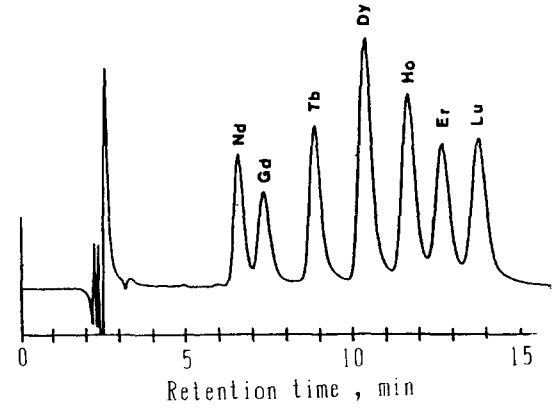

Fig. 3. HPLC separation of RE–TPP complexes. Column, TSK Gel ODS-80TM (150 × 4.6 mm i.d., 5 μm); mobile phase, methanol–water–Hacac–TEA (90:10:0.5:0.68, v/v); flow-rate, 0.8 ml min^{-1}; detection at 555 nm.

promising technique for the separation of several metal–TPP chelates. Accordingly, the most urgent need is to establish a suitable procedure for the preparation of these chelates. Several methods are available for the preparation of metal porphyrin chelates [32]. However, these are useful on a preparative rather than an analytical scale and the quantitative nature of the reaction has been little studied. Saitoh and Suzuki [33] described procedures for the quantitative formation of TPP chelates of Ni(II), Cu(II) and Zn(II) and the simultaneous determination of these metals in NBS SRM bovine liver. The metal ions were extracted as their diethyldithiocarbamate (DDC) chelates from an aqueous solution into carbon tetrachloride. The extract, after removal of the solvent, was treated with TPP in benzyl alcohol at 140°C for 60 min. Quantitative conversion of the DDC chelate into the TPP chelate was obtained over the range 0.25–4.5 μg of each metal by use of 3 μmol of TPP. The conversion procedure may be demonstrated as follows:

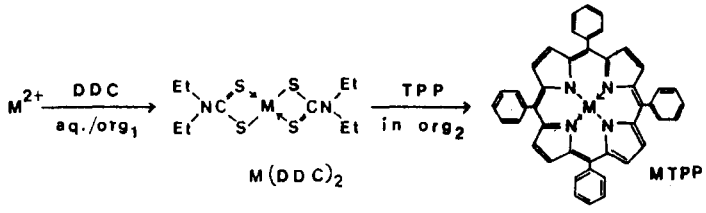

Saitoh and Suzuki's extraction step with DDC not only facilitates metal–TPP chelate formation but also pre-separates the metal ions of interest from a complicated real sample. However, the extraction and conversion procedure is complicated and time-consuming. Accordingly, a high level of operator skill is required to minimize the loss of metal ions during the sample preparation procedure. It appears that an easier procedure for the formation of metal–TPP chelates is needed.

After the extraction and conversion step, TPP and its Ni(II), Cu(II) and Zn(II) chelates were separated on a LiChrosorb RP-18 column (250 × 4 mm i.d. 7 μm) with acetone–acetonitrile (40:60, v/v) as the mobile phase. The flow-rate was 1.3 ml min^{-1} and the eluates were detected at 412 nm.

Liu and Huang [34] reported another feasible procedure for the quantitative formation of TPP chelates with Cu(II), Pb(II), Zn(II) and Cd(II). First, the metal ions reacted with TPP in *N,N*-dimethylformamide (DMF) at 100°C for 25 min with solid NaOH as catalyst. After the solution had cooled to room temperature, pure benzene was used to extract the MTPP chelates from the DMF solution.

The HPLC separation was achieved on a Micropak MCH-5 column (150 × 4 mm i.d.). The mobile phase was methanol–water–chloroform (94:1:5, v/v) and the eluates were detected at 425 nm. The detection limits were 0.04 ng for Cd(II), 0.16 ng for Pb(II), 0.20 ng for Cu(II) and 0.005 ng for Zn(II). The method was applied to the determination of metal ions in electroplating waste liquor and tin alloy.

From the papers that have been published on the HPLC of TPP chelates, we can see that most research work has been focused on the retention behavior of the chelates from theoretical viewpoints. As the TPP reagent is insoluble in water, the quantitative formation of the TPP chelates is difficult to achieve. Thus the application of the HPLC determination of metal ions with TPP as chelating reagent is limited.

2.2.2. TTP

Kobayashi et al. [35,36] investigated the migration behavior of metal–TTP complexes in HPTLC systems with cellulose, silica gel and octadecyl-bonded silica gel thin layers. Although the central metal atom is small in size relative to the porphyrin molecule and accordingly it is surrounded by the large cyclic organic structure of porphyrin, the mobility of metal–TTP complexes depends considerably on the central metal ion. It is considered that the central metal of a TTP complex influences the π-electron system of the metalloporphyrin with which the polar adsorbent

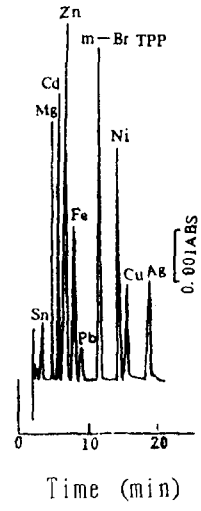

Fig. 4. Chromatogram of metal–*m*-BrTPP complexes. Column, YQG-C_{18} (150 × 5 mm i.d., 5 μm); mobile phase, methanol–acetonitrile (65:35, v/v); flow-rate, 1.0 ml min^{-1} and 3.0 ml min^{-1} after Pb has eluted; detection at 420 nm; sensitivity, 0.05 a.u.f.s; injection volume, 20 μl containing 10 ng Mg and Zn, 55 ng Cd and Fe, 65 ng Sn, 80 ng Ni, 85 ng Pb, 130 ng Cu and 145 ng Ag.

interacts. From the work of Kobayashi et al., we can conclude that a C_{18}-silica plate with a non-aqueous eluent is more convenient and effective for the separation of metal-TTP complexes.

On the basis of the HPTLC studies, Kobayashi et al. [37] successfully separated the TTP complexes of Mg, VO, Ni, Cu, Zn and Pd in about 10 min on a LiChrosorb RP-18 column (250 × 4 mm i.d., 7 μm) with acetone–acetonitrile (70:30, v/v) as mobile phase at a flow-rate of 1 ml min^{-1}; detection was achieved at 420 nm.

The above work has further confirmed the feasibility of the reversed-phase separation mode using a non-aqueous solution as mobile phase for the separation of metal chelates with water-insoluble porphyrins.

2.2.3. *m*-BrTPP

Cheng et al. [38] synthesized *m*-BrTPP and for the first time used it as chelating reagent for the reversed-phase HPLC separation and determination of Sn, Mg, Cd, Zn, Fe, Pb, Ni, Cu and Ag with a non-aqueous mobile phase. The chromatogram is shown in Fig. 4. This method can determine more metal ions than any other HPLC method using porphyrins as chelating reagents. It is unfortunate that these authors did not apply their method to the determination of metal ions in practical samples.

2.2.4. THPP

Igarashi et al. [39] described the simultaneous determination of small amounts of Cu(II) and Zn(II) with THPP by HPLC. The chelation procedure is as follows: place a sample solution containing up to 2.0 μg of Cu(II) and Zn(II) in a 100 ml round-bottomed flask and add 5 ml of ethanol, 1 ml of pH 8.0–8.5 buffer solution and 5 ml of 5×10^{-5} mol l^{-1} THPP ethanol solution. Heat and reflux the mixture for 10 min and allow to cool to room temperature, then dilute to 25 ml with water.

The metal chelates were separated on a Radial Pak C_{18} column (100 × 8 mm i.d.) with ethanol–water (75:25, v/v) as mobile phase; the eluates were detected at 420 nm. The method was successfully applied to the determination of Cu and Zn in tap water; 0.70 ppb of Cu(II) and 91. 5 ppb of Zn(II) were detected.

As THPP is slightly soluble in water, the quantitative formation of the MTHPP complexes can be easily performed in aqueous solution. The HPLC determination can be achieved using the conventional reversed-phase mode.

2.2.5. TMPyP

Igarashi et al. [40] reported on the simultaneous determination of Cu(II), Zn(II) and Pd(II) by HPLC with TMPyP as chelating reagent. The recommended procedure is as follows: place a sample solution containing up to 2.0 μg of metal ions in a 50 ml beaker and add 1 ml of 1×10^{-4} mol l^{-1} TMPyP solution and 2 ml of buffer solution (pH 5.0–7.0). Boil the mixture for 30 min, allow to cool to room temperature and then dilute to 25 ml with water.

Separation was performed on a Radial Pak column (silica, 100 × 8 mm i.d.). The mobile phase was H_2O-CH_3COOH (1:1, v/v) containing 0.35 mol l^{-1} of sodium dodecy sulfate (SDS) at a flow-rate of 1.0 ml min^{-1}; the eluates were detected at 430 nm. The peak height calibration

curves for these metal ions were linear in the range 0–0.08 μg ml^{-1}.

2.2.6. TCPP

Igarashi et al. [41] described the simultaneous determination of small amounts of Cu(II), Zn(II), Co(II) and Mn(II) with water-soluble TCPP by reversed-phase HPLC. The procedure is as follows: prepare a sample solution containing up to 1.6 μg of Cu(II), Zn(II), Mn(II) and Co(II) in a 25 ml amber-colored volumetric flask, then add 2 ml of 1×10^{-4} mol l^{-1} TCPP, 0.25 ml of 1 mol l^{-1} pyridine solution, 0.5 ml of 0.1 mol l^{-1} sodium tetraborate buffer solution (pH 9.3) and 1 ml of 1×10^{-4} mol l^{-1} mercury(II) solution. Leave to stand at room temperature for 30 min and dilute to 25 ml with water.

For HPLC, the mobile phase was a 1:1 (w/w) mixture of acetonitrile and acetic acid–sodium acetate buffer solution (pH 3.5) at a flow-rate of 0.5 ml min^{-1}. The column was a Merck CGC glass cartridge of LiChrosorb RP-18 (150 × 3.2 mm i.d., 5 μm). The absorbance was measured at 420 nm. The peak height calibration curves for these metal ions were linear over the range of 4×10^{-8}–1×10^{-6} mol l^{-1}. The method was applied to the determination of Cu(II), Zn(II) Co(II) and Mn(II) in water.

2.2.7. $TPPS_4$

Xu et al. [42] used $TPPS_4$ as a chelating reagent and proposed a new method for the rapid separation and determination of trace amounts of Cu(II), Zn(II), Fe(II) and Mn(II) by reversed-phase ion-pair HPLC. The chelation procedures are as follows: place 0–0.6 ml of standard solution containing Cu(II), Zn(II), Fe(II) and Mn(II) at concentrations of 10 μg ml^{-1} in a 25 ml amber-colored volumetric flask, add 3.0 ml of 1.4×10^{-4} mol l^{-1} $TPPS_4$, 5.0 ml of acetate buffer (pH 4.1), 1.0 ml of 0.01% beryllium II and 2.0 μg of Hg(II) and dilute the solution to 15 ml with water. Heat the solution for 45 min in boiling water, allow it to cool to room temperature and dilute to 25 ml with water.

The chelates were separated on a LiChrosorb RP-18 column (200 × 4.6 mm i.d., 5 μm). The mobile phase was acetonitrile–water (40:60, v/v) containing 8 mmol l^{-1} tetrabutylammonium bromide (ion-pair reagent) and 10 mmol l^{-1} acetic acid-sodium acetate buffer (pH 4.1). The eluates were detected at 420 nm. The chromatogram is shown in Fig. 5.

The authors claimed that the detection limits for Mn, Zn, Cu and Fe were 3.6, 0.93, 0.70 and 1.8 ppb, respectively. This method was successfully applied to the determination of Cu, Zn, Fe and Mn in a standard sample of peach leaves and the analytical results were in agreement with standard reference values.

Similar work was done by Leiet al. [43]. The chelation reaction of $TPPS_4$ with Cu(II), Co(II), Mn(II) and Zn(II) was optimized by catalyzing it with Hg(II) and in the presence of pyridine. For the HPLC separation of the metal ions, the authors employed benzyltriethylammonium chloride as counter ion. They proposed a rapid method for the determination of Cu(II), Co(II), Mn(II) and Zn(II) within 12 min. The detection limits were 0.42, 0.28, 0.23 and 0.09 ppb for Cu, Co, Mn and Zn, respectively.

These authors found that the peak of $CoTPPS_4$ was not good and overlapped that of $MnTPPS_4$ when pyridine was not added to the mobile phase.

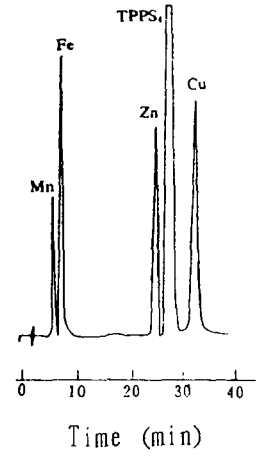

Fig. 5. Chromatogram of $TPPS_4$ and its metal chelates. Column, LiChrosorb RP-18 (200 × 4.6 mm i.d., 5 μm); mobile phase, acetonitrile–water (40:60, v/v), containing 8 mmol l^{-1} TBABr and 10 mmol l^{-1} HOAc–NaOAc buffer (PH 4.1); flow-rate, 1.0 ml min^{-1}; detection at 420 nm; sensitivity, 0.002 a.u.f.s; injection volume, 10 μl.

It was deduced that pyridine participates in the pre-column chelation process. Adding pyridine to the mobile phase can suppress the breakaway of pyridine from $CoTPPS_4$ and make the peak of $CoTPPS_4$ sharp and separated from that of $MnTPPS_4$.

In subsequent papers, Lei and co-workers applied the method to the determination of Cu(II) and Zn(II) in peanuts [44] and Mn(II), Zn(II) and Cu(II) in tea [45].

2.2.8. *m-BrTPPS*$_4$

Xu et al. [46] synthesized a new water-soluble porphyrin reagent, *m*-$BrTPPS_4$, and successfully used it as a pre-column chelating reagent for the determination of Mn(II), Fe(III), Zn(II), Pd(II) and Cu(II) by reversed-phase ion-pair HPLC.

The complexes were quantitatively formed according to the following procedure: add 3 ml of 1.5×10^{-4} mol l^{-1} *m*-$BrTPPS_4$, 5.0 ml of 1.0 mol l^{-1} acetate buffer (pH 4.1), 1.0 ml of 0.01% (w/w) beryllon II and 2.0 μg of Hg(II) to a sample containing Cu(II), Zn(II), Pd(II), Mn(II) and Fe(II), dilute the mixture to about 15 ml and heat the solution in boiling water for 45 min.

For HPLC analysis, a LiChrosorb RP-18 column (200 × 4.6 mm i.d. 5 μm) was employed. The mobile phase was CH_3CN-H_2O (45:55, v/v) containing 2.0 mmol l^{-1} tetrabutylammonium bromide and 10 mmol l^{-1} acetate buffer (pH 5.0), at a flow-rate of 1.0 ml min^{-1}. The detection wavelength was 420 nm. The authors claimed that the limits of detection (20 μl injected) were 160 pg for Mn, 79 pg for Fe, 70 pg for Pd, 36 pg for Cu and 31 pg for Zn.

Xu and co-workers also used *m*-$BrTPPS_4$ as a chelating reagent. For the quantitative determination of metal ions by reversed-phase HPLC, they used tetraethylammonium iodide (TEAI) as counter ion. This method was applied to the determination of trace amounts of Co(II), Zn(II) and Cu(II) in river water [47], tangerine skin and purple rice [48].

2.2.9. *T(4-MOP)PS*$_4$

Xu et al. [49] published a reversed-phase ion-pair HPLC method for the determination of Co(II), Zn(II) and Cu(II) in tangerine skin and purple rice with $T(4\text{-MOP})PS_4$ as pre-column chelating reagent. The chelation procedure was performed as follows: add 0–3.0 μg of Co(II), Zn(II) and Cu(II), 3.0 ml of $T(4\text{-MOP})PS_4$, 2.0 ml of pH 4.0 buffer, 1.0 ml of 0.2% hydroxylamine and 1.0 ml of 0.03% 8-hydroxyquinoline-5-sulfonic acid to a 10 ml colorimetric tube and heat the tube in boiling water for 12 min. A Zorbax ODS column (150 × 4.6 mm i.d., 5 μm) was used with acetonitrile–water (31:69, v/v) containing 0.040 mol l^{-1} TEAI and 0.020 mol l^{-1} HOAc-NaOAc buffer (pH 6.0) as mobile phase at a flow-rate of 1.0 ml min^{-1}. The column temperature was 40°C and the eluates were detected at 418 nm. The complexes and porphyrin were separated within 12 min. The authors claimed that the detection limits for Co, Zn, and Cu were 0.12, 10.12 and 0.35 ng, respectively.

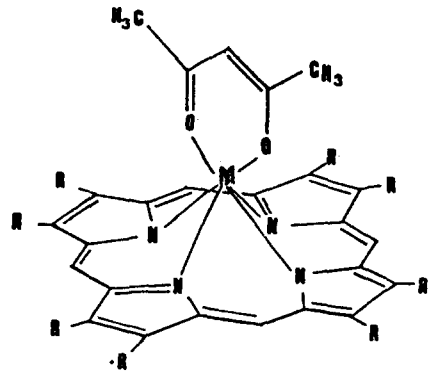

Fig. 6. Structural formula of RE(OEP)(acac) (R = ethyl).

2.3. *Porphyrins with substituents on the pyrrole rings*

2.3.1. *Octaethylporphyrin*

Octaethylporphyrin (OEP) is a kind of water-insoluble porphyrin which has been frequently used as a model porphyrin similarly to TPP in studies relating to porphyrins. In OEP, eight ethyl groups are bonded to eight β-pyrrole positions.

Shibata et al. [50] studied the reversed-phase HPLC behavior of the complexes of OEP with 11 trivalent REs viz., Y, Sm, Eu, Gd, Tb, Dy, Ho, Er, Tm, Yb and Lu, on an octadecyl-bonded silica gel column. The complexes were prepared in the form of RE(OEP)(acac) as shown in Fig. 6.

All these complexes can be eluted without decomposition with a methanol–water mixture that contains a small amount (about 1%) of acetylacetone (Hacac) and an amine. A amine added to the mobile phase with a small amount of Hacac functions as a base which enhances the stability of the RE(OEP)(acac) complexes and accordingly suppresses their undesirable adsorption on the stationary phase material. The second useful function of the amine is with regard to the selectivity and the elution sequence for the RE-OEP complexes. The retention selectivity depends on the amine used. The effect of dialkylamines in particular on the retention sequence of RE-OEP complexes is different from that for RE–TPP complexes [30].

OEP has not been used for the quantitative determination of rare earth elements owing to the difficulty of chelate formation. More research work should be focused on the quantitative formation and determination of RE–OEP complexes.

2.3.2. Hematoporphyrin IX (Hp)

Hp is well known as the first porphyrin to be isolated from natural materials. Hp and its metal complexes have been of increasing interest from the medical point of view because of their usefulness in the diagnosis and chemotherapy of malignant tumors [51–53]. The general structure of a metal (II)–Hp complex (MHp) is illustrated in Fig. 7.

Suzuki et al. [54] described the behavior of Hp and its complexes with Ni(II), Cu(II) and Zn(II)

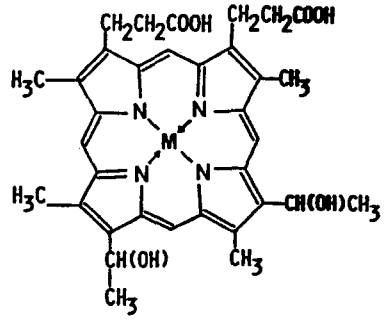

Fig. 7. Structural formula of a metal(II)–hematoporphyrin IX complex.

in a reversed-phase system. These four compounds were successfully separated within about 8 min on a Lichrosorb RP-18 column (250 × 4 mm i.d.) with methanol–phosphate buffer (pH 3) (85:15, v/v) as the mobile phase, at a flow-rate of 1 ml min^{-1}. The elution of the compound was monitored spectrophotometrically at 398 nm. The retention order was ZnP < (Hp) < NiP < CuP. This metal order with respect to the increase in retention is comparable with those observed for metal complexes of porphyrins more hydrophobic than Hp, such as TPP, TTP and porphine, on LiChrosorb RP-18 column with a non-aqueous polar mobile phase.

It was suggested that the retention order of the central metals of the metal porphyrin complexes shown above would be valid for various metalloporphyrins irrespective of whether the porphyrin ligand contains hydrophobic functional groups. It is unfortunate that the authors did not apply their method to the quantitative determination of metal ions.

3. Conclusions

Because of the widespread occurrence and biological importance of metalloporphyrins in plants and animals, the chemistry of these compounds are of interest to workers in a variety of fields. Porphyrins are attractive from the analytical point of view because of their very high molar absorbance. The main problem in utilizing a porphyrin as a chelating reagent for the HPLC determination of metal ions is that the formation of the metal chelates is often difficult. To enhance the rate of metalloporphyrin formation, the following procedures have been employed: (i) heating; (ii) the use of reducing agents such as hydroxylamine and ascorbic acid; (iii) addition of an aromatic heterocyclic base such as pyridine and imidazole; (iv) the use of a substitution reaction with cadmium or mercury porphyrins; (v) the use of porphyrins with substituents at the pyrrole nitrogens; and (vi) the introduction of functional groups binding metal ions in the vicinity of the porphyrin nucleus.

Among the porphyrin compounds, the water-insoluble type are relatively easy to synthesize in reasonable yields. As they are not soluble in water, the preparation of metal chelates cannot be accomplished in aqueous solution and complicated extraction procedures are often needed. Moreover, the porphyrins and their metal chelates are not easy to separate using the conventional reversed-phase HPLC mode. From papers that have been published on the separation of water-insoluble metalloporphyrins, we can see that non-aqueous reversed-phase HPLC has been employed by most workers.

Water-soluble porphryins are relatively difficult to synthesize and the yields are much lower, but their solubility in water makes it easy to prepare metal chelates in aqueous solution and the metal chelates can be separated by ion-pair reversed-phase HPLC. However, water-soluble porphyrins are usually synthesized by binding hydrophilic groups with water-insoluble porphyrins, thus making the molecule large and difficult to separate on a normal column.

To solve the above problems, more research work should be conducted. The following are the aspects that should be addressed in the future:

(i) study of easier procedures for the preparation and purification of porphyrins;

(ii) synthesis of new porphyrins which have superior chromatographic properties and high sensitivities;

(iii) study of new methods for the quantitative formation of metal porphyrin chelates, with special attention to the quantitative reaction of water-insoluble porphyrins with metal ions in aqueous solution;

(iv) extension of HPLC to the determination of more metals as their porphyrin chelates;

(v) application of porphyrins to speciation studies;

(vi) application of published methods to the determination of metal ions in practical samples; and

(vii) enhancement of the application of HPLC to the separation and determination of naturally occurring complexes.

References

[1] J.F.K. Huber, J.C. Kraak and H. Veening, Anal. Chem., 44 (1972) 1554.
[2] Y. Zhao and C.G. Fu, Chem. J. Chin. Univ., 10 (1989) 534.
[3] Y. Zhao and C.G. Fu, Anal. Chim. Acta, 230 (1990) 23.
[4] Y. Zhao and C.G. Fu, Analyst, 116 (1991) 621.
[5] Q. Liu, J. Liu, Y. Tong and J. Cheng, Anal. Chim. Acta, 269 (1992) 223.
[6] Y. Nagaosa, H. Kawabe and A.M. Bond, Anal. Chem., 63 (1991) 28.
[7] M.L. Marina, P. Andres and J.C. Masa, Chromatographia, 35 (1993) 621.
[8] S. Dilli, P.R. Haddad and A.K. Htoon, J. Chromatogr., 500 (1990) 313.
[9] S. Ichinoki and M. Yamazaki, J. Chromatogr. Sci., 28 (1990) 258.
[10] J.W. O'Laughline, J. Liq. Chromatogr., 7 (1984) 127.
[11] Y.X. Yuan, Chin. J. Anal. Chem., 18 (1990) 87.
[12] K. Robards, P. Star and E. Patsalides, Analyst, 116 (1991) 1247.
[13] Z. Yi, G.S. Zhuang and P.R. Brown, J. Liq. Chromatogr., 16 (1993) 3133.
[14] J.K. Cheng, Chem. J. Chin. Univ., 16 (5) (1995) 696.
[15] T. Makino and J. Itoh, Clin. Chim. Acta, 111 (1981) 1.
[16] S. Igarashi, T. Saeki and T. Yotsuyanagi, Bunseki Kagaku, 32 (1983) 39.
[17] Q.D. Ni and Y.H. Zhang, Chin. J. Anal. Chem., 22 (1994) 980.
[18] Y.H. Zhang, Q.D. Ni and Y.P. Liu, Anal. Lab. (Chinese), 14 (1995) 58.
[19] F.Z. Luo and G.P. Wei, Chin. J. Anal. Chem., 22 (1994) 1118.
[20] Z.T. Pan, Z.S. Jin, Y. Zhao, F.L. Cui and M.Y. Xu, Anal. Lab. (Chinese), 13 (1994) 12.
[21] C.K. Lim, J.M. Rideout and T.J. Peters, J. Chromatogr., 317 (1984) 333.
[22] C.J. Boreham and C.J.R. Fookes, J. Chromatogr., 467 (1989) 195.
[23] J.W. Ho and L.Y.F. Candy, J. Liq. Chromatogr., 17 (1994) 549.
[24] Y. Wakui, K. Saitoh and N. Suzuki, Chromatographia, 22 (1986) 160.
[25] K.S. Hui, B.A. Davis and A.A. Boulton, J. Chromatogr., 115 (1975) 581.
[26] K. Saitoh, M. Kobayashi and N. Suzuki, Anal. Chem., 53 (1981) 2309.
[27] K. Saitoh, M. Kobayashi and N. Suzuki, J. Chromatogr., 243 (1982) 291.
[28] N. Suzuki, T. Takeda and K. Saitoh, Chromatographia, 22 (1986) 43.
[29] W. Buchler, in K.M. Smith (Ed.), Porphyrins and Metalloporphryins, Elsevier, Amsterdam, 1975, p. 191.
[30] N. Suzuki, K. Saitoh and Y. Shibata, J. Chromatogr., 504 (1990) 179.

[31] K. Saitoh, Y. Shibata and N. Suzuki, J. Chromatogr., 542 (1991) 351.
[32] J.W. Buchler, in D. Dolphin (Ed.), The Porphyrins, Vol. 10, Chp. 10, Academic Press, New York, 1978.
[33] K. Saitoh and N. Suzuki, Anal. Chim. Acta, 178 (1985) 169.
[34] W.Y. Liu and J.H. Huang Chin. J. Chromatogr., 4 (1986) 206.
[35] M. Kobayashi, K. Saitoh and N. Suzuki, Chromatographia, 18 (1984) 441.
[36] M. Kobayashi, K. Saitoh and N. Suzuki, Chromatographia, 20 (1985) 49.
[37] M. Kobayashi, K. Saitoh and N. Suzuki, Chromatographia, 20 (1985) 72.
[38] J.K. Cheng, X.J. Xu and H.S. Zhang, Chem. J. Chin. Univ. (Engl. Edn.), 4 (1988) 17.
[39] S. Igarashi, T. Hashimoto, Y. Matsumoto and T. Yotsuyanagi, Bunseki Kagaku, 32 (1983) 591.
[40] S. Igarashi, M. Nakano and T. Yotsuyanagi, Bunseki Kagaku, 32 (1983) 67.
[41] S. Igarashi, A. Obara, H. Adachi and T. Yotsuyanagi, Bunseki Kagaku, 35 (1986) 829.
[42] X.J. Xu, H.S. Zhang, C.Y. Zhang and J.K. Cheng, Chem. J. Chin. Univ., 11 (1990) 947.
[43] C.H. Lei, F.L. Tang, M.R. Tang and X.H. Chen. Chin. J. Chromatogr., 12 (1994) 276.
[44] C.H. Lei, F.L. Tang, L.H. Wang and M.R. Tang, Chin. J. Anal. Chem., 22 (1994) 552.
[45] C.H. Lei, F.L. Tang, L.H. Wang and X.Q. Mao, Chin. J. Instrum. Anal., 13 (1994) 9.
[46] X.J. Xu, H.S. Zhang, C.Y. Zhang and J.K. Cheng, Anal. Chem., 63 (1991) 2529.
[47] F. Xu, L. Ying, B. Hu and F.L. Tang, Chin. J. Chromatogr., 12 (1994) 208.
[48] F. Xu, L. Ying, J.R. Chen and F.L. Tang, Chin. J. Instrum. Anal., 14 (1995) 46.
[49] F. Xu, J.R. Chen, L. Ying and B.L. Chen, Chin. J. Anal. Chem., 22 (1994) 970.
[50] Y. Shibata, K. Saitoh and N. Suzuki, J. Chromatogr., 598 (1992) 73.
[51] T.J. Dougherty, J.E. Kaufman, A. Goldfarb, K.R. Weishaupt, D. Boyl and A. Mittelman, Cancer Res., 38 (1978) 2628.
[52] A. Dahlman, A.G. Wile, R.G. Burns, G.R. Mason, F.M. Johnson and M.W. Berns, Cancer Res., 43 (1983) 430.
[53] D. Kesel and M.L. Cheng, Cancer Res., 45 (1985) 3053.
[54] N. Suzuki, K. Saitoh and Y. Sugiyama, Chromatographia, 22 (1986) 132.

ELSEVIER

Talanta 44 (1997) 605–615

Talanta

Renewable liquid film-based electrochemical sensor for gaseous hydroperoxides

Huiliang Huang, Purnendu K. Dasgupta *

Department of Chemistry and Biochemistry Texas Tech University, Lubbock, TX 79490-1061, USA

Received 16 July 1996; received in revised form 16 August 1996; accepted 16 August 1996

Abstract

Electrochemical sensors for hydroperoxides based on thin flowing films were investigated. The sensor is composed of two segments of Nafion tubing put on a silver wire. A small portion of the silver wire is exposed and is chloridized to function as the reference electrode. One Nafion segment has a Pt-wire coil wrapped on it to function as the counter electrode and the other has a similar Pt-Rh wire coil that functions as the working electrode. A collection solution flows as a thin film on the sensor surface and also functions as the collection medium. Hydrogen peroxide and cumene hydroperoxide were examined as test compounds. The former can be oxidatively determined with a Pt-Rh electrode over a large range (ppb–ppm) without any significant influence of relative humidity. By using a technique to stop the liquid flow, the sensitivity can be further improved. Cumene hydroperoxide, an industrially important hydroperoxide, can be determined easily with a relative precision of better than 5% in the vapor phase over simulated process reaction mixtures containing percentage levels of the analyte by reduction on a Pd electrode. The sensor is simple and inexpensive to fabricate and requires only a suitably equipped personal computer for operation. © 1997 Elsevier Science B.V.

Keywords: Electrochemical sensor; Hydroperoxides; Renewable liquid film

1. Introduction

In recent years, we have been fascinated by utility of small liquid drops and thin films for sample collection in biphasic systems, such as the collection of a gaseous analyte or solvent extraction, with analysis either in situ or on-line [1–7]. While much of this work has focused on the use of optical detectors, is was realized from the inception [1] that electrochemical detection should provide a very powerful means of in situ detection in these systems. Liquid drops and films have had a long history in electrochemistry in particular, the recognition that falling drops continuously provide a highly reproducible and renewable surface led to the dropping mercury electrode (DME) [8]. The invention of the DME ushered in the modern era of instrumental analytical methods and resulted in the 1959 Nobel Prize in Chemistry, the first related to instrumental analysis [9].

The DME itself operates best in the analytical concentration range 10^{-3}–10^{-5} M. Below an analyte concentration of 10^{-5} M, the background current becomes comparable with the diffusion

* Corresponding author.

PII S0039-9140(96)02069-3

current due to the analyte, thus restricting any further improvement in the limits of detection (LODs) in classical polarography. On the other hand, if a renewable liquid film is made to cover conventional metallic electrodes, it may be possible to determine much smaller analyte concentrations in the liquid. Mercury film electrodes, for example, have been extensively used to improve sensitivities and detection limits over those attainable with conventional solid electrodes [10–14], although the stability of such electrodes may be a problem [15]. Looking at more conventional liquids for forming a film for electrochemical sensing, if the liquid film is of suitable composition, such a film can be used for the collection of gaseous analytes, with the film serving as a miniature sampler/preconcentrator. If the analytes collected into the film are electroactive, electrochemical sensing would be simple and attractive.

Hydrogen peroxide is an important atmospheric oxidant [16] and we have been interested in the atmospheric measurement of H_2O_2 for some time [17,18]. Hydrogen peroxide is also used as a sterilizing agent in bioreactors and for safety reasons it is desirable to have a means for monitoring residual concentrations after sterilization has been completed. Hydroperoxides (of which H_2O_2 is the simplest member) are reactive oxidants that are electroactive. Some organic peroxides are also industrially important as polymerization initiators and cross-linking agents, dicumenyl peroxide (DCP) being particularly important [19]. DCP is typically produced from cumene hydroperoxide ($CumHO_2$). A typical reactor mixture may contain an aromatic alcohol (such as phenylpropan-2-ol) or phenol, a ketone such as acetone or acetophenone and cumene. $CumHO_2$ itself may also be used for the radical polymerization of methacrylates [20] and the acid hydrolysis of $CumHO_2$ to yield acetone and phenol is a major means of production of the latter two compounds, necessitating the use of $CumHO_2$ in quantities of many thousands of kilograms [21]. In a typical industrial application, it may be desirable to control the concentration of $CumHO_2$ at the levels below 10%. Rather than sampling the complex liquid mixture, monitoring the vapor phase in the reactor is an attractive alternative for monitoring the $CumHO_2$ content. Electrochemical sensors for H_2O_2 are well known [22]. In the present work, we explored the utility of a renewable film-based electrochemical sensor for measuring hydroperoxides from low ppb levels of gaseous H_2O_2 to vapor phase $CumHO_2$ present in percentage levels over the liquid.

2. Experimental

2.1. Reagents and materials

A stock solution of 1 M H_2O_2 was prepared from 30% H_2O_2 (Fisher) and standardized by iodimetry [23]. Lower concentrations of H_2O_2 were prepared fresh daily from this stock solution. Nafion tubing (dry dimensions 1 mm o.d., 0.8 mm i.d.) was obtained from Perma-Pure Products (Toms River, NJ, USA). Non-conductive epoxy adhesive was obtained from Decon (Danvers, MA, USA). Platinum, palladium, platinum/rhodium (30%) and silver wires were obtained from Aesar (Ward Hill, MA, USA).

2.2. Instrumentation

Fig. 1 shows a computerized electrochemical analyzer consisting of a potentiostat and a current to voltage converter. An LF353N (National Semiconductor) dual BiFET operational amplifier (A1 and A2) integrated circuit forms the basis of a potentiostat to provide a constant potential for conventional amperometry or a pulsed potential for pulsed amperometry. The A3 amplifier functions as a current to voltage converter to monitor the sensor current. The reference electrode R, the counter electrode C and the working electrode W in the electrochemical sensor S are connected to the non-inverting input of A2, the output of A1 and the inverting input of A3, respectively. The rotary switch P selects the feed back gain resistor (10 KΩ–10 MΩ). An 80486 class PC operating at 33 MHz is interfaced with the electronic circuit via a 12-bit A/D–D/A board (Flash-12 high speed analog and digital I/O card, Strawberry Tree, Sunnyvale, CA, USA) for controlling instru-

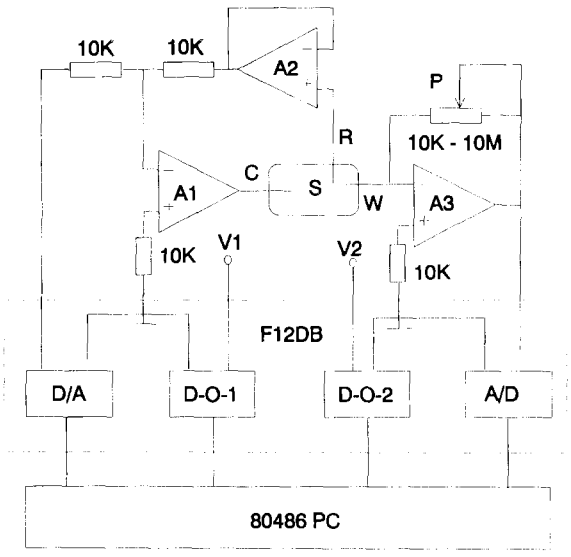

Fig. 1. PC-based electrochemical detection system. A1–A3 = FET-input operational amplifier; S = sensor (C, R, W = counter, refernece and working electrodes); F12DB = Flash-12 and daughter board housing D/A and A/D units and digital output-controlled relays (D-O-1, D-O-2) that govern valves V1 and V2.

ment operation and data acquisition. The digital to analog converter (D/A) can generate a constant voltage for amperometric measurements or any desired pulsed waveform for pulsed amperometric measurements. The analog to digital converter (A/D) acquires data from the A3 output. The digital outputs D-O-1 and the D-O-2 provide independent means for controlling valves V1 (see Fig. 2) and V2 (valve for stopping liquid flow, see below). Instrument control and operation are conducted by software written in-house in C and available from the authors on request. The operational details are given below.

2.3. Test arrangement

The sampling manifold and test gas generation device (reactor–simulator) are shown in Fig. 2. All gas flows are metered by mass flow controllers (Model FC-280, Tylan General, Torrance, CA, USA). Compressed house air is fed through a pressure regulator and purified by column C, containing sequential beds of silica gel and activated carbon. The pure air flow is then divided into three streams. One stream, metered through M4 (maximum 500 cm^3 min^{-1}), flows into the gas generator. For H_2O_2, the gas generator is a length of porous hydrophobic membrane immersed in H_2O_2 solution of known concentration; the exit gas is in Henry's law equilibrium with the solution. Details of such an H_2O_2 source are given elsewhere [24]. The exit H_2O_2 concentration is readily computed from published Henry's law data for H_2O_2.

To test the feasibility of monitoring $CumHO_2$ in a reactor that may typically contain 49% phenol, 23% acetone, 15% cumene and 3% $CumHO_2$ by weight, we mimicked this composition in the generating liquid except that acetontirile was substituted for cumene. The amount of $CumHO_2$ was varied by varying the $CumHO_2$ and acetonitrile content, maintaining a constant amount of phenol and acetone. Approximately 150 ml of this liquid was put in a 500 ml capacity Erlenmeyer flask, with the air inlet tube located 1 cm above the liquid surface and the exit tube 1 cm below the silicone-rubber stopper. The gaseous $CumHO_2$ output from this source was stable, but the exact gas phase concentration was not determined.

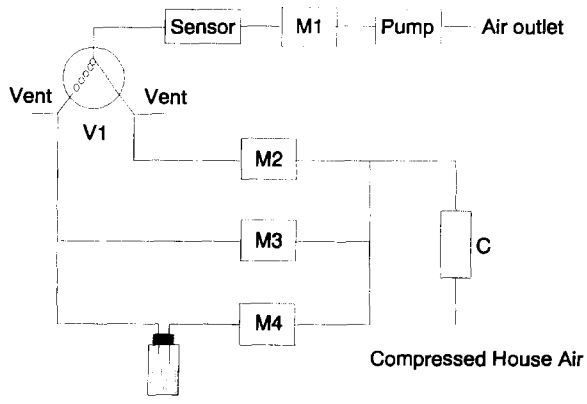

Fig. 2. C = silica gel/activated carbon column for air pruification; M1-M4 = mass flow controllers (M1 controls sampling rate, M2 controls zero (pure) air flow, M3 controls dilution air (may be partially humidified, see text) and M4 controls flow through the test gas generator (depicted as a bottle)); V1 = three-way PFA Teflon solenoid valve.

The exit gas from the generator is diluted by pure dry air metered by M3. The gas concentration generated in the merged stream is thus controlled by choosing an appropriate flow-rate ratio of M4 and M3. The humidity of the test gas was varied by dividing the stream after M3 into two parts and putting a controlled amount through a water bubbler, then recombining the wet and dry streams before addition to the gas generator output. The humidity of the final mixture was measured by a capacitance-type relative humidity probe.

Either the test gas stream or the purified air metered by M2 is selected by three-way perfluoroalkoxy (PF) Teflon valve V (Flouroware, Chaska, MN, USA) to be sampled by the sensor. The gas is aspirated by the air pump P at a flow-rate determined by M1 (1 l min^{-1}, unless stated otherwise). All remaining flow streams are vented.

2.4. Sensor fabrication

Fig. 3 shows the sensor construction. Two 15 mm long segments of Nafion tubing are slipped over a 1 mm diameter silver wire, leaving a 1.5 mm segment of bare silver surface exposed between the two tube segments. The exposed silver is anodically chloridized for 10 min in a solution of 0.01 M HCl. This functions as the reference electrode (RE). A 0.2 mm diameter platinum wire is coiled on to one segment of the Nafion tubing to function as the counter electrode (CE) and a 0.25 mm diameter Pt/Rh (30% Rh) or a Pd wire (127 μm) is coiled on to the other, downstream, segment of the Nafion tubing to function as a working electrode (WE). The assembly is then put into a polypropylene T-fitting T1 (3/32 in 1.8 mm i.d.), leaving the working electrode exposed outside the bottom end of the fitting. Epoxy adhesive is then liberally applied to cover up the top end of the fitting with the electrode connections protruding. Liquid (see below) is pumped by a syringe pump (Model 341, Sage Instruments) through the tee arm and flows as a thin film on the surfaces of the CE, the RE and the WE, forming eventually a drop at the tip of the sensor that periodically falls. The sensing arm of T1 is inserted through a hole drilled into another, larger, tee T2 (6.5 mm i.d.), directly on the top of the vertical arm of the latter. The sample gas enters through both the horizontal arms of T2, connected to a common inlet. The sample is aspirated concurrent to the liquid flow, first coming directly in contact with the film covering the WE. (Because the incoming sample gas directly contracts the bottom Nafion segment, it is advantageous to have the working electrode located on this segment. If the sensor

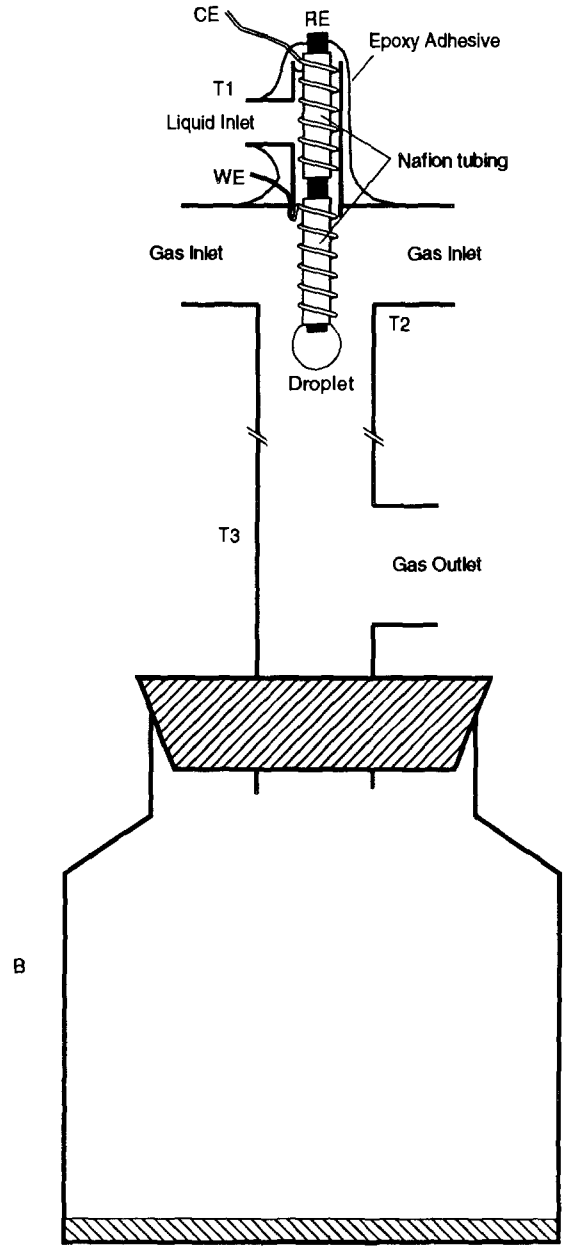

Fig. 3. Sensor arrangement. T1 = sensor tee; RE = reference electrode; CE = counter electrode; WE = working electrode; T2 = gas inlet tee (connected to V1, Fig. 2); T3 = gas outlet tee (connected to M1, Fig. 2); B = waste bottle.

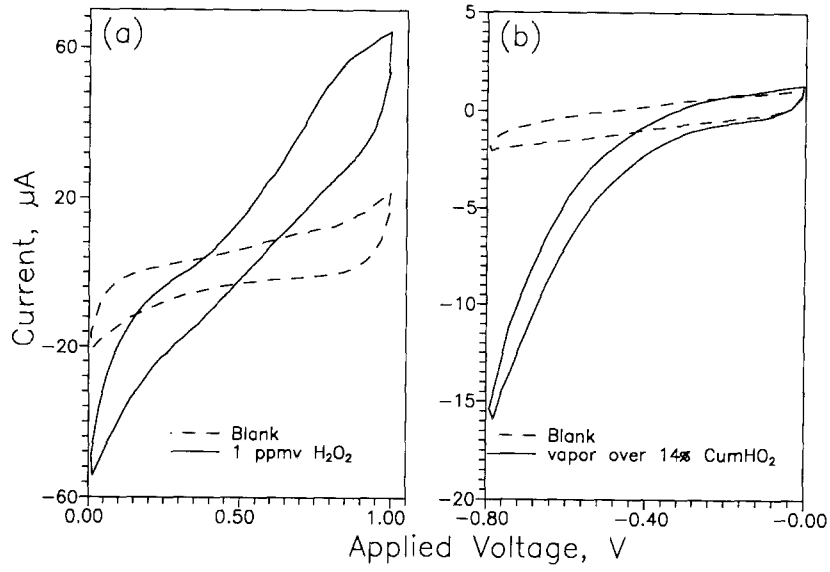

Fig. 4. Cyclic voltammograms of gas phase (a) H_2O_2 and (b) $CumHO_2$. Sensor construction and film composition are indicated in the text. Liquid and gas flow-rates are 15.3 μl min^{-1} and 1 l min^{-1}, respectively.

assembly were to be placed further down T1 such that the entering sample gas first contacts the top Nafion segment, the working electrode would be best placed on the top segment). Following a short length of connecting PFA tubing, the gas exits at the bottom through another tee T3 while waste liquid is collected in a bottle B.

3. Results and discussion

3.1. Sensor parameters

H_2O_2 can be determined either by oxidation to O_2 or reduction to water, while other hydropeoxides are determined by reduction. In atmospheric samples, to avoid interference from other concurrently present oxidants, H_2O_2 is preferably determined by oxidation. Sensor parameters that are readily selected include the choice of the electrode material, the film-forming solution and the nature of the reference electrode. In the present work, many combinations of the sensing and counter electrode materials were investigated. For the oxidation of hydrogen peroxide, the best working electrode was found to be Pt/Rh (30% Rh), while Pd was found to be the best electrode material for the reductive determination of $CumHO_2$. Regarding the choice of a reference electrode, a silver/silver chloride electrode is convenient, inexpensive and easily miniaturized. A minimum concentration of chloride is necessary for the electrode to maintain a constant reference potential; this can be accomplished by incorporating some constant concentration of chloride in the film-forming solution.

As a suitable sink for H_2O_2, water itself is sufficient. To promote the formation of a smoothly flowing film, a surfactant such as Triton X-100 (TX-100), 0.3% in concentration, is effective. Thus, for H_2O_2, we use a solution of 0.3% Triton X-100 and 1 mM HCl, the latter providing for a stable reference potential.

Unlike H_2O_2, $CumHO_2$ is very poorly soluble in water. Several water-miscible organic solvents such as acetonitrile, dimethylformamide, dimethyl sulfoxide, ethylene glycol and glycerol, in mixtures with water and salt solutions, were investi-

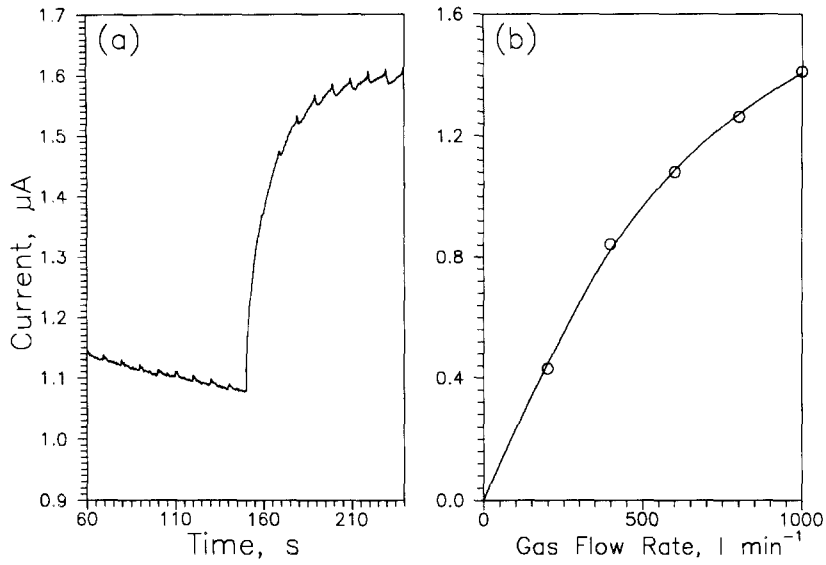

Fig. 5. (a) Sensor output during the sampling cycle, ca. 20 ppbv H_2O_2, flow-rates as in Fig. 4; (b) dependence of the signal on the gas flow-rate, liquid flow-rate 15.3 μl min^{-1}. The solid line is the best fit to Eq. (3).

gated. The best results were obtained with a 30% glycerol–70% saturated $CaCl_2$ solution for monitoring $CumHO_2$. The $CaCl_2$ serves as a humectant.

Fig. 4(a) shows the cyclic voltammogram obtained when 1 ppmv H_2O_2 is sampled in a flowing film of TX-100-HCl. A current plateau is reached above 0.86 V. An applied potential of 0.95 V was therefore chosen for the oxidative determination of H_2O_2. We did not notice any significant interference from common atmospheric gases under these conditions; NO_2 and HCHO produce a response but only when present at very high (ppm) levels, not relevant to ambient air studies.

Fig. 4(b) shows the cyclic voltammogram obtained when $CumHO_2$ is sampled. In this case, the cathodic current continues to increase with increasing cathodic potential within the range tested and never reaches a plateau. Since increasing the cathodic potential much further increases the background current significantly, a potential of −0.80 V was chosen for the reductive determination of $CumHO_2$. All potentials reported are relative to the Ag/AgCl reference electrode in the sensor. Since the two film-forming solutions have different chloride activities, the reference potential is not the same in the two cases.

3.2. Hydrogen peroxide

3.2.1. Sampling cycle and data acquisition

For H_2O_2, valve V1 (Fig. 1) was programmed to switch continuously between zero air and the sample gas for periods of 2.5 and 1.5 min, respectively, thus resulting in a sampling cycle of 4 min. No data were acquired for the first minute, allowing the system to attain a stable zero air response. The background current was then acquired for the next 1.5 min (Fig. 5(a)), at the end of which the valve was switched to the sample gas. The current rose to a stable plateau value over the next 30–60 s and the value for the 210–240 s period was taken to be the sample current. The valve was then switched back to zero air and the cycle repeated. During each sampling cycle, the temporal electrochemical protocol involves pretreating the electrode for 5 s at −0.1 V and then maintaining it at the sensing potential of +0.95 V for the remaining 235 s. The results were interpreted either in terms of current (averaged current

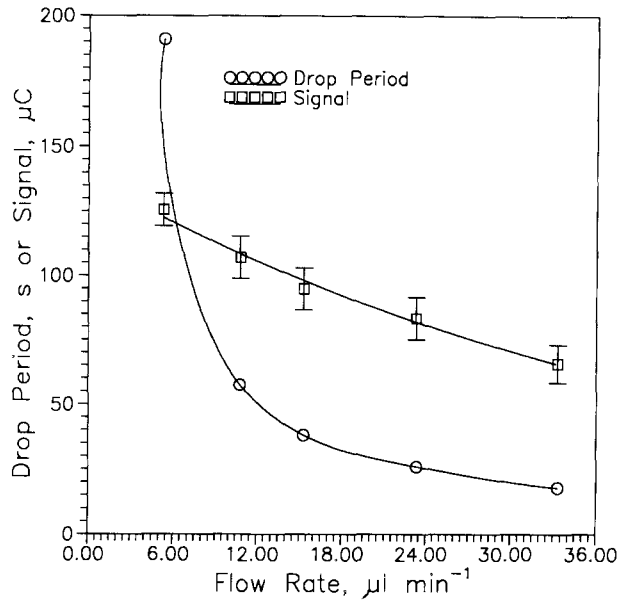

Fig. 6. Decrease in drop period and analytical signal with increasing liquid flow-rate. The collected sample is diluted.

during 210–240 s, less the averaged background current over 120–150 s) or charge (integrated charge in μC, less the background, over the same periods as above). There was no significant difference in the quality of the results using either approach.

3.2.2. Signal dependence on gas flow-rate

With 200 ppbv H_2O_2, the gas flow-rate was varied from 200 to 1000 ml min^{-1}, at a constant liquid flow-rate of 15.3 μl min^{-1}. The analytical signals increased with increasing the gas flow-rate, as shown in Fig. 5(b). When a gas is collected by diffusion to the walls of a tube, the collected fraction f is related to the flow-rate Q by an exponential relationship of the type [25]

$$1 - f = a\, e^{-b/Q} \quad (1)$$

Although the present geometry is not exactly the same, an equation of the same general form should be applicable to the present case. Consider that the total amount of the analyte collected is the product of the flow-rate Q and the collection efficiency f and the analytical signal S should be linearly related to this product, hence

$$f = kS/Q \quad (2)$$

where k is a proportionality constant. Eqs. (1) and (2) can be transposed to the form

$$S = Q(1 - a\, e^{-b/Q})/k \quad (3)$$

The solid line in Fig. 5(b) is the best fit of the experimental data to Eq. (3). The numerical values also suggest that at the lowest sampling rate tested of 200 ml min^{-1}, the collection efficiency is nearly 95%. In other experiments, a gas flow-rate of 1 l min^{-1} was used, except where stated otherwise.

3.2.3. Dependence on liquid flow-rate

With 200 ppbv H_2O_2 sampled at 1 l min^{-1}, the liquid flow-rate was varied from 5.3 to 33.3 μl min^{-1}. The analytical signals and the drop period decrease with increasing liquid flow-rate, as shown in Fig. 6. Both the analytical signal and the drop period are approximately linearly related to

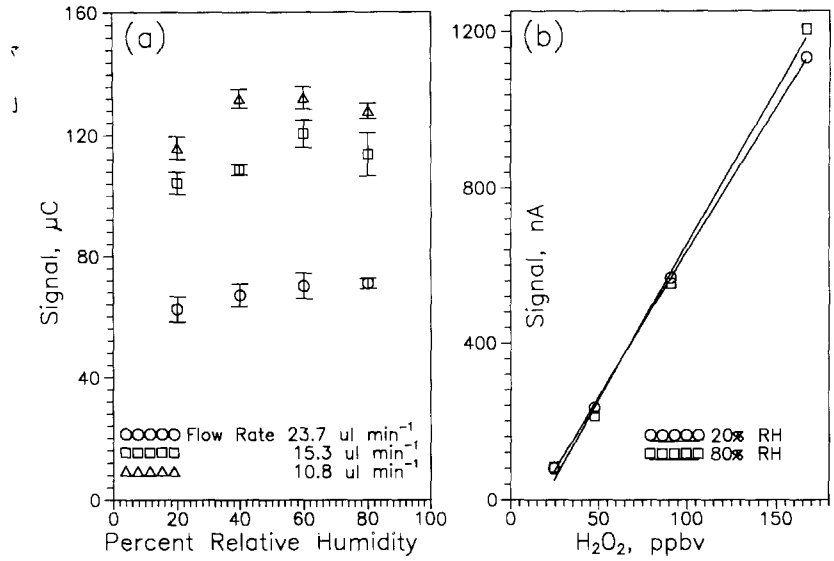

Fig. 7. Effect of relative humidity: (a) signal for 167 ppbv H_2O_2 at three different liquid flow-rates at four different RH levels; (b) calibration plots at 20 and 80% RH showing insignificant difference in slope.

the reciprocal of the liquid flow-rate. At high liquid flow-rates, the linear relationship holds well, but at low liquid flow rates, the signal or the drop period begins to increase more than linearly with decreasing flow-rate, as evaporative losses become important. Unless stated otherwise, a liquid flow-rate of 15.3 μl min^{-1} was used in the experiments.

3.2.4. Effects of relative humidity (RH)

The effects of RH on aqueous drop- or film-based sensors can be very important [1,4]. The present sensor showed no major dependence on RH. Fig. 7(a) shows signals obtained at four different relative humidities for a 167 ppbv H_2O_2 sample at three different liquid flow-rates. At the highest liquid flow-rate (lowest signal levels), the effect of evaporation is the least prominent and the signal is essentially constant over the RH range tested. Even at the other liquid flow-rates, the scatter in the data is larger but there is no consistent RH effect. A calibration plot was conducted at 20 and 80% RH over the range 24–167 ppb H_2O_2. These data (Fig. 4(b)) show virtually identical calibration plots, with no significant difference between the calibration slopes.

3.2.5. Analytical range

The sensor was calibrated for its response in the range 12–200 ppbv H_2O_2. The response was linear with concentration and followed the equation

$$\text{signal}(\mu C) = 0.42[H_2O_2, \text{ppbv}] + 13.66 \quad (r^2 = 0.9988) \quad (4)$$

Based on experiments conducted at 12 ppbv H_2O_2, the estimated LOD at a signal-to-noise ratio of 3 is ≤ 2 ppbv. Although atmospheric H_2O_2 levels frequently exceed this value, it would be desirable to improve upon this LOD for routine use. In the same manner that a hanging mercury drop electrode or an electrode bearing a thin mercury film provides better analytical sensitivity than that attainable with a DME, by stopping the liquid flow during sampling to form a stationary film (and thereby to increase the analyte concentration), one can dramatically improve the sensitivity. Stopped-flow experiments were conducted using gravity-induced liquid flow (at

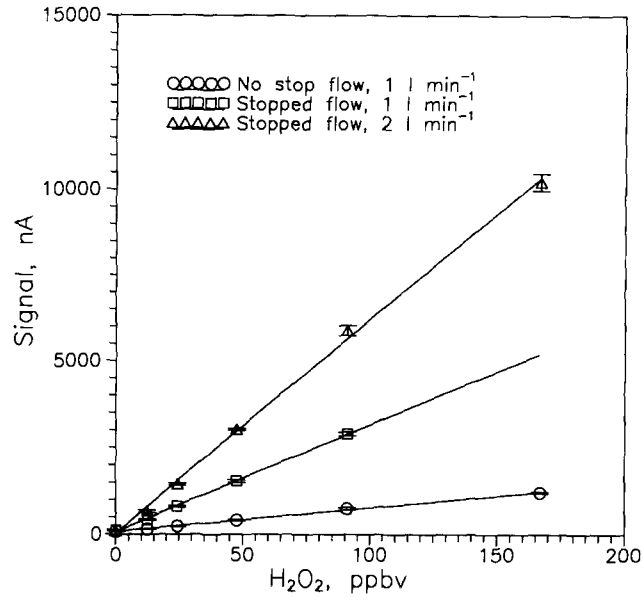

Fig. 8. Improvement in sensitivity by using stopped flow, especially at high gas sampling rates. (○) Response under conventional conditions, gas sampling rate 1 l min^{-1}; (□) response with the liquid flow stopped; (△) response under stopped-flow conditions with a gas sampling rate of 2 l min^{-1}.

ca. 50 μl min^{-1}) during the zero air sampling period and stopping the liquid flow altogether by means of a solenoid valve (V2 in Fig. 1) when the test gas was sampled. Fig. 8 shows calibration plots (at 50% RH) for: (i) normal conditions, liquid flow and gas flow 15.3 μl min^{-1} and 1 l min^{-1}, respectively, sensitivity 6.9 nA $(ppbv)^{-1}$; H_2O_2; (ii) stopped liquid flow, gas flow 1 l min^{-1}, sensitivity 31.2 nA $(ppbv)^{-1}$; and (iii) stopped liquid flow, gas flow 2 l min^{-1}, sensitivity 61.8 nA $(ppbv)^{-1}$. There is nearly an order of magnitude increase in sensitivity on going from operating mode (i) to (iii). The long-term stability of the sensor was studied with 167 ppbv H_2O_2. Over a ca. 8 h period (108 measurements), the relative standard deviation (RSD) was 2.7% under experimental mode (i) above, obviously, this includes not only the imprecision of the sensor but also that of the source output and all the other associated flow/temperature control systems. The measurement precision was slightly worse for experimental protocol (iii): over a period of ca. 10 h ($n = 137$), the RSD was 4.7%.

3.3. Cumene hydroperoxide

In this case, the output of the gas generator was continuously monitored using an electrochemical protocol in which the sensor was alternately cleaned at a potential of +0.1 V for 0–5 s and then maintained at the sensing potential of −0.8 V for 5–−95 s. The current was recorded for the period 65–95 s during each cycle. The response of the sensor to the $CumHO_2$ content of the simulated reaction mixture was highly linear:

$$\text{signal}(\mu C) = 10.54 \pm 0.18[CumHO_2, \%] + 33.79 \pm 1.46 \quad (r^2 = 0.9984) \qquad (5)$$

The precision of the data also indicated that such would readily provide a means for process

monitoring of $CumHO_2$ in a reactor at the 2.5% level with a relative precision of better than 5%.

4. Conclusion

We have demonstrated that in situ electrochemical sensing is a simple and sensitive complement to the drop- or film-based collection of analyte gases and vapors. The technique is obviously not limited to any given electrochemical sensing technology, or to any particular collection liquid. It should be possible to extend the approach to any biphasic system, e.g. in a liquid–liquid system where the film-forming liquid is different from and is immiscible with the liquid constituting the analyte matrix. In general, we believe that this general concept has great potential utility for the sensing of gases.

Acknowledgements

This research was partially supported by the US Environmental Protection Agency through grant No. R 8201117-01-1. However, this paper has not been subject to review by the agency and no endorsements should be inferred.

References

[1] S. Liu and P.K. Dasgupta, Anal. Chem., 67 (1995) 2042.
[2] A. Cardoso and P.K. Dasgupta, Anal. Chem., 67 (1995) 2562.
[3] S. Kar and P.K. Dasgupta, Anal. Chem., 67 (1995) 3853.
[4] H. Liu and P.K. Dasgupta, Anal. Chem., 67 (1995) 4221.
[5] H. Liu and P.K. Dasgupta, Anal. Chem., 68 (1996) 1817.
[6] H. Liu and P.K. Dasgupta, Anal. Chim. Acta, 326 (1996) 13.
[7] S. Kar and P.K. Dasgupta, J. Chromatogr., 739 (1996) 379.
[8] J. Heyrovský, Chem. Listy, 16 (1922) 256.
[9] M. Heyrovska, in P. Zuman and I.M. Kolthoff (Eds.), Progress in Polarography, Vol. 1, Wiley, New York, 1962, pp. 1–19.
[10] M.M.P.M. Neto, M.M.G.S. Rocha and C.M.A. Brett, Talanta, 41 (1994) 1957.
[11] E.P. Gill, R.M.G.-M. Carra and A. Sanchez-Misiego, Anal. Chim. Acta, 315 (1995) 69.
[12] R.M.G.-M. Carra, A. Sanchez-Misiego and A. Zirino, Anal. Chem., 67 (1995) 4484.
[13] S.B.O. Adelojou and F. Bablo, Electoranalysis, 7 (1995) 476.
[14] J.-M. Zen and M.-J. Chung, Anal. Chim. Acta, 320 (1996) 43.
[15] L. Nyholm and F. Bjo|amacron|refors, Anal. Chim. Acta, 327 (1996) 211.
[16] D.W. Gunz and M.R. Hoffmann, Atmos. Environ., 24A (1990) 1601.
[17] P.K. Dasgupta, S. Dong, H. Hwang, H.-C. Yang and Z. Genfa, Atmos. Environ., 22 (1988) 949.
[18] G. Zhang, P.K. Dasgupta and A. Sigg, Anal. Chim. Acta, 260 (1992) 57.
[19] J. Zawadiak, D. Gilner, Z. Kulicki and S. Baj, Analyst 118 (1993) 1081.
[20] P. Beunez, G. Helary and G. Sauvet, J. Polym. Sci., Part A, 32 (1984) 1471.
[21] J.I. Kroschwitz and M. Howe-Grant (Eds.), Kirk-Othmer Encyclopedia of Chemical Technology, Vol. 7, Wiley, New York, 4th edn., 1991, p. 735.
[22] J. Wang, L. Agnes, C. Liang and O. Evans, Talanta, 38 (1991) 1077.
[23] A.I. Vogel, A Textbook of Quantitative Inorganic Analysis, Longmans Green, London, 3rd edn., 1961, p. 363.
[24] H. Hwang and P.K. Dasgupta, Environ. Sci. Technol., 19 (1985) 255.
[25] P.K. Dasgupta, ACS Adv. Chem. Ser., 232 (1993) 41.

ELSEVIER

Talanta 44 (1997) 617–620

Talanta

The ionic product of water in concentrated tetramethylammonium chloride solutions

P. Sipos *, I. Bódi [1], P.M. May, G.T. Hefter

School of Physical Sciences Engineering and Technology, Murdoch University, Murdoch, WA 6150, Australia

Received 4 April 1996; received in revised form 6 August 1996; accepted 9 August 1996

Abstract

The ionic product of water, $pK_w = -\log[H^+][OH^-]$ has been determined in aqueous solutions of tetramethylammonium chloride over the concentration range of 0.1–5.5 M at 25°C using high-precision glass electrode potentiometric titrations. pK_w data relating to aqueous potassium and sodium chlorides at ionic strengths up to 5 M are markedly lower than the tetramethylammonium chloride results. These differences are almost certainly due to weak associations between potassium and (especially) sodium and hydroxide ions. © 1997 Elsevier Science B.V.

Keywords: Ionic product; Tetramethylammonium chloride solutions; Water

1. Introduction

Tetraalkylammonium salts, such as tetramethylammonium chloride (TMACl) are widely utilised as background electrolytes for solution speciation studies, mostly in bioinorganic chemistry and in the study of ion-selective electrodes [1]. This is because the tetraalkylammonium cations are expected to have little complexing ability. This 'inertness' makes them suitable as background electrolytes for studying interactions such as ion-pairing which despite being weak, can be of considerable importance in concentrated electrolyte solutions.

Thermodynamic characterisation of highly concentrated aqueous electrolytes is of interest in understanding and simulating the behaviour of seawater, geological brines and many industrial process streams [2,3]. Of all the reactions in aqueous solution the ionization of water

$$H_2O = H^+_{(aq)} + OH^-_{(aq)}$$

is undoubtedly the most important. Accurate values of the ionic product of water, $pK_w = -\log[H^+][OH^-]$, are essential for determining formation constants of most other reactions especially those occurring at relatively high pH. As noted in a recent paper from our laboratories [4] the value of pK_w tends to be rather poorly characterized at very high ionic strengths in most electrolyte solutions.

* Corresponding author. Fax: +61 9 3606237. On secondment from CSIRO Division of Minerals.

[1] On leave from Department of Inorganic and Analytical Chemistry, Attila József University, Szeged, H 6701, PO Box 440, Hungary.

PII S0039-9140(96)02074-7

Osmotic coefficients for aqueous solutions of different alkylammonium salts at 25°C have been systematically measured over a wide range of concentrations [5–7], whereas the corresponding pK_w data are scarce. As a minor part of a theoretical study [8], Lucas compared measured and calculated pK_w data in aqueous TMACl but provided almost no details about the experimental technique employed. Anderegg [9] has reported pK_w 14.11 at 20°C corresponding to 13.96 at 25°C in 1 M (TMACl) which is significantly different from that of Lucas (13.88). These observations clearly indicate a need for the systematic measurement of pK_w in TMACl over a range of ionic strength. Accordingly this paper describes the determination of the ionic product of water by glass electrode potentiometry in aqueous TMACl solutions over the concentration range 0.10–5.50 M at 25°C.

2. Experimental

2.1. Materials

TMACl (Sigma-Aldrich, 97% pure) was used as received for some experiments (see below) or was recrystallised from dry analytical grade ethanol and dried in vacuo at room temperature. The titrant was either NaOH (made from pellets, analytical grade, Ajax, Australia) or TMAOH (nominally 25 w/w% aqueous solution, analytical grade, Sigma-Aldrich). The carbonate content of the base solutions was minimised by adding solid CaO (0.5 g, analytical grade, Ajax) to the titrant solution (250 ml) which contained the necessary amount of NaOH or TMAOH (~ 0.1 M) and TMACl. The solution was agitated for at least 48 h in an airtight Pyrex glass container and then filtered on a supported membrane filter (0.45 μm). The calcium content of the solutions was measured and checked by ICP AES and was found to be less than 1 ppm. Gran-analyses of the glass electrode potentiometric titrations indicated that the resulting base solutions were practically carbonate free (accounting for less than 0.2% of the total alkalinity). The acid solutions were prepared from commercial volumetric ampoules (BDH Convol).

2.2. Apparatus and procedure

The ionic product of water in TMACl was determined by potentiometric titration of HCl (0.0400 M) dissolved in TMACl ($c - 0.04$)M with both TMAOH and NaOH (0.1 M) in TMACl (c). Measurements were performed at ionic strengths of $0.10\ \text{M} \leq c \leq 5.50$ M. At $c < 0.50$ M the measurements were of poor reproducibility (probably due to unsteady liquid junction potentials between the salt bridge and the test solutions) so these results should be regarded as less reliable than the values at $c \geq 0.50$ M. Nevertheless, even at these low ionic strengths the trend of the curve is reasonably consistent with both our other data and the values for NaCl and KCl media. The titrations were performed using glass (Metrohm, model 6.0101.000) and Ag/AgCl electrodes (of in house construction [10]) in a standard jacketed glass cell using the high precision automated titration system previously developed in our laboratories [10–12]. The solutions were blanketed by high purity nitrogen delivered through a carbon dioxide trap and a presaturator containing the TMACl concentration of interest. The burettes (calibrated precision 0.1%) were Metrohm 665 Model Dosimat units driven by an IBM microcomputer. All volumetric glassware was grade 'A' and calibrated. The cell emf was measured to ± 0.1 mV by high impedance digital voltmeters of in-house construction, connected to the computer. The temperature in the cells was maintained at 25.0 ± 0.02°C by use of a circulator thermostat (Heto Model 04 PT 623). Temperatures were periodically checked with a calibrated ITS 90 platinum resistance thermometer.

The titrations involved measuring the potential of a cell that may be represented schematically as (at the beginning of the titration)

$$\text{Ag|AgCl(s)|NaCl(aq)(5 M)}\,\|_{E_{j1}}\,\text{NaCl(aq)(5 M)}\,\|_{E_{j2}}$$

$$\text{HCl(0.04 M), TMACl}(c - 0.04)\text{M|GE}$$

where GE represents a hydrogen ion responsive glass electrode and E_{j1} and E_{j2} are liquid junction potentials. Following considerations previously presented [4], the relationship between the cell potential and the hydrogen ion concentration at 25°C is

Table 1
The ionic product of water in aqueous tetramethylammonium chloride solutions as a function of the salt concentration

I (M)	pK_w (S.D.)	OBJT[a] ($\times 10^{-8}$)	No. of titrations/no. of points	Real S.D.[b]	Data from ref. [8]
0.10[e]	13.7265 (11)	2.6	9/415	0.0027	
0.25[e]	13.6944 (12)	2.3	8/329	0.0031	
0.50	13.7324 (09)	1.3	7/336	0.0032	
1.00[c]	13.9111 (10)	0.4	4/140	0.0043	
1.00	13.9259 (08)	0.2	4/153	0.0041	13.88
1.00[d]	13.9295 (12)	2.0	9/415	0.0028	
1.50	14.0849 (06)	0.3	6/267	0.0036	
2.00	14.2592 (07)	0.3	7/272	0.0031	14.28
2.50	14.4715 (08)	0.3	7/268	0.0032	
3.00	14.6903 (10)	0.5	8/312	0.0030	14.72
3.50[c]	14.8721 (12)	1.3	9/359	0.0030	
3.50	14.9034 (15)	2.0	9/391	0.0030	
3.50[d]	14.0328 (16)	3.3	8/354	0.0031	
4.00	15.0845 (22)	5.7	8/357	0.0031	15.38
4.50	15.5984 (10)	1.6	8/418	0.0037	15.80[f]
5.00[c]	15.7254 (24)	10.0	8/386	0.0037	
5.00	15.9433 (17)	4.9	9/521	0.0032	
5.00[d]	15.9965 (18)	5.6	10/480	0.0033	
5.50	16.2332 (33)	10.2	9/367	0.0033	

(S.D., standard deviation, OBT, objective function with respect to the total concentrations).
[a]Overall values of sum of least squares residuals in total analytical concentration of hydrogen ion.
[b]Calculated by ESTA3B from a Monte Carlo error analysis [15].
[c]Measurements using non-recrystallised tetramethylammonium chloride.
[d]Measurements using tetramethylammonium hydroxide as base.
[e]These data are less reliable (see comment in text).
[f]$I = 4.6$ M.

$$E_{cell}/mV = E^{0\prime}/mV + 59.16 \log([H^+]/M) \quad (1)$$

where $E^{0\prime}$ is the formal cell potential.

3. Results and discussion

The titrations were carried out over the pH range of 1.5–12.0. At least 4 and usually 8, titrations were performed at each individual ionic strength. The titration curves were evaluated by means of the ESTA library of computer programmes [13–15]. Computer simulation of the titration data routinely consisted of the following steps.

(1) Calculation of Gran-plots for a given group of titrations gave the base concentration (which was then used without further optimisation), the estimated level of carbonate (or other weak acid or base) contamination and the general condition of the electrochemical cell (in terms of linearity of the plots), in this way the best sets of data were selected.

(2) Least-squares analyses of the emf data given by Eq. (1) were then carried out with respect to either the values of the potential (to obtain an estimate of the formal potential) or of the concentration of the H^+ ions (to obtain an estimate of pK_w), the results of these optimisations are summarised in Table 1 and Fig. 1.

(3) Simulations were carried out to calculate the likely magnitude of the real errors in the equilibrium constants using our standard Monte Carlo error analysis (Table 1).

Initial titrations using TMACl and TMAOH as supplied, revealed two artifactual protonation steps in the pH-range of 6–10 associated with ill-defined equivalence points. These effects became larger as the ionic strength increased and presumably correspond to minor amounts of sec-

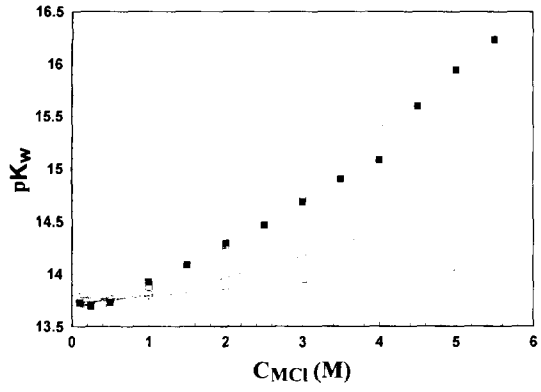

Fig. 1. The ionic product of water, pK_w, as a function of the ionic strength: tetramethylammonium chloride (■: present data; □, Ref. [8]). NaCl (△, Ref. [4]) and KCl (○, Ref. [4]).

ondary and/or tertiary amine impurities that are expected to be the main contaminants in quaternary ammonium compounds. Recrystallization of the TMACl eliminated the main discrepancy (the 'extra' inflexions virtually disappeared). Subsequent Gran-analyses showed that minor proton active substances (accounting for up to 0.5% of the total alkalinity) were still present. These most probably stem from the TMAOH stock solution and resulted in pK_w values with relatively high standard deviations and objective functions (Table 1). As purification of TMAOH stock solution is experimentally difficult, we decided to use NaOH instead. Although this means that a small fraction ($< 5\%$) of the tetramethylammonium cations is exchanged for sodium ions, this has no practical effect on pK_w particularly at higher ionic strengths. With NaOH as the titrant, the least squares analyses yielded pK_w values with acceptable standard deviations and objective functions (Table 1). It is noteworthy that at $c > 3$ M these characteristics become progressively worse, although still acceptable. This is almost certainly because even repeated recrystallization is unable to sufficiently lower trace impurities and also because of increasing experimental difficulties associated with the manipulation of the highly viscous TMACl solutions. In spite of these complications, there are grounds for confidence that the results are not adversely affected by any significant systematic error since the calculated equilibrium constants (pK_w) and their internal standard deviations are practically the same regardless of the objective function used (ESTA2B tasks OBJT or OBJE) [14].

It is noteworthy that pK_w data relating to aqueous potassium and sodium chlorides at ionic strengths up to 5 M[4] are markedly lower than either of these TMACl results (Fig. 1). These differences are almost certainly due, at least in part, to the weak association between K^+ and (especially) Na^+ and OH^- [2,4,16].

Acknowledgements

This work was funded by the Australian alumina industry through the Australian Mineral Industry Research Association Project P380A and the Australian Government under its Cooperative Research Centre Programs.

References

[1] A.E. Martell and R.M. Smith, Critical Stability Constants, Plenum, New York, 1976.
[2] C.F. Baes and R.E. Mesmer, The Hydrolysis of Cations, Wiley, New York, 1976.
[3] K.S. Pitzer (Ed.), Activity Coefficients in Electrolyte Solutions, CRC, Boca Raton, FL, 2nd edn., 1991, p. 75.
[4] I. Kron, S.L. Marshall, P.M. May, G.T. Hefter and E. Koenigsberger, Monatsh. Chem., 126 (1995) 819.
[5] O.D. Bonner, J. Chem. Eng. Data, 27 (1982) 62.
[6] O.D. Bonner, J. Chem. Soc., Faraday Trans. 1, 77 (1981) 2515.
[7] S. Lindenbaum and G.E. Boyd, J. Phys. Chem., 68 (1964) 911.
[8] M. Lucas, Bull. Soc. Chim. France, (1967) 3842.
[9] G. Anderegg, Helv. Chim. Acta, 50 (1967) 2333.
[10] P. Verhoeven, G.T. Hefter and P.M. May, Miner. Metal. Proc., 5 (1990) 185.
[11] G.T. Hefter, J. Electroanal. Chem., 39 (1972) 345.
[12] B.W. Clare, G.T. Hefter and P.M. May, unpublished.
[13] P.M. May, K. Murray and D.R. Williams, Talanta, 35 (1988) 825.
[14] P.M. May and K. Murray, Talanta, 35 (1988) 927.
[15] P.M. May and K. Murray, Talanta, 35 (1988) 933.
[16] A. De Robertis, S. Sammartano and C. Rigano, Thermochim. Acta, 74 (1984) 343.

ELSEVIER

Talanta 44 (1997) 621–626

Talanta

Determination of trace amounts of dipyridamole by stripping voltammetry using a Nafion modified electrode

Zhenhui Wang *, Hongzhong Zhang, Shuping Zhou

Department of Chemistry, Henan Normal University, Xinxiang 453002, China

Received 14 March 1996; received in revised form 26 August 1996; accepted 27 August 1996

Abstract

This paper presents a new method for determination of dipyridamole by anodic stripping voltammetry using a Nafion modified glassy carbon electrode. The stripping peak current was proportional to the concentration of dipyridamole over the range of 1.0×10^{-9}–8.0×10^{-8} M in (pH 1.7) Britton–Robinson buffer with 1 min accumulation. The detection limit has been estimated as 8.0×10^{-11} M with 4 min accumulation. The method has been successfully applied to the determination of dipyridamole in human serum. © 1997 Elsevier Science B.V.

Keywords: Anodic stripping voltammetry; Dipyridamole; Nafion modified electrode

1. Introduction

Dipyridamole[2,6-Bis(diethanolamino)-4,8-di-piperidinopyrimido-(5,4-d)pyrimidine] is a dilatation agent of coronary artery used for the treatment of angina pectoris and myocardial infarction.

Various methods have been employed for the determination of dipyridamole, including spectrotrophotometry [1,2] high-performance liquid chromatography [3,4] and polarography [5]. Zeng et al. have studied the determination of dipyridamole by adsorptive cathodic stripping voltammetry with a hanging mercury drop electrode [6]. The detection limit is 1.0×10^{-9} M with a 5 min preconcentration. However, the electroanalytical method for this drug with a non-mercury electrode has not yet been reported up to now.

This paper describes the determination of trace amounts of dipyridamole in human serum by anodic stripping voltammetry with a Nafion modified glassy carbon electrode. The Nafion film shows an excellent natural barrier to interferences from negatively charged compounds. So, this method exhibits its high sensitivity and selectivity in comparison with the pioneer work [6]. The detection limit of 8.0×10^{-11} M has been estimated with 4 min preconcentration. In addition, the regeneration of the electrode surface is quite easy, and the environmental pollution caused by mercury is also avoided.

* Corresponding author.

PII S0039-9140(96)02078-4

2. Experimental

2.1. Apparatus

A Model 79-1 voltammeter (Jinan No. 4 Radio Fctory) equipped with a X-Y recorder (LZ3-104) was used for electroanalytical measurements at a scan rate of 100 mv s^{-1}. A three-electrode system comprises a Nafion glassy carbon working electrode, platinum counter-electrode and Ag-AgCl (saturated KCl) reference electrode. Stirring was performed using a Model Gsp-76-02 magnetic stirrer. Voltammetric studies were performed with a PAR 174A polarography.

2.2. Reagents

A stock standard solution of dipyridamole in ethanol (1.0×10^{-2} M) was prepared and keep in brown volumetric flask. Dipyridamole working standard solutions were prepared daily by serial dilution of the stock standard solution.

Nafion were purchased from Aldrich. The Nafion stock solution was 0.05% absolute ethanol solution.

Trichloroacetic acid: 20% aqueous solution.

All reagents were of analytical-reagent grade quality. Deionized distilled water was used throughout to prepare solutions.

2.3. Preparation of modified electrode

The glassy carbon electrodes (GCE) having a geometric area of 0.126 cm^2 were used to prepare the Nafion modified electrode. The modified procedure was in the following.

The glassy carbon working electrode was polished with 0.05 μm α-alumina particles, ultrasonicated in absolute ethanol and de-ionized distilled water, respectively, and allowed to dry in air. The electrode was then coated with 4 μl of 0.05% (V/V) Nafion solution to cover the electrode surface, dried by infrared lamp. A uniform film was formed over the entire surface. The modified electrode was rinsed with de-ionized distilled water, and then cyclic scanned between 0.0 and + 1.0 V in Britton–Robinson (B.R. pH = 1.7) buffer solution for a few times before use.

2.4. Procedure

A 10 ml volume of (pH = 1.7) B.R. buffer solution containing a suitable amounts of dipyridamole was added to the sample cell. The Nafion modified electrode was kept at the desired accumulation potential for a given time period, while the solution was stirred at about 400 rpm throughout the entire period. The stirring was then stopped and the solution was allowed to rest for 30 s, after which a positive-going scan was initiated at 0.0 V (scan rate 100 mv s^{-1}). The scan was terminated at + 1.0 V, and the second derivative voltammogram was recorded.

2.5. Renewal of electrode surface

After each electrochemical measurement, the electrode was cycled two times between 0.0 and + 1.0 V in B.R. buffer to renew the electrode surface. There should be no peaks in the potential scan range, otherwise the regeneration must be repeated.

2.6. Serum treatment

Pipette 0.50 ml of human serum containing dipyridamole into a 5 ml centrifugal tube, add 0.50 ml of water and 1.00 ml of 20% trichloroacetic acid, mix thoroughly and stand for 2 min centrifuge at 4000 rpm in a high speed centrifuge, transfer 0.10 ml of centrifugal solution on superior layer, then follows the procedure described above.

3. Results and discussion

3.1. Second derivative voltammograms

The derivative technique is a significant advance in linear-sweep voltammetry. The higher the derivative order, the larger the peak current. Therefore, the sensitivity of using second-derivative stripping voltammetry is higher than that of conventional stripping methods [7].

Fig. 1 shows the second-derivative voltammograms for dipyridamole at 4.0×10^{-8} M level

Fig. 1. Second derivative voltammograms for 4.0×10^{-8} M of dipyridamole in B.R. (pH = 1.7) buffer. Accumulation potential: 0.0 V. Accumulation time: 80 s; (a) Nafion modified GCE; (b) GCE.

after 60 s preconcentration at 0.0 V from a stirred B.R. buffer. A larger stripping peak (peak a), which increased linearly with increasing of dipyridamole content, was found at +0.75 V measured with the Nafion modified electrode, and a smaller stripping peak (peak b) was appeared at the similar potential with a bare glassy carbon electrode under the same conditions. The results indicate that the Nafion film enhance the preconcentration of dipyridamole on the electrode surface.

Table 1 shows the results for determination of three concentration levels of dipyridamole with Nafion modified electrode (MGCE) and bare glassy carbon electrode (GCE), respectively.

It can be seen from Table 1 that the lower the determined concentration, the greater the difference of the peak currents. Contrasted the peak currents determined on Nafion modified electrode with the unmodified one, the former greatly improves the sensitivity for determination of trace amounts of dipyridamole.

The effect of the volume of Nafion which added to GCE surface on the peak height was studied. The results showed that the presence of 4 μl 0.05% of Nafion was sufficient for obtaining the maximum current. However, the stripping current is too small to be useful as using a bare glassy carbon electrode for determination of this drug (Fig. 1, curve b). The reproducibility and stability of the electrode were examined in ten parallel determinations. For 4.0×10^{-8} M of dipyridamole with a preconcentration time of 60 s, the relative standard deviation was 3.72%. The result indicates that the Nafion modified glassy carbon electrode has a good reproducibility and stability. The electrode lasted for 1 week at least before it needed remodifying.

3.2. Cyclic voltammetry

In order to understand the electrochemical process occurring on modified electrode, cyclic voltammetry of the system was carried out. Fig. 2 shows the repetitive cyclic voltammograms for dipyridamole stirring accumulation the analyte for 60 s gave a large anodic peak. No peak was observed on the cathodic branch, indicating irre-

Table 1
Comparison results

No.	Concentration (M)	Time (s)	Current (MGCE) (μA)	Current (GCE) (μA)	Rate (MGCE/GCE)
1.	4×10^{-6}	60	0.92	0.48	1.9
		120	0.99	0.57	1.7
		240	1.06	0.65	1.6
2.	4×10^{-7}	60	0.48	0.062	7.7
		120	0.50	0.090	5.6
		240	0.51	0.116	4.4
3.	4×10^{-8}	60	0.20	0.008	25.0
		120	0.24	0.010	24.0
		240	0.27	0.012	22.5

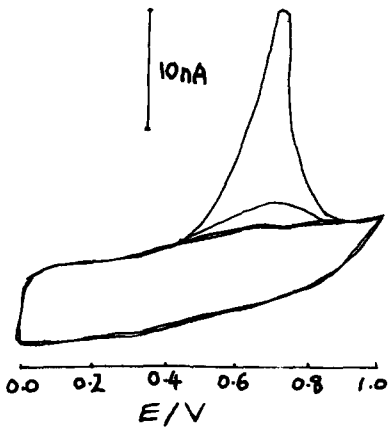

Fig. 2. Cyclic voltammograms for 4.0×10^{-8} M of dipyridamole recorded continuously at the Nafion modified electrode in B.R. (pH 1.7) buffer scan rate 100 mv s^{-1}; accumulation time: 60 s.

versibility of the oxidation. A rapid decrease in the anodic peak was observed in subsequent scans, such behaviour indicated the analyte which accumulated on the Nafion modified electrode surface rapid stripping.

3.3. Selection of experimental conditions

Various supporting electrolytes, such as HCl, H_2SO_4, HNO_3, H_3PO_4, HCl-NaAc, tartaric acid–tartarate, citric acid–citrate, NaOH and B.R. buffer solution were tested in order to optimize the response for dipyridamole at a Nafion modified electrode. The anodic stripping peak of dipyridamole was not found in alkaline and neutral medium. A well-defined and sensitive anodic stripping peak was appeared at $+0.75$ V when B.R. buffer was used as electrolyte. No reduction peak was obtained in the similar experimental conditions.

The solution pH has a strong effect on the stripping response (Fig. 3). For example, increasing the pH from 1.4 to 1.7 results in a sharp increase in the peak current. Further increasing the pH beyond 1.8, a rapid decrease in the response was observed. Therefore, a B.R. buffer solution (pH = 1.7) was selected for maximum sensitivity.

The stripping peak current of dipyridamole is affected by the preconcentration potential. Experiments showed that the peak current was increased with negative shifting of the start potential in the range $+0.4$–0.0 V. The stripping currents appeared stable values as the accumulation potential varied between 0.0 and -0.4 V. As the accumulation potential was beyond -0.4 V, the current signal was depressed, immediately. The selected accumulation potential was 0.0 V.

The stripping peak current increased linearly with increasing accumulation time up to 80 s for 2.0×10^{-8} M of dipyridamole. As the time longer than 90 s, the increment of peak current showed a deviation from linearity, indicating that complete coverage of the Nafion modified electrode was gradually being achieved. The choice of optimum accumulation time depends on the range of concentration studied, and requires a compromise between sensitivity and speed. The chosen accumulation time was 60 s for all further studies. The stripping signal was also affected by surfactants. Experiments proven that cation and neutral surfactants strongly depressed the peak current. The effect of cation surfactant, such as cetyltrimethylammonium bromide (CTMAB) was greater. However, the presence of a suitable amounts of anion surfactant did not affect the stripping signal. It can be deduced that protonated dipyridamole exists as cation form in solution.

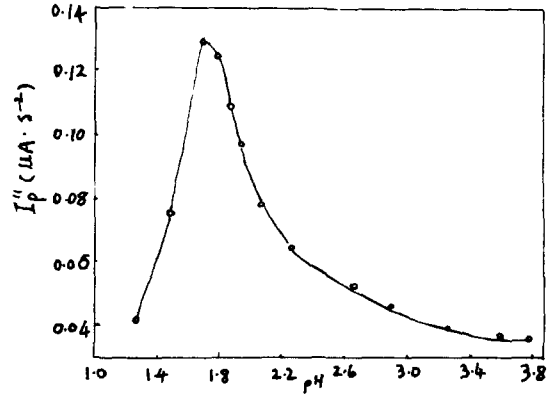

Fig. 3. Reltionship between stripping signal and pH values for 2.0×10^{-8} M of dipyridamole. Other conditions as in Fig. 1.

Table 2
Analytical results[a]

Determined values in human serum (μg/ml)	R.S.D. (%)	Added (μg)	Found (μg)	Recovery (%)
3.78	4.76	0.80	0.81	101
		0.80	0.82	103
		1.60	1.58	98.8
		1.60	1.67	104
		2.40	2.32	96.7

[a] The data were checked identical with the results determined by HPLC ($n = 5$).

3.4. Calibration graph

The serum sample pretreatment step is required owing to high protein content in human serum. In addition, the loss of determined dipyridamole is unavoidable in the process of serum treatment. So it is necessary to prepare the calibration graph in human serum, and the following procedure was described elsewhere [8].

Under the optimum conditions described above, the linear range of peak current versus the concentration of dipyridamole is $1.0 \times 10^{-9} \sim 8.0 \times 10^{-8}$ M (accumulation 1 min) with a correlation coefficient of 0.9998 and a slope of 6.9 nA per 10^{-9} M. the detection limit has been estimated as 8.0×10^{-11} M with 4 min accumulation.

3.5. Effect of foreign ions

Foreign ions were added together with 4.0×10^{-8} M of dipyridamole as in the recommended procedure. Measurement of the stripping signal for each solution was repeated three times and the average values of the three stripping currents were obtained. The relative error was less than $\pm 5\%$. The results showed that 20 000-fold excess of Na^+; 1000-fold excess of K^+; 2500-fold excess of Zn^{2+}; 1200-fold excess of Mg^{2+}; 1000-fold excess of Pb^{2+}; 500-fold excess of Ca^{2+}, Al^{3+}; 200-fold excess of Fe^{3+}, Se (IV); 100-fold excess of Cu^{2+}; 3000-fold excess of Cl^-; 2000-fold excess of PO_4^{2-}; 75-fold excess of I^-; 120-fold excess of gelatin; 1700-fold excess of ascorbic acid; 17-fold excess of albumin; 4-fold excess of dopamine; 16-fold excess of dopamine hydrochloride; 3-fold excess of nor-adrenaline; 9-fold excess of perphenazine; 12-fold excess of DL-tyrosine and DL-serine did not have a substantial effect on the determination of dipyridamole.

3.6. Application

The proposed method was applied to the determination of trace amounts of dipyridamole in human serum. The determination was performed by the standard-addition method. The determination results and recoveries of known amounts of dipyridamole added to serum sample were given in Table 2.

4. Conclusion

The anodic stripping voltammetry at a Nafion modified glassy carbon electrode has been shown to be suitable for the determination of trace amounts of dipyridamole in human serum. The sensitivity is significantly enhanced by accumulation of the drug on the modified electrode surface. Compared with the pioneer work [6], this method not only increases the sensitivity of assay the drug, but also reduces the pollution caused by mercury.

The preconcentration mechanism of dipyridamole at a Nafion modified glassy carbon electrode is probable a cation exchange process between the protonated dipyridamole and the active group of Nafion. The electro-oxidation mechanism is not fully understood. Studies are continuing on the mechanism of the oxidation reaction.

Acknowledgements

This work was supported by the nature science foundation of Henan province, China.

References

[1] M.H. Barary, M.A.H. El-Sayed, M.H. Abdel-Hay and S.M. Mohamed, Anal. Lett., 22(7) (1989) 1643.
[2] A.S. Issa, M.S. Mahrous and M.A. Salam, Talanta, 34(7) (1987) 670.
[3] C. Deballon and M. Guernet, J. Pharm. Biomed. Anal., 6(6–8) (1987) 1045.
[4] A. Nishitani, Y. Tsukamoto, S. Kanda and K. Imai, Anal. Chim. Acta, 251(1–2) (1991) 247.
[5] M. Tuncel, Y. Yanzan and D. Dogrukol, Anal. Lett., 24(10) (1991) 1837.
[6] X. Zeng, S. Lin and N. Hu, Talanta, 40(8) (1993) 1183.
[7] W. Jin and X. Li, Anal. Chim. Acta., 236 (1990) 453.
[8] Z. Wang, H. Zhou and S. Zhou, Talanta, 40(7) (1993) 1073.

ELSEVIER

Talanta 44 (1997) 627–631

Talanta

Estimation of cephalosporin antibiotics by differential pulse polarography

G.V. Subba Reddy, S. Jayarama Reddy *

Department of Chemistry, S.V. University, Tirupati-517 502, India

Received 28 May 1996; received in revised form 27 August 1996; accepted 27 August 1996

Abstract

Differential pulse polarographic (DPP) method of determination of cephalosporins has been developed based on the electrochemistry of the azomethine group in the drugs in universal buffers of pH 2.0–12.0. Quantitative measurements were successful in the concentration range of 1.0×10^{-5} M–2.5×10^{-8} M, the lower concentration representing the detection limit by DPP. The described procedure has been applied for the determination of these drugs individually in pharmaceutical formulations and urine samples as well as for simultaneous determination in a single run. © 1997 Elsevier Science B.V.

Keywords: Azomethine; Cephalosporin; Polarographic

1. Introduction

Cephalosporins are widely used in clinical therapy for the treatment of severe infections, because of their convenient antibacterial activity, β-lactamases resistance and pharmacokinetic properties [1–5]. Ceftazidime is known to be not metabolised in body and excreted 80–90% unchanged in active form in urine. Chromatographic [6,7] and spectrophotometric [8] method of determination of cephalosporins has been reported. Electrochemical techniques [9–11] have been widely used for the determination of azomethine containing compounds. In view of the known electroactivity of cephalosporins, application of electroanalytical methods also acquires importance due to their simplicity, selectivity and accuracy in this type of compounds. DPP has been widely used over the years to determine the drugs in pharmaceutical preparations and body fluids [12–19].

Cephalosporins such as Ceftazidime (I), Ceftizoxime (II) and Ceftriaxone (III) having the same >C=N– group with the different environment which have extensive use as antibiotics have not been determined electrochemically.

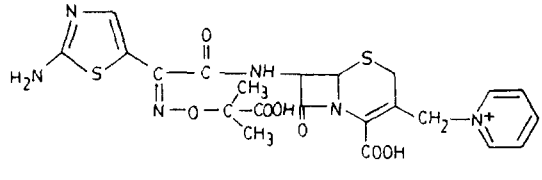

I

* Corresponding author. Fax: +91 8574 228009.

PII S0039-9140(96)02081-4

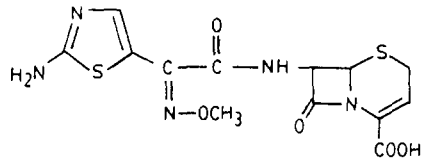

II

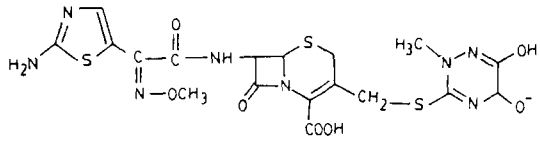

III

This communication describes a simple and rapid technique for the determination of the compounds I–III using DPP.

2. Experimental

The compounds (I–III) were obtained from Glaxo India Limited, Bombay. All chemicals used were AnalaR grade reagents. Stock solutions were prepared by dissolving the required quantity of the compound/pharmaceutical formulations in 100 ml pure methanol for getting a concentration of 1 mM (10^{-3} M). The desired concentrations of solutions were prepared by diluting the stock solution with the supporting electrolyte. The supporting electrolytes were prepared by from 0.05 M citric acid, 0.2 M boric acid and 0.1 M tri sodium orthophosphate over the pH range of 2.0–12.0. Aliquots of solutions diluted with supporting electrolyte and deoxygenated with oxygen free nitrogen for 15 min prior to measurements. Urine samples were analysed for drugs without any prior digestion or extraction.

Metrohm E506 polarecord connected to E612 VA-Scanner was used for differential pulse Polarographic experiments. The three electrode assembly consisted of a dropping mercury electrode of an area 0.0324 cm^2 as working electrode and a platinum foil as the auxiliary electrode. pH measurements were made using Elico L1 digital pH meter. All measurements were carried out at 25 ± 1°C.

3. Results and discussion

From the experimental results obtained by DPP, the reduction of the azomethine functional group in all the cephalosporins under investigation is found to proceed in a single step with a four electron addition in pH 2.0–12.0 of universal buffer system. The total number of electrons involved in the reduction process was calculated from the results obtained with millicoulometry [20] and found to be four [21]. The probable general half-reaction is given in: (Scheme 1).

As the pH of the buffer system increased, the peak potentials are found to be shifted towards more negative values within the range of − 0.564– − 1.34 V. In basic buffers of pH > 8.0, the reduction of azomethine is difficult due to non-availability of protons and it is not useful for analytical purpose. The investigated compounds were found to exhibit well resolved peaks which are suitable for the analysis in pH 4.0 and 6.0.

The electrode process for all the three electroactive species are found to be free from adsorption and diffusion controlled in nature which is confirmed through the linear plots of i_m vs. concentration, i_m versus $t^{2/3}$ passing through origin.

3.1. Analysis

Standard addition and calibration methods were employed for quantitative estimation of the compounds in pharmaceutical formulations and in urine samples. The peak currents vary linearly with the concentration of the drug over the range 1.25×10^{-5} M to 2.5×10^{-8} M with the slope of 0.03 and lower detection limit of 2.4×10^{-8} M. The correlation coefficient and standard deviation were 0.996 and 1.04, respectively. The lower detection limit was calculated using the expression

$$dl = 3\ S.D.\ m^{-1}$$

where S.D. = standard deviation, m = slope of calibration plot.

3.2. Recommended analytical procedure

Standard solutions of the investigated compounds (1.0×10^{-5} M) were prepared in pure

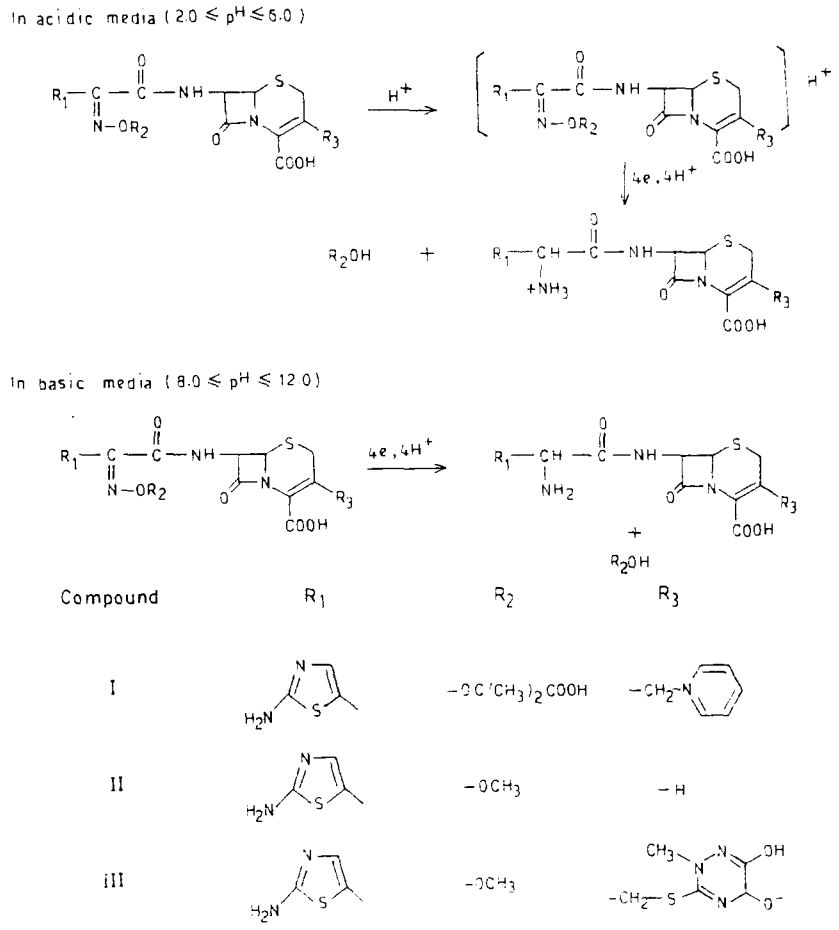

Scheme 1.

methanol. In polarographic cell, 1 ml of standard solution was transferred and made up with 9 ml of the supporting electrolyte (pH 4.0) and then deoxygenated with nitrogen gas for 10 min. After recording the polarogram small increments (0.2 ml) of standard solutions were added and polarograms were recorded after each addition under the similar conditions. The optimum conditions for the determination of cephalosporins in pH 4.0 was found to be a drop time of 2 s, a pulse amplitude of 60 mV and applied potential of -0.608 V, -0.65 V, and -0.72 V with the relative S.D. and correlation coefficient for 10 replicants 1.44, 1.58 and 1.34%, and 0.989, 0.996, 0.954 for I, II, III, respectively. The described analytical procedure was used for the determination of the Ceftazidime, Ceftizoxime and Ceftriaxone in its pharmaceutical formulations.

Tablet and injection formulations containing a nominal 100 mg of any compounds under investigation in a total mass approximately 300 mg were analysed in order to examine the applicability of the method. Not less than 10 tablets/injections were thoroughly ground and mixed. Portions equivalent to 5, 10, 15, 20 and 25 mg of compound were accurately weighed, dissolved in pure methanol and transferred in to 10 ml calibrated flasks. A 0.5 ml aliquot of the clear supernant liquid was diluted to 10 ml with the supporting electrolyte and subjected to polarography. The amount of the compound in portion of the sample taken was calculated by reference to the calibra-

Table 1
Polarogrpahic assay of selected cephalosporins by differential pulse polarography in pH 4.0

Pulse amplitude: 60 mV		Drop time: 2 s		
Sample	Labelled amount (mg)	Amount found (mg)	Recovery percentage	S.D.
Ceftazidime (powder)	25.0	24.96	99.82	0.021
Ceftazidime (powder)	15.0	14.97	99.89	0.019
Ceftizoxime (powder)	10.0	09.95	99.60	0.021
Ceftriaxone (powder)	25.0	24.89	98.89	0.022
Fortum (injection)	15.0	14.98	99.92	0.016
	10.0	09.97	99.89	0.016
Cefizox (injection)	10.0	09.98	99.60	0.021
	05.0	04.98	98.20	0.015
Monocef (injection)	25.0	24.85	98.74	0.025
	10.0	09.98	99.92	0.016
Oframax (injection)	25.0	24.97	99.89	0.019
	10.0	09.98	99.92	0.016

tion plot. The assay results for the formulations in pH 4.0 are given in Table 1.

In order to determine, the amount of a particular drug in urine sample, calibration plots constructed in accordance with the limits at which the unchanged drugs are excreted are employed. Different amounts of I were added to a fixed volume of urine. Aliquots of these spiked urine samples were diluted with the supporting electrolyte and the polarograms recorded. The calibration plots ranging from 2.4 to 60 ng ml^{-1} was linear passing through the origin. Using the same procedure calibration plots were constructed for II and III. Using the calibration plot ranging from 2.4 to 60 ng ml^{-1} compound I was determined in urine. The analysis of numerous samples indicates a relative S.D. of 2.0% at the lowest concentration and 1.5% at concentration 8 ng ml^{-1} and higher. II and III were determined in urine with the same concentration range and the relative S.D. at the lowest concentration were 1.48 and 1.46%, respectively. Typical differential pulse polarogram of Ceftriaxone in urine sample is given in Fig. 1.

Further the method is selective for simultaneous determination of cephalosporins because of wide separation in their E_m values (Fig. 2). The wide range of concentrations over which the drugs can be determined indicates great utility of the method. The determinations of higher concentrations in pharmaceutical formulations are possible. The proposed supporting electrolyte permits high sensitivity in polarographic quantitative determination of these compounds. The method is sensitive enough to measure concentrations as low as those encountered after therapeutic dosage.

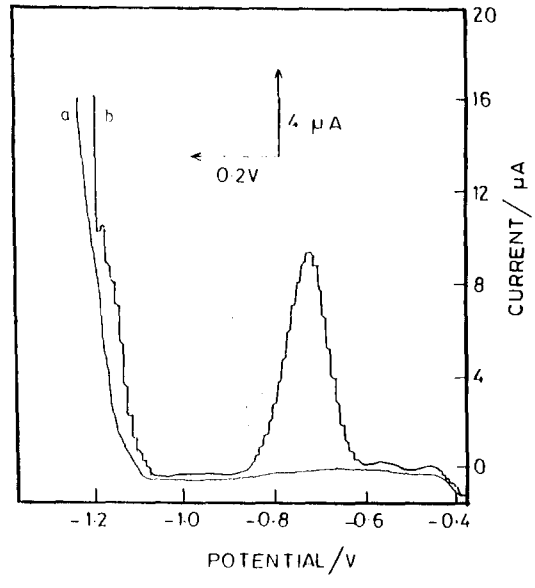

Fig. 1. Typical differential pulse polarogram of ceftriaxone in urine sample in pH 4.0. Concentration = 20 ng ml^{-1}; drop time = 2 s; and pulse amplitude = 60 mV. a = Urine blank + buffer, b = ceftriaxone in urine + buffer.

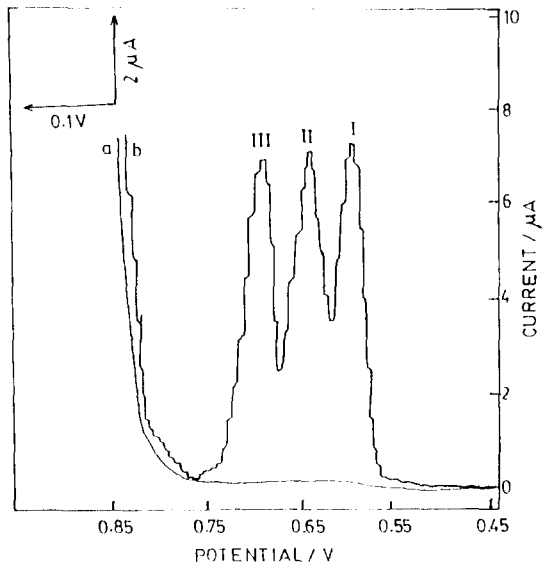

Fig. 2. Typical differential pulse polarogram of 0.01 mM I + 0.01 mM II + 0.01 mM III (I = Ceftazidime, II = Ceftizoxime and III = Ceftriaxone) in pH 4.0. Drop time = 2 s; and pulse amplitude = 60 mV. a = Blank solution, b = [I + II + III] + buffer.

Acknowledgements

The authors are thankful to UGC, New Delhi for providing financial assistance.

References

[1] P. Garzone, J. Lyon and V.L. Yu, Drug. Intell. Clin. Pharm., 17 (1983) 507.
[2] P. Garzone, J. Lyon and V.L. Yu, Drug. Intell. Clin. Pharm., 17 (1983) 615.
[3] B. Vanklingeren (Letter), J. Antimicrob. Chemother., 6 (1980) 674.
[4] T. Kaminura, Antimicrob. Agents Chemother., 16 (1979) 540.
[5] K.P. Fu and H.C. Neu, Ibid, (1980) 583.
[6] J. Martin-Villacorta and R. Mendez, J. Liq. Chromatogr., 13 (16) (1990) 3269.
[7] C.M. Moore, K. Sato and Y. Rasumata, J. Chromatogr., 539 (1) (1991) 215.
[8] P. Corti, E. Dreassi, G. Cerumelli, S. Lonardi, R. Viviani and S. Gruvina, Analusis, 19 (7) (1991) 198.
[9] H. Benadikova and K. Kalvoda, Anal. Lett., 17 (13) (1984) 1519.
[10] W.U. Malik, R.N. Goyal and R. Jain, Talanta, 24 (1977) 588.
[11] M. Subbalakshmamma and S.J. Reddy, Electroanalysis, 6 (1994) 612.
[12] A.G. Fogg, N.M. Fayed, C. Burgess and A. Mcglynn, Anal. Chim. Acta., 108 (1979) 205.
[13] A. Ivaska and F. Nordstrom, Anal. Chem. Acta, 87 (1983) 146.
[14] F.I. Sengun, T. Gurkan, I. Fedai and S. Sungur, Analyst, 110 (1985) 1111.
[15] B. Ogoreva, V. Hundnik and S. Gomiscek, Fresenius. Z. Anal. Chem., 23 (1988) 113.
[16] E. Munoz, L. Camcho, J.L. Avila and F. Garcia-Blanco, Analyst, 113 (1988) 23.
[17] D.W. Mason and B. Sandmann, J. Pharm. Sci., 65 (1976) 599.
[18] J.S. Burmicz, W. Franklin Smyth and R.F. Palmer, Analyst, 101 (1976) 986.
[19] J. Chodkowski and D. Gnalemska-Ludwicka, Pol. J. Chem., 54 (1980) 567.
[20] T. De Vries and J.L. Kroon, J. Am. Chem. Soc., 75 (1953) 2484.
[21] C. Sridevi and S.J. Reddy, Electroanalysis, 3 (1991) 435.

ELSEVIER

Talanta 44 (1997) 633–639

Talanta

Rapid and accurate determination of chlorpheniramine maleate, noscapine hydrochloride and guaiphenesin in binary mixtures by derivative spectrophotometry

Nora B. Pappano [a], Yolanda C. De Micalizzi [b], Nora B. Debattista [a,*], Ferdinando H. Ferretti [a]

[a] *Department of Chemistry, San Luis National University, Chacabuco 917 5.700- San Luis, Argentina*
[b] *Department of Pharmacie, San Luis National University, Chacabuco 917 5.700- San Luis, Argentina*

Received 15 April 1996; received in revised form 26 August 1996; accepted 27 August 1996

Abstract

Rapid and accurate binary mixture resolution of chlorpheniramine maleate–noscapine hydrochloride and chlorpheniramine maleate-guaiphenesin, was performed. Derivative spectrophotometry, by the zero-crossing measurements, was used due to the drugs closely overlapping absorption spectra. Neither sample pretreatment nor separation were required. Linear calibration graphs of first derivative values at 268.0 and 261.0 nm for chlorpheniramine-maleate-noscapine hydrochloride and at 273.2 and 261.0 nm for chlorpheniramine-guaiphenesin were obtained vs. concentration with negligible intercept on the y-axis. Thus, the derivative spectrophotometry method was applied to the determination of these drugs in binary mixtures obtaining selectivity, accuracy and precision. © 1997 Published by Elsevier Science B.V.

Keywords: Binary mixture; Chlorpheniramine maleate; Noscapine hydrochloride; Guaiphenesin

1. Introduction

Chlorpheniramine maleate (1) is an alkylamine derivative with the actions and uses of the antihistamines [1]. It is one of the most potent antihistamines and causes a moderate degree of sedation. It is used alone or with noscapine hydrochloride (2) [2] and guaiphenesin (3) [3] for the symptomatic treatment of coughs due to acute or chronic bronchitis and bronchial allergic conditions, Fig. 1. Bronchodilation has been produced by nebulized chlorpheniramine in children with asthma. Adverse effects have been reported: smell and taste alterations; thrombocytopenic purpura; and progressive left-sided facial dyskinesia [4]. Chlorpheniramine maleate in compound preparations cannot be directly determined by conventional spectrophotometric methods because of the significant overlapping in the spectra. The derivative technique in UV-vis spectrophotometry offers a powerful approach for the enhancement of sensitivity and specificity. It has frequently been em-

* Corresponding author. Fax: +54 652 30224.

PII S0039-9140(96)02083-8

ployed to overcome the problem of interference due to irrelevant spectral overlapping, which may be caused either by substances other than analytes or by excipient matrices commonly present in pharmaceutical formulations. In derivative spectroscopy, the conventional spectrum is rapidly and simply transformed to a function of its first derivative ($dA/d\lambda$), by an analogue or digital device as the spectrum is scanned. Consequently, fine structural features are sharpened to give improved resolution of overlapping peaks and potentially greater sensitivity. The main advantages and limitations of this technique have been described by O'Haver et al. [5].

Derivative spectrophotometry on the basis of zero-crossing measurements has been employed for the simultaneous determination of substances of clinical interest [6–8] and rapidly gained applications in the fields of pharmaceutical analysis, biochemistry, analytical chemistry and clinical chemistry [9,10].

The described first derivative UV spectrophotometric method is simple, direct and accurate and has been applied to determine chlorpheniramine maleate, noscapine hydrochloride and guaiphenesin, in the synthetic chlorpheniramine-noscapine and chlorpheniramine-guaiphenesin mixtures.

2. Experimental

2.1. Reagents

Stock chlorpheniramine maleate solution, 558.86 μg ml^{-1}, prepared by dissolving chlorpheniramine maleate (Sigma Chemical Products) in water.

Stock noscapine hydrochloride solution, 1954.5 μg ml^{-1} prepared by dissolving 2 (Sigma Chemical Products) in water.

Stock guaphenesin solution, 1070.0 μg ml^{-1}, prepared by dissolving 3 (Sigma Chemical Products) in water. The stock solutions were kept refrigerated at about 4°C, in the dark. Solutions of the desired concentration were obtained by diluting the stock solutions to volume with water. All experiments were performed with solvent grade Milli-Q-water (Millipore Corporation).

2.2. Apparatus

Ordinary and derivative spectrophotometric analyses were performed on a Shimadzu UV-vis Spectrophotometer UV-160 A with standard 1.0 cm quartz cuvettes. The UV-160 A is a microcomputer-controlled double-beam recording spectrophotometer which has the following features: this very compact instrument combines a monochromator, keyboard, CRT and graphic printer; it permits various spectral processing such as the expansion/compression of spectra, peak-pick, derivative, smoothing, data storage and arithmetic calculation between spectra.

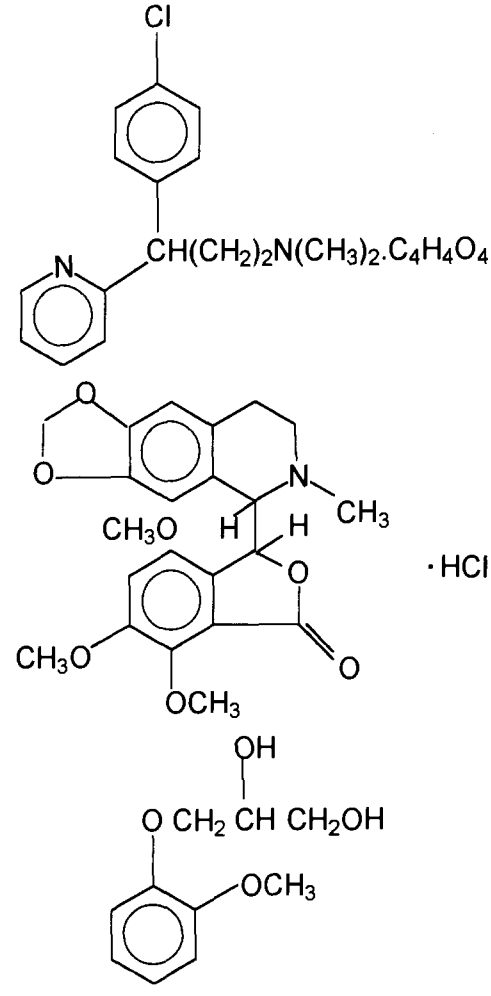

Fig. 1. Structural formulae of chlorpheniramine maleate (1), noscapine hydrochloride (2) and guaiphenesin (3).

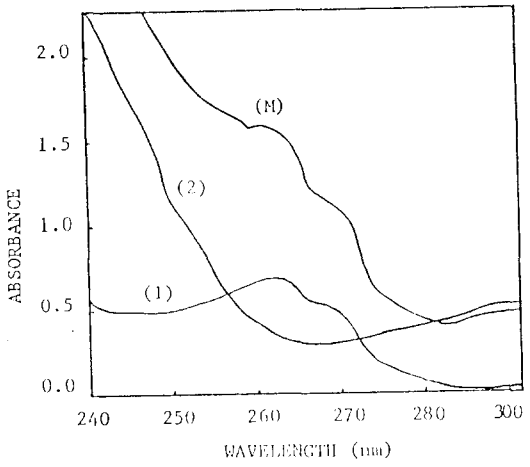

Fig. 2. Absorption spectra of chlorpheniramine maleate (1) 45.2 μg ml^{-1}, noscapine hydrochloride (2) 91.6 μg ml^{-1} and their 1:1 mixture (M), in distilled water.

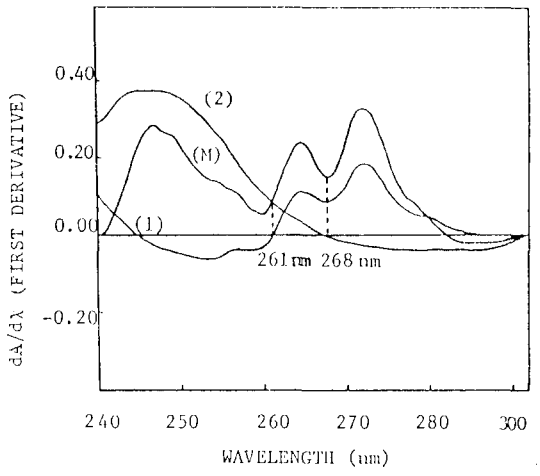

Fig. 4. First derivative spectra of chlorpheniramine maleate (1), noscapine hydrochloride (2) and their 1:1 mixture (M).

Absorption spectra of samples were recorded at a scan speed of about 480 nm min^{-1} between 230–300 nm for 1–2 mixtures and 220–320 nm for 1–3 mixtures.

The first derivative spectra were recorded with a $\Delta\lambda = 7.2$ nm.

2.3. Sample preparation and procedure

Samples (5 ml) were prepared in 8 ml test tubes containing 20.0–160.0 μg ml^{-1} of 1, 20.0–140.0 μg ml^{-1} of 2, and 20.0–140.0 μg ml^{-1} of 3 or their binary mixtures.

The absorption spectra of the samples were recorded against a reagent-blank (water). The calibration graphs were constructed on the chart paper against the corresponding concentrations. The absolute values of the derivative were obtained by a zero-crossing technique with measurements at 268.0 nm for 1 and 261.0 nm for 2 in the 1–2 mixtures and 273.2 nm for 1 and 261.0 nm for 3 in the 1–3 mixtures, respectively.

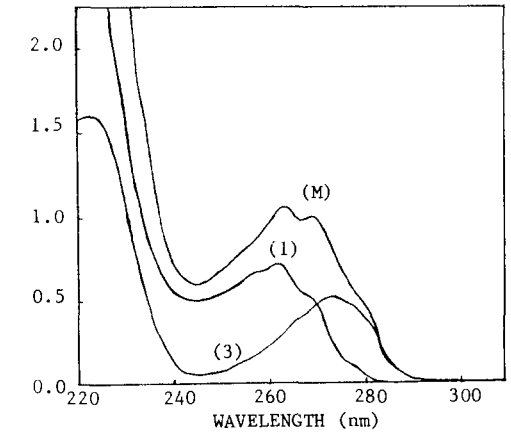

Fig. 3. Absorption spectra of chlorpheniramine maleate (1) 50.1 μg ml^{-1}, guaiphenesin (3) 43.9 μg ml^{-1} and their 1:1 mixture (M), in distilled water.

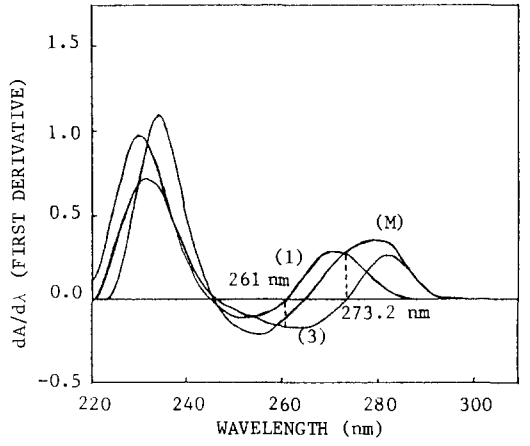

Fig. 5. First derivative spectra of chlorpheniramine maleate (1), guaiphenesin (3) and their 1:1 mixture (M).

Table 1
Analysis of calibration graphs in the determination of chlorpheniramine maleate (20.0–160.0 μg ml^{-1}) in the presence of noscapine hydrochloride (h_{268}) by first derivative spectrophotometry

C 2 (μg ml^{-1})		Slope	Intercept	Correlation coefficient
0.0	p_0	1.85×10^{-3}	2.28×10^{-3}	0.999
83.3	p_1	1.87×10^{-3}	-6.51×10^{-3}	0.999
106.0	p_2	1.68×10^{-3}	1.02×10^{-3}	0.999
129.0	p_3	1.78×10^{-3}	-3.14×10^{-3}	0.999
164.0	p_4	1.87×10^{-3}	-7.01×10^{-3}	0.999

LOD (the lower limits of detection) = 0.033 μg ml^{-1}.
C 2: noscapine hydrochloride concentration.

2.4. Sample analysis

The proposed method was applied to the determination of 1–2 or 1–3 in synthetic mixtures of different proportions, using the calibration graphs.

3. Results and discussion

Fig. 2 shows the closely overlapping absorption spectra of 1 (45.2 μg ml^{-1}) and 2 (91.6 μg ml^{-1}) together with M, a mixture of both compounds, in the region of 240–300 nm.

Similar behavior was observed for compounds 1 and 3 (Fig. 3).

This fact makes it extremely difficult to determine 1 in the presence of noscapine hydrochloride or guaiphenesin by conventional UV spectrophotometry. This problem has been solved satisfactorily by derivative spectrophotometry. When derivative UV spectra were recorded, sharp bands of large amplitudes of chlorpheniramine maleate were produced which may offer more selective identification and specific determination of this drug.

Fig. 4 shows the first derivative spectra of 1, 2 and their mixture, M. Fig. 5 shows the first derivative spectra of 1, 3 and their mixture, M. The zero-crossing value for 1 appears at 261.0 nm; for 2 at 268.0 nm and for 3 at 273.2 nm, respectively. From among these wavelengths, these values were selected as optima to determine 1 and 2 and 1 and 3 in their mixtures.

In order to test the mutual independence of the analytical signals of 1 and 2 or 1 and 3 compounds, the following experiments were performed.

Five calibration graphs were constructed from the first derivative signals by measuring at 268.0 nm for standard samples containing between 20.0 and 160.0 μg ml^{-1} of 1, in the absence of noscapine hydrochloride (p_0) and in the presence of 83.3 μg ml^{-1} (p_1), 105.8 μg ml^{-1} (p_2), 128.7 μg ml^{-1}

Table 2
Analysis of calibration graphs in the determination of noscapine hydrochloride (20.0–160.0 μg ml^{-1}) in the presence of chlorpheniramine maleate (h_{261}) by first derivative spectrophotometry

C 1 (μg ml^{-1})		Slope	Intercept	Correlation coefficient
0.0	q_0	8.65×10^{-4}	2.60×10^{-3}	0.999
23.4	q_1	9.29×10^{-4}	-0.58×10^{-3}	0.999
46.5	q_2	9.09×10^{-4}	5.27×10^{-3}	0.999
67.6	q_3	9.65×10^{-4}	-0.72×10^{-3}	0.999
90.1	q_4	10.0×10^{-4}	-0.24×10^{-3}	0.999

LOD (the lower limits of detection) = 0.031 μg ml^{-1}.
C 1: chlorpheniramine maleate concentration.

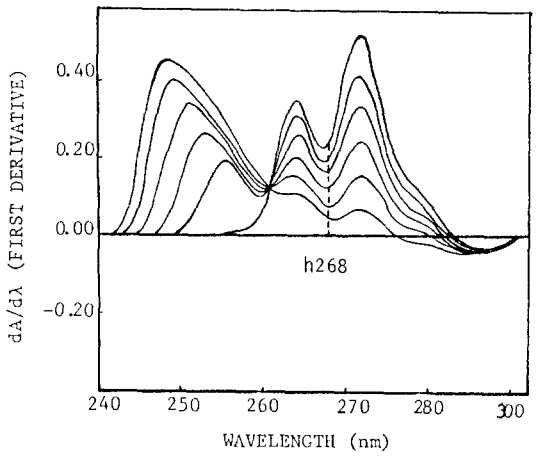

Fig. 6. A series of first derivative spectra with concentration of chlorpheniramine maleate varied from 23.8 to 140.5 μg ml^{-1} at a constant concentration of noscapine hydrochloride (129.0 μg ml^{-1}).

(p_3) and 164.1 μg ml^{-1} (p_4) of noscapine hydrochloride. The 'p' terms (p_0, p_1, p_2, p_3 and p_4) represent the calibration graphs corresponding to five sample series of chlorpheniramine maleate. The lower limits of detection (LOD) were calculated (Table 1).

Fig. 6 exhibits a series of first derivative spectra where the concentration of 1 is increased from 23.8 to 140.5 μg ml^{-1} at a constant concentration of noscapine hydrochloride (129.0 μg ml^{-1}). The experiments showed that the height at 268.0 nm

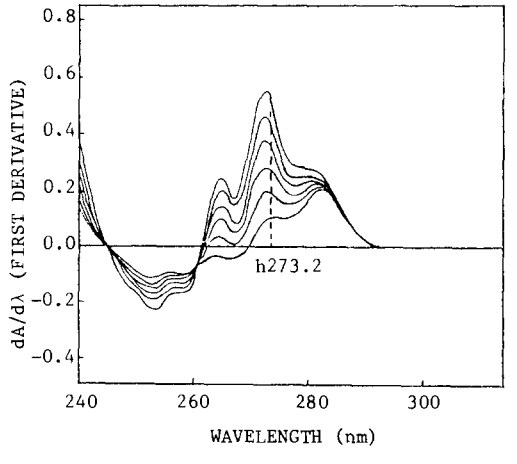

Fig. 7. A series of first derivative spectra with concentration of chlorpheniramine maleate varied from 24.9 to 146.0 μg ml^{-1} at a constant concentration of guaiphenesin (44.0 μg ml^{-1}).

($h_{268.0}$) was proportional to the chlorpheniramine maleate concentration.

It can be verified (Fig. 6) that all curves which contain the same concentration of noscapine hydrochloride converge to an abcissa value corresponding to the zero-crossing wavelength of the chlorpheniramine maleate (261.0 nm).

Similarly, five calibration graphs were prepared from the first derivative signals by measuring at 261.0 nm for standard samples containing between 20.0 and 300.0 μg ml^{-1} of 2, in the absence of 1 (q_0) and in the presence of 23.4 (q_1), 46.5 (q_2), 67.6 (q_3) and 90.1 μg ml^{-1} (q_4) of chlorpheniramine maleate. The 'q' terms (q_0, q_1, q_2, q_3 and q_4) represent the calibration graphs corresponding to five sample series of noscapine hydrochloride (Table 2).

Since, experiments with compounds 1 and 3 were performed at 273.2 and 261.0 nm for the determination of these compounds in their mixtures. Fig. 7 exhibits a series of first derivative spectra where the concentration of 1 is increased from 24.9 to 146.0 μg ml^{-1} at a constant concentration of guaiphenesin (44.0 μg ml^{-1}). The experiments showed that the height at 273.2 nm ($h_{273.2}$) was proportional to the chlorpheniramine maleate concentration.

It can be verified (Fig. 7) that all curves which contain the same concentration of guaiphenesin converge to an abcissa value corresponding to the zero-crossing wavelength of the chlorpheniramine maleate (261.0 nm).

The calibration graphs were constructed from the first derivative signals by measuring at 273.2 nm for standard samples containing between 20.0 and 120.0 μg ml^{-1} of 1, in the absence of guaiphenesin (p_0) and in the presence of 24.2 μg ml^{-1} (p_1), 65.3 μg ml^{-1} (p_2), 85.7 μg.

ml^{-1} (p_3) and 106.0 μg ml^{-1} (p_4) of guaphenesin. The 'p' terms (p_0, p_1, p_2, p_3 and p_4) represent the calibration graphs corresponding to five sample series of chlorpheniramine maleate (Table 3).

Similarly, five calibration graphs were prepared from the first derivative signals by measuring at 261.0 nm for standard samples containing between 20.0 and 120.0 μg ml^{-1} of 3, in the absence of 1 (q_0) and in the presence of 36.1 (q_1), 65.4 (q_2), 80.2 (q_3) and 115.3 μg ml^{-1} (q_4) of chlorpheni-

Table 3
Analysis of calibration graphs in the determination of chlorpheniramine maleate (20.0–120.0 μg ml^{-1}) in the presence of guaiphenesin ($h_{273.2}$) by first derivative spectrophotometry

C 3 (μg ml^{-1})		Slope	Intercept	Correlation coefficient
0.0	p_0	3.81×10^{-3}	7.60×10^{-5}	0.999
24.2	p_1	3.76×10^{-3}	7.51×10^{-5}	0.999
65.3	p_2	3.77×10^{-3}	7.58×10^{-5}	0.999
85.7	p_3	3.80×10^{-3}	7.82×10^{-5}	0.999
106.0	p_4	3.75×10^{-3}	7.53×10^{-5}	0.999

LOD (the lower limits of detection) = 0.048 μg ml^{-1}.
C 3: guaiphenesin concentration.

ramine maleate. The 'q' terms (q_0, q_1, q_2, q_3 and q_4) represent the calibration graphs corresponding to five sample series of guaiphenesin (Table 4).Tables 1–4 show the results of the statistical analysis of the experimental data for chlorpheniramine maleate, noscapine hydrochloride and guaphenesin, respectively. The linearity of the calibration graphs and the conformity of the systems to Beer's law are proven by the high value of correlation coefficients of regression equations. The lower limits of detection (LOD) were calculated by the expression LOD = 3 Sb/b [11].

The traditional Vierodt's method [12] was also applied, which involves the use of two simultaneous equations, for the determination of chlorpheniramine and guaiphenesin in unknown mixtures, with previous construction of four calibration graphs (absorbance vs. concentration). The results obtained were of poor accuracy and reproducibility with errors higher than 2%, if the ratio of guaiphenesin to chlorpheniramine maleate and noscapine hydrochloride to chlorpheniramine maleate is greater than one. This is due to close overlapping of the absorption spectra of the compounds.

Thus, the use of the first derivative spectrophotometry permits to eliminate the problem of closely overlapping spectra [13]. This method was applied for resolving the determination of clorpheniramine maleate-noscapine hydrochloride and clorpheniramine maleate-guaiphenesin in synthetic mixtures of different proportions. The results obtained are summarized in Table 5. In addition, the relative standard deviations (RSD) for five determinations at each concentration level are satisfactorily low (0.25–0.81%) and indicate the good reproducibility of the proposed method.

A rigorous analysis of the results indicated that the presence of one of the components does not interfere with the determination of the other.

Prior sample preparation, such as solvent extraction or column chromatography, is not necessary for the analysis of formulations containing mixtures of these compounds. Elimination of these steps saves considerable analysis time. It is worthy of mention that no expensive or toxic solvents or reagents are used.

Table 4
Analysis of calibration graphs in the determination of guaiphenesin (20.0–120.0 μg ml^{-1}) in the presence of chlorpheniramine maleate (h_{261}) by first derivative spectrophotometry

C 1 (μg ml^{-1})		Slope	Intercept	Correlation Coefficient
0.0	q_0	1.86×10^{-3}	1.94×10^{-4}	0.999
36.1	q_1	1.84×10^{-3}	1.87×10^{-4}	0.999
65.4	q_2	1.88×10^{-3}	1.96×10^{-4}	0.999
80.2	q_3	1.87×10^{-3}	-1.90×10^{-4}	0.999
115.3	q_4	1.84×10^{-3}	1.85×10^{-4}	0.999

LOD (the lower limits of detection) = 1.28 μg ml^{-1}.
C 1: chlorpheniramine maleate concentration.

Table 5
Determination of chlorpheniramine maleate-noscapine hydrochloride and chlorpheniramine maleate-guaiphenesin in synthetic mixtures by using the first derivative spectrophotometry

C 1 (μg ml^{-1})				C 2 (μg ml^{-1})			
	M_1	M_2	M_3		M_1	M_2	M_3
$A_{268.0}$	0.268	0.192	0.154	$A_{261.0}$	0.128	0.127	0.084
Known	61.97	107.4	86.31	Known	133.6	132.7	87.24
Found	61.65	108.1	87.06	Found	133.4	132.4	87.35
Recovery (%)	99.48	100.6	100.9	Recovery (%)	99.85	99.77	100.1
RSD (%)	0.571	0.742	0.635	RSD (%)	0.750	0.811	0.571

C 2/C 1 (w/w) ratio in the mixtures: M_1: 2.16; M_2: 1.24 and M_3: 1.01, respectively.

C 1 (μg ml^{-1})				C 3 (μg ml^{-1})			
	M_1	M_2	M_3		M_1	M_2	M_3
$A_{273.2}$	0.122	0.078	0.283	$A_{261.0}$	0.059	0.154	0.139
Known	31.97	20.72	75.48	Known	31.44	83.63	74.15
Found	32.34	20.68	75.02	Found	31.75	82.88	74.81
Recovery (%)	101.1	99.81	99.39	Recovery (%)	101.00	99.10	100.9
RSD (%)	0.411	0.253	0.292	RSD (%)	0.350	0.305	0.341

C 3/C 1 (w/w) ratio in the mixtures: M_1: 0.98; M_2: 4.04 and M_3: 0.98, respectively.

Thus, this method has a significant advantage over other techniques and is extremely suitable for routine pharmaceutical analysis.

References

[1] J.E.F. Reynolds, Martindale The Extra Pharmacopoeia 29th Edn., Pharmaceutical Press, London, 1989, p. 444.
[2] K. Florey, Analytical Profiles of Drug Substances, Academic Press, New York, 1982, p. 407.
[3] J.E.F. Reynolds, Martindale The Extra Pharmacopoeia 29th Edn., Pharmaceutical Press, London, 1989, p. 910.
[4] J.E.F. Reynolds, Martindale The Extra Pharmacopoeia 29th Edn., Pharmaceutical Press, London, 1989, p. 448.
[5] T.C. O'Haver, Anal. Proc., 19 (1982) 22.
[6] J.A. Murillo, J.M. Lemus and L.F. García, Anal. Lett., 24 (1991) 683.
[7] J.A. Murillo, J.M. Lemus and L.F. García, J. Anal. Chem., 347 (1993) 114.
[8] J.A. Murillo, J.M. Lemus and L.F. García, Anal. Lett., 27 (1994) 1875.
[9] A.R. Lee, Chin. Pharm. J., 44 (1992) 87.
[10] A.R. Lee and T.M. Hu, J. Pharm. Biom. Anal., 12 (1994) 747.
[11] G.L. Long and J.P. Winefordner, Anal. Chem., 55 (1983) 712.
[12] H.S.I. Tan and G.C. Salvador, Anal. Chim. Acta, 12 (1985) 71.
[13] G. Talsky, H. Mayring and H. Kreuzer, Angew. Chem. Int. Ed. Engl., 17 (1978) 785.

ELSEVIER

Talanta 44 (1997) 641–647

Talanta

Rapid determination of ribonuclease and microanalysis of heparin with a SAW/conductance sensor

Ronghui Wang [a], Qingyun Cai [a], Wei Wei [a], Lihua Nie [a], Shouzhuo Yao [a,*], Chunlin Liu [b], Tieshan Jiang [b]

[a] *Department of Chemistry and Chemical Engineering, Hunan University, Changsha 410082, China*
[b] *Hunan Agriculture University, Changsha 410128, China*

Received 10 June 1996; received in revised form 27 August 1996; accepted 27 August 1996

Abstract

A new method using a surface acoustic wave (SAW)/conductance sensor has been described in this paper for rapid determination of ribonuclease (RNase) and microanalysis of heparin. The assay of RNase is based on the change in conductance of the solution caused by enzymatic reaction between ribonucleic acid (RNA) and RNase and the analysis of heparin is based on its inhibitory action on RNase. A linear relationship between frequency response and enzyme concentration is obtained and the detection limit of RNase is evaluated to be 0.17 μg ml^{-1}. The recovery of the sensor system ranges from 95.8 to 105.0%. The inhibition of heparin is a competitive one and the possible inhibition mechanism is discussed. The kinetic parameters and inhibition parameters are estimated. The calibration graph is rectilinear for ≤ 8 μg ml^{-1} of heparin and the detection limit is 0.1 μg ml^{-1}. The influence of pH value on the inhibition of RNase by heparin has been investigated and the effects of Ca^{2+}, Mg^{2+} are also discussed. © 1997 Elsevier Science B.V.

Keywords: Heparin; Microanalysis; Ribonuclease; Surface acoustic wave

1. Introduction

The ribonuclease (RNase) is important in the anabolism and catabolism of ribonucleic acid (RNA) of the cytoplasm and nucleus. Various qualitative [1,2] and quantitative [3,4] assays for RNase activity have been described. Most utilize the differential solubility in acid or ethanol of the substrate and product of enzyme digestion. Heparin, a polymer of glucosamine and uronic acids, possess wide biological activities. It is important as a blood anticoagulant and is of clinical significance [5]. It has been widely used in medicine and pharmacology. The normal physiological concentration of heparin in human plasma is 9 μg dl^{-1} [6]. Several reports have covered the structure, function and quantitation of heparin [7,8]; up until now the main method to determine heparin is using its chromogenic substrates [9]. Heparin can greatly inhibit the enzymatic reaction of RNA/RNase and the inhibitory action is used to determine heparin in this paper. Although cur-

* Corresponding author.

PII S0039-9140(96)02088-7

rently available methods are fairly sensitive, many are time-consuming and require harsh analytical conditions [10]. The present investigation was prompted by the need to develop more reliable, simple and less time-consuming methods for quantitative analysis of heparin. In this paper, a new liquid-purpose SAW/conductance sensor system has been described to rapid determination of RNase and microanalysis of heparin.

This new type of SAW/conductance sensor system proposed in our laboratory recently [11,12] is composed of a 61 MHz SAW resonator and a pair of parallel platinum electrodes. The frequency of the SAW/conductance sensor can be measured within ± 1 Hz. The device is based on the principle that oscillation is only generated and supported when the sum of the phase angles of a loop circuit containing resistive, capactive and inductive elements in series with an amplifier and a SAW device is a multiple of 2π rad and the loop gain is greater than 1. If any element in the circuit imparts a phase delay change, the oscillation frequency will change. Therefore, it can response to any changes in the physical/chemical properties of the medium between two electrodes as they cause variations in the loop parameters. By analysing the frequency shift response much information about the liquid system can be obtained.

For such a SAW/conductance sensor system, frequency shifts (ΔF) are related to the change of the electrolyte conductance (ΔK): $\Delta F = a\Delta K + b$. Here, a and b are constants depending on the SAW device, amplifier circuit and experimental conditions. So, the frequency of the SAW/conductance sensor shifts according to the conductance change of the substrate solution caused by enzymatic reaction between RNA and RNase, and it is possible to correlate the enzymatic reaction rate with the frequency change. This is the fundamental principle for the RNase determination in this study.

The proposed SAW/conductance sensor has some advantages. One advantage over more conventional oscillator circuit is the high frequency, stability and narrow band-width obtainable with SAW oscillators versus other crystal-controlled and RC/RLC/LC circuits. Another advantage is that the interferences caused by mass, viscoelastic or electroacoustic properties can be avoided. Only the alternation of conductance in test solution can produce the frequency shift of the sensor. We also found that in a medium conductivity region, the higher the conductivity, the higher the sensitivity of the SAW/conductance sensor system. So, the SAW system seems more attractive than the normal a.c. conductometry and a.c. impedance measurement. In addition, the SAW/conductance sensor is advantageous in its rapid determination, simplicity in construction and low noise levels. Since there is no report on SAW devices applied to RNA/RNase reaction and the analysis of heparin, in this paper, the SAW/conductance sensor has been successfully applied in enzymatic analysis of RNase and microanalysis of heparin.

2. Experimental

2.1. Apparatus

The experimental set-up was same as described in the previous paper [11,12]. The 61 MHz SAW resonator used in this study was manufactured on an Y,Z-cut lithium niobate piezoelectric crystal and the whole SAW device was sealed for protection against atmosphere with an epoxide lid. Without touching the solution directly, the device was electrically connected to a pair of parallel platinum electrodes, which were set in the 5 ml detection cell. During the experiments, the detection cell was placed in an air-bath thermostating equipment in which the temperature was monitored and controlled by a WMZK-01 temperature controller (Medical Instrument Co., Shanghai). The temperature was thermostated at 25 ± 0.2°C throughout the experiments. The solution in the cell was stirred with a magnetic stirrer at a constant stirring rate 6.5 V d.c. power was delivered to the circuit board (self-made) by an adjustable dual-track d.c. power supply. A universal frequency counter (Model SC-7021, Iwatsu) was used to measure the oscillation frequency of the SAW resonator at a resolution of 1 Hz and data were collected at 6 points min^{-1}.

2.2. Materials and reagents

All reagents were of analytical grade or better. Doubly distilled water was used throughout. Working buffer was 2.0 mM Tris–HCl at pH 7.0. RNase [EC 3.1.27.5] and heparin sodium (140 units mg^{-1}) were obtained from Shanghai Biochemical Products Institute and Hunan Chemical Products Institute, respectively. RNA extracted from *E. coli* was supplied by Hunan Agriculture University. The method of extracting RNA was a convenient one according to the literature [13]. The RNA extract was measured spectrophotometrically in absorbancy at 230, 260 and 280 nm, and the concentration of RNA was evaluated to be 8.2 mg ml^{-1}.

2.3. Procedures

The detection cell was filled with 5 ml of the RNA, or RNA and heparin (in 2.0 mM Tris–HCl buffer, pH 7.0) under magnetic stirring and the stable frequency of the SAW/conductance sensor was measured (F_0). Then, a small volume of the enzyme solution was transferred into the cell and the enzyme catalyzed reaction was started. Changing with the time, the resulted frequency shift was recorded as $\Delta F = F - F_0$, where F was the frequency after adding the enzyme solution. A frequency shift versus time graph was obtained and the initial response rate was calculated from its initial linear section. Then, an initial response rate versus RNase concentration calibration curve was constructed and a linear relationship between initial response rate and RNA concentration was also obtained. All experiments were repeated more than three times and the average value was used for calculation. The experiments were performed at 25 ± 0.2°C.

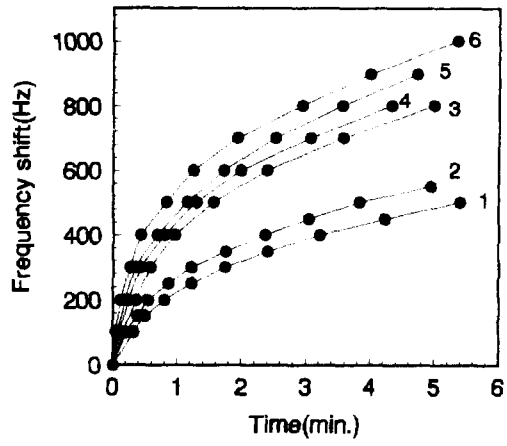

Fig. 1. Frequency response curves (frequency shift vs. time) corresponding to 15 μg ml^{-1} RNase and different concentration of RNA (μg ml^{-1}): (1) 16.5; (2) 32.9; (3) 65.9; (4) 98.8; (5) 131.7; and (6) 164.6.

3. Results and discussion

3.1. Estimation of kinetic parameters

Keeping the concentration of RNase constant at 15 μg ml^{-1}, the RNA concentration was

Table 1
Recovery determined with the SAW/conductance sensor system

Enzyme (μg ml^{-1})		V_0 (Hz min^{-1})	Recovery (%)	Mean (%)	R.S.D. (%)
Added	Found				
1.3	1.29	69	99.4		
2.6	2.49	119	95.8		
5.2	5.36	198	103.0		
7.8	8.19	280	105.0	100.1	2.4
10.4	10.29	388	98.8		
11.7	11.53	435	98.6		
13.0	12.97	475	99.7		

Experimental conditions: 165 μg ml^{-1} RNA, pH 7.0, 25°C.

ranged from 16.5 to 165 μg ml^{-1} to obtain a typical Michaelian curve. The experimental data is given in Fig. 1. The initial rate can be calculated from its initial linear section and the results show a linear relationship between the RNA concentration and the initial rate. A corresponding regression equation was described as follows: $V_0 = 3.3[RNA] + 9.2$ ($r = 0.993$, $n = 6$), where the RNA concentration was expressed in μg ml^{-1} and V_0 in Hz min^{-1}. According to the Lineweaver–Burk equation, the K_m value was estimated to be 2.6 mg ml^{-1} for RNA and a corresponding maximum initial rate (V_{max}) was 9973 Hz min^{-1}.

3.2. Assay of the enzyme concentration

At a fixed substrate concentration, the initial rate of an enzyme-catalyzed reaction is directly proportional to the concentration of that enzyme [14]. In this experiment, the substrate RNA was kept constant at 165 μg ml^{-1} and the enzyme concentration was in the range up to 13 μg ml^{-1} of RNase, at 25°C and pH 7.0. A correlation of $V_0 = 34.5[E] + 24$ ($r = 0.998$, $n = 7$) is obtained, where V_0 refer to the initial rate (in Hz min^{-1}) and $[E]$ to the concentration of the RNase solution (in μg ml^{-1}). Under our experimental condition, the detection limit of RNase is evaluated to be 0.17 μg ml^{-1} based on three times the signal-to-noise ratio (S/N = 3).

The average recoveries for RNase shown in Table 1 ranged from 95.8 to 105.0%. The data were obtained with seven different experiments and each obtained value was the mean of three measurements.

3.3. Inhibition action of heparin upon RNase

We have observed that heparin shows an inhibitory action on RNase activity. When heparin is introduced into a solution containing RNase and RNA, the enzymatic activity decreases by the concentration of heparin present in the solution. This process provided a possibility for detecting or assaying extremely low concentration of a wide range of heparin by comparing the alternation of the RNase-catalysed reaction rate which is followed by the SAW/conductance sensor. As shown in Fig. 2, the frequency response of the sensor decreases evidently when heparin is present.

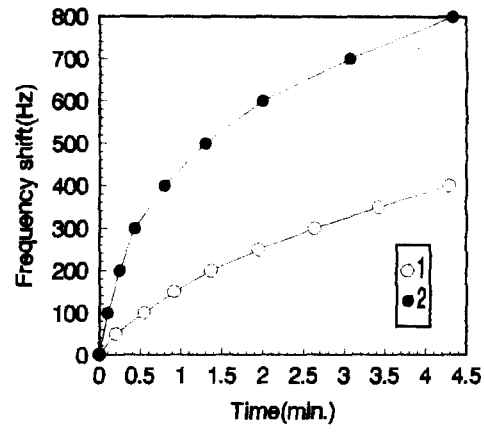

Fig. 2. Influence of heparin on the frequency response curves: (1) in the presence of 4 μg ml^{-1} heparin; and (2) in the absence of heparin. RNA concentration: 98.8 μg ml^{-1}; RNase concentration: 13 μg ml^{-1}.

The effect of substrate concentration on the inhibitory action of heparin has been investigated and the results are shown in Table 2. From the data, we can observe that the effect of the inhibitor depends on the substrate concentration. The higher the substrate concentration, the lower the inhibition. These results have implied that the inhibition is a competitive one.

Table 2
The effect of substrate concentration on the inhibitory action of heparin

Heparin concentration (μg ml^{-1})	RNA concentration (μg ml^{-1})	Inhibition (%)
8	98.8	97.7
	164.6	91.9
	247.0	84.3
4	98.8	61.0
	164.6	54.7
	247.0	45.8

The experimental conditions: 18 μg ml^{-1} RNase, pH 7.0, 25°C.

Table 3
Kinetic parameters and inhibition parameters of heparin

[heparin] (μg ml^{-1})	0	0.8	2	4	5	6
K'_m (mg ml^{-1})	2.4	3.60	5.1	7.6	8.8	10.1
V'_{max} (kHz min^{-1})	9.85	10.18	10.06	9.99	9.92	10.03
K_i (mg ml^{-1})			2.1×10^{-3}			
K_m (mg ml^{-1})			2.6			
V_{max} (kHz min^{-1})			9.97			
I_{50} (μg ml^{-1})			3.7			

The experimental conditions: 13 μg ml^{-1} RNase, pH 7.0, 25°C.

3.4. The possible inhibition mechanism of heparin

Heparin is a natural polysaccharide and resembles RNA in some respects. Because of this structural similarity the heparin can compete for the same binding-site on the enzyme. The enzyme-bound inhibitor then either lacks the appropriate reactive group or it is held in an unsuitable position with respect to the catalytic-site of the enzyme or to other potential substrate for a reaction to take place. In either case a dead-end complex is formed, and the inhibitor must dissociate from the enzyme and be replaced by a molecule of substrate before a reaction can take place at that particular enzyme molecule. So, the inhibition mechanism of heparin can be described as follows:

$$\begin{array}{ccccc} \mathbf{E} + \mathbf{S} & \underset{k_{-1}}{\overset{k_1}{\rightleftharpoons}} & \mathbf{ES} & \xrightarrow{k_2} & \mathbf{E} + \mathbf{P} \\ -\mathbf{I} \Big\| \Big\downarrow +\mathbf{I} & & & & \\ \mathbf{EI} & & & & \end{array} \quad (1)$$

The dissociation constant K_i, which is also called the inhibitor constant, is expressed as:

$$K_i = \frac{[E][S]}{[ES]} = \frac{[E][I]}{[EI]} \quad (2)$$

By using the steady-state assumption, the following expression can be derived:

$$V_0 = \frac{V_{max}[S_0]}{[S_0] + K_m(1 + [I_0]/K_i)} \quad (3)$$

where V_0 and V_{max} are the initial rate and intrinsic maximum rate of the RNase-catalysed hydrolysis reaction of RNA respectively, $[S_0]$ and $[I_0]$ are the initial concentration of substrate RNA and inhibitor heparin respectively. K_m is intrinsic Michaelis constant.

Eq. (3) has the same form as the Michaelis–Menten equation. The only difference being that K_m has been increase by a factor $(1 + [I_0]/K_i)$. So, the apparent Michaelis constant $K'_m = K_m(1 + [I_0]/K_i)$ and V_{max} is unchanged ($V'_{max} = V_{max}$).

The Lineweaver–Burk equation in the presence of heparin will be:

$$\frac{1}{V_0} = \frac{K'_m}{V'_{max}} \frac{1}{[S_0]} + \frac{1}{V'_{max}} \quad (4)$$

The calculated kinetic parameters (apparent kinetic parameters, K'_m and V'_{max}; intrinsic kinetic parameters, K_m and V_{max}) and inhibition parameters (inhibitor constant, K_i; inhibitor concentration necessary to produce 50% inhibitor, I_{50}) are summarized in Table 3, which are measured under the following conditions: 13 μg ml^{-1} RNase, 2.0 mM Tris–HCl buffer, pH 7.0 and 25°C.

3.5. Relationship between frequency response and heparin concentration

Under the present experimental conditions (98.8 μg ml^{-1} RNA, 13μg ml^{-1} RNase, 2.0 mM Tris–HCl, pH 7.0, 25°C), the calibration curve of initial rate or inhibition ratio against heparin concentration was linear for ≤ 8 μg ml^{-1} (Fig. 3). They are also described by the following regression equation:

$$V_0 = -49.8[\text{heparin}] + 388.4 \quad (5)$$

$$P = 12.0[\text{heparin}] + 6.1 \quad (6)$$

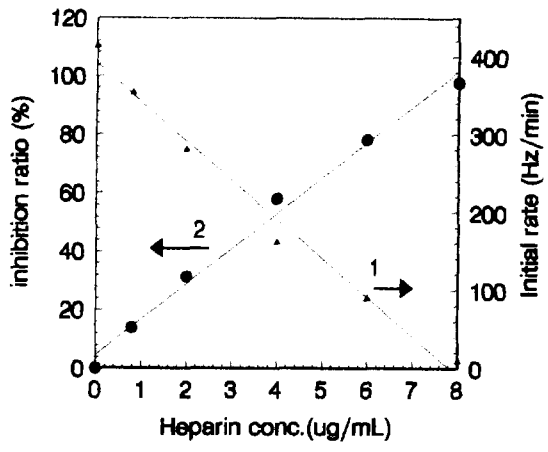

Fig. 3. Calibration graphs for heparin with SAW/conductance sensor: (1) initial rate against inhibitor heparin concentration; and (2) inhibition ratio against inhibitor heparin concentration. Experimental conditions: 13 μg ml^{-1} RNase, 98.8 μg ml^{-1} RNA, pH 7.0 and 25°C.

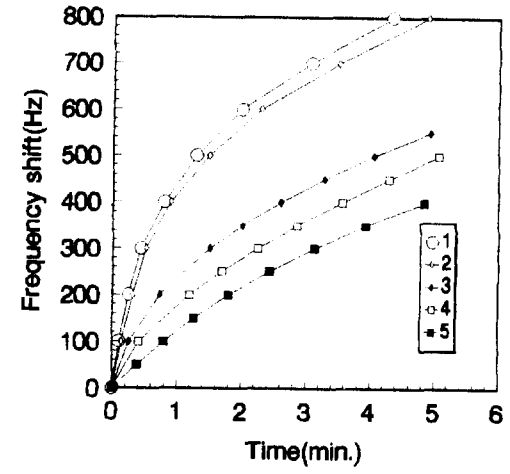

Fig. 4. Influences of Ca^{2+} and Mg^{2+}. (1) In the absense of Ca^{2+} or Mg^{2+}. (2) 2×10^{-4}M Ca^{2+}. (3) 2×10^{-4}M Mg^{2+}. (4) 2×10^{-4}M Ca^{2+} plus 2 μg ml^{-1} heparin. (5) 2×10^{-4}M Mg^{2+} plus 2 μg ml^{-1} heparin. 98.8 μg ml^{-1} RNA and 13 μg ml^{-1} RNase were selected for this measurement.

where V_0 is initial rate calculated in Hz min^{-1}, [heparin] in μg ml^{-1} and P refers to inhibition ratio (%). The regression coefficient is -0.989 ($n = 6$). The detection limit is 0.1 μg ml^{-1} or 0.014 units ml^{-1} of heparin. The standard deviation is 2.7% for four determinations of 2 μg ml^{-1} heparin.

3.6. The effect of pH on the inhibition of RNase by heparin and the influences of Ca^{2+}, Mg^{2+}

The pH value can affect the inhibition ratio of heparin and the results are shown in Table 4. The experimental conditions are: 98.8 μg ml^{-1} RNA, 13 μg ml^{-1} RNase, 4 μg ml^{-1} heparin, at 25°C. The data indicate that heparin has a minimum inhibitory effect on RNase between pH 7.5 and 8.5.

Table 4
The effect of pH on the inhibition of RNase by heparin

pH value	V_i (Hz min^{-1})	V_u (Hz min^{-1})	Inhibition (%)
6.0	145	406	64.3
6.5	148	403	63.3
7.0	161	414	61.1
7.5	248	417	40.5
8.0	290	413	29.8
8.5	252	405	37.8

V_i refers to the inhibited initial rate and V_u refers to the uninhibited initial rate.
Experimental conditions: 98.8 μg ml^{-1} RNA, 13 μg ml^{-1} RNase, 4 μg ml^{-1} heparin at 25°C.

The influences of Ca^{2+} and Mg^{2+} have also been investigated (98.8 μg ml^{-1} RNA, 13 μg ml^{-1} RNase, 2 μg ml^{-1} heparin, pH 7.0 and 25°C). The results are shown in Fig. 4. Although Ca^{2+} or Mg^{2+} can inhibit RNase, the inhibitory effect are greatly increased when Ca^{2+} plus heparin or Mg^{2+} plus heparin is added.

3.7. Comparison of the SAW-sensing method with other methods

Since the SAW/conductance sensor can respond to the conductance change of the substrate solution caused by enzymatic reactions and this is really a conductance measurement, a comparative study was carried out of the SAW/conductance sensor and the conductimetric method. The experimental conditions were the same as above. The detection limit of the conductimetry was 1.1 μg ml^{-1} of heparin and the detection limit of the

Table 5
Comparison of methods for analysing heparin

Method	Detection limit of heparin	Reference
Chemiluminescent method	90 μg l^{-1}	[5]
High-performance liquid-chromatographic-mass-spectrometric method	1 μg ml^{-1}(in plasma) 0.2 μg ml^{-1}(in urine)	[15]
Thrombin-clotting-time technique	0.05 unit ml^{-1} (in plasma)	[16]
Conductimetry	1.1 μg ml^{-1}	This paper
SAW method	0.1 μg ml^{-1} or 0.014 unit ml^{-1}	This paper

SAW-sensing method was only 0.1 μg ml^{-1} of heparin. So, the proposed SAW-sensing method was much more sensitive than the conductimetric one. A comparison of the SAW-sensing method with previously reported techniques [5,15,16] is given in Table 5. The sensitivity of both the SAW method and the overall method are good. Taking into consideration the advantages of the SAW/conductance sensor system (rapid determination, simplicity in operation and enough sensitivity), it appears to be an efficient techniques for the assay of enzyme and microanalysis of heparin.

Acknowledgements

We are grateful for the financial support from the National Natural Science Foundation and the State Education Commission Fund of China.

References

[1] T.P. Karpetsky, G.E. Davies, K.K. Shriver and C.C. Levy, Biochem. J., 189 (1980) 277–284.
[2] W.F. Burke Jr. and B.S. Slinker, Anal. Biochem., 108 (1980) 320–324.
[3] R. Shapira, Anal. Biochem., 3 (1962) 308–320.
[4] S.B. Zimmerman and G. Sandeen, Anal. Biochem., 10 (1965) 444–449.
[5] R.A. Steen and T.A. Nieman, Anal. Chim. Acta, 155 (1983) 123–129.
[6] S. Wang, Diagnostics, Ch. 5, People's Hygiene Press, China, 1990.
[7] J. Ehrlich and S.S. Stivala, J. Pharm. Sci., 62 (1973) 517.
[8] W.D. Comper, Heparin (and Related Polysaccharides), Gordon and Breach, New York, 1981.
[9] T. Zhang and H. Gao, Yaoxue Tongbao, 22 (12) (1987) 709–712.
[10] M.Y. Khan and S.A. Newman, Anal. Biochem., 187 (1) (1990) 124–128.
[11] S. Yao, K. Chen, and L. Nie, Anal. Chim. Acta., 289 (1994) 47–55.
[12] S. Yao, K. Chen, F. Zhu, D. Shen and L. Nie, Anal. Chim. Acta., 287 (1994) 65–73.
[13] J. Sambrook, E.F. Fritsch and T. Maniatis, Molecular Cloning, 1.33–1.41, Cold Spring Harbor Laboratory Press, 1989.
[14] T. Palme, Understanding Enzymes, Ch. 7, Ellis Horwood, Chichester, 1981.
[15] L. Silvestro, I. Viano, A. Naggi, G. Torri, R. Da Col and C. Baiocchi, J. Chromatogr., 591 (1–2) (1992) 225–232.
[16] J.D. Phillips, Med. Lab. Sci., 36 (2) (1979) 141–145.

ELSEVIER

Talanta 44 (1997) 649–656

Talanta

Gas chromatography–mass spectrometric determination of fthalide and heptachlor epoxide in environmental samples

Tameo Okumura, Yoshinori Nishikawa, Hitoshi Yamamoto, Hiroe Konishi

Environmental Pollution Control Center, 1-3-62, Nakamichi, Higashinari-ku, Osaka City 537, Japan

Accepted 30 August 1996

Abstract

Methods were developed to determine traces of 4,5,6,7-tetrachlorophthalide (fthalide) and 1,4,5,6,7,8,8-heptachloro-2,3-epoxy-2,3,3a,7a-tetrahydro-4,7-methanoindene (heptachlor epoxide) in environmental samples such as river water, sediment and fish. The samples were cleaned up by using convenient disk type solid phase extractors and cartridges and analyzed by GC/MS with selected ion monitoring. Fthalide and heptachlor epoxide in water samples could be determined in the range 0.1–0.3 ng ml^{-1} with relative standard deviations (RSDs) of 1.0–4.8%. The estimated detection limits were 0.020–0.031 ng ml^{-1}, 5.1–7.3 ng g^{-1} and 2.7–4.2 ng g^{-1} in water, sediment and fish samples, respectively. The recoveries were 96–103, 99–101, 66–85 and 67–77% with RSDs of 4.3–10.2, 2.4–2.5, 4.6–5.2 and 2.1–3.8% in river water, sea water, sediment and fish samples, respectively. © 1997 Elsevier Science B.V.

Keywords: Fthalide; Gas chromatography; Heptachlor epoxide; Mass spectrometric

1. Introduction

A large number of chemicals have so far been found in the environment, increasing with progress in industrial science and improvement in living. Accurate information is necessary on environmental pollution due to hazardous agents so as to take appropriate measure to avoid actual damage. The Japan Environmental Agency has surveyed to check the safety of the chemical agents distributed in the environment. So far, our laboratory has developed GC/MS–selected ion monitoring (SIM) methods [1–6] to determine some of the chemical listed by the Japan Environmental Agency.

4,5,6,7-Tetrachlorophthalide (fthalide) and 1,4,5,6,7,8,8-heptachloro-2,3-epoxy-2,3,3a,7a-tetrahydro-4,7-methanoindene (heptachlor epoxide), used as fungicide or insecticide, are selected as target compounds in the priority list. GC/MS–SIM allows the identification and the determination of the target compounds [7–9]. GC–electron capture detection (ECD) is also able to determine them because of their several chlorine atoms [10,11]. However, GC-ECD is problematic due to various kinds of interfering substances coexisting in actual samples. The final results of the analysis might thus be subject to considerable errors with an insufficient clean-up procedure, even if the analysis is made using sensitive and sophisticated detection systems. Recently, solid phase extraction systems have been developed using a cartridge [12–15] or a filter disk [8,15–19] instead of the solvent extraction in a separatory funnel.

PII S0039-9140(96)02097-8

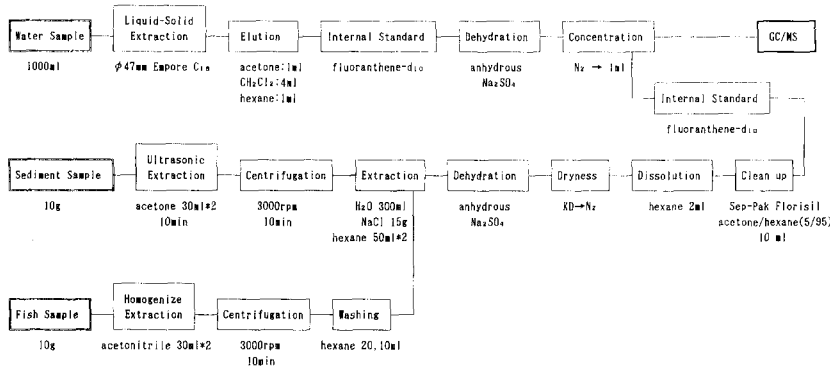

Fig. 1. Flow scheme for the determination of fthalide and heptachlor epoxide in the environmental samples.

This paper reports a convenient method to determine fthalide and heptachlor epoxide in water, sediment and fish samples at sub ng ml^{-1} or low ng g^{-1} levels. The samples are enriched and cleaned up by using a filter disk followed by capillary–GC/MS–SIM analysis.

2. Experimental

2.1. Reagents and apparatus

Fthalide ($C_8H_2Cl_4O_2$) and heptachlor epoxide ($C_{10}H_5Cl_7O$) of pesticide standards grade, and hexane, acetone, dichloromethane, acetonitrile, methanol, anhydrous sodium sulfate, sodium chloride of pesticides grade were obtained from Wako (Osaka, Japan). [$^2H_{10}$] Fluoranthene (fluoranthene-d_{10}) as an internal standard was from MSD Isotopes (Montreal, Canada). Solid phase extraction disk C_{18} (SPED-C18) for water samples was a 47 mm diameter Empore disk (3 M, from GL Science, Tokyo, Japan). The disk was washed with 10 ml of acetone and 10 ml of dichloromethane, and then conditioned with 10 ml of methanol and 10 ml of pure water before use. Glass fiber filter GF/C (47 mm d., Whatman, UK) and high density glass beads (3 M Filter Aid 400) were used on the disk to achieve smooth filtration in the case that water samples contain a lot of suspended substances. Se-Pak Florispil cartridges (Waters, Milfor, MA) for clean-up of sediment and fish samples were prewashed with 10 ml of hexane before use.

A Branson (Shelton, CT, USA) B-220 ultrasonic extractor and a Poly Toron PT10-30 homogenizer were used to extract analytes from sediment and fish samples, respectively. A Tomy Seiko LC06-SP (Tokyo, Japan) centrifuge was employed for phase separation of sediment and fish samples.

2.2. Gas chromatography–mass spectrometry

Employed were a Hewlett-Packard (Avondale, PA, USA) HP 5790 GC and a Nihondenshi (Tokyo, Japan) JEOL-DX303 MS equipped with DA-5000 data processing system. The analytical column was Ultra-2 crosslinked 5% phenyl methylsilicone (25 m × 0.32 mm i.d., 0.52 μm film thickness). The GC temperature program was as follows: initial temperature was 70°C and increased at 20°C min^{-1}–270°C. The temperature of the injector, transfer line and ion source were 250°C respectively. The carrier gas was helium at the following rate of 61 cm s^{-1} (column head pressure, 7.5 psi). The mass spectrometer was operated at 70 eV of ionization energy and 300 μA of ionization current in the electron-impact mode using scan or SIM. Monitor ions (m/z) for fthalide, heptachlor epoxide and their internal standard were as follows: fthalide; 242.9 (for quantitative determination), 244.9 (for qualitative determination), heptachlor epoxide; 352.8 (Quantification), 354.8 (Identification), fluoranthene-d_{10} (internal standard); 212.0.

Table 1
Degradation of fthalide and heptachlor epoxide at pH 5, 7 and 9

Compound	pH[a]	Conc. (mg l^{-1})	Recovery (%)		
			After 1 h	After 5 days	
				Dark	Light
Fthalide	5	0.096	112	113	—
	7	0.096	122	32	12
	9	0.096	118	1	—
Heptachlor epoxide	5	0.095	84	96	—
	7	0.095	87	100	88
	9	0.095	99	97	—

[a] pH 5: 65 mM-KH_2PO_4. pH 7: 65 mM-KH_2PO_4/65 mM-Na_2HPO_4 (4/6). pH 9: 65 Mm-Na_2HPO_4.

2.3. Analytical procedure

The clean-up and enrichment of environmental samples is outlined in the flow chart in Fig. 1. A 1000 ml volume of water sample was passed through the SPED-C18 by using an aspirator or a suction pump. Glass fiber filters and/or high density glass beads (10 g) were preferable to use on the disk in the case that the sample contains much suspended material. The pesticides adsorbed on the disk were eluted with 1 ml of acetone, 4 ml (in case of using the glass beads, 6 ml) of dichloromethane and 1 ml of hexane in that order. A 0.5 ml volume of internal standard solution (fluroanthene-d_{10}, 1 μg ml^{-1} in acetone) and 4 g (in case of using the glass fiber filter, 6 g) of anhydrous sodium sulfate were added to the eluate. As it is difficult to dehydrate polar solvent such as acetone and dichloromethane with anhydrous sodium sulfate, 1 ml of hexane was added to acetone–dichloromethane mixed solvent in order to lower polarity. Completion of the dehydration could be recognized by transparency of the eluent. The eluent was evaporated to 1 ml under a nitrogen stream, and 2 μl of the aliquot was analyzed by GC/MS.

Sediment (10 g) was mixed with 30 ml of acetone and stirred. The muddy suspension made was placed in a ultrasonic extractor for 10 min and then centrifuged at 3000 rpm for 10 min. The acetone extract was then removed. After twice repeating the procedure, the acetone extracts were combined and put into a separator funnel. A 300 ml volume of pure water and 15 g of NaCl were placed into the funnel. The solution was extracted twice with 50 ml of hexane. The organic phase was combined, dehydrated with anhydrous sodium sulfate, concentrated to 3–5 ml by a Kuderna-Danish evaporative concentrator and further evaporated to dryness under a nitrogen stream. The residue was dissolved with 2 ml of hexane, poured into the Sep-Pak Florisil cartridge, washed with 10 ml of hexane and then eluted with 10 ml of acetone/hexane (5/95). The internal standard was added to the eluate. The eluate was evaporated to 1 ml and then 2 μl of aliquot was analyzed by GC/MS.

Fish tissue (10 g) was homogenized, extracted with 30 ml of acetonitrile and centrifuged at 3000 rpm for 10 min. The extraction was performed twice. The acetonitrile phase was combined and washed with 20 ml and then with 10 ml of hexane. Followed procedures were similar to those employed for sediment sample.

3. Results and discussion

3.1. Degradation test

Degradation of fthalide and heptachlor epoxide was investigated at pH 5, 7 and 9 for 1 h and 5 days. Table 1 shows that fthalide degraded under neutral (pH 7) and alkaline (pH 9) conditions

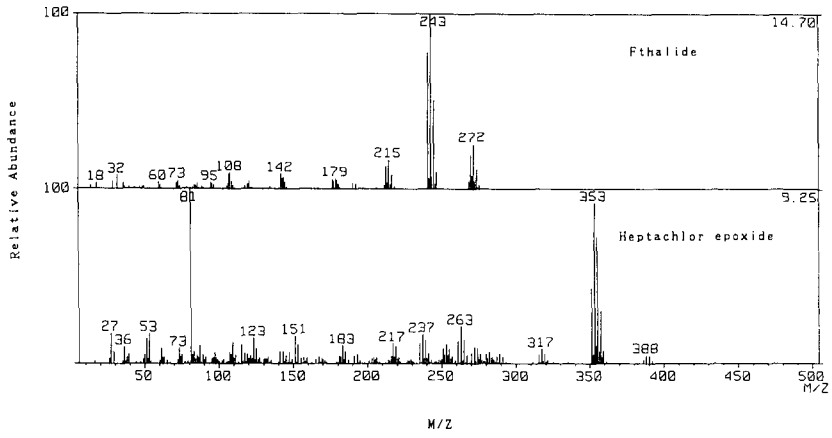

Fig. 2. GC/MS spectra of fthalide and heptachlor epoxide.

after 5 days. Fthalide is a cyclic ester, so it probably undergoes alkaline-catalyzed hydrolytic cleavage. On the other hand, heptachlor epoxide was stable under the pH conditions investigated and even stable in sunlight at pH 7.

3.2. Mass spectra, GC/MS–SIM chromatograms and calibration

The mass spectra of fthalide and heptachlor epoxide are shown in Fig. 2. The ions monitored for quantitative determination and identification were selected for optimum selectivity and sensitivity.

Typical GC/MS–SIM chromatograms of fthalide and heptachlor epoxide standards are shown in Fig. 3. Their retention time was 9–10 min at this analytical conditions.

The calibration graph for the compounds was obtained by plotting the concentration ratio (X) of the analyte to the internal standard against the corresponding peak area ratio (Y). An example is shown in Fig. 4. Excellent linearity was obtained in the calibration graphs by using five different concentrations. The equations of calibration for fthalide and heptachlor epoxide were $Y = 0.183\ X$ and $Y = 0.165\ X$ with correlation coefficients of 0.998 and 0.996, respectively.

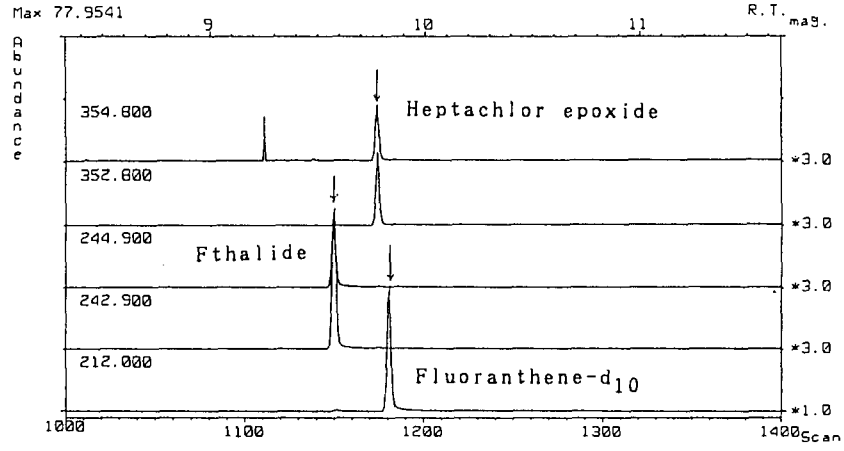

Fig. 3. Typical GC/MS–SIM chromatograms for the standards. R.T. = Rentention time in min; mag = magnitude; fthalide (m/z at 242.9 and 244.9), heptachlor epoxide (m/z at 352.8 and 354.8) fluroanthene-d_{10} (internal standard, m/z at 212.0).

Table 2
Analytical precision and detection limits for fthalide and heptachlor epoxide in environmental samples

Compound	Pure water			DL_w^a (ng ml^{-1})	Sediment		DL_s^b (ng g^{-1})	Fish		DL_f^b (ng g^{-1})
	Analytical precision				Analytical precision			Analytical precision		
	Concn. (ng ml^{-1})	Response ($n=4$)	RSD (%)		Conc. (ng g^{-1})	Found $\pm$ S.D. (ng g^{-1}, $n=7$)		Concn. (ng g^{-1})	Found $\pm$ S.D. (ng g^{-1}, $n=7$)	
Fthalide	0.10	446	1.0	0.020	50.0	33.0 ± 1.63	5.1	50.0	38.5 ± 0.85	2.7
	0.20	893	2.0							
	0.30	1352	2.6							
Heptachlor epoxide	0.10	193	4.1	0.031	50.0	42.6 ± 2.33	7.3	50.0	33.5 ± 1.34	4.2
	0.20	361	1.5							
	0.30	562	4.8							

[a] Detection limits of the water (DL_w) sample were calculated from the sensitivity of response estimating standard deviation as follows: $D = t(n-1, 0.05)\sigma/\sqrt{n}(dC/dR)$. $DL_w = 3\bar{D}$, where D is detection power at trace concentration of the compounds (three different concentration in this experiment). $\bar{D}$ is the average value of D calculated from different concentration (DL_w were defined as three times of the detection power). $t(n-1, 0.05)$ is the t-distribution at 95% reliability. σ is the standard deviation of the response, n is the number of replicates. C is the concentration of the compounds and R is the response (the peak area ratio of analyte to internal standard).

[b] For sediment and fish samples, detection limits ($DL_{s\&f}$) were calculated from the following equation. $DL_{s\&f} = t(n-1, 0.02)Sc$, where $t(n-1, 0.02) = 3.143$ ($n=7$) is the t-distribution at 98% reliability and Sc is the standard deviation of the seven replicate analyses.

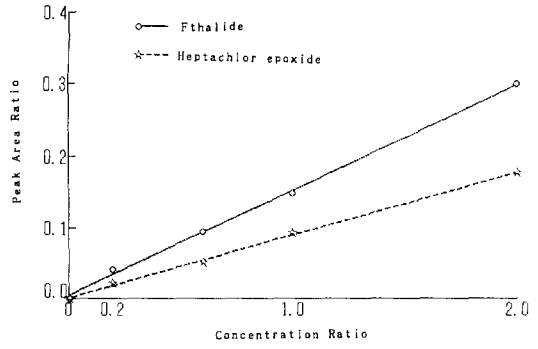

Fig. 4. Typical calibration graphs for fthalide and heptachlor epoxide. X-axis = concentration ratio (analyte/internal standard), Y-axis = peak area ratio (analyte/internal standard).

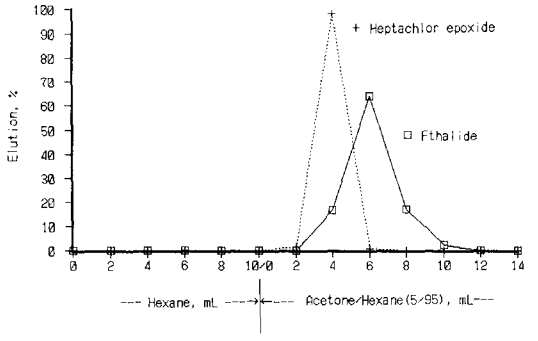

Fig. 5. Typical eluation patterns of fthalide and heptachlor epoxide on Sep-Pak Florisil cartridge. Eluent = acetone/hexane (5/95).

3.3. Solid phase disk extraction

Solid phase extraction depends on the principle of partition or adsorption of organic compounds on a solid non-polar material. The solid materials were used in a column or a cartridge at the early applications. Filter disk recently developed is most appropriate for extraction of pollutants from an environmental water sample. This technique is superior to conventional liquid–liquid extraction because it causes no emulsification, uses only small volume of extraction solvents and produces rapid procedure with less labour. The use of membrane extraction disks provide excellent recoveries for pesticides analysis even when a water sample is passed fast and small volume of an eluent is employed.

3.4. Clean-up procedure of Sep-Pak Florisil

The clean-up of sediment and fish extracts was carried out by using a Sep-Pak Florisil cartridge. Fig. 5 shows typical elution patterns of fthalide and heptachlor epoxide with hexane and acetone/hexane (5/95) as eluents. The chemicals were not eluted with 10 ml of hexane, but completely eluted with 10 ml of acetone/hexane (5/95).

3.5. Analytical precision and detection limits

Table 2 reports analytical precision and detection limits for fthalide and heptachlor epoxide in water, sediment and fish samples throughout the analytical procedures. Fthalide and heptachlor epoxide in water samples were determined in the range 0.1–0.3 ng ml^{-1} levels with relative standard deviations (RSDs) of 1.0–4.8%. Detection limits (DL_W) of water samples were calculated from the sensitivity of the response estimation

Table 3
Recovery of fthalide and heptachlor epoxide added to the environmental samples

	Sample	Sample vol.	Added (ng)	Recovery (%)	Number of sample (n)	RSD (%)
Fthalide	River water	1000 ml	500	96	4	10.2
	Sea water	1000 ml	500	99	4	2.4
	Sediment	10 g	500	66	7	4.6
	Fish	10 g	500	77	7	2.1
Heptachlor epoxide	River water	1000 ml	500	103	4	4.3
	Sea water	1000 ml	500	101	4	2.5
	Sediment	10 g	500	85	7	5.2
	Fish	10 g	500	67	7	3.8

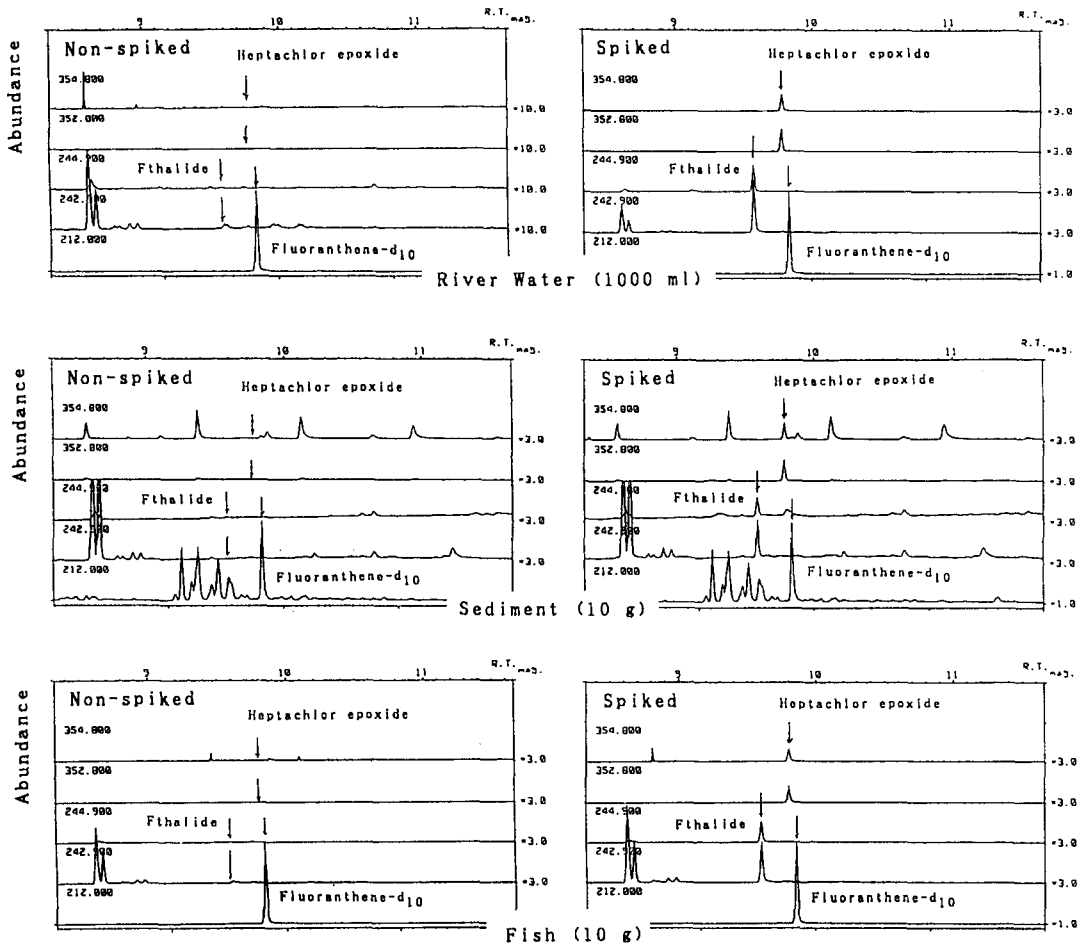

Fig. 6. Determination of fthalide and heptachlor epoxide in non-spiked and spiked river water (1000 ml, Okawa River), sediment (10 g Tokyo Bay) and fish (10 g, pearch in Osaka Bay) samples.

standard deviation. DL_W of fthalide and heptachlor epoxide were 0.020 and 0.031 ng ml^{-1} for 1000 ml of water samples, respectively. For the sediment and fish samples, detection limits (DL_S and DL_f) were calculated from the standard deviation of the seven replicated analyses. DL_S and DL_f were 2.7–5.1 and 4.2–7.3 ng g^{-1} for 10 g of samples, respectively.

3.6. Recovery test

Analyte recovery was investigated for 1000 ml of river water, 1000 ml of sea water, 10 g of sediment, and 10 g of fish samples, spiked with 500 ng of fthalide and heptachlor expodie. Table 3 shows their recovery from these environmental samples.

Fthalide and heptachlor epoxide were recovered in the range 96–103% with RSDs of 2.4–10.2% from the river and the sea waters. The recoveries of the chemical were 66–85% with RSDs of 2.1–5.2% from sediment and fish samples. The chromatograms of the chemical are shown in Fig. 6, as to non-spiked and spiked river water, sediment and fish samples.

4. Conclusions

The GC/MS–SIM method, involving SPED-C18 extraction of Sep-Pak Florisil clean-up pretreatment, are useful for routinely determining fthalide and heptachlor epoxide in the environmental samples at sub ng ml^{-1} or low ng g^{-1} levels.

Acknowledgements

This work was supported by Environmental Health and Safety Division, Japan Environmental Agency (Project for Development of Analytical Method).

References

[1] Y. Nishikawa and T. Okumura, J. Chromatogr., 690 (1995) 109.
[2] Y. Nishikawa and T. Okumura, Anal. Chim. Acta, 312 (1995) 45.
[3] T. Okumura and Y. Nishikawa, J. Chromatogr., 709 (1995) 319.
[4] T. Okumura, K. Imamura and Y. Nishikawa, Analyst, 120 (1995) 2675.
[5] T. Okumura, K. Imamura and Y. Nishikawa, J. Chromatogr. Sci., 34 (1996) 190.
[6] T. Okumura and Y. Nishikawa, Anal. Chim. Acta, 325 (1966) 175.
[7] F. Mangani, G. Crescentini, P. Palma and F. Bruner, J. Chromatogr., 452 (1988) 527.
[8] A. Kraut-Vass and J. Thoma, J. Chromatogr., 538 (1991) 233.
[9] B. Hans-Rudolf and D.M. Markus, Environ. Sci. Technol., 27 (1993) 1211.
[10] A. Bacaloni, G. Goretti, A. Lagana, B.M. Petronio and M. Rotatori, Anal. Chem. 52 (1980) 2033.
[11] I. Saito, N. Kawamura, K. Uno and Y. Takeuchi, Analyst, 110 (1985) 263.
[12] M.J.M. Wells and J.L. Michael, J. Chromatogr. Sci., 25 (1987) 345.
[13] G.A. Junk and J.J. Richard, Anal. Chem., 60 (1988) 451.
[14] A. DiMuccio, R. Dommarco, D.A. Barbini, A. Santilio, S. Girolimetti, A. Ausili, M. Ventriglia, T. Generali and L. Vergori, J. Chromatogr., 643 (1993) 363.
[15] J. Beltran, F.J. Lopez and F. Hernandez, Anal. Chim. Acta, 283 (1993) 297.
[16] D.F. Hagen, C.G. Markell, G.A. Schmitt and D.D. Blevins, Anal. Chim. Acta, 236 (1990) 157.
[17] S.A. Senseman, T.L. Lavy, J.D. Mattice, B.M. Myers and B.W. Skulman, Environ. Sci. Technol., 27 (1993) 516.
[18] J.S. Salau, R. Alonso, G. Batllo and D. Barcelo, Anal. Chim. Acta, 293 (1994) 109.
[19] S.A. Sensenman, T.L. Lavy and J.D. Mattice, Anal. Chem., 67 (1995) 3064.

ELSEVIER

Talanta 44 (1997) 657–662

Talanta

Separation study of cadmium through an emulsion liquid membrane

Quanmin Li [a], Qi Liu [a], Kean Li [b], Shenyang Tong [b]

[a] *Department of Chemistry, Henan Normal University, Xinxiang 453002, People's Republic of China*
[b] *Department of Chemistry, Peking University, Beijing 100871, People's Republic of China*

Received 10 June 1996; received in revised form 11 September 1996; accepted 11 September 1996

Abstract

A study of the transport of Cd^{2+} ions through a tri-*n*-octylamine(TOA)—sorbital monooleate (Span 80)—oxylene liquid membrane has been performed with varying concentrations of HCl, KI, TOA, Span 80 and NaOH in the feed, membrane and stripping solutions. Maximum transport was observed at 0.01 M KI, 0.025 M HCl, 0.015 M TOA, 3% (w/v) Span 80 and 0.025 M NaOH. With this system, cadmium could be completely separated from Zn^{2+}, Fe^{2+}, Co^{2+}, Ni^{2+}, Cr^{3+} and Mn^{2+}. The transport mechanism of this metal ions through the membrane has been discussed. © 1997 Elsevier Science B.V.

Keywords: Cadmium; Emulsion liquid membrane; Metal ions; Stripping solution

1. Introduction

The emulsion liquid membranes (ELM) are the subject of widespread investigation [1–4] as a potential method of separation and preconcentration for both technical and analytical purposes, because of their advantage of high efficiency and low expense. Tri-*n*-octylamine (TOA) has been studied as emulsion liquid membrane mobile carrier to separate metal ions [5–8], but it has not applied for the separation of cadmium from other metal ions, and no transport studies has been made. TOA is an important extractant and can complex with CdI_4^{2-} ions [8].

In this paper, an emulsion liquid membrane with TOA as mobile carrier will be studied for the transport of cadmium. Various parameters influencing the transport of cadmium across the membrane have been optimized to separated cadmium from Zn^{2+}, Fe^{2+}, Co^{2+}, Ni^{2+}, Cr^{3+} and Mn^{2+}, and the transport mechanism of this metal ion has been discussed.

2. Experimental

2.1. Reagents

A standard (1 mg ml^{-1}) solution of cadmium was prepared from metal cadmium (99.99%), and distilled, deionized water. TOA (analytical grade) was obtained from Fluka. Sorbital monooleate (Span 80; chemical grade) was obtained from Tianda Experimental Factory (Tianhing, People's

PII S0039-9140(96)02098-X

Republic of China). A 0.1 M solution of TOA and a 3% (w/v) solution of Span 80 in oxylene were used in this work.

2.2. Apparatus

The following instruments were used: a motor-driven emulsifier (range 0–6000 rev min^{-1}); motor-driven stirrers (range 0–600 rev min^{-1}); and a model 722 spectrophotometer (Shanghai Analytical Instrument Factory, People's Republic of China).

2.3. Procedures

2.3.1. Preparation of ELM

Solutions, 20 ml portions, of TOA and Span 80 in oxylene were emulsified at a stirring speed of 2000 rev min^{-1}. Stripping solution was added at a rate of 20 ml min^{-1} until the volume ratio of organic membrane solution to stripping solution was 1:1. The solution was then stirred continuously for 15 min to obtain a stable while ELM.

2.3.2. Transport of metal ions

Then 2 ml of ELM was added to small beakers containing 10 ml metal ion feed solutions and the contents stirred at 200 rev min^{-1} for a given transfer time; the phases were allowed to separate. Clear feed solution was pippetted into a 25 ml volumetric flask and analyzed for the amount of cation remaining.

2.3.3. Determination of cadmium [9]

3 ml of 5×10^{-4} M 4-(2-Pyridylazo) resorcinol (PAR) alcohol solution was added to 5 ml of 0.1 M $Na_2B_4O_7 \cdot 10H_2O$ buffer solution in a 25 ml volumetric flask containing cadmium ions, after diluting to the mark the absorbance was read at 495 nm against the reagent blank.

In separation experiment, the concentration of cadmium as well as other cations was determined by inductively-coupled plasma atomic emission spectrometry (ICP-AES).

3. Results and discussion

3.1. The effect of KI, KBr, KCl and KSCN in the feed solution

TOA is called liquid anion-exchanger. Only in the form of anions, can cadmium associate with TOA and transport into stripping phase, so it is very important of the ability of different anions associating with cadmium. With a suitable acid concentration of the feed solution, an increase in the concentration of KI increased the extraction of Cd^{2+}, 0.01 M KI resulted in complete transport of Cd^{2+}, and Cd^{2+} transported into the stripping solution in the form of CdI_4^{2-}. If KI was replaced by KBr and KSCN in turn, the extraction of Cd^{2+} decreased. According to Ref [10], Cd^{2+} can form a 1:4 complex with I^-, Br^- and SCN^-, the logarithm of its accumulating stability constant ($\log \beta_4$) is respectively, 5.35, 2.93 and 2.91. This shows that the more stable the anion complex, the higher the extraction of Cd^{2+} is (see Fig. 1).

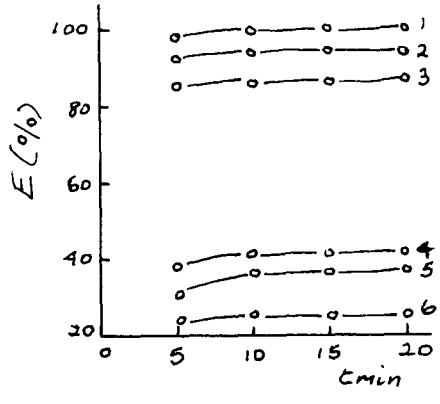

Fig. 1. The effect of KI, KBr, KSCN concentration in the feed on the percent extraction of Cd^{2+}. Feed phase: 50 μg ml^{-1} Cd^{2+} + 0.01 M HCl + agents:1- 0.01 M KI, 2- 0.005 M KI, 3- 0.05 M KBr, 4- 0.01 M KBr, 5- 0.05 KSCN, 6- 0.01 M KSCN; stripping phase: 0.025 M NaOH; and membrane phase: 3% (w/v) Span 80 + 0.015 M TOA + oxylene.

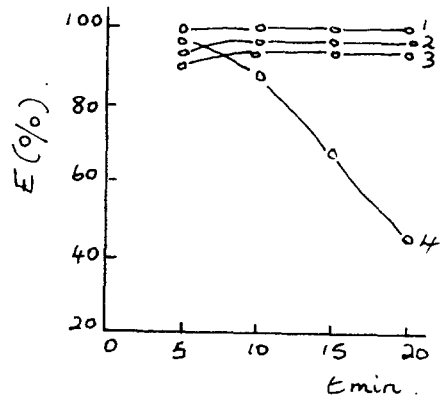

Fig. 2. The effect of HCl concentration in the feed on the percent extraction of Cd^{2+}. Membrane phase: 0.015 M TOA + 3% (w/v) Span 80 + oxylene; stripping phase: 0.05 M NaOH; and feed phase: 100 μg ml^{-1} Cd^{2+} + 0.010 M KI + HCl(M): 1- 0.01–0.025, 2- 0.05, 3- 0.1, 4- 0.005.

3.2. The effect of hydrochloric acid concentration in the feed

The relationship between the concentration of hydrochloric acid in the feed solution and extraction of cadmium is shown in Fig. 2. An acid concentration of 0.025 M was found to be the best for Cd^{2+} transport. The H^+ concentration in the feed solution was measured and it was found that with transport of cadmium into the stripping phase, the H^+ concentration in the feed solution decreased. This proved that H^+ transport into the stripping phase also occurs. In the presence of HCL and KI in the feed solution, the transport process of cadmium through an ELM is illustrated by the following equations

1. TOA (shown as R_3N) in the membrane phase reacts with hydrochloric acid in the feed phase.

$$\underset{\text{(membrane)}}{R_3N} + H^+ + \underset{\text{(feed)}}{Cl^-} = \underset{\text{(membrane)}}{R_3NH^+Cl^-}$$

2. In the feed, CdI_4^{2-} exchanges with Cl^- of $R_3NH^+Cl^-$ in the membrane phase.

$$\underset{\text{(feed)}}{CdI_4^{2-}} + 2\underset{\text{(membrane)}}{R_3NH^+Cl^-} = \underset{\text{(membrane)}}{(R_3N)_2CdI_4} + 2\underset{\text{(feed)}}{Cl^-}$$

3. NaOH in the stripping solution reacts with $(R_3NH)_2CdI_4^{2-}$ to strip cadmium into the stripping solution

$$\underset{\text{(membrane)}}{(R_3HN)_2CdI_4} + 2\underset{\text{(feed)}}{Cl^-} = \underset{\text{(membrane)}}{R_3N} + \underset{\text{(feed)}}{CdI_4^{2-}} + 2H_2O$$

The expected mechanism of cadmium transport in the present case is shown in Fig. 3. Cd^{2+} and H^+ were transported from the feed solution to the stripping solution where H^+ was neutralized by NaOH. The transport of H^+ along a concentration gradient supplied the energy for the transport of cadmium against a concentration gradient. It was discovered that the decrease of H^+ in the feed solution was more than that of cadmium. This was due to the formation of $R_3NH^+Cl^-$-type species and transport into the stripping phase. At an HCl concentration in the feed of >0.05 M, more Cl^- competed with CdI_4^{2-} to associate with protonated TOA, the extraction of cadmium decreased. When the concentration of HCl was <0.005 M, transport of cadmium abruptly decreased with time. This is because less H^+ is available to protonate R_3N, and precipitation of Cd^{2+} as $Cd(OH)_2$ blocks the transport of cadmium. In Fig. 4, it is also found that the transport of cadmium can be completed in 5 min, this is because extraction and back-extraction occur simultaneously, and the degree of dispersion of the ELM in the feed solution is high [11].

3.3. The effect of concentration of NaOH in the stripping solution

The NaOH in the stripping solution functioned as a back-extractant. When the composition of emulsion was fixed an increase in the hydroxyl

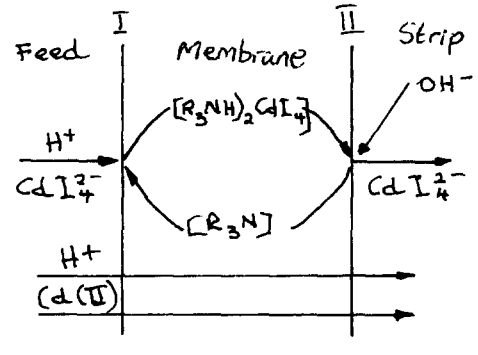

Fig. 3. Possible scheme for CdI_4^{2-} transport from HCl solution to NaOH solution through TOA-Span 80-oxylene liquid membranes.

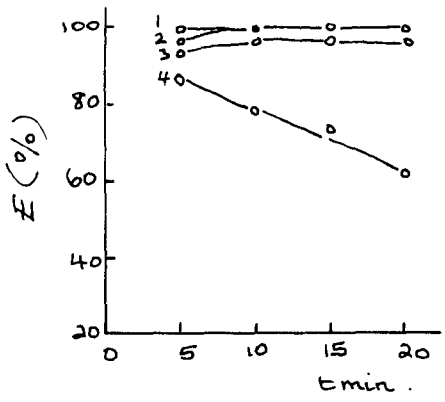

Fig. 4. The effect of NaOH concentration in the stripping phase on the percent extraction of Cd^{2+}. Feed phase: 50 μg ml^{-1} Cd^{2+} + 0.01 M KI + 0.01 M HCl; membrane phase: 3% (w/v) Span 80 + 0.15 M TOA + oxylene; and stripping phase: NaOH (M): 1- 0.01, 2- 0.025, 3- 0.05, 4- 0.1.

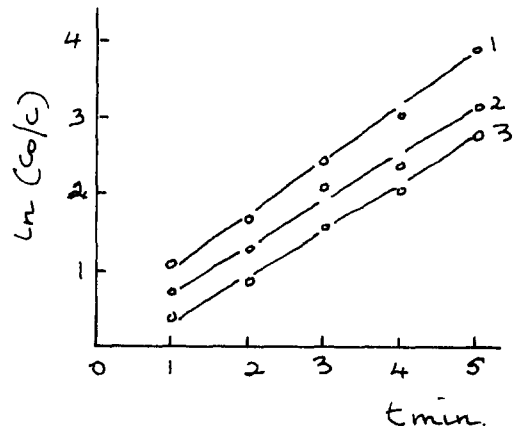

Fig. 5. The kinetic curve line of transport of Cd^{2+}. Feed phase: 50 μg ml^{-1} Cd^{2+} + 0.01 M KI + 0.01 M HCl; membrane phase: 3% (w/v) Span 80 + 0.015 M TOA + oxylene; and stripping phase: NaOH (M):1- 0.01, 2- 0.025, 3- 0.05.

ions results in faster decomposition of the cadmium complex and removal of protons from the amine molecules, thus resulting in higher extraction. However, it has been observed that above a concentration of 0.1 M NaOH, the extraction of cadmium decreased (see Fig. 4). This may be because the CdI_4^{2-} precipitated $Cd(OH)_2$ at higher NaOH concentration and clogged the membrane. This can be proved by found white $Cd(OH)_2$ precipitation in the stripping solution after demulsification.

The maximum extraction was obtained in different stripping solution at 0.01–0.1 M NaOH (shown in Fig. 4). In the experiment, 0.025 M NaOH was selected. When the concentration of NaOH was 0.01, 0.025 and 0.05 M, by changing transfer time (from 1 to 5 min) measured the natural logarithm of the ratio of initial concentration (C_0) to given time concentration (C) of cadmium the kinetic curve can be obtained (see Fig. 5). $\ln C_0/C \sim t$ curve line is a good straight line, they are (1) $\ln C_0/C = 1.103 \times 10^{-2}t + 0.4260$, $R = 0.9940$; (2) $\ln C_0/C = 1.008 \times 10^{-2}t + 0.1222$, $R = 0.9909$; (3) $\ln C_0/C = 1.012 \times 10^{-2}t - 0.3550$, $R = 0.9949$ respectively, this shows that transport of cadmium is near kinetic pesudo-first-order reaction. The transport rate constant of Cd^{2+} was 0.01103 s^{-1}, 0.01008 s^{-1} and 0.01012 s^{-1}, they are similar. This shows that the transport rate of Cd^{2+} was controlled only by $(R_3NH)_2CdI_4$ concentration on the feed-side interface, the concentration of hydroxyl ions in the stripping solution did not interfere. Its kinetic equation are illustrated by the following equation

$$-\mathrm{d[Cd(II)]} = k[(R_3NH)_2CdI_4]\,\mathrm{d}t$$

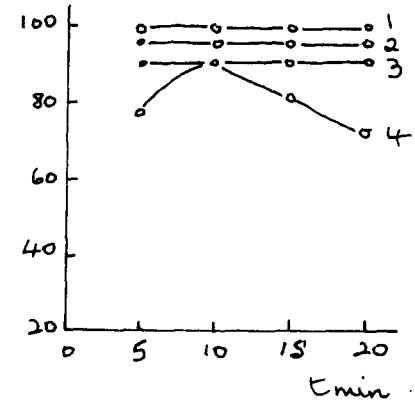

Fig. 6. The effect of TOA concentration in the membrane phase on the percent extraction of Cd^{2+}. Feed phase: 50 μg ml^{-1} Cd^{2+} + 0.01 M KI + 0.01 M HCl; stripping phase: 0.025 M NaOH; and membrane phase: 3% (w/v) Span 80 + TOA (M): 1- 0.015, 2- 0.01, 3- 0.0075, 4- 0.005.

Table 1
Separation of Cd^{2+} from mixed solution of co-ions

Initial amount of each ion (μg ml^{-1})	Percent extraction						
	Fe	Mn	Cr	Zn	Co	Ni	Cd
10.0	0	0	2	2	0	0	96.4
50.0	0	0	1	0	0	2	96.0
100	1	0	1	0	2	2	95.0

Feed phase: 50 μg ml^{-1} Cd^{2+} + 0.01 M KI + 0.01 M HCl; membrane phase: 3% (w/v) + Span 80 + 0.015 M TOA + oxylene; stripping phase: 0.025 M NaOH; and transfer time: 10 min.

3.4. The effect of the concentration of TOA

The effect of the concentration of TOA (mobile carrier) in the organic phase on the extraction of cadmium is shown in Fig. 6. The optimum concentration range of TOA was 0.015–0.02 M. A decrease of the concentration of TOA decreased the extraction of cadmium, this proved that the extraction of cadmium was controlled only by the concentration of $(R_3NH)_2CdI_4$ in the membrane phase. When the concentration of TOA was < 0.005 M, the transport of cadmium would decrease with transfer time, the reason was that less H^+ was transported into the stripping solution by TOA, cadmium precipitated $Cd(OH)_2$ (like curve line 4 in Fig. 2). In experiment 0.015 M TOA was selected for a rapid and complete transport of cadmium.

3.5. The effect of the concentration of surfactant

Both the stability of the emulsion and the viscosity of the liquid membrane were altered by the proportion of surfactant in the organic phase. An increase in the concentration of Span 80 (surfactant) increased the stability of the emulsion; however, the extraction of cadmium decreased. When the concentration of Span 80 was less than 2% (w/v) in the organic phase, the ELM was easy to break as transfer time increased. A concentration of 3% (w/v) in the organic phase resulted in good extraction and stability.

3.6. The effect of other reagents in the feed

When 0.05 M KNO_3, K_2SO_4, $KClO_4$ and $KClO_4$ were added to above system in turn, the results shown that NO_3^-, SO_4^{2-} and Cl^- did not interfere the transport of cadmium, but ClO_4^- was larger anion, associated with TOA more easily, it would form R_3NHClO_4 and repress the transport of cadmium. 0.05 M $KClO_4$ made the extraction of cadmium decrease 15%.

3.7. Separation of cadmium from other ions

Under suitably conditions, transports of Zn^{2+}, Fe^{2+}, Co^{2+}, Ni^{2+}, Mn^{2+} and Cr^{3+} were studied in the mixed solution. Results for the competitive transport of cadmium and other common cations are shown in Table 1. (Note that the data of Table 1 comes from ICP, all other data are from colorimetric measurements.) Selective transport of cadmium was excellent and the transports of Zn^{2+}, Fe^{2+}, Co^{2+}, Ni^{2+}, Mn^{2+} and Cr^{3+} were found to be negligible.

The TOA-Span 80-oxylene liquid membrane is feasible to separate cadmium from Zn^{2+}, Fe^{2+}, Co^{2+}, Ni^{2+}, Mn^{2+} and Cr^{3+}, specifically from Zn^{2+}. Because character of Zn^{2+} is similar to that of Cd^{2+}, quantitative separation of Cd^{2+} from Zn^{2+} is significant.

4. Conclusion

In this paper, transport of cadmium through TOA-Span 80-ocylene ELM was studied. The mechanism of transport of cadmium was discussed and presented in Fig. 3, it is based on the association of metal anions (CdI_4^{2-}) with protonated TOA molecules at the feed-side interface, diffusion through the membrane, decomposition of the comples at the strip-solution-side membrane interface under alkaline condition, and back-diffusion of TOA molecules. The optimum condition of transport has been found and are 0.01 M KI and 0.025 M HCl in the feed solution, 0.015 M TOA and 3% (w/v) Span 80 in the liquid membrane, and 0.025 M NaOH in the stripping solution. It is concluded that this method can be applied for the separation of cadmium from Zn^{2+}, Fe^{2+}, Co^{2+}, Ni^{2+}, Mn^{2+} and Cr^{3+} or as a preconcentrating step for measuring cadmium. Small amounts of carriers are involved and the extraction efficiency is high.

References

[1] Z.H. Zhang, Liquid Membrane Separation Technique, Jiangxi People Press, Nanchang, R.P. China, 1983, pp. 153–160.
[2] Q.M. Li, K.A. Li, C.Y. Zhou and S.Y. Tong, Chem. J. Chin. Univ., 14(2) (1993) 171.
[3] E. Lachowicz, Talanta, 39 (1992) 1031.
[4] Y. Li, A.X. Wang, J.C. Van Loon and R.R. Barefoot, Talanta, 39 (1992) 1337.
[5] Y. Zhang, Liquid Membrane Separation Technique, Atomic Energy Press, Beijing, R.P. China, 1983, pp. 210–219.
[6] Q.H. Cai, Z. Yan and H.J. Chao, Membr. Sci. Tech., 9(4) (1989) 33.
[7] D.S. He, Membr. Sci. Tech., 9(4) (1989) 44.
[8] C. Malik and A. Li, Sep. Sci. Tech., 25(3) (1990) 263.
[9] F. Liu, K.A. Li, J. Lu, Y.P. Shuen and S.Y. Tong, Ion-Exch. Adsorption, 8(5) (1992) 400.
[10] W.B. Chang and K.A. Li, A Concise Handbook of Analytical Chemistry, Peking University Press, Beijing, R.P. China, 1981, pp. 126–130.
[11] T.L. Largman and S. Sifniades, Hydrometallurgy, 3 (1978) 153.

ELSEVIER

Talanta 44 (1997) 663–672

Talanta

Development and application of new ion-exchange techniques for the separation of the platinum group and other siderophile elements from geological samples

M. Rehkämper *, A.N. Halliday

Department of Geological Sciences, The University of Michigan, Ann Arbor, MI 48109-1063, USA

Received 6 February 1996; received in revised form 4 October 1996; accepted 8 October 1996

Abstract

Two new anion-exchange techniques have been developed for the separation of the platinum group elements Ru, Pd, Ir, Pt and the siderophile metals Re, Ag, Zn and Cd from geological samples following a NiS fire assay digestion procedure. Both methods are simple and permit the isolation of these elements in sufficient purity for quantitative analysis by isotope dilution-inductively coupled plasma mass spectrometry (ID-ICPMS) at yields of 75–95%. The high affinity of the considered elements to anion exchange resins allows the use of small (1.25 ml) columns even for the processing of 5–10 g sized silicate rock samples. Following fire assay digestion and dissolution of the NiS buttons in aqua regia, the samples are loaded onto the resin bed as solutions in 1 M HCl. After elution of the bulk sample matrix with dilute HCl and HNO_3, Zn and Cd are stripped from the column using 0.8 M HNO_3. Small amounts of bromine water are added to the dilute mineral acids for the stabilization of strongly retained Ir(IV). Following this, the ion-exchange techniques permit the sequential elution of Ag, Re and the PGE using 11 M HCl, 8 M HNO_3 and 13.5 M HNO_3. The ion-exchange methods have been applied to separation of Ru, Pd, Re, Ir and Pt from the geological reference material SU-1a prior to concentration measurements by ID-ICPMS. Our analytical results are in good agreement with previously published data for this sample and display an external reproducibility (based upon repeat dissolutions) of approximately 2–10% for the elements considered in this study. © 1997 Elsevier Science B.V.

Keywords: Ion-exchange; Platinum group; Siderophile elements; ICP-MS

1. Introduction

Abundance measurements for the platinum group elements (PGE) in natural samples such as waters, rocks, sediments and extraterrestrial materials have received particular attention in recent years and are of relevance to a wide range of geo- and cosmochemical studies. Reliable concentration data for the PGE in meteorites and terrestrial samples provide constraints for theories on the accretion of the Earth, core formation and the origin of the Moon and are of importance in mineral exploration, environmental research, sedimentary studies and the identification of impact craters.

* Corresponding author.

PII S0039-9140(96)02100-5

Inductively coupled plasma mass spectrometry (ICP-MS) has become a preferred method of elemental trace analysis in geochemistry and, being characterized by excellent detection limits, is ideally suited for the determination of PGE abundances [1–3]. The precision and accuracy of standard ICP-MS techniques that use absolute signal intensities to determine elemental concentrations are, however, generally inferior to isotope dilution (ID) measurements for the same elements by thermal ionization mass spectrometry. Significant improvements, particularly for low-abundance elements such as the PGE, can be achieved by a combination of ID with ICP-MS [4,5]. A chemical separation of the elements of interest is desirable for high-precision ID analysis in order to increase analytical sensitivity and eliminate isobaric interferences from other elements and their oxides [5,6]. Following full spike-sample equilibration during sample dissolution, the preconcentration procedure need not be quantitative, however, and this permits the use of relatively simple separation techniques [7].

The new multiple collector inductively coupled plasma mass spectrometer (MC-ICPMS) at the University of Michigan combines the ionization efficiency of a plasma source with the superior peak shapes and improved transmission of a magnetic sector mass spectrometer [8,9]. The instrument permits isotopic composition and ID concentration measurements to be performed by static multiple collection with Faraday cups at a level of precision and accuracy hitherto not achievable by ICP-MS [10]. This paper summarizes our recent efforts in the development of new ion-exchange procedures for the separation of the PGE, Re and other siderophile elements from geological samples prior to concentration measurements by isotope dilution MC-ICPMS.

A number of ion-exchange techniques for the separation of the PGE from geological samples have been published in the past. These procedures, however, were not considered to be fully adequate for our purposes since they are generally characterized by one or more of the following drawbacks: (1) they achieve only a group separation of the PGE from rock samples with no separation of the elements from one another [11–13]; (2) they only consider the separation of one or two of the PGE [14–16]; (3) they use unnecessarily large resin columns and/or large volumes of eluent [17,18]; or (4) they require the use of acids or reagents (such as $HClO_4$ or thiourea) that are difficult to purify or remove from effluent fractions by evaporation [19,20].

In this study we have developed two new anion-exchange separation schemes that permit the sequential isolation of the PGE Ru, Pd, Ir, Pt and the siderophile elements Re, Ag, Zn and Cd from geological samples following sample digestion by the NiS fire assay technique. This dissolution procedure is commonly used in the analysis of rocks for PGE abundances since it achieves the complete digestion of resistant, PGE containing phases and ensures full spike-sample equilibration for isotope dilution concentration measurements. The new ion-exchange methods are characterized by simplicity, high elemental yields and require relatively small volumes of reagents. While the procedures have been developed and used for the processing of 5–10 g sized geological samples, they can easily be adapted to the treatment of larger or smaller samples.

2. Experimental

2.1. Apparatus

The inductively coupled mass spectrometer employed in this study was the new VG Elemental Plasma 54. Since this instrument has recently been described in detail elsewhere [8,9], only a brief introduction is given here. The Plasma 54 is a new type of ICP-MS instrument that combines a conventional inductively coupled plasma (ICP) source with a multiple collector magnetic sector mass spectrometer. Following extraction of the ions generated in the Ar-plasma, a d.c. quadrupole lens system and an electrostatic analyzer are used to focus the ion beam before entering the magnetic sector analyzer. The collector assembly consists of nine Faraday cups and a Daly detector with ion counting for the measurement of small ion beams. Sample delivery was performed with a peristaltic pump and a Fisons Instruments Mistral

high efficiency nebulizer, operated at an uptake rate of approximately 0.15–0.20 ml min^{-1}. The ion-source consisted of a Fassel-type ICP torch and a solid-state radio frequency generator, operating at 1.35 kW. The nebulizer, auxiliary and coolant Ar-flows were set at approximately 0.9, 1.5 and 13 ml min^{-1}, respectively.

2.2. Materials and reagents

The acids used in this study were purified by subboiling distillation in quartz stills. 18 MΩ-grade water from a Millipore purification system was used throughout. Saturated bromine water was prepared by the equilibration of approximately 5 ml of high-purity bromine (99.998%, Alfa-AESAR) with approximately 100 ml of purified water in a 125 ml Teflon bottle. Sodium tetraborate (Alfa-AESAR, 99.5%, anhydrous), sodium carbonate (Fluka, 99.5%, anhydrous), as well elemental Ni (Alfa-AESAR, 99.996%) and S (Alfa-AESAR, 99.999%) were used as obtained, without further purification.

All ion-exchange separations were performed using quartz-glass columns (inner diameter 6 mm) fitted with acid-cleaned quartz-wool plugs for the support of the resin bed. The columns were filled with 1.25 ml of Bio-Rad AG1X8 (200–400 mesh) anion-exchange resin to a bed height of approximately 4.4 cm.

The standard reference material SU-1a, obtained from the Canadian Centre for Mineral and Energy Technology (CANMET), was used for all experiments performed in this study. The bulk material of SU-1a constitutes a Ni-Cu-Co ore from the Sudbury region (Canada) and consists of 23% chlorite, 12–16% of each of quartz, feldspar, mica and amphibole and less than 4% of each of calcite, siderite, pyrrhotite, pentlandite and chalcopyrite [21]. This sample was chosen for the present study since certified reference concentrations and/or high-quality ICP-MS literature data are available for the PGE. Additionally, it is well suited for elution experiments because it is characterized by relatively high precious metal abundances (Table 3) and, since the mineralogy of SU-1a is predominantly silicate, the results are expected to be valid for silicate rocks in general [22].

2.3. Nickel sulfide fire assay digestion

Sample digestion was performed using the nickel sulfide fire assay digestion technique [23,24]. The fusion charge composition was chosen in accordance with the results of a detailed study conducted by Paukert and Rubeska [25]. Powder splits, 5–10 g sized, of the sample SU-1a were weighed directly into 50 ml Coors fireclay crucibles. To this were added 6 g sodium tetraborate, 3 g sodium carbonate, 500 mg nickel powder and 400 mg sulfur for every 5 g of rock sample present. The fusion charges were then thoroughly mixed in the crucible and fluxed in a muffle furnace for 75 min at 1000°C.

Following cooling, the NiS beads were removed from the crucibles, placed into 15 ml Savillex beakers with screw cap lids, and refluxed with 6 ml of concentrated (11 M) HCl for approximately 24 h on a hotplate. Concentrated (13.5 M) HNO_3, 2 ml, were then added and the beakers placed back on the hotplate for a further 24 h. After this step the beads were generally completely dissolved. If an undissolved residue still persisted, however, the solutions were evaporated to incipient dryness and the residue was again refluxed with 4 ml of freshly prepared aqua regia for approximately 24 h.

Following complete dissolution of the NiS buttons in aqua regia and evaporation of the solutions to dryness, 5–10 ml of 1 M HCl and 500–1000 μl of saturated bromine water (this mixture is abbreviated as 1 M HCl + 10% Br_2 hereafter) were added to the samples. The beakers were placed on a hotplate with lids closed for at least 12 h and the solutions then dried completely.

2.4. Ion-exchange separation

Approximately, 1.25 ml of fresh anion-exchange resin were transferred as a slurry into a quartz column and the resin bed was cleaned and equilibrated prior to use with the following reagents: 20 ml of 0.8 M HNO_3 (elution of Zn, Cd), 10 ml 11 M HCl (elution of Ag and Ru), 25 ml 13.5 M HNO_3 (elution of residual Ru and Re, Pd, Pt, Ir), 40 ml 6 M HCl (reconversion of the resin into the chloride form), 4 ml 1 M HCl +

10% Br_2, backwash with 1 M HCl + 10% Br_2, 2 × 2 ml 1 M HCl + 10% Br_2 (equilibration of the resin prior to sample loading).

Samples prepared as described above were dissolved in 5–10 ml of 1 M HCl + 10% Br_2 for 24 h on a hotplate prior to ion-exchange chemistry. Centrifugation of the sample solutions before loading of the columns was not necessary because clear solutions, with no undissolved residue, were obtained in all cases during this study. Following loading of the solutions onto the columns, sample elution was initially performed using a variety of different procedures and acids in an effort to determine the best separation conditions. Effluent fractions with volumes of 2–10 ml were collected in Teflon beakers for the determination of elemental concentrations and dried down at low heat on a hotplate. After the development of satisfactory separation protocols had been completed, the reliability and performance of these techniques were further verified and documented by additional elution experiments. One of the optimized ion-exchange procedures ('Method 1', see Section 3.1) was finally used for the separation of Re and the PGE Ru, Pd, Ir, Pt prior to ID concentration measurements by MC-ICPMS.

2.5. Analysis of ion-exchange fractions from elution experiments

Prior to analysis, the dried effluent fractions were redissolved in approximately 60 μl of aqua regia and dried down slowly to a volume of approximately 5 μl. This residue was then taken up in 2–5 ml of H_2O, and the solutions thus obtained were analyzed by MC-ICPMS.

The absolute signal intensities for each element and fraction was measured using either a Faraday cup (concentrations > 1 ppb) or the Daly detector (concentrations < 1 ppb), depending on the abundance of the analyte in the respective fraction. The following isotopes, chosen for the absence of isobaric interferences, were used in these measurements: ^{66}Zn, ^{99}Ru, ^{105}Pd, ^{107}Ag, ^{111}Cd, ^{185}Re, ^{189}Os, ^{191}Ir and ^{195}Pt. Matrix induced signal suppression was monitored and corrected for by the addition of U to the sample solutions.

Elution curves, based upon the relative signal intensities of each element in the different fractions, were constructed with these data. The accuracy of this semiquantitative procedure is estimated to be ± 10%. This was judged to be adequate for the construction of elution curves and no effort was made to employ a more accurate, but time consuming, measurement and calibration technique.

2.6. Isotope dilution concentration measurements

Enriched stable isotopes of ^{99}Ru, ^{105}Pd, ^{185}Re, ^{191}Ir and ^{198}Pt from the Oak Ridge National Laboratory were used to determine the concentrations of these elements in the standard reference material SU-1a. The preparation and calibration of the spike solutions will be described in detail in a forthcoming publication. It should be mentioned, however, that the ^{99}Ru and ^{191}Ir spike solutions have hitherto been calibrated only against gravimetric standard solutions prepared from $(NH_4)_2RuCl_6$ and $(NH_4)_2IrCl_6$, respectively. Any deviation of the composition of the employed compounds from perfect stochiometry will thus result in systematic errors in the calibration of the tracer solutions. Until the calibration of the spike solutions is further verified using gravimetric standard solutions prepared from the pure metals, the analytical results presented in this paper for Ru and Ir are considered to be provisional only. Any errors are unlikely to be larger than approximately 5%, however.

For isotope dilution analyses appropriate aliquots of the tracer solutions were added directly to the sample powders in the fireclay crucibles prior to the fire assay digestion. The samples were then digested as described above and an optimized ion-exchange procedure ('Method 1'; see Section 3.1) was used for the separation of Ru, (Re, Pd) and (Pt, Ir) fractions from the sample solutions. Following collection, the three precious metal fractions were evaporated to complete dryness on a hotplate, dried again with approximately 30 μl of concentrated HNO_3 and then redissolved in an appropriate volume of H_2O (generally approximately 5–20 ml) for analysis. All isotope dilution concentration measure-

ments were performed by static multiple collection using Faraday cups only. While the (Re, Pd) fractions were split into two parts prior to analysis (because Re and Pd must be analyzed sequentially with different collector positions due to the large mass difference between these elements), Pt and Ir were determined simultaneously with the same Faraday cup configuration. Further details of the measurement procedures (e.g., choice of isotopes monitored, collector configurations, mass discrimination correction, detection limits, etc.) are outside the scope of this paper and will be described in detail in a further publication.

3. Results and discussion

3.1. Elution experiments

A variety of different organic and mineral acid types and elution procedures were initially tested to find an optimal separation protocol for the PGE and other siderophile elements from geological samples following a NiS fire assay digestion. These experiments led to the development of two optimized anion-exchange separation procedures that are suitable for the isolation of Zn, Cd, Ag, Re, Ru, Pd, Ir and Pt from 5 to 10 g sized silicate rock samples. The experimental details of the two new elution protocols are summarized in Tables 1 and 2.

Table 1
Elution sequence of ion-exchange procedure 'Method 1' for the separation of Zn, Cd, Ag, Re and the PGE Ru, Pd, Ir and Pt from geological samples

Eluent	Volume (ml)	Eluted
Sample solution in 1 M HCl + 10% Br_2	~5–10	Bulk matrix
0.5 M HCl + 10% Br_2	2	Bulk matrix
0.8 M HNO_3 + 10% Br_2	0.5	Bulk matrix
0.8 M HNO_3 + 10% Br_2	5	Zn, Cd
11 M HCl	2	Ag
11 M HCl	10	Ru
8 M HNO_3	10	Pd, Re
13.5 M HNO_3	14	Ir, Pt

Table 2
Elution sequence of ion-exchange procedure 'Method 2' for the separation of Zn, Cd, Ag, Re and the PGE Ru, Pd, Ir and Pt from geological samples

Eluent	Volume (ml)	Eluted
Sample solution in 1 M HCl + 10% Br_2	~5–10	Bulk matrix
0.5 M HCl + 10% Br_2	2	Bulk matrix
0.8 M HNO_3 + 10% Br_2	0.5	Bulk matrix
0.8 M HNO_3 + 10% Br_2	5	Zn, Cd
8 M HNO_3	10	Ru, Re
13.5 M HNO_3	14	Pt, Ir
11 M HCl	2	Ag
11 M HCl, 13.5 M HNO_3	8, 5	Pd

Figs. 1 and 2 display the different elution patterns of the siderophile elements for the new ion-exchange methods. Plotted in these figures are the normalized elemental signal intensities for each fraction and element on a relative scale from 0–1000. An arbitrary value of 1000 was assigned to the fraction of each element that displayed the highest signal intensity in each experiment, permitting a direct visual comparison of the results for the two ion-exchange separation methods.

Both separation procedures use the same ion-exchange columns (see Section 2.2) and the same acids (see Tables 1 and 2) for loading of the sample solutions (5–10 ml 1 M HCl + 10% Br_2) and the initial rinse (2 ml 0.5 HCl + 10% Br_2, 0.5 ml 0.8 M HNO_3 + 10% Br_2). The rationale behind this choice of mineral acids is that the major cationic constituents of the sample solution (particularly Ni^{2+}, but also Fe^{3+}) are virtually unretained on the anion-exchange resin under these conditions [26–29]. Therefore only small columns are required for the processing of the NiS beads derived from approximately 5 to 10 g sized silicate rock samples. Additionally, small eluent volumes suffice to achieve a nearly quantitative elution of the bulk sample matrix. An oxidant must be added to the dilute HCl and HNO_3 eluents, however, to ensure efficient retention of Ir. On-column reduction of the Ir(IV) present in the sample solutions will otherwise lead to the formation of virtually unretained Ir(III). A number of oxidizing agents such as Ce(IV), H_2O_2 or chlorine

gas are recommended for this purpose in the literature [29]. In this study, saturated bromine water was used as the oxidant, since this achieves reliable oxidation of Ir, introduces no cations (such as Ce) that may form interfering isobars [5] and is conveniently prepared, purified and handled.

Following these initial steps, Zn and Cd are quantitatively stripped from the resin by elution with 5 ml of 0.8 M HNO_3 + 10% Br_2 (Figs. 1 and 2). The other siderophile elements considered in this study are not removed from the column. This was initially somewhat surprising in the case of Ag, since published distribution coefficients and separation procedures predict that Ag should be eluted from the column by 0.8 M HNO_3 [26,30]. No significant amounts of Ag could be detected in the 0.8 M HNO_3 + 10% Br_2 effluent fractions,

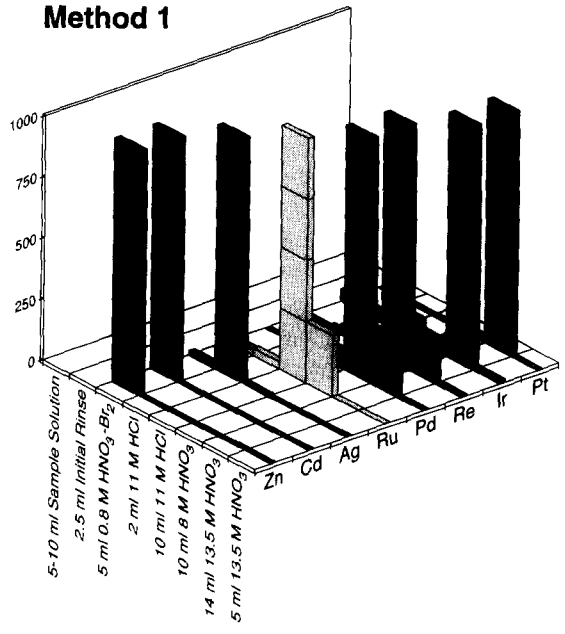

Fig. 1. Elution of Zn, Cd, Ag, Re and the PGE Ru, Pd, Ir and Pt during anion-exchange separation of standard rock SU-1a using 'Method 1'. Plotted are the normalized signal intensities for each element and effluent fraction on a scale of 0–1000. For each element the data are normalized by assigning an arbitrary value of 1000 to the signal intensity of the fraction that displays highest intensity. Effluent fractions with no data where not analyzed. 2.5 ml Initial rinse = 2 ml 0.5 M HCl + 10% Br_2 followed by 0.5 ml 0.8 M HNO_3 + 10% Br_2 (see Table 1).

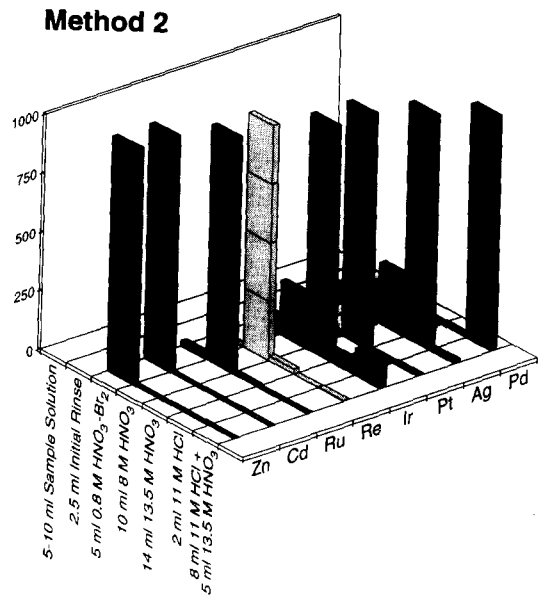

Fig. 2. Elution of Zn, Cd, Ag, Re and the PGE Ru, Pd, Ir and Pt during anion-exchange separation of the standard rock SU-1a using 'Method 2'. The figure displays the normalized elemental signal intensities (on a scale of 0–1000) for each element and effluent fraction. Normalized signal intensities were obtained with the same procedure used in Fig. 1. Effluent fractions with no data where not analyzed. 2.5 ml Initial rinse = 2 ml 0.5 M HCl + 10% Br_2 followed by 0.5 ml 0.8 M HNO_3 + 10% Br_2 (see Table 2).

however. This is most likely due to complex formation of Ag with trace amounts of Br^- in the eluent or with residual Cl^- present in the resin bed [30]. Since the elution protocols of the two new ion-exchange procedures are different after these initial steps, the two methods will be discussed separately in the following.

Ion-exchange procedure Method 1 (Table 1 and Fig. 1) continues with the elution of Ag and Ru using 2 and 10 ml of 11 M HCl, respectively. Addition of bromine water to the 11 M HCl eluent for the stabilization of Ir(IV) is not necessary, because significant amounts of Ir were not detected in the respective effluent fractions (Fig. 1) and is not desirable in any case, since this will lead to the elution of Re, as was demonstrated in additional experiments. The column yield for Ru is only marginally improved if larger volumes of 11 M HCl are used for the recovery of this

element. Additionally, this will result in increased losses of Re and Pd by premature elution.

In the next step of Method 1, Pd and Re are eluted from the anion-exchange column using 8 M HNO_3. With this acid, 10 ml are generally sufficient to achieve a yield of greater than approximately 85–90% for both elements (Fig. 1). Previous publications suggested using hot (approximately 80–100°C) nitric acid for the elution of the PGE from anion-exchange resins [5,31]. While no temperature controlled column was available for this study, the 8 M HNO_3 eluent was heated to a temperature of approximately 90°C prior to introduction of the acid into the column reservoir. Additional separation experiments confirmed that this procedure achieves a somewhat more efficient elution of Pd than use of 8 M HNO_3 at room temperature.

Although only small amounts of Ir and Pt are eluted from the resin with up to 20 ml of hot 8 M HNO_3, these elements can be efficiently stripped from the column with concentrated (approximately 13.5 M) nitric acid. While approximately 8–10 ml of 13.5 M HNO_3 are sufficient for the elution of Pt, approximately 10–15 ml are required for near-quantitative removal of Ir (Fig. 1). Elution with further 13.5 M HNO_3 leads to no significant improvements in elemental recovery for these metals (Fig. 1). The efficiency of the Pt, Ir elution is nearly identical for acids introduced into the column at approximately 90°C or at room temperature.

While ion-exchange procedure Method 2 (Table 2 and Fig. 2) uses the same acids as Method 1 (Table 1) they are applied in a different order to obtain a different elemental elution sequence. This can be of significance, e.g., to achieve a separation of Pd from Ru, which is not possible with Method 1. Following loading of the sample solutions, the initial rinse and the elution of Zn and Cd (which are identical to Method 1), Method 2 involves the elution of Ru and Re with 8 M HNO_3 at approximately 90°C. While the Ru recovery of this technique is somewhat better than for Method 1, significant amounts of Ir were eluted prematurely during this step and this could not be prevented even by the addition of bromine water to the eluent (Fig. 2). Significant amounts of Pd, however, were not detected in this effluent fraction. This result is somewhat surprising, since the same acid (8 M HNO_3) is used in Method 1 for the recovery of Pd.

Method 2 continues with the elution of Ir and Pt using 14 ml of 13.5 M HNO_3 (Fig. 2). Significant amounts of Ag accompany these elements in this procedure, however. The main Ag and Pd fractions are hereafter rinsed from the column using 2 ml of 11 M HCl and 8 ml of 11 M HCl followed by 5 ml of 13.5 M HNO_3, respectively (Fig. 2). Again the behavior of Pd was unexpected since only small amounts of this element were eluted from the resin in Method 1 with 12 ml of 11 M HCl. The reasons for the different ion-exchange properties of Pd in Methods 1 and 2 are not fully understood, but they are probably related to either complex-forming reactions of Pd with Cl^- and NO_3^- or different oxidation states of the cation (Pd^{2+} vs. Pd^{4+}) on the resin.

While our new ion-exchange techniques have hitherto only been applied to the separation of the PGE and other siderophile metals from 5 to 10 g sized geological samples they can easily be applied to the processing of even larger samples, through the use of larger resin beds and proportionally larger reagent volumes.

3.2. Elemental yields

The elution curves of Figs. 1 and 2 permit a rough, semiquantitative estimate of the elemental yield for the column chemistry. This is possible by comparing the signal intensity of, e.g., Ru in the main Ru fraction with the sum of the signal intensities of Ru in the all of the collected fractions. This estimate, however, is based upon the assumption that Ru is not eluted from the column in effluent fractions that are not analyzed and that no fraction of the element remains bound on the column after completion of the ion-exchange separation.

The semiquantitative results obtained by this procedure (estimated accuracy $\pm$ 10%) suggest that both methods generally achieve chemical yields of greater than approximately 80% for all considered elements with the exception of Ru in Method 1 (approximately 70%) and Ag and Ir in

Table 3
Re and PGE concentrations (in ppb) from this study and the literature for the geological reference material SU-1a

Element	MC-ICPMS this study	1σ	RSD (%)	n	Certified values [21]	ICP-MS Ref. [3]
Ru	54.4	1.6	2.9	4		44 ± 4
Pd	354	15	4.3	5	370 ± 30	327 ± 27
Re	40.9	1.4	3.4	5		14 ± 6
Ir	31.3	0.7	2.2	5		24 ± 2
Pt	370	41	11.1	5	410 ± 60	367 ± 40

$1\sigma = 1$ standard deviation; RSD = relative standard deviation; n = number of individual determinations, based upon repeat dissolutions. The certified values [21] are quoted with the $\pm 95\%$ confidence interval. Data of Ref. [3] are shown with 1σ external precision.

Method 2 (approximately 65%). No significant amounts of Os were detected in any of the ion-exchange fractions separated from reference material SU-1a. This indicates that Os is lost from the sample solutions as volatile OsO_4 during the dissolution of the NiS buttons with aqua regia.

After Method 1 was chosen for the separation of the PGE and Re from geological samples prior to concentration measurements by MC-ICPMS, the elemental yields of the analytical procedure were determined more rigorously. For this purpose two 5 g splits of a granitic rock sample (with negligible PGE concentrations and a known Re abundance) were doped with approximately 1 μg each of Re, Ru, Pd, Ir and Pt. The samples were then digested using the NiS fire assay technique and elemental fractions of Ru, (Re, Pd) and (Pt, Ir) were separated from the solutions of the NiS buttons using the ion-exchange procedure Method 1. After evaporation of the fractions to dryness, these were spiked with precisely weighed aliquots of stable isotope tracer solutions, refluxed for approximately 24 h on hotplate with 4 ml of aqua regia to ensure spike-sample equilibration and dried down again. The elemental yields of the complete analytical procedure were then determined by isotope-dilution analysis of the fractions with the Plasma 54. The results of the ID measurements are in good agreement with the semi-quantitative data obtained from the evaluation of the elution curves and indicate total procedural yields of approximately 85–95% for Re, Pd, Ir and Pt and of approximately 70–75% for Ru.

The high procedural yields for the PGE and Re also demonstrate that these elements are nearly quantitatively extracted into the NiS buttons during the fire assay sample digestion. In the case of Re, this result is in contradiction to reports of other investigators [3,32]. Our data, however, are further confirmed by the analyses of two fire assay fusion glasses from reference sample SU-1a, with both glass samples being characterized by negligible Re concentrations.

3.3. Isotope dilution analyses

The concentrations of Re and the PGE Ru, Pd, Ir and Pt were determined in five (four in the case of Ru) separate powder splits of the geological reference material SU-1a by isotope dilution measurements with the Plasma 54. The analytical results of these analyses are summarized and compared with certified reference values and other literature data in Table 3. The 1 σ external precision obtained by our technique varies between approximately 2 to 5% for all elements considered in this study, except Pt. The comparatively low precision of our Pt data (approximately 11%) is due to just one anomalously low result. Exclusion of this 'outlier' (Pt concentration 303 ppb) from the dataset results in a mean concentration of 387 ppb Pt for SU-1a, with a relative standard deviation of 5%. Since the other elemental concentration data of this particular sample split showed no irregularities, we suggest that the single outlier of our Pt dataset is due to the inhomogeneous distribution of a Pt-rich phase in the sample powder and is not caused by an analytical error such as incomplete spike-sample equilibration. This interpretation is supported by the fact that the previ-

ously published Pt data for reference material SU-1a (Table 3) are also characterized by relatively large analytical uncertainties in comparison to the results for other elements.

The new MC-ICPMS data are in excellent agreement with previously published values for the high-concentration elements Pt and Pd (Table 3). No certified reference concentrations are available for the elements Ru, Re and Ir, but our results are significantly higher than the ICP-MS data of Jackson et al. [3]. In the case of Re, this is probably due to incomplete recovery and loss of this element during the sample preparation procedure of Jackson et al. [3], as indicated by these authors in their publication. The discrepancies for Ru and Ir, where our data are approximately 20% higher compared with the results of Jackson et al. [3], are unlikely to be due solely to errors in the calibration of the spike solutions or blank problems. The total procedural blank of our analytical procedure was carefully monitored throughout and was found to be insignificant ($< 1\%$) for all elements considered in this study. Consequently no blank correction was applied to the analytical results. The excellent analytical precision that was obtained for the PGE as well as Re furthermore demonstrates that full spike-sample equilibration was routinely achieved during sample digestion, ruling out another potential pitfall. Since our isotope dilution technique does not require full elemental recovery during sample digestion and ion-exchange chemistry, we suggest that the differences in the concentrations are not a result of our analytical procedure but are due to other factors such as heterogeneity of the sample powders.

Acknowledgements

Der-Chuen Lee, Marcus Johnson, John Christensen and the other members of the RIGL team provided valuable technical assistance and advice. Becky Lange is thanked for making her lab and furnace available for these studies. The constructive comments of two anonymous reviewers were highly appreciated and led to significant changes and improvements in the manuscript. This research was supported by grants from DOE, NASA and NSF.

References

[1] D.C. Gregoire, J. Anal. At. Spectrom., 3 (1988) 309.
[2] A.R. Date, A.E. Davis and Y.Y. Cheung, Analyst, 112 (1987) 1217.
[3] S.E. Jackson, B.J. Fryer, W. Gosse, D.C. Healey, H.P. Longerich and D.F. Strong, Chem. Geol., 83 (1990) 119.
[4] J.W. McLaren, D. Beauchemin and S.S. Berman, Anal. Chem., 59 (1987) 610.
[5] D.C. Colodner, E.A. Boyle and J.M. Edmond, Anal. Chem., 65 (1993) 1419.
[6] W.M. White, Earth Planet. Sci. Lett., 115 (1993) 211.
[7] K.G. Heumann, Isotope dilution mass spectrometry, in F. Adams, R. Gijbels and R. van Grieken (Eds.), Inorganic Mass Spectrometry, Wiley, New York 1988, p. 301.
[8] A.J. Walder, I. Platzner and P.A. Freedmann, J. Anal. At. Spectrom., 8 (1993) 19.
[9] A.N. Halliday, D.-C. Lee, J.N. Christensen, A.J. Walder, P.A. Freedman, C.E. Jones, C.M. Hall, W. Yi and D. Teagle, Int. J. Mass Spectrom. Ion Processes, 146/147 (1995) 21.
[10] D.-C. Lee and A.N. Halliday, Int. J. Mass Spectrom. Ion Processes, 146/147 (1995) 35.
[11] J.G. Sen Gupta, Talanta, 36 (1989) 651.
[12] R.A. Nadkarni and G.H. Morrison, Anal. Chem., 46 (1974) 232.
[13] Y.S. Chung and R.M. Barnes, J. Anal. At. Spectrom., 3 (1988) 1079.
[14] J.H. Crocket and G.B. Skippen, Geochim. Cosmochim. Acta, 30 (1966) 129.
[15] J.W. Morgan and R.J. Walker, Anal. Chim. Acta, 222 (1989) 291.
[16] J. Enzweiler and P.J. Potts, Talanta, 42 (1995) 1411.
[17] R.R. Brooks and L.H. Ahrens, Spectrochim. Acta, 16 (1960) 783.
[18] L.G. Cilindro and D.S. Martin Jr., J. Radioanal. Chem., 3 (1969) 195.
[19] R.K. Petrie and J.W. Morgan, J. Radionanal. Chem., 74 (1982) 15.
[20] J.H. Crocket, R.R. Keays and S. Hsieh, Geochim. Cosmochim. Acta, 31 (1967) 1615.
[21] H.F. Steger and W.S. Bowman, Canada Centre for Mineral and Energy Technology (CANMET), Rep. No. 80-9E, Ottawa, 1980.
[22] M.M. Totland, I. Jarvis and K.E. Jarvis, Chem. Geol., 124 (1995) 21.
[23] R.V.D. Robért, E. van Wyk and R. Palmer, National Institute for Metallurgy South Africa, Rep. No. 1371, Randburg, 1971.
[24] E.L. Hoffmann, A.J. Naldrett, J.C. van Loon, R.G.V. Hancock and A. Manson, Anal. Chim. Acta, 102 (1978) 157.

[25] T. Paukert and I. Rubeska, Anal. Chim. Acta, 278 (1993) 125.
[26] J.P. Faris and R.F. Buchanan, Anal. Chem., 36 (1964) 1157.
[27] K.A. Kraus and F. Nelson, Anion Exchange Studies of the Fission Products, International Conference on the Peaceful Uses of Atomic Energy (Geneva, 1955), United Nations, New York, 1956, p. 113.
[28] J. Korkisch and H. Klakl, Talanta, 15 (1968) 339.
[29] J. Korkisch, Handbook of Ion Exchange Resins: Their Application to Inorganic Analytical Chemistry, Vol. III, CRC Press, Boca Raton, Florida, 1989.
[30] W.R. Kelly, F. Tera and G.J. Wasserburg, Anal. Chem., 50 (1978) 1279.
[31] V. Hodge, M. Stallard, M. Koide and E.D. Goldberg, Anal. Chem., 58 (1986) 616.
[32] C.E. Martin, Earth Planet. Sci. Lett., 93 (1989) 336.

ELSEVIER

Talanta 44 (1997) 673–683

Talanta

Comparative study of the zero-crossing, ratio spectra derivative and partial least-squares methods applied to the simultaneous determination of atrazine and its degradation product desethylatrazin-2-hydroxy in ground waters

R. Corbella Tena, M.A. Rodríguez Delgado, Mª J. Sanchez, F. Garcia Montelongo *

Department of Analytical Chemistry, Nutrition and Food Science, University of La Laguna, 38270-La Laguna, Spain

Received 29 December 1995; received in revised form 28 June 1996; accepted 16 September 1996

Abstract

The application of the ratio spectra derivative and partial least-squares methods to the simultaneous determination of atrazine and its degradation product desethylatrazin-2-hydroxy is presented. When the different methods are applied to the determination of these products in ground waters, PLS method gives the best results due to the presence of interfering substances with overlapping spectra. © 1997 Elsevier Science B.V.

Keywords: Atrazine; Derivative spectra; Desethylatrazin-2-hydroxy; Ground waters; Partial least squares; Ratio spectra derivative; Spectrophotometry

1. Introduction

Triazine herbicides, developed in the early 1950s [1], have been used for nearly 20 years in agriculture all over the world. Due to filtration through soil, atmospheric deposition or surface run-off most of these triazine herbicides have been reported as common contaminants in aquatic environments, including rivers, lakes, estuaries, rain water and both surface and ground waters [2–8].

Investigation of the impact of the agricultural non-point source concentration necessitates the development of rapid and accurate methods for the determination of these pesticides. Common multimethods are mainly based on gas chromatography with selective detection using electron capture, nitrogen–phosphorous, flame photometric detectors and mass selective detector. Other chromatographic techniques used in pesticide analysis are reversed-phase high performance liquid chromatography (RP–HPLC) with UV-Vis or diode array detectors and thin layer chromatographic methods [9–16]. Antibody-based assays represent an effective alternative to chromatographic methods, but discrimination of chemically similar structures is usually inferior to instrumental analysis [17,18]. However, these techniques are considerably time-consuming and expensive. UV-

* Corresponding author.

PII S0039-9140(96)02104-2

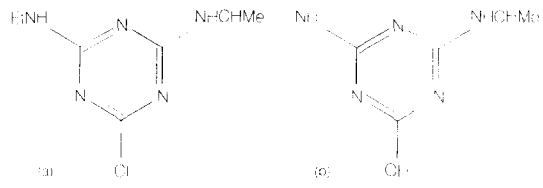

Fig. 1. (a) Atrazine; (b) desethylatrazin-2-hydroxy.

Vis analysis offers a fast and reliable method to obtain information about the distribution of these pesticide residues in waters. Furthermore, costs for UV-Vis determinations are far below of other instrumental methods.

The European Union (EU) has imposed rigid limits for pesticides in drinking water. So the maximum level allowed for a single pesticide is 0.1 μg l^{-1} while for a pesticide and its degradation products a limit of 0.5 μg l^{-1} has been established [19,20]. Although the use of UV-Vis methods do not allow to determine these pesticides for the established limits, these can be reached using the enrichment procedures described in the literature for *s*-triazines and their metabolites, such as liquid–liquid extraction [21] and solid-phase extraction (SPE) [22,23].

UV-Vis quantitation methods traditionally used involve measuring the analyte absorbance at a given wavelength. However the analyte of interest is often accompanied by other compounds absorbing in the same spectral region. In these cases, spectral overlapping is a serious limitation and requires resolution by mathematical procedures such as derivative techniques or multivariate statistical analysis, in this way, partial least squares, PLS, have been successfully applied to spectroscopic data [24–26]. Recently PLS has been applied to electroanalytical techniques, such as indirect voltametric of differential pulse polarographic (DPP) [27,28].

Considering that in real environment situations, the atrazine (Fig. 1a) degrades and the dealkylated and the hydroxylated metabolites are formed, [29,30] the present paper reports different quantitation methods such as zero crossing, ratio spectra derivative and PLS for the determination of atrazine and a hydroxy-dealkylated degradation product, desethylatrazin-2-hydroxy (Fig. 1b) in ground water samples.

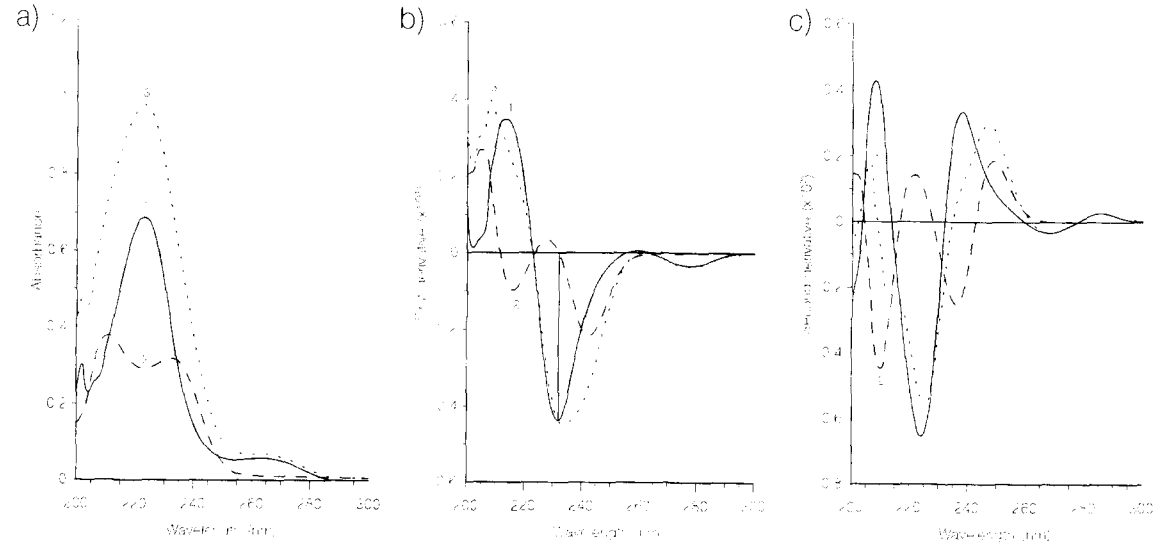

Fig. 2. Absorption spectra of (1) atrazine, 2 μg ml^{-1}, (2) desethylatrazin-2-hydroxy and (3) their mixture: (a) zero-order spectra, (b) 1st derivative spectra, and (c) 2nd derivative spectra.

2. Experimental

2.1. Reagents

Stock solutions, 100 μg ml^{-1} of atrazine (AT) and desethylatrazin-2-hydroxy (DAH) (Riedel-de Haën, Seelze Germany) were prepared in methanol. The pH of the working solutions was adjusted to pH = 5.8 with 1 ml of 0.1 M acetic/acetate buffer solution and the final percentage of methanol was 8% v/v. The ionic strength was maintained constant at 0.25 M with $NaClO_4$.

All reagents used were of analytical reagent grade and water deionized.

2.2. Apparatus

All absorption spectra were acquired on a Hewlett–Packard HP-8452A diode array spectrophotometer, furnished with a quartz cell of 1 cm path length, coupled on a Hewlett–Packard Vectra ES Computer equipped with a Hewlett–Packard Think Jet printer.

Absorption spectra were recorded and processed with the aid of the spectrophotmeter's bundled software. A PC/AT 46 computer provided with a mathematical coprocessor, equipped with the Unscrambler II [31] software package was used for the statistical treatment of the data and the application of multivariate methods.

A PHM 84 Radiometer digital pH meter equipped with a combined glass calomel electrode, was used to measure pH.

A Swinny Stainless 13 mm (Millipore) equipped with cellulose 0.45 μm filter (Millipore) was used to filter ground water samples.

2.3. Procedures

2.3.1. Zero crossing method

To 25 ml calibrated flasks were added 2.5 ml of 2.5 M $NaClO_4$ solution, 1 ml of acetic/acetate pH = 5.8 buffer solution, atrazine and desethylatrazin-2-hydroxy both in the range 25–150 mg, enough methanol to obtain a final composition of 8% v/v and made up to volume with deionized water.

To determine atrazine in presence of desethylatrazin-2-hydroxy first derivative of the spectra were obtained and calibration graph was prepared at the zero-crossing point ($\lambda_{AT} = 232$).

2.3.2. Ratio spectra derivative

To determine atrazine, the adsorption spectra of the solutions (prepared as in Section 2.3.1) were recorded between 200–350 nm and divided by the standard spectrum of a 2 μg ml^{-1} desethylatrazin-2-hydroxy solution. From the ratio spectra thus obtained, first derivatives were calculated. The concentration of atrazine is proportional to the amplitude at 216 nm.

To determine desethylatrazin-2-hydroxy, the adsorption spectra of the solutions were recorded between 200–350 nm and divided by the standard spectrum of a 2 μg ml^{-1} atrazine solution. From the ratio spectra thus obtained, first derivatives were calculated. The concentration of desethylatrazin-2-hydroxy is proportional to the amplitude at 236 nm.

2.3.3. PLS method

Eleven solutions were prepared for the corresponding multivariate calibration used to apply PLS-1 method. The optimized calibration matrix calculated by application of the PLS-1 method was then applied to analyze the 1st and 2nd derivative spectra of the samples in the range 240–280 nm.

2.3.4. Procedure to determine atrazine and desethylatrazin-2-hydroxy in ground waters

Ground waters from mountain sources were filtered and spiked with variable amounts of atrazine (50–125 mg) and desethylatrazin-2-hydroxy (50–150 mg) and analyzed according to the procedures outlined above.

3. Results and discussion

Fig. 2a shows the absorption spectra corresponding to atrazine, desethylatrazin-2-hydroxy and a mixture of them, at pH = 5.8, methanol-water 8% v/v and I = 0.25 M. The absorption maxima for atrazine are at 226 nm and 264 nm, and

Table 1
Equations for the calibration graphs in the determination of atrazine (AT) and desethylatrazin-2-hydroxy (DAH)

Compound	Equation[a](y = a + bx)	r^2	RSD[b]	Detection limit[c]
AT				
232 nm	Fd[d] = $(-1.07\cdot1^{-2}\pm8.01\cdot10^{-5})$[AT] + $(-7.50\cdot10^{-4}\pm3.58\cdot10^{-4})$	0.9996	$6.59\cdot10^{-4}$	0.18
216 nm	RSDS[e] = $(6.27\cdot10^{-2}\pm5.21\cdot10^{-4})$[AT] + $(-7.26\cdot10^{-3}\pm2.33\cdot10^{-3})$	0.9995	$4.29\cdot10^{-3}$	0.21
DAH				
236 nm	RSDS = $(5.56\cdot10^{-2}\pm4.95\cdot10^{-4})$[DAH] + $(-1.70\cdot10^{-4}\pm2.29\cdot10^{-3})$	0.9995	$4.06\cdot10^{-3}$	0.22

[a] μg ml^{-1}.
[b] Residual standard deviation.
[c] DL = (3·RSD/b).
[d] FD: first derivative signal.
[e] RSDS: ratio spectra derivative signal.

Table 2
Statistical data for the simultaneous determination in a synthetic mixture containing 2.00 μg ml^{-1} of atrazine (AT) and desethylatrazin-2-hydoxy (DAH)

Compound	Mean value found ($n = 11$)	Standard deviation	Coefficient of variation	t^a_{value}
AT				
FD[b], 232 nm	2.01	0.053	2.62	0.16
RSDS[c], 216 nm	2.05	0.033	1.60	0.90
HDA				
RSDS, 236 nm	2.10	0.030	1.42	1.97

[a] $t_{tabulated} = 2.23$ ($P = 0.05$).
[b] First derivative signal.
[c] Ratio spectra derivative signal.

no changes were observed in the spectra in the pH range 1–11. the absorption maxima for desethylatrazin-2-hydroxy are situated at 212 and 234 nm. In this case, at the same operatory conditions, the adsorption spectra are slightly influenced by variations of pH. It was observed that pH = 5.8 offers the best conditions to study the mixture of both pesticides.

3.1. Zero-crossing method

The adsorption spectra of desethylatrazin-2-hydroxy is completely overlapped with the spectrum of atrazine (Fig. 2a) and thus the determination of atrazine in presence of desethylatrazin-2-hydroxy, or vice-versa, can not be carried out by direct absorbance measurements. Fig. 2b shows the first derivative adsorption spectra of solutions of both pesticides and of their mixture. It can be seen that in spite of the overlapped O-order spectra of these compounds, the zero-crossing method could be suitable to obviate that problem. To quantitate atrazine in presence of desethylatrazin-2-hydroxy, the measurements were made at the zero-crossing point of desethylatrazin-2-hydroxy, at 212 and 232 nm. The best results were obtained at 232 nm (Table 1). However, the quantitation of desethylatrazin-2-hydroxy, in presence of atrazine at 256 nm zero-crossing point of atrazine is not satisfactory. Although the second derivative spectra of atrazine and desethylatrazin-2-hydroxy (Fig. 2c) produce some zero-crossing points for both pesticides that could permit their quantitation, the corresponding calibration graphs at 212 and 232 and 216, 228 and 242 nm for the quantitation of atrazine and desethylatrazin-2-hydroxy, respectively, do not allow good results. Similar results are obtained with higher order derivative spectra.

Thus, the zero-crossing method using first derivative spectra can only be used to quantitate atrazine in presence of desethylatrazin-2-hydroxy (Tables 1 and 2).

3.2. Ratio spectra derivative method

In the ratio spectra derivative method, overlapping of the spectra in a certain region is actually desirable because in division of spectrum by another, the error increases when one of absorbance approaches zero [32]. Fig. 3a shows the ratio spectra derivative of different amounts of atrazine, first derivative of the spectra of atrazine standard solutions divided by the standard spectrum of a 2 μg ml^{-1} solution of desethylatrazin-2-hydroxy. The first derivative amplitude at any given wavelength is proportional to the atrazine concentration, and the wavelength corresponding to the maximum at 216 nm was selected. Fig. 3b shows the ratio spectra derivative for different standard solutions of desethylatrazin-2-hydroxy, using the spectrum of a 2 μg ml^{-1} solutions of atrazine as the divisor. In this case, the optimum results were obtained at 236 nm.

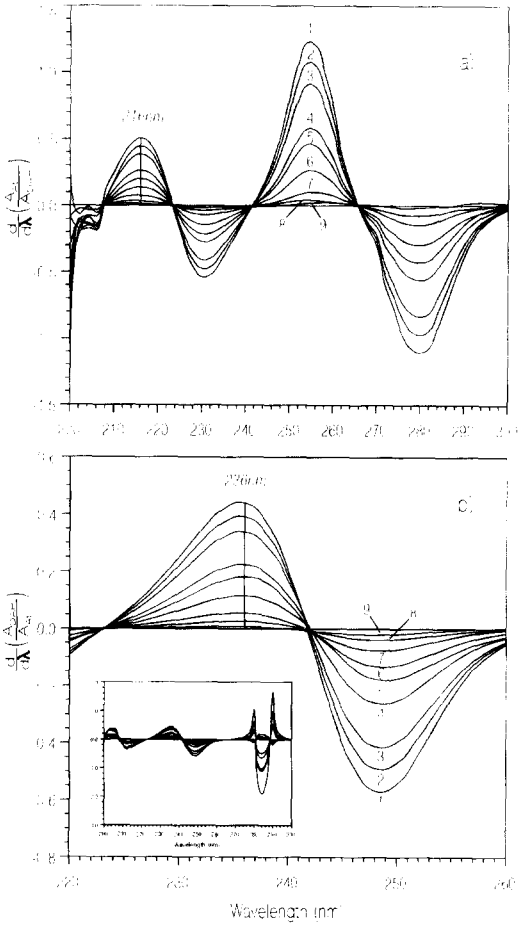

Fig. 3. First derivative of the ratio spectra of (a) atrazine, (b) desethylatrazin-2-hydroxy, using a 2 μg ml^{-1} divisor, solutions: (1–9) 0.2–8 μg ml^{-1}.

The ratio spectra derivative method allow to use different concentrations as the divisor to obtain the calibration graphs Thus, to quantitate atrazine, concentrations of desethylatrazin-2-hydroxy in the range 0.2–8.0 μg ml^{-1} were used and in order to minimize the standard error of the estimations and a concentration of 2 μg ml^{-1} of DAH was selected as divisor, Fig. 4. Similarly, a 2 μg ml^{-1} solution of atrazine was selected as divisor to quantitate desethylatrazin-2-hydroxy, Fig. 4.

Once the optimum working conditions has been established, calibration graphs were obtained at 216 nm (AT) and 236 nm (DAH), and showed that the proposed method is applicable over the ranges 0.30–8.0 μg ml^{-1} for atrazine and 0.22–8.0 μg ml^{-1} for desethylatrazin-2-hydroxy. The detection limit was calculated as the intercept of the calibration graphs plus three times the estimated standard deviation. The results obtained are included in Table 1. As can be seen, the corresponding r^2 values, which are an indication of the quality of the fitting of the data to the straight line, were higher than 0.9995.

To check the precision of the method, the signals for eleven replicates, containing 2 μg ml^{-1} of atrazine and 2 μg ml^{-1} of desethylatrazin-2-hydroxy were measured. The statistical parameter obtained for the simultaneous determination of both herbicides are shown in Table 2.

The proposed method was applied to several synthetic binary mixtures of atrazine and desethylatrazin-2-hydroxy in the range 1.0–6.0 μg ml^{-1}. The results obtained are summarized in Table 3.

Table 3
Results obtained for the determination of atrazine (AT) and desethylatrazin-2-hydoxy (DAH) in synthetic mixtures by the zero crossing at first derivative (FD), ratio spectra derivative (RSD) and PLS-1 methods

Composition of mixture		AT						DAH			
		FD, 232 nm		RSD, 216 nm		PLS-1[a]		RSD, 236 nm		PLS-1[b]	
AT μg ml^{-1}	DAH μg ml^{-1}	Found μg ml^{-1}	Recovery %	Found μg ml^{-1}	Recovery %	Found μg ml^{-1}	Recovery %	Found μg ml^{-1}	Recovery %	Found μg ml^{-1}	Recovery %
1.0	2.0	0.88	88	0.97	97	0.96	96	1.90	95	2.04	102
1.6	3.2	1.48	93	1.50	94	1.55	97	3.10	97	3.14	98
2.0	1.0	1.96	98	2.07	103	1.94	97	1.00	100	1.01	101
2.0	2.0	1.98	99	2.04	102	2.00	100	2.02	101	2.10	105
2.0	4.8	1.91	95	1.88	94	1.99	100	4.67	97	4.90	102
2.0	6.0	1.91	96	1.92	96	1.92	96	5.88	98	6.06	101
2.6	3.2	2.51	96	2.52	97	2.57	99	3.21	100	3.20	100
3.0	4.4	2.90	97	2.89	96	2.93	98	4.46	101	4.53	103
3.6	1.2	3.54	98	3.66	102	3.59	100	1.35	112	1.33	111
4.0	4.0	3.95	99	4.03	101	3.97	99	3.93	98	4.00	100

[a] 240–280 nm first derivative signal.
[b] 240–280 nm second derivative signal.

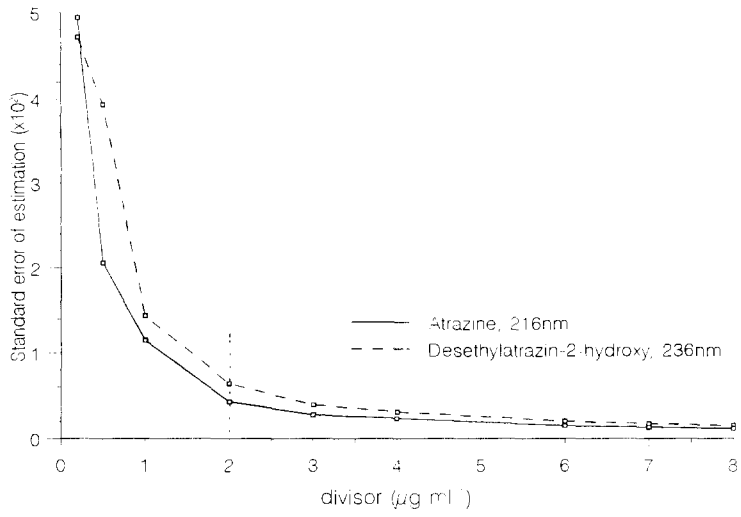

Fig. 4. Influence of divisor concentration on the standard error of estimation in the determination of atrazine and desethylatrazin-2-hydroxy.

3.3. Partial least squares method

Partial least-squares (PLS) modeling is a powerful multivariate statistical tool that has been successfully applied to quantitative analysis in spectrophotometric methods. PLS is a mathematical procedure that simultaneously includes spectral intensities at multiple selected wavelengths and allows to extract full useful complementary information from all of the spectra data, thus improving the quantitative analysis of mixtures.

It is also well known [33,34] that the quality of the results obtained in multi-component analysis from extensively overlapping spectra depends on the wavelength selection and the spectral mode used. PLS-1 and -2 types have been described. The difference between both types is that PLS-1 performs the optimization of the number of factors for only one component at a time and PLS-2 calculates the number of factors on all the components simultaneously and one pondered number of factor is optimized.

A training set of eleven representative binary mixtures, Table 4, of atrazine and desethylatrazin-2-hydroxy was prepared and the absorption spectra were recorded under the selected experimental conditions.

The PLS-1 method was applied to the quantitation of atrazine and desethylatrazin-2-hydroxy using first and second derivative adsorption spectra respectively, in the range 240–280 nm. By application of the PLS-2 algorithm no better results were obtained.

After the data were autoscaled to the mean value of the variables, the selection of the optimum number of factors in the PLS algorithm as to model the system without overfitting the concentration data, was carried out using the cross-validation method leaving out one sample at a time. Validation variance parameter was used to select the optimum number of factors, Table 5. In this sense, for atrazine the number of factors that minimizes the residual variance (optimal model) were two, corresponding to the local minimum. For desethylatrazin-2-hydroxy, two factors were selected also, because a higher number of factors does not minimize significantly the residual variance and could produce a overfitted model.

The root mean square difference (RMSD), which indicates the average error in the analysis and (R^2) which is an indication of the quality of fit of all the data to straight line were calculated.

$$\mathrm{RMSD} = \left[\frac{1}{N}\sum_{i=1}^{N}(\hat{x}_i - x_i)^2\right]^{1/2}$$

$$R^2 = 1 - \frac{\sum_{i=1}^{N}(x_i - \hat{x}_i)^2}{\sum_{i=1}^{N}(\bar{x}_i - x)^2}$$

where N is the total number of samples, $\hat{x}_i$ = predicted concentration, x_i = standard concentration and $\bar{x}$ = mean of true concentrations. The results are summarized in Table 6.

The calibration model was applied to a series of synthetic mixtures, Table 3, and the analytical precision of the optimized model was evaluated by using the relative error of prediction (REP).

Table 4
Training calibration set

Standard	AT μg ml^{-1}	DAH μg ml^{-1}
1	1.48	1.48
2	3.48	1.48
3	5.48	1.48
4	1.48	3.48
5	1.48	5.48
6	4.00	4.00
7	4.48	2.48
8	2.48	4.48
9	1.48	2.48
10	2.48	1.48
11	3.00	3.00

Table 5
Y-variable residual variance of the validation

Factor	AT	DAH
0	1.307	1.307
1	$0.1976\cdot10^{-1}$	$0.4349\cdot10^{-1}$
2	$0.8880\cdot10^{-3}$	$0.2517\cdot10^{-2}$
3	$0.1109\cdot10^{-2}$	$0.1717\cdot10^{-2}$
4	$0.1047\cdot10^{-2}$	$0.1455\cdot10^{-2}$
5	$0.1381\cdot10^{-2}$	$0.1840\cdot10^{-2}$
6	$0.3222\cdot10^{-2}$	$0.1812\cdot10^{-2}$
7	$0.5005\cdot10^{-2}$	$0.3392\cdot10^{-2}$

Table 6
Statistical parameters for the optimized models

AT		DAH	
RMSD	R^2	RMSD	R^2
0.03592	0.9993	0.04325	0.9990

Values of 1.93 and 2.49% for atrazine and desethylatrazin-2-hydroxy, respectively, indicate that the model proposed is satisfactory.

3.4. Determination of atrazine and desethylatrazin-2-hydroxy in ground water

When working on synthetic mixture, no significant advantages are found in the application of the different methods developed. Because of this, for the analysis of ground waters samples only the ratio spectra derivative and PLS-1 methods, were applied to the simultaneous determination of atrazine and desethylatrazin-2-hydroxy. Spiked samples were prepared from ground waters coming from mountain sources in the highest part of Orotava Valley (Tenerife, Canary Islands), in order to be sure that they were not contaminated with the named herbicides.

The results obtained are shown in Table 7. As can be seen the results obtained by application of ratio spectra derivative method gives such errors, specially for atrazine, that it can not be applied to the determination of these herbicides, in ground water samples. These results can be justified on the basis of the absorption spectra of the ground water, which show a maximum probably due to the presence of humic acids and related compounds, Fig. 5, overlapping those of the analytes.

However, when the PLS-1 method was applied to the first and second derivative spectra of the samples in the range 240–280 nm, as stated above, all the spiked samples of ground water were correctly resolved, Table 7.

4. Conclusions

A comparative study of the utilization of zero-crossing method, ratio spectra derivative and PLS approaches for the determination of mixtures of atrazine and desethylatrazin-2-hydroxy in ground waters samples has been carried out. These methods gave good results when applied to the resolution of synthetic binary mixtures. However, derivative methods are not suitable for the resolution of mixtures of both pesticides in ground waters samples due to the presence of spectral

Table 7
Results obtained for determination of atrazine and desethylatrazin-2-hydroxy (DAH) in ground waters mixtures by the ratio spectra derivative (RSD) and PLS-1 methods

Composition of mixture		Atrazine				Desethylatrazin-2-hydroxy			
		RSD, 216 nm		PLS-1[a]		RSD, 236 nm		PLS-1[b]	
Atrazine μg ml^{-1}	DAH (μg ml^{-1})	Found μg ml^{-1}	Recovery %	Found μg ml^{-1}	Recovery %	Found μg ml^{-1}	Recovery %	Found μg ml^{-1}	Recovery %
2.00	2.00	0.50	25	2.08	104	2.06	103	2.04	102
2.00	4.00	0.40	20	1.99	100	2.20	55	3.97	99
2.48	3.48	0.05	2	2.57	104	3.30	95	3.55	102
2.48	5.48	0.22	9	2.44	98	1.48	27	5.36	98
3.00	2.00	0.51	17	3.05	102	4.33	216	1.97	99
3.48	3.00	1.12	32	3.49	100	5.16	172	3.01	100
4.00	2.00	1.63	41	4.09	102	1.07	54	1.97	99
4.00	3.48	1.71	43	3.96	99	6.44	185	3.37	97
4.48	2.48	2.17	48	4.63	103	4.80	193	2.42	98
5.00	3.00	2.86	57	5.00	100	3.41	114	2.99	100

[a] First derivative spectra, 240–280 nm.
[b] Second derivative spectra, 240–280 nm.

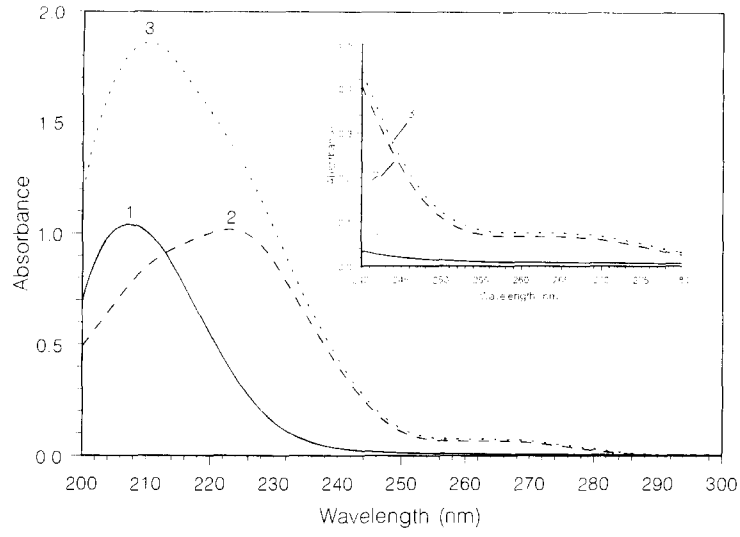

Fig. 5. Absorption spectra of (1) ground water, (2) 2 μg ml^{-1} atrazine and 2 μg ml^{-1} desethylatrazin-2-hydroxy mixture and (3) ground water spiked with atrazine and desethylatrazin-2-hydroxy mixture.

interfering substances, probably humic acids, while PLS-1 based method gave rise to good results.

Acknowledgements

Authors acknowledge financial support of this work by CICYT, Spain, AMB 92-0515. One of us, R.C.T., thanks the Consejeria de Educacion, Cultura y Deportes, Gobierno Autonomo de Canarias, for a scholarship.

References

[1] E. Knusli, in F.A. Gunther and J.D. Gunther (Eds.), Residue Reviews, Vol. 32, Springer-Verlag, New York, 1970, pp. 1–9.
[2] R.A. Leonard, in R. Grover (Ed.), Environmental Chemistry of Herbicide, CRC Press, Boca Raton, FL, 1988, p. 45.
[3] E.M. Thurman, D.A. Goolsby, M.T. Meyer and D.W. Koplin, Environ. Sci. Technol., 25 (1991) 1794.
[4] W.E. Pereira and C.E. Rostad, Environ. Sci. Technol., 24 (1990) 1400.
[5] E.M. Thurman, M. Meyer, M. Pomes, C.A. Perry and A.P. Schwab, Anal. Chem., 62 (1990) 2043.
[6] H.-R. Buser, Environ. Sci. Technol., 24 (1990) 1049.
[7] T.L. Wu, Water Air Soil Pollut., 15 (1981) 173.
[8] R.P. Richards, J.W. Kramer, D.B. Baker and K.A. Krieger, Nature, 327 (1987) 129.
[9] G.A. Junk and J.J. Richard, Anal. Chem., 60 (1988) 451.
[10] P. Cabras, M. Melis, L. Spanedda and C. Tuberoso, J. Chromatogr., 585 (1991) 164.
[11] L.M. Davi, M. Baldi, L. Penazzi and M. Liboni, Pestic. Sci., 35 (1992) 63.
[12] H.J. Stan and A. Bockhorn, Lebensmittelchemie., 45 (1991) 40.
[13] V. Coquart and M.C. Hennion, J. Chromatogr., 585 (1991) 67.
[14] P. Vitali, E. Venturini, C. Bonora, R. Calori and R. Raffaelli, J. Chromatogr., 660 (1994) 219.
[15] R.N. Lerch, W.W. Donald, Y.-X. Li and E.E. Alberts, Environ. Sci. Technol., 29 (1995) 2759.
[16] S. Butz and H.J. Stan, Anal. Chem., 67 (1985) 620.
[17] A. Brecht, J. Piehler, G. Lang and G. Gauglitz, Anal. Chim. Acta, 311 (1995) 289.
[18] M. Franek, V. Kolar, S.A. Eremin, Anal. Chim. Acta, 311 (1995) 349.
[19] EU Directive 80/778/EEC, Commision of the European Union, 15 July, 1980.
[20] M. Fielding, D. Barcelo, A. Helweg, S. Galassi, L. Tortenson, P. van Zoonen, R. Wolter and G. Angeletti, Pesticide Ground and Drinking Water, Water Pollution Report, N_{27}, Commision of the European Community, Brussels, 1992, pp. 1–36.
[21] K.A. Ramsteiner and W.D. Hormann, J. Agric. Food Chem., 27 (1979) 934.
[22] K. Farber, K. Nick and H.F. Scholer, Fresenius J. Anal. Chem., 350 (1994) 145.
[23] S.A. Senseman, T.L. Lavy, J.D. Mattice, B.M. Myers and B.W. Skulman, Environ. Sci. Technol., 27 (1993) 516.

[24] P. Geladi and B.R. Kowalski, Anal. Chim. Acta, 185 (1986) 1.
[25] M.M. Galera, J.L. Martinez and A. Garrido, Talanta, 41 (1994) 1545.
[26] E.V. Thomas and D.M. Haaland, Anal. Chem., 62 (1990) 1091.
[27] A. Guiberteau, T. Galeano, F. Salinas and J.M. Ortiz, Anal. Chim. Acta, (1995) 219.
[28] A. Guiberteau, T. Galeano, A. Espinosa-Mansilla, P.L. Lopez-de-ALba and F. Salinas, Anal. Chim. Acta, 302 (1995) 9.
[29] I.G. Ferris and B.M. Haigh, J. Chromatogr., 456 (1988) 121.
[30] V. Pakova, K. Stulik and M. Prihoda, J. Chromatogr., 442 (1988) 147.
[31] Unscrambler II extended memory version 4.0, CAMO A/S, Trodheim, Norway, 1992.
[32] F. Salinas, J.J. Berzas Nevado and A. Espinosa, Talanta, 37 (1990) 347.
[33] P.D. Sanchez, A.J. Ordierez, A.C. Garcia and P.T. Blanco, Electroanalysis, 2 (1990) 303.
[34] M. Blanco, J. Coello, H. Iturriaga, S. Maspoch, M. Redon and J. Riba, Anal. Chim. Acta, 259 (1992) 219.

ELSEVIER

Talanta 44 (1997) 685–695

Talanta

Preparation of a polypyrrole electrode modified with a nickel phthalocyanine complex. Application to the determination of an antioxidant (propylgallate) in foods

C. de la Fuente [a], J.A. Acuña [a], M.D. Vázquez [a], M.L. Tascón [a], M.I. Gómez [b], P. Sánchez Batanero [a,*]

[a] *Department of Analytical Chemistry, Faculty of Sciences, University of Valladolid, Valladolid, Spain*
[b] *Department of Analytical Chemistry, Faculty of Sciences, UNED, Madrid, Spain*

Received 16 February 1996; received in revised form 18 September 1996; accepted 19 September 1996

Abstract

In this paper a study of the electrocatalytic oxidation of propylgallate (PG) by using a polypyrrole electrode modified with tetrasulfonate nickel (II) phthalocyanine complex (Pt/PPy/NiPcTs) was carried out. Several parameters of this polymeric electrode, such as: (a) its stability in hydroorganic solution, by using an indium tin oxide (ITO) electrode and spectrophotometry; and (b) its thickness using electrochemical techniques, have been studied. In addition, several parameters affecting the PG voltammetric peak, such as pH, methanol/water ratio, potential scan rate and analyte concentration, were considered. Finally, the developed method was applied to the determination of PG in spiked potato flakes and cornflakes, showing its validity. © 1997 Elsevier Science B.V.

Keywords: Antioxidant; Nickel phthalocyanine; Polypyrrole electrode

1. Introduction

During the last decade, numerous and considerable advances concerning the development of polymeric materials in order to prepare redox complex modified electrodes with electrocatalytic properties, have been carried out. In this sense we can underline the work of Lyons [1] where an interesting theoretical review of electrocatalysis using electroactive polymers, electroactive composites and microheterogeneous systems was made. These electrodes have permitted the enhancement of the selectivity and sensitivity of many interesting electroanalytical reactions and the use of conducting polymer films in amperometric biosensors [2] and in potentiometric sensors [3].

Electrochemical synthesis of polymeric films has been carried out by different authors [4–8], showing that both the rate and the extension of the polymerisation process, as well as the physicochemical properties of the polymer, can be controlled, by a careful selection of experimental conditions.

* Corresponding author.

PII S0039-9140(96)02108-X

From an electroanalytical point of view, one of the compounds more widely used for electrode modification is pyrrole, mainly due to the important amount of counterions incorporated during the electropolymerisation step [9–11]. Moreover, polypyrrole is easily synthesised from different solvents, such as acetonitile [12–14] or water [4,5].

One of the counterions used for the modification of polypyrrole electrodes is the nickel (II) phthalocyanine tetrasulfonate complex (NiPcTs) [15], which allows us to take advantage of the electrocatalytic properties of this type of molecules. Examples of electron transfer reactions catalysed by these polymeric films electrodeposited on a solid electrodes can be found in the review of Cox [16] and Leidner [17]. Food products, mainly those containing a high amount of fat, can be involved in degenerative processes which can produce an important loss of their nutritional value (for example oxidative degeneration of vitamins), the appearance of an unpleasant smell or even the formation of toxic compounds [18]. Consequently, in order to keep the food quality, several antioxidant compounds [18]. Consequently, in order to keep food quality, several antioxidant compounds are added to food products. Antioxidants act against lipidic oxidation by means of different mechanisms.

An important group of oxidants is that of phenolic compounds, which can be either natural compounds or synthetic substances. Regarding synthetic antioxidants, one can consider, among other, the following: TBHQ (tert-butylhydroquinone), BHA (tert-butylhydroxyanisole), BHT (tert-butylhydroxytoluene), PG (propylgallate) and OG (octylgallate).

The use of these synthetic antioxidants is limited by the legislation of different countries [19] and their toxicity studies have been reported [20,21]. As other food additives, their inclusion in the corresponding positive catalogue implies an exhaustive evaluation of the ingestion risks in order to establish the admissible daily dose (ADD). The latter is the daily amount of antioxidant with no toxic effect in animals and is expressed in mg kg^{-1} of animal weight and divided by a security factor, usually 100.

The electrochemical methods used for the determination of antioxidant are numerous and they have been summarised in the review of Mannino and Wang [22]. It is important to emphasize that the electroanalytical methods are very useful for the determination of organic compounds, due to their sensitivity, selectivity and accuracy, as well as to the important information on the electrochemical mechanisms which sometimes are comparable to those taking place in metabolic processes in living organisms. In this sense, we can mention the reviews of Bersier and Bersier [23,24], and Kalvoda [25].

In this paper, a study of the anodic electrocatalysis of propylgallate at a nickel (II) phthalocyanine polypyrrole electrode deposited on a Pt wire is carried out. The stability of the modified electrode in the analytical solution used (Britton–Robinson 0.1 M) was checked by using a spectrophotometric method. Several analytical and electrochemical parameters have been considered and the characteristics of the developed method for the determination of PG established. This method has been applied to several commercial food products, such as spiked potato flakes and cornflakes.

2. Experimental

2.1. Reagents

Sodium nickel (II) phthalocyanine tetrasulfonate, NiPcTs, (Aldrich); sodium p-toluenesulfonate, TsNa, (Fluka); pyrrole (Merck); propylgallate (Riedel de Häen); boric acid (Merck); acetic acid (Merck); orthophosphoric acid (Panreac); sodium hydroxide (Panreac); methanol (Merck); aluminium oxide (Metrohm 6.2802.000); sodium dichromate (Panreac). All reagents were of analytical grade. Ultrapure water was obtained from a Barnstead System.

2.2. Instrumentation

Potentiosatat AUTOLAB PSTAT 10 ECO-CHEMIE (Holland) using the GPES software; spectrophotometer UV-Visible PU 8700, Unicam

(UK); ultrasonic bath P-Selecta (Spain). Mechanical stirrer vibromatic 384 P-Selecta (Spain); rotary vacuum evaporator Büchi (Italy); thermostatic bath P-Selecta (Spain).

2.3. Electrodes

Ag/AgCl/KCl (sat) reference electrode; Pt wire (home made) auxiliary electrode; Pt electrode, 0.076 cm^2 (Metrohm); optically transparent Indium and Tin oxide (ITO) electrodes (5 × 0.8 cm).

3. Procedure

3.1. Electrogeneration of modified polypyrrole electrodes

In all cases, modified polypyrrole electrodes were prepared by chronoamperometry at constant potential (0.8 V vs. Ag/AgCl/KCl (sat) for 60 s) from an aqueous solution onto an ITO or Pt substrate. The working electrode was polished on a polishing cloth with alumina and then cleaned by ultrasonication prior to use. Monomer solutions containing pyrrole (0.1 mol l^{-1}) and NiPcTs (10^{-4} mol l^{-1}), or pyrrole (0.1 mol l^{-1}) and TsNa ($4 \cdot 10^{-4}$ l^{-1}), were deoxygenated with nitrogen for 10 min prior to use.

3.2. Treatment of commercial food samples

A procedure similar to that proposed by King [26] was followed for the determination of PG in spiked potato flakes. The sample was powdered in an agate mortar. Then, 1 g of this sample, to which 100 μl aliquot of a 0.5 mol l^{-1} PG standard solution in methanol was added, was placed in a 20 ml centrifuge tube. Extraction was carried out with three 5 ml portions of a 50% v/v water:methanol mixture. The tube was mechanically shaken for 5 min, and after centrifugation at 5000 r.p.m. for 12 min, all the extracts were combined in a 100 ml vessel of a rotary vacuum evaporator, and concentrated up to a final volume of 3 ml. This extract was transferred into a 25 ml volumetric flask, and then diluted to the mark with a Britton–Robinson buffer solution of pH 1.05. This solution, with a PG theoretical concentration of $2.0 \cdot 10^{-3}$ mol l^{-1}, was transferred to the electrochemical cell, where PG was voltammetrically determined using the standard additions method (10 μl of a 0.5 mol l^{-1} PG standard solution were added, and the Britton–Robinson solution degassed, each time).

To modify the pH, maintaining the other parameters, a Britton–Robinson solution was employed. Therefore, to vary the pH, a 2 mol l^{-1} NaOH solution was added to the Britton–Robinson solution in sufficient amount to reach the necessary pH values.

All the experiments were carried out at constant temperature (20°C).

4. Results and discussion

Electrochemical polymerisation provides a simple means of incorporating counterions A^- into polypyrrole, according to Eq. 1.

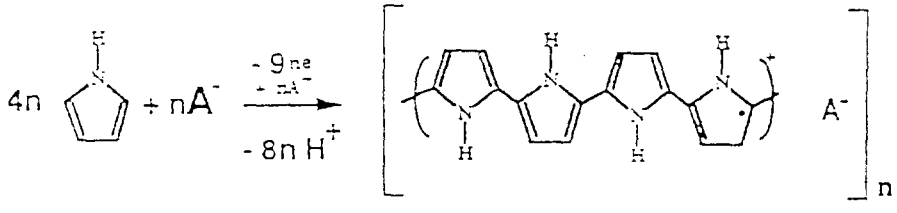

eq.1.

It was found that our NiPcTs could be incorporated directly into poplypyrrole using this method. Polymer growth could be initiated from an aqueous solution containing just the pyrrole monomer and the NiPcTs. When the platinum electrode in monomer solution was subjected to a 800 mV potential step a chronoamperometric response was observed, as shown in Fig. 1, similar to that previously described by other workers in galvanostatic experiments [27,28]. In this figure we can see that, after a great increase of the anodic current density at the potential jump, the current density decreased quickly, but 1 s after the potential step the current density rose again. As NiPcTs is the only other species present, it must be incorporated as the anion (A^-) in the polymer structure.

In order to achieve charge balance, the polymer reduction process in the analyte solution must be accompanied by immigration of cations from Britton–Robinson solution or immigration of anions from polypyrrole electrode. The relatives rates of these competitive processes will determine the outcome. These rates can in principle be understood in terms of diffusion coefficients and partition coefficients. In this way one might rationalize the difference between a conventional PP^+/X^- and our PP^+/NiPcTs where X^- is a more little and faster diffusing species than NiPcTs. So it's reasonable to think that the cations from Britton–Robinson solution move in and out of the polymer

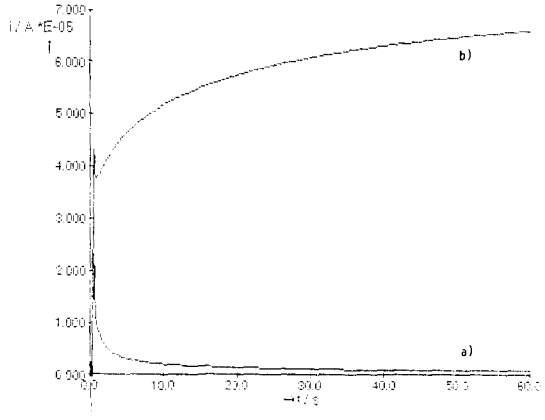

Fig. 1. Chronoamperometric response of a Pt electrode maintained to a constant potential potential of 800 mV during 60 s in 10^{-3} mol l^{-1} NiPcTs in water solution: (a) without pyrrole; and (b) with 0.1 mol l^{-1} pyrrole.

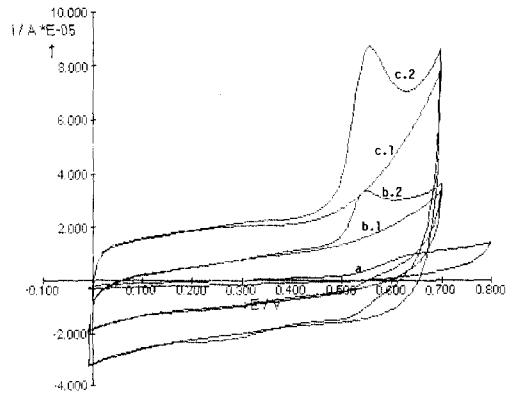

Fig. 2. Cyclic voltammograms obtained in a Britton–Robinson 0.1 mol l^{-1} solution (pH = 1.0; 5.6% methanol; $v = 100$ mV s^{-1} at different working electrodes: (a) WE Pt: with $2 \cdot 10^{-4}$ mol l^{-1} PG; $E_p = 0.631$ V, Ip = 1.87 μA; (b) WE Pt/PPy/Ts: without (I) and with (II) $2 \cdot 10^{-4}$ mol l^{-1} PG; $E_p = 0.554$ V, $I_p = 13.07$ μA; and (c) WE pt/PPy/NiPcTs: without (I) and with (II) $2 \cdot 10^{-4}$ mol l^{-1} PG; $E_p = 0.547$ V, $I_p = 38.29$ μA.

to provide charge compensation and the NiPcTs tends to stay in the reduced film [29].

4.1. Catalytic effect

In order to ascertain if PG is electrocatalytically oxidised at the Pt/PPy/NiPcTs electrode, voltammograms of PG were obtained in a Britton–Robinson 0.1 M solution of pH 1.05 (control solution), at different working electrodes: Pt, Pt/PPy/Ts and Pt/PPy/NiPcTs, where Ts is p-toluenesulphonate, a counterion with no electrocatalytic properties. These voltammograms are displayed in the Fig. 2. As can be seen the best results were obtained when working with a Pt/PPy/NiPcTs electrode, showing a higher PG peak intensity and demonstrating that an electrocatalytic effect is produced (Fig. 2 curve c.2).

It is necessary to remark that the cyclic voltammogram produced, when using a Pt/Ppy/NiPcTs electrode in pure (blank) electrolyte, show a high background current. The electrochemical reaction of the polypyrrole film in the supporting electrolyte was previously mentioned; this polypyrrole reaction is quite sensitive to the nature of the electrolyte and of the counterion incorporated into the polymer, since it involves movements of ions in and out

of the film. A. Díaz et al. [30] describe that the observed background currents are dependent on the potential region, the polarity of the solvent, the sweep rate and perhaps the nature of counterions incorporated. But the large background observed do not interfere with the electrochemical measurements using cyclic voltammetry. No signal of Ni(II) oxidation is produced because NiPcTs is an example of a redox inactive transition metal phthalocyanines [31].

4.2. Spectrophotometric control of the polymer stability

In order to verify that the NiPcTs film remained adsorbed onto the Pt electrode, a series of polymeric electrodes modified with NiPcTs were prepared on transparent Indium and Tin oxide (ITO) electrodes in the conventional way described in experimental section. The presence of the modifier onto these electrodes was studied by using molecular absorption spectroscopy. The spectra were compared with those recorded with NiPcTs in Britton–Robinson solution and the following results were obtained:

4.2.1. Study of the stability of the ITO/PPy/NiPcTs electrostatic finding in aqueous media

We have prepared several polypyrroles on ITO as mentioned above. These electrodes were subjected to the following spectrophotometric tests: (a) molecular absorption spectra of a freshly prepared electrode introduced into the control solution; (b) molecular absorption spectra of the control solution in which the polymer modified electrode was immersed for 15 min; and (c) molecular absorption spectra of the control solution in which the polymer modified electrode was immersed for 30 min. These experiments were carried out at three different pH values: 1.0, 7.20 and 11.30. The spectra of pH 1.05 are shown in Fig. 3 showing the others pH similar spectra. From these, it can be deduced that the polymer did not leak into the control solution.

The absorption spectra recorded after rinsing the electrodes with water are compared with those of the NiPcTs dissolved in Britton–Robinson solution at corresponding pH values, showing both a similar absorption spectrum. So we can conclude that the NiPcTs are retained by polypyrrole film, owing to electrostating binding. Because of the incorporation into the polymer films, a red shift of a few nanometers is observed for the Soret band. This red shift can likely be attributed to the aggregation and stacking of NiPcTs molecules in the polymer [32,33].

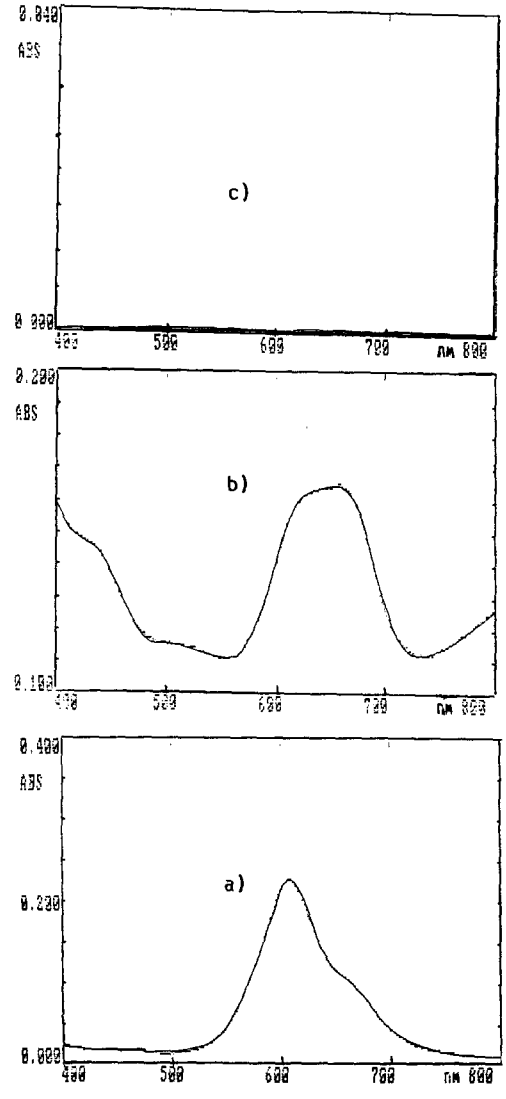

Fig. 3. Molecular absorption spectra of: (a) NiPcTs dissolved in a Britton–Robinson 0.1 mol l^{-1} solution of pH 1.05 (control solution); (b) an ITO/PPY/NiPcTs electrode freshly prepared; and (c) the control solution in which the polymer modified electrode was immersed for 30 min.

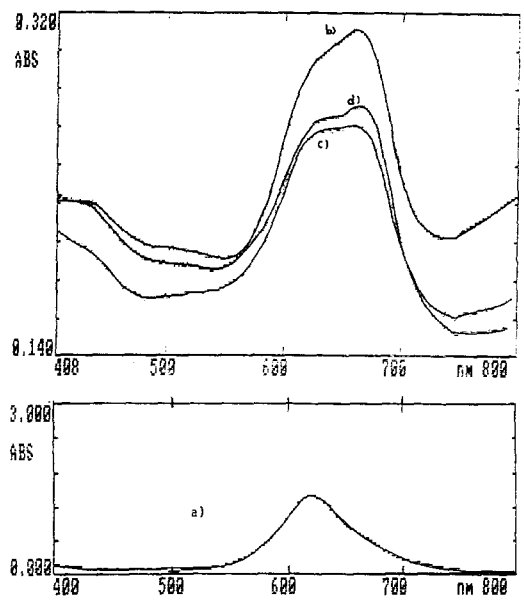

Fig. 4. Molecular absorption spectra of (a) NiPcTs solution in Britton–Robinson 0.1 mol l^{-1} solution; (b) ITO/PPy/NiPcTs electrode freshly prepared; (c) ITO/PPy/NiPcTs electrode after anodic pretreatment for 50 s at 0.9 V in Britton–Robinson 0.1 mol l^{-1} solution; and (d) ITO/PPy/NiPcTs electrode after cathodic pretreatment for 50 s at −0.1 V in Britton–Robinson 0.1 mol l^{-1} solution.

4.2.2. Study of the stability of the ITO/PPy/NiPcTs electrostatic binding after several oxidation–reduction cycles

Several experiments with the ITO/PPy/NiPcTs electrodes in Britton–Robinson 0.1 M solution were achieved with: (i) recently prepared electrode; (ii) after an anodic pretreatment at 0.9 V during 50 s; and (iii) after a cathodic pretreatment at −0.1 V during 50 s. The obtained spectra are plotted in Fig. 4.

In this figure it can be observed that the polypyrrole electrode immersed in the control solution retains its activity after a cathodic pretreatment, although after an anodic pretreatment the polypyrrole activity decreases. Therefore we can conclude that in these experimental conditions the polypyrrole modification with NiPcTs is efficient in general and that in principle, these electrodes can be used to carry out electrochemical reactions from an analytical point of view.

4.3. Effect of the polymerisation time on the PG voltammetry peak: estimation of the PPY/NiPcTs film thickness

As the polymer electrogeneration was carried out by chronoamperometry at controlled potential in the presence of the modifier, the amount of NiPcTs incorporated into the polymer matrix will depend upon the time of electrolysis. Therefore, in order to know this influence, different electrodes were prepared by varying the electropolymerisation time. We calculate the polymerisation charge by integrating the respective chronoamperometric curves I-t. Assuming that all the charge was used to form the polymeric film, it is possible to have an estimation of the polymer thickness. According to [4], we were considered that 0.1 μm = 24 mC cm^{-2}. Furthermore, taking into account the charge values involved in the electropolymerisation process, it is possible to calculate the number of NiPcTs moles incorporated into the polypyrrole matrix. By assuming that for each four pyrrole units one positive charge is created, and that phthalocyanine is tetravalent, the number of NiPcTs moles can be calculated by Faraday's equation, that is to say $N = Q_i/16 \times 96.500$, according to the expression:

$$16\,Py + NiPcTs^{-4} - 4e^- \rightarrow (Py_4)^{+4}NiPcTs^{-4}$$

The modified polymer electrodes, prepared with different electropolymerisation times, were washed with deionised water and immersed in a $4 \cdot 10^{-4}$ mol l^{-1} PG solution in Britton–Robinson buffer of pH 1.2. The values of polymerisation charge, moles of NiPcTs into the polymer, polymer thickness and PG peak current, are summarised in Table 1. From these data, it can be concluded that peak current increased as the electropolymerisation time increased up to 60 s, and then I_p decreased. This can be explained taking into account that the electron transport through the polymer slows down as the thickness of the polymer film becomes larger. An optimum electropolymerisation time of 60 s at +0.8 V was chosen for further experiments.

Table 1
Polymerisation charge, nanomoles of NiPcTs, polymer thickness and peak current for different modified polymer electrodes prepared with different electropolymerisation times

T_p (s)	Q_p (mC)	nmol NiPcTs	s (μm)	I_p (μA)
10	0.577	0.37	0.034	35.98
20	1.231	0.80	0.073	32.85
30	1.902	1.23	0.112	44.87
40	2.807	1.82	0.165	48.83
50	3.402	2.02	0.200	50.54
60	4.259	2.76	0.251	55.96
70	4.950	3.20	0.292	54.70
80	6.011	3.89	0.354	52.99
90	6.675	4.32	0.393	51.68
100	7.618	4.93	0.449	42.05

4.4. Electrochemical control of the polymer stability

Successive cyclic voltammograms of $1 \cdot 10^{-4}$ mol l^{-1} PG in a buffer solution of pH 1.05 recorded at 100 mV s^{-1} are shown in Fig. 5. As can be observed, the peak current decreases dramatically from the first to the second scan. Nevertheless, if a rest period of a few minutes with stirring is allowed (at a potential of 0.3 V), the first voltammogram is again obtained.

Another experiment consisted to record the PG oxidation current after having introduced a

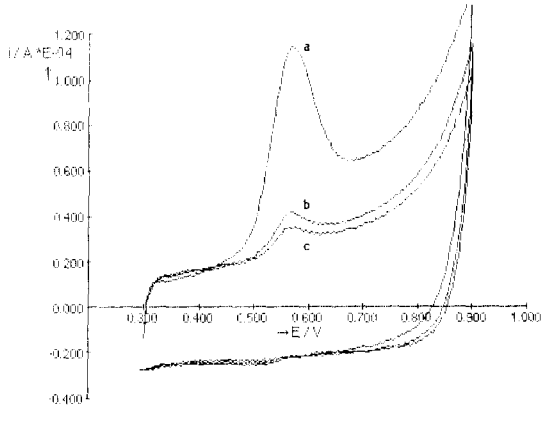

Fig. 5. Successive cyclic voltammograms of 10^{-4} mol l^{-1} PG obtained in a Britton–Robinson 0.1 mol l^{-1} solution (pH = 1.05; 5% methanol; v = 100 mV s^{-1}): (a) first voltammogram; (b) second voltammogoram|bdprime|; and (c) third voltammogram.

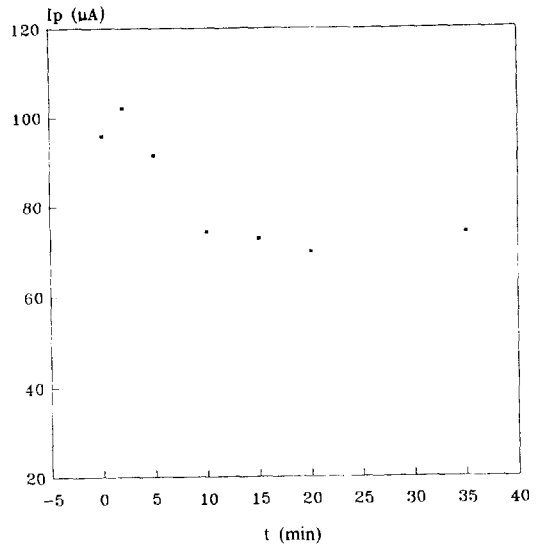

Fig. 6. Effect of working electrode permanency time into the analyte solution on PG peak current for cyclic voltammetry. PG $2.3 \cdot 10^{-4}$ mol l^{-1}; 0.5% methanol; 0.1 mol l^{-1} Britton–Robinson buffer; $v = 100$ mV s^{-1}.

freshly modified polymer electrode into the analyte solution for different times. By plotting the peak heights, I_p, (μA) c.s. time (min) the Fig. 6 was obtained. After an increase of PG anodic current from $t = 0$ to 5 min, an I_p exponential decrease with time up to $t = 10$ min was observed. Then, I_p remain approximately constant with time. For $t = 10$ min, the PG peak intensity is 21% lower than that registered on the first voltammogram ($t = 0$ min).

In order to check the reproducibility in the construction of the modified polypyrrole electrodes, ten Pt/PPy/NiPcTs were prepared under the same experimental conditions (60 s at 0.80 V). Two PG voltammograms were recorded: the first, immediately after the electrode was immersed in the analyte solution (time zero) and the second after immersing the electrodes for 3 min in the analyte solution (time three). The polymerisation charge was calculated by integrating the corresponding i-t curves, giving a Q mean value of 2.3 ± 0.2 mC. PG peak current mean values of 30.4 ± 0.60 and 36.9 ± 0.8 μA were obtained for time zero and time three, respectively. These results are good if we consider that reproducibility with this type of electrodes is not easy to achieve

since, during the electropolymerisation procedure, dimers, trimers, tetramers, etc, are formed. These forms consume polymerisation charge and are very difficult to control and quantify.

4.5. Effect of control solution composition containing PG

4.5.1. Influence of pH on voltammetric peak height and peak potential

In all cases the PG concentration was $2.3\ 10^{-4}$ mol l^{-1}, containing 0.5% of methanol. The potential scan rate was 100 mV s^{-1}.

The variation of E_p with pH shows a linear cathodic shift of 60 mV pH^{-1} units ($y = 0.62 + 0.06x$, $r^2 = 0.996$) indicating that an equal amount of protons and electrons are involved in the oxidation process [34].

The effect of pH on the PG peak height is displayed in Fig. 7. Initially, a decrease in I_p is observed up to pH 3 and then a levelling was produced. Finally, from pH 5 to peak height decreased and disappeared at pH 11. In order to obtain good sensitivity and to simplify the procedure, a pH of 1.05 was chosen for further studies.

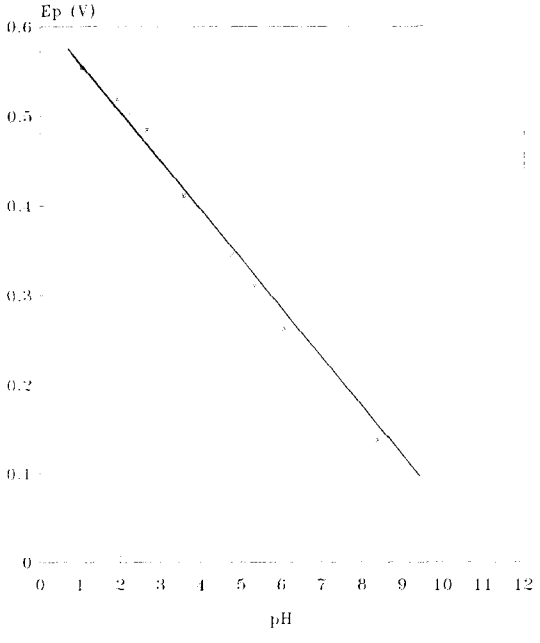

Fig. 7. Effect of pH on PG peak current for cyclic voltammetry at a nickel (II) phthalocyanine tetrasulfonate modified polypyrrole electrode (Pt/PPy/NiPcTs). PG $2.3 \cdot 10^{-4}$ mol l^{-1}; 0.5% methanol; 0.1 mol l^{-1} Britton–Robinson buffer; $v = 100$ mV s^{-1}.

4.5.2. Influence of the methanol/water ratio on the PG voltammetric peak

In order to study the influence of the presence of a non aqueous solvent, such as methanol, on the PG voltammetric peak obtained at Pt/PPy/NiPcTs electrodes, different electrodes were prepared under the experimental conditions mentioned above, and tested in $2.4\ 10^{-4}$ mol l^{-1} PG solutions prepared with different Britton–Robinson/methanol ratios. There is no significant pH change by adding methanol. We observed a gradual decrease of I_p with about 50% between 0.5 and 12% methanol. A solution with a 0.5% of methanol was selected as the optimum value.

4.5.3. Influence of scan rate

Cyclic voltammograms of $1.0 \cdot 10^{-4}$ mol l^{-1} PG solutions were recorded at different scan rates between 5 and 103 mV s^{-1}. We can deduce, as the scan rate was increased the peak current increased, as well as the background current and the peak potential. A clear shift of E_p was produced as expected for irreversible electrochemical reactions. On the other hand, I_p changed linearly with the square root of the scan rate, showing that the current is diffusion controlled. The PG oxidation can involve two electrons, as another similar substituted phenols [35]. We also can see that the current function, $I_p/Cv^{1/2}$, increases with potential scan rate. With these results a scan rate of 100 mV s^{-1} was chosen for further experiments.

4.6. Interferences

Different substances commonly present in commercial antioxidant mixtures, such as tert-butylhydroquinone (TBHQ), tert-butylhydroxyanisole (BHA), citric acid and ascorbic acid were tested by cyclic voltammetry at the NiPcTs modified electrode in order to check whether they interfere with the PG oxidation peak. Under the experi-

mental conditions used for the PG determination citric acid showed no oxidation peak in the potential range scanned (0–0.8 V), whereas BHA, TBHQ, and ascorbic acid gave rise to well-defined oxidation peaks at 566, 340 and 313 mV, respectively.

The closeness among the peak potentials for BHA with respect to that of PG (571 mV) gave rise to only one overall oxidation peak when voltammograms of mixtures of BHA and PG were registered. On the contrary, two well separated oxidation peaks were obtained for mixtures of PG with TBHQ or PG and ascorbic acid. In order to establish the degree of interference of each tested compound, voltammograms of solutions containing $1 \cdot 10^{-4}$ M PG and different concentrations of the interferent were registered. As expected, citric acid did not interfere even at 1/100 PG/citric acid ratio. Relative errors below 2.5% were obtained for a 1/1 PG/BHA ratio or higher, but for a 1/2 PG/BHA ratio the relative error was 22%. The presence of TBHQ affects the PG signal for a PG/TBHQ ratio of 1/10 or lower (a relative error of 4% was obtained for that ratio); this is because high TBHQ contents gave rise to a very high TBHQ peak whose descending part overlaps the PG peak yielding a flattened peak with decrease of its height. The interference of ascorbic acid is important for a PG/ascorbic acid ratio or lower (a relative error of 30% was obtained for a 1/55 ratio).

4.7. Influence of propylgallate concentration on its voltammetric signal

Using cyclic voltammetry under the optimised conditions, e.g. pH = 1.05, $v = 100$ mV s^{-1} and 0.5% methanol, linear relationships between peak intensity and concentration, summarised in Table 2, were obtained. The analytical characteristics of the method are included in this table. The detection and determination limits can be calculated according to the Miller and Miller criterium [36]. It can be observed that a detection limit of 1.53 mg l^{-1} of PG was reached, with better results than that obtained using a conventional Pt working electrode (linear range, $4–20 \cdot 10^{-4}$ mol l^{-1}; detection limit, 17 mg l^{-1}).

Table 2
Linear relationships detection limits (DL) and concentration limit (CL) obtained for propylgallate using cyclic voltammetry

Range (mol l^{-1}) $\times 10^4$	$r2$	DL	CL
4.0–44.0	0.998	$7.23 \cdot 10^{-6}$ mol l^{-1}	$2.05 \cdot 10^{-5}$ mol l^{-1}
2.0–4.0	0.997	(1.53 mg l^{-1})	(4.34 mg l^{-1})
0.2–2.0	0.998		

4.8. Application of the analytical method to the propylgallate determination in commercial food samples

Recovery studies of PG in commercial spiked potato flakes and cornflakes not containing this antioxidant were carried out by applying the procedure described under experimental. First, the commercial samples were tested in order to check the absence of PG. Thus, the described procedure was applied to a 1 g potato flake blank sample and to a 0.5 g cornflake blank sample. The cyclic voltammetry at the modified electrode of this potato flake sample solution showed one little peak (Fig. 8), which may correspond to the oxidation of the other compound present in the sample. Therefore, the intensity of the PG analytical response in the recovery studies must be measured

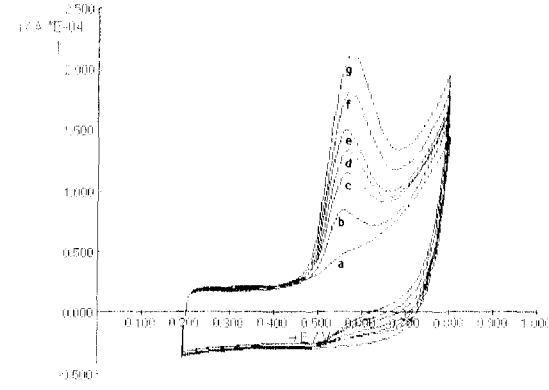

Fig. 8. Cyclic voltammograms at a nickel (II) phthalocyanine tetrasulfonate modified polypyrrole electrode (Pt/PPy/NiPcTs) for a commercial potato flake: (a) blank solution; (b)–(g) successive additions of 10 μl of a 0.5 mol l^{-1} PG standard solution.

against the blank background current. No signal was registered for the cornflakes blank sample.

Results obtained for three potato flake samples give a mean concentration in the analytical solution or $2.01 \pm 0.03 \cdot 10^{-3}$ mol l^{-1} PG, with a mean recovery of $100 \pm 1\%$. The experimental mean concentration obtained for three spiked cereal samples in the analytical solution was of $2.1 \pm 0.2 \cdot 10^{-3}$ mol l^{-1} PG, with a mean recovery of $103 \pm 9\%$. These results were for a significant level of 0.05 and demonstrate the validity of the proposed method for the determination of PG in samples of this kind.

5. Conclusions

The use of chronoamperometry at controlled potential is a rapid and efficient electrochemical procedure for the preparation of nickel (II) phthalocyanine tetrasulfonated modified polypyrrole electrodes. The species having electrocatalytic effect, NiPcTs, is incorporated as a counterion in the polymer film in order to maintain the electrical neutrality during the polymer formation by anodic oxidation of pyrrole. This modified electrode preparation procedure allows the control of the thickness film by varying the electropolymerisation time, t_p. This is of great importance to optimize the electrocatalytic reaction rate, because the higher the film thickness the slower the electron transfer, and consequently the analyte determination becomes more difficult. An optimum thickness of the polymer layer can be achieved. Voltammetry showed that the modified polymer electrode exerts an important electrocatalytic effect on the anodic oxidation of propylgallate, by comparing these voltammograms with those obtained by using a bare Pt electrode. When working with the modified polypyrrole electrode, Pt/PPy/NiPcTs, an E_p value 110 mV less positive than that at the Pt electrode was obtained, as well as an I_p value 2–3-fold higher. The modifier used is insoluble in the control solution employed, even after the electrode being immersed in this solution for 30 min and tends to stay in the film after cathodic or anodic treatment. A detection limit of 1.53 mg l^{-1} was found. The application of the proposed method to determine PG in spiked potato flake samples, using the standard addition method, gives a recovery of 100.3%, indicating that this electroanalytical method is suitable for the PG determination in this type of samples. The method was also applied to determine PG in spiked cereal samples (cornflakes) by using the same procedure. A mean recovery of 103% was obtained. Therefore, this method is also appropriate to analyse this type of sample, concerning the PG determination.

Acknowledgements

The authors thank the Ministerio de Educacion y Ciencia of Spain for the financial support granted to carry out this work (Project DGICYT PB 92-0259).

References

[1] M.E.G. Lyons, Analyst, 119 (1994).
[2] S.A. Emr and A.M. Yacynych, Electroanalysis, 7 (1995) 10.
[3] M. Josowicz, Analyst, 120 (1995).
[4] M.D. Imisides, M. John, P.J. Riley and G.C. Wallace, Electroanalysis, 3 (1991) 879.
[5] P. Heiduschka and J. Dittrich, Electroanalysis, 4 (1992) 223.
[6] L. Jin, W. Tong and Y. Fang, Fenxi Shiyanshi, 8 (1989) 42; Chem. Abstr. 111: 246803.
[7] A. Merz, Top. Curr. Chem., 152 (1980) 49.
[8] M. Josowick and J. Janata, Appl. Electroact. Polym., 310 (1993).
[9] L.F. Warren and D.P. Anderson, J. Electrochem. Soc., 134 (1987) 101–105.
[10] G.G. Wallace and Y.P. Lin, J. Electroanal. Chem., 247 (1988) 14–156.
[11] F. Beck and M. Oberst, J. App. Electrochem., 22 (1992) 332–340.
[12] R. Casas et al, Synthetic Metals, 39 (1990) 275–280.
[13] T. Otero and E. Angulo, J. App. Electrochem., 22 (1992) 369–375.
[14] M.L. Marcos, I. Rodriguez and Gonzalez-Velasco, J. Electrochim. Acta, 32 (1987) 1453–1459.
[15] C. de la Fuente, J.A. Acuña, M.L. Vázquez, M.L. Tascón, M.I. Gómez, Y. Castrillejo and P. Sánchez-Batanero, Química Analítica 13 (1994) 152–157.
[16] J.A. Cox, K.K. Jaworki and P.J. Kulesza, Electroanalysis, 3 (1991) 869–877.
[17] C.R. Leidner, Tech. Chem., 22 (1992) 313.

[18] O.R. Fennema (Ed.), Principles of Food Science. Part I. Food Chemistry, Marcel Dekker, New York, 1976.
[19] 'Positive list of food additives', Ministery of Health and Consume, General Direction of Public Health, General Subdirection of Food Hygiene, Madrid, Spain, 1986.
[20] A.L. Brannen, J. Assoc. Off. Anal. Chem., 52 (1975) 59.
[21] S.M. Barlow, Toxicological aspects of antioxidants used as food additives, in B.J.F. Hudson (Ed.), Food Antioxidants, Elsevier, London, 1990.
[22] S. Mannino and J. Wang, Electroanalysis, 4 (1992) 835–840.
[23] P.M. Bersier and J. Bersier, Analytical Voltammetry in Pharmacy in G. Svehla (Ed.), Comprehensive Analytical Chemistry, Vol. XXVII, Wilson and Wilson, 1992, p. 159.
[24] P.M. Bersier and J. Bersier, Analytical Voltammetry in Environmental Science II Organic and Organometallic Species, Comprehensive Analytical Chemistry, Vol. XXVII, Wilson and Wilson, 1992, p. 381.
[25] R. Kaldova, Electroanalytical Methods in Chemical and Environmental Analysis, Plenum Press, 1987.
[26] W.P. King and K.T. Joshep, J. Assoc. Off. Anal. Chem., 63 (1980) 137.
[27] A.F. Díaz, J. Crowley, J. Bargon, G.P. Gardini and J.B. Torrance, J. Electroanal. Chem., 121 (1981) 355.
[28] S. Asavapirryanont, G.K. Chandler, G.A. Gunawardena and D. Pletcher, J. Electroanal. Chem., 177 (1884) 245.
[29] Q.X. Zhou, C.J. Kolaskie and L.J. Miller, J. Electroanal. Chem., 223 (1987) 283–286.
[30] A. Díaz, J.M. Vasquez Vallejo and A. Martínez Duran, IBM. J. Res. Develop., 125 (1981).
[31] C.C. Leznoff and A.B.P. Leverl, 'Phthalocyanines' Vol. 1, V.C.H., New York, 1993, p. 27.
[32] I. De Gregory, M. Carrier, A. Derronzier, J.C. Moutet, F. Bedioui and J.J. Devynck, Chem. Soc. Faraday Trans., 88 (1992) 1567.
[33] F. Bedioui, Y. Bouhier, C. Sorel, J. Devynck, L. Coche-Guerente, A. Deronzier and J.C. Moutet, Electrochim. Acta, 38 (1993) 2485–2491.
[34] A.M. Bond, Modern Polarographic Methods in Analytical Chemistry, Marcel Dekker, New York, 1980.
[35] M. Baizer and H. Lund (Eds.), Organic Electrochemistry, Chp. 16, Marcel Dekker, New York, 1983, p. 486.
[36] J.C. Miller and N.N. Miller, Statistic for Analytical Chemistry, Ellis Horwood, New York, 1984.

ELSEVIER

Talanta 44 (1997) 697–704

Talanta

Development of highly sensitive cadmium ion-selective electrodes by titration method and its application to cadmium ion determination in industrial waste water

Satoshi Ito [a,b,*], Yasukazu Asano [a], Hiroko Wada [b]

[a] *R&D Division, DKK Corporation, 4-13-14 Kichijoji Kitamachi, Musashino, Tokyo 180, Japan*
[b] *Department of Applied Chemistry, Nagoya Institute of Technology, Gokiso, Showa, Nagoya 466, Japan*

Received 22 July 1996; received in revised form 16 September 1996; accepted 16 September 1996

Abstract

Characteristics of cadmium ion-selective electrode made cadmium sulphide (CdS)-silver sulphide (Ag_2S) mixture were studied. CdS-Ag_2S mixtures were obtained by gas/solid-phase reaction between silver-cadmium mixed powder and hydrogen sulphide gas (dry method) and by ionic reaction between cadmium-silver mixed ions and sulphide ion (wet method). As a result, it was found that the CdS-Ag_2S mixture had to be made in the condition of excess existence of sulfur and had better regulate the excess sulfur quantity minimum, for the CdS-Ag_2S pressed membrane gave a good Nernstian response against the cadmium ion concentration change. As the best way, CdS-Ag_2S mixture was obtained by adding sulphide ion solution to 5 mol% cadmium ion and 95 mol% silver ion mixed solution while measuring silver sulphide (Ag_2S) electrode potential as an indicator electrode. According to the reaction was stopped when the potential variation from the initial potential in the sulphide ion solution reached at 87–116 mV which the sulphide ion concentration became 10^{-3}–10^{-4} of the initial concentration, the cadmium ion membrane pressed diameter of 8 mm and thickness of 2 mm showed a Nernstian response from 10^{-8} to 10^{-1} M of cadmium ion concentration. Furthermore, aiming to its application for industrial waste water, masking buffer for interfering metal ions such as lead ion (Pb^{2+}) and copper ion (Cu^{2+}), which were possibly coexisted and to adjust total ionic strength and pH of sample was developed. The present Cd^{2+} ion-selective electrode was applied to the determination of Cd^{2+} in the industrial waste water. The good regression line with correlation factor of 0.984 was obtained compared with the conventional atomic absorption spectroscopy. © 1997 Elsevier Science B.V.

Keywords: Cadmium ion-selective; Cadmium sulphide; Electrodes; Silver sulphide

1. Introduction

Potentiometric, ion-selective electrodes are available in the field of chemical analysis because lots of specific ions are able to be measured easily and monitored, though nowadays of the development of many analytical instruments such as an ion chromatograph, a flame spectrophotometer, an atomic absorption spectrophotometer (AA), an inductively coupled radio frequency plasma (ICP)

* Corresponding author.

PII S0039-9140(96)02109-1

and so forth. In the case of measuring three divalent heavy metal ions such as Cd^{2+}, Cu^{2+} and Pb^{2+} in the industrial waste water, the ion-selective electrodes are very convenient because of their simplicity and selectivity. Though there have been some reports on the sensing materials of them, it has not become clear yet the relationship between the ion selective sensing materials and detection limit and high reproducibility, and also it is not to say sufficient discussions have been exhausted.

The books of Freiser [1] and Moody and Thomas [2] are very useful about the study of the divalent heavy metal ion selective membrane. Ross et al. [3,4] have reported the precipitate-based solid-state MS-Ag_2S mixture membrane by a stoichiometric reaction MS-Ag_2S mixture was made that mixed solution of $AgNO_3$ and $M(NO_3)_2$ with Na_2S. Also, Hirata et al. [5–7] have developed the ceramic solid-state MS-Ag_2S mixture membrane by baking the MS-Ag_2S mixed powder or its pressed membrane at 700°C. Up to now, some information concerning to the sensing membranes for the practical divalent heavy metal ion is as follows.

1. Mechanism of potential occurrence is based upon solubility equilibrium of MS compound. (M = Cd, Cu or Pb).
2. The sensing membrane had better be a solid state membrane consisted of MS-Ag_2S mixture. The ratio between MS and Ag_2S is not important to basic electrode characteristics.
3. Two methods have been reported. One is a coprecipitation method (wet method). Another is a baking method (dry method).
4. Whether electrode membrane is composed of homogeneous or heterogeneous is not important to basic electrode characteristics.

From information we have obtained to make the Cd^{2+} ion-selective electrode for the determination of Cd^{2+} ion of the industrial waste water, we found that CdS powder could not be moulded to a solid-state membrane by compression because of its fragility and CdS-Ag_2S mixture membrane moulded by commercialized CdS and Ag_2S compound had not shown Nernstian response mostly. However, it has not been clear that why CdS-Ag_2S mixture membrane can give Nernstian response till now. In the dry method, we found that CdS-Ag_2S mixture membrane could show the Nernstian response only under the next condition. (1) CdS-Ag_2S mixture was made by baking cadmium (Cd)-silver (Ag)-surpher (S) mixture at 500–650°C. (2) It was made by baking CdS-Ag_2S-S mixture or when it was made by baking these mixture in the hydrogen sulphide (H_2S) stream. In the wet method, we found that CdS-Ag_2S mixture membrane could show the Nernstian response when $Cd(NO_3)_2$-$AgNO_3$ mixed solution was added in Na_2S solution and the coprecipitation reaction had been ended in the condition of sulphide ion (S^{2-}) remained. In both methods, it seemed that the existence of sulphur was the key to get a good electrode performance. In comparison of the two methods, the wet method is better to control the ratio of each component and is more convenient to make easily and to obtain equal quality in the electrode characteristic.

The selectivity of the Cd^{2+} ion-selective electrode is affected by Cu^{2+}, Pb^{2+} and Fe^{3+} ions coexisted in industrial waste water. Also, it interfered by an oxidizer such as chlorine or hypochlorite ion. The detection limit and the calibration curve were slightly changed by pH of samples. In the basic solution, Cd^{2+} ion becomes cadmium hydroxide ($Cd(OH)_2$). In the acid solution, the detection limit becomes inferior owing to the increasing of solubility of CdS. All sample measurements should be performed in the best pH region. Therefore, the buffer solution for Cd^{2+} ion measurement such as Orion TISAB (total ionic strength adjustment buffer) [8] for the fluoride ion measurement which could mask the interfering substances was developed for the practical use. The present Cd^{2+} ion-selective electrode was applied to the determination of Cd^{2+} ion in the industrial waste water using the masking buffer mentioned above.

2. Experimental

2.1. Apparatus and reagents

A SEIWA Model FTO-5/TN-31C tube furnace was used for the heat treatment of CdS-Ag_2S

mixture. A DKK Model IOL-50 ion meter, a DKK Model EL7100 S^{2-} ion-selective electrode, and a DKK Model EL4083 double junction reference electrode (1M KNO_3 outer electrolyte, 3 M KCl inner electrolyte, Ag/AgCl inner electrode, glass sleeve junction) were used for monitoring of S^{2-} ion in making CdS-Ag_2S mixture in wet methods and for potential measurements of the Cd^{2+} ion-selective electrode. A Hitachi Model 208 atomic absorption spectrometer was used for the detection of cadmium, lead, copper and iron in the industrial waste water. Ag_2S of 99.99% purity, CdS of 99.9% purity and sulfur of 99.9% purity were obtained from Kojundo-kagaku (Tokyo, Japan). A silver disk, a silver wire and silver powder of 99.99% purity were obtained from Tokuriki (Tokyo, Japan), and silver paste SILVEST P-110 were obtained from Tokuriki Chemical (Tokyo, Japan).

Silver nitrate, cadmium nitrate, sodium sulphide, sodium acetate, disodium hydrogenphosphate, potassium nitrate, hydrogen nitrate, sodium hydroxide, salicylaldoxime and ethyl alcohol were obtained from Wako Chemicals (Osaka, Japan). All chemicals were of analytical reagent grade. Pure water obtained by a MILLI-Q SP Reagent Water System was used in this work. Argon cylinder gas and hydrogen sulphide cylinder gas were obtained from Nipponsanso (Tokyo, Japan).

2.2. Preparation of CdS-Ag_2S membrane by dry method

CdS-Ag_2S mixture was prepared the following two methods. The ratio between CdS and Ag_2S is 10:90 mol%, typically.

1. Stoichiometric amount of cadmium powder, silver powder and surfer powder was mixed well and was baked for 3 h at 700°C under hydrogen sulphide gas stream.
2. Stoichiometric amount of cadmium sulphide powder and silver sulphide powder and 5 mol% equivalent of surfer powder was mixed well and was baked for 3 h at 700°C under hydrogen sulphide gas stream.

The CdS-Ag_2S mixture produced was ground into powder (under 147 μm (100 mesh)) and was compressed under 200 kgf cm^{-1} in a 8 mm diameter die to form 2 mm thickness pellet or membrane. Furthermore the pellet was baked for 3 h at 700°C under hydrogen sulphide gas stream.

2.3. Preparation of CdS-Ag_2S membrane by wet method

CdS-Ag_2S mixture was prepared the following method. The ratio between CdS and Ag_2S is 10:90 mol%, typically. EL7100 sulphide ion-selective electrode and EL4083 reference electrode were soaked in solution of 0.1 M sodium sulphide. 1 M potassium nitrate was filled in outer chamber of the reference electrode not to outflow chloride ion from the liquid junction to the 0.1 M sodium sulphide. Solutions of 0.1 M cadmium nitrate and 0.2 M silver nitrate were mixed in 10:90 ratio. This mixed solution was added little by little in the 0.1 M sodium sulphide while the solution was strongly stirred and the change of the sulphide ion-selective electrode potential was measured. The co-precipitate reaction was stopped when the potential variation from the initial potential in the 0.1 M sodium sulphide reached at 116 mV, which the sulphide ion concentration became 10^{-4} of the initial concentration. After the solution kept being stirred for 1 h, the co-precipitate of CdS and Ag_2S was decanted and washed by sufficient amount of water for five times. Therefore the co-precipitate was filtered out and was washed by ethyl alcohol for three times and was dried at 80°C under argon gas stream. The final CdS-Ag_2S mixture powder was compressed under 200 kgf cm^{-1} in a 8 mm diameter die to form 2 mm thickness pellet or membrane not to touch the air so long time.

2.4. Electrode assembly

The structure of cadmium ion-selective electrodes fabricated is shown in Fig. 1. The CdS-Ag_2S membrane tablet is stuck in an epoxy resin body by epoxy bond. Two types of electrodes were measured. Type A electrode has inner solution (10^{-3} M cadmium chloride) and a Ag/AgCl inner electrode. The membrane of type B electrode is led out by a silver wire and a silver disk

which is stuck in opposite side of the membrane by silver paste. As these types of electrode were shown the same characteristics without the absolute value of the electrode potential, type B electrode was used throughout. The performance of the electrode was examined by measuring the e.m.f. against Model EL4083 reference electrode with a glass sleeve junction, 1M KNO_3 outer solution, 3M KCl inner solution and a Ag/AgCl inner electrode.

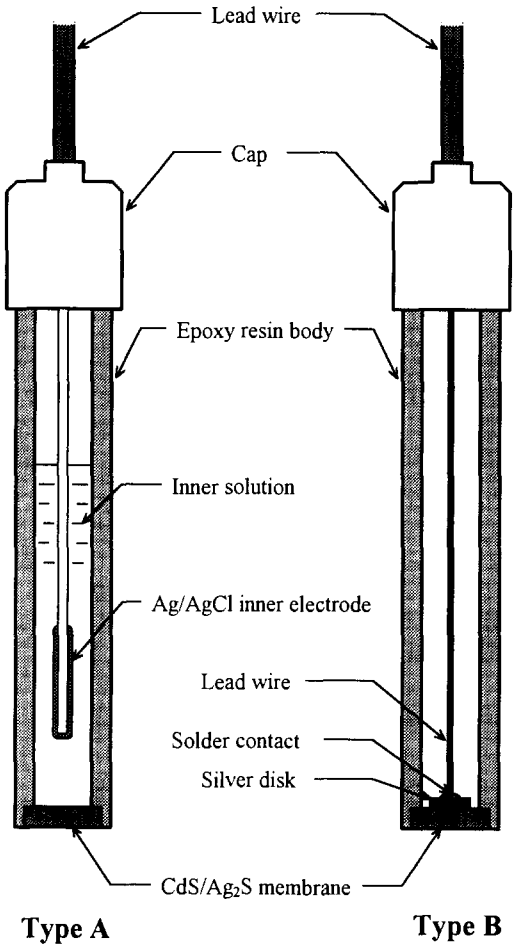

Fig. 1. Structure of Cd^{2+} ion-selective electrodes with CdS/Ag_2S solid state membrane.

2.5. Preparation of buffer solution

100 g of sodium acetate trihydrate, 100 g of disodium hydrogenphosphate 12 water, 100 g of potassium nitrate are dissolved in adequate quantity of water. The solution dissolved 10 g of salicylaldoxime in 50 ml of ethyl alcohol is added to the previous solution and adjusted in 6.15 pH by adding acetic acid using a pH meter and the whole quantity is adjusted by water in 1 l. When 1 vol.% of this buffer was added waste water of 5–8.5 pH it could be adjusted in about 6 pH.

2.6. Potential measurements and calibration curve

The Cd^{2+} ion-selective electrode fabricated and Model 4083 reference electrode were placed in 200 ml beaker. Sample of 100 ml in a beaker was stirred by a 300 mm length of magnet on a magnetic stirrer at about 400 rev min^{-1} during the measurement. The performance of the Cd^{2+} ion-selective electrode was examined by measuring the e.m.f. of the following electrochemical cell:

Ag |silver paste| CdS-Ag_2S |sample ‖1 M KNO_3‖ 3 M KCl |Ag/AgCl| Ag Each electrode was immersed in 10^{-9}–10^{-1} M l^{-1} Cd^{2+} standard solution of which the total ionic strength was adjusted with 0.1 M KNO_3 and calibration curves of each electrode were made. The electrode potentials were recorded after their values had stabilized within ± 0.1 mV min^{-1}. The potential-concentration curves were plotted as shown in Fig. 2.

2.7. Influence of pH

Each electrode was calibrated using standard solutions that changed pH from 2 to 11. The pH was adjusted by adding small volumes of HNO_3 or NaOH to the standard solution. The electrode potentials were recorded after their values stabilized, and were plotted as a function of pH values and Cd^{2+} concentration as shown in Fig. 3.

2.8. Influence of temperature

From 10^{-7}–10^{-1} M l^{-1} Cd^{2+} standard solution were prepared in a water bath at 5, 25 and

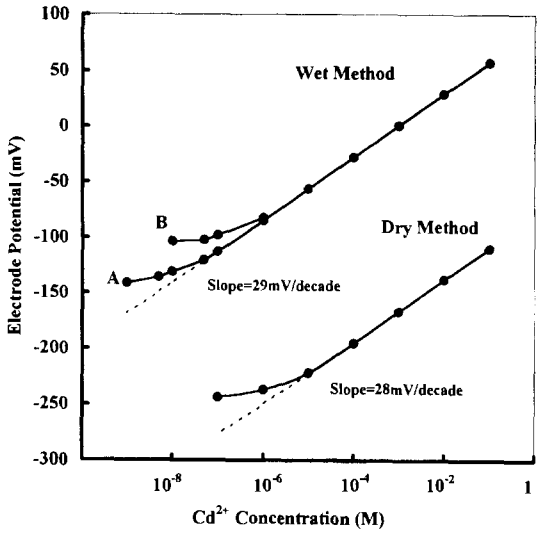

Fig. 2. Calibration curves for Cd^{2+} ion-selective electrodes with CdS/Ag_2S solid state membrane by a dry method and a wet method.

45°C, respectively. They were kept at a constant temperature within ±0.1°C. The calibration curves of the electrode were measured in standard solution at 5°C, and then, were measured at 25 and 45°C. The electrode potentials were recorded after their values stabilized, and were plotted as a function of temperature values and Cd^{2+} concentration.

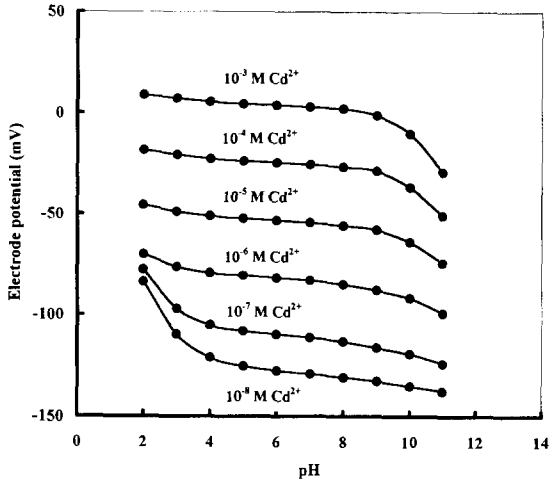

Fig. 3. Effect of pH on Cd^{2+} ion-selective electrodes with CdS/Ag_2S solid state membrane by a wet method.

2.9. Selectivity

Selectivity coefficients were determined by the mixed solution method, wherein the concentration of Cd^{2+} was fixed at 10^{-5} M l^{-1} of Cd^{2+} and the concentration of an interfering ion was varied. The selectivity coefficients, $K^{pot}_{A,B}$, were calculated according to the relation $K^{pot}_{A,B} = C_A^{(zB/zA)}/C_B$, where C_A and C_B are the total concentration of Cd^{2+} and that of an interfering ion obtained graphically in the sample solution, respectively. zA and zB are the charges of Cd^{2+} and the interfering ions, respectively.

3. Result and discussion

3.1. Detection limit of calibration curve

Calibration curves with the dry method membrane and the wet method membrane A and B are shown in Fig. 2. In the wet method, the membrane A is one that the co-precipitate reaction was stopped when the potential variation from the initial potential in the 0.1 M sodium sulphide reached at 116 mV, which the sulphide ion concentration became 10^{-4} of the initial concentration, the membrane B is one that the co-precipitate reaction was stopped when the potential variation reached at 38 mV, which the sulphide ion concentration became 5% of the initial concentration. Detection limits, which are the lowest point of Cd^{2+} concentration that their calibration curves showed Nernstian response, are 10^{-6}, 10^{-8} and 10^{-7} M l^{-1}, respectively. The characteristics of dry method electrodes on detection limit were varied between 10^{-5} and 10^{-3} M l^{-1} independently of whether departure materials of CdS-Ag_2S production were Ag-Cd-S or Ag_2S-CdS-S. This seems to be resulted from inhomogeneities of powder mixing, unequal heating, etc. In the wet method, the potential variation of S^{2-} ion-selective electrode became more, the detection limit of the membrane tended to be lower. However, as S^{2-} ion-selective electrode potential became unstable when the potential variation goes up to over 87 mV, which the sulphide ion concentration became 10^{-3} of the initial concentration,

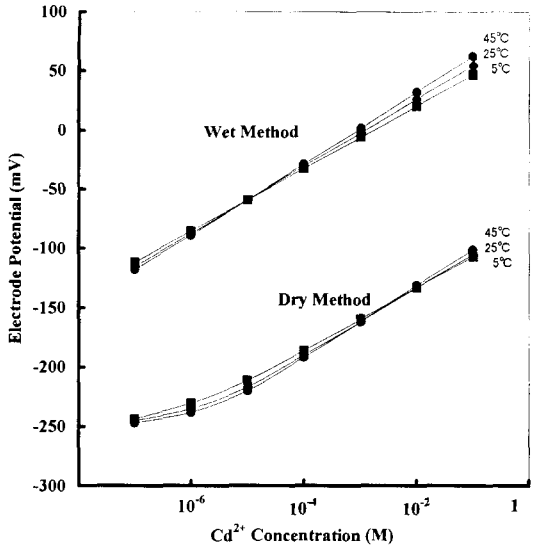

Fig. 4. Effect of temperature on Cd^{2+} ion-selective electrodes with CdS/Ag_2S solid state membrane by a dry method and a wet method.

it would be difficult to make the membrane with lower detection limit than the membrane A.

3.2. Effect of pH

pH dependence of the $CdS\text{-}Ag_2S$ membrane (the wet method membrane A) is shown in Fig. 3. There are not much differences between methods to make the membranes. Cd^{2+} ion-selective electrode potential is mostly independent of pH from 2 to 9. It is slightly interfered for pH values down to 4 for extremely low cadmium concentration (under 10^{-7} M l^{-1}). The detection limit comes to 10^{-7} M l^{-1} for pH 3 and 5×10^{-7} M l^{-1} for pH 2. However, as pH coefficient is calculated about -1.1 mV pH^{-1} (Cd^{2+} of 10^{-7}–10^{-3} M l^{-1}, pH of 2–9), calibration and sample measurement should be done at the same pH values.

3.3. Effect of temperature

Temperature dependencies of the $CdS\text{-}Ag_2S$ membrane (the dry method membrane and the wet method membrane A) at 5, 25 and 45°C were shown in Fig. 4. The isothermal point of the dry method membrane was calculated between 10^{-3} and 10^{-2} M l^{-1}. That of the wet method membrane was calculated at about 10^{-5} M l^{-1}. Although the slope (the electrode potential change per decade) increased according to Nernstian coefficient (0.0993 mV°C^{-1} at 25°C for divalent cation) when the temperature increased, detection limit became higher.

3.4. Effect of interfering compounds and its masking

Mercury (Hg^{2+}), silver ion (Ag^{+}), Cu^{2+}, Lead (Pb^{2+}), iron ion (Fe^{3+}) interfere with Cd^{2+} ion-selective electrode potential. Although under coexistence of interfering ions the Cd^{2+} ion-selective electrode potential is not stable and the selectivity coefficients could not be correctly measured, the interference of ions mentioned above were shown in Table 1. The approximate errors (S.D.) of the selectivity values were 50–200% in ten repeated measurements. These interfering result was independent of how to make the $CdS\text{-}Ag_2S$ membrane.

In the application for industrial waste water, practical selectivity could be improved by using masking reagents of interfering ions. By the use of 1% of the buffer solution (10 wet% of sodium acetate trihydrate, 10 wet% of disodium hydrogenphosphate 12 water, 10 wet% of potassium nitrate, 1 wet% of salicylaldoxime, pH 6.15), practical selectivity coefficients were obtained as shown in Table 1.

Table 1
Selectivity coefficients of Cd^{2+} membrane

Ions	Selectivity coefficients of Cd^{2+} membrane	
	In aqueous solution	In 1% buffer solution
Hg^{2+}	10^3	0.2
Ag^{+}	10^2	10^{-3}
Cu^{2+}	10	10^{-3}
Pb^{2+}	1	10^{-3}
Fe^{3+}	1	10^{-3}

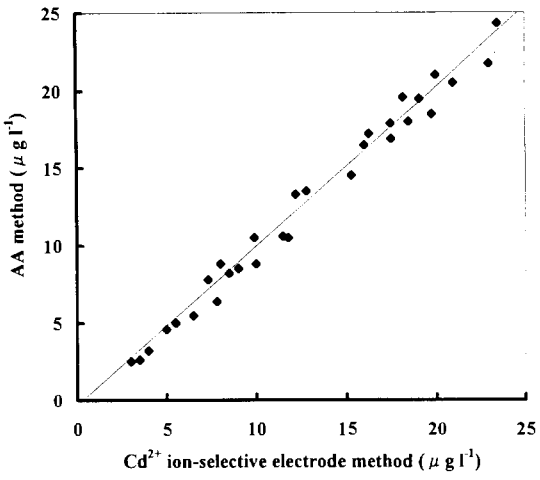

Fig. 5. Correlation between the value of Cd^{2+} ion-selective electrodes and that of AA in the industrial waste water.

4. Analysis of industrial waste water

We applied the present Cd^{2+} ion-selective electrode for the determination of the Cd^{2+} ion in the industrial waste water. Fig. 5 shows the correlation between the value of the Cd^{2+} ion-selective electrode and that of AA in the industrial waste water. The wet method membrane A was used in the analysis and 1% of buffer solution was added to sample solution for masking of Cu^{2+}, Pb^{2+} and Fe^{3+} ions. Concentrations of Cu^{2+}, Pb^{2+} and Fe^{3+} ions in the industrial waste water were 0.1–1, 0.1–0.5, and 0.2–2 mg l^{-1}, respectively. The values with Cd^{2+} ion-selective electrode are good agreement with those with AA ($r^2 = 0.984$, $y = 1.035x - 0.629$). In the analysis of industrial waste water under coexistence of 20–100 fold of Cu^{2+}, Pb^{2+} and Fe^{3+} ions against Cd^{2+} ion, low concentration range of 2.5–25 μg l^{-1} (2.5×10^{-8}–2.5×10^{-7} M) Cd^{2+} ion could be successfully measured. From these data, it is clear that the present Cd^{2+} ion-selective electrode was useful for the simple and speedy control of Cd^{2+} ion in the industrial waste water with sufficient sensitivity compared with AA.

5. Conclusion

New highly sensitive Cd^{2+} ion-selective electrode was developed by titration method using S^{2-} ion-selective electrode as the indicator electrode compared with the dry method. In the dry method, in the case S or H_2S was not used, the CdS-Ag_2S membrane was entirely not or little shown a Nernstian response. Also, in the wet method, in the case the sodium sulphide solution was added into Ag^+ and Cd^{2+} mixed solution and the co-precipitate reaction was stopped at about 400 mV of S^{2-} ion-selective electrode potential, which S^{2-} ion was not existed at all the CdS-Ag_2S membrane was entirely not shown a Nernstian response, too. Although Hirata et al. [6] reported to relationship between the electrode characteristics and the existence of intermediate phases: $Ag_{1.55}Cu_{0.45}S$, etc., in the study of ceramic copper (II) ion-selective electrode membrane in a X-ray microanalysis, we obtained good characteristics of the CdS-Ag_2S membrane without a heat treatment in the present wet method. As shown in Fig. 2, electrode potentials on the same concentration of Cd^{2+} standard solution are different the dry method membrane from the wet method membrane. Furthermore, as shown in Fig. 4, isothermal points are different each other. Because the each CdS-Ag_2S membrane obtained in dry method and in wet method has more or less different characteristics. However, it is sure that a sulphide in a CdS-Ag_2S procedure plays an important role for its good characteristic. As a result, we could make a Cd^{2+} ion-selective electrode of the best characteristics by titration method. Data by the present method was good agreement with those from AA.

References

[1] Freiser, Ion-Selective Electrodes in Analytical Chemistry, Vol. 1, Plenum Press, NY, (1978), 171–178.
[2] J. Moody and J.D.R. Thomas, Selective Ion Sensitive Electrodes, Merrow Technical Library, (1971) 83–87.
[3] W. Ross, in R.A. Durst (Ed.), Ion-selective electrodes, NBS special publication No. 314, Government Printing Office, Washington 1969.

[4] S. Frant, J.W. Ross, U.S. Patent No. 3 591 464, July 6 1971.
[5] Hirata, K. Higashiyama and K. Date, Anal. Chin. Acta. 51, (1970) 209.
[6] Hirata et al., Z. Abstracts of IUPAC International Congress on Analytical Chemistry, (1972) 213.
[7] Hirata et al., Z. Anal. Chem. 257, (1971) 104.
[8] Orion Research Inc., Appicatons Bullein No. 5A, 1969.

ELSEVIER

Talanta 44 (1997) 713–723

Talanta

Application of sequential injection analysis to anodic stripping voltammetry

Ari Ivaska [a,*], Wladyslaw W. Kubiak [b]

[a] *Laboratory of Analytical Chemistry, Åbo Akademi University, FIN-20500, Turku-Åbo, Finland*
[b] *Faculty of Materials Science and Ceramics, Academy of Mining and Metallurgy al. Mickievicza 30, PL 30-059 Krakow, Poland*

Received 2 July 1996; received in revised form 4 October 1996; accepted 4 October 1996

Abstract

Sequential injection analysis (SIA) technique has been applied to anodic stripping voltammetry (ASV). The sample and reagent volumes can easily be controlled by SIA. The technique also allows plating of the mercury film on-line and therefore substantially reduces generation of mercury containing waste. Repeated sample passage through the detector was used during the deposition step to enhance the sensitivity. The way solution handling is done in SIA allows an easy and effective medium exchange procedure increasing the selectivity of the method. This has been demonstrated by changing the stripping medium and having different complexing agents in the stripping solution. The observed potential shifts of the stripping peaks could theoretically be explained in the cases where the complexation constants are known. Calibration and the standard addition methods are discussed and demonstrated by determining copper in tap water as a method of testing the procedure. © 1997 Elsevier Science B.V.

Keywords: Anodic stripping voltammetry; Copper; Mercury; Sequential injection analysis

1. Introduction

Sequential injection analysis (SIA) is a new generation of flow injection analysis (FIA) [1]. The method is based on the same principle as FIA i.e., controlled dispersion, reproducible injection of the sample and exact timing of the different operations. The way how solutions are handled makes SIA more versatile than FIA. The enhanced versatility of SIA is due to the instrumental units of the system. A precise, in reversal directions functioning and digitally controlled pump as well as a multiposition and digitally controlled valve are needed [2]. Timing has to be precise, accurate and easily adjustable and therefore the system requires computer control. Remaining parts of the system i.e., detector, tubing and additional arrangements are similar as in FIA. One additional requirement in SIA is the response time of the detector. In FIA the flow is continuously pumped through the detector. In SIA, however, the flow is stopped while the sample and reagents are aspirated into the holding coil. Therefore the detector in SIA has to reach a stable baseline very fast after the flow is again directed through the detector. This is especially

* Corresponding author. Fax: + 358 2 2654479.

PII S0039-9140(96)02115-7

important when using potentiometric and voltammetric detectors where the response is based on interaction of the compounds in the flow and the sensor surface. The advantages of SIA are:

(i) reduced reagent consumption

(ii) easy and fast change of solutions and their handling: change of concentration and volume ratio, dilution, change of reagents

(iii) easy and fast change of system operating parameters: flow rate, number of reagents and their aspirated volumes

The last two points can easily be done by adjusting the proper parameters in the computer program.

The way how the sample and reagent solutions are handled in SIA makes the technique ideal for ASV at mercury film electrodes (MFE) in flow systems. ASV [3] is the method of choice for determination of heavy metals. Because the thin film electrode has a high ratio of surface area to volume, the mercury film electrodes exhibit a higher sensitivity than the bulk mercury electrode such as the hanging mercury drop electrode (HMDE) and its modern variants. Glassy carbon is an often used substrate for MFE, due to the lack of interaction between the substrate and mercury and the substrate and the deposited metals. Mercury, however, is not forming a real film on the glassy carbon substrate but the layer rather consists of very small drops of mercury. In contrast, metallic substrates such as silver, gold, platinum, copper, iridium give the possibility to obtain a real mercury film. However, depending on the metal substrate some interfering factors are possible such as: intermetallic compounds, substrate amalgamation or problems with mercury deposition because of an oxide film at the substrate surface. Two different electrochemical methods are normally used to generate a film of mercury on the substrate. One method is to preplate the mercury film during a separate plating step and in a separate mercury solution. Usually this method is used to make a thick film to be used in a number of subsequent analytical determinations. The second method is an 'in situ' preparation of the film where the mercury film is formed together with the metals to be determined [4].

The easy solution handling in FIA and the small sample volume used in assays have made FIA technique attractive also for anodic stripping voltammetry (ASV) [5–13]. The aim of the present paper is to show how the technique of SIA can be used with ASV in flow systems to improve the process of making a mercury film electrode, to enhance the sensitivity and selectivity of the method and how the analytical procedure can be carried out with reduced reagent consumption.

2. Experimental

2.1. The system

The SIA system used is shown in Fig. 1. The peristaltic pump is of type C4-V from Alitea, USA. The eight-ports multiposition valve with a home made controller of type MV-8 is from Pharmacia, Sweden. The whole system is controlled by a 486 PC computer (Compaq) with FIALab software (Alitea USA) via an ADA 1100 card (RTD, USA) and a home made connecting box. Parts of the flow system were connected together with PVC tubing with 0.8 mm i.d. and 4.0 mm o.d. Holding and auxiliary coils were fabricated by coiling up 1.5 m of tube on a plastic rod of 25 mm

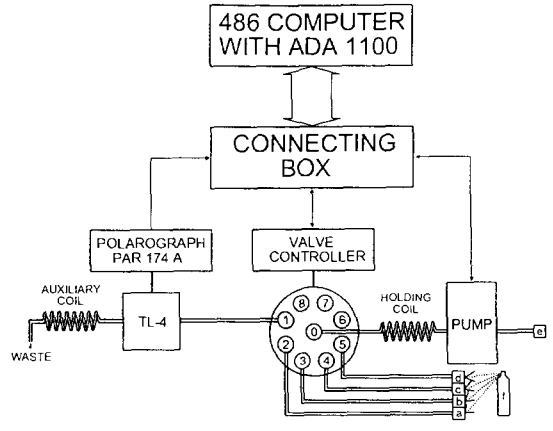

Fig. 1. Schematic diagram of the SIA system for ASV. Solutions: a, 0.1 M HCl; b, sample solution; c, Hg plating solution; d, stripping medium; e, carrier 0.1 M HCl. N_2 was used for deaeration of the solutions, f.

Table 1
Schedule of the medium exchange experiment

Event	Time s	Duration s	Pump speed %	Valve position	Potential V	Data acquisition	Operation
1	0	20	60	1	+0.5	Off	Cleaning
2	20	15	−30	5	+0.5	Off	Stripping medium
3	35	5	−30	2	+0.5	Off	0.1 M HCl
4	40	8	−30	3	+0.5	Off	Sample
5	48	8	−30	4	+0.5	Off	Hg plating
6	56	5	−30	2	+0.5	Off	0.1 M HCl
7	61	50	30	1	−1.0	Off	Deposition
8	111	10	0	2	−1.0	Off	Equilibration
9	124	45	0	3	Scan −1→0	On	Stripping
10	166	30	30	1	+0.5	Off	Cleaning

o.d.. The detector was a thin layer cell TL-4 from BAS, USA, with glassy carbon working electrode, saturated silver–silver chloride 3 M NaCl reference electrode and the stainless steel upper body of the detector serving as the auxiliary electrode. Potential control and current measurements were done by the polarographic analyzer model 174A, PAR, USA. Data were collected from the polarograph by an ADA 1100 card, visualized and stored with FIALab software. Interpretation of data was carried out with MicroCal Origin (MicroCal Software, USA). Deaeration of the solutions (sample, mercury plating solution, stripping solution) was performed outside the flow system by purging the solutions with nitrogen. Carrier solution was not deaerated.

2.2. Reagents

Carrier solution was 0.1 M HCl (Merck). Metal ion stock solutions were: Cd(II) 1000 ppm—cadmium shot (Merck 7398) dissolved in nitric acid (Merck suprapur); Cu(II) 1000 ppm—copper shot (Riedel De Haan 12809) dissolved in nitric acid; Hg(II) 50 mM—$HgSO_4$ (Merck) in 5% H_2SO_4; In(III) 5 mM—$InCl_3 \cdot 4H_2O$ (Fluka AG, puriss) in 0.1 M HCl; Pb(II) 1000 ppm—$Pb(NO_3)_2$ (Merck) in 2% nitric acid; Sn(II) 5 mM—$SnCl_2 \cdot 2H_2O$ (Baker, pure) in 0.1 M HCl; Tl(I) 5 mM—CH_3COOTl (BDH, general purpose) in 0.1 M HCl. The stripping solutions were: ammonia buffer 0.01 M, pH 9.2 (NH_4Cl—Merck, ammonia solution 25%—Merck suprapur); 2M ethylenediamine (Merck, for synthesis) in 0.1 M HCl; 0.2 M citric acid (Merck) in 0.1 M HCl and 0.1 M EDTA (Merck–Titriplex III) in 1 M ammonia buffer pH 9.0. The mercury plating solution was 1×10^{-5} M $HgSO_4$ in 0.1 M HCl. In the experiments where a thicker mercury film was required 1×10^{-4} M $HgSO_4$ was used. If not stated otherwise, purity of reagents were of the quality 'pro analysis' and they were used without additional purification. All solutions were prepared using Millipore water.

2.3. Procedure

Whole flow system is operated under computer control via an ADA 1100 card and FIALab software. Table 1 shows the schedule for an experiment with medium exchange. The first and last events are flushing the flow system with carrier solution. In this case carrier is pumped through port 1 to the detector. Next five steps are subsequent aspirations of the stripping solution, deaerated HCl, the sample, the plating solution and again the deaerated HCl solution. These five steps prepare the system for the actual analysis. In the seventh event the electrode potential is switched to plating potential (usually −1.0 V) and the solutions stacked in the holding coil are then pumped via port 1 of the valve to the detector. Solutions reach the detector in a reverse sequence than when they were aspirated in the holding coil. Generation of the Hg film at the electrode is followed by deposition of the components in the

sample. Concentration profiles of the solutions as they pass the detector during the event # 7 are shown in Fig. 2. The profiles were determined by using 1 mM $K_3Fe(CN)_6$ in 1 M acetate buffer pH = 4.5 as the zone which profile was to be measured. In such experiment all the other zones injected were 0.1 M HCl. The current was measured amperometrically at + 0.2 V by using the differential pulse mode with 25 mV pulse amplitude. In the actual experiment with the sample the flow is stopped when the maximum concentration of the stripping solution has reached the detector. After a short rest and stabilization period, step # 8, the stripping step is started in the event # 9 where a differential pulse potential scan is initiated. The scan rate is 20 mV s^{-1} and the pulse amplitude 25 mV. The stripping current is measured with a data acquisition frequency of 5 Hz. Event # 9 is terminated when the electrode potential reaches 0 V. During event # 10 the carrier solution is pumped through the detector. Potential scan is still continued without data collection until the electrode potential reaches + 0.5 V. By this time the mercury film has been removed from the electrode, waste solutions are removed and the system has been washed. The system is then ready for the next cycle. Potential + 0.5 V is also applied to the working electrode during events # 1–# 6.

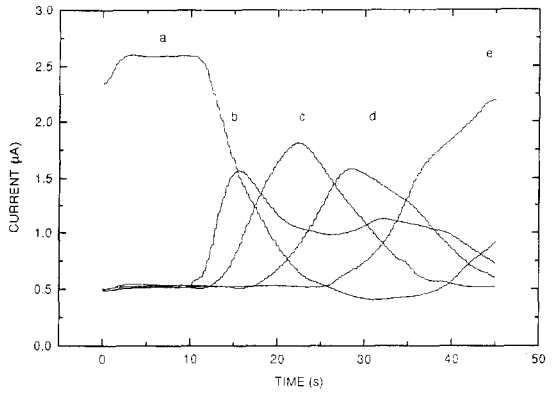

Fig. 2. Concentration profiles for the medium exchange experiment. Solutions: a, carrier 0.1 M HCl; b, deaerated 0.1 M HCl; c, Hg plating solution; d, sample; e, stripping medium. 1 mM $K_3Fe(CN)_6$ in 1 M acetate buffer pH = 4.5 was used as the solution for the zone which profile had to be measured.

Data collected by the FIALab software were stored in MATHLab format and after initial processing by MATHLab they were exported to Microcalc Origin, by which program the data were interpreted, graphically presented and archived.

3. Results and discussion

3.1. Reagent consumption

Increasing requirements on environment protection as well as economic reasons cause the demand to develop analytical methods with minimal reagent consumption and waste production. SIA is a technique that fulfils these requirements to a great extent. Even in comparison with FIA, a method of which one basic advantage is low reagent consumption, SIA shows substantial reagent savings.

3.2. Carrier solution

The role of carrier solution in SIA is to transfer the aspirated zones to the detector and flush the system. In most SIA application distilled water can be used as the carrier. By using distilled water as carrier not only the reagent consumption is reduced but the life time of the pump is also prolonged because in SIA only carrier is in contact with the pump. If peristaltic pumps are used the tubing will last longer lowering the maintenance costs of the system. In the present work it was necessary to assure a certain conductivity in the carrier solution and therefore 0.1 M HCl solution was used. During the entire experimental work required for this paper only 1.5 l of the carrier solution was consumed.

3.3. Sample

The main part of the sample consumed in a FIA system with injection valve goes to rinse the sample loop with a new sample prior to each new assay. Volume of the sample required is therefore 3–5 times higher than the actual volume of the sample loop. In a SIA system the sample is aspirated directly into the holding coil and therefore

only an exactly defined volume of the sample is used, minimizing the consumption of the sample. Assuming that a typical volume of sample in an ASV determination by SIA is 200 μl and three replicate determinations are done, SIA consumes only 0.6 ml, whereas consumption in FIA is 1.8–3.0 ml. Consumption during the sample change is similar in both flow methods and depends on the length of the tubing that delivers the sample to the valve.

3.4. Mercury plating solution

Reduction in consumption of the plating solution is especially important due to the toxicity of mercury salts. Direct comparison with FIA is not simple because in FIA mercury plating is done by a more complicated way. The consumption in FIA is low when the mercury film is generated in situ. In that case the sample is usually made to 50 μM in respect to the mercury salt. Then the consumption of the sample containing mercury salts for three replicate determinations is 1.8–3.0 ml plus the volume (about 2 ml) necessary to wash the delivery tube when the sample is changed. This makes it to 3.8–5.0 ml altogether. Assuming the same volume for cleaning the delivery tube, consumption in SIA is 2.6 ml. But when using the method of film generation as used in this work, i.e., the mercury solution is aspirated through a separate port, the consumption is only 0.6 ml. During the entire experimental work in this paper less than 100 ml of a 10 μM $HgSO_4$ solution was used. Other methods to generate a mercury film in FIA as well as in batch methods generally consume much more of the mercury salt.

3.5. Generation of mercury film

Generation of the mercury film electrode in a flow system needs usually a special procedure. Simplest way is the in situ generation [4]. In many cases, however, a preplated mercury film is used. In those cases the MFE is generated in batch conditions outside the flow system, or by a separate arrangement to deliver the mercury solution to the detector for plating. When a troublesome generation procedure has to be used the same film is then used for several assays. The principles of SIA allows an easy and versatile way to generate a thin mercury film electrode. In SIA it is possible to generate a MFE both by in situ and ex situ method without changing the system manifold.

The same procedure as in FIA can also be used in SIA to generate a mercury film electrode by the in situ method. The sample is made to 5×10^{-5} M with respect to a Hg(II)-salt and the mercury film is formed simultaneously with reduction and amalgam formation of the metals in the sample. Reproducibility of such an electrode was found to be 4.8% measured as the relative standard deviation in the lead stripping peak of a 1 μM Pb(II)-solution with deposition at −1.0 V for 40 s. In that time the leading plug of carrier, the sample and the second plug of carrier have passed the detector, so that the actual efficient deposition time was somewhat shorter.

Generation of a preplated film to be used in several determinations requires a separate SIA solution handling procedure. Mercury plating solution is aspirated first. The next step is deposition of the mercury film and exchange of the solution in the cell. Reproducibility of a preplated film measured with the same lead stripping procedure as mentioned earlier was found to be 5.3% with five determinations. The repeatability was slightly better, 4.3%. A preplated film could be used in generally in more than 15 determinations but the number varied and was difficult to predict in advance.

The third possibility is to generate a mercury film in each analytical run in combination of the metal deposition. As can be seen in Fig. 2 the zones of the mercury plating solution and the sample overlap each other resulting in a mixed zone where plating and deposition could be performed. Only mercury is deposited first and then both mercury and the metals and finally only the metals in the sample. The best results were obtained when the film was removed after each determination by anodic dissolution at +0.5 V and by keeping all the other conditions the same. With this procedure the reproducibility measured with 12 subsequent films was 4.2%. This is the procedure described in Table 1.

In some cases overlapping of the plating solution and the sample may be not advisable because of some possible chemical reactions with the components in the sample and the plating solution. In such cases a small volume of deaerated carrier may be aspirated between the sample and the plating solution. Reproducibility of such an electrode is the same as described above, but analysis time is naturally slightly longer.

3.6. Sensitivity

Sensitivity of ASV depends mainly on the deposition time and effectiveness of charge and mass transfer during the deposition step. In the injection techniques deposition takes place only during a certain effective time [6], i.e., the time during which the sample passes through the detector. With a constant sample volume the sensitivity can, to a certain degree, be enhanced by controlling the flow rate. By decreasing the flow rate the deposition time can be increased, but at the same time, unfortunately, transport of the metal ions from the sample to the electrode surface for amalgam formation is decreased due to increase in the thickness of the diffusion layer at the electrode. For each detector system there is an optimal flow rate which gives the maximal sensitivity. It is possible to improve the sensitivity further by increasing the sample volume or passing the same sample several times through the detector during the deposition step. Both approaches are easy to accomplish in a SIA system.

Sample volume can be increased by increasing the time of aspiration. Fig. 3 shows dpp stripping peaks of 0.5 μM lead and 0.48 μM cadmium in 0.1 M HCl for different aspiration times, i.e., sample volumes. The peak height is linearly dependent on the time of aspiration. The regression lines for both peaks go through the origin and the slopes are 0.204 and 0.153 μA s^{-1} for lead and cadmium, respectively. The correlation coefficient in both cases is 0.999.

Wang et al. demonstrated that when the sample plug in an ASV flow experiment was passed several times through an electrochemical detector with a cylindrical microelectrode the sensitivity could significantly be enhanced [9]. In their study

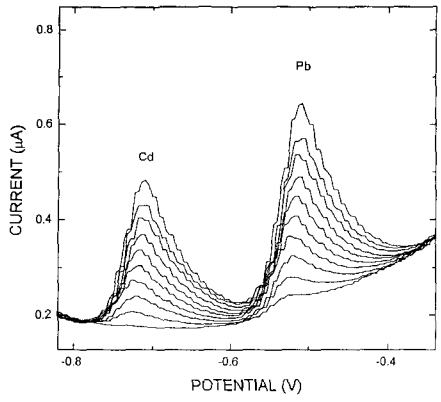

Fig. 3. Dpp stripping peaks of 0.5 μM lead and 0.48 μM cadmium in 0.1 M HCl for different times of aspiration: 0, 2, 4, 6, 8, 10, 12, 14, 16 and 20 s.

with a thin layer cell only 2.5-fold enhancement was reached even with 20 cycles of forward–backward sample passing. However, the following simple arrangement in the manifold used in the present work increased the sensitivity three times already after four forward–backward cycles. A second outlet was fabricated in the thin layer cell. An auxiliary coil of 1.5 m and i.d. of 0.8 mm was connected to this outlet. Flow through the original outlet where the reference electrode is sitting was stopped after the tubings were filled with the carrier solution. During the deposition step the sample was cycled between the auxiliary coil and the thin layer cell. Significant reduction of the sample dilution and dispersion could be achieved by this simple arrangement. Fig. 4A shows the deposition current and therefore also the concentration profiles during several passages of a 200 μl sample of 0.5 μM Pb(II) in 0.1 M HCl through the detector. Fig. 4B shows the dependence of the height of the lead peak on deposition time during which the sample has gone through the detector in both direction. The whole procedure of sample cycling is controlled by the computer and can therefore easily be modified, e.g., number of cycles can be changed depending on the sample. To take the maximum advantage of this repeated sample passage procedure the concentration profile of the sample in the cell has to be known in order to chose the best moment to reverse the flow and duration of each event.

3.7. Selectivity

3.7.1. Theory

Overlapping stripping peaks of different metals is a sever problem in ASV. Peak separation can sometimes be achieved by choosing a proper electrolyte. In ASV it is often enough to change the electrolyte only for the stripping step, a procedure usually referred to as the medium exchange method [14]. In a SIA system the solution in the cell can easily be exchanged. Stripping medium is aspirated as the first solution and the system timing must be organized in such a way that the flow is stopped for the stripping step exactly when the maximum concentration of the stripping medium is in the detector (Fig. 2).

During the stripping step the metal amalgam is oxidized:

$$M(Hg) \rightarrow M^{n+} + ne^- + Hg \quad (1)$$

If the stripping medium contains a ligand with which the metal forms a complex, the following reaction takes place:

$$M + pL \rightleftharpoons ML_p \quad (2)$$

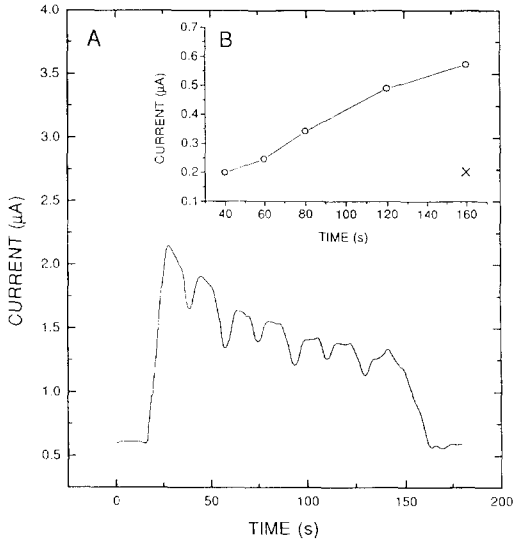

Fig. 4. Repeated sample passage procedure. A: concentration profile of the sample during multiple passages through the detector. B: dependence of the peak of lead on deposition time (during forward–backward cycles). Point 'x' represents the peak current with 160 s deposition time when the solution has flown in the forward direction only.

For simplicity the charges of the species are omitted. The notations to be used in this work are according to Ringbom [15]. The stability constant of the complex ML_p is given as:

$$K^{M,pL}_{ML_p} = \frac{[ML_p]}{[M][L]^p} \quad (3)$$

Potential and the current of a dc polarogram of the complex ML_p can approximately be expressed by the following equation [16]:

$$E = E^M_{1/2} - \frac{RT}{nF} \ln K^{M,pL}_{ML_p} - \frac{RT}{nF} p \ln[L] - \frac{RT}{nF} \ln \frac{i}{i_d - i} \quad (4)$$

$E^M_{1/2}$ denotes the half wave potential of the dc-wave of the free metal ion. As can be seen in Eq. (4), the half wave potential, which is approximately the same as the potential of the stripping peak, will be shifted due to complexation of the metal ion. The magnitude of the shift, ΔE, depends on the stability constant of the complex, coordination number of the metal ion and the concentration of the ligand:

$$\Delta E = -\frac{RT}{nF} \ln K^{M,pL}_{ML_p} - \frac{RT}{nF} p \ln[L] \quad (5)$$

The shift of the peak potential ΔE due to complexation of the metal ion may also be expressed as [15]:

$$\Delta E = -\frac{RT}{nF} \ln \alpha_{M(L)} \quad (6)$$

where $\alpha_{M(L)}$ is defined as:

$$\alpha_{M(L)} = \frac{[M']}{[M]} \quad (7)$$

where [M'] is the sum of the concentrations of the free metal ion and all the different species containing M and L. [M] is the concentration of the free metal ion. It can be shown that Eqs. (5) and (6) are practically equivalent.

If the metal ion, the ligand and the complex take part in some side reactions besides the main reaction Eq. (2), the stability constant according to Eq. (3) has to be recalculated to a conditional stability constant. This can be done by using the side reaction coefficients α_M, α_L and α_{ML_p}:

$$K'_{(ML_p)'} = \frac{\alpha_{ML_p} K^{M,pL}_{ML_p}}{\alpha_M (\alpha_L)^p} \quad (8)$$

where α_L is the side reaction coefficient for the protonation reaction of the ligand, i.e., $\alpha_{L(H)}$. The primed indexes indicate that side reactions of those species have been considered. The side reaction coefficient α_M is:

$$\alpha_M = \sum_{i=1}^{n} \alpha_{M(X_i)} + \alpha_{M(OH)} - n \quad (9)$$

where $\alpha_{M(X_i)}$ is the side reaction coefficient for the reaction where M reacts with ligands X_i and $\alpha_{M(OH)}$ is the side reaction coefficient for the reaction of the metal with hydroxide ions. The term $\alpha_{M(OH)}$ is presented here separately in order to emphasis the importance of the metal-hydroxide complexes. If the complex ML_p takes part in any side reactions, e.g., in forming acidic or basic complexes or any mixed ligand complexes α_{ML_p} should also be considered. In this work we assume that such complexes are not formed and therefore $\alpha_{ML_p} = 1$. When side reactions are considered Eq. (7) can be expressed in the following way:

$$\alpha_{M(L)} = \frac{[M']}{[M]} = 1 + \sum_{j=0}^{p} [L'] K^{M',jL'}_{ML_j} \quad (10)$$

where [L'] is the total concentration of the ligand in the solution. The values of the stability constants and the α-coefficients can be found in the reference [15] or can be calculates according to the theories presented in the same reference. If side reactions have to be considered the appropriate primed parameters should be introduced in Eq. (5).

3.8. Experimental

When 200 μl of a standard solution of 1.25 μM Cd(II) and 2.0 μM In(III) in 0.1 M HCl was aspirated in the SIA system and then processed according to the protocol in Table 1 the stripping peaks of Cd and In overlap each other and only one peak at ca 690 mV can be observed, Fig. 5A curve a. The stripping medium in this case was 0.1 M HCl. The peaks of the two metals could, however, be separated when the stripping medium was changed to 0.01 M EDTA in 2 M NaOH, Fig. 5B curve b. The cadmium peak is visible at ca

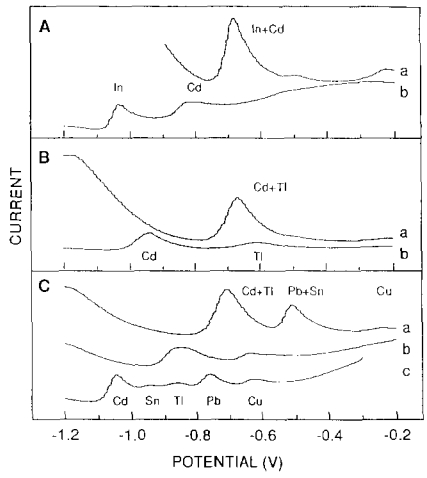

Fig. 5. Resolution of overlapping peaks by the medium exchange of 200 μl sample solution containing: A, 1.25 μM Cd(II) and 2.0 μM In(III), stripping in: (a) 0.1 M HCl; (b) 0.01 M EDTA in 2 M NaOH; B, 1.25 μM Cd(II) and 2.5 μM Tl(I), stripping in: (a) 0.1 M HCl; (b) 2 M ethylenediamine in 0.1 M HCl; C, 0.2 μM Cu(II), 1.0 μM Pb(II), 4.0 μM Tl(I), 10 μM Sn(II) and 2.0 μM Cd(II), stripping in: (a) 0.1 M HCl; (b) 0.1 M EDTA in 1 M ammonia buffer (pH = 9); (c) 0.05 M EDTA, 1 M ethylenediamine, 1 M ammonia buffer (pH = 9).

− 820 mV and the indium peak at − 1030 mV. A certain mixing of the stripping medium with the carrier solution is inevitable during the SIA procedure before the plugs reach the detector. Consequence of this is that concentrations in the stripping medium will be slightly changed. In the experiment shown in Fig. 5A and curve b the concentrations in the actual stripping media can be approximated to 0.008 M EDTA, 1.6 M NaOH and 0.02 M NaCl. The pH of such a mixture is ca 14.

The theoretical shifts of the peak potentials can be calculated by using Eqs. (6)–(10) and the values of the constants and α-coefficients as given by Ringbom [15]. Stability constants for Cd and In with EDTA are $10^{16.5}$ and $10^{25.0}$, respectively. These values have to be corrected for the side reactions of the metal ions and the ligand. At pH = 14 the ligand is completely deprotonated and $\alpha_{L(H)}$ is unity. The metal ions, however, form complexes with hydroxide ions. The following values, valid at pH = 14, can be found in [15]: lg $\alpha_{Cd(OH)} = 12.0$ and lg $\alpha_{In(OH)} = 7.0$. The metal complexes are assumed not to react further with

Table 2
Details of calculations of the potential shifts

Metal	p	lg $K_{ML}^{M,L}$	lg $\alpha_{L(H)}$	lg $\alpha_{M(OH)}$	lg $K_{ML}^{M',L}$	lg $\alpha_{M(L)}$	ΔE, mV calc.	ΔE, mV exp.
0.008 M EDTA, 1.6 M NaOH, pH = 14 Fig. 5A								
Cd	1	16.5	0	12.0	4.5	2.5	−75	−130
In	1	25.0	0	7.0	18.0	15.9	−320	−340
1.6 M ethylenediamine in 0.1 M HCl, pH = 11.7 (Fig. 5B)								
Tl	0	Very weak complex with OH^-					0	0
Cd	3	12.1	0	3.3	8.8	9.4	−280	−270

hydroxide ions to form any basic complexes and therefore the conditional stability constants for Cd-EDTA and In-EDTA complexes can be calculated according to Eq. (8) to $10^{4.5}$ and $10^{18.0}$, respectively. Concentration of EDTA is approximately 0.008 M and with this value and Eq. (10) the following values can be calculated: lg $\alpha_{Cd(L)} = 2.4$ and lg $\alpha_{In(L)} = 15.9$. When these values are used in Eq. (6), the theoretical shifts of the peak potentials can be calculated: −75 mV for cadmium and −340 mV for indium. The shift of the indium peak is the same as observed in Fig. 5A within the experimental uncertainties. There is, however, a larger discrepancy in the shift of the cadmium peak. This can be explained by the strong complexes cadmium forms with hydroxide ions. Even small variations in pH result in large changes in the $\alpha_{Cd(OH)}$ values. At pH = 13 the value is lg $\alpha_{Cd(OH)} = 8.1$ and would give $\Delta E = -190$ mV. The shift of the peak potential −130 mV, as experimentally found for cadmium, would be observed at pH 13.5. Such a change in pH in the vicinity of the electrode surface where the complex formation reaction takes place is quite possible. Indium, on the other hand, does not form as strong complexes with hydroxide ions as cadmium and pH 13.5 would give a shift of −330 mV in the peak potential. These calculations are presented in Table 2.

The stripping voltammogram for aspiration of 200 μl of a standard of 1.25 μM Cd(II) and 2.5 μM Tl(I) and the determination performed according to the protocol is shown in Fig. 5B. When the stripping medium is 0.1 M HCl only one peak can be observed at −680 mV, curve a. This peak has a small shoulder on the positive side. In 2 M ethylenediamine, En, and 0.1 M HCl, however, two separate peaks can be observed: cadmium at −940 mV and thallium at −610 mV. Thallium is not know to form any complexes either with hydroxide ions or ethylenediamine. Therefore the stripping peak of thallium is not shifted in this medium and the small shoulder observed on the peak on curve a in Fig. 5B is obviously the thallium peak. Cadmium forms a strong 1:3 complex with ethylenediamine with the stability product $10^{12.1}$. Concentration of ethylenediamine in the flow cell can be approximated to 1.6 M and pH of the solution to 11.7. At this pH ethylenediamine is totally deprotonated and therefore $\alpha_{En(H)} = 1$. The value of the side reaction coefficient for the reaction of cadmium with hydroxide ions can be calculated to lg $\alpha_{Cd(OH)} = 3.3$. With Eqs. (10) and (6) a ΔE value of −280 mV can be calculated. This value is in a good agreement with the experimentally found value of −270 mV. These calculations are also shown in Table 2.

The third example is the stripping analysis of 200 μl of a standard solution of 1.0 μM Pb(II), 2.0 μM Cd(II), 4.0 μM Tl(I), 0.2 μM Cu(II) and 10.0 μM Sn(II). When the stripping medium is 0.1 M HCl two peaks can be seen on the voltammogram, Fig. 5C curve a. The more positive peak is formed by overlapping of the peaks of lead and tin. The more negative peak is formed of cadmium and thallium peaks. When 0.1 M EDTA in 1 M ammonia buffer at pH = 9 is used as the stripping medium no further separation of the peaks could be accomplished. The overlapping peaks only shifted to more negative potentials but remained still overlapped. When the stripping medium was changed to a solution which in the

detector had the following concentrations: 0.04 M EDTA, 0.8 M ethylenediamine, 0.8 M ammonia buffer pH = 9.8, the stripping voltammogram c in Fig. 5C was observed. Five separate stripping peaks can be seen in the voltammogram showing that by selecting a proper stripping medium good separation of the individual peaks can be obtained even in such a complex mixture as in the experiment in Fig. 5C. Similar calculations of the shifts of the stripping peaks as done for the voltammograms in Fig. 5A and B and shown in Table 2 would give less good agreement between the theoretical and the experimentally found values. One of the reasons is that there is a possibility for formation of mixed ligand complexes because of the low concentration of the metal ions and the high concentration of the ligands: EDTA, ammonia and ethylenediamine. Constants of such mixed complexes are not known and therefore a number of approximations have to be made. Calculations of the α coefficients would therefore be difficult and give only too inaccurate values.

3.9. Analytical applications

Both the calibration curve and the standard addition method can be used with ASV with SIA. For determination of lead with a sample volume of 200 μl and by using forward flow with flow rate 0.85 ml min^{-1} during the deposition step, a linear calibration line was obtained in the concentration range 30–175 nM with the slope of 0.421 ± 0.016 nA nM^{-1}, intercept 71.9 ± 1.4 nA, limit of detection (by the error propagation method [17]) 25 nM and correlation coefficient $r = 0.9994$.

The standard in the standard addition method may be added directly to the sample, but it is also possible to do the standard addition in the flow system. The standard solution is connected to a separate port in the multiposition valve and aspirated into the holding coil either before or after the sample. The amount of the standard can be controlled by the aspiration time. This procedure has been shown to function well but the running parameters such as flow rate and deposition time have to be optimized separately for each case.

Calibration of the standard addition method in SIA is necessary to determine the correlation between the aspiration time of the standard solution, dispersion of the sample and the standard zones, mixing of the zones and the total amount of analyte in the zones. This can be done by aspirating different volumes of a standard, i.e., by using different aspiration times. In our work where 500 nM standard of lead was used, the correlation was found to be 180 ± 5 nM s^{-1}, i.e., aspiration of the standard for 1 s increased the concentration in the sample by 180 nM. Concentrations in this experiments were determined by comparing the stripping current observed with the current from a calibration plot. The shortest aspiration time that still gave reproducible results was 0.2 s. When this method was applied to a sample of 60 nM lead solution, standard addition with three aspirations gave a result of 56.4 nM, i.e., error of 6%.

In the procedure of repeated sample passage the standard addition method as described above is not convenient because the method requires that both the sample and the standard zones have to pass the detector entirely during each cycle. Therefore when ASV with SIA in the repeated sample passage mode was tested, a traditional standard addition method was used. Two additions of the standard was made in the sample prior to aspiration into the SIA system. The method was tested in determination of copper in tap water of the laboratory. The results were 12.2 ± 4.8 ppb and 63.0 ± 8.6 ppb in the cold and hot water, respectively.

4. Conclusions

SIA has shown to be a powerful technique in performing ASV experiments. SIA has several advantages over FIA in ASV. Solution handling in SIA is more simple than in FIA. It is easy to change the solutions in a SIA system and in that way to have the right solution zone in the detector during each step in the ASV protocol. In order to increase sensitivity the repeated sample passage method can easily be applied. The medium exchange procedure to increase the selectivity of the stripping method can also easily be performed. Generation of the mercury film on the substrate

electrode can be done more conveniently and effectively in SIA than in FIA. The same manifold can be used in SIA to perform different analyses. Change of the manifold is normally required in FIA when the analysis protocol is changed. Because only small volumes are used in SIA, consumption of reagents and the problem with waste solutions, such as mercury waste, are of less importance than in ordinary batch ASV experiments or when FIA is used. By improving the existing software it would be possible to automate the method even further and include all data collection and processing procedures in one run.

References

[1] J. Ruzicka and G.D. Marshall, Anal. Chim. Acta, 237 (1990) 329.
[2] A. Ivaska and J. Ruzicka, Analyst, 118 (1993) 885.
[3] J. Wang, 'Stripping Analysis: Principles, Instrumentation and Applications', VCH Publishers, Deerfield Beach, FL, 1985.
[4] T.M. Florence, J. Electroanal. Chem., 27 (1970) 273.
[5] J. Wang, H.D. Dewald and B. Green, Anal. Chim. Acta, 146 (1983) 45.
[6] J. Wang and H.D. Dewald, Anal. Chim. Acta, 162 (1984) 189.
[7] J.A. Wise, W.R. Heineman and P.T. Kissinger, Anal. Chim. Acta, 172 (1985) 1.
[8] E.B.-T. Tray, S.-B. Khoo, and S.-W. Loh, Analyst, 114 (1989) 1039.
[9] J. Wang, H. Huiliang and W.W. Kubiak, Electroanalysis, 2 (1990) 127.
[10] C. Hua, K.A. Sugar, K. McLaughlin, M. Jorge, M.P. Meaney and M.R. Smyth, Analyst, 116 (1991) 1117.
[11] Z. Lukaszewski and W. Zembrzuski, Talanta, 39 (1992) 221.
[12] F.-M. Matysik and G. Werner, Analyst, 118 (1993) 1523.
[13] D.W. Bryce, A. Izquierdo and M.D. Luque de Castro, Anal. Chim. Acta, 308 (1995) 96.
[14] R. Neeb, 'Inverse Polarographie und Voltammetrie', Verlag Chemie, Weinheim, 1969.
[15] A. Ringbom, Complexation in Analytical Chemistry, Wiley, New York, 1963.
[16] Allen J. Bard and Larry R. Faulkner, Electrochemical Methods, Fundamentals and Applications, Wiley, New York, 1980, p. 164.
[17] G.J. Long and J.D. Winefordner, Anal. Chem., 55 (1983) 712A.

ELSEVIER

Talanta 44 (1997) 725–727

Talanta

Announcement

MUACC: A 50 year heritage that continues to grow

Visionary analytical chemists strive to make enduring contributions to their field, contributions usually thought of as breakthrough research, innovative use of base elements, or improved testing and refining procedures.

As shown by the soon-to-be 50 year history of the Midwestern University Analytical Chemistry Conference (MUACC), enduring traditions sometimes are made of different stuff.

MUACC, an informal gathering of top chemistry faculty from throughout the Midwest, has clearly made its mark, changing lives, careers, teaching methods and research outcomes since 1947.

"It started out with Hobart Willard, an analytical chemistry professor from the University of Michigan and two of his very precocious students, G. Frederick Smith and Harvey Diehl", explains long-time MUACC attendee Professor Emeritus Carl Moore from Loyola University. "After Smith and Diehl earned their doctorates, the three kept a close, almost family relationship. Somehow, they got the idea to get together about once a year, visit, talk chemistry, talk about on-going work, talk 'blue sky' work, and engage in graduate student 'horse trading'".

Thus, MUACC was born. Its first meeting was held in December, 1947 at Northwestern University, with a dozen attendants from Syracuse to Iowa and in between. From the very beginning, MUACC separated itself from the multitude of other conferences available to academia.

The group differed, in part, because presentations must be informal discussions on research in progress. No slides or formal final work were permitted, just 'chalk talks'. Further, no specialized segments were held—all participants took part in the ongoing discussion, no matter their field of expertise.

"The topics covered were so broad, and all right on the forefront", explains retired professor A.A. Schilt who participated in MUACC for over 30 years. "Often, you would read the results of the research problems presented in the following year's research journals. We heard from people right on the fringe of scientific breakthroughs, detailing research problems in chromatography, mass spectrometry, polarimetry, all the different modifications in voltammetry, and a great deal in atomic spectroscopy".

Professor James Taylor from the University of Wisconsin, who has become known as the 'constant first', always volunteering to take the lead in presentations, explains:

"When you are asked to talk without slides about a project you have not finished, you are forced to go directly to the heart of why you are doing what you are doing. Sometimes, you end up with absolutely fabulous suggestions on how to resolve roadblocks from individuals working completely outside your subject area. When I first started, many presentations focused on electrochemistry. Now, it is shifted toward mass spectrochemistry. This field is so dynamic, and you can taste that at every MUACC meeting".

MUACC's emphasis on innovation does not stop at the lab door. It also enters the classroom.

PII S0039-9140(96)02128-5

"I am at an institution where we do not undertake a lot of research, but I have found MUACC as a group is wide-ranging, discussing problems that touch faculty and graduate students in all facets of their professional and academic life", says Professor Rod Olson at Hamline University in Minnesota. "Way back in the 1960s, I developed tape and slide curricula, something commonplace now but very different then. I shared preliminary versions of these materials with MUACC, and received enough positive feedback to keep me going on it. One segment was later published by the American Chemical Society".

"Everyone gave advice and encouragement, that is what I always remember about MUACC", notes Professor Bruno Jaselskis from Loyola University. "My first meeting was in the fall of 1995. Through the years, I have discussed issues like xenon chemistry, sometimes hilariously, some seriously. Xenon was very novel at one time, and while the analytical significance was not great, it did offer some very interesting characteristics. Some comments I received from founder G. Frederick Smith urged me to explore applications in an entrepreneurial nature".

MUACC participants mutually agree that the three founders of the group left a strong personal imprint upon it. Professor James Carr of the University of Nebraska has even spent time researching the "genealogy" of MUACC.

"In large measure, MUACC is comprised of the academic descendants of Hobart Willard's students and their students", he explains. "An enormous number trace their background to Willard, and subsequently to Diehl and Smith".

Schilt agrees. "MUACC is and was mainly built by Smith, Willard and Diehl. In one sense, though, the group flows back even further to critical research leaders like Fresenius. Like most family trees, it has just grown abundantly. We could probably tie it back to the first experiments of Adam".

Part of the imprint includes what group participants now jokingly call "their anonymous benefactor", G. Frederick Smith. Smith is one of a handful of academic chemists who successfully ventured into the commercial world. He founded G. Frederick Smith Chemicals with his brothers Allyne and Clarence Smith, in Columbus, Ohio, in 1928. As the company prospered, Smith and his brothers quietly financed all or a portion of MUACC's cost.

"Part of our success has always stemmed from making the meeting as affordable to participants as possible", says Dr Alexander Scheeline, Associate Professor of Chemistry at the University of Illinois, and host of the 1996 meeting. "Professor Smith, and now GFS Chemicals, assist with event costs, and help us achieve that goal".

MUACC also has extended far beyond just the "Midwest". Over its 50 year history MUACC meeting sites have included the University of Colorado, and the University of Alberta, in Edmonton, Canada.

"We stretch like a rubber band", notes Jaselskis". "We are very flexible and we have drawn people from Pittsburg, Mississippi and around the country".

Schilt remembers participants from places as far as Birmingham, England. He also notes that MUACC has spawned similar groups in the US, including SWAP, Southwest Analytical Professors, and SAC, Southeast Analytical Chemists.

What draws participants today to MUACC is the same draw created 50 years ago, says Steel Hutchinson, continuing event sponsor, grandson of Allyne Smith, and Vice President of Marketing for GFS Chemicals.

"The uniqueness of MUACC—and its number one reason for survival—is its ability to help participants step outside of their own paradigm, avoid myopic vision, and find a fresh approach to problem-solving in an atmosphere of openness and mutual support", says Hutchinson. "We believe in the spirit of MUACC's founders. Our business strives to carry on their traditions, by maintaining our independence as a privately-owned concern in a marketplace dominated by large corporations, by producing catalogs and other materials to educate and inform the industry, and by sponsoring MUACC, a group which clearly fosters great science".

"The informality remains, but the role of MUACC has expanded", summarizes Scheeline, who hosted the 1996 MUACC at the University

of Illinois. "We are a place where analytical faculty from both small colleges and large can go, where we can share our differences and our commonalities, whether an emphasis on classroom teaching or an emphasis on research, and we can meet and cross-fertilize".

With 50 years of cross-fertilization, it is no wonder that MUACC continues to grow.

For further information please contact:
Melinda Taylor Swan, GFS Chemicals Inc., P.O. Box 245, Powell, Ohio 43065, U.S.A.

ELSEVIER

Talanta 44 (1997) 729–732

Talanta

Construction and evaluation of a novel In(III) liquid ion-selective membrane electrode

Cunxiong Li[a,*], Jing-Guo Hou[b]

[a]*Department of Chemistry, Guizhou Normal University, Guiyang 550001, China*
[b]*Department of Chemistry, Northwest Normal University, Lanzhou 730070, China*

Received 17 January 1996; accepted 10 June 1996

Abstract

A liquid ion-selective membrane electrode containing a chloroform–acetonitrile (10:1) solution of the complex of In(III) with 1-benzyl-3-methyl-4-benzoyl-5-pyrazolone (PMBP) and diphenylguanidine is described. The basic electrode performance characteristics were evaluated according to IUPAC recommendations. The slope of the calibration graph (electrode potential v. concentration) was 18.7 mV $(pIn)^{-1}$ in the pIn range 4.5–1 (pH 6). Direct potentiometric determination of In(III) showed an average recovery of 99.1% with a standard deviation of 1.2%. The method is recommended for the precise direct potentiometric assay of In(III) in metals and minerals without a prior separation.

Keywords: Indium(III); Liquid ion-selective membrane electrode

1. Introduction

A number of electrodes sensitive to Ca(II), Fe(II), Bi(III) and La(III) cations [1] have been developed and employed as indicator electrodes in potentiometric titrations. The commonly known electrodes sensitive to Indium ion feature low selectivity and the slope of calibration graphs is different from Nernstian slope [2].

In the present paper, a new electrode sensitive to In(III) ion is proposed, the liquid ion exchanger being a complex of In(III) with 1-benzyl-3-methyl-4-benzoyl-5-pyrazolone (PMBP). PMBP with In(III) forms an $In(PMBP)_3$ complex, which is well extracted into the organic phase of choroform–acetonitrile in the presence of diphenylguanidine (DPG). These properties of the $In(PMBP)_3$ complex led us to develop a simple potentiometric method for In(III) with sufficiently high accuracy, selectivity and speed.

2. Experimental

2.1. Reagents and materials

All reagents were of analytical reagent grade. Doubly distilled water from a quartz still was used. The composition of the ion-exchange solu-

* Corresponding author.

PII S0039-9140(96)02015-2

tion was 1×10^{-3} M $In(PMBP)_3$ and 1×10^{-4} M diphenylguanidine in choroform–acetonitrile (10:1). A solution of concentration 1×10^{-3} M $In(PMBP)_3$ was obtained by shaking a solution of indium salt with PMBP in the mixed solvent (in the ratio 1:3) [3,4].

2.2. Apparatus

The liquid membrane was stabilized on a porous circular plate. A silanized filter disc saturated with ion-exchange solution was used as the liquid membrane. The composition of the inner solution of electrode was 1.0×10^{-3} M In(III) and 1×10^{-2} M KCL.

An Ag/AgCl electrode (Orion 90-02), containing 10% (w/v) potassium nitrate in the outer compartment, was used as the reference electrode. An Orion Ross combination pH electrode (Model 81-02) was used for pH adjustment.

3. Results and discussion

3.1. Effect of pH

The effect of pH on the potential of the electrode system was studied. The response of this electrode is hardly affected by changes in pH in the range 5.0–7.0 (Fig. 1).

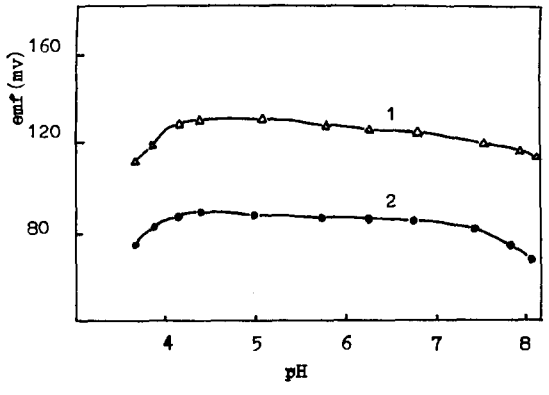

Fig. 1. Effect of pH on the Indium electrode. (1). 10^{-2} M; (2). 10^{-4} M.

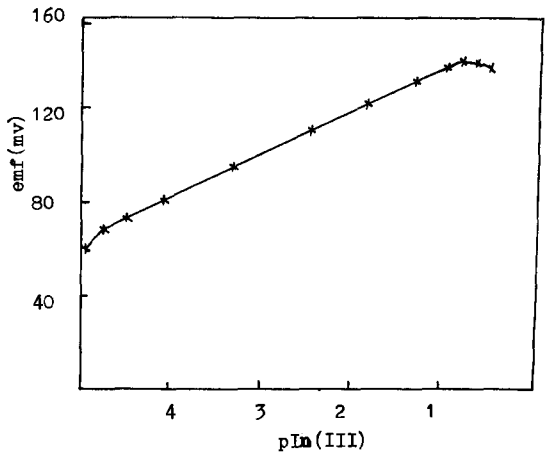

Fig. 2. Calibration graph for the indium-electrode.

3.2. Interference effects

The interference effect of different inorganic cations on the electrode response was evaluated. The potentiometric selectivity coefficients K^{pot} for the In(III) electrode was studied by the separate solutions method [5,6]. The selectivity coefficients were calculated using the extended Nernst equation:

$$\log K^{pot}_{In,M} = \frac{E_2 - E_1}{2.303RT/n_1F} + \left(1 - \frac{n_1}{n_2}\right) \log C_1 \qquad (1)$$

where E_1 and E_2 are the potential readings observed after 1 min due to the same concentration of In(III) and interferents, respectively, n_1 and n_2 are the charges of In and interferent ions, respectively, and C_1 is the concentration of In(III).

The values of the selectivity coefficients obtained are presented in Table 1. In most cases, up to a 100-fold excess of the interferent did not have a significant influence on the electrode performance. Electrodes sensitive to In(III) are not selective against Ga(III) and Ge(II) ions. However, they exhibit high selectivity against Ca(II), Al(III), Ni(II), Cu(II), Sn(II), La(III), Lu(III) and Nd(III).

3.3. Calibration graph

The calibration graph in Fig. 2 exhibits a Nernstian response for 3.2×10^{-5}–1×10^{-1} M In(III) with slope of 18.7 ± 0.5 mV per decade change in concentration. The dynamic response time of the electrode system was tested for the concentration range 1×10^{-1}–3.2×10^{-5} M In(III). The measurement sequence was from low to high concentration and back. The time required for the electrode to reach values within ± 0.2 mV of the final equilibrium potential after increasing the In(III) concentration level 10-fold is fairly short; it reaches 97% of its final steady potential after 30 s for In(III) $> 10^{-3}$ M and 1 min for In(III) $< 10^{-3}$ M.

The potential displayed by the In electrode did not vary by more than ± 1 mV ($n = 10$) on the same day. The calibration slope did not vary by more than ± 0.5 mV per decade change of concentration. The reproducibility and stability of the potential were evaluated over 2 months by constructing replicate calibration graphs ($n = 10$). The detection limit, linear range, response time and selectivity coefficients were almost constant for this liquid membrane electrode during this period. The critical response characteristics of the indium liquid membrane electrode are given in Table 2.

Table 1
Selectivity coefficients of the indium liquid membrane electrode[a]

M	$K^{pot}_{In,M}$
Sn(III)	1.3×10^{-5}
Cu	5.4×10^{-3}
Al	3.2×10^{-3}
Ni	1.0×10^{-3}
Ca	2.8×10^{-3}
Cd	1.2×10^{-3}
Sc	0.9×10^{-2}
La	1.2×10^{-2}
Lu	1.3×10^{-2}
Nd	1.0×10^{-2}
Ga	0.84
Ge	0.53

[a] In and M concentrations both 1×10^{-4} M.

Table 2
Critical response characteristics of indium electrode

Parameter	Value
Slope [mV (Log c)$^{-1}$]	18.7 ± 0.5
Correlation coefficient, r	0.995
Limit of detection (M)	1×10^{-1}–3.2×10^{-5}
Working pH range	5.0–7.0
Response time, 10^{-3} M In(III) (s)	30
Lifetime (days)	60

3.4. Analytical application

The direct potentiometric determination of In(III) using the indium liquid membrane electrode was performed by the standard addition method in a solution containing In(III) at concentrations of 10^{-2}–10^{-4} M in the presence of Cu(II), La(III) and Cd(II) at a concentration of 10^{-3} M. The results showed an average recovery of 99.1% and a standard deviation 1.2%.

A real sample was also analysed. A sample of Stannum (provided by the Metal Company, Human, China) were treated by the method in Ref. [7]. The method was compared by using the 5,7-dibromo-8-hydroxyquinoline (I) spectrophotometric method as follows:

The simulated or real sample solution was transferred into a 25 ml calibration flask, 2 ml of a chloroform solution of I and 10 ml of sodium acetate–acetic acid buffer solution (pH 4.0) were added and the volume was made up to the mark with water. The solution was transferred to a separating funnel, 10 ml of a chloroform solution of I were added twice and the organic layer was separated.

The absorbance of the organic extract was measured at 415 nm against the reagent blank using 1 cm glass cells. The results are given in Table 3.

The proposed electrode system was selected as it showed the most successful characteristics. This method is recommended for the precise direct potentiometric assay of In(III) in metals and minerals without a prior separation.

Table 3
Determination of In(III) by direct potentiometric and spectrophotometric methods

[In(III)] (M)	Direct potentiometry		Spectrophometric method	
	Recovery[a] (%)	RSD (%)	Recovery[a] (%)	RSD (%)
3.0×10^{-4} (Cu, 9.5×10^{-2})	99.4	1.4	97.2	1.8
2.0×10^{-2} (Cu, 4.0×10^{-3})	98.9	1.2	99.5	1.1
9.0×10^{-3} (La, 5.0×10^{-2})	100.2	1.5	97.3	0.9
5.0×10^{-3} (La, 9.0×10^{-3})	100.5	1.4	99.2	1.4
6.5×10^{-3} (Cd, 7.3×10^{-2})	97.7	0.9	95.2	2.0
4.2×10^{-3} (Ca, 2.3×10^{-3})	99.2	0.6	99.7	0.8
Sn sample (In, 2.2×10^{-3})	98.2	1.2	98.0	1.8

[a] Average of eight measurements.

References

[1] P. Gabor, K. Toth and E. Pungor, Symposium on Ion Selective Electrodes, Matrafured, Hungary, 23–26 October 1972.
[2] M. Wei, Chem. Sensors, 5 (1986) 55.
[3] H. Bauer, J. Am. Chem. Soc., 86 (1964) 5125.
[4] C. Li, J. Guizhou Normal Univ., 2 (1995) 61.
[5] K. Camman, Working with Ion-Selective Electrodes, Springer, Berlin, 1977.
[6] IUPAC, Analytical Chemistry Division, Commission on Analytical Nomenclature, Pure Appl. Chem., 48 (1976) 127.
[7] Z.S. Wei, Application of the Organic Reagents in Analytical Chemistry, Science Press, Beijing, 1981, Chapter 8.

ELSEVIER

Talanta 44 (1997) 733–742

Talanta

Anodic stripping voltammetry with carbon paste electrodes for rapid Ag(I) and Cu(II) determinations

Ch. Labar, L. Lamberts

Laboratoire d'Electrochimie et de Chimie Analytique, Facultés Universitaires Notre-Dame-de-la-Paix, 61 rue de Bruxelles, Bruxelles B-5000, Belgium

Received 14 July 1995; received in revised form 16 July 1996; accepted 23 July 1996

Abstract

The simultaneous determination of silver(I) and copper(II) is realized for the routine analysis of trace levels of these elements by anodic stripping voltammetry (ASV) at the carbon paste electrode (CPE). The electrochemical response is studied in 14 different supporting electrolytes, ranging from acidic solutions (pH 0.1) to neutral and basic (pH 9.7) media, and the parameters governing electrodeposition and stripping steps are characterized for each medium by the use of pseudo-voltammograms. Comparison between different modes of matter transport mechanisms is also given. The dynamic range of the method is 0.05 to 150 μg l^{-1} Ag(I) in the majority of the media studied and can be extended to 400 μg l^{-1} in selected media, with a general reproducibility in the ±2% range for five replicate measurements. The total analysis time lies between approximately 30 s and 10 min. Activation of the CPE surface has been studied, but this pretreatment is demonstrated to be unfavourable and is replaced by a simpler unique 'cleaning' procedure of dipping the CPE in diluted nitric acid. © 1997 Elsevier Science B.V.

Keywords: Anodic stripping voltammetry; Carbon paste; Copper; Silver; Trace element

1. Introduction

Stripping techniques are among the most frequently used enhancers of the key analytical parameters, namely sensitivity and selectivity [1]. Enhancements are achieved in the preconcentration step involved in such processes [2–4]. The most classical technique, i.e. stripping with a slow, linear potential scan (ASV), has recently be superseded by more modern methods [5]. Despite this, no potentiostatic method solves definitively the problem of the relatively poor selectivity of the measurement [3], and galvanostatic methods, including no-current methods [6,7] have been studied and applied to trace element analysis [8,9]. However, the classical ASV methodology remains the more practicable method used in routine analysis; it displays rapidity and feasibility, and uses relative low-cost commercial instrumentation that has been developed for non-electrochemists. Carbon paste electrode (CPE) takes a increasing importance in ASV [10]. On the other hand, the pyrolytic graphite electrode and the glassy carbon electrode are not suitable for the determination of small amounts of silver, as are wax-impregnated electrodes with a surface renewed on emery paper;

PII S0039-9140(96)02053-X

however carbon paste electrodes are used for this purpose, permitting 25 determinations without refilling [11]. Consequently, the main goal of this work is to improve a simple, rapid and efficient electrochemical method for the trace element determinations of Ag(I) and Cu(II) in routine analysis, based on CPE with commercial low-cost instrumentation and without the need for time-consuming sample/electrode pretreatment.

Silver does not normally occur in animal or human tissue but is found in different materials of general use [12]. The level of this metal in natural waters and in biological fluids is generally very low, so, analytical methods with great sensitivity are required. Electrochemical determinations of silver within the scope of this study has been reported in review articles: Vydra and co-workers [2] (until 1976), Mannino and Wang [13] and, more recently, Rivas and Ortiz [14]. In the recent literature, the use of modified carbon-based materials has attracted much interest [15]. However, the proper choice of the supporting electrolytes and of the parameters governing accumulation, electrodeposition and stripping are not always clearly defined and systematically studied. Furthermore, the necessity of time-consuming pretreatment, defining optimum electrode composition and the drift of signals observed over long-time use complicates the question of finding (for routine measurements) a simple, rapid and efficient technique, using a stable working electrode, in a wide concentration range, which can be used by non-electrochemists on low-cost instrumentation. Finally, the electrochemical measurement should be directly compatible with a variety of chemical dissolution media used in the analysis of real samples (water, effluents, sewage, minerals, biological fluids, alloys and metals).

2. Experimental

2.1. Reagents

All chemicals are AR quality and the solutions were prepared with Millipore MilliQ System's water. Stock solutions of silver nitrate and copper sulphate are checked weekly by classical volumetric analysis [16]. Supporting electrolyte solutions are checked by contamination tests developed for polarographic analysis [17].

2.2. Instrumentation

ASV measurements are made with a PAR EG and G scanning potentiostat coupled to a Phillips PM 9848 XY-t recorder. The electrochemical cell is the Radiometer TTA 80 and electrodes are Radiometer F 4551 (SCE) and Radiometer F 5155 (platinum counter electrode), respectively. For studies with a rotating CPE, the PAR EG and G Model 616 RDE is adapted to the configuration of the home-made CPE.

2.3. Carbon paste electrode

Despite the fact that the electrochemical characteristics of the CPE depend upon paste composition [18–21], for routine analysis we used the commercial Metrohm mixture (74 wt.% C, 26 wt.% mineral oil, abbreviated as CPE 74:26). Carbon paste sensors (tip configuration) are made as follows. The paste is packed under pressure into 1 ml polyethylene syringes (5 mm diameter), the tip of which is cut off in the conical region to obtain the desired geometric area (2–3 mm diameter); the electrical contact is established by a stainless steel wire, the diameter of which is chosen so it can be forced into the top of the syringe. The paste is furthermore compacted by polishing the tip of the CPE on filter paper (Whatman GF/C ultrafine glass fibre paper) and visualizing the final surface by microscopic examination to avoid edge effects. After an initial stabilization period (see below), the CPE can be used continuously for up to 2–3 weeks without alteration of its electrochemical response, if it is kept in 0.20 M HNO_3 between experiments and overnight. When working with metal ion concentrations in the ppm range, some memory effects [19,20] are observed; these are eliminated by dipping the CPE into 0.20 M HNO_3 for 15 min. and examining the background characteristics of the renewed CPE in the actual supporting electrolyte. We have not observed any significant differences between the signals obtained with and without oxygen removal

from the solutions; consequently, we consider that oxygen removal is not necessary for the present experiments.

The CPE is centred in the sample vessel and the stirring rod placed so that the angular velocity is zero but the circular motion maximum; the tip of the CPE is positioned close to the SCE. As previously demonstrated [21,22], the deposition current in stirred solutions obeys the semiempirical equation:

$$i_d = Knr_o^2 D^{\frac{2}{3}} C\,(\mathrm{RPM})^{\frac{1}{2}} + 4\pi r_o nFDC$$

where r_o is the CPE's radius, RPM is the velocity of stirring (rev min^{-1}) and n, F, D and C have their usual meaning [23]. The sensitivity of the method is thus related to cell geometry and stirring. Furthermore, the rest period required between the deposition and stripping steps is another parameter that affects the sensitivity [7–9,24]. To keep the results of this work within the scope of classical instrumentation, we choose a stirring rate of 3000 rev min^{-1} and a rest period of 30 s, which are compatible with conventional stirring devices and routine analysis times.

3. Results and discussion

3.1. Silver quantification

In 0.10 M $HClO_4$, by cycling between -0.40 and $+0.80$ V, a low cathodic current is observed from $+0.10$ to -0.40 V and, during the reverse scan, an oxidation peak appears in the anodic region at $+0.250$ V (E_{p_a}). A very high enhancement of the oxidation current (i_{p_a}) is observed if silver electrodeposition is made under potentiostatic control at a determined potential (E_d) during a fixed time (t_d) under stirring. In this work, the electrodeposition step will be conducted as follows: potentiostatic control at E_d during a time t_d under stirring, followed by the same potentiostatic control during a rest period of time ($t_r = 30$ s). In such conditions, the ASV signals appear as illustrated in Fig. 1, for a 0.10 M $HClO_4$, 30 μg l^{-1} Ag(I) solution.

Until now, stripping determinations of silver on carbon materials have been restricted to some definite media (0.15 M NH_3–0.15 M NH_4^+, 0.10 M KNO_3, 0.01 M H_2SO_4–0.05 M K_2SO_4 [2.5] despite the fact that such experiments can be conducted in a very wide variety of supporting electrolytes, ranging from acidic solutions to neutral media and basic pH buffers. In the majority of these media, the reproducibility and the magnitude of the oxidation current for low t_d values and Ag(I) concentration is such that silver quantification is predicted at the CPE. For instance, a relative standard deviation (RSD) of $\pm 0.2\%$ for i_{p_a} magnitudes is observed for five successive measurements in 0.018 M HAc–0.018 M NaAc for 30 μg l^{-1} Ag(I), where Ac stands for acetate. However, in identical electrodeposition conditions (E_d, t_d), the observed i_{p_a} values can be quite different from one medium to another, so that optimization of electrodeposition and stripping steps must be studied independently for each medium.

The only way to determine exactly the optimum electrodeposition potential and to see the influence of the nature and concentration of the supporting electrolyte on i_{p_a} is the observation of the corresponding ASV pseudo-voltammogram, e.g.

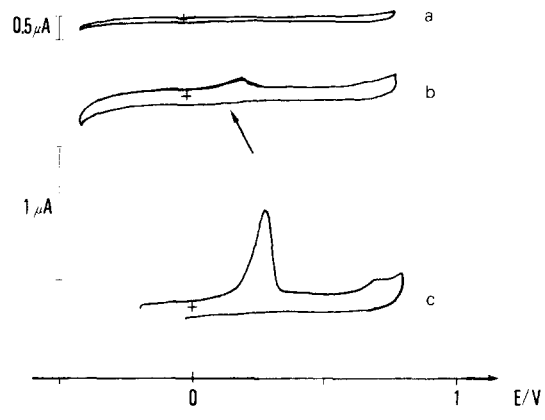

Fig. 1. (a) Cyclic voltammogram at the CPE in 0.10 M $HClO_4$; (b) cyclic voltammogram in 0.10 M $HClO_4$ + 30 μg l^{-1} Ag(I), same conditions as (a); (c) anodic portion of ASV voltammogram of medium (b), with $E_d = -0.20$ V, $t_d = 30$ s, $t_r = 30$ s, stirring rate: 3000 rev min^{-1}, same conditions as (a). The reduction wave (see arrow) is actually not detected but inferred by visualizing the corresponding reoxidation peak.

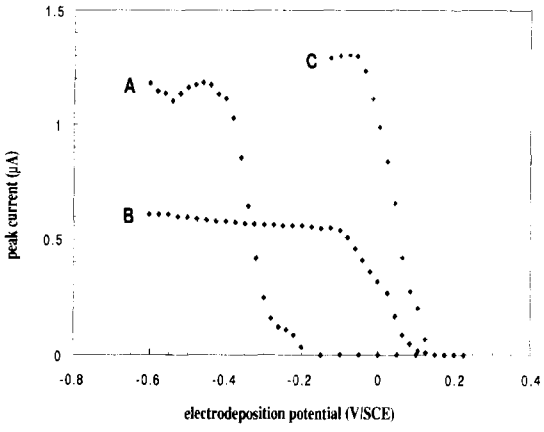

Fig. 2. ASV pseudo-voltammograms of 30 µg l^{-1} Ag(I) in various supporting electrolytes: (A) 0.10 M NH_3–0.10 M NH_4^+, pH = 9.7; (B) 0.10 M KNO_3, pH = 6.9; (C) 0.10 M $HClO_4$, pH = 1.1. Operating conditions: t_d = 60 s, t_r = 30 s, stirring rate: 3000 rev min^{-1}, scan rate: 50 mV s^{-1}.

the function $i_{p_a} = f(E_d)$ with all other parameters constant. Fig. 2 is an example of such ASV pseudo-voltammograms obtained in three typical media for a 30 µg l^{-1} Ag(I) concentrations and a low (60 s) electrodeposition time. One can see that the optimum electrodeposition potentials regions are rather different for each medium (− 0.010 V in 0.10 M $HClO_4$, − 0.45 V for 0.10 M NH_3: 0.10 M NH_4^+ and from − 0.20 to − 0.60 V for 0.10 M KNO_3) and that the corresponding i_{p_a} values differs by one order of magnitude depending upon the medium and the E_d selection. Furthermore, the optimum E_d values differ significantly from those given in the literature for the already studied media [2,5]. Selecting an E_d value of − 0.60 V for all media illustrated in Fig. 2 will, for instance, decrease the i_{p_a} value in 0.10 M $HClO_4$ because proton reduction is markedly altering the Ag(I) deposition. When interference problems are encountered, selection of E_d values from − 0.20 to − 0.60 V in 0.10 M KNO_3 medium can directly circumvent the problem (see below).

Table 1 gives a general overview of the ASV electrochemical responses of Ag(I) in 14 different supporting electrolytes. The choice of the media selected in Table 1 is governed by three reasons: (1) comparison with previous studies [2,5]; (2) a large pH range to correspond to the dissolution steps of the various materials containing silver; and (3) comparison of the ASV method with Ag(I) determinations observed in chemical potentiometric stripping analysis on CPE (with Fe(III) as the oxidizing agent) [23] or by adsorptive stripping voltammetry (media 5, 6 and 7, for instance) [18–20]. In identical operating conditions, a Ag(I) level of 30 µg l^{-1} gives oxidation currents ranging from 0.36 µA (0.10 M Na_2HPO_4) to 1.92 µA (0.08 M acetate buffer). Low differences in oxidation currents are observed with pH variations, but qualitatively, the method gives similar responses from pH 0.1 to pH 9.7 if the E_d value is correctly selected. These procedures avoid the use of exchange matrix solutions and the need for sample chemical pretreatment leading to contamination risks and time-consuming measurements. As a general conclusion, the choice of the correct electrodeposition potentials range is the primary problem to be solved for a determined supporting electrolyte. When the corresponding pseudo-voltammogram is determined, all the media selected in Table 1 can be used for Ag(I) analysis on a classical CPE. The position of the oxidation signal on the potential scale (E_{p_a}) is also dependent of the nature and pH of the supporting electrolyte and this last parameter must be considered for interference studies (see below).

Ag(I) quantification is also determined by the response of the oxidation signal with electrodeposition time, or more precisely, by the dynamic linear range of this response. We studied this parameter for a low concentration of Ag(I) (3 µg l^{-1}) in the media of Table 1. Typical responses are illustrated in Fig. 3, which gives the functions $i_{p_a} = f(t_d)$ in the two first media of Table 1. For 0.10 M NH_3–0.10 M NH_4^+, the linearity (equation order $N = 1$) is observed at this Ag(I) level for electrodeposition times up to 10 min. For a 0.10 M KNO_3 medium, apart from the fact that i_{p_a} is lower (Table 1), the function follows a second-order equation ($N = 2$) for the same electrodeposition times range. This is an illustration of the relative facility of metal electroplating from a medium where the metal ion is in a complexed form. When observing oxidation responses similar to those illustrated in Fig. 3, one can conclude that media 3, 4, 8, 9 and 10 of Table 1 offer a

Table 1
Electrochemical characteristics of silver in various supporting electrolytes at a 74:26 CPE

	Medium	pH	E_d(V/SCE)[a]	i_{p_a} (μA)[b]	E_{p_a} (V/SCE)
1	KNO_3 0.10 M	6.9	−0.20–0.65	0.52	+0.310
2	NH_3 0.10 M–NH_4^+ 0.10 M	9.7	−0.50–0.75	1.15	0
3	$HClO_4$ 0.10 M	0.9	−0.05–0.13	1.23	+0.250
4	$HClO_4$ 0.010 M	1.9	−0.15–0.25	1.19	+0.280
5	$HClO_4$ 0.001 M	2.9	−0.25–0.35	1.40	+0.320
6	$HClO_4 \pm 10^{-4}$ M	4.0	−0.32–0.45	1.36	+0.340
7	$HClO_4 \pm 10^{-5}$ M	5.6	−0.35–0.53	0.90	+0.380
8	KNO_3 0.10 M–HNO_3	1.7	−0.05–0.28	1.36	+0.270
9	KNO_3 0.10 M–HNO_3	0.7	0–0.15	1.60	+0.260
10	$HClO_4$ 0.10 M–HNO_3	0.1	0–0.15	0.52	+0.180
11	HAc–Ac^- 0.08 M	4.0	−0.20–0.45	1.92	+0.150
12	Na_2HPO_4 0.10 M	9.3	−0.20–0.50	0.36	+0.190
13	NaH_2PO_4 0.10 M	4.7	−0.20–0.55	1.40	+0.280
14	$NaHCO_3$ 0.10 M	8.7	−0.20–0.65	0.93	+0.260

Operating conditions: 30 μg l^{-1} Ag(I); $t_d = 60$ s; $t_r = 30$ s; stirring rate: 3000 rev min^{-1}; scan rate: 50 mV s^{-1}.
[a] As selected from the corresponding pseudo-voltammograms.
[b] i_{p_a} values given for three successive measurements in the optimum electrodeposition potential range.

linear relationship, whereas all the other media selected in Table 1 give a second-order relationship, in the 0–10 min electrodeposition time range. As this conclusion is valid only for this Ag(I) level and for the actual CPE geometry and composition, it must be noted that, for routine quantitative analysis of Ag(I), the standard addition procedure is recommended.

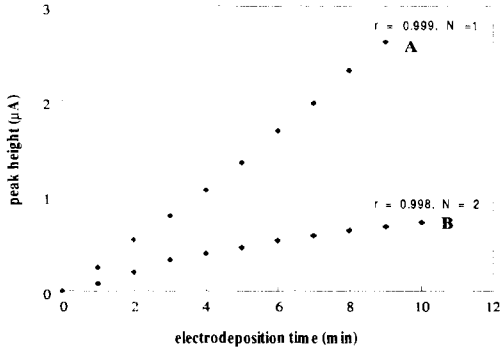

Fig. 3. Relationships between oxidation current and electrodeposition time in two supporting electrolytes: (A) 0.10 M NH_3–0.10 M NH_4^+, $E_d = -0.60$ V; (B) 0.10 M KNO_3, $E_d = -0.25$ V. [Ag(I)] = 3 μg l^{-1}; stirring rate: 3000 rev min^{-1}; cyclic voltammetry from E_d to +0.80 V at 50 mV s^{-1}. The oxidation current is corrected by subtracting the current component corresponding to $t_r = 30$ s in a quiescent solution from the observed value.

Calibration curves were established at different electrodeposition times for two modes of matter transport: linear diffusion (stationary electrode mode) and diffusion-convection, at a Ag(I) concentration of 12 μg l^{-1}. The oxidation currents observed, for diffusion during 90 s are practically similar to those obtained under diffusion-convection with an electrodeposition time three times lower. Currents corresponding to 30 s diffusion (0.037 μA) and 90 s diffusion-convection (0.323 μA), differ by a factor of approximately 10. At this Ag(I) concentration, all the calibration curves are linear, and the sensitivities of the ASV method (defined as the slope of a set of calibration curves corresponding to a defined matter transport, in μA s^{-1} μg^{-1} l Ag(I)) are 1.05×10^{-4} (linear diffusion) and 3.05×10^{-4} (diffusion-convection) respectively.

Fig. 4 indicates that, for a CPE used in normal electrodeposition conditions (say, stirring the medium during the electrodeposition time t_d), the linearity is respected in the range 0–400 μg l^{-1} Ag(I). This linearity range varies somewhat with the nature of the supporting electrolyte but, for all the media described in Table 1, the linearity is realized over a minimum concentration range 0–250 μg l^{-1} Ag(I). For comparison, the behavior

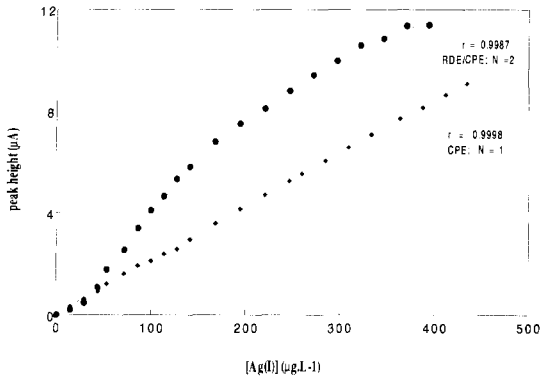

Fig. 4. Calibration curve for Ag(I) ions in 0.10 M KNO_3: high concentration range (0–450 μg l^{-1}). Operating conditions: $E_d = -0.25$ V; $t_d = 30$ s; $t_r = 30$ c; stirring rate: 3000 rev min^{-1} for the normal CPE; rotating rate: 5000 rev min^{-1} for the rotating CPE during t_d; cycling at 50 mV s^{-1}; number of measurements: 5.

of a rotating CPE (say, a CPE of the same geometrical area fixed at the rotating axis of a rotating disk electrode device) is also shown in Fig. 4, for identical electrodeposition conditions. This last electrode gives somewhat higher oxidation currents (by the fact that diffusion-convection is more efficient than forced convection in the deposition step), but the linearity region is narrower (0–150 μg l^{-1} Ag(I)) (electrode saturation more rapidly attained). The rotating CPE also permits the verification of the Levich's relation, indicating that diffusion is governing the electrodeposition of Ag(I). As the detection limit of both CPEs is approximately 0.05 μg l^{-1} (for measurements with a global duration of ±10 min, a value considered as compatible with routine analysis), the dynamic range of the method is approximately stated at 0.05–250 μg l^{-1} Ag(I). Such results can be compared with corresponding measurements made on chemically modified carbon paste electrode (CMCPEs): for instance, Yeom and co-workers [19] obtained a linear response up to 100 mg l^{-1} Ag(I) by linear sweep voltammetry and 1 μg l^{-1} Ag(I) by differential pulse polarography with a CPE modified by 2-imino-cyclopentane-dithiocarboxylic acid.

The question of the reproducibility of the CPE for quantitative analysis of metal ions by a (direct) preconcentration step has been tested [24,25]. It has been claimed that such a sensor needs electrode pretreatment or conditioning as a necessary preliminary step before it can offer reproducible electrochemical signals. Yet such pretreatment annuls the general gain in analysis time which is possible by direct electrodeposition. Applying a pretreatment will place this procedure among time-consuming measurements, such as needed by chemically modified electrode [2,5,25] or by adsorptive stripping voltammetry [18–20] (where pretreatment of the CMCPE or accumulation of the adsorbed species enhance the measurement duration).

The way to obtain a satisfying repeatability of the CPE (same electrode) without the need for tedious pretreatments that are incompatible with routine analysis is demonstrated as follows. First, the CPE is cycled in the studied supporting electrolyte at 50 mV s^{-1} during 3 min and the background curve is determined (as, for instance, in Fig. 1a). After this, the supporting electrolyte is subjected to electrodeposition/stripping cycles in the same manner as in the presence of metal ions (Fig. 5a) for 3–4 cycles. The metal concentration is finally spiked in the medium and electrodeposition/stripping steps are repeated: the oxidation signal is enhanced during the first cycles (Fig. 5b) (behavior already mentioned for modified CPEs) [2,5,30] and reaches a reproducible value after 8 to

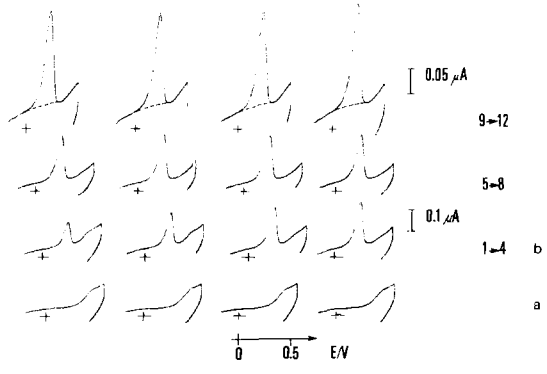

Fig. 5. Stabilization procedure of a freshly prepared CPE for Ag(I) analysis, in 0.10 M KNO_3 supporting electrolyte and operating conditions as in Fig. 4. (a) 0.10 M KNO_3 background curves; (b) same solution spiked with 14.2 μg l^{-1} Ag(I). The last eight electrodeposition/stripping cycles of Fig. 5b correspond to the first calibration point of Fig. 4.

12 cycles. In Fig. 5 the last eight cycles are considered to be reproducible (note the different current scales) and the mean of the i_{pa} values is the first point of the calibration curve of Fig. 4 (0.314 ± 0.008 μA, the RSD value considered to be acceptable for the corresponding Ag(I) concentration, 14.2 μg l^{-1}). Once this initial stabilization procedure is finished, further measurements can be made by repeating the first five electrodeposition/stripping cycles. Continuous measurements can be made with the same electrode for up to two to three weeks, the first alteration of the CPE behavior being suggested by an enhancement of the background curve (Fig. 1a). The reproducibility of different new CPEs, submitted to the described procedure, give, in a standard Ag(I) solution, a RSD of $\pm 2.1\%$ (five independent measurements, five electrodes). This value is mostly attributed to the difficulty in obtaining the same electrode geometric area (cutting pipette tips) than to the inherent behavior of the CPE itself. As the stabilization step is completed within ± 20 min, the question of the reproducibility of classical CPEs for quantitative analysis of metal ions by a direct preconcentration step does not seem to be a major problem for routine analysis.

The detection limit is related to a number of operational parameters (electrode surface, electrodeposition potential and time, stirring mode of solution and/or electrode, coulometric or amperometric recording). Consequently, considering that the maximum measurement time that can be devoted to low metal ions levels (< 1 μg l^{-1}) in routine analysis is of the order of 10–15 min, the corresponding concentration level has been measured: the current value (0.026 μA) corresponds, in such conditions, to the 50 ng l^{-1} Ag(I) level. For comparison, Yeom and co-workers [19] obtained, with CM-CPEs, a detection limit of 1×10^{-7} M and 1×10^{-9} M Ag(I) at 20 min deposition in linear sweep voltammetry and differential pulse polarography, respectively, with an electrode body made of 1 ml polyethylene syringes (5 mm diameter), the tip of which had been cut off.

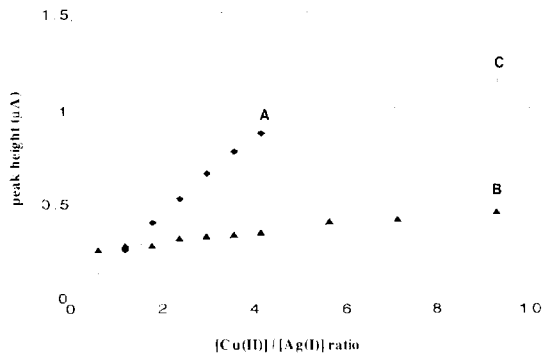

Fig. 6. Effect of Cu(II) interference on Ag(I) analysis in various supporting electrolytes: (A) 0.10 M KNO_3, [Ag(I)] = 8 μg l^{-1}, $E_d = -0.25$ V, $t_d = 60$ s, $t_r = 30$ s, stirring rate: 3000 rev min^{-1}; (B) 0.10 M Na_2HPO_4, [Ag(I)] = 8 μg l^{-1}, $E_d = -0.550$ V, $t_d = 60$ s, $t_r = 30$ s, rotating rate: 3000 rev min^{-1}; Ag(I) oxidation current at $E_{p_a} = +0.080$ V; (C) same conditions as (B): Cu(II) oxidation current at $E_{p_a} = +0.295$ V.

3.2. Interferences

The interference effects of other metal ions as Cd(II), Mg(II), Zn(II), Ni(II), Co(II), Fe(II), Pb(II), Bi(III) and Cu(II) was also studied.

Only Cu(II) and Bi(III) interfere during Ag(I) analysis. In the majority of the media described in Table 1, Ag(I) and Cu(II)/Bi(III) oxidation peaks appear close together, despite the selection of the proper E_d value: direct determination of mixtures of Ag(I), Cu(II) and Bi(III) is thus impossible. In basic media (Table 1, media 2, 12 and 14), where the different complexation characteristics of Cu(II), Bi(III) and Ag(I) with NH_3 and OH^- can be taken into account (as it can experimentally be visualized by the pseudo-voltammograms), the two oxidation signals appear at different E_{p_a}, values and the Cu(II)/Bi(III)-Ag(I) interference drops out. This is the case, for instance, for the 0.10 M Na_2HPO_4 supporting electrolyte, and, more generally, for the basic media of Table 1 (media 2, 12 and 14). In 0.10 M Na_2HPO_4, for $E_d = -0.50$ V, where both metal ions are reduced at the optimum reduction current (Table 1), the Ag(I) oxidation current is approximately independent of the Cu(II) concentration (Fig. 6b) and the Cu(II) signal presents a normal relationship with the metal ion content (Fig. 6c). Unfortunately, in this medium, the Ag(I) signal is somewhat lower

than in acidic electrolytes (Table 1) and this fact can be attributed to a partial precipitation of Ag(I) as Ag_3PO_4 ($K_s = 2.6 \times 10^{-18}$) or Ag_2O ($K_s = 3.8 \times 10^{-18}$) [26]. Nevertheless, the method remains applicable to the simultaneous determination of both ions in one analysis step. Cu((II)–Bi(III) interference must, for its part, be eliminated by specific complexation of one metal. The classical CPE sensor shows here its lack of specificity vs. the chemically modified carbon paste or adsorptive stripping mode [5,18–20].

3.3. Activation of the carbon paste surface

Among the various activation procedures, we select the method of Motta and Guadalupe used for biosensors [27] (cycling the electrode throughout the oxidative potential region at a relatively high scan speed during a determined time (t_a, activation time)) because this procedure is compatible with the requirements of routine analysis. The procedure was made directly in the supporting electrolyte, and the potential scan was extended by 0.9 V more positive than the actual anodic potential limit. Processing activation in basic solutions can appear quite surprising: however, recent studies [10,28] have demonstrated that electrochemical graphitic oxide can be formed in basic solutions, but is unstable only in highly basic media (pH > 12); furthermore, different potential regions must also be considered [28]. Considering the results of recent studies [10], the model developed by McCreery [29] thus needs to be reconsidered for a more effective understanding of the activation process. In such conditions, it is not unusual to examine the effect of activation on CPE in the various electrolytes studied in Table 1, whose pH values range between 0.1 and 9.3.

Upon activation, the equilibrium potential of the electrode becomes more positive, the reduction current is enhanced and the reversibility of the Ag(I)/Ag system increases. However, as indicated by Fig. 7, the silver oxidation signals show enhancements of i_{p_a} and back-ground currents, so that the signal/noise ratio is lowered. A possible explanation is that the electrochemically oxidized CPE is reduced at E_d and that the corresponding reoxidation component (quinone formation), the paraffin removal, porosity and edge effects enhancements more greatly affect the background signal than the silver one. The same conclusion is obtained with some variations, for the various (acidic, neutral and basic) electrolytes studied in Table 1; the value of the signal-to-background ratio depends upon the nature of the medium and the value of the activation time. Consequently as a general conclusion, the activation (as used in the conditions mentioned) of the CPE surface is unnecessary and quite unfavourable in the ASV technique, by opposition with chemical reoxidation as visualized by, f.i., potentiometric stripping analysis [23].

3.4. Method validation

The method is evaluated by determining the Ag(I) and Cu(II) contents of two NBS reference materials: the gelatine multicomponent Trace Element Reference Materials TEG 50 B and TEG 50 C. Observing the NBS recommendations, a sample aliquot ($\geqslant 250$ mg, dried) is treated with 6 ml

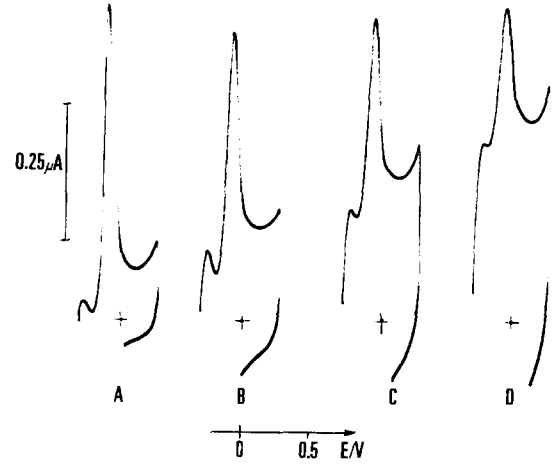

Fig. 7. Partial cyclic voltammetric measurements for [Ag(I)] = 8 μg l^{-1} in 0.10 M NH_3–0.10 M NH_4^+: (A) without activation; (B) after activation of 30 min; (C) after an additional activation time of 240 min; (D) after another additional activation time of 240 min. Activation: cycling between + 0.30 and + 1.20 V at 0.5 V s^{-1}, stationary conditions. ASV conditions: $E_d = -0.550$ V, $t_d = 60$ s, $t_r = 30$ c, stirring rate: 3000 rev min^{-1}.

Table 2
Comparison between measured and certified Ag(I) and Cu(II) concentrations in reference materials

Material	Element	Certified value (ppm)	Measured values (ppm)[a]					Mean (ppm)	RDS (ppm)
TEG 50 B	Cu	49 ± 2	51	52	53	50	50	51.2	1.9
	Ag	56 ± 7	61	61	60	58	56	59.2	3.3
TEG 50 C	Ag	51 ± 2	50	52	53	49	48	50.4	2.8

[a] Operating conditions: CPE 74:26; $E_d = -0.550$ V; $t_d = 45$ s; $t_r = 30$ s; stirring rate: 3000 rev min^{-1} 1.0×10^{-4} M $HClO_4$.

of a 2:1 volume mixture of HNO_3 (Ultrapure Grade, Merck): water at ± 80°C under reflux for approximatively 1 h; after cooling the solution is diluted to 10 ml and 2 ml aliquots are mixed with the supporting electrolyte ($HClO_4$) and analysed by the standard addition method.

Table 2 illustrates the results obtained; the correlation between the certified and measured Ag(I) and Cu(II) concentrations is good, for a total measurement time of ± 10 min. The final value was the mean of five replicate measurements.

4. Conclusion

Trends in electrochemical stripping analysis today make great use of CMCPEs and ASV. However, few applications appear in the routine determination of trace elements. By widening the choice of supporting electrolytes and selecting more precisely the electrochemical parameters by pseudo-voltammograms, a classical CPE is comparable in many ways with the more elaborate sensors and methodologies. If this electrode shows an inherent lack of selectivity, the direct (potentiostatic) preconcentration mode still presents unique advantage in routine analysis: low analysis time, low-cost instrumentation, friendly procedure and avoidance of matrix exchange and/or exotic electrolytes (as is generally the case for CMCPE and adsorptive stripping). The dynamic range of the method is 0.05 μg l^{-1} and this can be extended to 400 μg l^{-1} for a total analysis time between 30 s and 10 min. The reproducibility lies between 2 and 5% for five replicate measurements. Activation of the CPE appears unnecessary and only a first stabilization period of 20 min maximum is needed.

References

[1] J. Wang, Stripping Analysis, VCH, Deerfield Beach, Florida, 1985.
[2] F. Vydrá, K. Studik and E. Julakova, Electrochemical Stripping Analysis, Wiley, New York, 1976.
[3] H.W. Nürnberg, B. Kastening, in F. Korta (Ed.), Methodum Chimicum, Polarographic and Voltammetric Techniques, Vol. 1A, Academic Press, New York, 1974, pp. 584–607.
[4] R. Oilewicz, Z. Stojek and Z. Kublik, J. Electroanal. Chem. Interfacial Chem., 96 (1979); 29 (1979).
[5] J. Wang, Analytical Electrochemistry, VCH, New York, 1994.
[6] D. Jagner, Analyst, 107 (1981) 593.
[7] C. Labar and L. Lamberts, Anal. Chim. Acta, 132 (1981) 29.
[8] C. Labar and L. Lamberts, Anal. Chim. Acta, 39 (1994) 317.
[9] C. Labar and L. Lamberts, Anal. Chim. Acta, 38 (1994) 807.
[10] A.L. Beilby, T.A. Sasaki and H.M. Stern, Anal. Chem., 67 (1995) 976.
[11] H. Monien, H. Specker and Z. Zinke, Z. Anal. Chem., 225 (1967) 342.
[12] Cassantl and Doull's Toxicology, The Basic Science of Poisons, 2nd edn., McMillan, New York, 1990.
[13] S. Mannino and J. Wang, Electroanalysis, 4 (1992) 835.
[14] G.A. Rivas and P.I. Ortiz, Anal. Letters, 27 (1994) 751.
[15] M. Khodari, M.M. Abou Krisha and R. Fandy, Talanta, 41 (1994) 2179.
[16] W. Wagner and C.L. Hull, in J. Jordan (Ed.), Treatise in Titrimetry, Vol. 1, Inorganic Tritrimetry Analysis, Contemporary Methods, Marcel Dekker, New York, 1971.
[17] E. Yeager and A.J. Salkind (Eds.), Techniques of Electrochemistry, Vol. 1, Wiley, New York, 1972, p. 73.
[18] E.D. Jeong, M.S. Won and Y.B. Shim, Electroanalysis, 6 (1994) 887.
[19] J.S. Yeom, M.S. Won, S.N. Choi and Y.B. Shim, Bull. Korean Chem. Soc., 35 (1991) 545.
[20] M.S. Won, J.H. Park and Y.B. Shim, Electroanalysis, 5 (1993) 421.
[21] M.A.T. Gilmatin and J.P. Hart, Analyst, 119 (1994) 2431.
[22] E. Strafelda, Coll. Czech. Chem. Commun. 25 (1960) 862.
[23] C. Yarnitzky, Anal. Chem., 57 (1985) 2011.

[24] J.M. Kauffmann, A. Laudet and G.J. Patriarche, Anal. Chim. Acta, 135 (1962) 153.
[25] D.A. Anjo, M. Khan, M.M. Khudabaksk, S. Nowinski and B. Anger, Anal. Chem., 61 (1989) 2603.
[26] L. Meites, Handbood of Analytical Chemistry, 7th edn., McGraw-Hill, New York, 1971.
[27] N. Motta and A.R. Guadalupe, Anal. Chem., 66 (1994) 566.
[28] A. Beilby and A.R. Carlson, J. Electroanal. Chem., 248 (1988) 283.
[29] R.L. McCreery, in A.J. Bard (Ed.), Electroanalytical Chemistry, Vol. 17, Marcel Dekker, New York, 1991, pp. 221–374.
[30] T. Melina-Hidalgo, J.M. Pinilla-Maciàs and L. Hernàndez-Hernàndez, Anal. Chim. Acta, 309 (1995) 117.

ELSEVIER

Talanta 44 (1997) 743–748

Talanta

Reversed-phase ion-pair high performance liquid chromatographic determination of Co(III)-, Ni(II)-, V(V)- and Fe(III)-2-(2-benzothiazolylazo)-5-(3-sulforpropyl)aminophenol chelates

Zhi-Ling Ma *, Yan-Ping Wang, Chun-Xu Wang, Feng-Zhi Miao, Wei-Xin Ma

Department of Environmental Engineering, Hebei University of Science and Technology, Shijiazhuang, 050018, China

Received 22 April 1996; received in revised form 23 July 1996; accepted 8 August 1996

Abstract

The separation and determination of Co(III), Ni(II), V(V) and Fe(III) chelates with 2-(2-benzothiazolylazo)-5-(3-sulfopropyl)aminophenol (BTASPAP) by reversed-phase ion-pair HPLC was investigated. In the presence of the oxidant potassium iodate, BTASPAP reacts with Co(III), Ni(II), V(V) and Fe(III) to form stable, negatively charged, water-soluble chelates. The chelates were separated on a C_{18} siloxane bonded phase and eluted within 7 min with acetonitrile-acetate-water (36:1:63 v/v) containing 0.2 mol l^{-1} acetic acid-sodium acetate buffer (pH 3.0) and 1.0 mmol l^{-1} tetrabutylammonium bromide. The detection limits of Co(III), Ni(II), V(V) and Fe(III) at 565 nm are 0.3, 0.8, 0.3 and 1.0 ng (signal-to-noise ratio = 2), respectively. The method was applied to the determination of Co, Ni, V and Fe in four samples of standard alloys. © 1997 Elsevier Science B.V.

Keywords: Metal chelates; Reversed-phase ion-pair high-performance liquid chromatography

1. Introduction

Precolumn derivation HPLC is not only a sensitive but also a selective and rapid method for the separation and determination of metal ions. Many spectrophotometric reagents have been widely used in HPLC, such as 2-(5-bromo-2-pyridylazo)-5-diethylaminophenol(5-Br-PADAP) [1], 4-(2-pyridylazo)resorchinol (PAR) [2], 2-pyridyl-β-azonaphthol (PAN) [3] and others [4–6]. However, the use of thiazolazo reagents for the separation and determination of metal ions by means of HPLC has seldom been reported [7]. 2-(2-benzothiazolylazo)-5-(3-sulfopropyl)aminophenol (BTASPAP) is a sensitive spectrophotometric reagent.

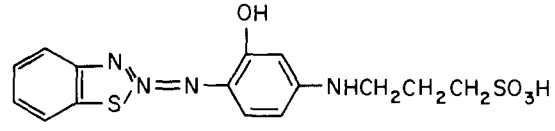

which can react with many metal ions, such as Fe, Co, Ni, V, Cu and Zn [8,9] to form stable, nega-

* Corresponding author.

PII S0039-9140(96)02061-9

tively charged, water-soluble, purplish red complexes, has been used in spectrophotometric determinations of these metal ions [8,10]. The spectrophotometric determination of any one of these metals ions is difficult when they are present together in a mixture, as a result of the spectral overlap of the BTASPAP complexes of these metal ions. The selectivity of BTASPAP is poor in the determination of metal ions by spectrophometry. Precolumn derivatization HPLC, which combines the high sensitivity of spectrophotometric reagents with the selectivity of HPLC, is a highly sensitive and selective method for the simultaneous determination of some metal ions. This paper reports for the first time the use of BTASPAP as a precolumn derivatization reagent to separate and determine Co(III), Ni(II), V(V) and Fe(III).

The reported reversed-phase HPLC methods for the separation and determination of heavy metals using chelating reagents such as PAR, 5-Br-PADAP and 2-(2-thiazolylazo)-5-dimethylaminophenol (TAM), have the disadvantage that they require the mobile phase to contain a high proportion of an organic solvent or surfactant owing to the poor water solubility of their chelates. In contrast, the BTASPAP chelates of metal ions are very water soluble, and therefore they can be separated from each other with a mobile phase containing a lower proportion of organic solvent. The BTASPAP chelates approach described here has the advantages of high sensitivity, good resolution in a short analytical time and good column efficiency.

2. Experimental

2.1. Apparatus

A Pye Unicam PU4015 HPLC system (Philips, Cambridge, UK) with a Spherisorb ODS C_{18} column (5 μm particle size, 250 × 4.6 mm i.d.), equipped with a PU 4025 UV-Visible detector and an SP4290 integrator (Beijing, China) was used.

2.2. Chemicals

Stock solutions of Co(III), Ni(II) and Fe(III) in 1 mol l^{-1} nitric acid were prepared from their pure metals (99.99%). Stock solution of V(V) was prepared by dissolving the desired amount of divanadium pentoxide (V_2O_5) (99.99%) in water containing few drops of nitric acid. Working solutions of Co(III), Ni(II), V(V) and Fe(III) of 5.00 mg l^{-1} each by dilution. Solution 1.0 mmol l^{-1} of BTASPAP (synthesized as desented earlier [11]) was prepared in water containing 40% (v/v) acetonitrile. The mobile phase was acetonitrile-acetate-water (36:1:63, v/v) containing 0.2 mol l^{-1} acetic acid–sodium acetate buffer (pH 3.0) and 1.0 mmol l^{-1} tetrabutylammonium bromide (TBA Br). All reagents used were of analytical-reagent grade and doubly distilled water was used for all solution preparations.

2.3. Procedure

2.3.1. Preparation of standards

A set of solutions containing different concentrations of Co(III), Ni(II), V(V) and Fe(III) ions were prepared in 10 ml volumetric flasks with 2.0 ml of acetic acid–sodium acetate buffer solution (pH 3.0), 1.0 ml of 0.4% (w/v) potassium iodate (KIO_4) solution and 3.0 ml of 1.0 mmol l^{-1} BTASPAP solution, then heated for 7 min at 70°C and, after cooling, diluted to volume with doubly distilled water. After thorough mixing, the solutions were allowing to stand for 20 min and filtered through a 0.45 μm filter membrane. At a column temperature of 40°C, 20 μl of the prepared test solution were injected on to the column and the complexes were eluted with acetonitrile-acetate-water (36:1:63 v/v) containing 0.2 mol l^{-1} acetic acid–sodium acetate buffer (pH 3.0) and 1.0 mmol l^{-1} TBABr at a flow-rate of 1.0 ml min^{-1}. The peak heights were measured at a detection wavelength of 565 nm.

2.3.2. Sample preparation

A known amount of accurately weighed alloy sample (0.1 g) was dissolved in about 15.0 ml of hydrochloric acid (1:1), the resulting solution was evaporated nearly to dryness, a few drops 37.5% nitric acid were added and the excess of nitric acid was removed by heating. The solution was trans-

Table 1
Optimum conditions for the spectrophotometric determination of the four metal ions

Metal ion[a]	pH range	Amount of buffer (ml)	Amount of 1.0 mmol l^{-1} BTASPAP (ml)	Amount of 0.4% (w/v) KIO_4 (ml)	Heating	
					Time (min)	Temperature (°C)
Co(III)	3.0–6.5	2.0–10.0	3.5–6.5	0.5–1.0	5–10	50–70
Ni(II)	3.0–7.5	2.0–10.0	4.0–6.0	–	–	–
V(V)	3.0–4.5	2.0–10.0	2.5–6.0	–	–	–
Fe(III)	2.5–4.2	5.0–10.0	2.0–5.0	0.5–1.0	5-10	50–70
All metal ions	2.5–4.0	5.0–10.0	5.0–10.0	0.5–1.0	5–10	50–70

[a] Co(III) 5 μg/25 ml; Ni(II) 5 μg/25 ml; V(V) 5 μg/25 ml; Fe(III) 5 μg/25 ml; 'all metal ions' contained 3.0 μg/25 ml of each.

ferred in to a 100 ml volumetric flask and diluted to the mark with water, then the experiments were continued in the same manner as for the preparation of standards.

3. Results and discussion

3.1. Precolumn derivatization conditions and detection wavelength

In the requisite medium in the presence of the oxidant KIO_4, BTASPAP reagent reacts with Co(III), Ni(II), V(V) and Fe(III) to form stable, negatively charged, water-soluble, purplish red chelates. The ratios of Co(III), Ni(II), V(V) and Fe(III) to BTASPAP are 1:2, 1:2, 2:3 and 1:2, respectively. The negative charges of the chelates for Co(III), Ni(II), V(V) and Fe(III)-BTASPAP are 1, 2, 4, and 1, respectively.

The optimum conditions for chromogenic reactions of BTASPAP with these metal ions were studied in detail by the spectrophotometric as shown in Table 1. We found by experiment that Co(III) reacted initially with BTASPAP to form the Co(II)-BTASPAP complex in the presence of only air at room temperature, the Co(II)-BTASPAP complex was gradually oxidized by oxygen in air to form the stable Co(III)-BTASPAP complex and strong oxidants and higher temperature could accelerate the oxidation. Under optimum HPLC conditions, Co(II)-BTASPAP and Ni(II)-BTASPAP complexes could not be separated. If the Co(II)-BTASPAP complex was oxidized to the stable Co(III)-BTASPAP complex, the complete separation of Co(II)-BTASPAP and Ni(II)-BTASPAP complexes could be achieved by changing the HPLC separation conditions.

For precolumn derivatization reactions, the optimum conditions were 5.0 ml of acetic acid-solium acetate buffer (pH 3.0), 3.5 ml of 1.0 mmol l^{-1} BTASPAP, 1.0 ml of KIO_4 solution and 3 μg each of the four metal ions per 10 ml. After the solution had been heated for 7 min at 70°C, all the metal ions complexes were stable for at least 24 h.

The absorption spectra of the four complexes are shown in Fig. 1. The wavelength of maximum absorption for the Co(III), Ni(II), V(V) and Fe(III) complexes and the reagent were 570, 560, 585, 580

and 528 nm, respectively. A optimum wavelength of 565 nm was chosen for the determination.

3.2. Chromatographic separation conditions

3.2.1. Selection of organic solvents in mobile phase

The effects of acetonitrile–water and methanol–water as mobile phases on the separation of Co, Ni, V and Fe were studied. It was found that acetonitrile–water was the most suitable mobile phase. The effect of the ratio of acetonitrile to water on capacity factor (k') is shown in Fig. 2.

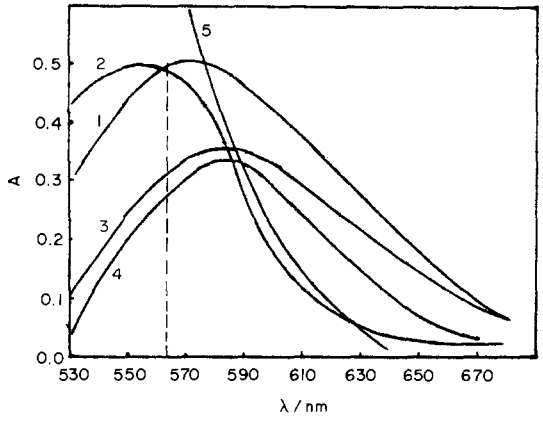

Fig. 1. Absorption spectra. Derivatization conditions: 10.0 ml HAc-NaAc buffer (pH 3.0), 5 ml 1.0 mmol l^{-1} BTASPAP, 1.0 ml KIO_4/25 ml. (1) 5.0 μg/25 ml Co(III); (2) 5.8 μg/25 ml Ni(II); (3) 5.0 μg/25 ml V(V); (4) 7.0 μg/25 ml Fe(III); (5) BTASPAP. Spectra 1–4 measured vs. reagent blank and 5 vs. water blank.

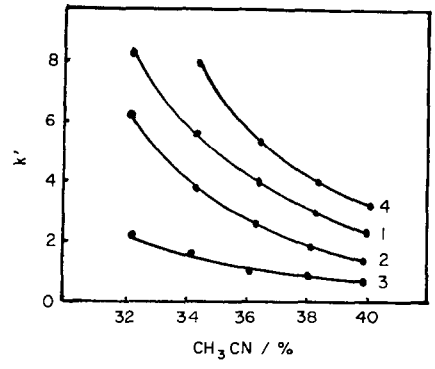

Fig. 2. Effect of content of acetonitrile on capacity factor, k' (1% acetone, 0.8 mmol l^{-1} TBABr and pH 3.0 were fixed). (1) Co-BTASPAP; (2) Ni-BTASPAP; (3) V-BTASPAP; (4) Fe-BTASPAP. Concentration of metal ions = 3.5 μg/10 ml.

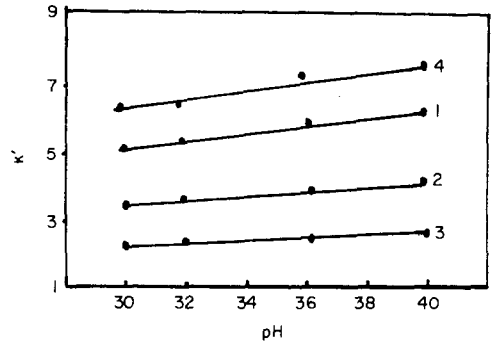

Fig. 3. Effect of pH of the mobile phase on k' (acetonitrile-water-acetone (36:63:1 v/v), 0.8 mmol l^{-1} TBABr, 20% HAC-NaAC buffer). (1) Co-BTASPAP; (2) Ni-BTASPAP; (3) V-BTASPAP; (4) Fe-BTASPAP.

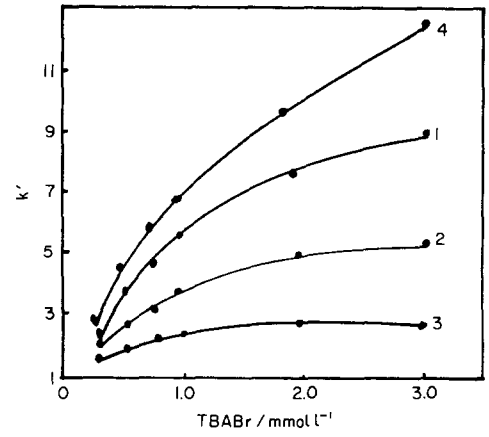

Fig. 4. Effect of the concentration of TBABr in the mobile phase on k' (acetonitrile-water-acetone (36:63:1, v/v), pH 3.0 20% HOAC-NaOaOAC buffer). (1) Co-BTASPAP; (2) Ni-BTASPAP; (3) V-BTASPSP; (4) Fe-BTASPAP.

The k' values of the four metal ion complexes decreased gradually with increase in the content of acetonitrile in the mobile phase. A 1% addition of acetone to the mobile phase was the most favorable for improving the chromatographic peak shapes and enhancing the peak heights. Acetonitrile–acetone–water (36:1:63, v/v), separated the Co(III), Ni(II), V(V) and Fe(III) complexes in the least time.

3.2.2. Effect of the pH of mobile phase

To prevent the four complexes from decomposing on the column, the mobile phase had to contain requisite amount of inorganic buffer. When the pH of the mobile phase was much lower than 3.0, it

would destroy the column, and if the pH was higher than 5.0 or lower than 3.0, the complexes would be unstable and decompose, with a decrease in chromatographic peak heights. With an increase in the pH of mobile phase, the k' values of the four metal ions only showed small changes. We examined the effect of the pH of the mobile phase on the retention volumes of the complexes only over a small pH range, as shown in Fig. 3. Based on the results we adopted pH 3.0 in subsequent work.

3.2.3. *Effect of added ion-pair reagent*

For better separation of the four metal ion complexes, an ion-pair reagent was added to the mobile phase. Three ion-pair reagents, tetramethylammonium bromide (TMABr), cetyltrimethylammonium bromide (CTMABr) and tetrabulylammonium bromde (TBABr) were examined for improving the separation of the complexes. The results showed that TMABr could not improve the separation of the chelates and the use of CTMABr could extend the retention times of the chelates. It was found that TBABr was the most suitable ion-pair reagent. The k' values of the four complexes increased slowly with increasing content of TBABr, as shown in Fig. 4. The optimum concentration range of TBABr was 0.8–1.0 mmol l^{-1}.

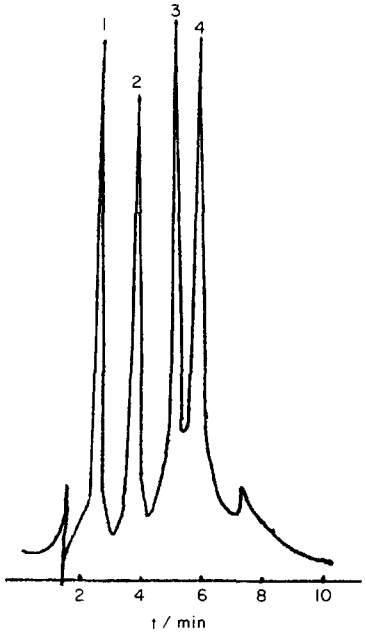

Fig. 5. Seperation of Co^-, Ni^-, Vi^- and Fe^- BTASPAP complexes by HPLC under the optimun conditions. (1) V–BTASPAP; (2) Ni–BASPAP; (3) Co–BTASPAP; (4) Fe–BTASPAP.

Table 2
Linear regression analysis of metal ion concentration (μg ml^{-1}) and chromatographic peak height (mm)

Metal ion	Linear equation[a]	Linear regression coefficient
Co	H = 18.7[Co] + 0.079	0.9978
Ni	H = 11.4[Ni] + 0.086	0.9999
V	H = 22.2[V] − 0.109	0.9992
Fe	H = 8.61[Fe] − 0.117	0.9916

[a] H = peak height; [Co], [Ni], [V] and [Fe] concentrations of Co(III), Ni(II), V(V) and Fe(III), respectively.

Table 3
Effect of foreign ions

Foreign ion added	Amount of foreign ion tolerated (μg)
K^+, Na^+, SO_4^{2-}, Cl^-	100 000
F^-, Br^-	80 000
Citrate, tartrate	45 000
Ca^{2+}, Mg^{2+}, Ba^{2+}, Sr^{2+}	15 000
Mo(VI), W(VI), Al^{3+}, Hg^{2+} (in presence of NH_4F)	1500
Cd^{2+}, Pb^{2+}, Cr^{3+}, Nb(IV)	500
Ta(V), Zr(IV)	500
Zn^{2+}, Cu^{2+}	100
Ti(IV)	50

3.3. *Separation of the Co, Ni, V and Fe complexes*

The developed procedure gave excellent resolution with sharp and symmetrical peaks of Co, Ni, V and Fe complexes, as shown in Fig. 5. Their linear regression equations and regression coefficients are given in Table 2. The linear ranges for Co, Ni, V and Fe are 0–0.8, 0–1.5, 0–0.6 and 0–1.2 μg ml^{-1}, respectively and the detection limits are

Table 4
Separation and determination of the metal ions in four alloys

Sample	Composition (%) (certified value)	Added	Found (%)[a]				RSD (%)[b]			
			Co	Ni	V	Fe	Co	Ni	V	Fe
Al alloy	Si 1.47, Fe 0.39, Mg 0.305, Mn 0.16, Ni 0.064, Cu 5,74, Zn 0.66, Co 0.12, V 0.23	Co, V	0.12	0.067	0.24	0.37	0.98	1.21	0.84	2.67
Al alloy	Si 9.74, Fe 0.70, Cu 0.24, Mg 0.14, Zn 0.18, Ni 0.731, Mn 0.30, Co 0.504, V 0.36	Ni, Co, V	0.51	0.74	0.352	0.76	0.54	0.85	0.96	2.46
Fe alloy	C 0.51, Si 0.823, Mn 0.622, Ni 1.602, Cr 4.045, Mo 4.34, Nb 0.319, V 5.04, W 6.246, Al 1.32, Co 1.978	–	2.055	1.251	5.088	–	1.47	2.08	3.68	–
Fe alloy	Co 0.014, V 0.036, Cu 0.123, Mo 0.002, Mn 1.07, Ti 0.094, Ni 0.027, Sb 0.0041, Cr 1.10	–	0.015	0.029	0.038	–	3.91	2.47	3.22	–

[a] Average of five determinations.
[b] Relative standard deviation ($n = 5$).

0.3, 0.3, 0.8 and 1.0 ng, respectively (signal-to-noise ratio = 2).

3.4. Effect of foreign ions

The potential interference of numerous ions was studied by spectrophotometry. Different amounts of ionic species were added to a mixture of Co, Ni, V and Fe containing 3 μg/25 ml of each. The starting amount of each foreign ion added was 100 mg, and if interference occurred the amount of the foreign ion were gradually reduced until interference ceased to occur. The tolerated limits were taken as the concentrations within which the errors caused were not greater than $\pm$ 5% in the determinations.

The tolerance limits are given in Table 3. All of the foreign ions in Table 3 have higher allowable amounts by the spectrophotometric method. In fact, none of the foreign ions gave a peak at 565 nm, but they consumed more BTASPAP reagent.

3.5. Analyses of some standard samples

The method was applied to the determination of Co, Ni, V and Fe in four standard alloys. The results are given in Table 4 together with the certified values, and demonstrate the good accuracies and precisions of the results obtained with the procedure proposed.

References

[1] X. Zhang and W. Liu, Fenxi Huaxue, 16 (1988) 122.
[2] D. Roston, Anal. Chem., 56 (1984) 241.
[3] Yu. S. Nikitin, N.B. Morozova and S.N. Lanin, Talanta, 34 (1987) 223.
[4] H. Hoshino and T. Yotsuyanagi, Anal. Chem., 57 (1985) 625.
[5] J.N. King and J.S. Fraus, Anal. Chem., 59 (1987) 703.
[6] M. Kobayaschi, K. Saitio and N. Suzuki, Chromatographia, 20 (1985) 72.
[7] L.-Y. Li, G.-M. De and Y.-Q. Zhao, Talanta, 42 (1995) 89.
[8] W.-X. Ma and Z.-P. Wang, Physical Testing and Chemical Analysis, Part B: Chem. Anal., 32 (1996) 36.
[9] Z.-L. Ma, Y.-P. Wang and F.-Z. Miao, J. Hebei Inst. Chem. Technol. Light Ind., 17(1) (1996) 37.
[10] W.-X. Ma and Z.-P. Wang, Yejin Fenxi, 15 (1995) 15.
[11] Z.-P. Wang and W.-X. Ma, J. Nanjing Inst. Chem. Technol., 12(3) (1990) 1.

ELSEVIER

Talanta 44 (1997) 749–753

Talanta

Analytical applications of graphite electrode modified with Bis(diisopropyloxithiophosphon)Disulphide

Zhivko I. Denchev [a,*], Nikola K. Nikolov [a], Liliana Ilcheva [b]

[a] *Department of Analytical Chemistry, University of Plovdiv, 24 Tzar Asen St., 4000 Plovdiv, Bulgaria*
[b] *Department of Analytical Chemistry, University of Chemical Technology and Metallurgy, 1000 Sofia, Bulgaria*

Received 24 October 1995; accepted 14 August 1996

Abstract

A modified graphite electrode was produced by adsorption the bis(diisopropyloxythiophosphone)disulphide {(i-PrO-)$_2$P(S)S-}$_2$ under vacuum. Its electrochemical characteristics in flowing stream were described. The modified electrode has been used for simultaneous determination of Cu(II), Ag(I) by flow injection anodic stripping voltammetry. © 1997 Elsevier Science B.V.

Keywords: Anodic stripping voltammetry; Chemically modified electrode; Copper; Flow injection analysis; Silver

1. Introduction

Chemically modified electrodes enlarge the scope of electroanalytical determinations. They improve the selectivity and the sensitivity of analysis. This is due to different ligands immobilized on their surfaces by various methods [1–3]. Different organic ligands have been used for graphite electrodes modification aiming at the simultaneous determination of inorganic ions (for example copper and silver).

Some authors have immobilized dithiocarbamate ligands on platinum and graphite electrode [4,5], but they have determined only copper in the presence of nickel, lead and zinc. It is proposed a paste graphite electrode for simultaneous determination of copper and silver [6]. The poor reproducibility of the electrode's surface is the main problem here.

It is known from the literature that the organic ligands which have a disulphide group (–S–S–) extend amazingly by the selectivity of extractive spectrophotometrical determination of Cu(II) and Ag(I) [7]. Their synthesis was described for the first time in [8,9]. There the alkaline salts of the ditiophosphonate acids are oxidized by slight oxidizers according to the equation:

$$2(RO_2)P(S)SK + Ox_2 = (RO)_2P(S)S - S(S)P(RO)_2 + 2\mathrm{Red} \quad (1)$$

where R is alkyl or aryl.

A modified graphite electrode produced by adsorption of bis(diisopropyldithiophosphate) disulfide is described. Its application to flow

* Corresponding author.

PII S0039-9140(96)02070-X

injection analysis (FIA) of metal ions is presented as well.

The equipment used includes a potentiostat-galvanostat 'Bi-Pad'; a generator of lineal voltage 'Servovit'; a recorder 'Sefram' (Tacussel, France), a peristaltic pump (P-1 Sweden), a flow voltammetric cell (home made [10]) and an injection valve (home made [13]). It is important to underline that the working part of the graphite electrode is of 0.6–0.8 mm diameter and its length is of 1.4–1.8 mm.

The following reagents were used: potassium diisopropyldithiophosphate $\{(i\text{-PrO})_2\text{P(S)SK}\}$ p.a., and bis(diisopropyloxythiophosphone)disulphide $\{(i\text{-PrO-})_2\text{-P(S)S-}\}_2$ which has been triply recrystallizated from ethyl alcohol. The concentration of the standard solution of Cu(II) and Ag(I) are of 1 g l^{-1}. All other reagents used were of an analytical grade (Merck). Doubly distilled water was used for solutions preparation and dilution.

1.1. Procedures

1.1.1. Preparation of a reagent for modification.

It has been prepared, according to the described Eq. (1), by dissolving potassium diisopropyldithiophosphate in doubly distilled water and has been oxidized with iodine solution. In this way the synthesizing disulphide has been recrystallisated into ethyl alcohol to get a product with a purity p.a. which has been controlled by chromatographic analysis.

1.1.2. Graphite electrode production.

The graphite electrode was prepared from spectroscopically pure graphite manufactured by Czechoslovak Ceramics Corporation, Praha, Czehia. The electrode's body was shaped to fit the dimensions pointed above by metal cutting machine and then glued to plastic holder.

1.1.3. Electrode modification.

The prepared electrode was placed in a vacuum vessel where a definite amount of the modifying reagent had been initially introduced. The system was then sealed and put into a water bath which was heated up to $T = 90$–95°C. At this temperature range the reagent was melted, the vacuum pump was turned on and a residual pressure of 13.3 HPa was created. In this way the thermal destruction of the modifier was avoided. The modification was carried out for 3 h at the same pressure and the same temperature. The electrode was then taken out of the melt and left over it at the same temperature and pressure for 30 min for homogenization of the coating.

2. Design of the analytical module

The flow injection system, created in our laboratory, is shown in Fig. 1. The electrochemical characteristics of the modified electrode were studied on varying of the type of the flow carrier and its rate and the parameters of electrochemical apparatus. The experiments were carried out in a flowing stream of a solution (0.2 M $KNO_3/10^{-3}$ M HNO_3).

3. Results and discussion

Cyclic voltammetry has been applied Fig. 2 shows cyclic voltammograms of graphite electrodes modified in different ways.

The electrode modified under vacuum (curve 1) is characterized by the widest working range (− 0.6– + 0.7 V) and the least residual current. It can be used for quantitative determination of ions of the precious metals because their anodic peaks appear in this range of potentials. The modified reagent favours the electrode's properties (curve 1) by decreasing the value of the residual current

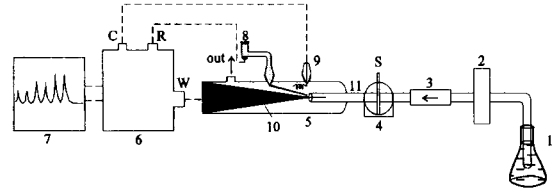

Fig. 1. Flow injection system. (1) Flow carrier; (2) peristaltic pump; (3) pulse damping system; (4) injection valve; (5) flowthrough cell; (6) potentiostat-galvanostat; (7) recorder; (8) reference electrode (SCE); (9) auxiliary electrode—platinum spiral; and (10) working electrode—MGE.

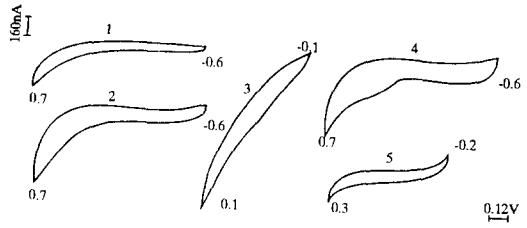

Fig. 2. Polarization curves for graphite electrode. (1) Graphite electrode modified under vacuum; (2) modified by dipping in a melt of the reagent; (3) modified by glycerine solution of the reagent; (4) pure graphite electrode in a flow carrier 0.2 m KNO_3; and (5) a graphite electrode modified in vacuum, in a flow carrier 0.1 M HNO_3; flow rate 1.3 ml min^{-1}; linear sweep potential rate 1 V min^{-1}.

when compared with that of a pure graphite electrode (curve 4). Curve 5 corresponds to a graphite electrode modified under vacuum, but the flow carrier used is 0.1 M HNO_3. Curve 5 shows also that the cathodic range becomes more narrow which is due to the disulfide reduction in presence of H^+.

3.1. Selectivity and sensitivity

The electrochemical behaviour of bis(diisopropyloxythiophosphone)disulphide $\{(i\text{-PrO-})_2P(S)S\text{-}\}_2$ on a mercury dropping electrode was described in detail [11]. It is reasonable to assume that the disulphide immobilized of the graphite electrode will have the same behaviour in the process of the electrochemical analysis in accordance with the following scheme:

$$\{(i\text{-PrO})_2P(S)S\}_{2ads} + 2e = 2\{(i\text{-PrO})_2P(S)S\text{-}\}_{ads} \quad (2)$$

$$2\{(i\text{-PrO-})_2P(S)S^-\}_{ads} + Me^{n+} = 2\{(i\text{-PrO})_2P(S)S\}Me_{ads} \quad (3)$$

$$\{(i\text{-PrO-})_2P(S)S\}Me_{ads} - 2e = Me^{n+} + \{(i\text{-PrO-})_2P(S)S\text{-}\}_{2ads} \quad (4)$$

The capabilities of modified graphite electrode (MGE) in respect to its sensitivity and selectivity, under the conditions of the flow injection analysis by anodic stripping voltammetry were tested by injections of samples containing the metal ions of interest. The results of those determinations are shown in Fig. 3.

Curves 1 and 2 show the sensitivity of a modified and unmodified graphite electrodes, respectively in the anodic stripping voltammetry analysis of the mercury ions present in the sample. The difference sensitivity in this is obvious. The modified electrode's sensitivity is two and a half times that of the unmodified electrode under the same experimental conditions. It is due to the complexation effect of the modifier which provides a stronger analytical signal than that observed at the unmodified graphite electrode. Curve 3, in the same figure can be treated as an anodic stripping voltammetric characteristics obtained on the oxidation of the products deposited upon the MGE during the electrolysis of the sample solution containing copper and silver ions. The two well outlined peaks, at potentials of -0.23 V for copper and -0.09 V for silver, coincide with values for the single peaks of copper or silver ions, correspondingly on the same MGE under identical experimental conditions. Curve 4 refers to the oxidation of the products deposited on the unmodified graphite electrode during the electrolysis of the sample containing copper and silver ions. An intensive peak with a maximum at a potential of -0.2 V is observed here. This intermediate value indicates that the separation under the conditions of FIA ASV is impossible. It follows that the modified graphite electrode shows a high selectivity towards this couple and a joint determination of both elements is possible. Thus, it can be used for quantitative analysis.

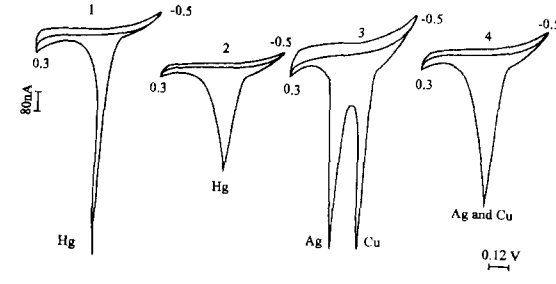

Fig. 3. ASV polarization curves of graphite electrodes. $E_{dep} = -0.5$ V; Carrier flow rate {0.2 M KNO_3/10^{-3} M HNO_3}-0, 13 ml min^{-1}; sample volume injected—800 μl; t_{dep}—10 min; concentration of the elements, 1 ppm.

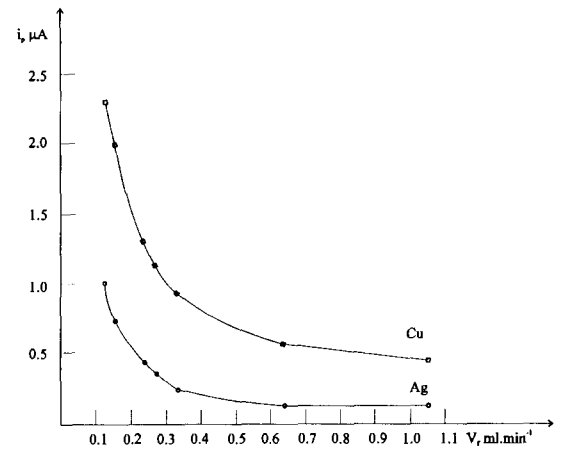

Fig. 4. Dependence of stripping peak on flow rate of copper and silver. $E_{dep} = -0.5$ V; $t_{dep} = 10$ min; $s_v = 800$ μl; $V_E = 33.3$ mV min^{-1}; flow carrier—0.2 M $KNO_3/10^{-3}$ M HNO_3; concentration of analyzed ions 1 ppm.

3.1.1. Optimization parameters of the FIA by modified graphite electrode

The basic parameters which may be optimized allow to find the most suitable conditions for a quantitative analysis. The analytical signal depending on the flow carrier rate should be followed. Fig. 4 shows analytical signals at different flow carrier rates.

The analytical signal is optimal for both analyzed cations at low flow carrier rates (0.10–0.25 ml min^{-1}). The reasons for the signal decrease with the flow carrier rate increase, is explained in the following way. The amount of the electrolysis products decreases practically with the increase of the flow rate because most of it is carried away by the flow prior to the electrolysis itself. Another factor of the FIA is the analytical signal dependence on the injection sample volume. For the anodic stripping voltammetric analysis the sample volume which will be injected in to the system depends on the analyte concentration, flow carrier rate and the time of electrolysis. For our determinations the injection sample volume is between 800 and 1000 μl the deposition time is of 10 min, the electrolysis potential is of -0.5 V, flow carrier rate is of 0.13 ml min^{-1}, linear sweep rate is of 33.3 mV s^{-1}.

The range used was determinated in the following way: a series of standard solutions containing both of the analyzed ions with different concentrations (0.10, 0.25, 0.50, 0.75 and 1 ppm) were prepared. The volume of the sample injected was 800 μl, the flow carrier rate (0.2 M $KNO_3/10^{-3}$ M HNO_3) was kept constant at 0.13 ml min^{-1} so that the electrolysis time was within of 10 min and the deposition potential was -0.5 V (SCE). After this period the flow carrier rate was increased to 1.3 ml min^{-1} and the linear sweep potential with rate of 33.3 mV s^{-1} was performed. The obtained anodic peaks are in the interval from -0.5 to 0.7 V. Their height was measured in μA and the dependence of the current on the analyzed elements concentration was followed. From time to time an empty sample solution was injected to the system aiming at the elimination of the hindering effect. Each analysis was carried out five times. Then the data for the calibration line were treated statistically [12]. The obtaining correlation coefficients of both curves are $r = 0.999$ for the copper and $r = 0.998$ for the silver. The equations of each line are $i_p = 0.044 + 3.42\ C_{Cu}$ and $i_p = 0.022 + 2.20\ C_{Ag}$, respectively $L.O.D._{Cu} = 0.05$ ppm and $L.O.D._{Ag} = 0.06$ ppm.

Application of modified graphite electrode to flow injection stripping voltammetry analysis of synthetic mixtures, containing copper and silver ions.

The synthetic mixture analysis was carried out in the following way. Three samples of different contents of side ions were prepared from an initial standard solution which had a concentration of 1 g l^{-1}.

The modified graphite electrode was inserted into the flow cell, the flow carrier was started (0.13 ml min^{-1} rate) and the cyclic voltammogram in the interval from -0.6 to 0.7 V was recorded. Then the indicator electrode potential was reduced to -0.5 V, the sample solution was injected and electrolysis was conducted for 10 min. After the corresponding deposition time linear sweep potential with a rate of 33.3 mV s^{-1} was applied. The anodic peaks recorded were measured in μA and the analyzed ions concentration was found from the calibration plot. The results are given in Table 1.

The hindering elements studied were selected because they could deposit and give respective

Table 1
A FI ASV with MGE of synthetic mixture containing 250 ppb silver ions and 250 ppb copper ions ($n = 5$; $P = 95\%$)

Added	Silver			Copper		
	$x \pm t_x$	S_r	RSD%	$x \pm t_x$	S_r	RSD%
Tl, In, Sn, Bi, Pb, Cd						
10 ppm from each elements	250 ± 10.3	4.2	1.7	250 ± 8.7	3.5	1.4
20 ppm from each elements	250 ± 16.5	6.7	2.7	250 ± 10.3	4.2	1.6
30 ppm from each elements	250 ± 17.0	6.8	2.7	250 ± 13.1	5.3	2.1

peaks in the potential range of interest. Table 1 shows that the modified graphite electrode did not react with them and therefore both metal ions can be simultaneously determined in their presence. The modified graphite electrode was tested in the determination of silver ions content in shampoos. The results are compared with the data from emission spectral analysis with inductively couple plasma—Table 2.

It is seen from Table 2 that both methods have one and the same precision and reproducibility.

4. Conclusion

A modified graphite electrode was prepared using a new reagent bis(diisopropyloxytiophosphone)disulphide. A method for its modification by heat treatment under vacuum was applied. A firm, homogeneous film of a modifier was obtained on the graphite surface. The advantages of the modified electrode when compared with the unmodified one, in respect to its electrochemical characteristics and behaviour towards the copper–silver couple were shown. The modified graphite electrode was used for champoo analysis and the results obtained were compared with those from ICP-AE.

Table 2
An analysis of shampoo for silver content ($n = 5$)

Sample	FI-ASV		ICP-AE	
	ppm	RSD%	ppm	RSD%
Ch-20 Ag	4.48	8.87	4.66	8.20
G-20 Ag	3.99	4.00	4.17	4.28

Acknowledgements

The authors would like to thank the National Fund 'Scientific Research', for the financial support of this work.

References

[1] J. Labuda, Zhurn. Analyt. Khim., 45 (1990) 629–642 (in Russian).
[2] J. Weng, Anal. Chim. Acta, 243 (1990) 41–48.
[3] A.A. Kaplin, N.P. Pikula and E.J. Newman, Zhurn. Analyt. Khim., 45 (1990) 2086–2120 (in Russian).
[4] G.G. Wallace, D.M.T. O'Riordan, Abs. Pap. Pitsburgh Conf. and Expo. Anal. Chemistry and Applied Spectroscopy, Atlantic City, N.J., March 10–14, 1986, S.I.S.A., 180 p.
[5] D.M.T. O'Riordan and G.G. Wallace, Anal. Proc., 23 (1986) 14.
[6] G.A. Rivas and P.I. Ortiz, Anal. Lett., 27 (4) (1994) 751–753.
[7] N.K. Nikolov and A.I. Bussev, Zhurn. Analyt. Khim., 31 (1976) 454–459 (in Russian).
[8] N.I. Zemlianski and V.P. Kalachnikov, Zhurn. Ob. Khim., 39 (1969) 616 (in Russian).
[9] B. Miller, Tetrahedron, 20 (1964) 2069.
[10] N. Elenkova, L. Ilcheva and Zh. Denchev, 31st International Congress of Pure and Applied Chemistry, Juli 13–18, 1987, Sofia, Bulgaria.
[11] A. Schischkov, J. Dentschev and Ch. Malakova, Talanta, 3 (1984) 69.
[12] J.N. Miller, Analyst, 116 (1991) 3.
[13] J. Ruzicka and E.H. Hansen, Flow Injection Analysis, Wiley, New York, 1981.

ELSEVIER

Talanta 44 (1997) 755–763

Talanta

Solubility of metal chelates and their extraction from an aqueous environment via supercritical CO_2

Mehdi Ashraf-Khorassani [a,*], Michael T. Combs [b], Larry T. Taylor [b]

[a] *Analytical Division, Durability Inc., Blacksburg, VA 24060, USA*
[b] *Department of Chemistry, Virginia Tech, Blacksburg, VA 24061, USA*

Received 21 May 1996; received in revised form 20 August 1996; accepted 20 August 1996

Abstract

Solubility of nickel(II), copper(II), and chromium(III) hexafluoroacetylacetone and chromium(III) acetylacetone chelates was measured in supercritical CO_2 at two different pressures (200 and 400 atm) and 60°C. Solubility of fluorinated acetylacetone chelates was at least an order of magnitude higher than the non-fluorinated complexes. These pre-formed metal chelates as well metal diethyldithiocarbamate (DDC) and metal bis(trifluoroethyl)dithiocarbamate (FDDC) have also been extracted from aqueous environment using pure supercritical CO_2. It was demonstrated that metal HFA chelates while exhibiting higher solubility in supercritical CO_2 compared with metal FDDC chelates, exhibited lower extraction efficiency using the same extraction conditions. This behavior of metal HFA chelates is related to their stability in an aqueous environment. Direct extraction of Ni^{+2} and Cu^{+2} from an aqueous matrix was also achieved via in-situ chelation using diethyldithiocarbamate and bis(trifluoroethyl)dithiocarbamate as the ligands. Bis(trifluoroethyl)dithiocarbamate proved to be a more effective ligand for direct extraction of metal ions from aqueous environment using supercritical CO_2. © 1997 Elsevier Science B.V.

Keywords: Aqueous environment; Extraction; Metal chelates; Solubility; Supercritical CO_2

1. Introduction

Metal ions and metal-ligand complexes are usually extracted from liquid matrices via formation of a neutral chelate combined with solvent extraction [1]. After complexation using a suitable ligand, toxic organic solvents are required to extract the complex. The toxic organic solvent, often in relatively large volume, usually causes a hazardous environment in terms of both solvent handling and solvent disposal.

Supercritical fluids have become an alternate solvent for extractions in the past decade. The high diffusivity, low viscosity and variable solvent strength as a function of density (P, T) are some of the attractive features of supercritical fluids [2]. Extraction of hydrated metal ions using pure supercritical CO_2 is not feasible due to the weak interaction of ionic solute and non-polar fluid [3]. However, metal ion extractions can be obtained via binding of the positive metal ion to an anionic

* Corresponding author. Fax: + 1 540 2313327.

PII S0039-9140(96)02075-9

organic ligand which forms a stable neutral metal complex provided the metal complex exhibits reasonable solubility in supercritical CO_2.

The literature regarding solubility of metal chelates in supercritical CO_2 is very limited. Recently, Wai et al. [4,5] measured the solubility of different metal (Ni^{+2}, Co^{+3}, Cu^{+2}, Na^{+}, Bi^{+3}, and Hg^{+2}) diethyldithiocarbamate (DDC) and bis(trifluoroethyl)dithiocarbamate (FDDC) chelates in supercritical CO_2. It was demonstrated that metal FDDC chelates have approximately 2–3 orders of magnitude higher solubility than metal DDC chelates in supercritical CO_2. Also it was demonstrated that the solubility of $Cu(FDDC)_2$ increased significantly as the density of the supercritical CO_2 increased at constant temperature [4]. They also measured solubility of $Hg(FDDC)_2$ and $Hg(DDC)_2$ in methanol modified CO_2. It was demonstrated that 5% methanol modified CO_2 enhanced the solubility of $Hg(FDDC)_2$ and $Hg(DDC)_2$ by an order of magnitude [5].

Knowing this information, Laintz et al. [6] were able to extract quantitatively Cu^{+2} ion from both a solid sorbent and an aqueous matrix using supercritical CO_2 saturated with LiFDDC as a chelating agent. Extraction efficiency of Cu^{+2} ion from both matrices was greater than 95% at density above 0.35 g/ml and 35°C. The same group also reported extraction of other divalent and trivalent metal ions from aqueous and solid matrices. Extraction efficiencies of greater than 90% were reported for Cd^{+2}, Pb^{+2}, Pd^{+2}, Zn^{+2}, As^{+3}, Au^{+3}, Ga^{+3} and Sb^{+3} from sand and filter paper using LiFDDC ligand [9]. Similar recovery was also obtained for extraction of Cd^{+2}, Pb^{+2} and Zn^{+2} from aqueous solution [9]. Wai et al. have reported [5] extraction of mercuric ion (Hg^{+2}) from cellulose-based filter paper using LiFDDC as a chelating agent. Extraction efficiency of Hg^{+2} was less than 12% from the dry filter paper. The low extraction efficiency of mercury ion was reportedly due to strong interaction of Hg^{+2} with the cellulose matrix. However, by addition of a small amount of water (10 μl) directly to the matrix, extraction efficiency of mercury increased to 84%. When using 5% methanol modified CO_2, the extraction efficiency of Hg^{+2} was increased from 84 to 95%. This increase in extraction efficiency was mostly due to enhanced interaction between the solute and the modified solvent.

Extraction of similar heavy metals from different matrices has been achieved using again supercritical CO_2 saturated with LiFDDC. Liu et al. [8] reported extraction of Co^{+3}, Cd^{+2}, Zn^{+2} and Cu^{+2} from solid matrices (sand, soil and filter paper). Recovery of ions ranged from 70 to 100%. They reported that metal impurities in the stainless steel extraction vessel can form a metal chelate with the ligand and positively affect percent recovery of analytes. They suggested using a non-metal containing apparatus such as polyether ether ketone (PEEK). Recently Wang et al. [10] used different dithiocarbamates such as tetrabutylammonium dibutyldithiocarbamate (TDBDTC), tetrabutylammonium diethyldithiocarbamate (TDEDTC), sodium diethyldithiocarbamate [Na(DEDTC)] and ammonium pyrollidinecarbamate (APDTC) ligands for in-situ chelation and SFE of Zn^{+2}, Cd^{+2} and Pb^{+2} from aqueous media. It was demonstrated that extraction efficiency of Zn-DBDTC is much greater than Zn-DEDTC or Zn-PDTC. The high extraction efficiency of Zn-DBDTC was related to the high solubility of the chelate. Solubility ratios of Zn-DBDTC/Zn-DEDTC and Zn-SDDTC/Zn-PDTCin SF CO_2 were measured to be 20 and 139, respectively.

Beside dithiocarbamates, other ligands such as tetra-butyl-substituted dibenzobistriazolo-crown ether have been used for extraction of similar heavy metal ions (Cd^{+2}, Co^{+3}, Pb^{+2}, Ni^{+2}, Mn^{+2}, Au^{+3} and Zn^{+2}) from sand and filter paper [7]. Extraction efficiency of most metal ions, except Au^{+3}, from wet matrices was less than 4% using 5% methanol modified CO_2. The efficiency of extracted Au^{+3} from wet filter paper using 5% methanol modified CO_2 was 79%. Bistriazol-crown ether was also used for extraction of Hg^{+2} [7]. It was demonstrated that 5% methanol modified CO_2 saturated with a bistriazol-crown ether can extract only 78% of Hg^{+2} from sand, while the same fluid after addition of 10 μl water to the sample improved extraction efficiency to more than 95%.

The objective of our study was first to measure solubility of different metal acetylacetone and metal hexafluoroacetylacetone complexes in supercritical CO_2. Second, obtain extraction efficiency of different pre-formed metal acetylacetone, metal hexafluoroacetylacetone, metal diethyldithiocarbamate, and metal bis(trifluoroethyl)dithiocarbamate chelates from an aqueous environment using pure CO_2. No results have been reported regarding solubility or extraction efficiency of Cr^{+3}, Ni^{+2}, and Cu^{+2} acetylacetone or hexafluoroacetylactone chelates from an aqueous environment using supercritical CO_2. Finally we were interested to learn if metal ions (Ni^{+2}, and Cu^{+2}) could be extracted from an aqueous environment via in-situ chelation using supercritical CO_2.

2. Experimental

2.1. Apparatus

A Suprex (Pittsburgh, PA) Prepmaster equipped with an Accutrap™, variable flow restrictor, and a 10 ml extraction vessel modified for use with aqueous samples [11–13] was used for all extractions. The stainless steel frits which were part of the fitting seals were removed in order that 1/16 inch stainless steel tubing (0.01 inch i.d.) could pass through either end of the vessel. The stainless tubing inserted through the top of the vessel extended to within 1 cm of the bottom, and vice versa. Standard 1/16 inch fittings and ferrules (Valco, Houston, TX) were used to obtain reliable seals.

A Suprex 200A supercritical fluid chromatographic pump, Waters (Milford, MA) 6000 high performance liquid chromatographic pump, a Micropump (Concord, CA) recirculating pump, a 6 port-2 position valve, a 4 port-2 position valve, and Kratos Spectroflow 757 UV absorbance detector were used for all on-line solubility measurement. A 0.5 ml stainless steel extraction vessel was used for solubility determination.

2.2. Reagents

Bis(acetylacetonato)nickel(II) $Ni(AcAc)_2$, tris(acetylacetonato)chromium(III) $Cr(AcAc)_3$, bis(acetylacetonato)copper(II) $Cu(AcAc)_2$, bis(hexafluoroacetylacetonato)nickel(II) $Ni(HFA)_2$, bis(hexafluoroacetylacetonato)copper(II) $Cu(HFA)_2$, copper nitrate hydrate, chromium nitrate hydrate, nickel nitrate hydrate, and sodium diethyldithiocarbamate (NaDDC) were purchased from Aldrich (Milwaukee, WI). Lithium bis(trifluoroethyl)dithiocarbamate (LiFDDC) was prepared according to a procedure outlined in the literature [14]. Bis(diethyldithiocarbamato)nickel(II) $Ni(DDC)_2$, bis(diethyldithiocarbamato)copper(II) $(Cu(DDC)_2$, and bis(bis(trifluoroethyl)dithiocarbamato)nickel(II) $Ni(FDDC)_2$ and bis(bis(trifluoroethyl)dithiocarbamato)copper(II) $Cu(FDDC)_2$ were synthesized according to a procedure outlined in the literature [6]. HPLC grade methanol and chloroform were purchased from EM Science (Gibbstown, NJ). SFE/SFC grade CO_2 (helium head pressure) was used for both supercritical fluid extraction and solubility studies and was obtained from Air Products and Chemical Co. (Allentown, PA).

2.3. Solubility measurement apparatus

Fig. 1 shows the apparatus and positions of valves at each step for measuring solubility of organic and inorganic compounds under supercritical conditions. In each measurement, the 0.5 ml extraction vessel was filled with metal chelate. Next, the system was pressurized to 200 atm using pure CO_2. After pressurization of the system, the three way valve was closed and the recirculating pump was activated (A). The function of the recirculating pump was to ensure complete saturation of supercritical fluid with the chelate of interest. After 30 min of equilibration, the 4 port-2 position valve with 1 μl sample loop was rotated such that the solubilized chelate in supercritical CO_2 was directed from the 1 μl loop to the liquid chromatographic (LC) system (B). The LC flow then washed the chelate from the injection loop

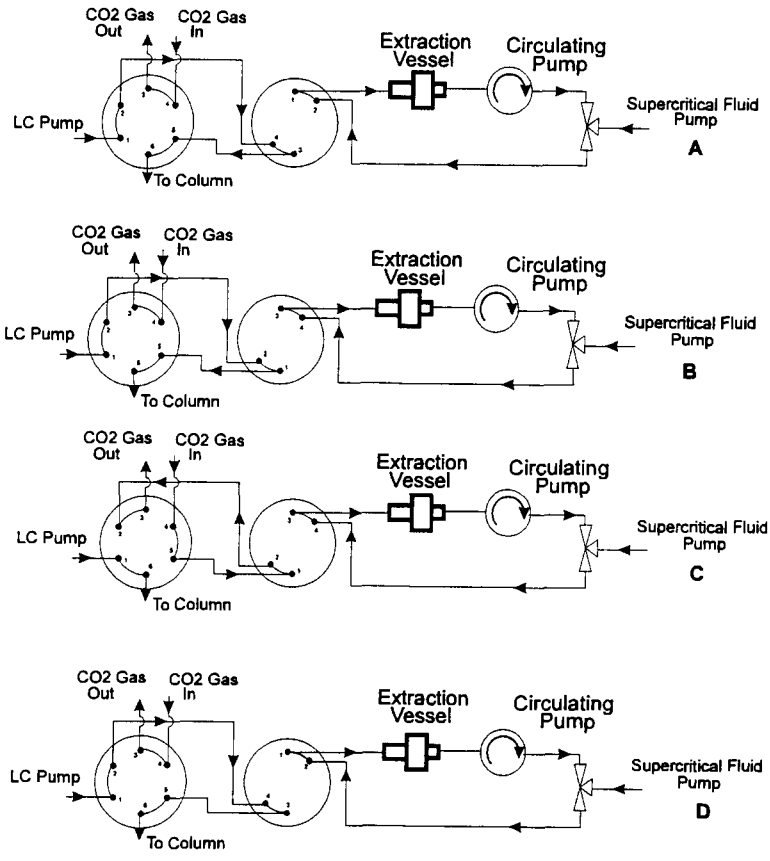

Fig. 1. Schematic diagram of apparatus for measuring solubility of inorganic compound in supercritical fluid.

through the column to a multi-wavelength UV absorbance detector operated at 280 nm for AcAc and HFA complexes and at 416 nm for DDC and FDDC complexes. By employing a second valve (6 port-2 position valve), a stream of carbon dioxide could then be passed through the sample loop to remove the chromatographic mobile phase from the loop, thus avoiding modification of supercritical fluid composition (C). Next, the 4 port-2 position valve was rotated to the load position and the procedure was repeated (D). Replicate determinations were made on each metal chelate to ensure reproducibility of the system. After measurement of analyte solubility at 200 atm, the system was pressurized to 400 atm and the same experiments were repeated.

2.4. SFE procedure

For each extraction, 5 ml of distilled water was added directly to the modified extraction vessel. Next, 200 μl of individual metal chelate standard with a concentration range of 15–22 μg μl^{-1} was spiked directly in to the distilled water. The system was operated at either 200 or 400 atm and 60°C for 10 min static and 30 min dynamic period using pure supercritical CO_2 at flow of 2 ml min^{-1}. For studies of in-situ chelation, 200 μl of metal salt standard with a concentration range of 6–8 μg μl was spiked into the vessel containing 5 ml of distilled water saturated with chloroform followed by addition of excess chelating ligand. The sample was then extracted under the same

Table 1
Solubility of different metal β-diketone and metal dithiocarbamate chelates in supercritical CO_2 at different conditions

Chelate	Mole l^{-1}, 200 atm, 60°C	Mole l^{-1}, 400 atm, 60°C	[a]Mole l^{-1}, 100 or 150 atm, 60°C
$Ni(HFA)_2$	$(8.0 \pm 0.1) \times 10^{-3}$	$(9.9 \pm 0.2) \times 10^{-3}$	
$Cu(HFA)_2$	$(8.7 \pm 0.2) \times 10^{-2}$	$(8.5 \pm 0.1) \times 10^{-2}$	
$Cr(HFA)_3$	$> 8.0 \times 10^{-2}$	$> 8.2 \times 10^{-2}$	
$Cr(AcAc)_3$	$(2.0 \pm 0.04) \times 10^{-3}$	$(3.5 \pm 0.2) \times 10^{-3}$	
Na(FDDC)			$(4.7 \pm 0.3) \times 10^{-4}$
Na(DDC)			$(1.5 \pm 0.1) \times 10^{-4}$
Cu(FDDC)2			$(9.1 \pm 0.3) \times 10^{-4}$
Cu(DDC)2			$(1.1 \pm 0.2) \times 10^{-6}$
Ni(FDDC)2			$(7.2 \pm 1.0) \times 10^{-4}$
Ni(DDC)2			$(8.5 \pm 1.0) \times 10^{-7}$
Co(FDDC)3			$(8.0 \pm 0.6) \times 10^{-4}$
Co(DDC)3			$(2.4 \pm 0.4) \times 10^{-6}$
Bi(FDDC)3			$(7.3 \pm 1.0) \times 10^{-4}$
Bi(DDC)3			$(9.0 \pm 0.6) \times 10^{-6}$
Hg(FDDC)2			$(5.0 \pm 0.4) \times 10^{-3}$*
Hg(DDC)2			$(8.2 \pm 0.6) \times 10^{-6}$*

[a] From Ref. [4,5].
*Pressure 150 atm.

conditions specified previously. The extracts were then collected in 5 ml of a 50/50 mixture of methylene chloride/methanol at ambient temperature. The analysis of the sample extracts for each metal was performed by atomic absorption spectroscopy (using either a nitrous oxide or acetylene flame) by REIC Laboratory (Beaver, WV).

3. Results and discussions

3.1. Solubility measurements

Solubility of $Ni(HFA)_2$, $Cu(HFA)_2$, $Cr(HFA)_3$, and $Cr(AcAc)_3$ was determined using the apparatus described in the Section 2. Table 1 shows the solubility of each analyte in CO_2 at 200 and 400 atm and 60°C. Due to low solubility of $Cu(AcAc)_2$ and $Ni(AcAc)_2$ in supercritical CO_2 and their poor chromatographic behavior [15], solubility measurements of these chelates via our system were not feasible. Even, increasing pressure from 200 to 400 atm did not drastically effect solubility of $Ni(AcAc)_2$ or $Cu(AcAc)_2$. It is important to note here that solubility of $Cr(HFA)_3$ in supercritical CO_2 was very high. It is believed that during our solubility measurement saturation of fluid was not achieved (due to limited mass of $Cr(HFA)_3$) since no chelate remained in the extraction vessel upon completion of the experiment. Therefore it is expected that solubility of $Cr(HFA)_3$ is greater than or equal to that reported here. The solubility of $Cr(HFA)_3$ in pure CO_2 at either 200 or 400 atm was at least an order of magnitude higher than the corresponding non-fluorinated complex. Also results showed that solubility of all metal HFA chelates was at least two order of magnitude higher than solubility of those metal FDDC chelates ($Ni(FDDC)_2$, $Cu(FDDC)_2$, $Co(FDDC)_3$, NaFDDC, $Bi(FDDC)_3$, and $Hg(FDDC)_2$) reported previously by Wai et al. [4,5].

Table 2
Percent recovery of different metal acetylacetone complexes from an aqueous environment using supercritical CO_2. Extraction period: 10 min static and 30 min dynamic with flow of 2 ml min^{-1}

Metal complex	% Recovery, 200 atm	% Recovery, 400 atm
$Ni(AcAc)_2$	2 (55)[a]	1.5 (3)
$Cu(AcAc)_2$	12 (66)	9 (18)
$Cr(AcAc)_3$	66 (10)	82 (1)

Extraction temperature: 60°C.
[a] % RSD for triplicate extractions are noted in parentheses.

3.2. Recovery of metal acetylacetone complexes from water

Extraction efficiency of Ni^{+2}, Cu^{+2}, and Cr^{+3} acetylacetone complexes from an aqueous matrix was obtained at two different pressures (200 and 400 atm) at 60°C. Table 2 shows the recovery of each analyte at the different pressures. Recovery of $Ni(AcAc)_2$ from water at either 200 or 400 atm was less than 2%, while recovery of $Cu(AcAc)_2$ from water using the same extraction conditions was less than 12%. The low recoveries and poor precision in extraction efficiency of chelates can be explained by either the low solubility of metal chelates in supercritical CO_2 or changes in composition of the chelates at low pH's caused by CO_2 passing through water thus producing carbonic acid. Hedrick et al. have demonstrated extraction of phenols and organic bases from aqueous matrices. They observed strong interaction of basic compounds with aqueous acidic matrices [16–18]. Similar results were reported by Combs et al. [13] on a series of phenols in buffered aqueous solutions. $Ni(AcAc)_2$ and $Cu(AcAc)_2$ are known as kinetically labile complexes. Therefore, it is possible that these labile complexes lose one of the anionic ligands bonded to the metal and which makes the resulting cationic complex less extractable in supercritical CO_2 as shown below.

$$[ML_n]^0 \Leftrightarrow L^- + [ML_{(n-1)}]^+$$

Recovery of $Cr(AcAc)_3$ increased from 66 to 82% by increasing CO_2 pressure from 200 to 400 atm. The $Cr(AcAc)_3$ exhibited higher solubility in supercritical CO_2 compared with $Ni(AcAc)_2$ and $Cu(AcAc)_2$, thus, accounting for the higher extraction efficiency from an aqueous environment. Also, $Cr(AcAc)_3$ is known as a kinetically inert complex which means that the complex is not prone to hydrolysis or ligand displacement.

3.3. Recovery of metal hexafluoroacetylacetone complexes from water

Table 3 shows the extraction efficiency of $Ni(HFA)_2$, $Cu(HFA)_2$, and $Cr(HFA)_3$ samples from an aqueous environment. Percent recovery of $Ni(HFA)_2$ at either 200 or 400 atm was less than 12%. Recovery of $Cu(HFA)_2$ and $Cr(HFA)_3$, however, increased to above 50% at both pressures. The higher percent recovery of HFA complexes, compared with AcAc complexes, is due to enhanced solubility of fluorinated complex compared with non-fluorinated complex in supercritical CO_2. It was expected that full recovery of all chelates from water could be obtained since all of the HFA complexes in this study exhibited high solubility in supercritical CO_2. However, it was concluded from our solubility measurement and extraction efficiency results that the stability of these complexes was very much dependent on the extraction environment. It is believed that carbonic acid produced during the extraction promotes partial dissociation of the HFA complexes to yield less soluble species via acid catalyzed hydrolysis. Similar factors may have also caused poor precision in the extraction recovery. Further studies are being pursued to show these effects.

Table 3
Percent recovery of different metal hexafluoroacetylacetone complexes from aqueous environment at different pressures using supercritical CO_2

Metal complex	% Recovery, 200 atm	% Recovery, 400 atm
$Ni(HFA)_2$	6.4 (35)[a]	11 (40)
$Cu(HFA)_2$	49 (1)	51 (9)
$Cr(HFA)_3$	61 (10)	52 (9)

Extraction conditions: same as Table 2.
[a] % RSD for triplicate extractions are noted in parentheses.

3.4. Recovery of metal diethyldithiocarbamates from water

The results from extraction of both pre-formed $Ni(DDC)_2$ and $Cu(DDC)_2$ chelates from an aqueous environment and the recovery of Ni^{+2} and Cu^{+2} from an aqueous matrix by in-situ chelation using supercritical CO_2 under various conditions are given in Table 4. Extraction efficiency of $Ni(DDC)_2$ from water after 30 min at both pressures was 5.9 and 8.4% respectively, which was lower than the extraction efficiency of $Cu(DDC)_2$ using the same extraction conditions

(e.g., 10% at 200 atm and 38% at 400 atm). The low recovery and poor precision in the extraction efficiency of metal DDC complexes from water can be explained by the low solubility of DDC chelates in supercritical CO_2. $Ni(DDC)_2$ and $Cu(DDC)_2$ possess solubility of 8.5×10^{-7} and 1.1×10^{-6}, M respectively, in supercritical CO_2 at 100 atm and 50°C [4]. The higher extraction efficiency of $Cu(DDC)_2$ maybe due to its higher solubility in supercritical CO_2. A stepwise extraction for 120 min of $Cu(DDC)_2$ and $Ni(DDC)_2$ chelates spiked separately into water is shown in Fig. 2. The profiles obtained for the extraction of $Cu(DDC)_2$ and $Ni(DDC)_2$ suggest a solubility limited process. Therefore, an extended extraction time was deemed necessary to achieve a quantitative extraction of these chelates.

Similar results were obtained when excess DDC ligand was added to the water for direct in-situ chelation and extraction of Ni^{+2} and Cu^{+2}. Extraction efficiencies of Ni^{+2} and Cu^{+2} via in-situ chelation were less than 20% after 30 min of extraction (Table 4). A stepwise extraction profile of both $Ni(DDC)_2$ and $Cu(DDC)_2$, at 400 atm and 60°C, formed by in-situ chelation can be observed in Fig. 3. Total extraction of each in-situ chelate after 120 min equalled 48% for $Ni(DDC)_2$ and 42% for $Cu(DDC)_2$, while total recovery of spiked pre-formed $Cu(DDC)_2$ from water after 90 min was 109%. The lower recovery and poor precision in the supercritical CO_2 extraction of $Ni(DDC)_2$ and $Cu(DDC)_2$, obtained by in-situ

Table 4
Percent recovery of $Ni(DDC)_2$ and $Cu(DDC)_2$ pre-formed complexes and Ni^{+2} and Cu^{+2} via in-situ chelation from aqueous environment using supercritical CO_2

Metal DDC	% Recovery, 200 atm	% Recovery, 400 atm
$Ni(DDC)_2$	6 (97)[a]	8 (37)
$Ni(DDC)_2$, in-situ	—	11 (18)
$Cu(DDC)_2$	10 (26)	38 (6)
$Cu(DDC)_2$, in-situ	5.6 (35)	20 (20)

—No measurement was obtained.
[a] % RSD for triplicate extractions are noted in parentheses.

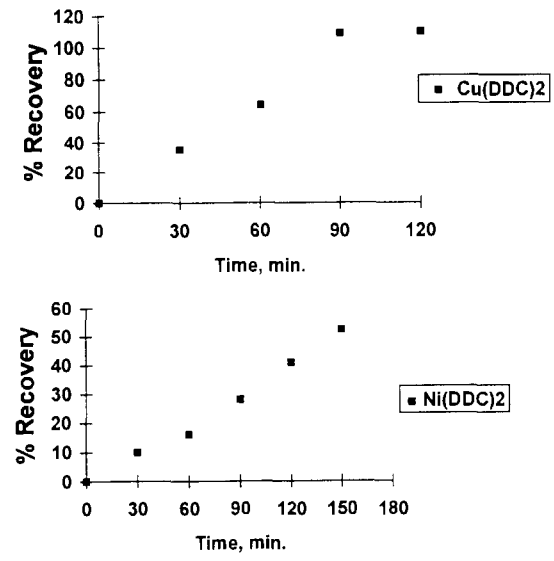

Fig. 2. Extraction profile for $Cu(DDC)_2$ and $Ni(DDC)_2$ complexes spiked separately into the water. Extraction conditions: 400 atm, 60°C, 2 ml min^{-1} liquid CO_2.

chelation can be explained by the fact that diethyldithiocarbamate ligand may decompose to produce CS_2 at low pH's. Our previous studies have demonstrated that the pH of aqueous solutions can easily drop to below 4 by continuous

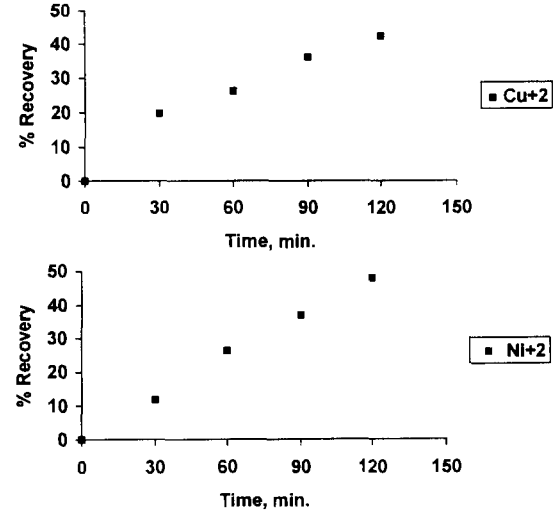

Fig. 3. Extraction profile for Cu^{+2} (A) and Ni^{+2} (B) ions via DDC in-situ chelation from water. Extraction conditions: 400 atm, 60°C, 2 ml min^{-1} liquid CO_2.

Table 5
Percent recovery $Ni(FDDC)_2$ and $Cu(FDDC)_2$ pre-formed complexes and Ni^{+2} and Cu^{+2} via in-situ chelation from an aqueous environment using supercritical CO_2

Metal FDDC	% Recovery, 200 atm	% Recovery, 400 atm
$Ni(FDDC)_2$	93 (7)[a]	103 (9)
$Ni(FDDC)_2$, in-situ	—	101[b]
$Cu(FDDC)_2$	95 (6)	94 (8)
$Cu(FDDC)_2$, in-situ	—	90[b]

—No measurement was obtained.
[a] *% RSD for triplicate extractions are noted in parentheses.
[b] Only two measurements were obtained due to limited mass of ligand.

bubbling of SF CO_2 through water [13]. Thus, if a large portion of the ligand in solution has decomposed during extraction, quantitative recovery of metal ion will not be possible since all metal ion would have not been fully chelated. As evidence for decomposition of DDC, a strong odor of CS_2 was noticed during extraction.

3.5. Recovery of bis(trifluoroethyl)dithiocarbamate complexes from water

Table 5 shows the recovery of both pre-formed metal FDDC complexes and Ni^{+2} and Cu^{+2} via in-situ chelation from water. Quantitative recovery of both pre-formed $Ni(FDDC)_2$ and $Cu(FDDC)_2$ at both 200 and 400 atm and 60°C was obtained. The increased metal complex solubility allowed quantitative recovery to occur in a short time period. Laintz et al. [6] have reported similar results. They concluded that high extraction efficiency of metal FDDC was related to large solubility of metal FDDC complexes in supercritical CO_2 and their high formation constant. In-situ chelation studies were performed by adding excess FDDC ligand directly to the aqueous extraction vessel containing Ni^{+2} or Cu^{+2}. After 30 min of extraction at either 200 or 400 atm, quantitative recovery of the metals was obtained. It was demonstrated that bis(trifluoroethyl)dithiocarbamate is the most effective ligand tested in this study for extraction of Ni^{+2} or Cu^{+2} from water. Unlike extraction of metal ions via in-situ chelation using DDC as a ligand, no decomposition of FDDC occurred during in-situ chelation of metal ions.

4. Conclusion

Solubility of Ni^{+2}, Cu^{+2}, and Cr^{+3} hexafluoroacetylacetone, and Cr^{+3} acetylacetone were measured in pure supercritical CO_2. Solubility of fluorinated chelates (e.g. $Cr(HFA)_3$) was at least an order of magnitude higher than the non-fluorinated (e.g., $Cr(AcAc)_3$) complexes and two orders of magnitude higher than metal FDDC complexes. Due to the low solubility of $Ni(AcAc)_2$ and $Cu(AcAc)_2$ in supercritical CO_2 and their poor chromatographic behavior, solubility measurements of these chelates was not feasible. Results from extraction efficiency of metal chelates from water demonstrated that fluorination of the ligand improved extraction efficiency by increasing volatility and solubility of the complex. However, stability of the ligand under supercritical conditions and aqueous acidic environments is very important. Extraction efficiency of metal DDC and metal FDDC showed quantitative recovery of chelate is feasible. However, longer extraction time is required to obtain quantitative recovery of metal DDC complexes. Also it was demonstrated that metal ions dissolved in aqueous solution can be extracted by supercritical CO_2 via in-situ chelation. However the extraction efficiency of ions is very much dependent on the type of ligand used as the chelating agent. Finally it was demonstrated that higher solubility of metal chelates in pure CO_2 does not necessarily mean a higher extraction efficiency of chelates. Extraction efficiency of chelates not only depends on their solubility in supercritical CO_2, but also depends on the matrix in which the chelates are located and the stability of the chelates in the surrounding environment.

Acknowledgements

This work was supported by a SBIR program of the United State Department of Energy under grant application no. 35158-95-I. Also we wish to thank Suprex Corp. for loan of their instrument and Air Products and Chemical Inc. for providing SFE grade CO_2.

References

[1] C.M. Wai, in Z.B. Alfassi and C.M. Wai (Eds.), Preconcentration Technique for Trace Elements, Ch. 4, CRC Press, Boca Raton, FL, 1991, 101–132.
[2] D.R. Gere, R. Board and D. McManigill, Anal. Chem., 54 (1983) 740–745.
[3] Y. Lin, R.D. Brauer, K.E. Laintz and C.M. Wai, Anal. Chem., 65 (1993) 2549–2551.
[4] K.E. Laintz, C.M. Wai, C.R. Yonker and R.D. Smith, J. Supercrit. Fluid, 4 (1991) 194–198.
[5] C.M. Wai, Y. Lin, R.D. Brauer, S. Wang and W.F. Beckert, Talanta, 40 (1993) 1325–1330.
[6] K.E. Laintz, C.M. Wai, C.R. Yonker and R.D. Smith, Anal. Chem., 64 (1992) 2875–2878.
[7] S. Wang, S. Elshani and C.M. Wai, Anal. Chem., 67 (1995) 919–922.
[8] Y. Liu, V. Lopez-Avila, M. Alcaraz, W.F. Beckert and E.M. Heithmar, J. Chromatogr. Sci., 31 (1993) 310-316.
[9] K.E. Laintz, J.J. Jya and C.M. Wai, Anal. Chem., 64 (1992) 311–315.
[10] J. Wang and W.D. Marshall, Anal. Chem., 66 (1994) 3900–3907.
[11] J.L. Hedrick and L.T. Taylor, Anal. Chem., 61 (1982) 1986–1988.
[12] A. Daneshfar, M. Barzegar and M. Ashraf-Khorassani, J. High Resolu. Chromatogr., 18 (1995) 446–448.
[13] M.T. Combs, M. Ashraf-Khorassani and L.T. Taylor, J. Supercrit. Fluids, 9 (1996) 122–127.
[14] L. Sucer and W. Jennings, Anal. Lett., 13 (1980) 497–500.
[15] C.A. Tooinche and T.H. Risby, J. Chromatogr. Sci., 16 (1978) 448–454.
[16] J.L. Hedrick and L.T. Taylor, J. High Resolu. Chromatogr., 15 (1992) 151–154.
[17] J.L. Hedrick, L.J. Mulcahey and L.T. Taylor, ACS Symp. Ser., 488 (1992) 206–220.
[18] J.L. Hedrick and L.T. Taylor, J. High Resolu. Chromatogr., 13 (1990) 312–316.

ELSEVIER

Talanta 44 (1997) 765–770

Talanta

Catalytic flow-injection determination of copper at nanogram levels by using color formation of *N*-phenyl-*p*-phenylenediamine with *m*-phenylenediamine in the presence of pyridine and ammonia as activators

Shigenori Nakano [a,*], Keiko Nakaso [a], Kazunori Noguchi [a], Takuji Kawashima [b]

[a] *Chemical Institute, Faculty of Education, Tottori University, Koyama-cho, Tottori 680, Japan*
[b] *Laboratory of Analytical Chemistry, Department of Chemistry, University of Tsukuba, Tsukuba 305, Japan*

Received 26 July 1996; received in revised form 30 August 1996; accepted 30 August 1996

Abstract

A spectrophotometric flow-injection method for determining copper(II) has been developed. It is based on the catalytic effect of copper(II) on the oxidative coupling of *N*-phenyl-*p*-phenylenediamine with *m*-phenylenediamine in the presence of hydrogen peroxide. Pyridine and ammonia as activators increased the absorbance for the copper(II)-catalyzed coloration, and the dye formed was stabilized by adding a non-ionic surfactant. The working range of the method was 0.1–2.0 ng ml^{-1} of copper(II) with a relative standard deviation 2.4% at a sampling rate of 30 h^{-1}. Interference from iron(III) was effectively suppressed by citric acid. Copper in natural water samples can be determined easily. © 1997 Elsevier Science B.V.

Keywords: Flow-injection photometric method; Catalytic reaction; Copper(II) determination; *N*-Phenyl-*p*-phenylenediamine; *m*-Phenylenediamine

1. Introduction

The application of catalyzed reactions to the trace analysis of metal ions is very attractive. By using an appropriate indicator reaction, nanogram and/or subnanogram amounts of a metal ion acting as a catalyst can be determined. The presence of ligands as activators increases the rate of the catalyzed reaction. High sensitivity and/or selectivity of catalytic methods can be achieved [1,2]. Furthermore, a surfactant having the ability to form organized assemblies can control reaction pathways and change reaction mechanisms [3]; its addition to the reaction system can improve sensitivity.

There have been many batchwise methods for the catalytic determination of copper, based on catalysis of various redox reactions [4–18]. These methods are able to determine the element at sub- and/or nanogram per ml levels; especially, by oxidative coupling of 3-methyl-2-benzothiazolinone hydrazone (MBTH) with *N*-ethyl-*N*-(2-hy-

* Corresponding author.

PII S0039-9140(96)02096-6

droxy-3-sulphopropyl)-3,5-dimethoxyaniline which, in the presence of hydrogen peroxide, allowed as little as 2 pg ml^{-1} of copper(II) to be determined [18]. However, their analytical conditions should be strictly controlled and the procedures are time-consuming.

Flow-injection analysis is an important technique in the development of kinetic-based methods, because control of the reagent addition and the reaction time is easy [2]. Thus, catalytic methods offer better reproducibility and sampling frequency as well as higher sensitivity by the aid of flow-injection mode. Some indicator reactions catalyzed by copper(II) were applied to flow-injection systems [19–21]. The oxidation of thiosulfate with iron(III) was employed for the determination of 0–180 ng ml^{-1} of copper [19]. Satoh et al., [20] reported a flow-injection determination for copper based on the catalytic effect on the oxidative coupling of MBTH with *N,N*-dimethylaniline by hydrogen peroxide. The detection limit of this method was 0.05 ng ml^{-1} of copper(II). A chemiluminescent reaction of 1,10-phenanthroline with hydrogen peroxide was adapted to the flow-injection determination of ultratrace levels of copper(II) [21].

In the previous paper [22], we have developed a catalytic flow- injection method for the determination of 0.5–30 ng ml^{-1} of iron using an oxidative coupling of *N*-phenyl-*p*-phenylenediamine (PPDA) with *m*-phenylenediamine (PDA) in the presence of hydrogen peroxide and polyoxyethylene(20) sorbitan monooleate (Tween 80) as a surfactant. This indicator reaction was also catalyzed by trace amounts of copper(II). Furthermore, pyridine and ammonia acted as activators in the copper(II)-catalyzed reaction system. This paper describes the highly sensitive flow-injection photometric determination of copper(II) based on catalysis of the coloration system of PPDA, PDA and hydrogen peroxide. In order to obtain higher sampling frequency and prevent the adsorption of the reaction product on the inner wall of the reaction coil, Tween 80 was also added to the present system. The interference of iron(III) was effectively eliminated with citric acid as a masking agent. Copper(II) in the range 0.1–2.0 ng ml^{-1} can be determined with a sampling rate of 30 h^{-1}.

2. Experimental

2.1. Reagents

All solutions were prepared from analytical grade reagents and deionized water purified with a Millipore Milli-Q system.

A copper(II) standard solution (1.0 mg ml^{-1}) was obtained from Wako Junyaku, Japan. The working standard solutions were prepared daily by diluting the standard solution with 0.1 mol l^{-1} hydrochloric acid.

N-Phenyl-*p*-phenylenediamine hydrochloride (PPDA) obtained from Aldrich was used as received. A 1.0×10^{-3} mol l^{-1} PPDA solution containing 0.5% w/v polyoxyethylene(20) sorbitan monooleate (Tween 80) was prepared. *m*-Phenylenediamine dihydrochloride (PDA) was purified by recrystalization from hydrochloric acid and a 1.0×10^{-2} mol l^{-1} PDA stock solution was prepared. A hydrogen peroxide solution (0.5 mol l^{-1}) was prepared by dilution of a commercial solution (30%, Mitsubishi Gasu Kagaku) with water. Acetic acid (1.0 mol l^{-1}), pyridine (1.0 mol l^{-1}), ammonia (2.0 mol l^{-1}) and citric acid (0.1 mol l^{-1}) stock solutions were also prepared.

A working mixed solution of PDA (3.0×10^{-3} mol l^{-1}), acetic acid (0.1 mol l^{-1}), ammonia (0.5 mol l^{-1}) and citric acid (2.0×10^{-3} mol l^{-1}) was prepared by mixing the stock solutions; the pH of the mixed solution was adjusted to about 5.6 with 1.0 and 0.1 mol l^{-1} hydrochloric acid.

2.2. Apparatus

A schematic diagram of the flow-injection system used for the determination of copper(II) is shown in Fig. 1. All connecting lines and reaction coil were made from 0.5 mm i.d. Teflon tubing. Carrier and reagent solutions were propelled by two double-plunger micropumps (Sanuki Kogyo, DMX-2400T). Sample solutions were introduced into the flow-line by a sixway injection valve (Sanuki Kogyo SVM-6M2) with a loop. The reaction coil was immersed in a circulating thermostated bath (Toyo LH-l000C). A spectrophotometer (Soma Kougaku S-3250) with

a 10-mm micro flow-cell (8 μl) and a recorder (Nippon Denshi Kagaku V1250) were used for detecting and recording the absorbance of the reaction product. An Hitachi 200–10 double-beam spectrophotometer with 10-mm cells and a Toa Model HM-5S pH meter were also used.

2.3. Procedure

Carrier (R1, 0.1 mol l^{-1} hydrochloric acid) and reagent solutions in the reservoirs R2 (hydrogen peroxide), R3 (PPDA and Tween 80) and R4 (PDA, acetic acid, pyridine, ammonia and citric acid) were pumped into the analytical line at a flow rate of 1.0 ml min^{-1} (Fig. 1). An aliquot of the sample solution (215 μl) was introduced into the carrier stream by a loop-valve injector (*S*), and then merged in the reagent solutions. The color formation of PPDA with PDA took place in the reaction coil (RC, 8 m) submerged in the thermostated bath at 55.0 ± 0.1°C. The absorbance of the colored product was continuously monitored at 620 nm.

3. Results and discussion

PPDA reacts with PDA to form a blue dye in the presence of hydrogen peroxide. The dye produced is thought to be *N*-phenyl-*N*′2′,4′-diaminobenzene-1,4-benzoquinone diiminonium ion and has a absorption maximum at 620 nm in the presence of Tween 80, as described previously [22]. The rate of coloration is catalytically accelerated by trace amounts of copper(II) in the slightly acidic medium.

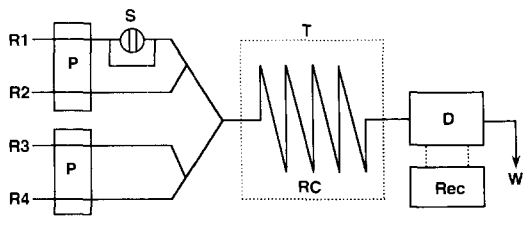

Fig. 1. Flow diagram for the determination of copper(II). R1, carrier (0.1 mol l^{-1} HCl); R2, 0.5 mol l^{-1} H_2O_2; R3, mixture of 1.0×10^{-3} mol l^{-1} PPDA and 0.5% w/v Tween 80; R4, mixture of 3.0×10^{-3} mol l^{-1} PDA, 0.5 mol l^{-1} ammonia, 0.2 mol l^{-1} pyridine and 2.0×10^{-3} mol l^{-1} citric acid; P, micropump (1.0 ml min^{-1}); S, sample injector valve (215 μl); RC, reaction coil (8 m); T, thermstated bath (55°C); D, detector (620 nm); Rec, recorder; and W, waste (pH 4.6–4.7).

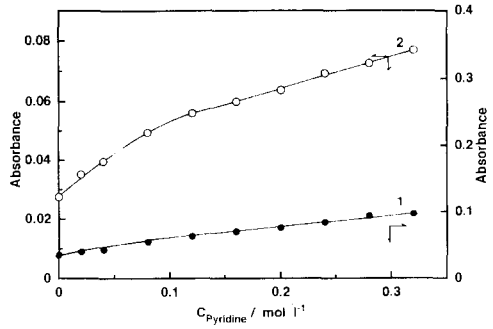

Fig. 2. Effect of pyridine concentration on the uncatalyzed (1) and catalyzed (2) reactions. Conditions as in Fig. 1 except for pyridine concentration. $C_{Cu(II)}$, 2.0 ng ml^{-1}.

3.1. Choice of activator and surfactant

The catalytic action of metal ion can be modified with an activator. It yields better sensitivity and lower limit of detection in a catalytic method [1,2]. Ammonia was used as an activator and an alkaline in the present system, because it is known as an activator for the copper(II)-catalyzed reaction [5]. By using the present flow system, the effect of other ligands such as pyridine, 2,2′-bipyrine (bpy) and 1,10-phenanthroline (phen) on the catalyzed reaction were examined in the presence of ammonia; these ligands enhanced the catalytic activity of copper(II). However, bpy and phen acted as activators for iron(III) which interfered with the copper(II) determination. Thus, pyridine was chosen as an activator for the copper(II)-catalyzed reaction. Fig. 2 and Fig. 3 show the effect of pyridine and ammonia concentrations on the uncatalyzed and catalyzed reactions. The peak heights increased with increasing the concentrations of these ligands. The concentrations of pyridine and ammonia were fixed at 0.2 and 0.5 mol l^{-1}, respectively.

As descried previously [22], the presence of a surfactant at concentrations above the critical micelle concentration (CMC) accelerated the catalyzed reaction and stabilized the dye produced. In

addition, the surfactant suppressed the adsorption of the dye on the inner surface of Teflon tubing. It led to higher sensitivity and sampling frequency. Cationic and non-ionic surfactants were examined since sodium dodecylsulphate (SDS) was observed to precipitate from the reaction system. The tested surfactants were tetradecyltrimethylammonium bromide (TTAB), tetradecyldimethylbenzylammonium chloride (zephiramine, TDBAC), hexadecyltrimethylammonium bromide (HTAB), hexadecylpyridinium chloride (HPC), polyoxyethylene(23) dodecanol (Brij-35), polyoxyethylene(9.5)p-1,1,3,3,-tetramethylbutylephenol (Triton X-100), polyoxyethylen(20) sorbitane monolaurate (Tween 20) and Tween 80. In the presence of cationic surfactants such as TTAB, TDBAC, HTAB and HPC, peak heights for the catalyzed reaction were almost constant and/or decreased with increasing surfactant concentration. On the other hand, the presence of non-ionic surfactants such as Brij-35, Triton X-100, Tween 20 and 80 at concentrations above the CMC increased peak heights and decreased peak tailing. In the present copper(II)-catalyzed coloration system, 0.5% w/v of Tween 80 was used.

3.2. Effect of reaction variables

The flow manifold and chemical variables were optimimized for the determination of copper(II). The baseline and the peak height increased with longer reaction time, i.e., lower flow rates and longer coil. The baseline was due to the uncatalyzed reaction and the peak height was due to the catalyzed reaction. The higher the height of baseline, the poorer its stability. The flow rate of streams and the reaction coil length were selected as 1.0 ml min^{-1} and 8 m, respectively, for the procedure. The peak height and peak width increased with increasing sample volume. A 215-μl sample solution was injected into the flow-line. As the reaction temperature was elevated, the higher rates of uncatalyzed and catalyzed reactions were observed. Considering sensitivity and baseline stability, the reaction coil was kept at 55°C.

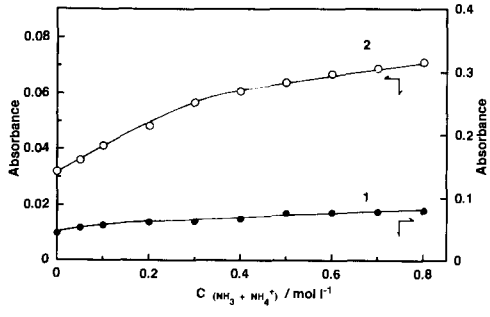

Fig. 3. Effect of total ammonia concentration on the uncatalyzed (1) and catalyzed (2) reactions. Conditions as in Fig. 1 except for ammomia concentration. $C_{Cu(II)}$, 2.0 ng ml^{-1}.

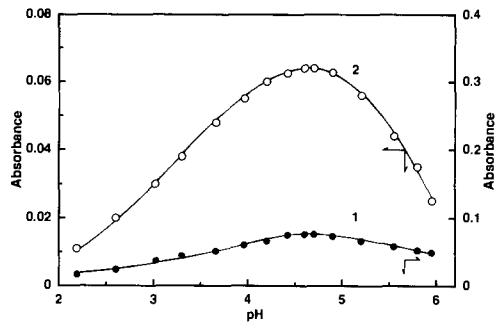

Fig. 4. Effect of pH on the uncatalyzed (1) and catalyzed (2) reactions. Conditions as in Fig. 1 except for reaction pH. $C_{Cu(II)}$, 2.0 ng ml^{-1}.

Fig. 4 shows the effect of pH on the copper(II)-catalyzed reaction over the range 2–6; a maximum peak height is obtained in the pH range 4.6–4.7. The reaction mixture in the coil was adjusted in this pH range. Acetic acid was chosen as a buffer because the acid up to 0.2 mol l^{-1} did not affect the peak heights. The concentration of acetic acid was fixed at 0.1 mol l^{-1} for the procedure.

The effects of PPDA, PDA and hydrogen peroxide concentrations were examined. An increase in the PPDA concentration caused an increase in the rate of uncatalyzed and catalyzed reactions. The concentration of PPDA was selected at 1.0×10^{-3} mol l^{-1} because of baseline stability due to the uncatalyzed reaction. With the increase in the PDA concentration, the rate of the catalyzed reaction increased, but it reached its maximum at concentrations above 2.0×10^{-3} mol l^{-1}. A 3.0×10^{-3} mol l^{-1} of PDA solution was used. As

the hydrogen peroxide concentration increased, the heights of baseline and peak also increased. A 0.5 mol l^{-1} of hydrogen peroxide concentration was selected being considered with the height of baseline.

3.3. Calibration graph

The calibration graphs for copper(II) were prepared by the recommended procedure. The relationship between peak height and copper(II) concentration was linear from 0.1 to 2.0 ng ml^{-1}. The detection limit for a signal to noise ratio of two was 0.05 ng ml^{-1}. The reproducibility was satisfactory; the relative standard deviations for ten determinations of 1.0 and 2.0 ng ml^{-1} of copper(II) were 2.4 and 1.6%, respectively. The sample throughout was about 30 h^{-1}.

3.4. Effect of diverse ions

Iron(III) also catalyzed this indicator reaction described previously [22]. Some complexing agents such as citric acid, diphosphate and malonic acid, which did not act as activators for iron(III), were examined in order to eliminate the interference of the element. Among them, citric acid was found to be the most effective masking agent for iron(III). At citric acid concentrations above 1.0×10^{-3} mol l^{-1}, 100 ng ml^{-1} iron(III) can be effectively masked in the determination of 1.0 ng ml^{-1} copper(II). A concentration of 2.0×10^{-3} mol l^{-1} citric acid was used as a masking agent for iron(III).

Table 1 summarizes the tolerance limits of other diverse ions on the determination of 1.0 ng ml^{-1} copper(II) in the presence of citric acid; an error of 5% are considered. Most of ions examined did not interfere with the copper(II) determination in concentrations up to at least 100-fold excesses. Chromium(VI) at the amount of 100 ng ml^{-1} gave positive interference; it did not interfere at amounts below 10 ng ml^{-1}. The levels of these metal ions normally presented in the natural water samples were tolerable.

3.5. Application

To evaluate the applicability of the proposed flow-injection method, it was applied to the determination of copper in river, lake and seashore water samples. These samples were filtered through a 0.45-μm Millipore filter and then concentrated hydrochloric acid was added to the filtrates (about pH 1). These filtrates were injected into the flow line after appropriate dilution; both calibration curve and standard addition methods were carried out. The results are summarized in Table 2. The values obtained from the calibration curve and the standard addition methods are in good agreement with each other. For the filtrates except for seashore waters, an aliquot of 50 ml was digested with nitric and perchloric acids because some copper species in the samples did not catalyze the indicator reaction [5]. As can be seen in Table 2, the copper contents in the digested samples were larger than those without digestion; reactive and non-reactive copper species in the fresh water samples could be found.

4. Conclusions

A simple and rapid catalytic flow-injection method is proposed for the determination of copper(II) at levels as low as 0.05 ng ml^{-1}, based on

Table 1
Tolerance limits for diverse ions in the determination of 1.0 ng ml^{-1} copper(II)

Tolerance limit/ ng ml^{-1}	Ion added
100 000	Ba(II), Hg(II), K(I), Na(I), Sr(II), BO_3^{3-}, ClO_4^-, CO_3^{2-}, NO3−, PO43−, SO_4^{2-}, Tartrate
10 000	As(III), Ca(II), Cd(II), Mg(II), Mn(II), Pb(II), Se(IV), Sn(II), Sn(IV), Te(IV), Br^-, F
1 000	Ag(I), As(V), Ce(III), Ce(IV), Co(II), Cr(III), Mo(VI), Ti(IV), W(VI), Zn(II), I^-, NO_2^-, Oxalate
100	Al(III), Bi(III), Fe(II), Fe(III), Ni(II), V(IV), V(V)
10	Cr(VI)

Table 2
Determination of copper in river, lake and seashore water samples

Sample[a]	Copper in sample[b]/ng ml^{-1}		
	(I)[c]	(II)[d]	Acid digestion[c]
River water			
Shiomi-gawa	0.57 ± 0.02	0.54 ± 0.01	1.10 ± 0.02
Hosyouji-gawa	0.56 ± 0.03	0.59 ± 0.01	1.57 ± 0.04
Shinkamo-gawa	3.07 ± 0.05	2.97 ± 0.08	4.96 ± 0.01
Lake water			
Koyama-ike	1.15 ± 0.03	1.24 ± 0.08	3.07 ± 0.03
Mizushiri-ike	2.71 ± 0.08	2.86 ± 0.07	6.93 ± 0.05
Togo-ike	0.79 ± 0.04	0.75 ± 0.02	4.41 ± 0.02
Seashore water			
Utai	2.78 ± 0.05	2.68 ± 0.09	—
Houjou	1.86 ± 0.03	1.79 ± 0.04	—
Yonago	0.98 ± 0.07	0.95 ± 0.02	—

[a] Collected at Tottori Prefecture, Japan.
[b] Corrected for addition ($n = 3$).
[c] Calibration curve method.
[d] Standard addition method.

its catalytic effect on the color-forming system of PPDA, PDA and hydrogen peroxide. The presence of pyridine, ammonia and Tween 80 in the reaction system led to higher sensitivity and sampling frequency. The selectivity of the method was improved by adding citric acid. The method was successfully used for the determination of reactive and non-reactive copper species in natural water samples with and without acid digestion. Due to easy operation and inexpensive instrumentation, the present method should be useful for monitoring natural water.

References

[1] D. Perez-Bendito and M. Silva, Kinetic Methods in Analytical Chemistry, Horwood, Chichester, 1988.
[2] T. Kawashima and S. Nakano, Anal. Chim. Acta, 261 (1992) 167.
[3] D. Perez-Bendito and S. Rubio, Trends Anal. Chem., 12 (1993) 9.
[4] S. Nakano, M. Tanaka, M. Fushihara and T. Kawashima, Microchim. Acta [Wien], I (1983) 457.
[5] S. Nakano, H. Ihara, M. Tanaka and T. Kawashima, Microchim. Acta [Wien], I (1985) 445.
[6] E. Casassas, A. Izquierdo-Ridorsa and L. Puignou, Talanta, 35 (1988) 199.
[7] A. Velasco, M. Silva and M. Valcarcel, Anal. Chim. Acta, 229 (1990) 107.
[8] T. Kamidate, K. Itoh and H. Watanabe, Anal. Sci., 6 (1990) 769.
[9] R. Marin Saez, F.J. Lopez Benet and M.J. Mezquita Cases, Analusis, 18 (1990) 358.
[10] M. Kamaya, I. Ohuri, K. Kaga, E. Ishii and T. Murakami, Fresenius Z. Anal. Chem., 338 (1990) 918.
[11] E. Gomez, J.M. Estela and V. Cerda, Thermochim. Acta, 165 (1990) 225.
[12] V.P. Dedkova and E.A. Likhonina, Zh. Anal. Khim., 46 (1991) 193.
[13] M.L. Lunar, S. Rubio and D. Perez-Bendito, Talanta, 39 (1992) 1163.
[14] F.H. Hernandez, M.T. Castillo, J.V. Sancho and J. Beltran, Analusis, 20 (1992) 275.
[15] A. Katayama, K. Itoh, M. Furukawa, T. Kamidate and H. Watanabe, Nippon Kagaku Kaishi, (1992) 318.
[16] C. Sanchez-Pedreno, J.A. Ortuno and J. Martine-Rodenas, Fresenius J. Anal. Chem., 344 (1992) 100.
[17] S. Nakano, M. Hayashi and T. Kawashima, Anal. Sci., 9 (1993) 695.
[18] S. Ohno, N. Teshima, T. Watanabe, H. Itabashi, S. Nakano and T. Kawashima, Analyst, 121 (1996) 1515.
[19] S. Kawakubo, T. Katsumata, M. Iwatsuki, T. Fukasawa and T. Fukasawa, Analyst, 113 (1988) 1827.
[20] K. Satoh, N. Iwamura, N. Teshima, S. Nakano and T. Kawashima, J. Flow Injection Anal., 10 (1993) 245.
[21] M. Ishii, M. Yamada and S. Suzuki, Bunseki Kagaku, 35 (1986) 373.
[22] S. Nakano, K. Tsujii and T. Kawashima, Talanta, 42 (1995) 1051.

ELSEVIER

Talanta 44 (1997) 771–780

Talanta

Simplex optimisation of conditions for the determination of antimony in environmental samples by using electrothermal atomic absorption spectrometry

Iris Koch [a], Christopher F. Harrington [a], Kenneth J. Reimer [b], William R. Cullen [a,*]

[a] *University of British Columbia, Department of Chemistry, 2036 Main Mall, Vancouver, British Columbia V6T 1Z1, Canada*
[b] *Environmental Sciences Group, The Royal Military College of Canada, Kingston, Ontario K7K 5L0, Canada*

Received 15 April 1996; received in revised form 12 September 1996; accepted 12 September 1996

Abstract

Analysis of the total antimony in plant material was unsuccessful using the electrothermal atomic absorption spectrometry (ETAAS) conditions recommended by the instrument manufacturer. For this reason, an optimisation procedure utilising the Plackett–Burman method, simplex optimisation and visualisation of the generated response surface via principal components analysis, was carried out. The Plackett–Burman method was used to eliminate four of the initial variables chosen. Four variables (atomisation temperature, atomisation time, ash temperature and modifier concentration) were subsequently optimised using the composite modified simplex method and the results were visualised as a contour diagram, after reduction to two principal components. The optimised conditions were used for the analysis of both an acid digested pine needle standard reference material (NIST 1575) and a pond weed sample, collected from a contaminated site at Yellowknife Bay, Yellowknife, NWT, Canada. The total concentration of antimony present in the pine needles was statistically indistinguishable from the non-certified value, as was the value for the pond weed sample, compared with a value determined by neutron activation analysis (NAA). The results for the analysis of the pond weed sample by ETAAS agreed with those obtained from a subsequent analysis by inductively coupled plasma-mass spectrometry. © 1997 Elsevier Science B.V.

Keywords: Antimony; Electrothermal atomic absorption spectroscopy; Environmental samples; Simplex optimisation and Plackett–Burman design

1. Introduction

Antimony has been found in biological, geological and water samples [1–4], and its toxicity has led the United States Environmental Protection Agency (US-EPA) to consider it and its compounds priority pollutants [5]. Common techniques for determining the total amount of antimony include: inductively coupled plasma mass spectrometry (ICP-MS) or atomic emission spectroscopy (ICP-AES) and hydride generation, followed by different atomisation methods such as electrothermal or flame heated quartz tube atomic

* Corresponding author. Tel.: +1 604 8222938; fax: +1 604 8222847.

PII S0039-9140(96)02101-7

Table 1
Plackett–Burman design ($n = 12$) for the determination of significant variables to optimise by using simplex optimisation
Designation:

Code	Variable	Lower level (−)	Upper level (+)
Dt	Dry time (s)	30	70
DT	Dry temperature (°C)	60	90
At	Ash time (s)	1	3
AT	Ash temperature (°C)	1000	1300
Att	Atomisation time (s)	1	3
AtT	Atomisation temperature (°C)	1800	2300
AtR	Atomisation ramp (° s^{-1})	260	1400
MC	Modifier concentration (mg l^{-1} Pd)[a]	100	700
D	Dummy	No change	No change
D	Dummy	No change	No change
D	Dummy	No change	No change

Matrix:

Expt	Dt	DT	At	AT	Att	AtT	AtR	MC	D	D	D
1	+[b]	+	−	+	+	+	−	−	−	+	−
2	−	+	+	−	+	+	+	−	−	−	+
3	+	−	+	+	−	+	+	+	−	−	−
4	−	+	−	+	+	−	+	+	+	−	−
5	−	−	+	−	+	+	−	+	+	+	−
6	−	−	−	+	−	+	+	−	+	+	+
7	+	−	−	−	+	−	+	+	−	+	+
8	+	+	−	−	−	+	−	+	+	−	+
9	+	+	+	−	−	−	+	−	+	+	−
10	−	+	+	+	−	−	−	+	−	+	+
11	+	−	+	+	+	−	−	−	+	−	+
12	−	−	−	−	−	−	−	−	−	−	−

[a] Experiments were carried out with a constant injected volume of 10 µl.
[b] '+' and '−' symbols correspond to the upper and lower levels of variable values, as defined by the preceding table.

absorption spectroscopy (HG-QT-AAS) [1–3]. The preconcentration of antimony hydride in a graphite furnace, followed by atomisation has recently been developed as another method of analysis [6,7].

All these methods give low detection limits, but ICP based methods are expensive for routine analysis. Hydride generation may not give 100% recovery when non-hydride forming species are present in the sample and is labour intensive. Electrothermal atomic absorption spectroscopy (ETAAS) is a widely used analytical tool for the determination of many trace metals, including antimony, in a wide variety of sample matrices [8–11]. The use of ETAAS for the determination of total antimony is cost effective and simple, but no formal optimisation of conditions has been reported for plant samples.

The very first studies [12] on the graphite furnace technique showed that the sample matrix has a pronounced effect on the absorbance signal observed for a particular element. These effects often lead to systematic errors when determining metals in complex organic matrices and result from substances not being fully volatilised prior to atomisation of the metal. Optimisation of instrumental conditions is therefore a prerequisite for development of an environmental analytical protocol using electrothermal AAS.

Until recently it was usual to optimise a system using a one-factor-at-a-time-approach, in which each variable but one is held at a low level and

Table 2
Plackett–Burman design ($n = 8$) for the determination of additional significant variables to optimise by using simplex optimisation
Designation:

Code	Variable	Lower level (−)	Upper level (+)
Dt	Dry time (s)	30	70
DT	Dry temperature (°C)	60	90
At	Ash time (s)	1	3
D	Dummy	No change	No change
AT	Ash temperature (°C)	800	1400
AtT	Atomisation temperature (°C)	1800	2300
D	Dummy	No change	No change

Matrix:

Expt.	Dt	DT	At	D	AT	AtT	D
1	+[a]	+	+	−	+	−	−
2	−	+	+	+	−	+	−
3	−	−	+	+	+	−	+
4	+	−	−	+	+	+	−
5	−	+	−	−	+	+	+
6	+	−	+	−	−	+	+
7	+	+	−	+	−	−	+
8	−	−	−	−	−	−	−

[a] '+' and '−' symbols correspond to the upper and lower levels of variable values, as defined by the preceding table.

the response is evaluated at the lower and the upper level of the factor being tested. Each variable is treated in turn, until the response is maximised or minimised, depending on the system. This approach is far from adequate because there is no guarantee that an optimum response will be found, it requires a large number of experiments to be carried out and the presence of inter-relationships between the variables (e.g., modifier concentration and ash temperature) means that the optimum obtained will depend on the initial conditions chosen. Factorial experiments, in which all the factors are varied simultaneously according to a pre-set design, have also been used to optimise analytical systems. However, this approach is highly dependent on the levels of each factor and thus, it works best when some prior knowledge of the system is available. It also requires a large amount of experimentation when more than three variables are investigated.

Simplex optimisation is a highly efficient, multifactor, empirical feedback, optimisation procedure, that does not require the large number of experiments nor the initial variable information that is necessary with the two methods outlined above. This procedure 'homes in' on the optimum response region by driving the experiments in the direction of steepest ascent of the response surface. The optimum thus obtained is generally a local optimum, but some assurance that it is the overall optimum can be obtained by repeating the search from different starting conditions to see if the same conditions are reached.

Simplex optimisation is now routinely used as a method of maximising a response [13,14] or reducing interferences [15,16] in the analysis of trace elements. In the present work the use of the instrument manufacturer's recommended operating conditions [17] for the determination of antimony by ETAAS were completely unsuccessful, yielding no absorbance maximum. These conditions were: dry at 75°C for 5 s, then at 90°C for 60 s, then at 120°C for 10 s, hold at 120°C for 2 s, ramp to 2000°C in 1 s (maximum ramp rate), atomise at 2000°C for 3 s, clean at 2000°C for 1 s.

A two stage approach was used to optimise the experimental conditions used for the determination of antimony in plant material. The first part

Table 3
Range and stepsize of the variables being optimised by the composite modified simplex method

Variable	Lower limit	Upper limit	Stepsize[a]
Atomisation temperature (°C)	1400	2700	100
Atomisation time (s)	0	4	1
Ash temperature (°C)	800	1600	50
Modifier concentration (mg l^{-1})[b]	100	900	100

[a]Same units as variables.
[b]Experiments carried out with a constant injected volume of 10 μl.

of the investigation involved the use of the Plackett–Burman method to screen a number of potential variables to select the most appropriate to optimise using the composite modified simplex method [18,19]. The principle advantages of this approach are that information concerning the significance of each variable is obtained (Plackett–Burman method) and the optimum conditions are efficiently reached, with less experimentation than would be necessary if none of the variables had been eliminated. Additionally, visualising the response surface eliminates the need for univariate searches around the optimum, which are often carried out to check that the optimum is correct. These goals are not possible using a one-step-at-a-time-approach, or a factorial experiment.

To check the accuracy of the developed methodology the concentration of antimony in a pine needle standard reference material (SRM), NIST 1575, was determined. The pond weed sample was acid digested and methanol extracted and these samples were statistically compared with results obtained by ICP-MS, as well as by neutron activation analysis (NAA).

2. Experimental

2.1. Reagents

Concentrated nitric and hydrochloric acids (both double sub-boiling distilled, Seastar Chemicals Inc., Sidney, BC), concentrated sulphuric acid (Analytical grade, BDH Chemicals, Toronto, ON), and glacial acetic acid (Reagent grade, Fisher Scientific, Nepean, ON). Hydrogen peroxide (30%) (Assurance grade, BDH Chemicals, Toronto, ON), D-tartaric acid (Reagent grade, Allied Chemical Canada Ltd., Canada), palladium nitrate ($Pd(NO_3)_2.2H_2O$, Reagent grade, Sigma Chemical, St. Louis, MO), citric acid (Certified, Fisher Scientific, Fairlawn, NJ).

Water was purified to a final resistivity of better than 1 M ohm (Barnstead Mega-Pure system, Barnstead/Thermolyne, Dubuque, IA). Methanol (HPLC grade, Fisher Scientific, Nepean, ON). A methanol/water (1/1 v/v) solvent mixture was used to extract the aqueous antimony species. Antimony metal (Certified, Fisher Scientific, Fair Lawn, NJ) and 1000 mg l^{-1} indium (Spectroscopy standard, High-Purity Standards, Charleston, SC).

The freeze dried pine needle standard reference material 1575, was obtained from the National Institute of Standards and Technology (NIST, Washington, DC). The pond weed sample (*Potomogetan pectinatus*) was collected from a site contaminated with mine tailings (Yellowknife Bay, NWT, Canada) as described previously [20] and freeze dried. The pine needle SRM (NIST 1575) was chosen as a representative standard reference material because it contains an uncertified antimony concentration of 0.2 mg kg^{-1}.

2.2. Preparation of samples and standards

The pine needles (1575), and pond weed were dried to constant weight and then acid digested. Acid digestions were carried out in duplicate by adding 3 ml of concentrated nitric acid, 3 ml of 30% hydrogen peroxide, and 1 ml of concentrated sulphuric acid to a 250 ml round bottom flask containing pine needles (0.5 g) or pond weed (0.25–0.40 g) and refluxed for 3 h as described

Table 4
Simplex experiments and responses

Expt. no.	Atomisation temp. (°C)	Atomisation time (s)	Ash temp. (°C)	Modifier conc. (mg l^{-1})[a]	Point type[b]	Response[c] (absorbance)
1	1800	0	1400	500	I	0.103
2	1800	3	800	500	I	0.056
3	2200	0	1000	900	I	0.085
4	2400	0	1400	200	I	0.179
5	2400	3	1400	200	I	0.026
6	2100	0	1100	500	R	0.145
7	2700	0	1050	200	R	0.139
8	2500	0	1600	100	R	0.000
9	2300	0	800	600	C	0.116
10	2700	0	1050	100	R	0.138
11	2600	0	1600	100	R	0.000
12	2400	0	1050	400	C	0.155
13	2100	0	1450	500	R	0.264
14	1800	0	1600	600	E	0.055
15	1700	0	1600	700	R	0.048
16	2400	0	1200	300	C	0.217
17	2300	0	1600	300	R	0.009
18	2200	0	1250	500	C	0.204
19	2000	0	1600	500	R	0.043
20	2300	0	1200	400	C	0.167
21	2000	0	1300	700	R	0.105
22	2300	0	1400	300	C	0.266
23[d]	2200	0	1350	400	F	0.280
24	2000	0	1250	600	R	0.129
25	2300	0	1350	300	C	0.258
26	2300	0	1350	400	F	0.262
27	2300	0	1450	300	R	0.214
28	2200	0	1400	400	C	0.270
29	2000	0	1550	500	R	0.128

[a] Constant volume of 10 μl.
[b] Initial (I), reflection (R), contraction (C), extension (E) and fit (F).
[c] Response is mean of 3 determinations.
[d] Optimum conditions.

elsewhere [21]. An additional pine needle digestion was carried out by heating 1 g of material with the above acid/hydrogen peroxide mixture, in a vial on a hot plate, at 90°C for 3 h. After the digestions were complete, the partially evaporated samples were diluted to 5 ml (pine needles) and 10 ml (pond weed) using deionised water.

Extraction of the pondweed was carried out by sonicating 0.5 g dry material with 10 ml methanol/water (1/1 v/v) for two samples, and 10 ml 0.2 M acetic acid for one sample. The sample and solvent were sonicated for 20 min, the mixture was centrifuged at 3000 rpm for 10 min. and the supernatant was decanted. This was repeated five times and the combined extracts were evaporated under reduced pressure to dryness and made up to 5 ml with water.

A stock solution of 1000 mg l^{-1} antimony solution was prepared by dissolving 0.1000 g antimony metal in aqua regia and diluting to 100 ml with 1% D-tartaric acid. The 50 and 25 μg l^{-1} solutions for use in the standard additions determinations were prepared fresh daily from the stock.

The palladium modifier solution was prepared by dissolving 0.1083 g palladium(II) nitrate dihy-

Table 5
t values for 12 and 8 variable designs used in the Plackett–Burman experiments

Variables	Dt	DT	At	AT	Att	AtT	AtR	MC
12	−1.58	2.55	−0.97	1.74	−4.46*	−0.83	−2.46	3.49*
8	−0.54	−0.79	−2.34	14.90*	—	18.20*	—	—

* Indicates that the variable is significant at the 95% confidence level.

drate in 0.5 ml of concentrated nitric acid and diluting to 100 ml with 2% citric acid solution to give a 1000 mg l^{-1} Pd solution. This stock solution was then diluted further with 2% citric acid solution to give the various concentrations needed for the experiments.

Indium solution was used as an internal standard in the ICP-MS determinations and was prepared by diluting an appropriate volume of a 200 μg l^{-1} standard solution so that the final concentration was 10 μg l^{-1} in each sample.

2.3. Instrumentation

An atomic absorption spectrometer (Varian Techtron Model 1275, Australia) fitted with an auto-sampler, graphite furnace and programmer (GTA-95) was used throughout this work. The antimony hollow cathode lamp (SpectrAA, Varian, Australia) was operated at 10 mA with a slit corresponding to a spectral bandwidth of 0.2 nm and the 217.9 nm line was monitored. Continuous background correction was by a deuterium lamp (Varian, Australia). Pyrolytically coated graphite tubes (Varian, Germany) were used.

The ICP-MS measurements were carried out using a VG PlasmaQuad 2 turbo plus instrument (VG Elemental, Fisons Scientific Equipment, Winsford, Cheshire, UK), operated at 1350 W RF power. Cooling, auxiliary and nebulizer gases (Ar) were at flow rates of 13.82, 0.69 and 1.00 l min^{-1}, respectively. Masses were monitored in the peak jumping mode by using m/z 115 (In) and 121 (Sb).

A real sample (pond weed digest diluted four times with deionised water) was used for the optimisation procedure outlined below. This sample was chosen, rather than an antimony standard, so that matrix and species dependent effects could be minimised and the antimony signal maximised.

The OPTIMA3 computer program [18,19] was used for the simplex calculations and the generation of experimental conditions. The principal components analysis was carried out by using Systat® 5.03 for windows (SYSTAT, Inc.). Both of these programs were run under Windows® 3.1, on a DELL 466/M personal computer.

NAA was carried out as described elsewhere [20,22].

2.4. Plackett–Burman experiments

The initial variables chosen to be screened using the Plackett–Burman method were: dry time (Dt), dry temperature (DT), ash time (At), ash temperature (AT), atomisation ramp (AtR), atomisation time (Att), atomisation temperature (AtT) and modifier concentration (MC). This allowed for the use of three dummy variables and so had 3 df (see Table 1). Initial experiments carried out using longer ash and atomisation times (up to 15 and 7 s, respectively) resulted in a short graphite tube lifetime (60 firings), thus limits for these variables were chosen to minimise tube deterioration. The limits for all the variables were chosen so as to show a change in measured absorbance, which was the response measured, rather than to reflect conditions usually used for ETAAS.

After the first design was carried out, three variables (atomisation ramp, atomisation time and modifier concentration) were kept constant, whilst the effect of the other five variables were investigated using a $n = 8$ design (two dummy variables, 2 df) (see Table 2). The matrix designs, adapted from the method of Jones et al. [23], accompany the designations of variables in Table 1 and Table 2.

2.5. Simplex optimisation

The composite modified simplex (CMS) optimisation method described previously [18,19] was employed during this work. Having screened out the variables that did not have a significant effect on the response, the remaining four factors (atomisation temperature, atomisation time, ash temperature and modifier concentration) were optimised to provide the maximum antimony absorbance signal from a pond weed digestate. The upper and lower limits used in the CMS procedure as well as the stepsize for each variable are given in Table 3.

Five initial experiments were conducted and the conditions for each factor, as well as the resulting absorbance, were entered into the OPTIMA3 computer program. The next set of experimental conditions were generated and carried out, and the response was entered. The simplex progressed via a series of reflections, expansions, contractions or fit points, towards the optimum absorbance (see Table 4). The process was continued until the S.D. of the five highest responses was less than the value of the stepsize of the absorbance (0.010), three times sequentially. To prove that the optimum values determined were not due to a local region of maximum response, the procedure was repeated with different starting conditions; the same optimum conditions were found.

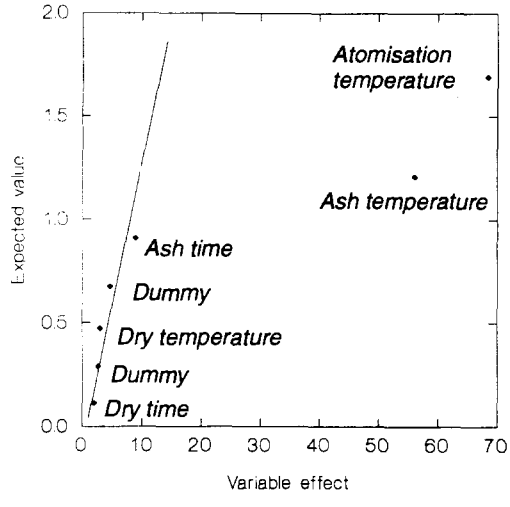

Fig. 1. Birnbaun plot for the second Plackett–Burman, showing the significance of the two variables atomisation temperature and ash temperature.

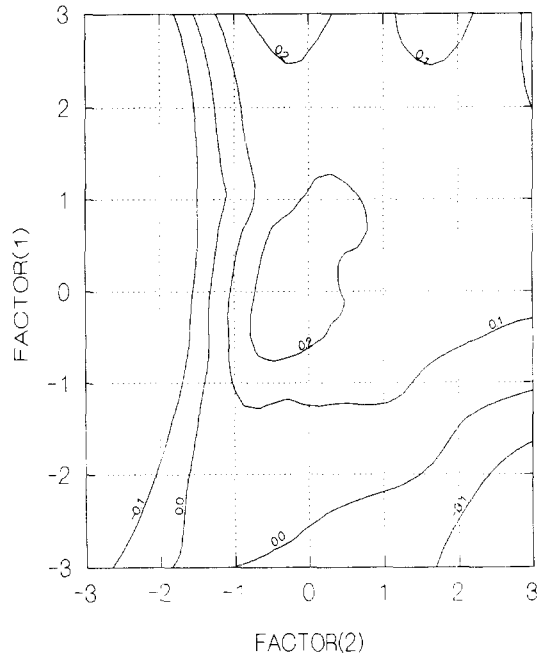

Fig. 2. Contour diagram showing the response surface for the first optimisation.

2.6. Visualisation of the response surface

The experimental results were analysed by using principal components analysis, as described in detail and with examples by Molinero [24]. Briefly, principle components analysis was used to reduce the four variables from the simplex optimisation to two new variables (principle components 1 and 2). The scores of these principle components give coordinates for all the experimental vertices. Thus, the vertices of the simplex previously represented by n variables, are now represented by two variables, and the responses are plotted against these variables, to generate the response surface. The relative significance of the effects of the original variables on the reponses can be evaluated by considering the loading of each variable on each principle component, which indicates to what degree each principle component is influenced by each of the original vari-

Table 6
The optimised furnace program, used for quantitation of antimony in plant samples (400 mg l^{-1} or 4 μg Pd as modifier was used)

Step no.	Temperature (°C)	Duration (s)	Gas flow (l min^{-1} Ar)	Function
1	90	30	3	Dry/ramp
2	120	10	3	Dry/ramp
3	1350	1.9	3	Ash/ramp
4	1350	2	3	Ash/hold
5	1350	1	0	Ash/gas off
6	2200	0.5	0	Atom/ramp[a]
7	2200	3	3	Clean

[a] 2000°C s^{-1} ramp from 1350 to 2200°C, integration during this step.

ables. This approach provides visual information on the optimum and the response surface, which is not possible with the simplex search alone. The response surface can be studied to determine more information such as the presence or absence of ridge features or local maxima. It also helps to show other factor levels that could provide better experimental conditions in terms of lower temperature operating conditions, or less modifier, thus resulting in a more cost effective procedure.

3. Results and discussion

3.1. Plackett–Burman experiments

The results for the first Plackett–Burman experiment were used to obtain a minimum t value of 3.18 for a 95% confidence interval. Only the atomisation time and modifier concentration give t values above this and so are the only significant variables at this confidence level (Table 5). Birnbaun plots can be used to confirm or help clarify results obtained from such experiments, as explained in more detail elsewhere [23]. Briefly, deviance of points from a straight line indicate large variable effects [14]. In this instance, the Birnbaun plot (not shown) gives essentially a straight line and therefore does not help with the further interpretation of this experiment.

The second Plackett–Burman experiment was carried out by holding three factors constant and hence utilised five of the original variables and two dummies (2 df). The atomisation time and modifier concentration shown to be important by the first experiment were held constant at 0 s and 500 mg l^{-1}, respectively, in the hopes that any other significant variables might be revealed. The ramp rate was observed in these and preliminary experiments to give maximum results at higher speeds, as noted by Pergantis et al. [11] in their optimisation for arsenic. Instrumental constraints limited the ramp to 2000°C s^{-1} and this value was used for all subsequent experiments.

The results for the second experiment produced a minimum t value at the 95% confidence interval of 4.3 and the t values for the two variables, ash and atomisation temperature were greater, indicating that these variables have a significant effect on the antimony response. The Birnbaun plot in Fig. 1 shows that the ash and atomisation temperatures deviate from a straight line because of large variable effects, which confirms the significance of these variables.

Table 7
Concentration of antimony (mg kg^{-1} dry weight) in Pine Needles (NIST 1575) after analysis by ETAAS

Sample	ETAAS analysis ± S.D.[a]	Comparison to SRM[b]
Total digest 1[c]	0.220 ± 0.012	nsd[d] at 98%
Total digest 2	0.208 ± 0.019[e]	nsd at 95%
Total digest 3	0.231 ± 0.044	nsd at 95%

[a] Precision expressed as S.D. based on five analytical replicates, except where indicated.
[b] Antimony concentration (0.2 mg kg^{-1}).
[c] Hot plate digestion.
[d] nsd: not significantly different at confidence level indicated.
[e] Four analytical replicates.

Table 8
Comparison of the concentrations of antimony (mg kg^{-1} dry weight) in pond weed samples from Yellowknife, NWT, Canada

Sample	Determined by ETAAS ± SD[a]	Determined by ICP-MS ± SD[b]	Comparison[c]
Extract 1[d]	0.28 ± 0.04	0.222 ± 0.003	nsd at 95%
Extract 2	0.26 ± 0.02[e]	0.221 ± 0.002	nsd at 95%
Extract 3	0.28 ± 0.02	0.179 ± 0.003	nsd at 98%
Total digest 1	39 ± 5	32.6[f]	nsd at 98%
Total digest 2	40 ± 5	41.8[f]	nsd at 95%

Determination by optimised ETAAS and ICP-MS.
[a] Precision expressed as S.D. based on five analytical replicates, except where indicated.
[b] Two analytical replicates except where indicated.
[c] nsd: not significantly different at confidence level indicated.
[d] Acetic acid/water extraction.
[e] Four analytical replicates.
[f] No replication.

Four variables: atomisation time, atomisation temperature, ash temperature and modifier concentration, were subsequently optimised by using the composite modified simplex procedure (CMS).

3.2. Simplex optimisation

A total of 29 experiments were carried out and the maximum response was reached after 23 experiments (see Table 4). The optimum parameters were found to be: atomisation temperature, 2200°C; atomisation time, 0 s; ash temperature, 1350°C; and modifier concentration, 400 mg l^{-1}. The simplex analysis was repeated from different initial conditions and the maximum response was: atomisation temperature, 2200°C; atomisation time, 0 s; ash temperature, 1450°C; and modifier concentration, 400 mg l^{-1}. These conditions were reached after 22 experiments from a total of 27. The conditions from the first optimisation are considered to be better for routine use, because the lower ash temperature is less destructive to the graphite cuvette.

The response surfaces generated from both searches are not identical, but the characteristic ridge feature of high absorbance is present in both (see Fig. 2 for the response surface generated from the first simplex). The results for the principle components analysis (PCA) indicate that the first and second principle components (PC) retain 43.8 and 31.5%, respectively of the original variance of the data. This is similar to values reported in previous work [24]. The results also demonstrate that the atomisation temperature and modifier concentration have the greatest influence on the first PC, whereas ash temperature has the greatest influence on the second PC. Generation of the response surface also eliminates the need to carry out univariate searches around the optimum to establish that it is correct.

Therefore, after carrying out the simplex optimisation twice, from two different starting conditions and then analysing each response surface using principle components analysis, it was felt that further univariate investigates of the optimum were unnecessary.

3.3. Analysis of samples by using the optimised temperature program

The optimised procedure (Table 6) was used to determine the antimony concentration in pine needle SRM and pond weed, by using ETAAS and the method of standard additions. The results obtained for analysis of the pine needles are shown in Table 7, along with a comparison to the reference value. The concentrations for pine needles, with an average observed concentration of 0.220 mg kg^{-1}, do not differ significantly from the non-certified concentration of 0.2 mg kg^{-1}.

The pond weed sample is from a contaminated site near a gold mine in the Northwest Territories, Canada. The concentration of antimony in this sample was determined by ICP-MS to verify the

values obtained by ETAAS and the results are given in Table 8. The results for the two methods do not differ significantly, as shown by the statistical comparison. The concentration of antimony for each digestion does not differ significantly (95% level) from the value determined by neutron activation analysis of 41.2 mg kg^{-1}.

The aqueous phase soluble antimony species were extracted from the pond weed sample with 1/1 methanol/water (V/V), so that further analysis by speciation techniques such as HPLC-ICP-MS or HG-GC-MS [24] can be carried out. However, prior to this it is important to establish the total antimony concentration, both hydride and non-hydride forming, present in the extract. Although the values obtained for the methanol/water extracts after analysis by ETAAS and ICP-MS do not differ statistically, consistently lower values for the ICP-MS results were observed. This is probably due to matrix or solvent effects, as the ETAAS analyses were carried out by using the method of standard additions, whereas the ICP-MS analyses were carried out using external calibration with aqueous standards.

By the analysis of the SRM and the methanol/water extract the optimised ETAAS procedure for the determination of antimony has been shown to overcome any interferences due to the sample matrix and any differences due to the different antimony species present. In addition, the method can be used for any total antimony determinations in samples of plant origin.

Acknowledgements

The authors would like to thank Dr M. Dodd for provision of the pond weed samples and NAA results, Mr B. Mueller for help with ICP-MS analysis, Ms M. Winters for assistance with sample preparation and Dr A. Wade for comments on the manuscript. We would like to acknowledge Dr K.J. Reimer, Environmental Sciences Group, Kingston, Ontario and the Natural Sciences and Engineering Research Council of Canada for financial assistance.

References

[1] M.O. Andreae, J.-F. Asmode, P. Foster and L. Van't dack, Anal. Chem., 53 (1981) 1766.
[2] X. Lu, J. Li, S. Chen and D. Guosheng, Acta Ocean. Sinica, 9 (1990) 255.
[3] R. Kantin, Limnol. Oceanogr., 28 (1983) 165.
[4] H. Onishi and E.B. Sandell, Geochim. Cosmochim. Acta, 8 (1955) 213.
[5] L.H. Keith and W.A. Telliard, Environ. Sci. Technol., 13 (1979) 416.
[6] M. Walcerz, S. Garbos, E. Balska and A. Hulanicks, Fresenius J. Anal. Chem., 350 (1994) 662.
[7] R.E. Sturgeon, S.N. Willie and S.S. Berman, Anal. Chem., 57 (1985) 2311.
[8] R.E. Sturgeon, Can. J. Spectros., 32 (1987) 79.
[9] J.G.S. Gupta and J.L. Bouvier, Talanta, 42 (1995) 269.
[10] M.T. Perez-Corona, M.B. De La Calle-Guntinas, Y. Madrid and C. Carmara, J. Anal. At. Spectr., 10 (1995) 321.
[11] S.A. Pergantis, W.R. Cullen and A.P. Wade, Talanta, 41 (1994) 205.
[12] B. Welz, Atomic Absorption Spectrometry, 2nd edn., VCH, Wenheim, 1985, p. 64–159.
[13] M.J. Ford, L. Ebdon, R.C. Hutton and S.J. Hill, Anal. Chim. Acta, 23 (1994) 23.
[14] D.J. Roberts and K.V. Kahokola, J. Anal. At. Spectr., 4 (1989) 185.
[15] T. Van der Velde-Koerts and J.L.M. de Boer, J. Anal. At. Spectr., 9 (1994) 1093.
[16] S.J. Hill, M.J. Ford and L. Ebdon, J. Anal. At. Spectr., 7 (1992) 719.
[17] T. Mackenzie, in E. Rothery (Ed.), Analytical Methods for Graphite Tube Atomizers, Varian, Australia, Publication No. 85–100447-00, 1982, pp. 43.
[18] D. Betteridge, A.P. Wade and A.B. Howard, Talanta, 32 (1985) 709.
[19] D. Betteridge, A.P. Wade and A.B. Howard, Talanta, 32 (1985) 723.
[20] D.A. Bright, W.T. Dushenko and K.J. Reimer, Aquat. Bot., 50 (1995) 141.
[21] S. Bajo, B. Suter and B. Aeschliman, Anal. Chim. Acta, 149 (1983) 321.
[22] D.A. Bright, B. Coedy, W.T. Dushenko and K.J. Reimer, Sci. Tot. Environ., 155 (1994) 237.
[23] K. Jones, Int. Lab., November (1986) 32.
[24] M.L. Molinero, Anal. Chim. Acta, 297 (1994) 417.

ELSEVIER

Talanta 44 (1997) 781–786

Talanta

Europium complexation by an aquatic fulvic acid - effects of competing ions

Maria Nordén, James H. Ephraim, Bert Allard

Department of Water and Environmental Studies, Linköping University, S-581 83 Linköping, Sweden

Received 15 December 1995; received in revised form 10 September 1996; accepted 16 September 1996

Abstract

Effects of competing ions, Fe^{2+}/Fe^{3+} and Al^{3+}, on Eu^{3+} complexation with an aquatic fulvic acid (FA), have been investigated using an ion exchange technique. The influence of different concentrations (10^{-6}, 10^{-4} M) of the competing ions on the distribution coefficient for Eu was measured, and the overall complex formation function, β_{ov}, was resolved for the Eu systems with Fe and Al. All systems showed pH-dependent β_{ov}-functions. The presence of 10^{-4} M concentration of competing ion reduced the resolved complex formation function ($\log \beta_{ov}$) for Eu complexation with fulvic acid by 0.6 and 0.4 log units at pH 5 for Fe and Al, respectively. This indicates that Fe has a more perturbing effect on Eu–FA complexation than Al. In similar competition studies Sr and Eu were found not to perturb each others complexation with fulvic acid, suggesting therefore that the two metals probably bind to different sites on the fulvic acid molecule. © 1997 Elsevier Science B.V.

Keywords: Competing ions; Europium; Fulvic acid; Ion exchange technique

1. Introduction

Humic substances are ubiquitous in natural waters and have significant effects on metal speciation and mobility in aquatic environments [1]. The metal complexes formed with humic substances are influenced by pH, ionic strength, concentrations of metal and humic matter and presence of competing ions. Few studies that investigate the effects of competing metals have been carried out [2–5]. The influence of Ca^{2+} [2–4], Mg^{2+} [2,3] and Cd^{2+} [5] on Cu^{2+} binding by naturally occurring dissolved organic matter are some of the few investigations where competition effects are considered. Usually in these studies only minor effects are observed. In a more recent work Al^{3+} was found to compete with Cu^{2+} for binding sites in a fulvic acid [6].

The overall objective of this study has been to quantify the perturbing effects of Fe, Al and Sr on the Eu-FA complexation. Europium was chosen as a model element for trivalent radionuclides that might be released into the environment from, e.g. radioactive waste in geologic deposits [7]. Aluminium and Fe are common metals in the environment, and therefore likely competitors. Aluminium can be found in fresh waters in the concentration range of 10^{-6}–10^{-4} M and Fe in the concentration range of 10^{-7}–10^{-4} M [1]. Strontium is present in radioactive waste and its

PII S0039-9140(96)02102-9

competition with Eu is therefore of interest. The conditions of the experiments (e.g. FA concentration, ionic strength) were chosen to resemble the experimental conditions in an earlier paper [8] in order to facilitate a meaningful comparison (Table 1). It has not been the goal to determine the selectivity coefficients for Eu, Al and Fe over the ion-exchange resin.

2. Experimental

2.1. Materials

A well-characterised aquatic fulvic acid (FA), extracted from the surface water of a bog area (Bersbo, Sweden), was used in all experiments. The potentiometric properties of the FA molecule have previously been described by assuming five predominant acid sites [9]. The Fe and Al content of the Bersbo FA was 0.18 and 1.87 mg g^{-1}, respectively (by Atomic Absorption Spectrophotometry). Other characteristics of the Bersbo FA are given elsewhere [8,9].

Radionuclides (^{152}Eu and ^{85}Sr; from Amersham) and analytical grade chemicals with Milli-Q water were used for all solutions. The non-radioactive Eu and Sr were prepared from Eu_2O_3 and $Sr(NO_3)_2$ (Merck), respectively, and the Al and Fe mixtures from $AlC_3 \times 6H_2O$ and $FeCl_2 \times 4H_2O$. The sodium form of a Dowex 50WX8 (mesh 50–100) cation exchange resin was used as adsorbent (see below). A radiometer pHM 82 standard pH-meter (precision ± 0.02 pH units) and a pH-combination glass electrode, GK 2401C, were employed for pH determinations. Calibration was carried out with two buffer solutions and the pH values are given as concentrations. Radioactivity measurements were made using a LKB (Wallac) 1282 Compugamma counter.

2.2. Procedures

The ion exchange distribution experiments were carried out batch-wise by a radiotracer technique (^{152}Eu and ^{85}Sr). The additional competing ions (Fe, Al, Eu or Sr) were non-active (no radiotracer), and the activities in the solutions with and without competing ions were compared. The ion exchange procedure for studies of metal complexation with humic substances, and the mode of computation of the overall complex formation function, β_{ov}, from the distribution coefficient, D, have been outlined in a previous work [8].

Constant ionic strength (0.10 M $NaClO_4$), constant total concentration of FA (120 mg l^{-1}, corresponding to a total acid capacity of 5.6×10^{-4} eq l^{-1} and 6.9×10^{-5} M with $M_n = 1750$) and constant concentrations of the complexed elements Eu and Sr were selected. The competing elements (Fe, Al, Eu or Sr) were added without absolute exclusion of air, and therefore some of the Fe would be oxidised to the trivalent state in the absence of FA and consequently Fe(III) hydrolysis products will form with increasing pH. Since FA is known to reduce Fe(III) to Fe(II) it is expected that the Fe(II) will be maintained in the divalent state in the FA systems, even in the presence of air [10–14]. The metal and metal-FA solutions were pH adjusted with $HClO_4$ or NaOH and left to equilibrate for 20 ± 3 h prior to addition to the ion exchange resin. This mode of pH adjustment is different from the one used in an earlier paper [8], where the pH was adjusted after aliquots of bulk solutions had been added to the resin. The pH adjustment was altered to accomplish an equilibrium between metal ions and ligands before the ion exchange reaction with the resin. The pH values that were determined after the equilibrium with the resin were used in calculations of log D and log β_{ov}. Samples of 5 ml were

Table 1
Experimental systems

(a) Complexing metal	Eu, 5.0×10^{-9} M (including ^{152}Eu)
Ligand	FA, 5.6×10^{-4} eq l^{-1} (120 mg l^{-1})
Competing metal	Fe; 10^{-6}, 10^{-4} M
	Sr; 10^{-8}, 10^{-6}, 10^{-4} M
Ion exchange resin	1.0 g l^{-1}
(b) Complexing metal	Sr, 3.0×10^{-6} M (including ^{85}Sr)
Ligand	FA, 5.7×10^{-4} eq l^{-1} (122 mg l^{-1})
Competing metal	Eu; 10^{-8}, 10^{-6}, 10^{-4} M
Ion exchange resin	10.0 g l^{-1}

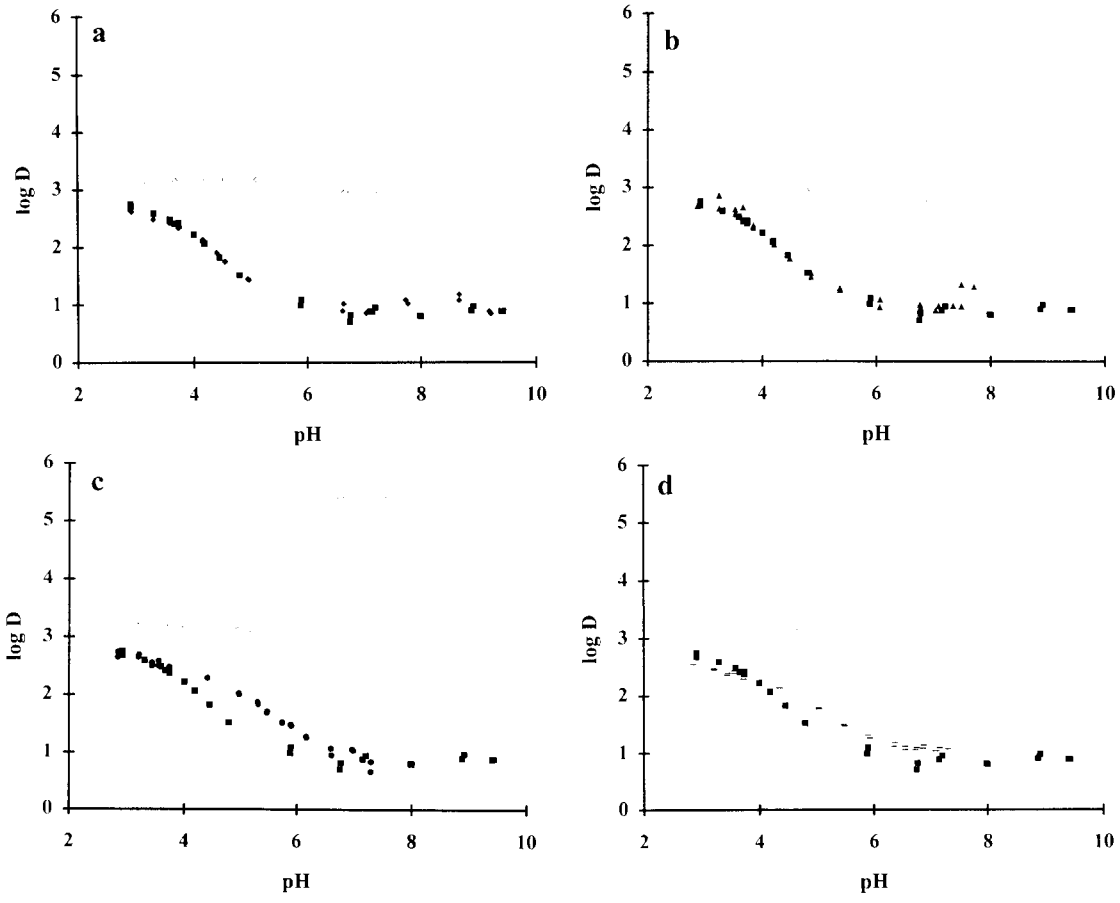

Fig. 1. The effect of different Fe and Al concentrations on the distributions of Eu over a cation exchange resin in the absence and presence of FA. □ Eu; ■, Eu + FA; (a) Fe(10^{-6} M), ◇ Eu; ◆ Eu + FA; (b) Al(10^{-6} M), △ Eu; ▲ Eu + FA, (c) Fe(10^{-4} M), ○ Eu; ● Eu + FA; and (d) Al(10^{-4} M), + Eu; − Eu + FA.

transferred from each container to three tubes (duplicate samples and one control with no resin). The tubes were equilibrated for 20 ± 3 h on a shaking-table (~ 110 rpm) at ambient temperature (20 ± 1°C). After equilibrium, the pH of each metal-resin mixture was determined. The mixture was centrifuged for about 10 min at 2000 rpm (~ 350 g), and 1 ml of the clear solution was withdrawn for radioactivity measurement. Duplicate samples were taken. The experimental systems are summarised in Table 1.

3. Results and discussion

The distribution of Eu over the ion exchange resin is illustrated in Fig. 1. Data from the Eu and Eu + FA series (without competing ions) are given in all diagrams for comparison. The distribution coefficient, D, was independent of pH in the pH-range 3–9 for Eu in the absence of FA. This observation differs form an earlier observation where log D decreased with an increase in pH [8]. The discrepancy in the results is attributable to the difference in the method of pH adjustment.

In the Eu + FA series the distribution coefficient decreased from 2.8 log units in the pH range 3–6 to a constant value of 0.8 log units at pH > 6.

3.1. The effects of Fe on the Eu distribution

The effects of Fe at 10^{-6} and 10^{-4} M, respectively, are shown in Fig. 1a and c. In the presence of 10^{-6} M Fe the distribution coefficient of Eu was the same as in the absence of Fe in the pH range of 3 to 5.5. However, at pH > 5.5 the decrease in log D (0.1 to 0.4 log units) was increasing with an increase in pH (Fig. 1a); i.e. more Eu stayed in solution in presence of 10^{-6} M Fe at pH > 5.5. The Fe would be present predominantly in the trivalent state, and the decrease may be caused by the formation of colloidal $Fe(OH)_3$ that can adsorb Eu and keep it in solution. Studies of Eu adsorption on colloidal $Fe(OH)_3$ have previously shown a pronounced Eu adsorption at pH > 5 [15]. The present centrifugation procedure to separate the ion exchange resin from the solution would not be sufficient to completely separate colloids from the true solution [15].

For the higher Fe concentration (10^{-4} M) the distribution coefficient was increasing at pH > 5–6 (Fig. 1c). This increase reached a maximum of 2.2 log units at a pH around 7. This would be due to aggregation of colloids and the formation of solid $Fe(OH)_3$ which together with the resin can serve as the adsorbing surface for Eu. Additionally, the increase in log D at higher pH could be attributable to the interaction of the solid $Fe(OH)_3$ with the ion exchange resin to produce a new surface with a higher affinity for Eu. Calculations of the amount of solid $Fe(OH)_3$ at the two total concentrations (10^{-6} and 10^{-4} M Fe) indicate that at the low concentration the solid phase would be only approximately 0.01% (pH-range 5–9) of the weight of the ion exchange resin, while at the higher concentration the corresponding value would be 1.0% for the same pH range (assuming $K_{sp} = 4 \times 10^{-38}$) [16].

3.2. The effects of Al on the Eu distribution

Aluminium seemed to influence the adsorption of Eu on the resin in a similar way as Fe (Figs, 1b and d). In absence of FA 10^{-6} M Al decreased log D of Eu by 0.3 log units in the pH interval 3 to 9. At the higher Al concentration (10^{-4} M) a sharp increase in the distribution coefficient was obtained at pH > 6 (Fig. 1d), with a maximum of 2.1 log units at a pH around 7.5. The effect was similar to that of Fe(10^{-4} M). A plausible explanation to the increase can be the formation of solid $Al(OH)_3$ (similar to the formation of $Fe(OH)_3$) that can act as an adsorbent for the Eu. Calculations indicate that the formation of solid $Al(OH)_3$ at the low Al concentration would be up to 0.007% (pH-range 5.5–9) of the weight of the ion exchange resin. For the higher concentration in the same pH range the formation of $Al(OH)_3$ would be 0.7% of the resin weight (assuming $K_{sp} = 2 \times 10^{-32}$) [16].

3.3. The effects of competing metals on Eu-FA and Sr-FA complexation

No difference in distribution coefficient was discernible for the Eu-FA system in the presence of 10^{-6} M Fe (Fig. 1a). This could imply that 10^{-6} M Fe does not affect the complexation of Eu with FA. However, it could also imply that since there is excess of FA both Fe and Eu can be complexed without effecting each other. At the higher concentration of Fe (10^{-4} M) there was a slight increase in log D (0.1 to 0.6 log units) between pH 4 and 7 which may be explained by the competition of Fe for the FA binding sites (Fig. 1c).

In the presence of FA at the lower Al concentration (10^{-6} M) no influence was discernible (Fig. 1b), just as for Fe at the same concentration. With FA and 10^{-4} M Al in the system there was a slight increase in log D (0.1 to 0.4 log units) in the pH range 4–7 (Fig. 1d).

In another competition study the influence of Sr on the Eu-FA complex, but also the influence of Eu on the Sr-FA complex, were investigated (Fig. 2). In one set of experiments inactive Sr^{2+} was added to active Eu^{3+} plus FA solution, in a typical ion exchange experiment as described earlier [8]. In the other set inactive Eu^{3+} was added to active Sr^{2+} plus FA solution, in a similar ion exchange distribution experiment. In the case of

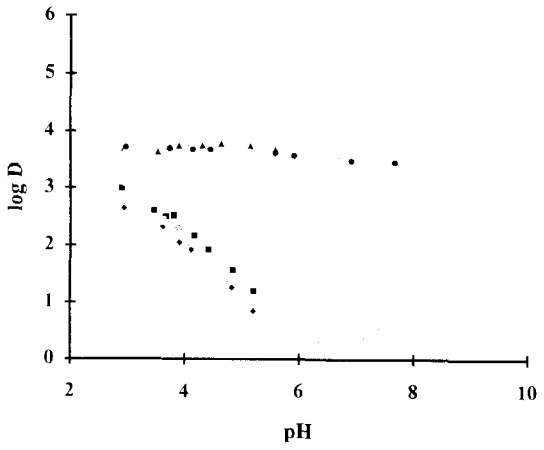

Fig. 2. The effect of different Sr concentrations on the distribution of Eu and the effect of different Eu concentrations on the distribution of Sr, over a cation exchange resin in the presence of FA. ◇ Eu + FA; ◆ Eu + Sr(10^{-8} M) + FA; □ Eu + Sr(10^{-6} M) + FA; ■ Eu + Sr(10^{-4} M) + FA; ○Sr + FA, ● Sr + Eu(10^{-8} M) + FA; △ Sr + Eu(10^{-6} M) + FA; ▲ Sr + Eu(10^{-4} M) + FA.

Eu-FA complexation Sr affected the observed log D of Eu only when its concentration was increased to 10^{-4} M, suggesting that competition was only significant at that concentration level. When Eu acted as the competing ion no effects of increasing concentration were noticed for the distribution of Sr on the ion exchange resin. This indicates that neither Eu nor Sr influences the others complexation with FA.

The relationship between the overall complex formation function, β_{ov}, and pH, calculated from distribution data are summarised in Table 2. Iron

Table 3
Comparison of formation constants for iron, aluminium and europium fulvic acid complexes

Metal ion	pH	log β (l eq^{-1})	Reference
Fe(II)	4.5	5.4	[17]
	6.0	5.6	
	3.5	5.06	[18]
	5.0	5.77	
Al(III)	2.35	3.7	[19]
	n.g.[a]	5.44	[20]
Eu(III)	4.5	6.90	[21]
	4	6.65	[22]
	6	8.15	
	4–7	5.10	
	2.7–6.5	6	[23]
	3.0	6.06	[8]
	3.5	6.43	
	4.5	7.17	
	5.0	7.54	
	6.0	8.28	

β implies both conditional stability constants and overall complex formation functions.
[a] n.g., not given.

at 10^{-4} M disturbs the Eu-FA binding more than Al at the same concentration in the pH interval 4 to 6, e.g. log $\beta_{ov} = 4.60$ for Fe and 4.86 for Al, as compared with the original value of 5.22. At a concentration of 10^{-6} M both Fe and Al seem to disturb the Eu-FA binding to an equally low degree, log $\beta_{ov} = 5.03$ and 5.04 for Fe and Al, respectively.

It is difficult to make a meaningful comparison of the stability constants of Fe, Al and Eu complexes with fulvic acids because of a number of

Table 2
The overall complex formation function, β_{ov}, for five Eu + FA systems described by polynomials (120 mg l^{-1} FA, I = 0.10 M $NaClO_4$ M)

System	pH	r	n	log β_{ov} (pH)[b]	log β^{c}_{ov} (pH = 5)
Eu + FA	3–9	0.997	30	$10.683-6.267\ pH+2.000(pH)^2-0.2452(pH)^3+0.01043(pH)^4$	5.22
Eu + Fe(10^{-6} M) + FA	3–9	0.998	28	$15.159-10.084\ pH+3.109(pH)^2-0.3813(pH)^3+0.01637(pH)^4$	5.03
Eu + Al(10^{-6} M) + FA	3–7	0.998	30	$22.221-16.804\ pH+5.359(pH)^2-0.7000(pH)^3+0.03259(pH)^4$	5.04
Eu + Fe(10^{-4} M) + FA	3–7	0.992	30	$5.593-1.233\ pH+0.2861(pH)^2-0.01584(pH)^3$	4.60
Eu + Al(10^{-4} M) + FA	3–7	0.996	30	$7.225-2.257\ pH+0.5341(pH)^2-0.03544(pH)^3$	4.86

r, correlation coefficient and n, number of experimental points.
[b] For the best fit of the polynomials (indicated by r) to the experimental points all given decimal points of the coefficient must be used.
[c] As an example the log β_{ov} function described with a polynomial is used for calculating log β_{ov} at pH = 5.

factors, e.g. pH, ionic strength, method, mode of computation and the origin of the FA. However, in Table 3 an attempt is made to compare literature values for Fe^{2+} and Al^{3+} fulvic acid complexes with the Eu-FA complexation data. The conditional stability constants for the Eu-FA complex are in general apparently greater than the constants for the Fe^{2+} and Al^{3+} complexes.

The conditional stability constant for Fe^{2+} yields a mean value of 5.5 in the pH interval 3.5–6.0, which is considerably lower than most values for Eu-FA in the same pH interval (Table 3). However, the concentration of Fe (10^{-4} M) in the present study is much greater than for Eu (5×10^{-9} M) which can explain the observed competition from Fe.

4. Conclusions

The experimental results from this work corroborate the observation that an increased pH augments the complexation between FA and Eu, but that the Sr complexation is insensitive to pH (in the pH range 3–8) [8].

Iron and Al exhibited some influence on the Eu-FA complexation. However, the effect was minor at 10^{-6} M. The concentration 10^{-4} M gave a clear effect (e.g. reduction of log β_{ov} by 0.6 and 0.4 log units at pH 5 for Fe and Al, respectively). Known formation constants for FA with Fe^{2+}, Al^{3+} and Eu^{3+} suggests that Eu^{3+} forms stronger complexes with FA than Fe^{2+} and Al^{3+}. This may explain why as much as 10^{-4} M of the competing ions is needed to affect a clear disturbance of the Eu-FA complex. Another feasible conclusion for the high concentration of competing ions required is that Eu and, Fe and Al, do not necessarily complex to the same site on the FA molecule. Since Sr did not influence the Eu-FA complex, nor did Eu influence the Sr-FA complex, it is also postulated that Sr and Eu probably bind to different sites on the FA molecule. However, these conclusions need to be supported by further experiments, e.g. investigation of the effect of different FA concentrations. Such exercises are in progress.

Acknowledgements

This work was supported by the Swedish Nuclear Fuel and Waste Management Company and the Swedish Natural Science Research Council. The assistance by Mr Anders Düker in performing the metal analysis of the fulvic acid is gratefully acknowledged.

References

[1] J. Buffle, Complexation Reactions in Aquatic Systems, Ellis Horwood, Chichester, 1988.
[2] W.G. Sunda and P.J. Hanson, in E.A. Jenne (Ed.), Chemical Modeling in Aqueous Systems, American Chemical Society, Washington DC, 1979, p. 147.
[3] S.E. Cabaniss and M.S. Shuman, Geochim. Cosmochim. Acta, 52 (1988) 185.
[4] J.G. Hering and F.M.M. Morel, Environ. Sci. Technol., 22 (1988) 1234.
[5] W. Fish, Ph.D. Modeling the interactions of trace metals and humic materials, Dissertation, MIT, Cambridge, MA, 1984.
[6] S.E. Cabaniss, Environ. Sci. Technol., 26 (1992) 1133.
[7] International Atomic Energy Agency, IAEA Yearbook 1991, Vienna, 1991.
[8] M. Nordén, J.H. Ephraim and B. Allard, Talanta, 40 (1993) 1425.
[9] J.H. Ephraim, H. Borén, C. Pettersson, I. Arsenie and B. Allard, Environ. Sci. Technol., 23 (1989) 356.
[10] D.T. Waite and F.M.M. Morel, Anal. Chim. Acta, 162 (1984) 263.
[11] C.H. Langford, R. Kay, G.W. Quance and T.R. Khan, Anal. Lett., 10 (1977) 1249.
[12] R.K. Skogerboe and S.A. Wilson, Anal. Chem., 53 (1981) 228.
[13] J.H. Ephraim, A.S. Mathuthu and J.A. Marinsky, SKB TR 90-28, Swedish Nuclear Fuel and Waste Mangement, Stockholm, 1990.
[14] C.J. Miles and P.L. Brezonik, Environ. Sci. Technol., 15 (1981) 1089.
[15] A. Ledin, S. Karlsson, A. Düker and B. Allard, Radiochim. Acta, 66/67 (1994) 213.
[16] D.A. Skoog and D.M. West, Fundamentals of Analytical Chemistry, Holt-Saunders, Philadelphia, 1982.
[17] R.L. Malcolm, in B.W. Nelson (Ed.), Environmental Framework of Coastal Plain Estuaries, Memoir 133, The Geological Society of America, Boulder, 1972, p. 79.
[18] M. Schnitzer and S.I.M. Skinner, Soil Sci., 102 (1966) 361.
[19] M. Schnitzer and E.H. Hansen, Soil Sci., 109 (1970) 333.
[20] M. Adhikari and G. Chakrabarti, J. Indian Chem. Soc., 54 (1977) 573.
[21] E.L. Bertha and G.R. Choppin, J. Inorg. Nucl. Chem., 40 (1978) 655.
[22] J.H. Ephraim, Sci. Tot. Environ., 108 (1991) 261.
[23] G. Bidoglio, I. Grenthe, P. Qi, P. Robouch and N. Omenetto, Talanta, 38 (1991) 999.

ELSEVIER

Talanta 44 (1997) 787–796

Talanta

Complexometric determination of some toxic mixtures of ions using bromo-cresol orange with visual endpoint indication

Medhat A.H. Hafez *, Magdi E. Khalifa

Chemistry Department, Faculty of Science, Mansoura University, El-Mansoura, Egypt

Received 10 April 1996; received in revised form 22 August 1996; accepted 17 September 1996

Abstract

A rapid and simple general complexometric method was presented for the determination of lead, cadmium and thallium or mercury or arsenic(V) in laboratory synthesized mixtures similar to those of some ores, minerals and alloys of such metals. The precision and accuracy attainable in successive titrations of Pb^{2+}, Cd^{2+} and Tl^{3+} or Hg^{2+} or AsO_4^{3-} (As^{5+}) with 0.05 and/or 0.01 mol l^{-1} solutions of disodium ethylenediaminetetraacetate (Na_2EDTA) and standard $Pb(NO_3)_2$ of the same concentration using Bromo-Cresol Orange (BCO) as a new metallochromic indicator with visual endpoint indication were studied. For the analysis of a three component mixtures of the aforementioned ions, Tl^{3+} was at first directly titrated with Na_2EDTA at pH 0.5–1 (HNO_3) using BCO as indicator. At the thallium endpoint an excess of Na_2EDTA was added and the pH was adjusted at pH ~ 4.8 using hexamine-HNO_3 buffer (solution A). The excess EDTA was back-titrated with standard solution of $Pb(NO_3)_2$. 1,10-Phenanthroline (1,10-phen) was added to release the EDTA combined with Cd^{2+}, while thiosemicarbazide (TSC) was used to liberate the EDTA from the mercury-EDTA chelate. To determine AsO_4^{3-} ion in such type of mixtures the pH of (solution A) was raised to a value of 10 using ammonia buffer. Excess standard Mg^{2+} solution was added and the formed precipitate of $MgNH_4AsO_4$ was separated, dissolved and its magnesium content equivalent to AsO_4^{3-} was determined complexometrically using Eriochrome Black-T (EBT) indicator. The interference caused by different anions, cations and organic acids was investigated. A comparison of the indicators BCO and Xylenol Orange (XO) for successive titration of the studied metal ions was carried out. The proposed successive titration method was applied successfully to some real samples of ores, minerals and alloys of the studied metal ions and the results were satisfactory and agreed with those obtained by AAS. © 1997 Elsevier Science B.V.

Keywords: Bromo-cresol orange (BCO); Cadmium; Lead; Mercury and arsenic determination; Thallium; Visual complexometric titration

1. Introduction

The toxicity of most of the investigated cations are due to the retardation of the brain growth and damage of the nervous system e.g., Pb^{2+} and Hg^{2+} [1–6]. Some of them accumulate in liver and kidneys e.g., Cd^{2+} [7–10]. Other metal ions combine with cell membrane altering the permeability of the membrane [6]. Some of such metals

* Corresponding author.

PII S0039-9140(96)02106-6

have also been shown to produce dangerous breaks in chromosomes of somatic cells, thus, causing mental retardation for children born to mothers exposed to excessive amounts of such metals [6] e.g., Hg^{2+}. Arsenate compounds find extensive use in agriculture as herbicides for weeds and pest control. The use of arsenic compounds is however limited because most of arsenicals are poisonous.

Although Tl^{3+}, Hg^{2+}, Cd^{2+}, Pb^{2+} and AsO_4^{3-} are very toxic ions, yet very little methods have been used for the determination of some of them together [20]. Usually rapid and simple general methods for their analysis have encountered difficulties especially in presence of AsO_4^{3-} ion. The selection of specific physical conditions for carrying out such an analysis complicates the determination by the use of a group of reagents for separating mixtures and for the determination of such individual ions. Körbl and Přibil [11] in 1957 prepared BCO (I) as a new metallochromic indicator by condensation of formaldehyde, iminodiacetic acid and bromo phenol red. No further work was reported to such indicator until 1970. Cherkesov et al. [12,13] in 1971 prepared the indicator again named it Bromo-phthalexon-S and studied its complexes with few metal ions. In 1977 Vytřas determined some values of its acid-dissociation constants potentiometrically and spectrophotometrically [14]. From that time until now no further detailed work was reported either for Bromo-Cresol Orange (BCO), (I) or its semi-form (II).

The aim of this work is to present a rapid and simple general complexometric method for the determination of Pb^{2+}, Cd^{2+} and Tl^{3+} or Hg^{2+} or AsO_4^{3-} if only three of such ions are present together in one aliquot solution successively with high precision and accuracy. At first some artificial solution mixtures similar to those of such ores, minerals and alloys were determined by visual endpoint indication using BCO as a metallochromic indicator followed by an application of the proposed procedures for real naturally occurring samples containing one or some of such metals.

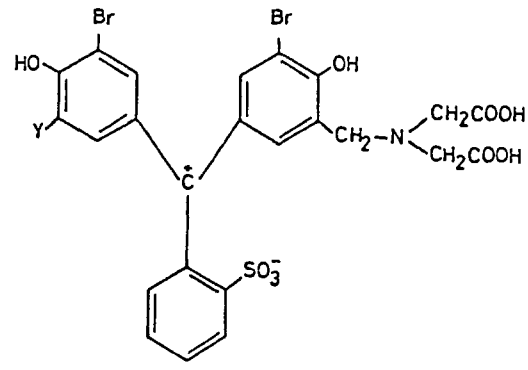

I Y= CH_2-N(CH_2COOH)$_2$
II Y=H

2. Experimental

2.1. Reagents and solutions

A 0.05 mol l^{-1} solution of disodium ethylenediaminetetraacetate (Na_2EDTA) was prepared by dissolving the required mass of $Na_2EDTA.2H_2O$ (analytical reagent grade, BDH, Poole, Dorset, UK) in redistilled water and diluting to the necessary volume. Standard Hg(II), Cd(II) and Pb(II) nitrate solutions were prepared by dissolving highly pure (99.99%-BDH) carbonates of such metals in concentrated nitric acid (BDH) and diluting to the necessary volume with 0.5 mol l^{-1} nitric acid. AsO_4^{3-} solution was prepared by oxidizing the corresponding mass of Na_3AsO_3 (BDH) with bromine water in 1 mol l^{-1} nitric acid. The excess bromine was removed by heating the solution on a steam bath for 15 min until the appearance of faint green colour of AsO_4^{3-} ion. Tl(III) nitrate solution was prepared by boiling the corresponding mass of Tl_2O_3 (BDH) in concentrated nitric acid and diluting to the necessary volume with 1 mol l^{-1} nitric acid. Na_3AsO_4 was standardized by precipitation as $MgNH_4AsO_4$ using standard $Mg(NO_3)_2$ solution and back titrating the excess Mg^{2+} with Na_2EDTA using Erichrome Black-T (EBT) as indicator (pH 10). The Na_2EDTA solution ($\sim$ 0.05 mol l^{-1}) was standardized by the spectrophotometric titration of 0.005 mol l^{-1} Pb(II) nitrate using XO as indicator in hexamine–HNO_3 buffer solution (pH 5, 520 nm). All other salts were prepared by dissolving the calculated mass of each salt (BDH) in the required

volume of redistilled water. In this work highly purified sample of the free acid form of BCO indicator obtained by liquid-liquid extraction procedures was used [17,18]. The product formed by Mannich condensation at 55°C (10 h) of bromophenol red, iminodiacetic acid and paraformaldehyde was extracted several times with pure *n*-butanol (organic phase) and 0.1 mol l^{-1} $NaHCO_3$ (aqueous phase). The component in the aqueous-phase (Semibromo-Cresol Orange (SBCO), and Bromo-cresol orange (BCO)) were extracted several times using n-butanol (organic phase) and 0.1 mol l^{-1} hydrochloric acid (aqueous phase). SBCO was isolated in the organic phase (raffinate) and BCO was extracted into the aqueous one. Further details of separation of SBCO and BCO have been described elsewhere [18]. The purity of the obtained BCO indicator was ascertained using HPLC (LKB-Bromma-Switzerland) instrument using *n*-butanol-acetic acid–water (4:1:2) by volumes as a mobile phase. For freshly preparing a 0.01 mol l^{-1} solution of the BCO indicator, the corresponding masses of the free acid form of the indicator was dissolved in redistilled water. 0.05 mol l^{-1} solution of 1,10 phen and TSC (Merck, Germany) were prepared by dissolving the required mass of reagent in pure methanol. Computation of experimental data and its statistical evaluation were as reported earlier [15,16]. If necessary, some outlier statistical tests such as *Q*-test were used to eliminate values of the determined metal ions, x_i, showing a statistically significant deviation from other experimentally determined values [15,16].

2.2. Decomposition of samples

The process of crushing, grinding (150 mesh), decomposition with different fusion mixtures and dissolution of various real samples were carried out as described earlier [19,20]. Some samples were fused with an approximately 0.5–1 g of Na_2CO_3 at 800°C for 1.5 h in an electric muffle furnace and dissolved after the described pretreatment in a 100 ml calibrated flask. Silica must be completely removed in each case by treating the fused ore in platinum crucible with an excess of hydrofluoric acid and small volume of concentrated sulphuric acid. The silica was expelled as volatile silicon tetrafluoride. The different cations present in the ore were first converted into the fluorides, which passed into the sulphates in contact with the less volatile sulphuric acid. Subsequent brief ignition at 700°C for 15 min converted the sulphates back into the oxides. The latter oxides were boiled with concentrated nitric acid nearly to dryness, cooled and diluted to 100 ml in a volumetric flask. The sulphate ores e.g., anglesite ($PbSO_4$) was treated in the same way after its fusion at 850°C for 30 min to convert the sulphate ore into PbO. The sulphides ores of some metals e.g., cinnabar (HgS), greenockite (CdS), realgar (As_4S_4) and orpiment (As_2S_3) were boiled with aqua regia and hydrofluoric acid until near dryness, cooled, diluted with redistilled water, filtered from the suspended sulphur and completed to the necessary volume with redistilled water. Other experimental procedures and apparatus were described earlier [21–24]. The proposed successive back-titration method for the determination of the elements under investigation was compared with the atomic absorption spectrometry (AAS). A Perkin-Elmer Model 2380 atomic absorption spectrometer (USA) was used with Pye Unicam (England) hollow-cathode lamps for Pb, Cd, As, Hg and Tl. Absorbance values were taken after an average integration time of 1 s. The optimum conditions used for the determination of the investigated elements were described elsewhere [25].

3. Results and discussion

3.1. Successive titrations of Cd^{2+}, Pb^{2+} and Tl^{3+} or Hg^{2+} or AsO_4^{3-} by visual endpoint indication using BCO

Different series of samples containing different proportions of Cd^{2+}, Pb^{2+} and Tl^{3+} or Hg^{2+} or AsO_4^{3-} were analysed. The same procedure was used for real samples of ores and alloys. In one of such series (series I_a), 5 ml of 0.1 mol l^{-1} Tl^{3+}, 5 ml of 0.1 mol l^{-1} Cd^{2+} and 5 ml of 0.1 mol l^{-1} Pb^{2+} solutions were transferred into a 250 ml conical flask containing about 85 ml of doubly distilled water. The mixture was adjusted to pH 0.5–1 (according to Tl^{3+} concentration) by dropwise addition of HNO_3 solution (5 mol l^{-1}). A few drops of BCO indicator (10^{-3} mol l^{-1}) to allow

the endpoint to be easily detected visually were added. The whole mixture was titrated with 0.05 mol l^{-1} Na_2EDTA solution. At the endpoint the colour changed from bright red to lemon yellow. This step gave Tl^{3+} only. At the Tl^{3+} endpoint 30 ml of 0.05 mol l^{-1} Na_2EDTA were added and the excess Na_2EDTA was back-titrated versus 0.05 mol l^{-1} $Pb(NO_3)_2$ solution after controlling the pH of solution to ~4.8 (hexamine–HNO_3 buffer). At the endpoint the colour reversibly changed from lemon yellow to red. 1,10-phen (25 ml of 0.05 mol l^{-1} solution) was added to the latter endpoint and the liberated EDTA equivalent to Cd^{2+} was titrated against the same $Pb(NO_3)_2$ solution. The process of addition of 1,10-phen and continuous stirring of solution should be repeated several times until permanent endpoint i.e., permanent existance of red colour. Pb^{2+} was found by difference. The feasibility of the proposed successive titration (ST) method for one aliquot sample containing Tl^{3+}, Cd^{2+} and Pb^{2+} was studied using different ratios of the components. Five series of titrations (series a) were done with different molar ratios of the investigated metal ions. The results for five series of parallel determinations of Tl^{3+}, Cd^{2+} and Pb^{2+} using the proposed ST method are given in Table 1 (series a). In another mixture containing Hg^{2+}, Cd^{2+} and Pb^{2+} (series 2_b), 1 ml of 0.1 mol l^{-1} Hg^{2+}, 9 ml of 0.1 mol l^{-1} Cd^{2+} and 5 ml of 0.1 mol l^{-1} Pb^{2+} solution were transferred into 250 ml conical flask and the whole solution was completed to about 100 ml with redistilled water. An excess of 40 ml of Na_2EDTA of concentration 0.05 mol l^{-1} were added and the excess Na_2EDTA was indirectly titrated against 0.05 mol l^{-1} $Pb(NO_3)_2$ solution using BCO indicator after adjusting the pH to ~4.8 (hexamine–HNO_3). At the endpoint thiosemicarbazide (TSC), 4 ml of 0.1 mol l^{-1} solution, were added to release the EDTA equivalent to Hg^{2+}. The released EDTA was titrated with $Pb(NO_3)_2$ again until the same endpoint. The process of addition of TSC should be done many times with continuous stirring until permanent endpoint.

At the Hg^{2+} endpoint 1,10-phen was added to release the EDTA combined with Cd^{2+}. Lead in the mixture was found by difference. The feasibility of the suggested ST method for one aliquot sample containing Hg^{2+}, Cd^{2+} and Pb^{2+} was studied using five series and the results are shown in Table 1 (series b).

For a third mixture containing AsO_4^{3-} (As^{5+}), Cd^{2+} and Pb^{2+} (series 3_c), 5 ml of 0.1 mol l^{-1} AsO_4^{3-}, 9 ml of 0.1 mol l^{-1} Cd^{2+} and 1 ml of 0.1 mol l^{-1} Pb^{2+} were transferred into 250-ml conical flask and the whole solution was diluted in the usual manner. An excess of 30 ml of 0.05 mol l^{-1} of Na_2EDTA was added. The pH of the solution was adjusted to pH 10 ($NH_4OH + NH_4Cl$ buffer) and an excess of 10 ml of standard 0.1 mol l^{-1} $Mg(NO_3)_2$ was added. The solution was boiled for 15 min, cooled and filtered. The white precipitate of $MgNH_4AsO_4$ was washed several times with doubly distilled water. AsO_4^{3-} was determined by directly titrating the magnesium equivalent to AsO_4^{3-} in the precipitate after its dissolution in boiling dilute nitric acid, controlling the pH to 10 (NH_4OH) using EBT indicator and adding both hydrazine hydrochloride and KBr to reduce the arsenic (V) to (III). The pH of the filtrate solution after the complete separation and determination of AsO_4^{3-} was lowered to pH ~4.8 using concentrated nitric acid and hexamine buffer. Both Cd^{2+} and Pb^{2+} were determined by the usual proposed procedure. The presence of Mg^{2+} ions do not cause interference at such lower pH. The feasibility of the proposed ST method for one aliquot sample containing AsO_4^{3-}, Cd^{2+} and Pb^{2+} was studied using five series and the results are shown in Table 1 (series c). Generally it was necessary to determine the value of the blank by titrating the same volume of a solution containing all the constituents with the exception of the metal ions at the selected pH value.

3.2. Interference of foreign species

It was found that NO_3^- and ClO_4^- at molar concentration of up to 1000 times that of Tl^{3+}, Hg^{2+}, Cd^{2+}, Pb^{2+} or AsO_4^{3-} did not interfere. SO_4^{2-} and Cl^- at 100-fold molar concentration of Pb^{2+} did not interfere. Iodide at the same molar concentration led to the complete reduction of Tl^{3+} to Tl^+ and converts Hg^{2+} to HgI_4^{2-} complex. PO_4^{3-} started to interfere when present at a molar concentration at least 100 times that of any of the metal ions studied. Higher concentrations of PO_4^{3-} (more than 100-fold) led to the formation of

Table 1
Statistical evaluation and tests of experimental data for five series of successive titrations of Cd^{2+}, Pb^{2+}, and Tl^{3+} or, Hg^{2+} or AsO_4^{3-} by visual detection of end-point using BCO and/or EBT indicators, pH = 0.5–1 for Tl^{3+}, 4.8 for Hg^{2+}, Cd^{2+} and Pb^{2+} and 10 for AsO_4^{3-} $C_{Na_2EDTA} = C_{Pb(NO_3)_2} = 0.05$ and/or 0.01 mol l^{-1}. The number of titrations in a series (n) = 5

Series No.	Metal ion	C_M^d mmol per 100 ml	Metal taken, μ mg per 100 ml	Mean, $\bar{x}_1$ mg per 100 ml	s_1/mg	s_{r_1} (%)	Recovery (%)	$\lvert t\rvert_1^+ = \frac{(\bar{x}_1-\mu)\sqrt{n}}{s}$
1a	Tl^{3+}	0.50	102	103[a]	0.9	0.9	101	2.48
	Cd^{2+}	0.50	56.2	55.8[b]	0.4	0.7	99.3	2.24
	Pb^{2+}	0.50	104	104[c]	0.9	0.7	100	2.48
2a	Tl^{3+}	0.10	20.4	20.0	0.4	2.0	98.0	2.24
	Cd^{2+}	0.50	56.2	55.5	0.6	1.1	98.8	2.61
	Pb^{2+}	0.90	186	186	0.5	0.3	100	0.00
3a	Tl^{3+}	0.50	102	103	0.9	0.9	101	2.48
	Cd^{2+}	0.9	101	101	0.9	0.9	100	0.00
	Pb^{2+}	0.10	21.0	20.5	0.5	2.4	97.6	2.24
4a	Tl^{3+}	0.90	184	183	0.9	0.3	99.5	2.48
	Cd^{2+}	0.10	11.2	10.8	0.4	3.7	98.2	2.24
	Pb^{2+}	0.50	104	104	0.6	0.6	100	0.00
5a	Tl^{3+}	0.25	51.1	50.5	0.5	1.0	98.8	2.68
	Cd^{2+}	0.50	56.2	55.5	0.6	1.1	98.8	2.61
	Pb^{2+}	0.75	155	154	0.9	0.6	99.4	2.48
1b	Hg^{2+}	0.50	100	100	0.4	0.4	100	0.00
	Cd^{2+}	0.50	56.2	56.0	0.3	0.5	99.6	1.49
	Pb^{2+}	0.50	104	104	0.6	0.6	100	0.00
2b	Hg^{2+}	0.10	20.1	20.0	0.7	3.5	99.5	0.32
	Cd^{2+}	0.50	56.2	55.6	0.5	0.9	98.9	1.79
	Pb^{2+}	0.90	186	185	0.9	0.5	99.5	2.24
3b	Hg^{2+}	0.50	100	99.5	0.8	0.8	99.5	1.40
	Cd^{2+}	0.90	101	100	0.9	0.9	99.0	2.48
	Pb^{2+}	0.10	20.7	20.2	0.8	4.0	97.6	1.40
4b	Hg^{2+}	0.90	181	180	0.9	0.5	99.5	2.48
	Cd^{2+}	0.10	11.2	10.8	0.5	4.6	96.4	1.79
	Pb^{2+}	0.50	104	103	0.9	0.9	99.0	2.48
5b	Hg^{2+}	0.25	50.2	49.5	0.5	1.0	98.6	3.13
	Cd^{2+}	0.50	56.2	55.5	0.4	0.7	98.8	3.90
	Pb^{2+}	0.75	155	155	0.6	0.4	100	0.00
1c	As^{5+}	0.50	37.5	37.0[e]	0.6	1.6	98.7	1.86
	Cd^{2+}	0.50	56.2	56.0	0.5	0.9	99.6	0.89
	Pb^{2+}	0.50	104	103	1.0	1.0	99.0	2.24
2c	As^{5+}	0.90	67.4	68.0	0.6	0.9	101	2.24
	Cd^{2+}	0.10	11.2	11.0	0.6	5.5	98.2	0.75
	Pb^{2+}	0.50	104	103	0.9	0.9	99.0	2.48
3c	As^{5+}	0.10	7.5	7.2	0.5	7.0	96.0	1.34
	Cd^{2+}	0.50	56.2	56.0	0.7	1.3	99.6	0.64
	Pb^{2+}	0.90	187	187	0.8	0.4	100	0.00
4c	As^{5+}	0.50	37.5	38.0	0.3	0.8	101	3.73
	Cd^{2+}	0.90	101	102	0.9	0.9	101	2.48
	Pb^{2+}	0.10	20.7	20.2	0.9	4.5	97.6	1.24
5c	As^{5+}	0.75	56.2	56.0	0.5	0.9	99.6	0.89
	Cd^{2+}	0.25	28.1	28.0	0.4	1.4	99.6	0.56
	Pb^{2+}	0.50	104	104	0.4	0.4	100	0.00

$^+$, $|t|_1$ for the comparison of the determined experimental mean with the standard given value, μ for $P = 0.05$ and $n = 5$ (4 degrees of freedom) is equal to 2.78[16].

[a] Endpoint from bright red to yellow.

[b] Endpoint from yellow to red.

[c] Pb was determined by difference.

[d] Titrated concentration of metal ion.

[e] Endpoint from wine red to blue (EBT).

turbidity that spoiled the titration completely. Citric, tartaric and acetic acid at molar concentrations of up to 1000 times that of Tl^{3+}, Hg^{2+}, Cd^{2+}, Pb^{2+} and AsO_4^{3-} did not interfere. Formic acid at the same concentration interfered owing to the complete reduction of Tl^{3+} to Tl^{+} and Hg^{2+} to Hg^{+}. Mg^{2+}, Ca^{2+}, Sr^{2+} and Ba^{2+} did not interfere at such lower pH. Zn^{2+}, Co^{2+}, Mn^{2+}, Al^{3+}, Ni^{2+}, Cu^{2+} and Fe^{2+} interfere at equal molar concentration to Cd^{2+} in the mixture. Fe^{3+}, Zr^{4+}, Bi^{3+}, Ti^{4+}, Th^{4+} and Sc^{3+} interfere at equal molar concentration to Tl^{3+} in the mixture. Fortunately most of interfering cations are rarely found in Tl^{3+}, Hg^{2+}, Cd^{2+}, and Pb^{2+} mineral, but iron is only sometimes present with As^{5+} ores and minerals and could be easily masked by triethanolamine (pH 10).

3.3. Successive titrations of Cd^{2+}, Pb^{2+} and Tl^{3+} or Hg^{2+} or AsO_4^{3-} by visual endpoint indication using XO

As for BCO, five series of successive titrations were performed with molar ratios of Tl^{3+}:Cd^{2+}:Pb^{2+}, Hg^{2+}:Cd^{2+}:Pb^{2+} and Cd^{2+}:Pb^{2+}:AsO_4^{3-} of 1:5:9, 5:9:1, 9:1:5 and others for each mixture using XO as indicator in order to obtain a reasonable comparison of the accuracy, precision and detection limits with the two indicators. The experimental procedure was the same for both indicators. The results of five series of parallel determinations for each mixture of the three investigated ions are shown in Table 2. The statistical evaluation showed that the detection limit (2s + blank) [26,27] is nearly the same for both indicators. The detection limit per 100 ml of solution is 2 mg for Tl^{3+}, 1.2 mg for Cd^{2+}, 3 mg for Pb^{2+}, 2.8 mg for Hg^{2+} and 1.4 mg for As^{5+}. Comparison between the experimental mean value of each metal ion (for both indicators) with the given standard value, μ, by applying the null hypothesis of $|t|_1$ for $P = 0.05$ and $n = 5$ in order to estimate systematic error was carried out.

From Table 1, it is found that for BCO indicator $|t|_1 = 0.00–2.68$ for all the three metals with the exception of mercury and cadmium in series 5b, and arsenic in series 4c for which have $|t|_1 = 3.13, 3.9$ and 3.73, respectively. This means that mercury and cadmium in series 5b and arsenic in series 4c are subjected to systematic error (the null hypothesis of $|t|_1$ for $P = 0.05$ and $n = 5$ for the specified metals in these series are rejected). For all the other metals ions the null hypothesis of $|t|_1$ for $P = 0.05$ and $n = 5$ is retained where the calculated experimental values of $|t|_1$ are less than the tabulated value ($|t|_1 = 2.78$) [16]. From Table 2, it is found that for XO indicator $|t|_1 = 0.00–2.48$ for all three metals in different series with the exception of lead in series 4a and 1b and cadmium in series 5b. This means that these metals ions in these series are the only determinations subject to systematic error. For all other metal ions determined the null hypothesis of $|t|_1$ for $P = 0.05$ and $n = 5$ is retained, which can be explained as mentioned before.

Comparison between the experimental means for the two studied indicators was carried out using the null hypothesis of $|t|_2$ for $P = 0.05$ and $n = 10$ (Table 2). It was found that for both indicators $|t|_2 = 0.0–2.20$ for all the three metals ions with the exception of thallium in series 4a, lead in series 4a, 5a, 1b and 2b. This means that the observed experimental values of $|t|_2$ are less than the tabulated value ($|t|_2 = 2.31$) [16] and $|t|_2$ is retained for all determinations with the exception of the referred to series for thallium and lead. In the latter series the null hypothesis of $|t|_2$ for $P = 0.05$ and $n = 10$ is rejected and the determined metals in these cases have unacceptable means or recoveries compared with the other accepted series (Table 2).

Comparison between the experimental means for the two studied indicators to estimate random errors of the two sets of data (Table 1 and Table 2) was carried out using the two-tailed F-test [16]. From Table 2, it is clear that all the experimental $F_{4,4}$ values are between 0.16 and 5.06 for all the series of determinations. These values are less than the tabulated value of $F_{4,4}$ for $P = 0.05$ and $n = 10$ (9.6) [16]. This proves that there is no significant difference between the two standard deviations at $P = 0.05$ for both BCO and XO indicators or that the two indicators give the same precision have in such determinations. In addition, all series are not subject to random errors for both investigated indicators.

The success of this ST method depends on the fact that Pb^{2+} ion does not react with neither 1,10-phen nor TSC and can be determined easily by difference. Also, Cd^{2+} ion does not react with TSC in case of

Table 2
Statistical evaluation and tests of experimental data for five series of successive titrations of Cd^{2+}, Pb^{2+} and Tl^{3+} or Hg^{2+} or AsO_4^{3-} by visual detection of end-point using XO and/or EBT as indicators

Series No.	Metal ion	C_M^e, mmol per 100 ml	Mean taken, μ mg per 100 ml	Mean, $\bar{x}_2$ mg per 100 ml	s_2/mg	s_{r_2} (%)	Recovery (%)	$\|t\|_1$	$\|t\|_2^a$	Two-tailed F-test $(F_{4,4})^a$
1a	Tl^{3+}	0.50	102	103[b]	0.9	0.9	101	2.48	0.00	1.00
	Cd^{2+}	0.50	56.2	55.8[c]	0.4	0.7	99.3	2.24	0.00	1.00
	Pb^{2+}	0.50	104	104[d]	0.9	0.9	100	0.00	0.00	1.00
2a	Tl^{3+}	0.10	20.4	20.2	0.4	2.0	99.0	1.12	0.79	1.00
	Cd^{2+}	0.50	56.2	56.0	0.6	1.1	99.6	0.75	2.20	1.00
	Pb^{2+}	0.90	186	185	0.9	0.5	99.5	2.48	2.17	0.31
3a	Tl^{3+}	0.50	102	102	0.9	0.9	100	0.00	1.76	1.00
	Cd^{2+}	0.90	101	100	0.9	0.9	99.0	2.48	1.76	1.00
	Pb^{2+}	0.10	21.0	20.5	0.5	2.4	97.6	2.24	0.00	1.00
4a	Tl^{3+}	0.90	184	185	0.9	0.5	101	2.48	3.51	1.00
	Cd^{2+}	0.10	11.2	11.3	0.4	3.5	101	0.56	1.98	1.00
	Pb^{2+}	0.50	104	103	0.6	0.6	99.0	3.73	2.64	1.00
5a	Tl^{3+}	0.25	51.1	50.9	0.5	1.0	99.6	0.89	1.27	1.00
	Cd^{2+}	0.50	56.2	56.0	0.6	1.1	99.6	0.75	0.83	1.00
	Pb^{2+}	0.75	155	156	0.9	0.6	101	2.48	3.51	1.00
1b	Hg^{2+}	0.50	100	99.5	0.5	0.5	99.5	2.24	1.10	0.64
	Cd^{2+}	0.50	56.2	55.9	0.3	0.5	99.5	2.24	1.33	1.00
	Pb^{2+}	0.50	104	103	0.7	0.7	99.0	3.19	2.43	0.56
2b	Hg^{2+}	0.10	20.1	20.0	0.7	3.5	99.5	0.32	0.00	1.00
	Cd^{2+}	0.50	56.2	55.9	0.5	0.9	99.5	1.34	0.95	1.00
	Pb^{2+}	0.90	186	186	0.5	0.3	100	0.00	2.77	3.24
3b	Hg^{2+}	0.50	100	99.6	0.8	0.8	99.6	1.12	0.20	1.00
	Cd^{2+}	0.90	101	100	0.9	0.9	99.0	2.48	0.00	1.00
	Pb^{2+}	0.10	20.7	20.5	0.8	3.9	99.0	0.56	0.59	1.00
4b	Hg^{2+}	0.90	181	180	0.9	0.5	99.4	2.48	0.00	1.00
	Cd^{2+}	0.10	11.2	11.0	0.5	4.5	98.2	0.89	0.63	1.00
	Pb^{2+}	0.50	104	103	0.9	0.9	99.0	2.48	0.00	1.00
5b	Hg^{2+}	0.25	50.2	50.0	0.4	0.8	99.6	1.12	1.75	1.563
	Cd^{2+}	0.50	56.2	55.5	0.4	0.7	98.8	3.91	0.00	1.00
	Pb^{2+}	0.75	155	154	0.9	0.6	99.4	2.48	2.67	0.44
1c	As^{5+}	0.50	37.5	37.8	0.6	1.6	101	1.12		
	Cd^{2+}	0.50	56.2	56.0	0.5	0.9	99.6	0.89	0.00	1.00
	Pb^{2+}	0.50	104	103	1.0	1.0	99.0	2.24	0.00	1.00
2c	As^{5+}	0.90	67.4	67.8	0.6	0.9	101	1.49	–	––
	Cd^{2+}	0.10	11.2	11.0	0.6	5.5	98.2	0.75	0.00	1.00
	Pb^{2+}	0.50	104	104	0.4	0.4	100	0.00	2.27	5.06

Table 2 (continued)

Series No.	Metal ion	C_M^e, mmol per 100 ml	Mean taken, μ mg per 100 ml	Mean, $\bar{x}_2$ mg per 100 ml	s_2/mg	s_{r_2} (%)	Recovery (%)	$\|t\|_1$	$\|t\|_2^+$	Two-tailed F-test $(F_{4,4})^a$
3c	As^{5+}	0.10	7.5	7.3	0.6	8.2	97.3	0.75	—	—
	Cd^{2+}	0.50	56.2	56.4	0.8	1.4	100	0.56	0.84	0.77
	Pb^{2+}	0.90	186	186	0.9	0.5	100	0.00	1.86	0.79
4c	As^{5+}	0.50	37.5	37.0	0.5	1.4	98.7	2.24	—	—
	Cd^{2+}	0.90	101	101	0.8	0.8	100	0.00	1.86	1.27
	Pb^{2+}	0.10	20.7	20.5	1.0	4.9	99.0	0.45	0.50	0.81
5c	As^{5+}	0.75	56.2	55.8	0.6	1.1	99.3	1.49	—	—
	Cd^{2+}	0.25	28.1	27.9	0.5	1.8	99.3	0.89	0.35	0.64
	Pb^{2+}	0.50	104	103	1.0	1.0	99.0	2.24	2.08	0.16

Conditions a+s in Table 1.

In case of As^{5+} EBT indicator was used only for all series.

$^+$, $|t|_2 = \bar{x}_1 - \bar{x}_2/s_p\left(\sqrt{\frac{1}{n_1}+\frac{1}{n_2}}\right)$ is for the comparison of the means of both BCO and XO indication for $P = 0.05$ and $n = 10$ for the two indicators (8 degrees of freedom) and is equal 2.31; s_p is the pooled estimate of the standard deviation $= \sqrt{(n_1-1)s_1^2+(n_2-1)s_2^2/(n_1+n_2-2)}$.

[a] $F_{4,4} = s_1^2/s_2^2$ for $P = 0.05$ is equal to 9.605 (two-tailed test)[16].

[b] Endpoint from red to lemon yellow.

[c] Endpoint from yellow to bright red.

[d] Pb was determined by difference.

[e] Titrated concentration of metal.

Table 3
Results of determination of lead, cadmium, thallium, mercury and arsenic in ores, minerals and alloys by the proposed successive titration method (ST) and atomic absorption spectrometry (AAS)

Sample, description and/or location	Pb (%)[g]		Cd (%)[g]		Tl (%)[g]		Hg (%)[g]		As (%)[g]	
	AAS	ST	AAS	ST	AAS	ST	AAS	ST	AAS	ST
Cerussite mineral, Patagonia, Arizona (USA)[h]	50.0	50.2	—	—	—	—	—	—	—	—
Anglesite mineral, Chihuahua (Mexico)[h]	42.8	43.0	—	—	—	—	—	—	—	—
Galena ore, Kansas (USA)[h]	25.6	25.4	—	—	—	—	—	—	—	—
Mimetesite mineral, eastern desert (Egypt)[h]	20.9	20.5	—	—	—	—	—	—	4.5	4.6
Solder alloy (Sn + Pb)[h]	55.3	55.7	—	—	—	—	—	—	—	—
Babitt alloy (Sn + Sb + Pb)[h]	75.4	75.0	—	—	—	—	—	—	—	—
White alloy (Sn + Sb + Pb)[h]	40.8	41.4	—	—	—	—	—	—	—	—
Greenockite mineral[a]	—	—	0.5	0.5	—	—	—	—	—	—
Hawleyite on sphelerite Eureka, Nevada (USA)[a]	—	—	43.6	44.1	—	—	—	—	—	—
Crooksite mineral[b,24]	—	—	—	—	18.2	18.0	—	—	—	—
Lorandite mineral[b,24]	—	—	—	—	59.5	59.2	—	—	—	—
Hutchinsonite mineral[b,24]	—	—	—	—	20.5	20.2	—	—	—	—
Vrbaite mineral[b,24]	—	—	—	—	30.5	30.3	—	—	—	—
Marcasite mineral[b,24]	—	—	—	—	0.8	0.8	—	—	—	—
Lead-cadmium-thallium alloy (20 + 25 + 55), (laboratory synthesized by fusion)[c]	20.0	19.7	24.8	24.7	54.8	54.7	—	—	—	—
Lead-cadmium-mercury (20 + 15 + 65), (laboratory synthesized amalgams)[d]	19.9	19.6	15.0	14.8	—	—	65.5	65.2	—	—
Cinnabar (red) Winnemucca, Nevada (USA)[e]	—	—	—	—	—	—	52.5	52.2	—	—
Cinnabar (grey), Huitzura (Mexico)[e]	—	—	—	—	—	—	22.9	22.7	—	—
Allemomite (arsenic metal-grey), Moctezuma, Sonora (Mexico)[f]	—	—	—	—	—	—	—	—	95.1	95.6
Realgar ore (reddish yellow), Gumma preparation (Japan)[f]	—	—	—	—	—	—	—	—	41.5	42.1
Loellingite mineral (yellowish grey), Dolni Borg, West Moravia (Czech Republic)[f]	—	—	—	—	—	—	—	—	22.1	22.5
Orpiment mineral (yellowish orange flakes), Nevada (USA)[f]	—	—	—	—	—	—	—	—	69.2	69.8
Arsenic (faint brown), Edwards island, lake superior antario (USA)[f]	—	—	—	—	—	—	—	—	96.2	96.5

Relative standard deviation (s_r) = 1.0–2.5% (n = 6).
[a] Samples contain cadmium.
[b] Samples contain thallium.
[c] Samples contain lead, cadmium and thallium.
[d] Samples contain lead, cadmium and mercury.
[e] Samples contain mercury.
[f] Samples contain arsenic.
[g] Average for two weighed samples (0.5–1 g per 100 ml).
[h] Samples contain lead and/or arsenic.

Hg^{2+} determination. The se quence of determination of metal ions should be adopted exactly to have perfect results. Trials to determine Hg^{2+} using KI instead of TSC as demasking reagent for EDTA did not succeed specially in presence of 1,10-phen in the second step for the determination of Cd^{2+} where a white turbidity was found. The use of $Pb(NO_3)_2$ instead of $Zn(NO_3)_2$ as titrant proceeded easily because it was found that Zn^{2+} ion reacted with 1,10-phen present in the titrating solution and no endpoint was observed or the solution was over titrated. The ST method is preferred for AAS in the fact that, it is relatively rapid, has no standard curves and conditions and of little interference.

3.4. Application of the proposed successive titration method

The results of the determination of Pb^{2+}, Cd^{2+} and Tl^{3+} or Hg^{2+} or As^{5+} in a series of naturally occurring ores, minerals and alloys containing one or any of three ions either together or with other metals are shown in Table 3. These results (average of three determinations of two different weighed samples) are in a good agreement with the values obtained by AAS. The relative standard deviation estimated using the range method [16] was found to be 1–2.5% for the proposed ST method. From the results obtained, it is clear that the titration of any of the three metal ions in different real samples is simple and reliable and can be used with good reproducibility.

Acknowledgements

We express our sincere gratitude to Mr Mohamed Salah El-Din Zaki, Chief of the Geological Museum, Geology Department, Faculty of Science, Mansoura University, for providing the real ore and mineral samples investigated and for constructive comments.

References

[1] N.N. Greenwood and A. Earnshaw, Chemistry of the Elements, Pergamon Press, Oxford, England, 1985, pp. 246–290.
[2] J. Emsley, The Elements, Clarendon, Oxford, 1989, pp. 190, 114, 102, 36 and 20.
[3] C.T. Polson, M.A. Green and M.R. Lee, Clinical Toxology, 1983, Pitman, London, p. 607.
[4] R.M. Harrisson and D.P.H. Laxon, Lead Pollution, Causes and Control, 1981, Chapman and Hall Methum, London, pp. 60.
[5] K.W. Smidle and K. Wards, Heavy metals accumulation in crops on sweage sludge amended with metal salts, Plant Soil, 62 (1981) 3–14.
[6] Encyclopedia of Environmental Science, 4th edition, McGraw-Hill, New York, 1974, pp. 254–256.
[7] R. Jones, Zinc and Cadmium in Lettuce and Radish grown in soils collected near electrical transmission (hydro) towers, Water, Air Soil Pollut., 19 (1982) 389–395.
[8] V. Hiatt and J.E. Huff, The Environmental Impact of Cadmium, Int. J. Environ. Studies, 7 (1975) 277–285.
[9] J. Doull, C.D. Klassen and M.O. Amdur, Toxicity, 1980, pp. 60, McMillan, New York.
[10] R.E. Train, Quality Criteria for water, 1979, pp. 256, U.S., Environmental Protection Agency, Castle-house Publication, Washington DC.
[11] J. Körbl and R. Přibil, Chem. Ind. (London), (1957) 233.
[12] A.I. Cherkesov and V.N. Ryzhov, Zh. Anal. Khim; 26 (1971) 1461.
[13] A.I. Cherkesov, A.I. Argisheva, N.K. Astakhova and A.A. Konyakhina, Izv. Vyssh. Ucheb. Zaved., Khim. Khim. Tekhnol., (1971) 14.
[14] K. Vytřas, Unpublished results, University of Pardubice, Czech Republic, 1977.
[15] K. Eckschlager, Errors, Measurement and Results in Chemical Analysis, Van Nostrand Reinhold, New York, 1969, pp. 88, 107 and 114.
[16] J.C. Miller and J.N. Miller, Statistics for Analytical Chemistry, Ellis Horwood, Chichester, 1st edn, 1986, pp. 43, 53, 59, 189 and 192.
[17] M.A.H. Hafez, I.M.M. Kenawy and M.A.M. Ramadan, Egypt. J. Anal. Chem., 4 (1994) 55.
[18] M.A.H. Hafez, Egyptian Patent No. 93 120 767 in Academy of Technology and Scientific Research, Egypt, December 1993, 4.
[19] R. Richard, Sample Pretreatment and Separation, Wiley, New York, 1987, pp. 60.
[20] A.I. Vogel, Text Book of Quantitative Inorganic Analysis, Longman, London, 4th edn., 1978, pp. 333, 502.
[21] M.A.H. Hafez, Talanta, 39 (1992) 1189.
[22] M.A.H. Hafez, I.M.M. Kenawy and M.A.M. Ramadan, Analyst, 119 (1994) 1103.
[23] M.A.H. Hafez, I.M.M. Kenawy and M.A.M. Ramadan, Anal. Lett., 27(7) (1994) 1383.
[24] M.A.H. Hafez, I.M.M. Kenawy and M.A.M. Ramadan, Analyst, 119 (1994) 2467.
[25] W.J. Price, Spectrochemical Analysis by Atomic Absorption, Heyden, London, England, 1979, pp. 290, 295, 316, 321 and 346.
[26] H. Kaiser, Fresenius'Z. Anal. Chem., 209 (1965) 1.
[27] H. Kaiser, Anal. Chem., 42 (1970) 24A.

ELSEVIER

Talanta 44 (1997) 797–803

Talanta

The stabilization of manganese(III) by azide ions in aqueous solution

Horacio Dorigan Moya [b], Eduardo Almeida Neves [a], Nina Coichev [b,*]

[a] *Departamento de Química, Universidade Federal de São Carlos, C.P. 676, CEP 13.565-905, São Carlos, Brazil*
[b] *Instituto de Química, Universidade de São Paulo, C.P. 26.077, CEP 05599-970, São Paulo, Brazil*

Received 20 May 1996; received in revised form 20 September 1996; accepted 23 September 1996

Abstract

The evidences of spontaneous oxidation of Mn(II) by the dissolved oxygen in azide buffer medium, which is dependent on the N_3^-/HN_3 concentration, suggested a formation of stable Mn(III) complexes due to marked colour changes. Spectrophotometric studies combined with coulometric generation of Mn(III), in presence of large excess of Mn(II), showed a maximum absorbance peak at 432 nm. The molar absorptivity increases with azide concentration (0.44–3.9 mol l^{-1}) from 3100 to 6300 mol^{-1} l cm^{-1}, showing a stepwise complex formation. Potential measurements of the Mn(III)/Mn(II) system in several azide aqueous buffers solutions: 1.0×10^{-2} mol l^{-1} HN_3, (0.50–2.0 mol l^{-1}) N_3^- and 5.0×10^{-2} mol l^{-1} Mn(II) and constant ionic strength 2.0 mol l^{-1}, kept with sodium perchlorate, leads to the conditional potential, $E^{0'}x$, in several azide concentrations at 25.0 ± 0.1°C. Considering the overall formation constants of Mn(II)/N_3^-, from former studies, and the potential, $E^{0'}s = 1.063$ V versus SCE, for Mn(III)/Mn(II) system in non-complexing media, it was possible to calculate the Fronaeus function, $F_0(L)$, and the following overall formation constants: $\beta_1 = 1.2 \times 10^5$ M^{-1}, $\beta_2 = 6.0 \times 10^8$ M^{-2}, $\beta_3 = (2.4 \pm 0.7) \times 10^{11}$ M^{-3}, $\beta_4 = (1.5 \pm 0.5) \times 10^{11}$ M^{-4} and $\beta_5 = (9.6 \pm 0.8) \times 10^{11}$ M^{-5} for the Mn(III)/N_3^- complexes. These data give important support to understand the importance of Mn(II) and Mn(III) synergistic effect on the analytical method of S(IV) determination based on the Co(II) autoxidation. © 1997 Elsevier Science B.V.

Keywords: Azide; Manganese; Stability constants

1. Introduction

It is well known that some ligands are able to stabilize Mn(III) complexes. Analytical applications, for instance, come from the use of pyrophosphates in manganese determination due to its formation of manganese(III) complexes [1]. The reaction of permanganate with the reducing agent oxalate is an interesting example of participation of Mn(III) as an intermediate in such redox reaction [2,3].

Former studies of manganese(II) in azide buffers solutions, N_3^-/HN_3, have shown a tendency to change colour of the solution with a possible formation of brownish manganese(III) azide complexes [4,5]. Spontaneous oxidation by

* Corresponding author. E-mail: ncoichev@quim.iq.usp.br

PII S0039-9140(96)02112-1

dissolved oxygen takes place specially at azide concentrations higher than 1.0 mol l^{-1} and it is markedly dependent on HN_3 concentration. We are concerned about the stabilization of Mn(III) in azide medium in order to better understand the role of the Mn(III)/Mn(II) system in previous kinetics studies on the autoxidation of Mn(II) induced by S(IV) and its synergistic effect on the similar studies of Co(II) and Fe(II) ions. These studies are of special relevance in environmental chemistry [5–10].

The synergistic effect of the Mn(II) and Mn(III) ions on the autoxidation of Co(II) induced by S(IV) allowed the development of an alternative analytical determination method of S(IV) in environmental samples [6,7]. The concentration of Co(III) azide complex formed was a linear relationship with the initial S(IV) concentration. As the molar absortivity of Co(III) in 365 nm is high ($\epsilon \approx 22\,000$ mol^{-1} l cm^{-1}), it was possible to determined S(IV) in the range of 10^{-6}–10^{-4} mol l^{-1}.

The present study deals with some spectrophotometric characteristics of Mn(III) azide complexes. The Mn(III) was generated by anodic oxidation of Mn(II) in azide medium at constant ionic strength. The parallel potentiometric measurements allowed to obtain the redox potential of Mn(III)/Mn(II) system at some azide concentrations in which stabilization of Mn(III) takes place. The potentiometric measurements in the $MnO_2/H^+/Mn^{2+}/Mn^{3+}$ system, by combination with data on the Fe(III)/Fe(II) system, were used to estimate the conditional potential, $E^{0'}s$, of the Mn(III)/Mn(II) in non complexing medium at the same ionic strength. Analysis of the potentiometric data led to the equilibrium constants in the Mn(III)/N_3^- system.

2. Experimental

2.1. Reagents and standard solutions

All reagents were from AR or CP specification from Merck or Fluka A.G.

Sodium azide was prepared directly from the salt. Standardization was carried out by adding a known volume of standard sulfuric acid solution, boiling to remove volatile hydrazoic acid, HN_3, followed by back titration of the remaining strong acid with standard sodium hydroxide solution.

Manganese(II) perchlorate solution was prepared from direct reaction of excess carbonate with 6.0 mol l^{-1} perchloric acid, under stirring for 2 days at room temperature. After filtering, free perchloric acid was added to adjust pH to 5.5, in order to avoid hydrolysis. Standardization was carried out by complexometric titration with EDTA [11].

Sodium perchlorate solution 5.0 mol l^{-1} utilized to make up the ionic strength of working solutions was standardized by taking small volume solution and dried in an oven at 120°C until constant weight.

Standard perchloric acid solution was added to the working solutions to displace hydrazoic acid from the azide ions.

2.2. Working solutions

The working solution for preparation of Mn(III) consisted of 100 ml of 1.0×10^{-2} mol l^{-1} HN_3, 5.0×10^{-2} mol l^{-1} Mn(II) and NaN_3 ranging from 0.50 to 2.0 mol l^{-1}. Electrolysis was performed at constant current (10 mA) as a function of time. After each period of applied current, the potential measurements of platinum indicator electrode, versus the Hg/Hg_2Cl_2 electrode, were done as described in former work [12]. Simultaneously UV-visible absorption spectra were recorded with a HP-8452 spectrophotometer equipped with a thermostatic cell holder. All measurements were performed at 25.0 ± 0.1°C.

3. Results and discussion

3.1. Evidences of the spontaneous oxidation of Mn(II) in azide medium

Fig. 1 shows the spectra changes, due to the spontaneous oxidation of Mn(II), by dissolved oxygen, in azide solutions containing Mn(II) in presence of some air and a small and constant hydrazoic acid concentration. The higher the

azide concentration the faster and more effective is the oxidation. In solutions previously bubbled with nitrogen the oxidation is almost non existent such small HN_3 concentration, such as 5.0×10^{-2} mol l^{-1}. The concentration of hydrazoic acid is also an important parameter in such oxidation, as the lowering pH favours the process. The following redox systems can well explain the oxidation power of hydrazoic acid [13]:

$$HN_3 + 3H^+ + 2e^- \rightleftharpoons N_2 + NH_4^+ \quad E^0 = 1.96\ V \tag{1a}$$

$$HN_3 + 11H^+ + 8e^- \rightleftharpoons 3NH_4^+ \quad E^0 = 0.695\ V \tag{2a}$$

These reactions can be better considered in the adequate form for the azide buffer:

$$4HN_3 + 2e^- \rightleftharpoons N_2 + NH_4^+ + 3N_3^- \tag{1b}$$

$$12HN_3 + 8e^- \rightleftharpoons 3NH_4^+ + 11N_3^- \tag{2b}$$

3.2. Determination of the potential of the Mn(III)/Mn(II) in non complexing medium

An important data to calculate the equilibrium constants of $Mn(III)/N_3^-$ complex is the value of the conditional potential, $E^{0'}s$, of the Mn(III)/Mn(II) system in non complexing medium at 2.0 mol l^{-1} ionic strength in perchlorate medium. The difficulties to obtain it are the tendencies of the trivalent cation to hydrolyze [14] and to disproportionate Eq. (3) at lower acidity medium [15], so it is required studies at high acidic medium.

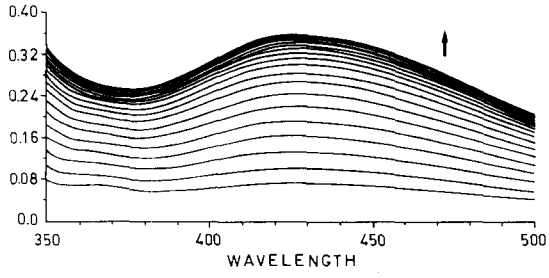

Fig. 1. Successive spectra, every 60 s, of $Mn(II)/N_3^-$ solutions in presence of dissolved oxygen with Mn(III) spontaneous formation. $Mn(II) = 1.0 \times 10^{-1}$ mol l^{-1}, $HN_3 = 5.0 \times 10^{-2}$ mol l^{-1}, $N_3^- = 1.6$ mol l^{-1} (path length = 1.00 cm).

$$2Mn^{3+} + 2H_2O \rightleftharpoons Mn^{2+} + 4H^+ + MnO_2$$
$$K \sim 10^9 \tag{3}$$

The literature refers to 1.5 V versus N.E.H. as the conditional potential of the Mn(III)/Mn(II) system in 3.0 mol l^{-1} perchloric acid or 7.5 mol l^{-1} sulfuric acid medium [16,17]. These data, in virtually non complexing medium, can not obviously be used in combination with the present potentiometric data in azide medium due to the very different experimental conditions of both experiments, such as ionic strength and acidity.

To calculate the conditional potential value, measurements were carried out initially in the following cell:

$$Hg|Hg_2Cl_2, NaCl(sat): 2.0M\ HClO_4, 5.0 \times 10^{-1}\ M\ Mn(ClO_4)_2, z[Mn^{3+}]|Au \tag{4}$$

The Mn^{3+} concentration was initially generated by coulometric oxidation up to 10^{-3} mol l^{-1} order. Measurements of the potential in several solutions led to non reproducible $E^{0'}$ data due to the low current electrode efficiency and slow oxidation of water by the trivalent cation formed.

Another way to obtain the conditional potential value of Mn(III)/Mn(II) system at this acidity medium was performed by reversion of the disproportioning Eq. (2a) by adding to a solution of 2.0 mol l^{-1} $HClO_4$ and 5.0×10^{-1} mol l^{-1} Mn(II) a large excess of manganese dioxide in order to form about 10^{-3} mol l^{-1} of Mn(III). To evaluate the Mn(III) concentration in the final solution, an excess of I^- was added and the I_2 formed was titrated with standard solution of $Na_2S_2O_3$. Measurements of the potential of the cell (4) led to the conditional potential value of 1.077 0.003 V versus the saturated calomel electrode (SCE). Gold electrode is more inert than the platinum one and is preferentially used for measurements in highly oxidizing medium as happens in this Mn(III)/Mn(II) system.

The evaluation of the conditional potential at 2 mol l^{-1} $NaClO_4$ and lower acidity was done by using the Fe(III)/Fe(II) redox system as a potentiometric pilot system. Equivalent experiments were performed with a solution having a similar cell compartment, described by cell (4): 2 mol l^{-1}

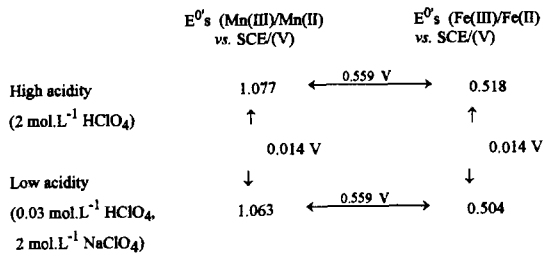

Scheme 1. Estimation of the conditional potential value, $E^{0'}s = 1.063$ V, for the Mn(III)/Mn(II) system, in 2.0 mol l^{-1} perchlorate medium based on the Fe(III)/Fe(II) system used as a potentiometric pilot system.

$HClO_4$ 0.5 mol l^{-1} Mn(II), and both Fe(III) and Fe(II) at 5.0×10^{-3} mol l^{-1} level, led to a conditional potential of Fe(III)/Fe(II) system equal to 0.518 V versus SCE. Further experiment at lower acidity solution, 3.0×10^{-2} mol l^{-1} $HClO_4$ 5.0×10^{-1} mol l^{-1} Mn(II) and both Fe(III) and Fe(II) at 5.0×10^{-3} mol l^{-1} and $NaClO_4$ to make up the ionic strength 2.0 mol l^{-1}, gave the value of 0.504 V versus SCE. This datum differs only 0.014 V from the other condition of higher acidity and different ionic medium, a difference that could be used as a correction to estimate the $E^{0'}s$ for the Mn(III)/Mn(II) system.

As both redox systems are constituted by the ratio of metal ion(III)/metal ion(II), a reasonable assumption is to attribute the same ratio of activity coefficients, γ_{III}/γ_{II} for both trivalent/divalent cations. On this basis, the Fe(III)/Fe(II) system can be used as a potentiometric pilot system which permits to estimated $E^{0'}s$ value of Mn(III)/Mn(II) at the 2.0 mol l^{-1} ionic strength ($NaClO_4$) by discounting 0.014 V from the 1.077 V value, becoming 1.063 V versus SCE. The Scheme 1 shows the estimation of this conditional potential by using the Fe(III)/Fe(II) redox system as a potentiometric pilot system. As there is a marked change in the potential of the Mn(III)/Mn(II) system in azide medium, compared with a non complexing medium, an uncertainty of even 10 mV resulting from this artifice is relatively small.

3.3. Determination of the conditional potential of the Mn(III)/Mn(II) in azide medium

Fig. 2 shows the spectrophotometric data of the average molar absortivity at 432 nm of Mn(III) azide complexes generated coulometrically in increasing azide concentration solutions. The Mn(III) concentration was calculated by Faraday's law.

The results suggest that a mixture of stepwise complexes are formed. The average molar absortivity tends to a constant value ranging from 3100 to 6300 mol^{-1} l cm^{-1}, in azide solutions from 0.439 to 3.85 mol l^{-1}. At this wavelength the average molar absortivity Mn(II) azide complexes is very small and can be neglected.

The potentiometric measurements data in the complexing medium were carried out with the following cell:

$$Hg|Hg_2Cl_2, NaCl(sat)5.0 \times 10^{-2}\ M\ Mn(ClO_4)_2, y\ M\ NaClO_4, x\ M\ NaN_3, 1.0 \times 10^{-2}\ M\ HN_3, z[Mn(III)]|Pt \quad (5)$$

The measured potential, E_x, is related to the conditional potential, $E^{0'}x$, and the Mn(III)/Mn(II) concentration ratio by the following Nernst equation, at fixed free ligand concentration:

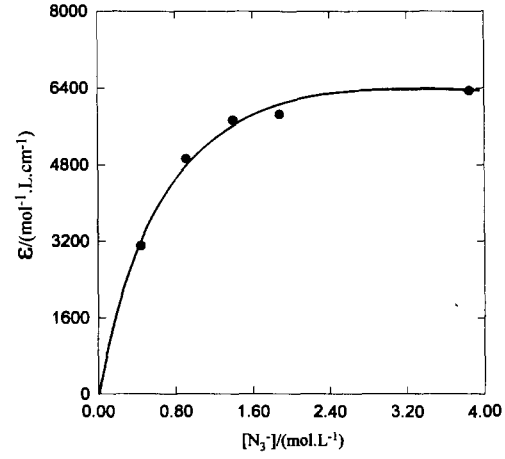

Fig. 2. Average molar absortivity of the Mn(III)/N_3^- complexes, at 432 nm, as a function of free azide concentration ($HN_3 = 1.0 \times 10^{-2}$ mol l^{-1}).

$$E_x = E_x^{0'} + 0.05916 \log \frac{[Mn(III)]}{[Mn(II) - Mn(III)]} \quad (6)$$

The data treatment was done, as described in a previous work, in order to obtain the conditional standard potential of the Mn(III)/Mn(II) system at different free azide concentration, $E^{0'}x$, due to the formation of different complexes in the two oxidation states [4].

Measurements in lower than 0.4395 mol l^{-1} free azide concentrations were not considered as the Mn(III) complexes system becomes unstable, the brownish colour fades and the potentiometric data drift to lower values.

In similar experiments carried out at high acidity (0.1 mol l^{-1} HN_3), the data treatment was not possible due to the high contribution of the spontaneous oxidation of Mn(II) by the HN_3 and by dissolved oxygen.

3.4. Determination of the equilibrium constants of the Mn(III)/N_3^- complex

Equilibrium data can be obtained by the Fronaeus function, $F_0(L)$, for several ligand concentrations [18] Eq. (7):

$$F_0(L) = 1 + \sum_{n=1}^{n} \beta_n [N_3^-]^n \quad (7)$$

The $F_0(L)$ values, for each free azide concentration, can be related to the change of $E_s^{0'}$, in non complexing perchlorate medium, to a less positive $E_x^{0'}$, in presence of the ligand Eq. (8). When the element is in two oxidation states, as Mn(III/Mn(II) or in a similar Co(III)/Co(II) system [12], the $E^{0'}$ refers to a ratio of the $F_0(L)$ values. Table 1 presents several experimental potentiometric data of $-\Delta E^{0'} = -(E^{0'}x - E^{0'}s)$ of the Mn(III)/Mn(II) system, in the range from 0.4395 to 1.936 mol l^{-1} of free azide concentration at 2.0 mol l^{-1} constant ionic strength in $NaClO_4$.

$$-\Delta E^{0'} = -(E_x^{0'} - E_s^{0'}) = 0.05916 \log \frac{F_0(L)_{ox}}{F_0(L)_{red}} \quad (8)$$

The $F_0(L)_{red}$, referred to the complexes of Mn(II) with azide, can be calculated for the several azide concentrations with the overall formation constants of the four stepwise complexes, β_n, determined in our previous work [19]:

Table 1
Potentiometric data of $-E^{0'} = -(E^{0'}x - E^{0'}s)$ of the Mn(III)/Mn(II) system, at different free azide concentration at ionic strength 2.0 mol l^{-1} ($NaClO_4$) and 25.0 ± 0.1°C

$-E^{0'}$/(V)	$[N_3^-]$/(mol l^{-1})	$F_0(L)_{red}$	$F_0(L)_{ox}/10^{10}$
0.5959	0.4395	4.407	5.210
0.6007	0.4760	4.865	6.933
0.6061	0.5283	5.578	9.808
0.6119	0.5875	6.471	1.426
0.6178	0.6492	7.505	20.81
0.6232	0.7076	8.586	29.37
0.6273	0.7539	9.519	38.20
0.6339	0.8323	11.26	58.42
0.6375	0.8764	12.33	73.61
0.6400	0.9087	13.16	86.59
0.6450	0.9757	15.02	119.9
0.6492	1.034	16.77	157.8
0.6541	1.106	19.14	218.5
0.6576	1.162	21.14	275.9
0.6627	1.248	24.50	389.9
0.6658	1.306	26.97	484.4
0.6700	1.390	30.87	652.8
0.6726	1.446	33.69	788.3
0.6779	1.578	41.06	1182
0.6804	1.653	45.75	1450
0.6824	1.724	50.52	1731
0.6858	1.877	62.04	2426
0.6867	1.936	66.96	2712

$E^{0'}s$ = 1.063 V.

$$F_0(L)_{red} = 1 + 4.15[N_3^-]^1 + 6.61[N_3^-]^2 + 3.33[N_3^-]^3 + 0.63[N_3^-]^4 \quad (9)$$

The $F_0(L)_{ox}$ at the same free ligand concentration, corresponding to the Mn(III) complexes, can be calculated by introducing in the Eq. (8) the $F_0(L)_{red}$, $E^{0'}x$ and $E^{0'}s$ data.

Average ligand number estimation for manganese(III), n_{III}, is based on $\Delta E^{0'}/\Delta \log[N_3^-]$, where potentials $E^{0'}x_1$ and $E^{0'}x_2$ refer to the ones in solutions with small increments in azide concentrations, $[N_3^-]_1$ and $[N_3^-]_2$, respectively, as described by Eq. (10). The average ligand number for manganese(II), n_{II}, can be calculated with de β_n for Mn(II)/N_3^- system [19]. The n_{III} values are in the range from 3.6 to 4.4 ligands and indicates that at least five stepwise complexes are formed.

$$n_{III} = (E^{0'}x_2 - E^{0'}x_1) / 0.05916(\log[N_3^-]_2 - \log[N_3^-]_1) + n_{II} \quad (10)$$

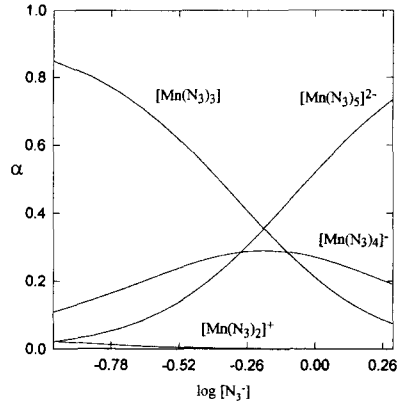

Fig. 3. Distribution diagram of the Mn(III)/N_3^- complexes calculated with the equilibrium constants.

The potentiometric data obtained in this concentration range of the azide ions are inadequate to permit the equilibrium data calculation for the species with less than three ligands. The reason for that is the instability of Mn(III) complexes in azide concentration lower than 0.4 mol l^{-1} azide concentration.

The conventional graphic treatment of $F_0(L)$ data could not be applied for the present system [18]. Matrix solution of the weighed simultaneous equations indicated only five ligands, neglecting a solution for six ligands [20]. These experimental data were also inadequate for the direct calculation of β_1 and β_2, because there were no potentiometric data at lower than 0.44 mol l^{-1} ligand concentration, due to experimental problems of Mn(III) stabilization. The limited concentration range of the ligand led to exclude the terms referred to β_1 and β_2, in the matrix of simultaneous equations. A set of weighed simultaneous equations was prepared and solved in a sophisticated computer program written in Quick BASIC-4.50—Microsoft®: the matrix solution gave the following data for the overall formation constants with 95% of confidence: $\beta_3 = (2.4 \pm 0.7) \times 10^{11}$ M^{-3}, $\beta_4 = (1.5 \pm 0.5) \times 10^{11}$ M^{-4} and $\beta_5 = (9.6 \pm 0.8) \times 10^{11}$ M^{-5}.

A reasonable estimation of β_1 and β_2 was taken by extrapolation in a linear plot of the $(\log \beta_n)/n$ versus $n (n = 3–5)$. This procedure is based on the proportionality of the average free energy with the ligand number attachment to the higher complexes. Data of β_1 and β_2 were found to be 1.2×10^5 M^{-1} and 6.0×10^8 M^{-2}, respectively.

Fig. 3 shows the distribution diagram of the Mn(III)/N_3^- complexes. The contributions of the $[Mn(N_3)]^{2+}$ and $[Mn(N_3)_2]^+$ complexes are negligible at free azide concentration of 0.5 mol l^{-1}.

Acknowledgements

The authors gratefully acknowledge financial support from the Brazilian Foundations (CNPq and FAPESP).

References

[1] A.I. Vogel, A textbook of quantitative inorganic analysis—Theory and practice, Longmans, 2nd ed., London, 1951, p. 713.
[2] J.W. Ladbury and C.F. Cullis, Chem. Rev., 58 (1958) 403.
[3] H.A. Laitinen and W.E. Harris, Chemical Analysis—An advanced text and reference, Series in Advanced Chemistry, McGraw-Hill, 2nd ed, (1975) p. 325.
[4] N. Coichev, E.A. Neves and R. van Eldik, Inorg. Chim. Acta, 179 (1991) 133.
[5] N. Coichev and R. van Eldik, Inorg. Chim. Acta, 185 (1991) 69.
[6] J. Gebert, E.A. Neves and D. Klockow, Fresenius Z. Anal. Chem., 331 (1988) 260.
[7] E.A. Neves, N. Coichev, J. Gebert and D. Klockow, Fresenius Z. Anal. Chem., 335 (1989) 386.
[8] K.B. Reddy, N. Coichev and R. van Eldyk, J. Chem. Soc. Chem. Commun., 481–483 (1991).
[9] N. Coichev and R. van Eldik, New. J. Chem. Chem., 18 (1994) 123.
[10] C. Brandt and R. van Eldik, Chem. Rev., 95 (1995) 119.
[11] H.A. Flaschka, EDTA Titrations, Pergamon Press, London, 1959, p. 77.
[12] N. Coichev and E.A. Neves, Polyhedron, 8 (1989) 641.
[13] A.J. Bard, R. Parsons and J. Jordan, Standard potentials in aqueous solution, Marcell Deckker, New York, 1985, p. 834.
[14] D.D. Perrin, Ionisation constants of inorganic acids and bases in aqueous solution, Pergamon Press, IUPAC Chemical Data Series No. 29, 2nd ed., 1982, p. 69.
[15] C.F. Baes, Jr. and R.E. Mesmer, The hydrolysis of cations, Wiley, New York, 1976, p. 221.
[16] L. Ciavatta and M. Grimaldi, J. Inorg. Nucl. Chem., 31 (1969) 3071.
[17] K.J. Vetter and G. Manecke, Z. Phys. Chem., 195 (1950) 270.

[18] M.T. Beck, Chemistry of Complex Equilibria, Van Nostrand, London, 1970, p. 285.
[19] H.D. Moya, E.A. Neves, M.E.V. Suarez-Iha and N. Coichev, Talanta, 43 (1996) 67.
[20] E.F.A. Neves, I.G.R. Gutz and R.G. Tavares, J. Eletroanal. Chem., 179 (1984) 91.

ELSEVIER

Talanta 44 (1997) 805–809

Talanta

The role of selected cations in the formation of pseudomicelles in aqueous humic acid

R. von Wandruszka *, C. Ragle, R. Engebretson

Department of Chemistry, University of Idaho, Moscow, Idaho, ID 83844-2343, USA

Received 1 August 1996; received in revised form 7 October 1996; accepted 7 October 1996

Abstract

The fluorescence intensity enhancement of a pyrene probe in aqueous humic acid solutions was assessed in terms of added lanthanide and thorium cations. Among the trivalent ions it was found that size played a role, with the small Lu^{3+} ion producing the greatest increase in pyrene emission. This was attributed to its superior ability to cause pseudomicellization in the humic acid polymer. Slow kinetic effects were observed, leading to substantial fluorescence enhancement over a period of 7 h. This was ascribed to a continuous aggregation process in aqueous humic acid, leading to ever more viscous microenvironments for the probe molecule. © 1997 Published by Elsevier Science B.V.

Keywords: Cations; Humic acid; Pseudomicelles

1. Introduction

Recent investigations conducted in this laboratory [1–5] have shown that aqueous solutions of certain soil humic acids respond to the addition of cations by the formation of molecular microdomains of relatively low polarity [6–8]. These domains, which can be looked upon as intramolecular aggregates, are referred to as pseudomicelles in view of their similarity to detergent micelles with regard to structure and polar character. It was found that humic acid molecules consisting of long flexible polymers, have a tendency to coil up in the presence of cations, especially metals. This is thought to be due to a combination of charge neutralization and functional group bridging. The former arises because the humic acid molecule, which requires neutral to basic conditions for solubilization, contains numerous carboxyl and hydroxyl groups that are negatively charged in these solutions. Mutual repulsion among these functional groups causes the humic acid polymers to adopt a stretched configuration, providing few association sites for nonpolar species in solution. Upon the addition of cations this effect is minimized and they fold and shorten, forming compact structures with relatively hydrophobic interiors and hydrophilic surfaces. Functional group bridging is considered to enhance this effect, especially with multivalent cations, by drawing together various groups on the humic acid chain. It should also be noted that all humic acid solutions are polydisperse, and that

* Corresponding author. Fax: +1 208 8856173.

PII S0039-9140(96)02116-9

the interaction of segments of different sizes leads to a degree of intermolecular aggregation that further augments pseudomicellization.

Evidence for the model described above was derived from the fluorescence behavior of small nonpolar species such as pyrene and diphenyloxazole which were added to humic acid solutions. As would be the case with detergent micelles, these molecules were found to partition into the hydrophobic domains of the humic acid structure. Sequestered in this manner, they are protected from solution borne fluorescence quenchers (e.g., bromide ion) and are unaffected by the presence of these species. It was also found that the increased microviscosity of the humic acid pseudomicelles strongly reduced dynamic quenching of the encapsulated fluorescent probe, producing an increase in fluorescence intensity upon the addition of salts. This is reminiscent of the effect of metal ions on fluorescent probes in bile salt solutions [9]. Fluorescence anisotropy measurements were consistent with these observations, showing that the rotational diffusion of humic acid/probe aggregates was directly linked to the degree of sequestration of the latter. When the ability of humic acids to coil up was reduced by photolytic cleavage of the chains, the effects described above disappeared. Likewise, when aquatic humic acids were used, which size exclusion chromatography showed to be considerably smaller than soil humic acids, the effects were absent or greatly diminished.

2. Experimental

The pyrene excitation and emission wavelengths used in this work were 240 and 373 nm, respectively. The former was chosen to minimize interference by humic acid fluorescence. Typical humic acid excitation extends from 250 to 420 nm, while emission is strong from 380 to beyond 500 nm [10,11]. The emission of pyrene dissolved in a humic acid solution will therefore be attenuated and must be appropriately corrected. While humic acid fluorescence can be subtracted from the total fluorescence by the use of a blank, the inner filter effect remains operative and requires additional treatment. A correction developed by Gauthier et al. [12] which incorporates the absorbances at the wavelengths in question was implemented:

$$\frac{F_{corr}}{F_{obsd}} = 2.3\frac{dA_{ex}}{1-10^{-dA_{ex}}}\,10^{gA_{em}}\,\frac{2.3sA_{em}}{1-10^{-sA_{em}}} \qquad (1)$$

Here F_{obsd} is the observed intensity, F_{corr} the corrected intensity, A_{ex} the absorbance at the excitation wavelength per cm of solution, A_{em} the absorbance at the emission wavelength cm^{-1} of solution, d the distance between the edge of the excitation beam and the inside wall of the cuvette, and s the width of the excitation beam (all in cm). The treatment corrects for absorption at both the excitation and emission wavelengths.

The humic acid used in this study was deashed Latahco silt-loam humic acid, extracted in our laboratory from a local soil (Argiaquic Xeric Argialbolls) by the procedure outlined by the International Humic Substances Society (IHSS, 1985). Its elemental analysis and characterization have been reported previously [2]. The humic acid was dissolved in 0.01 M NaOH (Fisher Scientific) to give a 1000 ppm stock solution. A subsequent dilution to 10 ppm was made with doubly deionized water. Pyrene was purchased from Sigma (98%), recrystallized from ethanol, and twice sublimed onto a cold finger. Aqueous pyrene solutions at 1×10^{-7} M were prepared by introducing an aliquot of a 0.01 M pyrene solution in cyclohexane into a volumetric flask, evaporating the cyclohexane, adding water, and sonicating for 2–3 h. The resulting solutions were stored in the dark at room temperature. Magnesium chloride (Baker), the hexahydrates of lanthanum chloride (Strem Chemicals), samarium chloride (Aldrich), lutetium chloride (Strem), and thorium nitrate (Spectrum Chemical) were used without further purification. The deionized water used for all solutions were brought to a resistivity of 18 MΩ cm by passing through a 0.22 μm Millipore filter system.

Fluorescence measurements were taken with a Hitachi F-4500 fluorescence spectrophotometer equipped with a thermostatted cell holder. Slits were set at a 5 nm bandpass. The data reported as a function of salt concentration were obtained by adding consecutive aliquots of a concentrated salt

solution to a known volume of humic acid solution containing pyrene [2]. A blank was also measured, which consisted of an aqueous humic acid solution (not containing pyrene) to which the same aliquots of salt solution were added. Dilution of the humic acid was insignificant over the range studied. The solutions were held at 19°C, open to the air. They were stirred with a magnetic stirrer using a stainless steel stir bar for 2 min after each addition of salt, and then left to equilibrate in the dark for 5 min before the fluorescence was measured.

3. Results and discussion

One of the central observations in previous studies [2,5] was the pyrene fluorescence enhancement obtained when salts were added to aqueous solutions containing soil humic acids. The effect of the cation followed the order $Na^+ < K^+ < Cs^+ < Mg^{2+}$, while the anion had no observable influence. In the present study, cations of the lanthanide series were investigated to evaluate the impact of more highly charged species and assess the role of ionic size. For comparison, Th^{4+} was included as a tetravalent species. Kinetic aggregation effects were also measured.

Fig. 1. shows the change in pyrene fluorescence intensity upon the addition of three lanthanide ions in comparison with mono- and divalent cations. It is clear that higher ionic charge generally leads to greater fluroescence enhancement,

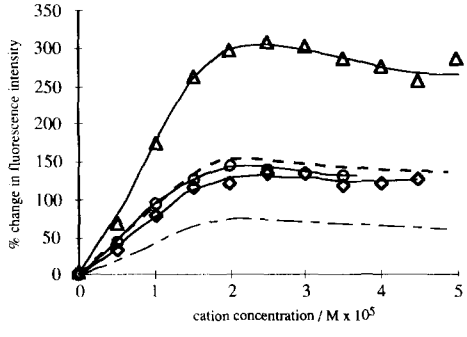

Fig. 1. Variation of pyrene fluorescence intensity in a 10 ppm humic acid solution containing salts. ○, $SmCl_3$; ◇, $LaCl_3$; △, $LuCl_3$; – – –, $MgCl_2$ (Ref. [2]); — — —, KCl (Ref. [2]).

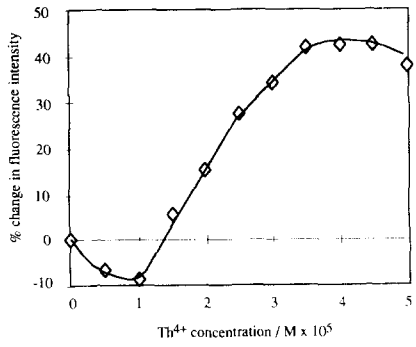

Fig. 2. Variation of pyrene fluorescence intensity with Th^{4+} concentration in a 10 ppm humic acid solution.

which must be ascribed to a tighter, more viscous interior of the humic pseudomicelles. Interestingly, however, La^{3+} and Sm^{3+}, the larger lanthanides (ionic radii 1.016 and 0.964 Å, respectively) [13] produced effects that were little different from each other and from Mg^{2+}. Lu^{3+} (radius 0.85 Å), on the other hand, gave a pyrene emission intensity twice as large as that of Sm^{3+}. In a separate experiment it was shown that aqueous pyrene solutions containing the various metal ions but no humic acid, produced no discernible trends in emission intensity. This indicates that neither cation quenching, nor metal-probe sensitization was responsible for the variations in fluorescence in the presence of humic acid. The effect of Th^{4+} (radius 1.02 Å) is shown in Fig. 2. It is evident that the extent of pyrene fluorescence enchancement is considerably less, and that there is an initial slight decrease in intensity when the salt is added. To assess the possible influence of the anion (thorium nitrate was used here, while all the other salt were chlorides), a side-by-side comparison of $MgCl_2$ and $Mg(NO_3)_2$ was carried out. Pyrene fluorescence enchancement was found to be virtually identical for the two salts.

It was found in earlier work that the kinetics of humic acid configurational adjustments can be slow. To evaluate the role this may play in the behavior of the Th^{4+} containing solution, extended measurements were carried out for 16 h. In this, a single addition of $Th(NO_3)_4$ was made to a humic acid/pyrene solution, bringing the salt concentration to 5×10^{-5} M. Repeated measure-

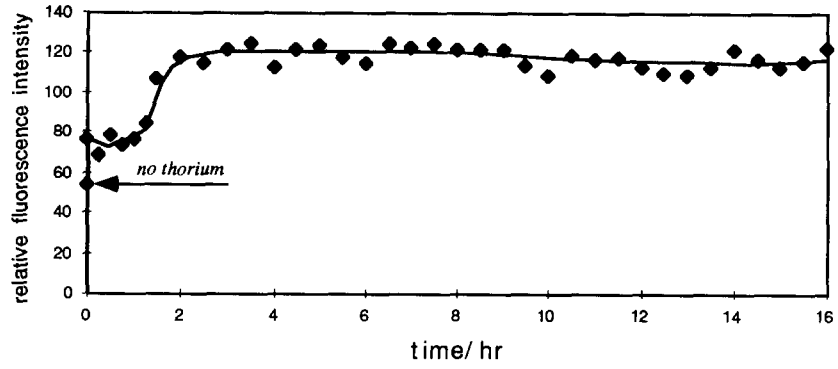

Fig. 3. Variation of pyrene fluorescence with time in a solution containing 10 ppm humic acid and 5×10^{-5} M $Th(NO_3)_4$.

ments were then carried out as shown in Fig. 3. These indicated that the initial rise in pyrene fluorescence intensity occurred as expected and persisted for approximately 90 min. After this period, a further rise in emission intensity was observed, reaching a maximum level after about 2 h. The conclusions drawn from this result are two-fold: (1) slow kinetics are indeed operative, and the pyrene probe finds a stable environment only after 7 h; and (2) the initial decrease in pyrene fluorescence intensity (Fig. 2) is unlikely to be affected by this. Comparisons with lanthanide salt kinetics were made to shed light on the long-term fluorescence enhancement (vide infra).

In the above discussion it was implied that ionic size is a factor in the cation-assisted pseudomicellization of humic acid. The information available on the lanthanide ions provides their crystalline radius (cf. the familiar lanthanide contraction), and as the prime distinguishing feature it is reasonable to invoke this to explain their different behavior vis-à-vis humic acid. It may be suggested that the small, densely charged Lu^{3+} (albeit hydrated) is most effective in pulling the humic acid into a structured cage. La^{3+} and Sm^{3+} are large and similar in size, especially when hydrated, and consequently interact in a similar fashion with humic acid. Comparison with Mg^{2+} and Th^{4+} is more tenuous since charge becomes a distinguishing factor with these ions. The crystal ionic radius of Mg^{2+} is 0.82 Å, similar to that of Lu^{3+}, but its lower charge renders its interactions with humic acid similar to those of the larger but more highly charged La^{3+} and Sm^{3+}. Th^{4+} is about the same size as La^{3+}, but carries an additional charge. It is possible that it is set apart from the others by its very large hydrated radius [14] of 11 Å. The singly charged potassium ion clearly has a much smaller effect.

The kinetics of pyrene fluorescence in a humic acid solution to which Sm^{3+} was added provided an interesting insight. Shown in Fig. 4, the time profile appears similar to that of the Th^{4+} solution in Fig. 3. Again the initial rise in fluorescence intensity after the addition of 5×10^{-5} M $SmCl_3$ and its persistence for about 2 h are evident. Then, over a period of another 2 h, a further doubling of the emission intensity was observed. In this case, however, this was accompanied by the gradual formation of a visible precipitate in the cell. Because of the optical configuration of the Hitachi 4500 fluorimeter, which excites a horizontal cross-section of solution near the bottom of the cell, the precipitate settling under gravity in that region gave rise to the increased fluorescence. This indicates that the macroscopic humic acid aggregates carry the (already microscopically sequestered) pyrene down with them, lending further credence to the association model. Furthermore, a parallel can be drawn between the precipitation process and the results shown in Fig. 3. No visible precipitate was observed with Th^{4+}, but it must be remembered that the coagulation process of dissolved humic acid should be viewed as a continuum of aggregation events, starting with intramolecular coiling of the polymer chains. It is therefore reasonable to suggest that the aggregation of humic acid under the influence of

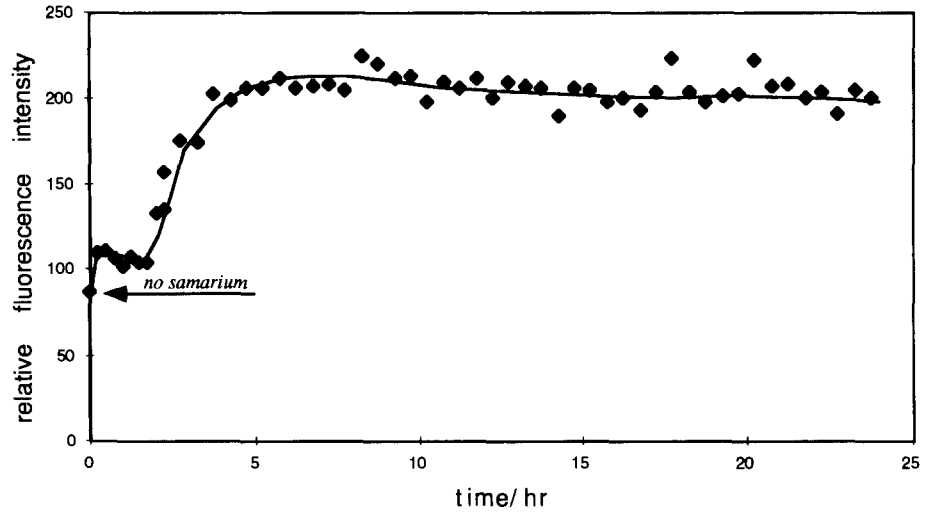

Fig. 4. Variations of pyrene fluorescence with time in a solution containing 10 ppm humic acid and 5×10^{-5} M $SmCl_3$.

Th^{4+}, while producing no precipitate, proceeded to an intermediate stage. The aggregates thus formed slowly settled to the bottom of the cell, like their larger counterparts, concentrating the sequestered pyrene in that region.

4. Conclusions

Ionic size and charge appear to exert a combined effect on the ability of cations to cause pseudomicellization in dissolved humic acid, with higher charge densities being more effective. Macroscopic and microscopic coagulation processes proceed slowly, taking 7 h to reach a final state of aggregation.

Acknowledgements

The authors thank the EPA and the NSF (EPSCoR program) for financial support.

References

[1] M.J. Morra, M.O. Corapcioglu, R. von Wandruszka, D.B. Marshall, and K. Topper, Soil Sci. Soc. Am. J., 54 (1990) 1283–1289.
[2] R. Engebretson and R. von Wandruszka, Environ. Sci. Technol., 28 (1994) 1934–1941.
[3] R. Engebretson, T. Amos, and R. von Wandruszka, Environ. Sci. Technol., 30 (1996) 990–997.
[4] R. Engebretson and R. von Wandruszka, Environ. Sci. Technol., in review.
[5] C. Ragle, R. Engebretson, and R. von Wandruszka, Soil Sci., in review.
[6] C.T. Chiou, R.L. Malcolm, T.I. Brinton and D.E. Kile, Environ. Sci. Technol., 20 (5) (1986) 502–508.
[7] R.L. Wershaw, K.A. Thorn, D.J. Pinckney, P. MacCarthy, J.A. Rice, and H.F. Hemond, C.H. Fuchsman (ed.), In Peat and Water, Elsevier Applied Science, Barking, 1986.
[8] R.L. Wershaw, Environ. Sci. Technol., 27 (5) 1993 814–816.
[9] K. Nithipatikom and L.B. McGown, Anal. Chem., 60 (1988) 1043–1045.
[10] P. MacCarthy and J.A. Rice, spectroscopic methods (Other than NMR) for determining functionality in humic substances, in G.R. Aiken, G.R., McKnight, R.L. Wershaw and P. MacCarthy (Eds.), Humic Substances in Soil, Sediment, and Water–Geochemistry, Isolation, and Characterization, Wiley, NY, 1985.
[11] N. Senesi, Application of electron spin resonance and fluorescence spectroscopies to the study of soil humic substances, in J. Kubat (Ed.), Humus, its Structure and Role in Agriculture and Environment, Elsevier, NY, 1992.
[12] T.D. Gauthier, T.D., E.C. Shane, W.F. Guerin, W.R. Seitz and C.L. Grant, Environ. Sci. Technol., 20 (1986) 1162–1166.
[13] Hanbook of Chemistry and Physics, 54th edn., R.C. Weast (Ed.), CRC Press, Cleveland, OH, 1973.
[14] J.A. Dean, in Lange's Handbook of Chemistry, 14th edn., McGraw-Hill, New York, 1992.

ELSEVIER

Talanta 44 (1997) 811–816

Talanta

Zirconium and hafnium determination by energy dispersive X-ray fluorescence with solid phase preconcentration

Patricio Peralta-Zamora *, Lorena Cornejo-Ponce, Maria Izabel Maretti S. Bueno, José Walter Martins

Universidade Estadual de Campinas, Instituto de Química, CP. 6154, CEP 13083-970, Campinas-SP, Brazil

Received 20 May 1996; accepted 25 September 1996

Abstract

Two preconcentration methods has been developed for simultaneous determination of zirconium and hafnium by energy dispersive X-ray fluorescence (EDXRF). The first method is a liquid–solid extraction procedure with the use of an anionic exchange resin modified with xylenol orange. The second is a precipitation procedure carried out in the presence of lanthanum. Both methods permit significant enhancement of sensitivity in comparison with direct measurement in the aqueous phase. The applicability of both procedures for the preconcentration of Zr and Hf prior to their determination by EDXRF was demonstrated by analyzing synthetic mixtures and a sample of zirconium ore. The results obtained with the use of the modified resin show relative standard deviation of about 4% and good agreement with those obtained by spectrographic analysis. © 1997 Published by Elsevier Science B.V.

Keywords: Hafnium; Preconcentration; X-ray fluorescence; Zirconium

1. Introduction

The simultaneous determination of zirconium and hafnium is one of the most difficult problems of analytical chemistry, because the close similarity of their chemical properties hinders the use of classical analytical methods [1–5]. Colorimetric techniques do not have any interesting application due to unavailability of specific chromogenics agents. The principal contribution of these techniques is reduced to the existence of several differential methods, based on differences between zirconium and hafnium complexes under different acidic conditions [6] or in the presence of specific masking agents [7].

The classic configuration of flame atomic absorption or emission techniques shows little application for this determination due to the heat-resistant characteristics of both species and the high complexity of the emission spectra [1–4]. The use of more energetic atomization systems (i.e., plasma, arc and spark) permits more suitable results only for determination of the concentration ratios [1]. Absolute determinations can be performed by using special calibration methods, typically chemometric tools for correction of mutual spectral interferences [1]. The individual de-

* Corresponding author.

PII S0039-9140(96)02117-0

termination of zirconium in silicate rocks by inductively-coupled plasma emission spectrometry were reported by Uchida et al. [8]. However, the results show poor precision (relative standard deviation, RSD, between 14 and 38%).

Due to the great spectral resolution of the instrumental system, energy dispersive X-ray fluorescence permits the determination of Zr-Hf mixtures without important interference problems. However, the low sensitivity of the technique can be resolved only by the use of preconcentration methods [9–21]. The determination of a great number of metallic species by EDXRF is usually preceded by concentration steps which involve the use of ion exchange resins [9,10,12,16], activated charcoal [9,10,17], naphthalene [14], polyurethane [15], modified silica [21] and coprecipitation procedures using ferric hydroxide as a collector [18–20]. The great selectivity reached by the use of chelating resins [22] has contributed to its popularization as solvents system. Xylenol orange has been used for modification of ionic exchanger resins, and for determination of zirconium by solid phase spectrophotometry [23–25].

In this work we propose the use of an ion exchange resin modified with xylenol orange or a lanthanum coprecipitation procedure for preconcentration and simultaneous determination of zirconium–hafnium mixtures by EDXRF.

2. Experimental

2.1. Instrumental

Spectrophotometric determinations were performed with an Intralab DMS-100 UV-Vis Spectrophotometer. X-ray fluorescence measurements were executed on a Spectrace 5000 Energy Dispersive X-ray Fluorescence Spectrometer, equipped with a rhodium tube and a Si(Li) semiconductor crystal detector (irradiation time, 60 s; tube voltage, 30 kV; tube current, 0.20 mA; atmosphere, air; filter, 0.127 mm rhodium film). The measurements were realized at 15.744 KeV for Zr (Kal) and 7.898 KeV for Hf (Lal). The samples were introduced on a cylindrical plastic device from Chemplex, of about 2 cm of height and 3 cm of internal diameter, using a X-ray Mylar film as sample support.

Spectrographic measurements were carried out on Carl Zeiss PGS-2 Emission Spectrometer, equipped with a linear array of photodiodes [26].

2.2. Chemicals and solutions

The zirconium standard solution was prepared by direct dissolution of $ZrOCl_2 . 8H_2O$ (99.5%, Riedel-de Haen) in H_2SO_4 (1:5 v/v). Zirconium hydroxide was precipitated with an aqueous solution of NH_3. The solid was recovered by filtration, thoroughly washed with deionized water and dissolved in HCl (final concentration of HCl, about 2 mol l^{-1}). The hafnium standard solution was prepared from HfO_2 (Specpure, Johnson, Mathey and Co.). The oxide was dissolved with a HF-H_2SO_4 (1:1 v/v) mixture, heating several times almost to dryness with successive additions of concentrated H_2SO_4. The solid residue was dissolved in H_2SO_4 and the hydroxide precipitated with an aqueous solution of NH_3. The solid was recovered by filtration, thoroughly washed with deionized water and dissolved in HCl (final concentration of HCl, about 2 mol l^{-1}). Both solutions were standardized by a gravimetric procedure using mandelic acid [27].

The lanthanum standard solution (40 g l^{-1}) was prepared from La_2O_3 (99%, Carlo Erba). Amberlite IRA-400 anion resin (Koch-Light Laboratories, 100–200 mesh) and Xylenol orange (Fluka A.G., Bucks S.G.) were used without further purification.

The natural sample, purchased from the Energetic and Nuclear Research Institute (IPEN, São Paulo-Brazil), corresponds to a mixture of zirconium and hafnium hydroxides obtained by physical and chemical treatment of a zirconium ore.

2.3. Preparation of modified resin

Dried resin, 40 g, were added to 400 ml of an aqueous solution of xylenol orange (4.3×10^{-3} mol l^{-1}, pH 7.0) and the mixture was vigorously stirred for 6 h. After this impregnation time, the

solid mass was filtered, thoroughly washed with deionized water, dried at 60°C and stored in amber glass flasks.

2.4. Extraction with modified resin

Suitable volumes of solution of Zr and Hf were placed in 200 ml beakers, diluted up to 50 ml with deionized water and adjusted to adequate pH values with aqueous solutions of HCl or NH_3. To these solutions were added 0.5 g of the modified resin. The mixture was stirred for a convenient time and the solid was recovered by filtration in Whatman 41 filter paper, washed with deionized water and dried at 60°C for 2 h. In preliminary studies, the Zr and Hf recuperation was evaluated by colorimetric determination [28] of the remained amounts in the filtrate. For this determination, the filtrate (approximately 50 ml) was led to almost dryness in a water bath, dissolved in 3.0 ml of 0.3 mol l^{-1} HCl, and added of 2.0 ml of xylenol orange 0.05% in HCl 0.3 mol l^{-1}. The concentration of zirconium or hafnium was determined spectrophotometrically at 550 nm, using analytical curves obtained between 0.2 and 2.0 mg l^{-1}. Further determinations were carried out by direct analysis of the solid mass by EDXRF. The concentration of Zr and Hf was determined through external calibration using standard solutions submitted to analogous extraction procedures.

2.5. Preconcentration by precipitation in the presence of lanthanum

Aqueous solutions, 50 ml, containing adequate amounts of Zr and Hf were added to 10 ml of the standard lanthanum solution. The hydroxides were precipitated by addition of an aqueous ammoniacal solution. After 5 min of stirring the precipitate was recovered by filtration and dried at 100°C for 2 h. The recuperation degree was evaluated by colorimetric analysis in the filtrate. Further determinations by EDXRF were directly carried out on the solid fraction.

3. Results and discussion

3.1. Impregnation of the resin

Colorimetric determination of the remaining amount of xylenol orange after the impregnation procedure verified that the efficiency of the impregnation process is very close to 100%. Relating the amounts used of resin (0.5 g) and the xylenol orange amount present in this solid fraction (0.043 ml mol), it is possible to estimate a maximum extraction capacity of about 2000 μg for Zr or 3500 μg for Hf.

3.2. Extraction with modified resin

The extraction of both species is almost complete at similar pH values (pH 4.0–8.0). Although the zirconium and hafnium hydrolysis is favored at these pH values, precipitation was not observed probably due to the low concentration of the analytes used in this study (approximately 2 μg ml^{-1}) and due to the presence of large amounts of sulfate ion, which can displace the hydroxyl groups from hydrolyzed species [1]. The procedure is not selective in this pH region, a result resembling those obtained by the application of other extraction procedures [29,30]. For subsequent determinations, a pH of 7.0 was selected. A X-ray fluorescence spectrum of zirconium and hafnium on the xylenol orange modified resin is presented in Fig. 1.

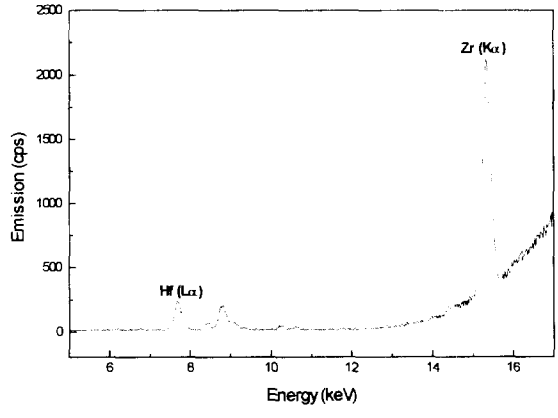

Fig. 1. X-ray fluorescence spectrum of zirconium and hafnium on the xylenol orange modified resin.

Table 1
Zr-Hf determination from synthetic samples with modified resin

Added (mg)		Found (mg)	
Zr	Hf	Zr (difference, %)	Hf (difference, %)
10.0	50.0	9.7(3.0)	51.5(3.0)
50.0	50.0	49.1(1.8)	52.3(4.6)
100.0	50.0	100.8(0.8)	52.5(5.0)
100.0	100.0	101.2(1.2)	100.7(0.7)
100.0	300.0	101.9(1.9)	303.1(1.0)
500.0	100.0	497.3(0.5)	105.9(5.9)
Average difference		1.5%	3.4%
RSD ($n = 5$)		3.0%	4.0%

The quantitative recuperation of Zr and Hf is completed with stirring times of about 15 min. The complete extraction of the analytes in a short time like this, and the great convenience of the involved operations, implies a very important economy of time, mainly when compared with the times required for other preconcentration procedures. Liquid–liquid extraction procedures and liquid–solid methodologies executed in column systems, for example, are slower techniques because of the difficulty in reaching equilibrium conditions and long time elution stages, respectively. For posterior determinations stirring times of 20 min were selected.

Using sample volumes between 50 and 200 ml, the extraction of Zr and Hf is quantitative. With higher volumes the recuperation of the analytes is decreased, presumably due to excessive dilution of the solid extractor and consequently inefficient contact of the phases during the selected stirring time. If we consider the complete transference of the Zr or Hf amounts present in this high volume of aqueous phase for a small mass of resin, it is possible to perceive the great preconcentration potentiality of the proposed method. For subsequent determinations maximum volumes of 200 ml were selected.

Is known that the particle size have a great importance on the X-ray fluorescence measurements, nevertheless preliminary studies shown that for ours experimental conditions insignificant differences are obtained by using resin of size equivalent to 41–60 or 150–190 mesh.

Executing the extraction procedure in the optimized conditions and measuring the EDXRF emission directly on the solid mass, linear calibration curves are obtained for a large concentration range (10–800 μg for zirconium, and 50–800 μg for hafnium) with typical correlations higher than 0.999. Considering the sensibility of the determination as a function of the inclination of the analytical curves, we observed that the proposed method permits sensitivity increases of about 25 times for Zr and 40 times for Hf, in relation to direct measurement in the aqueous phase.

3.3. Analysis of synthetic samples

The results obtained for synthetic mixtures of diverse composition (Table 1) indicate high concordance between added and found amounts. The precision of the methodology, expressed as relative standard deviation for five determinations (about 3% for Zr and 4% for Hf), is very similar to that obtained by other techniques [9,10].

3.4. Precipitation in the presence of lanthanum

This method appears as a very simple alternative for preconcentration of metallic species because it depends on but a few experimental variables. The added amount of lanthanum, for example, is not a critical parameter. The selected value was defined only to facilitate the filtration and transference operations and as a function of the capacity of the sample compartment. Prelimi-

Table 2
Zr-Hf determination from synthetic samples by precipitation in the presence of lanthanum

Added (mg)		Found (mg)	
Zr	Hf	Zr (difference, %)	Hf (difference, %)
100.0	100.0	100.8(0.8)	101.2(1.2)
100.0	150.0	98.7(1.3)	150.9(0.6)
100.0	200.0	99.5(0.5)	201.9(1.0)
300.0	200.0	297.4(0.9)	203.4(1.7)
500.0	200.0	498.7(0.3)	205.6(2.8)
Average difference		0.8	1.5%
RSD ($n = 5$)		4.0%	4.0%

nary experiments indicated 300 ml as a maximum sample volume; with higher volumes the recuperation of the metallic species is incomplete.

The calibration curves show good linearity ($r > 0.999$) over a large concentration range (300–1000 μg ml^{-1}). However, the sensitivity is lower than that obtained by extraction on the modified resin. In any case, the sensitivity is enhanced about 4 times in relation to the directly measurement in the aqueous phase.

The results for the Zr-Hf determination from synthetic mixtures (Table 2) show high coherence with the added amounts, with typical standard deviations of about 4%. The accuracy of the proposed method is better than those obtained by Ricci [18] (5–10%) through a coprecipitation procedure using ferric hydroxide as a collector agent.

3.5. Zr-Hf determination from natural samples

Both proposed preconcentration procedures were evaluated for determination of Zr-Hf mixtures from natural samples, which result from physical and chemical treatments of zirconium ore. The results for zirconium determination using the modified resin and the coprecipitation procedure (Table 3) show a high coherence with those obtained by spectrographic analysis. By applying the statistical Student's test for 95% of confidence, we verify that for hafnium determination, only the modified resin provides comparable results. The results obtained by the coprecipitation procedure shows significant differences with those obtained by spectrographic analysis and by using the modified resin.

4. Conclusions

Both preconcentration procedures permit the quantitative recuperation of Zr and Hf from large volumes of aqueous samples. For this motive they represent a potential and simple alternative for determination of metallic species by EDXRF. The procedure based on the use of a modified resin permits a significant increase of the sensitivity of

Table 3
Zr-Hf determination from zirconium ore using the proposed methods

Run	Extraction with modified resin (%)		Precipitation (%)		Spectrography (%)	
	Zr	Hf	Zr	Hf	Zr	Hf
1	95.4	4.6	96.5	3.5	95.0	5.0
2	95.2	4.8	97.1	2.9	95.3	4.7
3	95.6	4.4	96.7	3.3	95.2	4.8
Average	95.4 ± 0.4	4.6 ± 0.4	96.8 ± 0.6	3.2 ± 0.6	95.2 ± 0.3	4.8 ± 0.3
RSD (%)	0.2	4.3	0.3	9.5	0.2	3.2

the determination and can be used in analyses of low concentration samples. The non-selectivity of the extraction procedure with the use of modified resin is not a significant inconvenient, because can be compensate for the great selectivity presented for the EDXRF technique.

References

[1] A.K. Mukherji, Analytical Chemistry of Zirconium and Hafnium, Pergamon Press, Oxford, 1970.
[2] R.J.H. Clark, D.C. Bradley and P. Thornton, The Chemistry of Titanium, Zirconium and Hafnium, Pergamon Press, Oxford, 1975.
[3] V.V. Serbinovich, V.P. Antonovich and N.A.J. Pshetakovskaya, J. Anal. Chem. USSR, 41 (1986) 867.
[4] A. Brookes and A. Townshend, Analyst, 95 (1970) 529.
[5] U.G. Senin, A.M. Asavin, L.N. Lazutkina and N.V. Korsakova, J. Anal. Chem. USSR, 44 (1989) 1348.
[6] S.V. Elinson and N.A. Mirzoyan (in A. Brookes and A. Townshend), Analyst, 95 (1970) 529.
[7] K.L. Cheng, Talanta, 3 (1959) 81.
[8] H. Uchida, K. Inasaki and K. Tanaka, Anal. Chim. Acta., 134 (1982) 375.
[9] A.T. Ellis, D.E. Leyden, W. Wegscheider, B.B. Jablonski and W.B. Bodnar, Anal. Chim. Acta, 142 (1982) 73.
[10] A.T. Ellis, D.E. Leyden, W. Wegscheider, B.B. Jablonski and W.B. Bodnar, Anal. Chim. Acta, 142 (1982) 89.
[11] I.F. Seregina, G.T. Tsizin, A.M. Shilnikov, A.A. Formanovski and Y.A. Zolotov, J. Anal. Chem. USSR, 48 (1993) 122.
[12] A.N. Masi and R.A. Olsina, Talanta, 40 (1993) 931.
[13] L. Oi-Wah and H. Sing Yiu, Anal. Chim. Acta, 280 (1993) 269.
[14] V. Bhagavathy, L.P. Reddy, R. Prasada and A.D. Damodaram, J. Radioanal. Nucl. Chem., 49 (1991) 35.
[15] M.S. Carvalho, J.A. Medeiros, A.W. Nóbrega, J.L. Mantovano and U.P. Rocha, Talanta, 42 (1995) 45.
[16] H. Knote and V. Krivan, Anal. Chem., 54 (1982) 1858.
[17] V. Bhagavathy, L.P. Reddy, P.S.T. Sai, R. Prasada and A.D. Damodaram, Anal. Chim. Acta, 242 (1991) 215.
[18] E. Ricci, Anal. Chem., 52 (1980) 1708.
[19] V. Bhagavathy, P.S.T. Sai, R. Prasada and A.D. Damodaram, Anal. Lett., 22 (1989) 197.
[20] H. Qing-Lie, T.C. Hughes, M. Haukka and P. Hannaker, Talanta, 32 (1985) 495.
[21] C.L. Ponce, P.P. Zamora and M.I.M.S. Bueno, Química Nova, 19 (1996) 30.
[22] C. Cordeiro, M. Gonzalez de la Barrera, J. Rosas, J. Ma. Pinilla and L. Hernandez, An. Quím., 89 (1993) 230.
[23] L.F. Capitán Vallvey, J.M. Bosque Sendra and M.C. Valencia, Analusis, 17 (1989) 601.
[24] L.F. Capitán, L.F. Capitán Vallvey, M.C. Valencia, J.M. Bosque Sendra and I. de Orbe, Analusis, 19 (1991) 177.
[25] G.D. Brykina, G.G. Lebedeva and G.F. Agapova, J. Anal. Chem. USSR, 45 (1990) 1322.
[26] C.R. Bellato, J.J.R. Rohweder, I.M. Raimundo Jr. and C. Paquini, XVIII Reunião Anual da Sociedade Brasileira de Química, Livro de Resumos, QA-47 (1995).
[27] R.S. Barbiéri, J.C. Rocha, V.R. Terra and A. Marques Neto, Eclét. Quím., 14 (1989) 101.
[28] K.L. Cheng, Talanta, 2 (1959) 61.
[29] F.L. Moore, Anal. Chem., 28 (1956) 947.
[30] Z.P.G. Peralta, Tese de Doutorado, Instituto de Química Universidade Estadual de Campinas, Campinas-SP (Brazil), 1995.

ELSEVIER

Talanta 44 (1997) 817–822

Talanta

Determination of tin in canned foods by UV/visible spectrophotometric technique using mixed surfactants

Xirong Huang *, Wenjuan Zhang, Shuhan Han, Xinqian Wang

Department of Chemistry, Shandong University, Jinan 250100, People's Republic of China

Received 11 June 1996; received in revised form 23 September 1996; accepted 27 September 1996

Abstract

The complex of tin(IV) with bromopyrogallol red (BPR) in the presence of nonyl phenoxy polyethoxyethanol (OP) and cetyltrimethylammonium bromide (CTAB) has a sensitive absorption peak at 304 nm. Under the optimal conditions, Beer's law is obeyed over the range 0.1–2.5 μg ml^{-1} Sn(IV) with molar absorptivity being 8.2×10^4 l mol^{-1} cm^{-1} and detection limit 0.018 μg ml^{-1}. As compared with the visible method which also uses BPR as chromogenic reagent ($\lambda_{max} = 550$ nm), our method is sensitive and selective because of the complex's high, sharp absorption peak. In addition, the present method is simple and rapid, no heating or standing is needed. By means of the mixed surfactants the precipitation caused by the ion association of cetyltrimethylammonium cation and I_3^- anion is avoided if iodide is used for separating micro amounts of tin(IV) from a sample matrix. An application of the proposed method to the determination of Sn(IV) in a canned food was made with satisfactory results. © 1997 Elsevier Science B.V.

Keywords: Spectrophotometry; Tin determination; Bromopyrogallol red; Surfactant; Canned food

1. Introduction

It is of great importance to establish a method for the determination of the inorganic tin at μg or sub μg levels. Because micro amounts of tin have an adverse effect on deep-drawing steels [1], the amount of tin present in these steels must be monitored. In addition, studies on marine antifouling coatings also need a method for tin determination in seawater [2]. If a tin-plated iron can is used for package, the content of tin in food is indicative of the quality of the food in storage although inorganic tin is nontoxic for living systems. It is also worth a mention that a sensitive method for inorganic tin determination could be used as an alternative for organic tin (toxic)determination after proper modifications.

To date, there are many spectrophotometric methods for tin determination such as extraction spectrophotometry [3], solid phase spectrophotometry [4,5] and micelle spectrophotometry [6–14]. In the case of micelle spectrophotometry, each chromogenic system has its advantages and disadvantages with respect to sensitivity, selectivity and rapidity due to using different chromogenic reagents and surfactants. As the chromogenic

* Corresponding author.

PII S0039-9140(96)02119-4

reagents used for tin determination are almost all anionic dyes, and, hence, the surfactants are only cationic ones such as cetyltrimethylammonium bromide (CTAB) and cetylpyridinium bromide (CPB), precipitates often occur, especially at low room temperature [13] or after heating, due to the interaction of anionic dyes with cationic surfactants (CSF). In view of the properties of mixed surfactants such as low critical micelle concentration (CMC) (ion-association, and hence sensitisation, occurred only above CMC [1,15]), we substituted a mixed surfactant solution composed of CTAB and nonyl phenoxy polyethoxyethanol (OP) for single CTAB (Systems in the presence of CTAB and sodium dodecylsulfate (SDS) were turbid even if not heated). Preliminary tests showed that the use of the mixed surfactant solution could not only get rid of the drawbacks occurred when single CSF was used, but also enhance the sensitivity. In this paper, we developed a spectrophotometric method for Sn(IV) determination with bromopyrogallol red (BPR) in the presence of OP and CTAB as well as applied it to the determination of tin in canned foods.

2. Experimental

2.1. Apparatus

The UV-vis absorption spectra were recorded on a Shimadzu UV-240 spectrophotometer using a matched pair of 1 cm quartz cuvettes. The pHs of solutions were measured using a model PHS-2 pH meter.

2.2. Reagents

Unless otherwise stated, all reagents used were of analytical grade and their solutions were prepared by weighing with distilled water as solvent.

The concentration of each reagent was as follows:

(1) bromopyrogallol red (BPR), from Merck, 0.01%,

(2) cetyltrimethylammonium bromide (CTAB), from Jining Institute of Chemical Industry, China, 0.1%,

(3) nonyl phenoxy polyethoxyethanol (containing approximately 10 moles of ethylene oxide) (OP), from Wuhan Tongxing Chemical Reagent Plant, China, 0.2%,

(4) tin(IV) stock solution, 100 μg ml^{-1}, prepared by dissolving 0.1000 g of granulated tin metal (Baker) in 10 ml of concentrated H_2SO_4, and then diluting to 1 l with concentrated H_2SO_4 and water so that the concentration of H_2SO_4 was 0.1 mol l^{-1}; tin(IV) working solution, 10 μg ml^{-1}, prepared fresh, when required, by diluting 10 ml of 100 μg ml^{-1} tin(IV) stock solution to 100 ml with water.

2.3. Procedure

Pipette to a 10 ml colorimetric tube 3.0 ml of 0.01% BPR, 0.8 ml of 0.2% OP, 0.2ml of 0.1% CTAB, 2.0 ml of 95% ethanol, in that order. After mixing, add a portion of the working solution, (or sample solution) and dilute to the mark with 0.10 mol l^{-1} H_2SO_4. Finally, transfer the resulting solution to the quartz cuvettes and record the absorption spectrum using corresponding blank as reference.

3. Results and discussion

3.1. Absorption spectra

The complex of Sn(IV) with BPR in the presence of OP + CTAB had two sensitive absorption peaks in the UV/Visible zone (see Fig. 1). Under any circumstances, the peak height and half-band width of each ultraviolet absorption peak were better than those of corresponding visible absorption peak, respectively. So we chose the ultraviolet peak for tin determination. It is worth mentioning that in the visible range the absorption peak of Sn(IV)-BPR complex in the presence of single CTAB was much similar in peak position and half-band width to that in the presence of cetylpyridinium bromide (CPB) [6].

3.2. Selection of experimental conditions

3.2.1. Composition of mixed surfactant solution and its volume

Let the total volume of 0.2% OP + 0.1% CTAB be equal to 1.0 ml and change the relative volumes of the OP and the CTAB (other conditions as in Fig. 1). We found that 0.8:0.2 (0.2% OP:0.1% CTAB) was the optimum volume ratio and 1.0 ml was none other than the optimum volume of the mixed surfactant solution prepared in the optimum ratio. The peak under such conditions was the highest with its position being at 304 nm.

3.2.2. Effect of acidity

With the decrease of the pH of the system (conditions as in Fig. 1(1) except the volume of 0.1 mol l^{-1} H_2SO_4), the absorbance of the system at 304 nm first increased gradually (pH = 2.3–1.6) then changed little (pH = 1.6–1.0). After that, it decreased by a big margin (pH = 0.8–0.5). For the above system, maximum absorbance occurred at 1.42 (pH of the final solution) where 1.3 ml of 0.10 mol l^{-1} H_2SO_4 was added for adjusting the acidity of the system. Owing to the effect of pH on the absorbance of the system was very small over the pH range 1.0–1.6, we controlled the final pH of each system used for the calibration curve of tin(IV) simply by diluting with 0.1 mol l^{-1} H_2SO_4 to the mark (strong acid (pH < 2) itself is a buffering agent).

By the way, ionic strength, adjusted with up to 1.0 ml of 1.0 mol l^{-1} KCl, had almost no influence on the absorbance (if 2 ml of 0.1 mol l^{-1} H_2SO_4 was added, then the ionic strength from the solution itself to which the standard procedure was applied was roughly 0.06). A detailed investigation into the influence was not made.

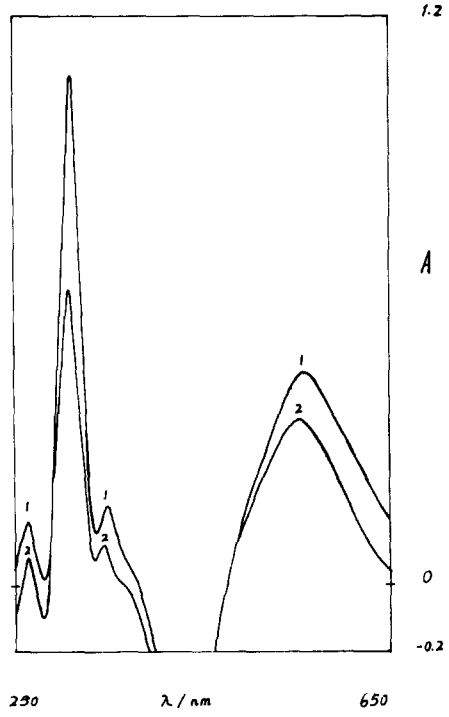

Fig. 1. Absorption spectra of Sn(IV)-BPR complex in the presence of OP + CTAB(1) and CTAB(2). Conditions: 3.0 ml of 0.01% BPR + 1.0 ml of a mixed surfactant solution (V_{OP}/V_{CTAB} = 8/2)(1) or 1.0 ml of 0.1%CTAB(2) + 2.0 ml of 95% ethanol + 15 μg Sn(IV) + 1.3 ml of 0.1 mol l^{-1} H_2SO_4.

3.2.3. Volume of 0.01% BPR

For a system containing 20 μg Sn(IV) (conditions as in the procedure except the volume of 0.01% BPR), with the increase of the volume of 0.01% BPR, the absorbance increased first rapidly then very slowly. After that, it dropped slowly. The optimal volume of 0.01% BPR was 3.0–4.0 ml. Taking into account the absorption of corresponding reagent blank at 304 nm, we chose 3.0 ml as optimum (the molar ratio of BPR to Sn was ca. 3.5:1).

3.2.4. Effect of ethanol

Ethanol had a sensitizing effect on the determination of Sn. For the system composed of 3.0 ml of 0.01% BPR, 1.0 ml of the mixed surfactant solution, 1.0 ml of 0.10 mol l^{-1} H_2SO_4 and 20 μg Sn(IV), the absorbance of the system increased rapidly with the increase of the volume of ethanol followed by remaining almost unchanged. The optimum amount of 95% ethanol was 2–3 ml. An excess of alcohol over the optimum could cause the absorbance to decrease. It was reported [6] that CPB was the optimal one among several cationic surfactants. However, we found that both CPB and CTAB have almost the same effects. This discrepancy lies in the solvent used for the

preparation of CSF (In Ref. [6], the solvent for CPB was 20% methanol in water, while that for CTAB was pure water).

Ethanol also had a stabilizing effect on the micellar system used for tin determination [16]. This effect is the reason their system [6] was not turbid even if heated in a water bath at 80–90°C (if alcohol was not added in CPB, we found their system would be turbid especially when a slight excess of Sn(IV) was present). In our system, however, this effect became insignificant because of the presence of OP (when heated our system was not turbid even if ethanol was not added).

3.2.5. The order of addition of the reagents

The order of addition of the reagents was studied. Results demonstrated that the order has a great effect on the absorbance. The chromogenic reagent and the surfactants must be added before the Sn(IV) or sample solution (see Procedure in Section 2).

3.2.6. Stability of the complex

The chromogenic reaction completed immediately after all reagents were added in the given order, and the chromogenic system could stabilize for at least 4 h.

3.3. Composition of the complex

The composition ratio of the Sn(IV)-BPR complex obtained using the mole-ratio method and the method of continuous variations was 1:3 (Sn(IV):BPR). We did not obtain the 1:1 ratio even if small amounts of BPR were added, which was not in accord with the results in Ref. [6]. A possible explanation for this difference was that the polyoxyethylene ether chains of OP molecules in a micelle could form a 'cage' like a crown ether molecule to capture Sn(IV) [17].

3.4. Analytical characteristics

Under the optimal conditions, Beer's law was obeyed over the range 0.1–2.5 μg ml^{-1} Sn(IV) with molar absorptivity being 8.2×10^4 l mol^{-1} cm^{-1} and detection limit (based on three times the standard deviation ($n = 11$) of the blank solution) being 0.018 μg ml^{-1}. For 15 μg Sn(IV), the relative standard deviation (R.S.D.) of seven replicate determinations was 1.6%.

3.5. Interference study

Under the optimal conditions, the effects of various foreign ions on the determination of 10 μg Sn(IV) were examined separately. With a relative error being less than ± 3%, the tolerance limits (μg) for various metal ions were as follows: Ca(II), Mg(II), As(III), Fe(II), Cr(III), Pb(II)(1000); Ni(II), Zn(II), Cu(II), Co(II), Mn(II)(200); Fe(III), W(VI), V(V)(10); Mo(VI), Sb(III), Cr(VI)(5). The tolerance limits for anions (used as complexing or reducing agents or media): lactic acid, oxalic acid, ascorbic acid, citric acid, NH_2OH HCl (2 g); iodide (13 mg)(26 mg (if 1.0 ml of 2% ascorbic acid was added)); chloride (100 mg); sulfate (200 mg). Nitrate and EDTA caused serious positive and negative interferences, respectively. Incidentally, when the volume of 0.1 mol l^{-1} EDTA exceeded 1.0 ml, the system became turbid (the white precipitate may be the ion-association complex of EDTa with CTAB). Sn(II), as $SnCl_2$ $2H_2O$, had almost the same results as Sn(IV) with respect to peak shape and peak position; for equal amounts of tin, however, the peak height of Sn(II) was a little lower than (ca. 93%) that of Sn(IV).

The interferences caused by Cr(VI), Fe(III), Sb(III), W(VI), Mo(VI) and V(V) could be reduced by reduction with 1 ml of 2% ascorbate (for Cr(VI) from 5 to 1000 μg and Fe(III) from 10 to 1000 μg) and by masking with 1 ml of 2% citrate (for Sb(III) from 5 to 20 μg and W(VI) from 10 to 30 μg [8]) as well as 1 ml of 2% lactate (for Mo(VI) from 5 to 30 μg and V(V) from 10 to 30 μg [1]).

3.6. Sample analysis

An application of the proposed method to canned meat, produced by Jinan Meat Packing Plant was made. It was told that the packing material was tin-plated iron sheet; so the main interferent was Fe(III), which could be eliminated readily by its reduction with 1.0 ml of 2% ascorbic acid.

Table 1
Recovery assays of Sn(IV) in canned foods

Added (μg)	Found[a] (μg)	R.S.D. (%)	Recovery (%)
0	11.3 (10.9)[b]	2.7	—
5	16.7	2.1	108.0
10	21.6	1.9	103.0
15	26.1	2.3	98.7

[a]Mean of five replicate determinations.
[b]Datum in parentheses was the value obtained by hydride generation [9]-atomic absorption spectrometry [18].

Prior to the determination, the sample was pretreated in the following way:

Weigh ca. 2.0 g of the meat; dry and ash it at 600°C. After that, dissolve the ash with 10 ml of concentrated HCl and dilute to 50 ml with distilled water and 1 mol l^{-1} NaOH so that the final pH was ca. 1. Pipette 1.0 ml of the digest for the determination.

The tin content (mean of five replicate determinations) obtained was 282.5 mg kg^{-1} (R.S.D. = 2.7%).

In order to check the accuracy of the proposed method, a recovery study was carried out on 1.0 ml of the digested solution. The average recovery was 103.2% (see Table 1), which is acceptable.

Usually, the iodide extraction method was used for separating micro amounts of Sn(IV) from interfering matrices. However, this sample pretreatment method could hardly be combined with other micelle spectrophotometric methods, in which a single CSF was used, owing to the precipitation of CSF by I_3^- introduced from extract. Probably because of the solubilization of the mixed micelles composed mainly of OP [16], the present method could preclude the precipitation even if no ascorbic acid was added (it was reported that ascorbic acid could preclude this phenomenon [1,11,19]).

In order to demonstrate that the proposed method could be compatible with the iodide extraction method, we digested the ashed sample, according to Ref. [1], first with concentrated HCl then concentrated H_2SO_4 (to drive off remaining HCl because chloride interfered in the extraction of SnI_4). As the contents of Cu(II) and Pb(II) were very low, their interferences (due to reactions with iodide) were not significant. After digestion, Sn(IV), as SnI_4, was extracted into toluene, then back-extracted into 0.2 mol l^{-1} HCl (a detailed procedure see Ref. [1]). Prior to the determination, no ascorbic acid was added to the extracts to preclude iodine (not Fe(III)). The amount of Sn(IV) found in this method was 11.0 μg ml^{-1}, which was satisfactory to us.

3.7. Conclusions

First, the proposed method is simple and rapid. The chromogenic reaction completed immediately after all reagents were added. No heating [6] or standing [1,2,14] was needed.

Second, the proposed method is sensitive. Its molar absorptivity at 304 nm was nearly three times as much as that in Ref. [6] ($\varepsilon = 3.0 \times 10^4$ l mol^{-1} cm^{-1} at 550 nm), which also used BPR as chromogenic reagent, more than five times as much as that in Ref. [3] ($\varepsilon = 1.6 \times 10^4$ mol^{-1} cm^{-1}), which was lately obtained by extraction spectrometry, and comparable to the latest result reported in Ref. [14] ($\varepsilon = 1.03 \times 10^5$ l mol^{-1} cm^{-1}). In terms of detection limit, the result of our method was as good as that obtained by hydride generation-flame AAS [20].

Third, the selectivity of our method is high because of its narrow half-band width. In addition, the linear range of our method is about three times as wide as that in Ref. [6].

Last but not the least, difficulties (precipitation of CSF by I_3^-) experienced by other researchers [11,16] in combining the proposed method with the selective extraction of SnI_4 have been overcome by means of the mixed surfactants.

References

[1] A. Ashton, A.G. Fogg and D. Thorburn Burns, Analyst, 98 (1973) 202.
[2] V.H. Kulkarnl and M.L. Good, Anal. Chem., 50 (1978) 973.
[3] S.P. Arya and A. Bansal, Mikrochim. Acta, 116 (1994) 63.
[4] M.C. Valencia, D. Gimeno and L.F. Capitan-Vallvey, Anal. Lett., 26 (1993) 1211.

[5] L.F. Capitan-Vallvey, M.C. Valencia and G. Miron, Anal. Chim. Acta, 289 (1994) 365.
[6] T.H. Con, I. Nemcova, I. Nemec and V. Suk, Anal. Chim. Acta, 115 (1980) 279.
[7] D. Thierig and F. Umland, Fresenius Z. Anal. Chem., 221 (1966) 229.
[8] G.H. Xu and H.X. Shen, Fenxi Huaxue, 10 (1982) 334.
[9] X.Y. Yu, Yejin Fenxi, 13 (1993) 27.
[10] Z.B. Li and Q.H. Xu, Fenxi Huaxue, 16 (1988) 390.
[11] R.M. Dagnall, T.S. West and P. Young, Analyst, 92 (1967) 27.
[12] C. Wyganowski, Mikrochim. Acta, I (1979) 399.
[13] Y.H. Zhou and C.W. Ma, Fenxi Huaxue, 11 (1982) 435.
[14] A.C. Spinola Costa, L.S.G. Teixeira and S.L.C. Ferreira, Talanta, 42 (1995) 1973.
[15] B.W. Bailey, J.E. Chester, R.M. Dagnall and T.S. West, Talanta, 15 (1968) 1359.
[16] G.X. Zhao, Physical Chemistry of Surfactants, 2nd edn., Beijing University Press, Beijing, 1991, p. 262.
[17] R.G. Vibhute and S.M. Khopkar, Indian J. Chem., 28A (1989) 1080–1083.
[18] R.V.C. Peddy, G. Kalpana and V. Koshy, Analyst, 117 (1992) 27.
[19] H.B. Corbin, Anal. Chem., 45 (1973) 534.
[20] X.W. Guo and S.Z. Wang, Fenxi Huaxue, 9 (1981) 258.

ELSEVIER

Talanta 44 (1997) 823–830

Talanta

Differential pulse voltammetric enzyme-linked immunoassay for the determination of *Helicobacter pylori* specific immunoglobulin G (IgG) antibody

Ya-nan He [a], Hong-yuan Chen [a,*], Jin-juan Zheng [b], Guang-yu Zhang [b], Zeng-Lan Chen [b]

[a] *Department of Chemistry, Institute of Coordination Chemistry, Nanjing University, Nanjing 210093, People's Republic of China*
[b] *Nanjing Children's Hospital, Nanjing 210008, People's Republic of China*

Received 15 April 1996; received in revised form 11 September 1996; accepted 26 September 1996

Abstract

A differential pulse voltammetric enzyme-linked immunoassay for the determination of *helicobacter pylori* (*H. pylori*) specific IgG antibody in human serum has been developed. The method is based on coupling the oxidation reaction of 3,3′,5,5′-tetramethylbenzidine (TMB)-H_2O_2 that is catalysed by horseradish peroxidase-IgG(HRP-IgG) conjugate with the electro-reduction of the enzymatic product to measure the activity of HRP-IgG. The latter reaction exhibits a sensitive differential pulse voltammetric response at 0.1 V (versus Ag/AgCl) in pH 4.0 acetate buffer solution. So, the *H. pylori* specific IgG antibody could be detected. The detection limit of present method for *H. pylori* specific IgG antibody was 1.0 units ml^{-1}, which was about seven times lower than that obtained by traditional spectrophotometric ELISA procedure. © 1997 Elsevier Science B.V.

Keywords: *Helicobacter pylori*; Immunoglobulin G (IgG) antibody; Serum

1. Introduction

H. pylori is a curved bacillus in close contact with gastric epithelium in biopsy samples from patients showing active chronic gastritis. *H. pylori* can cause acute gastritis and may lead to chronic gastritis [1]. The determination of *H. pylori* is valuable in diagnosis of gastritis and peptic ulcers. The current method for the determination of *H. pylori* is enzyme-linked immunosorbent assay (ELISA). In the ELISA, antibody production against *H. pylori* is studied, the presence of high IgG titer specific to *H. pylori* may show active *H. pylori* infection. Antibodies in the serum sample are allowed to react immunologically with the purified *H. pylori* antigens that are immobilized on the microwells. After washing off the unbound materials, the bound antibodies are quantitated by an enzyme labelled second antibodies specific to human IgG. A substrate is added and the intensity of the color generated is directly proportional to the concentration of the specific IgG that reacted with the *H. pylori* group specific antigens. Although ELISA is a popular assay in clinical examination, the relatively

* Corresponding author. Fax: +86 25 3317761. Email: HYChen@public1.ptt.js.cn.

PII S0039-9140(96)02120-0

poor detection limit with absorbance spectrophotometry is one cause of its lack of sensitivity [2,3].

Immunoassay with electrochemical detection appears to have some inherent advantages over the more widely used spectrophotometric techniques [4]. Lower detection limits and wider working detection range can be achieved with Morden electrochemical techniques. One approach used in such techniques is to employ an enzyme label that generates an electrochemically active product. Many of the recent studies have utilized amperometric detection of electroactive species, as *p*-aminophenol [5], the reduced form to 2,6-dichloroindophenol [6], 1-naphthol [7] and NADH [8] generated catalytically by an enzyme label. But to our knowledge, voltammetric immunoassay method was reported much less than amperometric immunoassay method.

In this paper, we established a voltammetric enzyme-linked immunoassay for *H. pylori* specific IgG antibody using HRP as labeled enzyme and TMB-H_2O_2 as substrate. The enzymatic product 4,4′-di(3,5-dimethyl-4-amino),2,2′,6,6′-tetramethylazobenzene is electroactive and can be detected by differential pulse voltammetry. The assay shows high sensitivity and accuracy, and the electrochemical detection can be done within half a minute.

The enzymatic coupling reaction scheme and the electrochemical reaction scheme are as follows.

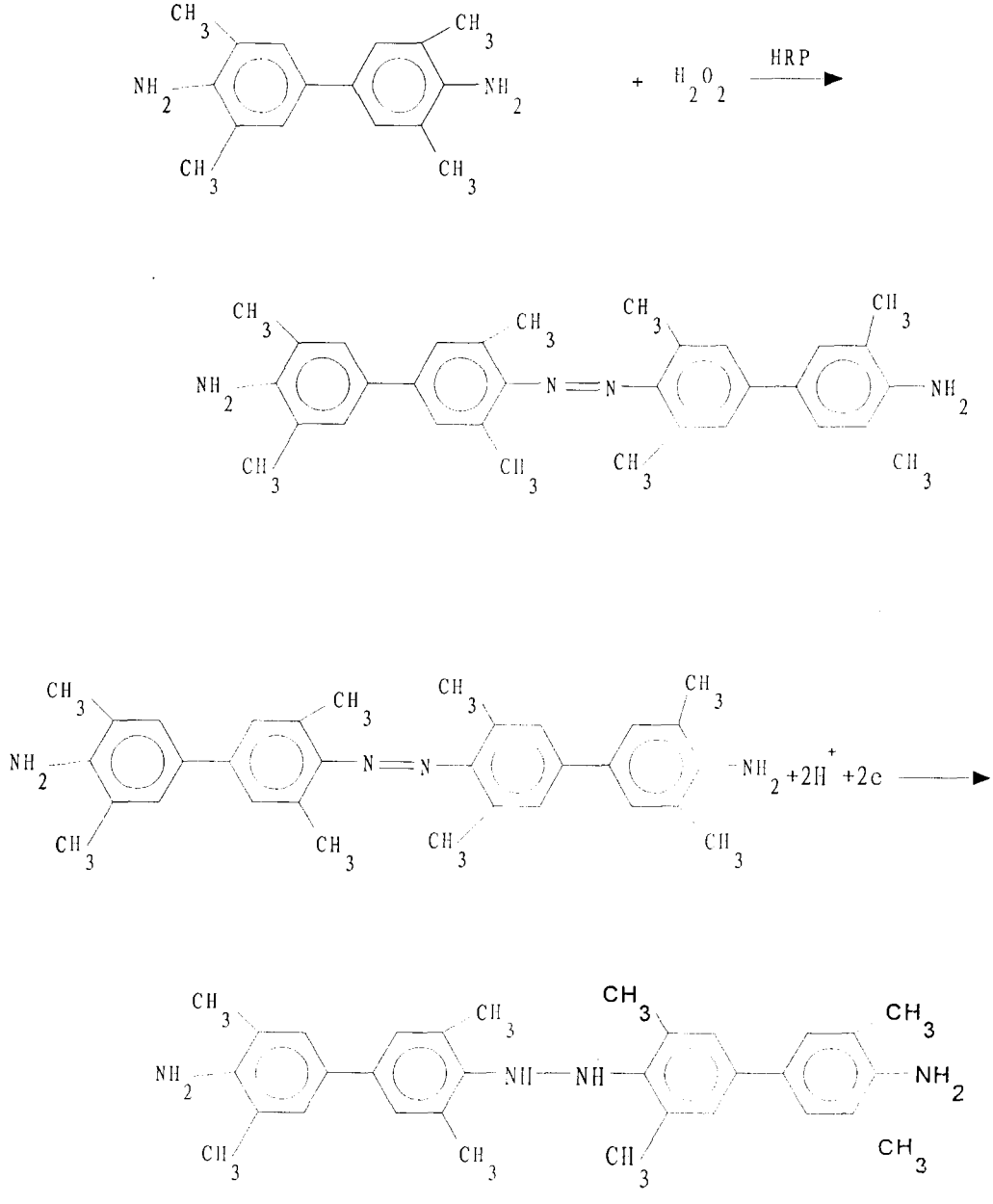

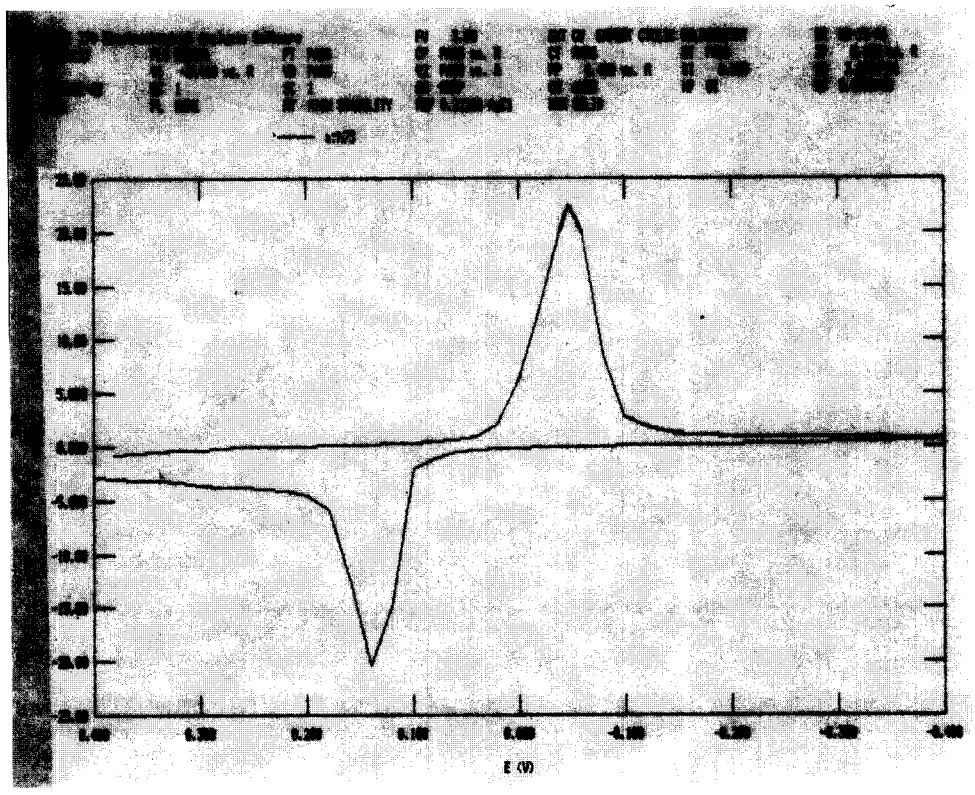

Fig. 1. Cyclic voltammogram of the enzymatic product in 0.2 mol l^{-1} pH 4.0 acetate/DMSO buffer solution. TMB: 0.5×10^{-3} mol l^{-1}, H_2O_2: 0.8×10^{-3} mol l^{-1}, HRP-IgG: $1{:}5.0 \times 10^{6}$ scan rate: 300 mV/S.

2. Experimental

2.1. Reagents and apparatus

A ELISA test kit for *H. pylori* specific IgG antibodies measurement was purchased from BIO-RAD laboratories (USA) and was used accordance with manufacture instructions [9]. In the kit, the serum diluent concentrate was pH 7.4 phosphate saline with PEG, Tween, 0.002% Thimerosal and 0.01% sodium azide. The substrate solution was TMB-H_2O_2 in pH 5.0 acetate/DMSO buffer solution. The ratio of the DMSO to the acetate buffer was 1%, and it was constant in all the experiments. The wash buffer concentrate was pH 7.4 phosphate buffered saline with Tween 20, 0.02% Thimerosal and 0.01% Gentamicin. The stop solution was 1 mol l^{-1} H_2SO_4. The voltammetric determination was done with an electrochemical system (Model 270, EG and G, USA). The working electrode was a home made gold disk electrode. The diameter of it was 0.5 mm. The counter electrode was a platinum wire and the reference electrode was a Ag/AgCl electrode with 0.1 mol l^{-1} KCL. Before use, the electrode was prepared as follows: first, polish the electrode by rough and fine sand paper, respectively. Then, polish it to a mirror smoothness on silk by successively fine grade of alumina, the final diameter of which was 0.05 μm. Finally, clean the electrode by ultrasonic waves.

The absorbancies were detected by a DYNATECH MR7000 microplate readers (USA).

2.2. H. pylori specific IgG antibody immunoassay

A series of human serum *H. pylori* specific IgG

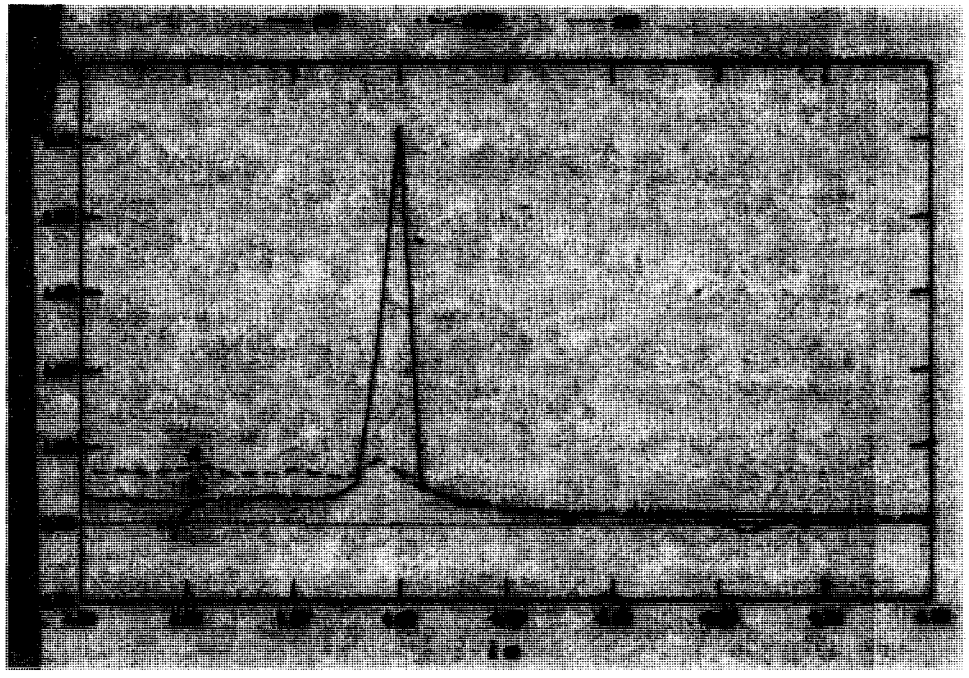

Fig. 2. Differential pulse voltammogram of the enzymatic product. 1. 0.2 mol l^{-1} pH 4.0 acetate/DMSO buffer solution. 2. $1 + 0.5 \times 10^{-3}$ mol l^{-1} TMB + 0.8×10^{-3} mol l^{-1} H_2O_2. 3. 2 + HRP-IgG($1:5.0 \times 10^6$). Pulse height: 60 mV, pulse width: 0.05 S, scan rate: 300 mV/S.

antibody calibrators that covered the clinically relevant range (0–100 units ml^{-1}) was supplied with the ELISA test kit. A standard curve for the spectrophotometric procedure was produced by following manufacture's protocol. Concentrations of *H. pyroli* specific IgG antibody were detected spectrophotometrically by measuring absorbance changes at 450 nm.

2.3. Voltammetric H. pylori specific IgG antibody immunoassay

After the H_2SO_4 termination in the ELISA procedure, 22 ul 2 mol l^{-1} NaOH was added to the well of an ELISA plate to return its pH to 4.0. Without separation, the small three-electrode system was directly inserted in the well for voltammetric determination. The scan rate was 300 mV/S,the initial potential was 0.40 V, the final potential was −0.40 V. For DPV detection, the pulse height was 60 mV, the pulse width was 0.05 S.

3. Results and discussion

3.1. Cyclic voltammetry of the enzymatic product

Fig. 1 is a cyclic voltammogram of the enzymatic product formed by H_2O_2 oxidizing TMB catalysed by HRP in 0.2 mol l^{-1} pH 4.0 acetate/DMSO buffer solution. It shows that enzymatic product could give a quasi-reversible current response. A pair of well-defined cathodic and anodic peaks appeared. E_{pc} and E_{pa} were −0.04 V and 0.14 V, respectively. The existence of the anodic peak suggests that the product of electroreduction of the enzymatic product can be oxidized again at the electrode when the scan direction is reversed. The influence of scan rate on the peak current was studied, the response of peak current was linear with respect to the scan rate between 50 and 300 mV/S, suggesting the adsorption of the enzymatic product and the electroreduction process of the enzymatic product is adsorption controlled [10].

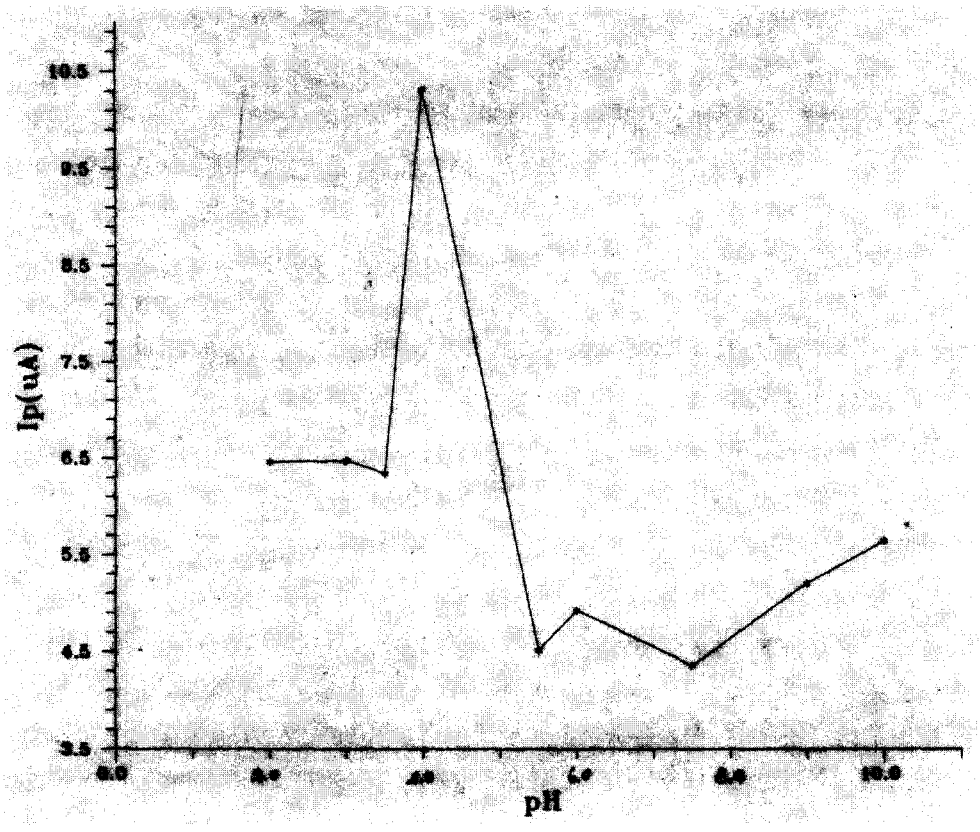

Fig. 3. Effect of pH on differential pulse voltammetric response of the enzymatic product. Conditions are the same as Fig. 2.

3.2. *Differential pulse voltammetric response of the enzymatic product*

The linear sweep voltammetry, the modern square wave voltammetry, the normal pulse voltammetry and the differential pulse voltammetry (DPV) all have excellent voltammetric peaks in the detection of the enzymatic product. Among these methods, DPV has the advantages of the highest sensitivity and the lowest detection limit. Fig. 2 shows the result of the differential pulse voltammetry. Curve 1 shows the situation that in the coupling reaction process there is nothing but acetate buffer solution that has no DPV response. Curve 2, which presents a lower DPV peak at 0.1 V (versus Ag/Ag CL) potential, shows the situation that the coupling reaction process has acetate buffer solution + TMB + H_2O_2. There is a blank peak that is due to a slow oxidation of TMB by H_2O_2 and the high sensitivity of this method. Curve 3 shows the situation at the time when HRP was added to the former solution. Owing to the addition of HRP, the product of the enzymatic reaction produced a high well-shaped DPV peak. Comparing curve 3 with curve 2, we could find that the peak potential did not move practically, but the peak current increased sharply. This means that HRP could highly speed up the oxidizing reaction of TMB by H_2O_2. With this electroreduction peak, free HRP and different labelled HRP can be detected. By means of immunoassay, different antibodies and antigens can also be identified.

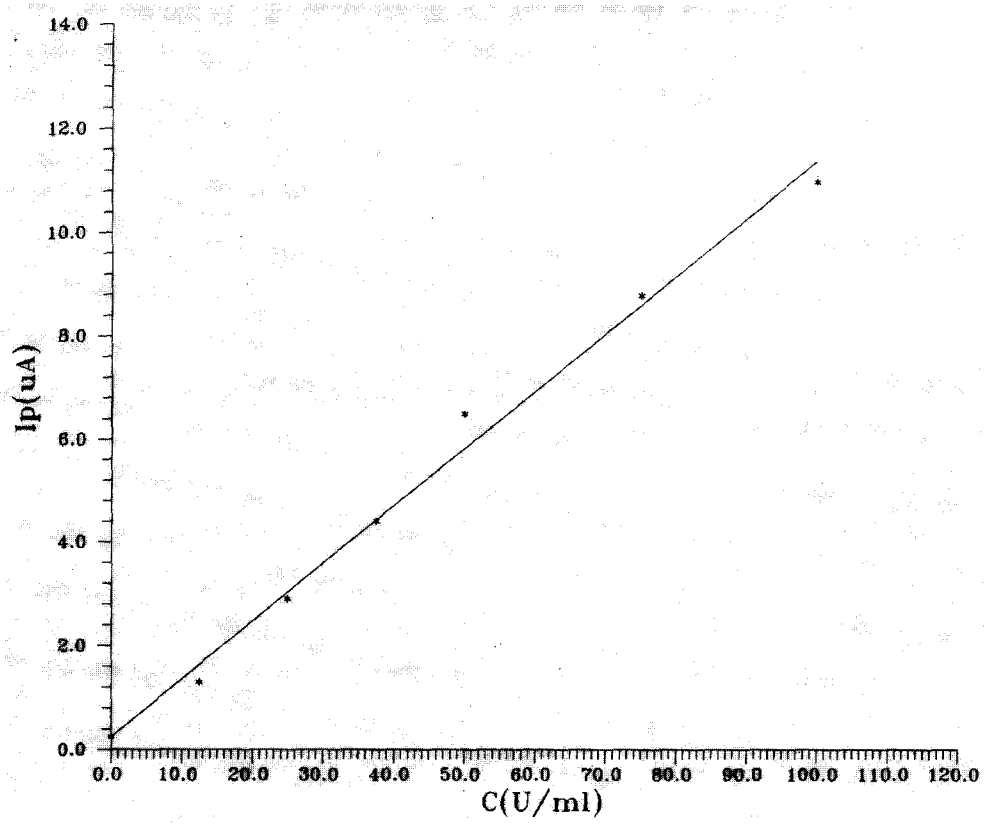

Fig. 4. Calibration curve for the determination of *H. pyroli* specific IgG antibody by differential pulse voltammetry. Conditions are the same as Fig. 2.

3.3. Optimum conditions for the determination of the enzymatic product

To check the effect of pH on the DPV response of the enzymatic product, successively increased volume of 2 mol l^{-1} NaOH was added to adjust the pH of the determination system after the enzymatic product formation and H_2SO_4 termination in the ELISA procedure. As shown in Fig. 3, the peak current I_p remains relatively low value between pH 1.5–3.5 and 5.5–10.0, but I_p increases sharply in pH 3.5–4.0, and reaches maximum value at pH 4.0, then it decreases at higher pH. So, pH 4.0 was selected as the working pH considering the response sensitivity.

DPV parameters were adjusted to optimize the instrument condition. Although I_p was greater for higher pulse height between 10–100 mV, a sharper peak was found at 60 mV using pulse width 0.05 S. A scan increment of 20 mV and a step time of 55 mS were selected.

3.4. Quantitative test for the detection of H. pylori specific IgG antibody

Under the selected conditions described above, the DPV response of the enzymatic product is proportional to the concentration of *H. pylori* specific IgG antibody in the serum. A linear calibration curve for the detection of *H. pyroli* specific IgG antibody in serum was produced over the range of 0–100 units ml^{-1} as shown in Fig. 4. The linear regression equation was $C_{HP} = 8.88\ I_p - 1.57$ with the linear relation coefficient (r) 0.996. The relative standard deviation (RSD) for the determination of 25 units ml^{-1} *H. pylori*

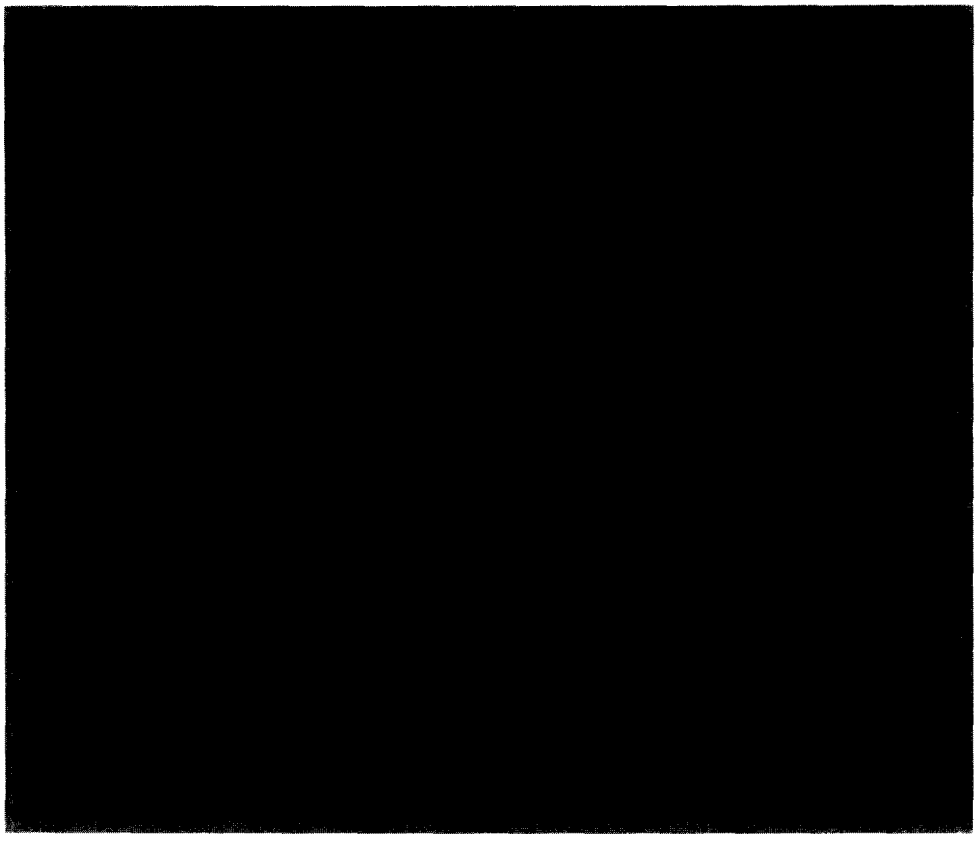

Fig. 5. Calibration curve for the determination of *H. pyroli* specific IgG antibody by ELISA.

specific antibody was 7.6% (eight replicates).

The ELISA procedure was also carried out as described, absorbance changes were plotted against the corresponding *H. pylori* specific IgG antibody concentration and a calibration curve was constructed. (Fig. 5, $C_{HP} = 54.03\ A - 9.16$, $r = 0.980$), the RSD for the determination of 25 units ml^{-1} *H. pylori* specific antibodies was 8.4% (eight replicates).

From Fig. 4 and Fig. 5, we could observe that DPV immunoassay has wider detection range than ELISA procedure in the higher and lower IgG concentration range. Taking the detection limit to be the concentration that gives a signal three times the standard deviation (S.D.) of the blank, we could calculate the detection limit from the calibration curve of these two methods. The S.D. of the blank for DPV and ELISA was 0.095 and 0.10, respectively (eight replicates). So, the calculated detection limit for DPV and ELISA procedure is 1.0 and 7.1 units ml^{-1}, respectively.

This result shows that DPV detection limit is about seven times more sensitive than that of the spectrophotometric method.

Acknowledgements

This project was supported by the National Natural Science Foundation of China.

References

[1] A. Morris and G. Nicholson, Amer. J. Gastroenterol, 82 (1987) 192.
[2] A.M.G. Bosch, H. Van Hell and J. Brands, Schuurs RHWM. In Proc Int Symp on Enzyme Labeled Immunoassay of Hormoues and Drugs (Ulm, F.R.G.), SP Pal, Ed., Walter de Gruyter, Berlin, 1978, pp. 175–187.
[3] A. Tsuji, M. Maedes and H. Arakawa, ibid pp. 327–339.

[4] W.R. Heineman and H.B. Halsall, Anal. Chem., 57 (1985) 1321A.
[5] C. Duane and M.E. Meyerhoff, Anal. Chem., 66 (1994) 1369.
[6] H. Yao, S.H. Jenkins, A. Pesce, H.B. Halsall and W.R. Heineman, Clin. Chem., 39 (1993) 1423.
[7] D. Athey, M. Ball and C. McNeil, J. Ann. Clin. Biochem., 30 (1993) 570.
[8] P. Manning, D. Athey and C. McNeil, Anal. Lett., 27 (1994) 2443.
[9] Quantitative Test for the detection of H. Pyroli specific IgG antibodies (Instruction Manual) MARCH 1995.
[10] E. Laviron, J. Electroanal. Chem., 100 (1979) 263.

ELSEVIER

Talanta 44 (1997) 831–836

Talanta

Direct electrochemical redox of tyrosinase at silver electrodes

Baoxian Ye, Xingyao Zhou *

Department of Chemistry, Wuhan University, Wuhan 430072, People's Republic of China

Received 30 April 1996; received in revised form 18 September 1996; accepted 26 September 1996

Abstract

The direct electron transfer reactions between tyrosinase and silver electrode were investigated by using cyclic voltammetry and potential-step chronoamperometry as well as current-step chronopotentiometry techniques. The kinetics of these reactions is quasi-reversible with two electron transfer reactions and 0.030 s^{-1} apparent electrode reaction rate constant. The results demonstrate that neither electrode surface modification nor the inclusion of mediators is necessary to study the electron transfer reactions of tyrosinase at silver electrodes. Moreover, both the anodic and the cathodic currents are linear relationship with the tyrosinase concentration in the range of $1 \times 10^{-9} \sim 5 \times 10^{-8}$ mol l^{-1}. It is possible to be used as a method of analyzing tyrosinase concentration. © 1997 Elsevier Science B.V.

Keywords: Direct electrochemistry; Silver electrode; Tyrosinase

1. Introduction

The electrochemical behavior investigations of biomacromolecules, such as proteins and enzymes, have been a major research area in recent years [1,2]. These investigations are important not only for fundamental reasons but also for the development of electroanalytical methodology [3]. It is because some analogies exist between the reactions of biomacromolecules at electrodes and their interaction in biological redox system [4]. However, although many proteins and enzymes possess functional groups that can be readily oxidized or reduced by chemical redox agents, it is rare for the biomacromolecules to undergo facile redox at electrodes, for reasons ascribed both to their extended three-dimensional structure and the resulting inaccessibility of the electroactive centers as well as their strong adsorption onto electrode surface for subsequent passivation. Most biomacromolecules exhibit so slow electron transfer reactions at electrode surface that no useful currents appear even when rather large overpotentials are applied. For our knowledge, only a few proteins with quasi-reversible redox are obtained at some chemically modified electrodes or by the presence of some promoters so far [5–10]. Few of these redox reactions could be used for analytical possibility.

A few papers about electrochemical redox of blue copper proteins were reported previously. Gray et al. [11,12] reported the direct electro-

* Corresponding author.

PII S0039-9140(96)02121-2

chemistry of *Bean plaslocyanin*, *Rhus vernicifera stellacyanin* and *Pseudomonas averuginosa azurin* at modified gold electrodes. The direct electrochemistry of *Spinach plaslocyanin* at graphite electrodes promoted by $Pt(NH_3)_6^{4+}$ were studied by Hill et al. [13]. Tyrosinase (Tyr) is one of blue copper proteins. It is an important enzyme with biofunction for catalyzing oxidation of Tyrosine and Catechol. The only report about the direct electrochemical behavior of Tyr was by Kelly et al. [3]. They modified glass carbon electrodes using Nafion mixed with copper chelate and obtained the redox reactions of Tyr. In our experiments, we found that Tyr occurred quasi-reversible redox reactions at bare silver electrodes with two electron transfer and 0.030 s^{-1} apparent reaction rate constant. More importantly, both the anodic currents and the cathodic currents are linear relationship with the concentration of Tyr in the range of $1 \times 10^{-9} \sim 5 \times 10^{-8}$ mol l^{-1}.

2. Experimental

2.1. Reagents and materials

Tyrosinase was obtained from Sigma with purity of 99% and without further purification. Tyr solid was stored under 0°C. Tyr solution, prepared fresh everyday, was stored under 5°C. Other reagents were of analytical grade and were used as received. All solutions were prepared using distilled water.

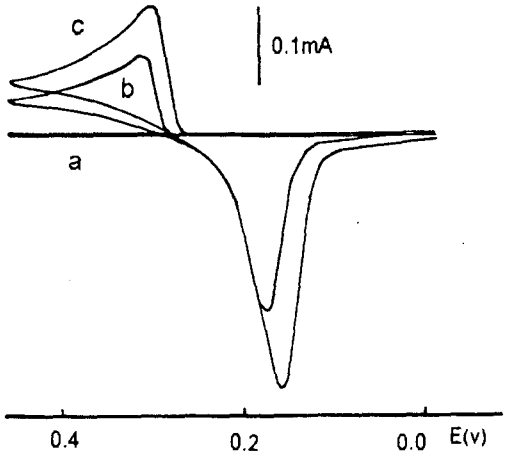

Fig. 1. The voltammograms of Tyr on bare Ag electrode (a) 0.50 mol l^{-1} KH_2PO_4; (b) (a) + 5×10^{-9} mol l^{-1} Tyr; (c) (a) + 1×10^{-8} mol l^{-1} Tyr v = 20 mV s^{-1}; pH = 5.0.

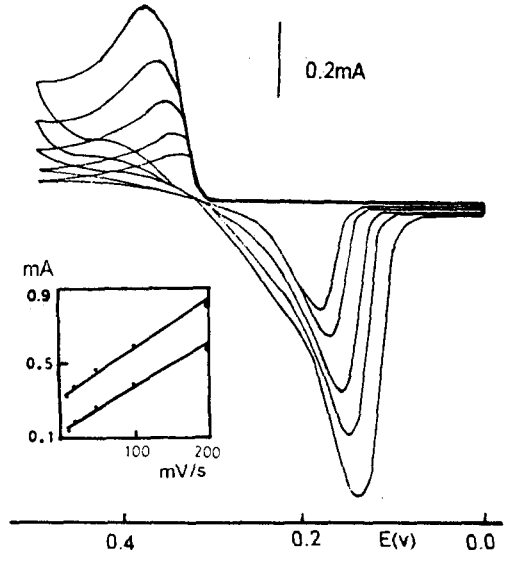

Fig. 2. The effect of v on I_p (from inner to exterior) v = 10, 20, 50, 100, 200 mV s^{-1}. Inset shows the dependence of observed I_{pa} and I_{pc} on v. The solution same as Fig. 1(c).

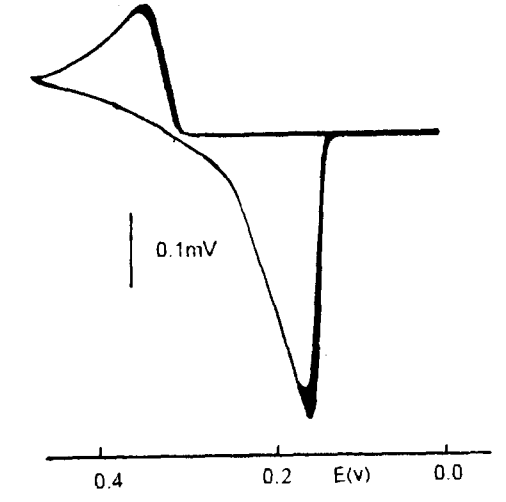

Fig. 3. The cyclic voltammogram for continuing scan 30 min. The solution same as Fig. 2. v = 20 mV s^{-1}.

Table 1
Detection of electron transfer number n ([Tyr] = 5×10^{-9} mol l^{-1})

v(mV s^{-1})	E_{pa}(mV)	E_{pc}(mV)	I_{pc}(mA)	Qc(mC)	n
10	342	179	0.1645	0.8192	2.06
20	346	171	0.2050	0.5101	2.06
30	348	169	0.2330	0.4020	1.98
40	352	164	0.2640	0.3527	1.92

2.2. Apparatus and procedures

Model 270 electrochemical system (EG and G Princeton Applied Research, USA) was employed along with an IBM 386 computer to control and treat data for cyclic voltammetry, potential-step chronoamperometry and current-step chronopotentiometry. A standard three-electrode electrochemical cell was used for all electrochemical experiments. The electrodes consist of bare silver electrode (area of 3.14 mm^2) as working electrode, platinum slice (area of 1.0 cm^2) electrode as counter electrode and SCE as reference electrode. The Ag electrodes were polished to a mirror smoothness on silk impregnated with 0.3 μm alumina powder suspension and then cleaned with ultrasonic waves. All experiments were performed under undeoxygen at room temperature.

3. Results and discussion

3.1. The direct electrochemical behavior of tyrosinase on silver electrodes

Fig. 1 shows the cyclic voltammograms of Tyr on bare silver electrodes. In medium of 0.5 mol l^{-1} KH_2PO_4 (pH = 5.0), with potential range of 0.00 ~ +0.5 V(versus SCE) and scan rate of 20 mV s^{-1}, the silver electrode does not occur redox reaction itself [Fig. 1(a)] and a pair of redox peaks are obtained when 5×10^{-9} mol l^{-1} Tyr is added in the medium with $E_{pc} = 171$ mV and $E_{pa} = 346$ mV ($\Delta E_p = 175$ mV) respectively [Fig. 1(b)]. Increasing Tyr concentration to 1×10^{-8} mol l^{-1}, both anodic currents I_{pa} and cathodic currents I_{pc} are multiplied with $E_{pc} = 155$ mV and $E_{pa} = 335$ mV ($\Delta E_p = 180$ mV). It is clear that the peak potentials (E_{pa} and E_{pc}) are related to Tyr

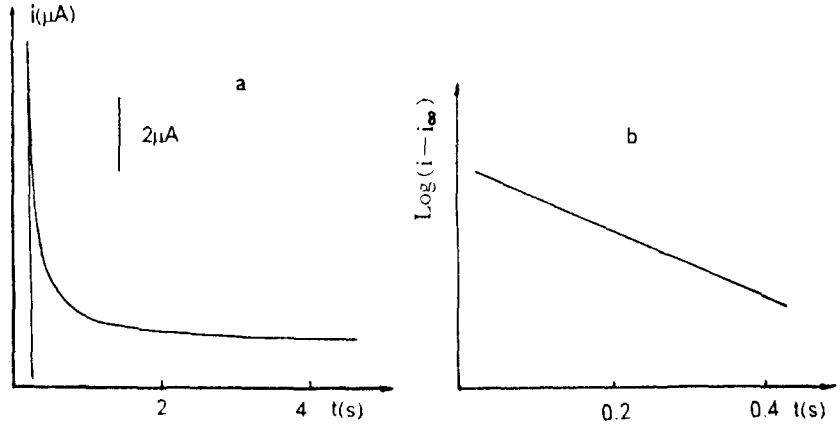

Fig. 4. Potential step experiment (ΔE = 5 mV). (a) $I \sim t$ curve; (b) $\mathrm{Log}(i - i_\infty) \sim t$ curve.

Table 2
The relationship between adsorbance and Tyr concentration ($\Delta i = 0.1$ mA)

Tyr(mol l^{-1})	Adsorbance(mol mm^{-2})
1.0×10^{-9}	7.7×10^{-13}
5.0×10^{-9}	1.1×10^{-12}
1.0×10^{-8}	2.57×10^{-12}
1.5×10^{-8}	3.71×10^{-12}
2.0×10^{-8}	4.64×10^{-12}
2.5×10^{-8}	5.56×10^{-12}

concentration. Both E_{pa} and E_{pc} are shifted negatively with increasing Tyr concentration. But the E_{pc} is shifted more quickly than that of E_{pa}, which results in the multiplication of ΔE_p, for reason ascribed to the I_{pc} larger than I_{pa} ($I_{pc} \cong 2I_{pa}$). The peak currents (I_{pa} and I_{pc}) are linear relationship with scan rate in range of $10 \sim 200$ mV s^{-1}[Fig. 2]. This exhibits that both Tyr and its redox product are adsorbed on electrode surface. In fact, if we immerse an Ag electrode in a solution containing Tyr for a moment and then put it in 0.5 mol l^{-1} KH_2PO_4 solution for cyclic scan, the redox peaks of Tyr are obtained still. Moreover, we had a silver electrode adsorbed Tyr on its surface be exposed in air for 30 min and then performed cyclic scan in background solution. The same voltammograms were obtained as that of performing in containing Tyr solution. This result suggests that the redox reactions of Tyr possess good stability. For this consideration, we performed the cyclic scan in a solution containing Tyr 1×10^{-8} mol l^{-1} for continuing 30 min [Fig. 3]. The electrode reactions exhibit so good a stability that the peak currents change by less than 8.0% (cathodic current)and 6.5% (anodic current), respectively.

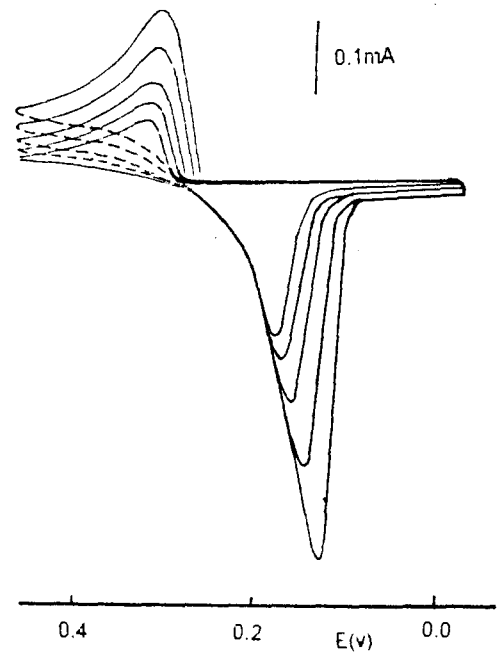

Fig. 6. The relationship between peak currents and Tyr concentration (from inner to exterior) 1×10^{-9}; 5×10^{-9}; 1×10^{-8}; 2×10^{-8}; 3×10^{-8} mol l^{-1}, $[KH_2PO_4] = 0.5$ mol l^{-1}, pH = 5.0, v = 20 mV s^{-1}.

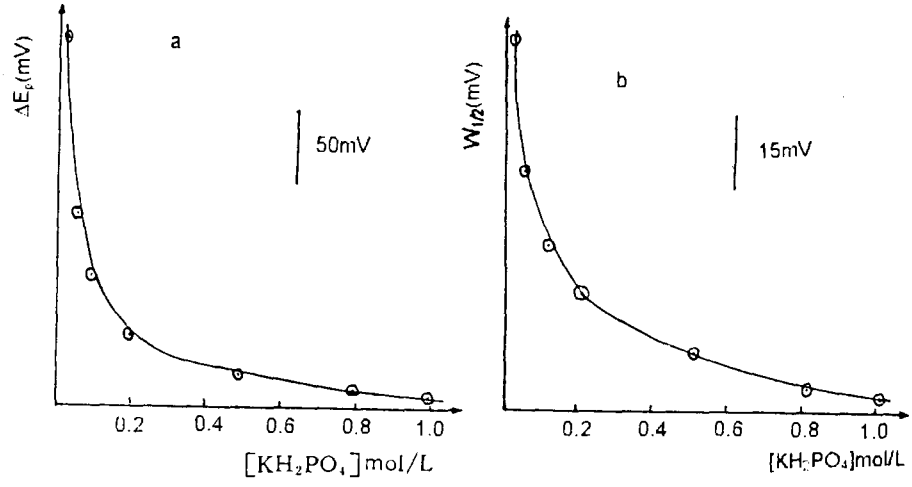

Fig. 5. The effect of KH_2PO_4 concentation on ΔE_p(a) and peak half – width $W_{1/2}$(b). [Tyr] = 1×10^{-8} mol l^{-1}, v = 20 mV s^{-1}.

3.2. The reaction rate of Tyr on bare silver electrodes

Cyclic voltammetric technique was employed to study the redox reactions between Tyr and bare silver electrodes. According to Laviron's theory [14], when the adsorption obeys the langmuir isotherm, the peak currents are linear relationship with scan rate. That is:

$$I_p = n^2F^2A\Gamma v/4RT = nFQv/4RT$$

Γ is the total surface concentration of electrode reaction substance (mol cm^{-2}). A is the electrode area(cm^2) and Q is the peak area of voltammogram (coulomb). I_p is here expressed in unit of amperes. n, F, R, T have their usual significance. The above equation shows that as long as Q is obtained under certain v, then n can be calculated. Table 1 shows the results on this basis. So, the redox of Tyr at bare silver electrodes is a two electron transfer reaction. The electrode reaction rate constant k_s was calculated using the method demonstrated by Laviron [15]. The transfer coefficient α can be obtained with $E_p \sim f(\log v)$ relation. Here when scan rate is 20 mV s^{-1}; $\Delta E_p = 175$ mV, that is $\Delta E_p > 200\ n^{-1}$ mV. K_s can be obtained with following equation:

$$\log k_s = \alpha\log(1-\alpha) + (1-\alpha)\log\alpha - \log(RT/nFv) - \alpha(1-\alpha)nF\,\Delta E_p/2.3RT$$

From this, we figured out $\alpha = 0.61$ and $k_s = 0.030\ s^{-1}$. It shows a quasi-reversible reaction.

3.3. The electrode reaction parameters R_r, C_d and electrode surface adsorbance

For an electrode reaction controlled by electrochemical step, when a low amplitude potential step ($\Delta E < 10$ mV) exerts on the electrode and continues for a short time, the concentration polarization will not occur. The controlling potential transient technique can be used to detect solution resistance R_l (including electrode inner resistance), electrode reaction resistance R_r and electrical double layer capacitance C_d. For this system, we used $\Delta E = 5$ mV as potential step to exert on electrode and record $i \sim t$ curves (Fig. 4). At this condition, we can consider that the R_r is not relation to potential, that is R_r = constant. According to Macdonald's [16] theory:

$$i_{max} = \Delta E/R_l$$

$$i = i_\infty + A\,e^{-t/R_{ll}C_d}$$

(R_{ll} is the parallel combination of R_r and R_l)

$$\mathrm{Log}(i - I_\infty) = \mathrm{Log}\,A - t/2.3\,R_{ll}\,C_d$$

If the i_∞ is selected suitably, the $\mathrm{Log}(i - i_\infty) \sim t$ curve is a straight line (Fig. 4b.) So: /slope/ = $(1/R_l + 1/R_r)/2.3\,C_d$ and $R_r = \Delta E/i_\infty - R_l$ We obtained $R_l = 1442\ \Omega$; $R_r = 8408\ \Omega$; and $C_d = 12.8\ \mu F$. The real electrode surface is $S_{real} = C_d/C_N = 12.8/20 = 0.64\ cm^2$. It is much larger than its apparent surface.

The electrode surface adsorbance have been investigated using transient current-step chronopotentiometry technique. In different Tyr concentration solutions, a fixed current-step exerted on electrode and different transitional times τ were obtained. Then, the charges (Q) were calculated from $Q = \tau \times t$ and the adsorbance were calculated from $\Gamma = Q/nFA$. Table 2 shows the results on this basis.

From the results, we know that the adsorbance are enhanced with increasing Tyr concentration. It predicts that it may possesses a linear relationship between electrode reaction currents and Tyr concentration. This has been confirmed by following experiments. We also know that there is an adsorption equilibrium between adsorbed Tyr molecules and Tyr molecules in solution. For reasons ascribed that Tyr molecule is a macromolecule. The adsorbed Tyr molecules impede the further adsorption of dissolved Tyr molecules. Although the adsorbance on electrode surface does not reach saturation, it cannot be enhanced further, unless the Tyr concentration be increased. This may be explained that the adsorbance are linearly multiplied with increasing Tyr concentration.

3.4. The relationship between peak currents and Tyr concentration

Several salts have been examined as electrolyte. The results indicate that the KH_2PO_4 is the best choice. The solution pH and KH_2PO_4 concentration have been carefully tested for affecting I_p and E_p. The results are that pH do not affect I_p but affect the E_p. Both E_{pa} and E_{pc} are shifted negatively (about 12 mV pH^{-1}) with decreasing pH, but the ΔE_p is a constant at different pH (ΔE_p = 180 mV with 1×10^{-8} mol l^{-1} Tyr). This suggests that the H^+ ions do not participate in the reaction. Fig. 5 shows the affect of ΔE_p(a) and the peak half-width $W_{1/2}$(b) by KH_2PO_4 concentration. Both ΔE_p and $W_{1/2}$ are decreased with increasing KH_2PO_4 concentration. This suggests that the KH_2PO_4 concentration affects the Tyr conformation and reaction activation energy. Fig. 6 is the voltammograms of different Tyr concentration. Both the anodic currents and cathodic currents are multiplied with increasing Tyr concentration and linear relationship with it in the range of $1 \times 10^{-9} \sim 5 \times 10^{-8}$ mol l^{-1}. The linear regression equations are:

$$I_{pa(A)} = 4.64 \times 10^{-5} + 2434.7C(\text{mol}\,l^{-1})$$

$$I_{pc}(A) = 9.77 \times 10^{-5} + 5514.4C(\text{mol}\,l^{-1})$$

with correlation coefficients $\Upsilon_a = 0.9960$ and $\Upsilon_c = 0.9976$. The detection limit is up to 5×10^{-10} mol l^{-1} estimated by signal/noise = 1.

4. Conclusion

The existence of Tyr are of tetramers, each of which contains an electroactive center (copper) and may be experiencing electron transfer individually. The tetramers are negatively charged at pH 5. Some kind of 'adsorption bond' may be formed between Tyr and the 5s orbit of Ag atom (a half-full orbit of Ag). But the tetramers are a macromolecules with molecular weight of 119 000 (from mammal tissues). One side of the tetramers is adsorbed on the electrode surface and exchanges two electrons with the electrodes. Essentially, the redox reactions of Tyr in the process are the redox between Cu^{2+} and Cu^+.

Acknowledgements

The support of the National Natural Science Foundation of China is greatly appreciated. The authors especially appreciate discussions with Prof. Wuming Zhang regarding this work.

References

[1] H.A.O. Hill, Pure Appl. Chem. 59 (1987) 743.
[2] A. Merz, Top. Curr. Chem. 152 (1990) 49.
[3] J.W. Furbee, Jr. C.R. Thomas, R.S. Kelly and M.R. Malachouski, Anal. Chem. 65 (1993) 1654.
[4] M.J. Eddowes, H.A.O. Hill, K. Uoski, J. Am. Chem. Soc. 101 (1979) 7117.
[5] D.E. Reed, F.M. Hawkridge, Anal. Chem. 59 (1987) 2334.
[6] K.B. Koller, F.M. Hawkridge, J. Electroanal. Chem. 239 (1988) 281.
[7] S. Dong, S. Song, Acta Chim. Sinca 49 (1991) 493.
[8] J. Han, H. Chen, H. Gao Acta Chim. Sinca 51 (1993) 683.
[9] C. Cai, H. Ju, H. Chen, Chem. J. Chin. Univ. 16(1) (1995) 31.
[10] A.I. Manuel, D.S. Rolf, Bioelectrochem. Bioenerg. 33 (2) (1994) 191.
[11] V.T. Taniguchi, S.S. Napopan et al., Pure Appl. Chem. 52 (1980) 2275.
[12] N. Sailasuta, F.C. Anson, H.B. Gray, J. Am. Chem. Soc. 101 (1979) 455.
[13] F.A. Armstrong, H.A.O. Hill, N.J. Walton, Acc. Chem. Res. 21 (1988) 407.
[14] F. Laviron, J. Electroanal. Chem. 100 (1979) 263.
[15] F. Laviron, J. Electroanal. Chem. 101 (1979) 19.
[16] D.D. Macdonald, Transient Techniques in Electrochem. Chapter 4 and 6, Plenum Press, New York, 1977.

ELSEVIER

Talanta 44 (1997) 837–842

Talanta

Spectrophotometric determination of palladium after solid–liquid extraction with 1-(2-Pyridylazo)-2-naphthol at 90°C

Jinzhang Gao *, Bo Peng, Haiyan Fan, Jingwan Kang, Xudong Wang

Department of Chemistry, Northwest Normal University, Lanzhou, 730070, People's Republic of China

Received 26 February 1996; received in revised form 17 September 1996; accepted 27 September 1996

Abstract

An effective spectrophotometric determination of palladium with 1-(2-pyridylazo)-2-naphthol (PAN) using molten naphthalene as a diluent has been studied. A green complex of palladium with PAN is formed at 90°C. In the range of pH 1.5–7.5, the complex is quantitatively extracted into molten naphthalene. The organic phase is anhydrously dissolved in $CHCl_3$ to be determined spectrophotometrically at 678 nm against the reagent blank. Beer's law is obeyed over the concentration range of 0.5–10 ppm. The molar absorptivity and Sandell's sensitivity are 1.2×10^4 l mol^{-1} cm^{-1} and 0.0070 mg cm^{-2}, respectively. The optimum conditions for determination are obtained. The interferences of various ions are observed in detail. The method has been applied to the determination of palladium in synthetic samples. © 1997 Published by Elsevier Science B.V.

Keywords: Molten naphthalene; Palladium; Spectrophotometric

1. Introduction

Solvent extraction of precious metals is widely employed in chemistry and industry for many years. Normally, it is difficult for metals such as palladium, platinum, rhodium, etc., to form complex with extractant at the room temperature, while at a high temperature the water-insoluble complex can form easily and rapidly. In 1969, Fujinaga et al. [1] developed a method involving the extraction of the complex at high temperature followed by the solid–liquid separation at room temperature. In recent years, much work was done on the solid–liquid extraction in our lab [2–4]. In this technique, organic substances which are solid at room temperature such as naphthalene, biphenyl and paraffin waxes are used as a diluents. The water-insoluble complex is extracted into the molten diluent at the high temperature to achieve distribution equilibrium. The phase separation is obtained by cooling the extraction system to room temperature. This technique is also applied for the concentration and separation of precious metals. Solid–liquid extraction spectrophotometric determination of palladium [5], platinum [6], rhodium [7], iridium [8], osmium [9] and ruthenium [10] are reported. The organic extractants used are mainly focused on 8-hydroxyquinolines, oximes and dioximes, cuprals and xanthates [5].

* Corresponding author.

PII S0039-9140(96)02122-4

For the solid–liquid extraction spectrophotometric analysis of platinum group metals, there are some shortages. The sensitivities of some system are lows and molar absorptivity are usually around 10^{-3} level [11,12], others have a relatively high sensitivities, but are not suitable to be extracted and detected for a wider acidity [13,14].

As a highly sensitive and selective indicator of polydentate organic reagents, PAN forms intensively coloured and water-insoluble complexes with many metals [15] which can be extracted into an organic solvent. However, there is no application of PAN for solid–liquid extraction of platinum group metals at a high temperature. The liquid–liquid extraction of palladium with PAN into $CHCl_3$ has been reported [16,17], but it has a narrow pH range for the determination and is time consuming.

In this paper, PAN is first used for the solid–liquid extraction of palladium (II) into molten naphthalene. High sensitivity of detection and a wider pH range of extraction are obtained. Time consumption is decreased and procedures are more convenient.

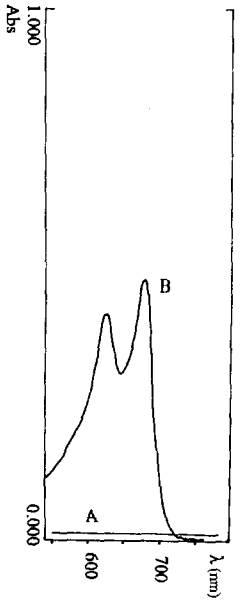

Fig. 1. Absorption spectra of PAN-Pd(II) complex and PAN in naphthalene–chloroform solution. (A) reagent against naphthalene–chloroform, (B) PAN-Pd(II) complex against reagent.

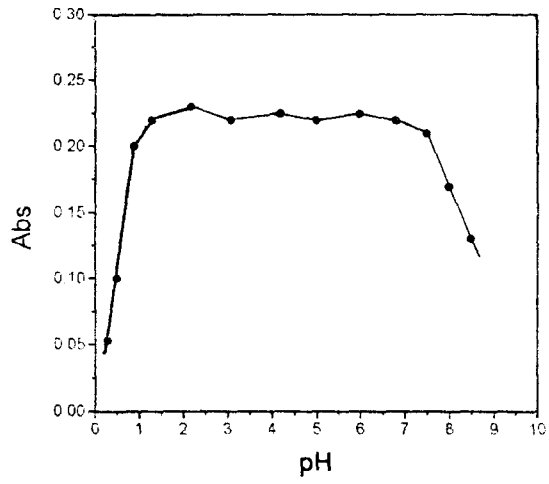

Fig. 2. Effect of pH on the extraction. Pd(II): 20 μg, PAN(1×10^{-3} M): 0.5 ml, V_{aq}: 20 ml, naphthalene:1.0 g (1.3 ml), $I = 0.1$ M $NaClO_4$.

2. Experimental

2.1. Apparatus

A model U-3400 Hitachi spectrophotometer (Japan), a Model pHS-10A digital acidity/ionometer (Xiaoshan, China) and a Model HHS21-4 super thermostatic water bath (Beijing, China) were used in this study.

2.2. Reagents

2.2.1. Standard palladium solution

A standard palladium solution was prepared by dissolving 0.08866 g of palladium chloride (99.99%) in 10 ml of concentrated hydrochloric acid and diluting to 500 ml with water. The content of palladium was also standardized gravimetrically by the method reported elsewhere [18]. The solution contains 106.4 μg ml^{-1} of palladium. Solutions of lower concentration required were prepared by diluting standard solution.

2.2.2. (2-pyridylazo)-2-naphthol solution (PAN)

A 1×10^{-3} M solution in acetone is prepared by dissolving 0.02490 g PAN (Baker Analyzed) in 100 ml pure acetone and stored in an amber bottle.

2.2.3. Buffer solution

0.1 M of solution acetate–acetic acid and 0.1 M of ammonium chloride–ammonia are used for the experiment.

2.2.4. Naphthalene (m.p. 80–82°C)

The purity of naphthalene is checked spectrophotometrically before use in the range 300–800 nm.

Distilled-deionized water was used throughout. All other reagents are of analytical reagent grade.

2.3. General procedure

All solid–liquid extractions were carried out at 90 ± 0.1°C as follows: a certain amount of standard palladium solution was pipetted into a 250 ml Erlenmeyer flask. 5.0 ml of NaAc–HAc buffer solution and 1.0 ml of 1×10^{-3} M PAN-acetone solution were added sequentially. The total volume of the aqueous phase was diluted to 20 ml with water. The mixture in the flask was warmed on a water bath of 90 ± 0.1°C for 3 min after addition of 1.0 g of naphthalene and continued to be warmed until naphthalene melted completely. The flask was shaken vigorously for 30 s, cooled to room temperature until naphthalene coagulated completely. The solid phase was collected dried at 50°C dissolved in 10 ml chloroform. Palladium was determined spectrophotometrically by measurement of the colour complex of 678 nm against a reagent blank.

3. Results and discussion

3.1. Absorption spectra

The absorption spectra of the palladium complex in naphthalene–chloroform are measured against a reagent blank, that of the reagent, treated in a similar manner against a chloroform–naphthalene blank (Fig. 1). The palladium complex has two absorbance peaks at 678 and 625 nm, respectively, where the absorbance of the reagent is negligible. The intensity of the peak at 625 nm is slightly smaller than that at 678 nm. Therefore, the following determinations performed at 678 nm.

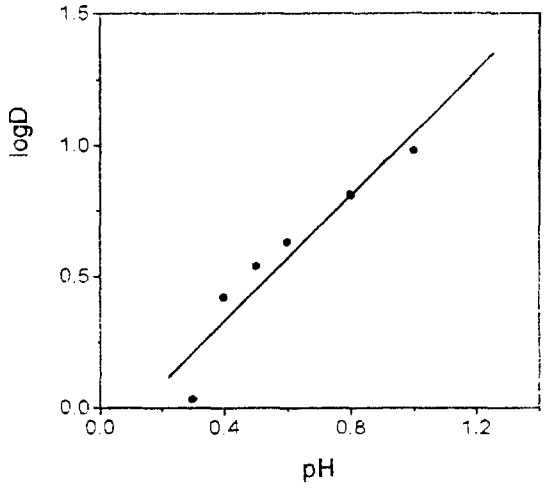

Fig. 3. Relationship between log D and pH value; conditions shown are the same as in Fig. 2.

3.2. Effect of pH value

The effect of pH value in aqueous phase on the absorbance is examined and showed in Fig. 2. In the pH value range from 1.5–7.5, quantitative

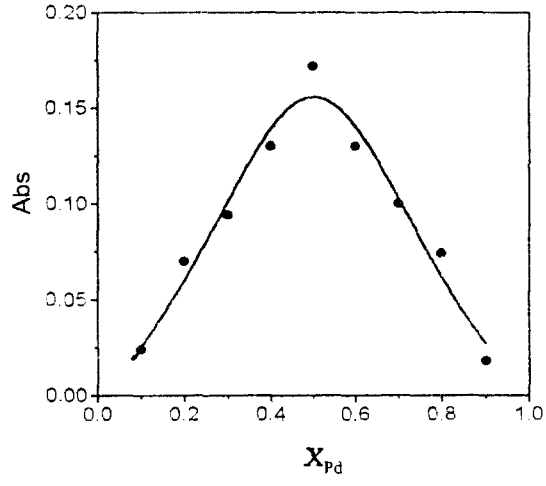

Fig. 4. Plot of composition of the extracted species by Job's continuous variation method. Pd(II): 1×10^{-4} M, PAN: 1×10^{-4} M, pH:4.40, total content of Pd(II) and PAN: 0.4×10^{-6} mol, V_{aq}: 20 ml, naphthalene: 1.0 g (1.3 ml), I = 0.1 M $NaClO_4$.

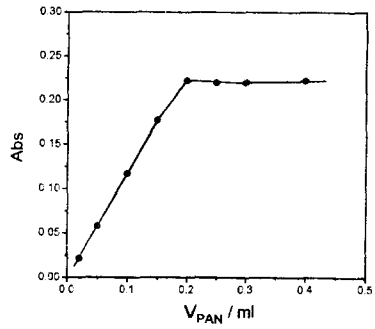

Fig. 5. Plot of composition of the extracted species by Molar ratio method. Pd(II): 20 μg, PAN: 1×10^{-3} M, pH: 4.40, V_{aq}: 20 ml, naphthalene: 1.0 g (1.3 ml), I = 0.1 M $NaClO_4$.

extraction of palladium occurs and the absorbance is found to be constant. Although PAN in the aqueous solution displays different colours at different acidity, no interference is found for the measurement. A NaAc–HAc buffer of pH 4.40 is employed for the following experiments.

3.3. Effect of volume of the aqueous phase and naphthalene

When the volume of the aqueous phase is varied from 10–150 ml, the absorbance remains constant up to 45 ml. Above this volume, it begins to decrease due to excessive ratio of two phases and incompleted extraction of palladium occurs. Thus, in the following experiments a volume of 20 ml was maintained. It was found that the absorbance has a slight increase when the amount of naphthalene was varied from 0.2–2.0 g. Excessive naphthalene was detrimental to the determination of palladium because of its low solubility in chloroform and volatilization. An optimum of 1.0 g of naphthalene is employed for this work.

3.4. Effect of heating, shaking and standing times

The extraction system is heated about 3–4 min at the temperature of the experiment. After naphthalene is completely molten, 30 s of vigorous shaking can achieve extraction equilibrium. The absorbance of the palladium complex in naphthalene–chloroform solution is constant for more than 24 h.

3.5. Mechanism of extraction

As a weak organic acid, the degree of dissociation of PAN increases with the decreasing acidity in the aqueous phase. At the given acidity, the metal ion Pd (II) reacts with PAN (HL) in the presence of anion A^-, giving an uncharged chelate which is distributed between two phase according to the equation:

$$Pd^{2+} + nHL_{(o)} + (2-n)A \rightleftharpoons PdL_nA_{(2-n)(o)} + nH^+ \quad (1)$$

the equilibrium constant of the above reaction is defined as:

$$K_{ex} = [PdL_nA_{(2-n)}]_{(o)}[H^+]^n/[HL]^{n(o)}[Pd^{2+}][A^-]^{(2-n)} \quad (2)$$

Assuming that the species of Pd(II) in the aqueous phase and $PdLnA_{2-n}$ in the organic phase mainly exist respectively, there is:

$$K_{ex} = D[H^+]^n/[HL]^n[A^-]^{(2-n)} \quad (3)$$

where D is the distribution ratio of the palladium between two phase as defined by Eq. (4),

$$D = [PdL_nA_{(2-n)}]/[Pd^{2+}] \quad (4)$$

Expressing Eq. (3) in the equivalent logarithmic form, there is called:

$$\log D = \log K_{ex} + npH + n\log[HL]_{(o)} - (2-n)\log[A^-] \quad (5)$$

Under the conditions of experiments, the relationship between the distribution ratio D and absorbance A is expressed as:

$$D = [A_i/(A_{max} - A_i)](V_{aq}/V_o) \quad (6)$$

Eq. (6) may be simplified into the form:

$$D = A_i/(A_{max} - A_i) \times r \quad (7)$$

where A_{max} denotes the mean maximum absorbance of determination, A_i denotes the absorbance of single determination, r denotes the ratio of to phase.

Log D at different pH values keeping $[HL]_o$ and $[A^-]$ constant are obtained. The plot log D versus

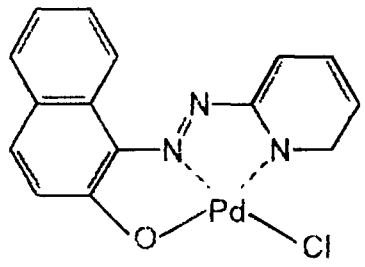

Fig. 6. A suggested structure of palladium complex.

pH (Fig. 3) gives a straight line with a slop of 1, i.e., $n = 1$. One proton is released in the extraction reaction.

The composition of the extraction species is studied by means of Job's method (Fig. 4) and the Molar Ratio method (Fig. 5). The results show that the molar ratio of Pd (II) to PAN in the extracted species is 1:1. The palladium and PAN in the extracted species is demonstrated to be [Pd(PAN)]Cl in the presence of large amount of Cl. Fig. 6 shows a possible structure. Therefore, the extraction reaction can be rewritten as follow:

$$PAN_{(o)} + Pd^{2+} + Cl^{-} \overset{463K}{\rightleftharpoons} Pd(PAN)Cl_{(o)} + H^{+} \quad (8)$$

3.6. Beer's law and sensitivity

Under the optimum conditions described above, Beer's law is obeyed over the concentra-

Table 1
Effect of coexisting ions

Coexisting ions	Addition (mg)	Amount of Pd(II) found (μg)	Recovery without masking agent (%)	Recovery of with masking agent (%)
NO_3^-	50.0	20.0	100	
Cl^-	50.0	20.0	100	
CO_3^{2-}	40.0	20.0	100	
PO_4^{3-}	20.0	19.8	98.9	
SO_4^{2-}	25.0	20.2	101	
$C_2O_4^{2-}$	4.0	20.0	100	
I^-	25.0	22.0	100	
SCN^-	25.0	22.0	110	
$B_4O_7^{2-}$	1.25	18.0	90.0	
$Mo_2O_4^{2-}$	0.5	12.0	60.0	
EDTA-Na^2	6.0	20.2	101	
$C_{10}H_{14}O_8^{2-}$ (tartrates)	25.0	20.0	100	
$C_6H_5O_7^{3-}$ (citrates)	25.0	20.0	100	
Pt(IV)	0.08	20.2	101	
Rh(III)	0.12	20.1	101	
Au(III)	0.05	20.1	100	
Ag(I)	0.05	20.0	100	
Nl(II)	0.02	12.0	60.0	98.9
Co(II)	0.03	22.8	114	98.5
Cu(II)	0.16	17.7	88.7	98.5
Fe(II)	0.01	22.4	112	98.0
Fe(III)	0.01	22.4	112	98.0
Zn(II)	0.01	22.9	123	101
La(III)	0.02	20.2	101	100
Al(III)	0.10	20.6	103	100
Hg(II)	0.05	20.4	102	99.0
Cr(III)	0.05	20.4	102	98.9
Cd(II)	0.04	20.3	102	100

Pd(II): 20 μg.

Table 2
Determination of Pd(II) in synthetic mixtures

Samples	Composition of mixture (μg)	Pd(II) found by present method (μg)	Average (μg)	RSD
1	Pd(II)(20), Pt(IV)(40), Au(III)(20)	20.0, 19.7, 19.8, 20.1, 19.7	19.86	0.182
2	Pd(II)(20), Pt(IV)(40), Rh(III)(50)	19.8, 19.9, 19.7, 20.2, 20.1	19.94	0.207
3	Pd(II)(20), Pt(IV)40, Rh(III)(50), Ir(III)(30), Os(VIII)(20), Ru(III)(20)	19.9, 20.2, 20.0, 20.1, 20.1	20.06	0.114
4	Pd(II)(20), Ir(III)(30), Ru(III)(20)	20.0, 20.1, 20.1, 19.9, 19.9	20.00	0.100

tion range from 0.5–10.0 ppm. The molar absorptivity and Sondell's sensitivity are 1.2×10^4 l mol^{-1} cm^{-1} and 0.0070 μg cm^2, respectively.

3.7. Effect of coexisting ions

Tolerance limits of various cations and anions were investigated on the extraction of palladium. The results are listed in Table 1. It is found that large amount of NO_3^{-1}, Cl^{-1}, CO_3^{2-}, tartrates and citrates do not interfere in the determination. I^{-1}, SCN^{-1} have positive effects on the absorbance. This implies that sensitivity can be improved by choosing I^- or SCN^{-1} as diverse ion in a suitable system. But the reducibility of I^- and chelation of SCN^{-1} also produce disadvantageous at the same time.

Cations were tested by comparing in the presence/absence of masking agents EDTA and citrate sodium. It is found that Pt(IV), Rh(III), Au(III), Ag(I) do not interfere. Ni(II), Fe(II), Fe(III) interfere seriously. However their interferences are masked efficiently by addition of 0.5 ml of 0.1 M EDTA and 1 ml 0.05 M sodium citrate.

3.8. Applications

The propose method was applied to the determination of palladium in synthetic mixtures. A suitable aliquot of synthetic mixture was analyzed by the procedure described above and the results displayed in Table 2.

Acknowledgements

This research was supported by the Gansu Province Natural Science Foundation of China.

References

[1] T. Fujinaga, T. Kuwamoto and E. Nagayama, Talanta, 16 (1969) 1225.
[2] Jinzhang Gao, Guanglin Hu, Jingwan Kang and Guanbi Bai, Talanta, 40 (1993) 195.
[3] Jinzhang Gao, Guanglin Hu, Haiyan Fan and Jingwan Kang, Talanta, 41 (1994) 541.
[4] Jinzhang Gao and G.R. Choppin, Solvent Extraction Ion Exch., 13 (3) (1995) 495.
[5] P. Riyazuddin, Curr. Sci., 51 (8) (1982) 413.
[6] Y. Shigetomi, T. Kojima, E. Iwamoto, and Y. Yamamoto, Anal. Chim. Acta, 152 (1983) 301.
[7] A. Wasey, R.K. Bansal, M. Stake and B.K. Puri, Bull. Chem. Soc. Jpn., 56 (1983) 3036.
[8] A. Wasey, R.K. Bansal and B.K. Puri, Mikrochim. Acta. I, 211 (1984).
[9] B.K. Puri, M. Gautam, A. Kumar, A. Wsaey, M.F. Hussain and C.L. Sethi, Chim. Scripta, 22 (1983) 19.
[10] B.K. Puri, R.K. Bansal, A. Wasey and C.L. Sethi, Russ. Anal. Chem., 37 (1981) 662.
[11] T. Fujinaga, M. Stake and T. Yonekubo, Anal. Chem. (Jpn.) W, 1255 (1971).
[12] L.F. Chang, M. Stake, T. Kumamoto and B.K. Puri, Microchem. J., 33 (1986) 46.
[13] A. Wasey, R.K. Bansal, B.K. Puri and M. Stake, Analyst, 109 (1984) 601.
[14] B.K. Puri, A. Kumar and C.L. Sethi, Chem. Script., 19 (1982) 205.
[15] K.L. Cheng, Organic Analysis Reagents (Chinese version), Geology Press of China, 1985.
[16] H.A. Flaschka, Chelates in Analytical Chemistry, Vol. 4, Marcel Dekker, NY, 1972.
[17] W. Berger and H. Elvers, Z. Anal. Chem., 17 (1959) 256.
[18] A.I. Vogel, A Text Book of Quantitative Inorganic Analysis, 3rd edn., Longmans, London, 1969.

ELSEVIER

Talanta 44 (1997) 843–848

Talanta

Extraction and separation of mercury(II) using triisobutyl phosphine sulfide (TIBPS/Cyanex 471X) as an extractant and its application to industrial effluent

Rashmi Singh, S.N. Tandon *

Department of Chemistry, University of Roorkee, Roorkee-24766, India

Received 1 April 1996; received in revised form 20 September 1996; accepted 27 September 1996

Abstract

Studies have been carried out on the extraction of Hg(II) along with Cr(III), Fe(III), Mn(II), Co(II), Ni(II), Cu(II), Zn(II), Cd(II), Pb(II) and Ag(I), from mineral acid media using TIBPS. The effect of different variables influencing extraction of Hg(II), such as, mineral acid used, nature of diluent, concentration of metal ion and extractant has been investigated. Based on the partition data some binary separations from Hg(II) have been achieved. The potential of the extractant for decontaminating Hg from paper industry effluent has been assessed. © 1997 Elsevier Science B.V.

Keywords: Extraction; Paper industry effluent; Mercury; Triisobutyl phosphine sulfide

1. Introduction

Mercury is one of the most toxic elements and has a tendency to concentrate in the human system because of its affinity to the sulphydryl group. Thus the removal of Hg from waste streams assumes a paramount importance. Also Hg readily forms amalgams with a number of metals and therefore its separation from them has been a subject of great analytical interest. Over the years a number of sulfur containing ligands have been proposed as extractants for Hg(II). Most of these reagents lack selectivity and for separations a strict control of aqueous phase conditions, namely pH [1–6] and/or the presence of masking reagents are required [7–11]. In the recent past, triisobutyl phosphine sulfide (TIBPS) has been marketed under the trade name Cyanex 471X. Because of a lower pKa value it will be able to extract metal ions at a higher acidity than trioctyl phosphine oxide (TOPO). Moreover, the branching in the chain may introduce selectivity in extraction. It is a soft Lewis base and will readily complex with soft acids e.g., Ag(I), Au(III), Hg(II) and Pd(II). Salvado et al. [12] have employed TIBPS for the extraction of gold from chloride solutions. A number of workers have recovered silver by using this reagent [13–15]. Mathur et al. [16] have reported the probable Pd(II)–TIBPS extracting species. Employing this extractant, Baba et al. [17] reported the extraction of Hg(II) from hydrochloric acid solutions.

* Corresponding author. Fax: +91 1332 73560.

PII S0039-9140(96)02124-8

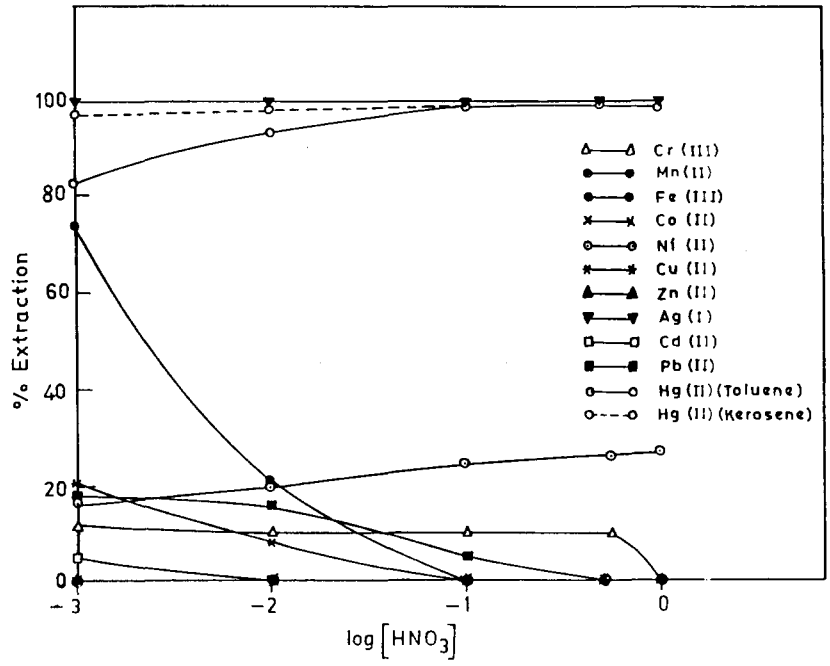

Fig. 1. Extraction behaviour of some metal ions (1.0×10^{-4} M) in toluene solution of 0.10 M TIBPS.

In view of the reported extractability by TIBPS of Hg(II), a detailed study has been planned. The present paper reports the extraction behaviour of Hg(II) in TIBPS from mineral acid media. The effect of various parameters, namely type of mineral acid used, nature of diluent, concentration of metal ion and extractant has been investigated. The probable extracting species has been identified by log–log plot of distribution ratio versus extractant concentration and mole ratio method. The behaviour of other metal ions namely Cr(III), Fe(III), Mn(II), Co(II), Ni(II), Cu(II), Zn(II), Cd(II), Pb(II) and Ag(I) has been studied to achieve separations. Based on the distribution data the separation of Hg(II) from other metal ions is reported. Hg(II) is recovered quantitatively from the organic phase by various stripping agents. The method has been used successfully to quantitatively remove Hg(II) from paper industry waste effluent.

2. Experimental

2.1. Instruments and reagents

The nitrates/chlorides of Cr(III), Fe(III), Mn(II), Co(II), Ni(II), Cu(II), Zn(II), Cd(II), Pb(II), Hg(II) and Ag(I) were used to prepare the stock solutions which were standardised by the usual complexometric titrations. TIBPS was procured from American Cyanamid, USA and used after purification [18]. The purity was checked by GC. The distribution studies were carried out by solutions labelled with ^{51}Cr, ^{54}Mn, ^{58}Co, ^{59}Fe, ^{65}Zn, ^{110m}Ag and ^{203}Hg radioisotopes. A well type NaI(Tl) scintillation counter was used for the measurement of gamma activity of ^{51}Cr, ^{54}Mn, ^{58}Co, ^{59}Fe, ^{65}Zn, ^{110m}Ag and ^{203}Hg. ICP-AES (8040 PLASMA LABTAM, Australia) and AAS (Perkin Elmer 3100) were used for obtaining the distribution data of Ni(II), Cu(II), Cd(II) and

Table 1
Extraction of Hg(II) (1.0×10^{-4} M) in TIBPS (0.10 M) from 0.010 M HNO_3 with different solvents as diluents

Serial No.	Solvent	Dielectric constant	Percentage extraction (%E) of Hg(II)
1.	*n*-Hexane	1.89	2.0
2.	Kerosene (160–200°C)	2.02	98.1
3.	Xylene	2.20	32.8
4.	Toluene	2.44	93.1
5.	Chloroform	4.81	99.1
6.	Cyclohexanone	18.3	99.2

Pb(II), checking the yield in the separations and analysis of the industrial waste.

Equal volumes of aqueous phase (metal ion in mineral acid) and organic phase (Cyanex 471X in an appropriate diluent) were shaken at room temperature (25 ± 3°C) for 5 min to ensure complete equilibration. The two phases were separated and suitable aliquots of each phase were removed to determine the concentration of the metal ion by the assay of radioactivity or using ICP-AES/AAS.

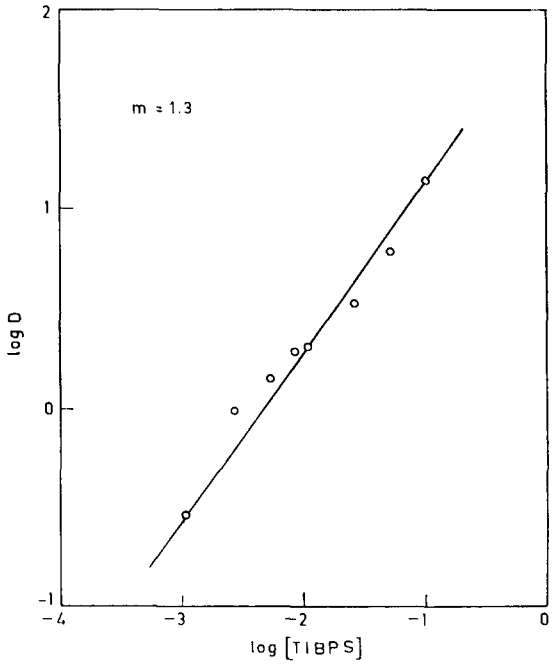

Fig. 2. Effect of concentration of TIBPS on the distribution of Hg(II) in 0.010 M HNO_3.

3. Results and discussion

3.1. Extraction behaviour

The extraction behaviour of different metal ions in toluene solution of TIBPS from nitric acid solution is shown in Fig. 1. Ag(I) and Hg(II) are more or less quantitatively extracted over the entire investigated range of acid molarity. Mn(II), Co(II), Zn(II) and Cd(II) show negligible extraction (< 5%) while Cr(III), Ni(II), Cu(II) and Pb(II) show poor extraction with a maximum of ~ 20%. In the case of Fe(III), the percentage extraction increases with decreasing acid molarity reaching a value of ~ 70% at 1.0×10^{-3} M HNO_3. Thus Hg can be quantitatively separated from almost all the metal ions except Ag(I) with a high decontamination factor. It was observed that the extraction behaviour of Hg(II) remains practically the same (within ± 3%) on changing the aqueous phase from nitric acid to hydrochloric or sulfuric acid. All further studies regarding the effect of different variables were carried out with nitric acid as the aqueous phase. The results of the change in the nature of diluent are shown in Table 1. The extraction increased with the increase in the dielectric constant of the diluent; kerosene being an exception. The extraction of Hg(II) is > 90% with toluene, kerosene (160–200°C), chloroform and cyclohexanone whereas it shows poor or negligible extraction when xylene and *n*-hexane are used as diluents. Further studies were carried out using nitric acid as aqueous phase and toluene as diluent.

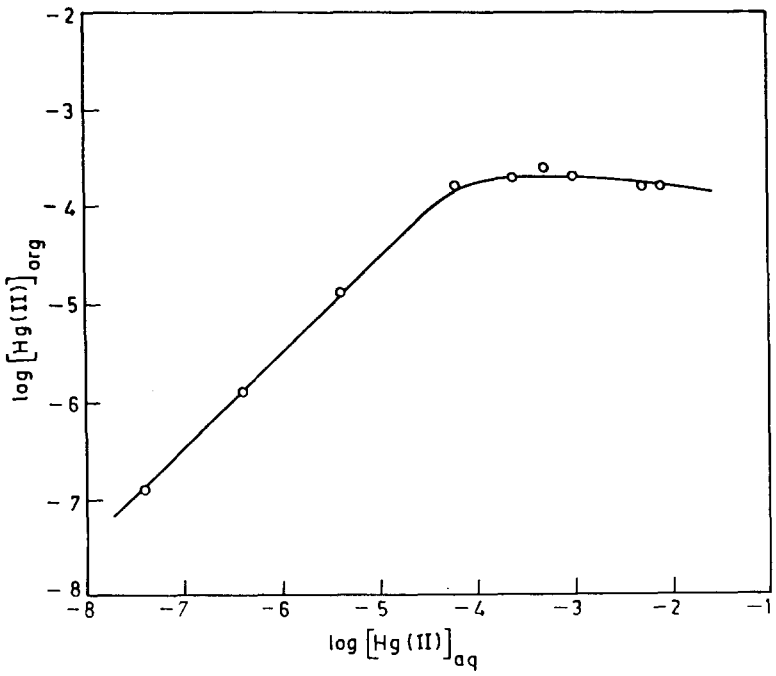

Fig. 3. Extraction isotherm of Hg(II) (1.0×10^{-7} to 5.0×10^{-3} M) from 0.10 M HNO_3 by TIBPS in toluene (1.0×10^{-3} M).

3.2. Effect of the concentration of metal ion

The effect of the concentration of the metal ion as studied in the range 1.0×10^{-7} to 5.0×10^{-3} M shows that the distribution is more or less independent of the concentration. This suggests that the extracting species is not changing in this metal ion concentration range. For subsequent studies on identification of extracting species the metal ion concentration was confined to this range. In most of other experiments 1.0×10^{-4} M was chosen as the working concentration.

Table 2
Stripping efficiency for Hg(II) (1.0×10^{-4} M) with different reagents (1.0×10^{-2} M)

Serial No.	Reagent	%Recovery of Hg(II)
1.	Ammonium thiocyanate	0.0
2.	Disodium salt of ethylenediammine tetraacetic acid	0.0
3.	5% NH_4Cl in 1:10 NH_3	99.1
4.	DL-pencillamine	99.5
5.	Potassium thiocyanate	0.0
6.	Sodium sulfite	0.0
7.	Sodium thiosulfate	99.9
8.	Sodium citrate	0.0
9.	Thiourea	99.5
10.	Thiosemicarbazide	0.0

3.3. Nature of the extracted species

The effect of concentration of the TIBPS (1.0×10^{-3} to 0.10 M) as studied for Hg(II) from 0.010 M HNO_3 is shown in Fig. 2. There is an increase in extraction with the increase in the concentration of the extractant. The variations of distribution ratio with the concentration of the extractant can be utilized for the identification of the extracting species. A straight line with a slope of around one suggests the involvement of one molecule of the extractant in the formation of the Hg(II) complex. The results of loading the extractant (TIBPS) with varying concentration of Hg(II) are shown in Fig. 3. The concentration of Hg in the organic phase first increases linearly with the increase in the aqueous phase but as the extrac-

Table 3
Separation of Hg(II) (1.0×10^{-4} M) from Cr(III), Fe(III), Mn(II), Co(II), Ni(II), Cu(II), Zn(II), Cd(II) and Pb(II) by 0.10 M TIBPS in 0.10 M HNO_3

Serial No.	Metal ions	Ratio	%Recovery of Hg(II)[a,b]	Cr(III)/Mn(II)/Fe(III) Co(II)/Ni(II)/Cu(II)/ Zn(II)/Cd(II) and Pb(II) in aqueous phase (%)[a]	Separation factor (β)
1.	Hg(II)–Cr(III)	1:1	95.1	91.5	3.3×10^3
		1:10	96.0	90.0	1.5×10^3
		10:1	96.1	92.1	2.3×10^3
2.	Hg(II)–Mn(II)	1:1	99.3	96.4	3.3×10^3
		1:10	99.0	92.2	1.3×10^3
		10:1	97.4	96.8	2.7×10^3
3.	Hg(II)–Fe(III)	1:1	99.3	100.0	$> 10^4$
		1:10	98.6	99.0	$> 10^4$
		10:1	98.0	100.0	$> 10^4$
4.	Hg(II)–Co(II)	1:1	99.4	95.5	$> 10^4$
		1:10	99.4	91.0	$> 10^4$
		10:1	98.0	94.8	4.5×10^3
5.	Hg(II)–Ni(II)	1:1	98.0	91.0	2.5×10^3
		1:10	98.8	84.0	7.5×10^2
		10:1	98.5	91.0	1.3×10^3
6.	Hg(II)–Cu(II)	1:1	99.1	98.0	5.5×10^3
		1:10	99.3	93.0	4.4×10^3
		10:1	100.0	100.0	$> 10^4$
7.	Hg(II)–Zn(II)	1:1	99.0	100.0	$> 10^4$
		1:10	98.0	91.0	2.5×10^3
		10:1	100.0	100.0	$> 10^4$
8.	Hg(II)–Cd(II)	1:1	99.5	100.0	$> 10^4$
		1:10	98.7	85.0	6.9×10^2
		10:1	97.9	95.0	9.4×10^3
9.	Hg(II)–Pb(II)	1:1	95.0	87.0	9.5×10^2
		1:10	95.7	83.4	4.3×10^2
		10:1	95.4	91.2	1.2×10^3

[a] Average of three determinations.
[b] Hg(II) was recovered from the organic phase by washing with 5% NH_4Cl in 1:10 NH_3.

tant gets saturated, the Hg content in the organic layer tends to assume a constant value. This result clearly indicates a 1:1 stoichiometric ratio of metal ion to extractant which is in conformity with the slope analysis data. The extracting species can be proposed as $Hg(NO_3)_2$ (TIBPS). This is similar to the one reported by Mathur et al. for palladium, i.e. $Pd(NO_3)_2$ (TIBPS) [16].

3.4. Stripping agent

Various stripping agents of different concentrations were examined for the back-extraction of the metal ion from the organic phase (Table 2). Hg(II) is stripped almost quantitatively by DL-pencillamine, thiourea, sodium thiosulfate and 5% NH_4Cl in 1:10 NH_3.

3.5. Separations

Partition data indicate that separation of Hg(II) from metal ions such as Cr(III), Fe(III), Mn(II), Co(II), Ni(II), Cu(II), Zn(II), Cd(II) and Pb(II) can be easily achieved by carrying out extraction with 0.10 M TIBPS at 0.10 M HNO_3. Under these conditions Hg(II) is quantitatively extracted in the organic phase, leaving other metal ions in the aqueous phase. The results of separation of Hg(II) from other metal ions are shown in Table 3. Due to the similar extraction behaviour and response to stripping reagents it was not possible to separate Hg(II) from Ag(I).

3.6. Determination of Hg(II) in industrial effluent

The proposed method was applied for the removal and recovery of Hg(II) from paper industry wastewater (0.75 ppm Hg). 50.0 ml Sample was boiled with 5.0 ml HNO_3 and evaporated on a hot plate to reduce the volume and then finally made up to 50.0 ml [19]. 10.0 ml Of the prepared sample were extracted with 10.0 ml of 0.10 M TIBPS in toluene. Hg was quantitatively removed from the aqueous phase and subsequently recovered from the organic phase by washing it with 5% NH_4Cl in 1:10 NH_3 and determined by ICP-AES.

The investigations reveal that the reagent offers a convenient method for the separation of Hg(II) from a number of metal ions. Since the extraction of Hg is more or less quantitative over the entire acidity range of different mineral acids it does not require a rigid control of aqueous phase conditions for separation. Moreover, Hg(II) can be recovered quantitatively by a variety of reagents depending upon the need for its further processing. Kerosene (160–200°C) can replace toluene as diluent without any change in the extraction behaviour of Hg (Fig. 1) thereby offering a possibility to reduce the cost of the separation process.

Acknowledgements

The authors are grateful to American Cyanamid, USA for providing the samples of the extractant. The financial assistance from Council of Scientific and Industrial Research (CSIR) and Society for Participatory Research in Asia (PRIA), New Delhi, India is gratefully acknowledged.

References

[1] H. Bode, Z. Anal. Chem., 144 (1955) 165.
[2] O.V. Singh and S.N. Tandon, Radiochem. Radioanal. Lett., 19(5–6) (1974) 371–376.
[3] O.V. Singh and S.N. Tandon, Sep. Sci., 10(4) (1975) 359–370.
[4] O.V. Singh and S.N. Tandon, Anal. Lett., 9(10) (1976) 921–927.
[5] Devendra Singh, O.V. Singh and S.N. Tandon, Sep. Sci. Technol., 13(7) (1978) 625–632.
[6] R. Sahu, S.M. Sondhi and B. Gupta, J. Radioanal. Nucl. Chem. Lett., 200(6) (1995) 509–520.
[7] H. Friedeberg, Anal. Chem., 27 (1955) 305.
[8] S.N. Tandon, P.K. Srivastava and S.R. Joshi, J. Radioanal. Chem., 8 (1971) 123–126.
[9] S.R. Joshi, C.B. Gupta and S.N. Tandon, Acta Chim., 77(2) (1973) 147–153.
[10] C.B. Gupta and S.N. Tandon, J. Radioanal. Chem., 11 (1972) 56–66.
[11] S.R. Joshi, P.K. Srivastava and S.N. Tandon, J. Radioanal. Chem., 13 (1973) 343–347.
[12] V. Salvado, M. Hidalgo, A. Masana, M. Munoz, M. Valiente and M. Muhammed, Process Metall., 7B (Solvent Extr. 1990, Part B), (1992) 1511.
[13] Y. Abe and D.S. Flett, Process Metall., 7B (Solvent Extr. 1990, Part B) (1992) 1127.
[14] W.A. Rickelton and A.J. Robertson, Miner. Metall. Process., 4(1) (1987) 7–10.
[15] M. Munoz, X. Ribas and M. Valiente, Quim. Anal., 10(1) (1991) 110.
[16] J.N. Mathur, G.H. Rizvi, M.S. Murali, R.H. Iyer, D.S. Deshingkar and T.K. Theyyunni, 10th ISAS Nat. Symp. on Strategic and Hi-Tech Metals Extraction and Process Characterisation, Udaipur (India), 21–23 March, 1994, 240 pp.
[17] Y. Baba, Y. Umezaki and K. Inoue, Solvent Extr. Ion Exch., 4(1) (1986) 15–26.
[18] Publication from American Cyanamid Company, No.: SPT-041 entitled CYANEX471X Extractant.
[19] APHA AWWA WPCF, Standard Methods for the Examination of Water and Wastewater, APHA publication, Washington, DC, 1985, 148 pp.

ELSEVIER

Talanta 44 (1997) 849–853

Talanta

Consecutive thin-layer chromatographic separation of Zr(IV), Hf(IV) and many other ions on silica gel in nitric acid–hydrogen peroxide media

Yoichi Takeda, Koji Ishida *

Laboratory of Chemistry, Nippon Medical School, Kosugi, Nakahara-ku, Kawasaki, Kanagawa 211, Japan

Received 5 April 1996; received in revised form 4 October 1996; accepted 8 October 1996

Abstract

The thin-layer chromatographic (TLC) behaviour of 64 ions including Zr(IV) and Hf(IV) has been surveyed on systems composed of silica gel and of nitric acid and nitric acid–hydrogen peroxide media. In the 0.5 mol l^{-1} HNO_3–3% (w/v) H_2O_2 solution, only Hf(IV) adsorbed very strongly, whereas Zr(IV) and many other ions showed no or weak adsorption. Stepwise development with diluted nitric acid and subsequently with nitric acid–hydrogen peroxide solution allowed the consecutive separation of three-component mixtures consisting of Zr(IV), Hf(IV) and one of many other accompanying elements, such as Mo(VI), Nb(V), Th(IV), Ti(IV), U(VI) and rare earths(III), to be conducted simply and effectively. © 1997 Elsevier Science B.V.

Keywords: Hydrogen peroxide; Nitric acid; TLC separation; Silica gel

1. Introduction

Considerable data regarding the thin-layer chromatographic (TLC) separation of Zr(IV) and/or Hf(IV) from other metals have been compiled [1–3], though most of these data have been obtained only within systematic investigations of the chromatographic behaviour of inorganic ions on a number of systems composed of various combinations of stationary and mobile phases. Little has, however, been reported about the simultaneous separation of Zr(IV) and Hf(IV), because of the remarkable similarity in the chemistry of both elements, based on their similar outer electronic configurations and ionic radii.

Several TLC methods [4–7] for separating Zr(IV) and Hf(IV) have been proposed, but they are often time-consuming, and/or applicable only to mixtures containing limited amounts of both metals and a few or no other ions. The best resolution for the separation of both metals has been obtained by Olsina et al. [6] in the system composed of silica gel and of an HCl–H_3PO_4–H_2O (10:1:9, v/v/v) mixture, in which Zr(IV) remains near the starting point and Hf(IV) migrates up to the solvent front. However, this TLC method of separation requires some experience and special care in preparing the sample solutions.

* Corresponding author. Fax: +81 44 7221231.

PII S0039-9140(96)02125-X

Furthermore, the separation of Zr(IV) and/or Hf(IV) from other metals has not been demonstrated, whereas the R_f data of 41 ions are given on silica gel and cellulose in the same solvent. Recently, we [7] have also revealed that the systems composed of silica gel and of mineral acid–hydrogen peroxide media provide separation factors large enough to resolve Zr(IV) and Hf(IV) from each other, present in large amounts and ratios, though the adsorption sequence is reversed from that in the system developed by Olsina et al. [6]. However, the TLC behaviour of other metals has not been investigated. Thus, effective methods for the separation of Zr(IV) and Hf(IV) from each other and from other ions are still lacking.

In this paper, the TLC behaviour of a number of inorganic ions including Zr(IV) and Hf(IV) is surveyed in systems composed of silica gel and of nitric acid–hydrogen peroxide media, and simple and useful procedures for the specific separation of three-component mixtures of Zr(IV), Hf(IV) and another inorganic ion by means of one-dimensional, stepwise development with nitric acid and subsequently with a nitric acid–hydrogen peroxide solution are presented.

2. Experimental

2.1. Materials

2.1.1. Stock solutions

Stock solutions of Zr(IV) and Hf(IV) were prepared from their oxychlorides (99.99% purity) similarly to that described earlier [7], so as to give a concentration of 0.05 mol metal l^{-1} of 6 mol l^{-1} HNO_3. For most other metals, appropriate amounts of their nitrates were dissolved in 0.1 mol l^{-1} HNO_3 to give a concentration of 0.01 to 0.1 mol metal l^{-1}. For Au(III), Bi(III), Ir(IV), Os(IV), Pd(II), Pt(IV), Rh(III), Ru(III), Sb(III), Sn(II) and Tl(III), their chlorides were dissolved in 3 mol l^{-1} HCl to give a 0.01 to 0.1 metal l^{-1} solution. For As(III), As(V), Mo(VI), Re(VII), Se(IV), Se(VI), Te(IV) and W(VI), their oxysalts were dissolved in distilled water to give a 0.005 to 0.01 mol l^{-1} solution. For V(IV), the oxychloride was dissolved in 1 mol l^{-1} HCl to give a 0.1 mol l^{-1} solution. For Ge(IV), the oxide was dissolved in a 1 mol l^{-1} NaOH solution, and the resulting solution was acidified with 1 mol l^{-1} HCl and then diluted with distilled water to a 0.005 mol l^{-1} solution. For Nb(V) and Ta(V), their chlorides were dissolved in hydrofluoric acid and a small amounts of H_2SO_4, and the resulting solutions were evaporated until sulfur trioxide fumes were evolved. The residues were taken up with a 1 to 2 mol l^{-1} tartaric acid solution to give a 0.005 mol l^{-1} metal solution. For Ti(IV), the sulfate was dissolved in 0.5 mol l^{-1} H_2SO_4 to give a 0.02 mol l^{-1} solution.

Test solutions for the measurement of R_f values were prepared, if necessary, by diluting the respective stock solutions with 6 mol l^{-1} HNO_3 or with the solvent used for the preparation of each stock solution. Sample solutions used for the separation were prepared by mixing appropriate amounts of the respective stock solutions of Zr(IV), Hf(IV) and another ion, or by diluting the resulting mixtures with 6 mol l^{-1} HNO_3. The concentrations of Zr(IV) and Hf(IV) in the test and the sample solutions were adjusted to 0.005 mol l^{-1} with respect to each metal. When the sample solution contained Sn(II), oxychloride solutions of Zr(IV) and Hf(IV), dissolved in 6 mol l^{-1} HCl, were used to prevent the production of metastannic acid.

2.1.2. Preparation of thin-layer plates

A 20-g portion of silica gel without binder (Wakogel B-0; Wako, Osaka, Japan) was thoroughly blended with 41.5 ml of distilled and deionized water. The slurry was spread to a thickness of 0.375 mm on glass plates (20×20 cm^2) with an applicator. The plates were allowed to stand for 30 min at room temperature and then dried in an oven at approximately 70°C for 30 min.

In order to remove inorganic impurities from the silica gel, the plate was thoroughly washed by developing up to the upper edge of the plate by means of the ascending technique with 30 ml of a 1 mol l^{-1} HNO_3–3% (w/v) H_2O_2 solution, using a sandwich type chamber made of plastic. Subsequently, the plate was dried on a hot-plate at approximately 90°C for 20 min. After cooling, the

Table 1
Chromogenic reagents for detection of ions

Reagent (solvent)	Ion detected
0.05% aqueous arsenazo III and 1 mol l^{-1} CH_3COOH	Zr(IV), Hf(IV), Al(III), Ba(II), Bi(III), Ce(III), Dy(III), Er(III), Eu(III), Ga(III), Gd(III), Ho(III), In(III), Ir(IV), La(III), Lu(III), Nd(III), Pb(II), Pd(II), Pr(III), Sc(III), Sm(III), Tb(III), Th(IV), Tl(I), Tl(III), Tm(III), U(VI), Y(III), Yb(III)
and 1 mol/l NH_3	Ag(I), Ca(II), Cd(II), Co(II), Cr(III), Cu(II), Fe(III), Mg(II), Nb(V), Sr(II), Zn(II)
0.1% aqueous thioacetamide	As(III), As(V), Hg(II), Pt(IV), Re(VII), Rh(III), Ru(III), Se(IV), Se(VI)
0.1% aqueous pyrocatechol violet	Ge(IV), Mo(VI), Sn(II), W(VI)
0.05% bromopyrogallol red (in 50% v/v ethanol)	Au(III), Mn(II), Ni(II)
3% (w/v) H_2O_2	Ti(IV), V(IV)
0.05% 4-(2-pyridylazo)resorcinol (in 0.1 mol l^{-1} NaOH)	Ta(V), Os(IV)
3 mol l^{-1} $(NH_4)_2S$	Sb(III)
0.1% aqueous xyrenol orange	Be(II)
1% aqueous bismuthiol II	Te(IV)

plate was stored in a desiccator containing a saturated sodium chloride solution, until ready for use.

2.2. Procedure

A 0.5 μl portion of the test solution was applied to each plate by means of a microcap (Drummond, Broomall, PA) at a point 2.5 cm from one edge, and the spots were dried in air for 10 min. The plate was placed in a chromatographic chamber ($20 \times 10 \times 22$ cm^3) equipped with a small tank ($21 \times 5 \times 4$ cm^3) containing 30 ml of a developing solvent, and developed up to 10 cm from the starting point by the ascending technique at room temperature. It took about 20 min to develop with the solvent. The solvents used were 0.5 mol l^{-1} HNO_3 and a 0.5 mol l^{-1} HNO_3–3% (w/v) H_2O_2 solution. In the case of the sample solution containing Sn(II), a 0.5 mol l^{-1} HCl–3% (w/v) H_2O_2 solution was also used as a solvent.

For the separation of the sample solutions of the three-component mixtures, a new developing technique was applied. The plate, on which a 0.5 μl portion of the sample solution was spotted, was immersed first in 0.5 mol l^{-1} HNO_3 in a similar manner to that described above, and developed up to a distance of 3 cm from the starting point (development time approximately 4 min). Immediately, the plate was transferred to a different chromatographic chamber with a tank containing 30 ml of a 0.5 mol l^{-1} HNO_3–3% (w/v) H_2O_2 solution, and developed up to a distance of 10 cm from the first starting point by the ascending technique (development time approximately 16 min). When the sample solution contained Ti(IV), nitric acid of 2 mol l^{-1} was used as the first developing solvent to prevent the hydrolysis of the metal during chromatography.

2.3. Detection

After the second development, the plate was dried on a hot-plate at approximately 90°C, and the locations of the respective ions were visualized by spraying with various solutions of chromogenic reagents, as indicated in Table 1.

3. Results and discussion

3.1. Adsorption behaviour

HNO_3 system: The R_f values of all of the ions tested on silica gel in 0.5 mol l^{-1} HNO_3 are summarized in Table 2. Most of the ions did not show any adsorption, because of specific adsorption of protons on silica gel in the acidic solution [8]. Contrarily, Zr(IV) and Hf(IV) adsorbed very strongly, as noted previously [7]. Oxyanions, such

Table 2
$R_f \times 100$ values of 64 ions on silica gel in HNO_3–H_2O_2 media

Ion	Solvent (developing distance)		
	0.5 mol l^{-1} HNO_3 (10 cm)	0.5 mol l^{-1} HNO_3–3% (w/v) H_2O_2 (10 cm)	0.5 mol l^{-1} HNO_3 (3 cm) and 0.5 mol l^{-1} HNO_3–3% (w/v) H_2O_2 (7 cm)
Zr(IV)	1–4	94–100 (93–100)[c]	29–52 (26–50)[d]
Hf(IV)	1–4	1–10 (0–7)[c]	1–8 (0–13)[d]
56 ions[a]	93–100[b]	92–100[b]	89–100[b]
As(III)	37–52	68–78	56–67
Ge(IV)	20–45	23–39	20–40
Mo(VI)	50–83	98–100	54–84
Sn(II)	2–57	0–95 (11–45)[c]	1–90
Ti(IV)	0–78	90–100	38–67 (83–100)[d]
W(VI)	7–38	97–100	54–86

[a] All the ions listed in Table 1, except for Zr(IV), Hf(IV), As(III), Ge(IV), Mo(VI), Sn(IV), Ti(IV) and W(VI).
[b] Average of $R_f \times 100$ values of 56 ions.
[c] Developed with 0.5 mol l^{-1} HCl–3% (w/v) H_2O_2 (10 cm run).
[d] Developed with 2 mol l^{-1} HNO_3 (3 cm run) and then with 0.5 mol l^{-1} HNO_3–3% (w/v) H_2O_2 (7 cm run).

as As(III), Ge(IV) and Mo(VI), adsorbed to a moderate extent, probably owing to the anion exchange of silica gel in the strong acidic solution [8]. Sn(II) and W(VI) showed long tailing, due to the formation of insoluble species, metastannic acid and tungustic acid, respectively. Furthermore, Ti(IV) also showed long tailing, because of the hydrolysis of the metal during chromatography. It is clear that the nitric acid system is suitable for the separation of both Zr(IV) and Hf(IV) from many other ions except Sn(II) and Ti(IV).

HNO_3-H_2O_2 system: The R_f values of the ions tested are also given in Table 2. Zr(IV), Mo(VI), Ti(IV) and W(VI), which easily produce peroxso complexes, migrated up to the solvent front, and furthermore almost all of the others (56 ions) showed no adsorption, so that Hf(IV) could be separated from all the ions, except for Sn(II) which exhibited long tailing. This system is not favorable for the separation of Zr(IV) from many other ions, but is suitable for the separation of three-component mixtures consisting of Zr(IV), Hf(IV), and As(III) or Ge(IV). In addition, As(III) gave somewhat higher R_f values in this system than in the nitric acid system, because of the oxidation of As(III) to As(V) during chromatography.

Stepwise development: Inspection of the adsorption behaviour of a large number of ions tested in the nitric acid and the nitric acid–hydrogen peroxide media suggests that many effective procedures for the consecutive separation of Hf(IV), Zr(IV) and another inorganic ion in the described order can be established by a combination of these two solvents. In order to separate three-component mixtures of Zr(IV), Hf(IV) and another ion from each other, the stepwise development first with 0.5 mol l^{-1} HNO_3 (3 cm run) and then with a 0.5 mol l^{-1} HNO_3–3% H_2O_2 solution (7 cm run) was attempted as a new technique. The results are summarized in Table 2. The R_f data indicate that this technique enables the complete separation of three-component mixtures containing Zr(IV), Hf(IV), and one ion among 56 ions other than Ge(IV), Sn(II), and Ti(IV). It should be noted that in applying this developing technique, the plate should not be dried on a hot-plate just after the first development, because Zr(IV), if dried, gives irregular and long tailing.

3.2. Separation

Typical chromatograms of three-component mixtures, obtained by the stepwise development,

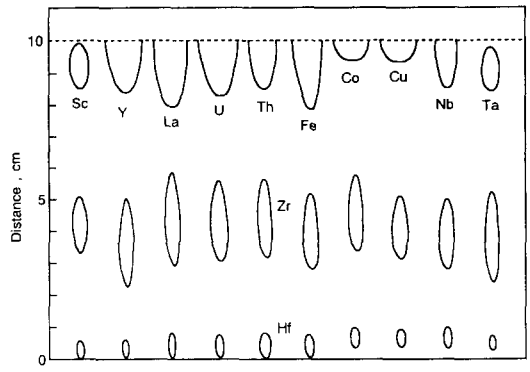

Fig. 1. Separation of Zr(IV), Hf(IV) and other metals (Zr(IV): the middle spot; Hf(IV): the lowest spot). Solvent: 0.5 mol l^{-1} HNO_3 for the first development (3 cm run); 0.5 mol l^{-1} HNO_3–3% (w/v) H_2O_2 for the second development (7 cm run), Loading amount: 2.5×10^{-9} mol for Zr(IV), Hf(IV), Nb(V) and Ta(V); 5.0×10^{-7} mol for Sc(III), Y(III), La(III), U(VI), Th(IV), Fe(III), Co(II) and Cu(II), - - -: solvent front.

are given in Fig. 1. As expected from the R_f data, Zr(IV) and/or Hf(IV) were easily and simultaneously separated from 56 ions except Ge(IV), Sn(II), and Ti(IV). For the separation of Zr(IV), Hf(IV), and Ge(IV) or Sn(II), the stepwise development technique was not applied. The three-component mixture containing Ge(IV) or Sn(II) was simply separated by developing upwards to 10 cm with the 0.5 mol l^{-1} HNO_3–3% (w/v) H_2O_2 solution, or with the 0.5 mol l^{-1} HCl–3% (w/v) H_2O_2 solution, respectively. The R_f values of each metal are given as numerical values in parentheses in Table 2. Furthermore, the complete separation of the three-component mixture containing Ti(IV) was achieved by the stepwise development first with 2 mol l^{-1} HNO_3 (3 cm run) and subsequently with the 0.5 mol l^{-1} HNO_3–3% (w/v) H_2O_2 solution (7 cm run). The first developing solvent was effective in preventing the formation of long tailing. The R_f values of each metal, obtained with this development, are also given in Table 2.

Hence, the present TLC systems composed of silica gel and of nitric acid and/or hydrogen peroxide enabled the specific separation of Zr(IV) and/or Hf(IV) from many other accompanying elements, such as Mo(VI), Nb(V), Th(IV), Ti(IV), U(VI) and rare earths(III), present in natural ores, reactor materials, and fission products. In addition, it can be expected that the present systems will offer a number of useful procedures effective for the separation of three-component mixtures, and furthermore will be applicable not only to TLC separation, but also to the column separation of three-component mixtures coexisting in a wide range of amounts and ratios.

References

[1] J. Korkisch, Modern Methods for the Separation of Rarer Metal Ions, Pergamon Press, Oxford, 1969, p. 415.
[2] J. Michal, Inorganic Chromatographic Analysis, translated by J.F. Tyson, Van Nostrand Reinhold, London, 1973, p. 75.
[3] A. Mohammad and K.G. Varshney, Handbook of Thin-Layer Chromatography, in: J. Sherma and B. Fried (Eds.), Marcel Dekker, New York, 1991, p. 463.
[4] K. Ishida and M. Miyazaki, Bunseki Kagaku, 21 (1972) 1518.
[5] T. Shimizu and A. Muto, J. Chromatogr., 88 (1974) 351.
[6] R. Olsina, R. Dapas and C. Marone, J. Chromatogr., 75 (1973) 93.
[7] K. Ishida, S. Ninomiya, Y. Uchida and M. Osawa, J. Chromatogr., 539 (1991) 169.
[8] S. Ahrland, I. Grenthe and B. Noren, Acta Chem. Scand., 14 (1960) 1059.

ELSEVIER

Talanta 44 (1997) 855–858

Talanta

Fluorescent reaction between ascorbic acid and DAN and its analytical application

Jinghe Yang [a,*], Changlun Tong [b], Nianqin Jie [a], Guiling Zhang [a], Xuezhen Ren [a], Jingtian Hu [a]

[a] *Department of Chemistry, Shandong University, Jinan 250100, China*
[b] *Hangzhou Everlong Biotechnics, China*

Received 9 April 1996; accepted 11 October 1996

Abstract

Fluorescent reaction between ascorbic acid (AA) and 2,3-diamino-naphthalene (DAN) was studied. The experimental results showed that AA could react with DAN at pH = 10.2–10.5, and form the fluorescent heterocyclic condensation products which emitted strong fluorescence. The fluorescence intensity was measured in a 1 cm quartz cell with excitation and emission wavelengths of 400 and 520 nm, respectively. The relationship was obtained between the fluorescence intensity and AA concentration in the range of 2–300 μg ml^{-1}, the regression coefficient is 0.9993. The detection limit (signal-to-noise = 2) is 0.4 μg ml^{-1}. © 1997 Elsevier Science B.V.

Keywords: Ascorbic acid determination; Fluorescent reaction

1. Introduction

Many different methods for the determination of ascorbic acid (AA) have been reported in the literature. They concentrated on spectrometry [1], redox reaction [2], derivatization reaction [3], electrochemical method [4], enzymatic method [5], and chromatographic method [6], but few fluorometric estimation methods of AA were reported. A classic fluorometric method with *o*-phenylenediamine (OPDA) as fluorescence reagent was used to determine AA [7]. This method needed to treat with redox reagent beforehand and then reacted AA with OPDA, its detection limit was 2 μg ml^{-1}. Our experiments indicated that at the pH = 10.2–10.5, AA could react with 2,3-diaminonaphthalene (DAN) which didn't need pretreatment, its detection limit was 0.4 μg ml^{-1}. So the proposed method is more simple and sensitive than OPDA method.

2. Experimental

2.1. Apparatus

All fluorescence intensities were measured on a 850 fluorescence spectrophotometer (Hitachi, Japan).

* Corresponding author.

PII S0039-9140(96)02129-7

2.2. Reagents

1. 2,3-diaminonaphthalene (DAN) solution (0.1%, v/v): it is prepared by dissolving 0.1 g DAN in 100 ml 0.1 mol l^{-1} HCl, then treated with cyclohexane, rejected organic phase, the remained water phase repeated 2–3 times with cyclohexane according to the above procedure.
2. Ascorbic acid solution: it is prepared by dissolving 0.100 g AA in 100 ml distilled water. The stock solution was 1.00 mg ml^{-1}.
3. Aminoacetic acid buffer solution: it is prepared by dissolving 3.8 g aminoacetic acid in 100 ml distilled water and adjusting pH to 10.3 with 6 mol l^{-1} NaOH.

2.3. Procedure

To a 25 ml test tube, solutions were added according to the following order: AA solution, 0.5 ml 0.5 mol l^{-1} NaOH, 1 ml 0.1% DAN solution, 2 ml aminoacetic acid buffer. The mixture was diluted to 10 ml with distilled water, thoroughly mixed by shaking and then allowed to stand for 40 min. The fluorescence intensity was measured in a 1 cm quartz cell with excitation and emission wavelengths of 400 and 520 nm, respectively.

3. Results and discussion

3.1. Fluorescence spectra

The excitation and emission spectra of AA-DAN-aminoacetic acid (1), DAN-aminoacetic acid (2) are shown in Fig. 1. From Fig. 1, it can be seen that the wavelength of emission peak is 520 nm, the wavelengths of excitation peak are 370, 400 nm. Since DAN itself is a strong fluorephore with excitation and emission wavelengths of 340 and 390 nm, if the excitation wavelength is 370 nm, the excess of DAN in the reaction will interfere with the emission of the fluorescence products, therefore, the excitation wavelength of 400 nm was chosen in our experiments and a low and stable reagent blank was obtained.

3.2. Effect of pH

The effect of pH on fluorescence intensity of the system was shown in Fig. 2. From Fig. 2, it can be seen that the fluorescence intensity is the strongest and remains stable in the range of pH = 10.2–10.5.

In this paper, the following buffers were examined: Na_2CO_3, borax–NaOH, NH_3–NH_3Cl, K_2HPO_4, aminoacetic acid. The results showed that 2 ml of 0.5 mol l^{-1} aminoacetic acid buffer was the most suitable.

3.3. Effect of DAN concentration

The effect of DAN concentration on fluorescence intensity of the system was studied. The results were shown in Fig. 3. From this figure we can see that the suitable concentration of DAN was 0.01%.

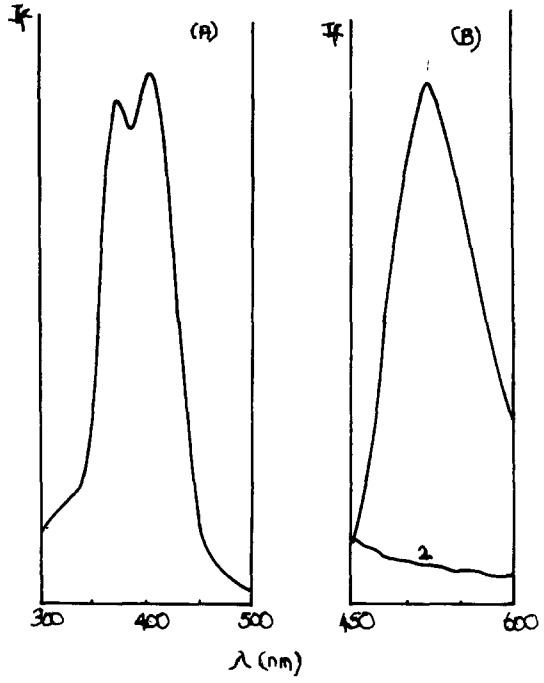

Fig. 1. Fluorescence spectra (a) excitation spectrum (λ_{em} = 520 nm), (b) emission spectrum (λ_{ex} = 400 nm). (1) AA-DAN-aminoacetic acid, (2) DAN-aminoacetic acid conditions: ascorbic acid: 0.2 mg ml^{-1}, DAN: 0.01%; aminoacetic acid: 0.5 mol l^{-1}, 2 ml, pH = 1.03.

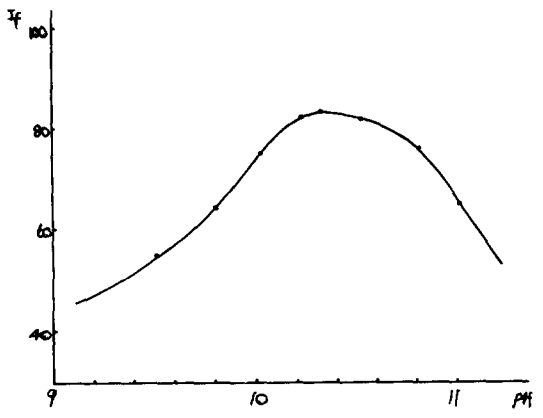

Fig. 2. Effect of pH. Conditions: ascorbic acid: 0.05 mg ml^{-1}, DAN: 0.01%; aminoacetic acid: 0.5 mol l^{-1}, 2 ml.

3.4. Effect of temperature

High temperature could destroy the structure of AA and quench the fluorescence of the system. Our experiments indicted that when the temperature was higher than 50°C, the fluorescence intensity of the system was completely quenched. The suitable temperature was 30°C or so.

3.5. Stable tests

The experiments indicated that at room temperature the fluorescence intensity of the system reached a maximum after 40 min and remained stable at least for 1 h. In addition, effect of surfactants of fluorescence intensity of the system was examined, the results showed the enhancement effect was not obvious.

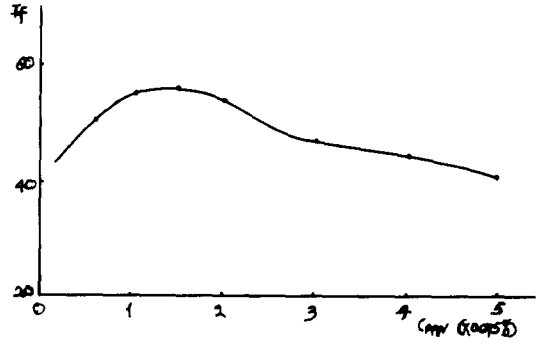

Fig. 3. Effect of DAN concentration. Conditions: ascorbic acid: 0.25 mg ml^{-1}; aminoacetic acid: 0.5 mol l^{-1}, 2 ml, pH = 10.3.

3.6. Calibration curve and detection limit

The calibration curve was made according to the procedure in the optimum conditions. The results indicated that the fluorescence intensity of the system was a linear function of AA concentration in the range of 2–300 μg ml^{-1}, the regression coefficient is 0.9993, the detection limit (S/N = 2) is 0.4 μg ml^{-1}.

3.7. Recovery test

In the serum, recovery tests of AA were made. The results were shown in Table 1. From Table 1, it can be seen that recovery ratios were upwards of 90% and serum didn't need complicated biological treatment. Therefore, the proposed method for determining AA was satisfactory.

3.8. Sample determination

The proposed method was used to determine AA in Vc tablets (Jilin Tonghua Baishan Medicine Factory of China) and compared with the most commonly used OPDA method [8]. The results were shown in Table 2. From Table 2, it can be seen that the accuracy and precision of the method are satisfactory.

3.9. The characteristics of the proposed method

In comparison with the most commonly used OPDA method, the proposed method possesses the following characteristics:

1. The detection limit is 0.4 μg ml^{-1}, which is obviously lower than that of OPDA method [8]. so the sensitivity of the proposed method is higher.

2. In OPDA method, the redox reagent, such as norit (carbon), 2,6-dichloroindophenol, *N*-Bromosuccinimide and iodone, must be used to oxidize AA to DHAA, while in this method it is unnecessary to add a redox reagent to the reaction system. We think that AA will not be transferred to DHAA in the absence of the oxidizer

Table 1
Recovery test in the serum

Added Vc (μg ml^{-1})	Found Vc (μg ml^{-1})	$\bar{X} \pm S$	Recovery (%)
20.0	18.92, 17.95, 18.33, 18.92, 18.95	18.6 ± 0.45	93.1
100.0	94.8, 96.1, 94.3, 93.4, 95.2	94.8 ± 1.01	94.8

Table 2
Determination of samples

The proposed method		OPDA method (8)	
Found Vc (%)	$\bar{X} \pm S$	Found Vc (%)	$\bar{X} \pm S$
52.3, 50.9, 54.6		52.4, 50.5, 50.9	
50.9, 52.3	52.2 ± 1.5	53.4, 54.2	52.3 ± 1.6

and there is a tautomeric between enediol and 2-hydroxy carbonyl groups in the alkaline medium. Therefore, the possible mechanism is illustrated as follows.

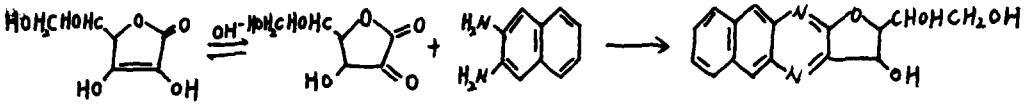

Since the conjugate π-bond system of the condensate product in the proposed method is larger than that in the OPDA method, the sensitivity of the proposed method is higher than that of OPDA method.

References

[1] S.H.R. Davis and S.J. Masten, Anal. Chim. Acta, 248 (1991) 225.
[2] B. Jaselskis and J. Nelapaty, Anal. Chem., 44 (1972) 379.
[3] M.J., Deutsch and C.E. Weeks, J. Assoc. Off. Agric. Chem., 48 (1965) 1248.
[4] L. Falat and H.Y. Cheng, Anal. Chem., 54 (1982) 2108.
[5] J.O. Schenk, E. Miller and R.N. Adams, Anal. Chem., 54 (1982) 1452.
[6] E.S. Wagner, B. Lindley and R.D. Coffin, J. Chromatogr., 163 (1979) 225.
[7] A.P. Lawrence, L.R. Donald and T.K. Peter, J. Assoc. Off. Anal. Chem., 68 (1985) 1.
[8] R.B. Roy, A. Conetta and J. Salpeter, J. Assoc. Off. Anal. chem., 59 (1976) 1244.

ELSEVIER

Talanta 44 (1997) 859–866

Talanta

Amperometric biosensor with physically immobilized glucose oxidase on a PVA cryogel membrane

Lucio Doretti [a,*], Daniela Ferrara [a], Paola Gattolin [a], Silvano Lora [b]

[a] *Ufficio Sicurezza e Prevenzione del CNR, Corso Stati Uniti 4, 35127 Padova, Italy*

[b] *Istituto di Fotochimica e Radiazioni d'Alta Energia del CNR, Sezione di Legnaro, Via Romea 4, 35020 Legnaro (Padova), Italy*

Received 22 July 1996; received in revised form 30 September 1996; accepted 14 October 1996

Abstract

A new method of physically immobilizing a biomolecule of analytical interest in poly(vinyl alcohol) cryogels was developed to obtain suitable biosensors. An amperometric glucose sensor was constructed using glucose oxidase immobilized on membranes obtained by a freezing-thawing cyclic process. No chemical cross-linking agent was used. Sensor behaviour was evaluated electrochemically with a hydrogen peroxide electrode. The glucose content in standard solutions was determined and linear calibration curves in the 5×10^{-5}–3×10^{-3} mol l^{-1} range were obtained. Temperature and pH effects on the electrochemical response were described and kinetic parameters in the immobilized system were evaluated. © 1997 Elsevier Science B.V.

Keywords: Biosensors glucose oxidase; Physical immobilization; PVA cryogels

1. Introduction

Amperometric enzyme-based biosensors continue to generate much interest in clinical, environmental and quality control analyses. The performance of enzyme electrodes are strongly dependent on enzyme immobilization techniques. Generally, entrapment of enzyme molecules in polymeric membranes is considered an attractive procedure because it is regarded as a mild coupling method that preserve quaternary protein structure and most of its activity, even if in some cases it can be reversible.

A method has been developed for the physical immobilization of enzymes in poly(hydroxyethylmethacrylate)(HEMA) membranes and glucose [1] and choline [2] sensors have been studied and characterized. The immobilization procedure, based on low-temperature γ induced polymerization of an aqueous solution of monomer and enzyme, produced a matrix characterized by a porous cross-linked structure, with both features of hydrophilicity and biocompatibility.

Pursuing our interest for biocompatible membrane electrodes with good electrochemical performances, we immobilized glucose oxidase (GOD) in poly(vinyl alcohol)(PVA) cryogels obtained by freezing-thawing cyclic processing.

* Corresponding author. Fax: + 39 49 8295662.

PII S0039-9140(96)02130-3

Poly(vinyl alcohol) is a biocompatible polymer [3], that is considered an appropriate matrix for sensor preparation. Lactate oxidase was incorporated in a PVA network prepared by cross-linking the reactive nucleophilic groups (as hydroxyl and amino) with aromatic tri-isocyanates [4]. Other authors demonstrated the possibility of immobilizing glucose oxidase [5] and lactate oxidase [6] in a PVA matrix on platinized graphite electrodes by γ irradiation, obtaining an enzyme layer sandwiched between two polymer layers. Enzymes were entrapped in a PVA membrane that was cross-linked by means of UV light [7]. Immobilization of microorganisms with phosphorylated PVA gel was also reported [8]. Recently a mixture of PVA and polyhydroxy cellulose was used to immobilize tyrosinase on a glassy carbon electrode [9] and a glucose sensor was realized by immobilizing glucose oxidase in a composite membrane of silk fibroine and PVA [10].

Acetogenium kivui cells were immobilized in PVA cryogels [11] to obtain biocatalytic reduction of CO_2 and *Pseudomonas sp.* cells were immobilized to construct an L-Proline biosensor [12].

The proposed method of enzyme immobilization in PVA hydrogels is characterized by the absence of chemical cross-linking agents that could compromise its biocompatibility or of physical agents, such as γ radiation that could deactivate the biological substrates, due to damage caused mostly by the indirect effect of water radiolysis.

The exposition of aqueous PVA solutions to several freezing-thawing cycles leads to reinforced gels owing to a densification of the macromolecular structure [13,14], that is function of the cycling time and temperatures. After the freezing-thawing process, the chains are physically cross-linked by semipermanent entanglements, molecular associations or crystallites. These novel networks are of significant interest in the biomedical field because they are nontoxic for organisms, contain no impurities and their water content matches that of biological tissue.

In this paper, GOD immobilized in PVA cryogel was used to assemble an amperometric sensor measuring hydrogen peroxide produced in the enzymatic reaction. The parameters that could affect the electrode performances were evaluated and the electrochemical features of the system are also described.

2. Experimental

2.1. Reagents

Glucose oxidase (EC 1.1.3.4, type II-S from *Aspergillus niger*, 18 000 units g^{-1} solid), peroxidase (POD, EC 1.11.1.7, type VI from Horseradish, 250 purpurogallin units mg^{-1} solid), o-dianisidina dihydrochloride (ODA) and β-glucose were obtained from Sigma Chemical (St. Louis, USA). Stock solutions were prepared in bidistilled water or buffer solution and stored in the dark at 4°C. Glucose solutions were allowed to mutarotate overnight at room temperature before use.

PVA with an average Mw = 50 000 and Mw = 124 000–186 000 both with a degree of hydrolysis of 99% were purchased from Aldrich Chemie (Stenheim, Germany) and used without further purification. All others analytical grade chemicals were purchased from Carlo Erba (Milano, Italy) or Merck (Darmstadt, Germany).

Control serum was manufactured by Technicon Instruments (Tarrytown, USA) and marketed by Bayer Diagnostics (Oreq-Tournai, Belgium).

2.2. GOD immobilization and sensor preparation

PVA solutions in 0.1 M phosphate buffer at pH 6 were heated in an oven at 90°C for a time no longer than 5 h to achieve complete polymer dissolution. When the solution had cooled to 30–35°C the appropriate amounts of GOD dissolved in few μl of buffer was added. The viscous honey-like solution was carefully mixed and then sonicated to remove air bubbles at a temperature below than 37°C. After partial filling with PVA solutions, polyethylene vials (5 mm i.d.) were sonicated again and left at −25°C for 12 h. After this first freezing process, they were allowed to thaw at 4°C for up to 12 h. Five freezing-thawing cycles were used for the PVA gel preparation. The sponge-like material obtained with this procedure

was cooled at −20°C and sliced into about 120 micron discs with a microtome. The discs were carefully washed six times with a phosphate buffer (20 ml, pH 6) for 12 h at 4°C.

The apparent GOD activity was determined by dipping a membrane in a 0.1 M glucose solution (2.8 ml, 0.1 M in phosphate buffer, pH 6) and incubating for 1 min, with stirring at 25°C. After removal of the membrane, a solution of 100 μl POD (50 purpurogallin units ml^{-1}) and 20 μl ODA (1% m/v in water) was added and the solution transferred to a glass cells to read the absorbance value at 460 nm.

The working electrode was a platinum wire (0.5 mm diameter) sealed in a glass tube and polished with alumina powder to ensure a flat surface. A membrane disc, placed on the electrode surface and fixed with a teflon cap having a 3 mm hole, gave the active sensor. When not in use the membranes were stored at 4°C in 0.1 M phosphate buffer at pH 6.

2.3. Apparatus

The determination of hydrogen peroxide was performed in an electrochemical cell with a working volume of 20 ml, in a three-electrode configuration. The three electrodes were connected to an AMEL (Milano, Italy) 559 model potentiostat. A saturated calomel electrode and a platinum foil with large surface area were used as the reference and counter electrode, respectively. All the experiments were carried out in a temperature-controlled cell using a Haake F3-C thermostatic bath.

Spectrophotometric measurements were carried out with a Hitachi U-3200 spectrophotometer equipped with a 1 cm thermostated cell.

The scanning electron microscopy was performed with a Cambridge Stereoscan 250 (Cambridge, UK) operating at a 20 kV accelerating voltage.

2.4. Electrochemical measurements

Glucose determination was carried out electrochemically by measuring the hydrogen peroxide production as a result of the enzymatic reaction. This was done by immersing the sensor in stirred 0.1 M phosphate buffer at pH 6 and applying an oxidative potential of +600 mV against a saturated calomel electrode. When the backround current had stabilized, an appropriate amount of glucose solution was introduced to give a preselected concentration. All measurements were carried out using a thermostated bath at 25°C, unless otherwise mentioned.

3. Results and discussion

The procedure described produces a matrix of a physically cross-linked polymer containing uncrossed-linked polymer and water. The porous, hydrophilic and permeable membranes had interesting mechanical characteristics and can be handled easily. The properties of this gel depended, under the same conditions of temperature and freezing time and number of cycles, on the molecular weight of the uncrossed-linked polymer and its concentration in an aqueous solution.

In fact, the characteristics of hydrogels are determined by the size of particles that make up the supermolecular structure and these small spheres increased in diameter with each freezing-thawing cycle. Freezing time and freezing temperature are very important in determining the cryogel structure. The stability and strength of gels increased with an increase in freezing time. Stable gels were formed even when solutions were frozen at −20°C for only 1 h, but the strongest gels resulted after 24 h. When the freezing temperature was changed to 0°C, the ensuing gel could not hold their weight even after four freezing-thawing cycles. Thawing temperature was not very important for the final structure of gel, provided it is above 0°C.

In water, the PVA gel is essentially insoluble, but undergoes significant swelling [15]. Experimental measurements related to swelling behaviour of the gel demonstrated that a significant densification of the structure was obtained after five freezing-thawing cycles and with a thawing time of approximately 4 h [14]. The increase of mechanical strength as the number of cycles increased was probably due to the increased degree of crystallinity [16].

Although even a solution of 10% wt of PVA led to a gel formation, stronger structures with high stability were obtained from solutions of at least 15% wt.

The features of two kinds of polymers were examined: *A*, obtained from an aqueous solution of 24% wt of PVA with an average Mw = 50 000 and *B*, from a solution of 15% PVA (highest solubility grade) with an average Mw = 124 000–186 000.

Fig. 1 shows the scanning electron micrographs of these two matrices. Although both PVA solutions led to stable polymers, stronger gels were obtained with the higher molecular weight. The structure looked closer and the pores were smaller.

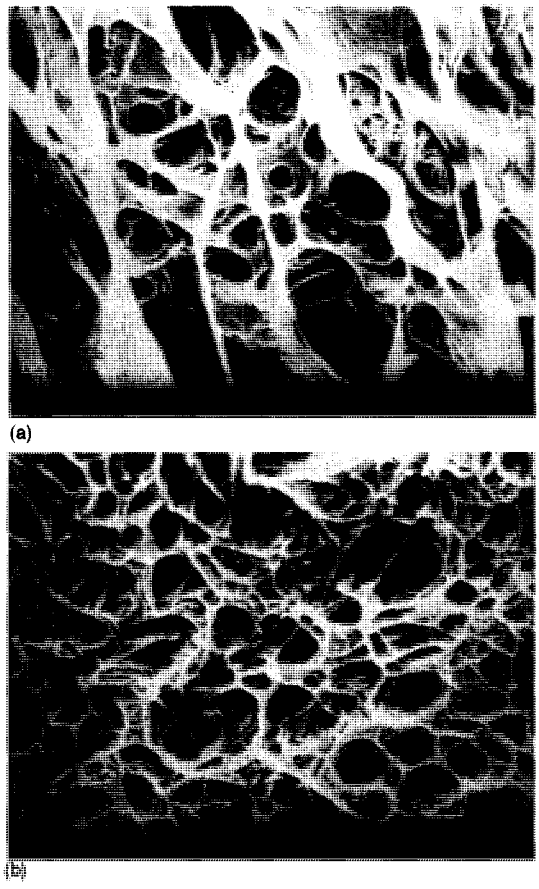

Fig. 1. Scanning electron microphotographs of PVA membranes. *A*, 24% PVA with an average Mw = 50 000; *B*, 15% PVA with an average Mw = 124 000–186 000.

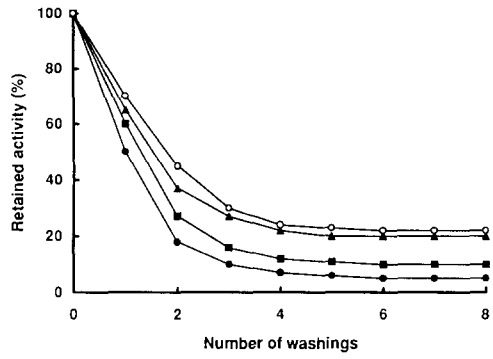

Fig. 2. Activity retention curves for the immobilized enzyme after repeated washings. (●) Membrane *A* with a 6 mg g^{-1} enzyme loading; membrane *B* with a (■) 6 mg g^{-1}, (△) 3 mg g^{-1} and (○) 1.5 mg g^{-1} enzyme loading.

In order to measure the apparent activity truly fixed, important to forecast its analytical performance as a sensor, and to determine the percentage leakage from the gel, the following method was used. Several pieces with a total weight of about 1 g were washed with a phosphate buffer (20 ml, pH 6) for 12 h, then the washing solution was assayed for enzyme activity. This process was repeated eight times, using the same matrix sample. After the last washing, the matrix was also assayed for apparent enzyme activity. The results are shown in Fig. 2. With an enzyme loading of 6 mg g^{-1} of monomer solution, the greater part of the total activity introduced passed into the solution in the first three washings and only 5–6% and 9–10% for polymer *A* and *B*, respectively were really fixed permanently. In order to verify the effect of the enzyme loading on the amount of activity truly fixed, the specific activity of polymer *B* was also measured using initial amounts of 1.5 and 3 mg g^{-1} of solution. The detected activity corresponded to a percentage immobilization of up to 22 and 20%, respectively. As shown in Fig. 2, this means that the percentage of fixed activity with respect to the introduced amount became less upon increasing the enzyme loading, whereas the specific activity seemed to increase very little for values higher than 3 mg g^{-1}. Moreover it is important to evaluate either the total weight of enzyme introduced or its molecular weight because these are all important factors in the understanding of the immobilization process.

All the following measurements were carried out with membranes obtained from an enzyme loading of 6 mg g^{-1} and washed six times with buffer solutions and so that all not fixed GOD had been rinsed out.

The apparent activity of immobilized GOD in measured membranes (120 μm thickness and 5 mm diameter) used for the amperometric analysis were found to be about 90 and 150 mU cm^{-2} for the polymers *A* and *B*, respectively. The enzyme was retained in the network of the polymer *B* in larger amounts than *A* and this was compatible with the stronger structure observed for the hydrogel obtained from the kind of PVA with higher molecular weight.

Typical calibration graphs for GOD-modified *A* and *B* polymer electrodes, measured by anodic oxidation of H_2O_2, are shown in Fig. 3. The response to glucose gave linear patterns in the 5×10^{-5}–3×10^{-3} M range with a linear regression equation of $y = 0.099x + 0.003$, $R^2 = 0.9992$ for electrode *A* and $y = 0.141x + 0.004$, $R^2 = 0.9994$ for electrode *B*, where y was the current (μA) and x was the substrate concentration (mmol l^{-1}). A detection limit of 3×10^{-5} M was estimated with a signal-to-noise ratio > 3. The relative standard deviation for five replicate determinations of 1 mM glucose solution was 2.5%.

As expected, the response increased with the amount of apparent enzyme activity immobilized in the membrane. These changes, however, were not directly proportional to the enzyme content. In fact, the slopes of the resulting calibration

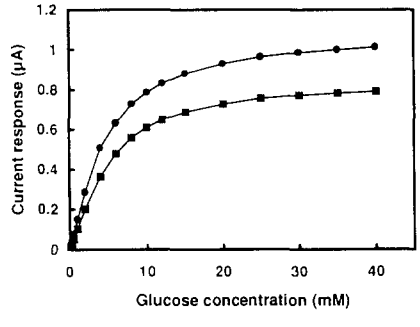

Fig. 3. Calibration graphs for glucose obtained at pH 6 and 25°C. (■) sensor with membrane *A* (lower Mw); (●) with membrane *B* (higher Mw).

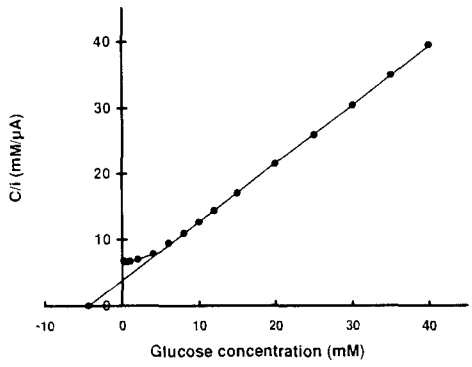

Fig. 4. Hanes plot of the calibration data for a glucose oxidase electrode with membrane *B*.

graphs in the linear range, and hence the sensitivities, were 0.099 and 0.141 μA l $mmol^{-1}$ for the electrodes *A* and *B*, respectively.

The glucose response curves can be described by the Michaelis–Menten equation, expressed in the electrochemical Hanes form:

$$C/i = (C + Km_{(app)})/i_{max}$$

where C = glucose concentration, i = steady-state current, i_{max} = maximum steady-state current and $Km_{(app)}$ = apparent Michaelis-Menten constant.

The linear portion of the curve (Fig. 4), corresponding to the response in the kinetic regime for electrode *B*, gave values of 4.5 mM for $Km_{(app)}$ ($-x$ intercept) and 1.126 μA for i_{max} (reciprocal of the slope). The response for electrode *A* gave the same value for $Km_{(app)}$ and 0.890 μA for i_{max}.

Surprisingly, the apparent Michaelis–Menten constant calculated was very low. Generally, an increase in K_m value for immobilized enzyme systems was observed, owing to the effect of conformation changes in the enzyme as a result of the chemistry of cross-linking and the effect of the diffusion of substrate towards the active sites. The gel material obtained through the process of freezing-thawing cycles is a physically cross-linked polymer containing uncrossed-linked polymer and water [13]. The enzyme is retained in the network but it behaves as it were freely soluble and maintained the same active conformation. Moreover the presence of a high water content and hydroxyl groups in the polymer provides microenvironmental conditions particularly favorable for glucose

oxidase. The structure of this matrix and its hydrophilicity reduces the mass-transport resistance to the diffusion of a substrate.

The poor linearity observed in Fig. 4 seems to imply diffusional limitations for lower glucose concentrations. An attempt was made to analyse the same data with the method proposed by Albery, Bartlett and coworkers [17–19], even though Albery's theoretical model does not take into consideration the concentration polarization in the enzyme layer and therefore these conclusions should to be considered correct as regards mass-transport limitations, but only approximate as regards the real experimental situation.

From this model, the k'_S/k'_{ME} ratios were calculated, where k'_S was the mass-transport rate constant for the substrate diffusion through the membrane and k'_{ME} was the effective electrochemical rate constant for the enzyme electrode. Values of 1.4 and 1.3 for electrodes *A* and *B* were obtained respectively, indicating that transport of glucose through membrane was partially rate limiting, mostly at low substrate concentration [20].

A low value for the apparent Michaelis–Menten constant implies more favorable conditions for GOD activity, but lowers the upper limit of the linear response range.

The pH influence on the sensor *B* was also investigated and Fig. 5 shows the sensor response to glucose solution in the pH range of 4–8. It can be seen that the optimum pH was found at 5.5, the same value reported for the free enzyme [21,22]. The lack of the typical shift toward more alkaline values upon immobilization procedures, confirmed the hypothesis that GOD in this matrix behaved as if it were free.

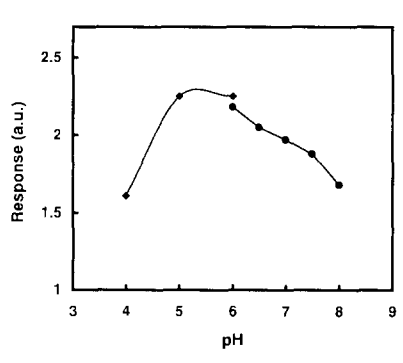

Fig. 5. Biosensor *B* response dependence on pH in 1 mM glucose solution at 25°C. (■) 0.1 M citrate buffer; (●) 0.1 M phosphate buffer.

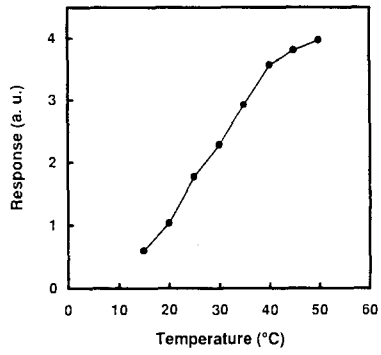

Fig. 6. Biosensor *B* response dependence on temperature in 1 mM glucose solution, pH 6.

Fig. 6 shows the trend of the electrode *B* response as a function of temperature. The response increased with a temperature increase from 15 to 50°C. In this range there were no irreversible modifications to the system; measurements carried out at 25°C with the same electrode again showed the original signal.

Response is modulated by the mass-transport through the membrane and therefore the electrode signal is considerably influenced by the thickness of the enzyme layer. Hence this parameter must be carefully controlled. The electrode signal of ten membranes with the same diameter, average weight and presumably the same thickness showed a relative standard deviation less than 5%.

The response time, for the examined biosensors *A* and *B*, was within 120 s and it remained unchanged for the entire life of the membranes.

The long term stability of the GOD modified polymer was good. In order to examine the effect of storage, the membranes were detached and washed after each assay in buffer solutions and kept at 4°C. After 2 months the electrode signal decreased by about 10% in comparison with the initial value measured at a single concentration in the linear response range.

Physical immobilization procedures are always connected with protein leaking on long term storage or exposures over large volumes, mainly if there are modifications of ionic strength or pH values.

Some membranes of an interesting batch (about 0.5 g) in buffer solution (25 ml) for a 2 months period were kept under control and an enzyme leaking of about 1–2% with respect to the original enzyme loading, corresponding to a 5–10% respect to the activity measured in the membranes after six washings, was actually observed.

From our results it could be claimed that this kind of leakage has no effect on normal, analytical biosensor performances, but it could otherwise be a problem when proposing the biocompatibility of the system.

The electrode *B* was used to determine glucose in a real sample and the results, relative to the analysis of a control serum, were compared with those obtained for the same sample by the enzymatic-spectrophotometric method which is generally used in routine biomedical analysis.

Nominal value of serum = 4.17 mmol l^{-1} (scattering range 3.67–4.67 mmol l^{-1}); mean value found by spectrophotometric method (triplicate) = 3.87 ± 0.04 mmol l^{-1}; mean value found by amperometric method (triplicate) = 3.95 ± 0.08 mmol l^{-1}.

4. Conclusions

This work supports the results that PVA cryogel produced by a cyclic freezing-thawing process is a suitable material for the immobilization of GOD on electrode surfaces and has some advantageous characteristics over other immobilization methods. The hydrogel membranes resulting from this treatment have interesting mechanical properties and the immobilization is achieved without use of chemical or reinforcing cross-linking agents.

In particular, the following considerations may be made.

(a) The PVA cryogel with higher molecular weight offers better performances owing to the closer structure, higher amount of immobilized enzyme and magnitude of the electrode signal.

(b) The data obtained indicate that the PVA hydrogel provides very favorable environmental conditions for glucose oxidase and the enzyme behaves as if it were virtually free.

(c) The low $Km_{(app)}$ value of the system limits the linear range and the possibility of extending the upper limit to higher values should be investigated.

(d) The response time and the long term stability of this glucose sensor are good.

(e) The immobilization method needs to be further improved so as to prevent all the enzyme leaking.

Acknowledgements

The authors are grateful to C.U.G.A.S. for the valuable support in carrying out scanning electron micrographs, and to Mr Gilberto Barison for his skilfull technical assistance.

References

[1] L. Doretti, D. Ferrara and S. Lora, Biosens. Bioelectron., 8 (1993) 443.
[2] L. Doretti, P. Gattolin and S. Lora, Anal. Lett., 27 (1994) 2455.
[3] N. Minoura, in T. Tsuruta, T. Hayashi, K. Kataoka, K. Ishihara and Y. Kimura (Eds.), Biomedical Applications of Polymeric Materials, CRC Press, Boca Raton, 1993.
[4] K. Hajizadeh, H.B. Halsall and W.R. Heineman, Talanta, 38 (1991) 37.
[5] C. Galiatsatos, C. Ikariyama, J.E. Mark and W.R. Heineman, Biosens. Bioelectron., 5 (1990) 47.
[6] K. Hajizadeh, H.B. Halsall and W.R. Heineman, Anal. Chim. Acta, 423 (1991) 23.
[7] K. Imai, T. Shiomi, K. Uchida and M. Miya, Biotechnol. Bioeng., 28 (1986) 1721.
[8] K.C. Chen and Y.F. Lin, Enzyme Microb. Technol., 16 (1994) 79.
[9] Q. Deng, Y. Guo and S. Dong, Anal. Chim. Acta, 319 (1996) 71.
[10] H. Lin, J. Qian, Y. Lin, T. Yu and J. Deng, Bioelectrochem. Bioenerg., 39 (1996) 303.
[11] E.I. Rainina, M.A. Pusheva, A.M. Ryabokon, N.P. Bolotina, V.I. Lozinsky and S.D. Varfolomeyev, Biotechnol. Appl. Biochem., 19 (1994) 321.
[12] A.L. Simonian, E.I. Rainina, V.I. Lozinsky, I.E. Badalian, G.E. Khachatrian, S.S. Tatikian, T.A. Makhlis and S.D. Varfolomeyev, Appl. Biochem. Biotechnol., 36 (1992) 199.
[13] N.A. Peppas and S.R. Stauffer, J. Control. Release, 16 (1991) 305.
[14] S.R. Stauffer and N.A. Peppas, Polymer, 33 (1992) 3932.
[15] N.A. Peppas, Makromol. Chem., 176 (1975) 3433.

[16] N.A. Peppas, N.K. Mongia and C.A. Bugest, Proc. 23th Intern. Symp. Control Rel. Bioact. Mater., Kyoto, Japan, July 7–10, 1996, p. 157.
[17] W.J. Albery and P.N. Bartlett, J. Electroanal. Chem., 194 (1985) 211.
[18] P.N. Bartlett, in A.E.G. Cass (Ed.), Biosensors: A Practical Approach, IRL Press, Oxford, 1990, p. 47.
[19] P.N. Bartlett, V.Q. Bradford and R.G. Whitaker, Talanta, 38 (1991) 57.
[20] W.J. Albery, P.N. Bartlett, M. Bycroft, D.H. Craston and B.J. Driscoll, J. Electroanal. Chem., 218 (1987) 119.
[21] R. Wilson and A.P.F. Turner, Biosens. Bioelecron., 7 (1992) 165.
[22] G.G. Guilbault and G.J. Lubrano, Anal. Chim. Acta, 64 (1973) 439.

ELSEVIER

Talanta 44 (1997) 867–875

Talanta

Flow injection determination of Pb and Cd traces with graphite furnace atomic absorption spectrometry

M. Colognesi, O. Abollino, M. Aceto, C. Sarzanini, E. Mentasti *

Department of Analytical Chemistry, University of Turin, Via P. Giuria n. 5, 10125 Turin, Italy

Received 14 May 1996; received in revised form 14 October 1996; accepted 15 October 1996

Abstract

The preconcentration and recovery of lead and cadmium traces at ng l^{-1} level were evaluated in standard solutions and natural aqueous samples using a FIAS (Flow Injection Atomic Spectrometry) apparatus. The method is based on retention of the complex formed between Pb or Cd and 1,2-dihydroxy-3,5-benzendisulphonic acid (Tiron) on a macroporous anion-exchange resin. The recovery of the analytes was obtained by elution with 0.1 M HCl and their determination was performed by Graphite Furnace Atomic Absorption Spectrometry (GFAAS). The detection limits were 9 and 7 ng l^{-1} for Pb and Cd respectively. The effects of sample solution pH and composition and of interfering agents as well as reagent purity are discussed. The technique was applied to the analysis of natural waters. © 1997 Elsevier Science B.V.

Keywords: Cadmium; Flow injection atomic spectrometry; Lead; Natural waters; Preconcentration; Tiron

1. Introduction

Two important features distinguish heavy metals from other toxic pollutants: they are not biodegradable and their toxicity is controlled by their physico-chemical form. Heavy metals can be found in waters (fresh, sea, lake, waste), food (fruit, fish, milk), soils, sediments and biological samples [1].

Several studies concerning determination of ultratraces of metal ions in water samples with preconcentration and/or separation of the analyte from its matrix have been reported [2–7].

The aim of this study was to determine very low concentrations of metal ions, namely lead and cadmium, in liquid samples. Lead and cadmium commonly occur in the environment due to the contribution of anthropogenic sources, such as waste incineration and combustion of coal and oil, and are among the most toxic heavy metals for human health.

Fang et al. [5,6] and Sperling et al. [7] determined cadmium and lead in sea-water and drinking water with a preconcentration system based on on-line sorbent extraction. A micro-column packed with silica C-18 and sodium diethyldithiocarbamate (DDTC) as ligand were used in conjunction with a flame atomic absorption spectrometer.

* Corresponding author.

PII S0039-9140(96)02131-5

A flow injection preconcentration technique and atomic spectrometry were coupled in this study; this allows several advantages such as minimised interference effects, enhanced sensitivity, ease of automation and matrix removal [8]. The method is based on the complexation of Pb and Cd with Tiron, 4,5-dihydroxy-1,3-benzendisulphonic acid, which forms negatively charged complexes, then retained by a macroporous anion-exchange resin. Metal complexation with Tiron takes place via the two hydroxylic moieties which allow a reversible chelation, whereas the two sulphonic groups allow the retention of the complex on the anion exchange resin. The total metal recovery from the resin was then obtained with a small volume of 0.1 M HCl, which was immediately analysed using graphite furnace atomic absorption spectrometry (GFAAS). Alternatively, it is possible to drive the eluate to the nebulizer of a flame atomic absorption spectrometer.

An advantage of the proposed method is the use of an anion exchange resin, which has a wider operating pH range (0–14) with respect to the C-18 sorbent (2–8) and allows the use of an acidic eluent, more suitable than an organic one in GFAAS determinations. In fact we verified in our laboratory that the measured metal concentrations in ethanol media decreased with time, probably due to absorption on the walls of the vessel. Moreover Tiron has a greater stability than DDTC and can be stored for a long time without degradation.

The method proposed in this paper is one of the approaches developed in our laboratory [3,4,9,10] for trace metal preconcentration. Advantages of the present technique over previous systems [9,10] coupled to inductively coupled plasma atomic emission spectrometry (ICP-AES) are slightly lower detection limits, reduced sample and reagents consumption and lower running costs (in the case of ICP-AES, the torch is powered during all the analysis cycle).

On the other hand the formerly developed GFAAS preconcentration technique [3], which was based on the direct insertion of the enrichment column in the autosampler arm, has lower detection limits than the present one and reasonable running costs. Anyway the alignment of the column tip with the graphite furnace is a delicate task and requires frequent readjustments. The present method based on FIAS system is more straightforward, does not require trained operators or expensive consumables.

Table 1
Heating cycle program for lead determination by GFAAS

Temperature °C	Ramp time (s)	Hold time (s)
90	1	10
130	50	20
1100	20	10
20	5	5
1800	0	4
2600	1	5

2. Experimental

2.1. Instrumentation

A Perkin-Elmer Model 5100 atomic absorption spectrophotometer with Zeeman-effect background correction was used for Pb and Cd determinations. Pyrocoated graphite furnaces with L'Vov platforms were used and measurements were performed at 283.3 nm Pb and 228.8 nm Cd analytical lines with a 0.7 nm slit. The heating cycle programs are reported in Table 1 and Table 2.

The preconcentration manifold used (Fig. 1(a)), a Perkin-Elmer FIAS-200, is composed of two peristaltic pumps and a four-way switchable valve.

Table 2
Heating cycle program for cadmium determination by GFAAS

Temperature °C	Ramp time (s)	Hold time (s)
90	1	5
130	30	30
900	40	20
20	5	5
1600	0	5
2700	1	2

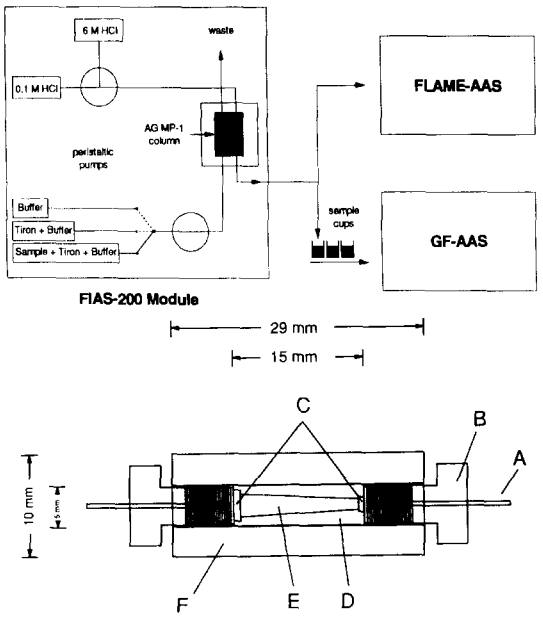

Fig. 1. (a) Scheme of the instrumentation utilised. (b) Microconic column. A, PTFE tubings with flanged ends; B, threaded fittings; C, 75 mesh Teflon filters; D, conical column with lid; E, AGMP-1 packing; and F, column housing.

The pump rate (range 1–12 ml min^{-1}) and valve position are completely software-controlled. Tygon pump tubings were used (i.d. 1.40 mm for Tiron and sample solutions and i.d. 0.76 mm for HCl).

UV-VIS Absorption measurements were performed with a double-beam spectrophotometer Hitachi 150–200.

A Mettler Delta 320 pH-meter equipped with a combined glass-calomel electrode was used for pH measurements.

High-purity acids and ammonia were obtained with a sub-boiling quartz still (K. Kurner).

All polyethylene labware was washed by immersion in 1 M HNO_3 for 48 h and stored in 1×10^{-2} M HCl until the moment of use.

Eppendorf dispensers or Gilson micropipets were used to prepare solutions. The accuracy of the dispensed volumes was periodically checked by weighing.

All sample manipulations were performed under a laminar flow hood in a laboratory provided with filtered air.

2.2. Reagents and materials

Analytical grade 100–200 mesh, macroporous anion-exchange resin AGMP-1(Bio-Rad) was used in Cl^- form for preconcentration.

Analytical grade 100–200 mesh, iminodiacetic functionalised resin Chelex-100 (Bio-Rad) and silica RP-C18 (40–63 μm, Merck) were used for reagent purification.

The microconic column used for preconcentration, loaded with 0.03 ml of AGMP-1 (Fig. 1(b)), was prepared by filling the column with a suspension of resin dispersed in 1 M HCl, using the slurry technique. Two 75-mesh Teflon filters were placed on both ends of the column.

The columns used for purification were prepared by filling short Tygon tubes (1.5 cm; i.d. 3.90 mm) with a suspension (total weight 0.05 g) in 1 M NH_4OH for Chelex-100 and in methanol for silica RP-C18 respectively, using the slurry technique. The particles were kept in place with two plugs of Teflon net inserted at the ends of the column.

High-purity water (HPW) was produced with a Milli-Q system and used to dilute all reagent solutions.

4,5-dihydroxy-1,3-benzendisulphonic acid (Tiron), monohydrate disodium salt (Merck) was dissolved in water at the desired pH and used after purification (see below).

Ammonium acetate buffer (prepared by mixing the appropriate amounts of concentrated acetic acid and ammonia previously purified by sub-boiling distillation) at pH values in the range 4.0–6.0 was used. Concentrated ammonia and a 3×10^{-2} M ammonium borate buffer were employed in pH range 7.0–9.0. For pH lower than 4.0 a 0.1 M trichloroacetic acid solution was used.

Lead and cadmium standard solutions were prepared from 1000 mg l^{-1} stock solutions of $PbCl_2$ and $CdCl_2$ (Merck) and diluted as required with HPW.

A matrix modifier for Cd and Pb AAS determinations (prepared by mixing 0.2 g $NH_4H_2PO_4$ and 0.01 g $Mg(NO_3)_2$ in 10 ml of HPW) was used.

Drinking water was collected from the hydric distribution of the city of Turin. Lake and sea-water were collected in Antarctica during the X

Table 3
FIAS-program for sample preconcentration

Step	Time (s)	Pump 1 (ml min^{-1})	Pump 2 (ml min^{-1})	Valve position	Description
1	60	1	0	Inject	Loading sample
2	20	0	0	Inject	Pause[a]
3	60	1	0	Inject	Loading (1×10^{-2} M Tiron)
4	20	0	0	Inject	Pause[a]
5	60	1	0	Inject	Loading (buffered HPW)
6	240	0	1	Fill	Elution
7	20	0	4	Fill	Rinsing (6 M HCl)
8	60	2	4	Inject	Column rinsing (buffered HPW)

[a] Technical delay necessary to replace sample container with Tiron or HPW container.

expedition within the Italian Antarctica Project. The samples were immediately filtered through 0.45 μm filters and kept frozen during transportation and storage.

2.3. Procedure

The method is based on retention on a macroporous anion-exchange resin of the negatively charged complex formed between Pb or Cd and Tiron; elution is obtained with 0.1 M HCl.

Proper volumes of sample, buffer solution and Tiron were pre-mixed and fluxed through a microcolumn filled with the resin; since a subsequent washing with buffered HPW only gave reduced recoveries ($73.0 \pm 0.5\%$ for Pb; $64 \pm 6\%$ for Cd), due to a partial retention of Pb and Cd on the surface of tubings; this step was modified and for the optimised procedure 1 ml of 1×10^{-2} M Tiron solution was used. Finally buffered HPW was loaded in order to drive the sample and Tiron through the column. The metal was eluted in countercurrent with 0.1 M HCl. The column was washed with 6 M HCl and conditioned with HPW buffered at the pH of the following experience. The eluate (0.5–1.0 ml) was directly collected in a sampling cup for GFAAS determination. The autosampler of the GFAAS was programmed to inject 20 μl of sample and 10 μl of matrix modifier for each analysis.

In order to load the desired sample volume through the column and elute the retained metal, a FIAS program consisting of eight steps was designed (see Table 3).

3. Results and discussion

The preconcentration procedure was optimised evaluating the percentage recoveries of each metal (10 μg l^{-1} Pb, 1 μg l^{-1} Cd) as a function of the pH of sample solution (that is pre-mixed ligand, buffer and metal solutions), of ligand concentration and of eluent type.

All these experiments were carried out with a sample and eluent volume of 1 ml, i.e., a preconcentration ratio of 1, in order to obtain a high sample throughput. In each determination the loading and elution volumes may slightly change (and usually do) and their values strongly depend upon the wear of the tubings. These factors were controlled, by weighing the sample bottle before and after loading and weighing the elution cup before and after elution. After calculating the loaded and eluted volumes a correction factor was applied to the percentage recovery. The formula used was:

$$\{(A/B \times C) - (A1/B1 \times C1)\}/D \times 100$$

where:

A and A1 are the volumes of the sample and blank eluates;

B and B1 are the loaded volumes of the sample and blank;

C and C1 are the concentrations of the sample and blank eluates;

D is the metal standard concentration.

3.1. Recovery as a function of type of eluent

Two different eluents, namely 0.1 M HCl and 1 M HNO_3, gave the best results for metal ion recoveries. The recovery was higher when eluent was 0.1 M HCl (Pb: 94 ± 4%, Cd: 76 ± 2%), since Cl ions have a greater affinity for Pb and Cd than NO_3 (Pb: 87 ± 12%, Cd: 74 ± 3%).

The presence of chloride influenced the subsequent GFAAS determination of lead. In fact when lead is vaporised and atomised from a chloride matrix, the presence of $PbCl_2$ (g) has been observed [11] prior to the appearance of Pb (g); a small amount of chlorine in the graphite furnace will bind lead to form $PbCl_2$ (c) or $PbCl_2$ (g). The proposed mechanism of atomisation is as follows:

$$PbCl_2(ad) \rightarrow PbCl_2(g) \rightarrow Pb(g) + Cl_2$$

where 'ad' stands for 'adsorbed' in agreement with [11]. Chloride matrix interference is due to the formation and loss of volatile lead chloride species (PbCl (g) and $PbCl_2$ (g)) in the gas phase.

This effect was taken into account by evaluating sample concentrations with standards prepared in 0.1 M HCl and using a matrix modifier which inhibits sample volatility (see Fig. 2(a) and (b)). The same modifier was used for cadmium determination as advised in the literature.

3.2. Recovery as a function of loading and elution flow-rate

The recovery yield of analytes was investigated for several loading and elution flow-rates; while the loading rate was kept constant to 1 ml min^{-1} and then 2 ml min^{-1}, the elution rate was varied from 1 ml min^{-1} to 3 ml min^{-1}. The best recoveries (Pb: 94 ± 4%; Cd: 76 ± 2%) were found at a loading and elution rate of 1 ml min^{-1} (Fig. 3 and Fig. 4), because it allows for a long contact period between resin and solution (metal-Tiron complex in the load step and 0.1 M HCl in the elution step).

3.3. Effect of pH and Tiron concentration

Using a load and elution rate of 1 ml min^{-1} the pH range of 3.0–9.0 was tested. The recovery increases with increasing pH in accordance with the values of the conditional stability constants for the metals, and pH 9.0 gave the highest recoveries.

Different ligand concentrations were investigated (5×10^{-3}–5×10^{-6} M). The recovery increases with increasing ligand concentration, since the equilibrium is shifted toward complex formation. Higher Tiron concentrations were not tested in order to avoid competition between complex and free ligand for the exchange sites on the resin.

Figs. 5–8 show the recovery behaviour (%) of Pb and Cd respectively as a function of the above cited parameters. The reduced recovery of Cd in respect to Pb is essentially due to a lower stability constant, which in turn is related to the presence of negatively charged oxygen-donor groups in Tiron molecule. The effect of these groups on complex stability

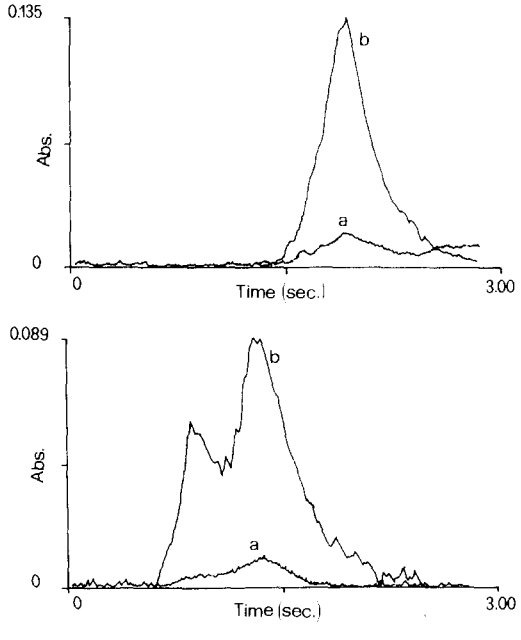

Fig. 2. (a) Atomic absorption spectrometry signal of lead in the presence of matrix-modifier. a, background; b, analyte. (b) Atomic absorption spectrometry signal of lead in the absence of matrix-modifier. a, background; b, analyte.

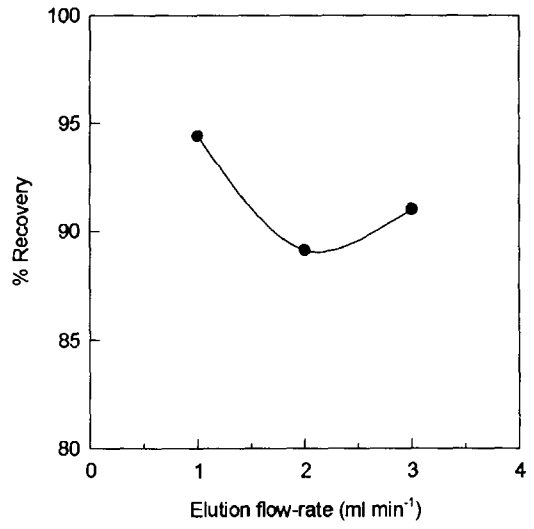

Fig. 3. Percentage recovery of lead as a function of elution flow-rate (ml min^{-1}) at a constant loading-rate (1 ml min^{-1}).

appears to depend on the acidity of the metal ion concerned. When acidity increases, the affinity of the metal ion towards negative O^--donor ligand, e.g., the OH^- ion, is also increased [12]. Anyway the recovery of cadmium is reproducible and the procedure can be used for analytical purpose.

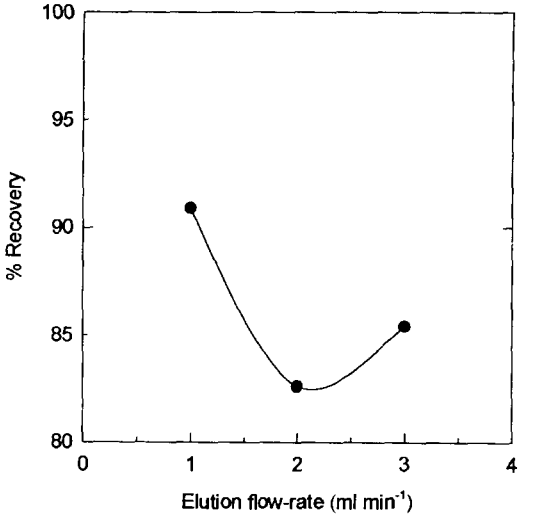

Fig. 4. Percentage recovery of lead as a function of elution flow-rate (ml nim^{-1}) at a constant loading-rate (2 ml min^{-1}).

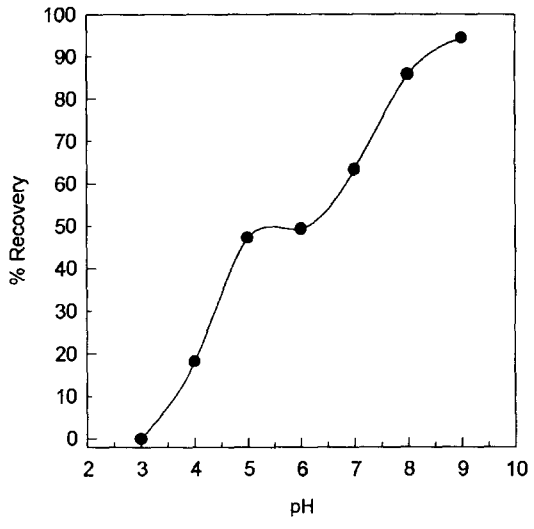

Fig. 5. Percentage recovery of lead as a function of pH (Tiron concentration 5×10^{-3} M).

3.4. Interfering agents

The effects of ionic strength (0.5 and 1.0 M NaCl), surfactants (10 and 100 mg l^{-1} polyoxyethylene-23-laurylether (Poly) and the concomitant presence of 20 mg l^{-1} Ca and 2 mg l^{-1} Mg were investigated. The chosen interferents are those likely to be present in natural waters. The

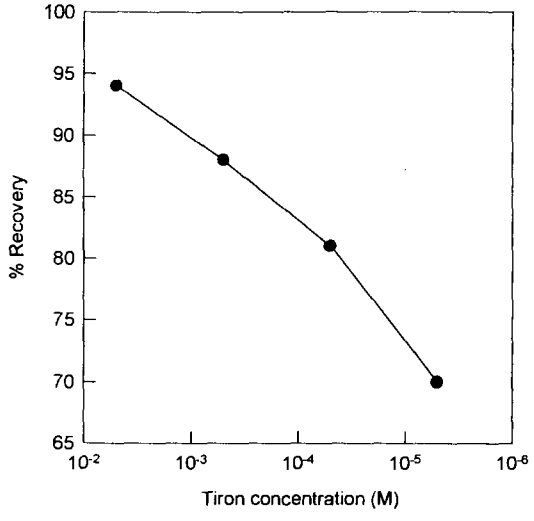

Fig. 6. Percentage recovery of lead as a function of Tiron concentration (pH = 9.0).

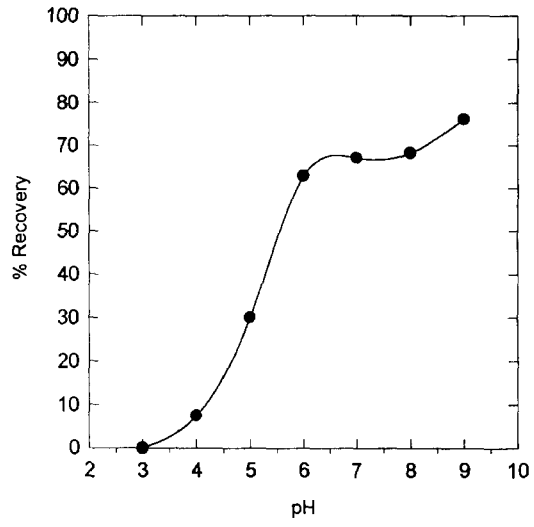

Fig. 7. Percentage recovery of cadmium as a function of pH (Tiron concentration 5×10^{-3} M).

experiments were carried out at pH 9.0, at a ligand concentration of 5×10^{-3} M and a flow rate of 1 ml min^{-1} corresponding to the maximum recovery. A 2 M NaCl solution (pH 9.0) was purified from Pb and Cd impurities (about 1.5 μg l^{-1}), before preconcentration and then diluted to the desired concentrations: NaCl solution was eluted through a microcolumn packed with Chelex-100 in NH_4^+ form.

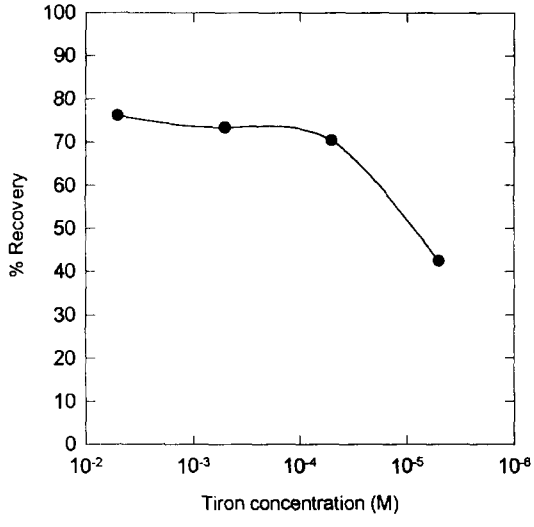

Fig. 8. Percentage recovery of cadmium as a function of Tiron concentration (pH = 9).

Table 4
Effect of different interfering agents on lead and cadmium recovery

Interfering agent	Recovery %	
	Pb	Cd
1 M NaCl	83 ± 1	52 ± 2
0.5 M NaCl	93.4 ± 0.9	70.8 ± 0.7
10.0 mg l^{-1} Poly	90.4 ± 0.9	73 ± 3
100.0 mg l^{-1} Poly	78 ± 3	60 ± 7
20.0 mg l^{-1} Ca + 2.0 mg l^{-1} Mg	82 ± 2	78 ± 2

Three replicates.

Table 4 shows recoveries obtained in the presence of the different interfering agents. The trend of the recoveries in the presence of NaCl is due to a competition between Cl^- and the metal complexes for the exchange sites of the resin, whereas Ca and Mg compete with the analytes for complexation. For all the agents considered the recovery was lower at higher interferent concentrations, but the interferences were not so large to hinder the use of the method for natural samples. In particular the method can be used for the analysis of sea water, whose ion strength is approximately 0.5 M.

3.5. On line procedure

The former experiments were performed by batch mixing ligand and sample. On-line mixing of sample and Tiron solutions allows a satisfactory recovery (92.7 ± 0.4%) of lead, but very low recoveries for Cd (28 ± 1%). This fact could be explained by considering the low kinetic of reaction for Cd-Tiron.

3.6. Enrichment and detection limits

Lead enrichments were initially evaluated for a preconcentration ratio of 10 (from 1 to 10 μg l^{-1} Pb). The recovery was highly satisfactory (95 ± 2) for this kind of samples and blank signals were under the detection limit. Recovery for a preconcentration ratio of 50 was also evaluated. Solutions containing 50 ng l^{-1} of Pb were preconcentrated up to 2.5 μg l^{-1} and the recovery

resulted 95.5%. In this case the blank levels were at 13 ng l^{-1} before preconcentration.

A similar approach was considered for Cd. Solutions (100 ng l^{-1}) were preconcentrated to 1 μg l^{-1} and gave a satisfactory recovery (76.0 ± 0.4%). The recovery percentage in solution containing 50 ng l^{-1} Cd and preconcentrated to 2.5 μg l^{-1} was slightly inferior: 69.1%.

For these enrichment procedures the blanks were purified using a method below detailed.

The detection limits of the technique, evaluated as three times the standard deviation of the blank (for the experiments with a preconcentration ratio of 50), were 9 ng l^{-1} for Pb and 7 ng l^{-1} for Cd.

3.7. Analysis of real samples

This preconcentration method was used for the analysis of Antarctic lake water and Turin drinking water. For these experiment the preconcentration ratio was 50 and purified Tiron was used (see below).

Pb and Cd were determined with the standard addition method in drinking water to be 218 ± 6 and 51 ± 2 ng l^{-1}, respectively. In Antarctic lake water (Carezza Lake, Ross Bay) Pb was found to be 22 ± 1 ng l^{-1} for Pb, while Cd resulted lower than the detection limit.

The accuracy of the method was checked by analysing a sample of uncontaminated sea-water from Antarctica spiked with 1 μg l^{-1} of Pb and 250 ng l^{-1} of Cd. The analysis was performed by standard addition method. The signal given by the original metal content, which is in the order of few tenths of ng l^{-1}, was subtracted as a blank signal.

The concentrations found were 950 ± 87 ng l^{-1} of Pb and 281 ± 6 ng l^{-1} of Cd, in good agreement with the expected values. The deviations (− 5.0% for Pb, + 12.4% for Cd) could be due to the sum of errors occurring during the procedure, i.e., in metal standard dilution, in loaded and eluted volumes and in the GFAAS measurements. Anyway the results are satisfactory, especially if the low concentration levels involved are taken into account.

These data confirm the applicability of the method to the determination of ultra-traces of metal ions in natural samples.

3.8. Tiron purification

The main source of contamination was found to be the impurity content of Tiron. Therefore the following methods for its purification were investigated: (1) crystallisation; (2) Chelex-100 treatment; (3) elution through silica RP-C18 after addition of 1 M 8-hydroxyquinoline to Tiron solution; and (4) elution through AGMP-1 functionalised with Tiron.

The crystallisation of Tiron was obtained taking advantage of its lower solubility in an acid medium. Concentrated HCl was gradually added (1 ml every day) to a saturated solution of Tiron (2.5 g in 6 ml of HPW) in order to obtain long thin crystals and to facilitate purification. In fact a flock precipitate would not be suitable for purification because of co-precipitation phenomena.

By the second method the metal impurities were bound to the resin owing to iminodiacetic groups.

Method (3) is based on the ability of 8-hydroxyquinoline to form neutral complexes with the metal ions which could be removed from Tiron solution by retention onto a C-18 microcolumn.

In the AGMP-1 method the resin exchange sites were saturated with Tiron. The saturation of the resin (10 ml of 1×10^{-2} M Tiron for 0.05 g resin) was evaluated spectrophotometrically by monitoring (at 290 nm) the concentration of Tiron in the effluent. Since the stability constants for metal-ligand complexes are greater for Tiron bound onto the resin than for the free one (solution) [13], it was possible to remove metal ions impurities by fluxing the solution of Tiron through a microcolumn filled with the so modified AGMP-1 resin.

These purification methods were formerly studied in our laboratory for the preconcentration of iron (see results in Table 5).

Table 5
Purification percentage efficiency

	Method 1	Method 2	Method 3	Method 4
% Efficiency	94.3	68.9	100	100

The last method was chosen because it is quick, simple, it does not require the addition of any reagent, it could be performed on-line and gives the best performance.

For this reason it was used also for Pb and Cd, whose concentrations in 1×10^{-2} M Tiron were about 5–6 μg l^{-1} (after 50-fold enrichment); using the last method the metal impurities in Tiron were reduced below the detection limit.

4. Conclusions

The preconcentration method developed to determine traces and ultratraces of Cd and Pb allows a precise and accurate determination of metal ions at low concentration (ng l^{-1}) in natural samples, and in the presence of interfering agents. Blanks are very low and detection limits are satisfactory.

The time required for preconcentration and determination of lead and cadmium levels close to the detection limit is about 30 min; the sample throughput increases if there is no need to reach such low concentrations. For instance it is possible to analyze nine samples in an hour at 100 ng l^{-1} level by loading 2.5 ml of the sample and eluting the analyte in 0.25 ml. This small volume is enough for several GFAAS determinations.

The method described can be used for several applications, not only for natural water samples but also for environmental or industrial samples. The procedure has been adapted in our laboratory also for the determination of aluminium [4] and iron.

References

[1] K. Robards and P. Worsfold, Analyst, 116 (1991) 549.
[2] J. Ruzicka and A. Arndal, Anal. Chim. Acta, 216 (1989) 243.
[3] V. Porta, O. Abollino, E. Mentasti and C. Sarzanini, J. Anal. At. Spectrom., 6 (1991) 119.
[4] M. Aceto, O. Abollino, C. Sarzanini, E. Mentasti and F. Mariconti, At. Spectrosc., 15 (1994) 237.
[5] Z. Fang, T. Guot and B. Welz, Talanta, 38 (1991) 613.
[6] Z. Fang, M. Sperling and B. Welz, J. Anal. At. Spectrom., 5 (1990) 639.
[7] M. Sperling, X. Yint and B. Welz, J. Anal. At. Spectrom., 6 (1991) 295.
[8] Z. Fang, Flow Injection Separation and Preconcentration, VCH, Weinheim, 1993.
[9] V. Porta, C. Sarzanini, O. Abollino, E. Mentasti and E. Carlini, J. Anal. At. Spectrom., 7 (1992) 19.
[10] V. Porta, C. Sarzanini, E. Mentasti and O. Abollino, Anal. Chim. Acta, 258 (1992) 237.
[11] G.F.R. Gilchrist, C.L. Chakrabarti, J. Cheng and D.M. Hughes, J. Anal. At. Spectrom., 8 (1993) 623.
[12] R.D. Hancock and A.E. Martell, Chem. Rev., 89 (1989) 1875.
[13] C. Sarzanini, E. Mentasti, M.C. Gennaro and E. Marengo, Anal. Chem., 57 (1985) 1960.

ELSEVIER

Talanta 44 (1997) 877–884

Talanta

Separation and preconcentration of iron(II) and iron(III) from natural water on a melamine-formaldehyde resin

Hayati Filik [a], Birsen Demirata Öztürk [b], Melek Doğutan [a], Gülçin Gümüş [b], Reşat Apak [a]

[a] *Department of Chemistry, Faculty of Engineering, Istanbul University, Avcılar, Istanbul, Turkey*
[b] *Department of Chemistry, Faculty of Science and Letters, Istanbul Technical University, Maslak, Istanbul, Turkey*

Received 24 April 1996; received in revised form 14 October 1996; accepted 14 October 1996

Abstract

A combined method for the preconcentration and selective spectrophotometric determination of both valencies of iron, i.e., Fe(II) and Fe(III), down to 0.4 μg l^{-1} has been developed. Iron(III) from synthetic and natural water samples has been concentrated on a melamine-formaldehyde resin at pH 5; iron(II) was not retained under identical conditions. The oxidized iron was concentrated on a second resin column. The iron in both columns was eluted with 1 M HCl solution and separately analyzed by the 1,10-phenanthroline-citrate spectrophotometric method. The effect of pH, adsorption and elution rates, and interferences on the developed procedure were investigated. Metal ions that can be retained by the resin at moderate concentrations, e.g., Al^{3+}, do not cause interference in more dilute solutions encountered in natural water samples. At least 160-fold volume enrichment can be easily obtained using an adsorption flowrate of 50 ml min^{-1}. A hydrothermal water sample was analyzed by the recommended procedure and by a literature method, and the results were statistically compared by *t*- and *F*-tests. © 1997 Elsevier Science B.V.

Keywords: Iron(II) and iron(III); Melamine-formaldehyde resin; Preconcentration; Separation

1. Introduction

Spectrophotometric determination of iron in different oxidation states in water has been a matter of concern in analytical chemistry since the mid 1950s [1]. The low concentration of iron present in natural waters (at mg l^{-1} levels) necessitates the selection of a suitable preconcentration procedure [2].

Most of the published spectrophotometric methods for the simultaneous determination of Fe(II) and Fe(III) involve the measurement of either valency in one sample portion, and of total iron, after oxidation or reduction, in another sample portion; the concentration of the other species is obtained by difference [3]. Such a procedure requires the usage of a selective photometric reagent capable of determining one of the valencies, usually the lower valency, of iron.

1,10-Phenanthroline has been shown to be a reliable colorimetric reagent for Fe(II) [4], but errors can arise in the presence of Fe(III) which can form a yellow complex with phenanthroline [1]. In this case, the absorbance of the Fe(II)-com-

PII S0039-9140(96)02132-7

plex is not stable due to the slow reduction of the ferric complex [5]. However when phenanthroline is used along with citrate, the latter as the masking reagent for Fe(III), both ferrous ion and total iron (after reduction with hydroxylamine or ascorbic acid) can be determined using this procedure [6].

Another reagent which selectively forms a coloured complex with Fe(II) but not with Fe(III) is ferrozine [3-(2-pyridyl)-5,6-bis(4-phenylsulphonic acid)-1,2,4-triazine] [7]. On the other hand, a ferric ion-specific reagent is tiron which may also enable the determination of total iron after catalyzing the autooxidation of Fe(II) to the ferric state in aerated solution [3].

On-line separation and preconcentration of both valencies of iron by a rapid and selective procedure is very important in flow injection analysis (FIA) which has received considerable attention in recent years [8,9]. For example, the Fe(II)-specific ferrozine may be used in this regard, enabling direct feeding of Fe(III) contained in the sample to AAS while the Fe(II)-ferrozine formed in-line is temporarily retained on a C_{18}-modified silica column and subsequently eluted with methanol [9]. This work aims to utilize the inexpensive and conventional phenanthroline–citrate reagent in conjunction with a melamine–formaldehyde preconcentrating resin column for developing a FIA-compatible spectrophotometric procedure for the simultaneous determination of Fe(II) and Fe(III) in natural waters.

The preconcentration and separation of elements by the use of chelating resins have been extensively reported and recently summarized [10]. Polyacrylonitrile [11], epoxypropyl methylacrylate grafted into a polyvinyl fiber with tannin [12], polyether foam [13], and polyether-type polyurethane foam [14,15] have been utilized as effective preconcentration agents for selectively retaining Fe(III) from water.

Melamine–formaldehyde resins having the methylol melamine functional groups [16], which have been used for long in textile-finishing and leather tanning operations [17] have recently been utilized in Cr(VI) preconcentration [18] and Cr(III)/Cr(VI) separation prior to AAS analysis [19]. Preliminary experiments showed that this resin could serve the purpose of selective preconcentration of the higher valency of iron, thereby giving rise to this work.

2. Experimental

2.1. Reagents

All chemicals used were of analytical grade (E. Merck), and distilled water was used throughout.

The melamine–formaldehyde resin was prepared from formaldehyde, NaOH and melamine according to the procedure set by Gams et al. [20], washed with 0.1 M HCl, 0.1 M NaOH and sufficient water in this order, dried, grounded, and classified to a particle size range of 500–600 mesh as described elsewhere [18]. The IR Spectrum of the resin was compared with that of the literature, and essential band assignments were made from the observed wavenumbers.

The stock solutions were prepared as follows:

Fe(III), 1000 ppm: 4.320 g of ammonium ferric alum was dissolved in 10 ml concentrated HCl and some water, and diluted to 500 ml with water.

Fe(II), 1000 ppm: 3.510 g Mohr's salt, i.e., $(NH_4)_2SO_4 \cdot FeSO_4 \cdot 6H_2O$, was dissolved in 2 ml concentrated HCl and some water, and diluted to 500 ml with water. (Deaerated water purged with N_2 was used for the Fe(II) solution) The Fe(II) stock solution was freshly prepared every week, and stored in the dark for inhibiting oxidation to Fe(III).

Both solutions were standardized by EDTA titration [21].

Phenanthroline, %0.2 (w/v): 0.2 g of 1,10-phenanthroline hydrochloride was dissolved in 100 ml hot water and cooled to room temperature.

2.2. Procedure for the preconcentration of iron(III) and iron(II) ions

A double-column procedure was used for preconcentrating iron(II) and iron(III) from synthetic and natural water samples. Two grams of the resin suspended in water was slurry-packed in each glass column (i.d. 1.0 cm) at a height of 8 cm and rinsed thoroughly before use.

The water sample containing up to 2 ppm of ferric ion and adjusted to an optimal pH of 5.0 (using acetic acid/sodium acetate buffer) was passed through the first column at a rate of 20–25 ml min^{-1}. The sample volume was usually taken as 250 ml. To the effluent of the first column were added several drops of concentrated (14 M) HNO_3 and concentrated H_2O_2 in hot solution so as to oxidize the Fe(II) to Fe(III) [22].

After oxidation, the pH was readjusted to five with sodium acetate and acetic acid, and the solution was passed through the second column as before. The originally present Fe(III) and Fe(II), the latter after oxidation, was retained by the first and second columns, respectively.

The iron retained in each column was eluted with 25 ml of 1.0 M HCl at a flow rate of 3 ml min^{-1} and analyzed by the phenanthroline method. The used resins were washed with water, 0.1 M NaOH, and finally with sufficient water until neutral prior to next use.

The effects of possible interferent ions were investigated under identical conditions with those of iron uptake. The interferent ions were added in varying amounts to 250 ml of 2 ppm Fe(III) solution, and the final mixture was passed through the resin column with subsequent analysis. The effect of the essential interferent, i.e., Al^{3+}, was further studied as a function of total metal concentration and pH. The dependence of iron recovery on pH, and on solution flowrates at adsorption and desorption were separately analyzed while keeping the other parameters constant.

2.3. Procedure for the simultaneous determination of iron(II) and iron(III) in synthetic and natural samples

The spectrophotometric method developed by Nigo et al. [6] was followed for determining both ferrous and total iron in a sample. To the acidic column eluate containing preferably 1–50 mg iron, 5 ml of 10% NH_2OH. HCl was added and the mixture was titrated dropwise with 5 M NH_3 solution until a pH of 2–3 was reached. After letting stand for 2 min, 10 ml of 25% diammonium hydrogen citrate solution was added to bring the pH to ~ 5. After the addition of 5 ml of 0.2% phenanthroline solution, dilution to a final volume of 50 ml was made. The absorbance at 512 nm of the resulting solution was measured against a reagent blank within 30 min. The acidic eluates of the first and second columns, when analyzed by this procedure, yielded the Fe(III) and Fe(II) concentrations, respectively, originally present in the water sample. All spectrophotometric analyses were accompanied by flame AAS for confirmation using the analytical wavelength of Fe at 248.3 nm; a spectral bandpass of 0.5 nm and a lamp current of 10 mA was selected with an air-acetylene flame for atomization.

The real sample containing both valencies of iron was collected from Yalova Termal hydrothermal water reserves, acidified with HCl (10 ml concentrated HCl to 1 l of water) before being brought to the laboratory, and immediately analyzed on the day of sample collection. An independent analysis for confirming the Fe(III) and Fe(II) results of the developed method was carried out by ion-exchanger colorimetry using the procedure set by Nigo et al. [6]. For this purpose, the phenanthroline–citrate reagent was used without and after the addition of hydroxylamine hydrochloride for the determination of Fe(II) and total Fe in two different sample aliquots, respectively, using Dowex 50W-X2 resin as the iron-concentrating medium from relatively large volumes of water. In the case of Fe(II) analysis alone where NH_2OH. HCl addition was omitted, dropwise neutralization of the acidic water sample with 5 M NH_3 solution was made after the addition of the citrate buffer so as to prevent any local hydrolytic iron precipitation possibilities.

2.4. Procedure for measuring the batch capacity of the resin for iron

Iron(III) solutions of concentration $(2.0–10.0) \times 10^{-4}$ M were contacted batchwise with the resin at a liquid-to-solid ratio of 200, i.e., 10 ml of solution per 50 mg of resin, in stoppered flasks placed in a thermostatic (25 ± 0.1°C) shaker/water bath for 4 h. The highest (saturation) amount of iron bound per unit mass of resin was noted.

2.5. Instruments

A Perkin-Elmer 300 atomic absorption spectrometer and a Hitachi 220 A UV-Visible spectrophotometer were used for iron determinations. The pH measurements were made with a Metrohm Herisau E-512 pH-meter equipped with a glass electrode. The infrared spectrum of the resin in KBr pellet was recorded with a ATI Unicam (Mattson 1000) FT-IR spectrometer within the wavenumber range of 4000–500 cm^{-1}.

3. Results and discussion

3.1. The resin functional groups and Fe(III) uptake

The IR-spectral band assignments (in cm^{-1}) showing the presence of—NH CH_2OH groups bound to carbon atoms of the resin were made as follows:

–O–H (OH bending): 1346.1 (s), C–OH (C–O stretch): 1061.5 (s), NH: 3346–3360 (m), NH: 1500 (w).

The selective uptake of Fe(III) over Fe(II) by the resin may partly be associated with the fact that ferric iron is a harder acid in the sense of HSAB Theory [23] showing a higher affinity to the hard O– and N– donor Lewis bases of the trimethylolmelamine structural units of the resin molecule. It has been well established in the literature that transition metal ions in high oxidation state tend to coordinate to hard σ donor-π donor ligands, and that in selective adsorption, inner-sphere complex formation may be preferred over ion-exchange [24]. Considering the predominantly hydrolytic complex environment of Fe(III) at the working pH (i.e., pH 5), the capability of mixed complex formation of Fe(III) (e.g., some Schiff-base-type bidentate N,O–donor ligands (L) form mixed hydroxo-complexes with ferric iron having the formula Fe^{III} $L(OH)_2$ constituting the predominant species in the neutral region) may reasonably explain the selective uptake of Fe(III) over Fe(II) on the resin having N– and O–donors [25]. Due to the complex nature of the melamine-formaldehyde polymer, it is quite difficult to exactly identify the mechanism of Fe(III) uptake, as in the case of polyether-type polyurethane foam where ether-like solvent extraction, ligand addition or exchange, anion exchange and cation chelation mechanisms could be involved [14,15,26].

3.2. Selection of optimal pH of preconcentration

The optimal pH of iron preconcentration was chosen in regard to both prevention of hydrolytic precipitation of Fe(III) at the ppm level and of Fe(II) oxidation to the ferric state. The percentage recovery of iron achieved when 250 ml of 1 ppm Fe(III) at various pH was passed through 2.0 g of resin in column is shown in Fig. 1. On the other hand, the non-retention of Fe(II) was clearly demonstrated where Fe(II) was not held by the resin between pH 2.0 and 5.9 (tested at 0.5 pH unit intervals). The influent and effluent pH were the same at pH 5 (where 100% Fe(III) recovery was observed) which was selected as the optimal pH in the successive experiments. Since the conjugate acid of the trimethylol melamine moiety has a pK_a of ~ 4 [16], the amine group should be available for iron binding at this pH.

The species distribution diagrams for the hydrolytic Fe(III) complexes, i.e., $FeOH^{2+}$, $Fe(OH)^{2+}$ and $Fe_2(OH)_4^{4+}$ in the heterogeneous

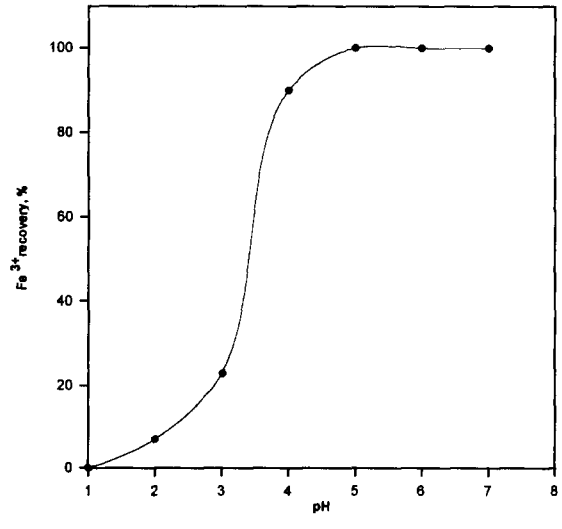

Fig. 1. Percentage recovery of iron as a function of pH.

system show that the solution becomes oversaturated with respect to solid amorphous $Fe(OH)_3$ over most of the pH range. However, additional polynuclear hydrolysis species occur as kinetic intermediates in the usually slow transition to $Fe(OH)_3$ (s) in the weakly acidic pH range [27]. Moreover, the upper limit of Fe(III) concentration that can remain in solution at a predetermined pH is also a function of total iron concentration. Thus, due to the slow character of the phase transition and to the additional iron complexation effect of acetate [28] used in the buffer for adjusting the pH of synthetic solutions, the uptake of Fe^{3+} ions at several ppm level from aqueous solutions of pH 5 could be investigated free from interference of hydrolytic precipitation within the relatively short time period of the experiments. Furthermore, iron(III), but not iron(II), has a tendency to form mixed hydrolysis complexes with N, O–donor ligands [25], which may also apply for the uptake by the resin. Besides hydrolytic equilibrium expectations, the selected pH is suitable from a kinetic standpoint as the oxidation of Fe(II) is very slow below pH 6 [27]. The rate of oxidation of Fe(II) in solutions of pH ≥ 5 has been reported to be first-order with respect to the concentrations of both Fe(II) and O_2 [27], and second-order with respect to the OH^- ion concentration [29]. Therefore Fe(II) present in a water sample may be safely determined along with Fe(III). However, it is still advisable to add at least ten-fold NH_2OH. HCl to the ferrous analyte solutions to prevent its oxidation to Fe(III) before the addition of phenanthroline [21] when the analyte does not originally contain Fe(III).

3.3. The flowrate at iron adsorption and elution, and eluant acid concentration

The uptake of ferric ions is very rapid as observed from nearly 100% recoveries with flow rates up to 50 ml min^{-1}. A precautious value of 25 ml min^{-1} was chosen as the adsorption flowrate in further experiments.

It was seen that 25 ml of 1.0 M HCl could effectively elute (with 100% recovery) the 250 mg Fe (III) retained in the column using a flowrate of 3 ml min^{-1}. In order to find out an optimal concentration factor (of iron from natural waters), two different eluant volumes, i.e., 10 and 25 ml, were selected using 0.1–2.0 M HCl as the eluant (Fig. 2). The effect of elution rate on recovery (Table 1) was tested using 25 ml of 1.0 M HCl as eluant; a precautious value of 3 ml min^{-1} was adapted in further experiments. As a conclusion, it may be deduced that iron(III) from relatively large amounts of natural water may be concentrated on the resin and eluted as described above with a high volume reduction factor useful for increasing analytical sensitivity.

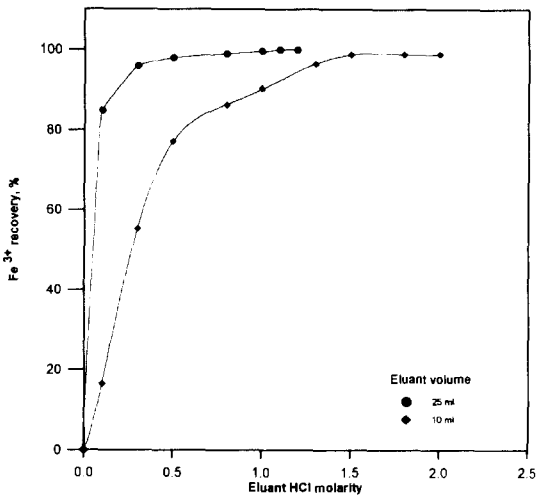

Fig. 2. Percentage recovery of iron as a function of eluant acidity.

Table 1
The effect of elution rate on iron recovery (eluant: 25 ml of 1.0 M HCl)

Elution rate (ml min^{-1})	Iron recovery, %
1–5	100
6	92
7	90
10	88

Table 2
Recovery and precision of the preconcentration and analysis of synthetic Fe(II)-Fe(III) mixture solutions at varying proportions (eluate volume = 25 ml)

A: Moderate concentrations (infiltrate volume = 250 ml)		B: Small concentrations (infiltrate volume = 4 l)	
C(mg l^{-1}) Fe(II)/Fe(III) in infiltrate	Recovery, % Fe(II)/ Fe(III)	C(μmol l^{-1}) Fe(II)/Fe(III) in infiltrate	Recovery, % Fe(II)/ Fe(III)
1.0/2.0	101/101	1.0/20[a]	96.0/96.5
1.0/1.0	100.6/100	0.6/12[a]	94.9/96.2
1.0/0.5	98.7/100	0.2/4.0[a]	95.8/98.4
0.5/3.0	100/100.3	0.2/0.2	96.0/97.1
0.5/0.5	100/100	4.0/0.2	98.7/97.2
RSD = 0.7%		RSD = 1.3%	

[a] A ratio of 1:20 Fe(II)/Fe(III) is meaningful in simulated natural water samples [9].

3.4. Preconcentration/analysis of Fe(II)-Fe(III) synthetic mixtures and precision

The analysis results of synthetic Fe(II)-Fe(III) mixture solutions at moderate and dilute concentrations are depicted in Table 2 using 250 ml^{-4} l infiltrate and 25 ml eluate volumes. The precision data for 8 determinations of Fe(II) + Fe(III) mixtures (at varying proportions) between 0.5–2.0 mg l^{-1} concentrations yielded an average relative standard deviation (RSD) of 0.7%, whereas the RSD was ca. 1.3% for mixture solutions between 0.2–20 μmol l^{-1}. At least 160-fold volume enrichment (from 4 l to 25 ml) could be easily achieved without serious loss of recovery efficiency and precision.

3.5. Calibration and precision

The calibration curves were perfectly linear, and when the factors of molar absorptivity, recovery and volume enrichment were taken into account, these calibration equations were found as:

$A_{512\ nm} = 1.94 \times 10^{-3}$ C for 500 ml

$A_{512\ nm} = 1.51 \times 10^{-2}$ C for 4 l samples, where C is the concentration of iron in the sample solution in μg l^{-1}. These curves were essentially identical for column-retained 'original' Fe(III) and first oxidized, then column-retained or 'converted' Fe(II). When the standard deviation of blank absorbance, calibration sensitivity (i.e., slope of the calibration equation) and literature coefficients [30] were considered together, the detection and quantification limits for 4 l samples were 0.4 and 1.3 μg l^{-1}, and for 500 ml samples 2.8 and 9.3 μg l^{-1} , respectively. Although adsorption from water volumes greater than 4 l was not employed, it is envisaged that lower detection limits may be attained. The developed method is probably capable of determining iron in most spring and coastal [31] waters, but not sensitive enough as required by oceanographic environments [29]. Since a preconcentration step is involved, the precision of the method is better than those of a great many direct spectrophotometric procedures [3,7].

3.6. Batch capacity of the resin for Fe(III) ions

The resin exhibited a Langmuir-type adsorption isotherm for iron (not shown). The saturation capacity was 7.2 mg Fe/g-resin. Naturally saturation would not be attained even with relatively large volumes of natural waters passed through the resin column.

3.7. Interferent ions and analysis of a real (hydrothermal water) sample

The following cations did not interfere at 100 ppm concentrations in the preconcentration and determination of 1 ppm Fe^{3+} ion: Mg^{2+}, Ca^{2+}, Cr^{3+}, Ni^{2+}, Co^{2+}, Zn^{2+}, Cu^{2+}, Cd^{2+}, Pb^{2+}. Aluminium(III) at 5 ppm level interfered, but

could be masked with phosphate or fluoride, necessitating higher concentrations of the latter (See Table 3). Probably Al^{3+} was retained in a similar binding mode as Fe^{3+}. The excessive amounts of Cl^-, NO_3^-, ClO_4^-, SO_4^{2-}, PO_4^{3-} and CH_3COO^- did not interfere provided that the pH did not exceed 5. Thus, most ions that bear the potential of accompanying iron in natural waters were either interference-free or could be masked easily without prolonging the time required for the recommended procedure.

Since Al^{3+} showed the potential of being the essential interferent in natural waters, it needed special treatment. Batch equilibration tests carried out by agitating 100 mg resin in 50 ml aqueous solution at pH 5 for 2 h yielded different results for iron and aluminium uptake whereas equilibration could not be attained under dynamic conditions. According to batch results, the ratio of the distribution coefficients (D) of Fe(III) and Al(III) on the resin, i.e., selectivity defined as D_{Fe}/D_{Al},determined separately, in binary mixtures and in ternary mixture solutions containing 3.6 ppm Fe^{3+}, 1.8 ppm Al^{3+} and 12.5 ppm F^- were 12.0, 10.2 and 38.4, respectively. When the initial metal concentrations were reduced prior to batch contact, i.e., to 0.4 ppm Fe^{3+} and 0.05 ppm Al^{3+}, either in separate solutions or in combination, iron retained its uptake efficiency on the resin while aluminium was not retained at all probably due to the increased abundance of the chemically inert polyhydroxo complexes in Al speciation [32].

Table 3
Aluminium interference and its elimination by masking (amount of iron(III) taken: 2 ppm)

Ion added, ppm			Fe recovery %
Al^{3+}	PO_4^{3-}	F^-	
1	—	—	70.0
2	—	—	69.5
5	—	—	69.5
10	—	—	57.7
—	100	—	100.0
—	—	100	100.0
5	100	—	100.0
5	—	100	100.0

Column experiments showed a different picture since 0.5 ppm Al^{3+}, either alone or in the presence of 10 ppm F^-, was not retained on the resin. When 0.4 ppm Fe^{3+} alone, in combination with 0.05 ppm Al^{3+}, or in a ternary mixture containing 0.05 ppm Al^{3+} and 0.35 ppm F^-, were passed through the resin, iron uptake was 100% in all three cases, and Al^{3+} did not pose any problems. These observations lead to a hypothesis capable of explaining the competition of Al^{3+} on the selective resin sites responsible for Fe^{3+} uptake and of the elimination of Al interference: ferric iron forms the more stable hydroxo-complexes while Al^{3+} forms the more stable fluoride complexes ($\log \beta_3$ values of F^- are 12 and 15 for Fe^{3+} and Al^{3+}, respectively. Moreover the Al^{3+}-F^- system has a $\log \beta_4$ value of 17.8) [28]. In batch experiments, iron uptake is slightly increased in the presence of fluoride as Fe(III) gets undersaturated with respect to the colloidal ferric hydroxide precipitation, and as polyhydroxo-iron(III) complex formation is diminished as a result of F^- complexation. Iron most probably binds to the resin-methylolamine moieties in the form of mixed complexes, and one or two sites around its coordination sphere are sufficient to anchor iron to the resin even if the other sites are preoccupied by OH^- or fluoride. Al^{3+} interference, normally observed at elevated concentrations, is eliminated with F^- due to selective complexation with this anion. On the other hand, Al^{3+} may not compete at reduced concentrations—without necessitating F^- - due to coordinative saturation and kinetic inertness of its polyhydroxo-complexes [32]. Aluminium should also form less stable complexes with N– and O–donor groups of the resin, because the complexing affinity of Fe(III) toward such donors involves the use of d-electrons (e.g., d^5) while Al(III) lacks such valence electrons. Considering the reduced concentration levels of Fe(III) and Al(III) in natural waters and similar samples, no interference from Al was expected (and actually observed) under dynamic column conditions; 100% iron recoveries were easily recorded without a secondary aid such as fluoride.

Hydrothermal water as the real sample was selected because of its known Fe (II) content[27],

which may sometimes be as high as 0.5 μM. This water was analyzed in 5 l volumes both by the recommended procedure and by ion-exchanger colorimetric literature method [6] yielding Fe^{3+}: 21.5 μg l^{-1}, Fe^{2+}: 34.4 μg l^{-1}, and total iron: 56.1 μg l^{-1} as the mean values ($n = 8$). The population means and standard deviations were compared by two-tailed t- and F-tests within 95% confidence limits [33]. The two procedures were not essentially different in precision and accuracy.

References

[1] A.E. Harvey, Jr., J.A. Smart and E.S. Aims, Anal. Chem., 27 (1955) 26.
[2] R.B. Willis and D. Sangster, Anal. Chem., 48 (1976) 59.
[3] M. Endo, I. Sasaki and S. Abe, Fresenius J. Anal. Chem., 343 (1992) 366.
[4] A.A. Schilt, Analytical Applications of 1,10-Phenanthroline and Related Compounds, Pergamon, Press, New York, 1967.
[5] G.S.R. Krishnamurti and P.M. Huang, Talanta, 37 (1990) 745.
[6] S. Nigo, K. Yoshimura and T. Tarutani, Talanta, 28 (1981) 669.
[7] M.M. Gibbs, Water Res., 13 (1979) 295.
[8] Z. Fang, Flow Injection Separation and Preconcentration, VCH Publishers, Weinheim, 1993.
[9] S. Krekler, W. Frenzel and G. Schulze, Anal. Chim. Acta, 296 (1994) 115.
[10] Z. Su, X. Chang, G. Zhan, X. Luo and Q. Pu, Anal. Chim. Acta, 310 (1995) 493.
[11] A.R. Türker, N. Arık and O. Şanlı, Ondokuzmayıs University, Bull. Faculty Sci., 2 (1990) 179.
[12] M. Kin, J. Appl. Polym. Sci., 39 (1990) 855.
[13] M. Drtil, J. Tölgyessy, and T. Braun, Fresenius J. Anal. Chem., 338 (1990) 50.
[14] K.F.G. Brackenbury, L. Jones and K.R. Koch, Analyst, 112 (1987) 459.
[15] T. Braun, Fresenius J. Anal. Chem., 333 (1989) 785.
[16] J.K. Dixon, N.T. Woodberry and G.W. Costa, J. Am. Chem. Soc., 69 (1947) 599.
[17] Kirk Othmer's Encyclopedia of Chemical Technology, Vol. 2, Wiley-Interscience, New York, 1978.
[18] B. Demirata, Fresenius J. Anal. Chem., 343 (1992) 357.
[19] B. Demirata, I. Tor, H. Filik and H. Afşar, Fresenius J. Anal. Chem., in press.
[20] A. Gams, G. Widmer and W. Fisch, Helv. Chim. Acta, 24 (1941) 309.
[21] Y. Okura, Bunseki Kagaku, 27 (1978) 477.
[22] S. Palagyi, T. Braun, Z. Homonnay and A. Vertes, Analyst, 117 (1992) 1537.
[23] R.G. Pearson, Hard and Soft Acids and Bases, Dowden, Hutchinson and Ross, Stroudsburg, Pa., 1973.
[24] C. Lepetit and M. Che, J. Mol. Catal., 100 (1995) 147.
[25] H. Cankurtaran, Ph.D. Thesis, Yıldız Technical University, Istanbul, 1996.
[26] S. Palagyi and T. Braun, in Z.B. Alfassi and C.M. Wai (Eds.), Preconcentration Techniques for Trace Elements, CRC Press, Boca Raton, FL, 1992.
[27] W. Stumm and J. Morgan, Aquatic Chemistry, Wiley-Interscience, New York, 1981.
[28] J.A. Dean, Lange's Handbook of Chemistry, 12th Edn., McGraw-Hill, New York, 1979.
[29] D.W. King, J. Lin and D.R. Kester, Anal. Chim. Acta, 247 (1991) 125.
[30] D.A. Skoog and J.J. Leary, Principles of Instrumental Analysis, 4th Edn., New York, 1992.
[31] H. Hong and D.R. Kester, Limnol. Oceanogr., 31 (1986) 512.
[32] J. Kragten, Atlas of Metal-Ligand Equilibria in Aqueous Solution, Ellis Horwood (Wiley), 1978.
[33] J.C. Miller and J.N. Miller, Statistics for Analytical Chemists, Ellis Horwood PTR Prentice Hall, New York, 1994.

ELSEVIER

Talanta 44 (1997) 885–890

Talanta

Self-assembled biotinylated disulfide derivative monolayer on gold electrode for immobilizing enzymes

Pingang He [a], Jiannong Ye [a], Yuzhi Fang [a,*], Junichi Anzai [b], Tetsuo Osa [b]

[a] *Department of Chemistry, East China Normal University, Shanghai 200062, People's Republic of China*
[b] *Pharmaceutical Institute, Tohoku University, Aobayama, Sendai 980, Japan*

Received 28 June 1996; accepted 10 October 1996

Abstract

Based on self-assembled biotinylated disulfide derivative monolayer on gold electrode, the sensors immobilized monolayer or multilayer membranes composed of avidin and biotinlabeled glucose oxidase (B·GOD) or of avidin-B·GOD complex (ABC) and B·COD were prepared. The present technique may be useful for controlling the enzyme content of the sensors in molecular level by repeating the deposition of enzyme layers. The sensors have the characteristics of shorter response time, higher sensitivity. The linear range is from 6.0×10^{-6}–5.0×10^{-3} M. The sensor can be used for more than 1 month and can be reactivated. The sensor was used to determine glucose in human blood serum, and the results are satisfactory. © 1997 Elsevier Science B.V.

Keywords: Avidin; Biotin; Enzyme sensors; Glucose oxidase; Immobilization; Self-assembled monolayer

1. Introduction

In order to fabricate enzyme sensors, considerable effort has been devoted to the development of various techniques for immobilizing enzymes. Recently, much attention has been devoted to molecular-level modification of electrode surface with enzymes [1–3]. Self-assembled monolayers are widely used to modify solid electrode surface in molecular-level [4–6]. We have recently reported to prepare multilayer enzymes based on self-assembled aminoethanethiol monolayer and the advantage of strong affinity between avidin-biotinlabeled enzyme on ITO electrode [7,8]. In this paper we present that based on self-assembled biotinylated disulfide derivative monolayer on gold electrode monolayer or multilayer enzyme membranes composed of avidin and biotinlabeled glucose oxidase (B·GOD) or of avidin and B·GOD complex and B·GOD (ABC-B·GOD) are prepared. The sensors have the characteristics of shorter response time, and higher sensitivity.

2. Experimental section

2.1. Materials

Biotinlabeled glucose oxidase (B·GOD, 200 units mg mg^{-1} protein, biotin content: 5.1 mol

* Corresponding author. Fax: +86 21 2576217.

PII S0039-9140(96)02133-9

mol^{-1} protein) were purchased from Sigma Chemical (St. Louis, USA). Avidin (13.2 units mg^{-1}, from chicken egg white) was obtained from Calzyme Lab. (Csan Luis Obispo, USA). Bis(*N*-biotinylhydrazidoethyl) disulfide (BDS) obtained from Dojindo Chem. Lab. (Japan). Glucose was obtained from Wako (Japan). Dulbecco's phosphate buffer saline (PBS) (PH = 7.4) was used throughout. 0.1 M BDS solution was prepared with DMSO, and diluted to 1.0×10^{-4} M with ethanol.

2.2. Electrode preparation

Gold electrodes (0.7 mm diameter, 0.5 cm length, 0.11 cm^2 area). The Gold electrode was washed with 1: HNO_3, acetone and water in ultrasonic waves, then was pretreated by electrocycling in 1.0 M H_2SO_4 (1.7 V–(−0.2)V versus Ag/AgCl) with scan rate of 10 V/S for 5 min [9]. The procedure for the modification of the surface of gold electrodes is schematically illustrated in Fig. 1. The gold electrode was immersed in 1.0×10^{-4} M BDS/ethanol for 14 h for electrode 1. Electrode 2 was prepared by immersing electrode 1 in avidin (50 mg ml^{-1}) and B·GOD (50 mg ml^{-1}) alternately for 30 min. For the construction of electrodes 3–6, a multiple Avidin-B·GOD Complex (ABC) solution which was prepared by mixing an equal volume of avidin (50 mg ml^{-1}) and B·GOD (25 mg ml^{-1}) solution was used. Electrode 3 was prepared by immersing the electrode 1 in ABC solution for 2 h. Electrodes 4, 5 and 6 were prepared by the modification of electrode 1 with ABC for 2 h and then B·GOD (50 mg ml^{-1}) for 30 min alternately each.

2.3. Determination method

All electrochemical measurements were made with Model 173 potentiostat/Galvanostat and Model 175 Universal Programmer (EG and G Princeton Applied Research). A conventional three electrode setup was employed with the enzyme modified gold electrode as the working electrode, Pt wire as auxiliary electrode, and Ag/AgCl as the reference electrode. The oxidation current of H_2O_2 produced by enzyme reaction was measured at 0.65 V versus Ag/AgCl. All measurements were performed at room temperature. When checking the long-term stability of the sensors, the sensors were stored in PBS buffer at 4°C if not use.

3. Results and discussion

3.1. Electrochemical characteristic of electrode 1

The biotin-functionalized self assembled monolayers on gold can change the property of the electrode surface [10]. Fig. 2 shows the cyclic voltammograms of $Fe(CN)_6^{3-}$ ions at bare gold electrode and electrode 1. The biotin-functionalized self-assembled monolayer can increase the electrode reaction of $Fe(CN)_6^{3-}$ ions at gold electrode surface. This is different from self-assembled *n*-alkylthiol monolayers which prevent the electrode reaction of $Fe(CN)_6^{3-}$ ions at the electrode surface [11]. Fig. 3 plots the oxidation current of the bare and electrode 1 at 0.65 V versus Ag/AgCl as a faction of H_2O_2 concentration. The results show that the biotin functionalized self-assembled monolayer also increase the transport of H_2O_2 molecules to gold electrode surface where H_2O_2 should oxidized. It suggests that electrode 1 is useful for construction of enzyme sensors which detect H_2O_2 produced by the enzyme reaction.

3.2. The responses of electrodes 2–6 to glucose

We and other groups have recently reported the use of an avidin-biotin complexation technique for immobilizing enzymes on the electrode surface [7,8,12–14]. Electrodes 2–6 were prepared by utilizing the strong affinity among avidin, biotinlabeled enzyme and biotin monolayer which was self assembled on gold electrode surface. Fig. 4 shows a typical response of electrodes 2–6–10 mM glucose. Electrode 2 which has a single layer of B·GOD bridged by avidin layer exhibited evident current response to glucose. However, the response was low because of monolayer of B·GOD. In order to enhance the response, a much large amount of B·GOD can be expected to be immobilized directly in the form of ABC.

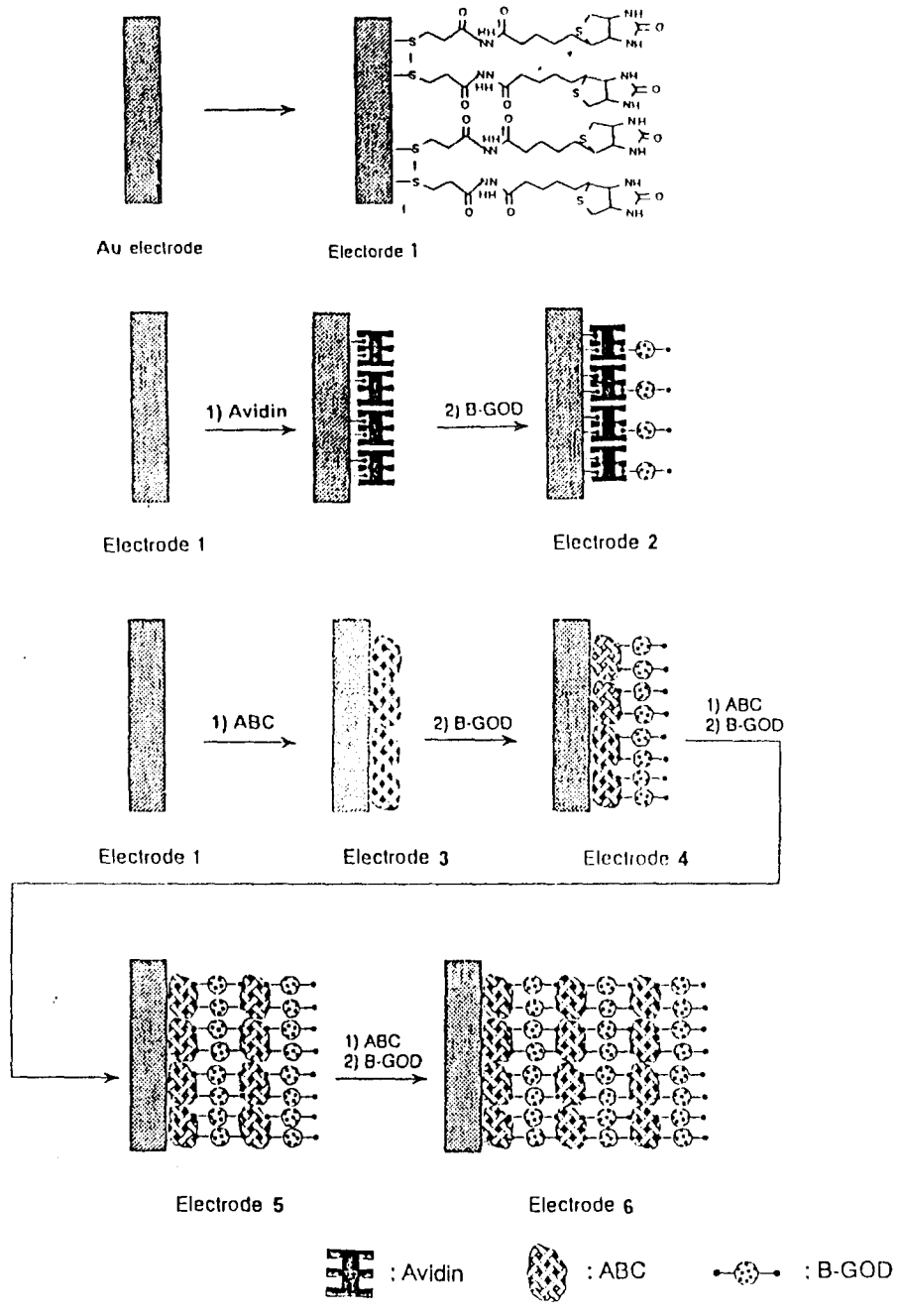

Fig. 1. Preparation of electrodes 1–6.

Electrode 3, which was prepared by immobilizing ABC membranes through complexation with biotin monolayers of electrode 1, showed a higher current response to glucose than electrode 2 (see Fig. 4b), indicated that more enzyme molecules were immobilized on gold electrode surface. On

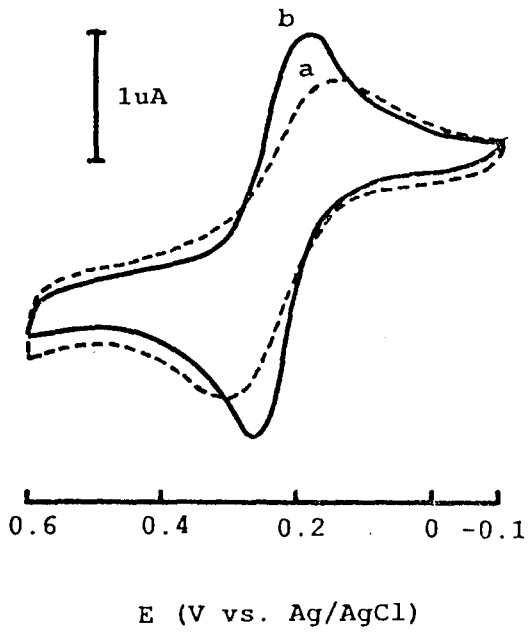

Fig. 2. Cyclic voltammograms of 1.0×10^{-3} M $K_3[Fe(CN)_6]$ on the bare gold electrode (a) and the electrode 1 (b). Scan rate: 100 mV s^{-1}.

the other hand, because each avidin protein contains four sites to biotin and the B·GOD used is substituted with an average 5.1 biotin residues per molecule, in principle, ABC membrane surface

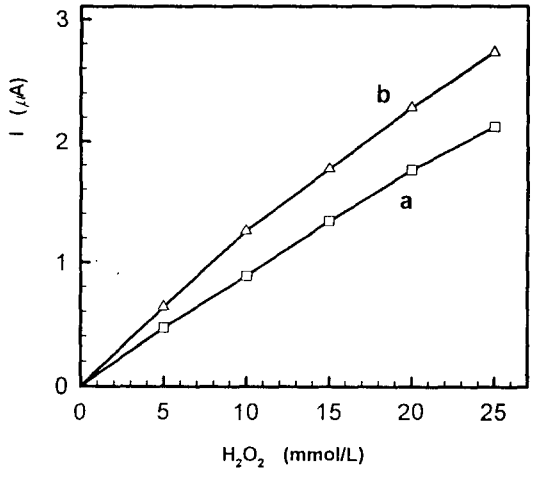

Fig. 3. Current response of bare gold electrode (a) and electrode 1 (b) to H_2O_2. Applied potential: 0.65 V (versus Ag/AgCl).

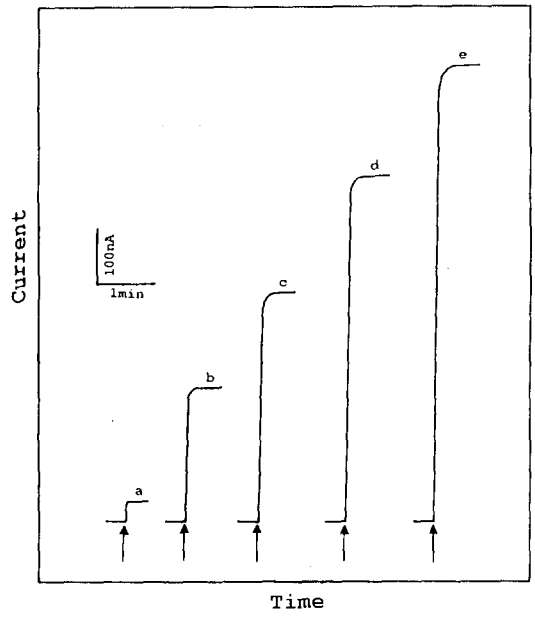

Fig. 4. Typical respone of electrode 2(a), 3(b), 4(c), 5(d), and 6(e) to 10 mmol l^{-1} glucose. Glucose was added to the sample solution at the time indicated by arrow.

can further load B·GOD. When electrode 3 was immersed in B·GOD solution, more B·GOD was immobilized on the electrode surface. Therefore, the current response of electrode 4 to glucose was further increased (as shown Fig. 4c). Electrode 5 and electrode 6 were prepared by depositing ABC and B·GOD alternately on the electrode for 2 times and 3 times, respectively. As shown in Fig. 4(d, e) the current values of the electrodes depend linearly on the number of ABC-B·GOD layers. For the reason, the alterant and repeated deposition of ABC and B·GOD thus provides a useful method for regulating the response sensitivity of enzyme sensors.

Fig. 5 shows the calibration curves for electrodes 2–6. The electrode 6 was most sensitive among the electrodes and the linear range of glucose was $6.0 \times 10^{-6} - 5.0 \times 10^{-3}$ M. On the other hand, although the electrodes 2–5 showed less sensitive than did electrode 6, the linear range of glucose was higher. The useful calibrations were over more than 30 mM which covers the blood glucose level of diabetic patients. This means that the technique may be useful for con-

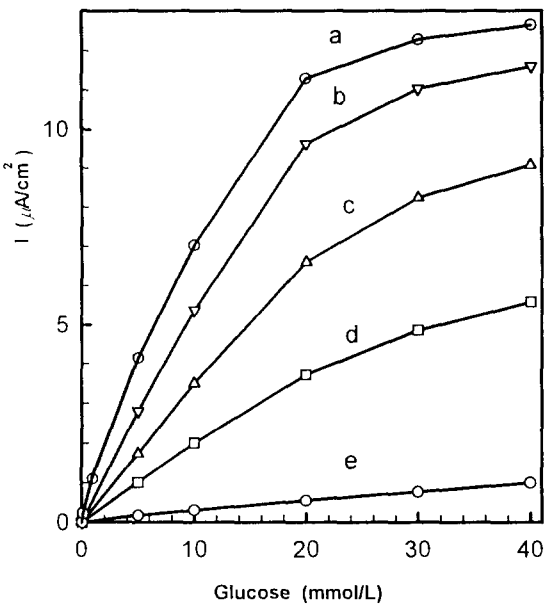

Fig. 5. Calibration curves of electrodes 2–6. Electrode: 6(a), 5(b), 4(c), 3(d) and 2(e).

trolling the performance characteristics of enzyme sensors such as low and up detection limit and magnitude of the output current by simply changing the number of deposition of the enzyme layer on the electrode surface.

3.3. Response time of electrodes

Table 1 shows the response time of electrodes 2–6–10 mM glucose. The results confirm that for all sensors the amperometric response are very rapid and response time is independent of the amount of B·GOD on the electrode surface.

3.4. Stability

In order to evaluate the long-term stability of the sensors, we measured the current response of

Table 1
Response time to glucose of electrodes 2–6

Electrodes	2	3	4	5	6
Response time(s)	2.1	3.1	2.8	3.7	3.0

Table 2
Comparison of response to glucose between before and after reactivation for electrodes 4–6

Electrodes	Beginning (nA)	After 2 weeks (nA)	
		No reactivation	Reactivation
4	385	294	404
5	589	437	570
6	782	571	758

the sensors to 10 mM glucose for 35 days. Although decrease in out-put current was observed in the first 5 days, after that period, the current values remained almost constant. This tendency in long-term stability was common to all electrodes 2–6. Meanwhile, the sensitivity of sensors preserved for long-term or/and used for many times could be recovered by immersing in 50 mg ml^{-1} avidin and 25 mg ml^{-1} B·GOD mixed solution for 30 min. In Table 2 comparison with the current values between before and after reactivation for the electrodes 4–6 which were preserved for 2 weeks conforms that the electrodes can be repeatedly reactivated.

3.5. Determination of glucose in blood serum

Human blood serum, 100 ml, was added in 8 ml PBS solution, and the current response of glucose at electrode 6 was determined. The results of glucose in three human blood serum samples are shown in Table 3. They are approached by the results determined by spectroscopic method and the recovery is among 90–110%.

4. Conclusion

We have demonstrated that the self-assembled biotinylated disulfide derivative monolayer is useful for constructing monolayer or multilayer enzyme membranes through avidin–biotin complexation. The method for the enzyme immobilization in molecular-level has the characteristics of fabricating enzyme sensors which have fast

Table 3
The determination results of glucose in blood serum

Glucose content 10^{-4} mol l^{-1}	Glucose added 10^{-4} mol l^{-1}	Total Glucose measured 10^{-4} mol l^{-1}	Recovery (%)	Glucose content in blood serum (10^{-3} mol l^{-1})	Value of Glucose by spectroscopic method (10^{-3} mol l^{-1})
0.95	1.0	2.04	109.0	7.60	7.45
1.01	1.0	2.11	110.0	8.08	7.86
1.12	1.0	2.02	90.0	8.96	8.74

response to glucose, simply regulating the response sensitivity of the enzyme sensors by changing the number of deposition of the enzyme layers, and repeatedly recovering the sensitivity of sensors with avidin and biotinlabeled enzyme complex solution. The sensors were used to determine glucose in human blood serum and the results are quite satisfactory.

Acknowledgements

This work was partially supported by Grants-in-Aid for scientific research from the National Commission of Education of P.R. China.

References

[1] A.P.F. Turner, I. Karube and G.S. Wilson, Biosensors: Fundamentals and Applications, Oxford University Press, Oxford, 1987.
[2] C. Bourdiooln, J.P. Bourgeois and D. Thomas, J. Am. Chem. Soc., 102 (1980) 4231.
[3] P. Bianeo, J. Haladjian and C. Bourdidon, J. Electranal. Chem., 293 (1990) 151.
[4] C.E.D. Chidsey, C.R. Bertozzi, T.M. Putuinski and A.M. Mujsee, J. Am. Chem. Soc., 112 (1990) 4301.
[5] M.A. Ryrant and J.E. Pemberton, J. Am. Chem. Soc., 113 (1991) 8284.
[6] A.J. Bard, H.D. Abruna, C.E. Chidsey, L.R. Faulkner, S.W. Feldberg, K. Itaya, M. Majda, O. Melroy, R.W. Murray, M.D. Porter, M.P. Soriaga and H.S. White, J. Phys. Chem., 97 (1993) 7147.
[7] P.G. He, T. Takahashi, J. Anzai, Y. Suzuki and T. Osa, Pharmazie, 49 (1994) 8.
[8] P.G. He, T. Takahashi, T. Hoshi, J. Anzai, Y. Suzuki and T. Osa, Pharmazie, 49 (1994) 8.
[9] S. Tamagaki, K. Fukada, H. Sunita and H. Tagaki, W. Chem. Exp., 6 (1991) 695.
[10] L. Haussling, H. Ringdorf, F.J. Schmitt and W. Knoll, Langmuir, 7 (1991) 1837.
[11] M.D. Porter, T.B. Bright, D.L. Allara and C. Chidsey, J. Am. Chem. Soc., 109 (1987) 3559.
[12] M. Snejdarkove, M. Rehak and M. Offo, Anal. Chem., 65 (1993) 665.
[13] P. Pantano and W.G. Kuhr, Anal. Chem., 65 (1993) 623.
[14] T. Osa, Appl. Biochem. Biotechnol., 41 (1991) 41.

ELSEVIER

Talanta 44 (1997) 891–896

Talanta

Potentiometric study of the protonation equilibrium of Tris(Hydroxymethyl) aminomethane in aqueous sodium perchlorate solutions at 25°C: construction of a thermodynamic model

R. Gil, M.S. Corbillón, M.A. Olazabal *, J.M. Madariaga

Kimika Analitikoaren Departamentua, Euskal Herriko Unibertsitatea, 644 P.K., E-48080, Spain

Received 15 December 1995; received in revised form 10 September 1996; accepted 17 October 1996

Abstract

The protonation equilibrium of the Tris(Hydroxymethyl)aminomethane (TRIS) has been studied using an automated potentiometric system. The temperature was kept constant at 25°C and the ionic strength was 0.1, 0.5, 1.0, 2.0 and 3.0 mol dm^{-3} in $NaClO_4$. The experimental constants, obtained at different ionic strengths, were correlated by means of the modified Bromley methodology (MBM) and the thermodynamic protonation constant found to be $\log {}^0\beta = 8.07 \pm 0.01$. Those values together with some others for NaCl medium were used to construct a thermodynamic model on both molal and molar scales for the protonation equilibrium of TRIS. © 1997 Elsevier Science B.V.

Keywords: Acid-base equilibria; Bromley's parameters; Ionic medium influence; TRIS

1. Introduction

A previous work [1] about fluoride determination by ion selective electrode in samples with high Al^{3+} concentrations has shown the high stability of aluminium-Tris(hydroximethyl)aminomethane (TRIS) complexes, although such complexes are not quantitatively described in the literature.

Metal-ligand complexes have been studied by the potentiometric technique using glass electrodes when the acid-base behavior of both, the metal and the ligand, is well established, i.e., when a proper chemical model (thermodynamic stability constant values and an estimation method for the activity coefficients computation of all the species) is defined. Such model is available for aluminium in pure sodium perchlorate using an approach developed by Baes and Mesmer [2] to estimate the ionic medium effects. Other approach used to estimate activity coefficient values is the Modified Bromley Methodology (MBM) [3,4] used by our working group for the last 5 years, that requires the knowledge of the interaction parameters of all the cations and anions present in the solution.

* Corresponding author.

PII S0039-9140(96)02134-0

In relation to the protolysis equilibrium of Tris(hydroxymethyl)aminomethane some works have been found in the literature but their results are not useful enough for our study. The use of single NaCl medium is reported in two papers [5,6], giving stoichiometric formation constant values which coincide within their random errors. From other papers, the thermodynamic constant value seems to be well defined [7,8]. However values in $NaClO_4$ medium reported by several authors are not enough information to have knowledge of the behavior of the system in our experimental conditions.

In order to define this system, i.e., to confirm the thermodynamic constant and calculate the Bromley's interaction parameters in a pure ionic medium, a systematic potentiometric study of the protonation constant of tris(hydroxymethyl)aminomethane at different ionic strengths has been performed using $NaClO_4$ as the ionic medium.

The protonation constants obtained in this work, together with data found in the literature will be used to build up a chemical model by the Bromley's methodology which will explain the behavior of this acid–base system in perchlorate and chloride media.

2. Experimental

2.1. Reagents and solutions

The chemicals used were all of analytical grade and used without further purification. Sodium perchlorate monohydrate (Fluka p.a.) was employed as the ionic medium. A stock solution of $NaClO_4$ was prepared and its concentration was tested gravimetrically after evaporation of an aliquot at 110°C. All solutions of this study have been prepared in a single $NaClO_4$ medium.

The following stock solutions were prepared and used as titrants:

$$C_{T1} = A_1 \text{ mol dm}^{-3} HClO_4 + (I - A_1) \text{ mol dm}^{-3} NaClO_4$$

$$C_{T2} = A_2 \text{ mol dm}^{-3} NaOH + (I - A_2) \text{ mol dm}^{-3} NaClO_4$$

where I is the total ionic strength. The ionic strengths studied were 0.1, 0.5, 1.0, 2.0 y 3.0 mol dm^{-3}. The C_{T2} solutions were prepared in N_2 atmosphere to avoid CO_2 contamination.

These solutions were standardized against tris(hydroxymethyl)aminomethane [9] and potassium acid phthalate [10], respectively.

The test solution were prepared with the following general composition:

$$C_B = B \text{ mol dm}^{-3} \text{ tris(hydroxymethyl) aminomethane} + I \text{ mol dm}^{-3} NaClO_4$$

where the values of B were 10^{-1}, 5×10^{-2}, 10^{-2} or 5×10^{-3} mol dm^{-3}.

2.2. Apparatus and experimental technique

The experiments were carried out as potentiometric titrations with constant ionic strength using an automated system developed in our laboratory which can control up to three titrations at the same time [11].

The titration cell with magnetic stirring was immersed in a thermostatic bath at 25.0 ± 0.1°C. The titrations were performed in a N_2 atmosphere to avoid CO_2 contamination during the experiments. The glass electrode (Methrom 6.0101.100) and the double-junction reference electrode [Ag-AgCl(s), Methrom 6.0726.100] were connected to an operational preamplifier in order to adapt the electric signal to the voltmeter. The electromotive force measurement was carried out with a Hewlett-Packard VXI E1326B voltmeter (resolution of six decimal digits and accuracy of 0.008% of the read + 15 μV) connected to a computer. The titrant additions were performed with a Metrohm Dosimat 665 burette with a precision of ± 0.01 ml. The potentiometric measurements were made with the following galvanic cell:

$$\text{Ag, AgCl(s)}/I \text{ mol dm}^{-3} NaClO_4 \text{ sat} \in \text{AgCl//Test solution/Glass electrode} \quad (1)$$

where I is the ionic strength of the solutions. As can be seen reference electrode has been designed including $NaClO_4$ as inert solution to minimize liquid junction potential.

Each titration took around 15 h and at least three different concentration were carried out for each ionic strength studied. Each titration was repeated at least twice in order to ensure the reproducibility of the data. For each titration it was considered that equilibrium was reached when the electromotive force measurement was kept constant during 5 min in a $\pm$ 0.05 mV interval.

2.3. Determination of h

The free hydrogen ion concentration, $[H^+] \cong h$, was determined by measuring the emf. of cell Eq. (1) in the course of the titrations. At 25°C the emf of the cell may be expressed as in Eq. (2) and Eq. (3).

$$E = E_0 + g \log h + E_j(h) \quad (2)$$

$$E_j(h) = j_{ac}\, h + j_{bas}\, k_w\, h^{-1} \quad (3)$$

E_0 value is specific for each titration carried out and is calculated in the first points (acid plateau) of each titration where no TRIS equilibrium is present. The value of the autoprototolysis constant of water (k_w) was determined previously for each ionic medium by means of potentiometric ionic media titrations. These parameters (E_0 and k_w) were calculated using a derivation of Gran's method and numerically refined by the non linear least squares computer program Model Function version [12] of Letagrop.

Acid and basic liquid junction potential coefficients (j_{ac} and j_{bas}, respectively) were determined from potentiometric ionic media titrations [13] as well. As liquid junction potential values depend only on the ionic strength, they can be considered as constant for each ionic strength in the latter potentiometric titrations with tris(hydroxymethyl)aminomethane.

3. Results

The protonation equilibria of tris(hydroxymethyl)aminomethane can be written as in Eq. (4)

$$H^+ + Tr \rightleftharpoons HTr^+ \quad (4)$$

and the corresponding stoichiometric protonation constant for a given medium of constant ionic strength can be expressed as in Eq. (5) where the superscript indicates the ionic strength.

$$^I\beta = \frac{[HTr^+]}{[H^+][Tr]} \quad (5)$$

The data were treated by means of graphical and numerical methods.

In a first approach to know the value of the protonation constant and to search some possible systematic errors in the total concentration of the reagents used, a graphical treatment was carried out [14]. The experimental $\bar{n}$ values ranged between 0 and 1 in the interval $1 < pH < 11$, which confirm the presence of one protonation step and the absence of systematic errors in the experiments. As an example, Fig. 1 shows an example of $\bar{n}$ function when $I = 2$ M.

The values obtained in the graphical treatment were numerically refined with two different programs the Nytit version [15] of the Letagrop program and Bstac11 program [16], minimizing the absolute square error sum of the measured

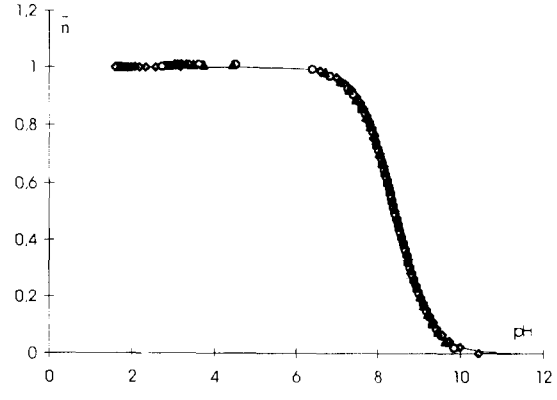

Fig. 1. Experimental $\bar{n}$ values plotted as a function of pH in 2 M $NaClO_4$ medium at different tris(hydroxymethyl)aminomethane concentrations levels.

Table 1
Stoichiometric protonation constant for tris-(hydroxymethyl)aminomethane protonation at different ionic strengths in $NaClO_4$ medium, obtained by the different numerical methods

Ionic strength (mol dm^{-3})	$\log {}^0\beta$		
	NYTIT	BSTAC	Proposed values
0.1	$8.06_5 \pm 0.01$	8.056 ± 0.008	8.06 ± 0.01
0.5	8.04 ± 0.05	8.091 ± 0.004	8.091 ± 0.004
1.0	8.199 ± 0.004	8.216 ± 0.002	8.207 ± 0.008
2.0	8.422 ± 0.002	8.418 ± 0.001	8.420 ± 0.002
3.0	8.64 ± 0.01	8.650 ± 0.006	8.65 ± 0.01

potential (U_E). Both programs have different minimization algorithms and different systematic error detection strategies.

The values obtained by this two numerical treatment programs are compared in Table 1. As it can be seen, the values from the different numerical treatments are equal within the limits of experimental error. The proposed value of the stability constants for $I = 0.1$, 1, 2 and 3 M ionic strengths have been calculated averaging the values obtained by the two numerical treatment programs (Nytit and Bstac). However for $I = 0.5$ M the error associated to the formation constant value was completely different with the two programs. As precision with Nytit is more than ten times larger, only the result obtained by Bstac has been considered. Fig. 1 also shows the fit between the experimental curves $\bar{n} = f(-\log h)$ and the theoretical plot of $\bar{n}$ versus $(-\log h)$ constructed with the protonation constant in $NaClO_4$ at the different ionic strengths, proposed in this work and listed in Table 1.

4. Discussion

As stated in the introduction, one of the aims of this work is to develop a thermodynamic model in order to explain the behavior of the protolysis of tris(hydroxymethyl)aminomethane in single $NaClO_4$ media. There are several literature references to the protonation constant of tris(hydroxymethyl)aminomethane at 25°C in $NaClO_4$ and NaCl media [5,6].

The chemical model has been constructed by means of the Modified Bromley Methodology, MBM [3,4]. In this method, it is necessary the knowledge of at least three stoichiometric constant values, in the same media, at different ionic strengths in order to calculate the thermodynamic constant value of the equilibria and the corresponding interactions parameters for each species taking part in the equilibrium.

The thermodynamic constant ${}^0\beta_i$ for the protonation equilibria of tris(hydroxymethyl)aminomethane can be expressed as Eq. (6):

$$ {}^0\beta_i = \frac{\{HTr+\}}{\{Tr\}\{H^+\}} = \frac{[HTr^+]\gamma_{HTr+}}{[Tr]\gamma_{Tr}[H^+]\gamma_{H+}} \quad (6) $$

where γ is the molar activity coefficient and $\{\}$ indicates activity. Combining Eq. (5) and Eq. (6), the expression to correlate the stoichiometric protonation constant can be written as:

$$ \log {}^0\beta = \log {}^I\beta + \log \gamma_{TrH+} - \log \gamma_{H+} - \log \gamma_{Tr} \quad (7) $$

The individual activity coefficients on the molar scale of the charged species, γ_i, can be substituted using the Bromley function, Eq. (8), where $A = 0.5111$ $dm^{3/2}$ $mol^{-1/2}$, I is the ionic strength on the molar scale, z_M the ionic charge of M, z_M the charge of the ionic species with the opposite sign to M and C_X its molarity.

$$ \log \gamma_M = -\frac{Az_M^2 I^{1/2}}{1+I^{1/2}} + \sum \mathring{B}_{MX}(|Z_M| + |Z_X|)^2 \frac{C_x}{4} \quad (8) $$

The parameter $\mathring{B}_{MX}$ can be expressed as in Eq. (9), where B_{MX} is the interaction parameter of the ion pair MX on the molar scale.

$$\mathring{B}_{MX} = \frac{(0.06 + 0.6B_{MX})|z_M z_X|}{[1 + (1.5I/|z_M z_X|)]^2} + B_{MX} \quad (9)$$

In the case of uncharged species the activity coefficient is expressed by means of the molar salt coefficient S by using an expression similar to that proposed by Long and Mc Devit (Eq. (10)) [17]:

$$\log \gamma_{MX} = S_{MX,\text{ionic medium}} I \quad (10)$$

Rearranging Eq. (7) and making use of Eq. (8) Eq. (9) Eq. (10) it is possible to obtain expression Eq. (11) to correlate the protonation constant at different ionic strength

$$\log^0\beta = \log^I\beta + \mathring{B}_{TrH^+,ClO_4^-} I + \mathring{B}_{H^+,ClO_4^-} I + S_{Tr,NaClO_4} I \quad (11)$$

This expression depends only on the value of the thermodynamic constant for the equilibrium taking place and the interaction parameters (B) or salt coefficient (S) of the different ionic or neutral species.

The value of $B_{H^+,ClO_4^-} = 0.1815 \pm 0.0005$ was previously determined [3] while the thermodynamic constant and the rest of the interaction parameters have to be calculated. The correlation of our proposed values in Table 1 was made by means of the program Model Function version [12] of Letagrop The results obtained from Eq. (11) are the following:

$$\log^0\beta = 8.07 \pm 0.01,\ B_{TrH^+,ClO_4} = 1.02 \pm 0.02 \text{ and } S_{Tr,NaClO_4} = 1.05 \pm 0.02$$

Fig. 2 shows the fit between our proposed $\log^I\beta$ values and the theoretical curve obtained with these results. The obtained thermodynamic constant value coincide with the values reported by Bates and Hetzer [7] (8.069) and by Datta et al. [8] (8.074).

The data collected in Table 1 and those bibliographic stoichiometric constants reported for NaCl [5,6] were finally used to define the thermodynamic model in Cl^- as well as ClO_4^- medium, by correlating both systems at the same time [14]. The results on both molal and molar scales are collected in Table 2 and the fit for molar data can be observed

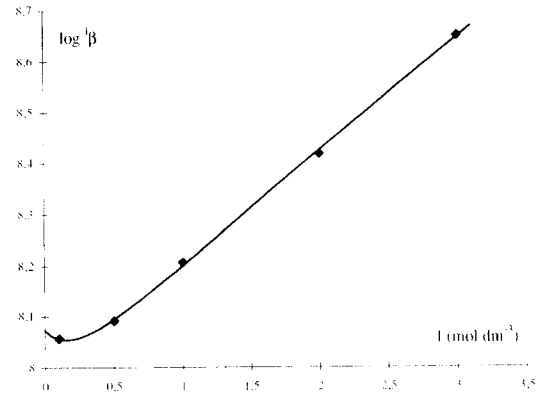

Fig. 2. Variation of log β with ionic strength together with the theoretical function.

in Fig. 3. With this model the stoichiometric constant for the protonation of TR1S can be obtained in both Cl^- or ClO_4^- salt medium or mixture of both at any ionic strength lower than 3 mol dm^{-3}. The uncertainty in the B and S parameters is similar for both media (NaCl and $NaClO_4$) although their values are quite different.

As it can be observed in Fig. 3, even if the stoichiometric values proposed in both media could be considered similar, the general shift of both system is different, showing a slight convex distribution for NaCl medium and a concave one in the $NaClO_4$ medium. The behavior of this system is similar to those obtained for other compounds having a amine group in their structure, as can be seen in the diethanolamine case [18].

Table 2
Thermodynamic protonation constant and Interaction parameters on molal and molar scales obtained with the Modified Bromley Theory in $NaClO_4$ as well as NaCl media

$\log^0\beta \pm 3\sigma(\log^0\beta)$	Molar scale 8.071 ± 0.006	Molal scale 8.067 ± 0.007
$NaClO_4$ medium	$B_{TrH^+,ClO_4} = 1.01 \pm 0.06$	$B_{TrH^+,ClO_4} = 0.77 \pm 0.06$
	$S_{Tr,NaClO_4} = 1.04 \pm 0.06$	$S_{Tr,NaClO_4} = 0.76 \pm 0.06$
NaCl medium	$B_{TrH^+,Cl} = -0.06 \pm 0.06$	$B_{TrH^+,Cl} = -0.23 \pm 0.04$
	$S_{Tr,NaCl} = -0.02 \pm 0.06$	$S_{Tr,NaCl} = -0.19 \pm 0.04$
U	6.47×10^{-4}	4.52×10^{-4}

Where U is the square cuadratic errors.

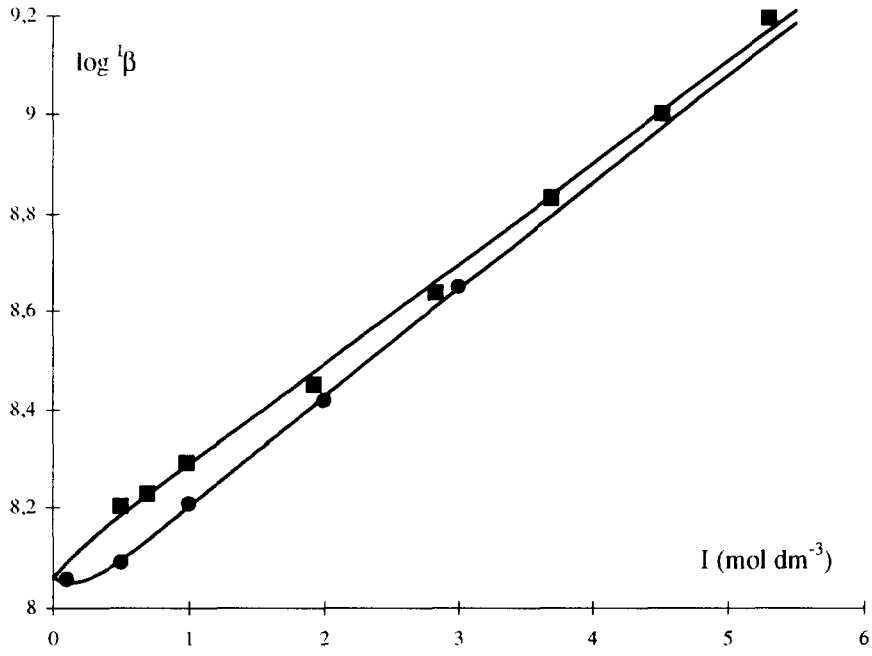

Fig. 3. Graphical representation of the experimental values of the constants in NaCl (■) and $NaClO_4$ (●) media together with the theoretical function.

Although somebody can argue the small difference between the two lines in Fig. 3, especially at high ionic strengths, the different behavior is important from the methodological point of view. For example we have observed that a convex shape is directly related with low or even negative values of the interaction parameters (B or S). A concave shape is always obtained with positive B and S values for all the species playing the equilibrium; as the B values increase, the concavity of the $\log \beta/I$ plot is more pronounced. A near linear shape seems to be related with similar values of the B and S parameters, where the corresponding estimated γ_i values of the different species are nearly equal at high ionic strengths; in such situations the slope of the $\log \beta/I$ plots is directly related to the activity coefficient of the third species participating in the equilibrium.

References

[1] M.S. Corbillón, M.P. Carril, J.M. Madariaga and I. Uriarte, Analyst, 120 (1995) 2227.
[2] C.F. Baes and R.E. Mesmer, The Hydrolysis of Cations, 1976, Wiley, New York.
[3] G. Borge, R. Castaño, M.P. Carril, M.S. Corbillón and J.M. Madariaga, Fluid Phase Equilibria, 121 (1996) 85.
[4] L.A. Bromley, AIChEJ, 19 (1973) 313.
[5] M. Izaguirre and F. Millero, J. Sol. Chem., 16 (1987) 827–834.
[6] D. Palmer and D. Wesolowski, J. Solution Chem., 16 (1996) 7, 571.
[7] G. Bates and H.B. Hetzer, Anal. Chem., 65 (1961) 667.
[8] S.P. Datta, A.K. Grzzybowski and BA Weston, J. Chem. Soc., (1963) 792.
[9] G. Bates and H.B. Hetzer, Anal. Chem., 33 (1961) 1285.
[10] H. Jeffery, J. Basset, J. Mendham and R.C. Denney, 'Vogel's Textbook of Quantitative Chemical Analysis', Wiley, Longman, London, 1989, p. 293.
[11] R. Cazallas, L.A. Fernandez, N. Etxebarria and J.M. Madariaga, Lab. Robotics Automation, 15 (1993) 161.
[12] L.G. Sillen, Acta Chem. Scand., 16 (1969) 159.
[13] F.J.C. Rossotti and H. Rossotti, The Determination of Stability Constants, 1961, McGraw-Hill Book Company, New York.
[14] R. Castaño, N. Etxebarria and J.M. Madariaga, J. Chem. Soc. Dalton Trans. (1994) 2729.
[15] L.G. Sillén, Acta Chem. Scand, 25 (1971) 1521.
[16] C. de Stefano, P. Mineo, C. Rigano and S. Sammartano, Annali di Chimica, 83 (1993) 243.
[17] F.A. Long and W.F. McDevit, Chem. Rev., 51 (1952) 119.
[18] A. Lopategi, R. Castaño, N. Etxebarria and J.M. Madariaga, J. Chem. Soc. Dalton Trans., (1995) 3843.

ELSEVIER

Talanta 44 (1997) 897–907

Talanta

Divalent cations speciation with three phosphonate ligands in the pH-range of natural waters

Véronique Deluchat, Jean-Claude Bollinger *, Bernard Serpaud, Claude Caullet

Laboratoire des Sciences de l'Eau et de l'Environnement, Faculté des Sciences, 123 avenue Albert Thomas, 87060 Limoges, France

Received 11 April 1996; received in revised form 18 October 1996; accepted 21 October 1996

Abstract

AMP and HEDP complexation constants for seven divalent cations (Ca, Cu, Cd, Fe, Ni, Pb and Zn) have been determined by acid–base titrations at 25 ± 0.5°C, at constant ionic strength (0.1 M KNO_3) with Martell and Motekaitis's computer programs. Speciation diagrams enable us to compare AMP, HEDP and TPP complexing properties. AMP complexes more strongly all seven divalent cations than HEDP and TPP, which have similar ligand behavior. Among the divalent cations studied here, the ligands have lowest affinity with calcium and usually higher with copper. In all the cation/ligand systems, the major species are ML and MHL which are charged species. The uncharged ionic species Ca_2Y^0, CaH_4X^0 and CdH_2Y^0 (H_6X = AMP and H_4Y = HEDP) which can potentially exist in solid phase, cannot be neglected. Moreover hydroxide complexes have to be taken into consideration in the complexation constant determinations and in the environmental impact. © 1997 Elsevier Science B.V.

Keywords: Complexation; Divalent cations; Phosphonic acids; Speciation

1. Introduction

Common washing powders contain surfactants, builders, peroxides and enzymes. Sodium tripolyphosphate (TPP) is the oldest builder, but phosphorus is now known to be a major factor in the eutrophication of lakes and rivers. The phosphorus in TPP detergents can account for 50% of the phosphorus in natural waters [1]. To combat eutrophication, the phosphate content in natural waters must be decreased and the most effective way to do this would be to decrease the amount of phosphorus in detergents.

The main TPP substitutes are zeolites, nitrilotriacetic acid, citrate, phosphonates and polycarboxylates [1,2]. Phosphonates or polycarboxylates improve the action of zeolites and other detergent compounds by their complexing behavior, especially with calcium and heavy metal cations. This is of interest because calcium deactivates the surfactants, and heavy metal cations catalyse peroxide decomposition. The EEC has recently established ecological criteria (decision no. 95/365/CE [3]) for the attribution of an 'Ecolabel' to formulations for textile detergents. In this study, we determine protonation and complexation constants with various cations for two phosphonic acids frequently encountered in detergent formu-

* Corresponding author. Fax: + 33 555 457459.

PII S0039-9140(96)02136-4

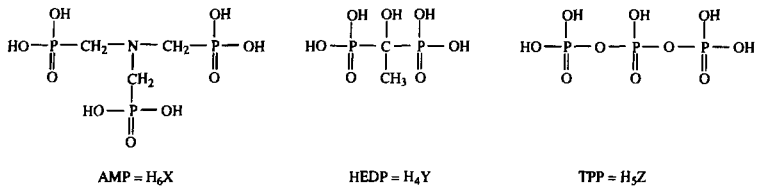

Scheme 1. Phosphonic acid formulas.

lations: nitrilotris(methylenephosphonic acid) AMP and 1-hydroxyethane-1,1′-diphosphonic acid HEDP (see Scheme 1).

Like TPP, these compounds will enter the ecosystem with domestic waste waters. Although AMP and HEDP have a very low biodegradability, HEDP is almost totally decomposed in surface waters when exposed to sunlight [4] and AMP is totally decomposed into various primary products [5]. However, before this abiotic degradation process begins, they are able to participate in cation mobilisation from river sediments. Thus we determine AMP and HEDP complexing properties with cations normally present in natural waters (Ca(II), Fe(II)), and with heavy metal cations (Cu(II), Zn(II), Ni(II), Cd(II), Pb(II)) able to come from industrial wastes. Some complexation constants have been previously published, and in some cases with a great number of figures, however most authors do not indicate precisely the nature of all complexed species taken into account in their calculations. The present study was carried out to determine these equilibrium constants paying special attention to the reproducibility of the calculated values and with a special emphasis on the computational process.

Stability constants were used to draw up speciation diagrams indicating major species present in natural waters (pH range from 5 to 9), thereby enabling us to determine the interference of hydroxide ligands. AMP and HEDP complexing behaviors are compared with that of TPP, in order to evaluate their environmental impact. In fact if the complexing properties of these compounds have already been studied with some cations, a forecast of their complexing behavior in the natural media has never been done.

2. Materials and methods

Equilibrium constants were calculated from data obtained by potentiometric titrations. pH titrations were done with a Metrohm 716-DMS automatic titrator. The combined glass electrode (Ag-AgCl, Metrohm 6.0233.100) was calibrated by hydrochloric acid titration with sodium hydroxide. Martell and Motekaitis [6] computer programs were used to analyse the pH data. Our stability constants were determined according to IUPAC recommended procedure [7] for testing the potentiometric apparatus and its technique for the pH measurement of metal-complex equilibrium constants with the glycine/nickel(II) system ($I = 1$ mol l^{-1} NaCl, 25°C). Experiments were carried out twice, and in duplicate by two manipulators (eight experiments with each system, protonation and complexation). Our protonation constants coincide exactly with IUPAC values. Taking into account standard deviations, our values for complexation constants are in good agreement with, though always slightly higher than, IUPAC values.

AMP and HEDP are pure grade Fluka products. Metal salts (nitrate) are pure grade compounds. The cation salt solutions were standardised with EDTA according to classic methods. The phosphonic acid and cation concentrations were 2.10^{-3} mol l^{-1}.

All the potentiometric titrations were performed at 25 ± 0.5°C in 0.1 mol l^{-1} KNO_3 solution and under purified nitrogen stream. Each

Table 1
Protonation constants ($I = 0.1$ mol l^{-1} (KNO_3), 25 ± 0.5°C)

	AMP		HEDP	
	Literature[a]	Present work	Literature[a]	Present work
$\log K_1$	12.1	12.5 ± 0.2	11.2	11.0 ± 0.2
$\log K_2$	7.3	7.22 ± 0.03	7.00	6.9 ± 0.1
$\log K_3$	5.86	5.90 ± 0.02	2.79	2.7 ± 0.1
$\log K_4$	4.64	4.59 ± 0.03	1.8	1.6 ± 0.2
$\log K_5$	1.5	1.6 ± 0.3		
$\log K_6$	0.3	0.5 ± 0.3		

i, is the number of acid functions, $K_i = [H_iL]/\{[H^+][H_{i-1}L]\}$.
[a] Taken from [10,11].

experiment was carried out at least three times, each one in triplicate.

3. Determination of equilibrium constants

When determining equilibrium constants various data must be taken into consideration:

- experimental data: concentrations, volume, pH,
- theoretical data: water ionic product, activity coefficients.

The protonation and complexation constants are obtained using an iterative method. The computer program calculates a pH value as close as possible to the observed pH:

$pH_{calc} = f$(experimental and theoretical data, equilibrium constants) = experimental pH.

The main difficulty is deciding when the iteration should stop, because in most cases the values of the calculated equilibrium constant keep varying but at levels not significant with respect to the uncertainty on the pH measurements.

The uncertainty of each one of these parameters leads to the uncertainty of equilibrium constants. The main problem is caused by the pH because it is difficult to calibrate precisely the electrode, especially at $pH \geq 10.5$. Water ionic product in 0.1 mol l^{-1} KNO_3 medium at 25°C is taken as $10^{-13.78}$ [8].

The data treatment is carried out according to the following systematic procedure:

- first, the data are analysed considering every species (phosphonate or hydroxyde complexes) which might exist;
- secondly, speciation diagrams are drawn up to show the complexed species present in solution;
- finally, the data treatment is performed again considering only the interfering species, and in the pH-range where phosphonate complexed species are present.

The use of this procedure allows to obtain reliable stability constants. Moreover, the treatment of more than ten experiments contributes also to determine a reliable standard deviation ($\sigma_{(n-1)}$) of the calculated stability constants.

Protonation constants were determined with the PKAS computer program [6] (Table 1). Considering i as the number of acid functions, we define

$$K_i = [H_iL]/\{[H^+][H_{i-1}L]\}$$

for the equilibrium

$$H^+ + H_{i-1}L \rightleftarrows H_iL$$

where the charges are omitted for easier printing.

There is good agreement between calculated and experimental pH, and between literature and present protonation constants values. The high uncertainty in $\log K_1$ is linked to the pH uncertainty in basic media. Whole protonated species represent a very low amount in the pH-range of the experiments, thus it is difficult to determine precisely their stability constants. Anyway, Grenthe [9] considers stability constant uncertainty of 0.05 (in log units) as a very high precision.

Complexation constants were determined with the BEST computer program [6] (Table 2). For each equilibrium:

$$MH_{(i-1)}L + H^+ \rightleftarrows MH_iL$$

Table 2
Complexation constants ($I = 0.1$ mol l^{-1} (KNO_3), 25 ± 0.5°C), $K_{MH_iL}^{MH_{(i-1)}L} = [MH_iL]/\{[MH_{(i-1)}L][H^+]\}$ $\beta_{MH_iL} = [MH_iL]/\{[M][L][H^+]^i\}$

		AMP				HEDP			
		Literature[a]		Present work		Literature[a]		Present work	
		log K	log β	log K	log β	log K	log β	log K	log β
Cu(II)	ML	17.4		17.4 ± 0.2		11.84		12.0 ± 0.2	
	MHL	6.4	23.8	6.35 ± 0.09	23.78 ± 0.06	7.47	19.31	5.4 ± 0.2	17.3 ± 0.2
	MH2L	4.7	28.5	4.57 ± 0.06	28.36 ± 0.06	4.80	24.11	3.0 ± 0.4	20.1 ± 0.5
	MH3L	3.5	32.0	3.46 ± 0.09	31.8 ± 0.1				
	MH4L	0	32.0	1.4 ± 0.6	33.3 ± 0.6				
Ni(II)	ML	11.1		11.3 ± 0.3		5.64		8.62 ± 0.09	
	MHL	8.3	19.4	8.28 ± 0.08	19.6 ± 0.2	9.14	14.78	6.96 ± 0.04	15.6 ± 0.1
	MH2L	5.8	25.2	5.67 ± 0.02	25.3 ± 0.2	6.08	20.86	4.8 ± 0.1	20.3 ± 0.2
	MH3L	4.5	29.7	3.4 ± 0.4	28.5 ± 0.6				
Cd(II)	ML	11.6		12.2 ± 0.2		5.98		8.7 ± 0.1	
	MHL	7.0	18.6	7.16 ± 0.06	19.4 ± 0.2	9.33	15.31	7.5 ± 0.1	16.3 ± 0.1
	MH2L	5.7	24.3	5.68 ± 0.05	25.0 ± 0.2	5.58	20.89	4.5 ± 0.2[b]	20.7 ± 0.3
	MH3L	4.8	29.1	4.13 ± 0.08	29.2 ± 0.2				
Pb(II)	ML			15.8 ± 0.1					
	MHL			6.7 ± 0.2	22.5 ± 0.2				
	MH2L			5.16 ± 0.06	27.7 ± 0.2				
	MH3L			3.8 ± 0.1	31.4 ± 0.3				
	MH4L			1.9 ± 0.6	33.6 ± 0.4				
Zn(II)	ML	16.4		16.3 ± 0.2		8.19		10.3 ± 0.1	
	MHL	6.1	22.5	6.1 ± 0.1	22.5 ± 0.1	8.01	16.2	6.27 ± 0.04	16.6 ± 0.2
	MH2L	5.1	27.6	4.89 ± 0.05	27.3 ± 0.2			3.8 ± 0.3	20.2 ± 0.5
	MH3L	4.1	31.7	4.0 ± 0.2	31.38 ± 0.05				
	MH4L	1.7	33.4	2.5 ± 0.2	33.8 ± 0.2				
Ca(II)	ML	7.5		7.6 ± 0.2		6.04		6.2 ± 0.2	
	MHL	9	16.5	8.9 ± 0.1	16.6 ± 0.1	8.16	14.2	7.67 ± 0.07	13.9 ± 0.1
	MH2L	6.6	23.1	6.30 ± 0.07	22.9 ± 0.06	7.63	21.83		
	MH3L	5.5	28.6	5.1 ± 0.1	28.0 ± 0.1				
	MH4L			4.1 ± 0.4	32.1 ± 0.4				
	M2L			2.9 ± 0.4	10.5 ± 0.4	3.63	9.67	4.5 ± 0.2	10.7 ± 0.2
Fe(II)	ML	13.5		12.7 ± 0.2				12.9 ± 0.3	
	MHL	6.49	19.99	6.4 ± 0.3	19.2 ± 0.3			4.87 ± 0.05	17.8 ± 0.3
	MH2L	5.41	25.4	6.30 ± 0.3	25.88 ± 0.08			3.3 ± 0.3	21.0 ± 0.4
	MH3L	4.2	29.6						

[a] Taken from [10,11].
[b] Occurrence of the insoluble complex species $CdH_2L_{(s)}$ [12].
[c] Immediate formation of an insoluble compound $Pb_2L_{(s)}$ [12].

we define a stepwise formation constant:

$$K_{MH_iL}^{MH_{(i-1)}L} = [MH_iL]/\{[MH_{(i-1)}L][H^+]\}$$

and an overall stability constant:

$$\beta_{MH_iL} = [MH_iL]/\{[M][L][H^+]^i\}$$

Although omitted, the electrical charges on MH_iL species are not the same depending on the ligands X^{6-}, Y^{4-} and Z^{5-} (see Scheme 1).

The greater interference of hydroxide/cation complexes with HEDP than with AMP might explain the better agreement obtained with AMP. There is a higher disagreement between experimental and calculated pH at basic pH, especially with Cu, Zn and Pb. This might be due to difficulties in the pH calibration at basic pH and uncertainties concerning the hydroxide/cations formation constants (which were not determined from our experimental data, but taken from the literature [10,11]). It is difficult to estimate constants for species representing less than 18% for the whole pH-range.

During our previous study [12], hydroxide/cation formation constants were also calculated, which explains the gap between complexation constant values. The Zn/HEDP complexation constants determined then are not fully reliable because of a zinc solution purity problem.

Sawada et al. [13,14] neglected the interference of hydroxide/cation/phosphonic acid ternary complexes and also the presence of higher complexes such as M_2L or ML_2, but such species can perturb the pH adjustment. It is very difficult to evaluate the contribution of such complexes under our experimental conditions. We usually worked only with ratio M/L = 1, and therefore could precisely determine the stability constants of the common species such as ML, MHL...

Since the concentrations of calcium cations are probably higher than those of phosphonic acids in natural waters, we also studied the complexation behavior for a ratio Ca/L = 2, thus enabling us to determine M_2L complexation constants. We also studied the possibility of CO_2 interaction with the Ca^{2+}/phosphonic acid system [15]. Atmospheric CO_2 does not lead to pertubations on the complexation properties.

4. Discussion

Our values of complexation constants with AMP confirm previous observations by Sawada et al. [13,14]:

- In the case of transition-metal complexes, the K_{MHX} constants for Cu, Zn and Pb are similar and always smaller than the second protonation constant of AMP (7.22), but Ni and Cd data do not follow such a rule.
- In the case of calcium complexes, K_{MHX} is higher than K_{HX} and K_{MX}.

The M–N bond of the transition metal complexes would be strong and not affected by the first protonation of the complex which would occur on the O^- of the phosphonate group. On the other hand, the M–N bond of the alkaline earth metal complexes would be mainly ionic and thus, very weak, therefore the first protonation of the complex would rupture this weak bond and occur on the nitrogen atom [13,14].

In any case, differences between MH_iX and $MH_{i-1}X$ logarithmic constants ($i \geq 1$ with Cu, Zn, Cd and Pb; $i \geq 2$ with Ca and Ni) are close (1– 2 log units), indicating that they correspond to a protonation on a free O^- of the phosphonate group. This is confirmed since this is also observed for HEDP cations stability constants. The gap from 1 to 2 log units between these differences can be explained by electrostatic interactions occurring during the various protonations.

The HEDP hydroxyl group might interfere in the cation complexation [16,17], explaining the higher difference between MY^{2-} and MHY^- logarithmic constants with Cu, Zn and Fe. This interference is also used to explain the special behavior of HEDP with calcium where $K_{MHY} > K_{MY}$ [18,19].

4.1. Ligand affinity towards various cations

Complexing classification was estimated by considering the total fraction of cation linked to the ligand, calculated from our AMP and HEDP stability constants. TPP stability constants were taken from studies [20,21] with similar experimental conditions (temperature and ionic strength). The ligand complexation properties with the various cations are determined in the pH-range of natural waters (5–9), with ligand and cation concentrations corresponding to our experimental conditions (2.10^{-3} mol l^{-1}), and also with phosphonate concentrations nearer to those encountered in natural media (2.10^{-7} mol l^{-1}), always with a cation/ligand ratio M/L = 1.

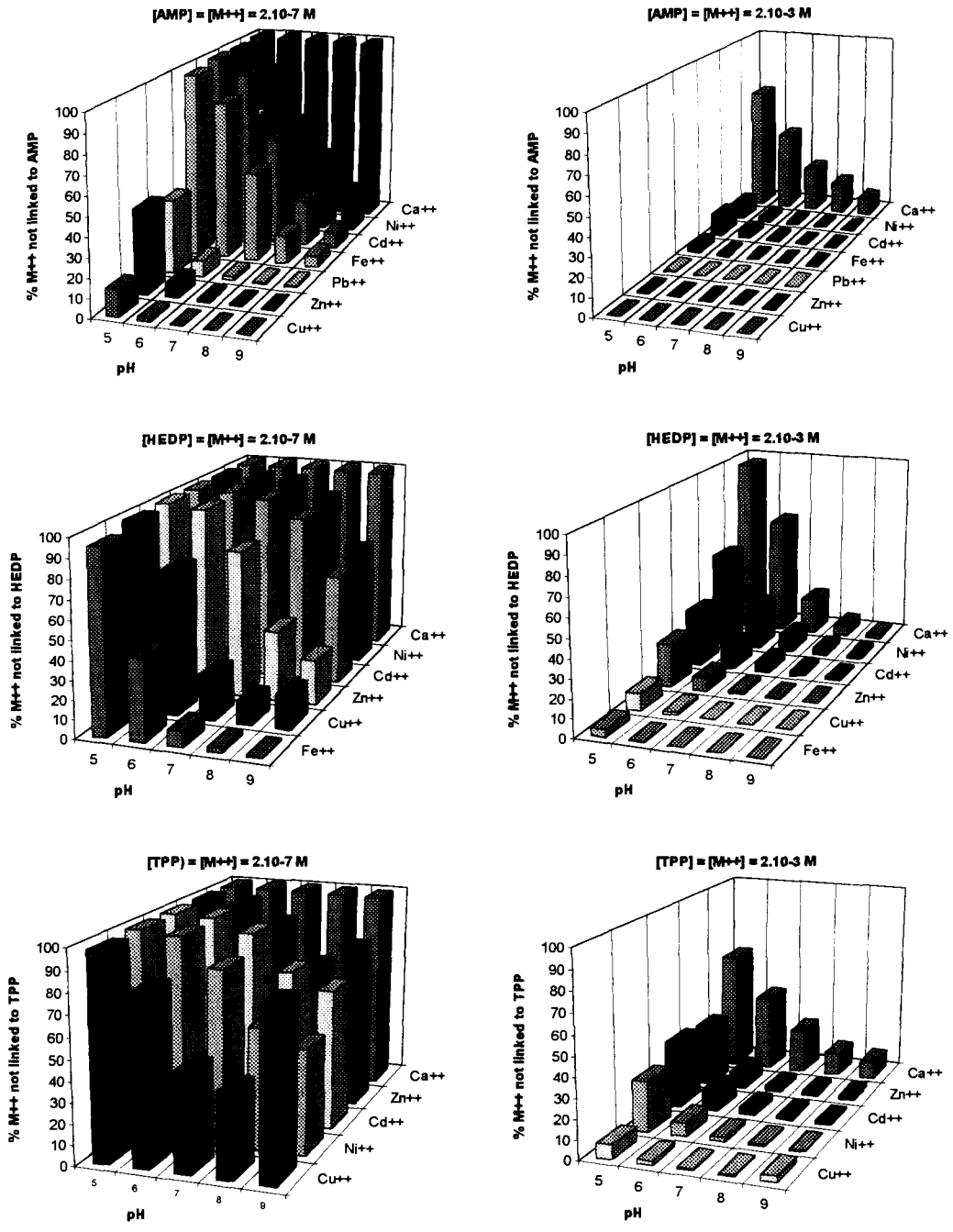

Fig. 1. Comparison of the ligands affinity classification with the various cations.

Fig. 1 shows the fraction of cations not linked to the ligand (= free cation + cation linked to hydroxide ions) at various pH. The following classifications can be made:

AMP Cu(II) > Zn(II) ≈ Pb(II) > Fe(II) > Cd(II) ≈ Ni(II) ≫ Ca(II)

HEDP Fe(II) > Cu(II) ≫ Zn(II) > Cd(II) > Ni(II) ≫ Ca(II)

TPP Cu(II) > Ni(II) ≈ Zn(II) ≈ Cd(II) > Ca(II)

The decrease of complexed cation at low concentrations is coherent with equilibrium rules. This phenomenon is less marked with AMP, but much more so with HEDP and TPP. At basic pH, with all the cations except Ca, 99% of the metal cations are linked to AMP at high concentrations, whereas at low concentrations only Cu, Zn and Pb complexes represent at least 98%. In the same pH range, at high concentrations 98% of Cu, Fe and Zn cations are linked to HEDP and 97% of all metal cations except Ca are complexed by TPP. At low concentrations these percentages decrease to 23% for Zn and 92% for Fe with HEDP, and to 47% for Cu and to 93% for Cd with TPP at pH 7.

Complexing classifications are similar at high and low concentrations. There is usually an increase in the complexed cation level with pH. TPP with Cu and Zn and HEDP with Cu do not follow such a rule. The percentage of cation linked to the ligand decreases from pH 8. This indicates that hydroxide complexation properties with these cations are stronger than those of TPP and HEDP at pH 9. This hydroxide complexes interference appears from pH 7 at low concentrations and makes affinity classification with TPP difficult. The three ligands, however, have the lowest complexing properties with Ca and usually highest with Cu. AMP has similar complexation properties with Cd, Ni and Fe, somewhat lower than those of Zn and Pb. The same is true of TPP with Ni, Zn and Cd. We cannot distinguish a family of cations with similar behavior with HEDP.

This classification is very similar to the Irving-Williams series of stabilities for chelates formed by metal ions with ligands [22]:

Zn < Cu > Ni > Co > Fe > Mn

In electrostatic terms, we would expect that the smaller the size of the metal ion, the greater the stability of the complex species. For Fe(II), Zn(II), Cu(II) and Ni(II), we did not obtain such a correlation with any of the three ligands studied, but observe that Zn always has higher complexing properties than Cd. This concept has been verified for alkaline-earth cations with HEDP [16] and AMP [13]. This phenomenon could be easily evaluated only with cations from a same column in the periodic table but is difficult to observe with cations from the same line, because the ionic radii are closer.

4.2. Complexation property classification of ligands

AMP is a stronger complexing agent than HEDP and TPP. We verified this with three typical cations of great interest in natural media. Ca is a major cation in water. Cu is often present in water because of its extensive use in farming, and its wide range of toxicological effects increases its interest. Both Ni and Cd have an intermediate behavior, but cadmium has a greater environmental impact because it is highly toxic. Furthermore, although Ni ore consumption is greater than that of Cd (18 000 and 800 000 tons year^{-1}, respectively), Cd concentrations in nonpolluted waters are of the same order of magnitude than those of Ni (ca. 1, and 2–13 μg l^{-1}, respectively) [23]. Zn and Fe complexing behaviors are similar with those of Cu and Cd.

Fig. 2 shows the complexation property classification of the three ligands with Ca, Cu and Cd at a molar ratio M/L = 1, in the pH-range of natural waters (5 to 9) at two concentration levels, 2.10^{-3} and 2.10^{-7} mol l^{-1}.

The complexation behaviors of HEDP and TPP are similar and much lower than that of AMP with copper and cadmium. HEDP has slightly stronger complexation properties than TPP, except at pH 5 with copper and for pH ≥ 6 with cadmium at high concentrations. AMP, HEDP and TPP have similar behaviors with calcium. This ligand classification is affected by pH only at high concentrations (2.10^{-3} mol l^{-1}).

AMP therefore appears to be the stronger ligand, the evolution of the complexation level with pH makes it difficult to draw a classification

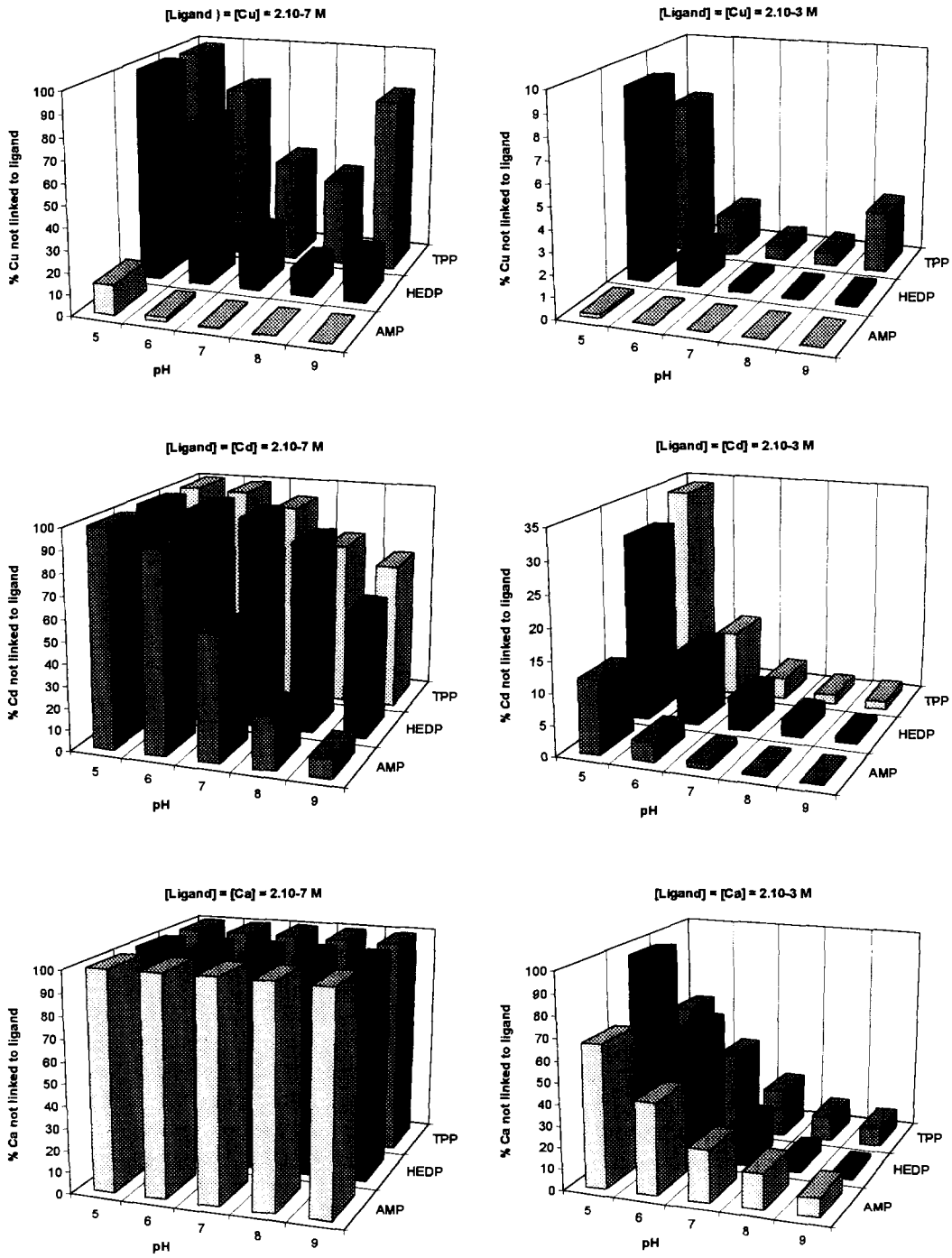

Fig. 2. Complexation properties classification of ligands.

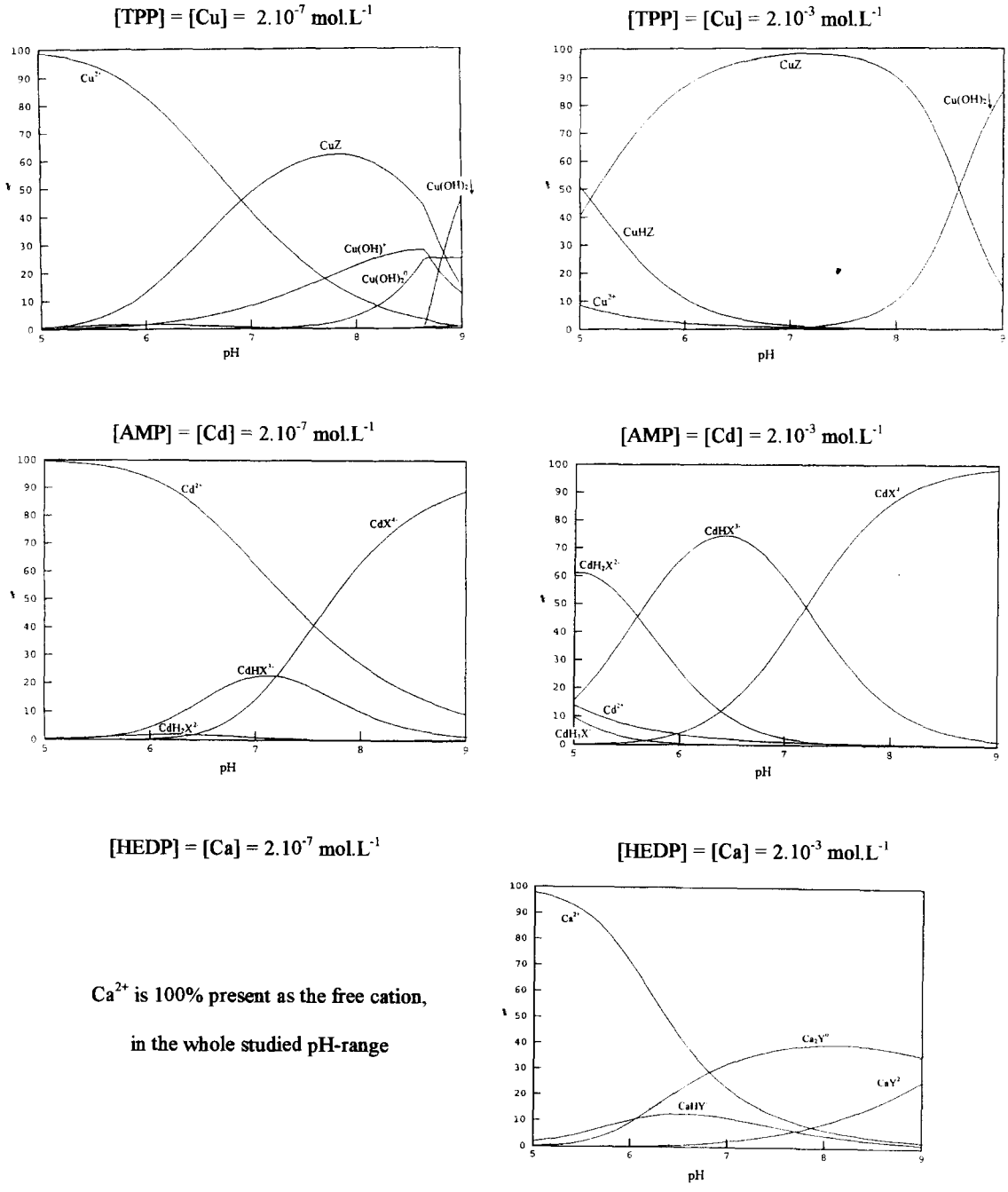

Fig. 3. Cation/ligand speciation diagrams determined with SPE computer program [6], calculated with our stability constants.

between HEDP and TPP. Therefore AMP might modify the heavy metal cations speciation in natural medium, more than HEDP and TPP.

4.3. Speciation diagrams

In natural aquatic and geological environments, the mobility and toxicity of a metal are determined by the thermodynamic activity of the species causing the toxic effect and not by the total soluble concentration of the metal [23,24]. A complete knowledge of speciation is therefore essential in order to assess the total environmental impact. Speciation diagrams were calculated with the SPE computer program [6] (Fig. 3). They are representative of ligand behavior with each cation.

At high concentrations, in our pH range, all the complexed species studied occur, except CaH_2Y^0, CdH_4X^0, CuH_4X^0, CuH_3X^- and CuH_2Y^0. The major species are $CaHX^{3-}$, Ca_2Y^0 and CaZ^{3-} in the Ca/ligand systems. CuL and CdL with $CdHX^{3-}$ and $CdHY^-$ are the major species in the Cu/ligand and Cd/ligand systems, respectively. Free cations are significant in every system except Cu/AMP. Hydroxide complex species are negligible at high concentrations, but $CdOH^+$, $CuOH^+$, $Cu(OH)_2^0$ and $Cu(OH)_3^-$ are present with HEDP and TPP at low concentrations ($[M] = [L] = 2.10^{-7}$ mol l^{-1}). At such concentrations, ligand interference decreases sharply. The percentage of free cations is higher, and it is the only metallic species in the Ca/ligand system. With each ligand, ML is the major species with Cu and Cd. Lamson et al. [25] studied the Ca/HEDP system in physiological conditions (pH 5.5–7.0, 25°C, $I = 0.1$ mol l^{-1}). They calculated speciation diagrams which are similar to ours, the same complexed species are present with similar proportions.

There is a high probability that all the charged species will stay in the liquid phase. Moreover in the natural water pH-range, all these phosphonate complexed species are anionic, as are natural ligands (such as humic substances, clays...), thus, no electrostatic adsorption phenomena will occur. Uncharged ionic species such as Ca_2Y^0, CaH_4X^0 and CdH_2Y^0 can potentially exist as a solid phase.

5. Conclusion

AMP is a stronger complexing agent with the seven divalent cations than HEDP and TPP which have similar ligand behavior. These phosphonic acids have higher affinity with Cu and lowest with Ca. HEDP will not modify heavy metal cations speciation more than TPP, whereas AMP might contribute to mobilize cations from sediments. A toxicologic study of MX^{4-}, MHX^{3-}, MH_2X^{2-}, MY^{2-} and MHY^- should be done to estimate AMP and HEDP potential harm to aquatic fauna and flora. Speciation diagrams, at low concentrations, confirm the hydroxide complexes significance in the HEDP and TPP systems with Cu and Cd. This is why hydroxide species have to be taken into consideration when determining complexation constants and, moreover, for an assessment of the impact of toxic cations on ecosystems.

Acknowledgements

The authors are grateful to Mrs A.K. Bourg, for her careful correction of the English text.

References

[1] R. Carbiener, Compositions Lessivielles avec ou sans Phosphates et Protection des Milieux Aquatiques, (Rapport), 1990, p. 77, 78, 131.
[2] P. Zini, Polymeric Additives for High Performing Detergents, Technomic, Lancaster PA, 1995.
[3] J. Off. Comm. Eur., Nr. L-217, p. 14–30, 13 Sept, 1995.
[4] J. Steber and P. Wierich, Chemosphere, 15 (1986) 929; K. Fischer, Water Res., 27 (1993) 485.
[5] J. Steber and P. Wierich, Chemosphere, 16 (1987) 1323.
[6] A.E. Martell and R.J. Motekaitis, Determination and Use of Stability Constants, 2nd Ed., VCH, New-York, 1992.
[7] A. Braibanti, G. Ostacoli, P. Paoletti, L.D. Pettit and S. Sammartano, Pure Appl. Chem., 59 (1987) 1721.
[8] M. Maeda, O. Hisada, Y. Kinjo and K. Ito, Bull. Chem. Soc. Jpn, 60 (1977) 3233.
[9] I. Grenthe, 7th International Symposium on Solubility Phenomena, Oral Communication, Leoben (Austria), (23–25 July 1996).
[10] L.D. Pettit and H.K.J. Powell, IUPAC Stability Constants Database, version 2.61, Academic Software, Otley (UK) 1995.
[11] R.M. Smith and A.E. Martell, Critical Stability Constants, Vol. 1 to 6, Plenum Press, New-York, 1974 to 1989.

[12] V. Deluchat, B. Serpaud, C. Caullet and J.C. Bollinger, Phosphorus Sulfur and Silicon, 104 (1995) 81.
[13] K. Sawada, T. Araki and T. Suzuki, Inorg. Chem., 26 (1987) 1199.
[14] K. Sawada, T. Araki, T. Suzuki and K. Doi, Inorg. Chem., 28 (1989) 2687.
[15] V. Deluchat, B. Serpaud, E. Alves, C. Caullet and J.C. Bollinger, Phosphorus Sulfur Silicon, 109–110 (1996) 209.
[16] E.N. Rizkalla and T.M. Zaki, Talanta, 27 (1980) 715.
[17] M.I. Kabachnik, R.P. Lastovskii, T.Y. Medved', V.V. Medyntsev, I.D. Kolpakova and N.M. Dyatlova, Proc. Acad. Sci. USSR, 177 (1967) 1060.
[18] R.L. Carroll and R.R Irani, Inorg. Chem., 6 (1967) 1994.
[19] R.A.M.J. Claessens and J.G.M. Van Der Linden, J. Inorg. Biochem., 21 (1984) 73.
[20] M. Taqui-Khan and P. Reddy, J. Inorg. Nucl. Chem., 35 (1973) 79.
[21] H. Ellison and A. Martell, J. Inorg. Nucl. Chem., 26 (1964) 1555.
[22] H. Irving and R.J.P. Williams, J. Chem. Soc., 162 (1953) 3192.
[23] H.G. Seiler, A. Sigel and H. Sigel, Handbook of Metals in Clinical and Analytical Chemistry, Dekker, New-York, 1994.
[24] F.M.M. Morel and J.G. Hering, Principles and Applications of Aquatic Chemistry, Wiley, New-York, 1993.
[25] M.L. Lamson, J.L. Fox and W.I. Higuchi, Int. J. Pharm., 21 (1984) 143.

ELSEVIER

Talanta 44 (1997) 909–915

Talanta

Comparative voltammetric studies of immunoglobulins and DNP-labelled immunoglobulins

M.D. Sánchez-Suárez, A. Costa-García *

Departamento de Química Física y Analítica, Universidad de Oviedo, 33006 Oviedo, Asturias, Spain

Received 2 April 1996; received in revised form 18 October 1996; accepted 21 October 1996

Abstract

A comparative electrochemical study of human immunoglobulins IgG_1 and IgG_3 carried out at a hanging mercury drop electrode shows that mechanisms other than the reduction of interchain disulphide linkages are responsible for the cathodic peaks observed for such proteins. Considering that the nature of the electrochemical process observed for immunoglobulins are poorly defined and not fully understood, a new approach to the electrochemical determination of such proteins, involving the use of 2,4-dinitrophenol (DNP) as a label, has been developed. Dynamic linear ranges of nearly two magnitudes and detection limits below 10^{-10} M were achieved. © 1997 Elsevier Science B.V.

Keywords: DNP-labelled immunoglobulins; Hanging drop mercury electrode; Immunoglobulins; Voltammetry

1. Introduction

The immunoassay is a technique that exploits an antibody as an analytical reagent capable of selective determination of an antigen species. Because of the advantages associated to immunoassay as high selectivity, low detection limits, speed, simplicity and relatively low cost these analytical methods are currently used in clinical chemistry.

The trend away from radioimmunoassays has resulted in a proliferation of immunoassays using a wide range of non-radioisotopic labels. The use of either electroactive species or enzymes as labels have been two different approaches to developing electrochemical immunoassays. A more direct method, involving no label, has been reported based on monitoring the changes in the electrochemical response of an antibody (or antigen) when its specific binding partner is added to the solution [1,2].

Studies of the electrochemical behaviour of antibodies on mercury electrodes are important for the development of new electroanalytical techniques which use antibodies, immunoglobulins, as analytical reagents.

Proteins are adsorbed on mercury electrodes because of the interaction of disulphide bonds with the mercury surface. This adsorptive behaviour has been used by several authors [1–4] for the electrochemical determination of proteins by adsorptive stripping voltammetry (AdSV).

* Corresponding author.

PII S0039-9140(96)02137-6

The reduction currents observed for proteins containing disulphide linkages in their structure have always been ascribed solely to the reduction of this bond [5–14]. Some results more recently reported [15,16] make difficult to agree with the assumption usually made in the literature, and other possible mechanisms as conformational changes of the adsorbed protein or reorientation of the molecule leading to some perturbation of the double layer have been suggested [17,18].

Following the controversy about the nature of the voltammetric behaviour reported for such proteins, as well as the bad definition of these peaks, Costa et al. [19] proposed a different approach to the electrochemical determination of proteins by means of the use of electroactive species as labels for these macromolecules. The 2,4-dinitrophenol (DNP) was studied. Several reasons were supporting this choice, first the DNP can be easily covalently bound to proteins by nucleophilic substitution achieving a high substitution grade (which leads to a significant increase in sensitivity). Moreover, the DNP presents a suitable electrochemical behaviour, its reduction involving a great number of electrons.

The starting point of this investigation was a comparative study of the electrochemical behaviour of two human immunoglobulins, which differ in the number of interchain disulphide linkages, to elucidate the role these bonds play in the electrochemistry of this type of proteins. A second stage involved the labelling of a mouse immunoglobulin with DNP, the DNP-labelled immunoglobulin electrochemical behaviour was studied and also was its ability to undergo an immunochemical reaction with anti-DNP and anti-mouse IgG_1 antibodies.

2. Experimental

2.1. Apparatus

Differential pulse voltammetric experiments were performed with a Metrohm Polarecord E-506. The working electrode was a hanging mercury drop electrode (HMDE), the surface of the mercury drop was 0.32 mm^2. A platinum wire was used as auxiliary electrode and all potentials were measured versus an Ag/AgCl/saturated KCl reference electrode.

A magnetic stirrer (Selecta Asincro) and a stirring bar (7 × 4 mm) provided the convective transport during the accumulation step, the rotation speed was 300 r.p.m.

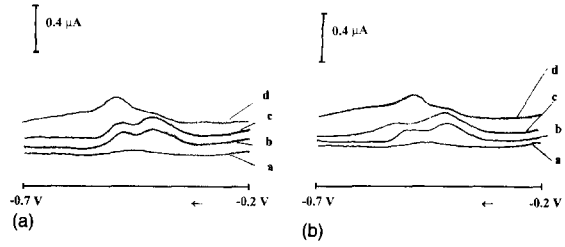

Fig. 1. (A) Differential pulse voltammetry responses of human IgG_1 at a HMDE: (a) background electrolyte, (b) 10^{-9} M IgG_1, (c) 10^{-8} M IgG_1, (d) 10^{-7} M IgG_1; (B) Differential pulse voltammetry responses of human IgG_3 at a HMDE: (a) background electrolyte, (b) 10^{-9} M IgG_3, (c) 10^{-8} M IgG_3, (d) 10^{-7} M IgG_3; $\Delta E = -50$ mV, $v = 10$ mV s^{-1}, $t_{acc} = 300$ s, at open circuit.

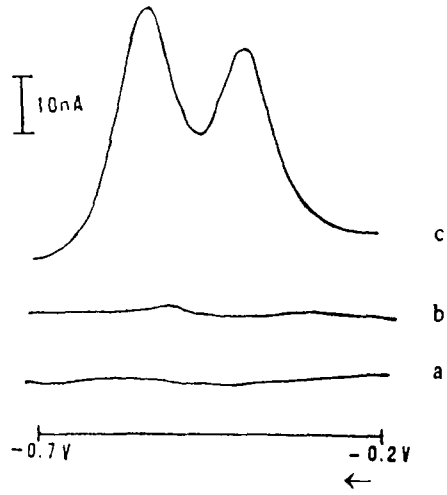

Fig. 2. Voltammetric responses of mouse IgG_1 and DNP-mouse IgG_1 at a HMDE: (a) background electrolyte, (b) 1×10^{-8} M mouse IgG_1, (c) 1×10^{-8} M DNP-mouse IgG_1; $\Delta E = -50$ mV, $v = 10$ mV s^{-1}, $t_{acc} = 240$ s, at open circuit.

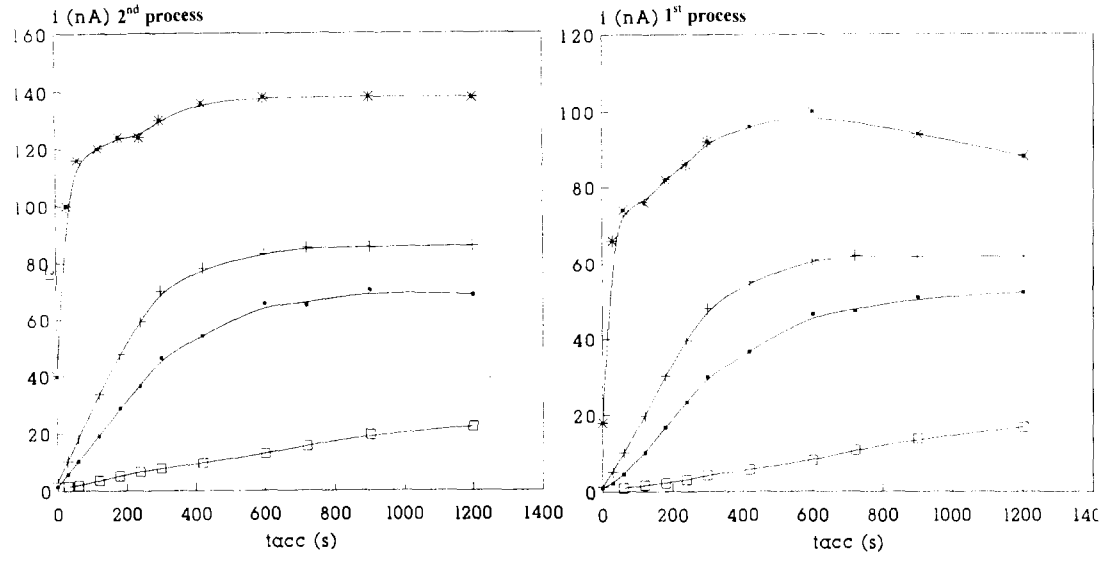

Fig. 3. Effect of the accumulation time at open circuit on the first and second processes peak currents for: (□) 1×10^{-10} M, (■) 5×10^{-10} M, (+) 1×10^{-9} M, (*) 1×10^{-8} M DNP-mouse IgG_1; $\Delta E = -50$ mV, $v = 10$ mV s^{-1}.

2.2. Reagents

All compounds used were of analytical reagent grade. The electrolyte solution was 0.01 M phosphate buffer, pH 7.2, prepared by using phosphoric acid and sodium hydroxide in deionized water (obtained by passing distilled through a Milli-Q Millipore water purification system).

Human IgG_1 and IgG_3 were purchased from Sigma (St. Louis, MO, USA) and both proteins were reconstituted in 0.01 M phosphate buffer, pH 7.2 and stored at 4°C.

Mouse IgG_1 (clon: 8.4a9.13), was a gift from Dr Juan Toyos (Dpto. Biología Funcional, Universidad de Oviedo, Spain) and was supplied as 1 mg ml^{-1} stock solution in 0.01 M phosphate buffer saline (PBS) with 0.1% sodium azide as preservative.

2,4-dinitrobenzenesulfonic acid, sodium salt (DNBS) was purchased from Aldrich (Gillingham-Dorset, UK).

Goat anti-mouse IgG_1 (clon: LO-M61-2) was obtained from ICN Biomedicals, and rat anti-DNP (clon: 04-8300) was purchased from Zymed Laboratories.

Nitrogen N-48 (SEO) was used to remove dissolved oxygen.

2.3. Procedures

Before each voltammetric experiment the electrolyte was purged with oxygen-free-nitrogen for 30 min. After addition of the sample the solution was purged for a further 5 min. A preconcentration is carried out for the required accumulation time (t_{acc}) at open circuit, with stirring at 300 rpm. The stirring was stopped and, after 10 s equilibration time, the potential was scanned in the differential pulse (DP) mode in the cathodic direction, with a pulse amplitude of -50 or -100 mV and a scan-rate of 10 mV s^{-1}. All experiments were carried out at room temperature.

2.3.1. DNP-labelling reaction of proteins

The conjugation of DNP to a mouse IgG_1, was carried out according to the procedure described by Little et al. to obtain 2,4-dinitrophenylproteins [20]. The conjugate was purified by dialysis against ultrapure water using cellulose membrane (MW 12 400). The Bio-Rad micro-Bradford assay [21] was used for measuring total protein concen-

tration in the solutions obtained from dialysis. DNP-mouse IgG_1 solutions were stored at 4°C in the dark.

2.3.2. ELISA procedure

The enzyme-linked-immunosorbent-assay (ELISA) plates were precoated with 100 μl of the antigen (10 μl ml^{-1}) diluted in 50 mM bicarbonate buffer, pH 9.6 and incubated during 3–4 h at 37°C. They were washed (× 4) in PBS, pH 7.3, containing 0.05% Tween 20. the plates were blocked by incubation with 1% (w/v) BSA in 10 mM PBS, pH 7.3, 0.1% NaN_3, for 1 h at 37°C and overnight at 4°C. The plates were rewashed as before. Dilutions of mouse IgG_1 (1 μg ml^{-1}), used as positive control and DNP- labelled mouse IgG_1 (1 μg ml^{-1}) were then made up and incubated in the wells for 3–4 h at 37°C. The plates were washed and then 100 μl of HRP-conjugated goat anti-mouse (Sigma) are incubated in the wells for 3–4 h at 37°C. The substrate used for HRP was 100 μl of *o*-phenylendiamine dihydrochloride (Sigma) and H_2O_2 (0.3% (v/v)) in 0.1 M citrate buffer, pH 4. Absorbance was read at 492 nm.

3. Results and discussion

3.1. Electrochemical behaviour of human IgG_1 and IgG_3

To elucidate the role disulphide linkages play in the electrochemical behaviour described for this type of protein on mercury electrodes, the electrochemistry of two human immunoglobulins G, which differ in the number of interchain disulphide bonds, has been compared. Immunoglobulin G_1 (IgG_1) and immunoglobulin G_3 (IgG_3) contain, respectively, 2 and 15 interchain disulphide bonds in their structure [22].

This investigation was carried out by differential pulse voltammetry (DPV) on a HMDE in the potential range -0.2– -0.7 V. The IgG_1 and IgG_3 concentrations were varied from 10^{-9} to 10^{-7} M and the voltammograms obtained for them under the same experimental conditions (pulse amplitude (ΔE) -50 mV, scan-rate (v) 10 mV s^{-1}, and accumulation time at open circuit (t_{acc}) 300 s) are shown in Fig. 1. Both human immunoglobulins gave rise to a badly defined cathodic peak at -0.5 V versus Ag/AgCl as reported in the literature.

Because of the considerable difference in the number of interchain disulphide linkages, a higher current intensity would be expected for IgG_3 than for IgG_1 if the voltammetric response were due to the reduction of these linkages. Actually, the IgG_1 peak current is slightly higher than that obtained for IgG_3. From this and other studies [15,16], it follows that the voltammetric peaks obtained for these immunoglobulins on mercury electrodes are due to processes other than the simple reduction of disulphide linkages.

3.2. Electrochemistry of the DNP-mouse IgG_1

Considering that the electrochemical processes giving rise to those peaks are still not fully understood, the electrochemistry of the immunoglobulins was studied by using an electroactive molecule as a label for immunoglobulins. The 2,4-dinitrophenol (DNP), which had been proposed by Costa et al. [19] as label for proteins, was used. The procedure followed to obtain DNP-mouse IgG_1 has already been described in the experimental section.

Reaction parameters as DNBS, K_2CO_3 concentrations and temperature were varied to study their influence on the substitution grade achieved in the labelling reaction, and the specificity of the DNP-mouse IgG_1 to the antigen.

It was observed that the substitution grade increases by increasing DNBS and K_2CO_3 concentrations and better results were obtained using 37°C than room temperature. Regarding to the specificity of the DNP-mouse IgG_1, the ability of the conjugate to undergo an immunochemical reaction with the antigen was evaluated by comparison of the absorbance readings obtained for this molecule with those obtained for the mouse IgG_1 in an ELISA. According to these readings, high substitution grades in the labelling reaction were associated with more significant loss of specificity to the antigen.

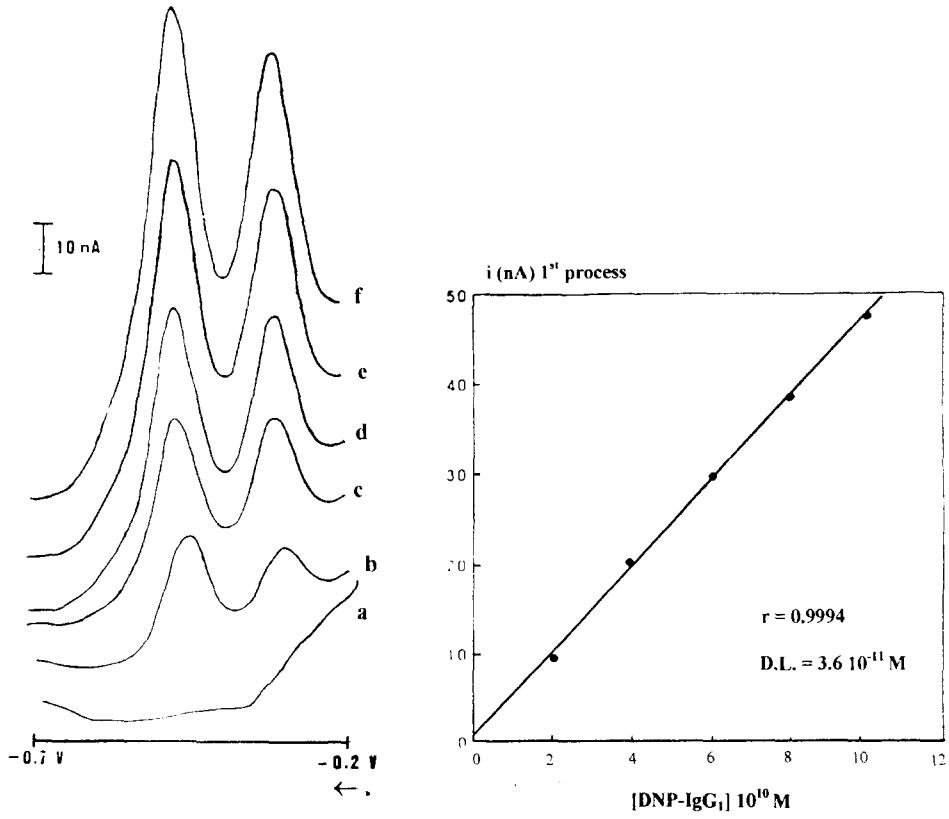

Fig. 4. Effect of concentration on the DP voltammetric current for DNP-mouse IgG_1: (a) background electrolyte, (b) 2×10^{-10} M, (c) 4×10^{-10} M, (d) 6×10^{-10} M, (e) 8×10^{-10} M, (f) 1×10^{-9} M DNP-mouse IgG_1; $\Delta E = -100$ mV, $v = 10$ mV s^{-1}, $t_{acc} = 600$ s at open circuit.

The DNP-immunoglobulin used in the following studies was obtained under that reaction conditions leading to higher substitution grade, i.e., 6.4 mg DNBS and 22.8 mg K_2CO_3, dissolved in 1 ml of 1 mg ml^{-1} mouse IgG_1, kept in the dark at 37°C for 48 h. The fact that its specificity is lost is not significant as the labelled immunoglobulin do not take part as an antibody in any of those immunochemical reactions described further on.

The electrochemical behaviour of the DNP-mouse IgG_1 was studied by differential pulse voltammetry (DPV) on a HMDE and the results have been compared with those obtained under the same conditions for the mouse IgG_1. The voltammograms recorded for 1×10^{-8} M solutions of each species, using $\Delta E = -50$ mV, $v = 10$ mV s^{-1} and $t_{acc} = 240$ s, are shown in Fig. 2. The mouse IgG_1 yields a poorly defined cathodic peak at -0.5 V versus Ag/AgCl, meanwhile the DNP-mouse IgG_1 gives rise to two peaks at -0.32 and -0.46 V versus Ag/AgCl. It is clear that those peaks obtained for the conjugate are analytically more useful signals than the one obtained for mouse IgG_1.

The accumulation curves for increasing concentrations of DNP-mouse IgG_1 (Fig. 3) were obtained by varying the preconcentration time from 0 to 1200 s and plotting this parameter against peak currents. The accumulation was carried out at open circuit under constant stirring. As expected, for each concentration, peak currents increase with accumulation time until saturation of the electrode was reached.

The analytical signal was optimized with respect to pulse amplitude as foreseen, increasing pulse amplitude gave rise to better analytical sig-

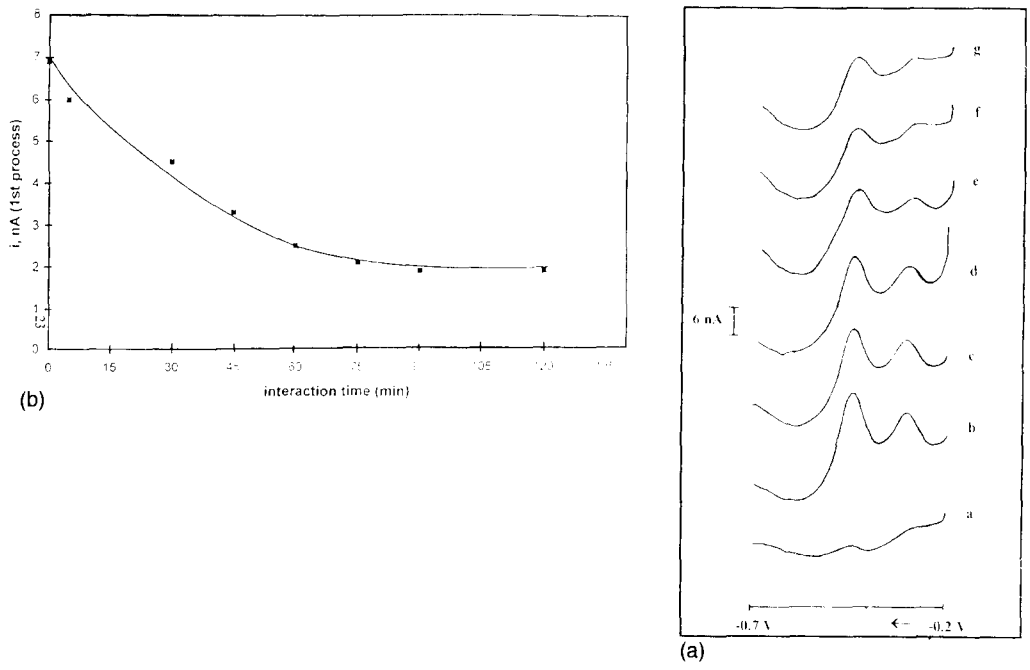

Fig. 5. Electrochemical response of 1×10^{-9} M DNP- mouse IgG_1 in the presence of 2×10^{-9} M anti-DNP: (a) background electrolyte, (b) 1×10^{-9} M DNP-mouse IgG_1, (c) 5 min (d) 30 min, (e) 1 h, (f) 1 h 30 min, (g) 2 h 15 min, anti-DNP and DNP-mouse IgG_1 interaction times. $\Delta E = -100$ mV, $v = 10$ mV s^{-1}, $t_{acc} = 240$ s at open circuit.

nals. A pulse amplitude of -100 mV was used for the remainder of the study.

The repeatability of the analytical signal was calculated for DNP-mouse IgG_1 from successive measurements ($n = 10$) of a 1×10^{-9} M solution, using a 240 s accumulation time at open circuit. The relative standard deviation was 2.6% for the first electrochemical process and 2.3% for the second one Fig. 4.

The DNP-immunoglobulin gave rise to current responses that increased linearly with respect to increasing concentration. Using an accumulation time of 600 s, the curve for the first electrochemical process was found to be linear between 2×10^{-10} M and 1×10^{-9} M ($r = 0.999$, $n = 5$). The detection limit achieved ($\sigma = 3$) was 3.6×10^{-11} M.

3.3. Interaction of DNP-mouse IgG_1 with anti-DNP and anti-mouse IgG_1 antibodies

The interaction in solution, at room temperature, of DNP-mouse IgG_1 and rat anti-DNP was monitored by DPV on a HMDE, using a pulse amplitude of -100 mV, a scan-rate of 10 mV s^{-1} and an accumulation time at open circuit of 240 s. The cell and the electrodes were equilibrated with the appropriate DNP-mouse IgG_1 solution for 2 h, so changes in the electrochemical response of the DNP-immunoglobulin could not be ascribed to a bulk concentration change by adsorption of DNP-mouse IgG_1 on the cell walls or salt-bridge tips, etc. A voltammogram of a 1×10^{-9} M DNP-mouse IgG_1 was recorded under the conditions indicated above. The solution was deareated for 5 min before each potential scan and the changes experimented by this signal, when the rat antibody anti-DNP was added at a concentration of 2×10^{-9} M to that solution, are monitored at different interaction times. It can be observed (Fig. 5A) that the peak currents of both first and second processes, registered for the DNP-immunoglobulin, decrease gradually with interaction time until a steady signal, (unvarying with reaction time), is obtained after 1 h 30 min (Fig. 5B).

When goat anti-IgG_1, instead of rat anti-DNP, was added at a concentration of 1×10^{-9} M no change in peak currents was observed in the different voltammograms recorded at different interaction times during a 4 h study. However, if the interaction was performed at 37°C the first and second reduction peaks both decrease with reaction time and after 2 h disappear.

Anti-DNP antibodies show a high affinity constant for DNP, this could be the reason these antibodies undergo immunochemical reaction at room temperature, meanwhile for an anti-mouse IgG_1 a 37°C temperature is necessary.

4. Conclusions

From the comparative study of the electrochemistry of human immunoglobulins IgG_1 and IgG_3 it can be concluded that the cathodic process observed for immunoglobulins on mercury electrodes involves some mechanism other than reduction of interchain disulphide linkages.

Immunoglobulins can be electrochemically determined by labelling these proteins with DNP using DPV dynamic linear ranges of nearly two orders of magnitude and detection limits below 10^{-10} M have been achieved.

The decrease in peak currents observed for DNP-labelled mouse IgG_1 in presence of anti-DNP and anti-mouse IgG_1 antibodies could support the monitoring of immunochemical reactions using electrochemical techniques.

Acknowledgements

We wish to express our gratitude to Dr Juan Toyos and Dr Segundo González for their technical assistance in the preparation of ELISA and Bradford assays, respectively.The authors gratefully acknowledge the financial support of the FISss (Spain) project No. 93/0017.

References

[1] J. Rodríguez Flores and M.R. Smyth, J. Electroanal. Chem., 235 (1987) 317.
[2] M.R. Smyth, E. Buckley, J. Rodríguez Flores and R. O'Kennedy, Analyst, 113 (1988) 31.
[3] J. Rodríguez Flores, R. O'Kennedy and M.R. Smyth, Anal. Chim. Acta, 212 (1988) 355.
[4] J. Rodríguez Flores, R. O'Kennedy and M.R. Smyth, Analyst, 113 (1988) 525.
[5] M.T. Stankovich and A.J. Bard, J. Electroanal. Chem., 75 (1977) 487.
[6] M.T. Stankovich and A.J. Bard, J. Electroanal. Chem., 85 (1977) 173.
[7] M.T. Stankovich and A.J. Bard, J. Electroanal. Chem., 85 (1977) 189.
[8] I.M. Kolthoff and C. Barnum, J. Am. Chem. Soc., 63 (1941) 520.
[9] I.M. Kolthoff, W. Stricks and N. Tanaka, J. Am. Chem. Soc., 77 (1955) 4739.
[10] I.M. Kolthoff and C. Barnum, J. Am. Chem. Soc., 62 (1940) 3061.
[11] B. Breyer and F.J. Radcliff, Nature, 167 (1951) 79.
[12] R. Cecil and P.O.J. Weitzman, Biochem. J., 93 (1964) 1.
[13] U. Forsman, Anal. Chim. Acta, 166 (1984) 141.
[14] M. Fontaine, C. Rivat, C. Ropartz and C. Caullet, Bull. Soc. Chim. Fran., 6 (1976) 1873.
[15] J.M. Fernández Alvarez, M.R. Smyth and R. O'Kennedy, Talanta, 38 (1991) 391.
[16] E. Buckley, J.M. Fernández Alvarez, M.R. Smyth and R. O'Kennedy, Biosensors, 3 (1991) 43.
[17] W. Hertl, Bioelectrochem. Bioenerg., 17 (1987) 89.
[18] H. Emons, G. Werner and W.R. Heineman, Analyst, 115 (1990) 405.
[19] A. Costa García, M.T. Fernández Abedul and P. Tuñón Blanco, Talanta, 41 (1994) 1191.
[20] S.R. Little and H.N. Eisen, Methods Immunol. Immunochem., 1 (1967) 128.
[21] M. Bradford, Anal. Chem., 72 (1976) 248.
[22] Ivan Roitt, J. Brostoff and D. Male, in Immunology, Gower Medical, London.

ELSEVIER

Talanta 44 (1997) 917–922

Talanta

Differential derivative spectrophotometric determination of phenobarbitone and phenytoin sodium in combined tablet preparations

C.V.N. Prasad, A. Gautam, V. Bharadwaj, P. Parimoo *

Department of Pharmacy, Birla Institute of Technology and Science, Pilani- 333031, India

Received 12 March 1996; received in revised form 16 October 1996; accepted 18 October 1996

Abstract

A pH-induced differential derivative spectrophotometric procedure has been developed for the simultaneous determination of Phenobarbitone (PBT) and Phenytoin sodium (DPH Na) in tablet preparations. The method comprized of measurement of difference absorptivities derivatized in second order(ΔD_2) of a tablet extract in 0.01 N NaOH relative to that of an equimolar solution in 0.01 N HCl at wavelengths of 244.8 and 252.8 nm respectively. The presence of identical zero-crossing points for pure drug and tablet extract solutions established the non-interference of the excipients in the absorption at these wavelengths. The compliance of Beer's law was adhered over a concentration range of 7.5–25 μg ml^{-1} for both PBT and DPH. © 1997 Elsevier Science B.V.

Keywords: Phenobarbitone; Phenytoin sodium; Spectrophotometric

1. Introduction

Derivative spectrophotometry has received increased attention in recent years in the assay of drugs alone or in combination from their formulations [1–3]. The procedure has been found to be successful in resolving two overlapping spectra, in the identification and quantification of drugs with low absorptivity values and in eliminating non-specific interferences from formulation matrix [4–6].

Difference spectrophotometry based on pH changes has also been reported to be useful in the determination of binary mixtures [7]. In our earlier work, we have described the successful application of later technique for the determination of combination preparations [8–10].

There are few reports on utilization of the above two combined techniques for the estimation of individual drug substances [11] and for combined preparations [12]. In the present work an effort has been made to utilize the combined techniques for simultaneous determination of phenytoin (DPH) and phenobarbitone (PBT) in the presence of each other as well as the excipients.

* Corresponding author. Fax: +91 1596 12112; e-mail: cvnp@bits.soft.net

PII S0039-9140(96)02139-X

The combination of PBT and DPH Na in the form of tablet preparation is widely used for major epilepsy and psychomotor seizures. The official monographs describe the procedure for individual assay of PBT and DPH Na [13]. A differential titrimetric method [14] and a derivative compensation technique [15] has been reported for simultaneous determination of above mixtures.

2. Experimental

2.1. Apparatus

A JASCO model 7800 double beam UV-visible autoscan spectrophotometer with 1 cm quartz cells was used. Suitable settings were scan speed of 480 nm min^{-1}, chart speed of 10 nm min^{-1}, ordinate maximum and minimum were adjusted to the magnitude of derivative values.

2.2. Standard solutions

The stock solutions of pure PBT and DPH Na (Anglo-French, Bangalore, India) were prepared by dissolving 25 mg each of the pure drugs in 50 ml of methanol. Appropriate volume aliquots of the stock solution were transferred to 25 ml volumetric flasks in duplicate. The volumes were made up with 0.01 N HCl and 0.01 N NaOH to give a series of equimolar solutions containing 7.5–25 μg ml^{-1} of both PBT and DPH. Similarly three series of 25 ml each of equimolar solutions of mixtures of PBT and DPH Na in 0.01 N HCl and 0.01 N NaOH were also prepared by using the stock solutions. The first series contained a constant concentration of PBT (7.5 μg ml^{-1}) and a varying concentration of DPH Na (7.5–25 μg ml^{-1}).

The second and third series contained a constant concentration of DPH Na (15/25 μg ml^{-1}) and a varying concentration of PBT (7.5–25 μg ml^{-1}). The absorbance of the solutions were taken within 3 h of their preparation. All reagents used were of analytical grade.

2.3. Sample preparation

Tablets, 20, of Phenytal 30 (Intas, India) labeled to contain 30 mg of PBT, 100 mg of DPH Na and excipients, 20 tablets of Phenytal (Intas, India), labeled to contain 50 mg of PBT, 100 mg of DPH Na and excipients, were accurately weighed, well powdered and a weight of the powder equivalent to 25 mg of DPH Na(corresponding amount of PBT 7.5 or 12.5 mg depending on the chosen marketed preparation) was dissolved in methanol by thorough mixing and made up to volume in a 50 ml volumetric flask. The sample solution of 25 ml each in 0.01 N HCl and 0.01 N NaOH were prepared by using 0.375 ml aliquots of the filtrate so as to obtain concentration 7.5 μg ml^{-1} of PBT and corresponding amount of DPH Na (15 or 25 μg ml^{-1} depending on the chosen preparation). The difference spectra between the acidic solution and equimolar 0.01 N NaOH solution of pure drugs and sample were recorded from 230–275 nm by placing the acidic solution in the reference compartment and the 0.01 N NaOH solutions in the sample compartment. A second derivative spectrum of each of the differential curves was subsequently recorded. The solutions were measured at 252.8 and 244.8 nm for DPH Na and PBT, respectively.

3. Results

The zero order spectrum of pure PBT (7.5 μg ml^{-1}) and DPH Na (15.0 μg ml^{-1}) either in 0.01 N NaOH or in 0.01 N HCl were very similar (Fig. 1). However, the difference absorption spectrum of two drugs and a mixture of PBT and DPH Na (7.5 and 15 μg ml^{-1}, respectively) showed significant alteration (Fig. 2).

The second derivative differential curves of both the drugs (Fig. 3) offered an advantage for their simultaneous determination by having zero crossing points. In particular absorbance at 244.8 nm for PBT and at 252.8 nm for DPH were considered as the optimum working wavelengths for their determination. The derivative differential curves showed the best linear response to analyte concentrations used at these wavelengths.

The proportionality of the ΔD_2 values and concentrations of PBT and DPH were found by measuring ΔD_2 of ten pairs of solutions of each containing 7.5–25 μg/ml of PBT at 244.8 nm and for DPH Na solutions at 252.8 nm, respectively. The linear regression equations were obtained by using the method of least squares. The linear regression for PBT was

$$Y = 0.001066X - 0.00041 \quad (1)$$

with a correlation coefficient of $r = 0.9999$ at 244.8 nm. The linear regression equation for DPH Na was as

$$Y = 0.000124X - 0.00013 \quad (2)$$

with a correlation coefficient of $r = 0.9999$ at 252.8 nm.

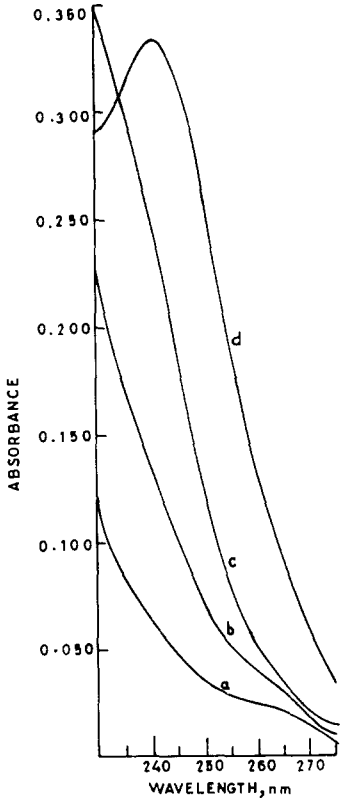

Fig. 1. Absorption spectra of (a) Phenobarbitone (7.5 μg ml^{-1}), (b) Phenytoin Na (15 μg ml^{-1}) in 0.01 N HCl and (c) Phenytoin Na (15 μg ml^{-1}), (d) Phenobarbitone (7.5 μg ml^{-1}) in 0.01 N NaOH, respectively.

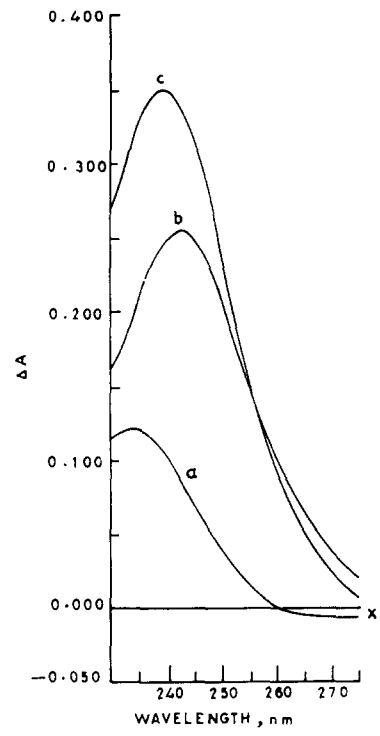

Fig. 2. Difference spectra of (a) Phenobarbitone (7.5 μg ml^{-1}), (b) Phenytoin Na (15 μg ml^{-1}) and (c) mixture of Phenobarbitone (7.5 μg ml^{-1} and Phenytoin Na 15 μg ml^{-1}) in 0.01 N HCl versus 0.01 N NaOH.

For establishing the specificity of the method for drug samples, three series each of ten solutions as mentioned under standard preparation were examined at the zero crossing wavelengths. The solution of the first series gave a regression equation of

$$Y = 0.000123X - 0.00018 \quad (3)$$

with a correlation coefficient of $r = 0.9999$ at 252.8 nm. The detection limit (LOD) [16] was 1.5 μg ml^{-1} and with a quantitation limit (LOQ) [16] of 2 μg ml^{-1}. The similarity of Eq. (3) with Eq. (2) and with a distinct isosbestic point at 244.8 nm (Fig. 4) suggested that the presence of PBT didn't affect the absorptivity of DPH Na at 252.8 nm.

The linear regression equations for second series was

$$Y = 0.001067X - 0.00019 \quad (4)$$

with a correlation coefficient of $r = 0.9999$ at 244.8 nm. The detection limit was 0.32 μg ml^{-1} and quantitation limit of 1 μg ml^{-1}. Similarly, the regression equation for third series was

$$Y = 0.001074X - 0.00001 \quad (5)$$

with a correlation coefficient of $r = 0.9999$ at 244.8 nm. The detection limit was 0.49 μg ml^{-1} and quantitation limit of 1 μg ml^{-1}.

The similarity of Eq. (4) and Eq. (5) with Eq. (1) and the presence of distinct isosbestic point at 252.8 nm (Fig. 5 and Fig. 6), the zero crossing point of PBT suggested a non-interference of absorptivity of DPH with that of PBT at 244.8 nm. The ΔD_2 values of standard solutions of PBT (7.5 μg ml^{-1}) and DPH Na (15 or 25 μg ml^{-1}) relative to ΔD_2 of tablet sample solution were used for the determination of PBT and DPH in the tablet preparation. The results are given in the Table 1.

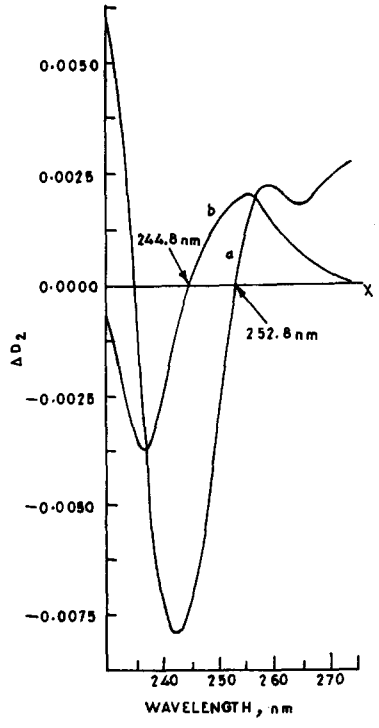

Fig. 3. Differential derivative spectra of (a) Phenobarbitone (7.5 μg ml^{-1}) and (b) Phenytoin Na (15 μg ml^{-1}) in 0.01 N HCl versus 0.01 N NaOH.

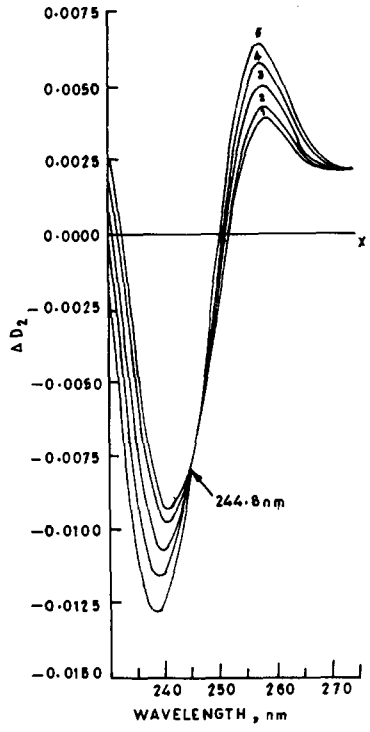

Fig. 4. Differential derivative spectra of Phenobarbitone (7.5 μg ml^{-1}) and Phenytoin Na (7.5, 10, 15, 20 and 25 μg ml^{-1}) in 0.01 N HCl versus 0.01 N NaOH in curves 1–5, respectively.

4. Discussion

The application of difference spectroscopy for the quantification of two component formulations depends on the fortuitous juxtaposition of the isosbestic points. As already pointed out in the text, the difference spectroscopy alone didn't produce the required isosbestic points. However, derivatization of the difference curves resulted in zero crossing points, which enabled the successful determination of both the drugs. The second derivative difference curves were relatively better for the estimation of drugs compared with the first derivative difference curves. In the latter, the zero crossing point of DPH Na had fallen closer to the 230 nm, which is the boundary limit of selected wavelength range. Hence the second derivative difference curves were chosen. The combined technique offers a distinct advantage as it involved refinement of spectra at two levels and

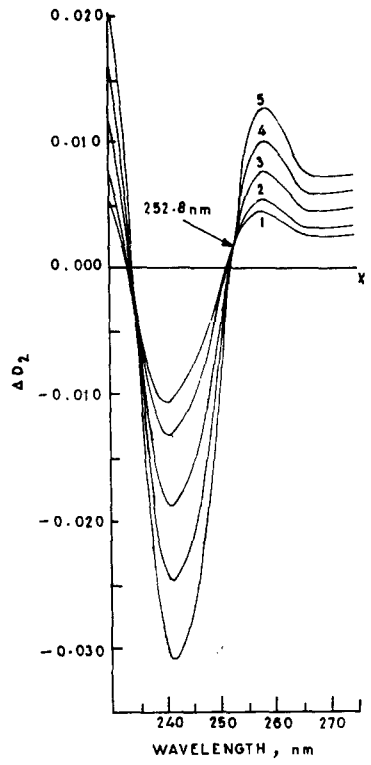

Fig. 5. Differential derivative spectra of Phenobarbitone(7.5, 10, 15, 20 and 25 μg ml^{-1}) and Phenytoin Na (15 μg ml^{-1}) in 0.01 N HCl versus 0.01 N NaOH in curves 1–5, respectively.

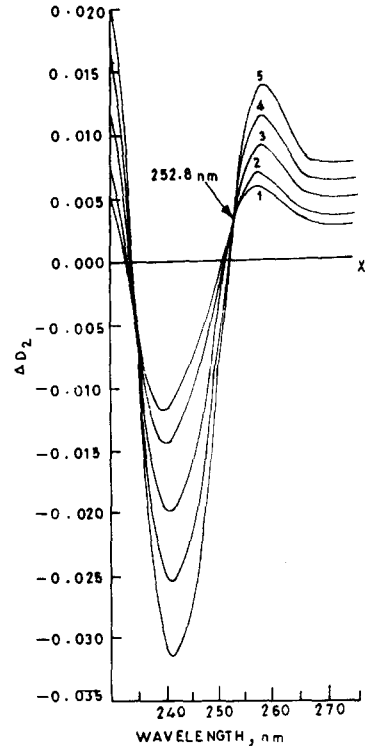

Fig. 6. Differential derivative spectra of Phenobarbitone (7.5, 10, 15, 20 and 25 μg ml^{-1}) and Phenytoin Na (25 μg ml^{-1}) in 0.01 N HCl versus 0.01 N NaOH in curves 1–5, respectively.

the interference from formulation matrix if any, will be at its minimum. The similarities between the linear regression equation, the detection and quantitation limits demonstrated the usefulness of derivative difference spectrophotometry in the quantitation of drug mixtures with overlapping spectra.

The procedure developed is simple and reproducible. In the absence of an official method for the simultaneous determination of PBT and DPH Na, the proposed method, if properly used can prove to be useful for routine analysis of the two drug combined formulations.

Acknowledgements

The authors express their gratitude to M/s The Anglo-French Drug Co (Eastern) Ltd, Bangalore, India for samples of pure DPH Na and PBT.

Table 1
Assay results of PBT and DPH Na in commercial formulations by differential derivative spectroscopy

Sample	PBT		DPH Na	
	mg tablet^{-1}	% w/w stated[a]	mg tablet^{-1}	% w/w stated[a]
Brand A	49.21	98.42 ± 0.92	99.65	99.65 ± 0.32
Brand B	29.59	98.63 ± 0.25	99.78	99.78 ± 0.71

[a] Five replicative measurements.

References

[1] B. Morelli, J. Pharm. Sci., 77 (1988) 615.
[2] B. Morelli, J. Pharm. Sci., 77 (1988) 1042.
[3] B. Morelli, J. Pharm. Sci., 84 (1995) 34.
[4] G. Talsky, L. Maryingand and H. Kreuzer, Angew. Chem. Int. Ed. Engl., 17 (978) 785.
[5] T.C. O'Haver, Anal. Chem., 51 (1979) 91A.
[6] F.S. Rojas, C.B. Ojedaand and J.M.C. Pavon, Talanta, 35 (1988) 753.
[7] T.D. Doyle and F.R. Fazzari, J. Pharm. Sci., 63 (1974) 1921.
[8] P. Parimoo, Drug Dev. Ind. Pharm., 13 (1987) 127.
[9] P. Parimoo, P. Umapathi and K. Ilango, Int. Jr. Pharm., 100 (1993) 227.
[10] P. Parimoo, C.V.N. Prasad and R. Vineeth, J. Pharm. Biomed. Anal., 14 (1996) 389.
[11] A.M. Wahbi, M. Barary, H. Mahgab and M.A. El. Sayed, J. Assoc. Off. Anal. Chem., 68 (1985) 1045.
[12] A.G. Davidson and L.M.M. Mkoji, J. Pharm. Biomed. Anal., 6 (1988) 449.
[13] U.S. Pharmacopeia, United States Pharmacopeial Convention, Rockville, MD., 23 (1995) 1202–1218.
[14] S.P. Agarwal, Anal. Chem., 41 (1969) 1105.
[15] A.M. Wahabi, H.M. Barary, F.A. El. Yazbi and S.M. Sabri, Analyst, 117 (1992) 785.
[16] D.A. Skoog and J.L. Leary, Principles of Instrumental Analysis, 4th Ed., Saunders, New York, 1992, p. 7.

ELSEVIER

Talanta 44 (1997) 923–930

Talanta

A linear regression method for the study of the Coomassie brilliant blue protein assay

Yong-ju Wei, Ke-an Li *, Shen-yang Tong

Department of Chemistry, Peking University, Beijing 100871, People's Republic of China

Received 11 June 1996; received in revised form 16 September 1996; accepted 18 October 1996

Abstract

The interactions of Coomassie brilliant blue G-250 (CBB) with bovine serum albumin (BSA) and γ-globulin at low pH are investigated by a spectrophotometric method. It is considered that the binding of CBB to protein is because of the weak interactions (ionic, van der Waals, hydrogen bonding, and hydrophobic). The solution equilibria involving the binding of three dye species (blue, green, and red) to protein are treated in the same way as Ringbom model used in the treatment of complexation in analytical chemistry. Based on this treatment, the formation of an isosbestic point in the absorption spectra of CBB-BSA mixtures is discussed, two mathematical models for the description of the CBB protein assay are developed. The first model is a nonlinear equation which is rigorous in theory but unreliable in use because of its optimization procedure. The second model based on an approximation is a linear equation, it allows to estimate apparent binding constant, maximum binding number, and molar absorptivity of bound dye from assay data by a linear regression method. The results of the linear regression operations are reasonable and in agreement with experimental findings. Factors which influence the sensitivity of the CBB protein assay are studied using this method. Ionic strength and acidity are found to have significant effect on the binding of CBB to protein. © 1997 Elsevier Science B.V.

Keywords: Coomassie brilliant blue protein assay; Solution equilibria; Spectrophotometry

1. Introduction

The Coomassie brilliant blue G-250 (CBB) protein assay [1] has been commonly used in biochemical and clinical laboratories because of its high sensitivity and convenience. In practice, the assay is conducted by adding a protein sample to a fixed quantity of dye reagent and measuring the increase in absorbance at 595 nm as a blue dye-protein complex forms. Though the performance of the assay is simple, its mechanism and solution equilibria are still under investigation [2–8]. A further theoretical study on the assay should be beneficial not only with regard to the quantitation of proteins but also to a deep understanding of the interactions between macrobiomolecules and small ions or molecules.

Previous authors have made great efforts in the study of the nature of the CBB protein assay. Compton and Jones [2] pointed out that CBB

* Corresponding author.

PII S0039-9140(96)02140-6

exists in three forms at the usual pH of the assay: cationic (red), neutral (green), and anionic (blue). A spectral study made by Chail et al. [4] shows that the three dye forms have markedly different visible spectra from one another and that none of these spectra correspond exactly to the spectrum of the dye-protein complex. The blue dye form is generally considered to be the form that complexes with protein [2,4,5], since its negative charge argues in favor of electrostatic attraction to arginine and lysine side chains on protein. However, there are indications of the existence of nonelectrostatic interactions between CBB and proteins in addition to the electrostatic interactions. Compton and Jones [2] estimated that the nonionic binding energies account for about 58% of the total binding energy of the CBB-protein complex. Therefore, Atherton et al. [8] recently proposed a dye-binding scheme in which it is assumed that all the three dye species can bind to protein to form dye-protein complexes.

The determination of binding constant and number of dye-binding sites on protein is a major difficulty in the theoretical study of dye-binding protein assays. The Scatchard equation [9] has long been considered to be a basic equation for the study of the interactions between macrobiomolecules and small ions or molecules. But there are reports pointed out that the Scatchard equation is not suitable for the description of some interactions between proteins and acid–base indicators such as T-azo-R [10], Chromazurol S [11], bromophenol blue [12], and bromocresol green [13] in acidic solutions. Though modified Scatchard equation was used to study high-affinity dye binding sites of the CBB protein assay at very large protein/dye molar ratios [6], there is no report on the use of this equation in the study of the CBB protein assay under normal conditions.

The number of dye-binding sites on protein could be estimated from the slope of the CBB protein assay plot [5,7], but binding constants cannot be found by this way. Recently, Atherton et al. [8] developed a mathematical model for the description of the CBB protein assay under normal conditions. Assay data may be fit to this model using curve-fitting techniques and thereby values of binding constant and number of binding sites could be estimated simultaneously for a particular protein. This model is quite rigorous in theory, but it seems that the optimization (curve-fitting) procedure is somewhat inconvenient in use.

In Ref. [12], the interaction of bromophenol blue with proteins in acidic solution is studied theoretically. As proposed by Kaler and Gavrilov [14], both dye species, protonated and deprotonated forms, are considered to be able to combine with protein by intermolecular forces (mainly electrostatic force). Two conditional constants, apparent binding constant and maximum number, are defined to express the binding ability of the dye to protein under a given set of conditions. These two parameters can be estimated by a linear regression method developed in that paper.

In the present work, the linear regression method proposed in reference [12] is extended to the study of the CBB protein assay. All the three dye species are treated to be able to combine with protein by weak interactions (ionic and nonionic) though their binding abilities are different. The solution equilibria are treated in the same way as Ringbom model [15] which is familiar to analytical chemist. A linear regression equation based on this treatment is developed to estimate apparent binding constant and maximum binding number from spectral data measured under normal conditions. The results obtained are in agreement with experimental findings.

2. Experimental

2.1. Reagents

BSA, 99%, was obtained from Sigma (fraction five, essentially fatty acid free). All calculations reported for BSA are in terms of a molecular weight of 65 000. The BSA solution (1.52×10^{-6} mol l^{-1}) was prepared by dissolving 0.100 g BSA reagent in 1000 ml deionized water. γ-Globulin human (γ-G) was obtained from Serva (Germany). Calculations reported for γ-G are in terms of a molecular weight of 160 000. The γ-G solution (6.2×10^{-7} mol l^{-1}) was prepared by dis-

solving 0.100 g γ-G reagent in 1000 ml deionized water. CBB was purchased from Fluka and purified by following a procedure reported by Wilson [6,16]. The CBB stock solution (1.17×10^{-3} mol l^{-1}) was prepared by dissolving 0.100 g purified dye in 50 ml 95% ethanol, and then diluting to 100 ml with deionized water. The operating solution of CBB was prepared by diluting the stock solution with water properly. All other reagents were of analytical or guaranteed reagent grade.

2.2. Apparatus

A Shimadzu Model UV-265 double-beam spectrophotometer was used for recording absorption spectra, and a Shimadzu UV-120-02 spectrophotometer for the measurement of absorbance at a given wavelength.

2.3. Method

Aliquots of 5% NaCl solution, phosphoric acid (7.3 mol l^{-1}) or standard HCl solution, and CBB operating solution were transferred into a series of 25 ml volumetric flasks, and then protein solution was added to each flask in different amounts. The mixtures were diluted to the mark with water and mixed thoroughly. After 20 min, spectra or absorbances of these solutions were measured with reference to water. The pH values of these solutions were calculated according to the concentrations of the acid used, ignoring activity effect.

3. Results and discussion

3.1. Absorption spectra and binding equilibria

Fig. 1 shows the absorption spectra of CBB at various pH values [4]. As the pH is raised a red form of the dye ($\lambda = 470$ nm) is replaced by a green form ($\lambda = 650$ nm) in the vicinity of pH 1. Further pH elevation results in a shift of the dye species from green form into a blue form ($\lambda = 585$ nm) at about pH 2. No isosbestic point is formed, indicating that three distinct dye species are present:

$$H_2L + \rightleftharpoons HL + H^+ \quad HL \rightleftharpoons L^- + H^+ \qquad (1)$$

with dissociation constants $pK_{a1} = 1.15$, and $pK_{a2} = 1.82$ [4].

Fig. 2 shows the absorption spectra of CBB-BSA mixtures [3]. They were obtained by keeping the CBB concentration and pH constant and changing the BSA concentration. With the increase in BSA concentration, the absorption peaks at 470 and 650 nm are replaced by a new absorption peak at 595 nm. An isosbestic point is formed at 530 nm. This spectral feature indicates that the free dye species are transformed into bound ones.

According to the study made by previous workers [2–6], the formation of CBB-BSA complexes is because of the weak (noncovalent) interactions (ionic, van der Waals, hydrogen bonding, and hydrophobic), all the three dye forms are being able to combine with protein although their binding abilities are different [8]. But, on account of the anion L^- has an advantage in binding to positively charged amino acid residues on protein by electrostatic force, we take this form as the main binding species and use the Ringbom model [15] for the description of the dye-binding equilibria (omitting electrical charges):

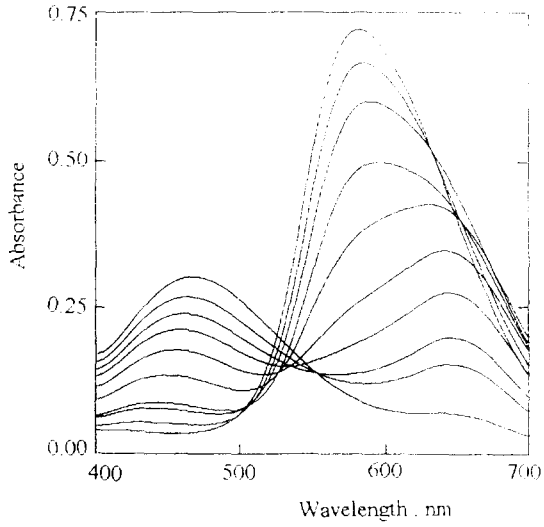

Fig. 1. CBB absorption spectra at various pH values. CBB concentration constant at 1.46×10^{-5} mol l^{-1}. In order of increasing absorbances at 595 nm, pH values are 0.27, 0.65, 0.80, 1.00, 1.17, 1.35, 1.65, 1.80, 2.17 and 2.65.

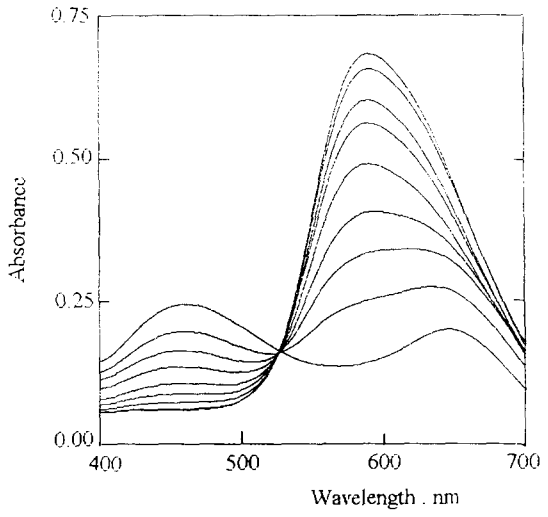

Fig. 2. Absorption spectra of CBB–BSA mixtures. 0.158 mol l^{-1} HCl medium, pH 0.80, CBB concentration constant at 1.46×10^{-5} mol l^{-1}. In order of increasing absorbances at 595 nm, BSA concentrations are 0.0, 3.0×10^{-8}, 6.0×10^{-8}, 9.1×10^{-8}, 1.5×10^{-7}, 2.1×10^{-7}, 2.7×10^{-7}, 3.6×10^{-7} and 4.6×10^{-7} mol l^{-1}.

$$\begin{array}{ccccc} L & + & P & \rightleftharpoons & L' \\ H\downarrow\uparrow & & A\downarrow\uparrow & & H\downarrow\uparrow \\ HL & & A' & & HL' \\ H\downarrow\uparrow & & & & H\downarrow\uparrow \\ H_2L & & & & H_2L' \end{array} \quad (2)$$

where P represents dye-binding sites on protein, A refers to co-existing anion(s) having unfavorable effect on the binding of dye to protein, the primed symbols, A′, L′, HL′, and H_2L' refer to bound A, L, HL, and H_2L, respectively. These equilibria may be described by proton dissociation constants for free and bound dye species and by binding constants for dye-protein and anion-protein complexes equilibria, as follows.

$$K_{a1} = [H][HL]/[H_2L];\ K_{a2} = [H][L]/[HL] \quad (3)$$

$$K'_{a1} = [H][HL']/[H_2L'];\ K'_{a2} = [H][L']/[HL'] \quad (4)$$

$$K_{L'} = [L']/[L][P] \quad (5)$$

$$K_{A'} = [A']/[A][P] \quad (6)$$

where [P] represents the total concentration of free dye binding sites on all protein molecules.

3.2. Explanation of the formation of the isosbestic point

The formation of the isosbestic point in Fig. 2 can be explained based on model Eq. (2). Define {L} as the total concentration of free dye, {L′} as the total concentration of bound dye, and c_L as the analytical concentration of dye, that is:

$$\{L\} = [L] + [HL] + [H_2L] \quad (7)$$

$$\{L'\} = [L'] + [HL'] + [H_2L'] \quad (8)$$

$$c_L = \{L\} + \{L'\} \quad (9)$$

The absorbance of the dye-protein mixture is (with 1 cm cell)

$$A = \epsilon_L[L] + \epsilon_{HL}[HL] + \epsilon_{H_2L}[H_2L] + \epsilon_{L'}[L'] + \epsilon_{HL'}[HL'] + \epsilon_{H_2L'}[H_2L'] \quad (10)$$

where ϵ_L, ϵ_{HL}, ϵ_{H_2L}, $\epsilon_{L'}$, $\epsilon_{HL'}$ and $\epsilon_{H_2L'}$ are molar absorptivities (mol^{-1} 1 cm^{-1}) of L, HL, H_2L, L′, HL′, and H_2L', respectively.

Define distribution coefficients as

$$\delta_L = [L]/\{L\} \quad (11)$$

$$\delta_{HL} = [HL]/\{L\} \quad (12)$$

$$\delta_{H_2L} = [H_2L]/\{L\} \quad (13)$$

$$\delta_{L'} = [L']/\{L'\} \quad (14)$$

$$\delta_{HL'} = [HL']/\{L'\} \quad (15)$$

$$\delta_{H_2L'} = [H_2L']/\{L'\} \quad (16)$$

Substituting Eq. (7) and Eq. (3) into Eq. (11) gives:

$$\delta_L = [L]/([L] + [HL] + [H_2L]) = K_{a1}K_{a2}/(K_{a1}K_{a2} + [H]K_{a1} + [H]^2) \quad (17)$$

Similar substitution leads to

$$\delta_{HL} = [H]K_{a1}/(K_{a1}K_{a2} + [H]K_{a1} + [H]^2) \quad (18)$$

$$\delta_{H_2L} = [H]^2/(K_{a1}K_{a2} + [H]K_{a1} + [H]^2) \quad (19)$$

$$\delta_{L'} = K'_{a1}K'_{a2}/(K'_{a1}K'_{a2} + [H]K'_{a1} + [H]^2) \quad (20)$$

$$\delta_{HL'} = [H]K'_{a1}/(K'_{a1}K'_{a2} + [H]K'_{a1} + [H]^2) \quad (21)$$

$$\delta_{H_2L'} = [H]^2/(K'_{a1}K'_{a2} + [H]K'_{a1} + [H]^2) \quad (22)$$

Note that distribution coefficients are merely the functions of pH and are independent of dye concentration. Substituting Eq. (11) Eq. (12) Eq. (13) Eq. (14) Eq. (15) Eq. (16) into Eq. (10) gives:

$$A = (\epsilon_L\delta_L + \epsilon_{HL}\delta_{HL} + \epsilon_{H_2L}\delta_{H_2L})\{L\} + (\epsilon_{L'}\delta_{L'} + \epsilon_{HL'}\epsilon_{HL'} + \epsilon_{H_2L'}\delta_{H_2L'})\{L'\} \quad (23)$$

Let

$$\epsilon = \epsilon_L\delta_L + \epsilon_{HL}\delta_{HL} + \epsilon_{H_2L}\delta_{H_2L} \quad (24)$$

$$\epsilon' = \epsilon_{L'}\delta_{L'} + \epsilon_{HL'}\delta_{HL'} + \epsilon_{H_2L'}\delta_{H_2L'} \quad (25)$$

where ϵ and ϵ' are the mean (distribution coefficient-weighted) molar absorptivities of free and bound dye at the assay pH. They are constants when pH and measuring wavelength are given. So Eq. (23) may be simplified as

$$A = \epsilon\{L\} + \epsilon'\{L'\} = \epsilon c_L + (\epsilon' - \epsilon)\{L'\} \quad (26)$$

Where ϵc_L is the absorbance of the CBB blank solution.

Fig. 2 shows that the maximum values of ϵ and ϵ' are at 470 nm and 595 nm, respectively. We could deduce that there should be a wavelength between 470 and 595 nm where ϵ equals ϵ'. As we can see from Fig. 2 this particular wavelength is 530 nm. It is at this wavelength that $\epsilon = \epsilon'$, Eq. (26) becomes $A = \epsilon c_L$, which is a fixed value, unchanging with increase of BSA concentration, so the isosbestic point appears.

The above discussion gives an explanation to the appearance of the isosbestic point in Fig. 2. The appearance of the isosbestic point in Fig. 2, in reverse order, provides an evidence for the above theory. And furthermore, based on the above discussion two mathematical models for the description of the CBB protein assay could be developed, as follows.

3.3. A nonlinear equation for the description of the CBB protein assay

In Eq. (26), both A and ϵc_L can be measured, ϵ' and ϵ are constants under certain conditions. Let

$$\Delta A = A - \epsilon c_L \quad (27)$$

$$\Delta\epsilon = \epsilon' - \epsilon \quad (28)$$

then Eq. (26) may be written as

$$\{L'\} = \Delta A/\Delta\epsilon \quad (29)$$

where ΔA is measurable, $\Delta\epsilon$ is a constant under certain conditions.

The total concentration of free dye binding sites [P] may be expressed as

$$[P] = (Nc_P - \{L'\}) \quad (30)$$

where c_P is the analytical molar concentration of protein, N the total number of binding sites per protein molecule. Substituting Eq. (30), Eq. (11) and Eq. (14) into Eq. (5) gives

$$K_{L'} = \delta_{L'}\{L'\}/[\delta_L\{L\}(Nc_P - \{L'\})] \quad (31)$$

Since $\delta_{L'}$ and δ_L have fixed values under certain conditions, we can define a new constant

$$K = K_{L'}\delta_L/\delta_{L'} = \{L'\}/[\{L\}(Nc_P - \{L'\})] \quad (32)$$

Substituting Eq. (29) and Eq. (9) into the above equation gives

$$K = (\Delta A/\Delta\epsilon)/[(c_L - \Delta A/\Delta\epsilon)(Nc_P - \Delta A/\Delta\epsilon)] \quad (33)$$

Rearranging this equation yields

$$\Delta A = K\Delta\epsilon^{-1}(\Delta\epsilon c_L - \Delta A)(\Delta\epsilon N c_P - \Delta A) \quad (34)$$

If the experiment is conducted by keeping the dye concentration c_L and other conditions constant and changing the protein concentration c_P, a group of $c_P \sim \Delta A$ data can be measured. These data may be fit to Eq. (34) using optimization method and, at the same time, the values of K, $\Delta\epsilon$, and N can be calculated.

But, unfortunately, in our experiment the optimization results are not satisfactory. Although Eq. (34) is a theoretically rigorous equation, its mathematical properties require further investigation. In the following section, a simple linear regression equation based on an approximation is proposed for studying the CBB protein assay.

3.4. A linear regression method for the study of the CBB protein assay

Define distribution coefficient of P as

$$\delta_P = [P]/Nc_P \quad (35)$$

Suppose δ_P is a constant over the entire c_P range studied when c_L and other conditions are fixed (this supposition is not rigorous in theory, but it leads to an easy mathematical treatment and it practically holds under normal conditions). Substituting Eq. (35), Eq. (11) and Eq. (14) into Eq. (5) gives

$$K_{L'} = \delta_{L'}\{L'\}/(\delta_L\{L\}\delta_P N c_P) \quad (36)$$

Under a given set of experimental conditions, $\delta_{L'}$, δ_L, δ_P and N are constants. Thus, we can define a new constant:

$$K_c = NK_{L'}\delta_L\delta_P/\delta_{L'} = \{L'\}/\{L\}c_P \quad (37)$$

K_c is a conditional constant. It is a measure of the CBB binding ability of a protein under certain conditions. We call K_c the apparent binding constant [12].

Substituting Eq. (29) and Eq. (9) into Eq. (37) gives

$$K_c = (\Delta A/\Delta\epsilon)/[(c_L - \Delta A/\Delta\epsilon)c_P]$$

Rearranging this equation yields

$$\Delta A = \Delta\epsilon c_L - K_c^{-1}\,\Delta A/c_P \quad (38)$$

where K_c and $\Delta\epsilon$ are conditional constants. If the experiment is conducted by keeping c_L constant and changing c_P, there should be a linear relationship between ΔA and $\Delta A/c_P$. From the slope ($-K_c^{-1}$) and the intercept ($\Delta\epsilon c_L$) of the regression line, K_c and $\Delta\epsilon$ (then $\epsilon' = \Delta\epsilon + \epsilon$) can be calculated.

Using the data measured at 595 nm in Fig. 2, a linear regression equation was obtained:

$$\Delta A = 0.771 - 1.78 \times 10^{-7}\Delta A/c_P \quad R = 0.9973$$

From the slope and the intercept of above equation, $K_c = 5.62 \times 10^6$, and $\Delta\epsilon = 5.28 \times 10^4$ mol^{-1} l cm^{-1} were obtained.

This example demonstrated that the linear regression method proposed above is feasible in the study of the CBB protein assay. This feasibility will be examined further in the following sections.

3.5. Maximum binding number and the Sandell index

The maximum binding number n and the Sandell index s (μg cm^{-2}) can be calculated respectively by the following equations [12]:

$$n = K_c c_L \quad (39)$$

$$s = F/n\,\Delta\epsilon \quad (40)$$

where F is the molecular weight of the protein assayed.

Using the K_c and $\Delta\epsilon$ values obtained above, $n = 82$, and $s = 0.015$ μg cm^{-2} were calculated. Both n and s values are reasonable.

3.6. Influence of experimental conditions on the binding of CBB to protein

The influence of ionic strength on the binding of CBB to protein is shown in Table 1. An increase in salt concentration causes a significant decrease in K_c and n values, thus decreasing the sensitivity of the CBB protein assay. This effect can be explained as a competition between anions and dye species for the same binding sites on BSA, see reaction model (2).

The influence of acidity on the binding of CBB to protein is shown in Table 2. From this test we can see that in the pH range studied a decrease in acid concentration causes an increase in K_c and n values, thus, increasing the sensitivity of the assay. This effect is due to the fact that an increase in pH causes an increase in L^- concentration thereby promoting the main reaction in model (2). But, the assay pH cannot be too high because a decrease in $\Delta\epsilon$ value occurs when pH is higher than pH 1.13. From Table 2 we can see that the best acidity for the CBB protein assay is at about pH 1.13 (0.73 mol l^{-1} H_3PO_4), which is slightly different from the acidity suggested by earlier workers (pH 0.97, 1.46 mol l^{-1} H_3PO_4) [1,3].

Table 1
Effect of sodium chloride concentration on binding of CBB on BSA

NaCl (%)	$\Delta\epsilon$	K_c	n	s	R
0	3.0×10^4	5.0×10^6	82	0.026	0.997
0.1	3.1×10^4	4.0×10^6	65	0.032	0.997
0.3	3.0×10^4	3.5×10^6	56	0.038	0.997
0.5	2.5×10^4	3.3×10^6	53	0.048	0.996
0.8	2.1×10^4	3.1×10^6	51	0.059	0.998

$c_L = 1.63 \times 10^{-5}$ mol l^{-1}, $c_{H_3PO_4} = 1.46$ mol l^{-1}, pH = 0.98, at 595 nm.

Table 2
Effect of acidity on binding of CBB on BSA

H_3PO_4 (mol l^{-1})	pH	$\Delta\epsilon$	K_c	n	s	R
1.46	0.98	2.5×10^4	3.3×10^6	53	0.048	0.996
1.02	1.06	4.6×10^4	3.9×10^6	64	0.021	0.999
0.88	1.09	4.6×10^4	4.5×10^6	73	0.019	0.993
0.73	1.13	5.2×10^4	5.2×10^6	85	0.014	0.991
0.58	1.18	5.1×10^4	5.4×10^6	88	0.014	0.997

$c_L = 1.63\times10^{-5}$ mol l^{-1}, 0.5% NaCl, at 595 nm.

Table 3 shows the influence of CBB concentration on the binding reaction. From this test we can see that an increase in dye concentration causes an increase in n values, while $\Delta\epsilon$ and K_c remain practically constant. Therefore an increase in dye concentration makes a higher sensitivity. This is an obvious result since more binding sites would be bound when the dye concentration increases. But the dye concentration cannot be too high in assay practice because of the restriction of spectral measurement.

3.7. Binding of CBB on γ-globulin

The binding of CBB on γ-globulin was investigated by using the linear regression method. Some results are listed in Table 4.

4. Conclusions

The combination of CBB with proteins at low pH is due to the weak interactions (ionic, van der Waals, hydrogen bonding, and hydrophobic). All the three dye forms (red, green, and blue) are able to combine with protein by nonelectrostatic forces. The anionic blue form of the dye has an advantage over other two forms in binding to protein by ionic attraction, which is the key point of the entire binding and color changing process.

Table 3
Effect of CBB concentration on CBB protein assay

c_L (mol l^{-1})	$\Delta\epsilon$	K_c	n	s	R
1.31×10^{-5}	2.3×10^4	3.2×10^6	42	0.068	0.990
1.63×10^{-5}	2.5×10^4	3.3×10^6	53	0.048	0.996
1.96×10^{-5}	2.6×10^4	3.9×10^6	78	0.032	0.994

$c_{H_3PO_4} = 1.46$ mol l^{-1}, pH = 0.98, 0.5% NaCl, at 595 nm.

The Ringbom model [15] used in the treatment of the complexation between metal ions and ligands is suitable in the expression of the dye-binding equilibria of the CBB protein assay. In this model, the influence of side reactions (dye's protonation and the competition of co-existing anions for the dye-binding sites on protein) on the main reaction (binding of the anionic blue form of the dye to protein) is expressed explicitly. By this model, the effects of acidity and ionic strength on the binding of CBB to protein are easier to understand.

The concepts of mean molar absorptivities defined in Eq. (24) and Eq. (25) for free and bound dye (ϵ and ϵ') are different from the usual concept of molar absorptivity for single species. They are distribution coefficient-weighted parameters, so that they are functions of pH. The sensitivity of the CBB protein assay depends greatly upon the difference of these two parameters ($\Delta\epsilon$). If the assay pH is higher than pH 1.2, its sensitivity will decline due to the decrease in $\Delta\epsilon$ value although more dye species may be bound to protein under such conditions.

The linear regression equation is able to give a reasonable description of the CBB protein assay. Both the apparent binding constant and the maximum binding number are conditional constants, so their values vary along with experimental conditions. The maximum value of the maximum binding number determined in this paper ($n = 88$) is about the same as that determined previously ($n = 82$–105) [5–8]. This value is consistent with the total number of arginine and lysine side chains on BSA ($n_{arg} + n_{lys} = 86$), lending credence to the

Table 4
Binding data of CBB on γ-globulin at different pH

H_3PO_4 (mol l^{-1})	pH	$\Delta\epsilon$	K_c	n	s	R
1.46	0.98	2.4×10^4	4.9×10^6	81	0.082	0.995
0.88	1.09	4.4×10^4	8.7×10^6	141	0.025	0.995

$c_L = 1.63\times10^{-5}$ mol l^{-1}, 0.5% NaCl, at 595 nm.

idea that arginine and lysine residues are the primary binding sites for CBB.

To use this method, one should first prepare a series of dye-protein mixtures containing the same amount of dye and having the same pH and ionic strength but different in protein concentration. Then measure the absorbances of these mixtures at a given wavelength (595 nm, for example). Finally, do a linear regression operation according to Eq. (38) and calculate $\Delta\epsilon$, K_c, n, and s, respectively. Compared with other methods used before, this new method is simple to use.

Acknowledgements

This research was supported by National Natural Science Foundation of China.

References

[1] M.M. Bradford, Anal. Biochem., 72 (1976) 248.
[2] S.J. Compton and C.G. Jones, Anal. Biochem., 151 (1985) 369.
[3] A.G. Splittgerber and J. Sohl, Anal. Biochem., 179 (1989) 198.
[4] H.J. Chial, H.B. Thompson and A.G. Splittgerber, Anal. Biochem., 209 (1993) 258.
[5] H.J. Chial and A.G. Splittgerber, Anal. Biochem., 213 (1993) 362.
[6] R.W. Congdon, G.W. Muth and A.G. Splittgerber, Anal. Biochem., 213 (1993) 407.
[7] H.J. Chial, R.W. Congdon and A.G. Splittgerber, J. Chem. Educ., 72 (1995) 76.
[8] B.A. Atherton, E.L. Cunningham and A.G. Splittgerber, Anal. Biochem., 233 (1996) 160.
[9] G. Scatchard, Ann. NY Acad. Sci., 51 (1949) 660.
[10] M. Pesavento and A. Profumo, Talanta, 38 (1991) 1099.
[11] Y.J. Wei, S.Y. Tong and K.A. Li, Acta Chim. Sinica, 53 (1995) 83.
[12] Y.J. Wei, K.A. Li and S.Y. Tong, Talanta, 43 (1996) 1.
[13] Y.J. Wei, K.A. Li and S.Y. Tong, Chin. J. Anal. Chem. (FenXi HuaXue), 24 (1996) 387.
[14] G.V. Kaler and V.B. Gavrilov, Mol. Biol. Engl. Transl., 28 (1994) 140.
[15] A. Ringbom, Complexation in Analytical Chemistry, Interscience Publishers, New York, 1963, p. 38.
[16] C.M. Wilson, Anal. Biochem., 96 (1979) 263.

ELSEVIER

Talanta 44 (1997) 931–937

Talanta

Voltammetric study of ketorolac and its differential pulse polarographic determination in pharmaceuticals

J.C. Sturm, H. Canelo, L.J. Nuñez-Vergara, J.A. Squella *

Bioelectrochemistry Laboratory, Chemical and Pharmaceutical Sciences Faculty, University of Chile, P.O. Box 233, Santiago 1, Chile

Received 15 July 1996; received in revised form 18 October 1996; accepted 18 October 1996

Abstract

A differential pulse polarographic method for the quantitative determination of ketorolac is described. Ketorolac is an antiinflamatory-analgesic agent that is directly electroreducible at the mercury electrode. The polarographic reduction is due to the reduction of the benzoyl moiety in the ketorolac molecule. For analytical purposes, a very well resolved diffusion controlled differential pulse polarographic peak obtained at pH 9 was selected. This peak was used to develop a new method for the determination of ketorolac in pharmaceutical dosage forms. Recovery study shows that the method is sufficiently accurate and precise to be applied in the individual tablet assay of commercial samples.

Keywords: Differential pulse polarography; Drug analysis; Ketorolac; Voltammetry

1. Introduction

Ketorolac tromethamine, (±)-5-benzoyl-2,3-dihydro-1H-pyrrolizine-1-carboxylic acid (Fig. 1), is a nonsteroidal anti-inflammatory analgesic agent [1]. Its rapid onset of action, effectiveness, lack of opiate action and safety make it an attractive agent for general purpose analgesia. Ketorolac is a non narcotic analgesic of great efficiency, that does not produce lateral effects on the central nervous system and does not provoke dependency [2–4]. It also possesses antipyretic properties, being indicated that it is 20 times more potent than the aspirin [5]. Furthermore some studies of its inhibitor action of the plaquelet aggregation have been described [2]. The mechanism of action consists of inhibiting the enzyme cyclooxygenase, involved in the synthesis of derivatives of the arachidonic acid, that is translated to a decrease in the metabolic products that trigger the inflammatory processes [6].

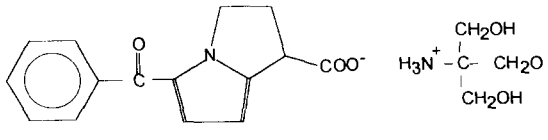

Fig. 1. Molecular structure of ketorolac tromethamine.

* Corresponding author. Fax: +56 2 7378920; e-mail:asquella@ll.ciq.uchile.cl

0039-9140/97/$17.00
PII S0039-9140(96)02143-1

Ketorolac is manufactured as the tromethamine salt for enhanced solubility in form of tablets and intramuscular injectables. The recommended initial loading dose is 30–60 mg given via intramuscular injection, followed by additional doses of 15 or 30 mg every 6 h [2]. When ketorolac tromethamine is absorbed after oral ingestion, or following intravenous injection, it is rapidly dissociated into the anion form of ketorolac at neutral pH. The major metabolic pathway in humans is glucuronic acid conjugation. The products appear in the urine, but not in the plasma.

Several analytical techniques for the determination of ketorolac tromethamine from the bulk drug are described. These include non-aqueous titration, TLC, UV spectrophotometry and HPLC methods [7,8]. Ketorolac has been determined in blood after a solid-phase extraction, by gas chromatography-mass spectrometry after derivatization using diazopropane [9]. Other studies in human serum have been performed by HPLC [10,11]. A flow injection analysis (FIA) method with spectrophotometric detection after derivatization with dichloronitrophenol in pharmaceutical formulations was published recently [12].

However, to our knowledge no information about the electrochemical redox properties of ketorolac and its analytical application have appeared in the literature. In this work we have carried out a study of the electrochemical reduction behavior of ketorolac by differential pulse(dpp) and tast polarography and cyclic voltammetry.

A dpp method is recommended for the quantitative determination of the pure drug and for commercial preparations.

2. Experimental

2.1. Apparatus

Differential pulse polarography (DPP), tast polarography and cyclic voltammetry (CV) were carried out in an Inelecsa® assembly containing a pdc1212 potentiostat-scan generator attached to an Acer® 500 + PC with suitable software for totally automated control of the experiments and data acquisition. A 25 ml capacity Metrohm® thermostated cell equipped with a three-electrode system was used. The working electrodes were a dropping mercury electrode (DME) and a hanging mercury drop electrode (HMDE), Metrohm® model EA-290, for polarographic and cyclic voltammetric experiments, respectively. As reference electrode, a silver–silver chloride electrode and a platinum wire counter-electrode were used.

Spectrophotometric measurements were carried out with a UV–Vis Spectrophotometer (Unicam® model UV-3) using 1 cm quartz cells and equipped with a 486 computer with a Vision® acquisition and treatment program (Unicam®).

2.2. Reagents and drugs

Ketorolac tromethamine standard (100% pure drug) was obtained from Laboratorio Saval® (Santiago, Chile). Stock solutions 2×10^{-3} M were prepared in distilled water. Netaf® tablets containing 10 mg of ketorolac tromethamine (Lab.Chemopharma S.A., Santiago, Chile) were commercially obtained.

All reagents employed were of analytical grade.

2.3. Buffer solutions

The solutions under study were buffered using Britton–Robinson buffer (0.04 M phosphoric acid/0.04 M acetic acid/0.04 M boric acid) adjusted with NaOH to the desired pH. The ionic strength was kept constant at 0.3 M with KCl.

2.4. Working solutions

An aliquot (1.25 ml) of the drug stock solution was diluted to a final volume of 25 ml with buffer (pH 9.0) to obtain a final concentration of 1.0×10^{-4} M.

3. Methods

3.1. Cyclic voltammetry

For obtaining cyclic voltammetric curves a 1×10^{-3} M, pH 9 KT solution was used. Scan rates

were varied between 0.1 and 10 V s^{-1}. Potential range was −1300 mV (initial potential) to −1800 mV (switching potential) versus Ag–AgCl.

3.2. Calibration curve

A calibration curve was produced adding different volumes of standard solution to 20 ml of buffer solution (pH 9.0) within the polarographic cell. The concentrations ranged between 4.9×10^{-5} and 4.2×10^{-4} M.

3.3. Synthetic samples

Synthetic samples for recovery studies were prepared by weighing 10 mg ketorolac tromethamine standard plus suitable excipients according to the manufacturer's batch formulas for 10 mg tablets. The excipients tested were. Lactose, magnesium stearate, hydroxy-propylmethyl-cellulose, polyethylenglicol, titanium dioxide, starch and microcrystaline cellulose. All the components were suspended in 6 ml distilled H_2O and sonicated for 3 min, then diluted to 100 ml with pH 9, 0.04 M Britton–Robinson buffer, obtaining a final concentration of 2.7×10^{-4}. Prior to the spectrophotometric experiment each sample was centrifuged at 4000 rpm for 10 min. The samples were assayed by polarography and spectrophotometry.

Tablet assay procedure.

3.4. Polarography

Ten series of one tablet of Netaf®, Lab.Chemopharma S.A. Santiago, Chile (declared amount 10 mg per tablet) were suspended in 5 ml of distilled water and then diluted to a final volume of 100 ml with Britton–Robinson Buffer pH 9.0.

Then, not less than 10 ml of each solution was transferred to a dry polarographic cell and a deaeration performed for 5 min with nitrogen. The DP polarogram is then recorded at the DME between −1200 and −1700 mV. The current is measured at the peak potential of ketorolac at ca. −1530 mV and the amount of ketorolac in the sample solution calculated from prepared standard calibration curve.

3.5. Spectrophotometry

Ten series of one tablet of Netaf® (declared amount of ketorolac per tablet, 10 mg) were suspended in 5 ml of distilled water and diluted to a final volume of 100 ml. A portion of this solution was centrifuged at 4000 rpm for 10 min, then an aliquot of 2 ml was taken and diluted up to 25 ml with pH 9.0 buffer. Then, the sample solution absorbance was measured at 324 nm using buffer solution as a blank. The amount of ketorolac in the sample solution was calculated from a prepared standard calibration curve.

4. Results and discussion

Ketorolac trometamine (KT) appears to be an electroactive drug. Specifically, the drug is capable to be both, oxidable and reducible. However, tromethamine did not shows neither reduction waves nor oxidation peaks when submitted to a voltammetric experiment. Consequently we can conclude that the electroactivity was not due to the tromethamine moiety. As a first step KT was subjected to a polarographic study in the tast and differential pulse modes, and to a cyclic voltammetric study with the aim of characterizing its electrochemical reduction behavior. When KT was subjected to reduction in the differential pulse polarographic mode (dpp), three well-defined peaks were observed (Fig. 2, peaks I, II, and III). The appearance of these peaks was pH-dependent and the evolution of the DPP signals between pH 1.8 and 11 are shown in the E_p versus pH graph in Fig. 3. Peak (I) appears between pH 1.0 to 3.0, peak II is present between pH 1.0 and 7.0 while peak III is seen between pH 7.0 to 12.0. A totally analogous behavior is observed by tast polarography (Fig. 2) and the corresponding i_l versus pH graph is showed in the insert of Fig. 3. The limiting current of peak I (or wave I), that appears only at acidic pHs, is strongly dependent on pH and appears just before the signal of the supporting electrolyte. This characteristic suggests a catalytic wave due to the catalytic proton discharge, commonly found in compounds with heterocyclic nitrogen in the molecule [13]. Considering

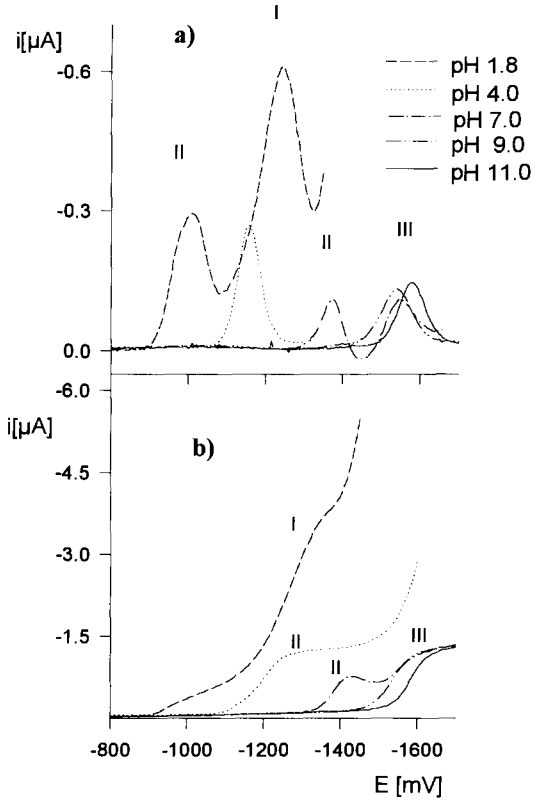

Fig. 2. Differential pulse (a) and Tast (b) polarograms of 1×10^{-4} M ketorolac at different pH values.

the molecular structure of KT the only possibility of obtaining a polarographic reduction signal is the reduction of the carbonyl group close to the benzene ring and the heterocyclic moiety. Consequently, peaks (or wave) II and III are due to the well-known two-electron carbonyl group reduction [14]. Peaks (or wave) II appears between pHs 1.8 and 6, shifting towards more negative potential values when pH increases. In Fig. 4 is clearly appreciated as the wave II that is observed at pH 5 is unfolded at pH 7 to be converted into a new wave III at pH 9. Between pHs 6 and 8 both waves II and III are present indicating the presence of two different reducible species. As can be seen the ratio of the wave heights (II and III) change with pH, however, the total height of these waves (II + III) remains constant. This phenomena is a very clear example of the general pattern that has been well-described by Zuman [15]. This

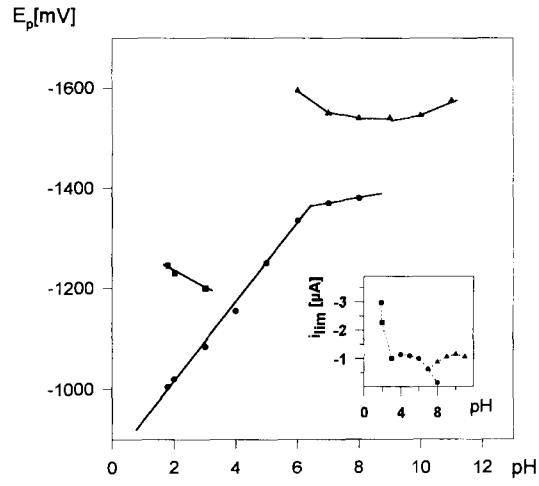

Fig. 3. Potential peaks and limiting current dependence with pH for 1×10^{-4} M ketorolac solutions. ■, peak (or wave) I; •, peak (or wave) II; and ▲, peak (or wave) III.

general pattern is described with the following scheme:

$$R + H^+ \rightleftharpoons RH^+ \quad (1)$$

$$RH^+ + n_1e^- \rightarrow P_1 \quad (2)$$

$$R + n_2e^- \rightarrow P_2 \quad (3)$$

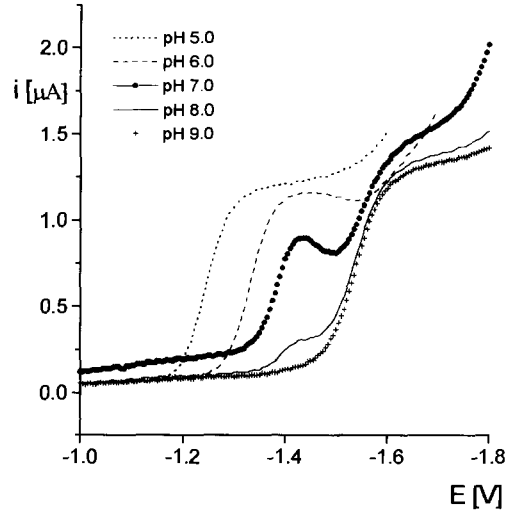

Fig. 4. Tast polarograms showing the unfolding of the benzoyl reduction wave of ketorolac between pHs 5 and 9.

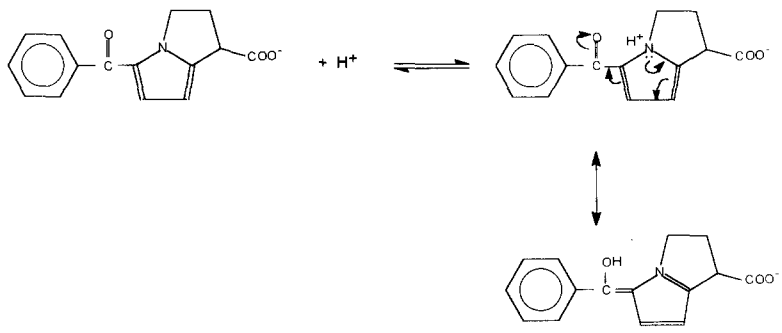

Scheme 1. Antecedent acid–base reaction and keto-enolic equilibria affecting the benzoyl reduction in ketorolac molecule.

At pH values $< pK_a$ the reduced specie would be RH^+ at the potential E_1, meanwhile at pH $> pK_a$ the non-protonated form is reduced at a more negative potential, E_2. In the zone ± 2 pH units around the pK_a, the two species coexists giving two polarographic signals. In our case, R is the KT molecule and RH^+ is the protonated KT. Specifically, the RH^+ specie corresponds to the KT molecule with the heterocyclic nitrogen protonated Scheme 1). The protonation on the heterocyclic nitrogen affect the reduction of the neighboring carbonyl group due to the existence of the keto-enolic equilibria as is shown in Scheme 1. According to the i_l versus pH behavior the pK_a value, that is defined as the pH value at which the heights of the waves II and III are equal. was 6.5. Consequently, at acidic pH the reduction occurs via Eq. (2) and at basic pH, the reducible specie is the non-protonated according to Eq. (3). Furthermore, the acid–base reaction can be qualified as a surface reaction. The phenomena that allows us to distinguish the surface character of the acid–base process involved is a decrease of the limiting current (pH 7 curve in Fig. 4) similar to that described for this type of surface processes [16].

We found that between pH 4.0 and 5.0 and at pH higher than 9.0 there is only one wave present, which is well resolved and appears suitable to be investigated for analytical use. But by comparing the electrocapillary curves (Fig. 5), it is observed that only the pH 9 condition did not show adsorption interferences in the potential range where the drug is reduced. Consequently, a pH of 9.0, buffered with the Britton–Robinson buffer, is selected to develop an analytical procedure. Furthermore, considering that tromethamine (TRIS buffer) was a normal constituent of the pharmaceutical form, the possibility of using TRIS buffer also was evaluated. However this buffer is ade-

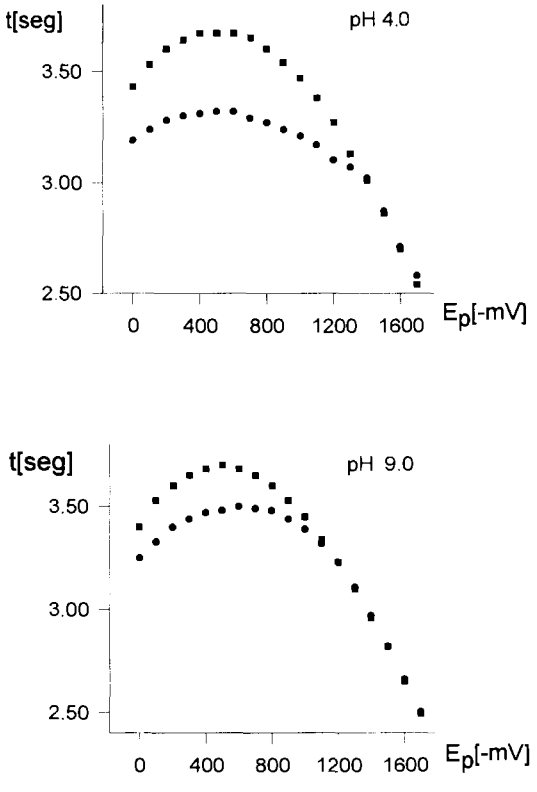

Fig. 5. Electrocapillary curves of ketorolac at pH 4 and 9. •, 1×10^{-4} M ketorolac solutions; and ■, only buffer solutions.

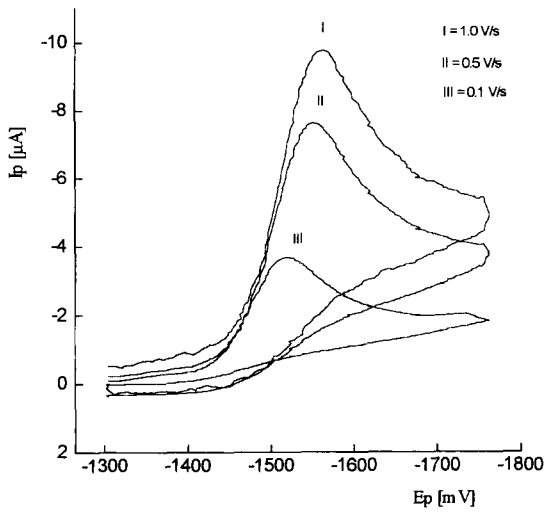

Fig. 6. Linear sweep cyclic voltammograms of 1×10^{-3} M, pH 9 ketorolac solution at different sweep rates.

quate only at physiological conditions (around pH 7.4).

In order to clarify the nature of the limiting current we have obtained a linear relationship between the limiting current and the height of the mercury column. From the dependence between the limiting current and the temperature a temperature coefficient of 2%°C^{-1} was obtained. Both of these results are indicative of a diffusion control of the limiting current. Moreover, also we have obtained a linear relation between the limiting current and the concentration of KT (linear range 2×10^{-3}–6×10^{-6} M) also showing a diffusion control.

From the cyclic voltammograms observed in Fig. 6, we can confirm that the reduction of KT at pH 9, appears to be irreversible with a linear relation between i_p and the square root of the sweep rate confirming a diffusion controlled process.

In order to develop a polarographic methodology for determining the drug, we have selected the differential pulse mode. For quantitation the calibration curve method, with concentrations ranging between 4×10^{-5} and 4×10^{-4} M, was used. The calibration curve is described by the following regression curve:

$$i_p(\mu A) = 1104.47C(M) - 0.00574 \quad (4)$$

(correlation coefficient = 0.999, $n = 10$, pH = 9, $T = 25$°C), where i_p is the peak current and C is the KT concentration. The repeatability (intra-day) and the reproducibility (inter-day) of the measurement was calculated from ten independent runs of a 1×10^{-4} M KT solution obtaining a RSD of 0.5 and 0.8%, respectively. The detection and quantitation limits were 4.04×10^{-6} and 6.15×10^{-6} M, respectively. The detection or quantitation limits were calculated as the blank response plus three times or ten times, respectively the blank standard deviation divided by the slope of the calibration curve. In order to check the accuracy and precision of the developed method, we have also carried out a recovery study (Table 1), obtaining a recovery of 98.25% with a RSD of 0.94%, concluding that the proposed method is sufficiently accurate and precise in order to be applied to pharmaceutical forms. The result for the individual tablet assay (Table 2) for commercial tablets containing 10 mg ketorolac tromethamine shows a mean of 9.81 with a RSD of 1.85% for ten individual tablets.

Furthermore, to obtain comparative results an UV spectrophotometric method was also applied. This spectrophotometric method was very similar to that described the U.S. Pharmacopeia [17] for the analysis of KT tablets. However, in order to

Table 1
Recovery of synthetic samples[a] of ketorolac

Sample	Recovery, %
1	97.08
2	97.76
3	97.40
4	98.12
5	98.87
6	98.51
7	98.12
8	98.50
9	97.74
10	100.38
Mean	98.25
R.S.D.	0.94

[1] Each synthetic sample contained 10 mg ketorolac tromethamine standard plus excipients.

Table 2
Individual tablet assay of ketorolac tablets[a]

Tablet	Polarographic, mg tablet^{-1}	Spectrophotometric, mg tablet^{-1}
1	9.77	9.50
2	10.15	9.64
3	10.0	9.60
4	9.81	9.60
5	9.81	9.52
6	9.51	9.68
7	9.85	9.50
8	9.81	9.18
9	9.59	9.50
10	9.77	9.64
Mean	9.81	9.54
R.S.D, %	1.85	1.49

[a] Netaf®, Chemopharma Lab., Santiago, Chile. Declared amount, 10 mg per tablet.

use the same sample that in the polarographic analysis we have performed the spectrophotometric analysis at pH 9. KT absorption spectra exhibit two well—resolved maxima at 250 and 324 nm in pH 9.0 solution. The maxima at 324 nm presents better absorbility and shows a linear dependence with the KT concentration. For analytical determination the calibration curve method, with concentrations ranging between 6.46×10^{-6} and 4.04×10^{-5} M, was used. This curve is described by the following regression line:

$$A = 21038.82C(M) + 5.014 \times 10^{-3} \quad (5)$$

(correlation coefficient = 0.9999, $n = 10$), where A is the absorbance of pH 9.0 solution of KT at 324 nm. The results of the recovery study (97.39, 0.5% RSD) and the individual tablet assay (9.54 mg tablet^{-1}, 1.49% RSD) are in accord with the polarographic results.

Although both, polarographic and UV spectrophotometric, showed similar accuracy and precision, the principal advantage of the proposed polarographic method over the spectrophotometric one is that the excipients do not interfere and the separation procedure is not necessary. Consequently, the above presented method is a good analytical alternative for determining ketorolac in tablets.

Acknowledgements

This research was funded by FONDECYT, project No. 1950480 and DTI Universidad de Chile.

References

[1] W.H. Rooks, A.J. Tomolins, P.J. Maloney, M.B. Wallach and M.E. Schuler, Agents Actions, 12 (5,6) (1982) 684–690.
[2] J.R. Prous, Drugs Today, 28 (1) (1992) 41–61.
[3] Drugs of the Future. Ketorolac, Vol. 11, No. 10 (1986) 889–890.
[4] Drugs of the Future. Ketorolac. Vol. 12, No. 10 (1987) 991–992.
[5] Drugs of the Future. Ketorolac, Vol. 9, No. 10 (1984) 789.
[6] Drugs of the Future. Ketorolac, Vol. 14, No. 10 (1989) 1010–1011.
[7] R.T. Sane, V.B. Tirodkar, A.J. Desai, M.K. Patel and U.D. Kulkarni, Indian Drugs, 29(11) (1992) 489–493.
[8] B. Pardhasaradhi-Reddy, M.V. Suryanarayana, S. Venkatraman and G.L. Krupadanam, Sastry, C.S.P. Indian Drugs, 30(4) (1993) 176–179.
[9] B.K. Logan, P.N. Friel, K.L. Peterson and D.B. Predmore, J. Anal. Toxicol., 19 (2) (1995) 61–64.
[10] R.S. Chaudhary, S.S. Gangwal, K.C. Jindal and S. Khanna, J. Chromatogr. Biomed. Appl., 125 (1993) 180–184.
[11] A.T Wu and I.J. Massey, J. Chromatogr. Biomed. Appl., 99 (1990) 241–246.
[12] B.V. Kamath, K. Shivram and A.C. Shah, J. Pharm. Biomed. Anal., 12 (3) (1994) 343–346.
[13] W.F. Smyth, in Voltammetric Determination of Molecules of Biological Significance. Wiley, New York, 1992, p. 33.
[14] M.M. Baizer, in H. Lund and M.M. Baizer (eds.), Organic Electrochemistry 3rd. Edn., Dekker, New York, 1990, pp. 433–460.
[15] P. Zuman in The Elucidation of Organic Electrode Processes, Academic Press, New York, 1969, pp. 45–46.
[16] P. Zuman in The Elucidation of Organic Electrode Processes, Academic Press, New York, 1969, p. 49.
[17] United States Pharmacopeia 23, Supp. 1, (1995) p. 2474.

ELSEVIER

Talanta 44 (1997) 939–945

Talanta

Dialysis membrane to prevent cadmium ion specific electrode fouling

Susan J. Fish, Pierre Brassard *

Department of Chemistry, McMaster University, 1280 Main St. West, Hamilton, Ontario, L8S 4M1, Canada

Received 31 May 1996; accepted 8 October 1996

Abstract

We present a simple method of protecting a Cd(II) ion-selective electrode from fouling using a dialysis membrane. Drift due to fouling is inevitable during continuous exposure of the electrode to the bulk solution. It presents a major problem in the case of automated titrations because recalibration is not possible. The drift is due to natural organic matter present in the sediment, and the membrane prevents its accumulation on the electrode surface. This was verified by calibrating a Cd electrode exposed to sediment for varying times, both with and without a membrane covering. There are two types of time dependent biases. A primary drift occurs without exposure to sediments and is probably caused by oxidation of the surface. A more important effect due to natural organic matter accumulation causes additional drift and deteriorates the Nernstian response of the electrode. From these results, it is possible to predict the uncertainty associated with measurements of binding constants and surface site densities for a Langmuir model. In general, the biased electrode overestimates the total metal concentration, reduces the value of the stability constants and increases estimates of maximum surface site densities. © 1997 Elsevier Science B.V.

Keywords: Cadmium ISE; Dialysis membrane; Fouling; Natural organic matter

1. Introduction

The interference of organic matter with electrode response is not a new phenomena. In 1931, Heyrovsky developed the 'adsorption analysis' technique, which takes advantage of the natural adsorption or organics to a mercury electrode. This adsorption of natural surface active organics suppresses the streaming maxima around a mercury drop electrode, and can be quantified. Some difficulties with this technique were noted by Pleše and Žutic [1], who attributed irregular surfactant aggregates with the mercury electrode/aqueous solution interface.

More recently, Ochs et al. [2] studied the extent of adsorption of humic substances onto a hydrophobic mercury electrode surface by measuring directly the change in double layer capacitance due to adsorption. They determined that these humic substances adsorbed significantly to both hydrophobic and hydrophillic surfaces, over varying pH. It was suggested that the adsorbed mate-

* Corresponding author.

PII S0039-9140(96)02144-3

rial could influence the chemical characteristics and reactivity of a surface, and therefore, its affinity for metal ions.

A silver based ion-selective electrode (ISE) is biased by complexones such as EDTA [3] and also by humic acids [4]. But even in the absence of organic matter, it will undergo ion exchange reactions in the presence of light which causes silver halide crystal growth on, and out of the membrane [5]. Scanning electron microscopy has also identified metallic silver on the active surface. This metallic silver leads to silver sulphide or silver oxide deposits on the electrode [6].

With the advent of automatic titrators, constant monitoring is required. Since the electrodes are not removed between readings, no recalibration is possible and some drift or fouling, due to contact with humic substances, is inevitable. These interferences can cause significant bias which could be removed by preventing natural organic matter (NOM) from contacting the electrode surface and, at the same time, allowing metal ions to react with the electrode.

We present here a series of experiments to evaluate the use of a dialysis membranes as a shield to isolate the electrode surface from NOM of high molecular weight. This approach is similar in concept but opposite in application from using dialysis membranes to retain enzymes near the electrode surface, as was done recently in the development of enzyme specific electrodes [7].

2. Experimental

2.1. Titrations

All titrations were done under CO_2 free air, obtained by filtering incoming instrument air through an ascarite column and followed by a water wash bottle. The reactor consisted of a 150 ml pyrex beaker. A plexiglass lid held reference and pH electrodes with also the tubing required for titrant addition and CO_2 free air. This method allowed rapid insertion and removal of electrodes to the reactor and thus, minimized exposure to ambient CO_2.

The following procedure was followed for all titrations. The electrode assembly was first calibrated against standard buffers immediately before the titration. The titration vessel was then filled with the titration solution and lowered in a constant temperature jacket (25°C) held over a magnetic stirrer. The titration was carried out after a 30 min equilibration time. After recalibration, blank titrations without cadmium and/or sediment followed. Because titration profiles for the blanks did not necessarily fall on the same pH points as the analyte, blank titration data were interpolated to the corresponding pH value of the analyte using cubic spline method. The difference between analyte and interpolated blank titrant addition at the same pH values yielded charge excess in the suspension.

Titration profile was controlled by a computer driven titrimeter (Tanager Scientific Systems, model 8901) and done at equal 0.1 pH intervals, based on estimates of the buffer capacity obtained from the previous titration point.

2.2. Sediment samples

Surficial sediments from Coote's Paradise (Cootes sediments) were collected with a square dredge from the deck of a scow in the western part of Hamilton Harbour at a depth of less then 3 m. The shallow depth of the embayment and strong winds maintain oxic conditions year round. Cootes sediments consist of erosion debris, mostly clays, coated with a small layer of organic matter arising from the very active algal and bacterial populations. Previous work on these sediments and at other locations in the harbour are given in Brassard et al. [8]. Loadings in Coote's Paradise come mainly from creek erosion (47 050 kg day^{-1} in 1987) and farming operations.

Surficial sediments were stored in polyethylene bottles at 4°C until decanted. We used a settling procedure designed to remove the coarse particulates, a necessary step to prevent grinding in the reactor and wear of electrode surfaces. Raw sediment, 50 g, was diluted in 500 ml water, stirred vigorously and then allowed to settle for 1 min. The top 1.5 cm was collected. The volume was replaced with water and the process repeated until

approximately 1 l of solution was collected. The concentration was determined by filtering an aliquot on 0.45 μm (Millipore) and weighing the dried filter until constant weight. A 1 g l^{-1} suspension was prepared by performing the appropriate dilution of the stock. Calculations from Stoke's settling equations predict the size distribution of the collected suspension to be less than 16 μm.

2.3. Electrodes

The Cd(II) ISE membrane was formed by thoroughly blending an equimolar ratio of CdS and Ag_2S powders under argon. A 6 mm die was loaded with this blend and subjected to 8000 kg cm^{-2} pressure [9,10]. A temperature controlled jacket held the die at 150 ± 5°C during a 16 h curing period. The resulting pellet was mounted at the end of a glass tube and sealed with a thermoplastic sleeve. A strip of platinum mounted at the end of a small spring established electrical contact between the inner surface of the pellet and a copper wire.

The Cd(II) ISE was polished before every use with 1.0 μm followed by 0.5 μm Al_2O_3 powder on a felt pad. A Radiometer pH glass electrode and Fisher Scientific Calomel reference electrode were calibrated with standard buffers before every use. The Cd(II) ISE was calibrated both automatically, and manually with standard $Cd(NO_3)_2$ solutions, ranging from $10^{-5.5}$ M to 10^{-3} M.

2.4. The membrane

Regenerated cellulose (viscose process) dialysis tubing (Viskase Canada) with a molecular weight cutoff of 12 000–16 000 Da was cut into 10 cm strips, three times boiled (30 min), and rinsed in deionized H_2O. The wet tubes were slip open and stored in deionized H_2O and used within 3 days. After cleaning the electrode, a square of tubing was pulled tightly over the end of the Cd electrode and an O-ring was rolled over it from one end, up to the edge of the tubing to hold the membrane in place. The arrangement is stable and the membrane could maintain a tight contact with the membrane surface for a week.

2.5. Exposure to sediment

The response of the electrode with and without membrane were examined under three operational conditions: (1) a pH edge titration where the amount of metal sorbed on the sediment was measured over a range of pH conditions; (2) drift of electrode potential with time due to NOM accumulation on the surface; and (3) offset in Nernstian calibration due to NOM accumulation.

For pH edge experiments, 1.1 g l^{-1} sediment was resuspended in 100 ml containing about 10^{-4} M Cd in 0.05 M KCl and brought to pH 3 by addition of 0.1 M HCl. The mixture was equilibrated in the titration reactor for 30 min in presence of precalibrated pH and ISE electrodes. Titration commenced with addition of 0.1 M NaOH at equal pH intervals until pH 10 where precipitation of Cd hydroxides dominated the system.

Eight experiments were performed in order to determine electrode drift. In each case, an ionic strength of 0.01 M $NaNO_3$ and a pH of 4.5 were maintained. The value of pH was determined from previous exposures to NOM and corresponds to the point of maximum electrode bias. Sediment were monitored, both with 10^{-4} Cd and without, and both with and without a membrane. Control solutions containing deionized H_2O in place of the sediment suspension were also monitored under the same conditions.

For offset in Nernstian calibration, the electrode was placed in a sediment solution, prepared as described above, and the suspension was adjusted to a particular pH, ranging from 4 to 6. This range corresponds to the greatest deviation in electrode response from the edge experiments. The total exposure time ranged from 0 to 3 h. The 'fouled' electrode was then placed in a series of $Cd(NO_3)_2$ standards at the same pH as the sediment and the Cd responses were measured. A similar series of experiments were performed with the electrode covered with the membrane.

3. Results and discussion

3.1. pH edge titrations

At low pH, sediment exists in a protonated form. As the pH of a sediment and metal suspension increases, protons on the sediment exchange with metal ions in solution and the total free metal concentration should decrease. However, free cadmium concentration appeared to increase with pH during a pH edge titration and suggested that more cadmium was present in the system than was originally added (Fig. 1a,b). In this experiment the exposure of the electrode to NOM was controlled by increasing the time interval between titrant addition. This additional cadmium did not come from the sediment since ICP-MS analysis of the sediment indicated cadmium at 14 μg g^{-1} [8], which is equivalent to 0.0485 μmol $^{-1}$ l and is not significant. A control experiment without cadmium (not shown) resulted in a similar increase in electrode potential for the same pH range, indicating electrode bias. In contrast (Fig. 1a,b), the membrane-coated electrode showed Cadmium to be free until pH 6.7 and progressively bound afterwards.

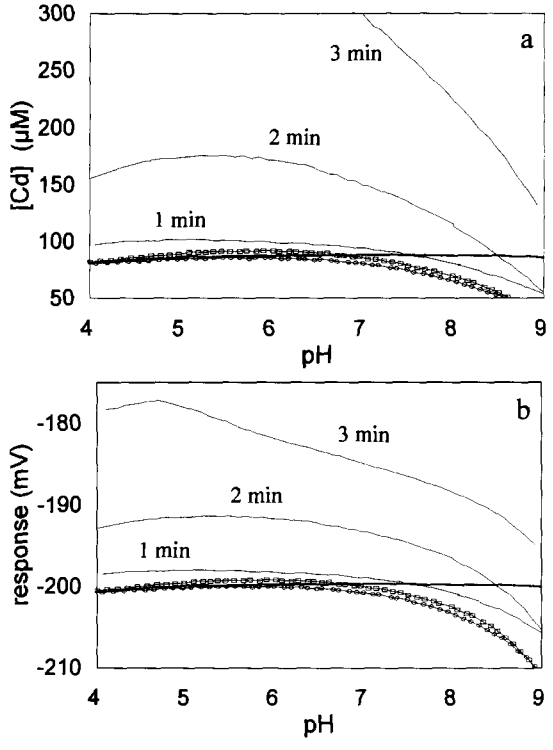

Fig. 1. Distortion of pH edge profile for Cd adsorption on 1 g l^{-1} suspended sediments. (a) Concentration expressed as molarity; and (b) concentration as electrode potential. Titrations were done with both an unprotected, and a membrane protected electrode. Thin lines: unprotected electrode at the indicated time interval. Symbols: membrane protected electrode at [○], 2 min, and [□], 5 min intervals. The thick line is a control without membrane and without sediments. Parameter optimization for Langmuir fit is shown in Table 1.

Similar results by Qi et al. [3] for Cd ISE exposed to complexing agents showed an enhanced electrode response above the total amounts added. Exposure to the complexones EDTA, EDTA and NTA without Cd addition showed a Nernstian response to ligand concentration. But the response did not work with weaker ligands such as citrate, tartrate or NH_3, suggesting that the Cd binding constant of the ligand must be very high to produce a bias. Sekerka and Lechner [4] found the same Nernstian behaviour using Cu ISE exposed to the above three complexones and also with humic acids. Gulens [11] proposed that the artificially high Cu concentration is caused by the ligand inducing dissolution of the electrode surface. In our case, for Hamilton harbour suspended sediments, the low molecular weight NOM that would pass through the membrane is either absent or, if present, would not be a ligand strong enough to produce the Nernstian response observed for complexones.

3.2. Drift

Our results show two distinct alteration processes occurring at the membrane surface. The first one is possibly oxidation of the exposed surface and occurs any time the electrode is exposed to molecular oxygen [6]. The drift is constant in time (Fig. 2) and shows a small increase in drift slope when Cd concentration is increased ten-fold.

The second process arises from exposure of the electrode to NOM. In Fig. 2, both solutions with and without sediments containing 10^{-4} M cadmium show a linear increase in electrode response with time. In the sediment suspension, the drift is

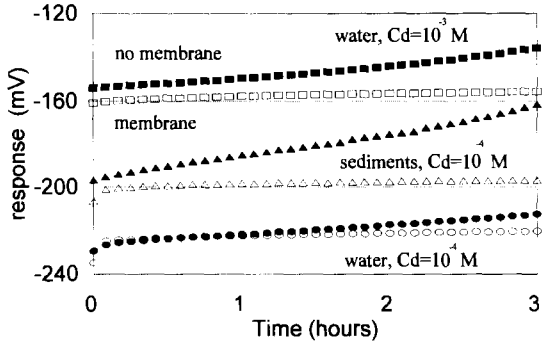

Fig. 2. Effect of drift on the Cd(II) ISE for water and sediment solutions at 10^{-4} M Cd, both with and without a dialysis membrane. [●], water blank without membrane; [○], water blank with membrane; [▲], sediment suspension without membrane; [△], sediment suspension with membrane; [■], 10^{-3} M Cd standard without membrane; and [□], 10^{-3} M Cd standard with membrane. The 10^{-4} M water blank was shifted by −30 mV for clarity.

more extreme, the difference owing entirely to the presence of NOM. Drift due solely to NOM is estimated to be 6.4 mV h^{-1} by difference from the water control. Since this offset disappears when the membrane is in place, the interference to the electrode surface can be attributed to colloidal NOM, above the 12 000–16 000 MW cut-off of the dialysis tubing.

Organic matter affecting the surface of the electrode would alter the Nernstian response as well. Fig. 3 demonstrates the degradation of the Nernstein response after exposing the Cd(II) ISE to

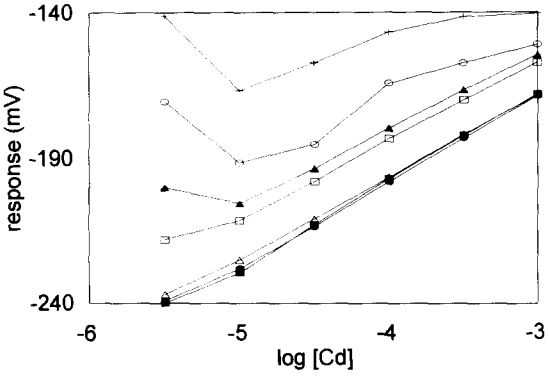

Fig. 3. Calibration without dialysis membrane. Exposure conditions: [+], pH 4, 3.5 h exposure; [○], pH 6, 3 h exposure; [▲], pH 5, 2 h exposure; [□], pH 4, 1.25 h exposure; [●], natural pH, 5 min exposure; [△], no exposure, with membrane; and [■], no exposure, no membrane.

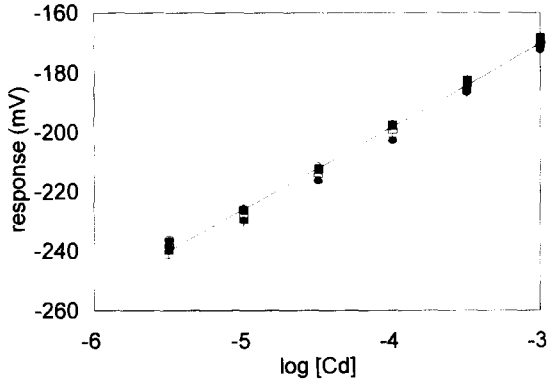

Fig. 4. Calibration with the dialysis membrane. Exposure conditions: [■], no exposure, no membrane; [●], no exposure, with membrane; [▲], pH 4, 2 h; [+], pH 4, 0.5 h; [□], pH 6, 1.25 h; [○], pH 6, 3.5 h; and [△], pH 5, 2 h.

sediment for extended periods of time, without membrane protection. As both exposure time and pH increase, the deviations from the expected Nernstian response increase. In contrast, Fig. 4 demonstrates that the membrane prevents NOM contamination regardless of solution pH or exposure time.

If we assume that the electrode surface is an adequate model for the surface of a resuspended natural sediment particle, it follows that only large molecular NOM, presumably humic acids, can significantly alter surface properties of aquatic suspensions. This effect is important since coatings of NOM on suspended particles are recognized as an important agent in metal exchange with the bulk solution and in controlling surface charge [12–14].

Generally, the membrane appears to reduce significantly the drift due to oxidation and NOM fouling. We do not know how this occurs. It is also unclear what kind of binding occurs between the organic matter and the surface but the fact that only colloidal substances have an effect suggests that NOM act as surfactant on natural particles.

3.3. *Effect on adsorption parameters*

Electrode drift during a continuous titration can introduce unaccounted biases in the profile

causing erroneous parameter evaluation. For pH edge titrations, adsorption on surfaces is generally a Langmuirian exchange between protons and free metal. Fu and Allen [15] have tested adsorption models based on 1:1 and 2:1 exchanges and found the predominant sites to follow a 1:1 exchange. Similar conclusions were reached by Bourg and Mouvet [16]. We therefore assume:

$$\equiv SOH + H^{2+} = \equiv SOM^{+} + H^{+} \quad (1)$$

and ignore the electrostatic terms associated with surface charge. The profile for adsorbed metal, Γ, is therefore:

$$\Gamma = M_T - [M^{2+}] = \frac{\Gamma_{MAX}[M^{2+}]}{\frac{[H^{+}]}{K} + [M^{2+}]} \quad (2)$$

where Γ_{MAX} is the total available surface site concentration (M), K is the stability constant for the equation I, M_T is the total exchangeable metal, and H^{+} is the proton concentration.

Of interest is how this function is distorted when we introduce a drift in the measurement of metal concentration. To do so, Eq. (2) is expressed as a function of the free metal:

$$[M^{2+}] = M_T - \frac{\Gamma_{MAX}[M^{2+}]}{\frac{[H^{+}]}{K} + [M^{2+}]} \quad (3)$$

We then adjust Eq. (3) to a series of pH edge titration data of suspended sediments (Fig. 1), under an increasing time interval, and for both electrode conditions. Non-linear curve fitting (Levenberg-Marquard minimization method) was used to obtain optimized values for $[M_T]$, Γ_{MAX} and K (Table 1). In spite of our lower sediment concentration (1 g l^{-1} versus 50 g l^{-1}), K and Γ_{MAX} in this experiment are both greater by about two orders of magnitude than the samples analyzed by Fu and Allen [15]. We attribute this difference to the air-drying step they used to remove reduced materials. We think that drying of the sediment could have decomposed some of the organic matter and/or forced the floc structure of the sediment particles to collapse. This would cause a reduction in the available surface sites for metal binding.

Fig. 3 shows that a greater time interval increases the duration of titration and, therefore, allows a greater bias due to fouling. Thus, although the unprotected electrode at 3 min time interval shows distorted estimates for M_T (Table 1), the protected electrode can still match the control at 5 min interval. The results are consistent with Fig. 1 and Fig. 2.

3.4. Sensitivity analysis

Adjustment of parameters by the Levenberg-Marquard method returns a sensitivity analysis useful for determining the pH range where a particular parameter is more important. Fig. 5 expresses sensitivity as a dimensionless ratio of the change in Eq. (3) resulting from a unit change in the value of the parameter. The binding function is essentially dominated by estimates for total metal at pH values lower than the binding constant. Past this point, its influence decreases somewhat and the other two parameters increase their influence only at a pH near 9. However, the titration would loose its value at that point since the precipitation of cadmium oxides becomes a

Table 1
Parameter optimization for Cd adsorption profiles (Eq. (3)) as biased by electrode fouling

ΔT	Fit %	$M_T \times 10^{-5}$	$\Gamma_{MAX} \times 10^{-5}$	pK	r^2
Control					
1	—	8.6 (0.2)	0	—	—
With membrane					
2	1.76	8.4 (0.1)	6 (1.1)	4.2 (0.1)	0.992
5	2.96	8.9 (0.3)	8 (2.7)	4.4 (0.2)	0.978
Without membrane					
1	1.71	10.0 (0.2)	5 (1.1)	4.1 (0.2)	0.987
2	3.53	17.0 (0.6)	13 (3.2)	4.1 (0.2)	0.982
3	37.8	40 (12)	40 (44)	4.5 (2)	0.732

Fit, overall goodness of fit expressed in percent deviation from data.
Values in parenthesis show percent uncertainty.
ΔT, time interval between titrant addition (min) for a fixed pH change of 0.1 units; M_T, total Cd concentration (M); Γ_{MAX}, total available surface sites (mol g^{-1}); K, stability constant for 1:1 exchange between proton and Cd; and r^2, square of correlation coefficient between model simulation and data.

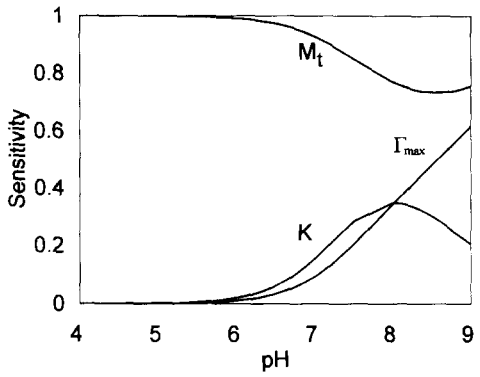

Fig. 5. Sensitivity analysis for adjusted parameters in Table 1. The curves shown represent a run at 2 min time interval, without membrane. M_T, total Cd concentration (M); Γ_{MAX}, total available surface sites (M); and K, stability constant for 1:1 exchange between proton and Cd.

factor. Fig. 5 nevertheless shows why large uncertainties in Γ_{MAX} and K (Table 1) can still arise in spite of a good overall fit. This analysis exemplified the false security in using goodness of fit or correlation as sole indicators of the suitability of a parameter.

4. Conclusions

Metal binding studies using ISE electrodes as indicators of free metal are biased by a drift in potential probably caused by oxidation of the surface and by NOM coating the surface. The drift increases linearly in time and causes serious distortions to estimates from binding models. Effects are small if the electrode is inserted in the suspension only for short periods of time, and if regularly cleaned and calibrated between measurements.

The impact is severe when the electrode is part of an automated titration procedure since recalibration and cleaning are no longer possible. In this case, the use of a membrane to protect the electrode surface reduces both kinds of drift. The membrane probably prevents the first kind by hindering the flow of oxidant from the bulk solution to the electrode surface. In the second case, the membrane protects the electrode surface from contact with the high molecular weight colloidal fraction. The low molecular weight NOM has no effect and, presumably, does not coat the surface. By analogy, results suggest that only organic matter greater than 12 000–16 000 Da in size would be found on the surface of natural aggregates.

Acknowledgements

The paper has benefited from reviewers comments. We thank Dr Ron Smark for insights on the role of low molecular weight organic matter and their interaction with sulfide based electrodes.

References

[1] T. Plese and V.J. Zutic, Electroanal. Chem., 175 (1984) 299.
[2] M. Ochs, B. Cosovic and W. Stumm, Geochim. Cosmochim. Acta, 58 (1994) 639–650.
[3] D. Qi, T. Yin and X. Wu, Huaxue Xuebao, 40 (3) (1982) 243–250 (abstract).
[4] I. Sererka and J.F. Lechner, Anal. Lett., A11 (1978) 415–427.
[5] R. DeMarco, R.W. Cattrall, J. Lisegang, G.L. Nyberg and I.C. Hamilton, Anal. Chem., 62 (1990) 2339–2346.
[6] J. Gulens and B. Ikeda, Anal. Chem., 50 (1978) 782–787.
[7] H. Bu., S.R. Mikkelsen and A.M. English, Anal. Chem., 67 (1995) 4071–4076.
[8] P. Brassard, J. Kramer and P.V. Collins, J. Great Lakes Res., (1996) submitted.
[9] I. Sererka and J.F. Lechner, J. Electroanal. Chem., 69 (1976) 339–344.
[10] I. Sekerka and J.F. Leckner, Anal. Lett., 9 (1976) 1099–1110.
[11] J. Gulens, Ion-selective Electrode Rev., 2 (2) (1980) 117–157.
[12] K.A. Hunter, Limnol. Oceanogr., 25 (1980) 807–822.
[13] K.A. Hunter and P.S. Liss, Nature, 282 (1979) 823–825.
[14] R. Neihof and G. Loeb, J. Mar. Res., 32 (1974) 5–12.
[15] G. Fu and H.E. Allen, Water Res., 26 (1992) 225–233.
[16] A.C.M. Bourg and C. Mouvet, A heterogeneous complexation model of the adsorption of trace metals on natural particulate matter, in C.J.M. Kramer and J.C. Duinker (Eds.), Complexation of Trace Metals in Natural Waters, Martinus Nijhoff, Dordrecht, 1984, pp. 267–278.

ELSEVIER

Talanta 44 (1997) 947–950

Talanta

Short communication

Use of dichloromethane with dithizone as an alternative solvent to carbon tetrachloride restricted by Montreal Protocol

A.M. Kiwan

Department of Chemistry, Faculty of Science, United Arab Emirates University, P.O. Box: 17551, Al-Ain, United Arab Emirates

Received 24 June 1996; received in revised form 17 October 1996; accepted 21 October 1996

Abstract

The spectral characteristics of dithizone and its metal complexes were measured in dichloromethane as an alternative solvent to carbon tetrachloride which will be illegal to manufacture by the year 2000, according to the revised Montreal Protocol. The extraction equilibria of its metal complexes were also reported and discussed. Dichloromethane was found to enhance the sensitivity of dithizone towards Co(II), Cu(II), Hg(II), Pb(II), Zn(II), Bi(III), Ag(I), In(III) and Tl(I). It was also found to be a better solvent than carbon tetrachloride for the separation of Cd(II) from Zn(II) and for the separation of Co(II) from Ni(II). © 1997 Elsevier Science B.V.

Keywords: Dithizone; Dichloromethane; Extraction; Metal Complexes

1. Introduction

In view of its unique position among organic analytical reagents, dithizone, (Ph–N=N–C(=S)–NH–NH–Ph); 3-mercapto-1,5-diphenylthiocarbazone; phenyl azothioformic acid 2-phenylhydrazide as is listed in the Chemical Abstracts, is a well known S, N chelating ligand. There is a very rich literature comprising over 3000 published articles, extended reviews and special chapters in books [1–8]. Two special books are also devoted to its wide applications in analytical chemistry [9,10].

Dithizone reacts with 20 metals and several organometals to form highly coloured chelate complexes [8,9]. As dithizone and its metal complexes are insoluble in water but soluble in organic solvents, carbon tetrachloride was extensively used with dithizone in liquid–liquid extraction techniques for the separation and spectrophotometric determination of trace metals and organometals in various matrices [6–10].

Although other analytical techniques such as atomic absorption, inductively coupled plasma, atomic fluorescence spectrometry are used due to their higher sensitivities and certainly require less technical skill and experience for successful operation, this tendency will continue. At the same time, however, the use of dithizone for preconcentration of trace metals prior to their determina-

PII S0039-9140(96)02135-2

tion by highly sensitive methods is continuing [11–15].

In view of its ozone-depleting property, carbon tetrachloride was included among the compounds controlled by the revised Montreal Protocol which was agreed upon in London revision meeting of 1990 [16]. According to the terms of agreement, the production of carbon tetrachloride was to be frozen at 1989 level starting 1991 and to be cut by 85% from 1995 and to become completely banned from 2000.

The present paper reports our results on the use of dichloromethane as an alternative safer solvent to carbon tetrachloride for analytical applications with dithizone. The environmental safety of dichloromethane may be attributed [16] to its very short atmospheric lifetime, so it does not rise into the atmosphere and cause the same problems as carbon tetrachloride or the CFC's.

The spectral characteristics of dithizone and its metal complexes in dichloromethane are described. The extraction equilibria and $pH_{1/2}$ values of metal dithizonates are also reported and discussed in comparison with the corresponding data in carbon tetrachloride.

2. Experimental

2.1. Reagents and materials

Dithizone, dichloromethane, sodium perchlorate, sodium acetate and metal salts were A.C.S. (Aldrich) reagent quality. Solutions of dithizone in dichloromethane were purified by applying a similar procedure to that used for purifying solutions of dithizone in carbon tetrachloride or chloroform [7,18,19]. Deionized water was used throughout. Buffered (pH < 7) sodium perchlorate solutions were purified from traces of metals by scrubbing with solutions of dithizone in dichloromethane prior to use.

2.2. General procedures

The spectral characteristics (λ_{max} and ε_{max}) of both dithizone in dichloromethane were determined, as was done with chloroform and carbon tetrachloride [7,20,21]. The visible spectra of dithizone and its metal complexes were recorded on a Shimadzu double-beam UV-visible scanning spectrophotometer model UV-2101 PC. Metrohm 691 pH-meter was used for pH measurements.

The extraction constants (K_{ext}) of metal complexes were determined by equilibrating 5 cm^3 aliquots of dichloromethane containing known amounts of dithizone in stoppered glass tubes with equal volumes of sodium perchlorate (0.5 M) sodium acetate (0.02 M) mixture at different pH values in the presence of known amounts of metal ions. Preliminary experiments showed that the equilibrium was attained in ca. 30 min for Ni(II) complex and ca. 15 min for the rest of metal complexes. The extraction constants of $Hg(HDz)_2$ and $Cu(HDz)_2$ were carried out in presence of potassium iodide and EDTA, respectively, according to methods suggested by Takei and Kato [17]. The equilibrium concentrations of the dithizone and its metal complexes were determined spectrophotometrically, whereas the concentrations of metal ions in aqueous solutions were determined by difference; $[H^+]$ was calculated from the pH of the aqueous phase.

3. Results and discussion

Dithizone dissolves readily in dichloromethane (12.6 g l^{-1}, 30°C) [9] to give green solution with two distinct absorption bands with maxima at 609 and 445 nm, respectively (Table 1). These λ values agree with those reported by Koskinen [22], but our values of ε_{max} (Table 1) are slightly higher. Both bands are slightly shifted to lower wavelengths compared to the corresponding λ_{max} values of 620 and 450 nm, respectively, in carbon tetrachloride [9,10]. The solution of dithizone in dichloromethane was found to be stable for at least six days if kept refrigerated.

The spectral data summarized in Table 1 indicate that ε_{max}, 1 and ε_{max}, 2 of dithizone are considerably higher than the corresponding values in carbon tetrachloride. These findings suggest also that dichloromethane is a superior solvent to carbon tetrachloride since it enhances its sensitivity as a spectrophotometric reagent. Its sensitivity

as measured by ε_{max}, 1 and ε_{max}, 2 is close to that in chloroform, the other solvent which has been used extensively as a solvent with dithizone [7,10]. Both solvents have higher dielectric constants and dipole moments than carbon tetrachloride which may be partially responsible for increasing the molar absorptivities of dithizone.

3.1. Spectral characteristics of dithizone metal complexes in dichloromethane

It is known that dithizone reacts with metal ions to give highly coloured neutral chelates according to Eq. (1).

$$n\mathrm{H_2Dz_{org.}} + \mathrm{M_{aq}^{n+}} \overset{K_{ext}}{=} \mathrm{M(HDz)_{n_{org.}}} + n\mathrm{H_{aq.}^{+}} \qquad (1)$$

which can be extracted into organic solvents. The spectral data of several metal dithizonate complexes in dichloromethane are also given in Table 1 together with the corresponding values in carbon tetrachloride [8,10]. These spectral data indicate that the λ_{max} values of Cd(II), Co(II), Cu(II), Pb(II), Zn(II) were slightly shifted to lower wavelengths whereas their ε_{max}, 1 values increased by ca. 2 to 24%.

Although λ_{max}, values of mercury(II), Bi(III), Ag(I) and In(III) have been slightly shifted towards longer wavelengths nevertheless, their ε_{max} values have also increased by ca. 3–46%. So, in addition to being a safer alternative solvent to carbon tetrachloride, dichloromethane was found to enhance the sensitivity of dithizone towards most metal ions.

3.2. Extraction equilibria of metal dithizonate complexes in dichloromethane

Table 1 gives the extraction constants and the $pH_{1/2}$ values for metal dithizonates in dichloromethane as well as in carbon tetrachloride for comparison and the following conclusions may be drawn from those data.

1. The much higher $pH_{1/2}$ value of dithizone in dichloromethane (10.35) than the corresponding value (8.88) in carbon tetrachloride suggests that dithizone has a higher partition coefficient in the former solvent.
2. The K_{ext} values of metal dithizonate complexes in dichloromethane are generally lower than the corresponding values in carbon tetrachloride. On the other hand, the $pH_{1/2}$ values of metal dithizonate complexes in dichloromethane are higher than the corresponding $pH_{1/2}$ values in carbon tetrachloride. The $pH_{1/2}$ values of metal-ligand complexes may be considered indicators of the bonding strength of dithizone towards a particular metal in a particular two phase system. These relatively lower values of K_{ext} and $pH_{1/2}$ in CH_2Cl_2 than the corresponding values in CCl_4 may be attributed to the lower dipole moment and lower polarity of the latter solvent (CCl_4) [22].
3. Dichloromethane was found to be a better solvent than carbon tetrachloride or chloroform in the separation of cadmium(II) from zinc(II) as shown in Fig. 1. This solvent effect in enhancing the separation of Cd(II) from Zn(II) dithizonate complexes may be also attributed to the relatively higher polarity of dithochloromethane as well as its higher dipole moments. It is known that both Zn(II) and

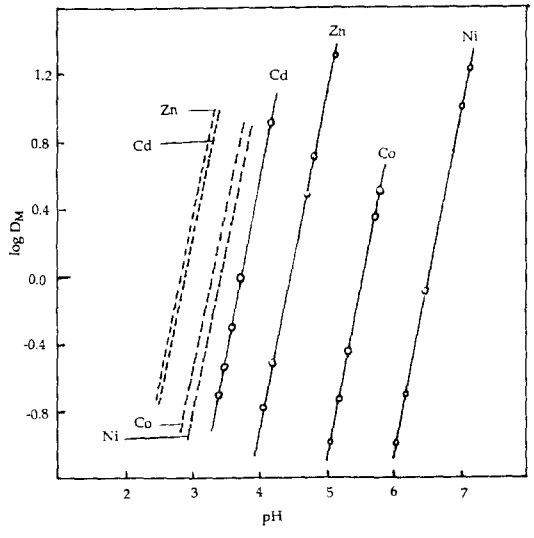

Fig. 1. log D_M (distribution coefficient), where M is Cd or Zn, Co or Ni vs. pH. Calculated from K_{ext} based on the assumption that 1.0×10^{-4} M dithizone is used as the extractant in CH_2Cl_2 (——) or CCl_4 (— - - —). Aq. phase: 0.5 M $NaClO_4$,–0.2 M sodium acetate.

Cd(II) have comparable electronic configuration viz., [Ar] $3d^{10}$ and [Kr] $3d^{10}$ respectively, through their different effective ionic radii viz., 74 pm and 95 pm [23] respectively seem to play a role in enhancing the selectivity of reaction with dithizone in dichloromethane. Similar results of improving the separation of Cd(II) from Zn(II) were reported by modifying the structure of dithizone by introducing certain substituents in the phenyl nuclei of dithizone, thus increasing the selectivity of the dithizone analogue towards one of the two metals [24–26].

4. Dichloromethane was also found to be a better solvent than carbon tetrachloride or chloroform for the separation of Co(II) from Ni(II) as shown in Fig. 1.
5. The $pH_{1/2}$ values (Table 1) also indicate that dichloromethane is a better solvent for the separation of Pb(II) from Ni(II) or Co(II). On the other hand, dichloromethane seems to be inferior to carbon tetrachloride for the separation of Cu(II) from Bi(III) or Zn(II) from Pb(II).

Acknowledgements

This work was supported by a research grant from the Scientific Research Council of United Arab Emirates University. Technical assistance from Mr B. Al-Hindawi is appreciated.

References

[1] I.M. Kolthoff and E.B. Sandell, J. Am. Chem. Soc., 63 (1941) 1906.
[2] B. Freiser and H. Freiser, Talanta, 1 (1970) 540.
[3] H.M.N.H. Irving, A.M. Kiwan, D. Rupainwar and S.S. Sahota, Anal. Chim. Acta, 56 (1971) 205.
[4] H.M.N.H. Irving and R.J.P. Williams, J. Chem. Soc., (1952) 356.
[5] G.H. Morrison and H. Freiser, Solvent Extraction in Analytical Chemistry, Wiley, New York, 1966.
[6] J. Stary, The Solvent Extraction of Metal Chelates, Pergamon Press, 1964, 138 p.
[7] E.B. Sandell and H. Onishi, Photometric Determination of Traces of Metals, Part I, Wiley, New York, 1978, Ch. 6G.
[8] K.L. Cheng, U. Keihei and T. Imamura, CRC Handbook of Organic Analytical Reagents, CRC Press, Florida, 1982, 363 p.
[9] H.M.N.H. Irving, Dithizone, Analytical Science Monograph, The Chemical Society, London, 1977.
[10] G. Iwantscheff, Das Dithizon und seine Anwendung in der Mikro und Spuren—Analyse, Verlag Chemie, Weinheim, 1972.
[11] M. Chikuma, H. Aoki and H. Tanaka, Anal. Sci., 7 (1991).
[12] A.G. Hamza, A.B. Farag, T.A. Amireh, Z.E. El-Bas and F.M. Al-Nowaiser, Anal. Sci., 6 (1990) 6.
[13] E. Beinrohr and H. Hofbauerova, Mikrochim Acta, 2 (1989) 1–3.
[14] E. Beinrohr, J. Rajcek and J. Garaj, Analyst, 113 (1988) 12.
[15] M. Chikuma, H. Aoki and H. Tanaka, Anal. Sci., 7 (1991) 1131.
[16] R. Stevenson, Chem. Br., (1992).
[17] S. Takei and T. Kato, Tech. Rep. Tohoku Univ., 26 (1962) 35(21) (1957) 319.
[18] S. Landry and S.F. Rodendo, Anal. Chem., 26 (1954) 732.
[19] H. Irving and J.J. Cox, Analyst (London), 83 (1958) 526.
[20] A.L. Koskinen, Finn. Chem. Lett., 2 (1985) 29.
[21] C. Goesling, A. Adason and A. Gutierrez, Inorg. Chim. Acta 29 (1978) 279.
[22] C. Reichardt, Solvent Effects in Organic Chemistry, Verlag Chemie, Weinheim, 1979, 271.
[23] N.N. Greenwood and A. Earnshaw, Chemistry of the Elements, Pergamon Press, Oxford, 1985, Ch. 29, 400 p.
[24] A.M. Kiwan, H.F. Ali and G. Wanas, Sep. Sci. Tech., 15(4) (1980) 1025.
[25] A.M. Kiwan and G.A. Wanas, Anal. Chim. Acta 144 (1982) 165.
[26] A.M. Kiwan, G.A. Wanas and F.M. Hassan, Anal. Sci. 9 (1993) 687.

ELSEVIER

Talanta 44 (1997) 951–957

Talanta

Cyclodextrin enhanced fluorimetric determination of malonaldehyde by the thiobarbituric acid method

Sofia Erazo Castrejón, Anatoly K. Yatsimirsky *

Facultad de Química, Universidad Nacional Autónoma de México, 04510 México D.F., México

Received 15 July 1996; received in revised form 14 October 1996; accepted 18 October 1996

Abstract

The enhancement effects of α-, β-, γ- and hydroxypropyl-β-cyclodextrins on the fluorescence of a 2:1 thiobarbituric acid/malonaldehyde adduct in acid aqueous solutions have been studied. The best characteristics as a fluorescence enhancement agent showed hydroxypropyl-β-cyclodextrin which bound the adduct sufficiently tightly ($K = 180$ l mol^{-1}) and caused a five-fold increase in its fluorescence. A kinetic-fluorimetric method of determination of malonaldehyde in the range 0.1–10 μM at room temperature with hydroxypropyl-β-cyclodextrin as the enhancement agent is proposed and applied for the analysis of raw and cooked meat samples. © 1997 Elsevier Science B.V.

Keywords: Cyclodextrin; Malonaldehyde; Thiobarbituric acid

1. Introduction

The thiobarbituric acid (TBA) method is the most widely used test for measuring the extent of oxidative deterioration of lipids [1–10]. In this method TBA reacts at 60–95°C with malonaldehyde (MA), a degradation product of lipid hydroperoxides, to give a red fluorescent 1:2 MA/TBA adduct (TMT), reaction Eq. 1, [11] which usually is quantified spectrophotometrically at 525-532 nm [2–11].

Although TMT possesses a very high, ca. 1.6×10^5 l mol^{-1} cm^{-1}, molar absorptivity [8], the method is considered not sufficiently sensitive [9]. To achieve a higher sensitivity a solid phase extraction method [9], different variants of extraction-fluorimetric [4,12–16], and, recently, a kinetic-fluorimetric [17] TBA methods of determination of MA have been proposed. The extraction fluorimetry allows one to determine as low as 0.1 μM MA and the kinetic–fluorimetric method even 15 nM (1.1 ng ml^{-1}), although the reasons of this enhanced sensitivity are not clear.

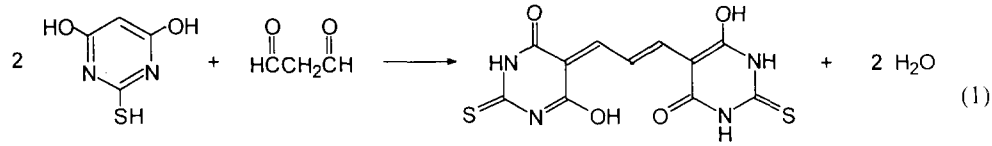

(1)

TBA MA TMT

* Corresponding author. Fax: +52 5 6162010; e-mail: anatoli@servidor.dgsca.unam.mx

PII S0039-9140(96)02141-8

Actually, the limit of detection of 0.1 μM is very close to that of the spectrophotometric procedure and therefore a simple fluorimetric determination of MA does not give any considerable improvement. However, a fluorimetric method frequently can be further improved by use of cyclodextrin (CD) solutions as reaction media due to the complexation-induced fluorescence enhancement effect [18,19]. A hydrophobic character of TMT, manifested in its extractability into organic solvents [4,8,14,15], is indicative of its ability to form the inclusion complexes. Therefore, it seems logical to test CDs as fluorescence enhancement agents for MA determination.

This paper reports a study of CD effects on the TMT fluorescence in aqueous acid medium. The expected enhancement effects have been observed and used for the development of a kinetic–fluorimetric method, which possesses the sensitivity of conventional fluorimetric or spectrophotometric determination with prolonged heating, but operates at room temperature. A method of MA determination avoiding the heating is desirable because it makes possible determination of free MA, unbound to proteins, amino acids and other sample components [1,5]. The bound forms of MA are thought to be destroyed by heating and, therefore, the conventional TBA methods measure total MA of a sample. Evidently, a combination of low and high temperature methods can be used when determination of both free and bound MA is necessary.

2. Experimental

2.1. Materials

TBA, malonaldehyde bis(diethyl acetal), α-, β-, and γ-cyclodextrins (Aldrich), butylated hydroxytoluene (Sigma), hydroxypropyl-β-cyclodextrin (HP-β-CD) (Amaizo), and 70% perchloric acid (Mallinkrodt) were used as obtained without further purification. All solutions were prepared in purified (Milli-Q Reagent Water System) water.

2.2. Instrumentation

Fluorescence measurements were made on a FluoroMax SPEX spectrofluorometer and absorption spectra were recorded on a Hewlett Packard 8452A diode array spectrophotometer. Both instruments were equipped with thermostated cell holders and magnetic stirrers.

2.3. Procedures

Fluorescence intensity was measured at 548–553 nm, depending on reaction conditions, with the excitation wavelength 520 nm. Absorption was measured at 532 nm. All fluorescence intensities and absorbances were corrected for the respective background signals by use of appropriate blanks.

A stock solution was prepared weekly by dissolving 22.0 mg malonaldehyde bis(diethyl acetal) in 100 ml of water. Working solutions of MA were made daily by diluting the stock solution with 0.1 M $HClO_4$ and subsequent heating in a boiling water bath for 5 min to ensure the complete hydrolysis of the acetal [6]. A 0.03 M standard solution of TBA was prepared by dissolving a weighed amount of solid TBA in water.

2.4. Cyclodextrin effects on TMT fluorescence

0.1 μM TMT solution was prepared by heating the mixture of 0.1 μM MA and 0.015 M TBA in 0.05 M $HClO_4$ in a boiling water bath for 15 min and subsequent cooling with cold tap water. Then a weighed amount of the solid CD was dissolved in a portion of TMT solution to obtain the highest concentration of a given CD and the intermediate concentrations were obtained by mixing this and initial TMT solutions at different proportions.

2.5. Analytical procedures

The basic procedure of the sample (raw beef and smoked pork) treatment was the same as in [9]. Ground meat (10 g) was homogenized with 40 ml of 0.1 M $HClO_4$ for 1 min. Butylated hydroxytoluene (20 mg) was added before the homogenization to prevent the autoxidation of the blend during homogenization. The blend was centrifuged (Damon/IEC HT Division) at 10 000 × *g* for 5 min, the supernatant was filtered through Whatman paper No. 5 into a 50 ml volumetric flask and the volume was adjusted to 50 ml with 0.1 M perchloric acid.

These extracts were analyzed by the conventional TBA spectrophotometric method, following in general the procedure described in [5], and by the new fluorimetric procedure proposed in this paper.

2.5.1. Spectrophotometric method

To 2.0 ml of the extract 2.0 ml of 0.03 M TBA were added and the mixture was incubated for 15 min at 94°C in a water bath. Then the mixture was cooled by tap water and its absorbance at 532 nm was measured. The calibration graph was constructed using the absorbances of the mixtures of 2.0 ml of 0.1–10 μM MA working solutions in 0.1 M perchloric acid with 2.0 ml of 0.03 M TBA treated as described above for the sample solution.

2.5.2. Fluorimetric method

A solution containing 0.03 M TBA and 0.07 M HP-β-CD was prepared by dissolving a weighed amount of HP-β-CD in TBA solution. To 1 ml of this solution, placed in a stirred fluorimetric cell, 1 ml of the working MA or sample solution, containing 0.1 M $HClO_4$, was added and the fluorescence recording started. Construction of the calibration graph is described in the text.

3. Results and discussion

3.1. Cyclodextrin effects on the fluorescence of TMT

Reported emission maxima for TMT vary from 547 to 553 nm [16], probably, due to some differences in reaction media. The excitation maximum should coincide with the absorption maximum (532 nm), but some authors [14,15,17] use shorter excitation wavelengths, between 515 and 525 nm, in order to minimize the effect of Rayleigh scattering, which strongly disturbs the emission spectra when the excitation wavelength lies near the emission maximum. We found that with the excitation wavelength 520 nm Rayleigh scattering does not disturb the region of the emission maximum and the fluorescence intensity is high enough to detect 0.1 μM TMT, which is a typical sensitivity of the fluorescence determinations.

Fig. 1 Fig. 2 Fig. 3 Fig. 4 show the effects of different cyclodextrins on the fluorescence of TMT in aqueous acid solution. The acid medium was used because reaction Eq. 1 is known to be acid-catalyzed and all variants of the TBA method employ acid solutions with pH values in the range 1–3 [4]. Evidently, all cyclodextrins cause a fluorescence enhancement. With α-cyclodextrin, Fig. 1, the effect is very modest, ca. 50% at the highest cyclodextrin concentration, and the fluorescence intensity versus cyclodextrin concentration plot does not show any tendency to saturation. On the contrary, it deviates from linearity in a way, which implies the involvement of a quadratic term in α-cyclodextrin concentration. The best fit of the results gives Eq. (2)

$$I(\text{cps}) = 1160 + 3160[\alpha\text{-CD}] + 35100[\alpha\text{-CD}]^2 \quad (2)$$

where I is the fluorescence intensity.

These observations indicate that the binding constant of TMT to α-cyclodextrin is very small and, probably, the inclusion complex has 2:1 α-CD/TMT stoichiometry.

Other cyclodextrins show higher enhancement effects and typical for the formation of 1:1 inclusion complexes hyperbolic plots [20], which fitted well to the theoretical Eq. (3)

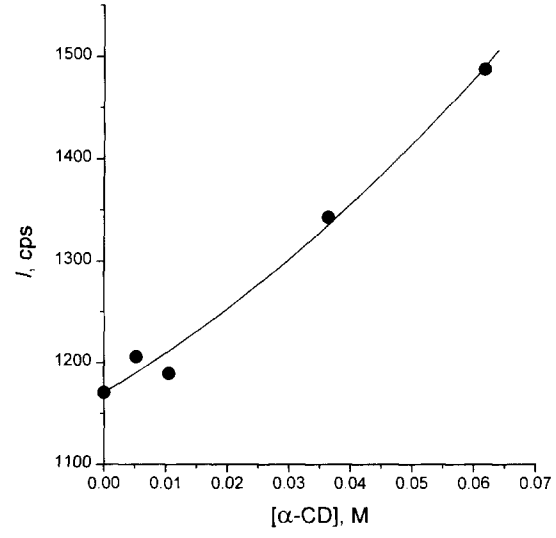

Fig. 1. The fluorescence intensity (counts s^{-1}, cps) of 0.1 μM TMT in 0.05 M $HClO_4$ at 553 nm (excitation wavelength 520 nm) versus α-CD concentration. The curve is the fitting profile calculated from Eq. (2).

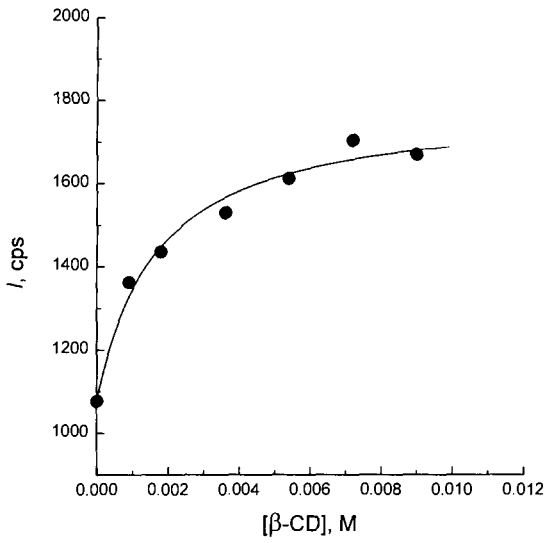

Fig. 2. The fluorescence intensity (counts s^{-1}, cps) of 0.1 μM TMT in 0.05 M $HClO_4$ at 544 nm (excitation wavelength 520 nm) versus β-CD concentration. The curve is the theoretical profile calculated from Eq. (3) with parameters given in Table 1.

$$I(\text{cps}) = \frac{I_0 + I_C K[\text{CD}]}{1 + K[\text{CD}]} \quad (3)$$

where I_0 and I_C are the fluorescence intensities of free and complexed TMT and K is the binding constant. The parameters of Eq. (3) for β-, γ- and HP-β-CD are given in Table 1.

Additions of these cyclodextrins induced both fluorescence enhancements and shifts in the emission wavelength maximum of TMT from 553 nm in water to 544 nm in the presence of β-CD and 548 nm in the presence of γ- and HP-β-CDs. Such blue cyclodextrin-induced shifts are typically observed for different analytes [19]. Also typical is a weaker binding of TMT to HP-β-CD than to unsubstituted β-CD [19]. The general trend in the binding constants, α-CD < γ-CD < HP-β-CD < β-CD, can be interpreted in such a way that the cavities of α-CD and γ-CD are, respectively, too small and too big for the complementary inclusion of TMT, which is a requisite for the tight binding. At the same time, the fluorescence enhancement factor, evaluated as the ratio I_C/I_0, Table 1, increases in the order β-CD < HP-β-CD < γ-CD, indicating the cavity volume and not the tightness of the binding to be the dominant factor. This observation is in agreement with a general conclusion regarding the mechanism of CD-induced fluorescence enhancement, which is attributed to the protection of the bound analyte from the quenching by water molecules [19].

The highest value of the ratio I_C/I_0 was found for γ-CD, but the use of this CD is impractical due to the very small binding constant of TMT and, consequently, the necessity to apply very high concentrations of this expensive CD. The highest binding constant is observed for β-CD, but the enhancement factor for this CD is less than 2. An optimum between the binding ability and the enhancement factor is reached with HP-β-CD. The standard calibration curve of the fluorescence intensity versus TMT concentration in the presence of 0.035 M HP-β-CD obeys the equation (obtained using seven different analyte concentrations and blank, each measured three times)

$$I(\text{cps}) = (120 \pm 10) + (37 \pm 2)[\text{TMT}] \quad (4)$$

where [TMT] is in nM. The limit of detection, calculated by 3 × (S.D. in the intercept)/(slope), equals 0.8 nM and the application range is between 1.5 and 50 nM.

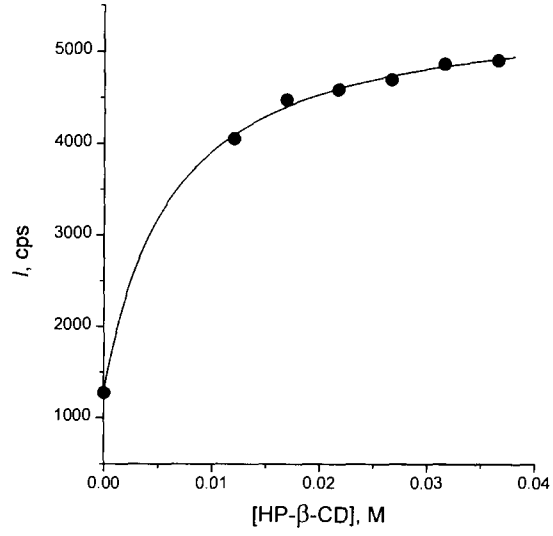

Fig. 3. The fluorescence intensity (counts s^{-1}, cps) of 0.1 μM TMT in 0.05 M $HClO_4$ at 548 nm (excitation wavelength 520 nm) versus HP-β-CD concentration. The curve is the theoretical profile calculated from Eq. (3) with parameters given in Table 1.

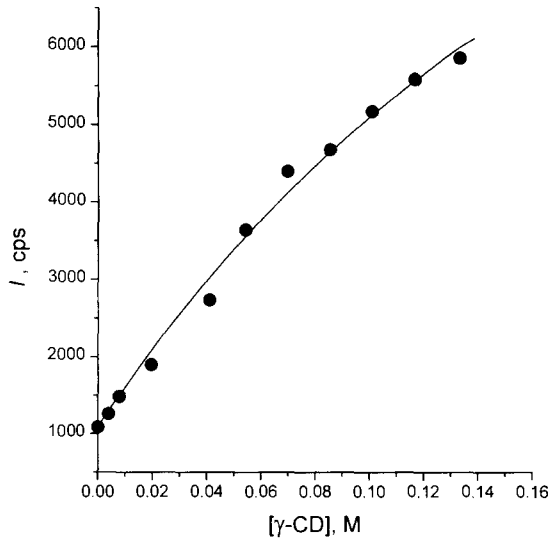

Fig. 4. The fluorescence intensity (counts s^{-1}, cps) of 0.1 μM TMT in 0.05 M $HClO_4$ at 548 nm (excitation wavelength 520 nm) versus γ-CD concentration. The curve is the theoretical profile calculated from Eq. (3) with parameters given in Table 1.

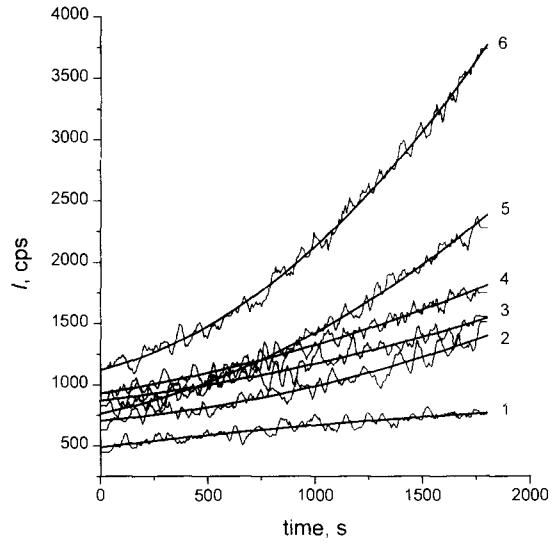

Fig. 5. The fluorescence intensity at 548 nm (excitation wavelength 520 nm) versus time profiles for the reaction of MA with 0.015 M TBA in the presence of 0.035 M HP-β-CD in 0.05 M $HClO_4$ at 25°C. Curves 1–6 correspond to MA concentrations 0; 0.08; 0.15; 0.3; 0.6 and 1.0 μM. Solid thick lines are the fitting profiles calculated with Eq. (5).

Such high sensitivity allows one to detect MA at a nM level, but it also can be useful for the development of a method with 'normal' sensitivity, i.e., in the range 0.1–10 μM, which would not need a prolonged heating for the conversion of MA into TMT. Reaction Eq. 1 is slow and the heating, usually at 60–95°C, is necessary to make the reaction time reasonably short, usually 10–60 min. The HP-β-CD enhanced fluorimetric method allows one, however, to detect 0.1 μM MA when only 1% of the aldehyde is converted into TMT. One can expect that such a low conversion can be achieved during 60 min or less even at room temperature and this prompted us to investigate such a possibility.

Table 1
Parameters of Eq. (3) for different cyclodextrins at 25°C in 0.05 M $HClO_4$

Cyclodextrin	I_0, cps	I_C, cps	K, $l \cdot mol^{-1}$	I_C/I_0
β-CD	1080 ± 30	1800 ± 40	600 ± 100	1.7
HP-β-CD	1100 ± 30	5500 ± 200	180 ± 30	5.0
γ-CD	1080 ± 30	16 400 ± 3000	3.5 ± 1.0	15.2

3.2. Kinetic-fluorimetric HP-β-CD enhanced determination of MA

In preliminary experiments we investigated the stability of TBA solutions in the presence of HP-β-CD in acid media. Unexpectedly, a slow formation of an unidentified yellow product was observed. Fortunately, this color did not interfere with TMT fluorescence under conditions employed.

Fig. 5 shows some typical fluorescence versus time profiles obtained in the presence of 0.035 M HP-β-CD at room temperature. In accordance with data of Espinosa-Mansilla et al. [17] the plots are curved downward. Such curvature may indicate a chain mechanism, autocatalysis or a mechanism which involves several consecutive steps, the colored TMT product being formed in the last of them. A detailed mechanistic study of reaction Eq. 1, which will be published elsewhere,

Table 2
Determination of MA in raw beef and smoked pork by the proposed kinetic–fluorimetric method at room temperature and by conventional spectrophotometry

Sample	Method	Equation of calibration graph	MA added, (mg kg^{-1})[a]	MA found,[b] (mg kg^{-1})[a]	Recovery, %
Raw beef	Kinetic –fluorimetric	Eq. (6)	0	0.15 ± 0.03	
			1.05	1.47 ± 0.07	126
			2.1	2.81 ± 0.07	125
		Eq. (7)	0	0.10 ± 0.01	
			1.05	1.10 ± 0.02	96
			2.1	2.45 ± 0.06	93
	Spectrophotometric		0	0.14 ± 0.01	
			1.05	0.85 ± 0.01	67
			2.1	1.48 ± 0.01	64
Smoked pork	Kinetic –fluorimetric	Eq. (6)	0	0.035 ± 0.002	
			1.14	0.98 ± 0.01	83
			2.3	1.97 ± 0.08	84
		Eq. (7)	0	0.041 ± 0.004	
			1.14	0.85 ± 0.01	71
			2.3	1.58 ± 0.07	67
	Spectrophotometric		0	0.084 ± 0.004	
			1.14	0.92 ± 0.01	73
			2.3	1.80 ± 0.02	75

[a] In mg kg^{-1} of the sample meat.
[b] Errors are the standard deviations from three measurements.

shows the last option to be correct. In any case, the curvature does not allow one to use the slopes of kinetic curves for the construction of the calibration graph. We used therefore the fixed time method in the following modification: the kinetic curves (I at 548 nm versus time (t) profiles) were fitted to a quadratic Eq. (5) and the values of ΔI at $t = 15$ min (ΔI_{15}) and $t = 30$ min (ΔI_{30}) were calculated as the differences between the respective calculated values of I and a_0 and used for the construction of calibration graphs represented by Eq. (6) and Eq. (7).

$$I = a_0 + a_1 t + a_2 t^2 \quad (5)$$

$$\Delta I_{15} = (150 \pm 20) + (0.65 \pm 0.04)[\mathrm{TMT}] \quad (6)$$

$$\Delta I_{30} = (320 \pm 50) + (2.2 \pm 0.1)[\mathrm{TMT}] \quad (7)$$

where [TMT] is in nM. The calibration graphs were obtained using 11 different MA concentrations and blank, each measured twice. The limits of detection, calculated by $3 \times$ (S.D. in the intercept)/(slope), equal to 90 and 70 nM for the calibration graphs Eq. (6) and Eq. (7), respectively, and the application range is between 0.1 and 10 μM for both graphs.

The fluorimetric determination of MA is known to be more selective than the spectrophotometric [17]. We tested as interferences glyoxal, 2-furfuraldehyde, 5-hydroxymethyl-2-furfuraldehyde, fructose and glucose taken at 100:1 molar ratio to MA and did not observe any interference in determination of 1 μM MA in accordance with data of Espinosa-Mansilla et al. for the selectivity of the kinetic-fluorimetric method without enhancement reagents [17].

The method was applied for the determination of MA in raw beef and smoked pork. Both samples were analyzed also by the conventional spec-trophotometric TBA method. The results are collected in Table 2.

In the case of raw beef both methods give close results, while the level of MA in smoked pork detected by the new method is considerably lower than that determined by spectrophotometry with heating. This difference cannot be attributed to the difference in recovery and, most probably, reflects the difference in concentrations of free and total (free + bound) MA of the sample, Section I. The TBA method usually gives low, 60–80%, recovery for meat samples [9]. The new method shows the same level of recovery for smoked pork, but higher levels for raw beef. The results obtained with 15 min interval, Eq. (6), differ considerably from those with 30 min interval, Eq. (7), for raw meat, but are reasonably close for smoked pork. Taking into account an obvious overestimation of MA with Eq. (6), one can consider the results with 30 min interval more confident.

In general, the results of this study shows HP-β-CD to be the best fluorescence enhancement reagent in agreement with conclusion of Frankewich et al. [19], and by using this cyclodextrin the sensitivity of MA determination can be improved to an extent that allows one to determine as low as 0.1 μM MA at room temperature.

Acknowledgements

The work was supported by DGAPA-UNAM, Project IN 205393.

References

[1] J.I. Gray and F.J. Monahan, Trends Food Sci. Technol., 3 (1992) 315.
[2] B.G. Tarladgis, B.M. Watts, M.T. Younathan and L.R. Dugan, J. Am. Oil Chem. Soc., 37 (1960) 44.
[3] K.S. Rhee, J. Food Sci., 43 (1978) 1776.
[4] R.P. Bird and H.H. Draper, Methods Enzymol, 105 (1984) 299.
[5] J. Pikul, D.E. Leszczynski and F.A. Kummerow, J. Agric. Food. Chem., 37 (1989) 1309.
[6] A. Schmedes and G. Holmer, J. Am. Oil Chem. Soc., 66 (1989) 813.
[7] H. Ikatsu, T. Nakajuma, N. Murayama and T. Korenaga, Clin. Chem., 38 (1992) 2061.
[8] Z. Du and W.J. Bramlage, J. Agric. Food. Chem., 40 (1992) 1566.
[9] S. Rajaro, J.N. Sofos and G.R. Schmidt, J. Agric. Food. Chem., 40 (1992) 2182.
[10] D.R. Janero, Free Radic. Biol. Med., 9 (1990) 515.
[11] R.B. Pegg, F. Shahidi and C.R. Jablonski, J. Agric. Food. Chem., 40 (1992) 1826.
[12] K. Yagi, Biochem. Res., 15 (1976) 212.
[13] K. Yagi, Methods Enzymol, 105 (1984) 328.
[14] M.-J. Richard, B. Portal, J. Meo, C. Coudray, A. Hadjian and A. Favier, Clin. Chem., 38 (1992) 704.
[15] W. Wasowicz, J. Néve and A. Peretz, Clin. Chem., 39 (1993) 2522.
[16] D. Yin, Clin. Chem., 41 (1995) 329.
[17] A. Espinosa-Mansilla, I.D. Merás and F.S. López, Analyt. Chim. Acta, 320 (1996) 125.
[18] S. Li and W.C. Purdy, Chem. Rev., 92 (1992) 1457.
[19] R.P. Frankewich, K.N. Thimmaiah and W.L. Hinze, Anal. Chem., 63 (1991) 2924.
[20] M.L. Bender and M. Komiyama, Cyclodextrin Chemistry, Springer-Verlag, Berlin, 1978.

ELSEVIER

Talanta 44 (1997) 959–965

Talanta

Kinetic determination of organic vapor mixtures with single piezoelectric quartz crystal sensor using artificial neural networks

Wan-Li Xing, Xi-Wen He *

Department of Chemistry, Nankai University, Tianjin 300071, People's Republic of China

Received 19 July 1996; received in revised form 17 October 1996; accepted 17 October 1996

Abstract

A single piezoelectric quartz crystal coated with one kind of crown ether was applied to the simultaneous determination of binary acid and amine vapor mixtures. From the adsorption and desorption curves of analytes, which were somewhat different in shape, frequency shifts from ten time windows were taken as inputs for artificial neural networks (ANN). Prediction results were satisfactory for ANN in both sample sets. The average relative errors, for formic acid and acrylic acid were 5%, for *n*-butylamine and aniline, they were 3% with ANN respectively. The effects of number of neurons in the hidden layer of ANN on the performance of the network are also discussed. © 1997 Elsevier Science B.V.

Keywords: Artificial neural networks (ANN); Hidden layer; Organic vapors; Piezoelectric quartz crystal

1. Introduction

Recently the piezoelectric crystal sensor has received much attention as a fast, convenient and sensitive analytical tool. Based on the linear relationship between the sensor frequency shift and the total mass change of the adsorptive coating, many sensitive analytical techniques have been developed for both vapors and liquids [1–3]. For multi-component analysis in gaseous phases, the use of piezoelectric crystal array has been proposed. Carey et al. [4] used a piezoelectric crystal array modified by different coating films to detect two and three component organic vapor mixtures. Chang et al. [5] identified odorants with a piezoelectric crystal sensor array through artificial neural network pattern recognition. Barko et al. [6] used an array of four piezoelectric crystal sensors each coated with a GC stationary phases to identify organic vapors, such as benzene, *n*-pentane, acetone, et al. using pattern recognition. Our laboratory has also detected some organic vapor mixtures with an array of nine piezoelectric crystal sensor coated with different crown ether derivatives [7]. The interaction between crown ethers and organic species, which leads to different response patterns of the analytes, is affected not only by the size of the ring, the type and

* Corresponding author.

PII S0039-9140(96)02142-X

basicity of the hetero atom (O, N, S), and the property of the substituent, but also by the molar mass, polarity, and steric hindrance of analytes [8]. In the process of measurement, we discovered that the adsorption and desorption model for some analytes had some differences. So in this paper, we only used one single piezoelectric crystal sensor coated with one kind of crown ether to detect organic vapor mixtures. Two groups of analytes each contained two components were detected with ANN. The frequency shifts from ten time windows were taken as inputs for ANN. This single crystal method makes the detection device more convenient and practical. We have also tested this method successfully to simultaneously determine the concentration of sulfuric dioxide and the relative humidity [9].

Artificial neural networks (ANN) are a form of artificial intelligence that mathematically simulate biological nervous system. Thay have been employed in chemistry since 1960 [10], for instance using data from a metal-oxide-semiconductor field-effect-transistors (MOSFETS) sensor array to determinate of individual components in a gas mixture, such as hydrogen, ammonia, et al. [11]. The approach is selected because of its adaptability to almost any mathematical function [12]. In this paper we deal with the signals from ten time windows of a single piezoelectric crystal sensor in two group of two-component mixtures. Our goal is not only to identify the gas mixtures, but also to determine independently and with sufficient accuracy the concentrations of the individual components, which is a somewhat more difficult problem than the identification of a gas mixture. It was proved by our experiment that our ANN model provided adequate prediction.

2. Experimental

2.1. Apparatus and reagent

The apparatus shown in Fig. 1 consisted of an AT-cut, 9 MHz piezoelectric quartz crystal, 12.5 mm in diameter, having two coated silver electrodes, 6.00 mm in diameter, was obtained commercially (Peking). The lead wires soldered to electrodes were connected to a TTL oscillator made in our laboratory. The frequency change was monitored by an N3165 frequency counter and the power was supplied by a PL2002A d.c. voltage regulator. The ANN data analysis program was written in Turbo C language by ourselves. All data analysis were treated by an PC-DX486 computer.

Analytes of formic acid, acrylic acid, *n*-butylamine and aniline were all of analytical-reagent grade. The coating material, crown ethers, were synthesized by Polymer Chemistry Institute in our school. Their molecular structure is showed in Fig. 2. The first one, *N*, *N'*-bis(4-methoxyl-phehyl)-1,10-diaza-18-crown-6, was used to detect the first sample set consisting of formic acid and acrylic acid. The second one, dibenzo-18-crown-6, was used to detect the second sample set consisting of *n*-butylamine and aniline. Coating solutions were prepared by dissolving about 100 mg of the substrate in 50 ml of chloroform or

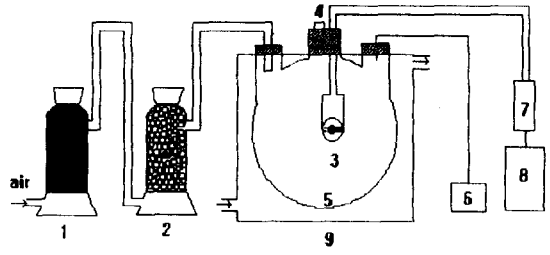

Fig. 1. Diagram of the experimental system: (1) active carbon; (2) silica gel; (3) piezoelectric crystal; (4) sample injection port; (5) 1 l glass flask; (6) vacuum pump; (7) oscillator; (8) frequency counter; and (9) water jacket.

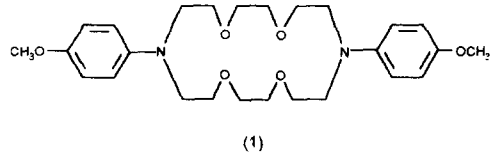

(1)

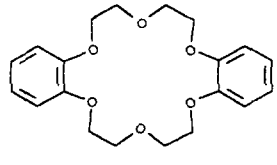

(2)

Fig. 2. Molecular structure of crown ether coating material.

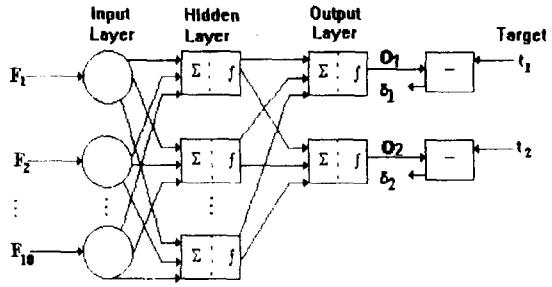

Fig. 3. Two layer back-propagation model.

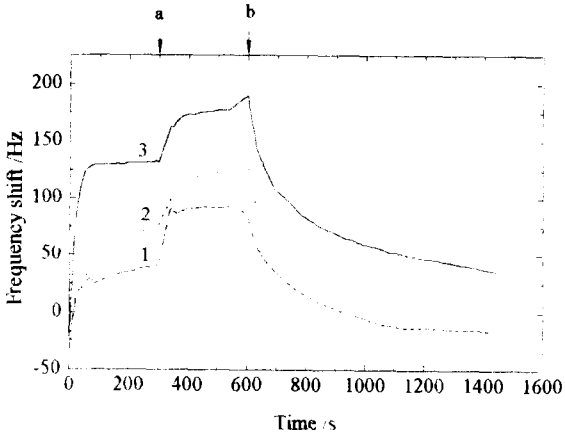

Fig. 4. Frequency shift patterns for formic acid and acrylic acid: (1) formic acid (0.87 mg l^{-1}); (2) acrylic acid (1.6 mg l^{-1}); and (3) sum of formic acid (0.87 mg l^{-1}) and acrylic acid (1.6 mg l^{-1}). (a) The air was introduced in and the pressure in the detection cell became normal. (b) The dectection cell was purged with dried and purified air.

methanol. The obtained concentrations of the solutions were about 2 mg ml^{-1}. Both sides of the crystals were coated with crown ethers via the dropping method using a microsyringe. The thin film of the coating was formed by solvent evaporation. The mass of the coating caused a frequency shift of about 5 kHz.

art2.2. Measurement procedure

The piezoelectric quartz was mounted in an 1.4 l flask which was thermostated at 30 ± 0.5°C. The stable oscillation frequency f_0 was recorded. Then we decreased the pressure in detection cell with an vacuum pump until it arrived about 5 mm Hg and the stable frequency f_1 was recorded. At this pressure, analytes evaporate completely in a very short time. After injecting a certain amount of mixture of analytes using a microsyringe, i.e., formic acid and acrylic acid or *n*-butylamine and aniline, the initial reaction time was recorded. After the injection, 5 min, the air was introduced in and the pressure in the detection cell became normal. The system was equilibrated for another 5 min, then the detection cell was purged with dried and purified air at 3 l min^{-1} till the frequency of the sensor was restored to its fundamental value. From the initial reaction time, the frequency values ($f(t)$) at every 10 s were injection of the samples and 15 min after purging the detection cell. In order to avoid too many input neurons leading much longer training time of ANN, in each sample set, every pure component with four concentrations covering the range of calibration set were detected under the same experiment conditions as other samples in the calibration set. Among the 150 $f(t)$, the average change rates of frequency shift of the four concentrations for every component at every time point, $\Delta f(t)_{\text{sample}(i)} = f(t)_{\text{sample}(i)} - f(t-1)_{\text{sample}(i)}$, were calculated. Then the differences of $\Delta f(t)_{\text{sample}(i)}$ between the two components of every sample set at the same time point were calculated. Among these differences, ten of the largest ones were selected.

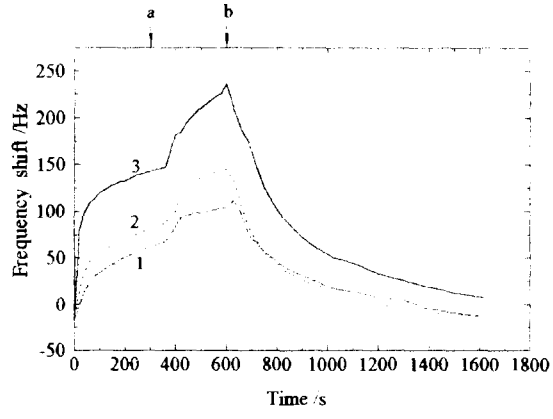

Fig. 5. Frequency shift patterns for *n*-butylamine and aniline: (1) *n*-butylamine (0.5 mg l^{-1}); (2) aniline (0.714 mg l^{-1}); and (3) sum of *n*-butylamine (0.5 mg l^{-1}) and aniline (0.714 mg l^{-1}). (a) The air was introduced in and the pressure in the detection cell became normal. (b) The dectection cell was purged with dried and purified air.

Table 1
Calibration sample concentrations

Sample No.	Set 1, mg l^{-1}		Set 2, mg l^{-1}	
	Formic acid	Acrylic acid	*n*-Butylamine	Aniline
1	0.87	0	0	0.71
2	0	1.60	0	1.43
3	0	3.20	0.50	0
4	2.61	0	1.00	0
5	0.87	1.60	0.50	0.71
6	2.61	3.20	1.00	1.43
7	1.74	4.00	0.75	1.79
8	3.48	2.40	1.25	1.07

The frequency shifts at these ten time points, which could reflect the characteristics of the components' adsorption and desorption process were taken as inputs for ANN. More inputs were tested, but they did not improve the prediction results obviously. Each sample was measured in triplicate in order to obtain an estimation of the precision of the sensor response.

2.3. Network design

Fig. 3 shows a generalized two-layer back-propagation network used in our experiment that has ten inputs (frequency shifts from ten time windows) in the input layer, an arbitrary number of artificial neurons in the hidden layer and two artificial neurons in the output layer (organic vapors). Each of the inputs is multiplied by an associated weight. The output signal y_i is further processed by sigmoid activation function F, so the neural output o_i is given by

$$o_i = 1/[1 + \exp(-y_i)] \tag{1}$$

and

$$y_i = \sum_{i=1}^{n} w_i x_i \tag{2}$$

The learning rules specify the initial set of weights and determine how these weights should change to improve the network performance. In all our parametric studies, we have used the BP algorithm and the delta learning rule, where the difference δ_i between target value t_i and actual neuronal output o_i is propagated back through the network to the input. The weights of the processing elements are thus iteratively changed until the output errors are be acceptable. A correction of Δ_i is made to the weights where

$$\Delta_i(m+1) = \eta\delta_i x_i + \alpha\Delta_i(m) \tag{3}$$

$$W_i(m+1) = W_i(m) + \Delta_i(m+1) \tag{4}$$

So the weights are adjusted by one term that is propagational to the error with a constant of the proportionality, called the learning rate. The second term is used to improve the stability of the learning process and is called the momentum term. The performance of each network and learning rule was determined by an error function, E, usually defined as the total squared error [10], from

$$E = \frac{1}{2}\sum_j \sum_k (t_{jk} - o_{jk})^2 \tag{5}$$

where j is the number of sensor response samples in the training and test set and k is the number of outputs in the output layer. After each iteration of the back-propagation process, the network error should gradually fall and converge to an asymptotic value.

In the our experiment, learning rate in the network training was set as 0.1, the momentum coefficient, 0.6. The number of neurons in the hidden layer was set as 6. The order of presentation of the training set samples was randomized at

Table 2
Multivariate prediction results for formic acid and acrylic acid mixture

	Actual concn, mg l^{-1}		ANN predicted concn, mg l^{-1}		Rel error %	
	A	B	A	B	A	B
1	2.61	2.40	2.56	2.16	2.15	9.67
2	3.05	3.20	2.85	3.03	6.70	5.40
3	1.74	2.40	1.59	2.34	8.35	0.95
4	2.18	2.80	2.11	2.65	3.14	5.42
Av.					5.08	5.36

Note: A, formic acid; and B, acrylic acid.

Table 3
Multivariate prediction results for *n*-butylamine and aniline mixture

	Actual concentration, mg l^{-1}		ANN predicted concentration, mg l^{-1}		Rel. error %	
	C	D	C	D	C	D
1	1.00	1.14	0.99	1.11	1.41	2.85
2	0.90	1.57	0.87	1.56	3.47	0.35
3	1.10	1.29	1.06	1.22	3.94	5.67
4	0.80	1.43	0.79	1.40	1.41	2.03
Av.					2.56	2.72

Note: C, *n*-butylamine; and D, aniline.

the beginning of each epoch to speed convergence. In order to avoid overtraining, a point when a network training should be stopped is determined by cross-validation method [13].

3. Results and discussion

It can be seen in Fig. 4 and Fig. 5 when the crystal under 5 mm Hg pressure, its frequency was higher than its fundamental frequency, this is because of the stress on the surface of crystal decreased, after injection of analytes, they evaporated and were adsorbed by the coating material on the surface of the crystal, leading to the decreasing of the frequency, and the rate of decreasing became slow gradually with time. After the pressure became normal, the sensor's frequency decreased further and became stable gradually. While purged with air, the analytes were desorpted from the coating material on the surface of crystal, the frequency of the sensor rose progressively to its fundamental value. The rate of increasing also became slow gradually with time.

As showed by the figures, the outlines of the adsorption and desorption curves for the analytes were similar. But there were some differences in detail because of the difference of interaction between the analytes and the coating material, crown ethers. For example, the desorption rate for formic acid was faster than that of acrylic acid. The interaction between the analytes and the crown ethers was explained in detail elsewhere [7].

In Fig. 4 and Fig. 5, the frequency shift patterns for the two groups of analytes were plotted to show the degree of similarity, which indicate that there are some differences between the components, but they are not very obvious. The frequency shifts at different time are basically proportional to the concentrations of the analytes but not strictly.

3.1. Sample analysis

In each group, eight mixtures of analytes of various concentrations were prepared as a calibration set according to factorial-design, as showed in Table 1, four other mixtures of analytes were prepared as a test set which were not contained in the calibration set and measured under the same experimental conditions.

The predicted concentration results are given in Table 2 and Table 3. For the first sample set of formic acid and acrylic acid, the average relative error was 5%. For the second sample set of *n*-butylamine and aniline, the average relative error was 3%. The great prediction capacity for ANN is due to its advantageous ability to treat nonlinear problem, since while analyzing vapor mixtures, several components simultaneously interacted with the coating, crown ether, which may lead to complex relationship between the responses of the sensor and the concentrations of the vapors.

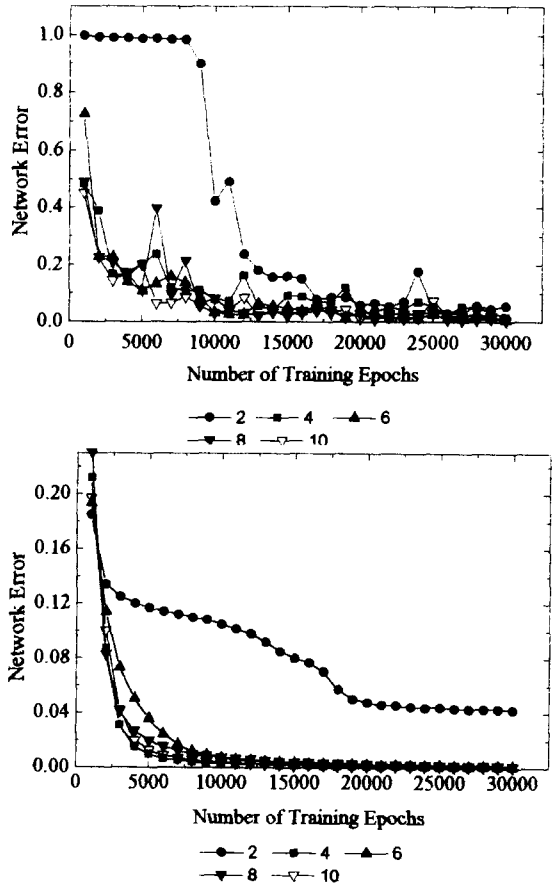

Fig. 6. (a) Effects of the number of neurons in hidden layer on the performance of neural networks in the first sample set. (b) Effects of the number of neurons in hidden layer on the performance of neural networks in the second sample set.

3.2. Network architecture and training

3.2.1. Number of neurons in the hidden layer

During the training phase for neural network analysis, we performed extensive experimentation to define appropriate network parameters. Although the selection of neurons in the hidden layers in a BP network was empirical, it is recognized that this choice can have a significant effect on network performance. A large number of hidden neurons can provide more predicting power, but the network will require more computation time and may also suffer in ability to generalize for an unknown data set [14]. In our experiment we tested different number of neurons in the hidden layer (from two to ten) for learning rate as 0.1 and momentum term as 0.6. Fig. 6(a, b) illustrates the relation between the network error and the number of training epochs for different number of neurons in the hidden layer. We can see that the performance of the network stabilized after inclusion of an adequate number of hidden units (more than four). The network with too few neurons in the hidden layer, e.g., in this experiment, two, can not converge effectively. This phenomena can also be found in our another work [7].

4. Conclusion

In this paper, we only used a single piezoelectric quartz crystal sensor to detect organic vapor mixtures using kinetic method. Compared with a piezoelectric quartz crystal sensor array, this detection system is more convenient and practical, although the sensor array method has its own advantages. This single crystal method can be extended to other analytes and detection systems

as long as there are some differences in the kinetic process. It is hopeful to become an practical method for multicomponent analysis. For quantitative analysis of the individual concentration in the vapor mixtures, it is important to keep the sensitivity of the coating material unchanged with time so as to ensure the precision of the frequency shifts. Crown ethers can satisfy this criterion because of its small volatility, long life-stan and reversible interaction with the analytes. In the data analysis of our study, the BP ANN model provided satisfactory prediction.

Acknowledgements

This work was supported by the National Natural Science Foundation of People's Republic of China.

References

[1] J.J. McCallum, Analyst, 114 (1989) 1173.
[2] J.F. Alder and J.J. McCallum, Analyst, 108 (1983) 1169.
[3] M. Thompson, A.L. Kipling, W.C. Duncan-Hewitt, L.V. Rajakovic and B.A. Cavic-Vlasak, Analyst, 116 (1991) 881.
[4] W.P. Carey, K.R. Beede and B.R. Kowalski, Anal. Chem., 59 (1987) 1529.
[5] S.M. Chang, Y. Iwasaki, M. Suzuki, I. Karube and I. Muramatsu, Anal. Chim. Acta, 249 (1991) 323.
[6] G. Barko, B. Papp and J. Hlavay, Talanta, 42 (1995) 475.
[7] W.L. Xing and X.W. He, Analyst, in press.
[8] C.J. Lu and J.S. Shih, Anal. Chim. Acta, 306 (1995) 129.
[9] H.M. Wei, L.S. Wang, W.L. Xing, B.G. Zhang, C.J. Liu and J.X. Feng, Anal. Chem., (in press).
[10] J.A. Burns and G.M. Whitesides, Chem. Rev., 93 (1993) 2583.
[11] H. Sundgrent, F. Winquist, I. Lukkarl and I. Lundstrom, Meas. Sci. Technol., 2 (1991) 464.
[12] R.P. Lippman, IEEE ASSP Mag., 4(2) (1987) 4.
[13] V. Tetko, D.J. Livingstone and A.L. Luik, J. Chem. Inf. Comput. Sci., 35 (1995) 826.
[14] H. Chow, H. Chen, T. Ng, P. Myrdal and S.H. Yalkowsky, J. Chem. Inf. Comput. Sci., 35 (1995) 723.

ELSEVIER

Talanta 44 (1997) 967–972

Talanta

An automatic back titration method for microchemical analysis

Aimin Tan *, Cailin Xiao

Department of Chemistry, Central South University of Technology, Changsha 410083, People's Republic of China

Received 9 September 1996; received in revised form 24 October 1996; accepted 25 October 1996

Abstract

An automatic back titration method for microchemical analysis is introduced, which is based on conventional volumetric analysis's principle and the use of flow injection analysis apparatus for the automation and microminiaturization of the process. The sample and a known, but excess amount of a calibrated reagent solution are injected and propelled into a titration cell, where their reaction takes place. The excess of the reagent is then titrated with a titrant containing an indicator and the end point is monitored photometrically. Since homogeneous mixing in the titration cell is obtained magnetically in the whole process, there is a linear relationship between the analyte's concentration and the volume of the titrant consumed. Nickel in the range of 10–70 g l^{-1} is determined by the above method, in which 30 μl of sample and 500 μl of EDTA are injected and the excess of EDTA is titrated with a standard zinc salt solution containing xylenol orange which could be blocked by nickel ion in a direct titration. This method is characteristic of low sample and reagent consumption, high sampling rate as high as 45 samples h^{-1}, negligible effect of sample's viscosity, small carry-over effect (lower than 0.14%), and very good precision, whose relative standard deviations are as small as 0.24%. © 1997 Elsevier Science B.V.

Keywords: Automatic titration; Back titration; Flow analysis; Microchemistry; Nickel

1. Introduction

In recent years, much attention is attracted to flow injection titration for its advantages over conventional automatic titrator, including high sampling rate, low reagent and sample consumption, simplicity in instrumentation, versatility in solution handling, and rich in information [1]. However, flow injection titration's precision and accuracy is not so satisfactory as its advantages since its readout is not directly related to analyte's concentration, but to the logarithm of the concentration. Several new methods have therefore been proposed to increase the precision by making the readout linearly related to the analyte's concentration and maintaining most of its advantages.

A majority of these methods are based on varying the flow rate ratio between titrant and sample stream to obtain the equivalence point. Martinez Calatayud et al. [2] proposed a flow method for the titration of weak acids or weak bases using linear titration plots. The method involves continuous titrations based on mixing of titrant, propelled at a constant flow rate, and titrant, propelled at a manually varied flow rate, and pH measurements in a flow cell. The depen-

* Corresponding author.

PII S0039-9140(96)02158-3

dence of the response of this potentiometric detector on the flow-rate requires calibration at each flow rate used. Extensive work has been developed by Valcarcel and co-workers discussing in depth the use of programmable flow rate gradients [3–6] and their application to acid–base [7], complexometric and redox titrations [8,9], as well as to calculating acidity [10] and kinetics constants [11]. All the titration procedure based on a single gradient need a previous calibration of the system, although this step can be avoided by using two successive and diametrically opposite gradients as in the automatic titration system proposed by Hernandez Corboda et al. [12].

Ruzicka et al. [13] present a simple and rapid continuous flow injection system equipped with a mixing chamber, which is actually a combination of automated titration and automated dilution. The balance can be tipped towards either end to meet the special requirements of a particular analysis. When the analyte concentration varies over a wide dynamic range, the dilution function should be emphasized so that the analysis time can be shortened. On the other hand, when analyte varies over a narrow concentration range, the titration function is emphasized to differentiate between samples better. In addition, they introduced two application cases with the readout is logarithmic in the first and linear in the second, respectively.

Fumio Sagara et al. [14] proposed a micro flow spectrophotometric titration method which is the same as conventional titration in principle, but different in apparatus. For example, fused-silica capillary tubes in gas chromatography is employed as microburettes. The solution in a microbeaker, as small as 500 μl, was circulated through the micro-flow cell of a spectrophotometer to determine the indicator endpoint. This method's main advantage is that the reagent and sample's consumption is reduced to as small as μl.

In addition, the linear pH-buffering single-point titration using potentiometric detection [15–17] allows for linear system response, too, though it is limited to diluted samples.

The above developments in flow titration methodologies imply a continued interest in this field. However, in all these methods, back titration is very difficult to be automated, and no example is yet reported, even though back titration procedures are widely used in conventional titrimetric analysis while a suitable indicator is not available or where the reaction between an anlyte and a titrant occurs too slowly. In addition, since titrimetric analysis methods are usually employed for the determination of concentrated components, which requires high precision, most of the above methods based on the adjustment of flow rate are thus not suitable because their precision, r.s.d. is as high as 2%. Furthermore, the fluctuation of sample's viscosity has large influence on the determinations; and the concentrated analytes are usually difficult to be titrated directly without predilutions.

Recently, we proposed an automatic micro-titration method [18] which is based on the injection of a very small volume of sample and homogeneous mixing in a titration cell of the injected sample with a titrant solution propelled at a constant flow rate by a peristaltic pump. The mixture in the titration cell is monitored by photometry for endpoint. On the basis of the above method, automatic back titration method for microchemical analysis is developed, in which both a sample and an excess of standard reagent solution are injected and the excess is then titrated with a titrant. Since the sample volume, albeit small as 30 μl, could be maintained unchanged for a long period, the reduction of sample and reagent consumption is achieved but without any loss of precision. In addition, the method's precision is further increased with the titrant propelled by a stepper motor driven syringe piston pump in place of a conventional peristaltic pump. Concentrated samples can be titrated directly without predilutions, while the influence of sample's viscosity on the determinations is negligible. Moreover, since the titration cell is drained, it eliminates the long washing out time accompanied with the mixing chamber titration system. Finally, the above method is employed for the determination of nickel, in which an excess of EDTA is injected to react with nickel and the excess is then titrated with zinc salt solution containing xylenol orange (XO) as the indicator, which could be blocked by nickel ion in a direct titration. End point is determined while a sharp increase of absorbance at the

wavelength of 560 nm occurs owing to the formation of the red zinc-XO complex.

2. Experimental

2.1. Reagents and solutions

R: 0.1000 mol l^{-1} Na_2-EDTA + 1.5 mol l^{-1} hexamine buffer at pH 5.5

T: 0.005000 mol l^{-1} zinc + 0.002% (w/v) xylenol orange + 1.0 mol l^{-1} hexamine buffer at pH 5.5.

Nickel sulphate solution containing 80.00 g l^{-1} of nickel and 1.0 mol l^{-1} H_2SO_4.

All the reagents except otherwise stated are of analytical grade.

3. Apparatus

The micro-titration system depicted in Fig. 1 were constructed from the following components: a 16-port rotary valve (Zhaofa Automatic Analysis Research Institute, Shenyang, China), two self-designed variable-speed, linear flow piston pumps, each equipped with two disposable plastic syringes of 10 ml (diameter 17 mm); a self-constructed titration cell; a photometer based on LED and phototransistor; a magnetic stirrer

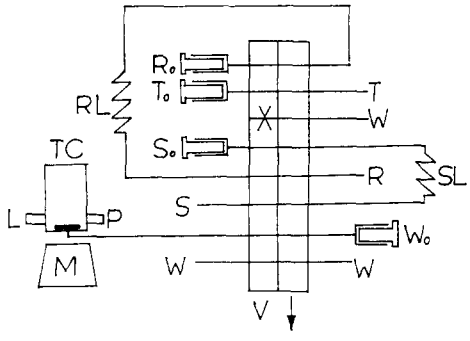

Fig. 1. The system configuration. Ro, So, To and Wo are the syringes for the calibrated reagent solution (R), sample (S), titrant (T), and the drainage of the titration cell (TC), respectively. *V* is the valve. *W* is the waste. *M* is the magnetic stirrer. SL is a 30 µl sample loop. RL is a 500 µl reagent loop. L and P are the LED and the phototransistor, respectively.

(Model GSP-80-04, Taixian Radio Factory, Jiangsu, China), and an intel 8031 based single-chip microcomputer system for the control of pump, valve, and stirrer, data acquisition and processing. The valve is driven by a stepper motor (Model 45BF3/3A, Shanghai Instrument Motor Factory, China) through two gears with a diameter ratio of 1:4.5. Through the control of the microcomputer, the valve can be turned to either load or inject position. The piston pumps, also driven by stepper motors, can be controlled to a precision of 2 µl. Since syringes need to be refilled, the pump's movements should be in accordance with the valve's position. The piston's forward movement requires the valve in inject position, while backward movement needs the valve in load position. Each determination always begins with the piston backward movement for filling the syringes, and ends with the piston's forward movement to deliver reagent. The titration cell, made of glass, has a volume about 12 ml. In its outside, near the bottom are mounted a green LED, whose emission maximum is at 560 nm, and a phototransistor, which, opposite to each other, are 18 mm apart. The titration cell together with the photometric components are put in a light-tight box to prevent the influence of ambient lights. For further details about the photometric detector, readers are referred to Ref. [19] and [20].

There are two distinct steps in the procedure, sampling and titration. During the first step, the valve turns to the load position, the syringes move backward, the titrant taken into the titrant syringe directly, while the sample flowing through the sample loop first and then to the sample syringe. The calibrated reagent solution is also loaded into the reagent loop. At the same time, the titration cell is drained by another syringe, which should be operated a little bit longer than the titrant syringes to secure the complete drainage of the titration cell. The blank signal for the following absorbance measurements is taken when the titration cell becomes empty. After sampling step, the valve is turned to inject position, followed by the forward movement of the syringes. The titrant delivered by syringe propels the loaded sample and the reagent solution into the titration cell one after the other. After the reagent

solution loaded in the reagent loop is propelled into the cell, stop the titrant's forward movement for a while until the reaction goes well to completion. Then restart the titrant pump to titrate the excess of the reagent and the endpoint is continuously monitored. Once a sharp increase in absorbance is detected, stop the addition of titrant, and read the volume of titrant delivered. Since homogeneous mixing of the solution in the titration cell is obtained by a magnetic stirrer, the principle is similar to that in conventional back titration methods, and the unknown concentration of a sample could be calculated similarly.

4. Results and discussion

4.1. Calibration curve and result calculation

As homogeneous mixing is employed in the titration, the principle of this method is quite similar to the conventional titration, except for that the sample's volume in this method is much smaller. The analyte's concentration in an unknown (C_X) can be calculated from the following equation,

$$C_X = (C_R V_R - C_T V_T)/V_0 \quad (1)$$

where C_R is the concentration of the calibrated reagent solution, i.e., the concentration of EDTA; C_T is the concentration of the titrant, zinc; V_R, V_0, and V_T are the volumes of reagent loop, sample loop, and titrant consumed, respectively. Since C_R and C_T are known, the unknown sample's concentration can be readily calculated if the volumes are determined accurately. Considering the difficulty in accurately determining the small volumes of sample and reagent loops, seven standard nickel solutions with increasing content of nickel from 10 to 70 g l^{-1} with 10 g l^{-1} interval are employed to calibrate these unknown volumes and other uncertainties altogether,obtaining the following regression equation,

$$C_X\ (\mathrm{g\ l^{-1}}) = 98.07 - 9.731 V_T\ (\mathrm{ml}) \quad (2)$$

whose regression coefficient is 0.9999. The linearity error, i.e., the relative difference between the known concentration and that calculated by the regression equation, in the whole range is below 0.21%. The relative standard deviation for delivering a known volume is 0.033%, which is much better than the linearity because of the small variations in the inner diameter of the syringe.

Since both the sample loop's volume and the reagent loop's volume, albeit small, can be maintained constant over a very long period, and the precision for delivering titrant by computer controlled piston pump does not fluctuate so easily as in peristaltic pump, frequent calibration is thus unnecessary.

5. The carry-over effect

As the titration cell and the tube connecting the cell to the valve is drained, the carry-over effect in this method depends mainly on the volume of the residual solution after drainage (V_r), its concentration (C_r), and the concentration of the next sample (C_x). The reagent's concentration in residual solution may be expressed as

$$C_r = T_e C_R V_R / V_s \quad (3)$$

where T_e is the titration error; V_s is the total volume of the mixture in the titration cell at endpoint. Therefore, the relative error (RE) caused by carry-over effect is as following,

$$\mathrm{RE} = (V_r T_e C_R V_R / V_S)/(V_0 C_X) \quad (4)$$

where V_0 is the volume of sample injected.

To determine the residual solution's volume approximately, a sample containing 100 g l^{-1} of cobalt is injected and diluted to 10 ml, the residual solution after drainage is then washed with distilled water and the cobalt content in the resulting solution is determined by spectrophotometry with nitroso *R* salt [21], from which the volume of the residual solution may be determined. The residual solution's volume, as the results of 11 measurements done this way determines, ranges from 0.01 to a maximum of 0.1 ml.

For the most unfavourable situation, V_S and C_X takes the minimum of 3.4 ml and 0.17 mol l^{-1}, respectively, the resulting relative error being as low as $\pm 0.14\%$ if the titration error is $\pm 0.5\%$.

To demonstrate by experiments: two samples with 10 and 70 g l^{-1} of nickel are titrated alternatively, no appreciable carry-over effect is found, since the titration error is practically smaller than 0.5%, and the residual solution's volume may be smaller than 0.1 ml, also.

6. The influence of sample's viscosity

In conventional FIA titration method, increased sample viscosity increases the pressure drop with the system and reduce the dispersion and mixing. The pressure drop increase is so predictable that it has been used by Betteridge et al. for the measurement of viscosity [22]. However, the influence of sample's viscosity in this method is greatly reduced because the length of the tube connecting the valve and the titration cell, i.e., the passage a sample transported, is as short as 10 cm, and homogeneous mixing is employed in the titration process. Even though the loaded samples with different viscosities might have increasing trailing, the analyte may be flushed to the titration cell completely by the reagent in the reagent loop as large as 500 μl. To demonstrate, when several samples containing 30 g l^{-1} of nickel but with increasing amounts of glycerin were determined, no appreciable viscosity effect is found even for the glycerin's content as high as 50% (V/V).

7. Sampling rate

The time for a typical analysis includes the time for draining the titration cell, the time for the analyte to react with the calibrated reagent solution, and the time to deliver the required volume of titrant, which depends on both the sample's concentration and the flow rates. The time for the sampling period should be kept constant, and large enough for draining the largest volume possible, since one may not know the titrant's volume consumed by the previous sample. During the titration, titrant is delivered quickly at first, and at a lower rate during the detection of end point. This is accomplished by comparing the measured absorbance with a set absorbance value (lower than the absorbance value corresponding to the equivalence point). Once the measured absorbance is larger than the set value, it is indicated that the equivalence point is approaching, slow down the titrant's delivering rate. The slower the titrant is delivered, the better the precision would be. Because the flow rates could be easily varied, the time for one determination varies, too. Here, to make a compromise between precision and sampling rate, 30 and 60 s are assigned for sampling and titration steps, respectively, whose sampling rate is 45 samples h^{-1}.

8. Sample analysis

Although the complex of nickel with EDTA is very stable, concentrated nickel can't be determined by direct titration since it will block most of the metal indicators (the nickel-indicator complex is more stable than the nickel-EDTA complex). In addition, sample dilution is necessary to reduce the influence of nickel ion's colour and NiY's colour on the endpoint determination in conventional titrimetric analysis. While this method is employed for the determination of nickel in the range of 10–70 g l^{-1}, the blocking to indicator is overcome by back titration; and the color's interference on endpoint detection is eliminated by dilution and the selection of a suitable wavelength far away from their absorption maxima. Several concentrated nickel sulphate solution samples from a metallurgical plant were determined by this method, whose results together with those obtained by manually performed back titration method with EDTA [17] are listed in Table 1. The results indicate that both the accuracy and precision in this method are quite good.

9. Conclusion

Automatic back titration method for microchemical analysis is achieved by injecting two accurately known small volumes of sample and a calibrated reagent solution, and the reagent consumption is thus, reduced. The excess of the

Table 1
The results of sample analysis (g l^{-1})

Sample No.	Manual titration	This method					Average	RSD
1	70.36	70.29	70.13	70.37	70.39	70.25	70.29	0.15%
2	45.09	45.03	44.91	45.10	45.11	44.97	45.02	0.19%
3	32.78	32.84	32.80	32.90	32.77	32.87	32.83	0.16%
4	13.48	13.52	13.47	13.49	13.54	13.55	13.51	0.24%

reagent after reaction with the analyte is then titrated by a titrant and the endpoint is determined photometrically. Although it is used for the complexometric determination of nickel, the method, in principle, could be employed for the determination of a wide variety of analytes by using different reagents and adjusting the volumes of two loops and the concentration of reagent solutions. Furthermore, if the small variations in the inner diameter of the titrant syringe could be adequately calibrated, high precision as good as 0.1%, or even higher, might be obtained. More related research work and its application to displacement titrations are in progress at our laboratory.

References

[1] J. Ruzicka and E.H. Hansen, Flow Injection Analysis, Wiley, New York, 1988, p. 56.
[2] J.M. Calatayud, P.C. Falco and R.M. Albert, Analyst, 112 (1987) 1063.
[3] A. Rios, M.D. Luque de Castro and M. Valcarcel, Talanta, 32 (1985) 845.
[4] M. Agudo, J. Marcos, A. Rios and M. Valcarcel, Anal. Chim. Acta, 239 (1990) 211.
[5] A. Rios and M. Valcarcel, Talanta, 38 (1991) 1359.
[6] J. Marcos, G. del Campo, A. Rios and M. Valcarcel, Fresenius' J. Anal. Chem., 342 (1992) 76.
[7] J. Marcos, A. Rios and M. Valcarcel, Anal. Chim. Acta, 261 (1992) 489.
[8] J. Marcos, A. Rios and M. Valcarcel, Anal. Chim. Acta, 261 (1992) 495.
[9] J. Marcos, A. Rios and M. Valcarcel, Analyst, 117 (1992) 1629.
[10] J. Marcos, A. Rios and M. Valcarcel, Anal. Chem., 62 (1990) 2237.
[11] J. Marcos, A. Rios and M. Valcarcel, Anal. Chim. Acta, 283 (1993) 429.
[12] I.L. Garcia, P. Vinas, N. Campillo and M.H. Cordoba, Anal. Chim. Acta, 308 (1995) 67.
[13] R. Chen, J. Ruzicka and G.D. Christian, Talanta, 41 (1994) 949.
[14] F. Sagara, T. Kobayashi, T. Tajima, H. Ijyuin, I. Yoshida, D. Ishii and K. Ueno, Anal. Chim. Acta, 261 (1992) 505.
[15] O. Astrom, Anal. Chim. Acta, 105 (1979) 67.
[16] B. Olsson, Anal. Chim. Acta, 209 (1988) 123.
[17] N. Ishibashi and T. Imato, Fresenius Z. Anal. Chem., 323 (1986) 244.
[18] A.M. Tan, W.P. Ma, Y.C. Xu, A.Z. Mao, J.L. Huang, J.H. Xu and X.N. Zhao, Fenxi Huaxue (Chin. J. Anal. Chem.), 22 (1994) 482.
[19] A.M. Tan, J.L. Huang, L.D. Geng, J.H. Xu and X.N. Zhao, J. Auto. Chem., 16 (1994) 71.
[20] J.L. Huang, H.H. Liu, A.M. Tan, J.H. Xu and X.N. Zhao, Talanta, 39 (1992) 589.
[21] S.Y. Shun, L.G. Ying, J.X. Ying and B. Fu, Handbook for the Analysis of Ores and Non-ferrous Metals, Metallurgical Industry Press, Beijing, 1990, pp. 68–71.
[22] D. Betteridge, W.C. Cheng, E.L. Daglass, P. David, T.B. Goad, D.R. Deans, D.A. Newton and T.B. Pierce, Analyst, 108 (1983) 1.

ELSEVIER

Talanta 44 (1997) 973–978

Talanta

Sol-gel based amperometric biosensor incorporating an osmium redox polymer as mediator for detection of L-lactate

Tae-Myung Park [a,b], Emmanuel I. Iwuoha [a], Malcolm R. Smyth [a,*], Rosemarie Freaney [c], Alan J. McShane [d]

[a] *BEST Centre, School of Chemical Sciences, Dubin City University, Dublin 9, Ireland*
[b] *Department of Environmental Engineering, Suncheon Technical Junior College, Suncheon 540-744, South Korea*
[c] *Department of Metabolic Medicine, St. Vincent's Hospital, Elm Park, Dublin 4, Ireland*
[d] *Department of Anaesthesia, St. Vincent's Hospital, Elm Park, Dublin 4, Ireland*

Received 22 August 1996; received in revised form 29 October 1996; accepted 6 November 1996

Abstract

A novel amperometric biosensor for the determination of lactate was constructed by first immobilizing lactate oxidase and an osmium redox polymer ($[Os(bpy)_2(PVP)_{10}Cl]Cl$; abbreviated Os-polymer) on the surface of a glassy carbon electrode, followed by coating with a sol-gel film derived from methyltriethoxysilane (MTEOS). The electrooxidation current of this electrode was found to be diffusion controlled. In the presence of lactate, a clear electrocatalytic oxidation wave was observed, and lactate could be determined amperometrically at 400 mV versus Ag/AgCl. The concentration range of linear response, slope of linear response and detection limit were 0.1–9 mM, 1.02 μA mM^{-1}, and 0.05 mM, respectively. Although L-ascorbate was electrooxidized at this potential, uric acid, paracetamol and glucose were found not to interfere. © 1997 Elsevier Science B.V.

Keywords: Amperometric biosensor; Lactate determination; Osmium polymer; Sol-gel

1. Introduction

Enzyme-based, amperometric biosensors have attracted much interest for clinical, environmental, agricultural, and biotechnological applications. An important area of biosensor research is the immobilization of enzymes at transducer surfaces. Conventional methods of enzyme immobilization include covalent binding, physical adsorption, encapsulation in polymers, or cross-linking to a suitable supporting matrix. Generally, supporting matrices are constructed of conductive and nonconductive polymers [1–3], conductive organic salts [4], and carbon-based composite materials [5–8], or layer of enzymes adsorbed onto electrode surfaces [9]. Recent research has demonstrated that silicate glasses obtained by the sol-gel method can provide such a supporting matrix and that biomolecules can be immobilized by this method [10–17]. These bioceramic materials have been further applied to produce silica-based photometric and FI detectors [18–22]. More recently, low temperature processing conditions, chemical inertness, negligible swelling effects, tunable

* Corresponding author.

PII S0039-9140(96)02164-9

porosity, thermal stability and the high purity of sol-gel-derived glasses make them ideal for many sensor applications [23,24]. The formation of sol-gel based sensors has been reviewed by Lev et al. [25]. Although most applications to date have been based on spectroscopic techniques, a few papers have emerged recently on the use of electroanalytical procedures. For instance, Narang et al. [26] have described a series of prototype tetraethylorthosilicate(TEOS)-derived sol-gel thin films for immobilization of glucose oxidase. Audebert et al. [27] have demonstrated the activity of glucose oxidase doped within a sol-gel-derived matrix(tetramethylorthosilicate; TMOS) using hydroxymethylferrocene as mediator. Glezer and Lev [28], however, prepared platinum electrodes with glucose oxidase entrapped within a vanadium pentaoxide gel and demonstrated the possibility of detection of glucose by cyclic voltammetry. Pankratov and Lev [29] have demonstrated the use of silica/carbon-based glucose sensor containing tetrathiafulvalene as mediator. In our previous study [30], we demonstrated the construction of a sol-gel based amperometric glucose biosensor incoporating an osmium redox polymer as mediator.

The rapid, accurate and selective assay of lactate is necessary in clinical and industrial food laboratories. Dempsey et al. [31] prepared a L-lactate biosensor immobilizing lactate oxidase in an *o*-phenylenediamine film. Mizutani et al. [32] prepared an amperometric enzyme electrode for lactate by immobilizing lactate oxidase in a polyion complex membrane. Spohn et al. [33] investigated the influence of different additives on the performance of a bienzyme carbon paste electrode for detection of lactate. Murr et al. [34] constructed an amperometric lactate biosensor by confining lactate oxidase and hydroxymethyl-ferrocene as mediator in a carbon paste electrode. Heller et al. [35] also demonstrated the use of a poly(1-vinylimidazole)-based lactate sensor containing $Os(4,4'\text{-dimethylbpy})_2Cl$ as a mediator. Zhang et al. [36] prepared an amperometric tetrathiafulvalene mediated reduced NADH sensor co-immobilizing lactate oxidase and lactate dehydrogenase on an Eastman-AQ-TTF-modified electrode. These methods result, however, in shorter linear response ranges than the method described in this paper.

This paper describes the feasibility of a sol-gel based amperometric L-lactate sensor based on lactate oxidase and an osmium redox polymer as mediator for the determination of L-lactate. We have investigated the electrochemical behaviour of this electrode and shown that L-lactate can be determined amperometrically with good analytical characteristics.

2. Experimental

2.1. Materials

The source of all chemicals used for experiments are given in parenthesis: methyltriethoxysilane (MTEOS, Aldrich), lactate oxidase (EC number, not assigned;from Pediococcus sp., 34 unit mg^{-1}, Sigma), L-lactic acid (Fluka), Glucose (Sigma), Uric acid (Aldrich), Paracetamol (BDH), L-ascorbic acid (Aldrich), Na_2HPO_4 and NaH_2PO_4 (BDH). All aqueous solutions were prepared in deionized water (Easypure RF, Branstead water purification system). The Os-polymer, $[Os(bpy)_2(PVP)_{10}Cl]Cl$, used as an electron transfer mediator, was prepared as described elsewhere [37].

2.2. Instrumentation

Cyclic voltammetry experiments and steady-state measurements were carried out using a BAS (W. Lafayette, USA) CV-100W voltammetric analyzer interfaced to an IBM-PC compatible computer. pH Measurements were performed using an RE 357 Microprocessor pH meter (EDT Instruments, UK).

2.3. Preparation of sol-gel derived electrode

The silica sol was prepared by mixing 4.5 ml of MTEOS, 1.6 ml of deionized water and 0.03 ml of 0.05 M HCl (which was used to catalyze the reaction) in a glass vial. After 3 h of mixing, a clear sol-gel solution resulted. The resulting molar ratio of MTEOS to water was 1:4. To prepare the

modified electrode, 3 μl of 1% Os polymer (in methanol) was coated on the surface of a glassy carbon electrode and dried at room temperature to evaporate off methanol, and then a 3 μl aliquot of LOD solution (680 units ml^{-1}; prepared in phosphate buffer, pH 6.8) was coated onto the surface of the modified electrode and allowed to air dry in a covered beaker. After 24 h a sol-gel layer was spin coated onto the surface.

2.4. Procedures

All measurements were carried out in a three-electrode system using a platinum wire and Ag/AgCl (sat'd KCl) as the auxiliary and reference electrode, respectively. All steady state measurement were performed at 400 mV versus Ag/AgCl in 0.1 M phosphate buffer, pH 6.8. Argon gas was passed through the cell to prohibit the competition of oxygen with the osmium redox centre [38]. The solution was stirred at 1000 rpm using a magnetic stirrer.

3. Results and discussion

3.1. Electrochemical behaviour of sol-gel derived electrode

Fig. 1 shows the typical voltammetric behaviour of a sol-gel based electrode containing LOD and Os-polymer as mediator in 0.1 M phosphate buffer, pH 6.8, at different scan rates. In the absence of lactate, the enzyme gives no response and only the Os-polymer electrochemistry is observed. Under the experimental conditions used in this study and over the range of potential scanned (− 100–550 mV) and range of potential scan rate ($v = 2$–200 mV s^{-1}), the dependence of peak current on the scan rate was investigated in order to identify the type of current. The current function ($i_p/v^{1/2}$) had a constant value at different scan rates. This means that the catalytic electrooxidation current of the sol-gel derived electrode is diffusion controlled current [39].

3.2. Bioelectrocatalytic oxidation of lactate

In the presence of L-lactate, a clear electrocatalytic oxidation wave was observed (Fig. 2). This means that lactate oxidase is reduced by the lactate penetrating the sol-gel film, electrons are transferred from the LOD-$FADH_2$ to the Os^{3+} site, Os^{3+} sites are reduced to Os^{2+}, followed by re-oxidation of this reduced form. The redox centre of LOD, i.e., FAD, is reduced by L-lactate as follows:

$$\text{LOD} - \text{FAD} + \text{L} - \text{lactate} + 2\text{H}^{+} \rightarrow \text{LOD} - \text{FADH}_2 + \text{pyruvate} \quad (1)$$

The Os^{3+} sites then oxidize the reduced LOD-$FADH_2$, regenerating LOD-FAD:

$$\text{LOD} - \text{FADH}_2 + 2\text{Os}^{3+} \rightarrow \text{LOD} - \text{FAD} + \text{Os}^{2+} + 2\text{H}^{+} \quad (2)$$

This is followed by the oxidation of reduced form of the mediator on the electrode surface:

$$2\text{Os}^{2+} \rightarrow 2\text{Os}^{3+} + 2\text{e} \quad (3)$$

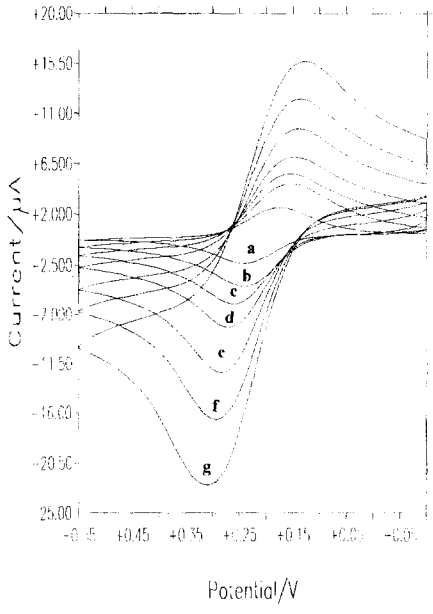

Fig. 1. Cyclic voltammograms of the sol-gel derived electrode in absence of lactate at various scan rate (mV s^{-1}) in 0.1 M phosphate buffer solution(pH 6.8): (a) 2, (b) 5, (c) 10, (d) 20, (e) 50, (f) 100, (g) 200.

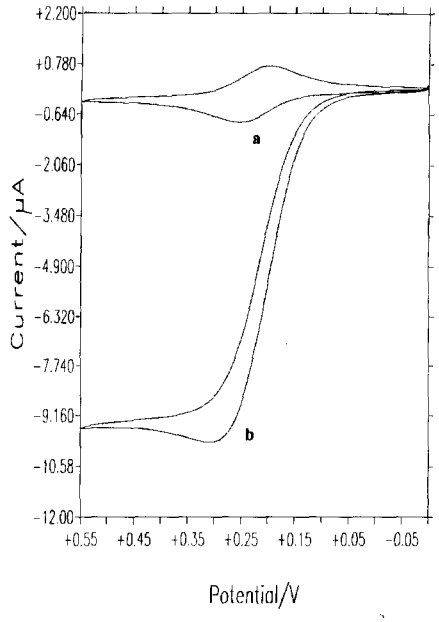

Fig. 2. Cyclic voltammograms of a sol-gel based lactate biosensor in 0.1 M phosphate buffer solution, pH 6.8: scan rate 2 mV s^{-1}, 1000 rpm, Ar; (a) no analyte, (b) 10 mM lactate.

The elimination of a reduction peak means that the reduced state of sol-gel film is maintained. Fig. 3 shows the potential dependence of the L-lactate electrocatalytic oxidation current at steady-state condition under argon. The L-lactate electrocatalytic oxidation current reached a plateau at 350 mV versus Ag/AgCl. In order to obtain constant and high electrocatalytic oxidation currents, the electrode potential was maintained at 400 mV versus Ag/AgCl for amperometric measurements.

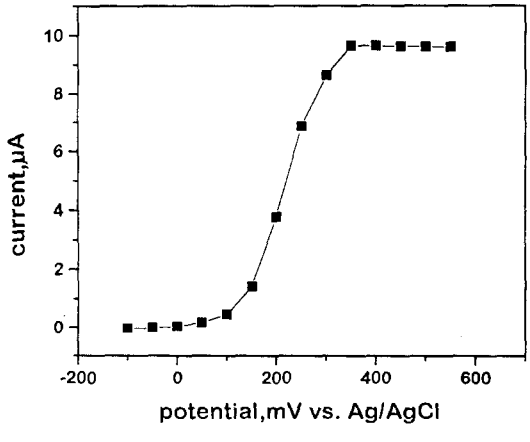

Fig. 3. Potential dependence of the steady-state current for the lactate electrode: 100 rpm, Ar, 10 mM lactate.

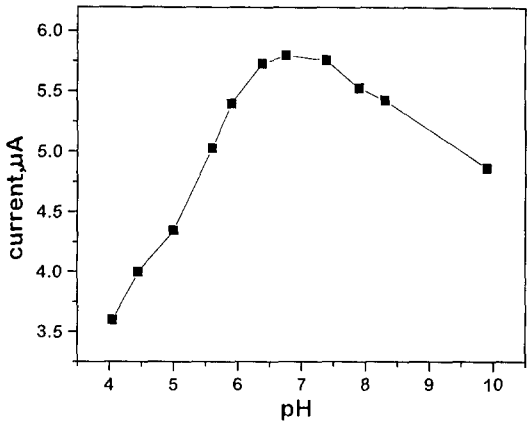

Fig. 4. Dependence of pH on electrocatalytic oxidation currents for a sol-gel based lactate electrode: 1000 rpm, Ar, 5 mM lactate.

3.3. pH studies

Fig. 4 shows the pH dependence of the catalytic current for the sol-gel based L-lactate electrode attained at a concentration of 5 mM lactate in 0.1 M phosphate buffer stirred at 1000 rpm under argon. The curves exhibit a plateau from pH 6.3 to 7.4. We selected a pH 6.8 for all further experiments in consideration of analytical sensitivity.

3.4. Steady-state current measurements

Fig. 5 shows the typical steady state current-time response of a sol-gel derived L-lactate biosensor. The electrode response time was about 10 s until steady state values were obtained. The fast response is attributed to the thin active film and short penetration depth of this electrode. The electrode response was found to be linear within the concentration range 0.1–9 mM with a correlation coefficient, $r = 0.9985$. The detection limit and slope of linear response were 0.05 mM and 1.02 μA mM^{-1} with 5.3% RSD, respectively. The

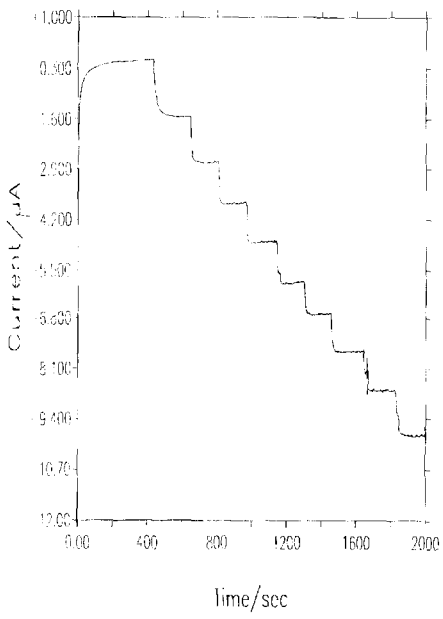

Fig. 5. Amperometric responses of a sol-gel based lactate biosensor on addition of lactate in 0.1 M phosphate buffer (pH 6.8): $E_{appl} = 400$ mV versus Ag/AgCl; 1000 rpm, Ar.

detection limit was calculated based on twice the value of the background currents. The short-term stability was shown to be within ± 5% RSD over a 1 week period.

3.5. Interferences studies

Interference effects were investigated by testing the response of the sol-gel derived electrode to L-ascorbic acid, paracetamol (4-acetamidophenol), uric acid, and glucose. As shown in Table 1 the presence of L-ascorbic acid greatly affects the response of the electrode, but uric acid, paracetamol and glucose did not interfere to any great extent. The use of an alternative mediator with a lower redox potential, a change in the composition of the sol-gel, or some form of prior separation, remains to be investigated to counteract this interference problem.

4. Conclusions

In this work we have demonstrated the feasibility of a novel sol-gel based amperometric L-lactate biosensor using an osmium redox polymer as mediator. Our results demonstrate that the electrocataytic oxidation current of a sol-gel film coated LOD/Os-polymer/glassy carbon electrode were diffusion controlled current. This electrode can be used as an amperometric lactate biosensor that provides a linear response and detection limit to lactate within the concentration range between 0.1 and 9 mM, and 0.05 mM, respectively. L-ascorbate was electrooxidized at this potential, but uric acid, paracetamol and glucose were found not to interfere. In previous studies [31–35], other authors obtained a smaller linear range than the sol-gel system described in this paper. This may be due to diffusional constraints caused by a lower permeability in the sol-gel layer described in this paper. The use of sol-gel immobilization may be useful for situations in which there are high lactate concentrations, e.g., in critical care monitoring. It may also prove to be a more robust method of immobilization compared with polymer-modified electrodes.

Table 1
Response of the sol-gel-based amperometric sensor to interferents

Interferents	5 mM lactate (μA)	Interferent + 5 mM lactate (μA)	% Diff.
1 mM acetaminophen	5.820	5.820	0
1 mM uric acid	5.813	5.813	0
0.1 mM ascorbic acid	5.823	5.963	2.4
1 mM ascorbic acid	5.823	7.395	23.7
1 mM glucose	5.820	5.821	0

Acknowledgements

The authors wish to acknowledge partial funding for this research from the Department of Anaesthesia, St. Vincent's Hospital. We also thank Dr Brian MacCraith for valuable discussions.

References

[1] N.C. Foulds and C.R. Lowe, Anal. Chem., 60 (1988) 2473.
[2] P.N. Bartelett and R.G. Whitaker, J. Electroanal. Chem., 224 (1987) 37.
[3] C. Malitesta, F. Palmisano, L. Torsi and P.G. Zambonin, Anal. Chem., 62 (1990) 24.
[4] J.L. Kawagoe, D.E. Niehaus and R.M. Wightman, Anal. Chem., 63 (1991) 2961.
[5] J.E. Frew, M.A. Harmer, H.A.O. Hill and S.I. Libor, J. Electroanal. Chem., 201 (1986) 1.
[6] L. Chen, M.S. Lin, M. Hara and G.A. Rechnitz, Anal. Lett., 24 (1991) 1.
[7] P.D. Hale, T. Inagaki, H.S. Lee, H.I. Karan, Y. Okamoto and T.A. Skotheim, Anal. Chim. Acta, 228 (1990) 31.
[8] S.A. Wring and J.P. Hart, Analyst, 117 (1992) 1215.
[9] W. Schuhmann, T.J. Ohara, H.L. Schmidt and A. Heller, J. Am. Chem. Soc., 63 (1991) 677.
[10] D. Avnir, D. Levy and R. Reisfeld, J. Phys. Chem., 88 (1984) 5956.
[11] S. Braun, S. Rappoport, R. Zusman, D. Avnir and M. Ottolenghi, Mater. Lett., 10 (1990) 1.
[12] I. Kuselman, B.I. Kuyavskaya and O. Lev, Anal. Chim. Acta, 256 (1992) 65.
[13] A. Schwok, D. Avnir and M. Ottolenghi, J. Am. Chem. Soc., 113 (1991) 3984.
[14] J. Gun, M. Tsionsky and O. Lev, Mat. Res. Soc. Symp. Proc., 346 (1994) 1011.
[15] J. Gun, M. Tsionsky, Y. Golan, I. Rubinson and O. Lev, J. Electroanal. Chem., 395 (1995) 57.
[16] J. Gun, M. Tsionsky and O. Lev, Anal. Chim. Acta, 294 (1994) 261.
[17] S. Barreau and J.M. Miller, Anal. Commun., 33 (1996) 5H.
[18] L.M. Ellerby, C.R. Nishida, F. Nishida, S.A. Yamanaka, B. Dunn, J.S. Valentine and J.I. Zink, Science, 255 (1992) 1113.
[19] D.D. Dunuwila, B.A. Torgerson, C.K. Chang and K.A. Berglund, Anal. Chem., 66 (1994) 2739.
[20] A. Schwok, M. Ottolenghi and D. Avnir, Nature 355 (1992) 240.
[21] J.E. Lee and S.S. Saavedra, Anal. Chim. Acta, 285 (1994) 265.
[22] Y. Tatsu, K. Yamashita, M. Yamaguchi, S. Yamamura, H. Yamamoto and S. Yoshikawa, Chem. Lett., (1992) 1619.
[23] B.D. MacCraith, C. McDonagh, G. O'Keeffe, A.K. McEvoy, T. Butler and B.D. Sheridan, Sens. Actuators, B29 (1995) 51.
[24] A.K. McEvoy, C.M. McDonagh and B.B. MacCraith, Analyst, 121 (1996) 785.
[25] O. Lev, M. Tsionsky, L. Rabinovich, V. Glezer, S. Sampath, I. Pankratov and J. Gun, Anal. Chem., 67 (1995) 22A.
[26] U. Narang, P.N. Prasad, F.V. Bright, K. Ramanathan, N.D. Kumar, B.D. Malhotra, M.N. Kamalasanan and S. Chandra, Anal. Chem., 66 (1994) 3139.
[27] P. Audebert, C. Demaille and C. Sanchez, Chem. Mater., 5 (1993) 911.
[28] V. Glezer and O. Lev, J. Am. Chem. Soc., 115 (1993) 2533.
[29] I. Pankratov and O. Lev, J. Electroanal. Chem., 393 (1995) 35.
[30] T.M. Park, E.I. Iwuoha, M.R. Smyth and B.D. MacCraith, Anal. Commun., 33 (1996) 271.
[31] E. Dempsey, J. Wang and M.R. Smyth, Talanta, 40 (1993) 445.
[32] F. Mizutani, S. Yabuki and Y. Hirata, Anal. Chim. Acta, 314 (1995) 233.
[33] U. Sphon, D. Narasaiah and L. Gorton, Electroanalysis, 8 (1996) 507.
[34] M. Boujtita, M. Chapleau and N.E. Murr, Electroanalysis, 8 (1996) 485.
[35] T.J. Ohara, R. Rajagopalan and A. Heller, Anal. Chem., 66 (1994) 2451.
[36] X. Zhang, H. Liu, X. Wu, D. Qi, Z. Zhang, M. Dai, J. Deng and F. Feng, Anal. Comm., 33 (1996) 111.
[37] R.J. Forster and J.G. Vos, Macromolecules, 59 (1990) 4372.
[38] B.A. Gregg and A. Heller, Anal. Chem., 62 (1990) 258.
[39] R.S. Nicholson and I. Shain, Anal. Chem., 36 (1964) 706.

ELSEVIER

Talanta 44 (1997) 979–983

Talanta

Flotation-spectrophotometric determination of trace of germanium with isochromatic dye ion-pairs formed by rhodamine 6G and tetrabromofluorescein

Zhao Xingru [a,*], Liang Shuxuan [b], Zuo Bencheng [b]

[a] *Department of Medico-chemistry, Hebei Medical College for Continuing Education, Baoding, 071000, People's Republic of China*
[b] *Hebei University, Baoding, 071002, People's Republic of China*

Received 31 July 1996; received in revised form 4 November 1996; accepted 5 November 1996

Abstract

A flotation spectrophotometric method for the determination of germanium with isochromatic dye ion-pairs is described. The molar ratio of germanium to rhodamine 6G to tetrabromofluorescein is 1:5:5. The apparent molar absorptivity is 5.8×10^5 l mol^{-1} cm^{-1} at 531 nm. Beer's law is obeyed over the concentration range of 5.0×10^{-8}–1.25×10^{-6} mol l^{-1}. The proposed method is sensitive and accuracy and can be applied satisfactorily to the determination of germanium in vegetables. © 1997 Elsevier Science B.V.

Keywords: Flotation-spectrophotometric; Germanium; Isochromatic dye

1. Introduction

Phenylfluorone [1–8] and its replacement [9–16] are commonly used as sensitive spectrophotometric reagents for determining germanium and their molar absorptivities do not in general exceed 1.8×10^5. High sensitivity characterizes methods based on the formation of sparingly water-soluble compounds of molybdogermanic acid with xanthene dye (e.g., Rhodamine B, Rhodamine 6G) [17,18]. These compounds can be dissolved in enthanol or acetone after flotation with toluene or butyl acetate [18,19]. Some other methods for the extractive-spectrophotometric and flotation-spectrophotometric determination of germanium are described in the literature [20–22], but the sensitivities of these methods are lower than this paper's.

In this paper, the flotation-spectrophotometric determination of germanium with isochromatic dye ion-pairs is studied. The isochromatric dye was formed by R6G($C_{26}H_{27}ClN_2O_3$) with TBF($C_{20}H_6Br_4Na_2O_5$) at acetate buffer (pH 5.5). TBF is similar in colour to R6G and they associated with the molar ratio TBF: R6G = 1:1 at pH 5.5. During the determination process, R6G formed a ternary complex with germanoalizarincomplexone first. The molar ratio of germanium to alizarincomplexone (AC) to R6G was 1:3:5 [23], and its absorptivity was 2.9×10^5. Then de-

* Corresponding author.

PII S0039-9140(96)02167-4

composed the ternary complex with NaOH, added TBF to the aqueous solution, the isochromatric dye ion-pairs of TBF with R6G was floated with toluene again, added acetate to dissolve the flotation. Owing to the isochromatic effect of ion-pairs, the sensitivity for the determination of germanium was enhanced and the molar absorptivity is achieved 5.8×10^5 at 531 nm. The proposed method has been applied to the determination of germanium in vegetables with good precision and accuracy.

2. Experiment

2.1. Apparatus

The absorbance was measured with a Model UV-265 spectrophotometer (Shimadzu Corporation, Kyoto, Japan). The pH measurements were made with a Model pHS-3C pH meter (Shanghai Leici Instrument Factory).

2.2. Reagents

All solutions were prepared with analytical reagent and deionized water. Standard solution, containing 1.00 mg ml^{-1} germanium, was prepared by dissolving 0.1000 g of Ge powder in 5.0 ml of 1 mol l^{-1} NaOH, acidified the solution with hydrochloric acid, and diluted to the mark in a 100 ml volumetric flask with water.

Acetate buffer solution, pH 5.5, was prepared by mixing 1 mol l^{-1} acetic acid and 1 mol l^{-1} sodium acetate solution. The pH was ultimately adjusted using a pH meter.

Tetrabromofluorescein (TBF) solution, 1.0×10^{-2} mol l^{-1}, was prepared by dissolving 1.7298 g of TBF in 500 ml of water.

Rhodamine 6G (R6G) solution, 1.0×10^{-3} mol l^{-1}, was prepared by dissolving 0.2935 of R6G in 500 ml of water.

Alizarine complexone (AC) solution, 0.0015 mol l^{-1}, was prepared by dissolving 0.1445 g of the reagent in 50 ml of water containing 0.5 ml of concentrated ammonia. Added 0.5 ml of glacial acetic acid, and diluted with water to exactly 250 ml.

2.3. Procedure for the determination of Ge

The solution containing not more than 1.5 μg of Ge, 3.0 ml of 1.0×10^{-4} mol l^{-1} AC solution, 5.0 ml of 1.0×10^{-4} mol l^{-1} R6G and 1 ml of pH 5.5 acetate buffer were added to a 30 ml separating funnel. The solution was shaken for about 30 min in a mechanical shaker with 5 ml toluene. Discarded the aqueous phase. Washed the flotation three times with 10 ml of 0.1 mol l^{-1} NaCl. Added 0.1 mol l^{-1} NaOH to the flotation, the ternary complex (the molar ratio Ge:AC:R6G = 1:3:5) [23] was then decomposed. Acidified the solution with 0.05 mol l^{-1} H_2SO_4. Added successively 3.0 ml of 1.0×10^{-4} mol l^{-1} TBF, 2.0 ml of pH 5.5 acetate buffer. Shook the solution for 3 min. The flotation of TBF with R6G was adhered on the wall of the separating funnel, discarded the solution, washed the flotation three times with 10 ml of 0.1 mol l^{-1} NaCl and the flotation was dissolved in 10 ml of acetone. The absorbance was measured at 531 nm in a 1.0 cm cell against reagent blank.

3. Results and discussion

3.1. Spectral characteristics

The absorption spectra of 1.0×10^{-5} mol l^{-1} TBF solution, of 1.0×10^{-5} mol l^{-1} R6G solution and of the 1.0×10^{-5} mol l^{-1} acetone solution of the isochromatic dye ion-pairs of TBF with R6G (the molar ratio of TBF to R6G was 1:1) are shown in Fig. 1.

All results showed that TBF and R6G were similar in colour in acetone and the sensitivity was enhanced by the use of isochromatic ion-pairs of TBF with R6G at 531 nm.

3.2. Select of organic solvents

The ion associate of germanoalizarincomplexone acid with R6G is insoluble in water. It cannot be extracted into polar or non-polar organic solvents, but it can be floated [23].

The isochromatic dye ion-pairs of TBF with R6G was floated with toluene at pH 5.5 acetate

buffer. Consequently, toluene was chosen as the optimum flotation agent.

3.3. Effect of pH

It was reported in literature [24] that the optimum pH range of the ternary complex was from 5 to 6. The range of pH was controlled in 3–11 with the acetate buffer and NaOH. A study of the complexation of TBF with R6G at different pH values showed that the isochromatic dye ion-pairs had a higher absorbance at the pH 5.5 (see Fig. 2). Consequently, a pH of 5.5 acetate buffer was chosen as the optimum for this work.

3.4. Effect of developer concentration

Fig. 3 shows the effect of TBF concentration. 2.5–4.0 ml of 1.0×10^{-4} mol l^{-1} TBF solution gave a maximum and constant absorbance with 5.0×10^{-7} mol l^{-1} of Ge, so that 3.0 ml of 1.0×10^{-4} mol l^{-1} TBF was used in the determinations. AC and R6G concentration were not less than 60 and 100 times of Ge concentration.

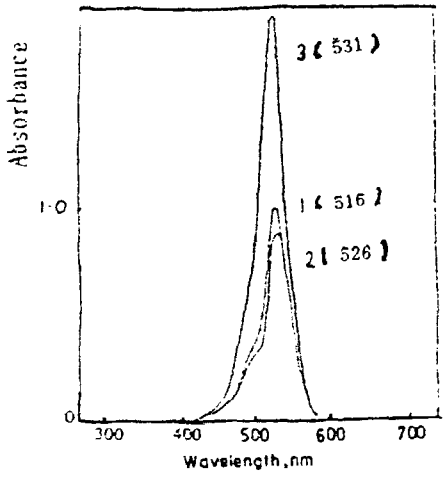

Fig. 1. Absorption spectra of TBF, R6G and TBF·R6G. (1) 1.0×10^{-5} mol l^{-1} TBF solution measured against water, (2) 1.0×10^{-5} mol l^{-1} R6G solution measured against water, (3) 1.0×10^{-5} mol l^{-1} TBF:R6G acetone solution against reagent blank.

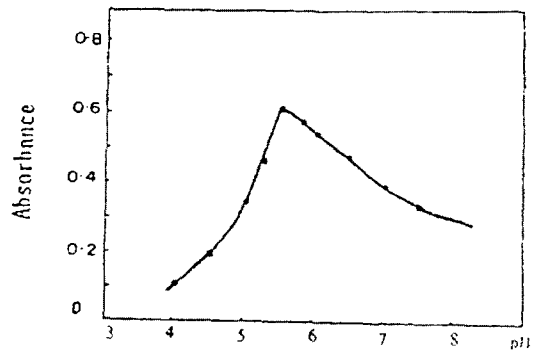

Fig. 2. Effect of pH on the isochromatic dye ion-pairs of TBF with R6G. R6G: 3.0×10^{-5} mol l^{-1}, TBF: 5.0×10^{-5} mol l^{-1}. Absorbance measured at 531 nm against corresponding reagent blank.

3.5. Composition of the ion-pairs

The composition of the complex were investigated by the continuous variations and equilibrium shifting methods. Both the molar ratio of TBF to R6G and R6G to AC were found to be 1:1.

3.6. Stability of the ion-pairs TBF·R6G and AC·R6G

Ksp was regarded as an association capacity of the complex [24]. It was found that Ksp of TBF·R6G and AC·R6G were 5.9×10^{-12} and 1.88×10^{-11}, respectively. The results showed

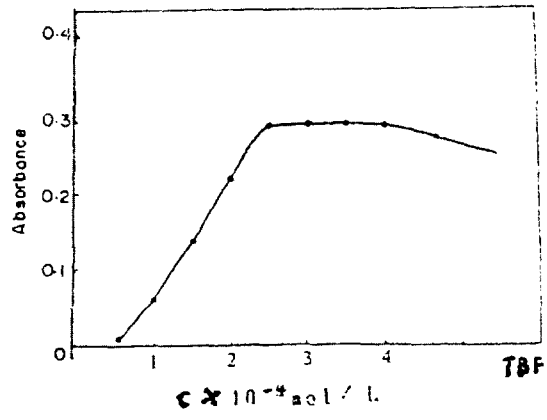

Fig. 3. Effect of reagent concentration. Germanium: 5.0×10^{-7} mol l^{-1}.

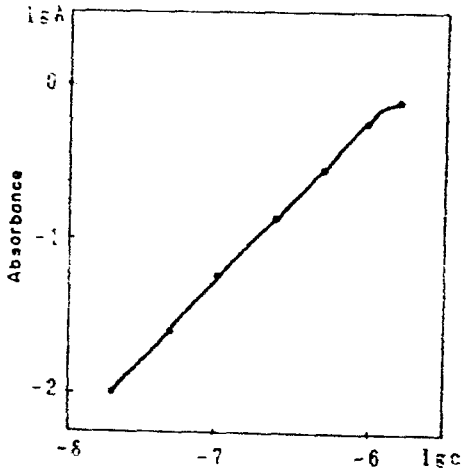

Fig. 4. Analytical curves of germanium.

that TBF associated extremely R6G of the ternary complex.

3.7. Analytical curves and sensitivity of the method

According to the recommended procedure outlined above, analytical curves were prepared by taking the appropriate amount of the standard germanium solution. During the flotation process, the TBF of adsorption on the precipitate was washed with 0.1 mol l^{-1} NaCl. Thus, good linearity was obtained at concentration of germanium between 5.0×10^{-8}–1.25×10^{-6} mol l^{-1} (Fig. 4). From this straight line the apparent molar absorptivity coefficient was 5.8×10^5 l mol^{-1} cm^{-1} at 531 nm.

3.8. Determination of germanium in samples

The contents of Ge in vegetables were determined. Washed thoroughly the vegetables with water, then with distilled water. Powered the vegetables after 24 h in oven at temperature 50°C. Samples (0.5000 g) were placed in pressure vessels, added 4 ml of HNO_3. The vessels were then sealed and kept at 120°C for 3 h. After cooling the vessels were opened. Ultimately the solution transferred into a 25 ml calibrated flask, diluted to the mark with deionized water. Then extractive separation of Ge, added sufficient concentrated hydrochloric acid to the sample solution to give a final acid concentration of at least 9.0 mol l^{-1}. Shook the acidic solution for 2 min in a separating funnel with two portions of CCl_4, and washed the combined organic extracts with 9.0 mol l^{-1} HCl. Stripped the Ge by shaking the CCl_4 solution with 10.0 ml of water followed by 5.0 ml of water containing 1 drop of 1 mol l^{-1} NaOH (shaking for 1 min) and determined by the proposed method. The results are given in Table 1.

3.9. Effect of diverse ions

The literature [24] had investigated the effects of 0.16 mol l^{-1} SO_4^{2-}, F^-, Cl^-, CH_3COO^-, Br^-, I^-, ClO_4^-, NO_3^- on the flotation under the optimum pH. SO_4^{2-}, F^- did not interfere in the absorbance of the complex. Cl^-, Br^-, NO_3^- decreased strongly the flotation, and I^-, ClO_4^- interfered seriously in the flotation. The diverse ions were not obtained in the following work.

Table 1
Determination of Ge in samples

Sample	By AAS method μg g^{-1} dry weight	By the present method μg g^{-1} dry weight	S.D.%	Number of determinations
Cabbage	0.2922	0.2915	4.2	5
Chives	0.2842	0.2850	4.4	5

References

[1] W.A. Schneider Jr. and E.B. Sandell, Mikrochim. Acta (1954) 263.
[2] C.L. Luke and M.E. Campbell, Anal. Chem., 28 (1956) 1273.
[3] P.V. Dhond and S.M. Khopkar, Anal. Chim. Acta, 59 (1972) 161.
[4] W.J. Frederick, J.A. White and H.E. Biber, Anal. Chem., 26 (1954) 1328.
[5] J. Gilles, J. Hoste and A. Claeys, Anal. Chim. Acta, 1 (1947) 302.
[6] F.G. Zharovskil and A.T. Pilipenko, Zavodsk. Lab., 24 (1958) 1192.
[7] J.D. Burton and J.P. Riley, Mikrochim. Acta (1959) 586.
[8] V.A. Oshman and V.M. Volkov, Zavodsk Lab., 27 (1961) 1341.
[9] C.A. Yao, G.H. Xu et al., Fenxi Huaxue, 19 (1991) 545.
[10] F.P. Wang, A.X. Hou et al., Fenxi Huaxue, 19 (1991) 577.
[11] M.Y. Xu, H.S. Zhang et al., Huaxue Shiji, 14 (1992) 46.
[12] J.Y. Zhung, D.J. Wang et al., Lihua Jianyan (Chem. Sect.), 19 (1983) 11.
[13] L.A. Egorova, Avramenko Sov. J. Water Chem. Technol., 136 (1991) 70.
[14] K. Kania, Chem. Anal. (Warsaw), 36 (5–6) (1991) 911.
[15] L.X. Bian, R.P. Chen et al., Lihua Jianyan (Chem. Sec.), 28 (1992) 93.
[16] X.A. Cao, X.P. Li et al., Lihua Jianyan (Chem. Sec.), 28 (1992) 28.
[17] Gr. Popa and I. Paralescu, Talanta, 16 (1969) 315.
[18] L.I. Ganago and I.A. Prostak, Izv. Vyssh. Ucheb. Zaved., Khim. Khim. Tekhnol., 14 (1971) 1165.
[19] L.I. Ganago and I.A. Prostak, Zh. Analit. Khim., 26 (1971) 104.
[20] C. Schlcich, G. Henze, Frescnius, J. Anal. Chem., 388 (1991) 140.
[21] A.K. Charykov, E.A. Alcksandrova et al., Ж. аНек ХИМ, 44 (1989) 1918.
[22] L.I. Gango, I. Vanova, IF, Zh. Anal. Khim., 47 (1992) 543.
[23] G.V. Flyantikova, L.I. Korolenko, L.I. Vinarova and T.N. Chekirda, Zh., Analit. Khim., 32 (1977) 1028.
[24] B.C. Buo, G.R. Chen et al., Fenxi Huaxue, 12 (1984) 1014.

ELSEVIER

Talanta 44 (1997) 985–1001

Talanta

Analysis of polyaromatic quinones in a complex environmental matrix using gas chromatography ion trap tandem mass spectrometry

Andrew A. Mosi [a], Kenneth J. Reimer [b], Guenter K. Eigendorf [a,*]

[a] *Chemistry Department, University of British Columbia, 2036 Main Mall, Vancouver, British Columbia, V6T 1Z1, Canada*
[b] *Environmental Sciences Group, Royal Military College, Kingston, Ontario, K7K 5L0, Canada*

Received 17 July 1996; received in revised form 5 November 1996; accepted 13 November 1996

Abstract

GC/MS and GC/MS/MS in a quadrupole ion trap were used to analyze for anthraquinone, alkyl anthraquinones, benz[a]anthracene-7,12-dione and 9-fluoranone in a sediment obtained from an aluminum smelter settling pond contaminated with polycyclic aromatic hydrocarbons. By standard GC/MS analysis many of these target compounds were either undetectable or their confirmation uncertain because of matrix interferences. Detection and identification were greatly improved by using GC/MS/MS. GC/MS/MS analyses were performed by selecting the molecular ion (M) of a target compound and fragmenting it via collision induced dissociation (CID) to yield product ions corresponding to loss of CO for unsubstituted compounds or CO plus CH_3 for alkylated compounds. The CID conditions were optimized using anthraquinone and 2-methylanthraquinone standards by varying the CID excitation energy and RF storage levels to yield optimum amounts of fragment ions. CID experiments were performed using both resonant and non-resonant wave forms. Although both excitation techniques gave comparable results for the removal of matrix interferences, non-resonant excitation provided more characteristic spectra for the alkylated anthraquinones. Monitoring of secondary fragmentation products, such as M-2CO, provided greater discrimination from matrix interferences than the use of primary fragmentation products, such as M-CO. © 1997 Elsevier Science B.V.

Keywords: Collision induced dissociation; Environmental analysis; Gas chromatography; Ion trap; Polycyclic aromatic hydrocarbons; Polyaromatic quinones; Tandem mass spectrometry

1. Introduction

Polycyclic aromatic hydrocarbons (PAHs) constitute a class of environmental contaminants that are produced in large amounts through incomplete combustion processes, pyrolysis, and via dispersion of petroleum products [1]. Because many PAHs are potent mutagens or carcinogens [2] numerous analytical techniques have been developed for determining their concentrations in environmental samples. However, toxicity of PAH contaminants is not exclusively dependent on the parent compounds. Air particulates contaminated with PAHs have been found to be more carcino-

* Corresponding author. Fax: + 1 604 8222847.

PII S0039-9140(96)02172-8

genic than can be accounted for by their PAH content alone [3]. This increased toxicity is potentially attributable to PAH oxidation products such as polyaromatic quinones [4,5]. For example, quinones of the non-mutagenic PAH pyrene, as well as some polyaromatic ketones (PAKs) of benzofluorenes and 7H-benz[d,e]anthracene have been found to be mutagenic [5,6].

Because the toxicological and environmental effects of a PAH can be significantly altered following a chemical transformation, such as oxidation, a full accounting of the impact of PAHs should also include their transformation products. However, since PAHs are often associated with complex matrixes, such as soils or sediments, the detection and quantification of trace level transformation products is often a difficult task, usually requiring extensive fractionation by liquid chromatography [7]. This in turn will generally lead to loss of analyte. In order to be able to routinely screen for trace level PAH transformation products together with their precursors, new methods which do not require extensive sample manipulation need to be developed. Such methods could involve simple extractions with minimal solvent workup followed by a rapid chromatographic step to remove highly polar impurities if gas chromatography is to be used.

Capillary GC/MS is usually the analytical technique of choice when analyzing complex mixtures of PAHs, as it combines efficient chromatographic separation with mass spectral information. Selectivity and sensitivity can be achieved by software extraction of the molecular or fragment ion chromatograms for a particular analyte, as long as coeluting matrix compounds do not interfere at the specific m/z values of the analyte. However, when analyzing for trace level substances, such as the transformation products of PAHs, their molecular or characteristic fragment ions are often obscured throughout the ion chromatogram by abundant matrix ions. Standards will generally not be available for many transformation products thus, a confirmatory spectrum has to be obtained, a difficult task when other coeluting interferences are present. To differentiate analytes obscured by coeluting interferences a GC tandem mass spectrometry method (GC/MS/MS) is required. In the first step molecular ions of the appropriate m/z value can be preselected, eliminating interfering ions with m/z values different from the analyte. The preselected molecular ions can then be fragmented via CID leading to characteristic fragments. If coeluting interferences of the same preselected m/z are also present they will likely lead to different fragment ions. Consequently, identification and quantitation of the target analyte can be performed using its characteristic CID product ions.

Although GC/MS/MS can be performed using multi sector [8,9] or triple quadrupole instruments, [10,11] the use of an ion trap affords better sensitivity since it eliminates losses of ions during transfer between different analyzers [12]. The recent availability of reliable commercial GC Ion Trap MS (GC/ITMS) systems has enabled GC/MS/MS experiments to be readily performed at pg–fg levels [13,14].

Besides improved sensitivity other advantages of an ion trap include the possibility of performing analyses in the field because of the compact nature of the instrument and significantly lower instrument cost when compared with other mass spectrometer systems [15].

The present work demonstrates a relatively simple yet powerful technique for the analysis of trace level PAH oxidation products in a complex matrix by performing GC/MS/MS in an ion trap. The ion trap used in this study has two modes of CID excitation, resonant excitation (RCID) and non-resonant excitation (NRCID). Resonant excitation involves the application of a high frequency RF potential to the end-caps, corresponding to the oscillation frequency of the selected ion. Non resonant excitation uses a low frequency dipole square wave which causes simultaneous excitation of all ions in the trap. The amount of energy imparted onto the excited ion will depend upon the amplitude of the CID waveform, its duration, the RF storage level and the nature and pressure of the collision gas. In our work the He mobile phase from the GC served as the collision gas. The CID amplitude and the RF storage level were the two parameters optimized to yield the maximum amount of the required fragment ions.

It is important to note CID in an ion trap leads to the formation of products via the lowest energy dissociation pathways, [16] resulting in non-standard MS/MS spectra, as compared with the higher energy CID MS/MS spectra obtained in triple quadrupole or multi sector instruments. Thus, the MS/MS spectra from ion trap experiments will not necessarily be identical to published reference electron ionization (EI) mass spectra, and the extent of fragmentation will depend upon the CID conditions. Nevertheless, all major fragments present in EI spectra should be observed under varying CID conditions.

Anthraquinone (AQ) and 2-methylanthraquinone (2-MeAQ) were selected as the target compounds for optimization of the CID method. These compounds can arise from the oxidation of anthracene, [17] and 2-methylanthracene respectively, substances that are present in high concentration in the contaminated sediment extract investigated here [18]. AQ yields two major fragment ions, m/z 180 and 152, corresponding to two successive losses of CO. In addition 2-MeAQ shows loss of a methyl radical.

By using the optimized resonant and non-resonant CID conditions established for AQ, and 2-MeAQ an extract from a contaminated sediment obtained from an aluminum smelter settling pond was analyzed for AQ, methyl AQs, C_2-AQs (dimethyl or ethyl) and C_3-AQs.

This work is part of an extensive investigation into the environmental effects of the large scale generation of PAHs in an aluminum smelter on the west coast of Canada and their disposal into the environment.

2. Experimental

2.1. Reagents

Anthraquinone, 2-methylanthraquinone, 9-fluoranone, and benz[a]anthracene-7,12-dione were obtained from Aldrich (Milwaukee, WI, USA). The internal standard D_{10}-anthracene was obtained from CIL (Woburn, MA, USA). All solvents used were of HPLC grade (Fisher Scientific, Nepean, ON, Canada).

2.2. Instrumentation

All experiments were performed on a Saturn 4D GC/MS/MS system (Varian, Walnut Creek, CA, USA) equipped with a Wave-Board for the generation of user-defined wave forms applied to the ion-trap electrodes. The software used for general operation of the instrument was the Saturn version 5.2. The 'Toolkit' version 1.0 software was used for performing sequential MS/MS experiments during the optimization procedure.

2.3. Analytical procedures

2.3.1. Sample preparation and quantitation

The contaminated sediment was obtained from a settling pond at the Alcan aluminum smelter in Kitimat, British Columbia, Canada, as described elsewhere [18]. The sediment was freeze dried and a 5 g sample was spiked with 4.5 μg of D_{10}-anthracene and extracted for 15 min with 40 ml of dichloromethane and acetone (5:1) using an Accelerated Solvent Extraction System (Dionex, Sunnyvale, CA, USA) operated at 125°C and 2000 psi. A 1 ml aliquot, containing 10 mg of crude extract, was placed on a column containing 5 g of silica and flushed with acetone to collect all the non polar (aliphatics, PAHs) and semi polar compounds (heteroaromatics). This acetone extract was used to perform all the analyses discussed in this paper.

Although partial fractionation of the aliphatic, PAHs and heteroaromatics can be performed using a gradient elution starting with hexane, no fractionation was attempted in this work in order to determine the viability of performing analyses on a single complex extract. The amounts of anthracene, anthraquinone, 2-methylanthracene and 2-methylanthraquinone in the sediment extract were determined by using the D_{10}-anthracene internal standard and appropriate relative response factors obtained by analyzing a mixture containing these four compounds together with D_{10}-anthracene under non-resonant CID conditions. Calibration curves were obtained for AQ, anthracene and D_{10}-anthracene to determine the dynamic range of the method. A series of control samples of uncontaminated sediment (as deter-

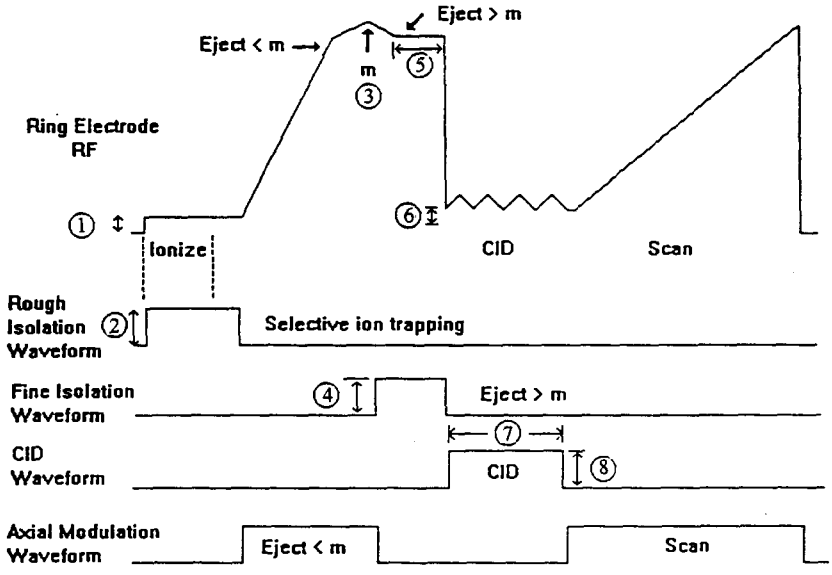

① Ionization low mass cutoff: 48 m/z

② Ejection amplitude: 20 volts

③ Parent ion selection: m/z 208 (AQ), 222 (Me-AQ), 236 (C_2-AQ)

④ Broadband amplitude: 30 volts

⑤ Dwell time prior to CID: 5 msec

⑥ CID Storage RF (SRF) low mass cutoff: 80 m/z

⑦ CID Time: 20 msec

⑧ CID Supplemental RF:

- Non-Resonant: 60 volts (AQ, Me-AQ and C_2-AQ)
- Resonant: 1.1 volts (AQ), 1.5 volts (Me-AQ and C_2-AQ)

Fig. 1. Ion trap MS/MS mass isolation and CID scan function.

mined by prior analysis) spiked with 20 μg of anthracene or AQ were also extracted to determine the extraction efficiency of AQ and to monitor for any oxidation of anthracene to AQ during the extraction or cleanup processes.

2.3.2. Gas chromatography

Samples were introduced via splitless injection of 1–2 μl of solution, at an injector temperature of 290°C, onto a DB5 capillary column (J&W, Folsom, CA, USA), 30 m × 0.25 mm I.D., 0.25 μm film thickness. The end of the column was inserted directly into the ion trap via a transfer line. The latter was held at 280°C and the ion trap temperature at 250°C. The GC column was held at 90°C for 0.1 min followed by a 6°C min^{-1} ramp to 280°C, holding at 280°C for 1 min and then ramping to 300°C at 20°C min^{-1} and holding for 20 min. Helium carrier gas (99.996% purity, Linde, ON, Canada) coupled to a carrier gas purifier (Supelco, ON, Canada) was adjusted to give a linear velocity of 32 cm s^{-1}, corresponding to a flow of approximately 1 ml min^{-1} into the ion trap.

2.3.3. Ion trap

Details on the operation of the trapping and scan functions for the Saturn ion trap have been described elsewhere [13,14]. All experi-

ments were performed under automatic gain control (AGC) with a target value of 30 000 for GC/MS and 10 000 for GC/MS/MS. The filament emission current was 40 μAmps and the multiplier voltage was set to give a gain of 10^5. The RF was ramped to produce a scan rate of 5600 amu s^{-1} over a mass range of 100–300 m/z. The MS/MS parameters used are indicated in Fig. 1. For all these experiments the storage RF (SRF) was maintained to store ions above m/z 80.

For the AQ and 2-MeAQ CID experiment the optimum excitation voltage yielding maximum production of fragment ions was determined by a series of multistep experiments in which the CID voltage (resonant or non-resonant) was increased in ten sequential steps. With a scan rate of 0.2 s per step a ten step experiment took 2 s allowing five experiments to be performed during the 10 s wide chromatographic band containing 50 ng of compound. The data obtained for each ion of interest were normalized as a percent of the total ion current (TIC).

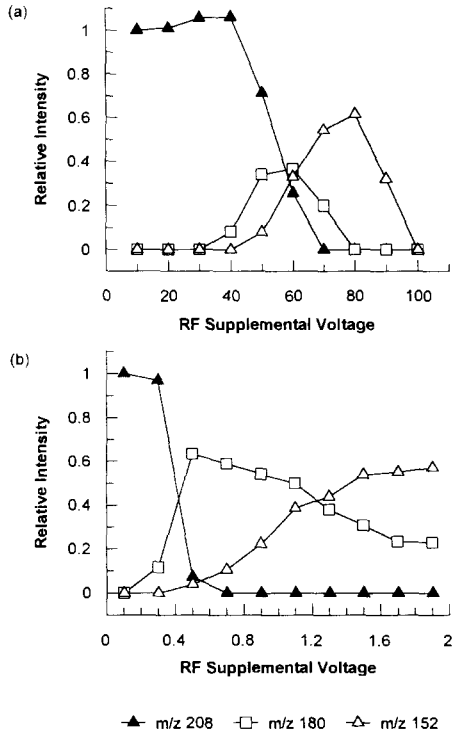

Fig. 2. Decomposition curves for anthraquinone molecular ion using (a) non-resonant excitation: parent mass = m/z 208, CID time 20 ms, CID energy 10–100 volts; and (b) resonant excitation: parent mass = m/z 208, CID time 20 ms, CID energy 0.1–1.9 volts.

3. Results and discussion

3.1. Optimization of CID conditions

The resonant and non-resonant decomposition curves for the molecular ions of AQ and 2-MeAQ are shown as a function of CID voltage in Fig. 2 and Fig. 3, respectively. From these curves CID voltages were selected to provide maximum information concerning characteristic fragmentation of these compounds. Under non-resonant excitation the CID voltage selected for both AQ and 2-Me AQ was 60 volts. At this voltage approximately 25% of the molecular ion signal remained and for AQ the M-CO (m/z 180) and M-2CO (m/z 152) fragment ions were present in approximately equal proportions. For 2-MeAQ the M-CH_3 (m/z 207), M-CH_3,CO (m/z 179) and M-CH_3,2CO (m/z 151) ions were present in significantly lower amounts than the M-CO (m/z 194) and M-2CO (m/z 166) ions. For resonant excitation the CID voltages chosen were 1.1 volts for AQ and 1.5 volts for 2-MeAQ. The latter voltage was the smallest value that yielded detectable amounts of the m/z 151 fragment.

For all experiments the CID excitation period was kept at 20 msec; variations from 10–40 ms did not significantly affect the fragmentation behavior of AQ and 2-MeAQ.

Although standards are available for AQ and 2-MeAQ allowing their identification in unknown samples via both mass spectral data and retention times, other alkylated AQs isomers for which standards were not available (i.e., 1-MeAQ and C_2-AQs) can only be identified by their mass spectral patterns. Consequently, it is necessary to obtain a good characteristic spectrum with enough fragmentation data to identify the compound.

3.2. Qualitative analysis of contaminated sediment

From the GC/MS analysis of the sediment extract, a portion (t_R = 18–20 min) of the total ion chromatogram and the mass chromatograms for

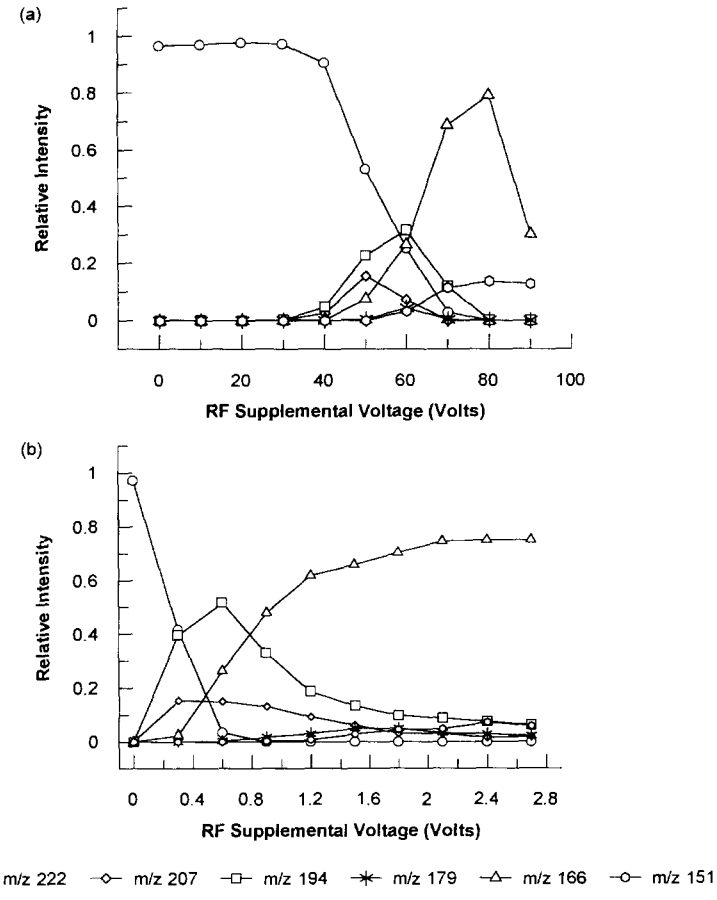

Fig. 3. Decomposition curves for 2-methylanthraquinone molecular ion using (a) non-resonant excitation: parent mass = m/z 222, CID time 20 ms, CID energy 0–90 volts; and (b) resonant excitation: parent mass = m/z 222, CID time 20 ms, CID energy 0–2.7 volts.

m/z = 208, 180 and 152 are displayed in Fig. 4a. The various signals observed in the chromatogram, during this retention period, originate from intact molecular ions and/or fragment ions of different compounds present in the sediment extract. The mass spectrum at the retention time of AQ (19.4 min) is reproduced in Fig. 4b. Although ions characteristic for AQ (208, 180, 152) are observable, the spectrum is dominated by a coeluting interference with m/z 204. By employing GC/MS/MS in non-resonant (Fig. 5a) or resonant (Fig. 6a) modes the m/z 180 and 152 mass chromatograms are 'cleaned up' significantly resulting in clear confirmatory spectra (Fig. 5b and Fig. 6b) for AQ.

The real advantage of the MS/MS technique is demonstrated in the search for MeAQs (MW = 222) and C_2-AQs (MW = 236) in the sediment extract. As indicated previously for 2-MeAQ, MeAQs yield in addition to the molecular ion (m/z 222) fragments at m/z 207, 194, 179, 166 and 151. The TIC and mass chromatograms corresponding to these masses in GC/MS, GC/MS/MS non-resonant and resonant modes are shown in Fig. 7a-c, respectively. The corresponding mass spectra extracted at positions 1 (t_R = 20.9 min) and 2 (t_R = 21.6 min) are reproduced in Fig. 8a-c. Position 2 corresponds to 2-methyl AQ as confirmed by the retention time of the standard. Because AQ appears to be the only dominant MW

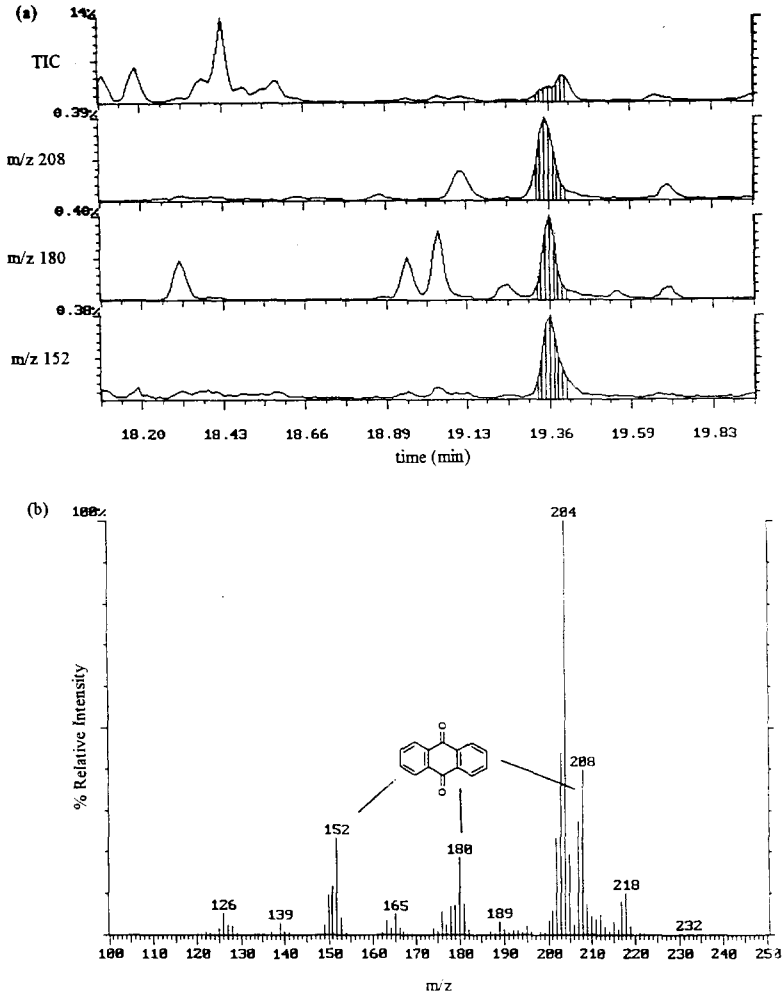

Fig. 4. GC/MS analysis of sediment extract. (a) TIC and m/z 208, 180, 152 ion chromatograms, (b) background subtracted mass spectrum at $t_R = 19.4$ min in (a).

208 quinone detected in the sediment extract, it is unlikely that the m/z (208 + 14) and m/z (208 + 28) alkyl isomers are not AQ in nature. The standard library reference spectra of 1,4-anthraquinone (NIST # 48 970), another possible anthraquinone isomer, displays an intense M-82 ion due to loss of COC_2H_2CO which is not observed in any of the spectra obtained in this work. The retention time of 9,10-phenanthrenequinone, another structural isomer of AQ, was found to be over 3 min longer than that of AQ.

Given that only two possible monomethyl isomers of AQ exist, the chromatographic signals at position 1 must correspond to 1-methyl AQ. The unavailability of a standard for this compound makes full mass spectral data necessary for structural confirmation.

Furthermore, when comparing Fig. 8b1 and 8b2 it is noticed that ions m/z 207 and 179 are absent in the former. This difference is most likely due to an interaction between the carbonyl oxy-gen and the methyl protons, similar to the ortho effect described by Schwartz [19], leading to the formation of the ion at m/z 177 (compound 1, Fig. 8b). This ion is not observed in the 2-MeAQ mass spectrum.

A number of small ions at m/z 202, 210 and 211 are also observed in the mass spectra shown in Fig.

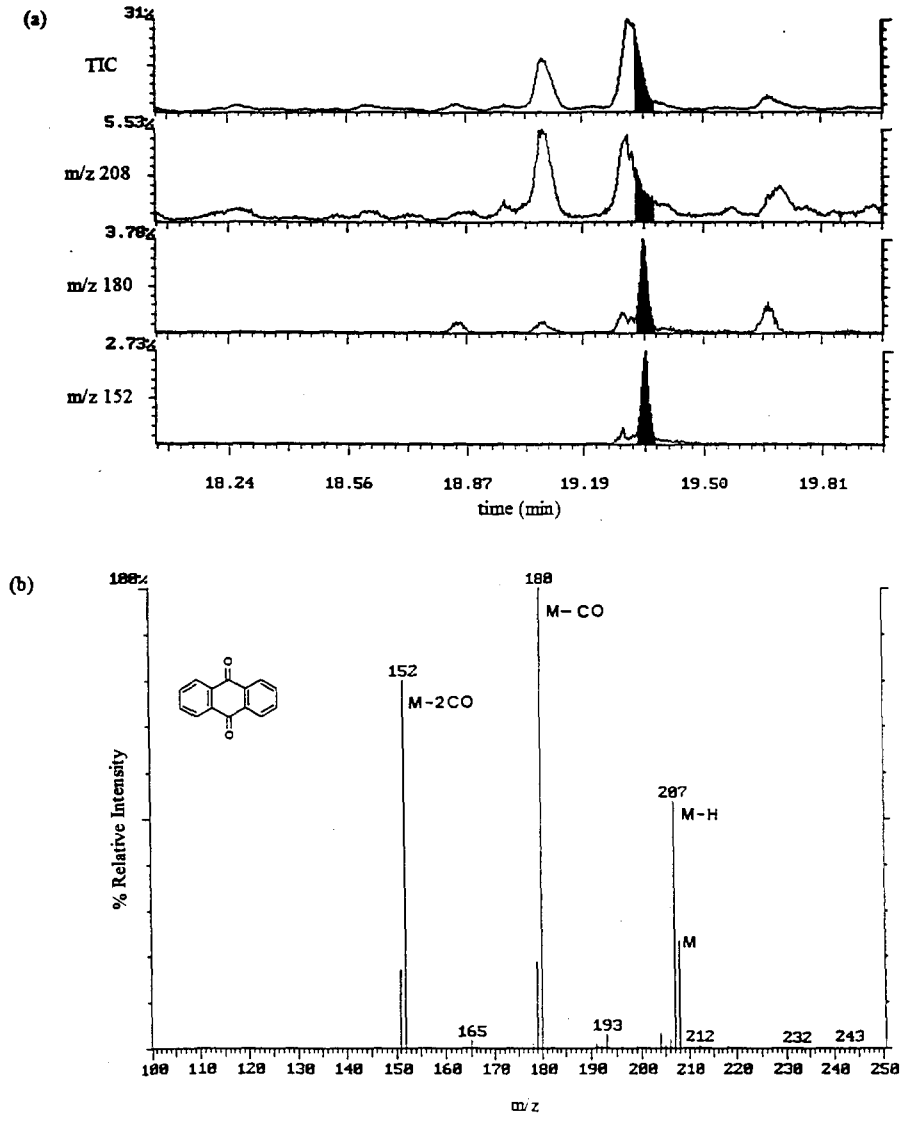

Fig. 5. Non-resonant GC/MS/MS analysis of sediment extract. (a) TIC and m/z 208, 180, 152 ion chromatograms, (b) background subtracted mass spectrum at t_R = 19.4 min in (a).

8b1. As these ions do not correspond to any logical losses from m/z 222, they are most likely due to co-eluting interferences. For example, the m/z 202 ion probably corresponds to pyrene (MW 202), since large amounts of this substance, present in concentrations two orders of magnitude higher than C1-AQ, are found to coelute in this region (t_R = 20.86 min). One has to recognize that during the CID process, (step 7, Fig. 1), eluants from the GC column are constantly entering the trap and can interact with the ions which have been isolated. Given that the ionization potential of anthraquinone and its fragmentation products is greater than that of pyrene [20] the m/z 202 pyrene ions may be formed via charge transfer reactions with the stored m/z 222 ions. Similarly, the m/z 210 and 211 ions could arise from ion molecule reactions between matrix molecules and stored ions.

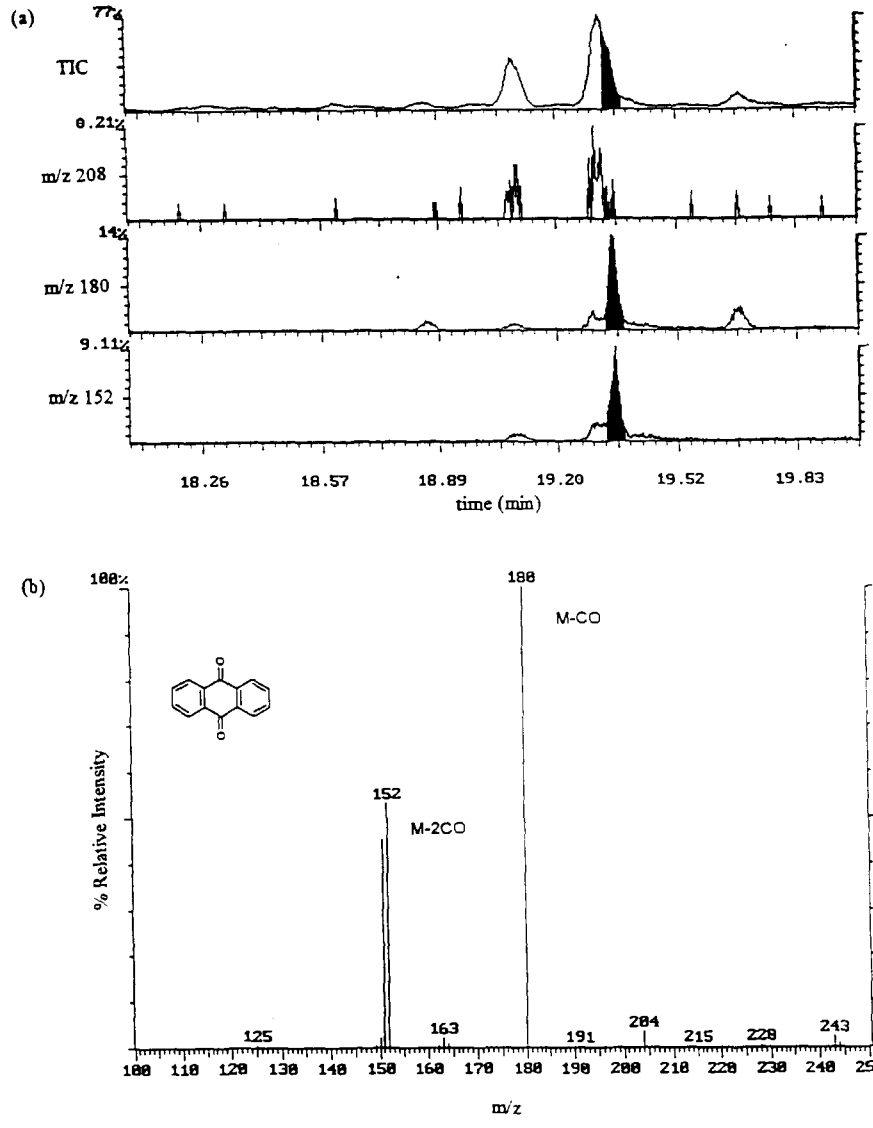

Fig. 6. Resonant GC/MS/MS analysis of sediment extract. (a) TIC and m/z 208, 180, 152 ion chromatograms, (b) background subtracted mass spectrum at $t_R = 19.4$ min in (a).

Although the isolation of m/z 222 for the CID experiments was performed with a 1 amu window, these data demonstrate that the presence of relatively large amounts of co-eluting substances can generate small spectral interferences.

Comparison of the mass chromatograms (Fig. 7b and c) and mass spectra (Fig. 8b and c), reveals that the non-resonant experiment does in general provide slightly cleaner chromatograms and more intense characteristic fragment ions. In addition, in the resonant mode at certain energies loss of H is also observed (m/z 165, Fig. 8c), regardless of position of the methyl substituent, thus, complicating the mass search. Consequently, for the C_2-AQs only data obtained in non-resonant mode were considered. C_2-AQ signals were not detectable by GC/MS analysis.

The non-resonant GC/MS/MS search for C_2-AQ (dimethyl or mono ethyl) used m/z 236 as a precursor

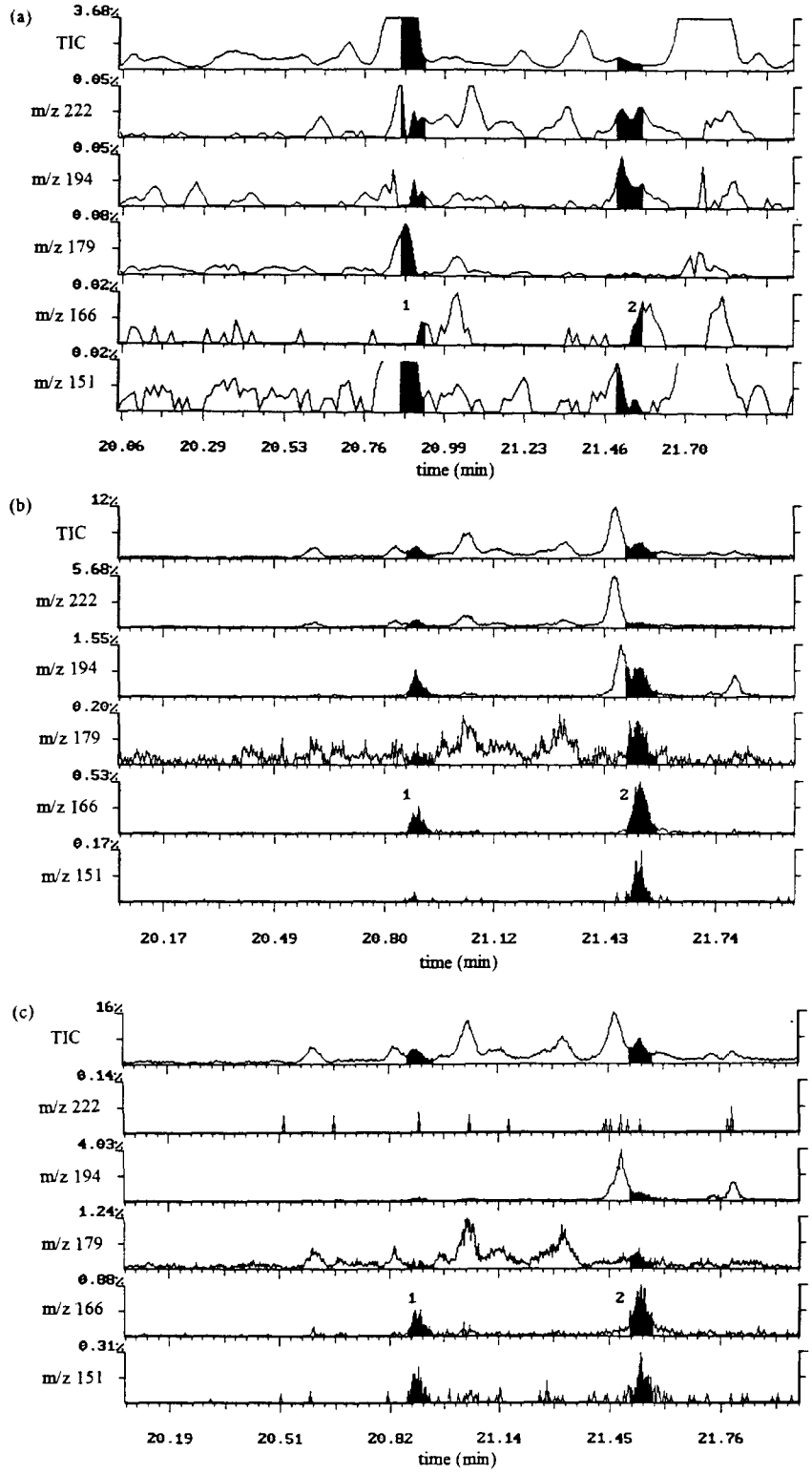

Fig. 7. TIC and m/z 222, 194, 179, 166, 151 ion chromatograms for sediment extract in (a) GC/MS, (b) non-resonant GC/MS/MS, (c) resonant GC/MS/MS modes.

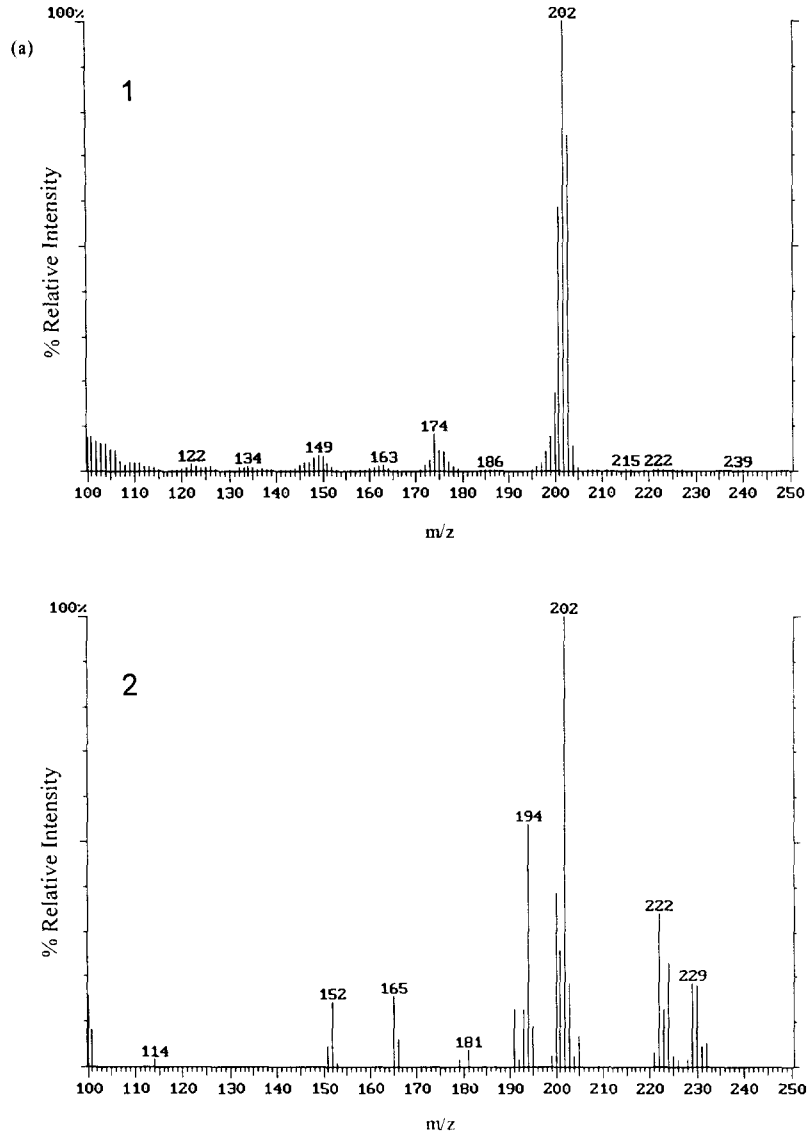

Fig. 8.

ion. Fragments at m/z 221 (M-CH_3), 208 (M-CO), 207 (M-C_2H_5 or M-HCO), 193 (M-CO, CH_3), 180 (M-2CO) and 165 (M-2CO, CH_3) could be expected. The corresponding ion chromatograms are shown in Fig. 9. Mass spectra extracted at positions 1 ($t_R = 23.1$ min) and 2 ($t_R = 23.6$ min) are shown in Fig. 10. The spectra confirm the presence of C_2-AQ in the sediment extract. Ions of m/z 207 at position 1 could be due to loss of C_2H_5 from the parent ion and/or loss of CO + H because of the close proximity of the carbonyl oxygen(s) and an alkyl group; the latter also applies to the m/z 179 in the spectra from positions 1 and 2. In consideration of the ion at m/z 165 in the spectra of the MeAQs in Fig. 8c (1 and 2) a dimethyl substitution is more likely than an ethyl substituent.

The three experiments outlined above, searching for presence of anthraquinone and its C_1 and C_2 alkylated analogues in the sediment extract, were carried out first individually to determine the

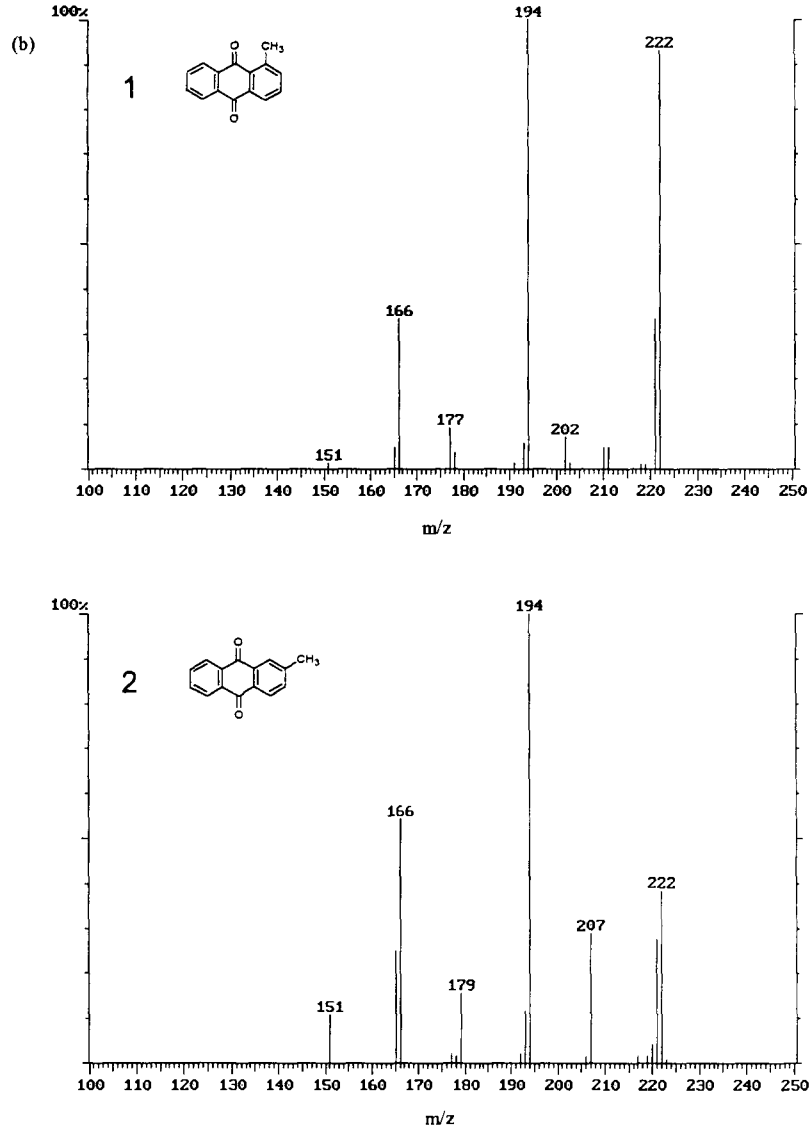

Fig. 8.

appropriate elution windows, followed by a single combined experiment in which the three time windows were defined for the three different CID precursor masses (m/z 208, 222, 236). As expected, there was no detectable difference in the results obtained. The ability to perform multiple CID experiments during a single GC run, either for method development or for analytical purposes, is advantageous especially if only small amounts of sample are available or if a large number of samples has to be analyzed.

3.3. Quantitation

Although a large number of fragment ions is desirable for compound identification, for quantification of the compounds discussed here it is important to remove as many coeluting interferences as possible, thus, GC/MS/MS would be the method of choice particularly if strong ion chromatograms are available from secondary fragmentation products such as the m/z 152 (M-2CO) ion of AQ, the m/z 151 (M-2CO, CH_3) and m/z 166

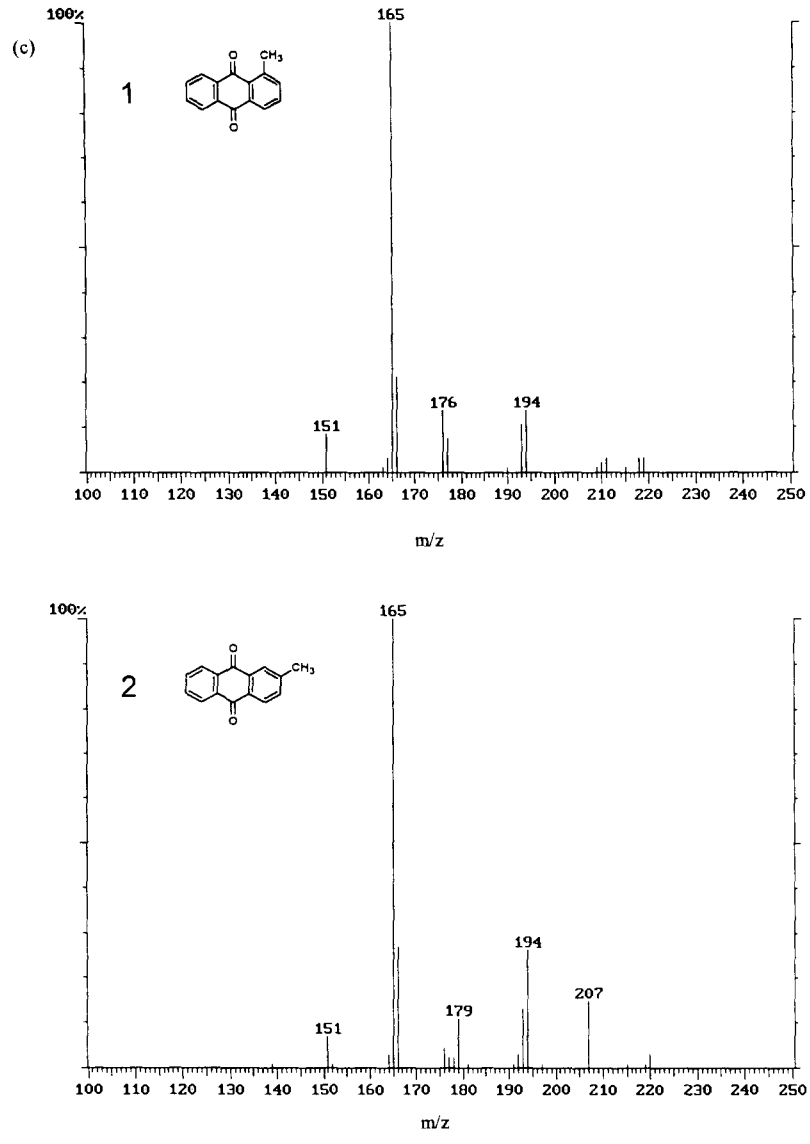

Fig. 8. Background subtracted mass spectra extracted at position 1 and 2 in Fig. 7. (a) GC/MS, (b) non-resonant GC/MS/MS, (c) resonant GC/MS/MS conditions.

(M-2CO) ions of MeAQs and the m/z 180 (M-2CO) and m/z 165 (M-2CO, CH_3) ions of C_2-MeAQs. As clearly demonstrated by the ion chromatograms in Fig. 7 and Fig. 9 these fragments provide the best selectivity over matrix interferences. Consequently, for quantitation purposes the CID conditions should be optimized to yield maximum amounts of these ions. For example, in the case of AQ and 2-MeAQ a non-resonant CID energy of 80 volts (see Fig. 2 and Fig. 3) provides the maximum yield of secondary fragments.

Calibration curves for AQ, obtained using the m/z 152, were linear ($r = 0.99$) over a range of 1 pg to 10 000 pg for both resonant and non-resonant CID analyses. The lowest detectable amount of AQ by GC/MS/MS was approximately 0.5–1.5 pg using the m/z 152 ion for quantitation.

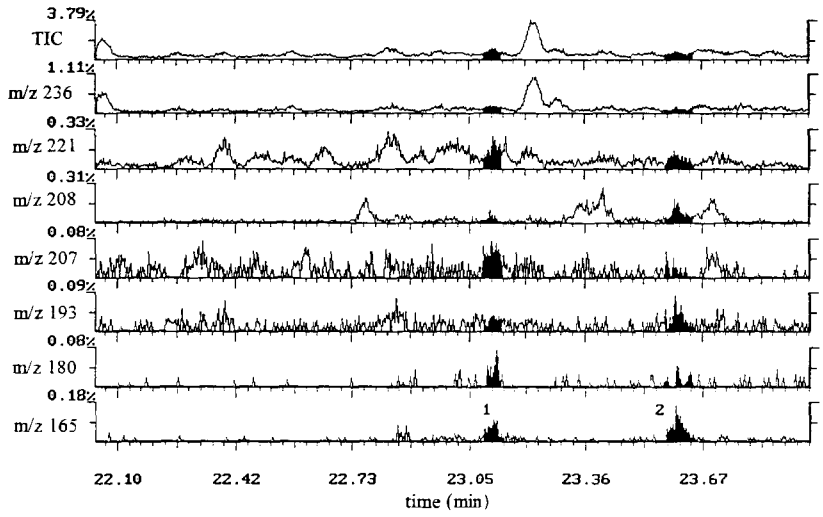

Fig. 9. TIC and m/z 236, 221, 208, 207, 193, 180, 165 ion chromatograms for sediment extract in non-resonant GC/MS/MS mode.

The extraction efficiency of AQ determined using a spiked uncontaminated sediment was approximately (70–130%). This is significantly higher than the recovery of anthracene and D_{10}-anthracene (50–70%). This large difference can be explained by the fact that acetone was employed in the extraction process, thus facilitating the extraction of the more polar components. Furthermore, from the sediment spiked with an thracene it was found that approximately 6% of the anthracene in a spiked sample was converted to AQ. Injections of pure anthracene revealed that oxidation to AQ did not occur in the injector. Consequently, this observed oxidation must have taken place during the extraction or cleanup procedures.

These results indicate the importance of monitoring for transformation products as part of an analytical protocol to determine if low extraction efficiencies are due to merely adherence to the matrix or due to actual loss of analyte through chemical transformation. The importance of the transformation of PAHs during extraction was recently indicated by Soheila et al. [21] who identified the presence of bianthracene as a polymerization product of anthracene.

The concentrations of anthracene, 2-methylanthracene, AQ and 2-MeAQ in the freeze dried sediment were determined using the internal standard anthracene-D_{10} m/z 188 molecular ion chromatogram and the M-2CO ion chromatograms for the quinones, together with the appropriate relative response factors. For the anthraquinone and 2-methylanthraquinone, a correction factor corresponding to 6% of the non oxidized compound, (anthracene or 2-methylanthracene), was employed to account for potential oxidation during the sample preparation. The results obtained from non-resonant analysis indicate concentrations in dry sediment of: 400–600 $\mu g\ g^{-1}$ anthracene, 40–60 $\mu g\ g^{-1}$ 2-methylanthracene, 6–24 $\mu g\ g^{-1}$ anthraquinone and 1–7 $\mu g\ g^{-1}$ 2-methylanthraquinone. For the other quinones analyzed, for which standards were not available, concentration values were estimated by using the response factor of 2-MeAQ. The values obtained were: 0.9–1.8 $\mu g\ g^{-1}$ 1-methylanthraquinone and 1.0–1.9 $\mu g\ g^{-1}$ for the sum of the two C_2-AQs (positions 1 plus 2 in Fig. 9).

4. Analysis of other PAH oxidation products

GC/MS and NRCID GC/MS/MS analyses were also performed for 9-fluoranone (MW 180) and benz[a]anthracene-7,12-dione (MW 258) for which standards were available to obtain retention times and develop optimum CID conditions. The former, being a monoketone, only offers one major fragment for identification (m/z 152, M-CO) while the latter

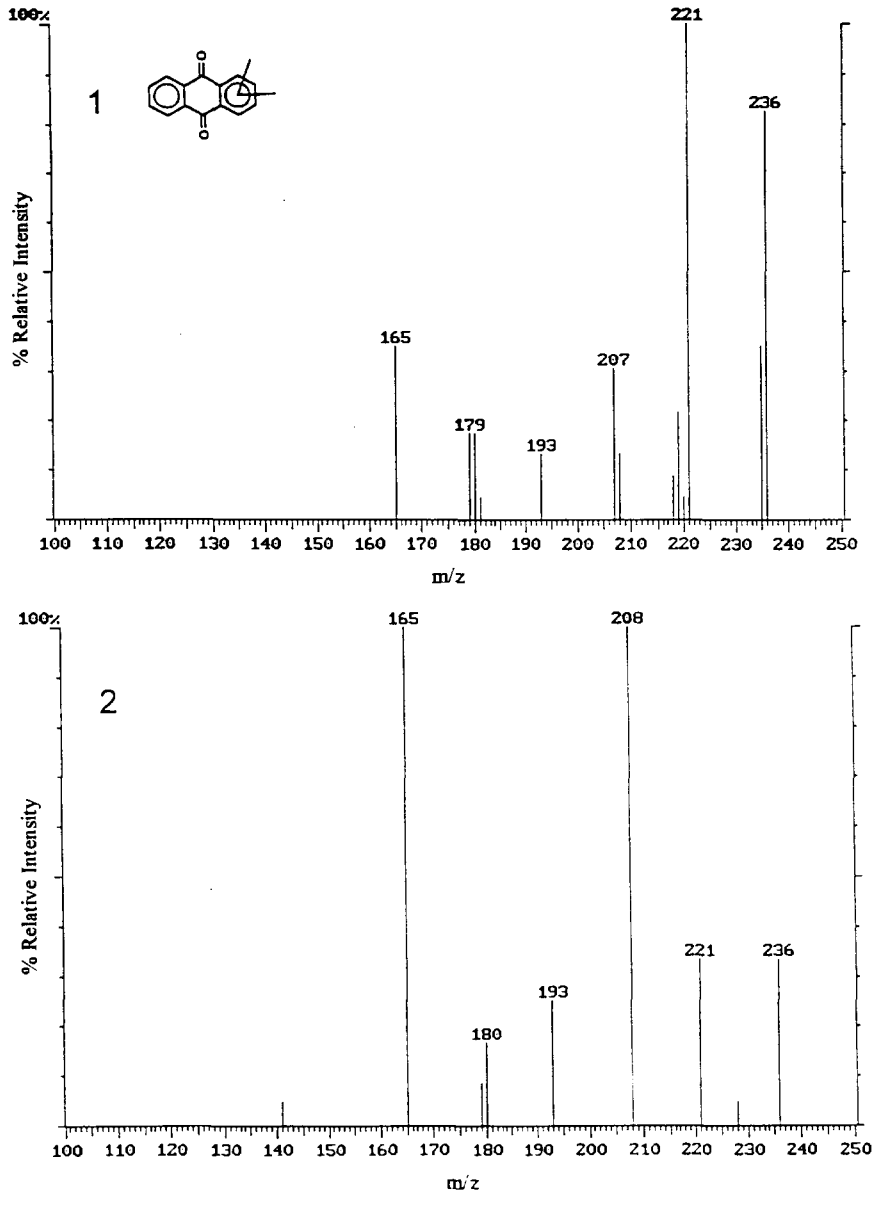

Fig. 10. Background subtracted mass spectra extracted at position 1 and 2 in Fig. 9.

offers two fragments (m/z 230, M-CO and m/z 202, M-2CO). Using the two standards the optimum NRCID fragmentation conditions to yield maximum amounts of m/z 152 for 9-fluoranone and m/z 202 for benz[a]anthracene-7,12-dione were 90 and 60 volts, respectively. Using these NRCID conditions, during the appropriate retention time windows, these two compounds were targeted in the sediment extract. The 9-fluoranone m/z 152 ion chromatogram and the benz[a]anthracene-7,12-dione m/z 202 ion chromatogram obtained for both GC/MS and GC/MS/MS analysis are shown in Fig. 11. The latter compound was only detectable by GC/MS/MS. Furthermore, comparison of the data reveals that the M-2CO ion chromatogram of benz[a]anthracene-7,12-dione does not contain any

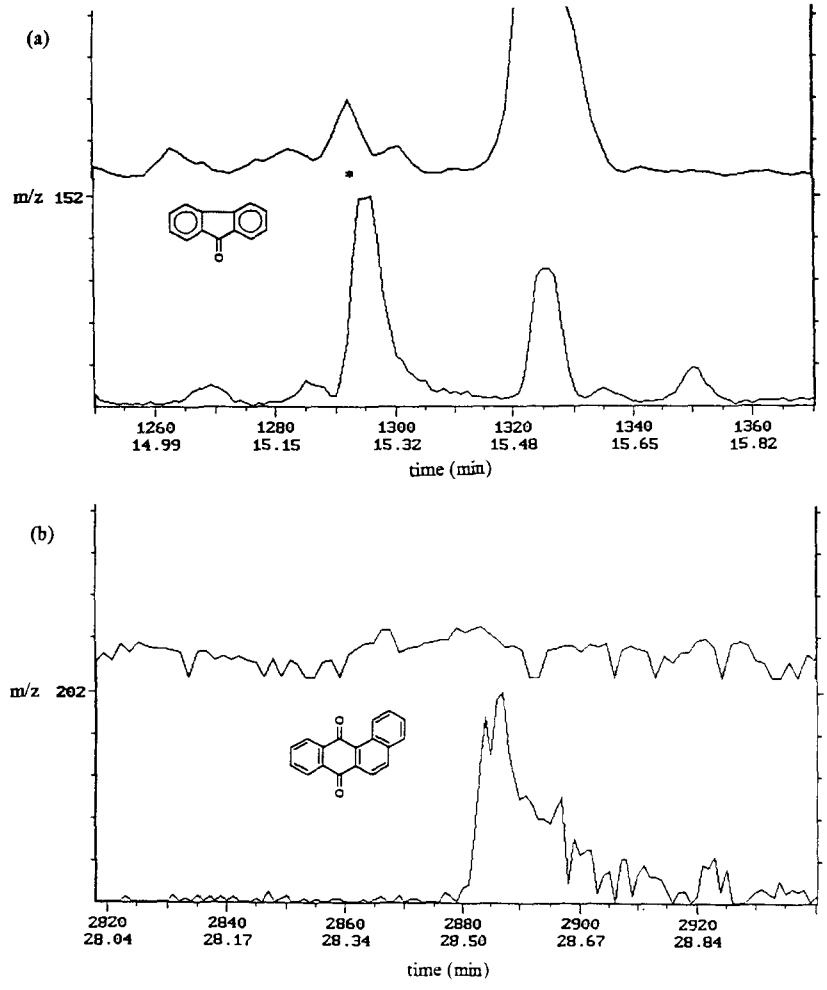

Fig. 11. GC/MS (top trace) and NRCID GC/MS/MS (bottom trace) ion chromatograms for (a) 9-fluoranone (m/z 152) and (b) benz[a]anthracene-7,12-dione (m/z 202) in sediment extract.

other eluting compounds while the M-CO ion chromatogram of 9-fluoranone contains several other eluting substances. Although the GC/MS/MS analysis results in a strong enhancement of the 9-fluoranone ($t_R = 15.3$ min) signal it does not completely eliminate other compounds from the chromatogram. These results further demonstrate the greater specificity obtained by monitoring secondary fragmentation products. From these analyses the concentrations in dry sediment of 9-fluoranone and benz[a]anthracene-7,12-dione were estimated to be 20–40 and 10–20 μg g^{-1}, respectively.

5. Conclusion

The data obtained in this study demonstrate the usefulness of ion trap GC/MS/MS experiments for detecting and quantifying trace amounts of polyaromatic quinones which would ordinarily be obscured by matrix interferences when using standard GC/MS techniques. Improvements are especially notable when secondary fragmentation products, such as M-2CO, are monitored. Non-resonant CID is preferred when characteristic spectra are required for confirmation, it provides intense fragment ions together with molecular ion information.

The development of techniques able to analyze for trace level transformation products of contaminants in complex matrixes, such as the one outlined in this work, are important tools in monitoring the recovery of contaminated ecosystems.

Acknowledgements

The authors thank Varian Canada for providing the MS/MS capabilities to the Saturn GC/MS system. We acknowledge financial support from the Department of Indian Affairs and Northern Development (DIAND) and the National Science and Engineering Research Council (NSERC) of Canada. We would also like to thank Dionex Canada Ltd. for providing access to the ASE system and C. Simpson for collecting the settling pond sediment.

References

[1] NRCC Publication No. NRCC 18981, Polycyclic Aromatic Hydrocarbons in the Aquatic Environment: Formation, Sources, Fate and Effects on Aquatic Systems, 1983.
[2] R.G. Harvey, Polycyclic Hydrocarbons and Carcinogens, ACS Symposium Series 283, American Chemical Society, Washington, D.C., 1985.
[3] N.J. Pitts Jr., D. Grosjean, T.M. Mischke, V.F. Simmon and D. Poole, Toxicol. Lett., 1 (1977) 65.
[4] R.C. Pierce and M. Katz, Environ. Sci. Technol., 10 (1976) 45.
[5] M.F. Salamone, J.A. Heddle, and M. Katz, Environ. Int., 2 (1979) 37.
[6] T. Ramdahl, Environ. Sci. Technol., 17 (1983) 666.
[7] T. Ramdahl, Environ. Sci. Technol., 17 (1985) 187.
[8] J.R.B. Slayback and P.A. Taylor, Spectra, 9 (1983) 18.
[9] P.A. D'Agostino and L.R. Provost, J. Chromatogr. A, 695 (1995) 65.
[10] K. Lindstrom and R. Shubert, J. High Res. Chromatogr. Comm., 7 (1984) 68.
[11] U. Hofmann, M.F. Fromm, S. Johnson and G. Mikus, J. Chromatogr. B, 663 (1995) 59.
[12] J.V. Johnson, R.A. Yost, P.E. Kelley and D.C. Bradford, Anal. Chem., 62 (1990) 2162.
[13] S. Schachterle, R.D. Brittain and J.D. Mills, J. Chromatogr. A, 683 (1994) 185.
[14] J.B. Plomley, C.J. Koester and R.E. March, Anal. Chem., 66 (1994) 4437.
[15] R.D. Brittain and C. Feigel, Am. Lab., (1994) 44.
[16] S.A. McLuckey, G.L. Glish and G.J. Van Berkler, Int. J. Mass Spectrom. Ion Proc., 106 (1991) 213.
[17] M.A. Fox and S. Olive, Science, 205 (1979) 582.
[18] C.D. Simpson, A.A. Mosi, W.R. Cullen and K.J. Reimer, Sci. Tot. Environ., 181 (1996) 265
[19] H. Shwartz, Topics Current Chem., 73 (1978) 231.
[20] R.D. Levin and S. Lias, Ionization potential and appearance potential measurements, U.S. Dept. of Commerce, National Bureau of Standards, Washington, D.C., 1982.
[21] K-L Soheila, M.A. Pickard and M.R. Gray, Environ. Sci. Technol., 30 (1996) 1145.

ELSEVIER

Talanta 44 (1997) 1003–1007

Talanta

Determination of tributyltin in toluene extract from sea water by graphite furnace atomic absorption spectrometry with a new matrix modifier

Benling Gong *, Yongming Liu, Yuli Xu, Tiezheng Lin

Dalian Institute of Chemical Physics, Academia Sinica, 161 Zhongshan Road, Dalian, People's Republic of China

Received 26 July 1996; received in revised form 4 November 1996; accepted 13 November 1996

Abstract

A new matrix modifier composed of calcium and chromium[VI] was proposed for the determination of tributyltin (TBT) in toluene extract from sea water containing sediment by graphite furnace atomic absorption spectrometry (GFAAS). Fourteen inorganic and organic compounds (barium, calcium, chromium[VI], lanthanum, magnesium, nickel, palladium, strontium, calcium–chromium[VI], calcium–strontium, nickel isocaprylate, 5%-, 10%-aqueous solution of ascorbic acid and toluene-saturated solution of ascorbic acid) as a matrix modifier were comparatively studied and a matrix modifier composed from 5 μg of calcium and 1 μg of chromium[VI] was found to give the best performance. The interference effects of co-existing elements in sea water containing sediment (aluminium, iron, magnesium, sodium and strontium) were studied. TBT in eight toluene extracts was determined by GFAAS with the proposed matrix modifier. The relative standard deviation was 3.0% for 63 ng ml^{-1} of TBT ($n = 11$). The recoveries were 88–104%. The characteristic mass was 7 pg. The linearity range was 0–250 ng mg^{-1}. © 1997 Elsevier Science B.V.

Keywords: Matrix modifier; Sea water; Toluene

1. Introduction

In recent 30 years, organotin compounds are widely used in industry and agriculture resulting in increasing influences on environment. Tributyltin (TBT) used as antifouling agents in paint formulation is released into sea-water, more or less degraded, adsorbed on floating particles and accumulated in marine sediments. This released TBT even in trace amounts could seriously impair marine organisms and becomes one of the most important pollutants in marine environment.

The objective environmental concentrations of organotin compounds are 8 ng l^{-1} for France and United Kingdom, 4 ng l^{-1} for Japan and USA.

Graphite furnace atomic absorption spectrometry (GFAAS) is a favourable method for the determination of TBT at very low concentration. But the tendency of tin to form volatile compounds during the drying and ashing steps, and

* Corresponding author.

PII S0039-9140(96)02174-1

Table 1
Instrumental parameters and operating conditions

Heating program	Step	1	2	3	4	5	6	7
	Temperature (°C)	130	1200	100	2200	100	2500	20
	Ramp time (s)	10	10	10	0	1	1	1
	Hold time (s)	40	20	3	4	3	3	3
	Read time (s)	—	—	—	−1	—	—	
	Internal gas flow Rate (ml min^{-1})	300	300	300	0	300	300	300
Instrumental parameters	Wavelength (nm)	224.6						
	Spectral band-pass (nm)	0.7						
	Lamp current (mA)	10						
	Integration time (s)	6						
	Mode	Peak height						
	Background corrector	Deuterium arc						
	Injected sample volume (μl)	5						

its interaction with the carbon of the graphite tube wall causes erratic results easily. Moreover the organotin compounds have different behaviours in the furnace from the inorganotin compounds. These problems could be resolved by use of a suitable matrix modifier. Up to now, several inorganic and organic compounds have been proposed for this purpose. For example, palladium was used by Kashin et al. [1]; 4-methylpentane-2-one solution of palladium was selected by Dadfarnia et al. [2]; 0.1% ammonium dichromate was chosen by Parks et al. [3]; 0.4% potassium dichromate–0.2% ammonium dihydrogenophosphate in 2% nitric acid was proposed by Pinel et al. [4]; 0.01% picric acid was reported by Astruc et al. [5].

The investigation for the adsorption character of TBT on marine sediment is necessary for understanding the contamination behaviour of TBT in marine environment. So we study the determination of TBT in toluene extract from sea water containing sediment by GFAAS. Several inorganic and organic compounds were compared as a matrix modifier. From the results obtained a new mixed matrix modifier composed of calcium and chromium[VI] was selected.

2. Experimental

2.1. Apparatus

A Perkin–Elmer Model 5000 Atomic absorption spectrometer equipped with a Model HGA 500 graphite furnace, a Data Station 10 and a PR 100 printer was used. An L233 type hollow cathod lamp made by Hamamatsu TV and a Perkin–Elmer pyrolytic tube were used. An eppendorf micropipette was used for injecting sample solution into graphite furnace.

Instrumental parameters and operating conditions were optimized by means of experiments, and shown in Table 1.

2.2. Reagents

All chemicals used were of analytical grade, and distilled, deionized water was used throughout.

A stock standard solution of TBT (1000 mg l^{-1}) was prepared by dissolving 122.2 mg tributyltin chloride and diluting to 100 ml with methanol. The working standard solutions were prepared by successive dilution of the stock stan-

dard solution to following concentrations (0, 50, 100, 150, 250 ng ml^{-1}) with toluene.

A 1 g l^{-1} solution of chromium[VI] was prepared by dissolving potassium dichromate in 0.2% nitric acid. A 1 g l^{-1} solution of calcium was prepared by dissolving calcium nitrate in 0.2% nitric acid. A mixed matrix modifier composed from 5 μg of calcium and 1 μg of chromium[VI] was prepared by the above-mentioned solutions of chromium[VI] and calcium.

1 g l^{-1} solutions of aluminium, barium, iron, lanthanium, magnesium, nickel, palladium, sodium and strontium were prepared by dissolving their nitrate or chloride salts in 0.2% nitric acid. A 1 g l^{-1} solution of nickel isocaprylate was prepared by dissolving nickel isocaprylate in toluene. 5%- and 10%-aqueous solutions of ascorbic acid were prepared by dissolving ascorbic acid in water. A toluene-saturated solution of ascorbic acid was prepared by dissolving ascorbic acid in toluene as much as possible.

These solutions were used as a matrix modifier for the comparative study of their performances or used as an interferent for the study of their interference effects.

2.3. Procedure

A certain amount of TBT methanol solution was added into 50 ml sea water containing 0.5 g sediment. This solution was oscillated 12 h at 200 rpm and centrifuged 20 min at 3000 rpm. The 20 ml supernatant liquid was transferred into a separatory funnel.

Toluene, 2 ml, were added, shaken vigorously for 2 min and allowed to stand for phase separation. After draining off the aqueous phase, the toluene phase was washed with 10 ml water three times in order to remove the remaining interferent such as sodium chloride and transferred into test tube.

A 5 μl aliquot of the sample solution in test tube at first and then a 10 μl solution of the mixed matrix modifier were injected into the graphite furnace consecutively, and the peak height was measured.

3. Results and discussion

3.1. Effects of heating rate mode in atomization step

The heating rate mode in atomization step influences appreciably on the analytical sensitivity of TBT.

The model HGA 500 graphite furnace has two heating rate modes: temperature-controlled maximum heating (ramp time = 0 s) and conventional voltage-controlled heating (ramp time ≥ 1 s).

The former without any matrix modifier can produce 23% of the absorption signal which is obtained with a calcium–chromium[VI] matrix modifier. But the latter can not produce any absorption signal even with a calcium–chromium[VI] matrix modifier. So the former was used.

3.2. Effect of ashing- and atomization-temperature

The effects of atomization temperatures were studied from 2500–1600°C. The results showed this temperature range to give the same effects. Under the condition of using a matrix modifier composed of calcium and chromium[VI], ashing temperature could be increased up to 1300°C. At 1350 and 1400°C, the absorbances obtained decreased about 13 and 40% of that at 1300°C, respectively. From the above results, 2200 and 1200°C were selected as atomization- and ashing-temperature, respectively.

3.3. Comparative study of the performances of 14 matrix modifiers

The authors have reported that the analytical sensitivity for TBT can be significantly improved by the addition of di(methylcyano) palladium [$PbCl_2(CH_3CN)_2$] [6]. But the compound was not available now, so an inorganic palladium compound was tried to replace it. The ordinary matrix modifiers such as lanthanum, magnesium, nickel, strontium and calcium salts were studied also.

Moreover, the analytical sensitivity of tin could be improved not only by a reducing agent such as ascorbic acid [7–10], but also by an oxidizing agent such as potassium dichromate [3].

Table 2
Relative enhancement ratios for the analytical sensitivity of TBT using 14 compounds as matrix modifier (relative to palladium)

Matrix modifier		Pd	Ba	Ca	Cr[VI]	La	Mg	Ni	Sr	Ca–Cr[VI]	Ca–Sr	$Ni(C_8H_{14}O_2)_2$	Ascorbic acid		
Concentration (mg ml^{-1})		1	1	1	1	1	1	1	1	0.5–0.1	0.5–0.5	1	0.5% aqueous	10% aqueous	Toluene-saturated
Enhancement ratio		1.0	0.8	1.0	1.3	0.1	0.4	0.4	1.1	1.7	1.6	0.7	0.7	0.8	0.5

Accordingly, the 14 inorganic and organic compounds (barium, calcium, chromium[VI], lanthanium, nickel, palladium, strontium, calcium–chromium[VI], calcium–strontium, nickel isocaprylate, 5%- and 10%-aqueous solution of ascorbic acid and toluene-saturated solution) were taken as a matrix modifier to study their performances for increasing the analytical sensitivity of TBT.

The results shown in Table 2, indicate the two mixed matrix modifiers (calcium–chromium[VI] and calcium–strontium) to give the higher sensitivities among 14 compounds. The precision of calcium–chromium[VI] (RSD = 1.0% for 100 ng ml^{-1} standard solution of TBT) is higher than that of calcium–strontium (RSD = 1.6% for the same TBT solution). So a mixed matrix modifier composed of calcium and chromium[VI] was selected.

3.4. Optimal composition of a calcium–chromium[VI] matrix modifier

The optimal amounts of each component of a calcium–chromium[VI] matrix modifier were studied.

The concentrations beyond 0.2 mg ml^{-1} of chromium[VI] cause blank value to increase, and the concentration range from 0.05–1 mg ml^{-1} of calcium gives the same sensitivity. So a mixture composed from 0.5 mg ml^{-1} of calcium and 0.1 mg ml^{-1} of chromium[VI] was chosen as a matrix modifier.

3.5. Interferences of coexisting elements

Calcium, magnesium, potassium, sodium, aluminium, iron and strontium contained in sea water and sediment may interfere on the determination of TBT. Though these elements could not be extracted in toluene phase, but the

Table 3
Permissible amounts of coexisting elements for 0.5 ng of TBT

Element	Al	Fe	Mg	Na	Sr
Permissible amount (ng)	100	100	50	5	1000

Table 4
Determination of TBT in toluene-extract from sea water containing different sediments

Sample number	Value found[a] (ng ml^{-1})	Recovery test		Recovery (%)
		Added (ng ml^{-1})	Found (ng ml^{-1})	
1	15	90	86	96
2	21	90	80	89
3	33	90	79	88
4	63	90	95	104
5	95	90	80	89
6	103	90	79	88
7	115	90	85	94
8	128	90	88	98

[a] Value of sample number 4 is means of 11 determinations. All the other values are means of three determinations.

trace amount might be mixed in toluene phase. So, the interference effects from the above elements except for calcium and potassium (because calcium and potassium were contained in a matrix modifier used) were studied with a matrix modifier composed of calcium and chromium[VI].

It is seen from Table 3 that sodium shows the severest interference effect among these coexisting elements. For example, under the coexistances of 5 and 10 ng of sodium the recoveries of TBT were 94 and 76%, respectively. This showed that the larger amounts of sodium than 5 ng cause the interference effect. So, the toluene phase should be washed with water three times to remove its remaining interferents, especially sodium [3].

3.6. Determination of TBT in toluene extract from sea water containing different sediments

The investigation of the adsorption character of TBT on sediment was carried out by using different sorts of marine sediments. A certain amount of TBT was added into sea water containing different sediments and the remaining TBT in sea water was measured by the proposed method after extracting with toluene. The results are shown in Table 4.

The relative standard deviation was 3.0% for 63 ng ml^{-1} of TBT ($n = 11$, 62, 69, 62, 63, 62, 64, 61, 64, 61, 63, 67). A characteristic mass was 7 pg. The linear range of the calibration curve was 0–250 ng ml^{-1} and its correlation coefficient was 0.999. The recoveries were 88–104%.

The above data demonstrate that the proposed method has good accuracy, precision and sensitivity.

References

[1] A.N. Kashin, E.T. Kabeshova and A.B. Volynskii, XXVI CSJ, July 2–7, Poster C-43, Abstract, Vol. 1, p. 95 (1989).
[2] S. Dadfarnia, K.C. Thompson and G. Hoult, J. Anal. At. Spectrom., 9 (1994) 7.
[3] E.J. Parks, W.R. Blair and F.E. Brinckman, Talanta, 32 (1985) 633.
[4] R. Pinel, M.Z. Benabdallah, A. Astruc and M. Astruc, Anal. Chim. Acta, 181 (1986) 187.
[5] M. Astruc, R. Pinel and A. Astruc, Mikrichim. Acta, 109 (1992) 73.
[6] Hui Li, Benling Gong, T. Ochiai and K. Matsumoto, Anal. Sci., 9 (1993) 707.
[7] M. Tominaga and Y. Umezaki, Anal. Chim. Acta, 110 (1979) 55.
[8] Jin Longzhu, At. Spectros., 5 (1984) 91.
[9] A.B. Volynskii, E.M. Sedykh, B.Ya. Spinakov and Yu. A. Zolotov, Anal. Chim. Acta, 177 (1985) 129.
[10] Benling Gong, Hui Li, Tiezheng Lin and K. Matsumoto, Anal. Sci., 9 (1993) 723.

ELSEVIER

Talanta 44 (1997) 1009–1016

Talanta

Flow injection analysis of sulphite by gas-phase molecular absorption UV/VIS spectrophotometry

A. Safavi *, B. Haghighi

Department of Chemistry, College of Sciences, Shiraz University, Shiraz 71454, Iran

Received 23 July 1996; received in revised form 6 November 1996; accepted 15 November 1996

Abstract

A flow injection gas-phase molecular absorption spectrophotometric method is described for the determination of sulphite in aqueous solution. The sulphite solution, 200 μl, is introduced into a stream of distilled water. The carrier stream containing a sulphite zone is reacted, in the first mixing coil, with a stream of sulphuric acid (1 M). The evolved sulphur dioxide is purged to the segments of nitrogen flow through the second mixing coil. The gaseous phase is separated from the liquid stream by the use of a purpose built gas-liquid separator and then is swept into a purpose built flow-through cell. The absorbance of the gaseous phase is measured at 200 nm using a UV/VIS spectrophotometer. Up to 440 μg of sulphite is determined. The limit of detection is 0.8 μg and the R.D.S. for the determination of 70 and 220 μg of sulphite are 1.02 and 0.76%, respectively. Up to 40 samples h^{-1} can be analyzed. The effect of several anions and cations on the determination of sulphite was studied and the results showed that the method is relatively free from interferences. The proposed method was applied to the determination of sulphite in a synthetic sample, water sample and lemon juice. © 1997 Elsevier Science B.V.

Keywords: FIA; GPMAS; Lemon juice; Sulphite

1. Introduction

Sulphite and sulphur dioxide are widely used as preservatives in the food and pharmaceutical industries because of their ability to prevent oxidation, bacterial growth and inhibit discolouration in order to improve the appearance of dried fruit [1]. Strict control over their concentrations in industrial products is mandatory because of their toxicity. Sulphur dioxide is also a major pollutant that has been causing environmental concern over recent decades. It has been identified as one of the main causes of increasing acidification of the environment through the generation of acid rain. Sulphur dioxide is released into the atmosphere primarily from the combustion of coal and petroleum, the smelting of sulphur-containing ores, production of sulphuric acid and the paper manufacturing industry. Its adverse effects on living organisms are well known [2].

Both sulphite and sulphur dioxide have been determined by a variety of analytical methods [3]. These include titrimetry [4], ion chromatography [5], coulometry [6], conductimetry [7], polarogra-

* Corresponding author.

PII S0039-9140(96)02184-4

phy [8], flame photometry [9], chemiluminescence [10], UV/VIS spectrophotometry [11], molecular-emission cavity analysis [12], kinetic analysis [13] and FIA [14].

The determination of anions and cations in solution by conversion of the determinant into a volatile molecular species followed by their molecular absorbance measurements in the gas phase has been thoroughly investigated in the past two decades. The gaseous product is carried by a stream of air or nitrogen to a flow-through absorption cell which is positioned in the light path of the spectrometer in the space normally occupied by the flame of an atomic absorption spectrometer. A narrow band of radiation from a hollow cathode or deuterium lamp corresponding to an absorption maximum of the evolved compound is passed through the cell and the absorbance signal of the compound is measured. The technique is known as gas-phase molecular absorption spectrometry (GPMAS). The GPMAS technique is sensitive, reproducible and a versatile non-flame molecular absorption method [15].

The GPMAS technique has been introduced by Syty [16,17], who utilized the characteristics UV absorption bands of sulphur dioxide for its determination in solution. In Cresser's laboratory [18,19], GPMAS was developed during a search for a rapid and reliable method for the determination of ammonium–nitrogen in digests of soil and plant samples using the Kjeldahl method. Their methods were manual and involved considerable manipulation. Later, Cresser et al. described a method for the determination of sulphite [15] by automated GPMAS with a similar procedure. However, the manifold is complex and the system needs the use of an atomic absorption spectrometer (AAS).

The introduction of diode-array detection systems in UV/VIS spectrophotometers allowed new developments in GPMAS by Sanz et al. for single [20,21] and multicomponent simultaneous determinations [22,23]. Cabredo Pinillos et al. [24] described a continuous method for the simultaneous determination of sulphide and sulphite by the use of GPMAS with diode-array detection.

The purpose of this study was to investigate the possibilities for developing a modification of the above method for simple, precise and fast determination of small amounts (μg) of sulphite with low reagents consumption, when small volumes of samples are available. The method utilizes a UV/VIS spectrophotometer instead of an AAS which has been used before [15] with a purpose built gas liquid separator and a simple flow injection manifold. The absorbance of the generated gas (SO_2) is measured at 200 nm as it is swept into a purpose built flow-through cell positioned in the space of the cell compartment of a UV/VIS spectrophotometer. Up to 440 μg of sulphite can be determined precisely with a sampling rate of 40 samples h^{-1}.

2. Experimental

2.1. Apparatus

A Philips PU8275 UV/VIS spectrophotometer interfaced to an IBM compatible computer (AUVA, 386 SX) via an RS-232C port was used for monitoring and collecting absorbance data at 1 s intervals.

The flow injection system consisted of a Desaga PLG-peristaltic pump with Desaga silicon tubing E, Rheodyne Teflon rotary valve type 50, Supelco Teflon tubing (0.5 mm i.d.) and couplings, a purpose built gas-liquid separator and a purpose built flow-thorough cell.

The gas-liquid separator (Fig. 1) was made of two coaxial glass tubes in which the outer glass tube is sealed around an inner glass tube. The separator chamber had about 2.3 ml inner volume with one inlet and two outlets. Placement of the inner glass tube in the separator chamber provides a large flat area, on which, the incoming gas–solution mixture from the mixing coil is dispersed and efficiently separated. Also, the inner glass tube provides a channel for circulating water so the temperature of the chamber could be easily controlled. More details and dimension of the separator chamber are shown in Fig. 1. The flow-through cell of the standard U-type design was made of a cylindrical block of polyethylene (50 mm length, 30 mm o.d. and 5 mm i.d.) with quartz windows.

A program written by the authors collected and saved data in the Excel format for further processing.

2.2. Reagents

Analytical reagent grade chemicals from Merck and deionized, triple distilled water were used. A stock solution of sulphite (2500 μg ml^{-1}) was prepared daily by dissolving 0.3935 g of anhydrous Na_2SO_3 in 100 ml of 0.02 M sodium hydroxide solution. Working solutions were prepared by the least number of dilution steps, immediately before use. A stock solution of sulphuric acid (2 M) was prepared by diluting 28.0 ml of concentrated H_2SO_4 (98% and 1.84 g ml^{-1}) to 250 ml. Working sulphuric acid solutions were prepared by appropriate dilution. Solutions of a range of interferent cations and anions were prepared from analytical reagent grade salts.

2.3. Manifold and procedure

The flow injection manifold is shown in Fig. 2. The streams of sulphuric acid (1 M) and triple distilled water were delivered by the pump at flow

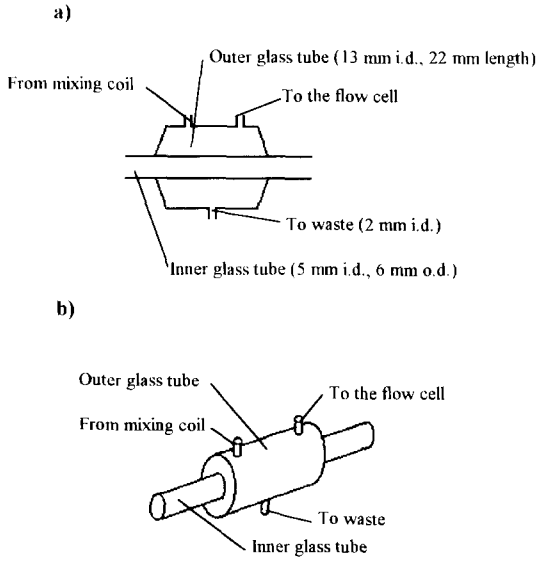

Fig. 1. Cross section view (a) and schematic diagram (b) of the purpose built gas-liquid separator.

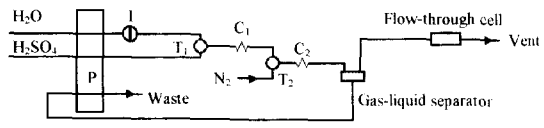

Fig. 2. The manifold design for the generation and measurement of sulphur dioxide; P, pump; I, injection port; C_1 and C_2, mixing coils; T_1 an T_2, 3-way connector.

rates of 1.9 ml min^{-1}. 200 μl Sulphite solution (100 μg ml^{-1}) was injected at I, via the six port rotary valve into a stream of triple distilled water and was mixed with a sulphuric acid stream at the first three-way connector (T_1). The reaction between the sulphuric acid and sulphite was completed in mixing coil C_1 (length 50 cm). Nitrogen gas at a flow rate of 17.0 ml min^{-1} was introduced to the stream containing the product of the reaction between sulphite and sulphuric acid at the second three-way connector (T_2). The evolved sulphur dioxide (SO_2) diffused into the nitrogen gas segments through the second mixing coil C_2 (length 30 cm). In the gas-liquid separator, the gas phase containing SO_2 was separated from the liquid phase and was passed through the flow cell. The molecular absorbance of the gaseous phase was recorded at 200 nm and at 1 s intervals. The temperature of the separator's stream of water was 25°C in all the experiments. All the optimization processes were performed on the determination of 200 μl of 100 μg ml^{-1} of sulphite.

3. Results and discussion

The spectrum of the SO_2 gas evolved in the process was obtained by a UV/VIS spectrophotometer which showed similar results to those cited in the literature [15]. The experimental variables influencing the performance of the proposed manifold were studied and optimized as discussed below.

3.1. Effect of N_2 flow rate

The influence of N_2 flow which carried the evolved SO_2 to the separator chamber and then to the flow cell was investigated. The results showed

that the absorbance increases with increasing N_2 flow rate from 6.2 to 17.0 ml min^{-1}, while further increase in N_2 flow rates up to 52.1 ml min^{-1} caused the signal to decrease (Fig. 3). Thus, a N_2 flow rate of 17.0 ml min^{-1} was selected for further studies. The effect of an auxiliary nitrogen flow for carrying SO_2 from the separator to the flow cell was also studied but no improvement in sensitivity was observed.

3.2. Effect of carrier solution flow rate

The effect of flow rates of carrier solutions was studied for flow rates of 0.4 up to 4.5 ml min^{-1}. Increasing the flow rates caused the peak width to decrease. The peak heights increased for carriers flow rates up to 1.9 ml min^{-1}, further increase in carriers flow rates did not affect the absorption signal intensities (Fig. 3). A flow rate of 1.9 ml min^{-1} was selected for further studies.

3.3. Effect of length of mixing coils C_1 and C_2

The effect of length of mixing coil C_1 on peak height was investigated. The results obtained indicate an increase in peak heights when the length of mixing coil C_1 was varied from 10 to 50 cm. Use of mixing coils longer than 50 and up to 450 cm did not increase the peak heights so the length of mixing coil C_1 was selected as 50 cm for further studies.

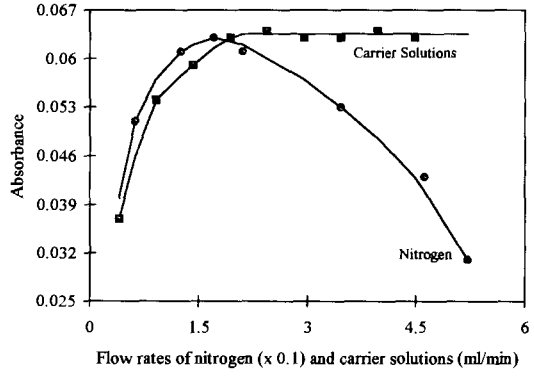

Fig. 3. Effect of N_2 and carrier solutions flow rates on the absorption signal intensities. Conditions: N_2 flow, 15.8 ml min^{-1} (for optimization of flow rates of carrier solutions); carrier solutions flow rates, 1.4 ml min^{-1} (for optimization of N_2 flow); mixing coil C_1, 96 cm; mixing coil C_2, 130 cm; sample volume, 200 μl, concentration of sulphite, 100 μg ml^{-1}; concentration of H_2SO_4, 2 M; λ_{max}, 200 nm; temperature, 25°C.

Studies on the effect of length of mixing coil C_2 on the peak height showed a small increase in peak heights with increasing length of mixing coil C_2 from 10 to 30 cm, while longer mixing coils up to 150 cm resulted in a slight decrease in peak heights. Therefore, the optimized length of mixing coil C_2 was selected as 30 cm.

Increasing the length of mixing coil C_1 had no significant effect on peak widths, while increasing the length of mixing coil C_2 increased the peak widths.

3.4. Effect of sample volume

It was found that by increasing the sample volume from 60 to 200 μl, with constant concentration of sulphite (100 μg ml^{-1}), the peak height was increased (absorbance changed from 0.027 to 0.064). However, further increase in sample volume up to 400 μl caused a slight decrease in absorption signal intensities (absorbance changed from 0.064 to 0.059). Also, the peak width was increased with increasing sample volume. A volume of 200 μl was therefore, chosen for further studies.

3.5. Effect of concentration of H_2SO_4

Increasing the concentration of H_2SO_4 from 0.2 to 2 M showed no significant improvement in absorption signal intensities. Also, the blank signal was not affected with increasing concentration of H_2SO_4. So, a concentration of 1 M H_2SO_4 was chosen for further studies.

3.6. Effect of temperature

The effect of temperature on the rate of evolution of SO_2 was investigated by placing the mixing coils C_1 and C_2 in a water bath and at the same time circulating water at the same temperature in the inner glass tube of the gas-liquid separator. The results showed that 40°C gives the highest signal (Table 1). However, 25°C was chosen for further studies as it is close to ambient temperature, making experimental manipulation easier.

Table 1
Effect of temperature on the absorption signal intensity

Temperature (°C)	Absorption signal intensity
24	0.064
29	0.071
5	0.074
40	0.080
45	0.078
50	0.075
60	0.071

Conditions: N_2 flow, 17.0 ml min^{-1}; carrier solutions flow rates, 1.9 ml min^{-1}; mixing coil C_1, 50 cm; mixing coil C_2, 30 cm; sample volume, 200 μl; concentration of sulphite, 100 μg ml^{-1} of sulphite; concentration of H_2SO_4, 1 M; λ_{max}, 200 nm.

3.7. Analytical performance of the manifold

The analytical performance achieved by the proposed manifold, including calibration equations and linear dynamic ranges are listed in Table 2. The presented calibration equations are obtained with similar operational parameters (optimum condition). As is obvious, three linear dynamic ranges are achieved. The theoretical detection limit calculated on the basis of three times the S.D. of the measurements of the blank signal [25],was obtained as 0.8 μg. Typical calibration traces are shown in Fig. 4. As can be seen, up to 40 samples h^{-1} can be analyzed.

Table 2
Analytical performance of the proposed manifold.

Linear dynamic range (μg)	Calibration equation	Correlation coefficient
≤120	$A = -1.744 \times 10^{-3} + 3.8345 \times 10^{-3} C$	0.9994
120–240	$A = 0.1546 + 2.6875 \times 10^{-3} C$	0.9995
240–440	$A = 0.3443 + 1.9722 \times 10^{-3} C$	0.9981

A, Absorbance; C, amount of sulphite in μg.

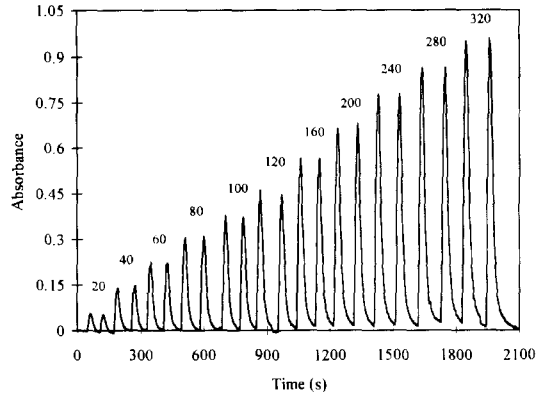

Fig. 4. Typical calibration trace for a series of standard sulphite solutions. Numbers above peaks denote amount of sulphite in μg.

3.8. Interferences

The effect of various anions and cations on the evolved SO_2 was studied. A range of solutions was prepared containing 50 μg ml^{-1} of sulphite and 3200 μg ml^{-1} of possible interfering anions (as K or Na salts). The solutions containing the sulphite sample plus the potential interferent anion (3200 μg ml^{-1}) were analyzed by the proposed method. The response was compared with those obtained from an uncontaminated sulphite solution. The results obtained are summarized in Table 3.

As expected, sulphide caused an enhancement effect on sulphite signal. This effect is due to the evolution of hydrogen sulphide which absorbs at 198 nm. An absorbance value of 0.016 was obtained when 25 μg ml^{-1} of sulphide were analyzed alone.

The interference effects of various cations (as SO_4^{2-} or NO_3^- salts) were investigated by a procedure similar to that used for anions. As it is shown in Table 3, the cations Na^+, K^+, Cr^{3+} and Mg^{2+} at a concentration of 1600 μg ml^{-1} had no effect on the determination of sulphite (50 μg ml^{-1}). The ions Mn^{2+}, Cu^{2+}, Co^{2+}, Ni^{2+}, Zn^{2+} and Cd^{2+} formed a precipitate after mixing with sulphite solution.

Preparation of similar solutions in EDTA (0.001 M of di sodium salt of EDTA) is effective in removing the interference effect of cations and

Table 3
Effect of anions and cations on 50 μg ml^{-1} of sulphite

Ion	Concentration (μg ml^{-1})	$\frac{S^{a}_{ion+sulphite}}{S_{sulphite}}$ (%)	$\frac{S_{ion+sulphite+EDTA}}{S_{sulphite+EDTA}}$ (%)
NO_3^-, I^-, CO_3^{2-}, SO_4^{2-}, PO_4^{3-}	3200	100	100
Br^-	3200	93	100
	1600	100	100
Cl^-	3200	53	100
	1600	100	100
S^{2-}	25	160	160
K^+, Na^+, Mg^{2+}, Cr^{3+}	1600	100	100
Mn^{2+}	1600	P[b]	30
	800	P	34
	160	P	39
Cu^{2+}	1600	P	97
	800	P	98
	160	P	100
Zn^{2+}	1600	P	78
	800	P	95
	160	P	100
Cd^{2+}	1600	P	90
	800	P	95
	160	P	100
Ni^{2+}	1600	P	93
	800	P	100
Co^{2+}	1600	P	72
	800	P	97
	160	P	100

[a] S, observed signal intensity.
[b] P, precipitate formed after mixing of solution.

anions. The addition of EDTA solution at a concentration of 0.001 M resulted in the dissolution of the above mentioned precipitates. Also the depressive interference effect of Cl^- and Br^- on sulphite is restored by the addition of EDTA (0.001 M) solution. However, Mn^{2+} and S^{2-} were the most severe interferents of the cations and anions investigated.

The results showed that introduction of EDTA in concentration ranges of 1×10^{-6} to 1×10^{-2} M into the sulphite solution not only stabilized the sulphite solution [15] and prevent the interference of some interferent cations and anions, but also, increases the sensitivity of the sulphite determination about two fold.

4. Application

To examine the reliability of the method certain amounts of standard sulphite solutions were added to a synthetic and water sample and analyzed according to the proposed method. The method was also applied to the determination of sulphite in lemon juice. Results obtained including recovery and precision are summarized in Table 4. It can be seen from the results that the method can be satisfactorily employed for the determination of sulphite.

5. Conclusion

By the use of a UV/VIS spectrophotometer for measuring the absorbance, a purpose built gas-liquid separator and a purpose built flow-through

Table 4
Analytical results of spiked samples

Sample[a]	Initially present (μg ml^{-1})	Added (μg ml^{-1})	Found (μg ml^{-1})	Recovery (%)	R.S.D.[b] (%)
1	0	350	342	97.7	1.02
2	0	1100	1087	98.8	0.76
3	0	1400	1384	98.9	1.12
4	0	30	29.63	98.8	2.01
		50	50.19	100.4	
		70	70.75	101.1	
		90	89.44	99.4	
5	0	40	38.09	95.2	1.83
		80	82.54	103.2	
		120	120.63	100.5	
		160	158.73	99.2	
6	0	50	48.75	97.5	1.35
		70	71.67	102.4	
		90	90.42	100.5	
		110	109.17	99.2	
7	29.21[c]	0	29.71	101.7	2.81
		18.85	49.51	105.0	
		37.58	66.53	99.51	
		56.87	86.66	102.0	
		74.67	103.68	99.3	

[a] Samples 1–3 were prepared from stock sulphite solution. Sample 4 was prepared from stock sulphite solution, 0.001 M EDTA and 400 μg ml^{-1} of interfering cations containing Cu^{2+}, Co^{2+}, Mg^{2+}, Ni^{2+}, Cd^{2+}, Cr^{3+} and Zn^{2+}. Sample 5 was prepared by adding certain amounts of stock sulphite solution to a water sample. Sample 6 was prepared by adding certain amounts of stock sulphite solution and 0.001 EDTA to a water sample. Sample 7 was prepared by adding certain amounts of stock sulphite solution to lemon juice.
[b] Relative standard deviation of six time analysis.
[c] Certified value given by the manufacturer.

cell, the determination of sulphite and dissolved sulphur dioxide is possible by the proposed flow injection gas-phase molecular absorption method. The proposed system is attractive because of its efficiency and simplicity. Interferences in the proposed method are few and are readily overcome by the addition of EDTA solution. Addition of EDTA solution to the sample solution also causes the sensitivity and selectivity of the proposed method to increase. Time saving, low reagent consumption, need of small sample volume, good precision, large dynamic range and high sample throughput (40 samples h^{-1}) are important features of the proposed system.

Acknowledgements

The authors wish to express their gratitude to Shiraz University Research Council for the support of this work.

References

[1] H.D. Belitz and W. Grosch, Food chemistry, Springer-Verlag, Berlin, 1987.
[2] Environmental Health Criteria 8 –Sulfur Oxide and Suspended Particulate Matter, WHO, Geneva, 1979.
[3] W.J. Williams, Handbook of Anion Determination, 1st edn., Butterworth, London, 1979, p. 587.
[4] C.M. Dos, Talanta, 38 (1991) 347.
[5] T. Imanori, K. Ogata, S. Tanabe, T. Todia, T. Kawanishi and M. Ichikawa, Chem. Pharm. Bull., 30 (1982) 375.
[6] P. Bruno, M. Casalli, M. Delle Monica and A. Di Fano, Talanta, 26 (1979) 1011.
[7] J. Janak and Z. Vecera, Mikrochim. Acta, Part III, 1990, 29.
[8] G. Raspi and G. Giantell (unir. pisa, Italy), Chim. Ind. (Milan), 47 (1965) 1325.

[9] S.S. Brody and J.E. Chaney, J. Gas Chromatogr., 4 (1996) 42.
[10] I.I. Koukli, E.G. Sarantonis and A.C. Calokerions, Analyst, 113 (1988) 603.
[11] N. Balasubramanian and B.S.M. Kumar, Analyst, 116 (1991) 207.
[12] T.A. Arowolo and M.S. Gresser, Talanta, 39 (1992) 1471.
[13] A. Safavi and A.A. Ensafi, Anal. Chim. Acta, 252 (1991) 121.
[14] C.A. Groom, J.H.T. Luong and C. Masson, J. Biotechnol., 27 (1993) 117.
[15] T.A. Arowolo and M.S. Cresser., Analyst, 116 (1991) 1135.
[16] A. Syty, Anal. Chem., 45 (1973) 1744.
[17] H.E. Winkler and A. Syty, Environ. Sci. Technol., 10 (1976) 913.
[18] M.S. Cresser, Proc. Anal. Div. Chem. Soc., 15 (1978) 68.
[19] M.S. Cresser, Eur. Spectrosc. News, 19 (1987) 36.
[20] J. Sanz, F. Gallarta, J. Galban and J.R. Castillo, Fresenius Z. Anal. Chem., 330 (1988) 510.
[21] J. Sanz, S. De Marcos, O. Muro and J. Galban, Microchim. Acta, 110 (1993) 193.
[22] J. Sanz, F. Gallarta and J. Galban, Anal. Chim. Acta., 225 (1991) 113.
[23] J. Sanz, S. De, J. Galban and F. Gallarta, Analusis, 21 (1993) 27.
[24] S. Cabredo Pinillos, I. Sanz Vicente, J. Sanz Asensio and J. Galban Bevnal, Talanta, 42 (1995) 937.
[25] J.C. Miller and J.N. Miller, Statistics for Analytical Chemistry, Ellis Horwood, New York, 1984.

ELSEVIER

Talanta 44 (1997) 1017–1023

Talanta

Determination of trace amounts of some metals in samples with high salt content by atomic absorption spectrometry after cobalt-diethyldithiocarbamate coprecipitation

Latif Elçi *, Uğur Şahin, Sibel Öztaş

Erciyes University, Art and Sciences Faculty, Chemistry Department, 38039 Kayseri, Turkey

Received 7 August 1996; received in revised form 18 November 1996; accepted 19 November 1996

Abstract

A method for determination of trace amounts of Cu, Fe, Pb, Mn, Zn, Cd, Ni, Bi and Cr in aqueous solutions by flame atomic absorption spectrometry after coprecipitation by using a combination of sodium diethyldithiocarbamate as a chelating agent and cobalt as a carrier element was introduced. Different factors including amounts of reagents, pH of sample solution, standing time, sample volume for the precipitation and matrix effects were examined. Under selected conditions, the relative standard deviation of the combined method of sample treatment, coprecipitation and determination with flame AAS ($n = 9$) is generally about 3.5–6.9%; the limits of detection (3 s, $n = 20$) for the analytes were found to be between 4 and 64 μg l^{-1}. The procedure was applied to the analysis of sea water and dialysis concentrate samples with quantitative recovery, ≥95%. © 1997 Elsevier Science B.V.

Keywords: Co-DDTC; Coprecipitation; Dialysis concentrate; Sea water

1. Introduction

Many techniques have been proposed to preconcentrate trace metals from matrices that adversely influence atomic absorption spectrometric detection. Separation methods used for this purpose include solvent extraction [1,2], ion exchange supports [3,4], chelating resins [5,6], sorbent extraction [7–9] and coprecipitation [10,11]. The combination of coprecipitation and filtration offer a simple and rapid preconcentration technique mainly in water analysis. Among coprecipitation precipitates, metal chelates are the most attractive gathering precipitate because of the excellent multi-elements trace recovery and sufficient separation factors especially for alkali and alkaline earth elements. Various procedures involving the use of metal-chelating precipitates are well documentated in the literatures [12,13]. Many metal ions, such as Co, Cu, Fe, Pb, Mn, Zn, Cd, Ni, Bi and Cr, form stable chelates with sodium diethyldithiocarbamate (NaDDTC). These chelates have been used for the extraction of some metal ions from aqueous solutions to an organic phase [12–14]. Co-DDTC is a considerably stable chelate [12]. Furthermore it is insoluble in water.

* Corresponding author.

PII S0039-9140(96)02186-8

We conclude from the data given above that the employment of Co-DDTC in the study of the coprecipitation of trace metal ions in aqueous solutions as a collector of intent.

The purpose of the present work was to study the conditions of coprecipitation of Cu, Fe, Pb, Mn, Zn, Cd, Ni, Bi and Cr at trace level in aqueous solutions including high salinity by aid of Co-DDTC chelate.

2. Experimental

2.1. Instrument

A Hitachi atomic absorption spectrometer (Model Z-8000) with an air/acetylene flame and a Zeeman background corrector was used throughout the determination of the metal ions in model solutions and samples. The analysing solutions as 100 μl were introduced into the nebulizer of flame AAS with an injection method [15]. The operating conditions suggested in the instrument data processor were followed for the determination of metals.

2.2. Chemicals

Analytical reagent grade pure chemicals were used throughout the experiments. Doubly de-ionized water was redistilled in a quartz apparatus. Stock solutions of 1000 μg ml^{-1} in 1 M HNO_3 for each element of interest were used for the preparation of standard and model solutions. A solution of NaDDTC (5%, m/v) was prepared by dissolving of solid NaDDTC (Merck) in the water. The solution should be filtered through a membrane filter with 0.45 μm pore size and then kept at 4°C for longer storage. A solution of cobalt (500 μg ml^{-1}) as a carrier element was prepared by dissolving of proper amount as nitrate salt in the water.

The buffer used were phosphoric acid/dihydrogenphosphate for pH 2, ammonium acetate/acetic acid for pH 4–6, ammonium hydroxide/ammonium chloride for pH 8 to 10. pH 1 was obtained with nitric acid.

The membrane filter used was made of cellulose nitrate (0.45 μm pore size, 47 mm diameter and Whatman Cat. No: 7184 004).

3. Procedures

3.1. Model working

In the experiments for the recovery of examined metal ions, 100 ml portion of an aqueous solution containing an appropriate amount of them, 5 μg for Cu, Ni, Fe, Mn, Bi, Cr and Pb, and 1 μg for Cd and Zn was placed in a glass vial. The pH and acid concentration of the solutions were adjusted with a appropriate buffer solution and concentrated nitric acid, respectively. Cobalt as a carrier element, 600 μg, was added to this solution. Then, the required volume of 5% NaDDTC solution for 200 mg NaDDTC was poured into the glass vial. After 10 min, the solution containing precipitate loaded with the analytes was filtered through a membrane filter made of cellulose nitrate by aid of vacuum. The precipitate was washed with the blank solution without cobalt. The precipitate together with the membrane were dissolved with 1–2 ml of conc. HNO_3 and the solution was evaporated almost to dryness. The residue was diluted up to 2 or 5 ml with 1 M HNO_3 solution. The analytes in the solution were determined with the injection method by flame AAS.

3.2. Analysis of sea water

Sea water sample, collected from the Mersin bay on east of the mediterranean sea, was immediately filtered through a 0.45 μm cellulose nitrate membrane, acidified to pH 3 with hydrochloric acid, and stored in precleaned polyethylene bottles. The procedure was applied to the sample within 15 days. Since the storage period was so short, it was considered that there was no apparent loss of the analytes. For the analysis, the sample containing 400 ml of acidified seawater were firstly neutralized and then pH of which was buffered to 6. Cobalt, 600 μg, and 200 mg NaDDTC were successively added to the buffered sample. Subsequent treatments were the same as

to those described in the model working. The volume of the final solution was 2 ml.

3.3. Analysis of dialysis concentrate

A 150 ml portion of a dialysis concentrate used for the hemodialysis of patients suffering from renal function deficiency, without pretreatments, was transferred into a 250 ml beaker. It was buffered to pH 6. After 600 μg cobalt and 200 mg NaDDTC were added, the concentration and determination steps were carried out as described above. The volume of the final analysing solution was 2 ml.

4. Results and discussion

4.1. Amount of coprecipitation reagents

The reason why cobalt as the carrier metal was used is that cobalt is a suitable matrix for the determination of elements of interest by AAS. This reason was tested with a preliminary experiment. The solution containing fixed amount of examined elements and preparing with increasing concentrations of cobalt was analysed by flame AAS without any pretreatment. As a result, no significant interference had been observed up to 350 μg ml^{-1} Co. The concentration of cobalt found is considerably higher than the concentration of cobalt, max. 300 μg ml^{-1}, in the final solution obtained after the coprecipitation. The another reason is that the compound NaDDTC forms a more stable chelate with cobalt than that of examined elements such as Cu, Ni, Bi, Pb, Zn, Fe, Cr ve Mn [12].

After the findings above, the influence of amount of cobalt as a carrier element and amount of NaDDTC as a chelating agent on the coprecipitation of metals of interest was examined. The influence of cobalt was investigated with the multielement test solutions containing different amounts of Co, ranging from 0 to 1250 μg (Table 1). Although high recovery yields would be expected with a high amount of cobalt, there was difficulty associated the filtration of test solutions including 1250 μg of cobalt. The results indicate that quantitative recoveries for Cu, Pb, Fe, Mn, Zn, Cd and Ni in aqueous solutions were easily obtained with the ranging of 500–1000 μg cobalt. In the same range of cobalt, the recoveries for Bi and Cr were found between 40 and 60%.

The experiments were also repeated without cobalt. In this case, the recovery yields were found to be as less than 60%. However, the repeatability of recovery values was considerably poor($s/\bar{x} \geq$ 25%). As the concentration of trace elements is at the μg ml^{-1} level or even lower, they can not form completely their own independent solid phases. Also, NaDDTC can not precipitate in water [12]. Probably, the low recoveries are due to these two reasons. Therefore, for the precipitation of the trace elements from aqueous solution, a solid phase must be formed.

In this procedure, NaDDTC performs two functions. Firstly, it forms the solid phase with cobalt. Secondly, it reacts with the trace element ions to form the chelates in aqueous solution. Therefore, the effect of NaDDTC amount on the coprecipitation was examined with the fixed amount of cobalt, 600 μg, in the model solution. The amount of NaDDTC was increased from 12.5 to 250 mg. To obtain quantitative recovery, the optimal amount of NaDDTC was found to be 200 mg for the examined metal ions. Consequently, 600 μg of cobalt and 200 mg of NaDDTC were used in subsequent studies. Also, it can be expected that the recoveries obtained with the experiments repeated without both cobalt and NaDDTC will be smaller than 20%.

Table 1
Effect of cobalt amount on coprecipitation of analytes ($n = 3$)

Co amount (mg)	Recovery, %						
	Cu	Fe	Pb	Mn	Zn	Cd	Ni
0	55	40	58	5	40	10	5
0.250	75	75	98	80	90	95	90
0.500	100	95	101	100	94	98	102
0.600	98	96	99	97	96	96	100
0.750	95	102	100	100	96	97	98
1.000	96	98	100	98	97	96	101
1.250	98	101	96	99	98	99	98

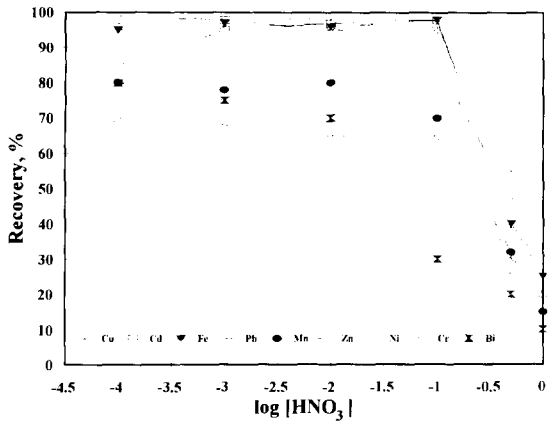

Fig. 1. Effect of HNO_3 concentration on coprecipitation of Cu, Cd, Fe, Pb, Mn, Zn, Ni, Cr and Bi.

4.2. Effect of acid concentration and pH on coprecipitation

Firstly, the effect of sample solution acidity on the coprecipitation of examined metal ions with Co-NaDDTC complex was investigated by use of HNO_3. As shown in Fig. 1, copper, lead and iron in range of 10^{-4}–10^{-1} M, zinc in a range of 10^{-4}–10^{-2} M and, cadmium and nickel in a range of 10^{-3}–10^{-1} M HNO_3 were quantitatively coprecipitated. The recoveries of Mn, Cr and Bi in a range of 10^{-4}–10^{-1} M HNO_3 were lower than 80%. However, the recoveries for the examined metals considerably decrease after 10^{-1} M HNO_3. This fact is probably connected with the stability of NaDDTC in acidic solution. It is well known that NaDDTC decomposes easily in acidic solution [12,16].

The coprecipitation of the metal ions was also studied with buffer solutions. As seen from Fig. 2, Cu, Fe, Pb in a range of pH = 1.0–10.0 and Ni, Zn and Cd in a range of pH = 1.0–8.0 were coprecipitated quantitatively. In contrast to HNO_3, buffer solutions in a range of pH = 4–8 are also suitable for the quantitatative recovery of Mn(II). The recoveries for Cr and Bi were lower than 80%. Due to the number of recovered elements, the model solution buffered to pH = 6 were used in subsequent experiments.

4.3. Standing time for coprecipitation

The standing time for precipitate formation was also optimized as it is an other important factor which influences the quality of coprecipitation. After 5 min, the quantitative recoveries for the all elements were obtained. Consequently, 5 min at least for the completion of coprecipitation were stood in all experiments. This period consists of the formation of preprecipitate and the adsorption of traces on the precipitate.

4.4. Sample volume

In the analysis of a real sample using preconcentration procedures, the sample volume is one of important parameters used to obtain a high concentration factor. Therefore, the recoveries of Cu, Fe, Pb, Mn, Zn, Cd and Ni from different sample volumes were tested in concentration range of 2–50 μg l^{-1} as depending on the elements. The results showed that the recoveries, except for Mn (up to 250 ml), were quantitative up to 450 ml. Due to two of the final solution volumes, the highest concentration factor was found to be 225.

4.5. Effect of matrix ions on coprecipitation

The effect of major components, such as Na^+, K^+, Ca^{2+}, Mg^{2+}, Cl^-, CH_3COO^-, Dextrose in

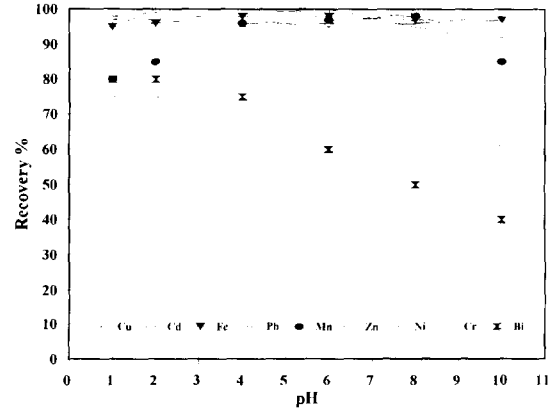

Fig. 2. Effect of pH on coprecipitation of Cu, Cd, Fe, Pb, Mn, Zn, Ni, Cr and Bi.

Table 2
Maximum tolerance limits for matrix ions on coprecipitation of analytes ($n = 3$, sample Vol. 100 ml)

Ions	Concentration, μg ml^{-1}	
	Tolerance limit	In the effluent
Na^+	≤100.000	65
K^+	≤5000	45
Ca^{2+}	≤5000	30
Mg^{2+}	≤5000	25
CH_3COO^-	≤110.000	n.d.
Cl^-	≤100.000	n.d.
Dextrose	≤200.000	n.d.

n.d. Not determined.

sea water and dialysis concentrate, on the coprecipitation were studied systematically. Various amounts of matrix ions were added to a solution containing fixed amounts of analytes and the present procedure was followed. The results were listed in Table 2. The tolerance limit is defined as the ion concentration causing a relative error smaller than ± 5% related to the coprecipitation and determination of examined elements. As seen from Table 2, the low recoveries for the matrix ions are helpful in the determinations of interest trace heavy metals. The tolerance limits are higher than the concentrations of Na^+, K^+, Ca^{2+} and Mg^{2+} in sea water [17], and of Na^+, K^+, Ca^{2+}, Mg^{2+}, Cl^-, CH_3COO^- and dextrose in dialysis concentrate [18,19]. The these results are desired in view of applications to these samples.

4.6. Analytical performance

The analytical performance of the proposed procedure was illustrated by the results from flame atomic absorption spectrometric measurements. The relative standard deviations, ($s/\bar{x}$, $n = 7$), in the case of 20–100 μg l^{-1} of examined metal ions for 100.0 ml of sample volumes were found to be as ≤7%. The recoveries obtained with model solutions in redistilled water and in the presence of an interferent up to a certain concentration were higher than 95%, thus confirming the accuracy of the procedure. Also, the correctness of present method was confirmed by the recoveries of spikes from the real samples including various salts at high concentration levels. For the sea water and dialysis concentrate analysis, the efficiency of recovery of metal spikes from a sea water sample and a dialysis concentrate was investigated. As seen from Table 3, the analytical errors for the all analytes in both two samples were always lower than 5%. Thus, the accuracy of the procedure and its independence from matrix effects were confirmed for high salinity solution. The detection limits ($s = 3$, $n = 20$) for Cu, Fe, Pb, Mn, Cd, Ni and Zn from the blank solution were found to be as 16, 54, 64, 15, 4, 18 and 20 μg l^{-1}, respectively [20].

4.7. Application of the method

In this work, the recommended procedure as described under experimental was applied to some samples with high salinity such as a sea water and a commercial dialysis concentrate. The results which are shown in Table 4 and Table 5 have been calculated on the assumption of 100% recovery of the analytes. The concentration factors for sea water and dialysis concentrate were 225 and 75, respectively. For the analysis, the relative standard deviation of the procedure varies in range of 3.5–6.9% ($n = 9$).

5. Conclusion

The coprecipitation procedure with Co-DDTC examined in this paper provides a very simple, fairly rapidly, precise, accurate and reliable technique for the preconcentration of some trace metal ions from aqueous solutions of high salinity. The recoveries obtained with model solutions in redistilled water and in the presence of the most common matrix elements including the alkaline and alkaline earth metals were always higher than 95% (Fig. 1 and Table 3), thus, confirming the accuracy of the procedure and its independence from matrix effects.

Future work will be focused on application to other sample types containing high salinity, such as urine and spring water.

Table 3
Recovery of metal spikes from 150 ml of dialysis concentrate and 250 ml of sea water, ($n = 3$)

Analyte	Added, μg	Dialysis concentrate		Sea water	
		Found, μg	Error, %	Found, μg	Error, %
Cu	1.00	0.96	−4	0.95	−5
	2.00	2.04	+2	1.92	−4
	4.00	3.80	−5	3.88	−3
Fe	1.00	1.90	−5	1.02	+1
	3.00	2.85	−5	2.88	−4
	5.00	5.05	+1	5.14	+3
Pb	2.00	2.03	+2	2.04	+2
	4.00	4.08	+2	4.12	+3
	10.00	9.60	−4	10.40	+4
Mn	1.00	1.02	+2	1.01	+1
	2.50	2.55	+2	2.54	+2
	5.00	5.10	+2	5.10	+2
Zn	0.50	0.53	+6	0.52	+4
	1.00	1.02	+2	1.02	+2
Cd	0.20	0.19	−5	0.22	+1
	0.80	0.78	−3	0.76	−5
	1.00	0.98	−2	0.96	−4
Ni	1.00	1.02	+2	0.98	−2
	4.00	4.06	+2	3.90	−3

Table 4
Analytical results for sea water

Analyte	Conc., μg l^{-1}, ($\bar{x} \pm t \cdot s/\sqrt{n}$)*	$s/\bar{x}$
Cu	1.94 ± 0.09	0.06
Fe	4.5 ± 0.2	0.07
Pb	1.2 ± 0.04	0.04
Zn	2.8 ± 0.1	0.06
Cd	0.37 ± 0.01	0.04
Ni	4.8 ± 0.2	0.06

* Uncertainty at 95% confidience level, $n = 9$.

Table 5
Analytical results for dialysis concentrate

Analyte	Conc., μg l^{-1}, ($\bar{x} \pm t \cdot s/\sqrt{n}$)*	$s/\bar{x}$
Cu	3.5 ± 0.1	0.05
Fe	6.9 ± 0.3	0.06
Pb	1.67 ± 0.05	0.04
Mn	3.04 ± 0.09	0.04
Zn	0.90 ± 0.03	0.04
Cd	0.83 ± 0.04	0.06
Ni	1.51 ± 0.08	0.07

* Uncertainty at 95% confidence level, $n = 9$.

References

[1] R.P. Mitcham, Analyst, 105 (1980) 43.
[2] R.G. Smith and H.L. Windom, Anal. Chim. Acta, 113 (1980) 39.
[3] D.E. Leyden, T.A. Patterson and J.J. Alberts, Anal. Chem., 47 (1975) 733.
[4] M. Kirk, E.G. Perry and J.M. Arritt, Anal. Chim. Acta, 80 (1975) 163.
[5] D.E. Lee, C.H. Eum, I.H. Lee and S.J. Jeon, Anal. Sci., 4 (1988) 505.
[6] L. Joseph and V.N.S. Pillai, Analyst, 114 (1989) 439.
[7] L. Elçi, Seval Işildar and M.Doğan, Anal. Chim. Acta, 293 (1994) 319.
[8] Ş. Tokalıoğlu, Ş. Kartal and L. Elçi, Anal. Sci., 10 (1994) 779.
[9] H.L. Lancester, G.D. Marshall, E.R. Gonzalo, J. Ruzicka and G.D. Christian, Analyst, 119 (1994) 1459.
[10] R. Eidecker and E. Jackwerth, Fresenius Z Anal. Chem., 328 (1987) 469.
[11] J. Zucheng and P. Schramel, Fresenius J. Anal. Chem., 343 (1992) 600.

[12] J. Minczewski, J. Chwastowska and R. Dybczynski, 'Separation and Preconcentration Methods in Inorganic Trace Analysis' Ellis Harwood, Chichester, 1982.
[13] A. Mizuike, 'Enrichment Techniques for Inorganic Trace Analysis', Springer-Verlag, Berlin, 1983.
[14] A. Wyttenbach and S. Bajo, Anal. Chem., 47 (1975) 1813.
[15] H. Berndt and E. Jackwerth, Spectrochim. Acta, 30B (1975) 169.
[16] M. Vircavs, A. Pelne, V. Rone and D. Vircava, Analyst, 117 (1992) 1013.
[17] V.L. Snoeying and D. Jenkins, 'Water Chemistry', Wiley, New York, 1980.
[18] M. Soylak, L. Elçi and M. Doğan, Anal. Lett., 9 (1993) 1997.
[19] M.R.P. Garcia, A.L. Garcia, M.E.D. Garcia and A. Sanz-Medel, J. Anal. At. Spectrom., 5 (1990) 15.
[20] IUPAC, Nomenclature, symbols, units and their usages in spectrochemical analysis, Pure Appl. Chem., 45 (1976) 105.

ELSEVIER

Talanta 44 (1997) 1025–1035

Talanta

Particle beam-mass spectrometric analysis of difluorophenyl triazole compounds using normal phase-HPLC

Colin S. Creaser [a,*], James W. Stygall [a], David V. Bowen [b], Frank S. Pullen [c]

[a] *Department of Chemistry and Physics, Nottingham Trent University, Clifton Lane, Nottingham, NG11 8NS, UK*
[b] *Preclinical Information Technology, Pfizer Central Research, Sandwich, Kent, CT13 9NJ, UK*
[c] *Physical Sciences, Pfizer Central Research, Sandwich, Kent, CT13 9NJ, UK*

Received 10 September 1996; received in revised form 18 November 1996; accepted 19 November 1996

Abstract

Normal phase liquid chromatography combined with particle beam mass spectrometry has been applied to the analysis of fluconazole, an anti-fungal agent, [2-(2,4-difluorophenyl)-1,3-bis(1H-1,2,4-triazol-1-yl)-propan-2-ol] and a related intermediate, UK-51060 [2-(2,4-difluorophenyl)-1-(1H-1,2,4-triazol-1-yl)-ethan-2-one]. Electron ionisation and chemical ionisation have been investigated in combination with quadrupole ion trap and magnetic sector mass spectrometers and the spectra obtained compared with those for direct probe analyis. A novel method for the introduction of the chemical ionisation reagent gas via the interface is described for particle beam-magnetic sector mass spectrometry. Multi-stage scan routines have been implemented on the ion trap for the selective storage of analyte species and removal of solvent ions. Detection limits for both spectrometers have been determined and are discussed in terms of interface geometry and analyte transport characteristics. Normal phase HPLC on silica provided a good separation of the intermediate from the later eluting fluconaole peak. © 1997 Elsevier Science B.V.

Keywords: Chemical ionisation; Fluconazole; High performance liquid chromatography; Ion trap; Mass spectrometry; Normal phase; Particle beam

1. Introduction

Fluconazole is a difluorophenyl bis-triazole compound, used in the treatment of superficial and deep-seated fungal infections caused by Candida and *Cryptococcus neoformans* [1,2]. Other applications include the treatment of fungal meningitus and endophthalmitus [3,4]. In-vivo and in-vitro fluconazole levels have been determined by HPLC with UV detection [5] and GC with nitrogen–phosphorus [6] and electron-capture [7] detection. The mass spectrometry of fluconazole and related compounds has also been investigated [8].

Of the currently available interfaces for LC-MS, only the particle beam (PB) device produces classical electron ionisation (EI) and chemical ionisation (CI) spectra for HPLC analytes, being a sample/solvent enrichment technique independent of the ionisation mechanism [9]. The EI and CI

* Corresponding author.

PII S0039-9140(96)02187-X

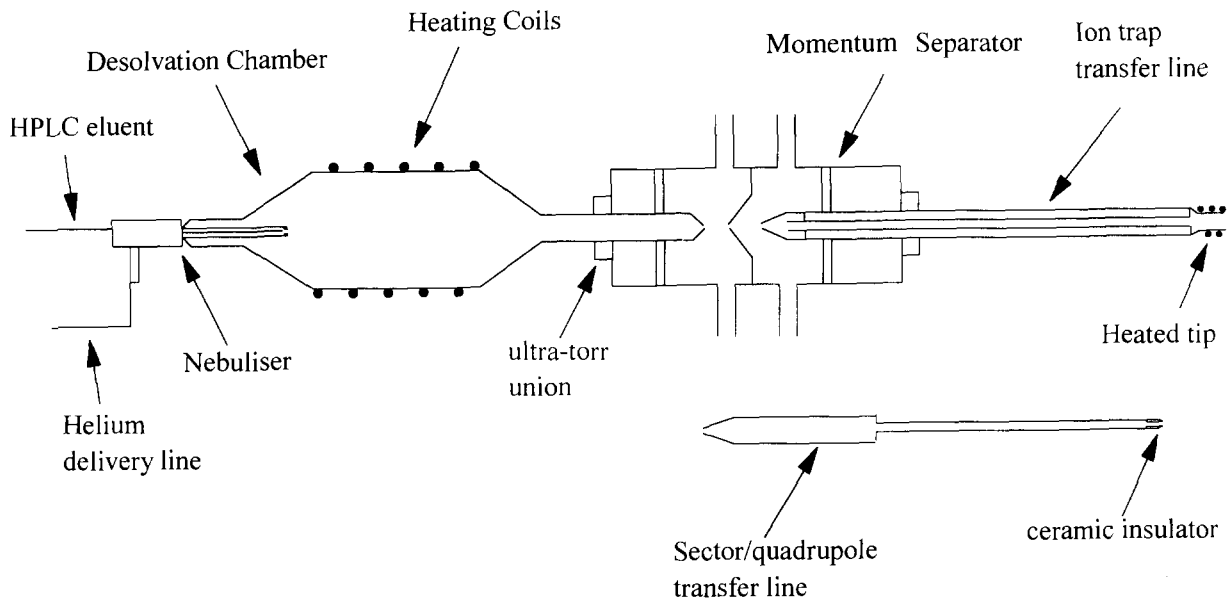

Fig. 1. Particle beam schematic.

spectra obtained contain useful structural information, as a result of fragmentation processes not observed using other interfacing techniques, and EI spectra can be compared with library spectra to confirm the presence of a target compound. These, and other, features have led to the successful use of the particle beam device for a wide variety of analyses, including many biomedical applications [9].

The separation of fluconazole and related compounds by reverse phase HPLC-PB-CI/MS has been reported [10] as part of an evaluation of on-line HPLC-NMR-MS. The determination of the triazole-containing compound [9-(4-methoxyphenylthiocarbamoyl)-6-(2-chlorophenyl) -1-methyl-4,7,8,10-tetrahydro-pyrido [4′,3′-4,5] thieno [3,2-f]—1,2,4-triazolo [4,3-a]-1,4-diazepine, a strong synthetic platelet activating factor antagonist, by reverse phase HPLC-PB-MS has also been discussed [11,12]. However, the use of normal-phase HPLC conditions for HPLC-PB-MS analyses of compounds of biomedical interest has not been extensively reported although the higher volatility of the mobile phase makes such separations well suited to the particle-beam interface [9].

We have recently reported a particle beam interface design that can be coupled to various beam and trapping mass spectrometers, yielding good mass spectral data for a number of different analytes [13]. In this paper we report the normal phase liquid-chromatographic separation of the anti-fungal drug fluconazole (1) and a reaction intermediate (2) combined with particle beam-mass spectrometric detection. This analysis has been used to compare various aspects of magnetic sector and ion trap HPLC-PB-MS instruments, using both EI and CI ionisation techniques.

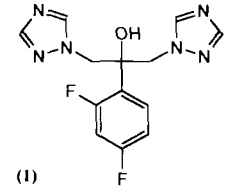

(1)

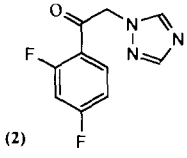

(2)

2. Experimental

Fig. 1 shows a schematic of the two-stage particle beam interface, fabricated to our design (ASH

instruments, Macclesfield, UK). Details of the design and construction of the device are given elsewhere [13]. The modular construction allowed various operational parameters to be optimised without disturbing vacuum conditions, and facilitated easy replacement or repair of components. The operational principle was similar to other PB interfaces [9].

The nebuliser was constructed using two concentric tubes of fused-silica (40 μm i.d.) and glass (approx. 250 μm i.d.), and the glass desolvation chamber was fitted with a resistively heated coil to aid vaporisation (approx. temperature 40°C). The momentum separator and transfer line were constructed from aluminium and stainless steel and coupled to two 18 m^3/h rotary pumps (Edwards high vacuum, Sussex, UK). A cold trap (Edwards) was fitted between the first vacuum chamber and the rotary pump. Nozzle-skimmer and skimmer–skimmer distances, adjustable from 0 to greater than 20 mm, were fixed using 'ultra-torr' unions (Cajon, OH, USA) at either end of the momentum separator body. Balanced gas flow was ensured by the use of two opposed pumping ports per chamber.

The ion trap spectrometer (Finnigan MAT ITMS, San Jose, CA, USA) was operated at 180°C and calibrated with perfluorotributylamine. The manifold pressure with the interface in position and both solvent and nebuliser helium gas flowing was 1.5×10^{-5} torr (uncorrected). Helium bath gas was added through the vacuum manifold fine metering valve (Meggitt Avionics, Portsmouth, UK) to give an operating pressure of 1.0×10^{-4} torr. The ion trap transfer line consisted of two concentric stainless steel tubes (3/8″ and 1/8″ i.d.). Connections for a heater and a thermocouple were passed between the tubes up to the transfer line tip. In operation, the heater was maintained at a temperature of approx. 240°C. The interface was introduced into the ITMS manifold via the probe lock and the tip placed approximately 0.5–1.0 mm from the face of the Roulon inlet to the trap. This was found to give best spectral quality with minimal space charging effects, and good sensitivity.

The magnetic sector spectrometer (VG 7070E-HF, VG Micromass, Altrincham, UK) was operated at a source pressure of 2.3×10^{-6} torr (uncorrected), as indicated by the source housing ion gauge, under particle beam operation. The source temperature was 300°C. Connection of the interface to the mass spectrometer was made via the probe lock, using a 3/8″ o.d. stainless steel transfer line (Fig. 1). This transfer line was not heated: rapid particle vaporisation was achieved by impact with the hot ion source. An insulating tip of machinable ceramic (Macor, Corning Glass) was fitted to the probe end to insulate the interface from the accelerating voltage of the ion source, which was operated at 4 kV.

Ammonia-CI spectra of 1 and 2 using probe introduction were obtained on a Kratos 1S double focusing magnetic sector spectrometer (Kratos Analytical, Manchester, UK). The instrument was tuned with PFK in the EI mode and then operated under ammonia CI conditions with a source housing pressure of 4×10^{-5} torr. The source temperature and accelerating potential were 120°C and 8 kV, respectively.

Normal phase HPLC separations were carried out on either a 2.1 mm × 250 mm × 5 μm silica column (Techsphere, HPLC technology, Manchester, UK) or a 4.6 mm × 250 mm × 5 μm silica column (Hypersil, Shandon, Runcorn, UK). The mobile phase, 60:40 hexane: 2% diethylamine in methanol, was delivered at a flow rate of 0.3 ml min^{-1} using a Milton Roy Constametric 300 pump (LDC Analytical, Staffordshire, UK). Injections were made using a Rheodyne 7125 injection valve (Cotati, CA, USA) fitted with a 20 μl loop. All solvents used were HPLC or AR grade and analytes were used as received without further purification.

3. Results and discussion

The EI spectra of 1 and 2, obtained on the magnetic sector and ion trap spectrometers using the same particle beam interface, are shown in Fig. 2. The spectra from magnetic sector and ion

trap instruments are similar and in both cases are good matches to spectra from the probe-EI analysis of these compounds [8], with little interference from solvent or other instrumental artifacts. Fragment ion structures are assigned tentatively in Scheme 1 based on accurate mass and linked-scan tandem mass spectrometric data [8]. The origin of the species at m/z 200 (18%) in the PB-ion trap spectrum of 1 is not assigned. Fig. 3 shows the selected ion chromatograms obtained for 1 (m/z 224) and 2 (m/z 141) using the 2.1 mm i.d. normal phase silica column-ion trap mass spectrometer combination, and illustrates the HPLC separation obtained in combination with the particle beam interface. A similar chromatographic separation

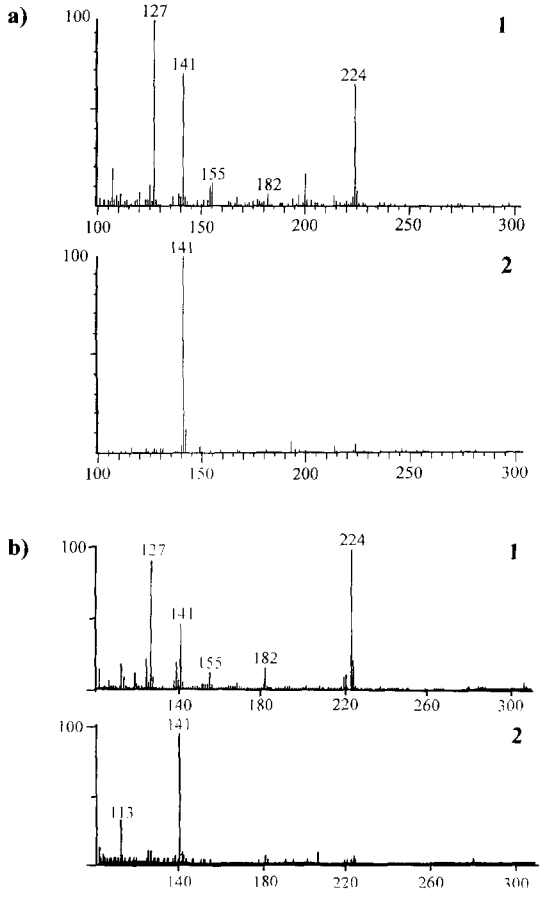

Fig. 2. EI spectra of 1 and 2 obtained from HPLC-PB-MS analysis: (a) ion trap; (b) magnetic sector.

of the analytes was achieved on the particle beam-magnetic sector spectrometer. Some peak tailing was observed in the chromatograms obtained from both spectrometers, a common feature of PB-MS systems [9], arising from sample hold-up in the momentum separator/transfer line and slow particle volatilisation off the source walls/heated probe tip.

In order to obtain good quality EI spectra on the PB-ion trap instrument, it was necessary to construct a scan routine consisting of several ion accumulation steps [13]. Each individual step consisted of an ionisation pulse (500 μs), with the operating conditions of the trap set to retain all ions with masses greater than a 20 amu low mass cut-off, followed by an increase in the RF voltage to give a 100 amu low mass cut-off. The low mass cut-off was then reset to 20 amu for the next ionisation pulse. These operating conditions corresponded to ion trap q_z values of 0.055 (20 amu) and 0.275 (100 amu) where the q_z parameter, derived from the Mathieu equation, is defined as:

$$q_z = \frac{-4eV}{mr^2\Omega_0^2}$$

for an ion of mass m and single charge e, held in a quadrupole ion trap of radius r_0, operating with an RF voltage of V and an RF drive frequency $\Omega/2\pi$. Ions having stable trajectories within the trap will possess q_z values of between 0 and 0.906, depending on the value of V, at any given time.

This ionisation method was found to improve the sensitivity for LC-PB-ion trap MS analysis [13]. The advantages of this complex routine were three-fold. Firstly, ions formed at low $q_{z(\text{ionise})}$ have low initial kinetic energy, and are therefore stored more efficiently in the trap volume than ions created at higher $q_{z(\text{ionise})}$ values [14]. Secondly, ionisation at low $q_{z(\text{ionise})}$ increases the initial trap ionisation volume [15] and lowers the electron energy [16], two factors which improve ion intensity. Finally, increasing q_z to a higher value after ionisation raised the low mass cut-off to a level high enough to ensure that all mobile phase derived ions were ejected from the trap before the next ionisation step. This prevented a high population of low mass solvent ions accumulating in the trap volume and causing space charg-

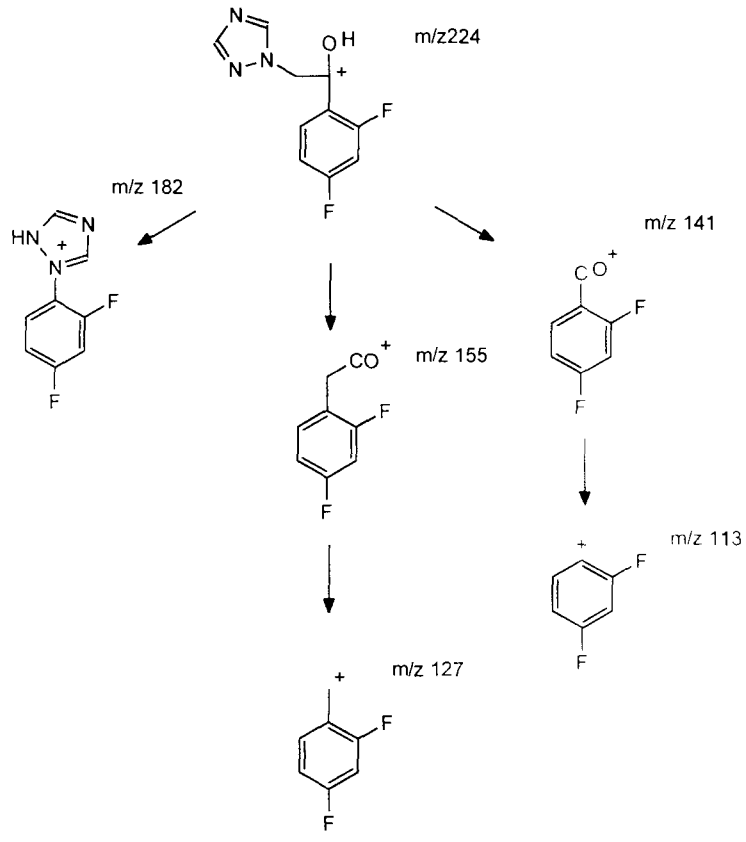

Scheme 1. EI fragmentation pathways for 1 and 2.

ing and solvent-CI effects, both of which lead to a deterioration in spectral quality.

Fig. 4 illustrates how the signal intensity for the m/z 224 ion of 1 changes as $q_{z(\text{ionise})}$ increases (Fig. 4a), and as ionisation pulse length increases at a constant total ionisation time (Fig. 4b). These show that the best ionisation conditions were $q_{z(\text{ionise})} = 0.06$ (low mass cut-off = 20 amu) and pulse width = 500 μs. The spectra obtained with a high $q_{z(\text{ionise})}$ or a single long ionisation pulse length (4 ms) compare poorly to the spectra in Fig. 2(b), with large noise peaks evident due to decreased S/N levels. In addition, ions derived from solvent CI processes (m/z 307, $(M + H)^+$ of 1) were observed for low $q_{z(\text{ionise})}$, long pulse length ionisation, due to the large population of solvent ions present. The importance of low $q_{z(\text{ionise})}$ conditions has been noted by other investigators [17].

Fig. 5 shows the UV and selected ion chromatograms obtained from HPLC-PB-magnetic sector MS analysis of a sample prepared containing 95% 1 and 5% 2 (4.6 mm i.d. silica column). The fluconazole peak exhibits some tailing in comparison with the UV trace, but the advantage of the normal phase separation used in these experiments, compared with the reverse phase analysis normally employed for pharmaceutical products, is that 2 elutes before the main product 1, avoiding the elution of a minor peak on the tail of a major one and thus allowing clear identification and quantitation of both compounds.

Sensitivity on the HPLC-PB-magnetic sector instrument was fairly typical for PB-MS analysis

[9], with injections of 18 ng of 1 (m/z 224) and 60 ng of 2 (m/z 141) in the full scan mode yielding single ion chromatographic peaks of S/N 3:1 (2.1 mm i.d. silica column). The HPLC-PB-ion trap instrument showed poorer sensitivity for these analytes, injections of 5 μg of 1 and 2 yielding peaks of S/N 18:1 (m/z 224) and 16:1 (m/z 141), respectively. This can probably be attributed to analyte hold-up in the narrow ion trap transfer line and to sample decomposition [9], which was particularly severe at high probe tip temperatures (approx. 300°C). Detection limits in the low nanogram range have been reported for this PB-ion trap configuration on a number of other analytes [13].

Ammonia CI was carried out on compounds 1 and 2 using the double-focusing spectrometer. The major ions observed are tabulated in Table 1, together with the results for direct probe introduction of 1 and 2 into a CI source, and those for HPLC-PB-solvent-CI ion trap MS of the same compounds (see below). All the spectra obtained on magnetic sector instruments show prominent $[M+H]^+$ ions for both 1 and 2. However, the results for PB-sector analysis demonstrate a large degree of fragmentation when compared with the probe data, with the base peak for 1 at m/z 222. This species was of very low intensity in the probe-CI spectrum, but similarly intense under

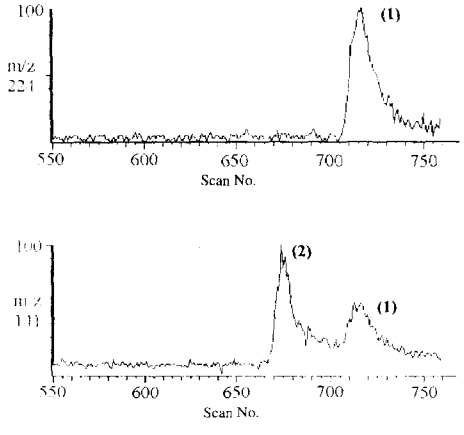

Fig. 3. Selected ion chromatograms for the separation of 1 and 2 obtained from HPLC-PB-ion trap MS analysis (250 ng μl^{-1} 1 and 2).

ammonia-CI conditions for a commercial PB-quadrupole MS system using reverse phase HPLC [10]. This suggests that under high pressure ammonia-CI conditions, some particles of analyte striking the hot source walls may undergo thermal degradation and the thermal fragments formed then react with reagent ions in the CI plasma. Anomalous ions due to thermal degradation in HPLC-PB-MS spectra have been reported in the literature, using both EI and CI techniques [9]. Full scan sensitivity for PB-magnetic sector CI was lower than that observed under EI operation, with injections of 120 ng 1 and 150 ng 2 yielding single ion chromatographic peaks of S/N 7:1 (m/z 307) and 2:1 (m/z 224) respectively.

The lower sensitivity under ammonia CI conditions, compared with EI, for the double focusing spectrometer may be due to the source geometry: CI gas at relatively high pressure was entering the source exactly opposite the particle beam entrance and was possibly affecting the efficiency of particle transmission into the source. Previous work on GC-CI/MS using a high resolution spectrometer [18] has shown that analyte peak area and sensitivity can be markedly improved by introducing the reagent gas co-axially to the eluent flow. Although this exact configuration could not be implemented on the PB-MS instrumentation during these experiments, it was possible to introduce the ammonia into the particle beam via an inlet between skimmers 1 and 2, which eliminated any detrimental turbulence in the source.

To characterise this new 'inter-skimmer' CI inlet technique, a comparison was made between the use of the normal source CI gas inlet and the 'inter-skimmer' CI approach. Post-column injections of 500 ng fluconazole were made under CI ionisation conditions using both inlet configurations at a variety of source housing pressures, set by adjusting the ammonia flow to the source or momentum separator. The resulting signal peak areas were recorded, using TIC and selected ion data. The results are illustrated in graphical form in Fig. 6. During the initial rise in source pressure, both sets of data show an increase in the intensity of CI-derived $[M+H]^+$ species, with a corresponding drop in EI-derived fragment ion strength. This trend continues at higher pressures

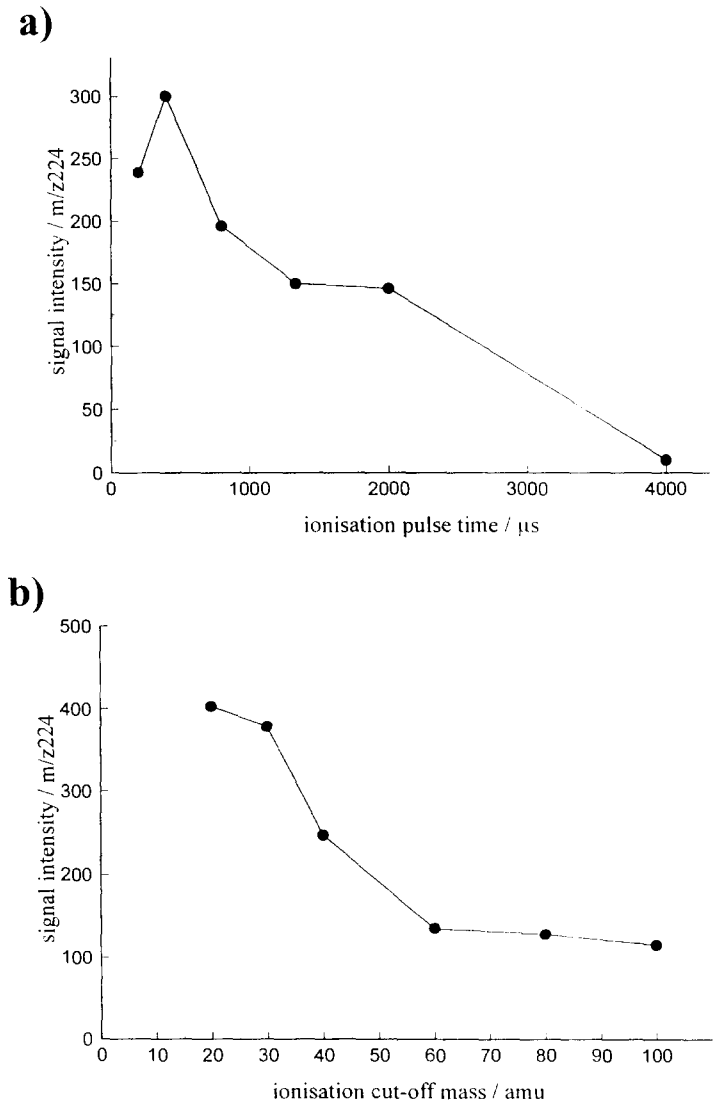

Fig. 4. Variation of m/z 224 peak area for fluconazole injections monitored by PB-ion trap MS with: (a) ionisation pulse length; (b) q_z (ionise) value.

using the inter-skimmer inlet technique (Fig. 6a), with only a small drop in the total ion current (TIC). However, using the standard source CI inlet (Fig. 6b) the intensity of both CI and EI ions decreases above a certain reagent gas pressure, with the TIC dropping significantly.

The inter-skimmer approach can therefore give measurable improvements in sensitivity for PB-CI/MS analysis. A CI inlet arrangement co-axial with the transfer line exit, rather than the second skimmer as in this approach, should not affect particle transmission in either the source or the momentum separator and therefore sensitivity in CI mode might be further enhanced by this approach.

In contrast to conventional 'beam' type instruments, ion trap chemical ionisation routines utilise low (10^{-5}–10^{-6} torr) pressures of reagent gas for

long (up to 100 ms) reaction times [19]. This presents few problems for inlet systems such as heated probes or gas chromatographs that impose little or no vacuum restrictions. However, for LC-MS inlets such as the particle beam, that transmit significant quantities of vapourised solvent into the analyser, ionising and storing a population of CI reagent ions can prove difficult, due to space charge limitations and reagent-solvent reactions, both of which will quickly deplete the number of stored reagent ions. This was found to be the case during experiments on a PB-ion trap system utilising a three stage momentum separator with inter-skimmer helium flushing to reduce solvent levels to an absolute minimum [20]. With the much simpler two-stage design used in this work the results were similar. A large ion count could be obtained easily for the RF/DC

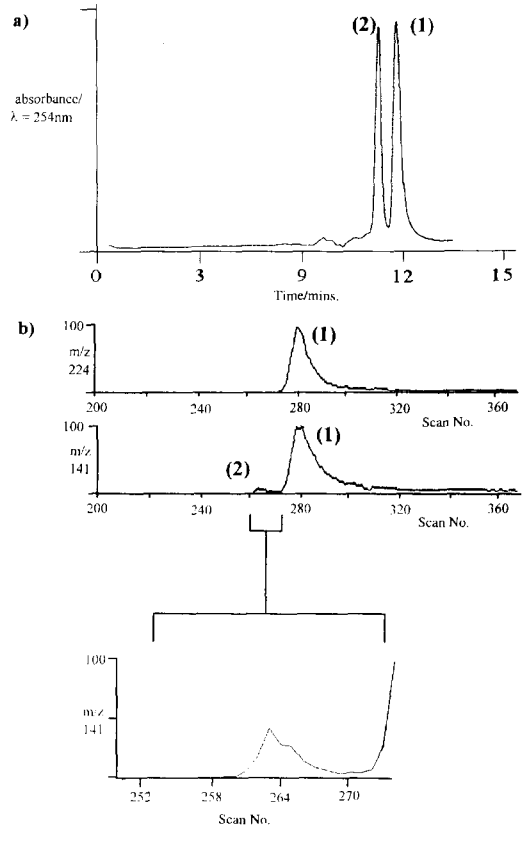

Fig. 5. (a) UV and (b) PB-MS chromatograms for the separation of a mixture containing 95% 1 and 5% 2.

Table 1
Major ions obtained from CI-MS analysis of 1 and 2, using different CI reagents and sample introduction methods

MS acquisition mode	Fluconazole (1)	UK-51060 (2)
NH_4^+ CI	307 (100%)	224 (100%)
Probe introduction	224 (35%)	141 (11%)
Magnetic sector	127 (5%)	
Spectrometer	83 (3%)	
NH_4^+ CI	307 (80%)	224 (100%)
Particle beam introduction	289 (18%)	141 (95%)
Magnetic sector	265 (24%)	
Spectrometer	224 (58%)	
	222 (100%)	
	141 (38%)	
$CH_3OH_2^+$ CI	307 (100%)	224 (100%)
Particle beam introduction	289 (14%)	
Ion trap spectrometer	238 (46%)	
	222 (32%)	

isolated NH_4^+ reagent ion from ammonia with the interface in place, but without solvent or sample introduction. However, with methanol/hexane/DEA solvent flows as low as 0.1 ml min^{-1}, the count was reduced to under 5% of its initial reading, with significant amounts of $[CH_3OH_2]^+$ ions derived from methanol solvent molecules being formed. Whilst the application of a notched broadband axial ejection signal [21] during ionisation might eliminate the space charge problem, the solvent-reagent ion reactions would still occur, particularly with less selective CI species such as CH_5^+. Consequently, standard CI ion trap routines seem not to be applicable to PB introduction.

However, chemical ionisation in the ion trap can be carried by using the solvent vapor itself as a source of reagent ions. Table 1 tabulates the solvent-CI spectra of 1 and 2, obtained on the HPLC-PB-ion trap instrument using the RF/DC isolated $[CH_3OH_2]^+$ reagent ion, derived from residual methanol mobile phase [19], as the proton donor. The spectra show strong $[M+H]^+$ ions with little fragmentation compared with the PB/MS CI data obtained with the sector instrument using the ammonium reagent ion, although an ion is observed at m/z 238, $[M\text{-}C_2N_3H_3]^+$, in

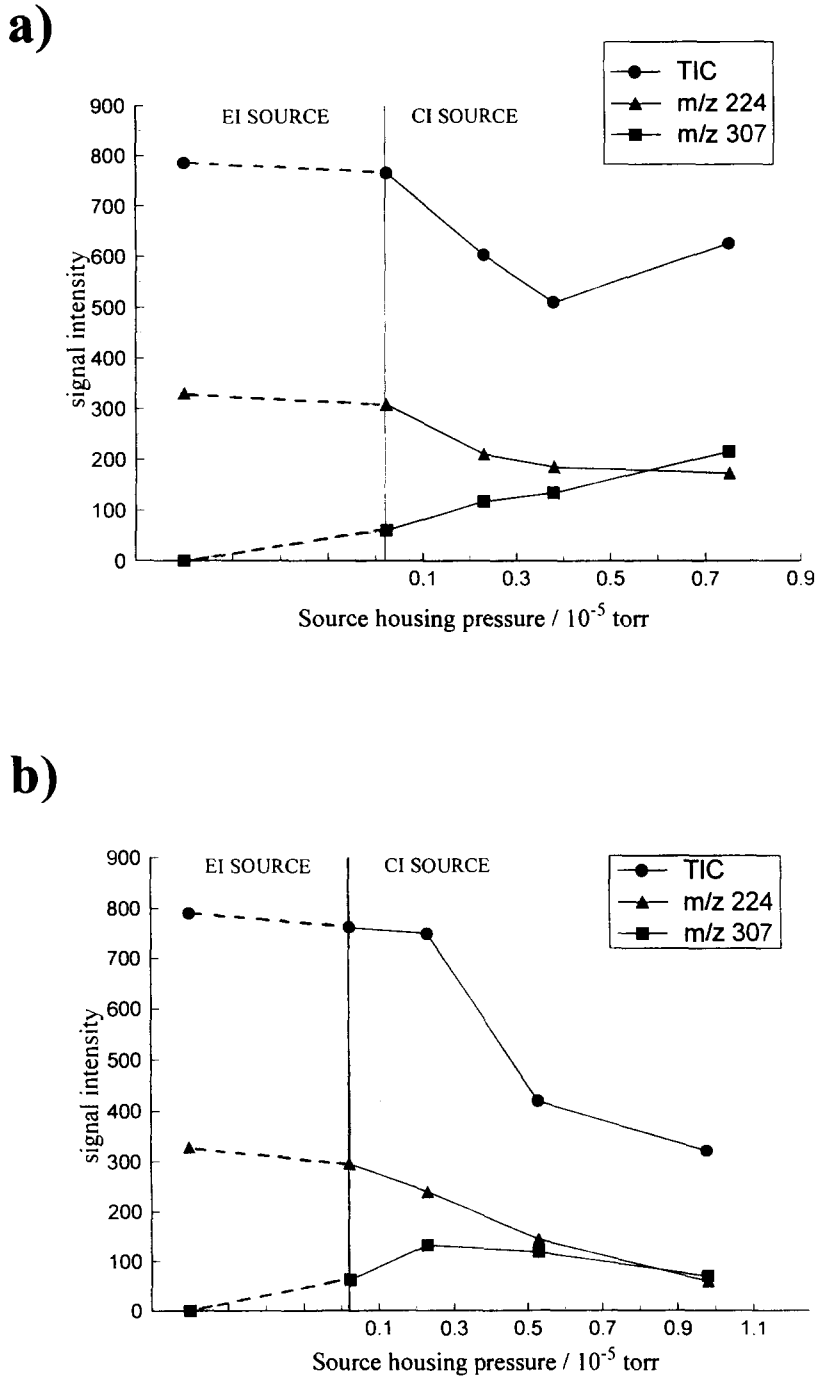

Fig. 6. Variation of fluconazole signal intensity (m/z 307, 224 and TIC) with CI source pressure using (a) PB inter-skimmer CI inlet (b) source CI inlet.

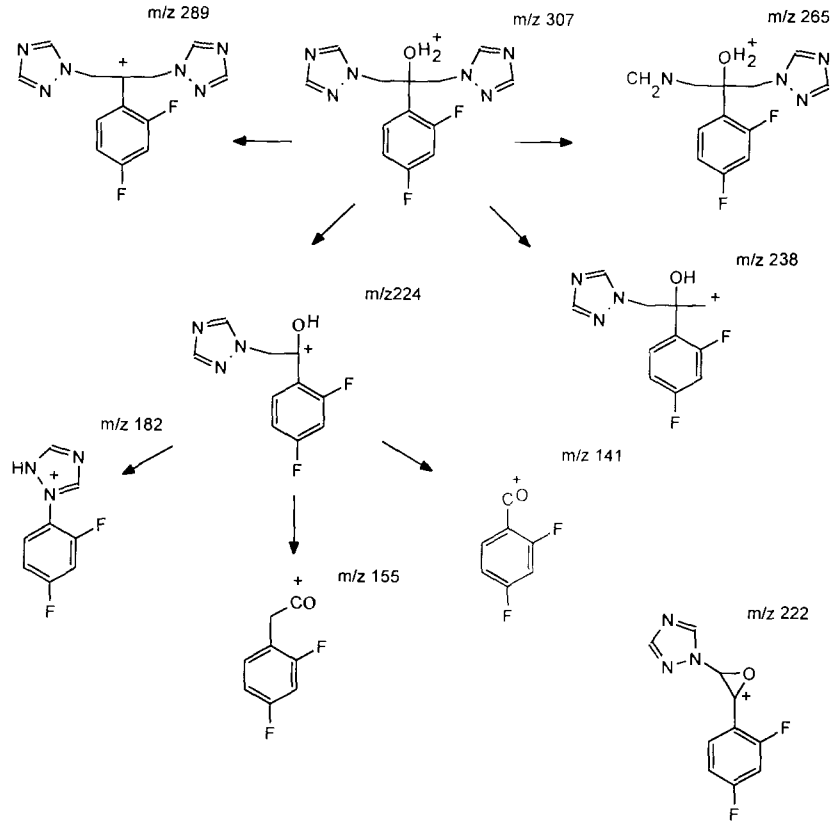

Scheme 2. CI fragmentation pathways for 1.

the methanol CI spectrum of 1, which is not observed in the ammonium CI spectrum. Scheme 2 shows the tentative assignment of ions observed in sector and ion trap CI spectra (those common to EI acquisition are show in Scheme 1) [8]. The absence of extensive fragmentation in the ion trap spectra is suprising, since methanol has a lower proton affinity than ammonia (761 and 854 kJ mol^{-1}, respectively [22]) and the methanol-CI reaction is therefore more exothermic. This suggests that competing processes other than proton transfer were occurring in the high temperature (300°C), high pressure magnetic sector CI source, but not in the ion trap where a single reactant ion can be isolated prior to analyte ionisation, and these processes can have a significant effect on the CI spectra obtained.

4. Conclusions

Normal phase HPLC separation of difluorophenyl triazoles has been monitored by magnetic sector and ion trap mass spectrometers using a two-stage particle beam interface fitted with an appropriate transfer line. EI and CI spectra were both obtained for these triazoles on both instruments. The sensitivity of the technique was system-dependent due to differences in particle transmission/volatilisation. Good EI spectral quality on the ion trap was achieved using a modified scan routine to minimise solvent ion interactions and maximise analyte ion populations. Introduction of CI reagent into the momentum separator for analysis in the double focusing spectrometer gave results comparable to those

obtained using introduction of reagent directly into the source volume.

Acknowledgements

We thank Mike Richardson of ASH instruments (Macclesfield, UK) for constructing the momentum separator, transfer lines and cold trap. We thank the Engineering and Physical Sciences Research Council (Swindon, UK) and Pfizer Central Research (Sandwich) for financial support.

References

[1] P.F. Troke, R.J. Andrews, K.W. Brummer and M.S. Marriot, Antimicrob. Agents Chemother., 28 (1985) 815.
[2] F.C. Odds, S.L. Cheesman and A.B. Abott, J. Antimicrob. Chemother., 18 (1986) 473.
[3] J.W. van't Wout, H. Mattie and R. van Furth, J. Antimicrob. Chemother., 21 (1988) 665.
[4] F.C. Odds, S.L. Cheesman and A.B. Abott, J. Antimicrob. Chemother., 18 (1986) 473.
[5] E.J. Kim, H.S. Lee, O.P. Zee and S.T. Lee, Arch. Pharm. Res., 11 (1988) 250.
[6] D. Debruyne, J.-P. Ryckelynck, M.-C. Bigot and M. Moulin, J. Pharm. Sci., 77 (1988) 534.
[7] A.B. Rege, J.Y. Walker-Cador, R.A. Clark, J.J.L. Lertora, N.E. Hyslop Jr. and W.L. George, Antimicro. Agents Chemother, 36 (1992) 647.
[8] V.C.M. Dale, M. Sc Thesis, University of East Anglia, UK (1991).
[9] C.S. Creaser and J.W. Stygall, Analyst, 118 (1993) 1467.
[10] F.S. Pullen, A.G. Swanson, M.J. Newman and D.S. Richards, Rapid Comm. Mass Spectrom., 9 (1995) 1003.
[11] C. Celma, Biol. Mass Spectrom., 23 (1994) 13.
[12] J. Girault, J.M. Malgouyat, D. Longueville, G. Lecomte, M. Revaud and J.B. Fourtillan, J. Chromatogr, 658 (1994) 289.
[13] C.S. Creaser and J.W. Stygall, Instrumen. Sci. Technol., 22 (1994) 185.
[14] P.H. Dawson, Quadrupole Mass Spectrometry and It's Applications, Elsevier, Amsterdam, 1976.
[15] G.C. Stafford, P.E. Kelly, J.E.P. Syka, W.E. Reynolds and J.F.J. Todd, Int. J. Mass Spectrom. Ion Processes, 60 (1984) 85.
[16] R.E. Pedder, J.V. Johnson and R.A. Yost, presented at the 40th annual meeting of the ASMS, Washington D.C., USA, 1991, p. 1761.
[17] B.L. Kleintop, D.M. Eades and R.A. Yost, Anal. Chem., 65 (1993) 1295.
[18] F.S. Pullen, unpublished results.
[19] C.S. Creaser, in R.E. March and J.F.J. Todd, (Eds.), Practical aspects of Ion Trap Mass Spectrometry, Vol. 2, CRC, Boca Raton, FL, USA, 1995.
[20] B.L. Kleintop, D.M. Eades and R.A. Yost, presented at the 40th annual meeting of the ASMS, Washington D.C., USA, 1992.
[21] A.V. Mordehai and J.D. Henion, Rapid Comm. Mass Spectrom., 7 (1993) 1131.
[22] A.G. Harrison, Chemical ionisation mass spectrometry, CRC press, Boca Raton, FL, USA, 1992.

ELSEVIER

Talanta 44 (1997) 1037–1053

Talanta

Equilibrium and kinetic properties of a fast iminodiacetate based chelating ion exchanger and its incorporation in a FIA-ICP-AES system

Payman Hashemi *, Åke Olin

Department of Analytical Chemistry, Uppsala University, P.O. Box 531, S-751 21 Uppsala, Sweden

Received 6 September 1996; received in revised form 22 November 1996; accepted 23 November 1996

Abstract

The equilibrium and kinetic properties of an iminodiacetate (IDA) based chelating ion exchanger with a crosslinked agarose, Novarose™, as support has been investigated. The second and third acidity constants and some complexation constants of the ligand were determined for adsorbents with metal binding capacities of 140, 55 and 18 μmol ml^{-1}, respectively. The adsorbent of medium capacity showed fast adsorption and desorption of Cu(II), Cd(II), Ni(II) and Ca(II) both in the batch and column mode. It was found to be about 50 times faster than Chelex-100 (50–100 mesh) in accumulation of these metal ions in the batch mode. Studies of the adsorbent in a flow system, using a 5 mm × 6 mm i.d. column, indicated quantitative accumulation of Cu(II), Cd(II), and Ni(II) at volumetric flow rates up to 110 ml min^{-1}. Linear calibration curves with $r > 0.999$ and signal enhancement factors up to 1300 were obtained. Preconcentration by a FIA system connected to an ICP-AES instrument will make simultaneous measurement of ultratrace concentrations of a number of metal ions possible within reasonable cycle times due to the high flow rates which can be used with the adsorbent. Trace amounts of cadmium and copper in tap water were determined successfully at 60 ml min^{-1}. However, copper and nickel in tap water are strongly complexed and do not accumulate quantitatively even at low flow rates. Hence a sample pretreatment is needed. Copper was completely adsorbed after UV-treatment of the sample. © 1997 Elsevier Science B.V.

Keywords: Flow-injection; Iminodiacetate-agarose metal adsorbent; Inductively coupled plasma atomic emission spectrometry; Tap water analysis

1. Introduction

Chelating ion-exchangers have been widely used for preconcentration in trace metal determinations by atomic spectrometry [1–5]. A separation from interfering alkali and alkaline earth metals can be achieved concurrently. More recently elimination of anions, such as chloride and sulphate, has become an important aspect of the ion-exchange preconcentration-separation procedure as these ions are precursors to some of the disturbing species in determinations by inductively coupled plasma mass spectrometry [6,7]. The most commonly used ligand in chelating ion-exchangers is

* Corresponding author.

PII S0039-9140(96)02189-3

no doubt the iminodiacetate group. It is attached by a $-CH_2-$ link to a styrene- divinylbenzene polymer in the much used adsorbent Chelex-100.

The preconcentration is usually performed in a flow system containing the adsorbent in a column [8,9]. Conditioning and washing of the column, loading of the sample, elution of the enriched sample and transport to the spectrometer are often carried out in a manifold under computer control [10–13]. The dimensions of the column holding the adsorbent are typically 2–3 mm i.d. × 50 mm corresponding to a volume of about 0.15–0.35 ml. A representative pumping speed is 5 ml min^{-1}. The calculated residence time of the sample in the column is then around 0.7–1.7 s for a void volume of 40%. Under these conditions most metal ions are quantitatively retained on Chelex-100 (100–200 mesh). However, an increase in the flow rate or in the particle size to 50–100 mesh, in order to diminish the backpressure, soon leads to losses [10].

The rate of removal of zinc, cadmium, lead and copper ions from solution by Chelex-100 has been studied in bulk experiments [14]. The observed first-order rate constants, corresponding to half-lives of about 1 min, did not differ by more than 10%, which indicates that mass transfer, rather than the rate of complexation, was the main resistance in the accumulation process. The recoveries obtained for a large number of metal ions, accumulated on a 0.1 ml column of Chelex-100 (50–100 mesh) and a flow rate of 9.5 ml min^{-1}, were around 55% with moderate variation [9]. This again suggests that mass transfer rather than the rate of a chemical reaction limits the quantitative accumulation of the metal ions. Related observations have been made by others [11].

Preconcentration ratios of the order of 100–1000 are required for trace and ultra-trace determinations of metals by inductively coupled plasma atomic emission spectrometry in tap water, ultra-pure waters, such as reactor waters in the nuclear power industry, etc. In order to diminish analysis time at high preconcentration ratios, much higher flow rates are needed than normally used with Chelex-100 and other adsorbents. Crosslinked agarose is a hydrophilic support with moderate resistance to flow. Covalent bonding of chelating ligands to this material has been studied in connection with the preparation of adsorbents for immobilised metal ion affinity chromatography (IMAC) [15]. As the iminodiacetate group appears to have fast kinetics both with respect to bonding and release of a metal ion, this group was selected in preference to others which may show stronger bonding but, at the same time, slower kinetics. We report here on the properties of a commercially available IMAC adsorbent based on a highly crosslinked agarose gel with attached iminoacetate groups, in particular with respect to the preconcentration of trace metals at high flow rates.

2. Experimental

2.1. Chemicals

The chelating ion-exchanger was obtained from Scand Inovata AB, Stockholm, Sweden. The support is a highly crosslinked agarose with the trade name of Novarose™. The adsorbent can be obtained with different metal binding capacities and exclusion limits. The ion-exchangers studied had an exclusion limit of about 200 000 and the bead size ranged between 30 and 60 μm. The ion-exchanger will be written IDA-Novarose in the following.

Standard solutions of hydrochloric acid and sodium hydroxide were prepared from ampoules (P.H. Tamm, Uppsala, Sweden) and further diluted when needed. Test solutions of metal ions were made by appropriate dilution of AAS standards (Referensmaterial AB, Sweden). Synthetic tap water samples were prepared by 200 times dilution of a stock solution containing 1 M Ca and respectively, 20, 2, 12, 12, 4 and 50 mg l^{-1} Al, Fe, Ba, Zn, Mn, and Sr. The chemicals used were of analytical grade (Merck) and all solutions made up with Milli-Q filtered distilled water.

2.2. Apparatus and analysis

The metal ion binding capacity and preconcentration measurements at flow rates below 8 ml min^{-1} were carried out with the TraceCon com-

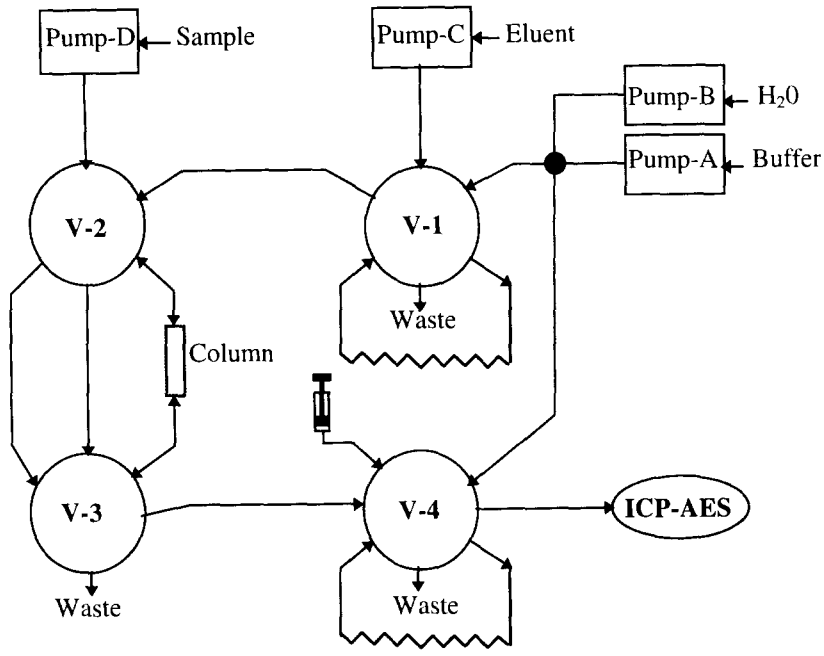

Fig. 1. Block diagram of the FIA-ICP-AES system with four pumps, four switching valves (V-1–V-4), acid and external standard loops and the IDA-Novarose column.

puter controlled flow analysis equipment (Knapp Logistics, Graz, Austria). At higher flow rates a variable reciprocating pump was used (Model-QD, Fluid Metering, NY).

Metal ion concentrations were determined by FAAS (Perkin-Elmer 2380) or by ICP-AES (Spectroflame, Spectro, Kleve, Germany). The instrumental settings of the manufacturers were followed. AC-R3A integrator (Shimadzu, Japan) was used for integration of the signals measured by FAAS.

GFAAS, with platform technique, was used for direct measurements of concentrations in tap water. Copper concentrations were measured by a Perkin Elmer 5000 instrument with deuterium background correction. A Zeeman GFAAS, Perkin Elmer 4100 ZL, was used for cadmium (multiple injection) and nickel (preconcentration by freeze-drying). The analysis made by MeAna-Konsult, Uppsala, Sweden.

The flow injection system shown in Fig. 1 was comprised of a Pharmacia FPLC manifold, four MV-7 seven port rotating valves (V-1 to V-4), two P-500 displacement pumps (Pump-A and Pump-B), one P-1 peristaltic pump (Pump-C) all from Pharmacia, and a reciprocating pump (Pump-D). The fittings and tubings were mostly from Tefzel material (Upchurch Scientific, WA). The FIA system, including the reciprocating pump and the integrator, were controlled from a Pharmacia LCC-500 LC controller.

The columns for holding the adsorbent were either of fixed length, 8 mm i.d. × 14 mm, (Inovata AB, Stockholm) or of variable length, 6 mm i.d. × 5 mm (min), (Omnifit).

The pH measurements were made with a Radiometer PHM 84 (Radiometer, Copenhagen, Denmark). For the potentiometric measurements a double junction (0.1 M $NaNO_3$) Ag/AgCl reference electrode and a pHG201 glass electrode (Radiometer) were used. The electrode was calibrated in the usual way on the concentration scale by adding strong acid to the ionic medium. In all other experiments a combined glass electrode was used and calibrated against certified pH buffers (Merck).

A home-build UV irradiation apparatus, equipped with a TQ 718 high pressure mercury lamp (Heraeus), was used for photo-digestion of the samples [16].

2.3. Water content and volume stability of IDA-Novarose

The IDA-Novarose columns were packed by gravity settling while a slight underpressure was applied at the outlet. Packed adsorbent, 1 ml, is the unit used for the amount of IDA-Novarose taken in an experiment. Accordingly, the analytical results are expressed per ml of packed adsorbent.

The pore volume of the adsorbent was estimated as follows. IDA-Novarose packed in a column was flushed with nitrogen gas until water was no longer expelled (5 min). The adsorbent was then extruded, weighed and dried to constant weight at 80°C. The pore volume was 0.60 ± 0.02 ml ml^{-1} packed adsorbent.

The volume change of IDA-Novarose with pH was studied by observing the change in column height when solutions of different pH were passed through the adsorbent. No volume change was observed between the extremes 1 M hydrochloric acid and 0.2 M potassium hydroxide.

2.4. Acid dissociation constants

A known volume of about 0.5 ml of IDA-Novarose in a column was converted to the fully protonated form by treatment with 5 ml of 1 M hydrochloric acid. The adsorbent was then washed with water until the effluent was neutral. This treatment changes IDA-Novarose to the zwitterion form. It was then extruded into 45 ml of 0.1 M sodium nitrate as ionic medium. The titrations were performed in an N_2 atmosphere by stepwise addition of sodium hydroxide to a pH of about 9. Back titrations with hydrochloric acid were also performed to obtain information on the reversibility of the acid–base equilibria. After each addition of titrant the emf was followed until a constant reading was observed (< 0.2 mV 10 min^{-1}), which generally took less than 15 min.

The degree of deprotonation, α, of the adsorbent was calculated from

$$\alpha = \{(V_O + V_{OH})[H^+] - [OH^-]) + V_{OH}C_{OH}\}/Qw - \alpha_{blank}$$

Here V_O is the initial solution volume and V_{OH} the added volume of base of concentration C_{OH}. Q is the concentration of IDA groups as determined from the inflection point on the titration curve and w the volume of IDA-Novarose. The proton concentration, $[H^+]$, was calculated from the glass electrode potential calibrated on the concentration scale. The expression for α neglects the amount of protons in the pore volume, which is difficult to find in an exact way but can be estimated to be negligible over most of the studied pH range. The underivatised Novarose showed a small acid–base capacity which was corrected for by α_{blank}.

2.5. Capacity determinations

The static metal ion binding capacity was determined in the column mode as described previously [5].

The dynamic capacity is defined here as the amount of metal ion captured by the adsorbent until the metal ion concentration in the column effluent has increased to 1% of the in-going solution. It was determined for an 8 mm i.d. × 14 mm column by continuously pumping a solution of the test ion through the column and directing the effluent into the nebulizer of the FAAS instrument. Since the loading flow rates used were higher than the normal aspiration rate of the FAAS instrument, a simple flow splitter was used after the column to yield a constant aspiration rate of 5 ml min^{-1}.

2.6. Sorption isotherms

A known volume of about 1 or 2 ml of the adsorbent was converted to the zwitterion form in a column and extruded into a 200 ml portion of 5 μM Ni^{2+} or Cd^{2+} in water or 0.1 M sodium nitrate. The initial pH of the solution was adjusted to about 6.7 by 1 M ammonium acetate. The magnetic stirrer used for mixing hanged in a

thin, freely rotatable Teflon string in order to avoid grinding of the adsorbent. The pH of the solution was changed by additions of 1 M acetic or hydrochloric acid and measured by a combined glass electrode. The solution was sampled 15 min after a change in pH had been made. A 3 ml portion was withdrawn by a pipette equipped with a 25 μm filter at the tip and further filtered through a 0.45 μm membrane filter into a test tube. Duplicates were collected at each pH and analysed by ICP-AES.

2.7. Adsorption and desorption kinetics

The kinetic measurements of the adsorption and desorption of the metal ions were performed in the batch mode. The experimental conditions were selected so that pseudo first order reaction conditions could be assumed [17]. A 200 ml portion of 5 μM Cd^{2+}, Ni^{2+}, Cu^{2+} and Ca^{2+} in 10 mM acetate buffer, pH 4.7, was prepared in a beaker and continuously sampled by a peristaltic pump. The sample was transported through a filter to the ICP-AES instrument at a constant flow rate of 2 ml min^{-1}. When the base lines had stabilised, 1.0 ml of IDA-Novarose or 1.6 ml of Chelex-100 (50–100 mesh) was quickly added to the rapidly stirred solution. The adsorption of the metals was followed by recording the emission signal every other second.

The metal loaded adsorbent and the virtually metal free solution after the adsorption measurement were then used to the study of the desorption profiles. The filter was cleaned from resin particles, the pump restarted, concentrated hydrochloric acid added to a final concentration of 1 M and the increase in metal ion concentrations determined by ICP-AES.

2.8. The FIA-ICP-AES procedure

The flow injection system is presented in Fig. 1. The column was first conditioned by 6 ml of a 0.1 M acetate buffer, pH 5.5, delivered by pump-A at a flow rate of 4 ml min^{-1}. The sample was then enriched, usually at a flow rate of 60 ml min^{-1} (unless otherwise stated), washed by 4 ml of the buffer and eluted by 1 ml of acid in the direction opposite to the enrichment flow. The acid was loaded in a 1 ml loop by pump-C and carried to the column by the flow from pump-A. A flow of Milli-Q water at 4 ml min^{-1} from pump-B bypassed the column and was aspirated into the plasma during sampling. The cycle time is 3 min plus the sample enrichment time (up to 10 min). The transient signals were recorded during the washing and elution steps by the ICP-AES computer software. The area and height of the elution peaks were evaluated using a home made program. The sample loop connected to valve-4 was used for introduction of an external standard as a check of the sensitivity of the instruments. The FIA system can also be connected to a FAAS instrument as was done here in the preliminary experiments.

For tap water analysis, the system was used also in an off-line mode. The eluted analytes were collected in about 6 ml and determined by ICP-AES, against matched standards.

2.9. Photo-digestion of tap water

Portions of tap water, 50 ml, were weighed into 12 quartz tubes and 50 μl 30% hydrogen peroxide were added. Six portions were acidified by 50 μl (0.012 M) and the others by 420 μl (0.1 M) of hydrochloric acid. The tubes were UV-irradiated with a mercury lamp, operated at 500 W, for 3 h. After the photo-digestion, the evaporated water (normally < 1 ml) was compensated by Milli-Q water.

3. Results and discussion

3.1. Acidity constants

Iminodiacetic acid is a three-protonic acid and the different forms of IDA-Novarose can be represented by $R\text{-}NH^{+}(CH_2COOH)_2$, $R\text{-}NH^{+}(CH_2COO^{-})(CH_2COOH)$ (zwitterion form), $R\text{-}NH^{+}(CH_2COO^{-})_2$ and $R\text{-}N(CH_2COO^{-})_2$. In equations further simplification to $R\text{-}H_3^{+}$ ... R_2^{-} will be made. The potentiometric titrations started from the zwitterion form, which appears to be the only form of IDA based ion exchangers which can

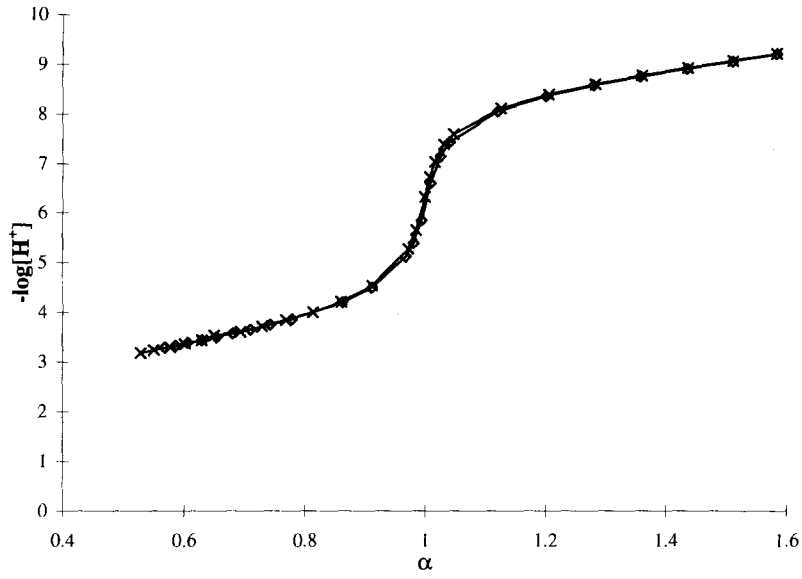

Fig. 2. Titration curve of the high capacity IDA-Novarose, showing the dependence of the degree of deprotonation (α) on $-\log[H^+]$. ×, forward and ◇, reverse titration. Adsorbent volume, 0.43 ml; temperature, 23(±1)°C; forward titrant, 10 mM NaOH; backward titrant, 10 mM HCl.

be obtained with a well-defined stoichiometry [18]. The titration curve exhibits a reasonably sharp equivalence point for the titration of the first proton in the zwitterion. It was used to calculate the number of IDA groups and the degree of deprotonation, α, of the zwitterion as exemplified in Fig. 2. The fair agreement between the forward and reverse titrations indicates that the acid–base equilibria are reversible and the attainment of equilibrium appears to be markedly faster than for Chelex-100 [19,20].

The equilibria and apparent acidity constants can be written

$$R-NH^+(CH_2COO^-)(CH_2COOH) = R-NH^+(CH_2COO^-)_2 + H^+(aq) \quad \text{(I)}$$

$$K_1 = \frac{\overline{\{R-H^-\}}[H^+]}{\overline{\{R-H_2\}}} = \frac{\alpha}{1-\alpha}[H^+] \quad (1)$$

and

$$R-NH^+(CH_2COO^-)_2 = R-N(CH_2COO^-)_2 + H^+(aq) \quad \text{(II)}$$

$$K_2 = \frac{\overline{\{R^{2-}\}}[H^+]}{\overline{\{R-H^-\}}} = \frac{\alpha-1}{2-\alpha}[H^+] \quad (2)$$

Square and curled brackets denote concentration and activity, respectively, and the bar is used for quantities in the ion-exchanger phase. While the apparent acidity constants are readily calculated from the experimental data, they are of somewhat limited usefulness because they depend on the degree of deprotonation and the ionic composition of the solution phase.

A number of approaches has been used to calculate the acidity constants in the resin phase [19,21,22]. The intrinsic acidity constants are defined by:

$$K_{1i} = \frac{\overline{\{R-H^-\}\{H^+\}}}{\overline{\{R-H_2\}}} \text{ and } K_{2i} = \frac{\overline{\{R^{2-}\}\{H^+\}}}{\overline{\{R-H^-\}}} \quad (3)$$

The method proposed by Pesavento et al. [19] has been used to estimate K_{1i} and K_{2i}. The relationship between K_n and K_{ni} is

$$K_{ni} = K_n \frac{\bar{\gamma}_H \bar{\gamma}_{RH_{n-1}}}{\bar{\gamma}_{RH_n}} \frac{\overline{\{H^+\}}}{\{H^+\}} \cong K_n \gamma_H \frac{\overline{\{Na^+\}}}{\{Na^+\}} \cong K_n \frac{\overline{\{Na^+\}}}{[Na^+]} \quad (4)$$

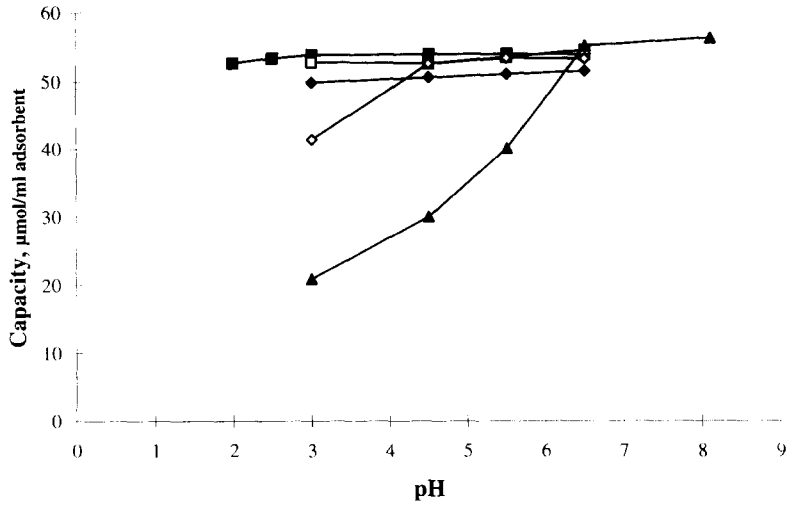

Fig. 3. Capacity of the medium capacity IDA-Novarose at different pH for Cu^{2+} (■), Ni^{2+} (□), Pb^{2+} (◆), Cd^{2+} (◇), and Ca^{2+} (▲). Adsorbent volume, 0.5 ml; buffer concentration, 0.01 M for Ca^{2+} and 0.1 M for the other ions.

The ratio of the activity coefficients (γ) in the resin phase is assumed to be 1. This assumption together with the Donnan equilibrium $\overline{\{H^+\}}/\{H^+\} = \overline{\{Na^+\}}/\{Na^+\}$ leads to the second step in Eq. (4). The last step assumes that the activity coefficients of H^+ and Na^+ cancel in the solution phase. The sodium ion concentration in the resin phase was calculated as suggested by Pesavento et al. [19] and $\bar{\gamma}_{Na}$ was taken from tabulated data of the mean activity coefficient of sodium nitrate [23].

Three IDA-Novarose preparations with the capacities 18, 55 and 140 μmol H^+ ml^{-1}, respectively, were studied. The titrations were stopped at about pH 9 since titrations on underivatised Novarose showed a substantial increase in the consumption of added base by the agarose support above this pH. The measurements covered a range in α from 0.5 to 1.9. The value of pK_{2i} obtained was 8.65 ± 0.1 and there was little or no variation of this value with the degree of deprotonation or with the capacity of the adsorbent. The result for pK_{1i}, on the other hand, showed a significant trend with α and increased from 2.95 to 3.20 when α increased from 0.5 to 0.9. Part of this trend may be caused by experimental errors since the trend became more pronounced with decreasing capacity of the ion-exchanger and for α values above 0.9. The value of pK_{1i} extrapolated to $\alpha = 0$ is 2.6.

The pK_{1i} value is similar to the result obtained for Chelex-100 [19,22], whereas pK_{2i} is lower by 0.5 units [21]. The attachment of the iminodiacetate group to the support is quite different in Chelex-100 and in IDA-Novarose. In the latter adsorbent the group is held by an alkyl chain containing hydroxyl groups. It may therefore be appropriate to compare the intrinsic acidity constants with the corresponding constants of *N*(2-hydroxyethyl)iminodiacetic acid. The reported values are $pK_1 = 2.2$ and $pK_2 = 8.73$ ($I = 0.1$ M) [24], of which the latter is quite similar to the results obtained for IDA-Novarose.

3.2. Sorption isoterms

The sorption of Cu^{2+}, Ni^{2+}, Cd^{2+}, Pb^{2+} and Ca^{2+} by the adsorbent of medium capacity was measured in the column mode. The result at different pH is shown in Fig. 3. The maximum capacity was about 55 μmol ml^{-1} adsorbent for all of the ions tested. The final capacity for Ca^{2+} was only reached at a pH higher than 6.5. After washing the column with 3, 10 and 20 ml of a 0.1 M acetate buffer, pH 5.5, the calcium remaining on the column decreased to 5.9, 0.3 and 0.2 μmol

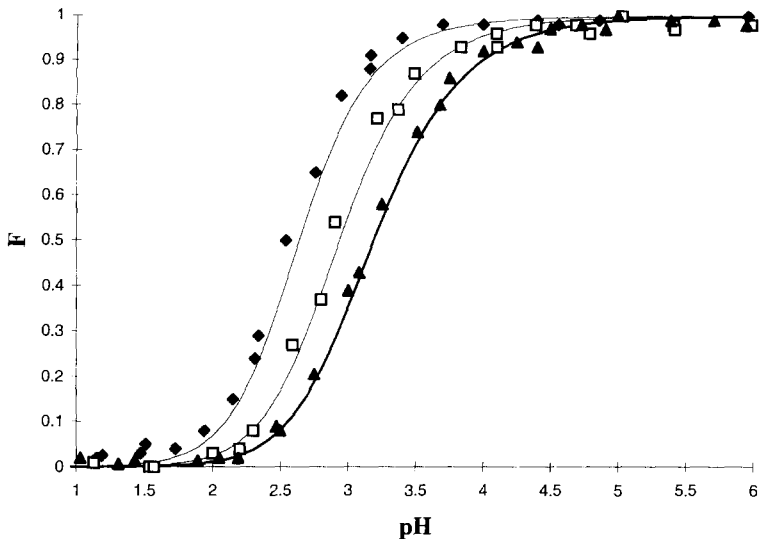

Fig. 4. Adsorption of nickel on high (◆), medium (□) and low (▲) capacity IDA-Novarose as a function of pH. The curves depict the calculated sorption isotherms from Eq. (7).

ml^{-1}, respectively. The other metal ions were not eluted by this treatment. This behaviour indicates that calcium can be removed from the enriched sample by washing the column with a buffer solution after enrichment but before the elution. The high capacity ion-exchanger (140 μmol ml^{-1}) also exhibited the same capacities for Cu^{2+}, Ni^{2+} and Cd^{2+}, whereas the capacity for Pb^{2+} was about 120 μmol ml^{-1}.

Sorption isotherms were studied more closely only for nickel and cadmium and at two ionic strengths, $I = 0.1$ and 0. Two sets of isotherms are presented in Figs. 4 and 5, which demonstrate the influence of the capacity of the sorbent. It has been shown that the iminodiacetate group binds nickel as a tridentate ligand in Chelex-100 [25] and the interpretation of the sorption isotherms was started on this hypothesis. The equilibrium reaction would then be

$$M^{2+} + \overline{R-H_2} = \overline{R-M} + 2H^+ \qquad \text{(III)}$$

with

$$\beta_1 = \frac{\overline{[R-M][H^+]^2}}{\overline{[R-H_2]}[M^{2+}]} \qquad (5)$$

The fraction sorbed, F, is

$$F = \frac{v\overline{[R-M]}}{V[M^{2+}] + v\overline{[R-M]}} \qquad (6)$$

in which v is the volume of the sorbent and V the volume of the surrounding solution. In the pH range studied, $R-H_2$ and $R-H^-$ predominate in the resin phase since the loading of the resin was small compared with its total capacity. Introduction of the total capacity, R_t, and the apparent acidity constant from Eq. (1) into Eq. (6) yields

$$F = \frac{1}{1 + \dfrac{V[H^+](K_1 + [H^+])}{\beta_1 v R_t}} = \frac{1}{1 + \varphi[H^+](K_1 + [H^+])} \qquad (7)$$

in which φ is a constant. The value of φ, of course, depends on the experimental conditions chosen and was determined by curve fitting. Curves, $F = f([H^+], K_1, \varphi)$, were calculated with K_1-values extracted from the acid–base titrations. Very good fits could be achieved between the experimental data and the calculated curves. However, the β_1-values obtained from the φ-values showed a more or less definite trend towards smaller values with decreasing total capacity.

It has been suggested that the following reaction

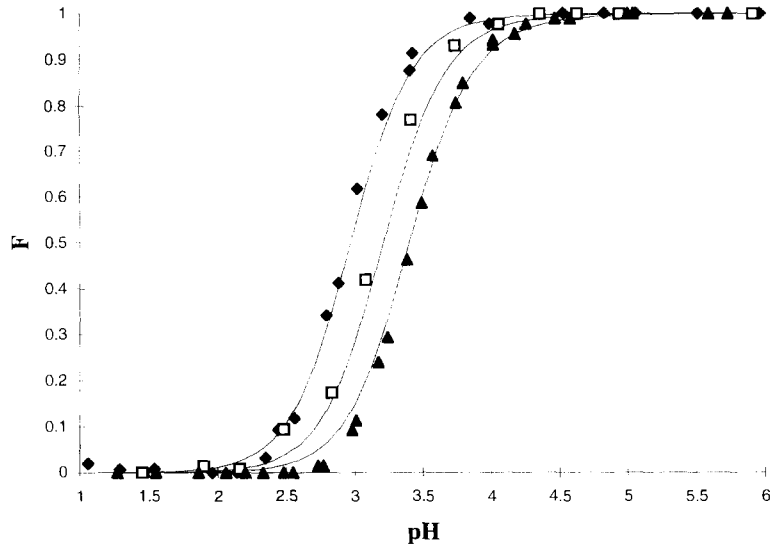

Fig. 5. Adsorption of cadmium on high (◆), medium (□) and low (▲) capacity IDA-Novarose as a function of pH. The curves depict the calculated sorption isotherms from Eq. (7).

$$M^{2+} + 2\overline{R-H_2} = \overline{M(RH)_2} + 2H^+ \qquad \text{(IV)}$$

plays a major part in the sorption in addition to reaction(III). Inclusion of this reaction, which can be envisaged also as an ion exchange reaction rather than as complexation by two bidentate ligands, removed some of the trend in the β_1-values. On the whole, however, no convincing evidence of the presence of the species $\overline{M(RH)_2}$ was found.

One reason for the trend in the value of the equilibrium constant might be that β_1 does not have a definite value in the resin phase but covers a range of values instead [26]. Some positions in the sorbent could allow further complexation to take place by adjacent carboxylate groups, which should lead to a stronger binding of the metal ion. If such a distribution of positions is present, it can be anticipated that the positions will be occupied in descending order of strength. In the sorption experiments, the relative loading of the sorbent increased with decreasing total capacity and hence, according to the hypothesis, the β_1-value would decrease with R_t as observed.

It is also known that the agarose matrix contains some sulphate and carboxylate groups and that additional carboxylate groups may be introduced by the crosslinking procedure [27]. These groups will probably contribute to the total capacity, which is measured at a pH of about 5 and a relatively high metal ion concentration, but they may contribute little in most of the pH range covered by the sorption isotherm measurements. The blank titrations on Novarose showed a base consumption corresponding to about 5 μmol ml^{-1} at pH 5 indicating that groups other than iminodiacetate could contribute to the capacity. As a consequence, the chelating capacity would be overrated. By subtracting 7.5 μmol ml^{-1} from the total capacities good agreement between experimental and calculated results were obtained for a constant value of β_1 as shown in Fig. 4 and Fig. 5. The results are summarised in Table 1. Since

Table 1
Stability constants, defined by reaction (III), of IDA-Novarose and *N*(2-hydroxyethyl)iminodiacetate complexes of Ni^{2+} and Cd^{2+}

	$\log \beta_1$		
	$I=0.1$	$I=0$	Ref. [23] ($I=0.1$)
Ni	-1.9_2	-1.8_0	−1.65
Cd	-2.8_5	-2.7_4	−3.41

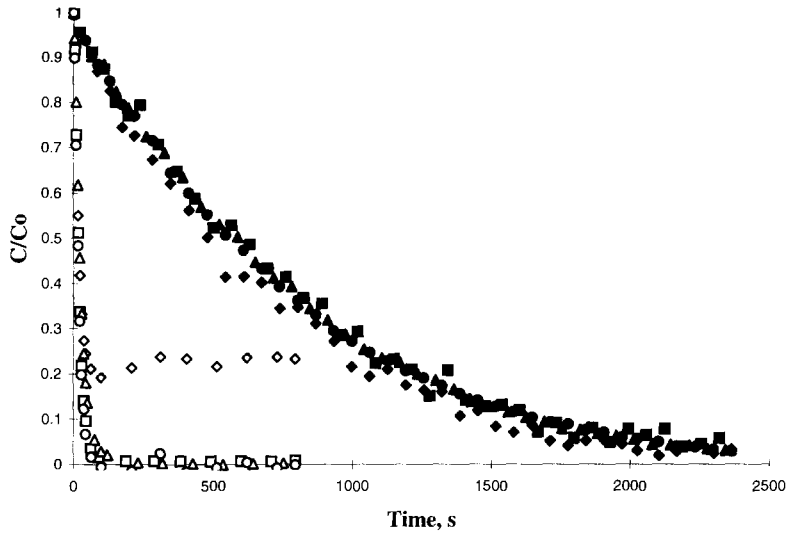

Fig. 6. Comparison of the adsorption rates on Chelex-100 (filled symbols) and medium capacity IDA-Novarose (open symbols). C/C_0 is the ratio between the current and initial concentrations. Ca^{2+} ◇; Cd^{2+} ○; Cu^{2+} △; Ni^{2+} □. Many experimental points have been omitted for clarity.

the applied correction is small for the sorbent with the highest capacity, the reported data are close to the values obtained for this sorbent without the correction. The value of β_1 for nickel is quite close to the value obtained for *N*(2-hydoxyethyl)iminodiacetic acid, whereas the constant for cadmium is about five times larger. It has been observed that the isotherms on Chelex-100 follow the same pattern. The sorption takes place at a lower pH than expected from the stability constants determined in homogeneous solution, particularly for weak complexes [19]. To account for the higher than expected sorption to Chelex-100, reaction(IV) was introduced into the sorption model. Although convincing evidence for this reaction could not be found here from the sorption isotherms of nickel and cadmium, it is likely that ion exchange mechanisms play a major role in the sorption of more weakly complexing ions.

3.3. Kinetic measurements

3.3.1. Batch experiments

The kinetics of the metal ion adsorption and desorption were studied in the batch mode for Chelex-100 and medium capacity IDA-Novarose. Different volumes of the adsorbents were taken in order to make the dry weight of each adsorbent equal to 0.2 g. This choice leads to an about five-fold larger exchange capacity in the experiments with Chelex-100, which is offset by a smaller surface area due to a larger particle size. Otherwise the experimental conditions were the same for the two adsorbents. Results from the adsorption experiments are shown in Fig. 6. The great difference in the rate of accumulation of the metal ions on the two adsorbents is evident from the graph. The enrichment is quantitative except for Ca^{2+} on IDA-Novarose. As the equilibrium concentration is expected to be inversely proportional to the square of the capacity, the sequestering of Ca^{2+} is more efficient, and even quantitative, by Chelex-100. There is little variation between the adsorption curves belonging to the same adsorbent, indicating that mass transfer is rate limiting. Conditional first order rate constant were calculated for the four metal ions studied and the average and standard deviation of the adsorption half-times were 10.7 ± 2.9 s for IDA-Novarose and 525 ± 30 s for Chelex-100. Thus the new adsorbent is about 50 times faster than Chelex-100, which appears too large to be attributed solely to the difference in particle size.

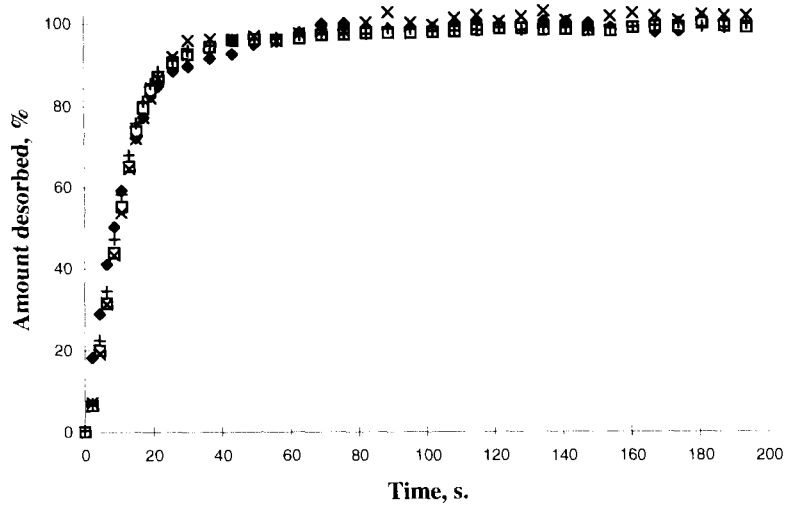

Fig. 7. Desorption of Ca^{2+} (◆), Cd^{2+} (□), Cu^{2+} (+) and Ni^{2+} (×) from medium capacity IDA-Novarose in the batch mode as a function of time. Many experimental points have been omitted for clarity.

Differences in the hydrophobicities and the anchoring of the chelating group to the support most likely play a role here. Schulze and Elsholz [14] determined the adsorption half-times of 15 sorbents and found substantial differences between them. The ratio between the half-times of Chelex-100 and the fastest adsorbent was about four. Due to the variation in the nature of the exchanging group in this study, it is difficult to discern the influence of the matrix but, in general, sorbents based on a hydrophilic support appear to be faster than those based on an organic polymer matrix.

The desorption profiles in 1 M hydrochloric acid are shown in Fig. 7 and Fig. 8. The curves for IDA-Novarose are similar and the average desorption half-time is 7.0 ± 0.8 s. The desorption and adsorption rates are thus rather equal and again point to the mass transfer characteristics of the experimental system as rate limiting. For Chelex- 100, the half-time for Cu^{2+} was similar to the result obtained for IDA-Novarose, whereas the values for Ca^{2+} and Ni^{2+} were 2–3 times larger. The slow desorption of Cd^{2+} is due to the composition of the eluent and may be explained as follows. At a high chloride concentration a large fraction of the cadmium is present as the anionic complexes $CdCl_3^-$ and $CdCl_4^{2-}$. Concurrently the high concentration of acid protonates the iminodiacetate group which becomes positively charged. The adsorbent will hence become a 'strong' anion exchanger leading to a delayed desorption determined by the rate of exchange of the complexes by the chloride ion. Evidence for this hypothesis was obtained by a change of the eluent to 1 M perchloric acid. In this medium no anionic complexes are formed and the behaviour of Cd^{2+} was normal. Lowering the concentration of the hydrochloric acid eluent to 0.25 M also substantially increased the desorption rate. We can thus conclude that the desorption from the two adsorbents proceeds at similar rates, at least for low loadings. The normal desorption process can, however, be affected by the charge rendered to the sorbents at low pH. Such complications would be less pronounced for low capacity sorbents as observed here.

3.3.2. Column experiments

The efficiency of the IDA-Novarose adsorbent for accumulation of metal ions at high flow rates was studied in the column mode. A 500 μg l^{-1} mixture of Cu^{2+}, Cd^{2+}, Ni^{2+}, and Sr^{2+} (as an alternative to Ca^{2+} with less risk of contamination) in 10 mM acetate buffer, pH 5.5, was passed through the 8 mm i.d. × 14 mm column at flow

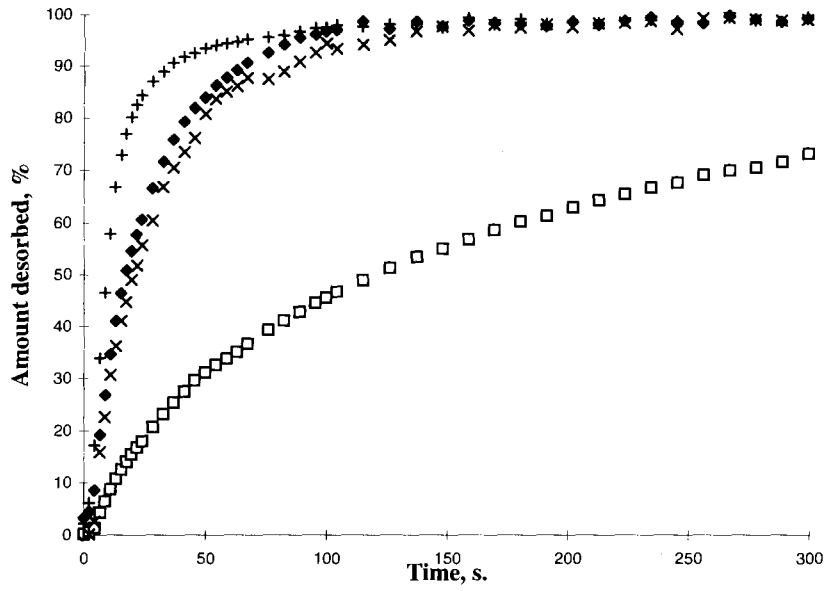

Fig. 8. Desorption of Ca^{2+} (◆), Cd^{2+} (□), Cu^{2+} (+) and Ni^{2+} (×) from Chelex-100 in the batch mode as a function of time. Many experimental points have been omitted for clarity.

rates between 10 and 100 ml min^{-1}. Analysis of the column effluent by ICP-AES indicated that greater than 99% of Cu^{2+}, Cd^{2+} or Ni^{2+}, was taken up by the column at all flow rates studied. In the case of Sr^{2+}, however, a breakthrough occurred after 40–50 ml of test solution. The high flow rates slightly compressed the adsorbent and decreased the bed volume. It is, hence, recommended to pack the column under pressure to avoid this problem or add more adsorbent to the column after compression. The exchange properties of the column were unaffected by the volume change.

The effect of the loading flow rate on the adsorption of Cu^{2+} has been studied for Chelex-100 by Liu and Ingle, Jr [10]. A 3 mm i.d. × 50 mm column, packed with the 100–200 mesh resin, adsorbed the metal ion quantitatively at flow rates up to 15 ml min^{-1}, the highest flow rate studied. For smaller particle sizes the packing collapsed because of the high back pressure. Other investigations generally report flow rates below 10 ml min^{-1} or unacceptable losses of analyte at high flow rates for IDA-based as well as some other chelating sorbents [9,28,29].

The influence of the flow rate was further investigated by a measurement of the dynamic capacity of the adsorbent for Cu^{2+}, Cd^{2+} and Ni^{2+} at input concentrations of 0.16 and 0.48 μM and the flow rates of 10 and 50 ml min^{-1}. The dynamic capacity, expressed in percent of the static capacity, was found to be dependent both on the sample flow rate and the concentration as exemplified in Fig. 9. The dynamic capacities decreased with increasing flow rate and increased with sample concentration. The capacities at 10 ml min^{-1} were 80–95% and at 50 ml min^{-1} 50–80% of the static capacity. These values are considerably better than for the previously studied polyethyleneimine-Novarose adsorbent [5]. The dynamic capacities of Cu^{2+}, Cd^{2+} and Ni^{2+} were 35, 10 and 2%, respectively, at a concentration of 1 g l^{-1} and a flow rate of only 5 ml min^{-1}.

3.4. The FIA-FAAS and FIA-ICP systems

The performance of IDA-Novarose in the FIA-FAAS and FIA-ICP configurations was very similar. Therefore, mainly the results from the experiments with ICP-AES detection will be re-

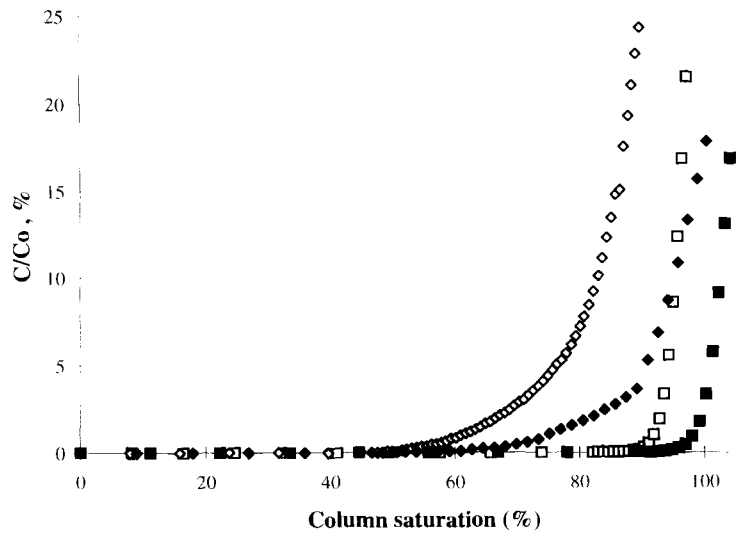

Fig. 9. Break through curves for cadmium at different sample concentrations and flow rates. □, 0.16 μM, 10 ml min^{-1}; ◇, 0.16 μM, 50 ml min^{-1}; ■, 0.48 μM, 10 ml min^{-1}; ◆, 0.48 μM, 50 ml min^{-1}.

ported. The increased backpressure caused by the tubing and valves of the FIA manifold necessitated a decrease in the column length to achieve high flow rates. The shortest column packing that could be realised in the adjustable holder was 5 mm (0.14 ml). The small packing was tested by passing 500 ng of Cd^{2+} at pH 5.5 through the column at flow rates between 10 and 110 ml min^{-1}. The absorbance signals of the eluates did not vary indicating complete accumulation of the test ion. This finding was corroborated by diminishing the active length of the 8 mm i.d. × 14 mm column packing to 3.5 mm. This was accomplished by replacing 10.5 mm of the IDA-Novarose packing by underivatised Novarose and repeating the test, which again indicated complete uptake. Hence, the 6 mm i.d. column with 5 mm packings was used in the following experiments.

The effect of the volume and concentration of the hydrochloric acid eluent on the transient analyte signal was investigated in the ranges 0.10–1.5 ml and 0.12–2 M, respectively. The area and height of the signal reached constant values for concentrations and volumes larger than 0.5 M and 500 μl, respectively, and 1 ml of 1 M HCl was used henceforth. The effect of the elution flow rate on the emission signals was studied at 2 and 4 ml min^{-1}. The signal height at the lower flow rate was greater by a few percent but the peaks tailed excessively. Thus, the higher flow rate, 4 ml min^{-1}, was used.

The elution profiles of Cu^{2+}, Cd^{2+} and Ni^{2+} obtained from 260 ng of each metal ion are presented in Fig. 10. Yttrium was added to the eluent and used to indicate the dispersion of the eluent plug. A comparison of the profiles demonstrates the similarity of the desorption kinetics. Cadmium, however, seems to desorb at lower concentrations of acid than the others, which probably reflects the lower binding strength of this element. The peak width of Y^{3+}, which estimates the final volume of the acid plug, was calculated to be about 2.5 ml, whereas the widths of the eluted peaks were about 1 ml.

Work at low concentrations increases the risk of contamination. Hence, the purity of the acetate buffer and Milli-Q water was tested by passing 600 ml portions through the column. No significant contamination problems were encountered for Cd^{2+} and Ni^{2+}. For Cu^{2+}, however, varying degrees of contaminations, up to 60 ng l^{-1}, were observed. The source of the contamination could not be identified but it was not due to a copper impurity in the acetate buffer. The effect of sam-

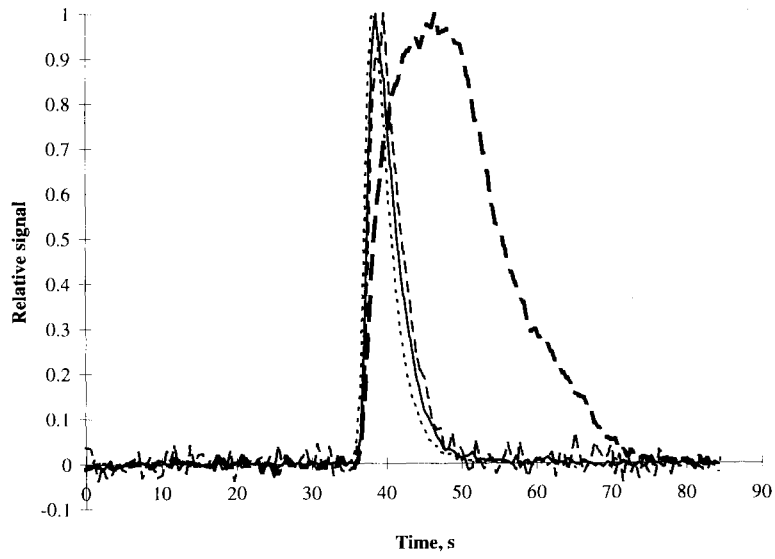

Fig. 10. Comparison of the elution profiles of Cd^{2+} (dotted line), Cu^{2+} (solid line), and Ni^{2+} (dashed line) in the FIA-ICP-AES system. Y^{+3} (thick dashed line) signal indicates the distribution of the 1 ml eluent plug. The first 35 s of the graph show the signals during the washing step.

ple volume and concentration on the recovery was investigated in the concentration range 50–500 ng l^{-1} for Cd^{2+}, 150–1500 ng l^{-1} for Cu^{2+}, and 300 to 3000 ng l^{-1} for Ni^{2+}. The volumes and concentrations were chosen so that constant amounts of the test ions were collected. No significant change was observed in the emission signals of Cd^{2+} and Ni^{2+} from the eluate. In the case of Cu^{2+}, however, a slight increase in the peak area with the volume of the sample was observed. The amount collected was 85 ng. This trend probably originates from the contamination problems met for this element and was not observed at the higher concentrations used with FAAS detection.

The linearity of the calibration curves for Cd^{2+}, Cu^{2+} and Ni^{2+} were studied in somewhat different concentration ranges depending on their relative sensitivities. Appropriate volumes of a standard solution were passed through the column and the peak area used to establish the calibration curves, which were linear ($r > 0.999$) in the studied loading ranges, respectively, 15–120, 45–350 and 90–700 ng. The detection limits, calculated as three times the standard deviation of the estimated noise contribution from the baseline, were for Cd^{2+}, Cu^{2+} and Ni^{2+}, respectively, 4, 7 and 22 ng (peak height) and 2, 5 and 10 ng (peak area).

Considering 10 min as a reasonable enrichment time, and 60 ml min^{-1} as an appropriate and practical sample flow rate, the peak area detection limits in ng can be transformed to the corresponding concentrations limits of 3, 8 and 16 ng l^{-1}. The signal enhancement for a 600 ml sample is estimated to about 1300. This estimate is based on a comparison of the peak height from an enriched sample of Cd^{2+} with the signal obtained by continuous aspiration of a 1 ppm solution of the element. Since the elution peak is present in a volume of about 1 ml, the preconcentration factor is numerically about equal to the enriched volume. The relative standard deviation of the peak area for four replicates was 1.8, 2.4 and 1.3% for Cd^{2+} (50 ng), Cu^{2+} (150 ng) and Ni^{2+} (300 ng), respectively.

The possible interference from calcium, a major matrix element in water samples, on the FAAS and ICP determinations was evaluated. Calcium can be removed from the column by washing with 0.1 M ammonium acetate. This treatment does not affect the test ions but will displace other

loosely held ions such as Mg^{2+} and Mn^{2+}. In FAAS, elimination of accumulated calcium by washing was unnecessary as the absorbance signal was unaffected at the concentration present in the effluent from the column. Enrichment of cadmium from solutions containing 5 mM calcium chloride, pH 5.5, yielded complete recovery, which shows that calcium does not disturb the adsorption.

3.5. Analysis of tap water

Cadmium and nickel are present in natural waters at ng l^{-1} levels and cannot be directly measured by ICP-AES and the copper concentration is close to the detection limit of the technique. Thus, preconcentration and determination of these elements in tap water was selected as an application. In the initial enrichment experiments on tap water and ICP detection, the column was washed with 2 ml of buffer solution before elution. The base line of the cadmium and nickel signals, were then found to be disturbed by the effluent from the washing step right up to the start of the analyte peaks. It is likely that the disturbance is caused by changes in the plasma from the relatively high concentrations of alkaline and alkaline earth metals present in the effluent. The same effect was observed for synthetic tap water as well as for samples containing Ca^{2+} as the only matrix element. Therefore, the effect of different washing volumes on the calcium and magnesium signals was studied. It was found that 4 ml of the 0.1 M acetate buffer sufficed to remove the majority of Ca^{2+} and Mg^{2+} from the column. Using this volume, the disturbed part of the cadmium and nickel base lines were well separated from the analyte peak. Experiments with blanks, containing only the tap water matrix, indicated that the remaining part of Ca^{2+} in the elution step does not change the background signal.

In order to study the effect of the tap water matrix on the recovery of the analytes, tap water was spiked with 0.5, 1.5 and 3.0 μg l^{-1} of Cd^{2+}, Cu^{2+} and Ni^{2+}, respectively, after acetate buffering to pH 5.5. Different volumes of the solutions were enriched on the column. Linear relationships ($r > 0.999$) were obtained between peak area and sample volume. The recovery of added Cd^{2+} was not significantly different from 100%, whereas the recovery of Ni^{2+} was about 90% and greater than 100% for Cu^{2+}. It can therefore be concluded that the first results for copper were due to an erroneous calibration curve caused by losses of copper in the solutions of pH 5.5 and low analyte and acetate concentrations. The results for nickel could be explained by the fact that, in presence of calcium and magnesium at relatively high concentrations, the adsorbent is mostly in the Ca^{2+}, Mg^{2+}, rather than H^+ or NH_4^+, form. This might affect the kinetics of the chelation of nickel. Experiments on the effect of the enrichment flow rate were in agreement with this hypothesis. A 2 μg l^{-1} Ni^{2+} sample, containing 10 mM Ca^{2+}, was loaded at flow rates of 60, 30 and 15 ml min^{-1}, and the recoveries obtained were 75, 92 and 101%, respectively.

For the determination of copper in tap water the column was enriched with 100 ml increments of the sample buffered at pH 5.0. The water sample contained 4.8 μg Cu l^{-1} as determined by GFAAS. The eluates were collected in the off-line mode in order to increase the accuracy, and analysed by ICP-AES. While a recovery of 99% was obtained for standard solutions of the same concentration run in parallel, only about 60% of copper was recovered from the tap water sample and the rest, 40%, was found in the column effluent. Loading flow rates of 60, 30 and 12 ml min^{-1} for a natural and a synthetic tap water resulted in quantitative uptake for the synthetic sample, while recoveries of 68, 72 and 78%, respectively, were obtained for the natural tap water. The effluent concentrations were in agreement with the recovery figures. The results for the synthetic sample clearly indicate that the matrix effects from inorganic constituents are negligible. Hence, the reason for the loss of copper is probably complexation with humic substances or other organic ligands present in the tap water. This was tested by a measurement of the recovery of a photo-digested tap water. The column was enriched with two tap water samples UV-irradiated at pH 2.3 and 1.2, respectively. No significant amounts of copper was found in the column

effluents indicating quantitative adsorption of the analyte from both samples (< 5% loss).

For nickel, it was necessary to enrich more than 400 ml of tap water to get reasonable signals in the FIA-ICP-AES system. The sample was buffered at pH 5.5 and enriched at flow rate of 60 ml min^{-1}. Enrichment of a 0.45 μg Ni l^{-1} tap water resulted in an uptake of only 0.22 μg l^{-1}. The effluent concentration was measured to be about 0.2 μg l^{-1} in agreement with the previous figure. Hence, the recovery of nickel at this flow rate is about 50%. This is less than obtained for spiked, synthetic tap water samples (see above). Thus, complexation of nickel with humic substances is indicated. Digestion experiments were not performed for this element due to the large sample volumes required.

For determination of the cadmium concentration, the column was enriched with 400 ml increments of a tap water at pH 5.5, 6.5 (adjusted) and 7.7 (natural). A mean value of 36 ± 6 ng l^{-1} ($n = 2 \times 3$) was obtained for the cadmium concentration. No trend in the result with pH could be discerned with the present precision, which, however, is not as good as could be expected from the estimated detection limit. Analysis by GFAAS, using multiple injections, resulted in the concentration 36 ± 4 ng l^{-1} in agreement with the result obtained from the preconcentration by IDA-Novarose. Analysis of the column effluent, resulted in cadmium concentrations below the detection limit (< 2 ng l^{-1}).

4. Conclusions

This work has demonstrated the rapid exchange of metal ions on IDA-Novarose. In particular, the adsorption appears to proceed much faster than on Chelex-100, the most common adsorbent with iminodiacetate groups. The new adsorbent can tolerate relatively high pressures with no change in adsorption properties. Metal ions, at least in an uncomplexed form, can be quantitatively sequestered at high volumetric flow rates on a small column. Large preconcentration factors can then be reached within a moderate accumulation time.

The large preconcentration factor, 500–1000, needed in ultra trace analysis with ICP-AES detection, will create an unbalance between the preconcentration and quantitation times even at high sample flow rates. Automated preconcentration off-line could then be considered. In case a preconcentration factor of 50–100 is needed, a more balanced situation is at hand, and the high flow rate permissible with IDA-Novarose will considerably increase the sample throughput.

Analysis of tap water indicates the capability of the adsorbent to quantitatively adsorb cadmium at high flow rates. Effects of humic substances and other matrix components on the kinetics of the adsorption of copper and nickel lead to incomplete recoveries even at low flow rates.

Acknowledgements

We would like to thank Dr Göran Lindgren (Scand Inovata AB, Stockholm, Sweden) for valuable discussion and the gift of the IDA-Novarose adsorbents.

References

[1] H.M. Kingston, I.L. Barnes, T.J. Brady, T.C. Rains and M.A. Champ, Anal. Chem., 50 (1978) 2064.
[2] F. Malamas, M. Bengtsson and G. Johansson, Anal. Chim. Acta, 160 (1984) 1.
[3] M. Torre and M.L. Marina, Crit. Rev. Anal. Chem., 24 (1994) 327.
[4] D.B. Taylor, H.M. Kingston, D.J. Nogay, D. Koller and R. Hutton, J. Anal. At. Spectrom., 11 (1986) 187.
[5] L. Steinmann, J. Porath, P. Hashemi and Å. Olin, Talanta, 41 (1994) 1707.
[6] L. Ebdon, A.S. Fisher, P.J. Worsfold, H. Crews and M. Baxter, J. Anal. At. Spectrom., 8 (1993) 691.
[7] M.J. Bloxham, S.J. Hill and P.J. Worsfold, J. Anal. At. Spectrom., 9 (1994) 935.
[8] S. Olsen, L.C.R. Pessenda, J. Ruzicka and E.H. Hansen, Analyst, 108 (1983) 905.
[9] S.D. Hartenstein, J. Ruzicka and G.D. Christian, Anal. Chem., 57 (1985) 21.
[10] Y. Liu and J.D. Ingle Jr., Anal. Chem., 61 (1989) 520.
[11] S. Caroli, A. Alimonti, F. Petrucci and Z. Horváth, Anal. Chim. Acta, 248 (1991) 241.
[12] Z. Fang, S. Xu and S. Zhang, Anal. Chim. Acta, 200 (1987) 35.

[13] Z. Fang, S. Xu and G. Tao, J. Anal. At. Spectrom., 11 (1996) 1.
[14] G. Schulze and O. Elsholz. Fresenius Z. Anal. Chem., 335 (1989) 721.
[15] J. Porath, Protein Expression Purif., 3 (1992) 263.
[16] G. Mattsson, L. Nyholm, Å. Olin and U. Örnemark, Talanta, 42 (1995) 817.
[17] Y. Lu, C.L. Chakrabarti, M.H. Back, D.C. Grégoire and W.H. Schroeder, Anal. Chim. Acta, 293 (1994) 95.
[18] J. Lehto, A. Paajanen, R. Harjula and H. Leinonen, React. Polymers, 23 (1994) 135.
[19] M. Pesavento, R. Biesuz, M. Gallorini and A. Profumo, Anal. Chem., 65 (1993) 2522.
[20] N.V. Jarvis and J.M. Wagener, Talanta, 41 (1994) 747.
[21] Y. Merle and J.A. Marinsky, Talanta, 31 (1984) 199.
[22] Ö. Szabadka, Talanta, 29 (1982) 183.
[23] R.A. Robinson and R.H. Stokes, Electrolyte Solutions, Butterworth, London, 1959, p. 492.
[24] G. Schwarzenbach, G. Anderegg, W. Schneider and H. Senn, Helv. Chim. Acta, 38 (1955) 1147.
[25] P.J. Hoek and J. Reedijk, J. Inorg. Nucl. Chem., 41 (1979) 401.
[26] R. Hering, Chelatbildende Ionenauscher, Academie-Verlag, Berlin, 1967, Ch. 5.
[27] A. Medin, Studies on Structure and Properties of Agarose, Ph.D. Thesis, Uppsala University, 1995.
[28] A.M. Naghmush, K. Pyrzynska and M. Trojanowicz, Talanta, 42 (1995) 851.
[29] S. Hirata, Y. Umezaki and M. Ikeda, Anal. Chem., 58 (1986) 2602.

ELSEVIER

Talanta 44 (1997) 1055–1061

Talanta

Sorptive behavior of Zn(II) on a lake sediment by sequential extraction-radiotracer technique

Ryoko Fujiyoshi *, Tomoo Gomei, Sadashi Sawamura

Faculty of Engineering, Hokkaido University, Sapporo 060, Japan

Received 9 July 1996; received in revised form 2 December 1996; accepted 3 December 1996

Abstract

A sequential extraction-radiotracer technique was applied to a sediment core sample collected from Lake Biwa (Japan) in order to evaluate relative importance of the fractionated solid components to sorb Zn(II) ions. The core was previously divided into three parts from the surface of the sediment: upper (0–6 cm), middle (6–12 cm) and bottom (12–18 cm). The solid residue after each chemical treatment was collected to perform a sorption experiment by using ^{65}Zn as a tracer. A difference in the amount of Zn(II) sorption was observed among original samples without any chemical treatments at each depth. The amounts were very small (10^{-5}–10^{-4} mol Zn(II) 100 g^{-1} of dry sample) in all fractions of the sediment. Electrochemical measurements of cadmium and copper ion sorption supported the results from the radiometric sorption experiment. The effects of several potential factors on zinc sorption were investigated. Ion exchange of zinc with protons on the mineral surfaces was a significant cause of the zinc sorption.

Keywords: Extraction-radiotracer; Fractionated solid; Lake sediment

1. Introduction

Factors controlling fates of pollutants like heavy metals and radionuclides in the aquatic environment have been extensively studied. They are found to be very complex, partly because there are several forms of pollutants themselves depending on in situ conditions as well as those of solid phases with which the pollutants interact [1,2].

In the previous papers [3,4], the authors investigated a sequential extraction-radiotracer technique to elucidate mineral phases of several natural samples with which pertinent pollutants would be taken up. Good results were obtained in those cases; the Zn(II) sorption was relevant to the amount and the properties of some solid components of the samples remaining after certain chemical treatments.

The technique is further applied to an oxic lake sediment collected from Lake Biwa (Siga Prefecture, Japan) to find possible scavengers and the sorbed amount of Zn(II) in the aquatic environment.

* Corresponding author. Fax: +81 11 7066675; e-mail: fuji@sun.hune.hokudai.ac.jp

0039-9140/97/$17.00
PII S0039-9140(96)02193-5

2. Experimental

2.1. Reagents and materials

The core sediment used in this study was supplied by the courtesy of Dr Masuzawa of Nagoya University (Japan). It was collected at a point south west of Chikubu Island in Lake Biwa (Siga Prefecture, Japan) on November 21 1985. The sample was cut into three portions from the top of the sediment; upper (0–6 cm), middle (6–12 cm) and bottom (12–18 cm). After drying at room temperature, those subsamples were then ground to homogeneous powders.

Zinc-65 was purchased from Japan Radioisotope Association in the form of chloride in 0.5 M hydrochloric acid(stock solution). The nominal sp. act. was 105 GBq gZn^{-1}, with a radionuclidic purity of 99.00% and a radiochemical purity of 99.00%. The $^{65}Zn(II)$ tracer solution (925 $kBqcm^{-3}$) was prepared from the stock solution by diluting with a standard zinc nitrate solution (1000 $mgZn\ dm^{-3}$) to avoid the Zn(II)-chloro complexation in the solution. Almost all zinc ions in the solution is to be in the form of nitrates which have lower complexing capacities with Zn(II) than chloride ions. The specific activity of this working solution was 2.36 GBq g^{-1} of zinc.

2.2. Instruments

GM counting system (Aloka Type 203B); X-ray diffractometer (Mac Science MXP); centrifuge (Kokusan Partner); ion analyzer (Orion EA940); pH meter (Horiba D-12); spectrophotometer (Hitachi 3000); mechanical shaker (Yamato Model SA-31); thermal analyzer (Shimazu DTA-50 and Shimazu TG-50).

2.3. Procedure

The sequential extraction of the lake sediment. A dried and ground original sample (F0) was treated sequentially with the following chemical reagents: (i) 1 M NaCl (F1); (ii) 25% CH_3COOH (F2); (iii) 0.04 M $NH_2OH \cdot HCl$ in 25% CH_3COOH (pH 2) (F3); (iv) 30% H_2O_2 (pH 2) (F4); and (v) 7 M HNO_3 (F5). In the previous works [3,4], 1 M CH_3COONH_4 was used in the first step treatment (i) to obtain ion exchangeable components. However, the treatment with ammonium acetate was not suitable for dissolving ion exchangeable components of this sediment with low zero point of charge (ZPC). Instead, 1 M sodium chloride solution was used for the purpose. Both carbonate and oxide phases contained in a sediment had been dissolved simultaneously into an acid/reductant mixed solution in the previous works [3,4]. The present sample was thus, treated first with (ii) 25% CH_3COOH and then with (iii) 0.04 M $NH_2OH \cdot HCl$ in 25% CH_3COOH. It is therefore to be six fractions (F0, F1, F2, F3, F4 and F5) of the sediment including the original sample without any chemical treatment (F0).

The sorption experiments were carried out as follows; a dried sample (F0–F5) was weighed and transferred to a centrifuge tube (10 cm^3). The total volume of the suspension was adjusted to 10 cm^3 with distilled water. A small amount of the $^{65}Zn(II)$ tracer solution (10–80 μl) was added to the suspension, which was shaken mechanically for 40 min. The suspension was then centrifuged (3000 rpm, 30 min). An aliquot (1 cm^3) of the supernatant solution was pipetted into an aluminum container, and dried completely for γ-counting.

The ^{65}Zn activity was measured using a GM counter. The specific activity of the $^{65}Zn(II)$ tracer solution used in this study was found to be 2.36 GBq gZn^{-1}, and the efficiency of the counting was 0.327% in total. Several standards of known activity were used to evaluate values obtained under the same counting conditions.

The cation exchange capacity (CEC) of each sample was measured electrochemically with an ammonia electrode (Orion 95-10); all the cation sites of a sample in an aqueous suspension were previously substituted with ammonium ions (1 M NH_4Cl). After centrifugation of the suspension, the residue was washed repeatedly with distilled water and then treated with 0.1 N NaCl solution. The amount of NH_4^+ ions released from the solid phase by the exchange with Na^+ ions was determined electrochemically.

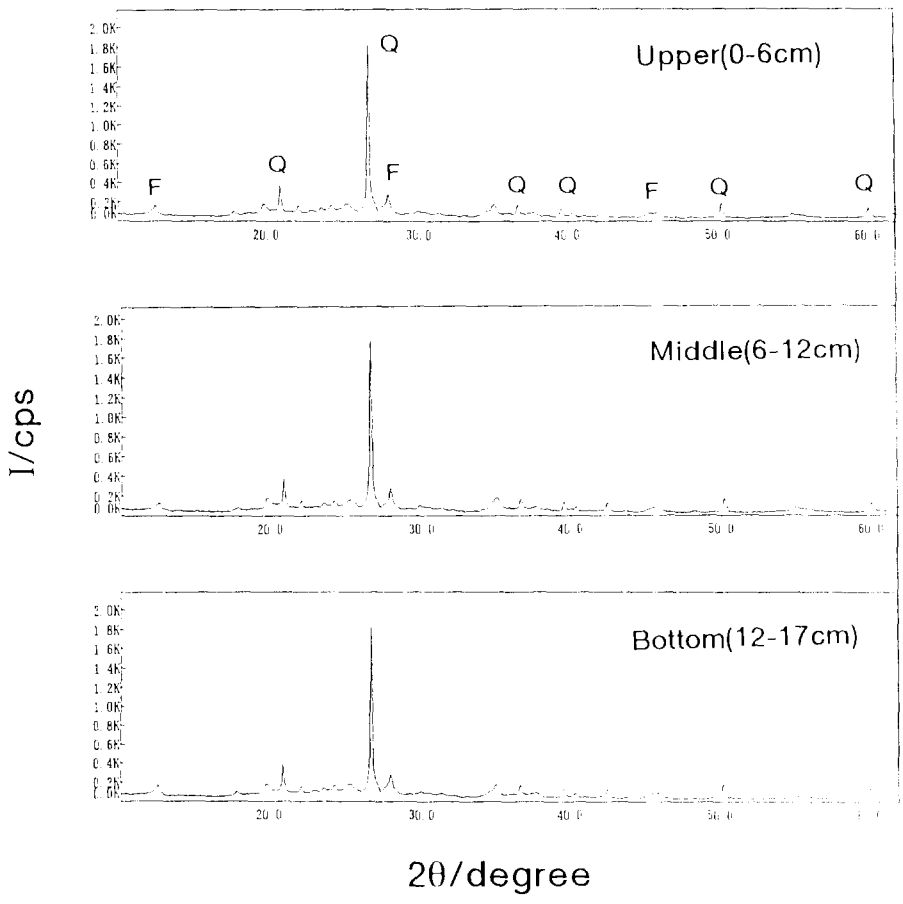

Fig. 1. X-ray diffraction patterns of the untreated fractions (F0) of the core sediment sample. Q: quartz, F: feldspar.

pH Effect was also investigated on Cd(II) and Cu(II) sorption by using ion selective electrodes of both ions (Orion 94-48 cadmium electrode and Orion 94-29 cupric electrode). It was actually evaluated from the emf measurement of a liquid phase before and after the sorption equilibrium in each system.

The mineral phases of the sediment samples after the various chemical treatments were identified by powder X-ray diffraction analysis [5].

The surface area of the sediment samples were measured spectrophotometrically by using methylene blue as a coloring agent [6].

Thermal analyses of the untreated samples were carried out by DTA and TG in which the initial heating rate was 10°C min^{-1}, and the temperature of the furnace was then kept constant at 450°C for 2 h. Weight loss of each sample after the combustion was calculated.

3. Results and discussion

The Lake Biwa is the largest lake in Japan, and many studies have been done on this lake ecologically and hydrodynamically so far [7]. However, information on the chemistry of bottom sediments of the lake seems to be rather scant.

Fig. 1 shows the X-ray diffraction patterns of untreated fractions (F0) of the three portions (upper, middle and bottom) of the core sample. There appear quartz and feldspars in all samples, and no apparent differences exist in the pattern among them. Similar patterns were observed in all

Table 1
Weight loss (%) of individual fractions of the sediment samples upon each chemical treatment

Chemical treatment	Upper (0–6 cm)	Middle (6–12 cm)	Bottom (12–17 cm)
Electrolyte	2.4	2.5	0.7
Weak acid	2.7	2.0	3.2
Reductant	1.3	1.8	1.8
Oxidant	5.2	4.9	5.1
Strong acid	4.2	3.7	2.4
Residue	84.2	85.1	86.8

All values are on a dry sediment weight bases. Possible errors of those values are estimated to be less than ± 5%.

other fractions of the sediment. It is considerable that major mineral components of the sediment may be stable enough not to be leached appreciably by any chemical treatments other than conc. HNO_3. Results on the weight loss of the sample upon each treatment supports this assumption (Table 1). It should be noted that there exist some clay minerals and also hydrous ferric oxides in the sediment sample [7]. Those minerals may play a role to sorb Zn(II) ions, however, as shown later, the sorbed amount was very small as a whole.

Sorption experiments were then carried out radiometrically on 15 fractionated samples by using ^{65}Zn as a tracer. Fig. 2 shows the sorption isotherm on three portions of the untreated sediments; upper (F0), middle (F0) and bottom (F0). The good linearity of the isotherms leads to calculate the sorbed amount of ^{65}Zn at maximum (A_m).

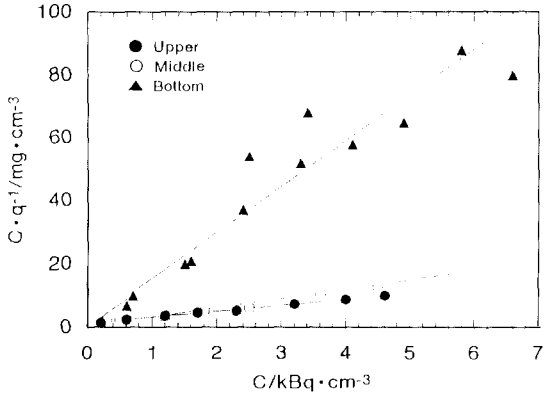

Fig. 2. Sorption isotherms on untreated fractions (F0) of the sediment sample. C and q denote the $^{65}Zn(II)$ activities in the aqueous and solid phases, respectively. ●: upper, ○: middle, ▲: bottom.

As shown in Table 2, the value is found to be highest at the surface (upper) and extremely low in the deepest portion (bottom) of the core sediment.

In order to elucidate possible reasons for such differences in the sorption, the surface area of each sample was measured colorimetrically. No clear relationship exists between the surface area and the A_m value of those samples (Table 2). The result suggests that the surface area is not a predominant factor controlling the Zn(II) sorption under the present experimental condition.

Fig. 3 shows the CEC of each fractionated sample of the sediment. The values are higher in all fractions of the upper portion than those in other portions of the sediment. As shown in Table 2, the CEC values on F0 samples are more than 30 times higher than the sorbed amount of ^{65}Zn at maximum (A_m). As described in the experimental section, the CEC was obtained electrochemically by using an ammonia electrode, in which the electrode potential caused by the ion exchange between Na^+ and NH_4^+ in the solution was measured. It is thus possible that the sites for Zn(II) ions to be sorbed may not be just the same as those for NH_4^+ ions, since there are differences in charge and also in ionic radius between them.

The CEC is obviously affected by surface states of solid phases, and it is closely related to the pH value at zero point of charge (pH_{ZPC}) of the solids. The apparent pH_{ZPC} of the untreated fractions (F0) of the sediment is estimated by pH change of the solid suspension before and after the sorption equilibrium [d(pH)]. Fig. 4 shows that the pH value at which d(pH) is to be zero on the curve may be approximated to be the pH_{ZPC}

Table 2
Comparative lists of data on surface area, sorbed amount of ^{65}Zn at maximum (A_m), CEC, pH_{ZPC} and ignition loss at 450°C of three portions (upper, middle and bottom) of the untreated sediment sample (F0)

	Upper (0–6) cm^{-1}	Middle (6–12) cm^{-1}	Bottom (12–17) cm^{-1}
Surface area ($m^2\ g^{-1}$)	15 ± 3	15 ± 3	10 ± 3
A_m (10^{-4} mol 100 g^{-1})	3.43 ± 0.07	2.21 ± 0.04	0.51 ± 0.01
CEC (meq 100 g^{-1})	9.59 ± 0.36	6.98 ± 0.49	6.73 ± 0.92
pH_{ZPC}	6.6 ± 0.1	6.3 ± 0.1	6.2 ± 0.1
Ignition loss at 450°C (%)	6.60 ± 0.01	6.29 ± 0.01	6.13 ± 0.01

of each F0 sample. As shown in Table 2, the resulting value is highest at the upper portion and the lowest at the deepest one of the sediment, which is consistent with the result obtained in the radio-metric ^{65}Zn sorption experiment. It is therefore possible that the Zn(II) sorption is related to the proton exchange on the sediment surfaces, i.e., the more negative solid surfaces provide more sites for cation sorption in the aqueous phase.

In order to evaluate the above results on other ions than Zn(II), the electrochemical approach was carried out by using ion selective electrodes of cadmium and copper. Fig. 5 shows the results of both cadmium (II) and copper (II) sorption on three portions of the nontreated sediment samples (F0) at pH_{ZPC}. The sorbed amount of Cu(II) is consistently larger than that of Cd(II) at any depth of the sediment samples. Such a difference in sorptive ability between two metal ions can be explained by considering their hydrated radii and coordination properties of aqua-complexes. The values are in the same order of magnitude as those of the sorbed amount of ^{65}Zn at maximum obtained from the tracer experiment (Table 2).

Those results suggest that the sorption of the divalent metal ions like Zn(II), Cu(II) and Cd(II) occur rather selectively through the ion exchange with protons on mineral surfaces of this lake sediment. A mineral which provides a surface with proton exchangeable sites thus, enables those metal ions to be sorbed to a great extent. This may also be true in the organic matter which will provide protons from carboxylic and phenolic groups. The organic contents of the non-treated sediments may be estimated from their ignition loss at 450°C. As shown in Table 2, the value is highest at the upper portion and the lowest at the bottom of the core.

The crucial role of protons is well known in biosorption. Shiewer and Volesky [8] observed biosorption of Cd^{2+}, Cu^{2+} and Zn^{2+} on a non-

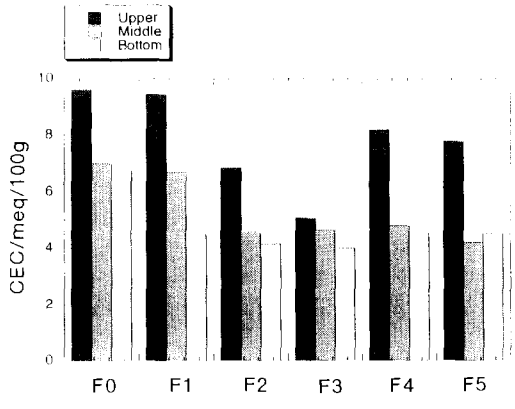

Fig. 3. CEC of each fraction of the sediment sample (F0, F1, F2, F3, F4, F5).

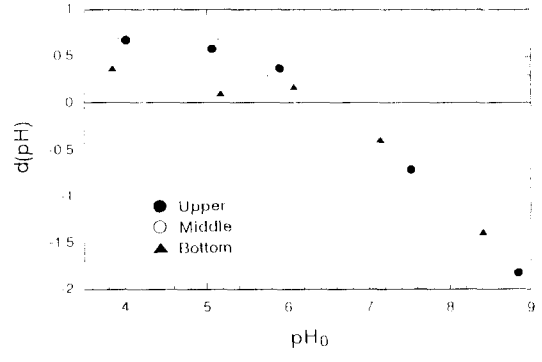

Fig. 4. Change in pH of the solid (F0) suspension before and after the sorption equilibrium [d(pH)] as a function of pH adjusted initially (pH_0). ●: upper, ○: middle, ▲: bottom.

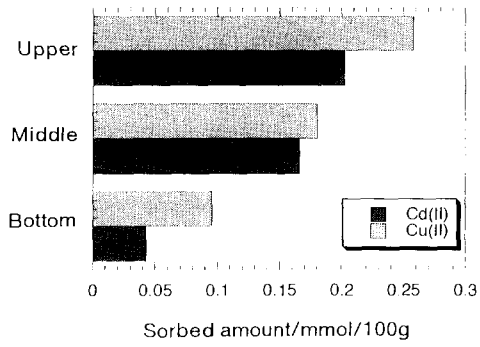

Fig. 5. Sorption of Cd(II) and Cu(II) on three portions of the untreated sediment sample (F0) at pH_{ZPC}.

living biomass of the marine alga (Sargassum fluitans). They modeled the sorption using a modified multicomponent Langmuir equation to describe metal ion-proton exchanges.

It is apparent that there are several factors controlling sorption behavior of the divalent metal ions on various sediments; chemical forms of metal ions, surface states of minerals especially on number of proton exchangeable sites, and probably the existence of organic matter as complexing agents with metals as well as usual in situ temperature, pressure and redox conditions. Chemical forms of metal ions are also dependent on pH value of the aqueous phase.

Sorption processes in natural environment are therefore intrinsically heterogeneous in nature. Weber et al. [9] reviewed sorption phenomena in subsurface systems in order to elucidate the behavior, transport and ultimate fate of contaminants. And then they introduced the distributed reactivity model which was derived on the basis of different distributions of sorption reactions and mechanisms for different solute–solid combinations [10]. They showed experimental evidence to conclude the model to be valid.

The sequential extraction-radiotracer technique should help to evaluate sorption capacities of individual components of a sediment, if they could be leached sequentially by suitable chemical treatments. The present authors previously reported the results on this technique applying to a scale sample collected from a water still and also a marine sediment [3,4]. The sorbed amount of Zn(II) was found to be clearly correlated with the kind and amount of mineral phases contained in the solid sample.

From the results obtained in a series of experiments, it is concluded that the Zn(II) sorption is significantly controlled by the proton concentration of both aqueous and solid phases. A solid phase containing much amount of acidic minerals (or organic matter with carboxylic groups) tends to release protons into the aqueous phase to result in its suspension with low pH. The amount of Zn(II) sorbed is to be very small in such a case. The sequential extraction-radiotracer technique is thus, useful to evaluate the capacity of each component of the sediment to scavenge toxic heavy metals, when its pH_{ZPC} is relatively high ($pH > 8$). Anyway, a sediment with low pH_{ZPC} has only a small capacity for scavenging as a whole.

Further experimental study should be continued to elucidate the reversibility of the sorption and also competitive sorption among metal ions with various ionic radius and complexing abilities.

Acknowledgements

The authors gratefully acknowledge Dr T. Masuzawa of Nagoya University for giving valuable suggestion and providing a sediment sample used in this study.

References

[1] H.R. von Guten and P. Benes, Speciation of Radionuclides in the environment. IUPAC Analytical Chemistry Division, Commission on Radiochemistry and Nuclear Techniques Paul Scherrer Institut No. 94-03: Villigen (Switzerland), 1994, p. 12.

[2] H. Haraguchi and A. Itoh, in Chemical Society of Japan (ed.), The Global environment and the analyses; Kagakusousetsu No. 29 (in Japanese), Gakkai Shuppan Center, Tokyo (Japan), 1996, p. 35.

[3] R. Fujiyoshi, T. Okamoto and M. Katayama, Appl. Radiat. Isot., 45 (1994) 165.

[4] R. Fujiyoshi, T. Gomei and M. Katayama, Appl. Radiat. Isot., 47 (1996) 165.

[5] B.F. Jones and C.J. Bowser, in A. Lerman (ed.), Lakes Chemistry, Geology, Physics, Springer-Verlag, New York, 1978, p. 248.
[6] C.P. Huang and E.A.J. Rhoads, Colloid Interface Sci., 131 (1989) 289.
[7] T. Fujinaga and T. Hori, Environmental Chemistry on Lake Biwa (in Japanese) Japan Society for the Promotion of Science, Japan 1982.
[8] S. Schiewer and B. Volesky, Environ. Sci. Technol., 29 (1995) 3049.
[9] W.J. Weber Jr, P.M. McGinley and L.E. Katz, Water Res., 25 (1991) 499.
[10] W.J. Weber Jr, P.M. McGinley and L.E. Katz, Environ. Sci. Technol., 26 (1992) 1955.

ELSEVIER

Talanta 44 (1997) 1063–1071

Talanta

Study of the selective extraction of iron (III) by silica-immobilized 5-Formyl-3-Arylazo-salicylic acid derivatives

Mohamed E. Mahmoud [a,*], Ezzat M. Soliman [b]

[a] *Chemistry Department, Faculty of Science, Alexandria University, P.O. Box 426, Ibrahimia, Alexandria 21321, Egypt*
[b] *Chemistry Department, Faculty of Science, El-Minia University, El-Minia, Egypt*

Received 16 July 1996; received in revised form 25 November 1996; accepted 2 December 1996

Abstract

A method for immobilization of 5-formyl-3-arylazosalicylic acid derivatives on the surface of silica gel is described. The new silica gel phases were synthesized by a very simple and rapid route which can be defined as a one-step reaction. The phases were proved to show an excellent improvement in the iron (III) extraction and the determined mmol g^{-1} values are in the range of 1.24–1.32. The metal-uptake properties of eleven metal ions were also evaluated at different pH values and shaking times. The process of selective extraction of iron (III), in presence of an interfering ion, by these phases was also studied by both column and batch equilibrium techniques in order to identify the possible type of interference of each metal ion in this process. Three divalent metal ions (Mg, Ca and Mn) exhibited a minimum interference in iron (III) extraction. A group of six divalent metal ions (Co, Ni, Cu, Zn, Cd and Pb) were found to be interfering in the selective extraction of iron (III) via the arylazo-moiety of the silica phase, while Cr(III) was found to show a specific interference type based on the affinity of Cr(III) for binding to the chelation centers of the salicylic acid moiety of the silica phase. © 1997 Elsevier Science B.V.

Keywords: Chelation centers; 5-Formyl-3-Arylazo-salicylic acid derivatives; Selective extraction

1. Introduction

Immobilization of chelating compounds on the surface of silica gel has received special interest in recent years because of the wide range of applicability of these phases in metal-ion uptake and pre-concentration [1–10], separation of transition and non-transition metal ions [11–15], solvent clean-up from undesired metal ions and selective extraction of metal ions from different solvent systems [16]. The selectivity incorporated and encountered in such phases is mainly attributed to the presence of donor atoms capable of metal-complex formation with certain metal ions [5,17]. The most commonly used donor atoms in metal complexes are oxygen, nitrogen and sulfur, which are bound to the metal ion in a certain fashion for forcing selective extraction of metal ions. A method for selective extraction of alkali-metal ions by silica-immobilized crown ether derivatives was reported [18]. Silica gel modified with γ-aminopropyltriethoxysilane was shown to be a

* Corresponding author.

PII S0039-9140(96)02194-7

selective phase for preconcentration of gold (III), Platinum (IV) and palladium (II) [19]. Oxygen- and nitrogen-donor-containing macro-cyclic compounds immobilized on silica gel surface showed high selectivity for copper (II) in presence of cobalt (II), nickel (II), zinc (II) and cadmium (II) [20]. Palladium (II) was selectively extracted from other interfering metal ions by the use of silica-immobilized thioaniline derivatives [21].

Recently, we have reported the method of immobilization of two isomeric formylsalicylic acid derivatives on the surface of silica gel modified with aminosylating agent through the Schiff base formation between the aldehydic and the amino groups. The phases were found to be highly selective for iron (III) extraction from a mixture of different interfering metal ions [22]. The selectivity of iron (III) through chelation with the two oxygen atoms furnished by the hydroxyl and the carboxyl groups [23].

In this paper, 5-formylsalicylic acid is derivatized to the corresponding arylazo derivatives via diazotization reaction with aniline, 2-aminophenol, 2-aminothiophenol and 2-aminobenzoic acid. This was done in an attempt to explore the phenomenon of selective extraction of iron (III) by silica-immobilized salicylic acid derivatives, increase the possibility of metal-ion uptake, especially iron (III), by the presence of additional chelating functional groups and study the influence of such additional chelating centers on the selective extraction process.

2. Experimental

2.1. Apparatus

Infrared spectra of 5-formylsalicylic acid arylazo-derivatives were recorded on a Perkin-Elmer 1430 ratio-recording spectrophotometer. Atomic absorption measurements of the different metal ions were carried out by using a Perkin-Elmer 2380 atomic absorption spectrophotometer operated at the specific wavelength of absorption of each metal ion. The pH values of the various buffer solutions were measured by using a Schott Geräte pH-meter calibrated against two standard buffer solutions of pH 4.0 and 9.2. Elemental analyses of the various 5-formyl-3-arylazosalicylic acid derivatives and modified phases were done at the microanalysis center at Cairo University.

2.2. Reagents and materials

5-Formylsalicylic acid was prepared according to previously reported method [24]. Aniline, 2-aminophenol, 2-aminothiophenol and 2-aminobenzoic acid were purchased from BDH Chemicals, Poole, England and used as received. 3-Aminopropyltriethoxysilane was purchased from Aldrich Chemical Company, USA. The silica gel used in this study is of TLC grade with 70–230 mesh size and 60 Å pore diameter, purchased from Woelm Pharma, Eschwege, Germany. Organic solvents were purified and dried according to conventional methods.

5-Formyl-3-arylazosalicylic acid derivatives of aniline, 2-aminophenol, 2-aminothiophenol and 2-aminobenzoic acid were synthesized by diazotization of the corresponding arylamine below 5°C with conc. HCl and sodium nitrite, followed by coupling with an alkaline solution of 5-formylsalicylic acid [25]. The separated azo-derivatives were filtered off, washed with water, air dried and recrystallized from methanol.

Silica-gel-bound arylazoderivatives were prepared by mixing 5.0 g of dry amino-modified silica gel with 10 mmol of the azo-derivative, already dissolved in 300 ml of hot dry toluene, and the reaction mixture was refluxed for 2 h. After completion of the reaction, detected by the colour stability of the silica gel, the product was filtered off, washed with toluene, alcohol and diethylether and dried under vacuum at 80°C for 6 h.

2.3. Surface coverage and metal capacity of modified silica

The surface coverage (mmol g^{-1}) of silica gel with arylazo-derivatives was determined on the basis of percent carbon of the modified silica phases. The metal capacity values (mmol g^{-1}) of the newly synthesized phases for the different metal ions in various buffer solutions (pH 1.0, 2.0,

3.8, 5.0 and 10.0) and in 1.0 M sodium acetate were determined in triplicate by the batch equilibrium technique. Of the dry phase, 30 mg was added to a mixture of 1.0 ml of 0.1 M metal ion and 9.0 ml of the selected buffer solution and automatically shaken for 30 min. After equilibration, the mixture was filtered, washed with 80 ml double-distilled deionized water and the unbound metal ions were subjected to complexometric titration using the proper indicator and/or atomic absorption analysis.

The effect of shaking time on the amount of extracted metal ion (mmol g^{-1}) was also studied by the batch equilibrium technique. Of the dry phase, 30 mg were added to 1.0 ml of 0.1 M metal ion and 9.0 ml of the buffer solution which showed the maximum metal capacity value in the previous section and the mixture was automatically shaken for the selected time and the metal capacity value (mmol g^{-1}) was determined as above.

2.4. Selective extraction of iron (III)

Selective extraction of iron (III) in presence of an interfering metal ion was evaluated by using both column and batch equilibrium technique. In the column technique, a column identical to that previously reported [1] was established and packed with 30 mg of the required phase in slurry of 5 ml double-distilled deionized water. A mixture containing 0.1 M iron (III) and the interfering metal ion, 1.0 ml each, was mixed with 15 ml of 1.0 M sodium acetate and drawn through the column with a flow rate of approximately 0.5 ml min^{-1}. The column was then flushed with double-distilled deionized water and the eluents were collected and diluted with double-distilled deionized water to a total volume of 100 ml in a volumetric flask. The mixture was subjected to further dilution to meet the requirements of the linear dynamic range of the calibration curves set up by the atomic absorption analysis for each metal ion.

The batch equilibrium technique study of the selective extraction of iron (III) in presence of an interfering metal ion was accomplished by mixing 30 mg of the phase with 1.0 ml each of 0.1 M iron (III) and the interfering metal ion and 15 ml of 1.0 M sodium acetate in a 50 ml measuring flask. The mixture was automatically shaken for 30 min, filtered, washed with double-distilled deionized water and the total volume of the metal ion mixture was completed to 100 ml in a measuring flask and subjected to further dilution as above for the atomic absorption analysis.

3. Results and discussion

The structure of the arylazo-compounds was confirmed on the basis of IR analysis which showed the presence of the symmetric stretching vibration mode of the azo group in the range 1430–1491 cm^{-1}. The band correspond to the asymmetrical N=N stretching mode, near 1600 cm^{-1}, was not detected as it merged with strong C=C ring vibration [26]. The structure of silica-immobilized 5-formyl-3-arylazosalicylic acid derivatives is shown below in Scheme 1.

The IR studies of the modified silica gel Phases I–IV showed the evidence for the formation of a new band corresponding to the coupling between the 5-formyl group and the amino group of modified silica with 3-aminotriethoxysilane. The product of this coupling is the C=N Schiff base bond formation which is identified in the IR spectra of I-IV at $\nu_{C=N}$ 1525–1580 cm^{-1}. The other characteristic functional groups such as $\nu_{C=O}$ at 1600–1700 cm^{-1} and ν_{OH} at 3600 cm^{-1} were confirmed from the IR spectra of Phases I–IV.

It is important to declare here that the immobilization of arylazo-compounds on the surface of silica was accomplished in only one simple and fast reaction rather than the multi-step reactions reported by others [27–29]. The double bond nature of the Schiff-base-characteristic bond,

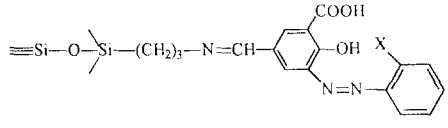

Phase I, X = H Phase III, X = SH

Phase II, X = OH Phase IV, X = COOH

Scheme 1.

C=N, is known to be strong enough and the hydrolysis of Phases I–IV by the studied buffer solutions was found to be insignificant based on the distinguished colour formation of filtrate solution of these phases with iron (III), a property that can be used for a wide range of pH application of these phases. Moreover, the surface coverage determined on the basis of percent carbon by elemental analysis was found to be in the range of 0.75–0.82 mmol g^{-1}, which is superior to the reported low values of silica gel surface coverage by azo-compounds [27,28].

3.1. Metal capacity study

The metal capacity values (mmol g^{-1}) determined for the twelve tested metal ions, namely Mg (II), Ca (II), Cr (III), Mn (II), Fe (III), Co (II), Ni (II), Cu (II), Zn (II), Cd (II), Hg (II) and Pb (II), by the newly modified silica gel Phases I–IV are compiled in Table 1. The values were determined in different buffer solutions to decide the optimum pH value for each metal ion extraction and evaluate the effect of the pH value on the metal capacity.

Several conclusions can be drawn from the data given in Table 1. The most important is the exceptionally high iron (III) metal capacity values demonstrated by the four phases. These values are 1.24, 1.32, 1.30 and 1.28 for Phases I, II, III and IV, respectively. Such high mmol g^{-1} values of iron extraction compared with our previously reported data [22] can only be interpreted on the basis of the additional chelating functional groups present in Phases I–IV from the arylazo-moiety. These chelating groups acted together with the salicylic acid moiety to enhance the metal capacity value of iron (III) and this trend suggests the participation of all chelating functional groups in iron (III) extraction by Phases I–IV, as shown in Scheme 1. The effect of pH variation on the process of iron (III) extraction is evident in Table 1, and can be summarized by the gradual increase of the mmol/g values with increasing the pH of the iron (III) solution to a maximum value in 1.0 M sodium acetate, which is determined to have a pH of 5.6 and known to be the highest pH-limit for iron (III) extraction in presence of a buffer solution. However, the mmol/g values determined in buffer solutions of pH 5.6 and 5.0 revealed no or minimal contribution of the iron (III) hydroxide.

The metal capacity values of the other metal ions listed in Table 1 can be classified into three categories. The first includes Mg(II), Ca (II) and Zn (II) ions, which were found to show little affinity for extraction by Phases I–IV in acidic buffer solutions. The metal capacity values for these metal ions ranged from 0.00–0.10 mmol g^{-1} which are very low compared with other metal ions. The use of basic buffer solutions, especially pH 10, was found to improve the metal capacity values of these three metal ions to the range of 0.10–0.30 mmol g^{-1}. The order of metal ion extraction is Mg (II) < Ca (II) < Zn (II).

The second category of metal ions involves Cr (III), Cu (II), Cd (II) and Hg (II) and shows maximum metal capacity values in 0.1 M sodium acetate solution (pH 5.8–6.2). The 0.40–0.52 mmol g^{-1} values of Cu (II), giving the following order of increasing metal capacity, Cd (II) < Cr (III) ≈ Hg (II) < Cu (II). The third category consists of Mn (II), Co (II), Ni (II) and Pb (II) ions. This group of metal ions showed an intermediate behavior between the first and second category. Mn (II) < Ni (II) ≈ Pb (II) < Co (II). A comparison between the metal capacity values of some of the tested metal ions by Phases I-IV and those previously reported [22] indicates a close similarity in the mmol g^{-1} range of Co (II), Ni (II), Cu (II) and Pb (II) by the two phase types, while the corresponding value of Cd (II) was improved by the new phases.

The effect of shaking time on the percent extraction of metal ions was studied because it is important to identify the discrimination order in the behavior of the newly synthesized Phases I–IV towards the metal ion extraction. Three representative metal ions from the previously classified categories, Fe (III), Cu (II) and Pb (II), were selected and tested at different shaking times. The results of this study are shown in Figs. 1–3 and designate the rapid interaction of Phases I–IV with metal ions, judging from the percent extraction of metal ions. As shown in Fig. 1 Fig. 2 Fig. 3, only 2 min shaking time was sufficient to force

Table 1
Metal capacity values (mmol g^{-1}) of different metal ions in various buffer solutions[a]

Phase	pH	Mg (II)	Ca (II)	Cr (III)	Mn (II)	Fe (III)	Co (II)	Ni (II)	Cu (II)	Zn (II)	Cd (II)	Hg (II)	Pb (II)
I	0.00	0.00	0.00	0.10	0.02	0.20	0.03	0.02	0.06	0.00	0.04	0.04	0.08
	2.0	0.00	0.02	0.13	0.06	0.29	0.16	0.03	0.12	0.00	0.12	0.06	0.10
	3.8	0.00	0.05	0.17	0.10	0.60	0.26[b]	0.06	0.14	0.00	0.18	0.12	0.12
	5.0	0.02	0.06	0.28	0.13	1.19	0.22	0.10	0.22	0.00	0.29	0.20	0.16[b]
	NaAc	0.05[b]	0.09[b]	0.28[b]	0.14[b]	1.24[b]	0.20	0.16[b]	0.40[b]	0.06[b]	0.36[b]	0.28[b]	0.08
II	1.0	0.00	0.01	0.05	0.00	0.21	0.06	0.02	0.06	0.00	0.10	0.02	0.10
	2.0	0.00	0.03	0.12	0.00	0.27	0.14	0.05	0.14	0.00	0.14	0.04	0.11
	3.8	0.00	0.06	0.20	0.02	0.60	0.30[b]	0.06	0.16	0.00	0.18	0.08	0.12
	5.0	0.03	0.08	0.28	0.05[b]	1.25	0.24	0.08	0.22	0.00	0.20	0.22	0.14[b]
	NaAc	0.05[b]	0.10[b]	0.30[b]	0.03	1.32[b]	0.21	0.18[b]	0.42[b]	0.05[b]	0.38[b]	0.30[b]	0.10
III	1.0	0.00	0.00	0.08	0.01	0.26	0.12	0.00	0.04	0.00	0.06	0.00	0.04
	2.0	0.00	0.02	0.15	0.06	0.33	0.18	0.10	0.14	0.00	0.10	0.04	0.10
	3.8	0.00	0.04	0.21	0.10	0.52	0.38[b]	0.16	0.16	0.00	0.14	0.16	0.12
	5.0	0.00	0.07	0.28	0.14[b]	1.28	0.25	0.20[b]	0.22	0.00	0.18	0.24	0.14[b]
	NaAc	0.02[b]	0.08[b]	0.31[b]	0.13	1.30[b]	0.22	0.14	0.52[b]	0.04[b]	0.32[b]	0.35[b]	0.04
IV	1.0	0.00	0.00	0.10	0.02	0.14	0.14	0.02	0.06	0.00	0.04	0.00	0.02
	2.0	0.00	0.02	0.15	0.07	0.20	0.20	0.03	0.12	0.00	0.14	0.02	0.04
	3.8	0.00	0.03	0.22	0.10	0.47	0.30[b]	0.06	0.18	0.00	0.20	0.12	0.08
	5.0	0.00	0.07	0.35[b]	0.13[b]	1.19	0.14	0.10	0.22	0.00	0.22	0.22	0.18[b]
	NaAc	0.04[b]	0.09[b]	0.32	0.12	1.28[b]	0.13	0.14[b]	0.42[b]	0.08[b]	0.30[b]	0.28[b]	0.06

[a] Standard deviation values are in the range of 0.00–0.01 based on $n = 3$.
[b] Maximum metal capacity values.

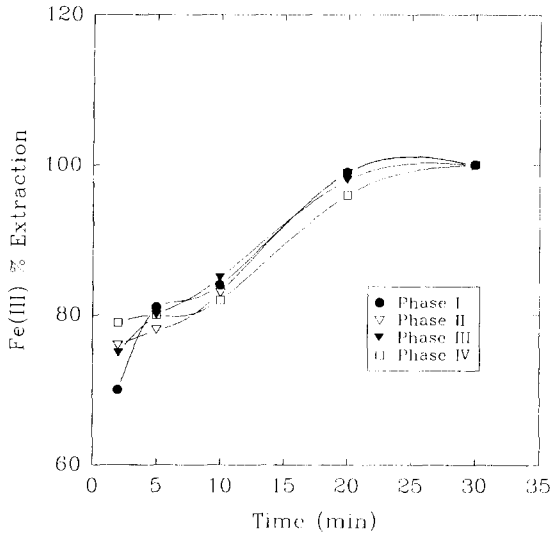

Fig. 1. Effect of shaking time (min) on the percent extraction of Fe (III) by Phases I–IV.

at least 70% of the total capacity determined in case of Fe (III) and Cu (II), while this shaking time affects 60% extraction of Pb (II). In addition, 20 min shaking time showed 98–99% of Fe (III) extraction, 90–95% of Cu (II) and 79–100% of Pb (II) extraction. It is clear from the data given that the metal ion—silica phase binding process is very fast, but no discrimination order can be

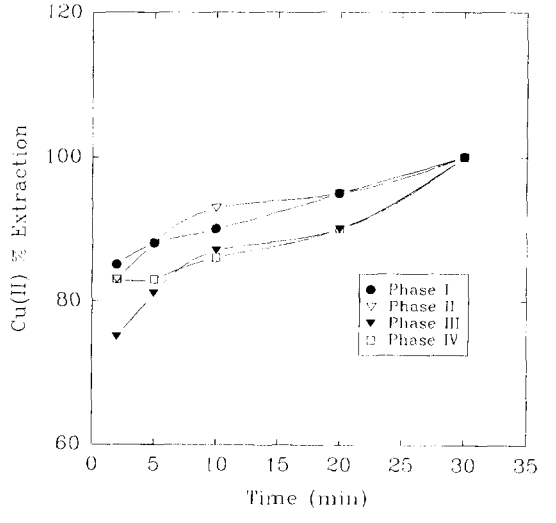

Fig. 2. Effect of shaking time (min) on the percent extraction of Cu (II) by Phases I–IV.

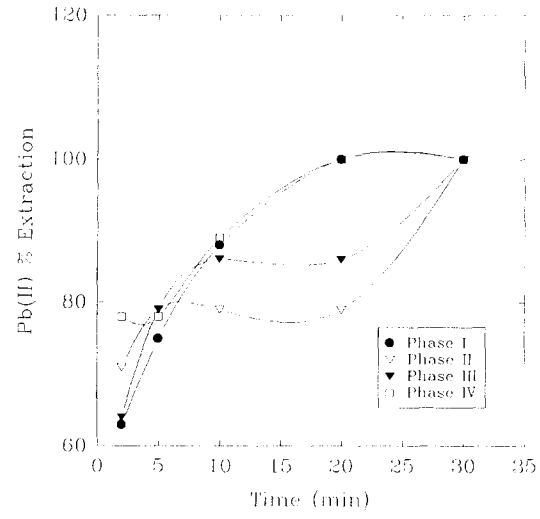

Fig. 3. Effect of shaking time (min) on the percent extraction of Pb (II) by Phases I–IV.

outlined from the effect of shaking time on the value of mmol g^{-1} and percent extraction of these metal ions.

3.2. Selectivity study

The determined values of metal capacity (mmol g^{-1}) of the various metal ions by Phases I–IV demonstrate that iron (III) is the most extractable metal ion amongst all tested metal ions, or, in other words, Phases I–IV can be successfully used for selective extraction of iron (III). In this study we preferred to evaluate the approach of selective extraction of iron (III) in presence of only one interfering species rather than a mixture of different interfering metal ions as we reported before [22], in an attempt to investigate the individual behavior of iron (III) in presence of only one interfering metal ion.

It is well known that the column technique is widely applicable in trace metal preconcentration from large-volume sample solution, in addition to the possibility of further separation of adsorbed or chemically bonded metal ions on the packing material surface [30]. This property is taken as an advantage over the batch equilibrium technique. However, the advantage of using the latter is the simplicity of operation and time saving compared with the column technique.

In the selectivity study, both column and batch equilibrium techniques were employed for the comparison. The experimental conditions such as dilution, washing and time of equilibration between the metal ion solution and the phases were almost identical. The results of this experiment are presented in Table 2. Values in Table 2 are expressed in mmol g^{-1} for simple and direct comparison with the values given in Table 1. Three different trends can be summarized from the mmol g^{-1} values of iron (III) in presence of an interfering metal ion. The first trend is the less- or non-interfering group of elements which includes Mg (II), Ca (II) and Mn(II), classified on the basis of the high metal capacity values of iron (III) which closely approaches the mmol g^{-1} value determined for iron (III) separately (Table 1), and the very low mmol g^{-1} values of the other three interfering metal ions. Therefore, Phases I–IV can be successfully used for selective extraction and separation of iron (III) in presence of Mg (II), Ca (II) and Mn (II). The second trend is demonstrated by the general behavior of Co (II), Ni (II), Cu (II), Zn (II), Cd (II) and Pb (II) metal ions. Although the metal capacity values of iron (III) given in Table 2 are high and considered in good agreement with those shown in Table 1, a strong evidence for the interference of this group of metals in the selective extraction of iron (III) comes from the similar good agreement of mmol g^{-1} values compiled in Table 1 and 2 for each metal ion, except Cu (II) which showed lower mmol g^{-1} values in Table 2. The number of accessible functional groups available for chelation and complex formation with the metal ion must be considered to account for this type of interference through selective extraction of iron (III), mainly by complex formation via the salicylic acid moiety, leaving the other chelating functional groups derived from the arylazo-moiety free for participation in the extraction of the interfering metal ion, thus, enforcing such type of interference denoted in Table 2 as arylazo chelation centers interference. This behavior of binding more than one metal ion is common and well known in the mixed metal complex formation by binucleating ligands [26,31–35].

The third trend in this study clearly shows another type of interference based on the selective extraction of iron (III) in presence of Cr (III). The metal capacity values of Cr (III) shown in Table 2 are consistent with those in Table 1, but those of Fe (III) given in Table 2 are dramatically lowered compared with those found in Table 1. The reason for this is attributed to the strong competition between iron (III) and Cr (III) ions for complex formation with the same chelating centers, namely the salicylic acid active chelating groups. This type of interference can be correlated to the similarity of the charge on both metal ions and the strong affinity of both cations to the same chelation sites.

Finally, the column and batch equilibrium data listed in Table 2 refer to the consistency between both techniques in evaluating metal uptake properties, metal ion extraction and interference processes, but the column technique is superior if further chromatographic separation between such metal ions is needed.

4. Conclusion

The studied silica-gel-bound 5-formyl-3-arylazosalicylic acid phases show very important and interesting results. The guide for designing new selective silica gel phases for metal ion extraction must be well defined on the basis of the number of interference types described in this study. The presence of an excessive number of chelating centers may enhance the chance of increasing the metal capacity of one or more metal ions, but undoubtedly will assist the possibility of strong interference by other metal ions, which diminishes the possibility of using such phases for selective extraction of a certain metal ion in presence of interfering metal ion(s). Therefore, it is important to design the new selective silica gel phases on the basis of the least number of chelating centers and selectively direct these centers to bind only the desired metal ion. Elimination of other factors which may cause any sort of interference is also recommended.

Table 2
Selective extraction of iron (III) in presence of an interfering metal ion

Phase	Fe (III)–Cr (III)				Interference type
	Fe (III)		Cr (III)		
	B	C	B	C	
I	0.90	0.95	0.28	0.30	Salicylic acid chelation centers interference
II	1.01	0.99	0.29	0.32	
III	0.96	0.93	0.33	0.34	
IV	0.94	0.94	0.36	0.31	

	Fe (III)–Mg (II)				Fe(III)–Ca(II)				Fe (III)–Mn (II)				Interference type
	Fe (III)		Mg (II)		Fe (III)		Ca (II)		Fe (III)		Mn (II)		
	B	C	B	C	B	C	B	C	B	C	B	C	
I	1.21	1.23	0.04	0.05	1.25	1.23	0.05	0.06	1.21	1.25	0.06	0.03	Minimum interference
II	1.28	1.24	0.05	0.05	1.33	1.29	0.07	0.02	1.31	1.31	0.02	0.01	
III	1.25	1.30	0.05	0.05	1.29	1.25	0.03	0.04	1.28	1.29	0.02	0.02	
IV	1.32	1.30	0.05	0.05	1.30	1.30	0.02	0.03	1.24	1.30	0.03	0.04	

	Fe (III)–Co (II)				Fe (III)–Ni (II)				Fe (III)–Cu (II)				Fe (III)–Zn (II)				Fe (III)–Cd (II)				Fe (III)–Pb (II)				Interference type
	Fe (III)		C (II)		Fe (III)		Ni (II)		Fe (III)		Cu (II)		Fe (III)		Zn (II)		Fe (III)		Cd (II)		Fe (III)		Pb (II)		
	B	C	B	C	B	C	B	C	B	C	B	C	B	C	B	C	B	C	B	C	B	C	B	C	
I	1.20	1.23	0.26	0.25	1.24	1.29	0.21	0.19	1.20	1.22	0.28	0.31	1.22	1.21	0.16	0.12	1.23	1.25	0.37	0.37	1.26	1.20	0.16	0.15	Arylazo chelation centers interference
II	1.32	1.31	0.23	0.22	1.30	1.27	0.22	0.23	1.30	1.34	0.29	0.32	1.31	1.36	0.25	0.19	1.29	1.27	0.39	0.36	1.28	1.25	0.12	0.13	
III	1.30	1.29	0.21	0.23	1.29	1.26	0.26	0.24	1.30	1.32	0.23	0.19	1.30	1.32	0.23	0.20	1.30	1.30	0.33	0.34	1.28	1.25	0.14	0.15	
IV	1.28	1.26	0.20	0.24	1.26	1.27	0.25	0.24	1.27	1.23	0.29	0.31	1.28	1.27	0.20	0.21	1.23	1.22	0.34	0.34	1.26	1.23	0.18	0.18	

[a] Values are expressed in mmol g^{-1}. B: batch equilibrium technique; C: column technique.

Acknowledgements

The authors wish to thank Dr Sherif Kholeif for his assistance.

References

[1] R.E. Sturgeon, S.S. Berman, S.N. Willie and J.A. Desaulniers, Anal. Chem., 53 (1981) 2337.
[2] J.C. Moriera and Y. Gushikem, Anal. Chim. Acta, 176 (1985) 263.
[3] M. Volkan, O.Y. Atman and A.G. Howard, Analyst, 112 (1987) 1409.
[4] P.Y.T. Chow and F.F. Cantwell, Anal. Chem., 60 (1988) 1569.
[5] A. Tong, Y. Akama and S. Tanaka, Analyst, 115 (1990) 947.
[6] V.A. Basiuk and E.G. Khil'chevskaya, Anal. Chim. Acta, 255 (1991) 197.
[7] T.I. Tikhomirova, V.I. Fadeeva, G.V. Kuryavtsev, P.N. Nesterenko, V.M. Ivanov, A.T. Savitchev and N.S. Smirnova, Talanta, 38 (1991) 267.
[8] H. Ince, S. Akman and Ü. Köklü, Fresenius Z. Anal. Chem., 342 (1992) 560.
[9] M.E. Mahmoud and G.A. Gohar, Alexandria Eng. J., 33 (1994) D159.
[10] M.E. Mahmoud, Anal. Lett., 29 (1996) 1791.
[11] T. Seshardi, U. Kampschulze and A. Kettrup, Fresenius Z. Anal. Chem., 300 (1980) 124.
[12] I.P. Alimarin, V.I. Fadeeva, G.V. Kudryavtsev, I.M. Loskutova and T.I. Tikkhomirova, Talanta, 34 (1987) 103.
[13] N. Simonzadeh and A.A. Schilt, Talanta, 35 (1988) 187.
[14] U. Pyell and G. Stork, Fresenius Z. Anal. Chem., 343 (1992) 576.
[15] Ü. Köklü, S. Akman, Ö. Gocer and G. Donor, Anal. Lett., 28 (1995) 357.
[16] M.M. Guedas, F.G. Rmer and B. Griepenik, Fresenius Z. Anal. Chem., 287 (1977) 19.
[17] (a) K. Terada, A. Inoue, J. Inamura and T. Kiba, Bull. Chem. Soc. Jpn, 50 (1977) 1060; (b) K. Terada, K. Morimoto and T. Kiba, Anal. Chim. Acta, 116 (1980) 127.
[18] M.L. Bruening, D.M. Mitchell, J.S. Bradshaw, R.M. Izatt and R.L. Bruening, Anal. Chem., 63 (1991) 21.
[19] A. Tong, Y. Akama and S. Tanaka, Anal. Chim. Acta, 230 (1990) 179.
[20] V. Dudler, L.F. Lindoy, D. Sallin and C.W. Schlaepfer, Aust. J. Chem., 40 (1987) 1557.
[21] T. Seshadri and H.J. Haupt, Anal. Chem., 60 (1988) 47.
[22] M. E. Mahmoud and E. M. Soliman, Talanta, 44 (1997) 15.
[23] P.H. Gore and P.J. Newman, Anal. Chim. Acta, 31 (1964) 111.
[24] M. Vidali, U. Casellato, P.A. Vigato, L. Doretti and F. Mada Losso, J. Inorg. Nucl. Chem., 39 (1977) 1985.
[25] A.I. Vogel, A Textbook of Practical Organic Chemistry, 3rd edn., Longmans, London, 1962.
[26] E.M. Soliman and M. El-Shabasy, J. Mater. Sci., 29 (1994) 4505.
[27] M.A. Marshall and H.A. Mottola, Anal. Chem., 55 (1983) 2089.
[28] V.I. Fadeeva, T.I. Tikhomirova, I.B. Yuferova and G.V. Kudryavtsev, Anal. Chim. Acta, 219 (1989) 201.
[29] U. Pyell and G. Stork, Fresenius Z. Anal. Chem., 342 (1992) 281.
[30] K. Unger, Porous Silica, Elsevier, Amsterdam, 1979.
[31] C. Policar, I. Artaud and D. Mansuy, Inorg. Chem., 35 (1996) 210.
[32] L. Chen, S.R. Breeze, R.J. Rousseau, S. Wang and L.K. Thompson, Inorg. Chem., 34 (1995) 454.
[33] S. Wang, Z. Pang, K.D.L. Smith and M.J. Wagner, J. Chem. Soc. Dalton Trans. (1994) 955.
[34] S. Wang, Z. Pang and K.D.L. Smith, Inorg. Chem., 32 (1993) 4992.
[35] D.J. Phillips, N.S. Rawat and S.K. Tiwari, J. Inorg. Nucl. Chem., 39 (1977) 797.

ELSEVIER

Talanta 44 (1997) 1073–1079

Talanta

Synergistic enhancement of the horseradish peroxidase-catalyzed oxidation of luminol by 4-substituted phenylboronic acids

Larry J. Kricka *, Xiaoying Ji

Department of Pathology and Laboratory Medicine, University of Pennsylvania Medical Center, Philadelphia, PA 19104, USA

Received 11 June 1996; received in revised form 2 December 1996; accepted 3 December 1996

Abstract

Combinations of 4-substituted phenylboronic acids [phenyl, iodo, bromo, and trans-4-(3-propenoic acid) substituents] have been discovered to have synergistic effects in the horseradish peroxidase (HRP) catalyzed chemiluminescent oxidation of luminol. Three types of effect have been observed: 1. synergistic reduction in the background light emission of a luminol-peroxide assay reagent to a value lower than the background obtained with either enhancer individually; 2. increase in signal to background ratio (S/B) in the presence of HRP to a value higher than the S/B obtained with either enhancer individually (synergy) or to a value higher than the combined S/B obtained with each enhancer (synergistic enhancement); and 3. for some combinations of enhancers, an increase in signal in the presence of HRP to a value higher than the signal obtained with either enhancer individually (synergy), or to a value higher than the combined signal obtained with each enhancer (synergistic enhancement). The magnitude of the effect was moderate but the synergistic decreases in background and increases in signal produced increases in S/B up to four-fold. Examples of synergistic pairs of enhancers included 4-biphenyl and 4-bromophenylboronic acid; 4-biphenyl and 4-iodophenylboronic acid; and trans-4-(3-propenoic acid) and 4-iodophenylboronic acid. Generally, synergy was obtained at several concentrations of all of the combinations of enhancers tested, and at different time points in the reaction due to the different light emission kinetics of the enhanced reactions. The mechanism of this synergistic effect has not been elucidated but may involve the enhancers acting at different points in the complex chemiluminescent peroxidase catalyzed oxidation reaction. © 1997 Elsevier Science B.V.

Keywords: Aryl boronic acids; Chemiluminescence; Horseradish peroxidase; Luminol

1. Introduction

The discovery that firefly luciferin enhanced light emission from the chemiluminescent horseradish peroxidase (HRP) catalyzed oxidation of luminol [1,2] led to a search for other molecules that would act as enhancers in this reaction. Subsequently, potent 4-substituted phenols [3,4], substituted naphthols [4], aromatic amines [5], phenylboronic acids [6,7], and a series of aromatic molecules (e.g., 4-hydroxyacetanilide) [8] have been identified as enhancers. In an effort to further improve the enhancement effect (increased

* Corresponding author. Fax: +1 215 6627529; e-mail: larry_kricka@path1a.med.upenn.edu

PII S0039-9140(96)02195-9

signal, decreased background) we have investigated the enhancement properties of combinations of enhancers and we describe here our results with combinations of 4-substituted phenyl boronic acids.

2. Experimental

2.1. Materials

Luminol (Aldrich, Milwaukee, WI) was purified as the sodium salt by recrystallization from sodium hydroxide as described previously [9]. Light emission was measured using either an Amerlite analyzer (Amerlite Diagnostics PLC, Amersham, UK), or ML-3000 microtiter plate luminometer (Dynatech Laboratories, Chantilly, VA). Horseradish peroxidase (HRP, type VI-A) and phenylboronic acid were purchased from Sigma (St Louis, MO). 1,1′-Biphenyl-4-yl boronic acid, hydrogen peroxide (30% w/v), and 3-aminophenylboronic acid were purchased from Aldrich. 4-Bromophenylboronic acid was purchased from Lancaster Synthesis (Windham, NH). 4-Iodophenylboronic acid and trans-4-(3-propenoic acid) phenylboronic acid were synthesized by Cookson Chemicals (Southampton, UK).

2.2. Experimental protocol

Matrix experiments were designed in which a range of concentrations of each enhancer were tested. The matrix experiments investigated combinations of 1,1′-biphenyl-4-yl boronic acid, 4-iodophenylboronic acid, 4-bromophenylboronic acid, and trans-4-(3-propenoic acid) phenylboronic acid. The enhancers were tested in: (i) a luminol-peroxide reaction to determine if combinations of the enhancers reduced the assay background; and (ii) a luminol-peroxide-HRP (type VI-A) reaction to determine if combinations of the enhancers increased the signal due to HRP. The signal to background ratio (S/B) was calculated to determine if combinations of the enhancers produced an improvement in the S/B for detection of HRP. For each combination of enhancers, a range of concentrations either side of the optimum concentration for each enhancer was tested.

2.3. Screening procedure

Two 11×4 matrix experiments were devised involving enhancer combinations as follows: enhancer 1 (0, 0.005, 0.01, 0.02, 0.05, 0.1, 0.2, 0.5, 1, 10, 20 mmol l^{-1}) and enhancer 2 (0, 0.01, 0.1, 1 mmol l^{-1}) or enhancer 1 (0, 0.01, 0.1, 1 mmol l^{-1}) and enhancer 2 (0, 0.005, 0.01, 0.02, 0.05, 0.1, 0.2, 0.5, 1, 10, 20 mmol l^{-1}). Stock solutions of enhancer 1 (20 mmol l^{-1}) and enhancer 2 (20 mmol l^{-1}) were prepared in DMSO, and then diluted in Tris buffer (0.1 mol l^{-1}, pH 8.6). The luminol—hydrogen peroxide reagent was prepared as follows: sodium luminol (12.5 mg) was dissolved in 50 ml of Tris buffer (0.1 mol l^{-1}, pH 8.6), and 15.5 μl of hydrogen peroxide (30% w/v) was mixed with 0.5 ml of Tris buffer (0.1 mol l^{-1}, pH 8.6). These two solutions were combined and diluted 1:10 in Tris buffer (0.1 mol l^{-1}, pH 8.6). Enhancer 1, 10 μL, 10 μl of enhancer 2, 10 μl of Tris buffer, and 100 μl of luminol-peroxide were mixed in a microwell and the light emission was measured using an Amerlite analyzer. The experiment was repeated, except that a sample of HRP (10 μl, 1:10 000 dilution of a 1 mg ml^{-1} stock solution in Tris buffer, pH 8.6) replaced the Tris buffer added to the microwell.

3. Results

3.1. Types of synergy and synergistic enhancement

Several analytically desirable effects may occur as a result of mixing together two enhancers. A. Assay reagent background may be reduced to a value lower than the background obtained with either enhancer individually. Low background light emission from a luminol-peroxide assay reagent is desirable because this is a major factor limiting the detection limit for HRP in this type of chemiluminescent assay. B. Signal in the presence of HRP may be increased to a value higher than the signal obtained with either enhancer individu-

Table 1
Synergy and synergistic enhancement of a peroxidase catalyzed oxidation of luminol using 1,1'-biphenyl-4-yl boronic acid and 4-iodophenylboronic acid

	Background rul		Signal rlu		Signal/background	
	a	b	a	b	a	b
Enhancer 1 1,1'-biphenyl-4-yl boronic acid (76.9 μmol l^{-1})	0.21	0.19	81.3	69.1	387.1	363.7
Enhancer 2 4-iodophenylboronic acid (76.9 μmol l^{-1})	0.38	0.38	2.8	3.9	7.4	10.3
Enhancer 1+2 (observed)	0.18	0.15	124.0	78.4	688.9	522.7
Synergy	Yes	Yes	Yes	Yes	Yes	Yes
Synergistic enhancement	—*	—*	Yes	Yes	Yes	Yes

* Not applicable rlu, relative light units, light emission was measured on Amerlite analyzer immediately after initiating the reaction.
a Experiment 1.
b Experiment 2.

ally (synergy). Alternatively, the light emission signal in the presence of HRP may be increased to a value higher than the combined signal obtained with either enhancer individually (synergistic enhancement). High signals in the presence of peroxidase are desirable because the measurement of high light levels is simple and convenient (e.g., wide range of light emission detectors can be used—photographic film, silicon photodiodes). C. S/B in the presence of HRP may be increased to a value higher than the S/B obtained with either enhancer individually (synergy). Alternatively, the S/B in the presence of HRP may be increased to a value higher than the combined S/B obtained with either enhancer individually (synergistic enhancement). An increase in the S/B can be achieved from an increase in the signal, a decrease in the background, or from combinations of these effects. For example, an increased S/B can be obtained from a combination of enhancers that lower the signal in the presence of HRP, but produce a major reduction in the assay background. Increased S/B in the presence of peroxidase is desirable because this improves assay sensitivity and hence the ability to discriminate between incremental amounts of peroxidase or a peroxidase label.

3.2. Matrix experiment

Table 1 illustrates data from two separate experiments for synergy and synergistic enhancement with a pair of enhancers (1,1'-biphenyl-4-yl boronic acid + 4-iodophenylboronic acid). Background light emission for the enhancer combination was lower than obtained with either enhancer individually, indicating synergy. The signal and S/B was higher than with either enhancer individually or the sum of values thus, indicating synergy and synergistic enhancement.

All combinations of enhancers produced a concentration dependent decrease in the assay background (synergy). The concentration dependence of the background reduction is illustrated for the combination of the 4-bromophenylboronic acid and 1,1'-biphenyl-4-yl boronic acid in Fig. 1. Generally, background light emission was reduced as the concentrations of the added 1,1'-biphenyl-4-yl boronic acid was increased. However, at high enhancer concentration (>0.1 mmol l^{-1} final concentration) the signal was reduced and thus, optimal signal is obtained at lower enhancer concentration (Fig. 1). The net effect of decreased background and increases signal was an improvement of the S/B by up to 4-fold (Fig. 1, 0.154 mmol l^{-1} 4-bromophenylboronic acid).

Combinations of enhancers that produced a synergistic enhancement in light emission and a synergistic enhancement in S/B in the presence of peroxidase included 1,1'-biphenyl-4-yl boronic acid in combination with trans-4-(3-propenoic acid) phenylboronic acid or 4-bromophenylboronic acid or 4-iodophenylboronic acid, and 4-iodophenylboronic acid combined with trans-4-

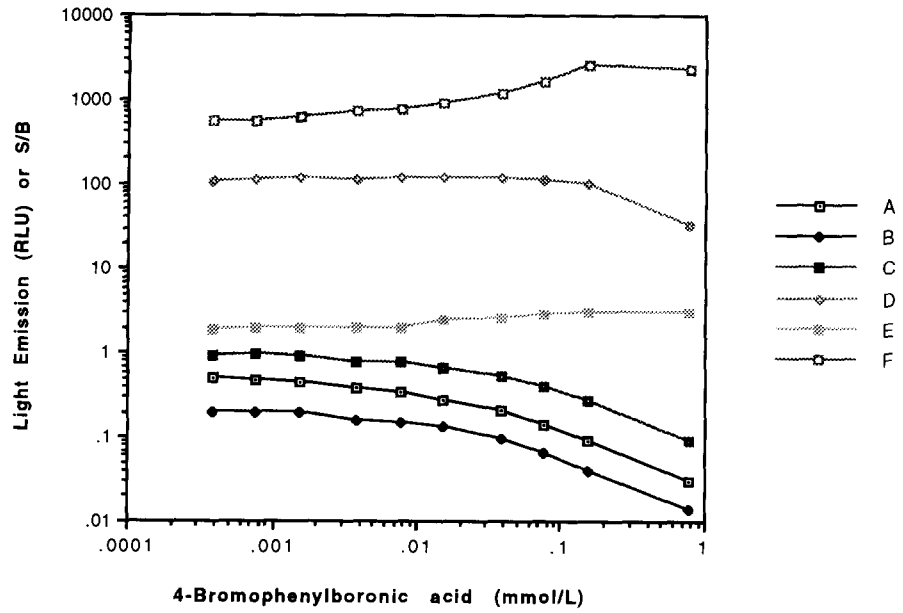

Fig. 1. Effect of 1,1′-biphenyl-4-yl boronic acid on luminol—peroxide—4-bromophenylboronic acid reaction background (A), signal (HRP 25 fmol) (C), and signal/background ratio (E) in absence of 1,1′-biphenyl-4-yl boronic acid; background (B), signal (HRP 25 fmol) (D), and signal/background ratio (F) in presence of 1,1′-biphenyl-4-yl boronic acid (76.9 μmol l^{-1}); light emission was measured immediately after initiation of the reaction using a Amerlite analyzer.

(3-propenoic acid) phenylboronic acid. Generally, synergy was obtained at several concentrations of all of the combinations of enhancers tested. An example of the effect of combining 1,1′-biphenyl-4-yl boronic acid and 4-iodophenylboronic acid is shown in Fig. 2. Successive addition of 1,1′-biphenyl-4-yl boronic acid reduced the background, increased the signal, and produced a significant improvement in S/B. Above 0.03 mmol l^{-1} of 1,1′-biphenyl-4-yl boronic acid (Fig. 2) there was no further improvement in S/B and at concentrations of 1,1′-biphenyl-4-yl boronic acid greater than 0.2 mmol l^{-1} a decline in S/B was observed.

The kinetics of the light emission from enhanced chemiluminescent reactions using different boronates show some differences. For example, the light emission kinetics with 4-bromophenylboronic acid rises slowly and then decays slowly. In contrast, 1,1′-biphenyl-4-yl boronic acid shows a more rapid rise and fall in light emission. Consequently in experiments that combine two enhancers, the presence of synergy or synergistic enhancement can vary over the time course of the reaction. This is illustrated in Fig. 3 that shows data from twelve replicate 1,1′-biphenyl-4-yl boronic acid and 4-iodophenylboronic acid synergy experiments performed in a microplate. The kinetics of 1,1′-biphenyl-4-yl boronic acid reaction are rapid compared with 4-iodophenylboronic acid, and thus the time taken to initiate the reactions in the wells and serial measurement significantly effects the observed synergy in the light emission signal. Panel A show the data for wells 1–12 immediately after initiation of the reaction ($t = 0$). Panel B in Fig. 3 shows light emission data 5 min after initiation of the reactions. The signal from the wells containing peroxidase and the mixture of enhancers varies at both time points (0, 5 min). This reflects the kinetics of the reaction and the time taken to measure light emission from each well in the plate. However, a synergistic enhancement of the light emission was observed for each of the replicate experiments. This temporal variability restricts its analytical utility because it would require very tight control of initiation and light measurement.

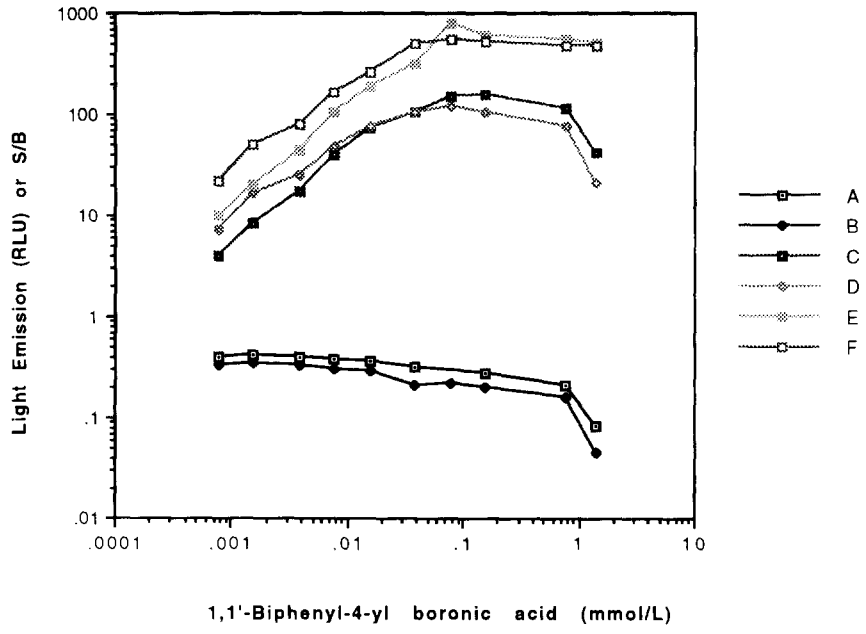

Fig. 2. Effect of 4-iodophenylboronic acid on luminol—peroxide—1,1′-biphenyl-4-yl boronic acid reaction background (A), signal (HRP 25 fmol) (C), and signal/background ratio (E) in absence of 4-iodophenylboronic acid; background (B), signal (HRP 25 fmol) (D), and signal/background ratio (F) in presence of 4-iodophenylboronic acid (76.9 μmol l^{-1}); light emission was measured immediately after initiation of the reaction using a Amerlite analyzer.

4. Discussion

The synergistic enhancement effect was unexpected and is complex. It is dependent on the particular pair of enhancers and on their relative concentrations and time of measurement of the light emission. Background reduction was the most important component of the synergy effect. The effect on signal is seen at enhancer combinations that are suboptimal and it is possible to obtain higher signals using one of the enhancers at its optimal concentration. However, in the presence of a second enhancer the background reduction exceeds any diminution in signal and a net improvement in S/B is obtained.

Some studies of the mechanism of boronate enhancement of the HRP catalyzed chemiluminescent oxidation of luminol have been undertaken (e.g., determination of rate constants for reactions with HRP compounds I and II) [10], but the precise mechanism remains unknown. Likewise, the mechanism of the background reduction by enhancers is not fully understood. Complexion of metal ions that catalyze the chemiluminescent decomposition of luminol is one possible mode of background reduction. The antioxidant properties of the enhancers (boronates are potent antioxidants) [11] may also be a contributing factor. In a previous study, we found some correlation between the electronic properties of the 4-substituent Hammett constant (σ_p^+) on the boronic acid and the enhancer properties of the molecule (e.g., σ_p^+ value for a 4-substituted aryl boronic acid ≥ -0.31 conferred enhancer properties) [12]. In this study we noted that the combination of an enhancer with a positive Hammett constant and an enhancer with a negative Hammett constant produced a synergistic effect (e.g., σ_p^+ Ph $= -0.18$, Br $= +0.15$, I $= +0.14$). We are currently studying other enhancers in an effort to clarify the mechanism and to identify superior combinations for analysis of peroxidase and peroxidase labels.

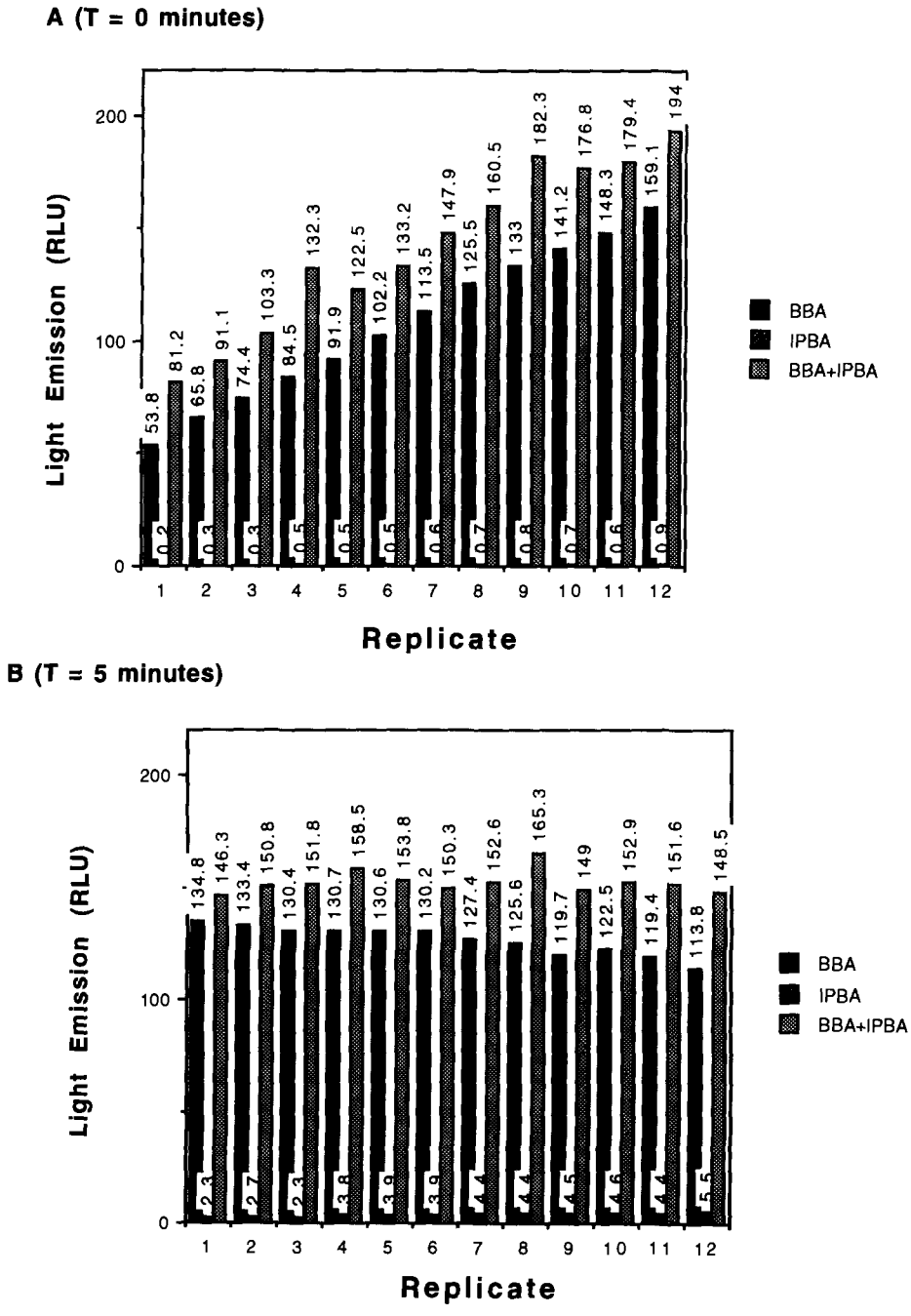

Fig. 3. Light emission from twelve replicate assays for peroxidase using 4-iodophenylboronic acid (IPBA 76.9 μmol l^{-1}), 1,1′-biphenyl-4-yl boronic acid (BBA 76.9 μmol l^{-1}) and a combination of these two enhancers. Light emission was measured immediately after initiation (Panel A) and 5 min after initiation (Panel B) using a ML-3000 microtiter plate luminometer.

Acknowledgements

The financial support of the British Technology Group (NRDC) is gratefully acknowledged. This work is the subject of patent applications assigned to the British Technology Group.

References

[1] T.P. Whitehead, L.J. Kricka and G.H.G.Thorpe, Eu. Patent 116 454, 1987.
[2] T.P. Whitehead, G.H.G. Thorpe, T.J.N. Carter, C. Groucutt and L.J. Kricka, Nature (London), 305 (1983) 158.
[3] G.H.G. Thorpe, L.J. Kricka, S.B. Moseley and T.P. Whitehead, Clin. Chem., 31 (1985) 1335.
[4] G.H.G. Thorpe and L.J. Kricka, Methods Enzymol., 133 (1986) 331.
[5] L.J. Kricka, A.M. O'Toole, G.H.G. Thorpe and T.P. Whitehead, U.S. Patent 4 729 950, 1988.
[6] L.J. Kricka and X. Ji, J. Biolumin. Chemilumin., 10 (1995) 49–54.
[7] L.J. Kricka, PCT Patent Application WO 93/16195.
[8] R.K. Thomas, U.S. Patent 5 279 940, 1994.
[9] G. Ham, R. Belcher, L.J. Kricka and T.J.N. Carter, Anal. Lett., 12 (1979) 535.
[10] W. Sun, X. Ji, L.J. Kricka and H.B. Dunford, Can. J. Chem., 72 (1994) 2159.
[11] A. Bergold and W. Scouten, Borate Chromatography, in W.H. Scouten (Ed.), Solid Phase Biochemistry, Wiley, New York, 1983, pp. 149–221.
[12] X. Ji and L.J. Kricka, in J.W. Hasting, L.J. Kricka and P.E. Stanley (Eds.), Chemiluminescence and Bioluminescence: Molecular Reporting with Photons, Wiley, Chichester, 1997, in press.

ELSEVIER

Talanta 44 (1997) 1081–1086

Talanta

Determination of aluminium in tree samples by cathodic adsorptive stripping voltammetry

Jadwiga Opydo

Institute of Chemistry, Poznań University of Technology, 60-965 Poznań, Poland

Received 20 May 1996; received in revised form 26 November 1996; accepted 3 December 1996

Abstract

This paper presents a method of determination of aluminium in tree samples (wood, leaves, roots) based on the cathodic adsorptive stripping voltammetry. Al(III) complexed with alizarin S was determined by ASV method using a hanging mercury drop electrode. Optimal conditions were found to be: accumulation time 30–90 s, accumulation potential −0.70 V versus SCE, supporting electrolyte 0.1 M ammonia–ammonium chloride buffer at pH 8.2 and concentration of alizarin 1×10^{-5} M. The response of the system, a linear current-concentration relationship was observed up to 8×10^{-6} M. The developed method has been tested by analysing international reference materials (BCR 62 Olive leaves and BCR 101 spruce needles). © 1997 Elsevier Science B.V.

Keywords: Adsorptive stripping voltammetry; Aluminium; Alizarin S; Tree samples

1. Introduction

The increasing process of soil acidification in recent years has caused the release of Al(III) ions in natural environment. This is the so-called exchangeable aluminium, which when taken up through plant roots may induce a number of phenomena unfavourable to the development and growth of plants [1,2]. This 'aluminium danger' in recent years has been conducive to intense studies on the development of new, rapid and reliable methods for monitoring aluminium in the environment.

Especially useful in this respect seems to be adsorptive stripping voltammetry. This method consists in producing an aluminium complex compound with organic ligands. This complex is accumulated adsorptively at a chosen potential on the cathode. Then, peaks of aluminium complexes, the currents of which are directly proportional to Al concentration, are registered. Solochrome Violet SR [3–6], calmagit [7–10], cupferron [11] and alizarin S (1,2-dihydroxy- anthraquinone-3-sulphonic acid) [12,13] are most frequently used for aluminium complexation. Out of all these complex compounds the most suitable seems to alizarin S. Its complex with aluminium is obtainable for several s at a room temperature, without heating. Alizarin S in BES buffer (*N,N'*-bis-2-hydroxyethyl-2-amino-ethane sulphonic acid) was used to determine Al in seawater [12,13]. However, the application of BES solution as a supporting electrolyte causes production of the aliz./Al peak at the potential of −1.25 V versus

PII S0039-9140(96)02198-4

Ag/AgCl, which causes interference by high concentrations of zinc (> 50 nM) [12]. The employment of this method for the analysis of samples containing not more than 50–100 nM Al was caused by the necessity to perform additional analytical operations, i.e., Zn(II) masking by the use of EDTA. This method, therefore, does not permit to determine Al in trees, where Zn concentration is on the level of 1–20 μM [1,14,15].

The objectives of the present work were: (i) to establish optimal conditions for aluminium determination by the method of cathodic adsorptive stripping voltammetry in differential pulse technique using alizarin S as a complexing factor and 0.1 M ammonia–ammonium chloride buffer as a supporting electrolyte; and (ii) to develop a method for aluminium determination in tree samples.

2. Experimental

2.1. Apparatus

Cathodic stripping voltammograms were obtained with a PA-4 polarographic analyzer, Laboratorni Pristroje (Czech republic). The electrochemical measurements were performed in a 3-electrode system: hanging mercury drop electrode (HMDE), produced by Laboratorni Pristroje, saturated calomel electrode (SCE) produced by Radiometer and Pt wire electrode. The differential pulse amplitude was 50 mV and the scan-rate was 10 mV s^{-1}.

Microwave digestion system were: low-pressure vessels type P/N 323000, CEM (USA); home microwave oven Sharp, 850 W (Japan).

2.2. Reagents

Nitric acid 'Suprapur' and alizarin S (Merck). Hydrogen peroxide, ammonia, ammonium chloride, analytical grade, were produced by POCh (Poland). Certified reference materials: BCR No. 62 Olive leaves and BCR No. 101 Spruce needles (Belgium).

Standard solutions of Al, Cd, Pb, Cu, Ni, Co and Zn containing 1 g l^{-1} were prepared from ampoules (Merck). Solutions with concentrations below 10^{-3} M were prepared just before use. Water was doubly distilled in a quartz still.

2.3. Procedure

Tree samples were taken from several oak trees *Quercus robur* L., on each investigated area. Wood samples were taken with a Pressler's bore at a height of 1.3 m above the ground. Roots samples were collected from the main and lateral roots. Leaves samples were at the end of the vegetation season—in September 1994.

0.1–0.2 g biological samples were placed in low pressure vessels and a mixture of nitric acid and hydrogen peroxide (1 ml each) was added. The vessels were put into a microwave chamber to perform mineralization: 2 min with 225 W, 3 min with 425 W, 5 min with 595 W and 5 min with 850 W. Intervals of 5 min were made after each cycle.

After mineralization in low pressure vessels the solution was transferred into a conical quartz cup and the excess of nitric acid was evaporated. The residue was dilluted in 0.1 M ammonia–ammonium chloride buffer pH 8.2 (in the amount providing the aluminium content to be within the range $1–5 \times 10^{-6}$ M) and 1×10^{-5} M alizarin S was added.

20 ml of the solution was transferred into a measuring vessel. After deaeration of the solution with purified nitrogen the aliz./Al complex was adsorptively accumulated for 30–90 s (depending on the amount of aluminium) at the potential of −0.7 V by stirring the solution. The stirrer was stopped and after 15 s voltammetric cathodic curves over the potential range −0.7– −1.2 V were registered, at a scan rate of 10 mV s^{-1}, with a pulse amplitude of 50 mV. The cycle was repeated three times. The content of aluminium was evaluated by the method of standard additions.

3. Results and discussion

3.1. Response characteristics

Alizarin adsorbed on a drop electrode forms a cathodic peak at the potential of −0.63 V and

two anodic peaks at the potentials of −0.63 and −0.55 V. A repeated cycle on the same mercury drop affects an increase in the peak height due to alizarin adsorption on the electrode and causes the appearance of one more cathode peak at the potential of −0.51 V. These voltammograms are consistent with the previous ones obtained in BES buffer at pH 7.1 [12]. They indicate a reversible reduction of free alizarin ligands on a mercury drop.

Introduction of Al(III) into the system causes the occurrence of cathode peak at the potential of −0.87 V, being the result of adsorptive reduction of the aliz./Al complex. Fig. 1 shows cyclic voltammograms for 0.1 M ammonia–ammonium chloride buffer at pH 8.2 containing 1×10^{-5} M alizarin S and 4×10^{-6} M Al(III). This reduction step is irreversible; no peaks are observed upon scanning in the positive direction. A repeated measuring cycle (dashed line) causes a very strong decrease in the reduction peak due to diffusion of the dye and the aluminium away from the electrode.

The process of adsorptive accumulation of aluminium depends on many parameters. One of them is the accumulation time. Being too long it causes competitive saturation of the electrode surface with free ligand and decreases the effectiveness of Al determination. This relationship for alizarin in ammonia–ammonium chloride buffer at pH 8.2 is presented in Fig. 2. It is linear within quite a wide range 15–180 s. According to it, the optimal time of adsorptive accumulation at alizarin concentration 1×10^{-5} M is within the range of 30–90 s.

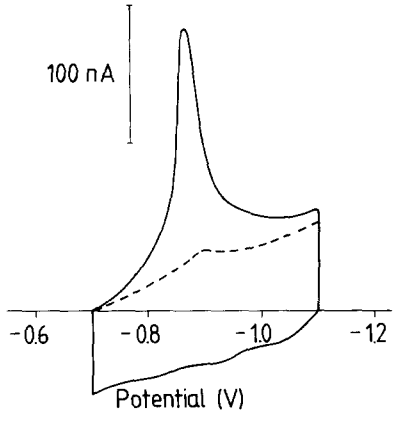

Fig. 1. Cyclic voltammograms for 1×10^{-5} M Alizarin S with 4×10^{-6} M Al(III) in unstirred 0.1 M NH_3-NH_4Cl buffer at pH 8.2. Conditions: scan rate, 100 mV s^{-1}; adsorption potential −0.7 V; adsorption time, 30 s. Solid line: scan on the new mercury drop. Dashed line: repetitive scan on the same drop.

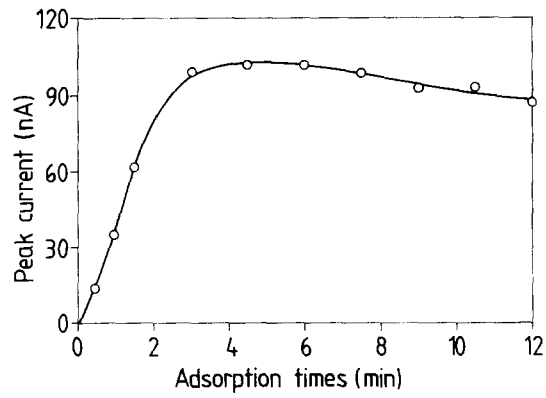

Fig. 2. Dependence of the differential-pulse peak height for the Aliz./Al complex on adsorption time. Al(III) concentration, 1.5×10^{-6} M. Supporting electrolyte, 0.1 M NH_3-NH_4Cl buffer at pH 8.2. Alizarin concentration, 1×10^{-5} M. Adsorption potential, −0.7 V; scan rate, 10 mV s^{-1}; pulse amplitude, 50 mV.

Another, not less important parameter is the adsorptive potential (Fig. 3). A decrease of the Al peak height is observed when performing accumulation in the range of free ligand adsorption (to the potential of −0.65 V); also under these conditions the peak of the aliz./Al complex is masked by free ligand adsorption.

The influence of electrolyte pH and alizarin concentration is illustrated in Fig. 4 and 5. Fig. 4 presents the dependence of Al peak height on pH of 0.1 M ammonia–ammonium chloride buffer, whereas Fig. 5 shows the dependence of Al peak on the concentration of alizarin obtained in 0.1 M ammonia–ammonium chloride buffer at pH 8.2.

The best analytical signal is obtained by complexing aluminium at pH 8.0 and 8.2 in the presence of 1×10^{-5} M alizarin. Changes in the solution pH and a reduction in alizarin concentra-

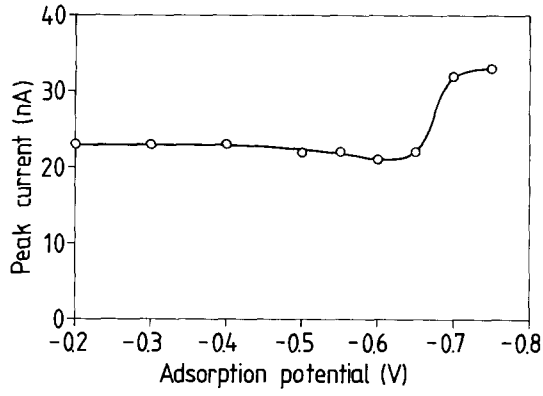

Fig. 3. Dependence of the differential-pulse peak height for the Aliz./Al complex on adsorption potential. Al(III) concentration, 1.5×10^{-6} M. Supporting electrolyte, 0.1 M NH_3-NH_4Cl buffer at pH 8.2. Alizarin concentration, 1×10^{-5} M. Adsorption time, 30 s; scan rate, 10 mV s^{-1}; pulse amplitude, 50 mV.

tion decrease the effectiveness of complexating, whereas an increase in alizarin concentration, likewise a long accumulation time, has a similar effect—it suppresses the Al peak.

On the basis of Figs. 1–5 the optimal conditions for aluminium determination are as follows:

- solution pH 8.2;
- alizarin concentration – 10 μM;

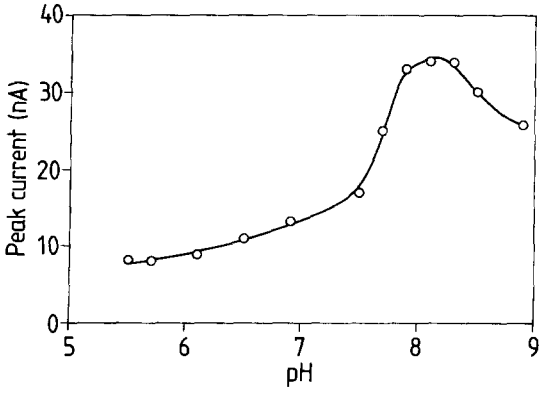

Fig. 4. Dependence of the differential-pulse peak height for the Aliz./Al complex on pH of the solution. Al(III) concentration, 1.5×10^{-6} M. Alizarin concentration, 1×10^{-5} M. Supporting electrolyte, 0.1 M NH_3-NH_4Cl buffer. Adsorption potential, – 0.7 V; adsorption time, 30 s; scan rate, 10 mV s^{-1}; pulse amplitude, 50 mV.

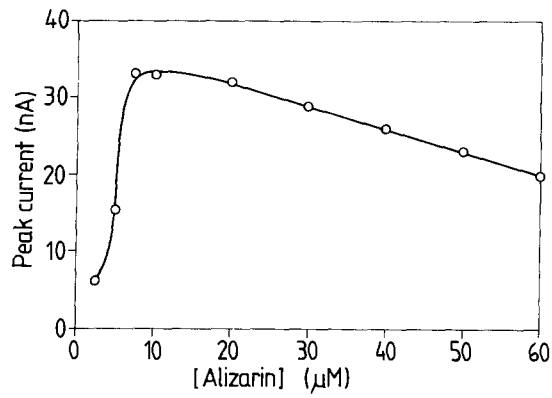

Fig. 5. Dependence of the differential-pulse peak height for the Aliz./Al complex on Alizarin concentration. Al(III) concentration, 1.5×10^{-6} M. Supporting electrolyte, 0.1 M NH_3-NH_4Cl buffer at pH 8.2. Other conditions as for Fig. 4.

- accumulation potential – 0.70 V;
- accumulation time 30–90 s.

Under the above conditions the dependence of the aliz./Al peak height on Al concentration is linear within the concentration range of $1–8 \times 10^{-6}$ M (Fig. 6). This range is incomparable with possibil-

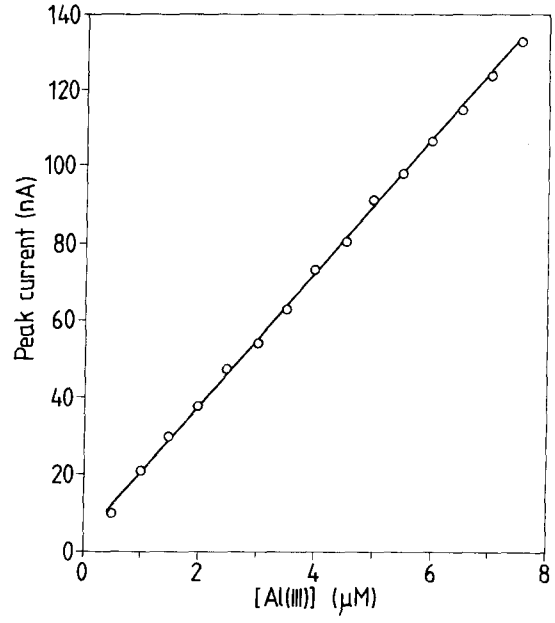

Fig. 6. Dependence of the differential-pulse peak height for the Aliz./Al complex on Al(III) concentration. Alizarin concentration, 1×10^{-5} M. Supporting electrolyte, 0.1 M NH_3-NH_4Cl buffer at pH 8.2. Other conditions as for Fig. 4.

ities of the methods developed in [12], where the limit of detectability is 1 nM. This however, is a sufficient (and even a more suitable) range for analysing biological materials, if 0.1–1.0 g samples are used (e.g., 5×10^{-6} M Al in 1 g sample 25 ml $^{-1}$ corresponds to 3.4 μg g^{-1} Al).

The limit of detectability can be reduced to 2.5×10^{-8} M. For that purpose the accumulation time should be extended to 3 min at a simultaneous decrease of alizarin concentration to 2.5×10^{-6} M. A linear dependence under these conditions was obtained for the range 2.5×10^{-8}–3.5×10^{-7} M Al(III).

3.2. Interferences

The influence of Zn(II), Cd(II), Pb(II), Cu(II), Ni(II), Co(III) and Fe(III) on the height of aliz./Al peak was examined.

As shown by the experiments, 1 μM of Zn, Cd, Pb, Cu and Ni or 25 μM Co and Fe have no effect on determination of 1.5 μM Al. An increase in the contents of Zn, Cd, Pb, Cu or Ni to 25 μM, causes a decrease in the height of Al peak, in some cases by 30%, but, however, it enables Al determination by the method of standard additions. Besides that, it should be emphasized that the contents on these ions on the level 25 μM l^{-1} correspond to 100–1000 μg g^{-1} in samples and, for instance, in biological materials they are very rare.

The influence of surfactants was tested on the example of sodium dodecylsulphate and Triton X-100. The both, one and another surfactants present in the amount of 1×10^{-4}% cause a very strong deformation and suppression of Al peak, making impossible its determination. Their influence can be completely eliminated by a thorough mineralization of samples.

3.3. Analytical applications

According to the procedure described in point 2.3. an analysis was carried out on samples collected from oaks *Quercus robur* L., growing under conditions of different pH of soils. Fig. 7 gives an example of aluminium determination in the wood of oaks by the method of standard additions. The

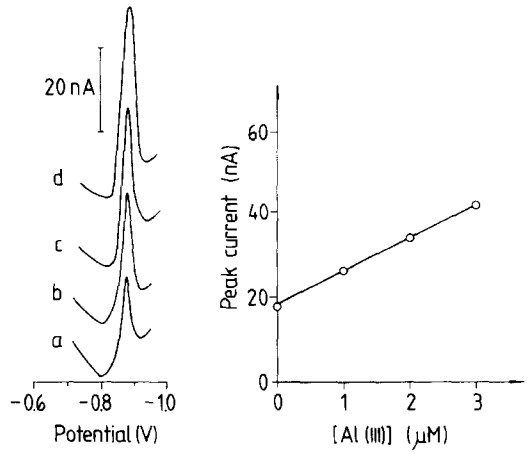

Fig. 7. Voltammograms and calibration curve from the determination of Al(III) in a sample in wood by the method of standard addition. Curve (a) is of the sample. Curves (b)–(d) result from the further addition of 1×10^{-6} M Al(III). Conditions as for Fig. 4.

standard addition plot was linear. The Al(III) content evaluated from it is 4.7×10^{-6} M.

Results of the oak analysis are presented in Table 1. The first studied oak stand is located in the region of the Głogów-Lubin copper basin, characterized by a very acid soil. This soil contains significant amounts of exchangeable aluminium. The second oak stand is located in Krakowsko-Częstochowska Upland, characterized by neutral soil and by the same lack of aluminium. The third oak stand belongs to the experimental forest of the Institute of Dendrology in Kórnik. The level of exchangeable aluminium content in soils is reflected in different Al absorption by trees. As seen from Table 1, the precision of the proposed method is satisfactory (the relative standard deviation ranged within 3.4–10.1%).

The accuracy of the developed method has been tested by analysing certified reference materials: BCR 62 Olive leaves and BCR 101 Spruce needles. The results are given in Table 2. They are satisfactory.

The developed method was used in estimation of the effect of industrial pollutions on the oak stand decline on the Krotoszyn Plateau (West-Central part of Poland) [16].

Table 1
Determination of Al in samples of oak trees

Sampling regions	pH of soil versus 1 M KCl	Exchangeable Al[a] mg 100 g^{-1}	Matrix	No. of tests	Content Al μg g^{-1}	S.D. μg g^{-1}	R.S.D. %
Copper basin	3.5	14.0	Wood	8	5.8	0.2	3.4
			Leaves	6	75.6	6.3	8.3
			Roots	7	482	19.8	4.1
Krakowsko	7.0	—	Wood	8	1.4	0.15	10.1
Częstochowska			Leaves	6	78.2	3.1	4.0
Upland			Roots	7	56.0	4.3	7.7
Experimental	4.0	7.0	Wood	8	3.8	0.2	5.3
Forest Kórnik			Leaves	6	60.1	5.9	9.8
			Roots	7	182	12.1	6.6

[a] Versus [16].

Table 2
Determination of Al in reference materials

Samples	Certified value μg g^{-1}	Found μg g^{-1}
Olive leaves BCR 62	450 ± 20	462 ± 32
Spruce needles BCR 101	173 ± 5	165 ± 8

Confidence intervals of means at a 95% confidence level, $n = 8$.

Acknowledgements

This work was supported by the Poznań University of Technology, Grant No. 31-474/95/DS

References

[1] Kabata-Pendias and H. Pendias, Trace Elements in Soils and Plants, 2nd edn., CRC Press, Boca Raton, Florida, 1992.
[2] Stienen and J. Bauch, Plant and Soil, 106 (1988) 231.
[3] Wang, P.M.A. Farias and J.S. Mahmoud, Anal. Chim. Acta, 172 (1982) 57.
[4] Romero, J.E. Tahan and A.J. Moronta, Anal. Chim. Acta, 257 (1992) 147.
[5] Stryjewska, S. Rubel and K. Kuśmierczyk, Chem. Anal., 37 (1992) 43.
[6] Downard, H.K.J. Powell and S. Xu, Anal. Chim. Acta, 262 (1992) 339.
[7] Stryjewska and S. Rubel, Electroanal., 3 (1991) 995.
[8] Stryjewska, S. Rubel and J. Wilgos, Chem. Anal., 36 (1991) 941.
[9] Stryjewska, M. Karpiuk and S. Rubel, Chem. Anal., 37 (1992) 729.
[10] Stryjewska, S. Rubel, J. Sadowska and M. Karpiuk, Chem. Anal., 38 (1993) 175.
[11] Wang, J. Lu and R. Setiadji, Talanta, 40 (1993) 351.
[12] Van den Berg, K. Murphy and J.P. Riley, Anal. Chim. Acta, 188 (1986) 177.
[13] Hernandez-Brito, M.D. Gelado-Caballero and J. Perez-Pena, Analyst, 119 (1994) 1593.
[14] Greszta, Frag. Flor. Geobot., 28 (1982) 29.
[15] Łukaszewski, R. Siwecki, J. Opydo and W. Zembrzuski, Trees, 7 (1993) 169.
[16] Opydo, to be published in Acta Soc. Bot. Pol.

ELSEVIER

Talanta 44 (1997) 1087–1094

Talanta

A novel potassium ion membrane sensor based on rifamycin neutral ionophore

Saad S.M. Hassan *, Wagiha H. Mahmoud, Abdel Hameed M. Othman

Department of Chemistry, Faculty of Science, Ain Shams University, Cairo, Egypt

Received 22 July 1996; received in revised form 6 November 1996; accepted 3 December 1996

Abstract

A novel potentiometric membrane sensor for potassium ion based on the use of rifamycin as a neutral ionophore is described. The sensing membrane is formulated with 2 wt.% rifamycin-SV, 69 wt.% dibutylsebacate plasticizer and 29 wt.% PVC. Linear and stable potential response with near-Nernstian slope of 56.7 ± 0.2 mV decade^{-1} are obtained over the concentration range 1×10^{-1}–3×10^{-5} M K^+. The detection limit is 0.3 μg ml^{-1} K^+, the response time is 10–30 s and the working pH range is 4–11. Responses of the sensor toward alkali and alkaline earth metal ions are in the order $K^+ > Rb^+ > Cs^+ > Na^+ > NH_4^+ > Ba^{2+} > Mg^{2+} > Ca^{2+} > Sr^{2+} > Li^+$. The selectivity coefficient data reveal negligible interference from transition metal ions. Direct potentiometric determination of K^+ in the presence of 10–50-fold excess of alkali and alkaline earth metals gives results with an average recovery of 99.1%, and a mean standard deviation of 1.2%. The data agree fairly well with those obtained by flame photometry.

Keywords: Dibutylsebacate plasticizer; Potassium PVC membrane sensor; Rifamycin neutral ionophore

1. Introduction

Potentiometric sensors for potassium ion are steadily replacing flame photometry and other assay techniques for monitoring potassium in various matrices and have been widely used in various analytical applications [1]. These sensors incorporate valinomycin [2–6], crown ethers [7–10] and nonactin [11] neutral ionophores as active membrane components. Nature and characteristics of various types of potassium ion membrane sensors have been reviewed [12]. Although valinomycin is, by far, the most successful ionophore for potassium ion, it is a very expensive reagent with potentiometric selectivity in the order: $Rb^+ > Cs^+ > K^+ \gg Na^+$. Crown ethers and nonactin based sensors respond to the alkali metals in the order: $Rb^+ > K^+ > Cs^+ > Na^+$ and $Cs^+ > Rb^+ > K^+ > Na^+$, respectively. It is evident from most of the published reports dealing with these ionophores that Rb^+ and Cs^+ are seriously interfere in the determination of K^+.

In the work reported here, attempts were made to use some derivatives of rifamycins as novel neutral carriers for K^+ ion, in PVC matrix membrane sensors. Rifamycins are a class of antibi-

* Corresponding author.

0039-9140/97/$17.00
PII S0039-9140(96)02199-6

otics known to stimulate the release of K^+ ion remarkably from isolated living mitachondria and from red blood cells [13]. This is attributed to the interaction of these compounds with the biological membrane causing a change in their permeability to K^+ ion. We have found that rifamycin-SV, a commercially available cheap antibiotic, has an excellent electrochemical response for potassium ion and a sensor based on it displays a potentiometric selectivity in the order $K^+ > Rb^+ > Cs^+ > Na^+ > Li^+$. Performance characteristics of rifamycin-SV based sensor including linear response range, calibration slope, lower detection limit, selectivity order, nature of solvent mediator, effect of pH and analytical application have been investigated.

2. Experimental

2.1. Reagents

Chemicals of analytical–reagent grade were used unless stated otherwise. Doubly distilled deionized water was used throughout. Rifamycin-SV, 3-formyl rifamycin, rifampicin, poly(vinyl chloride) powder (PVC), potassium tetra-*p*-chlorophenylborate (KT-pClPB) and tetrahydrofuran (THF) were obtained from Fluka. Dibutylsebacate (DBS), 2-nitrophenyloctylether (NPOE), dioctylphthalate (DOP) and dinonylphthalate (DNP) were purchased from Aldrich. Alkali, alkaline earth and transition metal salts in the form of chloride or nitrate were obtained from B.D.H. Standard solutions were freshly prepared with deionized doubly distilled water. Pharmaceutical preparations containing K^+ were obtained for local pharmaceutical companies.

2.2. Apparatus

Measurements of potassium were made at 25 ± 1°C with an Orion Ionalyzer (model 920 digital pH/mV meter) using rifamycin-SV PVC membrane sensor in conjunction with an Orion single junction Ag–AgCl reference electrode (Model 90-02). An Orion combination pH electrode (model 91-02) was used for pH adjustment. All spectrophotometric measurements were made on a Perkin Elmer Lambda 15 uv/vis spectrophotometer using 10 mm cuvettes. Flame photometry were made on Corning Clinical Flame photometer 410 C.

2.3. Potassium rifamycin PVC membrane sensors

The polymeric membranes were prepared by mixing 10 mg of rifamycin-SV, 190 mg PVC and 360 mg of DBS with 3 ml THF. The resulting homogeneous syrup was poured into a 50 mm diameter ground glass casting ring and the solvent was allowed to evaporate off slowly at room temperature over a period of 48 h. A semi transparent flexible membrane with a thickness of 0.25 mm was obtained. A disc (8 mm diameter) was cut using a cork borer and pasting using THF [14–17], to an interchangeable PVC tip which was clipped on to the end of the electrode glass body. A solution of potassium chloride 1×10^{-2} M was used as an internal reference solution and Ag–AgCl wire (1 mm diameter) was used as an internal reference electrode. The sensor was preconditioned after preparations by soaking for at least 24 h in 1×10^{-2} M potassium chloride solution and stored in the same solution when not in use. The sensor was washed with doubly deionized water and blotted with tissue-paper between measurements.

Sensor calibration was carried out by measuring the potential of 1×10^{-6}–1×10^{-2} MKCl solutions starting from the low to the high concentrations. The potentials were plotted as a function of potassium ion concentrations. The lower

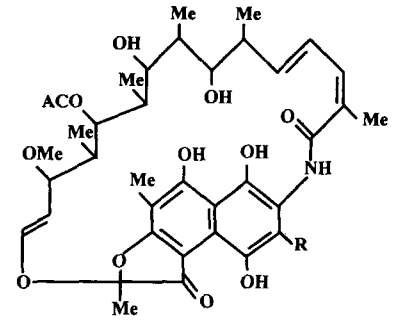

Rifamycin-SV : R = —H

3 - Formyl rifamycin : R = — CHO

Rifampicin : R = —CH = N —N N —CH_3

Fig. 1. Structure of some rifamycin ionophores.

Table 1
Potentiometric response characteristics of rifamycin-SV PVC (DBS) membrane sensor

Parameter	Value[a]
Slope, mV decade^{-1}	56.7 ± 0.2
Correlation coefficient, (r)	0.998
Intercept, (mV)	216.7 ± 0.5
Lower limit of linear range, (M)	3.5×10^{-5}
Detection limit, (M)	8.5×10^{-6}
Working range, (pH)	4–11
Response time for 10^{-3} M, (s)	10 ± 2
Recovery time for 10^{-3} M, (s)	40 ± 2

[a] Mean of five measurements.

detection limit was taken at the point of intersection of the extrapolated linear segments of the potassium calibration curve. Repeatability was measured by immersing the sensor alternatively into 10^{-2} and 10^{-3} M KCl solutions at 25°C. Sensor life span was examined by repeated monitoring of the slope of potassium calibration curve periodically. Selectivity coefficients of the sensor were determined using the separate solution method [1,18] and calculated from the rearranged Nicolsky equation:

$$\text{Log } K^{\text{pot}}_{\text{K,M}} = [E_{\text{K}} - E_{\text{M}}/S] + [1 + Z_{\text{K}}/Z_{\text{M}}] \text{ Log } \text{K}^{+}$$

Where E_{K} is the potential measured in 10^{-2} M KCl solution, E_{M} is the potential measured in a 10^{-2} M solution of the chloride of the interfering cation, Z_{K} and Z_{M} are the charges of the potassium and interfering ion, respectively, and S is the slope of the electrode calibration plot.

2.4. Determination of potassium in pharmaceutical products

The contents of potassium syrup solutions and the contents of ten tablets containing potassium salt were mixed well. An accurate weight equivalent to one tablet and a 5.0 ml aliquot of the syrup solution were transferred to 1 l volumetric flask, and completed to the mark with doubly distilled deionized water. A 3.0 ml aliquot of the solution was diluted to 25 ml and rifamycin-SV PVC (DBS) membrane sensor in conjunction with an Ag–AgCl reference electrode was immersed in the solution. The potential was measured before and after addition of 1.0 ml of 10^{-1} M KCl solution. The original concentration of K^{+} in the test solution was measured using the standard addition equation [1,18].

3. Results and discussion

3.1. Rifamycin neutral ionophore

Plasticized poly(vinyl chloride) membranes doped with three different derivatives of rifamycin, namely, rifamycin-SV, 3-formyl rifamycin and rifampicin (Fig. 1) were prepared and electrochemically evaluated as prospective sensors for potassium ion according to IUPAC standards [18]. Table 1 shows that rifamycin-SV based sensor displays the best performance char-

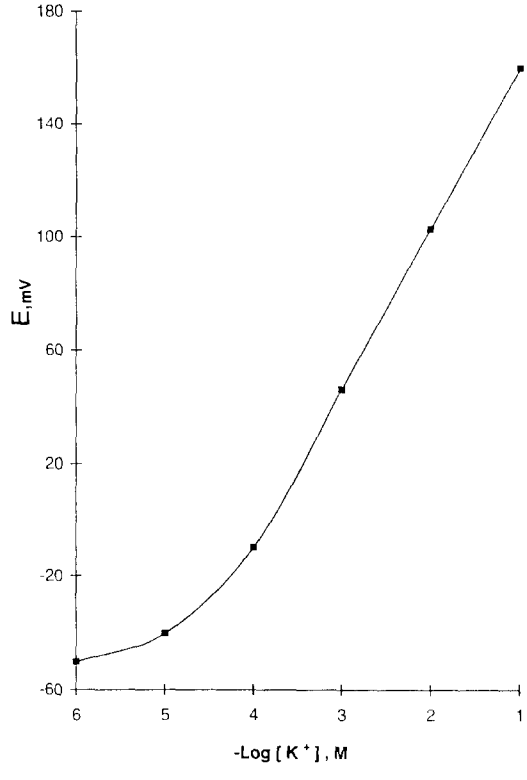

Fig. 2. Calibration curve for potassium PVC membrane sensor based on rifamycin-SV ionophore and dibutylsebacate (DBS) plasticizer.

Table 2
Effect of rifamycin ionophores on the response to K^+ using dibutylsebacate (DBS) as a solvent mediator

Ionophore	Slope, mV decade^{-1}	Linear range, M	Lower limit of detection, M
Rifamycin-SV	56.7 ± 0.2	1×10^{-1}–3×10^{-5}	8×10^{-6}
3-Formyl rifamycin	51.3 ± 0.3	1×10^{-1}–1×10^{-4}	3×10^{-5}
Rifampicin	42.2 ± 0.3	1×10^{-1}–1×10^{-4}	5×10^{-5}

acteristics for potassium ions compared with the other two derivatives. Optimization of membrane composition led to the composition of 28, 2 and 70 wt.%, poly(vinyl chloride), rifamycin-SV, and solvent mediator, respectively.

Typical calibration graph and response characteristics of potassium ion sensor based on rifamycin-SV ionophore and dibutylsebacate solvent mediator are reported in Fig. 2 and Table 2, respectively. At 25°C, the sensor displays a linear response for potassium ions over the concentration range 1×10^{-1}–3×10^{-5} M with a detection limit of 8.5×10^{-6} M and a calibration slope of 56.7 ± 0.2 mV decade^{-1} ($n > 6$). Repeated calibrations of the sensor over a period of 3 weeks with potassium chloride solutions show potential and slope stabilities within ±1 and 0.8 mV decade^{-1}, respectively. The extended linearity of the calibration plots without Donnan failure up to 10^{-1} M K^+ in solutions of KCl, KBr, KI, KNO_3 and KSCN indicates complete co-ion exclusion under the present conditions.

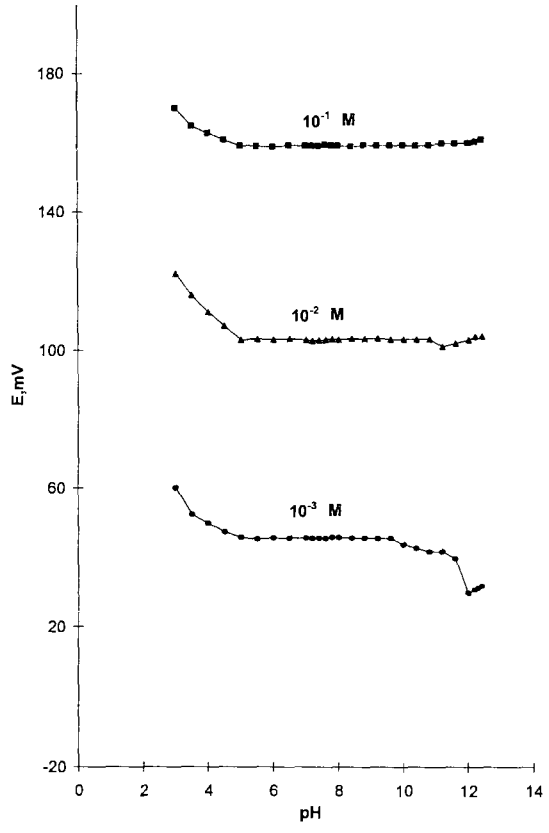

Fig. 3. Effect of pH on the response of rifamycin-SV PVC (DBS) membrane sensor for different potassium ion concentrations.

The response time (t_{95}) of rifamycin-SV potassium ion sensor was tested by measuring the time required to achieve a 95% steady potential for 10^{-4} and 10^{-3} M KCl solutions when their concentrations were rapidly increased by one decade. Fairly short response times of 10 s for $[K^+] > 10^{-3}$ M and 30 s for $[K^+] < 10^{-4}$ M, were obtained. Reasonably stable behaviour of the sensor was maintained during at least 6 weeks, then a drop of the sensitivity as a function of time was observed. This response decay could be attributed to leaching of the ionophore from the membrane.

The pH dependence of rifamycin-SV potassium sensor was examined using 10^{-1}, 10^{-2} and 10^{-3} M KCl solutions. Stable response over the pH range 4–11 was obtained (Fig. 3). Adjustment of pH was performed using dilute lithium hydroxide and hydrochloric acid. Below pH 5, the sensor response increases with the increase of the analyte acidity. At such high acidities the membrane may extract H^+ ion in addition to K^+ ions as rifamycin is also known to extract H^+ [13].

Table 3
Effect of solvent mediators on the response to K^+ using rifamycin-SV ionophore

Solvent mediators	Dielectric constant, ϵ	Slope, mV decade^{-1}	Linear range, M	Lower limit of detection, M
Dibutylsebacate (DBS)	4	56.7 ± 0.2	1×10^{-1} – 3×10^{-5}	8×10^{-6}
Dioctylphthalate (DOP)	7	44.6 ± 0.5	1×10^{-1} – 1×10^{-3}	1×10^{-5}
Dinonylphthalate (DNP)	9	38.3 ± 0.3	1×10^{-1} – 1×10^{-3}	5×10^{-5}
2-Nitrophenyl octylether (NPOE)	24	14.7 ± 0.4	1×10^{-1} – 1×10^{-2}	7×10^{-3}

3.2. Effect of solvent mediators

Potentiometric response of sensors based on neutral ionophores is greatly influenced by the polarity of the membrane medium, which is in turn defined by the dielectric constants of the major membrane components. Potassium PVC matrix membrane incorporating rifamycin-SV with four different plasticizers having dielectric constants over the range 4–24, namely dibutylsebacate (DBS), dioctylphthalate (DOP), dinonylphthalate (DNP) and 2-nitrophenyloctylether (NPOE) were prepared, tested and the results are shown in Table 3. Performance characteristics of membranes plasticized with DBS showed high sensitivity, reasonable selectivity, wide linear response range and near Nernstian slope. With DOP and DNP plasticizers, however, narrower linear response range (1×10^{-1}–1×10^{-3} M) and non-Nernstian slope (35 ± 1 mV decade^{-1}) were obtained. Poor response was detected with membranes plasticized with NPOE.

These data indicate that non polar ester type solvent mediators give a potassium ion sensor with more favourable potentiometric characteristics than polar solvents of the ether type with high

Table 4
Selectivity coefficient ($K^{pot}_{K,M}$) for rifamycin-SV PVC (DBS) matrix K^+ sensor

Interfering ion, M	$K^{pot}_{K,M}$
Li^+	1.4×10^{-4}
Na^+	3.9×10^{-3}
NH_4^+	3.1×10^{-3}
Rb^+	1.1×10^{-1}
Cs^+	4.1×10^{-3}
Sr^{2+}	2.3×10^{-4}
Ca^{2+}	3.7×10^{-4}
Mg^{2+}	3.9×10^{-4}
Ba^{2+}	5.3×10^{-4}
Cu^{2+}	5.7×10^{-3}
Ni^{2+}	3.9×10^{-3}
Co^{2+}	3.9×10^{-3}
Zn^{2+}	1.4×10^{-2}
Fe^{2+}	1.9×10^{-2}
Al^{3+}	1.4×10^{-2}

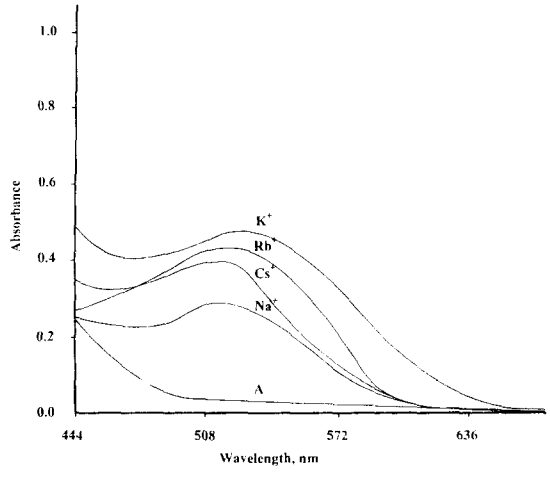

Fig. 4. Absorption spectra of rifamycin-SV in absence (A) and in the presence of various alkali metal cations.

Table 5
Determination of potassium in some pharmaceutical products using rifamycin-SV PVC (DBS) matrix membrane sensor and flame photometry

Pharmaceutical product	Nominal potassium content	Recovery[a], %	
		K-Sensor	Flame photometry
Slow-K (Swiss-Pharma)	600 mg tablet^{-1}	99.3 ± 0.6	98.8 ± 0.9
K-Syrup (El-Nile Pharm.)	150 mg ml^{-1}	101.5 ± 0.6	100.9 ± 1.1
KCl, 7.5% (W/V) solution (El-Nasr Pharm. Chem.)	75 mg ml^{-1}	99.5 ± 0.6	98.9 ± 0.8
KCl, 15% (W/V) solution (El-Nasr Pharm. Chem.)	150 mg ml^{-1}	99.2 ± 0.5	98.8 ± 0.9

[a] Average of five measurements.

dielectric constants. This is in good agreement with previous reports showing that the response characteristics and selectivities of monovalent cations are favoured by low dielectric constant solvents [5,19].

3.3. Selectivity of rifamycin membrane

The potentiometric selectivity coefficients K^{pot}_{KM} of potassium rifamycin-SV sensor were evaluated using the separate solution method [1,18] with 10^{-2} M concentration level of alkali, alkaline earth and transition metal ions. The results obtained (Table 4) show that the selectivity of the sensor with regard to alkali metal ions is in the order: $K^+ > Rb^+ > Cs^+ > Na^+ \gg Li^+$. Although the hydrophobicity and free energy of transfer (ΔG_t) data parameters of these metal cations are in the sequence: $Cs^+ > Rb^+ > K^+ > Na^+ > Li^+$ [20,21], selective complexation of K^+ with rifamycin-SV displaces Cs^+ and Rb^+ in respect of the above order of hydrophilicity and strict $\Delta G_t/K^{pot}_{K,M}$ correlation is no longer valid. Accordingly, the selective response of rifamycin-SV membrane towards K^+ could be mainly explained in term of interaction between rifamycin-SV and K^+ ions and a preferred extraction of K^+ ion into the plasticized membrane phase. Measurements of the electronic absorption spectra of rifamycin-SV in the presence of K^+, Rb^+, Cs^+ and Na^+ ions show absorption maxima at 536, 526, 524 and 515 nm, respectively.

As shown in Fig. 4, K^+ ions induce the greatest shift of the maximum absorption in the visible spectrum of rifamycin-SV and also induce the greatest change of the molar absorptivities when compared with the other alkali metal ions. This observation confirms the preferential complexation of K^+ ions over other metal cations with rifamycin-SV ionophore and supports a neutral carrier ion exchange mechanism. The electrostatic interactions between the ionic charge of K^+ ions and the dipoles of rifamycin-SV ionophore are primarily responsible for the fast and stable complex. The electrostatic interaction between potassium rifamycin-SV complex and the surrounding membrane solvent is a further contribution to the stability of rifamycin-SV complex in the membrane.

The influence of quaternary ammonium chlorides on K^+ based rifamycin-SV sensor was tested by soaking the membrane sensor for different time intervals (20–40 min) in 0.1 mM tetramethyl ammonium chloride (TMACl) before sensor calibration in KCl solutions. In contrast to K^+ based valinomycin sensor [22], the potentimetric response of the present sensor is less disturbed by quaternary ammonium salts. Potassium rifamycin-SV sensor pre-soaked in lipophilic TMA^+ cation exhibits near-Nernstian slope towards K^+ (40–45 mV decade^{-1}) depending on pre-soaking time without a significant variation in the lower detection limit. A membrane sensor pre-soaked in 10^{-2} M TMA^+ for 20 min exhibits a linear calibration slope of 32 mV decade^{-1} over

Table 6
Comparison of some potassium sensors

Ionophore	Price US $-g[a]	$(K^{pot}_{K,M})$[b]				References
		Na^+	Cs^+	Rb^+	NH_4^+	
Valinomycin	1862.8	2×10^{-5}	2.6×10^{-1}	0.2	1.2×10^{-2}	[2,3,25–27]
		2×10^{-2}	4	25	0.1	
Nonactin	709.8	6.6×10^{-3}	3.1	0.42	2.62	[11]
Dibenzo-18-crown-6	133.5	1.4×10^{-2}	9×10^{-2}	0.1	5.8×10^{-2}	[7,28,29]
		4.5×10^{-1}	1×10^{-1}	0.25	1.14	
Rifamycin-SV	36.6	3.9×10^{-3}	4.2×10^{-3}	1.1×10^{-1}	3.1×10^{-3}	Present work

[a] Fluka Chemika–Biochemica AG Cataloge, Switzerland, 1994–1995.
[b] High and low selectivity coefficient values reported in the literature.

the concentration range 10^{-3}–10^{-1} M with a lower limit of detection of 5×10^{-4} M TMA^+.

The cation response order of potassium rifamycin-SV sensor for alkaline earth ions is $Ba^{2+} > Mg^{2+} > Ca^{2+} > Sr^{2+}$. The response for Ba^{2+} is < 37 mV decade^{-1}, whereas response for other divalent cations are considerably less. The responses of the transition metal ions are poor with response order of $Zn^{2+} > Fe^{2+} > Co^{2+} = Ni^{2+} > Cu^{2+}$. The rejection of divalent and trivalent ions is favoured more in DBS than in NPOE plasticized membranes. Interferences caused by high concentrations (> 1000-fold excess) of Al^{3+}, Fe^{2+}, Fe^{3+}, and Zn^{2+} ions are completely circumvented by potentiometric measurements at pH 10, at which these metal ions are precipitated as hydroxides and–or converted into non interfering anionic species such as $[Al(OH)_4]^-$ and $[Zn(OH)_3]^-$.

An effort was also made to improve the response characteristics of rifamycin-SV sensor, by incorporating potassium tetra-*p*-chloro-phenylborate (KT*p*ClPB) in the sensor cocktail to act as anion excluder, to improve the selectivity for potassium, to reduce the membrane resistance and to reduce the activation barrier of the membrane–solution interface [23]. No improvement of the sensor selectivity for K^+ over other alkali metal cations was noticed. On the contrary, the response of the sensor for Rb^+ and Cs^+ cations was improved over K^+ ions; probably due to the stronger interaction of Rb^+ and Cs^+ with KT*p*-ClPB. Interaction of alkali metal ions with tetraphenylborate is known to increase with the increase of the ionic diameter of the alkali metals, that is in line with the ΔG_t sequence [24].

3.4. Analytical applications

Utility, sensitivity and selectivity of rifamycin-SV sensor were verified by determining 10 μg ml^{-1} of K^+ in synthetic mixtures containing 10–50-fold molar excess of different alkali (except Na^+) and alkaline earth metal cations using the standard addition (spiking) technique. Results with an average recovery of 99.1% and a mean standard deviation of 1.2% were obtained. The sensor was also used for the determination of potassium ions in some pharmaceutical products. The average recovery was 99.8% of the nominal and the mean standard deviation was 0.6% (Table 5). These results were compared with data obtained using flame photometry (average recovery 98.7%, mean standard deviation 1.3%). The *F*-test reveals that no significant difference between the means and variances of the two sets of results. The good agreement between potentiometric and spectrometric data demonstrates the applicability of the sensor for routine analysis of real samples containing potassium without a prior separation.

4. Conclusions

The most interesting features of rifamycin-SV based potassium ion sensor compared with those incorporating valinomycin, crown ethers and nonactin are: (a) better potentiometric selectivity for K^+ ion over Rb^+, Cs^+ and NH_4^+ ions; (b) fast and stable potentiometric response; (c) weak potential disturbant in presence of quaternary ammonium cations and (d) commercial availability of rifamycin-SV ionophore at a considerably cheap price. These characteristics (Table 6) make the use of the proposed sensor useful and convenient substituent for all other K^+ sensors except in cases when the Na^+-K^+ ratio is significantly high as in blood serum (Na^+-K^+ ratio >35).

References

[1] T.S. Ma and S.S.M. Hassan, Organic Analysis Using Ion Selective Electrodes, Vols. 1 and 2, Academic Press, London (1982).
[2] R.W. Cattrall, S. Tribuzio and H. Freiser, Anal. Chem., 46 (1974) 2223.
[3] H. Tamura, K. Kimura and T. Shano, Bull. Chem. Soc. Jpn., 53 (1980) 547.
[4] A. Bratov, N. Abramova, J. Munoz, C. Dominguez, S. Alegret and J. Bartroli, Anal. Chem., 67 (1995) 3589.
[5] D. Ammann, W.E. Morf, P. Anker, P.C. Merler, E. Pretsch and W. Simon, Ion Selective Electrode Rev., 5 (1983) 3.
[6] P. Oggenfuss, W.E. Morf, U. Oesch, D. Ammann, E. Pretsch and W. Simon, Anal. Chim. Acta., 180 (1986) 299.
[7] G.A. Rechnitz and E. Eyal, Anal. Chem., 44 (1972) 370.
[8] U. Oesch, D. Ammann and W. Simon, Clin. Chem., 32 (1986) 1448.
[9] M.A. Arnold and M.E. Meyerhoff, Anal. Chem., 56 (1984) 20R.
[10] A.S. Attyate, G.D. Chrsitian, R.Y.X. Wen and R.A. Bartsch, Electroanalysis, 4 (1992) 51.
[11] L.A.R. Pioda and W. Simon, Chemica, 24 (1979) 72.
[12] Y. Umezawa, Ion Selective Electrodes: Selectivity Coefficients, CRC Press, Florida, 1990, pp. 578–677.
[13] B. Inouye, Y. Uchinomi, T. Wachi and K. Utsumi, J. Antibiot., 30 (1977) 494.
[14] A. Craggs, G.J. Moody and J.D.R. Thomas, J. Chem. Ed., 51 (1974) 541.
[15] S.S.M. Hassan and F.Sh. Tadros, Anal. Chem., 56 (1984) 542.
[16] S.S.M. Hassan, R.M. Abdel Aziz and M.S. Abdel Samad, Analyst., 119 (1994) 1993.
[17] S.S.M. Hassan and S.A.M. Marzouk, Talanta, 41 (1994) 891.
[18] IUPAC, Analytical Chemistry Division, Commission on Analytical Nomenclature, Pure Appl. Chem., 67 (1995) 507.
[19] W.E. Morf, The Principles of Ion Selective Electrodes and Membrane Transfere, Elsevier, New York, 1981.
[20] R. Scholer and W. Simon, Helv. Chim. Acta., 55 (1972) 1801.
[21] G. Baum, J. Phys. Chem., 76 (1972) 1872.
[22] A. Lewenstam, E. Erkola and A. Lehmenkühler, Fresenius J. Anal. Chem., 346 (1993) 577.
[23] T. Okada, K. Hiratani and H. Sugihara, Analyst, 112 (1987) 587.
[24] H. Flaschka and A.J. Barnard, Adv. Anal. Chem. Instrum., 1 (1960) 1.
[25] M. Fiedler and J. Ruzicka, Anal. Chim. Acta., 67 (1973) 179.
[26] S. Lai and G.D. Christian, Anal. Lett., 3 (1970) 11.
[27] J.J. Griffin and G.D. Christian, Talanta, 30 (1983) 201.
[28] M. Mascini and F. Pallozzi, Anal. Chim. Acta, 73 (1974) 375.
[29] A. Rani, S. Kumar and N.B. Bannerjee, Fresenius'Z. Anal. Chem., 328 (1987) 33.

ELSEVIER

Talanta 44 (1997) 1095–1098

Talanta

Cold dissolution method for the determination of uranium in various geological materials at trace levels by laser fluorimetry

K. Ramdoss *, B. Gomathy Amma, V. Umashankar, R. Rangaswamy

Atomic Minerals Division, Department of Atomic Energy, Nagarbhavi, Bangalore 560 072, India

Received 23 September 1996; accepted 5 December 1996

Abstract

A cold dissolution procedure for the determination of uranium in various geological materials like rocks, minerals, soils etc., has been described. Samples are allowed to react with HF and HNO_3 at room temperature overnight. Boric acid is added to complex excess fluoride ions. From the clear solution thus obtained, uranium is determined directly in laser fluorimeter after the addition of fluorescence enhancing reagents. The results of few standard reference materials analysed by the present method agree with the certified values. This methodology does not require platinum or teflon ware, exhaust system and time consuming solvent extraction step. Hazardous acid vapours are not left in air, so there is no air pollution. Chemicals consumption is minimal. Therefore the method is economical. The method can be employed for high sample throughput which is the prerequisite for exploration geochemists. © 1997 Elsevier Science B.V.

Keywords: Geological materials; Laser fluorimetry; Uranium

1. Introduction

Exploration geochemists generate large number of samples for the delineation of anomalous zones, favourable for uranium. Therefore a rapid and economical feedback of the data is always desired. Among the various dissolution procedures for the determination of total uranium, in various matrices, dissolution [1,2] with HF and HNO_3 mixture in platinum dishes followed by Na_2O_2 fusion of residue, if any left, is practiced mostly. But this methodology requires platinum or teflon ware and exhaust system, for sample opening. So big batch analysis cannot be carried out rapidly and economically. The determination of different constituents of solid samples after aquaregia and HF attack at room temperature is well established [3–5]. Fluorescence of aqueous uranyl solution is quite weak, therefore intense excitation source in the presence of various fluorescence enhancing reagents [6–12] is used for very low level detection. Chloride ions in aquaregia quenches [13] uranium fluoresence even with intense excitation source and various known fluorescence enhancers. Also chloride ions leads to extraction [14] of Fe(III) in ethyl acetate which is a quenching agent in the fluorimetric determination of uranium. Therefore HCl (Aqua regia) is

* Corresponding author.

PII S0039-9140(96)02201-1

mostly avoided in the uranium determination by fluorimetry which is the most sensitive method for uranium.

In the present method samples of rock, mineral, soil and stream sediments are allowed to react with HF-HNO_3 at room temperature overnight in wide mouth screw cap polythene bottles and excess fluoride ions are complexed by the addition of H_3BO_3. From the clear solution uranium is determined [8] by laser excited fluorimetry after the addition of fluorescence enhancing reagents. To test the accuracy and precision of the present method standard reference materials (SRMS) and inhouse standards were analysed. The results obtained are in agreement with the certified and recommended values.

2. Experimental

Instrumentation: Scintrex UA-3. Uranium analyser (Scintrex, Canada). N_2-Laser pulse rate 16 times s^{-1}. Pulse duration 3–4 nanoseconds. Excitation wavelength 337.1 nm. Measurement wavelength 516 nm.

Reagents: all the reagents used are of analytical grade.

Fluoresence enhancing buffer mixture: $NH_4H_2PO_4$ (500 g) and H_3PO_4 (50 ml) made up to 2 l volume.

Plastic ware: 125 ml capacity wide mouth screw cap polythene bottles.

2.1. Procedure

Of each of the powdered (− 200 mesh) samples, 0.1 g, were weighed into polythene bottles. Reagent blank was also run simultaneously. Conc. HNO_3, 5 ml, and 5 ml of 40% HF were added. The bottles were tightly capped and allowed to stand at room temperature overnight. The demineralised water, 50 ml, and 15 ml of saturated boric acid added to the bottles and shaken for a few minutes with cap fixed tightly. The contents of the bottles were carefully transferred to 100 ml volumetric flasks quantitatively, diluted to volume with demineralised water and shaken thoroughly to get clear solution. An aliquot of 1 ml was transferred to a 10 ml volumetric flask, 4 ml of buffer mixture was added and made up to volume. Fluorescence readings were obtained using UA-3 Uranium Analyser. Using pure uranium standards calibration graphs were prepared for 0–2 and 2–20 ppb U. For higher Uranium content in sample, suitable dilution is made before drawing an aliquot of 1 ml for fluorescence measurement.

3. Results and discussion

Boric acid is added to neutralise fluoride ions which attack glass. Fluoborate does not interfere in uranium determination. Most of the elements that decrease the intensity of uranium fluorescence are taken care of by the dilution technique followed and total uranium is quantitatively determined in a variety of geological materials. Dolostone [15] and syenite [16] samples are associated with pitchblende and betafite, pyrochlore and monazite minerals respectively, which are the source for uranium. In these minerals [17] uranium is also present in tetra valency state. In the present method uranium tetrafluoride (UF_4) has not precipitated and lost but oxidised to hexavalency state and kept in solution. This is confirmed from the data presented in Table 1. Samples containing 50% of uranium in tetra valency state [18] have been analysed by the present method. The results obtained for total uranium compare favourably with the conventional method of dissolution [1,2] and estimation [9,14] demonstrating efficacy of the proposed method of dissolution for the determination of uranium. A variety of international standards (SRMS) rocks and minerals were analysed by the present method and the values obtained are in good agreement with the certified values [19] (Table 2).

Although Dolostone samples contain very high calcium, i.e., around 30% CaO [15] and Calcium precipitates as CaF_2, the uranium concentration obtained from the supernatant solution agreed very well with the inhouse standard values (Table 3). Luminescence of aqueous uranyl solution is quite weak and enhanced fluorescence yields have been achieved by using intense excitation source

Table 1
Comparison of total uranium obtained with the present method and with the conventional method of dissolution [1,2] and estimation [9,14]

Test sample No.	Present method	U_3O_8 (%)[a]		
		Conventional method		
	Total uranium	Total uranium	Tetra valent uranium [18]	Hexavalent uranium [18]
1	0.083	0.084	0.041	0.040
2	0.076	0.080	0.037	0.035
3	0.049	0.051	0.025	0.025

[a] Each value is an average of three determinations.

in the presence of various fluorescence enhancing reagents [6–12]. Fluran [9,10] sodium pyrophosphate, sodium dihydrogen phosphate [11] and sodium polysilicate [12] are reported fluorescence enhancing reagents. These are strongly pH dependent and at pH lower than seven their effect is greatly reduced. Tolerance for inorganic quenchers (Fe, Mn, Cu, Co) is also less. Orthophosphoric acid [6,7] has been extensively used as an enhancer of Uranyl fluorescence both as direct additive to U VI solutions and as a stripping agent for Uranylnitrate from ethyl acetate extractive phase. A mixture of orthophosphoric acid and ammonium dihydrogen phosphate [8] has a fairly high tolerance for inorganic quenching ions and for Ca, Mg, Nb, Ta, Ti, Al etc. Uranium in solid sample solution of 10% acidity prepared by the present cold dissolution is directly determined using this reagent [8]. It is not highly pH sensitive and has high tolerance for inorganic quenchers, while determining nanogram ml^{-1} of uranium.

The precision expressed as coefficient of variation is within $\pm$ 10%. This work is most suitable for Geochemical exploration of uranium where anomalous values are important, so a variation of 10% at these low values (Table 3) will be sufficient. The accuracy of the method is also within $\pm$ 10% at low concentration of uranium (Table 2).

4. Conclusion

The present cold dissolution technique and Laser fluorimetric method of uranium determination is highly useful for exploration Geochemists where speed, economy and high sample throughput are the prerequisite. The present method does not require costly platinum or teflon ware for sample dissolution, acid and other reagents used are minimal. Therefore it is highly economical. Since no defluoridisation step is involved by evaporation, air pollution is not there and there is no solvent extractive stage for removal of interferents and hence the method is eco-friendly also. Another advantage of this method of dissolution is the limited attention required at the dissolution stage, which decreases the likelihood of errors. The use of plastic ware, the avoidance of heating and after dilution with demineralised water, direct determination of uranium in laser fluorimeter renders the method adoptable for big batch analysis in geochemical exploration work in field conditions.

Acknowledgements

The authors thank Shri K.K. Dwivedy, Director, AMD for granting permission to publish the paper. Our sincere thanks are also due to, Head, Chemistry Group and Regional Director, SR for their encouragement, Dr R. Dhanaraju, Deputy Regional Director for petrological support and Dr D.S.R. Murthy, Senior Scientist for his critical and constructive comments.

Table 2
Uranium contents of standard reference materials determined using the present method

Sample No.	Rock–mineral	Uranium (ppm)	
		Present method	Certified values [19]
SY-2	Syenite	275	284
SY-3	Syenite	632	650
ASK-2	Schist	23	22
ZW-C	Zinwaldite	18.1	20
MA-N	Granite	12.9	12.5
GXR-1	Jasperoid	32.9	34.9
Mica-Fe	Biotite	76	80
NIST-120C	Phosphate rock (Florida)	120	114

Table 3
Comparison of results obtained with the present method and with the conventional method of dissolution [1,2] and estimation [9,14]

Test sample in-house standards	Uranium (ppm)	
	Present method[a]	Conventional method
Dolostone [15]	516	525
Dolostone [15]	945	927
Syenite [16]	360	365
Syenite [16]	949	932
Pink granite	4	4
Grey granite	2.8	3
Rhyolite	1.9	2
Dolerite	2.1	2
Dolerite pink granite and rhyolite	2.1	2
Andesite	4.6	5
Rhyolite porphyry	1.9	2
Granodiorite	8.4	9

[a] Each value is an average of three determinations.

References

[1] F.S. Grimaldi, F.N. Ward and R.K. Fuyat, US Geol. Survey Bull. (1954) 1006.
[2] M.D. Hassials and R.C. Musa, Proc. Intern. Conf. Peaceful Uses of Atom Energy, Geneva, 1955, Vol. 1 (VIII), p. 216.
[3] C.R.M. Rao and G.S. Reddi, Anal. Chim. Acta, 237 (1990) 251.
[4] G.S. Reddi, C.R.M. Rao, T.A.S. Rao and H.S. Muralidhar, Anal. Chim. Acta, 251 (1991) 205.
[5] C.R.M. Rao, G.S. Reddi and T.A.S. Rao, Anal. Chim. Acta, 268 (1992) 357.
[6] P.G. Whitkop, Anal. Chem., 54 (1982) 2475.
[7] A.T. Rhyswilliams and J.N. Miller, Anal. Chim. Acta, 154 (1983) 341.
[8] B.N. Tikoo and D.S.R. Murthy, Curr. Sci., 22 (1990) 861.
[9] Analytical techniques in uranium exploration and ore processing, International Atomic Energy Agency, Tech. Reports series No. 341, p. 74, Vienna, 1992.
[10] J.C. Robbins, Field techniques for measurement of uranium in natural waters, G.I.M. Bulletin, 61 (1978) 793.
[11] A. Creigzook, Linda H. Collins and Charles E. Pietri, Mikro Chim. Acta, 11 (1981) 457.
[12] G.I. Ramanovskaya, V.I. Pogoin and A. Chibsov, Talanta, 34(1) (1987) 207.
[13] R.K. Malhotra and B.N. Tikoo, Proceedings of the 5th National Symposium held at Hyderabad (India), Indian Society of Analytical Scientists, 1988.
[14] Horshi Onishi, Photometric Determination of Traces of Metals, Vol. 2, Part IIB, 4th Edn., Wiley Interscience, New York, 1989, p. 619.
[15] Petromineralogical investigations on carbonate hosted uranium mineralisation in the Tummalapalle–Gadankipalle prospect, Cuddapah district, Andhra Pradesh, India-1990, unpublished report.
[16] Atomic Minerals Division, DAE, India, Petrology Report No. AMD/SR/PET/19-94 dt 31.5.1995, personal communication.
[17] E. Wm. Heinrich, Mineralogy and Geology of Radioactive Raw Materials, P. 26, 35, 43 and 112, McGraw Hill, New York, 1958.
[18] Atomic Minerals Division, DAE, India Chemical Report No. AMD/SR/Chem/94-95/AR No. 51/95 dt. 5.6.1995, personal communications.
[19] K. Govindaraju, Geostandards News Letter 1994, XVIII Special Issue of Geostandards.

ELSEVIER

Talanta 44 (1997) 1099–1106

Talanta

Fluorometric fiber optic drop sensor for atmospheric hydrogen sulfide

Arnaldo A. Cardoso [1], Hanghui Liu, Purnendu K. Dasgupta *

Department of Chemistry and Biochemistry, Texas Tech University, Lubbock, TX 79409–1061, USA

Received 4 November 1996; received in revised form 4 December 1996; accepted 4 December 1996

Abstract

A fluorometric technique based on a liquid drop excited from its interior by an optical fiber is described for the measurement of low concentrations of atmospheric hydrogen sulfide (H_2S). A drop of alkaline fluorescein mercuric acetate (FMA) solution is suspended in a flowing air sample stream and serves as a renewable sensor. An optical fiber contained within the conduit that forms the drop, brings in the excitation beam; the fluorescence emission is measured by an inexpensive photodiode positioned close to the drop. As H_2S in the sample is collected by the alkaline drop, it reacts rapidly with FMA resulting in a significant decrease in fluorescence intensity, proportional to the concentration of H_2S sampled. The chemistry of this uniquely selective reaction has been well established for many years; the present technique permits a simple fast inexpensive near real-time measurement with very little reagent consumption. Even without prolonged sampling/preconcentration steps, limits of detection (LODs) in the double digit ppbv range is readily attainable. © 1997 Elsevier Science B.V.

Keywords: FMA; H_2S; Limit of detection; Optical fiber

1. Introduction

Sulfur gases and their reaction products have taken on a new significance in recent years due to their involvement in the formation of atmospheric aerosols, acid precipitation, planetary radiative equilibrium and a number of other issues, including the biogeochemical cycling of sulfur in the marine environment [1]. Sulfur dioxide is the only sulfur compound that is emitted with the sulfur in the +4 oxidation state. Most of the emitted sulfur compounds contain sulfur in the −2 oxidation state, these include dimethyl sulfide, carbonyl sulfide and H_2S. The natural emission of H_2S into the atmosphere was once believed to be the dominant sulfur emission [2]. But over the years, the importance of this contribution has been continuously revised downward and is now believed to be relatively small [3]. Except in remote regions, anthropogenic, mostly petroleum related, sources dominate H_2S emissions. Regardless of the decreased perceived importance of H_2S

* Corresponding author. Fax: +1 806 7421289; e-mail: VEPPD@TTACS.TTU.EDU

[1] Permanent address: Instituto de Quimica-UNESP, Dep. Quim Analitica Caixa Postal 355/CEP 14800–900, Araraquara-São Paulo, Brazil.

PII S0039-9140(96)02202-3

in the global sulfur cycle, it has long been known that at a local level even low levels of H_2S contributes to material corrosion, paint damage and troubles for the electronics industry [4]. In addition, of the sulfur gases mentioned above, H_2S is by far the most toxic. Here in West Texas, known for its oilfields, dead pigeons around oil storage tanks are a common sight; accidental human fatalities also occur.

The measurement of atmospheric H_2S has therefore received considerable attention and a number of analytical methods have been developed over the years [5–9]. In the following discussion, we confine ourselves to simple, field deployable, affordable methods. Most of these methods require a collection/preconcentration step (typically using a $Cd(OH)_2$ suspension to make CdS) before actual analysis is carried out [6–9]. Atmospheric oxidants can interfere in the collection step, the collected CdS photodecomposes and the physical design of the absorber can cause varied results, leading to conflicting, questionable and erroneous conclusions [10,11]. Post-sampling reactions can also occur with glass collection vessels [12].

In recent years, we have become enamored with the potential of liquid drops and films as analytical devices, notably as gas sensors. Such a sensor has a truly renewable collection surface like a wetted denuder [13,14] but requires much less collection liquid and can be produced in a compact form more conveniently and reproducibly. In the first drop based gas sampling system, an 18 μl static drop of diluted H_2SO_4 suspended in a sample stream was used to collect ppbv levels of NH_3 [15]. The drop contents were then withdrawn into a microscale elctroosmotically pumped sequential injection system for detection. Instead of withdrawing the drop for analysis elsewhere, in many cases it is possible to use a reagent in the drop that can result in a property change that can be followed in real-time, thus a selective reproducible sensor results. In this vein, a drop/film of Griess-Saltzman reagent suspended on a wire support forms the basis for sensing NO_2 at ppbv level using simple light emitting diode (LED) based interrogation of the drop/film [16]. Hydroperoxides were selectively detected using in-situ electrochemical sensing in a drop [17]. A gaseous chlorine sensor was developed with a continuously growing and falling drop of tetramethylbenzidine solution suspended in a sample stream and photometry with an LED based system [18].

It has occurred to us that a drop system is also particularly suitable for exciting fluorescence by placing a light source, such as an optical fiber terminus within the drop, because of the small optical path length, there is little attenuation of the excitation beam and efficient excitation of the liquid can take place. Further, such a scheme eliminates interfacial scattering of the excitation beam at the air/container wall interface. In this work, we demonstrate a near real-time fluorometric detection method for H_2S using a drop sampler. The H_2S is collected by a drop of alkaline fluorescein mercuric acetate (FMA) solution. This well known sensitive reaction, selective for sulfhydryl groups, results in a quenching of the native FMA fluorescence [7,8,19].

2. Experimental

2.1. Chemicals

All chemicals were reagent grade quality and used without further purification. Deionized water was used throughout. The FMA stock solution (20 μM) was prepared in 0.1 M NaOH. An FMA solution of 6.0 μM, diluted from the stock solution with 0.1 M NaOH, was used to form the drop sampler for gaseous H_2S.

2.2. Measurement system

The measurement system arrangement is shown in Fig. 1 (a) with the cross section view from the top shown in Fig. 1 (b). Silica optical fiber *F* (1000 μm core, fused silica, Ensign-Bickford Optics, Avon, CT) is positioned inside Teflon tube *T* (3.8 mm i.d., 4.8 mm o.d. and 27.0 mm in length) to carry the excitation beam. The axis of optical fiber F is 1 mm away from the axis of tube *T* and the end of the fiber is ~2 mm above the tip of tube *T*. A Teflon tube *C* (0.3 mm i.d. and 0.6 mm o.d.) is also inserted into tube *T* to deliver the

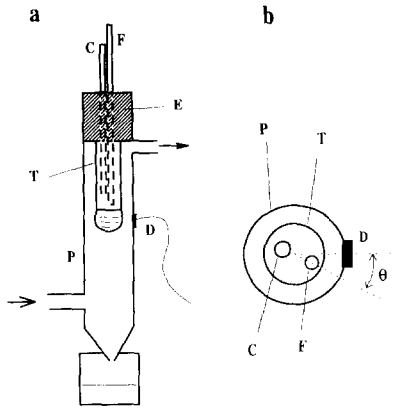

Fig. 1. Schematic diagram of the drop based sampling/detection chamber. *C*, Teflon tube for the delivery of FMA solution; *F*, silica optical fiber; *T*, Teflon tube for drop formation; *E*, fitting (the gas outlet arm is an integral part of this), *P*, opaque PVC tube; *D* photodiode. The drawing is not to scale.

FMA reagent. Tube *T* is fixed in a fitting *E* that is screwed into an opaque PVC tube *P* (12 mm i.d., 17 mm o.d. and 110 mm in length) through which the sample gas is aspirated. The FMA solution is allowed to flow by gravity through tube *C* to form a drop on the tip of tube *T*. A solenoid valve (SV in Fig. 2) is incorporated in the liquid inlet line. The FMA solution flow is stopped when the valve is shut off. The maximum drop volume of a drop for such an arrangement is about 60 μl, after that, the drop falls. The fall of a drop is readily discernible from the optical signal. Using the instant of drop detachment as a marker, keeping the solenoid valve on for a given period of time past this instant allows one to form a drop of desired size (up to the maximum) reproducibly. The beam from a 25 W Tungsten lamp source (Lamp source type 01 coupled to grating AMC1-03, PTR Optics, Waltham, MA) is coupled to optical fiber *F*, with the grating wavelength set at 495 nm. A small silicon photodiode *D* equipped with an interference filter centered at 530 nm (T5-STK-530, Intor, Socorro, NM, TO-5 package) is put into a hole on the wall of tube *P* (approximately on the same side as fiber optic *F*; vide infra) to detect the fluorescence emission from the drop. The center of the photodiode is in the same horizontal plane as the center of the drop. A home-built current detector, based on a low noise switched integrator [20] is used to convert the photocurrent detected to a voltage signal.

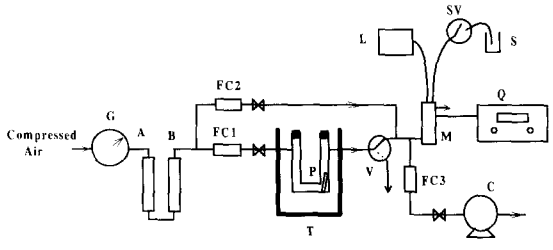

Fig. 2. Schematic diagram of the experimental arrangement. *A* and *B*, sequential columns for air purification; FC 1–3, mass flow controllers; *G*, pressure gauge and regulator; *T*, thermostated enclosure; *P*, permeation chamber; *V*, three-way Teflon solenoid valve; *L*, light source; *S*, FMA solution; SV, liquid on/off valve; *M*, drop based sampling/detection chamber; *Q*, signal processor and readout; *C*, air aspiration pump.

2.3. Gas generation and sampling

The arrangement for H_2S standard gas generation and sampling system is illustrated in Fig. 2. All gas flows are regulated by mass flow controllers FC1-3 (Model FC280, Tylan General, Torrance, CA). Air purified by sequential columns *A* (activated carbon) and *B* (silica gel/soda lime) is metered by flow controller FC1 through a permeation chamber *P* housed in a thermostated enclosure *T* maintained at 30°C. A permeation wafer device (VICI Metronics, Santa Clara, CA) emitting H_2S at ~ 100 ng min^{-1} is placed inside the permeation chamber. The H_2S gas stream from the chamber is diluted by pure air metered by FC2. Any excess flow of the standard gas, metered by FC3, is aspirated to waste, while the desired amount (FC1 + FC2 − FC3) flows through the sampling chamber. By activating three-way valve V, pure air, controlled by FC2, can be sampled instead of the analyte. Soda lime trap tubes are placed in all vent lines to avoid contamination of the laboratory atmosphere with the noxious gas.

Unless otherwise stated, the experiment procedures are as follows: (a) form a drop of ~ μl in volume and begin recording the fluorescence signal synchronous with the solenoid valve being shut off; (b) sample H_2S of desired concentration for 2 min at a flow rate of 0.16 l min^{-1}; (c)

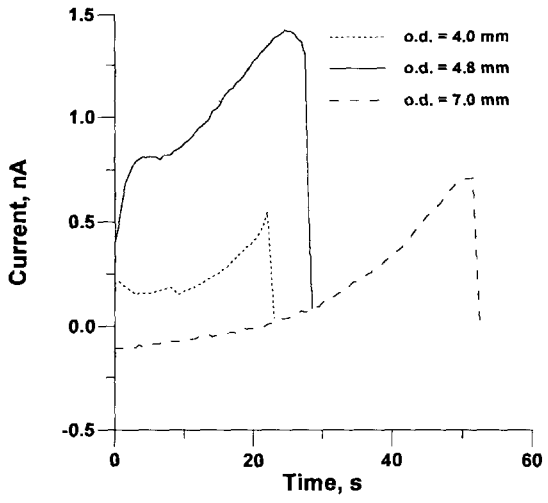

Fig. 3. Fluorescence signal in during the lifetime of a single drop for various diameters of Teflon tube T; liquid flow rate is held constant.

activate three-way valve V to flush the measurement chamber with pure air for 10 s; (d) cease all gas flow; and (e) reestablish liquid flow, form a new drop and begin a new cycle. A complete cycle takes ~ 5 min.

3. Results and discussion

3.1. Effect of drop size

As noted in the Section 2, the drop size can be varied by the timing of the solenoid valve. The maximum attainable drop size, on the other hand, can be changed by varying the diameter of the drop tube T. Experiments were conducted with different outer diameters of T with a drop continuously forming and falling while the fluorescence signal was monitored, the optical fiber being coaxial with tube T. The results are shown in Fig. 3. In each case, the fluorescence signal increases as the drop grows and reaches a maximum shortly before drop detachment occurs. The results do not show an unidirectional change with an increase in drop diameter, rather, the observed fluorescence intensity is substantially higher for the 4.8 mm tube. In these experiments, the observed fluorescence signal is a complex function of many factors. Some of the light launched from the fiber undergoes internal reflection at the drop/air interface; McMillan et al. have made an excellent and detailed analysis as to how such multiple internal reflections can occur in a drop [21]. In the present case, it is intuitive that the number of internal reflections should also be dependent on the convexity of the drop bottom, decreasing with increasing tube diameter. However, there is a substantially larger amount of liquid (and thence a substantially larger number of molecules) to be excited as the tube diameter increases. On the other hand, the detector position and photosensitive area remains fixed regardless of drop size, keeping its field of view fixed. Finally, the drop also behaves like a lens and its focus changes as a function of size; past a certain size, it may actually block the vision of the detector towards the most luminescent region.

Clearly, it is impossible to assess the contribution of each individual factor from the results in Fig. 3. The data however, allowed us to choose the intermediate tube diameter of 4.8 mm as the optimum in our specific experimental setup for further work. We also elected to choose a drop volume of 50 μl for further work, just short of the maximum drop volume (at which point the drop may be more subject to premature detachment due to shock/vibration).

3.2. Position of the optical fiber and the detector

Fig. 4 (a) shows the detector photocurrent as a function of the depth of protrusion of the fiber beyond the mouth of tube T, with negative values indicating that the fiber is inside tube T. Maximum photocurrent is observed with the fiber ca. 2 mm inside tube T. This is likely a function of the numerical aperture of the fiber and the consequent angular dispersion of the light as it enters the liquid as well as the drop size. Experiments also showed that maximum photocurrent is produced with the fiber slightly off the coaxial position within the tube T, the highest photocurrent being observed with the fiber axis in a position ~ 1 mm off the tube axis in the direction close to the detector. Light launched from an off-axis fiber and perpendicularly incident on the interior of the

drop surface encounters an area with greater curvature relative to when the fiber is concentric with tube T. We believe therefore that the off axis position of the fiber likely increases the extent of internal reflections, thus resulting in signal enhancement.

The emitted photon flux around the drop becomes anisotropic when the fiber is no longer coaxial with the tube. The position of the detector now becomes a variable. Referring to Fig. 1 (b), we can define its relative position by considering the angle θ between the center of the photodiode D, the axis of tube T and the axis of fiber F on an horizontal plane. With the detector D fixed on the wall of tube P, the above relative position can be changed by rotating tube P with respect to tube T (and vice-versa). For $\theta = 0°$ (F is in the closest possible position to D), the photocurrent was observed to be 1.18 nA, this increased to a maximum of 1.40 nA at $\theta = 30°$ and decreased to a minimum of 750 pA at $\theta = 180°$. Overall, relative to the coaxial position, the 1 mm off-axis position of the fiber and the 30° viewing angle of the detector led to a significant enhancement of the observed photocurrent. In addition, the amount of scattered excitation light registered by the detector (as measured by the signal when a NaOH solution was substituted for alkaline fluorescein) is also minimum at an observation angle of 30°.

Thus, with the optimum positioning of fiber F vertically, radially and relative to detector D, Fig. 4 (b) shows the photocurrent from a growing and falling drop (three sequential drop traces are shown) of (a) a NaOH blank solution and (b) a solution of 6 μM FMA in 0.1 M NaOH. Clearly, if we consider the ratio of the signal in case b versus the signal in case a as the index of the signal to noise ratio (the noise is assumed to be linearly related to the blank), this is maximized shortly before the drop grows to its maximum size. The choice of a static drop size of ~ 50 μl is thus further justified.

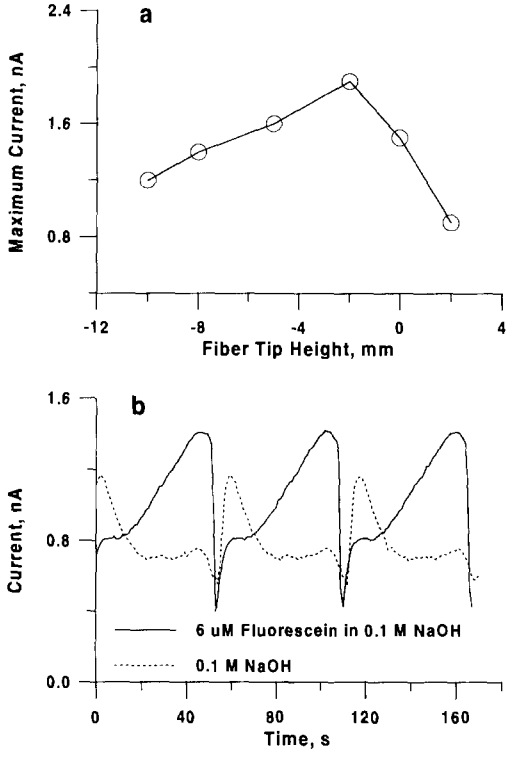

Fig. 4. (a) Fluorescence signal as a function of vertical position of the terminus of fiber F, zero connotes a position flush with the terminus of tube T and negative values indicate a position inside the tube. (b) Signals from an alkaline drop containing a fluorescent analyte and a drop containing only NaOH with optimized positions of the fiber and the detector, three successive drops are shown in each case.

3.3. Reduction of stray light with fiber in drop

Two experimental situations were compared. In the first, conventional setup, the excitation fiber was introduced through an aperture in the wall of the tube P in the same horizontal plane as the photodiode and the center of the drop. The fiber terminus was located 2 mm away from the drop boundary. The point of the fiber terminus, the drop and the photodetector formed a 90° angle in the same horizontal plane. In the second experiment, the optimized position of the fiber (1 mm off-axis, 2 mm inside the tube) and the detector (at an angle of 30°). Only a drop of water was used in the tube so that the signal registered by the photo detector is essentially due to stray/refracted light. The mean current due to stray light was 225% greater in the first vs. the second case, testifying to the advantage of the design.

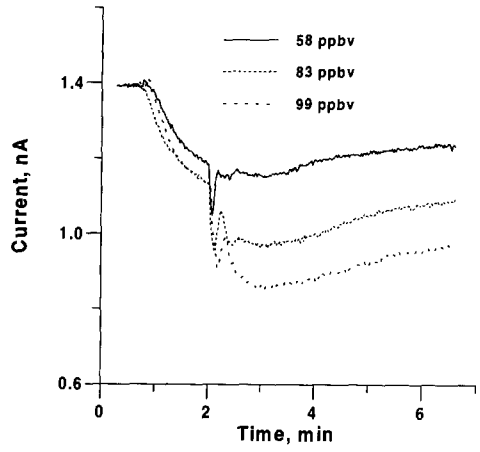

Fig. 5. Temporal profiles of the fluorescence signal for three different H_2S concentrations.

3.4. Response characteristics

A typical trace of the detector photocurrent as a function of time is shown in Fig. 5 for several different H_2S concentrations. A careful study of the traces will reveal that the length of this quiescent period is dependent on the H_2S concentration sampled, decreasing with increasing H_2S concentration. This can occur either because the reaction has an induction period that is dependent on the concentration of HS^- at the droplet surface (dependent in turn on the concentration of H_2S sampled) or more likely, the quiescent period reflects the time necessary for a finite concentration of the quenching species generated at the surface to travel to the region that is effectively probed by the exciting radiation. From first principles this period is likely to be related to the logarithm of the concentration sampled, this was not explored in the present study.

At a time of 2 min, the gas sampling is stopped and pure air flow is turned on for 10 s. This flow switching results in a perturbation in the status of dynamic mixing of the drop, apparently enhancing it momentarily and bringing in more of the quencher species in the most effectively probed region of the drop. (It should be noted that the mixing in the drop is not simply due to diffusion, the frictional drag of the gas moving past the liquid generates a circulatory motion on the surface that is very readily visible [15].) All gas flow is then ceased. The current initially increases after the cessation of all flow and decreases again to a minimum and then increases slowly to a stable plateau. The analytical signal ΔS can be taken to be the difference between the photocurrent at the beginning of the experiment and that at the minimum occurring between 2.3 and 3.5 min, leading to a linear relationship within the H_2S concentration range of 0–100 ppb H_2S:

$$\Delta S = 7.04(\pm 0.22) \times 10^{-3}[H_2S, \text{ppb}] - 0.1520 \pm 0.0154, \quad r^2 = 0.9991 \quad (1)$$

Alternatively, ΔS can also be taken to be the difference between the initial photocurrent and that at some point after cessation of sampling, e.g., when the difference between $t = 0$ and 4 min are considered, we obtain the following linear relationship:

$$\Delta S = 6.65(\pm 0.37) \times 10^{-3}[H_2S, \text{ppb}] - 0.1778 \pm 0.0254, \quad r^2 = 0.9967 \quad (2)$$

The lowest concentration tested was 28 ppbv H_2S, at this concentration, a detectable signal was observed. The relative standard deviation ranged from less than 2% to 12% in the 28–100 ppbv concentration range.

3.5. Effect of gas flow rate

If the collection of the gas by the drop is diffusion limited, the analytical signal ΔS should be related to the flow rate Q through a relationship of the type:

$$\Delta S = Q(1 - ae^{-b/Q})/c \quad (3)$$

where a, b and c are constants [17]. Fig. 6 (a) shows the experimental data for the flow rate range of 60–350 ml min^{-1}; a good fit ($a = 4.115$, $b = 1284$, $c = 1165$, $r^2 = 0.9969$) is obviously obtained.

3.6. Effect of water vapor and other gases

Relative humidity (RH) of the sample indirectly affects the measurements in that a low sample RH leads to greater evaporation of the droplet.

At this droplet size, as the droplet evaporates and there is greater concentration of FMA within the smaller droplet (probably the surface concentration is greater), the observed photocurrent increases. Fig. 6 (b) shows the situation when pure dry air is sampled at 0.16 l min^{-1}. Beyond a period of 5 min, the increase in photocurrent is sufficient to cause too great an analytical error if not compensated for. Of course, this is the worst case situation, a more humid sample will cause far less evaporation. In any case, this compensation can be provided by a second fluorescent dye incorporated into the drop which is inert to H_2S and fluoresces at a wavelength different from that for FMA when excited by the same incident beam. This fluorescence intensity can be read by a second, symmetrically placed photodiode, equipped with a suitable interference filter.

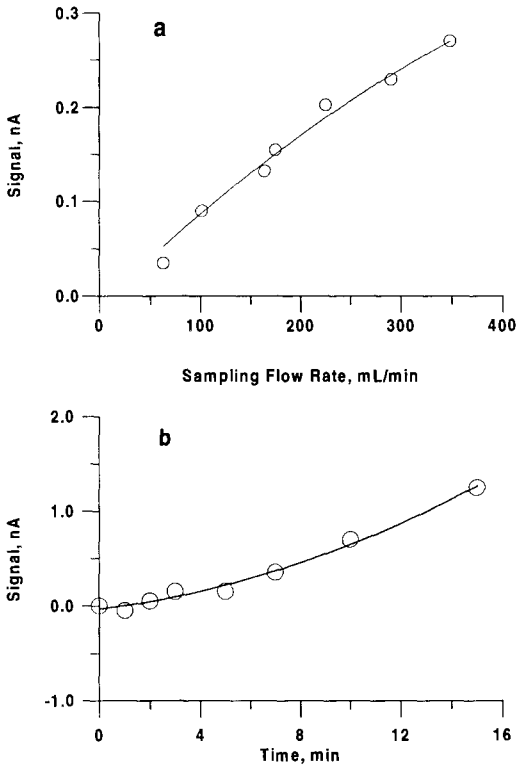

Fig. 6. (a) Analytical signal as a function of sampling flow rate. The sample gas concentration is 49 ppbv; (b) Signal observed for pure air as a function of sampling time.

As may be expected, the chemistry used in the present case responds to other gases bearing –SH groups such as CH_3SH. However, prolonged collection is not a feature of the present technique and oxidants such as NO_2 which was found to be a significant interference in early deployment of this chemistry [8] did not interfere. We found no interference in the determination of 49 ppb H_2S by 180 ppb NO_2.

In summary, the present application shows that a fluorescence based drop sensor can be configured simply and provide impressive limits of detection even with a photodiode detector. Initial experiments show that appropriately filtered blue LED sources can work as well or better in this application relative to the lamp/grating combination used in this work, thus further simplifying deployment.

Acknowledgements

A.A.C. acknowledges financial support from Conselho Nacional de Desenvolvimento Científico de Tecnológico, CNPq, Brazil. This research was supported by the U.S. Environmental Protection Agency, Office of Exploratory Research, through grant No. R-8201117-01-1.

References

[1] K.S. Johnson, K.H. Coale and H.W. Jannasch, Anal. Chem., 64 (1992) 1065A.
[2] E. Ericksson, Tellus, 12 (1960) 63.
[3] P. Warneck, Chemistry of the Natural Atmosphere, Academic Press, San Diego (1988) 484–542.
[4] J.E. Yocom and J.B. Upham, in A.C. Stern (Ed.), Air Pollution, 3rd edn., Vol. 2, Academic Press, New York, 1976, pp. 65–116.
[5] R.K. Stevens, J.D. Mulik, A.E. O'Keefe and K.J. Krost, Anal. Chem., 43 (1971) 827.
[6] J.B. Jacobs, M.M. Braverman and S. Hocheiser, Anal. Chem., 29 (1957) 1349.
[7] B.A. Hardwick, D.K.B. Thistlethwayte and R.T. Fowler, Atmos. Environ., 4 (1970) 379.
[8] D.H. Axelrod, J.H. Cary, J.E. Bonelli and J.P. Lodge Jr. Anal. Chem., 41 (1969) 1856.
[9] D.F.S. Natusch, H.B. Klonis, H.D. Axelrod, R.J. Teck, and J.P. Lodge Jr., Anal. Chem., 44 (1972) 2067.

[10] D.F. Adams, in A.C. Stern, (Ed.), Air Pollution, 3rd ed., vol. 2, Academic Press, New York, 1976, pp. 214–257.
[11] E.S. Saltzman and D.J. Cooper, in E.S. Saltzman, D.J. Cooper, D.J. (Eds.), Biogenic Sulfur in the Environment American Chemical Society, Washington DC, 1989, pp. 330–351.
[12] I. Devai and R.D. DeLaune, Anal. Lett., 27 (1994) 2403.
[13] P.K. Dasgupta, ACS Adv. Chem. Ser., 232 (1993) 41.
[14] Z. Ali, C.L. Paul Thomas and J.F. Alder, Analyst, 114 (1989) 759.
[15] S. Liu and P.K. Dasgupta, Anal. Chem., 67 (1995) 2042.
[16] A.A. Cardoso and P.K. Dasgupta, Anal. Chem., 67 (1995) 2562.
[17] H. Huang and P.K. Dasgupta, Talanta (in press).
[18] H. Liu and P.K. Dasgupta, Anal. Chem., 67 (1995) 4221.
[19] M. Wronski, Talanta, 15 (1968) 241.
[20] H. Liu, P.K. Dasgupta and H.J. Zheng, Talanta, 40 (1993) 1331.
[21] N.D. McMillan, E. O'Mongain, J. Walsh, L. Breen, D.G.E. McMillan, M.J. Power, J.P. O'Dea, S.M. Kinsella, M.P. Kelly, C. Hammil and D. Orr, Opt. Eng., 33 (1994) 3871.

ELSEVIER

Talanta 44 (1997) 1107–1112

Talanta

Investigation of conductometric humidity sensors

Jurgis Barkauskas

Department of General and Inorganic Chemistry, Vilnius University, LT-2734 Vilnius, Lithuania

Received 24 January 1995; received in revised form 31 March 1995; accepted 9 December 1996

Abstract

Sensors for determining humidity in air have been described and investigated. Sensing film of the devices was prepared from polyvinylalcohol and graphitized carbon black disperse phase. The composition, thermal treatment and design of sensing films were investigated and optimized. An optimized humidity sensor has better metrological parameters as compared with its prototype (response time ~45 s, detection limit 0.17%, slope 6.25 ± 0.05 Ω/R.H., standard deviation of measurement 0.15%, standard deviation of analytical signal in the graduation equation 8.29Ω). Such construction of sensors have prospects in analytical practice. © 1997 Elsevier Science B.V.

Keywords: Air; Conductometric humidity sensors; Graphitized carbon; Polyvinylalcohol

1. Introduction

Looking through the evolution in field of humidity sensors during the last years devices based on varying of resistance stand out. Majority of this kind are thin hydrophile polymer films sometimes including a disperse phase of first-class conductor [1–3]. The conductivity of thin film changes owing to the swelling process of hydrophile polymer layer [4]. First-class conductor dispersed in the polymer matrix improves metrological parameters of the sensor. There the resistance of thin film is significantly lower and the use of more simple and reliable measuring equipment is possible [5]. These sensors are used for measuring humidity in gaseous, liquid and solid phases [6,7].

Except named positive features these sensors are not lack of shortcomings limiting their application. The most distinct are: relatively long response time, hysteresis and high level of uncertainty. Notwithstanding, only a few sources directly dealing with metrological improvement problem its possible to discover [8,9]. Getting clear that further development of polymer-film sensors with first-class conductor will advance only after elimination of enumerated shortcomings this work is an attempt to make a step in this direction.

2. Experimental

Resistance of thin polymer film was measured using constant current ohmmeter (model V7-38, running voltage 1.0 V) and registered with recorder N 307. Thin polymer film (thickness of 30 μm) was formed by means of spin-coating

PII S0039-9140(96)02203-5

(device model OPn-8). The constant temperature in the system was maintained using thermostat MLW-UH. The air stream saturated up to fixed humidity was transported to the sensor by means of microcompressor (model AEN-3). Artificial aging of the sensors was carried out in device SKVS-4.5.4, 54/ZI-1. This device consists from an insulated camera with controlled level of relative humidity (R.H.) and temperature inside. Sensors were kept at the R.H. 100% and temperature 50°C in this camera for 10 h.

The chemicals used were analytical grade. Polyvinylalcohol, 10%, (PVA) (type PVS; av. mol. mass 60 000) solution was prepared after swelling and dissolving at 60°C. Graphitized carbon black (CB) for conducting disperse phase was synthesized according to Brauer [10] from gaseous carbon monoxide at 600 C using Fe as catalyst and purified by means of permanent hot extraction with HCl. The grain size of CB synthesized under above mentioned conditions is ~ 15 nm [10]. Dispersion of CB in PVA was observed using light microscope (Leitz-Wetzlar, type 307-107.002). There the conglomerates of inhomogeneity reaches 1.0–2.0 μm.

Connection between the sensor's design and metrological parameters was examined. For that purpose sensors of different structure were prepared (Fig. 1A, B). Both kind consisted from two electrodes and thin sensing film. The sensors were designed on the glass plate. Two electrodes were made from Al foil. In one of these modifications electrodes were coated with transition layer of high-concentrated CB dispersion in PVA, treated at 300°C (Fig. 1B). Etched glass (glass treated with 10% Na_2SiO_3 solution up to 300°C for 6 h; Fig. 1B) and heated PVA (at 300 C) sublayers were used to improve adhesion between polymer film and substrate. The morphology of etched glass was observed by means of light microscope. Surface roughness of etched samples reaches 0.5 mm, dimensions of chaotically scattered crystallites varies within 0.5–5.0 μm. Thin films heated at 300°C show gradual discoloration, embrittlement and reduction of water absorbency. There the polymer exists in cross-linked state incapable for swelling [11]. Thin films of PVA formed from aqueous solutions well when placed in contact with humid air. The state of polymer there is thermoplastic and swelling process is reversible. Humidity sensing CB/PVA film was prepared by means of spin-coating at 1000 turns min^{-1}. In the process of calibration, the stream of air was saturated up to indicated value of relative humidity (R.H.) by means of blowing it through bubblers (stream velocity 25 cm min^{-1}). The bubblers were filled with solutions of salts and in common with measurement cell were placed into thermostat at 20 C. Salts for solutions used and R.H. reached (pointed out in blackets) were as follows [12]: K_2SO_4 (99); $(NH_4)_2SO_4$ (81); NH_4NO_3 (67); $NaHSO_4 \cdot H_2O$ (52); $CaCl_2 \cdot 6H_2O$ (33); $LiCl \cdot H_2O$ (15); H_2SO_4 (0). Measurements were repeated five times.

3. Results and discussion

Parameters most often used for metrological description of humidity sensors are as follows [13]: response time (τ), detection limit (ΔX_{lim}), slope ± confidence limits ($b \pm \epsilon_b$), standard deviation of measurement (σ_X), standard deviation of analytical signal in graduation equation (σ_Y). The slope was linear in all cases inside investigated R.H. interval (Table 1). Named parameters are sensitive to the composition and design of humidity sensor and could be used for the optimization.

The contact quality between polymer film and substrate directly acts on the analytical signal. In the case of poor contact the sensor gradually becomes degraded at that time increasing the uncertainty of results (Table 1). Sublayers positively affect on the quality of sensor. This fact is evident comparing metrological parameters of the sensors after artificial aging: the one without sublayer degrades. There we can draw and conclusion that the sensors including sublayers are more stable in time.

Heating of PVA reduces the hydrophobity and swelling capacity of the film due to forming of cross-linked structure [11]:

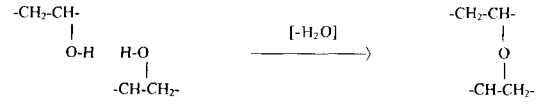

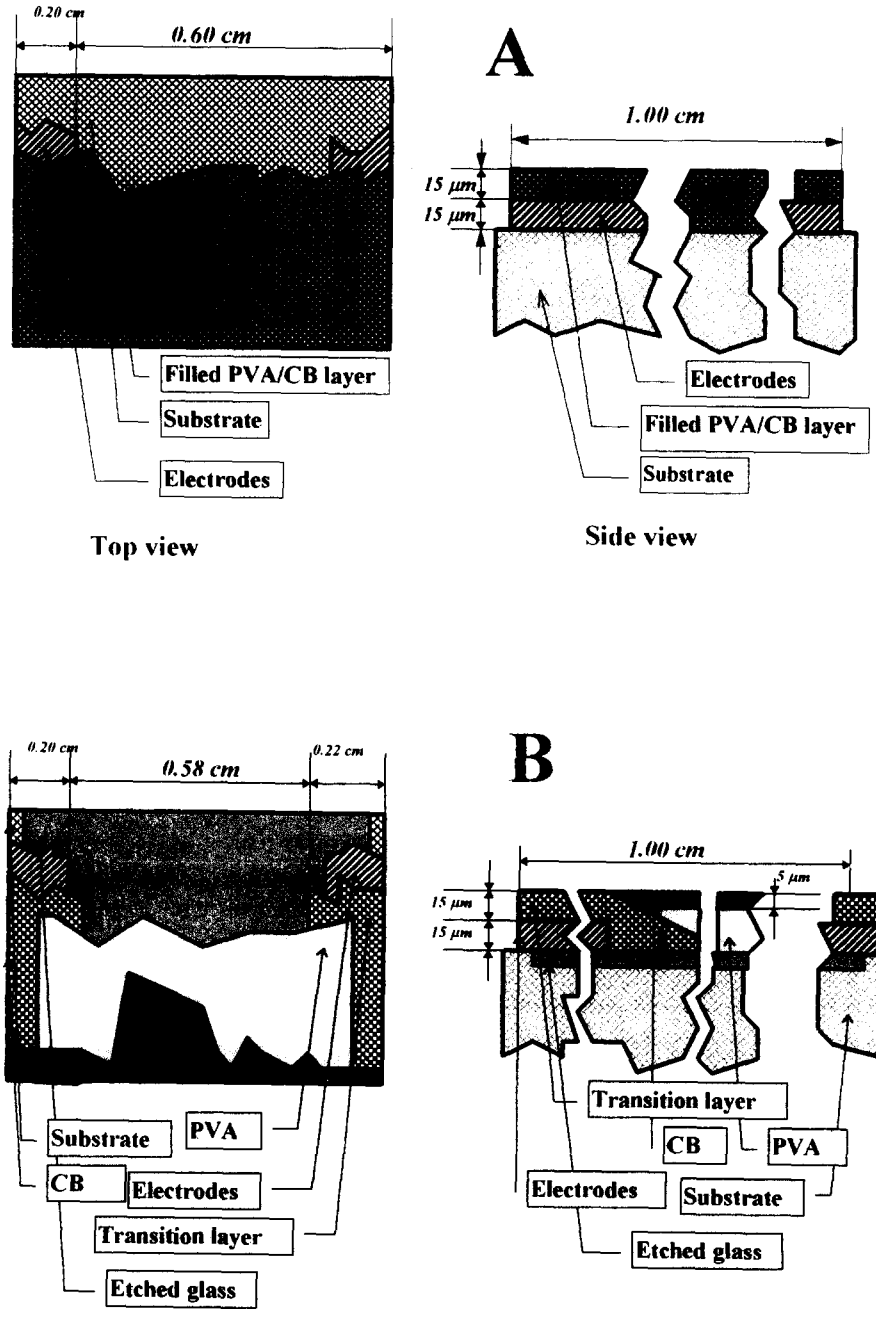

Fig. 1. Design of humidity sensors. (A) humidity sensing film consisting from CB dispersion in PVA matrix. (B) including composite two-layer humidity sensing film (optimized design of humidity sensor).

Table 1
Metrological parameters of humidity sensors prepared by different ways

Changed detail or construction and its parameters	Resp. time (τ); s	Detection limit (ΔX_{lim}); %	Slope and confidence limits ($b \pm \epsilon_b$); Ω/R.H.	Stand. dev. of signal (σ_Y); Ω	Stand. dev. of measurand (σ_X); %
Sublayers					
Without sublayer	50	1.17	119.50 ± 1.36	0.98	58.4
Aged sensor	240	43.4	40.48 ± 5.31	36.3	220.1
Etched glass	60	0.80	121.70 ± 1.02	0.67	43.8
Etched glass + aged	65	1.94	107.37 ± 1.43	1.62	61.3
Heated PVA sublayer	60	0.38	177.43 ± 1.13	0.32	48.5
PVA + aged	60	0.64	164.20 ± 1.40	0.54	60.0
Heated sensing film (temperature, °C)					
—	65	1.39	34.91 ± 0.42	1.17	18.03
100	30	0.58	10.54 ± 0.05	0.49	2.14
170	40	4.64	4.67 ± 0.02	3.88	0.86
240	40	8.04	0.31 ± 0.01	7.15	0.42
300	40	14.8	0.23 ± 0.01	12.4	0.42
CB amount in sensing film (%)					
53	120	>20	$12\,573 \pm 542$	>18	23 265
57	60	2.21	1842 ± 16	1.73	687
59	65	1.54	244.5 ± 2.5	1.30	107
66	40	—	10.7 ± 2.0	>80	86
Two-layer sensing film (Fig. 1B)	45	0.17	16.25 ± 0.05	0.15	8.29

Statistics and other results accompanying the heating of sensing film at various temperatures are presented in Table 1. These data show strict correlation between heating temperature and standard deviation of analytical signal. This could be explained taking into account interaction between CB grains and PVA matrix. At lower temperatures the chemical interaction is weak and CB grains are not fixed in the polymer matrix very steady. Working with humidity-sensing films prepared under these conditions we observe standard deviation of analytical signal reaching significant values. One of the possible explanation of this phenomena could be that during multiple process of swelling and contraction of the polymer matrix CB grains are affected by the irreversible process of spatial orientation. This could occur where bonds between PVA molecules and CB grains are weak. The conjecture is affirmed by the fact that standard deviation of humidity-sensing film prepared at higher temperatures reduces to insignificant values. Taking into account that under higher temperatures –OH groups from PVA chain reacts with surface of CB grains (see reaction above), these grains being fixed more steadily in the polymer matrix. Under these conditions we could expect that the irreversible process of grains spatial orientation has no place. The swelling capacity of humidity-sensing films, treated at higher temperatures, is reduced as well as their sensitivity. Detection limit being the function of slope reaches minimum values after heating at 100°C.

The amount of conducting CB phase in polymer matrix affects the metrological parameters of humidity sensors too (Table 1). In the case of less amounts CB grains are insulated by PVA matrix and resistance of the film is high. The standard deviation of analytical signal there is significant apparently due to lower reliability of equipment as well as to high values of resistance and less amounts of microcontacts between CB grains. In the case of greater amount when carbon grains prevails over polymer in the bulk of sensing film

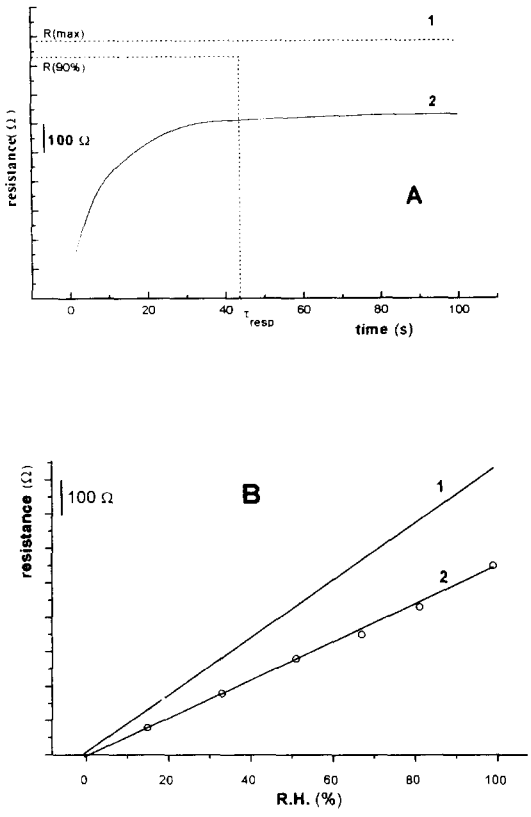

Fig. 2. Response transients (A) and calibration curves (b) of two-layer humidity sensor (1) and heated (at 100°C) sensing film (2).

the sensitivity to humidity falls abruptly. Mass, 57–59, percent amount of CB in PVA matrix is an optimum for humidity sensing films.

Design of this humidity sensor has some joints we could distinguish as 'weak points' in the circuit of resistance measurement. Those are (see Fig. 1A):

- Construction allows direct interaction between electrodes, e.g., by reaching a dew point. Electrode material should be insulated using an inert coating. Chemical inactive CB coating is used for improvement the sensor's quality.
- CB grains in PVA bulk are scattered and insulated by the polymer. During the swelling process positions of CB grains changes in three-dimensional coordinates. Limiting this process in two-dimensional coordinates the sensitivity should be improved. To solve this problem is possible using composite sensing film with separated CB and PVA layers.
- Quality of adhesion between sensing film and substrate affects on the sensor's metrological parameters (Table 1). For better adhesion the sublayer of etched glass is used.

Taking into account these notes above design of humidity sensor has been changed (Fig. 1B). New one included composite two-layer humidity sensing film. Additionally a sublayer of etched glass and inert transition layer on the electrodes were formed. Metrological parameters of the sensor are given in Table 1. Response transient and calibration curve of this sensor are presented comparing with analogous data of other sensor in Fig. 2. It's evident, that precision and sensitivity are increased using two layer humidity sensors. Thus, the conclusion about correction direction in sensor's design optimization could be done.

Acknowledgements

The author wishes to express his gratitude for Lithuanian Innovation Center (LIC) for the financial support.

References

[1] N. Yamazone and Y. Shimizu, Sens. Actuators 10 (1986) 379.
[2] S. Chandra and A. Hashmi, Solid State Ionics, 40, 41 (1990) 460.
[3] G. Myioshi, T. Sugihara and M. Hajikigawa, Pat. USA, 4902571, 1990.
[4] N. Hiromichi, U. Yasuzo, N. Akiro and M. Shin-Ichiro, J. Mater. Sci. Lett., 8 (1989) 1278.
[5] D.Yu. Godovski, E.A. Koltypin, A.V. Volkov and M.A. Moskvina, Analyst, 118 (1993) 997.
[6] D.R. Burfield, G.T. Hefter and S.P. Koh, J. Chem. Technol. Biotechnol., 34 (1984) 187.
[7] V.Yu. Dubnitski and V.L. Chernyawski, Pat. USSR 4348618/24-25, 1989.
[8] N. Inagaki and K. Suzuki, Polym. Bull., 11 (1984) 541.
[9] K. Takahashi, T. Itagaki and T. Susai, Mater. Raifu, 3 (1991) 110.
[10] G. Brauer et al., Handbuch der präparativen anorganischen Chemie. B. 2, S. 670, F. Enke Verlag, Stuttgart, 1978.

[11] R.L. Davidson, Handbook of Water-Soluble Gums and Resins. P. 20, McGraw-Hill, New York, 1990.
[12] Kohlrausch Praktische Physik 1. S. 398, Teubner Verlag, Stuttgart, 1985.
[13] P. Profos et al., Handbuch der industriellen Messtechnik. 2. Aufl., S. 25. Vulkan-Verlag, Essen, 1984.

ELSEVIER

Talanta 44 (1997) 1113–1121

Talanta

The reaction of glutamic acid and trinitrobenzenesulfonic acid—kinetic study and analytical application

E.R. Kiranas, S.M. Tzouwara-Karayanni, M.I. Karayannis *

Department of Chemistry, University of Ioannia, 451 10 Ioannina, Greece

Received 12 April 1996; received in revised form 10 December 1996; accepted 11 December 1996

Abstract

Some kinetic aspects of the reaction of glutamic acid (GLU) and Trinitrobenzenesulfonic acid (TNBS) were studied spectrophotometrically (420 nm), under pseudo-first order reaction conditions. The effect of GLU, TNBS, SO_3^{2-} and H^+ had been investigated. Working curves for the initial rates IR versus [GLU] are linear in the range 7.5–30.0 mM. The regression equation is $IR = (8 \pm 8)E - 6 + (39 \pm 0.5) \cdot [GLU]$ and the correlation coefficient $r = 0.9998$. The limit of quantitation is 1.5 μM GLU and the relative standard deviation of the method 1.2%. The kinetics of the interfering TNBS hydrolysis reaction in alkaline range of pH, as well as the effect of sulfite concentration on the main reaction, are also presented. The analytical application of the reaction for the kinetic spectrophotometric assay of GLU and other aminoacids, as well as TNBS, is presented and the relevant advantages and disadvantages of the method are discussed. © 1997 Elsevier Science B.V.

Keywords: Glutamic acid; Kinetic study; Kinetic determination; Trinitrobenzenesulfonic acid

1. Introduction

K. Satake and his group [1,2] applied the reaction of Trinitrobenzenesulfonic acid (TNBS) with α- and β-aminoacids (AM), amines and proteins for their assay in different samples. The same investigator found that this reaction belongs to the category of the bimolecular reactions of aromatic nucleophilic substitution and takes place according to the following general scheme [3]:

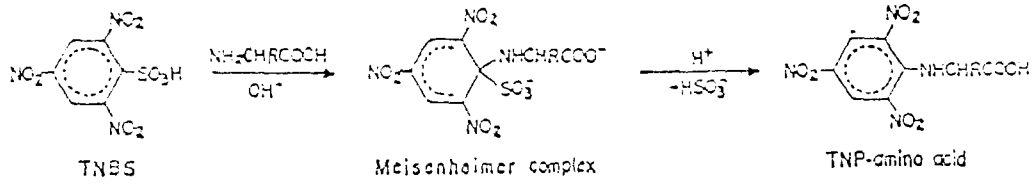

TNBS — Meisenheimer complex — TNP-amino acid

* Corresponding author.

PII S0039-9140(96)02205-9

Freedman and Radda [4] studied the rate of the reaction of TNBS and -SH, while Goldfard [5] the effect of SO_3^{2-} on the formation of its complex with the TNP-Am, at 420 nm.

R. Fields [6] made a detailed study of the reaction at 420 nm and observed the various factors affecting the value of the second order reaction rate constant k. Many investigators made use of this reaction: (i) for the spectrophotometric determination of aminoacids, amines, peptides, proteins and their mixtures [7–10]; (ii) for the measurement of the activity of enzymes [11]; (iii) for the inhibition of the activity of enzymes [12]; and (iv) for the construction and analytical applications of an ion selective electrode responding to trinitrobenzenesulfonic acid [13,14].

The use of a buffer of pH higher than 8.5 is necessary, because the reaction goes on the unprotonated aminogroup. All investigators who have so far used this reaction have observed, that at pH values over 10.0 the determination of the $-NH_2$ is problematic, because of side reactions mainly initiated by the hydrolysis of TNBS, itself.

In the present work we have studied the reaction of glutamic acid (GLU) and TNBS and its interfering hydrolysis of TNBS to picric acid.

2. Theoretical considerations

The reactions of TNBS with GLU as well as its alkaline hydrolysis to picric acid, are bimolecular (second order) aromatic nucleophilic substitutions. Both are taking place in two consecutive steps, the first of which is slow and reaction rate determining:

$$T + G \xrightarrow{k_1} MC1 \rightarrow P_1 \quad (1)$$

$$T + C \xrightarrow{k_2} MC2 \rightarrow P_2 \quad (2)$$

where T, G, C, MC, P_1 and P_2 stand for TNBS, GLU, OH^-, Meisenheimer complex, TNP-GLU and picric acid, respectively.

Under the conditions where T is in excess ($[T] \gg [G]$ and $[T] \gg [C]$) we have pseudo-first order reactions and the following equations are valid:

$$\frac{d[P_1]}{dt} = k_1[T][G] \quad (3)$$

$$\frac{d[P_2]}{dt} = k_2[T][C] \quad (4)$$

The absorbancies (A) of the reacting mixture are additive:

$$A_t = A_{p_1} + A_{p_2} = \epsilon_1 b P_1 + \epsilon_2 b P_2 \quad (5)$$

By differentiating Eq. (5) we receive:

$$\frac{dA_t}{dt} = \epsilon_1 b\left(\frac{dP_1}{dt}\right) + \epsilon_2 b\left(\frac{dP_2}{dt}\right) \quad (6)$$

and substituting Eq. (3) and Eq. (4) to Eq. (6) we finally receive:

$$\frac{dA_t}{dt} = \epsilon_1 b k_1[T][G] + \epsilon_2 b k_2[T][C]$$

or

$$\frac{dA_t}{dt} = k_{ob_1}[G] + k_{ob_2}[C] \quad (7)$$

where $k_{ob_1} = \epsilon_1 b k_1[T]$ and $k_{ob_2} = \epsilon_2 b k_2[T]$.In the above equations, [G] is the concentration of the unprotonated aminoacid, which can be determined from the dissociation constant k_2 of the aminoacid and the known $[H^+]$ using Eq. (8):

$$[G] = C_G \frac{k_2}{k_2 + [H^+]} = b C_G \quad (8)$$

where C_G is the analytical concentration of glutamic acid and the factor β represents the fraction of the unprotonated aminoacid.

The second order reaction rate constant k was calculated by dividing the observed rate constants, by the fraction of aminoacid with unprotonated aminogroup.

3. Materials and methods

3.1. Apparatus

Kinetic measurements for the reaction of GLU with TNBS were done with a filter spectrophotometer (Metrohm Model 662 Photometer) equipped with fiber optic for the transmission of the light and a 1 cm immersed-type optical cell.

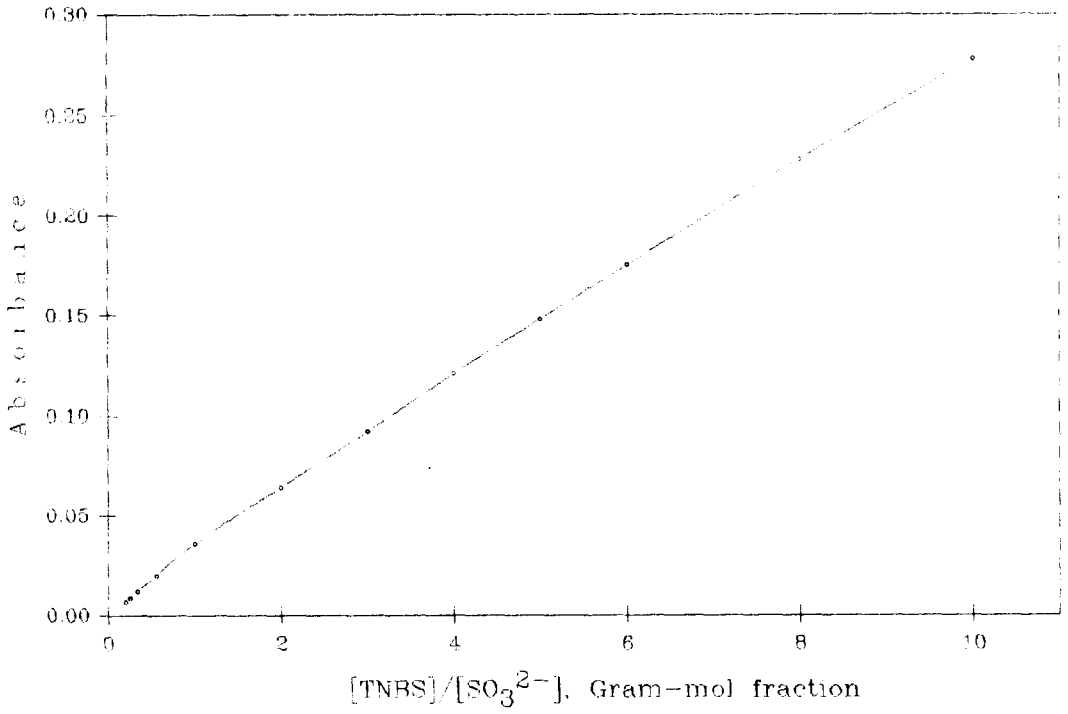

Fig. 1. Absorbance versus [TNBS]/[SO_3^{2-}] Gram-mol, fraction at pH 9.5 and $t = 25.0 \pm 0.1$°C, [SO_3^{2-}] = 1.0 mM.

The reaction cell was thermostatted at 25.0 ± 0.1°C. The measurements were carried out under stirring conditions with a mechanical stirrer (Radiometer TTA 80).

Spectra of the reagents and the products were taken with a double beam spectrophotometer (Perkin–Elmer Model Lambda 15).

A pH/pIon meter (Radiometer PHM 83) was used for pH measurements. Data acquisition was performed by an IBM data acquisition and control adaptor (Mendelson Electronics) and an IBM-compatible PC. Data collection and acquisition software was written in Microsoft Quick-BASIC. The program allows the collection of 2500 points, the plotting of the reaction curve $A_t = f(t)$, the determination of k_{ob} applying the infinite time method and the measurements of the slope $\delta A/\delta t$ in any point of the reaction curve.

4. Reagents

All the solutions were prepared in distilled water from p.a. grade reagents.

Buffers: the buffers used were 0.025 M $Na_2B_4O_7 \cdot 10H_2O$–0.1 M HCl for pH 8.5–9.0 and 0.025 M $Na_2B_4O_7 \cdot 10H_2O$–0.1 M NaOH for pH 9.5–11.0.

Na_2SO_3: a stock solution 0.4 M was prepared and stored at 4°C for 3 days.

GLU, TNBS and Picric Acid: aqueous stock solutions 0.004 M were prepared and stored at 4°C. For TNBS, fresh working solutions were prepared every 2 days.

4.1. Procedure

Borate buffer, 15.0 ml, 0.040 ml of sulfite stock 0.4 M solution and 0.100 ml of aminoacid work-

Table 1
Experimental results for the determination of the reaction rate constant k_1 at different pHs and sulphite

pH	$[SO_3^{2-}]$ mM	k_{ob} $s^{-1} \times 10^{-4}$	k_{ob2} $s^{-1} \times 10^{-4}$	k_{ob1} $s^{-1} \times 10^{-4}$	k_1 10^{-4} $M^{-1} \times s^{-1}$	$(\delta A/\delta t)_{in}$ A $s^{-1} \times 10^{-4}$
9.0	0.0	2.03	0.76	1.27	0.8	0.51
9.0	0.5	3.38	0.76	2.62	1.7	1.36
9.0	1.0	3.90	0.76	3.14	2.1	1.52
9.0	2.0	3.83	0.76	3.07	2.0	1.56
9.0	4.0	4.02	0.76	3.26	2.1	1.63
9.5	0.0	5.18	0.82	4.36	1.4	1.41
9.5	0.5	9.01	0.82	8.19	2.6	4.14
9.5	1.0	10.07	0.82	9.25	3.0	4.80
9.5	2.0	9.99	0.82	9.17	3.0	4.60
9.5	4.0	10.04	0.82	9.22	3.0	4.60
10.0	0.0	10.68	0.93	9.75	2.1	2.63
10.0	0.5	15.81	0.93	14.88	3.2	7.27
10.0	1.0	16.07	0.93	15.14	3.2	7.83
10.0	2.0	15.87	0.93	14.94	3.2	7.79
10.0	4.0	15.88	0.93	14.95	3.2	7.79

[TNBS] = 6.0×10^{-4} M, [GLU] = 1.2×10^{-5}, $t = 25 \pm 0.1$°C.

ing solution were pipetted in the reaction cell. The mixture was equilibrated at 25 ± 0.1°C, the wavelength set at 420 nm (except otherwise stated) and the transmittance adjusted to 100%. Then 0.100 ml of the TNBS working solution was rapidly injected in the reaction cell and the measuring system activated. The total measuring time and the interval between points were set accordingly. The reaction curve was plotted and the observed reaction constant k_{ob} and the initial reaction rate $(\delta A/\delta t)$ were calculated using the software.

For the study of hydrolysis of TNBS the same procedure was followed, except that GLU was omitted from the reaction cell. The observed reaction rate constant k_{ob} or other parameters were determined using the same software.

The reaction curve received by this procedure is the composite curve for both reactions leading to products P_1 and P_2 with k_{ob_1} and k_{ob_2}, respectively. The rate constant k_{ob} of the main reaction between TNBS, GLU and SO_3^{2-} may be calculated by the following equation:

$$k_{ob} = k_{ob_1} + k_{ob_2}$$

5. Results and discussion

5.1. Effect of sulfite concentration

By the addition of TNBS in a buffered solution of SO_2^{2-} a red product was formed very rapidly. Its absorption spectrum shows λ_{max} at 350 nm and absorptivities depending on the pH (Fig. 4, point A). This red product, already cited by previous investigators as a complex compound [5,6], is a meisenheimer like product of TNBS with SO_3^{2-}. An effort to determine its coordination number at pH 9.5, gave the results of Fig. 1. The almost linear dependence of its absorbance on the $[TNBS]/[SO_3^{2-}]$ ratio for a wide range of sulfite concentrations higher than 0.1 mM, denotes rather the formation of an equilibrium product. A small change of the slope in the range above 1 of $[TNBS]/[SO_3^{2-}]$ might mean the formation of a complex in a 1:1 ratio followed by the formation of a second equilibrium product with almost the same absorptivity.

The study of the effect of $[SO_3^{2-}]$ on the reaction rate constant of the main reaction between

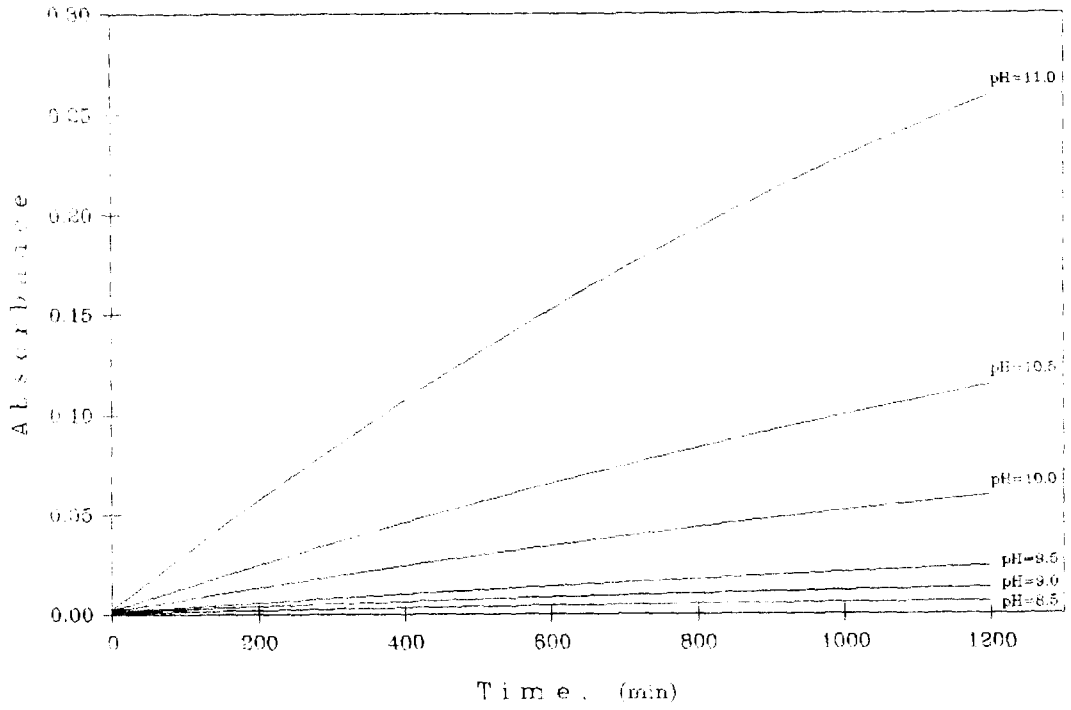

Fig. 2. Reaction curves, $A = f(t)$ for the reaction of hydrolysis of TNBS at different pHs. $\lambda = 420$ nm, $[SO_3^{2-}] = 1.0$ mM, [TNBS] = 0.73 mM, $t = 25.0 \pm 0.1$°C.

TNBS, GLU and SO_3^{2-}, shows that $[SO_3^{2-}]$ in the range 1.0–4.0 mM gives constant values for k_{ob}, k_{ob_1}, k_{ob_2} and initial rates $(\delta A/\delta t)_{in}$, as shown in Table 1.

5.2. Effect of TNBS hydrolysis to picric acid

The spectrum of picric acid shows maximum absorption at 360 nm and therefore contributes very little to the total absorption of the reaction mixture at 420 nm.

Fig. 2 shows the reaction curves (absorbance versus time) of the hydrolysis of TNBS at different pH values. The second order rate constant k_2 for the hydrolysis reaction of TNBS to picric acid at pH 9.5 was found to be $k_2 = 0.15$ s^{-1} M^{-1} (Fig. 3, Curve A), while $k_1 = 3.00$ s^{-1} M^{-1}. Therefore its interference with the main reaction seems to be significant only at pH values over 10.0, while at lower values it is negligible (Fig. 3). The big difference of molar absorptivities values between TNBS and picric acid at $\lambda = 420$ nm ($\epsilon_{TNBS} = 600$ cm^{-1} M^{-1} and $\epsilon_{p.ac.} = 7500$ cm^{-1} M^{-1}) and the increased contribution of the hydrolysis reaction at higher pHs might give a good explanation for the behaviour of the system, under these conditions.

5.3. The effect of pH

The pH of the reacting mixture TNBS-GLU-SO_3^{2-} affects the concentration of species participating in the reaction. It determines:

- The concentration of the unprotonated amino group ($K_2 = 3.39 \cdot 10^{-10}$ at pH 9.5).
- The addition of SO_3^{2-} on TNBS. TNBS is an electrophilic reagent and the degree of this substitution by SO_3^{2-} increases with pH ($K_{HSO_3^-} = 1.02 \cdot 10^{-7}$).
- The formation of the final coloured P_1, as shown in the proposed schemes of the reactions.
- The rate of hydrolysis of TNBS to picric acid at pH values higher than 10.0.

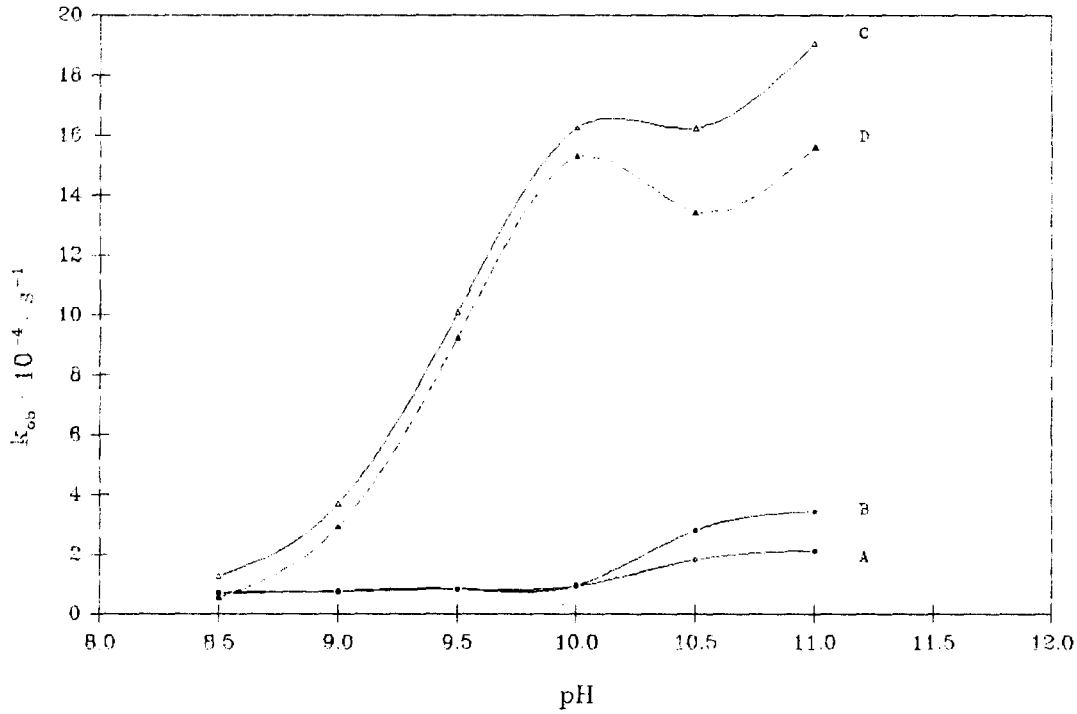

Fig. 3. Dependence of k_{ob}, k_{ob1}, k_{ob2} and k'_{ob} on the pH value at $t = 25.0 \pm 0.1$°C. Curve A: k'_{ob} for TNBS (0.6 mM) hydrolysis in the absence of SO_3^{2-}. Curve B: k_{ob2} for TNBS (0.6 mM) hydrolysis in the presence of SO_3^{2-} (1.0 mM). Curve C: experimental k_{ob}. [TNBS] = 0.6 mM, [GLU] = 0.01 mM, $[SO_3^{2-}] = 1.0$ mM. Curve D: k_{ob1} calculated after correction of k_{ob} ($k_{ob1} = k_{ob} - k_{ob2}$).

The reaction curves $A = f(t)$ for the reaction of GLU with TNBS at different pHs and $\lambda = 420$ nm, are shown in Fig. 4 (after point B). The reaction curves at $\lambda = 500$ nm show the same profiles. Our experimental results show that pH values in the range 9.5–10.0 ensure maximum value for the second order rate constant k_1, keeping the interference of the side reactions at negligible level. From our experimental results we are proposing the following sequences for the main and side reactions:

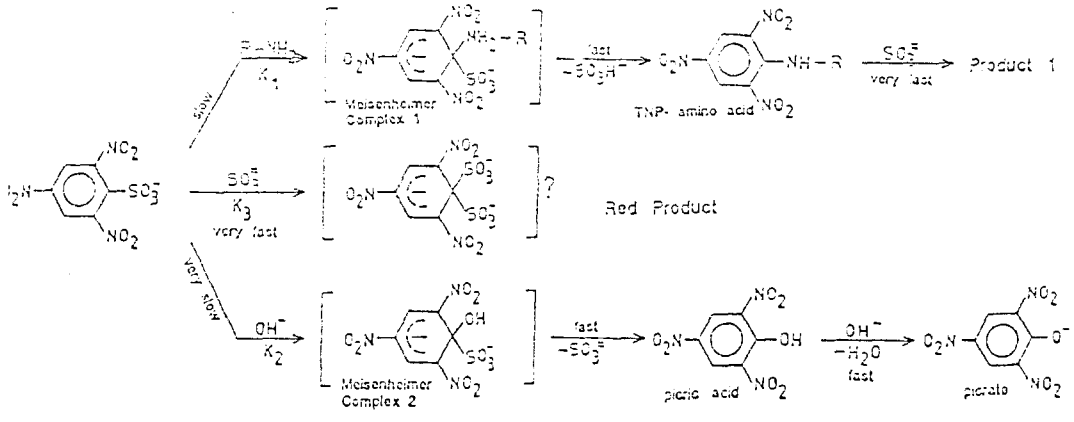

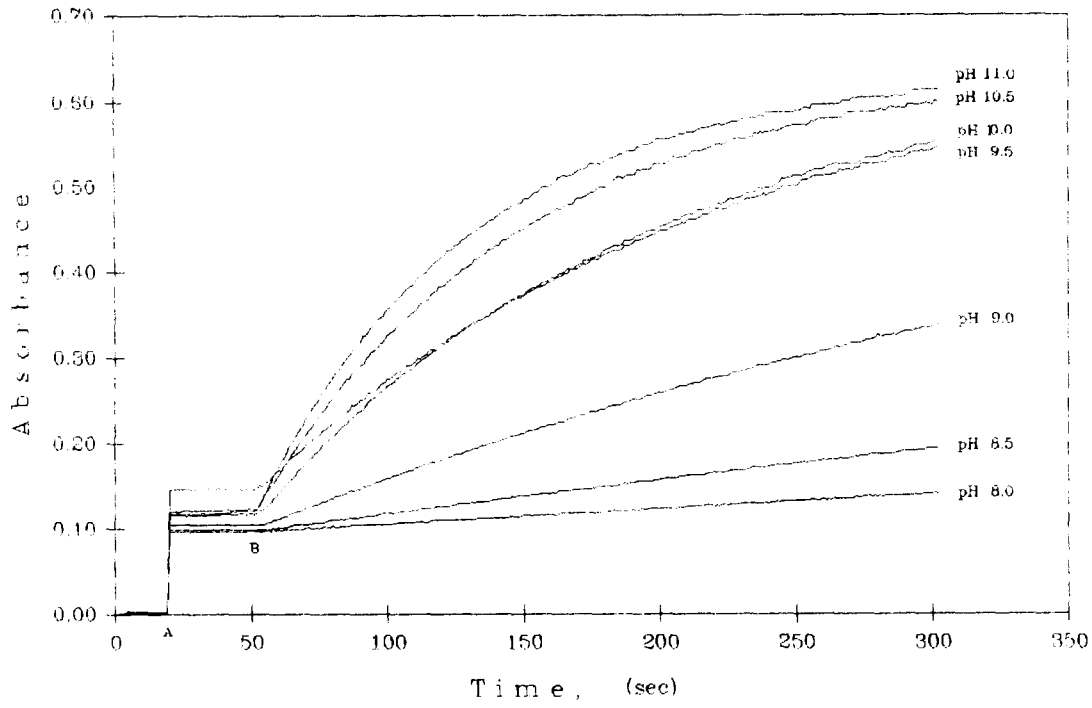

Fig. 4. Reaction curves, $A = f(t)$ for the main reaction between TNBS (4 mM) and GLU (0.066 mM) in the presence of SO_3^{2-} (1.0 mM), at different pH values. $\lambda = 25.0 \pm 0.1$°C. Point A: addition of TNBS in the reaction cell with the buffered sulfite solution. Point B: addition of GLU in the reaction cell with the buffered sulfite solution and TNBS.

5.4. Kinetic determination of GLU and TNBS

The effect of [GLU] or [TNBS] on the reaction rate was studied under pseudo-first order conditions and constant pH, $[SO_3^{2-}]$ and temperature. The results are presented in Table 2. The applicability of this procedure for the development of a reaction rate method for the determination of GLU, other aminoacids or TNBS in aqueous solutions, seems to have very good prospectives.

For [GLU] and [TNBS], in the range of 7.5–30 μM the working curves $(\delta A/\delta t)_{in} = f$[GLU] and $(\delta A/\delta t)_{in} = f$[TNBS] are linear, as shown in Fig. 5. The regression equations of the curves are:

$$(\delta A/\delta t)_{in} = (8 \pm 8)E-6 + (39 \pm 0.5)[\text{GLU}] \quad (9)$$

and

$$(\delta A/\delta t)_{in} = (7 \pm 6)E-6 + (36.7 \pm 0.4)[\text{TNBS}] \quad (10)$$

at pH = 9.5, $[SO_3^{2-}] = 1.0$ mM and $t = 25 \pm 0.1$°C. The correlation coefficient for both curves is $r = 0.9998$. Concentration of GLU and TNBS in Eq. (9) and Eq. (10) are applied in molar concentrations, M.

The accuracy of the method for both determinations is better than 1.5%. The limits of detection are 1.5 μM GLU and 1.2 μM TNBS. The method can be applied for the kinetic assay of many other amino acids in aqueous solutions, in combination with chromatographic separation. The kinetic method is more accurate, precise, sensitive, fast and therefore advantageous compared to the stoichiometric methods, because the initial rate is measured during the first 30–100 s after the injection of TNBS, where interference due to hydrolysis of TNBS is almost negligible. It can be also applied for the study of hydrolysis of various proteins and total of free aminoacids in mixtures. The method is not selective and cannot

Table 2
Experimental results for the determination of the rate constant k_1, for the reaction between Glutamic acid and Trinitrobenzenesulfonic acid ($\lambda = 420$ nm)

$M \times 10^{-4}$		k_{ob} $s^{-1} \times 10^{-4}$	k_{ob2} $s^{-1} \times 10^{-4}$	k_{ob1} $s^{-1} \times 10^{-4}$	$k_1 \times 10^{-4}$ $M^{-1} \times s^{-1}$	$(\delta A/\delta t)_{in}$ A $s^{-1} \times 10^{-4}$
[TNBS]	[GLU]					
6.00	0.075	10.04	0.82	9.22	3.0	2.92
6.00	0.100	9.97	0.82	9.15	3.0	4.10
6.00	0.120	10.02	0.82	9.21	3.0	4.75
6.00	0.150	10.02	0.82	9.20	3.0	5.92
6.00	0.300	9.95	0.82	9.13	3.0	11.77
0.075	6.00	9.50	0.047	9.45	3.0	2.81
0.100	6.00	9.46	0.047	9.41	3.0	3.78
0.120	6.00	9.49	0.047	9.44	3.0	4.40
0.150	6.00	9.49	0.047	9.44	3.0	5.65
0.300	6.00	9.55	0.047	9.50	3.1	11.08

$[SO_3^{2-}] = 1.0$ nM, pH = 9.5, $t = 25 \pm 0.1$°C.

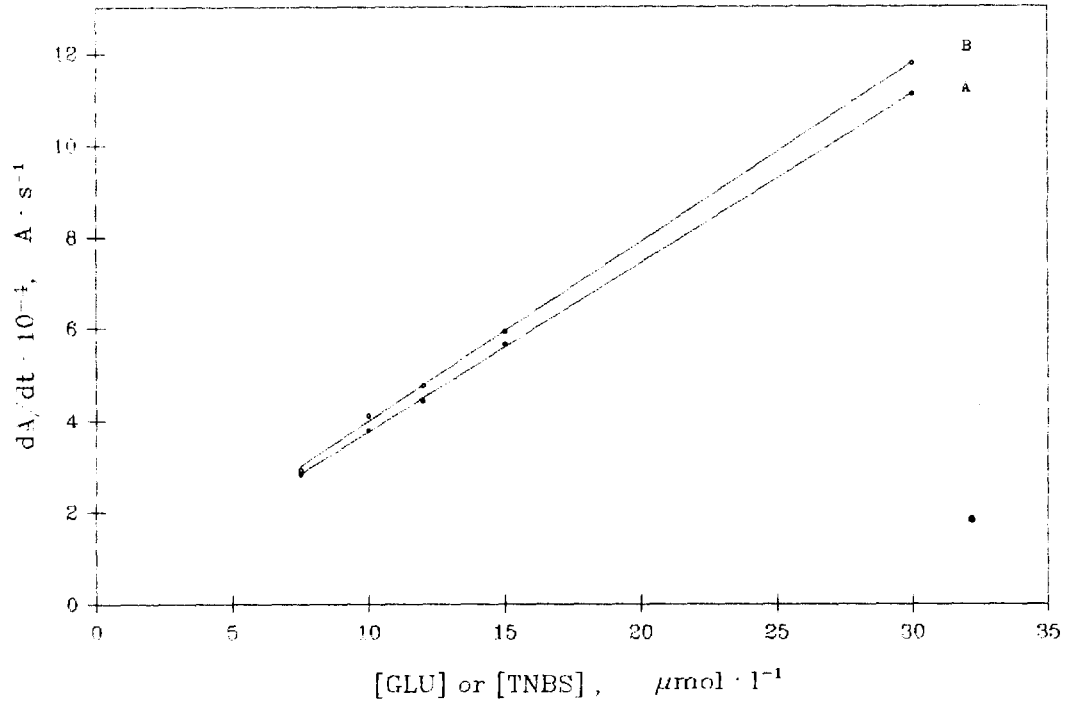

Fig. 5. Dependence of the initial rate on the concentration of GLU (curve A) or TNBS (curve B) at pH 9.5 and under pseudo-first order reaction conditions. [TNBS] or [GLU] = 0.6 mM, $[SO_3^{2-}] = 1.0$ mM.

differentiate the different aminoacids. It can be applied to samples which contain only one aminoacid. Since the reaction rate is almost the same for all aminoacids with one aminogroup [13] it can be applied for determination of total aminogroups of aminoacids.

References

[1] T. Okuyama and K. Satake, J. Biochem., 47 (4) (1960) 545–466.
[2] K. Satake, T. Okuyama, M. Ohashi and T. Shinoda, J. Bioch., 47 (5) (1960) 654–660.
[3] K. Satake, T. Tabe, A. Matsuo, K. Tazaki and Y. Hiraga, J. Biochem., 60 (1) (1966) 12–16.
[4] B.R. Freedman and K.G. Radda, Biochem. J., 108 (1968) 383–391.
[5] R.A. Goldfard, Biochemistry, 5 (8) (1966) 2570–2574.
[6] R. Field, Biochem. J., 124 (1974) 581–590.
[7] N.P. Evmiridis and M.I. Karayannis, Anal. Chim. Acta, 151 (1983) 211–219.
[8] F.J. Goodwin and S.Y. Choi, Clin. Chem., 16 (1970) 24–31.
[9] A.F.S.A. Habeeb, Anal. Biochem., 14 (1966) 328–336.
[10] C.L. Mokrasch, Anal. Biochem., 18 (1967) 64–71.
[11] A. Holm, Analyst, 105 (1980) 18–24.
[12] I. Flugge and H.W. Heldt, Bioch. Bioph. Res. Commun., 84 (1978) 37–44.
[13] E.G. Sarantonis and M.I. Karayannis, Anal. Biochem., 130 (1983) 177–184.
[14] G.E. Sarantonis, E.P. Diamantis and M.I. Karayannis, Anal. Biochem., 155 (1986) 129–134.

ELSEVIER

Talanta 44 (1997) 1123–1130

Talanta

Specific extraction behavior of amide derivative of calix[4]arene for silver (I) and gold (III) ions from highly acidic chloride media

Keisuke Ohto *, Hiroshi Yamaga, Emi Murakami, Katsutoshi Inoue

Department of Applied Chemistry, Faculty of Science and Engineering, Saga University, Honjo, Saga 840, Japan

Received 24 September 1996; received in revised form 3 January 1997; accepted 6 January 1997

Abstract

25,26,27,28-tetrakis(*N*,*N*-diethylaminocarbonylmethoxy)-5,11,17,23-tetrakis(1,1,3,3-tetramethylbutyl)calix[4]arene, a macrocyclic extraction reagent, and *p*-(1,1,3,3-tetra-methylbutyl)phenoxymethyl-*N*,*N*-diethylamide, an acyclic extraction reagent corresponding to the former one, were synthesized to investigate their extraction behavior for silver(I), gold(III), palladium(II), and platinum(IV) from highly acidic solution into chloroform. In the extraction of silver and gold from hydrochloric acid solution, a completely different extraction behavior was observed between these two types of the reagents. The extraction behavior was examined in detail for silver and was found to be dependent on whether silver ion was extracted as a cationic species or a anionic species complexed with chloride ion. This was supported by proton nuclear magnetic resonance study of the calix[4]arene derivative. As a result, the extraction of silver ion with calix[4]arene derivative was very peculiar which was attributable to the fitting between cyclic size of calix[4]arene and ionic radius of silver. © 1997 Elsevier Science B.V.

Keywords: Calixarene amide derivative; Chemical shift; Competition; Highly acidic chloride media; Silver ion; Solvent extraction

1. Introduction

Calixarenes and their derivatives have been attracting much attention as novel types of interesting host compounds [1–4]. Their recognition and discrimination ability for metal ions are one of the remarkable features as a specific receptor [5,6].

In the previous work, we synthesized 25,26,27,28-tetrakis(acetomethoxy)-5,11,17,23-tetrakis(1,1,3,3-tetramethylbutyl)calix[4]arene as a carbonyl compound to investigate the extraction behavior for silver (I) and palladium (II) from the highly acidic solution into chloroform. In nitrate media, the ketonic tetramer was found to selectively extract silver ion over palladium ion in the highly acidic region [7,8], suggesting, therefore, that carbonyl compounds are capable of extracting some metal ions from highly acidic solution.

* Corresponding author. Fax: +81 952 288591; e-mail: ultraman@ccs.ce.saga-u.ac.jp

PII S0039-9140(97)00019-2

Among carbonyl compounds, amide compounds have high dipole moment and tautomerize at high concentration of mineral acid [9–12]. Many authors have reported about the extraction of some metal ions with the amide compounds including diamide compound [10–29]. Recently, amides have been attracting much attention as good extractants for the recovery of actinides, in particular, which can alternate with tributylphosphate, a typical conventional extractant for actinides. The amide type derivatives of calixarenes have been also reported in relation to solvent extraction of some metal ions [30–33], though no paper have been reported on those from highly acidic solution.

In the present work, an amide type derivative of calix[4]arene have been synthesized to investigate the solvent extraction of some precious metal ions from acidic solution and compared with the extraction behavior of the corresponding monomeric amide.

2. Experimental

2.1. Reagent

The chemical structures of the extractants employed in the present work are shown in Fig. 1. Synthesis of carboxylate derivative of calix[4]arene ($\mathbf{2_4}$) was described in the previous paper [34]. The syntheses of the amide derivatives were carried out according to the similar manners with those of calixarene derivatives with *t*-butyl groups as alkyl radicals [35–37].

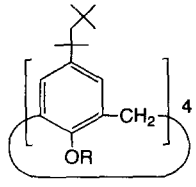

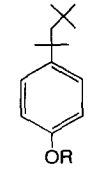

$\mathbf{1_4}$: R = CH_2CONEt_2 $\mathbf{1_1}$: R = CH_2CONEt_2

$\mathbf{2_4}$: R = CH_2COOH

Fig. 1. Chemical structures of the extractants.

25,26,27,28-tetrakis(*n*,*n*-diethylaminocarbonylmethoxy)-5,11,17,23- tetrakis(1,1,3,3-tetramethylbutyl)calix[4]arene (cone conformation) ($\mathbf{1_4}$)

Under a nitrogen stream, to 300 cm^3 of dry toluene were added carboxylate derivative $\mathbf{2_4}$ (15.67 g, 14.2 mmol) and thionylchloride (160 g, 1.34 mol). The solution was refluxed for 20 h. After cooling, the solvent was removed in vacuo. The residue was dissolved into 150 cm^3 of dry toluene and to the solution was carefully added diethylamine (16.5 g, 226 mmol) in 50 cm^3 of dry toluene in an ice bath. The mixture was stirred at 0°C for 2 h and at room temperature for 48 h. The solvent was removed in vacuo and to the residue was added 500 cm^3 of chloroform. The organic layer was washed three times with 1 $moldm^{-3}$ hydrochloric acid and with distilled water. After drying over anhydrous magnesium sulfate, filtration, and evaporation, to the residue was added acetone and distilled water to reprecipitate three times the desired compound. It was filtered to get white powder; 13.1 g (81%), m.p. 148°C, TLC(SiO_2, chloroform:methanol = 5:1 (v/v), $R_f = 0.91$); IR(KBr) $\nu_{C=O}$ 1664 cm^{-1}, $\nu_{C\text{-}N}$ 1434 cm^{-1}; ^{1}H-NMR (270MHz, $CDCl_3$, TMS, 27°C) δ 0.69 (36H,s,$C(CH_3)_3$), 1.09 (48H,m,$C(CH_3)_2 + (CH_2CH_3)_2$), 1.53 (8H,s,CCH_2C), 3.17 (4H,d,$ArCH_2Ar$(exo), J = 13.18 Hz), 3.31 (16H,m,$(CH_2CH_3)_2$), 5.00 (8H,s,OCH_2CO), 5.29 (4H,d,$ArCH_2Ar$(endo), J = 13.19 Hz), 6.74 (8H,s,ArH).

p-(1,1,3,3-tetramethylbutyl)

phenoxymethyl-*N*,*N*-diethylamide ($\mathbf{1_1}$)

N,*N*-Diethylchloroacetoamide was synthesized from chloroacetyl chloride and *N*,*N*-diethyl amine in toluene according to the paper reported by Cope and Ciganek [38].

Under a nitrogen stream, to 600 cm^3 of dry acetone were added sodium iodide (5.25 g, 35 mmol) *N*,*N*-diethylchloroacetoamide (10.47 g, 70 mmol), *p*-(1,1,3,3-tetramethylbutyl)phenol (10.32 g, 50 mmol), and potassium carbonate (13.82 g, 100 mmol) to reflux for 8 days. After cooling, the solvent was removed in vacuo. To the residue was added 400 cm^3 of chloroform to extract the desired compound. The organic layer was washed twice with 1 mol dm^{-3} hydrochloric acid and

three times with distilled water. After drying over anhydrous magnesium sulfate, filtration, and evaporation, to the residue was distilled in vacuo as pale yellow liquid; 12.35 g (77%), TLC(SiO_2, chloroform, $R_f = 0.73$); IR(neat) $\nu_{C=O}$ 1651 cm^{-1}, ν_{C-N} 1436 cm^{-1}; 1H-NMR (270 MHz, $CDCl_3$, TMS, 20°C) δ 0.70 (9H,s,$C(CH_3)_3$), 1.16(6H,m,$(CH_2CH_3)_2$), 1.33(6H,s,$C(CH_3)_2$), 1.69 (2H,s,CCH_2C), 3.39 (4H,s,$(CH_2CH_3)_2$)), 4.64 (2H,s,OCH_2CO), 6.86 (2H,d,O-ArH), 7.27 (2H,d,C-ArH).

2.2. Distribution equilibria

An organic solution was prepared by diluting each extractant into an analytical grade of chloroform to a desired concentration. An aqueous solution was prepared by dissolving metal salts to a desired concentration into aqueous hydrochloric acid or nitric acid solution. Chloroauric acid was employed as a gold salt. Equal volumes (10 cm^3) of both phases were mixed and vigorously shaken at 30°C for more than 48 h, which was sufficient enough to attain equilibrium in a preliminary experiment. After phase separation, the concentration of proton in the aqueous phase was determined by neutralization titration with sodium hydroxide aqueous solution using phenolphthalein as an indicator or by using a pH meter (Beckman, ϕ-45). Concentrations of metal ions were measured by atomic absorption spectrometer (Seiko Instruments, SAS-7500) and inductively coupled plasma atomic emission spectrophotometer (Shimadzu, ICPS-2000). The amount of extracted metal ions were calculated from the differences of the metal concentrations in the aqueous phase between before and after the extraction.

2.3. Proton nuclear magnetic resonance study

An organic sample solution was prepared by dissolving 1_4 into an analytical grade of deuterium chloroform to a desired concentration. An aqueous solution was prepared by dissolving silver nitrate or sodium nitrate into an analytical grade of deuterium oxide or distilled water. The initial concentration of sodium and silver were appropriately adjusted. Both phases were mixed and vigorously shaken at 30°C for more than 48 h. After phase separation, the peaks of $\mathbf{1_4}$ in the organic phase were measured by proton nuclear magnetic resonance spectrometer (Jeol, JNM-GX270).

3. Results and discussion

3.1. Distribution equilibria in the extraction from nitrate media

The effects of the concentration of nitric acid on percentage extraction of gold(III), silver(I), palladium(II) and platinum(IV) with $\mathbf{1_4}$ and $\mathbf{1_1}$ are shown in Fig. 2a and b, respectively. With $\mathbf{1_4}$, gold was quantitatively extracted over the whole concentration region of nitric acid except for at 10 mol dm^{-3} where the extraction decreased to 80%. The percentage extraction of silver was about 80% over the whole concentration region, though it reached about 100% at 10 $moldm^{-3}$. Palladium was extracted to the extent of only about 15% in the concentration region less than 4 $moldm^{-3}$ while it abruptly increased up to 100% in the region greater than 4 $moldm^{-3}$. The extraction of platinum was not observed in the concentration region greater than 0.1 $moldm^{-3}$. On the other hand, in the extraction with $\mathbf{1_1}$, the plots of the % extraction for gold appear to lie on a convex curve having a maximum of 68% at 1 $moldm^{-3}$, while the plots for silver appear to lie on concave curve having a minimum of 21% at 0.5 $moldm^{-3}$. Palladium was hardly extracted over the whole region. The extraction of platinum with $\mathbf{1_1}$ was similar to that with $\mathbf{1_4}$. As described above, the percentage extractions of all kinds of metal ions examined with $\mathbf{1_1}$ was much lower than those with $\mathbf{1_4}$, except for platinum. The higher extraction ability of $\mathbf{1_4}$ may be considered to be attributable to the following factors: size matching between the ring size of calix[4]arene and the ionic diameters of metal ions, aggregation of functional groups based on cone conformation.

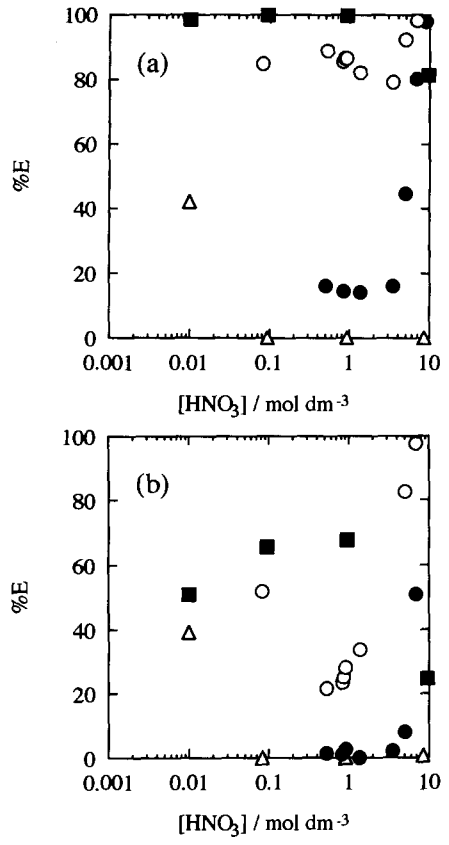

Fig. 2. Effect of the concentration of nitric acid on percent extraction. (a) $\mathbf{1}_4$; (b) $\mathbf{1}_1$; ■, gold; ○, silver; ●, palladium; △, platinum, $[\mathbf{1}_4] = 3.3 \times 10^{-3}$ moldm^{-3}, $[\mathbf{1}_1] = 1.33 \times 10^{-2}$ moldm^{-3}, $[Au^{3+}] = [Ag^{+}] = [Pd^{2+}] = [Pt^{4+}] = 1.0 \times 10^{-4}$ moldm^{-3}.

3.2. Distribution equilibrium in chloride media

The effects of hydrochloric acid concentration on percentage extraction of precious metals with $\mathbf{1}_4$ and $\mathbf{1}_1$ are shown in Fig. 3a and b, respectively. In the extraction of silver, since great majority was precipitated in the hydrochloric acid concentration region less than 3 moldm^{-3}, lithium chloride was added so as to maintain the total chloride concentration constant at 3 moldm^{-3} in the region of hydrochloric acid less than 3 moldm^{-3} to prevent the formation of the precipitate. In nitrate media, although the large difference in the extraction ability was observed between monomeric and tetrameric extractants, the order of selectivity for precious metals was the same between these two regents. In chloride media, however, the drastic change in the extraction of gold and silver ions was observed between $\mathbf{1}_4$ and $\mathbf{1}_1$. The tetrameric $\mathbf{1}_4$ can quantitatively extract gold, while the monomeric $\mathbf{1}_1$ scarcely extract gold over the whole concentration region of hydrochloric acid except for 10 moldm^{-3}, where gold was quantitatively extracted. Concerned with silver, although the percentage extraction with the tetramer is constant in the hydrogen ion concentration region less than 3 moldm^{-3} since total chloride ion concentration is maintained constant at 3 moldm^{-3}, it decreases with the increase of chloride concentration in the region greater than 3 moldm^{-3}, attributable to the suppression of ex-

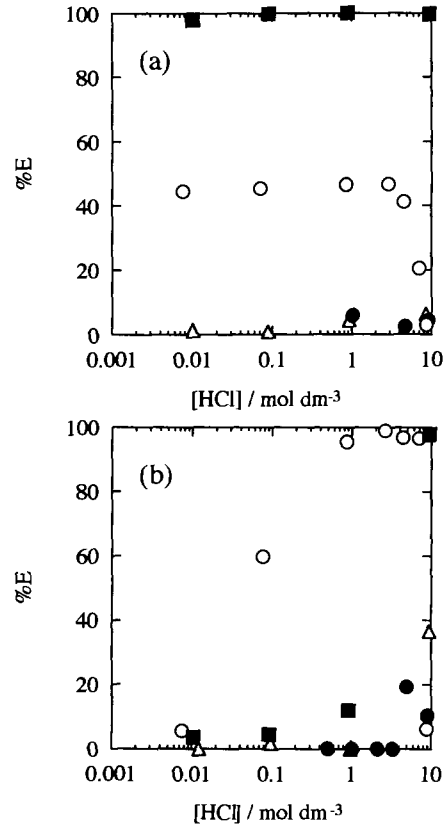

Fig. 3. Effect of the concentration of hydrochloric acid on percent extraction. (a) $\mathbf{1}_4$; (b) $\mathbf{1}_1$; ■, gold; ○, silver; ●, palladium; △, platinum; $[\mathbf{1}_4] = 3.3 \times 10^{-3}$ moldm^{-3}; $[\mathbf{1}_1] = 1.33 \times 10^{-2}$ moldm^{-3}; $[Au^{3+}] = [Ag^{+}] = [Pd^{2+}] = [Pt^{4+}] = 1.0 \times 10^{-4}$ moldm^{-3}.

traction due to the complexation of silver ion with chloride anions. Contrarily, the % extraction of silver with the monomeric analog increases with the increase of proton concentration, and attains to 100% extraction in the concentration region greater than 1 moldm^{-3}, though it abruptly and drastically decreases to nearly 0% at 10 moldm^{-3}. This extraction behavior is similar to the extraction of anionic metal complexes with protonated extractant such as high-molecular-weight amines, suggesting that the monomeric analog extracts silver as anionic species.

In order to clarify the extremely different extraction behavior between these two extractants, further experiment was carried out for silver ion in particular. The effect of the concentration of proton on percentage extraction of silver ion with $\mathbf{1}_4$ and $\mathbf{1}_1$ was compared in Fig. 4a and b, respectively. As described above, since the precipitate was formed in the concentration region of hydrochloric acid below 3 moldm^{-3}, lithium chloride was added so as to keep the chloride concentrations constant at 5 and 3 moldm^{-3} in the experiment of Fig. 4a and b, respectively. In the chloride concentration region above 5 or 3 moldm^{-3}, hydrochloric acid was added to increase proton and chloride concentration as in the previous case. The decrease of the added amount of chloride ion from 5 to 3 moldm^{-3} increases the percentage extraction of silver ion with $\mathbf{1}_4$, while only slightly decreased with $\mathbf{1}_1$, indicating the opposite extraction behavior between $\mathbf{1}_4$ and $\mathbf{1}_1$. As mentioned earlier, the difference in the extraction behavior is attributable to the difference in the species of silver extracted with each extractant. That is, since the calix[4]arene derivative $\mathbf{1}_4$ is suggested to extract silver ion as cationic species, the extraction is suppressed by the complexation of silver ion with chloride ion to form anionic species with the increase of chloride concentration. On the other hand, since the monomeric derivative $\mathbf{1}_1$ is considered to extract metals as anionic species, the percent extraction increases with the increase of chloride concentration in low acidic region, and it also increases with the increase of the concentration of the protonated extractant in highly acidic region. This result shows that the difference of the silver species

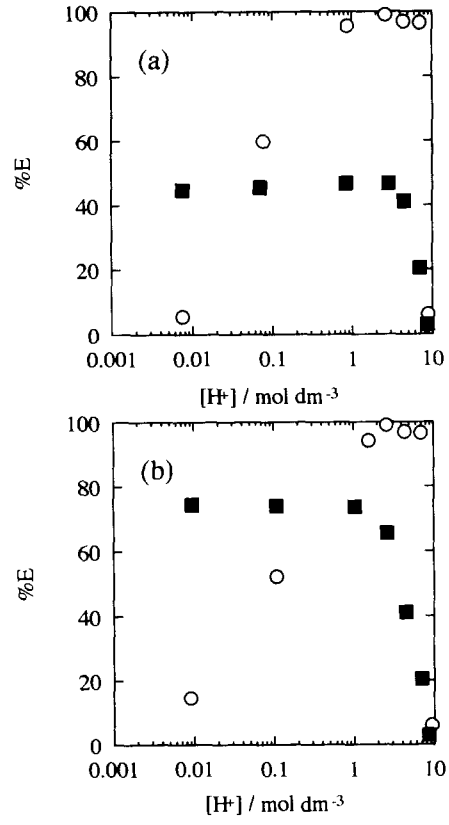

Fig. 4. Effect of the concentration of proton on percent extraction of silver ion with $\mathbf{1}_4$ and $\mathbf{1}_1$. (a) 5 moldm^{-3} of chloride ion and (b) 3 moldm^{-3} of chloride ion in the low hydrochloric acid concentration ■, $\mathbf{1}_4$; ○, $\mathbf{1}_1$; $[\mathbf{2}_4] = 3.3 \times 10^{-3}$ moldm^{-3}; $[\mathbf{2}_1] = 1.33 \times 10^{-2}$ moldm^{-3}; $[Ag^+] = 1.0 \times 10^{-4}$ moldm^{-3}.

extracted depends on whether the structure of the extractant is cyclic or acyclic and on the fitting between cyclic size and ionic radius in the case of cyclic compound.

The extraction of gold (III) ion with the amide extractants $\mathbf{1}_4$ and $\mathbf{1}_1$ shown in Fig. 3a and b seems to exhibit more significant difference of the metal species extracted. That is, the calix[4]arene derivative $\mathbf{1}_4$ and the monomeric derivative $\mathbf{1}_1$ are considered to extract gold as cationic and anionic species, respectively, similarly to the extraction of silver. However, different from the extraction of silver, the extraction of gold with the calix[4]arene derivative $\mathbf{1}_4$ is hardly suppressed by the complexation of gold ion with chloride ion due to the

strong affinity of gold ion with $\mathbf{1}_4$. The extraction of gold with the monomeric derivative $\mathbf{1}_1$ is very poor in the region of hydrochloric acid concentration less than 1 moldm^{-3}, while quantitatively extraction was observed at 10 moldm^{-3}. Thus, gold was suggested to be easily extracted as cationic species and to be scarcely extracted as anionic species less than 1 moldm^{-3} with $\mathbf{1}_4$ not with $\mathbf{1}_1$, and was extracted as anionic species at 10 moldm^{-3} with $\mathbf{1}_1$.

3.3. Dependency of the extraction of silver ion on the extractant concentration

The effect of the extractant concentration on the extraction of silver ion was examined for the purpose of clarifying the stoichiometry of the extracted complex as shown in Fig. 5. The plots for $\mathbf{1}_4$ appear to lie on a straight line with the slope of 1, while those for $\mathbf{1}_1$ appear to lie on a straight line with the slope of 2, suggesting the numbers of the molecules of the reagent species which takes part in the extraction of the silver ion to be 1 and 2 for $\mathbf{1}_4$ and $\mathbf{1}_1$, respectively.

3.4. Proton nuclear magnetic resonance study for the complex of 1_4 and silver ion

As the amide $\mathbf{1}_4$ effectively extracted silver ion as well as the tetrameric ketonic derivative [7,8],

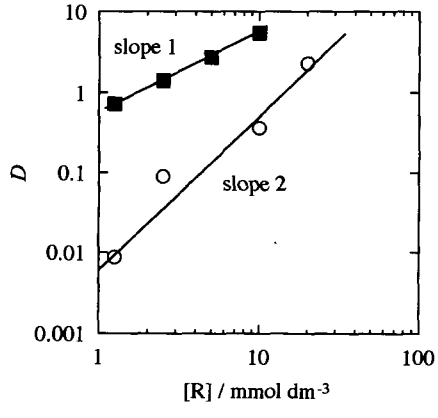

Fig. 5. Effect of the extractant concentration on percent extraction of silver ion with $\mathbf{1}_4$ and $\mathbf{1}_1$. ■, $\mathbf{1}_4$; ○, $\mathbf{1}_1$; [HCl] = 1 moldm^{-3}; [Ag$^+$] = 1.0×10^{-4} moldm^{-3}.

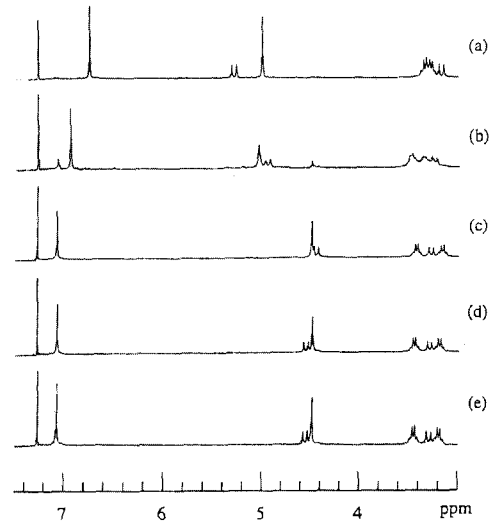

Fig. 6. Partial proton nuclear resonance spectra of $\mathbf{1}_4$. [$\mathbf{1}_4$] = 2.0×10^{-3} moldm^{-3}; $D_2O/CDCl_3$ = (1 cm^3/1.6 cm^3); (a) original, contacting with; (b) 5 moldm^{-3} hydrochloric acid solution; (c) 0.4 moldm^{-3} sodium ion in 1 moldm^{-3} hydrochloric acid solution; (d) 0.16 moldm^{-3} silver ion in 5 moldm^{-3} nitric acid solution; (e) 0.08 moldm^{-3} silver ion in deuterium oxide.

the participation of carbonyl groups in the extraction reaction should be taken into consideration. However, the extraction behavior of the monomeric derivative suggested the participation of the protonated form of the extractant in the extraction reaction in highly acidic region. In order to clarify the participation of the carbonyl groups and the protonation of the $\mathbf{1}_4$, the proton nuclear magnetic resonance study was also conducted. The partial proton nuclear magnetic resonance spectra of $\mathbf{1}_4$ was shown in Fig. 6. The chemical shifts for the peaks of $\mathbf{1}_4$ was observed in the sample prepared by only contacting with hydrochloric acid solution, suggesting the protonation of $\mathbf{1}_4$, since, as is well-known, amide compounds are protonated at carbonyl oxygens in highly acidic region. The addition of silver ion caused further chemical shifts of $\mathbf{1}_4$ through the extraction. The addition of sodium ion also caused similar shifts. However, the shifted peaks of ketonic derivative which extracted silver ion

appeared at approximately the same position as those which extracted sodium ion, whereas the position of the shifted peaks of amide derivative which coordinated silver ion was partially different from that which coordinated sodium ion. Therefore, it can be considered that the coordination of silver and sodium ions takes place at same sites with the ketonic derivative, while it takes place at slightly different sites with the amide $\mathbf{1}_4$. Since the peaks assigned to aryl proton were hardly shifted, the difference between the ketonic and amide extractants was considered to be attributable to that of the participation of carbonyl groups of amide compound and ketonic compounds to the coordination to metal ions; but, further detailed investigation should be conducted on this respect.

3.5. Extraction mechanism of silver

According to the above-mentioned experimental results, the extraction reactions of silver (I) were inferred to be expressed as follows; For $\mathbf{1}_4$,

$$H_4R^{4+}4Cl^- + AgCl_3^{2-} = RAg^+Cl^- + 6Cl^- + 4H^+ \quad (1)$$

,and for $\mathbf{1}_1$

$$2(HR^+Cl^-) + AgCl_3^{2-} = (HR)_2^+AgCl_3^{2-} + 2Cl^-. \quad (2)$$

where $H_4R^{4+}4Cl^-$ and HR^+Cl^- denote the protonated $\mathbf{1}_4$ and $\mathbf{1}_1$, respectively. Since the protonation of the extractant 1_4 was supported by the proton nuclear magnetic resonance study as described above, the extraction of silver ion with calixarene derivative is suppressed not only with the increase of the proton concentration but also with that of the chloride concentration.

The proposal structures of the complexes of silver ions formed with the extractants $\mathbf{1}_4$ and $\mathbf{1}_1$ are shown in Fig. 7a and b. The ionic diameter of silver (I) is about 1.94Å which fits for the ring size of calix[4]arene. However, the diameters of the chloride complexes of silver are much greater than that of the cationic species and no longer fits for the size of the calix[4]arene. Thus, the remarkably great difference of the specific extraction behavior between monomeric and tetrameric derivatives was suggested to be attributable to the fact that calix[4]arene derivative can extract silver ion only as a cationic species.

Acknowledgements

The authors are grateful to Saga Ceramics Research Laboratory for measurement of the concentrations of metals by using inductively coupled plasma atomic emission spectrometer. This work was financially supported in part by a Grant-in-Aid for Scientific Research No. 08875162 from Ministry of Education, Science and Culture, Japan.

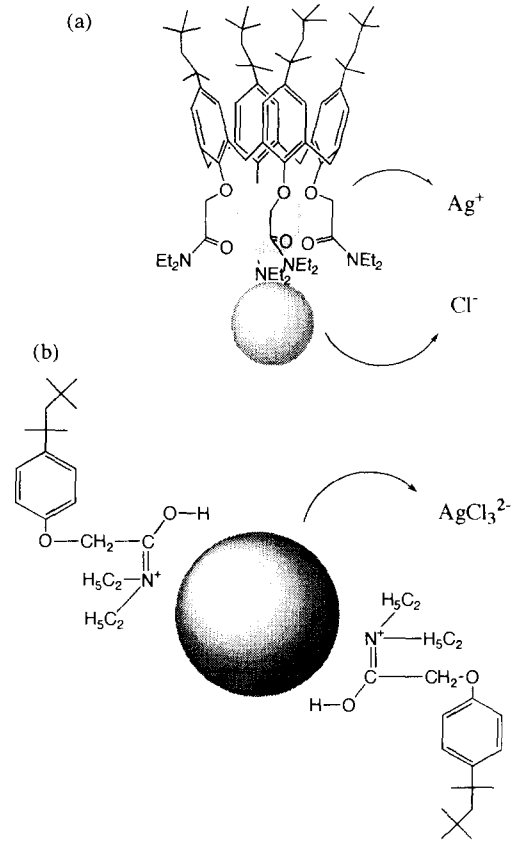

Fig. 7. Proposal structures of complex formed of silver ion with $\mathbf{1}_4$ and $\mathbf{1}_1$. (a) $\mathbf{1}_4$; (b) $\mathbf{1}_1$.

References

[1] C.D. Gutsche, 'Calixarenes', Royal Society of Chemistry, Cambridge, 1989.
[2] J. Vicens and V. Bohmer, 'Calixarenes: A Versatile Class of Macrocyclic Compounds', Kluwer Academic, Dordrecht, 1992.
[3] S. Shinkai, Tetrahedron, 49 (1993) 8933.
[4] V. Bohmer, Angew. Chem. Int. Ed. Engl., 34 (1995) 713.
[5] R. Ludwig, JAERI-Review 95–022, (1995) 1.
[6] D.M. Roundhill, Progr. Inorg. Chem., 43 (1995) 533.
[7] K. Ohto, E. Murakami, K. Shiratsuchi, K. Inoue and M. Iwasaki, Chem. Lett., (1996) 173.
[8] K. Ohto, E. Murakami, T. Shinohara, K. Shiratsuchi, K. Inoue and M. Iwasaki, Anal. Chim. Acta, in press, 1997.
[9] B.N. Laskorin, V.V. Yakshin, E.A. Filippov, G.M. Chumakova, V.A. Belov and G.G. Arkhipova, Radiokhimiya, 20 (1978) 511.
[10] Z. Taili, Z. Xiang, M. Rongjun, H. Zhuoshu, Q. Ming and Z. Zhonghua, Hydrometallurgy, 8 (1982) 379.
[11] H. Stephan, K. Gloe, J. Bager and P. Muhl, Solv. Extr. Ion Exch., 9 (1991) 435.
[12] N. Condamines and C. Musikas, Solv. Extr. Ion Exch., 10 (1992) 69.
[13] M.M. Kopechi and D.M. Petkovic, Solv. Extr. Ion Exch., 4 (1986) 435.
[14] M.C. Charbonnel and C. Musikas, Proceedings of Symposium on Solvent Extraction 1986, München, September 1986, Vol. 1, p. 261.
[15] H. Ohmori, J. Shibata, M. Sano and S. Nishimura, Solv. Extr. Ion Exch., 5 (1987) 227.
[16] C. Musikas and H. Hubert, Solv. Extr. Ion Exch., 5 (1987) 877.
[17] M.R. Tanasheva, Proceedings of Symposium on Solvent Extraction 1988, Moscow, July 1988, Vol. 1, p. 244.
[18] C. Cuillerdier, H. Hubert, P. Hoel and C. Musikas, Proceedings of Symposium on Solvent Extraction 1988, Moscow, July 1988, Vol. 1, p. 291.
[19] D.I. Skorovarov, G.M. Chumakova, L.I. Rusin, V.S. Uljanov, R.A.Sviridova and A.N.Sviridov, Proceedings of Symposium on Solvent Extraction 1988, Moscow, July 1988, Vol. 1, p. 287.
[20] G. Thiollet and C. Musikas, Solv. Extr. Ion Exch., 7 (1989) 813.
[21] H. Stephan, K. Gloe, J. Beger and P. Muhl, Solv. Extr. Ion Exch., 9 (1989) 459.
[22] C. Cuillerdier, C. Musikas, P. Hoel, L. Nigond and X. Vitart, Sep. Sci. Tech., 26 (1991) 1229.
[23] N. Condamines and C. Musikas, Solv. Extr. Ion Exch., 10 (1992) 69.
[24] Q. Tian and M.A. Hughes, Proceedings of Symposium on Solvent Extraction 1993, York, September 1993, Vol. 1, p. 404.
[25] J.S. Preston and A.C. Du Preez, Proceedings of Symposium on Solvent Extraction 1993, York, September 1993, Vol. 3, p. 1295.
[26] B. Bao, C. Shen, G. Wang and J. Qian, Proceedings of Symposium on Solvent Extraction 1993, York, September 1993, Vol. 1, p. 1821.
[27] C. Cuillerdier, C. Musikas and L. Nigond, Sep. Sci. Tech., 28 (1993) 155.
[28] S. Tachimori and S. Suzuki, Proceeding of Global '95, 2 (1995) 1171.
[29] Y. Suzuki and G.R. Choppin, Anal. Sci., 12 (1996) 225.
[30] F.A. Neu, E.M. Collins, M. Deasy, G. Ferguson, S.J. Harris, B. Kaitner, A.J. Lough, M.A. Mckervey, E. Marques, B.L. Ruhl, M.J.S. Weill and E.M. Seward, J. Am. Chem. Soc., 111 (1989) 8681.
[31] S.K. Chang and I. Cho, Chem. Lett., (1987) 947.
[32] F.A. Neu, M.J.S. Weill, K. Ziat, S. Cremin, S.J. Harris and M.A. Mckervey, New J. Chem., 15 (1991) 13.
[33] F.A. Neu, L. Guerra, W. McGregor, K. Ziat, M.J.S. Weill, G. Barrett, M.A. Mckervey, D. Marrs and E.M. Seward, J. Chem. Soc., Perkin Trans. 2, (1995) 113.
[34] K. Ohto, M. Yano, K. Inoue, T. Yamamoto, M. Goto, F. Nakashio, S. Shinkai and T. Nagasaki, Anal. Sci., 11 (1995) 893.
[35] A. Arduini, A. Pochini, S. Reveberi, R. Ungaro, G.D. Andreetti and F. Ugozzoli, J. Incl. Phenom., 6 (1988) 119.
[36] F.A. Neu, M.J. Schwing, K. Ziat, S. Cremin, S.J. Harris and M.A. McKervey, New. J. Chem., 15 (1991) 33.
[37] F.A. Neu, G. Barrett, S. Cremin, M. Deasy, G. Ferguson, S.J. Harris, A.J. Lough, L. Guerra, M.A. McKervey, M.J. Schwing-Weill and P. Schwinte, J. Chem. Soc., Perkin Trans. 2, (1995) 113.
[38] A.C. Cope and E. Ciganek, Org. Synth., 4 (1969) 339.

ELSEVIER

Talanta 44 (1997) 1131–1135

Talanta

Lead-selective poly(vinyl chloride) membrane electrodes based on acyclic dibenzopolyether diamides

Akira Ohki [a,*], Jong Seung Kim [b], Yoshihiro Suzuki [a], Takashi Hayashita [c], Shigeru Maeda [a]

[a] *Department of Applied Chemistry and Chemical Engineering, Faculty of Engineering, Kagoshima University, 1-21-40 Korimoto, Kagoshima 890, Japan*

[b] *Department of Chemistry, Konyang University, Nonsan, 320-800, South Korea*

[c] *Department of Chemistry, Saga University, 1 Honjo, Saga 840, Japan*

Received 20 June 1996; received in revised form 23 August 1996; accepted 30 December 1996

Abstract

Lipophilic acyclic dibenzopolyether diamides, 12 kinds, have been designed to prepare solvent polymeric membrane ion-selective electrodes (ISEs) for Pb^{2+}. The ionophores include 1,5-bis[2-(*N*,*N*-dialkylcarbamoylmethoxy)phenoxy]-3-oxapentanes **1**–**4**, 1,5-bis[2-(*N*,*N*-dialkylcarbamoylpentadecyloxy)phenoxy]-3-oxapentanes **5**–**8**, and 1,2-bis[2-(2′-*N*,*N*-dialkylcarbamoylpentadecyloxy)phenoxy]ethanes **9**–**12**. Linear response concentration range of the ISE based on **9** is $3 \times 10^{-2} - 1 \times 10^{-6}$ M of Pb^{2+} (average slope = 28.5 mV decade^{-1}). Potentiometric selectivities of the ISEs based on **1**–**12** for Pb^{2+} over other heavy metal cations, alkali metal cations, and alkaline earth metal cations have been assessed. These ISEs exhibit remarkably high selectivities for Pb^{2+} relative to heavy metal cations, such as Cu^{2+}, Fe^{2+}, and Ni^{2+}, the selectivity coefficients ($K^{Pot}_{Pb,Cu}$) being $5 \times 10^{-5} - 6 \times 10^{-5}$ for **1**–**4** and ca. 6×10^{-4} for **9**. For the Pb^{2+} selectivities over alkali metal cations, such as Na^+ and K^+, **9** which has an ethylene glycol spacer and a *N*,*N*-diethyl group is superior to other dibenzopolyether diamide ionophores **1**–**8** and **10**–**12**. © 1997 Elsevier Science B.V.

Keywords: Acyclic dibenzopolyether diamides; Electrode; Lead-selective ionophore; Poly(vinyl chloride) membrane

1. Introduction

Much effort has been placed on the development of ion-selective electrodes (ISEs) for various metal cations. However, relatively a little attention has been paid to development of Pb^{2+}-selective electrodes [1]. Several solid-state Pb^{2+}-ISEs based on PbS/Ag_2S have been reported [2–8]. However, the presence of some heavy metal cations, such as Cu^{2+} and Fe^{2+}, greatly interfered with the measurement of Pb^{2+} by the solid-state ISEs.

Some polymeric membrane ISEs based on neutral carriers for Pb^{2+} have been developed. Acyclic [9,10] and cyclic [11] oxamides which show selectivities for PbX^+ (X^-: OH^-, Cl^-,

* Corresponding author.

PII S0039-9140(97)00021-0

and NO_3^-) and Pb^{2+} have been examined. Malinowska et al. reported polymeric membrane ISEs based on thioamide functionalized calix[4]arenes for which the selectivity coefficients for Pb^{2+} relative to Cu^{2+} ($K^{Pot}_{Pb,Cu}$) were $10^{-3}-10^{-4}$ [12]. Polymeric membrane ISEs based on polyalkoxylates [13] and liquid ion-exchangers [14] for Pb^{2+} have been reported. Also a Pb^{2+} selective field effect transistor (FET) was developed [15].

Recently acyclic dibenzopolyether dicarboxylic acids, such as 1,5-bis[2-(2′-carboxyheptyloxy)phenoxy]-3-oxapentane, have been prepared as selective extractants for Pb^{2+} [16,17]. These extractants exhibited excellent selectivities for Pb^{2+} over Cu^{2+}. Condensation polymerization of the acyclic dibenzopolyether dicarboxylic acids provided effective chelating resins for Pb^{2+} separation [17,18]. In our short communication, we reported the synthesis of lipophilic *N,N*-dipentylamide derivatives of the dibenzopolyether dicarboxylic acids, such as 1,5-bis[2-(*N,N*-dipentylcarbamoylmethoxy)phenoxy]-3-oxapentane, and briefly described that a polymeric membrane ISE based on the ionophore showed remarkably high Pb^{2+}/Cu^{2+} selectivity [19].

In this study, we have made solvent polymeric membrane ISEs by using 12 kinds of *N,N*-dialkylamide derivatives of the dibenzopolyether dicarboxylic acids **1**–**12** (Fig. 1) as Pb^{2+}-selective neutral carriers. Potentiometric selectivities of the ISEs for Pb^{2+} over other heavy metal cations, alkali metal cations, and alkaline earth metal cations have been assessed. The effect of the length of ethylene glycol spacer which connects two benzene-ring in the ionophores and that of the length of alkyl group in the amide end-group upon the potentiometric selectivities will be discussed.

2. Experimental

2.1. Chemicals

Poly(vinyl chloride) (PVC) with an average polymerization degree of 1100 was purchased from Wako Pure Chemical Industries (Osaka, Japan). *o*-Nitrophenyl octyl ether (NPOE) and potassium tetrakis(*p*-chlorophenyl)borate (KTpClPB) were obtained from Dojindo Laboratories (Kumamoto, Japan). Metal nitrates including $Pb(NO_3)_2$ and tetrahydrofuran (THF) were reagent-grade chemicals. Deionized water was prepared by passing distilled water through an Organo G-10 cartridge.

Acyclic dibenzopolyether diamides with diethylene glycol spacers **4** and **8** are known compounds [19]. Other compounds **1**–**3**, **5**–**7**, and

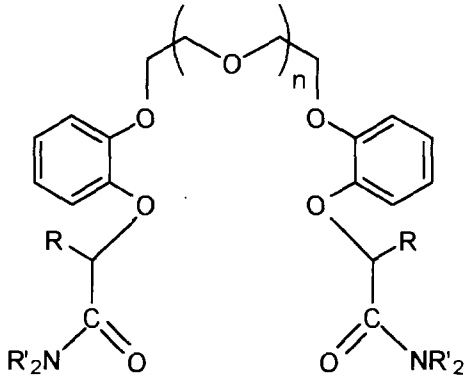

Dibenzopolyether diamide

Cmpd	n	R	R'
1	1	H	C_2H_5
2	1	H	C_3H_7
3	1	H	C_4H_9
4	1	H	C_5H_{11}
5	1	$C_{14}H_{29}$	C_2H_5
6	1	$C_{14}H_{29}$	C_3H_7
7	1	$C_{14}H_{29}$	C_4H_9
8	1	$C_{14}H_{29}$	C_5H_{11}
9	0	$C_{14}H_{29}$	C_2H_5
10	0	$C_{14}H_{29}$	C_3H_7
11	0	$C_{14}H_{29}$	C_4H_9
12	0	$C_{14}H_{29}$	C_5H_{11}

Fig. 1. Structures of dibenzopolyether diamides.

9–12 were prepared by adaptation of the reported compounds and their analytical data were provided elsewhere [20].

2.2. Preparation of PVC membranes

PVC (50 mg), NPOE (100 mg), the dibenzopolyether diamide (5.0 mg), and KTpClPB (1.0 mg) were dissolved in 1.5 ml of THF. An aliquot of the THF solution was poured onto a porous polytetrafluoroethylene (PTFE) membrane attached to a PVC tube and the solvent was allowed to evaporate for 15–20 min. Addition of the THF solution and evaporation were repeated eight or nine times. The resulting PVC tube with the coated PTFE membrane was fixed on a Denki Kagaku Keiki (DKK, Tokyo, Japan) number 7900 electrode body. An internal filling solution of 1 mM $PbCl_2$ was added to the electrode. The electrode was conditioned by soaking in a 1 mM Pb $(NO_3)_2$ solution for 12 h before use.

2.3. Measurements

Potentiometric measurements with a membrane electrode were carried out at 24–25°C with a voltage meter (DKK PHL-40 pH meter), a double junction Ag-AgCl reference electrode (DKK number 4083), and a magnetic stirrer to agitate the sample solution. The electrode cell was Ag-AgCl/1 mM $PbCl_2$/PVC membrane/sample solution/0.1 M $MgCl_2$/3 M KCl/Ag-AgCl. Single ion activities were obtained as described in our previous paper [21]. The selectivity coefficient ($K^{Pot}_{Pb,M}$) for Pb^{2+} over other metal cations were determined by the Fixed interference method [22]. The constant background concentration was made by the addition of 0.01–0.1 M of interfering metal nitrates.

3. Results and discussion

Acyclic dibenzopolyether diamides **1–12** were incorporated into solvent polymeric membranes in which PVC was the polymer and NPOE was the membrane solvent. For the ISEs prepared from these membranes, potentiometric selectivities for Pb^{2+} relative to other heavy metal cations, alkali metal cations, and alkaline earth metal cations were determined by the Fixed interference method [22].

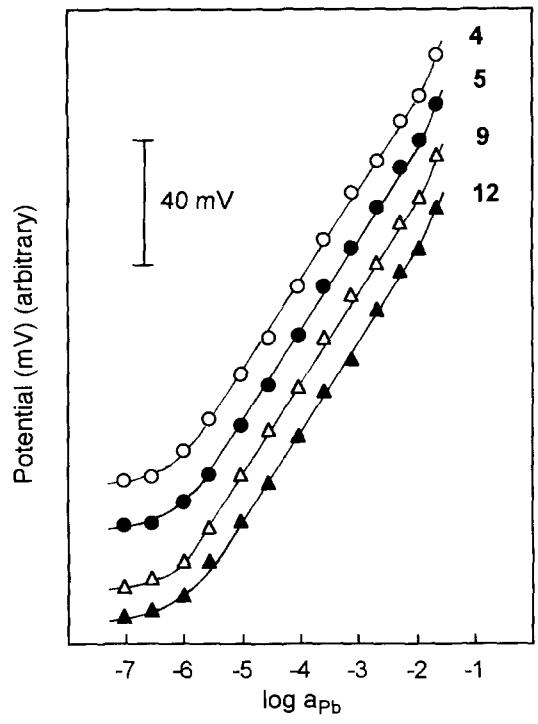

Fig. 2. Potential responses of ISEs based on **4**, **5**, **9** and **12** to the change of Pb^{2+} activity. $Pb(NO_3)_2$ solution was used.

3.1. Response of ISEs based on dibenzopolyether diamides

Typical responses of ISEs based on **4**, **5**, **9** and 12 to the change of Pb^{2+} activity are shown in Fig. 2. Nernstian responses or near Nernstian responses (average slope = 28.5 mV decade^{-1}) were observed for all of those ISEs in the ranges of $3 \times 10^{-2} - 1 \times 10^{-6}$ M for **9** and $3 \times 10^{-2} - 3 \times 10^{-6}$ M for **4**, **5** and **12**. It is found that dibenzopolyether diamides which have diethylene glycol spacers and ethylene glycol spacers provide good responses for Pb^{2+}. Other dibenzopolyether diamides **1–3**, **6–8**, **10** and **11**, gave similar good responses.

3.2. Potentiometric selectivities of dibenzopolyether diamides with diethylene glycol spacers

Selectivity coefficients expressed as $\log K^{Pot}_{Pb,M}$ for ISEs based on **1–4** are presented in Fig. 3. Compounds **1–4** are *N,N*-dialkylamide derivatives of 1,5-bis[2-(carboxymethoxy)phenoxy]-3-oxapentane. It was reported that the dibenzopolyether dicarboxylic acid exhibited a good selectivity for Pb^{2+} relative to Cu^{2+} in solvent extraction (ca. 100-fold selectivity in the extraction constant K_{ex}) [16]. The $\log K^{Pot}_{Pb,Cu}$ values of ISEs based on **1–4** are more negative than -4, which means the dibenzopolyether diamides have remarkably high selectivities for Pb^{2+} over Cu^{2+}.

Similarly the ISEs based on **1–4** exhibit quite high selectivities for Pb^{2+} relative to some divalent heavy metal cations, the $\log K^{Pot}_{Pb,M}$ values being -3.9– -4.7 for $M = Fe^{2+}$ and -3.6– -3.9 for $M = Ni^{2+}$. However, the selectivities for Pb^{2+} over alkali metal cations, such as Na^+ and K^+, for the ISEs are not good. The $\log K^{Pot}_{Pb,M}$ values are 0–0.1 when $M = Na^+$ and -0.7– -0.6 when $M = K^+$.

Compounds **1–4** are homologs which have ethyl, propyl, butyl, and pentyl groups, respectively, as *N,N*-dialky groups in the amide end-group. The selectivities for Pb^{2+} are not much dependent on the length of the alkyl group for most of interfering cations. However, lengthening the alkyl group from ethyl to pentyl provides

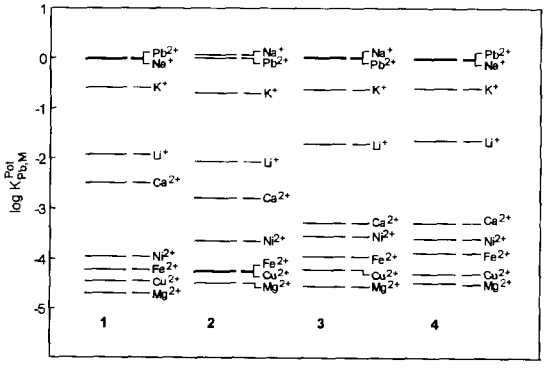

Fig. 3. Potentiometric selectivities expressed as $\log K^{Pot}_{Pb,M}$ of ISEs based on **1–4** for Pb^{2+} over other metal cations.

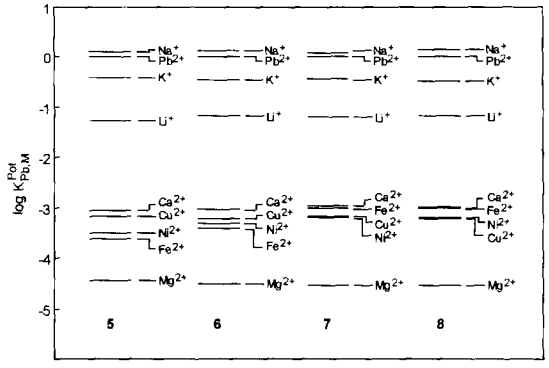

Fig. 4. Potentiometric selectivities expressed as $\log K^{Pot}_{Pb,M}$ of ISEs based on **5–8** for Pb^{2+} over other metal cations.

some increase in the Pb^{2+}/Ca^{2+} selectivity (0.8 unit in the $\log K^{Pot}_{Pb,Ca}$); whereas the same lengthening lowers the Pb^{2+}/Fe^{2+} selectivity (0.8 unit in the $\log K^{Pot}_{Pb,Fe}$).

Compounds **5–8** are tetradecyl-attached derivatives of **1–4** at the β-position of carbonyl group. The $\log K^{Pot}_{Pb,M}$ values of ISEs based on **5–8** are summarized in Fig. 4. Compared with **1–4**, the $\log K^{Pot}_{Pb,Cu}$ values for **5–8** are more positive by 1.0–1.1 unit. It appears that attachment of the long alkyl group reduces the Pb^{2+}/Cu^{2+} selectivity. This tendency is also observed for the Pb^{2+}/Fe^{2+} selectivity. The $\log K^{Pot}_{Pb,Fe}$ values for **5–8** are more positive than those for **1–4** by 0.9–1.1 unit. The Pb^{2+} selectivities over Na^+ and K^+ for **5–8** are about the same as those for **1–4**.

3.3. Potentiometric selectivities of dibenzopolyether diamides with ethylene glycol spacers

Compounds **9–12** possess ethylene glycol spacers which connect two benzene-ring instead of diethylene glycol spacers in **5–8**. The $\log K^{Pot}_{Pb,M}$ values of ISEs based on **9–12** are summarized in Fig. 5.

Compared with **5** which has a diethylene glycol spacer and a *N,N*-diethyl group, the $\log K^{Pot}_{Pb,M}$ values for **9** are more negative by 0.5 unit when $M = Li^+$, 1.3 unit when $M = Na^+$, and 0.8 unit when $M = K^+$. It is anticipated that the introduction of ethylene glycol spacer enhances the selectivities for Pb^{2+} relative to the alkali metal

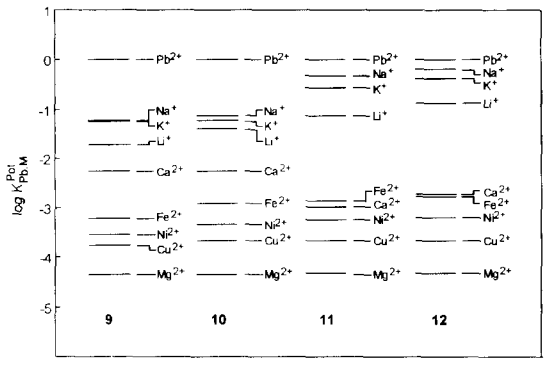

Fig. 5. Potentiometric selectivities expressed as log $K^{Pot}_{Pb,M}$ of ISEs based on **9**–**12** for Pb^{2+} over other metal cations.

cations. Lengthening the alkyl group in the amide end-group from ethyl to pentyl reduces the selectivities for Pb^{2+} relative to alkali metal cations by 0.9, 1.1, and 0.9 units in the values of log $K^{Pot}_{Pb,Li}$, log $K^{Pot}_{Pb,Na}$ and log $K^{Pot}_{Pb,K}$, respectively.

Also the introduction of ethylene glycol spacer provides an increase in the Pb^{2+}/Cu^{2+} selectivities by 0.4–0.6 unit in the log $K^{Pot}_{Pb,Cu}$ value. It is proposed that ethylene glycol spacers are good for the Pb^{2+} complexation compared with diethylene glycol spacers.

Taking into account the high selectivities for Pb^{2+} over alkali metal cations, such as Na^+ and K^+, as well as over heavy metal cations, compound **9**, which has an ethylene glycol spacer and a *N*,*N*-diethyl group, seems excellent as a Pb^{2+}-selective neutral carrier for polymeric membrane ISE. The log $K^{Pot}_{Pb,Cu}$ value for **9** is -3.8 which is somewhat worse than those for **1**–**4**; whereas the selectivity is still much superior to those for solid-state ISEs [3,5]. The ISE based on **9** show almost constant response (slope and selectivity) over 3 months with measurement every 2 or 3 days.

References

[1] Y. Umezawa, CRC Handbook of Ion-Selective Electrodes, CRC Press, Boca Raton, FL, 1990, pp. 466–479.
[2] G.A. Rechnitz and N.C. Kenny, Anal. Lett., 3 (1970) 259.
[3] M. Mascini and A. Liberti, Anal. Chim. Acta, 60 (1972) 405.
[4] P. Kivalo, R. Viertanen, K. Wickström, W. Wilson, E. Pungor, G. Horvai and K. Tóth, Anal. Chim. Acta, 87 (1976) 401.
[5] G.J.M. Heijne, W.E. van der Linden and G. den Boef, Anal. Chim. Acta, 100 (1978) 193.
[6] D. Midgley, Anal. Chim. Acta, 159 (1984) 63.
[7] A.K. Jain and C. Bala, Fresenius's Z. Anal. Chem., 319 (1984) 307.
[8] S.K. Srivastava, S. Kumar, C.K. Jain and S. Kumar, Talanta, 33 (1986) 717.
[9] E. Lindner, K. Tóth, E. Pungor, F. Behm, P. Oggenfuss, D.H. Welti, D. Ammann, W.E. Morf, E. Pretsch and W. Simon, Anal. Chem., 56 (1984) 1127.
[10] E. Malinowska, Analyst, 115 (1990) 1085.
[11] E. Malinowska, J. Jurczak and T. Stankiewicz, Electroanalysis, 5 (1993) 489.
[12] E. Malinowska, Z. Brzózka, K. Kasiura, R.J.M. Egberink and D.N. Reinhoudt, Anal. Chim. Acta, 298 (1994) 253.
[13] A.M.Y. Jaber, G.J. Moody and J.D.R. Thomas, Analyst, 113 (1988) 1409.
[14] S.E. Didina, L.L. Mitnik, N.V. Koshmina, A.L. Grekovich and K.N. Mikhelson, Sens. Actuators B, 18–19 (1994) 396.
[15] E. Davini, G. Mazzamurro and A.P. Piotto, Sens. Actuators B, 7 (1992) 580.
[16] T. Hayashita, T. Fujimoto, Y. Morita and R.A. Bartsch, Chem. Lett. (1994) 2285.
[17] T. Hayashita, K. Yamasaki, K. Kunogi, K. Hiratani, X. Huang, Y. Jang, D.E. McGowen and R.A. Bartsch, Supramol. Chem., 6 (1996) 347.
[18] T. Hayashita, K. Yamasaki, X. Huang and R.A. Bartsch, Chem. Lett. (1993) 1487.
[19] J.S. Kim, A. Ohki, N.S. Cho, I.Y. Yu, T. Hayashita and S. Maeda, Bull. Korean Chem. Soc., 17 (1996) 953.
[20] J.S. Kim, A. Ohki, M.H. Cho, I.Y. Yu, S.C. Lee, J.H. Lee and N.S. Cho, J. Korean Chem. Soc., 40 (1996) 706.
[21] A. Ohki, J.-P. Lu and R.A. Bartsch, Anal. Chem., 66 (1994) 651.
[22] Recommendation for Nomenclature of Ion-Selective Electrodes, Pure Appl. Chem., 48 (1976) 127.

ELSEVIER

Talanta 44 (1997) 1137–1140

Talanta

Short communication

On the feasibility of using molecularly imprinted poly (Hema) as a sensor component

K. Sreenivasan

Biomedical Technology Wing, Sree Chitra Tirunal Institute for Medical Sciences and Technology, Poojapura, Trivandrum 695 012, India

Received 8 September 1995; received in revised form 28 November 1996; accepted 6 December 1996

Keywords: Feasibility; Molecularly imprinted poly (Hema); Sensor component

1. Introduction

The recent years have witnessed a considerable growth in the usage of sensors for the detection of clinically and industrially relevant molecules. To achieve specificity, sensors normally employ molecules of biological origin like enzymes. The poor stability together with the high cost are perhaps the major drawbacks of the sensors containing biomolecules.

The systems based on stable chemicals, though look attractive, may not be specific which is indeed the most crucial factor of a sensor. The technique of molecular imprinting has emerged as a powerful method to impart specificity in common synthetic polymers [1–3]. During the last few years several molecularly imprinted polymers have been synthesised for a variety applications. The high degree of selectivity and specified functionality of this class of polymers have been demonstrated in several studies [4–7]. In spite of all these studies, however, the studies related to the use of molecularly imprinted polymers as sensor component have leastly been reported [8].

Normally molecularly imprinted polymers (MIPs) are synthesised either by thermal initiators or by photo polymerisation [9]. In both cases extra components are added as polymerisation aids. These additives may interfere with the rearrangement of monomers around the print molecules subsequently affecting the density of recognition sites. We have recently synthesised MIPs using—radiation method [10,11]. The radiation process appears to be more effective and simpler than the other methods.

The report discusses our preliminary results on the feasibility of using MIP as a sensing element. Radiation polymerised poly (2 hydroxy ethyl methacrylate) molecularly imprinted for the recognition of salicylic acid, is used in this study as a sensing component for sensing salicylic acid in urine.

PII S0039-9140(96)02204-7

2. Experimental

2-hydroxy ethyl methacrylate (HEMA) and ethylene glycol dimethacrylate (EDMA), obtained from Sigma Chemicals, St. Louis, USA were used after removing the stabiliser by vacuum distillation. All other chemicals (chromatographic grade or analytical grade) were obtained from EMerck, Bombay, India.

3. Synthesis of MIP

2 g HEMA, 300 mg salicylic acid and 1 g EDMA were dissolved in 10 ml methanol. The solution was placed in a polyethylene container, purged with nitrogen, sealed and subjected to γ-irradiation from a Co^{60} source (Panoramic batch irradiator, BARC, Bombay) to a total dose of 0.5 Mrad at a rate 0.25 Mrad/h. The polymer in the form of a film having a thickness of 0.1 mm was taken out and washed extensively used water followed by methanol for removing salicylic acid and unpolymerised monomer if any. The complete removal of salicylic acid was ensured prior to the use of the polymer for further studies. HEMA was also polymerised under the similar conditions without adding the print molecules (salicylic acid) to serve as control. Phthalic acid was used as a molecule of comparable shape and structure of salicylic acid to check the specificity of the MIP towards salicylic acid.

4. Instrumental

A Waters Assoc. High performance liquid chromatographic system consisting of a model 6000A solvent delivery pump model U6K injector and a model 486 tunable absorbance detector was used for the chromatographic studies. A μ-Bondapak C_{18} column in conjunction with methanol:water (90:10 v/v) was used as mobile phase at a flow rate of 1 ml min^{-1} for the chromatographic estimation of salicylic acid and phthalic acid. The column effluents were monitored at 236 and 254 nm for the estimation of salicylic acid and phthalic acid, respectively. The chromatograms were obtained on an omini scribe strip chart recorder (Houston Instruments, TX, USA).

5. Method

Standard solutions of salicylic acid in urine were prepared by dissolving appropriate amount of salicylic acid in freshly collected human urine. The solutions were filtered using 0.45 μm filters. Solutions of phthalic acid were also prepared in a similar fashion.

About 40 mg MIP was placed in 5 ml solution for 30 min at room temperature (26 ± 0.1°C). Calibration plot was constructed between the concentration and peak height of salicylic acid. The urine solutions were subjected to chromatographic analysis before and after placing the MIP. The amount of salicylic acid in the solutions were estimated using the peak height on the calibration plot. The difference in concentration of salicylic acid before and after placing MIP is taken as the amount of salicylic acid adsorbed by the polymer. Poly (HEMA) prepared under similar experimental conditions without print molecule was used as control. The extent of uptake of phthalic acid was also monitored by the chromatographic procedure as mentioned earlier.

6. Results and discussion

Table 1 summarises the extent of uptake of salicylic acid by MIP and control polymer. The amount of salicylic acid adsorbed by the control polymer is negligibly small. It may be reasonable to presume that salicylic acid molecules might

Table 1
Extent of adsorption of salicylic acid by MIP and control polymer

Amount adsorbed by MIP (μg)	Amount adsorbed by control polymer (μg)
7.5	1.6
14	2.6
18	3.5
20	3.7

Table 2
Extent of uptake of phthalic acid by MIP and control polymer

Amount adsorbed by MIP (μg)	Amount adsorbed by control (μg)
0.92	1.06
1.40	1.38
1.81	1.90

have trapped in the porous structure of the control polymer comparatively the higher uptake of salicylic acid by the MIP clearly point out the creation of recognition sites in the polymer. The sites favour the selective interaction of salicylic acid leading to the increased adsorption.

It is mandatory that a sensing element should have high degree of selectivity. In this study we used phthalic acid as a molecule of comparable features of salicylic acid. The uptake of phthalic acid by MIP and control polymer is summarised in Table 2. It can be seen that there is not considerable variation in the extent of adsorption of this molecule by MIP and control poly (HEMA). Indeed a small quantity of phthalic acid is adsorbed by MIP which is comparable with the amount of phthalic acid adsorbed by the control polymer forcing to conclude that the component is simply trapped in the polymer matrix. By comparing the extent of adsorption of salicylic acid and phthalic acid by MIP and control poly (HEMA), we could conclude that MIP does not have any specific affinity towards phthalic acid and this data further suggest that imprinted poly (HEMA) has a specific, recognising ability.

It is found that the equilibrium swelling of MIP and control poly (HEMA) in methanol are very less ($< 0.8\%$) by reflecting the extensive cross linking leading to the formation of rigid matrices. Moreover, nearly identical swelling of both MIP and control polymer (Equilibrium swelling of MIP—0.76%) point out that both these polymers have a nearly identical morphology.

Concentration dependent functionality is one of the prime factor of any sensing device. The uptake of salicylic acid vary as a function of concentration. This aspect is highlighted in Fig. 1. The extent of adsorption of salicylic acid is linear up to 300 μg ml^{-1} which is indeed higher than the normal concentration of drugs in a biological matrix like urine. The linearity up to this concentration, in fact, indicates that the MIP based system could be used as a sensing element.

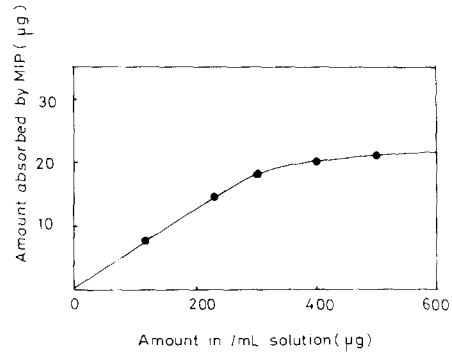

Fig. 1. A graphical representation of the extent of uptake of salicylic acid by MIP as a function of concentration.

The absorbed salicylic acid can completely be removed from the MIP by simply extracting with methanol reflecting the feasibility of reusing the MIP in a continuous manner.

The poor stability is the major drawback of any sensing element containing a biomolecule which is one of the additional advantage of MIP.

An ideal sensor should have high degree of selectivity together with the ability to visualise the event of binding of the molecule to be detected in the form of a visual colour change. This eventuality may be possible by incorporating additional reagents in the MIP which would be addressed in our forthcoming publications.

The results presented here are highly preliminary. Our aim is just to demonstrate the feasibility of employing MIPs in sensor construction. Further extensive studies are needed to optimise these synthetic systems to employ routinely in sensors.

References

[1] R. Arshady and K. Mosbach, Makromol. Chem., 182 (1981) 687.
[2] G. Wulf, ACS Symp. Ser., 308 (1986) 186.

[3] E. Selergren, B. Edberg and K. Mosbach, J. Chromatogr., 347 (1985) 1.
[4] M. Moradian and K. Mosbach, J. Mol. Recognit., 2 (1989) 167.
[5] G. Wulf and J. Harrer, J. Makromol. Chem., 192 (1991) 1329.
[6] L. Fischer, R. Mueller, B. Ekberg and K. Mosbach, J. Am. Chem. Soc., 113 (1991) 9358.
[7] G. Viatakis, L.I. Anderson, R. Mueller and K. Mosbach, Nature, 361 (1993) 645.
[8] E. Hedborg, F. Winquist, I. Lundstrom, L.I. Anderson and K. Mosbach, Sens. Actuators, A, 37–38 (1993) 796.
[9] K. Mosbach, Trends Biochem. Sci., 19 (1994) 9.
[10] K. Sreenivasan, Indian Patent, Pending approval.
[11] K. Sreenivasan, Communicated to J. Appl. Polym. Sci.

ELSEVIER

Talanta 44 (1997) 1141–1147

Talanta

Determination of trace thiocyanate in body fluids by a kinetic fluorimetric method

Guien Zhang *, Bin Li, Jing Fan, Suling Feng

Department of Chemistry, Henan Normal University, Xinxiang, Henan 453002, People's Republic of China

Received 20 June 1996; received in revised form 19 August 1996; accepted 20 August 1996

Abstract

A simple and very sensitive kinetic fluorimetric method is reported for the determination of trace amount of thiocyanate. The proposed method is based on the inhibition effect of thiocyanate on oxidation of rhodamine 6G by potassium bromate in sulfuric acid solution. The detection limit for thiocyanate is 1.63×10^{-6} mmol/l. The linear range of the determination is 4.82×10^{-6}–4.13×10^{-5} mmol/l. This method has been used to determine trace thiocyanate in urine and saliva of smokers and non-smokers. The results obtained are satisfactory. © 1997 Elsevier Science B.V.

Keywords: Body fluids; Inhibition; Kinetic fluorimetric method; Rhodamine 6G; Thiocyanate

1. Introduction

Thiocyanate is present in the human body as a metabolic degradation product of sulphur-containing compounds in tobacco. It is a detoxication product of cyanide and its content is higher in the body fluids of smokers. For this reason the concentration of thiocyanate has been considered to be a good indicator for distinguishing between smokers and non-smokers [1–3].

Thiocyanate is also administered as a drug in the treatment of thyroid conditions. In addition, the higher concentration of thiocyanate in the human body will lead to vertigo or unconciousness. Therefore, an accurate and reliable method for the determiantion of thiocyanate in biological sample is of medical interest.

Several methods for the determination of thiocyanate have been published. The spectrophotometric method is mainly based on the formation of the red iron(III)-thiocyanate complex [4,5]. It can meet the requirment of sensitivity for the determination of thiocyanate in body fluids, but does not possess sufficient selectivity. Flow injection method [2] is rapid and simple, but its sensitivity is lower. It can't meet other applications which require high sensitivity. The other methods such as linear sweep polarography [6], ion-selective electrodes [7,8], pulse-polarography [9] and gas chromatography [10,11] were also used for the determination of thiocyanate. Unfortunately, most of these methods are laborious to perform and involve use of hamful reagents. Also, some of those need more expensive instruments so that they can not easily be popularized.

* Corresponding author.

PII S0039-9140(96)02080-2

So far there is only one report on the determination of thiocyanate by catalytic fluorimetric photometry [12]. It is based on the catalytic effect of thiocyanate on oxidation of As(III) by Ce(IV). However, the compound of As(III) is toxic and therefore unfavourable for environmental reasons. Furthermore, the sensitivity of this method has been unsatisfactory.

In this work, a detailed study of the appropriate conditions for the inhibition effect of thiocyanate on the oxidation of rhodamine 6G by potassium bromate and of the best reagent concentration have been conducted. On the basis of this, a new way for the determination of trace thiocyanate with high sensitivity and selectivity was proposed. The method is simple, rapid and reliable. Its detection limit is 1.63×10^{-6} mmol/l, which is lower than that of any other method reported in the literature. This method has been applied for the determination of thiocyanate in urine and saliva of smokers and non-smokers. The result is satisfactory.

2. Experimental

2.1. Reagents and instruments

2.1.1. Thiocyanate solution

The solution was prepared from the potassium thiocyanate and standardized with standard silver nitrate solution by Volhard method [13]. The standardized concentration of thiocyanate is 1.0×10^{2} mmol l^{-1}. Working standards were prepared by suitable dilution.

Rhodamine 6G solution: 0.1 mmol l^{-1};

Potassium bromate solution: 1.0×10^{2} mmol l^{-1};

Sulfuric acid solution: 5.0×10^{2} mmol l^{-1};

Sodium acetate: 2.00×10^{3} mmol l^{-1};

RF-5000 (Japan) fluorophotometer;

Model 930 (Shang hai, China) fluorophotometer;

Model 501 super constant temperature meter.

All of the reagents used in the experiment were analytical grade or guaranteed reagent. Redistilled water was used to prepare solutions.

2.2. Procedure

Add proper amount of standard thiocyanate solution, 3.00 ml of 5.0×10^{2} mmol l^{-1} sulfuric acid and 0.30 ml of 0.1 mmol l^{-1} rhodamine 6G to a 25 ml measuring flask, then dilute the solution with water to 20 ml. Then add 0.70 ml of 1.0×10^{2} mmol l^{-1} potassium bromate into the flask, dilute up to the mark before shaking. After heating the sample in a thermostatted water bath (30 ± 0.2°C) for 9 min, add 1.00 ml of 2.0×10^{3} mmol l^{-1} sodium acetate to stop the reaction. Its fluorescence value I_F and blank value I_{F0} (I_{F0} is recorded when no thiocyanate is present) were determined at an excitation wavelength of 348.4 nm and emission wavelength of 548.4 nm. Then values of $\Delta I_F = I_F - I_{F0}$ was calculated.

3. Results and discussion

Rhodamine 6G is a triphenylmenthane dye. It emits very strong yellow-green fluorescent light. When oxidized by a strong oxidizer—potassium bromate, its molecular structure is destroyed and the fluorescence disappears. When trace amounts of thiocyanate are present, this oxidation reaction is inhibited (Fig. 1, 3–3′), as shown in Fig. 1. On the basis of this, a new kinetic fluorimetric method for the determination of trace thiocyanate has been proposed and the experimental conditions have been studied.

3.1. Choice of the best experimental conditions(with thiocyanate concentration being 2.07×10^{-5} mmol l^{-1} under all conditions).

3.1.1. Choice of medium and influence of its concentration level

The following media have been tried in the proposed experiments: sulfuric acid, phosphoric acid, hydrochloric acid. It was found that the sensitivity of reaction is very low in the medium of phosphoric acid. In hydrochloric acid, the reaction is interfered seriously because of the exit of a large amount of Cl^{-}. Only in sulfuric acid, the inhibition effect of thiocyanate is striking. The sensitivity is high and the reproducibility is good.

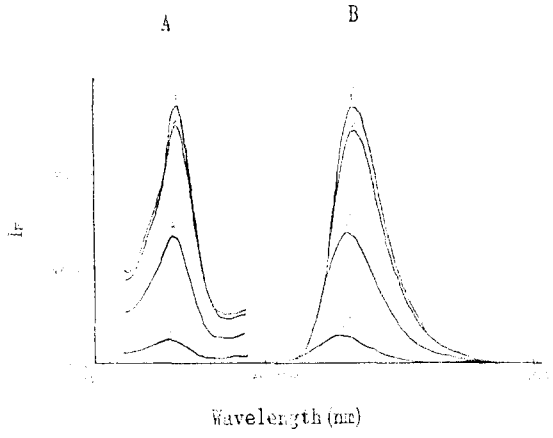

Fig. 1. Excitation (A) and emission (B) spectra of Rhodamine 6G in the presence of diferent reagents: $[SCN^-] = 3.44 \times 10^-$ 5 mM; 60 mM H_2SO_4; 1.2×10^{-3} mM Rh6G; 2.8 mM $KBrO_3$; Temperature: 30°C; Time: 9 min. 1-1′: Rh6G, H_2SO_4. 2-2′: Rh6G, $KBrO_3$. 3-3′: Rh6G, $KBrO_3$, H_2SO_4, SCN^-. 4-4′: Rh6G, $KBrO_3$, H_2SO_4. (1-1′,2-2′,3-3′,4-4′ pairs of curves were obtained through scanning different reaction systems, which were listed above).

Therefore, sulfuric acid was selected as the reaction medium.

The influence of the concentration level of 5.0×10^2 mmol l^{-1} sulfuric acid has been investigated. The results were shown in Fig. 2. It can be seen from this figure that ΔI_F value increases with

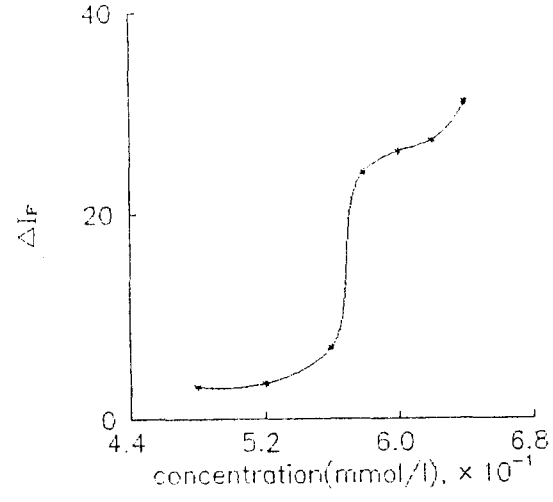

Fig. 2. Influence of sulfuric acid concentration upon I_F: 1.2×10^{-3} mM Rh6G; 2.8 mM $KBrO_3$; Temperature: 30°C; Time: 9 min.

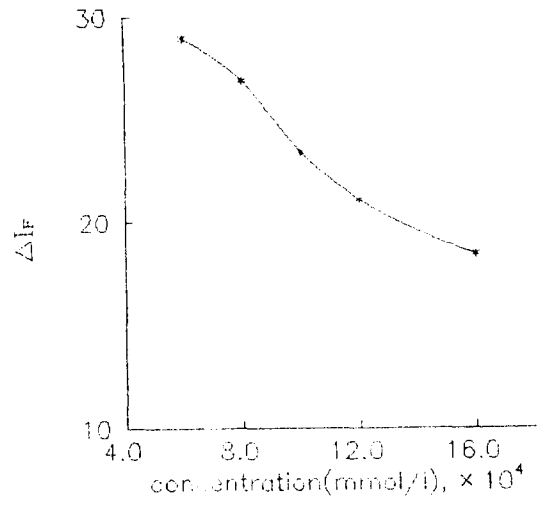

Fig. 3. Influence of Rh6G concentration upon I_F: 60 mM H_2SO_4; 2.8 mM $KBrO_3$; Temperature: 30°C; Time: 9 min.

increasing concentration of sulfuric acid. When the concentration is in the ranges of 48–56 mmol l^{-1} and 58–62 mmol l^{-1}, ΔI_F value changes slowly. But in the latter range, the sensitivity is higher. So 3.00 ml of 5.0×10^2 mmol l^{-1} sulfuric acid is chosen.

3.1.2. Influence of rhodamine 6G concentration level

Fig. 3 shows the influence of rhodamine 6G concentration upon I_F value. It is apparent that ΔI_F value decreases with increasing concentration of rhodamine 6G. On the contrary, the lower rhodamine 6G concentration is, the higher the test sensitivity is. However, the reproducibility is not good when the concentration of rhodamine 6G is low. So 0.30 ml of rhodamine 6G was used in this work.

3.1.3. Influence of concentration level of potassium bromate

The influence of potassium bromate upon I_F has been studied. The results obtained are shown in Fig. 4. Obviously, ΔI_F value increases with increasing concentration of potassium bromate. But a large amount of potassium bromate will result in bad reproducibility. So 0.70 ml of potassium bromate is best choice.

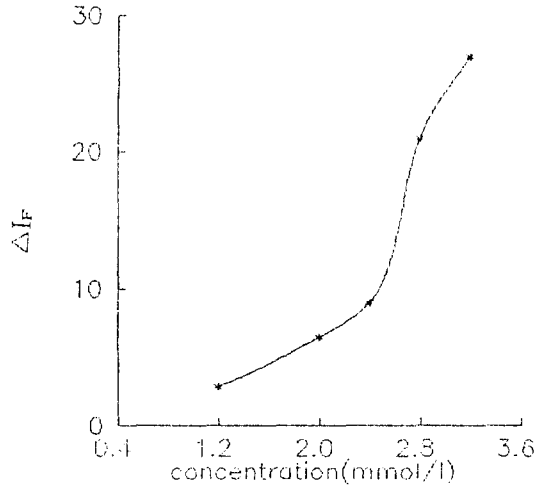

Fig. 4. Influence of potassium bromate concentration upon I_F: 60 mM H_2SO_4; 1.2×10^{-3} mM Rh6G; Temperature: 30°C; Time: 9 min.

3.1.4. Influence of reaction temperature

The effect of reaction temperature was studied in the range 20–35°. Fig. 5 shows that the reaction rate increases with increasing temperature up to 30°C. When the temperature is higher than 30°C, ΔI_F value diminishes. Thus, 30°C was used in this study.

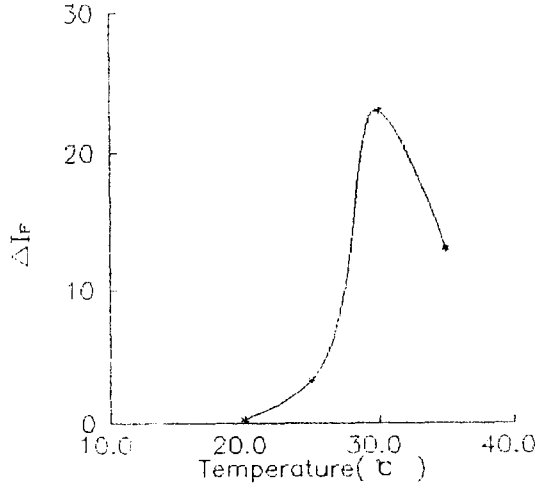

Fig. 5. Influence of temperature upon I_F: 60 mM H_2SO_4; 1.2×10^{-3} mM Rh6G; 2.8 mM $KBrO_3$; Time: 9 min.

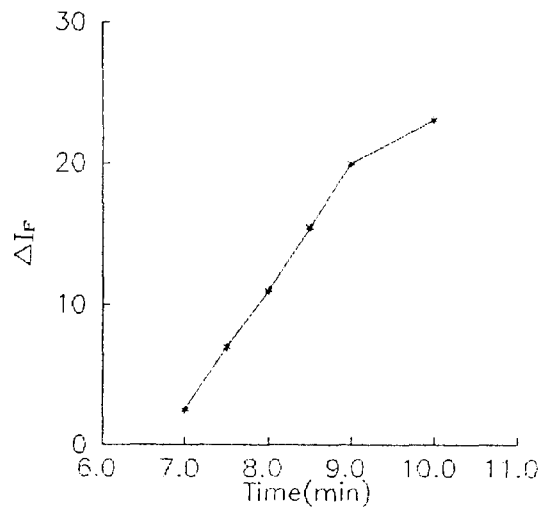

Fig. 6. ΔI_F-Reaction time curve of the system: 60 mM H_2SO_4; 1.2×10^{-3} mM Rh6G; 2.8 mM $KBrO_3$; Temperature: 30°C.

3.1.5. Influence of reaction time

The influence of reaction time upon fluorescence intensity was shown in Fig. 6. It can be seen that ΔI_F–t curve is linear in the range of 7–9 min. Thus, 9 min is taken as the reaction time.

3.1.6. The end of reaction

Considering the fact that the experiment was conducted by a fixed-time method, we have to find out an efficient way to end the reaction. In this study, the effect of PH on the reaction rate is notable. So 1.0 ml sodium acetate were added to end the reaction efficiently.

3.2. Relation between thiocyanate and I_F

According to the experimental method described above, values of I_F were determined and the calibration curve was drawn (Fig. 7). It can be seen that within the range of 4.82×10^{-6}–4.13×10^{-5} mmol l^{-1}, a linear relation was found between ΔI_F value and thiocyanate concentration. The linear equation obtained by a least-square analysis is found to be $\Delta I_F = 0.3967 + 1.065 \times 10^6$ C (mmol l^{-1}), with correlation coefficient $r = 0.9992$.

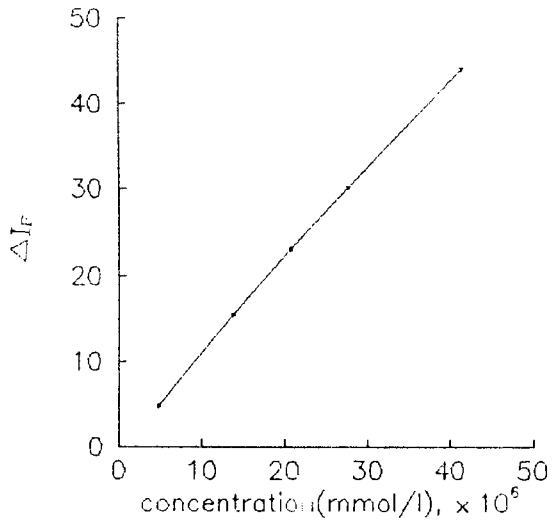

Fig. 7. Alibration graph.

3.3. Interference of coexistence ions

Under the chosen experimental conditions, an interference experiment was conducted on more than 30 common ions. When the permitted relative deviation from the I_F value is ±5%, the interference is listed in Table 1.

3.4. Sensitivity and accuracy of the method

Parallel experiments, 11, were made on the following test solutions. The results are as follows:

I_F values of the reagent blank: standard deviation S.D. = 0.58; detection limit: 1.63×10^{-6} mmol l^{-1}.

The measured I_F values for 6.89×10^{-6} mmol l^{-1} thiocyanate solution: standard deviation S.D. = 0.56; coefficient of variation: 0.89%.

The measured I_F value for 2.07×10^{-5} mmol l^{-1} thiocyanate solution: standard deviation S.D. = 1.13; coefficient of variation: 1.41%.

3.5. Sample analysis

The proposed method can be used successfully to determine thiocyanate in urine and saliva of smokers and non-smokers. The sensitivity of this system makes it possible to reduce the preparation procedures of samples. Samples only need centrifugate to be free from suspended matter. Then the samples were diluted and to be analysed directly. The results obtained have been compared with those of Ali A. Ensafi et al. [14] from catalytic photometric method.

3.5.1. Determination of trace thiocyanate in urine

Urine samples, 10, (five for smokers and five for non-smokers after getting up in the morning) were

Table 1
The influence of coexistence ions

Coexistence ions	Ratio [ion]/[SCN^-]	Coexistence ions	Ratio [ion]/[SCN^-]	Coexistence ions	Ratio [ion]/[SCN^-]
Na^+	4.32×10^3	K^+	5.15×10^3	Ca^{2+}	3.38
Mg^{2+}	1.66×10^4	Cu^{2+}	1.21×10^2	Pb^{2+}	4.35×10^3
Zn^{2+}	7.52×10^2	Ni^{2+}	3.60×10^3	Cd^{2+}	1.72×10^3
Mn^{2+}	1.67×10^4	As(III)	45.53	Sb(III)	65.73
Bi^{3+}	3.81×10^3	Cr^{3+}	24.5	Cr^{6+}	13.2
Fe^{3+}	3.33×10^2	Sn^{4+}	30.8	Si(IV)	67.9
Ge(IV)	10.0	Zr(IV)	3.47×10^3	V(V)	1.67
W(VI)	66.67	Mo(VI)	3.33×10^2	Se^{4+}	6.74×10^2
Co^{2+}	3.43×10^3	Al^{3+}	3.33×10^2	F^-	3.33×10^3
Cl^-	1.33×10^3	Br^-	0.67	I^-	0.27
SO_4^{2-}	9.01×10^3	NO_2^-	0.33	NO_3^-	8.18×10^3
PO_4^{3-}	3.33×10^3	$C_2O_4^{2-}$	3.33×10^3	ClO_3^-	1.33×10^5
CN^-	1.36×10^3				

[SCN^-] = 2.07×10^{-5} mmol l^{-1}.

Table 2
Measured results of the sample and the results of addition recovery test

Non-smokers Sample	SCN^- found (mmol l^{-1}, $n=6$)	RSD (%)	SCN^- added (mmol l^{-1}, $\times 10^6$)	Recovery (%)	C.P. method[a] (mmol l^{-1}, $n=5$)	Smokers Sample	SCN^- found (mmol l^{-1}, $n=6$)	RSD (%)	SCN^- added (mmol l^{-1}, $\times 10^6$)	Recovery (%)	C.P. method[a] (mmol l^{-1}, $n=5$)
Urine1	0.22	6.9	6.89	101,102	0.16	Urine6	0.60	8.8	6.89	105,97	0.46
Urine2	0.26	6.4	6.89	106,100	0.22	Urine7	0.50	4.6	6.89	102,95	0.45
Urine3	0.22	6.8	6.89	99,104	0.21	Urine8	0.44	5.8	6.89	98,93	0.35
Urine4	0.36	2.4	6.89	112,117	0.34	Urine9	0.82	3.7	6.89	108,98	—
Urine5	0.19	3.1	6.89	101,103	0.15	Urine10	0.41	4.2	6.89	97,97	—
Average	0.25					Average	0.55				
Saliva1	0.89	2.8	13.77	111,108	—	Saliva6	3.68	2.9	13.77	108,106	—
Saliva2	1.03	4.3	13.77	106,105	—	Saliva7	2.47	3.6	13.77	106,106	—
Saliva3	1.13	4.01	3.77	107,110	—	Saliva8	4.21	2.6	13.77	106,95	—
Saliva4	0.77	4.61	3.77	110,106	—	Saliva9	3.13	3.4	13.77	102,99	—
Saliva5	0.87	3.61	3.77	105,104	—	Saliva10	1.72	5.4	13.77	99,101	—
Average	0.94					Average	3.05				

[a] Catalytic photometric method [14].

collected, contrifugated for 5 min with the rate of 2000 r min^{-1}. Then the sample was diluted about 7000-fold and analysed using the procedures described before. At the same time, a blank test was conducted. Thus, obtained thiocyanate content in the urine sample and the result of addition recovery test are shown in Table 2. It is evident that the agreement between the results obtained from the two methods is reasonably good.

Determination of trace thiocyanate in saliva. The procedure of sample collection, centrifugation, dilution and determination is the same as described above. The result is also included in Table 2.

Densen et al. [1] reported that the thiocyanate levels in urine is 0.3 mmol l^{-1} for non-smokers and 0.6 mmol l^{-1} for smokers, and those in saliva were 0.9 mmol l^{-1} and 3.1 mmol l^{-1}, respectively.

Therfore, our results are in excellent agreement with those given by Densen et al. [1]

References

[1] P.M. Densen, B. Davidow, H.E. Bass and E.W. Jones, Arch. Environ. Health, 14 (1967) 865.
[2] B.B. Anders and H.H. Elo, Analyst, 116(6) (1991) 647.
[3] W.C. Butts, M. Kuehneman and G.M. Widdowson, Clin. Chem., 20 (1974) 1344.
[4] R.G. Bowler, Biochem. J., 38 (1944) 385.
[5] J.C.L. Meeussen, E.J.M. Timminghoff and M.G. Keizer, Analyst, 114(8) (1989) 959.
[6] X. Cai and Z. Zhao, Anal. Chim. Acta, 212 (1988) 43.
[7] M. Wojciechowski and J. Balcerzak, Anal. Chim. Acta, 237(1) (1990) 127.
[8] H. Below and H. Mueller, Pharmazie, 45(6) (1990) 416.
[9] J. Pasciak and J. Hurek, Chem. Anal., 29(5) (1984) 571.
[10] T. Chokamoto and T. Maitani, Anal. Sci., 2 (1986) 161.
[11] Z.M. Fu and K.M. Wu, J. Environ. Health China, 8(6) (1991) 271.
[12] A. Tanaka, Y. Imasaka and K. Hayashi, Anal. Chem., 36(11) (1987) 811.
[13] I.M. Kolthoff and V.A. Stenger, Volumetric Analysis, Vol. II p. 215.
[14] Ali A. Ensafi and J. Tajebakhsh-E-Ardakany, Anal. Lett., 28(4) (1995) 731.

ELSEVIER

Talanta 44 (1997) 1149–1157

Talanta

Equilibrium studies of organotin(IV) complexes with vitamin B_6

M.M. Shoukry *, E.M. Khairy, M.M.A. Mohamed

Department of Chemistry, Faculty of Science, Cairo University, Giza, Cairo, Egypt

Received 10 April 1996; received in revised form 23 September 1996; accepted 24 September 1996

Abstract

The complex-formation equilibria of dimethyltin(IV), trimethyltin(IV) and tributyltin(IV) with pyridoxamine were investigated in dioxane-water mixtures and at different temperatures using a potentiometric technique. The stepwise formation constants of the complexes formed in solution were calculated using the non-linear least-square program MINIQUAD-75. The effect of dioxane as a solvent on the protonation constants of pyridoxamine and the formation constants of organotin(IV) complexes was discussed. The thermodynamic parameters $\Delta H°$ and $\Delta S°$ calculated from the temperature dependence of the equilibrium constants were investigated. The concentration distribution of the various complex species was evaluated as a function of pH. © 1997 Elsevier Science B.V.

Keywords: Organotin(IV); Stability constants; Vitamin B_6

1. Introduction

Vitamin B_6 pyridoxol, pyridoxal and pyridoxamine and their phosphorylated derivatives form many complexes with metal ions [1,2]. Pyridoxamine, in particular, forms quite stable complexes in solution [3] and may act as a monodentate or bidentate ligand utilizing the *m*-oxy and amino-moiety of the *p*-aminomethyl group. Their complex formation equilibria may act as models mirroring the effects of exogenenous ligands in biological processes involving vitamin B_6.

In the context of studies on the antitumour properties of complexes involving organotin(IV) moieties with fragments of biological systems, the effect of organotin(IV) compounds with pyridoxamine against L 1210 leukemia has been investigated [4–6].

We considered that a systematic study of the coordination chemistry of organotin(IV) complexes with the pharmacologically active pyridoxamine might provide further information on their antitumour and cytotoxic activity. In conjunction with our research project directed to study the solution chemistry [7–10] of diorganotin(IV) and triorganotin(IV) complexes with amino acids and related compounds, the present paper aims to characterize the reaction of pyridoxamine with trimethyl-, dimethyl- and tributyltin(IV) chlorides. The effect of temperature and solvent on the

* Corresponding author.

PII S0039-9140(96)02113-3

complex formation equilibria were also investigated.

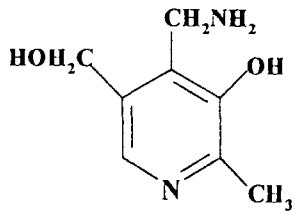

Pyridoxamine

2. Experimental

2.1. Materials and reagents

Pyridoxamine dihydrochloride [$Pm(HCl)_2$] provided by (Fluka AG) was used as supplied. Trimethyltin(IV) chloride [TMT], dimethyltin(IV) chloride [DMT] and tributyltin(IV)chloride [TBT] were from Merck Chem. Sodium hydroxide stock solutions were prepared by diluting the content of BDH concentrated volumetric solution vials. These solution were systematically checked by titration against potassium hydrogen phthalate. TBT solutions were prepared in dioxane. The other solutions were in deionized water.

2.2. Procedure and measuring techniques

The potentiometric titrations were performed using a Metrohm 686 titroprocessor equipped with a 665 dosimat (Switzerland-Herisaue). The titroprocessor and electrode were calibrated with standard buffer solutions, prepared according to NBS specifications [11]. The titrations were carried out in a purified nitrogen atmosphere using a titration vessel described previously [12]. The temperature was maintained constant by a Colora Ultrathermostat.

The following mixtures (A–C) were prepared and titrated potentiometrically with standardized NaOH solution (~ 0.1 M).

(A) 40 ml of a solution containing [$Pm(HCl)_2$] (2.5×10^{-3} M) and $NaNO_3$ (0.1 M).

(B) 40 ml of a solution containing [$Pm(HCl)_2$] (2.5×10^{-3} M), DMT (1.25×10^{-3} M) and $NaNO_3$ (0.1 M).

(C) 40 ml of a solution containing [$Pm(HCl)_2$] (2.5×10^{-3} M), TMT or TBT (2.5×10^{-3} M), and $NaNO_3$ (0.1 M).

All mixtures were titrated in different percentage (v/v) dioxane-water solutions (25.0, 37.5, 50.0, 62.5 and 75.0) and at different temperatures (15.0, 20.0, 25.0, 30.0 and 35.0°C).

The equilibrium constants were evaluated from titration data, defined by Eq. (1) and Eq. (2).

$$l(M) + p(L) + q(H) \rightleftharpoons (M)_l(L)_p(H)_q \quad (1)$$

$$\beta_{pqr} = \frac{[(M)_l(L)_p(H)_q]}{[M]^l[L]^p[H]^q} \quad (2)$$

where M, L and H represent organotin(IV), pyridoxamine and proton respectively. The calculations were performed using the computer program [13] MINIQUAD-75 by means of an IBM-4366

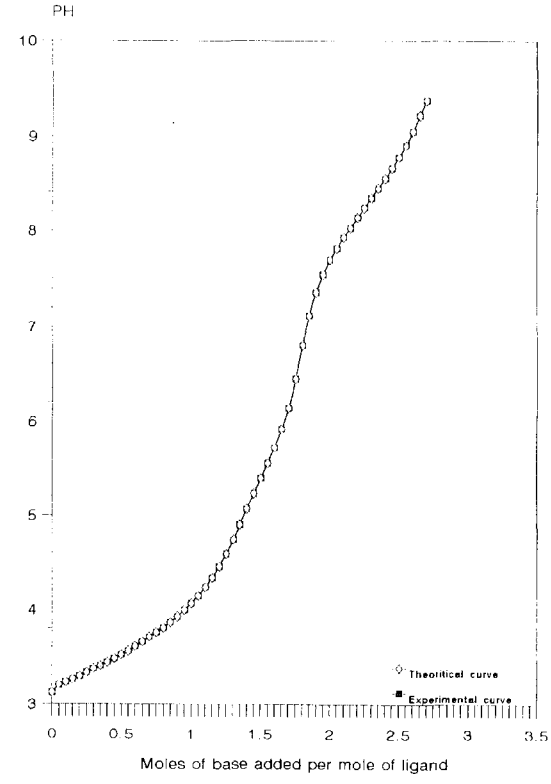

Fig. 1. Potentiometric titration curve for DMT-pyridoxamine system.

Table 1
Formation constants of pyridoxamine complexes

System	Temp. (°C)	l	p	q[a]	log β[b]	S[c]
Pm	15	0	1	1	11.08(0.02)	2.8E-7
		0	1	2	19.44(0.03)	
		0	1	3	22.88(0.05)	
DMT-Pm		1	1	0	12.99(0.06)	7.4E-8
		1	2	0	18.81(0.07)	
		1	1	1	18.77(0.02)	
TMT-Pm		1	1	0	8.27(0.03)	1.7E-7
		1	1	1	16.32(0.03)	
TBT-Pm		1	1	0	7.65(0.04)	2.3E-7
		1	1	1	15.02(0.09)	
Pm	20	0	1	1	10.68(0.01)	7.6E-8
		0	1	2	19.01(0.01)	
		0	1	3	22.52(0.02)	
DMT-Pm		1	1	0	12.66(0.05)	5.5E-8
		1	2	0	18.25(0.06)	
		1	1	1	18.38(0.02)	
TMT-Pm		1	1	0	7.82(0.03)	1.5E-7
		1	1	1	15.87(0.03)	
TBT-Pm		1	1	0	7.45(0.02)	8.3E-8
		1	1	1	14.70(0.06)	
Pm	25	0	1	1	10.61(0.01)	9.1E-8
		0	1	2	18.85(0.02)	
		0	1	3	22.20(0.03)	
DMT-Pm		1	1	0	11.93(0.03)	1.6E-8
		1	2	0	17.26(0.03)	
		1	1	1	17.68(0.01)	
TMT-Pm		1	1	0	8.21(0.06)	6.5E-7
		1	1	1	15.78(0.06)	2.2E-8
TBT-Pm		1	1	0	7.53(0.03)	6.8E-8
		1	1	1	14.76(0.05)	
Pm	30	0	1	1	10.53(0.01)	1.0E-7
		0	1	2	18.66(0.02)	
		0	1	3	21.64(0.03)	
DMT-Pm		1	1	0	11.86(0.05)	6.9E-8
		1	2	0	18.35(0.05)	
		1	1	1	17.31(0.03)	
TMT-Pm		1	1	0	8.37(0.03)	2.0E-7
		1	1	1	15.95(0.03)	
TBT-Pm		1	1	0	7.52(0.03)	1.3E-7
		1	1	1	14.81(0.06)	
Pm	35	0	1	1	9.94(0.01)	3.1E-7
		0	1	2	17.84(0.02)	
		0	1	3	21.00(0.05)	
DMT-Pm		1	1	0	11.68(0.08)	1.6E-7
		1	2	0	17.30(0.09)	
		1	1	1	17.31(0.03)	
TMT-Pm		1	1	0	7.66(0.02)	1.4E-7
		1	1	1	14.93(0.02)	
TBT-Pm		1	1	0	7.02(0.01)	3.1E-8
		1	1	1	14.12(0.03)	

[a] l, p and q are the stoichiometric coefficient corresponding to organotin(IV), pyridoxamine and H^+, respectively.
[b] Standard deviations are given in parentheses.
[c] Sum of square of residuals.

computer. The stoichiometries and stability constants of the complexes formed were determined by trying various possible composition models. The model selected gave the best statistical fit and was chemically consistent with the titration data without giving any systematic drifts in the magnitudes of various residuals, as described elsewhere [13]. The fitted model was tested by comparing the experimental titration data points and the theoretical curve (simulated) calculated from the values of acid dissociation constant of the ligand and formation constants of the corresponding complexes. Fig. 1 shows a comparison between the experimental data points of the titration of dimethyltin(IV)-pyridoxamine system, taken as a typical example, and the theoretical curve. Table 1 and Table 2 list the formation constants together with their standard deviations and the sum of square of residuals as was obtained from the program MINIQUAD-75. Concentration distribution diagrams were obtained using the program Species [14].

3. Results and discussion

3.1. Protonation equilibria

The acid dissociation constants of pyridoxamine were determined under the same experimental conditions of ionic strength and temperature which are used for the study of organotin(IV) complex equilibria. A maximum number of three protons can be released from pyridoxamine in the fully protonated form (H_3L^{2+}) on titration with strong base in the pH range (3.2–11.0). The titration data indicates the presence solely of simple HL, H_2L^+ and H_3L^{2+} complexes, where HL represents pyridoxamine in the neutral form. The overall protonation constants ($\log \beta_{011}$, $\log \beta_{012}$ and $\log \beta_{013}$) of pyridoxamine were calculated. The values obtained (Table 1) are in good agreement with the literature data [3], after considering changes in experimental conditions. The stepwise protonation constants in aqueous solution at 25°C can be represented by: $\log K_1^H = 10.61$, $\log K_2^H = 8.24$ and $\log K_3^H = 3.35$. These values correspond to the phenolic (OH), ammonium (NH_3^+) and protonated pyridine groups, respectively.

3.2. Complex formation equilibria

The potentiometric equilibrium titration curves of pyridoxamine in the presence and absence of trimethyltin(IV), taken as a representative example, are given in Fig. 2. The complex titration curve starts at pH ~ 3.10 and is significantly lower than the ligand curve. This may be conceived as a visual indication of complex formation through a release of hydrogen ions. The results of triorganotin(IV) complexes show the formation of the 1:1 (organotin:ligand) complex and the corresponding protonated complex species. On the other hand, the results in the diorganotin(IV) system show the formation of 1:1 and 1:2 complexes and of the protonated species of the 1:1 complex. The formation constants of the butyltin(IV) complexes, Table 1, were found to be lower than those of the methyl analogues. This may be due to steric crowding between the bulky butyl group and pyridoxamine. The formation constant of the 1:1 complex with DMT is higher than with TMT. This is explained on the premise that pyridoxamine binds to DMT and TMT as bidentate- and monodentate ligands, respectively. The coordination geometry around tin in $(CH_3)_3Sn(IV)$ in aqueous solution is believed to be trigonal bipyramidal in which the three methyl groups are situated in the equatorial plane. Complex formationwould then involve pyridoxamine binding in the apical site. The same behaviour was reported for $(CH_3)_3Sn(IV)$-pyridine complex [15]. Dimethyltin(IV), on the other hand, is able to form octahedral complex with the two methyl groups are probably colinear and placed vertically following the rules of group theory. A similar structure was reported for $(CH_3)_2Sn(IV)$-Br_2(pyridine)$_2$ complex [16]. Further studies are needed to support the structural elucidation of the coordination geometry of the organotin(IV) complexes, e.g., ^1H-^{119} Sn and/or ^{13}C-^{119} Sn nmr measurements. However such studies are not yet available and will be considered in the future.

The acid dissociation constants of the protonated complexes are given by relation Eq. (3)

$$pK^{(H)}_{M(L)(H)} = \log K^{M}_{M(L)(H)} - \log K^{M}_{M(L)} \quad (3)$$

Table 2
Effect of solvent on the equilibria of pyridoxamine complexes

System	Dioxane proportion (%)	l	p	q[a]	log β[b]	S[c]
Pm	Water	0	1	1	10.33(0.01)	1.5E-7
		0	1	2	18.39(0.02)	
		0	1	3	21.22(0.03)	
DMT-Pm		1	1	0	11.93(0.03)	1.6E-8
		1	2	0	17.26(0.03)	
		1	1	1	17.68(0.01)	
TMT-Pm		1	1	0	8.21(0.06)	6.5E-7
		1	1	1	15.78(0.06)	
Pm	25	0	1	1	10.83(0.01)	1.2E-7
		0	1	2	19.04(0.02)	
		0	1	3	22.69(0.03)	
DMT-Pm		1	1	0	12.02(0.04)	2.9E-8
		1	2	0	17.76(0.05)	
		1	1	1	18.06(0.02)	
TMT-Pm		1	1	0	7.40(0.02)	1.3E-7
		1	1	1	15.42(0.03)	
Pm	37.5	0	1	1	10.93(0.01)	1.3E-7
		0	1	2	19.08(0.02)	
		0	1	3	22.73(0.03)	
DMT-Pm		1	1	0	11.74(0.04)	2.7E-8
		1	2	0	17.46(0.05)	
		1	1	1	17.98(0.02)	
TMT-Pm		1	1	0	7.19(0.01)	6.7E-8
		1	1	1	15.15(0.02)	
Pm	50	0	1	1	11.12(0.01)	1.2E-7
		0	1	2	19.22(0.02)	
		0	1	3	22.86(0.03)	
DMT-Pm		1	1	0	12.09(0.03)	2.2E-8
		1	2	0	18.47(0.03)	
		1	1	1	18.13(0.01)	
TMT-Pm		1	1	0	7.38(0.01)	2.4E-8
		1	1	1	15.21(0.02)	
Pm	62.5	0	1	1	11.36(0.01)	1.9E-7
		0	1	2	19.41(0.02)	
		0	1	3	23.01(0.04)	
DMT-Pm		1	1	0	12.33(0.03)	1.8E-8
		1	2	0	19.24(0.03)	
		1	1	1	18.21(0.01)	
TMT-Pm		1	1	0	7.48(0.01)	1.8E-8
		1	1	1	15.24(0.01)	
Pm	75	0	1	1	11.57(0.01)	1.4E-7
		0	1	2	19.50(0.02)	
		0	1	3	23.07(0.03)	
DMT-Pm		1	1	0	12.46(0.05)	4.5E-8
		1	2	0	19.64(0.06)	
		1	1	1	18.10(0.02)	
TMT-Pm		1	1	0	7.47(0.01)	9.5E-9
		1	1	1	15.17(0.01)	

[a] l, p and q are the stoichiometric coefficient corresponding to organotin(IV), pyridoxamine and H^+, respectively.
[b] Standard deviations are given in parentheses.
[c] Sum of square of residuals.

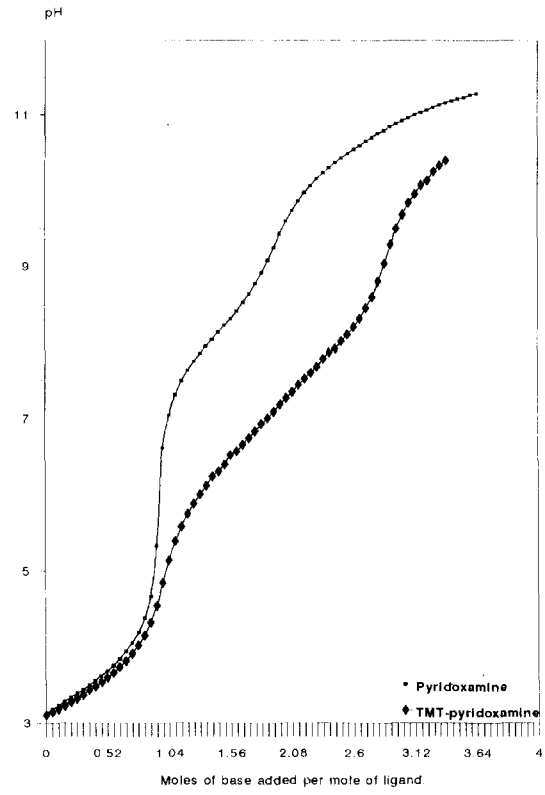

Fig. 2. Potentiometric titration curves of TMT-pyridoxamine sysytem.

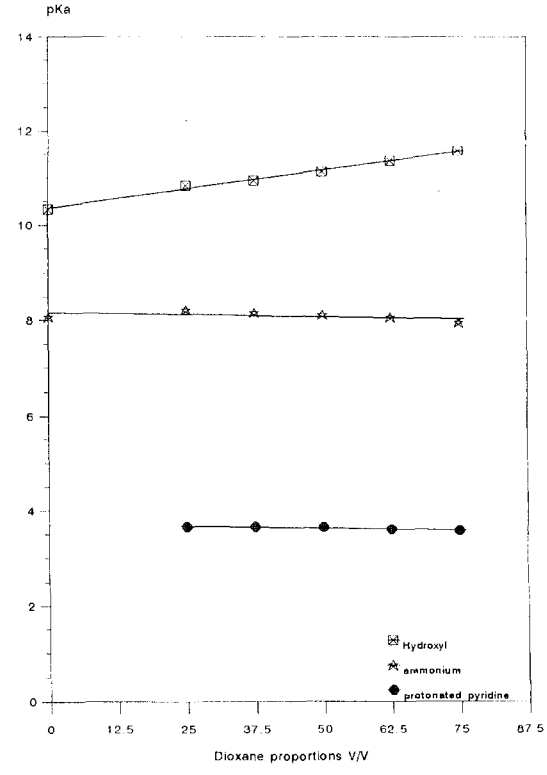

Fig. 3. Effect of dioxane proportions on pK_a of pyridoxamine.

The pK^H values are 7.57, 7.23 and 5.75 for trimethyltin(IV), tributyltin(IV) and dimethyltin(IV) complexes. The pK^H values of triorganotin(IV) complexes are in close agreement with the log K_2^H of the (NH_3^+) of the free pyridoxamine ligand. This indicates that the phenolic OH group is involved in complex formation through proton ionization, leaving the NH_2 group noncoordinated. The pK^H of the dimethyltin(IV) complex may be compared with that of pyridine after considering the increase in basicity as a result of proton ionization from pyridoxamine. This re-

Table 3
Thermodynamic parameters for the equilibria involving pyridoxamine and its organotin complexes

System	$\Delta H°$ kJ/mol^{-1}	$\Delta S°$ Jk^{-1} mol^{-1}	$-\Delta H°/R°$ K
$L^- + H^+ \rightleftharpoons HL$	−84.45(18.57)	−81.27	10.16
$HL + H^+ \rightleftharpoons H_2L^+$	−38.71(8.15)	+26.76	4.66
$H_2L^+ + H^+ \rightleftharpoons H_3L^{2+}$	−38.02(16.53)	−64.74	4.58
$M_a^{2+} + L^- \rightleftharpoons M_aL^+$	−118.87(22.64)	−165.40	14.31
$M_aL^+ + L^- \rightleftharpoons M_aL_2$	+19.22(54.62)	+174.93	−2.31
$M_a^{2+} + L^- + H^+ \rightleftharpoons M_aLH^{2+}$	−139.01(23.39)	−124.40	16.73
$M_b^+ + L^- + H^+ \rightleftharpoons M_bLH^+$	−93.15(37.01)	−10.97	11.21
$M_c^+ + L^- + H^+ \rightleftharpoons M_aLH^+$	−52.91(23.55)	+103.63	6.37

L^-, M_a, M_b and M_c denote pyridoxamine anion, dimethyltin(IV), trimethyltin(IV) and tributyltin(IV), respectively.
Standard deviations are given in parentheses and ($-\Delta H°/R$) is the vant Hoffisoohore.

veals that both -OH and NH_2 groups of pyridoxamine are involved in complex formation.

The values obtained for the thermodynamic parameters $\Delta H°$, $\Delta S°$ associated with the protonation of pyridoxamine and complex formation with the organotin(IV) species were calculated in the usual way from the temperature dependence of the data shown in Table 1. The values thus, obtained are reported in Table 3. These data can be employed to extrapolate the equilibrium constants to other temperatures. The main conclusions from the thermodynamic data can be summarized as follows:

(a) The protonation reaction of pyridoxamine associated with L^-, which corresponds to $\log K_1^H$, is more exothermic than those of $\log K_2^H$ and $\log K_3^H$. This may be explained on the basis of different coulombic forces between the proton and the pyridoxamine species (L^-, HL and H_2L^+).

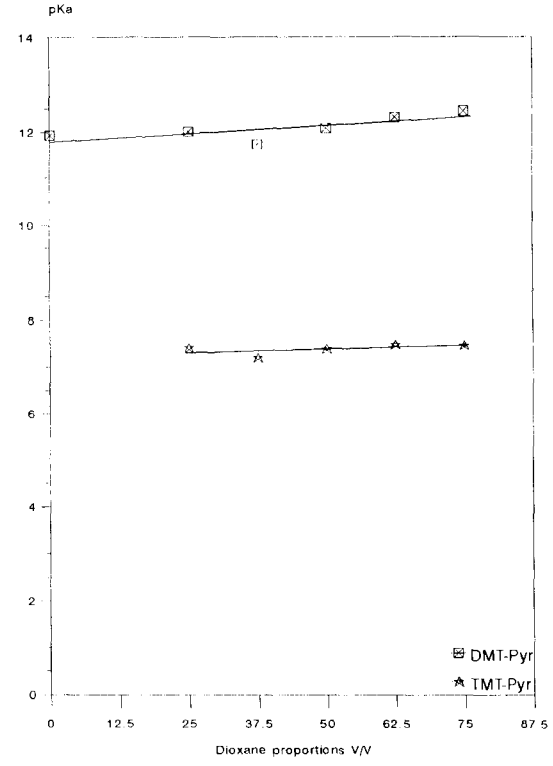

Fig. 4. Effect of dioxane proportions on the formation constants of the pyridoxamine complexes with dimethyltin(IV).

(b) The formation of the protonated 1:1 complex of pyridoxamine with TMT is more exothermic than with TBT. This means than the methyltin complex is more favoured than its butyltin homologue which suffers steric crowding between the bulky butyl group and pyridoxamine.

(c) The complex-formation of pyridoxamine with DMT is exothermic for the 1:1 complex and endothermic for the 1:2 complex. This may be explained statistically based on the presumption that more coordination sites are available for binding pyridoxamine in 1:1 than in 1:2 complexes.

3.3. Effect of solvent

It is well established that the 'effective' or 'equivalent solution' dielectric constants in proteins [17,18] or active site cavities of enzymes [19] are smaller compared with that in bulk water. Estimates for the dielectric constants in such locations range from ≈ 30 to 70 [17–19]. Hence by using aqueous solutions containing ≈ 10–50% dioxane [20], one may expect to simulate to some degree the situation in active site cavities [21], hence to extrapolate the data to physiological conditions. The variation of the pK^H values of pyridoxamine as a function of solvent composition is shown in Fig. 3. These values increase almost linearly with increasing the concentration of the organic solvent. However, the increase in the pK^H value of the -OH group is more significant. This may be correlated with the ability of a solvent of relatively low dielectric constant to increase the electrostatic forces between the ions in ($-O^- - H^+$) and to facilitate the formation of molecular species [22]. The variation of the formation constants of the pyridoxamine complexes with dimethyltin(IV) and trimethyltin(IV) as a function of solvent composition is exhibited in Fig. 4. The formation constant increases with increasing the dioxane content of the solvent. This behaviour can be explained by the variation of the protonation ability of the hydroxyl group of pyridoxamine, one of the binding sites in the complexes, as the organic solvent content increases.

Estimation of equilibrium concentrations of organotin(IV) ions and their pyridoxamine com-

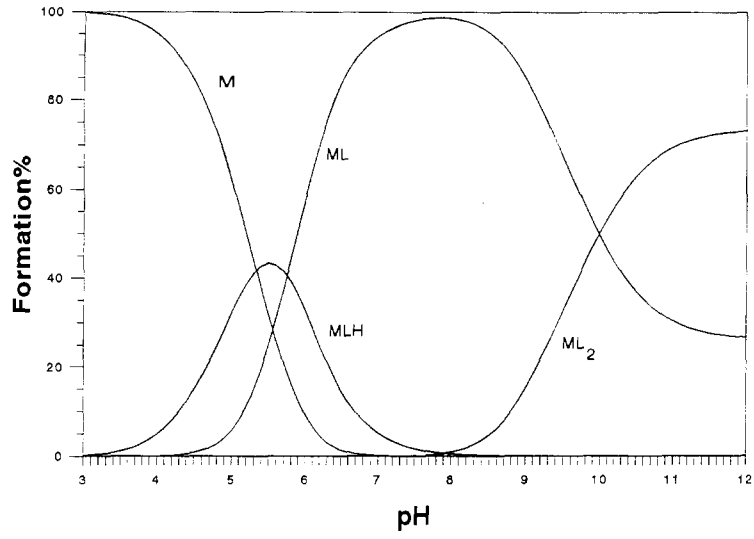

Fig. 5. Concentration of distribution of various species as a function of pH in the DMT-pyridoxamine system, where M = DMT; L = pyridoxamine; [L] = 2[DMT] = 0.0025 M.

plexes as a function of pH provides a useful picture of the organotin binding with pyridoxamine. The speciation diagrams obtained for di- and trimethyltin(IV) complexes are given in Fig. 5 and Fig. 6. The protonated complex with trimethyltin(IV) starts to form at pH = 4 and reaches a maximum concentration of 34.2% at pH = 7.30. The deprotonated complex concentration increases with increasing pH, predominating with a maximum concentration of 99% at pH = 10.00. For the diorganotin(IV) complexes, the concentration of the 1:1 complex species increases with increasing pH, attaining a maximum of 97.77% at pH = 8.20. Further increase in pH is accompanied by a decrease in the 1:1 complex concentration and increase in the 1:2 complex concentration

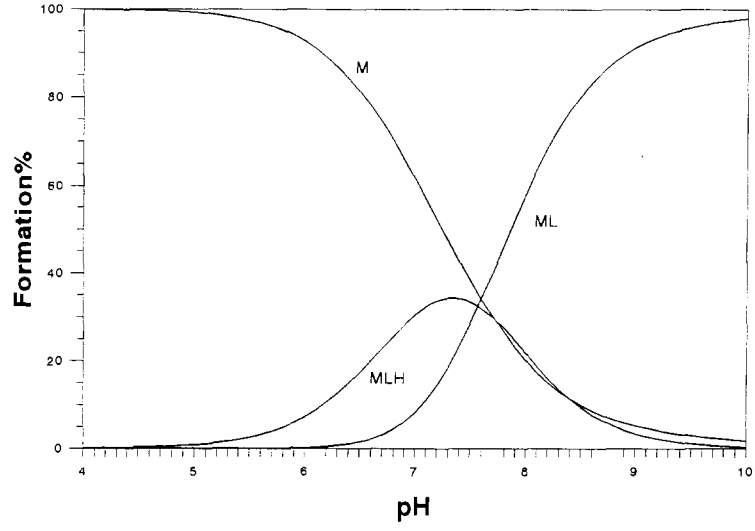

Fig. 6. Concentration distribution of various species as a function of pH in the TMT-pyridoxamine system, where M = TMT; L = pyridoxamine; [L] = [TMT] = 0.0025 M.

attaining a maximum of 73.20% at pH = 12.00. This reveals that in the physiological pH range, i.e., at pH 7.4, the (1:1) DMT-pyridoxamine complex is the predominant species and may have a chance to interact with DNA. This may provide some explanation for the reactivity of DMT-pyridoxamine complex against leukemia.

References

[1] M.S. El-Ezaby and F.R. El-Ziri, J. Inorg. Nucl. Chem., 38 (1967) 1901.
[2] M.S. El-Ezaby and N. Gayed, J. Inorg. Nucl. Chem., 37 (1975) 1065.
[3] H.M. Marafie, M.S. El-Ezaby, B.A. Abdel Nabey and N. Kihaneh, Transition Met. Chem., 7 (1982) 227.
[4] M. Gielen, R. Willem, T. Mancilla, J. Ramharter and E. Joosen, in J.J. Zuokerman (Ed.), Tin and Malignant Cell Growth, CRC Press, Cleveland, 1988.
[5] F. Kayser, M. Biesemans, M. Gielen and R. Willem, Magn. Reson. Chem., 32 (1994) 358.
[6] F. Kayser, M. Biesemans, M. Gielen and R. Willem, Main Group Met. Chem., 17 (1994) 559.
[7] M.M. Shoukry, J. Coord. Chem., 25 (1992) 111.
[8] M.M. Shoukry, J. Inorg. Biochem., 48 (1992) 271.
[9] M.M. Shoukry, Bull. Soc. Chem. Fr., 130 (1993) 177.
[10] M.M. Shoukry, Talanta, in press (1996).
[11] R.G. Bates 'Determination of pH-Theory and Practice' 2nd Edn., Wiley Interscience, New York, 1975.
[12] M.M. Shoukry, W.M. Hosny and M.M. Khalil, Transition Met. Chem., 20 (1995) 252.
[13] P. Gans, A. Sabatini and A. Vacca, Inorg. Chim. Acta, 18 (1976) 237.
[14] L. Pettit (University of Leeds), Personal Communication.
[15] R. Hulme, J. Chem. Soc., 1524 (1963).
[16] L.A. Aslanov, V.M. Innov, W.M. Atliya and A.B. Permin, J. Struct. Chem., 19 (1978) 166.
[17] D.O. Rees, J. Mol. Biol., 141 (1980) 323.
[18] N.K. Rogers, G.R. Roore and M.J.E. Strenberg, J. Mol. Biol., 182 (1985) 613.
[19] H. Sigel, R.B. Martin, R. Tribolet, U.K. Haring and R. Malini-Balakrishran, Eur. J. Biochem., 152 (1985) 187.
[20] G. Akerlof and O.A. Short, J. Am. Chem. Soc., 75 (1953) 6357.
[21] H. Sigel, Pure Appl. Chem., 61 (1989) 923.
[22] M.M. Shoukry, E.M. Shoukry and S.M. El-Medani, Monat. Chem., 126 (1995) 909.

ELSEVIER

Talanta 44 (1997) 1159–1162

Talanta

Determination of hafnium in air dust filters by inductively coupled plasma atomic emission spectrometry

Adam Hulanicki [a,*], Jolanta Surgiewicz [b], Irena Jaron [c]

[a] *Department of Chemistry, University of Warsaw, Warsaw, Poland*
[b] *Central Institute of Labour Protection, Warsaw, Poland*
[c] *State Institute of Geology, Warsaw, Poland*

Received 10 May 1996; received in revised form 22 October 1996; accepted 25 October 1996

Abstract

The procedure of hafnium determination in workplace air has been elaborated, which allows its determination at the level starting from 0.125 mg m^{-3}, which for a 400 l sample corresponds to the requirement for maximal allowable concentration. The method is based on excitation of the mineralized filter containing the analyte in inductively coupled plasma. © 1997 Elsevier Science B.V.

Keywords: Air analysis; Atomic emission spectrometry; Hafnium; Inductively coupled plasma

1. Introduction

Hafnium is used in production of highly resistant materials, as anticorrosive layers, explosives, special glasses and in ceramic industry. The dust containing hafnium is toxic through respiratory and alimentary tracks. The value of $LD_{50} = 76$ mg kg^{-1} has been evaluated for mice. Hafnium bound to transferrin was after 4 days detected in blood plasma in 95% [1]. The hafnium tetrachloride (for rats $LD_{50} = 2000$ mg kg^{-1}) results in renal degeneration and small intestine inflammation. In Poland the threshold limit value (TLV) for total hafnium in air has been proposed as 0.5 mg m^{-3} [2]. This corresponds to the value in other countries (Australia, Belgium, Danemark, France, Germany, UK, Switzerland, USA). In UK the short term exposure limit (STEL) equals 1.5 mg m^{-3}.

In the literature there are mainly spectrophotometric procedures for routine determination small amounts of hafnium [3], however other techniques have also been used [4]. Various materials have been analyzed using X-ray fluorescence and neutron activation analysis [5]. The atomic absorption spectrometry with flame atomization in nitrous oxide-acetylene flame has poor limit of detection and suffers interferences [6]. Atomic absorption spectrometry has been also proposed by OSHA [7] for hafnium determination at the workplace. In optimal conditions the limit of detection equals 2.0 μg ml^{-1} and the characteristic concentration 15 μg ml^{-1}.

* Corresponding author. Fax: +48 2 2225996.

PII S0039-9140(96)02152-2

The inductively coupled plasma optical emission spectrometry has been sugested for determination of hafnium in workplace air [8,9]. The limit of detection has been indicated at the level of a few ng ml^{-1}. It can be also used for hafnium determination in complex matrices [10], however in the case of complex matrices either the matrix should be separated or its effect compensated by matrix matched calibration solutions [11,12]. For determination of hafnium in geological samples also inductively coupled plasma mass spectrometry has been applied and the detection limit was found to be 20 ng g^{-1} [13].

In this paper the procedure was elaborated which makes possible determination of hafnium collected on filters from the workplace air.

2. Experimental

2.1. Instrumentation

The ICP-AES spectrometer Jobin-Yvon 70 Plus with a peristaltic pump (Instruments S.A.) was used for recording the emission spectra. Air aspirator with a constant air flow 20 l min^{-1} according to Polish Standard [14] was used for suction of air through the nitrocellulose membrane filters, Synpor 3, diameter 50 mm and porosity 0.6–0.8 μm.

2.2. Reagents

Hafnium metal (99.95%) purchased from Merck was used for preparation of stock solutions by dissolution of 1 g of metal in 40% hydrofluoric acid, and dilution up to 1 l with 5% hydrofluoric acid in a polypropylene flask. The working solution – 50 mg l^{-1} was prepared by appropriate dilution of the stock solution with 5% hydrofluoric acid.

Hydrofluoric acid – 40 and 5%, nitric acid – 65% and perchloric acid – 62% all of analytical grade were also purchased from Merck.

2.3. Procedure of determination

The samples should be taken according to Polish Standards [14] by aspiration of 400 l of air at the rate 20 l min^{-1}, through the membrane filter. The filters are mineralized in teflon crucibles using 3 ml of concentrated nitric acid. After evaporation till dryness, in the next step 3 ml of concentrated nitric acid and five drops of concentrated perchloric acid were used and again evaporated. In subsequent steps 3 ml of concentrated nitric acid + 5 ml of hydrofluoric acid and 1 ml of concentrated nitric acid + 5 ml hydrofluoric acid, respectively, were used. Finally the residue was dissolved in 3–5 ml of 5% hydrofluoric acid. In a 50 ml measuring flask the same acid should be added till the mark. The analyte line is measured at the wavelength 282.022 nm, with single point background correction. The experimental parameters of the ICP excitation are generally based on the manufacturers recommendations and are given in Table 1. The blank is obtained by using the pure filter of the same type mineralized as filters with sample dust.

The concentrations are read from the calibration graph, prepared with standards containing 1.0, 2.5,...10.0 ml of working hafnium solution, diluted with 5% hydrofluoric acid up to 50 ml.

3. Results and discussion

For determination of hafnium a few emission lines can be used. These are Hf II 282.022 nm, Hf II 277.336 nm, Hf II 264.141 nm and Hf II 232.247 nm. The 277.336 nm line is interfered in the case of the presence of iron and a number of

Table 1
Experimental conditions of excitation

Generator power	1.0 kW
Outer gas flow rate	12.0 l min^{-1}
Intermediate gas flow rate	1.0 l min^{-1}
Carrier gas flow rate	1.0 l min^{-1}
Sample uptake rate	1.3 ml min^{-1}
Observation height above coil	12 mm
Integration time	2 s

Table 2
Limiting concentrations of interferents at the ± 5% error level

Interferent	Interferent concentration in solution μg ml^{-1}	Interferent concentration in air[a] mg m^{-3}	Multiple of MAC in condition of sampling
Li	6	0.75	30
Na	120	15.0	30
K	120	15.0	30
Mg	150	18.8	~1 (for oxide)
Ti	25	3.1	—
V	5	0.6	~1
Cr	10	1.3	~13 (for Cr (VI))
Mn	15	1.9	~6
Fe	400	50	≈10 (for oxides)
Ni	5	0.6	~2.4
Cu	20	2.5	~2.5
Cd	1	0.1	~2.5
Sn	50	6.3	~3
Pb	4	0.5	10

Concentration of hafnium in solution = 5 μg/ml.
[a] In conditions of sampling air.

other concomitants. The measurements based on the line 264.141 nm, suggested by NIOSH [8], exhibit poor precision. The largest tolerance as well as best precision was found in the case of line 282.022 nm and this line was used in the elaborated analytical procedure. This line provided a sufficient limit of detection and lack of interference. The analytical signals were investigated in the presence of common concomitants and the maximum tolerable concentration was evaluated based on the limiting error of ± 5% (Table 2).

The figures of merit of the ICP-OES measurements were evaluated at the concentration level 4 mg l^{-1}, corresponding to the threshold limit value for 400 l air sample. Each of the five samples was measured nine times, and the relative standard deviation was in the range from 0.3 to 1.8%.

The calibration function is rectilinear with the equation C(mg l^{-1}) = −0.02254 + 0.000913 I (relative intensity readings). The calibration function was based on six model solutions, the first one not containing hafnium. For any calibration point the relative standard deviation was larger than 1.5%.

As there are no standard aerosol (dust) samples available containing the known content of hafnium, the recovery test was based on filters with known amount of added hafnium in the form of standard solution. Such procedure was assumed to give less uncertainty than using reference material with recommended Hf values but with a completely different matrices. The amount of hafnium on the filters was 0.100, 0.200 and 0.400 mg, which corresponds to 0.25, 0.50 and 1.00 mg m^{-3} of hafnium in air, which is below and above TLV (0.50 mg m^{-3}). The relative standard deviation was for all samples below 2%, and the recovery was in the range from 98 to 102%. The concentration of hafnium in the air (X) is calculated on the basis of the calibration function, relating the concentrations of hafnium (mg l^{-1}) in the sample (c), the concentration in the blank (c_0), the volume (l) of solution of the sample (v_1) and the volume (m^3) of the sampled air (v):

$$X = (c - c_0)v_1/v$$

4. Conclusions

The method of hafnium determination in the range from 50 to 500 μg has been developed using the inductively coupled plasma-optical emission spectrometry technique. This range, for a 400 l air

sample, corresponds to concentration of hafnium in air from 0.125 to 1.25 mg m^{-3}. This makes possible to use this procedure for determination of hafnium below and above the threshold limit value at the workplace (TLV = 0.5 mg m^{-3}). The hafnium containing dust is collected at the filter, dissolved and hafnium is excited in the ICP-OES technique. Accompanying elements which may potentially be present in the sampled air do not interfere.

Acknowledgements

The authors are grateful to Dr Piotr Paslawski, State Geological Institute, Warsaw, for his assistance in ICP-AES measurements. This work was partially supported by the BST 502/2/95 project.

References

[1] The Dictionary of Substances and their Effects, R. Soc. Chem., Vol. 4, Cambridge 1994, p. 735.
[2] Criteria for Recommended Standard for Occupational Exposure to Hafnium. Session of Experts for Chemical Agents, Łódź, 1995.
[3] Z. Marczenko, Separation and Spectrophotometric Determination of Elements, Ellis Horwood, Chichester 1986.
[4] R. Lobinski and Z. Marczenko, Spectrochemical Trace Analysis for Metals and Metaloids, Elsevier, Amsterdam, 1996.
[5] T. Mamuro, Y. Matsuda, A. Mizohota, T. Takeuchi and A. Fujita, Radioisotopes, 20 (1971) 117.
[6] V.K. Pany, Anal. Chim. Acta, 57 (1971) 31.
[7] Occupational Safety and Health Administration, Analytical Methods Manual, Vol. 1, Method ID-121, Salt Lake City, Utah, 1991.
[8] National Institute for Occupational Safety and Health, Manual of Analytical Methods, Vol. 1, Method S-194, Cincinnati, Ohio, 1991
[9] G. Wunsch and K. Pose, Fresenius Z. Anal. Chem., 322 (1985) 272.
[10] N. Korte, M. Kollenbach and S. Donivan, Anal. Chim. Acta, 146 (1983) 267.
[11] R. Łobinski, J.A.C. Broekaert, P. Tschöpel and G. Tölg, Fresenius J. Anal. Chem., 342 (1992) 569.
[12] F. Yokota, H. Morikawa and T. Ishizuka, Analyst, 119 (1994) 1023.
[13] G.E.M. Hall, J.C. Pelchat and J. Loop, J. Anal. At. Spectrom., 5 (1990) 339.
[14] Air purity protection, Sampling methods, Principles of air sampling in work environment and interpretation of results. Polish Standard PN-89/Z-04008/07.

ELSEVIER

Talanta 44 (1997) 1163–1171

Talanta

Determination of butyl- and phenyltin compounds in sediments by GC-FPD after $NaBEt_4$ ethylation

C. Carlier-Pinasseau, G. Lespes *, M. Astruc

Laboratoire de Chimie Analytique, CURS, Université de Pau et des Pays de l'Adour, Avenue de l'Université, 64000 Pau, France

Received 16 July 1996; received in revised form 16 October 1996; accepted 29 October 1996

Abstract

A reliable and rapid speciation method for the simultaneous determination of butyl- and phenyltin species in sediment samples has been developed. Two extraction procedures are compared: methanolic hydrochloric acid (at four different concentrations) and ethanoic acid leaching. Derivatization is carried out by the one-step ethylation/extraction procedure using the sodium tetraethylborate reagent directly in aqueous phase in the presence of an isooctane layer. Analysis is performed by capillary gas chromatography hyphenated to flame photometric detection (GC-FPD). Detection limits range from 0.5 to 1.5 ng(Sn) g^{-1}(dry weight). Analysis of environmental samples and certified reference materials demonstrate the accuracy of the analytical method. © 1997 Elsevier Science B.V.

Keywords: Butyltin; GC-FPD; $NaBEt_4$ ethylation; Phenyltin; Sediment

1. Introduction

Organotin compounds have been extensively used as biocides. Contamination of marine and fresh water environments by the highly toxic tributyltin (TBT) is primarily due to its use in antifouling paints on vessels [1]. The ecotoxicological impact of TBT has been demonstrated [1,2]. Triphenyltin (TPhT) compounds are used as agricultural fungicides in crop protection [3]. But TPhT was found to be a non selective pesticide, detrimental to fresh water fauna [4]. Moreover TPhT has been shown to have a high bioaccumulation potential [3]. In the aquatic environment, triorganotin compounds have low aqueous solubility and low mobility. They are easily adsorbed by particulate matter in the water, which, upon settling to the bottom, can be incorporated into the sediment [5]. Considerable concentrations of these compounds and their metabolites were detected in sediments of Swiss Lakes [6].

The recognition of organotin toxicity at low concentration levels has stimulated the development of accurate and sensitive analytical methods for organotin determinations. Many efficient analytical procedures combine chromatographic separation and various detection techniques such as atomic absorption spec-

* Corresponding author. Fax: + 33 59029377.

PII S0039-9140(96)02153-4

trometry (AAS) [7–10], mass spectrometry (MS) [4], atomic emission spectrometry (AES) [4,11] or flame photometric detection (FPD) [12–14]. Despite recent improvements in instrumentation, several limitations remain present especially in the sample preparation steps. Prior to gas chromatography (GC) organotin compounds need to be liberated from the sediment before being derivatized into forms suitable for chromatography. Extraction of organotin compounds after acid leaching from the matrix followed by hydridization using $NaBH_4$ or alkylation with Grignard reagent are the most common approaches. Alternatives to acid leaching are the use of super critical fluid [11,15] or soxhlet [4] extractions.

A new organotin derivatization procedure directly applied to aqueous extracts using sodium tetraethylborate ($NaBEt_4$) has been recently proposed. Ethylation and extraction of compounds are performed in a single operating flask [8,16–18]. It allows simultaneous speciation of butyl- and phenyltin and is much more simple and rapid than procedures using Grignard reaction.

The method of speciation associating this derivatization with GC-FPD was proved to be very performant in analysis of complex matrices [18]. This is due to the simplicity of the whole process and the specificity of the detector. Nevertheless, to our knowledge, it has never been used in the analysis of natural samples such as sediment. Moreover, it allowed the determination of several organotin species including the phenyltin compounds which are critical to determine.

In this paper, such a method has been developed for the simultaneous determination of butyl- and phenyltins. First, the optimal conditions for the extraction of these species have been evaluated on the BCR Certified Reference Material CRM 462 spiked with TPhT. Different approaches of organotin leaching from the material have been tested. Second, from the row extract, the in-situ derivatization with $NaBEt_4$ reagent and direct analysis using capillary gas chromatography and flame photometric detection (GC-FPD) were performed. The optimized method was applied to the analysis of the Canadian Reference Material PACS-1 and of fresh water sediment samples.

2. Experimental

All organotin concentrations reported in this paper are expressed as the mass of tin per sample mass or solution volume unit.

2.1. Apparatus

A Varian 3300 Gas Chromatograph (GC) was used for this study. It was fitted with a split/splitless injector, a J&W Scientific capillary column coated with polydimethylsiloxane (inner diameter 250 μm, length 30 m, film thickness 0.25 μm) and a Flame Photometric Detector (FPD). The detector was operated with a 610 nm optical filter (from MTO Optique Instrumentale) and an air/hydrogen flame. Nitrogen was used as carrier gas.

2.2. Reagents and standards

Tripropyltinchloride (TPT, 98%), monobutyltintrichloride (MBT, 95%), dibutyltindichloride (DBT, 97%), tributyltinchloride (TBT, 96%), monophenyltintrichloride (MPhT, 98%), diphenyltindichloride (DPhT, 96%) and triphenyltinchloride (TPhT, 95%) were purchased from Aldrich. Tetrabutyltin (TeBT, 98%) was obtained from Fluka. Stock organotin solutions (1000 mg l^{-1} as Sn) were prepared in methanol. Stored at +4°C in the dark, they are stable for several months [19]. Working standards were obtained by dilution in methanol weekly for 10 mg l^{-1} and daily for 100 μg l^{-1} and stored in the dark at +4°C.

Methanol and sodium ethanoate were purchased from Prolabo, nitric acid, hydrochloric acid, and ethanoic acid obtained from Merck, and isooctane from Fluka. The deionized water used was 18 MΩ (Millipore System).

Ethanoate buffer (pH 4.8, 0.2 mol l^{-1}) was prepared by dissolving 16.4 g of sodium ethanoate in 1 l of deionized water followed by pH adjustment with ethanoic acid. Sodium tetraethylborate ($NaBEt_4$) was obtained from Strem Chemical. Working solution was made up daily by dissolving 0.02 g $NaBEt_4$ in 1 ml of deionized water and stored in the dark at +4°C.

Glassware was rinsed in deionized water, decontaminated overnight in 10% (v/v) nitric acid solution and then rinsed again.

2.3. Samples

2.3.1. BCR certified reference material 462

It is certified to contain [20]:

70 ± 14 ng(cation) g^{-1}(dry weight) i.e., 29 ± 6 ng(Sn) g^{-1} for TBT

128 ± 16 ng(cation) g^{-1}(dry weight) i.e., 65 ± 8 ng(Sn) g^{-1} for DBT

It was found free of TPhT, so we spiked it before analysis with TPhT at the concentration of 50 ng(Sn) g^{-1}(dry weight). CRM 462 contains also MBT and MPhT but the concentrations of these species are not certified.

2.3.2. PACS-1 reference material

The PACS-1 reference sediment is a dry sample prepared by the National Research Council of Canada. It is certified for its DBT and TBT contents (Table 5).

2.3.3. Environmental sediments

Two different samples from Leman Lake (Swiss) were given by Dr Becker Van Slooten from Polytechnic Federal School of Lausanne. They were collected on different sites of Port d'Ouchy at different dates.

2.4. Extraction and analytical procedure

A scheme of the different procedures tested is shown on Fig. 1.

2.4.1. Extraction

Two extraction methods were tested on the spiked CRM 462 sample;

2.4.1.1. Methanolic/hydrochloric acid digestion. The action of HCl as leaching agent was tested at four different concentrations: from 0.1 to 3 mol l^{-1} in methanol using the following procedure:

1 g of sediment sample was introduced in a capped 50 ml polycarbonate tube with 0.5 ml of a 100 ng(Sn) ml^{-1} TPT methanolic solution as internal standard and 2.5 ml of methanol. Tubes were shaken at 420 rpm for 2 h to humidify the material. This rehumidification step was carried out only 1 h for wet samples. 12.5 ml of HCl at the appropriate concentration in methanol was then added and the mixture was treated ultrasonically for 1 h. The suspension was centrifuged at 3000 rpm for 15 min. The supernatant was then withdrawn.

2.4.1.2. Ethanoic acid digestion. Dry sediment sample, 1 g, was introduced in a capped 50 ml polycarbonate tube with 0.5 ml of a 100 ng(Sn) ml^{-1} TPT methanolic solution as internal standard and 20 ml of glacial ethanoic acid. Tubes were shaken at 420 rpm for 4 h. The suspension was centrifuged at 3000 rpm for 15 min. The supernatant was then withdrawn.

2.4.2. Derivatization and analysis

Extracts, 1–3 ml, were directly introduced in the derivatization reactor without any further

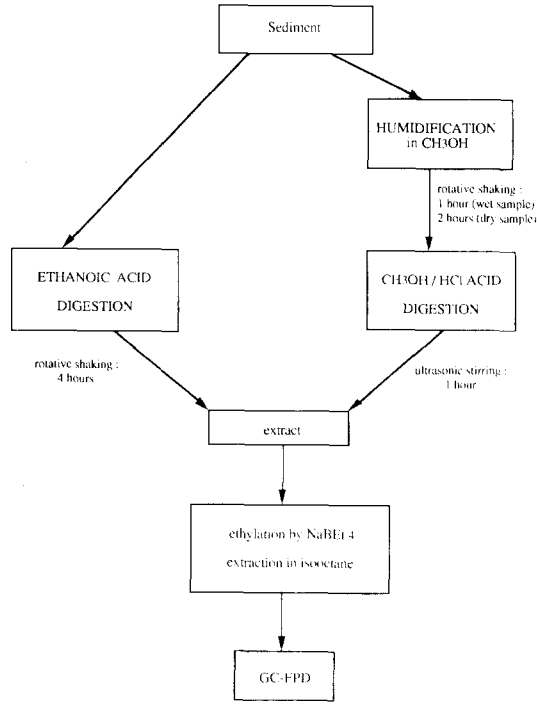

Fig. 1. Schematic representation of different sample preparation procedures used for isolation of organotin compounds from sediments.

Table 1
Analytical conditions for determination of organotin compounds by GC-FPD

Injector parameters			
	Sample amount		From 2 to 5 μl
	Injection temperature		290°C
	Relay	Initial relay	+1 (splitless)
		Relay time	1 min
		Final relay	−1 (split)
GC parameters			
	Carrier gras	Nitrogen	
		Flow rate	0.7 cm^3 min^{-1}
	Oven program	Initial temperature	70°C for 1 min
		1st heat up rate	30°C min^{-1}
		Intermediate temperature	190°C for 10 min
		2nd heat up rate	15°C min^{-1}
		Final temperature	270°C for 5 min
FPD parameters			
	Detection temperature		290°C
	Flame	Air/hydrogen	
		Hydrogen flow rate	185 cm^3 min^{-1}
		Air flow rate	250 cm^3 min^{-1}
	Make up	Nitrogen	
		Flow rate	30 cm^3 min^{-1}

treatment. Organotin compounds were ethylated in 100 ml of ethanoate buffer (pH = 4.8) with 0.1 ml of $NaBEt_4$ solution in the presence of 0.4 ml of isooctane. The mixture was shaken at 420 rpm for 30 min. Isooctane extracts, 2–5 μl, were directly injected into the GC-FPD. Analytical parameters were optimized and precisely described elsewhere [18]. Chromatographic conditions are summarized in Table 1.

The determination of organotin concentrations in samples were made on seven sediment extracts: two by standard additions and five else using TPT as internal standard (five replicates for each extract). This procedure allows a maximum reliability and accuracy without to be too time-consuming.

3. Results and discussion

3.1. Optimization of extraction and analytical performances

To our knowledge, acid leaching of sediments directly followed by $NaBEt_4$ derivatization for the determination of phenyltin compounds, as described in this paper, has not been previously reported in the literature. So, its influence on the analytical procedure has to be evaluated due to the possible disturbances on the derivatization step or on the GC-FPD signal.

Moreover, a such process appeared very simple. The number of sample handling steps was reduced, the clean-up step being found not necessary. We did not note any problem of column contamination or background interferences as indicated by Kuballa et al. [21] and Martin-Landa et al. [22].

Methanolic/HCl treatment is one of the most common way used to break the bonding between species and sediments. It has been especially employed in butyltin determination but does not seem to be applied to phenyltin extraction. Extraction experiments have been previously carried out with different HCl concentrations in methanol depending on their authors [22–24] and ranging between 0.48 and 6.7 mol l^{-1}. So, it was necessary to compare methanolic/HCl extractions at four different concentrations.

In most published works, organotin compounds are further complexed by ligands such as tropolone [10,14,22,24] to improve their extraction yields into an organic solvent before Grignard derivatization. Such procedures are more time and man-power consuming; losses and degradation may occur. So, we chose not to use any complexing agent.

Ethanoic acid digestion was developed by Desauziers et al. to analyse butyltin compounds in sediments [25], but it seems to have only been applied to leach butyltin compounds [9,25,26]. Therefore the efficiency of this extraction procedure as regards phenyltin species had also to be studied in this work.

3.1.1. Study of extraction

Recoveries of butyl- and phenyltin species presented in Table 2 are calculated by comparison with the certified reference butyltin values (DBT: 65 ± 8 ng(Sn) g^{-1} and TBT: 29 ± 6 ng(Sn) g^{-1}) or to the spiking TPhT concentration (50 ng(Sn) g^{-1}) TPhT.

3.1.1.1. Methanolic/hydrochloric acid digestion. Disturbances of the GC-FPD signal such as discontinuity of the baseline were observed when HCl concentration was used over 2 mol l^{-1}. More generally, random peaks could then appear. Baseline decreased or increased in the beginning of the chromatogram as showed in Fig. 2, whatever the HCl concentration was. These observations proved that a matrix effect could occurred according to the nature of the extraction solution.

Quantitative recoveries of DBT and TBT were obtained when using 0.1–2 mol l^{-1} methanolic HCl solutions while quantitative recovery of TPhT is obtained only for 0.1 mol l^{-1} HCl.

Simultaneously MBT and MPhT peak heights were maximum with 1 mol l^{-1} hydrochloric solution (Fig. 2), before disappearing when too concentrated HCl was used, probably due to inorganic tin occurrence.

In order to improve the knowledge of the behaviour of the organotin species during hydrochloric acid digestion, stability studies were carried out. First, in methanolic standard solutions containing either one of the six butyl- or phenyltin compounds, addition of HCl at different concentrations was made. Significant degradations were observed over 0.1 mol l^{-1} acid concentration. This phenomenon appeared all the more the organotin was substituted, the TBT and the TPhT being particularly subject to decompositions. The phenylated species were always less stable than the butylated ones. Second, according to these results, the trisubstituted standard solutions were submitted to the same conditions of extraction (data in brackets in Table 2). These experiments confirmed that the use of 0.1 molar HCl avoided any degradation and seemed convenient for extraction.

Moreover, it seems from Table 2 data that butyltin compounds are more stable in sediment matrix, especially TBT. This is in agreement with previous constatations [27]. It is well known that TBT half life times range from months to years in sediments instead of days to weeks for the water column [28].

At the difference of butyltins, phenyltin compounds had the same degradation behaviour either in sediment extracts or in standard solutions, indicating probably a difference in bonding sites. At HCl concentrations higher than 0.1 mol l^{-1}, TPhT was transformed directly into monophenyl-

Table 2
Recoveries of organotins after analysis of the spiked certified reference material 462 using different extraction procedures and, in brackets, recoveries from standard solutions of TBT and TPhT submitted to the same conditions

Extraction method	DBT% [a]	TBT% [a]	TPhT% [a]
HCl/methanol 0.1 mol l^{-1}	98	108 (100%)	92 (100%)
HCl/methanol 1 mol l^{-1}	109	91 (77%)	64 (60%)
HCl/methanol 2 mol l^{-1}	90	96 (71%)	64 (57%)
HCl/methanol 3 mol l^{-1}	71	109 (56%)	0 (29%)
Ethanoic acid	108	105 (100%)	103 (100%)

[a] Mean recovery ($n = 7$) calculated by comparison with the reference butyltin values (DBT: 65 ± 8 ng(Sn) g^{-1}, TBT: 29 ± 6 ng(Sn) g^{-1}) or the spiking TPhT concentration (50 ng(Sn) g^{-1}).

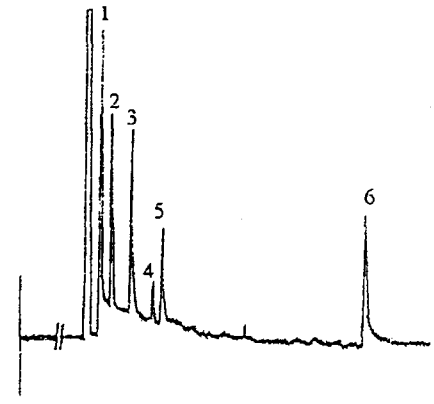

HCl/methanol extraction
with 0.1 mol/l HCl methanolic solution
(1 : MBT, 2 : TPT, 3 : DBT, 4 : MPhT,
5 : TBT, 6 : TPhT)

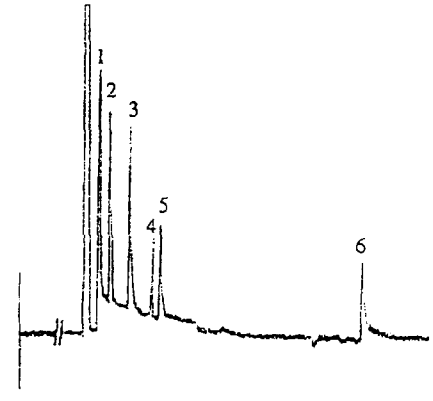

HCl/methanol extraction
with 1 mol/l HCl methanolic solution

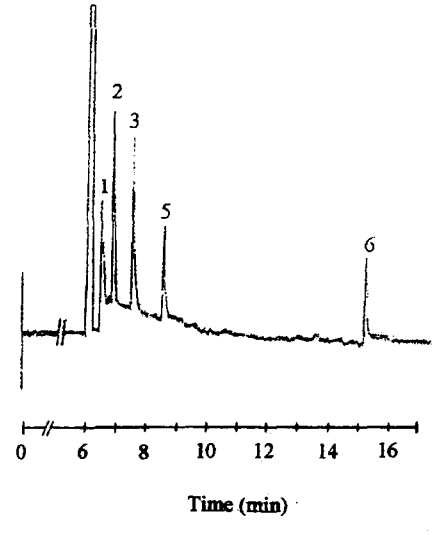

HCl/methanol extraction
with 2 mol/l HCl methanolic solution

Fig. 2. Typical chromatogramms of spiked CRM 462 analysis after HCl/methanol extraction (1: MBT, 2: TPT, 3: DBT, 4: MPhT 5: TBT, 6: TPhT).

Table 3
Relative standard deviation of seven different analysis of spiked CRM 462 extracts using each extraction method

Extraction method	MBT%	DBT%	TBT%	MPhT%	DPhT%	TPhT%
HCl/methanol 0.1 mol l^{-1}	4	4	4	13	7	6
HCl/methanol 1 mol l^{-1}	12	9	11	19	[a]	10
HCl/methanol 2 mol l^{-1}	17	12	13	[a]	[a]	11
HCl/methanol 3 mol l^{-1}	25	19	13	[a]	[a]	[a]
Ethanoic acid	6	6	6	12	7	9

[a] The compound was never detected.

and inorganic tin: the HCl/methanol extraction can not be successfully applied to leach phenyltin compounds from sediments except at very low (≤ 0.1 molar) HCl concentration.

3.1.1.2. Ethanoic acid digestion. Quantitative recoveries are obtained by ethanoic acid extraction. The possible decomposition of butyl- and phenyltin compounds during the extraction step was also checked by incubation of TBT and TPhT in ethanoic acid using leaching extraction conditions (Table 2). Analysis of the incubated standard solutions leads to a quantitative recovery of TBT and TPhT. These results agree with those reported in the literature for butyltin determination [9,25,26] but are new for TPhT.

Moreover, no disturbance of the GC-FPD signal was observed. Extraction and derivatization by $NaBEt_4$ are all the more compatible with this extraction procedure as the $NaBEt_4$ reaction needs an ethanoate/ethanoic acid buffer. So ethanoic acid leaching is preferred to analyse sediments. Butyl- and phenyltin compounds are determined simultaneously and quantitatively, without any noticeable degradation.

3.1.2. Performances of the analytical procedure

3.1.2.1. Reproducibility. Reproducibility was studied by evaluation of the relative standard deviation for the analysis of seven different extracts. Results obtained with different extraction procedures and for each compound are reported in Table 3. The reproducibility using methanolic HCl extraction is low except at very low HCl concentration. Ethanoic acid leaching is performant and results reproducible.

3.1.2.2. Detection limits. Detection limits (DL) reported in Table 4 were determined according to IUPAC recommendations with $k = 3$. They are calculated from the slope of calibration curves of all compounds and base line noise.

DL are slightly higher with the ethanoic acid method than with the 0.1 mol l^{-1} HCl/methanol one. However for phenyltin species, DL are generally lower than most of those reported in literature when organotin determinations are performed by GC-FPD following Grignard derivatization and HCl leaching or super critical fluid extraction (from 2.2 to 5.8 ng(Sn) g^{-1}(dry weight) [13,15]). As regards butyltin species, detection limits are close to those given for analysis performed by GC-FPD after Grignard derivatization (from 0.2 to 1.8 ng(Sn) g^{-1}(dry weight) [13–15]) and lower than those reported after $NaBEt_4$ ethylation: 25, 36 and 61 ng(Sn) g^{-1}(dry weight) for respectively TBT, DBT and MBT [7] using 2.2 molar HCl for the extraction and 0.44 ng(Sn) g^{-1}(dry weight) for TBT [8] using 0.5 molar HCl. Such differences may be due to the extraction procedure. From this study we retained the ethanoic acid extraction procedure for further studies.

3.2. Applications

The ethanoic acid leaching procedure was further validated by the analysis of three different environmental samples.

3.2.1. PACS-1 reference material

Mean concentrations obtained from five determinations are given in Table 5. Concentrations obtained are in agreement with the certified ones.

Table 4
Relative detection limits expressed in ng(Sn) g^{-1} (dry weight)

Extraction method	MBT	DBT	TBT	MPhT	DPhT	PhT
HCl/methanol 0.1 mol l^{-1}	0.5	0.7	0.7	1.1	0.9	1
HCl/methanol 1 mol l^{-1}	0.6	0.7	1	2.7	[a]	1.4
HCl/methanol 2 mol l^{-1}	0.6	0.7	0.9	[a]	[a]	1
HCl/methanol 3 mol l^{-1}	0.9	1.1	0.9	[a]	[a]	[a]
Ethanoic acid	1.2	1.2	0.8	1.8	0.8	1.5

[a] The compound was never detected.

Table 5
Concentrations of butyl- and phenyltin in the PACS-1 reference sediment expressed in ng(Sn) (dry weight)$^{-1}$

	DBT	TBT
Certified concentrations ± S.D.	1160 ± 180	1270 ± 220
Concentrations found ± S.D. ($n = 5$)	1174 ± 86	1044 ± 67

S.D., standard deviation.

According to the standard deviation values, the analytical method appears accurate.

3.2.2. *Sediments from Port D'Ouchy, Leman Lake, Switzerland*

Two different freshwater sediment samples were analysed and results obtained are reported in Table 6. They are compared with those determined by Dr Becker Van Slooten using a Grignard derivatization/GC-FPD procedure [29]. Results obtained by the two different analytical techniques are in very good agreement. Organotin concentrations in Port d'Ouchy sediments are quite high. This marina has a housing capacity of 603 places for pleasure boats staying all year round [6]. Every fourth boat is repainted annually. Becker Van Slooten and Tarradellas tentatively estimated the total number of boats protected by an organotin-containing antifouling paint to about 30% for the marinas of Leman Lake [6] and attributed the high sediment organotin pollution to boat paint leaching and the high stability of organotins in sediments.

4. Conclusion

After study of the operating conditions and comparison of two extraction methods, both butyl- and phenyltin species were determined in sediments.

Results show that ethanoic acid leaching is a convenient method to release simultaneously and

Table 6
Concentrations of butyl- and phenyltin in Leman Lake sediments

	Sediment 1		Sediment 2	
	Eth./GC-FPD	Ref. [29]	Eth./GC-FPD	Ref. [29]
MBT[a]	186 ± 7	n.c.	190 ± 13	n.c.
DBT[a]	295 ± 7	309	311 ± 13	246
TBT[a]	627 ± 50	632	632 ± 43	593
MPhT[a]	319 ± 23	n.a.	151 ± 2	n.a.
DPhT[a]	142 ± 10	n.a.	108 ± 9	n.a.
TPhT[a]	158	n.a.	112 ± 7	110

n.a., not analysed.
n.c., not communicated.
[a] Mean concentration ± S.D. ($n = 5$) in ng(Sn) g^{-1}(dry weight).

quantitatively butyl- and phenyltin compounds. Nevertheless, quantitative recoveries can also be reached with HCl/methanol solubilization if the HCl concentration is about 0.1 mol l^{-1} in methanol. Higher HCl concentrations lead to degradation of organotin compounds particularly of phenyltin ones.

The ethanoic acid extraction procedure is preferred because of its performances. Simple and rapid, it can be easily applied to a routine method. It is directly compatible with the one-step aqueous ethylation-extraction/capillary gas chromatography-flame photometric detection method. It allows an accurate simultaneous determination of butyl- and phenyltin compounds from fresh water and sea water sediments with detection limits in the ng(Sn) g^{-1} range.

Acknowledgements

This work was supported by the Agence de l'Eau Rhin-Meuse. Thanks are due to Dr Becker Van Slooten for the gift of sediment samples.

References

[1] K. Fent, Environ. Pollut., 76 (1992) 187.
[2] K. Fent and W. Meier, Arch. Environ. Contam. Toxicol., 22 (1992) 428.
[3] K. Fent, R. Lovas and J. Hunn, Naturwissenschaften, 78 (1991) 125.
[4] J.A. Stäb, W.P. Cofino, B. Van Hattum and V.A.T. Bunkman, Fresenius'J. Anal. Chem., 347 (1993) 247.
[5] L. May, D. Whalen and G. Eng, Appl. Organomet. Chem., 7 (1993) 437.
[6] K. Becker Van Slooten and J. Tarradellas, Arch. Environ. Contam. Toxicol., 29 (1995) 384.
[7] J.R. Ashby and P.J. Craig, Sci. Total Environ., 78 (1989) 219.
[8] Y. Cai, S. Rapsomanikis and M.O. Andreae, Talanta, 41 (1994) 589.
[9] W.M.R. Dirkx, M.B. De La Calle, M. Ceulemans and F.C. Adams, J. Chromatogr., 683 (1994) 51.
[10] S. Zhang, Y.K. Chau, W.C. Li and A.S.Y. Chau, Appl. Organomet. Chem., 5 (1991) 431.
[11] Y.K. Chau, F. Yang and M. Brown, Anal. Chim. Acta, 304 (1995) 85.
[12] H. Harino, M. Fukushima and M. Tasaka, Anal. Chim. Acta, 264 (1992) 91.
[13] J.L. Gomez-Ariza, R. Beltran, E. Morales, I. Giraldez and M. Ruiz-Bonitez, Appl. Organomet. Chem., 4 (1995) 51.
[14] I. Tolosa, L. Merlini, N. De Bertrand, J.M. Bayona and J. Albraiges, Environ. Toxicol. Chem., 11 (1992) 145.
[15] Y. Cai, R. Alzaga and J.M. Bayona, Anal. Chem., 66 (1994) 1161.
[16] J.R. Ashby and P.J. Craig, Appl. Organomet. Chem., 5 (1991) 173.
[17] M. Ceulemans, C. Witte, R. Lobinski and F.C. Adams, Appl. Organomet. Chem., 8 (1994) 451.
[18] C. Carlier-Pinasseau, G. Lespes and M. Astruc, Appl. Organomet. Chem., 10 (1996) 505.
[19] P.M. Sarradin, Thesis of University of Pau, France, 1993.
[20] Ph. Quevauviller, M. Astruc, L. Ebdon, V. Desauziers, P.M. Sarradin, A. Astruc, G.N. Kramer and B. Griepink, Appl. Organomet. Chem., 8 (1994) 629.
[21] J. Kuballa, R.D. Wilken, E. Jantzen, K.K. Kwan and Y.K. Chau, Analyst, 120 (1995) 667.
[22] I. Martin-Landa, F. De Pablos and I.L. Marr, Anal. Proc., 26 (1989) 16.
[23] Y. Cai, S. Rapsomanikis and M.O. Andreae, Mikrochim. Acta, 109 (1992) 67.
[24] I. Martin-Landa, F. De Pablos and I.L. Marr, Appl. Organomet. Chem., 5 (1991) 399.
[25] V. Desauziers, F. Leguille, R. Lavigne, M. Astruc and R. Pinel, Appl. Organomet. Chem., 3 (1989) 469.
[26] P.M. Sarradin, A. Astruc, R. Sabrier and M. Astruc, Mar. Pollut. Bull., 28 (1994) 621.
[27] K. Fent, J. Hunn and M. Sturm, Naturwissenschaften, 78 (1991) 219.
[28] S.J. de Mora, C. Stewart and D. Phillips, Mar. Pollut. Bull., 30 (1995) 50.
[29] K. Becker Van Slooten, Thesis. Federal Polytechnic School of Lausanne, Swiss, 1994.

ELSEVIER

Talanta 44 (1997) 1173–1182

Talanta

Utility of diphenylamine and *N*-bromosuccinimide for colorimetric determination of certain phenothiazine drugs

Abd El-Maaboud Ismail Mohamed

Department of Analytical Pharmaceutical Chemistry, Faculty of Pharmacy, Assiut University, Assiut, Egypt

Received 20 May 1996; received in revised form 27 August 1996; accepted 29 October 1996

Abstract

A sensitive colorimetric method for the quantitative estimation of 11 phenothiazine drugs was developed. The method was based on the interaction of phenothiazine compounds with diphenylamine in presence of *N*-bromosuccinimide and sulfuric acid. Most of studied phenothiazines yielded bluish green products with two absorption maxima, one in the range of 392–396 nm with higher molar absorptivity and the other in the range of 770–780 nm with lower molar absorptivity. Phenothiazine base, mepazine HCl and pericyazine yielded blue products with only one maximum at 655, 775 and 778 nm, respectively. The color was stable for at least 1 h. The reproducibility and recovery of the method were excellent. The method was applied successfully to the determination of some commercially available phenothiazines in different dosage forms. Results were comparable to those obtained by official and reported methods. © 1997 Elsevier Science B.V.

Keywords: Pharmaceuticals; Phenothiazines; Spectrophotometry

1. Introduction

Numerous methods used to assay phenothiazine drugs in bulk as well as in pharmaceutical preparations and biological fluids. Among these methods are titrimetric [1–5], chromatographic [6–14], electro-chemical [15–20], ultraviolet and visible spectrophotometric [21–34] and fluorimetric methods [35–38]. Many of these procedures suffer interference from excipients, coloring and flavoring agents, degradation and/or oxidation products of phenothiazine drugs. Thus, increasing selectivity and avoiding interferences was a main objective in this study.

The interaction between phenothiazine drugs and some selected amine compounds in presence of certain oxidants were investigated previously in our laboratory and some successful methods were developed [26–29]. The applicability of this reaction for developing more sensitive, selective and time saving procedures has been investigated. As a result of this investigation, a rapid, sensitive and reproducible colorimetric method for determination of 11 phenothiazine drugs has been developed.

PII S0039-9140(96)02154-6

Table 1
Absorption characteristics for the reaction products

Drugs	λ_{max1}	$\epsilon_{max1} \times 10^{-4}$ l mol^{-1} cm^{-1}	λ_{max2}	$\epsilon_{max2} \times 10^{-4}$ l mol^{-1} cm^{-1}	$\epsilon_{max1}/\epsilon_{max2}$	Concentration (μg ml^{-1})[a]
Phenothiazine base			655	1.63		50
Promethazine HCl	393	3.28	773	2.14	1.533	80
Promazine HCl	394	2.86	775	1.69	1.690	100
Alimemazine tartrate	394	8.19	776	5.57	1.470	50
Mepazine HCl			775	1.52		150
Perazine dimalonate	392	6.03	770	4.12	1.464	80
Chlorpromazine HCl	395	1.66	777	1.28	1.297	200
Thioridazine HCl	396	3.10	777	2.65	1.170	100
Methotrimeprazine maleate	395	9.78	776	7.20	1.358	30
Thiethylperazine maleate	396	3.06	780	2.01	1.522	200
Pericyazine			778	0.127		1500

[a] In the final working standard solution.

2. Experimental

2.1. Apparatus and reagents

(a) Apparatus: Uvidec-320 spectrophotometer (JASCO, Tokyo, Japan).

(b) Chemicals: pharmaceutical grade, phenothiazine base, promazine HCl, promethazine HCl, alimemazine tartrate, mepazine HCl, perazine dimalonate, chlorpromazine HCl, methotrimeprazine maleate, thiethylperazine maleate, thioridazine HCl, pericyazine, trifluoperazine HCl,

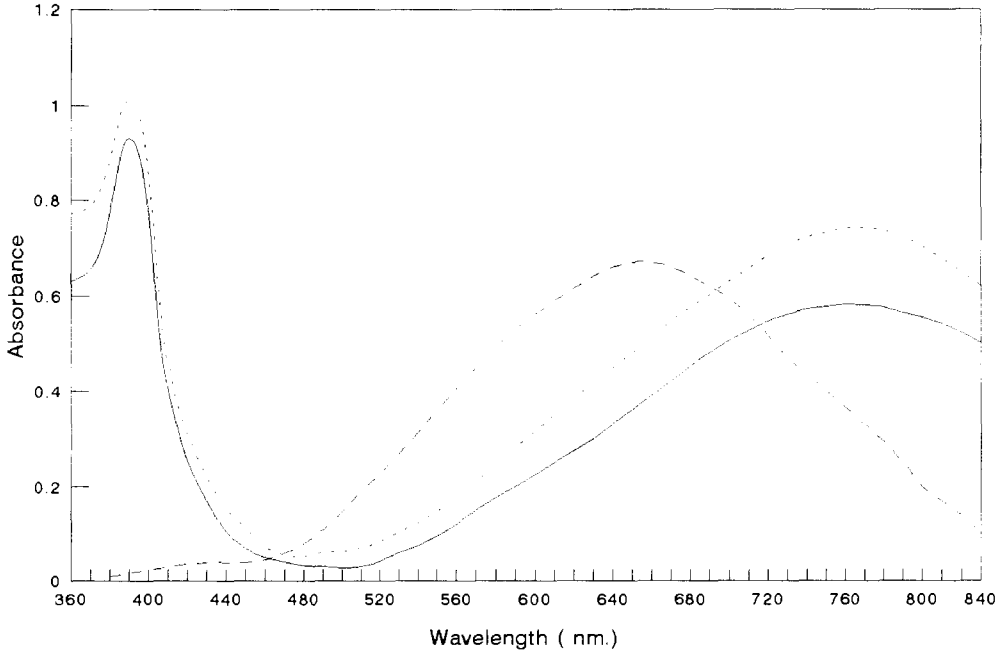

Fig. 1. Absorption spectra of colored products of promazine HCl (10 μg ml^{-1}), methotrimeprazine maleate (5 μg ml^{-1} and phenthiazine base (8 μg ml^{-1}).

Table 2
Comparative summary of some statistical data

Drugs	Lin. cal. range[a] μg ml^{-1}	Intercept ± S.D.	Slope ± S.D.	r^c	Lin. cal. range[b] μg ml^{-1}	Intercept ± S.D.	Slope ± S.D.	r^c
Phenothiazine base[d]					1–12	0.087 ± 0.007	0.073 ± 0.0006	0.9998
Promethazine HCl	1–10	0.153 ± 0.01	0.087 ± 0.001	0.9993	1–15	0.098 ± 0.01	0.057 ± 0.001	0.9989
Promazine HCl	1–12	0.142 ± 0.02	0.075 ± 0.001	0.9984	5–20	0.023 ± 0.003	0.050 ± 0.0001	0.9999
Alimemazine tartrate	1–10	0.077 ± 0.007	0.102 ± 0.0007	0.9998	2–15	0.037 ± 0.004	0.071 ± 0.0004	0.9998
Mepazine HCl					5–25	0.022 ± 0.003	0.039 ± 0.0001	0.9998
Perazine dimalonate	2–12	0.130 ± 0.02	0.097 ± 0.002	0.9991	2–12	0.053 ± 0.02	0.070 ± 0.001	0.9985
Chlorpromazine HCl	3–21	0.120 ± 0.01	0.035 ± 0.0003	0.9996	5–35	0.110 ± 0.02	0.025 ± 0.0005	0.9983
Thioridazine HCl	2–12	0.035 ± 0.003	0.073 ± 0.0006	0.9998	3–15	0.011 ± 0.001	0.064 ± 0.0002	0.9999
Methotrimeprazine maleate	1.5–5	−0.177 ± 0.01	0.238 ± 0.003	0.9993	2–8	−0.135 ± 0.008	0.175 ± 0.002	0.9995
Thiethylperazine maleate	3–20	0.078 ± 0.007	0.041 ± 0.0003	0.9998	5–40	0.062 ± 0.01	0.026 ± 0.0004	0.9990
Pericyazine					50–350	−0.043 ± 0.001	0.004 ± 0.00001	0.9999

[a] Measured at 392–396 nm.
[b] Measured at 770–780 nm.
[c] Correlation coefficient.
[d] Measured at 655 nm.

butaperazine maleate and oxomemazine tartrate were obtained as gifts from various manufacturers and were used as working standards without further treatment. Promazine sulfoxide was prepared by a reported procedure [39]. All solvents used throughout this work were analytical grade.

(c) *N*-Bromosuccinimide (NBS) solution: into 50 ml volumetric flask, add 250 mg NBS. Add about 40 ml of water and shake well. After complete dissolution dilute solution to volume with water. Mix well and use for 24 h.

(d) Diphenylamine solution: 1% w/v diphenylamine solution in methanol or ethanol.

(e) 2 M sulfuric acid solution.

(f) Dosage forms: various commercial preparations purchased from local sources and listed in Table 6.

2.2. Preparation of standards

Dissolve an accurately weighed amount of each phenothiazine drug as free base or its salt in methanol and dilute quantitatively with the same solvent to obtain the appropriate dilution for each drug (Table 1).

2.3. Preparation of samples

2.3.1. Tablets

Weigh 20 tablets and finely powder. Transfer accurately weighed amount of powder equivalent to 25 mg of studied drug to 100 ml volumetric flask and dilute to about 80 ml with methanol. Shake the mixture well for about 10 min, dilute to the mark with the same solvent and filter. Discard first portion of filtrate. Use clear solution obtained as stock solution. Dilute stock solution quantitatively with methanol to obtain the suitable working sample solution for studied drug (Table 1).

2.3.2. Liquid preparations (Syrups, Vials and Drops)

Dilute an accurately measured volume of each preparation equivalent to 25 mg of the declared drug quantitatively to obtain the suitable working sample dilution for studied drug (Table 1).

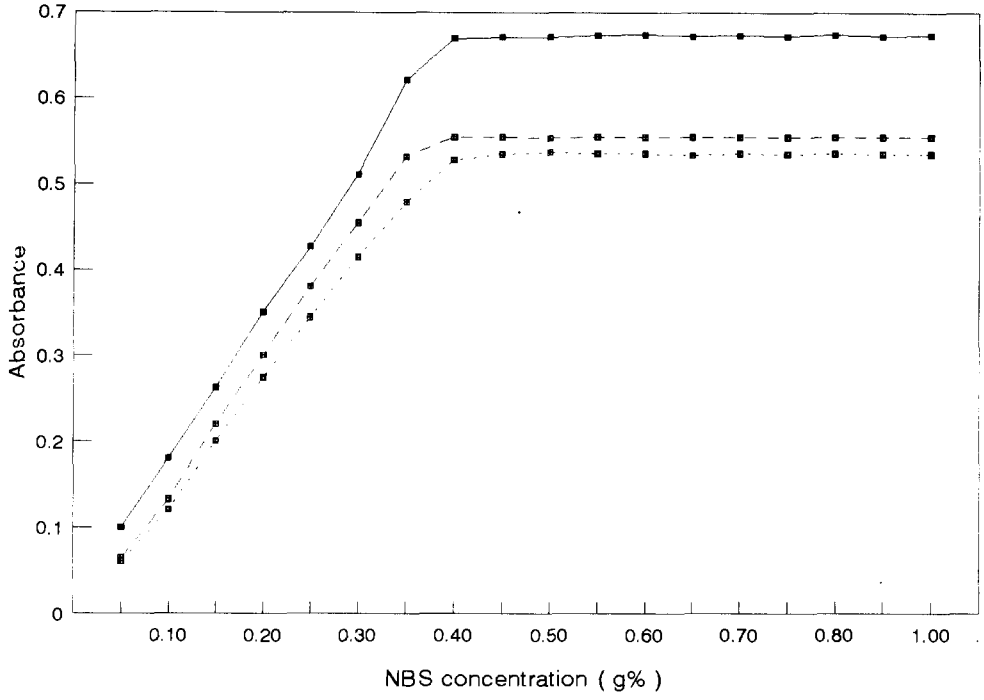

Fig. 2. Effect of NBS concentration on the absorbtion intensity of reaction products of 8 μg phenothiazine base, 10 μg promazine HCl and 4 μg methotrimeprazine maleate ml^{-1}.

2.3.3. Suppositories

Weigh and molten five suppositories. Transfer an accurately weighed amount of suppositories equivalent to 25 mg of chlorpromazine HCl or 10 mg of thiethylperazine to 50 ml volumetric flask. Add about 40 ml of methanol and warm to about 45°C. Shake well for about 10 min keeping the solution warm. Cool, dilute to the mark, shake and filter. Discard the first portion of the filtrate. Use the obtained filtrate as final sample dilution in the case of thiethylperazine or dilute quantitatively with methanol to obtain a working sample solution of chlorpromazine HCl containing 200 μg ml^{-1}.

2.3.4. Recovery study

Add an accurately weighed amount of declared drug for each preparation to 100 ml volumetric flask, containing accurately weighed quantity of the powdered tablets or moltened suppositories or accurately measured volume of liquid preparations. Either dissolve contents of flask in methanol and treat as described for tablets and suppositories or dilute quantitatively with methanol to obtain required concentration as described for liquid preparations.

2.4. Determination

To 1 ml of either standard or sample phenothiazine solution in 10 ml volumetric flask, add 1 ml diphenylamine solution followed by 1 ml NBS solution and 0.5 ml of sulfuric. Mix well and then dilute the solution to volume with methanol. Measure absorbance at either 392–396 or 770–780 nm through about 15 min against a blank treated similarly (measure phenothiazine base, mepazine HCl and pericyazine at 655, 775 and 778 nm, respectively).

Table 3
Effect of dilution by different solvents on the absorption intensity of developed colors from promazine HCl (10 μg ml^{-1}) and methotrimeprazine maleate (4 μg ml^{-1})

Solvent	Promazine HCl		Methotrimeprazine maleate	
	Wavelength (nm)	Absorbance[a]	Wavelength (nm)	Absorbance[a]
Methanol	394	0.886	395	0.764
	775	0.531	776	0.552
Ethanol	394	0.655	400	0.552
	777	0.421	772	0.385
Isopropanol	394	0.631	400	0.507
	778	0.399	778	0.389
Dioxane	398	0.772	404	0.558
	780	0.502	778	0.485
DMSO	418	0.181	420	0.154
	581	0.095	586	0.115
	897	0.102	900	0.112
Water[b]	—	—	—	—

[a] Average of four determinations.
[b] Complete color discharge and precipitation.

Table 4
Effect of the sequence of addition on the intensity of colored products

Sequence of addition	Promazine HCl (10 μg ml^{-1})		Methotrimeprazine maleate (4μg ml^{-1})	
	Wavelength (nm)	Absorbance[a]	Wavelength (nm)	Absorbance[a]
1-drug + amine + NBS + no acid	398	0.467	399	0.356
	610	0.235	612	0.301
	780	0.264	779	0.322
2-drug + amine + NBS + acid	394	0.891	395	0.771
	775	0.544	776	0.559
3-drug + amine + acid + NBS	352	0.797	355	0.698
	460	0.145	456	0.121
	800	0.151	789	0.132
4-drug + acid + NBS + amine	450	0.255	455	0.333
5-drug + NBS + amine + acid	395	0.305	395	0.354
	780	0.176	776	0.189
6-drug + acid + amine + NBS	462	0.171	455	0.201
	790	0.181	789	0.213
7-drug + amine + acid + no NBS	—[b]	—	—	—
8-drug + NBS + acid + amine	450	0.303	455	0.354

[a] Average of four determinations.
[b] No maxima was found in the studied range (390–800 nm).

3. Results and discussion

3.1. Absorption characteristics

The absorption spectra for the highly colored products of most phenothiazine drugs from reaction with diphenylamine and NBS reagents exhibit two maxima with different absorption intensities (Table 1 and Fig. 1). One absorption maximum is in the range of 392–396 nm, and the other in the 770–780 nm range. Each of phenothiazine base, mepazine HCl and pericyazine have one maximum at 655, 775 and 778 nm, respectively. The shorter wavelength peaks show higher

Table 5
Determination of promazine HCl in mixtures with promazine sulphoxide and alimemazine tartrate in mixtures with oxomemazine tartrate[a]

No.	Promazine HCl[b] μg ml^{-1}	Promazine sulphoxide[b] μg ml^{-1}	Recovery[c] % ± S.D.	Alimemazine tartrate[b] μg ml 1	Oxomemazine tartrate[b] μg ml^{-1}	Recovery[c] % ± S.D.
1	10	10	99.6 ± 1.2	5	5	100.6 ± 1.3
2	10	20	99.6 ± 1.6	5	10	99.7 ± 0.9
3	10	40	99.4 ± 1.2	5	20	99.6 ± 1.1
4	10	60	100.5 ± 1.7	5	40	100.2 ± 0.8
5	10	80	100.3 ± 0.9	5	50	99.8 ± 0.8
6	10	100	99.9 ± 1.5	5	100	100.3 ± 1.6

[a] All measurements are taken at the range of 770–780 nm.
[b] Average of five determinations.
[c] Concentrations in the final measured solutions.

absorption intensity compared with that of longer ones. Measurements were conducted at both wavelengths throughout this work. The ratio between absorptivities of the two maxima calculated at different concentration levels was found to be constant with small coefficients of variation. This ratio may be useful for identification of some drugs such as promazine HCl, chlorpromazine HCl and thioridazine HCl which have characteristic values (Table 1).

Beer's law was obeyed for all phenothiazines studied at the corresponding maxima. Table 2, shows typical linear regression correlations for the studied drugs with relative standard deviation of slope less than 2% in all cases.

3.2. Effect of diphenylamine concentration

Several solutions of diphenylamine in the concentration range from 0.2 to 2.0% w/v were prepared and tested with the studied drugs. Highest color intensities were obtained by using diphenylamine solution in concentrations ranging from 0.6 to 1.4% w/v. Therefore, 1 ml of 1% w/v diphenylamine solution was used throughout this work.

3.3. Effect of NBS concentration

Fig. 2 illustrates the effect of NBS on the absorption intensity of the colored products for phenothiazine base, promazine HCl and methotrimeprazine maleate. It is quite clear from the results that color formation could be maximized by using from 0.4 to 1.0% w/v NBS solutions. Therefore, 1 ml of 1% w/v NBS solution was used throughout this work.

3.4. Effect of acid concentration

Sulfuric acid solutions ranging from 0.2 to 5 M were prepared and tested with the studied phenothiazines. It was found that, maximum color intensity was obtained by using sulfuric acid concentrations more than 1 M. In this study, 0.5 ml of 2 M sulfuric acid solution was used throughout all of the work.

Table 6
Analysis of some phenothiazine drugs in commercial dosage forms by the proposed method and compendial or reported methods[a]

Product	Source	Content	Claimed mg	Found % ± S.D.	Added mg	Recovery % ± S.D.	USP, 1990 Found % ± S.D.
Phenergan tablets	Specia	Promethazine HCl	25 Tab^{-1}	98.4 ± 0.9 $t = 0.82$, $F = 1.78$	25	99.5 ± 0.9	98 ± 1
Phenergan syrup	Specia	Promethazine HCl	5/5 ml	97.3 ± 1.2 $t = 0.45$, $F = 1.19$	5	99 ± 1	98 ± 2
Sparine vials	Wyeth	Promazine HCl	50 ml^{-1}	99.0 ± 1.4 $t = 0.54$, $F = 1.15$	50	100 ± 2	99 ± 2
Promacid tablets	Cid	Chlorpromazine HCl	25 Tab^{-1}	97.7 ± 0.9 $t = 0.51$, $F = 2.09$	25	100 ± 1	98 ± 1
Promacid suppos.	Cid	Chlorpromazine HCl	25 $Supp.^{-1}$	97.4 ± 0.8 $t = 1.12$, $F = 1.89$	25	101 ± 1	98 ± 1
Neurazine drops	Misr	Chlorpromazine HCl	40 ml^{-1}	96.9 ± 1.1 $t = 0.60$, $F = 2.12$	40	99.2 ± 0.8	96 ± 2[c]
Melleril tablets	Sandoz	Thioridazine HCl	25 $Tab.^{-1}$	98.7 ± 1.7 $t = 0.53$, $F = 1.47$	25	100 ± 1	99 ± 1[b]
Torecan suppos.	Swiss-Pharma	Thiethylperazine	6.5 $Supp^{-1}$	98.9 ± 1.5 $t = 0.59$, $F = 1.86$	10	99 ± 1	98 ± 1
Nozinan tablets	Specia	Methotrimeprazine	25 $Tab.^{-1}$	99.0 ± 1.2 $t = 0.69$, $F = 1.78$	25	100.4 ± 0.9	100 ± 2[c]

[a] Average ± S.D. of five determinations, The t- and F-values refer to comparison of the proposed method with the official or reported methods. Theoretical values at 95% confidence limit $t = 2.36$, $F = 6.39$.
[b] According to BP 1988 method [22], p. 1011.
[c] According to reported method [29].

Table 7
Spot colors, Rf values and wavelengths of maximum absorption of eluted spots for products of phenothiazine base and promazine HCl under the specified reaction conditions

Color	Phenothiazine base		Promazine HCl	
	R_f^a	λ_{max}^b (nm)	R_f^a	λ_{max}^b (nm)
Green	—	—	0.93[c]	775
Blue	0.91[c]	655	—	—
Blue	0.87	655	0.73	670
Bluish violet	0.51	605	—	—
Violet	—	—	0.54	565
Orange	—	—	0.66	402

[a] Eluting system is ammonium acetate-water-methanol (3+20+100, w/v/v).
[b] Maxima of eluted spots.
[c] Major spots.

3.5. Effect of dilution by different solvents

Dilution of the colored products by different solvents showed that, there was no effect or slight effect on the position of absorption maxima in case of alcohols, but absorption intensities were influenced. Table 3, indicates that methanol is the suitable diluting solvent because it gave the highest and most stable absorption intensity.

3.6. Effect of time

The reaction time was determined by following the color development at ambient temperature (25 ± 2°C). It was found that, color intensity was maximum just after addition of sulfuric acid and remained stable for further 15 min and then decreased gradually. On the other hand, colored products were stable for at least 1 h when diluted with methanol immediately and this may reflect the stabilizing effect of the solvent. In this study, the reaction mixtures were diluted with methanol rapidly after addition of sulfuric acid and absorption measured through 15 min after dilution with solvent.

3.7. Effect of the sequence of addition

Table 4, indicates the different possibilities studied in this work. It is clear from the results that the only sequence of addition to be followed is drug, amine, NBS and finally the acid.

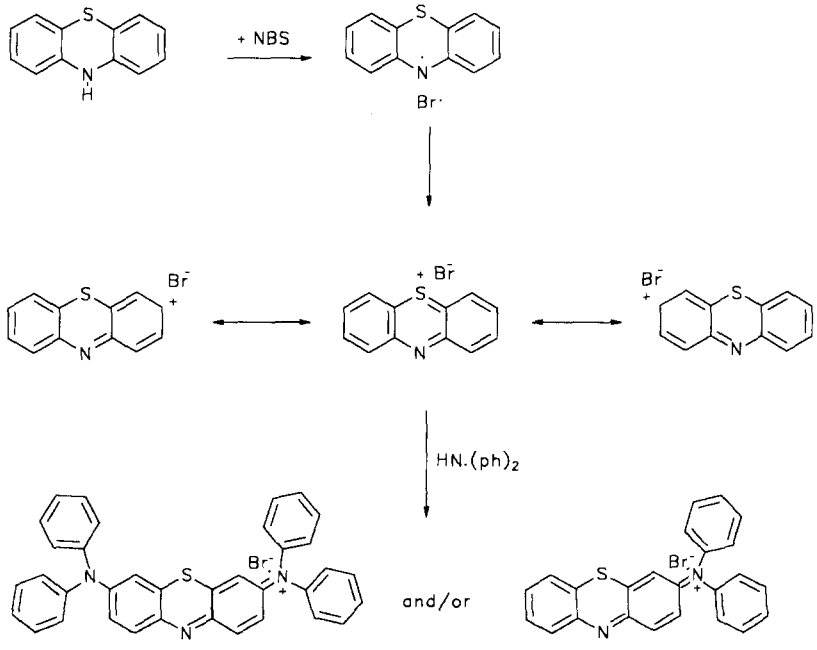

Scheme 1. Suggested sequence of reaction of phenothiazine with diphenylamine and *N*-bromosuccinimide reagents to form methylene blue-like dyes.

3.8. Specificity of the reaction

To assess the selectivity of the method to phenothiazines in presence of some oxidation products, the concentrations of promazine HCl and alimemazine tartrate were determined in several standard solutions containing promazine sulfoxide and oxomemazine tartrate (Alimemazine-5,5-dioxide), respectively. Excellent recoveries (99.4–100.5) of the intact drugs in these mixtures confirms that the assay is specific for unchanged drugs in presence of their oxidation products (Table 5).

The C-2 substituted phenothiazines with Hammett σ-values larger than 0.23 for the C-2 substituents, e.g., trifluoperazine HCl (0.54) and butaperazine maleate (0.48), gave no colored products under the studied reaction conditions.

3.9. Analysis of pharmaceuticals

The proposed method was applied for the determination of promazine HCl, promethazine HCl, chlorpromazine HCl, thioridazine HCl, thiethylperazine and methotrimeprazine as the drug entity in various pharmaceutical formulations. Recovery experiments were carried out for each drug in its respective pharmaceutical formulations. The results were compared with those obtained by applying the official or reported methods. As shown in Table 6, the results are in good agreement with those of official methods, and the recovery experiments indicate the absence of interferences from frequently encountered excipients, additives or coloring matter. It is better to use a larger volume of NBS solution (1.5 ml of 0.5% w/v solution) especially in the case of liquid preparations to overcome any interference due to the presence of antioxidants or any methanol soluble materials having strong reducing properties.

Application of Job's method of continuous variation [40] showed that all studied drugs reacted with diphenylamine in the molar ratio of 1:2 except promethazine HCl (2:3) and phenothiazine base (1:1). All other reagents and experimental conditions were kept constant.

Although the determined molar ratio for most phenothiazines was 1:2, the reaction was expected to be more complex, because at least three different spots were obtained when the reaction mixture was spotted on the thin layer chromatographic plates (Precoated silica gel, E. Merck, 0.25 mm with fluorescent indicators) as shown in Table 7.

Scheme 1 shows a suggestion for the possible pathway as predicted from literature reports [26–29,41,42] and from findings obtained in this work.

4. Conclusion

The method is simple, rapid and selective for analysis of intact phenothiazines without interference from the common oxidation and degradation products. Therefore, this method can be used as a measure for the rate of oxidation or degradation of phenothiazines (stability indicating assay). In addition, the use of diphenylamine in this work provides a higher sensitivity and better reproducibility compared with other similar previously used reagents. The method can be successfully used for the routine analysis of phenothiazine drugs in pure forms and in different pharmaceutical formulations.

References

[1] I.C. Shulka, J. Inst. Chem., 62 (1990) 159.
[2] S.M. Golabi and M. Showkati-Shishevan, Talanta, 38 (1991) 1253.
[3] U.M. Abbasi, M. Siddiqui and M.I. Bhangar, J. Chem. Soc. Pak., 13 (1991) 242.
[4] M.H. Pournaghi-Azar and J. Ordoukhanian, Talanta, 41 (1994) 611.
[5] C. Channegowda and S.M. Mayanna, Indian Drugs, 31 (1994) 574.
[6] O. Papp, I. Adam and I. Simonyi, Acta Pharm. Hung., 60 (1990) 204.
[7] T. Loennechen and S.G. Dahl, J. Chromatogr., 503 (1990) 205.
[8] H.-Y.P. Choo, Y.O. Shin and J. Park, J. Anal. Toxicol., 14 (1990) 116.
[9] P. Kintz, J.-M. Lamant and P. Mangin, Analyst, 115 (1990) 1269.
[10] S. Li and W.C. Purdy, J. Pharm. Biomed. Anal., 9 (1991) 409.

[11] H. Hattori, S. Yamamoto, M. Iwata, E. Takashima, T. Yamada and O. Suzuki, J. Chromatogr. Biomed. Appl., 117 (1992) 247.
[12] F. Garcia Sanchez, A. Navas Diaz and M.R. Fernandez Correa, J. Chromatogr., 655 (1993) 31.
[13] T.A. Berger and W.H. Wilson, J. Pharm. Sci., 83 (1994) 281.
[14] H.D. Revanasiddappa and P.G. Ramappa, Indian Drugs, 32 (1995) 73.
[15] K. Basavaiha and P.G. Ramappa, Indian J. Pharm. Sci., 51 (1989) 231.
[16] V.V. Cosofret, TrAC Trends Anal. Chem., 10 (1991) 290.
[17] J. Wang, Y.H. Lin, A.V. Eremenko, I.N. Kurochkin, M.F. Mineyeva, Anal. Chem., 65 (1993) 513.
[18] J.F. Fauvarque, G. Lepinasse, M. Mestre, P. Sarlande and O. Veyne, Analusis, 22 (1994) 373.
[19] O.I. Glukhova, V.I. Tkach and L.P. Tsyganok, Zh. Anal. Khim., 49 (1994) 1025.
[20] D.D. Schlereth and H.-L. Schmidt, J. Electroanal. Chem., 380 (1995) 117.
[21] United States Pharmacopeia XXII, National Formulary XVII, United States Pharmacopeial Convention, Inc. Rochville (1990).
[22] British Pharmacopoeia, H.M. Stationary Office, London (1988).
[23] P.G. Ramappa, H.S. Gowda and A.N. Nayak, Analyst, 105 (1980) 663.
[24] F. Buhl and M. Chwistek, Chem. Anal., 29 (1984) 581.
[25] P.G. Ramappa, A.N. Nayak and K. Basavaiha, Indian Drugs, 21 (1984) 448.
[26] S.R. El-Shabouri, A.F. Youssef, F.A. Mohamed and A.I. Rageh, Bull. Pharm. Sci. Assiut University, 8 (1985) 70.
[27] S.R. El-Shabouri, A.F. Youssef, F.A. Mohamed and A.I. Rageh, Bull. Pharm. Sci. Assiut University, 8 (1985) 144.
[28] S.R. El-Shabouri, A.F. Youssef, F.A. Mohamed and A.I. Rageh, J. Assoc. Off. Anal. Chem., 69 (1986) 821.
[29] A.F. Youssef, S.R. El-Shabouri, F.A. Mohamed and A.I. Rageh, J. Assoc. Off. Anal. Chem., 69 (1986) 513.
[30] K.M. Emara, Anal. Lett., 25 (1992) 99.
[31] Y. Fujita, I. Mori, M. Toyoda and K. Taguchi, Bunseki Kagaku, 42 (1993) T1–T5.
[32] M.M. El-Kerdawy, S.M. Hassan and S.M. El-Ashry, Mikrochim. Acta, 108 (1992) 323.
[33] M.M. El-Kerdawy, M.A. Moustafa, S.M. El-Ashry and D.R. El-wazzi, Anal. Lett., 26 (1993) 1669.
[34] S.L. Bhongade and A.V. Kasture, Talanta, 40 (1993) 1525.
[35] A.G. Davidson and E.O. Fadiran, Analyst, 115 (1990) 997.
[36] D. Chen, A. Rios, M.D. Luque de Castro and M. Valcarcel, Analyst, 116 (1991) 171.
[37] B. Laassis, J.J. Aaron and M.C. Mahedero, Anal. Chim. Acta, 290 (1994) 27.
[38] B. Laassis, J.J. Aaron and M.C. Mahedero, Talanta, 41 (1994) 1985.
[39] A.G. Davidson, J. Pharm. Pharmac., 28 (1976) 795.
[40] P. Job, Ann. Chim., 11(6) (1936) 97.
[41] A.R. Katritsky and A.J. Boulton, in 'Advances in Heterocyclic Chemistry', Vol. 9, Academic Press, New York, 1968, pp. 392–431.
[42] D. Barton and W.D. Ollis, in 'Comprehensive Organic Chemistry' Pergamon Press, Oxford, 1979, p. 1102.

ELSEVIER

Talanta 44 (1997) 1183–1193

Talanta

Analyte stabilization by electrodeposited palladium modifier for electrothermal atomic absorption spectrometry: characterization by scanning electron microscopy and anodic stripping voltammetry

J.P. Matousek [a,*], H.K.J. Powell [b]

[a] *Department of Analytical Chemistry, The University of New South Wales, Sydney 2052, Australia*
[b] *Department of Chemistry, University of Canterbury, Private Bag 4800, Christchurch, New Zealand*

Received 24 July 1996; received in revised form 31 October 1996; accepted 4 November 1996

Abstract

In electrothermal atomic absorption spectroscopy (ETAAS) effective stabilization of analytes can be achieved by an initial in situ electrodeposition of 0.2 μg of Pd. This amount of Pd is on average a factor of 50 lower than that typically used for conventional chemical modification. The surface features of this modifier have been characterized by scanning electron microscopy (SEM) measurements on sectioned pyrolytic graphite furnaces and contrasted with those for modifier produced from thermally reduced Pd salts. Electrodeposition produces a uniform array of Pd domains stretching approximately 2 mm from the centrally positioned Pt/Ir anode (which doubles as the autosampler sample delivery tube). In contrast, thermally reduced Pd salts produce a modifier which concentrates in domains near the drying edge of the modifier solution. Anodic stripping voltammetry (ASV) established that Pb electrodeposited onto Pd-modified pyrolytic graphite affixes to the Pd rather than the graphite. ASV measurements using a basal plane pyrolytic graphite working electrode also established that (i) the stripping potentials for monolayer and multilayer Pb are shifted anodically by 0.16 and 0.18 V, respectively by binding to Pd rather than graphite and (ii) deposition of Pb from dilute acidic medium (1% HNO_3) leads only to monolayer Pb, in contrast to deposition from acetate buffer (pH 4.0–4.4) which produces predominantly multilayer Pb. © 1997 Elsevier Science B.V.

Keywords: Electrodeposition; Palladium modifier; Stripping potential; Thermal stabilization

1. Introduction

Many analytical protocols in electrothermal atomic absorption spectroscopy (ETAAS) require stabilization of the analyte prior to, or within, the atomization phase. Often the objectives are to minimize the premature loss of volatile molecular analyte species, to improve separation of analyte and matrix components during the ashing phase and/or to increase the atomization temperature. The necessary stabilization can be achieved by

* Corresponding author. Fax: +61 2 93856141; e-mail: J.Matousek@unsw.edu.au

PII S0039-9140(96)02155-8

encapsulation of the analyte within a much larger mass of less volatile thermally produced matrix, e.g., MgO, or by alloying the analyte with a large mass of thermally produced metal, such as Ni or Pd [1]. Palladium is also used to preconcentrate hydrides of As, Sb, Se, Bi and Sn as compounds of low volatility prior to atomization from the pyrolytic graphite furnace [2].

A common problem with the use of chemical modifiers is the large mass required relative to the mass of analyte and therefore the associated risk of contamination. For example, the masses of Ni and Pd used are typically in the range 10–50 and 1–20 μg, respectively [1]. Recently we have reported the use of electrodeposited Pd as a modifier [3]. This modifier is significantly more effective than thermally reduced Pd at stabilizing the volatile analytes Pb, Cd, Cu [3] and H_2Se [4] to higher temperatures. Typically a mass of only 0.2 μg is required, being produced in situ in the pyrolytic graphite coated furnace. For example, our ETAAS results for stabilization of Pb by thermally generated (3.0 μg) and eletrodeposited (0.25 μg) Pd confirm more efficient stabilization by the latter: based on the ashing loss curves, stabilization of Pb by 500 K using electrodeposited Pd contrasts with only 150 K for thermally produced modifier [3]. The contribution of modifier contaminants with more negative reduction potentials is diminished by programming the autosampler to remove spent electrolyte after modifier deposition. The modifier blank can be further reduced by an acid wash. The modifier can be used for analysis of analytes by conventional methods, or by their electrodeposition onto the Pd. In the electrodeposition protocol the analyte can be quantitatively separated in 60 s deposition from such troublesome matrices as 0.5 M NaCl; the background absorption by NaCl is reduced by more than 99.5% [3].

In this paper we make a comparison of electrochemically and thermally produced Pd modifiers on the basis of their scanning electron micrographs. Modifiers produced from different electrolytes (HNO_3, HCl) are compared. Evidence is presented from differential pulse ASV that electrodeposited analytes affix to the Pd domains rather than to the much larger area of uncoated pyrolytic graphite. From ASV measurements on a basal plane pyrolytic graphite cathode it is established that the relative amounts of (the more highly stabilized) monolayer and bulk Pb deposited onto Pd (or graphite) depend on sample pH. The additional stabilization of Pb by deposition onto Pd rather than graphite is approximately $\Delta G = -31$ kJ mol^{-1}.

2. Experimental

2.1. Instrumentation

Scanning electron micrographs were taken with a Jeol JXA-840 scanning microanalyzer operating with an accelerating voltage of 30 kV and capable of 12–50 000 × magnification.

A GBC GF-3000 graphite furnace system, incorporated into a GBC 932 atomic absorption spectrometer was used to clean and condition miniature graphite furnace sections used for depositions. The standard graphite furnace tube (GBC Part No. G 19310121) was modified for this purpose by removing the internal central partitions so as to accommodate the furnace sections for cleaning and for thermal reduction of Pd.

ASV measurements were effected with a PAR 384B polarographic analyzer. Solution volumes of 6 ml were held in a perspex cell of 10 ml capacity designed for use with the PAR 303A stirrer and were stirred with a magnetic follower at 700 rpm. The working electrode (3 mm × 4 mm) was fabricated from a thin section of basal plane pyrolytic graphite mounted at the flanged base of a perspex tube (6 mm o.d.) by sealing in Araldite; electrical contact was via a drop of Hg on the reverse side. The auxiliary electrode was a 2 mm dia disk of high density graphite; the Ag,AgCl/Cl^- (3 M) reference electrode was separated from the test solution by a Vycor tip.

2.2. Reagents

Sodium acetate, HNO_3 and HCl were Aristar (BDH) quality. Acetic acid (BDH Analar) was further purified by isopiestic distillation. Stock solutions of Pd and Pb (100 mg l^{-1}) were pre-

pared by dissolving $PdCl_2$ (Aldrich 99.99%) and $Pb(NO_3)_2$ (BDH) in dilute Aristar HNO_3 or HCl. All dilutions were in Milli-Q water.

2.3. Procedure

For scanning electron microscopy (SEM) studies, electrodeposition was onto the concave surface of sections (9 × 3 mm) prepared by grinding pyrolytically coated miniature GBC GF-1000 furnaces (Ringsdorff Werke RWO/PyC) lengthwise to approximately half the original size. The sections were cleaned by heating twice inside a modified GF-3000 tube at 2500°C for 5 s with the internal Ar flow. The electrodepositions, at 5 V uncontrolled potential, were effected from 10 μl aliquots in the half furnaces, using a purpose-built stand in which the position of the Pt/Ir anode was controlled by an attached Agla micrometer. The anode-cathode separation was set at 0.7 mm, similar to that achieved in ETAAS experiments [3]. Following deposition of Pd (60 s, 20–30 mA) from 100 mg l^{-1} solution in 1% HNO_3 or 0.5% HCl, the furnace section was washed thoroughly in 0.1% Aristar HNO_3, then Milli-Q water and dried at 100°C. Lead was deposited over the Pd layer from 100–300 mg l^{-1} Pb in 1% HNO_3 or 0.03 M acetate buffer. Conditions were identical to those for Pd except the deposits were washed initially with Milli-Q water under applied voltage and then immersed in Milli-Q water prior to drying. For thermally produced modifier, 10 μl aliquots of 1000 mg l^{-1} Pd solution in 5% HCl were dried in half furnaces, followed by conditioning at 1200°C for 20 s.

ASV measurements were performed in a class 100 clean room. The electrode surface was initially cleaned by abrasion on an acid-soaked quantitative filter paper then by anodic polarization at 0.70 V for several minutes in stirred 1% HNO_3. Solution concentrations were: Pb, 120–225 μg l^{-1} in 0.03 M acetate buffer, pH 4.4, or in 0.1% HNO_3; Pd 5.0 mg l^{-1} in 0.05% HNO_3. Instrumental parameters were: N_2 flush 10 min, deposition time 60–1500 s, deposition potential −0.70 V (Pb) or 0.20 V (Pd), final potential 0.60 V, mode DPSV, modulation 25 mV, stripping speed 10 mV s^{-1}.

3. Results and discussion

3.1. Scanning electron microscopy

Surface distribution of thermally produced modifiers on pyrolytic graphite coated furnaces has been a subject of several SEM studies [5–7]. There is a general consensus that Pd or Ir modifier is concentrated towards the edges of the deposited solution. This is either ascribed to uneven distribution of the modifier during the drying step [5] or to its migration towards the edges during pyrolysis [6]. However, our experiments at 250 × magnification (not shown) confirm that the uneven distribution of Pd modifier stems from the drying process and is substantially maintained during pyrolysis up to 1200°C. In contrast, electrodeposited modifier is more uniformly and densely distributed. This difference in distribution is consistent with the observation that trapping of H_2Se injected through the furnace orifice following external generation is more efficient by Pd electrodeposited from 1% HNO_3 [4]. Modifier (Pd) electrodeposited from HCl contrasts with that from HNO_3. Evolution of Cl_2 at the anode leads to the dissolution of Pd [8] from the cathode area opposite the Pt/Ir probe.

Fig. 1(a)–(d) shows the scanning electron micrographs (2500 × magnification) and corresponding X-ray dot maps for Pd electrodeposited from 0.5% HCl and from 1% HNO_3. From HCl medium a more uniform, higher density of domains was achieved. At 2500 × magnification the Pd domains electrodeposited from HNO_3 medium appeared to fluoresce. Fluorescence (cathodoluminescence) is characteristic of non-conducting or semiconductor materials [9]. This suggests that under the conditions of vacuum and electron bombardment in the spectrometer the linkage between the Pd domains and the graphite substrate has a low electrical conductivity. As seen in Fig. 1(b), Pd deposits from HNO_3 indeed appear not to adhere as well to the pyrolytic graphite surface as those from HCl medium.

An additional feature associated with Pd deposited from HCl was a 'glazed' appearance. This feature is consistent with adsorption of Cl^- on the surface of the Pd domains (despite a 30 min

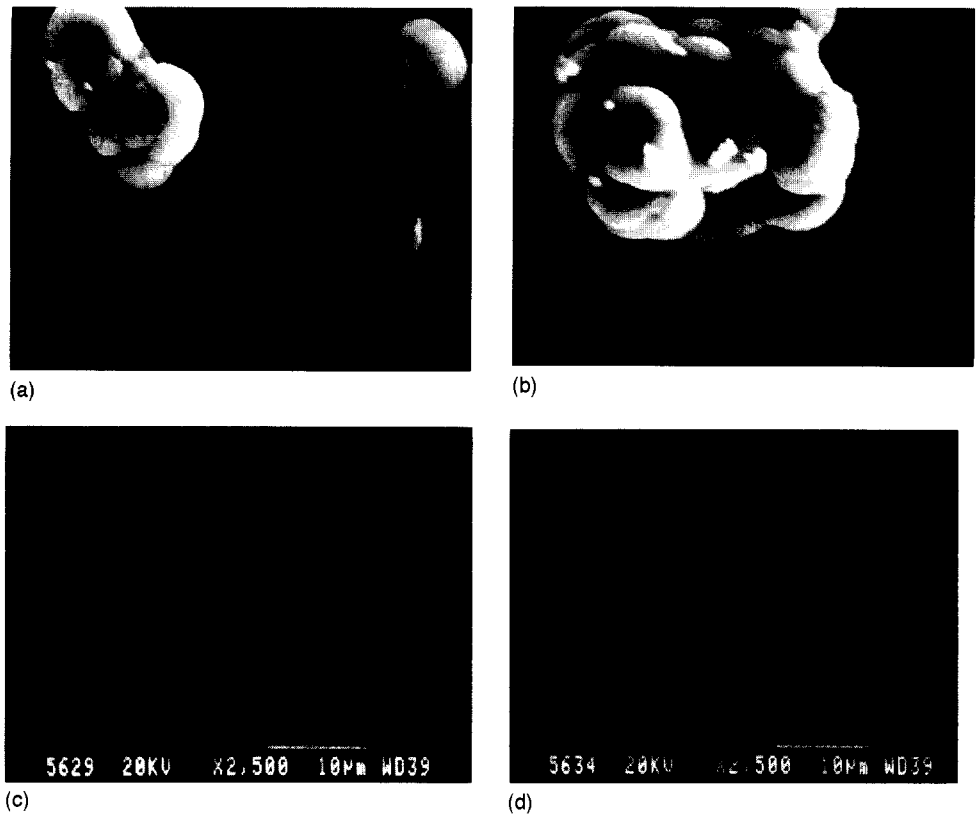

Fig. 1. Scanning electron micrographs at 2500 × magnification of 1 μg Pd electrodeposited from (a) 0.5% HCl and (b) 1% HNO_3 with corresponding X-ray dot maps measured at Pd $L\alpha_1$ 2.838 keV line (c) and (d), respectively.

wash in 0.1% HNO_3). An intense Cl fluorescence, its source physically coincident with Pd fluorescence, was observed in the SEM.

Although the mass of Pd used was well in excess of that required for a monolayer coverage (but of the same order as the amount required for the production of electrodeposited modifier), the Pd deposited from 0.5% HCl (Fig. 1(a) and (c)) is concentrated in a series of domains representing less than 20% of the surface area. Fig. 2 documents that, when viewed at the same magnification, thermally produced modifier provides a more uniform coverage (but less dense) relative to the same quantity of Pd electrodeposited from HCl. The scattered domains which arise from thermal evaporation and reduction of Pd salts (as documented previously [7]) indicate that sites with discrete activity are a feature of the adsorption and nucleation processes.

The formation of highly concentrated domains of Pd by electrodeposition on graphite surfaces, as observed for metal deposition on a glassy carbon electrode, indicates the presence of electroactive sites [10]. It may be expected that Pd electrodeposition is directed preferentially towards the most active sites. However, recent observations for thermally generated Ir modifier have confirmed that its distribution is non-reproducible even when carried out under the same conditions and that thermal pretreament results in modifier redistribution dictated by the surface features (rather than active sites) of the graphite tube [5].

Our observations confirm that surface morphology of the pyrolytic graphite coating plays a

significant role in determining the deposition pattern. The grade of graphite used displays a range of raised features and it is on these that preferential deposition takes place.

In ETAAS the amount of analyte determined is typically much smaller than the quantity of Pd modifier used. However, the low sensitivity of the XRF technique necessitates the use of unrealistically high amounts of analyte to obtain usable results. Despite using three orders of magnitude higher amount of Pb for SEM investigations (relative to the ASV work), detection still proved difficult. In order to highlight X-ray dot maps, these are presented in Fig. 3 and Fig. 4 as negative images. It appears from overlaps of X-ray dot maps for Pd and Pb that, for both HNO_3 and acetate buffer, these elements favour the same regions of the pyrolytic graphite surface. It should be noted that the dot maps are not exactly coincident, however, coincidence of the deposits is indicated by the displacement of the Pb ashing loss curve in the presence of electrodeposited Pd [3], and from the ASV results presented below. It was observed that the intensity of fluorescent radiation for Pd was noticeably weaker when Pb was deposited over the Pd layer (Fig. 3(b) and Fig. 4(b) compared with Fig. 1(c)).

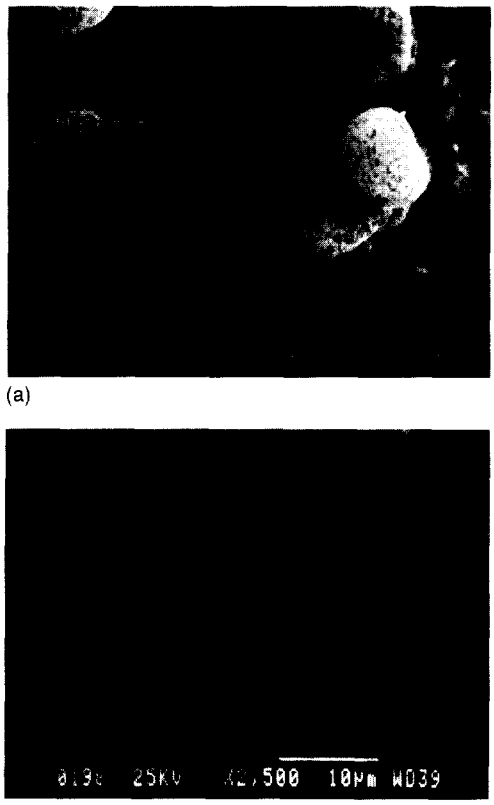

(a)

(b)

Fig. 2. Scanning electron micrographs at 2500 × magnification of 10 μg Pd in 5% HCl after drying and conditioning at 1200°C (a) and corresponding X-ray dot map measured at Pd $L\alpha_1$ 2.838 keV line (b).

3.2. Anodic stripping voltammetry

3.2.1. Deposition of Pb on graphite

Fig. 5 shows the differential pulse stripping voltammograms as a function of deposition time for Pb deposited at −0.80 V from a 120 μg l^{-1} solution in 0.03 M acetate buffer, pH 4.0. Broad stripping peaks are observed at $E_p = -0.45$, −0.06 and 0.21 V versus Ag,AgCl/Cl^- (3 M). The more cathodic peak at potential $E_p = -0.45$ V, is ascribed to the stripping of Pb from multilayer (bulk) deposits. For reference, the E° for Pb^{2+}/Pb is −0.32 V and $E_{1/2}$ for Pb^{2+}/(Pb/Hg) is −0.31 V, both relative to Ag,AgCl/Cl^- (3 M) [11]. The most anodic peak is ascribed to the stripping of monolayer Pb (designated Type I Pb). This indicates an underpotential of 0.66 V. The peak at −0.06 V may arise from Pb deposits at surface sites different from those at which the more stable monolayer is formed [12]. Szabo [13] has noted the energetic heterogeneity of substrate surfaces and thus the existence of multiple energy states for monolayers. Alternatively, the peak at −0.06 V may arise from stripping of the Pb layer next to that in direct contact with the graphite substrate. The atomic environment in this layer will be unique and the atoms will be partially stabilized by interaction with the electrode material.

Fig. 6 shows a plot of peak height versus deposition time for the three stripping peaks. The peak height for monolayer stripping increases systematically with deposition time, but much less rapidly than that for multilayer Pb. The peak at $E_p = -0.06$ V is almost invariant with deposition time. This is consistent with it representing monolayer deposition at sites for which the activation

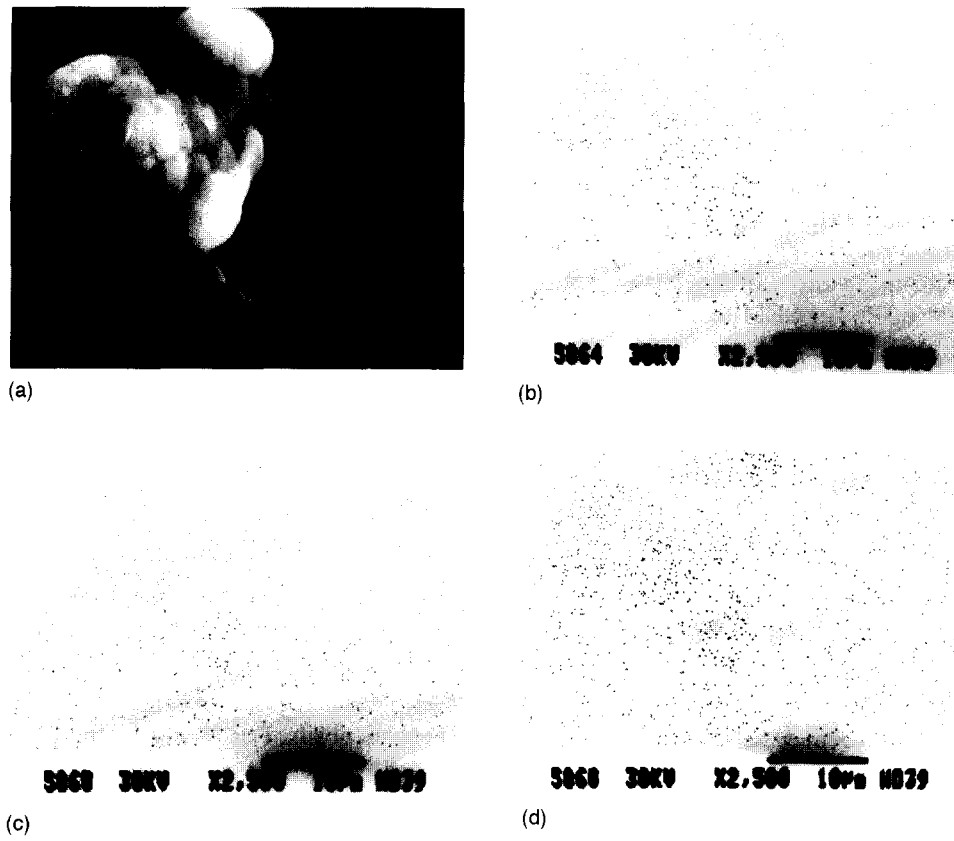

Fig. 3. Scanning electron micrographs at 2500 × magnification of 3 μg Pb electrodeposited from 1% HNO_3 over 1 μg Pd electrodeposited from 0.5% HCl (a) and corresponding X-ray dot maps measured at Pd $L\alpha_1$ 2.838 keV line (b) and Pb $M\alpha_1$ 2.346 keV line (c). X-ray dot map (d) is a composite of (b) and (c). Negative images are used for (b), (c) and (d).

energy for deposition is low and the number of sites is unaffected by the impact which cumulative deposition or gas evolution has on the surface properties. (This is designated Type II Pb.) It is not consistent with a unique second layer of Pb deposited over the expanding monolayer coverage. Both of the monolayer peaks are of significant magnitude after zero deposition time (70–90 s scan from −0.70 V in unstirred solution).

The unique stability of the monolayer Pb deposits is illustrated by the effect of a 20 s rinse of the electrode in 0.5% HNO_3 following a 360 s deposition at −0.80 V. Fig. 7, curve A indicates that all of the multilayer Pb (from 360 s deposition) is dissolved by the acid treatment. From the relative peak heights at 0.21 V and −0.06 V it is inferred that, compared with Fig. 5, a partial dissolution of the less stable Type II monolayer also occurs. Fig. 7, curves B and C show the stripping voltammograms following 60 s and 500 s depositions of Pb from a 0.1% HNO_3 solution, respectively. Only the more stable monolayer, Type I, accumulates; the monolayer Pb is more resistant to oxidative dissolution in the presence of O_2 [14], consistent with its more positive stripping potential. The E_p value for Type I Pb indicates a stabilization of $\Delta G° = -127$ kJ mol^{-1} $(= -zF\Delta E)$ relative to multilayer Pb. The resistance of the graphite-Pb monolayer to acid dissolution is consistent with the negative value of E for $Pb(C) + 2H^+ = Pb^{2+} + C + H_2$.

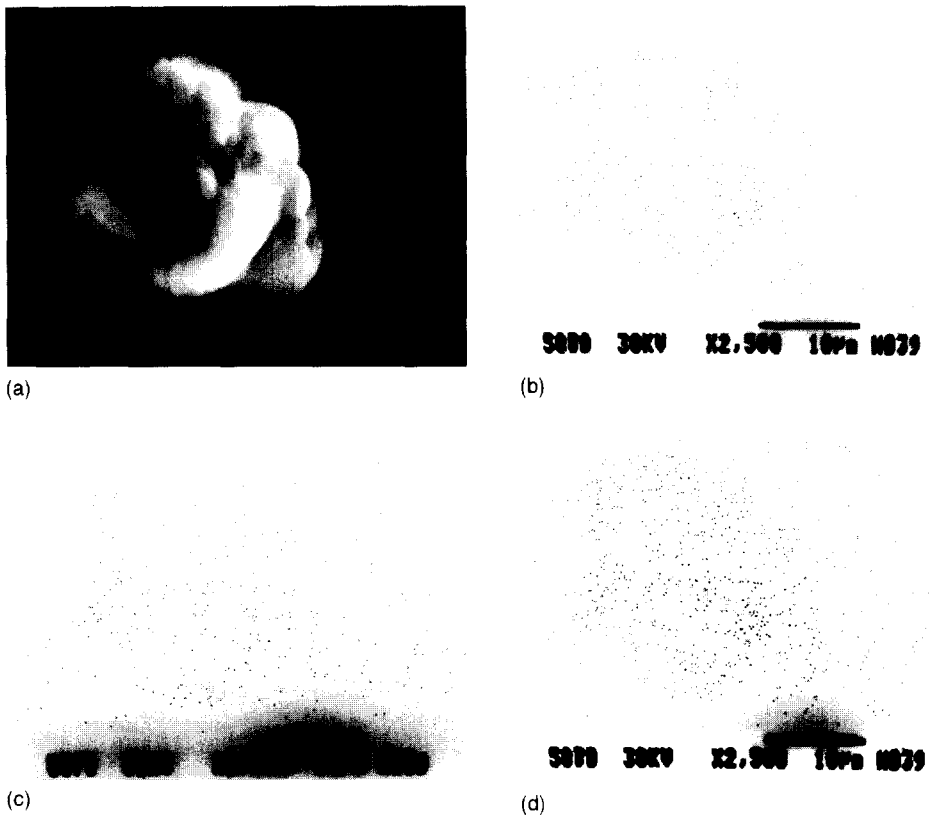

Fig. 4. Scanning electron micrographs at 2500 × magnification of 1 μg Pb electrodeposited from 0.03 M acetate buffer over 1 μg Pd electrodeposited from 0.5% HCl (a) and corresponding X-ray dot maps measured at Pd $L\alpha_1$ 2.838 keV line (b) and Pb $M\alpha_1$ 2.346 keV line (c). X-ray dot map (d) is a composite of (b) and (c). Negative images are used for (b), (c) and (d).

3.2.2. Deposition of Pd on graphite

Deposition of Pd onto pyrolytic graphite was effected at 0.20 V from a solution containing 5.0 mg l^{-1} Pd in 0.05% (0.08 M) HNO_3. The stripping voltammogram taken from −0.70 V, immediately following 100 s deposition showed a double peak with maxima at −0.18 V and approximately 0.00 V (Fig. 8, curve A). Because $E^{\circ}_{Pd^{2+}/Pd} = 0.95$ V (versus NHE) these peaks must involve a species other than (or in addition to) $Pd_{(s)}$. Possible assignments include the oxidation processes:

$$Pd_2H = 2Pd + H^+ + e^- \quad (1)$$

and

$$Pd(H_2) = Pd + 2H^+ + 2e^- \quad (2)$$

In contrast, stripping following a 60 s electrolysis at −0.70 V in acetate buffer gave a single peak at −0.16 V (Fig. 8, curve B). For the reduction process Eq. (1), the standard reduction potential $E^{\circ} = 0.048 - 0.059$ pH versus NHE [15], giving $E = -0.21$ V versus Ag,AgCl/Cl^- (3 M) at $[H^+] = 0.08$ M. For the reduction process Eq. (2), $E^{\circ} = 0.00$ V versus NHE, giving $E = -0.26$ V versus Ag,AgCl/Cl^- (3 M) at $[H^+] = 0.08$ M. These values are for bulk Pd; different values could be expected for small Pd domains on a graphite substrate [16]. As indicated below, the position of the peak(s) is very sensitive to the deposition of analyte (Pb) onto Pd.

3.2.3. Deposition of Pb on Pd

The electrode was precoated with Pd by 600 s deposition from 5.0 mg l^{-1} solution at 0.20 V. Deposition of Pb from 0.03 M acetate buffer (pH 4.4) onto electrodeposited Pd on pyrolytic graphite gave a stripping voltammogram with peaks at -0.27, -0.17 to 0.09 and 0.37 V (Fig. 9, curves A–E) for 0–1500 s depositions. The former was assigned to multilayer Pb and the latter to monolayer Pb on Pd. The shift in stripping potential for multilayer Pb (relative to E_p on graphite) was unexpected; it may be a consequence of the low mass of analyte involved, hence the proximity of all Pb atoms to the electrode (Pd) surface. The difference between E_p for monolayer Pb deposited on graphite and for monolayer deposition on Pd, $\Delta E_p = 0.16$ V, corresponds to a stabilization (on Pd) of $\Delta G° = -31$ kJ mol^{-1} ($= -zF\Delta E_p$). This is the energy difference for the processes

$$Pb(C) = Pb^{2+}_{(aq)} + 2e^- \quad (3)$$

and

$$Pb(Pd) = Pb^{2+}_{(aq)} + 2e^- \quad (4)$$

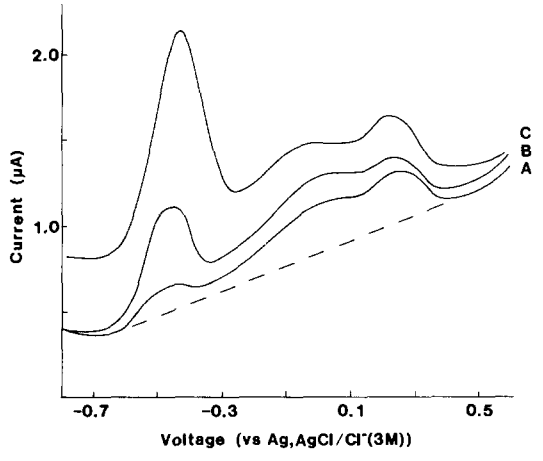

Fig. 5. Differential pulse stripping voltammograms for Pb deposited on pyrolytic graphite from acetate buffer (0.03 M, pH 4.0). Conditions: 120 μg l^{-1} Pb, conditioning potential 0.70 V, deposition potential -0.80 V. Voltammograms shown for (A) 60, (B) 180 and (C) 600 s deposition from stirred solutions.

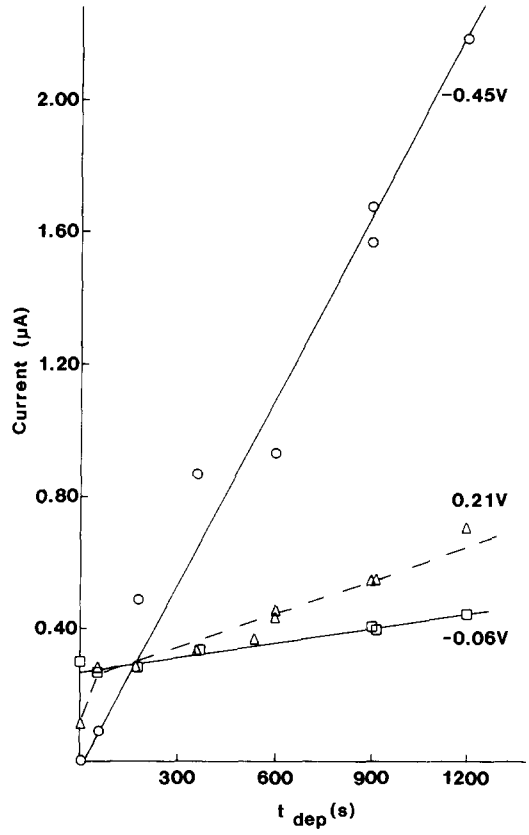

Fig. 6. Plot of differential pulse stripping peak height versus deposition time for bulk Pb ($E_p = -0.45$ V) and monolayer Pb bound to graphite, type I ($E_p = 0.21$ V) and type II ($E_p = -0.06$ V). Deposition conditions as for Fig. 3.

Yan and Ni [17] determined the activation energies for release (first order kinetics) of Pb from graphite and palladium surfaces (301 and 418–518 kJ mol^{-1}, respectively). They inferred that these energy terms are a measure of the analyte-surface interaction energy. If this is so, then the difference in stability of the two surface states of the analyte is c. -(100–200) kJ mol^{-1}. However these terms are kinetic parameters (activation energies) rather than thermodynamic parameters. Further, there is no guarantee that the process leading to the observed activation energy involves monolayer, as distinct from polylayer atomic species. For comparison, the stabilization of monolayer Pb on Pd relative to bulk Pb on Pd is calculated as $\Delta G° = -124$ kJ mol^{-1} from the shift in stripping potentials.

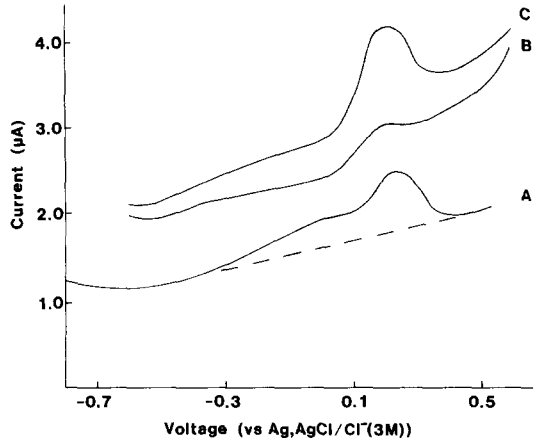

Fig. 7. Differential pulse stripping voltammograms for Pb deposited on graphite in acid (HNO_3) solution. Curve A, 200 s conditioning at 0.70 V, 360 s deposition from acetate buffer (0.03 M, pH 4.0) at −0.80 V, followed by 20 s in 0.5% HNO_3 before stripping. Curves B and C for deposition (60 and 500 s, respectively) and stripping in 0.1% HNO_3 (curve C at 1/3 sensitivity).

The position of the central stripping peak was very sensitive to plating time (mass of Pb deposited), Fig. 9, curves A–E. It shifted from −0.17 V for 0 s deposition to 0.09 V for deposition times greater than 1000 s, an effect which parallels that of Pb 'adatoms' on Pd catalysts; Mallat et al. [16] report the oxidation of H_2 from

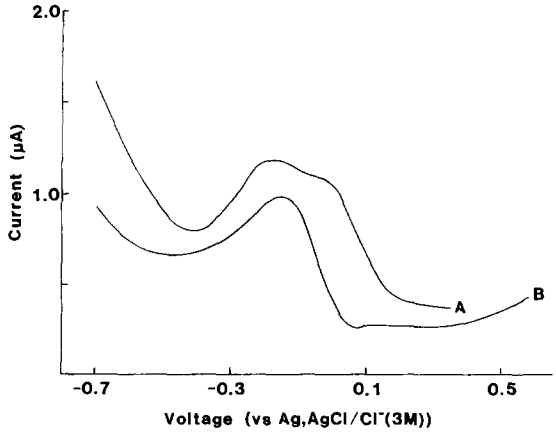

Fig. 8. Differential pulse stripping voltammograms for Pd deposited on pyrolytic graphite. Curve A: 100 s deposition from 5.0 mg l^{-1} Pd (0.05% HNO_3) at 0.20 V. Curve B: 60 s electrolysis at −0.70 V of Pd-coated pyrolytic graphite electrode (curve A) in 0.03 M acetate buffer (pH 4.4).

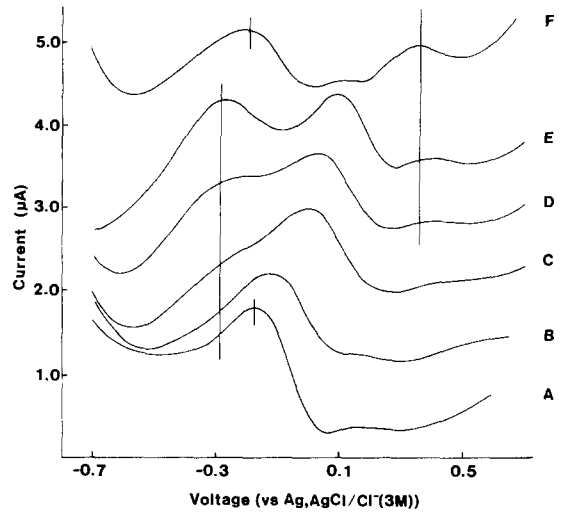

Fig. 9. Differential pulse stripping voltammograms for depositions from 225 μg l^{-1} Pb in 0.03 M acetate buffer (pH 4.4) onto pyrolytic graphite precoated with electrodeposited Pd. Curve A, blank (Pd only), B 60 s, C 240 s, D 480 s, E 1500 s deposition at −0.70 V. Curve F for 480 s deposition followed by 20 s in 1% HNO_3 before stripping.

β-Pd shifts from 0.15 V (versus NHE) for clean Pd to 0.30 V after Pb poisoning. In contrast, the stripping current was independent of plating time but was larger for scans in 0.5% HNO_3 than in acetate buffer. The stripping current increased with mass of deposited Pd. A 15 s wash with 1% HNO_3 following a 480 s deposition from pH 4.4 acetate buffer shifted this peak from 0.02 V back to −0.19 V (curve F). This wash also caused the loss of the −0.27 V peak. There was also an apparent three-fold increase in the monolayer peak at 0.37 V, presumably arising from the reactions:

$$2Pb + O_2 + 4H^+ = 2Pb^{2+} + H_2O \quad (5)$$

and

$$Pb^{2+} + Pd(H_2) = Pb/Pd + 2H^+ \quad (6)$$

Thus, analogous to deposition on graphite, only the Pb monolayer resists dissolution in dilute acid.

Deposition of Pb onto Pd from 1% (or 3%) HNO_3 gave monolayer Pb only (Fig. 10, curve A). The stripping current was proportional to $(t_{dep})^n$, where n is less than 1.0. The stripping voltammogram also showed the $Pd(H_2)$ oxidation peak

at −0.01 V. An interesting feature of this voltammogram is a ten-fold enhancement of the monolayer peak relative to that produced from acetate buffer for the same deposition time (Fig. 10, curve B). From this it may be inferred that in acetate buffer the rate (activation energy) for deposition of Pb onto Pb is greater (smaller) than that for deposition onto Pd. In the application of the electrodeposition—ETAAS technique it was found advantageous to effect 1% HNO_3 redeposition of Pb initially deposited from more weakly acidic acetate buffer solutions. This minimized losses during the subsequent rinsing stage (used to dilute matrix components such as NaCl). This can now be understood in terms of the dissolution of bulk Pb and its redeposition in more stable monolayer forms which resist dissolution during rinsing with air-saturated Milli-Q water.

A potential problem with quantitative deposition of analytes from dilute solutions is the competitive reaction from dissolved O_2, or other oxidants generated at the anode [14,18,19]. An advantage arising from monolayer deposition onto a Pd modifier is the substantial increase in stability of the Pb(s) phase. This will contribute to the success of the electrodeposition—ETAAS method.

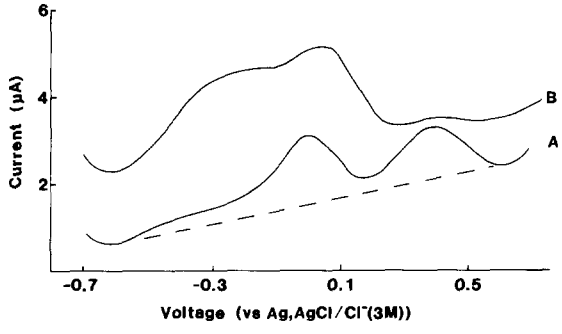

Fig. 10. Differential pulse stripping voltammograms for 225 μg l^{-1} Pb deposited on pyrolytic graphite coated with electrodeposited Pd. Curve A, 480 s deposition from and stripping into 1% HNO_3. Curve B, 480 s deposition from acetate buffer (pH 4.4).

3.2.4. Effect of analyte stabilization on appearance temperatures

Using a simplified approach it is possible to estimate the effect on the ETAAS appearance temperature of Pb (T_{app}) arising from its stabilization as a monolayer on Pd. From the relationship $\Delta(\Delta G^\circ) \cong -zF(\Delta E_p)$ applied to the redox reactions Eq. (7) and Eq. (8) the relative stability (Gibbs free energy) of the monolayers Pb(C) and Pb(Pd) can be estimated.

$$Pb^{2+} + 2e + C_{(s)} = Pb(C) \quad (7)$$

$$Pb^{2+} + 2e + Pd_{(s)} = Pb(Pd) \quad (8)$$

Using the relationship $\Delta(\Delta G^\circ) = -R\Delta(T \ln K_p)$ applied to reactions Eq. (9) and Eq. (10)

$$Pb(C) = Pb_{(g)} + C_{(s)} \quad (9)$$

$$Pb(Pd) = Pb_{(g)} + Pd_{(s)} \quad (10)$$

$\Delta(\Delta G^\circ)$ can be used to estimate:

(i) the ratio of partial pressures of Pb above the two monolayers at a given temperature, or

(ii) the shift in appearance temperature (T_{app}) corresponding to a specific vapour pressure of Pb,

$$\Delta(\Delta G^\circ) = -R\Delta(T_{app}) \ln P_{app}$$

However, some approximations are necessary. It is assumed that $\Delta(\Delta G^\circ)$ is not affected significantly by a change in temperature. If it is assumed that T_{app} corresponds to a mass of analyte similar to the characteristic mass (8 pg for Pb [3]) and that the effective volume occupied by the gaseous analyte at T_{app} is ca. 100 μl then at (say) 1000°C the ideal gas equation gives $P_{app} = 4 \times 10^{-8}$ atm. An ideal gas assumption is reasonable considering the high temperature involved. From the observed shift in stripping potentials (0.16 V) the calculated value for $\Delta(T_{app})$ is approximately 220 K, a value in reasonable agreement with the displacement of ashing loss curves by 250 K reported previously by Matousek and Powell [3]. Such calculations do not take cognisance of the kinetic factors involved in the atom release processes, nor the fact that the system may not be at equilibrium around the appearance temperature. However, they serve to indicate the insight to be gained about surface stabilization of analytes from measurement of their stripping potentials.

Acknowledgements

One of the authors (J.P.M.) gratefully acknowledges financial support from The University of New South Wales Special Studies Program and from Deutscher Akademischer Austauschdienst.

The authors are thankful to Miss V. Piegerova, School of Materials Science and Engineering, The University of New South Wales for assistance with measurement and interpretation of scanning electron micrographs.

References

[1] D.L. Tsalev, V.I. Slaveykova and P.B. Mandjukov, Spectrochim. Acta Rev., 13 (1990) 225.
[2] R.E. Sturgeon, S.N. Willie, G.I. Sproule, P.T. Robinson and S.S. Berman, Spectrochim. Acta, Part B, 44 (1989) 667.
[3] J.P. Matousek and H.K.J. Powell, Spectrochim. Acta, Part B, 50 (1995) 857.
[4] V. Smith, Selenium Analysis by Electrothermal Atomic Absorption Spectrometry Using Electrodeposited Metal Modifiers, M. Sc. Thesis, University of Canterbury, New Zealand, 1996.
[5] C.J. Rademayer, B. Radziuk, N. Romanova, N.P. Skaugset, A. Skogstad and Y. Thomassen, J. Anal. At. Spectrom., 10 (1995) 739.
[6] H. Qiao, T.M. Mahmood and K.W. Jackson, Spectrochim. Acta, Part B, 48 (1993) 1495.
[7] S. Sachsenberg, T. Klenke, W.E. Krumbein, H.J. Schellnhuber and E. Zeeck, Anal. Chim. Acta, 279 (1993) 241.
[8] S.I. Ginzburg, N.A. Ezerskaya, I.V. Prokof'eva, N.V. Fedorenko, V.I. Shlenskaya and N.K. Bel'skii, Analytical Chemistry of Platinum Metals, Translated by N. Kaner, Wiley, New York, 1975, pp. 18–19.
[9] J.I. Goldstein, D.E. Newbury, P. Echlin, D.C. Joy, A.D. Romig, Jr., C.E. Lyman, C. Fiori and E. Lifshin, Scanning Electron Microscopy and X-ray Microanalysis, 2nd edn., Plenum, New York, 1992, pp. 144–145.
[10] M. Stulikova, Electroanal. Chem. Interface Electrochem., 48 (1973) 33.
[11] CRC Handbook of Chemistry and Physics, in D.R. Lide (Ed.), CRC Press, New York, 76th edn., 1995, sect. 8–24.
[12] B.H. Vassos and H.B. Mark, Jr., Electroanal. Chem. Interface Electrochem., 13 (1967) 1.
[13] S. Szabo, Int. Rev. Phys. Chem., 10 (1991) 207.
[14] A. Ciszewski, J.R. Fish, T. Malinski and R.E. Sioda, Anal. Chem., 61 (1989) 856.
[15] J.F. Llopis and F. Colom, in A.J. Bard (Ed.), Encyclopedia of Electrochemistry of the Elements, Marcel Dekker, New York, 1976, Vol. VI, ch. 7, pp. 254–255.
[16] T. Mallat, Zs. Bodnar, S. Szabo and J. Petro, Appl. Catal., 69 (1991) 85.
[17] X.P. Yan and Z.M. Ni, Spectrochim. Acta, Part B, 48 (1993) 1315.
[18] J.L. Anderson and R.E. Sioda, Talanta, 30 (1983) 627.
[19] R.E. Sioda, Anal. Chim. Acta, 228 (1990) 323.

ELSEVIER

Talanta 44 (1997) 1195–1202

Talanta

Ion paired chromatography of iron (II,III), nickel (II) and copper (II) as their 4,7-Diphenyl-1,10-phenanthroline chelates

Mudasir [a,b,*], Naoki Yoshioka [a], Hidenari Inoue [a]

[a] *Department of Applied Chemistry, Keio University, 3-14-1 Hiyoshi, Kohoku-ku, Yokohama 223, Japan*
[b] *Chemistry Department, Gadjah Mada University, Sekip Utara, Bulaksumur, Yogyakarta, Indonesia*

Received 2 August 1996; received in revised form 24 October 1996; accepted 29 October 1996

Abstract

A reversed phase ion-paired chromatographic method that can be used to determine trace amounts of iron (II,III), nickel (II) and copper (II) was developed and applied to the determination of iron (II) and iron (III) levels in natural water. The separation of these metal ions as their 4,7-diphenyl-1,10-phenanthroline (bathophenanthroline) chelates on an Inertsil ODS column was investigated by using acetonitrile-water (80/20, v/v) containing 0.06 M perchloric acid as mobile phase and diode array spectrophotometric detection at 250–650 nm. Chromatographic parameters such as composition of mobile phase and concentration of perchloric acid in mobile phase were optimized. The calibration graphs of iron (II), nickel (II) and copper (II) ions were linear ($r > 0.991$) in the concentration range 0–0.5, 0–2.0 and 0–4.0 μg ml^{-1}, respectively. The detection limit of iron (II), nickel (II) and copper (II) were 2.67, 5.42 and 18.2 ng ml^{-1} with relative standard deviation ($n = 5$) of 3.11, 5.81 and 7.16% at a concentration level of 10 ng ml^{-1} for iron (II) and nickel (II) and 25 ng ml^{-1} for copper (II), respectively. The proposed method was applied to the determination of iron(II) and iron(III) in tap water and sea water samples without any interference from other common metal ions. © 1997 Elsevier Science B.V.

Keywords: Determination of iron (II,III); 4,7-diphenyl-1,10-phenanthroline; Ion-paired chromatography; Nickel (II) and copper (II)

1. Introduction

The simultaneous determination of metal ions as their chelates with organic reagents by high performance liquid chromatography (HPLC) has received increasing attention and has been used for inorganic analysis in recent years [1–4]. In particular, reversed-phase (RP) HPLC seems to offer excellent potential for the determination of many metals owing to its high efficiency and simplicity of operation [5]. Several reviews on this subject have appeared in the literature [6,7]. Many organic chelating agents such as dithiocarbamates [8], 8-hydroxy-quinoline [9], chlorophyll [10,11] and other highly sensitive azo dyes including PAR [12], PAN [13] and 1,10-phenanthroline [14,15] have been used for complexation prior to separa-

* Corresponding author. Fax.: +81 45 5630446; e-mail: c03027@educ.cc.keio.ac.jp

PII S0039-9140(96)02156-X

tion by HPLC. These reagents form either neutral or ionic chelates with a large number of metal ions, and the chelates in the eluate can be detected spectrophotometrically. Most recently, 1,10-phenanthroline also has been used for the determination of serum iron in human blood by high performance capillary electrophoresis (HPCE) after precipitation of serum proteins and reducing iron (III) to iron (II) with hydroxyl amine [16]. With this method, a single drop (10 μl) of serum would be sufficient to determine the serum iron concentration.

Some derivatives of 1,10-phenanthroline also have been developed for chelating reagents but most of them were only a little superior to the parent reagent. However, 4,7-diphenyl-1,10-phenanthroline (bathophenanthroline: Bphen) is an exception. Bathophenanthroline reacts with iron(II) and other metal ions very similarly to 1,10-phenanthroline. Both methods are of similar selectivity, but the bathophenanthroline method is twice as sensitive. The molar absorptivity of iron (II) bathophenanthroline at 534 nm varies between 2.24–2.56 ($\times 10^4$) depending upon the solvents used [17]. Colorimetric [18], spectrophotometric [19] and flow injection [20] methods using this reagent have been reported but their selectivity is still poor due to the interference from several metal ions such as Cu^{II}, Ni^{II}, Co^{II} and Zn^{II} which also form chelates with bathophenanthroline. So far, there has been still few reports regarding the use of bathophenanthroline as a pre-column reagents for the determination of metal ions by HPLC. If its chelates can be separated and detected spectrophotometrically by means of HPLC, the reagent could give a highly sensitive and selective HPLC method for simultaneous determination of some metal ions.

The aim of the present study is to develop a simple, selective and sensitive method for the determination of iron (II,III), nickel (II) and copper (II) using spectrophotometric detection with batho-phenanthroline as a pre-column reagent. The separation, identification and quantitation of different metals can be performed in one procedure by taking advantages of HPLC. The method was then applied to the direct determination of iron (II) and iron (III) at ppb level in tap water and sea water to demonstrate its applicability.

2. Experimental

2.1. Apparatus and reagents

A home-built HPLC system was used for the separation and determination of iron (II), nickel (II) and copper (II) as their bathophenanthroline chelates. Samples were injected into a Reodyne 7125 (100 μl loop) injector and passed through a filter and a guard column before passing to an Inertsil ODS AI525 column (5 μm, 4.6 × 250 mm from GL Sciences). The guard column of 4.0 mm was packed with 5 μm Inertsil ODS (GL Sciences). The pump (Jasco PU-980 intelligent pump together with LC-980-2 Ternary gradient unit and DG-980-50 3-line degasser) was adjusted so that the flow rate was 1.0 ml min^{-1}. The diode array spectrophotometer (Jasco Multi-340 multichannel) used as a detector was interfaced with a personal computer (NEC PC-980 VM) for the purpose of peak analysis and was operated between 250–650 nm. The mobile phase was prepared by volume and consisted of acetonitrile-water (80/20 v/v) and 0.06 M $HClO_4$ and was ultrasonically mixed for several minutes before use. The typical UV-Vis spectra were recorded by a Jasco V-550 UV/VIS spectrophotometer.

Bathophenanthroline was obtained from Aldrich and was used without further purification. Acetonitrile (special grade) and distilled water (HPLC grade) were purchased from Katayama Chemical Industries. Perchloric acid for counter ion and sodium acetate for buffer solution were obtained from Junsei and Wako, respectively. Stock solutions of iron(II), iron (III), nickel (II) and copper (II) were prepared from their corresponding salts which were purchased from the following sources: $FeSO_4$ $(NH_4)SO_4.6H_2O$ and $CuCl_2.2H_2O$ were from Wako Pure Chemical Industries, $NiSO_4.6H_2O$ from Showa and $Fe_2(SO_4)_3(NH_4)_2SO_4.12H_2O$ from Kokusan Chemical Works. All chemicals were analytical grade.

2.2. Preparation of metal chelates

Solid chelates of iron (II), nickel (II) and copper (II) bathophenanthroline were prepared as their perchlorate salts. The chelates were obtained by a modification of the procedure described by either Schilt and Taylor [21] or K. Miyoshi et al. [22]. The procedure, in general, consisted of dissolving corresponding metal salts and bathophenanthroline at a mole ratio 1:3 for iron(II) and nickel(II) and 1:2 for copper(II) in hot water (about 80°C) containing 50% of ethanol, followed by adding sodium perchlorate. The resulting crystals were washed with water and recrystallized from hot water and dried in vacuo. The crystalline complexes were then identified by elemental analysis and absorption spectroscopy.

2.2.1. Results of elemental analysis

$Fe(C_{24}H_{16}N_2)_3(ClO_4)_2$. Calculated: C = 69.06; H = 3.86; N = 6.71%. Found: C = 69.03, H = 3.66, N = 6.81%.$Ni(C_{24}H_{16}N_2)_3(ClO_4)_2.1/2H_2O$. Calculated: C = 68.35; H = 3.87; N = 6.70%. Found: C = 68.03, H = 3.83, N = 6.55%.$Cu(C_{24}H_{16}N_2)_2(ClO_4)_2$. Calculated: C = 62.17; H = 3.48; N = 6.04%. Found: C = 62.24, H = 3.50, N = 6.29%.

2.3. Analytical procedure

The HPLC of metal bathophenanthroline chelates was studied by using their aqueous solutions and the chelates were made up according to the following procedure. The required quantity of stock solution (100 mg ml^{-1}) of each metal ion was taken volumetrically into 25 ml calibrated flasks. After diluting the solution to about 10 ml with mobile phase, 2 ml of 5% sodium acetate and a sufficient amount (ca. 5 ml) of 0.002 M bathophenanthroline were added to the diluted solution. The solution was then heated to boiling for 15 min, cooled to room temperature and finally diluted to the mark with the mobile phase. The samples of tap water and sea water were filtered through 0.45 μm filter before treated as described above.

3. Results and discussion

3.1. Absorption spectra and pre-column derivatization conditions

The ultraviolet absorption spectra of free ligand and its metal chelates in chloroform are shown in Fig. 1. Both free ligand and its metal chelates give strong absorption in the ultraviolet region between 250–350 nm due to the conjugated structure of bathophenanthroline i.e., intra-ligand $\pi-\pi^*$ absorption. However the absorption maxima of the metal chelates are shifted towards longer wavelength compared with that of free ligand, proving the existence of coordination of ligand to metal ions. In addition, the absorption maximum of iron (II)-bathophenanthroline chelate is also observed in the visible region and corresponds to metal–to–ligand charge transfer ($d-\pi^*$) absorption. This strong visible absorption at 534 nm is the basis of the application of the ligand to colorimetric determination of iron [23]. The absorption maxima and molar absorptivity of ligand and metal chelates are summarized in Table 1. It is obvious from the table that all metal

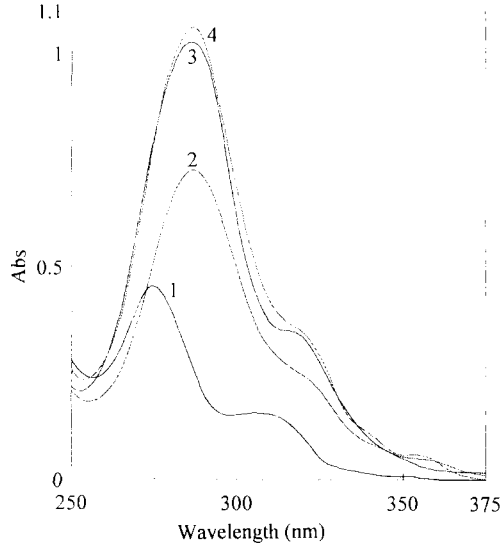

Fig. 1. Absorption spectra of metal bathophenanthroline chelates in ultraviolet region. (1) bathophenanthroline; (2) $Cu(Bphen)_2(ClO)_2$; (3) $Fe(Bphen)_3(ClO)_2$; and (4) $Ni(Bphen)_3(ClO)_2$.

Table 1
Absorption maxima (λ_{max}) and molar absorptivity (ϵ) of metal-bathophenanthroline chelates[a]

Compounds	λ_{max} (nm)	ϵ (cm^{-1} mol^{-1} l)
Bathophenanthroline(Bphen)	277	4.62×10^4
Tris(Bphen)Fe(ClO_4)$_2$	289	1.31×10^5
	534	2.26×10^4
Tris(Bphen)Ni(ClO_4)$_2$	290	1.35×10^5
Bis(Bphen)Cu(ClO_4)$_2$	289	9.28×10^4

[a] Dissolved in chloroform.

chelates have a maximum of detection sensitivity at about 290 nm. Therefore, a detection wavelength of 290 nm was selected for analytical purpose in the present study.

Bathophenanthroline reacts readily either with metal ions such as iron (II), nickel (II) and ruthenium (II) ions to form an octahedral chelate or with metal ions such as copper (II) ions to give a tetrahedral chelate over the wide range of pH 2–9 in acetate or tartrate buffer [17]. These differences in structure as well as their coordination numbers are considered to be the basis of chromatographic separation with a reversed phase column. We found by experiments that the concentration of bathophenanthroline in solution should be kept higher than 4.8×10^{-4} M for a solution containing 0.5, 2.0 and 4.0 μg ml^{-1} of iron (II), nickel (II) and copper (II) ions, respectively. Otherwise two peaks of nickel chelates which are assumed to be Ni(Bphen)$_2^{2+}$ and Ni(Bphen)$_3^{2+}$ will appear.

3.2. Separation of metal chelates

The separation of metal chelates Cu(Bphen)$_2^{2+}$, Fe(Bphen)$_3^{2+}$ and Ni(Bphen)$_3^{2+}$ on an Inertsil ODS column was studied using a combination of mobile phases such as water, methanol and acetonitrile. A good separation was achieved when the mobile phase consisted of acetonitrile–water (80/20 v/v) and 0.06 M perchloric acid was applied. All three peaks of metal chelates are resolved and well-separated from a peak due to the ligand, HBphen$^+$. The typical three dimensional chromatogram of metal chelates obtained by means of this composition of mobile phase is

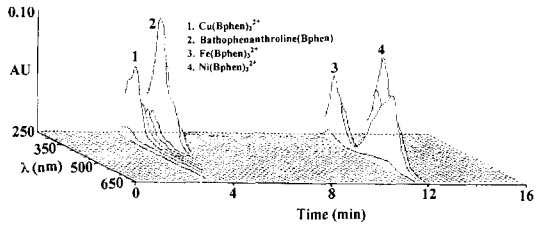

Fig. 2. Typical three dimensional chromatogram of metal bathophenanthroline chelates. Mobile phase, acetonitrile–water (80/20 v/v) containing 0.06 M $HClO_4$; column, Inertsil ODS; flow rate, 1.0 ml min^{-1}; and detection, 250–650 nm.

shown in Fig. 2. The retention time of all these species are 3.4, 4.7, 12.8 and 14.9 min for Cu(Bphen)$_2^{2+}$, HBphen$^+$, Fe(Bphen)$_3^{2+}$ and Ni(Bphen)$_3^{2+}$, respectively. The resolution (R_s) of Cu(Bphen)$_2^{2+}$, Fe(Bphen)$_3^{2+}$ and Ni(Bphen)$_3^{2+}$ from the ligand HBphen$^+$ calculated from the observed retention time (t_R) and measurements of peak widths (w_b) are 1.44, 12.46 and 13.60, respectively. The R_s values are quite sufficient for accurate quantification ($R_s > 1$) [24].

The retention behavior of metal chelates with acetonitrile based solvents was investigated as a function of the concentration of organic component and the plots of their capacity factor (log k′) against the composition of mobile phase are presented in Fig. 3. The retention time of all species were found to increase with the water content of the mobile phase. This tendency is consistent with

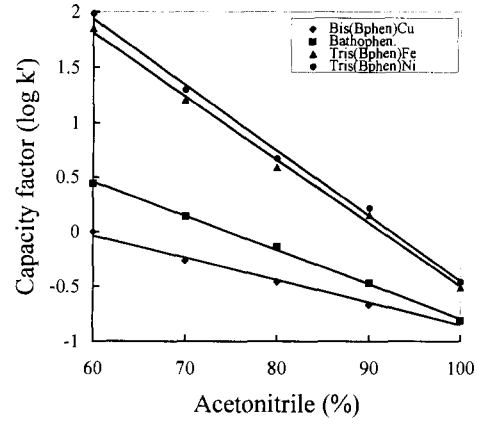

Fig. 3. Effect of acetonitrile concentration (%v) in mobile phase on capacity factor (log k′) of metal bathophenanthroline chelates

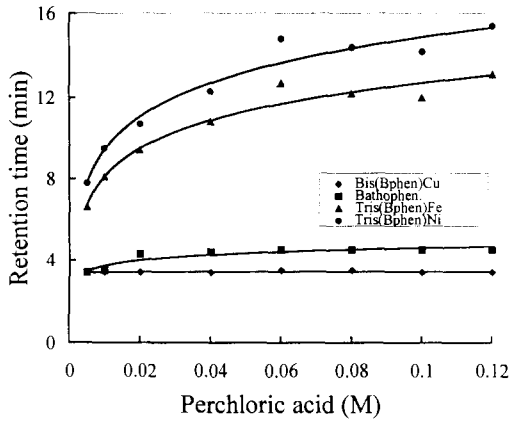

Fig. 4. Effect of perchloric acid concentration (M) in mobile phase on retention time of metal bathophenanthroline chelates.

what would be expected from the solvophobic theory. The optimum composition of mobile phase was reached at approximately 20% of water content. The resolution continued to increase at the higher concentration of water in acetonitrile but the metal chelates, except $Cu(Bphen)_2^{2+}$, gradually became insoluble and the retention time became too long for the purpose of practical analysis.

3.3. Effect of perchlorate concentration on retention time

From the previous work [25] on separation of iron (II) complexes of 1,10-phenanthroline and its derivatives, it was found that perchlorate ion was the most suitable counter ion for the separation compared with other counter ions such as alkylsulfonate and phosphate ion. The reason why perchlorate ion becomes the most suitable counter ion also has been discussed. On the basis of that results, perchlorate ion was selected as a counter ion for the separation of metal-bathophenanthroline chelates.

The relationship between perchlorate concentration and retention time of the chelates was studied by varying perchloric acid concentration in the mobile phase from 0.05 to 0.12 M. Fig. 4 shows that the retention time of metal chelates increases slightly with the perchlorate concentration up to 0.05 M and then becomes almost steady at the concentration greater than 0.05 M. This behavior indicates that a perchlorate concentration of about 0.05 M in the mobile phase was sufficient enough for the formation of ion-pair association so that further addition of perchlorate ion has no longer effect on retention time of the chelates. Even though the retention time is not influenced significantly, the use of perchloric acid concentration above 0.08 M was not suggested because it would decrease pH of the mobile phase. Probably column packing material could be damaged if the column is operated below the recommended pH of reverse-phase column operation (between 2–11). Moreover, protonation of the free ligand may occur at a lower pH of the mobile phase which can cause the metal chelates to dissociate due to the restoration of equilibrium conditions with the free ligands [26].

The effect of pH on the separation of metal chelates was not studied in the present work. Replacing perchloric acid in mobile phase (pH ca. 2) by lithium perchlorate (pH ca. 7) gave no significant effect on retention time, but the peak of $Cu(Bphen)_2^{2+}$ became broader and more tailing. This is probably due to the conversion of colorless $Cu(Bphen)_2^{2+}$ chelate to another species (yellow) as the mobile phase became neutral or alkaline [19]. For this reason and for its large solubility in the mobile phase compared with lithium perchlorate, perchloric acid was selected as a counter ion for further study.

3.4. Calibration graphs and interferences

In order to know the performance of the present method, a calibration graph for each metal ion was constructed according to the analytical procedure described in experimental section. The calibration graphs of peak area versus metal ion concentration were linear in the concentration ranges 0.05–0.5, 0.25–2.0 and 0.25–4.0 μg ml^{-1} for iron (II), nickel (II) and copper (II) ions, respectively. The correlation coefficients for all metal ions are above 0.991 ($n = 3$). The repeatability was examined with five injections at a concentration level of 10 ng ml^{-1} for iron (II) and nickel (II) ions and at a concentration level of 25 ng

Table 2
Analytical performance of the proposed method

Metal ion	Regression equation[a]	r	Detection limit (ng ml^{-1})[b]	RSD (%)[c]
Fe (290 nm)	$y = 2.94x + 0.03$	0.995	2.67	3.11
Fe (534 nm)	$y = 2.62x + 0.04$	0.992	5.15	7.37
Ni	$y = 1.94x + 0.08$	0.993	5.42	5.81
Cu	$y = 0.47x + 0.01$	0.998	18.20	7.16

[a] Where y is the peak area and x is the concentration (in μg ml^{-1}).
[b] Defined as the analyte concentration giving a signal equal to three times the standard deviation.
[c] Measured at 10 ng ml^{-1} for iron (II) and nickel (II) and at 25 ng ml^{-1} for copper (II) ($n = 5$).

ml^{-1} for copper(II) ion. The relative standard deviation of all metal ions was found to be below 7.5%. The detail analytical performance of the present method including regression equation, correlation coefficients (r), detection limit (for S/N = 3) and relative standard deviation (RSD) are listed in Table 2. Since $Fe(Bphen)_3^{2+}$ also gave an absorption maximum in the visible region at 534 nm, a calibration graph for iron(II) ion at this detection wavelength was also constructed for the purpose of comparison.

Because the analytical method developed is to be applied to the determination of iron (II) and iron (III) in natural water, possible interferences from other metal ions such as Ni^{II}, Co^{II}, Zn^{II}, Cu^{II}, Al^{III}, Sn^{II}, Mo^{IV} and Pb^{II} [4] which commonly exist in natural water should be aware. Among those metal ions, nickel (II) and copper (II) are reported to interfere strongly with the determination of iron (II) as bathophenanthroline chelate by spectrophotometry, while cobalt (II) and zinc (II) interfere slightly [17]. Fortunately, nickel (II) and copper (II) are well-separated from iron (II) under this analytical condition, and thus investigation was focused on cobalt (II) and zinc (II) ions. Aluminium (III), even though no interference is reported, was also investigated because this ion is most likely to be encountered in natural water in relatively high concentration.

Solutions of cobalt (II), zinc (II) and aluminium (III) (100 μg ml^{-1}) were prepared by dissolving their corresponding salts in distilled water. The concentration of each metal ion examined was adjusted 20 times higher than that of iron (II) so that it was also high enough compared with usual concentration encountered in real samples. The solution of bathophenanthroline chelate with cobalt (II), zinc (II) or aluminium (III) was prepared by the procedure described in experimental section and then injected into the HPLC system. No peaks other than those of iron (II) chelate and excess ligand were detected for cobalt (II), zinc (II) or aluminium (III) solution, suggesting that these chelates are probably decomposed during the separation process in the column because cobalt (II), zinc (II) chelates of bathophenanthroline are considered as labile chelate [15]. It was confirmed that the coexistence of cobalt (II), zinc (II) or aluminium (III) ions does not interfere with the present ion-paired chromatographic (IPC) determination of iron (II), nickel (II) and copper (II) in natural water.

3.5. Determination of iron (II) and iron (III)

The developed method was applied to the determination of iron (II) and iron (III) in tap water in Yokohama and sea water obtained from environmental chemistry laboratory, Keio University. Copper (II) and nickel (II) were not determined because their content in natural water is normally below the detection limit [2]. Iron (III) is also able to form chelate with bathophenanthroline but the stability of the chelate is very low compared with that of iron (II) chelate [17]. Preliminary investigation by injecting iron (III) chelate into the HPLC system showed that the chelate was eluted around 8 min before iron (II) chelate but the peak was very broad and tailing. Therefore, it is not possible to determine iron (III) and iron (II) simultaneously. Here, iron (II) and total iron were determined separately by reducing iron (III) to

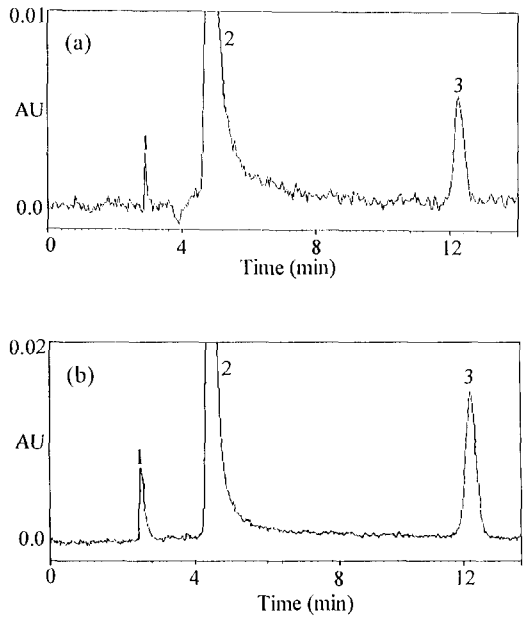

Fig. 5. Typical chromatograms for the determination of iron(II) in tap water sample (a) and total iron in sea water sample (b). Conditions as in Fig. 2 (1) solvent; (2) bathophenanthroline; and (3) $Fe(Bphen)_3^{2+}$.

iron (II) with hydroxyl amine hydrochloride for the total iron determination. Iron (III) content was then calculated by substracting iron (II) from the total iron content (iron (II) plus iron (III) ions).

Since bathophenanthroline is a very sensitive reagent toward iron (II), an extra-care should be taken against iron (II) contaminant from outside sources. Every determination should be corrected subsequently by blank solution especially for the determination of total iron because it is difficult to find a reducing agent free from iron (II). Total iron should be corrected with the blank solution also containing the reducing agent, and one fails to do so will have the result higher than it should be. Fig. 5 shows the typical chromatogram of iron (II) determination in tap water (a) and total iron determination in sea water (b). The results of the determination and their relative standard deviations are listed in Table 3, together with the analytical results obtained by spectrophotometry. It is clear that both sets of results (IPC and spectrophotometry) are comparable. A little higher results of spectrophotometry in sea water are attributed to the complexity of sea water matrix which slightly increases the measured absorbance. As a result, calculated concentrations of iron (II) and iron (III) in sea water are higher than they should be. In conclusion, it has been demonstrated that the developed IPC method is a simple and practical technique for the determination of iron (II) and iron (III) in tap water and sea water. The method may also be applied to the simultaneous determination of iron (II), nickel (II) and copper (II) in other samples containing these metal ions in the higher levels than those of limit detection.

Acknowledgements

The first author wishes to thank The Hitachi Scholarship Foundation, Tokyo Japan for financial support.

Table 3
Analytical results of iron (II) and iron (III) in tap water and sea water samples

Samples	Elements	IPC[a] (ng ml^{-1})	RSD (%)	Spectrophotometry[b] (ng ml^{-1})	RSD (%)
Tap water	Iron (II)	89.5	4.06	80.9	5.13
	Iron (III)	62.4	3.39	71.6	3.25
Sea water	Iron (II)	67.1	4.23	77.0	4.84
	Iron (III)	42.1	3.86	48.9	2.78

[a] Detected at 290 nm for $n = 4$.
[b] Detected at 533 nm for $n = 3$.

References

[1] M.Y. Khuhawar, S.N. Laujwani, Talanta, 43 (1996) 767.
[2] Y. Shijo, H. Sato, N. Uehara and S. Aratake, Analyst, 121 (1996) 325.
[3] A. Padarauskas and G. Schwedt, Talanta, 42 (1995) 693.
[4] C.Y. Zhou, J. Wu, H. Chi, M.K. Wong, L.L. Koh and Y.C.Wee, Talanta, 42 (1995) 415.
[5] H. Ohashi, N. Uehara and Y. Shijo, J. Chromatogr., 539 (1991) 225.
[6] K. Robards and P. Starr, Analyst, 116 (1991) 1247.
[7] J.W. O'Laughlin, J. Liq. Chromatogr., 7 (1984) 127.
[8] J.N. King and J.S. Fritz, Anal. Chem., 59 (1987) 703.
[9] E. Ryan and M. Meaney, Analyst, 117 (1992) 1435.
[10] S. Li and H. Inoue, Chromatographia, 33 (1992) 567.
[11] H. Inoue, H. Yamashita, K. Furuya, Y. Nonomura, N. Yoshioka and S. Li, J. Chromatogr., 679 (1994) 99.
[12] X.S. Zhang, X.P. Zhu and C.S. Lin, Talanta, 33 (1986) 838.
[13] H. Inoue and K. Ito, Microchem. J., 49 (1994) 249.
[14] J.W. O'Laughlin and R.S. Hanson, Anal. Chem., 52 (1980) 2263.
[15] J.W. O'Laughlin, Anal. Chem., 54 (1982) 178.
[16] P. Che, J. Xu, H. Shi and Y. Ma, J. Chromatogr., 669 (1995) 45.
[17] Z. Marczenko, Separation and Spectrophotometric Determination of Elements, Ellis Horward, Chichester, 1980, p. 333.
[18] L.C. Thomas, G.J. Chamberlin, Colorimetric Chemical Analytical Methods, The Tintometer, Salysbury UK, 1980, pp. 216, 405.
[19] L.J. Clark, Anal. Chem., 34 (3) (1962) 349.
[20] K. Yoshimura, S. Matsuoka, Y. Inokura and U. Hase, Anal. Chim. Acta, 268 (1992) 225.
[21] A.A. Schilt and R.C. Taylor, Inorg. Nucl. Chem., 9 (1959) 211.
[22] K. Miyoshi, T. Toura, C. Shimada and H. Yoneda, Bull. Chem. Soc. Jpn., 48 (6) (1975) 1783.
[23] D.F. Shriver, P.W. Atkins, C.H. Langford, Inorganic Chemistry, Oxford University Press, Oxford, 1980, p. 446.
[24] R.M. Smith, Gas and Liquid Chromatography in Analytical Chemistry, Wiley, Chichester, 1988, p. 30.
[25] Mudasir, N. Yoshioka and H. Inoue, Anal. Lett., 29 (12) (1996) 2239.
[26] M.V. Twigg, J. Chem. Educ., 49 (5) (1972) 371.

ELSEVIER

Talanta 44 (1997) 1203–1209

Talanta

Micellar enhanced cyanide ion determination in samples from synthetic organic processes

John O. Egekeze *, Thomas M. Dowling, Nelu Grinberg, Holly J. Perpall, Gary R. Bicker

Merck Research Laboratories, R80Y-115, P.O. Box 2000, Rahway, NJ 07065-0914, USA

Received 20 August 1996; received in revised form 21 October 1996; accepted 25 October 1996

Abstract

A method was developed for the recovery and determination of cyanide ion in organic sample matrices. To facilitate the solubilization of cyanide ions, cetyltrimethylammonium bromide (CTAB) was added at concentrations above the critical micelle concentration. Sample cyanation reaction products consisted of solvent mixtures of a hydroxynitrile in DMF-toluene or DMF-isopropylacetate (IPAC). Spectrophotometric determination of cyanide ion at 578 nm by the pyridine-barbituric acid method was automated by flow injection analysis. Recovery of cyanide ion from spiked samples was 93.2% in DMF-IPAC solvent matrix and 93.9% in DMF-toluene. Low alkali concentration was observed to favor solubilization of cyanide ion in the micellar solution. © 1997 Elsevier Science B.V.

Keywords: Cyanide determination; Micellar solution; Organic samples

1. Introduction

Cyanation is a commonly used synthetic organic reaction in the pharmaceutical and specialty chemical industries [1–4]. When this reaction is run on a pilot plant or factory scale, a product mixture generally results that is high in cyanide ion concentration. If the nitrile produced is an intermediate in the synthesis of a bulk drug candidate, the concentration of cyanide ion must be considerably reduced before the intermediate can be used in the next synthetic step. The high toxicity of cyanide ion at low doses and the environmental problem posed by cyanide waste disposal make accurate determination of this ion in organic sample matrices an important task. Published methods for cyanide ion determination have addressed cyanide (free/bound or HCN) assays in aqueous samples. A popular procedure in these methods involved distillation of the acidified sample solution to transfer evolved HCN into an aqueous sodium hydroxide solution where it was converted to cyanide ion. The cyanide ion produced has been determined by spectrophotometry [5–10], potentiometry [11], amperometry [12,13], fluorescence spectroscopy [14], and ion chromatography [15].

When the cyanide ion is present in a liquid organic sample, acidification and distillation to

* Corresponding author. Fax: +1 908 5945468.

PII S0039-9140(96)02160-1

evolve HCN leads to increased pressure in the distillation system due to production of a large volume of organic vapor. The distillation method is therefore unsafe for the analyst because of the likelihood for liquid boil over or explosion. Cyanide ion in an organic sample matrix can be made available for determination by the use of amphiphilic molecules (surfactants) each of which consists of a hydrophobic tail joined to a hydrophilic head. Surfactants are classified as anionic, cationic, or zwitterionic, depending upon the nature of the polar head [16]. When dissolved in water at concentrations equal to or above the critical micelle concentration (cmc), surfactants tend to form spherical aggregates called micelles or organized molecular assemblies. Micelles exhibit several properties which facilitate analytical measurements. These include their ability to solubilize and concentrate analytes, alter acidity and polarity of solutes, and modify reaction rates and chemical equilibria [17–19]. The most important of these properties is the ability of micelles to solubilize within their microscopic local environment compounds which are insoluble or sparingly soluble in water. Ionic micelles also provide charged structures where attractive or repulsive interactions with ionic solutes may take place. The use of an aqueous micellar medium to improve the spectrophotometric determination of cyanide ion with the organic disulfide 5,5′-dithiobis(2-nitrobenzoic acid), usually referred to as (DTNB), was reported by Hinze [20]. The problem with the use of DTNB is that the compound is sensitive to both cyanide and sulfite ions and is not ideal for a sample that contains both ions as is the case in this study.

This paper reports the use of aqueous micellar solutions of the cationic surfactant cetyltrimethylammonium bromide (CTAB) to facilitate the recovery of cyanide ion from a cyanation reaction product mixture. The samples used in the study were liquid hydroxynitrile concentrates from cyanation reactions between sodium cyanide and an organic sulfite. One group of nitrile samples was prepared in a solvent mixture consisting of 5% dimethylformamide (DMF) in isopropylacetate (IPAC), and the other group was prepared in a solvent mixture consisting of 12% DMF in toluene. Cyanide in these organic liquids is postulated to be in the form of HCN retained by dipole–dipole interactions with DMF [21]. The assay technique is based on the fact that the micellar solution of CTAB solubilizes the organic and inorganic components of the sample thereby facilitating cyanide ion determination. Cyanide ion was detected spectrophotometrically at 578 nm by the pyridine-barbituric acid method [18]. The effects of surfactant and alkali concentrations on cyanide ion recovery from these samples are discussed.

2. Experimental

2.1. Instrumentation

The instrumentation consisted of two Spectra Physics (San Jose, CA, USA) HPLC pumps, a Hewlett Packard (San Fernando, CA, USA) model HP1050 autosampler with 10 μl sample loop, a knitted teflon reaction coil (AURA Industries, Staten Island, New York, USA) 15 m × 0.5 mm internal diameter and total internal volume of 3 ml, and a model 759A variable wavelength UV/VIS absorbance detector with tungsten lamp (Applied Biosystems, Foster City, CA, USA). The data analysis was performed using a PE Nelson (Cupertino, CA, USA) Access*Chrom software.

2.2. Reagents for color development

All reagents were analytical grade chemicals purchased from Aldrich Chemical, Milwaukee, WI, USA.

Phosphate buffer (0.100 M) was prepared by dissolving 13.8 g of dibasic sodium phosphate monohydrate (MW = 138.0) in about 900 ml of deionized water and adjusting the pH of the resulting solution to 7.0 with sodium hydroxide. The final volume was brought to 1 l with deionized water.

Chloramine-T solution (0.044 M) was prepared by dissolving 10.0 g of chloramine-T (*N*-chloro-4-methylbenzene sulfonamide sodium salt, MW = 227.67) in about 500 ml of the previously prepared phosphate buffer and diluting to a final

volume of 1 l with the buffer. The prepared solution was filtered with 0.45 micron filter paper and stored in the refrigerator. The solution was allowed to warm up to room temperature before use.

Barbituric acid-pyridine solution (0.375 M) was prepared by dissolving 48.0 g of barbituric acid (MW = 128.09) in 240 ml of pyridine with constant stirring. Concentrated hydrochloric acid was added in four 12 ml portions while continuously stirring the solution. Each portion of hydrochloric acid was added in 5 min intervals. After adding all of the hydrochloric acid and allowing the solution to cool to room temperature, the final volume was brought to 1 l with deionized water. Stirring was continued until complete dissolution of solutes. The resulting solution was filtered with 0.45 μm filter paper and stored in the refrigerator when not in use. The solution was allowed to warm to room temperature before use.

2.3. Reagents for standard preparation

Sodium hydroxide solution (0.05 M) was prepared by dissolving 4.0 g of sodium hydroxide pellets in deionized water and bringing the final volume to 2 l with deionized water. Alkaline surfactant solution (0.001 M CTAB in 0.05 M NaOH) was prepared by dissolving 0.365 g of CTAB (MW = 364.46) in about 500 ml of 0.05 M NaOH. The final volume of the prepared solution was brought to 1 l with 0.05 M NaOH. The solution was filtered with 0.45 μm filter paper. For the preparation of a 0.002 M CTAB solution in 0.05 M NaOH, dissolve 0.730 g of CTAB l^{-1} of solution. A 200 μg ml^{-1} (ppm) cyanide stock solution was prepared by dissolving 0.07538 g of sodium cyanide in 100 ml of 0.05 M NaOH and bringing the final volume to 200 ml with 0.05 M NaOH. The solution was mixed thoroughly and stored at room temperature.

Cyanide standard solutions (0.25, 0.50, 1.00, 3.00, 4.00 and 5.00 ppm) were prepared by pipeting 0.125, 0.25, 0.50, 1.50, 2.00 and 2.50 ml, respectively, of the 200 ppm cyanide stock solution into a 100 ml volumetric flask. The final volume of each standard was brought to 100 ml with the appropriate alkaline micellar solution.

2.4. Sample preparation and handling

A 0.5 ml sample was diluted to volume in a 100 ml volumetric flask with the appropriate alkaline micellar solution. Reaction samples in DMF-IPAC or aqueous solvent matrices were diluted with 0.001 M alkaline CTAB. Reaction samples in DMF-toluene solvent matrix were diluted with 0.002 M alkaline CTAB. The volume of the sample diluted or the total volume of prepared solution could be adjusted to accommodate samples that are low or high in cyanide content. For accuracy, organic liquid samples were dispensed using volumetric pipets. The resulting solution was mixed thoroughly by vigorous stirring only after diluting to the final volume because foaming occurs when surfactant solutions are mixed.

2.5. Determination of cyanide

A schematic diagram of the flow-injection system is shown in Fig. 1. The sample was injected into a buffered chloramine-T stream R2 which then merged with a pyridine solution of barbituric acid R1 in a reaction coil C to provide mixing and reaction. Cyanide ion in the sample was oxidized by chloramine-T (Fig. 2) to form cyanogen chloride (CNCl), a compound which contains the CN^+ cation. Reaction between this cation and pyridine led to the formation of the *N*-cyanopyridinium ion which hydrolyzed to a conjugated dialdehyde, glutaconic aldehyde. Further reaction between the conjugated dialdehyde and the reactive tautomer of barbituric acid led to the formation of a reddish blue (purple) dye which was detected at 578 nm [22–24]. The flow injection response was processed by a PE Nelson data acquisition system.

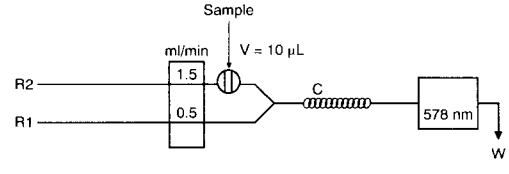

Fig. 1. FIA manifold for the determination of cyanide ion. R1 = pyridine-barbituric acid solution; R2 = chloramine-T solution in phosphate buffer.

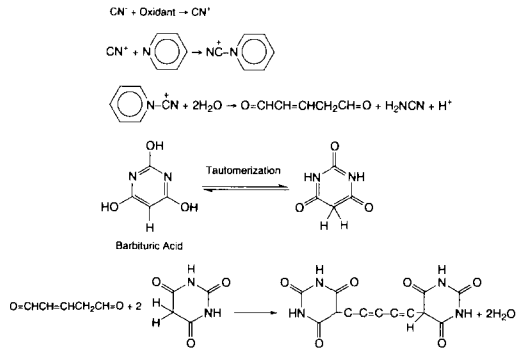

Fig. 2. Reaction sequence for color formation in the pyridine-barbituric acid method for cyanide analysis.

The average response factor (Rs) for a number (n) of cyanide standards, and the concentration (Cs) of cyanide ion in the sample are calculated according to Eq. (1) and Eq. (2), respectively.

$$Rs = \Sigma(\text{peak height of standard}/\text{concentration of standard})/n \quad (1)$$

$$Cs = (\text{Sample Peak Height} \times \text{Dilution Factor})/(\text{Response factor}) \quad (2)$$

Samples were diluted such that responses were within the linear range of the calibration graph. The FIA system was rinsed daily before shut down by pumping pyridine through the barbituric acid delivery tube and water through the chloramine-T delivery tube for a period of at least 30 min to prevent blockage by salts.

3. Results and discussion

3.1. NaOH as sample diluent

A basic solution with pH above 11.2 is required to completely ionize inorganic cyanide (pK_a of HCN = 9.2). Since samples analyzed in this study were cyanide-containing organic liquids, the mixture that resulted when samples were diluted with aqueous sodium hydroxide consisted of an organic layer and an aqueous layer. Cyanide ion is present in both layers even after prolonged mixing but higher levels of cyanide ion were detected in the aqueous layer as the concentration of the NaOH diluent decreased (Table 1). This observation was attributed to increased partitioning of cyanide ion from the organic layer into water as NaOH concentration decreased. The existence of two cyanide-containing layers makes aqueous sodium hydroxide an inappropriate diluent for organic liquid samples. There is therefore the need for a procedure that will incorporate an alkaline medium and also provide adequate solubilization of the organic and inorganic components of the sample.

3.2. Alkaline surfactant as sample diluent

Accurate cyanide ion determination in an organic liquid sample will only be possible if there is complete solubilization of the sample. A solution to the problem of solubilizing organic liquid samples was found by taking advantage of the role of surfactants as emulsifying agents. An alkaline solution of the cationic surfactant CTAB (0.001 M CTAB in 0.05 M NaOH) was observed to provide optimum solubilization of the reaction samples in the DMF-IPAC solvent mixture. A more concentrated surfactant solution (0.002 M CTAB in 0.05 M NaOH) was required to solubilize the reaction samples in the DMF-toluene solvent mixture. Higher CTAB concentration was required to solubilize the DMF-toluene solvent mixture (Table 2) as compared with the more polar DMF-IPAC solvent mixture. The degree of solubilization of the organic liquid sample by the surfactant was

Table 1
Effects of NaOH concentration on the amount of cyanide ion detected in samples

Nitrile sample matrix	Concentration of NaOH (M)	Cyanide ion detected (μg ml^{-1}) (Mean ± %RSD, $n = 3$)
DMF-toluene	0.05	182.0 ± 1.7
	0.1	125.0 ± 1.1
	0.5	49.0 ± 2.1
DMF-IPAC	0.05	122.0 ± 1.6
	0.1	104.0 ± 2.0
	0.5	81.9 ± 1.0

Table 2
Effects of surfactant concentration on cyanide ion detected in reaction samples

Sample matrix	Sample diluent	Cyanide concentration ($\mu g\ ml^{-1}$) (Mean ± RSD, $n = 3$)
DMF-toluene	0.05 M NaOH	14.3+2.6
	0.0005 M CTAB in 0.05 M NaOH	48.0+2.5
	0.001 M CTAB in 0.05 M NaOH	50.7+2.8
	0.002 M CTAB in 0.05 M NaOH	57.0+3.6
	0.003 M CTAB in 0.05 M NaOH	54.1+3.0
DMF-IPAC	0.05 M NaOH	132.1 ± 2.8
	0.0005 M CTAB in 0.05 M NaOH	137.0+2.0
	0.001 M CTAB in 0.05 M NaOH	155.0+3.2
	0.002 M CTAB in 0.05 M NaOH	149.4+3.1

determined by the concentration of cyanide ion detected in the surfactant-sample mixture.

The reported cmc of CTAB is 9.2×10^{-4} M in water [25] and 3.4×10^{-4} M in 0.05 M NaOH [26]. Micelle formation and solubilization of solutes were therefore expected at the alkaline CTAB concentrations of the two diluents used in this study. The organic constituents of the sample are preferentially solubilized by the hydrophobic chain of the cationic CTAB micelles resulting in a homogeneous mixture. Cyanide ion is electrostatically attracted to the micelles, thereby increasing the chance of reaction with solubilized chloramine-T and barbituric acid. The effects of the alkaline surfactant concentration on recovery of cyanide ion from organic samples are illustrated in Table 2. A general observation from this table is that the alkaline micellar diluents facilitated the detection of cyanide ion in organic liquid samples because of their ability to solubilize the sample as compared with aqueous NaOH.

3.3. Characteristics of the method

The dilution ratio of sample to alkaline micellar solution during sample preparation made the resulting solution aqueous in nature. The reagent volume ratio of 1:3 barbituric acid to chloramine-T provided excess barbituric acid required to assure complete reaction with cyanide ion and maximum absorbance for the reaction product. The pH of the mixed solution in the reaction coil was 5.8, a value within the pH range (5.4–6.0) reported in the literature for this reaction [27]. The use of flow injection analysis to automate the detection reaction provided a fast, precise and sensitive method for cyanide ion determination. On-line mixing of samples with reagents reduced analysis time and operator contact with the noxious pyridine reagent.

A typical flow injection response obtained for a series of cyanide standards in 0.002 M alkaline CTAB ranging in concentration from 0.25 to 5.00 ppm is shown in Fig. 3. Similar response was obtained for cyanide ion in 0.001 M alkaline CTAB but the linear range was from 0.25 to 10.0 ppm. Peak height (Y,mv) versus cyanide concentration (X, $\mu g\ ml^{-1}$) for cyanide ion in alkaline 0.002 M CTAB were related by the regression equation $Y = 18.8\ [CN^-] - 0.5$ with a correlation coefficient of 0.99878. In the 0.001 M alkaline CTAB solution, the regression equation was

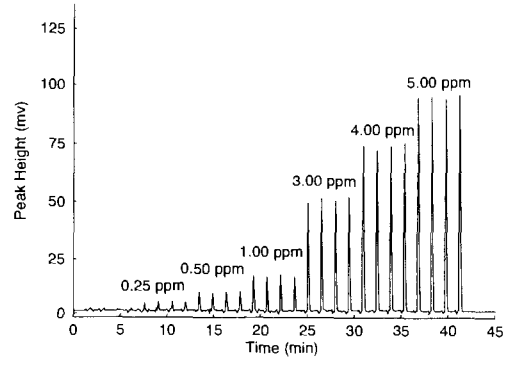

Fig. 3. FIA response for cyanide ion standards in alkaline 0.002 M CTAB.

Table 3
Recovery of added cyanide ion from reaction samples

Sample matrix	Cyanide concentration (μg ml^{-1})			
	Initial	Added	Found	Recovery (%)
DMF-IPAC				
1	105.0	198	184.5	93.3
2	79.5	74.8	68.8	92.0
3	119.1	100	91.5	91.5
4	489.0	76.6	73.7	96.2
Mean recovery ± %RSD				93.2 ± 2.3
DMF-toluene				
1	31.2	69.3	64.6	93.3
2	31.2	68.9	67.0	97.2
3	31.2	68.9	64.4	93.5
4	31.2	68.9	62.8	91.2
Mean recovery ± %RSD				93.8 + 2.6

$Y = 67.8\ [CN^-] - 8.6$ with a correlation coefficient of 0.99901. The detection limit for cyanide ion in both micellar solutions calculated as three times S/N was 0.10 ppm. The precision of injection for a 1.0 ppm cyanide standard solution was 2.1% ($n = 6$) in 0.002 M alkaline CTAB and 1.8% ($n = 6$) in 0.001 M alkaline CTAB. The FIA system performed 40 injections h^{-1}.

3.4. Recovery of cyanide ion from reaction samples

Reaction samples in DMF-IPAC or DMF-toluene solvent mixture were analyzed to determine the initial cyanide content, and then spiked with known amounts of cyanide ion. A 10 ml volume of spiked sample in DMF-toluene was diluted to 500 ml with the 0.002 M alkaline micellar CTAB solution and mixed by stirring before cyanide assay. For the spiked reaction sample in DMF-IPAC, 10 ml of the solution was diluted to 500 ml with alkaline 0.001 M CTAB and mixed by stirring before assay. Average recovery of added cyanide ion was 93.8 ± 2.6% RSD for nitrile in DMF-toluene and 93.2 ± 2.3% RSD in DMF/IPAC (Table 3). These results show that quantitative recovery of cyanide ion impurity from organic samples can be achieved by the use of alkaline micellar solutions as sample diluents.

4. Conclusions

A simple method based on the use of an alkaline micellar CTAB solution to improve solubilization and detection of cyanide ion in organic samples was developed. Automation of the method by flow injection analysis provided high sample throughput and reduced contact with noxious pyridine reagent used in the detection reaction. Recovery of cyanide ion spiked into pilot plant reaction samples was greater than 90%.

References

[1] K. Fredrich and K. Wallenfel, in Z. Rappoport (Ed.), The Chemistry of the Cyano Group, Interscience, New York, 1970, chapter 2, 67.
[2] I.T. Harrison and S. Harrison, Compendium of Organic Synthetic Methods, Interscience, New York, 1971, Vol. 1, chapter 13457.
[3] G. Simchen and H. Kobler, Synthesis, 1975, 605.
[4] D.A. White and N.M. Baizer, J. Chem. Soc. Perkin 1 (1973) 2230.
[5] M.W. Scoggins, Anal. Chem., 44 (1972) 1294.
[6] S. Nagashima, Anal. Chim. Acta, 99 (1978) 197.
[7] N.J. Csikai and A.J. Barnard, Anal. Chem., 55 (1983) 1677.
[8] A. Rios, M.D. Luque de Castro and M. Valcarcel, Analyst, 109 (1984) 1487.
[9] J.C.L. Meeussen, E.J.M. Temminghoff, M.G. Keizer and I. Novozansky, Analyst, 114 (1989) 959.
[10] J.C.L. Meeussen, M.G. Keizer and W.D. Lukassen, Analyst, 117 (1992) 1009.
[11] J.O. Egekeze and F.W. Oehme, J. Anal. Toxicol., 3 (1979) 243.
[12] B. Pihlar, L. Kosta and B. Hristovsk, Talanta, 26 (1979) 805.
[13] S.D. Nikolic, E.B. Milosavljevic, J.L. Hendrix and J.H. Nelson, Analyst, 117 (1992) 47.
[14] D. Chen, M.D. Luque de Castro and M. Valcarcel, Talanta, 37 (1990) 1049.
[15] Y. Liu, R.D. Rocklin, R.J. Joyce and M.J. Doyle, Anal. Chem., 62 (1990) 766.
[16] W.L. Hinze, in K.L. Mittal (Ed.), Solution Chemistry of Surfactants, Vol. 1, Plenum Press, New York, 1979, p. 79.
[17] J.L. Cline Love, J.G. Habarta and J.G. Dorsey, Anal. Chem., 56 (1984) 1133R.
[18] E. Pellizetti and E. Pramauro, Anal. Chim. Acta, 169 (1985) 1.
[19] F. Xia and R.M. Cassidy, Anal. Chem., 63 (1991) 2883.
[20] S. Spurlin, W. Hinze and D. A. Armstrong, Anal. Lett., 10 (1977) 997.

[21] R.S. Kittila, Dimethylformamide Chemical Uses, Du Pont De Nemours and Co., 1967, 92.
[22] E. Asmus and H. Garschagen, Fresenius Z. Anal. Chem., 138 (1953) 414.
[23] W. Konig, Z. Angew. Chem., 69 (1905) 115.
[24] J.L. Lambert, J. Ramasamy and J.V. Paukstelis, Anal. Chem, 47 (1975) 916.
[25] P. Mukerjee and K.J. Mysels, Critical Micelle Concentrations of Aqueous Surfactants Systems, National Standard Reference Data Series, 1971, Vol. 36, 57, U.S. National Bureau of Standards, Washington DC.
[26] C.A. Bunton and L.J. Robinson, J. Am. Chem. Soc., 90 (1968) 5973.
[27] H. Ma and J. Liu, Anal. Chim. Acta, 261 (1992) 247.

ELSEVIER

Talanta 44 (1997) 1211–1217

Talanta

Spectrophotometric methods for the determination of omeprazole in bulk form and pharmaceutical formulations

Chilukuri S.P. Sastry *, Petla Yerrayya Naidu, S.S.N. Murty

Foods and Drugs Laboratories, School of Chemistry, Andhra University, Visakhapatnam 530 003, India

Received 23 July 1996; received in revised form 24 October 1996; accepted 25 October 1996

Abstract

Four simple and sensitive methods for the assay of omeprazole (OMZ) were developed. These methods are based on the formation of colored species by treating OMZ with 3-methyl-2-benzothiazolinone hydrazone (MBTH) following oxidation with ferric chloride (method A) or *m*-aminophenol following oxidation with chloramine-*T* (CAT) (method B) or Folin–Ciocalteau reagent (F–C) (method D), or by oxidizing OMZ with excess *N*-bromosuccinimide (NBS) and determining the consumed NBS with a decrease in color intensity of Celestine blue (CB) (method C). All variables have been optimized. Regression analysis of Beer's plots showed good correlation in the concentration range of 1.0–10, 2.0–32, 0.4–2.4 and 0.8–10 μg ml^{-1} for methods A, B, C and D, respectively. No interference was observed for formulation additives and the validity of each method was tested by analysing capsules containing OMZ. Recoveries were 98.7–100.1%. © 1997 Elsevier Science B.V.

Keywords: Spectrophotometric; Omeprazole; Bulk form

1. Introduction

Omeprazole [5-methoxy-2-(4-methoxy-3, 5-dimethyl pyridin-2-yl-methyl sulphinyl)-1H-benzimidazole), a substituted benzimidazole compound and prototype anti-secretary agent, is the first of the 'proton pump inhibitors' widely used for the treatment of symptomatic gastro-oesophagal reflux. It is officially listed in the British Pharmacopoeia (B.P.) [1]. Two UV [2,3], one differential pulse polarographic [4], and three HPLC [5–7] procedures have been reported for its determination. In view of the fact that there is no visible spectrophotometric method for the determination of OMZ, sensitive and accurate visible spectrophotometric methods were viewed as essential to avoid interference due to UV absorbing compounds in the determination of OMZ in bulk samples or pharmaceutical dosage forms. This paper describes four visible spectrophotometric methods for the determination of OMZ utilizing its unique structural features.

Sawicki et al. developed a visible spectrophotometric procedure for determining phenols and amines by condensation with 3-methyl 2-benzothiazolinone hydrazone (MBTH) in the presence of an oxidant to form an intensely colored oxidized product [8,9]. Sastry et al. reported a visible spec-

* Corresponding author.

trophotometric method for the determination of indomethacin with *m*-aminophenol and chloramine-*T* [10]. Sastry et al. also developed a visible spectrophotometric procedure for the determination of a few drugs with *N*-bromosuccinimide and celestine blue (CB) [1-amino-carbonyl-7-diethyl amino-3, 4-dihydroxyphenoxazine-5-ium chloride; C.I. No. 51050] [11]. The Folin–Ciocalteau reagent was preferred by a number of workers for visible spectrophotometric determination of drugs exhibiting reducing reactivity [12].

We have applied these sensitive visible spectrophotometric procedures in the determination of OMZ in bulk samples and pharmaceutical formulations. Method A describes the determination of OMZ with MBTH following oxidation with ferric chloride (Fe III). Method B describes the determination of OMZ with *m*-amino phenol (*m*-AP) following oxidation with chloramine-*T* (CAT). Method C involves the addition of excess NBS of known concentration in the presence of 0.25 M HCl and unreacted NBS is determined by measurement of the decrease in absorbance of celestine blue. Method D describes the determination of OMZ with Folin–Ciocalteau reagent in the presence of sodium carbonate (Na_2CO_3).

2. Experimental

2.1. Apparatus

A systronics model 106 spectrophotometer with 1 cm matched glass cells and a Milton Roy spectronic 1201 spectrophotometer with 1 cm matched quartz cells were used for absorbance measurements in the visible and ultraviolet regions, respectively. An Elico-digital model LI-120 pH meter was used for pH measurements.

2.2. Materials and reagents

All reagents were analytical grade and all solutions were prepared with double-distilled water. Freshly prepared solutions were always used.

Aqueous solutions of 8.56×10^{-3} M MBTH (Aldrich) and 2.96×10^{-2} M iron (III) chloride hexahydrate (Wilson Laboratories) were prepared for method A. Aqueous solutions of 9.17×10^{-3} M *m*-aminophenol (BDH) in 0.025 M HCl, 0.03 M CAT (Loba-Chemic) and 0.05 M potassium acid phthalate (E. merck) were prepared for method B. Aqueous solutions of 100 μg ml^{-1} NBS (Loba), 100 μg ml^{-1} Celestine blue (E. Gurr) and 5 M hydrochloric acid (BDH) were prepared for method C. Aqueous solutions of 10% sodium carbonate (BDH), and commercially available 2*N* Folin–Ciocalteau (Loba-Chemic), reagent were used for method D.

2.3. Preparation of standard drug solutions

For method A: 10 mg of B.P. grade OMZ was dissolved and diluted to 200 ml with glacial acetic acid (50 μg ml^{-1}).

For methods B, C and D: 100 mg of B.P. grade OMZ was dissolved in 10 ml of 0.1 M NaOH solution and diluted with distilled water, to prepare working solutions of 200, 10, 50 μg ml^{-1} for methods B, C and D, respectively.

2.4. Procedures

2.4.1. Method A

To 20 ml graduated test tubes containing list volumes (0.4–4.0 ml) of 50 μg ml^{-1} OMZ solution was added 2.0 ml of MBTH solution and allowed to react for 2 min at room temperature. After that, 1.5 ml of iron (III) chloride solution was added, allowed to react for 5 min, and diluted to 20 ml with distilled water. Absorbances were measured during the next 20 min at 660 nm against a reagent blank prepared in a similar manner omitting the drug. The drug concentration was determined with a standard plot prepared under identical conditions.

2.4.2. Method B

To 25 ml graduated test tubes containing list volumes (0.25–4.0 ml) of 200 μg ml^{-1} OMZ solution was added 15 ml of 0.05 M potassium hydrogen phthalate solution, 3 ml each of CAT and *m*-AP solution and diluted to 25 ml with distilled water. The pH of the resulting solution was between 4.0 and 5.0. Absorbance was mea-

sured at 420 nm within 10 min against a reagent blank prepared in a similar manner. The omeprazole concentration was determined with a standard plot prepared with known solutions prepared under identical conditions.

2.4.3. Method C

To 25 ml graduated test tubes containing list volumes (1.0–6.0 ml) of 10 μg ml^{-1} OMZ solution was added 1.25 ml of 5 M HCl and 2.5 ml of 100 μg ml^{-1} NBS and the volume increased to 15 ml with distilled water. After 10 min, 10 ml of 100 μg ml CB was added and mixed thoroughly. After 5 min the absorbance was measured at 540 nm against distilled water. Blank was prepared similarly omitting the drug and its absorbance was measured against distilled water. The decrease in absorbance corresponding to consumed NBS and, in turn, to drug concentration, was obtained by subtracting the absorbance of the blank solution from that of the test solution. The calibration graph was drawn by plotting the decrease in the absorbance of the dye (CB) against the amount of drug. The drug concentration was determined with the above standard plot.

2.4.4. Method D

To 25 ml graduated test tubes containing list volumes (0.4–5.0 ml) of 50 μg ml^{-1} OMZ solution was added 2.0 ml of F–C reagent and 9.0 ml of Na_2CO_3 solution and allowed to react for 10 min at laboratory temperature. The solution was diluted to 25 ml with distilled water and the absorbance of each solution measured at 770 nm against reagent blank prepared simultaneously within the stability period (5 min–4 h). The drug content was determined with a standard plot.

2.5. Analysis of pharmaceutical formulations

Capsules, 20, were emptied and blended. Samples, 10 mg, for method A or 100 mg samples for methods B, C and D were massed and solutions prepared as described for the standard solutions and filtered if insoluble materials was present prior to analysis as described for pure samples.

2.6. Results and discussion

The optimum conditions for the development of methods A, B, C and D were established by varying parameters one at a time [13] and observing the effect produced on the absorbance of the colored species.

In order to establish experimental conditions for the determination of OMZ using method A, the applicability of MBTH in conjunction with various oxidizing agents such as Fe(III), Ce (IV), Cr (VI), IO_4^-, CAT, and $S_2O_8^{2-}$ were examined and Fe(III) was found to be the best. The effect of reagent concentrations [MBTH and Fe(III)], temperature, time, and order of addition of reagents with respect to maximum absorbance and stability were studied in preliminary experiments. For color development solutions of list volumes (1.5–2.5 ml) of MBTH, list volumes (1.0–2.0 ml) of Fe(III) and an ambient temperature of (28 ± 5°C) were found to be optimal. Reversing the order of addition, i.e., drug, plus iron (III) plus MBTH, resulted in considerable loss of sensitivity. Maximum color intensity was attained within 5 min after the addition of iron (III). The colored product was found to be stable up to 20 min after the attainment of maximum intensity at 660 nm.

Optimum conditions for method B were established after a thorough systematic study of parameters such as coupler–oxidant combination, acid strength (pH), reagent concentration, and order of addition of reagents. Of the various combinations of *o*-, *m*-, *p*- or *P*-*N*-methyl amino phenols, phenols (phenol, catechol, resorcinol, pyrogallol and phloroglucinol), and oxidizing agents [CAT, OCl^-, IO_4^-, IO_3^-, Cr (VI), Fe(III), $S_2O_8^{2-}$, and H_2O_2], examined for the development of color under acidic or alkaline conditions at laboratory temperature (28 ± 5°C), *m*-amino phenol-CAT was found to be superior. A volume of 15.0 ml of potassium hydrogen phthalate solution was found to be necessary to maintain the pH of the solution between 4.0 and 5.0. For color development, solutions of 2.5–3.5 ml of CAT and 2.5–3.5 ml of *m*-amino phenol were found optimal. Maximum color intensity was attained within 3 min after the addition of *m*-amino phenol solution. The colored product was found to be stable

Table 1
Optical and regression characteristics, precision and accuracy of the proposed methods

Parameters	Methods			
	A	B	C	D
λ_{max} (nm)	660	420	540	770
Beer's Law limit (μg ml^{-1})	10.0	32.0	2.4	10.0
Detection limit (μg ml^{-1})	0.074	0.104	0.023	0.039
Molar absorptivity (1 mol^{-1} cm^{-1})	2.10×10^{4}	1.19×10^{4}	7.58×10^{4}	2.85×10^{4}
Sandell's sensitivity (μg cm^{-2} per 0.001 absorbance unit)	0.045	0.028	0.005	0.012
Regression equation (Y)[a]				
Slope (b)	6.10×10^{-2}	3.46×10^{-2}	2.20×10^{-1}	8.26×10^{-2}
Standard deviation on slope (sb)	2.25×10^{-4}	7.39×10^{-5}	1.45×10^{-3}	8.79×10^{-4}
Intercept (a)	1.14×10^{-3}	-2.50×10^{-3}	-2.60×10^{-3}	3.0×10^{-3}
Standard deviation on intercept (Sa)	1.26×10^{-3}	1.62×10^{-3}	2.27×10^{-3}	5.83×10^{-3}
Standard error of estimation (Se)	1.49×10^{-3}	1.32×10^{-3}	2.44×10^{-3}	5.56×10^{-3}
Correlation coefficient	0.9999	0.9999	0.9999	0.9998
Relative standard deviation (%)[b]	0.69	0.53	0.73	0.48
% Range of error[b] (95% confidence limit)	0.72	0.56	0.77	0.50

[a]With respect to $Y=bC+a$, where C is concentration [μg ml^{-1}] and Y is absorbance.
[b]Six replicate samples, (concentration of 7.5, 16.0, 1.2 or 6.0 μg ml^{-1} of pure drug for methods A, B, C and D, respectively).

for 10 min after the attainment of maximum intensity at 420 nm.

In method C, the effect of reagent concentration (acidity, NBS and CB), reaction period in each step were studied by means of controlled experiments varying one parameter at a time. Studies of the variation of acid concentration indicated that a constant absorbance was obtained with 0.15–0.35 M HCl, 0.1–0.25 M H_2SO_4 or 0.3–0.5 M CH_3COOH with an NBS concentration of 8 μg ml^{-1}. Since the difference in absorbance between the sample and the blank was found to be highest for the addition of HCl, subsequent studies were performed in 0.25 M HCl. In order to obtain a linear relationship between the concentration of added NBS and the corresponding decrease in the absorbance of CB (40 μg ml^{-1}), experiments were performed on 0.25 M HCl with varying amounts of NBS. As the decrease in absorbances was found to be linear up to 10 μg ml^{-1} of NBS, subsequent studies were performed with 40 μg ml^{-1} of CB and 10 μg ml^{-1} of NBS in 25 ml of 0.25 M HCl. Time spans of 5–20 min for the reaction between the drug and NBS in the first step and 2–30 min between NBS and CB in the second step resulted in a constant and maximum difference in absorbance of the test and blank solutions. Hence, reaction periods of 10 and 5 min were maintained in subsequent studies of the first and second steps, respectively. The colored product was found to be stable for 5 h after the attainment of maximum intensity at 540 nm.

In order to establish the optimum volume of Na_2CO_3 solution in method D, the drug was allowed to react with F–C reagent in the presence of 1.0–13.0 ml of 10% Na_2CO_3. Constant absorbances were obtained with 8.0–10.0 ml, hence 9.0 ml was chosen as the routine addition. A volume of 2.0 ml of F–C reagent was found to be optimal. An increase in the volume of F–C reagent (> 2.0 ml) led to precipitation. Reversing the order of addition of reagents i.e., Na_2CO_3 plus F–C, had no influence on color formation. Maximum color intensity was attained within 5 min after the addition of Na_2CO_3 solution. The color product was found to be stable for 4 h after the attainment of maximum intensity at 770 nm.

The above optimum experimental conditions were incorporated in recommended procedures for color development. Beer's law was found to be valid over the concentration ranges given in Table 1 at appropriate λ_{max}.

Table 2
Assay and recovery of omeprazole in dosage forms

Pharmaceutical preparation[a]	Labelled amount (mg)	Amount found[b] (mg) using proposed methods				Found by reference Method 2[c]	% Recovery by proposed methods[d]			
		A	B	C	D		A	B	C	D
Capsule I	20	19.8 ± 0.17 $F = 2.52$ $t = 0.39$	19.9 ± 0.20 $F = 1.82$ $t = 1.66$	19.9 ± 0.18 $F = 2.25$ $t = 0.59$	19.8 ± 0.32 $F = 1.40$ $t = 0.83$	19.8 ± 0.27	99.2 ± 0.80	99.7 ± 0.92	99.6 ± 0.78	99.0 ± 0.46
Capsule II	20	20.0 ± 0.20 $F = 1.82$ $t = 0.50$	19.8 ± 0.16 $F = 2.84$ $t = 0.59$	20.1 ± 0.19 $F = 2.01$ $t = 0.44$	19.7 ± 0.28 $F = 1.07$ $t = 2.09$	19.9 ± 0.27	99.9 ± 1.00	99.2 ± 1.61	100.1 ± 1.18	98.7 ± 1.27
Capsule III	20	20.0 ± 0.11 $F = 1.19$ $t = 0.39$	20.0 ± 0.18 $F = 2.25$ $t = 0.81$	19.8 ± 0.09 $F = 1.77$ $t = 1.57$	20.0 ± 0.08 $F = 2.21$ $t = 0.69$	19.09 ± 0.12	99.9 ± 0.83	99.9 ± 0.84	98.9 ± 0.56	100.0 ± 0.90
Capsule IV	20	19.8 ± 0.12 $F = 1.36$ $t = 1.50$	19.96 ± 0.09 $F = 2.41$ $t = 0.88$	9.8 ± 0.10 $F = 1.96$ $t = 1.29$	20.0 ± 0.10 $F = 1.96$ $t = 0.80$	19.9 ± 0.14	99.2 ± 1.61	99.6 ± 1.72	99.3 ± 0.58	100.0 ± 0.54

[a] Capsules manufactured by four different pharmaceutical companies.
[b] Average ± standard deviation of six determinations; the F- and t values refer to comparison of the proposed method with the reference method. Theoretical values at 95% confidence limits $F = 5.05$, $t = 2.57$.
[c] UV reference method.
[d] Recovery of 10 mg added to the pharmaceutical formulations (average of three determinations).

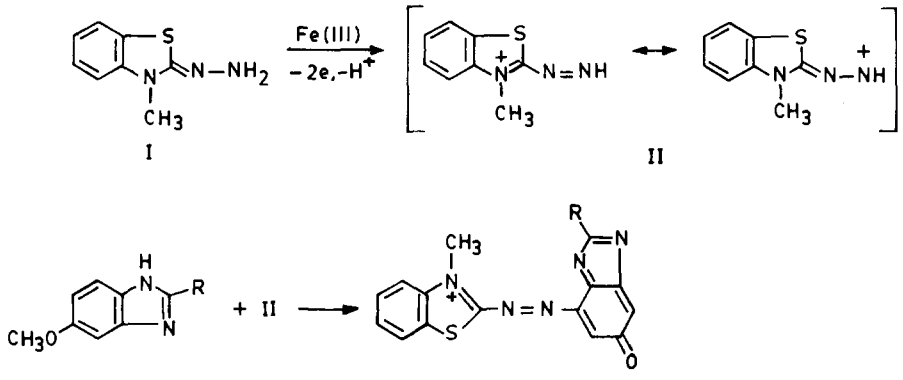

Scheme 1.

2.7. Analytical data

Beer's law limits, molar absorptivity, Sandell's sensitivity, detection limits [14], regression equation, and correlation coefficients obtained by least squares treatment of these results are given in Table 1. Precision of each method was tested by analysing six replicate samples containing (7.5, 16.0, 1.2 or 6.0 μg ml^{-1}) of pure drug for methods A, B, C and D, respectively. The percent standard deviation and the percent range of error at 95%, confidence level of each method are given in Table 1.

Commercial formulations (Capsules) containing OMZ were successfully analysed by the proposed methods. The value obtained by the proposed and reference methods for the pharmaceutical preparations were compared statistically by the *t*- and *F*-tests and found not to differ significantly. As an additional demonstration of accuracy, recovery experiments were performed by adding a fixed amount of the drug to the preanalysed formulations. These results are summarised in Table 2. The ingredients usually present in pharmaceutical preparations of OMZ did not interfere with the proposed analytical methods.

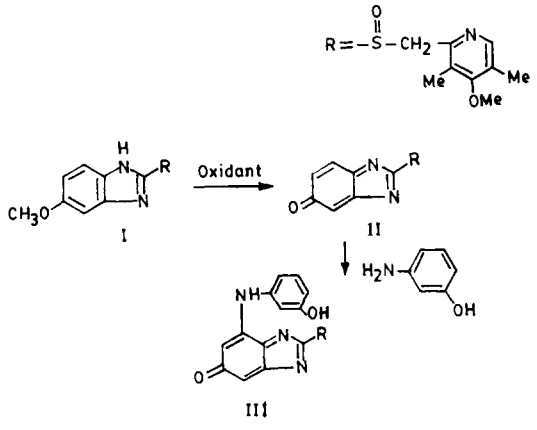

Scheme 2.

2.8. Chemistry of colored species

Several substituted Benzimidazoles [omeprazole (OMZ), albendazole (ABZ), mebendazole (MBZ), fenbendazole (FBZ) and astemizole (AZ)] were tested with reagents MBTH-Fe(III) (method A) or *m*-AP-CAT (method B). It was noticed that color development only occurred with OMZ. The failure of ABZ, MBZ, FBZ and AZ to develop colors with the proposed reagents indicate the necessity to have a 5-OMe group in the benzimidazole moiety.

Method A: under these reaction conditions MBTH (I) on oxidation with Fe(III) loses two electrons, and one proton forming an electrophilic intermediate (II), which is the active coupling species. Of this species, 1 mol, undergoes electrophilic substitution with OMZ to form a colored product (III), shown in Scheme 1.

Method B: omeprazole reacts initially with the CAT to produce the highly reactive and less stable intermediate as with *P*-Phenetidine (*P*-ethoxy aniline) [15]. The intermediate may react further with *m*-aminophenol to give 7-substituted product, as shown in Scheme 2.

Method C: NBS provides molecular bromine at low concentration in polar media [16]. This reacts with the drug resulting in either oxidation, substitution, or addition depending upon the functional group present in the drug. Probably a mixture of reproducible products are produced under the specified experimental conditions. The remaining molecular bromine is involved in bromination reaction with the dye (CB) to form a brominated dye which is colorless. The mole-ratio of the reaction between NBS and OMZ under the experimental conditions has been found to be 1:3.

Method D: color formation following the reaction of F–C reagent with OMZ in method D may be explained in the following manner based on the anology with reports of the earlier workers [12,17]. The mixed acids in the F–C preparation involve the following chemical species.

$3H_2O, P_2O_5 \cdot 13\ Wo_3 \cdot 5\ MoO_3 \cdot 10\ H_2O$ and

$3H_2O, P_2O_5 \cdot 14\ Wo_3 \cdot 4\ MoO_3 \cdot 10\ H_2O$

OMZ probably affects a reduction of 1, 2 or 3 oxygen atoms from tungstate and/or molydate in F–C reagent (Phosphomolybdotungstate), thereby producing one or more of the possible reduced species which have a characteristic intense blue color.

3. Conclusion

The order of sensitivity among the proposed methods and UV reference method (R) in the determination of OMZ is C > D > A > R > B. The λ_{max} order of D > A > C > B > R. Although the molar absorptivity of one of our methods (B) was somewhat less than that of the reference method, the λ_{max} of all the four proposed methods were considerably higher than that of the reference method. The higher λ_{max} of the proposed methods is a decisive advantage since the interference from the associated ingredients shall be far less at higher wavelengths. Moreover, no visible spectrophotometric method has been reported to date. Thus, all the proposed methods are simple, sensitive and useful for the determination of OMZ in pure samples and pharmaceutical formulations. They provide a wide choice, depending upon the need of the specific situation.

References

[1] British Pharmacopeia, HMSO, 1993 (Addendum 1995) London, p. 1590.
[2] Xe, Zhixum, Yaowu Fenxi Zazhi, 11 (5) (1991) 296.
[3] S.N. Dhumal, P.M. Dikshit, I.I. Ubhary and C.U. Gaitonde, Indian Drugs, 28 (12) (1991) 565.
[4] Oezaltin, Nuran, Temizer and Aytekin, Electronalysis (NY), 6 (9) (1994) 799.
[5] Pan Ti, Yu Zhenbang, Gan and Huifen, Zhongguo yiyao Gongye Zazhi, 24 (10) (1993) 466.
[6] Ray Satyabrata and De Prabirkumar, Indian Drugs, 31 (11) (1994) 543.
[7] Mary Mathew, V. Dasgupta and Rodney E. Bailey, Drug Dev. Ind. Pharm., 21 (8) (1995) 965.
[8] E. Sawicki, T.W. Stanley, T.R. Hauser, W. Elbert and J.L. Noe, Anal. Chim., 33 (1961) 722.
[9] M. Pays, R. Bourdon and M. Eeljean, Anal. Chim. Acta, 47 (1969) 101.
[10] C.S.P. Sastry, D.S. Mangala and K. Ekambareswara Rao, Analyst, 111 (1986) 323.
[11] C.S.P. Sastry, K.R. Srinivas and K.M.M. Krishna Prasad, Microchim. Acta, 122 (1996) 77.
[12] O. Folin and D. Ciocalteu, J. Biol. Chem., 73 (1927) 627.
[13] D.L. Massart, B.G.M. Vandegingte, S.N. Deming, Y. Michotte and L. Kaufman, Chemometrics, A Text Book, Elsevier, Amsterdam, 1988, p. 293.
[14] IUPAC, Spectrochimica Acta, 33 (1978) 241.
[15] D.R. Davis, A.G. Fogg, D. Thorburn and J.S. Wragg, Analyst, 99 (1974) 12.
[16] R.D. Tiwari and U.C. Pande, J. Indian Chem. Soc., 51 (1974) 112.
[17] G.L. Peterson, Anal. Biochem., 100 (1979) 201.

ELSEVIER

Talanta 44 (1997) 1219–1223

Talanta

Determination of mercury in urine by ET-AAS using complexation with dithizone and extraction with cyclohexane

C. Burrini [a,*], A. Cagnini [b]

[a] *Istituto Ricerche Cliniche 'M. Fanfani', Piazza Indipendenza 18 b, 50123 Firenze, Italy*

[b] *Università di Firenze Dipartimento di Sanità Pubblica, Epidemiologia e Chimica Analitica Ambientale, Via Gino Capponi 9, 50121 Firenze, Italy*

Received 11 July 1996; received in revised form 28 October 1996; accepted 29 October 1996

Abstract

A precise and accurate graphite furnace atomic absorption spectrometric method for the determination of mercury in urine was developed. Samples were subjected to hydrolysis with nitric acid. Then, mercury in the sample was complexed by dithizone and extracted by cyclohexane. Mercury concentrations were determined against a urine-matched calibration curve. Coated graphite notched partition tubes (Varian) and forked pyrolytic platforms (Varian) were used. The detection limit of the method ($x_{blank} + 3\ SD_{blank}$) was 1 μg l^{-1}. The between run precision CV's were 4.7 and 3.4% for urine with a mercury concentration of 48.2 and 156.2 μmol l^{-1}, respectively; the within run precision CV's were 8.9 and 2.9% for urine with a mercury concentration of 17.0 and 172 μg l^{-1}, respectively. © 1997 Elsevier Science B.V.

Keywords: Graphite furnace; Mercury; Pyrolytic platform

1. Introduction

In the past, mercury was an important constituent of drugs, but nowadays its use is gradually decreasing. Concentration of mercury in air, soil and water have been increasing because of greater utilisation of fossil fuels and for the expanded use in industry and agriculture. Apart from industrial exposure, the major source of elemental mercury for humans is dental fillings (Hg/Ag amalgam) [1]. A recent study [2] showed that amalgam fillings contribute considerably to plasma and urine mercury concentration.

The potential hazard of human exposure to mercury is well known. The novel 'Alice's adventures in wonderland' refers to 'Mad Hatters' who were hat makers gone mad due to exposure to mercury used in cleaning felt hats. With regard to toxicity, three major chemical forms of the metal must be distinguished: mercury vapours (elemental mercury); salts of mercury; and organic mercurials. Elemental mercury, salts of mercury and aryl mercurial compounds, containing a labile Hg–C bond, possess the same toxicity with formation of divalent mercuric cations. In contrast alkilmercurial (e.g., methylmercury) are metabolised slowly.

* Corresponding author.

PII S0039-9140(96)02162-5

There is a linear relationship between plasma concentration and urinary excretion of mercury after exposure to vapour [3]. The concentration of mercury in urine has been used as measure of the body burden of the metal. In contrast, the excretion of mercury in urine is a poor indicator of the amount of methylmercury in the blood, since it is eliminated mainly in faeces.

Mercury in urine can be measured using a potentiometric method [4], gas-chromatographic methods [5–7], cold vapour atomic fluorescence spectrometry method [8], and by atomic absorption spectrometry with the cold vapour technique [9–12]. The latter has several advantages such as lower detection limits, less time consuming sample preparation, higher sample throughput due to a shorter measurement cycle times and the procedure is full automated. But for this technique, additional accessories, specifically designed for measurement of mercury, are required. With our method we tried to determine Hg without this apparatus, but using the capacity of mercury to bind sulphidric groups. Dithizone was used successfully as stabilising agent in the furnace [13], and it is one of the complexing agents most commonly used for mercury [14–16]. The complex is generally extracted with chloroform or carbon tetrachloride. In this work we combined both the complexing capacity of dithizone with cyclohexane extraction. The latter was used because of its easier recovery due to its lower density with respect to water.

2. Materials and methods

2.1. Instrumentation and apparatus

For all measurements a Varian SperctrAA-300 atomic absorption spectrometer with graphite tube atomizer and programmable sample dispenser was used. The spectrometer was equipped with a Zeeman background corrector for the correction of non specific signal. Mercury hollow cathode lamp, graphite notched partition tubes and graphite forked pyrolytic platform were obtained from Varian (Torino, Italy).

2.2. Reagents and materials

Suprapur nitric acid, water pro analysis and cyclohexane were obtained from Merck (Milano, Italy). Diphenylthiocarbazone (dithizone) was obtained from Sigma, mercury (II) chloride 99.5%, mercury (II) nitrate monohydrate 98% and standard solution of mercury 995 μg ml^{-1} in 1% nitric acid were obtained from Aldrich (Sigma-Aldrich, Milano, Italy). Two stock standard solutions of 4 and 20 μg l^{-1} in 1% nitric acid using polypropylene tubes from PBI International (Milano, Italy) were prepared daily [17] from the latter.

Methylmercury (II) chloride (1 g l^{-1} standard solution in water) was purchased from Alfa Products (Karlsruhe, Germany). All glass tubes (PBI International) were acid-washed with 1 M nitric acid solution and rinsed three times with water.

2.3. Samples

Urine was collected at random time from a volunteer group of men and women (ages 20–40) with no professional exposure in polypropylene containers, 10 ml were put in polypropylene tubes, capped and stored at 4°C for a maximum of 48 h. The amount of creatinine ranged from 0.8 to 1.5 g l^{-1}. To monitor the accuracy and precision of analytical procedure a Lyphocheck Urine Metal Controls (Biorad, Milano, Italy) was used. The control is prepared from human urine with added trace elements and heavy metals. The lyophilised urine samples were reconstituted with distilled water and stored at 2–8°C for 5 days according the reported instructions.

2.4. Samples and standards preparation

Sample, 4 ml, were pipetted into glass tubes. Standard additions calibration curves were prepared adding different volumes of the stock standard solutions to 4 ml of urine from two donors without neither professional exposure nor dental fillings. Blank solutions were prepared using 4 ml of water. Nitric acid 65%, 500 μl were added to each tube, and, after mixing, were capped and incubated at 95°C for 90 min.

Table 1
Time/temperature program

Step no.	Temperature °C	Time s	Gas flow l min^{-1}	Read command
1	90	5.0	3.0	No
2	180	5.0	3.0	No
3	180	5.0	3.0	No
4	180	2.5	0.0	No
5	1400	1.0	0.0	Yes
6	1400	3.0	0.0	Yes
7	2700	1.1	3.0	No
8	2700	2.0	3.0	No
9	80	15.0	3.0	No

After cooling, 2 ml of a dithizone saturated solution in cyclohexane were added. The mixture was vigorously shaken for 30 s and then, after separation, the upper phase was transferred to a clean glass.

2.5. Instrument conditions

The monochromator was set at 253.7 with a slit width of 0.2 nm. Lamp current was 5 mA and measurements were recorded both in peak height and peak area mode. The samples were injected into the furnace at the temperature of 90°C (hot injection) with a rate of 0.7 μl s^{-1}. The volume of the injection was 25 μl.

3. Results and discussion

Usually the traditional furnace methods are not recommended for mercury because it is a very volatile metal. In order to decrease its volatility many matrix modificators have been proposed as palladium [18,19], strong oxidising agents [20] and complexing agent with sulphidric groups [13–16]. In our procedure, dithizone is responsible both of the extraction of the metal from a complex matrix (i.e., urine) and of a decreasing of volatility during the pre-atomisation step. In fact the determination of mercury in aqueous solution with the same time/temperature program do not give appreciable absorbance values. Every modification of time/temperature program do not increase the absorbance values. In Table 1 is presented the time/temperature program. As indicated on the char/atomisation curves in Fig. 1, the maximal char temperature that could be used without loss of sensitivity was 200°C, while the best atomisation temperature was 1300–1400°C.

We used coated graphite notched partition tubes and forked pyrolytic platforms. With the same time/temperature program a decreasing of the absorbance value was observed using coated graphite partition tubes. With such tubes the optimum of atomisation temperature was observed at 800°C. The resulting values were the same with respect to the values obtained with pyrolytic platform but they were characterised by a greater peak broadening (Fig. 2).

Dithizone forms hydrophobic complexes with most of the divalent or trivalent metal ions. Copper (10–70 μg 24 h^{-1}) and zinc (150–1300 μg 24 h^{-1}) are the most common metal ions in urine:

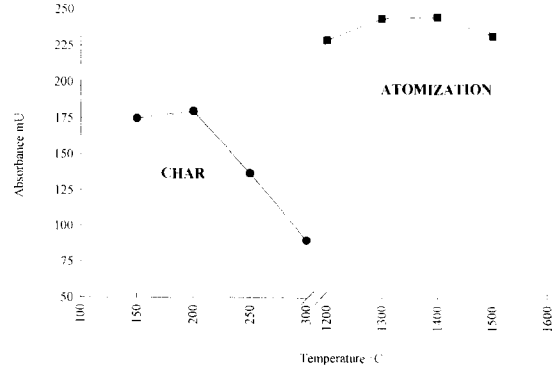

Fig. 1. Char and atomization temperature curves of the determination of mercury in urine.

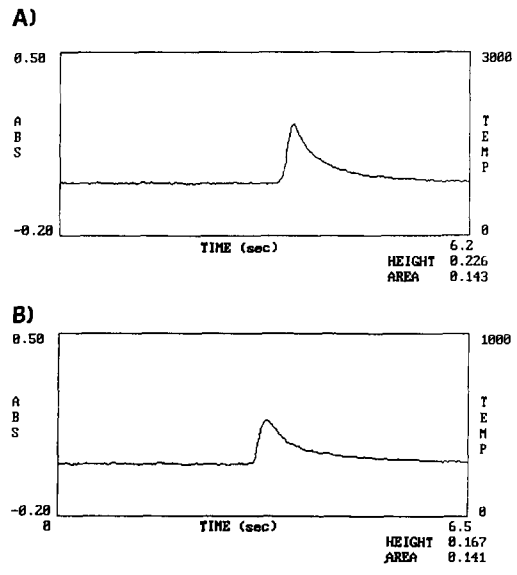

Fig. 2. (A) Atomic signal from pyrolytic platform (char temperature: 180°C, atomization temperature 1400°C); (B) Atomic signal from coated partition tube (char temperature: 180°C, atomization temperature 800°C). Height, A; Area, A·s.

but it was found that even high concentrations of both ions (300 μg l^{-1} for copper and 2000 μg l^{-1} for zinc) did not interfere with mercury determination with this method.

Nitric acid did not show an oxidising action to give dithizone a change in complexing capacity. But it was important to separate the organic phase from the urine after the extraction. In fact after 30 min the separated dithizone solution did not show significant absorbance variation, while the part in contact with urine showed a reduction of 10%.

The detection limit of the method, calculated as $X_{blank} + 3SD_{blank}$, was 1 μg l^{-1}. Solutions for 20 different calibration curves were prepared adding different volumes of the daily prepared stock standard solutions to urine from donors without neither professional exposure nor dental fillings. The recorded absorbances for no-spiked samples were below the threshold value. The results obtained in peak area and peak height mode were compared. The response was linear up to 200 μg l^{-1}. Both the systems give a good correlation factor (r) and reproducible slopes between the different calibration (peak area: average correlation factor $r =$ 0.9993, CV% = 0.08 and average slope 1.27, CV% = 0.07; peak height: average correlation factor $r = 0.9995$, CV% = 0.07 and average slope 1.74, CV% = 5.84). In order to test the proposed method in routine work, different furnaces with different degree of use were utilised. These furnaces were previously used both for mercury in urine determination and for determination of other analytes in different matrices (blood, urine, serum, plasma). The increase in life time of use led to wider peaks with lower peak heights, resulting in higher coefficient of variation. In Fig. 3 typical calibration curves are shown.

After 48 h of storage at 4°C no significant variation of concentration were measured. Urine added with Hg^{2+} in the linearity range and stored for the same time gave 98–101% recoveries. The within-run precision (measure of repeatability) and the between run precision (measure of reproducibility) were measured considering two concentrations of mercury with quality controls. For the between-run precision Bio Rad Lyphocheck Urine metal control Level 1 (Lot. No. 60901) and Level 2 (Lot No. 60902) were used. For the within-run precision Bio Rad Lyphocheck Level 1 (Lot No. 58501) and Level 2 (Lot No. 58502) were used. Results are reported in Table 2.

Accuracy was evaluated comparing data obtained with the Bio Rad quality controls (Table 2) and evaluating the recovery from urine of different subjects added with mercury. In the urine

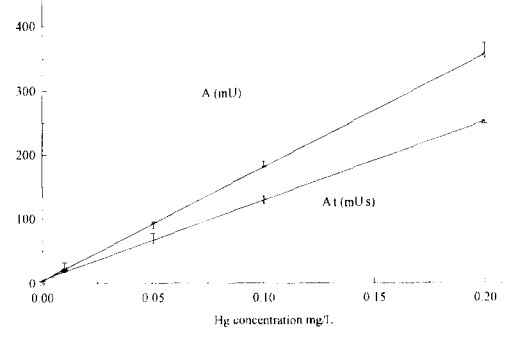

Fig. 3. Linearity of the calibration curve in urine in peak-area (□) and peak-height (○) modes using graphite tubes and platforms. Each point represents the mean ± S.D. of 20 calibrations. Char temperature, 180°C; atomization temperature, 1400°C. Instrumental settings as reported in the text.

Table 2
Precision

	Acceptable range (μg l^{-1})	Mean (μg l^{-1})	S.D. (μg l^{-1})	CV (%)
Between run ($n = 20$)				
Level 1	35.0--52.0	48.2	2.3	4.7
Level 2	116.0--174.0	156.8	5.3	3.4
Within run ($n = 4$)				
Level 1	13.0--20.0	14.9	1.3	8.9
Level 2	137.0--206.0	151.9	4.4	2.9

added with inorganic salts (mercury (II) nitrate and mercury (II) chloride) 98–101% of recoveries were obtained for all the concentrations in the linearity range. For metal organic compounds (methylmercury chloride), using the same procedure as for inorganic salts, the obtained recoveries were between 85–90% for 25 μg l^{-1}, 84–88% for 50 μg l^{-1} and 75–85% for 100 μg l^{-1} of methylmercury addition. During our work, 25 urine samples were tested. Results, ranging from 1 to 8 μg l^{-1} for 23 samples, collected from people with dental filling, were obtained while for two people without dental fillings results were below the detection limit. Though not statistically relevant, these results are in accordance with expected values and with other published papers [3,8,21].

All these data allow to consider this technique precise and accurate so that it makes possible a simple and fast quantification of mercury in urine even if the equipment necessary to the cold vapour technique is lacking.

References

[1] M.J. Vimj and F.L. Lorscheider, J. Dent. Res., 64 (1985) 1072–1075.
[2] M. Molin, B. Bergman, S.L. Marklund, A. Schutz and S. Skerfving, Acta Odontol. Scan., 48 (1990) 189–202.
[3] C.O. Klaassen, in A. Goodman Gilman and L.S Goodman (Eds.), The pharmacological basis of therapeutics, VII edition, Macmillan, New York, 1985, pp. 1605–1627.
[4] D. Jagner and K. Aren, Anal. Chim. Acta, 141 (1982) 157–162.
[5] P. Mushak, F.E. Tibbets, I.P. Zarnegar and G.B. Fisher, J. Chromatogr., 87 (1973) 215–226.
[6] P. Zarnegar and P. Mushak, Anal. Chim. Acta, 69 (1974) 389–407.
[7] L. Liang, N.S. Bloom and M. Horvat, Clin. Chem., 40 (4) (1994) 602–607.
[8] S.A. Winfield, N.D. Boyd, M.J. Vimy and F.L. Lorscheider, Clin. Chem., 40 (2) (1994) 206–210.
[9] A. Campe, N. Velghe and A. Claeys, At. Absorpt. Newslett., 17 (1978) 100.
[10] D.R. Boucier, R.P. Sharma and D.B. Drawn, Am. Ind. Hyg. Assoc. J., 32 (1982) 329.
[11] D.E. Shrader and W.B. Hobbins, Varian Ins. At Work, September, 1983, AA-32.
[12] T.E. Guo and J. Baasner, Anal. Chim. Acta, 278 (1993) 189–196.
[13] G.T.C. Shum, H.C. Freman and J.F. Uthe, Anal. Chem., 51 (3) (1979) 414–416.
[14] L.S. Clesceri, A.E. Greenberg and R.R. Trussel, Standards methods for the examination of water and wastewater, 17th ed., edited by APHA, AWWA and WPCF, American Public Health Association, Washington, 1989.
[15] S. Nobel and D. Nobel, Clin. Chem., 4 (1958) 150–158.
[16] S. Nobel, in D. Seligson (Ed.), Standard Methods in Clinical Chemistry, Vol. 3, Academic Press, New York, 1961, p. 176.
[17] J.M. Lo and C.M. Wai, Anal Chem., 47 (11) (1975) 1869–1870.
[18] L. Pingo, K. Fuwa and K. Matsumoto, Anal. Chim. Acta, 179 (1985) 279–284.
[19] B. Welz, G. Bozsai, M. Sperling and B. Radziuk, J. Anal. Atom. Spectr., 7 (3) (1992) 505–509.
[20] G.F. Kirkbright, S. Hsiao-Chuan and R.D. Snook, At. Spectrosc., 1(A) (1980) 85–89.
[21] V. Liengar and J. Walttier, Clin. Chem., 34 (3) (1988) 474–481.

ELSEVIER

Talanta 44 (1997) 1225–1230

Talanta

Kinetic spectrophotometric determination of traces of sulfide

Afsaneh Safavi *, Zahra Ramezani

Department of Chemistry, Faculty of Sciences, Shiraz University, Shiraz, 71454, Iran

Received 15 May 1996; received in revised form 25 October 1996; accepted 29 October 1996

Abstract

A method for the determination of sulfide based on the addition reaction of sulfide with magenta at pH 7 and 25°C is described. The decrease in absorbance of magenta at 540 nm, its λ_{max}, over a fixed time is proportional to the concentration of sulfide over the range of 25–2500 ng ml^{-1}. The limit of detection was found to be 15 ng ml^{-1}. Ten replicate analysis of a sample solution containing 1.5 μg ml^{-1} sulfide gave a relative standard deviation of 0.8%. The effects of various cations and anions on sulfide determination have been reported and procedures for removal of interferences have been described. © 1997 Elsevier Science B.V.

Keywords: Kinetic spectrophotometry; Magenta; Sulfide determination

1. Introduction

Determination of sulfide is important particularly from biological and industrial point of view. Its extreme toxicity as hydrogen sulfide is well known. Conversion of amino acids to sulfide occurs in most microorganisms [1]. Sulfur can be converted to sulfide fairly readily by non enzymatic reactions [2]. Sulfides are also present in industrial effluents. Sulfur metabolizing organisms are responsible, at least in part, for several types of corrosion [3–5]. Evidence was obtained that the sulfide was generated by the action of sulfate reducing organisms. So sulfide determination is a measure of corrosion. In agriculture, sulfur compounds influence to a considerable extent on soil fertility.

Different classical and instrumental methods were used for sulfide determination including argentiometric titration of alkaline solution [6], complexometry [7], spectrophotometry [8], flow injection analysis [9,10], molecular emission cavity analysis [11] and so forth, but few are convenient for modern routine analysis, or have sufficient sensitivity.

Kinetic methods of determination of micro amounts of sulfide have been described [12–15]. In some of these methods the catalytic action of sulfide is used for the determination while in others an addition reaction of sulfide with a specific reagent is described. However, most of these methods suffer from interfering effects of other sulfur anions, or poor sensitivity and low linear dynamic range. Thus, more selective as well as sensitive methods are still required.

* Corresponding author.

PII S0039-9140(96)02163-7

In this study a kinetic spectrophotometric method based on the addition reaction of sulfide to magenta at pH 7 is described.

2. Experimental

2.1. Reagents

All reagents were of analytical grade. Triply distilled water was used throughout. A stock solution of 1000 μg ml^{-1} sulfide was prepared daily by dissolving 0.3746 g of $Na_2S.9H_2O$ (Merck) in water and diluting to 50 ml. This solution was standardized using sulfide selective electrode. The results were consistent with those of iodometric titrations. Magenta solution (1.77×10^{-4} M) was prepared by dissolving 5.73 mg magenta in water and diluting to 100 ml. Phosphate buffer (pH 7) was used for pH adjustments.

2.2. Apparatus

Absorption spectra were recorded on a Philips PU 8750 UV-Vis spectrophotometer. Spectrophotometric measurements at a fixed wavelength were made on a PU 8625 spectrophotometer. The PU 8625 spectrophotometer was connected to a 386 personal computer through its RS-232C port. The change in absorbance by time was displayed on the screen. A mechanical stirrer (Janke and Kunkel GMBH KG, IKA-Werk) was used for mixing when using the procedure of data collection by computer. pH was adjusted by a 691 Metrohm pH meter. The temperature was kept constant at 25 ± 0.1°C by a thermostat (Colora, NB, Germany). All the solutions were previously brought to this temperature. The temperature was maintained constant in the reaction cell by circulating water at appropriate temperature around the cell compartment of the spectrophotometer during the experiment.

2.3. Recommended procedure

Two separate procedures were adopted. The first was based on the conventional fixed time method and the other was performed by direct data collection by computer and applying the slope method.

2.4. Fixed time method

Buffer, 1 ml, (pH 7) was added to the sample solution containing 0.125–12.5 μg sulfide in a 5 ml volumetric flask. The solution was diluted to about 4.5 ml and kept in the water bath at 25°C for 10 min. Then, 0.25 ml of 1.77×10^{-4} M magenta, previously brought to the same temperature was added to initiate the reaction and the solution was diluted to the mark with distilled water. The chronometer was turned on when the last drop of magenta was added to the solution. A portion of this solution was transferred to a glass cell within 30 s and the absorbance change at 540 nm was recorded for 2 min after initiation of the reaction.

2.5. Slope method using direct data collection by computer

Since the absorbance data was directly transferred to the computer, the solutions were prepared in 1 cm, 4 ml glass cell. In this case, 0.7 ml of phosphate buffer was added to a sample solution containing 0.09–8.75 μg sulfide in the cell. The solution was diluted to 3.3 ml by the addition of appropriate amounts of water. The cell was

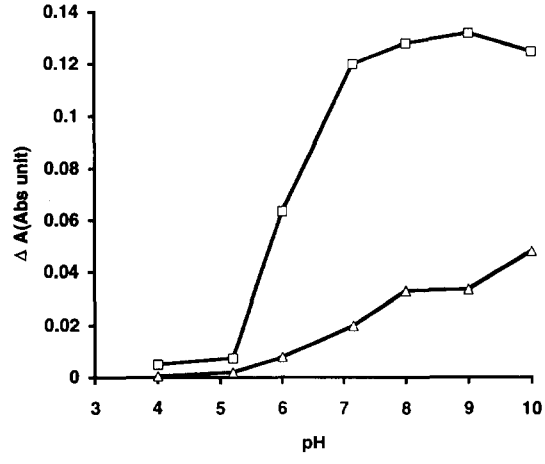

Fig. 1. Effect of pH on the reaction rate of 1 μg ml^{-1} sulfide (□) and blank (△).

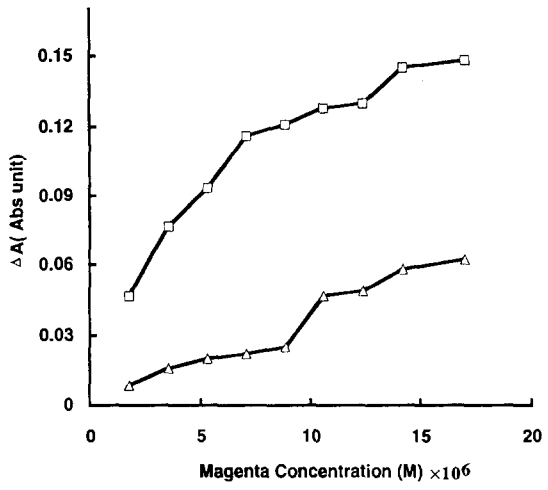

Fig. 2. Effect of magenta concentration on the reaction rate of 1 μg ml^{-1} sulfide (□) and blank (△).

inserted in the cell compartment of the spectrophotometer, where its temperature was kept constant at 25°C. A mechanical stirrer was used to mix the solution within the cell. After 10 min, 0.2 ml of 1.54×10^{-4} M magenta was added to the cell, and the absorbance versus time data were collected by the computer. The slope of the plot of absorbance versus time was found during the first 2 min after starting the reaction.

3. Results and discussion

Magenta is an acid base indicator and exists in two forms, R^+ and ROH, depending on the pH of the solution [16].

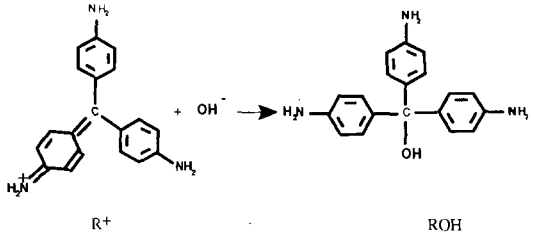

At pH 6–8 addition of sulfide to magenta occurs at room temperature [17]. This causes a relatively rapid change of the color from purple to colorless even in the presence of small amounts of sulfide (ng ml^{-1}). The following optimizations were undertaken to achieve maximum sensitivity and large linear dynamic range.

3.1. Effect of variables

The decrease in the absorbance of magenta with and without sulfide was measured in the pH range 4–10, using either titrisol buffer, hydrochloric acid or sodium hydroxide solutions for pH adjustments. The effect of variation of pH on the rate of the reaction of 7.08×10^{-6} M magenta in the presence of 1.0 μg ml^{-1} sulfide is shown in Fig. 1. As it is obvious from the figure, the difference between blank and sample reaction rate was increased with increasing pH from 4 through 7, whereas this difference was decreased for pH values greater than 7. So pH 7 was used as optimum pH because of maximum difference between the rate of blank and sample reactions. Above pH 7 the rate of blank reaction is increased owing to the formation of ROH and thus, pH values greater than 10 were not tested.

Effect of magenta concentration on the reaction rate at pH 7 was studied. As it is shown in Fig. 2, there was an increase in the reaction rate when the concentration of magenta was varied from 1.77×10^{-6} to 1.70×10^{-5} M while at higher concentrations of magenta no considerable change in the reaction rate was observed. However, the rate of the blank reaction was also increased above 8.84×10^{-6} M of magenta. Thus, the optimum final concentration of magenta was chosen as 8.84×10^{-6} M.

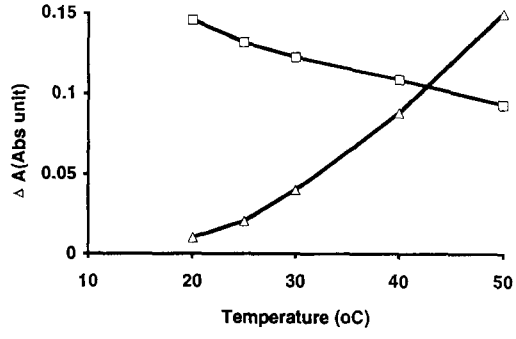

Fig. 3. Effect of temperature on the reaction rate of 1 μg ml^{-1} sulfide (□) and blank (△).

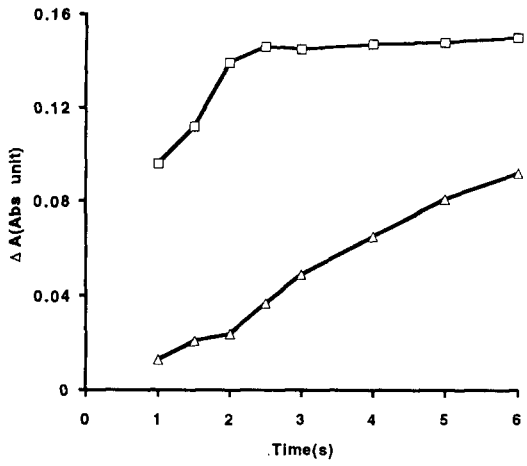

Fig. 4. Effect of measuring time on the reaction rate of 1 μg ml^{-1} sulfide (□) and blank (△).

The effect of ionic strength on the reaction rate was investigated. The ionic strength was varied from 0.02 to 0.7 M, using KCl solution. The results showed that this parameter had no effect on the reaction rate up to 0.2 M.

The effect of temperature was studied in the temperature range 20–50°C. Fig. 3 shows that the reaction rate of sulfide decreased with increasing temperature while the blank reaction rate increased. This deviation from Arrhenius equation could be due to instability of sulfide solution at higher temperatures or complexity of the reaction mixture [18]. Temperature of 25°C was used as the best working temperature, since at this temperature the difference between blank and sample reactions is large and 25°C is the ambient temperature at which it is very easy to work.

Table 1
Precision and accuracy of the method evaluated by fixed time analysis

S^{2-} (ng ml^{-1})	S^{2-}found (ng ml^{-1})	RSD% ($n = 10$)
150	134	2.10
400[a]	360	1.03
500	489	1.30
1000	950	1.00
1500	1460	0.80

[a] This amount of sulfide was added to a sample of tap water.

Table 2
Precision and accuracy evaluated by slope method

Sulfide concentration (ng ml^{-1})	Sulfide found (ng ml^{-1})	RSD (%)
50	50.8	1.80
500	536	1.12
1000	960	0.83
1500	1480	0.60

The effect of measuring time on the reaction rate was investigated (Fig. 4). The results showed that the first 2 min was the best working time at which maximum rate of reaction was achieved.

Optimum conditions chosen were as follows: pH 7; magenta concentration, 8.84×10^{-6} M; temperature, 25°C; measuring time, 2 min and λ_{max}, 540 nm.

4. Calibration

Calibration graphs were obtained by slope and fixed time methods. In fixed time method, the calibration curve was linear in the range 25–2500 ng ml^{-1} with equation of $\Delta A = 0.02925 + 0.097 \times 10^{-3}$ C and correlation coefficient (r) of 0.9986, where C is the concentration of sulfide in ng ml^{-1}. In the case of slope method, calibration curve is linear in the range of 25–2500 ng ml^{-1} with equation of $dA/dt = 1.128 \times 10^{-3} + 1.104 \times 10^{-5}$ C and correlation coefficient of 0.9991, where C is concentration of sulfide in ng ml^{-1} and dA/dt is the change in absorbance per second.

4.1. Precision and limit of detection

Both fixed time and slope methods were used to evaluate the precision, accuracy and detection limit. In each case a series of independent synthetic samples with fixed magenta concentration was used. In fixed time method the relative standard deviation, RSD, was in the range of 2.1–0.8% for sulfide concentration of 150–1500 ng ml^{-1} (Table 1). In the case of slope method, the RSD was in the range of 1.8–0.6% for sulfide concentration of 50–1500 ng ml^{-1} (Table 2). The

Table 3
The maximum tolerance value of various cations and anions on the measurement of 700 ng ml^{-1} S^{2-} by the suggested method

Interfering ions	Tolerance limit (μg ml^{-1})
Cl^-, SO_4^{2-}, $S_2O_8^{2-}$, $S_2O_7^{2-}$, $B_4O_7^{2-}$	1000[a]
CH_3COO^-, SCN^-, HCO_3^-, MoO_4^-, I^-,	
F^-, Br^-, BrO_3^-, CO_3^{2-}, NO_3^-, PO_4^{3-},	
$H_2PO_4^-$, HPO_4^{2-}, CN^-, Oxalate, $S_2O_3^{2-}$	
ClO_4^-	
K^+, Na^+, Ca^{2+}, V^{3+}, NH_4^+, Co^{2+}, As^{3+}	1000[a]
Mg^{2+}, Cd^{2+}, La^{3+}, W^{6+}	
Mn^{2+}	800
Cr^{3+}, Fe^{3+}, Fe^{2+}, VO^{2+}	200
Ni^{2+}, Al^{3+}	100
Cu^{2+}, Pd^{2+}	10
Hg^{2+}, Hg^+, Ag^+, Pb^{2+}, IO_3^-	1
SO_3^{2-}	Interfered

[a] Maximum concentration studied.

theoretical limit of detection, $Y_{DL} = Y_B + 3\ S_B$ [19] where Y_{DL}, Y_B, and S_B are signal of detection limit, blank signal and standard deviation of the blank, respectively, was 5 ng ml^{-1}. The experimental limit of detection was 15 ng ml^{-1} by both methods.

4.2. Interference study

To study the selectivity of the proposed method the effect of various cations and anions on the reaction rate of 700 ng ml^{-1} of sulfide at pH 7 was tested. The results are summarized in Table 3 with maximum tolerance limit for each ion.

4.3. Removal of interfering ions

Among the anions, sulfite and iodate interfere. Sulfite interference was eliminated by the addition of 1 ml of 0.1% formaldehyde to 5 ml of test solution prior to each measurement. The interfering effect of iodate was removed by the addition of 1 ml of 500 mg ml^{-1} I^- to 5 ml of test solution prior to each measurement.

Most of the cations that interfere in sulfide determination form insoluble metal sulfides. Interference effects of these cations were removed by the addition of iodide or hydroxide ions and filtering the solution prior to each measurement. Since cyanide did not interfere, the interfering effect of silver was removed by the addition of cyanide to form stable silver cyanide complex and thus preventing silver sulfide formation. The results are summarized in Table 4.

The proposed method offers good sensitivity for sulfide determination. As the results imply the fixed time and slope methods are comparable with each other. Higher precision of the latter may arise from the difference in data collection method. In the slope method large number of data was collected by the computer just after initiation of the reaction with two second time intervals. So the slope could be estimated with higher precision.

Table 4
The accuracy obtained after removal of interfering ions[a]

Interfering ion	Masking agent	S^2-found (μg ml^{-1})	RSD% $n = 3$
SO_3^{2-}(5)[b]	Formaldehyde(0.02%)	0.981	0.80
Ag^+(10)	CN^-(100)	0.970	0.72
Pb^{2+}(10)	OH^-(100)	1.03	1.63
Hg^{2+}(10)	I^-(100)	0.95	1.10
Hg^+(10)	I^-(100)	0.92	1.30
Cu^{2+}(20)	OH^-(200)	0.99	1.00
IO_3^-(10)	I^-(100)	0.974	0.98

[a] Sulfide concentration was 1 μg ml^{-1} in each case.
[b] The term in parenthesis are concentration of interfering ions or masking agent in μg ml^{-1} except for formaldehyde.

Table 5
Analysis of real samples by proposed method

Spring water	Proposed method (μg ml^{-1})	Standard method [20] (μg ml^{-1})	RSD %
Type 1	30.93	31.20	0.86
Type 2	29.07	29.41	1.00
Type 3	23.25	23.51	0.95

These are the results of ten replicate analysis.

5. Application

To evaluate the analytical applicability of the method, the recommended procedure was applied to the determination of sulfide in three different samples of spring water. The spring water sample was first treated with sodium hydroxide and filtered. The pH of the filtrate was then adjusted to about 7 with HCl. The recommended procedure was then applied using the standard addition method. The results (Table 5) show that the method is suitable for the analysis of real samples.

Acknowledgements

The authors wish to express their gratitude to Shiraz University research council for the support of this work.

References

[1] J.W. Roger and M.L. Edusin, The Encyclopedia of Biochemistry, Reinhold Publishing Corporation, 1967, pp. 77.
[2] A.B. Roy and P.A. Trudinger, The Biochemistry of Inorganic Compounds of Sulfur, Cambridge University Press, 1970, 175.
[3] C.D. Parker, Aust. J. Exp. Biol. Med. Sci. 23 (1945) 81.
[4] C.B. Taylor and G.H. Hutchinson, J. Soc. Chem. Ind., London, 66 (1947) 54.
[5] J. Pochon, O. Coppier and Y.T. Tchan, Chim. Ind. 65 (1951) 496.
[6] C.H. Liu and S. Shen, Anal. Chem. 36 (1964) 1652.
[7] S. Komatsu and A.J. Shundo, Chem. Soc. Jpn., Pure Chem. Sect. 84 (1967) 585.
[8] L.V. Bunikene, E.I. Ramanauskas and V.P. Karpavichene, Busilaite Zh. Analit. Khim. 23 (1968) 1679.
[9] J.L. Lambert and D.J. Manzo, Anal. Chim. Acta 59 (1969) 185.
[10] M. Roman Ceba, F. Vinagre Jara and J.A. Munoz Leyva, Analyst 107 (1982) 781.
[11] R. Belcher, S.L. Bogdsnski, D.J. Knowles and A. Townshend, Anal. Chim. Acta 77 (1975) 53.
[12] L.O. Sokolik, V.V. Markov and E.I. Viol, (UKHIN, USSR) Koks Khim. 4 (1983) 28–30 (Russ). (Chem. Abs. 98:209175d).
[13] K. Han and W.F. Koch, Anal. Chem. 59 (1987) 1016.
[14] W. Lei and P.K. Dasgupta Anal. Chim. Acta 226 (1989) 165.
[15] A.A. Ensafi, Anal. Lett. 25 (1992) 1525.
[16] E. Bishope, Indicators, Pergamon Press, 1972.
[17] R.V. Nauman, P. Wo West, F. Tron and G.C. Gaeke, Anal. Chem. 32 (1960) 1307.
[18] H.L. Plardue and B. Fields, Anal. Chim. Acta 124 (1981) 39.
[19] J.C. Miller and J.N. Miller, Statistics for Analytical Chemistry, Ellis Horwood, New York 1984.
[20] W.J. Williams, Handbook of Anion Determination, Butter Worth, Guildford, 1979, 568.

ELSEVIER

Talanta 44 (1997) 1231–1240

Talanta

The effect of pulsed amperometric detection on penicillin G concentration profiles in a flowing-stream environment

Mark W. Lehmann, Marcelle R. Fahr, Lawrence E. Welch *

Department of Chemistry, Knox College, Galesburg, Illinois, 61401, USA

Received 6 August 1996; received in revised form 4 November 1996; accepted 5 November 1996

Abstract

It is well known that alterations of the times and potentials of each step within a PAD waveform can alter the sensitivity of the amperometric response, peak shape has also been found to vary with waveform adjustments. This work studied the variation in both peak heights and peak tailing as a function of waveform alterations for penicillin G oxidation in flow injection analysis. Large variations were found when the detection step and adsorption time were altered and smaller changes were observed during alterations of the other parameters. The major contribution to the tailing profile was inefficient removal of adsorbed analyte, which was subsequently retained until further PAD cycles. Alterations that improved the desorption efficiency led to reduced peak tailing, whereas alterations that hindered desorption caused an increase in tailing. The ability to minimize peak tailing will be advantageous for PAD usage with separation methods featuring ever-increasing resolution capability. © 1997 Elsevier Science B.V.

Keywords: Alterations; PAD waveform; Penicillin G

1. Introduction

Pulsed amperometric detection (PAD) has developed into a mature technique for determination of various organic compounds following liquid chromatographic separation. PAD utilizes a regular waveform that incorporates potential steps to perform anodic and cathodic cleaning following current measurement at a constant potential, insuring a reproducible detection environment for each detection period, even when in the presence of potentially passivating adsorbates [1]. This detection technique was originally applied for carbohydrate detection following a cation-exchange separation and post-column addition of NaOH by Hughes and Johnson [2,3] and carbohydrates remain the major application area for PAD today [4–6]. Significant development work has also been done utilizing PAD for detection of amines and amino acids [7,8] and organosulfur compounds [9,10]. Many very specific and narrowly focused PAD applications are appearing in the current literature [11,12], illustrating the maturity of the technique. A series of related detection waveforms are often grouped together with PAD under the designation of pulsed electrochemical detection (PED) [13]. These methods are similar

* Corresponding author. Fax: +1 309 3417718; e-mail: lwelch@knox.knox.edu

PII S0039-9140(96)02166-2

to PAD except that their current measurements are taken during a period where the potential is changing rather than being held constant as in PAD. Another recent development has been the application of PAD following separation by capillary electrophoresis (CE). As with PAD use following HPLC, the original applications with CE have been for detection of carbohydrates [14,15].

The penicillins are the most popular class of antimicrobial agents, having proven to have a tremendous positive impact on human health [16]. Studies in this laboratory have determined that the penicillins could be electrochemically oxidized on noble metal electrodes [17]. It was found that PAD could be successfully applied for penicillin detection, in either a direct or an indirect manner. Further work determined that this detection mechanism would operate properly following a reversed-phase separation on a C-18 column [18]. The PAD system was found to be compatible with a gradient solvent program that could separate a mixture of nine different penicillins. Methodology of a similar type was applied for determination of penicillins within bovine milk samples, and an on-column concentration scheme was shown to allow improved detection limits for these compounds [19]. Alternative PAD waveforms with four potential steps rather than the standard three were demonstrated using the penicillins as a model electrochemical system [20]. Summarizing from previous studies [17,20] and using the description of a PAD waveform given in Table 1, the electrochemical oxidation mechanism of the penicillins is proposed to occur as described henceforth. E1 is the detection potential where catalytic oxide (AuOH) is grown on the electrode surface, allowing oxidation of the penicillins previously adsorbed. The oxidation is thought to occur via an oxygen transfer from the oxide to the sulfur group within the penicillin. The second stage is a step to a more positive potential to initiate oxidative cleaning. The electrode is stepped to a potential whereby the higher, non-catalytic oxide (AuO) is formed on the electrode surface, accompanied by the desorption of adsorbed material ranging from analyte to carbonaceous free radicals. E3 steps the potential to a much smaller value, where the surface oxide is reductively stripped. Adsorption of the penicillin G occurs at this stage, through the sulfide group. Only adsorbed analyte is subsequently oxidized upon the return to the detection step. A similar mechanism has been proposed for the PAD oxidation of other organosulfur compounds [21–23].

Table 1
The standard waveform

E1 = 1500 mV	T1 = 0.333 s
E2 = 1600 mV	T2 = 0.333 s
E3 = −200 mV	T3 = 0.167 s

It is not unusual for PAD response to be very non-Gaussian in nature, typically displaying a tailing profile. Some of this can be attributed to chromatographic conditions and extra-column broadening, but even flow injection analysis experiments can produce tailing well beyond what can be attributed to flow-cell dead volume, etc. Tailing has been shown to occur for fixed potential (dc) amperometry in addition to pulsed amperometric trials [24] for sodium thiophosphate, and detector waveform alterations were noted to change the peak shape. Examination of a non-adsorbing analyte under similar conditions gave a response much closer to Gaussian, suggesting that adsorption was critical. Peak tailing has also been observed for amino acids using pulsed electrochemical detection and the observation was made that waveform alterations could alter the observed peak shapes [25].

Vandeberg et al. [26] showed that PAD determination of thiourea could produce peaks varying greatly in breadth depending on the detection potential chosen. The original PAD investigation of penicillins [17] noted that peak tailing was clearly in evidence for flow injection trials. It was postulated that this was related to the rates of the adsorption/desorption processes for the penicillin adsorbates at the gold electrode. Further work [20] has shown that the addition of a fourth potential step for pre-growth of catalytic oxide prior to the PAD detection step allows a waveform to be constructed that had less tailing character than that seen with standard 3-step PAD. It was noted that tailing was a greater problem with indirect PAD compared with direct PAD and that

the peak asymmetry factor (PAF) was useful as a quantitative measure of the degree of peak tailing. Despite clear evidence that the PAD waveform altered peak shapes, no in-depth study elucidating the relationship between the various PAD waveform parameters and peak shape has been performed. Our intention with this work was to examine how each parameter of the standard PAD waveform affected the peak shape and to determine the relationship between peak shape and peak size for injections of penicillin G.

2. Experimental

Penicillin G was purchased from Sigma (St. Louis, MO). All other solutions were made from reagent-grade chemicals from Aldrich (Milwaukee, WI), Baker (Phillipsburg, NJ) or Fisher (Pittsburgh, PA). Water was distilled and deionized before use as a solvent.

Flow injection analysis was done with a Waters 625 LC system (Milford, MA) and a Waters 464 Pulsed Electrochemical Detector. A 75 μl sample injection loop was employed with this system, and a flow rate of 0.7 ml min^{-1} was standard. The solvent for all flow injection work was 0.200 M acetate buffer (pH 4.7). Injected penicillin solutions during flow injection analysis trials were all solvent matched with the mobile phase to avoid having a system peak overlapping with the analytical peak. All mobile phases were vacuum filtered through an Alltech (Deerfield, IL) 0.20 μm nylon filter. The mobile phase mixtures were degassed further using a 15 ml min^{-1} helium sparge during the flow injection trials.

A thin-layer cell was utilized with a single gold working electrode having a diameter of 0.25 cm. The counter electrode was a stainless steel block mounted opposing the thin-layer cell, with the flow channel created by a teflon spacer between the two. The reference electrode was a Ag/AgCl. A BAS MF-2060 Polishing Kit was used to polish the working electrode, in addition potential cycling to the voltage limits of the system, as defined by the onset of solvent breakdown, was helpful to restore electrode activity following temporary losses of sensitivity.

Current integration was always during the final 16.7 ms of the detection step, as required by the detector. Detector signal polarity was inverted so that increased anodic response would produce peaks rather than troughs on the output plots. Output data was collected by a PC using LabCalc software (Galactic Industries, Salem, NH). The collection interval was synchronized with the potentiostat, such that a single data point was collected per PAD cycle.

3. Results and discussion

Peak size was determined by measuring peak height and measurements of peak asymmetry factors (PAF) were utilized to quantitatively describe the degree of peak tailing [27,28]. To find the PAF, a vertical trace is drawn through the Y maximum, then bisected by a second segment drawn perpendicularly at 10% of the maximum peak height. The segment length of the bisecting line from the intersection point to the right edge is divided by the segment length from the intersection point to the left, with the resulting ratio giving the PAF value. Originally developed for theoretical plate measurements in chromatography, the PAF was ideal for quantitating detector-related tailing in flow injection analysis [20]. Not all of the tailing was solely related to electrochemical events, tandem detector experiments with downstream ultraviolet detection found that dispersion of the sample during passage through the electrochemical flow cell and its associated fittings was enough to induce a small degree of tailing. By using a single solvent mixture, maintaining a constant flow rate and identical injection volumes, and using a single flow cell without any modification, tailing from this source was assumed to be constant throughout all experiments, allowing peak height and PAF variations to be attributed solely to PAD waveform changes and any corresponding alterations in the electrochemistry.

Initial studies found that although peak heights for a series of repetitive trials were fairly precise, the PAF measurements were a great deal more variable. To be able to interpret trends in peak shape based on PAF measurements, maximum

precision within sets of experimental data was a necessity. Data was collected in sets of 12 replicate trials, with all sets varying a given waveform parameter done during the same session. There was a considerable degree of day-to-day variability, underlining the importance of collecting an entire data set during a single session. The overall PAF trends remained consistent on a daily basis even if the value for a given set of conditions varied from 1 day to the next. Foley and Dorsey [29] have noted that the precision of peak asymmetry measurements increases as the peak becomes more asymmetric, this was confirmed experimentally for penicillin G. Thus, a relatively high penicillin G concentration, 1.00×10^{-2} M, was chosen to improve precision. The relationship between concentration and peak shape will be discussed at length below. Detector noise varied significantly as a function of solvent flow rate due to the lack of pump back pressure. Optimal response was found at a value of 0.7 ml min^{-1}, which was incorporated for all subsequent trials.

Initial measurements were made by displaying each peak on the computer screen and manually using the cursors to determine the peak heights and segment lengths necessary to calculate the PAF. Adaptation of an algorithm to instruct the data collection computer to automatically calculate both peak height and PAF was successful at providing improved precision. Further study of the PAF algorithm found that measuring a bisecting line at a height greater than the standard 10% limited the effect of baseline perturbations, producing a more precise set of PAF measurements for a given series of peaks. Measuring chromatographic figures of merit at the standard 10% height has been defended as advantageous for a number of reasons [29], including precision and simplicity. With the computer program doing the measurements, the simplicity angle does not come in to play. It is possible that measurements at 10% might be better given more ideal conditions (i.e., less baseline noise), however, the precision clearly increased until a maximum was achieved at 20% for the system being tested. This 20% value was utilized thereafter for all PAF measurements.

Although previous chromatographic trials had required the addition of organic modifier to an aqueous mobile phase [18–20], for simplicity, unmodified acetate buffer was chosen for the flow injection studies. A standard waveform, shown in Table 1, was chosen as a starting point for this work and a systematic variation of each waveform parameter was initiated while all of the other parameters were held constant. Observations of each parameter are discussed in turn below.

Based on observation of PAD peaks for penicillin G with a wide variety of waveforms, it is theorized that the tailing profiles are an artifact of inefficient electrode cleaning during the E2 (oxidative cleaning) and E3 (reductive cleaning) potential steps. Some analyte material and likely other adsorbates depending on solution composition, are not removed during the cleaning steps, carrying them over to the following PAD cycle. Other workers [21] have noted the very strong adsorption of organosulfur compounds to gold via their sulfur group. A strong adsorption would be more likely to give rise to this carry-over effect than for more weakly adsorbed species. This carry-over would result in the oxidized analyte for each step being composed of two types, analyte freshly adsorbed, and analyte carried over from the previous PAD cycle. If the cleaning were 100% efficient, then the amount of analyte adsorbed and oxidized would be solely a function of solution concentration, giving a Gaussian peak shape. The delay caused by adsorbate carry-over causes the analyte material to spend a greater amount of time on the working electrode on average, shifting the peak's center of mass to a later time and creating the tailing profile much like that seen for slow mass transfer from a stationary phase. Typically, an increase in the amount of analyte carry-over would be expected to increase peak height, assuming that carry-over adsorbate augments rather than replaces fresh adsorbate, the greater amount of adsorbed material will lead to a larger anodic signal. The proportion of fresh versus carry-over adsorbate, and therefore the peak shape, ultimately depends on the waveform parameters selected. It has been noted in the literature [23] that adsorption sites of varying types and strengths are present on Au. Due to surface roughness, there are likely a few sites where catalytic oxidation is hindered due to ge-

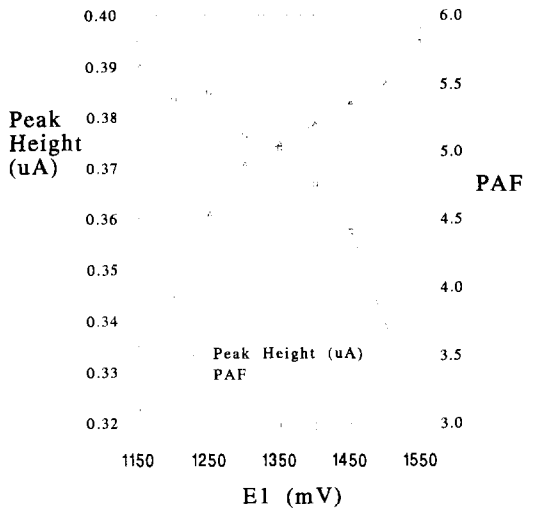

Fig. 1. Peak height and peak asymmetry factor (PAF) values for 1.00×10^{-2} M penicillin G injections as a function of E1. The other waveform parameters are held at their standard values (see Table 1). Relative standard deviation of peak heights = 0.00521. Relative standard deviation of PAF values = 0.0577.

ometry–desorption from here is presumably quite inefficient, creating severe tailing at the very end of each peak. This can be illustrated by observing peak shapes following mechanical polishing of the working electrode. Immediately following polishing, both the peak height and PAF values drop significantly. This is due to the polishing minimizing surface roughness, which cuts down on electrode surface area. The smaller surface area limits the degree of analyte adsorption and therefore reduces peak size. The peak shape improves because a more-level electrode surface allows the adsorbed penicillins greater access to active surface oxide groups. At greater times following the polish, both the peak height and PAF grow larger as the electrode surface regains its roughness.

3.1. E1

E1 was varied from 1150 to 1550 mV in 50 mV intervals. Average peak heights and PAF values for each voltage are displayed in Fig. 1. As expected, the peak heights became larger as E1 was increased. The rate of penicillin G oxidation is not particularly rapid [17], so by increasing E1, greater overpotential is applied, accelerating the reaction and producing a greater anodic signal. The PAF displays an inverse relationship with E1. The proposed oxidation mechanism for penicillin G predicts that analyte desorption accompanies oxidation. As E1 is increased and greater oxidation efficiency enabled, this should also result in more efficient analyte desorption. Less analyte is carried over to following PAD cycles, so the degree of tailing is reduced. Normally when the amount of carry-over adsorbate is reduced, the peak height would be expected to decrease as well, but in this circumstance the overpotential increase causes a large enhancement in oxidative efficiency, which more than offsets loss of carry-over material. At first glance, the trends seen in Fig. 1 suggest that the optimum value of E1 would be at an even greater value than the 1550 mV, as this gave the largest peaks and the smallest PAF values. This overlooks the fact that noise is not being considered along with the signal, and noise increases significantly as E1 is elevated. Reproducibility also suffers at large E1 values, as evidenced by a decrease in precision for the data sets. The reduced detector selectivity seen at larger E1 values might also be a concern for PAD usage in a chromatographic setting.

3.2. T1

T1 was varied from 0.166 to 0.516 s in intervals of 0.050 s. Average peak heights and PAF values for each time are displayed in Fig. 2. By holding at the detection potential for a longer time, it would be expected that a greater total amount of analyte would get oxidized during the detection step. Assuming desorption follows oxidation, this would result in less analyte carry-over to subsequent cycles, and therefore less tailing and a decrease in PAF as observed. The greater degree of oxidation would be expected to increase peak heights, but the experimental data shows a decrease, this can be attributed to the current sampling taking place only during the last 16.7 ms of the detection step. The oxidative current is well known to decay with time for PAD experiments [7], so a sampling at the very end of the detection step will yield smaller peaks as step length in

increased, even though a greater degree of oxidation takes place when the entire detection step is considered. One can interpret Fig. 2 to see a trade-off, where peak size and peak shape are antagonistic. LaCourse et al. [30] have observed the same trend in peak size while working with sugars in basic solution.

3.3. E2

E2 was varied from 1600 to 1800 mV in 50 mV intervals. Average peak heights and PAF values for each voltage are displayed in Fig. 3. As E2 is increased, the peak heights and the PAF values both were seen to increase. This would suggest that higher E2 values create a greater degree of analyte carry-over. Tailing would increase, and the peak height would also increase if this were indeed the case. This was a surprise, as the natural assumption was that increasing the E2 value would make the oxidative cleaning step more efficient, resulting in decreased carry-over of analyte to subsequent cycles. Although the trends are clear, it should be noted that the relative change of both peak height and PAF values as T2 is

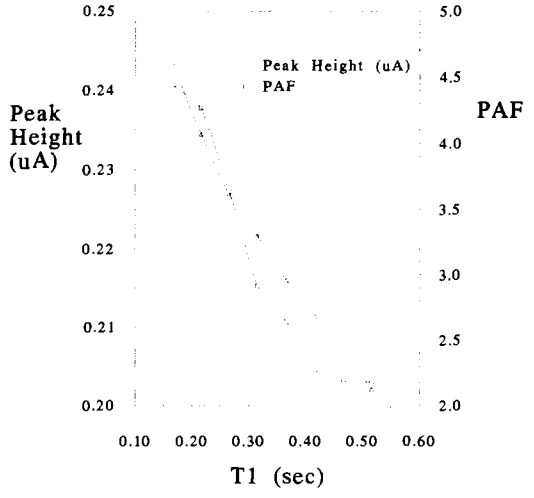

Fig. 2. Peak height and peak asymmetry factor (PAF) values for 1.00×10^{-2} M penicillin G injections as a function of T1. The other waveform parameters are held at their standard values (see Table 1). Relative standard deviation of peak heights = 0.00872. Relative standard deviation of PAF values = 0.0871.

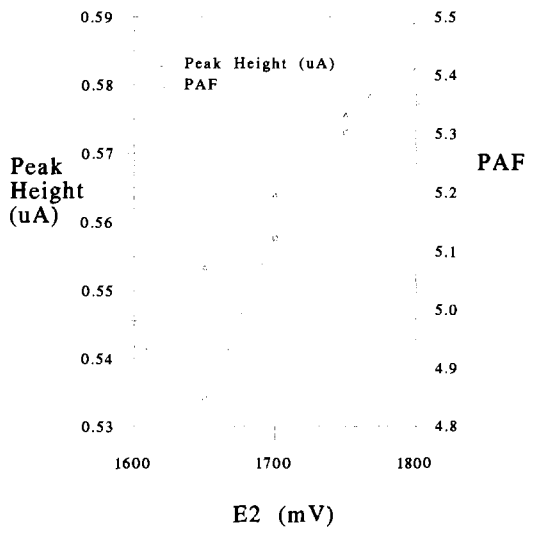

Fig. 3. Peak height and peak asymmetry factor (PAF) values for 1.00×10^{-2} M penicillin G injections as a function of E2. The other waveform parameters are held at their standard values (see Table 1). Relative standard deviation of peak heights = 0.00642. Relative standard deviation of PAF values = 0.0614.

altered is much smaller than that seen for either E1 or T1. Extension of the E2 range downward to 1350 mV demonstrates that very little change for either parameter occurs below 1600 mV. A clear upward trend follows this region of little change, as can be seen in Fig. 3.

It would appear that at high E2 values, where a large overpotential for the formation of the higher surface oxide (AuO) exists, that cleaning is less efficient and more carry-over results. The best cleaning potentials would be in the lower-potential region, which corresponds to a much greater surface coverage of the lower surface oxide (AuOH). This would suggest that in this range that the continued presence of catalytic surface oxide allows penicillin oxidation to overlap into the E2 step, producing less carry-over following desorption of the oxidized material. This would produce the observed smaller peak heights and PAF values. At larger E2 potentials, the high degree of inactive higher oxide insures that no further oxidation takes place during this step. The large E2 value, however, does not appear to remove much of the adsorbed analyte, so much is

carried over for possible oxidation during the next cycle. The strong adsorption of the penicillins to the gold surface appears to allow them to remain on the surface during E2 potentials that would cause the release of most other organic adsorbates.

The loss of oxidative activity resulting from higher oxide production was not observed during the E1 variation due to the lower potential range employed and the fact that the oxide was much 'younger', having been grown during the step rather than carried over from a prior step as with the E2 variation. Coupling a very large E1 and T1 would allow production of significant quantities of the higher oxide much like seen with the E2 trials, but these values are outside the range tested and impractical for proper detector performance.

3.4. T2

T2 was varied from 0.166 to 0.516 s in intervals of 0.050 s. Average peak heights and PAF values for each time are displayed in Fig. 4. For the T2 variation, as the length of the oxidative cleaning

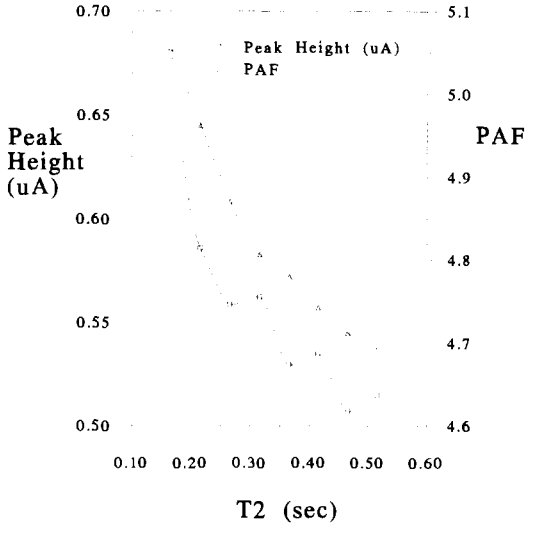

Fig. 4. Peak height and peak asymmetry factor (PAF) values for 1.00×10^{-2} M penicillin G injections as a function of T2. The other waveform parameters are held at their standard values (see Table 1). Relative standard deviation of peak heights = 0.00587. Relative standard deviation of PAF values = 0.0621.

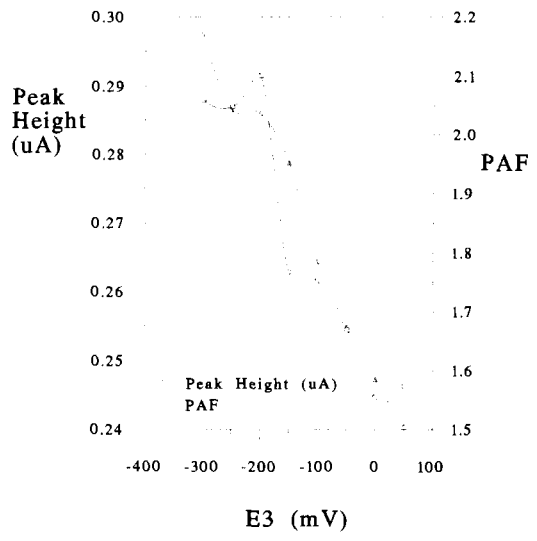

Fig. 5. Peak height and peak asymmetry factor (PAF) values for 1.00×10^{-2} M penicillin G injections as a function of E3. The other waveform parameters are held at their standard values (see Table 1). Relative standard deviation of peak heights = 0.0139. Relative standard deviation of PAF values = 0.0956.

period was increased, greater cleaning efficiency was expected. This would mean less carry-over of adsorbate, causing a decrease in peak height and less tailing at higher T2 values. The experimental data showed this behavior clearly. Short oxidative cleaning periods have been shown to produce greater tailing for amino acid samples in a prior study [25].

3.5. E3

E3 was varied from -300 to 50 mV in 50 mV intervals. Average peak heights and PAF values for each voltage are displayed in Fig. 5. As E3 was increased, the peak heights and the PAF values both showed a decrease. It was felt that all of the E3 values utilized were sufficiently small enough to not really alter the efficiency of reductive oxide removal. However, the amount of analyte adsorbed at this step was considered to be variable throughout this voltage domain. From the experimental data, both of the trends point out that the carry-over of adsorbed analyte is reduced as E3 is increased. The higher E3 voltages

lead to less efficient adsorption of analyte. If the cleaning efficiency is not changed, then making adsorption less efficient will create a smaller degree of carry-over, explaining the observed peak height and PAF trends. A more efficient adsorption will lead to greater electrode surface coverage of analyte, resulting in a change in response similar to what one would expect upon increasing analyte concentration, as discussed below.

3.6. T3

T3 was varied from 0.016 to 0.466 s in intervals of approximately 0.060 s. Average peak heights and PAF values for each time are displayed in Fig. 6. Prior studies have shown that peak size increases as the PAD adsorption step is extended to longer times, deviating only at very large time values as adsorbate saturation is approached [31]. The same trend is evident in Fig. 6, as both the peak height and the PAF are seen to increase. As with the E3 response, the trends are dictated by T3 alteration changing the efficiency of the adsorption without alteration of the cleaning effectiveness. Longer T3 values allow greater adsorption of analyte, so without a change in the cleaning, the analyte carry-over increases, resulting in larger peaks with a greater degree of tailing.

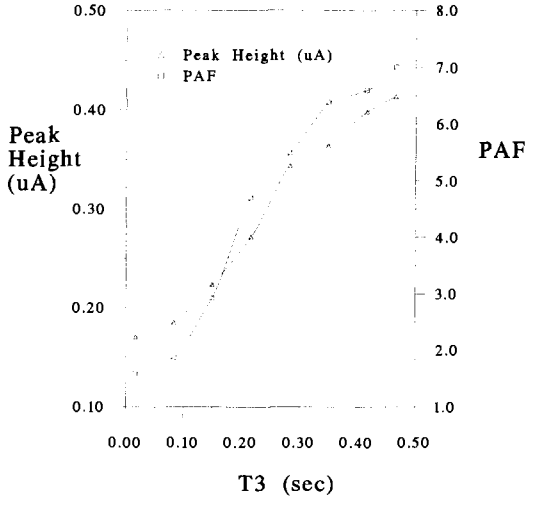

Fig. 6. Peak height and peak asymmetry factor (PAF) values for 1.00×10^{-2} M penicillin G injections as a function of T3. The other waveform parameters are held at their standard values (see Table 1). Relative standard deviation of peak heights = 0.00970. Relative standard deviation of PAF values = 0.0737.

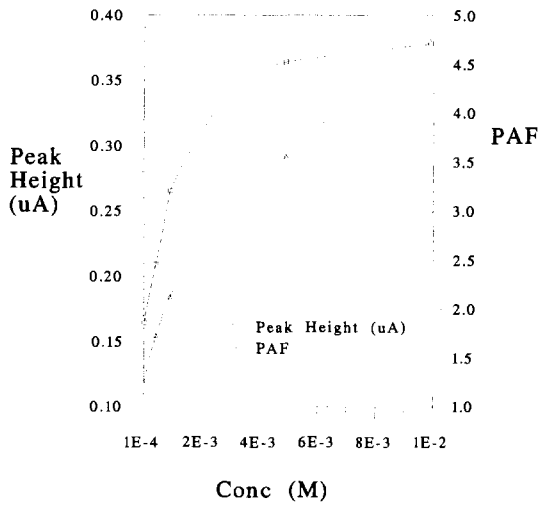

Fig. 7. Peak height and peak asymmetry factor (PAF) values for penicillin G injections as a function of concentration. The waveform parameters are held at their standard values (see Table 1). Relative standard deviation of peak heights = 0.00546. Relative standard deviation of PAF values = 0.0956.

3.7. Concentration

It is well known that the current versus concentration response for PAD is non-linear, except for examination of relatively small concentration ranges [32]. When viewed over a wide range, the response is linear at low concentrations, but then curvature occurs at higher concentrations as the current is less than the linear extrapolation. This is due to the crucial adsorption requirement for oxidation, creating an isotherm-like response resulting from the limited area available for adsorption. Our data confirmed that this type of response was present. The degree of peak tailing was also clearly a function of concentration, as can be seen in Fig. 7. Peak tailing was minimal at low concentrations, yet very significant at increased values. Variations in both peak height and PAF were present for low penicillin G concentrations as the various waveform parameters were

varied, but they were very slight and the data sets of low precision. Employing 1.00×10^{-2} M, as done above, allowed greater precision and easier visualization of the trends. The concentration dependence of the PAF is further evidence that the carry-over of adsorbed material is the root cause of peak tailing. At low penicillin G concentrations, the electrode surface coverage of adsorbed analyte will be quite small. The balance of the surface sites would be expected to grow surface oxide, which would be available for electrocatalytic oxidation via an oxygen transfer. At this low coverage value, there is a great likelihood that most of the adsorbed analyte has a nearby oxide site available to donate an oxygen, so the oxidation proceeds with great efficiency. Since the oxidative mechanism ends with desorption of the analyte, the efficient oxidation seen at these low concentration values would leave very little adsorbed analyte material behind, making carry-over minimal. Very little peak tailing results. However, as the concentration of analyte is increased, the penicillin G surface coverage becomes much larger. This leaves fewer sites available for oxide growth on the electrode surface. Under these conditions, the efficiency of oxidation is much lower, as many adsorbed analytes do not have an adjacent oxide available for oxidation. This contributes not only to the isotherm-like current versus concentration response, but it also results in fewer analyte molecules desorbed via the oxidative mechanism. The unoxidized analyte remains behind to be subjected to the E2 and E3 cleaning steps of the PAD waveform. Whereas the oxidative desorption process is very efficient, the cleaning from E2 and E3 is notably inefficient, and a clear function of waveform design. In any case, this inefficiency means that a good deal of the remaining adsorbate will not be removed and the carry-over to the following cycle is significant. As noted before, this carry-over is what leads to peak tailing. One can conclude that if all potential adsorbates are present at very low concentration, then there is little reason to be concerned with detector-generated tailing, but this will become an issue at higher concentrations.

4. Conclusion

As can be noted from the discussion above, waveform optimization in most cases makes size and shape antagonistic parameters, optimizing to maximize one will cause a degradation in the other. Optimizing for peak S/N instead of size tends to blur this relationship slightly, but it still exists most of the time. HPLC detector enthusiasts often try to maximize S/N, as detection limits are a common yardstick for detector performance. The antagonistic relationship between size and shape suggests that one might want to develop several waveforms, one featuring high sensitivity, one featuring minimized peak tailing and perhaps others of intermediate character.

While the trends determined within this study relate solely for direct PAD of a single analyte, it is expected that similar behavior would be observed for other PAD analytes that are detected via oxidation at the catalytic lower oxide of gold. The importance of the peak shape produced by a PAD waveform is likely to become a more significant issue. As HPLC efficiency increases and PAD is applied to capillary separation methods, detector response to narrow bands of analyte material, thus, greater detector resolution, will be required to keep pace. Avoiding detector-related peak tailing might be a crucial factor for such separations, and it should be noted that the high frequency waveforms necessary to accurately portray such narrow bands should suffer from worse peak shapes than the standard PAD waveforms for use with HPLC, especially given the PAF dependence on T1 and T2.

Acknowledgements

The generous donation of equipment from the Waters Chromatography Division of the Millipore Corporation is acknowledged with gratitude. Financial support for MWL was from a Ford Undergraduate Research Fellowship from Knox College, partially supported by The Ford Foundation. Additional support came from Knox College, and thanks to Jennifer Miller for programming assistance.

References

[1] S. Hughes, P.L. Meschi and D.C. Johnson, Anal. Chim. Acta, 132 (1981) 1.
[2] S. Hughes and D.C. Johnson, Anal. Chim. Acta, 132 (1981) 11.
[3] S. Hughes and D.C. Johnson, J. Agric. Food Chem., 30(4) (1982) 712.
[4] J. Prodolliet, E. Bugner and M. Feinberg, J. AOAC. Int., 78(3) (1995) 768.
[5] Y. Dauphin and F. Marin, Experientia, 51 (3) (1995) 278.
[6] M.P.H. Dunkel and R. Amado, Carbohydr. Res., 268 (1) (1995) 151.
[7] J.A. Polta and D.C. Johnson, J. Liq. Chromatogr., 6 (1983) 1727.
[8] L.E. Welch, W.R. LaCourse, D.A. Mead Jr. and D.C. Johnson, Anal. Chem., 61 (1989) 555.
[9] T.Z. Polta and D.C. Johnson, J. Electroanal. Chem., 209 (1986) 159.
[10] L.E. Welch and D.C. Johnson, J. Liq. Chromatogr., 13(7) (1990) 1387.
[11] R.M. Ianniello, J. Liq. Chromatogr., 15 (17) (1992) 3045.
[12] M.K. Park, J.H. Park, M.Y. Lee, S.J. Kim and I.J. Park, J. Liq. Chromatogr., 17 (5) (1994) 1171.
[13] D.C. Johnson and W.R. LaCourse, Electroanalysis, 4 (1992) 367.
[14] T.J. O'Shea, S.M. Lunte and W.R. LaCourse, Anal. Chem., 65 (1993) 948.
[15] W. Lu and R.M. Cassidy, Anal. Chem., 65 (1993) 2878.
[16] F. Jehl, P. Birckel and H. Monteil, J. Chromatogr., 413 (1987) 109.
[17] L. Koprowski, E. Kirchmann and L.E. Welch, Electroanalysis, 5 (1993) 473.
[18] E. Kirchmann and L.E. Welch, J. Chromatogr., 633 (1993) 111.
[19] E. Kirchmann, R.L. Earley and L.E. Welch, J. Liq. Chromatogr., 17 (1994) 1755.
[20] S. Altunata, R.L. Earley, D.M. Mossman and L.E. Welch, Talanta, 42 (1) (1995) 17.
[21] P.J. Vandeberg and D.C. Johnson, Anal. Chem., 65 (1993) 2713.
[22] A.J. Tudos, P.J. Vandeberg and D.C. Johnson, Anal. Chem., 67 (1995) 552.
[23] A.J. Tudos and D.C. Johnson, Anal. Chem., 67 (1995) 557.
[24] A. Ngoviwatchai, Ph.D. Dissertation, Iowa State University, 1988.
[25] L.E. Welch, Ph.D. Dissertation, Iowa State University, 1988.
[26] P.J. Vandeberg, J.L. Kowagoe and D.C. Johnson, Anal. Chim. Acta, 260 (1992) 1.
[27] L.R. Snyder and J.J. Kirkland, in Introduction to Modern Liquid Chromatography, 2nd Edn., Wiley-Interscience, New York, 1979.
[28] J.J. Kirkland, W.W. Yau, H.J. Stoklosa and C.H. Dilks, J. Chromatogr. Sci., 15 (1977) 303.
[29] J.P. Foley and J.G. Dorsey, Anal. Chem., 55 (1983) 730.
[30] W.R. LaCourse and D.C. Johnson, Anal. Chem., 65 (1993) 50.
[31] T.Z. Polta, D.C. Johnson and G.R. Luecke, J. Electroanal. Chem., 209 (1986) 171.
[32] D.C. Johnson, Anal. Chim. Acta, 209 (1988) 1.

ELSEVIER

Talanta 44 (1997) 1241–1251

Talanta

Simplex optimisation of conditions for the determination of antimony in environmental samples by using electrothermal atomic absorption spectrometry

Iris Koch [a], Christopher F. Harrington [a], Kenneth J. Reimer [b], William R. Cullen [a,*]

[a] *University of British Columbia, Department of Chemistry, 2036 Main Mall, Vancouver, British Columbia, V6T 1Z1, Canada*
[b] *Environmental Sciences Group, The Royal Military College of Canada, Kingston, Ontario, K7K 5L0, Canada*

Received 15 April 1996; received in revised form 12 September 1996; accepted 13 September 1996

Abstract

Analysis of the total antimony in plant material was unsuccessful using the electrothermal atomic absorption spectrometry (ETAAS) conditions recommended by the instrument manufacturer. For this reason, an optimisation procedure utilising the Plackett-Burman method, simplex optimisation and visualisation of the generated response surface via principal components analysis, was carried out. The Plackett-Burman method was used to eliminate four of the initial variables chosen. Four variables (atomisation temperature, atomisation time, ash temperature and modifier concentration) were subsequently optimised using the composite modified simplex method and the results were visualised as a contour diagram, after reduction to two principal components. The optimised conditions were used for the analysis of both an acid digested pine needle standard reference material (NIST 1575) and a pond weed sample, collected from a contaminated site at Yellowknife Bay, Yellowknife, NWT, Canada. The total concentration of antimony present in the pine needles was statistically indistinguishable from the non-certified value, as was the value for the pond weed sample, compared with a value determined by neutron activation analysis (NAA). The results for the analysis of the pond weed sample by ETAAS agreed with those obtained from a subsequent analysis by inductively coupled plasma-mass spectrometry. © 1997 Elsevier Science B.V.

Keywords: Antimony; Electrothermal atomic absorption spectroscopy; Environmental samples; Simplex optimisation and Plackett-Burman design

1. Introduction

Antimony has been found in biological, geological and water samples [1–4], and its toxicity has led the United States Environmental Protection Agency (US-EPA) to consider it and its compounds priority pollutants [5]. Common techniques for determining the total amount of antimony include: inductively coupled plasma mass spectrometry (ICP-MS) or atomic emission spectroscopy (ICP-AES) and hydride generation, followed by different atomisation methods such as electrothermal or flame heated quartz tube atomic

* Corresponding author. Tel.: +1 604 8222938; fax: +1 604 8222847.

PII S0039-9140(96)02168-6

absorption spectroscopy (HG-QT-AAS) [1–3]. The preconcentration of antimony hydride in a graphite furnace, followed by atomisation has recently been developed as another method of analysis [6,7].

All these methods give low detection limits, but ICP based methods are expensive for routine analysis. Hydride generation may not give 100% recovery when non-hydride forming species are present in the sample and is labour intensive. Electrothermal atomic absorption spectroscopy (ETAAS) is a widely used analytical tool for the determination of many trace metals, including antimony, in a wide variety of sample matrices [8–11]. The use of ETAAS for the determination of total antimony is cost effective and simple, but no formal optimisation of conditions has been reported for plant samples.

The very first studies [12] on the graphite furnace technique showed that the sample matrix has a pronounced effect on the absorbance signal observed for a particular element. These effects often lead to systematic errors when determining metals in complex organic matrices and result from substances not being fully volatilised prior to atomisation of the metal. Optimisation of instrumental conditions is therefore a prerequisite for development of an environmental analytical protocol using electrothermal AAS.

Until recently it was usual to optimise a system using a one-factor-at-a-time-approach, in which each variable but one is held at a low level and the response is evaluated at the lower and the upper level of the factor being tested. Each variable is treated in turn, until the response is maximised or minimised, depending on the system. This approach is far from adequate because there is no guarantee that an optimum response will be found, it requires a large number of experiments to be carried out and the presence of inter-relationships between the variables (e.g., modifier concentration and ash temperature) means that the optimum obtained will depend on the initial conditions chosen. Factorial experiments, in which all the factors are varied simultaneously according to a pre-set design, have also been used to optimise analytical systems. However, this approach is highly dependent on the levels of each factor and thus, it works best when some prior knowledge of the system is available. It also requires a large amount of experimentation when more than three variables are investigated.

Simplex optimisation is a highly efficient, multifactor, empirical feedback, optimisation procedure, that does not require the large number of experiments nor the initial variable information that is necessary with the two methods outlined above. This procedure 'homes in' on the optimum response region by driving the experiments in the direction of steepest ascent of the response surface. The optimum thus obtained is generally a local optimum, but some assurance that it is the overall optimum can be obtained by repeating the search from different starting conditions to see if the same conditions are reached.

Simplex optimisation is now routinely used as a method of maximising a response [13,14] or reducing interferences [15,16] in the analysis of trace elements. In the present work the use of the instrument manufacturer's recommended operating conditions [17] for the determination of antimony by ETAAS were completely unsuccessful, yielding no absorbance maximum. These conditions were: dry at 75°C for 5 s, then at 90°C for 60 s, then at 120°C for 10 s, hold at 120°C for 2 s, ramp to 2000°C in 1 s (maximum ramp rate), atomise at 2000°C for 3 s, clean at 2000°C for 1 s.

A two stage approach was used to optimise the experimental conditions used for the determination of antimony in plant material. The first part of the investigation involved the use of the Plackett-Burman method to screen a number of potential variables to select the most appropriate to optimise using the composite modified simplex method [18,19]. The principle advantages of this approach are that information concerning the significance of each variable is obtained (Plackett-Burman method) and the optimum conditions are efficiently reached, with less experimentation than would be necessary if none of the variables had been eliminated. Additionally, visualising the response surface eliminates the need for univariate searches around the optimum, which are often carried out to check that the optimum is correct. These goals are not possible using a one-step-at-a-time-approach, or a factorial experiment.

To check the accuracy of the developed methodology the concentration of antimony in a pine needle standard reference material (SRM), NIST 1575, was determined. The pond weed sample was acid digested and methanol extracted and these samples were statistically compared with results obtained by ICP-MS, as well as by neutron activation analysis (NAA).

2. Experimental

2.1. Reagents

Concentrated nitric and hydrochloric acids (both double sub-boiling distilled, Seastar Chemicals, Sidney, BC), concentrated sulphuric acid (Analytical grade, BDH Chemicals, Toronto, ON), and glacial acetic acid (Reagent grade, Fisher Scientific, Nepean, ON). Hydrogen peroxide (30%) (Assurance grade, BDH Chemicals, Toronto, ON), D-tartaric acid (Reagent grade, Allied Chemical Canada, Canada), palladium nitrate ($Pd(NO_3)_2 \cdot 2H_2O$, Reagent grade, Sigma, St. Louis, MO), citric acid (Certified, Fisher Scientific, Fairlawn, NJ).

Water was purified to a final resistivity of better than 1 M ohm (Barnstead Mega-Pure system, Barnstead/Thermolyne, Dubuque, IA). Methanol (HPLC grade, Fisher Scientific, Nepean, ON). A methanol/water (1/1 v/v) solvent mixture was used to extract the aqueous antimony species. Antimony metal (Certified, Fisher Scientific, Fair Lawn, NJ) and 1000 mg l^{-1} indium (Spectroscopy standard, High-Purity Standards, Charleston, SC).

The freeze dried pine needle standard reference material 1575, was obtained from the National Institute of Standards and Technology (NIST, Washington, DC). The pond weed sample (*Potomogetan pectinatus*) was collected from a site contaminated with mine tailings (Yellowknife Bay, NWT, Canada) as described previously [20] and freeze dried. The pine needle SRM (NIST 1575) was chosen as a representative standard reference material because it contains an uncertified antimony concentration of 0.2 mg kg^{-1}.

2.2. Preparation of samples and standards

The pine needles (1575), and pond weed were dried to constant weight and then acid digested. Acid digestions were carried out in duplicate by adding 3 ml of concentrated nitric acid, 3 ml of 30% hydrogen peroxide, and 1 ml of concentrated sulphuric acid to a 250 ml round bottom flask containing pine needles (0.5 g) or pond weed (0.25–0.40 g) and refluxed for 3 h as described elsewhere [21]. An additional pine needle digestion was carried out by heating 1 g of material with the above acid/hydrogen peroxide mixture, in a vial on a hot plate, at 90°C for 3 h. After the digestions were complete, the partially evaporated samples were diluted to 5 ml (pine needles) and 10 ml (pond weed) using deionised water.

Extraction of the pondweed was carried out by sonicating 0.5 g dry material with 10 ml methanol/water (1/1 v/v) for two samples, and 10 ml 0.2 M acetic acid for one sample. The sample and solvent were sonicated for 20 min, the mixture was centrifuged at 3000 rpm for 10 min and the supernatant was decanted. This was repeated five times and the combined extracts were evaporated under reduced pressure to dryness and made up to 5 ml with water.

A stock solution of 1000 mg l^{-1} antimony solution was prepared by dissolving 0.1000 g antimony metal in aqua regia and diluting to 100 ml with 1% D-tartaric acid. The 50 and 25 μg l^{-1} solutions for use in the standard additions determinations were prepared fresh daily from the stock.

The palladium modifier solution was prepared by dissolving 0.1083 g palladium(II) nitrate dihydrate in 0.5 ml of concentrated nitric acid and diluting to 100 ml with 2% citric acid solution to give a 1000 mg l^{-1} Pd solution. This stock solution was then diluted further with 2% citric acid solution to give the various concentrations needed for the experiments.

Indium solution was used as an internal standard in the ICP-MS determinations and was prepared by diluting an appropriate volume of a 200 μg l^{-1} standard solution so that the final concentration was 10 μg l^{-1} in each sample.

2.3. Instrumentation

An atomic absorption spectrometer (Varian Techtron Model 1275, Australia) fitted with an auto-sampler, graphite furnace and programmer (GTA-95) was used throughout this work. The antimony hollow cathode lamp (SpectrAA, Varian, Australia) was operated at 10 mA with a slit corresponding to a spectral bandwidth of 0.2 nm and the 217.9 nm line was monitored. Continuous background correction was by a deuterium lamp (Varian, Australia). Pyrolytically coated graphite tubes (Varian, Germany) were used.

The ICP-MS measurements were carried out using a VG PlasmaQuad 2 turbo plus instrument (VG Elemental, Fisons Scientific Equipment, Winsford, Cheshire, UK), operated at 1350 W RF power. Cooling, auxiliary and nebulizer gases (Ar) were at flow rates of 13.82, 0.69 and 1.00 l min^{-1}, respectively. Masses were monitored in the peak jumping mode by using m/z 115 (In) and 121 (Sb).

A real sample (pond weed digest diluted four times with deionised water) was used for the optimisation procedure outlined below. This sample was chosen, rather than an antimony standard, so that matrix and species dependent effects could be minimised and the antimony signal maximised.

The OPTIMA3 computer program [18,19] was used for the simplex calculations and the generation of experimental conditions. The principal components analysis was carried out by using Systat® 5.03 for windows (SYSTAT). Both of these programs were run under Windows® 3.1, on a DELL 466/M personal computer.

NAA was carried out as described elsewhere [20,22].

2.4. Plackett-Burman experiments

The initial variables chosen to be screened using the Plackett and Burman method were: dry time (Dt), dry temperature (DT), ash time (At), ash temperature (AT), atomisation ramp (AtR), atomisation time (Att), atomisation temperature (AtT) and modifier concentration (MC). This allowed for the use of three dummy variables and so had 3 df (see Table 1). Initial experiments carried out using longer ash and atomisation times (up to 15 and 7 s, respectively) resulted in a short graphite tube lifetime (60 firings), thus limits for these variables were chosen to minimise tube deterioration. The limits for all the variables were chosen so as to show a change in measured absorbance, which was the response measured, rather than to reflect conditions usually used for ETAAS.

After the first design was carried out, three variables (atomisation ramp, atomisation time and modifier concentration) were kept constant, whilst the effect of the other five variables were investigated using a $N = 8$ design (two dummy variables, 2 df) (see Table 2). The matrix designs, adapted from the method of Jones et al. [23], accompany the designations of variables in Table 1 and Table 2.

2.5. Simplex optimisation

The composite modified simplex (CMS) optimisation method described previously [18,19] was employed during this work. Having screened out the variables that did not have a significant effect on the response, the remaining four factors (atomisation temperature, atomisation time, ash temperature and modifier concentration) were optimised to provide the maximum antimony absorbance signal from a pond weed digestate. The upper and lower limits used in the CMS procedure as well as the stepsize for each variable are given in Table 3.

Five initial experiments were conducted and the conditions for each factor, as well as the resulting absorbance, were entered into the OPTIMA3 computer program. The next set of experimental conditions were generated and carried out, and the response was entered. The simplex progressed via a series of reflections, expansions, contractions or fit points, towards the optimum absorbance (see Table 4). The process was continued until the standard deviation of the five highest responses was less than the value of the stepsize of the absorbance (0.010), three times sequentially. To prove that the optimum values determined were not due to a local region of maximum response, the procedure was repeated with different starting

Table 1
Plackett-Burman design ($N = 12$) for the determination of significant variables to optimise by using simplex optimisation

Code	Variable	Lower level (−)	Upper level (+)
Designation			
Dt	Dry time (s)	30	70
DT	Dry temperature (°C)	60	90
At	Ash time (s)	1	3
AT	Ash temperature (°C)	1000	1300
Att	Atomisation time (s)	1	3
AtT	Atomisation temperature (°C)	1800	2300
AtR	Atomisation ramp (°/s)	260	1400
MC	Modifier concentration (mg l^{-1} Pd)[a]	100	700
D	Dummy	No change	No change
D	Dummy	No change	No change
D	Dummy	No change	No change

Expt	Dt	DT	At	AT	Att	AtT	AtR	MC	D	D	D
Matrix											
1	+[b]	+	−	+	+	+	−	−	−	+	−
2	−	+	+	−	+	+	+	−	−	−	+
3	+	−	+	+	−	+	+	+	−	−	−
4	−	+	−	+	+	−	+	+	+	−	−
5	−	−	+	−	+	+	−	+	+	+	−
6	−	−	−	+	−	+	+	−	+	+	+
7	+	−	−	−	+	−	+	+	−	+	+
8	+	+	−	−	−	+	−	+	+	−	+
9	+	+	+	−	−	−	+	−	+	+	−
10	−	+	+	+	−	−	−	+	−	+	+
11	+	−	+	+	+	−	−	−	+	−	+
12	−	−	−	−	−	−	−	−	−	−	−

[a] Experiments were carried out with a constant injected volume of 10 μl.
[b] '+' and '−' symbols correspond to the upper and lower levels of variable values, as defined by the preceding table.

Table 2
Plackett-Burman design ($N = 8$) for the determination of additional significant variables to optimise by using simplex optimisation

Code	Variable	Lower level (−)	Upper level (+)
Designation			
Dt	Dry time (s)	30	70
DT	Dry temperature (°C)	60	90
At	Ash time (s)	1	3
D	Dummy	No change	No change
AT	Ash temperature (°C)	800	1400
AtT	Atomisation temperature (°C)	1800	2300
D	Dummy	No change	No change

Expt.	Dt	DT	At	D	AT	AtT	D
Matrix							
1	+[a]	+	+	−	+	−	−
2	−	+	+	+	−	+	−
3	−	−	+	+	+	−	+
4	+	−	−	+	+	+	−
5	−	+	−	−	+	+	+
6	+	−	+	−	−	+	+
7	+	+	−	+	−	−	+
8	−	−	−	−	−	−	−

[a] '+' and '−' symbols correspond to the upper and lower levels of variable values, as defined by the preceding table.

conditions; the same optimum conditions were found.

2.6. Visualisation of the response surface

The experimental results were analysed by using principal components analysis, as described in detail and with examples by Molinero [24]. Briefly, principle components analysis was used to reduce the four variables from the simplex optimisation to two new variables (principle components 1 and 2). The scores of these principle components give coordinates for all the experimental vertices. Thus, the vertices of the simplex previously represented by n variables, are now represented by two variables, and the responses are plotted against these variables, to generate the response surface. The relative significance of the effects of the original variables on the responses can be evaluated by considering the loading of each variable on each principle component, which indicates to what degree each principle component is influenced by each of the original variables. This approach provides visual information on the optimum and the response surface, which is not possible with the simplex

Table 3
Range and stepsize of the variables being optimised by the composite modified simplex method

Variable	Lower limit	Upper limit	Stepsize[a]
Atomisation temperature (°C)	1400	2700	100
Atomisation time (s)	0	4	1
Ash temperature (°C)	800	1600	50
Modifier concentration (mg l^{-1})[b]	100	900	100

[a] Same units as variables.
[b] Experiments carried out with a constant injected volume of 10 μl.

Table 4
Simplex experiments and responses

Expt. No.	Atomisation temp. (°C)	Atomisation time (s)	Ash temp. (°C)	Modifier conc. (mg l^{-1})[a]	Point type[b]	Response[c] (absorbance)
1	1800	0	1400	500	I	0.103
2	1800	3	800	500	I	0.056
3	2200	0	1000	900	I	0.085
4	2400	0	1400	200	I	0.179
5	2400	3	1400	200	I	0.026
6	2100	0	1100	500	R	0.145
7	2700	0	1050	200	R	0.139
8	2500	0	1600	100	R	0.000
9	2300	0	800	600	C	0.116
10	2700	0	1050	100	R	0.138
11	2600	0	1600	100	R	0.000
12	2400	0	1050	400	C	0.155
13	2100	0	1450	500	R	0.264
14	1800	0	1600	600	E	0.055
15	1700	0	1600	700	R	0.048
16	2400	0	1200	300	C	0.217
17	2300	0	1600	300	R	0.009
18	2200	0	1250	500	C	0.204
19	2000	0	1600	500	R	0.043
20	2300	0	1200	400	C	0.167
21	2000	0	1300	700	R	0.105
22	2300	0	1400	300	C	0.266
23[d]	2200	0	1350	400	F	0.280
24	2000	0	1250	600	R	0.129
25	2300	0	1350	300	C	0.258
26	2300	0	1350	400	F	0.262
27	2300	0	1450	300	R	0.214
28	2200	0	1400	400	C	0.270
29	2000	0	1550	500	R	0.128

[a] Constant volume of 10 µl.
[b] Initial (I), reflection (R), contraction (C), extension (E) and fit (F).
[c] Response is mean of three determinations.
[d] Optimum conditions.

search alone. The response surface can be studied to determine more information such as the presence or absence of ridge features or local maxima. It also helps to show other factor levels that could provide better experimental conditions in terms of lower temperature operating conditions, or less modifier, thus resulting in a more cost effective procedure.

Table 5
t Values for 12 and 8 variable designs used in the Plackett-Burman experiments

Variables	Dt	DT	At	AT	Att	AtT	AtR	MC
12	−1.58	2.55	−0.97	1.74	−4.46*	−0.83	−2.46	3.49*
8	−0.54	−0.79	−2.34	14.90*	–	18.20*	–	–

* Indicates that the variable is significant at the 95% confidence level.

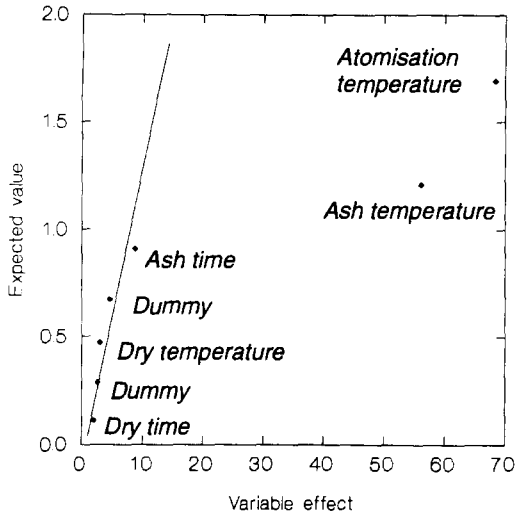

Fig. 1. Birnbaun plot for the second Plackett-Burman, showing the significance of the two variables atomisation temperature and ash temperature.

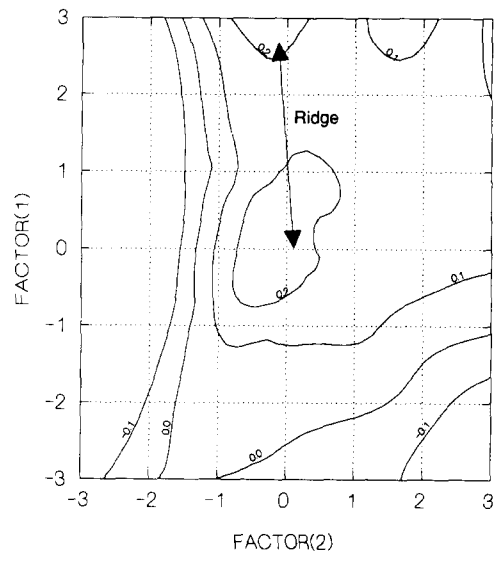

Fig. 2. Contour diagram showing the response surface for the first optimisation.

3. Results and discussion

3.1. Plackett-Burman experiments

The results for the first Plackett-Burm experiment were used to obtain a minimum t value of 3.18 for a 95% confidence interval. Only the atomisation time and modifier concentration give t values above this and so are the only significant variables at this confidence level (Table 5). Birnbaun plots can be used to confirm or help clarify results obtained from such experiments, as explained in more detail elsewhere [23]. Briefly, deviance of points from a straight line indicate large variable effects [14]. In this instance, the Birnbaun plot (not shown) gives essentially a straight line and therefore does not help with the further interpretation of this experiment.

The second Plackett-Burman experiment was carried out by holding three factors constant and hence utilised five of the original variables and two dummies (2 df). The atomisation time and modifier concentration shown to be important by the first experiment were held constant at 0 s and 500 mg l^{-1}, respectively, in the hopes that any other significant variables might be revealed. The ramp rate was observed in these and preliminary experiments to give maximum results at higher speeds, as noted by Pergantis et al. [11] in their optimisation for arsenic. Instrumental constraints

Table 6
The optimised furnace program, used for quantitation of antimony in plant samples (400 mg L^{-1} or 4 μg Pd as modifier was used)

Step No.	Temperature (°C)	Duration (s)	Gas flow (L min^{-1} Ar)	Function
1	90	30	3	Dry/ramp
2	120	10	3	Dry/ramp
3	1350	1.9	3	Ash/ramp
4	1350	2	3	Ash/hold
5	1350	1	0	Ash/gas off
6	2200	0.5	0	Atom/ramp[a]
7	2200	3	3	Clean

[a] 2000°C s^{-1} ramp from 1350°C to 2200°C, integration during this step.

Table 7
Concentration of antimony (mg kg^{-1} dry weight) in pine needles (NIST 1575) after analysis by ETAAS

Sample	ETAAS analysis ± S.D.[a]	Comparison to SRM[b]
Total digest 1[c]	0.220 ± 0.012	nsd[d] at 98%
Total digest 2	0.208 ± 0.019[e]	nsd at 95%
Total digest 3	0.231 ± 0.044	nsd at 95%

[a] Precision expressed as standard deviation (S.D.) based on five analytical replicates, except where indicated.
[b] Antimony concentration (0.2 mg kg^{-1}).
[c] Hot plate digestion.
[d] nsd: not significantly different at confidence level indicated.
[e] Four analytical replicates.

limited the ramp to 2000°C s^{-1} and this value was used for all subsequent experiments.

The results for the second experiment produced a minimum t value at the 95% confidence interval of 4.3 and the t values for the two variables, ash and atomisation temperature were greater, indicating that these variables have a significant effect on the antimony response. The Birnbaun plot in Fig. 1 shows that the ash and atomisation temperatures deviate from a straight line because of large variable effects, which confirms the significance of these variables.

Four variables: atomisation time, atomisation temperature, ash temperature and modifier concentration, were subsequently optimised by using the composite modified simplex procedure (CMS).

3.2. Simplex optimisation

A total of 29 experiments were carried out and the maximum response was reached after 23 experiments (see Table 4). The optimum parameters were found to be: atomisation temperature, 2200°C; atomisation time, 0 s; ash temperature, 1350°C; and modifier concentration, 400 mg l^{-1}. The simplex analysis was repeated from different initial conditions and the maximum response was: atomisation temperature, 2200°C; atomisation time, 0 s; ash temperature, 1450°C; and modifier concentration, 400 mg l^{-1}. These conditions were reached after 22 experiments from a total of 27. The conditions from the first optimisation are considered to be better for routine use, because the lower ash temperature is less destructive to the graphite cuvette.

The response surfaces generated from both searches are not identical, but the characteristic ridge feature of high absorbance is present in both (see Fig. 2 for the response surface generated from the first simplex). The results for the principle components analysis (PCA) indicate that the first and second principle components (PC) retain 43.8 and 31.5%, respectively of the original variance of the data. This is similar to values reported in previous work [24]. The results also demonstrate that the atomisation temperature and modifier concentration have the greatest influence on the first PC, whereas ash temperature has the greatest

Table 8
Comparison of the concentrations of antimony (mg kg^{-1} dry weight) in pond weed samples from Yellowknife, NWT, Canada

Sample	Determined by ETAAS ± S.D.[a]	Determined by ICP-MS ± S.D.[b]	Comparison[c]
Extract 1[d]	0.28 ± 0.04	0.222 ± 0.003	nsd at 95%
Extract 2	0.26 ± 0.02[e]	0.221 ± 0.002	nsd at 95%
Extract 3	0.28 ± 0.02	0.179 ± 0.003	nsd at 98%
Total digest 1	39 ± 5	32.6[f]	nsd at 98%
Total digest 2	40 ± 5	41.8[f]	nsd at 95%

Determination by optimised ETAAS and ICP-MS.
[a] Precision expressed as standard deviation (S.D.) based on five analytical replicates, except where indicated.
[b] Two analytical replicates except where indicated.
[c] nsd, not significantly different at confidence level indicated.
[d] Acetic acid/water extraction.
[e] Four analytical replicates.
[f] No replication.

influence on the second PC. Generation of the response surface also eliminates the need to carry out univariate searches around the optimum to establish that it is correct.

Therefore, after carrying out the simplex optimisation twice, from two different starting conditions and then analysing each response surface using principle components analysis, it was felt that further univariate investigates of the optimum were unnecessary.

3.3. Analysis of samples by using the optimised temperature program

The optimised procedure (Table 6) was used to determine the antimony concentration in pine needle SRM and pond weed, by using ETAAS and the method of standard additions. The results obtained for analysis of the pine needles are shown in Table 7, along with a comparison to the reference value. The concentrations for pine needles, with an average observed concentration of 0.220 mg kg^{-1}, do not differ significantly from the non-certified concentration of 0.2 mg kg^{-1}.

The pond weed sample is from a contaminated site near a gold mine in the Northwest Territories, Canada. The concentration of antimony in this sample was determined by ICP-MS to verify the values obtained by ETAAS and the results are given in Table 8. The results for the two methods do not differ significantly, as shown by the statistical comparison. The concentration of antimony for each digestion does not differ significantly (95% level) from the value determined by neutron activation analysis of 41.2 mg kg^{-1}.

The aqueous phase soluble antimony species were extracted from the pond weed sample with 1/1 methanol/water (V/V), so that further analysis by speciation techniques such as HPLC-ICP-MS or HG-GC-MS [24] can be carried out. However, prior to this it is important to establish the total antimony concentration, both hydride and non-hydride forming, present in the extract. Although the values obtained for the methanol/water extracts after analysis by ETAAS and ICP-MS do not differ statistically, consistently lower values for the ICP-MS results were observed. This is probably due to matrix or solvent effects, as the ETAAS analyses were carried out by using the method of standard additions, whereas the ICP-MS analyses were carried out using external calibration with aqueous standards.

By the analysis of the SRM and the methanol/water extract the optimised ETAAS procedure for the determination of antimony has been shown to overcome any interferences due to the sample matrix and any differences due to the different antimony species present. In addition, the method can be used for any total antimony determinations in samples of plant origin.

Acknowledgements

The authors would like to thank Dr M. Dodd for provision of the pond weed samples and NAA results, Mr B. Mueller for help with ICP-MS analysis, Ms M. Winters for assistance with sample preparation and Dr A. Wade for comments on the manuscript. We would like to acknowledge Dr K.J. Reimer, Environmental Sciences Group, Kingston, Ontario and the Natural Sciences and Engineering Research Council of Canada for financial assistance.

References

[1] M.O. Andreae, J.-F. Asmode, P. Foster and L. Van't Dack, Anal. Chem., 53 (1981) 1766.
[2] X. Lu, J. Li, S. Chen and D. Guosheng, Acta Ocean. Sinica, 9 (1990) 255.
[3] R. Kantin, Limnol. Oceanogr., 28 (1983) 165.
[4] H. Onishi, and E.B. Sandell, Geochim. Cosmochim. Acta, 8 (1955) 213.
[5] L.H. Keith, and W.A. Telliard, Environ. Sci. Technol., 13 (1979) 416.
[6] M. Walcerz, S. Garbos, E. Balska and A. Hulanicks, Fresenius J. Anal. Chem., 350 (1994) 662.
[7] R.E. Sturgeon, S.N. Willie and S.S. Berman, Anal. Chem., 57 (1985) 2311.
[8] R.E. Sturgeon, Can. J. Spectrosc., 32 (1987) 79.
[9] J.G.S. Gupta and J.L. Bouvier, Talanta, 42 (1995) 269.
[10] M.T. Perez-Corona, M.B. De La Calle-Guntinas, Y. Madrid and C. Carmara, J. Anal. At. Spectrom., 10 (1995) 321.
[11] S.A. Pergantis, W.R. Cullen and A.P. Wade, Talanta, 41 (1994) 205.

[12] B. Welz, Atomic Absorption Spectrometry, 2nd edn., VCH, Wenheim, 1985, p. 64–159.
[13] M.J. Ford, L. Ebdon, R.C. Hutton and S.J. Hill, Anal. Chim. Acta, 23 (1994) 23.
[14] D.J. Roberts and K.V. Kahokola, J. Anal. At. Spectrom., 4 (1989) 185.
[15] T. Van der Velde-Koerts and J.L.M. de Boer, J. Anal. At. Spectrom., 9 (1994) 1093.
[16] S.J. Hill, M.J. Ford and L. Ebdon, J. Anal. At. Spectrom., 7 (1992) 719.
[17] T. Mackenzie, in E. Rothery (Ed.), Analytical Methods for Graphite Tube Atomizers, Varian, Australia, Publication No. 85-100447-00, 1982, pp. 43.
[18] D. Betteridge, A.P. Wade and A.B. Howard, Talanta, 32 (1985) 709.
[19] D. Betteridge, A.P. Wade and A.B. Howard, Talanta, 32 (1985) 723.
[20] D.A. Bright, W.T. Dushenko and K.J. Reimer, Aquat. Bot., 50 (1995) 141.
[21] S. Bajo, B. Suter and B. Aeschliman, Anal. Chim. Acta, 149 (1983) 321.
[22] D.A. Bright, B. Coedy, W.T. Dushenko and K.J. Reimer, Sci. Tot. Environ., 155 (1994) 237.
[23] K. Jones, Int. Lab., November (1986) 32.
[24] M.L. Molinero, Anal. Chim. Acta, 297 (1994) 417.

ELSEVIER

Talanta 44 (1997) 1253–1259

Talanta

Determination of phenolic compounds in water using membrane inlet mass spectrometry

Marja Ojala [a,b,*], Raimo A. Ketola [a], Vesa Virkki [c], Harri Sorsa [a], Tapio Kotiaho [a]

[a] *VTT Chemical Technology, P.O. Box 1401, FIN-02044 VTT, Finland*
[b] *University of Helsinki, Laboratory of Analytical Chemistry, P.O. Box 55, FIN-00014, University of Helsinki, Finland*
[c] *VTT Automation, P.O. Box 1304, FIN-02044 VTT, Finland*

Received 7 May 1996; received in revised form 8 November 1996; accepted 13 November 1996

Abstract

Two membrane inlet mass spectrometric (MIMS) methods for determining phenolic compounds in water are described and compared, namely direct analysis and analysis after acetylation of the phenolic compounds. Direct analysis of phenolic compounds in water is a very simple and rapid method and detection limits are relatively low (from 30 μg l^{-1} for phenol to 1000 μg l^{-1} for 4-nitrophenol). Analysis of phenolic compounds after aqueous acetylation is also a very simple and rapid method, and the detection limits are even two orders of magnitude lower than in the direct analysis. For example the detection limit of phenol acetate is 0.5 μg l^{-1} and that of 4-nitrophenol is 10 μg l^{-1}. The acetylation method was also tested in the analysis of phenolic compounds from contaminated surface water samples. © 1997 Elsevier Science B.V.

Keywords: Membrane inlet mass spectrometry; Phenolic compounds; Water analysis

1. Introduction

Phenol and related compounds are used in large amounts in industry (total world production capacity 1993 was 5.5 million tons [1]). As a result of emissions, accidents and other releases they are also present in the environment. Phenols are highly toxic and can cause serious taste and odour contamination and therefore their analysis at low concentrations is very important [2,3]. However, the analysis of phenolic compounds is difficult due to their high polarity. The separation of phenolic compounds from water by solvent extraction is especially difficult and the recoveries are not satisfactory. Many different analysis methods have already been tested but there is still a need for methods which are applicable to rapid on-line analysis, especially directly from water samples.

Direct measurement of phenolic compounds in water using high performance liquid chromatography (HPLC) is possible, but the detection limits are rather high, about 100 μg l^{-1} [4]. Several concentration methods may be used to obtain better overall detection limits. Solid phases such as C_{18} [5], polymeric sorbents [6], carbon black [7]

* Corresponding author.

PII S0039-9140(96)02169-8

and alkaline anion exchanger [8] extraction enrichment are used to improve detection limits but these methods are all quite laborious. Continuous liquid–liquid extraction [9], on-line liquid chromatographic precolumn-based column-switching [10] and on-line membrane/liquid chromatographic analysis [11] have all given good results but special equipment is needed. Solid-phase microextraction [12,13] has also been applied to the analysis of phenolic compounds. Low detection limits with good precision were obtained, but the absorption time of one sample, about 40–50 min, limited the usefulness of the method for on-line applications. Various derivatives [14] have also been used to improve the chromatographic behaviour of phenolic compounds, mainly in gas chromatography. Acetylation of phenols after solvent extraction is one of the most frequently used derivatization techniques. Recent studies have shown that it is also possible to carry out acetylation in aqueous solution [15–17]. This derivatization method, followed by solvent extraction and gas chromatographic analysis, has produced much better results than the reversed order method, in which the phenols are first extracted and then derivatized, due to better recovery of the phenols. With the new method recoveries of about 100% could be obtained [15].

In this study the applicability of membrane inlet mass spectrometry (MIMS) to the analysis of phenolic compounds was studied. MIMS is an analytical method well suited to rapid on-line analysis. In the method the introduction of analyte into the mass spectrometer occurs through a polymer membrane, which is highly selective for organic compounds relative to water. MIMS is an excellent technique for monitoring gases and volatile organic compounds directly from aqueous solutions [18]. The main application fields are biochemical and environmental analysis [19–24]. Lauritsen et al. [25] have already used a modified MIMS method, Trap-MIMS, for the analysis of chlorophenols from water samples. In this method the membrane is kept cold during sample loading by the flow of sample, and when the sample flow is stopped the membrane is heated rapidly due to the heat of the filament, which subsequently causes rapid release of compounds adsorbed on the inside of the membrane into the ion source of the mass spectrometer. Good detection limits for larger chlorophenols (10 $\mu g\ l^{-1}$) were obtained, but the results for more volatile compounds such as phenol and 4-chlorophenol were less satisfactory.

In the present study the traditional MIMS method for the analysis of phenols from aqueous samples was characterized. Phenols were measured directly from aqueous solutions or after acetylation. Lower detection limits were obtained with the acetylation method. The acetylation method was also applied to the analysis of contaminated surface water samples and compared with a HPLC method.

2. Experimental

2.1. Reagents

The standard phenolic compounds: phenol [108-95-2], 3-methylphenol [108-39-4], 2,3-dimethylphenol [526-75-0], 2,4,6-trimethylphenol [527-60-6], 4-chloro-3-methylphenol [59-50-7], 2,5-dichlorophenol [583-78-8], 2,4,6-trichlorophenol [88-06-2], 2,3,4,6-tetrachlorophenol [58-90-2], pentachlorophenol [87-86-5] and 4-nitrophenol [100-02-7] were obtained commercially (from Riedel-de Haën, Merck, Analabs, Fluka and Dr Ehrenstorfer GmbH). For each standard compound a stock solution containing about 10 $g\ l^{-1}$ was prepared in methanol. Dilutions of the stock solutions were prepared using deionized water (Millipore, Milli-Q plus) as needed. Twice distilled acetic anhydride (Merck, distilled in the laboratory) and sodium bicarbonate (Riedel-de Haën) was used in the derivatization of samples and methanol (Rathburn, HPLC grade) was used as eluent in HPLC analysis.

2.2. Derivatization procedure

The derivatization procedure used was similar to that described by Coutts et al. [14]. Acetic esters of phenols were prepared in a 1000 ml separation funnel. $NaHCO_3$, 20 g, was dissolved in a water sample of 500 ml, and 1 ml of acetic

anhydride (twice distilled) was added. The separation funnel was shaken vigorously during the evolution of carbon dioxide (about 2 min), after which the samples were ready for analysis. The total derivatization time is about 5 min.

2.3. Mass spectrometric and liquid chromatographic conditions

Membrane inlet mass spectrometry: samples were analyzed using a Balzers QMG 421C mass spectrometer with a mass range of 1–500 amu and equipped with an open cross-beam electron impact (70 eV) ion source (Balzers Aktiengesellschaft, Balzers, Liechtenstein). Data were collected continuously either by measuring full mass spectra or by using a selected ion monitoring method. The latter method was used to determine detection limits and the linearity of response. The membrane inlet used was built at VTT Chemical Technology on the basis of the design of Lauritsen [26]. The membrane utilized was a methylsilicone sheet membrane (Specialty Silicone Products, Ballston SPA, NY, USA) with dimensions: thickness 100 μm and contact area 28 mm^2. During operation of the system a water stream was continuously supplied to the membrane inlet via a peristaltic pump (Ismatec IPS4, Ismatec SA, Switzerland), typically at a flow rate of 10 ml min^{-1}, and aliquots of sample solution (typically 50–100 ml) were injected into this stream as needed. Before passing of the flowing water stream through the membrane inlet, its temperature was equilibrated to 70°C using a heat exchanger, which in turn was heated with a circulating water bath (Lauda M3, MGW, Germany).

Liquid chromatographic experiments were carried out using a HPLC (HP 1090, Hewlett Packard, Palo Alto, CA, USA) in combination with an autoinjector, an autosampler and a diode array detector. A reversed phase analytical column (Hypersil 100 mm × 2.1 mm i.d., 5 μm) with a linear gradient elution (10% methanol/acidic water $\rightarrow$ 10 min 100% methanol, flowrate 0.4 ml min^{-1}) was used to separate compounds and a diode array detector (wavelength 225 nm) was used for detection.

2.4. Samples

Three surface water samples were analyzed using MIMS. The content of phenolic compounds in two of the samples was below the detection limit. The third sample was diluted 1:100 and acetylated before analysis. The pH of standard solutions measured without acetylation was about 5.5, the pH of deionized water. Pentachlorophenol was the only compound for which the pK_a value was lower than 5.5 and it was therefore partly ionized. This probably explains its poor detection limit without acetylation [27]. Before acetylation the pH of both standards and samples was adjusted to $\cong 8$ using $NaHCO_3$ [15].

3. Results and discussion

Electron ionization mass spectra of the standard compounds were measured by MIMS before and after acetylation (Table 1). Even at this early stage it was observed that the acetylated compounds could be measured at lower levels, since solutions of similar concentrations produced mass spectra with much better signal to noise ratios for the acetylated phenols than for the underivatized compounds. For underivatized phenols the base peak is most often the molecular ion, whereas in the case of acetylated phenols the base peak is the fragment ion formed by the loss of neutral ketene (CH_2CO). The relative abundance of the molecular ion of the acetylated phenols was typically in the order of 20% and it was lowest for pentachlorophenol and highest for 4-nitrophenol (4 and 70%, respectively). All the measured EI mass spectra agreed very well with the EI mass spectra published in reference mass spectral libraries [28]. As an example of this the EI mass spectra of 4-nitrophenol as measured by MIMS and redrawn from the Wiley reference library are presented in Fig. 1. The good agreement obtained in this case also demonstrated the good analytical capabilities of membrane inlet mass spectrometry. The typical fragmentation pathways of 4-nitrophenol acetate can easily be recognized from the spectra presented. The main fragmentation route starts with the loss of neutral ketene producing the fragment

Table 1
Standard compounds and their mass spectra measured by MIMS directly from water and after aqueous acetylation

Compound	MW[a]	Ions m/z (RA[b])
Phenol	94	94 (100), 66 (44), 65 (38), 63 (13), 50 (12), 55 (9), 95 (8) 62 (8), 51 (8), 53 (7)
Phenol acetate	136	94 (100), 136 (18), 66 (15), 65 (14), 95 (7), 51 (6), 63 (5)
3-Methylphenol	108	108 (100), 107 (87), 77 (45), 79 (36), 51 (21), 53 (15) 52 (12), 50 (12), 63 (11), 90 (10), 80 (10)
3-Methylphenol acetate	150	108 (100), 107 (40), 150 (23), 77 (15), 79 (11), 109 (8), 51 (7) 80 (6), 90 (6), 78 (5), 53 (5)
2,3-Dimethylphenol	122	107 (100), 122 (89), 77 (44), 121 (31), 91 (30), 79 (24), 51 (21) 78 (16), 65 (14), 53 (14)
2,3-Dimethylphenol acetate	164	122 (100), 107 (57), 164 (28), 121 (16), 77 (16), 91 (15) 123 (9), 79 (7), 51 (7), 78 (6), 65 (6)
2,4,6-Trimethylphenol	136	121 (100), 136 (89), 91 (37), 135 (29), 77 (19), 65 (13), 51 (11) 137 (9), 122 (9), 93 (9)
2,4,6-Trimethylphenol acetate	178	136 (100), 121 (82), 135 (26), 91 (24), 77(12), 137 (10) 122 (9), 178 (8), 65 (8), 79 (7), 51 (7)
4-Chloro-3-methylphenol	142	107 (100), 142 (97), 77 (63), 51 (41), 144 (32), 78 (18), 50 (17) 79 (15), 63 (15), 53 (14)
4-Chloro-3-methylphenol acetate	184	142 (100), 107 (43), 144 (33), 77(20), 184 (17), 51 (13), 143 (9) 186 (6), 141 (5), 78 (5), 63 (5)
2,5-Dichlorophenol	162	162 (100), 164 (65), 63 (59), 99 (22), 62 (20), 98 (19), 73 (15) 61 (13), 53 (12), 166 (10)
2,5-Dichlorophenol acetate	204	162 (100), 164 (65), 63 (18), 204 (16), 166 (11), 206 (11) 73 (9), 133 (8), 163 (8), 62 (7)
2,4,6-Trichlorophenol	196	196 (100), 198 (96), 97 (42), 200 (30), 132 (28), 62 (24) 61 (20), 134 (18), 99 (16), 53 (11)
2,4,6-Trichlorophenol acetate	238	196 (100), 198 (96), 200 (32), 238 (16), 240 (16), 97 (16) 169 (10), 167 (10), 199 (8), 132 (8), 62 (8)
2,3,4,6-Tetrachlorophenol	230	232 (100), 230 (86), 234 (48), 131 (47), 133 (31), 166 (30) 168 (29), 61 (26), 96 (24), 196 (16),194 (15)
2,3,4,6-Tetrachlorophenol acetate	272	232 (100), 230 (84), 234 (50), 274 (21), 272 (17), 131 (13) 236 (12), 203 (12), 276 (10), 201 (10), 74 (10)
Pentachlorophenol	264	266 (100), 268 (66), 264 (63), 165 (36), 167 (35), 202 (21) 95 (18), 230 (17), 130 (17), 132 (13), 237 (12), 169 (12)
Pentachlorophenol acetate	306	266 (100), 264 (63), 268 (63), 165 (26), 91 (25), 167 (25) 237 (20), 270 (20), 74 (16), 130 (16), 92 (15), 306 (4)
4-Nitrophenol	139	57 (100), 139 (99), 65 (75), 71 (62), 53 (61), 51 (58), 63 (53) 55 (46), 81 (44), 64 (43)
4-Nitrophenol acetate	181	139 (100), 109 (72),181 (70), 65 (55), 63 (43), 93 (34) 74 (32), 64 (27), 81 (19), 53 (14)

[a] MW, molecular weight.
[b] (RA) relative abundance.

ion m/z 139, which subsequently looses either neutral NO or NO_2 to produce fragment ions m/z 109 and 93, respectively.

The detection limits (Table 2) and the linear dynamic ranges for underivatized and acetylated phenols were measured using selected ion monitoring (SIM) method. Typically the base peak of the mass spectrum was used in the SIM method and a signal to noise ratio of 3 was used as a criterion for the detection limit determination.

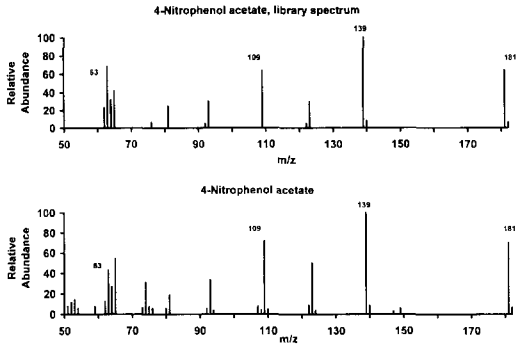

Fig. 1. Electron ionization mass spectrum of 4-nitrophenol acetate measured by membrane inlet mass spectrometry, and a mass spectrum redrawn from the Wiley mass spectra collection.

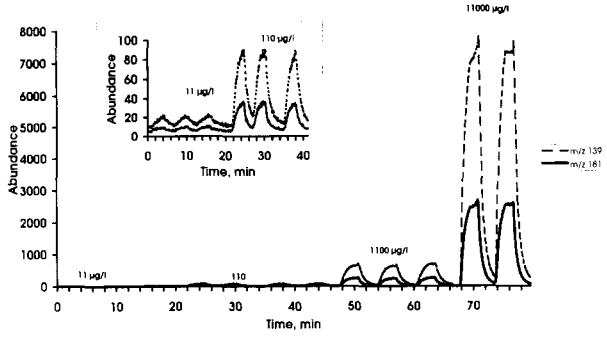

Fig. 2. Ion chromatograms of m/z 181 and 139 showing the MIMS response to successive injections of aqueous solutions of 4-nitrophenol (11, 110, 1100 and 11 000 µg l^{-1}).

Four or five different concentrations were used for the linear dynamic range determinations. From Table 2 it can be seen that acetylation significantly lowered the detection limits, especially in the case of 4-nitrophenol. The detection limit of four nitrophenol was lowered from 1000 to 10 µg l^{-1}. The effect is believed to be due mainly to two factors. Probably the most important of these is the change in the solubility of analytes in the methyl silicone membrane. The more polar underivatized phenols do not dissolve as well in the relatively non-polar membrane material as do the less polar acetylated phenols (i.e., the partition coefficient of acetylated compounds into the silicone is higher than that of underivatized phenols). Another effect is that the phenols with pK_a values below 5.5 (e.g., pentachlorophenol, pK_a 4.74 [13]) cannot be analyzed very well directly from water samples at the used pH values of the samples because they are in ionic form and ions do not dissolve in the methyl silicone membrane. This effect has earlier been reported in connection with SPME determinations of phenols from aqueous solutions [13]. For example pentachlorophenol was extracted by SPME 1.4-fold better at pH 2 than at neutral pH.

The linear dynamic ranges measured were typically about three orders of magnitude. An example of this is presented in Fig. 2, which shows

Table 2
Detection limits and linear dynamic ranges of some phenolic compounds measured by MIMS with and without acetylation

Compound	Detection limit µg l^{-1}	Linear dynamic range µg l^{-1}	Detection limit after acetylation µg l^{-1}	Linear dynamic range µg l^{-1}
Phenol	30	30–1000	0.5	0.5–300
3-Methylphenol	20	20–1000	1	1–300
4-Chloro-3-methylphenol	10	10–1000	1	1–300
2,5-Dichlorophenol	5	5–1000	1	1–300
2,4,6-Trichlorophenol	5	5–1000	1	1–300
2,3,4,6-Tetrachloropenol	10	nm	2	2–1000
Pentachlorophenol	60	nm	5	5–2500
4-Nitrophenol	1000	nm	10	10–10000

nm, Not measured.

selected ion monitoring data measured for successive injections of 4-nitrophenol acetate. The correlation coefficient of the calibration line calculated on the basis of the data was 1.00. The correlation coefficients of the calibration lines of all the other phenols were in the range of 0.996–1.00, demonstrating the good quantitative capabilities of membrane inlet mass spectrometry. It is also worthy of note that the average measurement time in Fig. 2 is about 7 min, which clearly demonstrates the potential of MIMS for rapid analyses.

Membrane inlet mass spectrometry was also tested in the analysis of complex phenol mixtures. A mixture mass spectrum of acetylated phenol, methylphenol, 4-chloro-3-methylphenol, 2,5-dichlorophenol, 2,4,6-trichlorophenol and pentachlorophenol is presented in Fig. 3. The concentration of each of the analyte was about 1 ppm. For all the analytes characteristics ions can be seen, i.e., the molecular ion and the ion formed by the loss of neutral ketene from the molecular ion. These ions are m/z 136 and 94 for phenol, m/z 150 and 108 for methylphenol, m/z 184 and 142 for 4-chloro-3-methylphenol, m/z 204 and 162 for 2,5-dichlorophenol, and m/z 238 and 196 for 2,4,6-trichlorophenol. For pentachlorophenol only the ketene loss ion, m/z 264, can been seen. These results clearly demonstrate that MIMS is capable of mixture analysis.

Some surface water samples taken from an area contaminated with phenolic resins were analyzed using both the acetylation method and the direct

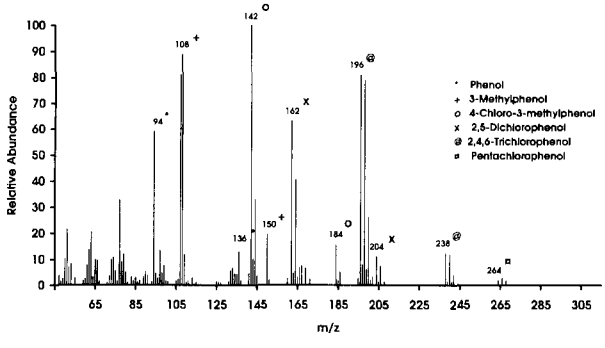

Fig. 3. Mass spectrum of a solution containing phenol, methylphenol, 4-chloro-3-methylphenol, 2,5-dichlorophenol, 2,4,6-trichlorophenol and pentachlorophenol. The characteristic ions of each compound are indicated.

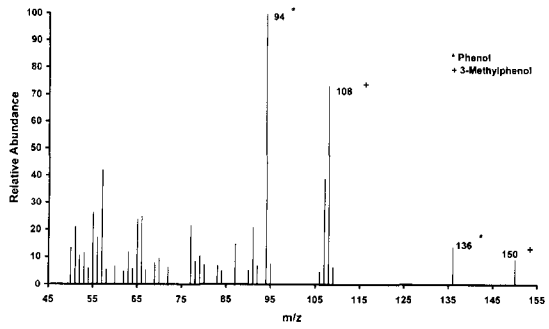

Fig. 4. Mass spectrum of a contaminated surface water sample measured after acetylation of the phenolic compounds.

HPLC method presented in the experimental section. The phenolic content of most of the samples were below the detection limits of both of the methods. Only in one sample measureable amounts of phenolic compounds were observed. For quantitative analysis this sample was diluted 1000-fold prior to analysis by MIMS, the HPLC analysis was carried out without any dilution. The mass spectrum measured for this sample is presented in Fig. 4. The characteristic ions of phenol actetate (m/z 94 and 136) and methylphenol acetate (m/z 108 and 150) can be recognized from the mass spectrum. The concentrations of these compounds were determined by an external standard quantitation method using the closest concentration of standard solution as calibrant. The concentrations of phenol and methylphenol in calibrant were 11.6 and 12.5 $\mu g\ l^{-1}$ and the peak heights of measured ions (m/z 94 and 108) were 13 300 and 6300 respectively. The peak heights of the same ions measured in diluted water samples were 39 000 and 13 000. The concentrations of phenol and methylphenol calculated on the basis of these numbers were 34 and 26 mg l^{-1}, respectively. With the HPLC method only phenol could be identified reliably, due to the large background eluting simultaneously with the methylphenols. The concentration of phenol obtained by the HPLC method was 36 mg l^{-1} which agrees very well with the MIMS determination.

In conclusion, acetylation of phenolic compounds directly in water with subsequent MIMS analysis is a very rapid and easy analytical method for the analysis of phenolic compounds in

aqueous solutions. The derivatization step adds only about 5 min to the direct MIMS analysis time of 5 min i.e., even with the derivatization step the analysis time of one sample is less than 20 min. The implementation of derivatization step in the flow injection analysis manner is also planned so that this method can also be used for on-line analysis. The detection limits obtainable with the acetylation method are 5–100 times lower than in the direct MIMS method in which phenols are not derivatized before analysis. For example detection limits of 0.5 μg l^{-1} for phenol and 10 μg l^{-1} for 4-nitrophenol were measured.

Acknowledgements

We thank Sirpa Vapaavuori for technical assistance.

References

[1] Chemical Economical Handbook database, SRI researchers.
[2] P.A. Realini, J. Chrom. Sci., 19 (1981) 124.
[3] R. Tyagi, Fresenius Environ. Bull., 4 (1995) 751.
[4] N.G. Buckman, J.O. Hill, R.J. Magee and M.J.J. McCormick, Chromatogr., 284 (1984) 441.
[5] Z. Vasilic, S. Fingler and V Drevenkar, Fresenius J. Anal. Chem., 341 (1991) 732.
[6] B. Gawdzik, J. Gawdzik and U.J. Czerwinska-Bil, Chromatogr., 509 (1990) 135.
[7] C. Borra, A. Di Corcia, M. Marchetti and R. Samperi, Anal. Chem., 58 (1986) 2048.
[8] P. Alarcon and A. Bustos, Chromatographia, 24 (1987) 613.
[9] J. Czuczwa, C. Leuenberger, J. Tremp, W. Giger and M. Ahel, J. Chromatogr., 403 (1987) 233.
[10] E.R. Brouwer and U.A. Th. Brinkman, J. Chromatogr. A, 678 (1994) 223.
[11] R.G. Melcher, D.W. Bakke and H.G Hughes, Anal. Chem., 64 (1992) 2258.
[12] K.D. Buchholz and J. Pawliszyn, Environ. Sci. Technol., 27 (1993) 2844.
[13] K.D. Buchholz and J. Pawliszyn, Anal. Chem., 66 (1994) 160.
[14] J. Hajslova, V. Kocourek, I. Zemanova, F. Pudil and J. Davidek, J. Chromatogr., 439 (1988) 307.
[15] R.T. Coutts, E.E. Hargesheimer and F. M. Pasutto, J. Chromatogr., 179 (1979) 291.
[16] V. Janda and H. Van Langenhove, J. Chromatogr., 472 (1989) 327.
[17] T.J. Boyd, J. Chromatogr. A, 662 (1994) 281.
[18] T. Kotiaho, F.R. Lauritsen, T.K. Choudhury, R.G. Cooks and G.T. Tsao, Anal. Chem., 63 (1991) 875A.
[19] H. Degn, J. Microbiol. Methods, 15 (1992) 185.
[20] F.R. Lauritsen and D. Lloyd, in C. Fenselau (Ed.), Mass Spectrometry for the Characterisation of Microorganisms, ACS Symposium Series, No. 541, American Chemical Society, Washington, DC, 1994, p. 91.
[21] F.R. Lauritsen, in Proceedings of the COMETT II Course 'Advanced Instrumentation, Data Interpretation, and Control of Biotechnological Processes', October 24–27, 1994, Gent, Belgium, Kluwer Academic Press.
[22] S.J. Bauer and R.G. Cooks, Am. Lab., 36 (1993).
[23] P.S.H. Wong, R.G. Cooks, M. Cisper and P.H. Hemberger, Environ. Sci. Technol., 29 (1995) 215A.
[24] M.A. Mendes, R.S. PimPim, T. Kotiaho and M.N. Eberlin, Anal. Chem., 68 (1996) 3502–3506.
[25] M. Leth and F.R. Lauritsen, Rapid Commun. Mass Spectrom., 9 (1995) 591.
[26] F.R. Lauritsen, Int. J. Mass Spectrom. Ion Proc., 95 (1990) 259.
[27] P.R. Brookes and A.G. Livingston, J. Membrane Sci., 104 (1995) 119.
[28] Wiley 138K Mass spectral library, Wiley, New York, 1990.

ELSEVIER

Talanta 44 (1997) 1261–1270

Talanta

Determination of equilibrium states in multi-phase systems

Jarosław Chojnacki *

Technical University of Gdańsk, 80-952, Gdańsk, Poland

Received 1 July 1996; received in revised form 7 November 1996; accepted 13 November 1996

Abstract

Volume corrections in calculation of equilibrium state for multi-phase systems, as an extension from one-phase systems, have been described. The algorithms can handle with one, two, three or more phases of different volumes. Several applications of the algorithms to calculation of equilibrium concentrations of all species in two- and three-phase systems have been presented. Different possibilities of the determination of equilibrium constants from extraction data have been discussed. © 1997 Elsevier Science B.V.

Keywords: Computer programs; Equilibrium; Extraction; Multi-phase systems

1. Introduction

In the literature one can find many programs for determination of equilibrium concentrations [1] and equilibrium constants, e.g., most popular SCOGS [2], SUPERQUAD [3], or more recent SPECA [4] and SIRKO [5]. Practical use of them also have been examined [6]. However, the programs are designed for processing spectroscopic or potentiometric data. Application of them to all extraction data is not possible. Although there are old extraction oriented programs e.g., LETAGROP-DISTR [7], other, interactive computer programs are required. Moreover, new programs are more general and can describe multi-phase systems.

Mathematical formalism describing multi-reaction equilibria has been described in details by Kostrowicki and Liwo [8]. The formalism, although general considering the types of equilibria, was worked out for systems with many reactions, but only one-phase. More precisely: heterogenic (solid–liquid) systems were allowed, but only concentrations in one liquid phase were calculated. However, one can be interested in equilibrium concentrations in several liquid phases. Such necessity is in extraction, whenever phases (organic and aqueous) are of different volumes. If the volumes were equal, the system would be regarded as one-phase using the existing programs. Sometimes one can meet stable three-phase liquid extraction systems (e.g., Zn distribution in H_2SO_4-1-penthanol-toluol [9]). Other examples of three phase systems are liquid–liquid extraction with a solid deposit (e.g., extraction of metals in $AlCl_3$-HCl-H_2O-diisopropyl ether system [10]) or bulk

* Corresponding author. Fax: +48 58 472694; e-mail: jarekch@chem.pg.gda.pl

PII S0039-9140(96)02170-4

liquid membrane with two aqueous phases separated by one organic phase.

In the previous algorithms concentrations were inserted into balance equations. In systems with several phases, moles instead of molar concentrations must be used in balances. The necessary modifications in procedures are described in this work.

Programs for determination of equilibrium constants from extraction data are much less common. Many researchers investigating extraction equilibria use graphical procedures (e.g., see Fletcher and Flett [11]). Some use commercial programs for linear or multiple regression to support graphical procedures. Berger and Graff describe one-species extraction equilibrium in [12], while mathematical analysis of multiple-species extraction appeared in their next paper [13]. Extraction of many species in liquid–liquid systems were first analyzed by a specialized program by Rydberg et al. [14] by fitting of the measured metal concentration to a polynomial. Analysis of the extraction data by multiple regression has been presented e.g., by Jaycock et al. [15] or Apostoluk [16].

In most of those procedures there are no corrections of concentrations for progress of reactions. It is assumed that the experiment is arranged in such a way that addition of excesses of some reagents allows to neglect concentration changes caused by run of reactions. The correction is not trivial if there are several reactions to consider. Liem overcome that by applying an iteration procedure for finding the equilibrium concentrations for two-phase extraction systems, in the program LETAGROP-DISTR [7].

Presented programs EXTRAFIT and EXTRAPH are an extension of LETAGROP-DISTR towards systems with more than two phases and towards more types of equilibria. The advantage of the algorithms is that they accept wider spectrum of different equilibria, e.g., solid deposit formation/dissolution and use actual equilibrium concentrations corrected for run of reactions. This means that we can investigate systems with small stoichiometric excesses of reagents. The balance equations are created automatically according to chemical equilibria specified. There is no restriction regarding the number of phases or the number of species, or the number, or the type of reactions other than the capability of the applied computer.

2. Determination of equilibrium concentrations

It has been shown that multiple equilibria most conveniently can be expressed in language of linear algebra [17,18]. One may also study the simple example given in the application section. Consider a system of n components involved in m reactions. The equilibrium concentrations must satisfy equilibrium condition Eq. (1)

$$\mathbf{A} \ln \boldsymbol{C} = \ln \boldsymbol{K} \tag{1}$$

where: $\mathbf{A}_{m \times n}$, stoichiometric matrix; $\boldsymbol{C}$, vector of concentrations, $\boldsymbol{C} = [C_1, C_2,..,C_n]^T$, ln $\boldsymbol{K}$-vector of natural logarithms from stability constants, ln $\boldsymbol{K} = [\ln K_1, \ln K_2,..,\ln K_m]^T$.Additionally for one phase systems the following balance equations set must hold

$$\mathbf{Q}\boldsymbol{C} = \boldsymbol{T} \tag{2}$$

where: $\mathbf{Q}_{n-m \times n}$, balance matrix; $\boldsymbol{T}$, balance constants vector $[T_1, T_2,.., T_{n-m}]^T$.For multi-phase systems Eq. (2) must be replaced by Eq. (3)

$$\mathbf{Q}\boldsymbol{N} = \boldsymbol{T} \text{ or } \mathbf{QV}\boldsymbol{C} = \boldsymbol{T} \tag{3}$$

where: $\boldsymbol{N}$, moles vector, $\boldsymbol{N} = [\mathbf{V}_1 C_1, \mathbf{V}_2 C_2,..,\mathbf{V}_n C_n]^T$, $\mathbf{V}$, diagonal volumes matrix $\mathbf{V} = [\delta_{i,j}\mathbf{V}_i]_{n \times n}$ V_i, volume of the phase in which i species exists, $\delta_{i,j}$, the Kronecker δ (0 if $i \neq j$, 1 if $i = j$). We assume here that transfer of solutes does not induce significant volumes change and activity coefficients are constant in all phases.

Solving the system (1) + (3) can be accomplished by analogy to one-phase systems (1) + (2). This is a non-linear system which can be solved using Newton-Raphson iterative method. In multi-phase systems the volume matrix must be introduced in balances and in derivatives in the iteration process as described below. Also initialization of vector $\boldsymbol{C}$ needs volume corrections when calculations are carried out by varying progress of reactions.

(a) adjusting equilibrium while balances are held

This method is based on run of reactions until concentrations satisfy Eq. (1). Technically it means variation of m reaction numbers ϵ_i. In this procedure balances are satisfied because run of reactions do not change the balances. Definition of concentration as a function of progress of reactions for one-phase systems:

$$\boldsymbol{C} = \boldsymbol{C}^0 + \mathbf{A}^T\varepsilon \tag{4}$$

for multi-phase systems must be rewritten as follows:

$$\boldsymbol{C} = \boldsymbol{C}^0 + \mathbf{A}^T\mathbf{V}^{-1}\varepsilon \tag{5}$$

where: $\mathbf{V}^{-1} = [\delta_{i,j}\mathbf{V}_i^{-1}]_{n\times n}$; ε, reaction number vector $= [\varepsilon_1, \varepsilon_2, \ldots \varepsilon_m]^T$; $\boldsymbol{C}^0$, any vector satisfying balance equation, usually initial composition.There is an important orthogonality Eq. (8), [19] $\mathbf{QA}^T = 0$ which expresses mutual dependence of stoichiometric and balance matrixes. Due to orthogonality of matrices $\mathbf{Q}$ and $\mathbf{A}^T$ balance equations are automatically satisfied for any vector ε, $\mathbf{QV}\boldsymbol{C} = \mathbf{QV}\boldsymbol{C}^0 (= \boldsymbol{T})$.

Inserting Eq. (5) into Eq. (1) we get the following system of m unknowns:

$$\mathbf{A}\ln(\boldsymbol{C}^0 + \mathbf{A}^T\mathbf{V}^{-1}\varepsilon) - \ln \boldsymbol{K} = 0 \tag{6}$$

This can be solved by the Newton-Raphson method according to equations

$$\rho^{(l)}\Delta\varepsilon^{(l)} = \ln \boldsymbol{K} - \mathbf{A}\ln \boldsymbol{C}^{(l)} \tag{7}$$

$$\boldsymbol{C}^{(l+1)} = \boldsymbol{C}^{(l)} + \mathbf{A}^T\mathbf{V}^{-1}\Delta\varepsilon^{(l)} \tag{8}$$

where:

$$\boldsymbol{\rho}^{(l)} = \mathbf{A}^T M^{(l)} A,\quad M^{(l)} = [\delta_{k,j}\boldsymbol{C}_k^{(l)-1}\mathbf{V}_k^{-1}]_{n\times n}$$

$$\text{or } \boldsymbol{\rho}_{i,j}^{(l)} = \sum_{k=1}^{n} \frac{a_{i,k}\,a_{j,k}}{\boldsymbol{C}_k^{(l)}\,\mathbf{V}_k} \tag{9}$$

Here l is the iteration number. In the multi-phases case the derivative $\boldsymbol{\rho}$ contains volume correction. As the stop test $\|\ln \boldsymbol{K}\text{-Aln}\boldsymbol{C}\|_1 = 10^{-4}$ was applied.

Now, to start the iteration process we need a positive concentration vector to calculate $\ln \boldsymbol{C}$. Usually in starting conditions we have some zero concentrations. To overcome this we can take a component of zero concentration and advance a reaction which produces it to an extend allowed by amount of substrates.The details are as follows:

(1) Find first component i of zero concentration;
(2) Find first non-zero element $a[j,i]$ of the stoichiometric matrix in the column i corresponding to its name (j reaction will be run);
(3) Determine maximum reaction number ε_j that can be accomplished:

$$\varepsilon_j = \min_k \left\{ \underset{a[j,k]<0}{\forall} \frac{-\boldsymbol{C}_k\mathbf{V}_k}{a[j,k]} \right\},\ \text{if } a[j,i] > 0 \tag{10}$$

$$\varepsilon_j = \min_k \left\{ \underset{a[j,k]>0}{\forall} \frac{\boldsymbol{C}_k\mathbf{V}_k}{a[j,k]} \right\},\ \text{if } a[j,i] < 0 \tag{11}$$

Eq. (10) describes reaction toward products, Eq. (11) towards substrates. If $\varepsilon_j = 0$ because all $\boldsymbol{C}_k\mathbf{V}_k/a[j,k]$ have $\boldsymbol{C}_k = 0$, then probably the substrates will be produced in next reactions. So we must skip it this time and return to this reaction again after initiating others. Another possibility, no negative $a[j,k]$ in Eq. (10) (or no positive $a[j,k]$ in Eq. (11)), indicates usually solid phase solution/deposition or solvent self-ionization take place. It can be overcome by introducing special initialization for those reactions as $\varepsilon_j := \ln K_j/(\Sigma_k\, a[j,k])$ (j is the index of such a reaction).
(4) Replace all $\boldsymbol{C}_k$ with

$$C_k + \frac{1}{a[j,i]m}\frac{a[j,k]\varepsilon_j}{\mathbf{V}_k}$$

for $k = 1..n$, where: m, total number of reactions. Note, that we proceed with mth fraction of the available limiting component.
(5) If there are still some $\boldsymbol{C}_i = 0$, then repeat the previous four steps.The method gave good results in practice and seems general for all chemical systems. It is a modified, volume-corrected, version of the algorithm introduced by Kostrowicki and Liwo [8].

(b) adjusting balances while equilibrium is held.

Second method proceeds by changing amounts of reagents while equilibrium is hold until balance equations are satisfied. This implies that parameters proportional to $\ln\mathbf{C}$ are being varied while equilibrium condition is hold. Concentrations, which satisfy equilibrium condition, can be rewritten as:

$$\ln \boldsymbol{C} = \ln \boldsymbol{C}^* + \mathbf{Q}^T\tau \tag{13}$$

for any vector τ, if $\ln C^*$ is an arbitrary chosen solution of Eq. (1). As the consequence of orthogonality equation $\mathbf{AQ}^T = 0$, the equilibrium condition is always valid $\mathbf{A} \ln C = \mathbf{A} \ln C^* (= \ln K)$. Insertion of Eq. (13) to Eq. (3) gives non-linear equations system of $n - m$ order:

$$\mathbf{Q}\,\mathbf{V}\,(\exp(\ln C^* + \mathbf{Q}^T\tau)) - T = 0, \tag{14}$$

In the one-phase version there is no matrix **V**. This implies that for multi-phase systems we will get also different derivative σ in the iteration scheme. By analogy to one-phase algorithm equilibrium concentrations can be calculated by the following iteration scheme:

$$\sigma^{(l)}\,\Delta\tau^{(l)} = T - \mathbf{Q}\,\mathbf{V}\,C^{(l)} \tag{15}$$

$$\ln C^{(l+1)} = \ln C^{(l)} + \mathbf{Q}^T\Delta\tau^{(l)} \tag{16}$$

where:

$$\sigma^{(l)} = \mathbf{Q}\,\Lambda^{(l)}\mathbf{Q}^T,\ \Lambda^{(l)} = [\delta_{k,j}\mathrm{V}_k C_k^{(l)}]_{n\times n}$$

$$\text{or } \sigma_{i,j}^{(l)} = \sum_{k=1}^{n} q_{i,k}\,q_{j,k}\,\mathrm{V}_k\,C_k^{(l)} \tag{17}$$

As the stop test $\|\Delta\tau\|_1 = 10^{-4}$ has been chosen.

The balance matrix **Q** is calculated automatically from stoichiometric matrix **A** as described elsewhere [8]. Additionally some minor modifications of initialization of vector $\ln C^*$ were made in presented programs.

3. Determination of equilibrium constants from extraction experiments

Once the concentrations have been determined they can be used for evaluation of equilibrium constants from experimental data. In the extraction research it is common to measure equilibrium metal distribution and to measure equilibrium pH values. Another, less common, approach is to add large excess of a buffer and resign measuring pH. Both situations can be processed with the use of multidimensional calculations.

1. In the first case we assume the pH values are error-free and that we can combine them with the equilibrium constants. So, for each pH we have a specific, apparent equilibrium constants set, log K′. The log K′ is a sum of the log K and pH multiplied by the stoichiometric coefficient of $[H^+]$ for each reaction (see the examples in the following text). In this manner $[H^+]$ is placed on the right-hand side of equation and is no longer changed during the iteration process. Hence $[H^+]$ column is removed from the stoichiometric matrix, the balance matrix must be accordingly modified. It is immediately found as $\mathbf{Q} = [-((\mathbf{A}^L)^{-1}\,\mathbf{A}^R)|\mathrm{I}]$, where we defined partition of the stoichiometric matrix **A** into left and right parts as: $\mathbf{A} = [\mathbf{A}^L_{m\times m} \mid \mathbf{A}^R_{(n-m)\times m}]$, $\det\{\mathbf{A}^L\} \neq 0$. Here A denotes stoichiometric matrix after removal the hydrogen ion column. For practical reasons (less complicated equations) it is more convenient to fit total organic phase metal concentration than logarithm from distribution ratio (log D). Thus, the minimized function ϕ can be defined as:

$$\phi = \sum_{i=1}^{pn} w_i\,(\hat{C}_i^{tot} - C_i^{tot})^2 \tag{18}$$

where: *pn*, number of measurements; C_i^{tot}, total metal concentration in one (e.g., organic) phase in *i* experiment, hat stands for experimental value; w_i, statistical weight of *i*th measurement. Total metal concentration can be calculated as:

$$C_i^{tot} = \sum_{k=1}^{n} \beta_k C_{i,k} = \boldsymbol{\beta}\mathbf{C}_i \tag{19}$$

where $C_{i,k}$ denote concentration of *k* species in *i* experiment and β_k denote the number of metal atoms in *k* species molecule, if present in the analyzed phase. Thus, for each experimental point we can define pH-dependent equilibrium constants set, calculate C_i^{tot} and add squares of differences between calculated and measured values for all points obtaining the desired sum of squares [18]. Once we have done that we need to find such constants that minimize the sum. Minimization of the sum can be carried out by the Marquardt method. Multi-dimensional calculation has a convenient property of the possibility of calculating derivative $\boldsymbol{J}_{i,j} = \partial C_i^{tot}/\partial \ln K_j$ analytically [8]. For each point *i* we calculate vector $\boldsymbol{J}_{i,j}$, $j = 1,..m$. The formula is the following:

$$\boldsymbol{J}_{i,j} = \frac{\partial C_i^{tot}}{\partial \ln \boldsymbol{K}_j} = (\rho_i^{-1} A\beta)_j \tag{20}$$

Table 1
Influence of aqueous phase volume on distribution ratio in two-phase, multi-reaction system

V_{aq}	AgR μM	Ag_2R_2 μM	Ag 10^{-16} M	AgT_2 μM	AgT_3 μM	HR mM	K_2H mM	KH_2 mM	$S_2O_3^{2-}$ M	H μM	Distribution ratio	
											D	lgD
0.05	15.6	6.14	5.266	27.56	16.60	1.972	19.94	20.06	0.0999	13.26	2.45	0.389
0.1	20.5	10.59	6.955	36.40	21.90	1.958	19.96	20.04	0.0999	12.04	4.09	0.612
0.2	25.1	15.81	8.553	44.74	26.91	1.943	19.97	20.03	0.0998	13.22	5.98	0.777
0.5	29.7	22.08	10.18	53.23	32.01	1.926	19.99	20.01	0.0998	13.20	8.21	0.914
0.8	31.2	24.48	10.75	56.19	33.79	1.920	19.99	20.01	0.0998	13.20	9.03	0.956
1.0	31.8	25.39	10.96	57.29	34.45	1.917	19.99	20.01	0.0998	13.19	9.35	0.971
2.0	33.1	27.45	11.43	59.71	35.90	1.912	19.99	20.00	0.0998	13.19	10.08	1.003

Organic phase volume 0.1 l, aqueous phase volume expressed in litres. Columns contain equilibrium concentration in the system: K_2H, abbreviates hydrogenphosphates; KH_2, dihydrogenphosphates. Programs EQU (ε) and EQUT(τ) were used. Final results were obtained in less than 13 iterations.
M, mole l^{-1}; mM, millimole l^{-1}; μM, micromole l^{-1}; and pM, picomole l^{-1}.

where: ρ_i is derivative Eq. (9) in experimental point i. The minimization is carried out by the following iteration scheme:

$$((\boldsymbol{J}^T\mathbf{W}\boldsymbol{J})^{(l)} + \lambda I)\,\Delta X^{(l)} = \boldsymbol{J}^{(l)\,T}\mathbf{W}\,(\hat{\mathrm{C}}^{\mathrm{tot}} - \mathrm{C}^{\mathrm{tot}^{(l)}})$$

$$\ln \boldsymbol{K}^{(l+1)} = \ln \boldsymbol{K}^{(l)} + \Delta X^{(l)} \tag{21}$$

Where l is the iteration number and $\mathbf{W}_{\mathrm{pn}\times\mathrm{pn}}$ is the matrix of weights ($\mathbf{W}_{i,j} = \delta_{i,j}\mathbf{W}_i$). As the stop test $\|\Delta \mathrm{X}\|_1 \leq 10^{-4}$ was applied. Program, realizing this algorithm have been worked out and named EXTRAPH.

(2) If we can assume that pH is not affected by unknown variables, we can simply use function Eq. (18) and not-modified system $\mathbf{A}\ln \boldsymbol{C} = \ln \boldsymbol{K}$ to solve the problem. It is possible to create a bigger model system and optimize just a few unknown constants. Again, iteration scheme Eq. (21) can be used for chosen number of constants to vary s ($s \leq m$) with a shorter Jacobian $\boldsymbol{J}_{\mathrm{pn}\times s}$. This algorithm is realized by the program EXTRAFIT.

Third method can minimize extended sum of squares

$$\phi = \sum_{i=1}^{pn} w(\mathrm{C})_i(\hat{\mathrm{C}}_i - C_i)^2 + w(\mathrm{pH})_i\,(\mathrm{p}\hat{\mathrm{H}}_i - \mathrm{pH}_i)^2 \tag{22}$$

where: $w_i(C)$,w_i(pH), statistical weights for each C or pH measurement; C, total metal concentration in one phase, hat stands for experimental values; i, indexes measurements. Although most justified for statistical point of view, it has not been implemented yet. The work is in progress.

4. Application section

In order to illustrate the applicability of the derived algorithms I tested them on data obtained from simulation as well as from real-life extraction experiments. The original code was written in Turbo-Pascal v 6.0 and run on a simple IBM PC 486-DX2 computer.

The use of the programs is intuitive for every chemist. One must define equilibria expected in the system (the equation and the appropriate constant for each reaction) and specify initial concentrations of all chemicals. All the reactions can be

Table 2
Simulation of liquid–liquid extraction with solid deposit formation

Initial	Equilibrium							
C_H M	[Ag] pM	$[Ag(SCN)_2]$ μM	[AgR(o)] mM	[SCN] mM	[HR(o)] mM	[H] mM	Total Ag soluted μmole	D
0.001	101.3	1.796	5.769	10.52	14.23	1.577	57.87	3210
0.01	105.9	1.719	1.238	10.12	18.76	10.12	12.55	720
0.10	107.0	1.700	0.1341	10.01	19.87	100	1.511	78.9
1.00	107.2	1.698	0.0135	10.00	19.99	1000	0.305	7.9 6

Influence of acidity on solubility and extraction of silver from solid AgSCN. Conditions as stated in the text.

entered manually from keyboard in the same way they are usually written down. All matrixes are created automatically by the programs, however they can be modified manually in the input files with any ASCII—text editor. In the case of multi-phase reaction additionally volumes of each phase are to be introduced.

4.1. Calculation of equilibrium concentrations in the case of multi-reaction, multi-phase system

Example 1. Example of stoichiometric, balance and volume matrixes.
For simple aminoacid HA—acid/base reactions with extraction of HA we have two equilibria:

$$H^+ + A^- = HA(o),\ K_1 = \frac{[HA(o)]}{[H^+][A^-]}$$

$$H^+ + HA(o) = H_2A^+,\ K_2 = \frac{[H_2A^+]}{[H^+][HA(o)]}$$

which can be denoted as matrix **A** (substrates negative, products positive coefficients, charges omitted for clarity):

$$\begin{bmatrix} HA(o) & H_2A & A & H \\ 1 & 0 & -1 & -1 \\ -1 & 1 & 0 & -1 \end{bmatrix}$$

One can see that equations obtained by taking natural logarithm from equilibria constants:

$$\ln K_1 = \ln [HA(o)] - \ln [A] - \ln [H]$$

$$\ln K_2 = \ln [H_2A] - \ln [HA(o)] - \ln [H],$$

are equivalent to matrix notation $\mathbf{A} \ln \mathbf{C} = \ln \mathbf{K}$.If the organic phase has twice more volume then the aqueous phase, the **V** matrix will get the following form:

$$\mathbf{V} = \begin{bmatrix} HA(o) & H_2A & A & H \\ 2 & 0 & 0 & 0 \\ 0 & 1 & 0 & 0 \\ 0 & 0 & 1 & 0 \\ 0 & 0 & 0 & 1 \end{bmatrix}$$

The balance equations in this case have the following form (one of many possibilities):

$$V_o[HA(o)] + V_a[H_2A] + V_a[A] = n_A$$

$$V_o[HA(o)] + 2V_a[H_2A] + V_a[H] = n_H,$$

where: V_a, volume of the aqueous phase; V_o, volume of the organic phase.This is equivalent to matrix equation $\mathbf{QVC} = \boldsymbol{T}$:

$$\begin{bmatrix} 1 & 1 & 1 & 0 \\ 1 & 2 & 0 & 1 \end{bmatrix}$$

$$\begin{bmatrix} V_o & 0 & 0 & 0 \\ 0 & V_a & 0 & 0 \\ 0 & 0 & V_a & 0 \\ 0 & 0 & 0 & V_a \end{bmatrix} \begin{bmatrix} [HA(o)] \\ [H_2A] \\ [A] \\ [H] \end{bmatrix} = \begin{bmatrix} n_A \\ n_H \end{bmatrix}$$

Note: EQUT transforms matrix **A** to its Hermite normal form [18] [I|P] so in output generally you

Table 3
Calculations of bulk membrane equilibrium states

Run		Na(1)	Na(3)	H(1)	H(3)	AH	ANa
1	Initial	0.1 M	0.1 M	0.0 mM	0.0 mM	0.01 M	0.0
	Equilibrium	0.0967 M	0.0967 M	0.3332 M	0.3332 mM	3.342 μM	9.997 mM
2	Initial	0.1 M	0.1 M	0.0	0.1 M	0.1 M	0.0
	Equilibrium	0.05813 M	0.1163 M	0.04187 M	0.08373 M	6.718 mM	93.28 mM
3	Initial	0.1 M	0.5 M	0.0	0.2 M	0.01 M	0.0
	Equilibrium	0.07327 M	0.5129 M	0.0273 M	0.1871 M	0.352 mM	9.648 mM

First run is a case of equal distribution, next cases are examples of counter-transport of Na-H where concentration of Na(3) is increased by so-called uphill transport. Volumes of phases are: (1) 0.1 l; (2) 0.01 l; and (3) 0.2 l.

will obtain information about the transformed stoichiometric matrix.

Example 2. Consider a complicated system of two-phase liquid–liquid extraction. It is very laborious to calculate equilibrium concentrations of all reagents and the distribution ratio. This is true even if one knows which equilibria take place, knows their equilibrium constants and knows all balance concentrations. In this example we use an equilibria set comprised of two complex-formation, one acid–base and two extraction equilibria.

$$\begin{aligned} 2Ag^+ + 2\,HR(o) &= (AgR)_2(o) + 2\,H^+, & \log K &= 17.0,\\ Ag^+ + HR(o) &= AgR(o) + H^+, & \log K &= 6.8,\\ HPO_4^{2-} + H^+ &= H_2PO_4^-, & \log K &= 6.88,\\ Ag^+ + 2\,S_2O_3^{2-} &= Ag(S_2O_3)_2^{3-}, & \log K &= 12.72,\\ Ag^+ + 3\,S_2O_3^{2-} &= Ag(S_2O_3)_3^{5-}, & \log K &= 13.5 \end{aligned} \qquad (28)$$

where: HR denotes a thiol (tri-*t*-butoxysilanethiol), (o) means organic phase. First two constants were taken from preliminary results of the author's research. The other constants are taken from literature [20]. Initial concentration profile was: $C(Ag) = 0.0001$ mole l^{-1}, $C(HR) = 0.002$ mole l^{-1}, $C(Na_2S_2O_3) = 0.1$ mole l^{-1}, $C(K_2HPO_4) = C(KH_2PO_4) = 0.02$ mole l^{-1}, organic phase volume 0.1 l.

Program called EQU (by varying ε) have been used. Nevertheless, method which varies balance parameters τ (EQUT) has been also tested and yielded identical results in similar iteration numbers. The test runs are summarized in Table 1.

Example 3. Liquid–liquid extraction with solid deposit

Let us take a system with three reactions. Complex formation in the aqueous phase:

$$Ag + 2\,SCN = Ag(SCN)_2 \quad \log \beta_2 = 8.2$$

dissolution of solid AgSCN

$$Ag + SCN = 0 \text{ (nothing)} \quad \log K_{SO} = -11.97$$

and extraction of silver by a thiol HR into an organic phase

$$Ag + HR(o) = AgR(o) + H \quad \log K = 6.8 \qquad (29)$$

First two constants were taken from the literature [20], last one from preliminary author's results. All charges were omitted for clarity. Organic phase volume was 0.01 l, whereas aqueous phase was 0.1 l. Initial concentrations were 0.01 M SCN in the aqueous phase and 0.02 M of HR in the organic phase. Table 2 summarizes results of different silver dissolution from AgSCN when different acidities of the aqueous phase were applied. Program EQU and EQUT both gave rapid convergence within 10–13 iterations. It should be emphasized that the results are obtained very fast, with no need of manual derivation of D from complicated set of equations. Lowering of partition ratio D and deposit formation at high acid concentration, when silver was introduced to the organic phase, were experimentally observed by the author.

Example 4. Three phase system. Bulk liquid membrane.

Let us take a system composed of two aqueous phases of volume 0.1 l (phase 1) and 0.2 l (phase

Table 4
Data on nickel extraction with decanic acid, all concentration in mole l^{-1}

Number	Initial		Equilibrium		
	$C^0(Ni)$	$C^0(HA)_2(o)$	Measured		Calculated
			pH	$C(Ni)(o) \times 10^4$	$C(Ni)(o) \times 10^4$
1	0.001	1	5.09	0.909	0.886
2	0.001	1	5.36	3.330	3.322
3	0.001	1	5.44	4.450	4.435
4	0.001	1	5.48	5.000	5.004
5	0.001	1	5.61	6.680	6.707
6	0.001	1	5.68	7.500	7.456
7	0.001	1	5.74	7.998	7.988
8	0.001	1	5.79	8.337	8.357
9	0.001	1	5.86	8.750	8.775
10	0.001	1	5.93	9.099	9.093
11	0.001	0.5	5.63	2.404	2.456
12	0.001	0.5	5.70	3.333	3.393
13	0.001	0.5	5.77	4.446	4.423
14	0.001	0.5	5.81	5.066	5.016
15	0.001	0.5	5.93	6.668	6.640
16	0.001	0.2	5.99	1.667	1.718
17	0.001	0.2	6.06	2.500	2.554
18	0.001	0.2	6.26	5.559	5.514
19	0.001	0.2	6.33	6.501	6.462
20	0.001	0.2	6.55	8.492	8.511

3), containing sodium and hydrogen ions, separated by a floating organic phase (phase 2) of volume equal to 0.01 l containing an organic ion carrier (in form of AH or ANa). Additionally assume two interface reactions:

$$Na(1) + AH(2) = ANa(2) + H(1),\ K = 10 \quad (30)$$

$$Na(3) + AH(2) = ANa(2) + H(3),\ K = 10 \quad (31)$$

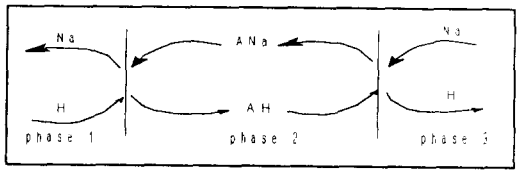

Phase numbers are specified in brackets. Equilibrium concentrations in all three phases were calculated starting from different initial compositions. Test runs are specified in Table 3. One can notice that uniform distribution of species is not always obtained at the equilibrium. It is so only in the first case where there was no hydrogen ion gradient. Second run starts from evenly distributed Na, whereas third run starts from more sodium in the (3) phase. In both last cases, as a result of hydrogen removal from (3) phase, Na(3) concentration must be increased in this phase as the result of ion exchange.

4.2. Determination of extraction equilibrium constants

(1) Method with pH combined with equilibrium constants. Test run of EXTRAPH. As a model let us regard data from extraction of nickel (II) with decanic acid. Extraction model together with relevant constants were taken from [21]. The authors concluded that experimental data is best described by assumption of two extraction reactions:

Table 5
Determination of extraction constants from non-equal volume extraction experiments

Initial buffer components concentrations		Total silver in the organic phase, μmole l^{-1}		
$C(K_2HPO_4)$	$C(KH_2PO_4)$	Simulated	Perturbed	Recalculated
0.002	0.038	733.5	734.5	733.58
0.004	0.036	573.2	572.4	573.30
0.006	0.034	453.9	454.9	453.99
0.008	0.032	360.4	359.4	360.56
0.010	0.030	285.8	286.8	285.86
0.012	0.028	225.6	224.6	225.71
0.014	0.026	177.2	178.2	177.26
0.016	0.024	138.3	137.3	138.37
0.018	0.022	107.3	108.3	107.30
0.020	0.020	82.58	82.48	82.61
0.022	0.018	63.06	63.16	63.07
0.024	0.016	47.66	47.56	47.67
0.026	0.014	35.56	35.66	35.56
0.028	0.012	26.07	25.97	26.07
0.030	0.010	18.64	18.74	18.63
0.032	0.008	12.83	12.73	12.83
0.034	0.006	8.307	8.317	8.30
0.036	0.004	4.795	4.78	4.79
0.038	0.002	2.083	2.09	2.08

Organic phase volume was set as 0.1 l, aqueous 1 l. Initial concentrations: C(Ag) = 0.0001 mole l^{-1}, C(HR(o)) = 0.002 mole l^{-1}, $C(Na_2S_2O_3)$ = 0.1 mole l^{-1}.

$$Ni^{2+} + 3(HA)_2(o) = [NiA_2 4HA](o) + 2\,H^+,\ \log K_1 = -11.34$$
$$2\,Ni^{2+} + 4(HA)_2(o) = [NiA_2 2HA]_2(o) + 4\,H^+,\ \log K_2 = -19.15 \quad (32)$$

Thus, instead of the stoichiometric matrix **A** and the ln ***K*** vector of

$$\begin{bmatrix} NiA_2 4\,HA & [NiA_2 2\,HA]_2 & (HA)_2 & Ni^{2+} & H^+ \\ 1 & 0 & -3 & -1 & 2 \\ 0 & 1 & -4 & -2 & 4 \end{bmatrix} \begin{matrix} \ln K \\ \ln K_1 \\ \ln K_2 \end{matrix}$$

we use its reduced version, **A′** and a corrected ln **K′**:

$$\begin{bmatrix} NiA_2 4\,HA & [NiA_2 2\,HA]_2 & (HA)_2 & Ni^{2+} \\ 1 & 0 & -3 & -1 \\ 0 & 1 & -4 & -2 \end{bmatrix} \begin{matrix} \ln K' \\ \ln K_1 + 2\,pH \\ \ln K_2 + 4\,pH \end{matrix}$$

Recalculating of the constants' values from data in Table 4 leads to $\log K_1 = -11.354 \pm 0.008$ and $\log K = -19.140 \pm 0.006$.

(2) Method with no pH measurements, but with an excess of a buffer applied. Test run of EXTRAFIT. As an example a set of simulated extraction data with two phases of different volume was created, total metal concentration was disturbed by 1% and then the equilibrium constants were backward evaluated. The values of the constants were perfectly redetermined as is shown in Table 5. The system contained five reactions and can be described by the equations set.

Simulation values of the constants were: log K = [6.30,17.00,12.72,13.50,6.88]. Fitting two first constants to the disturbed data gave back: $\log K_1 = 6.2995 \pm 0.005$ and $\log K_2 = 17.0004 \pm 0.005$ while $\log K_1 = 8$ and $\log K_2 = 15$ were taken as initial values.

Possibility of using the algorithms

If we investigate a system with multiple equi-

libria, some of the constants may happen to be determined in different physical-chemical conditions than others. Sometimes the difference is in ionic strength, sometimes in temperature or in different supporting electrolyte. This specially can happen when we take into consideration many independently determined constants (e.g., acid–base constants together with complex formation). One possible solution is to choose experimental conditions to match those declared for most of the constants, and recalculate the other constants together with the searched equilibrium. Thus, some of the equilibrium constants will be processed as unknowns during the iterations until they best fit to the experimental data. Such a possibility give both EXTRAFIT and EXTRAPH.

5. Final remarks

I hope wider use of the programs will help chemists to deal with complicated systems. The examples given do not show all possible applications of the programs. So far little attention is given to distribution of species in three phase systems, partly because of difficulty of mathematical description. This seems to be of diminishing significance. As mentioned before, all matrixes are generated internally by the programs. A chemist must just define the chemical model and the equilibrium concentrations are calculated automatically without time-consuming manual derivation. Moreover, the concentrations can be used for determination of unknown equilibrium constants, even if the system is very complicated.

The tentative versions of the programs EQU, EQUT, EXTRAFIT and EXTRAPH are available from the author along with the source Pascal code upon request. The source codes can be downloaded from Internet at http://www.pg.gda.pl/~jarekch/.

References

[1] J. Kostrowicki, A. Liwo and K. Sokołowski, Comput. Chem. 12 (1988) 293
[2] I.G. Sayce, Talanta, 15 (1968) 1397.
[3] P. Gans, A. Sabatini and A. Vacca, J. Chem. Soc. Dalton Trans., 1195 (1985).
[4] R. Cazallas, M.J. Citores, N. Etxebarria, LA Fernández and JM Madariaga, Talanta, 41 (1994) 1637.
[5] V.I. Vetrogon, N.G. Lukyanenko, M.-J. Schwing-Weill and F Arnaud-Neu, Talanta, 41 (1994) 2105.
[6] L. Łomozik, M. Jaskólski, A. Gasowska, J. Chem. Ed., 72 (1995) 27.
[7] D.H. Liem, Acta Chem. Scand., 25 (1971) 1521.
[8] J. Kostrowicki, A. Liwo, Comput. Chem., 8 (1984) 91.
[9] C. Heneczkowska and S. Kopacz, Communication on Seminar of Polish Chemical Society, Poznan, September 23–26, 1996.
[10] I. Gluch and M. Mojski, J. Anal. Chem., 51 (1996) 59–63.
[11] A.W. Fletcher and D.S. Flett, J. Appl. Chem., 14 (1964) 250.
[12] S.A. Berger and S. Graff, J. Inorg. Nucl. Chem., 37 (1975) 1031.
[13] S.M. Graff and S.A. Berger, J. Inorg. Nucl. Chem., 38 (1976) 863.
[14] J. Rydberg and J.C. Sullivan, Acta Chem. Scand., 13 (1959) 2057.
[15] M.J. Jaycock, A.D. Jones and C. Robinson, J. Inorg. Nucl. Chem., 36 (1974) 887.
[16] W. Apostoluk, Hydrometallurgy, 26 (1991) 223.
[17] A. Bauder and Hs. Gunthard, Helv. Chim. Acta, 55 (1972) 2263.
[18] G.R. Blakley, J. Chem. Educ., 59 (1982) 728.
[19] A. Bauder and Hs. Gunthard, Helv. Chim. Acta, 55 (1972) 2263.
[20] R.M. Smith and A.E. Martell, Critical Stability Constants, Vol. 6, Second Supplement, Plenum Press, New York, 1989.
[21] H. Yamada and M. Tanaka, Adv. Inorg. Nucl. Chem., 29 (1985) 143.

ELSEVIER

Talanta 44 (1997) 1271–1283

Talanta

Protonation equilibria of quinolone antibacterials in acetonitrile–water mobile phases used in LC

J. Barbosa *, R. Bergés, I. Toro, V. Sanz-Nebot

Department of Analytical Chemistry, Diagonal 647, 08028, Barcelona, Spain

Received 12 August 1996; received in revised form 22 November 1996; accepted 23 November 1996

Abstract

Ionization constants of nine quinolone antibacterials in acetonitrile–water mixtures containing 0, 5.5, 10, 16.3, 25, 30, 40, 50 and 70% (w/w) acetonitrile were obtained and assignment of these pK values to the several potentially ionizable functional groups was made. The variation of the pK values obtained over the whole composition range studied can be explained by consideration of the preferential solvation of electrolytes in acetonitrile–water mixtures. In order to obtain pK values in any of the unlimited number of possible binary solvent acetonitrile–water mixtures, relationships between pK values and different bulk properties (such as dielectric constant) were examined. The linear solvation energy relationships method, LSER, was applied to study the correlation of pK values with the solvatochromic parameters of acetonitrile–water mixtures. The equations obtained allow calculation of the pK values of the quinolone antimicrobials in any acetonitrile–water mixtures up to 70% (w/w) and thus permit the knowledge of the acid–base behaviour of these important antimicrobials in the widely used acetonitrile–water media. © 1997 Elsevier Science B.V.

Keywords: Acetonitrile–water mixtures; Liquid chromatography; Preferential solvation; Quinolones, dissociation constants

1. Introduction

Quinolone antibiotics are synthetic orally active, broad spectrum agents which are effective against resistant mutants of bacteria [1,2]. They all possess a carbonyl group in position '4', so are often referred to as 4-quinolones. These quinolone carboxylic acids are active against many gram-positive and gram-negative bacteria [3–5]. Increase in their antibacterial activity is greatly influenced by addition of the 6-fluoro and 7-piperazinyl groups to the molecule. The increased potency of the new fluoroquinolones has greatly expanded their potential clinical usefulness [6]. The antibacterial activity of quinolones is pH-dependent since they act by inhibition of bacterial DNA gyrase, a process which depends upon both the pH and concentration of the acid [7]. Therefore, the examination of protonation equilibria in quinolone solutions is essential in order to understand their antibacterial activity. Furthermore, the equilibrium constants of antibiotics are biologi-

* Corresponding author.

PII S0039-9140(96)02188-1

cally important physicochemical parameters. These data are important for a thorough understanding of absorption, transport and receptor binding of these drugs at the molecular level.

Traditionally, water has been considered the solvent which best represents the biological conditions. Although this is a general assumption, a lower polarity has been detected in some biochemical microenvironments, such as active sites of enzymes and side chains in proteins, sometimes hidden in lower dielectric cavities [8–10]. In these cases, the selection of other solvents seems more recommendable in order to emulate properly the medium's real features. Among the wide range of eligible solvents, hydroorganic mixtures have been found especially suitable because they show simultaneously a low polar character and a partially aqueous content, as do all biological systems. In this work, acetonitrile–water mixtures were selected because of the different nature of their constituents, which provides solvent mixtures offering a wide range of features and behaviour.

Acetonitrile–water mixtures are used in many branches of chemistry, ranging from hydrometallurgy to liquid chromatography, from reaction media for synthesis to capillary electrophoresis. The acid–base behaviour of substances in these mixtures are, therefore, of considerable interest.

However, the infinite number of different solvent compositions which can be prepared from a particular binary system (e.g., acetonitrile–water) precludes determination of the pK values in all the compositions. Therefore, an equation which connected the pK value of an acid or base to the solvent composition would be very useful. The relationship between equilibrium constants and solvent composition in mixed solvents is not straightforward. The electrolytes can be preferentially solvated by any of the solvents present in the mixture. Preferential solvation will produce higher pK values than expected if the 'preferred' solvent has the lowest relative permittivity, or lower pK values in the contrary instance. In general, preferential solvation is a composite effect determined by solute–solvent and solvent–solvent interaction [11].

In the last years we have reported acid–base studies in acetonitrile–water mixtures concerning the standardization of the glass electrode in these mixtures and the determination of their autoprotolysis constant [12], the determination of ionization constants of pH reference materials in these media [13], the assignment of reference pH-values to primary standard buffer solutions for standardization of potentiometric sensors in acetonitrile–water mixtures [14,15] and the application of the quasi-lattice quasi-chemical (QLQC) theory [16,17] to the study of the preferential solvation of the hydrogen ions in these mixtures in order to clarify the acid–base behaviour of the solutes in these media [11].

Central to the study of acid–base equilibria in organic-water mixtures is the problem of how the solute species react to changes in the solvent that forms their solvation sphere. In order to characterize this important zone of the solvent, a group of solvatochromic parameters was proposed (π^*, α, β and E_T^N) and reported for acetonitrile–water mixtures [18–21]. π^* measures the polarity and polarizability of these solvents; α and β measure the hydrogen bond acidity and hydrogen bond basicity, respectively; the normalized Dimroth and Reichardt solvatochromic parameter, E_T^N, has a mixed nature and is sensitive to many solvent–solvent interactions [21].

The purpose of the present study is the determination of pK values of nine quinolone antibacterials in 0, 5.5, 10, 16.3, 25, 30, 40, 50 and 70% (w/w) acetonitrile–water mixtures according to the rules and procedures endorsed by IUPAC [22]. The variation of the pK values obtained over the whole composition range studied can be explained by tacking into account the preferential solvation of electrolytes in acetonitrile–water mixtures. In order to obtain pK values in any of the unlimited number of the possible binary solvent acetonitrile–water mixtures, relationships between pK values and different bulk properties (such as dielectric constant) were examined and the linear solvation energy relationships method, LSER, was applied to study the correlation of pK values with the solvatochromic parameters of acetonitrile–water mixtures. The equations obtained allow calculation of the pK values of the quinolone antimicrobials in any acetonitrile–water mixtures up to 70% (w/w) and thus permit the knowledge

of the acid–base behaviour of these important antimicrobials in the widely used acetonitrile–water media.

2. Experimental

2.1. Apparatus

Values of the emf of the potentiometric cell were measured with a CRISON 2002 potentiometer (± 0.1 mV) using a Radiometer G 202 C glass electrode and a reference Ag/AgCl electrode prepared according to the electrolytic method [23] and directly immersed in the solution to avoid the residual liquid junction potentials [12].

The glass electrode was stored in water when not in use and soaked for 15–20 min in acetonitrile–water mixture before potentiometric measurements. The stabilization criterion for the emf readings was 0.2 mV within 150 s; in all instances the electrode system gave stable and reproducible potentials within 5 min.

The reference electrode was stable for three months of continuous work. The E^0 values used here are the average of at least 15 standardizations. The standardization of the electrode system was carried out each time solvent media or electrodes were changed and the constancy of E^0 values was ensured by continual surveillance by means of periodical calibrations. The cell was thermostatted externally at 25 ± 0.1°C. The potentiometric assembly was automatically controlled with a microcomputer.

2.2. Reagents

Analytical reagent grade chemicals were used, unless otherwise indicated.

All the solutions were prepared by mixing doubly distilled, freshly boiled water, the conductivity of which did not exceed 0.05 μS cm^{-1}, and acetonitrile (Merck, chromatography grade). The quinolones used in this study are shown in Fig. 1 and were purchased from different pharmaceutical laboratories: Pipemidic acid (Almirall, Prodesfarma); Nalidixic acid (Impex Química, Sterling Winthrop); Norfloxacin (Liade, Boral Química); Enoxacin (Almirall); Flumequine (Sigma); Fleroxacin (Roche); Ciprofloxacin (Lasa); Cinoxacin (Impex Química, Dista); Ofloxacin (Hoescht).

Stock 0.1 and 0.02 mol l^{-1} potassium hydroxide (Carlo Erba) solutions were prepared with an ion-exchange resin [12] to avoid carbonation and standardized volumetrically against potassium hydrogen phthalate.

Stock 0.1, 0.03 and 0.01 mol l^{-1} hydrochloric acid (Merck) solutions were prepared and standardized titrimetrically against tris(hydroxymethyl)aminomethane (Merck).

2.3. Procedures

The quinolone pK values were determined potentiometrically by different analytical methods:

(i) by titration of appropriate solutions of quinolones in the acetonitrile–water mixtures studied, which also contained approximately 5×10^{-3} M KCl solution for the correct response of the electrode system. KOH solutions were used in the same solvent as titrant. The KOH solutions used as titrants were of different concentrations (0.1 M–0.02 M) depending on the solubility of the quinolones.

(ii) by titration of appropriate solutions of quinolones in the acetonitrile–water mixtures studied, using HCl solution as titrant. Again, the concentration of HCl solution was different depending on the solubility of the quinolones.

(iii) by titration of appropriate solutions of quinolones in the acetonitrile–water mixtures studied, which contained a measured excess of HCl solution using KOH solution as titrant. In this way, the quinolones are fully protonated at the beginning of the titration.

The differences existing in the literature about the assignment of the ionizable function groups justify the use of these different analytical procedures [24,25].

pK values were obtained from systematic measurements of the emf of the cell

$$\mathrm{Pt/Ag/AgCl/}\ \underset{\text{in acetonitrile - water}}{\mathrm{HA + A + Cl^-}}\ \mathrm{/Glass\ Electrode} \quad \text{A}$$

where HA and A are the acid and basic species, respectively, involved in the dissociation equilibrium studied. The emf, E, of this cell is directly

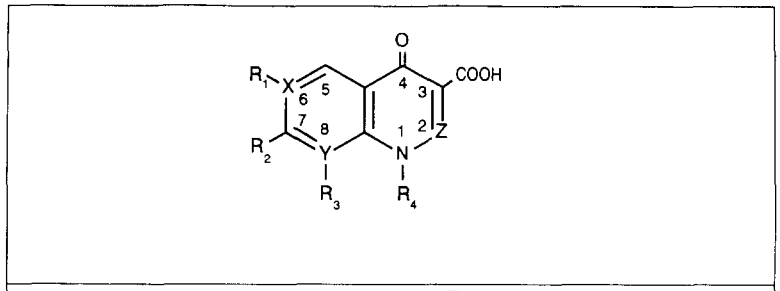

Compound	X	Y	Z	R_1	R_2	R_3	R_4
1.- Ciprofloxacin	C	C	C	F	-N(2' 3' 1' 4')NH	H	
2.- Norfloxacin	C	C	C	F	-N NH	H	$-CH_2-CH_3$
3.- Fleroxacin	C	C	C	F	-N N-CH_3	F	$-CH_2-CH_2F$
4.- Ofloxacin	C	C	C	F	-N N-CH_3	O - CH_2 - CH - CH_3	
5.- Enoxacin	C	N	C	F	-N NH	H	$-CH_2-CH_3$
6.- Pipemidic acid	N	N	C	H	-N NH	H	$-CH_2-CH_3$
7.- Cinoxacin	C	C	N	O - CH - O		H	$-CH_2-CH_3$
8.- Nalidixic acid	C	N	C	H	$-CH_2-CH_3$	H	$-CH_2-CH_3$
9.- Flumequine	C	C	C	F	H	CH_2-CH_2 - CH - CH_3	

Fig. 1. Structures of selected quinolones.

related to the activities of the hydrogen and chloride ions in solution:

$$E = E^{\theta} + k \log(a_{H+} a_{Cl-}) \quad (1)$$

where E^{θ} is the standard emf of the cell and $k = (\ln 10)RT/F$. E^{θ} values were determined as in a previous study [12].Taking into account the general expression for the dissociation equilibria studied

$$K = \frac{c_A y_A c_{H+} y_{H+}}{c_{HA} y_{HA}} \quad (2)$$

the functional Eq. (3), which permits pK calculation, is obtained:

$$\frac{E^0 - E}{k} + \log \frac{c_{HA} y_{HA} c_{Cl-} y_{Cl-}}{c_A y_A} = pK \quad (3)$$

where c_{HA} and c_A are the molar concentrations of acidic and basic species, respectively; c_{Cl-} is the molar concentration of the ion chloride; and y_x the molar activity coefficient of species x. These values can be calculated through an extrathermodynamic assumption, i.e., a form of the classical Debye-Hückel equation,

$$py = \frac{AI^{1/2}}{(1 + a_0 BI^{1/2})} \quad (4)$$

where A and B are the Debye-Hückel constants; a_0 is the ion size parameter in the solvent mixture; and I is the ionic strength.

In compliance with IUPAC rules [22,26] the value of the a_0B produce in Eq. (4) is assigned at temperature $T = 298.15$ K by an extension of the Bates-Guggenheim convention [22,27], in terms of

$$(a_0B)_T = 1.5(\epsilon^W\rho^S/\epsilon^S\rho^W)_T^{1/2} \quad (5)$$

where ϵ is the dielectric constant, ρ the densities and the superscripts W and S refer to pure water and to the appropriate solvent mixture, respectively. Values of Debye-Hückel parameters A and a_0B at 25°C at different percentages of acetonitrile in admixture with water were reported in previous works [12,28].

The difference between the two ionization constants of the quinolones is not very high. Therefore, pK values were calculated in two different ways: considering the two equilibria independently and considering them simultaneously. In the latter case the calculation made use of a program written in PASCAL, pKPOT [29]. The least-square computer program, PKPOT, determines thermodynamic acid–base constants in aqueous and non-aqueous media, taking into account the activity coefficients of the species. These mathematical procedures also allow the determination of pK_a values in overlapping ranges ($pK_i - pK_f < 2$) and dissociation constants in very alkaline conditions. The procedures are based on the postulation of a chemical model, that is, the postulation of an initial set of species defined by their stoichiometric coefficients and formation constants, which are then refined in least square minimization.

Moreover, pK_a values were obtained in pure acetonitrile solvent for two acid species of two NIST standard buffers (acetic and citric acids) in order to study preferential solvation in acetonitrile–water mixtures. For this purpose the potentiometric system described previously [30,31] was used and the standard potential of the cell was determined by titration of picric acid solutions in acetonitrile with tetrabutylammonium hydroxide, as in a previous study [30].

3. Results and discussion

The emf, E, of cell A was measured at different concentrations of acidic, HA, and basic, A, species of quinolones in 0, 5.5, 10, 16.33, 25, 30, 40, 50 and 70% (w/w) acetonitrile–water solvent. 5.5, 16.3 and 25% (w/w) correspond to 7, 20 and 30% (v/v), respectively. For each quinolone various series of measurements were performed, making a total of more than 5600 independent measurements over the solvent interval explored. To simplify the tabulation and as an example, one series of measurements for one titration of norfloxacin and HCl acid solution in 10% (w/w) acetonitrile–water using KOH solution in the same solvent as titrant is shown in Table 1, where V_0 is the initial solution volume, V_{ei} the equivalence volumes, c_t the titrant concentration and E^0 the standard emf of cell. For each point of titration, E is the emf value measured, [H_2A] the concentration of fully protonated species, [HA] the concentration of intermediate species, [A] the concentration of basic species and y the molar activity coefficient.

Table 2 shows the ionization constant values determined using the pKPOT program for the series of nine quinolones studied in 0, 5.5, 10, 16.3, 25, 30, 40, 50 and 70% (w/w) acetonitrile–water mixtures and the respective standard deviations, s, together with pK values reported in water [32–34].

Quinolone analogues have several potentially ionizable functional groups, Fig. 1. Although in the literature there is no agreement on the assignment of the obtained pK values in water [24,32,35], extensive experimental data obtained in this study by potentiometric titrations of quinolone solutions with KOH and HCl, and of quinolones and HCl solutions with KOH, are in perfect agreement with the protolytic equilibria expressed in Fig. 2.

Six of the quinolone derivatives studies (1–6, Fig. 1) have two relevant ionizable functional groups, which means that their acid base chemistry involves two protons. In contrast, nalidixic acid, flumequine and cinoxacin have only one relevant ionizable functional group within the pH ranges of pharmaceutical or physiological importance. All the quinolones have a carboxyl group that is normally stronger acid than the ammonium group, and have a pK value of 6 ± 1 in water rich solvents. Therefore pK_1 values can be associated with the carboxylic acid function [33,36].

Nalidixic acid, pipemidic acid and enoxacin have naphtyridine rings and the other analogues

Table 1
pK values of Norfloxacin in 10% (w/w) acetonitrile–water mixtures

V_0 (ml) = 50 V (ml)	V_{e1} (ml) = 4.02 E (mV)	V_{e2} (ml) = 6.05 [H_2A]	$c_t = 1.99 \times 10^{-2}$ [HA]	$E^0 = 394.76$ [A]	y	[H^+]
2.00	−60.6	7.86E−04	1.23E−05	2.14E−09	0.955	1.74E−05
2.10	−90.8	7.58E−04	3.85E−05	2.16E−08	0.955	5.39E−06
2.20	−98.7	7.21E−04	7.37E−05	6.69E−08	0.995	2.67E−06
2.32	−107.9	6.75E−04	1.17E−04	2.26E−07	0.995	1.57E−06
2.42	−129.8	6.36E−04	1.54E−04	4.15E−07	0.995	1.12E−06
2.62	−143.3	5.59E−04	2.28E−04	1.02E−06	0.955	6.71E−07
2.82	−154.5	4.83E−04	3.00E−04	2.05E−06	0.955	4.40E−07
3.02	−164.5	4.08E−04	3.70E−04	3.71E−06	0.955	3.01E−07
3.22	−174.2	3.34E−04	4.38E−04	6.34E−06	0.955	2.09E−07
3.42	−184.6	2.63E−04	5.03E−04	1.05E−05	0.955	1.43E−07
3.62	−196.3	1.95E−04	5.60E−04	1.77E−05	0.952	9.54E−08
3.82	−209.3	1.33E−04	6.07E−04	3.04E−05	0.952	6.03E−08
4.02	−223.5	8.27E−05	6.32E−04	5.34E−05	0.952	3.58E−08
4.22	−337.3	4.74E−05	6.26E−04	9.15E−05	0.952	2.07E−08
4.42	−249.7	2.69E−05	5.92E−04	1.43E−04	0.952	1.24E−08
4.62	−260.3	1.57E−05	5.39E−04	2.04E−04	0.952	7.99E−09
4.72	−265.2	1.21E−05	5.09E−04	2.37E−04	0.952	6.52E−09
4.82	−270.0	9.29E−06	4.76E−04	2.71E−04	0.952	5.34E−09
4.92	−274.7	7.11E−06	4.42E−04	3.06E−04	0.952	4.39E−09
5.03	−279.4	5.41E−06	4.07E−04	3.41E−04	0.952	3.63E−09
5.18	−286.7	3.55E−06	3.54E−04	3.94E−04	0.952	2.74E−09
5.34	−294.1	2.25E−06	3.00E−04	4.47E−04	0.952	2.05E−09
5.50	−302.3	1.35E−06	2.46E−04	5.00E−04	0.951	1.50E−09
5.60	−308.1	9.26E−07	2.10E−04	5.35E−04	0.951	1.20E−09
5.76	−318.1	4.71E−07	1.57E−04	5.86E−04	0.951	8.21E−10
5.86	−326.2	2.71E−07	1.22E−04	6.20E−04	0.951	6.05E−10
					pK_1 = 6.56 (0.01)	
					pK_2 = 8.56 (0.01)	

have quinolone rings. Their ring nitrogen does not have appreciable basicity in aqueous solutions [36] and neither in acetonitrile–water mixtures, as can be seen in the potentiometric titration curves of nalidixic acid, flumequine and cinoxacin. The pK_2 values can be associated to the presence of a piperazine ring (1–6, Fig. 1). Protonation occurs at N_4 of the piperazine ring over other apparently basic sites, as is proven by NMR measurements [36] and by the fact that N'_4-acetylnorfloxacin has only one proton binding group (carboxylate), since the molecule loses amine basicity due to the acetylation of N'_4 atom [36].

The pK_1 values associated with the carboxylic acid function for the compounds studied here were higher than those generally observed with carboxylic acids in water mixtures [13] (e.g., acetic acid in 30% (w/w) of acetonitrile has a pK = 5.63). This decrease in acidity can be attributed to an intramolecular H-bond formation with the neighbouring keto function resulting in stabilization of the protonation species [33]. The formation of an intramolecular hydrogen bond is supported by US and IR spectral data [37].

The pK_2 values of the four secondary amine type derivatives studied (ciprofloxacin, norfloxacin, enoxacin and pipemidic acid) are greater than those of the tertiary amines (ofloxacin and fleroxacin). These findings were consistent with reports in the literature for similar secondary and tertiary amines: piperazine, pK = 9.71 [38], and N-methylpiperazine, pK = 8.98 [39], in water. The more water molecules involved in the hydrate sphere of the protonated amine, the greater the

Table 2
pK values of quinolones in acetonitrile-water mixtures up to 70% at 298.15 K (values in parentheses are standard deviations)

		% Acetonitrile (w/w)								
		0%	5.5%	10%	16.3%	25%	30%	40%	50%	70%
Ofloxacin	pK_1	6.05	6.20 (0.03)							
	pK_2	8.11 (0.02)		8.17 (0.03)			8.35 (0.04)	8.37 (0.05)	8.76 (0.04)	9.87 (0.02)
Pipemidic acid	pK_1		5.58 (0.03)	5.76 (0.03)						
	pK_2			8.43 (0.05)			8.45 (0.04)	8.41 (0.04)	8.65 (0.04)	9.49 (0.03)
Norfloxacin	pK_1	6.22	6.26 (0.05)	6.57 (0.06)	6.81 (0.03)	7.20 (0.04)	7.45 (0.05)		7.98 (0.03)	
	pK_2	8.38		8.48 (0.03)	8.58 (0.01)	8.78 (0.02)	8.72 (0.02)	8.76 (0.05)	9.05 (0.04)	10.01 (0.02)
Enoxacin	pK_1	6.00	6.20 (0.02)							
	pK_2	8.50		8.51 (0.02)			8.38 (0.05)	8.61 (0.05)	8.95 (0.04)	9.81 (0.02)
Fleroxacin	pK_1	5.46	5.71 (0.02)	5.93 (0.05)	6.17 (0.04)	6.59 (0.03)	6.60 (0.02)		7.11 (0.03)	
	pK_2	8.00		7.95 (0.06)	8.07 (0.03)	8.05 (0.02)	7.94 (0.05)	8.06 (0.04)	8.39 (0.03)	9.44 (0.04)
Ciprofloxacin	pK_1	6.09	6.13 (0.05)							
	pK_2	8.62		8.38 (0.04)			8.41 (0.04)	8.61 (0.04)	8.95 (0.05)	9.84 (0.03)
Nalidixic acid	pK_1	5.95		6.57 (0.04)			7.42 (0.04)	7.76 (0.04)	8.31 (0.02)	9.55 (0.03)
Flumequine	pK_1			6.90 (0.04)	7.09 (0.03)	7.60 (0.03)	7.78 (0.02)	8.11 (0.02)	8.66 (0.02)	9.85 (0.02)
Cinoxacin	pK_1			5.05 (0.03)			5.87 (0.04)	6.13 (0.04)	6.72 (0.02)	7.85 (0.03)

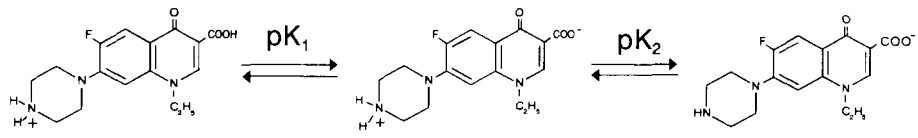

Fig. 2. Protolytic equilibria of Norfloxacin.

stabilization [40]. The protonated form of the secondary amine was stabilized by the greater number of water molecules involved in its hydration sphere when compared with the corresponding tertiary amine [33].

The variation of the pK_1 and pK_2 values of quinolones with dielectric constant is presented in Fig. 3 and Fig. 4, respectively. The variation is different for each substance although, in general, the pK values increase as the acetonitrile content increases. However, pK_1 values corresponding to dissociation of carboxylic acid vary differently from pK_2 ones.

The dissociation constant of a substance HA in a solvent S is related, by means of the Born model, with the dielectric constant of the medium, ϵ, by the following expression [41]

$$HA + S \leftrightarrows A^- + HS^+$$

$$pK_a = pK_a^0 - pK_{HS+}^0 - e^2(z-1)/(2.3r\epsilon kT) \qquad (6)$$

where K_a^0 and K_{HS+}^0 are the intrinsic dissociation constants of the substance and the protonated solvent in the vacuum, taken as standard state, r the average radius of the ions, e the electron charge, z the charge of the acid species HA and KT the energy of thermal agitation.

Eq. (6) shows that the medium affects the strength of an acid in two ways: when the acidity of the solvent, K_{HS+}^0, increases, K_a becomes smaller; and when the dielectric constant decreases, K_a decreases if $z \leq 0$, does not change if $z = 1$ and increases if $z > 1$.

For a series of solvents with similar acidity, the change in the dissociation constant can only be attributed to the change in dielectric constant, and Eq. (6) can be written as:

$$pK_a = A + \frac{B}{\epsilon} \qquad (7)$$

where A and B are constants for a given substance, assuming the radius of the ions, r, independent of the solvent composition.

Thus, the plot of the pK_a of neutral or anion acids versus the reciprocal of the dielectric constant in some solvents of similar acidity shows a straight line. These predictions are in agreement

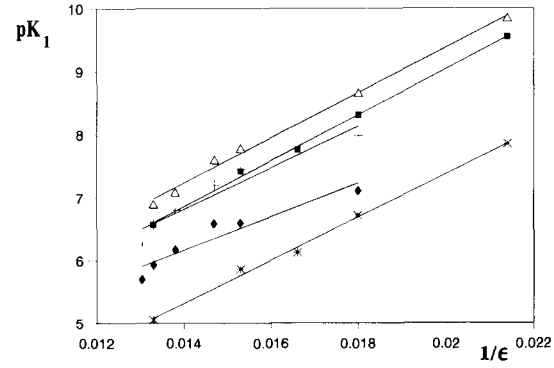

Fig. 3. Plot of pK_1 values of selected quinolones versus the reciprocal of the relative permittivity of solvent mixtures, $1/\epsilon$. △ Flumequine; ■ Nalidixic acid; + Norfloxacin; ◆ Fleroxacin; * Cinoxacin.

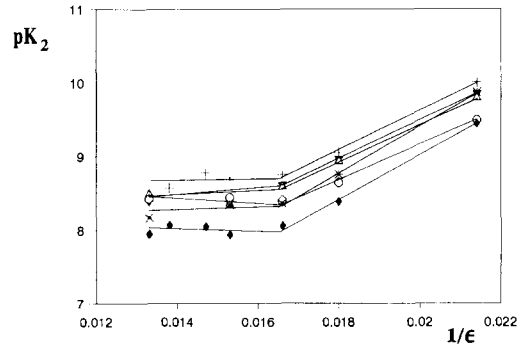

Fig. 4. Plot of pK_2 values of selected quinolones versus the reciprocal of the relative permittivity of solvent mixtures, $1/\epsilon$. + Norfloxacin; ▼ Ciprofloxacin; △ Enoxacin; * Ofloxacin; ○ Pipemidic acid; ◆ Fleroxacin.

with plots shown in Fig. 3 of the dissociation of carboxylic acids of the quinolones, pK_1 values.

In fact, Eqs. (6) and (7) apply only if all solvents show similar specific solute–solvent interactions, when changes in pK values can be attributed mainly to the change in dielectric constant.

For dissociation of the carboxylic acid of the quinolones, pK_1, the electrostatic interaction overwhelms the specific solvation and the pK_1 value increases with the percentage of acetonitrile, as Eq. (7) predicts.

However, in dissociation of a monocharged cation acid (such as the ammonium ions of the N'_4 of piperazine ring of quinolones, pK_2), there is no change in the number of charges ($HA^+ \rightleftharpoons H^+ + A$) and the change in the dielectric constant of the medium does not affect the dissociation process. In this instance, the dissociation depends only on the solvation of the different species by the solvents of the mixture.

The pK_2 values of quinolones in acetonitrile–water mixtures show low changes in the range 0% (w/w) to approximately 30% (w/w) of acetonitrile whereas at higher percentages of acetonitrile they increase with the percentage of acetonitrile, Fig. 4.

The change of pK_2 values corresponding to ammonium ions of quinolones with a percentage of acetonitrile could be explained by the fact that these dissociation constants depend on the solute–solvent interaction effects with the solvents of the mixture. Preferential solvation by water exists in acetonitrile–water mixtures [11] and is related to the structural features of these mixtures [42,43]. On the water-rich side, $x_{AN} < 0.15$, there is a region in which the water structure remains more or less intact: the acetonitrile molecules gradually occupy the cavities between water molecules without disrupting the water structure [43]. In this water-rich region there are not changes in the pK_2 of quinolones. This is in accordance with the previously obtained values of preferential solvation, δ_w, of hydrogen ions by water in acetonitrile–water mixtures [11]. The preferential solvation of hydrogen ions by water is positive, i.e., water molecules show a greater tendency to be in the immediate vicinity of a given hydrogen ion than acetonitrile molecules. In this water-rich region the structure of water remains constant, the solutes are preferentially solvated by water and the variations of pK_2 values are minimal.

In the range $0.15 \leq x_{AN} \leq 0.75$ there are clusters of molecules of the same kind surrounded by regions where molecules of both kinds are near each other. In this middle range of compositions there is also preferential solvation of hydrogen ions by water [11], which could explain the low slope of the linear variations of pK_2 values of quinolones versus x_{AN}. The boundaries of the regions are, of course, not sharp [18].

At $x_{AN} \geq 0.75$ the number of water clusters is low, and water–acetonitrile interactions that could be discounted in the middle range now become important. This may be considered as a region in which preferential solvation by water decreases [11].

Although the variation of the pK_1 values of quinolones obtained in acetonitrile–water mixtures with x_{AN} is linear with the mixtures studied, these pK_1 values, as well as pK_2 values, are lower than expected, giving the high pK value expected in the neat solvent acetonitrile. Preferential solvation in acetonitrile–water mixtures produce lower pK values than expected if the preferred solvent is water.

The deviation from the ideal dependence on the composition of the mixture indicates that the solvent composition in the neighbourhood of the solute may be different from that in the bulk. pK values of quinolones in acetonitrile neat solvent are not known, but in this study pK values of citric acid were determined in pure solvent and the pK value of acetic acid is obtained from literature [44]. These pK values were determined previously over the whole composition range of acetonitrile–water mixtures [13]. Fig. 5 and Fig. 6 show these pK values as a function of x_w, the bulk mole fraction of water, where the dashed line represents the expected variation of pK values between $x_{AN} \approx 0.5$ and pure acetonitrile solvent and the dotted straight line correspond to the ideal variation of the pK values. Fig. 5 and Fig. 6 also show pK_1 and pK_2 values of quinolones, respectively, versus x_w for comparison. The pK values obtained could be explained in terms of

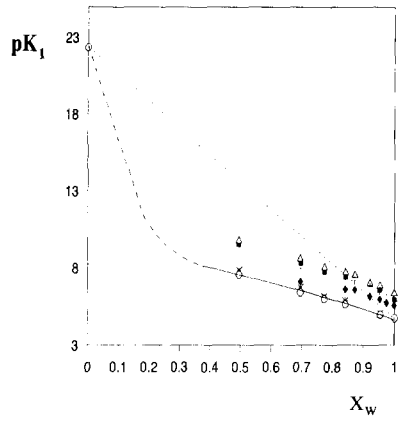

Fig. 5. pK_1 values versus mole fraction of water, x_w, in acetonitrile–water mixtures. ● Acetic acid; Remainder symbols as in Fig. 3.

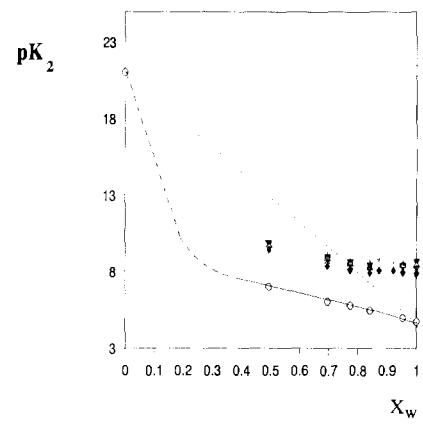

Fig. 6. pK_2 values versus mole fraction of water, x_w, in acetonitrile–water mixtures. ● Citric acid; $pK_1 = 14.86$ ($s = 0.04$), $pK_2 = 20.98$ ($s = 0.09$); Remainder symbols as in Fig. 3.

structural features and preferential solvation by water in acetonitrile–water mixtures. The slope of pK_1 values of quinolones versus x_w plot is greater than the pK_2 values versus x_w plot in the water-rich region because of the influence of ϵ.

In water-rich region $x_{AN} \leq 0.15$, pK_2 values do not vary in contrast with pK_1 values because of the influence of changes in ϵ. In the regions where water–acetonitrile mixtures show microheterogeneity $0.15 \leq x_{AN} \leq 0.75$, pK_1 and pK_2 values change but are lower than the theoretical ones because of the preferential solvation by water; a concave variation of pK versus x_w may be expected with an inflexion point at $x_w = 0.25$, where preferential solvation by water is maximal [11].

On the other hand, it is not self-evident that solvatochromic parameters are valid stand-ins for generalized solutes in binary solvent mixtures with regard to the properties they are supposed to measure. Preferential solvation in such mixtures may interfere more seriously with the ability of indicators to act as stand-ins for generalized solutes than in the case of single solvents. Progress has been made [18,45] and although this problem is not solved unequivocally, these investigations provide significant evidence of the general validity of the solvatochromic parameters. It is, therefore, of interest to examine the linear solvation energy

Table 3
Values of relative permittivity, autoprotolysis constants, and solvatochromic parameters for acetonitrile-water mixtures at 25°C

x_{AN}	wt% AN	ϵ	pK_{ap}	E_T^N	π^*	α	β
0.0000	0	78.36	14.00	1.00	1.14	1.13	0.58
0.0251	5.5	76.68	14.17	0.96	1.12	1.07	0.59
0.0465	10	75.01	14.26	0.93	1.10	1.03	0.59
0.0787	16.3	72.29	14.47	0.90	1.07	0.98	0.60
0.1277	25	68.06	14.74	0.86	1.03	0.94	0.61
0.1583	30	65.52	14.94	0.84	1.01	0.92	0.61
0.2264	40	60.38	15.33	0.81	0.97	0.91	0.61
0.3051	50	55.44	15.73	0.79	0.92	0.90	0.61
0.5059	70	46.82	16.81	0.76	0.84	0.89	0.59

Table 4
Linear solvation energy relationships for pK values of quinolones

Substance		
Ofloxacin	$pK_2 = 20.75 - 5.32\pi^* + 2.26\alpha - 15.04\beta$	$r = 0.994$
Pipemidic acid	$pK_2 = 17.92 - 2.75\pi^* + 1.51\alpha - 13.34\beta$	$r = 0.993$
Norfloxacin	$pK_1 = 8.82 - 6.21\pi^* - 1.60\alpha + 10.41\beta$	$r = 0.998$
	$pK_2 = 21.91 - 2.67\pi^* - 1.50\alpha - 14.91\beta$	$r = 0.998$
Enoxacin	$pK_2 = 13.84 - 7.84\pi^* + 7.38\alpha - 7.11\beta$	$r = 0.999$
Fleroxacin	$pK_1 = 7.29 - 4.69\pi^* - 1.67\alpha + 9.27\beta$	$r = 0.997$
	$pK_2 = 20.50 - 3.77\pi^* + 1.50\alpha - 16.48\beta$	$r = 0.990$
Ciprofloxacin	$pK_2 = 15.74 - 7.15\pi^* + 5.30\alpha - 8.20\beta$	$r = 0.999$
Nalidixic acid	$pK_1 = 22.60 - 10.30\pi^* + 0.59\alpha - 8.77\beta$	$r = 0.999$
Flumequine	$pK_1 = 17.94 - 13.32\pi^* + 4.43\alpha - 1.43\beta$	$r = 0.995$
Cinoxacin	$pK_1 = 19.59 - 10.02\pi^* + 1.00\alpha - 7.50\beta$	$r = 0.993$

relationships (LSER) which explain any solute property varying with solvent composition as a linear combination of the microscopic parameters of the solvent responsible. The Kamlet-Taft [46] expression states:

$$XYZ = (XYZ)_0 + s\pi^* + a\alpha + b\beta \quad (8)$$

where α, β and π^* are the microscopic parameters previously described, XYZ is the solute property, XYZ_0 the value of this property for the same solute in a hypothetical solvent for which $\alpha = \beta = \pi^* = 0$ and a, b and c are the susceptibilities of the solute property studied to changes in α, β and π^*, respectively. This equation can include additional terms or some of its terms can become equal to zero, depending on the property of the solute to be described [47]. Values of the Kamlet-Taft solvatochromic parameters π^* [18,20], α [18,47] and β [18,19] for acetonitrile–water mixtures over the entire range of composition are known. Table 3 gives the relevant solvatochromic parameter values for the mixtures studied.

Several attempts were made to find the best form of the Kamlet-Taft equation to describe the variation of pK_1 and pK_2 values of quinolones in acetonitrile–water mixtures. Multiple regression analysis was applied to the pK data. All possible combinations of solvatochromic parameters, including Dimroth and Reichardt normalized parameter E_T^N, Table 3, were checked. The best fit was obtained when the three solvatochromic parameters α, β and π^* were used, yielding the general equations in Table 4. The linear solvation energy relationships obtained, permit to know the pK values of quinolones in any acetonitrile–water mixture up to 70% (w/w) acetonitrile. It could be of great practical interest to apply multiple regression analysis to the whole set of pK values of quinolones and the usual concentration by volume %(v/v), v, and weight %(w/w), w, as the intercept variables. In these cases the second order polynomials shown in Table 5 are obtained. The equations in Table 4 and Table 5 enable the pK_1 and pK_2 values of the quinolones studied in any binary solvent acetonitrile–water mixture up to 70% (w/w) acetonitrile to be known, and thus permit the interpretation of their acid–base behaviour in these widely used hydrorganic mixtures.

Acknowledgements

Financial support of this project by DGICYT (Project PB94-0833) is gratefully acknowledged.

Table 5
Relationships between pK values of the quinolones and weight, w, and volume, v, % of acetonitrile

Substance		
Ofloxacin	$pK_2 = 8.20 - 1.76 \times 10^{-2}v + 5.06 \times 10^{-4}v^2$	$r = 0.985$
	$pK_2 = 8.18 - 1.43 \times 10^{-2}w + 5.41 \times 10^{-4}w^2$	$r = 0.991$
Pipemidic acid	$pK_2 = 8.77 - 3.13 \times 10^{-2}v + 5.28 \times 10^{-4}v^2$	$r = 0.986$
	$pK_2 = 8.68 - 2.75 \times 10^{-2}w + 5.55 \times 10^{-4}w^2$	$r = 0.991$
Norfloxacin	$pK_1 = 5.94 + 4.93 \times 10^{-2}v - 2.38 \times 10^{-4}v^2$	$r = 0.999$
	$pK_2 = 8.74 - 1.80 \times 10^{-2}v + 4.43 \times 10^{-4}v^2$	$r = 0.976$
	$pK_1 = 5.95 + 6.12 \times 10^{-2}w - 4.12 \times 10^{-4}w^2$	$r = 0.999$
	$pK_2 = 8.66 - 1.33 \times 10^{-2}w + 4.56 \times 10^{-4}w^2$	$r = 0.982$
Enoxacin	$pK_2 = 8.82 - 3.33 \times 10^{-2}v + 6.08 \times 10^{-4}v^2$	$r = 0.999$
	$pK_2 = 8.70 - 2.69 \times 10^{-2}w + 6.15 \times 10^{-4}w^2$	$r = 0.997$
Fleroxacin	$pK_1 = 5.42 + 4.27 \times 10^{-2}v - 2.33 \times 10^{-4}v^2$	$r = 0.996$
	$pK_2 = 8.43 - 3.64 \times 10^{-2}v + 6.42 \times 10^{-4}v^2$	$r = 0.983$
	$pK_1 = 5.44 + 5.25 \times 10^{-2}w - 3.83 \times 10^{-4}w^2$	$r = 0.996$
	$pK_2 = 8.31 - 3.15 \times 10^{-2}w + 6.77 \times 10^{-4}w^2$	$r = 0.988$
Ciprofloxacin	$pK_2 = 8.62 - 2.58 \times 10^{-2}v + 5.48 \times 10^{-4}v^2$	$r = 0.999$
	$pK_2 = 8.51 - 1.90 \times 10^{-2}w + 5.45 \times 10^{-4}w^2$	$r = 0.999$
Nalidixic acid	$pK_1 = 6.05 + 2.75 \times 10^{-2}v + 2.31 \times 10^{-4}v^2$	$r = 0.997$
	$pK_1 = 6.29 + 2.66 \times 10^{-2}w + 2.82 \times 10^{-4}w^2$	$r = 0.999$
Flumequine	$pK_1 = 6.48 + 2.67 \times 10^{-2}v + 2.20 \times 10^{-4}v^2$	$r = 0.998$
	$pK_1 = 6.57 + 3.22 \times 10^{-2}w + 2.05 \times 10^{-4}w^2$	$r = 0.998$
Cinoxacin	$pK_1 = 4.85 + 1.28 \times 10^{-2}v + 3.45 \times 10^{-4}v^2$	$r = 0.998$
	$pK_1 = 4.79 + 2.52 \times 10^{-2}w + 2.63 \times 10^{-4}w^2$	$r = 0.998$

References

[1] K. Hirai, H. Aoyama, T. Irikura, S. Tyobe and S. Mitsuhashi, Antimicrob. Agents Chemother., 31 (1987) 582.
[2] M.R. Lockley, R. Wise and J. Dent, J. Antimicrob. Chemother., 14 (1984) 647.
[3] B. Joos, B. Ledergerber, M. Flepp, S.D. Bettex, R. Luthy and W. Siegenthaler, Antimicrob. Agents Chemother., 27 (1985) 353.
[4] J. Smith, Pharm. J., 233 (1984) 299.
[5] K. Sato, Y. Inoue, T. Fujii, H. Aoyama and M. Inoue, Antimicrob. Agents Chemother., 30 (1986) 777.
[6] N. Desplaces, L. Gutmann, J. Carlet and J. Acar, J. Antimicrob. Chemother., 17 (1986) 25.
[7] M. Neuman, Clin. Pharmacokinet., 14 (1988) 96.
[8] H. Sigel, R.B. Martin R. Tribolet, H.K. Häring and R. Matini-Balakrishnan, Eur. J. Biochem., 152 (1985) 187.
[9] R. Kauski and C.J. Murray, Tetrahedron Lett., 34 (1993) 2263.
[10] Y.K. Li, A. Kuliopulos, A.S. Mildrais and P. Talalay, Biochemistry, 32 (1993) 1816.
[11] J. Barbosa and V. Sanz-Nebot, J. Chem. Soc. Faraday Trans., 90 (1994) 3287.
[12] J. Barbosa and V. Sans-Nebot, Anal. Chim. Acta, 244 (1991) 183.
[13] J. Barbosa, J.L. Beltrán and V. Sanz-Nebot, Anal. Chim. Acta, 288 (1994) 271.
[14] J. Barbosa, S. Butí and V. Sanz-Nebot, Talanta, 41 (1994) 825.
[15] J. Barbosa and V. Sanz-Nebot, Fresenius J. Anal. Chem., 353 (1995) 148.
[16] Y. Marcus, Aust. J. Chem., 36 (1983) 1719.
[17] Y. Marcus, J. Chem. Soc. Faraday Trans. 1, 84 (1988) 1465.
[18] Y. Marcus and Y. Migron, J. Phys. Chem., 95 (1991) 400.
[19] T.M. Krygowski, P.K. Wrona, U. Zielkowska and C. Reichardt, Tetrahedron, 41 (1985) 4519.
[20] W.J. Cheong and P.W. Carr, Anal. Chem., 60 (1988) 820.
[21] C. Reichardt, Solvents and Solvent Effects in Organic Chemistry, 2nd edn., VCH, Weinheim, 1988.
[22] S. Rondinini, P.R. Mussini and T. Mussini, Pure Appl. Chem., 59 (1987) 1549.

[23] D.J. Ives and G.J. Janz, Reference electrodes, Academic Press, New York, 1961.
[24] D.S. Lee, H.J. Han, K. Kim, W.B. Park, J.K. Cho and J.H. Kim, J. Pharm. Biomed. Anal., 12 (1994) 157.
[25] D.L. Ross and C.M. Riley, Int. J. Pharm., 63 (1990) 237.
[26] T. Mussini, A.K. Covington, P. Longhi and S. Rondinini, Pure Appl. Chem., 57 (1985) 865.
[27] A.K. Covington, R.G. Bates and R.A. Durst, Pure Appl. Chem., 57 (1985) 531.
[28] J. Barbosa and V. Sanz-Nebot, Mikrochim. Acta, 116 (1994) 131.
[29] J. Barbosa, D. Barron, J.L. Beltran and V. Sanz-Nebot, Anal. Chim. Acta, 317 (1995) 75.
[30] J. Barbosa and V. Sanz-Nebot, Talanta, 36 (1988) 837.
[31] J. Barbosa, V. Sanz-Nebot and E. Torrero, Talanta, 38 (1991) 425.
[32] D.L. Ross and C.M. Riley, J. Pharm. Biomed. Anal., 12 (1994) 1325.
[33] D.L. Ross and C.M. Riley, Int. J. Pharm., 83 (1992) 267.
[34] R. Kitzes-Chohen, Quinolone Bull., 3 (1987) 7.
[35] D.A. Buckingham, C.R. Clark and A. Nangia, Aust. J. Chem., 43 (1990) 301.
[36] K. Takács-Novák, B. Noszál, I. Hermecz, G. Keresztúri, B. Podányi and G. Szász, J. Pharm. Sci., 79 (1990) 1023.
[37] M. Jelikic, D. Veselinovic and P. Djurdjevic, Talanta, 39 (1992) 665.
[38] H.B. Hetzer, R.A. Robinson and R.G. Bates, J. Phys. Chem., 72 (1968) 2081.
[39] D. Enea, K. Honughossa and G. Berthon, Electrochim. Acta, 17 (1972) 1585.
[40] P. Nagy, J. Mol. Struct., 201 (1989) 271.
[41] O. Budewsky, Foundations of Chemical Analysis, Ellis Horwood, Chichester, 1979.
[42] Y. Marcus, J. Chem. Soc., Faraday Trans. 1, 85 (1989) 381.
[43] A.J. Easteal and L.A. Woolf, J. Chem. Thermodyn., 20 (1988) 693.
[44] M.K. Chantooni, Jr. and I.M. Kolthoff, J. Phys. Chem., 79 (1975) 1176.
[45] Y. Migron and Y. Marcus, J. Chem. Soc., Faraday Trans., 87 (1991) 1339.
[46] M.J. Kamlet, J.L.M. Abboud, M.H. Abraham and R.W. Taft, J. Org. Chem., 48 (1983) 2877.
[47] J.H. Park, M.D. Jang, D.S. Kim and P.W. Carr, J. Chromatogr., 513 (1990) 107.

ELSEVIER

Talanta 44 (1997) 1285–1290

Talanta

Liquid–liquid extraction separation of iron (III) with 2-ethyl hexyl phosphonic acid mono 2-ethyl hexyl ester

J. Jayachandran, P.M. Dhadke *

Inorganic Chemistry Laboratory, Department of Chemical Technology, University of Bombay, Matunga, Mumbai 400 019, India

Received 8 August 1996; received in revised form 21 November 1996; accepted 22 November 1996

Abstract

Liquid–liquid extraction separation of iron(III) with 2-ethyl hexyl phosphonic acid mono 2-ethyl hexyl ester (PC-88A) in toluene has been studied. Quantitative extraction of iron(III) with 5×10^{-3} M PC-88A in toluene is observed in the pH range 0.75–2.5. From the extracted complex species in the organic phase iron(III) was stripped with 1–4 M HNO_3, 1.5–4 M H_2SO_4 and 1.5–4 M HCl, and later determined spectrophotometrically by thiocyanate method. Separation of iron(III) was carried out with some of the first transition metals in binary and multicomponent mixtures. This method was extended for the determination of iron in real samples. © 1997 Elsevier Science B.V.

Keywords: Iron (III); Liquid–liquid extraction; PC-88A; Thiocyanate method

1. Introduction

During the last two decades, large number of workers have reported on the extraction of iron(III) from different aqueous media by organophosphorus extractants [1,2]. In recent years phosphonic and phosphinic acid extractants have been commercialised [3], and among these, the dialkylphosphonic acid, especially 2-ethyl hexyl phosphonic acid mono 2-ethylhexyl ester(PC-88A) has been widely studied [4,5]. It has been preferred as an extractant for the separation of rare earth elements due to the high separation factor between any two chemically similar rare earth elements [6,7].

The extraction of iron(III) from KSCN with tri-*n*-butyl phosphate(TBP) has been reported [8]. Bis-2-ethyl hexyl phosphoric acid (D2EHPA) is an excellent extractant for iron(III), though back extraction of iron(III) from organic phase is found to be very difficult [9,10]. The quantitative extraction of iron(III) was possible from nitrate media with 0.1 M mono-2-ethyl hexyl phosphoric acid in hexane [11]. The extraction of iron(III), iron(II) and titanium(IV) from acidic sulphate medium with Di-*o*-tolyl phosphoric acid in benzene-hexane-1-ol system was reported by Islam et. al [12].

Demopoulos et al. have reported synergistic extraction of iron(III) from H_2SO_4 solutions using mixtures of Kelex 100-PC-88A in varsol 140 [13], while Jiayong chen et al. carried out the extraction with the mixture of amine and PC-88A [14].

* Corresponding author. Fax: +91 22 4145614.

PII S0039-9140(97)02190-X

However, systematic investigation on the extraction of iron(III) with PC-88A are lacking.

2. Experimental

2.1. Apparatus and reagent

Elico model LI-120 pH meter with combined electrode was used for H^+ ion concentration and Elico model SL-150 UV/Visible spectrophotometer with 10 mm corex quartz cuvettes were used for absorbance measurements.

The stock solution of iron(III) was prepared by dissolving 8.634 g of $NH_4Fe(SO_4)_2\ 12H_2O$ in 1 l of distilled water containing concentrated sulfuric acid and it was standardised volumetrically [15]. The required concentration of iron(III) solution was prepared by appropriate dilution with double distilled water. PC-88A (2-ethyl hexyl phosphonic acid mono 2-ethyl hexyl ester) supplied by Daihachi Chemical Industry (Japan) was used without further purification. All other chemicals used were of analytical grade.

2.2. Procedure

An aliquot of the solution containing 5 μg ml^{-1} of iron(III) was taken for all experiments. For extraction studies, 10 ml of aqueous solution containing 50 μg of iron(III) was taken and its pH was adjusted with sulphuric acid and/or ammonium hydroxide. The solution was then transferred into a separating funnel and 10 ml of 5×10^{-3} M PC-88A in toluene was added to it and was shaken for 5 min. The two phases were allowed to separate. Iron(III) from the metal loaded organic phase was then stripped back with different mineral acids as stripping agents. The amount of iron(III) in aqueous phase was determined spectrophotometrically by thiocyanate method [16].

3. Result and discussion

3.1. Effect of pH on extraction

Iron(III) was extracted in the pH range of 0.1–5.0 with 5×10^{-3} M PC-88A in toluene. The extraction was found to be quantitative in the pH range 0.75–2.5, hence all extraction were carried out at pH 2.0. (Fig. 1).

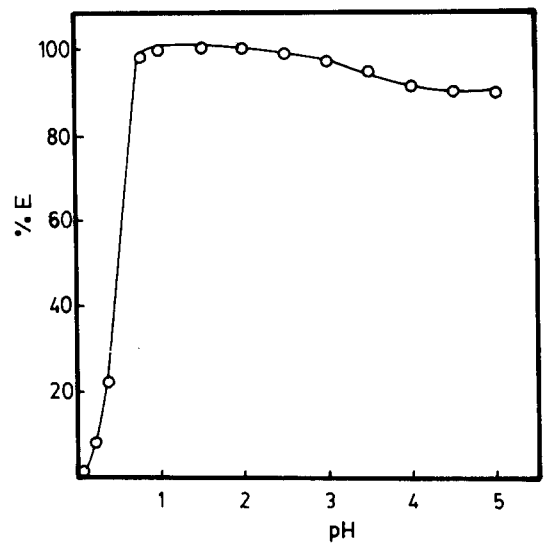

Fig. 1. Effect of pH on percentage extraction of iron(III) with 5×10^{-3} M PC-88A in toluene.

Table 1
Extraction as a function of PC-88A concentration

PC-88A conc (1×10^{-3} M)	% Extraction (E)	Distribution ratio (D)
0.10	7.5	0.08
0.25	11.3	0.13
0.50	16.5	0.20
0.75	30.1	0.43
1.0	45.9	0.85
2.5	60.9	1.56
3.0	65.4	1.89
3.5	88.7	7.87
4.0	90.9	10.09
5.0	99.2	132.0
10.0--100.0	99.9	999.0

Fe(III) = 50 μg, pH = 2.0.

Table 2
Effect of stripping agents on back extraction of iron

Stripping agents (M)	% Recovery								
	0.1	0.5	1.0	1.5	2.0	2.5	3.0	3.5	4.0
HNO_3	63.9	90.2	99.9	99.9	99.9	99.9	99.9	99.9	99.9
HCl	50.8	91.1	97.7	99.9	99.9	99.9	99.9	99.5	99.5
H_2SO_4	55.2	88.5	96.2	99.2	99.9	99.9	99.9	99.7	99.3

3.2. Effect of reagent concentration

Iron(III) was extracted with varying concentration of PC-88A in toluene from 1×10^{-4} to 1×10^{-1} M. The extraction was observed to be quantitative with 5×10^{-3}M of PC-88A in toluene (Table 1).

3.3. Extraction with various diluents

The extraction of Iron(III) was performed with 5×10^{-3} M PC-88A in different diluents. The extraction was found to be quantitative with toluene, xylene, benzene and chloroform as the diluents, while with hexane (90.9%), cyclohexane (96.2%), carbon tetrachloride (93.2%) and methyl-iso-butyl ketone (91.7%) the extraction was not quantitative. Toluene was preferred as best diluent for extraction, since it provided better phase separation.

3.4. Effect of various stripping agents

Iron(III) was back extracted from organic phase with various strength of mineral acids. The stripping of iron(III) was observed to be quantitative with 1–4 M HNO_3, 1.5–4 M HCl and 1.5–4 M H_2SO_4. Among these mineral acids HNO_3 was preferred as stripping agent as it facilitates the determination of iron(III) without the step of dry ashing (Table 2).

3.5. Equilibration study

The solution was shaken for a period ranging from 1 to 20 min. The extraction was quantitative with a minimum 4 min of shaking. Therefore, a 4 min period of equilibration was maintained.

3.6. Nature of extracted species

It was necessary to evaluate distribution constant (D) while varying extractant concentration to ascertain the nature of the extracted species. The composition of the extracted species was ascertained from the graph of log D versus log [PC-88A] at fixed pH 2.0. The slope obtained was 2.7 (Fig. 2). Hence the probable composition of the extractable species is 1:3 or $Fe(PC\text{-}88A)_3$.

3.7. Effect of various diverse ions

Iron(III) was extracted in the presence of a large number of metal ions. The tolerance limit was so set as the amount of foreign ion causing interference of $\pm 1\%$ in the extraction of iron. The alkali metals were tolerated a ratio of 1:50. Manganese(II), mercury(II), copper(II) and

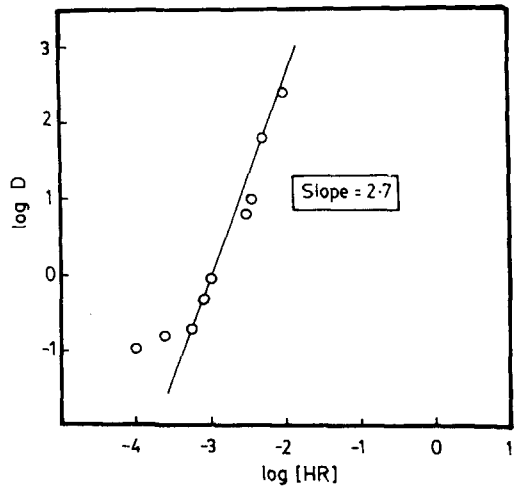

Fig. 2. Dependency of distribution ratio of iron(III) on PC-88A concentration in toluene (pH = 2.0)

Table 3
Separation from multicomponent mixtures

Sr No.	Mixture	Amt. taken (μg)	pH	Extractant PC-88A/toluene	Stripping agent	% Recovery
1	Fe(III)	50	2.0	0.005 M	1 M HNO_3	99.8
	Co(II)	25	0.3 M CH_3COONa	0.005 M	1 M HCl	99.5
	Cr(VI)	25	0.3 M CH_3COONa	Unextracted	Aq. phase	99.6
2	Fe(III)	100	1.0	0.05 M	1 M HNO_3	99.2
	Ti(IV)	100	1.0	0.05 M	2 M H_2SO_4 + 3% H_2O_2	98.8
	Cr(VI)	25	1.0	Unextracted	Aq. phase	99.8
3	Fe(III)	150	1.0	0.05 M	1 M HNO_3	99.5
	Ti(IV)	100	1.0	0.05 M	2 M H_2SO_4 + 3%H_2O_2	98.5
	Co(II)	25	1.0	Unextracted	Aq. phase	99.8
4	Fe(III)	50	2.0	0.005 M	1 M HNO_3	99.6
	Zn(II)	25	5.0	0.02 M	1 M HCl	98.6
	Co(VI)	25	5.0	Unextracted	Aq. phase	99.3
5	Fe(III)	50	1.0	0.05 M	1 M HNO_3	99.3
	Ti(IV)	100	1.0	0.05 M	2 M H_2SO_4 + 3% H_2O_2	98.3
	Zn(II)	50	1.0	Unextracted	Aq. phase	99.2
6	Fe(III)	50	2.0	0.005 M	1 M HNO_3	99.1
	Zn(II)	25	5.0	0.02 M	1 M HCl	98.9
	Cr(VI)	25	5.0	Unextracted	Aq. phase	99.8
7	Fe(III)	50	1.0	0.05 M	1 M HNO_3	99.6
	Ti(IV)	100	1.0	0.05 M	2 M H_2SO_4 + 3% H_2O_2	98.2
	Cu(II)	25	1.0	Unextracted	Aq. phase	99.3
8	Fe(III)	50	1.0	0.05 M	1 M HNO_3	98.6
	Ti(IV)	100	1.0	0.05 M	2 M H_2SO_4 + 3%H_2O_2	98.9
	Co(II)	25	0.3 M CH_3COONa	0.005 M	1 M HCl	99.1
	Cr(VI)	25	5.0	Unextracted	Aq. phase	99.6

Table 4
Analysis of samples containing iron

Samples	Metal present	Present	Found	% Recovery
Ilmenite ore	Fe, Ti	48.5%	48.2%	99.5
Pyrulosite ore[a]	Fe, Al, Mn	9.8%	9.7%	98.9
Monel metal[a]	Fe, Cu, Ni, Mn	1.5%	1.45%	96.6
Impheron injection	Fe	100 mg	99.9 mg	99.9
Fecontin-F tablets	Fe	100 mg	99.2 mg	99.2

[a] Al, Mn and Ni were separated after studying their extraction condition.

calcium(II) were tolerated in the ratio of 1:25. Chromium(VI), nickel(II) and lead(II) were tolerated up to a ratio of 1:10. Cobalt(II), vanadium(V), zinc(II), cadmium(II), rubidium(I), thallium(I), barium(II), indium(III) and osmium(VIII) were tolerated in the ratio of 1:4. Anions like chloride, sulphite, sulphate and perchlorate were tolerated at a ratio of 1:60 but acetate, EDTA, bismuth(III), silver(I) and arsenic(III) showed strong interference.

3.8. Separation of iron(III) from multicomponent mixtures

The mixture of iron(III), titanium(IV), cobalt(II) and chromium(VI) was resolved by first extracting iron(III) and titanium(IV) at pH 1.0 with 5×10^{-2} M PC-88A in toluene, during which cobalt(II) and chromium(VI) remain unextracted in the aqueous phase. From the organic phase iron(III) and titanium(IV) were separated by taking advantage of difference in stripping agents. Iron(III) was first stripped with 1 M HNO_3, followed by titanium(IV) with the mixture of 2 M H_2SO_4 and 3% H_2O_2 to get a quantitative separation. Cobalt(II) and chromium(VI) which remained unextracted in the aqueous phase were separated by first extracting cobalt(II) in acetate media with 5×10^{-3} M PC-88A in toluene. In acetate medium, chromium(VI) remained unextracted.

Copper(II) and zinc(II) were found to get extracted at pH 6.0 and 4.5, respectively with 2×10^{-2}M PC-88A in toluene [17]. Iron(III), zinc(II) and chromium(VI) from their mixture were separated by first extracting iron(III) at pH 2.0 with 5×10^{-3} M PC-88A in toluene and then zinc(II) at pH 5.0 with 2×10^{-2} M PC-88A in toluene where as chromium(VI) remain unextracted (Table 3).

4. Application

The proposed method was applied for the analysis of different samples containing iron (Table 4). The results conform to the labile claim and is free from interferences due to other excipient present in pharmaceutical formulation. Determination of iron in ilmenite ore and monel metal was carried out after separating titanium and copper respectively by the method given in Table 3.

5. Conclusion

The proposed method is simple, rapid and selective. It is advantageous over other existing method as follows:

1. Concentration of PC-88A (5×10^{-3} M) required is much less as compared with reagents like 8-hydroxyquinoline, acetylacetone and thenoyltrifluoroacetone.
2. Extraction is difficult with dithizone as iron(III) oxidizes the reagent and does not form a complex.
3. Various metals showed different extents of extraction with PC-88A in toluene at different pH and have difference in stripping power. These factor permitted the separation of iron(III) from commonly associated elements like titanium(IV), cobalt(II), chromium(VI), zinc(II) and copper(II) in binary, ternary and quaternary mixtures.
4. Equilibrium time required is much less, i.e., 4 min and much less concentration of stripping agent is required.

Acknowledgements

The authors are thankful to Professor S.M Khopkar, Emeritus Scientist (CSIR), Department of Chemical Technology, University of Bombay, for his help and inspiration in the research work and Dai-hachi Chemical Industries, Japan for the gift sample of PC-88A.

References

[1] S.K. Yadav, O.V. Singh and S.N. Tandon, Hydrometallurgy, 36 (1994) 53.
[2] C. Wang and D. Li, Solvent Extr. Ion Exchange, 13 (1995) 503.
[3] Z. Hubicki and H. Hubicka, Hydrometallurgy, 40 (1996) 65.
[4] C. Chen and T. Zhu, Solvent Extr. Ion Exchange, 12 (1994) 1013.
[5] D.B. Dreisinger and W.C. Copper, Hydrometallurgy, 12 (1984) 1.
[6] N.V. Thakur, D.V. Jayawant, N.S. Iyer and K.S. Koppiker, Hydrometallurgy, 34 (1993) 99.
[7] K. Fukiko, G. Masahiro and F. Nakashio, Solvent Extr. Ion Exchange, 11 (1993) 437.
[8] L.M. Melnick, H. Freiser and H.F. Beekly, Anal. Chem., 25 (1953) 856.
[9] H. Majima, T. Izaki and S. Sanuki, Metall. Trans., 16B (1985) 187.

[10] T. Sato and T. Nakamora, Hydrometallurgy, 15 (1985) 209.
[11] S.K. Yadav, O.V. Singh and S.N. Tandon, Indian J. Chem., 30A (1991) 982.
[12] M.F. Islam, R.K. Biswas and C.M. Mustafa, Hydrometallurgy, 13 (1985) 365.
[13] G.P. Demopolus, I.O. Mihaylov and G. Pouskouleli, Solvent Extr. Ion Exchange, 11 (1993) 67.
[14] J. Chen and S. Yu, Hydrometallurgy, 22 (1989) 1883.
[15] A.I. Vogel, A Text of Quantitative Inorganic Analysis, 3rd. edn., Longmans, London, 1964, p. 293.
[16] E.B. Sandell, Colorimetric determination of traces of metals. Interscience Publication, New York, Vol III, 1944, p. 263.
[17] A. Murakaini, Y. Akiyoshi, K. Kondo and F. Nakashio, J. Chem. Eng. Jpn., 15 (1982) 274.

ELSEVIER

Talanta 44 (1997) 1291–1298

Talanta

Silver(I)-selective membrane electrodes based on sulfur-containing podands

Sarah Chung [a], Wantae Kim [a], Sung Bae Park [a], Dae Yeon Kim [b], Shim Sung Lee [b,*]

[a] *Department of Chemistry and Research Institute of Basic Sciences, Inje University, Kimhae 621-749, South Korea*
[b] *Department of Chemistry and Research Institute of Natural Sciences, Gyeongsang National University, Chinju 660-701, South Korea*

Received 20 August 1996; received in revised form 25 November 1996; accepted 26 November 1996

Abstract

Some podands, acyclic polyethers, were utilized as membrane active components to prepare Ag^+-selective polymeric membrane electrodes. The thiapodand-based electrodes exhibited considerable selectivity toward Ag^+ over other heavy metal ions including Cd^{2+}, Pb^{2+}, Cu^{2+} and Hg^{2+}. Also, good selectivity over alkali and alkali earth metal ions were observed. Response slopes, pH effects, response time, and signal baseline return of the sensor systems were studied in static mode and/or in a flow-injection system. The Ag^+-selectivity was explained by the soft–soft interaction of the Ag^+ ion with the sulfur donor atoms as well as the stacking interaction between aromatic end groups of the host molecule on complexation. © 1997 Elsevier Science B.V.

Keywords: Electrode; Podands; Silver(I)-selective; Sulfur

1. Introduction

Among various metallic ions, alkali and alkali earth metal ions (Li^+, Na^+, K^+ and Ca^{2+}) have been routinely measured by ion-selective electrodes (ISEs) in clinical applications [1–4]. Active components (ionophores) for the related ion-selective membranes are usually macrocyclic polyethers that contain oxygen and nitrogen atoms. The remarkable selectivity of such membrane electrodes toward these metal ions reflects the high affinity of oxygen- and nitrogen-containing coordination sites toward the cations. Nitrogen- and oxygen-containing cryptands have also been exploited for the measurement of Zn^{2+} and other heavy metal ions [5–7].

On the other hand, the multi-purpose nature of silver makes its analysis in, and recovery from, waste material of importance [8]. Soft coordination sites like sulfur seem to generate great affinity toward the d^{10} transition metal ions such as Ag^+ and Hg^{2+}. A group of polythiacrown ethers and acyclic polythia compounds have been utilized for the measurement of Ag^+ [9–11]. It is also found that some sulfur and/or nitrogen-containing calixarene-based PVC membrane electrodes exhibit good selectivity toward Ag^+ ion over alkali metal ions [12].

* Corresponding author. Fax: +82 52 5219718.

0039-9140/97/$17.00
PII S0039-9140(97)00010-6

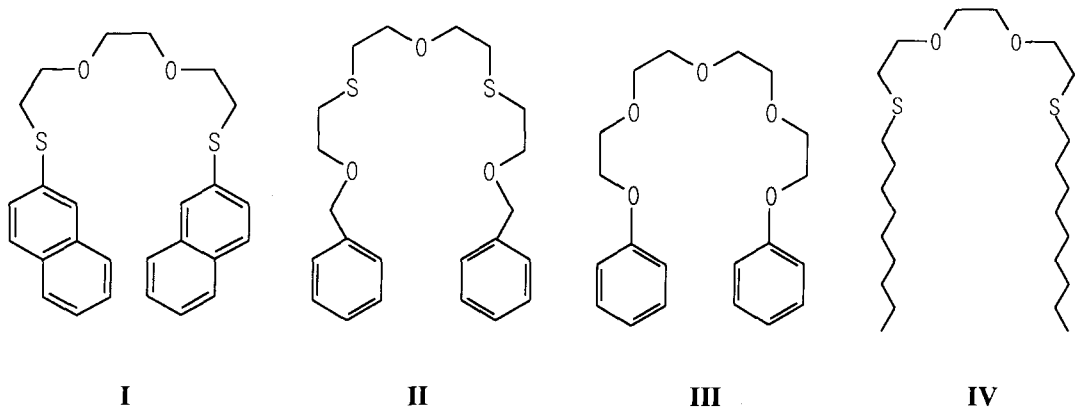

I II III IV

Fig. 1. Structures of some podand-type ionophores used in the preparation of Ag^+-selective membrane electrodes.

Here we describe the synthesis of some new podands, which contain two sulfur atoms in ether chain, and aromatic or lipophilic end groups (Fig. 1). These oxygen or sulfur-containing podands are employed as the active components for Ag^+-selective polymeric membranes. And the relation between the structure of ionophores and the selectivity are also discussed. The electrochemical properties of the podands as the Ag^+-selective ionophore are tested in static and flow-injection analysis (FIA) mode.

2. Experimental

2.1. Materials

The podands II and III were prepared as reported [13,14]. Podands I and IV were synthesized by the reaction of 1,8-dichloro-3,6-dioxaoctane with β-thionaphthol and n-nonylmercaptane in the presence of KOH in ethanol, respectively.

Podand I: β-thionaphthol and KOH were dissolved in boiling ethanol. Under reflux condition, 1,8-dichloro-3,6-dioxaoctane in ethanol was added dropwise. The mixture was refluxed for 12 h. After cooling to room temperature, the mixture was filtered and evaporated. The residue was dissolved in chloroform. To separate unreacted β-thionaphthol, the mixture was extracted several times with dilute NaOH. The organic layer was dried over $MgSO_4$, concentrated and purified by column chromatography over silica gel (eluent, n-hexane:ethylacetate 65:35 v/v; R_f value, 0.34; yield 50%; ^1H NMR ($CDCl_3$), 8.6–6.9 (m, 14H, aromatic C–H), 3.4–3.9 (m, 12H, CH_2OCH_2), 3.2–3.5 (m, 4H, $-SCH_2$); IR (KBr), 3010 (aromatic C–H, m), 2900 (aliphatic C–H, s) 1100 (alkyl C–O, s), 740 (allyl C–S, s) cm^{-1}).

Podand IV: n-nonylmercaptane and KOH were dissolved in boiling ethanol. Under reflux condition, 1,8-dichloro-3,6-dioxaoctane in ethanol was added dropwise. The mixture was refluxed for 16 h. The synthetic procedure was almost same as that used for podand I (eluent, n-hexane: ethylacetate 90:10 v/v; R_f value, 0.35; yield 65%; ^1H NMR ($CDCl_3$), 3.45–3.67 (m, 4H, OCH_2), 2.40–2.75 (t, 4H, SCH_2), 1.10–1.70 (m, 8H, CH_2), 0.83 (t, 3H, CH_3); ^{13}C NMR ($CDCl_3$), 70.98, 70.19 (OCH_2), 32.54, 32.42 (SCH_2), 22.43, 28.40, 29.63, 31.20 (CH_2), 13.93 (CH_3); IR (KBr), 2920 (aliphatic C – H, s), 1126 (alkyl C – O, s), 725 (allyl C – S, w) cm^{-1}).

Poly(vinyl chloride) (PVC) and potassium tetrakis(4-chlorophenyl)borate (KTpClPB) from Fluka (Ronkonkoma, NY) were used to cast the ISE membranes. A plasticizer, diisodecyl adipate (DIDA) was obtained from Scientific Polymer Products (Ontario, NY). Tetrahydrofuran (THF) was purchased from Aldrich (Milwaukee, WI) and purified over sodium before use. A Tris buffer solution consisting of 0.05 M Tris[hydroxymethyl]aminomethane (Trizma Base) (Sigma, St. Louis, MO) adjusted with HNO_3 solution to pH

Table 1
Formulation and electrochemical properties of podand-based Ag^+-selective membrane electrodes

Electrode ID	Podand[a,b]	PVC[a]	DIDA[a]	KTpClPB[a]	Detection limit (μM)[c]	Slope (mV per decade)[c,d]	
						Fresh	30 days
E1	6.0, I	31.7	62.3	–	1.0	54.5 ± 0.9	53.5 ± 2.2
E2	6.0, II	31.7	62.3	–	0.6	58.5 ± 1.0	57.7 ± 2.3
E3	4.0, I	31.7	64.3	–	1.2	53.1 ± 1.2	52.0 ± 2.7
E4	4.0, II	31.7	64.3	–	0.9	57.0 ± 1.3	56.5 ± 2.8
E5	1.0, I	33.0	66.0	–	1.5	51.0 ± 1.1	50.1 ± 2.5
E6	1.0, II	33.0	66.0	–	1.4	52.4 ± 1.3	49.5 ± 2.7
E7	5.9, I	30.9	60.6	2.6	2.2	54.0 ± 2.0	52.1 ± 3.2
E8	5.7, II	30.9	60.7	2.7	2.0	57.8 ± 1.9	53.5 ± 3.0
E9	6.0, III	31.7	62.3	–	1.0	49.3 ± 1.8	45.0 ± 2.0
E10	6.0, IV	31.7	62.3	–	1.4	55.0 ± 1.9	54.1 ± 2.5

[a] Numbers indicate wt.%.
[b] Roman numerals indicate the podands in Fig. 1.
[c] Data were obtained with three membranes. Slope values denote (mean ± S.D.).
[d] The slopes were calculated using the linear portion of the response curve (detection limits and 1 mM).

9.0 was used as the working buffer for the potentiometric measurements. Nitrate salts of analytical-reagent grade were employed for the preparation of metal ion standard solutions. The buffer and standard solutions were prepared with deionized water.

2.2. Preparation of polymer membranes and electrodes

PVC-based ISE membranes were prepared by the method of Simon et al. [15]. The membrane compositions in the present work are listed in Table 1. After allowing the membranes to cure, 5.5 mm diameter disks were cut out and placed in Phillis electrode bodies (ISE-561, Glasblaserei Moller, Zurich). As an internal filling solution, 1 mM $AgNO_3$ was used for all electrodes.

2.3. Static mode potentiometric measurements

Cell potentials were measured at ambient temperature (18°C). The potentiometric cell used was as follows: Ag/AgCl(s)/4M KCl saturated with AgCl/Tris buffer/sample solution/ion-selective membrane/1 mM $AgNO_3$/AgCl(s)/Ag. The ion-selective and Ag/AgCl reference electrodes were connected through a high impedance amplifier to an IBM AT-type computer equipped with an A/D converter. Sampling rate was adjusted to 1 Hz. This apparatus was used to determine the selectivity of each membrane toward Ag^+ ion over other cations in the static mode. Selectivity coefficients, $k^{pot}_{Ag/x}$, were obtained by using the separate solution method [16].

2.4. Flow-injection mode measurements

The arrangement shown in Fig. 2 was used to evaluate the performance of the podand-based PVC membrane electrodes in the IFA mode. A Phillips electrode body was fitted with a wall-jet type flow-through cap similar to that described

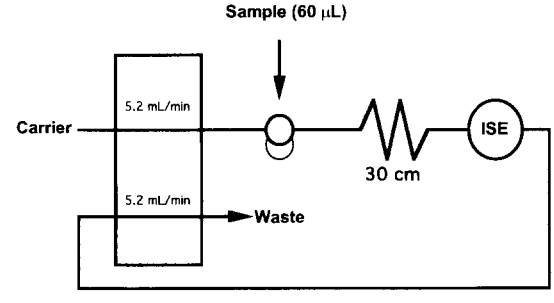

Fig. 2. Schematic of the membrane electrode-based flow-injection system.

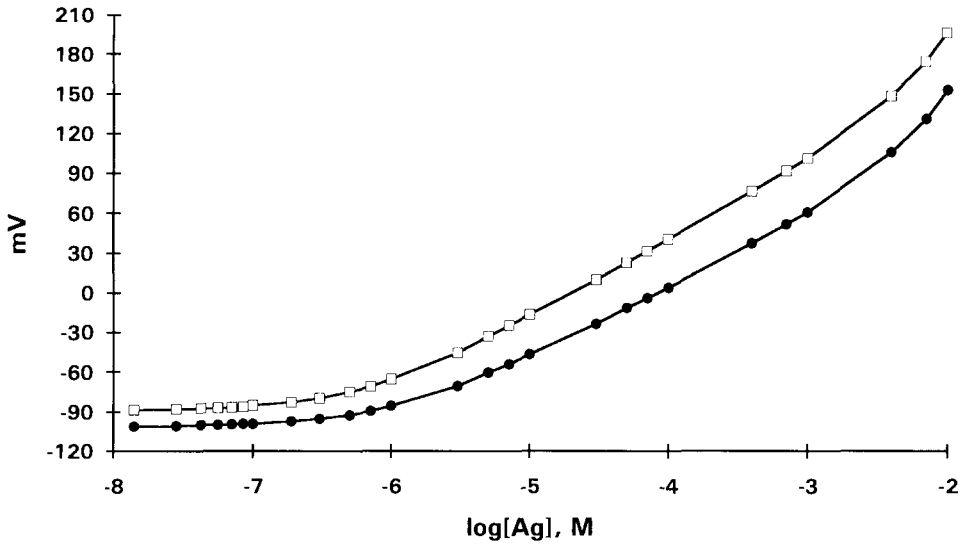

Fig. 3. Potentiometric Ag^+ ion response of the podand-based PVC membrane electrodes: (•) E1, (□) E2 in Table 1, respectively. Measurements were made in 0.05 M Tris buffer, pH 9.0.

previously [17]. The flow cap was connected to the injection valve by teflon tubing (0.012 in. i.d.). A peristaltic pump (Ismatech SA, Zurich) and a Rheodyne four-way rotary teflon valve (Model 7125) equipped with a 60 μl sample loop completed the flow-injection setup. The Tris buffer was used as the carrier stream. The Ag^+-selective and Ag/AgCl reference electrode were connected as described above. Sampling rate was adjusted to 2 Hz to observe delicate changes in the mV response.

3. Results and discussion

As with many ionophore-based membrane electrodes, the potentiometric response of the electrode toward Ag^+ ion depends on the concentration of the ionophore incorporated in the membranes. As shown in Table 1, increasing levels of the podand results in membrane electrodes (E1–E6) that exhibit larger slopes and lower detection limits. Approximately 6 wt.% of podands yielded electrodes with near-Nernstian response toward Ag^+ (55–60 mV per decade) over a wide range of Ag^+ concentrations. If the concentration of podand is higher than 6 wt.%, there was no clear advantage in terms of response slope and detection limits of the fresh membrane-based electrodes. Therefore, membranes doped with 6.0 wt.% podands were employed for further studies.

In addition, KTpClPB was used as an anionic additive in the membranes. KTpClPB is known to assist an ionophore's binding capability in many cation-selective membranes [18,19]. As can be seen in Table 1 for E7(I) and E8(II), however, there was no clear advantage of using the additive. Rather, it was revealed that those membrane electrodes showed slightly adverse effects in terms of detection limits and electrical signal to noise.

The equilibrium potentiometric response of the new podand-based PVC membrane electrodes E1(I) and E2(II) toward Ag^+ in the concentration range of 0–10 mM is shown in Fig. 3. Almost Nernstian slopes are observed in both type of electrodes. Surprisingly, unlike most membrane electrodes, the electrodes do not demonstrate a Donnan failure. Rather, there is an increase in slope at Ag^+ concentrations higher than 1 mM. These phenomena may indicate that there is a cooperative interaction between the ion and podand molecules as the concentration of podand-Ag^+ complexes increases in the membrane phase

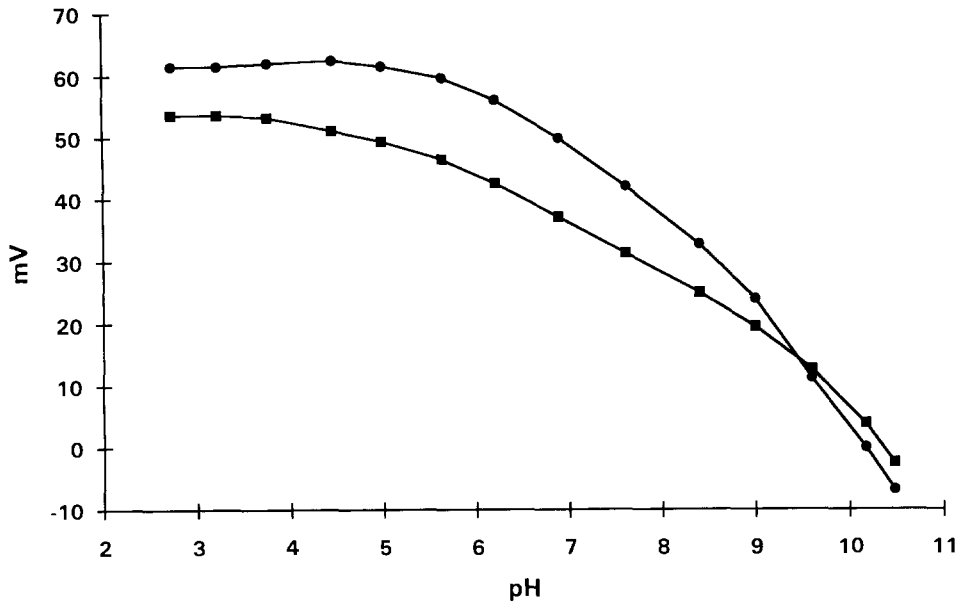

Fig. 4. Potentiometric pH response of the podand-based PVC membrane electrodes: (■) E1, (•) E2 in Table 1, respectively.

(see later discussion on mechanism). Response time of each electrode is short enough. Indeed time required to reach 90% of equilibrium mV values was less than 2 s.

Fig. 4 shows the pH response of E1(I) and E2(II) evaluated by titrating 0.05 M phosphoric acid with 0.1 M sodium hydroxide. These pH responses seem to ascribe to the competitive binding of proton (or hydrated water) to the ligands. Despite of the relatively minor pH response (< 10 mV per decade), 0.05 M Tris buffer, pH 9.0, was used throughout the whole work to dilute/carry sample standards to minimize H^+ interferences.

In terms of lifetime of the PVC membrane electrodes, more than 1 month of response stability was observed (see Table 1).

Table 2 provides the potentiometric selectivity coefficient data of some podand-based PVC membrane electrodes for the interfering cations relative to Ag^+. The data for thiapodand-based electrodes, such as E1(I), E2(II) and E10(IV) show the better response and selectivity to Ag^+ ion with respect to the most common monovalent and divalent metal cations than that of oxopodand, (III, E9). It is noted that oxopodands yield the lower selectivity toward each metal ion, undoubtedly reflecting the relatively poor coordination power of each oxygen donors toward Ag^+ ion.

Table 2
Static mode potentiometric selectivity coefficients[a], $\log k^{pot}_{Ag,x}$ of the podand-based membrane electrodes[b]

Cation	Electrode[c]			
	E1(I)	E2(II)	E9(III)	E10(IV)
Ag^+	0	0	0	0
NH_4^+	−3.5	−3.8	−1.3	−3.0
Na^+	−3.4	−3.7	−1.7	−3.0
K^+	−3.1	−3.4	−0.8	−3.1
Ba^{2+}	−4.9	−5.2	−3.3	−4.5
Ca^{2+}	−4.9	−5.2	−3.3	−4.5
Mg^{2+}	−4.5	−5.0	−3.3	−4.5
Cu^{2+}	−4.9	−5.1	−3.3	−4.4
Cd^{2+}	−4.4	−4.9	−2.9	−4.4
Co^{2+}	−4.9	−5.2	−3.0	−4.5
Pb^{2+}	−4.4	−5.1	−2.3	−4.2
Ni^{2+}	−4.8	−5.1	−3.1	−4.5
Hg^{2+}	−3.9	−3.9	−3.1	−3.9

[a] Measured by the separate solution method at 1 mM cation concentrations in 0.05 M tris-nitric acid, pH 9.0.
[b] Membrane composition (E1–E10) is listed in Table 1.
[c] Roman numerals in parentheses indicate the podands in Fig. 1.

Among thiapodands, O_3S_2 donor set podand with benzyl end group (II, E2) seems to show the best response and selectivity to Ag^+ ion. Values of $\log k_{Ag/x}$ range from -3.4 for K^+ to -5.2 Ba^{2+}, Ca^{2+} and Co^{2+}. For the Hg^{2+} ion, the selectivity coefficient ($\log k_{Ag/Hg}$) was -3.9. Generally the Hg^{2+} ion is known as the most severely interfering ion for the membrane electrodes based on the thia cyclic and acyclic ionophores [10,11].

The presence of O_2S_2 donor set, as occurs in I(E1) and IV(E10) results in good selectivity toward Ag^+ ion. There is no improvement in the performance of the electrode on attaching the long chain to the sensor molecules, as would be expected from their increased lipophilicity.

The relation between the structures of podands and the performance of electrodes from E1(I), E2(II), E9(III) and E10(IV) in Table 2 could be explained by the combination of following two reasons.

The high selectivity toward Ag^+ is due to the high affinity of sulfur atoms in the ionophores. It is well known that the $Ag^+(d^{10})$ exhibits strong affinity toward sulfur derived ligands and show a remarkable preference for linear coordination [8,20]. To explain the Ag^+ ion selectivity of the membrane electrode based on these thiapodands it is essential to take into account all these effect. The monovalent or divalent metal cation tested as interference do not show the strong sulfur affinity or linear coordination preference, except Hg^{2+}.

In addition, improved results were obtained by modifying the aromatic end groups with benzyl groups (II, E2). In our previous NMR [21] and the thermodynamic [14] works, it was suggested that podand II-Ag^+ ion complexes can be stabilized by the partial stacking interaction between two flexible aromatic end groups to give the pseudo-cyclization. This extra stabilization effect by the stacking interaction seems to lead the higher selectivity for Ag^+ ion in membrane electrodes. It is instructive to consider the position of two sulfur atoms, and the size or the length of ether chain in podand I, II, and IV. Podand II is distinguishable in both cases. The inner position of two sulfur in podand II act advantageously to improve the complexation affinity due to the flexible nature of the terminals. Otherwise, it is not a matter of size of the podands, because there is enough flexibility to fit the size of given metal cations.

In summary, two sulfur atoms and flexible benzyl end groups in podand II give rise to increased discrimination for Ag^+ ion, simultaneously.

Fig. 5A shows the typical flow-injection response to Ag^+ ion when an E2 electrode is used as the detector in the FIA arrangement shown in Fig. 2. In the nonequilibrium flow-injection system, response slopes toward Ag^+ ion tend to be somewhat less than observed in static mode experiments (50 mV per decade). In addition, the time required to return completely to baseline potential limits the throughput of the system (20 samples h^{-1}) particularly when the system is exposed to higher concentrations of Ag^+ ion (e.g., greater than 1 mM). Although it shows a limited throughput the reproducibility was satisfactory. For five repeated injections of 1 mM aqueous standard, RSD was 0.7%. As were in the static mode the podand-based electrodes were found to give high selectivities toward Ag^+ over other cations. A typical data is shown in Fig. 5B. Note that the peak heights (ΔmV) for a series of 1.0 mM $AgNO_3$ standards containing different interfering metal ions are essentially the same.

4. Conclusions

We have reported on the potentiometric Ag^+-selectivity of polymer membranes doped with several podands. Considerable response and selectivity toward Ag^+ ion are observed for membranes doped with podands that contain sulfur in their main chain and/or aromatic rings in the tail. When incorporated into an optimal FIA system, the podand-based membrane electrode may serve as a suitable detector for measuring Ag^+ levels in various samples. With further modification of the podand structure, additional enhancement in the potentiometric selectivity toward Ag^+ ion would be possible. Real sample measurements as well as more mechanistic studies (e.g., binding constant measurements) are also warranted.

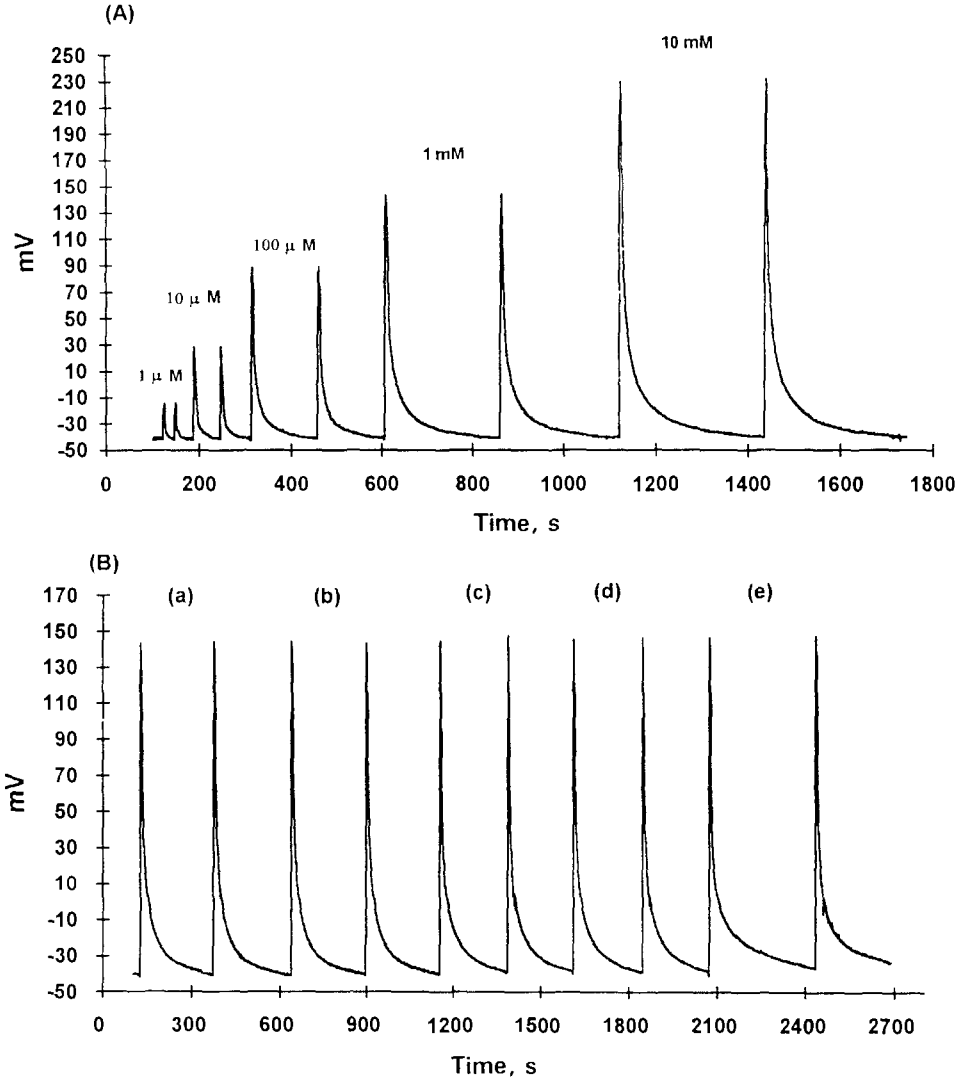

Fig. 5. (A) Potentiometric responses obtained for injections of Ag^+ standards in the FIA system with the podand II-based (E2 in Table 1) PVC membrane detector. (B) Responses for double injections of 1.0 mM $AgNO_3$ containing: (a) no other metal ion; (b) 1.0 mM $NaNO_3$; (c) 1.0 mM $Pb(NO_3)_2$; (d) 1.0 mM $Cu(NO_3)_2$; and (e) 1.0 mM $Hg(NO_3)_2$, respectively, using the Tris buffer, pH 9.0, as carrier stream.

Acknowledgements

S.S.L. and D.Y.K. are grateful to the Korea Science and Engineering Foundation (94-1400-10-01-3) for the financial support. D.Y.K. also acknowledges a fellowship from Seoam Academic Foundation in Korea. S.C., W.K., and S.B.P. acknowledge financial support from Korean Ministry of Education (BSRI-96-3446).

References

[1] F.N. Assubaie, G.J. Moody and J.D.R. Thomas, Anal., 114 (1989) 1545.
[2] K. Suzuki, H. Yamada, K. Sato, K. Watanabe, H. Hisamato, Y. Tobe and K. Kobiro, Anal. Chem., 65 (1993) 3404.
[3] S.R. Sheen and J.S. Shih, Anal., 117 (1992) 1691.
[4] S. Kitazawa, K. Kimura, H. Yano and T. Shono, J. Am. Chem. Soc., 10 (1984) 6978.

[5] S.K. Srivastava, V.K. Gupta and S. Jain, Anal. Chem., 68 (1996) 1272.
[6] N.G. Lukyanenko, N.Y. Titova, N.L. Nesterenko, T.I. Kirichenko and S.V. Scherbakov, Anal. Chim. Acta, 263 (1992) 169.
[7] G.G. Gross, T.M. Fyles and V.V. Sresh, Talanta, 41 (1991) 1589.
[8] R.M. Izatt, G.C. Lindh, R.L. Bruening, P. Huszthy, C.W. McDaniel, J.S. Bradshaw and J. J. Christensen Anal. Chem., 60 (1988) 1694.
[9] M. Oue, K. Akama, K. Kimura, M. Tanaka and T. Shono, J. Chem. Soc. Perkin. Trans. I, (1994) 963.
[10] F. Teixidor, M. Flores, L. Escriche, C. Viñas and J. Casabó, J. Chem. Soc. Chem. Commun., (1994) 963.
[11] J. Casabó, F. Teixidor, L. Escriche, C. Viñas and C. Pérez-Jiménez, Adv. Mater., 7 (1995) 238.
[12] K.M. O'Connor, G. Svehla, S.J. Harris, M.A. Mckervey, Talanta, 39 (1992) 1549.
[13] B.G. Tümmer, G. Maass, E. Weber, W. Weher and F. Vögtle, J. Am. Chem. Soc., 99 (1977) 4683.
[14] S.S. Lee, J.H. Jung, S.H. Yu and M.H. Cho, Thermochi. Acta, 259 (1995) 133.
[15] P. Schulthess, D. Ammann, W. Simon, C. Caderas, R. Stepanek and B. Krautler, Helv. Chim. Acta, 67 (1984) 1026.
[16] G. Moody and J. Thomas, Selective Ion-Selective Electrodes, Merrow, Watford, UK, 1971.
[17] M. Trojanowicz and M.E. Meyerhoff, Anal. Chem., 61 (1989) 787.
[18] U. Schefer, D. Ammann, E. Pretsch, U. Oesch and W. Simon, Anal. Chem., 58 (1986) 2282.
[19] E. Metzger, R. Dohner, W. Simon, D. Vonderschmitt and K. Hautschi, Anal. Chem., 59 (1987) 1600.
[20] J. Casabó, T. Flor, M.I. Romero, F. Teixidor and C. Pérez-Jiménez, Anal. Chim. Acta, 294 (1994) 207.
[21] J.H. Jung, S.B. Cho, J. Kim, J.S. Kim and S.S. Lee, Bull. Korean Chem. Soc., 14 (1993) 534.

ELSEVIER

Talanta 44 (1997) 1299–1305

Talanta

A highly water-soluble disulfonated tetrazolium salt as a chromogenic indicator for NADH as well as cell viability

Munetaka Ishiyama, Yoko Miyazono, Kazumi Sasamoto *, Yosuke Ohkura, Keiyu Ueno

Dojindo Laboratories, Tabaru 2025-5, Mashiki-machi, Kumamoto 861-22, Japan

Received 17 October 1996; received in revised form 31 December 1996

Abstract

A highly water soluble disulfonated tetrazolium salt, 4-[3-(2-methoxy-4-nitrophenyl)-2-(4-nitrophenyl)-2H-5-tetrazolio]-1,3-benzene disulfonate sodium salt, was synthesized. The compound is reduced by NADH in good yields at neutral pHs in the presence of 1-methoxy PMS to produce the corresponding formazan dye that absorbs at 460 nm. The formazan is soluble to water at concentrations higher than 0.1 M. The tetrazolium salt thus proved to be useful as a sensitive chromogenic indicator for NADH. It is also applicable to cell proliferation assays as a cell viability indicator. © 1997 Elsevier Science B.V.

Keywords: Cell viability; Formazan; Lactic acid; Lactate dehydrogenase; Tetrazolium salt; Water solubility

1. Introduction

Tetrazolium salts, which produce highly colored formazan dyes upon NADH reduction, have been of broad application as chromogenic reagents for NADH both in clinical and cell proliferation/cytotoxicity assays. These assays are based on colorimetric quantification of NADH as a detection signal. A major disadvantage of tetrazolium salts, which limits further applications in the both area, is that formazan dyes are extremely water insoluble; colorimetric assays using the tetrazolium salt/formazan system thus suffer from a poor data reproducibility possibly due to a solubilizing process, and are often accompanied by adsorption of the dyes to the assay instruments which resulted in contamination.

In previous work [1–3], we reported a novel disulfonated tetrazolium salt, 4-[3-(4-iodophenyl)-2-(4-nitrophenyl)-2H-5-tetrazolio]-1,3-benzene disulfonate sodium salt (WST-1 in Scheme 1), that produces highly water soluble formazan with a solubility greater than 0.1 M. WST-1 is currently employed as a chromogenic indicator for cell's bio-reducibility in viability assays [4–9], rather than for use in the area of clinical chemistry where a higher sensitivity for NADH is required. The sensitivity of WST-1 has been improved in an analogous compound, 4-[3-(4-iodophenyl)-2-(2,4-

* Corresponding author. Fax: +81 96 2861525; e-mail: sasamoto@dojindo.co.jp

PII S0039-9140(97)00017-9

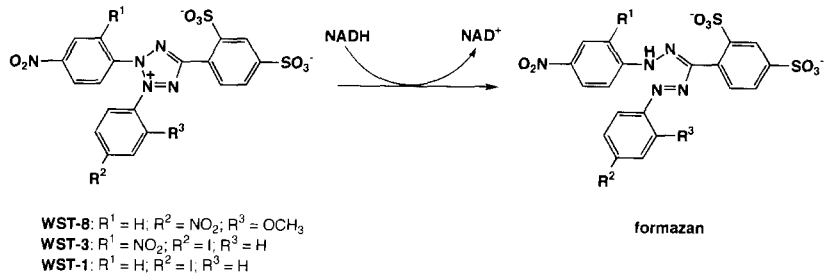

WST-8: R^1 = H; R^2 = NO_2; R^3 = OCH_3
WST-3: R^1 = NO_2; R^2 = I; R^3 = H
WST-1: R^1 = H; R^2 = I; R^3 = H

Scheme 1. NADH reduction of WST compound.

dinitrophenyl)-2H-5-tetrazolio]-1,3-benzene disulfonate sodium salt (WST-3) [10], that has a smaller reduction potential than WST-1 because of an additional nitro group (Scheme 1). The sensitivity of WST-3 for NADH is 2.5-fold greater than that of WST-1 at pH 7.4, and, in addition, it is less pH-dependent at important neutral pH range. [10] However, its stability, which is one of the key factors in exploring further applications, is much lower in aqueous solution, giving rise to a substantial increase of blank absorption even when refrigerated. An assumption that the lack of stability in WST-3 is attributable to the two nitro groups on the same benzene ring led us to design a new tetrazolium salt, 4-[3-(2-methoxy-4-nitrophenyl)-2-(4-nitrophenyl)-2H-5-tetrazolio]

-1,3-benzene disulfonate sodium salt (WST-8), that bears each nitro group at different ring as well as a methoxy group instead of the electron-withdrawing iodo group of WST-3 (Scheme 1).

We describe herein the synthesis and the potential applicability of WST-8, which proved to combine the both advantages of high stability of WST-1 and high sensitivity of WST-3.

2. Experimental

2.1. Apparatus

Thin-layer chromatography (TLC) was performed on Kieselgel 60 F_{254} (Merck, Darmstadt, Germany) using a mixture of *n*-butanol, acetic acid, pyridine and water (4:1:1:2, v/v) as a developing solvent. Absorbance spectra were taken on a Shimadzu UV-210A spectrophotometer. Proton nuclear magnetic resonance (^{1}H-NMR) spectra were measured on a Bruker AC-200P spectrometer at 200 MHz using sodium 3-(trimethylsilyl)-1-propanesulfonate as an internal standard. The splitting patterns were designated as follows: s, singlet; and m, multiplet. IR spectra were recorded in KBr disks on a Hitachi 270-30 spectrometer. Electrochemical measurements were carried out with a Cypress computer-controlled system, model CS-1090/1087 (Lawrence, KS, U.S.A.) in a Tris–HCl buffer (pH 8.0) at a scan rate of 20 mV s^{-1} using a glassy carbon working electrode. Uncorrected melting points were obtained on a Yamato MP-21 melting-point apparatus.

2.2. Materials

1-Methoxy-5-methylphenazinium methosulfate (1-methoxy PMS) was obtained from Dojindo Laboratories (Kumamoto, Japan). Lactic acid lithium salt of greater than 97% purity (enzymatic assay) was purchased from Sigma (St. Louis, MO, U.S.A.). Lactate dehydrogenase isoenzyme (LDH-1 H_4, 98 + % homogeneous)) from human erythrocytes was also from Sigma as a suspension of a 2.1 M $(NH_4)_2SO_4$ solution at pH 6.0. NADH and β-NAD^+ were purchased from Oriental Yeast (Osaka, Japan). The solutions of tetrazolium salts were all prepared as an aqueous solution at a concentration of 1 mM. The following buffers were used: 50 mM citrate (for pH 5–6), 50 mM Tris (for pH 7–9). These buffers were obtained from Dojindo Laboratories. HeLa cells (human uterus carcinoma, Dainippon Phar-

maceutical Co., Tokyo, Japan) were cultured in a Dulbecco's modified Eagle's medium (DMEM) (Gibco Laboratories, NY, U.S.A.) supplemented with 10% fetal bovine serum (Gibco Laboratories) at 37°C and under 5% CO_2 in a CO_2 incubator.

2.3. Assay procedure for NADH

To a mixture containing WST-8 (0.1 mM) and 1-methoxy PMS (5 μM) in 5 ml of 50 mM Tris–HCl (pH 8.0), 0–50 μl of NADH (5 mM) was added to yield a final concentration of 0–50 μM. After the solution was incubated at 22°C for 5 min, the absorbance at 460 nm was measured against a blank prepared in the same manner without NADH addition. The pH of the solution was then raised to 12.5 by adding 100 μl of 4 M NaOH and the absorbance at 640 nm was measured.

2.4. Assay procedure for lactic acid

To a mixture containing a tetrazolium salt (1 mM), 1-methoxy PMS (20 μM) and β-NAD^+ (200 μM) in 5 ml of 100 mM CHES buffer (pH 8.8) was added 0–50 μl of lactic acid lithium salt (10 mM in water) to give a final concentration of 0–100 μM. After the solution was pre-incubated at 30°C for 5 min, 100 μl of LDH (20 U ml^{-1}) was added (final concentration = 0.4 U ml^{-1}). The solution was incubated at 30°C for 10 min; the absorbance was measured at 455 nm (for WST-8), 440 nm (for WST-1), 435 nm (for WST-3) or 340 nm (for UV method).

2.5. Cell proliferation assay

A hundred μl of HeLa cell culture in the logarithmic phase was inoculated onto a 96-well microtiter plate, and the plate pre-incubated for 24 h in a CO_2 incubator at 37°C. A 10 μl of the working solution containing WST-8 and 1-methoxy PMS (0.5 mM and 20 μM, respectively, as the final concentration) was added to each well; it was incubated for an additional 2 h. The absorbance of each well was measured at 450 nm with a reference wavelength at 650 nm with an M-UVmax microplate reader (Molecular Devices Corp., Menlo Park, U.S.A.). An aliquot was taken from the medium to count the number of the cells with a Bürker–Türk haemacytometer (Nitirin, Tokyo, Japan).

2.6. Syntheses

2.6.1. Disodium 4-[1-(2-methoxy-4-nitrophenyl)-5-(4-nitrophenyl) formaz-3-yl]-1,3-benzene disulfonate

Concentrated HCl (4 ml, 48 mmol) was added to a stirred suspension of 5-nitro-*o*-anisidine (2.7 g, 0.016 mol) in water (30 ml), and the suspension was cooled to 0°C. To this suspension was added sodium nitrite (1.2 g, 18 mmol) in water (20 ml) at 0–5°C. After being stirred at approximately 0°C for 30 min, the solution was added to a pre-cooled solution of 2,4-disulfobenzaldehyde-4′-nitrophenylhydrazone, disodium salt [1] (6.7 g, 15 mmol) in water (200 ml). Sodium hydroxide (2.6 g, 64 mmol) in water (40 ml) was added dropwise to the mixture while the temperature was kept at 0–5°C. The solution was stirred at this temperature for 2 h and then at room temperature for an additional 2 h. The reaction mixture was acidified (pH 2) with 3 M HCl and treated with activated charcoal. The reaction mixture was concentrated to roughly one quarter of its volume, which resulted in precipitation of the crude formazan product. The precipitate was collected, dissolved in hot water (400 ml), and re-treated with activated charcoal. The filtrate was concentrated (not to dryness). Addition of isopropanol yielded 5.9 g (63%) of the title compound as a dark-reddish powder. mp: > 300°C (decomp.); TLC: $R_f = 0.60$; ^{1}H-NMR (D_2O): δ 3.78 (3H, s, OCH_3), 7.51–8.21 (10 H, m, Ar), 8.42 (1H, s, NH); FAB-MS: m/z = 624 $[M]^+$.

2.6.2. 4-[3-(2-Methoxy-4-nitrophenyl)-2-(4-nitrophenyl)-2H-5-tetrazolio]-1,3-benzene disulfonate, sodium salt (WST-8)

Concentrated HCl (6.7 ml, 0.08 mol) and *n*-butylnitrite (4.1 g, 0.04 mol) were sequentially added to the formazan as obtained as above (5.0 g, 8 mmol) in methanol (250 ml). After being

stirred at room temperature overnight, the mixture was treated with activated charcoal. The filtrate was concentrated to dryness to leave an oily residue, to which was added tetrahydrofuran to prompt crystallization. The crude product was re-dissolved in water and re-treated with activated charcoal. Concentration of the aqueous solution gave an oily residue. Addition of ethanol and tetrahydrofuran yielded crystals, which were collected to give 2.2 g (45%) of the title compound as a light yellow powder. mp: >300°C (decomp.); TLC: $R_f = 0.55$; IR (cm^{-1}): 1620 (C = N), 1540 (NO_2), 1350 (NO_2); ^{1}H-NMR (D_2O): δ 3.65 (3H, s, OCH_3), 7.99–8.47 (10 H, m, Ar); FAB-MS: m/z = 601 $[M+H]^+$. Anal. Calcd. for $C_{20}H_{13}N_6O_{11}S_2Na$: C, 40.00; H, 2.18; N, 14.00. Found: C, 39.96; H, 2.41; N, 14.27.

3. Results and discussion

WST-8 was synthesized in a similar way as described for WST-1 [1] in a moderate overall yield from 4-formyl-1,3-benzene disulfonic acid disodium salt. Unlike WST-1, however, for which chromatographic purification of the precursor formazan is needed, the formazan of WST-8 could be readily purified by single crystallization with a good recovery.

In the presence of a catalytic amount of 1-methoxy PMS, an electron mediator, WST-8 is readily reduced by NADH to give an absorption at 460 nm in proportion to the NADH concentration. The absorption maximum (λ_{max}) corresponds to λ_{max} of its formazan (Fig. 1). The λ_{max} was longer than that of WST-1 (438 nm) or WST-3 (433 nm), and was largely shifted reversibly to 640 nm when the pH was raised to $\sim$ 12.5, where the molar coefficient (e) value was roughly 1.7-fold greater than the value at 460 nm. Fig. 2 clearly indicates this pH-dependent color change which is characteristic to sulfonated tetrazolium salts. It appears to be reasonable by analogy to WST-3 [10] to assume that imide double bond isomerization of the formazan nucleus, rather than deprotonation, gives rise to the reversible color change. The formazan of WST-8 has a smaller ε value of 3.07×10^4 at pH 8.0 and 460 nm than does WST-1 (3.70×10^4 at pH 8.0 and 433 nm), but it is roughly equal to that of WST-3 (3.01×10^4 at 438 nm). In addition to the ε value, the yield of the product formazan (y) is another important factor that accounts for the sensitivity of tetrazolium salts toward NADH. In an overall NADH reduction expressed as:

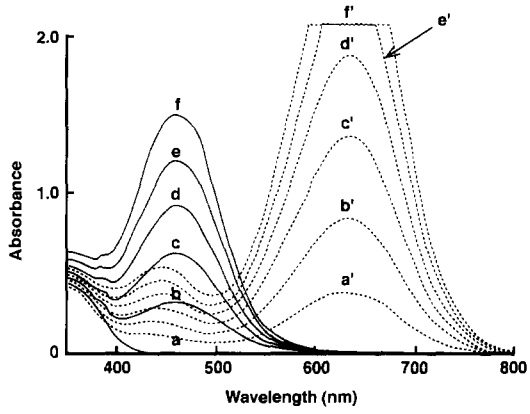

Fig. 1. Absorption spectra of WST-8 (0.1 mM) in the presence of increasing concentration of NADH and 1-methoxy PMS (5 μM). The spectra were taken after 5 min incubation at 22°C. Concentration of NADH (μM): a, 0; b, 10; c, 20; d, 30; e, 40; f, 50. Spectra a–f were taken at pH 8.0 and a'–f' are at pH 12.5.

$$T^+ + NADH \rightarrow F + NAD^+ ([T^+] > [NADH])$$

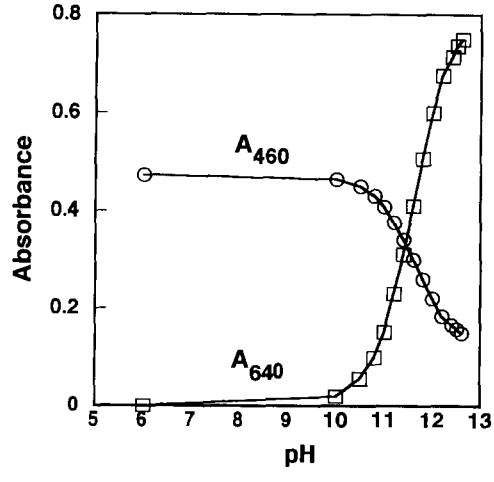

Fig. 2. Absorbance—pH profile of WST-8 formazan (15.4 μM) at different wavelengths. The pH was adjusted with 0.01 M NaOH.

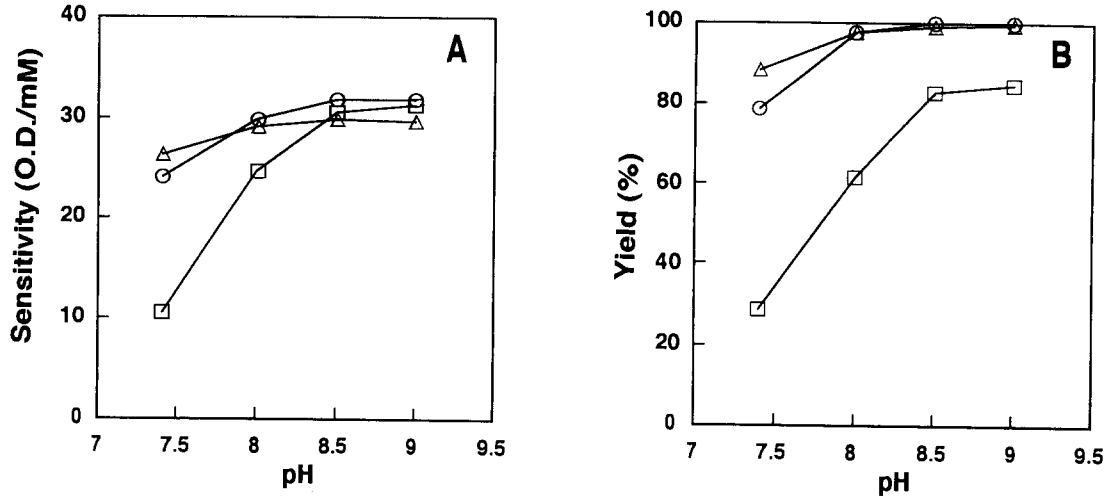

Fig. 3. Sensitivity—pH (A) and yield—pH (B) profiles of WST-8 in comparison with WST-1 and WST-3. ○: WST-8 (460 nm); □: WST-1 (438 nm); △: WST-3 (433 nm). The sensitivity ($\Delta A/\Delta$[NADH]) and the yield (Δ[F]/Δ[NADH]) of the NADH reduction were obtained based on the standard curves of absorbance (A) versus [NADH] that were taken as detailed in the experimental section.

in which T^+ and F stand for a tetrazolium salt and a formazan (= TH), respectively, the sensitivity for NADH is determined to be as follows:

$$\text{sensitivity} = \Delta A/\Delta[\text{NADH}] = \varepsilon(\Delta[\text{F}]/\Delta[\text{NADH}]) = \varepsilon y$$

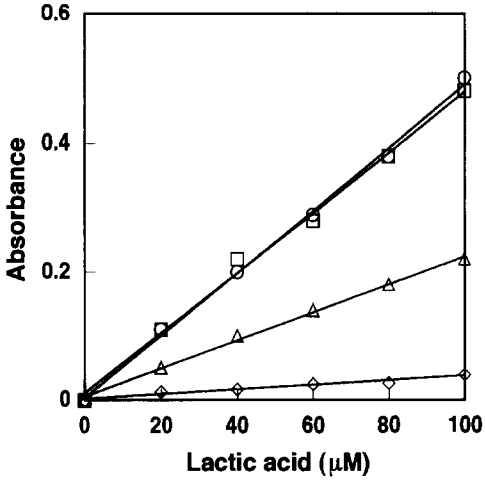

Fig. 4. Standard curves of lactic acid assays using WST compounds. See Section 2. ○: WST-8 (455 nm); □: WST-1 (440 nm); △: WST-3 (435 nm); ◇: UV method (340 nm).

where ΔA is the increase of the absorbance due to formazan formation. Accordingly, both the sensitivity and the yield of tetrazolium salts are given by the plot of the absorbance observed at λ_{max} of the formazan versus concentration of NADH. The sensitivities thus determined for WST-1, -3 and -8 at various pH values are shown in Fig. 3(A), in which good linearities of ΔA versus Δ[NADH] were observed ($r > 0.998$) for these tetrazolium salts, with within-assay coefficients of variation of less than 5% ($n = 5$) under conditions involving 0.1 mM tetrazolium salt and 0–50 mM NADH. Fig. 3(B) shows the yield of formazan as the function of pH, which is similar to the pH profile of the sensitivity (Fig. 3(A)) because ε values are almost constant at the observed pH range. In the figure, WST-8 is more readily reduced by NADH (larger yields) than is WST-1 particularly at important neutral pH range. At pH 8, for example, the NADH reduction of WST-8 takes place almost quantitatively whereas that of WST-1 is of approximately 60% efficiency. This greater reactivity of WST-8 compared with WST-1 toward NADH leads to a higher sensitivity of WST-8, despite the fact that it has a smaller ε value. Furthermore, the sensitiv-

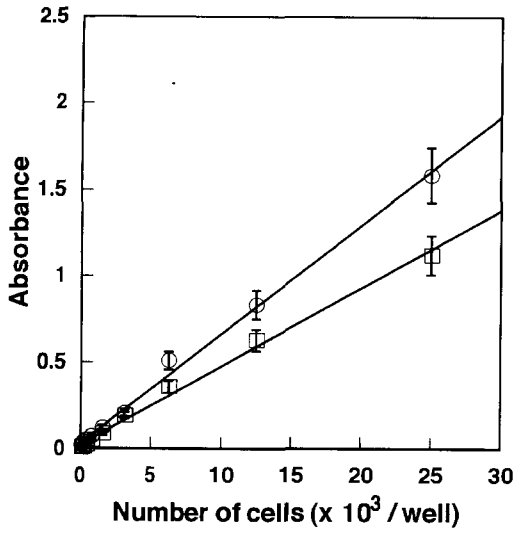

Fig. 5. Cell proliferation assays using WST-8 (○) and WST-1 (□) with HeLa cell line. The assay procedure is detailed in the experimental section.

ity of WST-8 is less pH-dependent. To our knowledge, WST-8 and -3 give the highest sensitivity for NADH among tetrazolium salts so far reported, with almost quantitative yields of reduction at pH higher than 8. However, electrochemical analyses did not support the greater reduction yield of WST-8, as its reduction potential was found to be nearly equal (− 0.37 V) to that of WST-1 (− 0.35 V).

Effects of addition of detergents and bovine serum albumin (BSA) on the sensitivity of WST-8 were also examined. Triton X-100, cetyltrimethylammonium bromide (CTMAB) and sodium dodecyl sulfate (SDS) were tested as a non-ionic, cationic and anionic detergent, respectively, in which SDS at the concentration of 0.1% (w/v) caused the sensitivity to be decreased 32%. The addition of BSA resulted in a similar decrease in the sensitivity; the presence of 1% (w/v) BSA caused a 22% decrease.

The reduction of WST-8 by NADH is very fast. Indeed, the reduction monitored at 460 nm completed within 5 min when it was run at pH 8.0 (50 mM Tris buffer) and 22°C using WST-8 (0.1 mM) and NADH (30 μM) in the presence of 1-methoxy PMS (5 μM); no decrease of the absorbance was observed once it reaches a plateau. The color thus developed was found to be stable for weeks at room temperature.

With the high sensitivity for NADH, we next examined the stability of WST-8 as an aqueous solution since the stability in aqueous solution becomes very important because of a growing demand to supply reagents as aqueous solution for ready use in clinical analyses. An increase of the blank absorbance of WST-8 (1 mM in 50 mM Tris buffer at pH 7.4) at 460 nm after 2 weeks at room temperature was 16% ($\Delta = 0.138$) of that of WST-3 at its λ_{max} under the same conditions, a value close to that of WST-1. The blank absorbance increase was less than 0.1 when the solution was refrigerated for 30 days. WST-8, therefore, combines advantages of the higher sensitivity from WST-3 and the greater aqueous stability of WST-1.

WST-8 was applied to the assay of lactic acid which is based on LDH-mediated dehydrogenation of the acid to pyruvic acid and NADH. Fig. 4 shows the standard curves of the tetrazolium salts for lactate, in comparison with a UV method that measures an increase of the absorbance of NADH directly at its λmax of 340 nm. Relative standard deviations for WST-8 determined by five separate runs for each point in the figure did not exceed 5%. The sensitivity of WST-8 toward lactic acid, as determined as $\Delta A/\Delta$[lactate] (O.D. mM^{-1}), was almost equal (4.86) to that of WST-1 (4.67), and was 2.2-fold larger than that of WST-3; it is sensitive enough to detect lactic acid in serum that ranges sub-mM to 2 mM. A poor sensitivity of WST-3 is partly due to a large background absorption as the sensitivity for NADH is comparable to those of WST-1 and -8.

We then turned our attention to using WST-8 as a viability indicator in cell proliferation assays. When HeLa cells were incubated with tetrazolium salts in the presence of 1-methoxy PMS, a linear colorimetric response was obtained in proportion to the number of viable cells with good correlation coefficients ($r = 0.9981$ and 0.9970 for WST-8 and WST-1, respectively) (Fig. 5). WST-8 gave 1.39-fold greater sensitivity than WST-1, for which increasing number of applications have been reported [4–9], under identical assay conditions.

In conclusion, WST-8 combines the best features of WST-1 and -3, being sensitive and stable. In addition, it is much easier to synthesize, which is a practical advantage to enable a cost-effective synthesis. We have also demonstrated that WST-8 has a great potential as a viability indicator in cell proliferation/cytotoxicity assays. Further application is currently underway.

References

[1] M. Ishiyama, M. Shiga, K. Sasamoto, M. Mizoguchi and P.-G. He, Chem. Pharm. Bull., 41 (1993) 1118.
[2] M. Ishiyama, H. Tominaga, M. Shiga, K. Sasamoto, Y. Ohkura, K. Ueno and M. Watanabe, In Vitro Toxicol., 8 (1995) 187.
[3] M. Ishiyama, H. Tominaga, M. Shiga, K. Sasamoto, Y. Ohkura and K. Ueno, Biol. Pharm. Bull., 19 (1996) 1518.
[4] T. Yano, K. Teruya, S. Shirahata, J. Watanabe, K. Osada, H. Tachibana, H. Ohashi, E.H. Kim and H. Murakami, Cytotechnology, 16 (1994) 167.
[5] K. Teruya, T. Yano, S. Shirahata, J. Watanabe, K. Osada, H. Ohashi, H. Tachibana, E.H. Kim and H. Murakami, Biosci. Biotech. Biochem., 59 (1995) 341.
[6] T. Iwaki, A. Iwaki, Y. Fukumaki and J. Tateishi, Brain Res., 673 (1995) 47.
[7] S.Q. Liu, K. Saijo, T. Todoroki and T. Ohno, Nat. Med., 1 (1995) 267.
[8] T. Takenouchi and E. Munekata, Life Sci., 56 (1995) 479.
[9] T. Kawase, S. Ogata, M. Orikasa and D.M. Burns, Calcif. Tissue Int., 57 (1995) 359.
[10] M. Ishiyama, K. Sasamoto, M. Shiga, I. Taniguchi, K. Nishiyama, Y. Ohkura and K. Ueno, Analyst, 120 (1995) 113.

ELSEVIER

Talanta 44 (1997) 1307–1312

Talanta

Solvent extraction, spectrophotometric and inductively coupled plasma atomic emission spectroscopic (ICP-AES) determination of lanthanum(III) with crown hydroxamic acid

Yadvendra K. Agrawal *, Pranav Shrivastav

Chemistry Department, School of Sciences, Gujarat University, Ahmedabad 380 009, India

Received 17 July 1996; received in revised form 7 January 1997; accepted 8 January 1997

Abstract

A new crown hydroxamic acid, 5,14-*N*,*N*′-hydroxyphenyl–4,15-dioxo-1,5,14,18-tetraaza hexacosane (NHDTAHA) for the extraction and spectrophotometric determination of lanthanum(III) is described. Lanthanum(III) forms a yellow coloured complex with NHDTAHA, which is extracted with chloroform, having molar absorptivity 7.7×10^3 l mol^{-1} per cm at 372 nm. The system obeys Beer's law in the range 1.2–20 ppm of lanthanum. The extract is directly aspirated for ICP–AES measurements, the limits for estimation are 5–140 ppb of lanthanum. Lanthanum has been determined in monazite sand and standard samples. © 1997 Elsevier Science B.V.

Keywords: Crown hydroxamic acid; Inductively coupled plasma atomic emission spectrophotometry (ICP-AES); Monazite sand; Lanthanum(III); Spectrophotometry

1. Introduction

Liquid–liquid extraction technique is widely used for preconcentration and separation of various metal ions from an interfering matrix. Hydroxamic acids are superior reagents for extraction and spectrophotometric determination of metal ions [1–5]. In recent years the macrocyclic ligands, crown ethers, have been reported for metal complexation [6–10]. However, the methods for the extraction and determination of lanthanum with crown ethers suffer from low sensitivity and interference of diverse ions [11,12]. The direct atomic absorption and inductively coupled plasma emission determination of lanthanum is reported, but a prior ion exchange separation is required [13,14]. The complexities of lanthanum emission lines with large number of strong ionic lines cause some difficulties over line selection thereby causes overlaps and reduces the detection limits considerably [15,16]. The very low levels at which the lanthanum is sought and potential interference from major elements, have led to the use of separation method to remove the bulk of major elements and at the same time to concentrate the lanthanum from the samples into small volume of solution.

* Corresponding author.

PII S0039-9140(97)00022-2

The use of strongly luminous flame is physically unpleasant and the photomultiplier receives high background radiation that can cause fatigue of the photo responsive surface of the cathode, even though the continuum radiation is not amplified. With this view a new crown hydroxamic acid is used for the extraction and simultaneous determination of lanthanum in presence of several diverse ions. The extraction removes the bulk of the major elements and at the same time concentrate the lanthanum into small volume of solution and the extract is directly injected into the plasma which increases the sensitivity and detection limit to several folds.

2. Experimental section

2.1. Apparatus

A Hitachi 3210 Spectrophotometer with matched 10 mm quartz cells was used for spectral measurements. Plasma Scan Model 710 Sequential Inductively Coupled Plasma Atomic Emission Spectrophotometer with Plasma Scan multitasking computer and peristaltic pump was used.

The following operating conditions were set for ICP–AES: Rf 27.12 MHz, incident power 2000 watts; GMK nebulizer; sample concentration 1 ng ml^{-1}; RF power 5 watts; observation height 14 mm; argon coolant flow rate 10 l min^{-1}; argon carrier flow rate 1 l min^{-1}; intergraph period 10 s; resolution 0.004 nm; peristaltic pump flow rate 1 ml min^{-1}; wavelength 394.91 nm.

2.2. Reagents

All chemicals used were of analytical grades of BDH or E. Merck. The ligand 5,14-*N*,*N*′-hydroxyphenyl-4,15-dioxo-1,5,14,18-tetraaza hexacosane (NHDTAHA) (Scheme 1) was synthesized by reacting 3,6-dioxoctane-1,8-diphenylhydroxylamine with 4,15-diamino-4,-13-dioxohexadecane-1,16-dioic acid chloride [17] in etherial medium in presence of suspended sodium bicarbonate as described elsewhere [18]. Its 0.2% stock solution was prepared in acetone. A standard lanthanum solution was prepared by dissolving 2.276 g of lanthanum acetate hydrate in a litre of double distilled water in the presence of HCl. Its final concentration 7.20×10^{-3} M was determined volumetrically [19]. It was further diluted as and when required. Buffer solution of pH 9 was prepared by mixing 40 ml of 1 M HNO_3 and 100 ml of 15% triethanolamine [20].

2.3. Extraction procedure

An aliquot of sample solution containing 30–500 ppm of lanthanum was transferred into a 60 ml separatory funnel. 10 ml of 0.2% NHDTAHA in acetone was added. pH 9 was adjusted with 2 ml of buffer solution and the mixture was shaken with 15 ml of chloroform for 1 min. The organic extract was collected, dried over anhydrous sodium sulphate and transferred into a 25 ml volumetric flask. To ensure the complete recovery of lanthanum, the extraction was repeated, adding 5 ml of NHDTAHA along with 5 ml of chloroform. The sodium sulphate was washed with chloroform and the combined extracts and washings were diluted to the mark with chloroform. The absorbance of the organic phase was measured against the reagent blank at 372 nm. For ICP-AES determination the lanthanum-NHDTAHA chloroform extract was introduced into the plasma by peristaltic pump.

The values of the percentage extraction (%E) and distribution ratio (D) of lanthanum was cal-

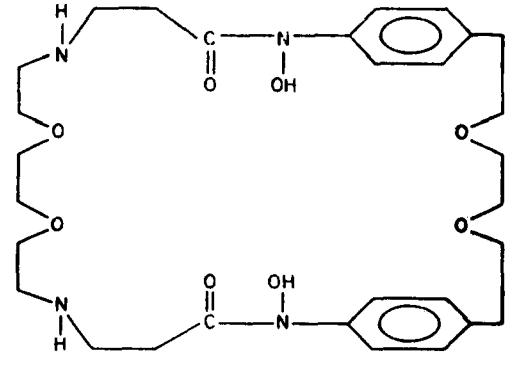

Scheme 1. 5,14-*N*,*N*′-hydroxyphenyl-4,15-dioxo-1,5,14,18-tetraaza hexacosane hydroxamic acid (NHDTAHA).

culated at different pH and NHDTAHA concentrations.

3. Results and discussion

3.1. Absorption spectra, Beer's law and precision

The Lanthanum(III)–NHDTAHA complex has a maximum absorbance at 372 nm and reagent blank does not absorb at this wavelength. The system obeys Beer's law in the range 1.2–20 ppm of lanthanum, sensitivity 0.018 ppm and the molar absorptivity is 7.7×10^3 l mol^{-1} cm^{-1}. The regression analysis represent Conc. = 18.8 × Absorbance with correlation coefficient 1.00.

Under the optimum conditions for ICP–AES determination, a linear calibration graph was obtained between 5 and 140 ppb of lanthanum. The determination of standard solution containing 20 ppb of lanthanum gave a relative standard deviation of 2.5%. The detection limit, expressed as the concentration of lanthanum giving a signal equivalent to three times the standard deviation of the blank plus the net blank intensity, was measured to be 0.18 ppb.

3.2. Effect of pH and shaking time

The percentage extraction and formation of chelate is also influenced by the pH of the solution. Maximum extraction of lanthanum with NHDTAHA was obtained in the pH range 8.5–9.5 (Fig. 1). At both lower and higher pH the extraction was incomplete (Table 1). The extraction is instantaneous, however, 1 min shaking is sufficient for quantitative extraction of lanthanum.

3.3. Effect of NHDTAHA concentration

The influence of NHDTAHA was studied by extracting lanthanum (1.78×10^{-4} M) with different amounts of NHDTAHA. It has been observed (Table 2) that 10 ml of 3.62×10^{-3} M reagent NHDTAHA is quite adequate for the complete extraction of lanthanum. The lower concentration of NHDTAHA reduces the percentage extraction, while a large excess of reagent can be used without any difficulty.

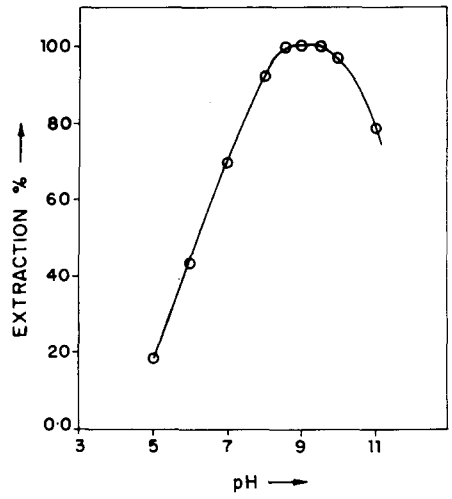

Fig. 1. Plot of percentage extraction of lanthanum against pH.

3.4. Stoichiometry of the complex

The composition of the Lanthanum(III)-NHDTAHA complex extracted into chloroform has been studied by slope ratio method [21] viz. by plotting a graph of logarithm of the distribution ratio of the metal ($\log D_M$) against the negative logarithm of ligand concentration ($-\log$ ligand).

Table 1
Effect of varying pH on the extraction of Lanthanum(III)–NHDTAHA complex

pH	Extraction (%)	Molar absorptivity (l mol^{-1} cm^{-1})
5.0	18.5	1.4×10^3
6.0	43.5	3.3×10^3
7.0	70.0	5.3×10^3
8.0	91.8	7.0×10^3
8.5	100.0	7.7×10^3
9.0	100.0	7.7×10^3
9.5	100.0	7.7×10^3
10.0	97.0	7.4×10^3
11.0	78.4	6.0×10^3

The lanthanum in the aqueous phase was determined by ICP-AES.
Solvent, chloroform; Lanthanum, 12 pm; NHDTAHA, 10 ml, 3.62×10^{-3} M in acetone; and λ_{max}, 372 nm.

Table 2
Effect of varying concentration of reagent for the extraction of Lanthanum(III)—NHDTAHA complex

NHDTAHA ($M \times 10^{-3}$)	$-\log$ (NHDTAHA)	Lanthanum conc. (M)		Log D_M
		$[La_{org}] \times 10$	$[La_{aq}] \times 10^{-4}$	
0.90	3.04	1.49	0.297	0.70
1.26	2.89	1.55	0.236	0.82
1.80	2.74	1.61	0.180	0.95
2.70	2.56	1.66	0.128	1.11
3.62	2.44	1.78	0.08	1.35
4.46	2.35	1.78	0.08	1.35

The detection limit for lanthanum is 8.0×10^{-6} M.
The lanthanum in aqueous phase was determined by ICP–AES.
Solvent, chloroform; pH, 9; and λ_{max}, 372 nm.

The extraction was carried out by taking a fixed amount of lanthanum with varying amounts of NHDTAHA. The plot of log D_M against $-\log$(ligand) gave a straight line of a slope 0.89 (Fig. 2), which indicates the composition of the complex is 1:1, thus 1 mol of ligand (NHDTAHA) is required for 1 mol of lanthanum. The NHDTAHA is having two hydroxamic groups (2L) and hence the expected structure of the complex is [La(OH)(2L)].

To get more information about the nature of the extracted complex, attempts were made to isolate it from chloroform extract. The extract was evaporated to dryness and subjected to elemental analysis. Further a known weight of the dry complex was digested with perchloric and nitric acid mixture and lanthanum content was determined by ICP–AES. The experimental results obtained for the complex are carbon 48.75%, nitrogen 7.41%, hydrogen 5.80% and lanthanum 18.65% and are comparable to the theoretical values for carbon 48.53%, nitrogen 7.54%, hydrogen 5.83% and lanthanum 18.71% which are in conformity with the complex formula [La(OH)(2L)].

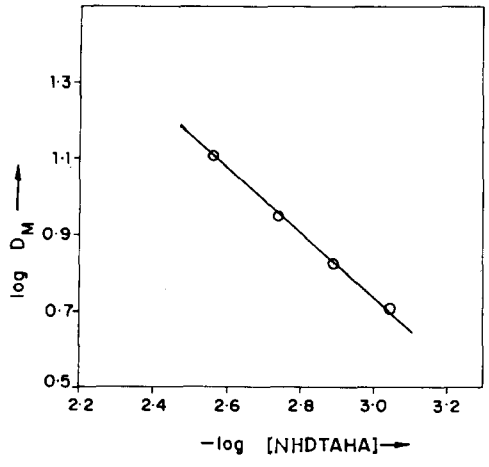

Fig. 2. Plot of distribution ratio of lanthanum [D_M] against crown hydroxamic acid [NHDTAHA].

3.5. Effect of solvents

The extraction was carried out with various solvents viz. chloroform, benzene, toluene and isoamyl alcohol. The results given in Table 3 show that the chloroform is the most appropriate solvent for the quantitative extraction of lanthanum.

Table 3
Effect of solvents on the extraction of Lanthanum(III)—NHDTAHA Complex

Solvent	Extraction (%)	Molar absorptivity ($l\ mol^{-1}\ cm^{-1}$)
Chloroform	100	7.7×10^3
Benzene	24	1.8×10^3
Toluene	29	2.2×10^3
Iso-amyl alcohol	[a]	—

Lanthanum, 2 ppm; NHDTAHA, 10 ml, 3.62×10^{-3} M in acetone; pH, 9; and λ_{max}, 372 nm.
[a] No extraction was obtained in iso-amylalcohol

Table 4
Effect of diverse ions on the extraction of Lanthanum(III)—NHDTAHA complex

Diverse ion	Added as	Amount added (mg)	Recovery of lanthanum (ppm)	
			Spectro-photometry	ICP- AES
Al^{+3}	$AlCl_3$	60	9.9 ± 0.05	9.95 ± 0.005
Sc^{+3}	SC_2O_3	50	9.9 ± 0.06	9.95 ± 0.003
Cr^{+3}	$CrCl_3$	60	9.9 ± 0.08	10.00 ± 0.001
Co^{+2}	$CoCl_2$	60	10.0 ± 0.06	10.00 ± 0.002
Hf^{+4}	$HfOCl_2$	60	10.0 ± 0.02	10.00 ± 0.001
Zr^{+4}	$Zr(NO_3)_4$	60	9.9 ± 0.03	9.90 ± 0.002
Ti^{+4}	$TiOCl_2$	60	9.9 ± 0.03	9.90 ± 0.003
Ta^{+5}	Ta_2O_5	60	9 9 ± 0 01	9.95 ± 0.003
Th^{+4}	$Th(N0_3)_4.6H_2O$	60	9.9 ± 0.02	9.90 ± 0.002
Tl^{+3}	$Tl(NO_3)_3$	50	9.9 ± 0.04	9.95 ± 0.007
Ga^{+3}	$GaCl_3$	60	9.9 ± 0.08	9.90 ± 0.006
In^{+3}	$In_2(SO_4)_3.5H_2O$	60	9.9 ± 0.02	10.00 ± 0.002
Sb^{+3}	$K(SbO)C_4H_4O_6.1/2H_2O$	60	9.9 ± 0.03	10.00 ± 0.002
Bi^{+3}	$Bi(NO_3)_3.5H_2O$	50	9.9 ± 0.04	9.95 ± 0.005
Fe^{+3}	$Fe_2(SO_4)_3$	60	9.9 ± 0.03	9.95 ± 0.002
Hg^{+2}	$HgCl_2$	60	10.0 ± 0.02	10.00 ± 0.001
Mg^{+2}	$MgS0_4.7H_20$	40	10.0 ± 0.02	10.00 ± 0.001
Pb^{+2}	$Pb(NO_3)_2$	30	10.0 ± 0.02	10.00 ± 0.002
Mn^{+2}	$MnSO_4.4H_2O$	40	9.9 ± 0.04	9.90 ± 0.003
Pd^{+2}	$PdCl_2$	60	9.9 ± 0.03	9.95 ± 0.002
Sn^{+4}	$SnCl_4$	60	10.0 ± 0.01	9.95 ± 0.001
V^{+5}	NH_4VO_3	60	9.9 ± 0.03	9.90 ± 0.001
Y^{+3a}	$Y_2(CO_3)_3$	40	9.9 ± 0.03	10.00 ± 0.001
UO_2^{+2}	$UO_2(CH_3COO)_2.2H_2O$	40	9.9 ± 0.04	9.95 ± 0.001
Pr^{3+b}	$Pr(ClO_4)_3$	40	10.0 ± 0.02	10.05 ± 0.001
Nd^{3+b}	$Nd(ClO_4)_3$	40	10.0 ± 0.01	10.00 ± 0.002
Ce^{4+c}	$(NH_4)_4Ce(SO_4).2H_20$	80	10.0 ± 0.03	10.00 ± 0.001

Solvent, chloroform; Lanthanum, 10 ppm; NHDTAHA, 10 ml, 3.62×10^{-3} M in acetone; pH, 9; and λ_{max}, 372 nm.
[a] Stripped with sodium fluoride.
[b] Stripped with sodium oxalate.
[c] Reduced with sodium nirite.

3.6. Effect of diverse ions

Lanthanum was selectively separated and determined in presence of various metal ions viz. Th(IV), U(Vl), Zr(IV), Hf(IV), Sc(III) etc. Scandium, being extracted at a considerably lower pH with hydroxamic acids, is not interfering in the extraction of lanthanum. However, yttrium(III) (> 20 ppm), cerium(IV) (> 10 ppm), praseodymium(III) (> 20 ppm) and neodymium(III) (> 20 ppm) do interfere in the determination of lanthanum. The interference of cerium(IV) can be eliminated by reducing it to cerium(III) with sodium nitrite. Lanthanum, 12 ppm, in presence of 40 mg each of yttrium, praseodymium and neodymium is extracted either masking these with fluoride (1:20) and oxalate (1:1000; 1:1500), respectively or after stripping yttrium with 0.1 M sodium fluoride and praseodymium and neodymium with 2.5 M sodium oxalate. The results obtained are given in Table 4.

3.7. Determination of lanthanum in standard samples

Standard lanthanum samples were analyzed to test the reliability of the present method. The samples were digested in a mixture of perchloric

Table 5
Determination of lanthanum in standard samples from the United States Geological Survey

Sample	Lanthanum present mg kg^{-1}	Lanthanum found mg kg^{-1}	
		Spectro-photometry[a]	ICP–AES[a]
BCR-1 (52/19)	26.0	25.7 ± 0.2	25.95 ± 0.06
ACV-1 (74/19)	35.0	34.9 ± 0.5	35.02 ± 0.05
GSR-1 (17/22)	190.0	190.8 ± 0.4	189.85 ± 0.07
G2 (108/15)	96.0	96.3 ± 0.5	96.15 ± 0.03
W1	9.8	9.7 ± 0.3	9.82 ± 0.09
Monozide sand (%)[b]	24.0	23.96 ± 0.7	23.90 ± 0.05

[a] The results are the average of eight determinations
[b] Samples from Travancore, India.

acid and nitric acid and evaporated to dryness. The residue was redissolved in 0.5 M perchloric acid and diluted to 250 ml with distilled water. An aliquot of this solution was taken for extraction and determination of lanthanum. The data are given in Table 5.

4. Conclusion

The present method is simple, sensitive and selective. Lanthanum(III) is first pre-concentrated by solvent extraction and then subjected to a versatile technique, ICP–AES, which enhances the sensitivity many folds (detection limit 0.18 ppb) compared with its non-extract estimation. The proposed method overcomes the problem of spectral interference due to matrix components, nebulizer blockage due to high solid content of the solution or analyte emission enhancement.

Acknowledgements

Financial assistance given by Department of Science and Technology is gratefully acknowledged.

References

[1] Y.K. Agrawal, Rev. Anal. Chem., 3 (2) (1980) 51.
[2] Y.K. Agrawal and S.A. Patel, Rev. Anal. Chem., 4 (4) (1980) 237.
[3] Y.K. Agrawal and R.D. Roshania, Bull. Soc. Chim. Belg., 89 (1980) 159.
[4] Y.K. Agrawal and R.K. Jain, Rev. Anal Chem., 6 (1982) 49.
[5] Y.K. Agrawal, Anal. Chem., 47 (1975) 940.
[6] W.J. McDowell, G.N. Case, J.A. McDonough and R.A. Bartsch, Anal. Chem., 64 (23) (1992) 3013.
[7] V.V. Yakshin and O.M. Viokova, Radiokhimiya, 34 (5) (1992) 68.
[8] J.N. Mathur and G.R. Choppin, Solvent Extr. Ion Exch., 11 (1) (1993) 1.
[9] D.J. Wood, S. Elshani, H.S. Du, N.R. Natale and C.M. Wai, Anal. Chem., 65 (10) (1993) 1350.
[10] H.S. Du, D.J. Wood, S. Elshani and C.M. Wai, Talanta, 7 (1993) 312.
[11] K. Nakagawa and S. Okada, Anal. Chem., 60 (1988) 2257.
[12] J. Tang and C.M. Wai, Anal. Chem., 58 (1986) 3233.
[13] J.N. Walsh, F. Buckley and J. Warker, Chem. Geol., 33 (1981) 141.
[14] J.G. Crock and F.E. Lichte, Anal. Chem., 54 (1982) 1329.
[15] J.A.C. Broekaert, F. Leis and K. Lague, Spectrochim. Acta, 34B (1979) 73.
[16] S. Nikdel, A. Massoumi and J.D. Winefordes, Microchem. J., 24 (1979) 1.
[17] B. Dietrich, J.M. Lehn, J.P. Sauvage and J. Blanzat, Tetrahedron, 29 (1973) 1629.
[18] Y.K. Agrawal, Tetrahedron, Communicated.
[19] J.S. Fritz, R.T. Oliver and D.J. Pietrzyk, Anal. Chem., 30 (1958) 1111.
[20] P.T. Thomas Kutty, Ph.D. Thesis, M.S. University, Baroda, 1988.
[21] J.H. Yoe and A.L. Jones, Ind. Eng. Chem. Anal. Educ., 16 (1944) 111.

ELSEVIER

Talanta 44 (1997) 1313–1317

Talanta

A new preconcentration method for platinum and gold based on a macropore anion resin HHY-10A

Chunsheng Li [a,b,*], Chifang Chai [a,b], Xuefeng Yang [c], Xiaolin Hou [a,b], Xueying Mao [a,b]

[a] *Institute of High Energy Physics, Chinese Academy of Science, Beijing, 100080, People's Republic of China*
[b] *Laboratory of Nuclear Analysis Technique, Chinese Academy of Science, P.O. Box 2732, Beijing, 100080, Perople's Republic of China*
[c] *Institute of Chemical Engineering and Metallurgy, China Nuclear Industry General Company, Beijing, 101149, People's Republic of China*

Received 28 August 1996; received in revised form 17 January 1997; accepted 20 January 1997

Abstract

The ion exchange behavior of Au and Pt on a new China-made macropore anion resin was studied using radiotracer technique. The conditions for adsorption and desorption, such as acidity, flow-rate and concentration of desorbing agents were studied carefully. Using the established method, the contents of Au and Pt in two Chinese ultrabasic SRMs were determined by ICP-MS and the results found in good agreement with the reference values.

Keywords: Au and Pt adsorption and desorption; HHY-10A macropore resin; ICP-MS; Radiotracer technique

1. Introduction

With an average concentration of 5 ppb [1] in the earth crust, platinum belongs to the category of the most rare naturally occurring elements. The omnipresent concentration of platinum in environmental and biological samples is estimated to lie in the ppt region, or even lower. There are only very few reliable data available about it, simply for the reason that no analytical procedures with sufficient detection sensitivity are yet existing.

Since the introduction of automobile exhaust catalytic cleaning, platinum has become a new environmental pollutant [2]. The concentration of Pt in ocean water has been reported to be higher than that existing in fresh water [3]. Thus, the concentration of Pt in ocean organisms is likely very high. Perhaps more and more intake of seafood will lead to an unexpected effect. This potential new impact to human health has initiated research to develop analytical methods for the Pt detection at very low levels.

Gold is an element coexisting with Pt generally in biological and environmental samples. Thus, it is convenient and hopeful to get the content of Au

* Fax: +86 10 68213374.

0039-9140/97/$17.00
PII S0039-9140(97)00027-1

simultaneously in analyzing Pt in a portion of sample.

Since the conventional analytical techniques, such as graphite furnace atomic absorption spectrometry (GFAAS) [4], instrumental neutron activation analysis (INAA) [5] and inductively coupled plasma-mss spectrometry (ICP-MS) [6] are not able to analyze Pt at such a low content, a preconcentration of Pt is necessary. Alt et al. [7] used MIBK extraction to preconcentrate Pt from biological and environmental materials, but this method is inconvenient in dealing with great amount of samples with low-level Pt. Parent et al. [8] reported an adsorption chromatography method with high recovery and minor interference of other elements, but the method is very time consuming. Ion exchange is a widely used method for separation due to its high adsorption capacity and unique selectivity, we selected it to preconcentrate Pt and Au from practical samples.

To develop the preconcentration procedures, radiotracer technique are very helpful because of its easy detection. ^{195m}Pt and ^{199}Au have suitable half-lives (^{199}Au 3.14d; ^{195m}Pt 4.02d) [9] and γ-ray energies(^{199}Au 158.38 keV; ^{195m}Pt 98.88 keV) [9] and can be produced from a kind of chemical only containing Pt. In this work, we studied the adsorption and desorption behaviors of ^{199}Au and ^{195m}Pt on a new China-made HHY-10A macropore anion resin. Since no biological or environmental reference materials with certificated values for Pt and Au is available up to date, we preconcentrated Au and Pt from China-made geological standard reference materials DZΣ-1 and DZΣ-2 and determined them by ICP-MS.

2. Experimental

2.1. Instruments and apparatus

A miniature nuclear reactor (China Institute of Atomic Energy); a γ-ray spectrometer system (HPGe detector of Nucleus, PCA-II-8000 multianalyzer, detection effect 25% and resolution 1.96 keV for 1332 KeV peak of ^{60}Co); a Teflon column (ϕ10 mm × 250 mm) with adjustable flow-rate and various plastic vials (ϕ5 mm × 35 mm; ϕ10 mm × 50 mm) for measuring the radioactivities.

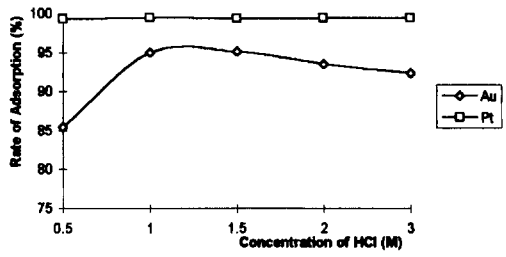

Fig. 1. Effect of HCl concentration on Au and Pt adsorption on HHY-10A resin (20 ml HCl, flow-rate 1.0 ml min^{-1}).

2.2. Radiotracers and other reagents

The radiotracers ^{195m}Pt and ^{199}Au are made of the same chemical reagent (H_2PtCl_6). The chemical, 300 mg was irradiated in the nuclear reactor for 5 h (neutron flux 5×10^{11} n cm^{-2} s), the ^{195m}Pt was formed via ^{194}Pt(n, γ) reaction, while the ^{199}Au via ^{198}Pt(n, γ)^{199}Pt, and followed by its β^- decay in the same time. After cooling for 24 h, the chemical was dissolved in 50 ml 0.5 M HCl as stock solution. All other reagents, such as HCl and thiourea, are A.R degree, and the water is deionized. The HHY-10A resin is a kind of macropore resin with Cl ionic form, it has a large exchange capacity (4.1 mmol g^{-1}) and a proper wet density (0.69 g ml^{-1}), its particle size, cross-linkage, specific surface, porosity and hole diameter are 0.3–1.2 mm, 4%, 38 m^2 g^{-1}, 0.54 cm^3 g^{-1} and 24.2 nm, respectively, and the functional group amido is bound to the polystyrene diethylenebenzene frame.

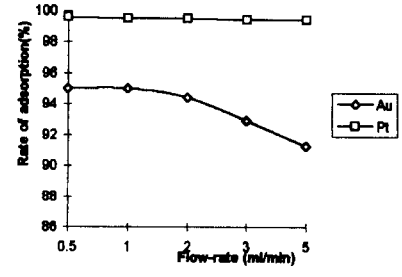

Fig. 2. Effect of flow-rate on adsorption of Au and Pt on HHY-10A resin (20 ml 1.0 M HCl).

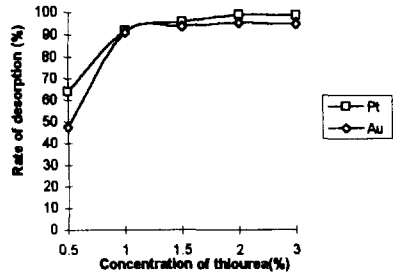

Fig. 3. Effect of thiourea concentration on desorption of Au and Pt on HHY-10A (20 ml thiourea, 1.0 ml min^{-1}).

2.3. Adsorption and desorption

The column was filled with about 1.0 g (20 mm high) pretreated HHY-10A resin, which was prebalanced with 0.5 M HCl overnight before use. Pipetted 1.00 ml of the stock solution into a 50 ml beaker, diluted it with 19.0 ml HCl which has a certain concentration. Transferred the diluted radiotracer solution into the column and adjusted the flow-rate to obtain a certain flow velocity, collected the eluent (2 ml each counting vial) and measured the radioactivity of ^{195m}Pt and ^{199}Au at the same time, 2 ml of the stock solution was used as the relative standard. Added the contents of Au and Pt in each vial together to get the total contents Au and Pt which were not been adsorbed, and then the contents of adsorbed Au and Pt could be calculated, the latter were used to calculate the adsorption rates of Au and Pt. After washing the column with 20 ml 0.5 M HCl at 2 ml min^{-1} velocity, desorbed Au and Pt with 20 ml thiourea solution of a certain concentration at a certain flow velocity, collected each 2 ml of the desorbed solution and measured ^{195m}Pt and ^{199}Au.

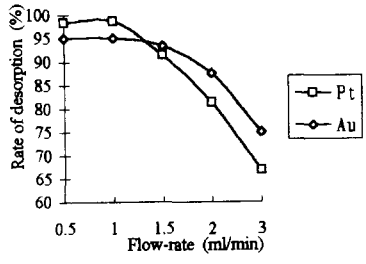

Fig. 4. Effect of flow-rate on the desorption of Au and Pt on HHY-10A resin (20 ml 2% thiourea).

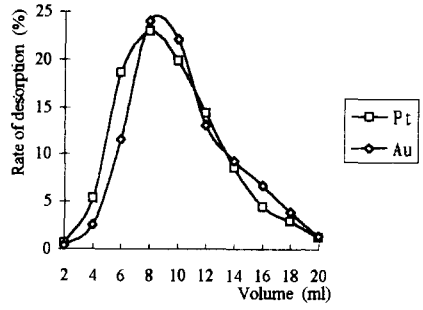

Fig. 5. Desorption curves of Au and Pt from HHY-10A resin (20 ml 2% thiourea at 1.0 ml min^{-1}).

Added the contents of Au and Pt in each vial together to get the total contents of Au and Pt desorbed, and then the desorption rates of Au and Pt were calculated. The stock solution, 2 ml, was used as the relative standard.

2.4. Analysis of SRMs

Pt and Au in some China-made geological standard reference materials ultrabasic DZΣ-1 and DZΣ-2 were preconcentrated using the above described method and determined with ICP-MS. Before preconcentration, 10.00 g of the samples were baked at 600°C for 1 h to oxide the organisms and dissolved in 100 ml aqua regia. Evaporated the solution to near dryness and drove HNO_3 off with 10 ml concentrated HCl, repeated twice. And then, dissolved the residue with 50 ml 1.0 M HCl and filtered it, washed the residue with another 50 ml 1.0 M HCl. After preconcentration, the solution containing Au and Pt was treated and the concentrations of Au and Pt were determined. The method of determination using ICP-MS was reported elsewhere [10].

3. Results and discussion

3.1. Adsorption acidity

The adsorption of Pt is almost complete in the range of 0.5–3.0 M HCl (1.0 ml min^{-1} flow-rate). Fig. 1 shows the effect of the HCl concentration on the adsorption percentage of Pt and Au. The

Table 1
The contets of Au and Pt in DZΣ-1 and DZΣ-2 ($n = 2$, ng g^{-1})

Samples	DZΣ-1 [10]		DZΣ-2 [10]	
	Experimental values	Reference values [10]	Experimental values	Reference values [10]
Pt	3.9	4	6.0	6
	4.8		7.1	
Mean	4.4 ± 0.5		6.6 ± 0.6	
Au	1.3	1.4	0.3	0.4
	1.9		0.8	
	1.6 ± 0.3		0.6 ± 0.3	

maximum adsorption of Au is at about 1.2 M HCl and the adsorption increases or decreases gradually with the concentration of HCl increasing before 1.2 M or decreasing after that. It is evident that the adsorption is less than 96% in any case, perhaps it is due to the change of Au valence during the nuclear decaying process. Most of the Au atoms exist as Au^{3+}, perhaps there is a minor existing in Au^{+}, whose ability to form complex ions is not as good as Au^{3+}. Thus, the adsorption rate of Au^{+} is less than Au^{3+} during the adsorbing stage. But generally speaking, the adsorption of Au is satisfactory.

3.2. Adsorption flow-rate

Each of the flow-rate tested (0.5–5.0 ml min^{-1}) has a almost complete adsorption of Pt (HCl concentration 1.0 M). Fig. 2 shows the recoveries of Pt and Au at different flow-rates. Obviously, Au can be adsorbed quantitively at a flow-rate of ≤ 2 ml min^{-1}.

3.3. Desorption conditions

Fig. 3 shows the recoveries of Au and Pt desorbed with 20 ml different concentration of thiourea (1.0 ml min^{-1} flow-rate) from the column. Evidently, Au and Pt can be desorbed quantitively by 20 ml 2% (w/w) thiourea and their recoveries are greater than 91% when 20 ml 1% thiourea is used as desorbent. Fig. 4 shows the effect of flow-rate on the desorption of Au and Pt (2% thiourea), it can be seen that the rate of desorption decreases dramatically when the flow-rate is greater than 1.5 ml min^{-1}, and the quantitative desorption happens only at the flow-rate not exceeding 1.0 ml min^{-1}. Fig. 5 describes the desorption curves of Au and Pt (20 ml 2% thiourea at 1.0 ml min^{-1}).

3.4. Precision and accuracy

At the optimum conditions (adsorption in 1.0 M HCl at 1.0 ml min^{-1}, desorption with 2% thiourea at 1.0 ml min^{-1}), using 1.0 ml radiotracer stock solution replicated the experiments for three times. The total recoveries of Au and Pt are $(92.3 \pm 2.6)\%$ and $(97.7 \pm 0.9)\%$, respectively. The analytical results for ultrabasic SRMs DZΣ-1 and DZΣ-2 are listed in Table 1, which are in good agreement with the reference values [10].

4. Conclusion

The radiotracer technique is very convenient and successful in establishing preconcentration procedure for Au and Pt. The HHY-10A anion resin is suitable for preconcentrating Pt and Au for the quantitative adsorption and easy desorption at the optimum conditions we experimented. The SRMs analytical results agreed with the reference values very well.

Acknowledgements

The authors express appreciation to Wang Ke, Dong Jinquan and Ouyang Hong for their help with the experimental work.

References

[1] Liu Yingjun, Cao Liming and Li Zhaolin, Element Earth Chemistry, Science Press, Beijing, 1984, p. 344.
[2] V. Hodge and M. Stallard, Environ. Sci. Technol., 20 (1986) 1058–1060.
[3] V. Hodge, M. Stallard and M. Koide, Anal. Chem., 58 (1986) 616–620,
[4] S.A. Wood and D. Vlassopoulos, Anal. Chim. Acta, 229 (1990) 227–238.
[5] S.J. Parry, M. Asif and H. Malik, Analyst, 117 (1992) 1351–1353.
[6] O. Nygren and G.T. Vaughan, Anal. Chem., 62 (1990) 1637–1640.
[7] F. Alt, K. Hoppstock and K. Camman, Fresnius Z. Anal. Chem., 355 (1989) 813–816.
[8] M. Parent, R. Cornelis and F. Alt, Biol. Tra. Elem. Res., 1994, pp. 109–195.
[9] Practical Aspect of Operating: A Neutron Activiation Analysis Laboratory, IAEA-TECDOC.564.
[10] H. Zeng and C. Ji, Chin. J. Rock Miner. Anal., 2 (15) (1996) 92–96.

ELSEVIER

Talanta 44 (1997) 1319–1327

Talanta

A selective optical chemical sensor for *o*-nitrophenol based on fluorescence quenching of curcumin

Ying Wang [1], Ke-Min Wang, Guo-li Shen, Ru-Qin Yu *

Department of Chemistry and Chemical Engineering, Hunan University, Changsha, 410082, People's Republic of China

Received 19 July 1996; received in revised form 10 January 1997; accepted 20 January 1997

Abstract

An optical chemical sensor has been prepared for the selective determination of *o*-nitrophenol in aqueous solutions based on the fluorescence quenching of curcumin in PVC membrane. The sensing mechanism of the proposed sensor for *o*-nitrophenol has been discussed in detail. The fluorescence changes of sensing membrane resulted from an associated complex formation between curcumin and *o*-nitrophenol. In pH 4.8 buffer solution, the sensor responds linearly in the measuring range from 1.0×10^{-2} mol l^{-1} to 1.5×10^{-4} mol l^{-1}, and the experimental detection limit is evaluated to be 8.0×10^{-5} mol l^{-1}. A stable signal was obtained within less than 1.5 min. Under the optimum conditions, the sequence of selective response to the sensing membrane is *o*-nitrophenol > 2,4-dinitrophenol > *m*-nitrophenol > *p*-nitrophenol > 2,4,6-trinitrophenol. Phenol, aniline as well as other ions have less effect on the fluorescence of the sensor. The reproducibility for the determination of *o*-nitrophenol is better than 1%, and the response is reversible. The sensor can be used for the determination of *o*-nitrophenol in water samples. © 1997 Elsevier Science B.V.

Keywords: Curcumin; Fluorescence quenching; Optical sensor

1. Introduction

In recent years, owing to the development of a large variety of devices and techniques of the optical fiber sensing and its potential advantages over electrochemical sensing, the interest in the development of optically based chemical sensors has been increasing considerably. A common feature of this kind of sensors is that an immobilized reagent phase changes the optical properties upon interaction with an analyte. Therefore, the selection of immobilized reagents plays the central role in the development of the optical chemical sensors. The sensing materials in optode membrane based on fluorescence described in the literature include polycyclic aromatic hydrocarbons [1,2], laser dyestuff compounds [3], hydroxyquinoline compounds [4], and some newly synthesized fluorescence reagents [5]. In this work, an organic chromogenic reagent curcumin widely used for the measurement of trace boron in various samples is employed as the sensing material in optode

* Corresponding author.

[1] On leave from the Southwest China Normal University, Chongqing, Sichuan.

PII S0039-9140(97)00028-3

membrane utilizing its excellent fluorescence property and high lipophilicity.

Though different kinds of optical fiber chemical sensors have been reported in the literature measuring various species important for environmental monitoring such as ammonia [6], sulfur dioxide [7], nitrogen dioxide [8], organochlorinated compounds [9], nitro-compounds [10,11], and humidity [12], to our knowledge, however, no sensors have been reported for the determination of *o*-nitrophenol.

The monitoring of nitrophenols is essential for environmental pollution control and industrial applications. In the past, after being reduced and transformed into azostuffs, the compounds formed were detected with spectrophotometry or polarography [13]. More recently, nitrophenols are determined with GC or HPLC [14–16]. Questions remain, however, as to how to realize the on line and continuous determination of *o*-nitophenol with a non-destructive device such as an optical chemical sensor.

We discovered that *o*-nitrophenol in buffer solution of pH = 4.8 can strongly quench the fluorescence of curcumin. A new sensor using curcumin as sensing material for the selective determination of *o*-nitrophenol has been prepared. The sensor can respond selectively, rapidly and reversibly to *o*-nitrophenol. These analytical characteristics make it possible to determine *o*-nitrophenol in mixtures containing appropriate amounts of other nitrophenols. The analytical results obtained by recovery measurement are satisfactory.

2. Experimental

2.1. Apparatus

All fluorescence intensities were measured with a Hitachi M-850 fluorescence spectrophotometer equipped with a xenon lamp. For measuring fluorescence quenching, the excitation and emission wavelengths were set to 426 and 512 nm, respectively.

2.2. Chemicals

Unless otherwise stated, all solutions were prepared from analytical-reagent grade with redistilled water. For membrane preparation, the following reagents were purchased and used without further purification: high relative molecular mass poly(vinyl chloride)(PVC)(Zhuzhou Chemical Plant), tetrahydrofuran(THF) (Shanghai Chemical Reagent Corporation), curcumin (The Third Reagent Plant of Shanghai), tricresyl phosphate (C.P. The First Reagent Plant of Shanghai). Test solutions of *o*-nitrophenol were prepared by dilution of the stock standard solution. Acetate buffer solution (pH = 4.8) was prepared by dissolving 50 g of sodium acetate trihydrate in 500 ml of water, adding 34 ml of 6 mol l^{-1} acetic acid and diluting to 1 l.

2.3. Procedure

2.3.1. Membrane preparation

A medium containing 4.0 mg of curcumin, 50 mg of PVC, 100 mg of tricresyl phosphate was dissolved in 2 ml of THF. By means of a spin -on device [1], a membrane of approximately 4 μm thickness was cast onto a 35 mm diameter quartz plate.

2.3.2. Measurement of o-nitrophenol

Two identical membranes were subsequently mounted in the specially designed flow-through measuring cell [1]. About 3.4 ml of sample solution was aspirated by a syringe. Fluorescence measurements were completed under batch condition. The limiting fluorescence intensities F_b and F_s of the optode membrane were detected in pH = 4.8 blank solution and in 4.0×10^{-2} mol l^{-1} *o*-nitrophenol, respectively.

For the selectivity evaluation, the separate solution method (SSM) [17] was used to estimate the selectivity of the *o*-nitrophenol sensor with respect to other nitrophenols. The effect of other potential interferents on sensing performance was also tested.

3. Results and discussion

3.1. Principle of operation and quenching mechanism of o-nitrophenol

We discovered that *o*-nitrophenol can strongly quench the fluorescence of curcumin in the PVC membrane. Fig. 1 shows the fluorescence spectra of the optode membrane incorporating curcumin in pH = 4.8 buffer solutions containing various concentrations of *o*- nitrophenol. The fluorescence spectra were recorded at excitation wavelengths from 360 to 480 nm and emission wavelengths from 460 to 600 nm. It is apparent that the increase of *o*-nitrophenol concentrations causes a significant decrease in the fluorescence intensity of curcumin.

In order to explain the aforementioned phenomenon in the view of complex formation, we supposed that curcumin in the plasticized PVC membrane phase (org.) with *o*-nitrophenol in the aqueous solution (aq.) forms a *m*:*n* complex, the over-all equilibrium can be described as:

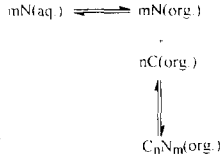

$$\text{i.e., } nC(org.) + mN(aq.) \rightleftharpoons C_nN_m(org.) \quad (1)$$

where C and N represent curcumin and *o*-nitrophenol, respectively. There is an equation as follows [1]:

$$\frac{\alpha^n}{1-\alpha} = \frac{1}{nKC_C^{n-1}[N]^m} \quad (2)$$

where C_C is the total concentration of curcumin in the membrane, [N] is the concentration of *o*-nitrophenol in aqueous solution, α (relative fluorescence value) is the ratio of the free curcumin concentration, [C], to the total concentration of curcumin present in the membrane, C_C, i.e.,

$$\alpha = \frac{[C]}{C_C} \quad (3)$$

and K is the equilibrium constant of the reaction described by Eq. (1). Relative fluorescence value α can also be derived from Eq. (3) that

$$\alpha = \frac{F - F_s}{F_b - F_s} \quad (4)$$

where F_b and F_s are the limiting fluorescence intensities when the optode membrane contacted with the blank solution and 4.0×10^{-2} mol l^{-1} *o*-nitrophenol solution, respectively. F is the fluorescence intensity of optode membrane exposed to the different concentrations of *o*- nitrophenol solutions. Obviously, Eq. (2) provides the basis for quantitative determination of *o*-nitrophenol.

It can also be seen from Eq. (2) that when the stoichiometric ratio of the complex changes, the relative fluorescence value α with various concentrations of *o*-nitrophenol has different functional relations. The fitted curves (1) in Fig. 2 by changing the ratio of *m* to *n* and adjusting the over-all equilibrium constant K was the best one to represent the experimental data. In other words, the complex ratio of *o*-nitrophenol to curcumin is 1:1.

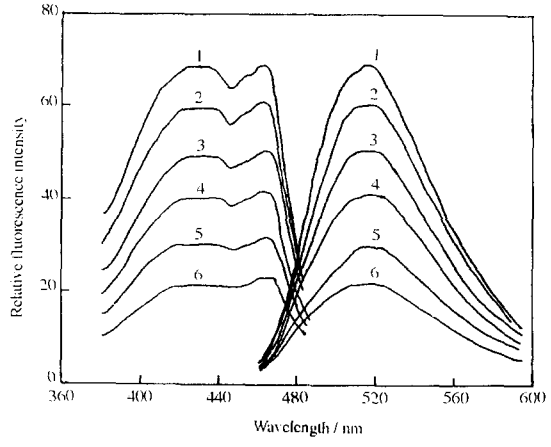

Fig. 1. Fluorescence spectra of the optode membrane after equilibrium with different concentrations *o*-nitrophenol solutions buffered at pH = 4.8. (5 nm bandwidth for excitation and emission, $\lambda_{ex} = 421$ nm and $\lambda_{em} = 520$ nm). 1. Reagent blank; 2. 2.5×10^{-4} mol l^{-1}; 3. 5.0×10^{-4} mol l^{-1}; 4. 1.0×10^{-3} mol l^{-1}; 5. 1.8×10^{-3} mol l^{-1}; and 6. 2.5×10^{-3} mol l^{-1}.

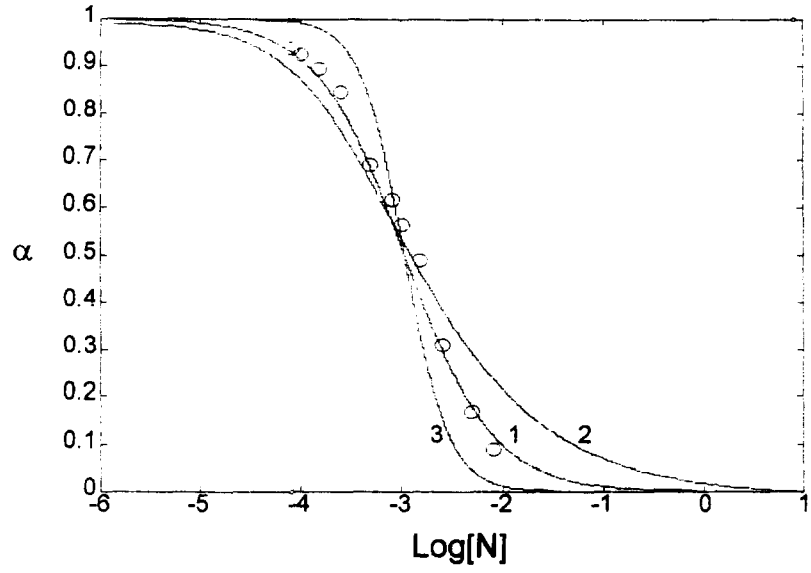

Fig. 2. Fitting the experimental data to Eq. (2). 1. $m:n = 1:1$, K = 800 (best fit); 2. $m:n = 1:2$, K = 150 000; and 3. $m:n = 2:1$, K = 650 000.

Curcumin is able to emit a strong yellow-green fluorescence. It usually exists in the keto (I) or enol (II) forms, i.e.,

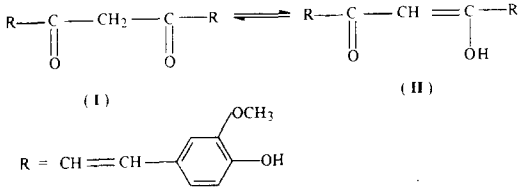

It is possible for hydroxyl or carbonyl groups to form associated complexes by the means of hydrogen-bonds with some compounds containing hydroxyl or nitro group.

As the stoichiometric ratio of *o*-nitrophenol to curcumin is proved to be 1:1 and *o*-nitrophenol exists mainly in the molecular form at pH 4.8, it seems that the hydroxyl and nitro-groups in *o*-nitrophenol simultaneously associate with the carbonyl and hydroxyl groups of II through hydrogen-bonds to form non-fluorescent ground state complex (III). i.e.,

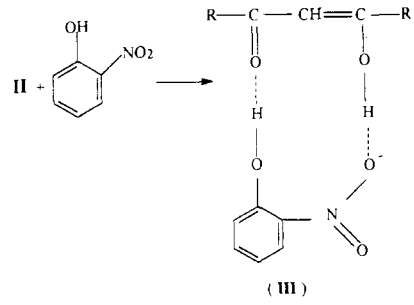

The formation of the cyclic structure III causes the fluorescence quenching of curcumin.

3.2. Membrane composition

The membrane composition was optimized by selecting appropriate plasticizers. Plasticizers must be selected so as to obtain a transparent and

flexible membrane, which has the maximum response to *o*-nitrophenol. The sensing membranes made of the different plasticizers such as tricresyl phosphate, dinonyl sebacate, butyl phthalate and didecyl phthalate were prepared. The membrane consisting of tricresyl phosphate shows the best results. The amount of curcumin giving the maximum sensitivity to *o*-nitrophenol is 2–4 mg. The optimum sensing membrane shows a linear response to *o*-nitrophenol in the range from 1.0×10^{-2} to 1.5×10^{-4} mol l^{-1}.

3.3. Influence of the acidity on o-nitrophenol sensitivity

The blank fluorescence of the sensing membrane itself was found to be independent of pH from 1.0 to 8.0. Solutions at pH > 8 caused the curcumin to be dissolved out from the PVC membrane. Fig. 3 shows the changes in relative fluorescence value α of the sensing membrane with the different pH in the presence of 1.0×10^{-3} mol l^{-1} *o*-nitrophenol. Because the ionization of *o*-nitrophenol was inhibited at pH < 6, α remained a constant. The extent of *o*-nitrophenol ionization was increased at pH > 6 so that the ability to form hydrogen-bonds with curcumin in the membrane was weakened and α increased. In our experiment, a HOAc–NaOAc buffer solution of pH 4.8 was used.

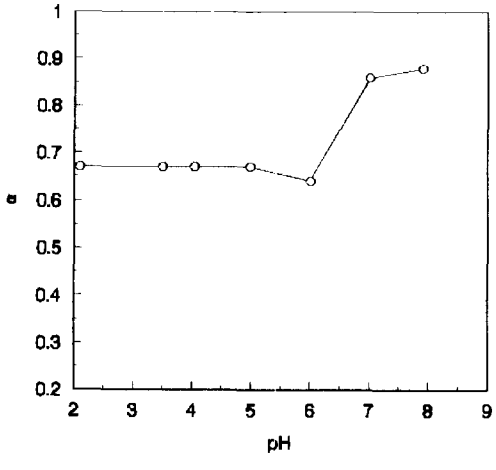

Fig. 3. Response of optode membrane at the different pH.

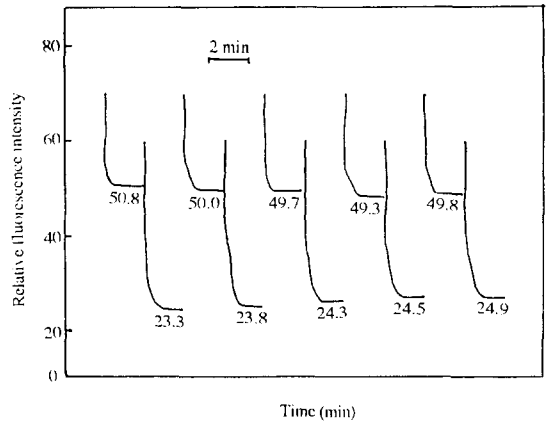

Fig. 4. Response of *o*-nitrophenol optode membrane versus time after a concentration step changing between 5.0×10^{-4} mol l^{-1} and 1.8×10^{-3} mol l^{-1}.

3.4. Reproducibility and response time

The reproducibility of the optode membrane consisting of curcumin in the determination of *o*-nitrophenol was evaluated by repetitively dipping the sensor into two sample solutions. Fig. 4 shows the fluorescence intensities change versus time recordings for the *o*-nitrophenol optode membrane. The present sensor shows good reproducibility and reversibility. Five determinations at 5.0×10^{-4} mol l^{-1} and 1.8×10^{-3} mol l^{-1} *o*-nitrophenol produced standard deviations of 0.55 and 0.62, respectively. Stable readings were obtained within ca. 1.5 min.

3.5. Short-term stability

Short-term stability for the optode membrane in 5.0×10^{-4} mol l^{-1} *o*-nitrophenol solution buffered at pH = 4.8 was measured over a period of 6 h. From the fluorescence intensities taken every 30 min ($n = 12$), a mean value of 48.3 and a standard deviation of 1.45 were obtained. During this period of time there was no evidence of significant leakage of reagent from the membrane and changed in response. The sensor was immersed in a HOAc–NaOAc buffer solution of pH 4.8 when not in use.

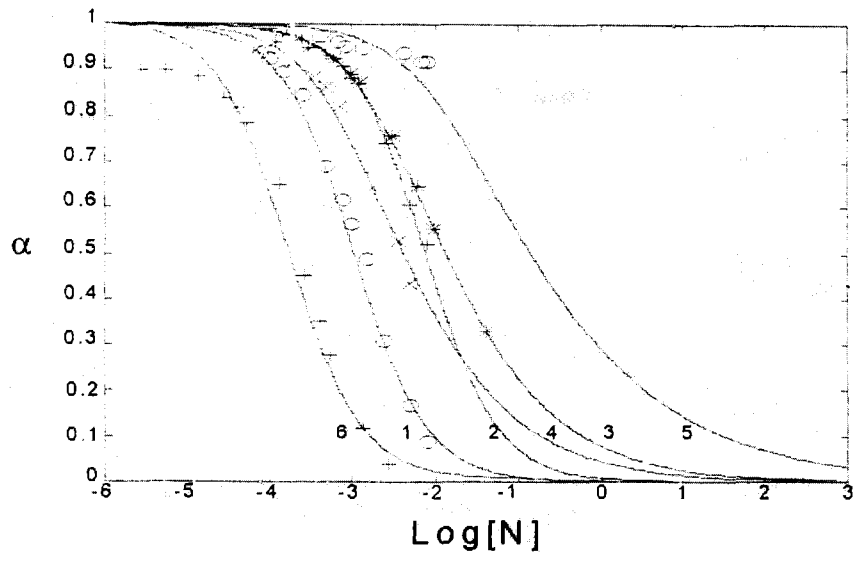

Fig. 5. Dependence of relative fluorescence values α on the various concentrations of nitrophenols. The curves were fitted according to Eq. (2). 1. *o*-nitrophenol (*m*:*n* = 1:1, K = 800); 2. *m*-nitrophenol (*m*:*n* = 1:1, K = 120); 3. *p*-nitrophenol (*m*:*n* = 1:2, K = 13000); 4. 2,4-dinitrophenol (*m*:*n* = 1:2, K = 4000); 5. 2,4,6-trinitrophenol; and 6. 2,4,6,-trinitrophenol (*m*:*n* = 1:1, K = 5000, 1.5 mol l^{-1} H_2SO_4 medium).

3.6. Measurement range, equilibrium constant and detection limit

As mentioned above, Fig. 2 shows that the curve referring to 1:1 complex ratio and K = 800 is the best one fitted to the experimental data. The best fitted curve can be served as the calibration curve for the determination of *o*-nitrophenol. A practically usable range for quantitative determinations covers 1.0×10^{-2}–1.5×10^{-4} mol l^{-1} of *o*-nitrophenol with a detection limit of 8×10^{-5} mol l^{-1}.

3.7. Selectivity

To investigate the influences of nitrophenols similar to *o*-nitrophenol structure on the optode membrane, the separate solution method (SSM) was employed. It is supposed that curcumin in plasticized PVC membrane phase (org.) forms *m*:*n* complexes with other nitrophenols in the aqueous solution (aq). According to the similar method as mentioned above, the best fitted curves (2), (3), (4), (6) for *m*-nitrophenol, *p*-nitrophenol, 2,4-dinitrophenol in the buffer solution of pH 4.8 and 2,4,6-trinitrophenol in 1.5 mol l^{-1} H_2SO_4 medium were obtained. The stoichiometric ratio for *m*-nitrophenol-curcumin complex is 1:1 and the complex compositions for *p*-nitrophenol and 2,4-dinitrophenol with curcumin are 1:2. It is obviously from Fig. 5 that the response sequence for nitrophenols to curcumin is *o*-nitrophenol > 2,4-dinitrophenol > *m*-nitrophenol > *p*-nitrophenol > 2,4,6-trinitrophenol under the experimental conditions tested.

As described above, *o*-nitrophenol can form an associated complex (III) with curcumin in the PVC membrane, while it is difficult for *m*-nitrophenol, *p*-nitrophenol and 2,4-dinitrophenol to form complexes similar to III owing to steric hindrance. From the view of stoichiometric ratios of *m*-nitrophenol, *p*-nitrophenol and 2,4-dinitro-

phenol to curcumin, one may assume that *m*-nitrophenol form the associated complex (IV) or (V) and *p*-nitrophenol and 2,4- dinitrophenol form the associated complex (VI) or (VII). i.e.,

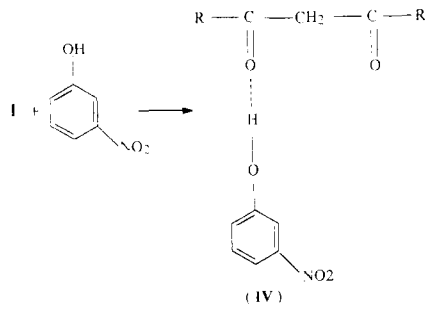

(IV)

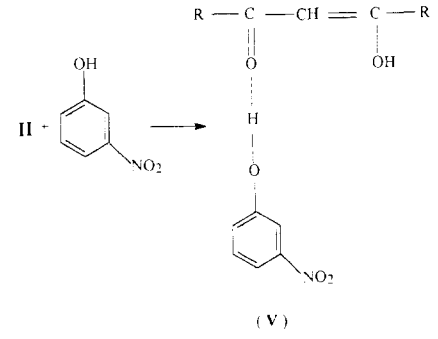

(V)

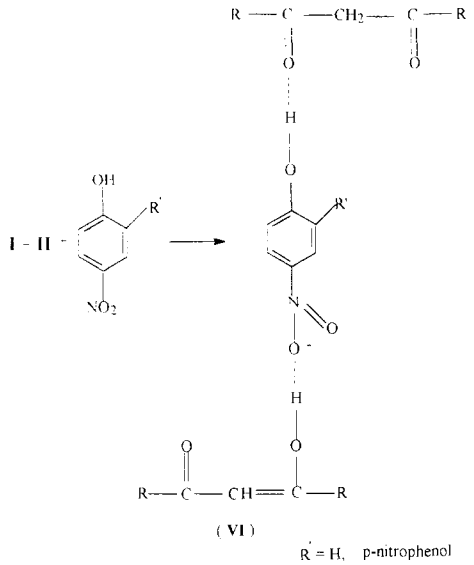

(VI)

R' = H, p-nitrophenol

R' = NO_2, 2,4-dinitrophenol

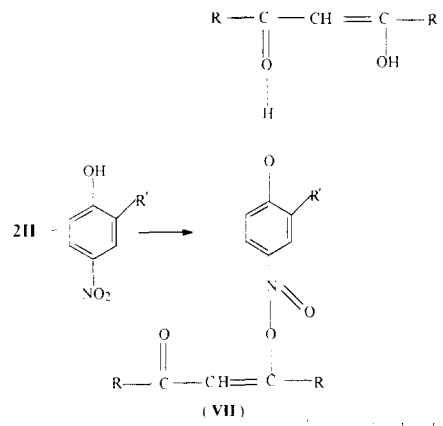

(VII)

R' = H, p-nitrophenol

R' = NO_2, 2,4-dinitrophenol

The quenching relatively strong by *o*-nitrophenol comparing to other nitrophenols seems to be related to more favorite complex forming sites for *o*-nitrophenol.

2,4,6-trinitrophenol has a structure similar to *o*-nitrophenol. However, it tends to dissociate more completely at pH 4.8 and is mainly in the anion form, which may not form associated complex with curcumin. The quenching effect of 2,4,6-trinitrophenol is much weaker than that of *o*-nitrophenol.

It was observed, however, 2,4,6-trinitrophenol can strongly quench fluorescence of the sensing membrane in 1.5 mol l^{-1} H_2SO_4 medium. In such medium, 2,4,6-trinitrophenol exists in the molecular form and forms an 1:1 associated complex with curcumin.

The effect of other potential interferents such as aniline, phenol and some ions were also tested for their possible co-occurrences in environmental samples with *o*-nitrophenol. No significant interferences were observed if a tolerance of less than $\pm$ 5% relative error in the determination of 1.5×10^{-3} mol l^{-1} *o*-nitrophenol was considered. Table 1 summaries the results obtained. The practical application of the optode membrane based on curcumin for the determination of *o*-nitrophenol seems really feasible.

Table 1
Effect of different interferents on the fluorescence signal of the optode membrane[a]

Interferent	Concentration (mol l^{-1})	Fluorescence change value $\Delta F = (F_2 - F_1)$[b]	Relative fluorescence change value(%) $(\Delta F/F_1) \times 100$
Phenol	4.50×10^{-3}	0.900	3.67
Aniline	6.00×10^{-3}	−0.500	−2.04
Nitrobenzene	1.00×10^{-3}	−0.700	−2.85
NaCl	1.00	−1.00	−4.08
KCl	1.00	0.300	1.22
$NaNO_3$	1.00	−0.300	−1.22
$CaCl_2$	0.80	−1.00	−4.08
$MgCl_2$	0.80	−1.10	−4.49
$Pb(NO_3)_2$	8.00×10^{-3}	0.900	1.23
$Cu(NO_3)_2$	7.00×10^{-3}	−0.200	−0.80
$CoCl_2$	5.00×10^{-2}	−0.600	−2.45
$FeCl_3$	1.00×10^{-2}	0.900	3.67
$ZnCl_2$	1.50×10^{-3}	0.900	3.67
$NiSO_4$	5.00×10^{-3}	−0.600	−2.45
$HgCl_2$	1.50×10^{-3}	0.300	1.22
$CrCl_3$	5.00×10^{-3}	−0.500	−2.04

[a] Each sample solution contained a fixed *o*-nitrophenol concentration 1.5×10^{-3} mol l^{-1}. The fluorescence intensities were recorded after the sample solutions have contacted with the membrane for 2 min.
[b] F_1 and F_2 are the fluorescence intensities of the optode membrane contacted with the 1.5×10^{-3} mol l^{-1} *o*-nitrophenol solutions without and with interferents, respectively.

Table 2
Determination of *o*-nitrophenol in tap water sample

Sample	Analyte and interferents added (10^{-3} mol l^{-1})					*o*-NP found[a] (10^{-3} mol l^{-1})	Recovery (%)
	o-NP	*m*-NP	*p*-NP	2,4-DNP	2,4,6-TNP		
1	1.00	0.80	1.20	0.50	1.50	1.08	108
2	1.00	0.50	1.20	0.30	1.50	1.04	104
3	1.00	0.20	1.20	0.15	1.50	1.01	101
4	0.50	0.20	0.60	0.15	1.50	0.501	104
5	0.50	0.50	0.60	0.15	1.50	0.50	108
6	0.50	0.20	0.60	0.30	1.50	0.505	110

o-NP, *o*-nitrophenol; *m*-NP, *m*-nitrophenol; *p*-NP, *p*-nitrophenol; 2,4-DNP, 2,4-dinitrophenol; 2,4,6-TNP, 2,4,6-trinitrophenol.
[a] An average of three determinations.

3.8. Determination of o-nitrophenol in water samples

To examine the recovery for the *o*-nitrophenol determination in the presence of other nitrophenols, the tap water samples with different amounts of nitrophenols added were analyzed. The recovery was 101 –108% (Table 2).

Acknowledgements

The authors thank the National Natural Science Fund of China for its support of this research

References

[1] H.H. Zheng, K.M. Wang, C.L. Liu and R.Q. Yu, Talanta, 40 (1993) 1569.

[2] O.S. Wolfbeis and A. Sharma, Anal. Chem. Acta, 208 (1988) 53.
[3] B.P.H. Schaffar, Otto S. Wolfbeis, A. Leitner, Analyst, 113 (1988) 693.
[4] K.S. Lee, W. Lee and D.W. Lee, Anal. Chem., 50 (1978) 225.
[5] K.M. Wang, K. Seiler, B. Rusterholz and W. Simon, Analyst, 117 (1992) 57.
[6] S. West, S. Ozawa, K. Seiler, S.S.S. Tan, W. Simon, Anal. Chem., 64 (1992) 533.
[7] Otto S. Wolfbeis, H.E. Posh and H.K. Kroneis, Anal. Chem., 57 (1985) 2556.
[8] T. Kobayashi, M. Hirama and H. Inaba, Appl. Opt., 20 (1981) 3279.
[9] F.P. Milanovich, D.G. Garvis, S.M. Angel and S.M. Klainer, Anal. Instrum., 15 (1986) 136.
[10] F.L. Dickert and S.K. Schreiner, G.R. Mages and H. Kimmel, Anal. Chem., 61 (1989) 2306.
[11] K.M. Wang, H.H. Zheng and R.Q. Yu, Chem. J. Chim. Univ., 15 (1994) 836.
[12] K.M. Wang, K. Seiler, J.P. Haug, B. Lehmann, S. West, K. Hartmann, W. Simon, Anal. Chem., 64 (1992) 533.
[13] Shanghai Sanitation and Antiepidemic, Environmental Protection Examination, Shanghai Science and Technology Press, Shanghai, 1977.
[14] J.J. Scanlon, P.A. Flagver, G.W. Robinson, G.E. O' Brien, P.E. Sturrock, Anal. Chim. Acta., 158 (1984) 169.
[15] B. Schaltz, J. Chromatogr, 269 (1983) 208.
[16] E. Tesarove, V. Packova, Chromatographia, 17 (1983) 269.
[17] K.M. Wang, Theories and Methods of Optical Chemical Sensor, Hunan Education Publishing House, Changsha, 1994.

ELSEVIER

Talanta 44 (1997) 1329–1331

Talanta

Book reviews

Stat-100, version 1.22 Biosoft, Cambridge, 1996. £99.00, US$199.00.

Stat-100 is a general purpose statistical analysis program for Microsoft Windows. It is accompanied by a comprehensive 161-page manual (with an index) and on-line help is available during program execution. The minimum requirements are: a 386 cpu, Windows 3.1 (or later), VGA monitor (or better), at least 4 Mb of ram and a minimum of 6 Mb of hard disk space for the program files. I installed the program, on a personal computer with a pentium cpu and Windows 3.1, plus the sample files without any problems. As the name implies, more than 100 procedures are offered for processing, analysing and presenting data. There is a STAT-100 native format but spreadsheet files can also be imported from, or saved as, Excel files. The maximum size of the STAT-100 spreadsheet is stated to be 262 144 cells.

The techniques covered include parametric and non-parametric analytical statistics, analysis of variance, linear regression analysis and survival data analysis. The usual set of descriptive statistics (mean, standard deviation, max and min values, skewness, etc.) is calculated in one easy operation. Numerous data transformations are possible, e.g. converting absorbance to log absorbance or temperature to reciprocal temperature - these are easily performed and include polynomial, probability and trigonometric transforms. In addition the expected range of spreadsheet operators and functions are also available.

Graph types include line, pie, bar, scatter, box-whisker charts and 3D plots. Fits can be made to polynomial, logarithmic, exponential and power functions. These numerous plots are easily annotated and various graph styles can be created. The graphs can be printed or saved and, if required, exported as Windows bitmaps or metafiles. The many options available for graph plotting take some time to explore and once the desired format is obtained it can be saved as a template. I found that this template worked well when the graph filled the whole screen. I also found it possible to incorporate several plots on the one set of axes.

I completed the tutorial in the manual with the correct results but occasionally found the indicator for a data range, e.g. $B$1:$B$10, appearing in the output. This caused no problems for graph labelling as editing options are comprehensive—in this case editing the 'legend text' removed the range label. Care is required to ensure that the order of data entry is correct, e.g. select X values first then Y values for line graph plotting but select Y values first then X values for simpler linear regression. I also tried many of the tests on offer (ANOVA, Student's t, Chi-squared, Mann-Whitney U, etc.) and found that the learning curve soon became horizontal. Producing the required results with this program is an easy task.

Overall an excellent program with a helpful manual that will enable you to quickly perform probably all the statistical calculations you will ever need. Try the free demonstration disk from Biosoft which can be downloaded from the Internet (http://www.cityscape.co.uk/biosoft/).

P.J. Cox

PII S0039-9140(96)02146-7

A Manual for the Chemical Analysis of Metals, by T.R. Dulski, ASTM, West Conshohocken, PA, 1996, xiv + 251 pp., US$89. ISBN 0-8031-2066-4.

This book is a comprehensive laboratory manual that deserves to become a best-seller in the metal analysis community. The book is a treasure trove of information, providing extensive and up-to-date references on all aspects of the analytical process. Furthermore, the author is a gifted writer and as evidence of this I confess to packing the book for my summer vacation. The book is divided into 5 sections that progress from Materials (laboratory design, equipment and reagents) to Samples (sampling, sample preparation and dissolution in acids) and thence to Separations followed by Measurement (gravimetry, titrimetry, absorption/emission spectroscopy etc.) and, finally, a section on Quality (reference materials, calibration, validation, statistics, good laboratory/administration practices and personnel). The book concludes with a series of Appendices that provide at-a-glance information on the chemical behaviour of analytes and strategies for their analysis.

It is the width of subject material and the depth to which it is treated that makes this book so valuable and unique. In addition to this the book is ruggedly bound—an important consideration for a laboratory manual. Finally, the really good news for cash strapped laboratories is that all this can be yours for a mere $89.

B.A. McGaw

PII S0039-9140(96)02147-9

EqCaL for Windows, by L. Lackman, Biosoft, 1996. £125.00.

The package supplied includes a well presented manual which accompanies the disk containing the program which is for use with Windows 3.1 or later versions. The terminology used, both in the manual and the disk, for accessing and using the program should present no problems to those who are familiar, with Windows 3.1. To operate the system the user will need a 386SX or higher processor with a minimum of 4 Mb of memory and 1 Mb of free disk space. Installation proved very straight forward. The system is well designed and does take the tedium out of the cumbersome, time consuming calculations required for determining the equilibrium concentrations of the individual components in, for example, buffer solutions, chelation or binding interactions and other complex multiple equilibria reactions. To use this program the user must have prior knowledge of both the equilibrium constant and the balanced chemical equation for each of the reactions involving the components of the solution from which all the species present at equilibrium are formed. It will not cope with the ionic strength effects on the equilibria of the addition of ionic components not taking part in the equilibria.

The readily understandable manual clearly explains both the conventions using the EqCal program and how to use EqCal. The instant 'user friendly' Help facility in the program supplies the operational answers to any difficulties the user may have with the program.

Data input is comparatively straight forward. The sample session included in the manual is a particularly good guide to the on screen information and data/calculation handling facilities. It would have been helpful to have included in the manual a typical screen output for the equilibrium and total concentration calculations for the components present. On screen editing of the data and equations, and the storage and retrieval of the final templates and calculated values is easily done. The final results can be customised using display fonts and then printed out. The on screen data can also be easily copied into the clipboard for future pasting into a spreadsheet or wordprocessor.

A high quality presentation which does exactly what it claims to do.

R.R. Moody

PII S0039-9140(96)02148-0

Biosensor and Chemical Sensor Technology - Process Monitoring and Control, edited by K.R. Rogers, A. Mulchandani and W. Zhou, American Chemical Society, Washington, DC, 1995, xii + 187 pp., US$52.95. ISBN 0-8412-3330-6.

This American Chemical Society symposium volume emphasizes the application of biosensors and chemical sensors to monitoring bioproceses. It is divided into two sections. The chapters in the first section describe sensor technologies in various states of development with the common feature that they involve a biological recognition element. The second section describes the application of sensor technologies to bioprocessing monitoring. Each section has a short introductory chapter by the editors.

The first section includes seven chapters on sensor technology. Chapter 2 describes the use of an acoustic immunosensor as an HPLC detector. However, the slow response of immunosensors is detrimental to the separating power of HPLC and the selectivity should render a prior separation unnecessary so it is difficult to see how this will emerge as an important methodology. Chapter 3 is a short but comprehensive review on antibody basics as they relate to immunosensing. Chapter 4 describes the application of evanescent wave fibre optic biosensor technology developed at the Naval Research Laboratory, under the supervision of Fran Ligler, to environmental monitoring. Chapter 6 describes a method for detecting polyaromatic carcinogens based on competitive intercalation with a fluorescent dye using a DNA segment as the recognition element. Chapter 7 describes a chemically modified electrode that involves hydrogen peroxide reduction catalyzed so that it can be carried out at low potential. This device can be coupled to oxidase enzymes that catalyze hydrogen peroxide to yield a family of biosensors. Chapter 8 describes the use of enzyme cycling procedures to make measurements at subnanomolar concentrations. Chapter 9 describes a fructose electrode based on fructose dehydrogenase. While far from comprehensive, the chapters in the first section provide a representative selection of current biosensor research.

The second section emphasizes the application of sensing technology to bioprocess control. It contains two chapters on spectroscopy, including chapter 9 on chemical sensors for pH and oxygen based on fluorescence lifetimes measured by phase techniques and chapter 12 showing that near infrared spectroscopy can selectively measure glutamine and asparagine in water and can potentially be used to measure these substances non-invasively in bioprocesses. It also contains two chapters on the automation of flow injection analysis systems for bioprocess monitoring. Chapter 13 involves automation of several enzymatic methods while chapter 16 describes immunoassay automation. Chapter 11 describes the use of a enzymatic penicillin sensor to monitor penicillin production by fermentation. Chapters 14 and 15 show how conventional measurements of turbidity and chemical concentrations can be used to optimize and predict the output of bioprocesses.

What is striking about this book is how rarely the biosensor technologies described in the first section appear in the section that emphasizes the practical. The only exception to this is the use of a penicillin electrode based on penicillinase and this was done off-line rather than directly in the formation. The lesson here is that biosensors are not yet the practical solution for most bioprocess applications.

The quality of the papers is generally good and the book is recommended for scientists who wish to keep abreast of recent developments in biosensor research and bioprocess monitoring.

W.R. Seitz

PII S0039-9140(96)02149-2

ELSEVIER

Talanta 44 (1997) 1333

Talanta

Announcement

28th ISEAC: 28th Annual International Symposium on Environmental Analytical Chemistry

Geneva, Switzerland,
2–5 March 1998

The aim of this 28th Symposium is to actively encourage progress in methods, instrumentation, applications and to facilitate the transfer of know-how in different fields. It is targeted at scientists, analysts, manufacturers, end-users and post-graduate students.

Tentative main topics of the Symposium:

—Analyzing trace polar products in the environment
—New extraction, separation and instrumental techniques
—Chiral separations in environmental analysis
—Micro-Total Analysis Systems (μTAS)
—In situ measurements and speciation
—Quality assurance issues for environmental analysis for harmonization within EC and non-EEC countries
—Environmental and education
—Other topics

All topics will be introduced in plenary lectures and invited research lectures followed by brief research presentations and posters. An exhibition of scientific equipment will also be organised.

A short course on Sample Handling and Analysis of Organic Pollutants will be organised in Archamps, France, 27–28 February 1988.

For further details contact:

Dr. M. Frei-Häusler,
IAEAC Secretariat,
Postfach 46,
CH-4123 Allschwil 2,
Switzerland.
Tel.: +41 61 4812789;
fax: +41 61 4820805.

PII S0039-9140(96)00007-0

ELSEVIER

Talanta 44 (1997) 1335–1352

Talanta

Fibre-optic pesticide biosensor based on covalently immobilized acetylcholinesterase and thymol blue

Roberto T. Andres, Ramaier Narayanaswamy *

Department of Instrumentation and Analytical Science, UMIST, P.O. Box 88, Sackville Street, Manchester M60 1QD, UK

Received 30 May 1996; accepted 16 August 1996

Abstract

A fibre-optic based on immobilized acetylcholinesterase is described and its application in the detection of carbamate and organophosphate pesticides through enzyme inhibition measurements is discussed. The bioactive component of the sensor consists of acetylcholinesterase covalently immobilized on preactivated isothiocyanate glass mixed with thymol blue indicator bound on aminopropyl glass and the sensor was constructed by packing a thin layer of the glass bead mixture at the tip of a bifurcated fibre-optic sensor head, which was then integrated with a flow-through cell. The response of the sensor to acetylcholine was highly reproducible (RSD < 2%) and readily reversible. The sensor exhibited a linear response to acetylcholine in the concentration range 2.5–25 mM ($r^2 = 0.992$). Inhibition plots obtained for test organophosphate (paraoxon) and carbamate (carbofuran) pesticides exhibited concentration-dependent behaviour and showed linear profiles in the concentration ranges 5×10^{-8}–5×10^{-7} M for carbofuran and 5×10^{-7}–5×10^{-6} M for paraoxon. The detection limits, calculated at $I_{10\%}$, are 1.5×10^{-8} M (3.1 ppb) and 1.1×10^{-7} M (24.7 ppb) for carbofuran and paraoxon, respectively. The regeneration of paraoxon-inhibited sensor was possible using 2-pyrimidine aldoxime, while repetitive substrate injection was necessary to reactivate the carbofuran-inhibited optrode. The factors affecting the inhibition and reactivation processes were investigated.

Keywords: Acetylcholinesterase; Enzyme inhibition; Fibre-optic biosensor; Pesticide biosensor

1. Introduction

The development of cholinesterase-based biosensors has been actively pursued in recent years. These devices have found use in the determination of acetylcholine, a biomolecule which plays an important role in nerve impulse transmission in the peripheral and central nervous systems. Some authors [1–3] have already demonstrated their practicability in real sample analysis, e.g. in the determination of acetylcholine in cerebrospinal fluid and brain tissue extracts. Their application to other biological materials such as plasma and erythrocyte samples is also widely envisioned [4–6].

A more major interest on cholinesterase-based biosensors lies in their applicability in the analysis

* Corresponding author. Tel.: +44 161 2004891; fax: +44 161 2004911; e-mail: naswamy@fs3.in.umist.ac.uk

PII S0039-9140(96)02071-1

of organophosphate and carbamate compounds. These are compounds that commonly find utility as pesticides in agriculture or household insecticide products and as chemical warfare agents. The toxicity of these compounds is commonly attributed to their inhibition effects on cholinesterase enzymes. In the development of pesticide biosensors based on cholinesterase enzymes, the measurement of inhibition also provides the analytical basis for the sensing of these toxic substances.

Two types of cholinesterase enzymes exist, both of which have proved useful for biosensor construction. They can be distinguished as acetylcholinesterase (also called true cholinesterase or choline esterase I) and acylcholine acylhydrolase (also referred as pseudocholinesterase or choline esterase II and comprises other cholinesterases, including butyrylcholinesterase) [7]. Physiologically, acetylcholinesterases exist in the erythrocytes, lungs and spleen, nerve endings and in the grey matter of the brain and they are involved in nerve impulse transmission. The second type of cholinesterases can be found in the liver, pancreas, heart, white matter of the brain and serum, although their biological role is unknown. Both types of enzymes display high sensitivity to the inhibition by organophosphate and carbamate compounds and have been found to be equally useful in the construction of pesticide biosensors.

The measurement of enzyme inhibition in pesticide biosensors has been performed using a variety of transducers and enzyme substrate systems. The most commonly used transducers have been pH-sensitive devices, such as glass pH electrodes [8–11], ion-selective field-effect transistors (ISFETS) [12–16] and metal–metal oxide electrodes [10]. These potentiometric devices monitor the changes of pH during an acetycholinesterase-catalysed hydrolysis of acetylcholine or butyrylcholine. Lower pH changes are detected for the enzyme sensors inhibited by pesticides. Another type of potentiometric sensor, based on a butyrylcholine-sensitive plasticized poly(vinyl chloride) membrane, has also been recently used as a transducer for an organophosphate pesticide biosensor [17]. The use of solution conductivity as a means of determining cholinesterase activity in pesticide sensors has also been exploited. A conductometric thin-film transducer [18] and an ion-responsive impedance sensor [19] have been utilized as transducers in these cases.

Amperometric devices have also become popular transducers for pesticide biosensors. Enzyme inhibition in these systems is normally assessed using either acetyl- or butyrylthiocholine as the substrate reagents, both of which hydrolyse to produce the electrochemically detectable species, thiocholine [20–24]. A different substrate, 4-aminophenyl acetate, which yields 4-aminophenol as the electroactive species, has also been shown recently to be a useful reagent for a pesticide biosensor [25]. Amperometric enzyme-based sensing of pesticides is more commonly performed, however, using a bi-enzymatic reaction (between acetyl- or butyrylcholinesterase and choline oxidase) and hydrogen peroxide detection [26–31], as described in the following equations:

$$\text{acetylcholine} + H_2 \xrightarrow{\text{acetylcholinesterase}} \text{acetic acid} + \text{choline} \quad (1)$$

$$\text{choline} + 2O_2 + H_2O \xrightarrow{\text{choline oxidase}} \text{betaine} + 2H_2O_2 \quad (2)$$

$$H_2O_2 \xrightarrow{\text{anodic oxidation}} O_2 + 2e^- + 2H^+ \quad (3)$$

Current is measured as a result of H_2O_2 oxidation; acetylcholinesterase inhibition by organophosphate and carbamate compounds leads to a decrease in the current.

Optical-based pesticide biosensors have also been described in recent years. However, accounts concerning these devices are not as numerous as those for electrochemical sensors despite the advantages they offer (e.g. no direct electrical connections, possibility of remote sensing and ease of miniaturization). Wolfbeis and Koeller [32] reported the first fibre-optic device based on immobilized acetylcholinesterase that has been applied for sensing pesticides, although this was not a biosensor in a 'true' sense. It consists of acetylcholinesterase immobilized on nylon beads and packed in a reactor column. A buffered proprietary substrate solution is passed through the column, where it is converted from a red solution into a blue dye upon action by the enzyme. The

colour change is detected, using a yellow LED as light source and a photodiode detector, as the effluent passed through a flow cell, fitted with optical fibres arranged in a transmittive mode. An analogous device was also later reported by Trettnak et al. [33], but activated aminopropyl glass was utilized as the immobilizing support for the enzyme and 2-(2-acetoxy-5-methylphenylazo)-*N*-methyl-1,3-thiazolium methosulphate was used as the specific chromogenic substrate for the assay.

Rogers et al. [34] reported the first fibre-optic anti-cholinesterase biosensor, which was constructed by immobilizing a fluorescein isothiocyanate-tagged acetylcholinesterase (FITC–AChE) on quartz fibres. During acetylcholine hydrolysis, the pH-dependent fluorescent signal generated by FITC–AChE present in the evanescent zone of the fibre surface is quenched by the protons produced, thereby allowing the measurement of enzyme activity. The biosensor was able to detect the carbamate insecticides bendiocarb and methomyl and the organophosphates echothiphate and paraoxon in the nanomolar to micromolar range, but malathion, parathion, and dicrotophos were not detected even at millimolar concentrations. Hobel and Polster [35] described another acetyclcholinesterase-based optical biosensor for pesticides. The enzyme, together with a FITC-modified dextran, were immobilized in a thin polyacrylamide gel layer, which was in turn covalently fixed in front of a functionalized bifurcated optical fibre. As before, the measurements were based on the fluorescence changes brought about by pH shifts during substrate hydrolysis. The detection of the carbamates aldicarb and carbofuran was demonstrated using this sensor.

In this paper, a fibre-optic pesticide biosensor different to those described above and based on an immobilized acetylcholinesterase and reflectance measurement is described. The bioactive reagent layer of the biosensor consists of acetylcholinesterase covalently bound on isothiocyanate glass mixed with thymo blue covalently immobilized on aminopropyl glass, and reflectance measurements are derived from the colour change of the pH-sensitive indicator during the enzyme action on acetylcholine. The response characteristics of the biosensor to acetylcholine are first presented, followed by its application to carbamate and organophosphate determination. The factors affecting the inhibition and reactivation processes are also discussed.

2. Experimental

2.1. Materials

Acetylcholinesterase (EC 3.1.1.7, Type VI-S from electric eel, lyophilized, 225 units mg^{-1} solid, AChE), acetylcholine chloride (AChCl), isothiocyanate glass (Sigma G4893, average pore size 50 nm, 200–400 mesh, 39 μmol isothiocyanate g^{-1} glass), aminopropyl glass (Sigma G4643, average pore size 50 nm, 200–400 mesh, 81 μmol amine g^{-1} glass) and tris(hydroxymethyl)aminomethane–HCl (Tris) were obtained from Sigma Chemical (St. Louis, MO, USA). Potassium dihydrogenphosphate, hydroxylamine, 2-pyrimidine aldoxime methiodide (2-PAM) (99%), thymol blue sodium salt, morpholineethanesulphonic acid (MES) and diethyl 4-nitorphenyl phosphate (technical 90%) (paraoxon) were purchased from Aldrich Chemical (Gillingham, Dorset, UK). Carbofuran was acquired from Riedel-de Haën (Seelze, Germany). Formaldehyde solution (37–40%) was obtained from BDH–Merck (Poole, Dorset, UK). All other reagents were of analytical grade, unless stated, otherwise, and were used as received.

2.2. Immobilization of indicator reagent and acetylcholinesterase

The bioactive reagent phase of the optical pesticide biosensor consists of covalently immobilized acetylcholinesterase enzyme and thymol blue indicator. The immobilization of acetylchoinesterase (AChE) was performed through covalent binding on preactivated isothiocyanate glass. A typical batch immobilization procedure consists of mixing 10 mg portions of the isothiocyanate glass, 50 μl of acetylcholinesterase solution (made by dissolving 0.5 mg of AChE in 1.5 ml of water) and 350 μl of 0.05 M borate buffer (pH 8.5) in a small

glass vial (5 × 1 cm i.d.). The mixture was then kept in a refrigerator for at least 2 h to allow the covalent binding of the enzyme. Subsequently, the glass material was repeatedly washed with cold distilled water and then with 0.1 M phosphate buffer (pH 7.0) to remove unbound enzyme reagent.

Thymol blue was immobilized on aminopropyl glass support through a condensation reaction with formaldehyde. About 200 μl of 10 mM formaldehyde, prepared in 0.1 M MES solution, was first added to a 10 mg portion of the glass beads, followed by 200 μl of 5 μM aqueous thymol blue solution, in a small, stoppered glass vial. The mixture was carefully swirled then stored in a preheated oven (50–60°C) for at least 48 h to effect the covalent binding of the indicator. Subsequently, excess indicator solution was carefully decanted, then the glass beads were thoroughly washed, first with 2 M NaCl then alternately with copious amount of buffer solutions of pH 10.0 and 2.0, followed by distilled water to remove weakly bound or unbound indicators. The glass beads were also subjected to intermittent (3–5 times) and short ultrasonic agitation (ca. 10 s) during the washing procedure to facilitate a more thorough removal of excess indicators.

2.3. Sensor construction and flow-cell configuration

The sensitive enzyme reagent phase of the optical biosensor was prepared by homogeneously mixing 10 mg portions of each of the glass-immobilized acetylcholinesterase and thymol blue indicator preparations. When not in use, this reagent mixture was stored in a refrigerator under 0.1 M phosphate buffer solution (pH 7.0). To construct the optical sensor, an aliquot of the reagent phase was pipetted out and deposited in the microwell (100–150 μm deep and 1.55 mm diameter) of a specially fabricated fibre-optic probe head (Fig. 1). The beads were blotted dry, then carefully packed until a thin and compact glass layer was produced. The glass materials were then retained in place using a fine nylon mesh, which in turn was supported by a plastic tube. The fibre-optic probe was inserted into a flow cell assembly, which was machined from a Perspex cylinder (1 cm diameter × 1 cm high). The flow cell device incorporated two 19G (20 × 1 mm o.d.) stainless-steel needles, positioned diametrically opposite each other, to serve as the solution inlet/outlet. The bottom end of the flow cell was also fitted with a white PTFE plug (at a 1.5 mm distance from the probe tip) to provide a reflective surface backing. The internal volume of the flow cell is approximately 25 μl.

2.4. Flow manifold configuration and measurement procedure

The flow manifold utilized for the characterization of the fibre-optic acetyklcholinesterase-based biosensor and for performing pesticide analysis is depicted in Fig. 2. For the initial characterization studies, the first two valves remained in the load position and only the third valve was activated for

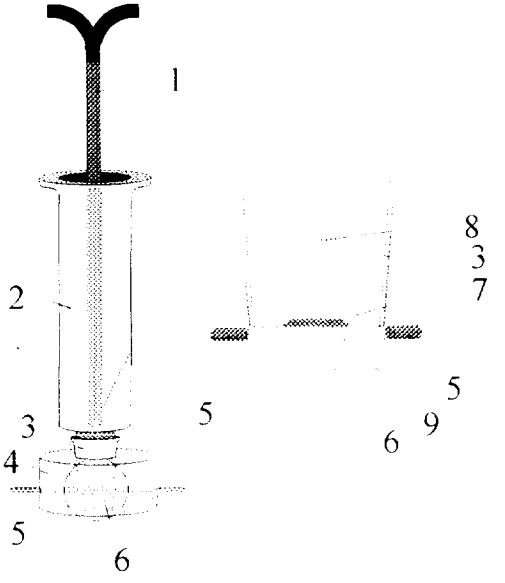

Fig. 1. Configuration of fibre-optic biosensor and flow cell set-up: 1, bifurcated optical fibre bundle; 2, plastic syringe cylinder; 3, plastic body of syringe needle; 4, poly(methacrylate) cylinder; 5, 19G gauge syringe needles; 6, white PTFE cylinder as reflector; 7, glass bead mixture (containing immobilized acetylcholinesterase and thymol blue) packed in a microwell; 8, bare 32-fibre plastic optical fibre bundle; 9, nylon mesh support.

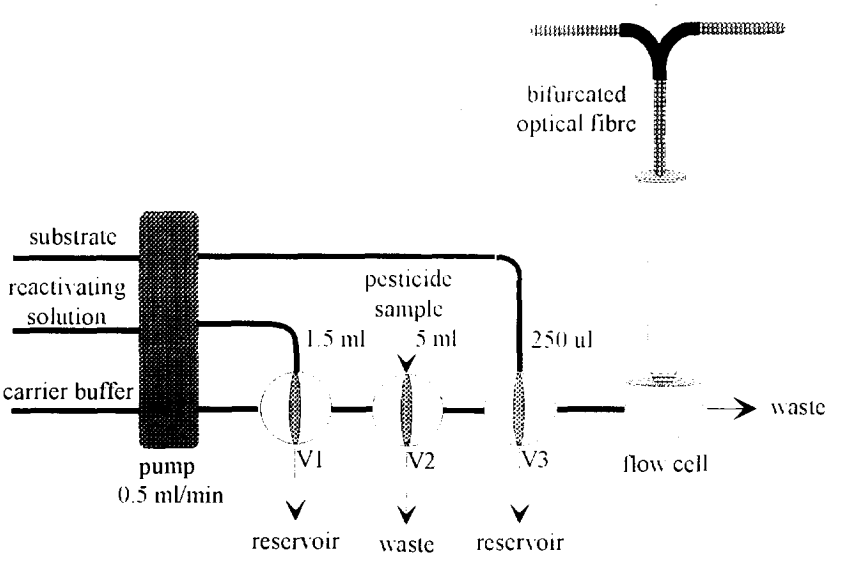

Fig. 2. Flow manifold used for sensor characterization and inhibition measurements. Carrier buffer = 7.5 mM Tris buffer (pH 7.5), reactivating solution = 0.1 mM 2-PAM; substrate = 100 mM acetylcholine; pump = Watson Marlow Model 202U Peristaltic pump; V1–V3 = injection valves (Rheodyne 5020); tubings used = Teflon of 0.8 mm i.d. except for the sample loop of V2 (1.6 mm i.d.).

the introduction of substrate solutions. Pesticide determination was performed using a measurement cycle involving the following: measurement of initial enzyme activity, pesiticide sampling, measurement of inhibited sensor signal, reactivation using a regenerating agent, measurement of reactivated sensor response and subsequent sampling of another pesticide solution. The detailed procedure is as follows: with all valves in the load position, the baseline signal was first allowed to stabilize by continuously pumping the carrier buffer solution (7.5 mM Tris buffer (pH 7.5)) across the sensor. The initial acetylcholinesterase activity was then measured by injecting replicate samples of the substrate solution (100 mM acetylcholine prepared in the Tris buffer) through valve 3. At the onset of peak recovery in the last substrate injection, valve 3 was returned to load position and the pesticide solution was injected to the flow system using valve 2. After the sample solution plug had completely passed through the flow cell (typically after 10–12 min) and when the baseline level had been regained, valve 2 was switched back to the load position and the substrate was injected through valve 3 to measure the inhibited enzyme activity. At the onset of peak recovery, valve 2 was returned to the load position and the regenerating solution was then introduced via valve 1. The baseline was allowed to recover and the 'regenerated' enzyme activity was measured again by the reintroduction of acetylcholine solution, while valve 1 was switched back to the load position. The whole measurement cycle was repeated for sampling other pesticide solutions. The percentage inhibition (or reactivation) at each measurement step was evaluated using the expression

$$\text{inhibition}(\%) = [(E_0 - E)/E_0] \times 100 \quad (4)$$

where E_0 is the initial uninhibited sensor response and E is the inhibited (or reactivated) sensor response.

The fibre-optic measuring system employed in these studies is the same as that described previously [36] and measured light intensities from the optical sensor are expressed as voltage output.

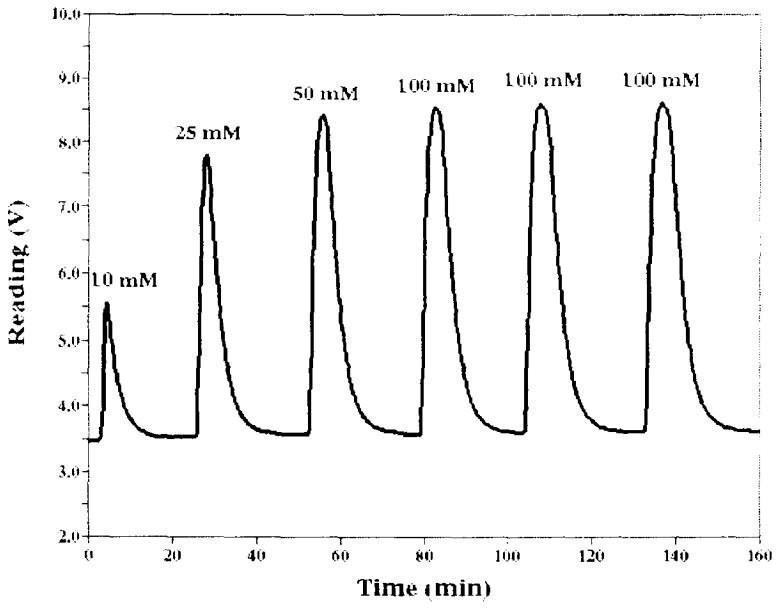

Fig. 3. Sample response curve of the acetylcholine optical biosensor.

3. Results and discussion

3.1. Sensitivity to acetylcholine

Acetylcholine was utilized as the test substrate for the characterization of the enzyme optrode and for the assay of its immobilized enzyme activity. Acetylcholine, introduced into the enzyme sensor, is biocatalytically hydrolysed into acetic acid and choline. It is generally accepted [37,38] that the hydrolysis of acetylcholine occurs in three steps and may be expressed by the following reactions:

$$\underset{\text{acetylcholine chloride}}{CH_3COOCH_2CH_2N^+(CH_3)_3Cl^-} + \underset{\text{acetylcholinesterase}}{AChE} \rightleftharpoons [\underset{\text{acetylcholine–acetylcholinesterase complex}}{CH_3COOCH_2CH_2N^+(CH_3)_3Cl\text{–}AChE}] \rightarrow \underset{\text{acetylated acetylcholinesterase}}{AChE\text{-}OOCHCH_3} + \underset{\text{choline chloride}}{HOCH_2CH_2N^+(CH_3)_3Cl^-} \quad (5)$$

$$\underset{\text{acetylated acetylcholinesterase}}{AChE\text{-}OOCHCH_3} \xrightarrow{H_2O} \underset{\text{acetic acid}}{CH_3COOH} + \underset{\text{free acetylcholinesterase}}{AChE} \quad (6)$$

The enzyme and the substrate first combine to form the Michaelis enzyme–substrate complex. The acetyl group then transfers to the serine group in the active site of the esterase molecule to form the acetylated enzyme and the first product (choline chloride). The third step involves the rapid hydrolysis of the acetylated enzyme to produce the free enzyme and the second hydrolytic product (acetic acid). The liberated acetic acid causes a pH decrease in the local environment of the enzyme optrode that can be detected by the immobilized pH indicator. This pH change is manifested as a colour change (blue green to yellow) in thymol blue, thereby leading to the increase in the reflected light intensity (measured at 600 nm) for the sensor.

A test sensor response curve illustrating the peaks obtained for varying concentrations of acetylcholine and replicate injections of the substrate is shown in Fig. 3. The concentration-dependent peaks and reproducible signals obtained here illustrate the feasibility of the measurement approach and the usefulness of the fibre-optic sensor design.

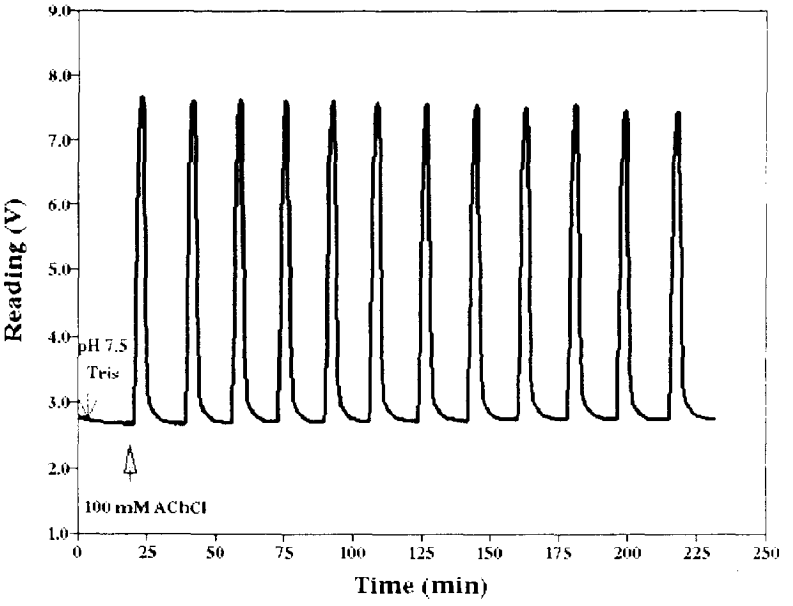

Fig. 4. Response of acetylcholine optrode to repetitive injection of 100 mM acetylcholine.

3.2. Reproducibility of response to acetylcholine

The reproducibility of the optrode response to repetitive injection of acetylcholine was then investigated. The applicability of the acetylcholinesterase-based sensor to pesticide determination depends on its reproducible response to the substrate solution. This requirement arises from the fact that the detection process involves the comparison of the enzyme activity before and after the exposure to the inhibitor. The change in sensor response should therefore be attributed to the inhibitor and not to the poor or non-reproducible sensor performance.

The response of the acetylcholine optical sensor on a periodic exposure to 100 mM acetylcholine chloride is depicted in Fig. 4. The response was fairly reproducible (RSD = 1.83% for $n = 12$), although it suffered from a small drift in the peak heights (about 1.6% h^{-1}). It was initially thought that the slow deterioration in the enzyme optrode response was due to product inhibition, brought about by drastic changes in pH during the enzyme reaction. Consequently, replicate measurements were also performed using a more dilute acetylcholine concentration (50 mM) and a reagent phase with a lower enzyme loading. However, no improvement was seen in the reproducibility tests for the optrode under these conditions. In fact, in some instances, the precision was worse for these sensors; although this was more attributable to the less perfect packing of the enzyme reagent phase at the fibre tip and the sporadic disturbances caused by bubbles that become entrapped in the flow cell and cause scattering in the light.

Nonetheless, provided that the reagent phase had been washed thoroughly (to remove weakly bound enzymes), that the glass beads are well packed at the sensor tip and that the bubbles in the flow stream were found to be absent or were carefully removed when they became entrapped in the flow cell, then the obtained precision of the sensor response is acceptable for inhibition measurements. The best precision achieved would already allow the distinct recognition of a pesticide sample that would cause at least a 3.7% inhibition in the response (2δ) of the enzyme optrode.

3.3. Acetylcholine calibration curve

The time–response curve of the enzyme op-

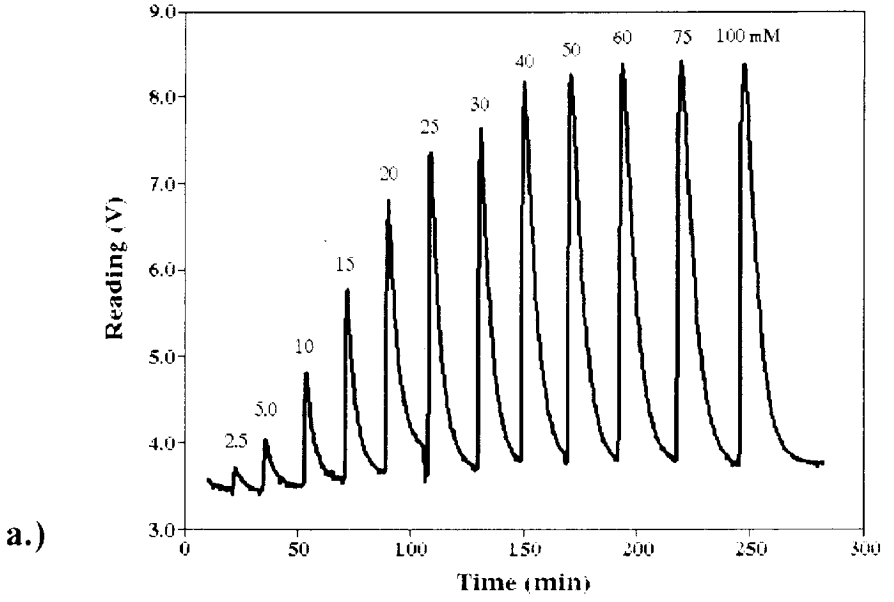

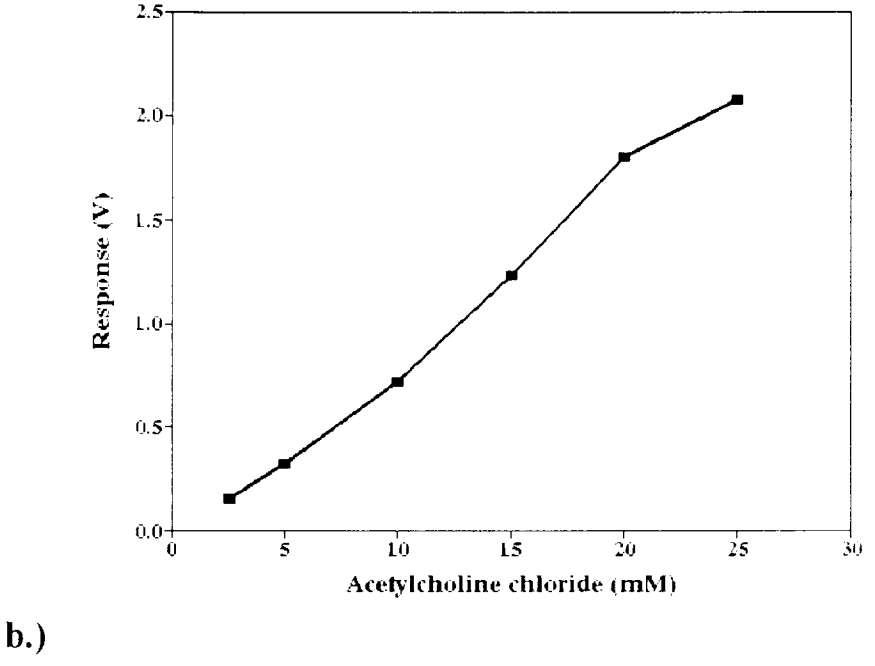

Fig. 5. (a) Time–response curve of acetylcholinesterase-based optrode to various concentrations of acetylcholine; (b) corresponding calibration curve in its linear response range.

trode during exposure to various concentrations of acetylcholine chloride is shown in Fig. 5(a) and the corresponding calibration curve is depicted in Fig. 5(b). Depending on the substrate concentra-

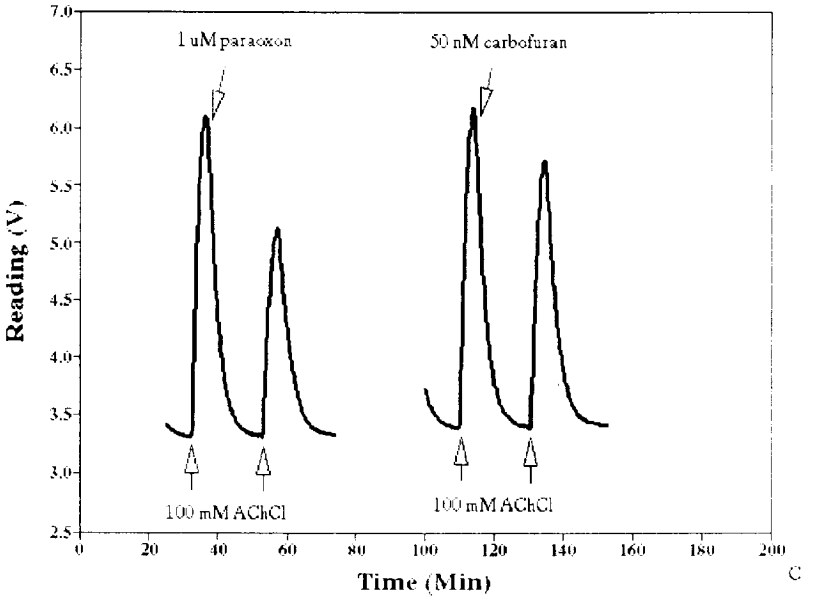

Fig. 6. Time–response curve of acetylcholine optrode before and after exposure to an organophosphate (paraoxon) and a carbamate (carbofuran) pesticide. The points of injection of the substrate and pesticides are indicated by the arrows.

tion, it takes around 1.3–2.5 min to reach the maximum peak signal and around 15–20 min to recover the baseline level. The signal response, measured as the peak height, was linear with respect to acetylcholine concentration in the range 2.5–25 mM ($r^2 = 0.992$) and levelled off at concentrations > 40 mM. There was no sign of inhibition due to excess substrate, within the concentration range 0–100 mM, contrary to the normally observed behaviour of solubilized acetylcholinesterase enzyme [39].

3.4. Determination of carbamate and organophosphate pesticides

3.4.1. Detection principle

Fig. 6(a) and (b) show the test response curves for the acetylcholinesterase-based optrode before and after the exposure to an organophosphate compound (paraoxon, 1 μM) and a carbamate (carbofuran, 50 nM). The reduced responses obtained after the introduction of the pesticides illustrate the possibility of detecting organophosphate and carbamate compounds using the acetylcholinesterase-based fibre-optic biosensor described here. The inhibition of acetylcholinesterase is normally attributed to the acylation of the serine –OH in the active site of the enzyme by these compounds [39,40]. The reaction with acetylcholinesterase is analogous to the enzyme–substrate reaction, whereby a Michaelis enzyme–pesticide complex is first formed, followed by the transfer of the pesticide acyl groups to the serine –OH of the enzyme, and the concomitant release of the side product HB, as depicted in Eqs. 7 and 8.

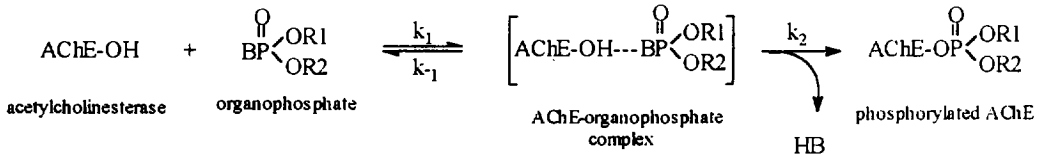

(7)

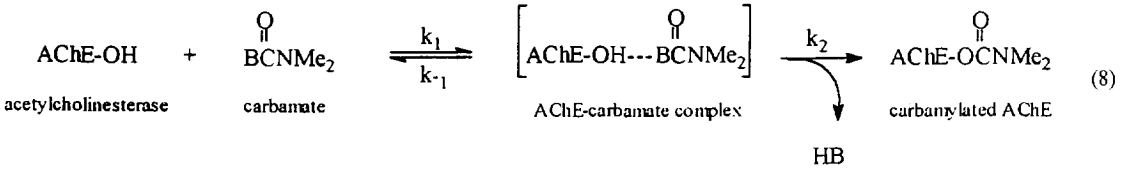

(8)

However, unlike the acylated ester formed from the choline ester, the rate of hydrolysis of the phosphorylated and carbamylated acetylcholinesterases was very slow. Consequently, when these acylated enzymes are reacted again with the natural enzyme substrate, acetylcholine, a lower pH change would be detected since the enzyme remains inhibited. The difference in the pH changes before and after the pesticide treatment of the sensor thus, provides information on the amount of the pesticide and can be utilized for its analysis.

3.4.2. Factors affecting the inhibition measurement

Substrate concentration can have a significant influence on the measured degree of inhibition for the acetylcholinesterase optrode, because both organophosphorus and carbamate pesticides act as competitive inhibitors and bind to the same active site of the enzyme on which the hydrolysis of the substrate (acetylcholine) takes place [39]. Thus, with a high concentration of the substrate, the inhibition by the pesticides may be hampered. This is obviously a concern in procedures wherein the inhibition and the measurement of enzyme activity are carried out simultaneously or where the pesticide sample and the substrate solution are both present in the reaction solution. In the procedure adopted in this work, however, the enzyme–substrate reaction is only initiated after a preincubation of the sensor in the pesticide sample. This ensures that there is no competition between acetylcholine and the pesticide and that the inhibition is maximized. High substrate concentrations can then be utilized for the enzyme assay. It also avoids the problem of having to contend with low optrode signals obtained at low substrate concentrations. In fact, in order to provide an accurate measure of the enzyme activity of the optrode, the substrate concentration should be high enough and into the saturation concentration range for the immobilized enzyme. In view, of this, an acetylcholine concentration of 100 mM is used for establishing the reference optrode signal and for the measurement of pesticide inhibition.

Flow-rate and sample volume are two of the experimental variables which are expected to have an effect on the sensitivity of the pesticide measurements. Large sample volumes favour greater contact time between the enzyme optrode and the pesticide sample, and thus can lead to higher enzyme inhibition. A similar situation is achieved when the flow-rate is low. However, as it has been observed that a low flow-rate results in longer sensor response times and consequently a low sample throughput, it is necessary to compromise the selected flow-rate condition for inhibition studies. It was therefore decided to adopt a flow-rate of 0.5 ml min^{-1} and a sample volume of 5 ml. This combination allows a reasonable sample contact time of 10 min between the sensor and the pesticide sample. Moreover, with these settings, the sample consumption is low, while the sensor response is maintained high and reasonably rapid.

3.4.3. Reactivation of pesticide-inhibited enzyme optrode

It is desirable for a pesticide-inhibited acetylcholinesterase-based optrode that its enzymic activity be recovered easily and efficiently. This will allow a more economical use of the sensor and facilitates its easier handling. However, results have shown that for an optrode that has been exposed to paraoxon, a spontaneous or rapid recovery of the enzyme activity was not very likely. Even a repetitive exposure to substrate solution did not provide a significant improvement in the enzyme reactivation. This can be ascribed, of course, to the strong ester linkage between the diethyl phosphate group and the serine moiety of the enzyme. Significant restoration in the enzyme optrode signal was only attained after the sensor has been treated with 2-PAM, which is a reagent commonly used for the

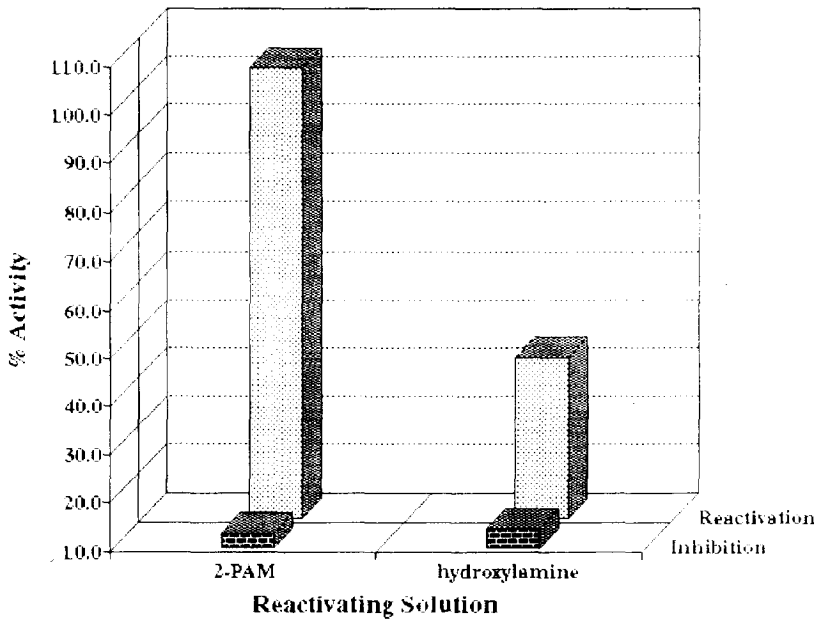

Fig. 7. Comparison of the reactivation efficiency of 2-PAM and hydroxylamine towards a paraoxon-inhibited acetylcholinesterase-based optrode.

reactivation of organophosphate-inhibited cholinesterase enzymes [37]. It is generally believed that the reactivating effect of this reagent is due to its strong nucleophilic character, which makes it reactive towards the electrophilic phosphorus atom of the phsophorylated enzyme. In doing so, it displaces the enzyme from its attachment to the phosphorus, hence yielding the free and active form of the acetylcholinesterase again. This is illustrated in Eq. 9.

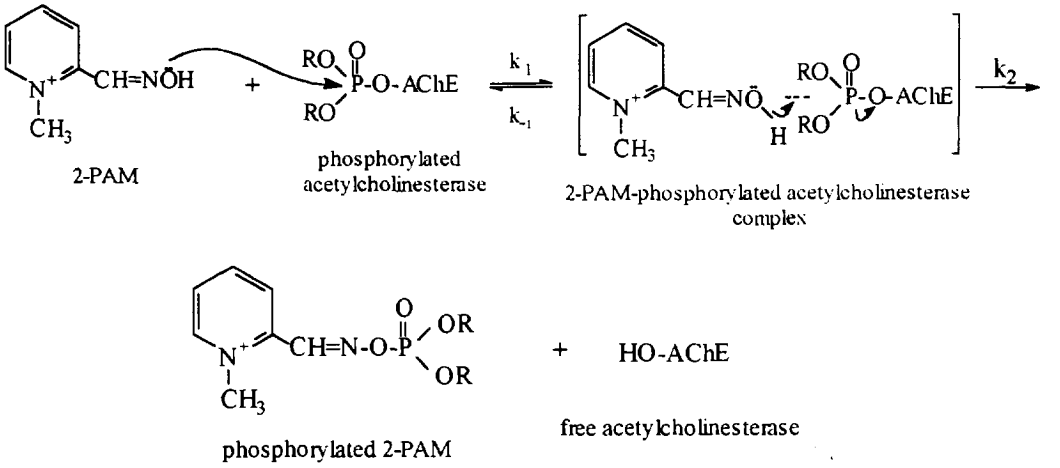

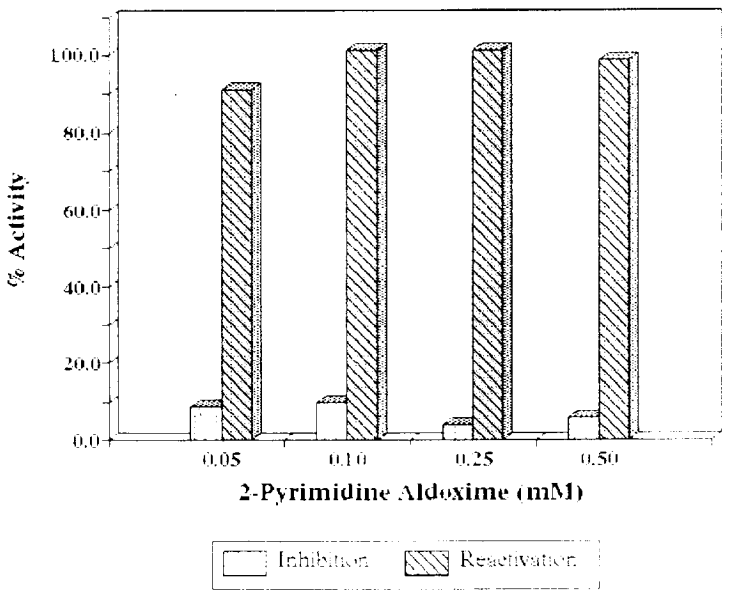

Fig. 8. Effect of the 2-PAM concentration on the efficiency of reactivation of acetylcholine optrode inhibited by 10 μM paraoxon.

However, as the phosphorylated oxime is known to be a potent inhibitor of the enzyme itself [37], it is necessary that a prolonged exposure of the immobilized enzyme with the former also be avoided, although with the relatively rapid decomposition of the phosphorylated 2-PAM and the continuous flow system employed in this study, the immediate removal or deactivation of the phosphorylated oxime is rather assured.

The efficiencies of hydroxylamine ($HONH_2$) and 2-PAM as reactivating reagents for a phosphorylated acetylcholinesterase optrode were also compared. A 10 μM paraoxon solution was used as the test pesticide solution and 2-PAM and hydroxylamine solutions, prepared at the same concentration (1 mM) and under similar pH conditions, were used as the reactivating agents. The results (Fig. 7) showed that 2-PAM is a more efficient regenerating agent than hydroxylamine. This can be traced to the better nucleophilic property of the oxime compared with the hydroxylamine. The good reactivating property of 2-PAM is also believed to be due to the cationic centre of the aldoxime [37]. This part can attach to the anionic site of the inhibited enzyme and thus arranges an easier and more proximate interaction between the nucleophilic –OH and the phosphorylated esteratic site.

Reactivation test were also performed on a carbamate-inhibited enzyme optrode. However, unlike the paraoxon-inhibited sensor, a recovery in the enzyme activity of the carbofuran-inhibited optrode is evident even on exposure alone to the substrate solution, albeit the reactivation was slow. This behaviour attests that the inhibition of the acetylcholinesterase optrode by the carbamate was reversible in nature, unlike that of the paraoxon inhibition. Unfortunately, however, the rate of regeneration of the carbofuran-inhibited optrode remained slow even after the introduction of 1 mM hydroxylamine or 2-PAM. A tenfold increase in the concentration of the nucleophilic reagents did not provide a significant improvement in the sensor regeneration either.

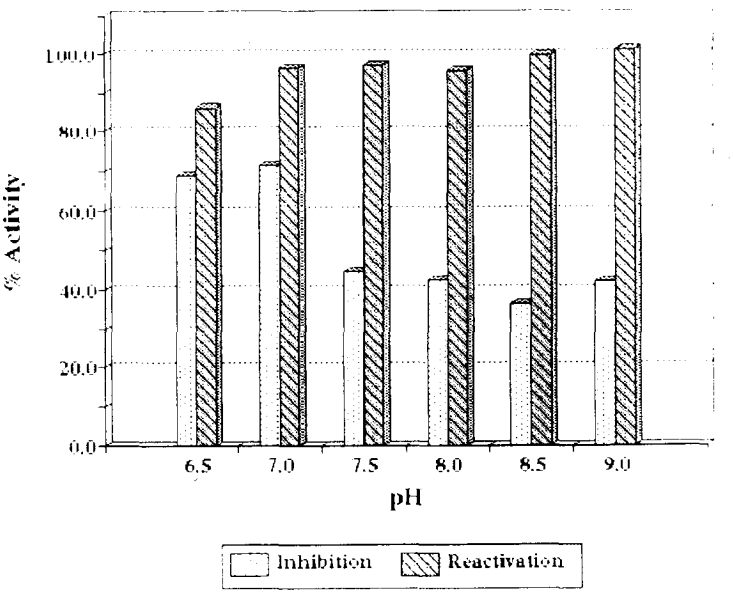

Fig. 9. Effect of pH on paraoxon (10 μM) inhibition and 2-PAM (1 mM) reactivation of the acetylcholinesterase-based optrode.

3.4.4. Factors affecting the reactivation

Having chosen 2-PAM as the reactivating reagent, solutions with various concentrations of this reagent were then prepared in order to compare its reactivating efficiency on the paraoxon-inhibited acetylcholinesterase-based optrode, using 10 μM paraoxon as the test inhibitor solution. The results (Fig. 8) suggest that 0.1 mM 2-PAM is sufficient to bring about a significant regeneration of a highly inhibited acetylcholinesterase optrode.

The influence of pH on the inhibition of the acetylcholine optrode by paraoxon and its reactivation by 2-PAM were also investigated. Tris buffers (7.5 mM) of varying pH (6.5–9.0) were made and were also used to prepare the various paraoxon (10 μM), 2-PAM (1 mM) and acetylcholine chloride (100 mM) working solutions. The results (Fig. 9) showed that the inhibition due to paraoxon increases with increasing pH and exhibits an apparent maximum at pH 8.5. The efficiency of reactivation by 2-PAM also improves with increase in pH. These changes can be attributed to the variation in the changes in ionization of the binding and catalytic sites of the enzyme, the inhibitor, the reactivator and the substrate as the pH is modified. As a result, the interaction between the enzyme and inhibitor of enzyme and reactivator is also expected to change. Although it seems that high pH (e.g. pH 8.5) appear to be favourable for the inhibition or regeneration reactions, the relative substrate response of the sensor at this pH is low. Measurements at this pH will thus be less precise. Furthermore, the prepared organophosphate and carbamate solutions are also unstable at high pH as they become more susceptible to hydrolysis [41]. Consequently, it was decided to conduct further inhibition and reactivation studies at pH 7.5, in order to maintain sensitive inhibition, efficient reactivation, high substrate response and stable pesticide samples.

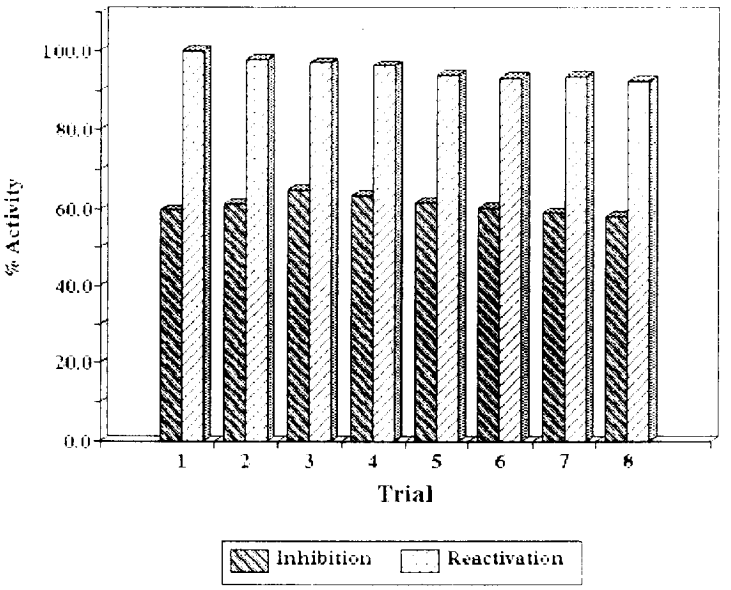

Fig. 10. Reproducibility of the inhibition of acetylcholinesterase-based optrode by 1 μM paraoxon and its reactivation by 0.1 mM 2-pyrimidine aldoxime.

3.4.5. Reproducibility of inhibition and reactivation

The reproducibilities of the inhibition measurement and the reactivation process for the acetylcholinesterase optical biosensor were also evaluated. The enzyme optrode was alternately reacted with 1 μM paraoxon and then regenerated using 0.1 mM 2-PAM. The results of the study are presented in Fig. 10. The inhibition and reactivation steps for paraoxon were fairly reproducible ($RSD_{inhibition} = 3.7\%$ for $n = 8$ and $RSD_{reactivation} = 2.8\%$ for $n = 8$). The precision and efficiency of the reactivation process can probably be improved by using 2-PAM solutions of slightly higher concentration.

An analogous inhibition and reactivation procedure for carbofuran (0.1 μM) yielded less reproducible responses ($RSD_{inhibition} = 5.8\%$ for $n = 4$ and $RSD_{reactivation} = 4.1\%$ for $n = 4$). These less precise inhibition data can be partly ascribed to the variations in the period allowed for sample and buffer stream elution before the substrate is again injected into the sensor. Ideally, a prompt introduction of the substrate, immediately after the tail of the sample stream has completely passed the sensor head, is necessary in order to obtain accurate inhibition measurement. However, in several instances, it was necessary to delay the substrate injection slightly to allow a more complete baseline recovery. Unfortunately during this delay, regeneration of the sensor can proceed owing to the reversible nature of the enzyme–carbamate interaction. Hence a slightly lower inhibition will be recorded.

3.4.6. Assay of organophosphate and carbamate pesticides

In order to demonstrate the usefulness of the acetylcholinesterase-based optical biosensor in the analysis of pesticides, its response to different concentrations of an organophosphate (paraoxon) and a carbamate (carbofuran) pesticide were determined. Stock pesticide solutions (1.5×10^{-3} M paraoxon and 1.0×10^{-3} M carbofuran) were prepared by dissolution of the reagents in acetone, and standard solutions were made by appropriate dilution in (7.5 mM) Tris buffer solution (pH 7.5). Response curves were obtained through a measurement cycle involving

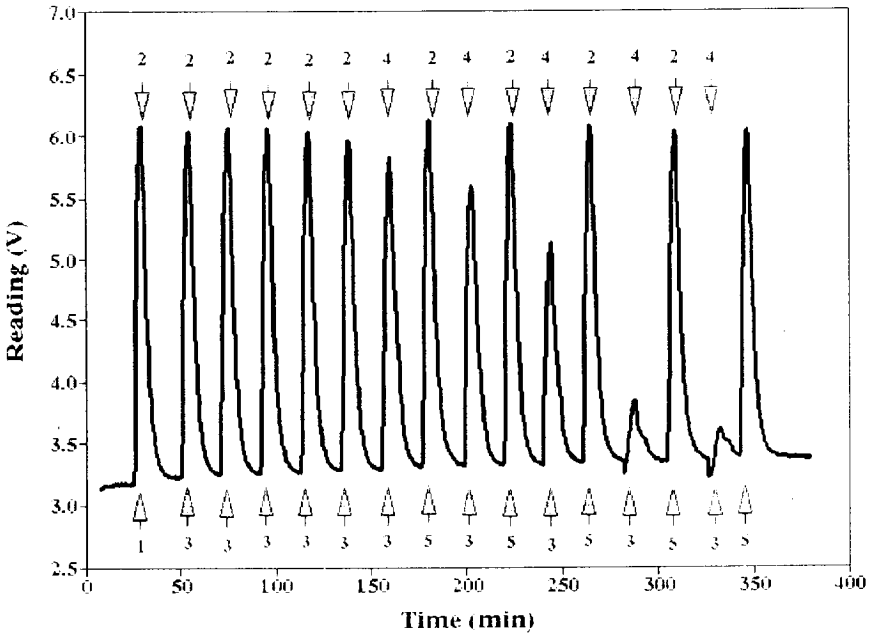

Fig. 11. Time–response curve of acetylcholinesterase-based optrode showing the inhibition by different concentrations of paraoxon and reactivation by 2-pyrimidine aldoxime. The arrows indicate the point of injection of substrate (1, 3, 5), pesticide (2) and reactivating agent (4). The measurement procedure generally consists of (1) preliminary measurement of uninhibited sensor response, (2) sampling of pesticide, (3) measurement of inhibited response, (4) reaction with reactivating agent, (5) measurement of reactivated response and (2) subsequent sampling of another pesticide sample.

the alternate determination of acetylcholinesterase activity, sample exposure, measurement of inhibited signal, reactivation and remeasurement of enzyme activity. The time–signal profile showing these measurement cycles for paraoxon determination is shown in Fig. 11. The corresponding calibration curves for paraoxon and carbofuran are illustrated in Fig. 12(a) and (b). Both plots appear sigmoidal and exhibit linear response in the concentration ranges 5×10^{-8}–5×10^{-7} M for carbofuran and 5×10^{-7}–5×10^{-6} M for paraoxon. The detection limits, taken as the concentration at which the inhibition is 10% [10], i.e. $I_{10\%}$, are 1.5×10^{-8} M for carbofuran and 1.1×10^{-7} M for paraoxon.

The plots also show the corresponding efficiency of the reactivation steps during the measurement cycles. A highly efficient recovery of acetylcholinesterase activity is obtained throughout a wide range of increasing paraoxon concentrations using 0.1 mM 2-PAM as the reactivating agent. On the other hand, the response of the biosensor was deteriorating during the determination of the carbamate, and this due to the incomplete reactivation at each regeneration cycle. However, the regeneration appears viable and can probably be improved by prolonging the sensor's exposure time to the substrate.

4. Conclusion

The construction and characterization of a fibre-optic biosensor based on controlled-pore glass-immobilized acetylcholinesterase and a colorimetric pH indicator (thymol blue) have been described and its application to pesticide analysis

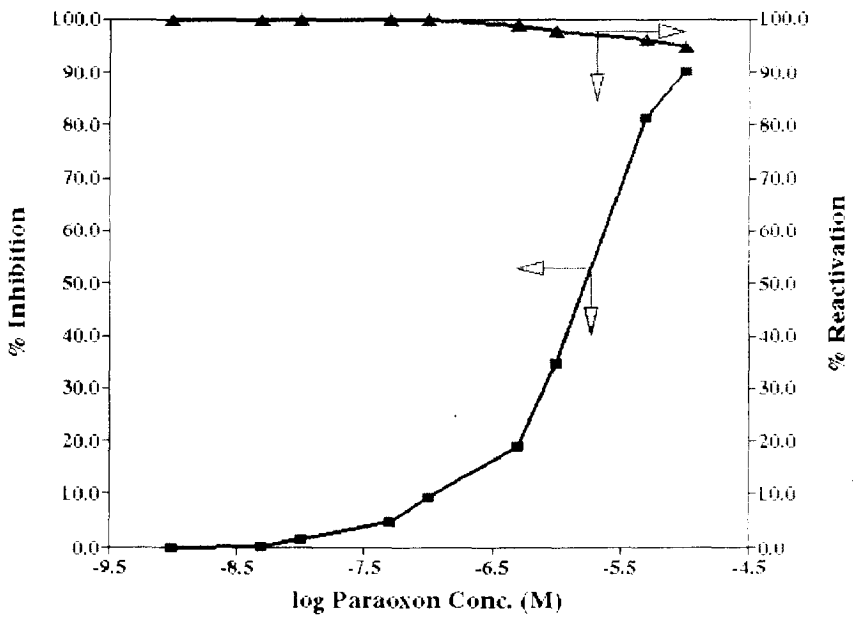

a.)

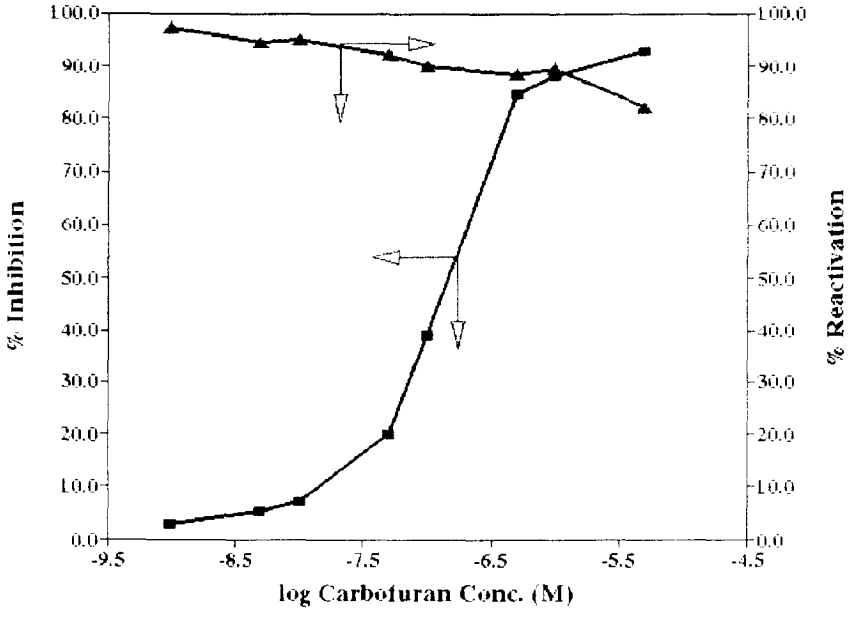

b.)

Fig. 12. Calibration plots showing the variation of percentage inhibition with pesticide concentration and the corresponding percentage reactivation at each pesticide concentration: (a) paraoxon; (b) carbofuran.

has been investigated. The enzyme optrode exhibited good sensitivity towards acetylcholine, with a linear response in the concentration range 2.5–25 mM. The response was fully reversible and highly reproducible (RSD < 2%), further meriting its employment in the determination of pesticides based on enzyme inhibition. Parameters such as pH, flow-rate, substrate concentration and sample volume were noted to affect the inhibition process thus need to be optimized. Inhibition measurements using carbofuran and paraoxon as representative carbamate and organophosphate pesticides proved successful. The log [pesticide] vs. percentage inhibition plots exhibited a concentration dependence and were linear in limited concentration ranges. The detection limits, measured at $I_{10\%}$, are 1.5×10^{-8} M (3.1 ppb) for carbofuran and 1.1×10^{-7} M (27.1 ppb) for paraoxon. To achieve better sensitivity in the sensing process, an increase in the pesticide incubation time, e.g. through an increase in the sample volume, decrease in sample flow-rate or performing stopped-flow operations, can be further explored. By utilizing other sources of cholinesterase enzymes, better detection limits may also be achieved. Alfthan et al. [42] observed that cholinesterase preparations of different mammalian origins differ in sensitivity to pesticide inhibition.

The regeneration of the inhibited enzyme optrode has been possible, permitting its practical utility as a pesticide biosensor. Inhibition by an organophosphate pesticide (paraoxon) was effectively rectified by treatment with 2-pyrimidine aldoxime. The regeneration of carbamate-inhibited enzyme optrode was simpler and only entailed treatment with the substrate solution. The rate of signal recovery was slow, however.

As with other cholinesterase-based biosensors, the enzyme optrode described in this work does not selectively respond to a particular pesticide species, but to a wide range of organophosphate and carbamate pesticides. Hence, when exposed to a mixture of pesticide samples, it will most likely respond to the sum of inhibitory effect of the different inhibitors. It is therefore more useful as a screening device for cholinesterase-inhibiting pesticides, rather than being concerned with the determination of a particular pesticide. It can be applied as a general monitor for pesticide contamination in environmental water samples, drinking water, agricultural products, foodstuffs and many other samples.

References

[1] M.F. Suaud-Chagny and J.F. Pujol, Analysis, 13 (1985) 25.
[2] L. Campanella, M.P. Sammartino and M. Tomassetti, Anal. Lett., 22 (1989) 1389.
[3] L. Campanella, M.P. Sammartino and M. Tomassetti, Ann. Chim. (Rome), 81 (1991) 639.
[4] Z.X. Huang, R.L. Vilarta-Snow, G.J. Lubrano and G.G. Guilbault, Anal. Biochem., 215 (1991) 31.
[5] M.G. Garguilo and A.R. Michael, Trends Anal. Chem., 14 (1995) 164.
[6] C. Eppelsheim and N. Hampp, Analyst, 119 (1994) 2167.
[7] D.W. Moss and A.R. Henderson, in C.A. Burtis and E.R. Ashwood (Eds.), Tietz Textbook of Clinical Chemistry, W.B. Saunders, Philadelphia, 2nd edn., 1994, pp. 877–882.
[8] P. Durand and D. Thomas, J. Environ. Pathol. Toxicol. Oncol., 15 (1984) 51.
[9] C. Tran-Minh, P.C. Pandey and S. Kumaran, Biosens. Biolelectron., 5 (1990) 461.
[10] S. Kumaran and C. Tran-Minh, Electroanalysis, 4 (1992) 949.
[11] S. Kumaran and M. Morita, Talanta, 42 (1995) 649.
[12] H. Sakai, N. Kaneki, H. Tanaka and H. Hara, Sens. Mater. 3 (1992) 145.
[13] H. Sakai, N. Kaneki and H. Hara, Sens Actuators B, 13–14 (1993) 578.
[14] C. Colapicchioni, A. Barbaro and F. Procelli, Sens. Actuators B, 6 (1992) 202.
[15] V. Vlasov, A. Bratov, S. Levichev and Y. Tarantov, Sens. Actuators B, 4 (1991) 283.
[16] A.M.N. Hendji, N. Jaffrezic-Renault, C. Martelet, P. Clechet, A.A. Shul'ga, V. Strikha, L. Netchiporuk, A.P. Soldatkin and W.B. Wlodarski, Anal. Chim. Acta, 281 (1993) 3.
[17] T. Imato and N. Ishibashi, Biosens. Bioelectron., 10 (1995) 435.
[18] S.V. Dzyadevich, A.P. Soldatkin, A.A. Shulga, V.I. Strikha and A.V. Elskaya, J. Anal. Chem., 49 (1994) 789.
[19] R.B.M. Schasfoort and T. Niedziela, Sens. Actuators B, 18–19 (1994) 175.
[20] J.L. Marty, N. Mionetto, T. Noguer, F. Ortega and C. Roux, Biosens. Bioelectron., 8 (1993) 273.
[21] M. Stoytcheva, Anal. Lett., 27 (1994) 3065.
[22] N. Mionetto, J.L. Marty and I. Karube, Biosens. Biolectron., 9 (1994) 463.

[23] D. Martorell, F. Cespedes, E. Martinez-Fabregas and S. Alegret, Anal. Chim. Acta, 290 (1994) 343.
[24] P. Skladal, M. Pavlik and M. Fiala, Anal. Lett., 27 (1994) 20.
[25] C. La Rosa, F. Pariente, L. Hernandez and E. Lorenzo, Anal. Chim. Acta, 295 (1994) 273.
[26] J.L. Marty, K. Sode and I. Karube, Electroanalysis, 4 (1992) 249.
[27] M. Bernabei, C. Cremisini, M. Mascini and G. Palleschi, Anal. Lett., 24 (1991) 1317.
[28] G. Palleschi, M. Bernabei, C. Cremisini and M. Mascini, Sens. Actuators B, 7 (1992) 513.
[29] M. Bernabei, S. Chiavarini, C. Cremisini and G. Palleschi, Biosens. Bioelectron., 8 (1993) 265.
[30] U. Wollenberger, K. Setz, F.W. Scheller, U. Loffler, W. Gopel and R. Gruss, Sens. Actuators B, 4 (1991) 257.
[31] L. Campanella, R. Cocco, M.D. Sammartino and M. Tomassetti, Sci. Total. Environ., 123/124 (1992) 1.
[32] O.S. Wolfbeis and E. Koeller, in R.D. Schmid and F. Scheller (Eds.), International Workshop on Biosensors: Applications in Medicine, Environmental Protection and Process Control, Verlag Chemie, Weinheim, 1989, pp. 221–224.
[33] W. Trettnak, I. Reininger, E. Zinterl and O.S. Wolfbeis, Sens. Actuators B, 11 (1993) 87.
[34] K.R. Rogers, C.J. Cao, J.J. Valdes, A.T. Eldefrawi and M.E. Eldefrawi, Fundam. Appl. Toxicol., 16 (1991) 810.
[35] W. Hobel and K. Polster, Fresenius' J. Anal. Chem., 343 (1992) 101.
[36] R.T. Andres and R. Narayanaswamy, Analyst, 120 (1995) 1549.
[37] M. Eto, Organoiphosphorus Pesticides: Organic and Biological Chemistry, CRC Press, Cleveland, OH, 1974.
[38] W.N. Aldridge and E. Reiner, Enzyme Inhibitors as Substrates: Interaction of Esterases with Esters of Organophosphrous and Carbamic Acids, North-Holland, Amsterdam, 1972.
[39] R.D. O'Brien, in C.F. Wilkinson (Ed.), Insecticide Biochemistry and Physiology, London, 1976, pp. 271–296.
[40] I.B. Wilson, in R.M. Hochster and J.H. Quastel (Eds.), Metabolic Inhibitors. A Comprehensive Treatise, Vol. 2, Academic Press, New York, 1963, pp. 193–204.
[41] I.I. Falah and W.E. Hammers, Toxicol. Environ. Chem., 42 (1994) 9.
[42] K. Alfthan, H. Kenttamaa and T. Zukale, Anal. Chim. Acta, 217 (1989) 43.

ELSEVIER

Talanta 44 (1997) 1353–1363

Talanta

Determination of enantiomeric excess using a chiral selective separation mode and polarimetric detection

Romulo G. Lodevico [a], Donald R. Bobbitt [a,*], Thomas J. Edkins [b]

[a] *Department of Chemistry and Biochemistry, University of Arkansas, Fayetteville, AR 72701, USA*
[b] *Analytical Development, The R.W. Johnson Pharmaceutical Research Institute, Spring House, PA 19477-0776, USA*

Received 24 May 1996; received in revised form 26 August 1996; accepted 26 August 1996

Abstract

The quantitative capabilities of a system that combines a chiral selective separation mode with polarimetric detection (CSS/PD) were investigated in terms of the ability to quantitate enantiomeric mixtures even under conditions of poor chromatographic resolution. The laser-based polarimetric detection system can provide a rotational sensitivity on the order of 10 μdeg corresponding to a minimum measurable quantity of 10 ng for a compound with a specific rotation of 100 deg $(g/ml)^{-1}$ dm^{-1}. For the chromatographic studies, peak height and peak area were measured as analytical descriptors of the bimodal response function of this polarimetric detector. Analyses of the dansylated enantiomers of the amino acids phenylalanine, threonine, and valine have shown that chromatographic resolution and specific rotation are important factors affecting the shape of the polarimetric response curve. With CSS/PD, enantiomeric materials can be quantitated at both low and high enantiomeric excess (ee) even at resolutions of 0.3–0.4. © 1997 Elsevier Science B.V.

Keywords: Chiral separation; Enantiometric mixtures; Polarimetric detection

1. Introduction

The 1980s proved to be an important decade in the development of chiral separations, particularly with respect to liquid phase-based methods. In spite of the usefulness of indirect methods that produce separable diastereomers via derivatization with a chiral reagent, direct methods that involve chiral mobile phase additives (CMPA) and chiral stationary phases (CSP), have been vigorously pursued. The primary advantages of these methods over diastereomer formation are the reduced time per analysis, and the greatly reduced sample handling requirements of the instrumental methods. A considerable amount of work has been devoted to the design and utilization of chiral stationary phases and recent developments have revolutionized this area of separation science. Chiral separation techniques have especially benefited research in biotechnology and the pharmaceutical industry due to the importance of precise characterization of pharmaceutical materials of interest.

* Corresponding author. Fax: +1 501 5754049.

PII S0039-9140(96)02082-6

Several recent reviews [1–5] have summarized the progress in the field of enantiomeric separations. The emergence of the concept of chirality developed from studies by Pasteur on the relationship between optical activity and the spatial arrangement of atoms in a molecule. With the initial formulation of the structural requirements of chiral recognition by Dalgliesh, subsequent studies on the theory of enantioselective complexation have spurred the development of chiral stationary phases. In systematic studies of chiral recognition, Pirkle et al. [6–9] have validated the 'three-point rule' by implicating a minimum of three simultaneous interactions that must take place between the chiral stationary phase and at least one of the enantiomers. One of these interactions must be associated with a stereochemical dependence, that is, at least one of the three is either absent or significantly altered by replacing one enantiomer with its antipode without any conformational changes in either component. As summarized in the reviews cited above, thousands of compounds have been studied and separated using primarily the five different categories of commercially available chiral stationary phases that include ligand exchange, affinity, helical polymer, Pirkle or 'brush type,' and chiral cavity phases.

While HPLC has become an efficient technique for enantiomeric separations, the importance of polarimetric detection [10–12] has been noted as an adjunct to chromatography in the improvement of a chiral separation, and in enantiomeric purity determinations when only partial separation can be achieved. Since the separation of sugar standards and pressed juice samples by Boehme [13] using a commercially available polarimeter, substantial improvements have been reported with the introduction of a laser-based polarimeter [14]. Detection limits as low as 11 ng for fructose have been reported by Bobbitt and Yeung [15,16] using a microbore reverse-phase system with an argon-ion laser-based polarimeter. Such improvement was due to the increased efficiency of the chromatographic system and high frequency modulation which made it possible to detect an optical rotation of 1 μdeg. In one of the first reports of the use of a polarimetric detection system for enantiomeric purity determinations, Yeung and Reitsma [17,18] studied samples of amino acids separated using a cation exchange column. It was shown that the laser-based polarimeter was more sensitive than the RI detector and that the sensitivity of the technique could be increased by precolumn derivatization of amino acids with dansyl chloride in order to increase their specific rotation. Subsequently, using a diode-laser polarimeter, Lloyd et al. [19] tested a laboratory prototype optical rotation (OR) detector using the enantiomers of tryptophan. Polarimetric detection limits of 1 μg and $\pm$ 1% purity determinations at the 50 μg injection level were reported using a Spherisorb ODS column.

Whether or not a chiral separation has occurred is perhaps the most fundamental information a polarimetric detector can provide due to the opposite signs of the resulting peaks. An enantiomeric separation can be confirmed by coupling the UV and polarimetric detectors in series and measuring the ratio of the peak areas (or heights) of the UV and OR signals. This ratio should be constant for the two probable enantiomeric peaks [20]. In dealing with measurements of enantiomeric purity, Mannschreck et al. [21], invoked the role of UV and OA detectors connected in-series with the purpose of having the UV detector respond to the total amount of analyte and using the chiroptical detector to assay the proportion of each enantiomer in a mixture. The calibration factors obtained using a polarimetric detector for the *R* and *S* enantiomers, however, are not necessarily identical in the analysis of compounds with small specific rotations, or for mixtures with small enantiomeric excess (ee) due to refractive index-related effects [22]. While response functions were linear, the negative and positive signals did not coincide at zero ee.

Many studies reported during the past two decades have designed CSPs for the optimum separation of compounds as either the free enantiomers or as derivatized forms. These CSPs, however, while exhibiting excellent performance specifications for the compounds for which they were optimized, tend to be expensive and limited in their application. The utility of these chiral HPLC techniques to ascertain enantiomeric ratios and optical purities in mixtures is appropriate

only when baseline, or near baseline separation of the enantiomeric pair is achieved. Even in situations when adequate resolution is available, peak shape and detector sensitivity can limit the quality of the enantiomeric determination. Further, column failure, as manifested by decreased resolution can occur through various mechanisms including irreversible adsorption and stationary phase conformational changes. When the resolution decreases below baseline or near baseline, the ability to accurately quantitate the enantiomeric pair is substantially compromised. To enhance the quantitative capabilities of conventional enantiomeric separation methods, a chiral selective separation mode was interfaced with a polarimetric detection system (CSS/PD). To test the combined CSS/PD system, a series of dansylated amino acids were used as models to test the effect of chromatographic resolution and specific rotation on the quality of the data. Both peak area and peak height will be evaluated as analytical descriptors in this quantitation scheme. The influence of chromatographic resolution and specific rotation on the accuracy and precision of the enantiomeric data will be determined.

2. Experimental

2.1. Reagents

The dansylated amino acids (Dns-D- and L-Phenylalanine, Dns-L-Threonine and Dns-L-Valine), as well as the underivatized forms (D-Threonine and D-Valine) were obtained from Sigma (St. Louis, MO). Dns-D- and L-Phenylalanine were available in the free acid form while Dns-L-Threonine and Dns-L-Valine were purchased as cyclohexylammonium salts. The derivatizing agent, 5-[Dimethyl-amino]naphthalene-1-sulfonyl chloride (DnsCl) and the HPLC solvents acetonitrile and methanol were also obtained from Sigma.

2.2. Derivatization of amino acids

The procedure for the derivatization of amino acids for use in UV detection was reported by Tapuhi et al. [23]. DnsCl was dissolved in acetonitrile (1.5 mg/ml) while the amino acid was dissolved in 40 mM lithium carbonate buffer adjusted to pH 9.5 with HCl. A 1 ml volume of the DnsCl solution was rapidly added to 2 ml of the amino acid solution, the mixture was shaken for 2 min and then allowed to stand overnight at room temperature (22–23°C). Termination of the reaction was accomplished by adding 100 μl of a 2% ethylamine hydrochloride solution. Containers were wrapped with aluminum foil to exclude light.

For polarimetric detection, the quantity of the derivatizing agent as well as the amino acid, was increased to 0.0500 and 0.0250 g, respectively. DnsCl was dissolved in 20.0 ml of acetonitrile while the amino acid was dissolved in 10.0 ml of 40 mM lithium carbonate buffer adjusted to pH 9.5. The mixture was heated to about 55°C for 1 h and reactions were terminated using the 2% ethylamine hydrochloride solution. Solvents were evaporated at the same temperature under a vacuum.

Concentrations for the derivatized samples (Dns-D-Threonine and Dns-D-Valine) were determined using known concentrations of the corresponding Dns-L-amino acid and UV absorption spectroscopy.

2.3. Determination of specific rotation

Samples of commercially available, dansylated amino acids (DNS-L- and D-Phenylalanine, DNS-L-Threonine and DNS-L-Valine) were dissolved in a 70/30 (v/v) acetonitrile/NH_4NO_3 solvent mixture at a level of 0.100 g/10.00 ml. Specific rotations were obtained using a conventional polarimetric system at a measurement wavelength of 488.0 nm. The specific rotation of each compound was calculated from α, the actual rotation measured, c, the concentration of the solute in grams per ml of solution, and l, the pathlength, in decimeters.

2.4. Chromatographic analysis

The 25 cm × 4.6 mm i.d. Cyclobond column was purchased from Astec, Inc. (Whippany, NJ). The stationary phase for this column is a chiral

β-cyclodextrin chemically bound to a spherical gel support through a non-nitrogen-containing spacer arm. The preparation and characterization of this stationary phase has been described by Armstrong and DeMond [24].

Enantiomeric mixtures of D and L dansylated amino acids were prepared using different D to L ratios: 1/0, 0/1/, 1/1/, 1/2/, 2/1, 1/3, 3/1, 1/4, 4/1. In these mixtures, the total amount (L + D) of amino acid dissolved in the methanol solvent was prepared such that the amount of material injected with the polarimetric detection system was 15 μg for phenylalanine, 40 μg for threonine and 60 μg for valine using a 20 μl injection loop. With UV detection, the concentration of all three samples was set at 1.50 mg/250.0 ml. All separations were achieved at a flow rate of 1.00 ml/min using a degassed solvent system consisting of combinations of acetonitrile and NH_4NO_3. Since baseline separation for DNS-D and L-Phenylalanine was obtained with a solvent system of 80/20 acetonitrile/NH_4NO_3 [25], other solvent systems were prepared, for example, 70/30, 50/50 and 40/60, to decrease resolution. For the 40/60 solvent, the [NH_4NO_3] was 0.10 M.

2.5. UV and polarimetric detection

The UV detector (Shimadzu, Kyoto, Japan, model LC-6), was equipped with a solvent delivery module, a UV-VIS spectrophotometric detector and a CR 601 integrator. The laser-based polarimetric detection system has been described in detail previously [14,26], a schematic of which is given in Fig. 1. Briefly, the light source was an argon ion laser, (Lexel, Palo Alto, CA, model 85), mounted on a 4 × 6 ft. optical bread board. The source light was polarized by passing through a pair of Glan–Thompson polarizing prisms (Karl Lambrecht, Chicago, IL, model MGT-E8) and modulated using an in-house constructed Faraday cell driven by a signal generator (Wavetek, model 190). The modulation and detection cells had volumes of 1.1 ml and 28.57 μl, and pathlengths of 0.850 and 0.3826 dm, respectively. The polarized light passing through the analyzer was detected with a photomultiplier tube (PMT (Hamamatsu, Middlesex, NJ, model 928) powered by a high-voltage supply (Bertran Associates, Associates, Hicksville, NY, model 215). The signal from the PMT was demodulated, amplified and digitized using a lock-in amplifier (Stanford Research Systems, Palo Alto, CA, model SR 510). The digitized data were transferred to a PC computer over an IEEE interface (National Instruments, Austin, TX, model PC-2A) for storage and analysis. The Faraday coil used as an internal standard was made from a 10 cm × 0.125 o.d. piece of stainless-steel tubing wrapped with 8000 turns of a 30 AWG magnet wire (Bendon, Geneva, IL). A DC current of 0.266 A produced a rotation of 2.86×10^{-4} degree, as determined by Faraday's Law [26].

A minimum of three determinations for each enantiomeric mixture were obtained for both the UV and polarimetric detectors at all resolutions and L/D mixtures tested.

3. Results and discussion

This study sought to explore the potential of polarimetric detection for the quantitation of enantiomeric mixtures partially separated by a chiral-selective separation mode. The unique bi-

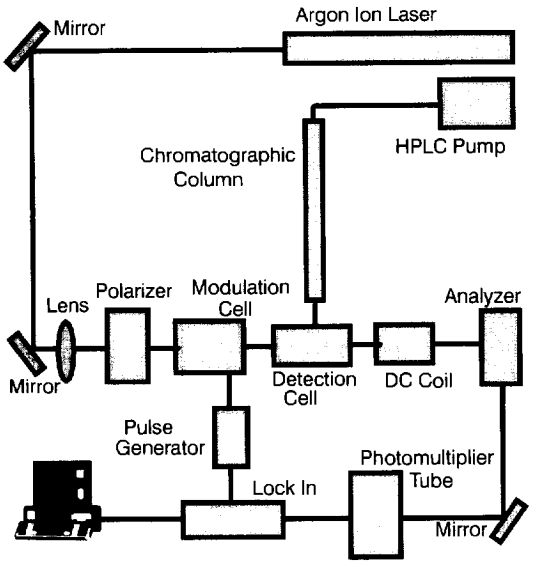

Fig. 1. Schematic of the laser-based polarimetric detection system.

modal response of the polarimetric system to the differing rotational properties of an enantiomeric pair may allow quantitative information to be obtained even under conditions of poor chromatographic resolution. This polarimetric response is expected to be equal in magnitude but opposite in sign for a given pair of enantiomers. Therefore, in contrast to a detection system which only provides a response in the same direction for an enantiomeric pair, the polarimeter provides a distinct and well defined zero crossing point which can be used to attribute peak area or height to the respective enantiomers in a quantitation protocol.

To evaluate the potential of this combined technology for enantiomeric quantitation, it is necessary to investigate the effect of specific rotation, chromatographic resolution and the mass ratio of the two enantiomers on the quality of the quantitative information extracted from the bimodal polarimetric response. Therefore, the dansylated derivatives of phenylalanine, threonine and valine were separated using a cyclodextrin column under varying conditions of chromatographic resolution. The three amino acid derivatives chosen provide specific rotations that vary by an order of magnitude, and in their sign of rotation.

Sample chromatograms obtained using either UV or polarimetric detection for the separated enantiomers of Dns-Phenylalanine are shown in Fig. 2 and Fig. 3. Fig. 2 shows the chromatograms of L and D Dns-Phenylalanine obtained from separate injections of the enantiomers with the L peak eluting earlier than the D peak. Fig. 2 also shows the DC reference signal that appears about 1 min after injection, and a peak disturbance due to the solvent at about 3 min. Fig. 3 shows the expanded chromatograms of the mixed enantiomers obtained using UV and polarimetric detection. The interesting feature of the polarimetric detector is seen in the unique bimodal response pattern, which is different from the unimodal response obtained with UV detection. As shown, since the L and D enantiomers rotate the plane of polarized light in opposite directions, the chromatograms obtained using polarimetric detection exhibit opposing signals for the L and D peaks. Unlike the unimodal response obtained using UV detection, the bimodal response pattern provides a

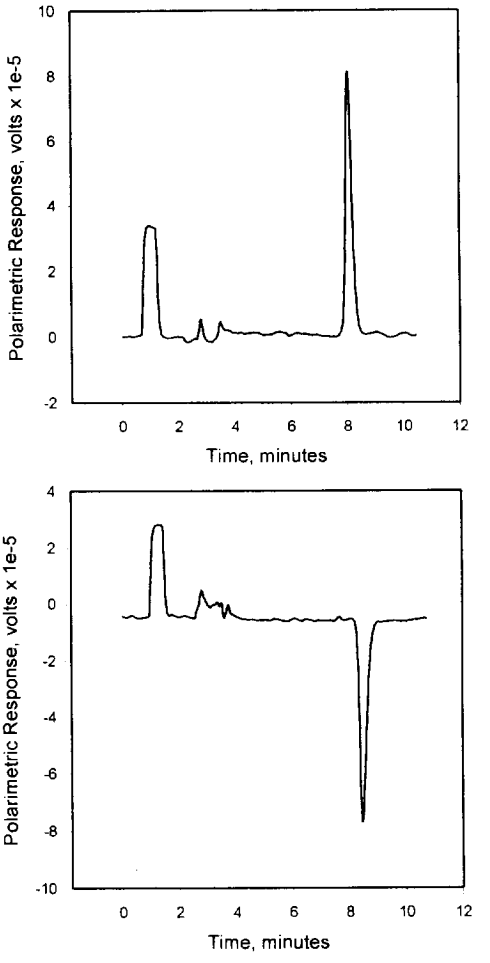

Fig. 2. Polarimetric detection of Dns-Phenylalanine. The peaks corresponding to the L and D enantiomers obtained using an 80/20 eluent system are shown in A and B, respectively. A DC reference signal produced by a DC coil appears at ~1 min and the peak disturbance due to solvent, at ~2 min.

well-defined crossing point between the two enantiomers that can serve as a reference in the determination of peak height and area. In combinations other than 1:1, such as 1:3 or 3:1 for the L and D enantiomers, the chromatogram obtained using polarimetric detection would clearly show this crossing point which would not be seen in a chromatogram obtained using UV detection. It should also be noted that the peaks obtained using UV and polarimetric detection as shown in the chromatograms in Fig. 3, do not elute exactly

at the same time due to differences in the length of connecting tubing and in the volumes of the cells used for the two detectors.

While a baseline separation of Dns-Phenylalanine enantiomers has been reported with the use of ACN/NH_4NO_3 [25] and MeOH/water [27] solvent systems, preliminary experiments identified conditions designed to decrease the resolution of the dansylated amino acid enantiomers by decreasing the organic content of the mobile phase.

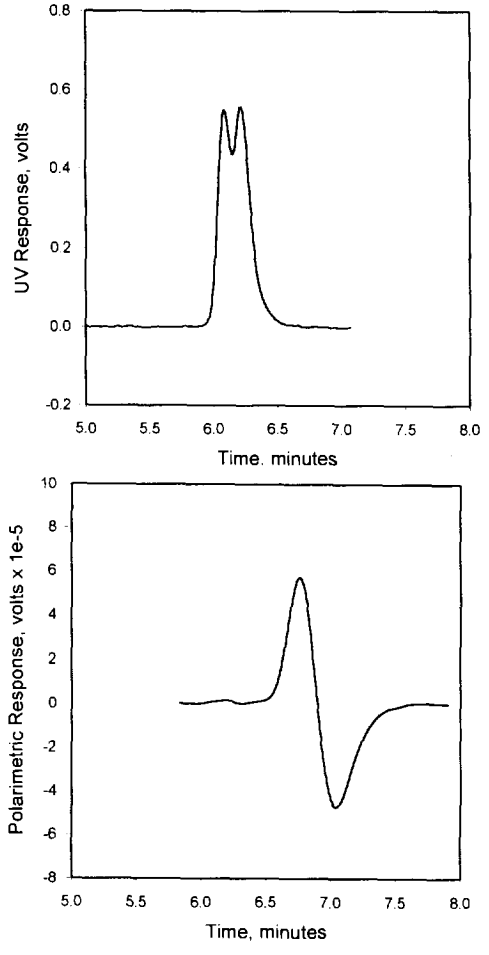

Fig. 3. UV and polarimetric response curves for Dns-Phenylalanine. The chromatogram in A was obtained using UV detection while B was obtained using polarimetric detection. Both chromatograms represent a 1/1 mixture of L and D enantiomers obtained with a 50/50 eluent system. Quantities injected were 0.12 and 15.0 μg for UV and polarimetric detection, respectively.

Tables 1–3 show the combinations of ACN/NH_4NO_3 used and the resulting retention time and resolution data for all pairs of enantiomers studied. The 60/40 combination was used with valine due to difficulties encountered in the elution of the enantiomers using the 80/20 eluent system. The decreased resolution available by decreasing the organic content of the mobile phase was an important part of this study and it allowed the capabilities of the CSS/PD system to be studied even under conditions of poor chromatographic resolution. As shown, the 80/20 eluent system was the most efficient in resolving the dansylated enantiomers of the amino acids as compared with the other eluent systems.

Peak height and area constitute the basic analytical descriptors utilized in many chromatographic analyses. While peak area has been generally considered a more 'fundamental' measurement as compared with peak height, uncertainties in the determination of baselines and peak boundaries have subjected peak area measurements to precision problems [28]. Studies have indicated that while peak area adequately correlates with the concentration of a component eluted from a column, the precision of a peak height measurement is significantly better than that of area even with the use of modern digital equipment [29]. Foley also noted that for tailed peaks of equal area, the errors in peak height are less than those in peak area [30]. In a 10:1 area ratio, it was found that a peak height measurement was more accurate than an area measurement when the small peak was eluted first, regardless of the tailing involved. When the small peak was eluted last, peak height determination was only superior if tailing was absent [31].

As analytical descriptors for the three dansyl amino acids, peak height and area were correlated with enantiomer fraction and these results are given in Table 4–6, and graphically presented in Figs. 4 and 5. Correlation coefficients were larger for peak height than for peak area, regardless of the magnitude of the chromatographic resolution. For Dns-L-Phenylalanine, the correlation coefficients for peak height and area using the 40/60 eluent were 0.993 and 0.981, respectively. With the 80/20 eluent where the resolution was higher,

Table 1
Retention time and enantiomeric resolution for Dns-Phenylalanine

Eluent[a]	Retention time, min		Resolution[b]
40/60	L	4.81 ± 0.02	0.32
	D	4.96 ± 0.00	
50/50	L	6.73 ± 0.01	0.34
	D	6.90 ± 0.00	
70/30	L	6.33 ± 0.02	0.66
	D	6.54 ± 0.02	
80/20	L	8.46 ± 0.02	1.00
	D	8.88 ± 0.04	

[a] ACN/NH_4NO_3 (0.025 M, pH 4.0) except for the 40/60 (0.10 M, pH 4.0).
[b] Resolution obtained using polarimetric detection.

Table 2
Retention time and enantiomeric resolution for Dns-Threonine

Eluent[a]	Retention time, min		Resolution[b]
40/60	L	4.83 ± 0.01	0.47
	D	5.03 ± 0.00	
50/50	L	7.91 ± 0.03	0.43
	D	8.14 ± 0.03	
70/30	L	8.64 ± 0.00	0.86
	D	9.10 ± 0.00	
80/20	L	12.5 ± 0.05	1.06
	D	13.3 ± 0.01	

[a] ACN/NH_4NO_3 (0.025 M, pH 4.0) except for the 40/60 (0.10 M, pH 4.0).
[b] Resolution obtained using polarimetric detection.

Table 3
Retention time and enantiomeric resolution for Dns-Valine

Eluent[a]	Retention time, min		Resolution[b]
40/60	L	4.70 ± 0.02	0.34
	D	4.84 ± 0.02	
50/50	L	6.40 ± 0.01	0.44
	D	6.60 ± 0.00	
60/40	L	5.73 ± 0.08	0.90
	D	6.13 ± 0.08	
70/30	L	6.80 ± 0.01	1.03
	D	7.15 ± 0.01	

[a] ACN/NH_4NO_3 (0.025 M, pH 4.0) except for the 40/60 (0.10 M, pH 4.0).
[b] Resolution obtained using polarimetric detection.

the correlation coefficients for the same parameters were 0.996 and 0.995. With the latter eluting D enantiomer, these numbers were 0.984 and 0.987 for the 40/60 eluent and 0.996 and 0.987 for the 80/20.

The larger correlation coefficient observed for phenylalanine is most likely due to its larger optical activity when compared with the other species studied and the reduced quantity of material injected into the chromatographic system. Using the 70/30 eluent system, the specific rotations of Dns-Phenylalanine, Dns-Threonine and Dns-Valine were (− 131), (− 18.7) and (+ 65.3) deg $(g/ml)^{-1}$ dm^{-1}, respectively. The amount injected for phenylalanine was 15.0 μg as compared with the 40.0 and 60.0 μg amounts for threonine and valine, respectively. The commercially prepared Dns-Phenylalanine enantiomers also were obtained in a more pure form than the Dns-Threonine and Dns-Valine, which were synthesized prior to study. The derivatizing agent may interfere with the elution of the enantiomers, although it is not visible in the chromatograms obtained with the polarimetric detection system because of the absence of a chiral structure in the derivatizing agent. The use of the 80/20 eluent with UV detection of Dns-Valine in a preliminary study showed the fusion of the peak corresponding to the unreacted derivatizing agent with the enantiomeric peaks. This overlap was severe enough such that an accurate determination of resolution was not possible with UV detection.

In order to assess the efficiency of the CSS/PD, limits of quantitation for the enantiomers of Dns-Phenylalanine, Dns-Threonine and Dns-Valine were determined at different regions of enantiomeric excess (ee). The (ee) is defined as the difference between the proportions of the two enantiomeric components in the mixture divided by their total. For example, a 0% ee is equivalent to a racemic mixture, whereas, a 60% ee represents an 80:20 or 4:1 ratio of enantiomers. In the interest of this study, a − 40% ee represents a 30:70 ratio of the L and D enantiomers.

Tables 7–9 show the limits of quantitation (LOQ) for the enantiomers of dansylated phenylalanine, threonine, and valine at the regions of ee cited above. The LOQ represents the allowable values of x based on a linear calibration

Table 4
Correlation coefficient (r) for peak height and area with mass fraction of enantiomer for Dns-Phenylalanine

Eluent[a]	L PK height	L PK area	D PK height	D PK area
40/60	0.993	0.981	0.984	0.987
50/50	0.997	0.990	0.996	0.992
70/30	0.997	0.993	0.995	0.986
80/20	0.996	0.995	0.996	0.987

[a] ACN/NH_4NO_3 (0.025 M, pH 4.0) except for the 40/60 (0.10 M, pH 4.0).

Table 5
Correlation coefficient (r) for peak height and area with mass fraction of enantiomer for Dns-Threonine

Eluent[a]	L PK height	L PK area	D PK height	D PK area
40/60	0.996	0.998	0.985	0.997
50/50	0.991	0.994	0.993	0.982
70/30	0.994	0.998	0.997	0.991
80/20	0.992	0.984	0.987	0.993

[a] ACN/NH_4NO_3 (0.025 M, pH 4.0) except for the 40/60 (0.10 M, pH 4.0).

Table 6
Correlation coefficient (r) for peak height and area with mass fraction of enantiomer for Dns-Valine

Eluent[a]	L PK height	L PK area	D PK height	D PK area
40/60	0.992	0.991	0.987	0.985
50/50	0.996	0.994	0.994	0.994
60/40	0.998	0.991	0.984	0.993
70/30	0.995	0.989	0.986	0.997

[a] ACN/NH_4NO_3 (0.025 M, pH 4.0) except for the 40/60 (0.10 M, pH 4.0).

model and the standard error of the slope. In the 80/20 eluent system with Dns-Phenylalanine as the analyte, a 0.30 L enantiomeric fraction would fall in the range of 0.30–0.32, a 50% L, 0.49–0.52 and 80%, 0.77–0.83, when analysis was made in terms of peak height. In the 40/60 eluent, these values would correspond to 0.29–0.32, 0.48–0.53, and 0.77–0.85, respectively. With peak areas, the ranges include 0.30–0.32, 0.50–0.54, and 0.78–0.84, respectively, for the 80/20 eluent, and 0.27–0.33, 0.47–0.57, and 0.77–0.85, respectively, for the 40/60 eluent. Values for the D enantiomer were comparable over these ranges. Based on the correlation studies concerning peak height and area for all three derivatized samples at all resolutions, the LOQ indicate a value of 1–2% ee at the −40% ee level for peak height and peak area regardless of the magnitude of the correlation coefficient. At 0% and 60% ee, where the L/D ratios were 1/1 and 4/1, respectively, the LOQ was at the 3–5% ee level.

The unique feature of this study lies in the precision of the quantitative information available at these % ee levels. A limit of quantitation of 0.30–0.32, for instance, signifies a minimum quantity of 2% ee that can be measured using either peak height or area as the analytical descriptor. This limit of quantitation suggests the usefulness of the CSS/PD in quantitating enantiomers in a mixture under conditions of poor chromatographic resolution. For these limits, the resolution between the enantiomeric pair was 0.32, 0.47, and 0.34 obtained using the 40/60 eluent for phenylalanine, threonine and valine,

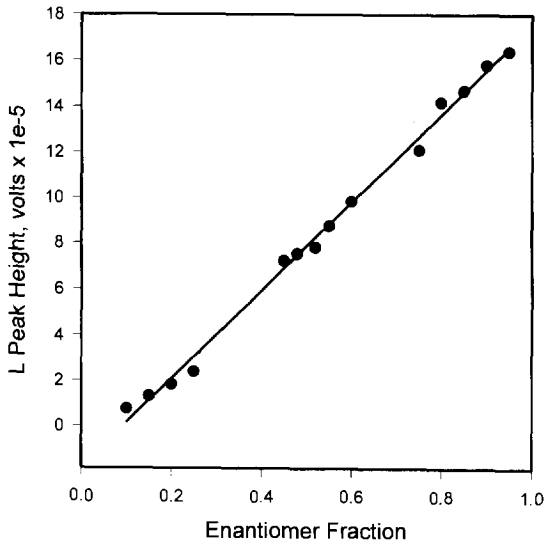

Fig. 4. Correlation of enantiomeric fraction and peak height for Dns-L-Phenylalanine. Eluent: 70/30 ACN/NH_4NO_3 (0.025 M, pH 4.0).

respectively. As compared with results obtainable using UV detection, where extensive overlap of the enantiomeric peaks precludes quantitation at these resolutions, the combination of the chiral selective separation mode with polarimetric detection, as demonstrated in this study provides significant advantages for the analysis of biological materials and pharmaceuticals. The limits of quantitation are at the level of injection reproducibility for manual injection. Further improvements would be expected in an automated injection system used with the CSS/PD technique.

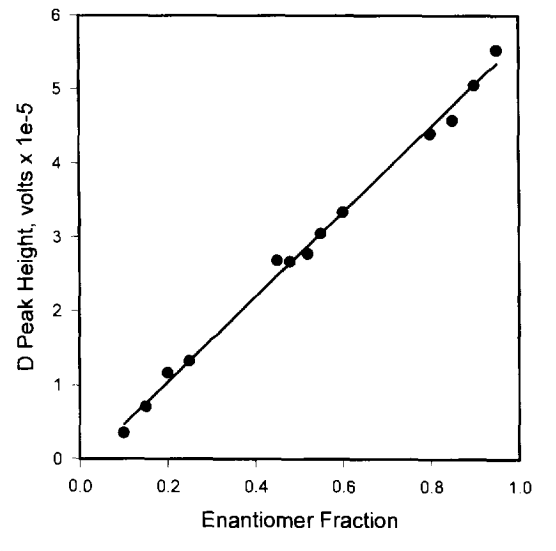

Fig. 5. Correlation of enantiomeric fraction and peak height for Dns-D-Phenylalanine. Eluent: 70/30 ACN/NH_4NO_3 (0.025 M, pH 4.0).

Table 7
Limits of quantitation for Dns-Phenylalanine enantiomers as a function of chromatographic resolution and enantiomeric excess

Eluent[a]	Parameter	−40% EE[b]	0% EE[c]	60% EE[d]
80/20	L, pk ht	0.30–0.32	0.49–0.52	0.77–0.83
	L, pk area	0.30–0.32	0.50–0.54	0.78–0.84
	D, pk ht	0.29–0.31	0.49–0.52	0.77–0.83
	D, pk area	0.28–0.32	0.47–0.54	0.75–0.86
70/30	L, pk ht	0.30–0.31	0.48–0.51	0.77–0.82
	L, pk area	0.29–0.32	0.49–0.54	0.77–0.84
	D, pk ht	0.30–0.33	0.50–0.54	0.78–0.84
	D, pk area	0.28–0.32	0.47–0.55	0.74–0.87
50/50	L, pk ht	0.29–0.31	0.50–0.53	0.79–0.83
	L, pk area	0.26–0.32	0.45–0.54	0.72–0.86
	D, pk ht	0.29–0.31	0.49–0.52	0.78–0.84
	D, pk area	0.29–0.32	0.47–0.52	0.77–0.86
40/60	L, pk ht	0.29–0.32	0.48–0.53	0.77–0.85
	L, pk area	0.27–0.33	0.47–0.57	0.73–0.89
	D, pk ht	0.29–0.34	0.46–0.54	0.73–0.88
	D, pk area	0.27–0.32	0.46–0.56	0.73–0.89

[a] ACN/NH_4NO_3 (0.025 M, pH 4.0) except for the 40/60 (0.10 M, pH 4.0).
[b] 30% L, 70% D.
[c] 50% L, 50% D.
[d] 80% L, 20% D.

This work has shown this technique to be useful for quantitating low levels of enantiomers ($\sim$ 1–2% ee), as compared to UV detection. What utility does polarimetric detection for incompletely resolved enantiomers have when compared with polarimetric detection with both no enantiomeric separation and with complete enantiomeric separation?

Polarimetric detection of enantiomers without separation is most useful when sufficient quantities of each enantiomer are available in pure form ($\geq$ 99.5% ee) for calibration purposes. Measuring the purity of these enantiomers requires an enan-

tiomeric separation, implying that the method of quantitating the enantiomers without separation may no longer be needed. A recent example illustrating the utility of enantiomeric quantitation without separation has been reported [32]. It may be true that enantiomeric quantitation without separation is often of limited utility as compared with these other two polarimetric detection modes.

The utility of polarimetric detection with complete enantiomeric separation is probably more clear cut: the bimodal signal is perhaps the most confirmatory evidence that an enantiomeric separation has indeed taken place. However, obtaining and maintaining baseline resolution of some enantiomers can be problematic, so there can be a complicated methods development strategy. Perhaps one clear advantage of polarimetric quantitation of partially resolved enantiomers is that it still provides a bimodal signal, just as with polarimetric detection with completely resolved enantiomers, but may permit shorter and simpler chromatographic methods development.

Table 8
Limits of quantitation for Dns-Threonine as a function of chromatographic resolution and enantiomeric excess

Eluent[a]	Parameter	−40% EE[b]	0% EE[c]	60% EE[d]
80/20	L, pk ht	0.28–0.32	0.48–0.53	0.75–0.84
	L, pk area	0.27–0.32	0.47–0.56	0.75–0.88
	D, pk ht	0.28–0.33	0.45–0.56	0.74–0.87
	D, pk area	0.30–0.33	0.47–0.52	0.76–0.84
70/30	L, pk ht	0.29–0.32	0.49–0.54	0.78–0.86
	L, pk area	0.30–0.31	0.49–0.52	0.77–0.81
	D, pk ht	0.29–0.32	0.49–0.53	0.78–0.84
	D, pk area	0.29–0.33	0.47–0.52	0.76–0.85
50/50	L, pk ht	0.28–0.32	0.47–0.54	0.75–0.86
	L, pk area	0.30–0.32	0.50–0.53	0.80–0.84
	D, pk ht	0.28–0.33	0.47–0.54	0.76–0.87
	D, pk area	0.28–0.34	0.46–0.56	0.76–0.92
40/60	L, pk ht	0.29–0.32	0.50–0.53	0.78–0.84
	L, pk area	0.29–0.31	0.49–0.51	0.79–0.83
	D, pk ht	0.31–0.36	0.46–0.54	0.74–0.87
	D, pk area	0.30–0.32	0.49–0.53	0.77–0.83

[a] ACN/NH_4NO_3 (0.025 M, pH 4.0) except for the 40/60 (0.10 M, pH 4.0);
[b] 30% L, 70% D;
[c] 50% L, 50% D;
[d] 80% L, 20% D.

Table 9
Limits of quantitation for Dns-Valine as a function of chromatographic resolution and enantiomeric excess

Eluent[a]	Parameter	−40% EE[b]	0% EE[c]	60% EE[d]
70/30	L, pk ht	0.28–0.31	0.48–0.53	0.77–0.86
	L, pk area	0.28–0.32	0.47–0.54	0.75–0.86
	D, pk ht	0.28–0.33	0.47–0.56	0.75–0.89
	D, pk area	0.29–0.31	0.48–0.51	0.78–0.84
60/40	L, pk ht	0.31–0.34	0.52–0.56	0.82–0.89
	L, pk area	0.29–0.32	0.48–0.54	0.77–0.86
	D, pk ht	0.28–0.33	0.46–0.54	0.74–0.88
	D, pk area	0.28–0.31	0.47–0.53	0.76–0.85
50/50	L, pk ht	0.28–0.32	0.47–0.53	0.76–0.85
	L, pk area	0.29–0.32	0.48–0.54	0.76–0.86
	D, pk ht	0.28–0.32	0.49–0.55	0.77–0.86
	D, pk area	0.29–0.32	0.48–0.53	0.76–0.85
40/60	L, pk ht	0.30–0.34	0.47–0.53	0.76–0.87
	L, pk area	0.28–0.32	0.47–0.54	0.76–0.87
	D, pk ht	0.27–0.32	0.47–0.55	0.75–0.88
	D, pk area	0.28–0.33	0.46–0.55	0.75–0.89

[a] ACN/NH_4NO_3 (0.025 M, pH 4.0) except for the 40/60 (0.10 M, pH 4.0).
[b] 30% L, 70% D.
[c] 50% L, 50% D.
[d] 80% L, 20% D.

4. Summary and conclusions

It has been shown that the combination of a chiral selective separation mode with polarimetric detection (CSS/PD) can be used to quantitate enantiomeric mixtures even under conditions of poor chromatographic resolution. The bimodal response function of the polarimetric detector provides a well-defined crossing point between the two enantiomers which can then be used as a reference in the determination of peak height and area.

Analyses of the dansylated enantiomers of the amino acids phenylalanine, threonine and valine have shown higher correlation coefficients for peak heights than for areas with mass fraction of enantiomer. In addition to the concentration ratio

of the L and D enantiomers, specific rotation and chromatographic resolution constitute the important factors that affect the shape of the polarimetric response curve. For most resolutions studied, the LOQ was at, or near the RSD of the injection method used.

Work on the pharmaceutical application of the CSS/PD technique involving the enantiomeric analysis of DOPA and propranolol is in progress.

Acknowledgements

The authors wish to acknowledge the Camille and Henry Dreyfus Foundation and the R.W. Johnson Pharmaceutical Research Institute for financial support.

References

[1] D.W. Armstrong, Anal. Chem., 59 (1987) 84A.
[2] R. Dappen, H. Arm and V.R. Meyer, J. Chromatogr., 373 (1986) 1.
[3] V.A. Davankov, Chromatographia, 27 (1989) 475.
[4] Y. Okamoto, Chem. Tech., (1987) 176.
[5] D.R. Taylor and K. Maher, J. Chromatogr. Sci., 30 (1992) 67.
[6] W.H. Pirkle and T.C. Pochapsky, Advanced Chromatography, in J.C. Giddings, E. Grushka and P.R. Brown (Eds.), Marcel Dekker, NY, 27 (1987) 73.
[7] W.H. Pirkle and T.C. Pochapsky, Chem. Rev., 89 (1989) 347.
[8] W.H. Pirkle and T.C. Pochapsky, Chromatogr. Sci., 47 (1990) 783.
[9] W.H. Pirkle, T.C. Pochapsky, J.A. Burke and K.C. Deming, Chiral Separations, in D. Stevenson and I.D. Wilson (Eds.), Plenum Press, NY 1988, 23.
[10] N. Purdie and K. Swallows, Anal. Chem., 61 (1989) 77A.
[11] A. Mannschreck, D. Ander, A. Eiglsperger, E. Gmahl and H. Buchner, Chromatographia, 25 (1988) 182.
[12] A. Mannschreck, M. Mintas, G. Becher and G. Stuhler, Angew. Chem. Int. Ed., 19 (1980) 469.
[13] W. Boehme, Chromatogr. Newslett., 8 (1980) 38.
[14] E.S. Yeung, L.E. Steenhoek, S.D. Woodruff and J.C. Kuo, Anal. Chem., 52 (1980) 1399.
[15] D.R. Bobbitt and E.S. Yeung, Anal. Chem., 59 (1984) 1577.
[16] D.R. Bobbitt and E.S. Yeung, Appl. Spectrosc., 40 (1986) 407.
[17] B.H. Reitsma and E.S. Yeung, J. Chromatogr., 362 (1986) 353.
[18] B.H. Reitsma and E.S. Yeung, Anal. Chem., 59 (1987) 1059.
[19] D.K. Lloyd, D.M. Goodall and H. Scrivener, Anal. Chem., 61 (1989) 1238.
[20] D.K. Lloyd and D.M. Goodall, Chirality, 1 (1989) 251.
[21] A. Mannschreck, M. Mintas, G. Becher and G. Stuhler, Angew. Chem. Int. Ed., 19 (1980) 469.
[22] R. Dappen, P. Voight, F. Maystre and A.E. Bruno, Anal. Chim. Acta, 282 (1993) 47.
[23] Y. Tapuhi, N. Miller and B.L. Karger, J. Chromatogr., 205 (1981) 325.
[24] D.W. Armstrong and W. DeMond, J. Chromatogr. Sci., 22 (1984) 411.
[25] Advanced Separation Technologies Inc., 'Cyclobond Handbook: A Guide to Using Cyclodextrin Bonded Phases,' Astec, Whippany, NJ, 1992.
[26] P.D. Rice, 'Analytical Applications of Laser-Based Polarimetry,' Ph.D. Thesis, University of Arkansas, 1992.
[27] W.L. Hinze, T.E. Riehl, D.W. Armstrong, W. DeMond, A. Alak and T. Ward, Anal. Chem., 57 (1985) 237.
[28] A. Papas, CRC Crit. Rev. in Anal. Chem., 20 (1989) 359.
[29] A. Janik, J. Chromatogr. Sci., 13 (1975) 93.
[30] J.P. Foley, J. Chromatogr., 384 (1987) 301.
[31] V.R. Meyer, LC-GC Int., 7 (1994) 94.
[32] T.J. Edkins, M. Fronheiser, D.R. Bobbitt, J.E. Mills and T.M. Rossi, Enantiomer (1996), In press.

ELSEVIER

Talanta 44 (1997) 1365–1369

Talanta

Potentiometric and conductometric studies on the binary and mixed ligand complexes in solution: M^{II}-dipicolinic acid–glycine systems

M.M. Khalil *, S.A. Mohamed, A.M. Radalla

Department of Chemistry, Faculty of Science, Cairo University, Beni-Suef Branch, Beni-Suef, Egypt

Received 13 June 1996; received in revised form 6 November 1996; accepted 13 November 1996

Abstract

The binary and mixed ligand complexes of some alkaline earth and transition metal (II) ions with dipicolinic acid (DPA) as a primary ligand and the biologically important secondary ligand (glycine), were studied using potentiometric technique. The acidity constants of the ligands were determined and used for determining the stability constants of the complexes formed in aqueous solutions under the experimental conditions ($t = 25°C$, $\mu = 0.1$ M $NaNO_3$). The dissociation constants of DPA were also determined in various water + dioxane mixtures under the same experimental conditions. It is concluded that a pronounced change in the pK values is observed as the solvent is enriched in dioxane. The values of $\Delta \log K$ have been evaluated and discussed. In addition, the chelation mode of ternary complexes was ascertained by conductivity measurements. © 1997 Elsevier Science B.V.

Keywords: Binary and ternary complexes; Dipicolinic acid; Potentiometric and conductometric studies

1. Introduction

Over the years there has been a steadily increasing interest in the complexes of pyridine derivatives [1–4] arises due in part to their physiological properties. The importance of pyridinecarboxylic acids stems from their presence in many natural products (alkaloids, vitamins, coenzymes, etc.). They are also of great interest to medicinal chemists because of the wide variety of their physiological properties displayed by the natural and synthetic acids. It is well known that complexes of metal ions are among the prominent interactions in nature [5,6], and the glycine residue is an important and versatile binding site of protein. Among pyridine dicarboxylic acids, dipicolinic acid seems to have the best chelating properties because it is terdentate.

As a continuation of our research program oriented to study binary and ternary complexes of biological importance, [7–11] the present work reports the formation and characterization of binary and mixed ligand complexes of the type M^{II}-DPA–glycine, where M = Mg, Ca, Sr, Ba, Cu, Co, Ni, Zn, Mn or Cd ions.

* Corresponding author.

PII S0039-9140(96)02173-X

2. Experimental

2.1. Materials and solutions

Dipicolinic acid was obtained from Fluka. The reagent was repeatedly recrystallized from water, dried at 115°C, and checked by its melting point (250°C). Stock solutions were prepared by dissolving precisely weighed amounts of the anhydrous acid in suitably bidistilled water. Glycine was also provided by Fluka. The metal salts were provided by BDH as nitrates or chlorides. All solutions of metal (II) ions were prepared and standardized complexometrically by EDTA using suitable indicators [12]. Dioxane was of high purity (spectro grade product). Carbonate-free sodium hydroxide (titrant, prepared in 0.1 M $NaNO_3$ solution) was standardized potentiometrically with KH-phthalate solution (Merck AG). Nitric acid and NaOH were from Merck p.a.

2.2. Apparatus

Potentiometric pH measurements were carried out on solutions in a double-walled glass vessel at 25°C ± 0.1°C using a Griffin pH J-300-010 G Digital pH meter. The temperature was controlled by circulating water through the jacket, from a constant temperature bath. The cell was equipped with magnetic stirrer and a tightly fitting rubber stopper, through which an Amel 882 delivery dispenser, readable to 1 μl, and electrode system were inserted. The electrode system was calibrated in terms of hydrogen-ion concentrations instead of activities. Thus, all constants determined in this work are concentration constants.

Conductance of solutions was measured with PTI-10 Mini Digital Conductivity and temperature meter.

2.3. Procedure and measuring techniques

The following solutions were prepared and titrated potentiometrically against standard carbonate- free NaOH (0.1053 M) solution:(a) 0.04 M HNO_3 (5 cm^3) + 0.50 M $NaNO_3$ (10 cm^3)(b) (a) + 0.01 M DPA (5 cm^3)(c) (b) + 0.01 M M^{II} (2 cm^3)(d) (a) + 0.01 M glycine (5 cm^3)(e) (d) + 0.01 M M^{II} (2 cm^3)(f) (a) + 0.01 M M^{II} (5 cm^3) + 0.01 M DPA (5 cm^3) + 0.01 M glycine (5 cm^3)The total volume was adjusted to 50 cm^3 by adding double-distilled water in each case. All pH-metric titrations were performed at 25°C and $\mu = 0.1$ M ($NaNO_3$). An Irving and Rossotti pH titration technique [13] with modifications [14,15] was used to determine the protonation constants of the ligands and formation constants of the metal complexes. The equilibrium constants were calculated from six independent titration curves. The errors given in Table 1 and Table 2 are three times the standard error of the mean or the sum of the probable systematic errors, whichever is the larger.

Mixture (g) was titrated conductometrically against 0.1 M NaOH solution: g, 0.01 M Cu^{II} (10 cm^3) + 0.01 M DPA (10 cm^3) + 0.01 M glycine (10 cm^3).

3. Results and discussion

Dipicolinic acid, H_2L, can be further protonated as the acidity of the medium increases forming a monopositive species, H_3L^+. However, in the pH range utilized, this cationic form always proved negligible as checked previously using spectrophotometric technique [16].

The first and second proton association constants of neutral DPA were determined potentiometrically in aqueous solutions, under the experimental conditions ($t = 25$°C, $\mu = 0.1$ M

Table 1
pK_a values of dipicolinic acid in aqueous dioxane media ($t = 25$°C, $\mu = 0.1$ M $NaNO_3$)

Solvent composition %v/v	pK_1	pK_2
0.00	2.32 ± 0.05	4.53 ± 0.06
10	2.68 ± 0.04	5.15 ± 0.07
20	2.81 ± 0.07	5.45 ± 0.04
30	3.02 ± 0.04	5.67 ± 0.08
40	3.28 ± 0.06	5.98 ± 0.05
50	3.65 ± 0.08	6.32 ± 0.06
60	3.96 ± 0.08	6.75 ± 0.05

The pK_a values were calculated from pH titration data without correction.

Table 2
Acidity constants of dipicolinic acid and stability constants of binary and mixed ligand complexes at 25°C, $\mu = 0.1$ M ($NaNO_3$)

Cation	$\log k_1^H$	$\log k_2^H$	$\log k_{MA}^M$	$\log k_{ML}^M$	$\log k_{MAL}^{MA}$	$\log \beta_{MAL}^M$	$\Delta \log k$
H	4.53 ± 0.06	2.32 ± 0.05					
Mg			2.50 ± 0.05	3.45 ± 0.08	3.92 ± 0.05	6.42	0.47
Ca			4.50 ± 0.08	5.12 ± 0.06	3.80 ± 0.04	8.30	−1.32
Sr			3.98 ± 0.06	3.90 ± 0.08	3.99 ± 0.06	7.97	0.09
Ba			3.60 ± 0.06	3.45 ± 0.04	3.73 ± 0.06	7.33	0.28
Cu			9.14[a]	7.85 ± 0.06	5.80 ± 0.07	14.94	−2.05
Co			6.65[a]	4.90 ± 0.05	3.10 ± 0.06	9.75	−1.80
Ni			6.95[a]	5.90 ± 0.06	4.77 ± 0.08	11.72	−1.13
Zn			6.35[a]	5.46 ± 0.06	3.58 ± 0.05	9.93	−1.88
Mn			5.01[a]	5.12 ± 0.04	3.74 ± 0.07	8.75	−1.38
Cd			6.75[a]	4.30 ± 0.05	1.65 ± 0.08	8.40	−2.65

[a] The values were previously determined by Anderegg using pCu-method [21], at 20°C, $\mu = 0.1$ M ($NaNO_3$).

$NaNO_3$). The values obtained (Table 1) are in a good agreement with the literature values [17].

In order to shed more light on the dissociation of DPA in various water + organic solvent mixtures, dioxane (an aprotic nonionizing coorganic solvent) was chosen. The observed increase in the pK_a values of DPA upon enrichment of the solvent with dioxane may be attributed to a lowering of the dielectric constant ($\varepsilon = 76.55$, 60.03 for 10 and 60% v/v solvent composition, respectively at 25°C) which increases in turn the fraction of associated ions to form Bjerrum ion pairs [18] and higher aggregates such as triple ions and dipole aggregates [19]. In this medium, free ions have very low concentration and acidity phenomena are governed largely by ionic association reactions, as previously reported by Kolthoff and Bruckenstein [20]. The pK_a values of DPA in aqueous dioxane media are listed in Table 1.

The stability constants of normal 1:1 binary complexes of DPA with alkaline earth metal ions have been determined. The values obtained (Table 2) agree well with those previously reported [21]. The stabilities decrease in the order Ca(II) > Sr(II) > Ba(II) > Mg(II).

In the cases of the 1:1 transition metal ions complexes with dipicolinic acid the acid strength of the complexing agent combined with the great stabilities of the complexes made the determination of stability constants by the pH method very inaccurate. The values of stability constants are taken from the work of Anderegg [21] using a copper amalgam electrode (p^{Cu}-method) as shown in Table 2.

The second association constant of glycine was determined, the obtained value (9.76) agree quite well with that previously reported [22].

The stability constants of glycine complexes with Mg, Cu, Co, Ni, Zn or Cd ions, agree well with literature values [22–25]. The disagreement found for the values of Ca, Sr, Ba or Mn complexes my be attributed to the different methods and ionic strength used for determination [23,26,27].

For the formation of the ternary complexes of the selected bivalent metal ions in presence of DPA = A and glycine = L, the following equilibria may be considered:

$$M + A \rightleftarrows MA$$

$$MA + L \rightleftarrows MAL$$

$$k_{MAL}^{MA} = \frac{[MAL]}{[MA][L]} \quad (1)$$

Here complex formation is considered to take place in a stepwise manner, i.e., the secondary ligand, glycine, starts complexation after the complete formation of the binary 1:1 complex of DPA. Representative titration curves for ternary systems investigated are shown in Fig. 1 and Fig. 2. The formation constants obtained are reported in Table 2.

The relative stability of the ternary complexes as compared with that of the corresponding binary complexes can be quantitatively expressed in different ways. The most suitable comparison is in terms of Δlog K, which represents the difference in stabilities for the addition of ligand L to the 1:1 MA complex and to the aquated metal ion as shown by Eq. (2) [28].

$$\Delta \log K = \log K^{MA}_{MAL} - \log K^{M}{}_{ML}$$

$$= \log K^{ML}_{MLA} - \log K^{M}_{MA} \quad (2)$$

The overall stability constant β^{M}_{MAL} which must be determined experimentally, is connected to K^{MA}_{MAL} by Eq. (3):

$$\log K^{MA}_{MAL} = \log \beta^{M}_{MAL} - \log K^{M}_{MA} \quad (3)$$

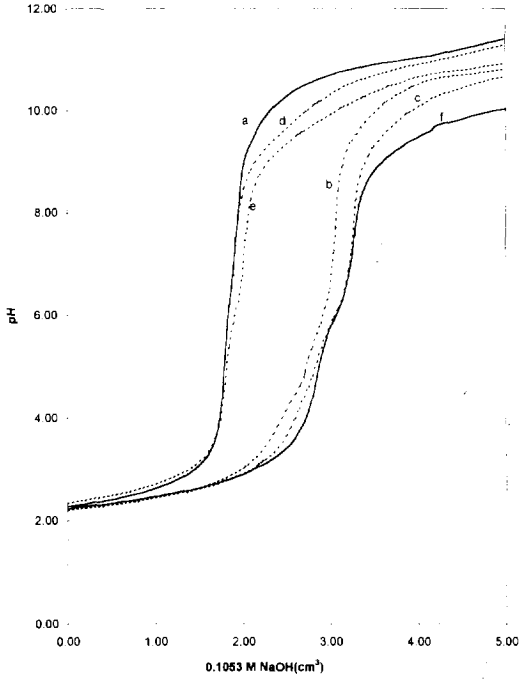

Fig. 1. Titration curves for the Ca^{++}–DPA–gly. system

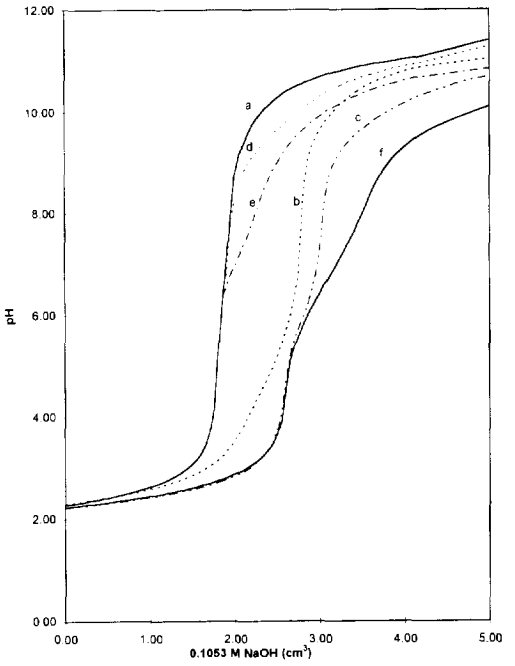

Fig. 2. Titration curves for the Ni^{++}–DPA–gly. system.

It is observed, that in general, Δlog K for the investigated ternary complexes is negative as expected from the statistical considerations (Table 2). There is π acidic character in the primary ligand (DPA), due to the possibility of M → Nπ bond formation. This behaviour is similar to that observed previously in [M-dipyridyl-L] complexes [14,29].

The conductometric titration curve of the ternary complex containing copper (II) with DPA and glycine (Fig. 3) shows an inflection at a = 2, probably corresponding to the neutralization of protons resulting from the formation of Cu-DPA binary complex. Between 2 < a < 3, the slight increase of conductance is due to the formation of the ternary complex and is associated with the release of a proton from the secondary ligand (glycine). Beyond a = 3, the conductance increases more uniformly due to the presence of excess sodium hydroxide.

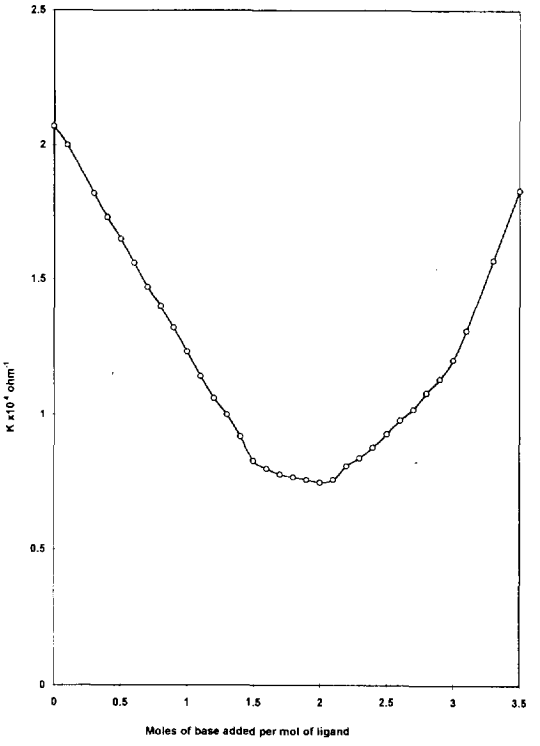

Fig. 3. Conductometric titration curve of Cu^{++}–DPA–gly. system.

References

[1] E. Casassas, G. Fonrodona and R. Tauler, Polyhedron, 6 (1987) 1517.
[2] E. Casassas and G. Fonrodona, Polyhedron, 7 (1988) 689.
[3] O. Jons and E.S. Johansen, Inorg. Chim. Acta 151 (1988) 129.
[4] M.M. Seleim, K.A. Idriss, M. Saleh and H. Sedaira, Analyst, 112 (1987) 1685.
[5] H. Sigel (Ed.), Metal Ions in Biological Systems (1973) Vol.2. Dekker, New York.
[6] J.M. Wood, Naturwissenschaften, 62 (1975) 357.
[7] M.M. Khalil, A.H.H. Elghandour, M. Mostafa and M.M. Shoukry, Polyhedron, 13 (1994) 3295.
[8] M.M. Khalil, A.H.H. Elghandour, E.M. Shoukry and A. Abdel Alem, Egypt. J. Chem., 37 (1994) 635.
[9] M.S. Abu-Bakr, M.M. Khalil, H. Sedaira and E.Y. Hashem, Indian J. Chem., 33A (1994) 644.
[10] E.M. Shoukry, M.M. Khalil, A.H.H. Elghandour and M.M. Shoukry, M. Monatshefte Chem., 126 (1995) 241.
[11] M.M. Shoukry, W.M. Hosny and M.M. Khalil, M. Transition Met. Chem., 20 (1995) 252.
[12] F.J. Welcher, The analytical uses of ethylendiaminetetraacetic acid, Van Nostrand, Princeton, 1965.
[13] H.M. Irving and H.S. Rossotti, J. Chem. Soc., 3397 (1954), J. Chem. Soc., (1953) 2904.
[14] M.V. Chidambaram and P.K. Bhattacharya, J. Inorg. Nucl. Chem., 32 (1970) 3271.
[15] B.H. Agrawal, K. Dwivedi, M. Chandra, B. Agrawala and K.A. Dey, J. Indian Chem. Soc., 54 (1977) 931.
[16] E. Chiacchierini, G. D'Ascenzo, G. De Angelis, A.L. Magri and V. Petrone, Ann. Chim. (Rome), 67 (1977) 195.
[17] A. Napoli and A.L. Magri, Ann. Chim., 77 (1987) 783.
[18] N. Bjerrum, Kgl. Danske Videnskab. Selskab., Mat. Fys. Medd. 7 (1926) 9.
[19] R.M. Fuoss and C.A. Kraus, J. Am. Chem. Soc., 55 (1933) 2387.
[20] I.M. Kolthoff, S. Bruckenstein, J. Am. Chem. Soc., 78 (1956) 1, S. Bruckenstein and I.M. Kolthoff, J. Am. Chem. Soc., 78 (1956) 2974.
[21] G. Anderegg, Helv. Chim. Acta, 52 (1960) 414.
[22] A. Gergely, I. Nagypal, J. Mojzes, Acta Chim. Acad. Sci. Hung., 51 (1967) 381.
[23] C.B. Monk, Trans. Faraday Soc., 47 (1951) 285;292;297;1233.
[24] A. Gergely, I. Nagypal, Acta Univ. Debrecen (1965) 113.
[25] G. Anderegg, Helv. Chim. Acta, 44 (1961) 1673.
[26] C.A. Colman-Porter and C.B. Monk, J. Chem. Soc., (1952) 4363.
[27] A. Albert, J. Biochem., 54 (1953) 646.
[28] R.B. Martin and R.J. Prados, J. Inorg. Nucl. Chem., 36 (1974) 1665.
[29] P.J. Patel, V.K. Patel and P.K. Bhattacharya, Indian J. Chem., Sect., A 21 (1982) 590.

ELSEVIER

Talanta 44 (1997) 1371–1378

Talanta

The separation of gold by selective extraction of $HAuBr_4$ using a poly(tetramethylene) ether glycol impregnated filter

Richard Oleschuk, Art Chow *

Department of Chemistry, University of Manitoba, Winnipeg, MB, R3T 2N2, Canada

Received 18 October 1996; received in revised form 2 December 1996

Abstract

The separation of gold(III) by selective extraction on an organic- impregnated filter (OIF) was studied. Gold was found to be rapidly extracted into the active polytetramethylene ether glycol (polyTHF) layer of the filter from strongly acidic solutions of HBr, as the $HAuBr_4$ complex. Quantitative extraction of gold from solution was obtained with flow rates up to 600 ml min^{-1} through the 10.75 cm^2 OIF and at ng ml^{-1} concentration levels. The extraction is shown to be dependent on the solution flow rate and HBr concentration as well as the filter pore size, thickness and porosity. Gold can be eluted from the filter by converting it into the $AuBr_4^-$ complex using a KBr solution. The separation of gold is demonstrated from simple binary metal mixtures involving iron and cadmium, as well as from a more complicated matrix, gold ore solution. © 1997 Elsevier Science B.V.

Keywords: Ether glycol; Gold; Selective extraction

1. Introduction

Classical solid phase extraction (SPE) is the selective partitioning of one or more components between a solid and liquid phase. Sorbent material can be made for a specific analyte or analytes in order to extract only certain components in a mixture, or it can be modified so that only the compounds of interest are not sorbed on the solid phase material. The extraction of metals is performed using either a chelating sorbent or by employing solution conditions to form complexes that are extractable onto the solid sorbent.

Extractable metal complexes can be formed using complexing agents such as crown ethers [1–4], or by attaching bulky ligands to a molecule followed by extraction onto a hydrophobic sorbent. The extent of formation for a complex is determined by the stability constant of the complex and the relative concentrations of the complexing agents present in solution. Gold(III) is a soft Pearson [5] acid so it prefers to form complexes with bulky non-polar ligands. Gold(III) in the presence of sufficiently high chloride and bromide concentrations forms either the $AuCl_4^-$ or $AuBr_4^-$ (Eq. (1)) complex, respectively [6,7]. These complexes are stable in aqueous solutions [8,9] at a pH lower than 6. Both complexes are weak acids that become protonated at sufficiently low

* Corresponding author. Fax: +1 204 2750905.

PII S0039-9140(96)02192-3

pH (Eq. (2)) to form the extractable $HAuCl_4$ [10,11] and $HAuBr_4$ complexes in the following equilibrium.

$$Au^{3+} + 4Br^- \rightleftharpoons AuBr_4^- \quad (1)$$

$$AuBr_4^- \rightleftharpoons HAuBr_4 \quad (2)$$

Gold has been shown to be extracted as either the $HAuCl_4$ or the $HAuBr_4$ complex by diethyl ether [12], isopropyl ether [13] and polyurethane ether-type foams [14] and elastomers [15]. Each of these compounds possess ether linkages (-O-) in their structures. Preliminary experiments have shown that gold is also extracted from an HBr solution into the compound polytetramethylene ether glycol (polyTHF) (Fig. 1) which also possesses an ether linkage in its structure.

By impregnating a porous polytetrafluoroethylene filter with polyTHF, the gold complex, $HAuBr_4$, can be rapidly extracted from solution as it passes through the impregnated filter. This device is termed an organic-impregnated filter (OIF). The immobilisation of polyglycols in the pores of a filter has also been used by Ho [16] to prepare supported liquid membranes for the removal of organics from aqueous solutions.

The rapid gold extraction is shown to be both selective and quantitative. Once extracted the gold can be eluted by an analogous process to the extraction. The gold complex is converted to the de-protonated $AuBr_4^-$ complex where it is stripped from the surface of the active layer and consequently removed from the filter. In this paper, the use of an organic-impregnated filter for the selective removal of gold from solution is demonstrated. The effects of the HBr concentration, the flow rate, the filter pore size and the filter porosity on the extraction of gold from HBr solutions will be described. The recovery of the gold, and the ability of the OIF to preconcentrate and separate gold in simple binary metal mixtures and from gold ore will be investigated.

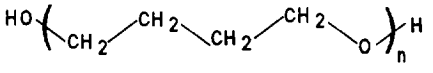

Fig. 1. Polytetramethylene ether glycol (polyTHF).

2. Experimental section

Polytetramethylene ether glycols (polyTHF's) of nominal molecular weights 650, 1000 and 2000 ± 50 g mol^{-1} were provided as samples by BASF. $NaAuCl_4$ was supplied by Johnson-Matthey and hydrobromic acid by Anachemia. Sodium hydroxide was purchased from Mallinckrodt and potassium bromide from British Drug Houses (BDH). All chemicals were reagent grade or better. Gold ore was obtained from Kirkland Lake Mine in eastern Ontario, Canada. All water used was purified by a Barnstead Nanopure™ II system using reverse osmosis-treated feedstock. A Varian Liberty 200 ICP emission spectrometer was used for the multi-element determinations made when performing the separation of gold from gold ore. Inter-element correction was used when overlapping emission lines were present. Atomic absorption was performed using a Varian SpectrAA-20 atomic absorption spectrometer equipped with an Instrumentation Laboratory Visimax™ hollow cathode lamp and an air-acetylene flame. The wavelength observed was 242.8 nm with a slit width of 1.0 nm. Two different types of polytetrafluoroethylene filters were used to prepare the OIF. Both filters were supplied by Millipore™ with the following specifications: pore size 5.0 μm, 47 mm diameter, 60% porosity and thickness 125 μm, (catalogue # LSWP04700) and pore size 3.0 μm, 47 mm diameter, 85% porosity and thickness 200 μm, (catalogue # FGLP04700).

The OIF was prepared by first liquefying the PolyTHF at 65°C in an oven for approximately 15 min. PolyTHF is a waxy solid at room temperature requiring softening to facilitate impregnation. The filter to be impregnated was first weighed and placed in a standard Millipore™ HPLC filtration device. Then 3–5 ml of PolyTHF was poured into the filtering receptacle. Vacuum was applied to the filter flask to pull PolyTHF through the filter until all the polymer in the filtering receptacle had been either passed through, or coated on the filter. The filter was then removed from the HPLC filtering apparatus and any excess PolyTHF beaded on the surface gently removed from the poly-

tetrafluoroethylene filter by pressing with a Kimwipe™. The organic-impregnated filter was weighed and was then ready to be used for extraction. The impregnation process yielded a filter with an active area of 9.6 cm^2 and requires less than 10 min of preparation time.

PolyTHF forms the active layer of the OIF in the gold extraction. The preparation process leads to an average loading of 50 and 100 mg of PolyTHF on the 5.0 and 3.0 μm pore size material, respectively. The larger loading on the 3.0 μm filter is due to the increased thickness and porosity of this filter compared with the 5.0 μm filter. PolyTHF coats the entire surface of the filter, penetrates into the pores of the filter and then solidifies. Scanning electron microscopy revealed that there are still holes visible on the surface of the OIF facilitating the passage of liquid through the filter. The presence of holes after the impregnation is essential for adequate flow through the filter because otherwise the filter would be clogged and unusable. Smaller pore size filters (0.2 and 0.5 μm) were impregnated and tested but the impregnation step led to clogging of the pores.

All gold solutions were prepared from a 500 mg l^{-1} standard prepared by dissolving $NaAuCl_4$ in 0.1 M HCl. The gold ore used in the gold ore separations is from the Kirkland Lake Mine in eastern Ontario, Canada. Gold ore solutions were prepared by first digesting the ore in aqua regia for a period of 1 week. The nitric acid portion of the mixture was then removed by evaporation while adding small aliquots of concentrated HCl. The acid content of the mixture was lowered by then boiling this solution while adding aliquots of deionised water. Finally the solution was filtered using Whatman™ No. 42 filter paper to remove the silicates not dissolved in the acid.

Samples were prepared and spiked with gold to the concentrations: 0, 1, 2, 5 mg l^{-1} Au. These solutions were made to 2.0 M HBr to facilitate the formation of the $HAuBr_4$ complex. The eluting solutions were prepared by dissolving KBr in deionised water and adjusting the pH with sodium hydroxide.

Once the OIF had been prepared it was placed in a standard HPLC filtration apparatus and clamped into place. The gold-containing solution was then placed in the filtering receptacle and a vacuum applied to the bottom filter flask to obtain the desired flow rate of the gold solution. The average flow rate was then calculated by dividing the time required for filtration by the volume of solution filtered. After the solution had passed through the OIF, an aliquot of the filtrate was taken for further analysis and the solution was placed again in the filtering receptacle and the filtration/extraction process repeated until the desired number of passes through the OIF had been completed. Once extracted the gold was eluted from the filter by passing the eluting solvent through the filter and collecting the filtrate for analysis.

3. Results and discussion

3.1. Extraction of $HAuBr_4$ with an OIF

Gold in the presence of suitable HBr concentrations forms the $AuBr_4^-$ complex [7]. The complex is a weak acid and at low pH becomes protonated.

$$HAuBr_4 \rightleftharpoons \overline{HAuBr_4}$$

*overline indicates the species present in the polyTHF layer of the OIF

We have shown previously [15] using polyurethane ether-type membranes that, the $HAuBr_4$ complex is responsible for the extraction of gold which is present at high HBr concentrations.

Fig. 2 shows the extraction of gold from several 100 ml solutions containing 5 μg ml^{-1} Au with increasing HBr concentrations. The solutions were each passed through the filter at 100 ml min^{-1}. The extraction of the solution containing 0.01 M HBr showed 50% of the gold still remained in the filtrate after one pass through the filter. Conversely, the extraction of gold from the solution containing 1.0 M HBr showed that the gold is quantitatively removed from the solution after only one pass through the OIF at 100 ml min^{-1}. The larger the HBr concentration, the greater the percentage of gold present in the extractable form. A greater percentage of the gold

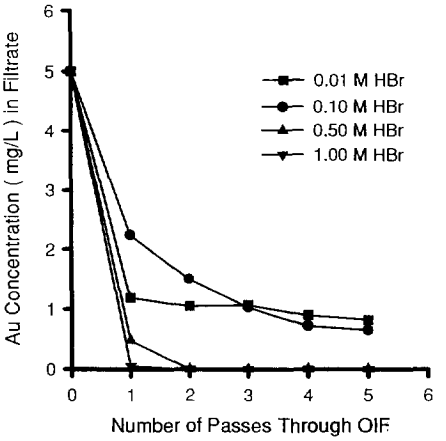

Fig. 2. The extraction of gold from solutions containing increasing HBr concentrations. Experiment was performed on 100 ml of solution at a flow rate of 100 ml min^{-1} through a 5.0 μm OIF.

being present in the extractable form leads to more of the gold being removed after one pass through the filter.

The extraction of gold can be followed both by the development, and loss, of an orange hue ($\lambda_{max} = 374$ nm) on the filter, and in the gold solution, respectively.

The effect of flow rate on the extraction of gold was tested using the 5.0 μm filter (Fig. 3). Several 100 ml solutions of 5 mg l^{-1} Au in 2.0 M HBr were passed through a 5.0 μm filter at different

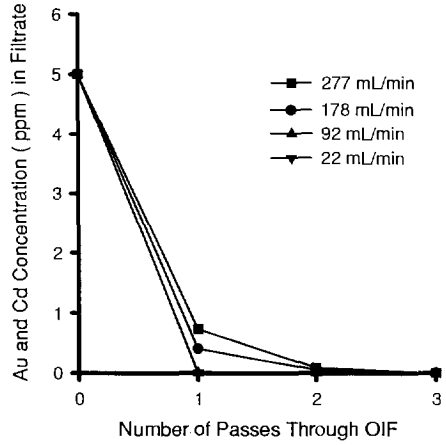

Fig. 3. The extraction of gold from 2.0 M HBr solutions using different flow rates with a 5.0 μm OIF.

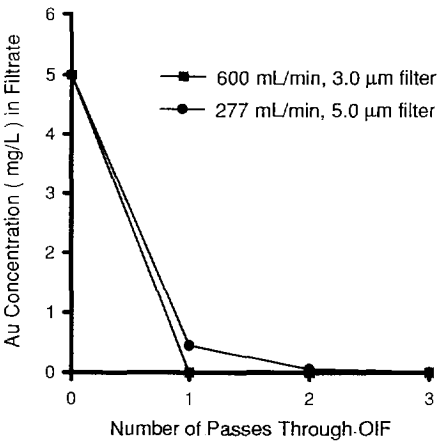

Fig. 4. The effect of using filters with different physical characteristics: ■ pore size 3.0 μm porosity 85% and thickness 200 μm, ● pore size 5.0 μm, porosity 60% and thickness 125 μm.

flow rates ranging from 22 to 277 ml min^{-1}. At flow rates of approximately 200–300 ml min^{-1}, 85–90% of the Au is removed from solution after one pass, and is quantitatively removed after two passes through the OIF. At flow rates of 92 ml min^{-1} and below the gold is quantitatively removed after only one pass through the OIF. The faster flow rates do not allow sufficient contact time for all of the gold to be extracted from solution. A comparison of the effect of flow rate on the extraction of gold for both the 5.0 and 3.0 μm filters is shown in Fig. 4. The 3.0 μm filter (thickness 200 μm, 85% porosity) has a greater thickness and porosity than the 5.0 μm filter, (thickness 125 μm, 60% porosity). The larger thickness and porosity leads to a greater loading of polyTHF on the surface of the filter which gives improved extraction performance. Even at a flow rate of 600 ml min^{-1}, the 3.0 μm OIF quantitatively removes the gold from solution. The extraction of gold is an extremely fast process as the actual contact time for the solution on the filter is extremely short. Filters with smaller pore sizes (i.e., 0.5 and 0.2 μm) were made but they became plugged after coating with polyTHF and did not allow sufficient solution flow.

Different molecular weights of polyTHF were tested ranging from 650–2000 g mol^{-1}. There appears to be no difference in extraction efficiency

between the different molecular weights. However, although there was no difference in the extraction efficiencies, the larger molecular weights had the advantage of being more viscous and more resistant to creep. Creep is the process by which a polymer undergoes a slow change of shape or a flowing action when subjected to a constant force. For the experiments performed in this paper, the polyTHF (M.W. 1000) used showed very little creep as measured by the slight weight loss incurred by an OIF for the duration of an experiment.

The capacity of the OIF was determined by passing several 100 ml solutions of 100 mg l^{-1} Au in 2.0 M HBr through the OIF until no further gold was extracted from solution. It was determined that greater than 0.5 mg of gold could be extracted for every mg of polyTHF loaded onto the filter.

3.2. Recovery of gold from the OIF

In solid phase extraction the recovery of an extracted analyte is important to the final analysis of a particular species. The gold can be recovered from the OIF in a similar manner to which it was extracted. The extraction of the gold into the active layer of the OIF dependent on the formation of the $HAuBr_4$ complex which is readily extractable into the active polyTHF layer held on the surface of the OIF. If the complex is not protonated it is not extracted into the organic layer. Conversion of the protonated complex at the surface of the polymer layer, to the deprotonated complex, leads to the elution of gold from the OIF.

$$\overline{HAuBr_4} \rightleftharpoons AuBr_4^- + H^+$$

* over line indicates species present in the polyTHF layer on the OIF.

The gold can be recovered with efficiencies of 95–100% at a flow rate of 10 ml min^{-1} using a solution of 0.5 M KBr adjusted to pH 10. The recovery of gold requires a flow rate that is substantially slower than that used for the extraction step. Once the $HAuBr_4$ is extracted, the complex diffuses throughout the polyTHF layer. Elution from the OIF requires the deprotonation of the gold complex. Only complexes present at the surface of the polymer layer are deprotonated by the change in elution solution and then subsequently removed, which induces a concentration gradient within the polyTHF layer. This gradient causes more gold complex to diffuse to the surface of the polyTHF layer where it can deprotonate and be subsequently removed. The recovery process is diffusion-limited, requiring flow rates of approximately 10 ml min^{-1}, roughly 10% of that of the extraction step. Eventually all of the gold on the filter is removed by the constant deprotonation of complexes that were formerly deeper within the polymer layer. The thin layer of polyTHF on the OIF is preferential to a disk made entirely of polyTHF. The thin layer allows faster elution of the extracted species. If the filter were made entirely of polyTHF or the applied layer made extremely thick, the filter would possess a greater capacity for the gold species, but would suffer from the extremely long elution times required to allow the complexes to diffuse to the surface.

The elution solvent was adjusted to a pH of 10 to neutralize any residual acid that was present on the filter. If this pH adjustment is not made then gold recoveries are not quantitative because the residual acid present on the filter and filter equipment lowers the pH of the eluting solution enough to inhibit the deprotonation of the $HAuBr_4$ complex. Consequently some of the gold will remain in the polyTHF layer.

The gold can also be removed from the filter by removing the entire polymer layer from the filter. Washing the filter with acetone will dissolve the polyTHF layer and remove it from the polytetrafluoroethylene filter. The filter can then be reused by impregnating it again with polyTHF.

3.3. Preconcentration using the OIF

Gold is usually found in low concentrations (μg l^{-1}) in natural waters and gold ore. Therefore it is often valuable to concentrate as well as separate gold from other species prior to analysis. The OIF can be employed to concentrate gold by extracting gold present at low concentrations in a large volume of solution, and then eluting the gold using a small volume of solution. A 2.0 l solution

of 125 μg l^{-1} Au in 2.0 M HBr was passed through a 5.0 μm OIF at a flow rate of 100 ml min^{-1}. The gold complex was then eluted from the filter using 100 ml of 0.5 M KBr adjusted to pH 10. Under these conditions the quantitative recovery of the gold should produce a gold concentration of 2.5 μg ml^{-1} in the eluting solvent. The concentration of the gold in the eluting solvent was found to be 2.4 μg ml^{-1}. This corresponds with a 96% recovery of the gold and a 20-fold increase in concentration compared with the original solution. The experiment shows that gold can be concentrated from solution onto the OIF even when initial concentrations are low.

3.4. Extraction of gold in the presence of other metals

Acyclic polyethers are relatively weak and unselective at complexing metal ions [17]. Only metals that can be made hydrophobic by either attaching hydrophobic ligands or by complexation can be extracted. The separation of gold from other metals in solution is possible if gold is the only metal that can form an extractable neutral complex with the HBr. Gold was shown to be quantitatively and selectively extracted from binary metal mixtures. An example of a binary mixture separation is gold from cadmium shown in Fig. 5,

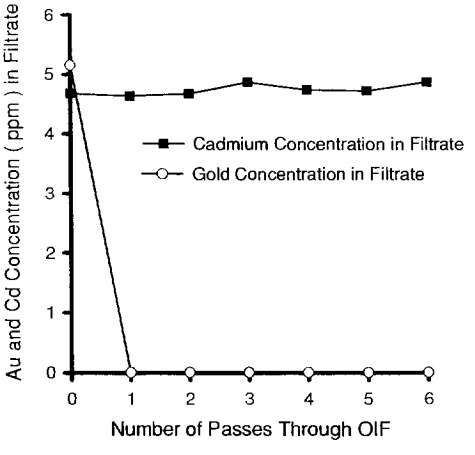

Fig. 5. The separation of gold from cadmium using an OIF. Experiment was performed on 100 ml of solution at a flow rate of 100 ml min^{-1} through a 5.0 μm OIF.

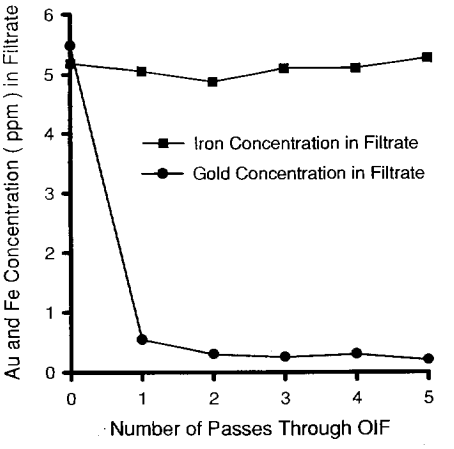

Fig. 6. The separation of gold from iron using an OIF. Experiment was performed on 100 ml of solution at a flow rate of 100 ml min^{-1} through a 5.0 μm OIF.

which demonstrates the effectiveness of the OIF as a separation device for the separation of gold from other metals. A 100 ml solution containing 5 mg l^{-1} Au, 5 mg l^{-1} Cd in 2.0 M HBr was passed through a 5.0 μm OIF at a flow rate of 100 ml min^{-1}. After one pass through the filter all of the gold was quantitatively removed from the solution and extracted onto the OIF, while none of the cadmium was extracted and it remained in the filtrate even after several passes of the solution through the OIF. The slight variation in cadmium concentration between each pass can be attributed to analytical errors. In this case gold is the only one of the two metals that is able to form an extractable complex under these conditions. In Fig. 6 the separation of gold from iron is shown. A 100 ml solution of 5 mg l^{-1} Au and 5 mg l^{-1} Fe in 2.0 M HBr was passed through a 5.0 μm OIF at a flow rate of 100 ml min^{-1}. In this case more than 95% of the gold is removed from solution after one pass through the OIF while the iron is left in the solution. In this binary metal mixture both Au and Fe are able to form hydrophobic extractable complexes in HBr. The stability constants of the $HFeBr_4$ complex dictate that much higher HBr concentrations [18] than those used would be required in order to form the extractable $HFeBr_4$ complex. Under these conditions gold is the only metal that can be extracted.

3.5. Separation of gold from gold ore

The ability to extract gold quantitatively and selectively in the presence of other metals has been demonstrated for relatively simple systems with binary metal mixtures. To demonstrate the ability of an OIF to separate gold from a more complicated matrix we attempted the separation of gold from a gold ore solution. The gold ore solution was prepared as described in the experimental section. The results of the separation of gold from a gold ore solution spiked with 1 mg l^{-1} Au are shown in Table 1. The metals analysed were chosen by performing an initial scan of several metals suspected of being present in the gold ore. If a metal was present in detectable concentrations it was further analysed for in the resulting samples. The gold ore from the Kirkland Lake Mine is known to possess a large concentration of pyrite which is indicated by the very large iron concentrations in the samples.

Fig. 7 shows the concentrations of gold and iron present in the spiked gold ore sample at different stages of the separation. Even though iron was present in concentrations 300 times as large as gold, the gold was still selectively extracted and removed from solution to the point where it was below the detection limits of the ICP after one pass through the filter. This indicates that the OIF can separate gold from solutions where large concentrations of possible interfering ions are present. The concentrations of the other metals do not change even after several passes through the OIF which demonstrates that none of these are extracted under the experimental conditions used. None of the metals present in the Canadian ore sample were co-extracted with the gold complex. Ore samples from different regions possess different metal compositions which may lead to interferences.

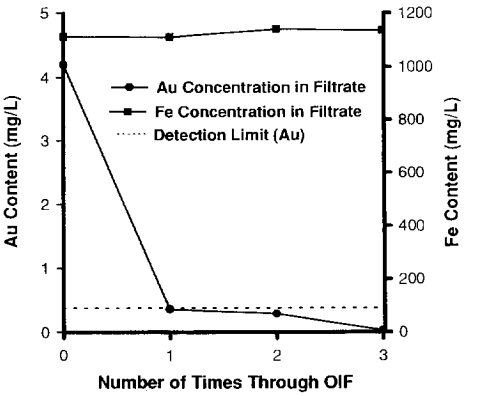

Fig. 7. The concentration of gold and iron present in the filtrate for the separation of gold from gold ore solution. Experiment was performed on 100 ml of solution at a flow rate of 100 ml min^{-1}.

Table 1
Concentration of metals present in the filtrate at different stages of the gold ore separation

No. of times through OIF	Metal concentration (mg l^{-1})			
	Au	Mn	Cu	Zn
Stock	4.2	26.78	1.03	1.41
1	0.36	26.45	1.05	1.40
2	0.30	27.36	1.15	1.48
3	0.03	26.58	1.13	1.49

The analysis of the eluting solution showed a 93% recovery of the extracted gold from the filter and virtually undetectable amounts of other metals present. The separation results of other gold ore solutions were similar. In each of the separations the gold was removed from solution by the OIF and the gold recovered using an eluting solution. The results of the gold ore separation indicates that there does not appear to be a competing ion effect between the other metals and gold, even though some of the metals are present in significantly higher and lower concentrations than gold.

4. Conclusions

A polytetrafluoroethylene filter impregnated with polyTHF can rapidly and quantitatively sep arate gold from HBr solutions that flow through it. The separation is due to the formation of the $HAuBr_4$ [7] complex in HBr solutions, and subse-

quent extraction into the PolyTHF layer on the OIF. The rate of extraction was found to increase with an increase in HBr concentration because of increased formation of the extractable species. The filter type effects the performance of the OIF with filters having larger porosity and greater thickness performing better because of the increased surface area and loading of PolyTHF.

The extracted gold can be removed from the OIF using an analogous process to the extraction. The protonated complex, $HAuBr_4$, can be eluted from the filter by converting it to the anionic, $AuBr_4^-$ complex using a 0.5 M KBr solution; the deprotonated form of the complex is not soluble in PolyTHF. Since only those complexes at the surface of the organic layer can be deprotonated, the elution process is diffusion-limited and requires reduced solution flow rates compared with the extraction to obtain recoveries greater than 95%.

The separation of gold from a number of other metals shows that the OIF can be used to separate gold from metals that cannot form extractable complexes in the presence of HBr. The separation of gold from gold ore solution demonstrates the ability of the OIF to separate gold from matrices that are quite complex. This method is inherently simple and rapid compared with other techniques currently available and can be expanded to include other metals.

Acknowledgements

This work is supported by the Natural Science and Engineering Research Council of Canada.

References

[1] S. Tsurubou, Anal. Chem., 67 (1995) 1465.
[2] S. Fang and L. Fu, Indian J. Chem., 33A (1994) 885.
[3] Y. Hongwu, Z. Zhixian, Z. Mingrui, Z. Xianxin and R. Boyang, Polyhedron, 10 (1991) 1025.
[4] R. Izatt, G. Clark, J. Bradshaw, J. Lamb and J. Christensen, Sep. Purif. Methods, 15 (1986) 21–72.
[5] R. Pearson, J. Chem. Educ., 45 (1968) 581.
[6] P. Pan and S. Wood, Geochim. Cosmochim. Acta, 55 (1991) 2365.
[7] P. Pan and S. Wood, J. Solution Chem., 22 (1993) 163.
[8] F. Fry, G. Hamilton and J. Turkevich, Inorg. Chem., 5 (1966) 1943.
[9] N. Bjerrum, Bull. Soc. Chim. Belg., 57 (1948) 432.
[10] S. Martinez, A. Sastre, N. Miralles and F. Alguacil, Hydrometallurgy, 40 (1996) 77.
[11] I. Villaescusa, N. Miralles, J. de Pablo, V. Salvadó and A. Sastre, Solvent Extr. Ion Exch., 11 (1993) 613.
[12] E. Souaya, M. Ramsis and S. Tobia, Microchem. J., 39 (1989) 194.
[13] D. Maljkovic, D. Maljkovic and A. Paulin, Solvent Extr. Ion Exch., 10 (1992) 477.
[14] R. Caletka, R. Hausbeck and V. Krivan, Anal. Chim. Acta, 229 (1990) 127.
[15] R. Oleschuk and A. Chow, Talanta, 43 (1996) 1545.
[16] S. Ho, P. Sheridan and E. Krupetsky, J. Membr. Sci., 112 (1996) 13.
[17] T. Okada, Analyst, 118 (1993) 959.
[18] R. Oleschuk and A. Chow, Talanta, 43 (1995) 957.

ELSEVIER

Talanta 44 (1997) 1379–1387

Talanta

New method of gold-film electrode preparation for anodic stripping voltammetric determination of arsenic (III and V) in seawater

Yuh-Chang Sun, Jerzy Mierzwa, Mo-Hsiung Yang *

Institute of Nuclear Science, National Tsing-Hua University, Kuang-Fu Rd., 30043 Hsinchu, Taiwan

Received 1 July 1996; received in revised form 18 November 1996

Abstract

A new method of efficient rotating gold-film glassy-carbon electrode preparation prior to the determination of As(III) and As(V) in seawater by anodic stripping voltammetry (ASV) is described. Factors affecting sensitivity and precision including pH, deposition time and potential, rotation and scan rate, and the nature of working electrode were investigated. Electroinactive As(V) was reduced to As(III) by gaseous SO_2 prior to ASV determination. For a deposition time of 4 min the determination limit was approximately 0.19 ppb. Precision of the proposed method was very good (RSD = 2–0.6% at 1–5 ppb) and a relatively good accuracy determined by analysis of certified reference seawater (CASS-1) and seawater samples spiked with an arsenic standard solution, was also obtained. © 1997 Elsevier Science B.V.

Keywords: Anodic stripping voltammetry; Arsenic; Gold-film plated electrode; Seawater

1. Introduction

The concentrations of As(III) and As(V) in the environmental samples are of considerable interest because of their potential toxicity, carcinogenic, and geochemical properties. The toxicological, physiological, and geochemical behavior of arsenic is dependent on its oxidation states [1,2]. Since the concentration of arsenic in normal natural water systems is in the range of ppb or sub-ppb levels, it is very important from the analytical point of view to develop a sensitive and reliable techniques capable to determine not only nanogram levels of arsenic but also their respective species.

Hydride generation techniques in conjunction with atomic absorption spectrometry and inductive-coupled plasma atomic emission spectrometry have been frequently used for the sensitive determination of arsenic [3,4]. Some environmental water samples have been reported [5–7] which contained methylated arsenic compounds in the amounts as high as 16–54% of total arsenic. The presence of methylated arsenic compounds can produce errors in speciation of inorganic arsenic(III) by hydride evolution directly into a

* Corresponding author.

PII S0039-9140(96)02197-2

spectral detector. The coexistence of metallic elements predominantly in periodic groups VIII and Ib and the mutual interactions of the volatile hydride-forming elements can cause interference as well [3]. On the contrary, electrochemical methods can distinguish between the different oxidation states of arsenic and have a great sensitivity. The instrumentation required is relatively simple and generally costs far less than that required for spectrochemical techniques. Arsenic determinations have been made using classical dc polarography [8], differential pulse polarography [9,10], single-sweep polarography [11], cathodic stripping voltammetry [12–14], and anodic stripping voltammetry [15–21]. All of the aforementioned approaches are subject to interferences and not sensitive enough for the direct determination of different arsenic species in seawater. The development of differential pulse anodic/cathodic stripping voltammetry considerably improved the sensitivity and accuracy of trace elements determination in various media.

Several different electrode materials have been used for the arsenic determination by stripping voltammetric techniques. Sadana [12] and Holak [13] used the hanging mercury drop electrode with the aid of Cu(II) or Se(IV) to preconcentrate As(III) by the way of forming intermetallic compounds on the electrode in the deposition step. Owing to the limitation of sensitivity of the method and the arsenic peak appeared as a shoulder on the hydrogen reduction wave, it was found to be of little analytical utility for seawater analysis. Davis et al. [19] reported a 'reductillation' process for separation of arsenic from possible interfering substances in the sample matrix prior to ASV determination using the pyrolytic graphite tube with a thin electroplated gold film as a working electrode. By the way of the reductillation-ASV procedure, the measurement of arsenic at the nanogram level was possible. This method seems to require too many manipulations that should be avoided in trace analysis. Kuwabara et al. [21] performed an anodic stripping voltammetric method for arsenic using co-deposition with copper on a rotating platinum electrode. A more complicated voltammogram was obtained and the calibration curve did not pass through the zero point. The anodic-stripping voltammetric determination of arsenic at copper-coated glassy-carbon electrode developed by Jaya et al. [15] still can not be used to analyze arsenic in seawater due to too high determination limit.

According to Forsberg et al. [22], gold is the most suitable electrode material for determination of arsenic because of high hydrogen overvoltage and better reversibility of the electrode reaction in both the plating and stripping step. However, the response of gold electrode is very strongly dependent on the past history, pretreatment, and the oxide films formation. Stationary glassy-carbon electrode coated with gold film [18] and rotating solid gold electrode [20] was used for determination of arsenic, and the detection limits obtained were 0.56 and 0.2 ppb, respectively.

Besides the mentioned limitations of the gold-film electrode, an extremely high chloride concentration in seawater samples is also a detrimental factor. In order to avoid the possible variation of the gold-film electrode sensitivity a new way of gold-film preparation is developed and applied to an anodic stripping voltammetric method for the direct determination of arsenic in seawater with a rotating gold-film glassy-carbon electrode. Factors likely to affect the stability of electrode response and method sensitivity, including: acidity, deposition potential, deposition time, rotation rate, scan rate, the electrode reaction, and the reduction step of As(V) to As(III) are investigated. Furthermore, the equation for the limiting current during deposition of As(III) onto the rotating gold-film electrode is discussed. The effect of dissolved organic substances which might interfere with the determination of arsenic and the sample preservation conditions are also reported.

2. Experimental

2.1. Reagents

High-purity sulphuric acid (18 M) and hydrochloric acid (9.5 M) were used without further purification. Both chemicals were Suprapur (Merck, Germany). Hydrazinium chloride was of analytical reagent grade (Merck).

Standard solutions of As(III) were made up by dissolving 0.132 g of primary As_2O_3 standard in the minimum amount of conc. NaOH (Suprapur, Merck), adjusting the pH to about 3.5 with HCl, and diluting to 100 ml with H_2O. A 5 ppm of hydrazinium chloride was added to prevent oxidation of As(III) to As(V). Solutions with 1000 ppm of As(III) stored at 4°C were stable for at least 1 month when checked against a freshly prepared standard solution. Standard solutions of As(V) were prepared from 1000 ppm As(V) Merck standard solution. The required standards were prepared daily by dilution of the stock solutions. The electrode was plated with 40 ppm gold chloride (atomic absorption standard, Fisher, USA) diluted with 1 M H_2SO_4.

2.2. Apparatus

All experiments were carried out with a BAS 100B Electrochemical Analyzer (BAS, West Lafayette, IN, USA) interfaced with an Intel 486DX personal computer. Data analysis was conveniently done with the software available with this instrumentation. The voltammograms were recorded with a FPG-310 color plotter. The electrochemical cell consisted of a 1/4" glassy-carbon electrode (GCE, BAS, USA), an Ag/AgCl with saturated KCl reference electrode (BAS, USA), and a platinum wire. The instrument was also fitted with a Teflon purge tube for deaerating of the solution with prepurified nitrogen and directing the nitrogen flow above the solution.

2.3. Gold-film electrode preparation

Before each deposition of a gold film, polish the electrode with alumina powder (0.5 μm diameter) and wash it successively with nitric acid and double-distilled water. Submerge the electrode in 40 ppm gold(III) solution and leave in open circuit during a 5 min purge with nitrogen. After ensuring that gas bubbles are not lodged on the surface of the glassy-carbon electrode (GCE), apply -0.2 V potential to the electrode for 4 min. Since the gold deposited on GCE as a brown powder from stirred solution and as a lustrous plate from quiescent solution, the plating was done in a quiescent solution. For optimum reproducibility, the electrode was replated (make-up) at 0.5 V for 10 s between each measurement and the electrode was washed with the same seawater sample before re-merge into the electrolytic cell.

2.4. As(III) determination

A 8 ml of seawater sample solution and 2 ml of conc. HCl were transferred to the cell and then the solution was deaerated with pure nitrogen for 5 min. After the gold film electrode has been prepared by aforementioned process, the sample cell was put into place for the determination, which was carried out at -0.3 V and the rotating rate of 5000 rpm for 4 min. After deposition, the rotation of electrode was turned off and left for 30 s at -0.3 V that the solution became quiescent. Stripping was carried out in the differential pulse mode starting at -0.3 V with a scan rate of 30 mV s^{-1} in positive direction. Other operation parameters of the polarographic analyzer included a pulse width of 50 ms and a pulse height of 50 mV. Duplicate determinations were performed on the sample solution before standard addition.

2.5. As(V) determination

Seawater sample solution, 40 ml and 10 ml of conc. HCl were transferred to a flask which is then closed with a Teflon stopper having holes for sulphur dioxide in- and outlet. The solution was heated in a water bath set at 80°C. Sulphur dioxide was passed through the solution for 10 min. The sample was then cooled to the room temperature and 5 ppm of N_2H_4 was added and bubbled with nitrogen for 30 min. Evaporation losses were made up with H_2O. The final volume of the solution was 50 ml. All of the operation parameters for voltammetric determination are the same as above (see Section 2.4).

3. Results and discussion

3.1. Characteristics of As(III) at gold-film plated electrode

Arsenic can occur in natural water in four

oxidation states (− III, 0, III, V), however, the main oxidation states of arsenic are As(III) and As(V) [23]. Generally, As(III) and As(V) are, respectively, electrochemically active and inactive in most media [23,24]. A number of supporting electrolytes was studied and HCl was found to be the most suitable, sensitive, and the narrowest peak was obtained (i.e., the charge-transfer reaction is fastest) [9,23,24].

From the cyclic voltammetry study of the gold-film plated electrode in seawater acidified with HCl, shown in Fig. 1, relatively well defined reduction and oxidation peaks were observed indicating the possibility of use such a gold-film electrode for the determination of As(III) in seawater by ASV.

The changes of peak current and peak potential in seawater acidified with various concentration of HCl are given in Fig. 2. The peak current increases and peak potential shifts to more negative with increasing HCl concentration. According to Arnold [25], the As(III) species present in aqueous solutions contained HCl at increasing concentration are found to be consistent with the existence of the following species:

H_3AsO_3, $As(OH)_2^+$, $As(OH)_2Cl$, $As(OH)Cl_2$, $AsCl_3$

Since $As(OH)_2Cl$ and $As(OH)Cl_2$ are though to be the actual species which take part in the electron-transfer reaction on the electrode [24], the deposition efficiency of As(III) become higher as the amount of $As(OH)_2Cl$ and $As(OH)Cl_2$ increases with increasing of HCl concentration. Moreover, it is noteworthy that more chloride ions tightly bound in double layer around the electrode act as a bridge between the arsenic ion and the electrode makes the redox reaction more reversible [24,26]. From above descriptions, the conversion of As(III) species and the occurrence of chloride ion-bridge may explain the corresponding positive shift of peak potential and increasing peak current. For analytical purposes, the optimum HCl concentration was ca. 2 M.

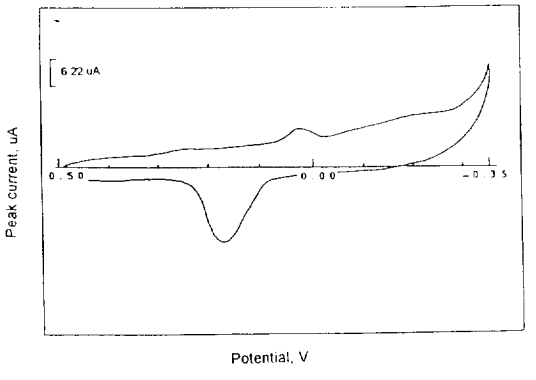

Fig. 1. Cyclic voltammograms of As (III) in seawater acidified with HCl. (8 ml seawater + 2 ml HCl, 5 ppb As (III)).

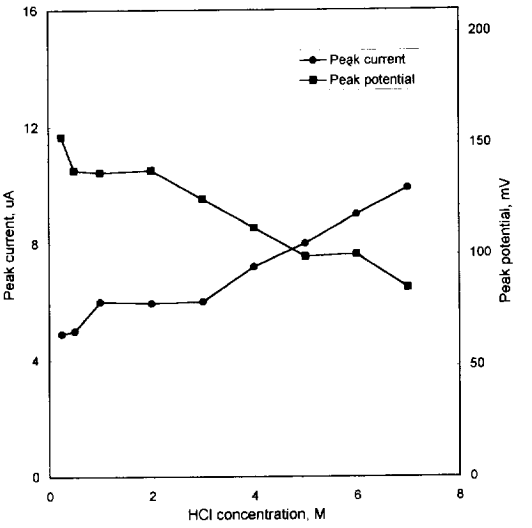

Fig. 2. Effect of HCl concentration on the peak current and peak potential. (8 ml seawater + 2 ml HCl, 5 ppb As(III), scan rate = 30 mV s^{-1}, rotation rate = 5000 rpm, deposition time = 30 s).

3.2. Gold-film electrode sensitivity

The decline of sensitivity of the gold electrode (solid or plated film) between each successive determination of the same solution has been widely discussed and many treatment procedures have been applied before or between sample runs [18,20,22,26–28]. However, all of the procedures applied were found to be unsatisfactory. From the obvious degradation of gold film on the used

electrode, it can be concluded that the gold film on the electrode was lost (dissolved) because of the tendency for complex formation between the gold and chloride ion. The same observation has also been reported by Baumann et al. [28] and Delahay [29]. The possible mechanism of declining sensitivity was deduced as follows: the plated gold film was oxidized in the sample solutions (seawater + HCl) contained high concentration of chloride ion to give the complex auric chloride ion ($AuCl_4^-$) [29], thus, the active gold surface for the deposition of arsenic was reduced and the reproducibility of the stripping peaks became disadvantageous. For the sake of solving the problem mentioned above, a 'make-up' procedure was developed, i.e., the original active surface area was restored between each run through replating the electrode with gold solution containing no chloride ion. Additionally, because impurities on electrode exert a profound effect on current-voltage curve when gold electrode was used for trace arsenic determination, gold electrode have to be pretreated. Among the possible interfering elements, copper was found to cause the most serious interference problem. In addition to having nearby oxidation peak (0.33 V), copper and arsenic have been shown to combine strongly [21], and the presence of even a slight excess of copper greatly reduces electrode response to arsenic [22]. In order to make up the gold-film on the electrode and get rid of codeposited copper simultaneously, 0.5 V potential was used as a make-up potential.

3.3. Effect of the deposition potential and deposition time

In fact, because anodic stripping voltammetry consists of a series of controlled-potential electrolysis steps, the sensitivity is dependent on the concentration of an interested element deposited on/in the electrode, and therefore the length and efficiency of the deposition (preconcentration) step becomes critical. The dependence of peak current on deposition potential was shown in Fig. 3. The deposition potential -0.3 V was chosen due to no apparent difference in peak current occurs in the range of -0.4– -0.2 V and the formation of H_2 bubbles become possible after -0.35 V.

Since elemental arsenic is a very poor conductor of electricity, the peak current of arsenic was found to be limited when the active surface of the electrode was fully covered with elemental arsenic [23]. The dependence of peak current on deposition time for seawater containing 5 ppb arsenic was shown in Fig. 4. The peak current reached a limiting height indicating the electrode surface saturated arsenic at the deposition time greater than 4 min. The levelling effect of peak current is concerned with the surface area of the electrode, the length of the deposition time, the stirring efficiency, and the concentration of arsenic(III). Owing to the concentration of arsenic in seawater is around 1.0–3.7 ppb [30], a deposition time of 4 min was used in this study to prevent possible error resulted from the electrode surface saturation.

3.4. Rotation rate effect

The sensitivity of stripping voltammetry strongly depends on the amount of substance deposited at the electrode, for which the rate of the substance flux from the bulk of the solution toward the electrode (i.e., the hydrodynamic conditions) is a predominant determinate. If a chemi-

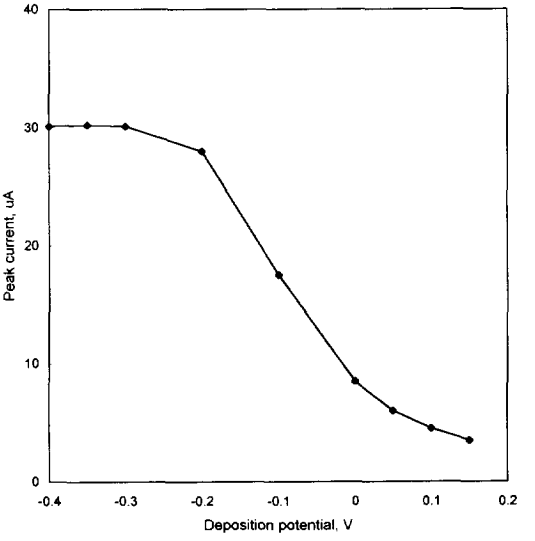

Fig. 3. Effect of the deposition potential on the peak current. (8 ml seawater + 2 ml HCl, 5 ppb As(III), scan rate = 30 mV s^{-1}, rotation rate = 5000 rpm, deposition time = 30 s).

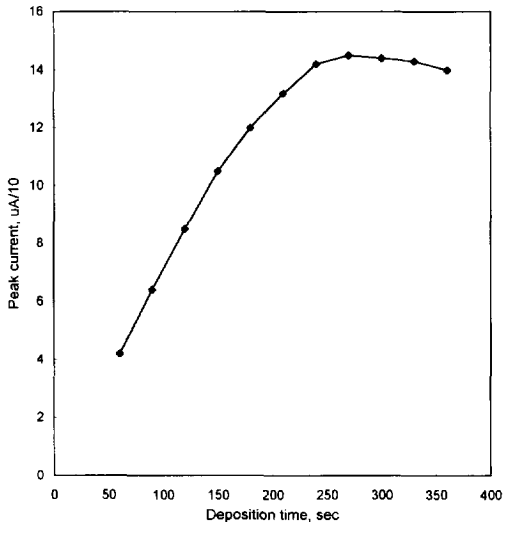

Fig. 4. Effect of the deposition time on the peak current. (8 ml seawater + 2 ml HCl, 5 ppb As(III), scan rate = 30 mV s^{-1}, rotation rate = 5000 rpm).

cal reaction is involved in the overall electrode process, it also affects the sensitivity through its reaction rate, the character of reaction products, and solubility of the compounds formed. According to Wang [31], the deposition current (I_L) as well as stripping peak current (I_P) at the rotating disk electrode is proportional to ω^{α} (where ω is the rotation rate and α is a constant dependent on the characteristics of the hydrodynamics and electrode configuration). For the laminar flow conditions, α usually ranges from 0.3 to 0.5. Frequently, α is found to be 0.5 when mercury film electrode is used and a reversible reaction is conducted [32]. In this study (as shown in Fig. 5) α was found to be 0.35 when gold-film electrode was used for As(III) deposition.

3.5. Scan rate effect

It was found that the stripping peak current was proportional to the square root of scan rate and agreed with the relationship between peak current (I_P) and scan rate (v) (in accordance with the equation $I_P = 2.74 \times v^{1/2}$) for mercury film electrode system [30]. Even if better sensitivity at higher scan rate was obtained, a broader and more ill-defined peak also resulted. For the determination of trace As in seawater, a scan rate of 30 mV s^{-1} was finally chosen to provide the necessary sensitivity and well-defined stripping peak.

3.6. Effect of hydrazinium chloride

Since As(III) can be oxidized in solution with a high Cl^- concentration and low pH [20], a continuous decrease of peak current was found during a series measurement of As(III) in the same samples with the proposed procedure. With the view of improving the poor reproducibility resulted from the oxidation of As(III) to As(V), different amount of hydrazinium chloride was added to the solutions. After an addition of hydrazinium chloride as the antioxidant, the reproducibility was apparently improved, but on the other hand, the background current elevated as more concentrated hydrazinium chloride was added. A 5 ppm of hydrazinium chloride addition of which the declining percentage of the peak current is 0.1% was chosen as compromise value. In seawater samples containing 5 ppm of As(III) the precision obtained was 6% for four duplicate analyses.

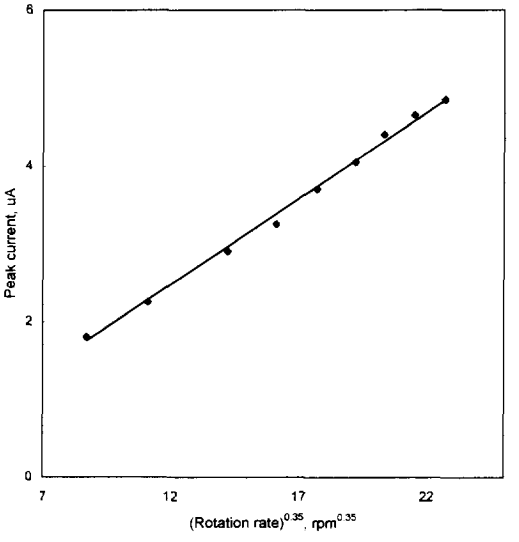

Fig. 5. Effect of the rotation rate on the peak current. (8 ml seawater + 2 ml HCl, 5 ppb As(III), scan rate = 30 mV s^{-1}, deposition time = 30 s).

According to the developed experimental procedure, a wide linear range for As(III) concentrations from 1 to 1100 ppb was achieved (in accordance with the linear equation $Y = 615.3 \times X - 7.4$, $R^2 = 0.999$). The determination limit was defined as the lowest concentration of As(III) which can be distinguished from the background current by the used measuring system. The concentration of As(III) in surface seawater is so low (0.05–0.02 ppb) that we can treat such a sample as 'blank'. The determination limit was obtained through addition of various concentration of As(III) into seawater sample and measured in the optimized conditions. The determination limit under the conditions used in this study was 0.19 ppb.

3.7. Interferences

Copper [21] and antimony(III) [30] have been found to present the most serious interference problem when gold-film electrode was used to determine As(III) by ASV. Fortunately, an observation that those elements contained in seawater do not interfere with the arsenic determination was reported [20]. Naturally occurring in seawater organic compounds such as humic acid and surfactant appeared to interfere in the determination of As(III), as shown in Fig. 6. Because the total amount of dissolved organic material in the open sea will not exceed 2 ppm and the concentration of humic acid is less than 0.11 ppm [33], no noticeable interference may be expected in open-seawater sample analysis according to the experimental data. With a view to avoid possible interference coming from the dissolved organic compounds and variation of the gold film electrode, the standard addition method was also used for a calibration.

Because the alkylated forms of arsenic are electroinactive, the determination of As(III) should be accurate. It is possible that the determination of As(V) can be interfere by the coexistent MMA (monomethylarsenic) after reduction [34]. However, because the concentration of MMA in surface seawater is extremely low (0.004 ppb) [2], the interference from reduced MMA can be negligible.

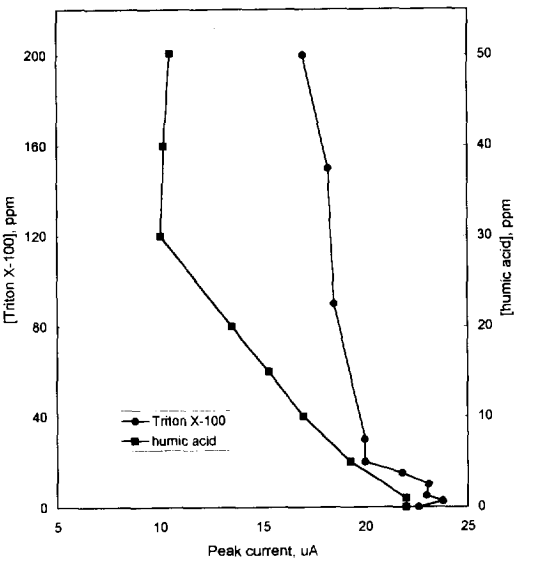

Fig. 6. Effect of the dissolved organic compound on the peak current: (a) humic acid; (b) Triton X-100. (8 ml seawater + 2 ml HCl, 5 ppb As(III), scan rate = 30 mV s^{-1}, deposition time = 30 s, rotation rate = 5000 rpm).

3.8. Sulfur dioxide reduction of As(V)

The same reduction procedure reported by Bodewig et al. [20] was used to reduce As(V) into As(III) in seawater. In order to ensure that no arsenic would be lost through splatter and volatilization, a closed system was used for reduction. However, the aforementioned make-up potential (0.5 V) used for the determination of 'natural' As(III) did not work here any more; meanwhile, the used gold-film plated on the electrode became tarnished and the analytical sensitivity got worse. Alternatively, −0.1 V was used as make-up potential, so that reproducible results could be obtained for SO_2 reduced samples.

Passivation may have involved adsorption of gold sulfite, $Au_2(SO_3)_3$, on the electrode during measurement, which resulted from the reaction between auric chloride ion around the electrode surface and dissolved sulfite originated from gaseous SO_2 reduction [35]. It has been reported that gold deposits in the form of discrete particles at active sites of a carbon surface and the condition of the substrate (i.e., glassy carbon electrode) can affect the activity of the gold deposition [36].

Table 1
Results of arsenic determination in water samples[a]

Sample	Added, ppb	Found, ppb	Recovery, %
Deionised water	5 ppb, As(III)	5.06 ± 0.04	101
Seawater	5 ppb, As(III)	5.00 ± 0.03	100
Seawater	5 ppb, As(V)	6.71 ± 0.03	101
Seawater	—	1.64 ± 0.01[b]	—
CASS-1	—	1.01 ± 0.02[b] (1.04 ± 0.07)[b]	97

Roman numerals in parenthesis indicate the certified value for CASS-1 sample (Nearshore Seawater Reference Material provided by National Research Council, Canada).
[a] 8 ml seawater + 2 ml HCL, 5 ppb As(III), scan rate = 30 mV s^{-1}, deposition time = 30 s, rotation rate = 5000 rpm.
[b] Total arsenic.

Through adsorption of gold sulfite on the electrode surface, some portions of the electrode become passivated (electrically isolated) and the sensitivity become worse. In view of restoring original activity -0.1 V was used as make-up potential instead of 0.5 V for the following experiments.

3.9. Preservation of seawater samples

Several studies [14,37–44] on the preservation of As(III) and As(V) in natural water prior to the analysis have been reported, but the different preservation methods appeared to be inconsistent. To the author's knowledge no suitable preservation conditions for As(III) in seawater sample have been reported until now. However, the preservation that maintains integrity and stability of samples is a prerequisite to the successful analytical determinations. In this study, the effective preservation conditions for As(III) and As(V) in seawater samples were established.

Adsorption on the wall of container, redox reactions, and the uptake by microorganisms present in the samples may cause the alteration of the distribution among arsenic species. It has been proven previously [44] that no adsorption occurs on the surface of polyethylene containers. In order to inhibit possible redox reactions and the activity of microorganisms, hydrazinium chloride and hydrochloric acid were used as preservatives for As(III) and As(V) in seawater. No significant loss of As(III) and no distinguishable reduction of As(V) into As(III) could be observed over a period of 6 days. For the analytical purposes, 5 ppm of hydrazinium chloride and 1:80 (V/V) hydrochloric acid were chosen as preservation media for the following experiments.

3.10. Analytical application

Andreae [45] has predicted that the concentration ratio of As(V) to As(III) of seawater is 10^{15}–10^{24} based on the thermodynamic equilibrium calculations. However, the redox reactions between As(III) and As(V) are biologically mediated and affected by complicated coexistent components [46]. In the oxygenated seawater, the As(V)/As(III) concentration ratio from 22 to 100 and the concentration of ca. 1.5 ppb of total arsenic in surface seawater were reported [6,47,48], therefore, the concentration range of As(III) in seawater could be presumed to be 0.05–0.02 ppb. Unfortunately, the proposed procedure was not sensitive enough for direct determination of As(III) in seawater, but the total amount of arsenic (As(III) + As(V)) can be certainly given, as shown in Table 1. The analytical results of standard reference seawater sample (CASS-1) and spiked samples are in a good agreement with the certified value and spiked concentrations. The open ocean water sample (Philippine Sea 3°45′ N, 124°01′ E), reported to contain 1.5 ppb arsenic [48], was analyzed by the described procedure and yielded 1.64 ppb of total arsenic (average of four independent determinations) with the standard deviation of ± 0.01 ppb.

4. Conclusion

In this study a new gold-film electrode preparation method for the determination of As(III) and total arsenic at the nanogram level in seawater by using rotating gold-film plated electrode for anodic stripping voltammetry was developed. An electrode make-up procedure was proved to be valid, and the extraordinary relationship of electrode rotating rate and deposition current for arsenic depositing from seawater onto a rotating gold-film electrode was observed. Additionally, efficient preservation conditions for As(III) and As(V) in seawater were established. The determination limit was 0.19 ppb of As(III) for a deposition time of 4 min and the precision, and accuracy of the method were very good. This technique has been successfully applied to the analysis of seawater samples and may be useful to study arsenic speciation in water samples.

Acknowledgement

The authors greatly appreciate the financial support of National Science Council of Republic of China (Taipei, Taiwan) for pursuing this research work.

References

[1] E. Merian, Metals and their Compounds in the Environment/Occurrence, Analysis and Biological Relevance, VCH Publishers, New York, 1991.
[2] J.E. Fergusson, The Heavy Element/Chemistry, Environmental Impact and Health Effect, BPCC Wheatons, 1990.
[3] B. Welz and M. Melcher, Anal. Chem., 57 (1985) 427.
[4] E. De Oliveira, J.W. McLaren and S.S. Berman, Anal. Chem., 55 (1983) 2047.
[5] R.S. Braman, D.L. Johnson, C.C. Foreback, J.M. Ammons and J.L. Bricker, Anal. Chem., 49 (1977) 621.
[6] M.O. Andreae, Anal. Chem., 49 (1977) 820.
[7] A.U. Shaikh and D.E. Tallman, Anal. Chem., 49 (1977) 1093.
[8] L. Meites, J. Am. Chem. Soc., 51 (1954) 5927.
[9] D.J. Myers and J. Osteryoung, Anal. Chem., 45 (1973) 267.
[10] M.A. Reed and R.J. Stolzberg, Anal. Chem., 59 (1987) 393.
[11] G.L. Whitnack and R.G. Brophy, Anal. Chim. Acta, 481 (1969) 123.
[12] R.S. Sadana, Anal. Chem., 55 (1983) 304.
[13] W. Holak, Anal. Chem., 52 (1983) 2189.
[14] J. Zima and C.M.G. van der Berg, Anal. Chim. Acta, 289 (1994) 291.
[15] S. Jaya, T.P. Rao and G.P. Rao, Talanta, 34 (1987) 574.
[16] P.C. Leung, U.S. Subramanian, and J.C. Meranger, Talanta, 29 (1982) 515.
[17] D. Jagner, L. Renman, and S.H. Stefansdottir, Electroanal., 6 (1994) 201.
[18] T.W. Hamilton, J. Ellis and T.M. Florence, Anal. Chim. Acta, 119 (1980) 225.
[19] P.H. Davis, G.R. Dulude, R.M. Griffin, W.R. Matson and E.W. Zink, Anal. Chem., 50 (1978) 137.
[20] F.G. Bodewig, P. Valenta and H.W. Nürnberg, Fresenius Z. Anal. Chem., 311 (1982) 187.
[21] T. Kuwabara, S. Suzuki and S. Araki, Bull. Chem. Soc. Jpn., 46 (1973) 1690.
[22] G. Forsberg, J.W. O'Laughlin, R.G. Megargle and S.R. Koirtyohann, Anal. Chem., 47 (1975) 1586.
[23] J.P. Riley and G. Skirrow, Chemical Oceanography, Vol. 1, Acdemic Press, 1975.
[24] L. Meites, J. Am. Chem. Soc., 76 (1954) 5972.
[25] J.P. Arnold and R.M. Johnson, Talanta, 16 (1967) 1191.
[26] R.S. Stojanovic, A.M. Bond and E.C.V. Butler, Anal. Chem., 62 (1990) 2692.
[27] D.C. Johnson and W.R. LaCourse, Anal. Chem., 62 (1990) 589A.
[28] F. Baumann and I. Shain, Anal. Chem., 29 (1957) 303.
[29] P. Delahay, New Instrumental Methods in Electrochemistry, Interscience Publishers, 1954.
[30] T.M. Florence and G.E. Batley, CRC Crit. Rev. Anal. Chem., 9 (1980) 219.
[31] J. Wang, Stripping Analysis/Principles, Instrumentation, and Applications, VCH Publishers, 1985.
[32] F. Vydra, K. Stulak, and E. Julakova, Electrochemical Stripping Analysis, Wiley, 1976.
[33] C.S. Wang, E. Boyle, K.W. Bruland, J.D. Burton, and E.D. Goldberg, Trace Metals in Sea Water, Plenum Press, 1983.
[34] F.T. Henry, T.O. Kirch and T.M. Thorpe, Anal. Chem., 51 (1979) 215.
[35] D.T. Burns, A. Townshend and A.H. Carter, Inorganic Reaction Chemistry, Wiley, 1981.
[36] T.W. Hamilton, J. Ellis, and T.M. Florence, Anal. Chim. Acta, 110 (1979) 87.
[37] M. Andreae, Anal. Chem., 49 (1977) 820.
[38] C. Feldman, Anal. Chem., 51 (1979) 664.
[39] V. Cheam and H. Agemian, Analyst, 105 (1980) 737.
[40] D.E. Tallman and A.V. Shaikh, Anal. Chem., 52 (1980) 196.
[41] J. Agget and G.A. O'Brien, Eviron. Sci. Technol., 19 (1985) 238.
[42] J. Agget and M.R. Kriegman, Analyst, 112 (1987) 153.
[43] S. Gohda, Bull. Chem. Soc. Jpn., 48 (1975) 1213.
[44] J.T. van Elteren, J. Hoegee, E.E. Van der Hoek, J. Radioanal. Nucl. Chem. (Letters), 154 (1991) 343.
[45] M.O. Andreae, Limno. Oceanogr., 24 (1979) 440.
[46] G. Bearman, Seawater: Its Composition, Properties and Behaviour, Pergamon Press, 1989.
[47] D.G. Waslenchuk, Marine Chem., 7 (1978) 39.
[48] T.M. Florence, Talanta, 29 (1982) 345.

ELSEVIER

Talanta 44 (1997) 1389–1396

Talanta

Validation of the determination of copper and zinc in blood plasma and urine by ICP MS with cross-flow and direct injection nebulization

J. Szpunar [a,*], J. Bettmer [b], M. Robert [c], H. Chassaigne [a], K. Cammann [b], R. Lobinski [a], O.F.X. Donard [d]

[a] *Laboratoire de Photophysique et Photochimie Moléculaire, URA 348, CNRS, Université de Bordeaux I, F-33405 Talence, France*
[b] *Institut für Chemo- und Biosensorik e.V., Mendelstrasse 7, D-48 149 Münster, Germany*
[c] *LABM Ruffié et Associés, 30, Allées de Tourny, F-33 080 Bordeaux, France*
[d] *Laboratoire de Chimie Bio-Inorganique et Environnement, EP 132, CNRS Université de Pau et du Pays de l'Adour, Helioparc, F 64 000 Pau, France*

Received 24 September 1996; received in revised form 16 November 1996; accepted 17 November 1996

Abstract

The simultaneous determination of copper and zinc in human plasma and urine by inductively coupled plasma mass spectrometry (ICP MS) is discussed. The performances of a cross-flow nebulizer and a direct-injection nebulizer (DIN) were compared. Flow-injection-DIN-ICP MS analysis of clinical samples using 1–2 μl samples was optimized. Isobaric interferences were discussed and were demonstrated to be eliminated for the ^{65}Cu and most of the Zn nuclides. The need for standard addition to compensate for signal suppression in the case of some serum samples was indicated. Results obtained by ICP MS using calibration with aqueous standard solutions were found to be in good agreement with those obtained by flame AAS for a batch of real blood plasma and urine samples. The methods developed were validated by analysis of several standard reference materials. © 1997 Elsevier Science B.V.

Keywords: Copper; FIA, Direct Injection Nebulizer; ICP MS; Serum; Urine; Zinc

1. Introduction

The levels of copper and zinc in plasma and urine have been extensively investigated for four decades and are now used for the early diagnosis of certain illnesses [1]. The mean values of Cu and Zn in healthy individuals are around 1 μg ml^{-1}. They can be readily determined by many instrumental methods; the analyses are usually done by flame or graphite furnace atomic absorption spectrometry (AAS) [2]. Inductively coupled plasma mass spectrometry (ICP MS) has been playing an increasingly important role in analytical laboratories owing to the possibility of direct, simultaneous and multielement trace analysis [3–5]. The determination of copper and zinc in clinical samples by this technique has been reported to be plagued by several spectral interferences and to be

* Corresponding author.

PII S0039-9140(97)00009-X

hard to be carried out with a quadrupole instrument [6–9]. The use of a high resolution magnetic sector instrument has been proposed but its high cost limits considerably its availability [9].

The objective of this paper is to consider a recent generation quadrupole ICP mass spectrometer for the simultaneous determination of copper and zinc in plasma and urine. A cross-flow and a direct injection nebulizer have been discussed in terms of sample throughput (flow-injection analysis), sample consumption and interferences. Particular attention has been given to the validation of the procedures developed in order to enable their use for routine analysis in a busy clinical laboratory.

2. Experimental

2.1. Instrumentation

The ICP mass spectrometer used in this work was the ELAN 6000 (Perkin-Elmer SCIEX, Concord, Ontario, Canada). The sample introduction systems used included a Ryton™ spray chamber fitted with a cross-flow nebulizer (Perkin-Elmer), and a model Microneb 2000 direct injection nebulizer (DIN) (CETAC, Omaha, NE). For the cross-flow nebulizer, the samples were fed by means of a Minipuls 3 peristaltic pump (Gilson) which also served for draining the spray chamber. For the DIN the samples were fed by means of a metal-free gas displacement pump (GDP) (CETAC) through a 50 μm i.d. capillary. Samples were injected using a six-port injection valve made of PEEK. A 20 μl sample loop was used. Smaller sample volumes (part of the sample loop volume) were injected by controlling the load time. Disposable polyethylene vials (OSI, France) were used.

Table 1
Signal acquisition and valve parameters for continuous-flow and flow-injection measurements using direct injection nebulization ICP MS

Parameter	Continuous flow	Flow injection
Scan mode	Peak hopping	Peak hopping
Sweeps/reading	10	3
Readings/replicate	3	25
Replicates	3	1
Dwell time per amu	100 ms	70 ms
Internal standard	10 μg l^{-1} Y	10 μg l^{-1} Y
Process signal profile	Average	Maximum Baseline readings: 5
Valve parameters		
Sample loop	250 ml	20 or 50 μl
Load time	45–60 s	5–8 s
Injection time	60 s	1–2 s
No. of injections	1	1–10

Flame AAS measurements were carried out with a Model 3100 PE atomic absorption spectrometer (Perkin-Elmer).

2.2. Samples and standards

Samples were prepared in disposable polyethylene vials under clean room conditions (Class 10 000). For all preparations, 18 MW Milli-Q water (Millipore, Bedford, MA) and Suprapure® HNO_3 (Merck, Darmstadt, Germany) were used. Standard stock solution of copper and zinc was prepared by a 250-fold dilution of the commercial standards (1 g l^{-1}) of Cu and Zn with a 2% nitric acid. The stock solution of yttrium was also obtained from Merck.

Reference materials. NYC S1 Human serum (Nycomed Pharma Norway, Seronorm™) was purchased from Promochem (Molsheim, France). Biotrol human serum and human urine (level 1 and 2) were purchased from BioRad (Ivry-sur-Seine, France) and Merck-Clevenot (Nogent-sur-Marne, France), respectively.

2.3. Analytical procedures

Cross-flow nebulizer. The RF source power used was 1.0 kW and the sample uptake rate was 1 ml min^{-1}. The torch X-Y position was adjusted manually to maximize the signal for yttrium. The operating ICP MS conditions (nebulizer gas flow and lens voltage) were optimized daily in the range of 0.7–1 l min^{-1} and 6–8 V, respectively, using a standard (incorporated in the software) automatic procedure. Calibration curve was pre-

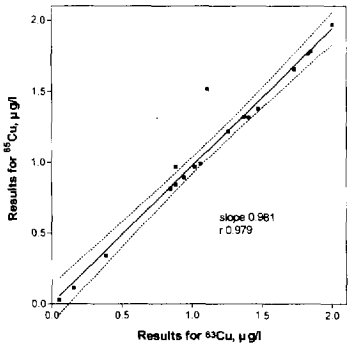

Fig. 1. Correlation ($\alpha = 0.95$) of the results obtained for the determination of copper in serum and urine by ICP MS using the different nuclides for quantification. ^{63}Cu versus ^{65}Cu.

pared by diluting the stock solution to obtain standard solutions at concentrations 0.2, 1, and 2 mg l^{-1}, respectively. Serum and urine samples were diluted 20-fold and 10-fold, respectively, with 0.05% HNO_3. Internal standard (Y-89) was added at the 10 µg l^{-1} level to the diluent.

Direct injection nebulizer. The RF source power used was 1.2 kW. The X-Y position of the ICP torch was adjusted first to maximize the signal for yttrium. Then, the position of the DIN capillary was optimized with the same objective. The fine-tuning was performed by the optimization of the GDP pressure (in the range 300–370 psi) and the nebulizer gas pressure (between 50–80 psi). The nebulizer makeup gas was optimized from the software of the ICP mass spectrometer between 0 and 300 ml min^{-1}. The lens voltage was tuned as described above. The DIN was operated either in the continuous-flow mode or in the flow-injection mode. For the latter the signal acquisition conditions were reoptimized. The parameters for data acquisition are summarized in Table 1. Calibration was performed as described above.

3. Results and discussion

Human serum is a rather difficult matrix for ICP MS. It contains 6–8% of proteins and about 1% of inorganic components, causing important spectral interferences up to m/z = 97. Urine contains less proteins, but also the concentrations of Cu and Zn are 5–20 times lower. The levels of Cu and Zn are sufficiently high to remain quantifiable by ICP MS after a 10–20-fold dilution. Standard precautions (class 10 000 clean room conditions and ultrapure water and acids) must be obeyed to avoid contamination problems. The choice of sample vials is critical. Among several types of polyethylene disposable vials tested those from OSI, France were found to produce the lowest (practically negligible) contribution to the blank signal. They could be used without the preliminary rinsing.

Serum and urine matrices affect strongly the element signal and are responsible for a considerable (up to 75%) signal suppression. Internal standard is thus necessary if external calibration with aqueous solutions is considered.

3.1. Isobaric interferences in ICP MS analysis for copper and zinc

Copper. Copper has two stable isotopes ^{63}Cu and ^{65}Cu with relative abundances of 69.2 and 30.8%, respectively. The former nuclide (m/z = 62.93) is interfered with the ion: $^{40}Ar^{23}Na$ (m/z = 62.95). This interference gives rise to an apparent concentration of Cu of ca. 10 µg ml^{-1} which is comparable with the actual concentration in plasma and is too large to be appropriately corrected for [4,8]. The latter nuclide (m/z = 64.93) is interfered by the ion: $^{32}S^{16}O_2^1H$ (m/z = 64.97)

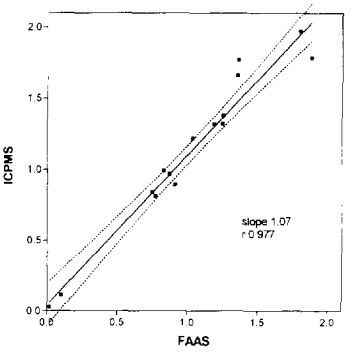

Fig. 2. Correlation ($\alpha = 0.95$) of the results for the determination of copper in serum and urine between flame AAS (another laboratory) and ICP MS.

Table 2
Simultaneous determination of copper and zinc by ICP MS in reference materials

Certified reference material	Copper concentration, mg ml^{-1}		Zinc concentration, mg ml^{-1}	
	Certified (range)	Found ± S.D.	Certified (range)	Found ± S.D.
Seronorm	1.26	1.17 ± 0.01	1.50	1.72 ± 0.03
		1.27 ± 0.03		1.6 ± 0.1
		1.19 ± 0.04		1.62 ± 0.03
Biotrol	0.84 (0.74–0.94)	0.81 ± 0.00	0.9 (0.8–1.0)	1.04 ± 0.00
		0.82 ± 0.01		0.84 ± 0.01
		0.87 ± 0.03		0.90 ± 0.09
Urine (level 1)	0.082 (0.066–0.098)	0.060 ± 0.002	0.202 (0.162–0.243)	0.225 ± 0.003
		0.050 ± 0.001		0.180 ± 0.006
		0.080 ± 0.002		0.202 ± 0.003
Urine (level 2)	0.266 (0.213–0.319)	0.266 ± 0.002	1.678 (1.342–2.013)	1.78 ± 0.01
		0.25 ± 0.03		1.84 ± 0.02
		0.25 ± 0.01		1.8 ± 0.1

Three independent series on different days.
Standard deviation calculated on the basis of five measurements.

which shows the apparent Cu concentrations of only 7% of the actual content of this element. High resolution (of 3000) was recommended to separate these interferences form the analyte peak [9]. An alternative is the use of size-exclusion LC to remove low-molecular-weight species ($ArNa^+$ and PO_2^+) that cause interference at m/e 63 [10].

Zinc. It has three major stable isotopes: ^{64}Zn (48.63%), ^{66}Zn (27.9%), and ^{68}Zn (18.75%). The determination of Zn in serum with quadrupole ICP MS is hampered by interferences caused by S-containing polyatomic ions for all the above nuclides. The most abundant ^{64}Zn is seriously interfered by $^{32}PO_2^+$ and $^{32}S_2^+$ [5]. In practice ^{66}Zn is chosen in the literature for which quadrupole ICP MS shows interferences by $^{34}S^{16}O_2^+$, $^{33}S^{16}O_2H^+$ and $^{32}S^{16}O^{18}O^+$, accounting for an apparent Zn content of around 0.66 μg ml^{-1} in serum which is half of the normal serum Zn level. ^{68}Zn was proposed alternatively [5].

3.2. Analysis using continuous cross-flow nebulization

Determination of copper. Fig. 1 shows that with the ICP mass spectrometer used in this work there is no difference between the results obtained using the different Cu isotopes. It means that, contrary to the literature [10], at the 1 μg l^{-1} level neither of the Cu nuclides is affected by the polyatomic interference probably owing to the PlasmaLok™ interface available on the instrument used. For the urine samples, however, results obtained using ^{63}Cu are ca. 20–30% higher than those with ^{65}Cu independent of the concentration level. This has to do with the fact that urine samples are run less diluted and the formation of the polyatomic ion of Ar with Na becomes more likely. Consequently, the ^{65}Cu should be chosen.

Fig. 2 shows that ICP MS gives consistent values with flame AAS. Table 2 shows that the Cu concentrations obtained for the certified sera and high level urine are in excellent agreement with the certified value. Also the low level urine is fully acceptable but in this case significant day to day variations are observed.

Determination of zinc. Fig. 3 shows that there is no difference in terms of result obtained regarding the nuclide chosen for quantification (^{66},^{67} or ^{68}Zn). Like in the case of copper, at the 1 μg l^{-1} level investigated none of the Zn nuclides is affected by the polyatomic interference probably owing to the PlasmaLok™ interface available on the instrument used. Contrary to copper, however, this is also true for the urine samples investi-

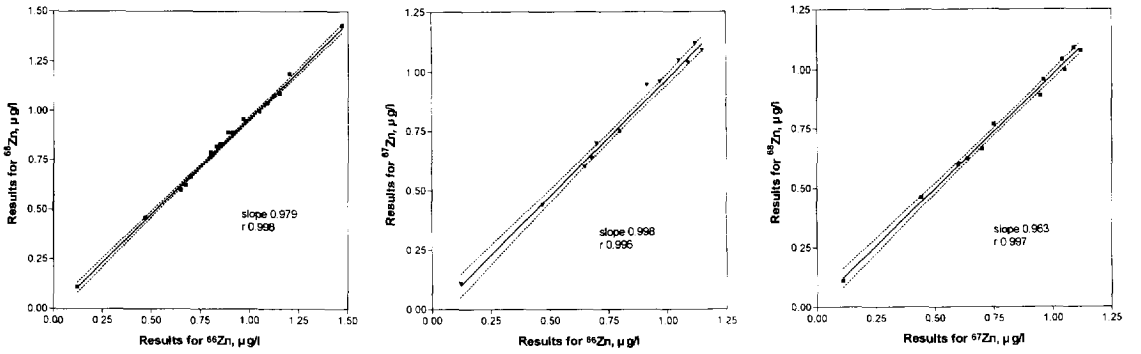

Fig. 3. Correlation ($\alpha = 0.95$) of the results obtained for the determination of zinc in serum and urine by ICP MS using the different nuclides for quantification. (a) ^{66}Zn versus ^{67}Zn; (b) ^{68}Zn versus ^{66}Zn; (c) ^{68}Zn versus ^{67}Zn.

gated. The ^{67}Zn and ^{68}Zn have been used in this work.

Fig. 4 shows that ICP MS gives consistent values with flame AAS. The reason for the few outliers was not established since it was not possible to re-run the samples with both techniques once again. Table 2 shows that the Zn concentrations obtained for the reference sera and reference urine are in agreement with the certified value.

3.3. ICP MS analysis with direct injection nebulization

The DIN is a microconcentric nebulizer with no spray chamber; it nebulizes the liquid sample directly into the central channel of the ICP torch [11]. Compared with conventional nebulizers it offers 100% sample introduction efficiency into the ICP, accommodation of low sample introduction flow rates (10–100 µl min^{-1}), an extremely small internal volume (< 2 µl) and fast sample washout with minimal memory effects.

Optimization of the DIN. The installation of the DIN required making a hole in the torch box of the ELAN 6000 mass spectrometer to enable the entrance of the nebulizer make-up flow. The virtual difference in the principle of operation between the DIN and the conventional nebulization systems makes it necessary to re-optimize the operational ICP MS parameters upon each and every installation of the DIN. Attempts to find a series of parameters once-for-ever were unsuccessful. The operational parameters (flow-rate, nebulizer gas flows, capillary position and lens voltage) were tuned on the every-day basis by the trial-and-error method to maximize the signal. RF source power was set at 1.2 kW which is higher than in the case of the cross-flow nebulization. Under the optimized conditions (Table 1) the sensitivity of the DIN-ICP MS for the nuclides: ^{23}Mg, ^{103}Rh, ^{134}Ba, ^{137}Cs and ^{208}Pb was a factor of two higher than that obtained with the cross-flow nebulizer. Note that the manufacturer's specification of the sensitivity is at 50% of that obtained with the cross-flow nebulizer. The relative standard deviation (for signals not limited by counting statistics) was 1–2%.

Analysis of clinical samples in the continuous-flow mode. It was found out that the introduction

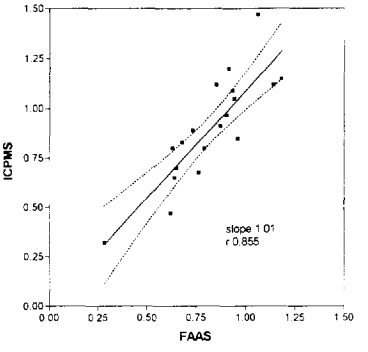

Fig. 4. Correlation ($\alpha = 0.95$) of the results for the determination of zinc in serum and urine between flame AAS (another laboratory) and ICP MS.

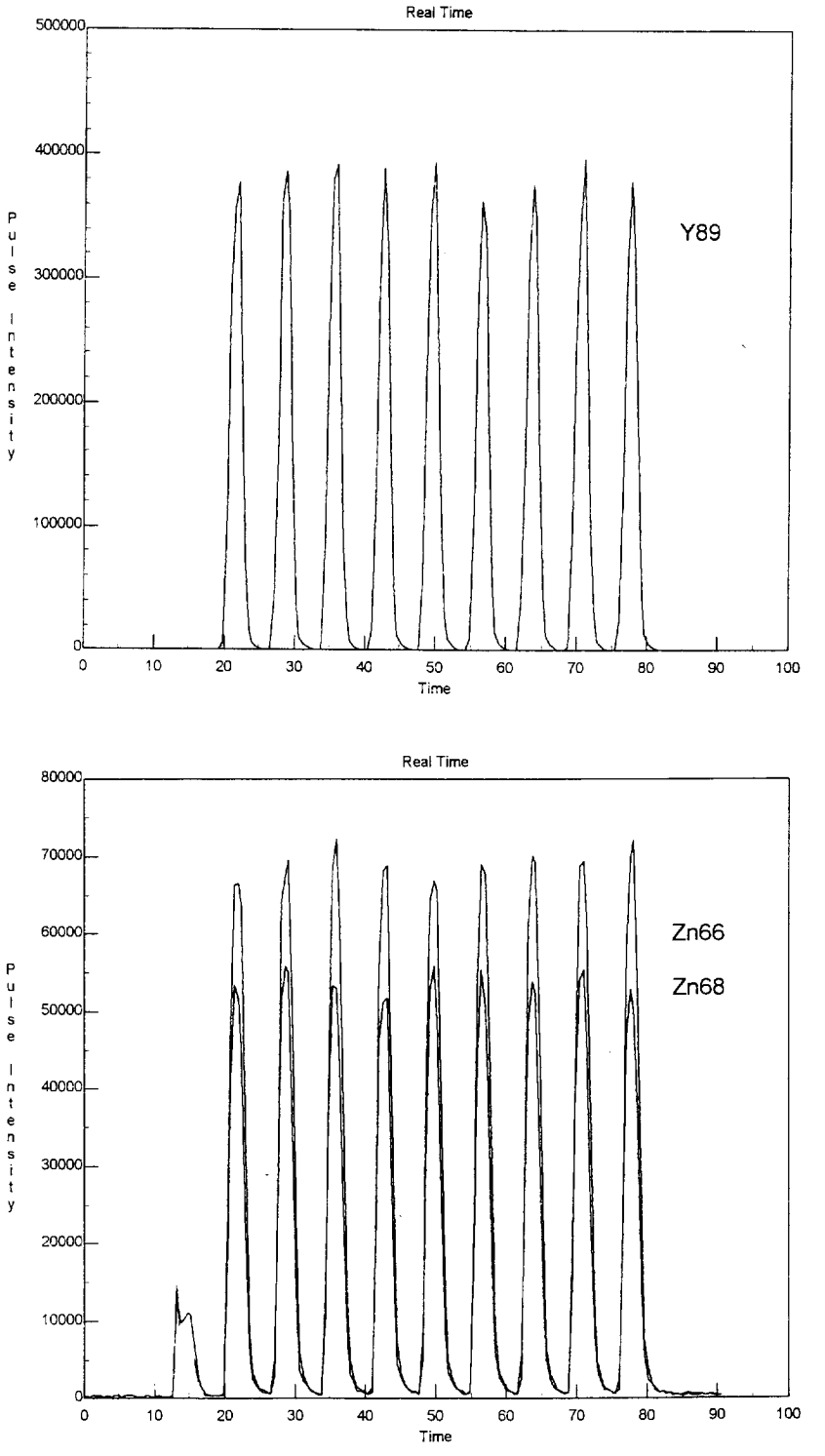

Fig. 5. Profile of the signal in a serum sample obtained by FIA-DIN-ICP MS for (a) zinc, (b) 10 ng ml^{-1} of Y (internal standard).

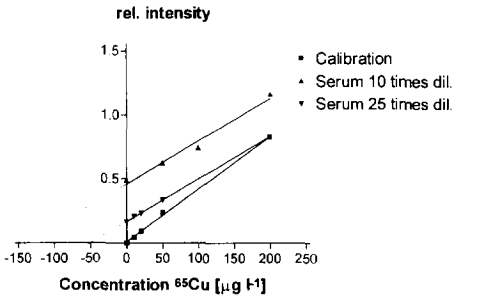

Fig. 6. External calibration and standard addition graphs for the determination of Cu in the Seronorm serum. (a) aqueous solution; (b) serum diluted ten times; (c) serum diluted 25 times.

of undiluted urine and, especially, of blood plasma samples led to the blockage of the DIN capillary after several seconds. Diluted (10–20-fold) samples could be fed for a couple of minutes but the signals decreased gradually and the results showed poor precision (RSD > 5%). This was found to be due to the adsorption of the serum proteins on the wall of the DIN capillary and thus to the gradual decrease in the nebulization efficiency. The use of the 0.1% Triton solution as the carrier and/or as the sample diluent was found to have no effect. It was therefore attempted to solve the above problems by discrete sample introduction (flow injection mode) with rinsing the capillary with the carrier solution between the subsequent injections.

Analysis of clinical samples in the FI mode. The injected volume was controlled by the sample load time from the sample loop. At the carrier flow-rate of 100 µl min^{-1} a 2 s load time (necessary to reach a peak height equal to the height of the continuous-flow signal) corresponds to a 2 µl injection. An example signal profile of a serum sample is shown in Fig. 5. The stability of signal measured as a relative standard deviation ($n = 5$) of the peak-height is 3–5%. If corrected for internal standard it can be reduced below 1%. The first peak should be, however, discarded since it may be due to some residual cross-contamination.

Matrix effects were investigated by comparing the slope of the calibration graph with that of the standard addition graph for ^{65}Cu and ^{68}Zn. A significant difference was observed for copper in the Seronorm serum sample which is illustrated in Fig. 6. Indeed, the value obtained with external calibration (0.94 ± 0.03 µg ml^{-1}) is different from that (1.17 ± 0.11 µg ml^{-1}) obtained by the method of standard additions. This suggests the existence of an interference which is characteristic to Cu and cannot be corrected by the internal standard. Indeed, for yttrium the slope of the straight line signal versus concentration is the same for aqueous and serum solutions. This interference cannot be removed by diluting the serum samples as shown in Fig. 6. The origin of this interference is hypothesized to be sorption of the protein-bound copper on the wall of the DIN capillary since once in the plasma protein-bound copper and free copper are ionized in the same way owing to the high temperature.

The results of the analysis of serum and urine samples using FIA-DIN-ICP MS were validated using the same reference materials as discussed above. The results (Table 3) show good agreement between the certified and obtained values when

Table 3
Results using flow injection DIN-ICP MS

Certified reference material	Copper concentration, mg ml^{-1}		Zinc concentration, mg ml^{-1}	
	Certified (range)	Found ± S.D.	Certified (range)	Found ± S.D.
Seronorm	1.26	1.2 ± 0.1[a]	1.50	1.4 ± 0.2
Biotrol	0.84(0.74--0.94)	0.91 ± 0.05	0.90(0.80--1.00)	0.90 ± 0.05
Urine (level 1)	0.082(0.066--0.098)	0.103 ± 0.005	0.202(0.162--0.243)	0.21 ± 0.02
Urine (level 2)	0.266(0.213--0.319)	0.31 ± 0.02	1.678(1.342--2.013)	1.87 ± 0.09

Standard deviation calculated on the basis of five independent measurements.
[a] Value obtained by the method of standard additions.

the eternal calibration with aqueous solutions was used except the copper concentration in the Seronorm serum for which standard addition is recommended.

4. Conclusion

It is concluded that ICP MS is a rapid and reliable technique for the determination of Cu and Zn in serum and urine. The spectral interferences evoked earlier in the literature are minimized with the latest generation of ICP MS instruments but nevertheless the agreement of data from obtained using different isotopes should be a prerequisite for the validation of the results obtained. In some cases matrix can affect the analyte and the internal standard in a different way so standard addition runs may be recommended. The most important advantage of ICP MS is its being the ideal technique for the validation of AAS data. Other advantages include lower detection limits, and lower sample consumption and higher sample throughput in flow-injection mode.

References

[1] J. Versieck and R. Cornelis, Trace Elements in Human Plasma or Serum, CRC Press, Boca Raton, FL, 1989.

[2] R. Lobinski and Z. Marczenko, Spectrochemical Analysis for Metals and Metalloids, Elsevier, Amsterdam, 1996.

[3] K.L. Nuttal, W.H. Gordon, K.O. Ash, Inductively coupled plasma mass spectrometry for trace element analysis in the clinical laboratory, Ann. Clin. Lab. Sci. 25 (1995) 264–271.

[4] H. Vanhoe, A review of the capabilities of ICP-MS for trace element analysis in body fluids and tissues, J. Trace Electrolytes Health Dis. 7 (1993) 131–142.

[5] C. Vandecasteele, H. Vanhoe, R. Dams, Inductively coupled plasma mass spectrometry of biological samples, J. Anal. At. Spectrom 8 (1993) 781–786.

[6] H. Vanhoe, C. Vandecasteele, J. Versieck, R. Dams, Determination of iron, cobalt, copper, zinc, rubidium, molybdenum, and cesium in human serum by inductively coupled plasma mass spectrometry, Anal. Chem. 61 (1989) 1851–1857.

[7] H. Vanhoe, J. Goossens, L. Moens, R. Dams, Spectral interferences encountered in the analysis of biological materials by inductively coupled plasma mass spectrometry, J. Anal. At. Spectrom. 9 (1994) 177–185.

[8] M. Gerotto, E. Dell'Andrea, A. Bortoli, M. Marchiori, M. Palonta, A. Troncon, Intereference effects and their control in ICP MS analysis of serum and saline solutions, Microchem. J. 51 (1995) 73–87.

[9] L. Moens, P. Verrept, R. Dams, U. Greb, G. Jung, B. Laser, New high-resolution inductively coupled plasma mass spectrometry technology applied for the determination of V, Fe, Cu, Zn and Ag in human serum, J. Anal. At. Spectrom. 9 (1994) 1075–1078.

[10] T.D.B. Lyon, G.S. Fell, Isotopic composition of copper in serum by inductively coupled plasma mass spectrometry, J. Anal. At. Spectrom. 5 (1990) 135–137.

[11] D.R. Wiederin, F.G. Smith, R.S. Houk, Direct injection nebulization for inductively coupled plasma mass spectrometry, Anal. Chem. 63 (1991) 219–225.

ELSEVIER

Talanta 44 (1997) 1397–1405

Talanta

A photo-cured coated-wire calcium ion selective electrode for use in flow injection potentiometry

Peter W. Alexander [a,*], Telis Dimitrakopoulos [a], D. Brynn Hibbert [b]

[a] *Department of Physical Sciences, University of Tasmania, P.O. Box 1214, Launceston, Tasmania, 7250, Australia*
[b] *Department of Analytical Chemistry, University of New South Wales, Sydney, 2052, Australia*

Received 5 September 1996; received in revised form 10 December 1996; accepted 23 December 1996

Abstract

A multi-sensor cell containing a new photo-cured calcium ion selective electrode sensor is reported. Four membranes containing different components are prepared to determine the one with optimum selectivity and sensitivity. This is shown to consist of the *N,N,N',N'*-tetracyclohexyl-3-oxapentanediamide ligand (ETH 129) as the ionophore, 2-nitrophenyl octyl ether as the plasticiser and tetradodecyl ammonium tetrakis(4-chlorophenyl) borate as the lipophilic additive. The photo-curing process is applied after coating a thin membrane on a silver wire as substrate transducer to produce the calcium sensor. The curing process is demonstrated to be faster (1 min) than previous methods and does not require a nitrogen atmosphere for reproducible production of membrane response characteristics. Four sensors constructed with the identical optimum membrane are shown to function reproducibly in a multi-sensor flow-through cell using the steady-state mode of flow measurement, and an average calibration slope of 28.5 ± 0.4 mV change per activity decade is observed over a log-linear concentration range between 0.01 and 10 mM. The sensor is also shown to respond to changes in pH. Hence, in the flow injection potentiometric mode, a constant carrier buffer composition of pH 8.3 is required for accurate potentiometric calcium determinations. The sensor is used to determine calcium in water samples by flow injection potentiometry. The accuracy of the electrode determination relative to atomic absorption spectroscopy was in the range 5–9% for three different water samples.

Keywords: Calcium selective electrodes; Flow injection potentiometry; Multi-sensor mode; Photo-cured membrane

1. Introduction

Multi-sensor potentiometric response has been previously reported to have advantages in potentiometric flow analysis cells [1–4]. Three modes of application are possible: (1) where additive response of multiple identical sensors provides improved sensitivity and detection limits; (2) where different ion sensors can be incorporated into a flow through cell to provide simultaneous determinations; and (3) for applications [5,6] in field-portable instrumentation for flow injection potentiometry (FIP). The application of membrane selective electrodes in a multi-sensor cell, however, have been less successful due to high

* Corresponding author. Fax: +61 3 63243839; e-mail: Peter.Alexander@physsci.utas.edu.au

0039-9140/97/$17.00
PII S0039-9140(97)00011-8

impedance ISEs and electronic problems of cross-talk between analog-to-digital channels caused by unshielded circuitry. Diamond et al [7] has discussed this problem, and has described successful multi-sensor potentiometric measurements using the batch injection analysis technique.

This study concerned the development of a new photo-cured membrane for a calcium ion selective electrode (ISE) which was tested in a multi-sensor flow-through cell for response characteristics. At present, the preferred liquid polymer membrane for manufacture of ISEs is poly(vinyl chloride) (PVC). Commercial companies have a considerable number of cation and anion selective electrodes available based on PVC membranes which are durable and flexible, and have been applied to solid-contact type electrodes [8].

Miniature electrodes referred to as 'coated wire electrodes' [8] have also been reported for a range of PVC based anion and cation selective electrodes. The disadvantages of PVC based liquid polymer membranes are that they can take up to 2 days to manufacture due to the solvent-cast method, they can experience significant electrode signal drifting when used as a solid-contact electrode, and they exhibit poor adhesion to a solid substrate surface [9]. The poor adhesion of a PVC membrane in a solid-contact configuration presents a problem with continuous on-line monitoring, when eventually the membrane peals-off.

The use of UV photo-curing of a bisphenol A epoxy diacrylate based membrane cross-linked with an acrylate ester is an alternative method for the rapid manufacture of liquid polymer membranes. These membranes are mechanically stronger than PVC membranes [10–19], but the photo-curing of acrylate based membranes can take up to 40 min and requires a nitrogen atmosphere.

Photo-cured membranes developed at present include calcium [10,11,16,17], potassium [12,15], pH [13], nitrate [14], lithium [18] and sodium [19]. Most of these were utilised in the FIP mode. Most of these have employed up to 30% (w/w) of plasticiser [10–13,16–19] compared with about 65% (w/w) of plasticiser required for PVC membranes [20]. The use of less plasticiser in photo-cured membranes leads to other advantages [3–6,10–13]. There is an increase in the mechanical strength of photo-cured membranes compared with PVC membranes, making photo-cured membranes more reliable for flow-through measurements. There is also a decrease in the water uptake of the membrane which minimises electrode signal drift, improves the adhesion to metallic substrates and eliminates the need for volatile solvents such as THF in the manufacture.

Plasticisers of a high dielectric constant, such as 2-nitrophenyl octyl ether ($e = 24.2$), are preferred for divalent-selective electrodes since they improve the determined selectivity over monovalent ions [21]. The major disadvantage with some of the above-mentioned photo-cured membranes, in particular the calcium-selective electrode, was their inability to employ 2-nitrophenyl octyl ether as the plasticiser. The nitro group is known to inhibit the photopolymerisation process by acting as a free radical scavenger when using the benzophenone type of photoinitiator [11,15]. This can be overcome by introducing a small drop of the 2-nitrophenyl octyl ether plasticiser onto the surface of the photo-cured membrane and allowing it to permeate the membrane [11,18,19]. This procedure improves the response and the selectivity of photo-cured membrane based ISEs, however, there is no control of the amount of plasticiser introduced into the photo-cured membrane.

Recently, there has been a report of a photo-cured nitrate ISE that employed 2-nitrophenyl octyl ether plasticiser in the pre-cured mixture, thereby controlling the amount of plasticiser in the membrane [14]. In this case, photo-curing was made possible by the use of a photoinitiator mixture that contained diaryliodonium chloride and 9,10-phenanthrenequinone, and the photo-curing process was completed in 1 min. This membrane was photo-cured on to a solid-contact electrode and was also photolithographically attached to an ion-sensitive field effect transistor.

This paper presents the evaluation of a new method for preparing a photo-cured calcium ISE, and the reproducibility is determined in a four-sensor flow-through cell for FIP. There are a number of advantages demonstrated for the method of membrane preparation using 2-nitrophenyl octyl ether as the plasticiser and

Table 1
Photo-cured membrane compositions investigated in this study

Membrane components	Ca1 (w/w %)	Ca2 (w/w %)	Ca3 (w/w %)	Ca4 (w/w %)
Ebecryl 600	50.0	49.2	49.0	48.4
HDDA	25.0	24.6	24.5	24.2
9,10-Phenanthrenequinone	0.5	0.8	0.6	0.7
Diphenyliodonium chloride	0.5	0.8	0.6	0.7
2-Nitrophenyl octyl ether	10.4	21.7	22.9	11.9
Bis(2-ethylhexyl)phthalate	10.4	—	—	11.9
ETH 129	1.4	1.4	1.4	1.3
TAClTPB	1.8	1.5	—	—
KClTPB	—	—	1.0	0.9

N,N,N′,N′-tetracyclohexyl-3-oxapentane diamide (ETH 129) as the ionophore. Although this is not a new ionophore, it was shown to be applicable in a faster preparation procedure in which the photo-curing process is completed in 1 min without the use of a nitrogen atmosphere. The photo-cured calcium ISE exhibited characteristics making it ideal for FIP measurements, and was applied successfully to determine calcium concentration in a range of water samples. Finally, reproducibility of the membrane preparation method and the precision of peak height measurements for four sensors in the multi-sensor mode of operation in FIP were demonstrated, without the problem of cross-talk.

2. Experimental

2.1. Materials

Metal chloride salts used in this study were all of analytical reagent grade. In addition sodium hydrogen carbonate (BDH, AnalaR), sodium acetate (BDH, AnalaR) and Ultrapure water (Barnstead Ultrapure water system, 18.0 MΩ) were used in this study.

The polymer mixture of the photo-cured membrane prepared in this study consisted of bisphenol A epoxy diacrylate (Ebecryl 600), obtained from UCB Chemical Sector (Belgium) and 1,6-hexanediol diacrylate (HDDA) obtained from Aldrich. The ionophore used was *N,N,N′,N′*-tetracyclohexyl-3-oxapentane diamide (ETH 129) and the lipophilic additives used were potassium tetrakis(4-chlorophenyl)borate (KClTPB) and tetradodecylammoniumtetrakis(4-chlorophenyl)borate (TAClTPB), the photoinitiator mixture consisted of 9,10-phenanthrenequinone and diphenyliodonium chloride and the plasticisers were 2-nitrophenyl octyl ether (NPOE) and bis(2-ethylhexyl)phthalate (BEHP), were all obtained from Fluka.

2.2. Electrode preparation

The composition of each of the pre-cured membrane mixtures prepared in this study are given in Table 1. The pre-cured membranes were each applied directly with a thin nylon brush onto four silver electrode substrates, each of 0.8 mm i.d., in the multi-sensor flow-through cell used in a portable battery-powered flow injection analyser described previously [5]. The coated electrodes were then exposed to UV radiation (250 W, $\lambda =$ 300 nm) for 1 min in the open atmosphere. A minimum of two membranes were prepared and evaluated for each of the compositions listed in Table 1, and identified as Ca1, Ca2, Ca3 and Ca4. All photo-cured membranes produced were hard and clear, and the resultant photo-cured calcium ISEs were conditioned in 100 mM calcium chloride solution overnight prior to any measurements.

2.3. Potentiometric measurements

Steady-state and FIP measurements were performed using four sensors in an eight-sensor flow cell developed in a previous study [5]. The multi-sensor flow cell contained two separate flow channels: (1) for the eight electrodes that were arranged in the wall-embedded configuration [22]; and (2) for the Ag/AgCl reference electrode that was prepared by anodising the silver electrode [23], and both flow channels were merged down stream.

Steady-state measurements were performed by continuously pumping each standard solution into the flow channel containing the photo-cured electrodes. The reference solution used was 10 mM potassium chloride with all steady-state measurements. The FIP measurements were performed by injecting a fixed sample volume into a carrier solution that travels over the surface of the photo-cured membrane and the reference solution was 10 mM sodium chloride. The carrier solutions used in FIP measurements were 10 mM sodium acetate buffer at pH = 5.5 and 7.0, and 10 mM sodium hydrogen carbonate buffer at pH = 8.3, whereby, the calcium standards solutions matched the carrier solutions. The injection sample volume used throughout this study was 200 μl.

In steady-state and FIP modes, electrode potentials were acquired using an analog-to-digital converter similar to that described previously [5,6,24] were displayed in real time and saved on a Macintosh Powerbook 145B computer. The data acquisition software was Satod© Ver. 1.46 and was written in Think C by J. Morgan (University of New South Wales, Sydney, Australia). Data was analysed and graphed by IGOR Ver.1.28 (AD Instruments, Sydney, Australia). The calcium ion activities were calculated using the Debye-Hückel equation [25].

2.4. Determination of membrane resistances

The membrane resistances of the photo-cured calcium ISEs were determined in a 100 mM calcium chloride solution, with each sensor connected to a Fluke 75 multimeter (John Fluke Mfg., USA) versus a platinum electrode. The 100 mM calcium chloride solution was continuously recirculated through the multi-sensor flow cell while measurements were performed.

3. Results and discussion

3.1. Calcium ion response

The four photo-cured membrane electrodes prepared (Ca1–Ca4, Table 1) were investigated to compare the response of each when exposed to calcium solutions. The characteristic performance of each of the ISEs is summarised in Table 2. Ca3 and Ca4 ISEs exhibited an inferior response to calcium in the steady-state mode compared with the Ca1 and Ca2 ISEs. Calibration curves for the four types of calcium ISEs are presented in Fig. 1.

The Ca3 and Ca4 ISEs were clearly sub-Nernstian when compared with the Ca1 and Ca2 ISEs in pure calcium chloride in the steady-state mode. The main difference in the membrane compositions of the photo-cured membranes was that Ca3 and Ca4 membranes both contained the lipophilic additive potassium tetrakis(4-chlorophenyl) borate, and the Ca1 and Ca2 membranes contained tetradodecyl ammonium tetrakis(4-chlorophenyl) borate. This observation indicates that tetradodecyl ammonium tetrakis(4-chlorophenyl) borate was more suited as an anion suppressing agent for photo-cured membranes that contain the NPOE plasticiser than the potassium tetrakis(4-chlorophenyl) borate.

The absence of anion suppressing agents in these photo-cured calcium membranes results in ISEs that respond to anions such as chloride. This observation was likely due to the formation of the

Table 2
Response behaviour of the photo-cured calcium ISEs prepared in this study

Calcium ISE	Electrode slope (RSD)	Log-linear range, mM
Ca1	27.7 (2.1%)	0.01–10
Ca2	28.8 (2.4%)	0.01–10
Ca3	20.7 (8.9%)	0.01–1
Ca4	13.5 (10.3%)	0.01–1

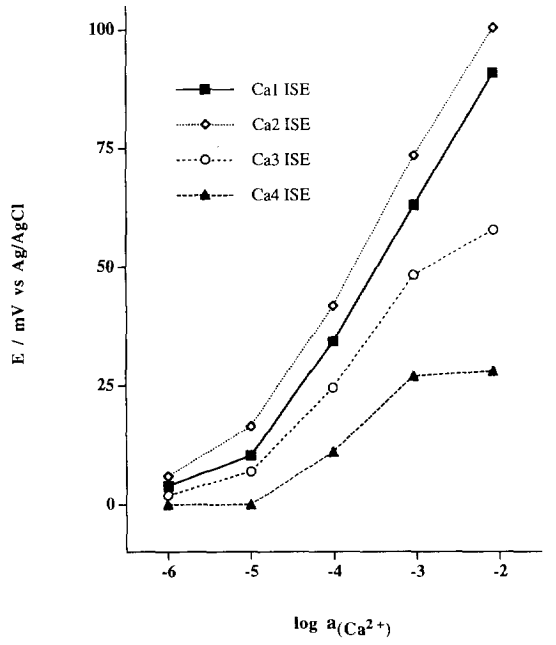

Fig. 1. Calibration curve observed for the photo-cured (Ca1–Ca4) calcium ISEs in the steady-state mode in pure calcium chloride solution.

positively charged calcium-ionophore complex in the membrane phase which electrostatically attracts sample anions, hence, the observed anion response. This also indicates that photo-cured epoxydiacrylate polymer contains no endogenous anionic sites to assist in counterbalancing the positively charged calcium-ionophore complex in the membrane phase.

The Ca1 and Ca2 electrodes were therefore used in further studies on FIP response characteristics in a multi-sensor flow-cell configuration used in a portable battery-powered flow injection system developed in our laboratories [5,6,24]. There was no observable cross-talk between the Ca1 and Ca2 membrane based ISEs, since the electronic circuitry employed in this study was contained in a single carry-case and shielded cables were used to carry the individual ISE signals which were displayed by the computer, as demonstrated in previous work [5,6]. Potentiometric application and evaluation of these photo-cured membranes of high resistance (greater than 10 MΩ) in either the steady-state or FIP modes was made possible employing the multi-sensor based portable flow injection analyser [5]. Typical membrane resistance for all the photo-cured calcium membranes produced in this study were in the range of 10 and 1 MΩ, depending on the thickness of the prepared membrane.

The Ca1 and Ca2 ISEs exhibited an electrode slope of 27.7 ± 0.6 and 28.8 ± 0.7 mV change per activity decade, respectively in pure calcium chloride solution. The log-linear range observed for the Ca1 and Ca2 ISEs were between 0.01 and 10 mM and a detection limit of 1.0 μM in pure calcium chloride solution in the steady-state mode. Fig. 2 illustrates a typical response curve for the step change in concentration for the Ca2 ISE. The time taken for Ca1 and Ca2 ISEs to achieve 90% steady-state were each 5 s making these photo-cured membranes ideal for FIP measurements. The observed baseline drifts for the Ca1 and Ca2 ISEs were about 5 mV per week,

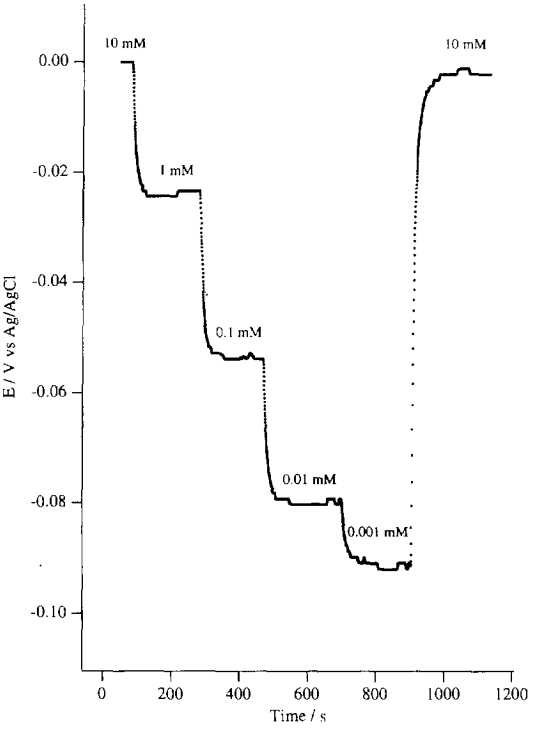

Fig. 2. Typical response curve observed for the Ca2 ISE for the step-change in concentration ranging between 0.001 and 10 mM calcium chloride.

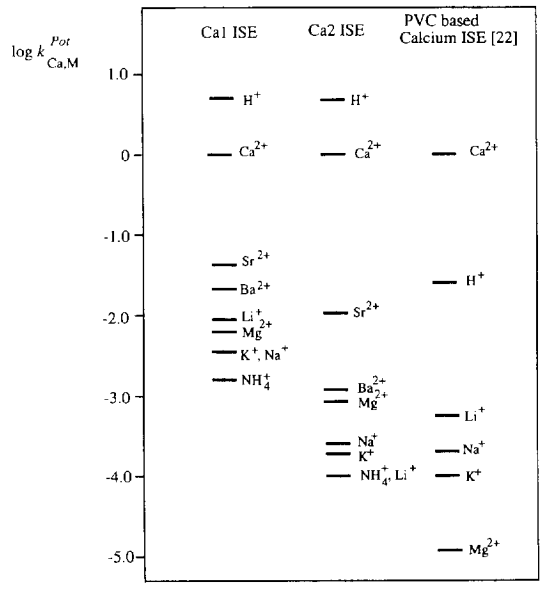

Fig. 3. The selectivity coefficients for the photo-cured Cal and Ca2 ISEs in this study compared to previously reported PVC based calcium ISE.

and both calcium ISEs were stored in 100 mM calcium chloride solution when not in use and were still operational after 3 months.

3.2. Selectivity of Cal and Ca2 ISEs

The selectivity coefficients for the Cal and Ca2 ISEs were determined using the matched potential method [26]. Fig. 3 shows the selectivity coefficients for the two photo-cured membrane based calcium ISEs Cal and Ca2 and a previously reported PVC based calcium ISE employing the same ionophore. The Ca2 ISE was generally more selective against interfering ions than the Cal. Generally, polar plasticisers such as NPOE having a high dielectric constant ($\varepsilon = 24.2$) are used in liquid polymer membranes of divalent cation ISEs in order to increase the selectivity of the determined ion over monovalent cations [21]. The plasticiser mixture employed for the Cal membrane consisted of 50% BEHP ($\varepsilon = 4.2$) and 50% NPOE, while the plasticiser used for the Ca2 membrane was NPOE alone as in Table 1. Since the overall polarity of the Cal membrane was lower than that of the Ca2 membrane, the inferior selectivity observed for the Cal ISE was expected.

The observed selectivities over the magnesium ion for the Cal and Ca2 based ISEs were inferior to a previously reported PVC membrane for calcium employing the same ionophore [27]. The Cal and Ca2 ISEs experienced severe interference from the hydrogen ion, but this was not detrimental to the calcium ion response. The Ca2 ISE exhibited adequate selectivity over sodium, potassium and magnesium ions for potentiometric calcium measurements in a range of water samples. However, the pH of the standards and samples must be the same.

Fig. 4 shows the calibration plot for the Ca2 ISE measured in the steady-state mode with solutions of different pH. Using a 10 mM sodium acetate buffer at pH = 5.5, there was a negligible response to calcium ions. In 10 mM sodium acetate buffer at pH 7.0 and in 10 mM sodium hydrogen carbonate buffer at pH 8.3, the electrode slopes were 22.5 ± 0.9 and 24.5 ± 0.5 mV

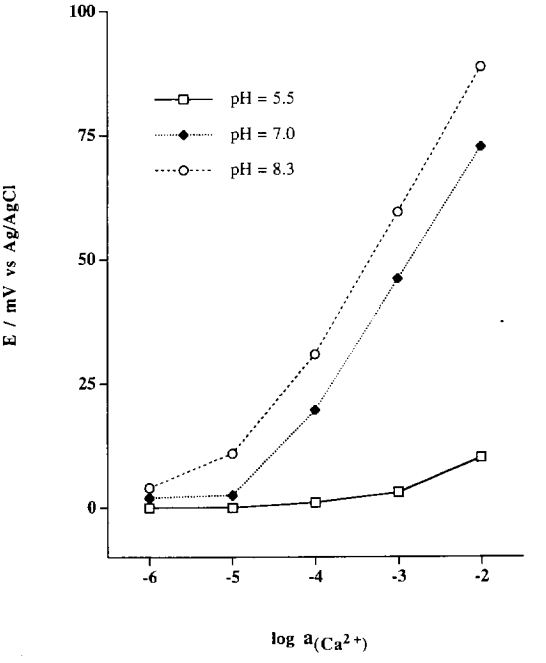

Fig. 4. Calibration curve observed for the photo-cured Ca2 ISE in the steady-state mode with calcium chloride solutions in 10 mM sodium acetate buffer at pH 5.5 and pH 7.0, and 10 mM sodium hydrogen carbonate buffer at pH 8.3.

per activity decade, respectively, and the observed log-linear range was between 0.5 and 10 mM calcium in the steady-state mode. Clearly, to perform reliable potentiometric measurements with this ISE, the pH must be ≥ 7.0 and there must be a pH match between the standards and the samples.

There are three possible sources of the hydrogen interference experienced by the Ca1 and Ca2 ISEs: (1) the epoxyacrylate membrane exhibited some pH sensitivity; (2) the lipophilic additive (tetradodecyl ammonium tetrakis(4-chlorophenyl) borate) was sensitive to pH; or (3) the ETH 129 ionophore was degraded after exposure to the UV radiation. Each point will be discussed in turn.

There have been numerous photo-cured epoxyacrylate based anion and cation-selective electrodes employing various ionophores and plasticisers (including NPOE), and none of these membranes have experienced any hydrogen interference [10–12,14–19]. A blank photo-cured membrane of similar composition to the Ca2 membrane, but without the ETH 129 ionophore, exhibited no pH response. It is therefore unlikely that the epoxydiacrylate polymer base and the lipophilic additive, tetradodecyl ammonium tetrakis(4-chlorophenyl) borate, contributed to the pH interference shown in this study. This eliminates the photo-cured epoxyacrylate polymer base for contributing to any pH interference of the Ca1 and Ca2 ISEs and the tetradodecyl ammonium tetrakis(4-chlorophenyl) borate additive.

In a previous study, oven-curing (90°C for 30 min) of a silicon rubber based calcium ISE which contained the ETH 129 ionophore resulted in an electrode response that was sub-Nernstian due to degradation of the ionophore [28]. In a different study, the room-temperature curing of a plasticised silicon rubber membrane employing the ETH 129 ionophore produced a calcium ISE that was comparable with the PVC based calcium ISEs [29].

A PVC calcium ISE based on the ETH 129 ionophore and the potassium tetrakis (4-chlorophenyl)borate lipophilic additive was prepared as described previously [27] and then exposed to UV radiation under the same conditions as the Ca1 and Ca2 ISEs. The PVC based calcium ISE exhibited a significant pH interference similar to that observed for the Ca1 and Ca2 ISEs. Clearly, curing of liquid polymer membranes containing the ETH 129 ionophore above room temperature results in a calcium ISE that shows some inferior electrochemical properties when compared with any liquid polymer membrane prepared at room temperature. We therefore believe that some degradation of the ETH 129 ionophore occurs on UV curing which raises the temperature of the membrane above room temperature and that this leads to the observed pH interference. The excellent selectivity observed against monovalent ions suggests that the extent of degradation is not great.

3.3. Flow injection potentiometric measurements with the Ca2 ISE

The photo-cured Ca2 ISE was fast responding, exhibited excellent adhesion to the silver substrate and was mechanically strong, thus making it ideal for FIP measurements. The carrier was 10 mM sodium hydrogen carbonate buffer (pH = 8.3). Typical peaks observed for four photo-cured Ca2 ISEs in the FIP mode are presented in Fig. 5 after baseline offsetting for each calcium ion electrode response. The precision of triplicate peak heights range between 1.0 and 4.0% (RSD). The mean electrode slope observed for the 4 Ca2 ISEs was 25.4 ± 0.4 mV change per activity decade which demonstrates the reproducible manufacture of the Ca2 membrane. The log-linear range observed for the Ca2 ISE was between 0.5 and 10 mM and the detection limit was 0.01 mM calcium in a 10 mM sodium hydrogen carbonate background in the FIP mode. The FIP response observed for the Ca2 ISE was 70% of the steady-state response.

To demonstrate the accuracy of the Ca2 ISE in the FIP mode, three types of water samples were analysed for their calcium content: (1) with low levels of calcium ions that would be near the detection limit of the Ca2 ISE (Tap water); (2) with similar levels of calcium and magnesium ions (Summit Mineral Water); and (3) with a higher calcium level than that of magnesium (Evian Mineral Water). Table 3 presents the results of the water analysis which were in agreement with atomic absorption spectroscopy measurements.

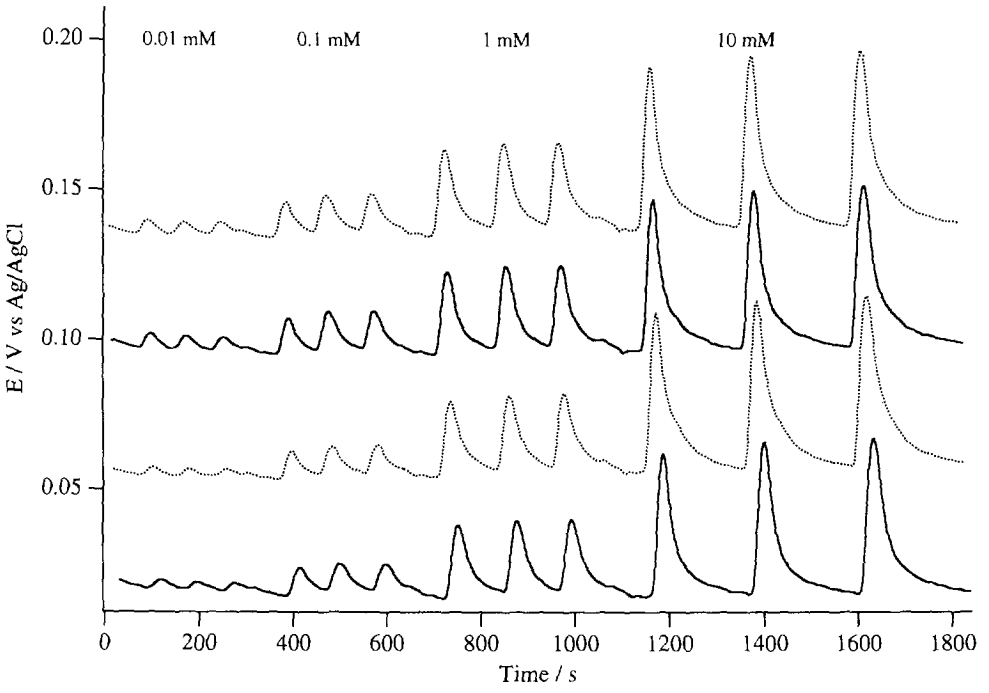

Fig. 5. Typical peak height responses observed for four photo-cured Ca2 ISEs, carrier stream was 10 mM sodium hydrogen carbonate (pH = 8.3) and reference stream was 10 mM sodium chloride, total flow rate was 2.5 ml min^{-1}, and the sample volume was 200 ml.

4. Conclusions

The development of a photo-cured Ca2 membrane using 2-nitrophenyl octyl ether as the plasticiser and tetradodecyl ammonium tetrakis(4-chlorophenyl)borate as the lipophilic additive has been shown to give superior potentiometric characteristics when compared with the other photo-cured calcium ISEs investigated in this study. A hard and transparent membrane was produced after a 1 min photo-curing process without the use of a nitrogen atmosphere compared with other reported photo-cured membranes which employ a benzophenone type photoinitiator requiring up to 40 min photo-curing under the nitrogen atmosphere [10–19]. Photo-curing membranes in ambient air which contained 2-nitrophenyl octyl ether plasticiser was made possible by employing a photoinitiator mixture containing 9,10-phenanthrenequinone and diphenyliodonium chloride. Good reproducibility of the calibration slope (1.4% RSD) was obtained in the multi-sensor flow cell design with four sensors coated with the same Ca2 membrane in the FIP mode. The peak height precision in the multi-sensor design for FIP ranged between 1 to 4% depending on the concentration injected.

Table 3
Calcium determination of various water samples by FIP and atomic absorption spectroscopy (AAS), ($n = 3$)

Water sample	Ca2 ISE mg l^{-1} (RSD)	AAS mg l^{-1} (RSD)	Labelled mg l^{-1}
Evian mineral water	71.2 (2.1%)	78.2 (0.3%)	78
Summit mineral water	16.0 (4.1%)	15.2 (0.3%)	18
Tap water	5.3 (4.2%)	5.6 (0.2%)	1–5[a]

[a] Expected range.

Significant interference by hydrogen ions was observed with all photo-cured membranes and it is proposed that a slight degradation of the ETH 129 ionophore in the photo-cured membranes after exposure to the UV light had occurred. The present photo-cured calcium ISE was used to determine calcium levels in various water samples in the FIP mode, whereby, a 10 mM sodium hydrogen carbonate (pH = 8.3) carrier was used. The results were in good agreement with atomic absorption spectroscopy.

Acknowledgements

We thank the Australian Research Council for financial support and the UCB Chemical Sector (Belgium) for kindly donating the Ebecryl 600 polymer.

References

[1] D.B. Hibbert, P.W. Alexander, S. Rachmawati and S.A. Caruana, Anal. Chem., 62 (1990) 1015.
[2] P.W. Alexander and D.B. Hibbert, Australian Patent, (Unisearch Ltd), No. PI 7728, April 1991.
[3] D.B. Hibbert, P.W. Alexander and P. Yatiman, Mikrochim. Acta, 108 (1992) 93.
[4] P.W. Alexander, L.T. Di Benedetto, T. Dimitrakopoulos, D.B. Hibbert, J.C. Nglia, M. Sequeira and D. Sheils, Talanta, 43 (1996) 915.
[5] P.W. Alexander, T. Dimitrakopoulos and D.B. Hibbert, Field Anal. Chem. Tech., 1 (1996) 31.
[6] T. Dimitrakopoulos, P.W. Alexander and D.B. Hibbert, Electroanalysis, 8 (1996) 438.
[7] D. Diamond, J. Lu, Q. Chen and J. Wang, Anal. Chim. Acta, 281 (1993) 629.
[8] R.W. Cattrall and I.C. Hamilton, Ion-Selective Electrode Rev., 6 (1984) 125.
[9] G.J. Moody, J.M. Slatert and J.D.R. Thomas, Analyst, 113 (1988) 103.
[10] R.W. Cattrall, I.C. Hamilton and P.J. Iles, Anal. Chim. Acta, 169 (1985) 403.
[11] T.J. Cardwell, R.W. Cattrall, I.C. Hamilton and P.J. Iles, Anal. Chim. Acta, 177 (1985) 239.
[12] T.J. Cardwell, R.W. Cattrall, I.C. Hamilton and P.J. Iles, Anal. Chim. Acta, 204 (1988) 329.
[13] F.R. del Mundo, T.J. Cardwell, R.W. Cattrall and P.J. Iles, Electroanalysis, 1 (1989) 179.
[14] C. Dumschat, R. Fromer, H. Rautschek, H. Muller and T.J. Timpe, Anal. Chim. Acta, 219 (1989) 179.
[15] A. Bratov, N. Abramova, J. Munoz, C. Dominguez, S. Alegret and J. Bartroli, Anal. Chem., 67 (1995) 3589.
[16] T. Dimitrakopoulos, J.R. Farrell and P.J. Iles, Electroanalysis, 8 (1996) 391.
[17] L.T. Di Benedetto, T. Dimitrakopoulos, J.R. Farrell and P.J. Iles, Talanta, in press (1996).
[18] T. Dimitrakopoulos, J.R. Farrell and P.J. Iles, Anal. Chim. Acta, in press (1996).
[19] T. Dimitrakopoulos, J.R. Farrell and P.J. Iles, Anal. Chim. Acta, in press (1996).
[20] G.J. Moody and J.D.R. Moody, in A. Covington (Ed.),'Ion-Selective Electrode Methodology', Vol. 1, Ch. 7, CRC Press, Florida, 1979.
[21] W.E. Morf, 'The Priniples of Ion-Selective Electrode and Membrane Transport', Elsevier, Amsterdam, 1981.
[22] J. Ruzicka and E.H. Hansen, 'Flow Injection Analysis', 2nd ed, Wiley, New York, 1988.
[23] R.G. Bates, 'Determination of pH, Theory and Practice', 2nd ed., John Wiley and Sons, New York, (1973), p. 330.
[24] T. Dimitrakopoulos, P.W. Alexander, D.B. Hibbert, L. Cherkson and J. Morgan, Electroanalysis, 7 (1995) 1118.
[25] D.A. Skoog and D.M. West, Fundementals of Analytical Chemistry, 4th edn., CBS Publishings, Japan, 1982, p. 118.
[26] Y. Umezawa, K. Umezawa and H. Sato, Pure Appl. Chem., 67 (1996) 507.
[27] U. Schefer, D. Ammann, E. Pretsch, U. Oesch and W. Simon, Anal. Chem., 58 (1986) 2282.
[28] H.D. Goldberg, R.B. Brown, D.P. Liu and M. Meyerhoff, Sens. Actuators, B 21 (1994) 171.
[29] B.K. Oh, C.Y. Kim, H.J. Lee, K.L. Rho, G.S. Cha and H. Nam, Anal. Chem., 68 (1996) 503.

ELSEVIER

Talanta 44 (1997) 1407–1412

Talanta

Spectrophotometric determination of hydrogen peroxide by using the cleavage of Eriochrome black T in the presence of peroxidase

Min Zhu, Xuemei Huang, Liuzhan Liu, Hanxi Shen *

Department of Chemistry, Nankai University, Tianjin, 300071, People's Republic of China

Received 28 August 1996; received in revised form 11 December 1996; accepted 23 December 1996

Abstract

A new hydrogen donor for peroxidase, Eriochrome black T, was reported for the first time. Steady-state catalytic velocity depends upon enzyme and substrate concentrations, and a Michaelis–Menten K_m value of 1.72×10^{-5} mol l^{-1} and a V_{max} value of 4.43×10^{-3} s^{-1} were measured at pH 8.6. Trace amount of hydrogen peroxide (2×10^{-7}–1.0×10^{-5} mol l^{-1}) was determined in aqueous solution by using the cleavage of Eriochrome black T catalyzed by peroxidase. The method is simple and practical, with high sensitivity and enzymatic activity. © 1997 Elsevier Science B.V.

Keywords: Catalytic cleavage; Eriochrome black T; Peroxidase; Spectrophotometric determination of H_2O_2

1. Introduction

The spectrophotometric determination of hydrogen peroxide by reaction with a chromogenic hydrogen donor in the presence of peroxidase has been widely accepted in the analysis of biological samples. Various kinds of hydrogen donors have been recommended for this purpose, such as phenol derivatives [1–6], aniline derivatives [7–12], and leuco dyes [13,14]. However, aniline-4-aminoantipyrine system proceeded only in an acidic medium, so its application was limited during the determination of hydrogen peroxide in the presence of oxidases, such as cholesterol oxidase. The maximum absorbance of phenol-4-aminoantipyrine system was located at 500–520 nm, which was often susceptible to interference by bilirubin in serum, that had an absorption band in a range of 380–530 nm [15]. In addition, its limited analytical sensitivity was a common disadvantage. The determination of hydrogen peroxide requires submicro molar limit of detection when hydrogen peroxide is produced from samples catalyzed by some oxidases, such as monoamine oxidase and uricase, or originated from the supermicro amount of sample. Leuco dye, such as leuco crystal violet and patent blue violet could be substituted for them with a spectacularly high sensitivity, but it also proceeded in acidic conditions (pH $\leq$ 4.5) for the reason of solubility and

* Corresponding author. Fax: +86 22 344853.

PII S0039-9140(97)00012-X

itself was easily oxidized by oxygen dissolved in water. In this paper, a new hydrogen donor for peroxidase, Eriochrome black T (EBT, 7-nitro-4-[(1-hydroxy-2-naphthonol)azo]

-1-naphthalenesulfonic sodium), was advocated for the first time. On the basis of oxidation cleavage of EBT, a simple and practical spectrophotometry was applied in the determination of hydrogen peroxide, with high sensitivity (ε_{max} is 5.51×10^4 l mol^{-1} per cm), wide working range and without coupling reagent.

2. Experiment

2.1. Chemicals

Horseradish peroxidase (HRP, E.C.1.11.1.7, ≥ 250 IU mg^{-1}, RZ > 3.0) was purchased from Sino-American Biotechnology Company and prepared to 2.5×10^{-7} mol l^{-1}. Hydrogen peroxide solution for analysis was freshly prepared by appreciate dilution of a stock solution, which was standardized by potassium permanganate. EBT was recrystaled twice before used and applied in 2.8×10^{-3} mol l^{-1} of stock solution and preserved at 4°C. 1-Phenyl-3-methyl-5-pyrazolone (PMP) was prepared in 0.01 M. Kolthoff [16], Tris–HCl and Glycine–NaOH buffer solutions were applied in pH 5.6–11.0. All other reagents were of analytical grade commercially available. All aqueous solutions were prepared in twice deioned water.

2.2. Apparatus

All spectrophotometric measurements were done with a Shimadzu UV-240 spectrophotometer in standard cells with 10 mm pathlength (Tokyo, Japan).

2.3. Procedure

In a 10 ml colorimetric tube, 2.5 ml buffer solution (pH 8.6), 0.4 ml EBT, 0.2 ml HRP, and a different amount of H_2O_2 standard solutions were added and diluted to the mark. The mixture was incubated at 50°C for 5 min, with the control sample without H_2O_2. The absorption spectra of both resulting solution and control sample were recorded and their absorbance differences at the wavelength of maximum absorbance (615 nm) were measured with the spectrophotometer.

3. Results and discussion

3.1. Reaction of EBT and H_2O_2 catalyzed by HRP

It was reported that 1-phenylazo-2-hydroxynaphthalene (Sudan I) was oxidized slowly by HRP/H_2O_2 to be the product of the oxidative splitting of this azo dye (30 min–3 h), which can be considered to lead to the formation of the benzenediazonium ion and quinone [17]. In our experiment, oxidation cleavage of EBT, which is the derivative of Sudan I, in the presence of HRP/H_2O_2, was investigated, as shown in Fig. 1. Absorption band of 615 nm at pH 8.6 (curve 1) disappeared immediately (0.5–3 min) at room

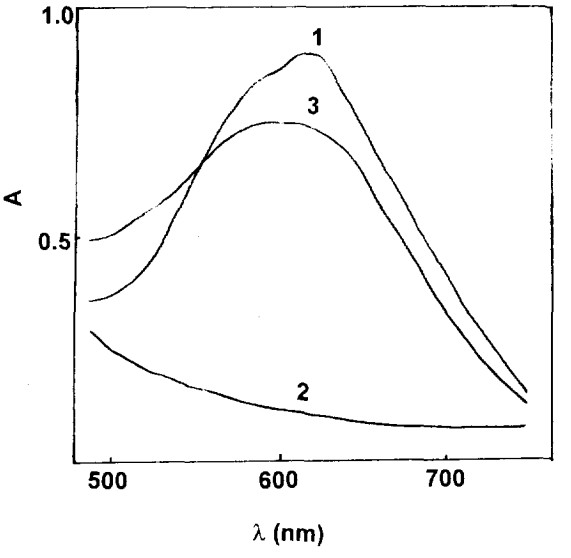

Fig. 1. Absorption spectra of EBT (1.0×10^{-4} mol l^{-1}) aqueous solution before (2) and after (3) addition of PMP (2×10^{-4} mol l^{-1}), in the precence and absence (1) of HRP (2×10^{-8} mol l^{-1}). The concentration of H_2O_2 was 2.5×10^{-5} mol l^{-1}. The solution was incubated at 50°C for 5 min, pH 8.6.

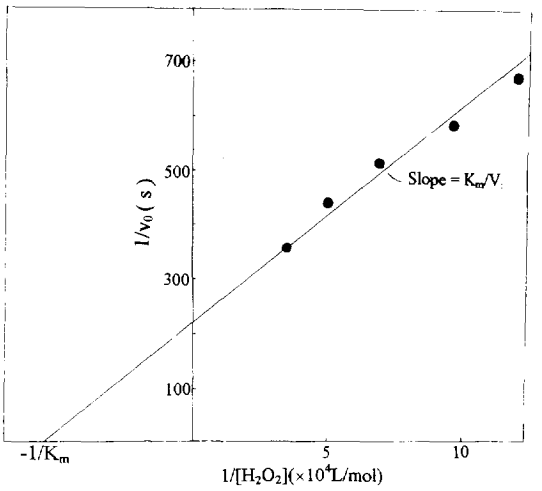

Fig. 2. Lineweaver–Burk plot The concentration of EBT was 1.1×10^{-4} mol l^{-1} at pH 8.6 and 25°C.

temperature or 50°C under the experimental condition, and no apparent absorption band was observed in the range of 500–750 nm (curve 2), which indicated that the conjugated double bond system was destroyed, probably due to the cleavage of covalent bond between –N=N– group and phenyl or naphthol group. The formation of the benzenediazonium ion in the EBT-HRP-H_2O_2 system was identified by its azo coupling with PMP. An absorption band at 550–650 nm was seen immediately after the benzenediazonium ion sensitive reagent, PMP, was added in the resulting solution (curve 3).

3.2. Determination of velocity and constants of enzyme reaction

The mechanism of enzyme action was not clear when EBT was used as the substrate for the peroxidase. It was necessary to measure velocity and constants of the enzyme reaction, in order to describe the enzyme mechanism further. The approach was to make the concentration of the substrate, EBT, excessive greatly and constant. Then the enzyme reaction was a single substrate reaction, and Michaelis–Menten behavior was observed. Thus, by Lineweaver–Burk plot, an approximately straight line is obtained, as shown in Fig. 2.

With its intercept and slope, it could be concluded that maximum velocity, V_{max} was $4.4(\pm 0.3) \times 10^{-3}$ s^{-1}, and Michaelis constant K_m was $1.7(\pm 0.2) \times 10^{-5}$ mol l^{-1}. Since $V_{max} = K_{cat}[E]_0$ ($[E]_0$ is the initial concentration of enzyme), the conversion constant K_{cat} was $2.0(\pm 0.1) \times 10^6$ $(\text{mol } l^{-1})^{-1}$ s^{-1}, and specificity constant K_{cat}/K_m was $1.2(\pm 0.1) \times 10^{11}$ $(\text{mol } l^{-1})^{-2}$ s^{-1}.

3.3. Optimization of experimental parameters

EBT is unstable in strong acid solution. As pH increased, the maximum wavelength shifted from 560 to 620 nm [18], and absorbances were measured at various maximum wavelengths. The effects of pH on relative enzyme activity and sensitivity were studied, with results shown in Table 1. Comparisons of the sensitivities would be made in terms of the following equation:

$$\frac{\Delta A_{\lambda\text{max of test pH}}}{\Delta A_{\lambda\text{max of pH 8.6}}} = \text{Factor} \quad (1)$$

Kolthoff, Tris–HCl and Glycine–NaOH buffer solution systems were compared and the EBT exhibited higher sensitivity and initial velocity at Kolthoff buffer solution. Measurement could be preceded in a range of pH 8.4–9.0. Both relative enzyme activity and relative absorbance differences were highest at pH 8.6, and the product of fading reaction was also more stable in a weakly basic condition.

There were few studies for the influence of temperature on enzyme activity [2–14], although there was much interest in horseradish peroxidase as a analytical reagent previously. Most of Trinder system and anline–aminoantipyrine system proceeded in the condition of 37°C [9–12] or at room temperature [5–8], following the Trinder's results in 1969 [1]. No experimental temperature was provided in literatures [13,14] when leuco dye was recommended as a substrate for routine assays. However, it was found by Bauminger [19] that higher absorbences were obtained at 45°C than at 37°C in phenol-4-aminoantipyrine system. In a previous paper [20], 40°C was identified as optimal when ascorbic acid was used as a substrate for the HRP.

Table 1
Effect of pH on initial rates and the sensitivity

	pH	λmax (nm)	v_0 ($\times 10^{-3}$ s^{-1})[a]	Factor[b]	t (min)[c]
Kolthoff	5.6	567	1.01	0.296	2
	7.0	604	2.76	0.515	2
	7.6	612	2.90	0.524	5
	8.2	612	5.25	0.702	5
	8.4	615	8.97	0.901	5
	8.6	615	10.7	1.00	10
	8.8	615	9.51	0.956	10
	9.0	617	5.55	0.915	10
	10.0	592	2.03	0.753	2
	11.0	592	0	—	—
Tris–HCl	7.6	612	2.51	0.508	2
	8.2	514	4.10	0.737	3
Glycine–NaOH	8.6	605	4.75	0.455	3
	9.2	605	5.04	0.633	3

[a] Initial rate, $[H_2O_2] = 1.0 \times 10^{-5}$ mol l^{-1}, $[HRP] = 5.0 \times 10^{-9}$ mol l^{-1}.
[b] Factor is defined in Eq. (1).
[c] Stable time of resulting fading product.

The impact of temperature on enzyme activity in the present system was examined when it varied from 20 to 70°C (Fig. 3). Enzyme lost more than 50% of its activity when temperature was above 70°C or below 20°C. Fig. 3 shows that relative enzyme activity increases with temperature, arriving at a maximum in the range of 45–60°C. Further increase in temperature leads to the decrease of velocity because of the partial denaturation of the enzyme. Thus, the reaction temperature for the following experiment was 50°C, and reaction was completed within 3 min.

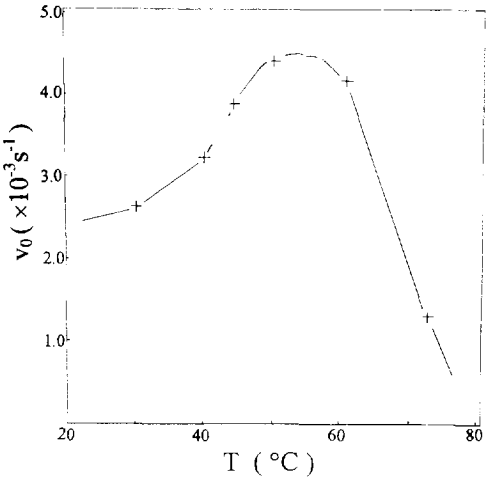

Fig. 3. Influence of temperature on relative enzyme activity. The concentration of HRP and H_2O_2 were 2.5×10^{-9} and 1.0×10^{-5} mol l^{-1}, respectively, pH 8.6.

Reaction time was directly related to HRP concentration. From experimental results, the reaction would be completed within 1 min when 1.0×10^{-8} mol l^{-1} enzyme was applied, and it would be completed within 10 min when 2.5×10^{-9} mol l^{-1} enzyme was used. So the concentration of HRP in a range of 2.5×10^{-9}–1.0×10^{-8} mol l^{-1} was recommended in the enzymatic assay.

The stability of the EBT stock solution was examined, and it was compared with Trinder reagent, aniline-4-aminoantipyrine system and leuco dye. Absorbance at experimental wavelength (505 nm) of phenol-4-aminoantipyrine

Table 2
Stability test of EBT

Day	A/A_0	$\Delta A/\Delta A_0$
1	1.00	1.00
10	0.93	0.99
30	0.88	0.99
60	0.80	0.96

Table 3
Results of recovery experiments

Sample	Added $\times 10^{-6}$ mol l^{-1}	Found $\times 10^{-6}$ mol l^{-1}	Recovery $\times 10^{-6}$ mol l^{-1}	%
1	0	4.12 ± 0.02	—	—
	2.00	6.06 ± 0.04	1.94 ± 0.02	97.0 ± 1.0
	4.00	8.16 ± 0.03	4.04 ± 0.01	101.0 ± 0.3
2	0	0.43 ± 0.01	—	—
	2.00	2.33 ± 0.02	1.90 ± 0.01	95.0 ± 0.5
	4.00	4.39 ± 0.02	3.96 ± 0.01	99.0 ± 0.3

stock solution was up to 0.075 from 0.030 after 15 days, and that of aniline-4-aminoantipyrine was up to 0.433 from 0.054 after 20 days [6]. High sensitive reagent, leuco dye was stable only for 24 h when stored in a dark bottle [14]. Table 2 shows the stability of EBT stock solution. A_0 is the absorbance at the maximum wavelength of EBT solution and ΔA_0 is the absorbance difference in the determination of 1.0×10^{-5} mol l^{-1} H_2O_2 with freshly prepared EBT reagent. A is the absorbance of EBT solution and ΔA is the absorbance difference with the EBT reagent which is stored for some day. From the results shown in Table 2, EBT exhibited good storage characteristics, in that there was no notable impact on measurement, although the absorbance at maximum wavelength decreased about 20% after 2 months.

3.4. Analytical characteristics

The calibration graph for the determination of H_2O_2 was obtained under the optimum reaction conditions. The range of linearity for the relationship between ΔA and concentration of H_2O_2 was 2×10^{-7}–1.0×10^{-5} mol l^{-1}. The regression equation and correlation coefficient of calibration graph for H_2O_2 was $\Delta A = 0.051(\pm 0.006) + 5.51(\pm 0.03) \times 10^4 C$ and $\gamma = 0.9987(\pm 0.0008)$, respectively. Calculated from the regression equation, the molar absorption coefficient of the EBT-HRP-H_2O_2 system was $5.51(\pm 0.03) \times 10^4$ l mol^{-1} per cm, which was 2.5–10 times better than that of the Trinder system [1,2]. The relative standard deviation was 0.4% for the determination of 1.0×10^{-5} mol l^{-1} H_2O_2 ($n = 8$).

Standard solutions of the test H_2O_2 were mixed to prepare mixture sample. The recovery experiments were carried out and the results were listed in Table 3.

The interferences of foreign ions to the determination of H_2O_2 (1.0×10^{-5} mol l^{-1}) in the EBT-H_2O_2-HRP system were studied, as shown in Table 4. When added at levels greater than those given, all the ions listed caused negative errors.

Acknowledgements

The authors thank the National Natural Foundation of Commission of China for the financial support.

Table 4
Interferences of foreign ions on the determination of 1.0×10^{-5} mol l^{-1} H_2O_2

Ion added	Maximum tolerance amount of ion (μg)	Ion added	Maximum tolerance amount of ion (mol l^{-1})
Cd^{2+}, Fe^{3+}	2	S^{2-}	1×10^{-7}
Mn^{2+}	3	SO_3^{2-}, SCN^-	3×10^{-4}
Fe^{2+}	10	SO_4^{2-}, NO^{3-}, PO_4^{3-}, $C_2O_4^{2-}$, Ac^-	2×10^{-3}
Cu^{2+}, Ca^{2+}, Mg^{2+}	40	HCO_3^-, Cl^-	1×10^{-2}
Ni^{2+}, Zn^{2+}	100	K^+	3×10^{-3}

References

[1] P. Trinder, Ann. Clin. Biochem., 6 (1969) 24.
[2] D. Barham and P. Trinder, Analyst, 97 (1972) 142.
[3] C.C. Allain, L.S. Poon, C.S.G. Cham, W. Richmond and P.C. Fu, Clin. Chem., 20 (4) (1974) 470.
[4] P.N. Tarbutton and C.R. Gunter, Clin. Chem., 20 (6) (1974) 924.
[5] P. Fossati, L. Prencipe and G. Berti, Clin. Chem., 26 (1980) 227.
[6] Wako Pure Chemical Industries, Ltd, JP pat 58 187 858.
[7] P. Kabasakalian, S. Kalliney and A. Westcott, Clin. Chem., 20 (5) (1974) 606.
[8] G.S. Rautela and R.J. Liedtke, Clin. Chem., 24 (1978) 108.
[9] T.T. Ngo and H.M. Genhoff, Anal. Biochem., 105 (1980) 389.
[10] K. Tamaoku, K. Ueno, K. Akiura and Y. Ohkura, Chem. Pharm. Bull., 30 (7) (1982) 2492.
[11] K. Tamaoku, Y. Murao, K. Akiura and Y. Ohkura, Anal. Clin. Acta., 136 (1982) 121.
[12] M. Shiga, M. Saito and K. Kima, Anal. Clin. Acta., 153 (1983) 191.
[13] H.A. Mottola, B.E. Simpson and G. Gorin, Anal. Chem., 47 (1970) 410.
[14] P.A. Clapp and D.F. Evans, Anal. Chim. Acta., 243 (1991) 217.
[15] G.W. Stavenson, S.L. Jacobs and R.J. Henry, Clin. Chem. 10 (1964) 95.
[16] Analytical Chemistry Group, Chemistry Department of Hangzhou University, 'Handbook of Analytical Chemistry', Part 2, P. 16, Chemical Engineer press, Beijing, 1979.
[17] M. Stiborova, B. Asfaw and P. Anzenbacher, FEBS Lett., 232 (2) (1988) 387.
[18] A.T. Pilipenko, L.I. Sarransky, Talanta, 34 (1987) 77.
[19] B.B. Bauminger, J. Clin. Pathol., 27 (1974) 1015.
[20] M. Zhu, X. Huang and H. Shen, R. Li, Anal. Chim. Acta, 1996, in press.

ELSEVIER

Talanta 44 (1997) 1413–1421

Talanta

Determination of carboxylic acid vapour by a thickness-sheer-mode acoustic wave sensor coated with crown ethers

Cao Zhong, Gao De, Lei Zheng-Gang, Lin Hui-Gai, Yu Ru-Qin *

College of Chemistry and Chemical Engineering, Hunan University, Changsha, 410082, People's Republic of China

Received 20 August 1996; accepted 2 January 1997

Abstract

The frequency response sensitivities for 39 organic vapours by thickness-sheer-mode (TSM) acoustic wave sensors coated with monobenzo-15-crown-5 (B15C5), monobenzo-18-crown-6 (B18C6) and dibenzo-30-crown-10 (DB30C10) have been reported. It shows that crown ethers are the most efficient adsorptively active material for sensing carboxylic acid vapour, particularly B15C5 can be used for sensing formic acid vapour. The B15C5 based sensor possesses good reproducibility, high stability and short response time with wide linear detection range and a low detection limit down to 0.0201 mg l^{-1} (about 5.70 ppm, V/V) of formic acid vapour while coating with 12 μg of B15C5. There is no significant interference from other organic vapours except for some nitrogen containing compounds such as diethylamine, pyridine and *N,N*-dimethylformamide, and carboxylic acid homologues such as acetic and propionic acids. The effect of humidity is easily controllable. Compared with acid–base titration method, the sensor can be used for the determination of HCOOH vapour with recovery rate of 98.4 ~ 103.8%, the analytical results are in good agreement with those obtained by the more time consuming acid–base titration method. © 1997 Elsevier Science B.V.

Keywords: Crown ethers; Organic vapours; Thickness-sheer-mode acoustic wave sensor; Carboxylic acid

1. Introduction

Carboxylic acids are toxic atmosphere pollutants, especially formic acid, which may be causing shock, pneumonitis, severe corrosive effects in the respiratory and gastrointestinal tract and irritative effects on eyes, skin and mucous membranes of human beings and animals. The maximum acceptable level of formic, acetic, and propionic acid vapours' exposure in the industrial atmosphere are 5 ppm (9 mg m^{-3}), 10 ppm (25 mg m^{-3}), and 10 ppm (30 mg m^{-3}), respectively [1,2]. Hence it is very important to develop sensitive analytical methods for monitoring carboxylic acids in particular formic acid. To date the existing methods for detecting formic and other carboxylic acids include acid–base titration [3,4], ion chromatography [5,6], high-performance liquid chromatography [7], capillary electrophoresis [7],

* Corresponding author. Fax: +86 731 8824525.

PII S0039-9140(97)00016-7

absorptiometry [8], spectrofluorimetry [9] and enzymatic assay [10,11]. Most of these methods are laborious and time-consuming and hardly applicable for on-line monitoring carboxylic acids including formic acid.

Recently, coated thickness-sheer-mode (TSM) acoustic wave sensors have shown promising potential to be used as simple, inexpensive, and portable devices with high mass sensitivity for the detection of toxic atmospheric pollutants such as acetic acid [12], formaldehyde [13,14], toluene [15], SO_2 [16], and NO_2 [17], etc. The principle of the TSM device is that the decrease in resonance frequency of an AT-cut quartz crystal vibrating in the thickness sheer mode (ΔF, Hz) is proportional to the increase in mass of a foreign substance adsorbed onto its surface (ΔM, g), derived from the Sauerbrey equation [18]

$$\Delta F = -2.3 \times 10^6 F_0^2 \frac{\Delta M}{A} \quad (1)$$

Here F_0 is the fundamental frequency of the quartz plate (MHz), A is the surface area of the quartz crystal coated (cm^2). From Eq. (1), a mass sensitivity of about 400 Hz μg^{-1} for a 9 MHz crystal and a sensitivity of 2600 Hz μg^{-1} for a 15 MHz crystal is obtained. The vibrating quartz crystal is in fact an extremely sensitive mass detector, whose theoretical detection limit is about 10^{-12} g for foreign substances absorbed [19].

The coated TSM acoustic wave gas sensors usually possess high sensitivities, low detection limits and long useful lifetimes with macromolecular compounds and polymers as adsorptive coating materials [20–24]. There is few attention paid to the analytical application of macrocyclic polyether such as crown ether coated TSM gas sensors [24–27]. In the presented paper, the response characteristics for 39 organic solvent vapours are investigated by TSM detectors coated with monobenzo-15-crown-5 (B15C5), monobenzo-18-crown-6 (B18C6) and dibenzo-30-crown-10 (DB30C10), respectively, showing that crown ethers are efficient adsorptively active materials for sensing carboxylic acid vapours, in particular B15C5 is very suitable for sensing formic acid vapour. Therefore, an inexpensive and portable TSM device coated with B15C5 may be used for detecting formic acid vapour with potential on-line or on-site applications.

2. Experimental

2.1. Apparatus and materials

The schematic diagram for the experimental assembly is shown in Fig. 1. The measuring chamber consist of a glass vessel with a volume of 535 ml. It included two way pipes with valves for incoming and outgoing gases, a stainless steel nozzle sealed and furnished with silicone rubber for injection of samples. A small customized magnetic fan was mounted on the bottom of the vessel that was used to homogenize the gas inside the chamber before detection, and a fixed magnetic stirrer (Model 78-1, Nanhui Telecommunication Equipment Factory, Shanghai) with its transformer and regulator placed outside the chamber for inductively driving the fan. The measuring chamber was kept at 24 ± 0.5°C by using a thermostatted water bath. The AT-cut quartz crystal (12.5 mm diameter) vibrating in the thickness sheer mode was placed in the sealed measuring chamber with a fundamental frequency of about

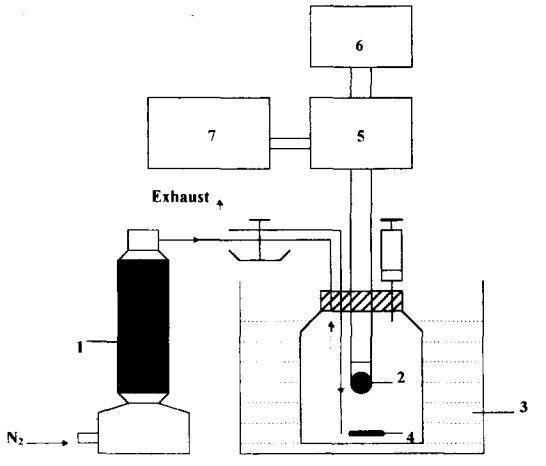

Fig. 1. The schematic diagram for the experimental assembly. 1, Anhydrous $CaCl_2$; 2, coated TSM acoustic sensor; 3, thermostatted water bath; 4, magnetic stirring fan; 5, TTL oscillator; 6, d.c. voltage regulator; 7, digital frequency counter.

9.3125 MHz, having silver-plated electrode (6 mm diameter) on each side (Model JA-5, Chengxing Radio Instruments, Beijing). The crystal electrode holder was direct connected to a laboratory-made oscillator build with a Transistor-Transistor Logic (TTL) circuit which was powered with a regulated power supply. The applied voltage was kept constant at 5 V dc for all measurements. The output frequency of the oscillating quartz crystal was monitored by using a digital frequency counter with a resolution capacity of 0.01 Hz (Model 1992/SS3380, Sijiazhuang Radio Instruments).

The adsorptively active materials applied to the crystal surface were monobenzo-15-crown-5 (B15C5), monobenzo-18-crown-6 (B18C6) and dibenzo-30-crown-10 (DB30C10) obtained from Neijiang Chemicals (Sichuan). All solvents were of analytical-reagent grade or laboratory-reagent grade which were refined and stored in sealed bottles with some pieces of drying anhydrous calcium sulfate before measurement.

2.2. Coating method

A solution about 1% by weight of each coating material was prepared using a high volatile organic solvent such as tetrahydrofuran. The solution was coated onto both sides of a crystal first by dipping and then by syringe dropping method in order to load desired amount of coating material and the solvent was evaporated with the aid of a blower. The process was repeated until a homogeneous film with an appropriate amount of coating ($4 \sim 50$ μg) dispersed on the crystal surface was formed. The coated TSM acoustic sensor was thus prepared, which was placed in a desiccator with anhydrous silica gel and activated charcoal holding while not used.

2.3. Detection procedure

In the measuring chamber, the stabilized coating fundamental frequency (F_1) of the coated TSM sensor was measured in an air or nitrogen atmosphere, which was dried and cleaned by passing through the anhydrous calcium chloride drying column. Then the appropriate amount of solvent sample was injected into the measuring chamber with a micro syringe. With the sensor coming into adsorption equilibrium with the sample vapour, the output frequency of the sensor was read (F_2). The frequency shift value of the sensor was obtained by the equation:

$$\Delta F = F_1 - F_2 \quad (2)$$

All measurements were performed at room temperature of 24 ± 0.5°C.

3. Results and discussion

3.1. Sensor's response sensitivities and selectivities

The TSM acoustic sensor coated with B15C5, B18C6, and DB30C10 were tested by exposure to 39 different organic solvent vapours. Their response sensitivities are listed in Table 1, showing that crown ethers are the efficient adsorptively active material for sensing of carboxylic acid vapours, in particular B15C5 possesses high sensitivity for formic acid vapour, which may be attributed to the formation of relatively strong hydrogen bonds RCOOH···O (crown ether) between carboxylic acid and crown ether resulting in greater adsorption than other organic solvents. With the molar mass of an acid molecule increased, the sensitivity of the sensor increases due to higher mass of individual molecule adsorbed on the coated TSM crystal. Similar regularity is true for other organic homologues of alcohol, ketone, acetate and aromatic hydrocarbon, etc., Fig. 2a–2c show that the sensitivity of the sensor response toward three carboxylic acid homologues in terms of the response curve slope has the following sequence: B15C5 > DB30C10 > B18C6. Compared with DB30C10 and B18C6, B15C5-coated sensor possesses excellent linear response characteristics for formic acid. It seems that this is due to monolayer adsorption, while possible multilayer adsorption might lead to non-linear responses to such species as acetic and propionic acids. B15C5 as the best adsorptively active material for the determination of formic acid vapour has taken as the subject of detailed investigation of the response characteristics of the TSM sensor of interest.

Table 1
Sensitivities of TSM acoustic sensor coated with crown ether exposing to different organic vapours

Organic compound (j)	Sensitivity (S_j, Hz mg^{-1} per l)[a]			Selectivity coefficient of B15C5 S_j/S_{HCOOH} (%)
	B15C5	B18C6	DB30C10	
Formic acid	47.18	19.92	38.62	100.00
Acetic acid	60.47	21.73	41.44	128.17
Propionic acid	105.30	22.09	59.30	223.19
Methanol	1.60	1.47	1.38	3.39
Ethanol	4.10	3.43	4.37	8.69
Propanol-1	4.50	3.90	4.40	9.54
Isopropanol	4.29	1.85	1.56	9.09
Butanol-1	7.11	6.93	4.53	15.07
Butanol-2	3.83	2.02	4.05	8.12
Isobutyl alcohol	6.31	6.32	4.21	13.37
Acetone	1.99	1.39	6.88	4.22
Butanone-2	3.28	2.44	2.72	6.95
Ethyl ether	1.60	1.52	2.79	3.39
Anisole	4.54	2.44	4.67	9.62
Phenetole	6.01	4.30	15.78	12.74
Tetrahydrofuran	3.18	2.35	5.30	6.74
Dioxane	8.56	4.82	9.13	18.14
1,2-Epoxy-3-chloropropane	4.91	2.62	6.34	10.41
Methyl acetate	0.43	0.30	0.59	0.91
Ethyl acetate	2.27	1.46	1.84	4.81
n-Propyl acetate	3.71	2.99	3.05	7.86
n-Butyl acetate	5.95	6.69	5.05	12.61
Ethyl propionate	4.59	4.21	4.78	9.73
Acetonitrile	4.26	2.65	3.00	9.03
Diethylamine	25.10	23.29	23.63	46.84
N,*N*-dimethylformamide	9.92	5.52	22.00	21.03
Pyridine	9.27	14.21	9.36	19.65
n-Hexane	3.58	3.76	4.04	7.59
Cyclohexane	3.31	3.52	4.56	7.02
Chloroform	3.61	1.37	6.42	7.65
Benzene	2.03	1.52	1.86	4.30
Toluene	3.82	4.25	3.37	8.10
o-Xylene	4.25	4.67	6.84	9.01
m-Xylene	1.98	4.76	8.05	4.20
p-Xylene	2.12	2.67	2.64	4.49
Ethylbenzene	3.94	1.61	4.70	8.35
Isopropylbenzene	4.78	5.79	8.50	10.13
Chlorobenzene	5.68	5.31	5.91	12.04
Nitrobenzene	6.31	5.54	4.19	13.37

[a] The coating mass of each crown ether was 12.5 μg.

For a TSM acoustic sensor, the selectivity coefficient (K_{ij}) for an organic species i with respect to interferant j may be simply defined as the ratio of corresponding sensitivities, i.e., $K_{ij} = S_j/S_i$. The selectivity coefficient of the B15C5 coated sensor for formic acid with respect to other organic compounds are given in Table 1. No significant interference is observed from organic solvent vapours such as alcohol, ketone, ether, ester, alkane, and aromatic hydrocarbon compounds except for some nitrogen containing compounds such as diethylamine, pyridine and *N*,*N*-dimethylformamide, and carboxylic acid homologues such as acetic and propionic acids.

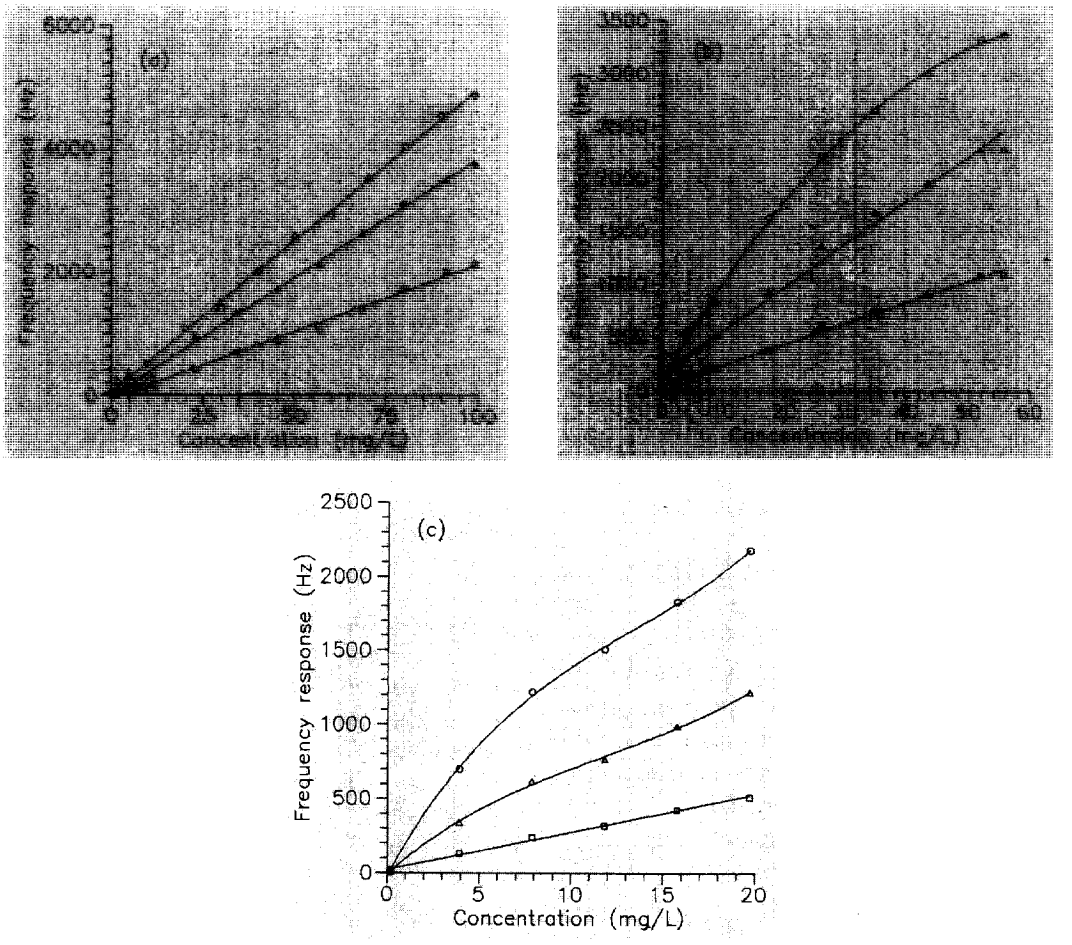

Fig. 2. The response curves of TSM acoustic sensors exposing to carboxylic acid vapours including; (a) formic acid; (b) acetic acid; and (c) propionic acid. The sensor surface was coated with 12.5 μg of B15C5 (○), B18C6 (□), or DB30C10 (△).

3.2. Relation between coating mass and linear response characteristics

The amount of B15C5 coated on the crystal surface had a significant influence on the linear response characteristics of TSM sensor for formic acid assay. The crystal with more B15C5 coated on its surface exhibited a larger frequency shift response for the same concentration of formic acid vapour. The optimum amount of B15C5 to be applied to the crystal was determined experimentally. Fig. 3 shows that the sensitivity of the B15C5 coated TSM acoustic sensor increases as the amount of the B15C5 coating increases due to an increased probability of interaction between the B15C5 coating material and the HCOOH molecules. One could not, however, take the full advantage of this phenomenon, as the increased amount of coating tended to lead poor linearity which seemed to be related to the thickness and homogeneity of the coating. The response curves of the TSM sensors coated with different amount of B15C5 exposing to formic acid vapour are shown in Fig. 4. It has been shown that about 12 μg of B15C5 coating is sufficient for obtaining satisfactory linear response characteristics. When TSM crystal with 12 μg of B15C5 coating was exposed to formic acid vapour, the linear response

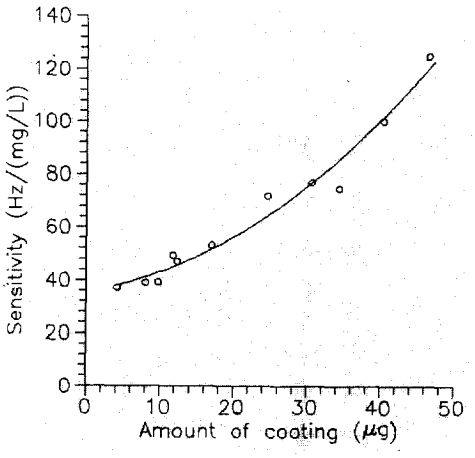

Fig. 3. Effect of coating mass on TSM sensor's sensitivity.

range of the sensor was 2.01 ~ 99.3 mg l^{-1} with the slope of 49.4 Hz mg^{-1} per l (24 ± 0.5°C), the regressive coefficient was 0.998 ($n = 12$). In addition, the same sensor could also be used for the determination of formic acid vapour of lower concentration. When the sensor was exposed to HCOOH vapour with the concentration of 0.100 ~ 2.01 mg l^{-1}, a roughly linear response could be obtained, though the regression line was

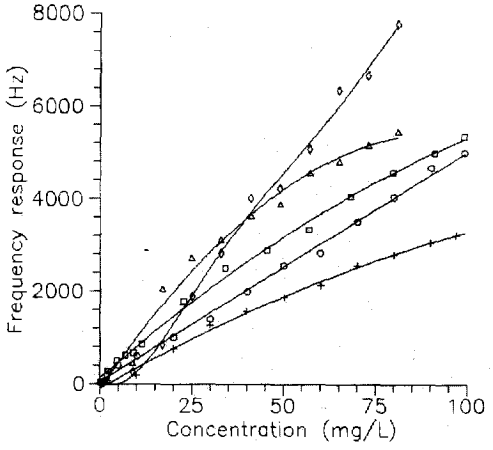

Fig. 4. The response curves of the TSM sensors coated with different amount of B15C5 exposing to formic acid vapour. Amount of coating are: 4.21 μg (+); 11.9 μg (○); 17.1 μg (□); 34.5 μg (△); and 40.5 μg (◇ >.

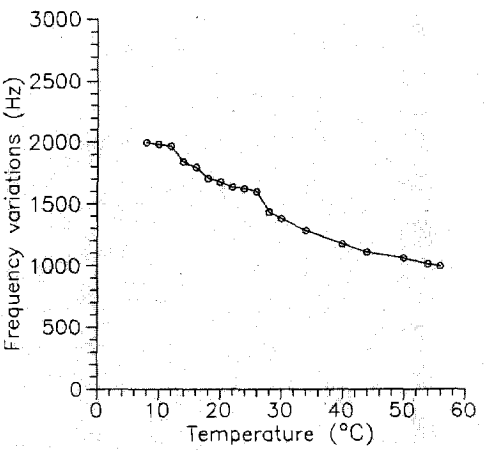

Fig. 5. Effect of temperature on the TSM sensor coated with 12 μg of B15C5 upon exposure to 30.1 mg l^{-1} HCOOH vapour.

only quasi-linear in this range and it was not the extrapolation of the aforementioned major lower concentration linear response range. The sensitivity in the lower concentration range was 103 Hz mg^{-1} per l (24 ± 0.5°C) with the regressive coefficient of 0.997 ($n = 11$), and the detection limit approached 0.0201 mg l^{-1} (equivalent to about 5.70 ppm, V/V).

3.3. Effect of cell temperature

The effect of temperature in the range of 8 ~ 56°C on the TSM crystal coated with 12 μg of B15C5 upon exposure to 30.1 mg l^{-1} HCOOH vapour is shown in Fig. 5. The frequency shift response decreased with increasing temperature from 8 to 56°C, indicating that the adsorption of HCOOH by the coating decreases with the increase of temperature. The variation of the sensor response within the temperature range from 18 to 26°C was relatively smooth. For all measurements in practical application, it is recommended that the temperature be controlled at 24 ± 0.5°C.

3.4. Influence of humidity

The effect of water vapour on the TSM sensor response was investigated in detail. Fig. 6 shows

the relation between relative humidity and the frequency shift responses when the TSM acoustic sensors coated with 11.9 and 12.4 μg of B15C5 were exposed to HCOOH vapours of different concentrations. The recorded lines were parallel to each other, which possessed good linearity with a slope of 3.84 ± 0.20 Hz/% RH ($n = 5$). The influence of moisture on the detection of HCOOH vapour seemed to be easily controllable.

3.5. Reproducibility and stability

The frequency response data of the TSM sensor coated with 12 μg of B15C5 alternatively (for nine times) exposing to HCOOH vapour of two concentrations of 10.0 and 20.1 mg l^{-1} are listed in Table 2. The relative standard deviations of the sensor response were 2.94% and 2.66%, respectively, showing that the sensor possesses good reproducibility for the determination of HCOOH vapour.

When the sensor was also exposed to 30.1 mg l^{-1} HCOOH vapour continuously for 3 h and the response data was recorded every 5 min, the standard deviation of the sensor response was ± 24.61 Hz ($n = 36$), the frequency drift of the sensor was less than ± 8.21 Hz/h (24 ± 0.5°C), showing that the sensor possesses good stability.

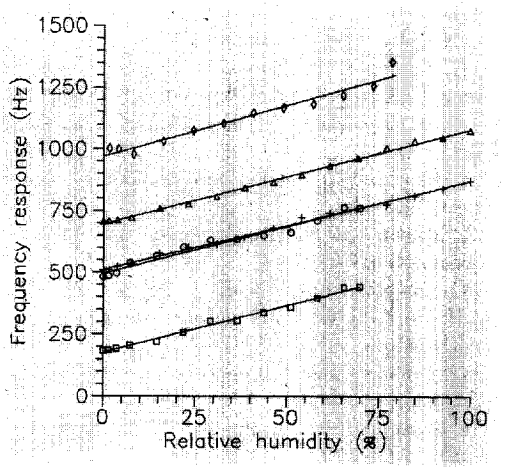

Fig. 6. Effect of relative humidity on the frequency response of the TSM acoustic sensor coated with B15C5: (i) 11.9 μg of B15C5: ○, [HCOOH] = 8.40 mg l^{-1}; △, [HCOOH] = 12.3 mg l^{-1}; and (ii) 12.4 μg of B15C5: □, [HCOOH] = 1.84 mg l^{-1}; +, [HCOOH] = 8.40 mg l^{-1}; ◇, [HCOOH] = 17.9 mg l^{-1}.

Table 2
Reproducibility of the TSM acoustic sensor coated with 12 μg of B15C5

No.	Frequency shift response (ΔF, Hz)[a]	
	10.0 mg l^{-1} HCOOH	20.1 mg l^{-1} HCOOH
1	622.66	1104.62
2	623.14	1109.23
3	613.60	1092.82
4	609.72	1104.07
5	604.94	1098.77
6	604.25	1096.70
7	573.99	1067.16
8	583.77	1109.63
9	584.47	1020.00
A.V.	602.28	1089.22
S.D.	17.70	28.97

[a] The sensor was alternatively exposed to low (left) and high (right column) HCOOH concentration samples.

3.6. Reversibility and useful lifetime

The response time of the TSM sensor coated with 12 μg of B15C5 was of the order of 2 min. When the HCOOH concentration was very low such as 0.2 mg l^{-1}, the sensor's response time was about 1 min. When the HCOOH concentration was very high such as 20.0 mg l^{-1}, the sensor's response time was about 3 min, as it took longer time for the adsorption of HCOOH vapour by the coating material to reach equilibrium. If the sensor was purged by dry nitrogen with the flow rate of 200 ml min^{-1}, it could restore to its initial coating fundamental frequency (F_1) in 2–4 min. The sensor seems to possess good reversibility. The sensitivity of the sensor decreased by 4.66% after 30 day continuous use. It decreased by 16.8% after 40 day continuous use. Therefore, the practical useful lifetime of the sensor was about 1 month.

3.7. Preliminary analytical application

The proposed sensor was applied to the determination of the HCOOH concentration in air

Table 3
Results of the determination of the formic acid concentration obtained by using the TSM sensor and by the acid–base titration method

HCOOH added (mg l^{-1})	HCOOH determined (mg l^{-1})[a]		Recovery of TSM sensor method (%)
	Acid–base titration method	TSM sensor	
1.00	1.03 ($\pm$0.03)	0.999 ($\pm$0.04)	99.9
2.00	1.97 ($\pm$0.08)	2.01 ($\pm$0.07)	100.5
3.00	3.04 ($\pm$0.09)	2.98 ($\pm$0.06)	99.3
5.00	5.08 ($\pm$0.04)	4.98 ($\pm$0.08)	99.6
10.00	9.85 ($\pm$0.06)	9.84 ($\pm$0.11)	98.4
20.00	19.58 ($\pm$0.05)	20.77 ($\pm$0.19)	103.8

[a] The data in the parenthesis are the standard deviations ($n = 4$).

with appropriate amount of HCOOH added, and the results were compared with those of acid–base titration method. Table 3 shows the results obtained by using the TSM sensor coated with 12 μg of B15C5 as well as by the acid–base titration method. The recovery of the TSM sensor method was from 98.4 to 103.8%, showing that the application of the proposed TSM sensor for monitoring HCOOH vapour in air is quite feasible. The accuracy of the sensor's method is comparable with that of the much more time-consuming chemical analysis method.

Acknowledgements

The work was supported by the National Natural Science Foundation of People's Republic of China and Electroanalytical Laboratory of Changchun Institute of Applied Chemistry, Academia Sinica.

References

[1] M. Sitting, Handbook of Toxic and Hazardous Chemicals, Noyes Publications, New Jersey, 1981, pp. 20, 343 and 571.
[2] E.R. Plunkett, Handbook of Industrial Toxicology, 3rd ed., Chemical Publishing Co., Inc., New York, 1987, pp. 3, 265 and 455.
[3] F.T. Weiss, Determination of Organic Compounds: Methods and Procedures, Wiley-Interscience, a Division of John Wiley & Sons, New York, London, Sydney, Toronto, 1970, pp. 63.
[4] D.C. Harris, Quantitative Chemical Analysis, 2nd ed., W.H. Freeman, New York, 1987, pp. 168.
[5] L. Groenbery, Y. Shen and J.A. Joensson, J. Chromatogr., 655 (1993) 207.
[6] B.J. Johnson, S.C. Huang, A. Wong and L. Yao, Microchem. J., 49 (1994) 78.
[7] D. Lagoutte, G. Lombard, S. Nisseron, M.P. Papet and Y. Saint-Jalm, J. Chromatogr. A, 684 (1994) 251.
[8] M. Pesez and J. Bartos, Talanta, 21 (1974) 1306.
[9] H.-H. Zeng, K.-M. Wang, X.-H. Yang and R.-Q. Yu, Anal. Chim. Acta, 287 (1994) 267.
[10] G.G. Guilbault, Handbook of Enzymatic Methods of Analysis, Marcel Dekker, New York, 1975, pp. 248.
[11] H. Li, J. Zhao and J.-Q. Deng, Chin. J. Anal. Chem., 23 (1995) 364.
[12] J.A. Munoz, J.L. Hidalgo and D. Garcia, Talanta, 40 (1993) 1725.
[13] J.A. Munoz, J.L. Hidalgo, D. Garcia and A.J. Fraidias, Talanta, 41 (1994) 159.
[14] G.G. Guilbault, Anal. Chem., 55 (1983) 1682.
[15] M.H. Ho, G.G. Guilbault and B. Reitz, Anal. Chem., 55 (1983) 1830.
[16] G.G. Guilbault and A. Lopez-Roman, Environ. Lett., 2 (1971) 35.
[17] T.E. Edmonds, M.J. Hepher and T.S. West, Anal. Chim. Acta, 207 (1988) 67.
[18] Z. Sauerbrey, Z. Phys., 155 (1959) 206.
[19] J. Hlavay and G.G. Guilbault, Anal. Chem., 49 (1977) 1890.
[20] J.J. McCallum, Analyst, 114 (1989) 1173.
[21] G.J. Moody, J.D.R. Thomas and M.A. Yarmo, Anal. Chim. Acta, 155 (1983) 255.

[22] K.-M. Wang, Z. Cao, H.-G. Lin, S.-H. Wang, B.-F. Wang and R.-Q. Yu, Analyst, 121 (1996) 259.
[23] K. Ren, Anal. Chim. Acta, 286 (1994) 197.
[24] R. Lucklum, B. Henning, P. Hauptmann, K.D. Schierbaum, S. Vaihinger and W. Göpel, Sens. Actuators A, 25–27 (1991) 705.
[25] S. Shinkai, M. Ishihara, O. Manabe, A. Mizumoto and Y. Osada, Chem. Lett., (1985) 1029.
[26] C.-J. Lu and J.-S. Shih, Anal. Chim. Acta, 306 (1995) 129.
[27] Z.-H. Huang, W. Xu, Y.-H. Xie, X.-Z. Lu and Y.-X. Lin, Huaxue Tongbao., 2 (1994) 41.

ELSEVIER

Talanta 44 (1997) 1423–1433

Talanta

Amberlite XAD resin solid-phase extraction coupled on-line to a flow injection approach for the rapid enrichment and determination of phenols in water and waste waters

Wen-lu Song [a], Zheng-liang Zhi [b,*], Lian-sheng Wang [a]

[a] *Department of Environmental Science and Engineering, Nanjing University, Nanjing 210093, People's Republic of China*
[b] *School of Chemical Engineering, Nanjing University of Science and Technology, Nanjing 210094, People's Republic of China*

Received 13 September 1996; received in revised form 3 January 1997; accepted 6 January 1997

Abstract

A novel and expeditious approach for direct determination of phenols in water and waste waters based on solid-phase extraction coupled on-line to a flow injection analysis (FIA) manifold is described. The method employs on-line preconcentration of the phenols in an acidified sample (pH = 2.0) onto a 3 cm × 3 mm column packed with Amberlite XAD-4 resin. The phenols are subsequently eluted from the resin into a flowing system with an alkaline solution (pH = 13) by actuating a switching valve; the eluted analytes were then quantified spectrophotometrically as the products of reaction with 4-aminoantipyrine (4-AAP) and potassium ferricyanide on passing through the flow-cell of a detector. The proposed method has a linear calibration range 0.01–1 μg ml^{-1} of phenol, with a detection limit of 0.004 μg ml^{-1} (S/N = 3) and a sample throughput of 12 h^{-1}, investigated with a 4.4 ml sample volume. The relative standard deviation is 2.4% for 0.2 μg ml^{-1} of the analyte. The sensitivity offered by the procedure was higher by a factor of 13 than that provided by a conventional flow injection analysis method. The analytical scheme of the proposed system is much simpler than its conventional manual counterpart due to the fact that it combines trace enrichment, sample clean-up, derivation and detection in one analytical set-up. The high speed, ease of use and automation, selectivity, and relative freedom from random contamination by sample handling make this method ideal for the phenols monitoring in water and waste waters. © 1997 Elsevier Science B.V.

Keywords: Amberlite XAD resin; Flow system; Phenols; Solid-phase extraction; Waste water

1. Introduction

Phenolic compounds are a sort of common and important water pollutants [1]. They are often taken up from waste waters discharged from a variety of industrial sources, e.g., the manufacture of dyes, papers, plastics, drugs and antioxidants. Phenol and its derivatives have been found toxic to most aquatic life and mammals, and could impart objectionable tastes and odors to both drinking water and fish even at very low concentrations; the adverse effects of phenols are even more hazardous when they are become chlori-

* Corresponding author. Fax: +86 25 4438513; e-mail: q1969130@public1.ptt.js.cn

PII S0039-9140(97)00018-0

nated. As a result, the maximum allowed levels of total phenolic compounds in a wide range of industrial wastes and natural waters are regulated by legislation in each country. The highest volatile phenols limits are normally set at a few ng ml^{-1}–sub-μg ml^{-1} range for different grades of environmental quality standards. For example, in China, maximum volatile phenols levels of 0.5 and 1 μg ml^{-1} are permitted for grade 1 and grade 2 standards of petroleum and chemical industrial effluents, respectively [2]. Hence, the development of new efficient assaying and monitoring methods for phenol and its derivatives in environmental waters to obtain reliable analytical data for regulatory and other purposes is of great interest.

A variety of analytical method for phenols determination have been established so far. Usually, chromatographic methods (HPLC [3,4] and GC [5,6], with or without derivation) are often applied for the selective determination of individual substituted phenols, but they normally involve solvent extraction for sample pre-treatment, which is complex, costly, time-consuming, and their use on-line for continuous monitoring or control is impractical. Electrochemical techniques such as cyclic voltammetry have also been used as suitable for the same purpose [7]. Spectrophotometric methods [8,9] are more conventionally and frequently employed for the determination of the sum of the compounds possessing a phenolic moiety (phenols index), among which the method based on the oxidative coupling of phenols with unblocked para-position and 4-aminoantipyrine (4-AAP) in an alkaline solution has been long-known. This method has been adopted by many countries as an approved official standard method for phenols assay [10,11]. While the method seems to be satisfactory, the procedure of which is rather complex and hazardous, and involves extensive sample clean-up processes such as stream distillation, liquid–liquid extraction, addition of masking agents etc., being time-consuming, tedious and sources of bias or accidental errors. Moreover, chloroform is used in color extraction in order to obtain desired sensitivity, which is expensive to disposal of and a major pollutant to the environment.

With the movement toward automation in phenols determination and monitoring, more and more research is being done with continuous flow systems in general and flow injection analysis (FIA) as coupled to continuous separation techniques such as distillation device and liquid phase extraction approach in particular [12–15]. These methods, however, have several limitations such as long start-up and line-out period, large on-line volume, low reproducibility etc., the sensitivity of the existing methods is not yet high enough to reliably measure phenols with concentration below a few parts per billion level in real samples; moreover, the use of chloroform is not avoided in most cases [13,14]. It is obvious that all these problems put serious constraints on the available phenols determination methods and that better analytical procedures are required.

Solid-phase extraction (SPE) appears to be a very promising alternative to the liquid–liquid extraction and related techniques, since it can be used for eliminating complex matrix and for trace enrichment [16]. The use of SPE for sample clean-up and enrichment of phenols from water for HPLC analysis, either in an on-line or off-line fashion, has achieved great success [17–21]. However, the combination of SPE and FI manifold is virtually exclusively related to the on-line enrichment of trace metal elements and species differentiations, as reviewed by Welz [22].

In a recent paper, Frenzel, et al. [23], have developed an FI method using solid sorbent (C_{18} bonded silica material) to retain the imine product of the oxidative coupling between phenols and 4-AAP, which is located in a flow-cell of on-column optical detector or in a mini-column in front of the detector. The sensitivity achieved is greatly enhanced due to the fact that all colors formed in the flow system was concentrated to a very small area of the support that was monitored in-situ by the detector or eluted to pass through the detector cell by a discrete volume of methanol. However, since the solid-phase absorbent located downstream of the reaction coil, it also retained the color formed by aromatic amines and related interfering substances. So the interference problem inherent in the standard method system was not efficiently eliminated there.

This paper describes a new FIA assembly with on-line SPE for phenols determination suitable for laboratory and field analyses. The aim of the present study is to develop a method being able to directly and accurately determine concentrations of the analyte over a range which spans the discharge consent levels, i.e., a few ng ml^{-1} to low μg ml^{-1} range. We have combined the simple chemistry of 4-AAP method with the ease of automation of flow injection analysis and the preconcentration abilities of Amberlite XAD-4 resin column. The sample is introduced by a volume-based injection fashion, and a mini-column loaded with Amberlite XAD-4 resin which is inserted into the FIA manifold is used for implementing trace enrichment and for undesired sample matrix removal, simultaneously. By introducing a relatively large sample volume, phenols are enriched onto the column from an acidified sample (pH = 2). Aromatic amines, dissociated at this pH, are not adsorbed by the resin, so they are isolated from the analytes; other inorganic substances are removed as well at this stage, rendering the procedure nearly specific toward the analyte. The elution is effected by taking advantage of the ionization properties of the phenolic compounds. By using a NaOH solution of pH 13.0, rapid and complete desorption can be achieved, so no organic solvent is required. The proposed procedure does not require complicated instrumentation and the operation is simple and fast. A critical evaluation of the optimal conditions for operation of the proposed method is present here with special emphasis on sensitivity, selectivity, responsibility to various phenol derivatives, and comparison of results provided by the proposed method and its manual standard counterpart for real sample analyses.

2. Experimental section

2.1. Apparatus

A Gilson Minipuls-2 peristaltic pump (France) was used throughout the investigation. A syringe was used for loading sample into the loop of an injection valve manually. A 756-UV/Vis spectrophotometer (Yixing, China) furnished with a Hellma 178.12 QS flow cell (18 μl inner-column, 10 mm path-length) and connected to an XWT-104 chart recorder (Shanghai, China) was used for absorbance measurements and for resulting transient FI signals recordings. One Rheodyne 5041 six-way injection valve fitted with a sample loop (volume adjustable) and another eight-port low-pressure rotary valve modified to a switching valve that fitted with two XAD-4 resin columns of the same dimensions were also used.

Teflon tubing of 0.8 mm (i.d.) was used to construct the flow manifold except sample loop was made of Tygon pumping tubes. Pumping tubes of various diameters were made of Tygon.

2.2. Reagents

All reagents used in this study were of analytical reagent grade and used as received. Water used was deionized distilled one. Carrier solution was of HCl solution at pH 2 unless notified especially. Eluent was of 0.1 M NaOH (pH = 13).

Stocking phenol solution and standard working solutions. Stocking solution containing 1000 μg ml^{-1} was obtained by initial dissolution of accurately weighed 1 g phenol (Shanghai Chemical Reagent Company) in a few ml of 1 M NaOH solution and diluting to 1000 ml with water. It was stored in a refrigerator at 4°C and was stable for at least 2 weeks. Standard working solutions of various concentrations were prepared daily by appropriate dilutions of aliquots of the stock with HCl solution at pH 2. Other phenolic compounds tested in this study were prepared similarly using commercially available products.

R_1-color reagent. 4-aminoantipyrine, 1.0 g (Shanghai Chemical Reagent Company) was dissolved in 1000 ml buffer solution.

Buffer solution (pH 8.5). A buffer solution of pH 8.5 was prepared by dissolving 10.7 g NH_4Cl and 4.0 g NaOH in 980 ml of water, the pH of which was carefully adjusted by adding a few ml of 1 M HCl or 1 M NaOH solution; the solution was made up to 1000 ml.

R_2-oxidant. 2.0 g of $K_3Fe(CN)_6$ (Shanghai Chemical Reagent Company) was dissolved in 1000 ml of water, a few drops of 1 M NaOH was added to adjust the pH to 11.0.

2.3. Column preparation

Amberlite XAD-4 resin was purchased from Fluka (Rohm and Hass) at 20–40 mesh, it was then ground and sieved to get 40–80, 80–120, and over 120 mesh, respectively, for testing. Glass tubes of 3 mm i.d. were cut into pieces of 2.5, 3.5 and 5.5 cm long. A typical procedure for the 3.0 cm long column preparation was as follows: to one end of the column a small glass wool plug was inserted, a water–ethanol (2:1) slurry of XAD-4 resin was then aspirated into the column to obtain a 3 cm long resin bed. A second portion of glass wool was plugged to another end to embed the loaded resin in order to prevent material losses. The column was connected with Teflon tubings (i.d. = 0.8 mm) and integrated into the FIA system, short pieces of suitable Tygon pumping tubes were used as connecting sleeves. The column so prepared was filled with water–methanol (2:1), any air bubbles possibly existed in the resin bed should be carefully driven out at this step. It was further washed successively with methanol, water, 0.01 M HCl, water, 0.01 M NaOH and water to remove impurities, and was made ready for FIA use. All columns thus remained serviceable for at least 4 months. The columns with 2.0, 3.0 and 5.0 cm length packed with different granularities (40–80, 80–120, over 120 mesh) of resin were made and tested in this study.

2.4. Sample pre-treatment

Water samples should be analyzed shortly after their collection (normally less than 4 h); otherwise, they should be stored at 4°C to minimise the possibility of biodegradation of the phenols. First, 100 ml of water was passed through a glass microfiber filter (Whatman) to remove any suspended particles; the clear filtrate was then adjusted to pH 2.0 using a few drops of 12 M HCl, and made ready for injection. For colored waste water sample, however, a predistillation step as described in [10] is recommended prior to analysis.

2.5. Manifold and proce dures

In Fig. 1, a schematic outline for the on-line solid-phase extraction/FIA manifold is given. The manifold consisted of two distinct blocks, namely, the preconcentration/separation unit for sample pretreatment and the flow assaying system for the phenols determination based on the 4-AAP method. The former was used to accomplish trace phenols enrichment and bulk sample matrix separation simultaneously. It was constructed from one peristaltic pump which produced the flow rates depicted in the manifold, and a Rheodyne 5401 six-port injection valve fitted with a 4.5 ml sample loop, a eight-port low pressure Teflon rotary valve accommodated two XAD-4 resin columns of the same dimensions in the two loops. The sample loading flow rate selected here was 1.8 ml min^{-1}. A flow-rate above this value is not recommended because the back-pressure from the column which is increased with the increase of flow rate may make the peristaltic pump difficulty to keep a constant value of the flow rate. Fig. 1 also shows the two positions the eight-port valve can take: one for retention and the other for elution. In the remainder of the manifold, the effluent from the preconcentration column was first confluenced with a 4-AAP (in buffer of pH 8.5) stream (denoted by R_1 in Fig. 1), then subsequently merged with an oxidant stream ($K_3Fe(CN)_6$, denoted by R_2 in Fig. 1). The high flow rate ratio of eluting stream to R_1 and R_2 (1.8:0.4:0.4) was chosen to minimise the diluting of the sample plug. The dye thus formed along reactor coil (RC) was monitored by a spectrophotometer at $\lambda = 490$ nm on passage through the flow cell. Peak height was used for the analytical measurements.

The operational scheme was as follows: in the first step, SV was set to loading position for column 1, elution position for column 2. The water sample or standard solution, containing 0.01–1.0 μg ml^{-1} of phenols at pH 2.0, was injected into the carrier stream of the flow system via injection valve (IV). The injected sample was thus driven and passed through the column 1, where adsorption of phenols took place, and the sample matrix was driven to waste on leaving the

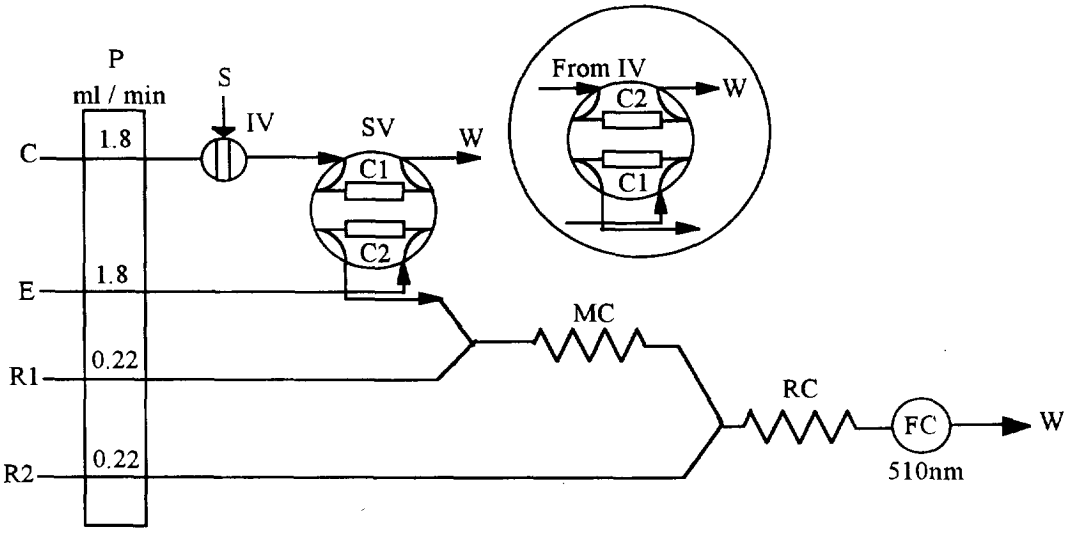

Fig. 1. Experimental setup for the direct enrichment and determination of phenols in water and waste waters with solid-phase extraction coupled on-line to a flow injection analysis system. Insert denotes the another valve position of SV. S, sample; C, carrier (HCl solution of pH 2.0); P, four channel peristaltic pump; W, waste; IV, injection valve; SV, switching valve fitted with two columns loaded with XAD-4 resin; FC, spectrophotometer fitted with a flow-cell; MC, 30 cm long mixing coil; RC, 60 cm long reacting coil; E, eluent (pH 13.0); R_1, 0.1% 4-AAP solution in buffer of pH 8.5; R_2, 0.2% $K_3Fe(CN)_6$ solution (pH 11.0).

column. Meanwhile, the eluting stream of pH 13.0 was pumped to flush column 2 continuously and merged to the phenols determination flowing system to give rise to a base-line zero-set on continuous passage through the detector cell. In the second step, SV was turned to eluting position for column 1, loading position for column 2; the eluent (0.1 M NaOH) back-flushed column 1 to desorb the phenols from resin and swept the analytes to the reaction and determination flowing system for measurement, within ca. 1.0 min, the eluted analyte is detected as a peak at the spectrophotometer and is quantified. Simultaneously, while column 2 was flushed by an acidified carrier, and the loop of IV was filled with the next sample, the loaded sample was injected into carrier and passed through column 2. After the signal of previous sample fell to the baseline, SV was switched again and the desorption of column 2 occurred, allowing the start of a new determination cycle.

3. Results and discussion

The chief advantage of the manifold used (Fig. 1) is that both trace enrichment and sample clean-up processes, as well as the determination procedures, were accomplished in the same setup. Adjustment of the sample pH to a suitable value enabling minimization of interference substances retention and maximization of retention of the analytes on the resin column is a key strategy for sensitive and selective determination of the analytes. To optimize the system, main efforts were focused on the conditions for sample loading and phenols eluting from the column, as well as the analytical flow system which was coupled on-line with the preconcentration and separation unit in order to obtain highly sensitive, accurate and reproducible results with minimal sample handling and maximal possible sample throughput.

Table 1
The analytical signals obtained at different sample pHs (phenol = 0.5 μg ml^{-1})

Sample pH	1	3	5	8	10	11	12	13
Signal (absorbance)	0.29	0.29	0.29	0.29	0.25	0.16	0.10	0.02

3.1. Preconcentration and separation system

3.1.1. Selection of the absorbent

The use of solid-phase sorbents as concentrating agents to adsorb and separate phenolic compounds from sample matrix has been well-documented. Commonly used sorbents are charcoal, alkylsilane-modified silica, macroreticular porous polymers. According to Galceran et al. [24], poly-(styrene-divinylbenene) (PS-DVB) offers better retention and selectivity for polar aromatic compounds such as phenols than C_{18} bonded silica, while Amberlite XAD resins is typical material of the former. In a previous paper [25], we have investigated the phenol collection efficiency of different types of XAD resins in terms of their breakthrough volume, and found XAD-4 resin offers the best sample capacity, the resin was then chosen in this study. In order to optimize the preconcentration and separation processes, we have studied the effects of sample pH, resin size, column length, and loading rate on the adsorption of phenols from water onto the resin.

3.1.2. Sample pH

The sample pH for the system was determined to satisfy two criteria: maximization of retention of the analytes and minimization of interferents retention on the column. Thus, the effect of varying the sample pH over the range 1–13 was studied by using a 3 cm × 3 mm column packed with 80–120 mesh XAD-4 resin, a standard solution of 0.5 μg ml^{-1} of phenol and a solution containing 1000 μg ml^{-1} of aniline was used separately at a loading flow rate of 1.8 ml min^{-1}. The results obtained are shown in Table 1. We found that the pH range for optimal phenol uptaking was at 1–10, at pH values above 10.0, the signals decreased obviously, and at pH 13.0, no retention of phenol on the column was observed, which fitted well to that reported previously [25]. While another test using 1000 μg ml^{-1} of aniline showed that the positive interference from this interferent decreased with decreasing sample pH; the effect was canceled at a sample pH below 3.0. Thus, in order to eliminate the aromatic amines and related substances, which are ionized and hence not retained on the resin at a low pH, a sample of pH 2.0 was chosen, and the same value was adopted for the carrier accordingly (washing cycle).

3.1.3. Column length and resin granularity

An optimal inside diameter of ca. 3.0 mm was adopted throughout according to Resing and Mottl [26]. Our initial experiments with a 10 cm long column packed with commercially available XAD-4 resin in the particle size range 20–40 mesh indicated there was less than 10% phenol uptake (recovery) when a 4.5 ml standard phenol solution (1.0 μg ml^{-1}) passed through the column at conditions mentioned above, possibly due to the channelling of water flow in the column and the short contact time between the resin and the sample containing phenols. This prompted us to test the ground resins as the absorbents for phenols enrichment. Thus, we constructed three columns of different lengths (2, 3 and 5 cm bed length), using 40–80, 80–120 and over 120 mesh XAD-4 resin, respectively, to assess the effect of column length and resin granularity on the retention of phenol. We evaluated the characteristics of these columns with respect to the sample capacity. The results are showed in Fig. 2. The data indicated that more sensitive with smaller granularity for phenol determination, however, due to high pressures produced during sample loading for an over 120 mesh resin column, which might influence the loading flow rate, an 80–120 mesh resin was preferred for further investigations. Fig. 2. also shows that a longer column resulted in a slightly reduced signal, indicating no break-

through occurred during sample loading. The reducing of the signal when a longer column was used compared with a shorter one (5 cm versus 3 cm) was believed to be a result of dispersion, but too short a column ($\leqslant 2$ cm) also resulted in the reduction of the signal, thus we have subsequently adopted a target column (3 cm) for all further studies.

3.1.4. Sample volume and washing time

In this study, we have selected a sample volume of 4.4 ml, a loading flow rate was set at 1.8 ml min^{-1}, thus it took ca. 2.5 min (taking into consideration the sample dispersion in the carrier and column) for complete concentrating the phenols onto the resin. With respect to the matrix removal, another 1.5 min washing period was kept in order to wash out the sample matrix and undesired co-existing interferents; adding a loop-loading time of ca. 1 min, a total period of 5 min was required before it was turned to eluting position. As mentioned above, two identical columns were equipped in the manifold allowing them to be operated in an alternative fashion, thus the time required for elution was overlapped with the loading time, resulting in an estimated sampling throughput of 12 h^{-1}.

3.1.5. Elution

According to literature [16], the adsorbed phenols could be recovered by elution with an organic solvent such as methanol, ether, acetone, ethyl acetate etc. However, in this study, we found these solvents were unsuitable for the system, since they provided abnormal signals resulting from the refractive disturbances when an interface between the continuously flowing organic solvent stream and the interstitial water volume present in the column passed through the detector cell. Thus, we tried to elute the adsorbed phenols from the resin using an aqueous solution of appropriate pH. The effect of the eluent pH was studied by varying this parameter at a range of 11–13, which were adjusted with 1 M NaOH solution. It was found that, at pH 11, the peak signal had a long tail, about 3 min was required for the signal to return to baseline, indicating the slow elution kinetics, moreover, low sensitivity was obtained; at pH 12.0, the peak was yet much wide; at pH 13.0, the peak became narrow, the signal returned to baseline within 40 s, and the sensitivity obtained was the highest. An eluent with pH 13.0 was adopted for rapid and sensitive measurement as a result. An eluent with pH higher than 13.0 was not recommended because it gave rise to a noise baseline.

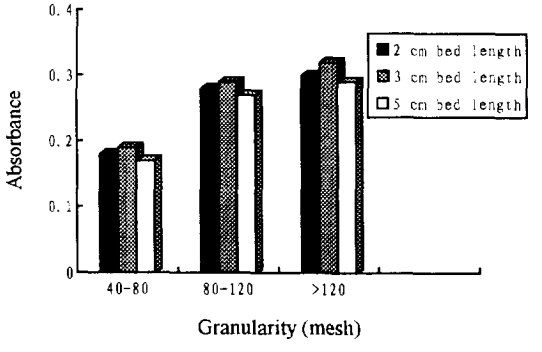

Fig. 2. Influence of the resin bed length and resin granularity on the determination of phenols. [phenol] = 0.5 μg ml^{-1}; sample volume = 4.4 ml.

3.2. Optimization of the flow analysis system

The effects of chemical and flow variables of the 4-AAP based flow system was similar to those observed in a normal FIA and independent of the sample treatment unit used. Consequently, such variables were optimized by using a three-channel flow injection manifold similar to that reported by Moller and Martin [13], except that a carrier was of an aqueous solution with pH 13.0, according to the eluting conditions as discussed above.

3.2.1. Oxidant (R_1)

$K_3Fe(CN)_6$ and $Na_2S_2O_8$ were tested in the concentration range of 0.1–2% (w/v) and 0.1–5% (w/v), respectively. When $Na_2S_2O_8$ was used as the oxidant, it provided less sensitive and reproducible results and very high concentration (saturated solution) was required for the maximal signal; while $K_3Fe(CN)_6$ was more conveniently adopted to give higher sensitivity. We found, at room temperature, MC = 30 cm, RC = 60 cm, and at a reasonably low concentration of the

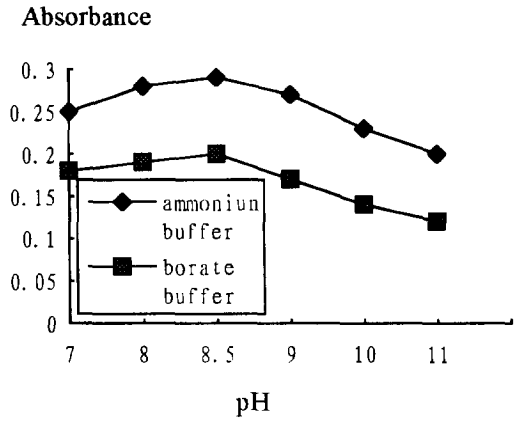

Fig. 3. Influnce of the buffer compositions and pH on the sensitivity for phenol determination. [phenol] = 0.5 μg ml^{-1}; NH_4Cl and borate: 0.2 M.

oxidant (0.2%, w/v), the reaction got complete shortly. A higher concentration resulted in no further increase of sensitivity, so a 0.2% $K_3Fe(CN)_6$ was preferred for great sensitive and reproducible results.

3.2.2. 4-AAP concentration

The effects of 4-AAP concentration was studied by varying it from 0.025 to 0.4%. It showed that the signal increased with the increment of 4-AAP concentration until 0.1%, after which, the sensitivity decreased slightly. It might be caused by the reaction between excess 4-AAP and the oxidant, leading to a high background absorbance. So a 0.1% 4-AAP concentration in buffer was set.

3.2.3. Buffer

According to literature, the optimal pH of the buffer must keep at 10.0 ± 0.2 in order to obtain reproducible results and keep interference minimum. The lower buffer pH used here (pH 8.5) is driven by the need to compensate the higher pH of the effluent containing the analyte. We have tested two kinds of buffers, $H_3BO_3 + NaHCO_3$ and NH_4Cl-$NH_3 \cdot H_2O$ at different composition concentrations. We found the optimal pH of buffer to be 8.5, but signal responses obtained by using ammonium buffer was generally higher than that when borate was used as a buffer, as shown in Fig. 3. A buffer containing 0.2 M NH_4Cl-$NH_3 \cdot H_2O$ (pH 8.5) proved to give the best reproducible results and highest sensitivity, the value was adopted as a result.

3.3. Response of phenolic derivatives

The response of the 4-AAP method to other phenolic compounds was the subject of several investigations [13,15]. The response factors of various phenol derivatives using 4-AAP in FI approach reported in literature are quite controversial. Moller and Martin reported that the relative responses of substituted phenols with respect to the phenol response were considerably lower under FIA dynamic conditions compared with the conditions of the manual assay [13]. Frenzel et al. argued that the response factors obtained under FIA conditions were almost identical with the literature values [15]. Our system differs with Frenzel only in that an on-line solid-phase extraction column was introduced in our manifold. Since the column uptake might show different kinetics for a variety of phenols, it is therefore of interest to re-exam how substituted phenols would be taken up on the column and reacted under the flowing condition compared with the available standard manual assays and normal FIA counterpart. Results of our studies are shown in Table 2, which indicates that the relative response of substituted phenols in percent with respect to the phenol on an equimolar basis by the proposed method is compared favorably with those obtained under both a standard manual method and a normal FIA method, except that the data provided by *o*-amino-phenol were generally lower for the proposed method compared with that of normal FIA without prior distillation, this was due to the presence of additional amino group in the parent compounds that were ionized at low pH (pH 2), thus was not extractable at all on the solid absorbent. Nevertheless, when a standard method including prior distillation procedure was applied, the result obtained agreed well with that provided by the proposed method.

Table 2
Comparison of response factors obtained for various phenols

Compound	Response (%)		
	Normal FIA	Proposed method	Standard method
Phenol	100	100	100
o-Chlorophenol	94	93	92
m-Chlorophenol	92	92	91
o-Cresol	88	85	85
m-Cresol	85	86	86
Salicylic acid	26	24	21
o-Nitrophenol	25	24	22
1-Naphthol	56	55	56
o-Aminophenol	55	<1	<1[a]

[a] With stream distillation.

3.4. Study of interferences

Some major inorganic and organic species usually present in water and waste water were studied as potential interferents with the phenol determination in order to testify the interference eliminating capability of the on-line solid phase extraction manifold. The limits were taken as the largest amount of foreign species yielding a relative error (with respect to pure standard phenol of 0.5 μg ml^{-1}) less than ± 5% in the peak height. Table 3 shows the tolerated limits for interferents accompanying phenol of 0.5 μg ml^{-1} using the proposed method and normal FIA. It allows us to conclude that almost none of the ions and common species tested at their usual concentrations in natural or treated waste waters interfered with the detection. While at least five kinds of species, i.e., aromatic amines, sulfide, sulfite, hypochlorite, and nitrite, were reported to be potential interferents in the standard method, which are normally eliminated by prior distillation at an acidified condition.

The lack of interferences exhibited in the proposed method is due to the adoption of a preconcentration and separation column as described above. When sample is adjusted to pH 2.0, interferents such as aromatic amines, if present in a given sample, may be dissociated and hence not retained onto the XAD column; other inorganic substances like sulfide, sulfite etc., are impossible to be retained on a non-ionic copolymer, XAD resin, they are feasibly removed during loading and washing cycles, and thus do not interfere at reasonably high concentrations. An exception was that when a colored sample is to be analysed, a predistillation step is yet required due to the color of bulk sample matrix would be irreversibly retained on the column and then interfere with the separation and detection.

Table 3
Study of interferences with the determination of 0.5 μg ml^{-1} of phenol by proposed method and normal FIA

Interferent	Normal FIA (ppm)	Proposed method (ppm)	Interferent	Normal FIA method (ppm)	Proposed method (ppm)
Aniline	<5	>500	PO_4^{3-}	20	>2000
3-nitro-aniline	<100	>2000	CO_3^{2-}	20	>2000
2,5-dichloroaniline	<10	>1000	NO_3^-	20	>2000
4-chloroaniline	<100	>2000	ClO^-	<1	50
3-amino phenylformic acid	<10	>1000	Zn^{2+}	<1	>1000
2-aminophenylamine	<1	>100	S^{2-}	<1	40
3-aminophenylamine (above added as R-NH_3^+ Cl^-)	1	>100	SO_3^{2-}	<1	40
Ca^{2+}	15	>2000	Fe^{3+}	10	>2000
Mg^{2+}	15	>2000	Fe^{2+}	10	>2000
Cu^{2+}	<1	>1000	NO_2^-	5	500
NH_4^+	20	>2000			

3.5. Calibration curves, detection limit and repeatability

When a sample volume of 4.4 ml was adopted, a calibration curve obtained could be expressed by a linear regression equation: $A = 0.547\ C\ (\mu g\ ml^{-1}) + 0.026$ ($n = 8$, $r = 0.993$, S.E. $= 7.35 \times 10^{-3}$), where A is the measured signal in absorbance; C the concentration of the analyte; n the number of standard samples tested; r the regression coefficient; and S.E. the standard error. The peak height obtained was proportional to phenol concentration from 0.01 to 1 $\mu g\ ml^{-1}$; the precision or repeatability, expressed as relative standard deviation (r.s.d.), was 2.4% ($n = 11$) for 0.2 $\mu g\ ml^{-1}$ of phenol standard solution. The detection limit was estimated to be 0.004 $\mu g\ ml^{-1}$ (S/N = 3). For comparison, we also constructed a normal FIA manifold which was similar to that reported by Moller and Martin [13] for phenol determination. A sample injection volume of 300 μl was set. We obtained a linear regression equation: $A = 0.0418\ C\ (\mu g\ ml^{-1}) + 0.012$ ($n = 8$, $r = 0.9997$, S.E. $= 8.16 \times 10^{-4}$); the calibration linear range was 0.05–15 $\mu g\ ml^{-1}$ of phenol; a detection limit of 0.02 $\mu g\ ml^{-1}$ and a r.s.d. of 2% were obtained. Thus, it could be concluded that a 13-fold increase of sensitivity compared with the normal FIA is achieved for the proposed method in which an on-line preconcentration and separation step was included, while repeatability is comparable with that of normal FIA.

3.6. Analysis of water and waste water samples

The ultimate test of the proposed method was to apply it to the analysis of real samples, so ten different local environmental water samples (including six industrial waste waters, three river waters, and one tap water) were tested in three different ways, i.e., the proposed method, normal FIA method, and approved standard manual method [10]. The correlation of phenols results obtained with the normal FIA and the approved standard method, as shown in Fig. 4a, yield $r = 0.940$, with an intercept of 0.19 ± 0.03 and a slope of 1.88 ± 0.10, indicated the results provided by the normal FIA method were generally higher,

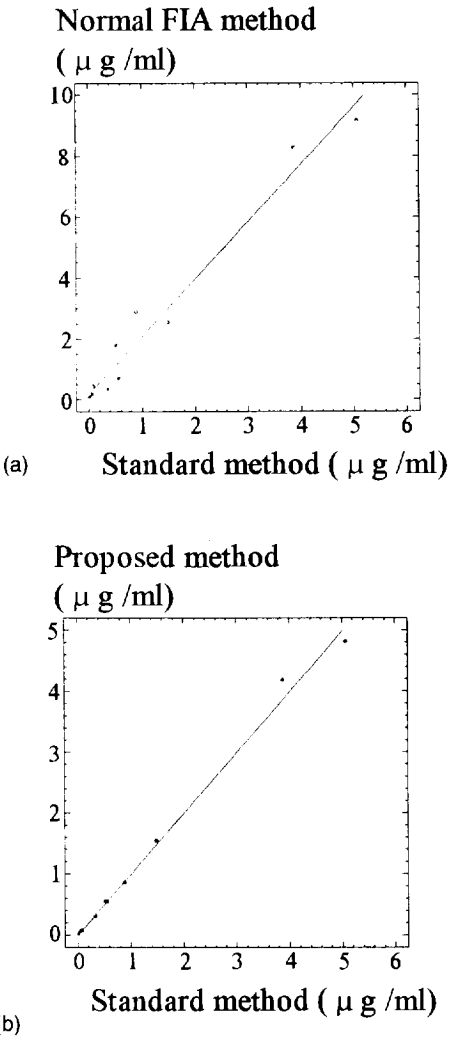

Fig. 4. Comparison of the phenols values measured by normal FIA method (4a), proposed method (4b) and a standard method for real samples.

thus suggesting the presence of systematic errors [27]. This is believed to be the results of interferences existing in the sample matrices contributing to the phenol index. While the correlation of phenols analyses by the proposed method and the approved official standard manual method, as shown in Fig. 4b can be described by a linear regression equation with a slope of 0.994 ± 0.027, an intercept of 0.0012 ± 0.0563, and a regression coefficient $r = 0.997$, which testifies the consis-

tency between two methods. Thus, it allows us to conclude that the proposed method could be reliably applied to the real sample analyses and provide the results in good agreement with those provided by the approved official standard method.

4. Conclusion

Flow injection with on-line solid-phase extraction approach resulted in significantly enhanced sensitivity and selectivity for the phenol index determination. It could provide the results in less than 5 min from sample introduction, which was ideally suitable for large-scale screening and on-site routine monitoring the trace pollutants in water and waste water samples. Detection limit achieved is similar to or better than that of the available standard method, even with liquid extraction. The method allows one to directly enrich and quantify phenols in a variety of waters in the presence of relatively high concentrations of interferents. It could eliminate pretreatment procedures such as distillation or extraction, which is required by other conventional methods due to the integration of the trace enrichment and sample clean-up into a single analytical scheme in an on-line fashion. The use of large quantities of expensive and environmentally harmful organic solvents is also avoided. We have found that the sensitivity for phenols essay was benefited from the using of a smaller particle size of the resin, but was worth nothing to use a longer preconcentration column. We also found that the major phenol derivatives have the response factors agreed well with those of available standard method.

Acknowledgements

The authors would like to thank Prof. Tian Liching from Center of Material Analysis of Nanjing University for providing instruments and Prof. Zhang Quanxing for providing treated waste water samples. The financial support of the Jiangsu (China) Science and Technology Committee is gratefully acknowledged.

References

[1] J.W. Moore and S. Ramamourthy, Organic Chemicals in Natural Waters–Applied Monitoring and Impact Assessment, Spring-Verlay, New York, 1984.
[2] Chinese National Standards, Effluent Standards for Pollutants from Petroleum and Chemical Industry, GB 4281–84, 1984.
[3] O. Busto, J.C. Olucha and E. Borrull, Chromatographia, 32 (1991) 566.
[4] L.J. Magee and J. Osteryoung, Anal. Chem., 62 (1990) 2625.
[5] H.J. Nea, W. Ziemer and W. Merz, Fresenius' J. Anal. Chem., 340 (1991) 65.
[6] H.D. Winkeler and K. Levsen, Fresenius' J. Anal. Chem., 334 (1989) 340.
[7] F. Canete, A. Rios, M.D. Luque de Castro and M. Valcarcel, Anal. Chim. Acta, 214 (1988) 375.
[8] H.O. Freietad, D.E. Ott and F.A. Gunther, Anal. Chem., 41 (1969) 1750.
[9] T.R. Crompton, Determination of Organic Substances in Water, Vol. 2, Wiley, Chichester, 1985, pp. 149–189.
[10] A.E. Greenberg (Ed.), Standard Methods for the Examination of Water and Waste Water, 15th edn., American Public Health Association, Washington, 1980.
[11] British Standards Institution, British Standard, 1 356 068, Section 2.12, 1990, p. 12.
[12] A.E. Goodwing and J.L. Marton, Anal. Chim. Acta, 152 (1983) 295.
[13] J. Moller and M. Martin, Fresenius' Z. Anal. Chem., 327 (1988) 728.
[14] C. Kwode, R. Voigtlander and K. Cammann, Fresenius' Z. Anal. Chem., 342 (1992) 426.
[15] W. Frenzel, J. Frenzel and J. Moeller, Anal. Chim. Acta, 261 (1992) 253.
[16] C.F. Poole and S.K. Poole, Chromatography Today, Elsevier, Amsterdam, 1991.
[17] D. Puig and D. Bareed, Chromatographia, 40 (1995) 435.
[18] E. Pocurull, M. Calull, R.M. Marce and F. Borrull, Chromatographia, 38 (1994) 579.
[19] L. Schmidt, J.J. Sun, J.S. Fritz, D.F. Hagen, C.G. Markell and E.E. Wisted, J. Chromatogr., 641 (1993) 57.
[20] J. Lehotay, M. Baloghova and S. Hatrik, J. Liq. Chromatogr., 16 (1993) 999.
[21] R. Infante, C. Gutierrez and C. Perez, Water Sci. Technol., 26 (1992) 2583.
[22] B. Welz, Microchem. J., 45 (1992) 163.
[23] W. Frenzel and S. Krekler, Anal. Chim. Acta, 310 (1995) 437.
[24] M. Teresa Galceran and O. Jauvegue, Anal. Chim. Acta, 304 (1995) 75 and references cited therein.
[25] Z. Zhi, A. Rios and M. Valcarcel, Analyst, 121 (1996) 1.
[26] J.A. Resing and M. Mottl, Anal. Chem., 64 (1992) 2682.
[27] J.C. Miller and J,N. Miller, Statistic for Analytical Chemistry, Ellis Horwood, Chichester, 2nd edn., 1988.

ELSEVIER

Talanta 44 (1997) 1435–1439

Talanta

Immobilization of uricase to gas diffusion carbon felt by electropolymerization of aniline and its application as an enzyme reactor for uric acid sensor

Shunichi Uchiyama *, Harukuni Sakamoto

Department of Environmental Engineering, Saitama Institute of Technology, 1690 Fusaiji, Okabe, Saitama 369-02, Japan

Received 28 August 1996; received in revised form 31 December 1996; accepted 3 January 1997

Abstract

Electropolymerizations of aniline and pyrrole solutions containing uricase at a neutral pH was performed to immobilize the enzyme on the surface of the gas diffusion carbon felt, and a selective uric acid sensor was fabricated by combining immobilized enzyme carbon felt and an oxygen electrode with oxygen gas permeable membrane. This carbon felt has a desirable feature for uricase sensing because an extremely efficient supply of oxygen for the enzymatic reaction can be realized due to its porosity permitting a transfer of oxygen. The current response time required from when sample is added until when current reaches the steady-state value is < 5 min. The calibration graph of uric acid showed a linear line in a concentration range from 1×10^{-5} to 4×10^{-4} M with a detection limit of 4×10^{-6} M. © 1997 Elsevier Science B.V.

Keywords: Aniline; Pyrrole; Uricase; Carbon felt

1. Introduction

Recently, an electropolymerization technique has been used to prepare the enzyme electrode [1–5]. In general, it is well known that an electropolymerization film is produced on the surface of electrode material such as glassy carbon, carbon paste or noble metals (Pt, Au) by electrooxidation of monomers such as pyrrole or aniline. Most of these electrodes can detect the reduced form of the enzyme, the electroactive enzymatic reaction product such as hydrogen peroxide or the consumed oxygen accompanied by an oxidase reaction. However, amperometric uric acid sensor with uricase membrane prepared by immobilization of enzyme during electropolymerization has not been reported, mainly because conducting polymer is not produced at a neutral pH and the electropolymerization electrode loses its electric conductivity. Furthermore, highly sensitive and selective detections of these species would be difficult because the side reactions of interferences might be occurring by amperometry at these electrode surface. Recently, poly(*o*-aminophenol)-modified carbon paste electrode for uric acid has

* Corresponding author. Tel.: +81 485 856839; fax: +81 485 856004.

PII S0039-9140(97)00023-4

been reported [6], but enzyme is not immobilized during an electropolymerization, because 0.1 M acetic acid (denature of enzyme may take place at pH 5) is used as an electrolyte.

A porous carbon felt used in this research consists of fine carbon fibers (diameter 10–20 mm) and has an excellent property for oxygen permeability because of its porosity. Recently, it has been demonstrated that amperometric response of glucose sensor using the gas diffusion carbon cloth electrode is much higher than that using gas impermeable electrode such as glassy carbon. The amplification of the current response is based on its extremely efficient supply of oxygen for the enzymatic reaction [7].

In this work, a carbon felt was chosen as a gas diffusion electrode material for electropolymerizations of aniline and pyrrole. Novel biosensing devices consisting of this porous enzyme reactor and a polarographic type oxygen electrode are fabricated to improve the selectivity and sensitivity. A carbon felt electrode has been employed as effective electrode material for controlled potential coulometry [8] and amperometry [9] by us, but the electrooxidation of hydrogen peroxide at this electrode material is highly irreversible [10], then the detection of oxygen is reasonable way for this type of biosensor.

2. Experimental

As an electrolyte for electropolymerization, 3 ml of 0.1 M KCl solution (pH 7) containing 0.1 M aniline or pyrrole and 2 mg of uricase (EC 1.7.3.3, Sigma, 4.53 U mg^{-1}, optimum pH 9.0) are used. A round porous carbon felt (Nippon carbon Ltd., GF-20-3F, baked at 2000°C, 0.5–2 mm thickness, 10 mm diameter) with platinum (0.5 mm diameter) wire lead and a gold wire (0.5 mm diameter) were used as working and counter electrodes, respectively, and a saturated calomel electrode was used as reference electrode. The electrode potential of the carbon felt was maintained at a constant potential (+ 0.7 V vs. SCE) by a potentiostat (Nikko Keisoku NPOT-1) and polymerization was performed by electrolyzing for 5 min. The electropolymerization carbon felt was washed with a distilled water and then fixed on the oxygen gas permeable membrane of an oxygen electrode by an electrode cap and this electrode was employed as an uric acid sensor. The electrode potential of the gold working electrode of Clark oxygen electrode (Denki Kagaku Keiki, Ltd.) was maintained at + 0.7 V vs. Ag/AgCl electrode. The solution in which the uric acid sensor is tested (0.1 M phosphate buffer solutions) was stirred with a magnetic stirrer. The chemicals used in this experiment were reagent grade. The carbon felt consists of the carbon fibers that possess a hydrophilic property and it has been estimated as an effective electrode material for rapid electrolysis [11].

3. Results and discussion

The sensing principle of uric acid electrode is schematically shown in Fig. 1. The oxygen consumed, accompanied by the enzymatic reaction occurred at the surface of the carbon fiber, is detected at a gold electrode of an oxygen electrode. Electropolymerization polyaniline prepared at a neutral pH is known to be an electroinactive polymer [12] in contrast to polypyrrole. In fact, the oxidation current of aniline decreases with electrolysis time because of the coating of this electroinactive polymer on the electrode surface

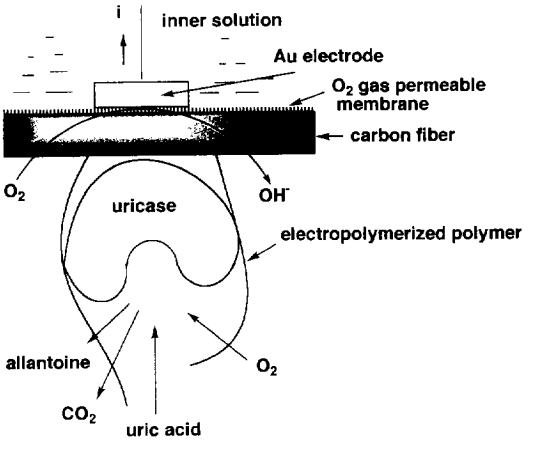

Fig. 1. Schematic sensing principle of uric acid by the present sensor.

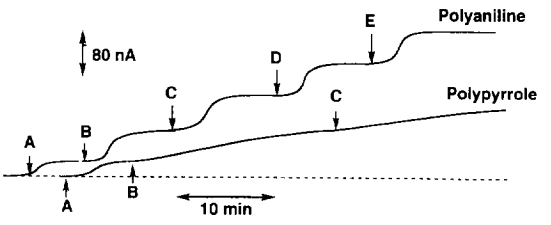

Fig. 2. Typical current responses of uric acid obtained by enzyme electrodes using carbon felts coated with polyaniline and polypyrrole. Addition of uric acid concentration, A: 0.01 mM, B–E: 0.02 mM.

and the oxidation current was decreased during electropolymerization from the initial current (several hundreds mA) to several mA after 20 min (total charges are about 0.1 coulomb) has passed. Therefore, this electropolymerization carbon felt is not adequate for an amperometric sensing device.

The typical current responses of uric acid obtained by the polyaniline and polypyrrole electrodes are shown in Fig. 2. These results show that uric acid gives the significant current responses in the case of polyaniline and it was found that uricase could be immobilized on the surface of the carbon fiber by electropolymerization of aniline. In the case of polypyrrole, the current responses of uric acid are also apparently observed, however, the rate of the current response is very slow and rapid sensing of uric acid has not been realized. This fact indicates that uricase can be immobilized to the surface of the carbon felt by an electropolymerization of pyrrole, as same as that of aniline, however, the current response time becomes very large, mainly because the transfer rate of uric acid to the active site of the immobilized enzyme is slow, probably due to a steric effect of polypyrrole coated on the surface. The current response of uric acid reaches the steady-state values after each addition of 2×10^{-5} M uric acid within 3 min when the thickness of the carbon felt is 0.5 mm. In contrast, no oxygen decrease was observed when uricase is not immobilized into the polyaniline or polypyrrole membrane, and it was confirmed that the present electrodes work as biosensor for uric acid. Uricase is well known to be the enzyme with an excellent specificity to uric acid, and no current responses of other species such as glucose or L-ascorbic acid were observed.

The current response of uric acid decreases linearly as decrease in oxygen concentration in the sample solution, then, the oxygen supply by the addition of buffer solution to the sample solution is needed to obtaine accurate analytical results for biological fluids such as urine.

From the results above, it can be recognized that an effective uric acid sensor can be fabricated by combining electropolymerization carbon felt and a Clark type oxygen electrode using aniline monomer. The uric acid electrode prepared using aniline polymerization retained its enzyme activity for 5 days and the activity was decreased at half value after 7 days. The calibration graph of uric acid exhibited an excellent linear concentration range from 1×10^{-5} to 4×10^{-4} M with a sensitivity of 2.5 μA mM^{-1}. The relative standard deviations of the steady state current responses are decreased according to increase in uric acid concentration, and the relative standard deviation ($n = 5$) of 1×10^{-4} M uric acid was found to be 3%.

The current response of uric acid is increased according to increase of the electrode potential of electroporimerization, but the side reactions such as oxygen gas evolution are increased and the electropolymerization was then carried out at + 0.7 V vs. SCE throughout the experiment.

It can be considered that the response time of the present electrode is highly dependent on the thickness of the carbon felt membrane, and the

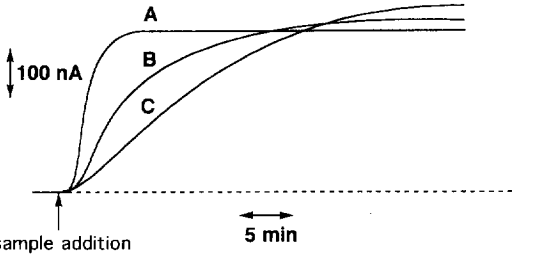

Fig. 3. Effect of the thickness of the carbon felt in the present sensor on the current response of 1×10^{-4} M uric acid.

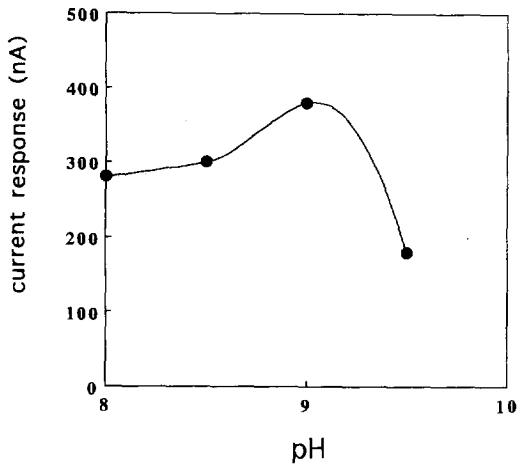

Fig. 4. Effect of pH on the 1×10^{-4} M uric acid response obtained by the present sensor. Thickness of the carbon felt: 0.5 mm.

effect of the thickness of the carbon felt on the current response is shown in Fig. 3. These results indicate that the rate of the current response of uric acid becomes larger as decrease of the thickness of the carbon felt, mainly because the mass transfer rates of oxygen and uric acid become faster. The time required from the sample addition to reach the steady state current response value of 1×10^{-4} M uric acid is found to be 5 min when 0.5 mm carbon felt was employed. Therefore, it has been estimated that the reasonable rapid responses can be obtained by the present sensor.

The effect of pH on the uric acid response is shown in Fig. 4, the maximum current response was obtained at pH 9.0 and this fact indicates that the structure change of enzyme due to an immobilization would not be occurring because the optimum pH of free uricase activity (pH 9.1) is about the same value. The current response characteristics of the present sensor are compatible with those of conventional uric acid electrodes with uricase membrane fabricated by the other methods [13,14].

The electropolymerization method has been found to be very powerful technique for enzyme immobilization during electropolymerization, but many electropolymerization polymers prepared at a neutral pH range are electroinactive and electrode becomes an insulator, although the electropolymerization polymers produced at acidic media (< pH 1), in which many redox enzymes unfortunately lose their activities, are electroactive. It is therefore desirable although not always essential, to use neutral aqueous solutions in the electropolymerization process [15]. In this work, the electropolymerization carbon felt was then used as a gas diffusion enzyme reactor and not an electrode of uric acid sensor, and oxygen electrode was used as an detector to avoid this problem.

From the results and discussion, it was found that the electropolymerization technique for immobilization of enzyme can be successfully applied to the biosensor based on gas sensing electrode with gas permeable membrane, using an enzyme reactor of porous carbon material. The combination of other gas sensing electrode such as ammonia or carbon dioxide electrode with the electropolymerization carbon felt would be expected to be an effective technique for fabricating various type of biosensors.

References

[1] S. Yabuki, H. Shinohara, Y. Ikariyama, M. Aizawa, J. Electroanal. Chem. 224 (1990) 37.
[2] M. Aizawa, G.F. Khan, H. Shinohara and Y. Ikariyama, in M. Aizawa (ed.), Chemical Sensor Technology, Vol. 5, Kodansha, Tokyo, 1994, pp. 157–175.
[3] M. Hidaka, M. Aizawa, Denki Kagaku 63 (1995) 1113.
[4] S. Cosrsinir, C. Innocent, J. Electroanal. Chem. 328 (1992) 361.
[5] S.L. Mu, J. Electroanal. Chem. 370 (1994) 135.
[6] E. Miland, A.J.M. Ordieres, P.T. Blanco, M.R. Smyth, C.O. Fagain, Talanta 43 (1996) 785.
[7] T.A. Zawodzinski Jr., C. Campbell, J. Davey, S. Gottesfeld, J. Search, M. Wilson, J. Rishpon, Electroanalysis 7 (1995) 1035.
[8] S. Uchiyama, Y. Kobayashi, S. Suzuki, O. Hamamoto, Anal. Chem. 60 (1988) 1835.
[9] S. Uchiyama, S. Suzuki, Sensors Actuators B 13/14 (1993) 76.
[10] S. Uchiyama, T. Obokata, S. Suzuki, O. Hamamoto, Anal. Chim. Acta 225 (1989) 425.

[11] O. Hamamoto, Y. Nakamura, S. Uchiyama, T. Hobo, Bunseki Kagaku 40 (1991) 617.
[12] A.F. Diaz, in H. Lund and M.M. Baizer (eds.), Organic Electrochemistry, Ch. 33, Marcel Dekker, New York, NY, 1991, pp. 1363–1396.
[13] M. Nanjo, G.G. Guilbault, Anal. Chem. 46 (1974) 1769.
[14] F. Yoshino, H. Osawa, Clin. Chem. 26 (1980) 1060.
[15] P.N. Bartlett and J. Cooper, in M.E.G. Lyons (ed.), Electroactive Polymer Electrochemistry, Part 2, Methods and Applications, Ch. 9, Plenum, New York, NY, 1996, pp. 233–267.

ELSEVIER

Talanta 44 (1997) 1441–1445

Talanta

Reproducibility of the nonlinear regression fit to the FTIR spectra of lysozyme[1]

Thomas F. Kumosinski *, Joseph J. Unruh, Harold F. Farrell Jr.

U.S. Department of Agriculture, ARS, Eastern Regional Research Center, 600 East Mermaid Lane, Wyndmoor, PA 19038, USA

Received 25 September 1996; received in revised form 22 January 1997

Abstract

Controversy exists concerning the influence of experimental artifacts on the number of component FTIR vibrational bands which may be resolved from the amide I and II envelopes of proteins in water. Whether these bands represent unique populations of vibrating protein groups in a particular global 2° structure or whether the bands are due to instrumental and environmental fluctuations has been addressed, T.F. Kumosinski and J.J. Unruh, Talanta, 43 (1996) 199–219. The repeatability of the methodology and the apparent uniqueness of the nonlinear regression fits are addressed in this study. We obtained a series of the spectra of lysozyme, and carried-out nonlinear regression analysis of each spectrum. Coefficients of variation (COV) were calculated for the wavenumber and area values of assigned component peaks obtained. Low COVs obtained attest to the precision of the methodology and the apparent uniqueness of the nonlinear regression fits. This methodology for acquisition and analysis of protein FTIR spectra yields results with good precision. © 1997 Elsevier Science B.V.

Keywords: FTIR; Fourier transform infra red spectroscopy; Lysozyme; Precision; Proteins; Protein secondary structure

1. Introduction

FTIR analysis of proteins and peptides as a method for estimation of their global secondary structure has become a valuable tool for protein biochemists [1,2]. While this methodology is used more frequently, controversy exists in the areas of how to carry out the experiments and analyze the results. Whether to obtain the spectra in the real-world environment of H_2O with a difficult subtraction routine, or in the potentially structure changing environment of D_2O [2,3] with an easier subtraction routine is still debated. The best method for analysis of the results is also in debate. Many methods and combinations for analysis are available to choose from; these include: nonlinear regression analysis; second derivative analysis; Fourier self-deconvolution; and basis-set factor analysis. The pros and cons of the above considerations have been discussed elsewhere [4,5].

* Corresponding author. E-mail: tkumosinski@arserrc.gov/junruh@arserrc.gov

[1] Reference to a brand or firm name does not constitute endorsement by the U.S. Department of Agriculture over others of a similar nature not mentioned.

PII S0039-9140(97)00025-8

Recently we reported an FTIR methodology with which we obtained the spectra of 14 proteins in H_2O, analyzed the data using the second derivative and nonlinear regression methods, and compared the results with the known X-ray crystallographic data [1]. Differences of 2–4% for the periodic structures of helix, extended, irregular and turn were observed between the FTIR and X-ray results. Thus the accuracy of the method is firmly founded. An additional consideration would be the reproducibility (overall precision) of the spectral acquisition and the uniqueness of the nonlinear regression analysis. Here we present a validation study showing the reproducibility and uniqueness of the results using our reported methodology [1] with the well characterized protein lysozyme.

2. Experimental

2.1. Materials and solutions

Water was Type I grade obtained from the NANOPURE system (Barnstead, Dubuque, IA). Lysozyme (chicken egg white) and PIPES (potassium salt) were from Sigma (St. Louis, MO). Any other chemicals were of reagent grade or better. The CaF_2 windows and 6 μm Mylar® spacer were from SPECAC (Smyrna, GA). The buffer solution was 25 mM PIPES (potassium salt) with pH adjusted to 6.65 using concentrated HCl. After pH adjustment the buffer was filtered through a 0.22 μm Nylon filter (Sigma), and stored at 5°C. Two Lysozyme solutions were made—one at 3% (w/w) and one at 1.5% (w/w)—in the PIPES buffer, then filtered through 0.22 μm DVDF filters (Sigma) and stored at 5°C. The concentration of the lysozyme solutions were verified by UV spectrometry (ϵ_{280} = 36000) [6] on a Beckman DU-7 (Fullerton, CA) instrument.

2.2. Infrared measurements

The procedures and equipment were as previously reported—collecting 4096 double-sided interferograms (each with 16384 data points), which were co-added, phase-corrected, apodized (Happ-Genzel function), and fast-Fourier transformed [1]. The following minor exceptions to the methodology were made: a 6 μm Mylar® spacer was used in place of the 12 μm Teflon spacer; the sample cell's temperature was controlled at 25°C using SPECAC's electrical heating jacket (part # 20707, SPECAC); and the lysozyme solution was 3% (w/w) in 25 mM PIPES·K, pH = 6.65 in place of 4% in an imidazole buffer. To test repeatability, a spectrum was acquired each day for 5 days with the sample cell being disassembled and cleaned daily.

2.3. Data analysis

The buffer subtraction procedure used to obtain the protein spectra has been reported elsewhere [1]. Briefly, after obtaining the absorbance spectra for the protein and buffer solutions the protein spectra (amide I and II region) were obtained by subtracting the buffer spectra from the respective protein solution spectra in the 2000–1350 cm^{-1} region. Subtractions were performed interactively using the subtraction function in the Sx software of the Nicolet 660 data system. The scaling factor (FCR) was individualized during each subtraction by adjusting the FCR parameter value until the region from 2000 to 1700 cm^{-1} was as flat as possible. Next, the water vapor absorption was subtracted from the protein spectra using the 2nd derivative method [7].

The data analysis procedure of our previously reported methodology was changed slightly [1]. Here, the Fourier-self deconvolution spectra were not calculated because the choice of values for the parameters is controversial and the results thus questionable. We found more acceptable analyses could be obtained using only the second derivatives and the nonlinear regression fits of the original spectra. As previously reported, the starting wavenumbers for the ABACUS [8][2] curve fitting program were chosen from the second derivative

[2] Version F.1 is available on the internet from QCPE (their program number 652) or directly from ERRC. Persons desiring the program may use FTP, connect to 'ceres.arserrc.gov', and use the account 'anonymous' which requires no password. They would then select directory 'abacusf' and download all files. Installation instructions and user documentation are also provided.

of the original spectrum. To increase the probability that the resulting fit was not a local minimum and the unique fit to the data, the original spectrum was fit twice, once starting from below the experimental values (where $Y_{exp} - Y_{theoretical}$ is positive) and once starting from above the experimental values (where $Y_{exp} - Y_{theoretical}$ is negative). Convergence to the same model from both starting positions was one criterion for an acceptable fit. The starting peak heights for the 'below fit' were chosen so that the composite sum was at least 25% below the original spectra absorbance plot, and the starting peak heights for the 'above fit' were similarly chosen to be 25% above the original spectra absorbance plot. The starting half-width at half-height was three for all peaks. While just the peak heights were adjusted to obtain two different starting points, it should be emphasized that all peak parameters (height, half-width at half-height, and wavenumber) as well as the baseline were permitted to float during the nonlinear regression analysis. A more detailed discussion of the nonlinear regression analysis can be found in our previous report [1].

Three criteria were required to be met before the results of the curve-fitting were considered acceptable. First, the lowest RMS (root-mean-square) value obtainable had to be reached. Acceptable RMS values were usually of magnitude 10^{-5} for spectra with maximum absorbance values in the 0.05–0.09 range. Second, the below and above fits should converge to the same model. Third, the second derivative of the composite sums should overlie the second derivative of the original spectra. Only when all three of the above criteria were met was the curve-fitting result considered acceptable.

χ^2 instead of the RMS could also be evaluated as a means to determine the best nonlinear fit, since it includes the effects of adding more parameters to the model. For our ABACUS program, χ^2 and the RMS are equivalent when the model has a fixed number of peaks as it does in our case for any individual fit of a model to the data. In the case where more or less peaks may be needed in the model, we use an F-test to statistically evaluate the change in the number of parameters (i.e., the number of peaks). This part of the methodology is discussed in more detail in our previous report [1].

3. Results and discussion

3.1. Spectral acquisition

Fig. 1 shows the spectra (amide I and II region) obtained on each of 5 different days for lysozyme. In all but one case the spectra are nearly identical. The one exception sample was prepared at half the concentration. This spectrum was included in the curve-fitting analysis to consider variance with concentration. With the exception of the 1.5% lysozyme spectra the upper four spectra nearly overlie each other, except in the 1500–1400 cm^{-1} region. We can not explain this but have not noticed differences in this region to effect the nonlinear regression analysis of the 1700–1500 cm^{-1} region. We have noticed though that small changes in the FCR during buffer subtraction have a greater effect in this region than the 1700–1500 cm^{-1} region.

During the 5 days of the study, the ambient temperature of the analysis room changed slightly (68–72°F) and the humidity changed greatly (27–56% relative humidity). As can be observed these environmental changes had little effect on the obtained spectra, and the presence of an H_2O vapor spectra are not observed in the final protein

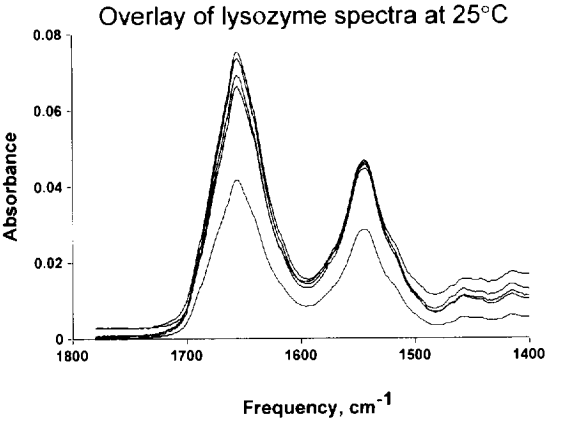

Fig. 1. Overlay plot of lysozyme spectra obtained as described in text.

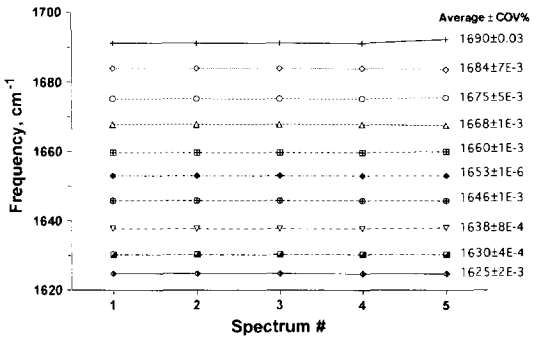

Fig. 2. Graph of the wavenumbers obtained from the nonlinear regression analysis of the spectra in Fig. 1 versus the day of acquisition.

spectra obtained. Daily cleaning and reassembly of the cell showed a variation in the pathlength to be approximately 1.5% Coefficient of variation (COV).

3.2. *Curve-fitting—nonlinear regression analysis*

Two points of evaluation were considered to determine if the curve-fitting procedure leads to repetitive results. First, if the resultant wavenumbers for the component peaks from the fit turned out to be the same for each of the five spectra; and second, if the resultant areas for the component peaks turned out to be the same for each of the five spectra.

Fig. 2 demonstrates the first case. There the wavenumbers found for the amide I of the spectra from each of the 5 days are plotted versus the day number. Nearly flat horizontal lines are obtained. This shows the repeatability of the curve-fitting procedure to obtain the same wavenumbers for different spectra of the same sample. Beside each plotted line is listed the average wavenumber ± COV%. The COV for the wavenumbers varies from 0.000002 to 0.03%—indicating very precise results for the wavenumbers. Repeatable wavenumbers show that defining the structural elements in the model for the secondary structure is precise for lysozyme, and will probably be precise for most other proteins analyzed. A more stringent test for repeatability of analysis will be found by comparing the areas for each wavenumber's component peaks.

Table 1 lists the areas of the component peaks obtained for each day's analysis. The standard deviations are good, an average COV of 7.86% (range 1.78–26.71%) is obtained for days 1–5. This shows acceptable repeatability. The greatest variation occurs in the day 5 results, where all the data for this day approach being considered outliers. Day 5 is the sample prepared at 1.5%, to test the effect of concentration on the results. If the results of day 5 are not included, the averages obtained only change slightly (last column in Table 1), while the average COV changes to 2.39% (range 1.36–4.97%). Eliminating the day 5 results greatly improves the precision of the methodology. Our first report [1] concerned itself with the accuracy of this methodology when comparing the results to X-ray crystallographic data. In that report we only analyzed 3–4% protein solutions. Therefore, until more data at lower concentrations is accumulated for a number of proteins, we suggest that a minimum absorbance value of 0.06 should be obtained for the amide I in order to ensure good repeatability of the nonlinear regression fit and ultimately the secondary structural model obtained for the protein.

4. Conclusions

FTIR analysis of lysozyme for its global secondary structural model in water (H_2O) using nonlinear regression to obtain the component wavenumbers and areas is a precise methodology. The only caution to be observed for the methodology is the absorbance value obtained for the amide I envelope. We found the absorbance of the amide I should be at least 0.06 in order to obtain precise results using the current instrumentation we have (the Nicolet model 740 spectrophotometer). Newer generation spectrophotometers (for example the Nicolet 860) have better signal-to-noise ratios, and would probably be capable of precisely analyzing protein spectra with the amide I absorbance at values less than 0.06.

Our previous work showed the methodology used in this report to be accurate for the 14 proteins studied [1] when compared with the X-ray crystallographic results. Combined with the

Table 1
Percent area values found

Wavenumber	Analysis day number					Average area ± cov	Average area ± cov
	1	2	3	4	5	Days 1–5	Days 1–4
1690	5.00	5.17	4.94	4.77	3.26	4.67 ± 17%	4.97 ± 3.4%
1684	11.67	11.49	11.96	12.01	11.73	11.77 ± 1.7%	11.78 ± 2.1%
1675	6.79	6.96	6.82	7.02	6.44	6.81 ± 2.9%	6.90 ± 1.6%
1667	11.61	11.16	11.47	11.50	11.70	11.49 ± 1.7%	11.44 ± 1.6%
1660	13.40	13.54	13.89	14.06	13.08	13.59 ± 2.9%	13.72 ± 2.3%
1653	13.34	13.75	12.99	13.25	15.67	13.80 ± 7.9%	13.33 ± 2.4%
1646	12.27	12.00	12.51	12.21	11.4	12.08 ± 3.1%	12.25 ± 1.7%
1638	12.52	12.46	12.05	11.86	15.27	12.83 ± 11%	12.22 ± 2.6%
1630	2.27	2.26	2.51	2.32	1.11	2.09 ± 33%	2.34 ± 5.1%
1625	11.11	11.21	10.86	11.00	10.34	10.90 ± 2.7%	11.05 ± 1.4%

precision analysis reported here, the methodology presented to analyze for the global secondary structure of proteins in H_2O is both accurate and precise. We recommend that researchers carrying out secondary structural analysis of proteins using FTIR of the protein in H_2O perform a validation analysis as reported here on a model protein (like lysozyme) before attempting to analyze proteins of unknown structure.

References

[1] T.F. Kumosinski and J.J. Unruh, Talanta, 43 (1996) 199–219.
[2] S.N. Timasheff, in H. Peeters (Ed.), Protides of the Biological Fluids, 20th Colloquium, 1973, pp. 511–519.
[3] J.L. Finney, Phil. Trans. R. Soc. Lond. B., 278 (1977) 3.
[4] W.K. Surewicz, H.H. Mantsch and D. Chapman, Biochemistry, 32 (1993) 389.
[5] E. Goormaghtigh, V. Cabiaux J.M. Ruysschaert, in: H.J. Hilderson and G.B. Ralston (Eds.), Subcellular Biochemistry, Vol. 23: Physicochemical Methods in the Study of Biomembranes, 1994, pp. 329–450.
[6] R.C. Davies, A. Neuberger and B.M. Wilson, BBA, 178 (1969) 294.
[7] A. Dong, P. Huang and W.S. Caughey, Biochemistry, 29 (1990) 3303.
[8] W. Damert, Quantum Chem. Program Exchange Bull., 14 (4) (1994) 61.

ELSEVIER

Talanta 44 (1997) 1447–1453

Talanta

Preparation and analytical properties of a chelating resin functionalized with 1-hydrazinophthalazine ligand

Rita Pathak, G.N. Rao *

Department of Chemistry, IIT Delhi, Hauz Khas, New Delhi-110016, India

Received 19 November 1996; received in revised form 13 January 1997; accepted 20 January 1997

Abstract

A poly[styrene-co-(divinylbenzene)] resin (XAD-4) functionalized with 1-hydrazinophthalazine ligand has been prepared and its analytical properties investigated. The pH dependence of sorption of metal ion on the resin has been determined for Cu(II), Ni(II), Co(II), Zn(II), Cd(II), Pb(II), Fe(III) and Cr(III). Trace amounts of these metal ions were quantitatively retained on the resin and recovered by eluting with 1 mol l^{-1} hydrochloric acid. The resin was found to be selective for Fe(III) and its separation from other metal ions was carried out effectively. Metal ions concentrations were determined using AAS. © 1997 Elsevier Science B.V.

Keywords: Atomic absorption spectrometry; Chelating resin; 1-hydrazinophthalazine; Iron(III); Metal sorption

1. Introduction

Chelating resins have found increasing utility for separation and concentration of metal ions at trace levels, because of their selectivity. A number of chelating resins containing various functional groups (e.g., ethylenediamine tetraacetic acid [1], iminodiacetic acid [2–4] etc.) have been reported. Vernon and Eccles used chelating resin formed with *N*-substituted hydroxylamine [5]. We have reported chelating resin containing bicine [6] functional group.

Polyamines like ethylenediamine, diethylenetriamine, etc., form an important class of chelating ligands. Several authors have studied the modification of synthetic resins with linear polyamine ligands [7–10]. More recently Blain et al. have applied a chelating resin, chelamine, for preconcentration of trace metals from sea water with high selectivity [11].

Synthesis of chelating resins having good selectivity is a subject of continuing interest and importance. 1-Hydrazinophthalazine, a hydrazino type ligand capable of chelating interactions utilizing the α-nitrogen of the hydrazine residue and the nitrogen doners of phthalazine substituent. Thus, it presents a favourable environment for coordination with the metal ion. 1-Hydrazinophthalazine has been reported to form stable complexes with Fe(III), Cu(II) and Zn(II), while it has negligible affinity for Ca(II), Mg(II) and Mn(II) [12]. Ruggieri et al. have used 1-hydrazinophthalazine as a sensitive reagent for the determination

* Corresponding author. Fax: +91 11 6862037.

PII S0039-9140(97)00026-X

of Fe(III) [13]. Takaoka et al. have reported a similar reagent, di-2-pyridylmethanone 2-(5-nitro)pyridyl hydrazone for sensitive and selective spectrophotometric determination of trace iron [14]. Hence it was considered interesting to incorporate this ligand on to a polymeric support and study its analytical potential. In the present work, the macroporous resin poly styrene-co-divinylbenzene (XAD-4) has been functionalized using 1-hydrazinophthalazine ligand. The resin have been characterized and sorption behaviour of different metal ions on the resin has been studied.

2. Experimental

2.1. Instrumentation

An ECIL (Hyderabad, India) AA 4139 microprocessor controlled atomic absorption spectrometer was utilized for determining metal concentration; an ELICO (Hyderabad, India) digital pH meter (LI-120) was used for pH measurements. A mechanical shaker with incubator (Scientific, New Delhi, India), 200 strokes min^{-1} was used for carrying out equilibrium studies. Infrared (IR) spectra were recorded on a Nicolet-5DX Fourier transform IR spectrophotometer (Madison, USA), in potassium bromide pellets.

2.2. Reagents

The stock metal ion solutions were prepared by dissolving analytical reagent grade metal nitrates, chlorides or sulfates in double distilled water or the matrix acid. All the metal ion solutions were standardized using standard methods [15]. Poly (styrene-co-(divinyl benzene)] resin (Amberlite XAD-4) was obtained from Fluka (Buchs, Switzerland) and 1-hydrazinophthalazine from Sigma (U.S.A.). The following buffers were used to control the pH of the solution: hydrochloric acid-glycine (pH 1–3), acetic acid-sodium acetate (pH 3–5); disodium hydrogen phosphate-potassium dihydrogenphosphate (pH 5–8); and sodium borate-hydrochloric acid (pH 8–9).

2.3. Synthesis of XAD_4-1-hydrazinophthalazine

Styrene divinyl benzene copolymer (XAD-4) was functionalized by a slight modification of the method reported by Fritz et al. [1], (Scheme 1). XAD-4 beads (10 g) were first acylated by refluxing with acetic anhydride (20 ml) and anhydrous aluminium trichloride (1 g) in petroleum ether (60–80°C) at 70°C for 30 h. The product was filtered off and washed with 50 ml of hexane. The intermediate product (II) was stirred in 500 ml of water containing 8.5 g of potassium permanganate and 10 g of sodium hydroxide at 40°C for 1 h. The product was filtered off, washed with water and then treated with (1 + 1) hydrochloric acid. The subsequent carboxylic form (III) was refluxed with 50 ml of thionyl chloride at 60°C for 0.5 h. The intermediate resin (IV) was refluxed with 1-hydrazinophthalazine (1.5 g) and sodium ethoxide (0.2 g) in dry dimethylformamide at 100°C for 12 h. XAD_4-1-hydrazinophthalazine resin formed, was filtered off, washed with methanol, water, acetone and dried. A pale yellow resin was obtained. A total of 20 g resin was prepared. The 200–250 mesh fraction of the resin was collected through standard sieve and was used for metal sorption studies.

2.4. Effect of pH on metal ion uptake

The effect of the pH on the metal ion uptake was studied by a batch equilibration technique.

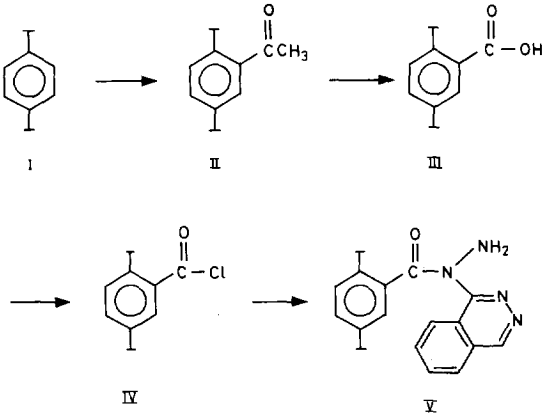

I II III IV V

Scheme 1.

Metal ion solution (50 ml, 50 μg ml^{-1}) was shaken with 100 mg of resin for 1 h. The pH of the metal ion solution was adjusted prior to equilibration over the range 2.0–9.0, with buffer solution. After the equilibration, the concentration of the metal ion remaining in the solution was determined by AAS. The concentration of metal ion was also determined in the eluent after desorbing the metal ion with 1 M hydrochloric acid. Sorption experiments were carried out in duplicate each time.

2.5. pH dependence of trace metal ion uptake

A 50 ml volume of buffered solution containing 5 μg ml^{-1} of metal ion was shaken with 100 mg of resin for 1 h in a glass stoppered bottle. The resin was filtered off and the concentration of the sorbed metal ions was determined after eluting out with 1 M HCl (10 ml) and diluting the resultant sample solution to 50 ml with distilled water.

2.6. Resin capacity

The capacity of the resin was determined by shaking the excess of metal ion [50 ml; 100 μg ml^{-1} for Cu(II), Ni(II), Fe(III), Zn(II), Cr(III) and Co(II) and 200 μg ml^{-1} for Pb(II) and Cd(II)] with 50 mg of resin for 6 h at the optimum pH of sorption. The resin was filtered off and the concentration of the remaining metal ion in the solution was determined by AAS. The capacity of the resin was also checked after soaking the resin in 1 M HCl–1 M NaOH for 24 h.

2.7. Equilibrium time

To determine the time of equilibrium for the metal ion under investigation, the metal ion solution (50 ml, 10 μg ml^{-1}) at a constant pH was sampled in six bottles. These bottles were removed from shaker at regular intervals of time and concentration of the sorbed metal ions was determined. The duplicate values agreed with a precision of $\pm 2\%$.

2.8. Effect of diverse ions

The effect of diverse ions viz. potassium, magnesium and calcium ions on the recovery of various metal ions from aqueous solution was studied. For this, standard solutions of 50 ml of Cu(II), Zn(II), Pb(II) and Fe(III) (1–5 μg ml^{-1} each) containing manifold amounts of the foreign ions as interferents were analysed.

2.9. Concentration and separation of metal ions

A batch equilibration method was used to concentrate the trace metal ions. Sample solutions (250–500 ml) containing 0.1 μg ml^{-1} metal ion were adjusted to the optimum pH of sorption with buffer solution. The solution was then shaken with 100 mg of resin for about 10 min. Sorbed metal ions were eluted with 1 M hydrochloric acid (10 ml) and the concentration of the metal ion in the eluent was determined using AAS.

Based on the sorption behaviour of metal ions on XAD_4-1- hydrazinophthalazine resin at different pH values, separation of Fe(III) from various other metal ions were carried out in binary mixtures by column method. A funnel-tipped glass column with a length of 6 cm and i.d. of 0.5 cm was used for separation purposes. The dry resin (0.5 g) was loaded into the glass column, immersed in the buffer solution and 50 ml of metal ion solution containing Fe(III) (10 μg ml^{-1}) and other metal ions (10 μg ml^{-1}) was passed through the column at a flow rate of 2.0 ml min^{-1}. The sorbed metal ion was desorbed from the resin with 1 M HCl (10 ml). Concentration of Ni(II), Cu(II), Co(II), Zn(II) or Pb(II) was determined in the effluent by AAS.

XAD_4-1-hydrazinophthalazine was also used for separation and analysis of Fe(III) in synthetic samples (N.B.S., SRM-1632 and NKK, No. 920).

3. Results and discussion

The resin was synthesized according to Scheme 1 and the incorporation of 1-hydrazinophthalazine into the polymeric matrix was established by IR spectra (Fig. 1) and chemical analysis.

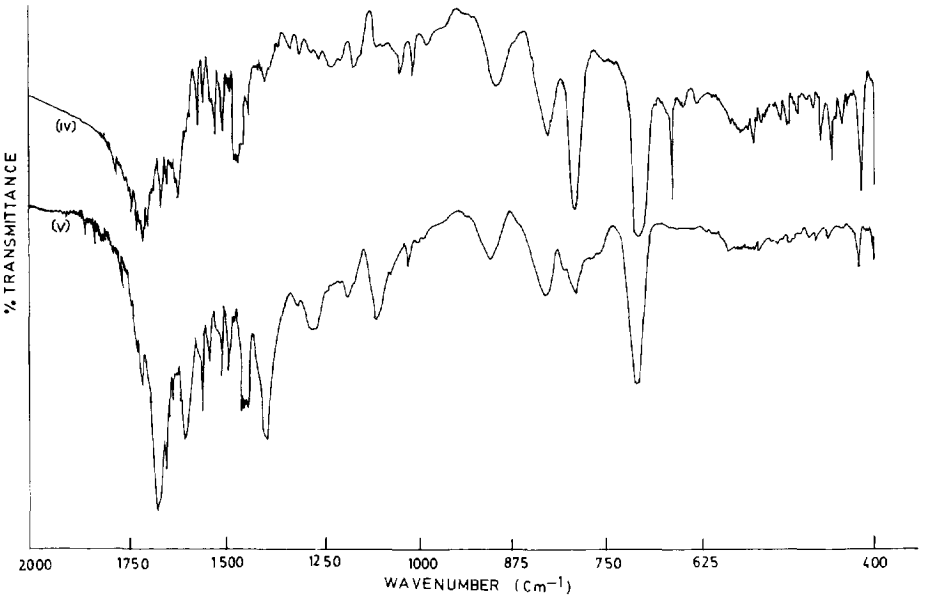

Fig. 1. Infrared spectra of resins (KBr disk): IV, acid chloride resin; and V, 1-hydrazinophthalazine resin.

The final resin (V) did not have C–Cl band at 670 cm^{-1} supporting Scheme 1. It is further indicated by a upper shift in the absorption band corresponding to a carbonyl group (1740–1765 cm^{-1}) in the spectrum of resin (IV) (acid chloride form) probably resulting from Fermi-resonance between the C=O band and the overtone of a longer wavelength band near 875 cm^{-1} [16]. The ligand is attached to the polymer through the secondary amine group. This is indicated by disappearance of the band corresponding to secondary aryl N–H (at 3220 cm^{-1}). All other characteristic band of pure ligand were present in the final resin(II).

Fig. 2 shows the scheme for coordination of the metal ion with the ligand. 1-Hydrazinophthalazine acts as bidentate ligand coordinating through α-nitrogen of the hydrazine moiety and one of the nitrogen of the phthalazine ring [17], resulting in the formation of a stable five membered ring.

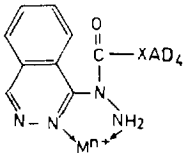

Fig. 2. Co-ordination of metal ion by the ligand.

Nitrogen analysis of the resin gave a value of 8.05% nitrogen. Assuming that all nitrogen is part of intact 1-hydrazinophthalazine group, the capacity for the metal ion should be 1.44 mmol g^{-1} of resin. The values actually obtained are reported in Table 1.

Fig. 3 shows the sorption behaviour of Cu(II), Ni(II), Zn(II), Co(II), Pb(II), Cd(II), Fe(III) and Cr(III) as a function of pH using XAD_4-1-hydrazinophthalazine resin. Sorption of Fe(III) be-

Table 1
Metal uptake capacity

Metal ion	pH	Capacity ($\pm$S.D.) mmol g^{-1} of resin)
Cu(II)	6.51	1.24(0.02)
Zn(II)	7.05	0.74(0.01)
Fe(III)	4.52	1.32(0.01)
Pb(II)	6.52	0.86(0.02)
Ni(II)	8.54	0.82(0.02)
Cd(II)	7.52	0.96(0.01)
Co(II)	8.03	0.85(0.02)
Cr(III)	8.84	0.62(0.02)

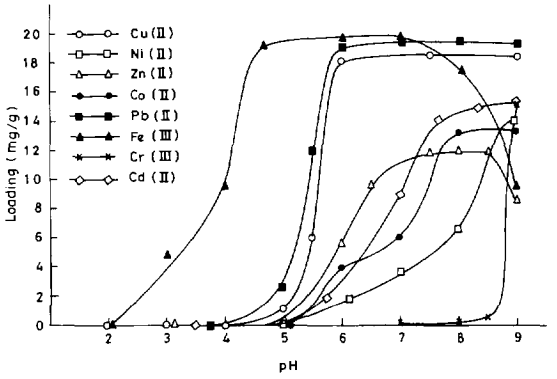

Fig. 3. Effect of pH sorption with 1-hydrazinophthalazine resin.

gins at lower pH (around pH 3) compared with other metal ions and attained a limiting value at pH 4. For Pb(II) and Cu(II) no uptake was observed till pH 5 but increases sharply beyond pH 5.5. Other metal ions showed gradual increase in sorption with increasing pH and the optimum uptake was observed in the higher pH region. These curves shows that the resin shows high selectivity for Fe(III) and its separation from other metal ions could be carried out by gradient elution. For example at pH 4.0 Fe(III) would remain on the resin while other metal ions would be eluted. Resin also shows fairly good selectivity for Pb(II) and Cu(II), and their separation from Ni(II), Co(II), Zn(II), Cr(III) etc., could be carried out by batch or column method.

Fig. 4 shows the effect of pH on the uptake of trace metal ions. This is to determine the pH value other than the optimum pH of metal sorption, at which metal ion can be quantitatively removed from the solution. Complete sorption was obtained in the following pH region for various metal ions, (4.2–8.5) for Fe(III); (5.8–9.0) for Cu(II); (6.5–8.5) for Zn(II); (7.7–9.0) for Co(II); (8.0–9.0) for Ni(II); (5.6–9.0) for Pb(II); (7.5–9.0) for Cd(II), and (> 9.0) for Cr(III).

The capacity of the resin for various metal ions was determined at optimum pH of sorption and data is listed in Table 1, along with the standard deviation. The capacity of the resin for Cu(II) was found to be 1.24 mmol g^{-1} which is higher than some of the previously used chelating resins having similar groups (e.g., chelamine resin [11], 1.0 mmol g^{-1}; 8-hydroxyquinoline on fractogel [18], 0.29 mmol g^{-1}; diamine on silica gel [19], 0.47 mmol g^{-1}).

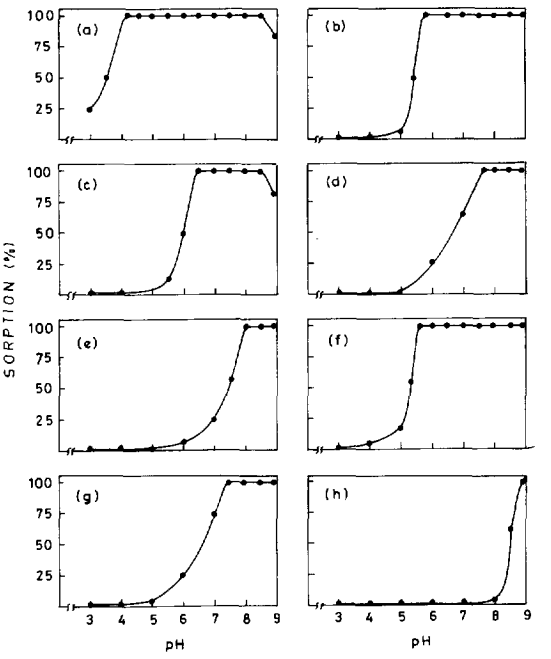

Fig. 4. PH dependence of the uptake of trace metal ions: (a), Fe(III); (b), Cu(II); (c), Zn(II); (d), Co(II); (e), Ni(II); (f), Pb(II); (g), Cd(II); and (h), Cr(III).

Equilibration time of the resin was determined for Cu(II), Ni(II) and Fe(III) and results are plotted in Fig. 5. Equilibration of the resin with

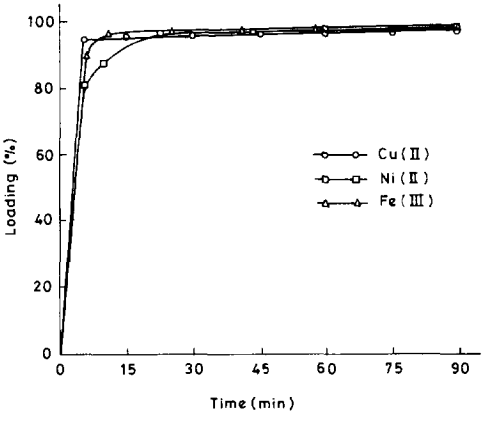

Fig. 5. Rate of uptake of metal ions.

Table 2
Effect of diverse ions

Interfering ions	Recovery (%)			
	Cu(II)	Pb(II)	Zn(II)	Fe(III)
Ca (50 μg ml^{-1})	98.5	99.4	98.9	98.4
Mg (50 μg ml^{-1})	101.0	99.2	99.1	100.2

the metal ion is sufficiently rapid, allowing the resin to be used in a packed column. Copper(II) and Ni(II) are extracted up to 90% within 5 min of their interaction with the resin, while Fe(III) reaches 81% extraction level in 5 min. Other metal ions also showed similar behaviour.

The presence of alkali and alkaline earth metals have no effect on the recovery of metal ion from the solution. Table 2 shows the recovery rates of metal ions in the presence of manifold amount of these foreign ions.

This suggests the suitability of this resin for trace concentration of metal ions from natural samples that have a high concentration of alkali and alkaline earth metals, e.g., sea-water, pond water, etc. The capacity of the resin is also high enough for use in the simultaneous concentration and determination of several metal ions. The resin has a high mechanical and chemical strength and no significant change in the hydrogen-metal exchange capacity was observed on using the resin after recycling.

The resin was used for preconcentration of various metal ions from aqueous solutions and the results are reported in Table 3.

Metal ions could be enriched up to 50 times with XAD_4-1- hydrazinophthalazine resin. Separation of Fe(III) has been carried out from other metal ions in various mixtures and the results are reported in Table 4.

At pH 4.2 resin selectively takes up Fe(III), while other metal ions viz Cu(II), Ni(II), Pb(II), Zn(II) or Co(II) passed through the column. Sorbed Fe(III) was eluted out with 1 M hydrochloric acid (10 ml). Analysis of sea water for Fe(III) is important and requires very rapid and sensitive method. Analytical methods like those involving solvent extraction-graphite furnace atomic absorption detection are time consuming and relatively inconvenient as large volumes of the sample solution have to be treated. The classical chemiluminescence method using luminol-H_2O_2 system along with chelating resin concentration was found to be promising [20]. But chemiluminescent detection is not specific for Fe(III) and ions like Cu(II), Co(II), Ni(II), Mn(II) etc., interfere. Therefore, chelating resin having good selectivity for Fe(III) over other metal ions are attractive. As Fe(III) was retained relatively at lower pH on XAD_4-1-hydrazinophthalazine (Fig. 3), its suitability for the separation of iron from other metal ions was evaluated by its application on various synthetic samples like coal (N.B.S., SRM- 1632) and Al alloy (NKK, No. 920).

3.1. Separation and determination of iron in synthetic samples

An aliquot of the pretreated sample solution was taken [21] and was passed through the column at pH 4.2. Iron retained on the column was eluted with 1 H HCl. The results are given in Table 5.

Amount of Fe(III) recovered agreed well with the certified value. Other metal ions were not detected in the eluent (1 M HCl) showing separation is possible.

Table 3
Preconcentration of metal ions (amount of metal ion taken 0.1 μg ml^{-1})

Metal ion	Sample volume (ml)	Metal ion found[a] (μg ml^{-1})
Cu(II)	250	2.45
Cu(II)	500	4.93
Fe(III)	250	2.42
Fe(III)	500	5.01
Pb(II)	250	2.48
Pb(II)	500	4.88
Ni(II)	250	2.50
Ni(II)	500	4.94

[a] Values agreed with a precision of ± 1%.

Table 4
Separation of Fe(III) from other metal ions performed at pH 4.2 (amount of Fe(III) 5 μg ml^{-1})

Metal ion	Amount of metal ion added (μg ml^{-1})	Amount of Fe(III) found (μg ml^{-1})[a]	Amount of metal ion found (μg ml^{-1})[a]
Cu(II)	10	4.96	9.82
Pb(II)	10	4.93	9.85
Ni(II)	10	5.01	9.92
Co(II)	10	4.98	9.89
Zn(II)	10	4.91	9.86

[a] Values agreed with a precision of ± 1%.

Table 5
Separation of iron in synthetic samples

Sample	Composition of synthetic sample (μg g^{-1})	Iron certified value (mg g^{-1})	Iron found (mg g^{-1})
Al Alloy (NKK No.92)	As,6.0: Cd,0.20; Cr,20.5; Cu,18; Pb,30; Mn,40; Hg,0.12; Ni,15; Se,2.9; V,35; Zn,37	8.7	8.69 ± (0.01)
Coal (NBS, SRM-1632)	Si,7800; Cu,7100; Mn,2000; Mg,4600; Cr,2700; Ni,2900; Zn,8000; Ti,1500; Sn,2000; Pb,1000; V, 1500; Bi,600; Ga,500; Co,1000; Sb,100; Ca,300	7.2	7.11 ± (0.02)

[a] Mean of three determinations.

4. Conclusion

The sorption studies of XAD_4-1-hydrazinophthalazine indicates its potential for enrichment and separation of various metal ions from aqueous solution. Resin has shown high selectivity for Fe(III) and its separation from other metal ions has been carried out effectively. Several other separation like Cu-Ni, Cu-Co, Cu-Zn, Pb-Co, Pb-Ni, etc., are feasible on resin by control of pH.

References

[1] E.M. Moyers and J.S. Fritz, Anal. Chem., 49 (1977) 418.
[2] M. Marhol and K.L. Cheng, Talanta, 21 (1974) 751.
[3] S. Tomoshige, M. Hirai and H. Ueshima, Anal. Chim. Acta, 115 (1980) 285.
[4] P. Figura and B. McDuffie, Anal. Chem., 49 (1977) 1950.
[5] F. Vernon and H. Eccles, Anal. Chim. Acta, 77 (1975) 145.
[6] Kapil Dev and G.N. Rao, Talanta, 42 (1995) 591.
[7] M.B. Shambu, M.C. Theodovakis and G.A. Digens, J. Polym. Sci., 15 (1977) 525.
[8] E. Marton-Schmidt, J. Inczedy, Z. Laki and O. Szabaolka, J. Chromatogr., 201 (1980) 73.
[9] T.M. Suzuki and T. Yokoyama, Polyhedron, 2 (1983) 127.
[10] D.E. Leyden, G.H. Luttrell, A.E. Sloan and N.J. DeAngelis, Anal. Chim. Acta, 84 (1976) 97.
[11] S. Blain, P. Appriou and H. Handel, Anal. Chim. Acta, 272 (1993) 91.
[12] H. Al-Falahi and M. Peter, Agents Actions, 14 (1) (1984) 113.
[13] R. Ruggieri, Anal. Chim. Acta, 16 (1957) 242.
[14] T. Takaoka, T. Taya and M. Otomo, Talanta, 39 (1992) 77.
[15] A.I. Vogel, Textbook of Quantitative Chemical Analysis, Revised by G.H. Jaffery, J. Bassett, J. Mandham and R.C. Denney, E.L.B.S., Longman, 5th edn, 1989.
[16] R.M. Silverstein, G.C. Bassler and T.C. Morrill, Spectrometric Identification of Organic Compounds, Wiley, New York, 1991, p. 120.
[17] S.N. Shaikh and J. Zubieta, Inorg. Chem., 27 (1988) 1896.
[18] W.M. Landing, C. Haraldsson and N. Paxeus, Anal. Chem., 58 (1986) 3031.
[19] D.E. Leydon and G.H. Luttrell, Anal. Chem., 47 (1975) 1612.
[20] H. Obata, H. Karatani and E. Nakayama, Anal. Chem., 65 (1993) 1524.
[21] P.D. Goulden, Environmental Pollution Analysis, Heyden, London, 1978.

ELSEVIER

Talanta 44 (1997) 1455–1462

Talanta

Steric effect of substituents on the extraction of lanthanoids(III) with *N*-*p*-(*n*-, *iso*- and *tert*-)butylbenzoyl-*N*-phenylhydroxylamine

Sadanobu Inoue [a,*], Qiangbin Zhang [a], Masayuki Uto [b]

[a] *Department of Material Science, Kitami Institute of Technology, Kitami 090, Japan*
[b] *Cooperative Research Center, Kitami Institute of Technology, Kitami 090, Japan*

Received 4 September 1996; received in revised form 20 January 1997; accepted 22 January 1997

Abstract

N-*p*-(*n*-, *iso*- and *tert*-)Butylbenzoyl-*N*-phenylhydroxylamine (HL) was synthesized to evaluate the steric effect of the substituent on the mutual extraction separation of representative lanthanoids(III) (Ln). Lanthanoids(III) were all found to be extracted with compounds as self-adducts of the form $LnL_3(HL)_2$. It was found that the structure of the substituents in *N*-*p*-butylbenzoyl-substituted *N*-phenylhydroxylamine is closely related to the separation factor for the pair of Yb/Eu. The separation factors for a pair of Eu/Yb with these compounds decreased in the order of *tert*-butyl derivative > *iso*- > *n*-, with a decreasing Taft's E_s value, that is, with an increasing steric effect of the substituent group. The correlation between the separation factor and the stereochemical shape of the substituent was also investigated. © 1997 Published by Elsevier Science B.V.

Keywords: *N*-*p*-(*n*-, *iso*- and *tert*-)Butylbenzoyl-*N*-phenylhydroxylamine; Lanthanoid; Steric effect; Stereochemical shape

1. Introduction

High-purity lanthanoid(III) metals are widely used as various functional materials such as electronic, optical and magnetic materials. The use of these metals is increasing annually [1]. However, it is very difficult to mutually separate lanthanoids(III), because of their similar chemical properties. The first general separation procedures, introduced in the 1950s, were based on complexation-enhanced ion exchange processes [2]. However ion exchange processes are costly as they require a chelating agent such as EDTA for stripping into the mobile phase, and these processes are also unsuitable for large-scale commercial production. In the mid-1960s, liquid–liquid extraction processes were introduced, and today all large-scale commercial production is performed by this process [2]. However, the extractant currently used is not sufficient for the mutual separation of lanthanoids(III). A large number of extraction steps in a continuous countercurrent process in a non-

* Corresponding author.

PII S0039-9140(97)00031-3

Table 1
Structures and nitrogen contents of *N*-benzoyl-*N*-phenylhydroxylamine and its butyl derivatives

Compound [a]	Substituent (R-)	N, % Found(Calc.)
n-Butyl-BPHA	$CH_3CH_2CH_2CH_2$-	5.26(5.20)
iso-Butyl-BPHA	$(CH_3)_2CHCH_2$-	5.18(5.20)
tert-Butyl-BPHA	$(CH_3)_3C$-	5.12(5.20)
BPHA	H-	-

a) Structure of compounds:

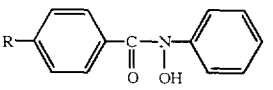

polar organic liquid are necessary to obtain high-purity lanthanoids(III), even with bis(ethylhexyl)hydrogen phosphate (D2EHPA) and 2-ethylhexyl hydrogen(2-ethylhexyl)phosphonate (PC-88A), which have been reported to have high separation efficiency [3].

Recently, the relationship between the steric effect of the extractant and separation efficiency was noted, and studies were mainly carried out with organophosphorus extractants having a bulky substituent [4–10]. Danesi et al. reported the effect of the structure of the alkyl substituents on the selectivity for the cobalt(II) and nickel(II) with dialkylphosphoric, alkyl alkylphosphonic and dialkylphosphinic acids [4]. Yuan et al. reported the steric effect of the extractant on the extraction behaviors of rare earth elements with a series of acidic organophosphorus extractants [5–7]. Ohto et al. reported the steric effect and the effect of ethereal oxygen on selectivity and extractability of rare earth elements with several kinds of new organophosphorus extractants [8,9]. Ishida et al. also reported the structural effect of extractants on the extraction behavior of rare earth metals with a series of alkyl cyclohexyl hydrogenphosphates [10].

In the present paper, we report the correlation of selectivity with Taft's E_s value, representing the steric effect of substituents, as well as the stereochemical shape of the substituent with *N*-*p*-(*n*-, *iso*- and *tert*-)butylbenzoyl substituted *N*-phenylhydroxylamine as the extractant.

2. Experimental

2.1. Reagents

The extractants were newly synthesized by the reaction of the corresponding acid chlorides with *N*-phenylhydroxylamine, as previously reported [11]. Crude products were purified by recrystallization from ethanol and water, and were dissolved in chloroform just prior to use. All the chemical formulas of *N*-benzoyl-*N*-phenylhydroxylamine (BPHA) and its butyl derivatives, and analytical results for nitrogen determined by the Kjeldahl method are shown in Table 1. Stock solutions containing lanthanoids(III) were prepared from chloride salts (Aldrich Chemical) and standardized by complexometric titration using Xylenol Orange as a indicator. Chloroform was washed three times with distilled water just prior to use. The buffer solution included 0.025 mol dm^{-3} tris(hydroxymethylamino)methane (THAM) and was prepared so as to cover a pH range of 7.4–9.1, and 0.085 mol dm^{-3} sodium tartrate solution was added to prevent the hydrolysis of lanthanoids(III). All other reagents were of analytical grade and were used without purification.

A Hitachi Model U-3210 spectrophotometer was used to determine metal concentrations after extraction. An Iwaki V-SN shaker was used to equilibrate the solutions. A Hitachi-Horiba F-7AD pH meter, calibrated daily at 4.01 and 6.86 using buffer solutions provided by Toa Denpa, was used for all measurements.

2.2. Procedure for distribution of lanthanoids(III)

The distribution of lanthanoids(III) between chloroform and water was examined as a function of each reagent and hydrogen ion concentration.

Table 2
Extraction results with butyl derivatives of BPHA

Plots	Metal	Slope	Corr. coeff.	No. of points
n-Butyl derivative	Pr	2.84	0.9990	7
log D vs. pH	Eu	3.09	0.994	9
	Yb	3.06	0.992	7
log *D*-3pH vs. log $[HL]_o$	Pr	5.24	0.998	7
	Eu	4.73	0.9985	5
	Yb	5.23	0.997	5
iso-Butyl derivative	Pr	3.21	0.9996	8
log D vs. pH	Eu	3.18	0.996	7
	Yb	2.83	0.996	7
log *D*-3pH vs. log $[HL]_o$	Pr	5.08	0.998	6
	Eu	5.01	0.9986	6
	Yb	5.07	0.997	4
tert-Butyl derivative	La	2.69	0.995	9
log D vs. pH	Pr	3.19	0.993	9
	Eu	3.20	0.998	7
	Ho	3.10	0.995	7
	Yb	2.77	0.998	5
log D-3pH vs. log $[HL]_o$	La	4.78	0.992	4
	Pr	5.23	0.996	6
	Eu	4.74	0.998	4
	Ho	4.72	0.992	4
	Yb	4.98	0.996	4

A 10 cm^3 portion of a buffered lanthanoid(III) solution with an initial concentration of 1.92×10^{-5} mol dm^{-3} containing 0.034 mol dm^{-3} tartrate ions and an equal volume of the reagent in chloroform solution was equilibrated in a 50-cm^3 vial by vigorous shaking for 1 h, a time period which was found to be adequate for the attainment of equilibrium. The pH at equilibrium was measured after phase separation. An aliquot of the organic phase was shaken with a 0.1 mol dm^{-3} sodium formate-formic acid buffer at pH 4.05. The concentration of the lanthanoid(III) back-extracted into the aqueous solution was determined by the Arsenazo III method [12]. The lanthanoid(III) concentration in the aqueous phase was calculated by using a material balance technique.

3. Results and discussion

3.1. Extraction equilibrium of lanthanoid(III)

The stoichiometries for chelate extractions and extraction constants of lanthanoids(III) with *N*-*p*-(*n*-, *iso*- and *tert*-)butylbenzoyl-*N*-phenylhydroxylamine were obtained based on the relationships of log D vs. pH and log D-3pH vs. $\log [HL]_O$, so-called 'slope analysis'. The results of slope analysis are summarized in Table 2 except the data for BPHA, which was already reported [13]. From these data, all of the slopes of log D vs. pH for the representative tervalent lanthanoids(III) (La, Pr, Eu, Ho and Yb) were found to be close to three, indicating that the extracted species contain three L^- ions, since three hydrogen ions are released during their formation. However, the ex-

Table 3
Extraction constant and $pH_{1/2}$ for the extraction of lanthanoids with butyl derivatives and comparison with BPHA

Compound	Log $k_{ex}\beta_{nHL}$ [a] and $pH_{1/2}$ [b]				
	La	Pr	Eu	Ho	Yb
n-Butyl	—	−12.01 (7.34)	−10.14 (6.71)	—	−9.24 (6.41)
iso-Butyl	—	−12.15 (7.38)	−10.34 (6.78)	—	−8.96 (6.32)
tert-Butyl	−13.18 (7.73)	−12.31 (7.44)	−10.46 (6.82)	−9.35 (6.45)	−8.69 (6.23)
BPHA[c]	−13.21 (7.07)	−12.05 (6.68)	−10.23 (6.08)	−9.42 (5.81)	−9.07 (5.69)

[a] $n = 1$ for BPHA and $n = 2$ for others.
[b] Calculated at $[HL]_o = 10^{-2}$ mol dm^{-3}; its values are given in parentheses.
[c] Ref. [13].

tracted species are not simple chelates. In Table 2, plots of log D-3pH vs. log $[HL]_O$ at a constant pH are linear with slopes close to five. As previously reported by Hori et al. [12], tartrate species, and lanthanoid(III) is present in the aqueous phase largely as its ditartrate complex, LnT_2^-. These results indicate that the stoichiometry for chelate extractions involving adduct formation can be expressed as

$$LnT_2^- + 5HL_O \rightleftharpoons LnL_3(HL)_{2,O} + 3H^+ + 2T^{2-} \quad (1)$$

where T^{2-} is the tartrate dianion and LnT_2^- is the tartrate complex of the lanthanoid(III), which exists in solution. The experiments were carried out at a constant concentration (C_T) of 0.034 mol dm^{-3}. The distribution ratio (D) of the lanthanoid(III) for chelate extraction equilibrium (Eq. (1)) is given by

$$D = \beta_3 K_{DC} K_a^3 \beta_{2HL} [HL]_o^5 / K_{DL}^3 K_f C_T^2 [H^+]^3 = K'_{ex}\, \beta_{2HL} [HL]_o^5 / [H^-]^3 \quad (2)$$

and

$$\log D = \log(K'_{ex}\, \beta_{2HL}) + 3pH + 5 \log [HL]_o \quad (3)$$

where K_a and K_{DL} are the acid dissociation constant and distribution constant of the reagents, respectively. β_3 and K_{DC} are the overall aqueous formation constant of LnL_3 and its distribution constant, respectively. K_f is the overall aqueous formation constant of LnT_2^- and β_{2HL} is the adduct formation constant of the following reaction:

$$LnL_{3,o} + 2HL_o \rightleftharpoons LnL_3(HL)_{2,o} \quad (4)$$

The conditional extraction constant (K'_{ex}) is related to the extraction constant (K_{ex}) in the following manner:

$$K_{ex} = K'_{ex}\, K_f\, C_T^2 = \beta_3\, K_{DC}\, K_a^3 / K_{DL}^3 \quad (5)$$

The values of log ($K_{ex}\, \beta_{2HL}$) and the pH values at half extraction ($pH_{1/2}$) for the reagents studied are given in Table 3 and compared with the values obtained for BPHA [13]. The separation factors (defined as the difference in log ($K_{ex}\, \beta_{2HL}$)) for the Pr/Eu and Eu/Yb pairs are also given in Table 4 along with that for BPHA. It was found that the lanthanoids(III) were extracted with each butyl derivative as a self-adducted chelate, $LnL_3(HL)_2$, containing two neutral adduct molecules in extracted species, although only one neutral adduct molecule for the BPHA system was found [13].

Table 4
Comparison of separation factor for Eu/Pr and Yb/Eu with BPHA and its butyl derivatives

Compound	Extracted species	Log (SF)		E_s value for substituent[a]
		Eu/Pr	Yb/Eu	
n-Butyl	$LnL_3(HL)_2$	1.87	0.90	−0.39
iso-Butyl	$LnL_3(HL)_2$	1.81	1.38	−0.93
tert-Butyl	$LnL_3(HL)_2$	1.85	1.77	−1.54
BPHA[b]	$LnL_3(HL)$	1.82	1.16	1.24

[a] Ref. [16].
[b] Ref. [13].

3.2. Correlation of extractability or separation factor with Taft's E_s value

For estimating the steric effect of the substituent in the organic reaction, the steric constant, E_s, was defined by Taft [14] as $E_s = \log(k_X/k_H)$, where k refers to the rate constant for the acid hydrolysis of esters of the $X-CH_2COOR$ type. Hence, $E_s = 0$ when $X = H$, i.e., when the group attached to the ester function is CH_3 [15]. The larger steric effect of the substituent, the smaller is the E_s value of the substituent. The steric constant, E_s, for each substituent [16] is shown in Table 4. As described above, since the same extraction stoichiometries with each butyl derivative hold, the values of $\log(K_{ex}\ \beta_{2HL})$ and log (SF) for each butyl derivatives can be directly compared with each other. The $\log(K_{ex}\ \beta_{2HL})$ values for Eu and Pr with these derivatives in Table 3 decrease with decreasing E_s values for the substituents, that is, with an increasing steric effect of the substituents: *n*-butyl derivative > *iso*- > *tert*-. However, the opposite order was found for the extraction of Yb with these derivatives: *n*-butyl derivative < *iso*, < *tert*-. If the $\log(K_{ex}\ \beta_{2HL})$ value is mainly influenced by a steric hindrance of the substituent, $\log(K_{ex}\ \beta_{2HL})$ values for Yb with these butyl derivatives should be still more same order as that of Eu and Pr, since Yb has the smallest ionic radii in the lanthanoids(III) studied. Probably the factors other than steric effect of substituent for the extraction of Yb may affect. These results suggest that selectivity in the extraction of lanthanoids(III) is influenced by introducing these butyl groups into BPHA. Separation factors (SF) for the two pairs Pr/Eu and Eu/Yb were chosen to represent selectivity in the lighter and heavier members of the lanthanoids(III). The log (SF) value for the pair Pr/Eu is approximately constant value (1.8) for *n*-, *iso*- and *tert*-butyl derivatives as shown in Table 4. However, the log (SF) values for a pair of Eu/Yb increase in the order of *tert*-butyl derivative > *iso*- > *n*-, with decreasing E_s values, that is, with an increasing steric effect of the substituent group. The steric effect of the substituent for the separation of lanthanoids(III) was observed for the pair Eu/Yb, which has smaller ionic radii than that of Pr.

3.3. Correlation of the separation factor with the stereochemical shape of the substituent

Taft's E_s constant is generally used as a numerical definition of the steric substituent effect in an organic reaction. However, this value is inappropriate as a parameter for representing the shape of the substituent. Verloop et al. have attempted a multiparameter approach to steric interaction of organic compounds with macromolecules or drug receptors [17]. They have selected five dimensions defined by the length and width of the substituent, and have developed a computer program using van der Waals radii, standard bond angles and length, and reasonable conformations to define the space requirements of the substituent. Fig. 1(a and b) illustrates a procedure for determining the

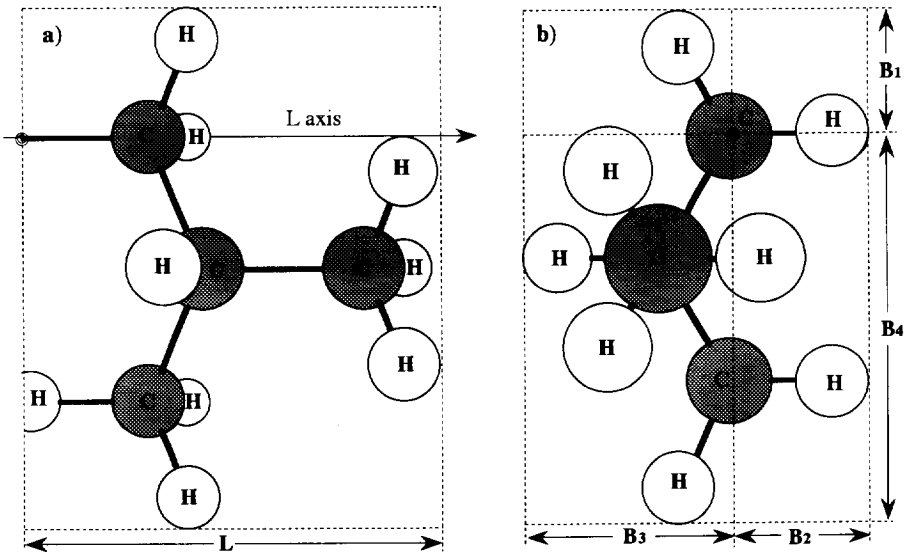

Fig. 1. Projection of the *iso*-butyl group: ◎ denotes the center of carbon in the benzene ring bonded to the *iso*-butyl group.

five dimensions by projecting an *iso*-butyl group. The length dimension, L, is defined as the length of substituent along the axis of the bond between the α-carbon atom of the *iso*-butyl group and the carbon atom in the benzene ring bonded to the *iso*-butyl group as shown in Fig. 1a. The four width dimensions, B_1–B_4, are determined from the distance at their maximum point perpendicular to this attachment bond axis and each other. B_1 is the smallest and B_4 is the largest width as shown in Fig. 1b. As these L and B values, we have employed the numerical values already reported by Verloop et al. [17]. The correlation between the E_s value and L or B_4 for butyl groups is shown in Fig. 2. L and B_4 parameters show relatively good correlations with the E_s value, indicating a steric effect of the branching of butyl substituents on the stereochemical shape of the substituent. However, a correlation of the E_s value with B_1, B_2 or B_3 was not observed. A relatively good inverse correlation between Log (SF) for Eu/Yb and L or B_4 for each butyl substituent was also observed as shown in Fig. 3. These results indicate the validity of the steric effect of branching of the butyl group on the selectivity of butyl derivatives and the possibility for evaluation of selectivity on the basis of L and B_4 for the substituent. Correlations of log (SF) with L/B_1 and log (SF) with B_4/B_1 are also shown in Fig. 4, where both L/B_1 and B_4/B_1 indicate asymmetry in the shape of the substituent. The log (SF) value for Yb/Eu gave the largest value

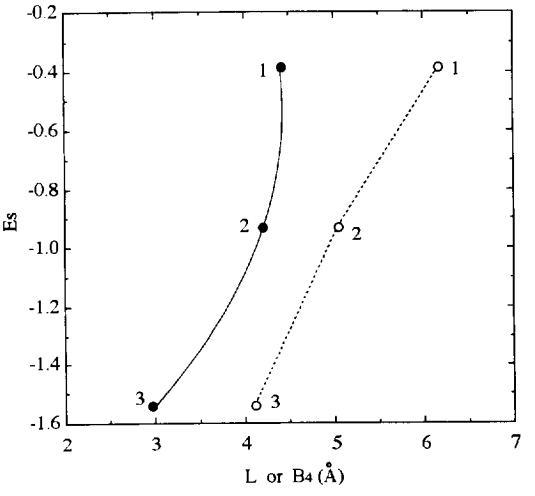

Fig. 2. Relationship between E_s and L or B_4. Dotted line, L; solid line, B_4; 1, *n*-butyl derivative; 2, *iso*-butyl; 3, *tert*-butyl.

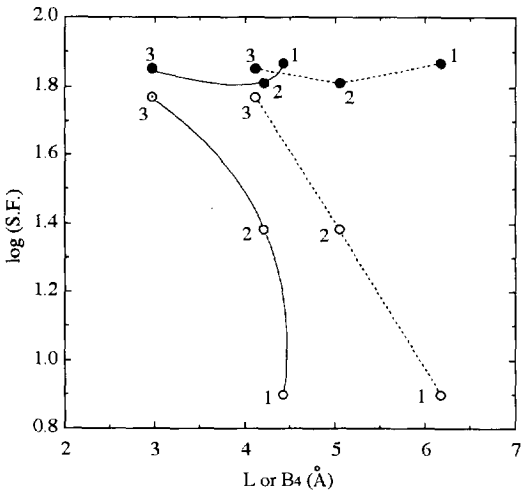

Fig. 3. Relationship between log (SF) and L or B_4. Dotted line, L; Solid line, B_4; white circle, Yb/Eu; black circle, Eu/Pr; 1, *n*-butyl derivative; 2, *iso*-butyl; 3, *tert*-butyl.

(1.77) with the *tert*-butyl derivative having developed branching structure and spherical in shape in the butyl derivatives studied. As is apparent from Fig. 3 and Fig. 4, introducing a substituent with the appropriate branching to BPHA that may cause a steric hindrance is a good means of improving the selectivity of HPHA for the extraction of heavy lanthanoids(III). Two neutral adduct molecules in the extracted species were included and these two neutral molecules may bond to metal ions with hydrogen bonds with the other ligands in some way. The configuration in space of neutral molecules may be expected to have an effect on the steric hindrance by substituent groups on the ligand. However, such an effect on steric hindrance was not considered in the present studies, although the effect of the length and width of the substituent on steric hindrance was investigated as shown in Fig. 1. The configuration in space of neutral adduct molecules will appear only by analysis with other separate experiments, such as X-ray diffraction.

In conclusion, the extractant plays an important role in mutual separation of lanthanoids(III). The results obtained in this study provide useful information on ligand design for the mutual extraction separation of lanthanoids(III).

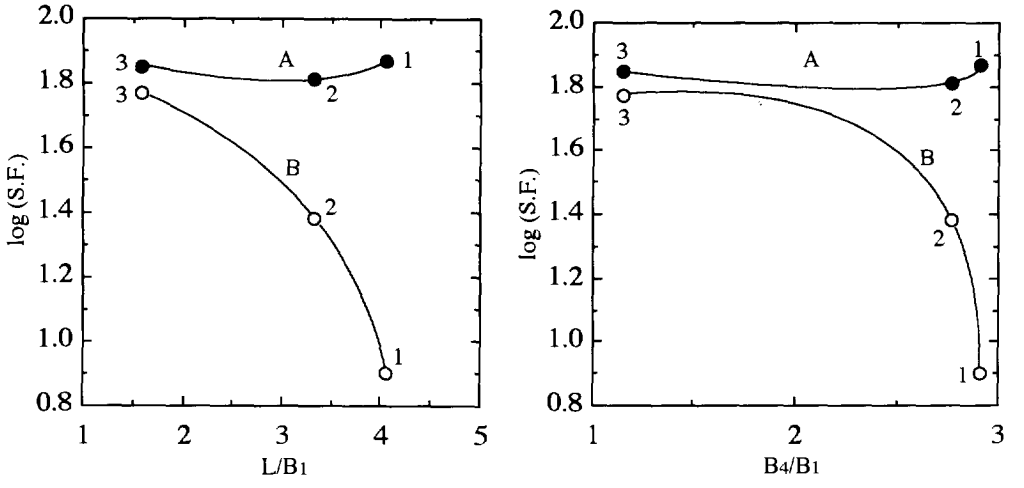

Fig. 4. Relationship between L/B_1 or B_4/B_1 and log (SF): Curve A, Eu/Pr; Curve B, Yb/Eu; 1, *n*-butyl derivative; 2, *iso*-butyl; 3, *tert*-butyl.

References

[1] G. Adachi's Laboratory in Osaka University, Kidorui Monogatari, in G. Adachi (Ed.), Rare-earth story, in Japanese, Sangyoutosho, Tokyo, 1991, pp. 17–18.
[2] F.A. Cotton and G. Wilkinson, Advanced Inorganic Chemistry, 5th Ed., Wiley, 1988, pp. 963–964.
[3] T.B. Pierce, P.F. Peck, Analyst (London) 88 (1963) 217.
[4] P.R. Danesi, L. Reichley-Yinger, G. Mason, L. Kaplan, E.P. Horwitz, H. Diamond, Solvent Extr. Ion Exch. 3 (1985) 435.
[5] C. Yuan, W. Ye, H. Ma, G. Wang, H. Long, J. Xie, X. Qin, Y. Zhou, Sci. Sin. Ser. B 25 (1982) 7.
[6] C. Yuan, J. Yan, H. Feng, H. Long, F. Wu, P. Jin, Sci. Sin. Ser. B 30 (1987) 7.
[7] C. Yuan, S. Hu, Sci. Sin. Ser. B 31 (1988) 137.
[8] K. Ohto, K. Inoue, M. Goto, F. Nakashio, T. Nagasaki, S. Shinkai, T. Kago, Bull. Chem. Soc. Jpn. 66 (1993) 2528.
[9] K. Ohto, S. Yoshida, K. Yoshizuka, K. Inoue, M. Ohtsuka, M. Goto, F. Nakashio, Anal. Sci. 11 (1995) 637.
[10] K. Ishida, T. Takahashi, M. Nakamura, T. Sato, Bunseki Kagaku 42 (1993) 655.
[11] C.A. Armour, D.E. Ryan, Can. J. Chem. 35 (1957) 1454.
[12] T. Hori, M. Kawashima, H. Freiser, Sep. Sci. Technol. 15 (1980) 861.
[13] T. Cecconie, M. Hojjatie, H. Freiser, Anal. Chim. Acta 193 (1987) 247.
[14] R.W. Taft, J. Am. Chem. Soc. 74 (1952) 3120.
[15] C. Hansch and A.J. Leo, Substituent Constants for Correlation Analysis in Chemistry and Biology, Wiley, NY, 1979, pp. 9.
[16] N. Inamoto, Kagaku Seminar 10, Hametto Soku, Chemical Seminar 10, Hammett rule (in Japanese), Maruzen, Tokyo, 1983, pp. 54.
[17] A. Verloop, W. Hoogenstraaten and J. Tipker, in E.J. Ariens (Ed.), Drug Design, Vol. VII, Academic Press, NY, 1976, pp. 165.

ELSEVIER

Talanta 44 (1997) 1463–1472

Talanta

Analytical assessment of the oscillating chemical reactions by use chemiluminescence detection

Rafael Jiménez-Prieto *, Manuel Silva, Dolores Pérez-Bendito

Department of Analytical Chemistry, Faculty of Sciences, University of Córdoba, E-14004 Córdoba, Spain

Received 27 November 1996; received in revised form 7 February 1997; accepted 10 February 1997

Abstract

This paper introduces the chemiluminescence (CL) detection in oscillating reaction-based determinations using the analyte pulse perturbation technique, a straightforward and expeditious approach to deriving quantitative analytical information from oscillating chemical reactions. The behavior of the H_2O_2–KSCN–$CuSO_4$-NaOH oscillating system in the presence of luminol was examined by using the proposed detection method and the classical potentiometric technique. Some analytical and practical aspects of both detection systems are discussed. A new analytical method for the determination of vitamin B_6 based on the sequential perturbation produced by different amounts of this substance on the oscillating chemical system was also developed in order to assess the potential of CL detection for routine analyses. The calibration curve thus obtained was linear over the range 0.5–2.0 μmol of vitamin B_6, and the precision and throughput were also quite good (3.04% as RSD and nine samples h^{-1}, respectively). The proposed method was validated by determining the vitamin in pharmaceutical preparations. © 1997 Elsevier Science B.V.

Keywords: Oscillating reaction; Analyte pulse perturbation technique; Chemiluminescence detection; Vitamin B_6; Pharmaceutical preparations

1. Introduction

Some far-from-equilibrium chemical systems exhibit an oscillating behaviour as a result of their complex mechanisms including and autocatalytic step [1]; such systems are usually referred to as oscillating reactions. The use of these reactions has been the focus of much research in the area of theoretical and experimental chemical kinetics in recent years [2,3]. From the first paper about the quantitative use of oscillating reactions published in 1978 by Tichonova et al. [4], some studies on the analytical applications of chemical oscillators have been developed [5–8].

The analyte pulse perturbation (APP) technique was developed fairly recently in order to facilitate the use of oscillating chemical reactions in routine quantitative analytical determinations [9]. It uses a continuous-flow stirred tank reactor (CSTR) to maintain oscillations for a long time (a few hours), thereby providing an inexhaustible indicator system for successively added analyte pulses; by contrast, classical determinations based on a closed system entail restarting the

* Corresponding author.

PII S0039-9140(97)00047-7

oscillating system for each new determination [4,6,7,10,11].

Research has shown that analytes exhibit various types of interactions with the H_2O_2–KSCN–$CuSO_4$–NaOH oscillation chemical system; thus, sodium thiosulphate [9] and vanillin [12] diminish its oscillating amplitude and period, whereas gallic acid [13] and ascorbic acid [12] increase its amplitude, and reduced glutathione [14] and paracetamol [12] increase its period. These responses are linearly correlated with the analyte concentration in the injected sample—those for glutathione and paracetamol fit a second-order polynomial equation, however. The APP technique also allows the resolution of mixtures of species such as gallic acid and resorcinol [15]. It has become a solidly established tool for quantitative routine determinations including those of vanillin, paracetamol and ascorbic acid in foods and pharmaceutical samples [12].

Oscillations are usually monitored potentiometrically (with a platinum electrode). However, the H_2O_2–KSCN–$CuSO_4$–NaOH system also exhibits oscillations in colour (between yellow and colourless), in the dissolved oxygen concentration [16] and, as shown more recently, in chemiluminescence in the presence of luminol [17,18].

The purpose of this work was to broaden the scope of application of the APP technique in oscillating reaction-based determinations by using a chemiluminescence (CL) detection system. To this end, we compared the performance of potentiometric and CL detection by use of the APP technique and then undertook the determination of vitamin B_6 in pharmaceutical preparations by use of this novel detection methodology in far-from-equilibrium dynamic systems.

2. Experimental

2.1. Reagents

All reagents used were supplied by Merck in analytical reagent grade. Bidistilled water was used to prepare the solutions: (1) (1.5 M hydrogen peroxide), (2) (0.15 M sodium thiocyanate, 0.15 M sodium hydroxide and 1.95×10^{-3} M luminol) and (3) [6.0×10^{-4} M copper(II) sulphate]. The analyte solutions (sodium thiosulphate, gallic acid and paracetamol) were also prepared in bidistilled water, as were vitamin B_6 solutions.

2.2. Apparatus

The instrumental set-up used is depicted in Fig. 1. The oscillating assembly comprised a 10-ml glass reaction vessel (CSTR) fitted with a thermostated jacked connected to a Selecta 6000484 thermostat, an Eyela RC-2 magnetic stirrer for homogenization, a Gilson Minipuls-3 4-channel peristaltic pump (3 of the channels were used to deliver the reactants and the fourth to keep the volume of reaction mixture in the CSTR constant), a remote control for operating the pump that allowed instantaneous switching between several preset flow-rates, and a Metrohm Dossimat 665 autoburette for injection of analyte pulses.

The CL detection system consisted of a Hitachi F-2000 fluorescence spectrophotometer the sample compartment of which was used to accommodate the CSTR and magnetic stirrer, and a PC-AT 12 MHz compatible computer equipped with a PC-Multilab PCL-812PG 12-bit analog-to-digital converter (ADC) for data acquisition and processing. Poly(vinyl chloride) pumping tubes and PTFE tubing for the manifold were also used.

2.3. General procedure for CL-based determinations

The CSTR, thermostated at 27.5°C, was loaded with the three reagent solutions (1–3), delivered by the peristaltic pump, to a final volume of 9.0 ml, and the mixture was homogenized by the magnetic stirrer. Then, the flow-rate was reset to the working conditions, viz. an overall reactant feed flow-rate of 0.9 ml min^{-1} (i.e. 0.3 ml min^{-1} through each reactant channel), the reaction products being removed at the same rate. After steady oscillating conditions were obtained, the system was perturbed by injecting micro-analyte volumes. Sodium thiosulphate, gallic acid and paracetamol were assayed in this way for comparison to potentiometric detection. Changes in the oscillation amplitude and period by effect of the perturbations

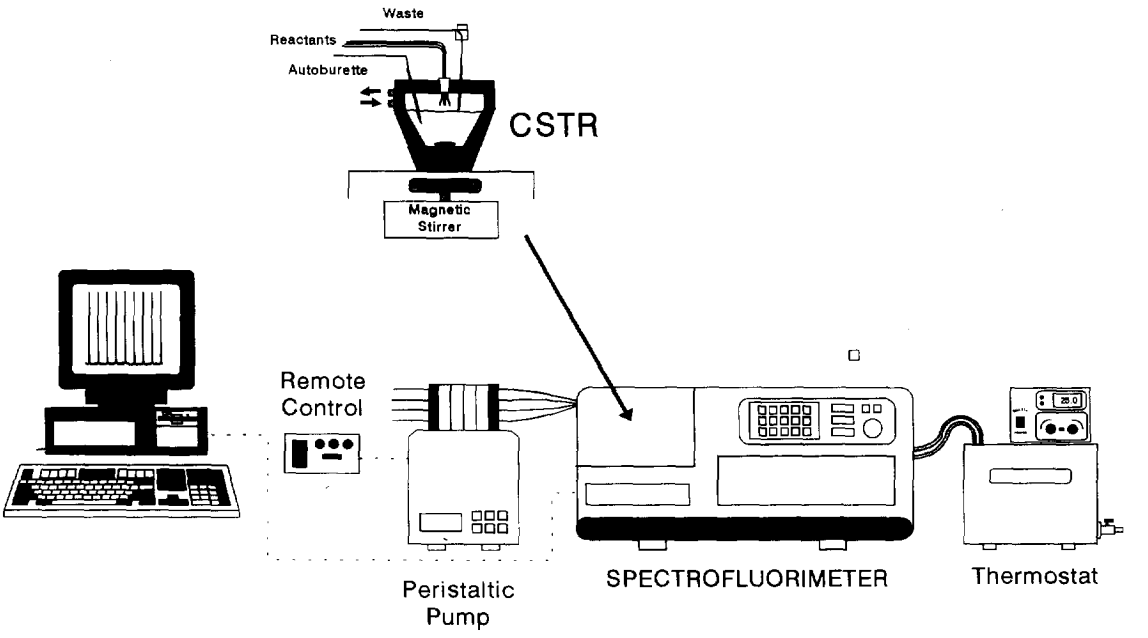

Fig. 1. Experimental set-up for implementation of CL oscillating reaction-based determinations.

were used as measurements in order to construct pertinent calibration graphs. Data were acquired and processed by using software developed by the authors in Microsoft QuickBasic v. 4.0 language.

2.4. CL determination of vitamin B_6

The CSTR, thermostated at 25°C, was filled, in this sequence, with 2.1 ml of 1.0 M hydrogen peroxide, 1.4 ml of 0.1 M sodium thiocynate, 1.05 ml of 0.1 M sodium hydroxide, 1.4 ml of 1.0×10^{-3} M copper sulphate and 1.0 ml of 7.0×10^{-3} M luminol, the mixture being homogenized by magnetic stirring. Without delay, the peristaltic pump was actuated to deliver the three reactant streams—the overall feed stream was 0.6 M in H_2O_2, 4.0×10^{-2} M in NaSCN, 3.0×10^{-2} M in NaOH, 2.0×10^{-4} M in $CuSO_4$ and 1.0×10^{-3} M in luminol—at a constant flow-rate of 1.8 ml min^{-1}. As soon as the signal and time increments for the oscillations levelled off, variable volumes (a few microlitres) of sample or standard containing also variable amounts of vitamin B_6 in the rage 0.5–20 μmol were sequentially injected. Perturbations decreased the amplitude of the oscillating cycle by a factor proportional to the amount of vitamin B_6 injected. After the system response was recorded, the flow-rate delivered by the pump was raised to 4.65 ml min^{-1} for 150 s in order to expedite restoration of the steady state. Then, the initial flow-rate (1.8 ml min^{-1}) was reset—such an abrupt rise was facilitated by the fact that the oscillating state was not lost under the working conditions used. After the steady state was regained, the system was ready for a new determination.

3. Results and discussion

The copper(II)-catalysed oscillating reaction between hydrogen peroxide and sodium thiocyanate has been widely studied by Orbán in 1986 and 1990 and Luo et al. in 1988 [16,19,20]; who propose that the mechanism for this oscillating reaction consists of 30 kinetic steps involving 26 independent variables [21]. The centerpiece of the mechanism of this reaction, which contains the key of the oscillation, is the positive and negative feedback loops on which the autocatalytic process

Table 1
Effect of experimental variables on the oscillating system, with potentiometric and CL detection

Variable	Range	Measured parameter				Selected value
		Amplitude		Period		
		E^a	CL	E^a	CL	
H_2O_2	0.4–0.8 M	↓	↑	↓	↓	0.5 M
NaSCN	$(3.0–9.0)\times10^{-2}$ M	↑	↑	↑	↑	5.0×10^{-2} M
$CuSO_4$	$(1.0–3.0)\times10^{-4}$ M	↓	↓	↓	↓	2.0×10^{-4} M
NaOH	$(1.0–7.0)\times10^{-2}$ M	↓	↓	↑	↑	5.0×10^{-2} M
Temperature	20–40°C	≈cons.	↑	↓	↓	27.5°C
Luminol	$(0.5–2.5)\times10^{-3}$ M	—	↑	—	↑	6.5×10^{-4} M

E, potentiometric detection.
Arrows pointing upward and downward indicate increase or decrease, respectively, in the oscillating amplitude and period with increase in the variable concerned over the stated range.
[a] Data from Jiménez-Prieto et al. [9].

relies. Thus, the positive feedback loop produces the yellow superoxy copper(I) complex:

$$OS(O)CN^* + Cu^+[SCN^-]_n \rightarrow OS(O)CN^- + Cu^{2+} + nSCN^-$$

$$H_2O_2 + Cu^{2+} + OH^- \rightarrow HO_2 - Cu(I)_{yellow} + H_2O$$

which disappears in the negative feedback loop:

$$HO_2 - Cu(I)_{yellow} + nSCN^- \rightarrow Cu^+[SCN^-]_n + HO_2^*$$

the concentration of species $Cu^+[SCN^-]_n$ being crucial for this feedback network.

The light-producing reactions of luminol have been the subject of much research and are thus widely documented [22–25]. However, oscillating chemiluminescence (viz. that produced by addition of luminol to the H_2O_2–KSCN–$CuSO_4$–NaOH oscillating system) is an intriguing phenomenon that was only recently described in the literature [17]. Although the information gathered from the few studies carried out so far on the interaction of luminol with this oscillating system necessitates some refining [18], it can be ascribed as:

$$HO_2 - Cu(I)_{yellow} + LumH^- \rightarrow Cu^{2+} + 2OH^- + Lum^{*-}$$

Such a peculiar oscillating system has not yet been used for analytical determinations. In this work, we examined its analytical performance in combination with the analyte pulse perturbation (APP) technique and compared it with that of potentiometric detection. As a result, a new analytical method for the determination of vitamin B_6 in pharmaceutical preparations was developed to validate the proposed use of CL oscillating-reaction based methods for routine analyses.

3.1. CL vs potentiometric detection of oscillating chemical reactions

The interaction of luminol with the H_2O_2–KSCN–$CuSO_4$–NaOH oscillating system was examined with a view to its subsequent use for developing analytical determinations in combination with the APP technique. Thus, the effect of experimental variables potentially influencing the system performance was thoroughly assessed and the results compared with those obtained with potentiometric detection. The oscillating amplitude and period were the two measured parameters used in both cases.

Table 1 shows the results of this comparative study. As can be seen, the oscillation period exhibited a similar behaviour with both potentiometric and CL detection; however, the oscillation

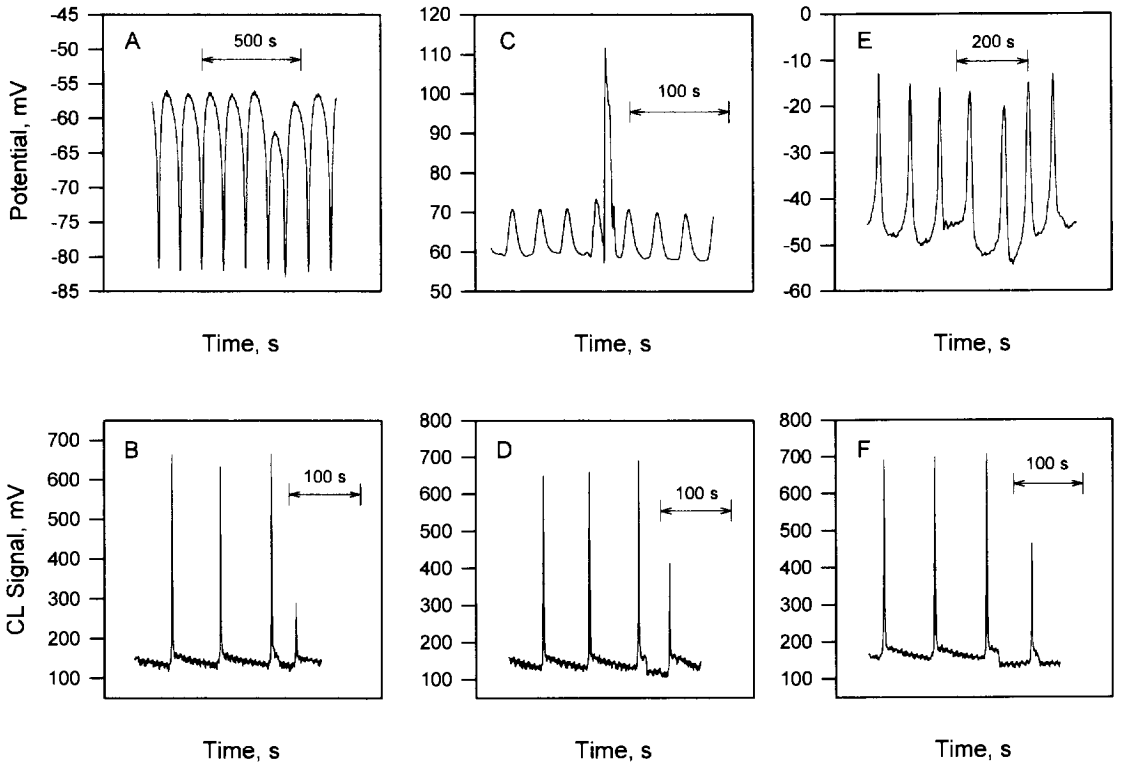

Fig. 2. Time course of oscillations for the H_2O_2–KSCN–$CuSO_4$–NaOH system in the absence and presence of perturbations with (A) and (B) sodium thiosulphate, (C) and (D) gallic acid, and (E) and (F) paracetamol, with potentiometric and CL detection in the presence of luminol.

amplitude response was different for hydrogen peroxide and temperature. The optimum value for each variable in the CL detection study was selected with three criteria in mind, namely: (a) maximizing the stability of the oscillating system over time; (b) maximizing the oscillation amplitude; and (c) ensuring that the oscillation period would allow the effect of perturbations on it to be accurately determined.

The high similarity in the behaviour of the oscillating period –the most important feature of an oscillating system whatever the detection system used—in relation to changes in the experimental variables suggests a coupled interaction between luminol and the oscillating system. In fact, considering that oscillations coincide in colour (between yellow and colourless) and in CL, then one can assume the yellow superoxy copper(I) complex to act as a catalyst in the oxidation of luminol by hydrogen peroxide. On the other hand, the differences observed for the hydrogen peroxide concentration and temperature in comparing the oscillation amplitude responses can be ascribed to a substantial effect of these variables on the optimization of the CL luminol reaction—the stability of the oscillating system over time is compromised in no way, however. The similar effects of copper on the oscillation amplitude and period with both potentiometric and CL detection, and hence the seemingly null influence of this variable on the CL luminol reaction—despite its catalytic effect on it—can be ascribed to the high concentration of copper in the reaction medium: the reaction was thus poisoned, so increasing the copper concentration decreased the CL amplitude, similarly as in potentiometric detection.

Under the selected experimental conditions, the oscillating curve was perturbed by using several

Table 2
Comparison of the performance of CL and potentiometric detection in the oscillating reaction-base determination of thiosulphate, gallic acid and paracetamol

Analyte	Determination method			
	CL detection		Potentiometric detection	
Thiosulphate	Amplitude	Period	Amplitude[a]	Period[a]
Dynamic linear range (μmol)	0.4–3.0		1.0–18	2.0–18
Detection limit (μmol)	0.10	0.15	0.28	0.73
Precision (RSD)[d] (%)	3.5[e]	2.5[e]	0.71[f]	1.33[f]
Throughput (samples h^{-1})	10		10–12	
Gallic acid	Amplitude	Period	Amplitude[b]	
Dynamic linear range	0.6–1.9		0.075–2.0	
Detection limit (μmol)	0.15	0.20	0.022	
Precision (RSD)[d] (%)	4.2[g]	2.1[g]	2.1[h]	
Throughput (samples h^{-1})	11		14	
Paracetamol	Amplitude		Period[c]	
Dynamic linear range	0.5–7.0		0.5–6.0	
Detection limit (μmol)	0.13		0.15	
Precision (RSD)[d] (%)	2.27[i]		0.95[i]	
Throughput (samples h^{-1})	7		8	

[a] Data from Jiménez-Prieto et al. [9].
[b] Data from Jiménez-Prieto et al. [13].
[c] Data from Jiménez-Prieto et al. [12].
[d] Relative standard deviation.
From 11 determinations of [e] 1 and [f] 10 μmol of thiosulphate, [g] 0.75 and [h] 0.3 μmol of gallic acid, and [i] 2 μmol of paracetamol.

amounts of various analytes, viz. sodium thiosulphate, gallic acid and paracetamol, which were chosen because each responded differently to perturbations of the oscillating system with potentiometric detection and thus afforded comparison with CL detection. Fig. 2 shows the typical responses thus obtained and their potentiometric counterparts. The responses were analysed in terms of the oscillation amplitude and period of the perturbed system for each analyte tested. Table 2 gives the analytical figures of merit for the proposed method and those obtained with potentiometric detection. Detection limits were taken to be the analyte concentrations giving analytical signals equal to three times the standard deviation ($n = 30$) of the oscillation amplitude or period in the absence of perturbation (blank) [26]; also, the throughput was calculated from the time needed for the system to recover after each perturbation.

The results shown in Fig. 2 and Table 2 allow one to draw several interesting conclusions, namely:

1. As a rule, the detection limit and dynamic linear range was similar or better with CL detection except for gallic acid. This analyte exhibited a peculiar behaviour; the large increase in the amplitude with potentiometric detection (Fig. 2C) was more likely the result of the electroanalytical properties of this compound, which presumably forms a complex with copper in the medium [13], than of its interaction with the oscillating system since a perturbation by itself can never increase the oscillation amplitude. In this respect, CL detection is a more reliable means for assessing interactions between analytes and the oscillating system. On the other hand, the reactivity sequence obtained for the analytes (sodium

thiosulphate > gallic acid > paracetamol) may be directly related to their reducing power.

2. CL detection provided poorer precision (as RSD) than potentiometric detection as the likely result of instrumental differences. Thus, the sharp change in CL signals (Fig. 2) results in some inaccuracy in locating its maximum. While the acquisition rate was more than adequate (the maximum A/D sampling rate was 30 kHz), the performance was constrained by the spectrofluorimeter's time constant, which directly influenced the analog signal provided by the instrument.

3.2. New approach to analytical determinations: the CL quantitation of vitamin B_6

After both detection methods were assessed, the potential of CL oscillating reaction-based determinations for routine analyses was evaluated with the determination of vitamin B_6 in pharmaceutical preparations.

The addition of variable amounts of vitamin B_6 to the CSTR where the H_2O_2–KSCN–$CuSO_4$–NaOH-luminol oscillating reaction was developed decreased the amplitude of the cycles following the perturbation to an extent proportional to the analyte concentration in the sample. Fig. 3 shows a typical oscillation sequence obtained for the proposed chemical system in the absence and presence of vitamin B_6 perturbations. Fig. 3 shows the system oscillating in the steady state (zone A), its response to the perturbations (zone B) and the situation after the steady state conditions were restored (zone C).

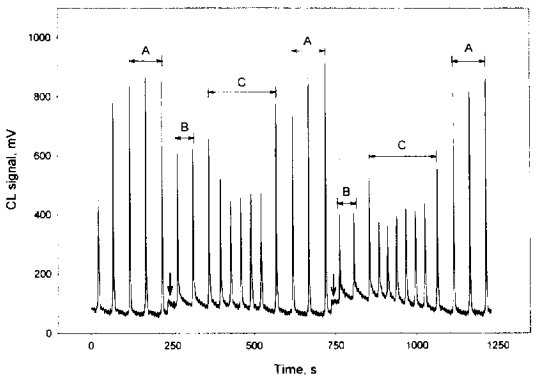

Fig. 3. Typical profiles for the proposed CL oscillating reaction in the presence and absence of a vitamin B_6 perturbation. Arrows indicate the times at which oscillations were perturbed. Zones A–C correspond to the oscillating steady state (A), the response of the oscillating system to the perturbation (B), and (C) recovery following the perturbation.

3.2.1. Influence of experimental variables

The effects of the variables potentially influencing the behaviour of the oscillating system were thoroughly studied in the presence and absence of perturbations. The measured parameter used for this purpose was the ratio of the oscillating amplitude before and after each injection. The optimum value of each variable met the following two conditions: (a) it allowed the system to oscillate undisruptedly and to recover its steady state after each perturbation; and (b) the system response to vitamin B_6 perturbations was maximal and so was the sensitivity of the method.

Fig. 4 illustrates the influence of the different variables studied—their optimum values are given in Section 2. Some selected values did not correspond to the maximum value of the measured parameter (e.g. 2.0×10^{-2} and 1.5×10^{-2} M as the concentration of NaSCN and NaOH, respectively) because a compromise between sensitivity in the determination of vitamin B_6 and stability of the oscillating system must be made. Thus, lower concentrations of both reactants caused the system to lose some stability on each injection.

One other influential variable—not shown in Fig. 4—was the reactant feed rate, the effect of which was examined over the range 0.44–5.31 ml min^{-1}. The oscillation amplitude of both the unperturbed and the perturbed system were found to decrease with increase in this rate, with no net effect on the amplitude ratio. The oscillating period also decreased with increase in the feed rate. Because the system response was not affected, the optimum flow-rate value was taken to be that resulting in an appropriate oscillation period in the steady state, viz. 1.8 ml min^{-1}. On the other hand, the flow-rate used to restore the steady-state conditions after each perturbation was the highest possible in order to shorten the restoration time with no loss of the oscillating state –

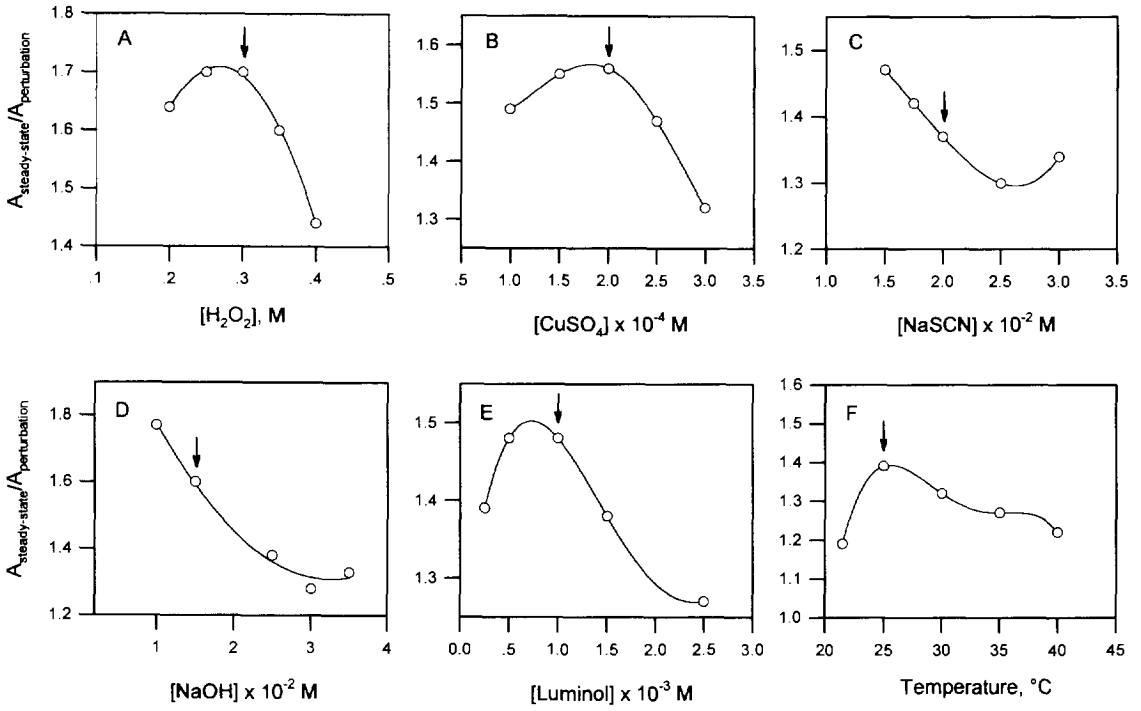

Fig. 4. Influence of the concentrations of hydrogen peroxide (A), copper sulphate (B), sodium thiocyanate (C), sodium hydroxide (D) and luminol (E), and of temperature (F), on the oscillating reaction in the presence of vitamin B_6. Arrows indicate the selected values for the variables.

not even with the most concentrated sample. As shown in the Experimental section, such a rate was set at 4.65 ml min^{-1} and applied for 150 s.

3.2.2. Determination of vitamin B_6

The oscillating system was perturbed with microvolumes of sample containing variable amounts of vitamin B_6 (pyridoxine) between 0.5 and 20 μmol as described in Section 2. The measured parameter was the amplitude of the second response cycle (see zone C in Fig. 3). A plot of oscillation amplitude against analyte concentration was linear throughout the range studied.

Table 3
Analytical figures of merit of the determination of vitamin B_6 with the proposed CL method

Dynamic linear range (μmol)	0.5–20
Detection limit (μmol)	0.1
Precision (RSD) (%)[a]	3.04
Throughput (samples h^{-1})	9

[a] From 11 determinations of 5 μmol of vitamin B_6.

Table 3 gives the analytical figures of merit for the determination. As can be seen, the proposed method is quite precise. Its throughput was calculated from the time needed for the system to regain its initial state after each perturbation; the result, 9 samples h^{-1}, confirms the goodness of the APP technique for the intended purpose.

The potential interfering effects of structurally related species was also investigated. To this end, a fixed amount of pyridoxine (5 μmol) was injected jointly with variable amounts of pyridoxylamine, pyridoxal-5-phosphate, pyridoxal and 4-pyridoxic acid. All were found to interfere with the determination—particularly pyridoxamine, above an interferent-to-analyte ratio as low as 0.0015; this can be ascribed to its reducing power and the presence of primary amino groups in its structure, which probably had a marked dis-

Table 4
Determination of vitamin B_6 in pharmaceutical preparations

Trade name	Nominal content (mg g^{-1})	Found[a] (mg g^{-1})	Error (%)
Pacium[b]	33.3	33 ± 9	−1.1
Vertigum[c]	275.1	247 ± 13	−10.1
Taurobetina[d]	112.4	104 ± 6	−7.4
Trofimilina[e]	387.1	370 ± 30	−4.5

[a] Average of three individual determinations ± S.D.
Other ingredients (in mg g^{-1}) included: [b] diazepam (16.7); [c] dixirazine (41.3), inositol nicotinate (275.1), wheat starch (33) and lactose (317.7); [d] taurine (224.7), adenosine phosphate dipotassium salt (11.2), uridine phosphate dipotassium salt (22.5), vitamin B_{12} (0.22) and sucrose (343.8); [e] 129 mg of total homogenate of neurohomologous phospholipids of cortical grey matter equivalent to 2.55 mg of lipid phosphorus in terms of its components (phosphatidylcholine, phosphatidylethanolamine, phosphatidylserine, phosphatidic acid, diphosphoinositic acid and sphingomyelin).

turbing effect on the oscillating reaction [21]. These results are of a high interest with a view to developing sensitive determination methods for various pyridoxine derivatives, which could be used as a useful alternative to other liquid chromatographic detection systems.

3.2.3. *Applications*

We assessed the potential of the proposed method for determining vitamin B_6 in real samples of special interest. For this purpose, we selected several pharmaceutical preparations including pyridoxine as the active principle or a secondary ingredient. The nominal value in each preparation was used as reference—with provision for potential errors made in the manufacturing process—because the basic aim was simply to demonstrate the usefulness of the method for routine analyses of this type of sample.

The sample preparation procedure was quite simple. Thus, solutions were all made in bidistilled water and the amount of sample used was dictated by its pyridoxine concentration. In those cases were dissolution was incomplete, the sole additional treatment required was filtration to a clear solution, an appropriate aliquot of which was subjected to the above-described procedure. The Trofimilina sample, a phospholipid homogenate and hence of oily texture, was dissolved in chloroform and then extracted for vitamin B_6 with bidistilled water.

The results obtained are given in Table 4. As can be seen, they were quite consistent with the nominal values. No separation of the species accompanying vitamin B_6 in the preparations studied was needed.

The simplicity, expeditiousness and precision of the proposed method as regards sample pretreatment, and the good results it provides, make oscillating chemical systems and chemiluminescence determination useful couples for determining species in real samples of interest.

Acknowledgements

The authors gratefully acknowledge financial support from the Spanish Dirección General Interministerial de Ciencia y Tecnología (DGICyT) for the realization of this work as part of Project PB91-0840.

References

[1] A.S. Tomlin, Anal. Proc. 30 (1993) 3072.
[2] R.J. Field and M. Burger, Oscillation and Travelling Waves in Chemical Systems. Wiley, New York, 1985.
[3] P. Gray and S.K. Scott, Chemical Oscillations and Instabilities. Clarendon Press, Oxford, 1990.
[4] L.P. Tichonova, L.N. Zakrevskaya, K.B. Yatsimirskii, Talanta 33 (1978) 1991.
[5] Z. Qinyuang, J. Chen, Fenxi Shiyanshi 7 (1988) 4.
[6] M. Jiang, Y. Li, X. Zhuo, Z. Zhao, H. Wang, J. Mo, Anal. Chim. Acta 236 (1990) 411.
[7] K.B. Yatsimirskii, P.E. Strizhak, T.S. Ivaschenko, Talanta 40 (1993) 1227.
[8] R.T. Echols, M.K. Caroll, J.F. Tyson, Anal. Proc. 32 (1995) 3.
[9] R. Jiménez-Prieto, M. Silva, D. Pérez-Bendito, Anal. Chem. 67 (1995) 729.
[10] Y. Liang, R. Yu, Gaodeng Xuexiao Huaxue Xuebao 9 (1988) 881.
[11] Q. Zhang, J. Chen, Fenxi Shiyanshi 7 (1988) 4.
[12] R. Jiménez-Prieto, M. Silva, D. Pérez-Bendito, Analyst 122 (1997) 287.
[13] R. Jiménez-Prieto, M. Silva, D. Pérez-Bendito, Anal. Chim. Acta 321 (1996) 53.
[14] R. Jiménez-Prieto, M. Silva, D. Pérez-Bendito, Analyst 121 (1996) 563.

[15] R. Jiménez-Prieto, M. Silva, D. Pérez-Bendito, Anal. Chim. Acta 334 (1996) 323.
[16] M. Orbán, J. Am. Chem. Soc. 108 (1986) 6893.
[17] J. Amrehn, P. Resch, F.W. Schneider, J. Phys. Chem. 92 (1988) 3318.
[18] S. Sattar, I.R. Epstein, J. Phys. Chem. 94 (1990) 275.
[19] M. Orbán, React. Kinet. Catal. Lett. 42 (1990) 343.
[20] Y. Luo, K. Kustin, I.R. Epstein, Inorg. Chem. 27 (1988) 2489.
[21] Y. Luo, M. Orbán, K. Kustin, I.R. Epstein, J. Am. Chem. Soc. 111 (1989) 4541.
[22] K.D. Gundermann and F. McCapra, in Chemiluminescence in Organic Chemistry. Springer-Verlag, Berlin, 1987, Ch. VII.
[23] A. Townshend, Anal. Proc. 22 (1985) 370.
[24] J.S. Lancaster, P.J. Worsfold, Anal. Proc. 26 (1989) 362.
[25] L.J. Kricka, P.E. Stanley, J. Biolumin. Chemilumin. 6 (1991) 203.
[26] G.L. Long, J.D. Winefordner, Anal. Chem. 55 (1983) 712A.

ELSEVIER

Talanta 44 (1997) 1473–1478

Talanta

The spectrophotometric determination of trace molybdenum (VI) after collection and elution as molybdate ion on protonated chitin

Suwaru Hoshi [a,*], Kiyotaka Konuma [a], Kazuharu Sugawara [a], Masayuki Uto [b], Kunihiko Akatsuka [a]

[a] *Department of Applied and Environmental Chemistry, Kitami Institute of Technology, 165 Koen-cho, Kitami-shi 090, Japan*
[b] *Department of Functional Materials, Kitami Institute of Technology, 165 Koen-cho, Kitami-shi 090, Japan*

Received 8 November 1996; received in revised form 24 January 1997; accepted 7 February 1997

Abstract

Collection and elution method for inorganic anion on protonated chitin has been applied to the spectrophotometric determination of molybdenum (VI). The molybdenum (VI) is collected as molybdate ion on a column of chitin in weak acidic medium which is easily eluted with a small volume of 0.1 M ammonia buffer solution (pH 10). The molybdenum (VI) in the eluent is determined by bromopyrogallol red-Zephiramine method spectrophotometrically. Beer's law is obeyed over the concentration range of 0.1–0.8 μg of molybdenum (VI) in 1 ml of eluent at 634 nm. The apparent molar absorptivity is 6×10^4 dm^3 mol^{-1} cm^{-1}. The tolerance limits for WO_4^{2-}, VO_3^-, CrO_4^{2-} and Fe (III) is low, that is, 1–100 times that of molybdenum (VI), but some metal ions and common inorganic anions do not interfere in concentration range of 1000–5000 times that of molybdenum (VI). The present method can be applied to the determination of molybdenum (VI) in natural water samples. © 1997 Elsevier Science B.V.

Keywords: Trace molybdenum; Chitin; Molybdate ion

1. Introduction

Molybdenum is one of the important elements for many organisms and has a wide distribution throughout nature. It is difficult, however, to determine molybdenum directly in natural samples, especially water samples because of its low concentration level. Therefore, the preconcentration methods for the determination of trace molybdenum have been developed using solvent extraction [1–6] and solid-phase extraction on various supports, including controlled pore glass [7], sephadex gel [8], anion-exchange resin [9,10], polyurethane foam [11], chelating resin [12–14], activated carbon [15] and silica gel [16].

Attention has been paid to the preconcentration of some inorganic ions as their various species on a natural polymer chitin. The spectrophotometric methods for some metal ions have been developed after the collection and elution of their colored

* Corresponding author. Fax: +81 157 2247719.

PII S0039-9140(97)00051-9

metal complexes on a chitin in the presence of suitable counter ions [17–20], in which their colored metal complexes were rapidly collected on chitin and readily eluted with a small volume of the suitable eluents. The functionalyzed chitin containing dithiocarbamate group has been also synthesized and used for preconcentration of some metal ions [21].

On the other hand, it is known that chitin acts as anion exchanger in acidic medium (Fig. 1). This property of chitin was applied to the determination of some metal ions with atomic absorption spectrometry after preconcentration as their maleonitriledithiolate [22] and 1-nitroso-2-naphthol-3,6-disulfonate [23–25] anionic chelates, and to the spectrophotometric determination of phosphate and iron after collection and elution as their phosphomolybdenum blue anion and 8-hydroxyquinoline-5-sulfonate anionic chelate [26,27].

In this paper we report on the spectrophotometric determination of molybdenum (VI) following the collection and elution as molybdate ion on protonated chitin, and the color reaction by bromopyrogallol red (BPR)-tetradecyldimethylbenzylammonium chloride (Zephiramine) method [28] in the eluent as shown in Fig. 1. The proposed method was applied to the determination of molybdenum (VI) in natural water samples.

2. Experimental

2.1. Reagents and apparatus

A commercially available purified chitin powder (FUNAKOSHI, Japan) was washed successively with a 1 M hydrochloric acid solution, distilled water and methanol; it was then kept at 40°C for 24 h in a vacuum dry oven.

Standard molybdenum (VI) solution (1 mg/ml) was prepared by dissolving accurately weighed 0.5044 g of analytical grade sodium molybdate dihydrate (Wako Pure Chemical Industries, Japan) in water and diluting to volume in a 200-ml standard flask and was further diluted as required. Bromopyrogallol red (DOJINODO LABORATORIES, Japan), Zephiramine (DOJINODO LABORATORIES, Japan) and other chemicals used were of analytical grade.

All absorbance measurements were made with a Hitachi U-2000 spectrophotometer with a black cell (light-path lengths 10 mm × light-path widths 2 mm, inner volume about 1 ml). A Hitachi-Horiba Model F-7_{AD} pH meter was used for all pH measurements.

2.2. Standard procedure

To a 100-ml of solution containing up to 0.8 μg of molybdenum (VI), add 1 ml of 0.1 M acetate buffer solution (pH 4.5). Then pass the solution through a chitin column (polyethylene column, 6 mm i.d. × 60 mm long, 50 mg of chitin) fitted with a porous polyethylene disk with a 20-μm pore size at a flow-rate of 10 ml min^{-1}. Elute molybdenum (VI) with 1 ml of 0.1 M ammonia buffer solution (pH 10) from chitin. To the eluent, add 0.05 ml of 10 M HCl, of 0.1 M Zephiramine and of 0.03 (w/v)% BPR with a micro-pipette, respectively, and then after 20 min, measure the absorbance of the solution at 634 nm against water.

3. Results and discussion

3.1. Overall capacity

The overall capacity for molybdenum (VI) as molybdate ion on protonated chitin at pH 4.5 was examined by batch equilibration of 50 mg of chitin with a 100-ml of solution containing 5×10^{-5} M of molybdenum (VI). The equilibration

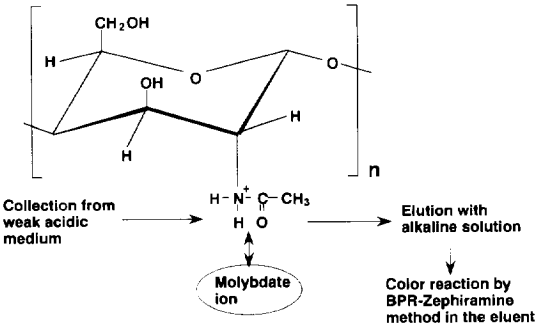

Fig. 1. Collection and elution scheme of molybdenum (VI) as molybdate ion on protonated chitin.

could be achieved by agitating for over 60 min. After filtration, the amounts collected for molybdenum (VI) were decided comparing the concentration of the solutions before and after equilibration by BPR-Zephiramine method spectrophotometrically. The overall capacity for molybdenum (VI) calculated on chitin were 50.56 μmol g^{-1}. The capacity is sufficient to collect a 0.01-μmol level of molybdenum (VI) (equal to 0.8 μg), though its capacity is less than that of common anion-exchange resin.

3.2. Color reaction in eluent

In preliminary work, some spectrophotometric methods for molybdenum (VI) were investigated. The BPR-Zephiramine method was selected for the determination of molybdenum (VI) in the eluent because of the simplicity for procedure and the sensitivity for the determination of molybdenum (VI). The optimum conditions for the color reaction by the BPR-Zephiramine method in the eluent were examined using the molybdenum (VI) standard solution. The maximal and constant absorbance of the eluent was obtained in the concentration over 0.04 ml of 10 M HCl, 0.04 ml of 0.1 M Zephiramine and 0.03 ml of 0.03 (w/v)% BPR, when used 1 ml of the eluent contained 0.8 μg of molybdenum (VI). These reagent conditions for the color reaction in the eluent were modified from original BPR-Zephiramine method [28], and chosen as described in the standard procedure. Fig. 2 shows the typical absorption spectra of the ternary complex of molybdenum (VI) and reagent blank. All absorption measurements were carried out at 634 nm as the ternary complex showed the maximum absorbance at 634 nm against water in this study.

3.3. Collection and elution of molybdenum (VI) as molybdate ion on chitin

Fig. 3 shows the effect of pH on the collection of molybdenum (VI) on chitin. The distribution curve of each species of molybdate, also shown in Fig. 3, was calculated using the acidic dissociation constants of H_2MoO_4 ($pK_{a1} = 2.4$ and $pK_{a2} = 3.8$) [29]. Molybdenum (VI) was quantitatively collected from aqueous solution over a pH range of 4–6. It is likely that the collection percentage for molybdenum (VI) on chitin decreases due to the decrease in the amount of the anionic species of molybdenum (VI) with protonation down to pH 4 as shown in Fig. 3, and due to the decrease in the amount of the effective protonated chitin beyond pH 6. In this study, the optimum pH of the solution for the collection was adjusted to be 4.5 by adding 1 ml of 0.1 M acetate buffer solution.

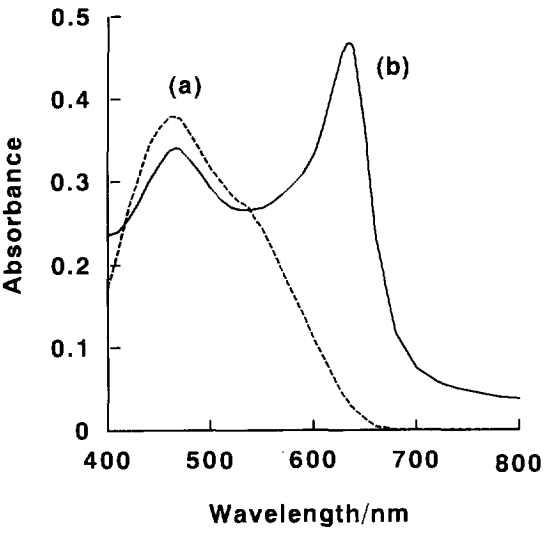

Fig. 2. Absorption spectra of the reagent blank and Mo-BPR-Zephiramine ternary complex in eluent. Condition as the standard procedure for 0.8 μg of molybdenum (VI): (a) reagent blank (Reference: water); (b) the ternary complex (Reference: water).

Collection from a 100-ml of solution containing 0.8 μg of molybdenum (VI) on a column with various amounts of chitin over the range of 10–65 mg was examined. Molybdenum (VI) was quantitatively collected on a column containing up to 40 mg.

The effect of flow rate on the collection was examined. The flow rate of sample solution for the collection was varied from 5 to 25 ml min^{-1}. The column was aspirated over 5 ml min^{-1}. Molybdenum (VI) was quantitatively collected up to 20 ml of the flow rate.

Recoveries of 0.8 μg of molybdenum (VI) from various volumes over the range of 100–500 ml of sample solution were examined. Molybdenum

(VI) was quantitatively collected in this range; up to 500-fold concentration could be easily achieved.

The elution of molybdenum (VI) collected on a column of chitin was examined using alkaline solution, mainly 0.1 M ammonia buffer solution over a pH range of 8–10 (Fig. 4), because molybdenum (VI) as molybdate ion was largely collected by the electrostatic interaction between the anionic species and the surface of the protonated chitin (Fig. 1). The elution of molybdenum (VI) was not quantitative with the ammonia buffer solution, pH 8 due to insufficient neutralization of the protonated chitin, while molybdenum (VI) was quantitatively eluted with the ammonia buffer solution, pH up to 8.5. In this study, 0.1M ammonia buffer solution, pH 10 was used. Molybdenum (VI) collected on the chitin was readily eluted with 1 ml of the eluent within 1 min.

Five successive collection and elution cycles with 0.8 μg of molybdenum (VI) on the same chitin gave almost identical results.

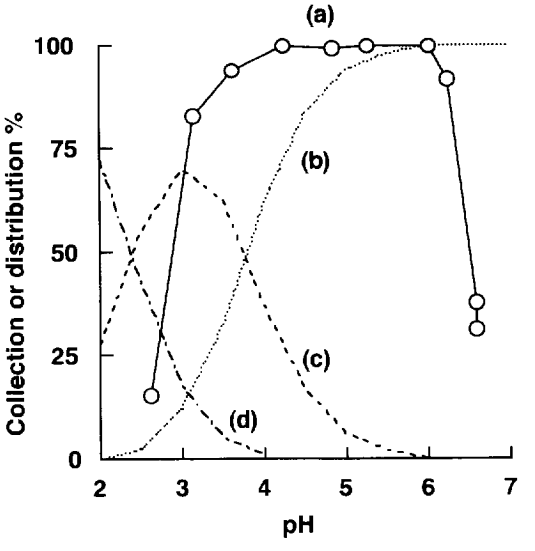

Fig. 3. Effect of pH on collection of molybdenum (VI) as molybdate ion, and distribution for molybdenum (VI) species as a function of pH. (a) Collection curve of Molybdenum (VI) (0.8 μg) on chitin; Distribution curves of (b) MoO_4^{2-}, (c) $HMoO_4^-$ and (d) H_2MoO_4 in solution.

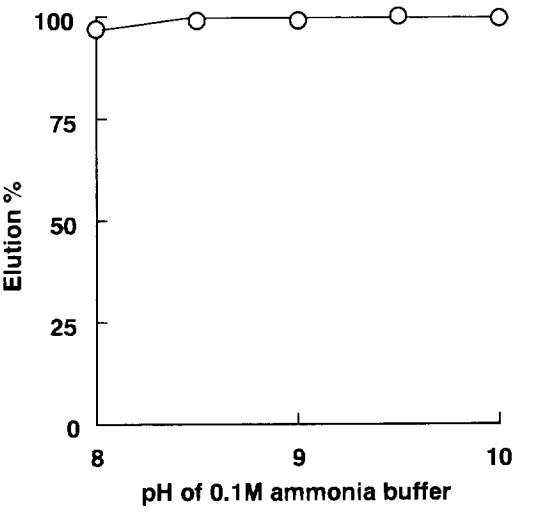

Fig. 4. Effect of pH of eluent on elution of molybdate ion from chitin. Eluent: 1 ml of 0.1 M ammonia buffer solution; Molybdenum (VI): 0.8 μg.

3.4. Calibration curve, and precision

The calibration curve obtained by the standard procedure was linear over the concentration range of 0.1–0.8 μg of molybdenum (VI) in 1 ml of the eluent. The apparent molar absorptivity was 6×10^4 dm^3 mol^{-1} cm^{-1}. The relative standard deviation was 2.31% for 0.4 μg of molybdenum (VI) (5 measurements).

Table 1
Effect of diverse ions on the determination of 0.4 μg of molybdenum (VI)

Ion added	Ion/Mo (VI) tolerated
F^-	5000
NO_3^-, EDTA	4000
Cl^-, ClO_4^-, SO_4^{2-}, PO_4^{3-}, AsO_4^{3-}, NO_2^-, Ca^{2+}, Mg^{2+}, Al^{3+}, Mn^{2+}, Cu^{2+}, Zn^{2+}, Pb^{2+} [a] NH_4^+, L-ascorbic acid	1000
Fe^{3+} [a]	100
CrO_4^{2-} [b]	10
WO_4^{2-}, VO_3^-	1

[a] 1600 μg of EDTA added.
[b] 400 μg of L-ascorbic acid added.

Table 2
Analytical results for molybdenum (VI) in tap and natural waters

Sample	Mo (VI) added (μg)	Mo (VI) found (μg)	Recovery (%)
Tapwater	0.00	ND	—
	0.10	0.105	105.0
	0.15	0.161	107.3
	0.20	0.211	105.5
Riverwater	0.00	0.097	—
	0.10	0.195	97.0
	0.15	0.245	98.7
	0.20	0.297	100.0
Spring water	0.00	ND	—
	0.10	0.102	102.0
	0.15	0.149	99.3
	0.20	0.197	98.5

Each sample volume, 100 ml; ND, not detected.

3.5. Effect of diverse ions

Table 1 shows the effect of diverse ions. The tolerance limit was taken as being the amount causing an error ± 3% in the absorbance of the eluent for molybdenum (VI) alone. For the determination of 0.4 μg of molybdenum (VI), Fe (III) in concentration up to 100-times, and CrO_4^{2-} in concentration up to 10-times that of molybdenum (VI) were tolerated when EDTA and L-ascorbic acid were added, respectively. The tolerance limits for WO_4^{2-} and VO_3^- were low, and it might cause the competitive adsorption on protonated chitin. The common anions, Al (III), Ca (II), Mg (II), Mn (II), Cu (II), Pb (II), Zn (II), NH_4^+, EDTA and L-ascorbic acid did not interfere in concentration up to 1000- to 5000-times that of molybdenum (VI).

3.6. Application

The method described was applied to the determination of molybdenum (VI) in tap water and natural water samples around our Kitami city. The samples were analyzed after filtration with a 0.45-μm cellulose acetate membrane filter. To a 100-ml of each sample, added a known amount of molybdenum (VI), and 1600 μg of EDTA to prevent the effect of Fe (III) and Pb (II), mainly. The percentage of recovery was estimated from the determination of molybdenum (VI) in the eluent. The results are summarized in Table 2. The recovery of molybdenum (VI) added for the each water sample was almost complete. Thus, this method is particularly effective for the determination of molybdenum (VI) in natural water.

In conclusion, the presented method has the advantages of simplicity, rapidity and a high concentration factor on the preconcentration procedure, and makes possible to determine molybdenum (VI) at ppb level. The proposed method may be also applicable to the spectrophotometric determination of other oxo-anions after the collection and elution on protonated chitin.

Acknowledgements

This work was financially supported by Grants-in-Aid for Scientific Research (No. 08640762) from the Ministry of Education, Science and Culture, Japan.

References

[1] H. Kohara, N. Ishibashi, K. Abe, Bunseki Kagaku 19 (1970) 48.
[2] S. Wakamatsu, Bunseki Kagaku 29 (1980) 472.
[3] M.P. Bermejo-Barrera, J.F. Vazqez-Gonzalez, F. Bermejo-Martinez, Analyst 112 (1887) 473.
[4] U. Dhingra, L.R. Kakkar, Analyst 113 (1988) 675.
[5] R. Dass, J.R. Mehta, Bull. Chem. Soc. Jpn. 67 (1994) 999.

[6] A.C. Basak, K.C. Ghosh, A.R. Paul, S. Bhattacharjee, L.P. Pandey, Talanta 42 (1995) 497.
[7] D.E. Leyden, G.H. Luttrell, W.K. Nonideg, D.B. Werho, Anal. Chem. 48 (1976) 67.
[8] K. Yoshimura, S. Hiraoka, T. Tarutani, Anal. Chim. Acta 142 (1982) 101.
[9] M.M.A. Shriadah, M. Kataoka, K. Ohzeki, Analyst 110 (1985) 125.
[10] L. Joseph, V.N.S. Pillai, Analyst 114 (1989) 439.
[11] R. Caletka, R. Hausbeck, V. Krivan, Talanta 33 (1986) 315.
[12] C-Y. Liu, P-J. Sun, Talanta 31 (1984) 353.
[13] M.H.H. Mahmoud, M. Kanesato, T. Yokoyama, T.M. Suzuki, Anal. Sci. 10 (1994) 929.
[14] X. Luo, Z. Su, G. Zhan, Analyst 117 (1992) 145.
[15] G.R. Boaventura, J. Da, R. Hirson, R.E. Santelli, Z. Anal. Chem. 350 (1994) 651.
[16] K. Sato, M. Suzuki, K. Hilman, T. Goto, Bunseki Kagaku 45 (1996) 175.
[17] S. Hoshi, Y. Kamada, S. Inoue, M. Matsubara, Anal. Sci. 4 (1988) 227.
[18] S. Hoshi, M. Yamada, S. Inoue, M. Matsubara, Talanta 36 (1989) 606.
[19] S. Hoshi, Y. Tanaka, S. Inoue, M. Matsubara, Anal. Sci. 5 (1989) 471.
[20] S. Hoshi, M. Yamada, S. Inoue, M. Matsubara, Anal. Sci. 7 (1991) 657.
[21] A. Hase, T. Kawabata, K. Terada, Anal. Sci. 6 (1990) 747.
[22] K. Komori, S. Igarashi, Y. Yotsuyanagi, Bunseki Kagaku 35 (1986) 890.
[23] H. Minamizawa, T. Hokazono, N. Arai and T. Okutani, Nippon Kagaku Kaishi (1993) 93.
[24] H. Minamizawa, N. Arai, T. Okutani, Bunseki Kagaku 42 (1993) 767.
[25] H. Minamizawa, N. Arai, T. Okutani, Anal. Sci. 11 (1995) 961.
[26] S. Hoshi, S. Kanagami, M. Uto, M. Matsubara, Anal. Sci. 8 (1992) 103.
[27] S. Hoshi, T. Tomizuka, C. Enjo, Y. Haga, M. Uto, K. Akatsuka, Anal. Sci. 11 (1995) 729.
[28] M. Deguchi, M. Iizuka, M. Yashiki, Bunseki Kagaku 23 (1974) 760.
[29] E. Hogfeldt, 'Stability constants of metal-ions complexes, Part A: Inorganic ligands', IUPAC Chemical Data Series, No. 21, Pergamon Press, 1979, p. 62.

ELSEVIER

Talanta 44 (1997) 1479–1485

Talanta

Determination of enantiomeric purity by simultaneous dual circular dichroism and ultraviolet spectroscopy

Péter Horváth, András Gergely, Béla Noszál *

Semmelweis University, Institute of Pharmaceutical Chemistry, Hôgyes Endre u. 9. Budapest H-1092, Hungary

Received 29 July 1996; received in revised form 3 February 1997; accepted 14 February 1997

Abstract

A method is described for the determination of enantiomeric composition. The ellipticity and absorbance of the sample are measured simultaneously by CD and UV spectroscopies, and the resulting G value is determined. G is an intensive physico-chemical parameter, a close derivative of anisotropy factor. Its magnitude is identical with opposite sign for enantiomers. The experimental G value is concentration-independent, as long as both absorption and ellipticity are linear functions of concentration. The analytical procedure introduced here is simple, rapid, and inexpensive, even though it includes calibration with standards of established enantiomeric composition. Provided the sample contains some UV-active contaminant(s), the method can be used after achiral chromatographic purification. By virtue, the method lacks several sources of error, arising normally from concentration inaccuracies. Applicability of the principles is tested by the example of phenylglycine and mandelic acid. Advantages of the method allowed the determination of phenylglycine enantiomer purity with an accuracy of 0.1%. © 1997 Elsevier Science B.V.

Keywords: Circular dichroism; Enantiomeric purity; Dual spectroscopy

1. Introduction

Optical purity is the state of matter in living organisms [1], with far-reaching consequences in life sciences. As such, it is an increasingly significant quality control criterion in pharmaceutical, biochemical and related industries.

The optical purity of substances can be determined with and without separation techniques.

Of the methods, using separation techniques, HPLC is certainly the most widely used one, as described by Souter (1991, pp. 418–421) [2]. All enantiomeric separations are based upon diastereomeric weak interactions with homochiral reactants. Such homochiral counter-molecules can be proteins [3,4] or chiral modifiers (amino acid- [5,6] or amine- and alcohol derivatives [6]) of the stationary phase, or asymmetric additives (cyclodextrin [7] and amino acid derivatives [8]) in the eluent. Chiral pre-column reagents can also be used to produce covalent diastereomeric derivatives [9–11], which can then be separated under achiral circumstances as well.

For the identification of asymmetric compounds, chiroptical detectors offer a relatively

* Corresponding author. Fax: +36 01 2170891; e-mail: nosbel@hogyes.sote.hu

PII S0039-9140(97)00058-1

new way. The combination of HPLC separation and CD or ORD detection has recently been reviewed [12,13]. Dual detector systems in a serial fashion have also been connected to HPLC. Such systems include a refractive index or UV spectrometer to measure the sum of the enantiomers, whereas polarimetric, CD or fluorescence-detected CD techniques monitor the enantiomeric excess [14–17]. Vibrational CD is a candidate to become a detector of high chiral and chemical identification capacity [18,19]. Other separation techniques, such as capillary zone electrophoresis was also shown to be appropriate to characterize enantiomeric composition, with the advantage of short analysis time, while remaining reasonably sensitive [20,21]. Thin layer chromatography can be an inexpensive alternative in some cases as well [22,23].

Concerning non-separation methods, NMR is the most frequently used one (Souter, 1991, pp. 422–423) [2], in which chiral shift reagents [24,25] serve to form diastereomeric complexes. Ladányi et al., have developed a thermoanalytical method to determine the enantiomeric composition of selegilin [26].

The inherently distinctive chiroptical methods, and the role of polarimetry has been summarized by Schurig [27]. The sensitivity of enantiomeric determinations can be enhanced by derivatization with chromophore groups [28]. Optical purity of amino acids was determined by ORD and CD spectroscopy of their mixed complexes formed with other chiral ligands [29]. Purdie et al., have developed a method based upon ligand substitution reaction, to characterize enantiomeric composition in epinephrine mixtures [30].

Here we describe the application of anisotropy factor, measured by single cell, single solution dual spectroscopy, to determine enantiomeric composition, without the physical separation of the enantiomers.

2. Experimental section

2.1. Reagents

Phenylglycine and mandelic acid isomers were obtained from Fluka. The enantiomeric purities were declared to be above 99% while the chemical purities were above 99.9%. No further purification was carried out. For the accurate determination of the enantiomeric compositions with HPLC, CHIREX D-Penicillamine chiral column (Phenomenex) was used. By this method, the L-phenylglycine impurity in D-phenylglycine was found to be 0.19%, whereas the D impurity in the L-isomer was below 0.05%. The L-isomer was therefore accepted as a standard reference material (SRM). In case of mandelic acid, the D-isomer contained 0.27% of L-isomer, while in the L-isomer, the quantity of the D-isomer could not be determined by the above method. The reason is that the peak of the minor D-isomer is highly covered by the peak of the earlier eluted major L-isomer. All solutions prepared for spectrometric measurement were made in 1 M HCl as solvent.

2.2. Instrument

The spectroscopic measurements were carried out on a JASCO J-720 type spectropolarimeter, using single cell technique, detecting simultaneously UV absorption plus ellipticity or optical rotation dispersion signals. The spectra of the materials were recorded in wavelength mode, while the ellipticity and the absorbance in 'Time' mode. The measurements in 'time' mode were carried out employing the following parameters:

Time for data registration: 60 s, resolution: 0.5 s, accumulation: 3 ×, cell: 10 mm cylindrical cell from Hellma, band width: 2 nm.

Following the threefold accumulation, the mean of 180 data points, the standard deviation as well as the G factor were calculated with MS Excel 5.0 program. The standard deviation of the ellipticity values were found to be approximately 0.25 mdeg, while a typical standard deviation of the absorption was 0.0005 absorbance unit. Further calculations were aided by the program-package STATISTICA 4.5 for Windows.

3. Theory

G-value, a concentration-independent parameter is a derivative of absorbance (see the denominator of Eq. (1)) and ellipticity (see the numerator). Also, it is proportional to the anisotropy factor, g [31,32], as given in Eq. (1).

$$G = \frac{[\Theta] \times c \times l}{\epsilon \times c \times l} = \frac{[\Theta]}{\epsilon} = 3298g \quad (1)$$

Eq. (1) shows that G is a wavelength-dependent intensive, intrinsic parameter of a chiral chemical entity. For the two enantiomers, it has the same numerical values with opposite sign. The value of G can be calculated if simultaneous determination of ellipticity and absorbance of the sample is feasible. Eq. (1) also shows the two most important features of G:

1. As long as both ellipticity and absorbance are linear functions of concentration (which is normally the case) the G value is independent of the concentration.
2. The G value is a function of enantiomeric composition.

Thus, we can conclude that CD/UV dual spectroscopy and the resulting anisotropy factor are a tool for concentration-independent determination of enantiomeric composition.

Concentration of the minor (contaminant) enantiomer ($C_{cont\%}$) can be calculated as follows:

$$C_{Cont\%} = \frac{G_{pure} - G_{obs}}{2G_{pure}} \times 100 \quad (2)$$

where G_{pure} is the G value for the pure, major enantiomer, G_{obs} is the actual observed value of the measurement in question.

This principle can be utilized for analytical purposes in a number of ways. For example, the use of single solution, single cell, double spectroscopy eliminates several traditional analytical errors arising normally from weighting and dilution, and also from differences in cell quality. If the sample contains some CD- or UV-active contaminant(s) previous purification or chromatographic separation is needed. The chemical and optical impurities of the substances, however, are also indicated by the experimental G value. The analytical exploitation and practical aspects of the principle will be illustrated by D- and L-phenylglycine and D- and L-mandelic acid, as described below.

4. Results and discussion

The experimental ellipticity and absorbance values are linear functions of concentration, unless association processes or technical artifacts occur. Taking into consideration that the observed ellipticity and absorbance are generally different in different state of protonation (Fig. 1), it is important to keep the compound studied in an unchanged protonation form. Also, the solvent must be chosen carefully, otherwise undesired homo- and heteroassotiations can be formed, resulting in distortion of linearity [33].

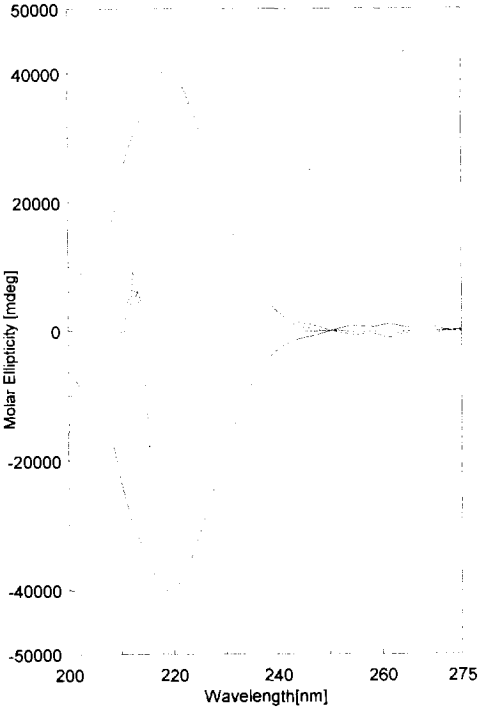

Fig. 1. CD spectra of phenylglycine and mandelic acid enantiomers. Spectrum extrema and molar ellipticities at extremum wavelengths are −40 153 at 218.6 nm for D-phenylglycine (——), 40 247 at 218.6 nm for L-phenylglycine (– – –), −35 903 at 221.6 nm for D-mandelic acid (• • •), 35 934 at 221.6 nm for L-mandelic acid (– • – – • –) and −22 950 at 218.6 nm for Na-D-mandelate (– ••– ••–), respectively.

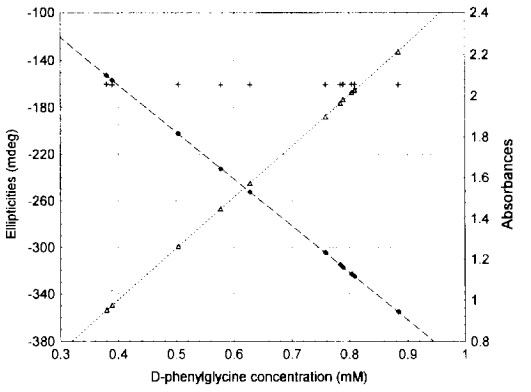

Fig. 2. Measured ellipticities (◆), absorbances (△) and calculated G values (+) vs. D-phenylglycine concentration in mM (C_D). Equations of the best fit are: $\Theta = -0.12 + (-401.56 \times C_D)$; $r = 0.99998$ (left axis). $A = -0.001 + (2.509 \times C_D)$; $r = 0.9999$ (right axis). Mean of $G = -160.3 \pm 0.2$; (left axis).

Fig. 1 shows the CD spectra of phenylglycine and mandelic acid. The chirally perturbed phenyl chromophore L_B band (250–270 nm) is of low intensity and provides poor conditions to determine the anisotropy factor. Around 220 nm, the Cotton effect is much more favorable, phenylglycine and mandelic acid were therefore measured at their 218.6 and 221.6 nm respective maxima in all subsequent measurements.

Concentration-independence of the anisotropy factor was verified as follows: L-phenylglycine solutions were in the dilution range of 0.2–1.0 mM, using 1.0 mM stock solution. The G parameters were calculated from the ellipticity and absorbance values in the same sample, yielding an unquestionably linear function in the 0.3–0.9 mM concentration range. For concentration above 0.9 mM, the absorbance was too high, and the concomitant background noise made the anisotropy factor also noisy. Data in the 0.3–0.9 mM range and the pertinent regression parameters are in Fig. 2. Clearly, the values are independent of concentration. Analogous results were found for D-phenylglycine.

The anisotropy factors for enantiomers were proved to be of identical magnitude with opposite sign, as theory predicts. The verification procedure was as follows: the actual molar ellipticity curves are in Fig. 1. The digitized spectrometer readings were divided by the actual molar concentrations. The resulting respective Θ_S, A_S standardized ellipticity and absorbance and G values are collected in Table 1. For phenylglycine, the A_S values of the isomer pairs do not differ significantly. This identity is also indicative of the similarity of their chemical purity. The Θ_S values show significant difference at $P = 0.1\%$ ($t = 4.56$), while the G values show significant difference at $P < 0.1\%$ ($t = 13.21$). The L-enantiomer impurity in the D-form was found to be 0.09% by ellipticity-difference measurement, whereas from difference of the G values is 0.15%. The latter result is in good agreement with the HPLC data (0.19%).

In the case of mandelic acid, none of the Θ_S, A_S or G values show significant differences. This suggest that the amount of D-isomer in the L-form is approximately the same as the L-isomer in the D-form (0.27%). Thus, on the basis of the G values, the enantiomeric composition can be determined directly.

D- and L-phenylglycine stock solutions ($C_D = 0.8097$ mM and $C_L = 0.7917$ mM) were mixed in various proportions. The G values of each solution are plotted against the % of the D isomer (Fig. 3(a)). The straight line intercepts the 'x' axis at 50% composition (racemic mixture). Linearity proves that no detectable homo- or heteroassociation takes place, and it can also serve as an analytical calibration curve. Since deviations from straight line are not discernible on Fig. 3(a), we also plotted residuals in Fig. 3(b). The random distribution of the residuals supports the hypothesis of linearity. The A_S value was also calculated with regards to the full concentration of the phenylglycine solutions. Thus, the obtained value of 2.505 ± 0.002 is practically the same as values given in Table 1.

For several analytical purposes, determination of small amounts of impurities have great importance. In many cases, however, highly purified standards of both enantiomers are not available. Instead, reasonably purified substances with validated amount of contaminants can be obtained. We have therefore made a test analysis under such circumstances.

A contamination standard was prepared containing 1.097% L-phenylglycine while L-impurity

Table 1
Standardized ellipticity (Θ_S), standardized absorbance (A_S) and G values for phenylglycine and mandelic acid enantiomers

	D-phenylglycine ($n = 65$)	L-phenylglycine ($n = 16$)	D-mandelic acid ($n = 59$)	L-mandelic acid ($n = 21$)
Θ_S	-401.8 ± 0.5	402.5 ± 0.6	-359.4 ± 0.5	359.6 ± 0.5
A_S	2.506 ± 0.004	2.503 ± 0.004	2.563 ± 0.005	2.568 ± 0.004
G	-160.3 ± 0.2	160.8 ± 0.1	-140.2 ± 0.3	140.1 ± 0.2

Θ_s, standardized ellipticities; A_S, standardized absorbances; G, Θ/A.

in the 'pure' D-isomer was 0.192%. After measuring ellipticities, absorbances and G values, calibration equations were found to be as follows: $\Theta = -325.305 + 42.994 \times C_L$ and $G = -161.949 + 9.45 \times C_L$ respectively, where C_L is the concentration of the L-isomer in percent. The analytes of known amounts of contaminants were prepared. After the measurements of the ellipticities and absorbances of these samples, the Θ and G values were substitued into the respective equations. As a result, calculated C_L values were obtained. The differences between the theoretical and experimental impurities are shown in Table 2. The maximum deviation is approximately 0.03%. The mean of deviations is irrespective of Θ or G function as a source, whereas the standard deviations favor the G values.

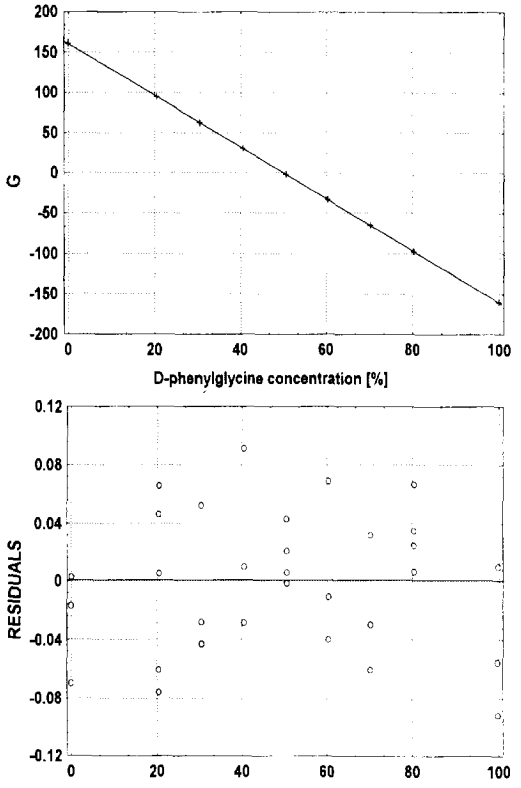

Fig. 3. G values against % of D-phenylglycine (top) and related residuals (bottom).

5. Conclusion

The method presented here is suitable for the determination of enantiomeric composition, including cases when the minor component is impurity only. This method determines anisotropy factor by using single cell, single solution dual spectroscopy, and its rapidity and accuracy makes it inexpensive, and eminently suitable for routine quality control purposes. Anisotropy, the measured quantity is a concentration-independent parameter, which eliminates concentration-related errors. Nevertheless, the measurement provides the traditional absorbance and ellipticity data as well, thus concentration values can also be obtained. Compared to HPLC, its disadvantage is that at least one standard of definite purity is needed for calibration.

Acknowledgements

This work has been supported by OTKA CO182/A, FEFA II/241 and OTKA T017570.

Table 2
Theoretical and experimental phenylglycine concentrations of test analysis

Solution	C_L	Θ	A	G	$C_L\Theta$	$C_L\Theta - C_L$	C_LG	$C_LG - C_L$
Stock d	0.192	−317.370	1.982	−160.134	0.192	0.000	0.192	0.000
9d+1dl	0.282	−313.120	1.968	−159.135	0.290	0.008	0.298	0.015
9d+1dl	0.282	−314.631	1.975	−159.346	0.255	−0.027	0.275	−0.007
8d+2dl	0.373	−308.745	1.950	−158.308	0.391	0.018	0.385	0.012
8d+2dl	0.373	−308.767	1.949	−158.407	0.391	0.018	0.375	0.002
7d+3dl	0.464	−304.934	1.937	−157.460	0.479	0.015	0.475	0.011
7d+3dl	0.464	−304.660	1.933	−157.626	0.485	0.021	0.457	−0.007
6d+4dl	0.554	−301.694	1.925	−156.714	0.554	−0.000	0.554	−0.000
6d+4dl	0.554	−302.745	1.934	−156.516	0.530	−0.024	0.575	0.021
5d+5dl	0.644	−296.227	1.900	−155.883	0.680	0.036	0.641	−0.003
5d+5dl	0.644	−296.631	1.905	−155.753	0.671	0.027	0.655	0.011
4d+6dl	0.735	−294.559	1.900	−155.015	0.719	−0.016	0.733	−0.002
4d+6dl	0.735	−294.158	1.897	−155.040	0.728	−0.007	0.731	−0.004
3d+7dl	0.825	−289.626	1.880	−154.096	0.833	0.008	0.831	0.006
3d+7dl	0.825	−289.404	1.879	−154.038	0.838	0.013	0.837	0.012
2d+8dl	0.916	−286.874	1.871	−153.286	0.896	−0.020	0.916	0.000
1d+9dl	1.006	−281.976	1.850	−152.426	1.009	0.003	1.007	0.001
1d+9dl	1.006	−282.388	1.852	−152.437	1.000	−0.006	1.006	−0.000
stock dl	1.097	−278.174	1.835	−151.577	1.097	0.000	1.097	−0.000
						0.0035*		0.0035*
						0.0175**		0.0078**

Stock d, stock solution of D-isomer; Stock dl, stock solution of D-isomer contaminated with L-isomer; C_L, amount of L-isomer in % (theoretical); Θ, measured ellipticities in mdeg; A, measured absorbances; $G = \Theta/A$; $C_L\Theta$, the L-isomer quantities derived from the calibration curve of ellipticities; C_LG, the L-isomer quantities derived from the calibration curve of G values.
* Mean of the entries above.
** Standard deviation of the entries above.

References

[1] D.E. Drayer, Clin. Pharmacol. Ther. 40 (1986) 125.
[2] R.W. Souter, The Determinnation of Isomeric Purity in Modern Methods of Pharmaceutical Analysis, 2nd edn., Vol. II, CRC Press, Boca Raton, Ann Arbor, Boston 1991, pp. 418–421, pp. 422–423.
[3] B. Herényi, S.J. Görög, Chromatography 592 (1992) 297.
[4] S.C. Jacobson, G. Guiochon, J. Chromatogr. 600 (1992) 37.
[5] N. Oi, H. Kitahara, R. Kira, J. Chromatogr. 592 (1991) 291.
[6] W.H. Pirkle, R.E. Field, G.S. Mahler, T.C. Pochapsky, J. Chromatogr. 348 (1985) 89.
[7] G. Ucello-Baretta, C. Chiavacci, C. Bertucci, P. Salvadori, Carbohydr. Res. 243 (1993) 1.
[8] G. Radeczky, Gy. Szász, Zs. Budvári-Bárány, Acta Pharm. Hung. 58 (1988) 267.
[9] T. Yamada, S. Nonomura, H. Fujiwara, T. Miyazawa, S. Kuwata, J. Chromatogr. 515 (1990) 475.
[10] Z.Y. Yang, R.Z. Xu, Chirality 1 (1989) 92.
[11] C.X. Gao, I.S. Krull, J. Pharm. Biomed. Anal. 7 (1989) 1183.
[12] A. Gergely, J. Pharm. Biomed. Anal. 7 (1989) 523.
[13] A. Gergely, in N. Purdie and H.G. Brittain (Eds.), The Use of Circular Dichroism as a Liquid Chromatographic Detector in Analytical Application of Circular Dichroism, Elsevier, Amsterdam, 1994, pp. 179–292.
[14] Z.C. Wu, D.M. Goodall, D.K. Lloyd, J. Pharm. Biomed. Anal. 8 (1990) 357.
[15] D.K. Lloyd, D.M. Goodall, Chirality 1 (1989) 251.
[16] D.M. Goodall, Trends. Anal. Chem. 12 (1993) 177.
[17] A.F. Drake, J.M. Gould, S.F. Mason, J. Chromator. 202 (1980) 239.
[18] K.M. Spencer, R.B. Edmonds, R.D. Rauh, Appl. Spectrosc. 50 (1996) 681.
[19] L. Hecht, A.L. Phillips, L.D. Barron, J. Raman. Spectroscopy 26 (1995) 727.
[20] K. Otsuka, S. Terabe, Trends Anal. Chem. 12 (1993) 125.
[21] M. M Rogan, K.D. Altria, D.M. Goodall, Chirality 6 (1994) 25.
[22] J. Martens, R.J. Bhushan, J. Pharm. Biomed. Anal. 8 (1990) 259.
[23] P. Slégel, G. Vereczkey-Donáth, L. Ladány, M. Tóth-Lauritz, J. Chromatogr. 5 (1987) 665.
[24] J.W. Jaroszewski, A.J. Olsson, J. Pharm. Biomed. Anal. 12 (1994) 295.

[25] G.M. Hanna, A. Lau-Cam, J. Pharm. Biomed. Anal. 11 (1993) 665.
[26] L. Ladányi, I. Szilágyi, I. Hermetz, Acta. Pharm. Hung. 62 (1992) 231.
[27] V. Schurig, Kontakte 1 (1985) 54.
[28] J.D. Weber, J. Pharm. Sci. 65 (1976) 105.
[29] Y. Fuji, Bull Chem. Soc. Japan 47 (1974) 2856.
[30] A.R. Engele, E.A. Lucas, N. Purdie, J. Pharm. Sci. 83 (1994) 1310.
[31] E. Charney, The Molecular Basis of Optical Activity, Wiley, New York, 1979.
[32] W. Kuhn, Annu. Rev. Phys. Chem. 9 (1958) 417.
[33] P. Horváth, A. Gergely, B. Noszál, J. Chem. Soc. Perkin Trans. 2 (7) (1996) 1419.

ELSEVIER

Talanta 44 (1997) 1487–1497

Talanta

Analysis of EDTA and DTPA

Mika Sillanpää *, Marja-Liisa Sihvonen

Helsinki University of Technology, Laboratory of Inorganic and Analytical Chemistry, FIN-02150 Espoo, Finland

Received 21 November 1996; received in revised form 28 January 1997; accepted 14 February 1997

Abstract

In this paper, analytical techniques for the determination of ethylenediaminetetraacetic acid (EDTA) and diethylenetriaminepentaacetic acid (DTPA) are reviewed. These compounds, especially EDTA, are used as metal chelating agents in several industries. As they are likely to be poorly degraded in waste water treatment plants, significant amounts of EDTA and DTPA are released into natural waters. The overview consists of comparing chromatographic, electrochemical, spectrophotometric, titrimetric and atomic absorption methods and their applicability to the determination of EDTA and DTPA in different matrices. © 1997 Elsevier Science B.V.

Keywords: EDTA; DTPA; Determination

1. Introduction

Aminopolycarboxylic acids, e.g. ethylenediaminetetraacetic acid (EDTA) and diethylenetriaminepentaacetic acid (DTPA), are widely used in industry, detergents, foods and agriculture. The industrial applications include metal, textile, leather, rubber, pharmaceutical, food and polymer production among others. In Finland, however, pulp and paper industry is obviously the dominant user of EDTA and DTPA.

Pulp and paper mills utilise EDTA and/or DTPA to inactivate metal ions which catalyze the decomposition of added bleach. If totally chlorine free (TCF) processes will be applied in wider extent, as the trend is at the moment, and if EDTA and DTPA are not replaced by other complexing agents, their use will significantly increase in the future. This raises concern of their ultimate release to the aquatic environment.

Complexing agents EDTA and DTPA have been analyzed by a variety of analytical methods. The earliest reports applied spectrophotometric and titrimetric methods, but later different forms of chromatography, being far more sensitive, have widely replaced these methods. Also, some electrochemical methods have been used for EDTA and DTPA analysis. The following review discusses and compares the applicability of the methods presented in the literature for the analysis of EDTA and DTPA with the main emphasis in waste and natural water applications.

* Corresponding author.

PII S0039-9140(97)00059-3

2. Liquid chromatography

EDTA has been determined in a wide variety of sample matrices by liquid chromatography (LC). These include waste waters [1–3], natural waters [1,4–7], sediments [7], fertilizers [8], chemical cleaning solutions [9], radioactive waste solutions [10], boiler water [11,12], drinking water [5], foodstuffs [13–17], vancomysin formulations [18], micronutrients [19], and anaesthetic parental solutions [20].

On the other hand, the LC applications for DTPA determination are much fewer in number: it has been analysed in natural waters [1], waste waters [2,3,21], fertilizers [8], and micronutrients [19].

In recent years, there has also been increasing interest in using these chelating agent for trace metal separations and metal–chelate analysis by reversed phase (RP)-HPLC or by ion chromatography (IC). This can be performed by utilising EDTA in sample pretreatment [20,22–26] and EDTA or DTPA solutions as eluents [27–34]. In addition, lanthanoid EDTA complexes have also been separated and determined by HPLC [35].

The separation of different metal-EDTA or metal-DTPA complexes in reversed-phase columns is analytically a challenging task due to the structural similarity of the complexes. However, some authors have succeeded in separating several metal complexes of EDTA [6,22,23].

Most common trace metal-EDTA complexes can be separated and determined at the $\mu g\ l^{-1}$ level in river water according to a recent report [6]. Unfortunately, in the case of the methods presented in Knox and Shibukawa [22] and Jen and Chen [23], the detection limits for different Me-EDTA compounds were not given [22], or were far too high for the natural water applications (ranging between 1.4–66 $mg\ l^{-1}$) [23]. Using the method presented in Jen can Chen [23], it is also unlikely that the other complexes than Fe(III)-EDTA could be detected even in waste waters, that is to say, without further preconcentration.

From the environmental point of view, the speciation of EDTA and DTPA complexes in aquatic media is of crucial importance. But, no HPLC speciation studies of metal-DTPA complexes exist until now, at least to our knowledge.

In LC methods, the separation of the analytes (EDTA and/or DTPA) are performed either by RP columns or by ion chromatography (IC). In the case of RP technique, ion-pair reagent is added to the mobile phase to convert the target compounds into neutral components. Usually, the increase in retention is achieved by this step. In the case of ion chromatography, EDTA and DTPA are polyvalent anions with high affinity to anion-exchange resin and can thus be analysed by IC.

Table 1 presents the characteristics of the LC methods described in the literature for the EDTA and DTPA analysis. It can be observed that in different methods, there exist extremely wide variety of detection limits ranging between 0.8 $\mu g\ l^{-1}$ and 0.8 $g\ l^{-1}$. However, usually the detection limits are at low $mg\ l^{-1}$ level.

EDTA and DTPA have been found at concentrations of few $mg\ l^{-1}$ in waste waters and 2–100 and 2–15 $\mu g\ l^{-1}$ in natural waters, respectively. Generally speaking, most methods are not suitable to natural water monitoring due to the lack of sensitivity. Two of the LC methods provide low enough detection limits (around 1 $\mu g\ l^{-1}$) for fresh and sea water applications [5,7], but the time-consuming enrichment step is required. On the other hand, LC can conveniently be applied to analysis of, e.g. foodstuffs, where low detection limits are not required.

Preconcentration is performed by evaporation [5,7]. In addition to preliminary enrichment, the increament of loop volume is another relatively simple way of lowering the detection limits. The loop volumes vary between 10 and 200 μl.

Ultraviolet (UV) detection is the most commonly used detector with three exceptions: Chinnick utilised visible light at 760 nm due to the matrix interferences caused by the other UV absorbing compounds [36]. Dai and Helz [1] analysed complexing agents in their free acid form and thus the detection was based on amperometric detection to minimise interferences of metal ions. Ye and Lucy [116,117] used fluorescence detection with postcolumn formation of a ternary complex, which proved to be relatively sensitive, as can be observed form Table 1.

Table 1
Characteristics of the LC methods for the determination of EDTA and DTPA in various matrixes

Reference	Analyte	Matrix	Complex	Loop (μl)	Method	Detector	L.O.D.
[38]	EDTA, DTPA	Water		10	RP	Visible light (760 nm)	584 mg l^{-1} for EDTA and 788 mg l^{-1} for DTPA
[4]	EDTA	Water	Fe(III)	50	IC	UV (258 nm)	0.2 mg l^{-1}
[40]	EDTA	Water	Fe(III)	10	RP	UV (255 nm)	0.6 mg l^{-1}
[41]	EDTA, DTPA	Water	Fe(III)	10	RP		
[42]	EDTA	Water		100	IC		0.8 mg l^{-1}
[11]	EDTA	Boiler water	Fe(III)	10	RP	UV (254 nm)	1 mg l^{-1}
[9]	EDTA	Chemical cleaning solution		20	RP	UV (254 nm)	3–5 mg l^{-1} (depends on eluent)
[43]	DTPA	Water	Gd(III)	20	RP	UV (200 nm) and radioactivity	5 mg l^{-1}
[10]	EDTA	Radioactive waste solution	Cu(II)	100	RP	UV (260 nm)	0.5 mg l^{-1}
[37]	EDTA, DTPA	Water		50	IC	UV (330 nm)	low mg l^{-1} level
[1]	EDTA, DTPA	Natural water		50	RP	Amperometric	0.15 mg l^{-1} for EDTA and 2.0 mg l^{-1} for DTPA
[18]	EDTA	Vancomysin formulation	Fe(III)	20	RP	UV (254 nm)	2.0 mg l^{-1}
[17]	EDTA	Canned mushroom	Cu(II)	20	RP	UV (300 nm)	10 mg l^{-1}
[6]	metal-EDTA	River water		120	IC	UV (250 nm)	12.5–33.3 μg l^{-1} depending on metal
[22]	metal-EDTA	Water		5	RP	UV (230 nm)	
[23]	metal-EDTA	Waste water		20	RP	UV (242 nm)	1.4–66 mg l^{-1}
[44]	EDTA, DTPA	Natural water	Fe(III)	5–150	RP	UV (260 nm)	10 μg l^{-1}
[2]	EDTA, DTPA	Waste and natural water	Fe(III)	50	IC	UV (290 nm)	10 μg l^{-1} (with enrichment step)
[20]	EDTA	Anaesthetic parental solution	Fe(III)	20	RP	UV (279 nm)	0.4 mg l^{-1}
[5]	EDTA	Natural and drinking water	Fe(III)	100	RP	UV (254 nm)	0.8 μg l^{-1} (preconcentration by evaporation)
[21]	DTPA	Waste water	Fe(III)	200	RP	UV (258 nm)	0.2 mg l^{-1}
[8]	EDTA, DTPA	Fertilizer	Fe(III)	50	RP	UV (330 nm)	1.7 mg l^{-1} for EDTA and 2.8 mg l^{-1} for DTPA
[19]	EDTA, DTPA	Micronutrient	Cu(II)	20	RP	UV (270 nm)	
[3]	EDTA, DTPA	Waste and natural water	Fe(III)	25/150	IC	UV (260 nm)	0.1 mg l^{-1} in waste water (loop: 25 μl); 0.01 mg l^{-1} in surface water (loop: 150 μl)
[26]	EDTA	Pore water	Co(II), Co(III)	25	IC	Visible light (535 nm) and electrical conductivity	0.18 mg l^{-1} for Co(II)-EDTA and 0.54 mg l^{-1} for Co(III)-EDTA

Table 1 (continued)

Reference	Analyte	Matrix	Complex	Loop (μl)	Method	Detector	L.O.D.
[115]	EDTA, DTPA	Waste water	Fe(III)	20	RP	UV (260 nm)	0.5 mg l^{-1} for both compounds
[116]	metal-EDTA	Natural water		50	RP	Fluorescence	0.1 μmol l^{-1} for Pb-, Zn-, Cu- and Cd-EDTA
[117]	EDTA	Ophthalmig drug	Cu(II)	20	RP	UV (250 nm)	
[118]	EDTA	Ophthalmic cleanser	Fe(III)		RP	UV (254 nm)	0.2 mg l^{-1}
[119]	EDTA, DTPA	Natural water	Lu(III)	50	RP	Fluorescence	7 μg l^{-1} for EDTA and 15 μg l^{-1} for DTPA
[7]	EDTA	Natural water and sediment	Fe(III)	200	RP	UV (258 nm)	0.9 μg l^{-1} (preconcentration step)

In most cases, however, EDTA and DTPA are converted into Cu(II) or Fe(III) complexes in sample pretreatment step and analysed at the UV region. It should be noted that, many authors have not, for some reason, analysed Me-EDTA or Me-DTPA complexes at their absorption maximum [2,8,17,19,20,22,37]. De Jong et al. reported that better selectivity was obtained at high wavelengh (300 nm), even though the response was weaker [17]. In addition, paying attention to the pH dependence of the stability of the metal complexes of EDTA and DTPA, unfavourable pH conditions were used in some papers [1,6,10,11].

Iron forms the strongest complexes with EDTA and DTPA [38,39] and thus in most applications the analytes are converted into their stable Fe(III) complexes [2–5,7–9,18,20,21,40,41,44]. Some authors have determined complexing agents as their Cu(II) complexes [10,17,19]. This procedure provides higher retention and thus better resolution of the analytes from the sample matrix, but is susceptible to the interferences arising from those metal ions, which form more stable complexes with EDTA and DTPA than copper.

In summary, LC determination of EDTA and DTPA can be applied in many matrices, as indicated in Table 1. However, without enrichment step, it is unlikely that LC is suitable for natural waters in which the concentrations are expected to be below detection limits. Interestingly, speciation study of metal complexes has received attention, which is of importance when estimating their environmental fate and ecotoxicological effects.

3. Gas chromatography

Gas chromatography (GC) requires volatility of the compounds to be determined. EDTA, DTPA and their metal complexes are most commonly converted into methyl, ethyl, propyl or butyl esters to obtain volatility. This makes sample preparation procedure time-consuming and labour intensive. In addition, need of manual work makes the pretreatment step susceptible to errors. Methyl esterification is most commonly applied (Table 2). Silylation is also reported by Suback and James [45], but difficulties arise when salts are present [46], as is the case, e.g. in sea water.

Table 2
Characteristics of the GC methods for the determination of EDTA and DTPA

Reference	Analyte	Matrix	Sample amount	Ester	Method	Garrier gas	Detector	L.O.D.
[47]	EDTA, DTPA	Waste water	5 ml	Methyl	GLC	Helium	FID	10 μg l^{-1}
[46]	EDTA	Steam propulsion system	10 ml	Butyl	GLC	Helium	FID	
[59]	EDTA	Pickled vegetable	10 g	Methyl	GLC	Nitrogen	FID	
[48]	EDTA	Natural water	25 ml	Ethyl	GLC	Nitrogen	FID	15 μg l^{-1}
[62]	EDTA	DTPA		Methyl	GLC	Helium	FID	0.05%
[49]	EDTA	Aqueous media		Methyl	GLC		FID	
[50]	EDTA, DTPA	Waste and natural water	5 ml	Methyl	GC	Nitrogen	FID	5 μg l^{-1} for EDTA and 40 μg l^{-1} for DTPA
[51]	EDTA	River water		Butyl	GC	Helium	MS	
[52]	EDTA	Aqueous rince	25–100 ml	Methyl	GC	Helium	FID	25 μg l^{-1}
[60]	EDTA	Tinned bean	25 g	Methyl	GC	Nitrogen	FID	5 mg kg^{-1}
[53]	EDTA	Aqueous media	Methyl/propyl		GC	Hydrogen	FID/NPD	
[54]	EDTA	Natural and drinking water	50 ml	Methyl	GC	Hydrogen	NPD	
[55]	EDTA, DTPA	River water		Propyl	GC	Nitrogen	MS	1 μg l^{-1} (enrichment step)
[2]	EDTA, DTPA	Waste and natural water	10 ml	Propyl	GC		MS	1 μg l^{-1}
[58]	EDTA	Mixed nuclear waste		Methyl	GC			
[56]	EDTA	Waste water	50 ml	Butyl	GC	Helium	MS	
[57]	EDTA	River water, sediment, fish	100 ml, 1–10 g	Methyl	GC	Helium	MS	6.2 μg l^{-1} level
[120]	EDTA, DTPA	Natural water	10 ml	Ethyl	GC	NItrogen	NPD	3 μg l^{-1} for EDTA and 12 μg l^{-1} for DTPA

Most GC methods were developed for EDTA analysis. There are only very few GC methods which provide the possibility for the simultaneous determination of EDTA and DTPA (Table 2). The reported object of the most existing gas chromatographic methods has been the determination of EDTA or EDTA and DTPA in natural and waste waters, as well as in aqueous solutions in general [47–58]. By GC, EDTA has also been determined in nuclear waste [59], foodstuffs [60,61], steam propulsion systems [46], as an impurity of DTPA [62] and in sediments and fishes [57].

Due to the evaporation to dryness of aqueous samples, the simpliest way to decrease detection limit is to increase sample volume. However, an increase in sample volume leads to prolonged sample preparation times. Evaporation step is required, as extraction of EDTA and DTPA into organic solvents is difficult due to their hydrophilic nature.

As a general trend, it can be conferred that the more recent GC methods provide lower detection limits than earlier ones. However, it must be remembered that also more sensitive mass selective (MS) and nitrogen phosphorus detectors (NPD) have widely replaced flame-ionization detectors (FID) which were applied in earlier reports (Table 2). The detection limits are approximately three decades lower than in HPLC methods in general (in other words, at low $\mu g\ l^{-1}$ level).

In conclusion, GC analysis is suitable when high sensitivity is required, i.e. for environmental samples. GC is also successfully applied for foodstuffs. The sample preparation procedures consist of several steps which increase the total analysis time. Total amount of complexing agents are measured as their esters. Therefore speciation studies are not possible, in contrast to LC. EDTA and DTPA form extremely stable complexes with metals, especially with Fe^{3+}. As these compounds are used to bind metal ions in industrial and agricultural applications, metals can interfere, at least to some extent, the esterification step. However, in many of the studies presented above, the interference of metal ions has not received sufficient attention.

4. Electroanalytical methods

Several electrochemical applications for EDTA determination has been developed. Only Horacek and Pribil [63] and Yoshimura [64–66], using potentiometry and voltammetry, have analysed EDTA and DTPA simultaneously. In addition, Yoshimura used PbO_2 electrode as an indicator electrode and observed that there is a linear relationship between the peak-to-peak heights and the stability constants of the lead complexes [64]. Therefore, it was inferred that the peaks were due to complex formation.

Methods for EDTA analysis include polarography [67–69], differential pulse polarography (DPP) [70,71], potentiometry [72,73], one-drop square-wave polarography [74], differential pulse anodic stripping voltammetry (DPASV) [75,76], differential pulse cathodic stripping voltammetry (DPCSV) [77] and potentiometric stripping analysis (PSA) [78]. The details of the methods described in literature are presented in Table 3.

Methods for natural and waste water analysis developed by Voulgaropoulos et al., provide the lowest detection limits ($0.1\ \mu g\ l^{-1}$) ever presented for EDTA determination [75,76]. Concentrations below this level have most likely only negligible environmental relevance. Unfortunately, the methods were developed for the nitrilotriacetic acid (NTA) and EDTA determination, while DTPA was excluded. In addition, it is reported that these methods are affected by the nature of the electrolyte present in solution and its concentration [78].

Generally speaking, the most recent methods [75–78] prove superiority to earlier ones in terms of sensitivity. If EDTA was found in natural waters by these methods, it was present at relatively low $\mu g\ l^{-1}$ level with one exception: the highest natural water concentration of EDTA ever presented in literature ($900\ \mu g\ l^{-1}$) was found in river water 1 km away from the point source [78].

The electrochemical methods presented in the literature for the EDTA and DTPA determination are well suited to the aquatic environment, such as waste and natural waters. Selectivity is poor in some electrochemical methods and simultaneous

Table 3
Characteristics of the existing elecrochemical methods for the analysis of EDTA and DTPA

Reference	Method	Analyte	Matrix	Indicator electrode	L.O.D.	Remarks
[63]	Potentiometry	EDTA, DTPA	Aqueous media		15 mg l^{-1}	Fe(III) complex
[69]	Voltammetry	EDTA	Aqueous media	Carbon	15 mg l^{-1}	
[73]	Potentiometry	EDTA	Detergent			Zn(II) complex, no differentiation between EDTA and NTA
[70]	DPP	EDTA	Phytoplancton media	DME	1.5 mg l^{-1}	Cd(II) complex
[71]	DPP	EDTA	Phytoplancton media	DME	0.6 0.9 mg l^{-1}	Cd(II) complex
[72]	Potentiometric	EDTA	Aqueous media	Perchlorate selective	2.2. mg l^{-1} catalytic titration	
[68]	Voltammetry	EDTA	Aqueous media	DME	15 μg l^{-1}	V(V) complex
[64]	Voltammetry	EDTA, DTPA	Aqueous media	MnO_2	30 mg l^{-1} for EDTA	
[65]	Voltammetry	EDTA, DTPA	Aqueous media	PbO_2	30 mg l^{-1} for EDTA	
[74]	One-drop square-wave polarography	EDTA	Aqueous media	DME/TFME	21 μg l^{-1}	
[66]	Voltammetry	EDTA, DTPA	Aqueous media	MnO_2 and PbO_2	30 mg l^{-1} for EDTA	
[75]	DPASV	EDTA	Natural waters	HMDE	0.1 μg l^{-1}	Bi(III) complex, indirect, Fe(III), Cu(II), Cl interfer
[77]	DPCSV	EDTA	Aqueous media	HMDE	3 μg l^{-1}	Cl, Br, Cu(II), Fe(III), Zn(II) interfere
[78]	PSA	EDTA	Natural and waste water	Glassy carbon	1 μg l^{-1}	Bi(III) complex, indirect
[76]	DPASV	EDTA	Natural and waste water	HMDE	0.1 μg l^{-1}	Indirect

Table 4
Characteristics of the spectrophotometric methods for the determination of EDTA and DTPA

Reference	Analyte	Matrix	L.O.D.	Remarks
[88]	EDTA	Fruit juice		Direct
[89]	EDTA, DTPA	Aqueous media		Indirect
[90]	EDTA	Aqueous media	0.3 mg l^{-1}	Direct, Fe(III) complex
[91]	EDTA	Freshwater	10 μg l^{-1}	Co(III) complex, preconcentration step
[92]	EDTA	Aqueous media	30 μg l^{-1}	Indirect, Mn(II) complex
[93]	EDTA	Aqueous media	750 μg	Direct
[94]	EDTA	Human urine	0.74 μg	Direct, interferences reported
[95]	EDTA	Aqueous media	3.0 mg l^{-1}	Indirect, Cu(II) complex
[96]	EDTA	Aqueous media	370 μg	Direct
[97]	EDTA	Aqueous media		Fe(III) complex
[98]	EDTA	Aqueous media	3 mg l^{-1}	Indirect
[99]	EDTA	Aqueous media	18.6 mg l^{-1}	Direct
[100]	EDTA, DTPA	Aqueous media	0.3 mg l^{-1}	Indirect
[101]	EDTA	Food	0.5 μg g^{-1}	Fe(III) complex, 20 g of sample
[121]	EDTA	Aqueous media		Cu(II) complex with chrome azurol S
[102]	EDTA	Food	3.4 μg l^{-1}	Zr(IV) complex with Alizarin Red S

detemination of chelating agents complicated. In natural waters, ligands, e.g. humic substances or other anthropogenic complexing agents than the analytes, can interfere. In addition, many anions and cations often present in natural waters also interfere [73,74]. On the other hand, most electrochemical methods are simple, inexpensive, rapid and sensitive.

5. Other methods

There exist several early reports [79–98] for EDTA determination by spectrophotometric procedures, but only few recent ones [99–101]. Again, only two of these methods can be directly applied to the DTPA determination [89,100]. These spectrophotometric methods are based on forming a metal–chelate complex and measuring its amount either directly or indirectly.

Most of these procedures do not differentiate between complexing agents, are subject to interferences and are not sensitive enough for trace analysis. On the other hand, the rapidity and simplicity are the unquestionable advantages.

The characteristics of the methods are presented in Table 4. In addition to aquatic media in general, EDTA has been determined in fruit juices [88], human urine [94] and foods [101]. Detection limits are usually at the low mg/l range and thus inappropriate for, e.g. natural water applications. However, the most recent paper presents the procedure which involves the reaction of EDTA with Zr(IV) and Alizarin Red S. This method gives a detection limit (3.4 μg l^{-1}) which is well compatible with chromatographic methods and thus should be paid attention in the case of natural water applications.

Some titrimetric methods are available for the determination of EDTA at low mg l^{-1} level [103–105]. These procedures have equal disadvantages as the colorimetric methods: interference by other complexing agents and low sensitivity.

Capillary electrophoresis (CE) is suited for the analysis of charged hydrophilic compounds. It offers efficient separation being relatively matrix-independent. However, the application of CE for EDTA and DTPA determination has not received sufficient attention so far.

EDTA has been used as a complexing agent in a carrier solution with the aim of alkali and alkaline–earth metal separation and determination by CE in tap and river waters as well as urine and serum samples [106,107]. Also, some heavy metals (Cr, Fe(III), Cu and Pb) have been simultaneously determined as their EDTA complexes

by CE in waste waters [108]. One paper presents a method for the determination of DTPA and its metal complexes (Fe(III), Bi, Cu, Pb and Ni) in waste waters [109]. With this procedure, it was found that Zn-DTPA, Ni-DTPA and Cu-DTPA comigrate and that the resolution between Pb-DTPA and Mn-DTPA is poor. Detection limits were found to be 0.2, 1.4, 0.7, 0.3 and 1.3 mg l^{-1} for Fe-DTPA, Bi-DTPA, Cu-DTPA, Pb-DTPA and Ni-DTPA, respectively. Chelating agents, including EDTA and DTPA, were separated and determined in tank waste simulant by CE as their Cu^{2+} complexes according to a recent report [122]. Detection limits were 2.9 mg l^{-1} for EDTA and 7.9 mg l^{-1} for DTPA. The free pentaacetic DTPA, as a major degradation product of the dianhydride of DTPA, has been determined using CE by another recent report [110]. UV absorbance detection was used in these methods.

The advantages of CE include the possibility for metal speciation studies, short analysis time and high separation efficiency. The applications include pharmaceutical use of DTPA and waste waters. Effective preconcentration procedure would make CE an important tool for heavy metal speciation investigations in natural water applications.

In addition, some procedures for indirect determination of EDTA by atomic absorption methods have been reported [111–114]. The lower limit of analysis is between 0.1–0.3 mg l^{-1} depending on method. Although they are relatively rapid and simple, they provide low selectivity, if other chelating agents are present. As a well-known fact, the speciation of heavy metals is of crucial importance when estimating their bioavailability and environmental fate in general. Hence, these methods can mainly be used for determining the complexing capacity of waste and natural water samples.

6. Conclusions

The chromatographic methods seem the most suitable for the EDTA and DTPA determination. There exists wide variety of matrices in which these compounds have been analysed either by LC or GC. However, waste and environmental samples as well as foodstuffs are the main objects. When the expected concentration is relatively high, as is the case with, e.g. foods, detergents and waste waters, HPLC might be favorable over GC. The sample preparation procedure for HPLC is simple and, in most cases, the required selectivity and sensitivity is achieved. In addition, no significant interferences were observed. Importantly also, the speciation of metal complexes, which is of vital importance from environmental point of view and in some industrial application, such as pulp and paper industry, could be studied by HPLC. The GC analysis of EDTA and DTPA is quite well-known and is very suitable for routine monitoring of complexing agents in natural waters due to high sensitivity. However, all GC procedures require a time-consuming sample preparation step and only the total concentration can be measured. On the other hand, there exist some relatively recent methods, based on either DPASV, PSA or spectrophotometry, which are well compatible with chromatographic methods in terms of sensitivity and simplicity. CE is also promising technique for the determination of EDTA and DTPA as well as their metal complexes in a variety of matrices. Other methods show relatively limited applicability.

References

[1] J. Dai, G.R. Helz, Anal. Chem. 60 (1988) 301.
[2] C. Randt, R. Wittlinger, W. Merz, Fresenius' J. Anal. Chem. 346 (1993) 728.
[3] C. Randt, J. Klein, W. Merz, Vom Wasser 84 (1995) 61.
[4] J. Harmsen, A. Van Den Toorn, J. Chromatogr. 249 (1982) 379.
[5] P.J.M. Bergers, A.C. De Groot, Wat. Res. 28 (1994) 639.
[6] W. Buchberger, P.R. Haddad, P.W. Alexander, J. Chromatogr. 558 (1991) 181.
[7] B. Nowack, F.G. Kari, S.U. Hilger, L. Sigg, Anal. Chem. 68 (1996) 561.
[8] I.V. Gucht, J. Chromatogr. A 671 (1994) 359.
[9] R.M. Cassidy, S. Elchuk, Anal. Chem. 57 (1985) 615.
[10] M. Unger, E. Mainka, W. König, Fresenius' Z. Anal. Chem. 329 (1987) 50.
[11] D.L. Venezky, W.E. Rudzinski, Anal. Chem. 56 (1984) 315.
[12] K.A.S. Hardy, J.C. Cooper, T.K. Ayres, W.E. Rudzinski, Proc. Int. Water Conf. Eng. Soc. West. Pa. 46 (1985) 245.

[13] G.A. Perfetti, C.L. Warner, J. Assoc. Off. Anal. Chem. 62 (1979) 1092.
[14] A. Yamaguchi, T. Yamaguchi, Y. Shiroishi, Y. Shimizu and N. Takasugi, Shokuhin Eiseigaku Zasshi 26 (1985) 253 (Ref. CA 104 (1985) 18 710 g).
[15] T. Hamano, Y. Mitsuhashi, K. Tanaka, Y. Matsuki, Y. Tonogai, K. Nakamura and Y. Ito, Shokuhin Eiseigaku Zasshi 26 (1985) 630 (Ref. CA 104 (1985) 223 716).
[16] M. Aihara, S. Okada, Fukuoka Joshi Daigaku Kaseigakubu Kiyo 18 (1987) 73.
[17] J. De Jong, A. Van Polanen, J.J.M. Driessen, J. Chromatogr. 553 (1991) 243.
[18] E.L. Inman, R.L. Clemens, B.A. Olsen, J. Pharm. Biomed. Anal. 8 (1990) 513.
[19] U. Göttlicher, R. Siegfied, H. Birke, Fresenius J. Anal. Chem. 352 (1995) 398.
[20] O. Stålberg, T. Arvidsson, J. Chromatogr. A 684 (1994) 213.
[21] D.E. Richardson, G.H. Ash, P.E. Harden, J. Chromatogr. A 688 (1994) 47.
[22] J.H. Knox, M. Shibukawa, J. Chromatogr. 545 (1991) 123.
[23] J.-F. Jen, C.-S. Chen, Anal. Chim. Acta 270 (1992) 55.
[24] J. Schöppenthau, L. Dunemann, Fresenius' J. Anal. Chem. 349 (1994) 794.
[25] J.-F. Jen, S.-M. Yang, Anal. Chim. Acta 289 (1994) 97.
[26] D.L. Taylor, P.M. Jardine, J. Environ. Qual. 24 (1995) 789.
[27] S. Matsushita, J. Chromatogr. 312 (1984) 327.
[28] T. Tanaka, Fresenius' J. Anal. Chem. 320 (1985) 125.
[29] M.L. Marina, J.C. Diez-Masa, M.V. Dabrio, J. High Res. Chromatogr. Chromatogr. Comm. 9 (1986) 300.
[30] W. Lien, B.K. Boerner, J.G. Tarter, J. Liq. Chromatogr. 10 (1987) 3213.
[31] G. Schwedt, B. Kondratenok, Fresenius' J. Anal. Chem. 332 (1989) 855.
[32] A. Nitsch, K. Kalcher, U. Posch, Fresenius' J. Anal. Chem. 338 (1990) 618.
[33] D. Yan, G. Schwedt, J. Chromatogr. 516 (1990) 383.
[34] M.L. Marina, P. Andres, J.C. Diez-Masa, Chromatographia 35 (1993) 621.
[35] H.-J. Götze, D. Bialkowski, Fresenius' Z. Anal. Chem. 323 (1986) 350.
[36] C.C.T. Chinnick, Analyst 106 (1981) 1203.
[37] J. Weiss, G. Hägele, Fresenius' Z. Anal. Chem. 328 (1987) 46.
[38] A.E. Martell and R.M. Smith, Stability constants. Chemical Society, Suppl. 1, Special publication No. 25, 865 p. London, 1971.
[39] G. Anderegg, Helv. Chim. Acta 47 (1964) 1801.
[40] A. Yamaguchi, A.R. Rajput, K. Ohzeki, T. Kambara, Bull. Chem. Soc. Jpn. 56 (1983) 2621.
[41] A. Yamaguchi, A. Toda, K. Ohzeki, T. Kambara, Bull. Chem. Soc. Jpn. 56 (1983) 2949.
[42] S.G. Chen, K.L. Cheng, C.R. Vogt, Microchim. Acta 31 (1983) 473.
[43] M.M. Vora, S. Wukovnig, R.D. Finn, A.M. Enram, T.E. Boothe, P.J. Kothari, J. Chromatogr. 369 (1986) 187.
[44] V.W. Huber, Acta Hydrochim. Hydrobiol. 20 (1992) 6.
[45] D.J. Subach, J.E. James, J. High. Resol. Chromatogr. & Chromatogr. Commun. 3 (1980) 309.
[46] P.J. Sniegoski, D.L. Venezky, J. Chromatogr. Sci. 12 (1974) 359.
[47] L. Rudling, Wat. Res. 6 (1972) 871.
[48] J. Gardiner, Analyst 102 (1977) 120.
[49] R.M. Cassidy, R. Harpur, S. Elchuk, J. Chromatogr. 190 (1980) 188.
[50] K. Momoki, T. Sakamoto, Bull. Fac. Eng., Yokohama Nat. Univ. 33 (1984) 51.
[51] F. Dietz, Wasser-Abwasser 128 (1987) 286.
[52] M.A. Ribick, M. Jemal, A.I. Cohen, J. Pharm. Biomed. Anal. 5 (1987) 687.
[53] St. Schürch, G. Düdendorfer, Mitt. Gebiete Lebensm. Hyg. Band 80 (1989) 324.
[54] H. Otteneder, B. Schleser, Lebensmittelchemie 46 (1992) 87.
[55] V.T. Wanke, S.H. Eberle, Acta Hydrochim. Hydrobiol. 20 (1992) 192.
[56] D.-K. Nguyen, A. Bruchet, P. Arpino, J. High Res. Chromatogr. 17 (1994) 153.
[57] Y. Nishikawa, T. Okumura, J. Chromatogr. A 690 (1995) 109.
[58] J. Pietsch, W. Schmidt, F. Sacher, S. Fichtner, H.-J. Brauch, Fresenius' J. Anal. Chem. 353 (1995) 75.
[59] A.P. Toste, T.J. Lechner-Fish, Waste Management 13 (1993) 237.
[60] D.T. Williams, J. Assoc. Off. Anal. Chem. 57 (1974) 1383.
[61] C. Retho, L. Diep, Z. Lebensm. Unters. Forsch. 188 (1989) 223.
[62] M.L. Blank, F. Snyder, J. Chromatogr. 170 (1979) 379.
[63] J. Horacek, R. Pribil, Talanta 16 (1969) 1495.
[64] T. Yoshimura, Fresenius' Z. Anal. Chem. 305 (1981) 364.
[65] T. Yoshimura, Fresenius' Z. Anal. Chem. 307 (1981) 197.
[66] T. Yoshimura, Bull. Chem. Soc. Jpn. 55 (1982) 2056.
[67] E.B. Barbolani, Inquinamento 16 (1974) 19.
[68] T. Kitagawa and Y. Kanei, Bunseki Kagaku 19 (1979) 482 (Ref CA 73 (1979) 41 631).
[69] T. Nomura, G. Nakagawa, J. Electroanal. Chem. 111 (1980) 319.
[70] R.J. Stolzberg, Anal. Chim. Acta 92 (1977) 139.
[71] R.J. Stolzberg, Electrochem. Stud. Biol. Syst. Symp. 38 (1977) 194.
[72] T.P. Hadjiioannou, M.A. Koupparis, C.E. Efstathiou, Anal. Chim. Acta 88 (1977) 281.
[73] B.M. Milwidsky, Soap. Cosmet. Chem. Spec. 47 (1971) 46.
[74] Z. Stojek, J. Osteryoung, Anal. Chem. 53 (1981) 847.
[75] A. Voulgaropoulos, P. Valenta, H.W. Nurnberg, Fresenius' Z. Anal. Chem. 317 (1984) 367.

[76] A. Voulgaropoulos, N. Tzivanakis, Electroanalysis 4 (1992) 647.
[77] M. Ciszkowska, Z. Stojek, Talanta 33 (1986) 817.
[78] M. Fayyad, M. Tutunji, Z. Taha, Analyt. Lett. 21 (1988) 1425.
[79] A. Darbey, Anal. Chem. 24 (1952) 373.
[80] T. Bersin, H. Schwarz, Schweiz. Med. Wochschr. 83 (1953) 765.
[81] G. Seris, Ann. Fals. Expert. Chim. 47 (1954) 29.
[82] P.J. Cherney, B. Crafts, H.H. Hagermoser, A.J. Boyle, R. Habin, B. Zak, Anal. Chem. 26 (1954) 1806.
[83] O. Menis, H.P. House, B. Rubins, Anal. Chem. 28 (1956) 1439.
[84] J. Vogel, J. Deshusses, Mitt. Gebiete Lebensm. Hyg. 53 (1962) 175.
[85] G.W.F. Brady, J.R. Gwilt, J. Appl. Chem. (London) 12 (1962) 79.
[86] R.E. Mosher, P.J. Burcar, A.J. Boyle, Anal. Chem. 35 (1963) 403.
[87] K. Saito, T. Hasuo and H. Nakano, Nippon Jozo Kyokai Zasshi 63 (1968) 1193 (Ref CA 71 (1968) 122 314).
[88] E. Bruno, R. Calapaj, G. Sergi, Ann. Fac. Econ. Commerc., Univ. Studi Messina 7 (1969) 3.
[89] R.M. Wallace, J.F. Hinton, Anal. Chim. Acta 51 (1970) 536.
[90] S.N. Bhattacharyya, K.P. Kundu, Talanta 18 (1971) 446.
[91] K.L.E. Kaiser, Wat. Res. 7 (1973) 1465.
[92] D.P. Nikolelis, T.P. Hadjiioannou, Anal. Chim. Acta 97 (1978) 111.
[93] M. Ternero, F. Pino, Anal. Chim. Acta 109 (1979) 401.
[94] S.Z. Qureshi, R. Bansal, Fresenius' Z. Anal. Chem. 308 (1981) 32.
[95] A. Yamaguchi, K. Ohzeki, T. Kambara, Fresenius' Z. Anal. Chem. 310 (1982) 30.
[96] T. Raya-Saro, D. Perez-Bendito, Analyst 108 (1983) 857.
[97] A. Yamaguchi, K. Ohzeki, T. Kambara, Bull. Chem. Soc. Jpn. 56 (1983) 2293.
[98] A. Rios, M. Valcarcel, Analyst 109 (1984) 1147.
[99] R. Parkash, R. Bansal, Analyt. Lett. 23 (1990) 1159.
[100] H. Itabashi, K. Umetsu, N. Teshima, K. Satoh, T. Kawashima, Anal. Chim. Acta 261 (1992) 213.
[101] T. Hamano, Y. Mitsuhashi, N. Kojima, N. Aoki, M. Shibata, Y. Ito, Y. Oji, Analyst 118 (1993) 909.
[102] A.M. Garcia Campaña, F Alés Barrero and M Romàn Ceba, Anal. Chim. Acta 329 (1996) 319.
[103] G.G. Clinckemaille, Anal. Chim. Acta 43 (1968) 520.
[104] J. Vanderdeelen, A. Van Der Hende, Chim. Anal. 50 (1968) 237.
[105] B.G. Blijenberg, B. Leijnse, Clinica Chim. Acta 26 (1969) 577.
[106] S. Motomizu, M. Oshima, S. Matsuda, Y. Obata, H. Tanaka, Anal. Sci. 8 (1992) 619.
[107] T. Wang, S.F.Y. Li, J. Chromatogr. A 707 (1995) 343.
[108] B. Baraj, M. Martinez, A. Sastre, M. Aguilar, J. Chromatogr. A 695 (1995) 103.
[109] W. Buchberger, S. Mulleder, Mikrochim. Acta 119 (1995) 103.
[110] J. Bullock, J. Chromatogr. B 669 (1995) 149.
[111] R. Kunkel, S.E. Manahan, Anal. Chem 45 (1973) 1465.
[112] D.R. Jones, S.E. Manahan, Anal. Lett. 8 (1975) 421.
[113] E.B. Milosavljevic, L. Solujic, J.L. Hendrix, J.H. Nelson, Analyst 114 (1989) 805.
[114] E. Farina, P.M. Bevinino, Boll. Chim. Igien. 41 (1990) 493.
[115] M. Sillanpää, R. Kokkonen, M.-L. Sihvonen, Anal. Chim. Acta 303 (1995) 187.
[116] L. Ye, C.A. Lucy, Anal. Chem. 67 (1995) 2534.
[117] A.S. Kord, I. Tumanova, W.L. Matier, J. Pharmaceut. Biomed. Anal. 13 (1995) 575.
[118] G. Tran, C. Chen, R.B. Miller, J. Liq. Chrom. Rel. Technol. 19 (1996) 1499.
[119] L. Ye, C.A. Lucy, J. Chrom. A 739 (1996) 307.
[120] M. Sillanpää, J. Sorvari, M.-L. Sihvonen, Chromatographia 42 (1996) 578.
[121] M. Shenker, Y. Hadar, Y. Chen, Soil Sci. Soc. Am. J. 59 (1995) 1612.
[122] N.E. Ballou, G.R. Ducatte, C. Qurang, V.T. Remcho, J. High Resol. Chrom. 19 (1996) 183.

ELSEVIER

Talanta 44 (1997) 1499–1500

Talanta

In Memoriam

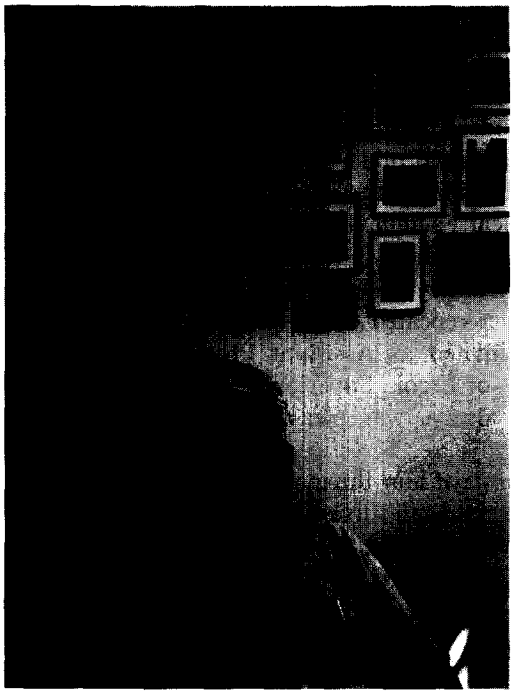

Professor Henrique Bergamin Filho

On December 14th 1996, a few days after receiving one of the highest Brazilian awards (Comenda da Ordem do Merito Cientifico), the scientist Henrique Bergamin Filho suddenly passed away, victim of a heart aneurysm. He was the intellectual mentor of the analytical chemistry group at CENA/USP, research father of several docents in different Brazilian Universities, lovely husband, father and grandfather, and exemplary citizen.

Professor Bergamin was internationally recognized, mainly for his research in the field of flow analysis, as he was concerned with the inception and development of Flow Injection Analysis (FIA). Without him, it is difficult to tell what FIA would have been today. Also, he experimented with atomic absorption spectroscopy (the first AAS instrument in South America was built by him in 1961, and was presented again at the First Rio Symposium on Graphite Furnace in 1988), and with atomic emission spectroscopy. Thus, his contributions evolved from atomic spectroscopy in the 1960s, to FIA-AAS and FIA-ICP-AES in the 1970s, and recently electrolytic dissolution spectroscopy. He liked to propose challenges, (e.g. automated merging zones, ion-exchange, solvent extraction, isothermal distillation, reagent immobilization, etc.), and this was the key to science development at CENA.

PII S0039-9140(97)00024-6

Besides science, his main hobby was photography. As he had his own laboratory since he was young, we believe that this feature had a large influence in his scientific comprehension of natural phenomena. Also, he was an expert in machining small pieces, both at home and in the laboratory.

Simplicity, creativity, intelligence, valorization of the human being, and availability to help were some of his personal characteristics, as can be realized from the following text, an adaptation of his autobiography prepared when he became a Member of the Brazilian Academy of Sciences [1]:

'Born in 1931. His father was a state civil servant and his mother a teacher in fundamental school. Home provided stimulating surroundings, as his father appreciated literature and music. There was in the house a hi-fi playing machine with an old motor: 10–12 turns of the handle sufficed for playing two 78 r.p.m. records! It was the first machine dismounted by him (actually, it was the second one, since the first was an alarm clock. His father became very angry and the clock remained dismounted). His father died when he was 11-years old, and his mother provided education for all their children and pushed them in the right direction. She died after her 91st birthday.

Dr Bergamin was a good student in fundamental and high schools. Before entering into University, his mother told him that his father would prefer if he became a doctor. This was a surprise, as Dr Bergamin was already looking for the best universities where he could learn chemistry. He did not get high enough a score to enter into the Medical Faculty. In Piracicaba, he was admitted in the Agricultural Faculty of the Sao Paulo University. He studied the four academic years with relative facility, mainly when disciplines such as physics, chemistry and mathematics were concerned. Other specific disciplines were more cumbersome, but he never repeated one.

After graduation, he was invited as Assistant Professor by R.A. Catani, full Professor of Chair # 10—Analytical Chemistry—of Escola Superior de Agricultura 'Luiz de Queiroz', USP, at Piracicaba. Dr Bergamin succeeded! He always was pleased with searching new things, solving problems, and teaching.

He married Therezinha who gave him three children: Henrique (today 36 years old), Denise (34) and Cynthia (32). They traveled abroad, and lived for one and a half years in Champaign-Urbana, Illinois, USA, working with H.V. Malmstadt, and about one year in Copenhagen, working with J. Ruzicka and E.H. Hansen. Back in Brazil, he worked at the Education Ministry and then organized the Analytical Chemistry Section at CENA/USP. Thereafter, he spent four years in the Amazon, directing the Instituto Nacional de Pesquisas da Amazonia. This was one of the most remarkable experiences of his life. He and his wife were always together, and his children visited him eventually, mainly during the holiday periods. Asked by J. Cousteau how and why a relatively successful chemist was directing a research institute in the Amazon region, he became astonished with his own answer: since he was a child, he was fascinated by explorers and explorations. And a secret wish: one day, to become one of them. Nowadays, he still lives well with the same wife, in the same house. He likes when the house is filled with children, grandchildren and friends, and hopes to live the next years in the same place in the same actual conditions'.

Elias Ayres G. Zagatto
Francisco Jose Krug

References

[1] Academia Brasileira de Ciencias, Academia Brasileira de Ciencias: organizacjo e membros, Commemorative edition to the 80 years of the Academy, Academia Brasileira de Ciencias, A Academia, Rio de Janeiro, 1996, p. 125.

ELSEVIER

Talanta 44 (1997) 1501–1504

Talanta

An analytical chemist of verve: George-Emil Baiulescu

J.D.R. Thomas [1]

4 Orchard Court, Gresford, Wrexham LL12 8EB, Wales, UK

Received 20 August 1996; accepted 3 September 1996

1. Introduction

Sixty-five is an age when distinguished people, like leading analytical chemists, are frequently honoured in one way or another. So it was in 1994 when I was asked to eulogize the contributions of Professor Richard P. Buck to electroanalytical chemistry [1]. It is my privilege to have been asked yet again to express appreciation of the contributions of another of the personalities of analytical chemistry. The honour of the special issue of Talanta on this occasion is Professor George-Emil Bailuescu, whose 65th birthday fell on August 4th, 1996.

George Baiulescu is well known for his work over a wide span of analytical chemistry, namely separations, colorimetry and spectrometry, ion-selective electrodes, environmental analysis and sampling. Additionally, he has been active in the field of education, and it was through such a contribution—as a plenary lecturer at The Royal Society of Chemistry's SAC 80: An International Conference on Analytical Chemistry at Lancaster, UK in July 1980, that I was to first meet George Baiulescu, but his works were known to me long before then. His lecture [2] with the esoteric title of 'Moral Ageing of Analytical Methods' reflected Baiulescu the philosopher, for George took on a broad view of analytical chemistry and reasoned the analysis of a sample in terms of the octahedron of analytical chemistry (Fig. 1) to demonstrate the areas of knowledge and experience demanded of a sound analyst.

Apart from the 'big slot' at Lancaster, George has filled many other significant engagements as plenary lecturer—at Sassari (Italy) (1976), Zaragoza (Spain) (1983), Chiba (Japan) (1991), Gdansk (Poland) (1986 and 1990) and Changchun (China) (1994). Doubtless, the list would be longer were it not for the frustrations of the ridiculous system of 'rationed' exit visas imposed by the former political system of Eastern Europe. George Baiulescu suffered from this, as illustrated by him being prevented from leaving Romania in

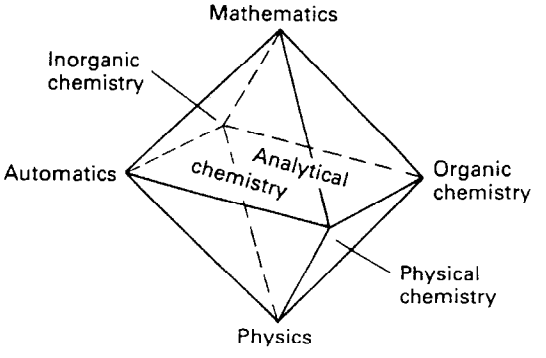

Fig. 1. The octahedron of analytical chemistry.

[1] The author is Emeritus Professor of Chemistry at the University of Wales, Cardiff; Visiting Professor at NEWI (An Associate College of the University of Wales), Wrexham; and Honorary Professor of the Faculty of Industrial Chemistry, University 'Politehnica', Bucharest.

PII S0039-9140(96)02178-9

November 1988 to deliver lectures on sampling for analysis at centres in the UK. This was not simply a case of an air ticket wasted, but rather—as also happened to others, an abuse of human dignity.

2. Education and experience

Baiulescu George-Emil took his BSc in 1954 from the Chemical Faculty of the University of Bucharest, and went on to be a researcher at the Centre of Chemical Researches (Department of Inorganic Chemistry) of the Romanian Academy of Sciences between 1954 and 1958. He then successively became assistant lecturer, reader and professor at the University of Bucharest, punctuated by a period at the National Institute of Chemistry. It was at the National Institute of Chemistry that I found him in September 1987, when I was the first British chemist to have visited Bucharest for some years. At the time George had just returned from Euroanalysis V which had been held in Paris.

After taking his PhD in 1960 and DSc in 1970, George—by the system in Romania, was in 1971 accorded with the authorization for directing PhD students. Twenty persons have completed this degree under his supervision.

3. Published works

In the field of separations, George's contributions are wide-ranging and relate to solvent extraction, ion-exchange, gas chromatography (GC), thin-layer chromatography (TLC), and HPLC. These are directed at advances in technique, such as new stationary phases in GC [3,4] and new vizualizing agents in TLC [5,6], as well as to the analysis of topical items and materials, such as PAHs [7], fruit extracts [8] and peptides [9].

Reaction analytical chemistry is an important feature of colorimetric and spectrophotometric analysis, and according to fashion of the time several of George's early papers are in this area, e.g. functional groups for osmium [10], palladium [11–13] and uranium (VI) [14,15]. Indeed, about a third of George's published titles relate to this area (mainly pre-1970), topped by some useful (post 1970) contributions in atomic absorption spectrometry [16,17], infrared spectrometry [18], spark mass spectrometry [19] and X-ray photoelectron spectroscopy [20].

While some of the spectrometric items relate to environmental analysis, e.g. analysis of lithium and manganese in Covasna and Harghita mineral waters [16] and colour measurement in the diagnosis of leaf diseases [21], George categorises his environmental analysis work as that of the analysis of gases in the air. Thus, there is the determination of ozone in ground level air [22] and various papers relating to determinations of atmospheric sulphur dioxide, such as by the use of reactive surfaces [23] and studies on reagents [24–26]. There are also papers relating to carbon monoxide [27,28] and nitrogen dioxide [29], and one on suspended particulates and their lead content [30]. Naturally, there is some reaction analytical chemistry and spectrophotometry underlying these items.

Potentiometry with ion-selective electrodes (ISEs) has attracted the attention of analytical chemists almost everywhere. It has led on from pioneering work—particularly in Hungary, Switzerland, UK and USA, and encouraged by the 1969 NBS Conference organized by Richard A. Durst in Washington, USA and the 1973 IUPAC Symposium organized by J.D.R. Thomas in Cardiff, Wales.

Further stimulation for researches on ISEs, as recently emphasized [31], has been given by the, by now, almost universal use of electrode-based blood electrolyte measurements seen as resulting from early work carried out in Philadelphia, Boston, Zürich and Cardiff. George Baiulescu was not to be left behind, and ISEs are to be seen as his equal second biggest area (with separations) of activity, enhanced by having Vasile Cosofret as an energetic partner. His attention, initially directed at metal cation ISEs, such as for copper(II) [32,33] and mercury(II) [34,35] has been given over to drugs and pharmaceutical systems, e.g. sulpha drugs [36], lidocaine [37], active components in intestopan [38] and imipramine [39].

4. Books

Ellis Horwood of Chichester did much to project East European analytical chemists to the world-wide community, and three of the five books co-authored by George Baiulescu were published by him. Among these, that on 'Applications of Ion Selective Membrane Electrodes in Organic Analysis' with V.V. Cosofret as co-author when published in 1977 (its Russian translation was published by Mir, Moscow in 1980) placed the Romanian group among world rankings in ISE research.

The two other books published by Ellis Harwood were 'Education and Teaching in Analytical Chemistry' by G.E. Baiulescu, C. Patroescu and R.A. Chalmers (1982) (Chinese edition in 1993), and 'Sampling' by G.E. Baiulescu, P. Dumitrescu and P.Gh. Zugravescu (1991) (Chinese edition in 1996). George's remaining two books are 'Physical Methods of Trace Analysis' co-authored by T. Nascutiu and published by Ed. Tehnica, Bucharest in 1974, and 'Stationary Phases in Gas Chromatography' co-authored by V.A. Ilie and published by Pergamon Press, Oxford in 1975.

5. Society and conference activities

To acknowledge his lecturing engagements at conferences outside of Romania, it is to be noted that George Baiulescu has taken on the role of organiser of several events in Romania. This has been facilitated by him being President of the Romanian Society of Analytical Chemistry—of which both he and Dr G.L. Radu have from time to time represented on the Working Party on Analytical Chemistry of the Federation of European Chemical Societies.

It was only on the occasion of the XIth National Conference on Analytical Chemistry in Ciuj-Napoca in 1992 that the first foreign lecturers were invited to these national Romanian events since that held in Brasov in 1971—the intervening 21 years being referred to as the 'dark period'. For the XIth, XIIth and XIIIth National Conferences at Ciuj-Napoca (1992), Constanza (1994) and Craiova (1996) respectively, George in his capacity as President and on behalf of SCAR (Societatea de Chimie Analitica din Romania) has welcomed many foreign lecturers of distinction, and these have been appreciative of their caring hosts.

The foreign guest lecturers have served to strengthen and add to the kind of international links, mentioned elsewhere [1], in which Richard P. Buck has been involved. The nature and extent of the involvement of these foreign lecturers invited by George Baiulescu on behalf of SCAR is summarized in a report [40] of the XIIth National Conference held in Constanza in 1994.

Having regard to the wide range of posters by Romanian analytical chemists at the SCAR National Conferences [40], it seems a pity that at least some of the Romanian authors are not encouraged to stand alongside the foreign guests on the lecturing podium in order to explain and enlarge on the work summarized in their posters. Now that George, through SCAR, has done the missionary work of having the international knowledge frontiers of analytical chemistry presented at these Conferences, there are indications that the XIVth Conference to be held in Piatra Neamt in 1998 (24–26th September) will have Romanian colleagues presenting their findings from the podium. The verve that George has for analytical chemistry will be well directed in promoting Romanian analytical chemistry by helping to bring this about.

6. Conclusion

Although his working life has been largely under a system where it was difficult to give vent to his kind of enterprising spirit, George-Emil Baiulescu has succeeded in adding to the status of analytical chemistry. In this, although it was by a quirk of circumstances, it has been an honour to have co-authored one of his papers [41].

By his enthusiasm and enjoyment of life, George has added a certain glitter to the pursuit of analytical chemistry. His qualities have assembled a wide circle of friends, spread over many countries. With him having now reached a significant milestone of life's journey, Professor George-

Emil Baiulescu is extended the best of good wishes. Long may his work prosper and friendship continue.

References

[1] J.D.R. Thomas, Talanta, 41 (1994) 837.
[2] G.E. Baiulescu, Analyst, 105 (1980) 1045; Pure Appl. Chem., 52 (1980) 2525.
[3] G.E. Baiulescu and V. Ilie, Anal. Chem., 44 (1972) 1490.
[4] G.E. Baiulescu and V. Ilie, Anal. Chem., 46 (1974) 1847.
[5] G.E. Baiulescu and T. Constantinescu, Rev. Chim. Bucharest, 25 (1974) 151.
[6] G.E. Baiulescu and T. Constantinescu, Rev. Chim. Bucharest, 26 (1975) 952.
[7] A. Medvedovici, G.E. Baiulescu, J. Chen and P. Sandra, Proc. XVth Int. Symp. on Capillary Chromatography, Riva del Garda, Italy, May 1993, p. 1118.
[8] A. Medvedovici, V. David, T. Tache, E. Baiulescu and P. Sandra, Proc. XVIth Int. Symp. on Capillary Chromatography, Riva del Garda, Italy, September 1994, p. 771.
[9] A.I. Colovai, N. Suiciu-Foca, G.E. Baiulescu and P.E. Harris, Tissue Antigens, 44 (1994) 65.
[10] G.E. Baiulescu, C. Lazar and C. Cristescu, Anal. Chim. Acta, 24 (1961) 463.
[11] Gr. Popa, D. Negoiu and Gh. Baiulescu, Zh. Anal. Chim., 14 (1959) 322.
[12] Gh. Baiulescu, C. Greff and F. Danet, Analyst, 94 (1969) 354.
[13] M.E.M. Khalifa, D. Stoicescu and G.E. Baiulescu, Microchim. Acta, 2 (1984) 169.
[14] Gh. Baiulescu and C.I. Ciurea, Z. Anal. Chem., 166 (1959) 5.
[15] Gh. Baiulescu, D. Marinescu and C. Greff, Analyst, 95 (1970) 661.
[16] G.E. Baiulescu, J. Fazakas, C. Manoliu and B. Tomi, Chim. Anal. Bucharest, 2 (1972) 184.
[17] J. Fazakas, A. Gherman, G.E. Baiulescu and C. Mullins, Rev. Chim. Bucharest, 25 (1974) 917.
[18] M. Draghici, S. Badilescu and G.E. Baiulescu, Spectrosc. Lett., 15 (1982) 583.
[19] M. Draghici, P. Dumitrescu and G.E. Baiulesicu, Anal. Lett., 16 (1983) 289.
[20] G.L. Radu and G.E. Baiulescu, J. Mol. Struct., 293 (1993) 265.
[21] D. Seracu and G.E. Baiulescu, Anal. Lett., 86 (1993) 2349.
[22] V. Magericu, Gh. Baiulescu and D. Popescu, Culegere de lucrari ale Institului Meteorologic pe anul, 1966 ,1968, p. 215.
[23] P. Marcuta, D. Marinescu si G.E. Baiulescu, Meteorol. Hydrol., 2 (1972) 61.
[24] G.E. Baiulescu, P.C. Marcuta and D.M. Marinescu, Int. J. Environ. Anal. Chem., 2 (1973) 203.
[25] G.E. Bailuscu and P. Marcuta, Rev. Chim. Bucharest, 24 (1973) 912.
[26] M. Biziuk, E. Kozlowski and G.E. Baiulescu, Anal. Lett., 14 (1981) 1377.
[27] V. David and G.E. Baiulescu, Rev. Roum. Chim., 33 (1988) 603.
[28] Y. David, P. Marcuta and G.E. Baiulescu, Rev. Chim. Bucharest, 40 (1989) 528.
[29] M.E.M. Rhalifa, C. Greff and G.E. Baiulescu, Anal. Lett., 14 (1981) 249.
[30] G.E. Baiulescu and D.M. Marinescu, Staub-Reinhalt Luft., 39 (1979) 79.
[31] M.S. Frant, Analyst, 119 (1994) 2293.
[32] G.E. Baiulescu and V.V. Cosofret, Rev. Chim. Bucharest, 26 (1975) 1051.
[33] G.E. Baiulescu, V.V Cosofret and F.G. Cocu, Talanta, 23 (1976) 329.
[34] G.E. Baiulescu and V.V. Cosofret, Talanta, 23 (1976) 677.
[35] V.V. Cosofret, P.G. Zugravescu and G.E. Baiulescu, Talanta, 24 (1977) 461.
[36] G.E. Baiulescu, G. Kandemir, M.S. Ionescu and C. Cristescu, Talanta, 32 (1985) 295.
[37] M.S. Ionescu, A.A. Abrutis, N. Radulescu and G.A. Baiulescu, Analyst, 110 (1995) 929.
[38] M.S. Ionescu, M. Lazarescu, A. Ionescu and G.E. Baiulescu, Talanta, 34 (1987) 887.
[39] R.I. Stefan, G.E. Baiulescu, M.S. Ionescu, I. Enachescu, A A. Bunaciu and V.V. Cosofret, Rev. Chem. Bucharest, 45 (1995) 837.
[40] J.D.R. Thomas, Analyst, 120 (1995) 6611.
[41] G.E. Baiulescu and J.D.R. Thomas, Anal. Proc., 26 (1989) 181.

ELSEVIER

Talanta 44 (1997) 1505–1508

Talanta

How to understand the response mechanism of ion-selective electrodes

Ernö Pungor

Institute for General and Analytical Chemistry, Technical University, Budapest, Hungary

Received 16 July 1996; received in revised form 23 October 1996; accepted 13 November 1996

Abstract

The present study breaks with the earlier mechanism of electrode potential on basis of experimental investigations and theoretical considerations. It rejects that the transport through the membrane produces the electrode potential and definitely proves that the electrode potential is created via surface chemisorption; i.e., the electrode potential is produced by a surface reaction. The reaction centres can be acid-base groups or complex formation groups (e.g., valinomycin or other alkaline earth metal complexing ligands). © 1997 Elsevier Science B.V.

Keywords: Chemisorption; Ion-selective electrodes; Surface reaction; Working mechanism of ISE-s

1. History

Nearly a century has passed since the time when it was found at some sorts of glass that they gave an electrochemical sign with respect to the acidity of the solution [1]. There was not found any explanation for this surprising discovery in the earlier theories. It was not clear, how a solid phase, at which any electron transitional reaction necessary to the potential response interpreted in case of metal phases cannot come true, gave an electrode potential response.

The researchers wished to find the answer for explanation by the first imaginable approach from a reaction of quite other type. In the experiment of Donnan [2], in which he separated two solutions—one of them was protein solution, the other was sodium–chloride solution—by a membrane, electrode potential was measurable, and it could be interpreted by supposition of equilibrium of charges and by supposition of ion equilibrium through the membrane. The entirely interpretable, clear picture of the Donnan reaction was adapted to the interpretation of the potential appearing on the glass electrode supposing appearance of charge transfer through the glass membrane. The external layer of the glass screen is swollen by the water solution in case of appropriate glass and through it was supposed the ion transport determining the potential. This transport idea has remained in the interpretation of glass electrodes with the difference that on the basis of precise layer analysis has been evident that the charge transporters can be only sodium ions, ion crystals.

In the 1930s a new change appeared in the interpretations in the way that Nicholski [3] introduced the term of ion exchange for the phenomenon observed by Lengyel and Blum [4]

PII S0039-9140(96)02183-2

potential given to high level of sodium ions in comparison to hydrogen ions. Nicholski interpreted it by that at certain ion concentration proportions the electrode responds to the activity of the formally not potential determining ionic species. By generalizing this idea the literature—first of all the educational literature—garbled this totally clear idea of the selectivity coefficient. The generalizing meant that it saw the basis of the effect of ion-selective electrodes in the ion exchange. Naturally, the Nicholski equation can be put down formally for the whole response function, and a wide domain of them, but in its mechanism the role of ion exchange gives only effect in the domain, where the two types of ions already disturb the response potential of each other. Even today there are in technical books equations attributing potential to the ion exchange, leaving aside that there is not any charge difference between the two sides of the equation being to put down. Although, if in a reaction new charges are not created or lost, then new potential response cannot emerge.

2. New phenomena

In the meantime several new electrodes were developed, and these were wished to be interpreted by the above principles, too. Transport through phase, as determinative process of potential was disclaimed by several experiences. One of the basic experiences is the response time figure determinable on the electrode investigation [5]. It was measurable that the response time of ion-selective electrodes is in general so short (20–40 ms) that this time is sufficient only for penetration onto the surface of the electrode through the fluid adhering to the surface of the electrode. Consequently, if we can speak about a kind of transport at such response times, it can contain in no way the ion transfer through the membrane phase.

A further result of experiments is that we separate space by a potassium-selective electrode so that on one side of the given surface potassium salt solution, on the other side distilled water can be found and considering the electrode membrane thickness as well as the ion transport being to calculate by the diffusion coefficient applied for one membrane phase, potassium ion does not appear on the water side of the membrane even during 8–10 times longer time, than could be calculated on the basis of the diffusion coefficient.

A further observation was, which we made with iodide membrane so that we prepared the electrode in a 'sandwich' form. We applied aluminium, platinum or silver, on the two sides iodide membrane electrodes. The speed of the potential response of such system was the same as that of the 'non-sandwich' membrane, and the E_0 value of the electrode remained the same.

We have proved by investigations of late years that the type of ions effecting potential of the glass electrode does not enter into the glass, but it takes part only in chemisorption on its surface [6]. Consequently it lies cross very fundamentally to the adaptation of analogies with the Donnan reaction.

We made experiments with help of reflection infrared spectrum [7], how deep does potassium ion penetrate into the potassium electrode. These penetration experiments of potassium ion in presence of very strongly lyophobic anion the depth of penetration is about 5–10 nanometre. Measurements of glass electrode by SIMS technique indicated the same depth adding that the depth distribution of gold atomized to the electrode was the same as that of the silver ion used at the experiment.

At the same time, if the lipophilic anion together with potassium is present, then the potassium ion can enter into the inside of the phase with help of a complexing agent. In this case at a high concentration of lyophobic anions we come to a condition, when the electrode is measuring the activity data of the lyophilic anions instead of that of potassium (Donnan maximum).

The observations concerning glass electrodes and electrodes with complexing agent can be attributed to the same experimental phenomena, namely to the chemisorption. In connection with chemisorption first of all the investigations of silver halides pointed out that by linkage of own ions onto the surface of the crystal a large electric field is emerging, which can considerably change the characteristics of the molecules adsorbed onto

the surface (constants of acid-base equilibrium, redox potential, face solubility product) and these data are measurable. Similarly the so-called related ions also establish adequate electric fields after their chemisorption [8]. In case of membranes with ion structure, the selectivity coefficients regarding the electrodes cannot only be interpreted, but also numerically defined on this basis [9].

In the new time of literature some authors are following the results described above. I have to emphasize the works of Umezawa et al. [10], P. Bühlmann et al. [11], who approached by the ATR-IR and SHG analyses the same phenomena, which we got earlier as results of ATT-IR.

Another question of ion-selective electrodes was analysed by Bakker et al. [12] and he interpreted the electrode selectivity coefficient. I would like to emphasize, too, that the selectivity coefficient bears only in that field an interpretation, where the disturbance function of the analysed ions arises. Therefore the equation, which can be written down without disturbing ion, can bear an interpretation only formally for the whole equation. At the same time Bakker et al. [13] analysed the interfacial potential method in details, too.

Specially remarkable is the publication, in which Buck et al. [14] deals with the transport mechanism. This publication is not understandable, because the potential through the membrane was described on a way, which was never controlled, but it was only assumed without any basis.

The results until now give that chemisorption developments on the surface of the membrane on the solution side, and hereby charge separation comes into being on the electrode and solution side. We demonstrated that the resistance of the membrane can be even infinitely high, but it changes the possibility of polarization only to such an extent that the input impedance of the measuring instrument will not be lower than the value of the measuring electrode system, about a 10 000-fold value.

Accordingly, the chemisorption will take place on the area of interface of the membrane electrode, the potential will emerge here, and the trajectories cannot be given through the membrane phase.

3. Interpretation of the phenomena

Specially remarkable is the result measured by us with help of valimomycin and bis crown ether membranes. It came out that the measured potential data were the same in case of both components. The energetics, which can be determined by the complex former, would have been different, if it had depended on the two complex formers. The energetics function is in connection with the charge separation energetics of the salt in the solution, and it can be expressed with help of the Gibbs function.

Accordingly, in case of lypophilic anion the chemisorption does not allow the penetration of the ion determining the potential into the membrane phase and in case of ion crystals it is from the beginning impossible that ion transport effected possibly by defect structure of the crystal plays a role in formation of electrode potential. The reaction itself producing potential is based upon charge separation in which the chemisorption regarding the given ion is bound on the electrode surface and the counter-ion is staying in the solution. We have to search for the energetic picture belonging to the establishment of the potential of the ion-selective electrode in the chemical potential of the ionic side in the solution, so we can put down, as follows:

$$-\Delta G = nFE$$

where ΔG is the chemical potential change, n is the charge of ion, F is the Faraday constant, E is the potential

The approach of Guggenheim established for ion-selective electrodes does not stand the proof. On the one hand the Guggenheim equation puts down two parameters changing in the same way and hereby the equation becomes fundamentally indefinable, because innumerable electrochemical potentials and galvanopotentials, which are, however, connected with each other, belong to the same chemical potential. On the other hand at the same time, if the components determining the potential can be found only on the surface of the membrane at the chemisorption, then there is no way to count with the potential data in the inside of the membrane.

The question arises that the Guggenheim approach is only then true, when we can put down the relation on the external layer of the membrane, as well as on the water phase and the area of interface closely connected with them.

If the ion determining potential can be forced through the membrane to pass the phase in form of ion transport, it is natural, if we apply an external electric field, which breaks down the potentials being established on the surfaces of the electrode, in this case the current intensity is adequate to the resistance of the electrode. Naturally, in this case the same component, which effects the chemisorption, as reagent can transport charges through the phase.

Acknowledgements

The paper is devoted to the birthday of my friend Professor G. Baiulescu, who made great progress for Analytical Chemistry in Romania.

References

[1] F. Haber and Z. Clemensiewitz, Z. Phys. Chem., 67 (1909) 385.
[2] F.G. Donnan, Z. Electrochem, 17 (1911) 572.
[3] B.P. Nicholsky, Acta Physicochem. USSR, 7 (1937) 797.
[4] B. Lengyel and E. Blum, Trans. Faraday Soc., 30 (1934) 461.
[5] K. Tóth, I. Gavallér and E. Pungor, Anal. Chim. Acta, 57 (1971) 131.
[6] E. Pungor, Electroanalysis, 8 (1996) 348.
[7] K. Tóth, E. Lindner, E. Pungor, E. Zippel and R. Kellner, Fresenius Z. Anal. Chem., 331 (1988) 448.
[8] E. Pungor, Acta Chim. Hung., 12 (1957) 265.
[9] E. Pungor and E. Hollos-Rokosinyi, Acta Chim. Hung., 27 (1961) 63.
[10] K. Umerawa, X.M. Lin, S. Nishizawa, M. Sugawara, Y. Umezawa, Anal. Chimi. Acta 282 (1993) 247.
[11] P. Bühlmann, S.Y.K. Tohda, K. Umerawa, S. Nishizawa and Y. Umezawa, Electroanalysis 7 (1995) 811.
[12] E. Bakker, R.K. Meruva, E. Pretsch and M.E. Mayerhoff, Anal. Chem., 66 (1994) 3021.
[13] E. Bakker, M. Nägele, U. Schaller and E. Pretsch, Electroanalysis, 7 (1995) 817.
[14] R.P. Buck, Tal M. Nahir, Vasile V. Cosofret, E. Lindner and M. Erdosy, Anal. Proc. Including Anal. Comm., 31 (1994) 301.

ELSEVIER

Talanta 44 (1997) 1509–1516

Talanta

Solids, flow systems and atomic spectroscopy[1]

M. Valcárcel *, M. Gallego

Department of Analytical Chemistry, University of Córdoba, 14004 Córdoba, Spain

Received 29 July 1996; received in revised form 7 October 1996; accepted 14 October 1996

Abstract

An overview of major combinations and recent applications of the solids/flow systems/atomic spectroscopy trinomial is presented. Several representative examples, classified according to the role played by the solids (sample or active component of a chemical reaction or separation) are described. © 1997 Elsevier Science B.V.

Keywords: Atomic spectroscopy; Flow systems; Solids

1. Introduction

As in other scientific and technical areas, interfaces play a role of paramount significance in contemporary analytical chemistry. Some, including those with separation techniques, instruments and computers, and cooperation with other professionals in defining analytical problems, are crucial in several aspects. It is therefore unsurprising that much R&D analytical endeavour is being focused on establishing such interfaces.

This paper deals with different facets of the triple association of objects (solids), methodologies (continuous flow systems) and techniques (atomic spectroscopy); to this end, it discusses the double interfaces shown in Fig. 1 and describes several representative approaches to the joint use of the three elements according to the role played by the solid (as sample or an active component in the methodology) by way of practical examples. It is not the intension of the authors to present a review, but to emphasize the importance of this topic in today's and tomorrow's analytical chemistry.

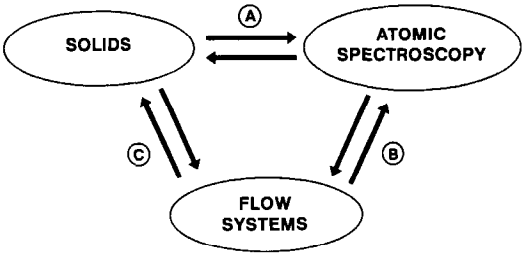

Fig. 1. Double (A, B and C) and triple (e.g., C-B-A) association among solids, flow systems and atomic spectroscopic instruments.

* Corresponding author.

[1] To our friend Professor Baiulescu in his 65th anniversary.

PII S0039-9140(96)02182-0

2. Solids/atomic spectroscopy coupling

This association (Fig. 1A) is gaining increasing interest because it can dramatically help improve, simplify and automate the preliminary operations of the analytical process, a pending goal of today's analytical chemistry [1,2]. No doubt, the direct introduction of solid samples into atomic spectroscopic instrumentation minimizes the number of preparation steps involved and hence reduces time, human participation, expenses and hazards. Although some analytical properties (e.g., accuracy, precision, selectivity) have not reached an average high level, the advantages involved make this alternative of great practical interest. The main problems arise from the sample itself. Thus, each type of sample requires distinct working conditions; also, there can be significant differences even between batches of the same type of sample or difficulties to find appropriate standards (CRM) for a given methodology. Nevertheless, recent advances in this field warrant continuing endeavour. Laser ablation and direct sampling of solids and slurries [3] are typical examples of the efforts made in this direction.

3. Flow systems/atomic spectroscopy coupling

This combination (Fig. 1B) has reached a high degree of maturity thanks to both easy implementation and the excellent results obtained [4,5]. Good proof of the importance of this interface is the increasing availability of commercial continuous-flow modules for implementing a variety of functions (e.g., standardization, preconcentration) that are being launched by major instrument manufacturers as a way of boosting sales of atomic instruments. Flow systems are being routinely used for sample introduction. Several overviews of the performance of the FI-FAAS, FI-ICP/AES and FI-ICP/MS combinations have been published [6]. However, use of FI with ETAAS dates from much later than that with FAAS, obviously because of the discrete nature of ETAAS operations. Currently, semi-on-line techniques where the autosampler acts as an interface are gaining momentum; with on-line systems, samples are introduced into the furnace, usually dispensed by a pump via a sampling probe [5].

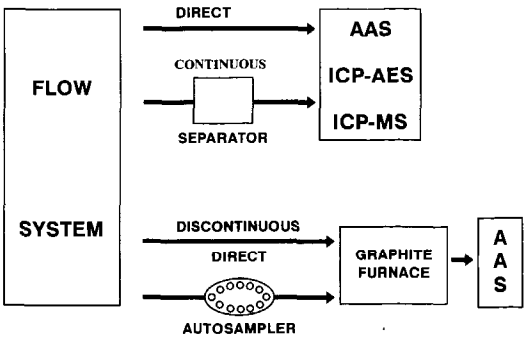

Fig. 2. Different ways of connecting (on-line or semi-on-line) flow systems and atomic spectrometers. For details, see text.

Fig. 2 shows different ways of connecting a continuous-flow system to an atomic spectrometer (AS). A direct combination is possible provided the two flow-rates involved are compatible. A continuous separator (gas–liquid, liquid–liquid, solid–liquid) can implement automatic preconcentration and interference removal. Somewhat more troublesome is connecting a flow system to an electrothermal atomization AS owing to the discrete functioning of the graphite furnace. Directly connecting the introduction arm to the flow system entails stopping the flow. On the other hand, the autosampler can be used as an interface between the continuous and discrete combined systems. Both choices can be considered semi-on-line connections.

4. Solids/flow systems coupling

The hydrodynamic character of flow systems make them theoretically incompatible with solids. However, solids and flow systems can be combined in many ways (see Fig. 3) because the former can act as samples, active components (sorbent, membranes, filters) of separations [7], ingredients (reagents, catalysts, products) of chemical reactions, and the sensing microzone of a flow-through sensor [8].

According to role, solids can be placed at different points in a flow-system, the most usual of which are as follows (Fig. 4):

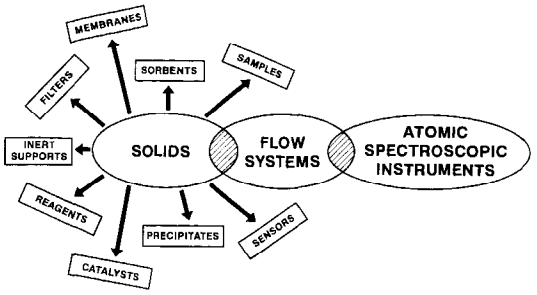

Fig. 3. Role of solids in flow systems connected to an atomic spectroscopic instrument.

1. Before the sample introduction point in order to condition the carrier (or reagent); prefilters, degassing units and redox minicolumns are usually placed in this zone.
2. Solid samples can be introduced on-line into a flow system in the form of slurries or by continuous leaching.
3. A minicolumn of sorbent material, and a dialysis or gas-diffusion unit can be placed in the loop of an injection valve through which the liquid sample or an accepting stream can be circulated.
4. A precipitate can be obtained in the reaction coil after mixing the analyte and reagent.
5. A separation unit (a liquid–liquid extractor, dialyser or sorption column, filter) furnished with an active solid (e.g., a membrane, sorbent, etc.) can be used between the mixing (reaction) coil and a continuous detector.
6. Finally, solids can be placed at the detection point in flow-through (bio)chemical sensors.

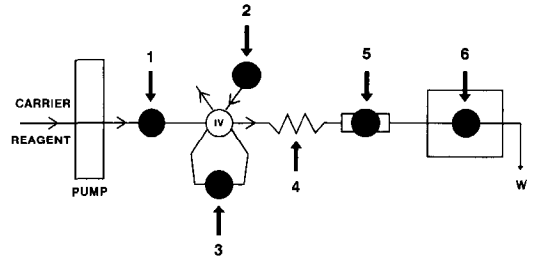

Fig. 4. Location of solids in flow (injection) manifolds. IV, injection valve; W, waste. For details, see text.

5. Solids/flow systems/atomic spectroscopy coupling

This triple association offers a great potential for solving analytical problems and enhancing basic and accessory analytical properties through a combination of the two above-described interfaces. Through representative approaches developed by our research group and applied to real samples, the most significant advances and prospects are discussed below, with special emphasis on the relevance of solids in this context.

5.1. Solids as samples

There are two general approaches to the direct introduction of solids into a coupled flow manifold/atomic spectrometer system. Continuous leaching of the analyte can be accomplished by applying electric or ultrasonic energy to a mini-reactor containing the solid sample. On the other hand, powdered or disperse solids can be introduced as slurries into the coupled flow system. It should be noted that the second alternative has been much more widely exploited.

Fig. 5 illustrates the ways real sample slurries can be introduced into a coupled flow system/electrothermal atomic absorption spectrometer (ETAAS) using an autosampler as interface; so, the sample from the flow system was collected in the cup of the autosampler instrument. According to the sample and analyte properties, a prior lyophilization step may be required. After the slurry is formed (e.g., by ultrasonic irradiation), a volume is introduced into the flow system, which can also receive several solution streams (e.g., carrier, digesting solution, chemical modifier, standards). This flow system can implement in an automatic way a variety of functions such as sample (slurry) volume measurement, dilution, addition of reagents, mixing (homogenization), standardization, filtration, and microwave digestion. The prepared sample is loaded into a cup of the ETAAS autosampler, where the metal ion concentration is determined in a discrete manner as usual.

Aluminium in milk dessert (yoghurt and custard) slurries can be determined by using an injec-

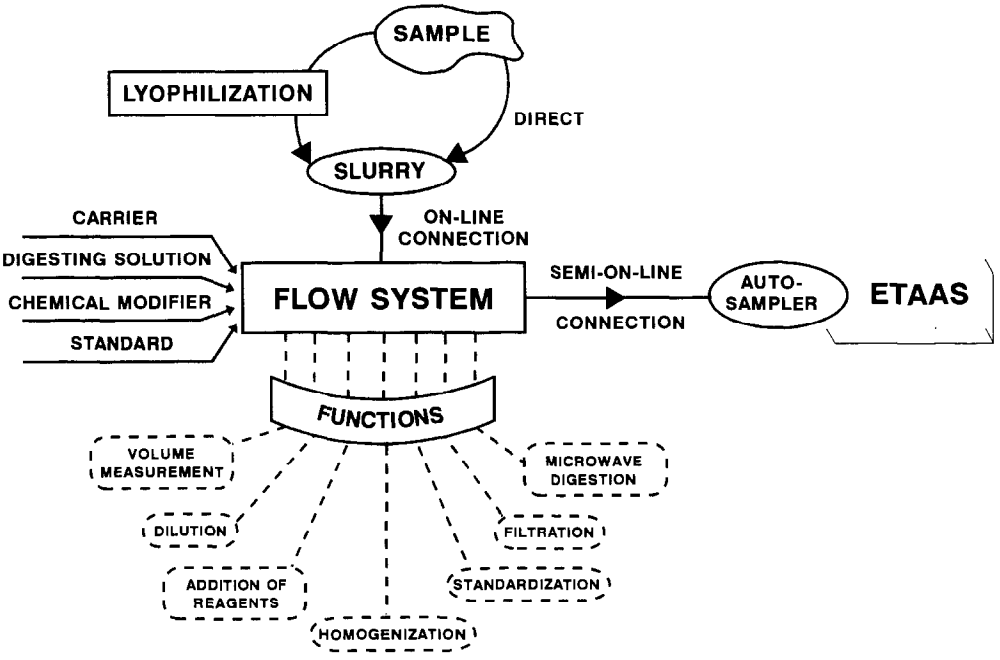

Fig. 5. Introduction of sample slurries into a flow system connected semi-on-line to an electrothermal atomic absorption spectrometer (ETAAS). For details, see text.

tor-commutator that facilitates the simultaneous introduction of two microvolumes (sample and standard) into two streams of 0.2% (v/v) nitric acid carrier that are merged with a chemical modifier (magnesium and palladium nitrate). The mixed solution (as slurry) is passed through a mixing chamber and then loaded into an autosampler cup for 120 s (2 ml). The turbulence arising from continuous dropping of the diluted/homogenized sample into the cups ensured adequate homogenization of the slurry. The results obtained are consistent with those provided by the classical dry ashing procedure and better than those of the wet ashing method, which exhibits severe contamination during sample preparation, as well as poor precision. The method was validated with a certified reference material (not-fat milk powder) from NIST [9].

The insertion of a paper disk sandwiched into a PTFE filter in the flow system allowed the direct speciation of aluminium [10] and selenium [11] in fruit and tomato juices, (i.e., the determination of the distribution of these elements in the suspended solids and in the aqueous phase of the foodstuffs). The ensuing methods are based on sequential, direct introduction of the juice slurry into two identical loops. In the first step, the contents of one loop are carried by a 0.2% HNO_3 stream, mixed with a magnesium (for Al) or palladium (for Se) nitrate chemical modifier solution and then filtered, the filtrate being loaded into an autosampler cup for determining the metal content in the liquid phase. In the second step, the contents of the other loop are flushed by the carrier and merged with the modifier stream, the mixture being loaded into another sample cup for the determination of the total metal content in the slurry; simultaneously, a stream of nitric acid washes the filter in the opposite direction. The metal content in the suspended solid is obtained by difference. The results obtained in the determination of the total metal content agree well with those obtained by the dry ashing method. This continuous methodology also allows one to dis-

criminate between the metal content in the solid and liquid phase; aluminium and selenium exist largely (60–90%) in combined forms in the liquid phase of fruit juices.

More complex samples entail implementing a new step in the flow system: microwave digestion of the slurry after mixing with a digesting plug (6 mol l^{-1} nitric acid). The use of air streams to transfer the sample to the microwave oven and an open system to collect the digested sample minimizes the well-know problems posed by digestion fumes. This methodology was successfully applied to the determination of aluminium [12] and selenium [13] in shellfish (mussels, clams, cockles, oysters and prawns) with excellent results. A parallel study was performed with lyophilized and unlyophilized samples of the same origin in order to check whether this typically tedious operation was necessary. The consistency between the two set of results revealed that the method can be directly applied with no lyophilization [13]. For aluminium, a correction factor must be used because the maximum recovery obtained was about 90%.

5.2. Solids as reaction ingredients

Solids can play an active role in analytical reactions taking place in coupled flow system, whether as reagents, catalysts or products (e.g., precipitates). Thus, they can be a permanent element of the flow system or be formed in situ. Analytes can be metal (ions) or organic species giving rise to direct or indirect determinations, respectively. Several examples illustrating these possibilities are described below.

The indirect determination of various oxidant drugs such as methadone [14], chloramphenicol [15] and chlordiazepoxide [16] can be accomplished by using a metal such as cadmium (uncoppered or coppered) or zinc packed in a minicolumn as reductant for specific organic groups such as keto, nitro and *N*-oxide to form alcohol, amine and azo functions, respectively. The stoichiometric amount of metal ion produced by passing the sample plug through the column is determined with an atomic absorption detector connected on-line to a straightforward flow injection manifold. The ensuing methods offer adequate sensitivity, selectivity and precision, and can thus be applied to pharmaceutical preparations and biological fluids. Recoveries range from 97 to 103%.

Over 90% of applications involving the formation, filtration, washing and dissolution of precipitates in continuous flow systems use an atomic absorption detector for direct or indirect determinations. The first such system was proposed by our research team in 1987 [17]. A variety of similar determinations have been reported ever since [5,18]. They are based on the reaction of a metal ion with an organic or inorganic anion and the retention of the precipitate on a filter. The continuous determination can be carried out on the metal excess in the filtrate (by measuring the difference between the initial concentration of the metal in the carrier and the concentration in the filtrate) or on quantitation of the metal contents in the precipitates. Thus, there are two different approaches depending on whether or not the precipitate is dissolved. Metal ions such copper, cobalt, nickel, lead, manganese and calcium, can be preconcentrated in these systems by forming a precipitate (a basic salt, or a quelate) and rapidly dissolving it after filtration; therefore, the procedure involves at least two steps. The indirect determination of halides in a variety of samples was achieved using silver ion as reagent; it even affords resolving a mixture of chloride and iodide ions in foodstuffs by selective dissolution of the silver chloride in ammonia [19]. A variety of organic anions of great practical interest can be indirectly determined in these continuous precipitation systems; typical examples include the determination of alkaloids (papaverine, strychnine and cocaine) using Dragendorff's reagent [20]; reducing sugars in wines using Fehling's reagents [21]; saccharin in mixtures of sweeteners with silver nitrate [22]; and tannins in wines and teas using the Folin-Ciocalteu reagent [23]. Coprecipitation without filtration was first reported by Fang et al., in 1991 [24]; the problems arising from the handling of a relatively large amount of precipitate in a flow system have been overcome by using knotted reactors as filterless precipitate collectors.

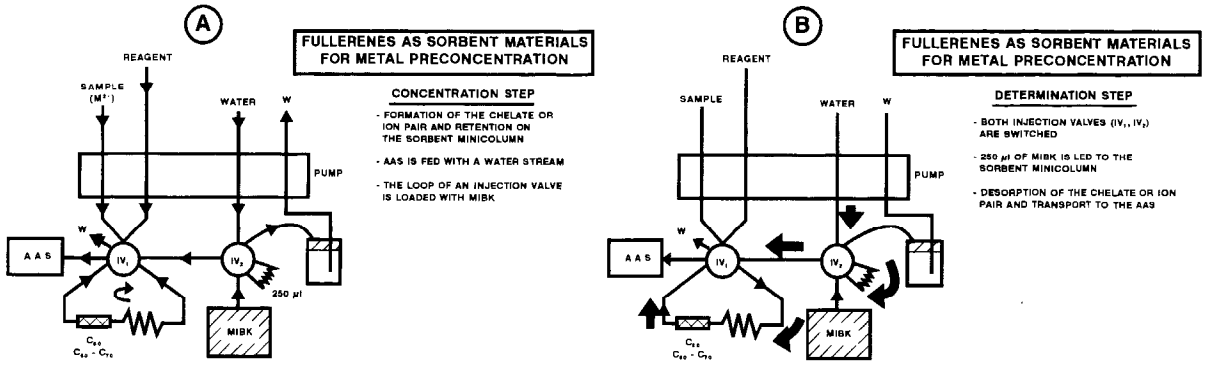

Fig. 6. Use of new sorbent materials (fullerenes) for the determination of metal traces by formation of chelates or ion-pairs. (A) concentration step; and (B) determination step. MIBK, methyl isobutyl ketone; IV, injection valve; W, waste; AAS, atomic absorption spectrometer. For details, see text. (Adapted from [25] and [26], with permission of the American Chemical Society).

5.3. Solids in continuous separations

The other way of using solids in flow systems coupled on-line to atomic spectroscopic instruments is by implementing non-chromatographic continuous separation techniques [7]. In this context, solids can act as filters in the above described continuous precipitation/dissolution systems; as membranes in dialysis, gas- diffusion and liquid–liquid extraction procedures; and as sorbents in solid-phase extractions. A detailed description of these approaches is beyond the scope of this paper (there are literally hundreds of publications on this topic) [2,5]. A survey of available literature can give the impression that innovation in such a widely explored field is virtually impossible. However, our group recently showed new ways for advancement. Thus, the use of new solid materials can open previously unexpected prospects. Such is the case of fullerenes as new sorbent materials for the concentration/determination of metal ions. Fig. 6 shows the manifold used for this purpose.

In the concentration step (Fig. 6A), the sample and ligand (and/or counter-ion) streams are continuously merged and passed through the loop of injection valve IV_1, and then sent to waste. A neutral chelate or ion-pair is formed in the reaction coil and retained on the sorbent minicolumn. The nebulizer of the atomic absorption spectrometer is continuously fed with a water stream. The loop of the second injection valve, IV_2, is loaded with methyl isobutyl ketone from a displacement flask. In the second step (Fig. 6B), both valves are simultaneously switched. The injected organic plug is led to the sorbent minicolumn, thereby effecting the rapid desorption of the chelate or ion-pair, which is directly transported to the nebulizer. A positive peak proportional to the concentration of the metal ion in the sample is obtained as a result.

Lead traces can be determined in this type of continuous manifold by using ammonium pyrrolidine dithiocarbamate (APDC) as ligand. For comparison, two systematic studies using C_{18} bonded silica and activated carbon as sorbents were also performed [25]. An amount of 50 mg of each sorbent material was packed into columns of 0.7–1.8 cm length (depending of the sorbent) and 3 mm internal diameter for all the experiments. The C_{60} fullerenes sorbent exhibited the highest preconcentration factor, lowest detection limit and widest pH range (at pH 0–5). The precision was similar for the three sorbents. Nevertheless, the most interesting feature of the new sorbent material is its selectivity. The effect of many common metal ions, that can form complexes with the chelating reagent (APDC), in the determination of cadmium and lead was listed in Table 1. In both

determinations the results obtained with C_{60} fullerene were compared with RP-C_{18} sorbent. As can be seen in Table 1, the selectivity was highest for C_{60} fullerene; this may have been the result of its larger surface area relative to C_{18}, in addition to its higher interstitial volume. The method is more favourable for the determination of cadmium than that for lead [25]. The selectivity of the fullerene sorbent was at least twice that of the C_{18} sorbent, for both elements. It is interesting to note that aluminium, iron, manganese and nickel are tolerated at concentrations thousands of times higher than that of lead, in contrast with the more modest ratios for RP-C_{18} [25].

The adsorptive potential of C_{60} and C_{70} fullerenes for the preconcentration of trace copper from aqueous solutions was also examined [26] using the formation of a neutral chelate with APDC, cationic chelates with 1,10-phenanthroline and neocuproine ligands forming ion-pairs with sodium dodecylsulphate, and an anionic complex with thiocyanate that in turn forms an ion-pair with dodecyltrimethylammonium bromide. The best analytical results (sensitivity and selectivity) were obtained with the neutral chelate and sorption on C_{70} fullerene thanks to its large surface area and high volume relative to C_{60} fullerene.

Table 1
Tolerated ratios of foreign cations to analyte in the determination of 10 or 50 ng ml^{-1} of cadmium or lead, respectively, with the APDC method

Foreign cation	Tolerated ratio			
	Cd determination		Pb determination	
	C_{60}	RP-C_{18}	C_{60}	RP-C_{18}
Al^{3+}	1000	600	1000	300
Zn^{2+}	1000	600	400	100
Pb^{2+}	1000	600	—	—
Mn^{2+}	1000	500	1000	200
Co^{2+}	1000	400	500	50
Cu^{2+}	1000	350	300	20
Fe^{3+}	1000	300	1000	20
Ni^{2+}	1000	200	1000	2
Sn^{2+}	800	400	400	100
Hg^{2+}	600	400	200	1
Cd^{++}	—	—	2	<1

6. Final remarks

The examples of the triple combination of solids, flow systems and atomic spectrometers briefly exposed in this paper, and many others not even mentioned for the obvious lack of space, demonstrate the possibility of expanding the scope of application of both flow systems and atomic spectroscopy, and of enhancing basic (sensitivity, selectivity and precision) and accessory analytical properties (expeditiousness, cost-effectiveness and personnel safety and comfort). The methodologies discussed have been validated by application to the resolution of real analytical problems.

Acknowledgements

The Spanish DGICyT is acknowledged for financial support awarded (Grant No. PB95-0977).

References

[1] M. Valcárcel, M.T. Tena and M.D. Luque de Castro, Anal. Proc., 30 (1993) 276.
[2] S.J. Hill, J.B. Dawson, W.J. Price, I.L. Shuttler and J.F. Tyson, J. Anal. At. Spectrom., 10 (1995) 199R and 11 (1996) 281R.
[3] M.A.Z. Arruda, M. Gallego and M. Valcárcel, Quim. Anal., 14 (1995) 17.
[4] J.L. Burguera (Ed.), Flow Injection Atomic Spectroscopy, Marcel Dekker, New York, 1989.
[5] Z. Fang, Flow Injection Atomic Absorption Spectrometry, Wiley, Chichester, 1995.
[6] Z. Fang, S.K. Hu and G.H. Tao, J. Anal. At. Spectrom., 11 (1996) 1.
[7] M. Valcárcel and M.D. Luque de Castro, Non-Chromatographic Continuous Separation Techniques, Royal Society of Chemistry, Cambridge, 1991.
[8] M. Valcárcel and M.D. Luque de Castro, Flow-Through (Bio)Chemical Sensors, Elsevier, Amsterdam, 1994.
[9] M.A.Z. Arruda, M. Gallego and M. Valcárcel, J. Anal. At. Spectrom., 10 (1995) 55.
[10] M.A.Z. Arruda, M. Gallego and M. Valcárcel, Anal. Chem., 65 (1993) 3331.
[11] M.A.Z. Arruda, M. Gallego and M. Valcárcel, J. Anal. At. Spectrom., 9 (1994) 657.
[12] M.A.Z. Arruda, M. Gallego and M. Valcárcel, J. Anal. At. Spectrom., 10 (1995) 501.

[13] M.A.Z. Arruda, M. Gallego and M. Valcárcel, J. Anal. At. Spectrom., 11 (1996) 169.
[14] R. Montero, M. Gallego and M. Valcárcel, Anal. Chim. Acta, 234 (1990) 433.
[15] R. Montero, M. Gallego and M. Valcárcel, Talanta, 37 (1990) 1129.
[16] R. Montero, M. Gallego and M. Valcárcel, Analyst, 115 (1990) 943.
[17] P. Martínez-Jiménez, M. Gallego and M. Valcárcel, Anal. Chem., 59 (1987) 69.
[18] V. Kubán, Fresenius J. Anal. Chem., 346 (1993) 873.
[19] P. Martínez-Jiménez, M. Gallego and M. Valcárcel, Anal. Chim. Acta, 193 (1987) 127.
[20] M. Eisman, M. Gallego and M. Valcárcel, J. Anal. At. Spectrom., 8 (1993) 1117.
[21] M.C. Yebra, M. Gallego and M. Valcárcel, Anal. Chim. Acta, 276 (1993) 385.
[22] M.C. Yebra, M. Gallego and M. Valcárcel, Anal. Chim. Acta, 308 (1995) 275.
[23] M.C. Yebra, M. Gallego and M. Valcárcel, Anal. Chim. Acta, 308 (1995) 357.
[24] Z. Fang, M. Sperling and B. Welz, J. Anal. At. Spectrom., 6 (1991) 301.
[25] M. Gallego, Y. Petit de Peña and M. Valcárcel, Anal. Chem., 66 (1994) 4074.
[26] Y. Petit de Peña, M. Gallego and M. Valcárcel, Anal. Chem., 67 (1995) 2524.

ELSEVIER

Talanta 44 (1997) 1517–1526

Talanta

Drug impurity profiling strategies[1,2]

S. Görög *, M. Babják, G. Balogh, J. Brlik, A. Csehi, F. Dravecz, M. Gazdag, P. Horváth, A. Laukó, K. Varga

Chemical Works of Gedeon Richter Ltd., P.O.B. 27, H-1475 Budapest, Hungary

Received 16 August 1996; received in revised form 1 October 1996; accepted 2 October 1996

Abstract

A general scheme is set up for the estimation of the impurity profile of bulk drug substances by the complex use of chromatographic, spectroscopic and hyphenated techniques. Several examples are presented as illustrations to the scheme from the authors' laboratory involving the use of chromatographic methods such as thin-layer-(TLC), gas-(GC), analytical and preparative high-performance liquid chromatography (HPLC), spectroscopic methods such as mass spectrometry (MS) and NMR spectroscopy as well as hyphenated techniques (HPLC/diode-array UV, GC/MS and HPLC/MS). In addition to summarizing earlier work, new examples are also presented: identification of an impurity (propyl 4-[diethylcarbamoyl(methoxy)]-3-methoxy phenylglyoxylate, **II**) in propanidid (**I**) and two unsaturated impurities in allylestrenol (**VII**) by GC/MS and HPLC/diode-array UV as well as estimation of the impurity profile of mazipredone (**III**) by HPLC/MS and HPLC/diode-array UV. © 1997 Elsevier Science B.V.

Keywords: Impurities; Propanidid; Allylestrenol; Mazipredone

1. Introduction

The estimation of the impurity profiles of bulk drug substances is one of the most important fields of activity in contemporary industrial pharmaceutical analysis [2]. In general impurities present in excess of 0.1% should be identified and quantified by sufficiently selective methods but drug registration authorities are increasingly interested in impurities in the range 0.01–0.1% [3] The main reasons for the increasing interest of drug manufacturers and drug registration authorities in the impurity profiles of bulk drug substances are as follows:

a. In the course of the development of a new drug or a new technology for manufacturing an existing drug it is essential to know the structures of the impurities: by possessing this information synthetic organic chemists are often able to change the reaction conditions in such a way that the formation of the impurity can be avoided or its quantity reduced to an acceptable level.

* Corresponding author.

[1] Presented at Euroanalysis IX, Bologna, September, 1996. This paper is Part 17 in the series 'Estimation of impurity profiles of drugs and related materials' and Part 52 in the series 'Analysis of Steroids'. For Parts 16 and 51, respectively, see Ref. [1].

[2] This paper is dedicated to Prof. G.-E. Baiulescu on the occasion of his 65th birthday.

PII S0039-9140(96)02179-0

b. Having suggested structures for the impurities, they can be synthesized and thus provide final evidence for their structures previously determined by spectroscopic methods.

c. The material synthesized (or in exceptional cases isolated by large scale preparative column chromatography) can be used as an 'impurity standard' during the development of a selective method for the quantitative determination of the impurity and the use of this method as part of the quality control testing of every batch.

d. In the case of major impurities the synthesized or isolated material can be subjected to toxicological studies thus greatly contributing to the safety of drug therapy.

e. The impurity profile of a drug substance depends on several factors such as the synthetic route, reaction conditions, source and quality of the starting materials, reagents and solvents used during the synthesis, the purification steps, conditions of crystallisation, distillation, drying and storage of the endproduct, etc. For this reason in the hands of drug authorities the impurity profile of a drug substance is a good fingerprint to indicate the level and constancy of the manufacturing process of the bulk drug substance: even minor changes of the above listed factors may cause dramatic changes in the impurity profile.

As a consequence of the above points the impurity profile of a bulk drug substance has to be checked repeatedly not only during the research and development period but in addition in all cases when changes take place in the factors listed under e. above. For this reason the estimation of impurity profiles of bulk drug substances is a frequent task, especially in industrial analytical research and quality control laboratories. Taking into account the large time and labour consuming nature of these studies it is essential to find a strategy which enables the results to be achieved within the shortest possible time with the greatest possible certainty. The aim of this study is to introduce a general scheme for the rational use of chromatographic, spectroscopic and hyphenated techniques in drug impurity profiling studies and to present several examples from the authors' laboratory as illustrations to the scheme.

2. Experimental

2.1. Instruments and methods

UV spectroscopy. Varian Cary 3 double beam instrument.

NMR spectroscopy (^1H and ^{13}C). Varian VXR-300 and Varian UNITYplus 500 spectrometers. Chemical shifts in the text are relative to $\delta_{TMS} = 0.00$.

Mass spectrometry. VG-TRIO-2 and Finnigan MAT 95 SQ tandem spectrometers.

Gas chromatography. Hewlett-Packard 5890A and Gas chromatography/mass spectrometry (GC/MS). Fisons MD-800. Column for GC and GC/MS DB-5 MS (J and W) fused silica capillary (30 m × 0.32 mm × 1.0 μm). EI^+ 70 eV. Ion source temperature 240°C.

Propanidid. Temperatures: column (150°C for 9 min, 150–260°C at 10°C min^{-1}, 260°C for 10 min, 260–300°C at 10°C min^{-1}, 30 min at 300°C), injector and FID (250 and 300°C, respectively); split ratio 1:50.

High-performance liquid chromatography (HPLC). Hewlett-Packard 1090A equipped with an HP 1040 diode-array UV detector.

Propanidid. Column: 250 mm × 4 mm packed with LiChrospher Si-60 5 μm (Merck); eluent: hexane–methanol–2-propanol (90:8:2, v/v/v) at a flow rate of 1 ml min^{-1} at ambient temperature. Diode array detector set at 210, 282 and 320 nm or used in the spectrum scanning mode.

Allylestrenol. Column: 150 mm × 4 mm packed with Hypersil ODS 5 μm (Shandon); eluent: acetonitrile–methanol–water (64:18:18, v/v/v) at a flow rate of 1 ml min^{-1} at ambient temperature. Diode-array detector set at 210 and 240 nm or used in the spectrum scanning mode.

High-performance liquid chromatography/mass spectrometry (HPLC/MS). Waters 600/ Finnigan MAT 95 SQ.

Mazipredone. Column: 100 × 4.6 mm packed with Hypersil BDS C8 3 μm (Shandon); eluent: 25 mM ammonium acetate–methanol (65:35, v/v) at a flow rate of 1 ml min^{-1} at ambient temperature. Diode-array detector set at 240 nm or used in the spectrum scanning mode. The

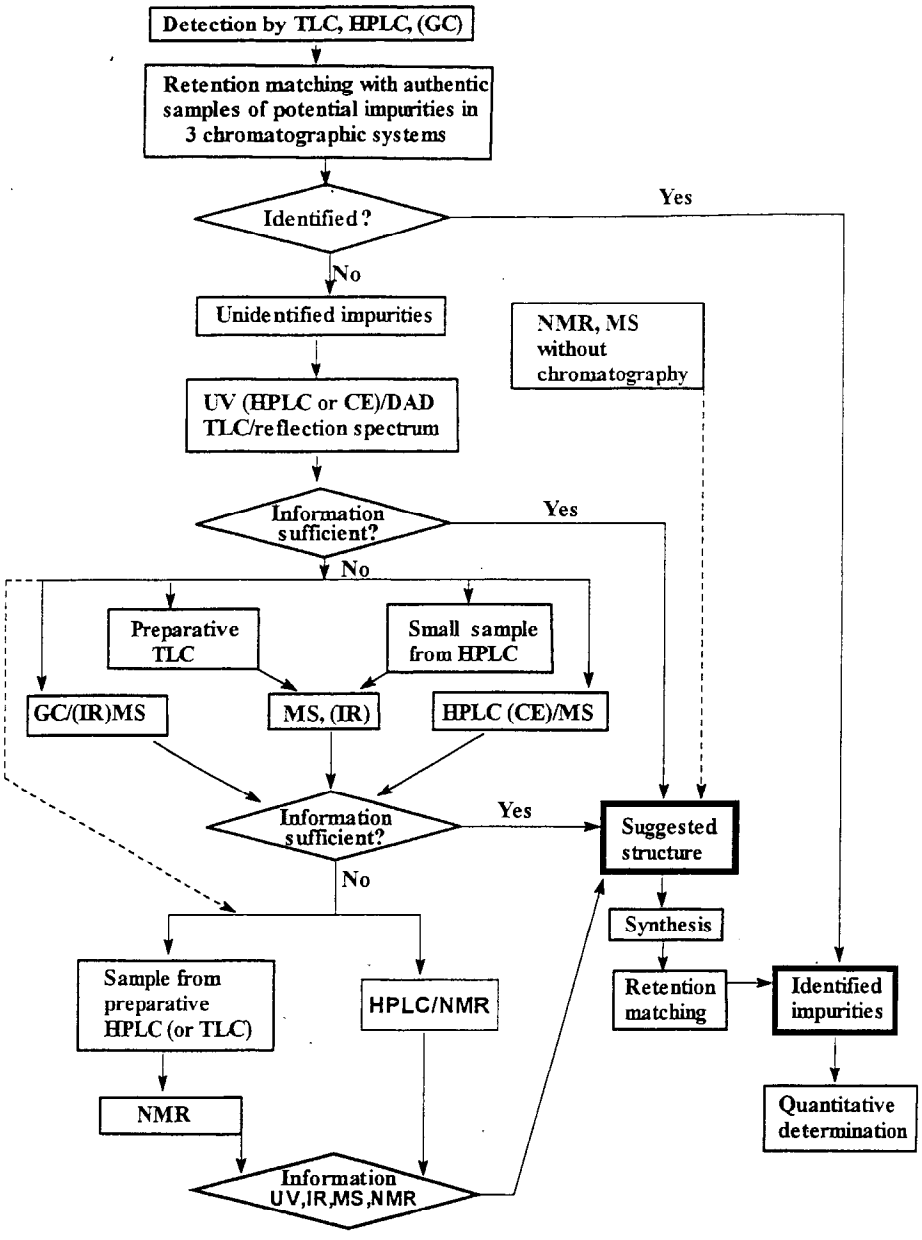

Fig. 1. A general scheme for drug impurity profiling.

mass spectrometer was used in the APCI (atmospheric pressure chemical ionisation) mode. Corona current: 4.8 μA. Temperatures: vaporizer 400°C, capillary 200°C. Sheath gas: nitrogen at 5.0 bar.

2.2. Samples

The investigated materials were laboratory or industrial samples from the Chemical Works of Gedeon Richter Ltd., Budapest.

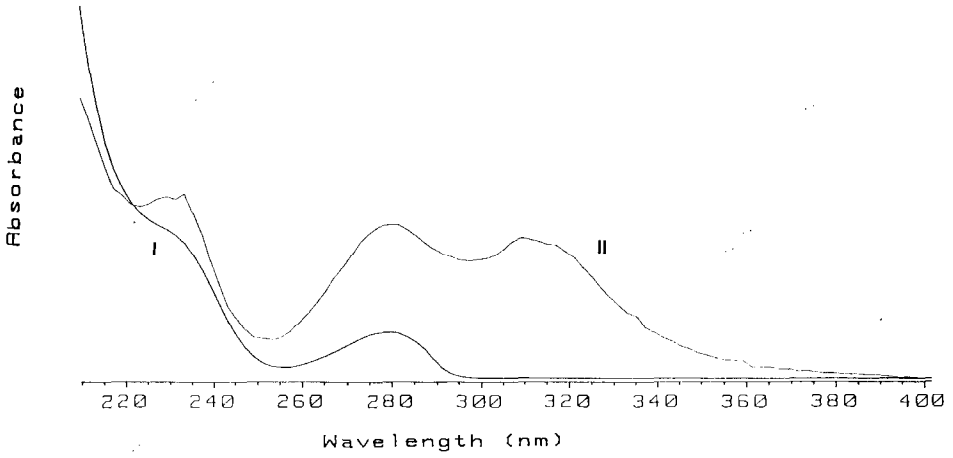

Fig. 2. Diode-array UV spectra of propanidid (**I**) and impurity **II**. See Section 2 for the HPLC conditions.

3. Results and discussion

3.1. General scheme for drug impurity profiling

As seen in Fig. 1 the procedure of impurity profiling begins with detecting the impurities on the thin-layer chromatograms, high-performance liquid chromatograms or gas chromatograms. (In the latter case caution is necessary since minor peaks originating from the thermal decomposition of the investigated drug material can easily be confused with real impurities.) The next step is to obtain as many potential impurity samples from the synthetic organic chemists as possible. These include the last intermediate of the synthesis, products of predictable side reactions and degradation reactions (if available). These samples should undergo retention matching with the previously detected impurities in the chromatographic systems where they were detected. The criterion for a positive identification is identical R_f or retention time in at least three different chromatographic systems selected in such a way that the separation mechanisms should be as different as possible. (In addition to the agreement of the retention data the TLC reflection spectra or the colour after visualization as well as the HPLC diode-array spectra, etc. should also be identical.)

In the case of unsuccessful identification with standard samples the most reasonable way to determine the structure of the impurity starts with the investigation of the UV spectra, easily obtainable with the aid of the diode-array detector in the case of HPLC and the densitometer with reflection spectrum scanning facilities in the case of TLC. Although in the majority of cases the UV spectra of the impurities do not markedly differ from that of the main component, in some instances even minor differences are of diagnostic value and hence because of the ease of obtaining the spectra by means of the standard HPLC and TLC instrumentation, it is reasonable to try to draw as much conclusions from the UV spectra as possible. In exceptional cases (with full knowledge of the synthesis of the drug material) it is even possible to propose a structure for the impurity exclusively on the basis of the UV spectrum thus saving much time and efforts or at least the information thus obtained can be a useful complement to those obtained from the mass- and NMR spectra [4].

If the information obtainable from the UV spectrum is not sufficient, the next step in the procedure of impurity profiling is usually to take the mass spectrum of the impurity. Of course the most effective way to do this is to make use of the on-line GC/MS or HPLC/MS facilities available in the majority of laboratories dealing with impurity profiling. A great benefit of these techniques is that data can be obtained simultaneously on

several impurities down to the 0.01% level. An advantage of the GC/MS method is that reliable molecular weight value is obtainable using chemical ionisation and, in addition, information on fragmentation necessary for the solution of more complicated structure elucidation problems can also be obtained using the electron impact ionisation technique. A disadvantage is that due to volatility and thermal stability problems the possibilities of this method are limited. (The use of derivatization reactions widely used in other fields of GC/MS analysis is problematic here because the side-products of the derivatization reaction can be confused with the impurities.) An advantage of the HPLC/MS method [5] is its general applicability. A disadvantage is, however, that the ionisation techniques used in association with the generally used instruments (the older thermospray and the more up-to-date electrospray and atmospheric pressure chemical ionisation (APCI) techniques) usually give only molecular weight information. To obtain the fragmentation pattern highly sophisticated HPLC/MS/MS facilities are necessary.

It is worth mentioning that capillary electrophoresis (CE) is increasingly used in drug impurity profiling as an alternative to the above chromatographic techniques [6]. This technique can also be coupled with mass spectrometry [5].

If the hyphenated GC/MS, LC/MS or CE/MS facilities are not available, mass spectra can be taken on samples obtained from preparative or—

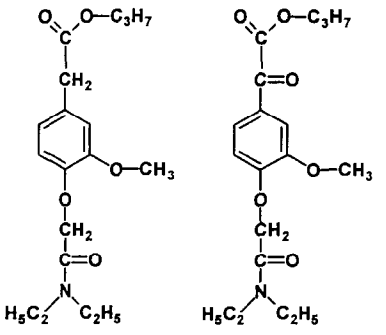

Scheme 1.

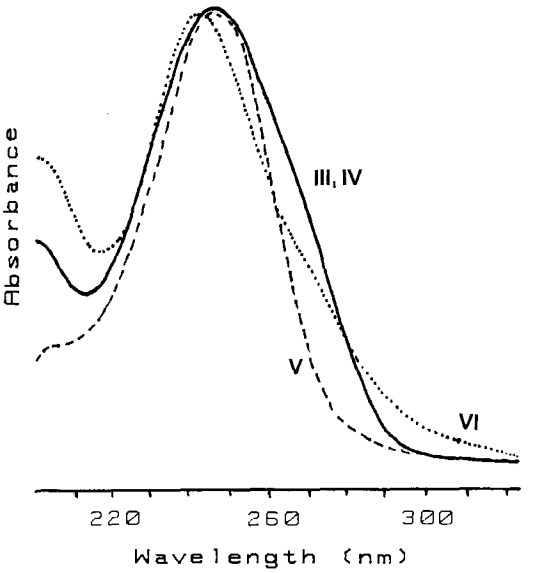

Fig. 3. Diode-array UV spectra of mazipredone (**III**) and impurities **IV**, **V**, **VI**. See Section 2 for the HPLC conditions.

due to the high sensitivity of mass spectrometry—analytical TLC or HPLC.

In the majority of cases the information from the mass spectrum (together with the previously taken UV spectrum) is sufficient to propose a structure for the impurity. If not, NMR spectroscopy is the ultimate method for elucidating the structure of the impurity. Due to the limited sensitivity of this method NMR spectra are usually obtained on samples from preparative HPLC (or TLC) separation. Quite recently on-line HPLC/NMR instruments became commercially available [7]. This new hyphenated technique will certainly have a bright future in various fields, among them in drug impurity profiling.

The next step in the impurity profiling is the synthesis of the material with the proposed structure. The retention and spectral matching of the synthesized material (impurity standard) with the impurity in question is carried out as outlined above. In the case of successful matching the procedure of impurity profiling is terminated by working out selective quantitative methods for the determination of the impurity making use of the impurity standard.

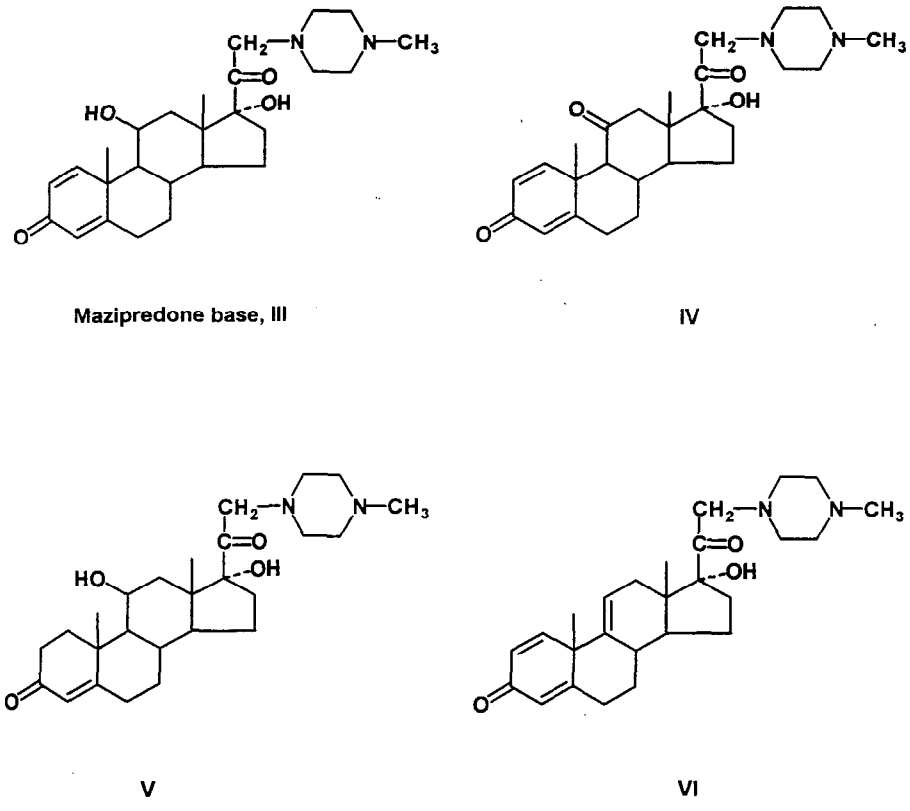

Scheme 2.

The possibilities of spectroscopic techniques in drug impurity profiling without chromatographic separation are also worth mentioning. Spectra obtained by using high-resolution, highly sensitive NMR spectrometers and mass spectrometers with FAB or electrospray/APCI facilities are suitable to provide a fingerprint-like picture regarding the purity of the sample. In addition to this, in advantageous cases (especially if there is only one major impurity in the sample), conclusions can be drawn from the minor NMR signals regarding the structure of the impurity. Making use of the above mentioned MS facilities the molecular weight of the impurity can be obtained, if it differs from that of the main component, and this can also be a useful information in the course of the impurity profiling procedure. It has to be emphasized, however, that investigations of this type by no means substitute for the systematic chromatographic analysis in the search for the structures of the impurities.

3.2. Practical examples from the authors' laboratory

Characteristic examples where the UV spectra obtained by the HPLC diode-array UV detector were of diagnostic value are the structure elucidation of 3,17α-diethinyl-13-ethyl-3,5-gonadien-17-ol (an impurity in norgestrel with the characteristic *trans*-dienine UV chromophore) [1], identification of 9(11)-dehydro derivatives as impurities in oestradiol [8], ethinyloestradiol [9] and mestranol [10], where the difference between the spectra of the phenol-type main component and its α,β-unsaturated impurity is remarkable and on the basis of the UV spectra even to differenciate between the three regioisomers (Δ^6, $\Delta^{8(9)}$ and

$\Delta^{9(11)}$) was also possible. The discrimination between 4-ene-3-keto- and 1-ene-3-ketosteroids was also possible on the basis of the rather large difference between their UV maxima (228 and 237 nm in the apolar eluent of the normal-phase HPLC system used in this study) [11]. However, even minor differences can be of diagnostic value such as in the case of the identification of 8(14)-dehydronorgestrel as an impurity in norgestrel where the slight hypsochromic shift (2 nm) of the band of the α,β-unsaturated 3-keto group together with the remarkable band broadening is characteristic of 'through-space' conjugation with the $\Delta^{8(14)}$ double bond [9]. Another example of this type is the identification of 6α- and β- as well as 10β-hydroxy derivatives as impurities in norgestrel [11].

In the following examples the diode-array UV spectra together with the off-line mass spectra afforded sufficient evidence for the structure elucidation of various impurities. In an impurity of oestradiol (4-chlorooestradiol) the mass spectrum indicated the presence of a chlorine atom in the phenolic ring while its position was established on the basis of the UV spectrum [8]. Another example is the identification of propyl 4-[diethylcarbamoyl(methoxy)]-3-methoxy phenylglyoxylate (**II**) impurity (oxidative degradation product) in propanidid (**I**). The molecule peak of **II** from a GC/MS scan was at m/z 351 (t_R = 34.6 min) while the molecular weight of **I** is 337 (t_R = 30.5 min). In the normal phase high-performance liquid chromatogram of propanidid **I** appears at 11.9 min, while the peak of **II** is at 16.4 min. It is evident from the diode-array UV spectra of **I** and **II** in Fig. 2 and Scheme 1 that the reason for the difference of 14 units between the molecular weights of **I** and **II** is that in the latter the active methylene group of **I** between the phenolic ring and the propyloxycarbonyl group is oxidized leading to a highly conjugated ketone derivative .

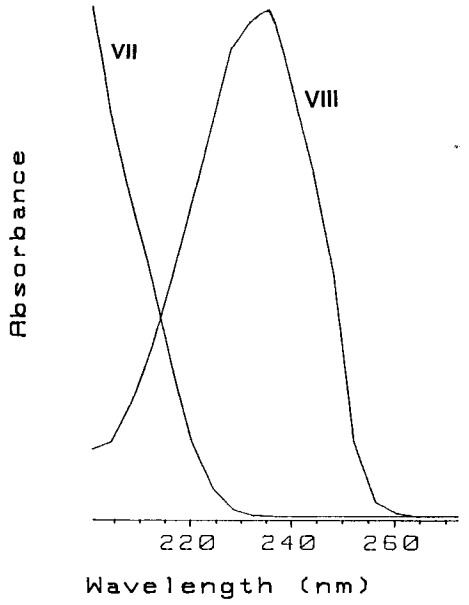

Fig. 4. Diode-array UV spectra of allylestrenol (**VII**) and impurity **VIII**. See Section 2 for the HPLC conditions.

In the following the potential of the LC/MS technique supplemented with information obtained from diode-array UV spectra will be demonstrated on the example of the impurity profiling of mazipredone (21-deoxy-21-*N*-methylpiperazinyl-prednisolone hydrochloride, **III**), the water-soluble prednisolone derivative of the Chemical Works of Gedeon Richter Ltd., Budapest. Under the HPLC conditions described in Section 2 the retention time of mazipredone (**III**) is 30.7 min. In addition to minor trivial impurities such as prednisolone (retention time 24.9 min) and prednisolone-21-mesylate, the last intermediate of the synthesis (retention time 48.5 min) we report on the identification of three main impurities present in the range 0.1–0.4%. It is to be noted that under the APCI conditions described in Section 2 only the molecular weights of the protonated compounds are obtainable. The molecular weight of **III** is 442 (MH^+ = 443). The molecular weight of 440 of impurity **IV** eluting at 28.2 min indicates that the 11-hydroxyl group in **III** is replaced by a 11-ketone group.This is supported by the full identity of the diode-array UV spectra of **III** and **IV** [12] (Fig. 3 and Scheme 2). Impurity V (29.9 min) has a molecular weight of 444. It can be seen from its UV spectrum that the additional hydrogen atoms are at the 1 and 2 positions: the absorption maxima of 1,4-diene-3-keto and 4-ene-3-keto steroids are known to be at nearly the same wavelength but the bandwidth of the latter is much smaller [12–15]. The molecular

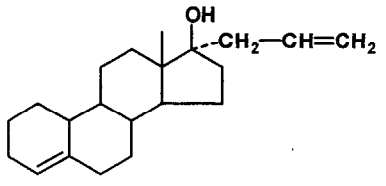

Allylestrenol, VII

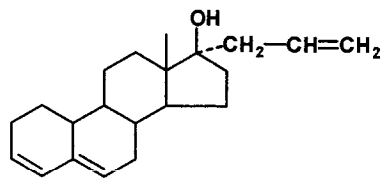

VIII

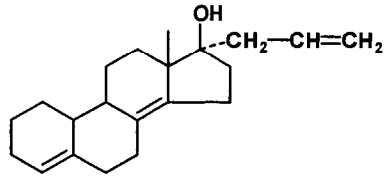

IX

Scheme 3.

weight of impurity **VI** (retention time 41.2 min) is 424. This indicates the loss of one molecule of water from the parent compound: either Δ^{16} or $\Delta^{9(11)}$ derivative. The hypsochromic shift observable in Fig. 3 is characteristic of the latter [12], the structure of which was proved by synthesis, retention and spectral matching. It is noteworthy that the characteristic molecular weights of the protonated forms of **IV–VI** (441, 445 and 425) could be estimated by direct APCI investigation of the contaminated sample of mazipredone without any chromatographic separation.

An example of the use of the GC/MS method is the impurity profiling of flumecinol (3-trifluoromethyl-α-ethyl-benzhydrol) [10,16,17]. This technique has also been successfully used (usually combined with other methods) in the impurity profiling of steroids, e.g. the identification of 3-deoxonorgestrel impurity in norgestrel [1], several impurities in 2-androstene-17-one (intermediate in the synthesis of pipecuronium bromide) [18] and in bulk cholesterol [19].

A recent example for the use of GC/MS supplemented by other spectroscopic techniques is the estimation of impurities **VIII–IX** in allyloestrenol (**VII**). The gas chromatographic retention times were as follows: **VII** 7.2 min, **VIII** 7.9 min, **IX** 6.3 min. The molecular weight of **VII** is 300 whereas those of **VIII** and **IX**, obtained from the GC/MS scans, is 298 indicating the presence of one additional double bond. The location of this in the structures of **VIII** and **IX** was estimated on the basis of the fragmentation pattern in the mass spectra and from NMR spectra obtained on samples isolated by preparative HPLC. The location of the additional double bond at the 8(14) position in **IX** is supported by a base peak at m/z 214 which is due to the cleavage of the C_{13}–C_{17} and C_{15}–C_{16} bonds (β-cleavage related to the 8(14) double bond). Further evidence is furnished by the NMR data. The chemical shifts (in $CDCl_3$) of the protons and carbons in the environment of the two bonds in the steroid nucleus are as follows. ^{1}H NMR: 1.09 (3 H, s, H-18), 5.44 (1 H, m, H-4); ^{13}C NMR: 21.7 (q, C-18), 120.1 (d, C-4), 130.8 (s,C-8), 136.2 (s,C-14), 140.0 (s,C-5). The base peak in the mass spectrum of **VIII** is the molecule peak. The intense fragment ion at m/z

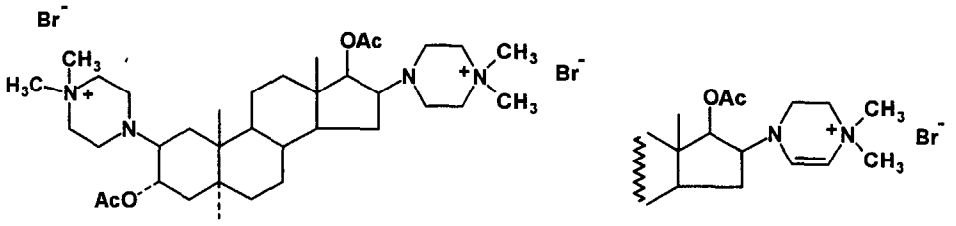

Pipecuronium bromide, X XI

Scheme 4.

199 (88%) is due to the cleavage of the C_{13}–C_{17} and C_{14}–C_{15} double bonds. NMR chemical shifts (in DMSO-d_6) supporting the 3,5-diene structure are as follows. ^{1}H NMR: 0.81 (3 H, s, H-18), 5.42 (1 H, m, H-6), 5.64 (1 H, m, H-3), 5.95 (1 H, m, H-4); ^{13}C NMR: 14.4 (q, C-18), 122.7 (d, C-6), 126.4 (d, C-3), 129.5 (d, C-4), 136.2 (s, C-5). In the case of **VIII** the HPLC/diode-array UV spectral scan (see Fig. 4 and Scheme 3) also contributed to the structure of this conjugated *trans*-diene type impurity; (retention times: **VII** 12.8 min, **VIII** 8.1, **IX** 10.0 min).

Some examples for the complex use of chromatographic and spectroscopic techniques including NMR spectroscopy are, for example, the identification of two isomeric impurities (Z and E ethynodiol-3-acetate-17-(3′-acetoxy-2′-butenoate) in ethynodiol diacetate [20], epimeric 17α-hydroxy-17β-ethinyl and ethinyl-bridged dimeric derivatives in norethisterone [9,17], impurities with a methyl group attached to the aromatic ring of the main component in hexoestrol [10] and enalapril [20], isodanazol in danazol [21], 3-[2-(diaminomethyleneamino)thiazol-4-ylmethylthio]-*N*-cyano-propionamidine in famotidine [17], 2,5-bis-[(*N*′-cyano-*N*″-methyl)guanidino-ethyl-thiomethyl]-4-methylimidazole and 1,8-bis-[(*N*′-cyano-*N*″-methyl)guanidino]-3,6-dithiaoctane in cimetidine [22] as well as 3,17α-diethinyl-13-ethyl-3,5-gonadien-17-ol in norgestrel [1].

The last example merits special attention. NMR spectroscopy not only played a predominant role in the structure elucidation of 2′-dehydropipecuronium bromide (**XI**) impurity in pipecuronium bromide (**X**) but (due to the absence of signals in the ^{1}H-NMR spectrum of the latter in the 5.2–6.3 ppm range) the estimation of the doublets of the vinylic protons at 5.26 and 6.29 ppm enabled the impurity to be detected and even quantitated (using the internal standard method) down to the level of 0.5% in **X** without chromatographic separation [20] (Scheme 4).

References

[1] P. Horváth, G. Balogh, J. Brlik et al., J. Pharm. Biomed. Anal., in press.
[2] J.C. Berridge, J. Pharm. Biomed. Anal., 14 (1995) 7.
[3] Note for Guidance on Impurities in New Drug Substances, (Guidelines prepared within the International Conference on Harmonisation (ICH) process.) The European Agency for the Evaluation of Medicinal Products, London, 1995.
[4] S. Görög, Ultraviolet-Visible Spectrophotometry in Pharmaceutical Analysis, CRC Press, Boca Raton, FL, 1995, pp. 135–153.
[5] W.M.A. Niessen and J. van der Greef, Liquid Chromatography—Mass Spectrometry, Marcel Dekker, New York, 1992.
[6] K.D. Altria, J. Chromatogr., 646 (1993) 245.
[7] J.C. Lindon, R.D. Farrant, P.N. Sanderson et al., Magn. Res. Chem. 33 (1995) 857.
[8] S. Görög, J. Brlik, A. Csehi et al., Anal. Methods Instrum., 2 (1995) 154.
[9] S. Görög and B. Herényi, J. Chromatogr., 400 (1987) 177.

[10] S. Görög, A. Laukó and B. Herényi, J. Pharm. Biomed. Anal., 6 (1988) 697.
[11] S. Görög, M. Bihari, É. Csizér, F. Dravecz, M. Gazdag and B. Herényi, J. Pharm. Biomed. Anal., 14 (1995) 82.
[12] L.L. Engel (Ed.), Physical Properties of the Steroid Hormones, Pergamon Press, Oxford, 1963, pp. 85–93.
[13] S. Görög and Gy. Szász, Analysis of Steroid Hormone Drugs, Elsevier, Amsterdam, 1978, pp. 176–177.
[14] S. Görög, Quantitative Analysis of Steroid Hormones, Elsevier, Amsterdam, 1983, pp. 24–25.
[15] S. Görög (Ed.), Steroid Analysis in the Pharmaceutical Industry, Ellis Horwood, Chichester, 1989, pp. 6–7, 226–227.
[16] A. Laukó, É. Csizér and S. Görög, Proc. 13th Int. Symp. on Capillary Chromatography, Vol. II (P. Sandra, Ed.), Huethig, 1991, pp. 1548–1556.
[17] S. Görög, G. Balogh, A. Csehi et al., J. Pharm. Biomed. Anal., 11 (1993) 1219.
[18] S. Görög, A. Laukó, B. Herényi et al., Chromatographia, 26 (1988) 316.
[19] A. Laukó, É. Csizér and S. Görög, Analyst, 118 (1993) 609.
[20] S. Görög, G. Balogh and M. Gazdag, J. Pharm. Biomed. Anal., 9 (1991) 829.
[21] G. Balogh, É. Csizér, Gy. G. Ferenczy et al., Pharm. Res., 12 (1995) 295.
[22] Zs. Halmos, Cs. Szántay Jr., J. Brlik et al., J. Pharm. Biomed. Anal., in press.

ELSEVIER

Talanta 44 (1997) 1527–1541

Talanta

Amperometric monitoring of lactate accumulation in rabbit ischemic myocardium

Sayed A.M. Marzouk [1,a], Vasile V. Cosofret [a], Richard P. Buck [a,*], Hua Yang [b], Wayne E. Cascio [b], Saad S.M. Hassan [c]

[a] *Department of Chemistry, University of North Carolina, Chapel Hill, NC 27599-3290, USA*
[b] *Department of Medicine, University of North Carolina, Chapel Hill, NC 27599-7075, USA*
[c] *Department of Chemistry, Ain Shams University, Cairo, Egypt*

Received 3 September 1996; received in revised form 29 October 1996; accepted 29 October 1996

Abstract

Fabrication and characterization of miniature, flexible, planar biosensors for monitoring L-lactate accumulation in an ischemic myocardium are described. Three configurations of Au-based electrodes were fabricated by a photolithographic technique on flexible polyimide Kapton® foil. All sensors are based on an immobilized lactate oxidase with amperometric detection of the enzymatically produced hydrogen peroxide at a platinum-electroplated-gold base electrode polarized at 0.5 V versus Ag/AgCl. An inner electropolymeric layer is used to prevent electrode fouling and to reject the interference effects of easily oxidizable molecules. In addition, a diffusion controlling outer layer that greatly enhances the linear dynamic range of the sensor, is obtained by casting a polyurethane external film. The developed sensor was evaluated in vitro and proved to have high selectivity, good operational stability, good accuracy and precision (average recovery = 102.3 ± 0.4% for control sera), fast response time (t_{95} = 20 s) and high upper limit of the linear dynamic range (25–80 mM, with sensitivity of 1.7–0.4 nA mM^{-1}, respectively at PO_2 = 15 mmHg). Subsequently, the sensor was brought into direct contact with the surface of the rabbit papillary muscle and used for continuous quantitative monitoring of extracellular lactate accumulation during no-flow ischemia. © 1997 Elsevier Science B.V.

Keywords: Amperometric biosensors; Ischemia; Lactate monitoring; Papillary muscle

1. Introduction

Lactic acid is an important metabolic product formed during anaerobic glycolysis as glucose is used for the generation of ATP [1,2]. Transsarcolemmal transport of lactate-anion and diffusion of lactic acid are believed to be important mechanisms regulating intracellular pH during cellular metabolic stresses such as anoxia, hypoxia, ischemia and chemical inhibition of mitochondrial function. Moreover, lactate anion-dependent mechanisms may contribute to cellular potassium loss during metabolic stress [3]. An understanding

* Corresponding author.

[1] On leave from the Department of Chemistry, Ain Shams University, Cairo, Egypt.

PII S0039-9140(96)02175-3

of the relation between lactate and K^+ efflux during ischemia is particularly important because accumulating extracellular K^+ contributes significantly to the occurrence of lethal ventricular arrhythmias during myocardial infarction [4]. Although extracellular lactate and K^+ have been measured independently, a notable absence of appropriate methods for measuring extracellular lactate accumulation in the absence of myocardial perfusion has prevented the study of their interdependence. Such an interdependence has been proposed [5] but remains controversial [6–8]. For this reason, we have sought a novel sensor to determine lactate in an ischemic myocardium with sufficient temporal and spatial characteristics as to allow the future measurement of extracellular K^+ simultaneously.

In the last two decades, enzyme-based amperometric biosensors have played an increasing role in solving analytical and clinical problems [9–11]. Several enzyme electrodes for the electrochemical determination of L-lactate have been developed by using immobilized enzymes, such as: lactate dehydrogenase (cytochrome b2) (EC 1.1.2.3) [12,13], lactate dehydrogenase (EC 1.1.1.27) [14], lactate 2-monooxygenase (EC 1.13.12.4) [15] and lactate oxidase (EC 1.1.3.2) [16].

Lactate oxidase (LOD) has attracted a considerable degree of attention. It is widely used with different immobilization techniques such as crosslinking with bovine serum albumin and glutaraldehyde [17,18], entrapment behind a polymeric membrane [19], attachment to a preactivated membrane [20], entrapment in an electropolymeric film [21,22], entrapment in a photopatterned poly-HEMA hydrogel membrane [23], entrapment in a polyion complex layer [24], and crosslinking with isocyanate [25]. There are also several LOD-based sensors that employ non-physiological electron acceptors, instead of O_2, to communicate electrons between the redox center of lactate oxidase and the electrode surface [26–28].

Some of the previously reported lactate biosensors have been successfully applied in real samples. Subcutaneous microdialysis [19], suction effusion fluid [18] and double lumen catheter [29] are collecting techniques and were coupled with lactate probes for lactate monitoring in subcutaneous rabbit tissue, and blood of healthy volunteers, respectively. In addition, some other implantable lactate sensors were successfully used for lactate monitoring in subcutaneous rat tissue [17] and in the blood stream inside the right atrium of an anesthetized dog heart [30]. However, none of the previously reported sensors can be adapted for direct surface monitoring of extracellular lactate accumulation in ischemic rabbit papillary muscle. The needle type sensor described by Wilson [17] offers several advantages in terms of size, selectivity and stability. However, the cylindrical geometry of the needle sensor is not suitable for measurement on the muscle surface. With the needle type sensor, the active electrode area varies widely depending on whether the muscle is perfused or not. Moreover, the linear dynamic range (20 mM) of the needle sensors may be not enough to cover the expected high lactate concentration formed during extended periods of no-flow ischemia. With direct contact between the sensor and myocardium, there is no chance to dilute the accumulated lactate with any fluid. This is the reason that the expected lactate level is significantly higher than the blood lactate. Limitations associated with the needle sensor were solved by constructing the sensor on miniature flexible planar substrate with the active part of the sensor localized on one side, facing the muscle. The flexible nature of the substrate ensured good contact to the muscle surface without interference with the rhythmic beating. A sensitive optimized enzyme layer, along with efficient diffusion control outer layer, significantly enhanced the linear range.

Microfabricated-planar amperometric biosensors have several advantages over conventional enzyme electrodes: small size, low cost and mass production capability. Additionally, they can be fabricated on flexible substrates. Photolithographic technique has been used already in the fabrication of many biosensors [18,31,32]. In the present work, three different configurations of planar microelectrodes were fabricated on a flexible polyimide substrate (Kapton® DuPont) by the standard photolithographic technique. Optimization of the sensor structure will be discussed.

The characteristics and the reliability of the sensor for lactate monitoring in control sera using both batch and flow setup are presented. Finally, measurements of the accumulation of extracellular lactate in rabbit ischemic myocardium are given. This study, using the developed sensor, permits cardiovascular scientists to gain better understanding of the lactate-dependent mechanisms of ionic homeostasis.

2. Experimental

2.1. Materials and reagents

Lyophilized lactate oxidase (LOD), E.C. 1.1.3.2., from *pediococcus* species, 34 U mg^{-1}, L-lactic acid (sodium salt), bovine serum albumin (BSA, fraction V), glutaraldehyde (GA), 25% aqueous solution, L-ascorbic acid, acetaminophen, uric acid (sodium salt), were obtained from Sigma, St. Louis, MO. Hydrogen hexachloroplatinate (IV) (99.9%), potassium silver cyanide, *m*-phenylenediamine (*m*-PDA), urea, *l*-cysteine, and 1,3-dihydroxyacetone were obtained from Aldrich Chemical, Milwaukee, WI. The medical grade aliphatic polyurethane (PU, Tecoflex SG-85A) was a gift from Thermedics, (Woburn, MA). All other chemicals were of analytical reagent grade.

Stock lactate solutions (0.5 M) were freshly prepared every week, in a 0.1 M phosphate buffer (PB) of pH 7.2 and stored at 4°C when not in use. Lactate standard solutions used in FIA measurements were prepared in a 0.1 M PB containing 100 mmole l^{-1} NaCl. This buffer was used as a carrier stream in FIA system as well. All solutions were prepared with water from a Barnstead Nanopure II system.

2.2. Apparatus

All electrochemical experiments were performed with a Princeton Applied Research Model 363 Potentiostat/Galvanostat connected to a Princeton Applied Research Model 175 Universal programmer for potential scanning. The potentiostat was modified to measure lower current values (sensitivities down to 1 V nA^{-1}). Current-time plots, cyclic voltammograms and FIA signals were recorded on a Hewlett Packard Model 7015B X-Y-T recorder. A temperature-controlled circulating water bath (Haake B3) was used throughout the work. A Rabbit peristaltic pump (Rainin Instrument) was used to pump the carrier solution through a single flow stream FIA system. A manual sample injection valve (Rheodyne, Model 7125), fitted with either 50 or 100 μl injection loop was used for sample injection.

2.3. Sensor fabrication

2.3.1. Wafer fabrication

Three configurations of planar gold electrodes were batch fabricated on a flexible polyimide (Kapton,® DuPont) substrate (125 μm thick) as shown in Fig. 1; single site electrodes (area = 0.06 cm^2) (used for all the optimization and characterization studies), two-electrode (1.75 × 3.5 mm) and three-electrode (3.5 × 4.5 mm) miniature chips, respectively. The two-electrode chip consists of a working electrode (area = 2.25 mm^2) and a reference electrode (area = 3.13 mm^2). This chip was used for all papillary muscle experiments. The three-electrode chip consists of a working, counter and reference electrodes of areas 3.75, 5.25 and 0.5 mm^2, respectively. This chip was used with the wall-jet FI analysis. The fabrication steps were described recently in more detail [33]. Two thin layers of chromium and gold, respectively were sputtered onto the Kapton substrate. The Cr layer enhances the adhesion of gold to the substrate. A layer of positive photoresist (JSR, 1 × 700 10 CP) was applied to the gold layer and then standard UV-lithographic technique was used to define the desired shape of the electrodes. The photoresist was developed, gold and chromium layers were etched, and the photoresist was then removed from the patterned metal surface. A photodefinable polyimide (Du Pont, PI2721) was used to define openings for the electrode sites and the bonding pads. Finally, each electrode (or cell) was cut from the wafer and connected, through the bonding pads, to electrical wire by means of Ag epoxy (Epoxy Technology,). The electrical contacts were insulated using silicone rubber coating seal (Dow Corning 3140 RTV). The base Au

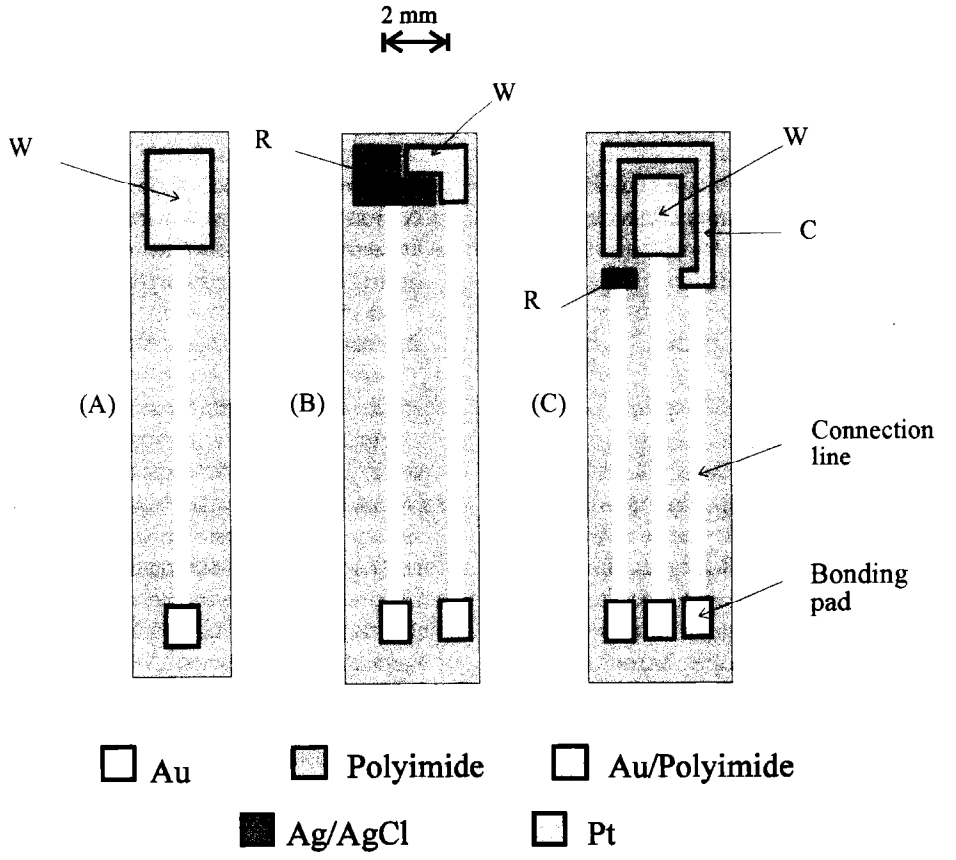

Fig. 1. Kapton-based substrates: single site electrode (A), two-electrode (B), and three-electrode chips. W, R and C refer to electrodes used as working, reference, and counter, respectively.

electrodes were then ready for further modification.

2.3.2. Electrochemical platinization

The platinization solution was prepared according to a well known method [34] as follow: 0.65 g $H_2[PtCl_6]$, 2.25 g $(NH_4)_2HPO_4$ and 4.73 g Na_2HPO_4 were dissolved separately each in ~10 ml water. The ammonium phosphate was added to the chloroplatinic acid with stirring. A yellow precipitate of $(NH_4)_2PtCl_6$ was formed; without filtering this solution, the sodium phosphate was added and the mixture was boiled gently with stirring for 2 h. The mixture was cooled and diluted to 50 ml with water. The electrodes for working or counter were electroplated by galvanostatic platinum deposition. A 5 cm diameter Pt mesh electrode was used as anode. Prior to plating, the gold electrodes to be platinized were cleaned by anodizing at 0.5 mA cm^{-2} for 25 s. in the same platinization solution. This bath was recommended for operation at 70°C with a current density of 2–5 mA cm^{-2} [34]. However, bright, smooth, and adherent platinum deposits were obtained at room temperature using a current density of 10–12 mA cm^{-2} for 5 min.

2.3.3. Electrochemical polymerization (inner layer formation)

Poly *m*-phenylenediamine film was prepared by electropolymerization using cyclic voltammetry. The film was grown from a gently stirred aqueous solution containing 10 mM *m*-PDA in 0.1 M PB pH 7.2. The potential was cycled from +0.2 to

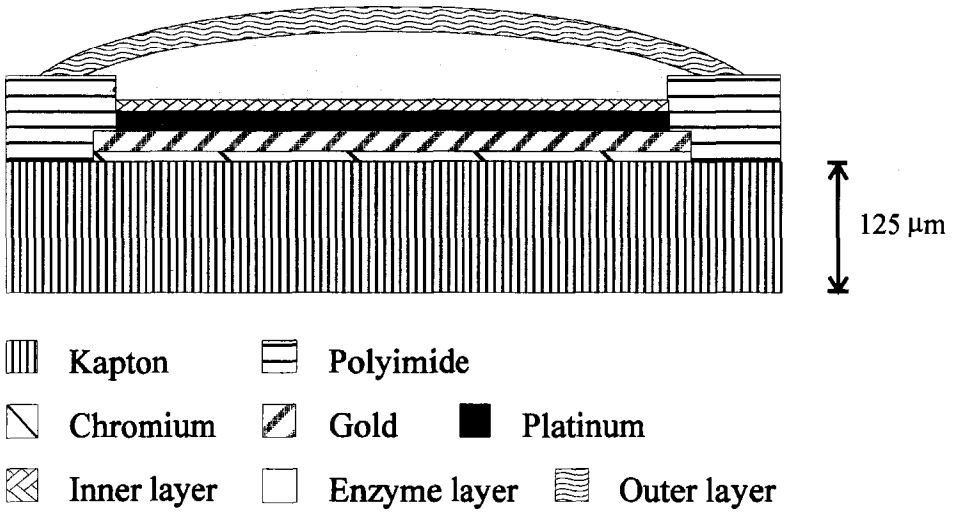

Fig. 2. Layer structure of the lactate biosensor.

+0.8 V versus Ag/AgCl at a scan rate of 2 mV s^{-1} for 12 cycles (2 h). The modified electrodes were washed with water and kept in 0.1 M PB at 4°C overnight. The selectivities of the electrodes towards common biological interferences, i.e., L-ascorbic acid, acetaminophen, uric acid, L-cysteine, urea, and 1,3-dihydroxyacetone were tested at 0.16, 0.16, 0.3, 0.1, 5.0, and 1.0 mM concentration level, respectively.

2.3.4. Enzyme layer (EL)

The immobilized enzyme layer was obtained by crosslinking LOD with BSA using GA. A 3 μl aliquot of a specified fresh enzyme mixture solution in PB was quickly syringed onto the electrode surface using a 5 μl syringe (Hamilton, Reno, Nevada). The enzyme layer was allowed to crosslink and to dry in air at room temperature for 1 h. The sensor was then washed thoroughly with water to remove excess reagents. The sensor was either stored in buffer at 4°C when not in use for EL optimization study, or dried in air for further modification with outer layer to complete the sensor construction.

2.3.5. Optimization of the enzyme layer

This study was done without inner polymeric layer. The term G/T was defined to reduce the number of variables to be investigated. G refers to the w/v% of glutaraldehyde and T refers to the total w/v% of LOD and BSA in the enzyme mixture solution. Initially, three sets of sensors (three in each) were prepared using different enzyme mixture solutions for which LOD was arbitrarily fixed at 6% (2 U μl^{-1}) and BSA was fixed at 5, 10, and 15% for the three sets, respectively. Among each set, G/T was adjusted to 0.03, 0.045 and 0.06, respectively. To study the effect of enzyme content, three different enzyme solutions were used containing 2, 4, and 6% LOD, respectively. BSA/LOD ratio was set at 1.4 and G/T ratio was set at 0.05. Finally, to study the effect of glutaraldehyde, three different compositions with 2% LOD—3% BSA and G/T of 0.05, 0.06 and 0.07, respectively were tested.

2.3.6. Outer membrane (OM)

To complete the construction of the sensor, a 3 μl aliquot of 1% w/v PU in pure THF was deposited above the enzyme layer by a microsyringe. The sensor was allowed to dry in air at room temperature for 5–10 min, washed with water and stored in PB at 4°C when not in use. A cross section of the whole layer structure of the sensor is shown in Fig. 2.

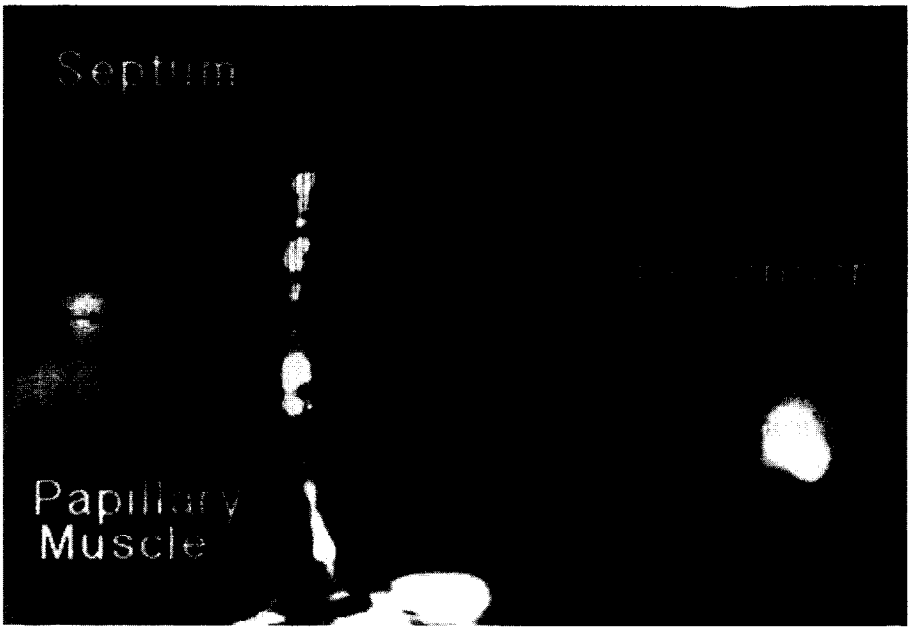

Fig. 3. The isolated arterially perfused RV rabbit papillary muscle is suspended in an artificial atmosphere and in contact with the two-electrode chip (the active part is behind the muscle). Pt counter electrode not shown in the field. The tendonous end of the muscle is fixed to a rigid hook with a suture. Electrical stimulation is delivered at twice diastolic threshold through a Pt wire affixed to the tendon. The scale bar represents 1 mm.

2.3.7. Miniature chips fabrication

The working and counter electrodes were platinized as before. The electrode that served as a pseudo reference was galvanostatically plated with silver from a 1% w/v solution of potassium silver cyanide using 5 mA cm^{-2} for 10 min. About 25% of this silver is electrochemically converted to AgCl in 0.1 M HCl. The inner polymeric film was grown on the working electrode as before. A 2 and 4 μl aliquot of the enzyme mixture solution (2% LOD-3% BSA-0.3%GA) was delivered by syringe onto the surface of two- and three-electrode chips, respectively, and spread with the syringe tip to cover all the electrodes. A 5 μl aliquot of PU solution was used for outer membrane formation.

2.4. Amperometric measurements

A conventional three-electrode system was used for all amperometric batch measurements. A Pt wire served as the counter electrode and a miniaturized Ag/AgCl electrode with flexible barrel (Cypress System, Lawrence, KS) was used as the reference, against which all potentials were referred in the present work unless otherwise stated. All experiments were performed in a 7 ml double-jacket-thermostated cell containing a magnetically stirred 4 ml PB at 25.0 ± 0.1°C. The working electrode was polarized at 0.5 V in all the measurement.

2.5. FIA setup

A three-electrode miniature chip was used in a single channel wall-jet flow injection system. A carrier solution consisting of 0.1 M PB containing 100 mmole l^{-1} NaCl was propelled by means of a peristaltic pump through PTFE tubings (0.8 mm i.d.) at the desired flow rate. The tubing ended with a horizontally mounted 8 cm glass capillary tube (6.6 mm o.d. and 1.0 mm i.d.). The length of the tubing from the injection valve to the capillary was 25 cm. The free end of the capillary was cut

at 90°. This end of the tube was brought into contact with the cell surface. The miniature chip was mounted in a vertical position with connection wires directed upward.

2.6. Lactate measurement in control serum

The human based control sera level I and II (Dade® Moni-Trol® ES Chemistry Control, Baxter Diagnostics) were constituted from the lyophilized preparation according to the manufacturer's recommendation. The manufacturer's mean values of lactate concentrations were 1.5 and 4.9 mM, respectively. A 3 ml PB aliquot was placed in the cell. After background current stabilization, a 0.5 ml aliquot of the serum sample without any treatment, was pipetted into the cell. When the current reached a steady value, the standard addition procedure was used to evaluate the lactate concentration level. The obtained results were compared with the results obtained with the established YSI 2700 SELECT Biochemistry analyzer equipped with YSI 2329 lactate membrane. For measurements with flow system, a 100 μl aliquot of the untreated serum sample was injected into the carrier stream and lactate concentrations were evaluated by direct calibration method.

2.7. Arterial perfusion of isolated papillary muscle

New Zealand white rabbits ($n = 5$) of either gender weighing 2–3 kg were heparinized (200 U kg^{-1}, i.v) and anesthetized with sodium thiopental (50 mg kg^{-1}, i.v.) in accordance with accepted guidelines for the care and treatment of experimental animals at the University of North Carolina at Chapel Hill. The heart was excised and arrested in cold Tyrode's solution (in mmol l^{-1}: Na^+, 149; K^+, 4.5; Mg^{2+}, 0.49; Ca^{2+}, 1.8; Cl^-, 133; HCO_3^-, 25; HPO_4^{2-}, 0.4; glucose, 20) for 20 s. The atria and left ventricle (LV) free wall were removed. The LV septal surface of the tissue was pinned to a wax plate in contact with Ag/AgCl ground electrode. The septal artery was visualized with a dissection microscope, cannulated and perfused with an perfusate composed of Tyrode's solution plus insulin (1 U l^{-1}), heparin (400 U l^{-1}), albumin (2 g l^{-1}), and dextran (M_r 70 000; 40 g l^{-1}). The time between cross clamping the aorta and perfusion was < 5 min in each experiment.

The cannula was fixed to the septal artery with a purse string suture and the septum was secured in a custom made experimental chamber [35]. The non-perfused portion of the right ventricle (RV) was excised and the papillary muscles were exposed. A long and symmetrical muscle was chosen and the tendon was attached to a rigid pin with a fine monofilament suture. The perfusate was pumped by a peristaltic pump (Digi-Staltic, Masterflex, Barrington, IL) through a custom made membrane gas exchanger in which partial pressures of O_2, N_2, and CO_2 of the perfusate were controlled [35]. The chamber was closed and the preparation was surrounded by humidified gas with the same composition as the perfusate. The pH of the perfusate was continuously monitored by a glass pH electrode positioned in the perfusion line before entering the septal artery. The amount of CO_2 was adjusted in the gas exchanger to yield a pH of 7.35 ± 0.05. The temperature of the papillary muscle was maintained between 36 and 37.5°C by passing the perfusate through a thermostated water bath before entering the cannula to the septal artery. The PO_2, PCO_2, HCO_3^- concentration and pH of the perfusate entering the cannula were confirmed by blood gas analysis (System 1304 pH/Blood Gas Analyzer, Instrumentation Laboratory, Lexington, MA). Intraarterial pressure was measured with a pressure transducer (Millar, Houston, TX) and continuously monitored on a strip chart recorder. The septal artery pressure ranged between 35 and 50 mmHg and was maintained by adjustment of the perfusion flow rate (approximately 1.0–1.5 ml min^{-1} g^{-1} tissue).

2.8. Measurement of extracellular lactate

Two-electrode chip with working electrode of (area 2.25 mm^2) and a Ag/AgCl pseudo reference electrode (area = 3.12 mm^2) was positioned in direct contact with the suspended muscle as shown in Fig. 3. A separate platinum wire, serving as a counter electrode, was positioned at the base of

the papillary muscle on the septal surface. A 0.7 Hz 5 pole Butterworth low pass filter was used to eliminate the noise resulting from the electrical pulse stimulation of the muscle. While the muscle is perfused the sensor is polarized at 0.5 V against the pseudo reference electrode. The background current was allowed to reach a stable value. Ischemia was induced by arresting flow. The volume fractions of O_2 and CO_2 in the recording chamber were measured using the gas analyzer. The magnitude of lactate accumulation was monitored by recording the change of the sensor output against the time after arrest of flow.

Ideally, the sensor should be calibrated under the same experimental conditions, namely, arrest of flow after infusion of a standard lactate solution. However, such a calibration will not be reliable because under no-flow conditions the muscle will generate lactate. In this way the standard value will be completely uncertain. For this reason the sensor calibration was performed under flow conditions. We believe that such in situ calibration is more accurate than the in vitro calibration approach which is accepted when a calibration under identical condition is not possible, e.g., with in vivo measurements. The sensor was calibrated in situ, by perfusing the muscle with perfusate containing lactate at 10 and 20 mM concentration levels, respectively. The current responses to the standard solutions were used to construct a two point calibration curve.

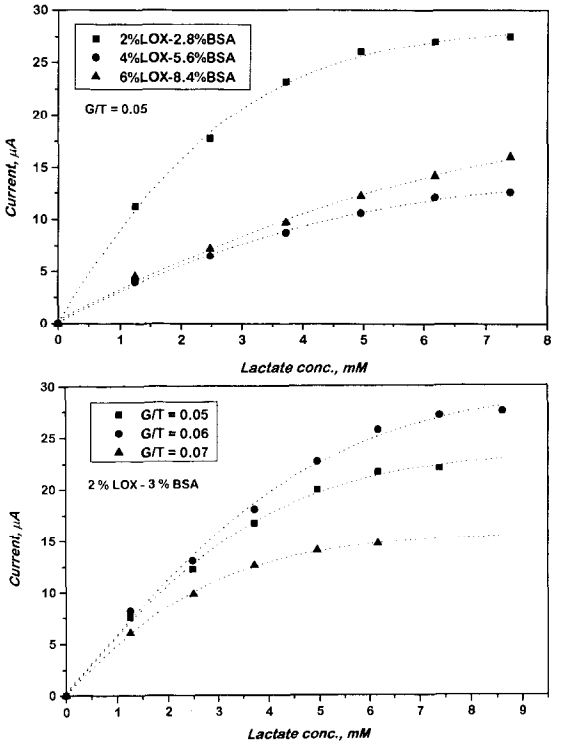

Fig. 4. (a) Effect of enzyme loading on the sensor response. (b) Effect of glutaraldehyde on the sensor response.

3. Results and discussion

3.1. Optimization of enzyme layer

Among many papers published for amperometric detection of lactic acid, only few papers [17,18,26,30,36] have adapted the crosslinking with BSA and GA as an immobilization technique for LOD. The reported ratios of LOD, BSA, and GA are widely varied, unjustified and sometimes incompletely mentioned [30]. In addition, Turner et al. [37] have published recently a paper on lactate, glutamate and glutamine biosensors. They immobilized LOD by mixing with hydroxyethylcellulose, and adapted glutaraldehyde crosslinking for the other two sensors. They apparently avoided crosslinking with glutaraldehyde as an immobilization technique. Moreover, Mulchandani et al. [38] have reported recently that LOD was not amenable to glutaraldehyde crosslinking. These observations suggested that LOD immobilization with glutaraldehyde crosslinking is not straightforward and requires a proper control of the enzyme mixture composition. This is the reason that the first step in this work was to find out the optimum composition of the enzyme layer. Enzyme layers obtained with BSA/LOD < 1 were found to be mechanically unstable and washed out from the electrode surface. BSA/LOD ratios in the range 1.4–1.5 showed very good mechanical stability and good adhesion to the polyimide substrate. With ratios greater than 1.7, the enzyme layer became undesirably thick and the response time became too long (50–60 s). The effect of enzyme concentration on the sensor response is shown in Fig. 4a. The response sensitivity is al-

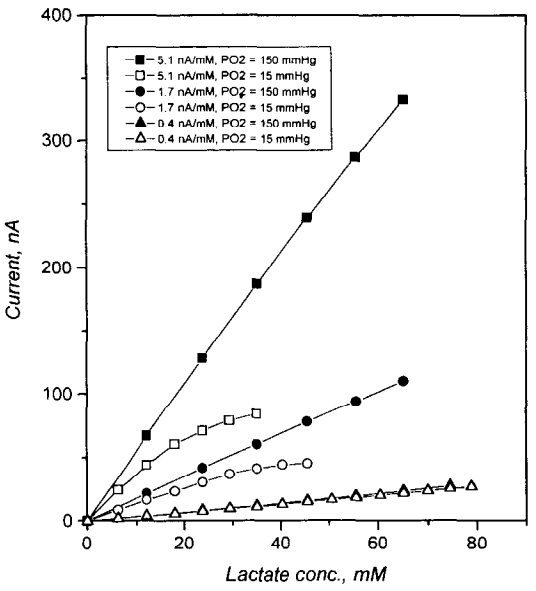

Fig. 5. Effect of sensitivity on the dependence of the sensor response on oxygen tension.

most halved on increasing the enzyme (and BSA) two-fold. This happens because the thickness of the enzyme layer is almost doubled as well. The decrease in sensitivity due to the increased enzyme layer thickness outweighs the increase in sensitivity due to the higher enzyme content. As a general trend, thicker enzyme layers lead to better linearity over a wide concentration range, but the response time is longer. A solution composition of 2% LOD-3% BSA was chosen for further work.

The effect of GA on the sensor response is shown in Fig. 4b. The trend shown in this figure is reproducible and G/T = 0.06 revealed the highest sensitivity. Smaller G/T ratio may lead to inefficient immobilization, while a higher ratio may lead to excessive crosslinking and blocking of some active sites of the enzyme. The critical dependence of the sensor response on the glutaraldehyde concentration in the enzyme solution is not a surprise if correlated with the above mentioned observations. Therefore, an enzyme mixture solution of composition 2% LOD-3% BSA-0.3% GA was proven to be the best among the ratios studied. Enzyme layers obtained with this ratios showed good adhesion to the substrate, high sensitivity (~ 8 μA mM^{-1}) and very short response time (< 5 s). These are the reasons that it is used throughout the subsequent work.

3.2. Interference rejection inner layer

Many approaches have been developed to enhance the selectivity of the H_2O_2 measuring system [24,39–42] in the presence of interferences. However, electropolymeric films provide many attractive features, such as self-limiting coverage, generation of very thin layers, strong adhesion to the electrode surface, ease of thickness control by changing the polymerization time, and convenience of automation. *m*-Phenylenediamine is one of the most successful monomers used for this purpose. Typical cyclic voltammograms (not shown) were obtained for oxidative electropolymerization of *m*-PDA from stirred 10 mM PB solution. The resulting film showed an efficient discrimination against ascorbic acid, uric acid, acetaminophen, etc., as we will discuss in the sensor selectivity section. On the other hand, a high permeability (80–90% of the bare Pt electrode response) to H_2O_2 was observed in comparison with the films obtained by casting cellulose acetate or Nafion solutions.

3.3. Diffusion control outer layer

Wilson et al. [17] have used a 5% PU solution in 98% tetrahydrofuran (THF)-2% dimethylformamide (DMF) and a wire loop technique to coat a needle-type lactate sensor with an outer diffusion layer. The described wire loop technique is not suitable for our planar sensors and 5% solution is too concentrated for the casting technique. The resulting sensor required very long time (10–20 days) to attain stable sensitivity and the upper limit of linear range is between 12 and 20 mM with sensitivity 2.8 and 1.1 nA mM^{-1}. On the other hand, we found that 1% PU solution in pure THF gives an efficient diffusion control outer layer and the sensor reached stable sensitivity in 12 h at 4°C. With almost the same sensitivity, the upper limit of the linear range is much higher as we will discuss below.

3.4. Characteristics of the sensor

Replicate sensors ($n = 30$) showed response sensitivities in the range of 1.5–3.6 nA mM^{-1} with a background current of 8 ± 3 nA. A typical sensor with sensitivity of 2.3 nA mM^{-1}, gave a linear dynamic range up to at least 140 mM in air equilibrated buffer, $r = 0.9997$. This high linearity is a result of a combination of a very sensitive enzyme layer and an efficient diffusion-controlling outer layer. The latter greatly reduces the flux of lactate ions that reach the enzyme layer. Sensors with higher and lower sensitivity ranges were prepared as well. In these cases, smaller (2 μl) or larger (4 μl) aliquots of PU solution (Section 2.3.6) were used, respectively, to form the outer layer. The sensor output is stable for 1 month when stored at 4°C when not in use. For longer periods, the linear range remains the same, but an increased sensitivity was observed due to the increase of permeability of the outer layer. About 10% increase in the sensor response was observed when the sensor is polarized in phosphate buffer at 37°C for 4 h. This is again due to the increased permeability of the outer layer. This relatively faster increase in the outer layer permeability is due to the higher temperature, because other sensors polarized for more than 8 h at 25°C did not show any significant change in the sensitivity. Operational stability at 37°C is adequate because the duration of the papillary muscle experiments does not exceed 2 h.

3.5. Effect of pH and temperature

The sensor output ($n = 3$) is stable to $3 \pm 0.5\%$ over the pH range 6.7–8.2. Outside this range, a relatively high background current was observed. The sensor showed a gradual increase in the sensitivity until it reached a maximum at 50°C. Then a slight decrease in sensitivity was observed from 50 to 60°C. The average temperature coefficient is 5%.

3.6. Sensor selectivity

The selectivity of the sensor towards some common interferences was tested. Addition of the combined maximum biological concentration of ascorbic acid, uric acid, acetaminophen, urea, L-cysteine and 1,3-dihydroxyacetone results in 6% increase of the signal obtained with 5 mM lactate solution with a sensor of 3 nA mM^{-1}. The high selectivity of the sensor is believed to be due to the combined effect of (1) the outer layer which reduces the flux of the analyte and interference molecules to the enzyme layer, and (2) the inner layer that selectively allows the small hydrogen peroxide molecules to reach the electrode surface to generate a signal nearly free from interferences. The sensor selectivity is maintained for about 12 days. For longer periods, the sensor started to show an increased response to the interferences (12–15% after 3 weeks).

3.7. Effect of oxygen tension

Since lactate oxidase catalyses the oxidation of lactate in the presence of oxygen as shown by the following equation:

$$\text{L} - \text{Lactate} + O_2 \rightarrow \text{Pyruvate} + H_2O_2$$

the sensor response should be oxygen dependent. Fortunately, the dependence of the sensor response on oxygen tension decreases with decrease of the sensor sensitivity [17,43,44]. Fig. 5 shows the calibration curves of three different sensors under high (150 mmHg) and low (15 mmHg) oxygen tension. Sensors with sensitivity of 5.1, 1.7 and 0.40 nA mM^{-1}, measured in air saturated buffers, showed linear dynamic ranges up to 8, 25, and 80 mM (at $PO_2 = 15$ mmHg), respectively. This is the reason that all the sensors used for extracellular lactate accumulation during induced ischemia experiments showed sensitivity < 1.7 mM nA^{-1} with linear dynamic ranges up to, at least, 25 mM under low oxygen tension required for the induced ischemia. Fortunately, such low sensitivities still allow successful measurement of the high extracellular lactate accumulation during no-flow ischemia under low oxygen tension which is the main objective of this work. However, sensors with reasonably higher sensitivies (5.0–11.0 nA mM^{-1}) obtained by using 2 μl aliquot of PU solution, will fit better any other application where no or fewer restrictions to the oxygen ten-

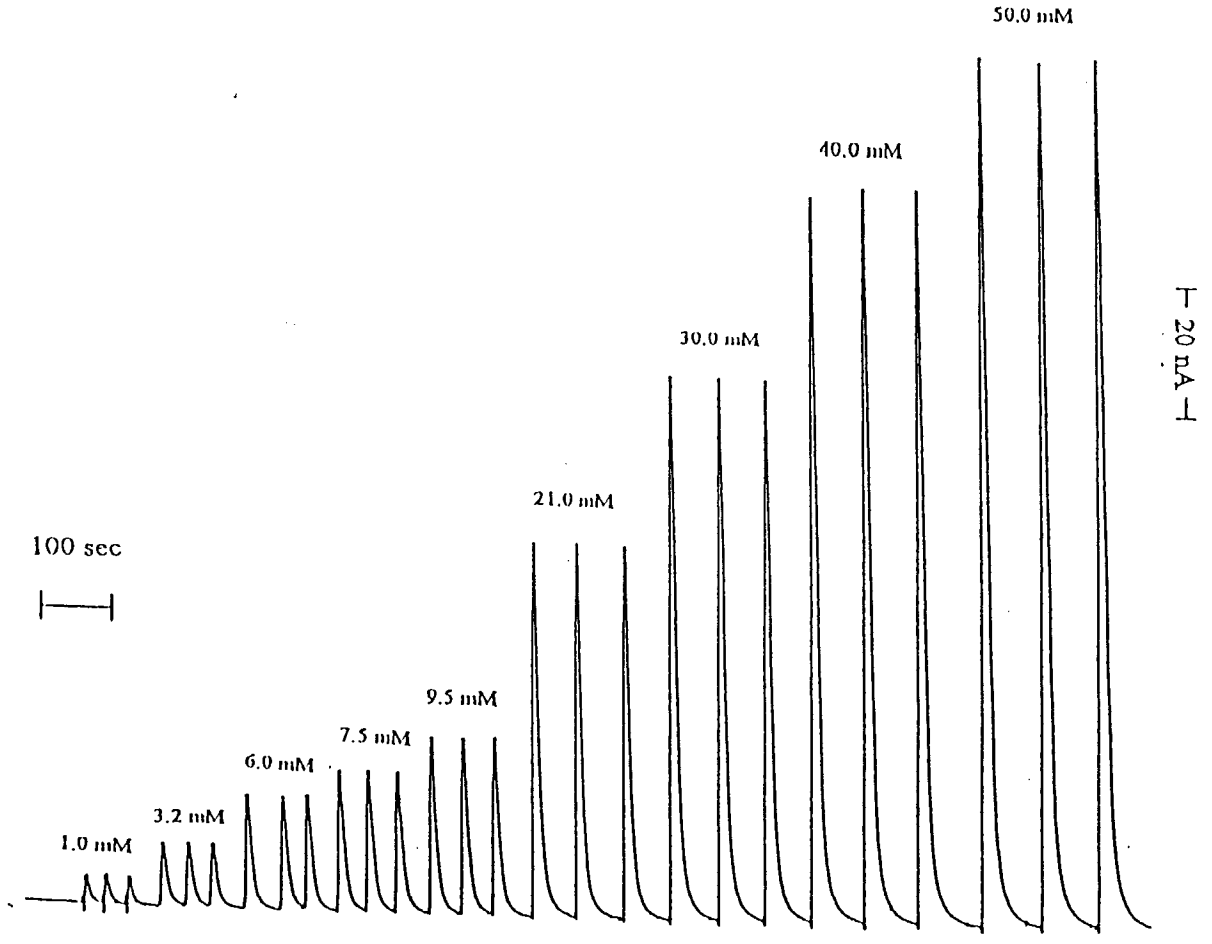

Fig. 6. Typical FIA signals.

sion and lactate concentration which is varying from sub- to several millimolar levels.

3.8. Flow injection analysis

A FIA setup, described in the experimental section, was used to evaluate the sensor response in a simulated wall-jet experiment similar to the setup described for lactate monitoring where the sensor is brought into direct contact with the muscle surface. A three electrode chip consisting of working, counter and reference electrodes was used in a single channel wall jet FIA setup. With a flow rate of 2 ml min^{-1}, and 100 μl injection loop size and a sensor sensitivity of 8.2 nA mM^{-1}, a linear range up to 30 mM was obtained. The sensor showed a good reproducibility ($1.5 \pm 0.5\%$), fast recovery time, and a very stable background current. Typical FIA peaks are shown in Fig. 6.

3.9. Lactate measurement in control sera

The reliability of the sensor for lactate monitoring in a biological complex matrix was assessed by determining lactic acid in a human based control sera which contain 42 constituents. The results obtained by both batch and FIA techniques were compared with those obtained with the YSI Biochemistry Analyzer. The excellent agreement (av-

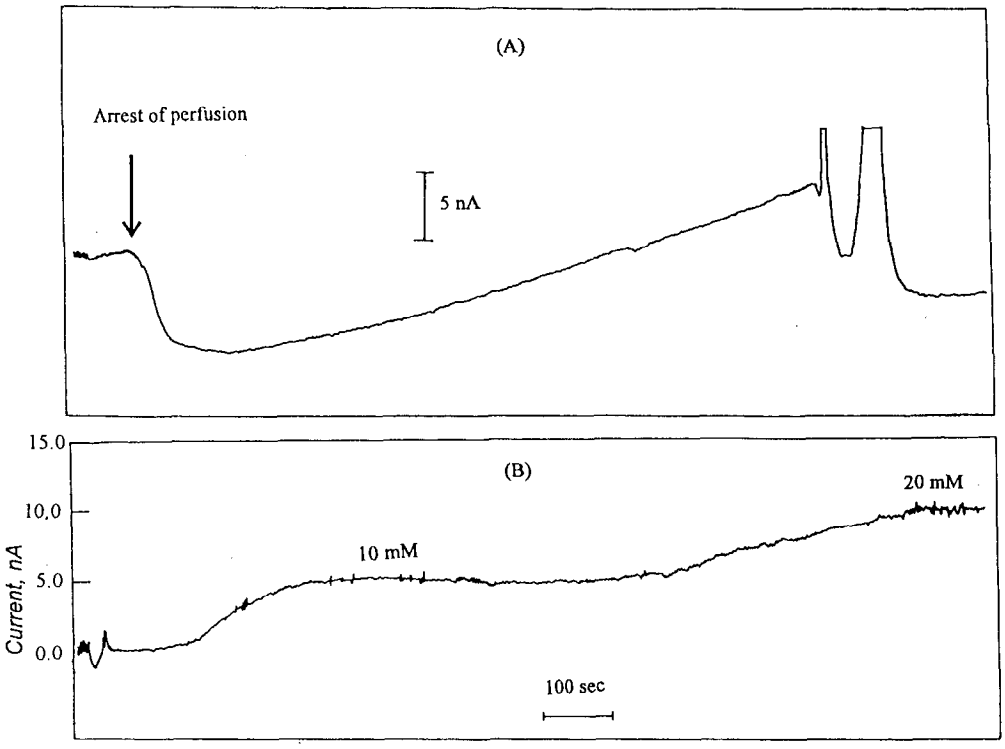

Fig. 7. Real time tracings of the sensor response during normal arterial perfusion, no-flow ischemia and reperfusion (A). An in situ sensor calibration (B).

erage recovery = 102.3 ± 0.4%) demonstrated that the sensor is reliable for simple, accurate, and rapid determination of lactic acid in real samples.

3.10. Time course and magnitude of the accumulation of extracellular lactate in rabbit ischemic ventricular muscle

The performance characteristics of the developed sensor, such as operational stability, high linearity under low oxygen tensions, high selectivity, fast response and reliability as a detector in a wall-jet flow system, suggest its successful use in continuous monitoring of the extracellular lactate accumulation in an ischemic rabbit papillary muscle. According to the authors' experience, this is the first report on continuous lactate monitoring using an amperometric sensor located in direct contact with the myocardium.

The layout of the two electrode chip (Fig. 1B) is designed to fit the dimensions of the papillary muscle. Within the same layout it is possible to make a three electrode pattern, however, the addition of the third electrode will lead to a smaller working and/or reference electrode area. At this stage of our work we sought a working electrode with a maximized area in order to measure lactate accumulation along the length of the entire papillary muscle.

The first attempt used the two-electrode chip in which the Ag/AgCl electrode served as both reference and counter. This configuration gave a very noisy and unstable response. However, when a separate Pt wire was connected to the muscle base, used as a counter, a stable response was obtained. The pseudo Ag/AgCl reference electrode was used successfully because the Cl^- ion concentration, in the solution perfusing the muscle, is nearly constant. The advantages of using

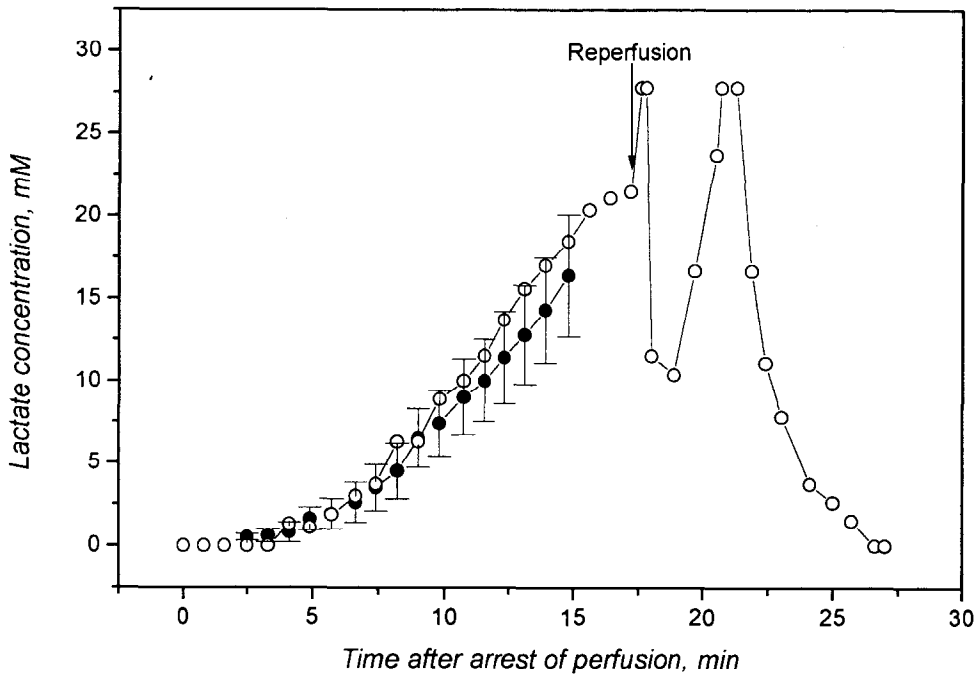

Fig. 8. Plot showing the accumulation of extracellular lactate during six episodes of 15 min of no-flow ischemia in five experimental animals. In these experiments PO_2 ranged from 24 to 250 mmHg but this did not significantly affect the accumulation of extracellular lactate. Reperfusion is shown for a single experiment for clarity because the time of repefusion differed among the individual experiments.

this arrangement are: (1) reproducible close position to the working electrode; and (2) saving the limited space around the muscle for other sensors such as oxygen, potassium sensors, etc., to be used for future studies (see Fig. 3). The sensitivity of the sensor chip placed on the papillary muscle was restricted to values < 1.7 nA mM^{-1}. The lactate content of the perfusate was measured and found to be zero prior to the onset of no-flow ischemia. As shown in Fig. 7, the arrest of perfusion resulted in an immediate shift in the baseline measuring 7.5 ± 1.5 nA. A new baseline was established within 1–1.5 min and this level was taken as the starting point for the measurement of the change in extracellular lactate concentration. Subsequently, lactate increased after a short delay. As shown in Fig. 8 the accumulation of extracellular lactate reached 16.4 ± 3.7 mM after 15 min of no-flow ischemia.

The maximal extracellular lactate concentration measured after 15 min of ischemia with the lactate sensor was substantially higher than the concentrations measured by microdialysis technique in ischemic canine heart (approximately 5 mM) [45]. This difference may be related to the methodologies or to the species studied. In contrast to the microdialysis technique, the developed lactate sensor does not damage the tissue and has direct contact to the extracellular compartment.

Reperfusion resulted in the prompt wash-out of the extracellular space. A transient increase in the current was noted after reperfusion and was similar in magnitude to the initial decrease observed immediately after arrest of perfusion. A second transient increase in current was measured 5–10 min after the onset of reperfusion. These phenomena were observed in each experiment. The mechanisms responsible for the initial decrease in current upon arrest of flow and the increase upon reperfusion are not fully understood at this time.

The second transient increase in current during reperfusion may result from washout of the lactate accumulation in the septum. Future studies will be needed to characterize these effects, although they do not interfere with the lactate measurement during the interval of no-flow ischemia.

4. Conclusion

The present miniature-three layered lactate biosensor, fabricated on a flexible planar substrate, shows many attractive features, such as miniaturization, flexibility, wide linear dynamic response range at low oxygen tensions, good stability, adequate sensitivity, fast response time and good selectivity. It was successfully used to monitor lactic acid in control sera by both batch and flow techniques and to measure extracellular lactate accumulation during no-flow ischemia. This novel lactate sensor will be a useful tool for further detailed studies in which both K^+ and lactate are monitored simultaneously for longer periods of ischemia, and to study lactate accumulation in hypoxic conditions, as well as conditions that simulate the boundary between normal and ischemic tissue. These conditions are characterized by low oxygen tensions and accumulation of potassium.

Acknowledgements

S. Marzouk gratefully acknowledges Ain-Shams University, Cairo, Egypt for providing resources for his stay at University of North Carolina. Authors like to acknowledge R.B. Ash for the wafer fabrication and D. Sandiford for technical assistance. This work was supported, in part, by grants RO1 HL48769 and P01 HL27430 from the NIH, HLBI, Bethesda, MD.

References

[1] J.R. Neely, J.T. Whitmer and M.J. Rovetto, Circ. Res., 37 (1975) 733.
[2] K. Kabayashi and J.R. Neely, Circ. Res., 44 (1979) 166.
[3] P.P. Mathur and R.B. Case, J. Mol. Cell. Cardiol., 5 (1973) 375.
[4] A.S. Harris, A. Bisteni, R.A. Russel, J.C. Brigham and J.E. Firestone, Science, 119 (1954) 200.
[5] A.G. Kleber, J. Mol. Cell. Cardiol., 16 (1984) 389.
[6] A.A.M. Wilde and G. Aksnes, Cardiovasc. Res., 29 (1995) 1.
[7] J.N. Weiss and R.-C. Shieh, Cardiovasc. Res., 28 (1994) 1125.
[8] R.-C. Shieh, J.I. Goldhaber, J.S. Stuart and J.N. Weiss, Circ. Res., 74 (1994) 829.
[9] F. Misutani and M. Asai, in D.L. Wise, (Ed.), Bioinstrumentation, Butterworths, Boston, 1990, p. 317.
[10] F. Scheller and F. Schubert, Biosensors, Elsevier, Amestrdam, 1992, p. 82.
[11] W. Schuhmann and H.-L. Schmidt, in Turner, A.P.T. (Ed.), Advances in Biosensors, Vol. 2, JAI Press, London, 1992, p. 79.
[12] D.L. Williams, A.R. Doig Jr and A. Korosi, Anal. Chem., 42 (1970) 118.
[13] J.J. Kulys and G.-J.S. Svirmickas, Anal. Chim. Acta, 117 (1980) 115.
[14] J. Wang and Q. Chen, Electroanalysis, 6 (1994) 850.
[15] E.B. Makovos and C.C. Lin, Biotechnol. Bioeng., 27 (1985) 167.
[16] I. Karube, T. Matsunaga, N. Teraoka and S. Suzuki, Anal. Chim. Acta, 119 (1980) 271.
[17] Y. Hu, Y. Zhang and G.S. Wilson, Anal. Chim. Acta, 281 (1993) 503.
[18] N. Ito, T. Matsumoto, H. Fujiwara, Y. Matsumoto, S. Kayashima, T. Arai, M. Kikuchi and I. Karube, Anal. Chim. Acta, 312 (1995) 323.
[19] G. Volpe, D. Moscone, D. Compagnone and G. Palleschi, Sens. Actuators, B, 24–25 (1995) 138.
[20] G. Bardelettti, F. Sechaud and P.R. Coulet, Anal. Chim. Acta, 187 (1986) 47.
[21] E. Dempsey, M.R. Smyth and J. Wang, Talanta, 40 (1993) 445.
[22] F. Palmisano, D. Centonze and P.G. Zambonin, Biosens. Bioelectron., 9 (1994) 471.
[23] G. Urban, G. Jobst, E. Aschauer, O. Tilado, P. Svasek, M. Varahram, Ch. Ritter and J. Riegebauer, J. Sens. Actuators, B, 18–19, (1994) 592.
[24] F. Mizutani, S. Yabuki and Y. Hirata, Anal. Chim. Acta, 314 (1995) 233.
[25] K. Hajizadeh, H.B. Halsall and W.R. Heineman, Talanta, 38 (1991) 37.
[26] H. Liu, J. Kong and J. Deng, Anal. Lett., 28 (1995) 563.
[27] J. Kulys, L. Wang and A. Maksimoviene, Anal. Chim. Acta, 274 (1993) 53.
[28] A.-L. Nguyen and J.H.T. Luong, Biosens. Bioelectron., 8 (1993) 421.
[29] C. Meyerhoff, F. Bischof, F.J. Mennel, F. Sternberg, J. Bican and E.F. Pfiffer, Biosens. Bioelectron., 8 (1993) 409.

[30] D.A. Baker and D.A. Gough, Anal. Chem., 67 (1995) 1536.
[31] I. Takatsu and T. Moriizumi, Sens. Actuators, 11 (1987) 309.
[32] M. Koudelka-Hep, D.J. Strike and N.F. deRooij, Anal. Chim. Acta, 281 (1993) 461.
[33] V.V. Cosofret, M. Erdosy, T.A. Johnson, R.B. Ash, M.R. Neuman, and R.P. Buck, Anal. Chem., 67 (1995) 1647.
[34] W. Blum and G.B. Hogaboom, in Principles of Electroplating and Electroforming, 3rd edn., McGraw-Hill, NY, 1949, p. 382.
[35] A.G. Kleber and C.B. Reigger, J. Physiol., 385 (1987) 307.
[36] G. Palleschi, M.H. Faridnia, G.J. Lubrano and G.G. Guilbault, Anal Chim. Acta, 245 (1991) 151.
[37] S.F. White, A.P.F. Turner, U. Bilitewski, R.D. Schmid and J. Bradley, Anal. Chim. Acta, 295 (1994) 243.
[38] A. Mulchandani, A.S. Bassi and A. Nguyen, J. Food Sci., 60 (1995) 74.
[39] L. Yang, E. Janie, T. Huang, J. Gitzen, P.T. Kissinger, M. Vreeke and A. Heller, Anal Chem., 67 (1995) 1326.
[40] D.L. Wang and A. Heller, Anal. Chem., 65 (1993) 1069.
[41] R.J. Geise, J.M. Adams, N.J. Barone and A.M. Yacynych, Biosens. Bioelectron., 6 (1991) 151.
[42] J. Wang, Electroanalysis, 3 (1991) 255.
[43] Y. Zhang and G.S. Wilson, Anal. Chim. Acta, 281 (1993) 513.
[44] Y. Hu, K.M. Mitchell, F.N. Albahadily, E.K. Michaelis and G.S. Wilson, Brain Res., 659 (1994) 117.
[45] J.A. Delyani, G.L. David and V. Wylen, Am. J. Physiol., 266 (1994) H1019.

ELSEVIER

Talanta 44 (1997) 1543–1550

Talanta

Calibration procedure for solid phase microextraction—gas chromatographic analysis of organic vapours in air

D. Gorlo, L. Wolska, B. Zygmunt, J. Namieśnik *

Department of Analytical Chemistry, Chemical Faculty, Technical University of Gdańsk, 80-952 Gdańsk, Poland

Received 16 August 1996; received in revised form 17 October 1996; accepted 13 November 1996

Abstract

A calibration procedure for solid phase microextraction—gas chromatographic (SPME-GC) analysis of organic vapours in air was described in which GC detector (MS in this case) signal is directly related to concentration of analytes of interest sampled by SPME. Gaseous standard mixtures used for the calibration were generated by means of a home-made permeation-type apparatus described elsewhere, W. Janicki et al., Chem. Anal., 38 (1993) 423 and modified to permit easy sampling of analytes on an SPME fibre. To establish sampling parameters, times for equilibrium partitioning of five selected organic compounds (carbon tetrachloride, toluene, chlorobenzene, *p*-xylene, *n*-decane) between gaseous mixtures and the fibre (fused silica fibre coated with 100 μm polydimethylsiloxane) were determined. For 10 min sampling time, the detector response and hence amount sampled on the fibre were linear functions of analytes concentration in a gaseous sample. © 1997 Elsevier Science B.V.

Keywords: Calibration; Gas chromatography; Microextraction; Organic vapours

1. Introduction

The dominant trend in present day environmental analytics can be related to the necessity to determine an increasingly wide range of pollutants on increasingly lower concentration levels in very complex matrices [2]. Hence, isolation and preconcentration of analytes of interest are usually necessary steps of the analytical procedure. Recently, a rapidly developing technique for this purpose is solid phase microextration (SPME) [3–10]. In the technique, sampling, isolation and enrichment are incorporated into a single step and use of solvents, which can be possible environmental pollutants, is eliminated. The technique can be applied to gases and relatively pure liquids by dipping an SPME fibre directly into an analysed medium; and to solid matrices and wastewater samples with grease, oil, and high molecular mass humic acids by analyte sampling from the headspace being at equilibrium with an original sample. The possible ways of sampling from different matrices are shown in Table 1.

In the case of SPME combined with gas chromatography, the fibre (with analytes extracted from the sample into stationary phase coated on it) is introduced into an injection port of a gas chromatograph. The analytes are thermally des-

* Corresponding author.

PII S0039-9140(96)02176-5

Table 1
Sampling in the case of different matrices

Sample type	Sampling is done
Gas	By fibre exposition directly to an analyzed sample
Liquid	By fibre exposition directly to a liquid sample
	From a gaseous phase being at equilibrium with an original sample
Solid	From a gaseous phase at equilibrium with an analyzed solid sample
	From a liquid extract

orbed from the fibre and transferred by a carrier gas into a GC column for separation and then to a detector for quantitation.

However, SPME is an equilibrium method and analytical methodologies based on it require calibration. It seems that the most reliable calibration approach would be to subject standard gaseous mixtures of precisely and accurately known analyte concentration to the complete analytical procedure (starting from sampling to final analysis) identical to the procedure for a real sample.

Standard gascous mixtures used for calibration as well as for studies on isolation and enrichment of trace analytes from gases in the above approach should satisfy the following requirements [11–13]:

- concentration of an analyte of interest should be constant for a required period of time;
- concentration should be known with an accuracy much better than the accuracy of a calibrated instrument or method;
- mixtures should be available in quantities sufficient to perform planned studies;
- analyte concentration can preferably be calculated from such basic quantities as mass, temperature, pressure, etc.

For environmental analytics in general and for these studies in particular (mixtures of very low analyte concentration: ppm, ppb, ppt levels required), dynamic methods based on permeation of vapours of volatile organic compounds through membranes (mainly PTFE, polyethylene and silicone rubber) into a stream of diluting gas seem the most adequate. In such methods very low analyte concentrations can be obtained. These concentrations can be varied within a wide range by changing such parameters as membrane thickness and area, flow rate of diluting gas and temperature of a permeation vessel. The dynamic permeation methods has been extensively studied and used, among them the apparatus designed in our laboratory [1,14,15].

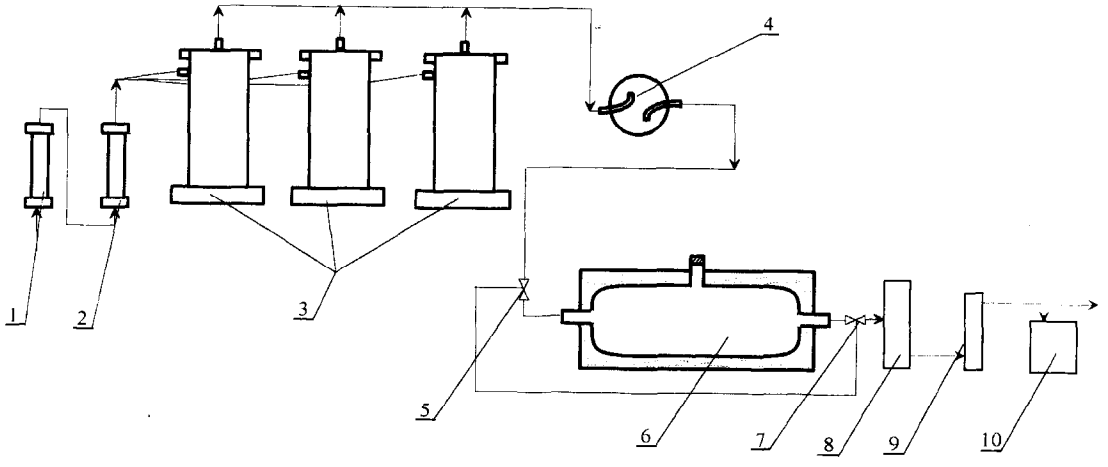

Fig. 1. The apparatus for generation of gaseous standard mixtures; 1- purifier, 2-drier, 3-generators, 4-preliminary mixing chamber, 5-teflon 3-way valve, 6-thermostated mixing glass chamber, 7-glass 3-way valve, 8-flowmeter, 9-rotameter, and 10-suction pump.

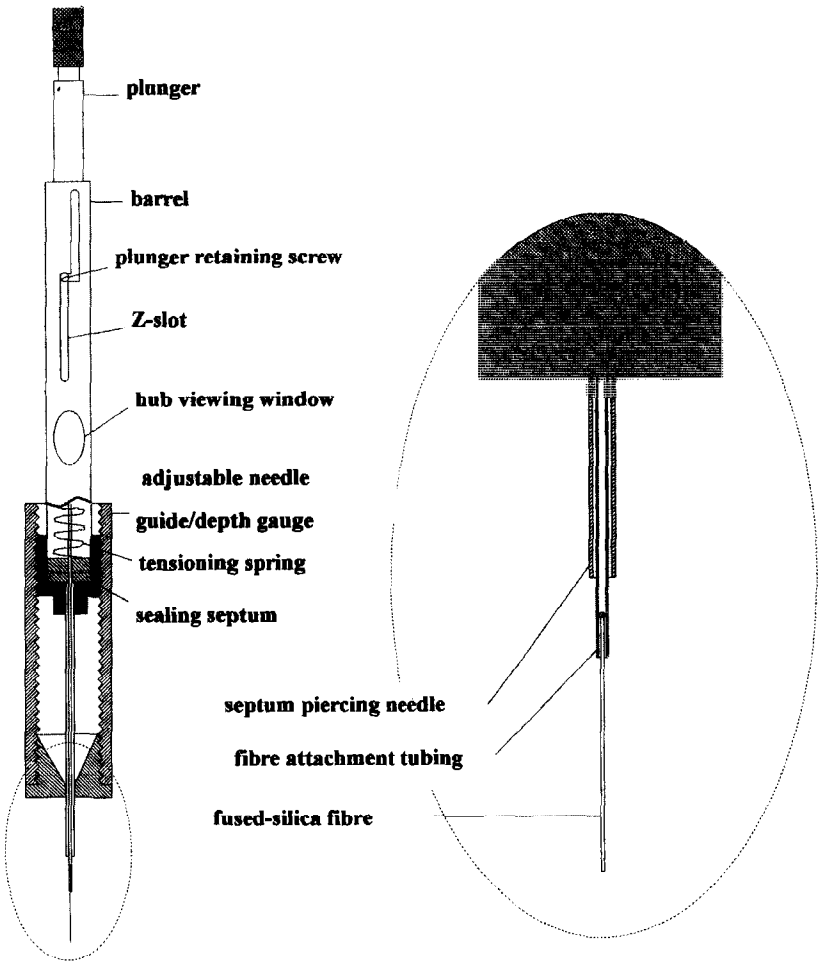

Fig. 2. SPME apparatus for manual sorption and injection [20].

The aim of this work was to develop a reliable method of SPME-GC-MS system calibration (output signal as a function of analyte concentration in gaseous sample) which can be used in analysis of different air samples (atmospheric, indoor and workplace air) for organic vapours. For the purpose we used the apparatus for permeative generation of standard gaseous mixtures described elsewhere [1] and modified to enable reproducible sampling of organic vapours present in the gaseous mixtures on an SPME fibre.

2. Experimental

2.1. Reagents and materials

n-Decane (pure) were from Merck, Germany, and carbon tetrachloride, chlorobenzene, toluene and *p*-xylene (all reagent grade) were from Polskie Odczynniki Chemiczne, Gliwice, Poland. PTFE foils of 50, 120 and 220 μm thickness (from Du Pont, USA) were used for the preparation of permeation membranes.

Table 2
Concentrations of organic compounds of interest in gaseous standard mixtures (purified air as a diluting gas)

Compound analyzed	Analyte concentration (mg m^{-3}) for different flow rates of diluting gas			
	25 cm^3 min^{-1}	50 cm^3 min^{-1}	100 cm^3 min^{-1}	150 cm^3 min^{-1}
Carbon tetrachloride	23.45	11.73	5.86	3.91
Toluene	2.33	1.17	0.58	0.39
Chlorobenzene	16.84	8.42	4.21	2.81
p-Xylene	1.22	0.61	0.3	0.2
n-Decane	0.75	0.38	0.19	0.13

2.2. Apparatus

The apparatus for the dynamic generation of gaseous standard mixtures with stop flow facility for sampling is given in Fig. 1. It consists of three generators (3) [1]. In each generator two or three permeation vessels are placed [1,16–19]. They are filled with liquid analytes of interest (carbon tetrachloride, toluene, chlorobenzene, *p*-xylene, *n*-decane). Diluting gas (atmospheric air purified from organic compounds) (1) is sucked by a suction pump (10) through purifier (1), drier (2) and generators (3) containing permeation vessels kept at a temperature of 28 ± 0.1°C. The stream of the gaseous mixture formed was then passed through a preliminary mixing chamber (4), Teflon 3-way valve (5), thermostated mixing glass chamber (6), glass 3-way valve (7), flowmeter (8) used for an accurate measurement of gaseous mixture flow rate and rotameter (9) with which flow rate is controlled. Mixing chamber (6) is equipped with a septum through which a needle of a SPME device can be inserted. During exposition the mixture flow through chamber (6) is stopped (the gas mixture by-passes the chamber).

GC-MS analysis was carried out with a Fisons GC-8000 gas chromatograph coupled with a Fisons MD-800 quadrupole mass spectrometer.

For SPME extraction an SPME holder for manual injection (SUPELCO, Bellefonte, PA, USA) with a 100 μm polydimethylsiloxane-coated fused-silica fibre (SUPELCO, Bellefonte, PA, USA) was used (Fig. 2) [20].

2.3. Calibration of permeation vessels

Permeation rates were determined by measuring vessel mass decrease (weighing) in a given time (1–30 days). When permeation rates became constant, permeation vessels were ready to use, and the concentration of a given analyte in a gaseous mixture was calculated from the permeation rate and diluting gas flow rate [1,19]. The concentrations of analytes in standard mixtures used in the studies are given in Table 2.

2.4. Analyte extraction (a) and injection into a gas chromatographic column (b)

(a) The membrane of the mixing chamber (Fig. 1) is pierced with an SPME syringe needle, the fibre is pushed out from the needle and exposed to a standard mixture for a given time and then withdrawn into the needle, whose tip is immediately closed by piercing it into a silicone septum to prevent the analytes from desorption.

Table 3
Parameters of fibre exposition

Exposition parameters	
Stationary phase	Polydimethylsiloxane
Thickness of stationary phase film	100 μm
Exposition temperature	25 ± 0.2°C
Mixture relative humidity	Dry air
Exposition time	0.5, 1, 2, 3, 10, 20 min
Flow rate of diluting gas (purified and dried air)	25, 50, 100, 150 cm^3 min^{-1}
Analyte concentration	as given in Table 2

Table 4
GC-MS parameters

Injection port	Splitless, (liner 1.2 mm I.D.)
Injector temperature	250°C
Desorption time	60 s
Analytical column	DB 5 MS 30 m × 0.32 mm I.D. 0.25 μm d_f (RESTEC, Bellefonte, USA)
Temperature program	30°C–2 min–5°C min^{-1} 50°C–15°C min^{-1} 230°C–10 min
Type of MS	SCAN
Ions for quantitation	Carbon tetrachloride 117, toluene 91, chlorobenzene 112, *p*-xylene 91, *n*-decane TIC
Ionisation	electron impact (70 eV)

(b) The device needle is quickly introduced into a splitless injector of a gas chromatograph, the fibre extended from the syringe for 20 s. At this time the analytes are desorbed and transferred into a GC column by carrier gas (parameters given in Table 3 and Table 4).

2.5. GC and MS parameters

The parameters of GC-MS are given in Table 4.

3. Results and discussion

Constancy of analyte concentration (after preconditioning) in gaseous standard mixtures, which is a basic requirement of the calibration method proposed, has been confirmed earlier [1]. Application of a mixing chamber of a special design makes SPME fibre exposition to a standard mixture simple and easy. Development of a calibration method requires the determination of minimum time necessary for equilibrium partitioning of analytes between a gaseous mixture and a fibre. For this purpose, the fibre was exposed to standard mixtures for different periods (0.5; 1.0; 2.0; 3.0; 5.0; 10 and 20 min). The fibre was exposed in the gaseous mixture at a temperature of 25 ± 0.2°C. Sorbed analytes were injected into a GC column and peak areas measured. It was found earlier that the injection parameters used (Table 4) ensure complete desorption of analytes from the fibre. In Fig. 3 plots of peak areas versus exposition time for different analytes concentrations are given. Each point is an average of five parallel measurements. For carbon tetrachloride, toluene, chlorobenzene, *p*-xylene and *n*-decane equilibration time ranges from 1.0 to 5.0 min (Table 5). The equilibration is relatively fast, and this step would extend the total time of an analytical procedure only slightly. A 10 min extraction time was selected for further experiments. For sampling at lower temperatures, e.g., outdoor air sampling on cold days, slightly longer extraction can be needed.

In the successive step, the relationship between SPME-GC-MS response and analyte concentration in the gaseous mixture (calibration curves) was studied. For each concentration five independent measurements were made.

The relatively high correlation coefficients (r) for linear regression ranging from 0.988 to 0.999 (Table 6) show that, in the examined concentration range, calibration curves can be assumed linear with high reliability. An example of a calibration curve is given in Fig. 4. Linearity of calibration curves, i.e., independence of partition coefficients on concentration, simplifies the analytical procedure. This was found for a fibre exposition temperature of 25°C, but should also be valid for other temperatures normally used during air sampling for organics.

However, partition coefficients (Kg) between the fibre coating and the gaseous phase are temperature dependent, which was quantitatively described for a number of organic compounds by Arthur et al. [8]. Therefore, the temperature of fibre extraction from the standard mixture (for calibration purposes) should be every time adjusted to a temperature of real sample extraction. Such an approach seems simpler and more accurate than the correction based on previously determined temperature variability of Kg. With the apparatus proposed this is easily done simply by changing the temperature of mixing chamber (6).

Humidity can affect sorption of organic compounds on the fibre but to small extent. As shown by Chai and Pawliszyn [10], the relative humidity reduces the amounts extracted at room temperature by less than 10% at up to 75%. The small

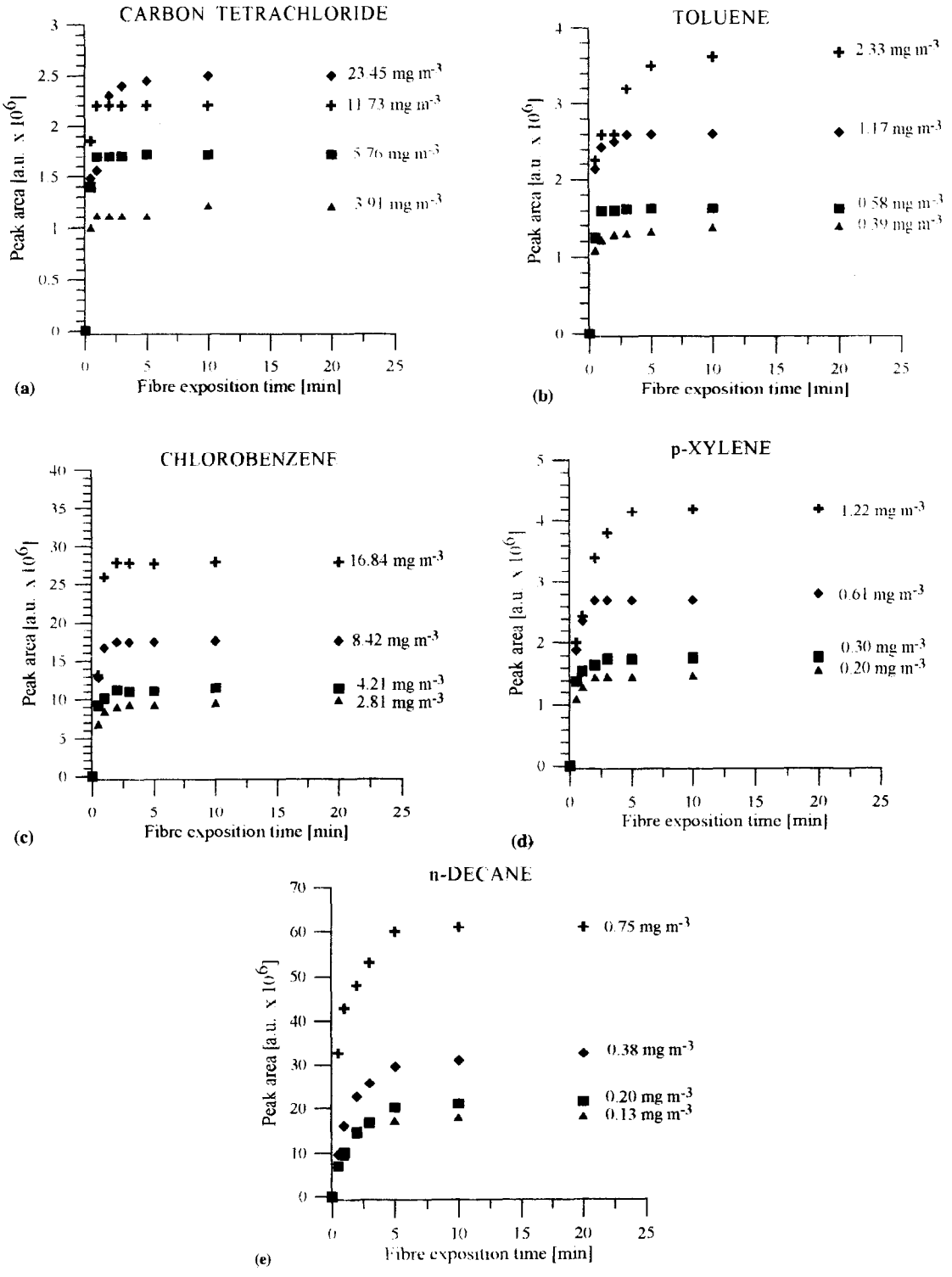

Fig. 3. Plots of GC-MS response (peak area in arbitrary units-a.u.) versus SPME fibre exposition time for different analyte concentrations in gaseous standard mixtures: (a) carbon tetrachloride; (b) toluene; (c) chlorobenzene; (d) *p*-xylene; and (e) *n*-decane.

Table 5
SPME equilibrium times for different organic compounds in gaseous mixture

Compound	Equilibration time [min] (concentration [mg m^{-3}])			
Carbon tetrachloride	1.0 (3.91)	1.0 (5.86)	1.0 (11.73)	2.5 (23.45)
Toluene	1.0 (0.39)	1.0 (0.58)	1.5 (1.17)	5.0 (2.33)
Chlorobenzene	1.5 (2.81)	1.5 (4.21)	1.5 (8.42)	1.5 (16.84)
p-Xylene	2.0 (0.20)	2.0 (0.30)	2.0 (0.61)	4.5 (1.22)
n-Decane	2.5 (0.13)	3.0 (0.20)	4.5 (0.38)	4.5 (0.75)

Table 6
Characteristies of calibration curves

Compound	*a* [a.u.]	S_a [a.u.]	*b* [a.u. mg^{-1} m^3]	S_b [a.u. mg^{-1} m^3]	Correlation coefficient *r*	Concentration range [mg m^{-3}]
Carbon tetrachloride	73×10^4	7.3×10^4	7.7×10^4	0.53×10^4	0.995	3.91 ÷ 23.45
Toluene	1.0×10^6	0.17×10^6	1.2×10^6	0.13×10^6	0.988	0.39 ÷ 2.33
Chlorobenzene	6.1×10^6	0.29×10^6	1.31×10^6	0.029×10^6	0.999	2.81 ÷ 16.84
p-Xylene	1.0×10^6	0.11×10^6	2.6×10^6	0.16×10^6	0.996	0.20 ÷ 1.22
n-Decane	0.3×10^7	5.2×10^7	8×10^7	1.2×10^7	0.980	0.13 ÷ 0.75

Each calibration curve consists of four calibration points and each point is an average of five measurements.
$y = bx + a$ (y—peak area in arbitrary unit (a.u.), x—analyte concentration in mg m^{-3}).

difference in humidity between a gaseous calibration mixture and an air sample analysed would influence the results but only slightly. The effect of humidity is nearly constant for the relative humidity range of 25–75%, which covers majority of indoor, outdoor and workplace air cases. Maintaining the humidity of standard gaseous mixtures within this range is relatively easy with the apparatus proposed.

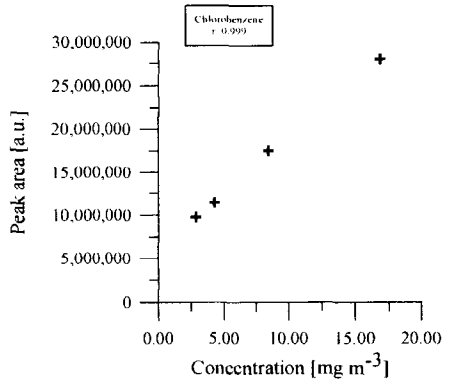

Fig. 4. The plot of SPME-GC-MS response versus concentration of chlorobenzene in a gaseous standard mixture.

4. Conclusions

The apparatus for the generation of standard gaseous mixtures with mixing and sampling chambers gives a mixture of uniform concentration and enables easy exposition of an SPME fibre to the mixture. Since the concentration can be easily controlled and calculated the easy and reliable calibration of SPME-GC system versus analyte concentration in gaseous sample is feasible.

The described calibration procedure should make the SPME technique a versatile, convenient and reliable tool for the determination of organic pollutants in various types of gaseous samples, such as indoor, atmospheric and workplace air. The determination would consist of two series of SPME-GC measurements: one for the sample studied and one for the standard mixture.

The analysis of the above types of samples using the SPME combined with the proposed method of calibration is relatively short and of

relatively low costs, since use of very pure solvents is eliminated, which is also important from environmental protection viewpoint.

Acknowledgements

This work has been financed by statutory funds of the Technical University of Gdañsk.

References

[1] W. Janicki, L. Wolska, T. Górecki and J. Namieśnik, Chem. Anal., 38 (1993) 423.
[2] J. Namieśnik, M. Biziuk, W. Chrzanowski, W. Wardencki and B. Zygmunt, Chem. Anal., 40 (1995) 115.
[3] C.L. Arthur and J. Pawliszyn, Anal. Chem., 62 (1990) 45.
[4] D. Louch, S. Motlagh and J. Pawliszyn, Anal. Chem., 64 (1992) 1187.
[5] C.L. Arthur, M. Chai and J. Pawliszyn, J. Microcol. Sep., 5 (1993) 1.
[6] C.L. Arthur, L.M. Killam, S. Motlagh, M. Lim, D.W. Potter and J. Pawliszyn, Environ. Sci. Technol., 26 (1992) 979.
[7] D.W. Potter and J. Pawliszyn, J. Chromatogr., 625 (1992) 247.
[8] C.L. Arthur, L.M. Killam, K.D. Bucholz and J. Pawliszyn, Anal. Chem., 64 (1992) 1960.
[9] Z. Zhang and J. Pawliszyn, Anal. Chem., 65 (1993) 1843.
[10] M. Chai and J. Pawliszyn, Environ. Sci. Technol., 29 (1995) 693.
[11] J. Namieśnik, Zeszyty Naukowe Politechniki Gdańskiej Nr 396, Chemia Zeszyt nr XXVIII, Gdańsk 1985.
[12] J. Namieśnik, J. Chromatogr., 300 (1984) 79.
[13] J.J. McKinley, Instrum. Technol., June 1974, 45.
[14] A.E. O'Keefe and G.C. Ortman, Anal. Chem., 38 (1966) 760.
[15] D.P. Lucero, Anal. Chem., 43 (1972) 1744.
[16] J.S.-Y. Ho, PH. A. Schlecht and P.C. Schlecht, Am. Ind. Hyg. Assoc. J., 42 (1981) 70.
[17] J.L. Perkins and A.D. Tippit, Am. Ind. Assoc. J., 46 (1985) 455.
[18] J. Namieśnik, L. Torres, E. Kozłowski and J. Mathieu, J. Chromatogr., 39 (1989) 281.
[19] J. Namieśnik, Chromatographia, 17 (1983) 47.
[20] Z. Zhang, M.J. Yang and J. Pawliszyn, Anal. Chem., 66 (1994) 844.

ELSEVIER

Talanta 44 (1997) 1551–1561

Talanta

Utilization of standards generated in the process of thermal decomposition chemically modified silica gel for a single point calibration of a GC/FID system

M. Prokopowicz [a], E. Luboch [a], J. Namieśnik [a,*], J.F. Biernat [a], A. Przyjazny [b]

[a] *Chemistry Faculty, Technical University of Gdańsk, 80-952 Gdańsk, Poland*
[b] *GMI Engineering and Management Institute, 1700 W. Third Ave., Flint, MI 48504, USA*

Received 16 August 1996; received in revised form 21 October 1996; accepted 21 October 1996

Abstract

The utilization of a multicomponent gaseous standard mixture, containing CO and CO_2 and obtained by thermal decomposition of a so-called immobilized compound, for a single point calibration of a GC/FID system are described. The generation of such a mixture takes place as a result of thermal decomposition of a sample of chemically modified silica gel placed in a heated chamber of thermal desorber coupled with the device being calibrated via a catalytic methanizer. The mean amount of the analyte librated from unit mass of the gel was 0.71 mg g^{-1} (RSD = 3%) for carbon monoxide and 0.86 mg g^{-1} (RSD = 3%) for carbon dioxide. © 1997 Elsevier Science B.V.

Keywords: Calibration; Carbon dioxide; Carbon monoxide; Modified silica gel; Standard gas mixtures

1. Introduction

Outdoor and indoor air, water, soil, food and the workplace atmosphere are polluted by an enormous number of toxic chemicals. In some cases, these hazardous chemicals cannot be detected by our senses, such as smell or sight. So far, Chemical Abstracts list about 13 million anthropogenic compounds. Of those, at least 100 000 are commonly used in various areas of life and technology, over 10 000 are considered to be especially hazardous, and about 200 are considered to be carcinogenic [1]. Separation, identification and determination of such a large number of compounds constitutes a difficult analytical problem, particularly if the analytes are volatile, unstable, toxic or malodorous.

Every analytical process consists of a number of steps, including sampling, sample storage and workup, calibration and final determination. Each of these steps is prone to errors, whose main sources are [2–4]:

- sample contamination,
- losses of analytes resulting from analyte evaporation or adsorption on the surface of a container,
- chemical reactions taking place in a sample,

* Corresponding author.

PII S0039-9140(96)02177-7

Table 1
Summary of studies on the method of preparation of gaseous standard mixtures by thermal decomposition of immobilized compounds

Type of immobilized compound	Volatile compound generated	Detector calibrated	Amount released per unit mass of gel [mg/g gel]	Reference
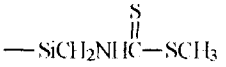	CH_3SH	FID	13.2	18
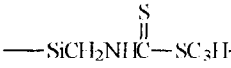	C_3H_7SH	FID, FPD	17.4*, 15.5*	18
	$CH_2{=}CHCH_2NCS$	FID	5.2	19
	C_4H_9NCS	FID	6.5	19
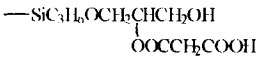	CO_2	NDIR	41	20
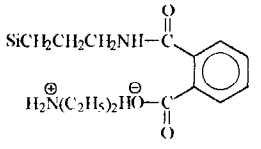	$NH(C_2H_5)_2$	NPD	3.1	21
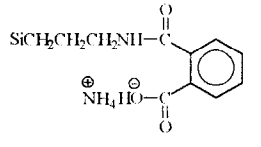	NH_3	Photometric detector (following absorption of the analyte)	1.2	21
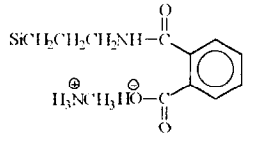	NH_2CH_3	Photometric detector (following absorption of the analyte)	1.6	21
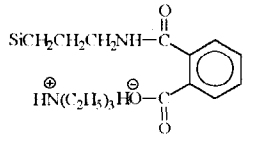	$N(C_2H_5)_3$	Photometric detector (following absorption of the analyte)	4.0	21

* results obtained for two different batches of silica gel

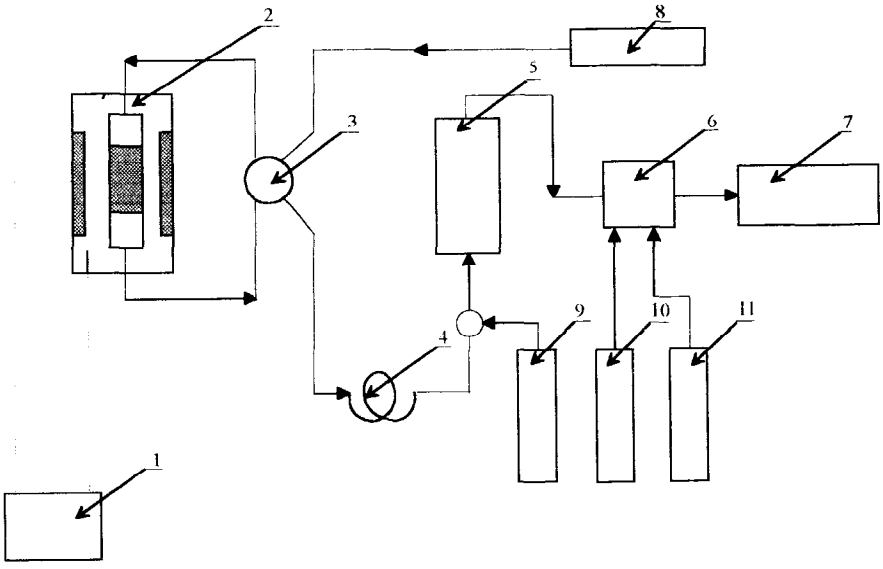

Fig. 1. Schematic diagram of the apparatus: 1—temperature controller, 2—desorber furnace, 3—six-port valve, 4—GC column, 5—methanizer, 6—FID, 7—recorder, 8—tank with carrier gas (nitrogen), 9—hydrogen tank, 10—hydrogen tank, 11—air tank.

- interference among trace components or with a matrix,
- erroneous measurements (biased), improper calibration associated with unacceptable extrapolation and/or improper or unstable standards.

In order to reduce or eliminate these errors, new reliable analytical procedures with an increasingly greater accuracy and precision are being sought. One vital step of these procedures is calibration of measuring devices, i.e., determination of the relationship between the output signal and the quantity being determined. The method of calibration depends on a number of factors, including [5,6]:

- type of a measuring device,
- number of samples to be analyzed,
- possibility of preparation of a wide range of concentrations of standards to check an entire measurement range,
- required accuracy of determination,
- degree of matrix complexity of the analyzed sample.

In the analysis of gaseous environmental pollutants, gaseous standard mixtures play a very important role in the calibration of gas analyzers. A number of methods of generation of these mixtures have been described both in original papers [3,7–15] and in reviews [16–19].

Calibration of analytical measuring devices can be accomplished in practice in two ways:

- by checking the entire measuring range (including zero point) using a set of gaseous standard mixtures with varying concentrations of the analyte, including a so-called zero gas and, sometimes, also a pure analyte;
- by verifying the reliability of an analytical device through checking its response at only one point within the measuring range (a so-called single point calibration).

The use of thermal decomposition of so-called immobilized compounds, chemically bonded to the surface of silica gel, is a new approach to the problem of preparation of gaseous standard mixtures [20–25]. In order to change physico-chemical properties of the surface of silica gel, it can be modified through the reaction of active sites (the -OH groups on the gel surface) with modifiers. This procedure is commonly used for the preparation of silica gel for liquid chromatography applications [26]. The group bonded to the gel surface can in turn become a reactant

for subsequent reactions. Using suitable sequences of such reactions, almost any functional group can be immobilized on the surface of silica gel [27]. Silica gel can be modified with a variety of inorganic compounds. Such a modification results in the coverage of the gel surface with mono- or multimolecular layers of, e.g.: Al_2O_3, Fe_2O_3, Cr_2O_3, B_2O_3, TiO_2, etc., [28]. Among commonly used organic reagents, one should mention amines (resulting in the formation of the Si–NR bonds), alcohols (resulting in the formation of the Si–OR bonds), and alkyl derivatives (resulting in the formation of the Si–C bonds). The most stable of the above bonds are Si–C; consequently, this kind of modification of the silica gel surface is most commonly used as the first step in a series of reactions of immobilized groups. Alkyl- or arylchlorosilanes and alkoxyalkyl- or alkoxyarylsilanes are used most frequently to form the Si–C bonds. A specific chemical compound bonded to the silica gel surface (and called an immobilized compound) then undergoes chemical rearrangement at an appropriate temperature, yielding gaseous analytes which combine with a stream of carrier gas generating a gaseous standard mixture. The major factors influencing the composition of standard mixtures are the method of modification of the gel surface, the carrier (diluent) gas flow rate, the bed temperature, the mass of modified gel and the time of the decomposition process. Evident advantages of this method of preparation of gaseous standard mixtures include:

- high stability of modified gels at room temperature as a result of significantly higher temperatures of liberation of analytes, which facilitates the storage of batches of modified gels without the danger of slow decomposition of the immobilized compound resulting in an increased background;
- the possibility of preparation of a standard mixture immediately before calibration of an analytical instrument, thus reducing memory effects associated with adsorption of the analytes on the inside walls of an experimental setup;
- suitability for the generation of standard mixtures containing unstable, toxic or malodorous compounds.

In addition to the above advantages, this approach to generation of gaseous standard mixtures has some inconveniences, the most important of which is the variability of analyte concentration in the diluent gas at the outlet of the tube with the modified silica gel. However, similarly to the classical exponential dilution method, this concentration can be calculated at any moment since the beginning of thermal decomposition [19].

Table 1 lists the methods of preparation of gaseous standard mixtures by thermal decomposition of chemically modified silica gel that have been developed thus, far.

The present paper describes the results of investigations of the possibility of utilization of thermal decomposition of samples of chemically modified silica gel for the generation of a multicomponent gaseous standard mixture which can be used for the single point calibration of chromatographic detectors. Substituted alkoxyalkylsilanes were used for chemical modification of

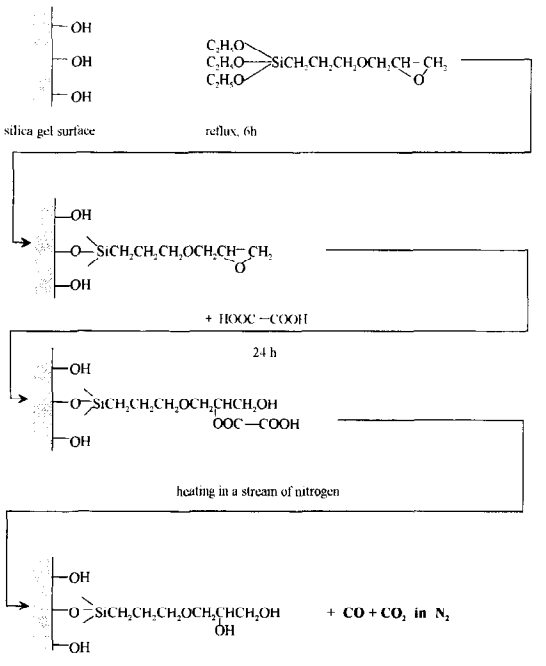

Fig. 2. Scheme of synthesis of a compound chemically bonded to the silica gel surface and its thermal decomposition.

Table 2
Results of determinations of the amount of methane in the primary standard mixture after methanization of carbon dioxide, obtained during preliminary studies of the output of an FID

No.	Volume of gaseous mixture injected [μl]	Peak area for methane (arbitrary units)	Amount of CO_2 [mg]	Equivalent amount of CH_4 [mmol]
1	50	107175	8.20×10^{-4}	1.86×10^{-5}
2	100	214967	1.64×10^{-3}	3.73×10^{-5}
3	200	432167	3.28×10^{-3}	7.45×10^{-5}
4	400	856133	6.56×10^{-3}	1.49×10^{-4}
5	700	1494667	1.15×10^{-2}	2.61×10^{-4}
6	1000	2073000	1.64×10^{-2}	3.73×10^{-4}

silica gel. Samples of the modified gel were then placed in a sorption tube and inserted into a thermal desorber connected on-line with the analytical device being calibrated (the detector), and the calibration of the detector output at a certain point of its measuring range was carried out in this way. In this work, thermal decomposition of the immobilized compounds yielding carbon monoxide and carbon dioxide was used to generate a multicomponent gaseous mixture. Utilization of the process of methanization of the two components (following their separation on a gas chromatographic column) results in the formation of two different amounts of methane in one cycle, which can be used to calibrate a flame-ionization detector, a common measuring device in a number of analyzers and monitors of gaseous mixtures.

2. Experimental

2.1. Apparatus

An HP 5830 A gas chromatograph equipped with a cold on—column, splitless injector, an FID detector ($T = 150$°C), and a methanizer ($T = 400$°C, catalyst—Raney nickel supported on silica gel) were used in the investigations. The process of catalytic methanization was carried out in a stream of nitrogen (carrier gas) with an addition of hydrogen (10 ml min^{-1}). A batch of the nickel catalyst was prepared according to the literature [29]. Separations were performed in a 100 × 0.3 cm column packed with Porapak Q, 80–100 mesh, (Hewlett Packard). The column temperature was 25°C. The carrier gas (nitrogen) flow rate was 20 ml min^{-1}. The gas chromatograph was coupled with a purpose-designed tube furnace in which a tube with the modified silica gel was placed. The tube (100 × 3.5 mm) was previously silanized (to minimize the wall-analyte interactions) using the following conditions [30]: silanizing mixture—hexamethyldisilazane: trimethylchlorosilane (5:1); time of silanization: 48 h; silanization temperature: 150°C. The apparatus used in the investigations is shown in Fig. 1.

2.2. Reagents

Silica gel (MN-Kiesegel 60, 35–70 mesh; specific surface area 200 m^2 g^{-1}; Macherey, Nagel, Germany) was modified using the following procedure: a solution of 2 ml of γ-glycidoxypropyltriethoxysilane in 30 ml of dried toluene was added to 20 g of silica gel dried at 120°C. The obtained mixture was refluxed for 6 h. The product was filtered, washed successively with toluene, acetone, and diethyl ether, and then suspended in a solution of 1.8 g of oxalic acid in 25 ml of diethyl ether. After 24 h the obtained product was filtered, washed with water and methanol, and dried. Fig. 2 shows chemical reactions used in the modification of silica gel.

2.3. Calibration of the GC/FID system

Prior to the investigation proper, the measuring device to be standardized (FID) was cali-

Table 3
Statistical evaluation of the obtained results using linear regression

Analyte determined	Slope of the line a	Intercept of the line b	Standard deviation of the slope S_a	Standard deviation of the intercept S_b	Correlation coefficient R
CH_4 (following methanization of CO_2)	5.59×10^9	13975	1236	0.24	0.99

brated by using a so-called primary gas standard mixture which was prepared in the laboratory by a volumetric method. To a conical flask of an exactly known volume (608 ml), which was previously purged with pure nitrogen and closed tightly, 5.2 ml of pure carbon dioxide was added using a gas-tight syringe, followed by 15 ml of nitrogen (to obtain overpressure). The primary standard mixture prepared in this manner contained 623 ml of nitrogen and 5.2 ml of CO_2 (10.296 mg). Calibration of the detector was carried out by a direct injection of a volume of the primary standard onto a GC column. After the separation and methanization of CO_2, a GC detector signal originating from methane was acquired. The amount of methane is directly proportional and equimolar to the amount of carbon dioxide in the primary standard mixture. It is not necessary to prepare a primary standard mixture for carbon monoxide, because the FID signal resulting from methane can be converted to the amount of carbon monoxide considering the fact that 1 mol of CO is also equivalent to 1 mol of methane. The results of calibration of an FID detector are compiled in Table 2.

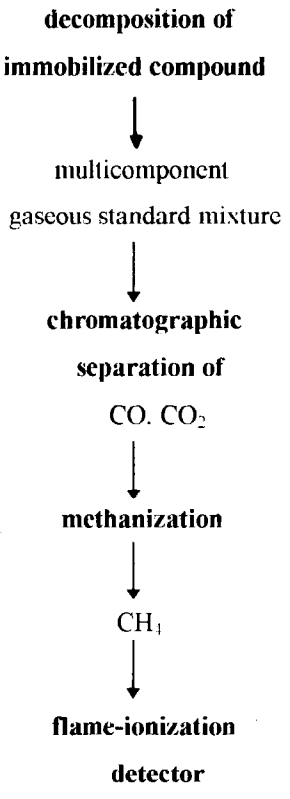

Fig. 3. Procedure used for the calibration of a flame-ionization detector employing two different amounts of methane in a single point calibration system.

Using the least-squares method, the relationship ($y = ax + b$) between a measured quantity y (the peak area) and the amount of methane x (mmol) was determined from the measurements carried out for a series of standards (Table 3).

2.4. Single point calibration of the GC/FID system utilizing the decomposition of immobilized compounds

A single point calibration of the GC/FID system was carried out by using methane formed from a standard mixture consisting of two volatile components: carbon monoxide and carbon dioxide generated in the process of thermal decomposition of the immobilized compound chemically bonded to the silica gel surface. The following procedure was used: a tube containing a weighed sample of chemically modified silica gel ($\pm$ 0.00001 g) was placed in desorber furnace (Fig. 1). Airtight connection was ensured by using PTFE washers. The tube was purged for 1

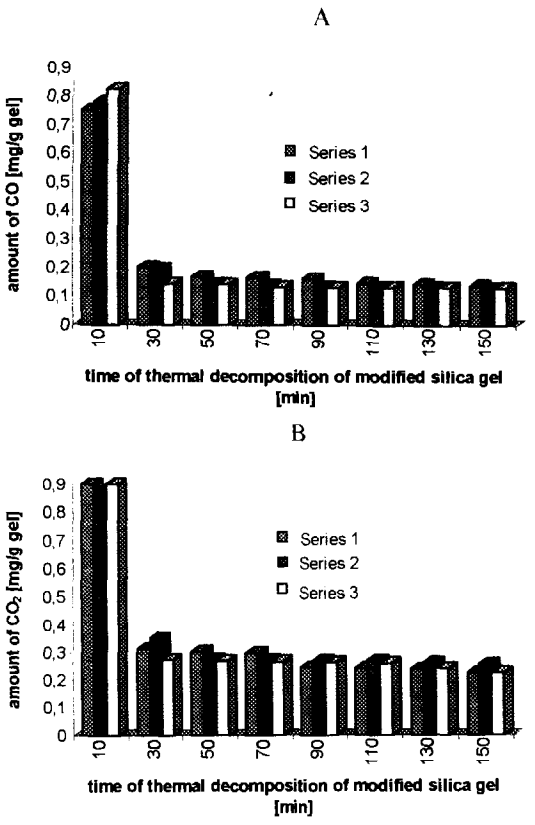

Fig. 4. Results of determination of the amounts of analytes liberated in the process of thermal decomposition of samples of modified silica gel (per unit mass of gel). Mass of silica gel: 1st series = 0.00797 g; 2nd series = 0.01302 g; 3rd series = 0.01247 g. A—determination of methane equivalent to the amount of liberated carbon monoxide. B—determination of methane equivalent to the amount of liberated carbon dioxide.

min at ambient temperature with a stream of carrier gas (nitrogen at 20 ml min^{-1}) to remove any air. Next, the furnace was heated electrically to a temperature of 300°C ($\pm$ 1°C), at which thermal decomposition of the silica gel sample was taking place. The conditions of thermal decomposition of the immobilized compound (temperature, time, and the diluent gas flow rate) have been previously determined using the same batch of chemically modified silica gel and were published elsewhere [22]. The time of thermal decomposition was measured from the moment of reaching by the bed the preset temperature. The measurements were performed by switching the position of a six-port valve, which caused the resulting standard mixture to be swept in a stream of carrier gas to the head of a GC column. Following the GC separation, the analytes (CO, CO_2) were passed in a stream of carrier gas (nitrogen) to a methanizer, where they were catalytically reduced in the presence of hydrogen to methane. After GC detection, a chromatogram was obtained which contained two peaks corresponding to methane, whose surface areas were directly proportional to the amounts of liberated analytes (1 mol of CO and 1 mol of CO_2 correspond to 1 mol of methane). A schematic diagram of the above procedure is shown in Fig. 3.

The described methodology of generation of more than one component, measured during thermal decomposition of a suitable immobilized compound followed by methanization of the analytes after their GC separation allows the use of single point calibration to check the readout of an analytical device simultaneously at two points within its measuring range.

Initially, the kinetics of thermal decomposition of chemically modified silica gel was examined, and the total amounts of the components generated as a result of this process (CO and CO_2) were determined. The total time of thermal decomposition of the immobilized compound at 300°C was 150 min; the first measurement was taken after 10 min from the initiation of the process, the next ones—every 20 min using the procedure described above. The measurements were carried out using three weighed samples of the same batch of chemically modified silica gel (with masses equal to 0.00797, 0.01302, and 0.01247 g, respectively). Fig. 4 (A, B, C) illustrates the course of thermal decomposition for each sample of the modified silica gel while the results of chromatographic determinations of total amounts of the liberated analytes (following their methanization) are listed in Table 4 and Table 5.

Subsequently, the amounts of analytes generated at a specific moment of thermal decomposition of the immobilized compound were determined. This will be of particular significance

Table 4
Results of determinations of total amounts of compounds liberated from the surface of chemically modified silica gel during its thermal decomposition ($T = 300°C$, $t = 150$ min)

Mass of gel sample [g]	0.0797		0.01302		0.01247	
Analyte	CO	CO_2	CO	CO_2	CO	CO_2
Total amount of the analte 10^{-4} [mmol]	5.71	4.73	8.64	8.04	8.46	7.43
Amount of the analyte per unit mass of gel [mg g^{-1} gel]	2.01	2.61	1.86	2.72	1.82	2.62
Percentage of the analyte in the mixture [%]	47.4	52.6	45.2	54.8	45.4	54.6

The compounds were determined in the form of equivalent amount of methane.

when using thermal decomposition of the immobilized compound the for single point calibration of an analytical system. Taking into consideration the fact that the largest amounts of the analytes are released in the initial phase of thermal decomposition (Fig. 4), the first 10 min of thermal decomposition were selected to generate sufficient quantities of CO and CO_2 (converted to methane) to accomplish a single point calibration of a GC/FID system. The objective of this investigation was to find the dependence of amounts of the analytes liberated from unit mass of the modified gel on the total mass of the gel used and thus, to determine the degree of homogeneity of coverage of the silica gel surface by the immobilized compound. At the same time, this is a test of the developed procedure for the preparation of modified silica gel. The determination of these properties is essential if chemically modified silica gels are to be used for the generation of standard mixtures employed in the calibration of measuring devices. The procedure followed was analogous to that used in the initial studies (kinetics of thermal decomposition of modified silica gel) and the amounts of the analytes liberated at 300°C during a 10 min decomposition were determined for 25 samples (of varying masses) of the same batch of chemically modified silica gel. The results of determinations of the amounts of liberated standards are listed in Table 6 and Table 7.

3. Discussion

On the basis of statistical analysis of the results of determination of methane formed in the process of methanization of carbon dioxide in the primary standard mixture (Table 3) it was established that the correlation coefficient ($R = 0.99$) obtained for a given number of samples ($n = 6$) is not significantly different from the critical value of the correlation coefficient (1.00 for $\alpha = 0.01$ which demonstrates a linear dependence of the detector output on the amount of the analyte.

The experimentally determined average total masses of the analytes liberated in thermal de-

Table 5
Statistical evaluation of the results of determination of total amounts of the two analytes obtained during thermal decomposition of the immobilized compound (following their methanization)

Analyte (determined as methane)	Confidence limit for the average $n = 3$, $P = 95\%$ $\mu = \bar{x} \pm \frac{t \cdot s}{\sqrt{n}}$		Relative standard deviation [%]
	mg g^{-1} gel	mmol g^{-1} gel	
CO	1.9 ± 0.2	0.07 ± 0.006	10
CO_2	2.7 ± 0.1	0.06 ± 0.003	5

Table 6
Results of determinations of the amount of carbon monoxide and carbon dioxide liberated during the first 10 min of thermal decomposition of chemically modified silica gel (following their methanization)

No.	Mass of gal [g]	Amount of CO [mmol]	Amount of CO [mg g^{-1} gel]	Amount of CO_2 [mmol]	Amount of CO_2 [mg g^{-1} gel]
1	0.00707	2.13×10^{-4}	0.75	1.50×10^{-4}	0.90
2	0.00445	1.15×10^{-4}	0.72	9.30×10^{-5}	0.92
3	0.01302	3.61×10^{-4}	0.78	2.60×10^{-4}	0.87
4	0.01247	3.64×10^{-4}	0.82	2.54×10^{-4}	0.90
5	0.01423	4.00×10^{-4}	0.78	2.84×10^{-4}	0.88
6	0.02923	7.43×10^{-4}	0.71	5.60×10^{-4}	0.84
7	0.01259	3.15×10^{-4}	0.70	2.20×10^{-4}	0.76
8	0.01016	2.46×10^{-4}	0.68	1.95×10^{-4}	0.85
9	0.01602	3.96×10^{-4}	0.70	2.98×10^{-4}	0.82
10	0.01403	3.52×10^{-4}	0.70	2.64×10^{-4}	0.83
11	0.01961	4.64×10^{-4}	0.66	3.50×10^{-4}	0.79
12	0.01105	2.76×10^{-4}	0.70	2.21×10^{-4}	0.88
13	0.01893	4.57×10^{-4}	0.68	3.23×10^{-4}	0.75
14	0.01900	4.75×10^{-4}	0.70	3.66×10^{-4}	0.85
15	0.04370	1.04×10^{-3}	0.66	7.66×10^{-4}	0.77
16	0.03049	8.25×10^{-4}	0.70	6.18×10^{-4}	0.89
17	0.02454	6.54×10^{-4}	0.74	5.16×10^{-4}	0.92
18	0.10937	2.76×10^{-3}	0.71	1.93×10^{-3}	0.78
19	0.01145	2.89×10^{-4}	0.71	2.32×10^{-4}	0.90
20	0.02529	6.11×10^{-4}	0.68	4.36×10^{-4}	0.76
21	0.02144	5.46×10^{-4}	0.71	4.18×10^{-4}	0.86
22	0.00592	1.48×10^{-4}	0.70	1.34×10^{-4}	0.99
23	0.01495	3.61×10^{-4}	0.67	3.09×10^{-4}	0.91
24	0.02808	7.46×10^{-4}	0.74	$5.86 - 10^{-4}$	0.92
25	0.00751	1.88×10^{-4}	0.70	1.67×10^{-4}	0.98

composition of the immobilized compound under the following conditions ($T = 300°C$, $t = 150$ min) per unit mass of the gel are 1.9 ± 0.2 and 2.7 ± 0.1 mg g^{-1} for carbon monoxide and carbon dioxide, respectively (Table 4). Relative standard deviations of the results for a given significance level ($\alpha = 0.05$) and $n = 3$ are about 10% and less than 5% for CO and CO_2, respectively (Table 5) which indicates a good precision. Based on the mole amounts of CO and CO_2 formed, which are equal to 0.07 ± 0.006 and 0.06 ± 0.003 mmol g^{-1} of gel, respectively, it can be concluded that in accordance with the reactions taking place on the silica gel surface, i.e., decarbonylation and decarboxylation (Fig. 2), equimolar quantities of the analytes are released (the experimental error is within 1%).

The process of thermal decomposition of the immobilized compound was found to have the highest yield during the first 10 min; afterwards, the amounts of the analytes released become progressively smaller which is understandable considering the finite amount of the immobilized compound on the surface of silica gel (Fig. 4). Relative standard deviations estimated from 25 determinations of the analytes liberated during the first 10 min of thermal decomposition of chemically modified silica gel at a given significance level ($\alpha = 0.05$) are within 3% (Table 7). The results obtained indicate that the amounts of the analytes liberated from unit mass of the gel do not depend on the mass of the gel used which means that the immobilized compound is bonded homogeneously to the surface of silica gel.

Table 7
Statistical analysis of the results of determinations of the amounts of carbon monoxide and carbon dioxide liberated during the first 10 min of thermal decomposition of samples of chemically modified silica gel expressed per unit mass of gel

Analyte (determined as methane)	Confidence limits for the average $n = 25$, $P = 95\%$ $\mu = \bar{x} \pm \frac{ts}{\sqrt{n}}$		Relative standard deviation [%]
	mg g^{-1} gel	mmol g^{-1} gel	
CO	0.71 ± 0.02	0.025 ± 0.0006	3
CO_2	0.86 ± 0.03	0.020 ± 0.0006	3

4. Conclusions

On the basis of experimental results one can draw the following conclusions:

- methanization of components following their chromatographic separation results in the formation of two different amounts of methane in one measurement cycle, thus yielding two data points in a single point calibration of a flame-ionization detector;
- a gaseous standard mixture generated through thermal decomposition of the immobilized compound can be used for the calibration of analytical devices in a very wide concentration range of the analyte (methane) because the amounts of the analytes liberated are directly proportional to the amount of silica gel used and,
- consequently, the amount of the analyte can be varied by changing the amount of modified silica gel;
- batches of chemically modified silica gel can be used not only as a source of analytes—components of gaseous standard mixtures but also as a source of small amounts of given analytes.

References

[1] K. Forowicz, 'My i Środowisko' (We and the Environment), Magazyn Rzeczpospolita, 11 (1995) 7.
[2] J. Namieśnik, J. Łukasiak and Z. Jamrógiewicz, 'Pobieranie próbek środowiskowych do analizy' ('Collection of environmental samples for analysis'), PWN Warszawa 1995.
[3] R.B. Denyszyn and T. Sassaman, ASTM STP, 957 (1987) 101.
[4] R.W. Gillham and S.F. O'Hannesin, ASTM STP, 1053 (1989) 108.
[5] P.L. Bonate, LC-GC Int., 10 (1992) 50.
[6] J.H. Kalivas and J.M. Sutter, J. Chemom., 5 (1991) 37.
[7] W.J. Woodfin, Am. Ind. Hyg. Assoc. J., 45 (1984) 138.
[8] J. Szulc and Z. Witkiewicz, Chem. Anal. (Warsaw), 26 (1981) 375.
[9] O. Grosjean, K. Fung, J. Collins, J. Harrison and E. Breitung, Anal. Chem., 56 (1984) 569.
[10] W. Muniak, Z. Witkiewicz, E. Woryna, E. Kusińska, A. Twardowski and B. Goca, J. Chromatogr., 436 (1988) 323.
[11] E. Eickeler and K.E. Prescher, Environ. Intern., 14 (1988) 19.
[12] J.C. Polasek and J.A. Bullin, Environ. Sci. Technol., 12 (1978) 708.
[13] R.A. Rasmussen and J.E. Lovelock, J. Geogr. Res., 88 (1983) 8369.
[14] J. Namieśnik and P. Konieczka, Chem. Anal. (Warsaw), 36 (1991) 357.
[15] W. Janicki, L. Wolska, T. Górecki and J. Namieśnik, Chem. Anal. (Warsaw), 38 (1993) 423.
[16] J. Namieśnik, P. Konieczka, W. Chrzanowski and J.F. Biernat, Chem. Anal. (Warsaw), 39 (1994) 245.
[17] J. Namieśnik, J. Chromatogr., 300 (1984) 79.
[18] J. Namieśnik and P. Konieczka, 'Preparation of gaseous standard mixtures using autodilution', Materials of the 4th National Chromatography Conference, Lublin, September 04–08, 1989, p. P-44.
[19] P. Konieczka, 'New method of preparation of gaseous standard mixtures', PhD Thesis, Gdańsk, 1994.
[20] P. Konieczka, J. Namieśnik and J.F. Biernat, J. Chromatogr., 540 (1991) 449.
[21] P. Konieczka, E. Luboch, J. Namieśnik and J.F. Biernat, Anal. Chim. Acta, 265 (1992) 127.
[22] P. Konieczka, J. Makarewicz, E. Luboch, J. Namieśnik and J.F. Biernat, Chem. Anal. (Warsaw), 39 (1994) 179.
[23] P. Konieczka, J. Namieśnik, A. Przyjazny, E. Luboch and J.F. Biernat, Analyst, 2041 (1995) 120.

[24] P. Konieczka, M. Prokopowicz, A. Skwierawska, A. Przyjazny, J. Namieśnik and J.F. Biernat (submitted to Anal. Chem.).
[25] P. Konieczka, L. Wolska, E. Luboch, J. Namieśnik, A. Przyjazny and J.F. Biernat, J. Chromatogr., (in print).
[26] Z. Witkiewicz, J. Chromatogr., 466 (1989) 37.
[27] J.F. Biernat, P. Konieczka, B.J. Tarbet, J.S. Bradshaw and R.M. Izatt, Sep. Purif. Methods, 23 (2) (1994) 77.
[28] V.A. Kasperskii, V.V. Pavlov, V.N. Plakhetnik and C.C. Chuiko, Dopov., Akad. Nauk Ukr. SSR, Ser. B. Geol., Khim. Biol. Nauki, 39 (8) (1983) 5.
[29] F.R. Cropper, D.M. Heinekey and A. Westwell, Analyst, 92 (1967) 436.
[30] M.L. Lee and B.W. Wright, J. Chromatogr., 18 (1980) 345.

ELSEVIER

Talanta 44 (1997) 1563–1571

Talanta

Sequential injection wetting film extraction applied to the spectrophotometric determination of chromium(VI) and chromium(III) in water

Yongyi Luo, Shigenori Nakano, David A. Holman, Jaromir Ruzicka, Gary D. Christian *

Center for Process Analytical Chemistry, Department of Chemistry, Box 351700, University of Washington, Seattle, WA 98195, USA

Received 16 August 1996; received in revised form 25 October 1996; accepted 4 November 1996

Abstract

The spectrophotometric determination of Cr(VI) and Cr(III) via sequential injection was used to demonstrate the sensitivity enhancement provided by a newly developed wetting film extraction system. The reaction product of Cr(VI) with 1,5-diphenylcarbazide was ion-paired with perchlorate and extracted into an organic wetting film consisting of octanol and 4-methyl-2-pentanone on the inner wall of a Teflon tube. The wetting film, with the extracted analyte, was then eluted with 100 μl acetonitrile and the analyte determined spectrophotometrically at 546 nm. Important optimized parameters were the selection of wetting film and elution solvents, the flow rate, the length and diameter of the extraction coil and the conditions for the formation of the ion paired chelate. Cr(III) was previously oxidized to Cr(VI) and calculated as the difference between total Cr and Cr(VI). An enrichment factor of 25 and a detection limit of 2.0 μg l^{-1} Cr(VI) were achieved with a sampling frequency of 17 h^{-1}. The calibration curve was linear up to 100 μg l^{-1} Cr(VI) ($r = 0.999$). The relative standard deviations were 2.8 and 2.0% at the 25 and 100 μg l^{-1} levels. © 1997 Elsevier Science B.V.

Keywords: Chromium; Extraction; Sequential injection; Spectrophotometry

1. Introduction

Recently, a flow injection extraction technique using replaceable organic wetting films on Teflon tubing was developed in our laboratory [1]. The value of this technique is that it has several key advantages over existing extraction methods, and it can be incorporated into many flow injection/sequential injection analyses to enhance sensitivity and selectivity. Compared with the long-standing segmented flow extraction methods, organic wetting film extraction is easier to apply because it does not involve phase segmentors, phase separators or discriminating on-tube detection of segmented flow streams [2]. Wetting film extraction furthermore consumes approximately ten times

* Corresponding author.

PII S0039-9140(96)02180-7

less organic solvent. The extracting phase is injected and discarded during each analysis cycle so that regeneration or reuse are not necessary, unlike tube wall adsorption [3,4] or reversed permeation membranes [5].

Historically, the development of wetting film extraction grew out of Lucy's segmented method of flow injection extraction [6]. Lucy and Yeung emphasized the usefulness of stationary organic wetting films to delay the average flow rate of extracted species in an aqueous/organic segmented flow system. The delayed flow rate was due to the partitioning of extracted analytes between the flowing organic segments and the stationary film. The differing flow rates achieved a separation of the extracted and unextracted species. Previously, stationary films were usually regarded as a source of unwanted dispersion in segmented flow systems. A logical extension of Lucy and Yueng's approach was to dispense completely with the flowing organic segments and attain the full benefit of the stationary wetting film.

In this paper, we demonstrate the use of organic wetting film extraction to enhance the sensitivity and selectivity in the sequential injection analysis of Cr(VI) and Cr(III) in natural waters. The colorimetric determination of chromium(VI) and (III) in water using 1,5-diphenylcarbazide was selected partly because it has been used to demonstrate various flow injection configurations [7–17]. The enhancement of sensitivity also makes the chromium determination more useful for trace environmental analysis. Yoshimura enhanced the sensitivity of the Cr(VI) determination 10-fold by solid phase spectrophotometry using cation exchange beads [18]. A detection limit of 0.5 ng ml^{-1} was achieved. Unfortunately, electrolytes present in natural water interfered. The sample solution must be passed through a hydrogen-form cation-exchange column, or matrix matched standard solutions must be used [19]. In this work, electrolyte interference is avoided by extracting the colored complex quantitatively as an ion pair into an organic wetting film, resulting in a similar enhancement of sensitivity.

2. Experimental

2.1. Apparatus

Fig. 1 illustrates the sequential injection manifold for the preconcentration and spectrophotometric determination of chromium(VI). Solutions were driven by two peristaltic pumps (Alitea USA, Medina, WA) with Masterflex # 13, # 14 and # 16 Norprene pump tubes (Cole-Parmer Instrument Company, Chicago, IL) for different flow rates. A six-port rotary selection valve V_1 (Valco Instrument Co., Houston, TX) was used to select the solutions. A 5.0 ml holding coil was used as an injection loop on an injection valve, V_2. The holding coil consisted of 5.6 m of 18 gauge Teflon tubing, 1.07 mm i.d. (Small Parts, Miami Lake, FL). The sample and reagent were loaded into the coil by pump P_2. Another injection valve, V_3, was used to inject the eluting solution via a Teflon 100 µl injection loop. Both injection valves were six-port, two position valves (Valco). The eluting solution was loaded into the loop manually with a syringe. The extraction coil, EC, consisted of a 3.5 m length of thick-walled Teflon (PolyTetraFluoroEthylene, PTFE) tubing (Small Parts, Miami Lake, FL) with an inner diameter of 1.07 mm (18 gauge) coiled on a 20

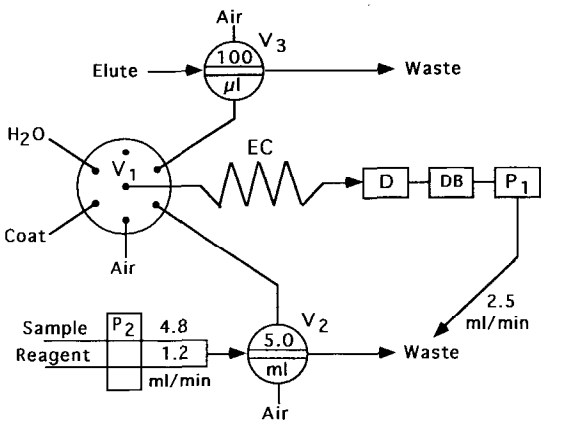

Fig. 1. Scheme of the sequential injection-wetting film extraction system. P_1, P_2 = peristaltic pumps, V_1 = selection valve, V_2, V_3 = injection valves, EC = extraction coil, D = detector, DB = displacement bottle, Coat = coating solvent, Elute = eluting solvent.

mm diameter rod. The extraction coil was connected to the common port of the selection valve, V_1. All other tubing connections were made with 0.8 mm i.d. Teflon tubing and Teflon nuts and ferrules (Upchurch, Oak Harbor, WA). A displacement bottle was placed between the detector and the pump P_1 to protect the pump tube from organic solvents. A Brinkmann colorimeter (PC-701, Brinkmann Analytical, Wesburg, NY) served as both the light source and detector. The transmittance cell was a sandwich cell with a 2.0 mm Teflon spacer [20]. The incident light passing through a 546 nm interference filter (Edmund Scientific) made two passes through 2.0 mm of solution for a total pathlength of 4 mm. Control of pump P_1 and valve V_1 and collection of data were performed with Atlantis software (Lakeshore Technologies, Chicago, IL).

2.2. Reagents and solutions.

All solutions were prepared in purified water (NANOpure II, Sybron Barnstead, Dubuque, IA). All chemicals were analytical reagent grade. Acetonitrile, acetone and methanol were used as received. All organic solvents that were immiscible with water were saturated with water before use.

Standard chromium(VI) solution (500 μg ml^{-1}) was prepared by dissolving potassium dichromate (Mallinchrodt) in water. Working solutions were made by step-wise dilution of the stock solution with water.

Standard chromium(III) solution was obtained by reducing 10.0 ml Cr(VI) stock solution with 25 mg Na_2SO_3 and 10 ml 6 M sulfuric acid. Excess sulfite was removed by boiling and then cooling the solution to room temperature. The solution was diluted to 100 ml with water. Working solutions were made by dilution of the obtained solution with water.

The colorimetric reagent was 1,5-diphenylcarbazide (DPC), also called 1,5-diphenylcarbohydrazide (Sigma). DPC solution was prepared by dissolving 0.1 g DPC in 10 ml acetone (J.T. Baker) and storing in a brown bottle at 4°C.

Sodium perchlorate solution was made by dissolving 61.2 g sodium perchlorate (Aldrich) and 1.0 ml of 6.0 mol l^{-1} sulfuric acid in water and diluting to 100 ml. Sodium perchlorate contains chromate impurities. The solution was purified by adding 1.0 ml of DPC solution and washing with aliquots of 4-methyl-2-pentanone (Aldrich) until the wash solution was colorless.

A color developing solution was prepared by mixing 2.5 ml DPC solution with 100 ml sodium perchlorate solution. This solution should be prepared daily.

A coating solution was made by mixing 10 ml octanol (J.T. Baker) with 20 ml 4-methyl-2-pentanone.

An ammonium cerium(IV) sulfate solution was made by dissolving 0.20 g ammonium cerium(IV) sulfate (Aldrich) in 2.5 mol l^{-1} sulfuric acid and diluting to 50 ml.

2.3. Sample preparation

For the determination of Cr(VI), the untreated, unfiltered water sample obtained just prior to analysis was loaded into the reaction coil. The same sample was then oxidized by Ce(IV) before aspirating into the reaction coil so that total Cr could be determined as Cr(VI). Samples were oxidized by adding 0.10 ml of the Ce(IV) solution to 9.9 ml sample then heating the mixture in a water bath for 5 min at 45°C. Samples were cooled to room temperature before loading. Lake, sea (Puget Sound) and drinking waters from Seattle were used as samples.

2.4. Procedure

The procedure, outlined in Table 1, is three chemical steps: (1) color development and ion pairing; (2) extraction into an organic wetting film; and (3) elution of the film to the detector. In the first step, the sample solution and reagent were merged in a T mixer and passed directly into a 5.0 ml reaction coil which was installed as an injection loop on valve V_2. The flow manifold and flow rates are given in Fig. 1. Before unloading the reaction coil into the extraction coil, the extraction coil, EC, had to be washed with water and coated with extraction solvent. A fresh film of organic solvent was formed on the extraction coil by switching valve V_1 to port 'Coat' and, aspirat-

Table 1
Analysis cycle

Step	Function	Time s^{-1}
1.*	Load sample and reagent into the reaction coil on the injection loop, V_2	56
2.	Aspirate H_2O to wash the extraction coil	30
3.	Aspirate extraction solvent into the extraction coil	4
4.	Aspirate air	2
5.	Aspirate the sample from the reaction coil	120
6.*	Aspirate elution solvent from injection loop, V_3	20

* Steps 1 and 6 were done concurrently to increase sampling efficiency.

ing with pump P_1. Next, a zone of air was aspirated from valve V_1 to separate the coating zone from the sample solution to follow. With a fresh extracting film on EC, the treated sample was aspirated from the reaction coil (on V_2) into the coil 'EC.' At this point, the complexed, ion-paired analyte was preconcentrated in the wetting film on EC. After the sample zone had passed, followed by a separating zone of air, the film was eluted to the detector by a zone of acetonitrile from the injection loop of valve V_3. Valve V_3 was switched manually, and pump P_1 was used to aspirate. Data was collected at 2 Hz.

3. Results and discussion

3.1. Coating solvent

Most critical to this work was the development of an organic thin film that could be formed and removed during each analysis cycle. The development of such a film required that we, firstly, identify solvents that extract our analyte well and, secondly, blend these solvents to optimize film characteristics. Extraction solvents were blended in order to satisfy the following necessary film characteristics: the film must be adequately insoluble in water, it must have a sufficiently high capacity for the analyte, it must be stable during extraction, and it must be eluted after sample perfusion.

Solvents containing hydroxyl and ketone functional groups were found to solvate the ion-paired chromium complex effectively. Other solvents tested were benzene, toluene, chloroform, carbon tetrachloride, dimethylsulfoxide, cyclohexane and hexadecane. All of these resulted in signals indistinguishable from those of blank solutions ($\sim$ 0.003 AU) when a 100 $\mu g\ l^{-1}$ Cr(VI) solution was used. Table 2 shows the absorbances resulting from various wetting film compositions.

The extraction solvents were blended to produce good wetting film characteristics according to some guiding principles. Operating properties were adjustable since ketone and alcohol extraction solvents have a range of physical properties. Film thickness was assumed to be the most critical film property. As a result, the strategy for finding the optimum mixture was straightforward. The solvent mixture was varied in order to vary the thickness of the film, while absorbance peak area was maximized. Film thickness was a guideline for optimization, but was not actually measured. Rather, the viscosity and surface tension of the solvent mixture were varied in the experiments since the film thickness is related to these, and their values are known for the pure solvents. Film thickness is directly proportional to viscosity and inversely proportional to surface tension [21]. The performance of the film was especially sensitive to viscosity.

There is a trade off between the capacity of the film for the analyte and the ease with which the

Table 2
Effect of coating solvent on the preconcentration of 100 $\mu g\ l^{-1}$ Cr(VI)

Coating solvent	Peak height/AU
No coating	<0.0030
2-Propanol	0.0055
1-Butanol	0.2282
1-Pentanol	0.2027
1-Octanol	0.2059
1-Decanol	0.1048
4-Methyl-2-pentanone (MIBK)	0.1515
75% Octanol+25% MIBK	0.2441
50% Octanol+50% MIBK	0.3213
33% Octanol+67% MIBK	0.3461
25% Octanol+75% MIBK	0.3337

film can be eluted to a detector. Both of these characteristics depend, predictably, on the thickness or viscosity of the film: thick films have high capacity but are more difficult to elute. As a lower limit, the film must be thick enough that it does not break up during sample perfusion. As an upper limit, it must be possible to remove the film quantitatively. Between these two limits, one should compromise between sensitivity and dynamic range. Lower capacity results in higher sensitivity because a smaller volume of extraction solvent yields higher enrichment factors. Higher capacity allows for a higher breakthrough concentration. A lower film thickness was chosen in this work. Although sensitivity was favored at the expense of dynamic range, the dynamic range was adequate for most water samples.

Film thickness and ease of elution were functions of the number of carbons for pure solvents. The solubility in water was a limiting factor for 2-propanol, 1-butanol and 4-methyl-2-pentanone. At five carbons or higher, alcohols were sufficiently insoluble in water, but they were too viscous so that the films were too thick. The perchlorate-Cr complex ion pair was completely extracted into the films, but the films could not be removed by satisfactory means. Excessive film thickness also decreased the sensitivity and enrichment factor by increasing the volume of the organic phase. Two selected extraction solvents, 1-octanol and 4-methyl-2-pentanone, had viscosities around the ideal value. These were blended to optimize film thickness. The highest sensitivity (peak area) was obtained with a mixture of 33% (volume) 1-octanol and 67% 4-methyl-2-pentanone.

The results shown in Table 2 verify that the perchlorate-paired complex did not adsorb onto the tubing wall. Without a wetting film, the absorbance of a 100 μg l^{-1} Cr(VI) standard solution was indistinguishable from that of a blank solution. Adsorption onto tubing walls has been used in the determination of ion-paired dye [3] and metal ion chelates [4].

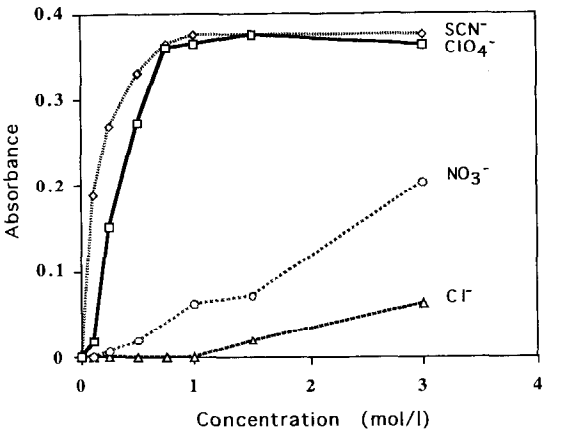

Fig. 2. Effect of pairing anion concentration on the extraction of Cr(VI).

3.2. Color development and ion-pairing conditions

Chromium(VI) forms an intensely colored complex with DPC in acidic solution. The reactions occurring were reported to be the simultaneously oxidation of DPC to diphenylcarbazone, the reduction of Cr(VI) to Cr(III), and the chelate formation of Cr(III) and diphenylcarbazone [22,23]. Although the structure of the chelate is still uncertain, it is evidently a cation [22]. The chelate can only be extracted into aqueous solution as a neutral ion pair in the presence of excess anions. Fig. 2 shows the performance of various counterions on the extraction of the colored chelate. The anion concentrations given are those of the extracting solution after flow manifold mixing. Thiocyanate and perchlorate were most efficient, but perchlorate was preferred based on interference studies (discussed later). The recommended perchlorate concentration, used for standards and samples, was 1 mol l^{-1}. Ion pairing did not alter λ max (540 nm) or the extinction coefficient.

The effect of sulfuric acid concentration was investigated by varying the concentration in the reagent solution. The peak heights were found to be highest and independent of sulfuric acid concentration over the range 0.005–0.1 mol l^{-1} (pH 0.7 ~ 2.0). It was also found that the acidity influenced the color development, but not the forma-

Table 3
Elution efficiency of 100 μl aliquots of various solvents

Solvent	Viscosity[b] η(m Pa s)	Surface tension[b] γ(mN m^{-1})	η/γ (Pa s mN^{-1})	Elution efficiency[a] (%)
Methanol	0.544	22.07	0.02465	51.0
Acetone	0.306	23.46	0.01304	77.5
Acetonitrile	0.369	28.66	0.01288	92.0

[a] The percentage of Cr(VI)-DPC complex eluted in the first aliquot. Complete elution was assumed for three successive aliquots.
[b] Data (25°C) from CRC Handbook of Chemistry and Physics, 75th Edition.

tion of ion paired complex. Sulfuric acid concentrations used for Cr(VI) and total Cr determinations in the proposed manifold were 0.012 mol l^{-1} (pH 1.6) and 0.032 mol l^{-1} (pH 1.2), respectively.

3.3. Elution solvent

Once the ion-paired chelate had been extracted into the 1-octanol 4-methyl-2-pentanone film, 100 μl of the elution solvent was injected into the extraction coil to disrupt the adhesion of the film to the Teflon and to elute it to the detector as one homogeneous segment. An ideal elution solvent is one which does not form a film or forms a very thin and unstable film. Such a solvent would be expected to have a low viscosity and a high surface tension [24]. The elution efficiencies of methanol, acetone and acetonitrile were investigated with 100 μg l^{-1} Cr(VI) standard solution. A small and adequate volume of elution solvent, 100 μl, was used throughout.

The efficiency of film elution after extraction was examined by measuring the peak areas of three sequential aliquots (100 μl each) of the elution solvent. Complete elution of the Cr(VI)-DPC complex was assumed for three aliquots. The percent recovered in the first aliquot is reported in Table 3 as the elution efficiency. With the smallest ratio of viscosity to surface tension, a single segment of 100 μl acetonitrile can elute 92% of the extracted analyte. The second and third aliquots, used for cleaning, eluted 7.4 and 1.3%, respectively.

3.4. Optimization of the manifold

Parameters of the manifold that were optimized were the flow rate, the sample volume and the length and diameter of the extraction coil. The oxidation of Cr(III) was also investigated.

Thickness of the wetting film is directly proportional to the inner diameter of the extraction coil. As a result, the extraction capacity (volume of the wetting film) is larger for wider and longer extraction coils. However, excessive coating solvent adsorbed on the coil requires excessive elution steps. The optimum extraction coil was PTFE tubing 3.5 m in length and 1.07 mm (18 gauge) inner diameter.

Wetting films formed much more readily on PTFE Teflon than on clear FEP Teflon. An equation predicting film thickness [21] that has long been cited in segmented flow extraction publications [24] neglects any consideration of the tubing material. Nevertheless, this equation was a useful guideline for predicting the effects of flow rate, viscosity and surface tension on film thickness.

Generally, a faster flow rate (pump P_1) results in a thicker film. In the range of 1.0–3.5 ml min^{-1} (1.8–6.5 cm s^{-1}), the peak areas were independent of the flow rate. Flow rates lower than 1.0 ml min^{-1} resulted in analyte breakthrough due to insufficient capacity because the film was too thin. Flow rates higher than 3.5 ml min^{-1} resulted in thick films with high capacity; however, analyte recovery was low partly because the contact time with the extraction solvent was shortened. Excessively high flow rates allowed even the elution solvent to form a film so that the elution of the analyte was incomplete.

To simplify the manifold, attempts were made to pump the aqueous sample and reagent directly into the extraction coil. The Cr(VI)-DPC reaction proved to be too slow [16]. The extraction efficiency was only 42% of that of the proposed system and conditions, as determined from relative peak areas. Having a separate reaction coil allowed as much time as needed for the ion paired chelate to form.

Different volumes of Cr(VI) standard solutions (100 μg l^{-1}) were injected into the extraction coil by changing the length of the reaction coil on valve V_2. The absorbances increased linearly with the injected sample volumes up to 6.0 ml (the total volume of sample plus reagent is 7.5 ml). Breakthrough occurred beyond 6.0 ml. A good compromise between sensitivity and sampling frequency was a sample volume of 4.0 ml.

The on-line oxidation of Cr(III) to Cr(VI) with Ce(IV) was reported to be incomplete [8,10]. The yield of Cr(VI) depended on the temperature, length of the reaction coil, flow rate, the concentrations of Ce(IV) and sulfuric acid, and the FIA manifold configuration. Coupling an oxidation system to the extraction system would make the manifold exceedingly complex. Therefore, water samples were pretreated. The oxidation was easily achieved by heating a mixture of 0.1 ml of Ce(IV) solution and 9.9 ml of water sample in a 45°C water bath for 5 min. Chromium(III) can be quantitatively oxidized to Cr(VI) and only one calibration curve is needed for the measurement of both Cr(VI) and total Cr.

3.5. System performance

Fig. 3A is a set of peaks observed for 25 and 100 μg l^{-1} Cr(VI) standard solutions as the eluted wetting film passed through the detector. The eluted film was preceded and followed by air. In contrast to most flow injection applications, the analyte signal was nearly constant as the zone passed through the detection cell. Extraction into a single homogeneous zone replaced the usual dispersion mixing. The irregular shoulders on the leading and following edges of the rectangular elution peak were due to light scattering at the solution/air interfaces. The light scattering was excluded by using only the absorbance measurements between 3.5 and 5 s, as in Fig. 3B. Fig. 3B shows absorbance versus time data of 27 runs of standard solutions ranging from 5 to 100 μg l^{-1} and two blanks.

The data shown in Fig. 3B was used to calculate a calibration curve. The average absorbance for each run was used. The data demonstrates a linear response to concentrations up to 100 μg l^{-1}. The y-intercept of the calibration line is indistinguishable from the blank absorbance value. The least squares line is absorbance =

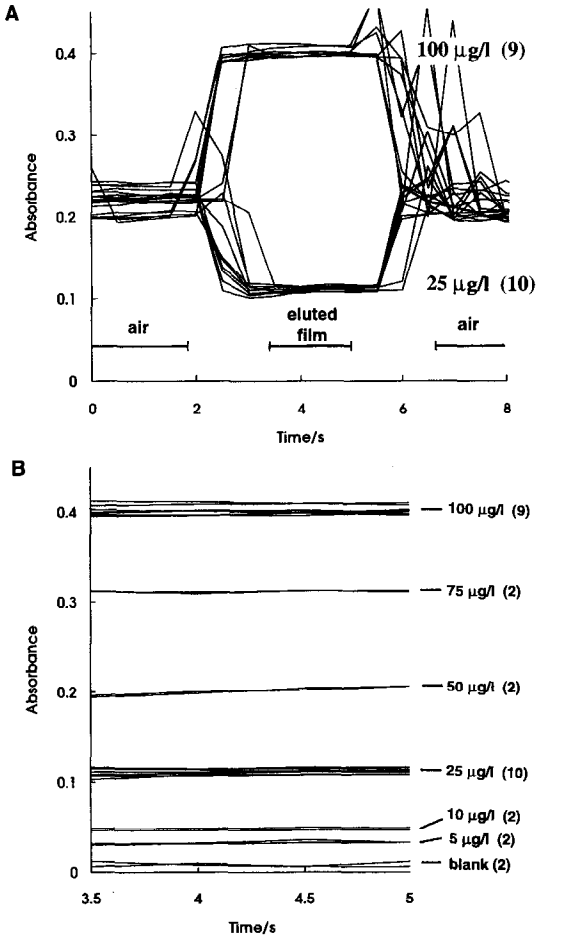

Fig. 3. (A) Observed peaks of 25 and 100 μg l^{-1} Cr(VI) standard solutions. (B) Absorbance vs. time for eluted wetting films between 3.5 and 5 s elapse times. Concentrations of Cr(VI) are indicated with the number of replications in parentheses.

Table 4
Effects of various pairing ions on the determination of 100 μg l^{-1} Cr(VI)

Ion	Concentration (mg l^{-1})	Cr(VI) found (μg l^{-1})	
		with SCN^-	with ClO_4^-
None	—	100	100
IIg(II)	10	98	102
Fe(III)	100	—	99
	10	449	—
	10*	104	—
	1	243	—
Cu(II)	100	246	103
	100*	98	—
	10	98	—
Co(II)	100	336	97
	10	143	98
	10*	98	—
	1	112	—
V(V)	10	57	70
	1	94	97
Mo(VI)	100	—	336
	10	—	96
	5	322	102
	2.5	243	—
	1.0	166	—

* In the presence of 0.02 mol l^{-1} EDTA.

$(3.913 \times 10^{-3})C—5.5 \times 10^{-3}$, $R^2 = 0.998$, where C is concentration in μg l^{-1}. The limit of detection, calculated on a 3σ basis, was 2.0 μg l^{-1} Cr(VI). The relative standard deviations of 25 μg l^{-1} and 100 μg l^{-1} Cr(VI) solutions were 2.8% ($n = 10$) and 2.0% ($n = 10$), respectively. The analysis can be performed at a rate of 17 h^{-1}.

3.6. Interference studies

Various ions were tested for interference in the determination of Cr(VI). No interference was observed for at least 1000 mg l^{-1} of Na(I), K(I), Ca(II), Mg(II), NH_4^+, Cl^-, NO_3^-, SO_4^{2-}, PO_4^{3-}, and 50 mg l^{-1} of Ni(II), Mn(II), Zn(II), Cd(II), Pb(II) on the determination of 100 μg l^{-1} Cr(VI). Analyses were performed using both thiocyanate and perchlorate as ion-pairing anions. However, thiocyanate resulted in positive interferences from Fe(III), Cu(II), Co(II) and Mo(VI). With perchlorate as the ion-pairing anion, all of the interferences were satisfactorily tolerated (Table 4) except V(V). Fortunately, V(V) is not likely to be encountered at such levels in most water samples.

3.7. Application

The method was applied to the determination of Cr(VI) and Cr(III) in tap water, lake water and Seattle area sea water samples. No interferences were found in three water samples tested by standard additions. The results of standard additions are given in Table 5.

4. Conclusion

The described wetting film extraction system is suitable for on-line preconcentration and separation. The method avoids the complications and performance limitations of segmented flow extraction which has been extensively studied for over two decades. With only μl scale organic solvent consumption, the sensitivity of an assay is enhanced in proportion to the enrichment factor. This extraction system can easily be coupled to detectors or subsequent analyzers because the analyte is uniformly distributed in a single segment of extraction solvent. Thus, it is possible to determine chromium at μg l^{-1} levels using simple spectrophotometric detection.

Acknowledgements

The authors would like to thank Dr Joseph Breen for his interest in this project and the US Environmental Protection Agency for financial support. We thank reviewer II for careful and constructive comments.

Table 5
Standard addition analysis of natural water samples

Sample	Added (μg l^{-1})		Found (μg l^{-1})		Percent found*	
	Cr(VI)	Cr(III)	Cr(VI)	Cr(III)	Cr(VI)	Cr(III)
Tap water	0	0	3.5	4.2	—	—
	10	50	12.3	49.2	88	90
	50	10	55.0	15.0	103	108
Lake water	0	0	<LOD	9.2	—	—
	10	10	10.8	19.3	108	101
	25	75	25.8	75.7	103	89
	50	50	48.8	55.1	98	92
	75	25	69.8	30.2	93	84
Sea water	0	0	<LOD	6.0	—	—
	10	10	9.3	14.2	93	82
	25	75	22.5	84.0	90	104
	50	50	45.3	48.6	91	85
	75	25	75.8	30.2	101	97

* $(D_{spiked}-D_{sample}) \times 100\%/$(amount added) where D_{spiked} and D_{sample} are amounts found in the spiked sample and sample.

References

[1] Y. Luo, R.A. Othman, J. Ruzicka and G.D. Christian, Analyst, 121 (1996) 601.
[2] Z. Fang, Flow Injection Separation and Preconcentration, VCH, Weinheim, 1993.
[3] C.C. Lindgren and P.K. Dasgupta, Talanta, 39 (1992) 101–111.
[4] H. Chen, S. Xu and Z. Fang, Anal. Chim. Acta, 298, (1994) 167–173.
[5] R.G. Melcher, P.P. O'Connor and M.W. Beach, Process Control Qual., 6 (1994) 167–185.
[6] C.A. Lucy and K.K.C. Yeung, Anal. Chem., 66 (1994) 2220–2225.
[7] S.S. Jørgensen and M.A.B. Aregitano, Analyst, 105 (1980) 292–295.
[8] B.P. Bubnis, M.R. Straka and G.E. Pacey, Talanta, 30 (1983) 841–844.
[9] R.A. Leach, J. Ruzicka and J.M. Harris, Anal. Chem., 55 (1983) 1669–1673.
[10] J.C. de Andrade, J.C. Rocha and N. Baccan, Analyst, 109 (1984) 645–647.
[11] C. Pasquini and W.A. de Oliveira, Anal. Chem., 57 (1985) 2575–2579.
[12] J. Ruz, A. Rios, M.D. Luque de Castro and M. Valcarcel, Fresenius'Z. Anal. Chem., 322 (1985) 499–502.
[13] J.C. de Andrade, J.C. Rocha and N. Baccan, Analyst, 110 (1985) 197–199.
[14] J. Ruz, A. Rios, M.D. Luque de Castro and M. Valcarcel, Talanta, 33 (1986) 199–202.
[15] J. Ruz, A. Rios, M.D. Luque de Castro and M. Valcarcel, Anal. Chim. Acta, 186 (1986) 139–146.
[16] A.N. Araujo, J.L.F.C. Lima, A.O.S.S. Rangel, J. Alonso, J. Bartroli and R. Barber, Analyst, 114 (1989) 1465–1468.
[17] J.A. Chamarro, J. Bartroli and R. Barber, Anal. Chim. Acta, 261 (1992) 219–223.
[18] K. Yoshimura, Analyst, 113 (1988) 471–474.
[19] M.D. Luque de Castro and M. Valcarcel, Int. J. Environ. Anal. Chem., 38 (1990) 171–183.
[20] J.L.P. Pavon, E.R. Gonzalo, G.D. Christian and J. Ruzicka, Anal. Chem., 64 (1992) 923–929.
[21] L.R. Snyder and H.J. Adler, Anal. Chem., 48 (1976) 1017–1022.
[22] R.T. Pflaum and L.C. Howick, J. Am. Chem. Soc., 78 (1956) 4862–4866.
[23] G.J. Willems, N.M. Blaton, O.M. Peeters and C.J. de Ranter, Anal. Chim. Acta, 88 (1977) 345–352.
[24] V. Kuban, Crit. Rev. Anal. Chem., 22 (1991) 477–557.

ELSEVIER

Talanta 44 (1997) 1573–1580

Talanta

Enzyme electrode for glucose determination in whole blood

T. Santoni [a], D. Santianni [a], A. Manzoni [b], S. Zanardi [b], M. Mascini [a,*]

[a] *Dipartimento di Sanità Pubblica, Epidemiologia e Chimica Analitica Ambientale, Università di Firenze, Via G. Capponi 9, 50121 Firenze, Italy*

[b] *Instrumentation Laboratory, Viale dell'Industria 3, Paderno Dugnano, 20037 Milano, Italy*

Received 30 July 1996; received in revised form 1 October 1996; accepted 2 October 1996

Abstract

The development of a glucose sensor suitable for use with whole blood is described. It is based on anodic oxidation at +700 mV of hydrogen peroxide with a platinum electrode covered with a gas permeable membrane. Glucose reacts with glucose oxidase immobilised on the external side of the membrane, and forms hydrogen peroxide which is able to cross the gas permeable membrane due to its high vapour tension, while other electroactive substances that are important interferents are completely blocked. This principle was discovered several years ago but no practical application was presented up to now. Therefore in this work a number of different commercial membranes were tested, in order to obtain a resistant, rapidly responding and interference free sensor to be used in conjunction with a blood gas measurement apparatus. Coimmobilisation of glucose oxidase and catalase was found to be useful for fast response and recovery of the electrode. Using some of the tested membranes, the linearity range is 1–15 mM, CV 5%, response time 90 s, recovery time for the next sample 120 s. The membrane's working life is 2–3 weeks. © 1997 Elsevier Science B.V.

Keywords: Biosensors; Glucose determination; Glucose oxidase; Gas permeable membranes

1. Introduction

Enzymes have been exploited for diagnostic purposes in several formats. In recent years enzymes have been coupled to electrochemical transducers, optical fibres, piezoelectric quartz and calorimetric devices in order to obtain biosensors for different chemical substances [1–3]. Great efforts have been made to find a glucose sensor for use in medical diagnosis. Most of the systems developed measure glucose by means of the anodic oxidation of hydrogen peroxide at +600 mV with a platinum electrode. However, several problems arise when the sample is whole blood. Glucose concentration can be up to 20 mM while the K_M of the glucose oxidase is around 1 mM, and the presence of other electrochemical active substances, like acetaminophen, ascorbic or uric acid are often important interferents in such samples [4–7]. Moreover, there is a pressing need in the medical community for an instrument which can measure glucose in whole blood at the same time as the blood gas parameters, like pH, pCO_2, pO_2 and electrolytes.

* Corresponding author. e-mail: Mascini@cesit1.unifi.it

PII S0039-9140(96)02181-9

One recent approach proposed [8] a new version of glucose sensor exploiting the vapour tension of hydrogen peroxide. In this case a gas permeable membrane was placed in front of the platinum electrode where oxidation takes place. The principle is simple. Glucose reacts with glucose oxidase and forms hydrogen peroxide which, due to its high vapour tension, is able to cross a gas permeable membrane and is oxidised at the platinum electrode.

The interest in this approach arises because the electroactive compounds generally present in whole blood (or serum), like ascorbic acid, uric acid or acetaminophen, are thus completely blocked and the sensor is completely interference-free. However, the teflon membrane proposed in the original paper was very fragile and only a few measurements could be obtained by the experimental apparatus described [8]. More recently the same principle was exploited for hydrogen peroxide determinations [9].

This paper reports the results of research to find a composite membrane formed of three layers, the first a gas permeable membrane supported in order to be strong enough to last several days without loss of selectivity, the second contains the immobilised enzyme and the third is an external membrane which protects the enzyme from microbial attack. Therefore the purpose of this work was very practical: to try to find a suitable membrane working on the principle of interference-free hydrogen peroxide diffusion by exploiting membrane materials that are commercially available.

The assembly of the biosensor was designed to be used in conjunction with blood gas measurement and the experiments were carried out in order to obtain reliable results within the analysis time of such parameters (120 s). This requirement was essential because the medical request was to measure glucose in whole blood during blood gas measurements. Therefore we tried to optimise the glucose sensor using the same cell and procedure of a well known commercial clinical chemistry analyzer.

It is reported that the immobilised enzyme layer should be formed with glucose oxidase and catalase directly coupled on the gas permeable membrane. The catalase catalyses the oxidation of hydrogen peroxide. The enzymatic decomposition of H_2O_2 is then a mean to consume less oxygen during the glucose oxidation (which is a limiting factor) and to decrease the response time.

2. Experimental

2.1. Reagents

Glucose oxidase (GOD, EC 1.1.3.4) from *Aspergillus Niger* (grade VII-s, 100 U mg^{-1}) and catalase (EC 1.11.1.6) from bovine liver (2800 U mg^{-1}) were from Sigma (Italy). Polycarbonate membranes (pore size 0.03 μm) were obtained from Nuclepore (Costar, Milan, Italy). Polycarbonate membranes (pore size 0.015 μm) were a gift from Poretics (PBI International, Milan, Italy). Polytetrafluoroethylene membranes (pore size 0.5 μm) with and without a polyethylene backing (Fluoropore), polyvinilydene difluoride membranes (Durapore hydrophobic, pore size 0.45 μm) and polypropylene membranes (AN hydrophobic prefilters, pore size 0.6 μm) were from Millipore (Vimodrone, Italy). Polytetrafluoroethylene membranes, backed with polypropylene (0.5 μm) were from Whatman (Springfield Mill, UK). Polypropylene membranes (Metricel, pore size 0.1 μm) were from Dasit (Milan, Italy). Nylon membranes (Magna SH, pore size 0.45 μm) were from MSI (Micron Separation, Inc., Bologna, Italy). Urethane/fluoropolymer membranes, backed with polyester (Repel 100, pore size 0.1 μm; these membranes are no longer commercially available), modified acrylic copolymer membranes backed with nylon (Versapor-200R, pore size 0.2 μm) and with polyester (Versapor-200TR, pore size 0.2 μm) were obtained from Gelman Sciences (Milan, Italy). All other reagents used were of analytical reagent grade.

2.2. Enzyme membranes

2.2.1. GOD membrane

1 mg of lyophilised glucose oxidase (GOD) was dissolved in 100 μl Dulbecco buffer (pH 7.04, with

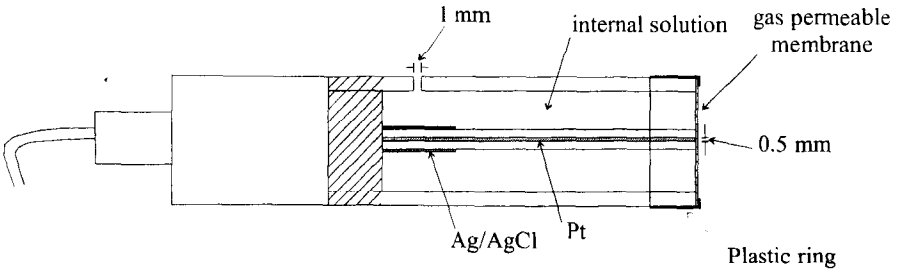

Fig. 1. A schematic representation of the I.L. modified oxygen electrode used as a glucose sensor.

composition 10 mM Na_2HPO_4, 1 mM KH_2PO_4, 2.7 mM KCl, 0.13 M NaCl). 5 μl of this solution were spread over a disk, 0.7 cm diameter, of gas permeable membrane. Immediately after, a solution of glutaraldehyde 2.5% in Dulbecco buffer was mixed over the same membrane. The membrane was left to dry at room temperature, then stored at 5°C.

2.2.2. God/catalase membrane

The membrane with coimmobilized GOD and catalase was prepared by spreading together over the disk 5 μl of GOD solution as described above, and 5 μl of a catalase solution in Dulbecco buffer, with an enzymatic activity equal to (or five times) the activity of the GOD solution. The same procedure as for the GOD membrane was followed.

2.3. Apparatus

The base sensor was an I.L. (Instrumentation Laboratory) modified oxygen sensor (P/N 70961-00), with the working electrode (platinum, diameter 0.5 mm) and the reference (Ag–AgCl) contained in the same jacket which was filled with Dulbecco buffer (Fig. 1). The electrode was used in the cell of a BGElectrolytes System, that is an automatic, microprocessor controlled, blood gas, electrolytes and hematocrit analyzer. Usually it is possible to measure pH, pO_2, pCO_2, Na^+, K^+,Cl^+, Ca^{2+} and hematocrit. The system has a constant temperature of 37°C. When a sampling cycle is initiated, the system aspires, preheats and analyses the blood sample. In our experimental work the glucose electrode replaced the calcium electrode, (Fig. 2) and was connected to an EG and G Electrochemical detector model 400. It was used for constant potential studies performed anodically at +700 mV.

2.3.1. Electrode assembly

The electrode jacket was closed by a plastic ring. The ring was used to keep the composite membrane in tight contact with the platinum surface. The composite membrane was formed of three layers, the inner layer was the gas permeable membrane, the second layer was the im-

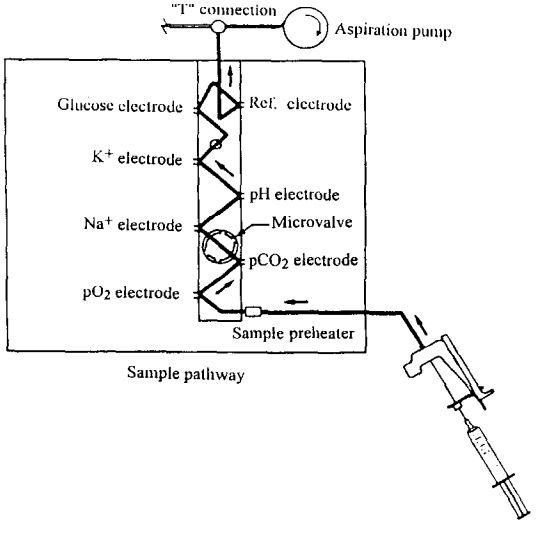

Fig. 2. Representation of the sample pathway. The glucose electrode substitutes for the calcium electrode of the original cell.

mobilised enzyme, and the outer layer was a polycarbonate membrane (pore size 0.03 μm). The side of the gas membrane on which the enzyme was layered and immobilised was mounted facing the outside of the electrode, in contact with the polycarbonate.

2.4. Measuring procedure

The apparatus had an automatic sampling cycle and it was started by the operator. About 240 μl of sample were aspirated into the cell (Fig. 2). Then the flow stopped and the sample remained in contact with the electrodes until the measurement was completed. The signals of the various electrodes were analysed by internal software. The glucose electrode in our system replaced the original calcium electrode and it was connected with the EG & G Electrochemical detector.

After 120 s, or before if all the standard electrodes reached an end point value or a peak value, the software started the washing cycle. The original washing solution, which contained a proteolytic enzyme, was substituted with Dulbecco buffer to protect the enzyme on the glucose sensor. The longest measurement, pCO_2, required about 2 min, and during this period the performance of the glucose sensor was evaluated. During this time the output current was recorded and the current values after 60, 90 and 120 s from the introduction of the sample into the cell were evaluated.

After washing a calibrating solution was aspirated into the cell and it was ready for a new sampling cycle. The time for washing and calibration is about 2 min. Therefore the glucose electrode had to revert to the base line during this time. The sensor was calibrated with 2–25 mM glucose concentration in Dulbecco buffer. The solutions were prepared daily from a 1 M stock solution. To check the integrity of the membrane we used a solution of 1 mM ascorbic acid in Dulbecco buffer. If the membrane was broken or impaired a high current value was obtained. An unimpaired membrane did not show any current increase with this ascorbic acid solution.

3. Results and discussion

3.1. Membranes

The aim of our research was to find commercial membranes with some ideal characteristics: a high permeability to H_2O_2 in order to give a high and quick response; good mechanical resistance, particularly required by the use of the electrode in the cell; and a surface on which the enzyme layer can link strongly (e.g. a certain roughness was found to be useful). For these reasons we tested various membranes, immobilising the enzyme glucose oxidase layer on them. The chosen membranes were all described as hydrophobic, water impermeable and only gas permeable.

For this kind of measurement it is essential to obtain a rapid return to base line during the washing step. To improve the behaviour of the tested membranes, we added catalase to the enzyme layer. The experiments were carried out with three types of membranes: Repel, Versapor-R and Versapor-TR.

Membranes with different GOD:catalase ratios were prepared, but we did not notice any significant difference, either in the signal intensity or in the response speed. In the experiments described we only used a 1:1 ratio.

3.1.1. Polytetrafluoroethylene membrane (Fluoropore, pore size 0.5 μm)

These membranes had a low mechanical resistance. They broke during assembly on the electrode, so they had a high response to ascorbic acid, and could not be used to measure glucose. (These membranes were the ones used in the original work [8].)

3.1.2. Polytetrafluoroethylene with polypropylene backing (Whatman, pore size 0.5 μm)

These membranes, too, had a low mechanical resistance. Generally the response to ascorbic acid rose after a few hours. None of these membranes could be used for more than a day. The response to glucose was high (5 mM of glucose gave, after 120 s, a current of 7.5 nA) but it rapidly reduced after a few hours. They gave a linear response over a 2–10 mM range. The return to base line after washing was rather poor (more than 5 min).

3.1.3. Polytetrafluoroethylene with polyethylene backing (Fluoropore, pore size 0.5 μm)

These membranes were very similar to the ones backed with polypropylene. Only few membranes were tested because of their low mechanical resistance.

3.1.4. Polypropylene membranes (AN hydrophobic prefilters, pore size 0.6 μm)

These membranes were not permeable to hydrogen peroxide so we were unable to take any measurement.

3.1.5. Nylon (Magna SH, pore size 0.45 μm)

Only a few membranes were tested. The response to glucose was good for intensity and reproducibility (the medium response to 5 mM glucose after 120 s was 1.99 nA, CV 1%) but the response was slow and the return to base line was very poor (more than 5 min, and longer times for high glucose concentrations). After only one day of use the membrane became sensitive to ascorbic acid.

3.1.6. Polyvinilydene difluoride membranes (Durapore hydrophobic, 0.45 μm)

These membranes had a good mechanical resistance so they did not have problems with interferences. They had good linearity in the range 2–10 mM. The response, however, decreases rapidly through the day resulting in very low reproducibility. On the second day of use there was no response to glucose.

3.1.7. Polypropylene membranes (Metricel, pore size 0.1 μm)

These membranes had a rather good mechanical resistance, and could be used for 2–4 days. The intensity of the response was quite variable between different membranes, going from 5 to 10 nA for a 5 mM glucose solution after 120 s. The CV was about 8%, but on the first day it could be under 1%. On the following days the response was reduced and the reproducibility got worse. The sensors were linear in the range 2–10 mM. The current did not reach a stable value in 120 s (Fig. 3) and the return to base line after washing was quite slow (more than 5 min).

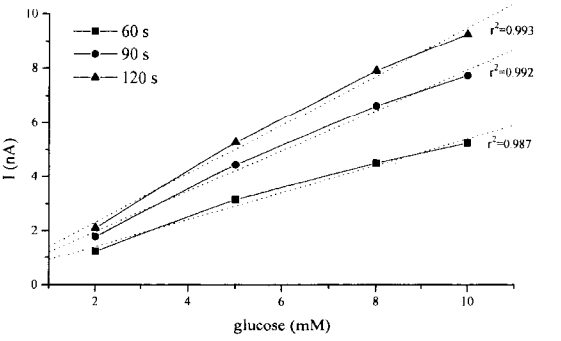

Fig. 3. Calibration curves after 60 (■), 90 (●) and 120 s (▲) from the introduction of the sample into the cell. The curves were obtained from a Metricel membrane with a GOD layer.

3.1.8. Urethane/fluoropolymer membranes, backed with polyester (Repel 100, pore size 0.1 μm)

This membrane was composed of two layers. The polyester had a backing function and it consisted of a felt adherent to the gas permeable part. This assured better mechanical stability. The enzyme solution was applied to the polyester side during immobilisation, and the roughness of the surface favoured the adsorption of the protein. Care was needed in mounting the membrane on the jacket. If the membrane was excessively drawn we got a small but measurable response to ascorbic acid (about a tenth for the same concentration of glucose). If the assembly was correct the membrane could usually be used for several days (7–15).

3.1.9. Experiments with GOD layer

The intensity of the current was variable from membrane to membrane (about 1 nA for a solution of 5 mM glucose after 120 s). The currents on the same day had good reproducibility with a CV of about 1.5%. The response rate was quite high, (Fig. 4a) and at low concentrations a plateau current was rapidly reached. The return to base line was rather quick (less than 5 min) but worse at higher concentrations (Fig. 4a). The current was linear up to 15 mM glucose.

3.1.10. Experiments with GOD/catalase layer

The membrane performance was improved using this layer. In Fig. 5 it is possible to see how

the response after 90 s was about the same as the one at 120 s, thus indicating reaching a plateau. The washing step was also quick at high concentration (return to base line was during the calibration step, i.e. about 2 min) while the sensitivity was similar to those for the corresponding GOD membrane. Fig. 4 compares a typical signal shape without (a) and with (b) the addition of catalase. As regards as the membrane working life, it ranged between 2–3 weeks. After some days we noticed a loss in linearity at concentrations over 10 mM, but return to the baseline remained good.

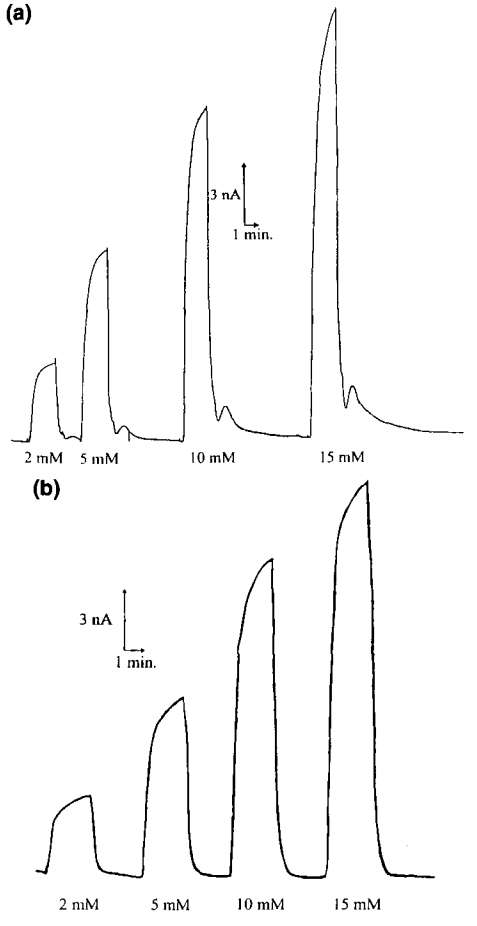

Fig. 4. Typical chart recordings obtained from a Repel membrane with: a, a GOD enzyme layer; b, a GOD/catalase enzyme layer.

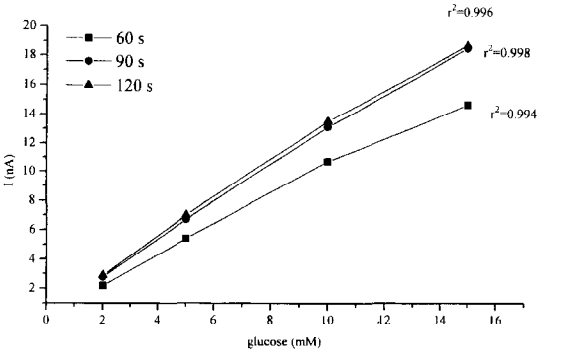

Fig. 5. Calibration curves after 60 (■), 90 (●) and 120 s (▲) from the introduction of the sample into the cell. The curves were obtained from a Repel membrane with a GOD/catalase enzyme layer.

3.1.11. Modified acrylic copolymer backed with nylon (Versapor-200R, pore size 0.2 μm) and with polyester (Versapor-200TR, pore size 0.2 μm)

We discuss the results for these two membranes together as they did not show any difference in behaviour. The structure was similar to the Repel membrane, with a hydrophobic polymer supported by polyester or nylon, but in this case, the hydrophobic layer was polymerised on both sides of the support, i.e. not separable. Both sides were treated to be hydrophobic. These results were with the enzyme layer composed of GOD/cata-

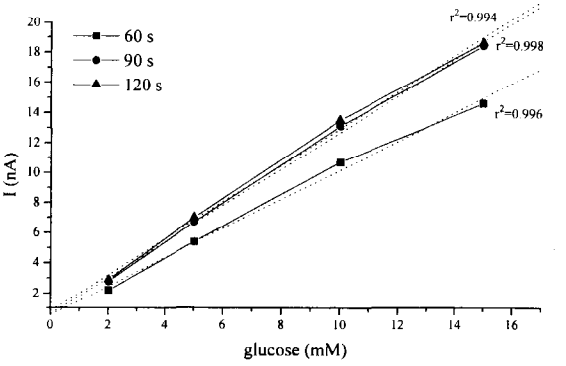

Fig. 6. Calibration curves after 60 (■), 90 (●) and 120 s (▲) from the introduction of the sample into the cell. The curves were obtained from a Versapor membrane with a GOD/catalase enzyme layer.

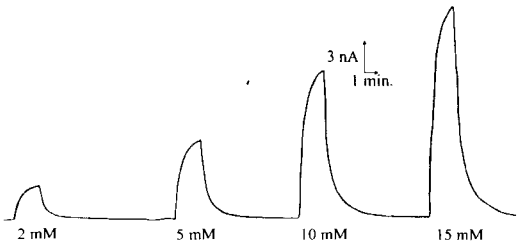

Fig. 7. Typical chart recording obtained from a Versapor membrane with a GOD/catalase enzyme layer.

lase. The signal was linear up to 15 mM (Fig. 6). The response rate was quite good, but return to baseline was worse than the Repel (compare Fig. 4b with Fig. 7). The medium intensity of the response was 10 nA for a solution 5 mM of glucose after 120 s, with a CV of about 5%. The calibration curve was constant for at least 2 weeks.

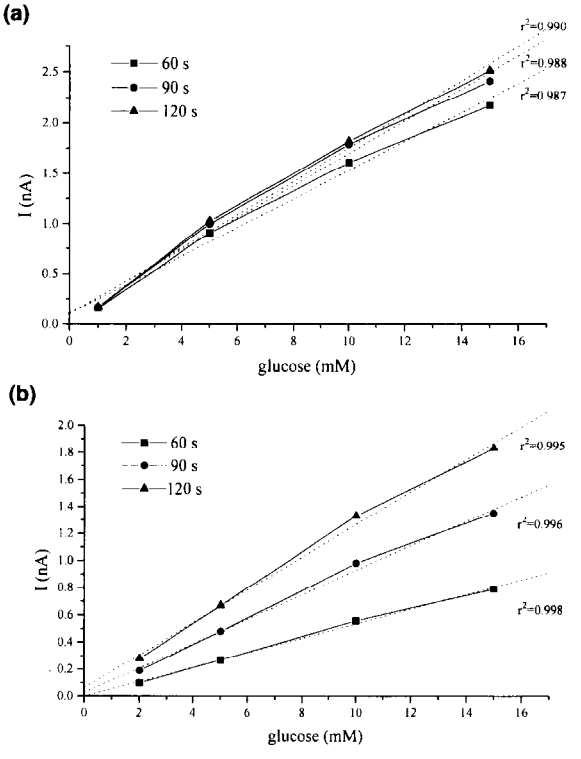

Fig. 8. Calibration curves after 60 (■), 90 (●) and 120 s (▲) from the introduction of the sample into the cell. The curves were obtained from a Repel membrane with a GOD enzyme layer. a, The external membrane was polycarbonate with a pore size of 0.03 μm; b, it was polycarbonate with a pore size of 0.015 μm.

4. Use of different polycarbonate membranes

Fig. 8 shows the results obtained with polycarbonate external membranes with pore size 0.03 μm and 0.015 μm. Using the 0.015 μm we noticed an increase in linearity (Fig. 8a) but at the same time the response rate and the washing rate greatly increased. Attention is drawn to the difference between the recorded current at 60, 90 and 120 s in Fig. 8a and b. With a 0.03 μm polycarbonate membrane, the current measured after 90 or 120 s were also very similar for the highest concentration, i.e. a plateau was reached. With the 0.015 μm, on the other hand, there was a large current variation during all the measuring intervals (Fig. 8a).

5. Conclusions

This research has shown that it is possible to obtain reliable results using the vapour tension of hydrogen peroxide and then completely eliminating interferences by any electrochemically active compound, namely ascorbic acid or acetoaminophen. However commercial membranes, generally used for separation purposes, are not completely suited for such a purpose. Thickness, pore size and hydrophobic treatment are very important features of the final membrane. In the composite membrane the presence of catalase mixed with glucose oxidase is of great importance for a practical glucose biosensor. The presence of it accelerates the response and return to base line. The results reported show it is possible to use this electrode in conjunction with and according to the measuring cycle of a well known commercial instrument developed for blood gas and electrolyte contents measurement of whole blood. Thus it is possible to answer the pressing medical need to develop an unique instrument measuring both blood gas parameters and glucose with a single

sample. It is our hope that in the near future such a sensor could be integrated into the same cell and exploited for glucose measurements in whole blood.

References

[1] A.P.F. Turner, I. Karube and G.S. Wilson (Eds.), Biosensors, Fundamentals and Applications, Oxford University Press, London, 1987.
[2] P. Vadgama and P.W. Crumps, Analyst, 117 (1992) 1657.
[3] S.J. Alcock and A.P.F. Turner (Eds.), Prospects for in vivo Sensors, Cranfield Press, 1995.
[4] J. Kulys, H.E. Hansen, T. Buch-Rasmussen, J. Wang and M. Ozsor, Anal. Chim. Acta, 288 (1994) 193.
[5] F. Cespedes, E. Martinez Fabregas and S. Alegret, Anal. Chim. Acta, 284 (1993) 21.
[6] Y. Zhang, Y. Hu, G. Wilson, D. Moatti-Sirat, V. Poltaut and G. Reach, Anal. Chem., 66 (1994) 1183.
[7] E. Csoregi, C. Quinn, D. Schmidtke et al., Anal. Chem., 66 (1994) 3131.
[8] G. Palleschi, M.H. Faridnia, G. Lubrano and G.G. Guilbault, Appl. Biochem. Biotech., 31 (1991) 21.
[9] S. Pan and M.A. Arnold, Anal. Chim. Acta, 283 (1993) 663.

ELSEVIER

Talanta 44 (1997) 1581–1604

Talanta

Analytical methodology for speciation of arsenic in environmental and biological samples

Marcela Burguera *, José Luis Burguera

IVAIQUIM (Venezuelan Andean Institute for Chemical Research), Faculty of Sciences, University of Los Andes, P.O. Box 542, Mérida 5101-A, Venezuela

Received 16 August 1996; received in revised form 18 February 1997; accepted 20 February 1997

Abstract

A literature search on the speciation of arsenic in environmental and biological samples shows an increasing interest of many researchers in the subject. Because of the low level of arsenic species in real samples, many problems related with its speciation remain unresolved: species instability during sampling, storage and sample treatment, incomplete recovery of all species, matrix interferences, lack of appropriate certified reference materials and of sensitive analytical methods, etc. These aspects are underlined in this paper. The continued development of new analytical procedures pretending to solve some of these problems claim for an up-to-date knowledge of the recent publications. Therefore, this paper pretends to review the latest publications on the chemical speciation of arsenic, emphasizing the increasing activity in the development of accurate and precise analytical methods. In most of the cases, separation and preconcentration is necessary, followed by element-specific detection for sensitivity improvement. Hydride generation following separation procedures (e.g., ion-exchange or high performance liquid chromatography) coupled to atomic absorption or atomic emission detectors proved to have sufficient sensitivity to monitor arsenic exposure, although restricts the analysis to hydride-forming species. Modified procedures including some kind of heating in the presence of highly oxidizing agents have proved successful to completely decompose the arsenic containing compounds to arsenate and so to extend the range of compounds which can be determined by these methods. On-line arrangements have the additional advantage of avoiding excessive sample handling, although some of them involve numerous steps and others are too costly to be recommended for routine use. The analytical figures of merits, specially detection limits are given for most of the methods in order to afford comparison and judge possible applicability. These studies, which have been approached in many different ways, would lead to knowledge that are determinant in the understanding of the cycle of this element in environment and of its physiological and toxicological behavior in the living organisms. © 1997 Elsevier Science B.V.

Keywords: Arsenic speciation; Environmental and biological samples; Analytical methodology

1. Introduction

The term 'speciation' in analytical chemistry, refers to the determination of different oxidation

* Corresponding author.

PII S0039-9140(97)00064-7

states of an element that prevail in a certain specimen or to the identification and quantification of the biologically active compounds to which the element is bound. Sparingly, in the investigation of toxic effects, the speciation of small molecules (organometallic compounds) is of concern, while for the study of the biological functions, the determination of large molecules has priority. This knowledge could help to explain the mobility, storage, retention and toxicity of the different species in different environments including the human body. The planning of the entire work, from sampling to the interpretation of data claim for an interdisciplinary research. Such studies require knowledge in the field of trace element analysis combined with experience in environmental and/or biochemical analysis [1].

Previously, the determination of total element concentrations was considered to be sufficient for clinical and environmental considerations. Although the total concentration of an element is still useful to know, and indeed is essential in many analytical schemes, the determination of species is an important task. The concentration of a toxic species is more relevant in the setting of environmental and biological standards than is the total elemental concentration. The collection, treatment and preservation of samples for quantitative analysis of species require careful consideration and planning. The nature of this task is very different from procedures for 'total' element determination, therefore analytical chemists are faced with very difficult problems in the acquisition of accurate data. Obviously, any procedure and apparatus adopted for sampling and the preservation of samples between the time of collection and the opportunity for analysis, should not disturb the equilibrium established among the species [2–4]. The introduction of biological contamination is equally undesirable, specially if the samples have to be stored for long periods; the presence of microorganisms and traces of oxygen might accelerate the deterioration of the sample, producing changes between species [4]. A holistic approach, which takes into consideration the various factors that influence the distribution of species of a given element before, during and after sampling is very much required. This is indeed essential if the results of experiments are to provide meaningful information that is indispensable for various studies. Speciation analysis involves a complex scheme of operations designed to simplify the analytical procedures to be implemented, but all, consist, in a way or another, in a separation step followed by the determination of the element in the different fractions. Despite the fact that the topic on speciation has been extensively documented in recent years in numerous publications, so far, there is no ideal method for any element speciation that unequivocally ensure high accuracy of the results. A closed look to the available literature on this subject shows the need for the availability of reference materials for quality control of particular species. Until now, most of the reference materials available for trace element determination in biological and environmental samples are only certified for the total element content [5,6].

A very tempting case to study for speciation is arsenic, which has an interesting behavior since: (1) it has different valence states, [As(III)/As(V)], interchangeable under certain conditions; (2) form small organometallic molecules which are biomarkers of exposure because, it is well known that in the mechanism of detoxification, inorganic arsenic is metabolized to monomethylarsonic acid (MMAA) and dimethylarsinic acid (DMAA); (3) is part of other organic compounds which remain unchanged in the body, like arsenobetaine (AsB), arsenocholine (AsC), arseno-sugars (AsS), arseno-lipids (AsL), etc.; (4) form macromolecular biomolecules, like those of arsenate bound to transferrin and hemoglobin [7]. The increasing interest in this topic is reflected in more than 500 papers, exhaustive reviews [8,9] and comprehensive monographs [3,10–12] published in recent years.

2. Concentration of arsenic species in biological and environmental samples

Arsenic is widely distributed in biosphere, thus the mobilization of the element by human activities (mining, smelting, glass making, refineries or pesticide manufacture) is estimated to exceed the

Table 1
Common arsenicals and their uses

Compound	Formula	Uses
Lead arsenate	$PbHAsO_4$	insecticide
Cupric arsenite (Schoele's green)	$Cu(AsO_2)_2$	pigment
Cupric acetoarsenate (Paris green)	$Cu(C_2H_3O_2)_2 \cdot 3Cu(AsO_2)_2$	insecticide
3-nitro-4-hydroxy phenylarsonic acid	$C_6H_6AsNO_6$	animal growth
Arsenilic acid	$C_6H_8AsNO_3$	animal growth and veterinary medicine
Arsenic oxides	As_2O_3 and As_2O_5	glass industry
Metallic arsenic	As	metallurgy
Arsenamide	$C_{11}H_{12}AsNO_5S_2$	veterinary medicine
Potassium arsenite (Fowler's solution)	$KASO_2$ (1%)	medicine
Arsenic sulfide	As_4S_4	fireworks
Gallium arsenide	GaAs	semiconductors
Diphenylchlorarsines (blue cross)	$(C_6H_6)_2AsCl$	chemical weapons
Alkyldichlorarsines (mustard gas)	$RAsCl_2$	chemical weapons
Melarsoprol	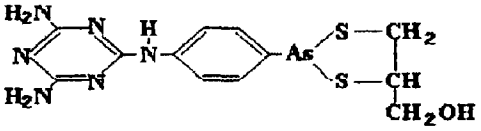	Medicine (sleeping sickness)
Carbarsone	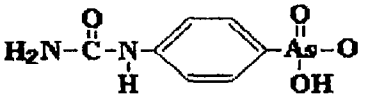	Medicine (intestinal amebiasis)

natural rate (from marine sedimentary rocks, weathering volcanic rocks or fossil fuels) by threefold; hence it might be anticipated that the distribution of the element in aquatic ecosystems and body fluids and tissues would be closely related to antropogenic activities [13,14]. As a result of the extensive use of the numerous arsenic compounds (Table 1), the element is found in a large variety of samples (fresh and sea waters, sediments, soils, plants, marine organisms, body fluids and tissues, etc.), in variable amounts and in a great variety of species.

In ground water, for instance, the levels of arsenic could exceed 20 mg l^{-1}, while in drinking water the concentrations may vary from 0.05 to over 60 mg l^{-1}. In some cases, these levels are two and even three orders of magnitude higher than those of most natural waters consumed by man [15,22]. Contamination of water and air near copper smelters in Argentina [15], Chile [16], USA [17] and Sweden [18] as well as the contamination of drinking water in Taiwan [19] and India [20–23] have been reported in numerous papers. In such samples, As(III) concentrations are normally only a small proportion of the total dissolved arsenic [24]. In an attempt to protect aquatic life as well as to establish a control over the implications of arsenic concentrations for public health, several international organizations [25–27], have prescribed a permissible dissolved, total arsenic

concentration in potable water between 0.008 and 0.05 mg l^{-1}. Despite the fact that it was known that different arsenicals exhibit very distinct toxicological properties, all regulations and reports related only to total arsenic and none differentiates between the toxic impacts of the various chemical species of arsenic [13]. Ingestion of contaminated ground water (containing arsenic of geological origin well above the maximum permissible limit), by people from several districts of West Bengal, India, resulted in excretion of inorganic arsenic and its metabolites in a proportion of more than 90%. It was reported that a daily intake of 1500 μg of inorganic arsenic (equivalent to drinking 1.5 l of water with an inorganic arsenic concentration of 1 mg l^{-1}) could produce signs of overt chronic arsenicism in some individuals [22]. Many of the affected people from India, usually drink more than 5 l per day and they showed serious signs of long-term arsenic exposure [20–23].

The concentration of arsenic in sea water is generally around 2 μg l^{-1} with the trivalent species being less than 10% of this level, while in normal soils the total arsenic concentration usually ranges from 1 to 40 μg g^{-1}, with higher levels in places where arsenicals are used for insect control or on disused mines tips. Certain plants growing on arsenic-enriched soils accumulate extremely high amounts of the element. Most human foods contain less than 0.5 μg g^{-1} arsenic, except those of marine origin which are more richer in arsenic than others. In marine animals and algae, because of biotransformation and accumulation, arsenic is present in organic forms and its concentration typically ranges from 1 to 100 μg g^{-1}. So, the total amount of arsenic ingested daily would be influenced by the amount and type of food included in the diet [28]. For instance, in rivers and soils it is present as arsenate, As(V), and arsenite, As(III); both inorganic species might be subjected to chemically and/or microbiologically mediated oxidation/reduction and methylation reactions, resulting in the transformation of inorganic arsenic in organic derivatives; simple methylated species (MMAA and DMAA) or more complex compounds (AsB, AsC, AsS, AsL, etc.) [29]. It is now certain that phytoplankton take up arsenate from aquatic environments, reduce it to arsenite and methylate the arsenite to produce MMAA and DMAA which are then excreted. This represents a mechanism of detoxification. Arsenobetaine, first reported as a major constituent of total arsenic in the tail muscle of the western rock lobster [30], the most frequently encountered water-soluble form of arsenic in higher aquatic organisms, is generally highly stable and is heavily bioaccumulated. This compound is believed not to be metabolized; after ingestion it is rapidly excreted unchanged in the urine [31]. Some studies, have however, demonstrated that arsenobetaine is unstable when irradiated with ultraviolet light alone [32] or in combination with an oxidizing agent [33]. Higher organisms also contain trimethylarsine oxide [29,34] and tetramethylarsonium ion [35,36]. There are also evidences of the presence of arsenocholine in seafood from polluted areas [37] and in dogfish reference material [38], although in lower concentrations than arsenobetaine. While some authors believe that this compound is also absorbed from the diet and it is partially transformed in arsenobetaine and trimethylarsine oxide [39], Shibata and Morita [36] demonstrated that trimethylarsonium ion and not arsenocholine was present in dogfish reference material. Undoubtedly, more work is necessary to solve these controversies. Arseno-sugars are others arsenic compounds in edible seaweed; there are evidences that the ingestion of seaweed may increase the urinary concentration of arsenic metabolites, one of which is DMAA [40]. Also the existence of arseno-lipids in marine and estuarine biota may be explained by the esterification of arseno-sugars. Although there is lack of evidence that the arsenicals present in foodstuff of marine origin do not cause any hazard to human health, the transformation among species might be taken into account and for reasons of toxicological reassurance should be determined by methods which can be routinely applied. From these statements, it seems clear that consumption of different kinds of food, water or beverages, as well as the amounts ingested, will affect differently the concentration of the different arsenic species in urine [34].

Arsenic is also present in the air at trace amounts, specially in the areas where its compounds are industrially used or where coal is burned. Its atmospheric concentration ranges from about 0.01 to 0.1 ng m^{-3} in clean areas such as Antarctica [41] and up to 500 ng m^{-3} near certain industrial environments such as copper smelters [42]. Particular attention must be paid to the measurement of these species while maintaining the initial As(III)/As(V) ratio during the sample collection, preparation and analysis steps. The average atmospheric concentrations of As(III) and As(V) were about 1.6 ± 1.4 and 5.4 ± 3.3 ng m^{-3}, respectively, in urban area of Los Angeles. Size-fractionated samples of atmospheric particulate matter were obtained employing a high-volume dichotomous virtual impactor as a sampler which allowed for the collection of a sufficient amount of sample so that both species could be routinely detected by HGAAS technique. Fine (< 2.5 μm aerodynamic diameter) and coarse ($>$ 2.5 μm) particles were collected employing different size filters with emphasis on the first fraction which is most efficiently collected in the lungs. This would help assess the impact of the potentially toxic species on human health. The data obtained indicate that both As(III) and As(V) species are present in ambient aerosol and that most of both species (about 75%) were found in the fine particle fraction. The primary source of arsenic in air is assumed to be As_4O_6, formed by the sublimation of As_2O_3 emitted from stationary high-temperature combustion processes (e.g., glass furnaces, primary metallurgical processes and fuel oil combustion) [43,44].

There are only limited studies on the arsenic distribution among different organs and body fluids. For example, the concentration of arsenic in urine of subjects without known exposure to arsenic is generally in the order of 10–20 μg l^{-1} while in the blood averages 0–12 μg l^{-1}, but intake of a meal of fish or shellfish may increase the total arsenic concentration to more than 50-fold, with no [45] or only two-fold [46] increase in excretion of methylated arsenic species. This invalidates the use of total urinary arsenic as an indicator of exposure to inorganic arsenic. In these cases it is advantageous to supplement the analysis with a more selective speciation. The results obtained by the application of such a method might be of interest if a person is suspected of being unable to methylate inorganic arsenic or of having a reduced ability to do so. One of the first studies of this kind determined the arsenic species (As(III), As(V), MMAA and DMAA) in urine of volunteers after ingestion of arsenite-rich wine (50 μg As), arsenate-rich drinking water (200 μg As) and crab meat (340 g) containing organo-arsenic compounds (about 2000 μg) [47]. Resulted that 10% of the arsenite was excreted as As(III), but the majority was methylated and excreted as MMAA and DMAA, 5 h after ingestion. Most of the arsenate was rapidly excreted without noticeable changes and only a small proportion was methylated, while the organic arsenic from the crab meat was quickly excreted without any change. Exposure to As_2O_3 in different industrial situations, results in increased urine arsenic concentrations, being inorganic arsenic, MMAA and DMAA the only relevant chemical forms; DMAA represented 60–70% of the total urinary arsenic elimination when comparing with the results from a reference population [45]. However, ingestion of seafood, even in such low amounts as 100 g, brings about a sharp increase in the total arsenic excretion; this is only confined to organic forms others than MMAA and DMAA. The time course of elimination of this dietary arsenic from the organism varies according to the load, but does not take more than 35–48 h. These results provide a simple tool to differentiate increases in urinary arsenic due to occupational or environmental exposure to inorganic arsenic from increases due to dietary intake of organic arsenic.

Some organic arsenicals have been extensively used as herbicides; it is likely to be present, together with inorganic arsenic species in soil samples. Extraction methods followed by spectroscopic detection have been applied with certain degree of success [48,49]. However, the differences between the soil types as well as the tedious clean-up of the arsenic residues are responsible for the low recoveries obtained.

The major problems in speciation studies are the immense hazards that exist due to contamina-

tion and losses of the element in the preparative steps of the sample for analysis. As these procedures require the use of various materials and reagents, highly pure materials and chemicals have to be made commercially available in order to exclude errors due to contamination. Large discrepancies are noted when comparing the data reported in the literature by different workers. The variations among workers may be due to two reasons: differences among the populations studied or inadequacy of the analytical methodology applied to the preparation of the samples for analysis. Although the first cause must be seriously taken into account, the latter seems more convincing; many researchers have experienced difficulties in the quantitative extraction of arsenic from the samples [13] while others claimed losses of volatile arsenic compounds during dry-ashing or heating with mineral acids [50]. To avoid these difficulties, investigators have also used nitric/sulfuric acids, both without catalysts [49] or in the presence of strong oxidizing agents like V_2O_5 [51,52], $K_2Cr_2O_7$ [51], $K_2S_2O_8$, H_2O_2, $K_2Cr_2O_7$, $KMnO_4$, V_2O_5, alone or in a mixture [53], claiming full recovery for all the species. Ultraviolet [33,39,53–56] or microwave [57–59] radiation and base hydrolysis [60] of the sample in highly oxidizing solutions have proved successful to completely decompose the arsenic containing compounds to arsenate. As photo-oxidation could result in the loss of potentially significant speciation information, less severe photolysis must be applied so that the presence of methylated arsenic compounds in marine waters could be detected in aqueous artificial samples [33,54], serum of uremic patients [55] or marine waters [56]. Also, to avoid the use of strongly reactive media resulted from digestion procedures, investigators developed methods for rapid solid-phase extraction of the non-toxic arsenic compounds from the matrix and the determination of the other arsenic species in the remaining portion [40,47].

Unless convincing evidence is given on the accuracy tests, the data obtained by any procedure could be dubious. Also it will be possible to reach solid conclusions only when sufficiently sensitive and selective analytical methods are developed. These methods must be capable to accurately distinguish between several forms of arsenic in different samples.

3. Analytical methodology for arsenic speciation

The numerous arsenic forms (Table 2) present in the environment and living organisms show large differences in their metabolism and toxicity [61]. Therefore, speciation studies are of critical importance. Also the arsenic species occur at very low concentrations so that reliable results are achieved only by means of very sensitive methods of analysis.

Table 2
Arsenicals of environmental and biological importance

Compound	Formula
Arsenious acid; arsenites; As(III)[a]	$HAsO_2$
Arsenic acid; arsenates; As(V)[a]	H_3AsO_4
Monomethylarsonic acid; (MMAA)[a]	$H_2(CH_3)AsO_3$
Dimethylarsinic acid; (DMAA)[a]	$H(CH_3)_2AsO_2$
Trimethilarsineoxide; (TMAO)[a]	$(CH_3)_3As^+O^-$
Tetramethylarsonium ion	$(CH_3)_4As^+$
Arsenobetaine; (AsB)	$(CH_3)_3As^+CH_2COOH$
Arsenobetaine; (AsC)	$(CH_3)_3As^+CH_2CH_2OH$
Arsenolipids; (AsL)	$(CH_3)_3As^+CH_2CHOHCOOH$ (trimethylarsoniumlactate)
Arsenosugars, (AsS)[b]	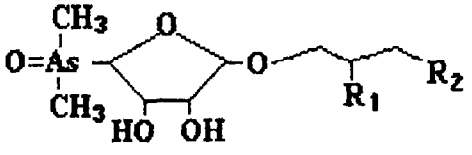

[a] Compounds forming gaseous species: As(III) and As(V) form AsH_3 (B.P. = −55°C); MMAA forms monomethylarsine (CH_3AsH_2 with B.P. = 2°C); DMAA forms dimethylarsine ($(CH_3)_2AsH$ with B.P. = 36°C); TMAO form trimethylarsine ($(CH_3)_3As$).

[b] R_1 = OH, R_2 = OH (Giant clams and algae); R_1 = OH, R_2 = SO_3H (Macroalgae); R_1 = NH_2, R_2 = SO_3H (Brown algae).

Arsenic (III) and (V) are the most often determined species in environmental waters, soils and sediments, while organic arsenic species are common constituents of biological tissues and fluids. Usually the concentration of these species is at low ranges and necessitates a preconcentration step because most of the available detectors still lack the sensitivity for direct determination. Moreover, these detectors are also deficient in selectivity, thus a separation step is required prior to determination. The most popular analytical methods used for arsenic speciation are based on a combination of a powerful separation process with an adequate element-specific detector. The methods frequently used for separation and preconcentration are solvent extraction, precipitation and coprecipitation, ion-exchange chromatography (IEC), gas chromatography (GC) and high performance liquid chromatography (HPLC).

Numerous instrumental methods have been developed either for the determination of total arsenic or its methylated and inorganic forms in soils and sediments, water, air and biological fluids and tissues. Among them, the most commonly used include ultraviolet spectrometry [62–67], electrochemical methods (EQ) [68–74], atomic absorption spectrometry (AAS) mainly coupled to hydride generation (HG-AAS) [75–111], in continuous flows or flow injection systems (FI), atomic emission spectrometry (AES), generally with inductively coupled plasma (ICP-AES) [111–130], ICP-mass spectrometry (ICP-MS) [111–114,124–130]], electrothermal-AAS in graphite furnace (ETAAS) [131–146], X-ray spectrometry [149,150], neutron activation analysis (NAA) [150,151], atomic fluorescence spectrometry (AFS) [152,153], capillary electrophoresis [155–157], etc. On-line combinations of some separation techniques (e.g., HPLC or IEC) with the most sensitive detection methods (AAS or ICP-AES) seem to be highly successful and lower detection limits are obtained, specially if HG is performed before detection.

3.1. Spectrophotometric and electroanalytical methods

The spectrophotometric methods used for the selective determination of arsenic, are usually applicable only to inorganic arsenic. They are based on the formation of colored complexes with certain ligands. For example, arsenic(III) forms a colored complex with silver diethylditiocarbamate [62–64] while As(V) forms arseno-molybdenum blue complex [65,66]. Based on the pH control and on the reduction characteristics of the borohydride ion, the former method was modified so that arsine was generated at pH 4.5 [63] or 6 [64] from As(III) and at lower pH from As(V) [63,64]. The resultant gaseous compound was quantitatively absorbed in silver diethylditiocarbamate solution and the molecular absorbance of the red complex was measured at 525 nm. This procedure is appropriate to determine 0.1 mg l^{-1} of arsenic, but it is susceptible to interferences from both, trace elements and methylated species. The latter method consists in the use of an oxidizing agent like permanganate [65] or iodate [66] to convert all arsenic present in the sample to As(V) used to form the blue compound and then measure the absorbance at 865 nm. As little as 0.005 mg l^{-1} of each species can be detected. Selectivity is achieved by on-line separation of the main interference phosphate, arsenate and silicate using a strong anion-exchange microcolumn located in the aspiration line of the FI system [65].

Also As(III) reacts quantitatively with potassium iodate in the presence of sulfuric acid releasing an equivalent amount of iodine which imparts a pink color to a carbon tetrachloride extract [67]. The absorbance is measured at 520 nm. The last procedure is more sensitive than the previously two already mentioned above; the amount of arsenic detected is 0.002 mg l^{-1}. Besides that the spectrophotometric procedures are less sensitive than other alternatives, they only apply to inorganic species, require long reaction times, and the procedures involve reduction, oxidation, chelation and sometimes extraction and evaporation steps which might disturb the equilibrium between species in the original sample leading to erroneous results and interpretations.

Among the electrochemical methods, differential pulse polarography seems to offer possibilities for quantifying arsenic in both oxidation states.

The procedure is based on the fact that only As(III) is electroactive and directly determined in perchloric or hydrochloric acids as supporting electrolytes [68,69], while total inorganic arsenic was determined after reduction with aqueous sulfur dioxide. As(V) was evaluated by difference. Sulfur dioxide was selected as reducing agent because it reduces As(V) rapidly and quantitatively and the excess reagent is readily removed from the reaction mixture. At low arsenic concentrations, which is really the case for environmental and clinical samples, the procedure is subjected to interferences from some elements present in the matrix {Fe(II) and Cu(II)}, therefore a separation step might be necessary; distillation of As(III) as $AsCl_3$ in concentrated HCl has proved appropriate [70]. Determination of methylated species is also possible by voltametric methods after separation by ion-exchange chromatography [68]. The detection limits of 18 and 8 $\mu g\ l^{-1}$ obtained for MMAA and DMAA, respectively, are far from being sufficiently low so that the procedure be applied for the direct determination of the arsenicals in natural waters. Additionally, before obtaining the analytical signal and after the separation of the species, there are other steps like digestion of each fraction in hot, concentrated perchloric acid, reduction with sulfur dioxide and removal of the excess reagent, each being a powerful source of errors. As As(V) is the stable oxidation state in natural waters and in biological digests, its reduction, at very low concentrations to the trivalent state is difficult and the use of reducing agents like iodide, hydrazine, Cu(I), etc., interfere with the stripping process. Therefore, oxidation of As(III) which takes place spontaneously in the presence of dissolved oxygen is preferred since some investigations on gold-coated platinum-fiber electrodes have shown that As(V) can also be reduced to elemental arsenic provided that extremely low reduction potentials are used (-1.60 V versus Ag/AgCl electrode) [71]. So, as As(III) is easily reduced at a gold electrode, it ought to be possible to determine As(III) in the presence of As(V) by suitable choice of the electrolysis potential. Some voltametric procedures for the determination of As(III) and As(V) have been considered in an expert system developed using KES (knowledge engineering system) [72].

However, given all the difficulties mentioned above, specially those concerning interferences due to complex matrixes or to the presence of certain reagents, the electrochemical methods are not used for routine analysis in the speciation and determination of arsenic in complex matrices samples.

A combination of electrochemical and spectrophotometrical detection for As(III) and As(V) following ion chromatographic separation, respectively, permitted the sequential determination of arsenite and arsenate in water samples [73]. The detection limits were found to be 2.9 and 13 $\mu g\ l^{-1}$ while the recoveries for spiked waste water samples were in the ranges 97.5–104% and 93.5–103% for As(III) and As(V), respectively. In a recent work, Boucher et al. [74] succeeded to differentiate six arsenic species (As(III), As(V), MMAA, DMAA, AsB and AsC) by ion-pair reversed-phase liquid chromatography coupled with amperometric and ultraviolet detection. Arsenobetaine and As(III) were not separated and only As(III) is amperometrically active. The limits of detection ranged from 0.1 μM for As(III) to 1.0 μM for As(V), the method being adequate for the detection of typical arsenical concentrations of 20–50 $\mu g\ l^{-1}$ in normal urine.

3.2. Hydride generation-atomic absorption spectrometry.

The most widely accepted procedures for the analysis of arsenic at $\mu g\ l^{-1}$ level exploit the reduction of some arsenic compounds to gaseous arsines (Table 2). The gas is then thermally decomposed to give elemental arsenic for atomic detectors like AAS, or ICP-AES. Early methods for arsine generation involved the dissolution of metals (Zn, Mg, Al) in mineral acids to form nascent hydrogen which reacts with As(III) to form AsH_3. Other hydride ion precursors that have found use in generating hydrides are $TiCl_3$ [75], $SnCl_2$ in concentrated HCl [76] or Al in basic medium known as Fleitmann reaction [77,78]. The effective reaction with $NaBH_4$ gained acceptance and is now almost universally used for the generation of hydrides ever since its introduced into analytical chemistry [79]. It is well known that

trivalent and pentavalent arsenic show different behavior in the generation process, although it was claimed that some procedures only measure the total content of As in the sample. However, it was demonstrated that even at high concentrations of borohydride and at optimized acid concentrations, the response obtained from As(V) is 10% lower than that of As(III) [80]. The process of formation of arsine from As(V) suggests that there are two steps in the reaction: the reduction of As(V) to As(III) and the subsequent formation of AsH_3. The rates of the redox reaction that involve electrons transfer are rather slow and pH dependent, therefore it appeared that it might be possible to differentiate between the two species provided that the first stage of the reaction is slower than the second at high pH values. Therefore, differentiation is made possible using pH-selective arsine generation technique, in which, for As(V) strongly acidic solutions are required ($pH \leq 1$), while for As(III) hydride formation occurs in solutions up to pH 5 [81–87]. MMAA and DMAA are also reduced to the corresponding hydrides at pH 1. Furthermore, it is not only the pH that affects the speciation, but other factors such as kinetics and complexation are also involved [88,89]. Several researchers, each using their own procedure, came to different conclusions concerning the redox stability of aqueous solutions containing arsenic species and the time scale on which spontaneous changes in species distribution occurred [83,88].

There are two major operation modes of hydride generation systems, batch and continuous modes; both involve reduction of an acidic sample followed by the transport of the hydride to the atomizer. In the batch mode, acidified sample and reducing reagent are injected into a reaction vessel and any hydride produced is purged and carried by a stream of an inert gas, while in continuous systems, acidified sample solution and reductant are continuously delivered for the production of hydride and the gas is separated from the liquid waste in a gas-liquid separator (GPS) also with the aid of a carrier gas. The last mode has two versions: continuous flow and FI.

The hydrides generated in batch systems are either directly delivered to the detector or collected either in a container under pressure together with the hydrogen gas produced in the reaction or in a cold trap for preconcentration when high sensitivity is required. Then, are directly swept into the atomizer or are released via a chromatographic column which separates the products [81–85]. In such systems, peak height and shape are critically dependent on some factors which are difficult to control. However, each instrumental setup can be optimized either to yield a high hydride concentration to attain a high sensitivity or to provide the appropriate conditions to eliminate or at least to suppress the effect of varying matrix components. A strict control of the experimental conditions permits the volatilization of hydrides from As(III) and from the methylated species in a single sample aliquot due to the differences in their boiling points (Table 2). The arsines, together with water vapors, carbon dioxide and any other vapor generated during the reduction reaction are freezed-trapped and sequentially volatilized for elemental determination by AAS. These features have been described by several researchers [81–87]. The use of liquid nitrogen traps has greatly improved the sensitivity of the technique since the volatile arsines are preconcentrated over a period of 5–10 min from a large volume of sample and ultimately passed as a 'plug' of analyte to the detector. Temperature-controlled selective volatilization from the trap makes it possible to differentiate between the different arsenic species, but the other frozen gasses are also released. To prevent freezing of the water vapors in the cold trap, some hygroscopic materials are used to dry the gases. Calcium chloride was mostly used but after several determinations become wet and thus impermeable to argon. This often causes a back-pressure which can blew off the system [90]. Frequent replacement is therefore necessary and loss of arsines is reported. Van Elteren et al. [82] interfaced a novel drying system composed by a commercially available hygroscopic ion exchange membrane and separates the organic compounds without losses of the arsines. The separation of the trapped compounds is carried out under non-isothermic conditions and the low-boiling gases volatilize out of the trap in 10–30 s. A slow heating rate is optimum since at

high heating rates the separation can become poorer and thermal decomposition might take place with subsequent loss in sensitivity [91]. However, the heating rate is greater than 100°C min^{-1} in any case, since the trap is heated from −195 to approximately 60°C in 1–2 min. Apart from being less precise than the selective reduction procedures, these approaches have other problems associated, like the molecular rearrangement during HG and incomplete collection of the hydrides. Insufficient selectivity during the reduction step is another drawback; at pH 5 only As(III) is reduced but MMAA and DMAA to a certain degree as well [82]. The complexity of the system makes on site speciation impossible which implies storage of sample prior to analysis; speciation alteration has to be faced then, in particular for As(III). The generally applied cold trap is U-shaped and made of glass; the relatively high thermal resistance of glass makes cooling and especially heating a slow process at room temperature. In order to achieve better trapping, the tube was half-filled with glass beads, although it was reported that arsines are irreversibly captured by this material [83,92]. Better, more efficient and more reproducible arsines separation was achieved when using the U-tube packed with a gas chromatographic support. The use of a Teflon-lined stainless steel U-tube with a gas chromatographic solid phase permits faster cooling and heating [82–85]. Some kind of electrical heating was also applied to volatilize the species. These systems are also subjected to interference effects and their precision and recovery are strongly dependent on the experimental conditions such as flow of carrier gas, rate of thermal desorption, type of absorbing phase and size of column. Most of these difficulties have been overcome by using an automated and on-line HG-cryogenic trapping followed by MW irradiation to release the hydrides for AAS detection [93].

The use of continuous systems allow minimum sample handling, being less likely to suffer from the problems of contamination or alteration of arsenic speciation. Also continuous flow methods, mainly flow injection, appear to be more tolerant to the presence of nitric acid and to be less prone to transition elements interferences. This effect, at least in part, is due to kinetic discrimination; the reduction of the element to its hydride is completed before reduction of the transition metal ion. The kinetic discrimination in flow systems is responsible for the pronounced difference in sensitivity between the two oxidation states (at least one order of magnitude), so that a pre-reduction step is mandatory. In some procedures, As(V) is reduced to As(III) prior to HG by the use of reducing reagents like: KI [94], thiosulphate [95], or mixtures of KI-ascorbic acid [95] and L-Cysteine [96–99] to achieve pre-reduction for the determination of total arsenic. L-Cysteine was found to be clearly superior as reductant and releaser since provides greater freedom from interference and much better stability of solutions with low concentrations of analyte. The reagent consumption and particularly the acid concentration are significantly lower, which permits the change from use of highly corrosive solutions to solutions of low acidity and low toxicity. This is of advantage for the operator and for the instrumentation, it reduces the cost per determination and produces less hazardous waste. However, controlling the acid nature and concentration, no prereduction is necessary to improve the kinetics of hydride from As(V) [93,100,101]. Such procedures were used to determine As(III), As(V), MMAA and DMAA [93,100], as well as total arsenic and inorganic As(III) and As(V) by either FI or continuous flow HG-AAS in water samples [101]. Although simpler to operate and easier to automate, these systems are limited in their ability to obtain a correct speciation of As. In the presence of MMAA and/or DMAA, As(III) or As(V) will be overestimated. The error will be function of the pH values chosen for the selective volatilization of the inorganic arsenic species and of the amount of organic arsenicals present.

Brannon and Patrick [102] inserted a H_2SO_4 trap between the hydride generator and the AAS to separate alkylarsines from inorganic arsines. While AsH_3 passed through, the alkylarsines were trapped. However efficient, this system does not allow for the identification of the organic arsenicals present. Improved sensitivity was obtained for all the arsine forming species after IEC separation [33,103–105]. The fractions containing ar-

senic species were submitted to hydride generation in batch [33], in a FI system [102,103] or in an on-line arrangement [104]. Although the detection limits, in all cases, are in the range of the ng levels, the methods are only applicable to studies related to arsenic exposure and its monitoring.

Determination of ultra-trace amounts of As(III) (detection limit = 0.003 μg l^{-1})was recently achieved by FI-HGAAS prior on-line preconcentration by coprecipitation with lanthanum hydroxide or hafnium hydroxide [106].

During the last decade HPLC methods have been reported to be capable of separating the most commonly found arsenic species in samples of different types. They offer the advantage of minimizing chemical interferences and rearrangement reactions. However, the time required for the overall analysis is in the range 10–300 min, limiting their usefulness for routine applications. Furthermore, due to the high dilution factors always associated with conventional chromatographic separations, the most sensitive and specific detection techniques such as HG coupled to Flame-AAS, ICP-AES or ETAAS are needed to compensate for dilution. Also the eluents typically contain high concentration of salts which quickly build up on the nebulizer, ICP torch and/or sampling cones of the ICP-MS interface, leading to instrumental drift. HG following HPLC separation, eliminates this problem because the arsenic is converted to its gaseous hydride which is separated without the associated dissolved solids. In the application of coupled techniques care must be taken in the design of the interface, so that the flow rate of a gas or liquid through the chromatographic column must be matched or adjusted in some manner to the gas or liquid uptake rate of a particular detector [2].

Several systems have been developed, based on post-column HG for the determination of the four arsine-forming species in natural waters [107], brawn algae [108], urine [109,110], etc. Hakala and Pyy [109] used an HPLC coupled to a continuous flow system for HG and tetrabuthylammonium ion in phosphate buffer as the ion-pairing agent in the C18 reversed-phase column to determine arsenic metabolites in urine. Matrix interferences from urine samples with different salt content occurring in the separation of arsenic species can be reduced by matching the samples with the mobile phase and by using a relatively low injection volume. The detection limits were 1.0, 1.6, 1.2 and 4.7 μg l^{-1} for As(III), As(V), MMAA and DMAA, respectively. An automated and direct HPLC-FI-HG-AAS method was developed and statistically validated for the assessment of inorganic arsenic and its metabolites in urine [110]. The detection limits of this procedure were compared with those obtained by directly coupling the HPLC column to an ICP spectrometer. The limit of detection of the FI-AAS system is approximately 35 times lower than that of the ICP-AES system, but still not low enough to be able to detect arsenic compounds in urine from non-exposed persons. Therefore, these methods are not applicable to the analysis of urine from normal persons, but could be useful in analysis for arsenic species in urine from highly exposed persons, or persons suspected of being unable to, or having a reduced ability to methylate inorganic arsenic compounds. The major limitation in using HG as a part of the HPLC separation-element specific detector is that many environmentally and biologically important organoarsenic compounds such as AsB, AsC, tetramethylarsonium ion, AsS, etc., do not form volatile arsines and would not be detected. To solve this problem, an appropriate decomposition procedure is required.

An on-line HPLC-microwave-oven (MWO) oxidation with persulphate and HGAAS detection has been successfully applied for the determination of arsenite, arsenate, MMAA, DMAA, AsB and AsC in environmental samples [55]. An anionic cartridge located before the HPLC anionic column, quantitatively retained arsenite, arsenate, MMAA and DMAA. The AsB and AsC which passed through, were separated in the HPLC column, eluted and, each fraction, microwave irradiated after mixing with persulfate for their oxidation to arsenate. The conversion efficiency was reported to be closed to 100%. The solution from the MWO was cooled in an ice bath and mixed downstream with acid and borohydride to form the arsine which was swept into an AAS atomization cell. To determine the anionic species, the same procedure was followed, except that the

anionic cartridge was removed, and water was introduced instead of persulfate. The detection limits were between 0.3 and 0.9 ng (for 100 μl sample). A similar procedure was developed by Le et al. [111] except that they used a dual system to avoid removal of the cartridge during the procedure. Comparable resolution was obtained by using HPLC-separation-MW-digestion with HGAAS or ICP-MS detection. Complete separation of five arsenicals was achieved on a reversed phase C18 column by using sodium heptanesulfonate as ion pair reagent and the detection limits were for example 10 μg l^{-1} for arsenite, DMAA and AsB, 15 μg l^{-1} for MMAA and 20 μg l^{-1} for arsenate.

3.3. Inductively coupled plasma-atomic emission spectrometry

The detection limits achieved in an ICP-AES system are far too high to allow detection of the low concentration of arsenic species present in urine of normal persons. Additionally, when ICP-AES is used for detection, a severe interference by background ions strongly degrades the detection limits. The single ^{75}As isotope has an interference from $^{40}Ar^{35}Cl$ species which has the same mass-to-charge ratio as that of monoisotopic arsenic [112–114]. The extent of this interference is such that the direct determination of the analyte is impossible. In the determination of total arsenic this interference has been eliminated by the addition of nitrogen to the argon carrier gas [115]. Nitrogen addition was found to reduce analyte sensitivity, which made the technique unsuitable for analysis at the required levels. A substantial increase in sensitivity has been reported when using HPLC in combination with HG-ICP-AES [112,116,117]. In the HG step, the concentration of the HCl used is relatively high; as a result, the conventional GLS produces a 'residual aerosol' which is transported to the torch and converted into the interferent. Therefore, HCl should be replaced by mild HNO_3 and L-Cysteine be used as reductant and releasing agent. In that way, the interference from Ar^+Cl^- is avoided and, based on the kinetical reduction, simultaneous determination of As(III) and As(V) in waters was possible without interferences from transition elements [99]. The detection limit for As(V) was 3.4 μg l^{-1} and for As(III) 0.7 μg l^{-1}. Also the effect of the 'residual aerosol' can be eliminated by using microporous membranes as GLS [118,119]. Some workers suggested that selectivity could be improved by an initial separation of the analyte from the matrix (e.g., solvent extraction) followed by the generation of the hydride directly from non-aqueous media and the detection of the analyte by ICP-AES [120,121]. There are some advantages of these applications: (i) a straightforward combination of liquid–liquid extraction with HG to overcome matrix interferences and (ii) the opportunity to determine hydride forming elements in organic samples and solvents directly, without resorting to lengthy re-extraction procedures. The introduction of organic solvents into ICP presents particular difficulties and therefore, the use of miscelles and other organized media with a hybrid aqueous/organic character, could prove advantageous. Arsine can be generated with sodium borohydride from a didodecyldimethylammonium bromide (DDBA) vesicular medium [122]. It was found that the analytical performance of this vesicles-enhanced method is superior to the HG from aqueous media. No speciation studies have been reported, although the detection limits were improved by a factor of two compared with those observed when arsine was generated from aqueous medium, and greater tolerance to interferences was observed [121,122].

However, the most direct method for dealing with this interference is to use a high resolution mass spectrometer. Since the advent of the combination of ICP with MS, exceptionally low detection limits have been achieved [99,111–114,124–127]. Coupling HPLC to ICP-MS, the simultaneous determination of up to six compounds was possible in about 10 min with detection limits in the range few picograms. These values are sufficiently low to study the chemical species at their naturally occurring concentration levels. Also the speciation of arsenosugars in marine reference materials by HPLC-ICP-MS has been recently reported [127].

The cost of an existing commercial ICP-MS instrument makes it one of the most expensive HPLC detector and it may not be realistic to use it in routine analysis or for environmental monitoring. Unless a previous separation technique is used prior to the detection by ICP-AES, the use of HG is mandatory, limiting the method, as in the case of HGAAS, to the speciation of arsine-forming compounds, thus leaving valuable information behind. So, coupling IEC with ICP-AES simplified the process and overcame the interference of Ar^+Cl^-, as it does when coupled to ICP-MS [128]. Optimizing the two systems and using an ultrasonic nebulizer, it was possible to reach detection limits in the range of ng l^{-1} for As(V) and MMAA [129]. The procedure was completely automated for sample retention, elution and regeneration of the resin.

3.4. Atomic absorption spectrometry with electrothermal atomization (ETAAS)

Although the detection of the separated species using on-line techniques, like those described above is ideal, ETAAS is still advantageous because of its sensitivity (two orders of magnitude higher when compared with flame-AAS) and ease of operation. Furthermore, the instrumentation is available in many laboratories. However, this technique has proved limited potential for speciation, apart from being prone to errors owing to pre-atomization losses and to the fact that different arsenic compounds produce different ETAAS responses. Larsen found that using conventional STPF furnace program, calibration for all species was possible with standards prepared from only one calibrant, e.g., arsenate, but the operation of the instrument is relatively slow [131]. He studied the conditions under which ETAAS gives equal and optimum sensitivities for all the arsenic species under study. To improve sample throughput, a fast furnace program that includes the use of a chemical modifier, shorten the time needed for analysis and makes calibration of all species possible using two arsenic species as calibrants, i.e., one for the quaternary arsonium compounds and one for the other species. However, systematic investigations on the behavior of arsenic species in graphite furnace are lacking. Krivan and Arpadjan [132] studied the influence of different matrices (HCl, NaCl, HNO_3 and urine) and of various chemical modifiers (W, Pd and a mixture of W + Pd + citric acid) on the behavior of As(III) and As(V) in the graphite furnace by means of an ^{75}As radiotracer. Different treatments of the pyrocoated tubes showed to thermally stabilize the arsenic species. Such is the case of Ce(IV) [133] and tungsten-carbide coated tubes [134] which improved the responses from arsenite, arsenate, MMAA, DMAA. No pronounced stabilizing effect was observed for AsB and AsC without the addition of palladium chloride to the treated tubes [134]. Aqueous and methanolic solutions of these species were studied because they are the main components of the various extraction systems and HPLC effluents. Attention was directed to a detailed investigation of the pyrolisis stage, which is the most critical step for the analysis of highly volatile species. An attempt to separate in situ As(III) from AsB in W-treated tubes failed because, the authors claim, of the presence of significant amounts of AsB under the conditions used for As(III) determination.

Nevertheless some of the arsenic species occur in some samples at such low concentrations that even ETAAS cannot provide sufficient sensitivity, so that preconcentration procedures have to be combined in order to achieve the required detection power. Attempts to preconcentrate water samples by evaporation before injection onto the furnace have resulted in losses of arsenic and in redox reactions affecting the ratio of species. Many separation-preconcentration schemes, followed by ETAAS detection, include thin-layer chromatography [135,136], or coordination of the species to organic molecules and extraction in organic solvents [137–141], precipitation or co-precipitation [142], adsorption on surfaces like those of ion-exchange resins [143,144] or HPLC columns [145,146].

Extraction as a means of separation and preconcentration of species has been applied most often to solids such as soils, sediments, particulate matter filtered from water and air or biological tissues. A number of extractants have been used by many researchers as a means of selectively

removing the species from the bulk of the sample and also as a means of preconcentration prior to the quantification by ETAAS. Since As(V) cannot be extracted from acidic media, only As(III) could form the ammonium tetramethylenedithiocarbamate complex which is extracted into chloroform and then, is selectively quantified. Prior to the extraction, however, As(V) can be reduced with potassium iodide, thiosulfate, L-Cysteine, or mixtures of hydrogensulfite–thiosulfate and iodide–ascorbic acid. In this case, both oxidation states are determined simultaneously and the As(V) concentration is quantified by difference. Ammonium pyrrolidinedithiocarbamate (APDC) and *o,o*-diethylditiophosphate have been also used as chelating agents for the extraction of As(III) into chloroform followed by back-extraction into an aqueous phase [137].

As(III) is also separated by solid–liquid extraction with sodium diethylditiocarbamate (NaDDC) into methyl isobuthyl ketone (MIBK). Aliquots of the organic phase are determined by ETAAS using palladium in MIBK as chemical modifier. Total arsenic is determined using slurry sampling and Pd-$Mg(NO_3)_2$ to stabilize the arsenic [138]. Extraction of arsenite with sec-butyl dithiophosphate followed by the determination of arsenic in the extract by ETAAS [139] is another mean of inorganic arsenic speciation. These procedures are time consuming because they involve multi-step procedures and usually permit only a moderate preconcentration because there is a limited ratio of organic to aqueous phase that can be reliably handled. The on-line combination of liquid–liquid extraction principles with sorption on a solid phase column material permits the use of a wide selection of functional groups. Rapid and complete elution prevents extensive dispersion of the sample, such as in chromatographic systems. The use of a flow injection on-line separation of As(III)-diethylditiocarbamate complex sorbed on a C18 reversed phase packing (bonded silica with octadecyl functional groups), reduction of As(V) with a sulfite-thiosulfate-iodide solution and preconcentration for ETAAS allows the determination of As(III) and total arsenic in a short time [89]. The fast complexation and sorption (approx. 100 ms) maintain the natural equilibrium between species and prevents their shift during the analysis. One of the main advantages of the on-line technique is that preconcentration takes place in a closed system, avoiding any exposure of the sample to atmosphere. Because of this greatly reduced risk of contamination, very low and reproducible blank values can be obtained. Sample loading, column washing, elution and sample transfer are operations on-line which leads to enhanced precision and accuracy compared with manual batch procedures for sample treatment. Equilibrium needs not be attained because of the exact timing of all process. The strict reproducibility of the process excludes interferences due to kinetic effects. The total time for sample treatment fits well into the running time of a standard graphite furnace program.

A reliable analytical procedure aimed to separate arsenic species in waste and potable waters: it involves a separation step on an extraction chromatographic column filled with a support modified with dioctyltin dichloride [140]. This arrangement selectively extracts As(V) which is eluted from the column with HCl. The effluate containing As(III) and the eluate containing As(V) are then determined by ETAAS in the presence of a mixed modifier of Pd, W and citric acid.

It can be concluded that the extraction procedures mentioned above apply only to inorganic arsenic species. A recent work [141], however, confirmed the suitability of the application of an extractive procedure to the methylated arsenic species. Only inorganic arsenic, MMAA and DMAA were quantitatively extracted in toluene from acidified urine samples, then were stripped from the organic solvent with diluted nitric acid and detected by ETAAS in the range 10–50 μg l^{-1}. None of the other known organic arsenicals were extracted. The results were in good agreement when compared with those obtained by HPLC-ICP-MS and the extractive procedure was recommended for the evaluation of occupational exposure to inorganic arsenic.

Chen et al. [142] determined As(V) and As(III) species in environmental samples by ETAAS after coprecipitation with zirconium hydroxide and were able to differentiate between As(III) and

As(V) by using different temperature programs in the graphite furnace.

Pacey and Ford [143] and Grabinski [144] used the strong affinity of arsenic species for certain ion-exchange resins to completely separate four arsenic species and measure the analyte content in each fraction by ETAAS. These systems gave better detection limits and/or shorter analysis times than the extraction procedures.

The fairly long time required for the analysis of a series of collected fractions may be inconvenient for practical analytical work. More work is needed in this direction to fully exploit the potentiality of ETAAS for speciation. Probably coupling ETAAS directly with HPLC might be the answer; interfacing a stepwise operational procedure (ETAAS) with a continuously flowing effluent from the HPLC column is a real analytical challenge. Although the work reported until now [145,146], do not give experimental details on the instrumental arrangement, making this type of coupling it is not impossible [147,148].

3.5. Other methods

Apart from the procedures described above, and which are massively studied, there are scarce data in the literature about other potential techniques, like neutron activation analysis, mass spectrometry, X-ray crystallography, NMR and IR spectroscopy, etc., which can be used in arsenic speciation. This is probably because the amount of sample per analysis for some of them, as well as the availability of sophisticated and costly instruments in many laboratories are the limiting factors.

Coprecipitation with dibenzildithiocarbamate(DBDTC) and hydrated iron(III) oxide for As(III) and As(V), respectively, followed by the determination of arsenic by X-ray spectrometry was reported [149,150]. Detection limits as low as 0.02 $\mu g\ l^{-1}$ have been obtained. These procedures are also limited to the inorganic species only, although investigations on the behavior of some other arsenic species, e.g., MMAA and DMAA, showed that MMAA is coprecipitated quantitatively with DBDTC when a strong reducing mixture of iodide and thiosulfate was used to reduce As(V) to As(III), while DMAA is not coprecipitated at all. This implies that MMAA interferes in the determination of As(V) [150]. The precipitates were collected successively on membrane filters and arsenic determined by NAA of the filters and subsequent γ-spectrometry.

Extraction and preconcentration of arsenic species prior to irradiation were deemed necessary in NAA methodology, because firstly, the oxidation states of arsenic in the original samples irradiated cannot be distinguished after radiochemical separation and secondly the use of large volumes of samples for irradiation without preconcentration is unsuitable due to the small concentration factor involved. The separation step is also ideal to create an interference-free environment in the matrix during the activation period. The selective extraction of the ammonium tetramethylenedithiocarbamate complex of As(III) into chloroform and the detection of arsenic by NAA after back-extraction was reported by Yusuf et al. [151]. Reduction of As(V) to As(III) was achieved with thiosulfate. Marine samples were subjected to microwave radiation choosing a suitable program to prevent the change in oxidation states of arsenic species during the heating process.

Contrary to AAS, AFS has not been widely used in speciation studies because of its low sensitivity when HG is coupled to introduce the analyte in the diffusion flames normally employed as atom cells for this technique. However, the detection limits have been recently improved, because high-intensity excitation sources e.g., boosted-discharge hollow cathode lamps, have become commercially available [152]. When coupled with HPLC, the fractions could be efficiently nebulized into the flame, and so, AFS becomes a powerful tool for arsenic speciation, achieving detection limits as low as 35, 50, 20 and 20 ng for As(III), As(V), DMAA and MMAA, respectively, in 250 μl of volume injected [153]. The analytical potential of such hybrid techniques has been recently illustrated on coupling vesicle-mediated HPLC to low-power argon microwave-induced plasma (MIP) for mercury and arsenic speciation. A HG technique was used as interface between the exit of the HPLC column and the MIP held in a

Table 3
Analytical details of arsenic speciation in different samples

As species (samples)	Matrix	Measurement technique	Some details of the procedure	D.L. ($\mu g\ l^{-1}$)*	Ref.
As(III), AsT	Waters, sediments, synthetic mixtures	UV-vis	Red complex with diethyldithiocarbamate ($\lambda = 525$ nm) Also arsine absorbed on ligand solution	100	[62–64]
As(V), AsT	Waters	UV-vis	Molybdenum blue complex ($\lambda = 865$ nm) Use of oxidizing agents.	5	[65,66,70]
As(III)	Polluted water	UV-vis	Indirect determination. Reaction with iodate in H_2SO_4-I_2 give a pink color to a CCl_4 extract. ($\lambda = 520$ nm)	2	[67]
As(III), AsT	Synthetic mixtures, SRM	EQ	In voltametric methods only As(III) is electroactive using $HClO_4$ or HCl as supporting electrolytes (As(V) is reduced with SO_2).	N.I.	[68,69]
MMAA, DMAA	Synthetic mixtures	EQ	Differential pulse polarography applied after separation by IEC	18, 8	[68]
As(III), AsT	Seawater, urine	EQ stripping	In the presence of As(V) by suitable choice of the electrolysis potential. (60 s electrolysis)	0.1	[71,72]
As(III), As(V)	Waters	EQ+UV-vis	Following IEC	2.9, 13	[73]
As(III), As(V), MMAA, DMAA, AsB, AsC	Urine	EQ+UV-vis	Coupled to ion-pair reversed phase liquid chromatography	0.1–1 μM	[74]
Soluble As	Soils	HG-AAS	Continuous flow HG-AAS. Selectivity based on pH selective reduction	0.90 all	[64]
As(III), As(V)	Sediment interstitial waters	HG-AAS	As(III) coprecipitated with dibenzyldithiocarbamate in methanol and As(V) with sodium molybdate and tetraphenylphosphonium chloride. (The filters were digested)	N.I.	[82]
As(III), As(V)	Waters	FI-HG-AAS with CT (Fleitmann reaction)	An electrically heated Al column was used to generate arsine in alkaline medium.	0.25	[77]

Table 3 (continued)

As species (samples)	Matrix	Measurement technique	Some details of the procedure	D.L. ($\mu g\ l^{-1}$)*	Ref.
MMAA, DMAA	Sediment interstitial waters	HG-AAS with CT	AsH_3 generated in continuous flow (released on progressive worming at room temperature)	0.05–0.13	[82]
As(III), As(V), MMAA, DMAA,	Interstitial water	HG-AAS with CT	AsH_3 generated in continuous flow using pH selective procedure, trapped in liquid nitrogen (released on progressive worming at room temperature)	0.019–0.061	[86]
As(III), As(V), MMAA, DMAA,	Waters	HG-AAS with CT	Arsines generated 'in batch' by pH selective procedure and trapped in liquid nitrogen (released on electric heating)	1 ng each (up to 70 ml sample)	[91]
Inorganic As, MMAA, DMAA	Waters	HG-AAS with CT, GC separation	Arsines generated 'in batch' by pH selective procedure and trapped in a GC column in liquid nitrogen (released on progressive heating up to 150°C)	0.01 each	[85]
As(III), As(V), MMAA, DMAA,	Soil extract, water	HG-AAS with CT and GC separation	Arsines generated 'in batch' by pH selective procedure and trapped in a GC column in liquid nitrogen (released on electric heating) (Flame-in-tube burner for AAS)	0.026	[84]
As(III), As(V), MMAA, DMAA	Urine	HG-AAS with CT and GC separation	Arsines generated by FIA, cryogenically trapped in a GC column and released on heating in water bath)	N.I.	[98]
As(III), As(V), MMAA, DMAA	Urine	IEC-FIA-HG-AAS	Separation on a GC column. Determination of As in the fractions by FIA-HG-AAS	2 each	[103,104]
As(III), As(V), MMAA, DMAA, AsB and AsC	Urine, waters, synthetic fish and sediment extracts	HPLC-HG-AAS	On-line HPLC, microwave oxidation of all species to As(V), HG-AAS detection. The column retains the anionic species, while AsB and AsC are determined after MW-$K_2S_2O_8$ decomposition.	4–6	[57,58]
As(III), As(V), MMAA, DMAA, AsB and AsC, o- and p-arsanilate, phenylarsonate, tetramethylarsonium	Synthetic mixtures	HPLC-HG-AAS	HPLC-persulfate-mediated photo oxidation with a low power UV-irradiation stage prior to HG-AAS	0.3	[54]

Table 3 (continued)

As species (samples)	Matrix	Measurement technique	Some details of the procedure	D.L. ($\mu g\ l^{-1}$)*	Ref.
As(III), As(V), MMAA, DMAA	Urine	HPLC-HG-AAS	Coupled techniques	1.0, 1.6, 1.2, 4.7	[109]
As(III), As(V), MMAA, DMAA, AsB		HPLC-HG-AAS HPLC-ICP-MS	Coupled techniques with comparable results.	10 for As(III), DMAA,AsB 15 for MMAA 20 for As(V)	[111]
As(III), AsT	Marine sediments	ETAAS	As(III) was chelated with sodium diethylditiocarbamate and extracted in MIBK	25–44 $\mu g\ kg^{-1}$	[138]
As(III), AsT	Bottled mineral water	ETAAS	Complexed As(III) extracted in organic solvents. As(V) must be reduced.	N.I.	[137]
As(III), AsT	Synthetic mixtures, sea waters	ETAAS on-line	FI-on-line separation and preconcentration. As(III)-NaDDTC complex is separated in a C18 reversed phase column	0.32, 0.43 ng	[89]
As(III), As(V), MMAA, DMAA	Waters	IEC-ETAAS	Separation on a dual column. Determination of As in the fractions by ETAAS	10 each	[144]
Total As, As(V), MMAA, DMAA	Synthetic mixtures	IEC-ETAAS	As is determined in collected fractions	4.0, 0.4, 2.0, 0.02	[143]
As(III), As(V)	Waters	HG-ICP	As(V) was reduced by L-Cysteine (use of a co-concentric generator without GLS)	0.7, 3.4, respectively	[99]
As(V), MMAA	SRM	IEC-ICP	On-line preconcentration with ultrasonic nebulization	0.015	[129]
As(III), As(V), MMAA, DMAA,	Synthetic fish extracts	HPLC-HG-ICP	On-line coupled techniques.	3.5, 9.2, 3.8, 21.3 (isocratic elution) 2.7, 11.4, 9.2, 9.4 (gradient elution)	[116] [117]
As(III), As(V)	Coal fly ash	HPLC-ICP-MS	Water and diluted acid extracts from the solid	N.I.	[126]

Table 3 (continued)

As species (samples)	Matrix	Measurement technique	Some details of the procedure	D.L. ($\mu g\ l^{-1}$)*	Ref.
As(III), As(V), MMAA, DMAA, AsB	Urine	HPLC-ICP-MS	Directly coupled techniques	N.I.	[141]
As(III), As(V), MMAA, DMAA, AsB and AsC	Waters	HPLC-ICP-MS	Directly coupled techniques	1.0–3.0	[118]
As(III), As(V), MMAA, DMAA, AsB and AsC	Simulated fish and sediment extracts	HPLC-ICP-MS	Coupled techniques	10–30 pg (20 μl)	[113]
As(III), As(V), MMAA, DMAA	Waters	HPLC-HG-ICP-MS	Coupled techniques	0.011–0.051	[114]
As(III), AS(V)	SRM	NAA	After sequential coprecipitation of As(III) with dibenzyldithiocarbamate	0.02 for both	[150]
As(III), AS(V)	Waters, marine species	NAA	Preconcentration of As(III) and As(V) by solvent extraction	N.I.	[151]
As(III), As(V), MMAA, DMAA		HPLC-AFS	Coupled techniques using ultrasonic nebulization	35, 50, 20, 20 ng	[153]
As(III), AsT		HG-direct current plasma	Modified hydride generator interfaced to a redesigned tube nebulizer	0.51	[90]
As(III), As(V), MMAA, DMAA	Tap, sea water and urine	HPLC-HG-MIP	Coupled techniques	1–6	[154]

* Unless otherwise stated. λ = wavelength; D.L. = detection Limit; N.I. = not indicated; AsT = total arsenic; MMAA = monomethylarsonic acid; DMAA = dimethylarsinic acid; AsB = arsenobetaine; AsC = arsenocholine; and other abbreviation as in Fig. 1.

surfatron at reduced pressure. Enhancements in the emission signals of about 100% were found in miscelles of cetyltrimethylammonium bromide and the detection limits for the arsenic species investigated (arseneous, arsenic, monomethylarsonic and dimethylarsinic acids) were in the range 1–6 ng l^{-1}. This novel methodology has been successfully applied for arsenic speciation in tap and sea waters and in human urine [154].

Also direct current plasma (DCP) atomic emission spectrometry coupled to a modified HG system proved successful for the determination of As(III) and As(V) [90]. Both species could be determined as total arsenic without the need for any prereduction step.

Mohan et al. [59] evaluated the capability of HG-DC helium emission spectrometry as an analytical tool in the speciation of arsenic in soils treated with arsenical herbicides. Due to differences in soil type and samples pore size, the method only permitted semicuantitative speciation.

The separation power of capillary electrophoresis has been widely demonstrated, most of the studies being focused on the optimization of separation parameters for complex mixtures of compounds of biochemical interest. Little effort has been devoted to quantitative studies and less to arsenic speciation. López-Sánchez et al. [155] separate arsenite, arsenate, MMAA, DMAA and phenilarsonic acid in a fused silica capillary filled with a phosphate buffer and detected the signals with an on-column UV detector operated at 190 nm. Capillary electrophoresis with conductivity [156] or AAS [157] detection was also used to speciate arsenic and selenium compounds in water. The samples were injected electrokinetically at 25 mbar for 12 s on to a pretreated fused silica column. The separation was carried out at 25 KV with triton X-100 and cyclohexil-amine-ethanesulfonic acid at pH = 9.4. The detection limit was 40 μg l^{-1} for As(V).

4. Conclusion

From this survey it can be concluded that the analytical techniques available for the detection and speciation of arsenic are diverse. A schematic diagram summarizing the different techniques and some of the most relevant information, such as samples type, procedure and detection limits, are given in Fig. 1 and Table 3, respectively. Each approach possesses both advantages and disadvantages that must be considered with respect to the scope of the study and also the laboratory facilities available. Adequate quantitative determination of complex matrices require the establishment of efficient separation and preconcentration processes, good recovery in clean-up procedures and precision and accuracy controls. All these problems can be partly solved by performing speciation studies with in vivo and in vitro labeled radioactive compounds followed by gamma or beta measurements. This would greatly eliminate the hazard of distorted results due to exogenous amounts of the element; which are not radioactive and will escape detection.

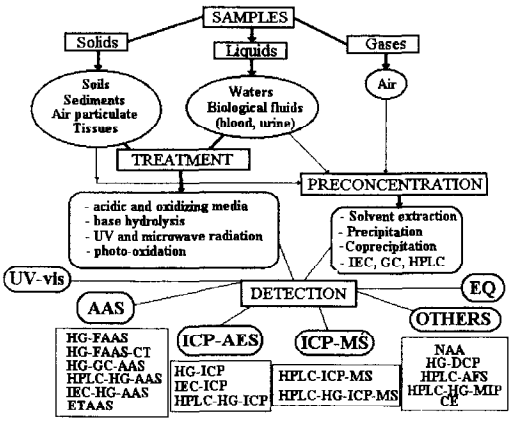

Fig. 1. Procedures for arsenic speciation in different matrixes. (UV-vis. = spectrophotometry; EQ = electrochemical methods; AAS = atomic absorption spectrometry; ICP-AES = inductively coupled plasma atomic emission spectrometry; ICP-MS = inductively coupled plasma mass spectrometry; HG = hydride generation; FAAS = flame atomic absorption spectrometry; CT = cryogenic trapping; GC = gas chromatography; HPLC = high performance liquid chromatography; IEC = ion exchange chromatography; ETAAS = electrothermal atomic absorption spectrometry; NAA = neutron activation analysis; DCP = direct current plasma; AFS = atomic fluorescence spectrometry; MIP = microwave induced plasma;and CE = capillary electrophoresis).

When environmental monitoring is used to asses the exposure to toxic compounds, it is important to be able to distinguish between the toxic species (arsenite, arsenate and the metabolites) and the non-toxic species (AsB and AsC). However, most of the methods outlined in this paper are unsuitable for routine analysis of real samples, although HPLC-HG-AAS, HPLC-ICP and HPLC-ICP-MS would appear to be a good choice in terms of sensitivity, selectivity and ease of operation. Their only disadvantage is that the instruments are expensive and not available in many laboratories.

Much work has to be conducted in order to understand first the natural distribution cycle of the element (the dynamics of its mobility through ecosystems) and to compare it with documented perturbations stemming from man's technological inputs and their impact on the public health. A balanced interdisciplinary approach is necessary, formed by analytical chemists, specialists in life sciences, statisticians, ecologists, etc. These multifaceted efforts would be able to respond questions regarding the biotransformation and redox reactions occurring in biological media as well as the interactions that could take place in the environment between arsenic compounds and other natural products to produce new organoarsenicals of perhaps totally different toxicity.

References

[1] R. Cornelis, F. Borguet, J. De Kimpe, Anal. Chim. Acta 283 (1993) 183.
[2] J.C. Van Loon, R.R. Barefoot, Analyst 117 (1992) 563.
[3] G.E. Batley (ed.), Trace Element Speciation: Analytical Methods and Problems, CRC Press, Boca Raton, Florida, 1989.
[4] P.H.E. Gardiner, J. Trace Elem. Electrolytes Health Dis. 7 (1993) 1.
[5] Ph. Quevauviller, Analyst 120 (1995) 597.
[6] R.K. Anderson, M. Thompson, E. Culbard, Analyst 111 (1986) 1153.
[7] R. Cornelis, J. De Kimpe, J. Anal. At. Spectrom. 9 (1994) 945.
[8] W.R. Cullen, K.J. Reimer, Chem. Rev. 89 (1989) 713.
[9] M. Morita, J.S. Edmonds, Pure Appl. Chem. 64 (1992) 575.
[10] Caroli (Ed.), Element Speciation in Bioinorganic Chemistry, Wiley, New York, 1996.
[11] J. Dêdina, D.L. Tsalev, Hydride Generation Atomic Absorption Spectrometry, Wiley, Chichester, 1995.
[12] R.M. Harrison, S. Rapsomanikis (Eds.), Environmental Analysis using Chromatography Interfaced with Atomic Spectroscopy, Ellis Horwood, Chichester, 1989.
[13] D.J.H. Phillips, Aquat. Toxicol. 16 (1990) 151.
[14] F.E. Brinckman, G.E. Parris, W.R. Blair, K.L. Jewett, W.P. Iverson, J.M. Bellama, Environ. Health Perspect. 19 (1977) 11.
[15] R.M. Bergoglio, Prensa Med. Argent. 51 (1964) 994.
[16] J.M. Borgono, R. Greiber, in: D. Hemphill (Ed.), Trace Substances in Environmental Health, University of Missouri, 1972.
[17] J.W. Southwick, A.E. Western, M.M. Beck, T. Whitley, R. Isaac, J. Petajan, C.D. Hansen, in: W.L. Lederer, R.J. Fensterheim (Eds.), Arsenic, Industrial, Biochemical and Environmental Perspectives, Van Nostrand, New York, 1983.
[18] L. Lindau, Environ. Health Perspect. 19 (1977) 25.
[19] W.P. Tseng, M.H. Chu, J.M. Fong, C.S. Lin, S. Yeh, J. Nat. Cancer Inst. 40 (1968) 453.
[20] D.N. Guha Mazumder, J. Das Gupta, A.K. Chakraborty, A. Chatterjee, D. Das, D. Chakraborti, Bull. World Health Org. 70 (1992) 481.
[21] A. Chatterjee, D. Das, D. Chakraborti, Environ. Pollut. 80 (1993) 57.
[22] A. Chatterjee, D. Das, B.K. Mandal, T.R. Chowdhury, G. Samanta, D. Chakraborti, Analyst 120 (1995) 925.
[23] D. Das, A. Chatterjee, B.K. Mandal, G. Samanta, B. Chanda, D. Chakraborti, Analyst 120 (1995) 917.
[24] L.E. Hunt, A.G. Howard, Mar. Pollut. Bull. 28 (1994) 33.
[25] U.S. EPA, Quality Criteria for Water, Report EPA 440/5-86-001, Office for Water Regulations and Standards, U.S. Environmental Protection Agency, Washington DC, 1986.
[26] World Health Organization, Environmental Health Criteria, 18. Arsenic, WHO, Geneva, 1981,
[27] G. Mance, C. Musselwhite, V.M. Brown, Water Research Center, Technical Report TR 212, Medmenham, U.K., 1984.
[28] A. Léonard, in: E. Merian (Ed.), Metals and their Compounds in the Environment: Occurrence, Analysis and Biological Relevance, VCH, New York, 1991.
[29] H.L. Windom, J.G. Sanders, Indian J. Mar. Sci. 10 (1981) 309.
[30] J.S. Edmonds, K.A. Francesconi, Nature 265 (1977) 436.
[31] M. Vahter, E. Marafante, L. Dencker, Sci. Total Environ. 30 (1983) 197.
[32] W.R. Cullen, M. Dodd, Appl. Organomet. Chem. 2 (1988) 1.
[33] R.H. Atallah, D.A. Kalman, Talanta 38 (1991) 167.
[34] M. Vahter, Clin. Chem. 40 (1994) 679.
[35] K.A. Francesconi, J.S. Edmonds, B.G. Hatcher, Comp. Biochem. Physiol. 90C (1988) 313.
[36] Y. Shibata, M. Morita, Anal. Chem. 31 (1989) 2116.

[37] H. Norin, A. Christakopoulos, L. Rondahl, A. Hagman, S. Jacobsson, Biomed. Environ. Mass Spectrom. 14 (1987) 117.
[38] D. Beauchemin, M.E. Bednas, S.S. Berman, J.W. McLaren, K.W.M. Siu, R.E. Sturgeon, Anal. Chem. 60 (1988) 2209.
[39] A. Christakopoulos, H. Norin, M. Sandstrom, H. Thor, P. Moldeus, R. Ryhage, J. Appl. Toxicol. 8 (1988) 119.
[40] X.-C. Le, W.R. Cullen, K.J. Reimer, Clin. Chem. 40 (1994) 617.
[41] W. Maenhaut, W.H. Zoller, R.A. Duce, G.L. Hoffman, J. Geophys. Res. 84 (1979) 2421.
[42] P.R. Walsh, R.A. Duce, J.L. Fasching, Environ. Sci. Technol. 11 (1977) 163.
[43] G.R. Cass, G.J. McRae, Source-receptor Reconciliation of South Coast Air Basin Particulate Air Quality Data, California Air Resources Board, Final Report, NTIS No. PB-82-250 093.
[44] E.S. Rábano, N.T. Castillo, K.J. Torre, P.A. Solomon, JAPCA 39 (1989) 76.
[45] V. Foá, A. Colombi, M. Maroni, M. Buratti, G. Calzaferri, Sci. Total Environ. 34 (1984) 241.
[46] H. Norin, M. Vahter, Scand. J. Work. Environ. Health 7 (1981) 38.
[47] E.A. Crecelius, Environ. Health Perspect. 19 (1977) 147.
[48] R. Iadevaia, N. Aharonson, E.A. Woolson, J. Assoc. Off. Anal. Chem. 63 (1980) 742.
[49] M.S. Mohan, R.A. Zingaro, P. Micks, P.J. Clark, Intern. J. Environ. Anal. Chem. 11 (1982) 175.
[50] L.M. Klevay, Pharmacol. Ther. A. 1 (1976) 189.
[51] D.R. Webb, D.E. Carter, J. Anal. Toxicol. 8 (1984) 118.
[52] J.F. Uthe, H.C. Freeman, J.R. Johnston, P. Michalik, J. Assoc. Off. Anal. Chem. 57 (1974) 1363.
[53] C.P. Hanna, J.F. Tyson, S. McIntosh, Clin. Chem. 39 (1993) 1662.
[54] A.G. Howard, L.E. Hunt, Anal. Chem. 65 (1993) 2995.
[55] X. Zhang, R. Cornelis, J. De Kimpe, L. Mees, Anal. Chim. Acta 319 (1996) 177.
[56] A.G. Howard, S.D.W. Comber, Appl. Organomet. Chem. 3 (1989) 509.
[57] M.A. López-Gonzálvez, M.M. Gómez, C. Cámara, M.A. Palacios, J. Anal. At. Spectrom. 9 (1994) 291.
[58] M.A. López-Gonzálvez, M.M. Gómez, C. Cámara, M.A. Palacios, Mikrochim. Acta 120 (1995) 301.
[59] X.-C. Le, W.R. Cullen, K.J. Reimer, Talanta 40 (1993) 185.
[60] A.M.M. De Bettencourt, Neth. J. Sea Res. 22 (1988) 205.
[61] R.J. Fielder, E.A. Dale, S.D. Williams, HMSO London, Toxicity Review of Inorganic Arsenic Compounds, Health and Safety Executive, London, 1986.
[62] American Public Health Association, American Water Works Association and Water Pollution Control Federation, Standard Methods for the Examination of Water and Waste Water, 13th Edn., American Public Health Association, Washington D.C., 1971.
[63] A. López, R. Torralba, M.A. Palacios, C. Cámara, Talanta 39 (1992) 1343.
[64] A.G. Howard, M.H. Arbab-Zavar, Analyst (1980) 105, 338.
[65] W. Frenzel, F. Titzenthaler, S. Elbel, Talanta 41 (1994) 1965.
[66] D.L. Johnson, M.E.Q. Pilson, Anal. Chim. Acta 58 (1972) 289.
[67] S.S. Sandhu, Analyst 101 (1976) 328.
[68] F.T. Henry, T.M. Thorpe, Anal. Chem. 52 (1980) 80.
[69] A. Brockmann, C. Nonn, A. Golloch, J. Anal. At. Spectrom. 8 (1993) 397.
[70] P.H. Davis, G.R. Dulude, R.M. Griffin, W.R. Matson, E.W. Zink, Anal. Chem. 50 (1978) 137.
[71] H. Huiliang, D. Jagner, L. Renman, Anal. Chim. Acta 207 (1988) 37.
[72] M. Esteban, C. Ariño, I. Ruisánchez, M.S. Larrechi, F.X. Rius, Anal. Chim. Acta 285 (1994) 193.
[73] Z.-l. Li, S.-f. Mou, Z.-m. Ni, J.M. Riviello, Anal. Chim. Acta 307 (1995) 79.
[74] P. Boucher, M. Accominotte, J.J. Vallon, J. Chromatogr. Sci. 34 (1996) 226.
[75] E.N. Pollock, S.J. West, At. Absorpt. Newsl. 12 (1973) 6.
[76] T. Maruta, G. Sudoh, Anal. Chim. Acta 77 (1975) 37.
[77] M. Burguera, J.L. Burguera, M.R. Brunetto, M. de la Guardia, A. Salvador, Anal. Chim. Acta 161 (1991) 105.
[78] M. Burguera, J.L. Burguera, J. Anal. At. Spectrom. 8 (1993) 229.
[79] R.S. Braman, L.L. Justen, C.C. Foreback, Anal. Chem. 44 (1972) 2195.
[80] H. Narsito, J. Agterdenbos, Anal. Chim. Acta. 197 (1987) 315.
[81] J. Dêdina, Fresenius J. Anal. Chem. 323 (1986) 771.
[82] J.T. Van Elteren, H.A. Das, C.L. de Ligny, J. Agterdenbos, D. Bax, J. Radioanal. Nucl. Chem. Articles 179 (1994) 211.
[83] P.H. Masscheleyn, R.D. Delaune, W.H. Partick Jr., Environ. Sci. Technol. 25 (1991) 1414.
[84] P.H. Masscheleyn, R.D. Delaune, W.H. Partick Jr., J. Environ. Qual. 20 (1991) 96.
[85] P. Michel, B. Averty, V. Colandini, Mikrochim. Acta 109 (1992) 35.
[86] A.G. Howard, S.D.W. Comber, Mikrochim. Acta 109 (1992) 27.
[87] S. Cabredo Pinillos, J. Sanz Asensio, J. Galbán Bernal, Anal. Chim. Acta 300 (1995) 321.
[88] R.K. Anderson, M. Thompson, E. Culbard, Analyst 111 (1986) 1143.
[89] M. Sperling, X. Yin, B. Welz, Spectrochim. Acta. 46B (1991) 1789.
[90] C. Boampong, I.D. Brindle, C.M. Ceccarelli Ponzoni, J. Anal. At. Spectrom. 2 (1987) 197.
[91] R.S. Braman, D.L. Johnson, C.C. Foreback, J.M. Ammons, J.L. Bricker, Anal. Chem. 49 (1977) 621.
[92] A.G. Howard, M.H. Arbab-Zavar, Analyst 106 (1981) 215.

[93] J.L. Burguera, M. Burguera, C. Rivas, P. Carrero, Talanta (1997) (in press).
[94] P.K. Hon, O.W. Lau, S.K. Tsui, J. Anal. At. Spectrom. 1 (1986) 125.
[95] K.S. Subramanian, J.C. Meranger, Anal. Chim. Acta 124 (1981) 131.
[96] B. Welz, M. Šucmanová, Analyst 118 (1993) 1417.
[97] B. Welz, M. Šucmanová, Analyst 118 (1993) 1425.
[98] X.-C. Le, W.R. Cullen, K.J. Reimer, Anal. Chim. Acta 285 (1994) 277.
[99] Y.-I. Feng, J.-p. Cao, Anal Chim. Acta 293 (1994) 211.
[100] R. Torralba, M. Bonilla, L.V. Perez-Arribas, M.A. Palacios, C. Cámara, Spectrochim. Acta 49B (1994) 893.
[101] R. Torralba, M. Bonilla, M.A. Palacios, C. Cámara, Analusis 22 (1994) 478.
[102] J.M. Brannon, W.H. Patrick Jr., Environ. Sci. Technol. 21 (1987) 450.
[103] O. Jiménez de Blas, S. Vicente González, R. Seisdedos Rodríguez, J. Hernández Méndez, J. AOAC Int. 77 (1994) 441.
[104] O. Jiménez de Blas, S. Vicente González, R. Muñoz Garrido, A. Martin Pascual, M.A. Sánchez Martin, Quím. Anal. 13 (1994) 138.
[105] J.L. Burguera, M. Burguera, C. Rivas, P. Carrero, C. Rondón, M.R. Brunetto, Quim. Anal. (1997) (in press).
[106] S. Nielsen, J.J. Sloth, E.H. Hansen, Talanta 43 (1996) 867.
[107] J. Stumneyer, B. Harazin, T. Wippermann, Fresenius J. Anal. Chem. 354 (1996) 344.
[108] M. Stoeppler, M. Burow, K. May, S. Padberg, G. Kloster, Mikrochim. Acta 109 (1992) 107.
[109] E. Hakala, L. Pyy, J. Anal. At. Spectrom. 7 (1992) 191.
[110] A.J.L. Mürer, A. Abildtrup, O.M. Poulsen, J.M. Christensen, Analyst 117 (1992) 677.
[111] X.-C Le, W.R. Cullen, K.J. Reimer, Talanta 41 (1994) 495.
[112] S.T.G. Anderson, R.V.D. Robert, H.N. Farrer, J. Anal. At. Spectrom. 9 (1994) 1107.
[113] C. Demesmay, M. Olle, M. Porthault, Fresenius J. Anal. Chem. 348 (1994) 205.
[114] C.-J Hwang, S.-J. Jiang, Anal. Chim. Acta 289 (1994) 205.
[115] S. Branch, L. Ebdon, M. Ford, M. Foulkes, P. O'Neill, J. Anal. At. Spectrom. 6 (1991) 151.
[116] G. Rauret, R. Rubio, A. Padró, Fresenius J. Anal. Chem. 340 (1991) 157.
[117] R. Rubio, A. Padró, J. Albertí, G. Rauret, Mikrochim. Acta 109 (1992) 39.
[118] P. Thomas, K. Sniatecki, J. Anal. At. Spectrom. 10 (1995) 615.
[119] S. Branch, W.T. Corns, L. Ebdon, S. Hill, P. O'Neill, J. Anal. At. Spectrom. 6 (1991) 155.
[120] M.L. Magnuson, J.T. Creed, C.A. Brockhoff, J. Anal. At. Spectrom. 11 (1996) 893.
[121] B. Huang, X. Zeng, Z. Zhang, J. Lin, Spectrochim. Acta 43B (1988) 381.
[122] A. Menendez-Garcia, J.E. Sanchez-Uria, A. Sanz-Medel, J. Anal. At. Spectrom. 4 (1989) 581.
[123] B. Aizpun Fernandez, C. Valdez-Hevia y Temprano, M.R. Fernandez de la Campa, A. Sanz-Medel, P. Neil, Talanta 39 (1992) 1517.
[124] X. Wang, M. Viczian, A. Lasztity, R. Barnes, J. Anal. At. Spectrom. 3 (1988) 821.
[125] C. Haraldsson, M. Pollak, P. Öhman, J. Anal. At. Spectrom. 7 (1992) 1183.
[126] J. Wang, M.J. Tomlinson, J.A. Caruso, J. Anal. At. Spectrom. 10 (1995) 601.
[127] E.H. Larsen, in: European Winter Conference on Plasma Spectrochemistry, Cambridge, UK, January 8–13, 1995.
[128] D. Jensen, W. Bloedorn, GIT Fachz. Lab. 39 (1995) 654, 657–658, 660–661.
[129] M. Ochsenkühn-Petropulu, P. Schramel, Anal. Chim. Acta 313 (1995) 243.
[130] D. Beauchemin, K.W.M. Siu, J.W. McLaren, S.S. Berman, J. Anal. At. Spectrom. 4 (1989) 285.
[131] E.H. Larsen, J. Anal. At. Spectrom. 6 (1991) 375.
[132] V. Krivan, S. Arpadjan, Fresenius J. Anal. Chem. 335 (1989) 743.
[133] D.L. Tsalev, P.B. Mandjukov, J.A. Stratis, J. Anal. At. Spectrom. 2 (1992) 135.
[134] V. Slaveykova, F. Rastegar, M.J.F. Leroy, J. Anal. At. Spectrom. 11 (1996) 997.
[135] R.R. Stanforth, Environ. Sci. Technol. 12 (1979) 1491.
[136] M. Styblo, M. Delnomdedieu, M.F. Hughes, D.J. Thomas, J. Chromatogr., B, Biomed. Appl. 668 (1995) 21.
[137] F. Puttemans, D.L. Massart, Anal. Chim. Acta 141 (1982) 225.
[138] P. Bermejo-Barrera, M.C. Barciela-Alonso, M. Ferrón-Novais, A. Bermejo-Barrera, J. Anal. At. Spectrom. 10 (1995) 247.
[139] D. Chakraborti, F. Adams, K.J. Irgolic, Fresenius J. Anal. Chem. 323 (1986) 340.
[140] E. Russeva, I. Havezov, A. Detcheva, Fresenius J. Anal. Chem. 347 (1993) 320.
[141] P. Bavazzano, A. Perico, K. Rosendahl, P. Apostoli, J. Anal. At. Spectrom. 11 (1996) 521.
[142] Y.K. Chen, W.G. Qi, J.S. Cao, M.S. Chang, J. Anal. At. Spectrom. 8 (1993) 379.
[143] G.E. Pacey, J.A. Ford, Talanta 28 (1981) 935.
[144] A.A. Grabinski, Anal. Chem. 53 (1981) 966.
[145] E.A. Woolson, N. Aharowsow, J. Assoc. Off. Anal. Chem. 63 (1980) 523.
[146] F.E. Brinckman, W.R. Blair, K.L. Jewett, W.P. Iverson, J. Chromatogr. Sci. 15 (1977) 493.
[147] J.L. Burguera, M. Burguera, J. Anal. At. Spectrom. 8 (1993) 235.
[148] M. Burguera, J.L. Burguera, C.E. Rondón, C. Rivas, P. Carrero, M. Gallignani, M.R. Brunetto, J. Anal. At Spectrom. 10 (1995) 343.
[149] D.E. Leyden, K. Goldbach, A.T. Ellis, Anal. Chim. Acta 171 (1985) 369.

[150] J.T. Van Elteren, H.A. Das, C.L. de Ligny, J. Agterdenbos, Anal. Chim. Acta 222 (1989) 159.
[151] A.M. Yusof, Z.B. Ikhsan, A.K.H. Wood, J. Radioanal. Nucl. Chem. Articles 179 (1994) 277.
[152] W.T. Corns, P.B. Stockwell, L. Ebdon, S.J. Hill, J. Anal. At. Spectrom. 8 (1993) 71.
[153] A. Woller, Z. Mester, P. Fodor, J. Anal. At. Spectrom. 10 (1995) 609.
[154] J.M. Costa-Fernández, F. Lunzer, R. Pereiro-García, A. Sanz-Medel, N. Bordel-García, J. Anal. At. Spectrom. 10 (1995) 1019.
[155] J.Γ. López-Sánchez, M.B. Amram, M.D. Lakkis, F. Lagarde, G. Rauret, M.J.F. Leroy, Fresenius J. Anal. Chem. 348 (1994) 810.
[156] D. Schlegel, J. Mattusch, R. Wennrich, Fresenius J. Anal. Chem. 354 (1996) 535.
[157] P.F. Reay, C.J. Asher, Anal. Biochem. 78 (1977) 557.

ELSEVIER

Talanta 44 (1997) 1605–1614

Talanta

Determination of trace Ag, Au, Ge, Pb, Sn and Te by microwave plasma torch atomic emission spectrometry coupled with an electrothermal vaporization sample introduction system

Qinhan Jin *, Hanqi Zhang, Wenjun Yang, Qun Jin, Yuhua Shi

Department of Chemistry, Jilin University, Changchun 130 023, People's Republic of China

Received 20 September 1996; received in revised form 4 February 1997; accepted 4 February 1997

Abstract

An electrothermal vaporization (ETV) sample introduction device tantalum filament was combined with microwave plasma torch atomic emission spectrometry (MPT-AES) for determination of several trace elements. Some operating parameters of the system were optimized. The effects of easily ionized elements (EIEs) on the emission intensities of the tested elements were studied in detail. It was revealed that there was no interference resulting from small amount of sample matrix; while with the existence of large amount of sample matrix, the method of standard addition could be used to determine trace elements in samples. So, no modifier was required in this method. The results indicated that ETV-MPT-AES not only has the advantage of micro sample consumption (a volume of 3 μl for each injection), but also offers high sensitivities for the determination of Ag, Au, Ge, Pb, Sn and Te as compared with those obtained with pneumatic nebulization (PN) MPT-AES. © 1997 Elsevier Science B.V.

Keywords: Atomic emission spectrometry; Electrothermal vaporization; Microwave plasma torch

1. Introduction

Because electrothermal vaporization (ETV) has some distinct advantages over solution nebulization as a means of sample introduction in plasma atomic spectrometry the ETV method has been investigated extensively. The ETV sample introduction systems have been applied to inductively coupled plasma atomic emission spectrometry (ICP-AES) [1–3], ICP-mass spectrometry (ICP-MS) [3], direct current plasma-AES (DCP-AES) [3], microwave induced plasma-AES (MIP-AES) [1,3,4] and MIP-MS [5,6]. Due to the inability of the low-powered microwave plasma (MWP) to readily tolerate the introduction of large amount of foreign materials, one of the most common and nearly optimal techniques for converting liquid samples into dry aerosols and introducing them into MWPs is the ETV. Graphite [7–14] and metals (tungsten, tantalum, platinum) [15–27] have been used as furnace materials for ETV devices in MIP-AES. Compared with graphite furnace manufactured for graphite furnace atomic absorption spectrometry, metal vaporizers are of

* Corresponding author.

PII S0039-9140(97)00065-9

low-cost and can work at low-power. Though in the development of ETV-MWP-AES, platinum filament was firstly used as a vaporizer [15], tungsten and tantalum were most often employed in latter studies [16–25]. The metal vaporizers used include tungsten loop [16,17], tungsten filament [18], tungsten boat [19,20], tantalum loop [21], tantalum filament [22], tantalum boat [23], and tantalum strip [24,15]. Brooks and Timmins [26,27] described a miniature device based on a heated tantalum filament which eliminated the dead volume and turbulence of the plasma gas was kept to minimum. Evans et al. [6] utilized a tantalum-tip electrothermal vaporizer. The vaporizer is such that the analyte is vaporized in the MIP, there by eliminating the dead volume.

Microwave plasma torch (MPT) was first developed by Jin et al. [28] as a new, attractive excitation source. The tolerance of it to the wet aerosols and molecular species is significantly improved as compared with conventional MWPs for the plasma formed with MPT is flame-like and has a central channel. Since the analyte is forced to pass through the central channel of the discharge, it is efficiently vaporized, atomized, excited and ionized, and causes minimal perturbation to the plasma [29]. MPT has been used as an excitation source for AES coupled with ultrasonic [30] or pneumatic [31] nebulization sample introduction system. Although these sample introduction systems are efficient, they consume relatively large amount of sample solution. In this work, a miniature ETV unit, based on a heated tantalum filament, has been designed to introduce micro aqueous samples into an MPT-AES system. The design of ETV was similar to that of Brooks et al. [26]. A desolvation system similar to that of Que et al. [32] was also set between the ETV unit and the MPT. The tantalum filament was surrounded by Ar carrier gas to avoid its exposure to the air. In addition, the drying time and drying temperature of the sample were strictly controlled to reduce or eliminate interferences caused by the matrix (it is especially important to remove water in samples at drying stage, because during vaporization stage the water can oxidize the tantalum filament at high temperature) and to minimize the vaporization of the tantalum. By doing so, no interference resulting from small amount of sample matrix was observed and no matrix modifier was needed. However, very large amount of the matrix did affect the emission intensities of the elements tested. In this case, the method of standard addition was necessary to be adapted.

Results obtained from our ETV-MPT-AES system proved that the method is not only sensitive, but also of low matrix effect, as well as less time and sample consuming. What is more, the whole instrumentation is compact and inexpensive.

2. Experimental

2.1. Apparatus

The MPT-AES system used is the same as described in our previous work [33]. The ETV system consists of a d.c. voltage stabilizer (maximum output voltage 10 V, laboratory built), a rheochord (maximum resistance 100 ohms) and an ETV atomizer (laboratory built, as shown in Fig. 1). Table 1 lists the operating conditions of the ETV-MPT-AES system used in this study.

2.2. Procedures

After ignition and stabilization of the plasma, 3 μl sample solution was injected onto the tantalum filament loop by using a micro-syringe through the sample inlet on the ETV introduction system. By applying different d.c. voltages across the terminals of tantalum filament, the sample was first dried for a while, and then vaporized and transported into the plasma by an Ar carrier gas. The emission intensity of the analyte was measured with a PMT (1P28) by the recorded peak height.

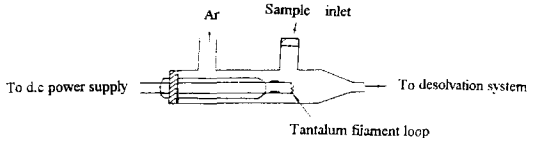

Fig. 1. Schematic diagram of ETV sample introduction system.

Table 1
Operating parameters of the ETV-MPT-AES system

MPT	Carrier and support gas	Ar
	Microwave frequency, MHz	2450
	Forward power, W	60
	Support gas flow rate, mL/min	400
	Carrier gas flow rate, mL/min	650
	Plasma viewing mode	Side-on
	Plasma viewing position	6–8 mm above the top of the torch
Monochromator	Slit-width, μm	25
	Slit height, mm	2
ETV system	Drying time, s	35–80
	Drying voltage, V	0.21–0.63
	Vaporizing time, s	3
	Vaporizing voltage, V	2.28–3.00

2.3. Sample preparation

Sediment sample, 0.5 g, was placed into a polytetrafluorethylene crucible. HF, 15 ml, and 8 ml of concentrated HBO_3 were slowly added in the crucible while it was being heated. When the sample was dissolved completely, 2 ml of $HClO_4$ was added into the crucible to get rid of the retained HF. Heated the solution till it was almost dry, then transported it to a 10 ml volumetric flask and diluted with de-ionized water to the mark.

3. Results and discussion

3.1. Solution medium

HCl, H_2SO_4, HNO_3, H_3PO_4 at various concentrations were used separately as the solution medium. It was observed that when the concentration of H_2SO_4, HNO_3 or H_3PO_4 exceeded 0.1 mol l^{-1} all emission intensities measured decreased, while the addition of HCl could increase the emission intensities of analytes.

The effects of HCl concentration on the emission intensities of different analytes are shown in Fig. 2. It seems that the enhancement effects of HCl are different for different elements. It was found that when the HCl concentration was in the range of 0.01 ~ 0.2 mol l^{-1}, the relative intensities reached a plateau. However, when the HCl concentration exceeded 0.2 mol l^{-1}, the enhancement effect began to reduce. It was also found experimentally that the background emission did not depend on the concentration of HCl. Thus, 0.1 mol l^{-1} HCl was selected as the solution medium in this work.

3.2. Flow rate of carrier gas

Fig. 3 shows the effects of flow rate of carrier gas on the emission intensities, which involves three aspects: (1) the carrier gas flow rate affects the residence times of the analytes in the plasma. The lower the carrier gas flow rate, the longer the residence time. As far as this aspect is concerned, low flow rate of carrier gas is better; (2) the process of the sample transportation to the plasma is also a process of sample diffusing in the carrier gas and depositing to the walls of vaporizer and transportation tube. The carrier gas flow rate affects the sample transportation and hence

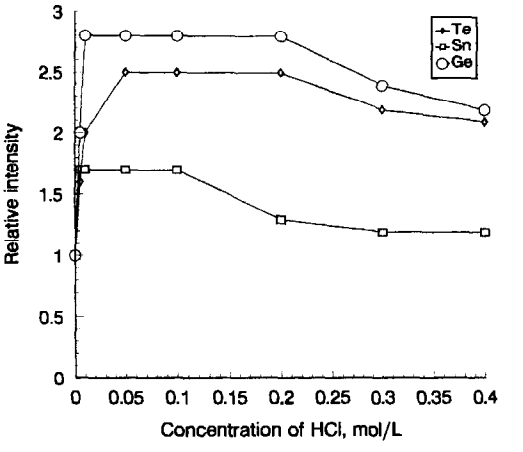

Fig. 2. Effect of HCl concentration on the emission intensities of different elements.

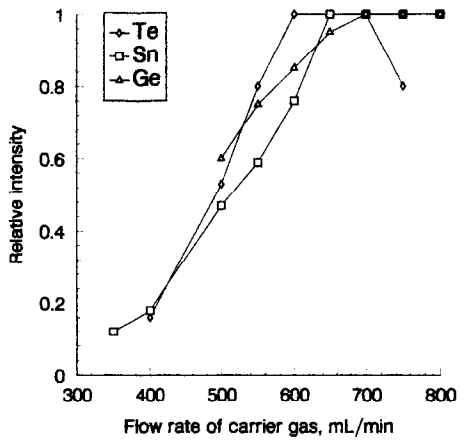

Fig. 3. Effect of carrier gas flow rate on the emission intensities.

the sample diffusion and deposition; (3) the change of the carrier gas flow rate results in a change of the plasma discharge status. It was observed that when the flow rate was relative low ($< 500 \sim 600$ ml min^{-1}), the emission intensities increased with the flow rate; when the flow rate went up to $600 \sim 700$ ml min^{-1}, the emission intensities reached maxima; however, with the further increase of the flow rate (> 700 ml min^{-1}), the emission intensities decreased or unchanged. Therefore, in this study a 650 ml min^{-1} carrier gas flow rate was chosen.

3.3. Flow rate of support gas

The effect of the flow rate of the support gas on the emission is shown in Fig. 4. For all elements tested the emission intensities reached maxima when the support gas flow rate goes up to about 400 ml min^{-1}.

3.4. Drying time and drying voltage

Water vapour can significantly absorb microwave at 2450 MHz, so if water in a sample is not removed, the excitation capability of the plasma will be affected. In addition, oxygen in water can oxidize tantalum filament under high temperature during the vaporization stage and hence reduce the lifetime of the ETV device. So it is necessary to remove water in samples as completely as possible during the drying stage.

Drying time and drying temperature are two correlative factors (the drying temperature was controlled by drying voltage). It was noticed that with the increase of the drying voltage, the optimum drying time became shorter. If drying voltage used is too high or drying time is too low, it will take longer time to remove water and takes longer time to complete the analysis.

For the determination of Te, a certain amount of reductant $SnCl_2$ was added into the sample solution (0.1% $SnCl_2$), thus Te will exist in Te^0 form. Since the boiling points of $TeCl_4$ and Te^0 are 390 and 990°C, respectively, the addition of $SnCl_2$ can minimize the loss of Te during drying stage. Fig. 5 shows the effect of drying time on the emission intensities of Te at different drying voltages.

Drying times and drying voltages of Sn, Ge, Ag, Au were also investigated and the optimum values are listed in Table 2.

3.5. Vaporization time and voltage

The sensitivities of ETV system for elements studied are better than that of PN system for the reason of higher solute transportation efficiency of the former. With the ETV system samples can

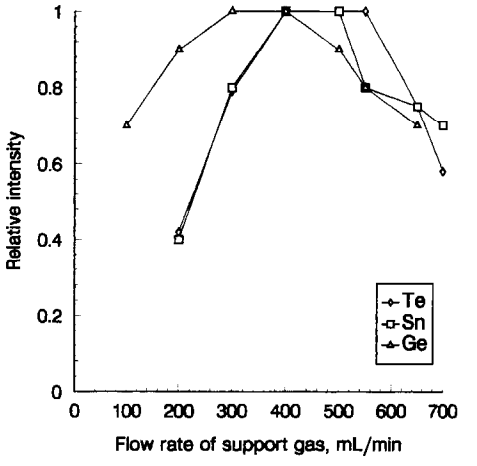

Fig. 4. Effect of support gas flow rate on the emission intensities.

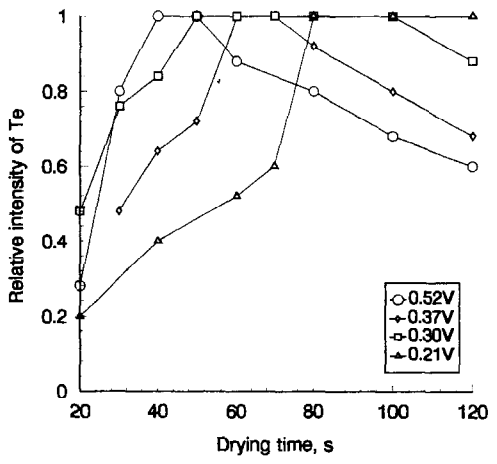

Fig. 5. Effect of drying time on the emission intensities of Te at different drying voltages.

be almost completely vaporized in a short time and transported into the excitation source by the carrier gas. In this study, to guarantee a complete vaporization of the element studied and an enough long lifetime of the tantalum filament, $3 \sim 4$ s was generally selected as the vaporization time. Fig. 6 presents the effect of vaporization voltages on the emission intensities. It is observed experimentally that the emission intensities increase with the mounting of the vaporization voltages when the vaporization voltages are low, while the vaporization temperatures (corresponding to the vaporization voltages) reach or exceed the boiling points of tested elements (their compounds), the emission intensities reach the maxima, and no more increase with the further increase of vaporization voltages will be observed because the analytes have been vaporized completely. What is more, too high vaporizing temperature can also shorten the lifetime of the tantalum filament. Therefore, to meet both requirements of vaporizing efficiency and lifetime of the tantalum filament, the vaporization voltages of different elements were optimized and shown in Table 2.

3.6. Effects of concomitant elements

3.6.1. Easily ionized element (EIE)

Since alkali metal elements, which are easily ionized elements (EIEs), especially Na and K are present in a wide variety of natural materials, the influence of EIEs upon the emission of analytes in the ETV-MPT-AES technique is of significant practical relevance. Fig. 7 illustrates the effects of some EIEs on the emission behaviour of the elements studied. Though the influences of the same EIE on the elements studied are not quite the same, they follow such general trends: (1) no obvious changes of emission intensities of the tested element occur with relatively low quantities of EIE (20 mg l^{-1} and less). (2) EIEs can cause either an emission enhancements (or suppressions) depending on EIE and element tested. The maximal emission enhancements (or suppressions) occur at EIE concentrations reaching around 500 mg l^{-1}. (3) When EIE concentrations go over about 500 mg l^{-1} the emission enhancements (or suppressions) reach plateaus. (4) The effects of EIEs on the emission intensities decrease when the concentrations of EIEs increase further to over about 1000 mg l^{-1}. (5) It is also observed that the extent of either suppression or enhancement correlates with the ionization potential(IP) of the EIE, i.e., Li > Na > K > Rb > Cs. This order is contrary to that reported by Matousek et al. [19] while is the same as that showed by our previous work (with PN introduction system) [17]. This phenomenon indicates that the mechanism of the effects of the same EIE on different line emission intensities may be similar. The mechanism involving enhanced collisional excitation was the most plausible explanation of the enhancement effect, and that the addition of EIEs may shrink the plasma and thus decrease the efficiency with which microwave energy is coupled to the plasma was said to be the reason for the suppression in the former work [30].

Effects of Na and K on the emission intensities of Sn with different sample introduction systems are shown in Fig. 8. It is observed that on the contrary to results obtained with ETV, the introduction of alkali metals will suppress rather than enhance the emission signals of Pb when a PN

Table 2
Drying time and voltage as well as vaporizing voltage for different analytes

Analyte	Ag	Au	Ge	Pb	Sn	Te
Drying time (s)	50–60	35–45	35–45	80–90	40–50	40–50
Drying voltage (V)	0.42	0.63	0.60	0.21	0.52	0.52
Vaporising voltage (V)	2.82	2.82	2.82	2.28	2.82	2.82

system is employed. The possible explanation for this may be that in the case of ETV the analyte is not transported into the plasma at the time while K and Na is vaporizing, and thus the effect caused by Na or K is reduced.

Some workers have investigated the mechanisms of EIE effect in an MIP with ETV sample introduction device [34,35]. In this work two experiments were performed to investigate the mechanism. Firstly, two different vaporization modes were employed. In the first mode, a 1.5 μl analyte solution and 1.5 μl of EIE (K) solution (both with 0.1 mol l^{-1} HCl) were injected onto two different sites of the tantalum filament loop, respectively. By this way the volatilization processes of the analyte and EIE were independent on each other. In the second mode, a 1.5 μl analyte solution containing EIE and a 1.5 μl HCl solution (0.1 mol l^{-1}) were injected onto the tantalum filament loop at the two sites the same as those in the former mode, respectively. Thus

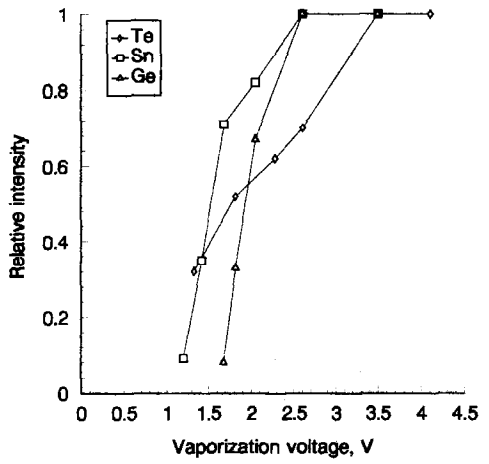

Fig. 6. Effect of vaporization voltage on the emission intensities.

the only difference between the two modes was that the analyte was vaporized separately from the EIE in the former while were vaporized together in the latter. The experimental results are shown in Fig. 9 and can be narrated as follows:

Generally speaking, EIEs can affect not only the vaporization behaviour but also the transportation process and the excitation behaviour of the analyte. When the concentration of EIEs are low, the results obtained from different vaporization modes are quite different. This indicated that, in this case, the EIE effects depends mainly on the vaporization process while the interference of EIE in excitation process in plasma is minor; with the increase of the concentration of EIEs, the two groups of results began to approach with each other (especially when the concentration of EIEs goes over 1000 mg l^{-1}). This reveals that when a large amount of EIEs is introduced into the system, their effects on transportation process and excitation process of the analytes will contribute more to the total EIE effect.

To understand the effect of EIE on vaporization, the time-resolved profiles of emissions for analyte and EIE were investigated. Curve 1 in Fig. 10 is the time-resolved profile of K obtained with KCl. Curves 2 and 3 in Fig. 10 are the time-resolved profiles of analyte Te obtained with a mixture solution of analyte $TeCl_4$ and KCl, and analyte ($TeCl_4$) alone, respectively. It is indicated from Fig. 10 that the addition of KCl shortened the time needed for the vaporization of analyte and the introduction of a certain amount of EIE can affect the vaporization of the element tested.

Over all, the EIE effect is a negative effect on the analyte determination and extremely complicated. It is related with many factors such as kind and amount of the analyte and EIEs themselves. However, EIE effect can also be making use of in

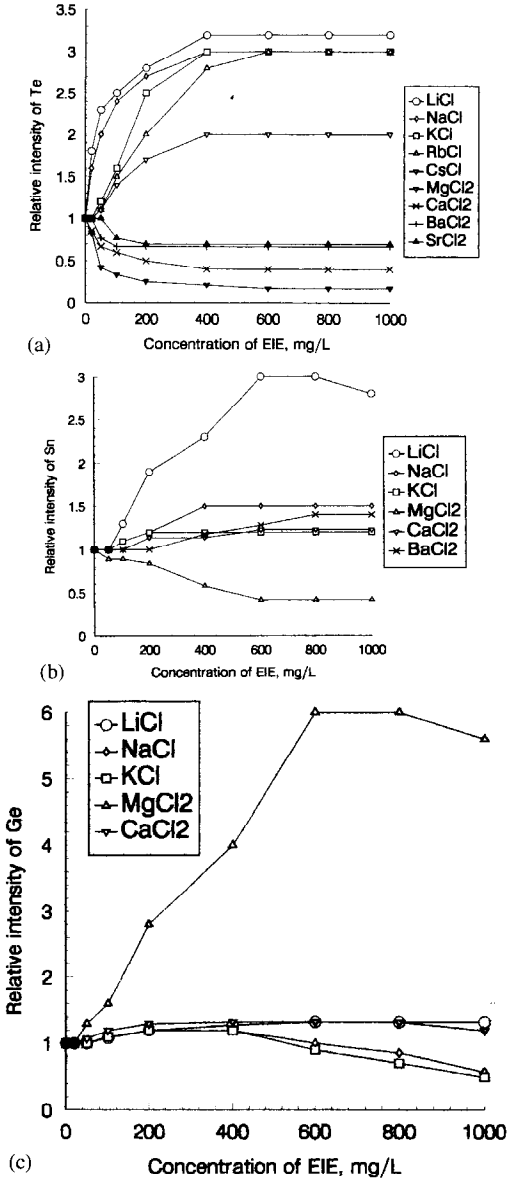

Fig. 7. Effect of EIEs on the emission intensities of (a)Te; (b)Sn; (c)Ge.

overcoming the matrix effects (including EIE effects themselves). For example, those EIEs with enhancement effects in a relatively wide concentration range can be used as matrix modifiers.

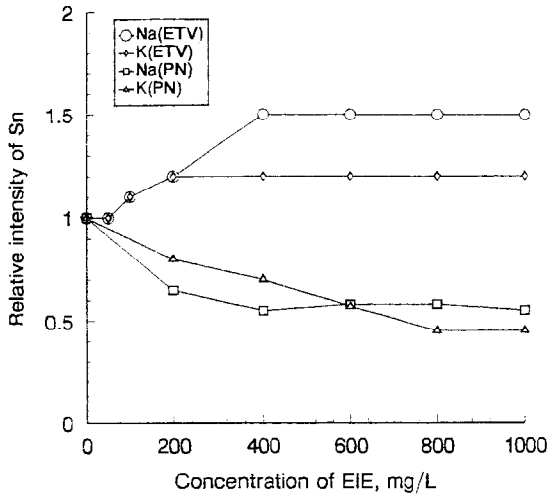

Fig. 8. Effect of Na and K on the emission intensity of Sn with two different sample introduction systems.

3.6.2. Alkaline earth metal element

For comparison, the effect of the alkaline earth metal element on the emission of analyte was also studied in the same manner as the above-mentioned method used in the studies for the effect of alkali metal elements. The effect of Mg, Ca, Sr and Ba on emission of Te, Mg, Ca and Ba on Sn as well as Mg and Ca on Ge are shown in Fig.

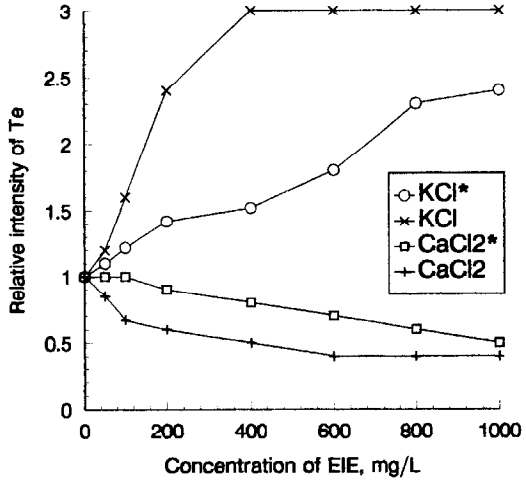

Fig. 9. Effects of Ca and K on the emission intensity of Te with different vaporization modes. *EIE and Te vaporized separately; the others, EIE and Te vaporized together.

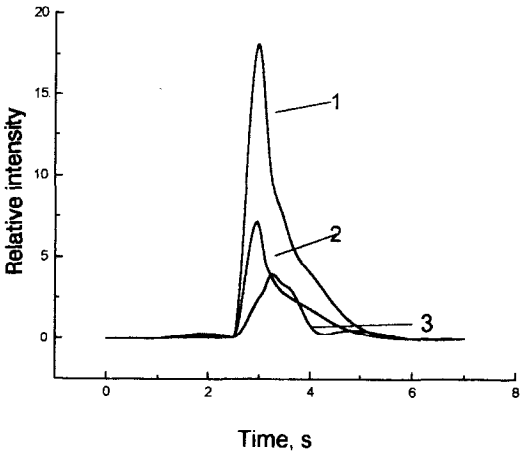

Fig. 10. Time-resolved profiles for K and Te. 1, 500 mg l^{-1} K, at K 404.72 nm; 2, 2 mg l^{-1} Te + 500 mg l^{-1} K, at Te 214.28 nm; 3, 1 mg l^{-1} Te, at Te 214.28 nm.

7(a, b and c), respectively. When two different vaporization modes were empolyed the effect of Ca on emission of Te was shown in Fig. 9. It was obvious from Fig. 7 and Fig. 9 that the effect of alkaline earth metal element on the same analyte is similar to that of alkali metal element.

3.6.3. Effect caused by other concomitant elements

Some concomitant element effects were observed. Table 3 shows some maximum concentrations values of coexistent elements including aluminum and iron allowed. Less than these concentration values the coexistant elements will not cause matrix effects on the determination of the analytes studied. For comparison, potassium and magnesium were also included in Table 3.

3.7. Analytical figures of merit

The detection limits, the linear dynamic ranges and relative standard deviations ($n = 11$) for elements studied by using the proposed technique were shown in Table 4. The standard deviation of the blank was used to calculate the detection limits (3σ). To make comparison the detection limits obtained with MPT-AES system with PN sample introduction are also included. It is obvious that the detection limits for easily volatile elements (Te, Ge, Sn, Pb) studied obtained with ETV-MPT-AES are lower than those obtained with PN-MPT-AES by 1–2 orders of magnitude, while detection limits for non-easily volatile elements (such as Ag and Au) are about the same as those obtained with PN-MPT-AES. The linear dynamic ranges are shown to be approximately three orders of magnitude. At the same time, a comparison of detection limits obtained in this work with those obtained in the literature is shown in Table 5.

3.8. Practical sample analysis

Several geochemical standard reference materials of China (GSD) were analyzed for the detection of Te, Sn, Ag with the proposed method and the results obtained were satisfactory, as shown in Table 6.

4. Conclusion

An ETV sample introduction device made of tantalum device has been coupled with an Ar MPT to determine several trace elements in environmental samples by AES without addition of any matrix modifier. The ETV-MPT-AES system has such advantages as high sensitivity, micro sample consumption, low matrix effect and low running cost. The studies reveal that EIE effects rely on not only the kind and amount of analytes and EIEs but also depend greatly on the sample introduction system (PN or ETV) and the sample introduction mode (whether EIE and analytes are vaporized together or separately). The analytical figures of merit show that the ETV-MPT-AES system is applicable to determination of trace elements in samples with low matrix. To those samples with relatively large amount of matrix, the method of standard addition can be employed. And also, suitable addition of large amount of certain EIE may be helpful because it was found experimentally that some EIE compounds (such as alkali chlorides) have constant enhancement effects in a fairly wide concentration range on most of the elements studied. The work in this direction is now in process.

Table 3
Maximum conncomitant conentration that does not affect determination of the analyte

Analyte (concentration mg l^{-1})	Maximal concomitant concentration (mg l^{-1}) not causing matrix effect			
	Fe	Al	K	Mg
Ag (0.1)	20	20	20	20
Au (0.1)	10	20	20	20
Ge (1)	100	800	100	50
Pb (1)	50	400	50	50
Sn (4)	100	100	100	100
Te (0.5)	50	50	20	20

Table 4
Analytical figures of merit of the proposed ETV-MPR-AES for some analytes

Analyte	Wavelength (nm)	Detection limit			Linear range (μg ml^{-1})	RSD* (%)
		ETV		PN (μg ml^{-1})		
		Absolute (pg)	Relative (μg ml^{-1})			
Ag	328.068	3.0	0.001	0.00074	0.01–10	2.0(0.1)
Au	242.795	6.0	0.002	0.0051	0.001–1	2.4(0.1)
Ge	267.100	24	0.008	0.039	0.08–60	3.8(1.0)
Pb	405.783	12	0.004	0.051	0.02–30	3.9(0.5)
Sn	326.234	147	0.049	0.20	0.2–20	2.8(5.0)
Te	214.283	9.0	0.003	0.25	0.03–10	3.8(0.2)

* Data in blankets are the analyte concentration (μg ml^{-1}) used in measurement of precision.

Table 5
Comparison of detection limits (pg) obtained with the proposed method and some other methods with ETV sample introduction

Element	This method	ETV-MIP-AES [4]	ETV-MIP-MS [6]	ETV-ICP-AES [3]	ETV-ICP-MS [3]
Ag	3.0	1.6–10	0.03	1–150	0.16
Au	6.0	10	—	10–20	0.002–0.5
Ge	24	5000	—	10–60	—
Pb	12	0.56–17	0.75	4–6500	0.002–0.5
Sn	147	300	—	20–2000	0.002–0.5
Te	9.0	125	—	50–4300	100

Table 6
Determination results of Te, Sn an Ag in sediment samples by ETV-MPT-AES

Analyte (samples)	Found (μg g^{-1})	Certified (μg g^{-1})	RSD ($n = 5$), %
Ag(GSD-6)	0.38	0.36	4.5
Sn(GSD-3)	3.6	3.4	6.1
(GSD-6)	2.9	2.8	4.1
Te(GSD-3)	0.16	0.15	5.0

References

[1] K.C. Ng, J.A. Caruso, Appl. Spectrosc. 39 (1985) 719.
[2] H. Matusiewicz, J. Anal. At. Spectrom. 1 (1986) 171.
[3] J.M. Carey, J.A. Caruso, Crit. Rev. Anal. Chem. 23 (1992) 397.
[4] H. Matusiewicz, Spectrochim. Acta. Rev. 13 (1990) 47.
[5] R.O. Satzger, J. Microwave Power Electromag. Energy 24 (1989) 132.
[6] E.H. Evans, J.A. Caruso, R.D. Satzger, Appl. Spectrosc. 45 (1991) 1473.
[7] F.L. Fricke, O. Rose Jr., J.A. Caruso, Anal. Chem. 47 (1975) 2018.
[8] C.I.M. Beenakker, P.W.J.M. Boumans, P.J. Rommers, Philips Tech. Rev. 39 (1980) 65.
[9] J.F. Alder, M.T.C. Da Cunha, Can. J. Spectrosc. 25 (1980) 32.
[10] A. Aziz, J.A.C. Broekaert, F. Leis, Spectrochim. Acta 37B (1982) 381.
[11] J.P. Matousek, B.J. Orr, M. Selby, Appl. Spectrosc. 38 (1984) 231.
[12] E. Beinrohr, E. Bulska, T. Tschopel, G. Tolg, J. Anal. At. Spectrom. 8 (1993) 965.
[13] M.M. Abdillahi, Appl. Spectrosc. 47 (1993) 366.
[14] E. Bulska, P. Tschopel, J.A.C. Broekaert, G. Tolg, Anal. Chim. Acta 27 (1993) 171.
[15] J.H. Runnels, J.H. Gibson, Anal. Chem. 39 (1967) 1398.
[16] K.M. Aldous, R.M. Dagnall, B.L. Sharp, T.S. Wost, Anal. Chim. Acta 54 (1971) 233.
[17] H. Kawaguchi, M. Hasegawa, A. Mizuike, Bunko Kenkyu 21 (1972) 36.
[18] T. Sakamoto, H. Kawaguchi, A. Mizuike, Bunko Kenkyu 25 (1976) 35.
[19] K. Chiba, M. Kurosawa, K. Tanabe, H. Haraguchi, Chem. Lett. (Japan) (1984) 75.
[20] N. Rait, D.W. Golightly, C.J. Massoni, Spectrochim. Acta 39B (1984) 931.
[21] R.G. Stahl, L. Brett, K.J. Timins, J. Anal. At. Spectrom. 4 (1989) 337.
[22] H. Kawaguchi, B.L. Vallee, Anal. Chem. 47 (1975) 1029.
[23] N.W. Barnett, G.F. Kirkbright, J. Anal. At. Spectrom. 1 (1986) 337.
[24] F.L. Fricke, O. Rose Jr., J.A. Caruso, Talanta 23 (1976) 317.
[25] H.P.J. Van Dalen, B.G. Kwee, L. de Galan, Anal. Chim. Acta 142 (1982) 159.
[26] E.I. Brooks, K.J. Timmins, Analyst 10 (1985) 557.
[27] K.J. Timmins, J. Anal. At. Spectrom. 2 (1987) 251.
[28] Q. Jin, C. Zhu, M.W. Borer, G.M. Hieftje, Spectrochim. Acta 46B (1991) 417.
[29] J. Dahman, ICP Inf. Newsl. 18 (1992) 104.
[30] Q. Jin, H. Zhang, Y. Wang, X. Yuan, W. Yand, J. Anal. At. Spectrom. 9 (1994) 851.
[31] H. Zhang, D. Ye, J. Zhao, J. Yu, R. Men, Q. Jin, D. Dong, Microchem. J. 53 (1996) 69.
[32] H. Que, H. Zhang, Q. Jin, Gaodneg Xuexiao Hanxue Xuebao 10 (1989) 897.
[33] D. Ye, H. Zhang, Q. Jin, Talanta 43 (1996) 535.
[34] H. Kawaguchi, I. Atsuya, B.L. Vaille, Anal. Chem. 49 (1977) 266.
[35] J.P. Matousek, G.J. Orr, M. Selby, Spectrochim. Acta 41B (1986) 415.

ELSEVIER

Talanta 44 (1997) 1615–1623

Talanta

On-line preconcentration with activated carbon for microwave plasma torch atomic emission spectrometry

Hanqi Zhang, Xianglin Yuan, Xiaojun Zhao, Qinhan Jin *

Department of Chemistry, Jilin University, Changchun 130023, People's Republic of China

Received 12 September 1996; accepted 4 February 1997

Abstract

This paper presents a method whereby trace elements are adsorbed in NH_4Cl–NH_3 medium on activated carbon and then determined by microwave plasma torch atomic emission spectrometry (MPT-AES). The working conditions (including microwave forward power, gas flow rate, NH_3–NH_4Cl concentration in the sample solution, HCl concentration in the eluant, sample introduction rate and preconcentration time) were investigated in detail. The effects of concomitant ions were studied. The experimental results for such analytes as Pb, Mn, Cd, Cu and Fe indicate that the procedure can eliminate fundamentally the interferences caused by alkali and alkaline earth metal elements and the application of it to the determination of iron in industrial silicon and tap water samples is successful.

Keywords: MPT; Activated carbon; FI; Preconcentration

1. Introduction

Although inductively coupled plasma atomic emission spectrometry (ICP-AES) has been widely applied to the determination of trace elements, the purchasing and operating costs are relatively high. Microwave induced plasma (MIP) has been receiving wide attention since it was used for spectrometric analysis in 1952 by Broida and Moyer [1] because it can provide high sensitivity for a large variety of elements with low operating costs. But traditional MIP sources have the disadvantages of low tolerance to the introduction of aqueous samples and significant interferences caused by easily ionized elements (EIEs), which limit its application to the practical sample analysis. In 1985, new microwave plasma supporting structure, microwave plasma torch (MPT) [2], was developed in the laboratory. It has been shown to have many attractive features such as the unique central channel which offers an easy way for sample introduction and enhances the interaction between the sample and plasma, the powerful excitation ability, and the less expensive running cost. Studies on the analytical performance of MPT in atomic emission spectrometry (AES) [3,4] have shown that the MPT discharge is a promising excitation source. However, the matrix effect is still a major factor that limits the MPT to be applied to the practical samples.

* Corresponding author.

0039-9140/97/$17.00
PII S0039-9140(97)00066-0

Activated carbon has been used as a trace collector for element preconcentration [5–24]. The mechanism involved in the adsorption of ions as trace compounds by the activated carbon is not completely known. Piperaki et al. [7] confirmed that sorption is quantitative when the chelate used contains systems of π-electrons in the molecule and when its centres for binding on carbon and those for the methyl ions are spatially separated so that their orbitals do not have a substantial influence with each other. Hutchinson and Schilt [8] considered there are two types of sites on activated carbon for adsorption, which are interpreted in terms of Langmuir parameters and ionic charge types of the adsorbates. Because activated carbon is a type of hydrophobic adsorbent which adsorbs nonpolar or little polar substances in aqueous solution, metal ions to be preconcentrated need to be transformed corresponding metal chelates [5–20], metal elements [21] or metal hydroxides [22–24] which could be adsorbed on activated carbon. Metal chelates could provide higher selectivity and high enrichment factors for such a preconcentration and separation. However, a strong acid is usually needed for elution and plasmas exhibit low tolerance to the introduction of strong acid. In addition, some noble metals can be reduced to elements being able to be adsorbed on activated carbon. In the literature [22,24], the pH of the solution was adjusted with NaOH, HCl or buffer solution $NaHCO_3$–Na_2CO_3, CH_3COONa–CH_3COOH, $Na_2B_4O_7$–(HCl or NaOH)–$NaClO_4$, and in general, higher pH value was adjusted with NaOH. It is obvious that the control and adjustment of pH are more difficult with NaOH than with buffer solution. In this work, the pH of solution was adjusted with buffer solution NH_4Cl–NH_3. Some trace elements are preconcentrated onto activated carbon in a NH_4Cl–NH_3 medium and then determined by flow injection (FI)-MPT-AES. It is evident from the experimental results that by using this ap-

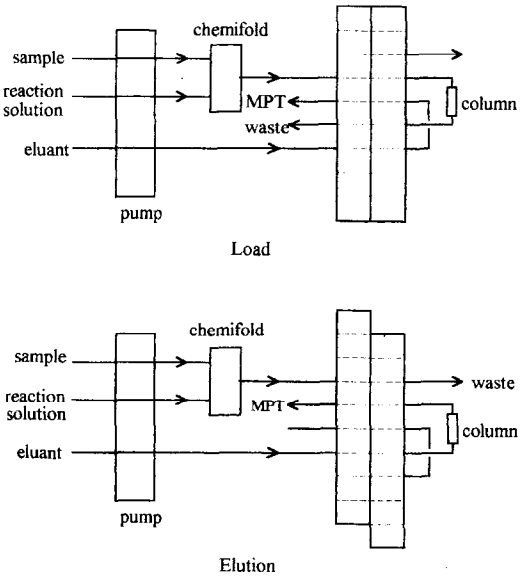

Fig. 1. Block diagram of flow injection system.

Table 1
Experimental components

Component	Model/size	Manufacturer
Microwave generator	DW-1 0–100 W	Beijing Geological Instrument Factory
Monochromator	WDG30 $f=30$ cm grating 1200 grooves mm^{-1}	The Second Beijing Optical Instrument Factory
High-voltage power supply	0–1000 V	Laboratory built
Photomultiplier	R456	Hamamatsu
Strip-chart recorder	056	Hitachi, Japan
Peristaltic pump	LZ-1010	Shenyang Zhaofa Institute of Automatic Analysis
Lens	20 mm diameter 70 mm focal length, quartz	
MPT		Laboratory built
Preconcentration column		Laboratory built

Table 2
Operating conditions

Parameter	Value
Microwave frequency (MHz)	2450
Forward power (W)	60
Plasma viewing mode	side-on
Plasma viewing position	8–9 mm above top of the torch
Support gas flow rate (ml min^{-1})	400
Carrier gas flow rate (ml min^{-1})	700
HCl concentration in the sample solution (mol l^{-1})	0.05
HCL concentration in the eluant (mol l^{-1})	0.5
NH_3 concentration in the reaction solution (mol l^{-1})	0.1
Loading time (s)	60
Washing time (s)	30
Sample introduction rate (ml min^{-1})	1.2
Eluant introduction rate (ml min^{-1})	1.2

proach the effects of alkali and alkaline earth elements on the determination of metal elements are eliminated efficiently.

2. Experimental

2.1. Apparatus

The block diagram of the experimental instrumentation used in this work is the same as that reported previously [25]. It consists of simple introduction system, desolvation system and MPT-AES system. The block diagram of sample introduction system is shown in Fig. 1. The desolvation system used in this work is the same as that used previously [3]. The components of the setup are listed in Table 1.

2.1.1. On-line preconcentration and elution

As shown in Fig. 1, the sampling loop in a regular FI set was replaced by an online preconcentration column, which was 4 mm i.d. and 40 mm long, filled with activated carbon and made of glass pipette. The activated carbon was limited in the column by two small plugs of plastic foam at either end. During the preconcentration step,

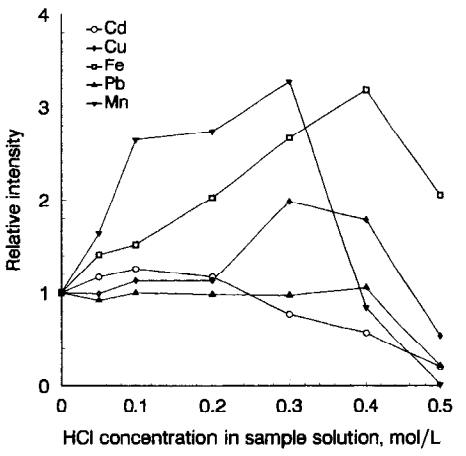

Fig. 2. Effect of HCl concentration in sample solution on emission intensity.

the eluant flowed from a peristaltic pump directly through the concentric pneumatic nebulizer to the plasma while the sample solution and reaction solution (certain concentration aqueous ammonia) were simultaneously pumped at the same rate separately into chemifold where they were mixed to form hydroxides. After the mixed solution passes through the activated carbon column, water was introduced to wash the activated carbon for a while, and then, the valve was rotated and

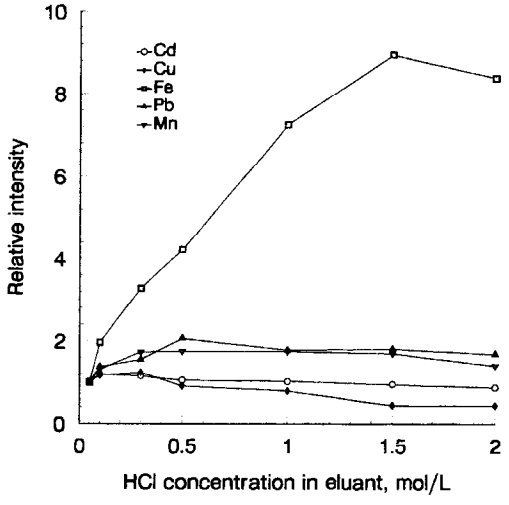

Fig. 3. Effect of HCl concentration in eluant on emission intensity.

the path of the eluant was redirected to flow through the preconcentration column, thereby the sample plug was carried into the MPT.

In addition, to make comparison, the system was also tested with regular flow injection (FI) and continuous pneumatic nebulization (CPN) sample introduction modes. In the FI mode, reaction solution was replaced by water and the preconcentration column was equivalent to a sample loop so there was no preconcentration. In the CPN mode, the FI on-line preconcentration setup was in the load position of the actuated injection valve and the sample was introduced into the MPT through the path of eluant.

2.1.2. Desolvation system

The desolvation system is similar to that of Ref. [3]. After the eluate was passed through the pneumatic nebulizer, it was desolvated by passing through a heating spray chamber, a tap-water cooled condenser and a concentrated sulfuric acid desiccator.

2.1.3. MPT

The MPT torch is similar to that of Ref. [26]. Its structure is like that of ICP torch, which consists of three concentric tubes. The central and intermediate tubes are made of copper and the outer tube is made of brass. The sample aerosol is introduced into the plasma through the central tube by a carrier gas. The plasma supporting gas is introduced through the intermediate tube. The plasma, a flame-like discharge, is formed between the central and intermediate tubes near the top of the torch and extended into the surrounding air.

2.2. Reagents

Activated carbon (Dalian Hongguang Chem. Eng. Factory, China) was soaked in 2 mol l^{-1} HCl for at least 24 h so as to remove the metal ions and other impurities sorbed on it.

Argon (99.99%) (Fushum Biousi., China) was used as both carrier gas and support gas. All reagents used were of superpure grade or analytical-reagent grade. De-ionized water was used in all experiments.

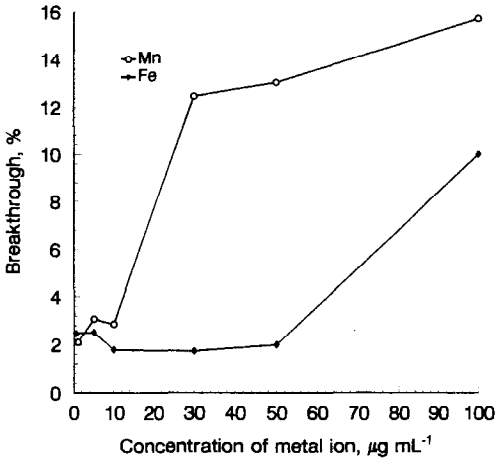

Fig. 4. Curves of breakthrough for Mn and Fe. The percentage of breakthrough is defined as the response of the element with the use of activated carbon column relative to the response without the column.

3. Results and discussion

3.1. Working conditions of MPT

The optimized operating conditions are given in Table 2.

3.2. Conditions for preconcentration and elution

The main experimental parameters influencing the process of preconcentration-elution for such analytes as Pb, Mn, Cd, Cu and Fe were investigated in detail.

3.2.1. Preconcentration time

The emission intensities of analytes increase with the increase of preconcentration loading time. The loading time selected in the experiment is 60 s.

3.2.2. HCl concentration in the sample solution and NH_3 concentration in reaction solution

To examine the effect of HCl concentration in sample solution, NH_3 concentration (0.5 mol l^{-1}) in reaction solution keeps constant. As shown in Fig. 2, the emission intensities increase or keep constant at first and then decrease with the increase of HCl concentration in sample solution.

Table 3
Analytical figures of merit of some elements obtained by this method

Element	Wavelength (nm)	Detection limit (ng ml^{-1})		Linear range (μg ml^{-1})	RSD (%)	EF
		a	b			
Cd	I228.8	1.0	10	0.01–50	1.7	6.4
Cu	I324.7	3.2	9.3	0.01–50	2.7	6.1
Fe	II259.9	4.7	12	0.02–50	1.7	6.2
Pb	I405.8	36	104	0.1–50	1.5	5.8
Mn	II257.6	2.4	9.1	0.01–10	2.2	4.3

a This work, ArMPT-AES, 60 W, FI on-line preconcentration with activated carbon.
b This laboratory, Ar-MPT-AES, 60 W, FI.

To examine the effect of NH_3 concentration in reaction solution, the HCl concentration (0.05 mol l^{-1}) in sample solution keeps constant.

In the present work, the pH value of the mixture solution (acidified sample + ammonia solution) was adjusted by concentration ration of HCl and NH_3. It is evident from above-mentioned experiments that the most intensive emission intensity was obtained when the NH_3 and NH_4^+ concentration in the mixture solution is approximately equal, and the corresponding pH value is about 9. The selected concentration of HCl in sample and NH_3 in reaction solution are 0.05 and 0.1 mol l^{-1}, respectively. The results are similar to that obtained in the absence of NH_3 [24]. In the present work, the mixture solution has an excess of ammonia (0.025 mol l^{-1}), Mn, Cd and Cu, especially Cd and Cu, are not precipitated under the conditions and mainly exist as the form of ammo complexes. Because the ammo complexes have positive charge and ammonia is a polar substance, it is difficult for them to be adsorbed on the activated carbon. However, because the hydroxides are preferably sorbed on activated carbon surface, the equilibrium is shifted, thus, hydroxides are sorbed on the surface anyway even if they are not present in solution.

3.2.3. HCl concentration in the eluant

To examine if the HCl concentration in eluant affected mainly on the process of elution of metal hydroxides on the surface of activated carbon or the process of emission of metal atoms in the plasma, the effect of HCl concentration in sample solution on emission intensities was investigated with CPN sample introduction mode. It was shown that there was no significant effect of HCl concentration on emission intensities of analytes directly introduced into the plasma. However, the effect of HCl concentration in the eluant on the emission intensities was obvious (see in Fig. 3). It is well known that $Fe(OH_3)$ precipitation can be formed at lower pH value than hydroxide precipitations of Pb, Mn, Cd, Cu when the metal ion concentrations are the same. So for most analytical lines studied, when the HCl concentration goes over 0.5 mol l^{-1}, the emission intensities are keeping constant or decreased slightly. But for iron, the emission intensity exhibits a maximum when HCl concentration in eluant is up to 1.5 mol l^{-1} because of the uneasy elution or iron hydroxide, thus 0.5 mol l^{-1} HCl for Pb, Mn, Cd and 1.5 mol l^{-1} HCl for Fe were selected as the eluant.

3.2.4. Breakthrough

The activated carbon in the column will be approaching a state of saturated adsorption little by little with the increase of the concentration of metal ions in the sample solution being studied. Fig. 4 shows a curve of breakthrough of the activated carbon column. It is obvious from the curves that the breakthrough volumes are basically constant when the concentrations of determined ions are low, and then increase sharply when the concentration of iron is higher than 50 μg ml^{-1} or the concentration of manganese is higher than 10 μg ml^{-1}. These experimental results are in agreement with the following results of

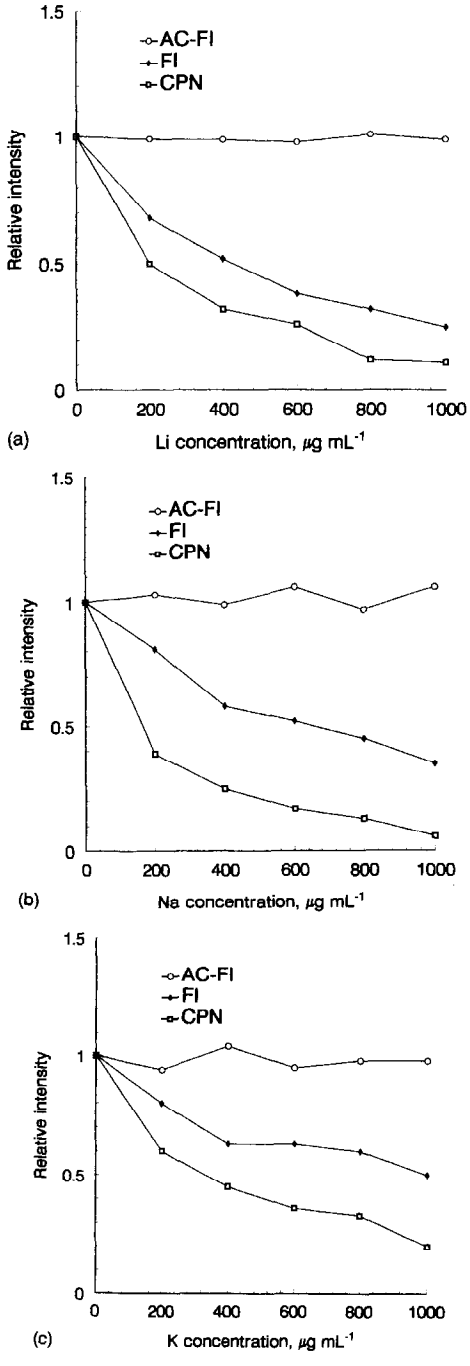

Fig. 5. Effect of EIEs (a, Li; b, Na; c, K) on emission intensity of Pb (405.8 nm)

dynamic linear range experiments (the dynamic liner range for Fe is 0.02–50 μg ml^{-1} and for Mn is 0.01–10 μg ml^{-1}).

3.3. Analytical figures of merit

The detection limits (3σ), dynamic linear ranges, precision and enrichment factors (EF) for elements studied obtained by this method are listed in Table 3. For comparison, Table 3 lists also detection limits obtained by FI-MPT-AES.

For all elements tested, the dynamic linear ranges are over 3 orders of magnitude and the relative standard deviations are in the range of 1.7–2.7%.

EF is a criterion used most often for evaluating preconcentration system. However, the precise meaning of the term is often not definite. Here EF [27] is defined as the ratio between the peak height with preconcentration and the peak height without preconcentration, a regular FI set-up was used.

3.4. Matrix effects

It has been shown that the interference caused by some concomitant ions is one of the major factors that limits the further development of MWP-AES [3,26]. Alkali and alkaline earth, Fe and Al exist in the nature in wide varieties, so the effects resulting from the elements were investigated in detail in this study.

3.4.1. Effect of easily ionized elements

It is clear from previous studies [28–30] that for traditional microwave induced plasmas the effect of EIEs on emission intensities is relatively significant. Additionally, the extent of interference depends on the sample introduction method adopted. To study the EIE effect, for this flow injection on-line preconcentration system with activated carbon (AC-FI), either FI or CPN sample introduction method was used. Fig. 5 shows that flow injection on-line preconcentration with activated carbon can eliminate fundamentally the interferences caused by EIEs. The reason is that EIEs are in existence of ions even in the basic solutions and can not be adsorbed by activated carbon. Flow injection alleviated the interferences

Table 4
Effects caused by EIEs

EIE[a]	EIE concentration ($\mu g\ ml^{-1}$)	Recovery (%)[b]				
		Cd (0.2 $\mu g\ ml^{-1}$)	Cu (0.3 $\mu g\ ml^{-1}$)	Fe (0.5 $\mu g\ ml^{-1}$)	Pb (4.0 $\mu g\ ml^{-1}$)	Mn (0.2 $\mu g\ ml^{-1}$)
Li	200	106	101	92	99	98
	400	106	104	96	99	97
	600	108	98	92	98	100
	800	102	72	102	101	98
	1000	97	71	101	99	98
Na	200	102	97	98	103	102
	400	94	97	98	99	101
	600	98	100	101	106	98
	800	93	98	104	97	104
	1000	102	99	104	106	96
K	200	100	105	100	94	102
	400	101	103	95	104	98
	600	98	98	99	95	99
	800	98	102	108	98	106
	1000	100	102	98	98	104

[a] EIEs were added in the form of chloride.
[b] The emission intensity of each element is taken as 100 when no EIEs are added.

compared with continuous pneumatic nebulization as a result of sample dilution in the FI system [31].

Table 4 lists the effect of a series of concentration changes of EIEs on emission intensities of elements studied. It is evident from Table 4 that the effect of EIEs is minimized because of the use of FI on-line preconcentration technique, and Cl^- does not affect the determination.

Table 5
Effect of alkaline earth metal elements, Fe and Al

Element	Concentration ($\mu g\ ml^{-1}$)	Fold of concomitant element of not causing interference
Cd	0.2	Mg(1000), Ca(1000), Ba(1000), Fe(100), Al(100)
Cu	0.3	Mg(1000), Ca(1000), Ba(1000), Fe(50), Al(50)
Fe	0.5	Mg(1000), Ca(1000), Ba(1000), Al(20)
Pb	4.0	Mg(500), Ca(500), Ba(500), Fe(20), Al(20)
Mn	0.2	Mg(1000), Ca(1000), Ba(1000), Fe(100), Al(100)

3.4.2. Effect of other concomitant ions

Table 5 lists the effect of alkaline earth elements, Fe and Al on the emission intensities of elements studied. The experimental results are explained under these experimental conditions that the hydroxides of alkaline earth elements are not formed and, therefore, they can not be adsorbed on activated carbon. Although the hydroxides of Fe^{3+} and Al^{3+} can be formed and adsorbed on the activated carbon, they do not affect the determination of these elements within the concentration ranges studied. Some anions, such as Cl^-, SO_4^{2-}, NO_3^-, exist in many natural

Table 6
Results of determination of iron in industrial silicon samples

Sample	RSD (%)	Content (%)	
		Certified	Determined
1	3.7	0.39	0.38
2	4.1	1.15	1.12
3	3.0	2.92	2.95
4	3.1	1.51	1.49

Table 7
Results of determination of iron in tap water samples

Sample	Determined concentration (μg ml^{-1})	RSD (%)	Recovery (%)
1	0.05	3.5	100
2	0.33	4.0	105

samples or can be introduced into sample solution in sample digestion. It is indicated from the experimental results that these anions do not affect the determination.

3.5. Practical sample analysis

To investigate the applicability of this method developed, the contents of iron in industrial silicon (Table 6) and tap water samples were determined. The obtained values are in good agreement with the certified values. The recoveries of iron in tap water are in the range of 100–109% (Table 7). The RSDs in all cases are less than 4.1%.

4. Conclusion

This work demonstrates that flow injection online preconcentration and preseparation with activated carbon not only improves the detection limits but also eliminates fundamentally the interferences caused by alkali, alkaline earth elements. The proposed procedure is beneficial to improving the analytical performance of MPT and applying MPT to the analysis of practical samples. However, in some specific cases for determination of Pb in iron or aluminium alloy, some further improvements to eliminate the interferences caused by excess iron and aluminium are necessary.

Acknowledgements

This work was supported by the National Natural Science Foundation of China and the Changchun Research Center for Applied Chemistry.

References

[1] H.P. Broida, J.W. Moyer, J. Opt. Soc. Am. 2 (1952) 37.
[2] Q. Jin, G. Yang, A. Yu, J. Liu, H. Zhang, Y. Ben, Pittsburgh Conference Abstracts, (1985) 1171.
[3] Q. Jin, H. Zhang, Y. Wang, X. Yuan, W. Yang, J. Anal. At. Spectrom. 9 (1994) 851.
[4] H. Zhang, D. Ye, J. Zhao, J. Yu, R. Men, Q. Jin, D. Dong, Microchem. J. 53 (1996) 69.
[5] K. Murakami, Y. Olamoto, T. Kumamara, J. Flow Injec. Anal. 9 (1992) 195.
[6] Y.P. de Peña, M. Gallego, M. Valcárcel, J. Anal. At. Spectrom. 9 (1994) 691.
[7] E. Piperaki, H. Berndt, E. Jackwerth, Anal. Chim. Acta 100 (1978) 589.
[8] D.J. Hutchinson, A.A. Schilt, Anal. Chim. Acta 154 (1983) 159.
[9] B.M. Vanderborght, R.E. Van Grieken, Anal. Chem. 49 (1977) 311.
[10] B.M. Vanderborght, R.E. Van Geieken, Talanta 27 (1980) 417.
[11] H. Berndt, J. Messerschmidt, Fresenius'Z. Anal. Chem. 308 (1981) 104.
[12] H. Berndt, J. Messerschmidt, E. Reiter, Fresenius'Z. Anal. Chem. 310 (1981) 230.
[13] H. Berndt, U. Harms, M. Sonneborn, Fresenius'Z. Anal. Chem. 322 (1985) 329.
[14] J. Ruzicka, A. Arndal, Anal. Chim. Acta 216 (1989) 243.
[15] P.R. Devi, G.R.K. Naidu, Analyst 115 (1990) 1496.
[16] A.J. Ambrose, L. Ebdon, P. Jores, Anal. Proc. 26 (1989) 377.
[17] E. Beinrohr, J. Rojcek, J. Garaj, Analyst 113 (1988) 1831.
[18] L.A. Monte, A.J. Curtiust, J. Anal. At. Spectrom. 5 (1990) 21.
[19] A.K. Avila, A.J. Curtius, J. Anal. At. Spectrom. 5 (1990) 21.
[20] R.E. Santelli, M. Gallego, M. Valcarcel, Talanta 41 (1994) 817.
[21] E.M. Hall, J.C. Pelchat, J. Anal. At. Spectrom. 8 (1993) 1059.
[22] H. Koshima, H. Onishi, Talanta 27 (1980) 795.
[23] M. Kimura, S. Egana, Talanta 29 (1982) 329.
[24] H. Koshima, H. Onishi, Talanta 33 (1986) 391.

[25] D. Ye, H. Zhang, Q. Jin, Talanta 43 (1996) 535.
[26] Q. Jin, C. Zhu, M.W. Borer, G.M. Hieftje, Spectrochim. Acta 46B (1991) 417.
[27] Z. Fang, Spectrochim. Acta, Rev. 14 (1991) 235.
[28] Q. Jin, H. Zhang, Y. Duan, A.Yu. Ren, X. Zhang, H. Lu, S. Yu, Microchem. J. 44 (1991) 153.
[29] M.H. Abdallah, S. Coulombe, J. Mermet, J. Hubert, Spectrochim. Acta 37B (1982) 583.
[30] M. Selby, R. Rezaaiyaan, G.M. Hieftje, Appl. Spectrosc 41 (1987) 761.
[31] Y. Madrid, M. Wu, Q. Jin, G.M. Hieftje, Anal. Chim. Acta 277 (1993) 1.

ELSEVIER

Talanta 44 (1997) 1625–1632

Talanta

Development of a diamine biosensor

Clarke X. Xu [a], Sayed A.M. Marzouk [a], Vasile V. Cosofret [a], Richard P. Buck [a,*], Michael R. Neuman [b], Robert H. Sprinkle [c]

[a] *Department of Chemistry, University of North Carolina, Chapel Hill, NC 27599-3290, USA*
[b] *Department of OB/GYN, Metro Health Medical Center, Case Western Reserve University, Cleveland, OH 44109-1998, USA*
[c] *School of Public Affairs, University of Maryland, College Park, MD 20742, USA*

Received 6 September 1996; received in revised form 26 November 1996; accepted 14 January 1997

Abstract

An amperometric diamine sensor is developed for clinical applications in diagnosis of bacterial vaginosis (BV). The sensor is based on crosslinked putrescine oxidase (PUO) which catalyzes the conversion of diamines (mainly putrescine and cadaverine) to products including hydrogen peroxide. The hydrogen peroxide is detected anodically at platinum electrode polarized at 0.5 V versus Ag/AgCl. Platinum-plated gold electrodes used as a substrate for the sensor construction, are batch-fabricated on a flexible polyimide foil (Kapton®, DuPont). A three-electrode cell configuration is used in all amperometric measurements. The sensor construction is based on three layers: an inner layer to reject the interference effect of oxidizable molecules, an outer diffusion controlling layer, and in addition, an enzyme middle layer. The enzyme layer was immobilized by crosslinking PUO with bovine serum albumin (BSA) using glutaraldehyde (GA). An optimization study of the enzyme solution composition was carried out. With the optimized enzyme layer, the biosensor showed a very high sensitivity and fast response time of ca. 20 s. The sensor has a linear dynamic range from (0.5–300 μM) for putrescine that covers the expected biological levels of the analyte. Details on sensor fabrication and characterization are given in the present work. © 1997 Elsevier Science B.V.

Keywords: Diamines; Biosensor; Bacterial vaginosis; Putrescine oxidase

1. Introduction

The three most common vaginal infections are: bacterial vaginosis (BV), candidiasis (yeast infection) and trichomoniasis (trich). BV, the most common type of vaginal infection, affects 35% of women visiting sexually transmitted disease clinics, 15–20% of pregnant women, and 5–15% of women visiting gynecologic clinics [1–3]. Women with symptoms usually have an increased, milk-like vaginal discharge with an unpleasant foul odor. However, about half of all patients may have no symptoms at all.

BV has become linked with increasing confidence to idiopathic premature labor which is the predominant cause of premature delivery in USA [4,5]. Despite the fact, BV is often unrecognized and diagnostically unsought in women without specific vaginal complaint. It is ordinarily not a screening target in women classically at risk for

* Corresponding author.

PII S0039-9140(97)00067-2

premature labor and in pregnant women generally. In the absence of typical BV symptoms, health providers may consider the current screening diagnostic options inadequate, neither sensitive enough nor specific enough to be reliable. Those procedures include examination of the vaginal odor, discharge character, density of clue cells (*bacillus* covered cells) microscopically, and nitrazine-paper pH measurement. The screening may not provide conclusive evidence and could unprofitably prolongs office visits. If a quick, reliable and low cost office-diagnostic test will be available, then BV screening would enter routine clinical practice, so a common complaint would be more cost-effectively managed.

The exact cause of BV is unknown, but is believed due to change of the natural balance of organisms found in the vagina. The more acidic *Lactobacillus* is replaced by high concentrations of *G. vaginalis*, anaerobes and *M. hominis*. The fishy odor of vaginal fluid with BV was reported mainly caused by putrescine (1,4-diaminobutane) and cadaverine (1,5-diaminopentane) [6,7], which are the decarboxylation products of arginine and lysine metabolism. These diamines are present in salt forms in the vagina. They become volatile and emit a fishy odor in alkaline pH. They are not detectable in women without a clinical diagnosis of BV. Although the exact cause of diamine production in vaginal fluid is not clear, its presence and association with BV have been widely confirmed. According to reported diamine screening test with TLC on population of more than 500 women, 88% of women with BV gave positive results while 92% of normal women gave negative results [7]. This convincing result predicts that diamine levels could be an effective marker in BV diagnosis. Trimethylamine has also been found only to be associated with BV patients, and not associated with normal women [8].

Detection of diamines in clinical samples currently requires time-consuming and relatively expensive electrophoretic [6], and chromatographic methods [7–10]. Enzymatic spectrophotometry has been used to study blood and urine samples where polyamines were served as cancer markers [11–17]. They provide good research tools, but are impractical to apply for routine clinical screening. An attractive alternative to these complicated analyses would be the miniature biosensors with electrochemical detection. In the last two decades, electrochemical biosensors have demonstrated their attractiveness in solving chemical and clinical problems [18–20]. Electrochemical polyamine biosensors have been reported [21–24]. They are mainly targeted at monitoring meat freshness [25–28] and plant growth-regulating activity [29,30]. No study has been reported with application of this sensor for BV diagnosis.

Until recently, pure and highly active polyamine oxidases were not readily available. Time-consuming protein purification procedures had to be taken to produce an analytically useful enzyme for amperometric sensors. However, putrescine oxidase [E.C. 1.4.3.10] from microorganisms is a pure active enzyme, and is also much more specific to putrescine and cadaverine than other polyamine oxidases (e.g., polyamine oxidase, E.C. 1.5.3.3; and diamine oxidase, E.C. 1.4.3.6).

Putrescine oxidase catalyzes the oxidation of diamines according to the following reaction:

$$H_2N(CH_2)_nNH_2 + O_2 + H_2O \rightarrow H_2N(CH_2)_{n-1}CHO + NH_3 + H_2O_2 \quad (1)$$

The generated H_2O_2 is detected amperometrically on the surface of the platinum-plated gold electrode.

Recent reports of amperometric sensors with PUO in homogeneous catalysis [25], and in immobilized form on substrates of graphite [30], thin layer gold [27], and thick layer graphite/TTF [28] showed that this enzyme is a promising one for the proposed work.

Growing interest have been shown to the flatform flexible biosensors. Some of the biomedical applications include monitoring pH, glucose, creatine, creatinine, and lactate levels [31–34]. The objective of this study is to develop a highly sensitive and selective, mass producible, and clinically acceptable diamine biosensor which will provide a screening device that meets the requirements for clinical diagnosis of BV. We present here a novel miniature diamine biosensor, based on crosslinked PUO, developed on a flexible sub-

strate. Its unique design is aimed at providing a sensor with high sensitivity and great selectivity against the potential interferences in vaginal fluid.

2. Experimental

2.1. Reagents

Putrescine oxidase [E.C. 1.4.3.10], 51.5 U mg^{-1} from *Micrococcus roseus* was received as a gift from Amano Pharmaceutical (Nagoya, Japan). Bovine serum albumin (fraction V), glutaraldehyde (25% aqueous solution), putrescine dihydrochloride (PUT), cadaverine dihydrochloride (CAD), spermine (SPM), tyramine (TYR), trimethylamine (TMA), L-lactic acid (sodium salt), fumaric acid, succinic acid, and pyruvic acid were purchased from Sigma (St. Louis, MO). The medical grade aliphatic polyurethane (Tecoflex SG 85A) was received as gift from Thermedics, (Woburn, MA). All other chemicals were of analytical reagent grade.

2.2. Apparatus and measurement procedure

2.2.1. Batch system

A computer controlled electrochemical measurement system was used throughout the experiments. The system contains an EG&G PARC M273A Potentiostat/Galvanostat, IBM PC-AT compatible computer, and M270 (v4.0) software for remote experimental control and data acquisition. All potentials were applied against a miniature Ag/AgCl reference electrode with flexible barrel (Cypress System, Lawrence, KS). The sensor was allowed to stabilize, and steady-state current values were obtained in all experiments. Data were collected at frequency of 1 Hz while a constant polarization potential of +0.5 V was applied on the putrescine sensor. All experiments were performed at room temperature (22 ± 1°C).

2.2.2. FIA system

The miniature diamine sensor was used in a single channel wall-jet flow system containing a manual sample injection valve (Rheodyne, Model 7125) fitted with a 20 μl injection loop. A carrier solution consisting of 0.1 M phosphate buffer (PB) of pH 7.2 was propelled by means of a Rabbit peristaltic pump (Rainin Instrument) through PTFE tubing (0.8 mm i.d.) at the desired flow rate. The tubing ended with a horizontally mounted 5 cm glass capillary tube (6.6 mm o.d. and 1 mm i.d.). The length of the tubing from the injection valve to the capillary was ~30 cm. The free end of the capillary was cut at 90° and polished with a fine emery paper. This end of the tube was brought into direct contact with the sensor surface. The sensor was mounted in a vertical position with connection wire directed upward. A Pt wire sealed to the glass capillary tube, 10 mm from the sensor, was used as a counter electrode. The reference electrode described above was inserted on the flowing stream, ca. 5 mm from the sensor, and sealed with epoxy. A schematic diagram for FIA is shown in Fig. 1. Sensor signals were recorded on a Yokogawa 3025 X-Y recorder.

2.3. Micro biosensor fabrication

2.3.1. Micro sensor substrate

Photolithographic technique has been used to fabricate the sensor substrate and details can be found in a recent publication [35]. Single-site planar gold electrodes (area = 0.06 cm^2) were batch-fabricated on flexible polyimide (Kapton®, DuPont) substrates (125 mm thickness). Two thin layers, chromium and gold, were sputtered onto the substrate. A layer of photodefinable polyimide

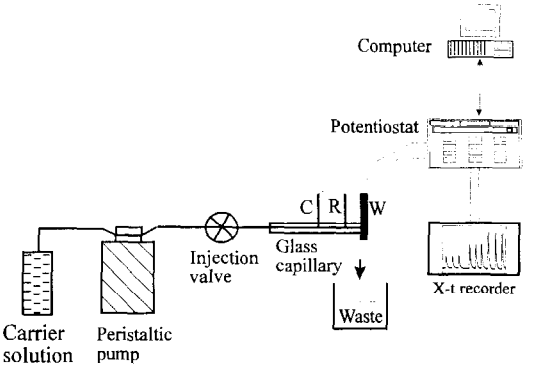

Fig. 1. Schematic diagram of single channel FIA setup.

was used to define both the electrode site and bonding pads. Each completed electrode substrate was cut from the wafer and connected through bonding pads to wires using silver epoxy (Epoxy Technology). Electrical contacts were insulated using silicone rubber (Dow Corning 3140 RTV). The gold substrate was further electroplated with a layer of platinum before the enzyme was immobilized. The platinization solution was prepared according to an early described method [36]. The surface was cleaned at $+500$ μA cm^{-2} for 30 s in the solution before a galvanostatic platinization current (~ 10 mA cm^{-2}) was applied for 5 min with a 5 cm diameter platinum mesh as counter electrode.

2.3.2. Modification of the sensor substrate

A thin film of poly *m*-phenylenediamine (*m*-PDA) was formed from 0.01 M *m*-PDA solution in PB by electrochemical polymerization using cyclic voltammetry. The potential was scanned between $+0.2$ to $+0.8$ V versus Ag/AgCl. The film forming process lasted about 2 h with scan rate of 2 mV s^{-1}. Then, the modified Pt electrodes were individually tested for interferences and sensors showing signals greater than 5 nA for 0.2 mM ascorbic acid were rejected. Less than 5% of the sensors were rejected in this test.

2.3.3. Immobilization of putrescine oxidase

The enzyme layer was immobilized on the electrode surface by crosslinking putrescine oxidase with bovine serum albumin using glutaraldehyde. To obtain an enzyme layer with high catalytic activity and good adhesion to the Pt and surrounding substrate, many sensors were prepared and tested with variable ratios of PUO, BSA, and GA. 1–3 μl aliquot of a freshly prepared enzyme mixture with specified composition in PB of pH 7.2 was quickly delivered onto the electrode surface with a micro syringe. The mixture was allowed to reticulate for an hour at room temperature.

2.3.4. Outer membrane layer

An outer layer was applied on the sensor by adding 2 μl of 1% polyurethane in pure THF solution. The sensor was allowed to dry in air for 10 min, washed with PB, and then stored at 4°C in phosphate buffer (pH = 7.2).

3. Results and discussion

3.1. Sensor calibration

A multilayer sensor is schematically represented in Fig. 2. Our results showed that membranes prepared with crosslinking 0.75 U PUO only gives a high quality sensor in comparison with ~ 15 U used for previous work reported by others. 1 μl aliquot of an enzyme mixture with final composition of 3% PUO-5% BSA-5% GA in phosphate buffer was used for all sensor preparations. The response of a typical putrescine sensor in phosphate buffer is illustrated in Fig. 3. The sensor has a detection limit of 0.5 μM for putrescine (S/N = 2), with linear response range up to 300 μM ($R^2 = 0.9997$). The sensor response to putrescine is very fast. An average response time of ca. 20 s ($t_{95\%}$) was obtained. The sensitivity of the sensor is 2.2 nA μM^{-1} within the linear concentration range. Sensors with enzyme layer only showed a narrower linear dynamic range (0.5–50 μM).

3.2. Sensor stability

Although they contain a small amount of enzyme, the sensors demonstrated very good stability. Fig. 4 showed the drifts of the sensor slope (S) relative to the initial slope (S_0), which was measured only a few hours after the sensor preparation. Approximately 200 measurements have been made for each sensor; they were kept in PB at 4°C when not in use. Sensors kept nearly 90% of the initial sensitivities in the first 10 days after a short period of conditioning. This period is long enough for disposable sensors in clinical applications.

3.3. The pH dependence of the sensor

The optimum catalytic activity of putrescine oxidase is known to be around pH 8.5 for homogeneous solution catalysis [37]. For diamine sensors with immobilized putrescine oxidase the

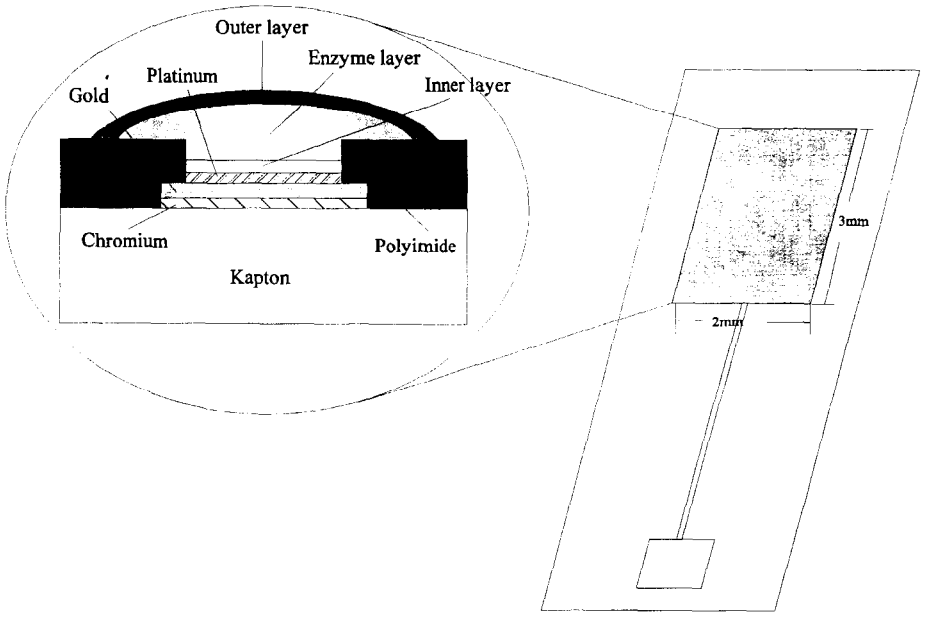

Fig. 2. Schematic diagram of a multilayer diamine sensor.

effects of pH of sample solution on sensor responses were studied with different buffers. Previous reports [27,28,30] have shown different pH profiles with maximum response in the range of pH 7–8.5. This is caused by different enzyme substrates and immobilization techniques used. In this study, three different buffers (0.1 M potassium phosphate, 0.1 M Tris–HCl + 0.1 M KCl, and 0.1 M H_3BO_3 + 0.1 M KCl + 0.1 M NaOH) were selected with pH ranging 6.5–9.5 to evaluate the sensor responses. In borate buffer the sensor gave the highest signal, and the maximum response of the enzyme sensor was observed at pH 8.5 with this buffer (Fig. 5). This agrees with the previous reported results [28]; however, we found that the sensor had the lowest background current and the fastest response time in phosphate buffer. In Tris–HCl buffer the sensor had the highest

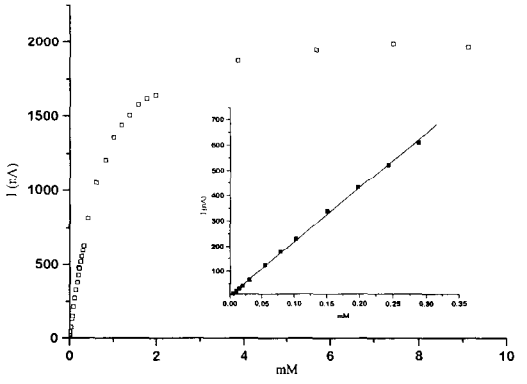

Fig. 3. Amperometric response of the diamine sensor to putrescine.

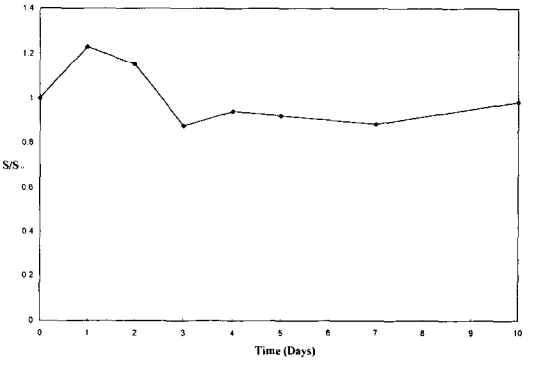

Fig. 4. Stability of diamine sensor (drift of the sensitivity).

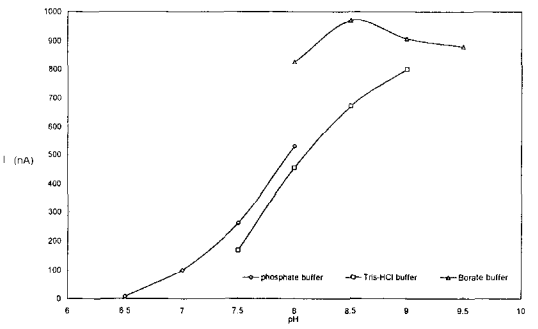

Fig. 5. Dependence of the response of the diamine sensor on sample pH in 0.1 M buffers (putrescine concentration = 100 μM).

background current and longest response time. In the following study, pH 8.5 borate buffer was used for all the subsequent work, but phosphate buffer of pH 7.4 was used for flow injection technique because of the fast response time of the sensors in this buffer.

3.4. Selectivity

3.4.1. Interference of other amines

The selectivity of the sensor toward other diamines (cadaverine), polyamine (spermine), monoamine (trimethylamine), and aromatic amine (tyramine) was investigated because most of these compounds are potential interferences in detection of putrescine in vaginal fluid for BV patients. Fig. 6 shows sensor responses to PUT, CAD and SPM. The sensor is more specific toward putrescine than CAD and SPE. For 10 μM

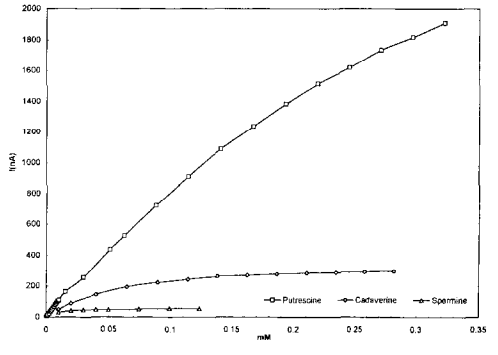

Fig. 6. Response of diamine biosensor to different amines.

substrate concentrations, sensor showed ~40 and ~20% response to CAD and SPM, respectively. However, those interference signals shown in Fig. 6 had very narrow dynamic range and the sensor responses became saturated (flat) at very low concentrations. The sensor did not respond to TMA up to 250 μM. The sensor showed response to TYR which is oxidized directly at the electrode surface under the applied potential.

To compare the enzymatic catalytic effect on those amines, their responses were studied at a bare Pt electrode without any modifications. Except TMA, all other amines showed slight signals at concentrations of 250 μM; however, these signals were negligible after coating a thin film of *m*-PDA on the Pt surface which rejected these interferences. To study the recovery of putrescine signal in the presence of various interferences, 10 μM of putrescine, interferences and mixture of putrescine with interferences were tested with the sensor, respectively. Additive signals were observed. Although this sensor also respond to cadaverine, it still could be used as a diamine indicator sensor, where total amount of diamines can be detected. It has been known that for normal women, both putrescine and cadaverine levels are undetectable in vaginal fluid, while significant amount of both diamines were found in sub-mM level with BV patients.

3.4.2. Interference of short chain organic acids existing in BV fluid

It has been well documented that normal women have a predominance of lactic acid in vaginal discharge produced by *Lactobacillus* [2], while BV patients lack lactic acid but have other short chain organic acids produced by anaerobes in the vaginal discharge. Further study showed that BV patients have high levels of succinate [6,38]. Later research, to directly measure the vaginal redox potential of the vaginal epithelial surface at the posterior fornix, showed that BV patients have an average E_h of −92 mV (on Pt electrode versus SHE), 78 mV lower than normal woman [39]. But the E_h were increased to normal level after the BV were successfully treated with metronidazole. They concluded the more reduced state of vaginal E_h for BV patients are caused by

the metabolism of anaerobic microbes, which in turn shifted the equilibrium of redox pairs such as lactate/pyruvate and succinate/fumarate (short chain organic acid produced by microbial metabolism).

To study the effects of these acids on the response of diamine sensor, 250 μM putrescine solution in the presence of 250 μM of L-lactic acid, fumaric acid, pyruvic acid and succinic acid, respectively were tested. The sensor did not respond to those acid and the putrescine signal were fully recovered.

3.5. FIA

The sensor was used as a detector in a single channel flow system. A flow rate of 2 ml min^{-1} was used throughout. With this flow rate, a good compromise between sensitivity and sample throughout was achieved. This system had a residence time of 16 s (time elapsed between sample injection to current peak maximum observed) with sampling rate of 60–80 h^{-1}. The system had very low background current, good peak reproducibility ($\pm$ 1.5%), and fast recovery time. A typical flow injection trace is presented in Fig. 7(a) along with a calibration curve in Fig. 7(b). The linear response range is up to 1 mM with sensitivity of 0.69 μA μM^{-1}. The detection limit for putrescine is below 25 μM.

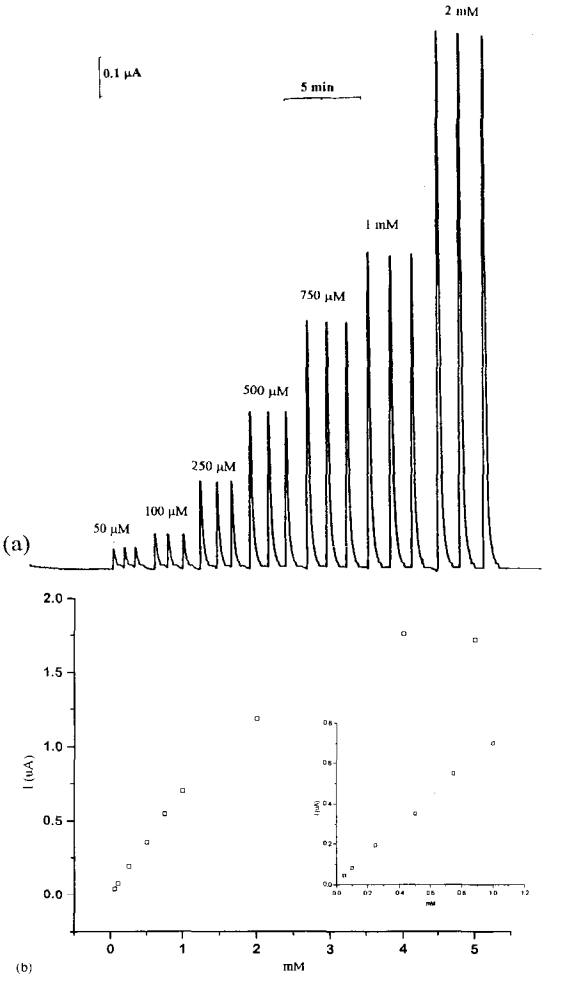

Fig. 7. Sensor response to putrescine with the flow injection technique (a) a typical FIA trace and (b) a calibration curve.

4. Conclusions

A miniature putrescine biosensor has been constructed with PUO on a flexible substrate. Besides its high analytical quality, each sensor contains only a minimum amount of enzyme and the substrates are batch fabricated. The system could eventually give any health provider a low cost, disposable sensor for routine clinic screening. Studies to detect the diamine levels in real samples by diamine sensors from normal and BV patients are scheduled. Further experiments, to study the reliability of the sensor acting as a clinical diagnosis tool for BV, are also under way. This test will be done by correlating the diamine (putrescine) levels detected by the sensors with diagnosis results obtained by current clinical screening procedures.

Acknowledgements

Authors would like to acknowledge Dr Kimiyasu Isobe of Amano Pharmaceutical Co. Ltd. for the donation of enzyme. This work was supported by NSF/Whitaker Foundation grant BES-9520526.

References

[1] C.A. Spiegel, Clin. Microbiol. Rev. 4 (1991) 485.
[2] D.A. Eschenbach, Am. J. Obstet. Gynecol. 169 (1993) 441.
[3] G.B. Hill, Am. J. Obstet. Gynecol. 169 (1993) 450.
[4] J.C. Hauth, R.L. Goldenberg, W.W. Andrews, M.B. Dubard, R.L. Copper, N. Eng. J. Med. 333 (1995) 1732.
[5] S.L. Hillier, N. Eng. J. Med. 333 (1995) 1737.
[6] K.C.S. Chen, P.S. Forsyth, T.M. Buchanan, K.K. Holms, J. Clin. Invest. 63 (1979) 828.
[7] K.C.S. Chen, R. Amsel, D.A. Eschenbach, K.K. Holms, J. Infect. Dis. 145 (1982) 337.
[8] J.M. Brand, R.P. Galask, Obstet. Gynecol. 68 (1986) 682.
[9] T.A. Smith, Anal. Biochem. 33 (1970) 10.
[10] S. Yamamoto, H. Itano, H. Kataoka, M. Makita, J. Agric. Food Chem. 30 (1982) 435.
[11] T. Matsumoto, O. Suzuki, Y. Katsumata, M. Oya, T. Suzuki, Y. Nimura, T. Hatlori, J. Cancer Res. Clin. Oncol. 100 (1981) 73.
[12] S. Kubota, M. Okada, K. Inahori, N. Ohsawa, Cancer Res. 43 (1983) 2363.
[13] S. Otsuji, Y. Soejima, K. Isobe, H. Yamada, S. Takao, M. Nishi, J. Cancer Res. Clin. Oncol. 109 (1985) 115.
[14] K. Isobe, H. Yamada, Y. Soejima, S. Otsuji, Biochem. Med. Met. Biol. 37 (1987) 110.
[15] K. Isobe, H. Yamada, Y. Soejima, S. Otsuji, Clin. Biochem. 20 (1987) 157.
[16] N. Mashige, N. Tanaka, T. Murakami, H. Shimosaka, S. Kamei, A. Ohkubo, Clin. Chem. 34 (1988) 2271.
[17] A.C. Rinaldi, E. Sanjust, A. Rescigno, A. Finazzi-Agro, A. Rinaldi, Biochem. Mol. Biol. Int. 34 (1994) 699.
[18] F. Misutani, M. Asai, in: D.L. Wise (Ed.), Bioinstrumentation, Butterworths, Boston, MA, 1990, p. 317.
[19] F. Scheller, F. Schubert, Biosensors, Elsevier, Amestrdam, 1992, p. 82.
[20] W. Schuhmann, H.-L. Schmidt, in: A.P.T. Turner (Ed.), Advances in Biosensors, vol. 2, JAI Press, London, 1992, p. 79.
[21] Z. Toul, L. Macholan, Collect. Czech. Chem. Commun. 40 (1975) 2208.
[22] L. Macholan, D. Jilkova, Collect. Czech. Chem. Commun. 48 (1983) 672.
[23] T. Yao, M. Satomura, T. Wasa, Anal. Chim. Acta 261 (1992) 161.
[24] F. Botre, C. Botre, G. Lorenti, F. Mazzei, F. Porcelli, G. Scibona, Sens. Actuators B15–16 (1993) 135.
[25] S. Todoriki, M. Tajima, M. Senda, Anal. Sci. 4 (1988) 583.
[26] R. Gaspaini, M. Scarpa, M.L. DiPaolo, R. Stevanato, A. Rigo, Bioelectrochem. Bioenerg. 25 (1991) 307.
[27] G.C. Chemnitius, M. Suzuki, K. Isobe, J. Kimura, I. Karube, R.D. Schmid, Anal. Chim. Acta 263 (1992) 93.
[28] U. Bilitewski, G.C. Chemnitius, P. Ruger, R.D. Schmid, Sens. Actuators B 7 (1992) 351.
[29] D. Wijesuriya, G.A. Rechnitz, Anal. Chim. Acta 243 (1991) 1.
[30] X. Yang, G.A. Rechnitz, Electroanalysis 7 (1995) 105.
[31] V.V. Cosofret, E. Lindner, T.A. Johnson, M.R. Neuman, Talanta 41 (1994) 931.
[32] S. Sakura, R.P. Buck, Bioelectrochem. Bioenerg. 28 (1992) 387.
[33] M.B. Madaras, S. Ufer, R.P. Buck, Anal. Chim. Acta 319 (1996) 335.
[34] S.A.M. Marzouk, V.V. Cosofret, R.P. Buck, H. Yang, W.E. Cascio, S.S.M. Hassan, Talanta, in press.
[35] V.V. Cosofret, M. Erdosy, T.A. Johnson, R.B. Ash, M.R. Neuman, R.P. Buck, Anal. Chem. 67 (1995) 1647.
[36] W. Blum, G.B. Hogaboom, in: Principles of Electroplating and Electroforming, 3rd ed., McGraw-Hill, New York, 1949, p. 382.
[37] In Toyobo Enzymes, Toyobo Co, Japan, 1994, p. 249.
[38] C.A. Spiegel, R. Amsel, D. Eschenbach, F. Schoen Knecht, K.K. Holmes, N. Engl. J. Med. 303 (1980) 601.
[39] K.K. Holmes, K.C.S. Chen, C.M. Lipinski, D.A. Eschenbach, J. Infect. Dis. 152 (1985) 379.

ELSEVIER

Talanta 44 (1997) 1633–1640

Talanta

Determination of the rodenticides warfarin, diphenadione and chlorophacinone in soil samples by HPLC-DAD

A. Medvedovici [1,a,*], F. David [b], P. Sandra [a]

[a] *Department of Organic Chemistry, University of Gent, Krijgslaan 281 (S4), B-9000, Gent, Belgium*
[b] *Research Institute of Chromatography, Kennedypark 20, B-8500, Kortrijk, Belgium*

Received 27 August 1996; received in revised form 28 October 1996; accepted 21 November 1996

Abstract

A HPLC-DAD method is described for the analysis of the rodenticides warfarin, diphenadione and chlorophacinone, together with the phenylurea herbicides isoproturon and diuron, in soil samples. The HPLC parameters have been optimised to provide baseline separation with symmetrical peakshapes in short analysis times. The sample preparation consists of Soxhlet extraction followed by SPE clean-up on cyanopropyl silica. © 1997 Elsevier Science B.V.

Keywords: Rodenticides; HPLC optimisation; Soil samples; Sample preparation

1. Introduction

Rodenticides act in animal organisms as depressors of prothombin formation and supressors of capillary fragility, leading to hemorrhages [1,2]. Rodenticides are widely used in agriculture, often together with pre- and post- emergence phenylurea herbicides, which explains the occurrence of residues of those formulations in water and soil samples.

The complex structure of warfarin (3α-phenyl-β-acetylethyl-4-hydroxycoumarin), containing an acidic enol group and a ketonic moiety led to extensive chromatographic studies concerning the relation between peakshape and mobile phase composition or injection volumes and matrix effects [3,4]. Because of the antitumoral action of warfarin [5], the chromatographic analysis in biological fluids and organ extracts is well documented [6,7]. Moreover, due to the fact that the S(−) enantiomer of warfarin is more active than the R(+) enantiomer, different enantioselective separations by LC [8–16] and SFC [17] have been reported. The analysis of warfarin, coumatetralyl, bromadiolone, difenacoum and brodifacoum in liver extracts has been described [18,19].

Diphenadione [(2-diphenylacetyl)-1H-indene-1,3(2H)-dione] also named diphacinone and chlorophacinone [2[(4-chlorophenyl)phenylacetyl]-1H-Indene-1,3-[2H]-dione] are rodenticidal agents which have not been intensively studied.

* Corresponding author.
[1] On leave from Department of Analytical Chemistry, Faculty of Chemistry, University of Bucharest, Blvd. Republicii 13, 70 346, Bucharest, Romania.

PII S0039-9140(97)00068-4

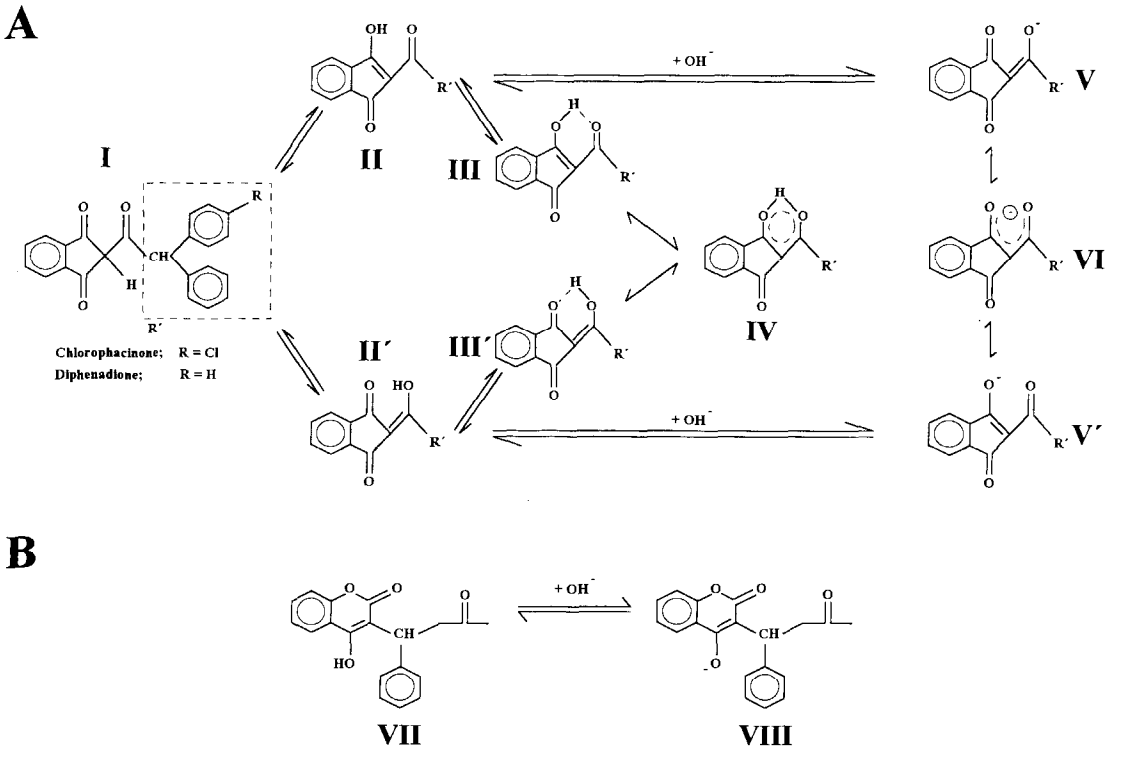

Fig. 1. Structure of W, DP and CP in relation with solvent polarity and/or pH.

Diphenadione and chlorophacinone analysis were determined in human serum and liver extracts, alone [20] or together with pindone and valone [21] or with warfarin [22]. Fluorescence detection of the diphenadione–Eu(III) complex was also reported [23].

The analysis of the rodenticides warfarin, diphenadione and chlorophacinone together with the phenylurea herbicides isoproturon and diuron in soil was the aim of the present work. The LC optimisation and the sample preparation steps are discussed.

2. Experimental

2.1. Chromatographic analysis

A Hewlett-Packard 1090 Model Liquid Chromatograph with automatic injector and Diode Array Detector was used. The chromatographic column was 20 cm L. × 4.6 mm i.d. packed with Hypersil ODS 5 mm (Hewlett-Packard). Injected sample volumes ranged from 5 to 250 ml. Detection was made at 310 nm for the rodenticides and at 247 nm for the phenylurea herbicides.

2.2. Materials

Warfarin (98%) was purchased from Aldrich. Diphenadione (99.9%), chlorophacinone (98.5%), isoproturon (99.9%) and diuron (99.9%) were obtained from Labor Dr. Ehrenstorfer GmbH, Germany. All solvents (water, acetonitrile, methanol) were HPLC grade from Lab Scan, Ireland. The other reagents were p.a. grade. SPE cartridges (ODS and CN, volume 3 ml, 500 mg adsorbent), were purchased from Analytichem International, UK.

Table 1
Solvents and gradient conditions applied in HPLC

Solvent System	A	B	C
Solvent (1)	Water	Aqueous 2 mM acetate buffer pH 4.2	Aqueous 0.5% phosphoric acid
Solvent (2)	Acetonitrile	Acetonitrile	0.5% phosphoric acid in acetonitrile
Gradient program	I	II	
Program	Solvent (2) programmed from 40% (5 min) to 60% at 4%/min, then to 100% in 0.1 min; flow rate 1 ml/min	Solvent (2) programmed from 40% (5 min) to 60% at 4%/min, then to 100% at 1%/min; flow rate increment from 1 to 2 ml/min between min 10 and 30.	

The soil sample was received for analysis and kept in the refrigerator at 4°C before analysis.

3. Results and discussions

3.1. Chromatographic optimisation

Diphenadione (DP) and chlorophacinone (CP) contain a β-tricarbonyl system, which results in ketoenolic tautomerism (Fig. 1A). The enolic structures are stabilised through an intramolecular hydrogen bond followed by delocalisation of the π electrons over the six atoms ring (structure IV). The enolic hydroxyl group can dissociate giving enolate formation (structures V,V'). Because of π electron conjugation in the enolate form, the negative charge is equally distributed over the two oxygen atoms resulting in structure VI. The global equilibrium can be summarised by:

keto form⇔enol form⇔enolate form

The rate of interconversion is pH dependent and is often catalysed by free silanols or metal ions residually present in HPLC column materials. The chemistry involved in β-carbonylic systems is very complex. For DP and CP some analogy can be found with α- and β-acids in hops and iso-α-acids in beer. The chemical transitions in those solutes has been studied [24] and the consequences for HPLC analysis have been described [25,26]. Good understanding of the equilibria between the different forms of DP and CP would require NMR experiments but this was not the aim of the present work. Nevertheless it is clear that the mobile phase composition will be of utmost importance for successful HPLC analysis. Dynamic interconversion between the different forms strongly affects the chromatographic partitioning process and peak distortion and retention irreproducibility can be anticipated. The mobile phase must inhibit chelating properties of the solutes in order to eliminate interactions with residual active centers in the column.

The same factors will influence the dissociation processes on the enolic group of warfarin (W), as shown in Fig. 1B.

Different mobile phase compositions and elution conditions have been evaluated (Table 1).

The chromatograms for a standard mixture containing the solutes of interest are presented in Fig. 2.

Warfarin and the phenylurea herbicides elute with good peak shape under all conditions. When the proton concentration in the mobile phase is, however, not controlled (gradient program I, solvent system A) the common anionic form may be present to a large extent giving rise to broad peaks with tailing (Fig. 2D). By lowering the pH to 4.2 (gradient program I, solvent system B) a slow equilibrium between the neutral keto and enol forms is probably established resulting in the observation of two distinct chromatographic peaks for each solute (Fig. 2C). At the low pH of

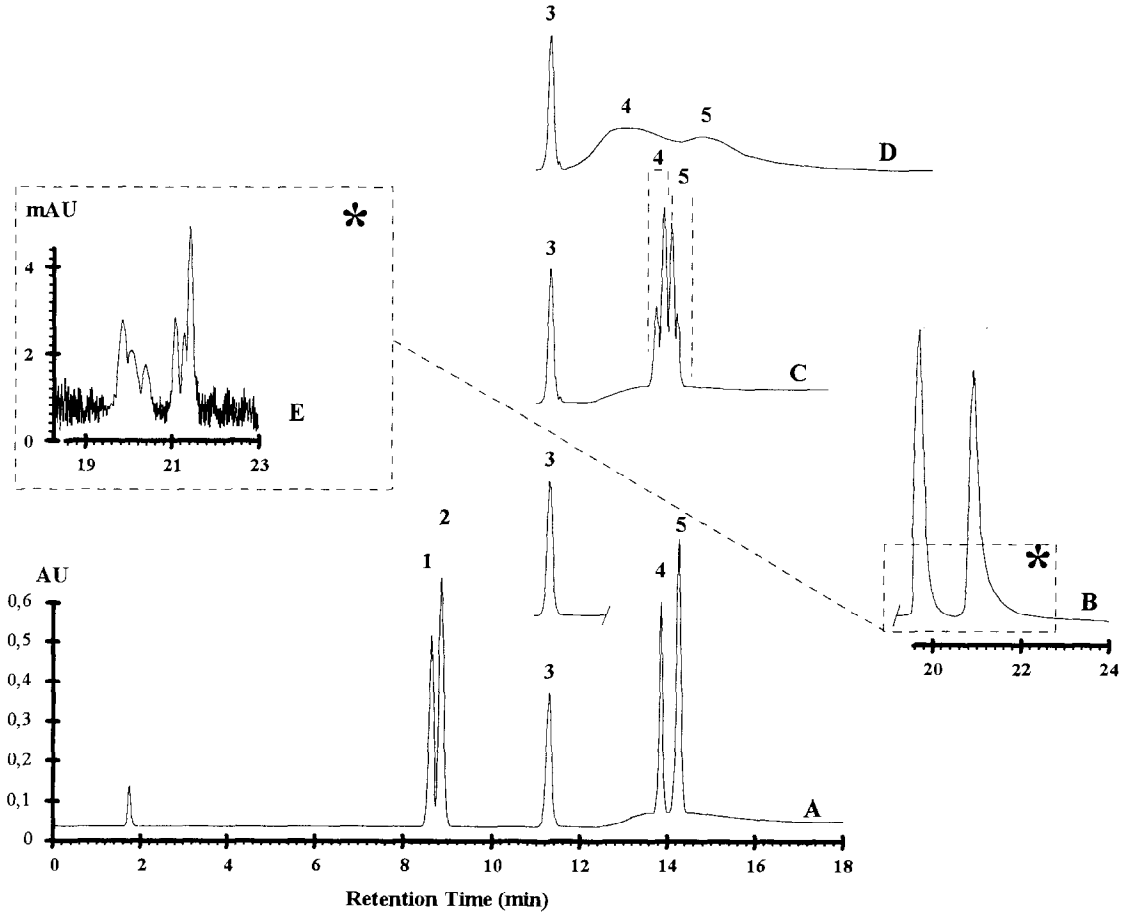

Fig. 2. Separation of isoproturon (1), diuron (2), W (3), DP (4) and CP (5) using different gradient elution profiles and solvent systems (conditions as described in text and Table 1).

the phosphoric acid solution (gradient program I, solvent system C), the rate of interconversion is fast relative to retention and only one single peak for each solute is observed (Fig. 2A). Increasing retention in the column by using gradient program II with solvent system C generates a better selectivity but peaks are slightly tailing (Fig. 2B). Moreover when the concentration of the solutes in the mobile phase is low, e.g., less than 10 ng, peak splitting is observed (Fig. 2E). This phenomenon must be related to the influence of residual silanolic groups or metal ion activity in the chromatographic system. Chromatogram 2E also suggests that the keto-enolic equilibrium constant K_T is pH independent, but the rate of interconversion obviously is pH dependent.

$$K_T = [\text{enol}]/[\text{keto}] = K_a^{\text{keto form}}/K_a^{\text{enol form}}$$

Under optimal elution conditions (gradient program *I*, solvent system *C*) the solute concentration no more influences the peak shape The minimal detectable amount corresponds to 1 ng of each solute injected onto the column. The sample loadability on the column depends on the solvent used. In pure acetonitrile containing 0.5% phosphoric acid, the loadability is restricted to 10 μl. Dilution in water/acetonitrile/phosphoric acid (49.75/49.75/0.5) allows injections up to 250 μl. For highly selective detection of W, DP and CP 310 nm is preferred for real samples, while 247 nm is the best wavelength for the detection of the phenylurea herbicides.

Table 2
Recoveries of isoproturon, diuron, W, DP and CP with Soxhlet extraction in function of time

Solvent	Extraction time (h)	Recovery (%)[a]									
		Isoproturon	RSD%	Diuron	RSD	Warfarin	RSD%	Diphenadione	RSD%	Chlorophacinone	RSD%
Methanol	1	78.8	1.5	116.1	2.5	54.9	2.9	45.4	2.3	16.4	4.9
Methanol	2	89.6	1.1	113.8	4.9	58.1	3.3	63.8	2.5	66.2	3.2
Methanol	16	24.8[b]	15.0	48.7[b]	13.3	56.8	4.0	66.4	1.0	89.1	2.6

[a] Values given are resulting by averaging data for three experiments.
[b] For longer periods at higher temperatures (Soxhlet extraction), isoproturon and diuron are decomposing.

3.2. Analysis of soil samples

Analysis of the rodenticides and phenylurea herbicides in soil samples requires a solid–liquid extraction step. Two procedures were evaluated: (a) ultrasonic extraction at room temperature; and (b) Soxhlet extraction. In order to study the extraction yields, 10 g of pure sea sand were spiked at the 10 ppm level with diuron, isoproturon, warfarin, diphenadione and chlorophacinone.

For ultrasonic extraction, 20 ml of solvent (acetone, methanol, acetonitrile, dichloromethane, as such and with 1% phosphoric acid) were added to the sea sand followed by ultrasonication during 15 min at 25°C. After filtration, the solvent was removed by evaporation and the residue taken up in 10 ml water/acetonitrile/phosphoric acid (49.75/49.75/0.5). Of this solution, 100 μl, were injected. Best recoveries were obtained with pure methanol: isoproturon 78%, diuron 104%, warfarin 69%, diphenadione 70% and chlorophacinone 68%. Repeating ultrasonic extraction with methanol on spiked blank soil, however, revealed that the recoveries for the phenylurea herbicides remained constant but dropped for the rodenticides to 44% for warfarin, 9.5% for diphenadione and 6.6% for chlorophacinone. All recoveries given are averaged values for five experiments and %RSDs were less than 5. This illustrates that specific solute-matrix interactions are extremely important and that extraction conditions have to be related with the characteristics of real samples. Ultrasonication at room temperature is definitely not efficient towards the extraction of the rodenticidal agents in real soil samples.

Soxhlet extraction was therefore carried out using the same spiked soil sample and 200 ml methanol as extracting solvent. The solvent selection was based on the recoveries obtained with the spiked sea sand samples. After extraction, the solvent was removed and replaced as described for the ultrasonic procedure. Recoveries in function of the extraction time for 10 ppm concentrations together with %RSD values for three experiments are enlisted in Table 2.

For the phenylurea herbicides, high recoveries are obtained for 1 and 2 h extraction time while longer extraction time results in decomposition of

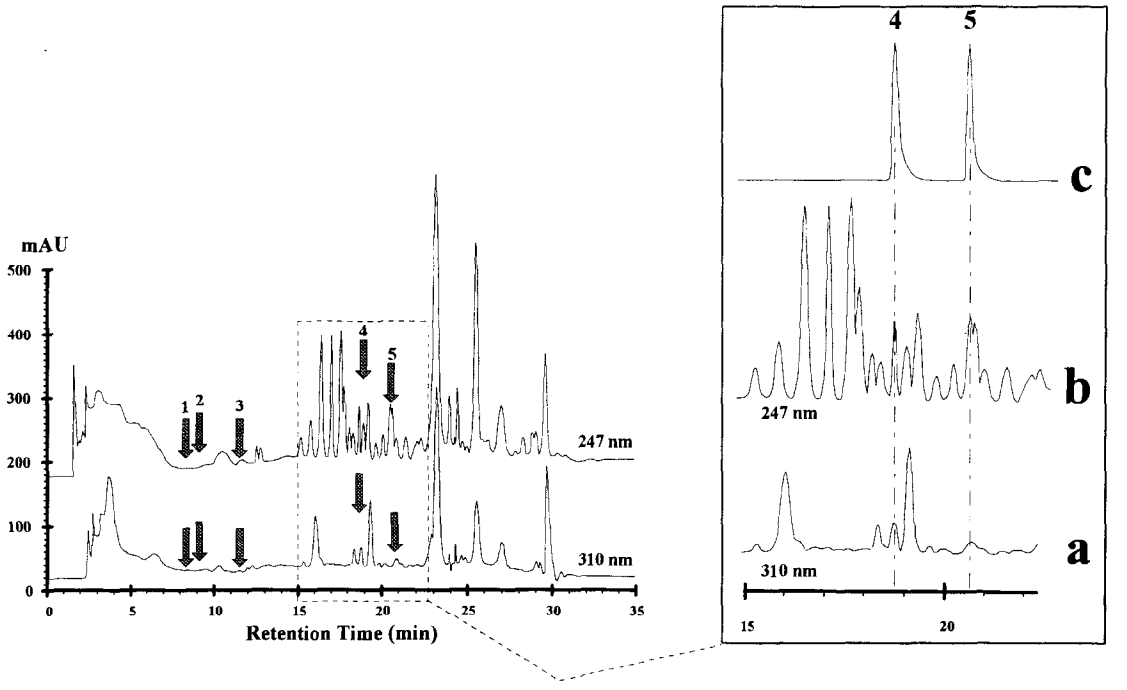

Fig. 3. Separation of rodenticides in extract of soil sample without clean-up.

these herbicides and thus low recoveries. For warfarin and diphenadione recoveries are constant over the 2–16 h extraction duration while for chlorophacinone extraction yields continuously increases with extraction time. As compromise 2 h were selected. Soxhlet extraction performed over 2 h at the 100 ppb level for each solute produced similar results i.e., 56.2% for W, 60.7% for DP and 65.2% for CP with RSD values in the order of 5% for three experiments.

Determination of the herbicides and rodenticides at low ppb level in real soil samples was, however, hindered by matrix interferences. Fig. 3 shows the analysis of a real sample analyzed with solvent C and program II and recorded at 247 nm for the phenylurea herbicides and at 310 nm for the rodenticides. As can be deduced from the Fig. 3, the phenylurea herbicides are absent but the presence of DP and CP can be elucidated. The strong background, however, did not allowed to confirm the presence of the rodenticides by means of their UV spectra and quantitation based on these data could be erratic.

Table 3
Recoveries of W, DP and CP on SPE-cyanopropyl silicagel as function of the composition of the washing solvent

	Recovery (%) on cyanopropyl silica[a]							
Washing solution ⇒ Compound ⇓	H_2O	RSD%	H_2O/ACN 9/1	RSD%	H_2O/ACN 3/1	RSD%	H_2O/ACN 3/2	RSD%
Warfarin	99.9	1.4	82.1	1.3	13.1	8.0	2.4	33.0
Diphenadione	90.5	1.8	89.2	1.3	88.0	1.1	18.1	13.8
Chlorophacinone	84.4	2.6	85.4	1.1	80.9	2.0	35.6	4.0

[a] Averaged results for three experiments.

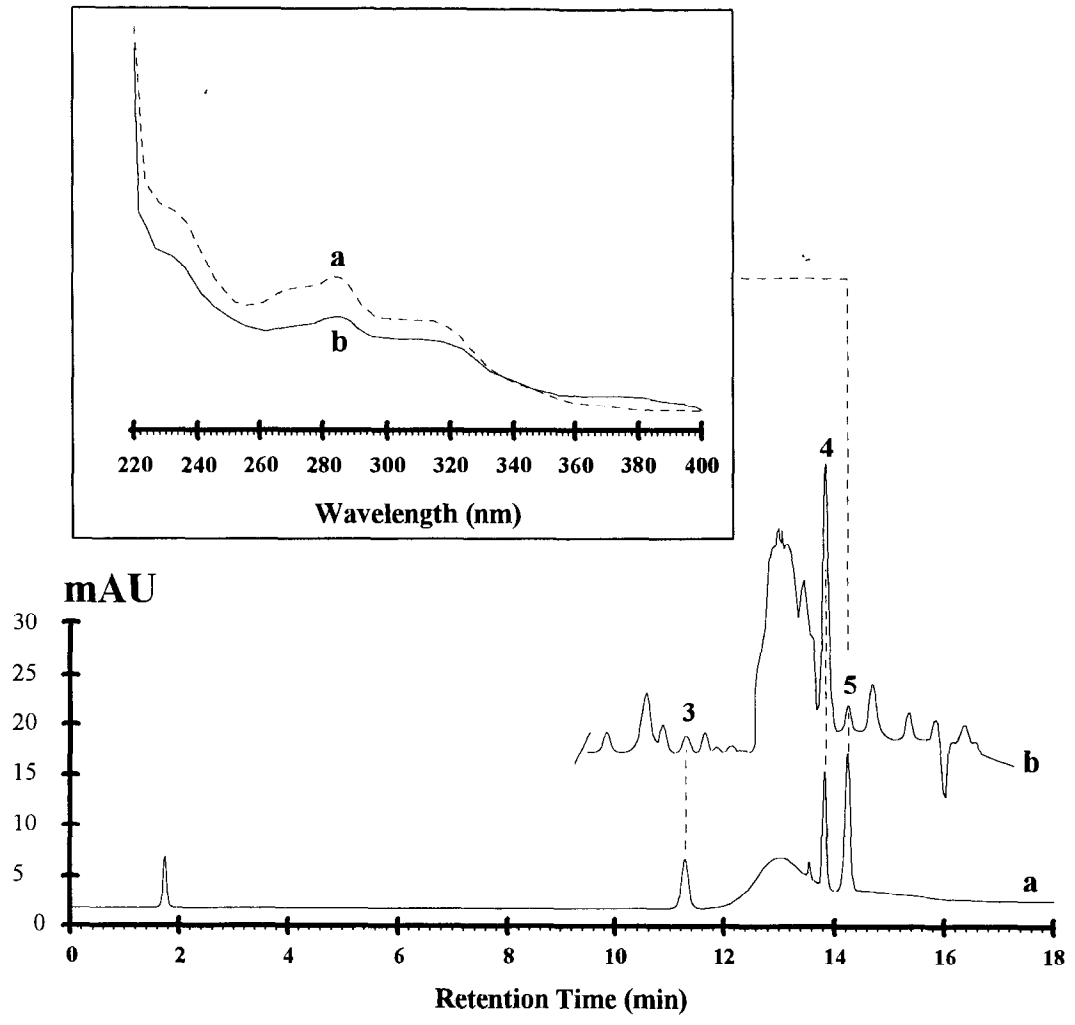

Fig. 4. Separation of rodenticides in extract of soil sample, after clean-up on cyanopropyl silicagel: (a) standard sample at the same concentration level; (b) real sample. Insert—a, recorded UV spectra of (5); b, reference spectra of CP.

To remove matrix interferences a clean-up procedure was therefore imposed to quantify the rodenticides. It is important to note that clean-up is not required for the analysis of the phenylurea at the 10 ppb level. In fact practical analysis is split in two parts. The first analysis consists of the injection of the sample as such at 247 nm for the determination of the phenylurea herbicides and analysis of the same extract but after clean-up at 310 nm for the determination of the rodenticides. Several SPE cartridges were evaluated but best results were obtained on cyanopropyl silicagel operated in the reversed phase mode. Preliminary experiments showed that washing conditions are extremely important, as outlined in Table 3.

There are no significant differences concerning recoveries of CP and DP when using water or water:acetonitrile 9:1 washing solutions. For W, recovery decreases with 20%, but results are still acceptable. Washing the adsorbent after sample loading with water:acetonitrile 9:1 results in a strong decrease of matrix interferences and those conditions were therefore considered optimal for the sample preparation procedure. The cartridge

was conditioned with 5 ml acetonitrile and dried during 4 min under vacuum. The dried residue from the Soxhlet extraction was retaken in 0.5 ml dichloromethane. An aliquot of 0.1 ml was loaded to the cartridge and the solvent was allowed to evaporate slowly. The adsorbent was then washed with 5 ml water/acetronitrile—9:1 containing 1% phosphoric acid. The adsorbent was dried under vacuum for 20 min and the rodenticides were desorbed with 4 ml acetone. The solvent was evaporated and the residue taken up in 0.5 ml water/acetonitrile/phosphoric acid—49.75: 49.75: 0.5. 250 μl were injected and the resulting chromatogram applying solvent C and gradient elution A is shown in Fig. 4.

The rodenticides can now easily be qualified through their UV spectra and quantified. The insert in Fig. 4 compares the UV spectra of chlorophacinone detected in the real sample (Fig. 4b) and in a standard solution (Fig. 4a). Measured concentrations of W, DP and CP were 3, 67 and 2 ppb, respectively. Reproducibility of the entire sample preparation process was satisfactory. Relative standard deviations for calculated concentration values are 1.2% for W, 4.6% for DP and 1.7% for CP, for a set of five experiments, carried out on a real sample over a 3 day period.

References

[1] R.J. Lewis, W.F. Trager, Ann. N.Y. Acad. Sci. 179 (1971) 205.
[2] J.V. Lloyd, Med. J. Aust. 142 (1985) 197.
[3] T. Nakagawa, Chem. Pharm. Bull. 36 (1988) 1930.
[4] A. Shibukawa, T. Nakagawa, M. Miyake, N. Mishimura, H. Tanaka, Chem. Pharm. Bull. 27 (1989) 1311.
[5] L.R. Zacharski, Cancer 53 (1984) 204.
[6] E.M. Koves, J. Wells, J. Forensic Sci. 37 (1992) 42.
[7] F.J. Diana, K. Veronich, A.L. Kapoor, J. Pharm. Sci. 78 (1989) 195.
[8] S.R. Carter, C. C Duke, D.I. Cutter, G.M. Hulder, J. Chromatogr. 574 (1992) 77.
[9] M. Aycard, S. Letellier, B. Maupas, F. Guyon, J. Liq. Chromatogr. 15 (1992) 2175.
[10] N. Mano, Y. Oda, N. Asakawa, Y. Yoskido, T. Sato, T. Miwa, J. Chromatogr. 623 (1992) 221.
[11] R.C. Williams, J.F. Edwards, M.J. Potter, J. Liq. Chromatogr. 16 (1993) 171.
[12] K.M. Kirkland, D.A. Mc Combs, J. Chromatogr. 545 (1991) 43.
[13] I. Marle, P. Erlandsson, L. Hansson, R. Isaksson, C. Petterson, G. Petterson, J. Chromatogr. 586 (1991) 233.
[14] N. Kornik, R.J. Prankerd, J.H. Perrin, Chirality 3 (1991) 124.
[15] V. Schurig, D. Wistuba, J. High Resolut. Chromatogr. 16 (1993) 215.
[16] N. Thuand, B. Sebille, A. Deratani, G. Lelievre, J. Chromatogr. 555 (1991) 53.
[17] W. Naidong, J.W. Lee, J.D. Hulse, J. Pharm. Biomed. Ann. 11 (1993) 785.
[18] W. Langseth, U. Nymoen, Fresenius'Z. Anal. Chem. 339 (1991) 249.
[19] L.J. Felice, T. Chalermchaikit, M.J. Murphy, J. Anal. Toxicol. 15 (1991) 126.
[20] P. Mura, Y. Papet, D. Lochon, D. Reiss, J. Anal. Toxicol. 16 (1992) 179.
[21] J.E. Houglum, R.D. Larson, R.M. Neal, J. Chromatogr. 481 (1989) 458.
[22] Z. Si, G. Shu, W. Zhu, Gaodeng Xuexiao Xuebao 11 (1990) 1138.
[23] T. Chalermchaikit, L.J. Felice, M.J. Murphy, J. Anal. Toxicol. 17 (1993) 56.
[24] M. Verzele, D. De Keukeleire, Chemistry and Analysis of Hop and Beer Bitter Acids, Elsevier Science, ISBN 0-444-88 165-4 (1991).
[25] M. Verzele, C. Dewaele, J. Chromatogr. 217 (1981) 399.
[26] M. Verzele, G. Steenbeke, C. Dewaele, L. Verhagen, J. Straling, J. High Resol. Chromatogr. 13 (1990) 737.

ELSEVIER

Talanta 44 (1997) 1641–1647

Talanta

Carbonate ion selective electrodes with trifluoroacetophenone derivatives in potentiometric clinical analyser

Magdalena Maj-Żurawska [a,*], Tomasz Sokalski [a], Joanna Ostaszewska [a], Dariusz Paradowski [a], Józef Mieczkowski [a], Zbigniew Czarnocki [a], Andrzej Lewenstam [b,c], Adam Hulanicki [a]

[a] *University of Warsaw, Department of Chemistry, 02 093 Warszawa, ul. Pasteura 1, Poland*
[b] *Department of Analytical Chemistry, Åbo Akademi, 20 500 Åbo (Turku), Finland*
[c] *Faculty of Material Science and Ceramics, University of Mining and Metalurgy, 30 059 Cracow, Poland*

Received 16 August 1996; received in revised form 23 November 1996; accepted 23 November 1996

Abstract

Properties of six derivatives of 1-trifluoroacetylbenzene: [4-(*n*-butyl)- (1), 4-(*n*-hexadecyl)- (2), 4-dodecyloxy- (3), 4-(*n*-dodecylsulfonyl)- (4), *N,N*-dioctyl-4-trifluoroacetylbenzamide (5), octyl-*p*-trifluoroacetylbenzoate (6)] as neutral carriers for carbonate ion were examined and compared. The sensitivity towards carbonate ion was for (3) pH dependent. This eliminates (3) from practical applications in clinical analysis. When measuring CO_3^{2-} within the physiological range of human blood using as carriers compounds 1 and 2 the interference of chloride must be taken into account. In the case of carriers 4, 5, 6 this effect is negligible. Electrodes with membranes containing as carriers 2, 4, 5 and 6 were tested in an automatic potentiometric clinical analyser Microlyte 6, KONE. To avoid contamination by atmospheric CO_2 of three aqueous standards (TES, NaCl, $NaHCO_3$), pH was adjusted by coulomeric generation of H^+ or OH^- in a system devoid of carbon dioxide. Recovery of HCO_3^- calculated from measured CO_3^{2-} and pH, was investigated in a series of aqueous solutions and spiked bovine serum samples. The correlation between added and recovered concentration of HCO_3^- was linear with the intercept close to 0 and slope equal to 1 in aqueous solutions for all ligands and in bovine serum samples only in the case of ligand (2). © 1997 Elsevier Science B.V.

Keywords: Carbonate; Trifluoroacetophenone derivatives; Ion-selective electrode; Serum analysis

1. Introduction

For many years there is an interest in determining carbon dioxide species in biological samples. In blood at pH 7.4 the dominating form is hydrogencarbonate ranging from 0.010 to 0.050 mol l^{-1}. These conditions define the concentration of carbonate ions in the range from 2×10^{-5} to 1×10^{-4} mol l^{-1}. Until now an ionophore for hydrogencarbonate useful in ion selective electrodes has not been described. However one can determine carbonate ions despite of their rela-

* Corresponding author.

PII S0039-9140(97)00069-6

tively small concentration. The group of possible ionophores are trifluoroacetophenone derivatives [1–11]. Their selectivity is related to electrophilicity of substituents, which is correlated to Hammett constant (σ) [8,10]. The lipophilicity of the compound plays also an important role mainly in respect of the detection limit of the ion selective electrode.

Until now, another potentiometric indirect method was used in clinical analysis for measuring hydrogen carbonate in blood. This method used pCO_2 and pH measurements with respective electrodes. The use of the carbonate electrode is an alternative method. The technology of carbonate electrode manufacturing is easier and simpler in respect to pCO_2 electrode. This makes possible miniaturisation and the use in a line of electrodes in an analyser using the same sample of blood.

In this paper the analytical characteristics of six trifluoroacetophenone derivatives in solvent-polymeric membranes containing bis(2-ethylhexyl)-sebacate (DOS) as plasticiser are reported as well as their application in a potentiometric clinical analyser. A new method of carbonate standards preparation is also proposed.

2. Experimental

2.1. Reagents

Doubly distilled water was used for preparing all solutions, additionally water for measurements of CO_3^{2-} and pH was freshly boiled and devoid of CO_2 by bubbling the purified argon. Salts used were pure for analysis or pure (POCh, Gliwice, Poland). Tetrahydrofuran (THF) was obtained from Merck (Darmstadt, Germany), poly(vinyl chloride) (PVC), bis(2-ethylhexyl) sebacate (DOS), tetradodecylammonium tetrakis(4-chlorophenyl)borate (ETH 500), 4-(*n*-dodecylsulfonyl)-1-trifluoroacetylbenzene (4) from Fluka (Buchs, Switzerland), methyltridodecylammonium chloride (MTDDACl) from Polysciences, (Niles, IL) and *N*-tris[hydroxymethyl]methyl-2-aminoethanesulfonic acid (TES) from Sigma (St. Louis, MO), 4-(*n*-butyl)-1-trifluoroacetylbenzene (1) from Orion (Espoo, Finland), Quality Serum Sample (LOT38001B) obtained from KONE Diagnostics (Espoo, Finland).

Ionophores 4-(*n*-hexadecyl)-1-trifluoroacetylbenzene (2) and 4-dodecyloxy-1-trifluoroacetylbenzene (3) were synthesised according to [11]. The synthesis of ionophores *N,N*-*n*-dioctyl-4-trifluoroacetylbenzamide (5), octyl-*p*-trifluoroacetylbenzoate (6) is given below. Each membrane contained 0.076 g PVC as matrix, 0.10 g of DOS as plasticizer, neutral ionophore (5.0×10^{-5} mole of 4-(*n*-butyl)-1-trifluoroacetylbenzene (1), 1.6×10^{-5} mole of 4-(*n*-hexadecyl)-1-trifluoroacetylbenzene (2), 1.6×10^{-5} mole of *p*-dodecyloxytrifluoroacetylbenzene (3), 1.6×10^{-5} mole of 4-(*n*-dodecylsulfonyl)-1-trifluoroacetylbenzene (4), 1.6×10^{-5} mole of *N,N*-dioctyl-4trifluoroacetylbenzamide (5), 1.6×10^{-5} mole of *n*-octyl-*p*-trifluoroacetylbenzoate (6)) and MTDDACl (40 molar percent versus ionophore).

After dissolution in 3 ml of THF the mixture of components was poured into a 28 mm diameter glass ring placed on a glass plate and the solvent was allowed to evaporate. After 48 h round pieces of the membrane were cut out and fixed in the Philips IS 561 electrode body. Alternatively the THF solution was poured into the KONE electrode body and left for the solvent to evaporate.

2.2. Methods and equipment

Measurements were made at 25 ± 1°C in cell set as follows:Ag;AgCl,$KCl_{(Sat)}$‖1 mol l^{-1} KCl‖sample solution|membrane|internal solution|AgCl,Ag or in Microlyte 6 clinical analyser (KONE, Espoo, Finland). The internal filling solution was: 0.1 mol l^{-1} NaH_2PO_4, 0.1 mol l^{-1} Na_2HPO_4, 0.01 mol l^{-1} NaCl.

Electrodes were stored in the conditioning solution: 0.1 mol l^{-1} $NaHCO_3$.

The external reference electrode was a double-junction Ingold 9811 electrode. For monitoring of pH glass electrodes Ingold 104711 or Hydromet ERH 11 (Warsaw, Poland) were used. In measurements with the clinical analyser all electrodes except carbonate electrode were commercially available from KONE.

Single-ion activities were calculated according to Debye-Hückel theory [12]. For carbonate solutions the concentration of each species was calculated from protonation equilibria at measured pH.

The emf measurements with electrodes using Philips IS 561 bodies were performed using a digital voltmeter Solartron LM 1604 DC (Farnborough, Hampshire, UK) with multi-electrode sampler. Each reading was carried out 20 min after change of sample solution, when no further significant emf drift (0.2 mV min^{-1}) was observed. The measurements were made in the unstirred solutions.

For determination of selectivity coefficients by the separate solution method 0.1 mol l^{-1} NaCl and 0.1 mol l^{-1} $NaHCO_3$ solutions were used [8]. The selectivity coefficient for chloride ions was always taken into account for recalculation of potential values. The Henderson equation [12] provided corrections for the liquid-junction potential.

Potential response characteristics of electrodes was determined by stepwise addition of weighed amounts of $NaHCO_3$ (to obtain lowest concentrations dilution was used instead) to 0.01 mol l^{-1} solution of TES. The pH was kept constant by the addition of dilute sulphuric acid.

The effect of pH change was investigated by addition of diluted sulphuric acid to 0.025 mol l^{-1} solution of $NaHCO_3$.

Analytical recovery investigation of hydrogencarbonate concentration in aqueous solutions and in spiked bovine serum (KONE Diagnostic Control Serum Sample LOT38001B) was made by Microlyte 6 clinical analyser in which the carbonate electrode was inserted.

Vacuum test tubes (Becton Dickinson Vacutainer Systems, England) were used for storing hydrogencarbonate solutions.

Hydrogencarbonate aqueous standard solutions were prepared using coulometric titrations to generate OH^- ions. In coulometric titration a potentiostat OH-404/A (Radelkis, Budapest, Hungary) and two-compartment coulometric cell equipped with the magnetic stirrer were used. The solutions were deaerated and kept under argon. The anode and cathode compartments were separated by two G-4 sintered-glass disks and the space between them was filled with 2% aqueous NaCl solutions in 2% agar–agar. The titrations were performed in constant current conditions ($I = 40$ mA). Nickel anode was immersed in 0.1 mol l^{-1} Na_2SO_4 acidified to pH 2 with 0.1 mol l^{-1} HCl (anodic reaction: $Ni \rightarrow Ni^{2+} + 2e$). Platinum cathode was immersed in the solution being titrated (cathodic reaction: $2H_2O + 2e \rightarrow H_2 + 2OH^-$). The pH of titrated solution was controlled using pH glass electrode Ingold 104 711 with external reference electrode double-junction Ingold 9811 (Ingold, Switzerland) and the PHM-64 pH-meter (Radiometer, Copenhagen, Denmark).

Hydrogencarbonate standards of the composition given in Table 1. were prepared in the following way: pH of the solution of NaCl, KCl and TES was adjusted to the value of about 7 then appropriate amount of sodium hydrogencarbonate was added and pH adjusted further to the required value. To avoid contamination of hydroxide solution by CO_2 from air, the standard was titrated coulometrically. Other aqueous hydrogencarbonate solutions were prepared in the same way.

Standard solutions prepared in the way described above were stored in vacuum test tubes in the refrigerator. The composition of standards remained stable over 1 year, within experimental error of carbonate determination, i.e., $\pm 3\%$.

2.3. Synthesis

2.3.1. General

IR spectra were recorded on a UR-20 spectrophotometer (Zeiss, Jena, Germany). ^{1}H-NMR

Table 1
Composition of the hydogencarbonate standards

	Low (mmol l^{-1})	Normal (mmol l^{-1})	High (mmol l^{-1})
NaCl	98	95	70
KCl	6	4.5	3
TES	30	50	50
$NaHCO_3$	10	25	50
pH	7.0	7.4	7.8

spectra were recorded on Bruker (Karlsruhe, Germany) AM 500 (at 500 MHz) and Varian 200 (at 200 MHz) spectrometers. ^{13}C-NMR spectra were performed on Bruker AM 500 (at 127 MHz) and Jeol (Tokyo, Japan) FX 90Q (at 22.5 MHz). In all cases TMS was used as an internal standard. Melting points were measured on Boetius hot-plate microscope and were uncorrected.

2.3.2. Trifluoroacetylbenzoic acid hydrate

This compound was synthesised according to the modified procedure for 4-trifluoroacetylbenzoic acid [8]. To a solution of 7.80 g (33.1 mmol) of 1,4-dibromobenzene in 75 ml of dry THF cooled to −78°C, a solution of 1.6 mol l^{-1} *n*-butyllithium in hexane (20.7 ml, 33.1 mmol) was added during 20 min. After 30 min of stirring a solution of 3.4 ml (33.7 mmol) of methyl trifluoroacetate in 20 ml of THF was added during 15 min. The resulted solution was treated again with 20.7 ml (33.1 mmol) of 1.6 mol l^{-1} *n*-butyllithium at −78°C. After additional 20 min of stirring the solution was poured on a slurry of 50 g of crushed dry ice in 100 ml of THF and allowed to stand overnight. Organic solvents were then removed in vacuo and the residue was quenched with 50 ml of water. The water layer was extracted twice with 25 ml portions of toluene and was made strongly acidic by addition of 20 ml of conc. hydrochloric acid. The resulted solution was evaporated under reduced pressure to approximately one-third of the volume and was left to stand in a refrigerator for 12 h. The product (4-trifluoroacetylbenzoic acid hydrate) was collected as white crystals in the yield of 6.33 g (88%).

M.p. 175–177°C; ^{13}C-NMR (22.5 MHz, DMSO-d_6, δ): 90.0 (q, J = 31 Hz), 123.4 (q, J = 289 Hz), 127.8, 128.8, 167.2.

2.3.3. N,N-dioctyl-4-trifluoroacetylbenzamide

A sample of 4-trifluoroacetylbenzoyl chloride, prepared from 4-trifluoroacetylbenzoic acid hydrate using the method of Behringer et al. [8], (1.25 g, 5.28 mmol) was added to a solution of 1.53 g (6.33 mmol) of dioctylamine in 25 ml of dry pyridine at 0°C and was left to stand overnight in a refrigerator. Pyridine was then evaporated and the residue was quenched with 25 ml of toluene. The organic layer was washed successively with brine, 0.1 mol l^{-1} hydrochloric acid, 0.1 mol l^{-1} sodium hydrogencarbonate and brine. After drying over anh. magnesium sulphate and evaporation, the residue was chromatographed on 230–400 mesh silica gel using chloroform as eluent. Evaporation of the solvent and drying for 24 h under vacuum (0.01 Torr) afforded compound (*N,N*-dioctyl-4-trifluoroacetylbenzamide) as colourless oil (1.84 g, 67.2%)

^{13}C-NMR (127 MHz, $CDCl_3$, δ, stable conformers present): 13.95, 22.53, 26.41, 26.99, 27.42, 28.58, 28.94, 29.17, 29.29, 31.62, 31.74,,44.83, 48.87, 116.51 (q, J = 289 Hz), 127.10, 130.03, 130.12, 130.24, 130.28, 144.09, 169.63, 179.85 (q, J = 35 Hz).

Other analytical data were the same as described by Behringer et al. [8].

2.3.4. Octyl-4-trifluoroacetylbenzoate

A sample of 4-trifluoroacetyl chloride [8] (1.25 g, 5.28 mmol) was added in one portion to 4 ml of freshly distilled 1-octanol and the mixture was stirred at room temperature for 12 h. The excess of 1-octanol was removed under reduced pressure and the residue was chromatographed on 230–400 mesh silica gel using benzene–hexane (1:1, v/v) as eluent. Evaporation of the solvents afforded octyl-4-trifluoroacetylbenzoate as a colourless oil (0.85 g, 41.5%).

IR ($CHCl_3$, cm^{-1}): 1720, 1280, 940.

^{1}H-NMR (200 MHz, $CDCl_3$, δ): 0.91 (t, 3H, J = 7.6 Hz), 1.25–1.52 (m, 10H), 1.76–1.84 (m, 2H), 8.11–8.21 (m, 4H).

^{13}C-NMR (22.5 MHz, $CDCl_3$, δ):14.1, 22.7, 26.1, 28.7, 29.3, 31.9, 66.1, 116.5 (q, J = 293 Hz), 130.1, 132.9, 136.4, 165.2, 180.2 (q, J = 37 Hz).

3. Results and discussion

3.1. Properties of compounds

Properties of six derivatives of 1-trifluoroacetylbenzene were investigated. The structure of the compounds is shown on Fig. 1. The summary of their properties is given in Table 2. Ligands with

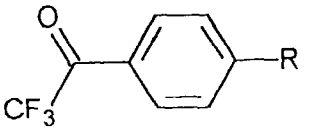

1. R=C_4H_9
2. R=$C_{16}H_{33}$
3. R=$OC_{12}H_{25}$
4. R=$SO_2C_{12}H_{25}$
5. R=$CON(C_8H_{17})_2$
6. R=$COOC_8H_{17}$

Fig. 1. Formulae of studied ionophores

strong electron acceptors as substituents improve carbonate selectivity [8]. The electrophilicity properties are reflected by Hammett constant (σ). The investigated ligands can be divided into two groups. The first one comprising ligands 1, 2, 3 having negative σ values and the second comprising ligands 4, 5, 6 having positive σ values. The first group of ligands is more sensitive towards chlorides. When measuring CO_3^{2-} within the physiological range of human blood for ligands 1, 2 and 3 one must take into account the chloride interference whereas for 4, 5, 6 this effect is negligible. Physiological chloride range in blood is from 0.08 to 0.13 mol l^{-1}. Lipophilicity measured as logarithm of partition coefficient between octanol and water gives us some indication about the value of the detection limit. Ligands 2 and 5 have the lowest detection limit in their respective groups which is consistent with their highest lipophilicity values, 11.1 and 8.0, respectively.

The sensitivity towards carbonates was for (3) pH dependent. The dependence of the electrode potential on pH changes were measured at total carbonate concentration of 25 mmol l^{-1} [11]. The slope of pH characteristic of an electrode containing ligand 3 was increasing with increasing pH.

Table 2
Properties of investigated compounds and the characteristics of electrodes with those ionophores

Ligand	Hammett const. (σ) [13]	Lipophilicity (log P)	Slope of el. charact. (S, mV dec^{-1})	Detection limit log ($a_{CO_3^{2-}}$))	Selectivity log $k^{Pot}_{CO_3^{2-},Cl^-}$
			pH from 7.0 to 7.8		
1	−0.17	5.6[a]	−31.3	−4.7	−2.0
2	−0.17	11.1[a]	−29.6	−5.3	−2.2
3	−0.27	8.4[a]	−29/−10 pH Dependent	−4.7/−3.5	−2.5
4	0.73	5.0 [8]	−30.2	−6.0	−4.0
5	0.36	8.0 [8]	−32.5	−6.5	−4.0
6	0.52	5.2 [8]	−30.9	−6.0	−4.0

[a] Calculated according to [14].

Table 3
Parameters of linear regression equations for selected electrodes

Ligand	Equation	
	Aqueous solutions	Serum samples
2	$Y = 1.00(\pm 0.07)X - 0.39(\pm 2.26)$ $r = 0.97$	$Y = 1.05(\pm 0.11)X - 0.65(\pm 2.02)$ $r = 0.96$
4	$Y = 1.09(\pm 0.07)X - 2.84(\pm 2.53)$ $r = 0.97$	$Y = 0.99(\pm 0.10)X + 13.25(\pm 3.27)$ $r = 0.97$
5	$Y = 0.97(\pm 0.07)X - 0.31(\pm 2.44)$ $r = 0.96$	$Y = 1.39(\pm 0.13)X + 0.68(\pm 3.49)$ $r = 0.97$
6	$Y = 1.00(\pm 0.07)X + 0.03(\pm 2.38)$ $r = 0.96$	$Y = 1.24(\pm 0.13)X + 0.48(\pm 3.43)$ $r = 0.96$

Y = Slope$X$ + intercept; (Y = recovery, X = added HCO_3^- in mmol l^{-1}).

This eliminates (3) from practical applications in clinical analysis.

3.2. Investigation of compounds in the clinical analyser

To estimate the possibility of application of carbonate electrode for biological samples, pH, Cl^- and CO_3^{2-} concentration were determined in clinical analyser. Carbonate concentrations were determined for the series of aqueous solutions, having: (i) ionic composition close to human serum; and (ii) bovine serum (Quality Serum Sample, KONE) spiked with $NaHCO_3$. The results are presented in Table 3. The graphical example of this correlation for ligand 2 is given in Fig. 2. The correlation of added and determined HCO_3^- both in aqueous solutions and in serum is satisfactory. In bovine control serum samples the slope of the recovery curve for some compounds (5, 6) is greater than 1 and for ligand 4 the intercept is not close to 0. This indicates additional unknown influences in serum samples. The only one electrode showing the same behaviour in aqueous solutions and in serum samples is that containing ligand 2.

4. Conclusions

Properties of six derivatives of trifluoacetophenone as neutral carriers for carbonate were examined.

Preliminary determination of carbonates in bovine serum was made using electrodes with investigated compounds (1, 2, 4, 5, 6) in potentiometric KONE Microlyte 6 clinical analyser. These results indicate that, at least, the sensor N° 2 can be used for rapid and simple potentiometric determination of HCO_3^- in blood. The response of this

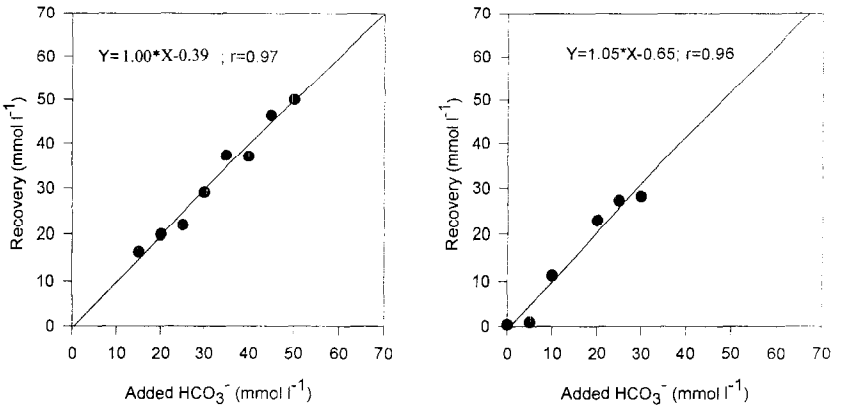

Fig. 2. Example of correlation between added and recovered HCO_3^- in aqueous solutions and in quality control serum for electrode with ligand 2.

sensor is not influenced by serum components. The poor selectivity against chloride ion can easily be compensated by simultaneous Cl^- concentration measurement.

Acknowledgements

This study was partially supported by project BW-1301/2/95 and KONE Instruments.

References

[1] W.M Wise, U.S. Patent 3 723 281 (1973).
[2] H.B. Herman, G.A. Rechnitz, Anal. Chim. Acta 76 (1975) 155.
[3] H.B. Herman, G.A. Rechnitz, Anal. Lett. 8 (1975) 147.
[4] J.A. Greenberg, M.E. Meyerhoff, Anal. Chim. Acta 141 (1982) 57.
[5] A.L. Smirnova, A.L. Grekovich, E.A. Materowa, Elektrokhimiya 21 (1985) 1221.
[6] A.L. Smirnova, A.L. Grekovich, E.A. Materowa, Elektrokhimiya 21 (1985) 1335.
[7] M.E. Meyerhoff, E. Pretsch, D.H. Welti, W. Simon, Anal. Chem. 59 (1987) 144.
[8] Ch. Behringer, B. Lehmann, J.P. Hang, K. Seiler, W.E. Morf, K. Hartman, W. Simon, Anal. Chim. Acta 233 (1990) 41.
[9] N.A. Ampilogova, V.S. Karavan, M.I. Beloshapko, Zh. Anal. Khim. 40 (1985) 895.
[10] Ya.T. Bart, V.S. Karavan, A.L. Grekovich, N.A. Ampilogova, V.E. Yurinskaya, V.A. Nikiforov, Zh. Anal. Khim. 45 (1990) 1364.
[11] T. Sokalski, D. Paradowski, J. Ostaszewska, M. Maj-Żurawska, J. Mieczkowski, A. Lewenstam, A. Hulanicki, Analyst 121 (1996) 133.
[12] P.C. Meier, D. Amman, W.E Morf, W. Simon,in: J. Koryta (Ed.), Medical and Biological Applications of Electrochemical Devices, chapter 2, Wiley, Chichester, 1980.
[13] D.H. McDaniel, H.C. Brown, J. Org. Chem. 23 (1958) 420.
[14] A. Leo, C. Hansch, D. Elkins, Chem. Rev. 71 (1971) 525.

ELSEVIER

Talanta 44 (1997) 1649–1658

Talanta

Size fractionation of metals in wine using ultrafiltration[1]

Anthony J. McKinnon, Geoffrey R. Scollary *

School of Chemistry, The University of Melbourne, Parkville, 3052, Australia

Received 13 August 1996; received in revised form 4 December 1996; accepted 6 December 1996

Abstract

Ultrafiltration has been used to examine the size fractionation of lead, copper, iron, aluminium, calcium, potassium and sodium in white and red wines. Fractionation patterns demonstrated that the behaviour of lead is significantly different to the other metals considered. In red wine, there was a sudden decrease for lead between 100 000 and 30 000 nominal molecular weight cut off (NMWCO) and in white wine, a gradual decrease in the lead concentration was observed from 100 000 NMWCO. Iron was the only other metal which showed, for red wine, a size distribution pattern with a reduction in the iron concentration between 30 and 50% from 100 000 to 1000 NMWCO. Potential binding agents for lead and iron are discussed. The absence of any fractionation pattern for the other metals examined has been interpreted in terms of the metals existing as aquated cations (potassium and sodium), metal tartrate complexes (aluminium, copper and calcium) and either tartrate or phosphate for iron in white wine. The possibility of ultrafiltration disturbing kinetically facile processes, particularly for copper and calcium, is identified.

Keywords: Size speciation; Ultrafiltration; Wine; Wine instability; Lead; Copper; Aluminium; Calcium; Iron; Potassium

1. Introduction

Various metals can induce spoilage reactions in wine. These spoilage processes include precipitation of hydrogen tartrate (potassium) or tartrate salts (calcium), enhanced rate of oxidation (copper, iron) and haze formation (copper, iron and aluminium). In attempting to understand these spoilage processes, most studies have adopted the approach of measuring the total metal concentration and developing a 'rule-of-thumb' to minimise the onset of the spoilage process [1]. Metal speciation studies are relatively few [2], although a detailed investigation of calcium speciation has recently been described [3]. The presence of toxic metals in foods and beverages is always of concern and this is particularly the case with lead in wine [4]. However, toxicity of a metal is related to its bioavailability which in turn is related to its speciation.

It is well-established that, for water bodies, knowledge of the physico-chemical forms is essential for a proper understanding of the bio-geo-

* Corresponding author. Tel.: +61 69 334030; fax: +61 69 332107; e-mail: gscollary@csu.edu.au

[1] Dedicated to Professor George E. Baiulescu on the occasion of his 65th birthday.

PII S0039-9140(97)00070-2

chemical cycling of metals and it can be argued that this knowledge is also required to understand the spoilage processes and potential toxicity associated with metals in wine. A range of experimental techniques have been used to examine the physical and chemical speciation of metals in aqueous systems [5] and ultrafiltration is one technique that frequently yields useful information on the physical (size) speciation of metals as well as organic species. Recent work on the size fractionation of metals in river water [6] and rain water [7] as well as humic substances and their metal complexes [8,9] has clearly demonstrated the usefulness of ultrafiltration for metal speciation. Ultrafiltration has long been used in the food industry as a process tool. For wine, it has been used for examining factors affecting stability [10] and peptide distribution [11] but not for metal speciation.

This work was undertaken to determine the suitability of ultrafiltration for examining the distribution of metals in different particle size fractions. The metals of interest were those which are associated with wine spoilage processes or are regarded as potentially toxic. The results of the size fractionation patterns are interpreted in terms of the compounds with which the metals may interact. Some preliminary observations on the suitability of ultrafiltration for one particular wine have been reported previously [12].

2. Experimental

2.1. Containers and wine samples

All containers were pre-conditioned in 10% (v/v) nitric acid and washed with copious amounts of Grade 1 water (resistivity greater than 18 Mohm cm^{-1}) prior to use. Grade 1 water was used for solution preparation and dilutions.

Wine samples were either obtained commercially or were provided by wineries supporting this project in standard 750 ml glass bottles. A non-commercial wine was collected in 1 l plastic bottles. A complete description of this wine is given elsewhere [12]. After opening the bottle and removal of part of the wine, the headspace was flushed with nitrogen, the bottle re-corked and stored at 4°C until subsequent use.

2.2. Ultrafiltration procedure

The bottled wines were shaken by hand for 5–10 min prior to opening to ensure that any solid material was dispersed prior to the initial filtration stage. An aliquot (500 ml) was taken from the bottle and filtered through a Sartorius 0.45 μm cellulose acetate membrane filter. Portions (60 ml) of this filtrate were then ultrafiltered in parallel using an Amicon (W.R. Grace, Danvers, Ma) model 8050 stirred cell with positive nitrogen pressure. Amicon disc membrane ultrafilters of nominal molecular weight cut-off (NMWCO) values of 100 000 (YM100), 30 000 (YM30) 10 000 (YM10), 5000 (YM5) or 3000 (YM3) and 1000 (YM1) were used. The first 5–8 ml of the ultrafilter permeate was discarded and approximately 5 ml of the sample was retained in the stirred cell to avoid large concentration gradients. The ultrafilter permeate (about 50 ml) was collected and stored in acid-washed plastic bottles at 4°C under nitrogen until required for analysis. Each ultrafilter was used for one wine sample only.

2.3. Procedure for metal determination in ultrafiltrates

Aluminium was determined by graphite furnace atomic absorption spectrophotometry using an Hitachi (Tokyo, Japan) Z7000 system with polarised Zeeman background correction [13]. Iron and copper were determined using an Hitachi (Tokyo, Japan) Z6000 flame atomic absorption spectrophotometer using in-house validated methods. Stripping potentiometry using a Radiometer Analytical SA (Lyon, France) TraceLab 20 system was applied to the measurement of lead [14]. Sodium and potassium were determined by flame photometry on a Beckman Klina flame photometer [15]. Metal determinations were performed on the unfiltered wine, the 0.45 μm membrane filtered wine and each ultrafiltrate fraction.

Absorbance measurements at 420 and 520 nm were made on an Hitachi (Tokyo, Japan) U2000

Table 1
Size fractionation patterns by ultrafiltration for Al, Ca, Fe, Na and K in various wines (in units of mg l^{-1})

		Al	Ca	Fe	Na	K
Dry white # 1	Unfilt	1.28	91	1.70	115	418
	0.45 μm	1.23	92	1.71	115	414
	10 000	1.26	92	1.76	115	426
	5000	1.26	93	1.74	115	418
	1000	1.17	91	1.70	115	426
Dry white # 2	Unfilt	0.23	57	0.07	ND	704
	0.45 μm	0.20	58	0.06	ND	665
	10 000	0.21	58	0.05	ND	704
	5000	0.20	58	0.05	ND	704
	1000	0.19	57	0.05	ND	547
Dry white # 3	Unfilt	0.78	95	1.84	69	383
	0.45 μm	0.74	95	1.82	69	383
	10 000	0.77	96	1.89	69	387
	5000	0.76	97	1.89	69	379
	1000	0.72	95	1.90	69	383
Dry red # 1	Unfilt	0.33	48	2.42	276	1482
	0.45 μm	0.34	49	2.55	276	1482
	10 000	0.33	44	1.86	276	1443
	5000	0.32	44	1.57	276	1482
	1000	0.31	43	1.23	299	1482
Dry red # 2	Unfilt	0.20	41		23	819
	0.45 μm	0.18	41		23	780
	10 000	0.16	38		23	663
	5000	0.17	37		23	741
	1000	0.16	37		23	741
Dry red # 3	Unfilt	0.28	47	3.45	23	1170
	0.45 μm	0.29	47	3.49	23	1170
	10 000	0.29	45	3.12	23	1131
	5000	0.29	45	2.97	23	1170
	1000	0.28	43	2.37	23	1170
Sweet white # 1	Unfilt	1.94	139	4.82		
	0.45 μm	2.05	109	4.79		
	10 000	2.04	104	4.72		
	5000	2.01	103	4.68		
	1000	2.20	109	5.10		

UV/Vis spectrophotometer using 2, 5 or 10 mm cells, as appropriate, and corrected to standard 10 mm path length. These wavelengths have been used for some time to describe red wine colour [16]. Manipulation of these absorbance values allows red wine colour density and colour hue to be calculated [17].

3. Results

The initial ultrafiltration procedure included an ultrafilter with a NMWCO value of 500 and, with some wines, a significant cut off with this ultrafilter was observed for aluminium, calcium and iron. However, analysis of a spiked model wine (12% v/v aqueous ethanol saturated with potassium hydrogen tartrate and adjusted to pH 3.2 with tartaric acid) and spiked aqueous samples showed up to 50% removal of the metal spike suggesting that the cut off may well be a conse-

Table 2
Size fractionation patterns by ultrafiltration for Al, Ca, Cu, Fe, and Pb in various wines

		Al (mg l^{-1})	Ca (mg l^{-1})	Fe (mg l^{-1})	Cu (mg l^{-1})	Pb (μg l^{-1})
Dry white # 4	Unfilt	0.79	97	0.96	0.29	9
	0.45 μm	0.81	101	0.93	0.24	19
	10 000	0.80	99	0.94	0.21	2
	3000	0.83	100	0.92	0.22	6
	1000	0.79	96	0.88	0.19	6
Dry white # 5	Unfilt	6.37	100	11.49	0.41	480
	0.45 μm	4.37	100	2.84	0.42	490
	10 000	4.41	95	2.73	0.39	50
	3000	4.45	92	2.66	0.38	20
	1000	3.80	91	1.90	0.35	40
Dry white # 6	Unfilt	2.07	109	3.44	0.33	126
	0.45 μm	2.02	110	3.44	0.32	136
	10 000	2.01	110	3.39	0.10	70
	3000	1.94	109	3.38	0.09	69
	1000	1.76	102	2.99	0.13	39
Dry white # 7	Unfilt	0.74	7	0.06	0.11	48
	0.45 μm	0.73	7	0.06	0.09	31
	10 000	0.72	7	0.06	0.09	29
	3000	0.71	6	0.06	0.09	25
	1000	0.68	6	0.03	0.07	21
Dry red # 4	Unfilt	0.58	47	5.14	0.40	86
	0.45 μm	0.55	47	5.51	0.03	98
	10 000	0.54	43	4.16	0.02	16
	3000	0.57	43	3.51	0.04	12
	1000	0.53	40	2.39	0.06	15
Dry red # 5	Unfilt	0.64	43	2.68	0.16	1100
	0.45 μm	0.64	42	2.61	0.08	980
	10 000	0.64	39	1.75	0.09	140
	3000	0.66	38	1.56	0.10	120
	1000	0.59	35	1.31	0.09	120

quence of metal retention by the ultrafilter rather than a size fractionation property of the wine. This differs from the observation of Cheng et al. [7] who found that, in their rain water analysis, a 500 NMWCO ultrafilter could be used. The reasons for this difference are not clear, but it was determined that the 500 NMWCO ultrafilter should not included in this wine metal profile study. The other ultrafilters used did not retain metals from spiked aqueous samples.

Apart from the sweet white wine, a botrytised Riesling, there was no difficulty in the ultrafiltration stage with the stirred cell arrangement, although some red wines proved to be a little difficult to pass through the 1000 NMWCO ultrafilter. *Botrytis*-infected wines generally contain a high concentration of glucans which would interfere with the filtration process, even in a stirred cell.

Table 1 and Table 2 present the metal distribution patterns for the first two studies. A change in the availability of the Amicon filters caused the use of 3000 NMWCO ultrafilter, in place of the 5000 NMWCO ultrafilter, for the data reported in Table 2. Copper and lead were included in the second study and sodium and potassium were excluded.

It is apparent from Table 2 that the distribution pattern for lead is significantly different from that of the other metals studied. This is clearly demonstrated in Fig. 1 where it is obvious that $\approx 80\%$ of the lead is cut off by the 10 000 NMWCO ultrafilter. As a consequence of these observations for lead (Table 2 and Fig. 1), the ultrafiltration proto-

col was modified to include ultrafilters with NMWCO values of 100 000 and 30 000. The values in Table 3 and Fig. 2 show that, for red wines, the cut off point for lead is between the NMWCO values of 100 000 and 30 000. For the white wines studied, there is a more gradual decrease in the lead concentration from 100 000 to 10 000 NMWCO.

Ultrafiltration also has a significant impact on the colour of red wine as is shown by the data in Fig. 3 and Table 4. Colour density ($A_{420} + A_{520}$) and colour hue (A_{420}/A_{520}) can be taken as two measures of red wine colour [16]. It is apparent from Table 4 that the colour density is affected markedly by ultrafiltration, but there is little effect on colour hue.

4. Discussion

4.1. Sodium and potassium

Within experimental error, there was no size fractionation observed for potassium for the six wines examined (Table 1) confirming earlier theoretical calculations that, at most, 1% of the potassium may be complexed with the hydrogen tartrate anion at wine pH [2]. The six wines used had been previously stabilised with respect to potassium hydrogen tartrate precipitation and this was verified by the similarity of the values obtained for the 0.45 μm membrane filtered wine compared with the unfiltered wine. Sodium complexes in wine have not been reported and it was not expected to see any size fractionation.

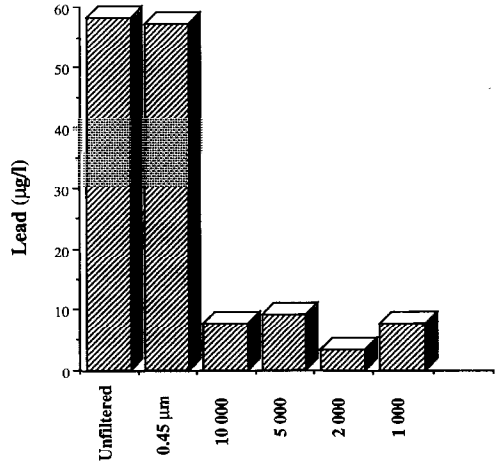

Fig. 1. Size fractionation of lead in Cabernet Sauvignon using 10 000, 5000, 2000 and 1000 ultrafilters. The unfiltered wine and 0.45 μm membrane filtered wine are included for comparison.

4.2. Aluminium

There was no noticeable size fractionation with the exception of Dry White # 5 where the reduction in the aluminium concentration between the unfiltered wine and the 0.45 μm membrane filtered wine is indicative of an aluminium haze. The high concentration of aluminium in this wine suggests that it has the potential for haze formation [17] and the cut-off between the unfiltered and 0.45 μm membrane filtered fraction is not surprising.

The absence of size fractionation is indicative of aluminium complexation with small molecules. In previous work on the speciation of aluminium in wine, there was tentative evidence [18,19] that aluminium is bound very strongly to tartaric acid and other related carboxylic acids found in wine such as malic and gallic acids and this correlates with the observed fractionation pattern.

4.3. Calcium

Similar to aluminium, there is essentially no variation in the calcium concentration with molecular size. For some red wines, there is an implication of a slow decrease in the calcium concentration with decreasing NMWCO value, although the change is not significant with respect to the experimental error.

These observations for calcium are surprising, as previous work has demonstrated that approximately 50% of the calcium in wine is complexed [20]. The possible complexing agents include the wine dicarboxylic acids, particularly tartaric and malic acids [21], as well as polyuronic acids [22]. As it is generally assumed that the polymer chain length of the uronic acid must be at least 10 units for significant interaction with calcium to occur [23], it is surprising that some size fractionation

Table 3
Size fractionation patterns by ultrafiltration for Al, Ca, Fe, Cu and Pb in white and red wine. Extended ultrafiltration procedure including 100 000 and 30 000 NMWCO filters

		Al (mg l^{-1})	Ca (mg l^{-1})	Fe (mg l^{-1})	Cu (mg l^{-1})	Pb (μg l^{-1})
Dry white # 8	Unfilt	1.84	85	7.48	0.290	39
	0.45 μm	1.84	83	7.45	0.162	43
	100 000	1.85	82	7.41	0.164	29
	30 000	1.82	79	7.22	0.154	17
	10 000	1.80	78	7.06	0.140	12
	3000	1.75	78	6.98	0.138	12
	1000	1.63	73	6.04	0.051	11
Dry white # 9	Unfilt	1.85	129	3.67	0.330	167
	0.45 μm	1.85	130	3.69	0.350	169
	100 000	1.87	128	3.62	0.260	142
	30 000	1.90	130	3.66	0.131	119
	10 000	1.88	128	3.63	0.144	90
	3000	1.87	128	3.65	0.078	94
	1000	1.71	123	3.39	0.067	74
Dry red # 6	Unfilt	0.54	51	1.83	0.095	30
	0.45 μm	0.51	52	1.87	0.104	20
	100 000	0.50	53	1.83	0.102	19
	30 000	0.50	49	1.68	0.095	8
	10 000	0.50	48	1.62	0.097	8
	3000	0.48	48	1.44	0.100	6
	1000	0.45	47	1.24	0.097	9
Dry red # 7	Unfilt	0.59	55	1.87	0.095	27
	0.45 μm	0.59	54	1.87	0.091	24
	100 000	0.61	54	1.85	0.098	25
	30 000	0.60	52	1.67	0.097	10
	10 000	0.55	51	1.64	0.091	3
	3000	0.59	52	1.62	0.094	13
	1000	0.55	49	1.25	0.086	6
Dry red # 8	Unfilt	0.72	63	3.04	0.320	129
	0.45 μm	0.65	64	3.02	0.078	120
	100 000	0.64	64	2.97	0.116	129
	30 000	0.65	62	2.88	0.078	48
	10 000	0.61	60	2.44	0.074	52
	3000	0.59	61	2.42	0.107	41
	1000	0.60	59	2.25	0.055	42

was not observed in the wines examined here. However, an alternative explanation is that the calcium interactions with its binding agents are weak (a ten-fold dilution of wine significantly decreases the proportion of complexed calcium [20]) and the physical agitation associated with the stirred cell ultrafiltration system used in this study may have been sufficient to disturb the calcium/complexing agent interactions. Less mechanical methods of size fractionation are presently being considered to solve this dilemma.

The *Botrytis*-affected Riesling (Sweet White # 1, Table 1) showed some loss of calcium between the unfiltered wine and the 0.45 μm membrane filtered wine. This wine did contain a haze which, on analysis, was shown to contain a significant amount of calcium. There is significant anecdotal evidence in the wine industry to suggest that calcium is involved in instability processes of *Botrytis*-affected wines and this point is the subject of an on-going study.

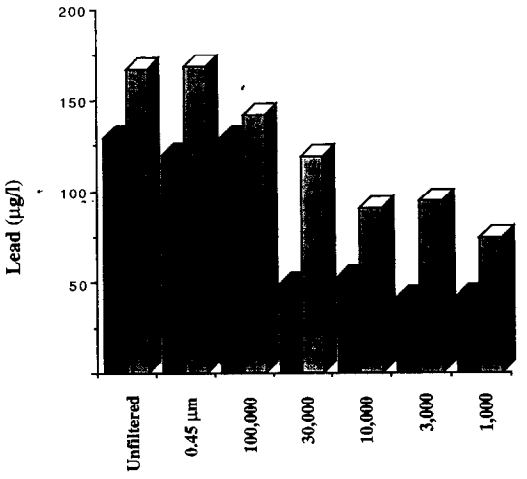

Fig. 2. Comparison of size fractionation patterns for lead in red (■) and white (▨) wine using 100 000, 30 000, 10 000, 3000 and 1000 ultrafilters together with the unfiltered wine and the 0.45 µm membrane filtered wine.

4.4. Copper

The distribution of copper is essentially independent of molecular size (Table 2 and Table 3), except for Dry Red # 4 where most of the copper is in the suspended phase. The chemistry of copper in wine is complex, but critical because of its role in enhancing the rate of oxidation. It is well established that copper can interact with catechin and caffeic acid [24–26] and, of course, with tartaric acid at wine pH [our unpublished observations]. In a non-wine system, Weber [24] has demonstrated that a copper/catechin complex is formed within a short time after mixing, but that this complex appears to breaks down as the mixture is allowed to age. Our work on copper-induced oxidation of catechin in a model wine has shown that there is a loss of ASV labile copper as the catechin oxidises and polymerises [26]. However, we have recently observed that the interaction of copper with the polymerised catechin is weak, as polyvinylpolypyrrolidone (PVPP) is capable of adsorbing the polymerised catechin which in turn releases all copper into solution in an ASV labile form [27].

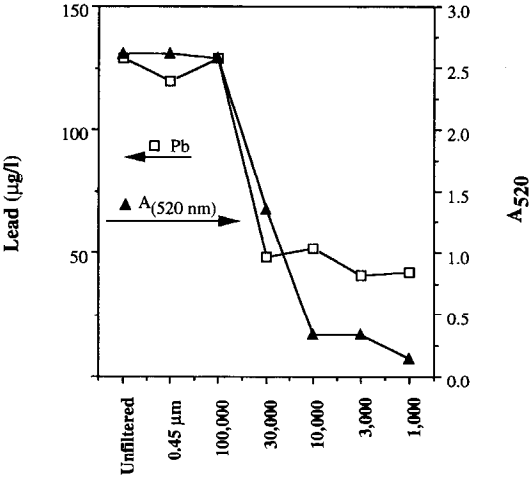

Fig. 3. Comparison of the size fractionation of lead and wine colour (A_{520}) for a red wine. Filtration pattern is the same as in Fig. 2.

These observations on the absence of any significant size distribution of copper may also be reflection of this weak interaction between copper and wine components such as catechin. That is, as proposed above for calcium, ultrafiltration may disturb the copper/organic polymer aggregates in solution.

4.5. Iron

The concentration of iron in white wine is independent of ultrafilter size, but there is a gradual decrease (a 30% reduction, on average) in concentration for red wine (Tables 1–3). The only exception is Dry White # 5, where most of the iron is in the insoluble phase (trapped by 0.45 µm membrane). The high iron concentration of the unfiltered wine would have induced the formation of a haze [28].

It is well recognised that iron binds strongly with humic substances (HS) and the tannin component of red wine has a distinct chemical resemblance to HS. In a study of aqueous HS by ultrafiltration, Burba et al. [8] noted that only iron showed a size distribution pattern similar to that of the HS itself. This observation was made at pH 3.7, approximate to the pH common for red wine. Thus, it is reasonable to assume that there is a some interaction between iron and the tannin component, but it must be also be recog-

Table 4
Effect of ultrafiltration on the absorbance at 420 and 520 nm for white and red wines and calculated colour properties for red wines

		A_{420}	A_{520}	Colour density	Colour hue
Dry white # 8	Unfilt	0.431	0.383		
	0.45 μm	0.410	0.365		
	100 000	0.400	0.356		
	30 000	0.311	0.263		
	10 000	0.163	0.120		
	3000	0.188	0.147		
	1000	0.045	0.022		
Dry white # 9	Unfilt	0.152	0.031		
	0.45 μm	0.151	0.031		
	100 000	0.147	0.031		
	30 000	0.146	0.030		
	10 000	0.139	0.027		
	3000	0.129	0.024		
	1000	0.063	0.009		
Dry red # 6	Unfilt	2.945	3.130	6.075	0.94
	0.45 μm	2.855	3.065	5.920	0.93
	100 000	2.910	3.100	6.010	0.94
	30 000	2.925	3.130	6.055	0.03
	10 000	0.875	0.845	1.720	1.04
	3000	0.775	0.703	1.478	1.10
	1000	0.216	0.150	0.366	1.44
Dry red # 7	Unfilt	2.510	2.915	5.425	0.86
	0.45 μm	2.485	2.915	5.400	0.85
	100 000	2.590	3.035	5.625	0.85
	30 000	1.830	2.100	3.390	0.87
	10 000	1.480	1.695	3.175	0.87
	3000	0.860	0.985	1.845	0.87
	1000	0.195	0.215	0.410	0.91
Dry red # 8	Unfilt	3.005	2.620	5.625	1.15
	0.45 μm	3.005	2.620	5.625	1.15
	100 000	2.960	2.575	5.535	1.15
	30 000	1.670	1.345	3.015	1.24
	10 000	0.575	0.335	0.910	1.72
	3000	0.585	0.336	0.921	1.74
	1000	0.338	0.149	0.487	2.27

nised that a significant proportion of the iron is still present at less than 1000 NMWCO. Obviously, iron can interact strongly with other wine components. Tartaric acid and phosphate must be considered to be potential binding agents: one form of iron-induced instability, especially in white wine, is thought to be iron phosphate precipitation [29].

4.6. Lead

Lead was determined by stripping potentiometry as this electrochemical stripping method has been shown to give results comparable with those obtained by graphite furnace AAS [14]. The particular advantages of stripping potentiometry for the measurement of lead in wine, especially with respect to alternative techniques such as anodic stripping voltammetry and graphite furnace AAS, have been described elsewhere [30,31].

The size fractionation of lead is markedly different to that observed for the other metals considered in this work (Tables 2 and 3 and Figs. 1 and 2). Even wines which are severely contaminated with lead (Dry Red # 5 and Dry White # 5; Table 2) show a very obvious cut off. Potential binding agents for lead in white wine include residual protein and procyanidins. Several wine proteins have sulfur groups in the active site which, of course, is a classic soft base ligand for the soft acid, Pb^{2+}. The gradual decrease in white wines is a reflection of the variation in molecular size of the proteins and procyanidins.

The marked cut off in the lead distribution in red wines indicates that a polymeric species, most probably tannin, is the binding species. It is already well established that lead binds with tannins and other polyphenols, for example, wattle tannin [32]. Addition of 'red tannin', a commercial wine making material, to a model wine has been shown to bind a significant proportion of the lead in the model wine [33].

The relationship between wine colour (A_{520}) and the lead size distribution (Fig. 3) is additional evidence for wine tannin being the binding agent. Further, the marked decrease in wine colour and colour density between 100 000 and 10 000 NMWCO (Fig. 3, Table 4) precludes any possibility of using ultrafiltration (for example, 10 000) as a method for removing lead from highly contaminated wines [12].

5. Conclusions

An obvious size fractionation pattern for lead in red and white wines is clearly discernible using ultrafiltration. However, with the exception of iron in red wine, ultrafiltration is limited in its ability to establish fractionation patterns for aluminium, calcium, copper and iron (in white wine). It is proposed that this limitation is a consequence of the mechanical action of ultrafiltration disturbing kinetically facile reactions, particularly for calcium and copper, where there is evidence that these metals exist in weakly associated complexes in solution. The effect of ultrafiltration on wine colour and colour density of red wine negates the application of ultrafiltration as a method of removing lead from contaminated wines.

Acknowledgements

This work was supported by the Australian Grape and Wine Research Development Corporation (project UM94/1) and The University of Melbourne through a special initiative grant.

References

[1] B. Rankine, Making Good Wine, Sun, Australia, 1991, p. 277.
[2] G.R. Scollary, Metal speciation in wine: measurement and consequences for instability, in: P.J. Williams, D.M. Davidson, T.H. Lee (Eds.), Proceedings of the Seventh Australian Wine Industry Technical Conference, Winetitles, Adelaide, 1990, p. 192.
[3] A.J. McKinnon, G.R. Scollary, D.H. Solomon, P.J. Williams, Colloids Surf. A: Physciochem. Eng. Aspects 82 (1994) 225.
[4] C.S. Stockley, T.H. Lee, J. Wine Res. 6 (1995) 5.
[5] P.G.C. Campbell, A. Tessier, Current Status of Metal Speciation Studies, in: J.W. Patterson, R. Passino (Eds.), Metals Speciation Separation and Recovery, Lewis Publishers, Michigan, 1987, p. 201.
[6] Y. Tanizaki, T. Maeno, M. Nakamura, M. Yamazaki, J. Environ. Sci. Health, Part A: Environ. Sci. Eng. Toxic Hazardous Substance Control 31 (1996) 913.
[7] J. Cheng, C.L. Chakrabarti, M.H. Back, W.H. Schroeder, Anal. Chim. Acta 288 (1994) 141.
[8] P. Burba, V. Shkinev, B.Ya. Spivakov, Fresenius J. Anal. Chem. 351 (1995) 74.
[9] B. Aster, P. Burba, J.A.C. Broekaert, Fresenius J. Anal. Chem. 354 (1996) 722.
[10] J.H. Flores, D.A. Heatherbell, M.R. McDaniel, Am. J. Enol. Vitic. 41 (1990) 207.
[11] M.I. Acedo, E. Pueyo, M.C. Polo, Am. J. Enol. Vitic. 45 (1994) 167.
[12] H.R. Eschnauer, G.R. Scollary, Vitic. Enol. Sci. 51 (1996) 6.
[13] R.W. Cattrall, A.J. McKinnon, G.R. Scollary, Am. J. Enol. Vitic. 43 (1992) 166.
[14] G.N. Chen, G.R. Scollary, V.A. Vicente-Beckett, Am. J. Enol. Vitic. 45 (1994) 305.
[15] G. Scollary, C. Skepper, Aust. Grapegrower Winemaker 244 (1984) 74.
[16] P. Sudrad, Ann. Technol. Agric. 7 (1958) 203.
[17] T.C. Sommers, M.E. Evans, J. Sci. Food Agric. 28 (1977) 279.

[18] H.R. Eschnauer, G.R. Scollary, Vitic. Enol. Sci. 50 (1995) 24.
[19] A.J. McKinnon, A comparison of analytical procedures for the determination of aluminium in wine, MSc Thesis, University of Melbourne, 1990.
[20] T.J. Cardwell, R.W. Cattrall, R.L. Mrzljak, L.M. Robins, G.R. Scollary, T. Sweeney, Electroanalysis 3 (1991) 573.
[21] A.J. McKinnon, G.R. Scollary, D.H. Solomon, P.J. Williams, Am. J. Enol. Vitic. 46 (1995) 509.
[22] A.J. McKinnon, P.J. Williams, G.R. Scollary, J. Agric. Food Chem. 44 (1996) 1382.
[23] A.J. McKinnon, An examination of factors affecting the precipitation of calcium tartrate in wine, PhD Thesis, University of Melbourne, 1994.
[24] G. Weber, Anal. Chim. Acta 232 (1990) 377.
[25] P.W. Linder, A. Voyé, Polyhedron 6 (1987) 53.
[26] G.R. Scollary, A.J. McKinnon, Studies on metal-induced wine spoilage processes: relevance to winemaking practice, in: C.S. Stockley, A.N. Sas, R.S. Johnstone, P.A. Leske, T.H. Lee (Eds.), Proceedings of the Ninth Australian Wine Technical Conference, Winetitles, Adelaide, 1996, 46.
[27] M. Mitri, V.A. Vicente-Beckett, G.R. Scollary, manuscript in preparation.
[28] E. Peynaud, Knowing and Making Wine, Wiley, New York, 1984, p. 324.
[29] B.W. Zoecklein, K.C. Gugelsang, B.H. Gump, F.S. Nury, Wine production and analysis, Chapman and Hall, New York, 1995, p. 202.
[30] C. Marin, P. Ostapczuk, Fresenius Anal. Chem. 343 (1992) 881.
[31] D. Jagner, L. Renman, Y. Wang, Electroanalysis 5 (1993) 283.
[32] N. Slabbert, Complexation of condensed tannins with metals ions, in: R.W. Hemingway, P.E. Laks (Eds.), Plant Polyphenols, Synthesis, Properties and Significance, Plenum Press, New York, 1992, p. 421.
[33] A.M. Green, G.R. Scollary, results to be published.

ELSEVIER

Talanta 44 (1997) 1659–1669

Talanta

Enzyme electrode probes obtained by electropolymerization of monomers with PMS and selected dehydrogenase enzymes

A. Curulli [a], I. Carelli [b], O. Trischitta [b], G. Palleschi [c,*]

[a] *Centro C.N.R. di Studio per l'Elettrochimica e la Chimica Fisica delle Interfasi, Via del Castro Laurenziano, 7 00161 Rome, Italy*
[b] *Dipartimento di ICMMPM Università di Roma 'La Sapienza', Via del Castro Laurenziano, 7 00161 Rome, Italy*
[c] *Dipartimento di Scienze e Tecnologie Chimiche Università di Roma Tor Vergata, Via della Ricerca Scientifica, 00133 Rome, Italy*

Received 1 August 1996; received in revised form 13 November 1996; accepted 21 November 1996

Abstract

5-methylphenazonium methylsulphate, (commonly named phenazine methosulphate, PMS) mediated electroxidation of β-nicotinamide adenine dinucleotide (phosphate), reduced form, (NAD(P)H), on platinum, gold and carbon electrodes has been studied by electropolymerization of 1,2-, 1,3-, 1,4-diaminobenzene (DAB), pyrrole-2-carboxylic acid (PY-2-COOH) and 4,4′-dihydroxybenzophenone (DHB) in presence of PMS using cyclic voltammetry. The electroxidation of ascorbic acid has been evaluated on the electrodes elctropolymerized in absence and in presence of PMS. The same experiments have been carried out with NAD(P)H in solution. Results showed that the NAD(P)H is oxidized by PMS coimmobilized with the polymer film on the electrode surface. NAD(P)H has been measured in the range 10^{-6}–10^{-2} mol l^{-1} with a detection limit of 5×10^{-7} mol l^{-1}. Amperometric measurements of NAD(P)H have been carried out at -0.10 V and the efficiency of different electrodes based on different materials has been studied. The electropolymerization has been also carried out in presence of PMS and selected dehydrogenase enzymes. The activity of these enzymes has been tested amperometrically at -0.1 V. Enzyme substrates such as glucose, lactate and glutamate have been measured in the range 5×10^{-6}–1×10^{-2} mol l^{-1} with a detection limit 1×10^{-6} mol l^{-1}. Also the stability of these probes during time has been evaluated. © 1997 Published by Elsevier Science B.V.

Keywords: Electropolymerization; Dehydrogenase enzymes; Electrochemical biosensors; Interferences

1. Introduction

The use of NAD(P)$^+$ dependent dehydrogenase enzymes in amperometric biosensors has been studied in the past decade [1–5].

The oxidation of NAD(P)H on several electrodic materials has received great attention and strong interest by the scientific community during these years. The main reason is the possibility to use more than 200 redox NAD(P)$^+$ dependent enzymes for assembling a novel class of biosensors.

In fact a reversible and efficient oxidation of enzimatically active NAD(P)H to NAD(P)$^+$ is the key to use any NAD(P)$^+$ dependent dehydrogenase enzymes electrodes probe.

* Corresponding author.

PII S0039-9140(97)00071-4

It is well known that the electrochemical oxidation of NAD(P)H involves a multi step (ECE) mechanism [6–8]. The electrochemical regeneration of $NAD(P)^+$ is affected by a degradation of the cofactor due to irreversible redox processes and overpotential constrains [9]. Moreover, the direct electron transfer between NAD(P)H and the electrode surface requires a relatively high overvoltage. Often electrode fouling and interfering background currents [10–12]: finally, the overvoltage leads to not enzimatically active $NAD(P)^+$ [13].

A way to overcome these problems has been the use of electron mediators which lower the working voltage to the formal potential of the mediator [4].

Mediators used for NADH oxidation are quinones [14], quinoid structures as phenoxazines [15], phenazines [16] or phenothiazines [17], polymetal lophthalocianines [18], ruthenium complexes [19] and quinoid redox dyes [20].

Mediators have been immobilized in many different ways, for example, by chemisorption [14], thus limiting the long-term stability of the biosensors due to the leaking of the catalyst from the electrode surface, by covalent attachment to the electrode or to functionalized conducting polymers [21], or to a polymer film deposited electrochemically onto the electrodic surface [22,23], mixed into carbon paste [24] or coupled with a polymer backbone mixed in a carbon paste, by electropolymerization of the mediator on the electrode surface [25–29]. One of these mediators is PMS, which acts as cofactor to mediate the electron transfer for many dehydrogenase enzymes.

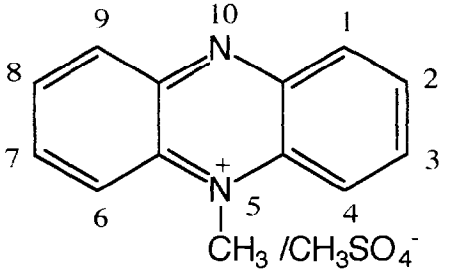

The electrochemical behaviour of PMS has been studied by our group in aprotic solvents and in aqueous buffered solutions [30].

Recently, a bioreactor [31] was constructed using the immobilized glucose-6-phosphate dehydrogenase (G6PDH) on graphite electrodes surface where PMS was previously absorbed.

Amperometric sensors were assembled with $NAD(P)^+$-dependent dehydrogenases and PMS or other quinoid redox dyes [32]. The ionic redox mediators could be immobilized as Reineckates salts in graphite-epoxy composite electrodes.

In the literature, to our best knowledge, there is only one example of immobilization of PMS and glutamate dehydrogenase in a conducting polymer [33], but this probe suffered in low term stability by the leaking of the mediator and the enzyme.

An example of methylphenazonium-zeolite-modified enzyme sensor is reported for subnanomolar detection of phenols, consisting of tyrosinase, immobilized on a novel poly-urethane hydrogel [34].

Our work consists in the immobilization of PMS in a polymeric matrix during the electrosynthesis of different non conducting polymers on platinum, gold and carbon electrodes.

These sensors have been evaluated for PMS mediated reoxidation of NAD(P)H.

The advantage of this system is that the resulting probes covered with non conducting polymers are interference-free. In fact the possible interferences such as ascorbic acid, uric acid and paracetamol have been minimized.

The biosensors based on the immobilization of enzymes in non-conducting polymers have some advantages over conducting films: the film thickness of the non-conducting polymer is self-controlled during electropolymerization and leads to very thin and uniform films.

These biosensors generally have the advantage of fast response time and high sensitivity because of relatively high enzyme loading [35].

Moreover, the non-conducting polymer films are generally found to be more effective in both preventing the biosensors from fouling and eliminating the interferences from electroactive species.

These electrodes assembled as dehydrogenase enzyme electrode probes by electropolymerization of monomers with PMS and selected dehydrogenase enzymes, allowed the measurements of glucose, lactate and glutamate.

Response time, stability, linear range, detection limits and interferences have been evaluated.

2. Experimental

2.1. Materials

β-Nicotinamide adenine dinucleotide, reduced form (NADH), β-Nicotinamide adenine dinucleotide (NAD^+), β-Nicotinamide adenine dinucleotide phosphate, reduced form (NAD(P)H) and β-Nicotinamide adenine dinucleotide phosphate ($NAD(P)^+$) from Sigma, St. Louis, MO, were used without further purification. 1,2-1,3-1,4-Diamminobenzene (1.2-, 1.3-, 1.4-DAB, FLUKA), pyrrole-2-carboxilic acid, 4,4′-dihydroxybenzophenone and PMS from FLUKA Buchs, Switzerland were used as received.

β-D-(+)-glucose, glutamic acid, lactic acid (as lithium salt), ascorbic acid (AA), uric acid, paracetamol were purchased from Sigma.

Glucose solutions were allowed to mutarotate overnight at room temperature before use.

All other chemicals were of analytical grade. Phosphate buffers (0.1 mol l^{-1}) were prepared with distilled-deionized water using sodium dihydrogen phosphate dihydrate (FLUKA Biochemica Microselect for molecular biology). The pH was adjusted to the suitable value with pellets of sodium hydroxide.

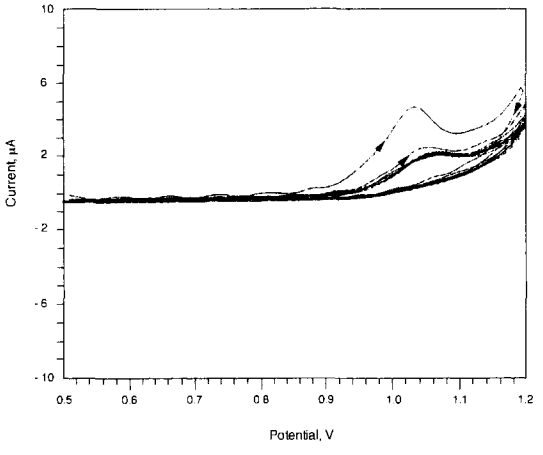

Fig. 1. Cyclic voltammograms for the oxidation of PPY-2-COOH 5 mmol l^{-1} at a gold electrode in a deoxygenated phosphate buffer (pH 8.1, I = 0.1). Scan rate 2 mV s^{-1}.

L-Lactic dehydrogenase type XI (EC 1.1.1.27; 700 units/mg) from rabbit muscle (LDH), glucose dehydrogenase (EC 1.1.1.47; 50–150 U mg^{-1}) from *Bacillus Megaterium* (GDH) and L-glutamic dehydrogenase type III (EC 1.4.1.3; 40 U mg^{-1}) from bovine liver (GlDH) were purchased from Sigma.

2.2. Apparatus

An AMEL polarographic system model 433A (AMEL, Milan, Italy) was used for voltammetric studies. The electrochemical cell consisted in a solid working electrode, a SCE reference electrode, and a Pt counter electrode. The gold (Au), platinum (Pt), glassy carbon (GC) working electrodes (surface nominal area 0.071 cm^2) were from AMEL.

Amperometric measurements were carried out with a 559 HPLC Detector from AMEL. Currents were recorded using a LKB 2210 strip chart recorder from Delft, Nederland.

All the measurements were carried out at 25 ± 1°C.

2.3. Procedure

The bare electrode used for the preparation of the sensors consisted of a Pt or Au or GC disks (2 mm diameter) sealed in a tygon tube.

The working electrode surface was polished with alumina (Al_2O_3, Buehler from Evanston, Illinois) powder of 1, 0.3 and 0.05 μm particle sizes just before use. After carefully rinsing with distilled water, electrodes were sonicated for almost 10 min. Moreover, the Pt and Au electrodes were pre-treated in 0.5 mol l^{-1} H_2SO_4 by potential cycling from −0.2 to +1.2V (vs. SCE) at a scan rate of 20 mV s^{-1}, until no changes in current were observed [36].

2.4. Electropolymerization with PMS in absence of enzyme

For the electropolymerization studies the following monomers have been used: 1,2-DAB, 1,3-

Table 1
Voltammetric data relative to polymers/electrodes in presence NAD(P)H and ascorbic acid

	ip_a (μA) at bare electrode	ip_a (μA) at covered electrodes	
		PPY-2-COOH	PDHB
Ascorbic acid (4 mM)			
(Pt)	7.14	1.04 (−86%)	0.91 (−87%)
(Au)	8.02	0.97 (−88%)	0.87 (−93%)
(GC)	7.51	0.92 (−87%)	0.98 (−88%)
NADPH (3 mM)			
(Pt)	3.98	0.38 (−95%)	0.44 (−88%)
(Au)	4.97	0.48 (−90%)	0.38 (−92%)
(GC)	4.23	0.42 (−90%)	0.41 (−90%)
NADH (3 mM)			
(Pt)	4.03	0.35 (−91%)	0.34 (−92%)
(Au)	5.01	0.43 (−91%)	0.41 (−95%)
(GC)	4.28	0.45 (−88%)	0.46 (−88%)

DAB, 1,4-DAB, PY-2-COOH and DHB. Each monomer was electropolymerized using a solution of sodium phosphate buffer 0.1 mol l^{-1}, which was deaerated for 30 min with Argon 99% (Air Liquide, France), in the presence of PMS.

Monomer and mediator concentrations have been varied from 5 to 9 mmol l^{-1} and from 0.8 to 4.0 mmol l^{-1} respectively. The electropolymerization has been carried out using cyclic voltammetry at pH values from 5.6 to 8.1. The scan rate has been varied from 20 to 2 mV s^{-1} and the potential has been continuously cycled from 0 to +0.8 V for 1.2-, 1.3-, 1.4-DAB, from +0.4 to +1.2 V for DHB and from +0.4 to +1.4 V for PY-2-COOH, until the current reached a value which remained constant after further cycling.

2.5. Voltammetric PMS and NAD(P)H measurements

To test the electrocatalytic behaviour of the entrapped PMS we used the following procedure: at the end of the electropolymerization the electrode was rinsed with the working buffer, then dipped in the same deaerated buffer solution and the potential scanned from +0.5 to −0.5 V.

Ascorbic acid, paracetamol at a concentration of 0.4 mmol l^{-1} and uric acid (saturated solution)

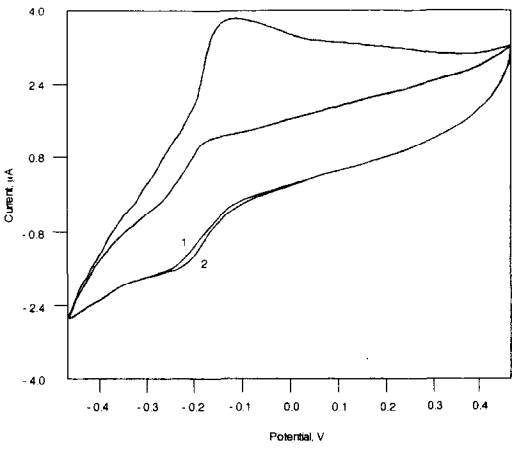

Fig. 2. Cyclic voltammograms at a PPY-2-COOH/PMS/gold electrode: (1) in a deoxygenated phosphate buffer (pH 8.1, $I = 0.1$); (2) in the presence of 0.5 mmol l^{-1} NADH. Scan rate 5 mV s^{-1},

were also tested in phosphate buffer pH 8.1, in the absence and presence of the polymer with the entrapped mediator. The same experiment was also carried out with solutions of NAD(P)H, ranging from 0.1 to 10 mmol l^{-1}.

Table 2
Catalytic efficiency of PMS for NAD(P)H oxidation from ratio of catalytic peak current I_{cat} to peak current I_{ox}, recorded in the same solution without NAD(P)H, in a buffer solution pH 8.1 $v = 10$ mV s^{-1}

Electrode	I_{cat} (μA)	I_{ox}(μA)	I_{cat}/I_{ox}
NADH 1 mmol l^{-1}			
(a) at a PMS/PPY-2-COOH/electrode			
Au	2.81	0.38	7.4
GC	0.88	0.35	2.5
Pt	2.64	0.36	7.3
(b) at a PMS/PDBH/electrode			
Au	3.12	0.37	8.4
GC	0.94	0.36	2.6
Pt	2.81	0.36	7.8
NADPH 1 mmol l^{-1}			
(a) at a PMS/PPY-2-COOH/electrode			
Au	3.24	0.38	8.5
GC	0.84	0.37	2.3
Pt	3.08	0.34	9.1
(b) at a PMS/PDHB/electrode			
Au	3.28	0.41	8.0
GC	0.83	0.32	2.5
Pt	3.13	0.41	7.6

2.6. Amperometric measurements

Interferences and NAD(P)H were also measured amperometrically at −0.1 V vs. SCE, using Au, Pt, GC electrodes, as follows: the polymer modified electrodes were dipped in a beaker containing 10 ml of phosphate buffer pH 8.1 and allowed to equilibrate at −0.1 V. After 10 min a stable current baseline was observed. Aliquots of NAD(P)H and/or interferences were added and changes in current recorded.

The response of the probe to the interferences and NAD(P)H has been measured weekly for 2 months and normalized to the initial response.

2.7. Electropolymerization with pms in presence of enzyme

The experimental conditions for the electropolymerization of the organic monomers in presence of the enzymes were the same of those carried out in absence of the enzyme.

We used gold and platinum electrodes. The electrodes were rinsed with the buffer solution to remove the non immobilized physically adsorbed PMS and stored in the same solution at 4°C.

The amount of enzyme used was 120 U ml^{-1}, for GDH, 160 U ml^{-1} for LDH and 80 U ml^{-1}, for GlDH.

Lower quantities of enzymes gave a signal current lower than that obtained with the amperometry reported above, higher quantities did not show any increase in current.

Amperometric measurements of glucose, lactate and glutamate were carried out using the procedure described for the NAD(P)H measurements, the difference being in $NAD(P)^+$ 1 mmol l^{-1} in the buffer solution and in the appropriate substrate injection aliquots.

3. Results and discussion

3.1. Electropolymerization studies

In previous works [37,38], we studied the electropolymerization of organic monomers together with oxidase and dehydrogenase enzymes on solid electrodes.

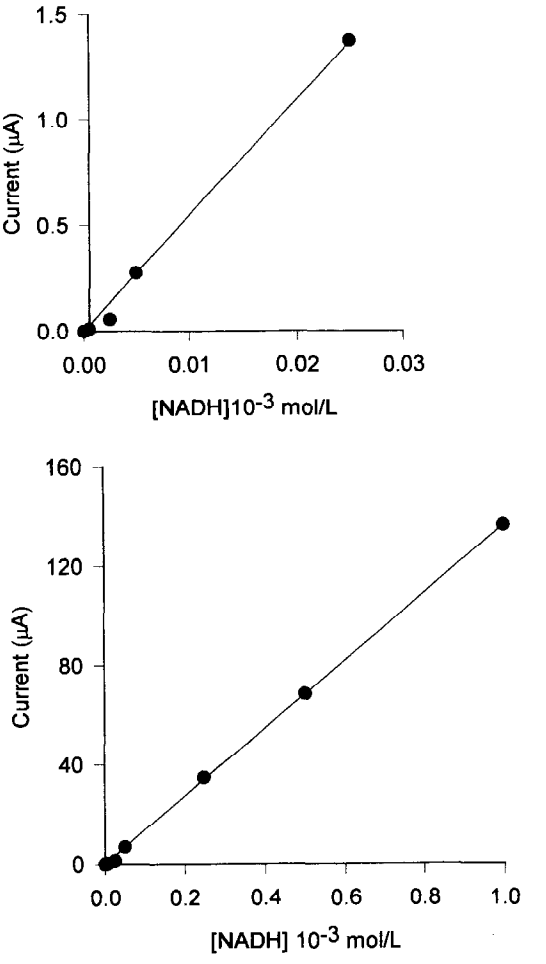

Fig. 3. Calibration curves of NADH at PMS/PPY-2-COOH/Au electrode: electrolyte: phosphate buffer 0.1 mol l^{-1}, pH 8.1; $E = -0.10$ V vs. SCE.

The generic reaction which involves the enzyme and PMS immobilized should have the following sequence:

$$\text{Substrate} + NAD(P)^+ + H^+ \rightarrow \text{Product} + NAD(P)H$$

$$NAD(P)H + PMS_{ox} \rightarrow NAD(P)^+ + PMS_{red} + H^+$$

$$PMS_{red} \rightarrow PMS_{ox} + 2e + 2H^+$$

All these reactions should occur at the electrode surface where the enzyme and PMS are immobilized and they make sense if the electrode surface is protected by the polymer film which should reject compounds electroactive at the potentials used to detect NAD(P)H/PMS mediated reaction.

3.2. Polymeric film formation

The first step of our study was the formation of the polymeric film on the electrode probes. Ascorbic acid was selected as interfering compound guide. Fig. 1 shows the effect of the electropolymerization of PY-2-COOH on a gold electrode. The potential was continuously cycled until a minimum current value was attained.

Results reported in Table 1 refer only to PPY-2-COOH and PDBH: data relative to the other polymers have been reported in previous works [37,38].

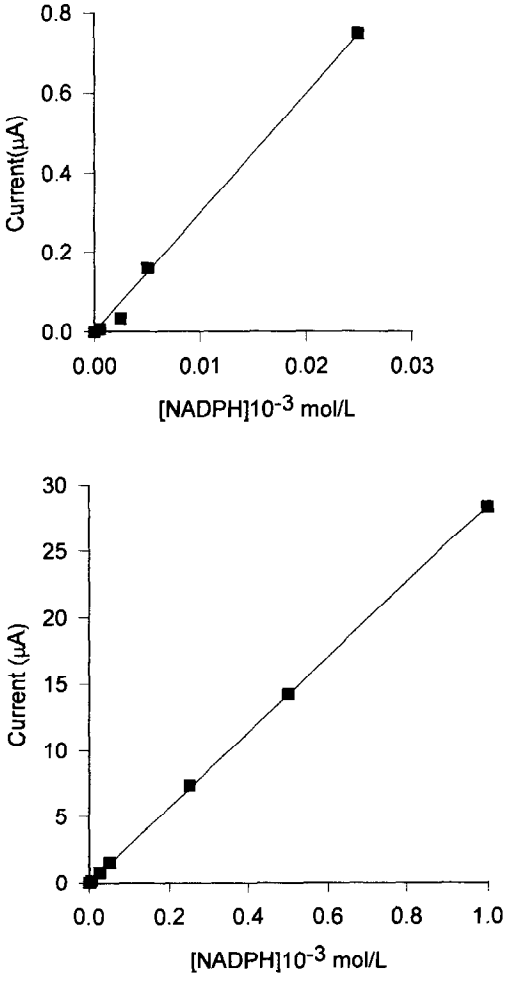

Fig. 4. Calibration curves of NADPH at PMS/PPY-2-COOH/Au electrode: electrolyte: phosphate buffer 0.1 mol l^{-1}, pH 8.1; $E = -0.10$ V vs. SCE.

3.3. Electropolymerization with PMS in absence of enzyme

In the second step the polymerization of the monomers in presence of PMS was carried out. In this case we evaluated the effects of the scan rate, pH and amount of PMS on the electropolymerization process. The optimum scan rate was 2 mV s^{-1}. Higher rates did not result in a mediator entrapment into the polymer [37,38], moreover we could hypothesize an unstable film formation because we observed that the response to ascorbic acid and to the other interferences increased after a week [39,40].

We investigated the ability of PY-2-COOH and DHB to form permselective films in aqueous buffered solution.

The permselectivity in these films can come from the deprotonated carboxylic groups for PPY-2-COOH [41] and from the carbonylic groups for DHB. Unlike the formation of overoxidized polypyrrole film, using these polymers, the overoxidation of the film and the introduction of the carbonyl groups by overoxidation is not needed.

3.4. pH study

The optimum pH value for the electropolymerization in presence of PMS was studied.

The pH value which gave a good result for the PMS electroactivity on the electrode surface was 8.1 and this value was used for further studies.

pH values from 5.6, reported as starting pH for electropolymerization study [42,43], to 7 did not show any entrapment of PMS on the surface of the electrodes. The minimum basic pH which gave a good result for the PMS electroactivity on the electrode surface was 8.1 and this value was used for further studies.

Table 3
Properties of PMS/PPY-2-COOH/enzyme electrodes probes

Enzyme	pH	Linearity range (mol l^{-1})	Slope (mA mmol $^{-1}$ l^{-1})	Response time (s)	Detection limit (mol l^{-1})	Reproducibility rsd% (4 measurements)
LDH	8.1	5×10^{-6}–1×10^{-2}	1.6	4–7	1×10^{-6}	3
GDH	8.1	5×10^{-6}–1×10^{-2}	1.1	5–9	1×10^{-6}	4
GlDH	8.1	5×10^{-6}–1×10^{-2}	1.9	6–10	1×10^{-6}	4

Moreover, this pH value was suitable for a good electropolymerization of PY-2-COOH because the monomer solubility at this pH is higher and the polymer itself shows the required permselectivity since the deprotonated carboxylic groups can repel, negatively charged compounds. Moreover, in the pH range from 5.6 to 7 the solubility of PY-2-COOH monomer is not sufficient to obtain a very compact film.

pH values higher than 8.1 were not used because the enzymes tested for the immobilization are less active at basic pH values (see Sigma Catalogue: pH 7.5 for GDH, pH 7.3 for GlDH and pH 7.5 for LDH).

The PMS amount was varied from 0.8 to 4.0 mmol l^{-1}. From the cyclic voltammetry we observed that the minimum concentration which gave an appreciable analytical signal was 0.8 mmol l^{-1}, then the current peak increased with the concentration of PMS and at a concentration higher than 3 mmol l^{-1} the current peak was constant. So we concluded that the amount of PMS entrapped was also constant.

Fig. 2 shows the voltammetric redox behaviour of PMS entrapped in PPY-2-COOH. Similar results were obtained with PDHB, while poly(1.2-DAB), poly(1.3-DAB) and poly(1.4-DAB) showed that the amount of PMS entrapped into the polymeric structure was not sufficient for the NAD(P)H catalytic oxidation.

The electrochemical behaviour of PMS at solid electrodes has been extensively studied and clarified in a previous paper [30].

In aprotic medium, the PMS reduction involves two quasi-reversible monoelectronic steps, in the potential range from $+0.5$ to -1.5 V.

In aqueous buffered solution, in the range of pH 4–10 a single reversible system is observed at -0.2 V vs. SCE, according to the following mechanism:

$$PMS_{ox} \underset{-2e^-,\ -H^+}{\overset{+2e^-,\ +H^+}{\rightleftarrows}} PMS_{red}$$

Unfortunately, the reduced form of PMS is strongly absorbed on the electrodic surface. Such an absorption disappears when a polymer modified electrode is used.

Table 4
Properties of PMS/PDHB/enzyme electrodes probes

Enzyme	pH	Linearity range (mol l^{-1})	Slope (mA $mmol^{-1}$ l^{-1})	Response time (s)	Detection limit (mol l^{-1})	Reproducibility rsd% (4 measurements)
GDH	8.1	1×10^{-5}–1×10^{-2}	1.4	4–8	5×10^{-6}	4
LDH	8.1	1×10^{-5}–1×10^{-2}	1.3	6–10	5×10^{-6}	3
GlDH	8.5	1×10^{-5}–1×10^{-2}	2.1	6–15	5×10^{-6}	3

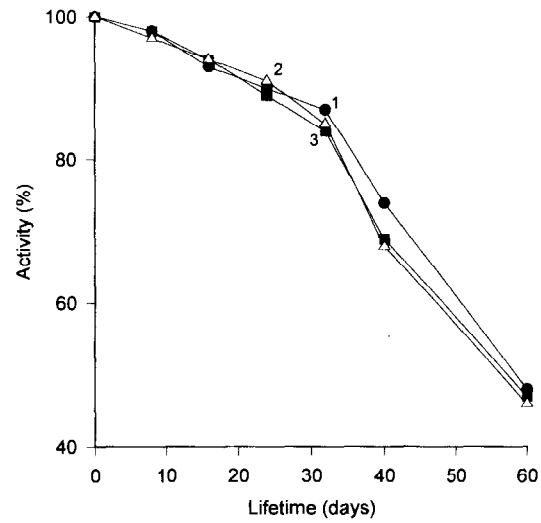

Fig. 5. response vs. time for (1) glucose at GDH/PMS/PPY-2-COOH/Au electrode; (2) lactate at LDH/PMS/PPY-2-COOH/Au electrode; (3) glutamate GLDH/PMS/PPY-2-COOH/Au electrode.

The voltammetric behaviour of PMS in a deaerated solution on a Au/PPY-2-COOH electrode in the range from $+0.5$ to -0.5 V vs. SCE shows a cathodic peak with the complementary anodic one.

The current is proportional to $v^{1/2}$ and to the PMS concentration.

The peak to peak separation (ΔE) is independent from the scan rate and its value of 30 mV is in reasonable agreement with the theoretical value of $56.6/n$ mV if $n=2$ for a two electron reaction.

The voltammetric results of PMS entrapped into the polymer film, showed that the peak to peak separation is similar than that obtained with PMS in solution. Moreover the difference (ΔE) between the anodic and cathodic peak potential is independent from v at low scan rates ($\Delta E \approx 29$ mV at $v = 10$ mV s^{-1}).

The peak current changed linearly with v, as expected for an entrapped redox species [44].

Similar results were obtained using Pt and GC electrodes.

The surface concentration of the electrochemically immobilized PMS on a gold electrode was evaluated by the integration of the peak (cathodic or anodic) and assuming a two electron mecha-

nism for the redox reaction [30]. The result was $(2.81 \pm 0.1) \times 10^{-7}$ mol cm^{-2} which is higher than those relative to PMS adsorbed on an electrode surface [15] or entrapped in a polypyrrole matrix [33].

3.5. NAD(P)H experiments

All the electrodes assembled with PPY-2-COOH or PDHB and PMS have been tested for NAD(P)H by cyclic voltammetry, then amperometrically.

The first step has been the voltammetric study of NAD(P)H with a modified electrode.

Voltammetric scans from -0.5 to $+0.5$ V have been carried out and the peak current was observed at -0.12 V for NADH and -0.14 V for NAD(P)H.

When the concentration of NAD(P)H was increased, the current peak increased linearly up to 1×10^{-2} mol l^{-1}. The peak current observed at -0.12 V for NADH and -0.14 V for NAD(P)H was a demonstration of the mediated reaction between PMS and NAD(P)H (Fig. 2). In fact the NADH oxidation at the naked electrode occurred at a potential around $+0.75$ V and the NADPH oxidation at $+0.77$ V [30] for all the electrodic materials tested.

So we can hypothesize the following mechanism:

$$NAD(P)H + PMS_{ox} \rightarrow NAD(P)^+ + PMS_{red} \quad (1)$$

$$PMS_{red} \rightarrow PMS_{ox} + 2e + 2H^+ \quad (2)$$

Table 2 reports the ratio I_{cat}/I_D of the anodic peak current of the mediator before (I_D) and after (I_{cat}) the injection of NAD(P)H 1 mmol l^{-1}. This was as a criterion for quantifying the electrocatalytic efficiency of NAD(P)H oxidation for different electrodic materials and for different polymeric films. This ratio was almost independent from the polymeric matrix, but strictly related to the electrodic materials, so we selected gold and Pt electrodes for further experiments. The differences observed are unclear and merit further investigation.

Probably, regarding the behaviour of GC, we have to consider different parameters such as the adsorption of PMS on the electrodic surface which lowers the catalytic activity of the mediator.

In fact, in a previous paper [30], we have studied and clarified, by CV, the electrochemical behaviour of PMS on solid electrodes and the trend of electrochemical parameters has indicated that the reduced form of PMS is strongly adsorbed on pyrolytic graphite and glassy carbon electrodes whereas no adsorption was observed on gold and platinum electrodes.

3.6. Amperometry of NAD(P)H

NAD(P)H has been detected in the range 10^{-6}–10^{-2} mol l^{-1} with a detection limit of 5×10^{-7} mol l^{-1}.

Figs. 3 and 4 report two calibration curves of NADH and NADH attained with a modified gold electrode. Same current changes were obtained when NAD(P)H was injected in a solution under Ar atmosphere or in a solution equilibrated with air.

The response time is about 10 s. After 10 h of repetitive measuring a decrease in response of 18% for NADH and of NADPH was observed. We have no direct information on how the mediator is entrapped by the polymer film but, from the data obtained, we can deduce that the mediator reacts rapidly with NAD(P)H so it should be entrapped in the external side of the polymer and the film layer should be sufficiently thin.

Injection of aliquots of paracetamol, uric and ascorbic acid, as reported in the Section 2, did not result in any currents change.

3.7. Electropolymerization in presence of enzyme

Only few examples are reported in the literature [45] of a dehydrogenase enzyme entrapment into a polymeric matrix.

In order to assemble electrochemical dehydrogenase enzyme electrode probes we polymerized the organic monomers (reported in the experimental) in presence of PMS and dehydrogenase enzymes. In this case, since NAD(P)$^+$ acts as cosubstrate for the enzymatic reaction, we used different concentrations of NAD(P)$^+$, to test the efficiency of the enzyme activity. The selected concentration of NAD$^+$ was 1 mmol l^{-1}: lower concentrations

resulted in a lower current output and higher concentrations did not show any increase in the current changes.

Tables 3 and 4 show the results obtained using different electrodes electropolymerized with two monomers together with different enzymes.

The analytical conditions of detection of glucose, lactate and glutamate are also reported in Tables 3 and 4. L-Lactic dehydrogenase type XI is NAD^+ dependent, but not $NADP^+$. In fact aliquots of lactate injected in a solution containing NADP+ did not result in any current change.

3.8. Stability

The probes were stored at 4°C when not in use. Every 10 days consecutive calibration curves were run to test the residual enzyme activity (Fig. 5). For all the probes used the enzyme activity showed a decrease of only 20% over 1 month period, then a more rapid decrease was observed, but a residual activity of about 40% over a period of 2 months was observed for all the three enzymes.

The main reason of the activity loss of the sensors during storage is due to the enzyme activity: this is because the lifetime of PMS/polymer/electrode was stable up to 3 months.

4. Conclusion

This work has shown for the first time the immobilization of dehydrogenase enzymes into non conducting films, together with PMS, thus resulted in the assembling of stable and interference free dehydrogenase enzyme electrode probes. Examples of detection of glucose, lactate and glutamate, showed a promising application for all dehydrogenase enzymes.

Acknowledgements

Authors thank MURST (60% Progetti d'Ateneo) for financial support.

References

[1] A. Schelter-Graf, H.L. Schmidt, H. Huck, Anal. Chim. Acta 163 (1984) 299.
[2] H. Huck, A.J. Schelter-Graf, P. Kirch, H.L. Schmidt, Analyst 109 (1984) 147.
[3] Z. Samec, P.J. Elving, J. Electroanal. Chem. 144 (1983) 217.
[4] L. Gorton, J. Chem. Soc. Faraday Trans. 82 (1986) 1245.
[5] L. Gorton, B. Persson, P.D. Hale, L.I. Boguslavsky, H.I. Karan, H.S. Lee, T.A. Skotheim, H.L. Lan, Y. Okamoto, ACS Symp. Series 487, in: P.G. Edelman, J. Wang (Eds.), Biosensors and Chemical Sensors-Optimizing Performance through Polymeric Materials, vol. 487, American Chem. Soc., Washington, 1992, p. 56.
[6] B.W. Carlson, L.L. Miller, J. Am. Chem. Soc. 105 (1983) 7453.
[7] B.W. Carlson, L.L. Miller, P. Neta, J. Grodkowski, J. Am. Chem. Soc. 106 (1984) 7233.
[8] A. Trazza, R. Andruzzi, I. Carelli, Electrochim. Acta 27 (1982) 347.
[9] M.A. Jansen, P.J. Elving, Biochim. Biophys. Acta 764 (1984) 310.
[10] R.W. Caughlin, M. Aizawa, B.F. Alexander, M. Charles, Biotechnol. Bioeng. 17 (1975) 515.
[11] C.O. Schmakel, K.S.V. Sauthanam, P.J. Elving, J. Am. Chem. Soc. 97 (1975) 5085.
[12] J. Moiroux, P.J. Elving, J. Electroanal. Chem. 102 (1979) 93.
[13] L. Bartalits, G. Nagy, E. Pungor, Anal. Lett. 17 (1984) 13.
[14] A. Torstensson, L. Gorton, J. Electroanal. Chem. 130 (1981) 199.
[15] L. Gorton, G. Johansson, A. Torstensson, J. Electroanal. Chem. 196 (1985) 81.
[16] J. Kulys, V. Bilitewskj, R.D. Schmid, Anal. Lett. 24 (1991) 181.
[17] J. Kulys, G. Gleixner, W. Schumann, H.L. Schmidt, Electroanalysis 5 (1993) 201.
[18] F. Xu, H. Li, S.J. Cross, T.F. Guarr, J. Electroanal. Chem. 368 (1994) 221.
[19] M. Somasunsrum, J. Hall, J.V. Bannister, Anal. Chim. Acta 295 (1994) 47.
[20] M.D. Smith, C.L. Olson, Anal. Chem. 46 (1974) 1544.
[21] C. Degrand, L.L. Miller, J. Am. Chem. Soc. 102 (1980) 5278.
[22] W. Schumann, R. Lammert, B. Uhe, H.L. Schmidt, Sensors Actuators B1 (1990) 537.
[23] W. Schumann, J. Huber, H. Wohlschlager, B. Strehlitz, B. Strehlitz, J. Biotechnol. 27 (1993) 149.
[24] L. Gorton, G. Breule, E. Csoregi, E. Csoregi, G. Jonsson-Petersson, B. Persson, Anal. Chim. Acta 249 (1991) 43.
[25] A.A. Karyakin, E.E. Karyakina, W. Schumann, H.L. Schimdt, Electroanalysis 6 (1994) 821.

[26] S. Cosnier, K. Le Lous, J. Electroanal. Chem. 406 (1996) 243.
[27] F. Pariente, E. Lorenzo, H.D. Abruna, Anal. Chem. 66 (1994) 4337.
[28] F. Pariente, E. Lorenzo, F. Tobalina, H.D. Abruna, Anal. Chem. 67 (1995) 3936.
[29] F. Pariente, F. Tobalina, E. Lorenzo, M. Darder, H.D. Abruna, Anal. Chem. 68 (1996) 3135.
[30] I. Carelli, I. Chiarotto, and A. Curulli, in: Current Topics in Electrochemistry, vol. 3, Ed. Council of Scientific Information Trivandrum, India, 1994, p. 141–57.
[31] O. Miyawaki, T. Yano, Enzyme Microb. Technol. 15 (1993) 197.
[32] B. Grundig, G. Wittstock, U. Rudel, B. Strehlitz, J. Electroanal. Chem. 395 (1995) 143.
[33] S. Yabuki, F. Mizutani, M. Asai, Biosensor and Bioelectronics 6 (1991) 311.
[34] H. Kotte, B. Grundig, K.D. Vorlop, B. Strehlitz, B. Stottmeister, Anal. Chem. 67 (1995) 65.
[35] Z. Zhang, H. Liu, J. Deng, Anal. Chem. 68 (1996) 1632.
[36] A. Capon, R.J. Parson, Electroanal. Chem. 65 (1975) 285.
[37] I. Carelli, I. Chiarotto, A. Curulli, G. Palleschi, Electrochim. Acta 41 (1996) 1793.
[38] A. Curulli, I. Carelli, O. Trischitta, and G. Palleschi submitted for the publication.
[39] S.E. Emr, A.M. Yacynych, Electroanalysis 7 (1995) 913.
[40] A.Q. Zhang, C.Q. Cui, Z.W. Thian, J. Phys. Chem. 7 (2) (1991) 146.
[41] C. Hsueh, A. Brajter-Toth, Anal. Chem. 66 (1994) 2458.
[42] C. Malitesta, F. Palmisano, L. Torsi, P.G. Zambonin, Anal. Chem. 62 (1990) 2735.
[43] R.J. Geise, J.M. Adams, N.J. Barone, A.M. Yacynych, Biosensors and Bioelectronics 6 (1991) 151.
[44] R.W. Murray, in: A.J. Bard (Ed.), Electroanalytical Chemistry, vol. 13, Marcel Dekker, New York, 1984, p. 191.
[45] P.N. Bartlett, J.M. Cooper, J. Electroanal. Chem. 362 (1993) 1.

ELSEVIER

Talanta 44 (1997) 1671–1682

Talanta

Metal-promoted shift of equilibrium between the two fluorescent forms of a synthetic macrocycloureide in view of designing chemical sensors

M. Dumaine-Bouaziz, D. Cordier *, P.R. Coulet

Laboratoire de Génie Enzymatique, UPRESA CNRS 5013, Université Claude Bernard Lyon 1, 43 Bd. du 11 Novembre 1918, 69622 Villeurbanne Cedex, France

Received 31 July 1996; received in revised form 24 February 1997; accepted 26 February 1997

Abstract

The emergence of the fiber-optic sensor era has stimulated investigations to create synthetic fluororeceptors capable of signaling the binding of metal ions. To fulfill this purpose, a new concept is presented: the metal-promoted shift of equilibrium between the two fluorescent forms of a synthetic receptor able to dimerize and to specifically recognize a metal ion by multiple non-covalent bonds. The thermodynamics of the dimerization itself and the dimer–zinc interactions are analyzed in terms of association constants. It is demonstrated that finely tuning the equilibrium between the monomeric and dimeric forms by controlling the pH, permits the alternate selective recognition and signaling of zinc or cadmium. © 1997 Elsevier Science B.V.

Keywords: Chemical sensors; Dimerization; Synthetic fluororeceptors

1. Introduction

For several years, there has been growing concern about heavy metals in the biosphere. Selenium, cadmium, mercury and lead are presently the most dangerous, owing to their increasing anthropogenic discharge in the environment and to their high toxicity. Although of less toxicity, copper, zinc and molybdenum are likely to pose a threat. The heavy metal pollution points out the need for reliable, fast and low-cost means for their aqueous detection.

Concerning zinc, the global excess burden on the environment due to mankind's activities is actually the result of smelting, refining and manufacturing processes, but domestic waste waters are also important sources and consequently high local concentrations are probable, especially in aquatic ecosystems [1]. According to its role as a cofactor of various enzymes, zinc is known as an important oligonutrient with strong physiological implications. Among others, including iron and manganese, the level of zinc is of importance in seawater [2,3] since this metal meets the needs of many species for survival, and for the productivity of plankton [4]. Therefore, it is not surprising that

* Corresponding author. E-mail: cordiesy@cismibm.univ-lyon1.fr.

PII S0039-9140(97)00072-6

several zinc measurement methods have been recently proposed, most of them combining, for instance, flow-injection analysis with an ion-exchange resin and fluorescence [3,5], or high-performance liquid chromatography (HPLC) and light absorption [6], or diffusive gradients in thin films and atomic absorption spectroscopy [7]. Besides, the function of zinc as a cofactor in enzymatic catalysis has been utilized in the design of enzyme-based zinc optical biosensors [2,8].

In parallel to the development of amperometric and optical biosensors [9], our group is now involved in the design and the study of stable artificial receptors for molecular recognition [10,11] with the purpose of elaborating new sensing layers usable in optodes (optical devices, by analogy with electrodes) for determining transition metal ions in water. A challenging goal is to get a signal, for instance fluorescent, when molecular recognition occurs. A previous work resulted in the synthesis of a promising water-soluble receptor, i.e., a macrocycloureide able to form a dimer at alkaline pH. Both the monomer and the dimer have distinctive fluorescence emission spectra. The dimer specifically complexes the zinc ion and the complexation induces a shift in the equilibrium between the monomer and dimer forms towards the dimer form. A fluorescence signal may thus be monitored which is the result of the (excited) dimer emission enhancement.

Basically, this is a metal-promoted shift of equilibrium between the two fluorescent forms of a receptor able to dimerize and specifically recognize a metal ion in water through a supramolecular process.

The emergence of the fiber-optic instrumentation, and the need for detection and quantification of heavy metals, in addition to the increasing interest of biologists for possible applications in their domain, have stimulated continuous investigations on artificial fluororeceptors able to complex metal ions with useful selectivity [12,13].

In the present article, an alternative to ion-promoted chelation-enhanced fluorescence (CHEF), at the origin of fluorescent chemosensors [13], is proposed for the detection of metal ion complexation.

2. Experimental procedure

2.1. Synthesis of the receptor

The synthesis of the macrocycloureide has been described elsewhere [10]. Starting from this procedure, the protocol has been improved to lead to the following accelerated process: in a typical experiment, trimethyl aluminium (1.12 cm^3 of a 2 M solution in hexanes, i.e., 2.24 mmol) was added in a closed vessel under nitrogen to 10 cm^3 of dry chloroform. The mixture was cooled down to $-10°C$ with salt and ice and 134 μl (1.12 mmol) of 1,5-diaminopentane were slowly added with a syringe through a septum. The mixture was stirred for 20 min at $-10°C$ and then for 45 min at room temperature. After addition of 160 cm^3 of dry chloroform, the temperature of the mixture was increased to 0°C and a solution of tetramethyl 2,2′-ureylenediterephthalate (100 mg, 0.225 mmol, synthesized in a previous step [10]) in chloroform (30 cm^3) was rapidly added. The reaction mixture was stirred overnight in an ice bath under nitrogen and then for 4 h at 50°C. After reaction, the chloroform was evaporated under vacuum. The product was redissolved in methanol and by-products were filtered off. The filtrate was dried under vacuum and redissolved in 20 cm^3 of a 50 mM sodium phosphate buffer, pH 6. Insoluble by-products were filtered off and colored residues were removed by a charcoal treatment. After filtration and evaporation of the water, the product was dried under vacuum, enabling 39 mg (0.081 mmol, 36%) of a white solid to be obtained.

2.2. ^1H-NMR studies

For the 300-MHz ^1H-NMR (nuclear magnetic resonance) experiments, the conditions were the following: a concentrated solution of the macrocycloureide in water was diluted with a 50 mM buffer solution (with phosphate at pH 6, borate at pH 9 and carbonate at pH 10, 11 and 12) to obtain 0.6 ml of a macrocycle solution at 2 mM concentration. The solution was then evaporated and dissolved six times with D_2O, under nitrogen, taken again by 0.6 ml D_2O and transferred in an

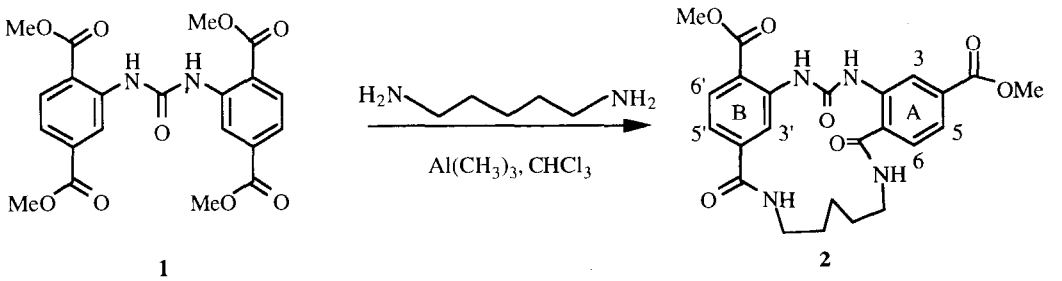

1 2

Fig. 1. Building-up and structure of the fluororeceptor **2** (for details see Section 2).

NMR tube for the analysis. All proton signals were stable within the NMR time scale.

2.3. Fluorescence measurements

The macrocycle complexation was monitored in aqueous solution by recording the increase in fluorescence emission of either the dimer (at 432 nm for the zinc complexation with excitation at 356 nm) or the monomer (at 380 nm for the cadmium complexation with excitation at 332 nm). The complexation of metal ions occurred when aliquots (1 or 2 μl) of the zinc or cadmium chloride solution were added and mixed in the cuvette with the macrocycle solution (concentration: 0.1–1 mM), in 50 mM sodium phosphate buffer (PO_4^{3-}/HPO_4^{2-}), pH 12, for zinc, or 50 mM carbonate buffer, pH 9.5, for cadmium. The equilibria of dimerization and complexation of metal ions were stable, as verified by the steady state of the fluorescence signal when monitored for several minutes.

2.4. Potentiometric pH and conductometry titrations

The macrocycloureide obtained by the synthesis described above was flash-chromatographed on silica with dichloromethane 80/methanol 20 as the eluent. After careful calibration, pH and conductance were measured and monitored in 1 cm^3 of a 15-mM macrocycloureide aqueous solution in which aliquots (1 μl) of a carbonate-free 1 M NaOH aqueous solution were successively added and mixed with an automatic pipette. All samples were extemporaneously prepared. The solution temperature was maintained at 25.0 ± 0.1°C. The NaOH concentration was determined by automatic titration with phthalic acid. The cell constant of the conductometry cell was previously adjusted to 12.88 mS cm^{-1}, using a 0.1 M KCl solution. Data were corrected for the volume addition.

3. Results

3.1. Structure and ionization properties of the fluororeceptor

The structure of the receptor is asymmetrical, bearing no chiral center (Fig. 1). Such a type of molecule is known to potentially recognize chiral guests. This property is not imperative in the perspective of metal ions recognition but was retained for further building of structures with increased complexity from this molecule. To achieve this goal starting from a symmetrical bis-substituted urea, the synthetic plan revolved around the regioselectivity of the cyclization of the tetramethyl 2,2′-ureylenediterephthalate with the 1,5-diaminopentane: owing to the length of the five-membered arm of the diamine, the cyclization between an *o*-methyl and a *m*-methyl ester group could only occur after rotation about the Ar–NH bonds.

Another characteristic of the receptor is that it implies a macrocyclophane combining urea and benzamide units. Clearly the amide group is paramount in the natural recognition and folding

processes that involve proteins, and the urea group has proven to be a powerful ligating moiety, as demonstrated in spherands containing cyclic urea units [14] or as a substrate in supramolecular processes through hydrogen bonding interactions [15]. These two types of chemical groups have been chosen as metal-binding elements of the fluororeceptor. Their presence in the chemical structure is also at the base of the properties of the molecule concerning its solubility and dimerization.

The fluororeceptor dimerizes in aqueous solution [10] and is then able to complex zinc. Such a spontaneous self-assembling leading to a dimer in water is not surprising with a molecule bearing aryl rings since association constants of arenes in water are usually large, owing to the favored $\pi-\pi$ interactions [16]. An interesting characteristic concerning the phenomenon of dimerization of this receptor is its modulation by the pH [11] and, hence, the formation of the dimer of **2** in water was first investigated by monitoring the fluorescence emission of the molecule under various pH conditions. Its behavior is characteristic of the formation of an intermolecular excited dimer at alkaline pH [17]: red shifting (380 → 432 nm) of the emission maximum and decreasing of the emission intensity, finally lowered at pH 11 to 60% of the initial value at pH 6. The amplitude of the red shift is indicative of a tight dimer formation which is stabilized by $\pi-\pi$ (hydrophobic) and

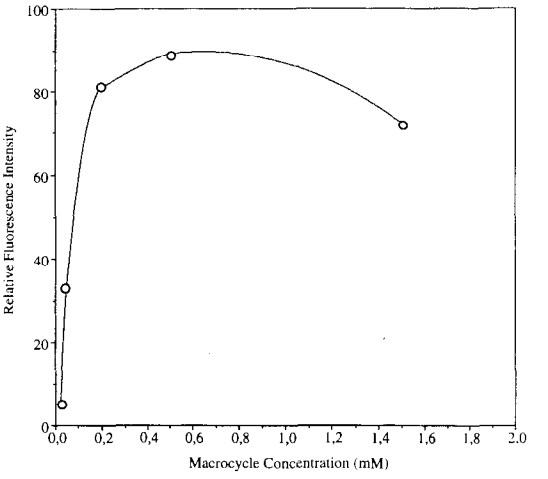

Fig. 2. Relative fluorescence intensity of an alkaline solution of the dimer as a function of its concentration ($\lambda_{ex} = 356$ nm, $\lambda_{em} = 432$ nm). Solvent: 50 mM aqueous sodium phosphate buffer (PO_4^{3-}/HPO_4^{2-}), pH 12.

polar interactions in alkaline medium. Fig. 2 illustrates the effect of the dimer concentration on the measure of the fluorescence intensity at pH 12. The curve exhibits the classical shape of the fluorescence versus concentration of any fluorophore solution: first increasing with a maximum steady level and then decreasing, owing to the concentration quenching which causes a fluorescence loss that is called the inner cell effect.

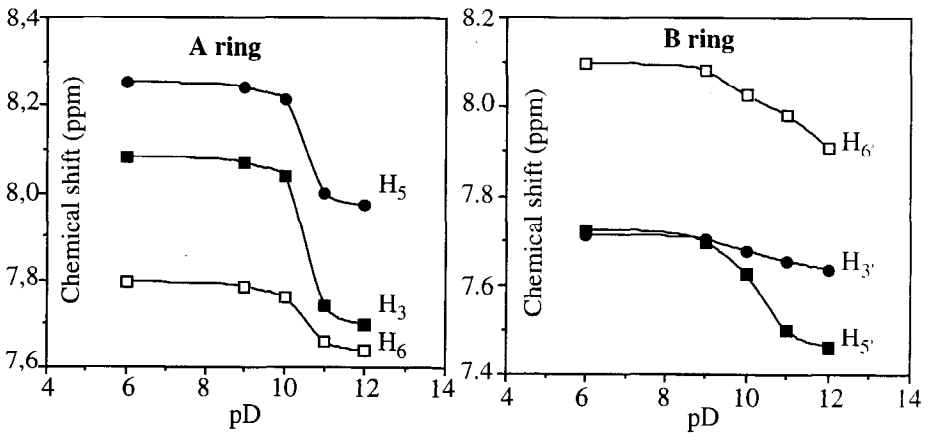

Fig. 3. Chemical shift of the aromatic protons of the two rings of **2** as a function of the pD; ([c] = 2 mM; 298 K).

Additional information required for a better comprehension of the dimerization process may be conveniently found by ^{1}H-NMR. Fig. 3, related to 300-MHz ^{1}H-NMR studies in parallel, shows the chemical shifts of the aromatic protons of the benzene rings A and B of fluororeceptor **2**, plotted as a function of the pD. All the signals are high-field shifted upon raising the pD of the medium. The well-defined discontinuity in the curves, approximately at the same pD value, characterizes the almost entire transformation of **2** into the dimer form. Below pD 9, the monomer form is predominant. Between pD 9 and 10, the monomer coexists with the dimer and the signals of the three protons of the A ring in the monomer are distinct from those of the dimer. All the signals of the A ring protons of the monomer coalesce with those of the dimer on and after pD 11. The simultaneous upfield shift of all the aromatic resonances upon alkalinization of the aqueous medium should be related to the dimerization of the receptor observed through the fluorescence change in the same conditions. The upfield shift of the resonances of the aromatic protons is usually the signature of a confinement of the nuclei in close proximity [18,19]. Hence these spectroscopic results indicate that the dimerization process occurs probably by a π-stacking process of the aromatic moieties of the molecules.

Taking into account the data of the NMR and fluorescence measurements, we inferred that a deprotonation of the molecule occurs at alkaline pH and thus we investigated the ionization behavior of the macrocycloureide, using a combination of potentiometry and conductometry techniques. With the macrocycloureide, the difficulty is increased by its insolubility above 20 mM in alkaline aqueous medium and, consequently, the pH measurements were made at 15 mM concentration. Furthermore, the weak acid–strong base titrations with a pH meter are highly inaccurate when the pK_a of the acid is high, especially when the solution is diluted, owing to the very gradual change of the pH around the equivalence point. Conductometry, under proper circumstances, can eliminate or at least minimize this problem. This is exemplified in Fig. 4, a typical titration curve of the macrocycle obtained by this method, in which

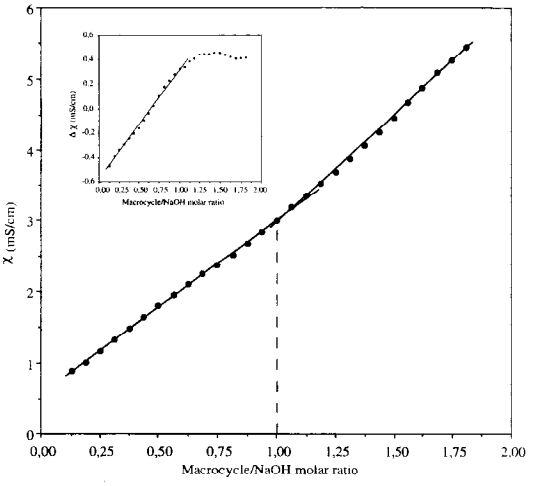

Fig. 4. Conductometric titration of a 15 mM solution of the macrocycloureide in water by a molar NaOH solution. Inset: differential conductivity between the 15 mM macrocycle solution and pure water as a function of the macrocycle/NaOH ratio.

the inset shown is obtained by subtraction of the values obtained with a 15 mM macrocycle solution to the values obtained with the water alone. It evidences the equivalence point obtained at 1 mole of sodium hydroxide per mole of macrocycle. Using the same experimental conditions with a pH meter, it was thus possible to measure the pH values at both the starting point and the semi-equivalence point of the titration. Computation led to an estimation of $pK_a = 12.4 \pm 0.7$. This value of the pK_a indicates that the macrocycloureide is a strong base, i.e., it is largely protonated in aqueous solution. Another point to be noted is the conductance of the 15 mM macrocycle solution which is significantly different from zero (0.72 ± 0.06 mS cm^{-1}) so that the solute should be a charged and very weak acid. These characteristics and data lead to the idea that the protonated macrocycle should be in a cationic form, MH^+. Among the chemical groups of the molecule which could act as an electron-donating group, the strongly basic carbonyl oxygen of the urea bridge is a good candidate (see Fig. 1). Its basicity is enhanced by the large dipole moment of the urea (4.6 D in unsubstituted urea) and the phenyl groups, which are directly connected to the

nitrogen atoms, could stabilize the cationic charge of the protonated molecule by a resonance effect through their π electrons. Another argument in favor of the implication of the urea group may be found in Fig. 3, which shows the largest high-field shift for the H_3 proton of the A ring of the molecule. This proton is in the closest vicinity of the urea group, pointing outside the molecule, and thus is not surrounded by other interacting chemical groups, like in the case of the H_3' proton. The largest pH-dependent chemical shift of the nuclei which is in proximity to the proton-binding site reflects undoubtedly its protonation state. A possible complementary intervening occurrence of the oxygen atom of one of the two amide bonds and of some water molecules, through a cluster involving hydrogen bonding, must also not be excluded.

3.2. Dimerization

Both NMR and fluorescence methods were used to determine the monomer (**2**) and dimer (**2·2**) concentrations at each pH value. At 298 K, the equilibrium of dimerization at the different pH values was almost instantaneously reached, as deduced from the monitoring of the fluorescence signal for several minutes. Therefore, association constants (K_{ass}, M^{-1}) and $-\Delta G^0$ values at 298 K for the equilibrium $\mathbf{2} + \mathbf{2} \rightleftarrows \mathbf{2 \cdot 2}$ were computed by employing the two methods. The monomer concentration at each pH value was calculated using limiting monomer peaks areas of both the Me protons and H_5 NMR signals and limiting fluorescence emission intensity of the monomer. Limiting values were estimated by extrapolation to pH 0 from the plots of the peaks areas or emission intensity of the monomer as a function of pH. K_{ass} values obtained by both methods were in good agreement and, hence, the mean values of K_{ass} and their corresponding errors could be computed.

The values vary with the pH, as summarized in Table 1, showing a large increase of K_{ass} at alkaline pH. On the other hand, it was observed that the dimer is thoroughly soluble in chloroform (though slightly soluble in alkaline aqueous medium where it forms aggregates above 20 mM [10]), whereas the monomer is especially soluble in water. This is the result of increased hydrophobic interactions between the molecules of **2** upon alkalinization of the medium. In water, these interactions shift $\mathbf{2} + \mathbf{2} \rightleftarrows \mathbf{2 \cdot 2}$ on right, increasing the dimer form, which is much less soluble in water. The dimer is soluble in chloroform because chloroform is a less polar solvent than water: its dielectric constant is only 4.806 against 78.5 for water. The monomer **2** has a structure which shows that two kinds of interactions may be expected: the ionic interactions, when the macrocycloureide is protonated, and the $\pi-\pi$ interactions, through the two aromatic rings. The large difference in the free binding energy ($\Delta\Delta G^0 = 4$ kcal mol^{-1}), observed in water upon raising the pH from 6 to 11, may be attributable to the enhancement of the strong aromatic interactions between two molecules of **2**, when the deprotonation of the macrocycloureide, decreasing the ionic interactions, turns the balance toward the $\pi-\pi$ interactions. The subsequent dimerization of **2** should also be largely favored by the desolvation, a consequence of the increased hydrophobicity of the molecule.

With the view to evaluating the effects of protonation (charge effect) and the effects of the van der Waals forces (hydrophobic effect) on the dimerization process, the solvent dependence of the binding strength in the dimerization was investigated at alkaline pH, using mixtures of 50 mM, pH 11 carbonate buffer and 1,4-dioxane. The latter was chosen owing to its miscibility with water and its very low dielectric constant (2.209). The polarity of such a mixed solvent may be easily modulated by changing the dioxane/buffer ratio. If the aromatic interactions are predomi-

Table 1
Association constants and free energy changes at 298 K of the dimerization of **2** as a function of the pH

pH	K_{ass} (M^{-1})	$-\Delta G^0$ (kcal mol^{-1})
6	137 ± 40%	3
9	1500 ± 40%	4
10	16 000 ± 30%	6
11	270 000 ± 30%	7

nant in the homodimer formation at alkaline pH, $2 + 2 \rightleftarrows 2 \cdot 2$ should be shifted to the left when the dioxane content increases, owing to enhanced competition between the dimer formation and the solvation of the deprotonated monomers by the dioxane. This is indeed what is observed. The electronic absorption spectrum of the monomer exhibits a maximum et 334 ± 1 nm that does not vary, even at a high dioxane ratio, whereas upon raising the dioxane proportion, the dimer maximum at 356 ± 1 nm in aqueous medium is progressively shifted to the monomer maximum absorption: at 84% 1,4-dioxane, almost all the dimer is dissociated. These results lead to the assumption that upon decreasing the polarity of the mixture of solvents, the dimer progressively dissociates, shifting the equilibrium toward the monomer form, which at alkaline pH is better solvated by dioxane than by water, owing to the increasing hydrophobicity of the macrocycle at alkaline pH (a consequence of the deprotonation of the amide and urea moieties). In other words, the competition between solvation (association of the monomer with the solvent) and dimerization (association of two monomers) turns to the advantage of the former when water is replaced by dioxane as a solvent.

The study of the thermodynamics of the dimerization reaction was found to be a useful way to investigate the part of the solvent during the dimerization process. Using ^{1}H-NMR data, values of K_{ass} (M^{-1}) for **2** dimerization at pH 11 changed with temperature as follows: 222 590 (308 K); 174 520 (318 K); 130 690 (328 K); 108 270 (338 K). The van't Hoff plot least-squares line ($\ln K_{ass} = -\Delta H^0/RT + \Delta S^0/R$, $r = 0.99$) of the data provided $\Delta H^0 = -5 \pm 2$ kcal mol^{-1} and $\Delta S^0 = 9 \pm 6$ eu. This behavior is similar to that found for complexation of substituted benzene guests by cyclophanes in water [20]. Calculating the free energy change at pH 11 and 298 K employing the equation $\Delta G^0 = \Delta H^0 - T\,\Delta S^0$ with ΔH^0 and ΔS^0 obtained by the van't Hoff analysis, leads to a value (-8 kcal mol^{-1}) in good agreement with the value of ΔG^0 at pH 11 obtained from of the association constant (Table 1).

A comparison between the enthalpy and entropy changes, taking into account the errors, leads to the conclusion that this is a predominantly enthalpy-driven process, which is probably the result of many van der Waals contacts between the two monomer units (the hydrophobic effect). Nevertheless, the van't Hoff plot least-squares line shows that the entropy dimerization term is not negligible and this signifies that the free energy change of the reaction is enhanced by the decollection of many solvent molecules from the macrocycle (they return to a less ordered state, enhancing the global entropy of the system). This desolvation of the macrocycle largely pays the entropy cost of the association of monomers units. In other words, the entropy gain, owing to the difference between the water molecules that solvate the monomer and those that solvate the dimer, amply pays the entropy cost of the association of the monomer into an homodimer. This observation completes and confirms the results obtained by forcing the equilibria by means of mixture of solvents. The dimerization mainly appears to be the consequence of two phenomena: first the deprotonation of the macrocycle leads to increased π–π interactions which give rise to stacking between aromatic parts of two monomer units (this is supported by the ^{1}H-NMR data in Fig. 3) and secondly, in parallel, the solvation by water decreases, owing to the non-ionic character of the macrocycle.

3.3. Analysis of dimer–zinc(II) interactions

The complexation of the zinc ion with the macrocycloureide occurs through a two-step process: a first equilibrium (Eq. (1)) involves the monomer and the dimer, and a second equilibrium (Eq. (2)) leads to the complex between the dimer and the zinc ion, keeping in mind that one zinc ion is associated with one molecule of dimer [11]. The equilibria and equations are considered to take place in the buffer region and to be reached and stable before the measurement. For simplification, charges and associated water are omitted in the following equilibria:

$$\mathbf{2} + \mathbf{2} \rightleftarrows \mathbf{2 \cdot 2} \quad (1)$$

$$\mathbf{2 \cdot 2} + \mathbf{Zn} \rightleftarrows \mathbf{2 \cdot 2 \cdot Zn} \quad (2)$$

The association constant of Eq. (1) has been determined at pH 11 (Table 1). The shift of Eq. (2) to the right is favored at pH > 10. This property of the interactions between the metal ion and the dimer has been utilized to quantify zinc at pH 12. Thus, determination of the association constant K_{Zn} between zinc and the dimer should be of interest. Since the equilibrium (Eq. (2)) is dependent on Eq. (1), both the association constants must be determined in the same physico-chemical conditions. However, it was not possible to determine with enough accuracy the association constant of Eq. (1) at pH 12, owing to the very low NMR signals then obtained. This led us to calculate the association constant of the dimer with zinc at pH 11. As pointed out below, the other metal ions which were tested do not bind significantly with the dimer at pH 12.

At the equilibrium, the ratio of the concentration of the dimer–zinc complex [**2·2·Zn**] to the product of the concentrations of the free dimer [**2·2**] and free zinc [**Zn**] defines the association constant K_{Zn}

$$K_{Zn} = \frac{[\mathbf{2\cdot 2\cdot Zn}]}{[\mathbf{2\cdot 2}][\mathbf{Zn}]} \quad (3)$$

Similarly, the equilibrium constant of Eq. (1) is

$$K_{ass} = \frac{[\mathbf{2\cdot 2}]}{[\mathbf{2}]^2} \quad (4)$$

The zinc and macrocycle mass balance leads to the two following equations at equilibrium:

$$[\mathbf{Zn}] + [\mathbf{2\cdot 2\cdot Zn}] = [\mathbf{Zn}]_{Tot} \quad (5)$$

$$\frac{[\mathbf{2}]}{2} + [\mathbf{2\cdot 2}] + [\mathbf{2\cdot 2\cdot Zn}] = \frac{[\mathbf{2}]_{Tot}}{2} \quad (6)$$

where $[\mathbf{Zn}]_{Tot}$ and $[\mathbf{2}]_{Tot}$, are respectively the initial total zinc and macrocycloureide concentrations. At equilibrium and fixed pH, between 0 and 1 mol zinc added per mole of dimer, [**2·2**] and [**2·2·Zn**] depend solely on the amount of zinc. These two variables are related to the increase of the fluorescence emission of the dimer upon addition of zinc ions. Hence, it is possible, knowing the amount of dimer before the addition of zinc, to estimate the amount of total dimer at equilibrium. This leads to the following last equation:

$$\frac{[\mathbf{2\cdot 2\cdot Zn}] + [\mathbf{2\cdot 2}]}{[\mathbf{Zn}] + [\mathbf{2\cdot 2\cdot Zn}]} = \frac{[\mathbf{2\cdot 2}]_0 + [\mathbf{2\cdot 2}]_{Sh}}{[\mathbf{Zn}]_{Tot}} \quad (7)$$

where $[\mathbf{2\cdot 2}]_0$ is the dimer concentration before the addition of zinc (Eq. (1)) and $[\mathbf{2\cdot 2}]_{Sh}$ is the increase of the dimer concentration induced by the shift of Eq. (2) upon zinc addition. This last parameter may be deduced from the least-square straight line of the dimer emission increase as a function of the amount of zinc added at pH 11 ($y = 98.49 + 52.99x$: y is relative fluorescence intensity, x is mole zinc added per mole macrocycloureide, $r = 0.98$).

Accordingly, numerical values are ascribed to the known parameters: $K_{ass} = 2.7 \times 10^5$ M^{-1}, $[\mathbf{2}]_{Tot} = 1 \times 10^{-4}$ M, $[\mathbf{Zn}]_{Tot} = 0.25 \times 10^{-4}$ M, $[\mathbf{2\cdot 2}]_{Sh} = 5.86 \times 10^{-6}$ M. Solving the system of Eqs. (3)–(7) gives the following concentrations at equilibrium of the system: $[\mathbf{2\cdot 2}] = 3.8 \times 10^{-5}$ M, $[\mathbf{Zn}] = 1.91 \times 10^{-5}$ M, $[\mathbf{2}] = 1.19 \times 10^{-5}$ M and $[\mathbf{2\cdot 2\cdot Zn}] = 0.59 \times 10^{-5}$ M. The association constant of the dimer with zinc at pH 11 is $K_{Zn} = 8 \times 10^3$ M^{-1}. This value is in close agreement with those reported elsewhere for complexes of zinc with imidazole-containing peptides derivatives [21,22].

3.4. Quantitative signaling of the complexation of metal ions

The shift of equilibrium of dimerization depends on the complexation of a metal ion by either the monomer or the dimer species. This property may be utilized to finely tune the conditions of the specific measurement of a metal ion. The dimer is formed at alkaline pH with two molecules of the fluororeceptor which associate at a relatively large distance, and this ensemble offers coordination possibilities for three of the four bonds of a tetrahedral ion (ion B in Fig. 5), the last one involving an external anion like a chloride ion. For instance, the dimer has the ability to form a complex with an ion that may be Zn(II), which is a tetrahedral coordinated ion [10]. With the optimal conditions for a B ion complexation, no A ion recognition signal is delivered, partly because the complexation of the B ion makes the receptor unable to recognize the A ion. This is exemplified by the inability of the Cd(II) ion to

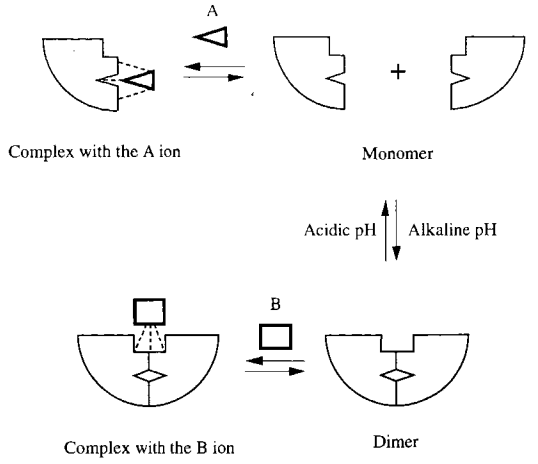

Fig. 5. Schematic representation of the selective complexation of the metal ions A and B with either the monomer or the dimer of the fluororeceptor whose equilibrium is first modulated by the pH. The A ion may be Cd(II) and the B ion may be Zn(II). Both the monomer and the dimer forms are fluorescent with different maximum emission wavelengths.

give a complexation signal with the fluororeceptor in the conditions of the recognition of the Zn(II) ion at pH 12. Cd(II) has the same coordination type as Zn(II) but has a larger ionic radius (0.92 Å instead of 0.74 Å). Conversely, there is no Zn(II) complexation with the monomer, which is able to recognize the Cd(II) ion in moderate alkaline pH conditions (pH 9.5).

Hence, in this example, for a signal of complexation to be delivered by the receptor, the amount of dimer must be significant, the ionic radius of the metal ion must fit with the available space between the two elements of the dimer and, finally, the coordination type of the metal ion should be recognized by the dimer. More generally, modifying the protonation of the molecule through the pH of the aqueous medium allows both the coordination geometry and the amount of receptor to be controlled, by the dimerization process. Since the coordination geometry together with the ionic radius is at the basis of the recognition process of the metal ion and since the fluorescence response is determined by the amount of the fluorescent species, one has the means to modulate both the receptor specificity for a given metal ion and the amplitude of the fluorescence signal.

3.5. Selectivity of the receptor

The specificity of the complexation governs the selectivity of the receptor. The specificity for zinc is illustrated by comparison with cadmium. No dimer emission enhancement can be obtained with this metal at pH 12. Further investigations on the protonation of the receptor have shown that a cadmium measurement was possible, using the monomer as the recognition element at pH 9.5, but the stoichiometry and equilibria of the complex receptor/cadmium are more complicated then in the case of zinc, probably owing to the intervention of water in multiple equilibria. Nevertheless determining the Cd(II) amount is possible upon the addition of the metal, by measurement of the slight increase of the fluorescence signal at the maximum emission wavelength of the monomer. The response is linear for the concentration range 75–375 μM. In the same conditions, no increase of the fluorescence of the monomer occurred with the Zn(II), Cu(II) and Hg(II) ions. An illustration of the differential response for cadmium and zinc is presented in Fig. 6. The slope of the straight line for zinc is much more important than for cadmium but the addition of

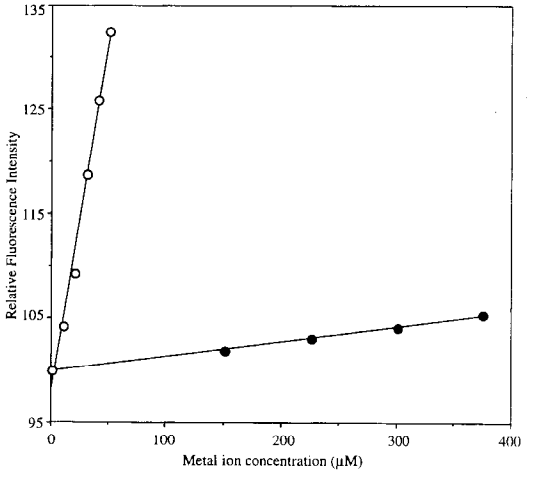

Fig. 6. Relative fluorescence intensity of the fluororeceptor as a function of metal ion concentration: (○) Zn(II), pH 12, $\lambda_{ex} = 356$ nm, $\lambda_{em} = 432$ nm, dimer emission); (●) Cd(II), pH 9.5, $\lambda_{ex} = 332$ nm, $\lambda_{em} = 380$ nm, monomer emission). Fluororeceptor concentration: 0.1 mM.

Table 2
Effect of interfering metal ions on the accuracy of the measure during the determination of 10, 20, 30, 40 and 50 μM zinc in phosphate buffer at pH 12 with the fluororeceptor concentration fixed at 0.2 mM

Interferent	Zinc conc. (μM)	Error (%) at 15 μM conc. of interferent	Error (%) at 100 μM conc. of interferent
Cd(II)	10	−1.8	0.9
Cu(II)	10	−2.5	−1.1
Hg(II)	10	0.0	0.9
Cd(II)	20	−1.5	0.6
Cu(II)	20	−2.4	−1.3
Hg(II)	20	0.3	0.4
Cd(II)	30	−3.8	−0.3
Cu(II)	30	−3.4	−2.2
Hg(II)	30	2.2	0.8
Cd(II)	40	−5.6	−1.1
Cu(II)	40	−3.9	−3.6
Hg(II)	40	2.3	−0.6
Cd(II)	50	−4.6	−0.6
Cu(II)	50	−2.8	−3.8
Hg(II)	50	4.9	0.8

the latter distinctly stresses the shift of the monomer/dimer equilibrium toward the monomer form. It is clear, however, that from an analytical point of view, the 5% amplitude variation observed in the range 75–375 μM, although reproducible, is not large enough. Fig. 6 exemplifies the utilization of the metal-promoted shift of equilibrium between the two fluorescent forms of a receptor and demonstrates that the conditions of the recognition may be adjusted to adapt to different ions. Preliminary results obtained in parallel with Cu(II) confirm this possibility (data not shown).

The selectivity of the zinc fluororeceptor (dimer at pH 12) was investigated by measuring the error on the determination of 10, 20, 30, 40 and 50 μM zinc ions mixed with 15 and 100 μM cadmium, copper or mercury ions. This panel of divalent metals was chosen with regard to their representativeness concerning their coordination type and size: cadmium displays predominantly the same geometry as zinc but is larger, copper has the same radius (0.71 Å) but is rather square coordinated and mercury, predominantly, has linear coordination with an ionic radius of 0.83 Å [23]. Mean results (six replicates in each case) are summarized in Table 2.

Since, for zinc measurement, the signal is correlated to the increase of the amount of dimer, a positive effect is the result of an interaction of the interfering ion with the receptor, thus shifting the dimer amount at a higher level. An opposite effect of the interferent species leads to a negative error. Cadmium, which forms a complex with the monomer, slightly decreases the signal then obtained. Copper has the same effect, while mercury causes an increase of the signal. Given the precision of the zinc measurement at 20 μM (1.5%, see below), the results point to no significant effect (e.g., $>3\%$) of the three interferents at 20 μM zinc concentration for both the interferent concentrations. With the other four zinc concentrations that were tested, the errors seem to be less important at 100 μM interferents concentration than at 15 μM. If this difference is significant, it might be explained by the effect of the interferents on the stability of the zinc–fluororeceptor complex, through a mechanism that remains to be determined.

Globally, the selectivity for zinc appears satisfying since at both 15 and 100 μM concentration of interferents, the errors are within 5%, except for the slightly higher value for 40 μM zinc in the presence of 15 μM cadmium. As pointed out

above, pH is the crucial variable that permits one to drive the specificity of the complexation for a given ion. Hence, defined conditions allow the metal-promoted shift of equilibrium to be initiated by the complexation of the ion, either with the monomer or with the dimer and this particular feature explains the performance in terms of selectivity of the fluororeceptor.

3.6. Detection limit and accuracy of the zinc measurement

Concerning these important parameters of a metal dosage, the zinc measurement at pH 12 with the fluororeceptor gave the following results: the fluorescence response was linear ($r = 0.99$, $n = 6$) from 5 to 50 μM added zinc, for a fluororeceptor concentration of 0.2 mM. The precision, based on the repeated analysis of samples containing 20 μM Zn, was 1.5% ($n = 6$). The detection limit, defined as the concentration of metal ions determined for three standard deviations above the mean of four replicate measurements of the zero standard, e.g., the control without any metal ion, was 5 μM.

4. Conclusion and trends

The metal-promoted shift of equilibrium between the two forms of a dimerizing fluororeceptor synthesized in our group was shown to be a promising tool for the aqueous detection and measurement of metal ions. By simply controlling, through the pH, the balance between the monomer and dimer forms, it is possible to turn on the complexation with zinc or with cadmium ions. Like in natural mechanisms, such supramolecular structures use the multiple noncovalent bonds for molecular recognition in aqueous solution. Recently, a system derived from a linear polyamine has been shown to self-assemble similarly upon metal complexation [13]. Such a strategy, exploiting the host–guest recognition in water by preorganized small molecules susceptible to large changes in their molecular conformation upon the binding event, is certainly of great promise. In our case, zinc measurement appears to be satisfying concerning both the selectivity and the detection limit. The specificity of the recognition process is the basis of the selectivity of the receptor. However, with the search for exquisite selectivity appearing more and more a costly task, the tendency is now toward sensor arrays combined with chemometrics which may provide the same results at a lower expense [24]. The two approaches are not exclusive and even may be complementary when a second-order instrumentation including an optode is designed around a fluororeceptor whose selectivity was proved to be satisfactory.

Opt(r)odes take a growing place in the development of chemical sensors. The utilization of optical fibers now allows a wide variety of chemical detection schemes to be proposed. These new perspectives should enlarge the means of quantification or detection of various molecules and ions [25].

Although chromogenic and fluorogenic devices are conceivable, the latter offers considerable advantage owing to the high sensitivity associated with fluorescence signal detection. The sensing element of the optode is mainly composed of the receptor which, in fluorogenic devices, will deliver a light emission signal upon recognition of the ion or molecule for which it has been designed.

The development of such an optode, based on the fluororeceptor properties, is under investigation, the first step consisting in the immobilization of the receptor on a waveguide. In parallel, the modification of the macrocycloureide by functionalizing the free methyl ester groups and the covalent bridging of the dimer, are underway. We also intend to design daughter molecules by refining the functionalization of this first-generation structure to achieve various chiral complexations. We are confident that this could open the way to new selective and promising sensing devices.

References

[1] J.O. Nriagu, Environment 32 (7) (1990) 7.
[2] R.B. Thompson, E.R. Jones, Analytical Chemistry 65 (1993) 730.
[3] J.L. Nowicki, K.S. Johnson, K.H. Coale, V.A. Elrod, S.H. Lieberman, Analytical Chemistry 66 (1994) 2732.

[4] L.E. Brand, W.G. Sunda, R.R.L. Guillard, Limnology and Oceanography 28 (1983) 1182.
[5] R. Compañò, R. Ferrer, J. Guiteras, M. Dolors Prat, Analyst 119 (1994) 1225.
[6] S. Zappoli, C. Bottura, Analytical Chemistry 66 (1994) 3492.
[7] H. Zhang, W. Davison, Analytical Chemistry 67 (1995) 3391.
[8] S.D. Kamtekar, R. Pande, M.S. Ayyagari, K.A. Marx, D.L. Kaplan, J. Kumar, S. Tripathy, Analytical Chemistry 68 (1996) 216.
[9] P.R. Coulet, Amperometric and optical biosensors, in: A.P.F. Turner (Ed.), Advances in Biosensors, vol. 2, JAI Press, London, 1992, p. 151.
[10] D. Cordier, P.R. Coulet, Journal of the Chemical Society, Perkin Transactions (2) 4 (1994) 891.
[11] D. Cordier, M. Dumaine-Bouaziz, P.R. Coulet, Analytical Letters 28 (6) (1995) 959.
[12] A.W. Czarnik, Accounts of Chemical Research 27 (1994) 302.
[13] J.A. Scalafani, M.T. Maranto, T.M. Sisk, S.A. Van Arman, Tetrahedron Letters 37 (13) (1996) 2193.
[14] J.A. Bryant, S.P. Ho, C.B. Knobler, D.J. Cram, Journal of the American Chemical Society 112 (1990) 5837.
[15] C.-Y. Hung, T. Höpfner, R.P. Thummel, Journal of the American Chemical Society 115 (1993) 12 601.
[16] D. Smithrud, F. Diederich, Journal of the American Chemical Society 112 (1990) 339.
[17] F. Diederich, in: J.F. Stoddart (Ed.), Cyclophanes (Monographs in Supramolecular Chemistry Series), The Royal Society of Chemistry, Cambridge, UK, 1991, pp. 7–14.
[18] J. Rebek, Jr., B. Askew, P. Ballester, C. Buhr, S. Jones, D. Nemeth, K. Williams, Journal of the American Chemical Society 109 (1987) 5033.
[19] A.D. Hamilton, S.-K. Chang, S. Goswami, A.V. Muehldorf, D. Van Engen, Design of artificial receptors for biochemically interesting substrates, in: S.M. Roberts (Ed.), Molecular Recognition—Chemical and Biochemical Problems, The Royal Society of Chemistry, Cambridge, UK, 1989, p. 241.
[20] J.F. Stoddart (Ed.), Cyclophanes (Monographs in Supramolecular Chemistry Series), The Royal Society of Chemistry, Cambridge, UK, 1991, pp. 90 and 252–287, as well as references cited therein.
[21] T. Gajda, B. Henry, J.-J. Delpuech, Journal of the Chemical Society, Perkin Transactions (2) 1 (1994) 157.
[22] E. Farkas, I. Sóvágó, A. Gergely, Journal of the Chemical Society, Dalton Transactions (1983) 1545.
[23] F.A. Cotton, G. Wilkinson, Advanced Inorganic Chemistry, 5th edition, Wiley Interscience, New York, 1988.
[24] Z. Lin, K.S. Booksh, L.W. Burgess, B.R. Kowalski, Analytical Chemistry 66 (1994) 2552.
[25] O.S. Wolfbeis (Ed.), Fiber Optic Chemical Sensors and Biosensors, CRC Press, Boca Raton, FL, 1991.

ELSEVIER

Talanta 44 (1997) 1683–1690

Talanta

A simple method for the trace determination of methanol, ethanol, acetone and pentane in human breath and in the ambient air by preconcentration on solid sorbents followed by gas chromatography

Tao Qin [a,*], Xiaobai Xu [a], Tomáš Polák [b], Věra Pacáková [b], Karel Štulík [b], Libor Jech [c]

[a] *The Research Centre for Eco-environmental Chemistry, Academia Sinica, Beijing 100085, People's Republic of China*
[b] *Department of Analytical Chemistry, Charles University, Albertov 2030, 128 40 Prague 2, Czech Republic*
[c] *Axys Varilab, Vrané n/Vltavou, Czech Republic*

Received 2 July 1996; received in revised form 21 November 1996; accepted 21 November 1996

Abstract

A simple technique has been developed for preconcentration of gaseous trace organic compounds on solid sorbents, followed by gas chromatography. The sorbent is packed in a cartridge prepared from a syringe needle placed in the gas chromatographic injector and the analytes previously adsorbed are thermally desorbed at the injector temperature and then directly swept by the carrier gas into the column. The system has been tested for a charcoal-based adsorbent and silica gel, with pentane, methanol, ethanol and acetone as the model analytes. The procedure is rapid, the detection limits vary from a few nmol l^{-1} to values below 0.1 nmol l^{-1} (i.e., a few ppb), the linear dynamic range amounts to at least five concentration decades and a typical relative standard deviation is 10% at the nmol l^{-1} concentrations. It has been shown that the method is readily applicable to determination of instantaneous concentrations of the analytes in natural and industrial atmosphere and to their monitoring in human breath which is important for medical and hygienic practice. In general, the procedure is applicable to low-molecular volatile organic compounds. © 1997 Elsevier Science B.V.

Keywords: Preconcentration; Air; Breath

1. Introduction

The increasing atmospheric pollution necessitates continuous improving of methods for monitoring of pollutants and checking the exposure of people to them. Gas chromatography belongs among the most common methods employed not only in industrial hygiene, but also in medicine in analysis of human breath [1–6].

The pollutant concentrations in the atmosphere and the contents of medically important organic compounds in exhaled air are usually too low for

* Corresponding author.

PII S0039-9140(97)00073-8

direct determination and preconcentration techniques are required, the most common being absorption of analytes in liquids, their freezing out or adsorption on solids at a decreased or ambient temperature [7–15]. Absorption in liquids has advantages in possible use of chemical reactions of the analytes with the liquid leading to their conversion into stable compounds and thus, to an improvement in the trapping efficiency and in the possibility of collecting samples with a relatively high humidity. The drawbacks involve analyte losses through evaporation and/or stripping by the test gas passed through the absorption liquid and the necessity of using poorly volatile solvents that complicate the subsequent GC analysis. The freezing out with, e.g., liquid nitrogen or helium, is advantageous in its capability of collecting all the analytes (including highly volatile ones), in exclusion of side reactions of the analytes and in selectivity of collection at various temperatures; on the other hand, a possibility of aerosol formation and high contents of water in liquefied samples are disadvantageous.

Preconcentration on solid sorbents belongs among the most frequent techniques (including recommended EPA and ISO methods [16,17]). The subsequent desorption may employ liquids or heat. Among the advantages are the possibility of regulating the selectivity and sorption capacity and of using mixed sorbents [12]. Problems may be caused by incomplete adsorption of highly volatile compounds, desorption of substances with higher molecular masses, chemical reactions of analytes with the sorbent and limited carrier gas flow rates.

The present paper compares preconcentration of model volatile compounds (pentane, methanol, ethanol and acetone) on a charcoal-based adsorbent and silica gel, followed by thermal desorption and GC determination, for analyses of the ambient air and human breath. Charcoal-based adsorbents are still the predominant choice for organic vapour trapping [11,13,18–22]. They have superior sampling capacities, but their properties depend on their origin and the method of preparation [13]. Silica gel is a suitable sorbent for polar organic compounds, e.g., alcohols and aldehydes [23]. The adsorbent can be packed in a modified syringe needle and desorption carried out in the injection port [23–25]. The experimental arrangement described below is very simple.

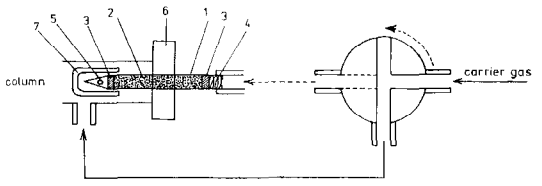

Fig. 1. Scheme of the sample introduction system: 1, syringe needle; 2, adsorbent; 3, glass wool; 4, spring; 5, outlet hole; 6, septum; and 7, sealed glass tube.

2. Experimental

2.1. Materials

All the chemicals were analytical grade, from Lachema, Brno, Czech Republic.

The charcoal adsorbent (trade name CNH charcoal), with a specific surface area of ca. 1050 $m^2\ g^{-1}$ (Slovenské Závody, Hnúšta, Slovakia), was made from wood filings and activated with water vapour. The fraction with a grain size from 0.1 to 0.25 mm was obtained by sieving, decanted in cold water, thoroughly washed with boiling distilled water and then dried for 40 min at 105°C.

Silica gel L (Merck, Germany), with a grain size of 0.2–0.3 mm, was washed with 5% hydrochloric acid and with water to neutral reaction and then activated for 8 h at 200°C.

Table 1
Solute specific retention volumes V_g (ml g^{-1}) on the CNH charcoal

Solute	V_g(20°C)	V_g(35°C)	V_g(300°C)	V'_R(35°C)[a]
Pentane	5.50×10^7	1.06×10^7	3.66	3.12×10^5
Methanol	4.34×10^4	2.02×10^4	2.25	0.62×10^3
Ethanol	1.54×10^5	6.82×10^4	3.20	2.09×10^3
Acetone	1.45×10^6	4.22×10^5	1.10	1.27×10^4

[a] V'_R: adjusted retention volume related to the packing weight in the cartridge.

Table 2
Solute specific retention volumes V_g (ml g^{-1}) on silica gel

Solute	V_g (20°C)	V_g(35°C)	V_g(300°C)	V_R (35°C)[a]
Methanol	9.36×10^4	3.16×10^4	1.22	9.50×10^2
Ethanol	2.76×10^5	8.91×10^4	2.24	2.62×10^3
Acetone	3.87×10^9	7.20×10^6	1.06	2.16×10^5

[a] V_R: adjusted retention volume related to the packing weight in the cartridge.

2.2. Apparatus

Adsorption cartridges were made according to ref. [23] from a stainless steel syringe needle 110 mm long, with an outer and inner diameter of 2.5 and 2.0 mm, respectively (Fig. 1). The needle tip was formed by fusion into a symmetrical, sharp point and a 0.5 mm hole was made circa 4 mm above the point. The needle was pushed through the septum of the chromatograph injection port and its end was connected to the carrier gas source through a three-way valve. The needle was packed with a defined amount of a sorbent (ca. 50 mg) and closed at both the ends with quartz wool. The sorbent bed was then fixed in place with a little metallic spring. Prior to sample collection, the cartridges were activated by passage of nitrogen at a flow rate of 30 ml min^{-1} and temperature of 300°C for 90 min. After the sample collection, before the thermal desorption step, the cartridges were briefly purged with nitrogen at room temperature, to remove atmospheric oxygen.

A CHROM 5 gas chromatograph (Laboratorní Přístroje, Prague, Czech Republic) was used with a glass column, 1.5 m long, 3 mm i.d., packed with Porapak Q (80-100 mesh, Waters, USA) and nitrogen carrier gas with a flow rate of 23 ml min^{-1}. The specific retention volumes of the solutes on the CNH charcoal and silica gel and their temperature dependences were measured with a glass column 20 cm long, 1 mm i.d., which contained 0.3123 g of CNH charcoal or 0.4646 g of silica gel. A FID was used with flow rates of hydrogen and air of 25 and 300 ml min^{-1}, respectively. The temperatures of the column, injector port and the FID were 160, 300 and 160°C, respectively.

The injection port was adapted according to Fig. 1 to permit thermal desorption of analytes from the cartridge. The three-way valve allowed by-passing of the carrier gas directly into the port, or its passage through the cartridge; after the time required for desorption (10 s), the valve was switched and the analytes were swept to the analytical column. To prevent the analytes from escaping during the desorption stage, the injection port liner was replaced by a glass tube with an external diameter of 5 mm, sealed at the bottom end (Fig. 1). This means that the losses of the analyte by diffusion are negligible, as experimentally verified. On passage of the carrier gas through the cartridge, the analyte desorbed is forced out of the sealed tube through the gap between the cartridge and the tube orifice. This causes, of course, a somewhat greater dispersion of the analyte zone, but this is not critical. It was further experimentally confirmed that no appreciable decomposition of the analytes occurred during the 10 s desorption period used [23].

The atmospheric samples were collected by pumping the test air through the cartridges at a defined flow rate regulated by a needle valve and measuring the sample volume either by a gas-tight syringe or a gas burette.

The samples of human breath were collected at the 3rd Internal Clinic, the 1st Faculty of Medicine, Charles University, Prague, in a 40 l plexiglass chamber. The chamber was provided with five outlets. Two of them were used to connect a respiration mask, one for supplying the oxygen consumed by breathing, one for connection of an expansion vessel and one for the collection of samples. The two inlets for connection of the tubes of a respiration mask were provided with a single-way valves permitting only a one-

Table 3
Recoveries (%) for selected compounds on the CNH charcoal and silica gel

Adsorbent	Methanol	Ethanol	Acetone	Pentane
Active carbon	92	95	90	85
Silica gel	99	97	98	—

Table 4
Comparison of analysis of human breath after preconcentration on the CNH charcoal and silica gel (concentrations in nmol l^{-1})

Solute	CNH charcoal	Silica gel	CNH charcoal* (after intake of alcohol)
Methanol	7.5 ± 0.5	6.2 ± 0.5*	8.7 ± 0.2
Ethanol	5.7 ± 0.9	52.6 ± 1.7*	6.5 ± 0.1
Acetone	3.3 ± 0.5	2.9 ± 0.4*	3.8 ± 0.1
Pentane	1.7 ± 0.5	—	—

* Breath of a person 2 h after consumption of 1 l of beer; sample volumes, 250 ml. The confidence interval was calculated from five parallel measurements for a 0.05 significance level.

way air circulation. The volume of the air exhaled was measured by a respirometer. The pressure balancing vessel was made of a 2 l glass cylinder, immersed upside down in a vessel with water; on breathing out, the air from the chamber expanded into the cylinder and on breathing in it was drawn back into the chamber. The oxygen consumed was replenished from a pressure cylinder, maintaining the atmospheric pressure all the time. A person breathed through the respiration mask for 4 min, which represents circa 80 l of exhaled air; hence, the air in the chamber was circa two-fold preconcentrated in the analytes. An air sample of a defined volume was then taken from the chamber by suction through the cartridge using and air pump. A $CaCl_2$ vent (3 mm i.d., bed length 50 mm) was placed before the cartridge to remove humidity. The samples with volumes of 20–500 ml were collected at a flow rate of 30 ml min^{-1}. The GC experiments carried out with the sample cartridges packed with $CaCl_2$ and a standard mixture of analytes confirmed that the $CaCl_2$ vent caused no change in the analyte contents.

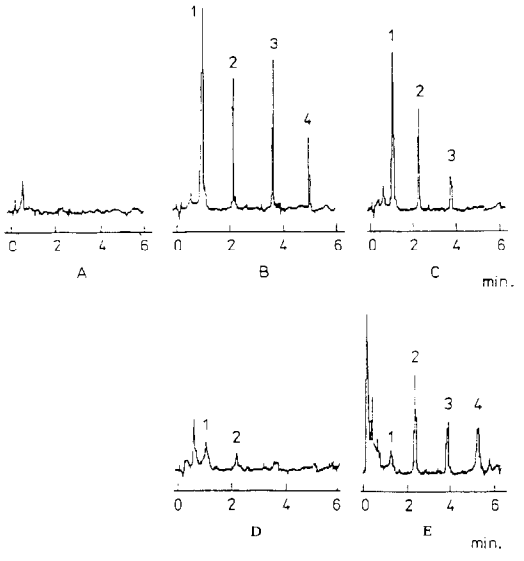

Fig. 2. Chromatogram of blank (A), standard mixture (B), air collected in the laboratory (C), air collected outside the building (D), human breath collected in the laboratory (E): 1, methanol; 2, ethanol; 3, acetone; and 4, pentane. The analyte concentrations determined (in nmol l^{-1}): Methanol: 17.0 (B), 13.0 (C), 1.9 (D), 1.6 (E); Ethanol: 8.7 (B), 6.7 (C), 1.2 (D), 6.5 (E); Acetone: 25.0 (B), 5.8 (C), 8.9 (E); Pentane: 6.4 (B), 4.2 (E). Sample volumes, 250 ml.

2.3. Procedures

Standard samples with defined analyte concentrations were prepared in two ways. For sampling of small volumes (up to 0.05 ml), a calculated amount of an analyte (max 10 μl of a liquid) was injected into a calibrated glass infusion bottle with a volume of 1200 ml. It was experimentally verified that gaseous samples prepared in this way retained a constant concentration for at least 6 h. For sampling of larger volumes (up to 0.5 l), a 50 l plexiglass chamber was used with a stirrer and a septum through which the cartridge was forced; the sample volumes collected were selected so that the maximum change in the analyte concentration did not exceed 0.2% and thus, the error could be neglected.

The breakthrough curves were measured with 800 mg of methanol per m^3 of air drawn from the 50 l plexiglass chamber through two cartridges connected in series. After passage of each 50 ml portion of the gas mixture, the methanol content in the downstream cartridge was determined and

oa new cartridge was connected; the measurement was continued until 50% breakthrough occurred whose relative value was obtained from the ratio of the inlet to the outlet concentration.

In the measuring procedure itself, a defined sample volume was passed through the precolumn, the precolumn was connected to the three-way valve in the bypass position, pushed through the septum of the injection port heated to 300°C and, after the desorption period (10 s), the three-way valve was switched for the carrier gas to sweep the desorbed analytes into the analytical column. The analytes were identified by comparing their retention times with those of standard substances. For quantitation, calibration plots were used obtained with standard mixtures of the analytes (see above).

3. Results and discussion

Pentane, methanol, ethanol and acetone have been selected as model analytes because they may occur in human breath. Pentane is formed by peroxidation of unsaturated fatty acids contained in tissues and its concentration in breath varies from 0.04 to 8 nmol l^{-1} [26–31], in dependence n different solubilities in fatty tissues and variations in the metabolism of individuals. Methanol and ethanol are contained in breath not only after intake of alcoholic beverages, but also as metabolic products and their concentrations vary between 1.3 and 8.5 nmol l^{-1} (without alcohol uptake), in dependence on the actual state of the organism [32–35]. The acetone concentration in breath of healthy individuals varies between 10 and 90 nmol l^{-1} and is several orders of magnitude higher for diabetics [32,36–38]. In view of these low concentrations, direct GC analysis is impossible.

When using solid sorbents for analyte preconcentration, a total recovery of at least 75% is required [1]. The sorption capacity is usually evaluated in terms of the breakthrough volume, which can either be calculated or determined experimentally (directly or indirectly) [39–42]. The direct experimental method is based on passage of a gas mixture of known concentration and its detection at the outlet, the indirect approach employs the specific retention volume V_g, related to 1 g of the sorbent, i.e., the gas volume from injection to the peak maximum, corresponding to a breakthrough of 50% of the analyte. The V_g value at a required sorption temperature is obtained by extrapolation of the log V_g dependence on the reciprocal of the temperature. An error of this method is caused by non-linearity of the log V_g versus 1/T dependence [42]. A disadvantage of indirect methods lies in their inability to describe the effect of the experimental conditions on the breakthrough volume. The real 'safe breakthrough volume' (usually given as a 1, 5 or 10% of the total breakthrough) must consider the atmospheric humidity, fluctuations in the solute flow through the sorbent, inhomogeneity of the gaseous solute sample, the mechanical properties of the sorbent (the grain size and the packing properties in the column) and the character of the sorption process [11]. Therefore, breakthrough volumes obtained indirectly are usually verified by direct methods.

The present paper compares the sorption properties of the CNH charcoal and silica gel. Carbopack C and Tenax GC were also tested, but the former was found unsuitable because of a generally poor sorption capacity due to a low specific surface area [43] (ca. 10 m^2 g^{-1}) and the latter exhibited a sufficient sorption only for pentane and acetone and not for the alcohols. The unsuitability of Tenax GC for volatile compounds has already been pointed out [4,23] (the breakthrough volume for methanol is only 0.4 l at 32°C). For the CNH charcoal and silica gel, the temperature dependences of the specific retention volumes were measured and extrapolated to 20, 35 and 300°C, corresponding to the temperatures of the atmosphere, of the human breath and of the desorption, respectively; for 35°C, the retention volumes were also extrapolated to the sorbent amount in the cartridge. The results are given in Table 1 for the CNH charcoal and in Table 2 for silica gel.

All the solutes tested are strongly adsorbed on the CNH charcoal. Silica gel does not adsorb pentane (the V_g value at 25°C is only 180 ml), while for methanol and ethanol are the breakthrough volumes at 35°C higher than those on the CNH charcoal, respectively.

Table 5
Concentrations of volatile compounds (nmol l^{-1}) in the air measured at different places and times (the CNH charcoal)

Solute	Chem. lab May, 17	Corridor May, 17	Chem. lab May, 21	Corridor May, 22
Methanol	690	240	21.5	22.5
Ethanol	500	111	10.9	66
Acetone	121	—	17	85
Pentane	—	—	4.2	2.8

Sample volume, 250 ml.

The reliability of the breakthrough volumes obtained from the retention volumes was verified by direct measurement for the CNH charcoal and methanol as the solute exhibiting the lowest adsorption; for the conditions Section 2. A breakthrough of 0.1, 10 and 50% occurred after passage of 850, 1000 and 1400 ml of a gas mixture containing methanol in the concentration of 800 mg m^{-3}, respectively, while a value of 1300 ml was obtained by the indirect measurement of V_g (50% breakthrough). This difference is caused by the different way of the CNH charcoal packing in the column and the cartridges and by the errors caused by extrapolation of the V_g values measured at higher temperatures to 20°C. The efficiency of the cartridge was approx. 20 theoretical plates.

The carrier gas flow rate and desorption temperature were optimized by the measurement of the analyte recovery (in %) for the CNH charcoal and silica gel, using a 10 s desorption time. The maximum recoveries were obtained at 25 ml min^{-1}, which was also the optimal flow rate for Porapak Q column. The desorption temperature was optimized in the same way, obtaining the highest recovery at 300°C; at higher temperatures, the injection septum was degraded. The recoveries for the CNH charcoal and silica gel are compared in Table 3. Higher values were obtained for silica gel.

Preconcentrations of analytes from human breath on active carbon and silica gel were compared and the results are given in Table 4. Two aliquots of the same sample were analyzed, one after adsorption on the CNH charcoal and the other after adsorption on silica gel; for illustration, an analysis of the breath of a person after intake of an alcoholic beverage is also given in Table 4. It follows from Table 4 that the values obtained after preconcentration on silica gel are $\approx 10\%$ higher than those obtained on the CNH charcoal, with the exception of pentane which is very little sorbed on silica gel (Table 1 and Table 2). The analysis of a human breath sample collected 2 h after consumption of 1 l of beer (containing ca. 36 g of pure ethanol) yielded a nine times higher value for ethanol compared with the other breath samples (see Table 4). A typical relative standard deviation of the determination was ca. 10% at a concentration level of units of nmol l^{-1}.

The detection limits for the volatile compounds studied (twice the absolute noise value) vary from a few nmol l^{-1} to well below 0.1 nmol l^{-1}.

Table 6
Analysis of human breath—comparison of effects of the surrounding environment (the CNH charcoal, nmol l^{-1})

Solute	Inside lab May, 17	Inside lab May, 19	Outside lab 1 h	Outside lab 2.5 h	Outside lab 15 h
Metanol	25	9.4	1.6	3.1	3.1
Ethanol	13	8.7	6.5	6.5	6.5
Acetone	14.3	14.3	8.9	8.9	7.1
Pentane	1.4	4.2	2.8	4.2	4.2

Sample volume, 500 ml.

Table 7
Comparison of the measured concentrations of volatile compounds (nmol l^{-1}) in breath with published data (the CNH charcoal)

Solute	Our results	Published data	References
Methanol, ethanol	1.6–8.7	1.3–8.5	[32–35]
Acetone	2.9–8.9	10–90	[32,36–38]
Pentane	0–4.2	0.04–8	[26–31]

Chromatograms of the analytes at concentrations close to the detection limits can be seen in Fig. 2. The blank recording was obtained on passage of pure nitrogen through the cartridge under the conditions of determination.

3.1. Applications

The concentrations of volatile compounds in the atmosphere inside and outside a chemical laboratory were measured on various days. The values obtained are given in Table 5. The high concentrations of methanol and ethanol on the 1st and 4th day were caused by HPLC experiments performed in the laboratory.

At the same time, the breath of a person exposed to this atmosphere (inside and outside the laboratory) was analyzed (Table 6). It follows from Table 6 that the values obtained depend on the ambient atmosphere. Rather high levels were found in the person who spent most of his time in the laboratory working with methanol and ethanol during HPLC experiments. The concentrations of volatile compounds in the breath of a person who left the laboratory, collected at different times after departure (1–15 h), were found to be constant, independent of the previous exposure in the laboratory.

We compared our results on breath analysis with the published data. As can be seen from Table 7, our results fall in the concentration range published by other authors with the exception of acetone, where lower values were found in this work; however, the variability of the data on the acetone content in the breath of healthy individuals is very large.

The industrial atmosphere in a dye factory was analyzed using the described method. The results are given in Table 8. High concentrations of solvents were found both in the production hall and in the solvent dispensing unit.

Table 8
Analysis of industrial environment in the Colorlak factory (the CNH charcoal, μmol l^{-1})

Solute	Production hall	Solvent dispensing unit
Acetone	0.33 ± 0.03	0.85 ± 0.05
Toluene	1.85 ± 0.05	0.35 ± 0.04
Ethanol	—	0.61 ± 0.06

Sample volume, 100 ml.

4. Conclusion

The method described makes it possible to measure instantaneous concentrations of volatile compounds in the air and human breath. It is thus, possible to monitor fluctuations in the pollutant concentrations in industrial atmosphere or in human breath during operations hazardous to health. This paper was not intended as a clinical study and thus, only a few men and women provided the breath samples to be analyzed.

The detection limits vary from a few nmol l^{-1} to less than 0.1 nmol l^{-1}. The main advantages of the proposed method lie in the very simple methodology and easiness and rapidity of the analyses. Its drawbacks involve the fact that the samples collected are not particularly large, the desorption temperature is limited by that of the chromatograph injection port and the elution curves are slightly dispersed in the collection cartridges.

Acknowledgements

We are indebted to MUDr. J. Poòka, CSc of the 3rd Internal Clinic of the 1st Faculty of Medicine, Charles University, for valuable discussions and kind permission to use the plexiglass chamber for the obtaining samples of human breath.

References

[1] J. Namiesnik, Talanta 35 (1988) 567.
[2] D.L. Fox, Anal. Chem. 65 (1993) 156R.
[3] Monitoring of airborne contaminants in workplace atmosphere using sampling device and GC or HPLC, Bulletin 769 F, Supelco 1995.
[4] W. Thain, Monitoring Toxic Gases in the Atmosphere for Hygiene and Pollution Control, Pergamon Press, New York, 1980, p. 64.
[5] S.M. Gordon, J. Chromatogr. 511 (1990) 291.
[6] J.F. Periago, C. Prado, I. Ibarra, J. Tortosa, J. Chromatogr. A 657 (1993) 147.
[7] J.P. Lodge (Ed.), Methods of Air Sampling and Analysis, 3rd ed., Lewis Publishers, Chelsea, MI, 1989, pp. 27–42, 190–214 and 427–449.
[8] J. Rudolph, K.P. Müller, R. Koppmann, Anal. Chim. Acta 236 (1990) 197.
[9] H.-J. Schaeffer, J. High Resol. Chromatogr. 12 (1989) 69.
[10] M.E. Rosen, J.F. Pankow, J. Chromatogr. 537 (1991) 321.
[11] Y.-Z. Tang, Q. Tran, P. Fellin, W.K. Cheng, I. Drummond, Anal. Chem. 1993 (1932) 65.
[12] D. Helmig, J.P. Greenberg, J. Chromatogr. A 677 (1994) 123.
[13] L. Senf, H. Frank, J. Chromatogr. 520 (1990) 131.
[14] R.G. Melcher, Anal. Chem. 55 (1983) 40R.
[15] A.J. Núnez, L.F. González, J. Janák, J. Chromatogr. 300 (1984) 127.
[16] L.T.H. Keith (Ed.), EPA's Sampling and Analysis Methods Database, Lewis Publishers, Boca Raton, 1990.
[17] NIOSH Manual of Analytical Methods, 4th ed., DHHS Publication no. (NIOSH), August 1994, pp. 94–113.
[18] J.E. Adkins Jr., N.W. Henry III, Anal. Chem. 65 (1993) 133R.
[19] Z. Witkiewicz, H. Grajek, J. Choma, J. Chromatogr. 556 (1991) 441.
[20] J. Rudling, J. Chromatogr. 503 (1990) 33.
[21] W.R. Betz, K.S. Ho, S.A. Hazard, S.J. Lambaiase, Dynamic Gas chromatographic techniques for the characterization of carbon based adsorbents utilized in air sampling, in: E.D. Wingard, L.H. Keith (Eds.), Sampling Anal. Airborne Pollution, Lewis, Boca Raton, 1993, pp. 91–100.
[22] A.K.W. Baughman, D.H. Love, Anal. Chem. 65 (1993) 480A.
[23] L. Jech, PhD Thesis, Charles University, Prague 1992.
[24] W.K. Fowler, C.H. Duffey, H.C. Miller, Anal. Chem. 51 (1979) 2333.
[25] S. Müller, J. Efer, W. Engewald, Chromatographia 38 (1994) 694.
[26] M. Dillard, J. Tomis, P. Narreb, Anal. Biochem. 162 (1981) 332.
[27] S. Morita, M.T. Schider, Y. Inada, Aneasthesiology 67 (1986) 730.
[28] J. Pincemail, C. Deby, A. Dethier, Y. Bertrand, M. Lismonde, M. Lamy, Bioelectrochem. Bioenerg. 18 (1987) 117.
[29] L. Massias, E. Postaire, C. Regnaulta, G. Hazenbroucq, Biomed. Chromatogr. 7 (1993) 200.
[30] S. Mendis, P.A. Sobotka, D.E. Euler, Clin. Chem. (Washington) 40 (1994) 1485.
[31] I.M. Moondie, D. Labadarios, J. High Resol. Chromatogr. 16 (1993) 437.
[32] M. Philips, J. Greenberg, J. Chromatogr. 422 (1987) 235.
[33] A.W. Jones, Clin. Sci. 63 (1981) 441.
[34] J. Dannecker, M. Philips, E.G. Shaksmann, Anal. Biochem. 114 (1981) 1.
[35] M. Falkensson, J. Wayne, B. Soergo, Clin. Chem. 35 (1989) 918.
[36] A.W. Jones, J. Anal. Toxicol. 426 (1985) 9.
[37] E. Anngard, J. Anal. Toxicol. 32 (1979) 212.
[38] J. Peinado, J. Lopéz-Soriano, J.M. Argiles, J. Chromatogr. Biomed. Appl. 415 (1987) 372.
[39] S. Van Tassel, N. Amalfitano, R.S. Narand, Anal. Chem. 53 (1981) 2130.
[40] D. van der Straeten, H. van Langenhove, N. Schamp, J. Chromatogr. 331 (1985) 207.
[41] J. Namiesnik, L. Torres, E. Kozlowski, J. Mathieu, J. Chromatogr. 208 (1981) 239.
[42] T. Tanaka, J. Chromatogr. 153 (1978) 7.
[43] K.J. Krost, E.D. Pellizzari, S.G. Walburn, S.A. Hubbard, Anal. Chem. 54 (1982) 810.

ELSEVIER

Talanta 44 (1997) 1691–1698

Talanta

A sensor for pH based on an optical reflective device coupled to the swelling of an aminated polystyrene membrane

Li Zhang [a], Margeret E. Langmuir [b], Mingqi Bai [b], W. Rudolf Seitz [a,*]

[a] *Department of Chemistry, University of New Hampshire, Durham, NH 03824, USA*
[b] *Covalent Associates, 10 State Street, Woburn, MA 01801-1064, USA*

Received 25 September 1996; received in revised form 7 March 1997; accepted 7 March 1997

Abstract

We have developed a low cost pH sensor based on an optical reflective device (ORD) coupled to a toughened, lightly crosslinked aminated polystyrene membrane. Protonation of the amine group causes the polymer to swell. This is accompanied by a decrease in the turbidity of the membrane. As a result, reflected intensity measured by the ORD is a function of pH. The resulting pH sensor is inexpensive and has modest power requirements. The sensor is stable, provided the membrane is not allowed to dry out and crack. Changing ionic strength affects response both by changing the turbidity of the membrane due to refractive index effects and also by reducing the extent to which the protonated polymer swells. Increasing temperature leads to a larger change in turbidity. © 1997 Elsevier Science B.V.

Keywords: Optical reflective device; pH sensor; Polystyrene

1. Introduction

We are interested in developing chemical sensors based on optical changes accompanying polymer swelling. The material that we have worked with is porous, lightly crosslinked polystyrene derivatized with a functional group that binds the analyte of interest. Analyte binding causes shrinking or swelling by changing the affinity of the polymer for the external solvent. In an earlier study we showed that porous derivatized polystyrene can undergo multiple swelling and shrinking cycles without cracking if it is toughened by adding Kraton G1652, a styrene–ethylene, butylene–styrene triblock copolymer [1]. In that study it was observed that aminated polystyrene beads became visibly clearer when protonation in acidic media caused them to swell. Based on this observation, we prepared a single fiber optical pH sensor based on reflectance changes accompanying polymer swelling [2] and pH sensitive membranes that could be coupled to multiple optical fiber measurements [3]. We also conducted an extensive study of the effects of formulation variables on polymer morphology and the rate and magnitude of its response to changes in pH [4]. More recently, we have proposed that the optical response of the membrane is due to reflection at the interface between the bulk polymer and water containing pores [5].

* Corresponding author.

PII S0039-9140(97)00080-5

When the polymer is exposed to acidic aqueous solutions that protonate the amine, it swells because the positive charge that arises from protonation increases the affinity of the polymer for the solvent. This process effectively dilutes the bulk polymer with water causing its refractive index to decrease so that it is closer to the refractive index of the water in the pore space. This reduces the reflectance at the polymer-pore interface resulting in a decrease in reflected intensity that is the basis for sensing.

In this manuscript we report that the optically sensitive membranes that we have developed can be coupled to an 'optical reflective device' (ORD) to make a robust, low cost sensor. An ORD is simply a light emitting diode (LED) and a phototransistor combined in the same package and configured to respond to the presence of a reflecting surface at or near the surface of the device. The retail cost of a currently available ORD is less than $5.

The objective that inspired this study was the development of a sensor that would be suitable for remote unattended measurements of pH in seawater. The ORD provides compactness, low power requirements and low cost while the membrane based on polymer swelling is stable with time. Thus, the combination of these two promises to be a useful sensing technology for applications of this sort. Because of the intended application to seawater measurements, information is included on the effects of ionic strength and temperature on response because these are both important issues for measurements in the ocean.

2. Experimental

2.1. Reagents

Vinylbenzyl chloride (98%, 30% para/70% meta) was obtained from Dow. Divinylbenzene (55%) and benzoyl peroxide were purchased form Polysciences, Warrington, PA. Kraton G1652, a styrene–ethylene/butylene–styrene triblock copolymer (29% styrene, 71% ethylene/butylene) was donated by Shell Chemical. Vinylmethoxysiloxane oligomer was obtained from Huls America. Dodecane, octadecane, polystyrene (MW 2500), xylene, piperidine, 1,4-dioxane, diethanolamine were obtained from Aldrich. Trihydroxyaminomethane hydrochloride (Tris) was obtained from Sigma. Other buffer reagents were from Fisher.

Acetate and ammonium buffers were used to adjust pH 4.0 and 10.0, respectively. Tris buffer was used in the experiments to evaluate response versus pH. The concentration of the buffer components was 0.10 M. The ionic strength of the buffer was adjusted with sodium chloride.

2.2. Apparatus

Models 710 and 710F ORDS were purchased from Optek Technology. Both models have an LED that emits a band of light centered at 930 nm. The 710F model has a filter to exclude ambient light over both the LED and phototransistor while the 710 is unfiltered. Fig. 1 shows both the ORD and the battery powered circuit used to power the LED and collect the signal from the phototransistor. The ORD is 5.6 mm in diameter and 3.8 mm thick.

A plastic light tight cell was constructed for optical measurements. The ORD was mounted in the cap of the cell such that the optically sensitive membrane was located ca. 1 cm below the bottom of the cap. The bottom of the cell was filled with sufficient solution to contact the membrane but not the leads from the ORD.

A Cary 5 uv-vis-nir spectrophotometer was used for direct membrane turbidity measurements using a membrane mounted in a cuvet in contact with buffer of the desired pH. A Brookfield viscometer was used to measure the viscosity during prepolymerization.

2.3. Membrane preparation

Membrane formulations were taken from earlier work [3]. The monomer for all experiments was vinylbenzyl chloride (VBC). The divinylbenzene level was 2 mol.% (moles DVB/moles monomer), and the Kraton level was 2 weight.% (g Kraton/g monomer). The formulation included

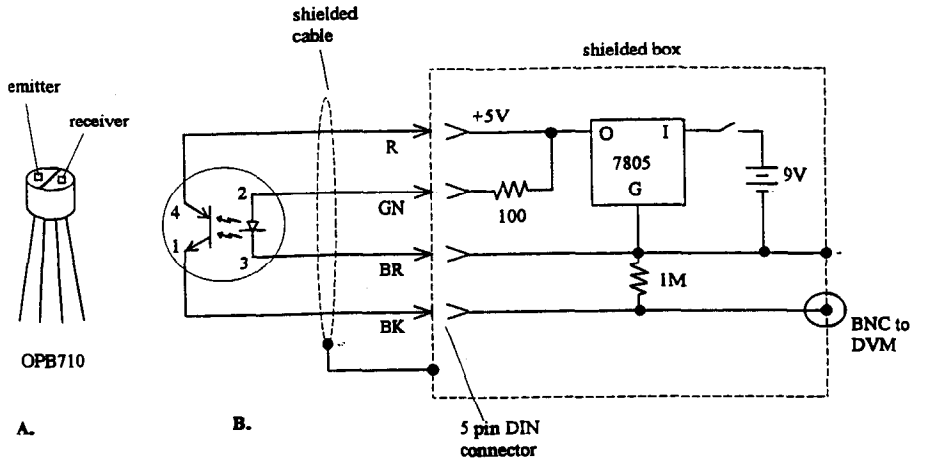

Fig. 1. Measurement apparatus including (A) Optek Technology 710 optical refective device and (B) schematic diagram of battery powered circuit for evaluation of sensors prepared by coupling the ORD and the polymer. Connections 1 and 4 are to the collector and emitter of the phototransistor. Connections 2 and 3 are to the LED.

2:1 xylene:dodecane as a porogenic solvent. In a few experiments, 2:1 polystyrene:octadecane was evaluated as the porogenic solvent. In all experiments, the level of porogenic solvent was 40 vol.% (volume porogenic solvent/volume monomer × 100). The initiator was benzoyl peroxide.

Membranes were prepared using a viscous partially polymerized solution, or prepolymer, as described previously [3]. The polymerization is initiated by heating a stirred solution of polymer and allowing the reaction to proceed to the point where there is a significant increase in viscosity. The reaction is then stopped by lowering the temperature of the solution. Membranes were formed by curing a small volume of prepolymer between two 1″ × 3″ glass microscope slides separated by a spacer. Prior to membrane formation, one of the slides was pretreated with vinylmethoxysiloxane oligomer to introduce vinyl groups onto the surface of the glass. The surface was first treated with 2.0 M HCl for 4 h. It was then silanized by refluxing the glass slides in a solution of 10 ml of vinylmethoxysiloxane oligomer and 30 ml of distilled toluene for 6 h. The other surface was sprayed with TFE release agent dry lubricant (Miller-Stephenson) to facilitate release of the membrane after polymerization. Membrane thickness was controlled using 25, 76 and 127 μm Teflon spacers (Berghof, Concord, CA). The two glass slides were held together by a spring clip and cured in an 85°C water bath for 6 h. After polymerization, the membrane adheres to the surface that was reacted with vinylmethoxysiloxane oligomer.

Diluents and unreacted monomer and crosslinker were removed by soaking in acetone for several hours, decanting, and then repeating the cycle. After air drying, the glass bound membrane was cut into smaller pieces that were just large enough to completely cover the ORD surface. Membranes were then derivatized by reacting them with 1:1 acetone:diethanolamine for 2 days at room temperature. The membranes were then washed with 0.1 M HCl three times to remove any unreacted diethanolamine and rinsed with deionized water. The membranes were preconditioned by soaking in pH 4 buffer (acetic acid/sodium acetate) for 24 h and cycled between pH 10 (ammonium/ammonia) and 4 at least three times prior to making any measurements on the membrane. The membranes were stored in distilled water when not in use.

The glass microscope slides with the membrane were attached to the ORD surface with transparent silicone RTV cement. The RTV cement was also used to pot the ORD connections to protect

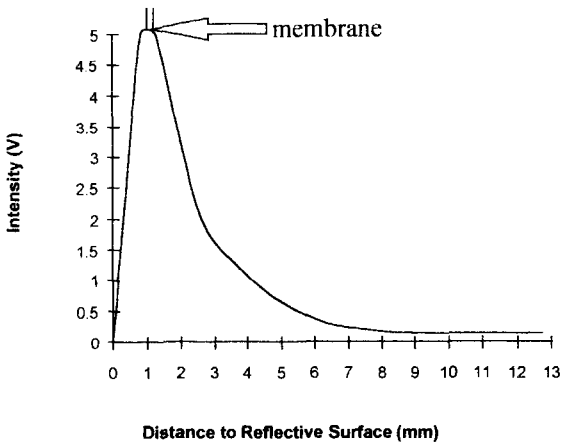

Fig. 2. The intensity measured by phototransistor of the ORD versus the distance between the ORD surface and a reflecting surface. This location of the polymer membrane on this curve is indicated by the arrow.

them from water during testing. The microscopy slide serves not only as a support for the membrane but also as a spacer to locate the membrane in the region where ORD is most sensitive. Fig. 2 illustrates this by showing where the membrane is located on a curve showing ORD signal versus distance between the ORD surface and a reflecting metal surface.

Unless otherwise specified all measurements were made at room temperature. In the experiment to evaluate the effect of temperature on response, the sensor temperature was raised above room temperature by placing it in a water bath at the desired temperature. To lower the temperature below room temperature, the sensor was placed in an ice bath. Response was measured when the sensor reached the desired temperature.

3. Results and discussion

3.1. General observations

All of our prepared membranes appear cloudy and reflect light. From previous work, we know that this is because the membranes contain pores with dimensions sufficiently large to reflect light [5]. In an aqueous environment, the pores are filled with water with dissolved solutes, which has a lower refractive index than the bulk polymer. The degree of cloudiness varies from batch to batch. One source of variability is the degree of prepolymerization. During prepolymerization, the solution becomes cloudy. As the polymer forms, the aliphatic component of the porogenic solvent separates into a distinct phase that eventually becomes pore space after polymerization is complete and the porogenic solvent is removed. Because the polymer components are stirred during the prepolymerization step, this may facilitate separation of the dodecane into smaller domains. Table 1 shows data from an experiment undertaken to assess the effect of the degree of prepolymerization on membrane cloudiness. The data show that a higher degree of prepolymerization is accompanied by a higher degree of cloudiness and smaller response.

When polymerization begins, it is very rapid as evidenced by an extremely rapid increase in viscosity with time. As a result, using our simplistic approach, it is difficult to stop the prepolymerization process at the same viscosity each time.

While membranes tend to be cloudy throughout, the degree of cloudiness is not uniform. This suggests that there may have been some large scale phase separation arising because the polymer is more dense than the monomer and the porogenic solvents. A relative standard deviation

Table 1
Effect of viscosity after prepolymerization on response

Viscosity (cp)	Signal at pH 4.0 (mV)	Signal at pH 10.0 (mV)	Change in signal (mV)
14.0	1300	2710	1410
35.5	4330	4780	450
100	4910	4920	10

of 11% has been observed for turbidance measurements at different locations in membranes from the same batch [6]. The relative standard deviation increases to 18% when membranes with the same formulation from different batches are compared [6]. These data emphasize the need to hold the membrane in a fixed position when it used for sensing. Sensor-to-sensor reproducibility is limited by membrane heterogeneity.

The results shown in this paper are for polyVBC derivatized with diethanolamine. The aminated polymer swells at low pH because protonation of the amine introduces a positive charge onto the polymer and increases its affinity for water. Previous work has shown that diethanolamine modified polymer beads are useful for sensing pH from 6.8–7.8 [1]. Because this is below the range of interest for seawater, attempts were make made to derivatize polyVBC with more strongly basic amines, e.g., piperidine, in the hopes that they would respond to higher pHs. However, the more strongly basic amines tended to attack the bond between the membrane and glass substrate causing the membrane to delaminate during the derivatization step.

A limited number of membranes were prepared using 2:1 styrene (M.W. 2500): ocatadecane as the porogenic solvent. This porogenic solvent has a lower affinity for the polymer than 2:1 xylene:dodecane. As a result phase separation occurs earlier in the polymerization process. These membranes responded more rapidly than membranes prepared using xylene: dodecane but were more 'brittle' and tended to flake.

3.2. Response to pH

Fig. 3 shows turbidity versus pH at four different ionic strengths measured in a spectrophotometer at 930 nm. As observed in previous work [2,3], there is a larger decrease in turbidity with decreasing pH. The polymer swells with water as it is protonated this dilutes the polymer chains with water, reducing its refractive index. As the refractive index of the bulk polymer gets closer to the refractive index of the water-filled pores, the turbidity of the membrane decreases.

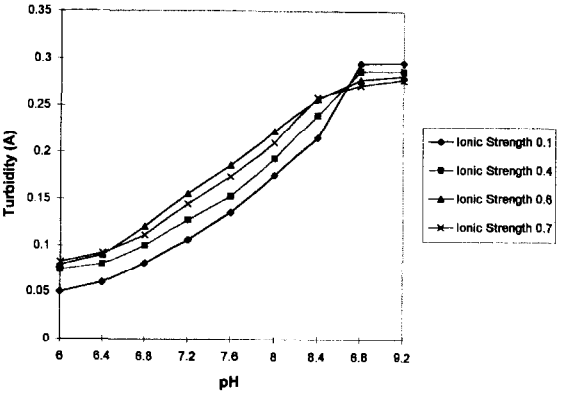

Fig. 3. Turbidity versus pH (in absorbance units) for a 75 μm thick membrane at four different ionic strengths measured at 930 nm with a spectrophotometer.

The magnitude of the change decreases with increasing ionic strength. Two effects contribute to this. First, the refractive index of the aqueous solution that occupies the pore space in the membrane is larger at the higher concentrations of sodium chloride that are used to adjust ionic strength. This in turn reduces the amount of light reflected at the interface between the bulk polymer and the aqueous solution in the pores. This explains why the turbidity decreases at high pH where the amine group is completely deprotonated.

The second effect of ionic strength is to reduce the extent of swelling of the protonated membrane. The swelling of charged crosslinked polymer networks can be viewed as an electrostatic repulsion effect or an osmotic pressure effect [7]. If it is viewed as arising from electrostatic repulsion, the effect of increased ionic strength is to shield adjacent positive charges such that the repulsive effect is reduced. Viewed as an osmotic pressure effect, swelling arises from the difference between the charge density on the polymer and the ionic strength in solution. Increasing ionic strength in solution reduces this difference and thus leads to less swelling.

In addition to affecting the degree of swelling and the membrane optical properties, increasing ionic strength also shifts the amine pK_a. Normally, increasing ionic strength favors the protonated form of the amine but the data in Fig. 3

show that the highest pK_a is observed at the lowest ionic strength. We suspect that this effect is related to the activity of water. At high ionic strength, there is less water in the polymer. This means the activity of water in the polymer is lower and the tendence of water to solvate a charged site on the polymer diminishes.

The data in Fig. 3 confirm earlier work showing that the diameter of aminated polyVBC beads depends on ionic strength [1]. If these materials are to be used for sensing in seawater or other high ionic strength media, provisions will have to be made for calibrating in media of equivalent ionic strength and correcting for any fluctuations in ion strength.

Fig. 4 shows reflected intensity versus pH measured with the ORD sensor. As expected it parallels the change in turbidity with pH measured in the spectrophotometer. Fig. 5 shows both the rate and range of response as a function of membrane thickness. The response rates shown are for a membrane exposed to a pH 4.0 buffer after it has equilibrated with a pH 10.0 buffer. As expected, the reflected intensity and response time both increase with membrane thickness. The 90% response times are 20, 180, 330 and 600 s for membranes that are 25, 75, 127 and 254 μm thick, respectively. As the membrane thickness is increased from 25–75 μm, the response time increases with the square of the membrane

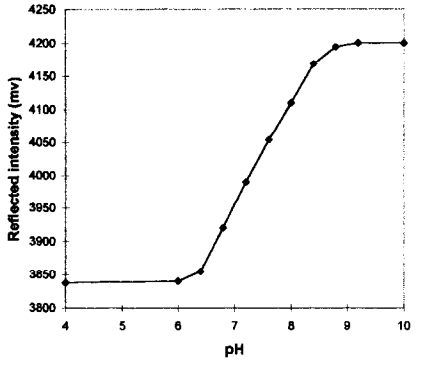

Fig. 4. Reflected intensity versus pH measured with the ORD coupled to a 75 μm thick aminated polystyrene membrane. The ionic strength is 0.1 M.

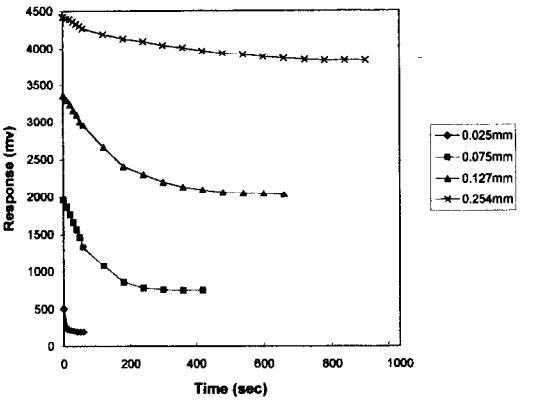

Fig. 5. Reflected intensity versus time for membranes of varying thicknesses initially equilibrated at pH 10.0 and then exposed to a pH 4.0 buffer. This curve shows not only the rate of response but also the magnitude of the intensity change. The ionic strength is 0.1 M.

thickness. This is expected if response is limited by the rate of diffusion into the membrane. This relationship does not extend to the thicker membranes, probably because these membranes have not completely equilibrated within the measured period.

The signal for the 25 micrometer thick membrane decreases by a factor of 2.74 from 0.52 to 0.19 volts. the signal for the 75 micrometer thick membrane decreases by a factor of 2.61 from 1.96–0.75 volts. Although the relative change is slightly smaller, the absolute change is larger so this thickness was used for the other measurements presented in this manuscripts. At membrane thicknesses greater than 75 μm, both the swollen and unswollen membranes are sufficiently turbid to reflect a large percentage of the incident light. As a results, the difference in signals for the swollen and unswollen membrane decreases at high membrane thickness.

Fig. 6 shows that reflected intensity decreases with increasing temperature. The largest effect is for the swollen polymer at pH 4.0. This is consistent with earlier data showing that the degree of swelling increases with temperature [1]. If the swelling is viewed as an osmotic pressure effect, then the explanation for the increase in swelling is that osmotic pressure is proportional to absolute

temperature. There is a smaller effect at pH 10.0. We do not have a ready explanation for this since previous work has shown that unprotonated aminated polyVBC shrinks slightly with increasing temperature. This should lead to a small increase in turbidity. Increasing temperature will also cause the refractive indices of both the solution in the pores and the polymer to change. Since the refractive index of liquids normally varies more strongly with temperature than the refractive index of solids, it is likely that the refractive index difference between the two phases is temperature dependent. However, this effect is expected to be smaller than the effect of temperature on swelling.

3.3. Membrane stability

Membrane stability is an important issue since one of our goals was to improve upon the stability of optical sensors based on indicator dyes. Consistent with previous work, we found that membranes that remain moist will respond for multiple swelling and shrinking cycles. One membrane was cycled between pH 4.0, 7.0 and 10.0 over 30 days with less than 2% drift. However, dried membranes tended to crack and then would degrade mechanically when rehydrated. When used for practical applications, we envision that each sensor would be individually calibrated and would have to be recalibrated at intervals. However, the low degree of drift indicates that recalibration intervals could be as long as a month, provided that the membrane is not allowed to dry out.

When the membrane was repeatedly cycled between pH 4 and 10, the relative standard deviation of intensity measurements at each pH was less than 1%.

If the membrane accumulates compounds that absorb at 930 nm, then this will interfere with sensor response. Fortunately, few compounds absorb at this wavelength so this is not expected to seriously limit sensor applicability.

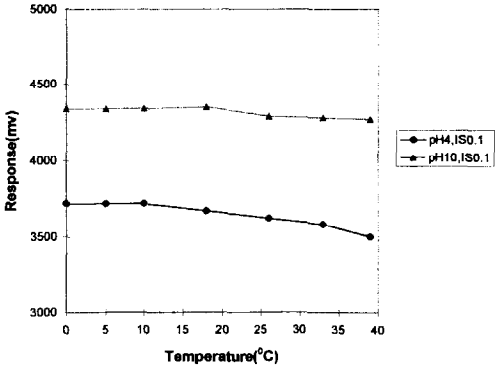

Fig. 6. Reflected intensity versus temperature for both the swollen (pH 4.0) and unswollen (pH 10.0) forms of a 75 μm thick membrane. The ionic strength is 0.1 M.

4. Conclusions

This study shows that turbidity changes accompanying the swelling of derivatized membranes may be coupled to optical reflective devices to make a chemical sensor that is inexpensive, has low power requirements and is stable with time if the membrane is not allowed to dry out. It also shows that response is affected by both ionic strength and temperature. These parameters must be accounted for when calibrating the sensor and a correction must be applied if there are variations in either ionic strength or temperature.

Acknowledgements

Partial support for the work reported here was provided by STTR grant DMI-9413616 from the National Science Foundation to Covalent Associates. The work was performed at the University of New Hampshire was under a subcontract from Covalent Associates.

References

[1] S. Pan, V. Conway, Z. Shakhsher, S. Emerson, M. Bai, W.R. Seitz, D.D. Legg, Anal. Chim. Acta 279 (1993) 195–202.

[2] Z. Shakhsher, W.R. Seitz, K.D. Legg, Anal. Chem. 66 (1994) 1731–1735.
[3] Z. Zhang, Z. Shakhsher, W.R. Seitz, Mikrochim. Acta 121 (1995) 41–50.
[4] Vicki L. Conway, Ph.D. Thesis, University of New Hampshire, 1994.
[5] Michael T. Rooney, Ph.D. Thesis, University of New Hampshire, 1996.
[6] Michael T. Rooney, unpublished data.
[7] P.J. Flory, Principles of Polymer Chemistry, Cornell University Press, Ithaca, NY, 1953, pp. 585–589.

ELSEVIER

Talanta 44 (1997) 1699–1703

Talanta

Hexaacetato calix(6)arene as the novel extractant for palladium

V.J. Mathew, S.M. Khopkar *

Department of Chemical Technology, University of Bombay, Bombay 400 019, India

Received 15 July 1996; received in revised form 10 December 1996; accepted 23 December 1996

Abstract

A novel method is proposed for the solvent extraction of palladium. A superamolecular compound, hexaacetato calix(6)arene in low concentration in toluene quantitatively extracts microgram concentration of palladium at pH 7.5. It can be stripped from the organic phase with 2 M nitric acid and determined spectrophotometrically as its stannous chloride complex at 635 nm. The probable composition of the extracted species is $Pd(HR)_2Cl$. As low as 1×10^{-3} M of extractant is adequate for quantitative extraction. Toluene was the best diluent. With nitric and perchloric acid (1.5–3 M) the stripping was complete. Palladium was separated in large ratios from alkali and alkaline earths (1:50). The main group elements were tolerated in higher ratios (1:25), but ions like zinc, cadmium, iron, nickel, platinium, thorium, vanadium and molydenum were tolerated at low concentrations (1:1). The ions showing strong interference were copper, chromium. The relative standard deviation is $\pm 1.1\%$. © 1997 Elsevier Science B.V.

1. Introduction

Calix(*n*)arenes [1] are superamolecular compounds which have a three dimensional network of 4–8 bridged phenolic units with varying annular space in which metals can be trapped due to the ionic interaction [2,3]. As the properties of calixarenes can be varied by chemical modification or effective substitution it was facinating to investigate the solvent extraction behaviour of metals. Calixarene form stable metal complexes [4]. The planar structures were obtained for complexes of crown ethers with alkali and alkaline earths [5], however, cryptands formed three dimensional structure with transition metals improving their selectivity [5]. The varying annular size ranging from 1.4–2.4 Å in calixarenes facilitated separation of metals with varying atomic sizes.

Calixarenes was used for solvent extraction of alkali and alkaline earths [6]. Calix(4)arene amides were also used for extracting and studying solution thermodynamics of complexation of s-block metals [7]. The ketone derivative of calix(4)arene was used for extraction of palladium and silver [8] from highly acidic nitrate media. A new calixarene, diphenylphosphino calix(4)arene methyl ether, was also used for extraction of alkali metals and few transition elements [9]. The carboxylate derivatives of calixarenes were used for the extraction of trivalent lanthanides [10–12]. *N*-Dimethyldithiocarbomoylethoxy-substituted calix(4)arene was used for extraction of the chlorocomplexes of divalent pal-

* Corresponding author. Fax: +91 22 57833245.

PII S00 9-9140(97)00013-1

ladium and platinum [13]. The thia crownether [14,15] and azacrown analogues [16] of dibenzo18crown6 were used for the separation of palladium from platinum, gold and iron. Some crownethers were also used in stripping voltametric studies of palladium [17]. The *p*-tertbutyl calix(6)arene was used for first time for extraction of palladium from ammonical alkaline solutions to ascertain nature of the extracted species [18] as 1:1.

Calix(6)arene occupies intermediate position between calix(4)arene and calix(8)arene in relation to conformational mobility. The orthosubstituted derivatives were effective in complexation, extraction and transport of metal ion. Our work on extraction of cobalt with hexaacetato calix(6)arene [19] promoted us to investigate similar method for extraction of palladium. Such method is described in this paper.

2. Experimental

The hexaacetato *p*-tertiary butyl calix(6)arene derivative (Fig. 1) was prepared by similar procedure as described earlier [19].

The product was characterised with IR, 1H NMR, 13C NMR spectroscopy. The m.p. and elemental analysis also furnished useful information. The solubility of the extractant in organic phase was reasonable at room temperature to facilitate solvent extraction studies.

A stock solution of palladium was prepared by dissolving 1.66 g of palladium chloride (Johnson Mathey, England) in 1 l of distilled water containing 5 ml of 11.5 M hydrochloric acid. The solution was standardised gravimetrically with dimethylglyoxine [20]. It contained 100 μg/ml of palladium. The solution containing 5 μg/ml of palladium was prepared by 20-fold dilution.

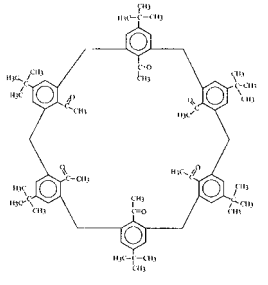

Fig. 1. Structure of calix(6)arene and acetyl derivative.

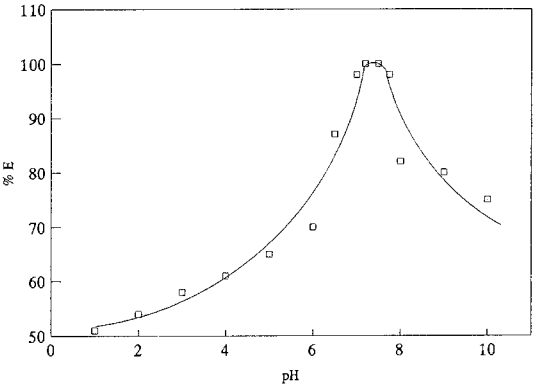

Fig. 2. Extraction as a function of pH.

3. General procedure

An aliquot of solution containg palladium was taken and its pH adjusted to 7.5 with diluted ammonia or hydrochloric acid. Then, the solution was made to 10 ml. It was transferred into a separating funnel; 10 ml 1×10^{-3} M of hexaacetato calix(6)arene in toluene was added to it. The resulting solution was equilibrated for about 10 min. The two phases were allowed to settle and separate. Palladium from organic phase was stripped with 2 M nitric acid. Palladium from the aqueous phase was determined spectrometrically [21] as its complex with stannous chloride at 635 nm. The amount of palladium was computed from the calibration curve.

4. Results and discussion

4.1. Extraction as the function of pH

The extraction of palladium was carried out at varying pH from 1.0–10.0 (Fig. 2). The extraction commenced at pH 1.0 (52.4%) and at pH 4.0 it was (60%). The extraction was quantitative between pH 7.0–7.4. shows the equilibrium in

Table 1
Extraction as the function of calix(6)arene concentration

Hexaacetato calix(6)arene (1×10^{-4} M)	*E* (% Extraction)	*D* (Distribution ratio)
0.1	2.5	0.30
0.5	35.0	0.50
1.0	46.3	0.86
2.0	62.2	1.64
5.0	89.0	8.11
8.0	95.1	19.54
10.0	99.9	999.00
50.0	99.1	110.10

pH range 7.0–7.4 is favourable for the formation of the complex. At higher pH of extraction there is the possibility of hydrolysis. This indirectly promotes competing equilibria with the formation of complex, resulting in a decrease in extraction.

The probable mechanism of extraction can be summarised as:-

1. $(HR)_{aq} = (HR)_{org}$, where HR = hexaacetato calix(6)arene
2. $Pd + 2HR = Pd(HR)_2 + 2H^+$ (in aqueous phase)
3. $Pd(HR)_2 + Cl^- = Pd(HR)_2Cl$ (Ion pair formation in aqueous phase)
4. $(Pd(HR)_2Cl)_{aq} = (Pd(HR)_2Cl)_{org}$ (Transformation to organic phase)

5. Extraction as a function of calix(6)arene concentration

Palladium was extracted at pH 7.2 with varying concentrations of hexaacetato calix(6)arene. The concentration was varied from 0.1×10^{-4} to 50×10^{-4} M. The extraction was 46.3% with 1×10^{-4} M of extractant. However, the extraction was quantitative with 10×10^{-4} M of extractant (Table 1). With increased concentration of extractant the phase separation is rendered difficult. We used 10×10^{-4} M of the extractant for routine work.

6. Extraction with various diluents

The different diluents with varying dielectric constant were used. The 0.001 M of calix(6)arene in various diluents was equilibrated at pH 7.2 with equal volumes of aqueous phase containing palladium (Table 2). Only with toluene as the diluent, the extraction was complete. The extraction never exceeded 80% with all other diluents. With cyclohexane and nitrobenzene the extraction was $< 40\%$. This showed non-polar diluents were best. This is because in polar solvents the association of cationic species with extraction is minimum, while in nonpolar solvents in absence of repulsive process the extraction is maximum. Toluene was preferred as the diluent as it has minimum toxicity and offers better phase separation.

Table 2
Extraction with various diluents

Solvent	Dielectric constant	*E* (% Extraction)	*D* (Distribution ratio)
Dichloromethane	9.08	78.0	3.55
Dichloroethane	10.50	74.4	2.90
Chloroform	4.80	78.0	3.55
Carbon tetrachloride	2.24	74.4	2.90
Benzene	2.28	90.2	9.24
Toluene	2.30	99.9	
Xylene	2.38	68.3	2.15
Cyclohexane	2.0	39.0	0.64
Nitrobenzene	34.8	36.6	0.68

Table 3
Effect of stripping agent

M	HCl		HNO_3		H_2SO_4		$HClO_4$	
	%E	D	%E	D	%E	D	%E	D
0.5	–	–	87.8	7.20	65.4	1.8	93.9	15.40
1.0	78.0	3.55	89.6	6.45	70.7	2.4	95.1	22.54
1.5	78.0	3.55	99.9	999.0	73.2	2.7	96.3	26.32
2.0	79.3	3.82	99.9	999.0	75.0	3.0	93.9	15.40
3.0	95.1	22.52	99.1	110.1	75.8	3.1	92.5	12.30

7. Effect of stripping agents

After extraction of palladium at pH 7.2 with 1×10^{-3} M of extractant it was stripped with various mineral acids as the stripping agents (Table 3). With 3 M hydrochloric the stripping was more than 95.1%, with 0.5 M sulphuric acid it was 85.36%, or 1.5 M perchloric acid it was 96.34%. With 2 M nitric acid the stripping was quantitative because at this molarity the optimum conditions of extraction were reversed. Hence 2 M nitric acid was used as the stripping agent.

8. Nature of extracted species

The nature of extracted species was ascertained by plotting graphs of Log D against Log (HR) at fixed pH 7.2. The slope was 1.9 (Fig. 3). Therefore the probable composition of the extracted species is 1:2, i.e. $Pd(HR)_2$. It may be assumed that the calix(6)arene derivative exists in the 'winged' conformation, i.e. '1,4-alternate' conformer. This situation gives rise to a conformation in which the aryl groups in the 1- and 4-positions project outward like a pair of wings perpendicular to the aryl groups in the 2-, 3-, 5- and 6-positions which are colinear, forming a channel into which other molecules might comfortably fit. The metal ion is probably held between two calixarene moieties by ionic attraction to the substituted oxygens. It is presumed that no true covalent bond formation exists, but an ion-dipole electrostatic attraction between the metal ion and oxygen atoms is possible.

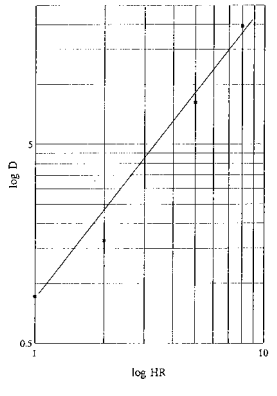

Fig. 3. Log D versus log calixarene concentration.

Table 4
Effect of diverse ions

Foreign ion	Amount tolerateed (μg)	Ratio
Li^+, Na^+, K^+, Cs^+	1500	1:50
Ca^{2+}, Sr^{2+}, Ba^{2+}	1500	1:50
Mg^{2+}, Al^{3+}, In^{3+}, Se^{4+}, Mn^{2+}	750	1:25
Zn^{2+}, Cd^{2+}	300	1:10
Mo^{6+}, V^{3+}, Th^{4+}	150	1:5
Fe^{3+}, Co^{2+}, Ni^{2+}, Pt^{2+}	30	1:1
Cu^{2+}, Cr^{3+}, Rh^{3+}, UO_2^{2+}, SCN^-	Nil	0
Cl^-, Br^-, SO_4^{2-}, SO_3^{2-}, $S_2O_3^{2-}$	3000	1:100

Pd, 30 μg; pH 7.2; 0.001 M in toluene.

9. Effect of diverse ions

Palladium was extracted in the presence of large number of diverse ions (Table 4). The tolerance limit was set as the amount of foreign ion causing $\pm 2\%$ error in recovery of palladium. All the anions (excepting thiocyanate which in fact is strong complexing ligand for palladium) were tolerated in the ratio exceeding 1:100. The alkali and alkaline earths were tolerated in the ratio of 1:50 while most of the main group elements were tolerated in the ratio of 1:25. Some transition metals were tolerated in ratios less than 1:10. While iron, cobalt, nickel, platinum were tolerated in ratios of 1:1, however, copper, chromium, rhodium, uranium showed strong interference.

The proposed method is compared with the existing methods of separations. The solvating solvents [22] like tributylphosphate did not permit extraction from nitric acid but it extracted it from thiocyanate media. The extraction with B-diketones was incomplete. The extraction with oxine and oxime offered weakly coloured complexes facilitating direct spectrophotometry. Thus, extraction with hexaacetato calix(6)arene was possible at very low concentration of reagent. The period of equilibrium was minimum. The use of non-toxic solvents like toluene was favourable. The method permitted separation of palladium from iron, cobalt, nickel and platinum which were commonly associated. The calixarene can be synthesised at low cost, with high yield and best purity. The proposed method is simple, rapid and selective. It permits separation and determination of palladium within 30 min. The relative standard deviation is $\pm 1.1\%$.

References

[1] C.D. Gutsche, Calixarenes, in: J.F. Stoddart (Ed.), Monograph on Superamolecular Chemistry, Royal Society of Chemistry, London, 1989.
[2] V. Bohmer, Angewante Chemi. 34 (1995) 713.
[3] Mayuri Gandhi and S.M. Khopkar, Bull. Assoc. Nucl. Chem., 10 (1994) 20.
[4] D.M. Roundhill, Progress in Inorg. Chem. 43 (1995) 533.
[5] Mayuri Gandhi and S.M. Khopkar, J. Sci. Ind. Res., 55 (1996) 139.
[6] K. Ohto, M. Yano, K. Inone, T. Yamamoto, M. Goto, F. Nakashio, T. Nagasaki, S. Shinkai, in: D.H. Logsdail and M.J. Slater (Eds.), Proc. Int. Conf. Solvent Extraction (York, England, 1993), Elsevier, Amsterdam, 1993, pp. 364.
[7] F. Arnaudneu, G. Barrett, S. Fanni, D. Marrs, W. McGregar, M.A. Mckervey, M.J. Schwingwelli, V. Vetrogen and S. Wechsler, J. Chem. Soc. Perkins Trans. 2, 113 (1995) 453.
[8] K. Ohto, E. Muakami, K. Shivatsuchi, K. Inoue, M. Iwasaki, Chem. Lett., 173 (1996).
[9] F. Hamada, T. Fukugaki, K. Murai, G.W. Orr, J.L. Atwood, J. Incl. Phenom. Mol. Recogn. Chem. 10 (1991) 57.
[10] F. Nakashio, S. Shinkai, T. Nagasaki, Anal. Sci. 11 (1995) 893.
[11] R. Ludwig, K. Inoue, T. Yamamoto, Solvent Extr. Ion Exch. 11 (1993) 311.
[12] R. Ludwig, K. Inoue, S. Shinkai, K. Gloe, in: D.H. Logsdail and M.J. Slater (Eds.), Proc. Int. Conf. Solvent Extraction (York, England, 1993), Elsevier, Amsterdam, 1993, pp. 273.
[13] A.T. Yordanov, J.T. Mague, D.M. Roundhill, Inorg. Chim. Acta 240 (1995) 441.
[14] E. Lachonig, M.C. Zapink, Talanta 37 (1990) 1011.
[15] O. Heitzsch, K. Gloe, H. Stephan, E. Weber, Solvent Extr. Ion Exch. 12 (1994) 475.
[16] M.K. Beklemische, S.E. Panfilova, A.B. Volyuskii, N.M. Kuzmin, Y.A. Zoltov, Yu. A. Ver. Musk. Uni. Ser. Z. Khim., 30 (1989) 168; AA18 (1990) 80.
[17] M.Y. Tsymbal, I.Y. Turjan, Z.A. Temerdshev, K.Z. Brainina, Electroanalysis 6 (1994) 113.
[18] Y. Masuda, T. Sawano, E. Sekido, Anal. Sci. 9 (1991) 31.
[19] Anita Gupta and S.M. Khopkar, Talanta 42 (1995) 1493.
[20] A.I. Vogel, Quantitative Inorganic Analysis, 3rd Edn., Wiley, New York, 1962, pp. 511.
[21] F.D. Snell, Photometric and Fluorimetric Methods of Analysis, Wiley, New York, 1978.
[22] A.K. De, S.M. Khopkar, R.A. Chalmers, Solvent Extraction Metals, Van Nostrand, London, 1970.

ELSEVIER

Talanta 44 (1997) 1705–1718

Talanta

On the behaviour of cysteine as ligand of cadmium(II)

Emilio Bottari *, Maria Rosa Festa

Dipartimento di Chimica, Università 'La Sapienza', P. le A. Moro 5, 00185 Roma, Italy

Received 13 September 1996; received in revised form 26 December 1996; accepted 29 December 1996

Abstract

The ability of cysteine to form complexes with cadmium(II) in aqueous solutions has been investigated at 25°C and in constant ionic medium NaCl at two different concentrations, 1.00 and 3.00 mol l^{-1}. The presence of chloride ions was necessary to avoid the precipitation of cadmium(II). Two kinds of measurements were carried out. The electromotive force of galvanic cells containing glass and cadmium amalgam electrodes was measured as a function of cadmium and hydrogen ion concentrations in acid or moderately alkaline solutions in order to obtain the free concentration of cadmium(II) and hydrogen ions. The experimental data obtained in 1.00 mol l^{-1} NaCl were explained by assuming the presence of CdHL and CdH_2L_2, while those obtained in 3.00 mol l^{-1} NaCl were accounted for with the formation of CdHL, CdH_2L_2, CdH_3L_3 and CdH_2L_3. Moreover, polarographic measurements were carried out under the same experimental conditions but in alkaline solutions, and the formation of CdL_2 and CdL_3 was assumed from the shift of E(1/2) of cadmium(II) with an excess of cysteine. The stability constants of the assumed species were determined. Protonation constants of cysteine in 1.00 and 3.00 mol l^{-1} NaCl have been also determined. A comparison with the behaviour of serine and α-aminopropanoate towards cadmium(II) is proposed.

Keywords: Cadmium(II) complexes; Cysteine complexes; Sulfur containing amino acids complexes

1. Introduction

Among aminoacids, the sulfur-containing aminoacids have raised interest in many respects. Hughes [1] showed that the sulfhydryl group of serum albumin combines with mercury(II) and Benesch et al. [2] that it forms complexes with silver. Klotz et al. [3], from absorption spectra studies, found that the order of affinity for the sulfhydryl group of bovine albumin is lead(II) > cadmium(II) > zinc(II) > copper(II).

The total concentrations for blood plasma models [4] show that among the amino acid components, cysteine (2-amino-3-mercaptopropanoic acid) is present at the highest concentration, reaching a value ≥ 100 μmol l^{-1}. The ratio between cysteine and cation concentration is higher than 2/1.

As it seems of interest to study quantitatively the equilibria between cysteine ($H_2NCH(CH_2SH)COOH = H_2L$) and cations, the main and more recent surveys of literature on this subject [5–7] report only few papers. In particular the behaviour of cysteine as ligand of cadmium(II) was studied very little.

* Corresponding author.

0039-9140/97/$17.00
PII S00 9-9140(97)00015-5

According to Li et al. [8], the formation of a precipitate prevents the determination of the stability constants of cadmium(II) cysteinate complexes at an ionic strength of 0.15 mol l^{-1} (KNO_3). Also Walker et al. [9] confirmed that the cadmium(II)—cysteinate system precipitated at 25°C and in 3.00 mol l^{-1} $NaClO_4$ even at very low concentration ($\sim 10^{-3}$ mol l^{-1}). They explained their potentiometric measurements with the formation of two species CdL and CdL_2 with $\log \beta = 12.88$ and 19.63, respectively. More recently, Cole et al. [10] asserted again that cadmium(II) forms an insoluble complex with cysteinate, but only in the range $5.0 \leq pH \leq 7.5$, thus, a large proportion of the formation curve could be obtained. They explain their potentiometric measurements at 37°C and 0.150 mol l^{-1} NaCl by assuming the presence of the species: CdL ($\log \beta_{1,1,0} = 10.3$), CdL(OH) ($\log \beta_{1,1,-1} = 2.42$), CdL_2 ($\log \beta_{1,2,0} = 16{,}92$), CdL_2H ($\log \beta_{1,2,1} = 24.97$), CdL_2H_2 ($\log \beta_{1,2,2} = 30.93$), CdL_3 ($\log \beta_{1,3,0} = 19.78$), CdL_3H ($\log \beta_{1,3,1} = 29.21$). The same authors determined the protonation constants of the ligand ($\log k_1 = 10.10$, $\log k_1k_2 = 18.03$ and $\log k_1k_2k_3 = 19.99$) by using potentiometric titrations carried out by means of a glass electrode. Most of the complexes found by Walker et al. [9] and Cole et al. [10] are different from one another. The latter authors propose the formation of complexes also with the participation of OH or H. These differences are probably due to the narrow pH range investigated because of the precipitation and the different experimental conditions.

More recently Berthon [11], by commenting upon the results obtained by the above researchers for investigating Cd(II)-cysteine, has proposed the constants of Cole et al. [10] as tentative.

Since cadmium(II) is one of the more toxic metals in the environment, the cases of cadmium poisoning are increasing and the assimilation of cadmium from man depends on the form under which the metal is present. It seems therefore very important to know the behaviour of aminoacids (in this case cysteine) present at high level in food and in blood towards cadmium(II). As cadmium(II) behaves similarly to zinc(II) its block of the normal process of zinc metabolism and its accumulation for the kidneys, liver and blood vessels can be supposed. On the other hand, as we have studied the complex formation between many amino acids (glycine, serine, histidine, ornithine, aspartate, glutamate) and cadmium(II) [12–15], we intend to investigate the behaviour of sulfur-containing aminoacids towards cations.

As the aim of this work was to study cysteine as ligand of cadmium(II) in a wide range of concentrations of the reagents, it was necessary to prepare all the solutions in a constant ionic medium. Use of an ionic medium of high concentration with respect to the reagents, allowed to assume as negligible the activity coefficients variations in spite of the change of the concentrations of the reagents [16].

By taking into account the results of earlier researchers [8–10] and looking for a suitable ionic medium, we found that, at high chloride concentration, it was possible to obtain clear solutions of cadmium(II) in the presence of cysteine. With 1.00 mol l^{-1} NaCl as an ionic medium, clear solutions were obtained in a limited range of hydrogen ion concentrations, but in 3.00 mol l^{-1} NaCl no precipitation occurred in the whole range of hydrogen ion concentrations, even after a day and at different ratios. It is reasonable to suppose that the high Cl^- concentration partially complexes cadmium(II) and avoids its precipitation.

For the above reasons we studied the behaviour of cysteine towards cadmium(II) at 25°C and in both 1.00 and 3.00 mol l^{-1} NaCl. The protonation constants of cysteine (L^{2-}) were also determined under the same experimental conditions.

2. Experimental

2.1. Method

Complexation between cadmium(II) and cysteine was studied assuming that the reagents Cd^{++}, H^+ and L^{2-} react according to the following equilibrium:

$$qCd + pH + rL \Leftrightarrow Cd_qH_pL_r \quad \beta_{q,p,r}$$

where charges are omitted, $q \geq 1$, $p \geq \leq 0$, $r \geq 1$ and the constant $\beta_{q,p,r}$ is defined according to the following relationship: $c_{Cd_qH_pL_r} = \beta_{q,p,r}\ c_{Cd}^{q}\ c_h^{p}\ c_L^{r}$. Here and in the following, small c_x and capital C_x stand for free and total concentration of the generic species x, respectively. C_H represents the analytical excess of hydrogen ion with respect to the ionic medium. Negative values of C_H correspond to hydroxyde ions concentrations and negative p values denote the presence of OH in the species formed.

To find the prevailing q, p and r values and the values of $\beta_{q,p,r}$, 2 kinds of approaches were performed. In the first one, electromotive force (e.m.f.) measurements of the following galvanic cells were performed:

$(-)$Cd(Hg)/SolutionS/R.E.$(+)$ (I)

$(-)$R.E./SolutionS/G.E.$(+)$ (II)

R.E. and G.E. are reference and glass electrodes, respectively, and Cd(Hg) the amalgam electrode. Solution *S*, prepared in the constant ionic medium, alternatively 1.00 or 3.00 mol l^{-1} NaCl, had the following general composition:

C_{Cd} mol l^{-1} in Cd^{2+}, C_H mol l^{-1} in H^+, C_L mol l^{-1} in cysteine, (Y-2C_{Cd}-C_H) mol l^{-1} in Na^+ and Y mol l^{-1} in Cl^-. Y is the concentration of the ionic medium, 1.00 or 3.00 mol l^{-1} NaCl.

The e.m.f. of the cells Eq. (I) and Eq. (II), at 25°C and in mV units, can be expressed, respectively, as follows:

$$E_I = E_I^\circ - 29.58 \log c_{Cd} - Ej;$$

$$E_{II} = E_{II}^\circ + 59.16 \log c_h + Ej$$

where E_I° and E_{II}°, 2 constants and Ej (the liquid junction potential) were determined in the first part of each e.m.f. measurement series, in the absence of the ligand, when $C_{Cd} = c_{Cd}$ and $C_H = c_h$. The liquid junction potential, which depends only on c_h [16], under these experimental conditions was found to be $Ej = -61c_h$ and $-16c_h$ in 1.00 mol l^{-1} and 3.00 mol l^{-1} NaCl, respectively. After the determination of E_I°, E_{II}° and Ej, the concentration of the ligand was increased gradually, whereas C_{Cd} and C_H were kept constant for each series of measurements. From the measurement of E_I and E_{II}, the values of c_{Cd} and c_h could be obtained for each point.

The analytical values of C_{Cd}, C_L and C_H and those measured c_{Cd} and c_h, are the experimental data provided by this approach.

In the investigation carried out at Y = 1.00 mol l^{-1}, titrations were interrupted at $-\log c_h \leq 5$, because precipitation occurred beyond this limit. E.m.f. measurements carried out in Y = 3.00 mol l^{-1} could be continued further but only until $-\log c_h \sim 8$, because of two different difficulties. The first was the response of the glass electrode which, in 3.00 mol l^{-1} of Na^+ agrees with that of the H_2 electrode only until $-\log c_h \leq 9$ as explained below. The second was the wrong response of the cadmium amalgam electrode, which does not reach stable e.m.f. values at high cysteine concentration and at $-\log c_h \geq 8$.

At very high $-\log c_h$ values, the polarographic approach was used. The shift of the $E_{(1/2)}$ of cadmium(II) induced by the addition of an excess of cysteine was measured at selected and constant $-\log c_h$ values. The $E_{(1/2)}$ value of a solution of the following general composition was determined in the absence of the ligand and at $-\log c_h \leq 3$:C_{Cd} mol l^{-1} in Cd^{2+}, C_H mol l^{-1} in H^+, (3-2C_{Cd}-C_H) mol l^{-1} in Na^+ and 3.00 mol l^{-1} in Cl^- = solution P.An excess of NaOH and ligand was added to solution P to reach the selected value of C_H in the same ionic medium. Keeping C_{Cd} and C_H constant, the concentration of the ligand was gradually increased.

Based on the protonation constants determined below, it was assumed that at $-\log c_h \geq 12$, $C_H = c_h$ or $C_{OH} = c_{OH}$ and $C_L = c_L$. Several series of measurements were carried out at different C_H and C_{Cd}. The experimental data $\Delta E_{(1/2)}$, C_{Cd}, C_H and C_L were elaborated according to De Ford and Hume [17,18] and Rossotti and Rossotti [19] to obtain the value of q, p and r and the relative stability constants in these experimental conditions.

Measurements of the e.m.f. of the cell:

$(-)$Pt,H_2/Solution T/R.E.$(+)$ (III)

were performed to obtain k_n, i.e., the protonation constants of L^{2-}, defined as follows: $c_{H_nL} = k_n\ c_h\ c_{H_{n-1}L}$. For cell (III), the liquid junction potential due to OH^- was calculated to be negligible in 3.00 mol l^{-1} NaCl, in 1.00 mol l^{-1} NaCl it was

determined as $E'j = -8c_{OH}$. Solutions T were prepared in 1.00 or 3.00 mol l^{-1} NaCl, respectively, so that protonation constants K_n could be determined at 25°C and in both ionic media. E.m.f. values of cell (III) reached equilibrium within 1 h after each addition and their value remained constant for several hours also in the presence of cysteine.

2.2. Reagents

Cadmium(II) chloride was prepared and analysed as described previously [14]. Hydrochloric acid, sodium hydroxyde and sodium chloride were prepared and analysed as described in ref. [20]. Preparation and behaviour of cadmium amalgam (0.01% weight of cadmium) have been described earlier [21]. Particular care had to be taken for the purification and conservation of cysteine in order to avoid its possible oxidation. A Sigma (DL-cysteine product) was twice recrystallized from bidistilled water. A DL-cysteine product was used because preliminary tests carried out with D-, L-, and DL-cysteine did not give significant differences and other D-, L, and DL-ligands (for example aspartate [22]) did not exhibit stereoselectivity. The purified product was dried by keeping it in a vacuum desiccator in the presence of P_2O_5 and under N_2 atmosphere. Its stoichiometric composition was checked by iodometric and thermometric analysis. The results of several determinations agreed within $\pm 0.1\%$ with the theoretical composition $H_2N\text{-}CH(CH_2\text{-}SH)COOH = H_2L$. However, from periodical check, it could be deduced that, in spite of the care paid to keep cysteine, it deteriorated after about 10 weeks of the purification. It was necessary to recrystallize again the product and to treat it as described above. Test solutions were prepared by checking cysteine the day before the use. The contact with air was minimized by using N_2 atmosphere during the preparation of the solutions and the measurements.

2.3. Apparatus

E.m.f. measurements of cells (I), (II) and (III) were carried out by using a Keithley mod. 199 or a Leeds and Northrup mod K5 and Radiometrer pHM64 or Metrohm mod. 654, respectively. The potentiometric salt bridge and the reference electrode (R.E. = Ag, AgCl/ Y mol l^{-1} NaCl, saturated with AgCl) were similar to those previously described [16]. The values of $E_I\text{-}E_I^\circ$ and $E_{III}\text{-}E_{III}^\circ$ were reproducible within ± 0.1 mV, while those of $E_{II}\text{-}E_{II}^\circ$ within ± 0.2 mV. The values of E_{III} were constant 30–45 min after each addition and remain constant within ± 0.1 mV overnight.

Voltammetric measurements (DP50) were carried out with a VA processor Metrohm mod. 646 connected with a Metrohm VA stand mod. 647. As the polarographic reference electrode was the same, $\Delta E_{(1/2)}$ could be calculated by subtracting the value of $E_{(1/2)}$ measured after the addition of the alkaline solution of the ligand, from that of the solution P. The $\Delta E_{(1/2)}$ values were reproducible within ± 3 mV. All measurements were performed at 25°C. Nitrogen and hydrogen used for the H_2 electrode for the determination of the protonation constants of cysteine (L^{2-}) were ultrapure gas 99.999%.

The response of the glass electrode was checked against that of the H_2 electrode assumed to be correct. Both measurements agreed within ± 0.1 mV until $-\log c_h \leq 9$, but beyond this limit the glass electrode value started to deviate from H_2 electrode markedly and consequently related e.m.f. measurements could not be considered reliable.

3. Results and calculations

Two kinds of experimental data have been obtained in this investigation: e.m.f. measurements at two ionic medium concentrations and polarographic data.

3.1. E.m.f. measurements

3.1.1. Protonation constants of cysteine

According to Berthon [11], the relatively high value of $\log k_1$ of cysteine, makes its accurate determination difficult since a pH range where the GE response becomes less reliable is investigated. Furthermore, value of $\log k_3$ must be deter-

mined at high C_H, with possible variation in the ionic strength. By using 3.00 mol l^{-1} NaCl as an ionic medium and the H_2 electrode we overcame both difficulties.

Measurements of e.m.f. of cell (III) were performed at 1.00 and 3.00 mol l^{-1} NaCl, respectively. From the knowledge of C_H, C_L and $-\log c_h$ obtained from the e.m.f. measurements, the protonation function Z was obtained for $C_L = 0.010$, 0.025 and 0.050 mol l^{-1}, in the range $1 \leq -\log c_h \leq 11$ and $0.3 \geq C_H \geq 0$. Since Z was independent of C_L for both ionic medium concentrations, polymeric species were not present in appreciable amount and then, from the dependence of Z *versus* $-\log c_h$, the values of protonation constants of cysteine were obtained. Refined k_n and k'_n values and their limits of error, obtained by using a computer program BSTAC [23], are collected in Table 1.

3.1.2. Complex formation in ionic medium 1.00 mol l^{-1} NaCl

Measurements were performed at different C_H (0.100, 0.070, 0.050, 0.035 and 0.025 mol l^{-1}) and different C_{Cd} (2.00, 1.00, 0.50 and 0.25) $\times 10^{-3}$ mol l^{-1}. Unfortunately, it was not possible to carry out measurements at higher C_{Cd} concentrations and even for $C_{Cd} = 2.00$ and 1.00×10^{-3} mol l^{-1}, e.m.f. values were not stable at $-\log c_h \geq 4.5$. The slow formation of precipitate precludes the increase in the ligand concentration.

Table 1
Protonation constants of cysteine in both ionic media studied at 25°C

NaCl	$\log k_1$	$\log k_1k_2$	$\log k_3$
1.00 mol l^{-1}	10.26 ± 0.02	18.48 ± 0.04	2.04 ± 0.10
3.00 mol l^{-1}	10.56 ± 0.02	19.09 ± 0.03	2.26 ± 0.10
Literature values			
KCl 0.2 mol l^{-1}	10.16	18.26	1.86 [29,30]
$NaClO_4$ 0.5 mol l^{-1}	10.37	19.14	2.50 [31]
$NaClO_4$ 1.0 mol l^{-1}	10.35	19.02	1.96 [31]
$NaClO_4$ 3.0 mol l^{-1}	10.69	19.40	2.40 [32]

For cadmium(II), the mass balance equation can be written as follows:

$$C_{Cd} = c_{Cd} + \Sigma\Sigma\Sigma q\beta'_{q,p,r} c_{Cd}^q c_h^p c_L^r \quad (1)$$

where q, p, r and $\beta'_{q,p,r}$ in this case are referred to 1.00 mol l^{-1} NaCl as an ionic medium. In Eq. (1) hydrolytic species of cadmium(II) were neglected based on the studies of Biedermann and Ciavatta [24].

The $\eta[=\log(C_{Cd}/c_{Cd})]$ function, calculated for each experimental point from Eq. (1), is plotted *versus* $-\log c_h$ in Fig. 1.

Fig. 1 shows that points obtained at the same C_H but at C_{Cd} 0.50 and 0.25×10^{-3} mol l^{-1} fall on the same curve. By increasing C_{Cd} small deviations could be observed. Based on the results obtained in 3.00 mol l^{-1} NaCl where precipitation does not occur, we supposed that these deviations can be attributed to e.m.f. measurements relative to solutions which do not attain real equilibrium.

To verify the presence of mixed species with protons, the free concentration of ligand, c_L, was calculated from the mass balance equation of C_H, which can be written as follows:

$$C_H = c_h + \Sigma n k'_n c_h^n c_L + \Sigma\Sigma\Sigma p\beta'_{q,p,r} c_{Cd}^q c_h^p c_L^r \quad (2)$$

where k'_n are the protonation constants of the ligand of Table 1, hydrolytic species of cadmium(II) are neglected and the constants refer to 1.00 mol l^{-1} NaCl, as an ionic medium. As only $C_{Cd} = 0.50$ and 0.25×10^{-3} mol l^{-1} points are considered, first approximation values of c_L for each point can be calculated by means of Eq. (2) by considering the last term as negligible.

By plotting η *versus* $-\log c_L$, points fall on different curves at different values of C_H. Since η is an increasing function of C_H, complexes containing protons ($p > 0$) are also formed. From the k'_n values and the $-\log c_h$ range investigated, it can be inferred that most of the cysteine is in the HL form. Thus, it can be supposed that cadmium(II) is bound to the form HL of cysteine. To verify this hypothesis, η is plotted *versus* $-\log(c_L c_h)$ in Fig. 2, where all the points fall on the same curve, independently of C_{Cd} and C_H.

The values of the constants obtained by applying the method of the normalized curves of Sillén

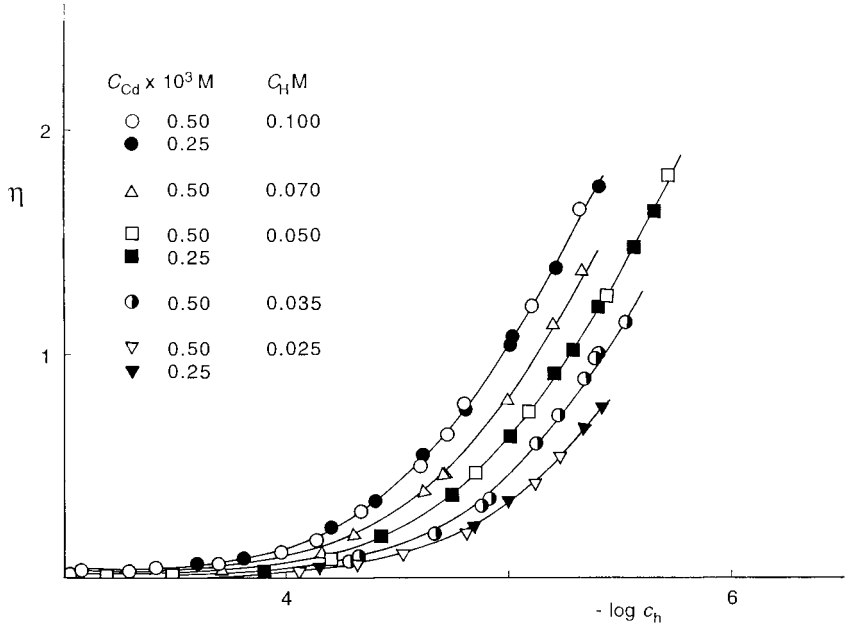

Fig. 1. Experimental data obtained in 1.00 mol l^{-1} NaCl, as ionic medium. Points at $C_{Cd} \geq 0.50 \times 10^{-3}$ mol l^{-1} are not plotted. Curves are calculated using constants in Table 2.

[25] and by using a computer program BSTAC [23] and practically coincident, are collected in Table 2.

3.1.3. Complex formation in ionic medium 3.00 mol l^{-1} NaCl

The high concentration of ionic medium was employed to study a wider range of concentration of the reagents and avoid the precipitation.

Measurements of e.m.f. of the cells (I) and (II) were performed in the range $1 \leq -\log c_h \leq 8$, at $C_H = 0.300$, 0.175, 0.100, 0.050 and 0.025 mol l^{-1} and at $C_{Cd} = (5.00,\ 2.50,\ 1.00,\ 0.50) \times 10^{-3}$ mol l^{-1} so that the formation of polynuclear or mixed complexes with a high ratio p/r could be favoured.

By applying the above explained procedure, the function η could be calculated. Fig. 3, where η is plotted *versus* $-\log c_h$, shows that points at the same C_H and different C_{Cd} fall on the same curve. Therefore, polynuclear complexes in cadmium(II) are not present in appreciable concentration and then $q = 1$. Since points obtained in the range $0.005 \geq C_{Cd} \geq 0.0005$ mol l^{-1} lie on the same curve, the deviations observed at 1.00 mol l^{-1} NaCl were to be attributed to starting precipitation. Thus the absence of polynuclear complexes even at ionic medium 1.00 mol l^{-1} NaCl is confirmed.

To find the prevailing values of p and r and the values of $\beta_{1,p,r}$, the free concentration of the ligand c_L, was calculated for each point by means of Eq. (2), by neglecting the last term and by using the k_n values determined in 3.00 mol l^{-1} NaCl. The c_L values obtained from Eq. (2) can be considered only as a first approximation. Although all the test solutions were prepared so that $C_{Cd} \leq 0.02\ C_H$, at the highest C_{Cd} values (i.e., 0.005 mol l^{-1}) refined $-\log c_L$ are different with respect to the first approximation $-\log c_L$. The difference never exceeds 0.02 units, but, the high number of protons participating to the complex formation implies significant differences in the calculation of the theoretical curves.

Fig. 4, where η is plotted as a function of $-\log c_L$, shows that points obtained at different C_H fall on different curves so that η is an increasing function of C_H. Therefore, protonated com-

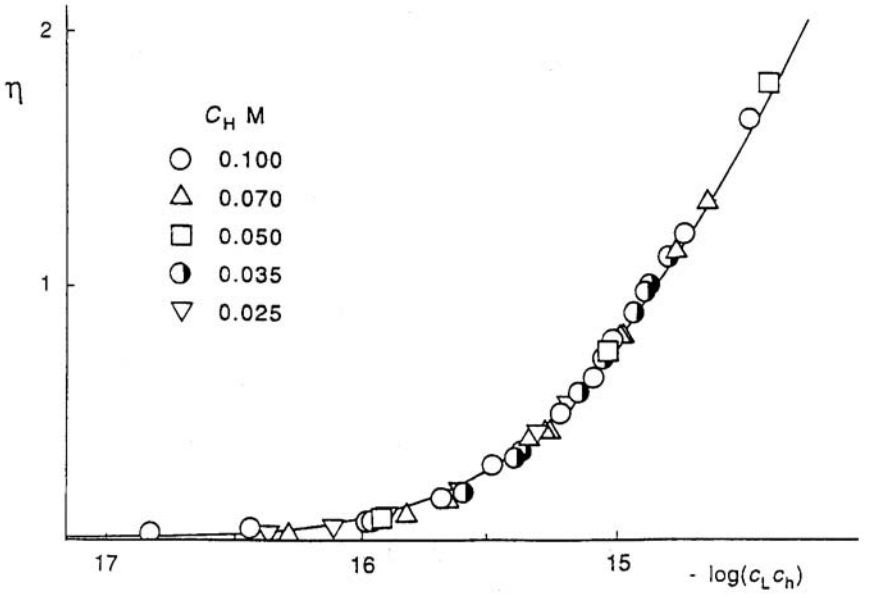

Fig. 2. Most of the experimental data plotted in the form $\eta[=\log(C_{Cd}/c_{Cd})]$ *versus* $-\log(c_L c_h)$. All the points fall on the same curve. The curve is calculated by means of the constants in Table 2.

plexes are formed and $p \geq 0$. The experimental data, treated as previously described [15], could be interpreted by assuming the presence of the species CdHL, CdH_2L_2, CdH_3L_3 and CdH_2L_3, with the relative stability constants.

Taking into account the complexity of the system, the $\beta_{1,1,1}$, $\beta_{1,2,2}$, $\beta_{1,3,3}$ and $\beta_{1,2,3}$ values obtained as first approximations and the values of $-\log c_L$ had to be refined. A computing procedure was applied. The BSTAC program was used in which the analytical and measured data were introduced. After a lot of different trials, such as the introduction of new species or the elimination of some the program interpreted the experimental data by assuming the species found with the graphic method. The differences between first approximation and refined constants are not very large and the proposed values are collected in Table 3. The error limits reported next to the β values are those given by the computer, because they are higher in the graphic treatment. Among a total of 310 points, 106 show a positive deviation with $[\eta_{ex}\text{-}\eta_{cal}]$ never bigger than 0.008, whereas the negative residual never exceeds 0.007.

The values of the constants in Table 3 are used to calculate the theoretical curves, which are drawn through the points on Fig. 3 and Fig. 4. The good agreement between points and curves supports the validity of our procedures and conclusions.

3.2. Results of the polarographic measurements

Since we were not able to obtain stable and reproducible e.m.f. measurements in cells (I) and (II) at high free concentration of cysteine and high $-\log c_h \geq 8$, it was not possible to collect information on the complex formation by means of potentiometric measurements.

From preliminary approaches, it was observed that by applying differential pulse polarography (DP50) a peak relative to cadmium was obtained, as expected, at -660 ± 2 mV versus R.E. By adding to a cadmium(II) solution an excess of cysteine and at $-\log c_h \sim 12$, a peak relative to the complex formation between cadmium(II) and cysteine was obtained. The response the polarographic measurements was very satisfactory, because the reduction of the complex took place at

a more negative and very different potential with respect to the cysteine peak.

It could be calculated that both the reduction of cadmium(II) in acid solution ($-\log c_h \leq 3$) and the reduction of the complex cadmium(II)—cysteine with ligand in excess and in alkaline solution ($-\log c_h \geq 12$) were relative to reversible processes. For the former the slope of 30 ± 1 mV and for the latter the slope 29 ± 1 mV could be calculated. Fig. 5 as an example, shows a polarogram of a solution of the composition:

$C_{Cd} = 10^{-3}$ mol l^{-1}, $C_H = -0.010$ mol l^{-1}, $C_L = 0.003$ mol l^{-1} in ionic medium 3.00 mol l^{-1} NaCl. The first peak is due to the presence of cysteine, while the second one is relative to the reduction of the complex.

As it was not possible to measure accurately $-\log c_h$ in our solutions, we selected high values of $C_{OH} = -C_H \geq 0.01$ mol l^{-1}. On the basis of the k_1 value, cysteine could be considered completely deprotonated (i.e., in the form L) and the equality $C_H = c_h$ was assumed for each series of measurements.

Several measurements were carried out at increasing concentration of cysteine and at different C_{Cd} and C_H values. Polarograms at $C_H = -0.010$, -0.020, -0.035, -0.070 and -0.100 mol l^{-1} were obtained.

For each C_H and C_{Cd} value, the total concentration of cysteine was increased to about 0.050 mol l^{-1}. By applying the method proposed by De Ford [17,18] and Rossotti [19], the composition of the complexes and their stability constants can be obtained. From the $\Delta E_{(1/2)}$ and the excess of cysteine with respect to cadmium(II), it can be calculated that the complex formation is independent of C_{Cd} and C_H (i.e., $q = 1$ and $p = 0$), but no evidence is found for the 1:1 complex. The formation of CdL_2 is assumed and a first approximation value $\delta_{1,0,2}$ is calculated, where it is supposed that:

$$\delta_{1,0,2} = \beta_{1,0,2} + \beta_{1,0,3} c_L \quad (3)$$

By increasing the concentration of cysteine could be observed an increase of $\delta_{1,0,2}$ and then the formation of CdL_3 had to be considered. By plotting $\delta_{1,0,2}$ *versus* C_L (Fig. 6), points fall all together independently of the C_H concentration, but a linear dependence of $\delta_{1,0,2}$ on C_L must be considered. All the points can be approximated with a straight line, thus the hypothesis of Eq. (3) is verified. The intercept on the ordinate and the slope give the $\beta_{1,0,2}$ and $\beta_{1,0,3}$ values, respectively. The values of $\log \beta_{1,0,2} = 14.40 \pm 0.08$ and $\log \beta_{1,0,3} = 16.0 \pm 0.1$ have been determined which are reported with others in Table 3. On the points of Fig. 6 the full line is calculated with the values proposed for the constants, while dashed lines are calculated by taking into account the proposed limits of error. It can be deduced that CdL is not present at appreciable concentration and polynuclear complexes or complexes with loss of protons are not present.

Table 2
Values of the stability constants ($\log \beta_{1,p,r}$) of the complexes assumed to explain the experimental data obtained in 1.00 mol l^{-1} NaCl

Species	Graphical	BSTAC	Proposed
$CdHL$ ($\log \beta_{1,1,1}$)	15.23 ± 0.1	15.20 ± 0.04	15.2 ± 0.07
CdH_2L_2 ($\log \beta_{1,2,2}$)	30.50 ± 0.1	30.47 ± 0.03	30.47 ± 0.05
Literature values			
	25°C and 3.00 mol l^{-1} $NaClO_4$		[9]
CdL ($\log \beta_{1,0,1}$)	12.88		
CdL_2 ($\log \beta_{1,0,2}$)	19.63		
	37°C and 0.15 mol l^{-1} NaCl		[10]
CdL ($\log \beta_{1,0,1}$)	10.3		
CdL_2 ($\log \beta_{1,0,2}$)	16.92		
$CdLH_{-1}$ ($\log \beta_{1,-1,1}$)	2.42		
$CdHL_2$ ($\log \beta_{1,1,2}$)	24.97		
CdH_2L_2 ($\log \beta_{1,2,2}$)	30.93		
CdL_3 ($\log \beta_{1,0,3}$)	19.78		
$CdHL_3$ ($\log \beta_{1,1,3}$)	29.21		

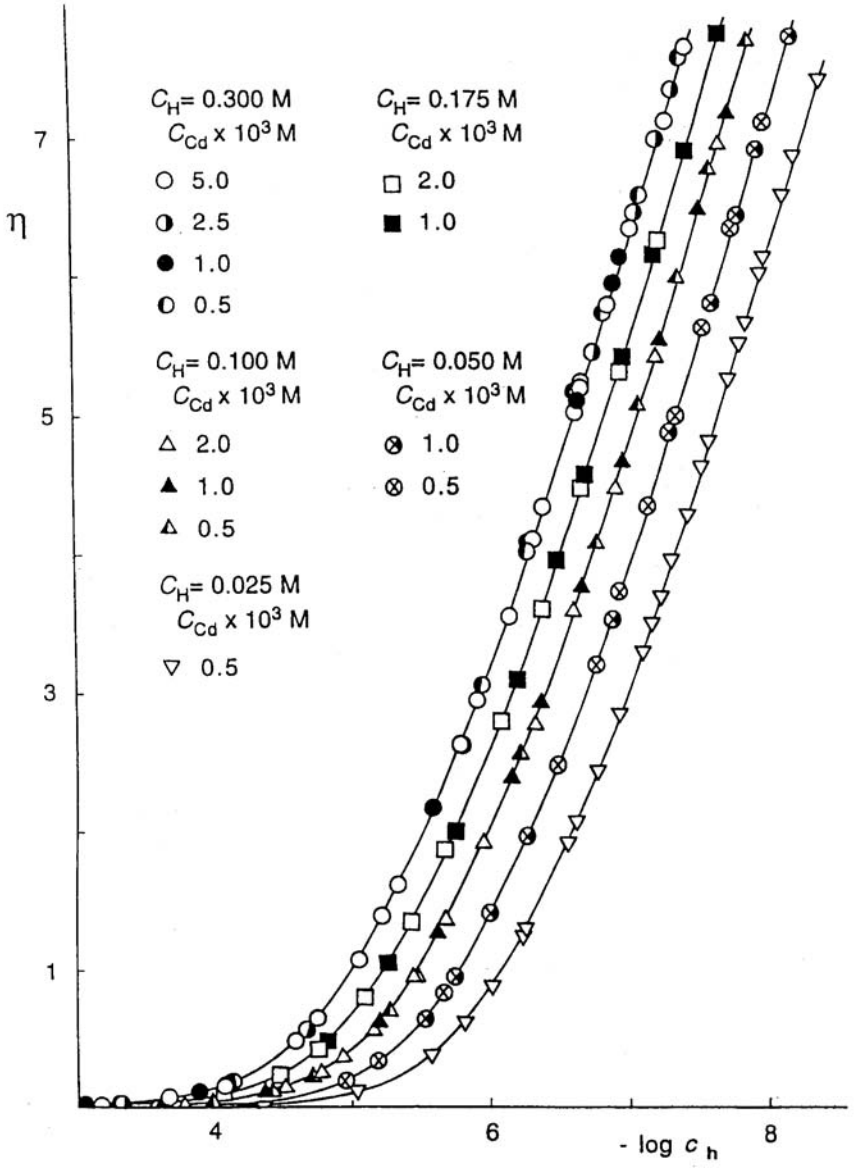

Fig. 3. Experimental data obtained in 3.00 mol l^{-1} NaCl as ionic medium. Curves are calculated using constants in Table 3.

4. Discussion

Complex formation of cysteine and cadmium(II) has been studied at 25°C and at two different concentrations of ionic medium NaCl. The use of 3.00 mol l^{-1} of NaCl was necessary to investigate a wide range of concentration of the reagents in clear solutions, i.e., without precipitation.

The Cl^- -complexing does not introduce, however, any significant complication but only the general limitations of a constant ionic medium [16], i.e., no distinction between species containing a different number of solvent salt ions and molecules. Thus the concentration of CdH_3L_3 really represents: $\Sigma_x\Sigma_y\Sigma_w\ c_{CdH3L3\ (Na+)x(Cl-)y(H2O)w}$ with $x \geq 0$, $y \geq 0$ and $w \geq 0$, unknown.

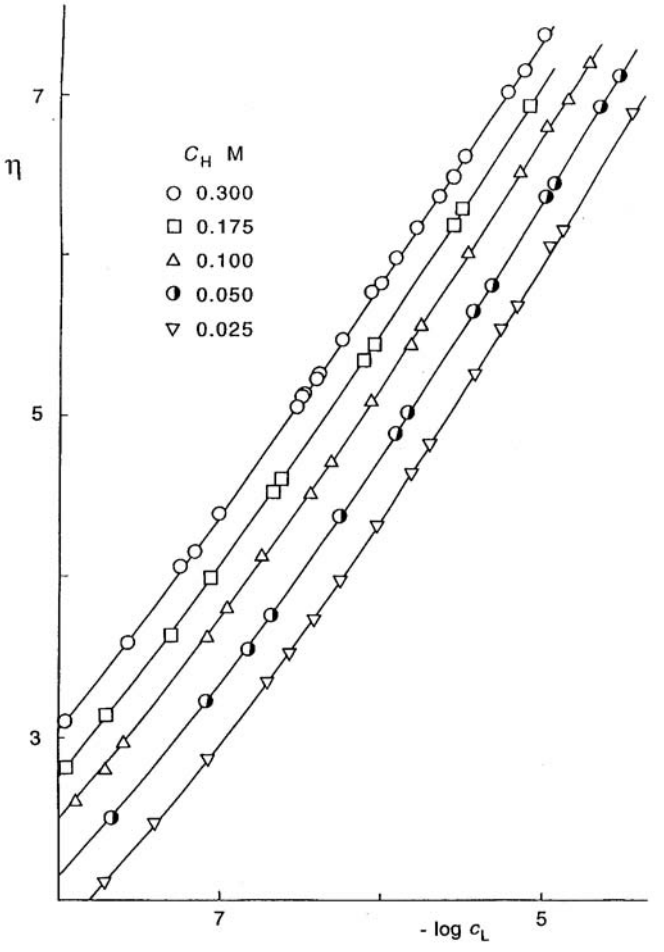

Fig. 4. Most of the experimental data plotted in the form $\eta(-\log c_L)$. The presence of protonated species is evident. The constants in Table 3 are used to calculate the curves.

Protonation constants of the ligand were determined in both ionic media. Their values increase by increasing the concentration of the ionic medium, according to the trend found by Ellilä [26] for the constant of acetic acid in NaCl at different concentrations.

Species and constants proposed here to explain the experimental data agree little with those of literature. This is to be attributed to the very different experimental conditions (temperature and ionic medium) and to the narrow range of concentrations previously investigated. The presence of the species CdH_2L_2 found by Cole et al. [10] is here confirmed. Its stability constant ($\log \beta_{1,2,2} = 30.62$) is not too far from that of Cole et al. ($\log \beta_{1,2,2} = 30.93$) by considering the very different experimental conditions.

Walker et al. [9] and Cole et al. [10] found the presence of CdL and CdL_2, even if with different stability constants. Both groups performed their experiments near the range of precipitation. Our data do not give appreciable evidence of CdL and the formation of CdL_2 takes place in alkaline solution where solutions with a high ratio cysteine/cadmium(II) (for instance 50:1) were investigated. The stability constant of CdL_2 is very different that found by Walker et al. [9] and Cole et al. [10] because they performed only e.m.f.

Table 3
Values of the stability constants ($\log \beta_{1,p,r}$) of the complexes assumed to explain the experimental data obtained in 3.00 mol l^{-1} NaCl

Species	Graphical	BSTAC	Proposed	Method
CdHL($\log \beta_{1,1,1}$)	15.46 ± 0.1	15.40 ± 0.08	15.40 ± 0.08	E.m.f.
CdH_2L_2 ($\log \beta_{1,2,2}$)	30.6 ± 0.1	30.62 ± 0.06	30.62 ± 0.06	E.m.f.
CdH_3L_3 ($\log \beta_{1,3,3}$)	44.72 ± 0.08	44.65 ± 0.05	44.65 ± 0.05	E.m.f.
CdH_2L_3 ($\log \beta_{1,2,3}$)	37.0 ± 0.2	36.80 ± 0.04	36.80 ± 0.05	E.m.f.
CdL_2 ($\log \beta_{1,0,2}$)	14.40 ± 0.06	—	14.40 ± 0.06	$\Delta E_{(1/2)}$
CdL_3 ($\log \beta_{1,0,3}$)	16.0 ± 0.12	—	16.0 ± 0.12	$\Delta E_{(1/2)}$

measurements and in alkaline solutions where the response of the glass electrode deviates with respect to that of hydrogen electrode. Moreover, the experimental conditions were very different.

The presence of other species is not found here in appreciable amount. The assumed complexes explain very well the experimental data, as it can be seen from the agreement between curves and experimental points. The species CdL(OH) can be excluded by considering the results obtained at $-\log c_h \geq 12$ polarographically, as proved also by the plot of Fig. 6.

It can be interesting to compare the results obtained in 1.00 and 3.00 mol l^{-1} NaCl. The latter ionic medium allows a complete investigation. The comparison of the results is limited to the constants of CdHL and CdH_2L_2. These constants of CdHL and CdH_2L_2 are higher in 3.00 mol l^{-1} than in 1.00 mol l^{-1} NaCl. The k'_n and k_n values provide an explanation for this surprising evidence. Cysteine behaves as a stronger base in 3.00 mol l^{-1} than in 1.00 mol l^{-1} NaCl. If the constants of the following equilibria are calculated at both concentrations of NaCl:

Table 4
Comparison among stability constants of the 1:1 and 1:2 complexes formed by α-aminopropanoate, serine, and cysteine with cadmium(II)

Species	CdL	CdL_2
Ligand		
α-Aminopropanoate (1.00 mol l^{-1} $NaClO_4$)	4.05	7.33
Serine (3.00 mol l^{-1} $NaClO_4$)	4.33	8.19
Cysteine (1.00 mol l^{-1} NaCl)	4.97	9.92
Cysteine (3.00 mol l^{-1} NaCl)	4.84	9.50

For cysteine and only in this table, L denotes HL.

$$Cd^{2+} + HL \Leftrightarrow CdHL \quad \beta_1$$

$$Cd^{2+} + 2HL \Leftrightarrow CdH_2L_2 \quad \beta_2 2$$

it is found that:

in 1.00 mol l^{-1} NaCl $\log \beta_1 = 4.97$ and $\log \beta_2 = 9.92$

in 3.00 mol l^{-1} NaCl $\log \beta_1 = 4.84$ and $\log \beta_2 = 9.50$.

The stability constants $\log \beta_1$ and $\log \beta_2$ in 1.00 mol l^{-1} are higher than in 3.00 mol $^{-1}$ NaCl because chloride forms complexes with cadmium(II) according to Biedermann et al. [27].

By using the constants of Table 3, distribution curves of the species found can be calculated as a function of $-\log c_h$ for $C_L = 0.100$ and 0.050 mol l^{-1} (Fig. 7(a) and (b), respectively). In the figures the percentage of each species corresponds to the

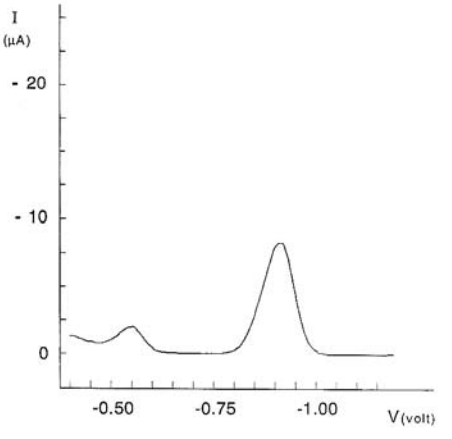

Fig. 5. A polarogram, as an example, of cadmium(II) with an excess of cysteine at $C_{OH} = 0.010$ mol l^{-1} and in 3.00 mol l^{-1} NaCl. I(μA) and V(volt) stand for current intensity and cathodic potential (*versus* R.E.), respectively.

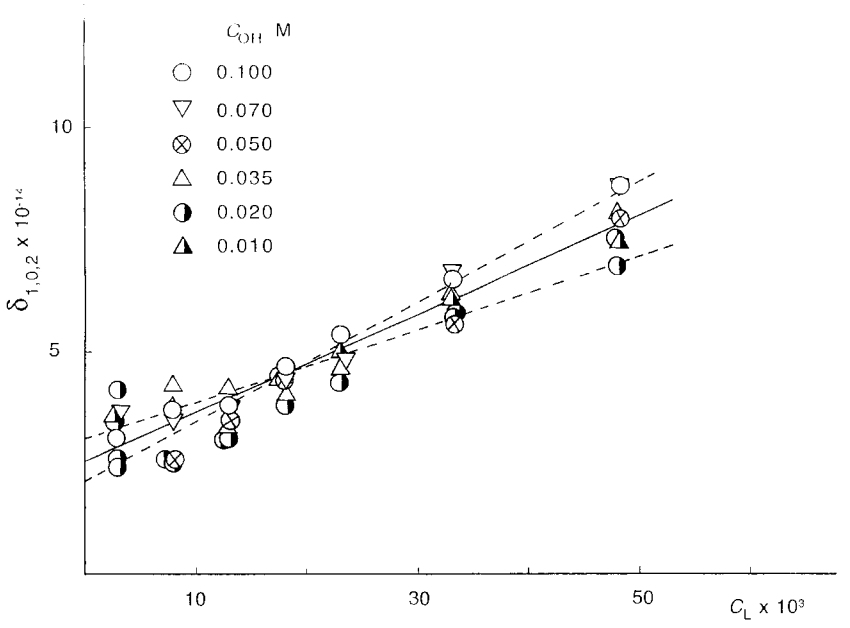

Fig. 6. The dependence of the value of $\delta_{1,0,2}$ on the concentration of cysteine. The full line corresponds to the values assumed for $\beta_{1,0,2}$ and $\beta_{1,0,3}$. Dashed lines correspond to error limits.

distance between the two curves which define the existence range of the species.

In both cases only the species CdHL, CdH_2L_2, CdH_3L_3, CdH_2L_3 are present, because even at $-\log c_h = 8$ and $C_L = 0.100$ mol l^{-1}, the contribution of CdL_2 is equal to or less than 1% of C_{Cd}. For both C_L values, the formation of complexes between cadmium(II) and cysteine starts at $-\log c_h \sim 4$ and the percentage of CdHL does not exceed 20%. The percentages of CdH_2L_2 and CdH_3L_3 are higher and CdH_3L_3 reaches at $-\log c_h \sim 7$ the percentage of 70%. At this value of $-\log c_h$, the species CdH_2L_3 represents 10% of the total cadmium(II), but at $-\log c_h \sim 8$ it becomes more than 50%.

Till $-\log c_h \sim 6.5$, cysteine bonds cadmium(II) in the HL form, i.e., by means of its monoprotonated form. The HL form can correspond to the protonation of NH_2 or S-. If it is supposed that the sulfhydrylic group is protonated first, CdHL, CdH_2L_2 and CdH_3L_3, could be five-membered chelate rings formed between aminic nitrogen and carboxylic group. At $-\log c_h \geq 7$, the contributions of sulfur and nitrogen must be considered. Thus, in CdL_2 and CdL_3 the bond between cadmium(II) and sulfur is also involved.

It becomes interesting to compare the behaviour of cysteine, serine, and α-aminopropanoate towards cadmium(II). Complex formation for the system cadmium(II) serine [12] and α-aminopropanoate [28] was previously investigated and the stability constants are collected in Table 4. The species CdL and CdL_2 of the other ligands correspond to CdHL and CdH_2L_2 for cysteine, respectively.

Although the constants for Cd(II)-cysteine have been obtained in NaCl as ionic medium, the order of stability is α-amino -propanoate < serine < cysteine. The presence of both oxygen and sulfur atoms give more stability to the complexes, and sulfur contributes more than oxygen. The values collected in Table 4 are relative to complexes formed by serine and cysteine with alcoholic sulfhydryl groups, respectively protonated. The stability constants of CdL_2 and

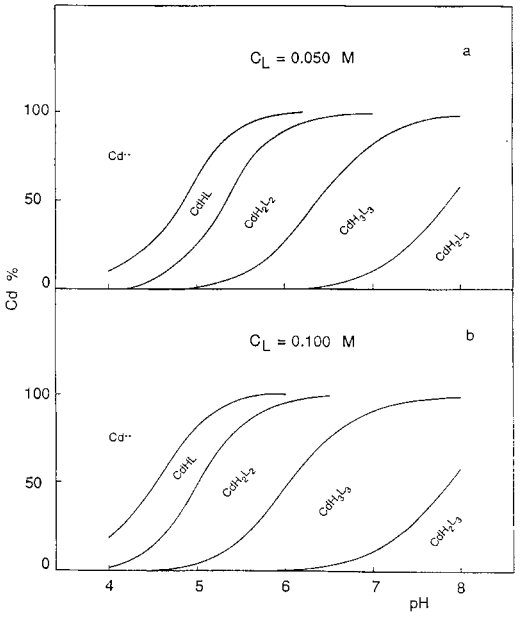

Fig. 7. Distribution curves of assumed species as a function of pH at two different C_L: (a) 0.050 and (b) 0.100 mol l^{-1}.

CdL_3 of cysteine (deprotonated), found at $-\log c_h \geq 12$ are of another order of magnitude.

In conclusion cysteine forms complexes with cadmium(II) in aqueous solutions. The ligand is mainly present as HL till $-\log c_h \sim 6$, but the ligand in its deprotonated form L, bonds cadmium(II) in alkaline solution. The stability of the complexes is high because it is reasonable to believe that the formation of stable chelate rings between cysteine and cadmium(II) takes place.

Acknowledgements

This work was supported by Consiglio Nazionale delle Ricerche (CNR) Ministero dell'Università e della Ricerca scientifica e Tecnologica (MURST) of Italy. Prof. S. Sammartano is gratefully acknowledged for helpful discussion on BSTAC.

References

[1] W.L. Hughes Jr., J. Am. Chem. Soc., 69 (1947) 1836.
[2] R. Benesch and R.E. Benesch, Arch. Biochem., 19 (1948) 35.
[3] I.M. Klotz, J.M. Urquhart and H.A. Fiess, J. Am. Chem. Soc., 74 (1952) 5537.
[4] Biochemists Handbook, C. Long (Ed.), Spon, London, 1961.
[5] A.E. Martell and L.G. Sillén, Stability Constants, Special Publications No. 17 and No. 25, The Chemical Society, London, 1964 and 1971.
[6] D.D. Perrin, Stability Constants of Metal Ion Complexes, Part B: Organic Ligands, IUPAC Chemical Data, Series No. 22. Pergamon Press, Oxford, 1979.
[7] L.D. Pettit and H.K. Powell, IUPAC, Stability Constants: Data Base, Academic Software 1993.
[8] N.C. Li and R.A. Manning, J. Am. Chem. Soc., 77 (1955) 5225.
[9] M.D. Walker and D.R. Williams, J. Chem. Soc. (Dalton) (1974) 1186.
[10] A. Cole, C. Furnival, Z.-X. Huang, D. Cerijones, P.M. May, G.L. Smith, J. Whittaker and D.R. Williams, Inorg. Chim. Acta, 108 (1985) 165.
[11] G. Berthon, Pure and Appl. Chem. 67 (1995) 1117.
[12] E. Bottari, Ann. Chim. (Rome), 66 (1976) 677.
[13] E. Bottari, M.R. Festa and R. Jasionowska, J. Coord. Chem., 17 (1988) 245.
[14] E. Bottari, M.R. Festa and R. Jasionowska, J. Coord. Chem., 20 (1989) 209.
[15] E. Bottari and M.R. Festa, Ann. Chim. (Rome), 83 (1993) 315.
[16] G. Biedermann and L.G. Sillén, Ark. Kem. 5 (1953) 425.
[17] D.D. De Ford and D.N. Hume, J. Am. Chem. Soc., 73 (1951) 5321.
[18] D.N. Hume, D.D. De Ford and G.C.B. Cave, J. Am. Chem. Soc., 73 (1951) 5323.
[19] F.J.C. Rossotti and H. Rossotti, The Determination of Stability Constants, Mc Graw-Hill, London, 1961.
[20] E. Bottari, Ann. Chim. (Rome), 66 (1976) 139.
[21] E. Bottari, Mh. Chemie, 106 (1975) 451.
[22] Yi-Chang Liang and Å. Olin, Acta Chem. Scand. 38A (1984) 247.
[23] C. De Stefano, P. Mineo, C. Rigano and S. Sammartano, Ann. Chim. (Rome), 83 (1993) 243.
[24] G. Biedermann and L. Ciavatta, Acta Chem. Scand., 16 (1962) 2221.
[25] L.G. Sillén, Acta Chem. Scand., 10 (1956) 803.
[26] A. Ellilä, Ann. Acad. Sci. Fennicae, A (1953), 51.
[27] G. Biedermann, J. Lagrange and P. Lagrange, Chem. Scripta, 5 (1974) 153.
[28] E. Bottari and O. Mancini, Ann. Chim. (Rome), 66 (1976) 663.

[29] B. Harman and I. Sovago, Inorg. Chim. Acta, 80 (1983) 75.
[30] I. Sovago, T. Kiss, K. Varnagy and B. Decock-Le Révérend, Polyedron, 7 (1988) 1089.
[31] C.L. Sharma and S.S. Narvi, Thermochim. Acta, 90 (1985)
[32] P. Bianco, J. Haladjian and R. Pilard, J. Electroanal. Chem., 72 (1976) 341.

ELSEVIER

Talanta 44 (1997) 1719–1728

Talanta

Liquid–liquid extraction of some lanthanide metal ions by polyoxyalkylene systems

A.M.Y. Jaber *, Abdul-Elah Al-Naser

King Fahd University of Petroleum and Minerals, Chemistry Department, Dhahran, 31261, Saudi Arabia

Received 11 September 1996; received in revised form 22 January 1997; accepted 23 January 1997

Abstract

Polyoxyalkylene systems, namely, polypropylene glycol (PPG-1025), polyethylene glycol (PEG-600) and polybutadieneoxide (PBDO-700) dissolved in either nitrobenzene or 1,2-dichloroethane have been tested as prospective extractants for some lanthanide metal ions (Eu^{3+}, Pr^{3+} and Er^{3+}) from their aqueous solutions in the presence of picrate anions. The metal ions were quantified before and after extraction using the inductively coupled plasma emission spectrophotometry technique. The percent extraction and the distribution coefficients have indicated that pH of the aqueous phase, picrate concentration and the organic solvent are the major parameters that affect the extraction efficiency of the metal ions. The optimum pH range was found to be 3.5–5.5 and the picrate concentration should be as high as possible; however, a picrate concentration of about 0.05 M proved to be adequate for a near quantitative extraction. In all cases, nitrobenzene enhanced a higher percent extraction compared to 1,2-dichloroethane. The efficiency of the polyoxyalkylene systems to extract certain lanthanide metal ions was in the order PBDO-700 > PPG-1025 > PEG-600 when nitrobenzene was the organic solvent and in the order PPG-1025 > PBDO-700 ≈ PEG-600 when 1,2-dichloroethane used as the solvent in the organic phase. The extractability of PPG-1025 towards the lanthanide metal ions was in the order $Pr^{3+} > Eu^{3+} > Er^{3+}$ irrespective of the organic solvent used. The stoichiometry of the extracted polyoxyalkylene ion-pairs with the lanthanide metal ions has been estimated. Each mole of metal ions is associated with three moles of picrate anions and 13 to 14 moles of propyleneoxide units in the case of PPG-1025, and about 9 to 10 moles of ethyleneoxide units in the case of PEG-600 and 10 moles of butadieneoxide units in the case of PBDO-700. © 1997 Elsevier Science B.V.

Keywords: Polyoxyalkylene; Lanthanides; Extraction; Picric acid

1. Introduction

Macrocyclic polyethers (crown ethers) have been given extensive attention in terms of their uses as selective and efficient extractants for some metal ions from their aqueous solutions and as active sensors in ion-selective membrane electrodes. The acyclic polyethers, for example, polyethylene and polypropylene glycols have proved to compete with the crown ethers for their use as metal ion extractants and active sensors in many instances.

* Corresponding author.

PII S00 9-9140(97)00033-7

Tetraphenylborate salts of polyoxyalkylene complexes with some metal ions gave successful electrodes for the respective metal ions like, for example, Ba [1,2], Ca [3], and Li [4], ion selective membrane electrodes.

Polyoxyalkylene nonionic surfactants having the poly(oxyethylene) chain have been tested as extractants for alkali and alkaline earth metal ions. Solvent extraction studies allowed also the assessment of the nature of the complex formed between the ligands and the metal ions in terms of complex stability and stoichiometry. The complexation equilibrium constant and the extraction efficiency of alkali and alkaline earth metal ions have been studied with high molar mass noncyclic poly(oxyethylene) ligands and their derivatives in either nitrobenzene [5,6] or chlorinated organic solvents such as dichloromethane, chloroform and carbon tetrachloride [7–13]. These studies proved that the extractability of polyoxyalkylene systems towards the metal ions is almost similar to the crown ethers and it is dependent on the nature of polyoxyalkylene and its organic solvent, size and charge of the metal ion, pH of the aqueous phase and nature of the anion associated with the ion pair extracted to the organic phase. The tendency for extraction was found to be more effective with bulkier anions like picrates and thiocyanates since they are less hydrophilic compared to small anions like chloride.

The rare earth metal ions have been mainly separated by solvent extraction methods using various extractants, for example, di-(2-ethylhexyl)phosphoric acid [14] and long-chain alkyl substituents of *N*-phenylhydroxylamine [15,16] which showed large separation factors among lanthanides(III). Ion-associate extraction systems [17], namely, 2,3-naphthalenediol as a diprotic chelating reagent and benzyldimethyltetradecylammonium chloride as ion-associate reagent have shown large separation factors for Pr^{3+}, Eu^{3+}, and Yb^{3+} ions at low pH values. Crown ethers, namely, 15-crown-5, 12-crown-4, and dibenzo-18-crown-6 in nitrobenzene phase have been tested as extractants for individual rare earth ions from aqueous solutions containing picrate anoins. Tb^{3+}, Eu^{3+}, Gd^{3+}, Nd^{3+} and Yb^{3+} have been extracted by 15-crown-5 [18]. Lanthanides have been also extracted from an aqueous phase containing trichloroacetate as a counter ion by 18-crown-6 in 1,2-dichloroethane [19]. The extraction selectivity towards lanthanides was enhanced when EDTA has been added to the aqueous phase.

Some lanthanide complexes with several polyethylene glycols and glymes were isolated and their properties were investigated by Hirashima et al. [20]. Stability constants and some other properties of lanthanide nitrate complexes with tri, tetra, and pentaethylene glycols have also been investigated [21]. It was found that stability of the complexes decreases with an increase in the atomic number of lanthanides. Further more, high molar masses polyethylene glycols in dichloromethane phase have been tested [22] as extractants in the liquid–liquid extraction of some actinides (U, Np and Pa). It has been reported that the extraction efficiency of the three actinides from acidic thiocyanate solution increases in the order U(VI) > Pa > Np.

It is obvious from the literature reports that the studies concerning application of the polyoxyalkylene nonionic surfactants as extractants for the rare earth metal ions are limited. The extraction facilitates preconcentration of these metal ions from their matrices and it may be imperative when these metal ions are to be determined by many experimental methods. Polyethylene glycols, polypropylene glycols of various ranges of molar masses and polybutadieneoxide in either 1,2-dichloroethane or nitrobenzene phase have been tested as extractants for three lanthanide metal ions, namely, praseodymium, Pr^{3+}, europium, Eu^{3+}, and erbium, Er^{3+}, from aqueous phases containing picrate anions.

1.1. Extraction equilibria and stoichiometry of extracted complex

Equilibria proposed in the literature for metal ion extractions by either crown ethers or acyclic polyethers were treated in different ways depending on the nature of the system since many parameters should be considered in such systems. The most possible equilibrium may be suggested for this study is

$$M^{z+} + b/nL^* + zX^- \rightleftharpoons ML_{b/n}X_z^* \quad (1)$$

where M^{z+} is the metal ion of charge z, L^* is the polyoxyalkylene ligand in the organic phase (the asterisk refers to the organic phase), b/n, is the number of moles of polyoxyalkylene ligand associated with one mole of metal ions, where b refers to the number of moles of alkylene oxide units (AOU) associated with a mole of metal ions and n is the average number of AOUs per mole of polyoxyalkylene. X^-, is the picrate anion associated with the ion-pair extracted to the organic phase. Assuming that dissociation of the ion-pair, $ML_{b/n}\,X_z^*$, in the organic phase is negligible, then the extraction equilibrium could be expressed as follows,

$$K_{ex} = \frac{[ML_{b/n}X_z^*]}{[M^{z+}][L^*]^{b/n}[X^-]^z} \quad (2)$$

The distribution ratio, D, is expressed by the ratio of the organic metal ion concentration, $C_{M^{z+}}{}^*$, to the aqueous metal ion concentration, $C_{M^{z+}}$, in all chemical forms, that is, $D = C_{M^{z+}}{}^*/C_{M^{z+}}$. Thus, D may be expressed as follows,

$$D = \frac{[ML_{b/n}X_z^*]}{[M^{z+}] + [ML_{b/n}^{z+}]}$$

Assuming that partitioning of the polyoxyalkylene into the aqueous phase is negligible, consequently, $[M^{z+}] > > [ML_{b/n}^{z+}]$. Hence, the distribution ratio will be expressed by the following equation,

$$D = \frac{[ML_{b/n}X_z^*]}{[M^{z+}]} \quad (3)$$

Introducing the term D into the K_{ex} expression in Eq. (2) gives,

$$K_{ex} = \frac{D}{[L^*]^{b/n}[X^-]^z} \quad (4)$$

Rearranging Eq. (4) and taking log of both sides gives,

$$\log K_{ex} + b/n \log [L^*] = \log \frac{D}{[X^-]^z} \quad (5)$$

Taking into consideration the dissociation of picric acid, HX, in the aqueous phase into H^+ and X^- ions and under the condition that $[HX] > > [M^{3+}]$, the concentration of picrate anion X^- in Eq. (5) may be expressed as follows,

$$[X^-] = (K_a[HX])^{1/2}$$

Inserting the value of $[X^-]$ into Eq. (5) gives,

$$\text{Log } K_{ex} + b/n \log [L^*] = \log \frac{D}{k_a^{z/2}\,[HX]^{z/2}} \quad (6)$$

Rearrangement of Eq. (6) gives,

$$\text{Log } D = \log K_a^{z/2} + \log K_{ex} + b/n \log [L^*] + z/2 \log [HX] \quad (7)$$

The terms, k_a and k_{ex} are expected to be constants under the extraction conditions, hence when $\log D$ is plotted against $\log [L^*]$ a straight line with a slope of b/n and intercept of, $\log K_a^{z/2} + \log K_{ex} + z/2 \log [HX]$, will be obtained. On the other hand, when the polyoxyalkylene concentration, [L*], is kept constant while the picric acid concentration, [HX], is varied and $\log D$ is plotted against $\log [HX]$, a straight line with a slope of $z/2$ is expected, where z is the number of moles of picrate anions associated with one mole of metal-picrate species. From the two plots, stoichiometry of the complex $ML_{b/n}\,X_z^*$ and $\log K_{ex}$ may be estimated.

2. Experimental

2.1. Materials

Polyethylene glycol (PEG-600), polypropylene glycol (PPG-1025 and PPG-2000) and polybutadiene oxide (PBDO-700) were all of reagent grade from Polyscience. Picric acid was of purum grade from Fluka. Praseodymium, europium, erbium and lanthanum stock solutions were obtained either from a spectroscopic grade (1000 ppm) stock solutions provided by Alfa products or prepared from high metal oxides provided by Fluke. Nitrobenzene and 1,2-dichloroethane were of purum grade provided by

Fluka. All other reagents used were of analytical grade and all standard solutions were prepared in distilled deionized water.

2.2. Instrumentation

A Perkin Elmer Plasma (400 ICP) spectrometer was utilized for the metal ion analysis after extraction. The spectra were measured at an observation height of 11 mm with an integration time of 100 ms and a photomultiplier voltage of 600 V. For all lines the built-in auto-background correction was applied. An Orion 720A pH meter in conjunction with a Corning combination pH glass electrode were used to measure the pH of the solutions. A mechanical shaker (Burrell, Model 75) was used to homogenize the samples during the extraction process.

2.3. Extraction procedure and measurements

The aqueous phase was prepared by mixing appropriate volumes of certain concentrations of both, picric acid and the metal ion solutions. The organic phase was prepared by dissolving the required amount ($<0.01-0.3$ M) of the polyoxyalkylenes (PEG, PPG or PBO) in either nitrobenzene or 1,2-dichloroethane solvents. Equal volumes (10 ml) of both phases were transferred to a separatory funnel and shaken mechanically for 30 min; a time found to be enough to get complete separation. The mixture was then left to stand for 30 min after which the aqueous phase was separated and analyzed for the metal ion concentration left using the ICP technique. Lanthanum, La^{3+}, at a level of 10 ppm was added as an internal standard into both, the sample and the calibration solutions. The correlation coefficients for all calibration curves were better than 0.9999. As a check experiment, the organic phase was separated and the metal ion was stripped to the aqueous phase by either 0.1 M HNO_3 or HCl. Results obtained indicated that the amount extracted into the organic phase is same as that lost from the aqueous phase, thus further analysis of the organic phase was not needed.

3. Results and discussion

3.1. Effect of picric acid concentration on extraction

The lanthanide metal ion extraction studies have been initiated by fixing the metal ion and the polyoxyalkylene concentrations at levels of about 100 ppm and 0.1 M, respectively. However, the picrate anion concentration was varied in the range of 0.01 M to about 0.055 M; the maximum picrate concentration was limited by its water solubility. The studies indicated that extraction is enhanced with the increase in the picrate anion concentration irrespective of the type of metal ion, polyoxyalkylene system or organic solvent. When picric acid concentration was increased from 0.017 to 0.052 M, the percent extraction of Eu^{3+}, for example, has increased from 9 to 52%, 6 to 45% and 2 to 20% when the polyoxyalkylene was PPG-1025, PEG-600 and PBDO-700, respectively, with nitrobenzene as the organic solvent. However, when 1,2-dichloroethane replaced nitrobenzene in the organic phase, the percent extraction of Eu^{3+} has increased from 3 to 31%, 7 to 38% and 1 to 5% in the case of PPG-1025, PEG-600 and PBDO-700 extractants, respectively.

3.2. Effect of pH on extraction

The optimum pH for a maxim percent extraction was determined by carrying out the extraction with fixed concentrations of polyoxyalkylenes (0.3 M), picric acid (0.055 M) and the metal ion to be extracted (100 ppm). However, the pH of the aqueous phase was varied by incremental additions of 0.1 M sodium hydroxide solution. It was not possible to raise the pH to values higher than 5.5 due to hydrolysis of the metal ions in the aqueous phase. In fact, the aqueous solutions became turbid at pH values higher than 5.5 and a decline in the percent extraction was observed.

Fig. 1 shows the extraction of Pr^{3+}, Eu^{3+} and Er^{3+} by PPG-1025 in nitrobenzene (curves 1, 2 and 4, respectively) under the conditions

mentioned above. Curve 3 of Fig. 1 shows the pH effect on the extraction of Eu^{3+}, for example, by PPG-1025 in 1,2-dichloroethane. It is obvious from all curves that the percent extraction increases by increasing the pH until it levels off at pH > 3.5 for all metal ions studied. This behavior has been noticed irrespective of the polyoxyalkylene system or the organic diluent used. Thus, the optimum pH for an efficient extraction lies within the range of 3.5–5.5. The low extractability at low pH values may be attributed to the proton extraction to the organic phase rather than the metal ion itself. However, the increase in pH facilitates the dissociation of picric acid and more picrate will be available for extraction.

3.3. Effect of polyoxyalkylene and the organic diluent on extraction

Extraction of metal ions has been caried out from aqueous solutions containing about 100 ppm of the metal ion, 0.055 M picric acid at pH 4.5, a value within the optimum pH range, using varying concentrations (from < 0.01 to ~ 0.3 M) of polyoxyalkylene. The percent extractions of Eu^{3+}, for example, by PPG-1025 and PEG-600 in

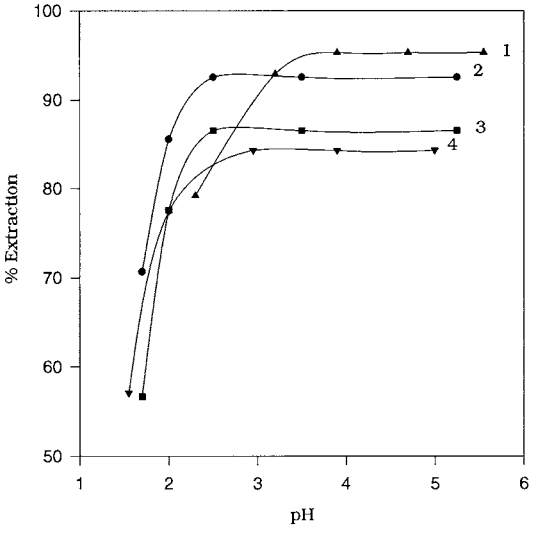

Fig. 1. Extraction of lanthanide metal ions from aqueous medium containing 100 ppm M^{3+}, 0.055 M picric acid at various pH values by 0.3 M PPG-1025. (1) Pr^{3+} into nitrobenzene, (2) Eu^{3+} into nitrobenzene, (3) Eu^{3+} into 1,2-dichloroethane, (4) Er^{3+} into nitrobenzene.

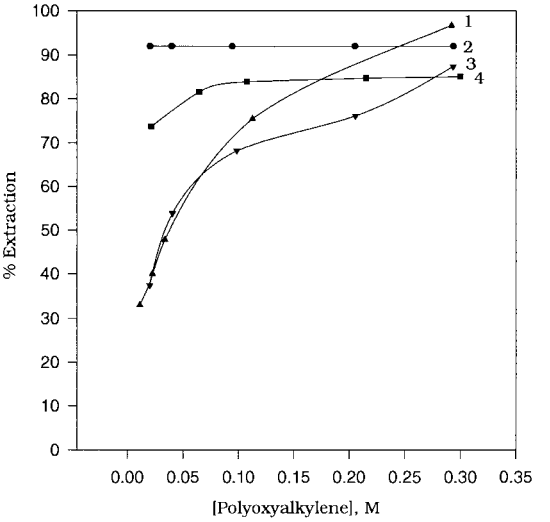

Fig. 2. Extraction of europium from aqueous medium containing 100 ppm Eu^{3+}, 0.055 M picric acid at pH 4.5 into organic phase containing various concentrations of polyoxyalkylenes in nitrobenzene or 1,2-dichloroethane. (1) PBDO-700 in nitrobenzene, (2) PPG-1025 in nitrobenzene, (3) PPG- 1025 in 1,2-dichloroethane, (4) PEG-600 in nitrobenzene.

nitrobenzene have reached their maximum values at polyoxyalkylene concentrations as low as $<$ 0.05 M (Fig. 2, curves 2 and 4). Same behavior has also been observed for Pr^{3+} extraction by PPG-1025 and PEG-600 under same conditions. However, the effect of polyoxyalkylene concentration on extraction efficiency was more significant in cases such as PBDO-700 in nitrobenzene (Fig. 2, curve 1) and all polyoxyalkylene systems in 1,2-dichloroethane (Fig. 2, curve 3 as an example). The percent extraction for these systems has increased as a function of concentration and became almost quantitative when its concentration in nitrobenzene became 0.3 M indicating the insignificance of a further increase in polyoxyalkylene concentration.

Table 1 shows the maximum percent extractions obtained at 0.3 M polyoxyalkylenes in the presence of 0.055 M picric acid in the aqueous phase at pH 4.5. The table indicates that the trend for extraction efficiency of Eu^{3+} by polyoxyalkylene in nitrobenzene organic phase was in the order PBDO-700 > PPG-1025 > PEG-600. This behavior may be attributed to the relative hydrophobic shielding of the alkyleneoxide units to the dehydrated metal ion when the ion-pair is

formed in the organic phase. The hydrophobicity may increase in the order of PEG (with the ethyleneoxide units, $-CH_2-CH_2-O$) < PPG (with propyleneoxide units, $-CH(CH_3)CH_2-O$) < PBDO (with butadieneoxide units $-CH_2-CH=CH-CH_2O$). However, the extraction of Eu^{3+} under same conditions but with 1,2-dichloroethane as the organic phase was in the order PPG-1025 > PBDO-700 ≈ PEG-600. Thus, the extraction selectivity with respect to PPG-1025 and PBDO-700 is reversed when a relatively low dielectric constant organic solvent is used.

The extraction efficiency has been found to be dependent, also, on the molar mass of the polyoxyalkylene system, that is, the number of alkylene oxide units surrounding the metal ion. The percent extractions of Pr^{3+}, Eu^{3+}, and Er^{3+}, from 0.055 M picric acid at pH 4.5 using 0.15 M of PPG have been found as 80.0, 82 and 75.0%, respectively, when PPG-1025 was used, meanwhile they have been increased to about 93, 94 and 84%, respectively, when PPG-2000 was introduced into the nitrobenzene organic phase. Same trend but with a higher relative increase has been observed when 1,2-dichloroethane was the diluent in the organic phase; for example, the percent extraction of Eu^{3+} has been increased from 40.0% in the case of PPG-1025 to 59% in the case of PPG-2000. A similar trend has been reported previously [7,13,24,25] for some transition metal ions, alkali and alkaline earth metal ions using various polyethylene glycols, polypropylene glycols, poly(oxyethylene) and poly(oxyethylene) derivatives of different molar masses. The enhancement of extraction has been ascribed [7] to the increase of hydrophobic property by the increase of the number of alkyleneoxide units.

Table 1
Percent extractions of Eu^{3+}, Pr^{3+} and Er^{3+} with various polyoxyalkylenes at the optimum conditions

Poly-oxyalkylene	M^{3+}	Organic phase	
		Nitrobenzene	1,2-Dichloroethane
PPG-1025	Eu^{3+}	92.7	87.4
	Pr^{3+}	95.8	91.2
	Er^{3+}	80.3	61.4
PEG-600	Eu^{3+}	85.0	60.0
PBDO-700	Eu^{3+}	96.7	61.1

[M^{3+}] 100 ppm, pH 4.5, $[\text{Picric acid}]_{\text{initial}}$ 0.055 M, [polyoxyalkylene] 0.3 M in nitrobenzene or 1,2-dichloroethane organic phase.

Table 1 also shows that percent extractions of the three metal ions by PPG-1025 in either nitrobenzene or 1,2-dichloroethane is in the order $Pr^{3+} > Eu^{3+} > Er^{3+}$. This trend is consistent with the ionic radii of the metal ions studied (ionic radii for Pr^{3+}, Eu^{3+} and Er^{3+} are: 1.013, 0.950 and 0.881 Å, respectively). A similar trend has been reported for the extraction of some lanthanide metal ions with crown ethers [18]. Since the ion-pair formation in the organic phase should be preceded by dehydration of the metal ions, Pr^{3+} with the relatively larger ionic size and the smallest relative hydration energy is expected to show the highest relative extractability.

All extractions studied were carried out using nitrobenzene and 1,2-dichloroethane as diluents in the organic phase. The percent extraction in the case of nitrobenzene was always higher than that of 1,2-dichloroethane regardless of pH of the aqueous phase, the polyoxyalkylene system or the metal ion. This behavior may be attributed to the configuration of the ion-pair formed in the organic solvent as suggested earlier [26]. The polyoxyalkylene molecule coordinates to the metal ion through the ether oxygen atoms and it wraps around the cation in a helical configuration which is stabilized in an organic solvent of high dielectric constant. Further more, the energy of solvation of picrate lipophilic anion by nitrobenzene is greater than that by 1,2-dichloroethane [26].

3.4. Effect of metal ion concentration on extraction

Europium has been extracted from aqueous solutions containing various concentrations of Eu^{3+}, 0.033 M picric acid at pH 4.5 into nitrobenzene or 1,2-dichloroethane containing 0.3 M PPG-1025. The percent extraction of Eu^{3+} was constant (about 92%) up to about 100 ppm Eu^{3+} (Fig. 3) then it showed a significant drop in either nitrobenzene or 1,2-dichloroethane; in fact, the percent extraction has dropped down to about 25% when the initial concentration of Eu^{3+} has reached 357 ppm (Fig. 3).

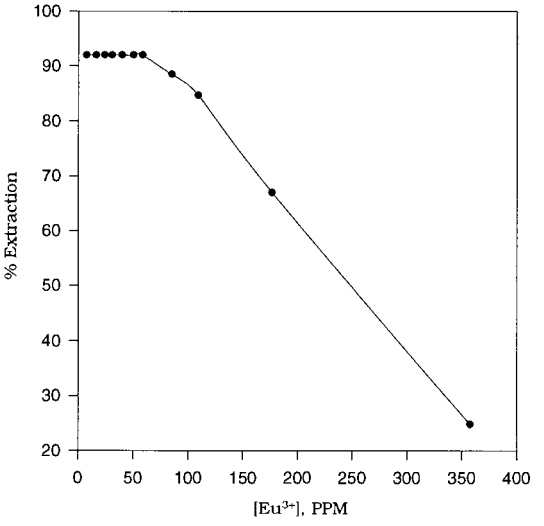

Fig. 3. Extraction of europium from aqueous medium containing various concentrations of Eu^{3+}, 0.033 M picric acid at pH 4.5 by 0.3 M PPG-1025 in nitrobenzene.

This behavior may be attributed to the depletion of picrate anion in the aqueous phase which is necessary to form the species, $M^{3+}.Pic^-$ which is readily extracted to the organic phase. Repetitive extraction experiments were carried out in which Eu^{3+} has been extracted from aqueous phases containing >100 ppm Eu^{3+} in the presence of 0.033 M picric acid at pH 4.5 into either nitrobenzene or 1,2-dichlorethane phase containing 0.3 M PPG-1025. In each experiment, a fresh organic phase has been added in the second extraction step; almost nothing has been extracted in the second step. This indicates the vital role of picrate which has been almost depleted in the first step. At high picric acid concentrations, some picrate may be transferred to the organic phase in the form of molecular picric acid [23] decreasing the chance for ion-pair formation with the metal ion M^{3+}.

3.5. Evaluation of ion-pair stoichiometry and extraction efficiency

In a series of experiments the initial concentration of polyoxyalkylene, $[L^*]_{initial}$ in 1,2-dichloroethane, was varied in the range of 0.01 to 0.3 M fixing the concentration of the metal ion, $[M^{3+}]$, at a level of 100 ppm (6.7×10^{-4} M), that of picric acid at 0.055 M and the pH at a value of 4.5 (a value within the optimum pH range for extraction). Thus, the conditions for Eq. (7) are met. Since $[L^*]_{initial} >> [M^{3+}]$ even with the lowest polyoxyalkylene concentration (~ 0.01 M), the equilibrium concentration of poloxyalkylene, [L*] in Eq. (7) may be replaced by the initial concentration, $[L^*]_{initial}$. Consequently, the number of moles of AOUs, required to combine with one mole of metal ions has been estimated from plots of log D against log $[L^*]_{initial}$. Plots for the ion-pairs of PPG-1025 ($n = 17.4$ propyleneoxide units, POU) with the M^{3+}-picrate species are shown in Fig. 4, curves 1, 2 and 3. The correlation coefficients for these curves were better than 0.99 in most cases. From the slopes of these curves it was possible to find that each mole of metal ions studied (Pr^{3+}, Eu^{3+} or Er^{3+}) is bound to about 13 to 14 moles of POUs (Table 2). However, when the data were plotted for extraction of Eu^{3+} with PEG-600 or PBDO-700 (Fig. 4, curves 4 and 5, respectively) it is found that number of ethyleneoxide units, EOU, estimated per a mole of

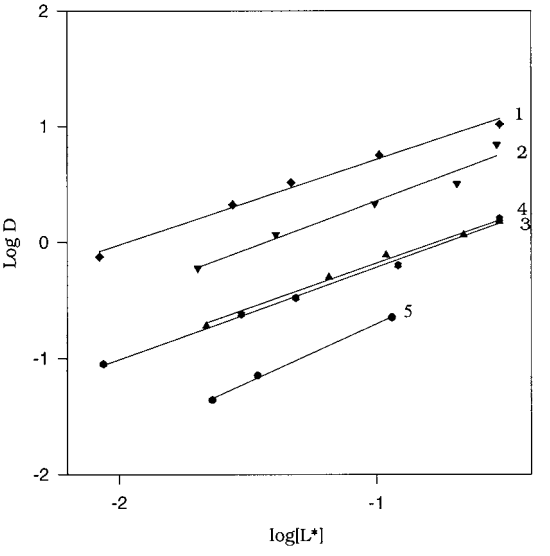

Fig. 4. Log D versus log [L*] for lanthanide metal ions extracted by PPG-1025, PEG-600 and PBDO-700 in 1,2-dichloroethane. [Picric acid] 0.055 M, $[M^{3+}]$ 100 ppm, pH 4.5. (1) Pr^{3+} by PPG-1025, (2) Eu^{3+} by PPG-1025, (3) Er^{3+} by PPG-1025, (4) Eu^{3+} by PEG-600, (5) Eu^{3+} by PBDO-700.

Table 2
Number of moles of alkyleneoxide units (AOU)[a] associated with a mole of M^{3+} extracted from an aqueous phase containing 0.055 M picric acid and 100 ppm of metal ion, into 1,2-dichloroethane containing varied concentrations of polyoxyalkylene

Polyoxyalkylene	M^{3+}	No. AOUs/metal ion[a]	Log K_{ex}
PPG-1025	Eu^{3+}	14.4	3.50
PPG-1025	Pr^{3+}	12.8	3.78
PPG-1025	Er^{3+}	13.8	2.91
PEG-600	Eu^{3+}	10.2	2.94
PBDO-700	Eu^{3+}	10.0	2.63

Log K^{a}_{ex} values for the ion-pairs $POA.M^{3+}.pic^{-}$ are also given.
[a] Number of AOUs and Log K_{ex} values for the ion-pairs are calculated, respectively, from the slopes and the intercepts of the curves in Fig. 4.

Eu^{3+} in the ion-pairs of PEG-600 ($n = 13.2$ EOU) is about 10 and number of moles of butadieneoxide units, BDOU, per a mole of Eu^{3+} for the ion-pairs of PBDO-700 ($n = 10$ PDOU) is also about 10 (Table 2). The curves for BBDO-700 were not linear thus only the linear portion of the curve was considered for the stoichiometry estimation as shown in Fig. 4, curve 5. Thus, the stoichiometry of the ion-pairs in the case of PBDO-700 is almost 1:1, PBDO:Eu^{3+}. These results are consistent with what has been reported earlier, where about 12 moles of EOUs or POUs are associated with a mole of alkaline earth metal ions [27].

On the other hand, another set of experiments have been carried out in which the concentration of the metal ion, M^{3+}, was fixed at 100 ppm (6.7×10^{-4} M), the picric acid concentration, [HX], was varied in the range of 0.01 to 0.055 M and the polyoxyalkylene concentration was fixed at 0.1 M in either nitrobenzene or 1,2-dichloroethane organic solvent. Since $[\text{picric acid}]_{initial}$ was $>> [M^{3+}]_{initial}$, hence the conditions for Eq. (7) are fulfilled. Thus log D was plotted against log $[\text{picric acid}]_{initial}$ according to Eq. (7). Typical plots are shown in Fig. 5 for the extraction of Eu^{3+} (curves 2 and 4) and Er^{3+} (curves 1 and 3) into PPG-1025 in nitrobenzene or 1,2-dichloroethane. All curves plotted indicate a linear relationship with a correlation coefficient better than 0.99 and a slope of about 3 (ranging from 2.7 to 3.2) regardless of the polyoxyalkylene system, the type of metal ion or the solvent in the organic phase. Consequently, M^{3+}-picrate species stoichiometry is consistent with what is expected for a trivalent metal ion with a univalent anion. This finding confirms the validity of the model assumed for extraction according to Eqs. (1)–(7) mentioned above.

Further more, Log K_{ex} values for the various metal ions with the polyoxyalkylenes studied have been estimated from Eq. (7) assuming that $z = 3$ and k_a of picric acid = 0.513; these values are shown in Table 2. It is obvious from Table 2 that Log K_{ex} values estimated under same conditions of pH indicate that the trend for extraction efficiency of Eu^{3+} into the 1,2-dichloroethane phase was in the order PPG-1025 > PEG-600 > PBDO-700. However, the extraction efficiency for the metal ions by PPG-1025 was in the order $Pr^{3+} > Eu^{3+} > Er^{3+}$.

The separation factors (K^{I}_{ex}/K^{II}_{ex}) for Pr^{3+}/Eu^{3+}, Pr^{3+}/Er^{3+} and Eu^{3+}/Er^{3+} were calculated from log K_{ex} values given in Table 2 and found to be 1.9, 7.4 and 4.0, respectively.

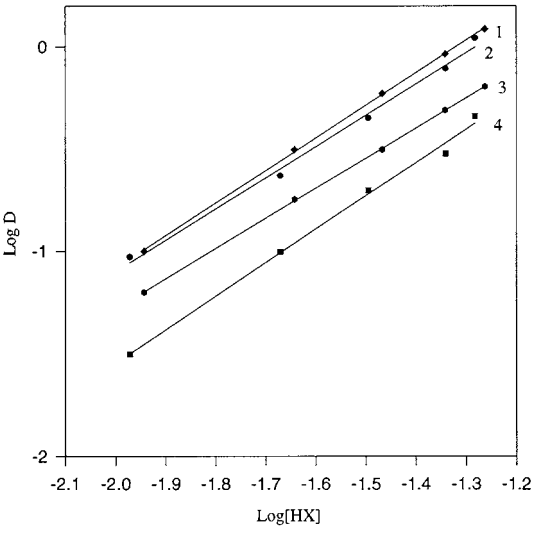

Fig. 5. Log D versus log [HX] for lanthanide metal ions extracted by PPG-1025. (1) Er^{3+} into nitrobenzene, (2) Eu^{3+} into nitrobenzene, (3) Er^{3+} into 1,2-dichloroethane, (4) Eu^{3+} into 1,2-dichloroethane. [Picric acid] 0.055 $[M^{3+}]$ 100 ppm, [Polyoxyalkylene] 0.1 M.

Attempts were made to apply similar extraction studies for the same systems under same conditions but in the presence of nitrobenzene as the organic diluent. Since the extraction has been carried out at the optimum pH (4.5), the percent extraction has reached its maximum values for most systems at the lowest polyoxyalkylene concentrations used. Thus, plots of $\log D$ against $\log [L^*]_{initial}$ were leveled off at very low polyoxyalkylene concentrations. Consequently, extraction experiments were carried out under same conditions but without pH adjustment. In fact, the pH measured was 2 or below where the extraction efficiency for all systems is very low. plots of $\log D$ against $\log [L^*]_{initial}$ under these conditions were in a similar fashion as those for 1,2-dichloroethane mentioned above. The slopes of the curves showed that each mole of metal ions (Pr^{3+}, Eu^{3+}, Er^{3+}) studied is bound to about 14 moles of POUs, 9 EOUs and 10 BDOUs. Log K_{ex} values estimated from Eq. (7) indicated that the efficiency of extraction for the metal ions studied by the polyoxyalkylene systems was in the same order as that in the case of 1,2-dichlorotethane organic phase diluent.

4. Conclusion

Lanthanide metal ions represented by europium, praseodymium and erbium can be extracted near quantitatively from their aqueous solutions in the presence of a lipophilic anion, namely, picrate anion, which forms an extractable species with the lanthanide metal ions. the extraction is facilitated by ion-pair formation with a polyoxyalkylene system in an organic solvent which should possess a fairly high dielectric constant. The optimum conditions for a maximum percent extraction are: [Picric acid] 0.05 M, pH 3.5–5.5, [Polyoxyalkylene] 0.3 M, as well as nitrobenzene as the organic phase. The extraction efficiency was in the order $Pr^{3+} > Eu^{3+} > Er^{3+}$. A larger number of alkyleneoxide units for the same type of polyoxyalkylene (higher molar mass) provides better extraction efficiency for these metal ions. The extraction efficiency under the optimum conditions mentioned above for the same metal ion by different polyoxyalkylenes was in the order PBDO > PPG > PEG in the case of nitrobenzene organic solvent, but when 1,2-dichloroethane was the organic solvent the extraction efficiency was in the order PPG > PBDO ≈ PEG. It has been found that 13 to 14 propyleneoxide units are associated with a metal ion in each ion-pair with PPG-1025 molecule. In the case of PEG-600, about 9 to 10 ethyleneoxide units were associated with a metal ion per an ion-pair. However, for the ion-pairs with PBDO-700 the stoichiometry was 1:1, M^{3+}:PBDO. In all cases the species extracted from the aqueous phase was M^{3+}:3 picrate confirming the validity of the proposed extraction equilibria.

The reproducibility of the extraction experiments has been checked for extraction of Eu^{3+} at the optimum conditions by PBDO-700 in nitrobenzene and found excellent; the relative standard deviation for 10 replicates was 0.27%.

Acknowledgement

King Fahd University of Petroleum and Minerals is thanked for the support of this research project.

References

[1] R.J. Levins, Anal. Chem. 43 (1971) 1045.
[2] A.M.Y. Jaber, G.J. Moody, J.D.R. Thomas, Analyst 101 (1976) 179.
[3] A.M.Y. Jaber, G.J. Moody, J.D.R. Thomas, Analyst 102 (1977) 943.
[4] V.P.Y. Gadskapo, G.J. Moody, J.D.R. Thomas, Analyst 110 (1985) 1381.
[5] J. Rais, E. Sebestova, P. Selucky, M. Kyrs, J. Inorg. Nucl. Chem. 38 (1976) 1742.
[6] A.M.Y. Jaber, M.Y.S. El-Issa, Analyst 106 (1981) 939.
[7] S. Yanaguda, K. Takahashi, M. Okahara, Bull. Chem. Soc. Jpn. 50 (1977) 1386.
[8] Y. Sakai, H. Nakamura, M. Takagi, K. Ueno, Bull. Chem. Soc. Jpn. 59 (1986) 381.
[9] Y. Sakai, M. Shinmura, H. Otsuka, M. Takagi, Bull. Chem. Soc. Jpn. 60 (1987) 545.
[10] A.M.Y. Jaber, G.J. Moody, J.D.R. Thomas, Inorg. Nucl. Chem. 39 (1977) 1689.
[11] L. Faveretto, B. Stancher, F. Tunis, Analyst 104 (1979) 241.

[12] H. Awano, K. Ono, K. Murakami, Bull. Chem. Soc Jpn. 55 (1982) 2530.
[13] T. Sotobayashi, T. Suzuki, S. Tonouchi, Chem. Lett. (1976) 585.
[14] S. Mutomizu, H. Freiser, Solvent Extr. Ion. Exch. 3 (1985) 627.
[15] K. Haragauchi, Y. Yamazaki, T. Saitoh, T. Kamidate, H. Watanabe, Anal. Sci. 6 (1990) 877.
[16] T. Saitoh, M. Okuyama, T. Kamidate, H. Watanabe, K. Haragauchi, Bull. Chem. Soc. Jpn. 67 (1994) 1002.
[17] T. Takayanagi, T. Yotsuyanagi, Bull. Chem. Soc. Jpn. 67 (1994) 1835.
[18] L. Tsay, J. Shih, S. Wu, Analyst 108 (1983) 1108.
[19] R. Frazier, C.M. Wai, Talanta 39 (1992) 211.
[20] Y. Hirashima, K. Kanetsuki, I. Yonezu, K. Kamakura, J. Shiokawa, Bull. Chem. Soc. Jpn. 56 (1983) 738.
[21] Y. Hirashima, K. Kanetsuki, I. Yonezu, N. Isobe, J. Shiokawa, Bull. Chem. Soc. Jpn. 59 (1986) 25.
[22] T. Sotobayashi, T. Suzuki, H. Kudo, J. Radioanal. Chem. 36 (1977) 145.
[23] J. Rais, P. Selucky, Collection Czechoslov. Chem. Commun. 36 (1971) 2766.
[24] T. Sotobayashi, T. Suzuki, K. Yamada, Chem. Lett. (1976) 77.
[25] Y. Skai, K. Nabeki, E. Uehara, M. Hiraishi, M. Takagi, Bull. Chem. Soc. Jpn. 66 (1993) 3107.
[26] M.D. Adams, P.W. Wade, R.D. Hancock, Talanta 37 (1990) 875.
[27] P.G. Delduca, A.M.Y. Jaber, G.J. Moody, Thomas, J. Inorg. Nucl. Chem. 40 (1978) 187.

ELSEVIER

Talanta 44 (1997) 1729–1733

Talanta

Effect of interfering ions on hexamethyldisiloxane microdiffusion method

R.W. Kahama *, D.N. Kariuki, L.W. Njenga

Department of Chemistry, PO Box 30197, University of Nairobi, Nairobi, Kenya

Received 21 June 1996; received in revised form 16 December 1996; accepted 3 February 1997

Abstract

Acid diffusion in the presence of hexamethyldisiloxane (HMDS) enables complete recovery of ionic fluoride from standards containing varying concentrations of aluminium as one of the main interfering ions. Acid diffusion without HMDS shows a decrease in fluoride recovery as aluminium ion concentration increases. The fluoride concentration in the trapping solution is determined directly on the diffusion cover with a combination fluoride electrode after neutralising and buffering. The same procedure was used for the analysis of fluoride in soil and plant materials containing high concentrations of aluminium ions. For the same samples, the concentrations of aluminium, iron and silicon were determined using atomic absorption spectrophotometer (AAS). © 1997 Elsevier Science B.V.

Keywords: HMDS microdiffusion; Interfering ions; GLC

1. Introduction

The determination of fluoride has been greatly facilitated by the increased adoption of diffusion procedures for the separation of fluoride from interfering substances and the introduction of suitable buffers. Severe problems still arise in separation methods for trace fluoride analysis in biological specimens due to interfering ions [1]. These ions have been removed by precipitation at pH 8–9 [2] and by the use of complexing agents such as Tiron, CDTA and EDTA [3].

In diffusion procedures, few authors have considered the effect of interfering ions, which form strong complexes with fluoride, on the rate of diffusion [4]. Some authors [5] have used sulphuric and perchloric acids for diffusion at 60°C for 20 h to find the effect of aluminium and silicon on fluoride recovery from standards. Both ions showed higher interference in sulphuric acid.

The use of HMDS in diffusion experiments have provided a more rapid method for fluoride separation at room temperature [6]. Its use has become widespread due to its simplicity and adaptability to fluoride determination in large number of samples. Several authors [7–9] have used and modified the method in the analysis of different biological samples. However, the effect of interfering ions on the rate of HMDS-aided

* Corresponding author. Current address: Academic Centre for Dentistry Amsterdam (ACTA), Dept. of Cariology, Endodontology, Pedodontology, Louwesweg 1, 1066 EA Amsterdam, The Netherlands.

PII S00 9-9140(97)00041-6

diffusion is not well documented. Aluminium levels in vegetables and plants have been reported to be in the range of 180–1350 μg g^{-1} [2] and this work addresses itself to whether such aluminium values would interfere with fluoride separation while using HMDS in standards, soils and plant materials. The effects of the presence of iron and silicon on fluoride recovery have also been considered.

2. Experimental

2.1. Apparatus

Combination fluoride ion-selective electrode (Orion, Cambridge, MA, USA, model 96-09), ion analyzer (Orion Model 407A and 920A), polystyrene Petri dishes 60 × 15 mm, Finn pippettes, polystyrene tips, shaker (GFL model 315), AAS Perkin Elmer model 2380, gas chromatograph (Chrompack model CP9001), and centrifuge.

2.2. Reagents

All chemicals were of analytical grade. Double distilled deionised water was used throughout the work. Reagents and solutions were freshly prepared and stored in plastic bottles except perchloric acid. Diffusion acid was prepared as reported by Kimarua et al. [10].

2.3. Aluminium standard solution

Aluminium standard solution was prepared by dissolving 13.90 g of hydrated aluminium nitrate $[Al(NO_3)_3 \cdot 9H_2O]$ in 250 cm^3 of water then made up to 1 l to make 1000 mg l^{-1}. It was stored in a plastic bottle.

2.4. Standard fluoride solution

First, 2.210 g of sodium fluoride (initially dried for 2 h at 120°C) was dissolved in 250 cm^3 of water, then made up to 1 l to give 1000 mg l^{-1}. This was stored in a plastic bottle.

2.5. Silicon standard solution

A solution containing 10 mg l^{-1} (500 mg l^{-1} for soil samples) was prepared by mixing 1.30 g of hydrated silicic acid powder ($SiO_2 \cdot nH_2O$) with 5 cm^3 of water. Then, 1.52 g of sodium hydroxide pellets were added to the mixture and shaken gently. After complete dissolution 30 cm^3 of water was added and allowed to cool. The solution was then diluted to 50 cm^3 with water and stored in a plastic bottle.

2.6. Iron standard solution

First, 1000 mg l^{-1} iron solution was made by dissolving 8.63 g of hydrated ammonium iron(III) sulphate $[NH_4Fe(SO_4)_2 \cdot 12H_2O]$ in water and diluted to 1 l. The solution was stored in a 1 l plastic bottle.

2.7. Procedure with ion-selective electrode

For fluoride analysis, polystyrene Petri dishes whose lids had been edged with acetone then rinsed with water were used. On each lid, a hole was made about 1.5 cm from the edge, using a soldering iron. The hole was for adding acid and sample using a Finn pipette. Then, 50 μl of 0.5 M sodium hydroxide was applied on the lid in form of eight drops. After replacing the lid, the Petri dish was sealed all round with a strip of parafilm. A 2.0-cm^3 aliquot of fluoride standard solution with a known amount of aluminium was put through the hole at the bottom of the Petri dish which contained 0.2 cm^3 of 1.0 M silver nitrate. Then, 2.0 cm^3 of 4.0 M perchloric acid was added and the hole quickly covered with a piece of parafilm. The dishes were placed on a shaker for 6 h at room temperature (20–23°C). After 6 h the lids were kept in a dessicator for the drops to dry. The dried up drops were dissolved in 50 μl of 0.5 M HCl and 50 μl TISAB II (pH 5.2) and the fluoride measured with a combination fluoride electrode. The same procedure was repeated using 0.1 g of plant materials and g of soil samples. Calibration standards and blanks were also subjected to the same diffusion procedures.

Table 1
Fluoride recovery from 1.0 and 2.0 μg ml^{-1} fluoride standard solution in the presence of 0.0–1000 μg ml^{-1} aluminium ions at room temperature with and without HMDS

Aluminium added (μg ml^{-1})	Mean percentage recovery			
	With HMDS		Without HMDS	
	A	B	A	B
0.0	100.0	99.0	6.2	6.0
100.0	103.0	102.0	1.8	1.6
200.0	102.0	98.0	1.4	1.2
500.0	102.0	99.0	—	0.7
800.0	100.0	100.0	—	—
1000.0	103.0	102.0	—	—

A, 1.0 μg ml^{-1} F.
B, 2.0 μg ml^{-1} F.
All concentrations are in μg ml^{-1}.
A dash (—) indicates that the fluoride concentration was below the detection limit.

2.8. Electrode calibration

NaF standards containing 0.1, 0.5, 1.0, 5.0, 10.0 and 20.0 μg ml^{-1} were prepared and treated the same way as the samples. Calibration of the electrode was done with two standards at a time on the 420A ion analyser (used for measurements in Table 1). At least five standards were used on the 920A concentration mode which then calculated the blank and the slope (used for measurements in Table 2). The measurement of the samples were carried out in a volume of 0.1 cm^3 and between measurements, the electrode was cleaned with water. The electrode was stored in 10 μg ml^{-1} NaF solution without any buffer. All the fluoride in the samples were concentrated above the detection limit of the electrode which was 0.02 μg ml^{-1}.

2.9. Procedure for gas liquid chromatography

Fluoride was determined on a CP9001 (Chrompack) gas chromatograph with a back flush system. It consists of a wide bore injection system, two wide bore columns of 10 and 25 m (WCOT Fused Silica with a coating of CP-SIL 5CB) and a flame ionisation detector [11]. The samples were weighed into 4 cm^3 borosilicate glass vials. Then, 0.5 cm^3 of water was added followed by 1 cm^3 of 8.0 M perchloric acid. The reagent solution was added which consists of 1 cm^3 toluene, 0.5% (v/v) trimethylchlorosilane (TMCS) and 0.0025% (v/v) iso-pentane (internal standard). The vial was closed immediately with a cap and septum. The reaction mixture was rotated overnight at 4°C then centrifuged for 2 min at 4000 rpm. A 1-μl sample was injected from the toluene layer to the column in duplicates and peak heights were determined and correlated to standard injections of known amounts of fluoride. Calibration curves were made with fluoride standards of 0.1–100 μg ml^{-1} from a stock solution of 1000 μg ml^{-1}. Straight lines were obtained with $r^2 = 0.999$.

Table 2
Concentration of fluoride in the sample

Sample	$[F^-]_1$	$[F^-]_2$	$[F^-]_3$	% Rec.	% CV
Tea bags	81.80	216.13	316.80	100.5	2.7
Green tea leaves	310.66	2280.00	2390.00	110.0	0.4
Terere Amaranthus	0.00	2.04	102.45	100.41	2.6
Spinach	0.00	4.64	105.09	100.45	5.7
Soil 113	15.56	100.00	200.33	100.33	2.2
Soil 118	22.17	229.75	338.00	108.25	1.2

$[F^-]_1$, fluoride levels in the absence of HMDS.
$[F^-]_2$, fluoride levels in the presence of HMDS.
$[F^-]_3$, fluoride levels in spiked samples (with 100 μg g^{-1} F) in the presence of HMDS.
CV, coefficient of variation for the recovery of spiked samples: S.D./Mean × 100.
All concentrations are in μg g^{-1}.

2.10. Aluminium, silicon and iron

Two procedures were follows:

1. Using hydrochloric acid and hydrofluoric acid for soil samples and concentrated nitric acid and perchloric acid for plant samples in the hot digestion method as reported in the AAS manual [12].
2. Using 4.0 M perchloric acid under the same conditions of the diffusion process. Then, 1.2 g of the samples were placed in plastic containers and 50.0 cm^3 of 4.0 M perchloric acid was added. The contents were placed on a shaker for 6 h. After filtering, the contents were analyzed for aluminium, iron and silicon using the AAS.

3. Results and discussions

In direct potentiometric analysis of fluoride, the tolerance limit of aluminium is 27 ppm at pH 6 and 2.7 ppm at pH 5.5 in the presence of Tiron as the masking agent [3], while in the indirect spectrophotometric method, the critical concentration is 22 ppm [13]. It is also indicated that the release of fluoride ion from aluminium varies with the masking reagent used, pH and the concentration of fluoride and aluminium ions. At the diffusion temperature of 60°C silicon forms a viscous gel in the presence of acids and thus reduces the rate of diffusion due to the trapping of the HF in the micellar spaces [5]. However, at room temperature, no gel is formed and the residue does not hinder the diffusion of trimethylflurosilane (TMFS). The documented interference during HF diffusion by Gustafsson and Njenga [5] indicates a decrease in fluoride recovery in standards as aluminium and silicon concentrations are increased. However, the literature on the effect of interfering ions on HMDS diffusion is scarce.

In the present study, the HMDS method was first tested with sodium fluoride standard solutions in the range 0.5–1.0 μg ml^{-1} with a recovery of 99.5–100.3% ($n = 4$) indicating high accuracy and precision of the method.

In the absence of aluminium and HMDS, acid diffusion at room temperature gave recoveries of about 5% added fluoride. This value does not change significantly for aluminium concentrations below 100 μg ml^{-1}. However, above 100 μg ml^{-1} aluminium, recoveries decreases and at 500 μg ml^{-1} no fluoride is recovered as shown in Table 1. It is stipulated that in the absence of HMDS, HF reacts with other HF molecules and with water to form higher molecular weight complexes which do not diffuse due to their high boiling points.

Table 1 also gives the recoveries of fluoride from 1.0 and 2.0 μg ml^{-1} fluoride standard solutions in the presence of 100–1000 μg ml^{-1} aluminium at room temperature in the presence of HMDS. Recoveries between 99.0–103.0% were realised indicating little or no interference from aluminium ions when HMDS is used.

The study was extended to four plant samples and two soil samples whose fluoride, aluminium, iron and silicon contents were determined. Table 2 shows the fluoride levels, recovery from spiked samples and analytical variations expressed as a coefficient of variation for the recovery of the added fluoride. Fluoride concentration ranges from as low as 2.0 μg g^{-1} in Terere (*Amaranthus*) to 2280 μg g^{-1} in green tea leaves. Regardless of the very high aluminium concentrations (Table 3), different levels of fluoride are obtained whose comparison with spiked samples gives acceptable recoveries with coefficient of variation between 0.4–5%. In the absence of HDMS, 10–15% fluoride was available for measurement except in tea bags which had 37%.

Table 3 gives the levels of aluminium, iron and silicon. Except for tea leaf samples, the aluminium levels during diffusion are lower than the total but high enough to have an effect during diffusion. The total levels of the ions are those obtained by extractions with acids different from the actual diffusion acids. To evaluate the actual concentrations of the ions during diffusion, perchloric acid was used for extraction and the levels determined by AAS.

The concentrations obtained are an indication of what is extracted by perchloric acid during diffusion. Such levels have been shown to fere with diffusion at 60°C but from the fluoride levels and recoveries, there is no interference in

Table 3
Concentration of aluminium, iron and silicon in the samples

Sample	$c(Al)_1$	$c(Al)_2$	$c(Fe)_1$	$c(Fe)_2$	$c(Si)_1$	$c(Si)_2$
Tea bags	0.67	0.45	0.50	0.08	<DL	0.09
Green tea leaves	4.98	5.04	0.60	0.11	<DL	0.32
Terere amaranthus	1.18	0.17	0.80	0.25	26.00	0.20
Spinach	1.54	0.12	1.10	0.30	9.00	0.12
Soil 113	77.00	3.83	67.30	3.45	204.00	0.64
Soil 118	74.33	3.14	48.60	1.97	166.00	0.66

$c(Al)_1$, $c(Fe)_1$, $c(Si)_1$, concentrations of iron and silicon after wet digestion using HF.
$c(Al)_2$, $c(Fe)_2$, $c(Si)_2$, concentrations of iron and silicon after digestion using $HClO_4$.
<DL, below detection limit.
All concentrations are in $\mu g\ g^{-1} \times 10^3$.

the presence of HMDS. The study clearly indicates that HMDS can be used for samples with high levels of interfering ions without any interference in the diffusion and the procedure can be applied to biological materials having high levels of aluminium, silicon and iron.

In order to validate the results, the fluoride concentrations of similar samples were also measured with a GLC. Table 4 gives the percentages of fluoride in the samples while using both GLC and HMDS microdiffusion. The data indicate that the two methods are comparable. The principle behind the extraction of fluoride is similar in both methods based on acid-promoted reaction trimethylchlorosilane (TMCS) in GLC and HMDS in microdiffusion with fluoride.

Table 4
Validation of the results of fluoride determination

Sample	GLC (% F)	FISE (% F)
Spinach	0.000473 ± 0.85	0.000534 ± 2.0
Tea bags	0.0204 ± 2.4	0.0199 ± 1.6
Terere	0.000593 ± 1.7	0.000622 ± 1.7
Soil 113	0.00864 ± 0.5	0.0119 ± 3.6
Soil 118	0.0205 ± 6.7	0.0244 ± 6.2
Tea leaves	0.291 ± 5.4	0.268 ± 8.1

GLC, liquid chromatography.
FISE, fluoride ion selective electrode after HMDS microdiffusion.

Acknowledgements

The authors acknowledge DAAD (The German Academic Exchange Services), the University of Nairobi for the financial support and the Department of Cariology and Endodontology (ACTA, Amsterdam) for the support during validation. We also thank Mark J. Buijs for helping in the analysis of the samples with the GLC and Dr Jan Damen for valuable comments.

References

[1] R.J. Hall, Analyst 93 (1968) 461.
[2] N.R. McQuaker, M. Gurney, Anal. Chem. 49 (1977) 53.
[3] A. Yuchi, N. Yanai, H. Wada, G. Nakagawa, Analyst 113 (1988) 1405.
[4] L.W. Njenga, PhD Thesis, University of Nairobi, 1989.
[5] L. Gustafsson, L.W. Njenga, Anal. Chim. Acta 212 (1988) 133.
[6] D.R. Taves, Talanta 15 (1968) 969.
[7] M. Hinoide, H. Koga, K. Inoue, S. Imai, Y. Takaesu, T. Nisizawa, J. Dent. Health 42 (1992) 239.
[8] M. Hinoide, K. Inoue, T. Nasizawa, J. Dent. Health 40 (1990) 254.
[9] R. Sara, E. Wannien, Talanta 22 (1975) 1033.
[10] R.W. Kimarua, D.N. Kariuki, L.W. Njenga, Analyst 120 (1995) 2245.
[11] J.J.M. Damen, M.J. Buijs, J.M. ten Cate, Caries Res. 30 (1996) 454.
[12] Analytical Methods for Atomic Absorption Spectrophotometry, Connecticut 06856, USA, Chpt. 3–4, 1976.
[13] R. Sandulescu, E. Florean, L. Roman, S. Mirel, R. Oprean, P. Suciu, J. Pharm. Biomed. Anal. 14 (1996) 951.

ELSEVIER

Talanta 44 (1997) 1735–1747

Talanta

The effect of the ion exchanger site-counterion complex formation on the selectivities of ISEs

V.V. Egorov *, N.D. Borisenko, E.M. Rakhman'ko, Ya.F. Lushchik, S.S. Kacharsky

Institute of Physico-Chemical Problems, Belarusian State University, Leningradskaya Str. 14, 220080 Minsk, Belarus

Received 18 June 1996; received in revised form 7 January 1997; accepted 3 February 1997

Abstract

Using the model of ideally associated solution, the effect of ion association of the ion exchanger sites with main and foreign counterions on the selectivity of ISEs based on liquid ion exchangers has been considered. Equations which describe the potentiometric selectivity coefficient as a function of ion association constants in the membrane phase and of standard free energies of transfer of the determined and foreign ions from water to the membrane are obtained for the following main cases: (a) the determined and foreign ions are single-charged; (b) the determined ion is double-charged and the foreign ion is single-charged. It is shown that in the case of single-charged main and foreign ions, the ratio of the ion association constants has a great effect on the potentiometric selectivity of membranes, only if the ion exchanger sites produce less strong associates with the determined counterion as compared with the foreign one. Otherwise, this effect is insignificant. The selectivity for double-charged ions should increase, other things being equal, as the first constant of association of these ions with the ion exchanger sites increases. The effect of producing ion triplets of the type $I_2R^{(\pm)}$ on the selectivity of ISEs is also considered. Experimental data are presented which illustrate the effect of the nature of the ion exchanger on the potentiometric selectivity. Some procedures employing the factor of ion association for increasing the potentiometric selectivity of liquid ion exchange membranes are considered. © 1997 Elsevier Science B.V.

Keywords: Electrodes; Ion association; Potentiometric selectivity

1. Introduction

The presence of relationship between the potentiometric selectivity of ISEs and the relative strength of binding main and foreign ions with the ion exchanger site follows directly from Sandblom, Eisenman and Walker's theory [1] and is one of the most important conclusions of Nikolsky-Schultz's general theory of glass electrodes [2], whose main statements are applicable to some extent to membanes based on liquid ion exchangers. Stover and Buck [3,4] have shown that apart from forming ion pairs, the ratio of mobilities of ion exchanger sites and counterions in the membrane phase can also have an important effect on the selectivity coefficient. It should be noted that this effect increases with ion association. Armstrong and co-workers [5–7] have shown that

* Corresponding author.

PII S00 9-9140(97)00042-8

mobilities of ion exchanger sites and counterions in plasticized polyvinylchloride membranes can differ by more than an order of magnitude. Thus, the possibility of exhibition of the mentioned effect seems quite realistic. On the other hand, experiments have shown that the nature of the ion exchanger usually does not have an important effect on ISE selectivity [8–11]. It is interesting to note that similar data were obtained both for fully dissociated nitrobenzene-containing membranes and for membranes with a relatively low dielectric constant. In general, this situation is consistent with results of the works on ion association [12,13], from which it follows that ion exchanger site-counterion association constants are almost independent of the ion nature. Moreover, Morf has shown [14] that even in those cases when charged ionophore tends to selective interaction with one of the ions, this property of the charged ionophore cannot be transformed completely into potentiometric selectivity. Therefore, for some time the concept prevailed that use of charged ionophores was not so promising as compared with neutral carriers as concerns achievement of high potentiometric selectivity.

However, for the recent 10–15 years the various anion-selective electrodes based on charged ionophores (derivatives of vitamin B_{12} [15–18], porphyrins [19–28], phthalocyanins [29], tin-organic, palladium-organic compounds [30–34] etc.) were described which were able to form sufficiently strong complexes with the determined ion. Selectivity of such electrodes differed substantially from selectivity of the Hofmeister series, which could not be explained reasonably within the formalism developed in [14]. Egorov and co-workers [35,36] have shown that the theoretical prohibition of the transformation of the selective ion exchanger affinity to the determined ion into potentiometric selectivity could be overcome, if the concentration of free ions of selective ion exchanger is stabilized in the membrane so that it could not change greatly in the course of the ion exchange reaction with the interfering ion. To do this, it was suggested to introduce into the membrane a lipophilic ionic additive having charge opposite to that of the ion exchanger sites and forming a rather well dissociating salt with the latter. It was shown experimentally that this procedure could, for example, increase substantially the selectivity to the cations of primary-tertiary amines as compared with quaternary ammonium cations which, according to [37], form less strong ion associates. The mechanism of functioning of the membranes based on highly selective ion exchangers (or charged carriers, according to the classification [38]) was thoroughly considered by Schaller and co-workers [39–41]. In particular, they showed that introduction of a lipophilic ion additive into the membrane was very important in the case of cation-selective electrodes but not so important in the case of anion-selective electrodes, since PVC membranes always contain anion admixtures that actually function as a lipophilic additive and provide selectivity close to optimal. Those authors obtained quantitative expressions for the electrode response and selectivity coefficients as a function of the membrane composition, solvation and complex formation parameters, which is important both for understanding of the functioning mechanism of such ISEs and for optimization of membrane compositions and measurements conditions.

In the present contribution the influence of the features of ion exchanger site-counterion interaction on the potentiometric selectivity of the membranes being in contact with sample solution containing both primary and interfering ions is discussed. New experimental data are presented which illustrate the effect of the ion exchanger nature on ISE selectivity.

2. Experimental

2.1. Reagents

2.1.1. Ion exchangers

Quaternary ammonium salts, namely, trinonyloctadecyl-ammonium (TNODA), dimethyldioctadecylammonium (DMDODA) and *N*,*N*,*N*-tridecyl-2-hydroxyethylammonium (TDHEA) were synthesized by stepwise alkylation of octadecylamine (the first two salts) and monoethanolamine, respectively, by halogen alkyls following the method of Veigand-Hilgetag [42].

The produced compounds were isolated and purified by extraction in the octane–dimethylformamide system [43]. For all compounds produced the contents of the main substance determined by nonaqueous potentiometric titration with respect to halogen ion was at least 99%. The contents of amine impurities in these compounds determined spectrophotometrically in the form of ion associates with picric acid following Lestchev et al. [44] did not exceed 0.01%. Trinonyloxybenzenesulphonic acid (TNBS) was produced by alkylation of pyrogallol by nonyl bromide followed by sulphonation [45]. The product was isolated and purified by extraction in the hexane–dimethylsulphoxide system. Di(2-decyloxyphenyl)phosphate (D(2DP)P) and di(3-nonyloxyphenyl)phosphate (D(3NP)P) were produced in the reaction of phosphorus chloroxide with the appropriate alkoxyphenol. These compounds were synthesized and purified following the procedure used for these kind of compounds [46]. For the last three compounds, the contents of the main substance determined by nonaqueous potentiometric titration amounted to at least 97%.

2.1.2. Plasticizers and solvents

Dibuthylphthalate (DBP), 1-bromnaphthalene (BN), *o*-nitrophenyloctyl ester (NPOE) and organic solvents toluene, nitrobenzene and cyclohexanone of reagent grade were purified by distillation. Dioctylphenylphosphonate (DOPP) was synthesized in the reaction of phenylphosphonedichloride with octanol following Cosolapoff [47]. Then, the product was isolated from the reaction mixture by extraction in the hexane and water/dimethylsulphoxide mixture (1:4). The isolated plasticizer was purified in the chromatographic column filled with S40/100 silicagel; the mobile phase was a chloroform/methanol mixture (9:1) [48]. Trihexylphosphate (THP) was purified from acid admixtures by treatment of hexane solution of the reagent with sodium hydroxide solution in the water/dimethylformamide mixture following [49]. 3-Nonyloxyphenol (NOP) was produced by alkylation of resorcinol by nonyl bromide. The product was distilled after extraction from the reaction mixture.

2.1.3. Polymer matrices and aqueous electrolytic solutions

Polyvinylchloride PZh-S70 was used as a polymer matrix of ISE membranes. Aqueous electrolytic solutions were prepared using distilled water. Dry salts used for these purposes were of at least analytical reagent grade.

2.2. Preparation of samples

Membranes of ISEs were prepared following the standard method [50]. The membrane compositions are presented in Table 1. Various interesting series of compounds of quaternary ammonium were obtained by ion exchange.

2.3. Measurements of ion exchange constants

Exchange of chloride for sulphate was studied at the constant temperature $T = 293 \pm 1$ K in the toluene-water system at an ion exchanger concentration of $1.7 \cdot 10^{-2}$ M. The contents of sulphate ions in the water phase varied in the range 0.005–1 M. After the system attained equilibrium the chloride ion concentration in the aqueous and organic phases was found by potentiometric titration by silver nitrate solution, and the sulphate ion concentration was found from the difference using the material balance equation. It was observed that the anion exchange constant depended substantially on the sulphate ion concentration, which is consistent with the available literature information [51] and can be ascribed to formation of the complex anion $NaSO_4^-$. Estimated concentration constants of anion exchange are given in Table 2.

2.4. Measurements of ion association constants

Ion association was studied at $T = 293 \pm 1$ K in the toluene–nitrobenzene system containing 10% v/v of nitrobenzene at constant current. Electric conductivities of a series solutions of quaternary amonium salts (QAS) were determined at concentrations of 10^{-2}–10^{-7} M. Then, the constants of ion association were calculated from the formula:

$$k_{ass} = (1 - \alpha)/(\alpha^2 \cdot C)$$

Table 1
The composition of produced ISE membranes

Membrane	PVC (%, w/w)	Plasticizer (%, w/w)				Ion exchanger (M)					NOP (w/w, %)
		DBP	THP	1-BN	NPOE	DOPP	TNODA	TDHEA	TNBS	D(3NP)P	D(2DP)P	DM-DODA	
I	33.3	66.6					$1.2\cdot10^{-1}$						
II	33.3		66.6				$1.2\cdot10^{-1}$						
III	33.3			66.6			$1.2\cdot10^{-1}$						
IV	33.3				66.6		$1.2\cdot10^{-1}$						
V	33.3	66.6						$1.2\cdot10^{-1}$					
VI	33.3		66.6					$1.2\cdot10^{-1}$					
VII	33.3			66.6				$1.2\cdot10^{-1}$					
VIII	33.3				66.6			$1.2\cdot10^{-1}$					
IX	28.5	57					$1.2\cdot10^{-1}$						14
X	28.5	57										$1.2\cdot10^{-1}$	14
XI	33.3					66.6			$2.5\cdot10^{-2}$				
XII	33.3					66.6				$2.5\cdot10^{-2}$			
XIII	33.3					66.6					$2.5\cdot10^{-2}$		

where α is the dissociation degree of QAS found with Stokes' method [52], C is the concentration of QAS in the solution.

2.5. Potentiometric measurements

Potentiometric measurements were taken at $T = 293 \pm 1$ K with an I-130 digital ionometer with an EVL-1M.3 silver–silver chloride reference electrode. Selectivity coefficients were determined with the method of mixed solutions for SO_4^{2-} ion selective electrode with a constant sulphate-ion background of 10^{-3} M and against the background of main ion of 0.1 M for the other ISEs. K_{ij}^{pot} was calculated from the equation:

$$K_{ij}^{pot} = \frac{a_i}{(a_j)^{z_i/z_j}} (10^{(E_2 - E_1)/\theta} - 1)$$

where a_i and a_j are the activities of the main and foreign ions; z_i and z_j are the charges of the main and foreign ions; E_1 and E_2 are the potentials of ISE in the background and mixed solutions; θ is the slope of the electrode function.

3. Results and discussion

3.1. The model of ideally associated solution. Single-charged ions

In media with low and moderate dielectric constants such as ISEs membranes (except those based on nitrobenzene or nitrogroup-containing plasticizers), liquid ion exchangers are present mainly in the form of ion associates with appropriate counterions, when the relative amount of free ions in the membrane is negligible. In these systems, the ion exchange constant determined experimentally is described by the equation:

$$K_{ij}^{(2)} = K_{ij}^{(1)} \cdot K_{jR}/K_{iR} \quad (1)$$

where $K_{ij}^{(2)}$ is the equilibrium constant of the ion exchange process, e.g., for cation-exchanger:

$$J_{aq}^{+} + \overline{RI} \xrightarrow{K_{ij}^{(2)}} I_{aq}^{+} + \overline{RJ} \quad (2)$$

$K_{ij}^{(1)}$ is the ion exchange constant only determined by standard free energies of transfer of ions I and J and is independent of the nature of the ion exchanger:

Table 2
The effect of the ion exchanger nature on the ion association, ion exchange and potentiometric parameters

Ion exchanger	Ion	Ion association constant	$K_{SO_4^{2-},Cl^-}$* for $C_{SO_4^{2-}}$		$K^{pot}_{SO_4^{2-},Cl}$
			$5\cdot10^{-2}$ M	1.0 M	
TNODA	SO_4^{2-}	$4.6\cdot10^{8}$	$4.8\cdot10^{1}$	$5.0\cdot10^{2}$	$1.5\cdot10^{3}$ (IX)
	Cl^-	$4.9\cdot10^{9}$			
	Pic^-	$3.1\cdot10^{8}$			
	$TPhB^-$	$4.1\cdot10^{7}$			
DMDODA	SO_4^{2-}	$4.8\cdot10^{8}$	$7.2\cdot10^{-1}$	5.0	$6.5\cdot10^{1}$ (X)
	Cl^-	$8.0\cdot10^{9}$			
	Pic^-	$5.9\cdot10^{8}$			
	$TPhB^-$	$2.7\cdot10^{7}$			

* $K_{SO_4^{2-},Cl^-}$ is the equilibrium constant of the process: $.2\ Cl^- + \overline{SO_4^{2-}\cdots(R^+)_2} \rightarrow 2\ \overline{Cl^-\cdots R^+} + SO_4^{2-}$

$$K_{ij}^{(1)} = \exp[(\Delta G_i^0 - \Delta G_j^0)/RT], \quad (3)$$

K_{iR} and K_{jR} are the constants of ion association of I^+ and J^+ counterions with the ion exchanger sites R^-. Thus, as it was shown by Eisenman [1], in highly associated systems, the ion exchange selectivity depends directly on the ratio of the constants of association of the ion exchanger sites with the corresponding counterions.

While considering the potentiometric selectivity, we restrict ourselves to the model including only the effect of the foreign ion J^+ on the interphase potential at the membrane–solution interface, assuming that for membranes based on liquid ion exchangers, the diffusion potential inside the membrane is unimportant. If the differences of the activities of ions I^+ and J^+ in the near-boundary layer and in the bulk of the sample solution are neglected, the effect of the foreign ion J^+ consists in changing the activity of the main ion I^+ in the membrane phase. In the first approximation this change may be described in terms of the concentration constants of ion exchange and of ion association. In the case of associated systems, concentrations of free (solvated by the solvent but not bound to the associates) ions is described by the equation:

$$\bar{C}_i = \frac{\bar{C}_{iR}}{K_{iR}\cdot\bar{C}_R} \quad (4)$$

where $\bar{C}_R$ is the concentration of the free ion exchanger site R^-. In the approximation of the model of ideally associated solution, this concentration is described by the equation

$$\bar{C}_R = \sqrt{\frac{\bar{C}_{iR}}{K_{iR}} + \frac{\bar{C}_{jR}}{K_{jR}}} \quad (5)$$

where $\bar{C}_{iR}$ and $\bar{C}_{jR}$ are the equilibrium concentrations of the corresponding ion associates described by the equations

$$\bar{C}_{iR} = \frac{\bar{C}_R^{tot}\cdot C_i}{C_i + K_{ij}^{(2)}\cdot C_j} \quad (6)$$

$$\bar{C}_{jR} = \frac{\bar{C}_R^{tot}\cdot K_{ij}^{(2)}\cdot C_j}{C_i + K_{ij}^{(2)} C_j} \quad (7)$$

where $\bar{C}_R^{tot}$ is the total concentration of the ion exchanger in the membrane.

It follows from Eqs. (4) and (5) that the change in the concentration of free counterions I^+ in the membrane that characterizes the interfering effect of the foreign ion J^+ is determined not only by completeness of the ion exchange process but also by the ratio of the ion association constants. Let the condition $K_{iR} > K_{jR}$ be satisfied. According to Eqs. (1) and (2) this should lead to a decrease in the concentration of the associate JR in the membrane. However, decrease in the portion of the less strong ion associate JR is compensated for, to a great extent, by its greater ability to generate free site R^-, which, according to Eq. (4), is accompanied by decrease in the concentration of the free counterion I^+ in the membrane. As a result, use of a selective ion exchanger producing stronger associates with the ion I^+ should not lead to appropriate increase in the potentiometric selectivity.

In this case the equation that expresses explicitly the experimentally determined potentiometric selectivity coefficient in terms of exchange parameters of the system can be easily obtained from the theory of ISEs based on liquid ion exchangers developed by Morf. According to [14], for an electrode immersed into the solution studied that contains simultaneously the determined and interfering ions the membrane potential is described by the equation:

$$E = E_i^0 + (1-\tau) \cdot RT/F \ln(a_i + K_{ij}^{(1)} a_j) + \tau \cdot RT/F \ln(a_i + K_{ij}^{(2)}) \quad (8)$$

where τ is the electric transport number of the ion exchanger site R^-, and $K_{ij}^{(1)}$ and $K_{ij}^{(2)}$ are physically the same as was defined above.

Assuming the diffusion potential to be zero, which is valid at $\tau = 0.5$ and combining Eq. (8) with Nikolsky's equation:

$$E = E_i^0 + RT/F \ln(a_i + K_{ij}^{pot} \cdot a_j) \quad (9)$$

we obtain

$$K_{ij}^{pot} = [(a_i + K_{ij}^{(1)} a_j)^{1/2} \cdot (a_i + K_{ij}^{(1)} \cdot K_{jR}/K_{iR})^{1/2} - a_i]/a_j \quad (10)$$

As follows from [3–7], neglect of the diffusion potential could hardly be considered quite reasonable. Nevertheless, to simplify the formalism, the assumption is ordinarily used in consideration of the effect of ion association on the potentiometric selectivity of the membrane [39–41,53].

If only foreign ions J^+ are presented in the solution analysed, Eq. (10) is reduced to the equation obtained in [39] for the separate solution method:

$$K_{ij}^{pot} = K_{ij}^{(1)} (K_{jR}/K_{iR})^{1/2} \quad (11)$$

When the association constants are equal ($K_{jR} = K_{iR}$), Eq. (10) is reduced to Nikolsky's ordinary equation.

In the general form analysis of Eq. (10) is rather difficult. Meanwhile, since this equation express explicitly the dependence of K_{ij}^{pot} on the constants of ion exchange and ion association, the effect of these parameters on K_{ij}^{pot} can be investigated in a simple way by mathematical modelling. The obtained results are presented in Fig. 1. It can be seen that $K_{ij}^{pot} \ll 1$ is the necessary condition for attainment of high selectivity for the ion I^+. In this case the ratio of ion association constants K_{iR}/K_{jR} is important only at $K_{iR} < K_{jR}$. On the contrary, at $K_{iR} \geq 10K_{jR}$ further increase in the constant of association of the ion exchanger site R^- with the main ion I^+ has actually no effect on K_{ij}^{pot} which tends to $(1/2)K_{ij}^{l}$. In the case when $K_{ij}^{l} \gg 1$, changes in the ratio K_{iR}/K_{jR} has some effect on K_{ij}^{pot} at $K_{iR} > K_{jR}$ as well. However, this case has no practical interest, since K_{ij}^{pot} is always larger than 1, tending to $(K_{ij}^{(1)})^{1/2}$.

Of course, by virtue of the assumptions made, the above scheme does not reflect the real situation quite rigorously. Nevertheless, it seems useful since it allows us to follow, at least qualitatively, the effect of ion association on K_{ij}^{pot}.

The present conclusions agree well with experimental data on the effect of the nature of the quaternary ammonium cation on K_{ij}^{pot}. The data are summarized in Table 3. It can be seen that an ISE based on salts of TDHEA containing a solvation-active OH group in the direct vicinity to the ion exchange centre, exhibit higher selectivity to sulphonate- and carboxylate-containing anions in the presence of perchlorate and picrate ions as compared with ISEs based on salts of TNODA. The observed effect can reasonably be explained

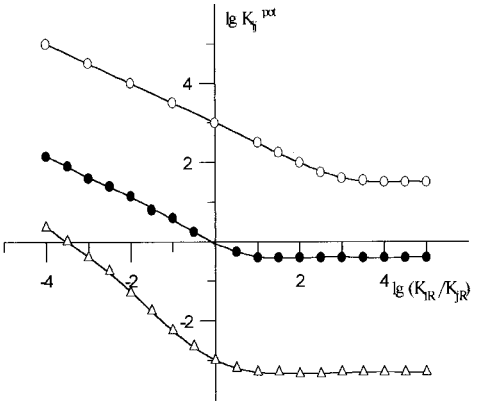

Fig. 1. Calculated selectivity coefficients for $I^{(\pm)}$ over $J^{(\pm)}$ for ion exchanger based membranes. To calculate the selectivity coefficients according to Eq. (10), the following assumptions were made: $a_i = a_j = 1 \cdot 10^{-2}$ M; $K_{ij}^{(1)}$ equals $1 \cdot 10^3$ (hollow circle); (filled circle); $1 \cdot 10^{-3}$ (hollow triangle).

Table 3
The effect of membrane components on the values of ISE selectivity coefficients in the presence of foreign ions

Determined ion	Plasticizer	Selectivity coefficients		$\frac{K_{ij}^{pot}(TNODA)}{K_{ij}^{pot}(TDHEA)}$
		Ion exchanger TNODA	Ion exchanger TDHEA	
Trichloroacetate	Dibuthylphthalate	ClO_4^-: $4.5\cdot10^1$ $(8\cdot10^{-1})$*	ClO_4^-: $2\cdot10^1$ $(4\cdot10^{-1})$*	2.25 (2.0)*
		Pic^-: $2\cdot10^4$ $(4\cdot10^2)$*	Pic^-: $1.5\cdot10^4$ $(2\cdot10^2)$*	1.3 (2.0)*
1-Naphthalenesulphonate	Dibuthylphthalate	ClO_4^-: 10 $(1.7\cdot10^{-1})$*	ClO_4^-: 4 $(1\cdot10^{-1})$*	2.5 (1.7)*
		Pic^-: $6\cdot10^3$ $(1\cdot10^2)$*	Pic^-: $4\cdot10$ $(6\cdot10^1)$*	1.5 (1.7)*
2,4-Dinitrobenzoate	Dibuthylphthalate	ClO_4^-: $1\cdot10^2$ $(9\cdot10^{-1})$*	ClO_4^-: $4\cdot10^1$ $(5\cdot10^{-1})$*	2.5 (1.8)*
		Pic^-: $5\cdot10^4$ $(5\cdot10^2)$*	Pic^-: $3\cdot10^4$ $(3\cdot10^2)$*	1.7 (1.7)*
Toluenesulphonate	Dibuthylphthalate	ClO_4^-: $8\cdot10^2$	ClO_4^- $2.5\cdot10^2$	3.2
Toluenesulphonate	Trihexylphosphate	ClO_4^-: $3\cdot10^2$	ClO_4^-: $1.4\cdot10^2$	2.1
Toluenesulphonate	1-Bromnaphthalene	ClO_4^-: $5.5\cdot10^2$	ClO_4^-: $2.5\cdot10^2$	2.2
Toluenesulphonate	*o*-Nitrophenyloctyl ester	ClO_4^-: $1\cdot10^3$	ClO_4^-: $3\cdot10^2$	3.3

* The membranes contain 14% w/w 3-nonyloxyphenol.

by increase in the strength of ion associates produced by anions with TDHEA cations as a result of formation of a hydrogen bond additional to electrostatic interaction. It is natural that the strength of this bond should depend on polarity of the anion, increasing from picrate and perchlorate to sulphonate- and carboxylate-containing anions. This effect results in a 10–20-fold increase in the ion exchange constants for exchange of benzoic acid derivatives for perchlorate and 2,4-dinitrophenolate ions [54]. However, K_{ij}^{pot} values change only by a factor of 1.5 to 3. It is noteworthy that the observed change in K_{ij}^{pot} is almost independent of the nature of the plasticizer and persists in the presence of the specific solvating additive resorcinol monononyl ester.

Selectivity of such ISEs can be increased somewhat, if the membrane is manufactured so that it functions as an indirect electrode, when only a small part of the selective ion exchanger (5–10%) is in the form of the determined ion I and the other part is in the form of more lipophilic ion A which is slightly capable of being displaced by the main ion to the near-electrode layer of the sample solution ($K_{iA}^{(2)} \geq 10^4$). If this electrode is immersed in solution of the determined ion I, the concentrations of the ion associates IR and AR in the membrane remain almost invariant. Thus, the concentration of the lipophilic ion A, that appears in the near-electrode layer as a result of ion exchange, is proportional to the concentration of the main ion I in the sample solution and the potential is a linear function of C_i. In this case the effect of the foreign ion J should be exhibited to the extent at which it leads to changes in the concentration of the ion associate IR in the boundary layer of the membrane, i.e. in accordance with the experimental ion exchange constant $K_{ij}^{(2)}$. We tested this method for a toluenesulphonate selective electrode based on TDHEA (picrate was used as a lipophilic anion) and found that in the presence of perchlorate as a foreign ion the electrode selectivity was two times higher as compared to ISE based on individual salt form of this ion exchanger. The electrode works effectively at least 6 month and its main analytical characteristics (the detection limit, the slope of the emf response, stability of the potential) are not inferior to ISEs based on individual salt form, because of which the suggested method can be recommended for practice.

If the ion to be determined produces less strong associates with the ion exchanger site as compared with the interfering one, as it follows from the results discussed, the potentiometric selectivity always can be improved by decreasing the ratio of ion association constants K_{jR}/K_{iR}. In the case of quaternary ammonium cations ions) and primary–tertiary ammonium cations or alkaline metal cations (foreign ions) the required effect can

be easily achieved by using plasticizers with high dielectric constant, that according to [55], results in leveling of ion association constants. The efficiency of this procedure is confirmed experimentally as when *o*-nitrophenyloctyl ester or nonyl ester of *o*-nitrobenzoic acid is substituted for dibutylphthalate or dioctylphthalate, selectivity to quaternary ammonium cations becomes 3–10 times higher [35].

3.2. The model of ideally associated solution. Double-charged ions

If the membrane contains liquid ion exchanger, which is the salt of single-charged site R^- with double-charged counterion I^{2+}, according to [14], the membrane potential in the solution containing both the main ion I^{2+}, and the foreign single-charged ion J^+ is described by the equation:

$$E = E_i^0 + (1-\tau) \cdot RT/F \ln\left[\sqrt{a_i + \frac{1}{4}K_{ij}^{(2)}a_j^2} - \sqrt{\frac{1}{4}K_{ij}^{(2)}a_j^2} + \sqrt{K_{ij}^{(1)}a_j^2}\right] + \tau \cdot RT/F \ln\left[\sqrt{a_i + \frac{1}{4}K_{ij}^{(2)}a_j^2} + \sqrt{\frac{1}{4}K_{ij}^{(2)}a_j^2}\right] \quad (12)$$

where

$$K_{ij}^{(1)} = (2K_{iRR}/K_{jR})^2 \cdot K_{ij}^{(2)} \quad (13)$$

$$K_{ij}^{(2)} = (K_{jR} \cdot k_j)^2/(2\bar{C}_R^{tot} \cdot K_{iR} \cdot K_{iRR} \cdot k_i) \quad (14)$$

K_{iR} and K_{jR} are the ion association constants characterizing the ion pairing of ion exchanger site R^- with counterions I^{2+} and J^+ respectively, K_{iRR} is the ion association constant characterizing the ion pairing of ion exchanger site R^- with single-charged complex IR^+, k_i and k_j are so-called individual distribution coefficients proposed by Eisenman [1], $\bar{C}_R^{tot}$ is the total concentration of ion exchanger sites in the membrane.

Neglecting the diffusion potential and assuming $\tau = 0.5$, we obtain

$$E = E_i^0 + RT/2F \ln\left[a_i + \sqrt{K_{ij}^{(1)}a_j^2}\left(\sqrt{a_i + \frac{1}{4}K_{ij}^{(2)}a_j^2} + \sqrt{\frac{1}{4}K_{ij}^{(2)}a_j^2}\right)\right] \quad (15)$$

Combining Eq. (15) with Nikolsky's expanded equation for single- and double-charged ions:

$$E_i = E_i^0 + RT/2F \ln(a_i + K_{ij}^{pot} \cdot a_j^2) \quad (16)$$

we find:

$$K_{ij}^{pot} = \sqrt{\frac{K_{ij}^{(1)}K_{ij}^{(2)}}{4}} + \sqrt{\frac{K_{ij}^{(1)}K_{ij}^{(2)}}{4} + \frac{K_{ij}^{(1)}a_i}{a_j^2}} \quad (17)$$

With account of Eqs. (13) and (14), Eq. (17) can be transformed to the following form convenient for analysis:

$$K_{ij}^{pot} = \frac{1}{2} \cdot \frac{K_{ij}^{(3)}K_{jR}}{\bar{C}_R^{tot}K_{iR}} + \sqrt{\left(\frac{1}{2} \cdot \frac{K_{ij}^{(3)}K_{jR}}{\bar{C}_R^{tot}K_{iR}}\right)^2 + 2\frac{a_iK_{ij}^{(3)}K_{iRR}}{a_j^2\bar{C}_R^{tot}K_{iR}}} \quad (18)$$

where $K_{ij}^{(3)}$, a hypothetic ion exchange constant in a fully dissociated system, is described by the equation:

$$K_{ij}^{(3)} = k_j^2/k_i \equiv \exp[(\Delta G_i^0 - 2\,\Delta G_j^0)/RT] \quad (19)$$

ΔG_i^0 and ΔG_j^0 are standard free energies of transfer of ions I^{2+} and J^+ from aqueous phase into membrane. Eq. (18) is equally valid for anion exchange membranes too.

It follows from Eq. (18) that increase in K_{iR} as well as increase in $\bar{C}_R^{tot}$ should always be accompanied by increase in the potentiometric selectivity for double-charged ions in the presence of single-charged ones. On the contrary, increase in $K_{ij}^{(3)}$ and increase in K_{jR} should always lead to increase in the interfering effect of single-charged ions. This situation seems quite reasonable. At first glance, it is surprising that increase in the second constant of ion association of the primary ion with the ion exchanger site (K_{iRR}) is accompanied by deterioration of the selectivity. Two oppositely directed factors act in this situation. On the one hand, in accordance with ion exchange equilibrium, increase in K_{iRR} should lead to decrease in the concentration of ion associate JR in the membrane. On the other hand, as K_{iRR} increases

the role of the ion associate JR in the production of free ion exchanger sites R^- becomes more important, so that even small concentration of ion associate JR is able to lead to an essential change in the concentration of free sites R^-, and, as a result, of free ions I^{2+} in the membrane. Eventually, the net action of these factors leads to a weak dependence of K_{ij}^{pot} on K_{iRR}.

If in the analysed solution foreign ions J^+ are only present, Eq. (18) is simplified to:

$$K_{ij}^{pot} = (K_{ij}^{(3)} \cdot K_{jR})/(\bar{C}_R^{tot} \cdot K_{iR}) \quad (20)$$

It can be easily shown that Eq. (20) fully agrees with the expression of K_{ij}^{pot} obtained in [39] for ions of different charges when it is determined by the separate solution method:

$$K_{ij}^{pot} = \frac{\bar{C}_i}{k_i}\left(\frac{k_j}{\bar{C}_j}\right)^{z_i/z_j} \quad (21)$$

where $\bar{C}_i$ and $\bar{C}_j$ are the concentrations of free ions I^{z_i} and J^{z_j} in the boundary layer of the membrane, which is in contact with the sample solution containing the only ions I^{z_i} or J^{z_j}, respectively. Since, as follows from the Eigen-Denison-Ramsey-Fuoss' theory [56], $K_{iR} \gg K_{iRR}$, the dissociation of single-charged associate IR^+ makes a negligible contribution to the concentration of free sites R^-. Therefore, according to the equation of electroneutrality, in the absence of ion J^+ $\bar{C}_R \cong \bar{C}_{Ri}$. As a result, the concentration of free ions I^{2+} in the membrane is described by the equation

$$\bar{C}_i = \frac{\bar{C}_{iR}}{K_{iR} \cdot \bar{C}_R} \cong \frac{1}{K_{iR}} \quad (22)$$

If the membrane is in contact with solution containing only the foreign ion J^+, the concentration of free ions J^+ in the membrane phase is described by the equation:

$$\bar{C}_j = \bar{C}_R = \sqrt{\frac{\bar{C}_R^{tot}}{K_{jR}}} \quad (23)$$

Bearing in mind that $k_j^2/k_i = K_{ij}^{(3)}$ and substituting Eqs. (22) and (23) into Eq. (21), we obtain Eq. (20).

The present theoretical conclusions agree qualitatively with experimental data. It can be seen from the data summarised in Table 2 that ion exchange affinity to sulphate-ion depends substantially on the nature of the ion exchanger: the sulphate–chloride exchange constant becomes 70–100 times lower in the case of substitution of DMDODA for TNODA. Meanwhile, the ratio of the second constants of association of sulphate-ion and of single-charged ions with cations of these ion exchangers changes slightly. It suggests a strong dependence of the first constant of association of sulphate-ion on the nature of the ion exchanger. This suggestion seems quite reasonable in view of the fact that the sulphate-ion whose charge is distributed uniformly among four oxygen atoms is able to interact specifically with positively charged hydrogen atoms nearest to the cation centre provided their steric accessibility. It is evident that the interaction in the case of atoms carrying negative and positive charges, oriented in an optimal way and located at the closest distance from one another, should be more effective in comparison with 'indifferent' electrostatic attraction of ions when this interaction is impossible because of steric hindrances. This should lead to increase in the sulphate-ion association constant and manifest itself in potentiometric selectivity, which agrees qualitatively with experimental results (see Table 2).

It is interesting that in the case of indirect electrode, when 10% of DMDODA is in the sulphate form, and 90% is in the form of lypophilic borohydride $B_{10}H_{10}^{2-}$, the value $K_{SO_4^{2-},Cl^-}^{pot}$ is 3.5 times lower as compared with ISE based on $(DMDODA^+)_2SO_4^{2-}$ [57].

3.3. Violation of the model of ideally associated solution. The effect of forming ion triplets on ISE selectivity

If the ion exchanger interacts with the determined ion not only following the electrostatic interaction mechanism, but is also able to form coordination bonds with them and this ability is partly preserved after forming an ion-pair, favourable conditions are provided for formation of ion triplets of the type $I_2R^{(\pm)}$:

$$IR + I^{(\pm)} \overset{K_s}{\rightarrow} I_2R^{(\pm)} \quad (24)$$

In this case the ion associate IR is a kind of neutral carrier for $I^{(\pm)}$ and the equilibrium constant of this process is formally similar to the complex formation constant.

The equation which expresses the experimentally determined potentiometric selectivity coefficient in terms of ion exchange, ion association and complex formation constants can be obtained as follows. In the solution of determined ion the membrane potential is described by the equation:

$$E_1 = E_i^0 \pm \theta \lg[(a_i)_1/\bar{C}_i^0] = E_i^{0'} \pm \theta \lg(a_i)_1 \quad (25)$$

where $\bar{C}_i^0$ is the initial concentration of the ion $I^{(\pm)}$ in the membrane.

In the presence of the foreign ion $J^{(\pm)}$ in the solution studied, the equation is valid:

$$E_2 = E_i^0 \pm \theta \lg[(a_i)/\bar{C}_i] = E^{0'} \pm \theta \lg(a_i + K_{ij}^{pot} \cdot a_j) \quad (26)$$

where $\bar{C}_i$ is the concentration of the free ion $I^{(\pm)}$ in the membrane being in contact with the mixed solution. Subtracting Eq. (25) from Eq. (26) and performing simple manipulations, we obtained:

$$K_{ij}^{pot} = a_i/a_j \cdot (\bar{C}_i^0/\bar{C}_i - 1) \quad (27)$$

If the total portion of ions in membrane is relatively small, i.e. the ion exchanger primarily occurs in the form of ion-pairs, without foreign ions the concentration of ion triplets is described by the equation

$$\bar{C}_{i_2R}^0 = \bar{C}_i^0 \cdot C_R^{tot} \cdot K_S \quad (28)$$

With account of the equation of electroneutrality we obtain

$$\bar{C}_R^0 = \bar{C}_i^0 + \bar{C}_{i_2R}^0) = \bar{C}_i^0 \cdot (1 + \bar{C}_R^{tot} \cdot K_S) \quad (29)$$

Finally, expressing the value of $\bar{C}_i^0$ in terms of the constant of ion association and substituting $\bar{C}_R^0$ from Eq. (29), we have

$$\bar{C}_i^0 = \frac{\bar{C}_R^{tot}}{K_{iR} \cdot \bar{C}_R^0} = \sqrt{\frac{\bar{C}_R^{tot}}{K_{iR} \cdot (1 + \bar{C}_R^{tot} \cdot K_S)}} \quad (30)$$

In the presence of the foreign ion J not tending to formation of ion triplets, the condition of electroneutrality becomes

$$\bar{C}_R = \bar{C}_i(1 + \bar{C}_R^{tot} \cdot K_S) + \bar{C}_j \quad (31)$$

In this case it is assumed that the addition of I to the ion associate RJ is characterized by the same equilibrium constant K_S. Otherwise, more bulky expressions are obtained but the essence of the conclusions remains basically the same.

Expressing the free ion concentrations $\bar{C}_i$ and $\bar{C}_j$ in terms of ion association constants, we obtain

$$\bar{C}_R = (1 + \bar{C}_R^{tot} \cdot K_S) \cdot \frac{\bar{C}_{iR}}{K_{iR} \cdot \bar{C}_R} + \frac{\bar{C}_{jR}}{K_{jR} \cdot \bar{C}_R} \quad (32)$$

Solving the above equation for $\bar{C}_R$ and substituting the obtained value in Eq. (4), we obtain:

$$\bar{C}_i = \frac{\bar{C}_{iR}}{\sqrt{K_{iR}}} \cdot \frac{1}{\sqrt{(1 + \bar{C}_R^{tot} \cdot K_S) \cdot \bar{C}_{iR} + \frac{K_{iR}}{K_{jR}} \cdot \bar{C}_{Rj}}} \quad (33)$$

Substituting Eqs. (30) and (33) into Eq. (27) and expressing equilibrium concentrations $\bar{C}_{iR}$ and $\bar{C}_{jR}$ by Eqs. (6) and (7), one can evaluate K_{ij}^{pot}.

The qualitative effect of forming ion triplets on K_{ij}^{pot} can be traced by comparison of the ratios $\bar{C}_i^0/\bar{C}_i$ for the case considered and for ideally associated solution, when there are no ion triplets. It follows from Eqs. (30) and (33) that

$$\frac{\bar{C}_i^0}{\bar{C}_i} = \frac{\sqrt{\bar{C}_R^{tot}}}{\bar{C}_{Ri}} \cdot \sqrt{\bar{C}_{Ri} + \bar{C}_{Rj} \cdot \frac{k_i}{k_j} \cdot \frac{1}{1 + \bar{C}_R^{tot} \cdot K_S}} \quad (34)$$

If ion triplets are absent, then

$$\bar{C}_i^0 = \sqrt{\frac{\bar{C}_R^{tot}}{K_{iR}}} \quad (35)$$

And according to Eqs. (4) and (5) we obtain:

$$\frac{\bar{C}_i^0}{\bar{C}_i} = \frac{\sqrt{\bar{C}_R^{tot}}}{\bar{C}_{Ri}} \cdot \sqrt{\bar{C}_{Ri} + \bar{C}_{Rj} \cdot \frac{k_i}{k_j}} \quad (36)$$

Comparison of Eqs. (34) and (36) shows that in the case of forming ion triplets the contribution of the second term in the expression under the radical sign decreases proportionally to the factor $(1 + \bar{C}_R^{tot} \sim \cdot \sim K_S)$, which should be exhibited in the appropriate increase in the potentiometric selectivity for I. To summarize, it can be stated that forming ion triplets leads to increase in the concentration of free ion exchanger sites in the membrane. As a result, the concentration of the free

Table 4
The effect of the nature of the ion exchanger on cation exchange membrane selectivity reversible to calcium cation

Membrane	Selectivity coefficients relative to cations							
	Li^+	Na^+	NH_4^+	K^+	Mg^{2+}	Fe^{2+}	Cu^{2+}	Zn^{2+}
XI	10^{-2}	$2\cdot10^{-2}$	10^{-1}	$7\cdot10^{-3}$	$2.5\cdot10^{-2}$	$2\cdot10^{-2}$	$1.6\cdot10^{-2}$	$1.3\cdot10^{-2}$
XII	$2\cdot10^{-1}$	$1.6\cdot10^{-2}$	$6\cdot10^{-2}$	$4\cdot10^{-3}$	$5\cdot10^{-3}$	10^{-2}	$1.3\cdot10^{-2}$	$1.3\cdot10^{-2}$
XIII	$5\cdot10^{4}$	$1.6\cdot10^{2}$	$8\cdot10^{2}$	6	10^{-1}	$4\cdot10^{-1}$	$1.6\cdot10^{-1}$	$2.5\cdot10^{-1}$

ions I is also stabilized and not subjected to strong changes when rather small numbers of low-strength associates RJ penetrate into the membrane. This mechanism is likely to be realized in some anion-selective electrodes based on charged carriers capable of forming coordination bonds with appropriate anions.

We have found a very strong effect of the nature of the ion exchanger on the ISE selectivity in the study of Ca^{2+}–ISEs based on derivatives or orthophosphoric acid (see Table 4). For membranes based on TNBS and D(3NP)P the selectivity series typical of membranes based on dialkyl(aryl) phosphoric acids is observed. On the contrary, for membranes based on D(2DP)P the selectivity for single-charged ions, especially, for Li^+, increases substantially (by 4 and more orders of magnitude).

At present, we have no experimental data that could give inequivocal and complete explanation of the mechanism of the observed phenomenon. However, a most probable reason seems to be exhibition of a kind of the crown effect by D(2DP)P molecules containing alkoxysubstitutents in the ortho-position, which provide favourable conditions for coordination of single-charged ions that results in forming ion triplets:

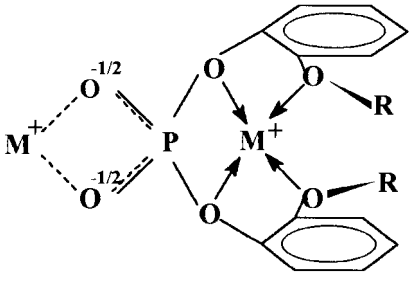

For double-charged cations solvated effectively by strong base dioctyl-phenylphosphonate, formation of such complexes should be less beneficial.

4. Conclusion

The present experimental and theoretical results indicate that feasibilities of transforming ion exchange selectivity into potentiometric one are substantially different for single- and double-charged ions. In ideally associated ion exchange membranes, that do not contain ionic admixtures, increase in the efficiency of interaction of the ion exchanger with determined single-charged ions has an important effect on the value of K_{ij}^{pot} only when $K_{iR} < K_{jR}$, which agrees with theoretical results [14]. However, if $K_{iR} > K_{jR}$, then without special procedures intended to stabilize the ion exchanger sites $R^{(\pm)}$ concentration in the membrane phase, which are described in [35,39–41], the gain in K_{ij}^{pot} is not high, as a rule. The case, when the ion exchanger sites form ion triplets of type $I_2R^{(\pm)}$ with the determined ion can be exception. In this case ion associate IR functions as a kind of a neutral carrier for determined ion $I^{(\pm)}$.

In the case of double-charged ions, increase in the first constant of ion association of the main ion with the ion exchanger sites (K_{iR}), all other things being equal, should always lead to benefit in potentiometric selectivity.

Acknowledgements

The has been carried out under financial support of the International Science Soros Foundation, Project MW 6000.

References

[1] J. Sandblom, G. Eisenman, J.L. Walker, J. Phys. Chem. 71 (1967) 3862.
[2] B.P. Nikolsky, M.M. Shultz, Vestnik LGU 4 (1963) 73.
[3] F.S. Stover, R.P. Buck, Biophys. J. 16 (1976) 753.
[4] F.S. Stover, R.P. Buck, J. Phys. Chem. 81 (1977) 2105.
[5] R.D. Armstrong, M. Todd, Electrochim. Acta 32 (1987) 155.
[6] R.D. Armstrong, Electrochim. Acta 32 (1987) 1549.
[7] R.D. Armstrong, G. Horvai, Electrochim. Acta 35 (1990) 1.
[8] A. Jyo, M. Torikai, N. Ishibashi, Bull. Chem. Soc. Jpn. 47 (1974) 2862.
[9] K. Kina, N. Maekawa, N. Ishibashi, Bull. Chem. Soc. Jpn. 46 (1973) 2772.
[10] A. Jyo, H. Mihara, N. Ishibashi, Denki Kagaku 44 (1976) 268.
[11] E.A. Materova, T. Ya. Bart, in: Ion Exchange and Ionometry, Vol. 4, Leningrad University Publishing House, Leningrad, 1984, p. 92.
[12] R.D. Armstrong, P. Nikitas, Electrochim. Acta 30 (1985) 1627.
[13] E.M.J. Verpoorte, A.D.C. Chan, D.J. Harrison, Electroanalysis 5 (1993) 845.
[14] W.E. Morf, The Principles of ISEs and of Membrane Transport, Mir, Moscow, 1985.
[15] P. Schulthess, D. Ammann, W. Simon, C. Caderas, R. Stepanek, B. Kräutler, Helv. Chim. Acta 67 (1984) 1026.
[16] P. Schulthess, D. Ammann, B. Kräutler, C. Caderas, R. Stepanek, W. Simon, Anal. Chem. 57 (1985) 1397.
[17] R. Stepanek, B. Kräutler, P. Schulthess, B. Lindemann, D. Ammann, W. Simon, Anal. Chim. Acta 182 (1986) 83.
[18] S. Daunert, L.G. Bachas, Anal. Chem. 61 (1989) 499.
[19] D. Ammann, M. Huser, B. Kräutler, B. Rusterholz, P. Schulthess, B. Lindemann, E. Halder, W. Simon, Helv. Chim. Acta 69 (1986) 849.
[20] S.C. Ma, N.A. Chaniotakis, M.E. Meyerhoff, Anal. Chem. 60 (1988) 2293.
[21] N.A. Chaniotakis, S.B. Park, M.E. Meyerhoff, Anal. Chem. 61 (1989) 566.
[22] X. Li, D.J. Harrison, Anal. Chem. 63 (1991) 2168.
[23] S.B. Park, W. Matuszewski, M.E. Meyerhoff, Y.H. Liu, K.M. Kadish, Electroanalysis 3 (1991) 909.
[24] E. Bakker, E. Malinowska, R.D. Schiller, M.E. Meyerhoff, Talanta 41 (1994) 881.
[25] E. Malinowska, M.E. Meyerhoff, Anal. Chim. Acta 300 (1995) 33.
[26] D. Gao, J.-Z. Li, R.-Q. Yu, G.-D. Zheng, Anal. Chem. 66 (1994) 2245.
[27] D. Gao, J. Gu, R.-Q. Yu, G.-D. Zheng, Analyst 120 (1995) 499.
[28] D. Gao, J. Gu, R.-Q. Yu, G.-D. Zheng, Anal. Chim. Acta 302 (1995) 263.
[29] J. Li, X. Wu, R. Yuan, G. Lin, R. Yu, Analyst 119 (1994) 1363.
[30] V.A. Zarinskij, L.K. Shpigun, V.M. Shkinjov, B.Ya. Spivakov, V.M. Trepalina, Yu.A. Zolotov, Zh. Anal. Khim. 35 (1980) 2137.
[31] S.A. Glasier, M.A. Arnold, Anal. Chem. 60 (1988) 2540.
[32] S.A. Glasier, M.A. Arnold, Anal. Lett. 22 (1989) 1075.
[33] N.A. Chaniotakis, K. Jurkschat, A. Rüchlemann, Anal. Chim. Acta 282 (1993) 345.
[34] I.H.A. Badr, M.E. Meyerhoff, S.S.M. Hassan, Anal. Chem.. 67 (1995) 2613.
[35] V.V. Egorov, V.A. Repin, T.A. Ovsyannikova, Zh. Anal. Khim. 47 (1992) 1685.
[36] V.V. Egorov, in: Conf. Chemical Sensors Proceedings Abstracts, St. Petersburg, 1993, p. 123.
[37] C.R. Witschonke, C.A. Krauss, J. Am. Chem. Soc. 69 (1947) 2472.
[38] Y. Umezawa, Handbook of Ion-Selective Electrodes: Selectivity Coefficients, CRC Press, Boca Raton, FL, 1990.
[39] U. Schaller, E. Bakker, U.E. Spichiger, E. Pretsch, Anal. Chem. 66 (1994) 391.
[40] U. Schaller, E. Bakker, E. Pretsch, Anal. Chem. 67 (1995) 3123.
[41] U. Schaller, E. Bakker, E. Pretsch, A.C.M. Models in Chemistry 131 (1994) 739.
[42] Veigand-Hilgetag, The Methods of the Experiment in Organic Chemistry, Khimia, Moscow, 1968.
[43] E.M. Rakhman'ko, G.L. Starobinets, V.V. Egorov, A.L. Gulevich, S.M. Lestchev, E.S. Borovski, Fresenius Z. Anal. Chem. 335 (1989) 104.
[44] S.M. Lestchev, E.M. Rakhman'ko, G.L. Starobinets, Zh. Anal. Khim. 34 (1979) 2244.
[45] Ya. F. Lushchik, Some Regularities of the Functioning and Analytical Application of Cation-Selective Electrodes based on Lipophilic Sulphonic Acids and their Compositions with Neutral Carriers, Dissertation Abstracts, Minsk, 1988.
[46] G.H. Griffiths, G.J. Moody, J.D.R. Thomas, J. Inorg. Nucl. Chem. 34 (1972) 3043.
[47] G.M. Cosolapoff, J. Am. Chem. Soc. 69 (1947) 2020.
[48] V.V. Egorov, E.A. Pavlovskaya, Ya.F. Lushchik, Zh. Anal. Khim. 47 (1992) 2011.
[49] T.M. Alkhazishvili, N.V. Astakhova, V.V. Egorov, Z.F. Kirpichnikova, L.V. Koleshko, E.M. Rakhman'ko, G.L. Starobinets, Yu. M. Tarasova, A.N. Khutsishvili, USSR Author Cert. N 1310401, IB, 1987, N 18.
[50] K. Cammann, Das Arbeiten mit ionselektiven Elektroden, Springer, Berlin, 1979.
[51] E.M. Rakhman'ko, N.A. Sloboda, S.A. Lagunovich, Zh. Neorg. Khim. 35 (1990) 2409.
[52] R.A. Robinson, R.H. Stokes, Electrolyte Solutions, Moscow, 1968.
[53] E. Bakker, M. Nägele, U. Schaller, E. Pretsch, Electroanalysis 7 (1995)
[54] A.L. Gulevich, V.V. Egorov, E.M. Rakhman'ko, A.P. Podterob, V.A. Repin, Vestsi Akad. Navuk RB, in press.

[55] A.L. Gulevich, Extraction of Alkylsulphates and Lypophilic Carbon Acids by Quaternary Ammonium Salts and its Analytical Application, Dissertation Abstracts, Minsk, 1982.
[56] E.G. Gordon, The Organic Chemistry of Electrolyte Solutions, Mir, Moscow, 1979.
[57] V.V. Egorov, N.D. E.M. Rakhman'ko, N.A. Sloboda, S.S. Kacharsky, Zh. Anal. Khim. in press.

ELSEVIER

Talanta 44 (1997) 1749–1755

Talanta

Spectrophotometric study of the charge transfer complexes of some pharmaceutical butyrophenones

Hassan F. Askal

Pharmaceutical Analytical Chemistry Department, Faculty of Pharmacy, Assiut University, 71 526-Assiut, Egypt

Received 13 September 1996; received in revised form 5 November 1996; accepted 4 February 1997

Abstract

The molecular interactions between haloperidol and droperidol as electron donors and each of iodine; 7,7,8,8-tetracyanoquinodimethane (TCNQ); 2,3-dichloro-5,6-dicyano-1,4-benzoquinone (DDQ); tetracyanoethylene (TCNE); 2,4,7-trinitro-9-fluorenon (TNF); and 2-3-5-6-tetrabromo-1,4-benzoquinone (Bromanil) as acceptors have been investigated spectrophotometrically. Different variables affecting the reaction were studies and optimized. Beer's law was obeyed in a concentration limit of 2.5–2500 μg ml^{-1} for the studied drugs with various acceptors used. Electron affinities (E_A) of the acceptors were found to correlate with both the time required for maximum colour formation and the molar absorptivities of haloperidol and droperidol. A Job's plot of the absorbance versus the molar ratio of the drugs to iodine indicated 1:1 ratio. The proposed methods were found to be rapid and sensitive and may be applied for estimation of named drugs in pharmaceutical dosage forms without interferences from the common additives encountered. Percentage recoveries ranged from 99.1–102.2%. © 1997 Elsevier Science B.V.

Keywords: Charge transfer complexes; Droperidol; Haloperidol; Spectrophotometry

1. Introduction

Different reported methods for the determination of haloperidol (I) and droperidol (II) butyrophenone neuroleptics have been reviewed [1,2]. The methods reported involve the following techniques: uv spectrophotometry [3], fluorometry [4,5], extraction photometry [6], condensation reaction with phenylhydrazine [7,8], reaction with 1,2-naphthoquinone-4-sulphonic acid [9], polarography [10,11], proton magnetic resonance spectroscopy [12] and high performance liquid chromatography [13–22]. USP XXII and NF XVII specify a non aqueous titrimetric method for the analysis of pure drugs and a uv spectrophotometric one for their dosage forms [23].

The molecular interactions between electron donors and acceptors are generally associated with the formation of intensely coloured charge transfer complexes, which absorb radiation in the visible region [24]. The photometric methods based on these interactions are usually simple and convenient because of the rapid formation of the complexes. Haloperidol and droperidol are good *n*-electron donors and will form charge transfer complexes with σ- or π-acceptors.

π-Acceptors such as TCNE, TCNQ, DDQ and *p*-Bromanil are known to yield charge-transfer

PII S00 9-9140(97)00043-X

complexes and radical anions with a variety of electron donors [24–26]. This donor-acceptor interaction has been investigated with two butyrophenones as electron donors (Scheme 1).

The reported spectrophotometric methods are either non specific, time consuming, indirect, or suffering from the disadvantage of low sensitivity. In addition, most of the published assay methods for butyrophenones were suggested for their determination in biological fluids rather than in pharmaceutical preparations.

This study describes simple, direct, sensitive and precise spectrophotometric methods for the determination of haloperidol and droperidol via complexation with σ and π-acceptors in their common dosage forms and irrespective of the presence of contaminants and additives.

2. Experimental apparatus

A Perkin-Elmer Lambda 3 B UV/VIS (Norwalk, CT, USA) and a Uvidec-320 (Tokyo, Japan) Spectrophotometers with 10 mm matched silica cells were used for all spectral measurements.

2.1. Chemicals and reagents

Haloperidol and droperidol were obtained from Gedeon Richter, Budapest, Hungary. Iodine resublimed, Riedel De-Haen AG, Germany, 8.5 mg ml^{-1} in 1,2-dichloroethane, the solution was stable for at least 1 week at 4°C.

7,7,8,8-tetracyanoquinodimethane (TCNQ), Aldrich Chem Co., Milwaukee, USA, 1 mg ml^{-1} in acetonitrile, the solution was stable for at least 1 week at 4°C.

2,3-Dichloro-5,6-dicyano-*p*-benzoquinone (DDQ), Merck-Schuchardt, Munich, Germany, 2 mg ml^{-1} in methanol, the solution was prepared fresh daily.

Tetracyanoethylene (TCNE), Nacalai Tesque, Kyoto, Japan, 1 mg ml^{-1} in acetonitrile, was prepared fresh daily.

2,4,7-trinitro-9-fluorenon (TNF), Fluka, Switzerland), 2 mg ml^{-1} in acetonitrile, was prepared fresh daily.

2,3,5,6-tetrabromo-1,4-benzoquinone (*p*-Bromanil), Hopkin and William, Essex, England, 5 mg ml^{-1} in methanol, was prepared fresh daily.

All solvents used are of analytical grade.

2.2. Pharmaceutical formulations

The following commercial formulations were subjected to the analytical procedures: Halodol® decanoas ampoules labelled to contain 70.52 mg decanoas ester of haloperidol equivalent to 50 mg haloperidol ml^{-1}, benzyl alcohol and sesame oil; Halodol® drops, labelled to contain 2 mg haloperidol ml^{-1} (Janssen Pharmaceutica I Beerse I, Belgium); Safinace® tablets; labelled to contain 5 mg haloperidol/tablet (Kahira Pharm. and Chem., Cairo, Egypt, under license of G.D. Searle, High Wycombe, England); Droperidol self prepared tablets, obtained by addition of 5 mg of droperidol to 50 mg each of starch and sucrose and 10 mg each of gum acacia, lactose, magnesium stearate and talc.

2.3. Standard solutions

Weigh accurately 1.25 g of either haloperidol or droperidol into a 50 ml calibrated flask. Dissolve the drug in methanol. Dissolve (DDQ or bromanil) in methanol, (TCNQ or TCNE) in acetonitrile and (iodine or TNF) in 1,2-dichloroethane give a final volume of 50 ml. Dilute quantitatively to obtain the suitable final concentration, Table 1.

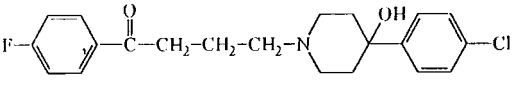

Haloperidol (I)

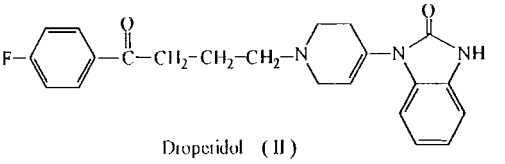

Droperidol (II)

Scheme 1

Table 1
Optimum reaction conditions for haloperidol and droperidol interaction with various acceptors

Parameter	Iodine	TCNQ	DDQ	TCNE	TNF	Bromanil
Conc., % (m V^{-1})	0.05	0.10	0.40	0.10	0.20	1.00
Solvent	A	B	C	B	A	C
Time, min	At once	60	15	10	90	70
λ_{max}, nm	295[a], 368[b]	842	460	414	413	454

A = 1,2-dichloroethane; B = acetonitrile; C = methanol.
[a] For haloperidol.
[b] For droperidol.

2.4. Procedure

2.4.1. General procedure for colour development

In 10 ml calibrated flasks, place aliquots volumes containing 25–15 000 and 25–25 000 μg for haloperidol and droperidol, respectively. Add 1 ml of the reagent and dilute to the mark with the corresponding solvent, Table 1. Measure the absorbance of the solution at the wavelength of maximum charge transfer bands after the appropriate time at 25°C ± 5 against reagent blank treated similarly.

2.4.2. Tablets

Tablets, 20, of the drug were weighed and powdered. A quantity of the powdered tablets equivalent to about 50 mg drug was transferred into a 50 ml calibrated flask. Then, the procedure is followed as under for standard solutions.

2.4.3. Drops

Dilute an appropriate volume of the solution in a volumetric flask so as to represent 1 mg ml^{-1}. Proceed as directed under tablets.

2.4.4. Injection solutions

A volume of the solution containing about 50 mg drug was transferred into a 50 ml calibrated flask. then the procedure is followed as directed under tablets.

2.4.5. Molecular ratio of reactants in complex

The Job's method of continuous variation [27] with 2×10^{-3} M iodine solution with either 4.24×10^{-4} M haloperidol or 2.12×10^{-4} M droperidol bases were prepared in 1,2-dichloroethane.

3. Results and discussion

The immediate change of the violet colour of iodine in 1,2-dichloroethane (520 nm) to a lemon yellow upon reaction with the investigated compounds was taken as suggestive of charge transfer complex formation which justified scanning in the uv range for the new bands (Fig. 1). The complex formation is distinguished from other slow oxidation or substitution reactions of the halogens with butyrophenones, by being practically instantaneous, in analogy to ionic reactions. Further confirmation of the charge transfer nature of the reaction was obtained on extracting the drugs from the complex by shaking with aqueous mineral acid, whereby the violet colour of iodine in 1,2-dichloroethane was restored.

All measurements with iodine were performed at 295 and 365 nm for haloperidol and only at 368 nm for droperidol due to interference from its native uv absorption (Fig. 1).

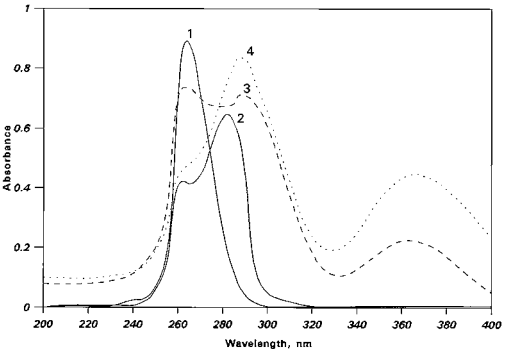

Fig. 1. Absorption spectra of: 1, haloperidol (15.2 μg ml^{-1}); 2, droperidol (10.3 μg ml^{-1}); and 3, 4 their reaction products with iodine respectively, all in 1,2-dichloroethane.

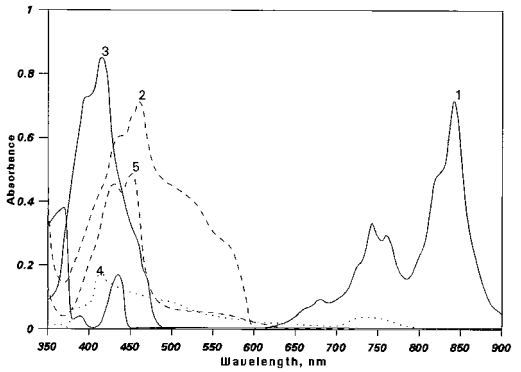

Fig. 2. Absorption spectra of the reaction products of haloperidol 125, 127, 25.5, 1500 and 216.5 μg ml^{-1} with each of TCNQ (1), DDQ (2), TCNE (3), TNF (4), and bromanil (5), respectively.

The interaction of haloperidol and droperidol with selective polyhaloquinones and polycyanoquinones π-acceptors was found to yield intensely coloured radical anions (Fig. 2). Butyrophenones interaction with TCNQ in acetonitrile solution was found to yield a deep colour causing characteristic long wavelength absorption bands. The predominant chromogen with TCNQ is the blue coloured radical anion which probably resulted through the dissociation of an original donor-acceptor complex with the drugs. The dissociation of the complex was promoted by the high ionizing power of acetonitrile solvent. Further support to this assignment was provided by the identity of the absorption maxima with those of TCNQ radical anion produced by the iodide reduction method in acetonitrile [28].

The resulting maxima of the investigated drugs with DDQ, bromanil and TNF are similar to that of radical anions of these acceptors obtained by the reduction method and coincide with the values reported in the literature [25,29].

With butyrophenones and TCNE, the characteristic shaped absorption band of TCNE radical anion with reported maximum in acetonitrile at 432 nm was not formed. Instead doplet at 394 and 414 in acetonitrile was formed which corresponds to the 1,1,2,3,3-pentacyanopropenide (PCNP) anion. From the quantitative point of view, PCNP anion is preferable to TCNE anion on grounds of its higher molar absorptivity [28]. The weak and small molar absorptivity in case of the reaction between TNF or bromanil and investigated drugs may be explained or due to the insufficient ionization of these relatively week π-acceptors which possess lower electron affinity than DDQ, TCNQ and TCNE [24].

The results for variation of reagent concentration, Table 1, indicated that 1.0 ml of either 0.05% iodine, 0.1% TCNQ, TCNE, 0.4% DDQ or 1.0% bromanil are suitable. The higher concentrations of the reagents may, on the other hand, be useful for rapidly reaching equilibrium, thus minimizing the time required to attain the maximum absorbance at the corresponding wavelength of charge transfer complex. Neither the studied drugs nor the reagents have a significant absorbances at the corresponding wavelengths of maximum absorbance except in case of droperidol.

3.1. Choice of solvent

Although, charge transfer complex as probably been formed in many solvents, the high cut-off points of some solvents obscured the scanning of the shorter wavelengths and therefore clear-cut spectroscopic evidence for charge-transfer formation could not be ascertained. Also the low solubility of the drugs in some other solvent restricted their use.

1,2-Dichloroethane may be used directly as an assay solvent in case of iodine and TNF. With iodine, haloperidol showed a major charge-transfer bands at 295 and 365 nm and for droperidol at 368 nm.

The formation of TCNQ radical was possible in methanol; however, response between absorbance and concentration was not linear. Furthermore, the molar absorptivity of the obtained chromogen was relatively lower compared with that in acetonitrile. The latter was considered as an ideal solvent because it offered excellent solvating power for TCNQ reagent and gave high absorbance.

Table 2
Quantitative parameters for the complexation of haloperidol (I) and droperidol (II) with different acceptors

Acceptors (E_A)[a]		Limits μg ml^{-1}	Molar absorptivity 1 mol^{-1} per cm	Slope b	Intercept a	Corr. coeff. r	Sandell's sensitivity μg cm^{-2}
Iodine,	I	2.5–2[b]	17700	0.04360	0.0455	0.9966	0.021
(2.7)	II	2.5–30[c]	17100	0.04250	0.0098	0.9996	0.022
TCNQ,	I	25–200	2200	0.00520	0.0650	0.9958	0.171
(1.7)	II	25–200	2080	0.00470	0.0720	0.9934	0.185
DDQ,	I	10–150	2100	0.00570	−0.0110	0.9988	0.179
(1.9)	II	10–150	2140	0.00550	0.0860	0.9984	0.179
TCNE,	I	2.5–30	12600	0.03230	0.0260	0.9983	0.029
(2.2)	II	2.5–20	15200	0.03940	0.0048	0.9920	0.023
TNF,	I	500–1500	43	0.00011	0.0013	0.9978	8.772
(1.1)	II	500–2000	60	0.00009	0.0695	0.9922	6.042
Bromanil,	I	25–500	866	0.00150	0.1611	0.9914	0.434
(1.37)	II	300–2500	120	0.00028	0.0328	0.9998	3.200

[a] Electron affinity of different acceptors (Ref. [24]).
[b] Measured at 295 nm.
[c] Measured at 368 nm.

In case of TCNQ and TCNE, as an assay solvent acetonitrile afforded maximum sensitivity owing to its high dielectric constant which promotes maximum yield of TCNQ radical anion. Methanol afforded maximum sensitivity in cases of DDQ and Bromanil, in spite, chloroform can also be used.

3.2. Reaction time

The reaction time was determined by following the absorbances of the developed colour at different time intervals. The development of colour was highest and immediate with iodine. Development time with other acceptors increase up to 90 min (in case of TNF). The developed colour for all cases remained stable thereafter 2 h at room temperature, Table 1.

3.3. Quantification

At fixed experimental conditions, the intensity of absorption at the specified wavelength was found a function of the concentration of the investigated drugs. In all cases studied, Beer's law plots were linear with very small intercept, in the general concentration range of 2.5–2500 μg ml^{-1}, Table 2.

3.4. Stoichiometric relationship

The application of the Job's method of continuous variation indicated 1:1 ratio for the two drugs with iodine. This indicates that only one nitrogen is responsible for the formation of the complex although droperidol has three nitrogen atoms, Scheme 1. This can be explained on the basis that a univalent, partially positively charged droperidol species may be formed initially during the charge-transfer process, which may not be easily engaged in additional complex formation. Both the two nitrogen atoms in the bezimidazolinone part are acidic. This suggestion is supported by the behaviour of this compound in non-aqueous medium where it was found to be titrated as a monobase (pK_a 7.64). In case of haloperidol (pK_a 8.30), [30] the ratio was found to be also 1:1.

3.5. Correlation between electron affinity of the acceptors with each of development time and sensitivity

The electron affinity (E_A) of the different acceptors varied with the sensitivity of the assay, expressed as (ϵ) values as well as development time (t), in a regular pattern.

Regression analysis of the above correlations by the method of least squares afforded:

Table 3
Determination of haloperidol and droperidol in commercial pharmaceutical preparations by proposed and official methods

Dosage form	Label claim mg unit^{-1}	Found, % ± S.D.[a]			
		Proposed methods			Reference methods
		Iodine	TCNQ	DDQ	
Safinace® tablets	5	100.0 ± 0.8 *t*: 1.32 *F*: 1.25	101.9 ± 0.9 *t*: 2.60 *F*: 1.71	99.4 ± 0.8 *t*: 2.54 *F*: 1.42	100.6 ± 0.7
Halodol® decanoas injection	50	99.7 ± 0.6 *t*: 2.01 *F*: 1.38	100.7 ± 0.6 *t*: 0.80 *F*: 1.29	99.5 ± 0.6 *t*: 2.59 *F*: 1.24	100.4 ± 0.5
Halodol® drops	2	99.5 ± 0.7 *t*: 2.33 *F*: 1.06	99.5 ± 0.9 *t*: 2.01 *F*: 1.62	101.0 ± 0.7 *t*: 1.14 *F*: 1.12	100.5 ± 0.7
Droperidol tablets[b]	5	100.8 ± 0.7 t: 0.45 F: 1.00	100.2 ± 0.8 t: 0.85 F: 1.24	99.6 ± 0.7 t: 2.28 F: 1.00	100.6 ± 0.7

[a] Average of five determinations.
[b] Self prepared tablets. Theoretical values at 95% confidence limit, *t*: 2.78 and *F*: 6.39.

$E_A = 2.42 - 0.0145\ t$ $(r = -0.9380)$
$E_A = 1.40 + 0.000072\ \epsilon$ $(r = 0.9203)$, for haloperidol
$E_A = 1.42 + 000066\ \epsilon$ $(r = 0.8998)$, for droperidol

3.6. Interference study

The presence of the fluoride atom acting as an electron withdrawing group does not affect the formation of the charge-transfer complex owing to the existence of tertiary basic electron donating group in the butyrophenone molecule. The energy of charge-transfer depends on the ionization potential of the donor and the electron affinity of the acceptor, hence the λ_{max} values of the other π-donors mostly differ of that of the investigated compounds if they are able to form charge-transfer complexes.

3.7. Analysis of dosage forms

The proposed charge-transfer spectrophotometric methods were applied to the determination of haloperidol in tablets, drops and injection solution in addition to droperidol in self prepared tablets. The results were compared statistically with those obtained by applying the official USP XXII and NF XVII methods for safinace tablets and halodol injection. These methods are based on measuring the absorbances of the solution from tablets or injections and standard solution after certain treatments at 245 nm. The results for halodol drops and droperidol prepared tables were compared with their respective uv-absorption. In the *t*: and *F*: tests, no significant differences were found between the calculated and theoretical values (95% confidence) of the proposed and reported methods. This indicates similar precision and accuracy. Data of Table 3 suggested that the present procedures could be applied to the assay of these drugs in their single dosage forms without interference. Frequently countered common ingredients of formulations were found not to interfere. Percentage recoveries ranged from 99.1–102.2%.

4. Conclusions

From the aforementioned results, the suggested procedures using σ and π-acceptors confirm their suitability for spectrophotometric analysis of named compounds in the micro range. The strongly red shifted bands combined with the intensity of absorption and very low reagent background obviously recommended these procedures for routine analysis of haloperidol and droperidol in bulk drugs and dosage forms with minimum interference.

References

[1] A.J. Casimir and K.G. Roger, in K. Florey (Ed.) Analytical Profiles of Drug Substances, Vol. 7, Academic Press, New York, 1978, pp. 172–192.
[2] A.J. Casimir and Y.K. Chan, in K. Florey (Ed.), Analytical Profiles of Drug Substances, Academic Press, Vol. 9, New York, 1980, pp. 342–369.
[3] V.V. Stefyuk, M.M. Turkevich, Farm. Zh. (Kiev) 6 (1984) 60.
[4] W. Baeyens, Analyst 102 (1977) 525.
[5] W. Baeyens, P. DeMoerloose, Pharmazie 32 (1977) 764.
[6] M.M. Kucher, V.P. Kramarenko, Farm. Zh. (Kiev) 5 (1984) 72.
[7] M.M. Kucher, V.P. Kramarenko, Farm. Zh. (Kiev) 4 (1985) 67.
[8] G. Misztal, Farm. Pol. 44 (1988) 206.
[9] G.R. Ramana, S. Raghuveer, Ind. Drugs 19 (1982) 408.
[10] J. Volke, L. Wasilewska, A.R. Kejharova, Pharmazie 26 (1971) 399.
[11] X. Guo, N. Hu, S. Lin, Huaxue Xuebao 50 (1992) 378.
[12] J.W. Turczan, C.A. Lau-CAm, Drug Dev. Ind. Pharm. 15 (1989) 112.
[13] A.R. Lea, D.M. Hailey, P.R. Duguid, J. Chromatogr. 250 (1982) 35.
[14] M. Dolezalova, J. Chromatogr. 286 (1984) 323.
[15] G. Mazzi, Chromatographia 24 (1987) 313.
[16] S.T. Tan, P.J. Boniface, J. Chromatogr. Biomed. Appl. 97 (1990) 181.
[17] C. Cahard, P.P. Rop, T. Conguy, A. Viala, J. Chromatogr. Biomed. Appl. 97 (1990) 193.
[18] D. Willhelm, A. Kemper, J. Chromatogr. 90 (1990) 218.
[19] J.E. Kountourellis, C.K. Markopoulou, J. Liq. Chromatogr. 14 (1991) 2969.
[20] R.T. Sane, J.K. Ghadge, A.B. Jani, A.J. Vaidya, S.S. Kotwal, Ind. Drugs 29 (1992) 240.
[21] J. Guichard, G. Panteix, J. Dubost, P. Baltassat, C. Roche, J. Chromatogr. Biomed. Appl. 123 (1993) 269.
[22] R.T. Sane, M.G. Gangrade, V.V. Bapat, S.R. Surve, N.L. Chonker, Ind. Drugs 30 (1993) 205.
[23] The US Pharmacopoeia, XXII and the National Formulary XVII, USP Convention, Twinbrok, Parkway, Rockville, 1990, pp. 484, 485, 628, 629.
[24] R. Foster, Organic Charge Transfer Complexes, Academic Press, London, 1969, pp. 51, 387.
[25] L.R. Melby, in S. Patai (Ed.), The Chemistry of the Cyano Group, New York, 1970.
[26] C.N.R. Rao, S.N. Bhat and P.C. Dwivedi, in E.G. Brame (Ed.), Applied Spectroscopy Reviews, vol. 5, Dekker, New York, 1972, pp. 1–170.
[27] P. Job, Ann. Chim., 16 (1936) 97, Through Advanced Physicochemical Experiments, 2nd Edn., Oliver and Boyd, London, 1964, p. 54.
[28] A. Taha, G. Rücker, Arch. Pharm. (Weinheim) 310 (1977) 485.
[29] A. Yamagishi, Bull. Soc. Jpan 48 (1975)
[30] S. Budavari (Ed), The Merck Index, Merck, Rahway, NJ, 1989.

.

ELSEVIER

Talanta 44 (1997) 1757–1763

Talanta

Amplified potentiometric determination of pK_{00}, pK_0, pK_1, and pK_2 of hydrogen sulfides with Ag_2S ISE

Y.S. Su, K.L. Cheng *, Y.C. Jean

Department of Chemistry, University of Missouri-Kansas City, Kansas City, MO 64110, USA

Received 28 June 1996; received in revised form 3 February 1997; accepted 4 February 1997

Abstract

The chemical capacitor theory has been applied to accurately determine dissociation constants of H_2S with the Ag_2S ion-selective electrode (ISE). The theory's principle is based on the measurement of the change in electrode charge density as a result of protonated or unprotonated sulfide adsorbed on the electrode surface. This charge density is related to the potential. Connection of each individual capacitor in series amplifies the potential according to the equation, $E_{total} = E_1 + E_2 + E_3 + \cdots E_n$. As the charges of individual capacitors are concentrated to one capacitor area, the charge density rises, and the potential increases. The pK_{00}, pK_0, pK_1, and pK_2 are reported as 1.8, 2.12, 7.05, and 12.0, respectively. The pK_{00} and pK_0 are reported here for the first time. The pK_1 agrees well with the literature values; however, the pK_2 differs from those reported recently under extreme conditions. Reasons for disproving the unreasonably high $pK_2 \gg 17$–19 values are given based on calculations. Mainly, when $pK_2 \gg 17$–19, the experimental results do not fit the equilibrium equations, $pH = (pK_1 + pK_2)/2$, $pK_1 = (pK_0 + pK_2)/2$, and $pH = pK_2 + \log(HS^-)/(S^{2-})$. © 1997 Elsevier Science B.V.

Keywords: Chemical capacitor; Hydrogen sulphides; Ion-selective electrode

1. Introduction

Electrode potential amplification has been explained by several authors [17,18] as the potential amplification of a cell. Cheng, Song, and Yang [15], however, have reported the theory of potential amplification of a chemical capacitor, emphasizing the difference between cells and capacitors [16]. The principle of the capacitor technique is to measure the potential change of protonated and unprotonated adsorbates on the electrode surface, which serves as a zwitterionic capacitor. The electrode net charge density varies with changes in the protonation and deprotonation, complexation, or dissociation: the dissociation constants are determined from these changes in charge density. At a certain pH, one may determine the species ratio in the solution based on the reversible equilibrium reaction. If two species of equal concentration are involved in the equilibrium, pH equals pK_a at the intersection. The dissociation constants, therefore, are easily determined. Amplification makes the technique more sensitive and accurate for the determination of dissociation constants of weak

* Corresponding author. Fax: +1 816 2355502.

PII S00 9-9140(97)00045-3

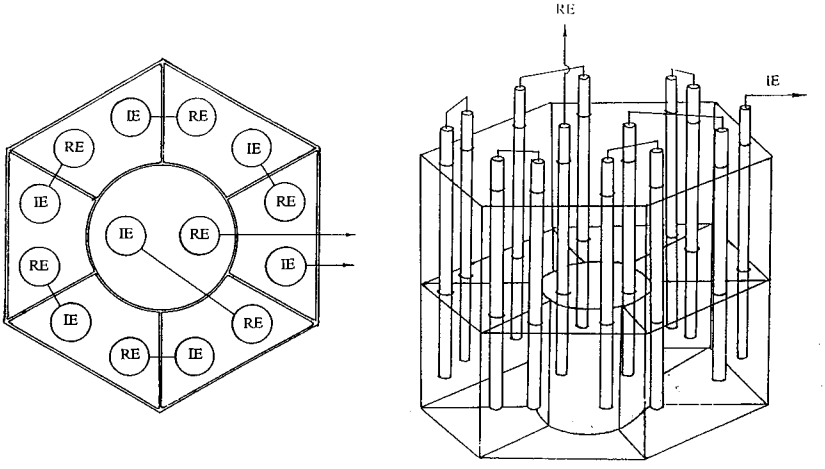

Fig. 1. Electrode assembly; (a) seven electrode connection; (b) measurement device.

acids, because it produces higher curve slopes than does unamplified potential.

In this paper, we report the application of the solid state Ag_2S ion selective electrode (ISE) as a capacitor to the amplified potentiometric determination of dissociation constants of H_2S. With appropriate ISEs, there may be applications for the determination of constants of other weak acids, complex reactions, and structural confirmation.

2. Experimental

The solid state Ag_2S ISE was prepared from Ag_2S precipitate pressed (under 12 tons cm^{-2} pressure) to produce a 1.0 mm × 10.0 mm disc. It was fixed atop a polymer electrode stem. Instead of an internal solution, the inner membrane surface was joined with liquid silver epoxy resin and silver wire. The potential was measured with a Fisher Model 825P pH meter and the pH was measured with a Chemtrix Model 430 pH meter. The experimental set-up is shown in Fig. 1. It should be stated that the test solution must be placed in each separate dish. Each indicator ISE and the Ag/AgCl reference electrode in each solution served as a capacitor unit. All capacitor units were connected in series (Fig. 1).

The 1×10^{-2} mol of Na_2S was dissolved in 100 ml of SAOB solution (salicylic acid–ascorbic acid oxygen buffer) and diluted to 1 l. A series of standard Na_2S solutions (10^{-2}–10^{-6} M) were prepared through dilution of the above standard solution containing 10 ml of SAOB 100 ml^{-1}. The SAOB solution contained 40 g of NaOH, 80 g of acetyl salicylic acid, and 35 g of ascorbic acid l^{-1}. Addition of SAOB solution prevents the oxidation of Na_2S. The Na_2S solution should be stored in a tightly stoppered plastic bottle with a shelf life of about 2 weeks. Discard it if it turns brown or dark.

For the determination of dissociation constants, 80 ml of water and 5 ml of 1.0×10^{-2} M Na_2S solution were mixed in a 150 ml beaker; the solution was adjusted to pH 13.5 or pOH 0.5 by adding 0.5 M NaOH solution. After each addition of 2 M HNO_3 through a burette, the pH and potential were recorded. The measuring interval is preferred to be about 0.2–0.4 pH unit difference. In the strong basic range the preferred interval would be kept about 0.1–0.15 pH unit. In order to avoid the loss of H_2S gas in an acid medium, the measurements were done quickly and the beaker was covered with a plastic paper. After addition of a base or acid, the solution was mixed; however, the solution was not stirred during pH and potential measurements.

3. Results and discussion

We have indicated that a membrane electrode acting as a parallel capacitor should follow the capacitance law. Therefore, the E_{total} resulting from connecting the capacitors in series with multimembrane electrodes is the sum of each capacitor potential (not cell potential) [15].

$$E_{total} = E_1 + E_2 + E_3 + \cdots E_n \quad (1)$$

When each capacitor is the same ISE in a same sample solution, the above equation becomes

$$E_{total} = \sum_{i=1}^{n} E_i \quad (2)$$

In the present experiment, $n = 4$. The amplification is illustrated in Fig. 2 and in acid and base with the pH glass electrode [15]. This capacitor potential amplification may find many applications, such as a simple portable voltameter without any electronic amplification, a device for surface charge measurement, etc. Here, we apply it to the accurate determination of dissociation constants of a dibasic acid, H_2S.

For titration of a Na_2S solution (already basic) with a HNO_3 solution, the potential versus pH relationship is shown in Fig. 3. The relationship indicates the distribution of each sulfide species on the Ag_2S electrode surface. The electrode surface charge density changes due to the protonation or deprotonation of electrode surface, resulting in the potential change.

At the beginning, the S^{2-} predominates; during the protonation, (S^{2-}) gradually decreases with

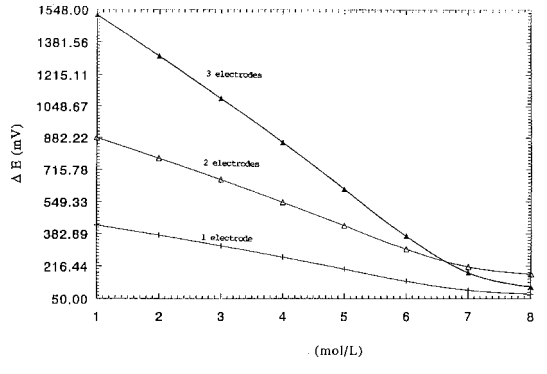

Fig. 2. Ampified calibration curves.

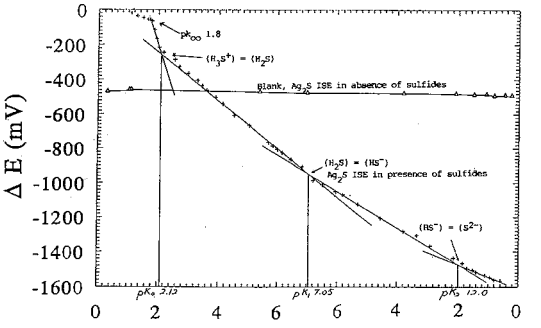

Fig. 3. Determination of pK_a with amplified Ag_2S ISE (four electrodes).

increasing (HS^-). There is a slope. At a point where one-half of the S^{2-} is protonated, further addition of H^+ starts to form $HS^- + H^+ \rightarrow H_2S$ with a different slope. An intersection is produced from the two slopes. At the intersection, $(S^{2-}) = (HS^-)$, $pH = pK_2$ or $pOH = pK_2$. Similarly, pK_1 and pK_2 are obtained from other intersections in Fig. 3. The results are shown in Table 1. When a single ISE was used, the pK_1 and pK_2 were found to be 6.98 and 12.3–12.5, respectively. When four ISEs were used, the pK_1 and pK_2 were found to be 7.05 and 12.0, respectively. Obviously, this is an electrode reaction resulting in changes of the electrode charge density and the electrode surface potential.

Cheng derived the capacitor electrode potential [16],

$$E = k\left(\sum q^+ - \sum q^-\right) \quad (3)$$

where q^+ and q^- are the charge density of positive charges and negative charges at the electrode surface. That is, only the net charge density is counted, even though both positive and negative charges are present, zwitterionic. The potential amplification is the addition of all charges together from each individual electrode (capacitor) to one electrode surface area. As a result, the charge density rises, and the potential also increases.

Our pK_1 of H_2S agrees well with most of the values in the literature. The pK_2 of H_2S has been widely in the literature (Table 1). In the

Table 1
Dissociation constants of hydrogen sulfides

Reaction	Present work		Reference												
			[1]	[2]	[3]	[4]	[5]	[6]	[7]	[8]	[9]	[10]	[11]	[12]	[13]	[14]
$H_4S^{2+} \rightleftharpoons H^+ + H_3S^+$	pK_{00}	1.8														
$H_3S^+ \rightleftharpoons H^+ + H_2S$	pK_0	2.12														
$H_2S \rightleftharpoons H^+ + HS^-$	pK_1	7.05	7.04	7.02	7.00	7.24	7.00	8.00	6.99	7.04	7.00				7.0	7.05
$HS^- \rightleftharpoons H^+ + S^{2-}$	pK_2	12.0	11.94	13.9	12.92	14.92	15.00	13.92	12.89	14.92	14.00	19 ± 2	17.2	16	17	12.4

recent literature, there seems to be an increasing tendency to believe the $pK_2 \gg 12$ is a better value [2,10–13]. Our $pK_2 = 12.0$ agrees well with the early reported values (Table 1). After carefully studying recently reported results ($pK_2 \gg 17$–19), we reached the following conclusions.

One of the reasons for obtaining the high pK_2 of H_2S may be attributed to the high concentrations of NaOH and/or Na_2S used. Experimental results might be misinterpreted. The equilibrium

$$HS^- \leftrightharpoons H^+ + S^{2-} \tag{4}$$

is not intended for the presence of highly-concentrated electrolytes which may form other side complexes or different equilibria. Indirect measurements and extrapolation are sometimes not reliable. Introduction of the term acidity function (H_-) instead of pH made their calculations and conclusions questionable [10,13]. It is also improper to use the terms activity and activity coefficient with high concentrations [10,12]. Our simple and sensitive measurements from a dilute solution are based on the direct measurement of the variation of $(HS^-)/(S^{2-})$ and charge density on the ISE electrode surface, which is the mirror of the test solution. When $(HS^-) = (S^{2-})$, $pOH = pK_b$ or $pH = pK_2 = pK_a$. The $pK_2 = 12.0$ obtained at the intersection in Fig. 3 is believed to be accurate.

Unlike other techniques, such as acid–base titration which requires a high purity sample for determining the 50% titration, the amplified potentiometric technique does not require a 100% pure sample, as it only measures the $(HS^-)/(S^{2-})$ ratio change.

Several means are available for testing the reliablilty of pK_2 values of H_2S.

1. Test with the equation

$$pk_2 = (pk_1 + pk_3)/2 \qquad \text{or}$$
$$pk_1 = (pk_0 + pk_2)/2 \tag{5}$$

(See Table 2)

$$pk_1 = (pk_0 + pk_2)/2 = (2.12 + 12.0)/2 = 7.06$$

$$pk_1 = (pk_0 + pk_2)/2 = (2.12 + 19)/2 = 10.6$$

Table 2
Calculated second dissociation constants from equation $pK_2 = (pK_1 + pK_3)/2$ or $pK_1 = (pK_0 + pK_2)/2$ (no protonated amine acids involved)

Acid	pK_1	pK_2 (experimental)	pK_3	pK_2 (calculated)
H_3BO_3	9.24	12.24	13.80	11.52
H_3AsO_4	2.24	6.96	11.50	6.87
H_3PO_4	2.14	7.20	12.35	7.20
Benzene-1,2,3,-tricarboxylic acid	2.88	4.75	7.13	5.0
H_3S^+	2.12	7.05	12.0[a]	7.06
	(pK_0)	(pK_1)	(pK_2)	
		13.0[a]	7.6	
		14.0[a]	8.1	
		17.0[a]	9.6	
		19.0[a]	10.6	

[a] These are pK_2 values of H_2S reported in the literature Table 1.

Calculation of pK_1 with $pK_2 = 19$ leads to an answer of 10.6, which does not agree with any known value.

Table 3
pH values of NaHS solution at different concentrations (T = 21.5°C)

Concentration (mol/l)	E (mV)	pH
0.008	−130.3	9.25
0.009	−131.6	9.27
0.01	−134.6	9.32
0.011	−135.8	9.37
0.0823	−152.2	9.76[a]
0.0927	−153.4	9.78
0.103	−156.3	9.83
0.113	−157.4	9.85
0.117	−158.6	9.87
0.123	−158.6	9.87
0.8	−195.8	10.34
0.9	−197.0	10.36
1.0	−200.0	10.41
1.1	−201.2	10.43
1.2	−203.6	10.47
2.9	−221.0	10.76
3.0	−224.0	10.81
3.1	−225.2	10.83
3.2	−227.0	10.86
3.3	−228.2	10.88

The *o*-phthalic acid is a dibasic acid with pK_1 2.95 and pK_2 5.41. Its KHP solution gives a pH of approximately 4.2 that is in good agreement with the equation $pH = (pK_1 + pK_2)/2$.
[a] This group of data was determined at 21.5°C.

2. Test with the equation

$$pH = (pk_1 + pk_2)/2$$

$$pH = (7.05 + 12.0)/2 = 9.5$$

$$pH = (7.05 + 19)/2 = 13.0$$

By using $pK_2 = 12.0$, the pH = 9.5 is in good agreement with the experimental value pH = 9.5 (NaHS solution), not pH = 13.0 with $pK_2 = 19$ (Table 3).

3. In the titration of Na_2S solution with an acid at the right part of Fig. 3,

$$S^{2+} + H_2O \rightleftharpoons HS^- + OH^- \quad (6)$$

$$pOH = pk_b - \log(S^{2-})/(HS^-) \quad (7)$$

When

$$(S^{2-}) = (HS^-),\ pOH = pk_b = pk_2 \quad (8)$$

The titration yields an intersection at pH 12 or pOH 2.0, not $pK_2 = 17$ or 19. This experiment shows that when Na_2S is dissolved in water it does not produce all OH^- in Eq. (6), as assumed by some of the authors [10].

4. The presence of O_2 in the solution, which interferes with the dissociation constant measurements, was overemphasized [10,13]. Kubli found no O_2 effect in his pK_2 determination [14]. Our experiment was done in the presence of SAOB to prevent oxidation of Na_2S. Meyers also misquoted (or misinterpreted) the titration of 0.04942

Table 4
Calculation of sulfide distribution ratio

NaOH estimated	pOH =	pK_b −	$\log(S^{2-})/(HS^-)$	$(HS^-)/(S^{2-})$	$(S^{2-})/(HS^-)$
10^5 M	3	2	(−1)	10	0.1
	2	2	(0)	1	1
	1	2	(1)	0.1	10
	0.1	2	(1.9)	1/80	80
	0	2	(2)	1/100	100
	−1	2	(3)	1/1000	1000
	−1.3	2	(3.3)	1/2000	2000
	−1.3	−3	(−1.7)	50	1/50
	−3 (calculated)	−3	(0)	1	1
	−1.3	−5	(−3.7)	5000	1/5000
	−5 (calculated)	−5	(0)	1	1

pOH = −1.3 18 M NaOH, pH 19 or pOH−5 would be equivalent to 10^5 M NaOH.

M NaOH solution in Kubli's pK_2 values of 12. Meyers' objection to Kubli's experiment was not justified, as Kubli titrated a solution of 0.04942 M Na_2S solution instead of 0.04942 M NaOH solution. As we know, Na_2S is not completely hydrolyzed in water all the way to produce OH^- (see Eq. (6)) even assuming $pK_2 > 14$ (See Table 4). Kubli just dissolved the Na_2S in water without adding any NaOH. Titration of OH^- as shown in Eq. (6) with 0.5223 N HCl by Kubli is an indication of how much OH^- is produced under the equilibrium.

The sulfide distribution ratio has been calculated according to Eq. (7) (Table 4). It is evident that the $(S^{2-})/(HS^-)$ ratio depends on the pH of the solution and pK_a or pK_b. For instance, at pOH 1 or pH 13, and $pK_2 = 12.0$ or $pK_b = 2.0$, the $(S^{2-}):(HS^-) = 10:1$. The Na_2S is far from the complete dissociation at pH 13. At pOH 0 or pH 14, and $pK_2 = 12.0$ or $pK_b = 2.0$, the $(S^{2-}):(HS^-) = 100:1$. If the $pK_2 = 17$, $(S^{2-}) = (HS^-)$, or $(S^{2-}):(HS^-) = 1:1$; this would require pOH-3 or 10^3 M NaOH. This calculation based on Eq. (7) disproves the possibility that $pK_2 \gg 12$. The figures in Table 3 also confirm that $pK_2 = 12.0$ is a reasonable value. Any questionable constant should be scrutinized by other techniques and calculations.

4. Conclusion

The dissociation constants of hydrogen sulfides have been determined by the sensitive amplified potentiometric Ag_2S ISE method: pK_{00}, pK_0, pK_1, and pK_2 are 1.8, 2.12, 7.05, and 12.0, respectively. The pK_1 agrees with the literature values. The pK_{00} and pK_0 from different acid media are reported here for the first time; the pK_{00} should be further studied. The pK_2 value has always been subject to considerable debate. Most textbooks have used values of $pK_2 \sim 12$–14, in general agreement with ours. However, some authors believe $pK_2 > 17$ or even 19, the value which has been accepted by the modern text. A few means have been applied to test the reliability of pK_2 values, and reasons for unreasonably higher pK_2 values are presented. One reason may be the high concentrations of NaOH or Na_2S used. The amplified potentiometric method to measure variation of sulfides adsorbates at the electrode surface due to protonation and deprotonation. The

present amplified potentiometric method may find applications for other weak acids and complexes with appropriate ISEs.

References

[1] R.C. Weast, Handbook of Physics and Chemistry, 72nd ed., CRC Press, Boca Raton, FL, 1991.
[2] D.C. Harris, Quantitative Chemical Analysis, 4th ed., p. AP25, Freeman, New York, 1995.
[3] I.M. Kolthoff, E.B. Sandell, E.J. Meehan and S. Bruckenstein, Quantitative Chemical Analysis, 4th ed., Macmillan, London, 1969.
[4] D.A. Day and A.L. Underwood, Quantitative Analysis, 6th ed., Prentice-Hall, Englewood Cliffs, NJ, 1991.
[5] D.A. Skoog and D.M. West, Fundamentals of Analytical Chemistry, 4th ed., Saunders, Philadelphia, PA, 1982.
[6] H.A. Flaschka, A.J. Barnard, Jr. and P.E. Starrock, Quantitative Analytical Chemistry, 2nd ed., Willard Grant Press, Boston, MA, 1980.
[7] T.R. Blackbarn, Equilibrium, Holt, Rinehart, and Winston, New York, 1969.
[8] E.H. Swift and E.A. Butler, Quantitative Measurements and Chemical Equilibrium, Freeman, 1972.
[9] R.L. Pecsok, L. Shields, T. Cains and I.G. McWilliam, Modern Methods of Chemical Analysis, 2nd ed., Wiley, New York, 1968.
[10] R.J. Myers, J. Chem. Educ. 63 (1967) 687.
[11] G. Yagil, J. Phys. Chem. 71 (1967) 1034.
[12] S. Licht, F. Forouzan, K. Longo, Anal. Chem. 62 (1990) 1356.
[13] A.J. Ellis, W. Giggenbach, Geochim. Cosmochim. Acta 25 (1971) 247.
[14] H. Kubli, Helv. Chim. Acta 29 (1946) 1962.
[15] K.L. Cheng, H.Z. Song and S.X.R. Yang, J. Chem. Soc. Chem. Commun., 1333 (1988).
[16] K.L. Cheng, Microchem. J. 42 (1990) 5.
[17] R. Stepak, Fresenius Z. Anal. Chem., 315 (1983) 629; 315 (1983) 29; 328 (1987) 268.
[18] K. Suzuki, K. Tohda, T. Shirai, Anal. Lett. 20 (1987) 1773.

ELSEVIER

Talanta 44 (1997) 1765–1771

Talanta

Polarographic determination of diffusion coefficient values of In(III) in potassium chloride and nitrate supporting electrolytes

Stephen Kariuki, Howard D. Dewald *

Department of Chemistry, Clippinger Laboratories, Ohio University, Athens, OH 45 701-2979, USA

Received 11 July 1996; received in revised form 9 September 1996; accepted 2 October 1996

Abstract

The diffusion coefficient values of In(III) in potassium chloride and potassium nitrate supporting electrolytes have been determined by polarography. Also, the half-wave potential, $E_{1/2}$, and the $|E_{3/4} - E_{1/4}|$ values have been calculated. The results show ionic strength and chloride concentration effects on electrode kinetics in the reduction of In(III). © 1997 Elsevier Science B.V.

Keywords: Adsorption; Complex formation; Diffusion coefficient; Dropping mercury electrode; Indium; Reversibility

1. Introduction

Under the influence of a chemical potential gradient, diffusion of an electroactive species involves the interdiffusion of the redox species, solvent molecules, and supporting electrolyte ions [1]. The diffusion velocity of a species in a given supporting electrolyte will be greatly influenced by the solution composition resulting from molecular and ionic interactions involved in the whole diffusion process. In spite of the complexities involved in the diffusion process, several methods for obtaining diffusion coefficient values for various species have been devised. Our recent review presents the diffusion coefficient values for a variety of metallic ions [2]. We pointed out that even when different studies have used the same techniques and supporting electrolytes for the diffusion coefficient measurement, the values may turn out to be different, sometimes quite substantially.

The electrochemical behavior of indium has been of interest to many. In recent years Doyle, et al. [3] developed a voltammetric immunoassay for proteins based on the anodic stripping voltammetric detection of an In(III) ion label. An aluminum alloy containing indium has been used as a sacrificial anode for the cathodic protection of steel structures in marine environments [4]. Indium has also been used to alter the electrochemical properties favorable for battery applications [5]. Liquid In/Ga alloy has been found useful by Sinclair, et al. when applied to the surfaces of glasses and ceramics for use as electrodes [6]. The electrocatalytic activity of an indium electrode for the reduction of CO_2 has also been demonstrated [7,8]. The diffusion coefficient of indium metal in mercury

* Corresponding author.

PII S00 9-9140(97)00046-5

was determined by means of the dropping mercury electrode by Stackelberg and Toome [9]. Turnham [10] has reported the In(III) diffusion coefficient values determined polarographically in several supporting electrolytes over the concentration range of 0.008–0.1 M. The diffusion coefficient values reported presently are for 0.5 mM In(III) in concentrations of 0.024–3 M KNO_3 and KCl and are compared with those obtained by Turnham [10]. Besides the determination of the diffusion coefficient values, we report the $E_{1/2}$ and $|E_{3/4} - E_{1/4}|$ values for In(III). These results present aspects of the reduction process of In(III) such as reversibility, complexation with chloride, and adsorption of chloride on the dropping mercury electrode.

2. Experimental

2.1. Equipment

The polarograms were obtained using an EG and G Princeton Applied Research Corporation (PARC) Model 264A Polarographic Analyzer/Stripping Voltammeter connected to an EG and G PARC Model RE 0089 X-Y Recorder. The dropping mercury electrode (DME) had an average drop time (t) in KNO_3 electrolytes of 2.29 s and an average mercury flow rate (m) of 3.44 mg s^{-1} with an applied potential of -0.75 V. At -1.20 V, the average t and m values were 2.06 s and 3.45 mg s^{-1}, respectively. At -0.75 V, the average values of t and m in KCl electrolytes were 2.23 s and 3.42 mg/s, respectively, while at -1.2 V the average values of t and m were 1.97 s and 3.43 mg/s, respectively. At each potential, the drop time was determined by measuring the time required for 20 drops of mercury to form and fall while the mass flow rate was determined by collecting mercury for not less than 10 min. The height of the mercury column above the capillary (EG and G PARC MCC0001) tip was 85 cm. The depth of the capillary immersion into the electrolyte was about 0.5 cm. The capillary had a length of about 25 cm while the radius of its lumen was about 0.16 mm. Besides the DME, the electrochemical cell (EG and G PARC K0066/K0060) was also equipped with a platinum wire auxiliary electrode and an aqueous saturated calomel electrode (SCE, EG and G PARC K0077). A resin cartridge (Barnstead D8902) connected to a glass still (Barnstead Fi streem2) was used to obtain doubly distilled deionized water. The pH of the solutions was measured using an Orion Research Digital Analyzer M501 and pH glass electrode (Orion Model 91-04).

2.2. Reagents and chemicals

The hydrated indium(III) nitrate (Alfa, Puratronic grade—99.999%), potassium chloride (Fisher Scientific, A.C.S. grade), potassium nitrate (Lab Chemicals, 99.99%), and Triton X-100 (Z.D. Gilman) were used as received. Mercury (Bethlehem Instrument, A.C.S. grade) was also used as received. High purity nitrogen gas was used for purging the In(III) solutions. The buffers of pH 4.00 and 7.00 used for calibrating the pH electrode had been obtained from Fisher Scientific.

2.3. In(III) reduction

0.5 mM $In(NO_3)_3 \cdot xH_2O$ in a given concentration of the supporting electrolyte was polarographed by scanning the potential from -0.1 V to about -1.8 V versus SCE. The baseline for each polarogram was extrapolated from which diffusion current measurements were made. To confirm that the plateau currents used for measurements were diffusion-limited, maximum current values for In(III) reductions at particular nitrate and chloride concentrations were plotted against the square root of the Hg-column height. The plots were linear with a correlation coefficient better than 0.99. The maximum diffusion current was measured either at -0.75 V or at -1.2 V. Reduction of In(III) in each supporting electrolyte containing 0.0002% Triton X-100 (w/v) was repeated four times from which the mean was taken. During the polarographic measurements, the temperature was maintained at 25 ± 0.1°C with the help of a water bath. $|E_{3/4} - E_{1/4}|$ values were determined directly from the polarogram. The $E_{1/2}$ were determined by using the Heyrovsky and Ilkovic equation [11].

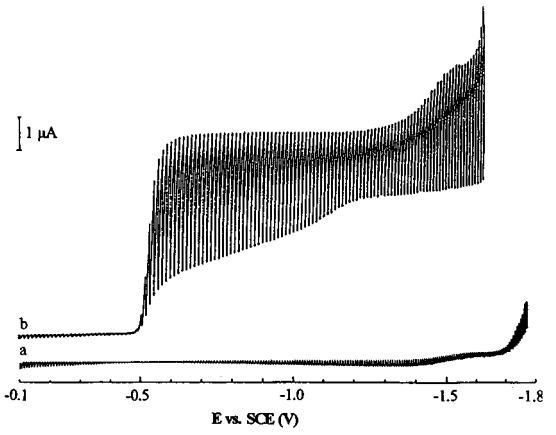

Fig. 1. Polarograms for (a) background and (b) 0.5 mM In(III) in 0.04 M KNO_3; scan rate = 5 m V s^{-1}; $E_i = -0.1$ V; Temp. = 25°C; 0.0002% (w/v) Triton X-100; At −1.2 V, m = 3.45 mg s^{-1} and $t = 2.06$ s.

3. Results and discussion

3.1. In(III) in presence of nitrate supporting electrolytes

3.1.1. Diffusion coefficients in KNO_3 supporting electrolytes

Solutions of In(III) in KNO_3 supporting electrolytes had a pH of 3.36 ± 0.10. The reduction of In(III) in KNO_3 supporting electrolytes gave waves, which at low supporting electrolyte concentrations, were characterized by large maxima of the first kind [12]. A concentration of 0.0002% (v/v) of Triton X-100 was used as a maxima suppressor. This concentration compares with the one Turnham [10] had previously used. Fig. 1 shows a typical polarogram of 0.5 mM In(III) in 0.04 M KNO_3. As seen from the polarogram, two reduction waves were obtained, the first one being for In(III). The second plateau arises from the reduction of hydrogen ions present in the solutions as indicated by their pH values. Any formation of In(Hg) at the electrode surface might also have catalyzed discharge of H_2 by the reduction of H_2O. This possibility was not explored further. The hydrogen reduction wave for solutions containing In(III) was observed at a less negative potential than without In(III).

The Ilkovic equation [13]

$$i_d = 708nD^{1/2}Ct^{1/6}m^{2/3} \quad (1)$$

was used to evaluate the diffusion coeffcient values. The symbol i_d is the diffusion limited current in μA, n is the number of electrons involved in the electrode reaction, D is the diffusion coefficient of the electroactive species in cm^2 s^{-1}, C is the concentration of the electroactive species in mM, t is the drop time of mercury in seconds, and m is the mass flow rate of mercury in mg s^{-1}.

The diffusion coefficient values of In(III) in KNO_3 are listed in Table 1 and Table 2. The diffusion current measurements in Table 1 were made at −1.2 V while those in Table 2 were made at −0.75 V. Changing of the potential for the current measurements was found necessary since at higher concentrations of the supporting electrolyte (0.2 M–3 M KNO_3), the hydrogen ion reduction appeared shifted to potentials less negative than −1.2 V. The choice of −0.75 V as the

Table 1
Diffusion coefficient values[a] (D), half-wave ($E_{1/2}$), and $|E_{3/4} - E_{1/4}|$ potentials for 0.5 mM In(III) in varying concentrations of KNO_3 supporting electrolyte having 0.0002% (w/v) of Triton X-100

[KNO_3] (M)	$E_{1/2}$ (V)	$\lvert E_{3/4} - E_{1/4}\rvert$ (mV)	D × 10^{-6} (cm^2 s^{-1})	Lit. [10] D × 10^{-6} (cm^2 s^{-1})
0.024	−0.526	39	4.28	4.409
0.04	−0.522	34	3.93	4.409
0.056	−0.528	39	3.86	4.138
0.06	−0.524	35	3.84	—
0.072	−0.528	32	3.83	4.258
0.08	−0.529	36	3.70	4.363
0.1	−0.530	37	3.72	—

[a] D calculated with diffusion current measurements at −1.2 V.

Table 2
Diffusion coefficient values[a] (D), half-wave ($E_{1/2}$), and $|E_{3/4}-E_{1/4}|$ potentials for 0.5 mM In(III) in varying concentrations of KNO_3 supporting electrolyte having 0.0002% (w/v) of Triton X-100

[KNO_3] (M)	$E_{1/2}$ (V)	$\lvert E_{3/4}-E_{1/4}\rvert$ (mV)	$D\times10^{-6}$ (cm^2 s^{-1})
0.2	−0.528	34	3.72
0.4	−0.529	25	3.70
1.0	−0.524	22	3.58
3.0	−0.524	54	1.55

[a] D value calculated with diffusion current measurements at −0.75 V.

potential at which all the diffusion coefficient current measurements would have been made would have been an ideal one. However, large maxima were observed at lower concentrations of supporting electrolyte and at 0.0002% Triton X−100. The maxima found in In(III) in 0.024 M KNO_3 required 0.0013% Triton X-100 to eliminate them, but this lowered considerably the diffusion currents at −0.75 V. A few of the diffusion coefficient values obtained are similar to the ones reported in the literature [10], while most vary from the reported values. All the values obtained are smaller. The diffusion coefficient values as seen in Table 1 and Table 2 tend to decrease with the increasing concentration of the supporting electrolyte.

The diffusion coefficient is related to the viscosity of solution [14]. However, any changes in viscosity for the concentrations of supporting electrolyte and maxima suppressor we used, are not expected to be large enough to cause a significant change in the diffusion coefficient values that we observed. The change in ionic strength for the concentrations of supporting electrolyte we used is however, major, and is therefore expected to significantly contribute to the diffusion coefficient values [15]. This effect of the ionic strength is particularly notable in 3 M $KN0_3$, where diffusion coefficient value at that concentration is much lower than at other concentrations of supporting electrolyte.

3.1.2. Half-wave potentials and $|E_{3/4}-E_{1/4}|$ values

The expression for the determination of the half-wave potential, $E_{1/2}$, was derived by Heyrovsky and Ilkovic [11]. It takes the form:

$$E = E_{1/2} - \frac{0.05915}{n}\log\frac{I}{I_d - I} \quad (2)$$

where E is the potential of the working electrode and I is the current at a given potential. By plotting E versus $\log[I/(I_d-I)]$, a straight line was obtained whose intercept gave the $E_{1/2}$ values. The $E_{1/2}$ values found in Table 1 and Table 2 appear shifted to more negative values with increasing ionic strength. An increase in the ionic strength of solution results in a decrease in the activity coefficient of the reducible ion. However, since it is the logarithm of the inverse of the activity coefficient of the reducible ion that is related to $E_{1/2}$ values [16], a considerable change in the activity coefficient should have only a small effect on the $E_{1/2}$ value. Our results qualitatively fit well with this theory since no significant changes are observed in the values of $E_{1/2}$ with the increasing concentration of the supporting electrolyte.

The $|E_{3/4}-E_{1/4}|$ values that were obtained are listed in Table 1 and 2. They seem higher than the predicted value of 18.8 mV [17,18] for a 3-electron reversible reduction process. These findings support that the reduction of In(III) in KNO_3 occurs in an irreversible manner.

3.2. Indium in presence of chloride supporting electrolytes

3.2.1. Diffusion coefficients in the KCl supporting electrolytes

Solutions of In(III) in KCl supporting electrolyte were found to have a pH of 4.15 ± 0.16. Polarograms of In(III) had two reduction waves as observed in KNO_3 solutions. Further, the reduction waves of In(III) in low concentrations of KCl supporting electrolytes had big maxima of the first kind [12]. However, the maxima were not as big as the ones found in KNO_3. The maxima found in In(III) in 0.024 M KCl required 0.0002% (w/v) Triton X-100 to eliminate them. Further, it was noted that the maxima found in In(III) diminished very rapidly with the increasing concen-

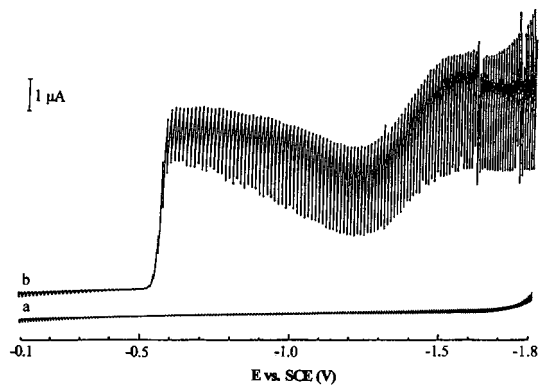

Fig. 2. Polarograms for (a) background and (b) 0.5 mM In(III) in 0.4 M KCl; scan rate = 5 mV s^{-1}; $E_i = -0.1$ V; Temp. = 25°C; 0.0002% (w/v) Triton X-100; at -1.2 V, $m = 3.42$ mg s^{-1} and $t = 2.23$ s. The polarogram exhibits a minimum at -1.25 V.

tration of the KCl supporting electrolytes. This was not so for In(III) in KNO_3 supporting electrolytes. A concentration of 0.0002% Triton X-100 was used to reduce the maxima found in In(III) in KCl supporting electrolyte to make easy measurements of the currents. However at higher concentrations of the KCl supporting electrolyte (from 0.2 to 3 M), a minimum (vice infra) could be observed (Fig. 2). Thus the maximum currents were made from the current measurements at -0.75 V.

The diffusion coefficient values of In(III) in the supporting electrolyte (Table 3) have an overall trend of decreasing with the increasing concentration of KCl up to 0.1 M. Just like the case of KNO_3 supporting electrolyte, the diffusion coefficient values in the KCl supporting electrolyte appear smaller than the literature values [10].

From 0.2 to 3 M KCl, the currents were found to appreciably increase with the increasing supporting electrolyte concentration, an effect that may be attributed to changes in electrode kinetics with the increasing concentration of the chloride [19–23]. Several groups have explained the increased currents of reducible species that form complexes that adsorb on the electrode [24–28]. These groups found that in solutions containing complex-forming molecules or ions adsorbable at the electrode surface, the metal cations can accumulate at the electrode-solution interface by entering into complexes with the adsorbed ligands. This accumulation of the metal cations leads to an enhancement of current or sensitivity, a feature that some groups [29,30] have taken advantage of in electroanalytical determinations. A plot of the current measured at -0.75 V of 0.5 mM In(III) versus the concentration of KCl supporting electrolytes from 0.2 to 3 M KCl suggests that as the concentration of the KCl is increased, some species whose reduction gives enhanced currents are formed each time. The observed currents for the reduction of In(III) in 0.2 to 3 M KCl appeared influenced by adsorption phenomena and were therefore not used to evaluate the diffusion coefficient values.

Engel, et al. [23] have also observed minima in the oxidation of indium amalgams polarographically in perchloric acid, sodium thiocyanate, hydrochloric acid, and sodium bromide solutions. They attributed the minima to the oxidation of

Table 3
Diffusion coefficient values[a] (D), half-wave ($E_{1/2}$), and $|E_{3/4} - E_{1/4}|$ potentials for 0.5 mM In(III) in varying concentrations of KCl supporting electrolyte having 0.0002% (w/v) of Triton X-100

[KCl] (M)	$E_{1/2}$ (V)	$\lvert E_{3/4} - E_{1/4} \rvert$ (mV)	$D \times 10^{-6}$ (cm^2 s^{-1})	Lit. [10] $D \times 10^{-6}$ (cm^2 s^{-1})
0.024	−0.529	22	4.44	4.733
0.04	−0.536	22	4.48	4.815
0.056	−0.541	21	4.42	4.306
0.06	−0.543	20	4.41	–
0.072	−0.542	19	4.37	4.586
0.08	−0.544	19	4.19	4.375
0.1	−0.550	22	3.95	–

[a] D calculated with diffusion current measurements at -1.2 V.

In(Hg) through the adsorbed halide. Moorhead, et al. [31] also reported observing minima in the reduction of the In(III) species in the presence of the 0.1 and 1 M KCl supporting electrolytes. Visco [32] described a minimum as a region of negative resistance in the reduction of the In(III) in the acidic solution of halides or pseudohalides. A further discussion about the minimum observed in the polarographic wave of In(III) in aqueous electrolyte solutions may be obtained from de Levie and Husovsky [33]. The minima we obtained increase in size with the increasing concentration of the potassium chloride showing that they are associated with the chloride concentration. The adsorption of the anion at the dropping mercury electrode also appears associated with the potential of the electrode.

3.2.2. Half-wave potentials, n and $|E_{3/4} - E_{1/4}|$ values

The $E_{1/2}$ values obtained for In(III) in KCl supporting electrolyte show definite shifts toward more negative values with the increasing concentration of the KCl. This contrasts with the pattern of $E_{1/2}$ values with the increasing concentration of the KNO_3 supporting electrolyte. Pines [34] earlier made observations that $E_{1/2}$ values of the metal ions shift to more negative values by complex formation.

The n values were also determined from the slope of the straight line obtained by plotting the potential of the dropping mercury electrode against the values of $\log[I/(I_d - I)]$. $|E_{3/4} - E_{1/4}|$ values were determined directly from the polarogram recorded. Lingane [35] obtained n values of three for the In(III) species reduction in 0.1 and 1 M KCl, respectively. Our values agree well with his. The $|E_{3/4} - E_{1/4}|$ values that we obtained are also close to the predicted one [17,21] of 18.8 mV for a 3-electron reversible system.

4. Conclusion

We were able to obtain the diffusion coefficient values for the polarographic reduction of In(III) in KNO_3 and KCl supporting electrolytes. The values are smaller than the reported ones [10] obtained under similar conditions. The calculated value of the diffusion coefficient using the Nernst–Einstein relation [36] is 5.94×10^{-6} cm^2 s^{-1}. This calculation, which is based on the molar conductivity of an ion, assumes that at infinite dilution intermolecular or interionic interactions do not exist. In real solutions this can never be the case. The values $|E_{3/4} - E_{1/4}|$ predicted reversibility of reduction of the In(III) in KCl supporting electrolyte. An irreversible behavior is observed for In(III) in KNO_3. Finally, we note that due to minima that occur in the reduction of the In(III) species in high concentrations of KCl, polarographic analysis of mixtures with other ions, such as gallium(III), would be more difficult.

References

[1] R.B. Bird, W.E. Stewart, and E.N. Lightfoot, Transport Phenomena, Wiley, New York, 1960, pp. 563–572.
[2] S. Kariuki, H.D. Dewald, Electroanalysis 8 (1996) 307.
[3] M.J. Doyle, H.B. Halsall, W.R. Heineman, Anal. Chem. 54 (1982) 2318.
[4] J.C. Lin, H.C. Shih, J. Electrochem. Soc. 134 (1987) 817.
[5] G. Burri, W. Luedi, O. Haas, J. Electrochem. Soc. 136 (1989) 2167.
[6] D.C. Sinclair, P.B. Morrison, F. Velasco, A.R. West, Solid State Ionics 37 (1990) 295.
[7] K. Hara, A. Kudo, T. Sakata, J. Electroanal. Chem. 391 (1995) 141.
[8] M. Todoroki, K. Hara, A. Kudo, T. Sakata, J. Electroanal. Chem. 394 (1995) 199.
[9] M. von Stackelberg, V. Toome, Z. Elektrochem. 58 (1954) 226.
[10] D.S. Turnham, J. Electroanal. Chem. 10 (1965) 19.
[11] J. Heyrovsky, D. Ilkovic, Collect. Czech. Chem. Commun. 7 (1935) 198.
[12] L. Meites, Polarographic Techniques, 2nd ed., Interscience, New York, 1965, pp. 304–312.
[13] A.J. Bard and L.R. Faulkner, Electrochemical Methods, Fundamentals and Applications, Wiley, New York, 1980, pp. l46–150.
[14] J.O. Bockris and A.K.N. Reddy, Modern Electrochemistry, Plenum, New York, 1970, vol. 1, pp. 379–381.
[15] M. Ciszkowska, J.G. Osteryoung, Anal. Chem. 67 (1995) 1125.
[16] I.M. Kolthoff, J.J. Lingane, Chem. Rev. 24 (1939) 1.
[17] J. Tomes, Collect. Czech. Chem. Commun. 9 (1937) 12, 150.
[18] L. Meites, Polarographic Techniques, 2nd ed., Interscience, New York, 1965, pp. 224–225.

[19] J.A. Schufle, H.M. Eiland, J. Am. Chem. Soc. 76 (1954) 960.
[20] J.A. Schufle, M.F. Stubbs, R.E. Witman, J. Am. Chem. Soc. 73 (1951) 1013.
[21] I.V. Nelson, R.T. Iwamoto, J. Electroanal. Chem. 6 (1963) 234.
[22] R.E. Connick, C.P. Coppel, J. Am. Chem. Soc. 81 (1959) 6389.
[23] A.J. Engel, J. Lawson, D.A. Aikens, Anal. Chem. 37 (1965) 203.
[24] R. Kalvoda, W. Anstine, M. Heyrovsky, Anal. Chim. Acta 50 (1970) 93.
[25] D.J. Barclay, F.C. Anson, J. Electrochem. Soc. 116 (1969) 438.
[26] B. Timmer, M. Sluyters-Rehbach, J.H. Sluyters, J. Electroanal. Chem. 18 (1968) 93.
[27] R.W. Murray, D.J. Gross, Anal. Chem. 38 (1966) 392.
[28] F.C. Anson, J.H. Christie, R.A. Osteryoung, J. Electroanal. Chem. 13 (1967) 343.
[29] R. Kalvoda, J. Ai-Chua, J. Electroanal. Chem. 8 (1964) 378.
[30] G. Donoso N., M.A. Santa Ana V., V.I. Chadwick W., Anal. Chim. Acta 42 (1968) 109.
[31] E.D. Moorhead, W.M. MacNevin, Anal. Chem. 34 (1962) 269.
[32] R.E. Visco, J. Electroanal. Chem. 10 (1965) 82.
[33] R. DeLevie, A.A. Husovsky, J. Electroanal. Chem. 22 (1969) 29.
[34] I. Pines, Collect. Czech. Chem. Commun. 1 (1929) 387, 429.
[35] J.J. Lingane, J. Am. Chem. Soc. 61 (1939) 2099.
[36] J.S. Newman, Electrochemical Systems, 2nd Prentice Hall, Englewood Cliffs, NJ, 1991, pp. 254.

ELSEVIER

Talanta 44 (1997) 1773–1781

Talanta

Potentiometric study of reaction between tetrabutylammonium periodate and phenothiazine in chloroform; application to the analysis of phenothiazine derivatives

M.H. Pournaghi-Azar *, Kh. Farhadi

Department of Analytical Chemistry, Faculty of Chemistry, University of Tabriz, Tabriz, Iran

Received 29 July 1996; received in revised form 8 January 1997; accepted 15 January 1997

Abstract

The reaction between tetrabutylammonium periodate and phenothiazine in the presence of the strong acids in chloroform was studied by potentiometry and the reaction pathways were determined. The oxidimetric titration conditions of phenothiazine derivatives using a standardized chloroform solution of tetrabutylammonium periodate were optimized and a potentiometric detection of end points was utilized. The relative standard deviation for the determination of 5 mg phenothiazines was obtained about 1–1.5%. The method was applied for the determination of phenothiazines in various pharmaceutical preparations after extraction into chloroform. © 1997 Elsevier Science B.V.

Keywords: Non-aqueous solvent; Phenothiazines; Potentiometry; Chloroform

1. Introduction

Several electroanalytical methods have been developed for the determination of phenothiazine derivatives in pharmaceutical preparations [1–10]. Usually, the potentiometric method can be simple and fast for pharmaceutical analysis. Ion selective membrane electrodes have been used for the potentiometric determination of some phenothiazine drugs [11]. Two-phase potentiometric titration was also reported [12]. Most of the employed methods for the determination of phenotiazine drugs in pharmaceutical preparations follow a preliminary separation by solvent extraction into an organic solvent, therefore direct application of potentiometric titration method in extracts is fast and sensitive when a suitable reagent and indicator electrode is available [9,13,14]. Golabi et al. [13] have applied the potentiometric titration for the determination of phenothiazine drugs using a chloroform solution of bromine. Since the bromine solution in chloroform suffer from a lack of stability and oxidizing strength, the use of a suitable oxidizing agent in chloroform seem to be interesting.

The aim of the present work is to study the reaction between tetrabutylammonium periodate and phenothiazines in chloroform in order to develop a potentiometric method of analysis on the basis of the oxidimetric titration for the deter-

* Corresponding author.

PII S00 9-9140(97)00048-9

Table 1
Determination of pure phenothiazines by potentiometry and the official USP method

Phenothiazines	Potentiometric method			USP method			F^c	t^c
	Taken (mg)[a]	Recovery[b]	RSD	Taken (mg)	Recovery	RSD		
Chlorpromazine HCl	5	100.4	1.2	75	101.5	0.7	2.9	1.4
Promethazine HCl	5	100.2	1.1	70	101.9	0.3	13.4	2.6
Thioridazine HCl	5	99.2	0.9	70	101.7	0.3	9.1	4.5
Perphenazine	5	99.2	1.6	40	100.7	0.5	10.2	1.5
Trifluoperazine HCl	5	101.8	1.6	50	102.4	0.9	2.8	0.6

[a] 5 ml extract pahase corresponding to the extraction of about 25 mg of phenothiazines in 25 ml chloroform.
[b] Mean of three titrations using a standardized solution of AIO_4.
[c] Theoretical values of F and t are 19 and 2.78 ($P = 0.05$) respectively.

mination of phenothiazine derivatives. The investigated phenothiazines are given in Table 1.

2. Experimental

2.1. Apparatus

A Video titrator Vit 90 (Radiometer) coupled with a Toshiba P321SL printer or an E 536 potentiograph equipped with an E 578 titration stand (Metrohm) were used to plot the normal and inflection forms of the titration curves.

2.2. Reagents

The solvent used was chloroform G.R. from E. Merck, tetrabutylammonium periodate (AIO_4), perchlorate ($ACIO_4$), chloride (ACl) and iodide (AI) were from Janssen. A 0.001 M solution of AIO_4 in chloroform was used. This solution was stable in refrigerator during the weeks. Concentrated perchloric acid 70% and *p*-toluenesulfonic acid (TSO_3H) from E. Merck was used as a suitable strong acid for acidifying the test solutions up to 0.1 M. A 0.005 M phenothiazine solution was prepared by dissolving the pure substance (Aldrich). Chloroform solutions of *N*-substituted phenothiazines such as promethazine, chlorpromazine, perphenazine, trifluoperazine and thioridazine were prepared from their pure hydrochlorides (purchased from local sources).

2.3. Electrodes

The reference electrode Ag/AgCl (sat'd), 0.05 M ACl and 0.5 M $ACIO_4$ in chloroform prepared in a separated compartment with a dense ceramic plug in the bottom was used. The indicator electrode was Pt wire or Pt disk.

2.4. Procedures

2.4.1. Extraction and separation of phenothiazines from pharmaceutical preparations

The pharmaceutical preparations were obtained from local sources in various forms (tablet, syrup and injection) and phenothiazines were extracted into chloroform as follows: An accurately measured volume of syrup and injection solutions or weighed portion of finely powdered tablets equivalent to about 50 mg of phenothiazine drugs (as their hydrochlorides)were transfered to a 125-ml separating funnel, 10 ml of 1 M NaOH, was added and extracted with three 20-ml portions of chloroform, shaking gently for 3 min to avoid emulsion formation. The extracts were combined in a 100-ml volumetric flask.

2.4.2. Standardization of AIO_4

A 10-ml portion of 0.01 M AIO_4 solution in chloroform was pipetted into a 125-ml separating funnel and the required amount of AI and a suitable strong acid such as *p*-toluenesulfonic or perchloric acid was added up to 0.1 M. The solution was shaken two times

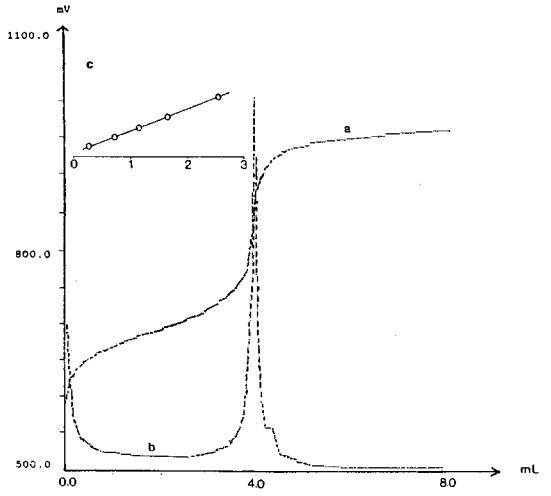

Fig. 1. Potentiometric titration of 5 ml 0.005 M phenothiazine + 5 ml 0.2 M *p*-toluenesulfonic acid with 0.0009 M AIO_4 solution (a) plots of E vs. V_{AIO_4}, (b) $\Delta E/\Delta V$ vs. V_{AIO_4} and (c) E vs. $\log[x/F(1-x)^2]$, delivery rate: 0.5 ml min^{-1}.

with a 10-ml portion of 1 M aqueous solution of KI for 2 min. The aqueous phases were separated and combined in a conical flask. The yielded I_2 according to the following reaction [14]:

$$7AI + AIO_4 + 8TSO_3H \rightleftharpoons 4I_2 + 8ATSO_3 + 4H_2O$$

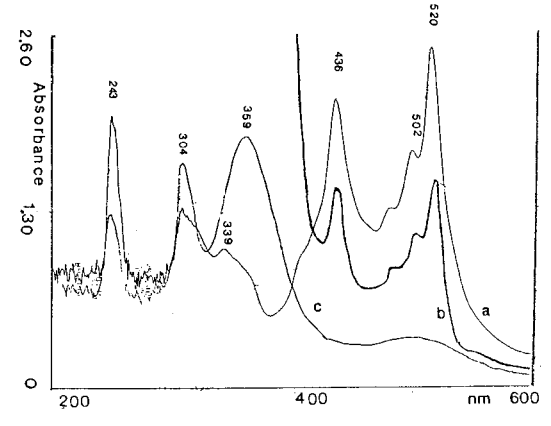

Fig. 2. Absorption spectra of (a) titrated solution of Ph with AIO_4 at the equivalence point, (b) partially oxidized Ph solution in chloroform with molecular oxygen and (c) acidified iodine chloroform solution.

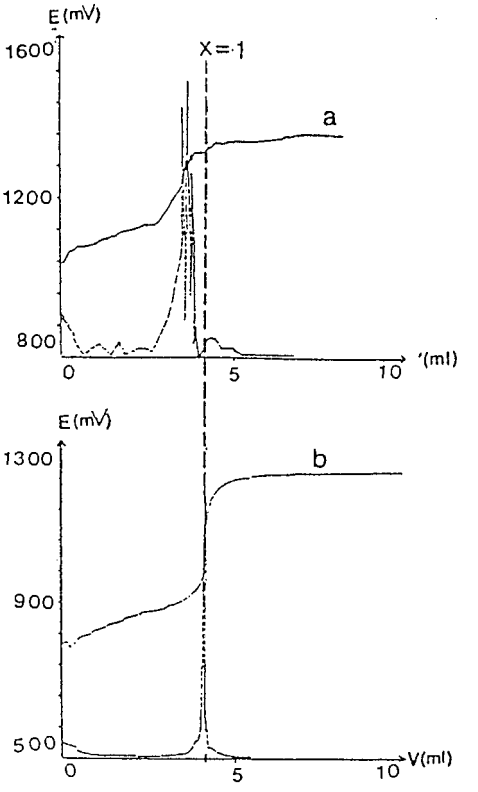

Fig. 3. Potentiometric titration of 5 ml 0.005 M phenothiazine with 0.0009 M AIO_4 solution in the presence of (a) 0.1 M sulfuric acid and (b) 0.1 M *p*-toluenesulfonic acid, delivery rate 0.5 ml min^{-1}.

which extracted in aqueous phase, was titrated with a 0.01 M standard solution of thiosulfate.

2.4.3. Titration of phenothiazine drugs

A 10-ml portion of chloroform extracts, obtained from the extraction of pharmaceutical preparation samples was pipetted into the reaction vessel and a required amount of strong acid such as *p*-toluenesulfonic acid or perchloric acid was added up to 0.1 M. The solution was titrated with AIO_4 solution (about 0.001 M) at a delivery rate of 0.5 ml min^{-1} using the autotitrator and the titration curve was plotted.The quantitative determination of phenothiazine drugs in the extracts is achieved in one of the following ways:

1. A standardized solution of AIO_4 is used in titration.

2. Another titration is carried out with a second 10-ml aliquot of pure *N*-substituted phenothiazine. The quantity of phenothiazine is calculated by comparison of the volumes of titrant used in 2 titrations.

2.4.4. Reaction pathways and stoichiometry

The results obtained from our previous works reveal that: (a) the potentiostatic oxidation of phenothiazines in chloroform occurs in two one-electron steps by forming the cation radical and dication respectively [9] and (b) the reaction between AIO_4 and AI gives rise to the formation of AI_3 and I_2, respectively [14]. Therefore on the basis of results mentioned above (a,b) the titration reaction may be proceeded according to one of the following schemes:

1. Oxidation of phenothiazines to cation radical involving a 3-step process.
   (a) $8Ph + AIO_4 + 8TSO_3H \rightleftharpoons AI + 8PhTSO_3 + 4H_2O$
   (b) $11AI + AIO_4 + 8TSO_3H \rightleftharpoons 4AI_3 + 8ATSO_3 + 4H_2O$
   (c) $7AI_3 + AIO_4 + 8TSO_3H \rightleftharpoons 11I_2 + 8ATSO_3 + 4H_2O$
2. Oxidation of phenothiazines to cation radical involving a one step process only.
   $14Ph + 2AIO_4 + 16TSO_3H \rightleftharpoons I_2 + 14PhTSO_3 + 2ATSO_3 + 8H_2O$
3. Oxidation of phenothiazines to dication involving a 2-step process.
   (a) $14Ph + 2AIO_4 + 16TSO_3H \rightleftharpoons I_2 + 14PhTSO_3 + 2ATSO_3 + 8H_2O$
   (b) $14PhTSO_3 + 2AIO_4 + 16TSO_3H \rightleftharpoons I_2 + 14Ph(TSO_3)_2 + 2ATSO_3 + 8H_2O$

   where Ph and A show phenothiazine and tetrabutylammonium cation, respectively.

Considering $x = (\text{added } AIO_4)/(C_o/8)$ (where C_o is the initial concentration of phenothiazine), according of scheme 1 the titration plots E vs. V_{AIO4} must show three inflection points at

$$x = 1\left(\frac{C_o/8}{C_o/8}\right),\ 1.09\left(\frac{3C_o/44}{C_o/8}\right)$$

and

$$1.14\left(\frac{C_o/7}{C_o/8}\right)$$

respectively. While on the basis of Scheme 2 only one potential rise is expected to appear at $x = 1$ where

$$x = \frac{\text{added } AIO_4}{C_o/7}$$

At least considering the Scheme 3, two equivalence points at $x = 1$ and $x = 2$ are expected to appear, where

$$x = \frac{\text{added } AIO_4}{C_o/7}$$

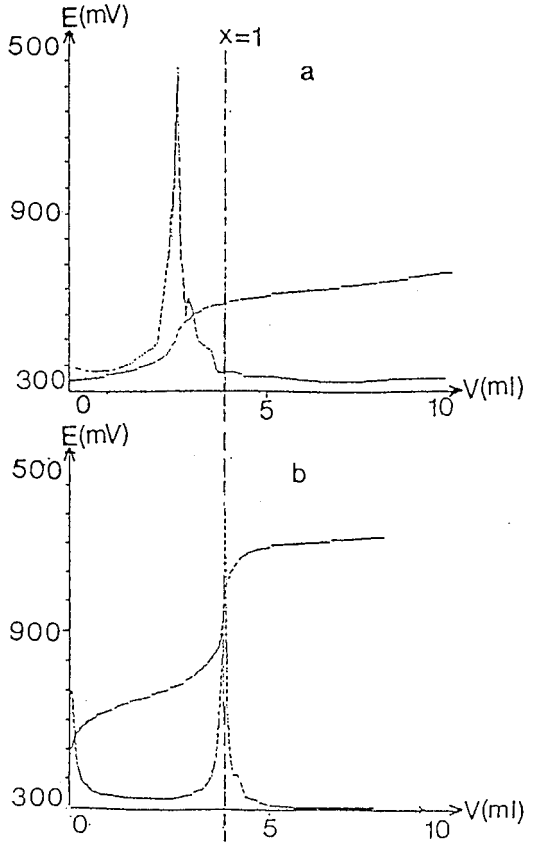

Fig. 4. Potentiometric titration of 5 ml 0.005 M phenothiazine with 0.0009 M AIO_4 solution in the presence of 0.1 M perchloric acid with delivery rate of (a) 1 ml min^{-1} and (b) 0.5 ml min^{-1}.

Table 2
Potentiometric determination of phenothiazines in pharmaceutical preparations

Phenothiazines[a]	Claimed	Added (mg)	Found[b]	RSD	Recovery[b]	RSD
Promethazine ampoule	50 mg 2 ml^{-1}	25	49.8	1.8	100.6	0.4
Promethazine tablet	25 mg $tablet^{-1}$	25	26.5	1.5	101	0.6
Chlorpromazine ampoule	50 mg 2 ml^{-1}	25	50.3	0.85	99.8	0.4
Chlorpromazine tablet	25 mg $tablet^{-1}$	25	24.9	1.1	101	0.3
Thioridazine tablet	10 mg $tablet^{-1}$	25	10.1	1.6	102.2	0.7
Perphenazine ampoule	5 mg ml^{-1}	25	5.23	1.6	99.9	1.1
Perphenazine tablet	8 mg $tablet^{-1}$	25	8.3	1.7	101.7	0.8
Trifluoperazine ampoule	1 mg ml^{-1}	15	1.2	1.3	101.8	1.4
Trifluoperazine tablet	5 mg $tablet^{-1}$	25	5.6	1.5	102.2	1.2
Promethazine syrup	5 mg 5 ml^{-1}	25	5.3	1.6	101	1.3

[a] Commercial names are their generic names.
[b] Mean of three determinations using a standardized solution of AIO_4.

3. Results and discussion

The potentiometric plot for the titration of 5 ml 0.005 M phenothiazine in chloroform with a standardized chloroform solution of AIO_4 (0.0009 M) in the presence of 0.1 M *p*-toluenesulfonic acid was shown in Fig. 1. As seen in this figure the potential ranges from 600 to 1000 mV vs reference electrode and only one inflection point appears at $x = 1$. On the other hand the plot of E vs. V_{I_2} during the addition of 0.001 M chloroform solution of I_2 to 10 ml 0.005 M phenothiazine shows that the potential remains unchanged. These observations lead us to conclud that the reduction product of AIO_4 by phenothiazine is I_2 and the titration reaction pathway corresponds to the Scheme 2. Alternatively, this can be tested by an analysis of the experimental titration curve. The electrode potential on the two sides of the equivalence point can be expressed as follows at 25°C.

Before the equivalence point:

$$Ph^+ + e \rightleftharpoons Ph$$

$$E = E^{o_{Ph}} + 0.059 \log \frac{[Ph^+]}{[Ph]} \quad (1)$$

because of the ion-pair formation, a dissociation equilibrium must also be considered for $PhTSO_3$ and $ATSO_3$ as follows:

$$PhTSO_3 \rightleftharpoons Ph^+ + TSO_3^-,$$

$$K_1 = \frac{[Ph^+][TSO_3^-]}{[PhTSO_3]} \quad (2)$$

$$ATSO_3 \rightleftharpoons A^+ + TSO_3^-, \qquad K_2 = \frac{[A^2][TSO_3^-]}{[ATSO_3]} \quad (3)$$

According to Eqs. (2) and (3) we can write:

$$[TSO_3^-] = [Ph^+] + [A^+] = \frac{K_1\,[PhTSO_3]}{[TSO_3^-]} + \frac{K_2[ATSO_3]}{[TSO_3^-]}$$

$$[TSO_3^-]^2 = K_1[PhTSO_3] + K_2[ATSO_3] \quad (4)$$

and from Eqs. (2) and (4) we have

$$[Ph^+] = \frac{K_1^2\,[PhTSO_3]^2}{K_1[PhTSO_3] + K_2[ATSO_3]} \quad (5)$$

$$E = E^{o_{Ph}} + \frac{0.059}{2} \log \frac{K_1^2[PhTSO_3]^2}{[Ph]^2(K_1[PhTSO_3] + K_2[ATSO_3])} \quad (6)$$

Considering

$$x = \frac{\text{added } AIO_4}{C_o/7}$$

on the basis of the reaction of Scheme 2, at any point of the titration we can write:

$[Ph] = F(C_o - xC_o)$, $[PhTSO_3] = FxC_o$

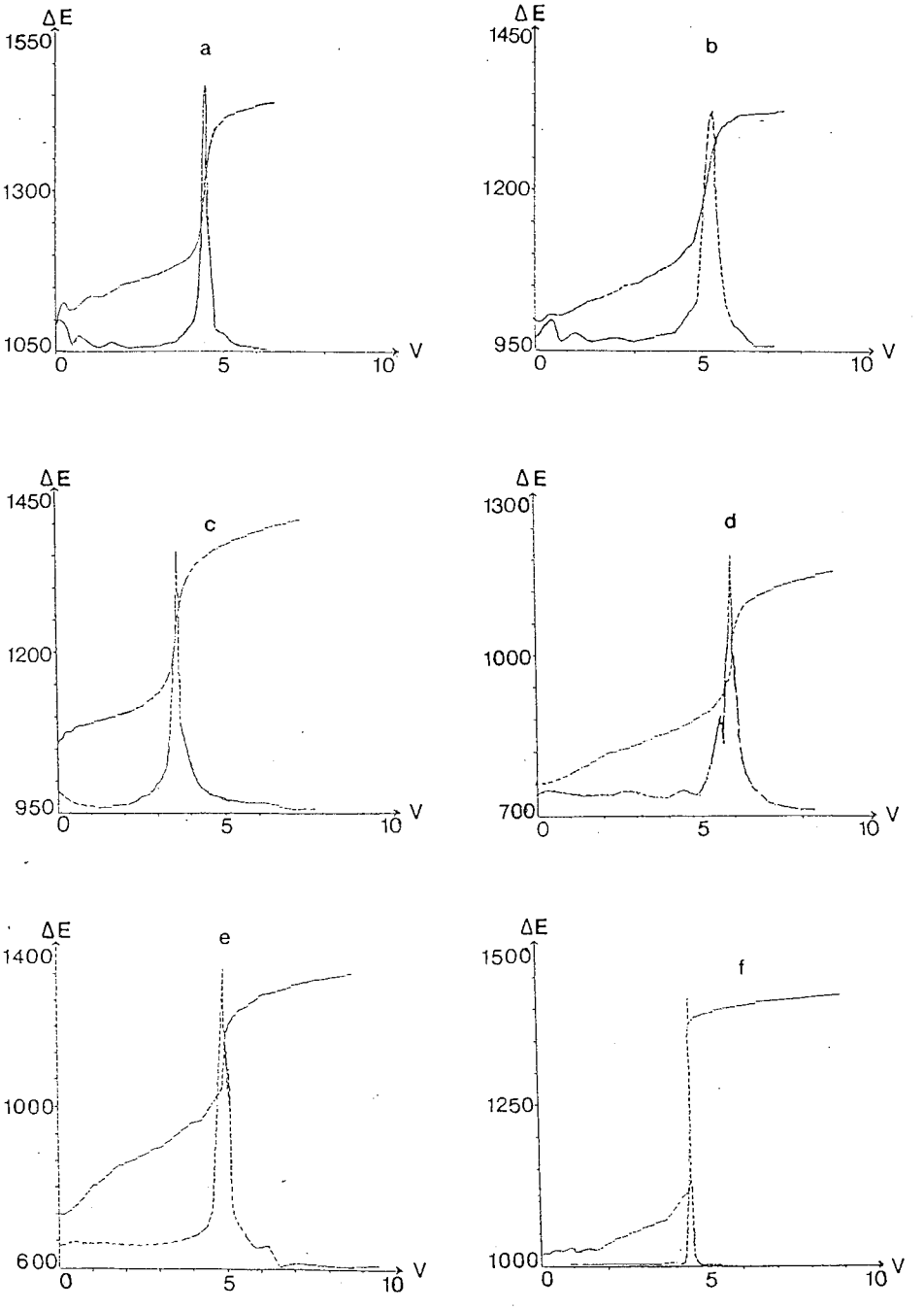

Fig. 5. Potentiometric titration curves of 10-ml portion of chloroform extracts containing about 5 mg of phenothiazine drugs with a 0.00085 M solution of AIO_4 in the presence of 0.1 M $HClO_4$. The extracts correspond to the extraction of about 25 mg of phenothiazine derivatives from (a) chlorpromazine 25 mg tablet^{-1}, (b) promethazine 25 mg tablet^{-1}, (c) thioridazine 10 mg tablet^{-1}, (d) chlorpromazine 50 mg 2 ml^{-1}, (e) promethazine 5 mg 5 ml^{-1}, and (f) perphenazine 5 mg 1 ml^{-1} into 25 ml (10, 10 and 5 ml) of chloroform.

Table 3
Determination of phenothiazinic drugs by potentiometric and USP methods

	Nominal content	Found[a]	
		Proposed method	USP method
Promethazine tablet	25 mg tablet^{-1}	26 ± 1	26.0 ± 0.6
Perphenazine ampoule	5 mg ml^{-1}	5.3 ± 0.2	5.5 ± 0.3
Trifluoperazine tablet	5 mg tablet^{-1}	5.5 ± 0.3	5.3 ± 0.2
Thioridazine tablet	25 mg tablet^{-1}	25 ± 1	25 ± 1

[a] Mean of three determinations and 90% confidence interval of the mean.

$[ATSO_3] = FxC_o/7$, $F = V/V + v$, where V is the initial volume of test solution, v is the volume of added AIO_4

$$E = a_1 + \frac{0.059}{2}\log\left(\frac{x}{F(1-x)^2}\right) \quad (7)$$

With:

$$a_1 = E^{oPh} + \frac{0.059}{2}\log\frac{7k_1}{C_o(k_1 + 7k_2)} \quad (8)$$

After the equivalence point

$2AIO_4 + 14e + 16TSO_3H \sim$

$\rightleftharpoons I_2 + 2ATSO_3 + 14TSO_3^-$

$$E = E^{oIO_4} + \frac{0.059}{14}\log\frac{[AIO_4]^2[TSO_3H]^{16}}{[I_2][ATSO_3]^2[TSO_3^-]^{14}} \quad (9)$$

Considering Eq. (4) and the concentration balance:

$[I_2] = FC_o/14$, $[ATSO_3] = FC_o/7$, $[PhTSO_3] = FC_o$

$[AIO_4] = FC_o(x-1)/7$, $[TSO_3H] = 0.2F$we can rewrite Eq. (9) as follows:

$$E = a_2 + \frac{0.059}{14}\log F^8(x-1)^2 \quad (10)$$

With: $a_2 = E^{oIO_4} + 0.067\log[TSO_3H]/C_o - 0.029\log(7k_1 + k_2) + 0.004$

The plot of E vs. $\log[x/F(1-x)^2]$ for $0 < x < 1$ and E vs. $\log[F^8(x-1)^2]$ for $x > 1$ gave straigth lines with slopes of 0.059/2 and 0.059/14 respectively (see Fig. 1C). This agree with the proposed stoichiometry for the titration reaction according to Scheme 2. The three replicate potentiometric titration plots of the phenothiazine solutions of various concentrations were analysed and the titration reaction pathway of Scheme 2 was confirmed. The same stoichiometry were observed for the titration reactions of the *N*-substituted phenothiazines investigated.

3.1. Spectrophotometric investigation

The absorption spectra of (a) diluted (10 times) of titrated solution of Ph (0.0025 M) with AIO_4 in the presence of 0.1 M TSO_3H at the equivalence point, (b) partially oxidized Ph solution by molecular oxygen ($Ph^+ + Ph$) and (c) violet coloured solution of 0.001 M iodine + 0.1 M TSO_3H in chloroform are given in Fig. 2. The absorption maxima appeared at visible region 600–400 nm (a and b) confirmed that the oxidation product of Ph with AIO_4 was Ph^+ (cation radical). On the other hand looking to spectrum (c) clears that the iodine solution in acidified chloroform has three absorption maxima at 502,359 and 3043 nm. In titrated solution of Ph by AIO_4 these absorption maxima of I_2 also appeared,while the first is overlapped by some absorptive maxima of Ph. Note that the absorptive maxima for yellow-red coloured AI_3 in chloroform appeared at 509 and 288 which differs from the spectrum of I_2. These findings shows that the reduction product of AIO_4 by Ph I_2 and the reaction pathway of Scheme 2 is confirmed.

4. Analytical aspects

4.1. Optimization of the titration conditions

In order to optimize the proposed potentiometric method the effect of some experimental variables were studied. Of the various acids tested, *p*-toluenesulfonic acid and perchloric acid were found to be the most suitable for phenothiazine (Fig. 3). But for *N*-substituted phenothiazines the titration reactions proceed according to scheme 2, only in the presence of 0.1 M perchloric acid. On the other hand the most reproducible and accurate result was obtained with a delivery rate of 0.5 ml min^{-1} (Fig. 4)

4.2. Performence characteristics

The precision and accuracy of the proposed method was evaluated by analysis of three pure samples of each phenothiazine investigated and comparing the results with those obtained by the official USP method [15] based on acidimetric titration in anhydrous acetic acid (Table 1). As shown by the recoveries and standard deviations ranging from 0.9 to 1.8% a satisfactory agreement between the results was obtained (except thioridazine). This was confirmed by statistical analysis, based on the variance ratio test (*F* test) and Student's *t*-test (see Table 1). The detection limit of the method depends on the oxidation ability of phenothiazine via molecular oxygen. On the other hand the reproducibility and accuracy of the determination at low concentration level, suffered from a lack of stability of the test solutions via molecular oxygen. However we have demonstrated that the satisfactory results with the relative S.D. of 0.8–2.5% for the determination of 0.0008–0.05 M of some phenothiazine derivatives such as chlorpromazine and trifluoroperazine ($n = 3$) can be obtained and a concentration range 0.001–0.02 M may be suitable for the titration of studied phenothiazines.

4.3. Application to dosage forms

Several phenothiazine drugs obtained from the local sourses were analysed by the present method. The results shown in Table 2 indicate that the phenothiazines in dosage forms of various claimed amount ranging from 5–25 mg per tablet and 1–25 mg ml^{-1} of injection can be conveniently determined by the proposed potentiometric method with good precision. Fig. 5 illustrates the potentiometric titration of some phenothiazines extracted from the dosage forms (tablet, ampoule or syrup) into chloroform (see experimental procedure).

We have evaluated the accuracy of the proposed method by performing experiments on the samples prepared from dosage forms and pure drugs. A mean recovery of 101% (ranging from 99.8 to 102.2%) was found (Table 2). Furthermore the results obtained for some typical pharmaceutical preparations by the present method were compared with those obtained by the time consumming official USP methods [15]. The results are given in Table 3. As can be seen, there is reasonable fair agreement between the present and official methods.

5. Conclusion

The proposed potentiometric titration method in chloroform is fast, precise, accurate and general. This method is suitable for the routine analysis of commonly used phenothiazine drugs in various commercial formulations (tablet, ampoule and syrup) of various amount of drugs ranging from 5 to 25 and 1 to 25 mg ml^{-1} for injections, instead of the tedious time consumming official methods. Interferences from common excipients are prevented by the selective extraction of phenothiazines into chloroform.

References

[1] G.J. Patriarche, J.J. Lingane, Anal. Chim. Acta 49 (1970) 25.
[2] G.J. Patriarche, J.J. Lingane, J. Pharm. Belg. 25 (1970) 57.
[3] G.J. Patriarche, J.J. Lingane, Pharm. Fr. 28 (1970) 511.
[4] F.W. Teare, R.N. Yadva, Can. J. Pharm. Sci. 13 (1978) 69.

[5] J. Wang, B.A. Freiha, Talanta 30 (1983) 837.
[6] F. Belal, J.L. Andersohn, Analyst 110 (1985) 1493.
[7] R.I. Baxter, G. Svehla, Anal. Chim. Acta 168 (1984) 171.
[8] N. Zimova, I. Nemec, Talanta 33 (1986) 467.
[9] S.M. Golabi, M.H. Pournaghi-Azar, M.B. Shabani, J. Pharm. Belg. 43 (1988) 19.
[10] S. Dermis, I. Biryol, Analyst 114 (1989) 525.
[11] V.V. Cosofret, R.P. Buck, Analyst 109 (1984) 1312.
[12] P.A. Johansson, R. Gustavic, Acta Pharm. Suec. 13 (1976) 407.
[13] S.M. Golabi, M. Showkati-Shishvan, Talanta 38 (1991) 1253.
[14] M.H. Pournaghi-Azar, Kh. Farhadi, Talanta (1995) 345.
[15] US Pharmacopeia XX, Mack Co., Easton, Pa., 1980.

ELSEVIER

Talanta 44 (1997) 1783–1792

Talanta

Determination of abscisic acid by cathodic stripping square wave voltammetry

P. Hernández, M. Dabrio-Ramos, F. Patón, Y. Ballesteros, L. Hernández *

Departamento de Química Analítica, Universidad Autónoma de Madrid, Madrid, Spain

Received 10 October 1996; received in revised form 15 January 1997; accepted 12 February 1997

Abstract

In this paper a study is accomplished on behavior in a mercury electrode, of the phytohormone abscisic acid and of the conditions of accumulation in a HMDE. A mechanism is proposed of reduction based on its electrochemical behavior and proving the product of the reduction through mass spectrometry of bulks. A method is proposed for the determination of Abscisic acid (ABA) with a quantification limit of 58 ng ml^{-1}. The procedure is applied wing determination of ABA in pears through the combination of high performance liquid chromatography (HPLC) with electrochemical quantification. © 1997 Elsevier Science B.V.

Keywords: Abscisic acid; Phytohormone; Mercury electrode

1. Introduction

Plant hormones or phytohormones are regulators that are produced by the plant itself. In low concentrations, they control the physiological processes. Phytohormones are classified into four groups: auxines, gibberellines, cytoquinines and inhibitors. Abscisic acid (ABA) belongs to the latter, which is quite different from the other groups of plant growth substances, as it inhibits or delays the physiological or biochemical process of plants [1].

Abscisic acid was isolated from young cotton fruit (*Gossypium hirsutum*) by a research group led initially by Corns and subsequently by Addicot [2]. Its structure, shown in Fig. 1, was determined by Ohkuma and associates [2].

The levels of concentration of this inhibitor vary considerably from one plant species to another and depend on environmental conditions [1]. Philips and Waring [2] studied this variation in *Acer pseudoplatanus* buds and leaves, finding

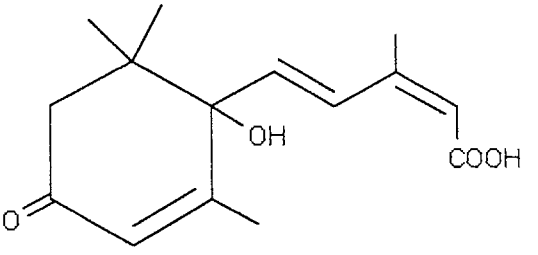

Fig. 1. Molecular structure of abscisic acid (ABA).

* Corresponding author.

PII S00 9-9140(97)00049-0

minimum levels of ABA in June in the terminal buds and maxima in winter, precisely the opposite of the leaves. This suggests that the inhibitor formed in the leaves in summer shifts to the terminal buds at the start of autumn.

Hormonal action depends on the hormone concentration, the presence and characteristics of the receptor and the elements involved in the signal transduction chain. The hormone-receiver complex, i.e., the activated receiver, is the first link in the signal transduction chain, which provokes a primary response. This in turn begins a series of changes which, as a whole, make up the complex physiological response.

In the case of abscisic acid, there is no single biological activity, which instead is manifested in several types of physiological response. The ABA has a great inhibiting effect on the growth of many types of plants. It is not the only growth-inhibiting substance, but it is the only one that is non-toxic. A seed treated with ABA, for example, can germinate once it is placed in another medium. With another inhibitor, this seed does not germinate [2].

Seed germination is regulated by the level of ABA and gibberellins (phytohormones that stimulate cell division or prolongation, or both). Gibberellins induce the synthesis of α-amylase, while the ABA inhibits this action, stopping cell division and hence growth [3].

Abscisic acid accelerates the abscission process in flowers and fruit, as well as in the reproductive organs of a wide variety of plant species [4], and ABA is also responsible for the closure of the stomas in the leaves of some plants such as *Triticum vulgare*, thus producing a reduction in transpiration [5].

In addition to plant activity, it has been suggested that abscisic acid inhibits reproduction in insects and the growth of tumours in some types of mice [2].

Given its importance, abscisic acid has been studied widely from an analytic perspective ever since its discovery. The first technique used to identify this acid, at the start of the 1960s, was paper chromatography (PC), which was soon replaced by thin layer chromatography (TLC). Detection was by means of UV spectroscopy because abscisic acid has an intense, well defined band [2]. As other techniques spread, however, TLC and PC was left as a mere technique for sample pre-purification. Gas chromatography (GC) and high performance liquid chromatography (HPLC) began to be used in the 1970s to study abscisic acid, and coupled to mass spectroscopy (MS) are an excellent method of identification [6,7]. The problem in HPLC analysis is the low specificity of the UV detector. GC-MS is a powerful method for identification, but the samples must be cleaned up. The lower limit of detection of ABA is 50 ng in HPLC. Before the analysis, crude samples should be purified by solvent partitioning and preparative TLC or by a short column such as the C_{18} Sep-pak cartridge [2]. Bioassay and immunoassay has been also used for determination and quantification of abscisic acid, and does not require pre-purification, although the experimental period tends to be very long due to the preparation of the antigen and the antiserum [8].

In recent times, the same techniques used in previous years have continued to be used for the determination and quantification of ABA, although additional techniques such as ELISA have arisen. We have not, however, found any literature on the electrochemical study of this phytohormone. This analysis, discussed in the present paper, is approached using square wave voltammetry (SWV), given that the coupling of an accumulation step to an impulse technique would enable us to obtain detection thresholds in the order of ng ml^{-1}. The use of an electrochemical measurement provides an additional selectivity which allows one to avoid the needed pre-purification steps used on other methods, such as GC or HPLC-UV. Likewise, the limit of detection obtained in this proposed method for quantification of ABA is similar to those obtained by using other traditional methods.

2. Experimental

2.1. Reagents and equipment

- A 0.2 mg ml^{-1} solution of abscisic acid (ABA) in methanol prepared from the crystallized

form supplied by SERVA (New York, USA). The solutions must by refrigerated and not exposed to light.

- Analysis quality reagents.
- Deionised water using Milliro-MilliQ (Water System) equipment.
- PAR polarographic analyser model 384B, equipped with a Ag/AgCl/KCl (3M) reference electrode and a platinum counter electrode. This polarograph was used for the square wave and cyclical voltammetry analyses using a hanging drop mercury electrode (HDME).
- Bioanalytical System Potentiostat BAS 100, equipped with a mercury pool electrode, a saturated calomel electrode as the reference electrode and a platinum electrode as the counter electrode. These were used for a coulometric analysis of the abscisic acid.
- HEWLETT PACKARD model 5890 Series II gas chromatograph with a HEWLETT PACKARD model 5971A spectrometry detector used to identify the coulometric reaction products.
- High performance liquid chromatography composed of a GILSON 302 pump connected to a GILSON 802C manometric module, with a GILSON 116 UV detector attached to the unit. The HPLC was used a the preparative separation method in a plant extract for subsequent electrochemical detection.

2.2. Procedure

The polarographic cell contains a 10-ml buffer solution at a previously adjusted pH and a known concentration of abscisic acid. The O_2 was eliminated by means of a stream of N_2 for 5 min in the first measurement and 30 s in the subsequent potential scans. An accumulation time (t_{ac}) was applied at an accumulation potential (E_{ac}) with a stirring speed of 400 r.p.m. The polarogram was recorded between -0.4 and -1.1 V for a mercury drop electrode of 0.0278 cm^2 average area, replaced for each measurement, against an Ag/AgCl 3M electrode and a platinum counter electrode. The equilibrium time was 5 s.

In order to establish the measurement conditions, the corresponding variable was modified in each analysis to find the optimum response value, establishing initial conditions of: square wave frequency (f) at 50 Hz with increments in the step wave potential (E) of 2 mV in each cycle, producing a scan rate of 100 mV s^{-1}. The pulse amplitude (a) was 20 mV.

2.2.1. Extraction procedure

The procedure used was as follows: 51.35 g of pears was pulverised after prior freezing with liquid nitrogen. Methanol (200 ml) was added, ensuring contact by constant stirring at 4°C for 24 h. The extract was vacuum filtered on a G4 filter plate, and the resulting extract was evaporated at 40°C in a rotary evaporator to a minimum volume. The extract was centrifuged to remove pigments and lipid phases, dissolved in methanol and levelled to 10 ml.

2.2.2. Methylation of the ABA carboxyl group [14]

100 μl of a 50 μg ml^{-1} ABA solution in methanol was taken and the solvent was evaporated by means of a N_2 stream. The dry residue was dissolved in 100 μl of a mixture containing acetonitrile:water:methanol:pyridine (7:1:1:1), adding 5 μl of methylchloroformate (MCF), which acted as the methylating agent, 100 μl of chloroform and 100 μl of 1M sodium bicarbonate. The abscisic acid was methylated in this medium, and afterwards the methylated compound was extracted in the chloroform, which remained at the bottom. After separating the two phases, the chloroform was removed by evaporation using a N_2 stream, leaving a dry residue that was dissolved in 100 μl of hexane.

3. Results and discussion

3.1. Influence of pH and accumulation potential on the abscisic acid reduction

The purpose of this study was to ascertain the conditions that facilitate the greatest adsorption of abscisic acid on the surface of the mercury droplet.

The measurements were made in different solutions containing 1.6 μg ml^{-1} of ABA in $HClO_4$, 1

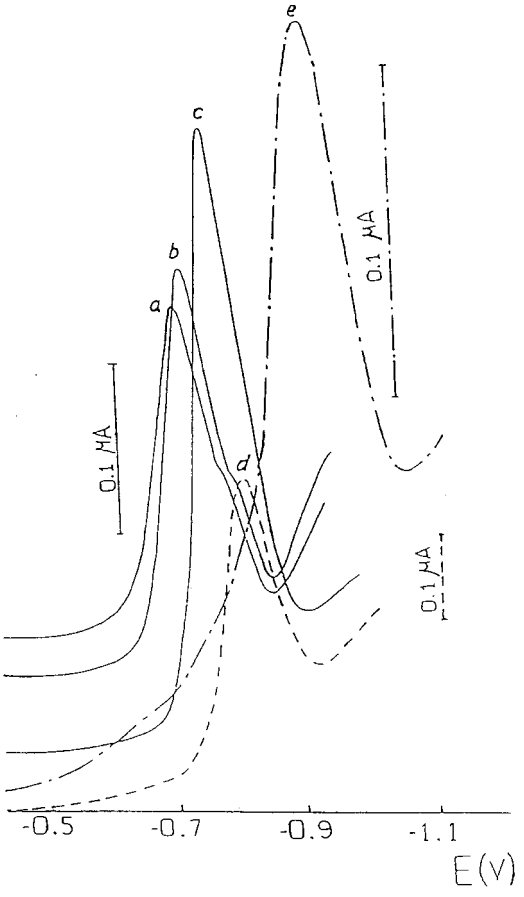

Fig. 2. Square wave voltammograms of abscisic acid reduction at different pH values: (a) pH 0; (b) pH 0.3; (c) pH 1; (d) pH 2 and (e) pH 3.

and 0.1 M, and H_3PO_4 0.04 M, obtaining the desired pH for the analysis in each case with KOH additions. An accumulation time of $t_{ac} = 30$ s was used, along with the rest of the conditions described in Section 2.2. The accumulation potential (E_{ac}) was varied for each pH value.

Fig. 2 shows the results for pH lower than 3. Beyond this pH, the width at half height grows considerably while the peak intensity diminishes, with a poor definition of the hormone reduction wave. In the concentrations at which it was found, the abscisic acid was not electroactive at basic medium.

Our results suggest that the pH is achieved at pH = 1, where the best wave definition and the highest peak intensity corresponding to the electroreduction of the phytohormone appear. We chose an accumulation potential of $E_{ac} = -0.4$ V and pH 1 for the subsequent analyses.

From the analysis of the variation in the pH, we obtain a shift in the peak potential towards more cathodic values, indicating an intervention of the protons in the reaction of the abscisic acid electroreduction. This shift shows two linear zones with differing slopes in the pH range under consideration. For pH levels between 0 and 2, the linear dependence fits the equation of the line:

$$E_p = -0.74 - 0.05 \text{ pH}; \quad r = 0.986$$

when the pH is between 2 and 4, the variation of the peak potential is linear, fitting the equation:

$$E_p = -0.64 - 0.1 \text{ pH}; \quad r = 0.993$$

in which peak potential is expressed in V.

The point of intersection between the two straight lines produces the value of pK corresponding to the abscisic acid system, obtaining a value of p$K = 1.9$.

A coulometric study was performed in a BAS-100 electrochemical analyser using a cell with a mercury pool electrode as the working electrode. A perchloric acid-sodium perchlorate solution at pH 1 containing 200 g of abscisic acid was placed in the cell. Applying a potential of -1.0 V, the ensuing number of electrons involved in the process was $n = 4$ [9].

To identify the product of the electrolysis, the solution was fed through a Sep-Pak C_{18} cartridge, after which the reduction product was eluted with methanol. The acid group of the molecule was methylated, and the product was injected into the GC-MS. The mass spectrum indicates the reduction of two double conjugated bonds (Fig. 3).

The proposed reduction mechanism for the ABA is in Fig. 4.

3.2. Influence of the scan rate

The scan rate was analysed in cyclic voltammetry over a 1.6 μg ml^{-1} solution of ABA in $HClO_4$ 0.1 M at pH 1. In all the measurements, the accumulation time was $t_{ac} = 30$ s, and accumulation potential was $E_{ac} = -0.4$ V.

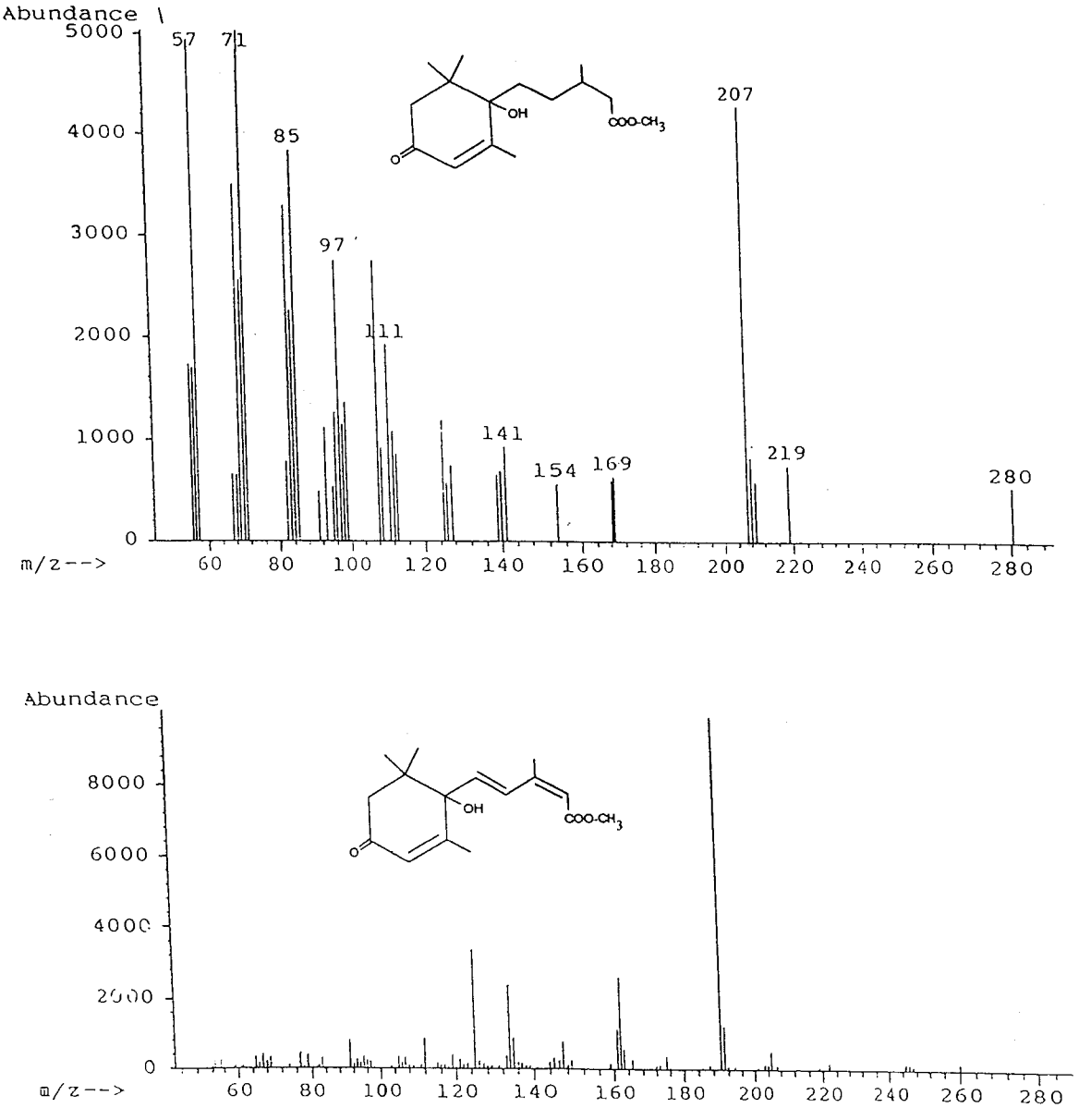

Fig. 3. Mass spectrum for the methylated ABA (down) and for the methylated product of the ABA electrolysis (up).

The data obtained with an increase in the scan rate indicate a shift in the peak potential towards more cathodic values. This variation of the peak potential in the abscisic acid reduction behaves linearly with the logarithm of the scan rate, following the equation

$$E_p = -0.7185 - 0.0422 \log v; \quad r = 0.996$$

where E_p is the peak potential expressed in V, and $\log v$ is the decimal logarithm the scan rate.

The intensity of the peak increases linearly with the scan rate, fitting the equation

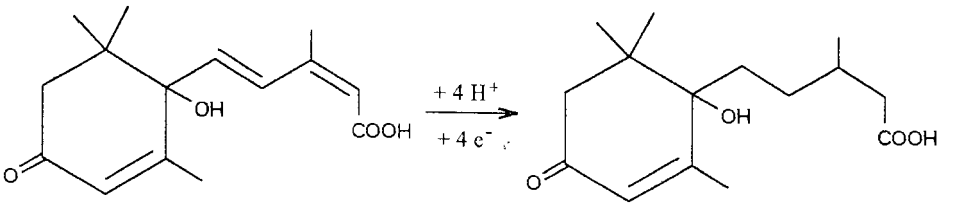

Fig. 4. The proposed reduction mechanism for the ABA.

$i_p = 0.0968 + 0.0021v; \quad r = 0.9994$

where the peak intensity is expressed in μA and the scan rate in mV s^{-1}.

This behaviour indicates that the abscisic acid reduction is produced by means of an adsorptive process controlled by diffusion [10] and is irreversible.

By representing the logarithm of the peak intensity at different scan rates against the peak potential, we obtain a linear relation that fits the equation

$\log i_p = -13.367 - 19.785E_p; \quad r = 0.995$

Using the value of the slope and knowing the number of electrons consumed in the electroreduction of the ABA, we can calculate the charge transfer coefficient, obtaining a value $\alpha = 0.31$ [11].

The influence of the square wave frequency was calculated under the conditions described in the Section 2.2, with the exception of the frequency variation. The results indicate that there is a linear dependency of the peak intensity on the frequency in accordance with the ratio:

$i_p = 3.059 \times 10^{-2} + 5.76 \times 10^{-3} f; \quad r = 0.9998$

expressing i_p in μA and where f is the square wave frequency expressed in Hz.

There is also a linear variation in the peak potential against the decimal logarithm of the frequency which fits the equation

$E_p = -0.72 - 0.044 \log f; \quad r = 0.997$

where E_p is the peak potential expressed in V and $\log f$ is the logarithm of the square wave frequency.

This analysis of the square wave frequency enables us to ascertain kinetic parameters of the electroreduction reaction of the abscisic acid in the mercury electrode. The value of the slope can be used to calculate the charge transfer coefficient (α), which can be calculated via the expression

$\Delta E_p / \Delta \log f = RT/Fn\alpha$

obtaining a value of $n = 1.58$. By means of coulometry, we found that the number of electrons exchanged by the molecule was $n = 4$. Hence, the value of the load transfer is $\alpha = 0.33$ [12].

Given that the peak intensity is linear with the square wave frequency, and that the peak potential is linear with the decimal logarithm of the square wave frequency, we can deduce that the electrochemical reduction process of the abscisic acid is of the adsorptive type controlled by diffusion. This concurs with the data obtained in the cyclic voltammetry analysis.

3.3. Influence of the square wave amplitude

From the variation in the square wave amplitude, we can obtain the degree of absorption of the ABA over the measurement electrode, i.e. the coating coefficient (Γ) of the mercury droplet used for measurement [12,13].

For this purpose we used an abscisic acid solution at 1.6 μg ml^{-1} concentration in $HClO_4$ at pH 1. We established an accumulation time of $t_{ac} =$ 30 s and the rest of the conditions as described in Section 2.2. The results are shown in Fig. 5.

In Fig. 5 we see an increase in the intensity of the peak with the amplitude of the square wave up to a value of $a = 40$ For higher values of the square wave amplitude, there is no significant increase in the peak intensity.

For square wave amplitude values lower than 20 mV, there is a linear increase in the value of the peak intensity that fits the equation:

$$i_p = 0.038 + 0.013a; \quad r = 0.992$$

where the peak potential is expressed in mV and the peak intensity in μA. On the basis of the slope of the line obtained for small square wave amplitudes, and knowing that the electrode has an surface area of 0.0278 cm^2, we can calculate a value for the coating coefficient of the mercury droplet of $1.9 \pm 0.7 \times 10^{-11}$ mol cm^{-2} [12,13].

3.4. Influence of the scan increment

Variations in the value of the scan increment produce changes in the intensity of the peak, which affect the sensitivity of the method. At the same time, however, the width at half height also varies, which affects its selectivity. A compromise must therefore be sought between the two factors.

In our measurements, we used a 1.6-μg ml^{-1} solution of ABA at pH 1 in $HClO_4$ 0.1 M, which acted as the supporting electrolyte. An accumulation time of $t_{ac} = 30$ s was set, using the rest of the initially established parameters.

Applying selectivity and sensitivity criteria, we took $E = 5$ mV as the optimum value for subsequent measurements as this combines a width at half height of $w_{1/2} = 95$ mV with a peak intensity of $i_p = 0.709$ μA.

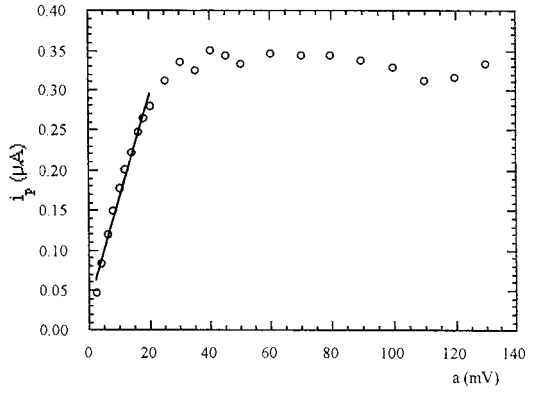

Fig. 5. Variation in peak intensity with square wave amplitude. Conditions in text.

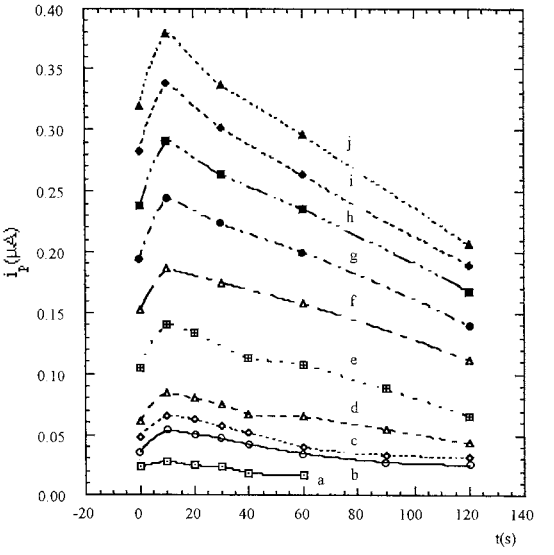

Fig. 6. Variation in peak intensity with accumulation time for different concentrations of ABA: (a) 0.1 μg ml^{-1}; (b) 0.2 μg ml^{-1}; (c) 0.3 μg ml^{-1}; (d) 0.4 μg ml^{-1}; (e) 0.6 μg ml^{-1}; (f) 0.8 μg ml^{-1}; (g) 1.0 μg ml^{-1}; (h) 1.2 μg ml^{-1}; (i) 1.4 μg ml^{-1} and (j) 1.6 μg ml^{-1}.

Fig. 6 graphs the results of varied accumulation times. In all cases, the adsorption of the hormone to the electrode reaches the highest peak intensity at an accumulation time of 10s. If this time is increased, the intensity of the peak diminishes. The optimum value is therefore $t_{ac} = 10$ s.

3.5. Influence of the buffer type

In the analysis of the influence of pH, the optimum working value was set at pH 1. On the basis of this condition, we tested different types of electrolytes: hydrochloric acid–sodium chloride, sulphuric acid–sodium sulphate, and finally perchloric acid–sodium perchlorate. Solutions of all these electrolytes at different concentrations were prepared to fix the ionic strength of the medium. Sulphuric acid–sodium sulphate solutions produce the highest peak intensities, the higher, the greater the concentration of electrolyte. This solution was thus used as a buffer medium and a support electrolyte at a 1 M concentration.

3.6. Influence of the ABA concentration

In the study of the effect of abscisic acid concentration on the peak intensity, the optimum conditions of the medium were set at those discussed in the previous sections.

The polarographic cell contained 10 ml of sulphuric acid-sodium sulphate solution at 1 M concentration, pH 1, which acted as a support electrolyte and different amounts of abscisic acid. An inert atmosphere was created by a stream of N_2 prior to each measurement. An accumulation potential $E_{ac} = -0.4$ V was applied for 10 s, with an equilibrium time of 5 s. The initial scan potential coincided with E_{ac}, and the final potential was set at -1.2 V to permit the full development of the wave.

Instrumental variables during the measurement stage were set at, pulse amplitude $a = 40$ mV, scan increment $E = 5$ mV, and square wave frequency $f = 120$ Hz, producing a scan rate of 600 mV s^{-1}.

There is an increase in the peak intensity with the concentration, shown in the superimposed voltammograms in Fig. 7.

This dependence of the peak intensity on concentration follows a linear relationship, which fits the expression

$$i_p = -1.76 \times 10^{-2} + 7.89 \times 10^{-4} C; \quad r = 0.999$$

The intensity of the peak is expressed in μA while the concentration is in ng ml^{-1}.

The relative error of the method ranges between 0.3 and 0.8% in absolute values and the relative standard deviation varies between 2.1 and 7.8%, producing a detection threshold of 30 ng ml^{-1} and a quantification threshold of 58 ng ml^{-1}.

4. Application

After optimising the abscisic acid determination method, it was applied to an extract of pears taken straight from the tree at the initial growth stage.

The extract obtained from little pears, like abscisic acid, contains many other compounds that interfere with voltammetric measurements, making purification necessary. For this purpose, HPLC was used as the preparatory technique in a 10-μm column of C_{18}, using a 0.01M mixture of methanol:phosphoric acid at pH 3 (1:2 v/v) as the eluent at a flow of 1.8 ml min^{-1}, and a UV detector at a wavelength of 270 nm. The retention time of the abscisic acid was 19.51 min. The corresponding fraction was collected at the column outlet.

For the purification process, we injected into the column a mixture containing 3 ml of extract and 6 ml of phosphoric acid with a 500 μl loop.

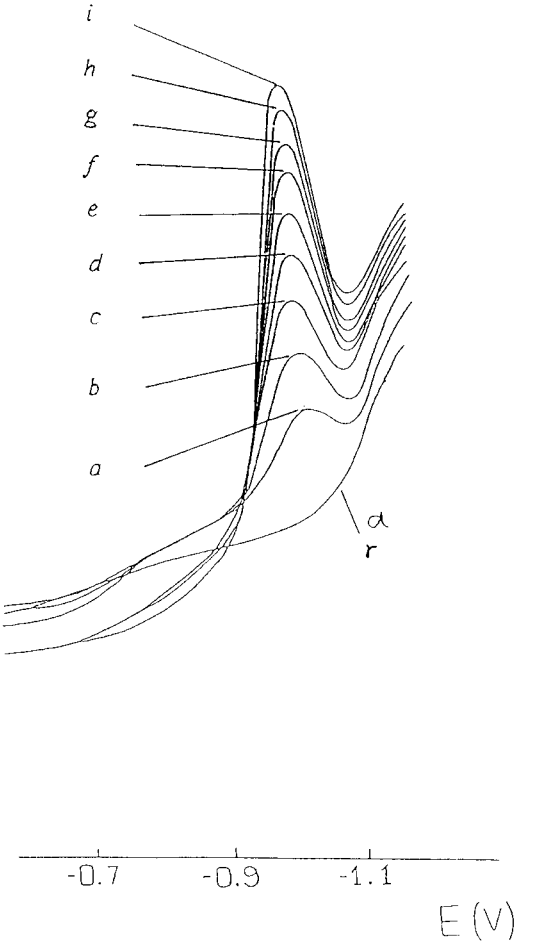

Fig. 7. Square wave voltammograms of abscisic acid reduction at different concentrations: r = residual current; (a) 75 ng ml^{-1}; (b) 125 ng ml^{-1}; (c) 150 ng ml^{-1}; (d) 250 ng ml^{-1}; (e) 300 ng ml^{-1}; (f) 350 ng ml^{-1}; (g) 400 ng ml^{-1}; (h) 450 ng ml^{-1} and (i) 500 ng ml^{-1}.

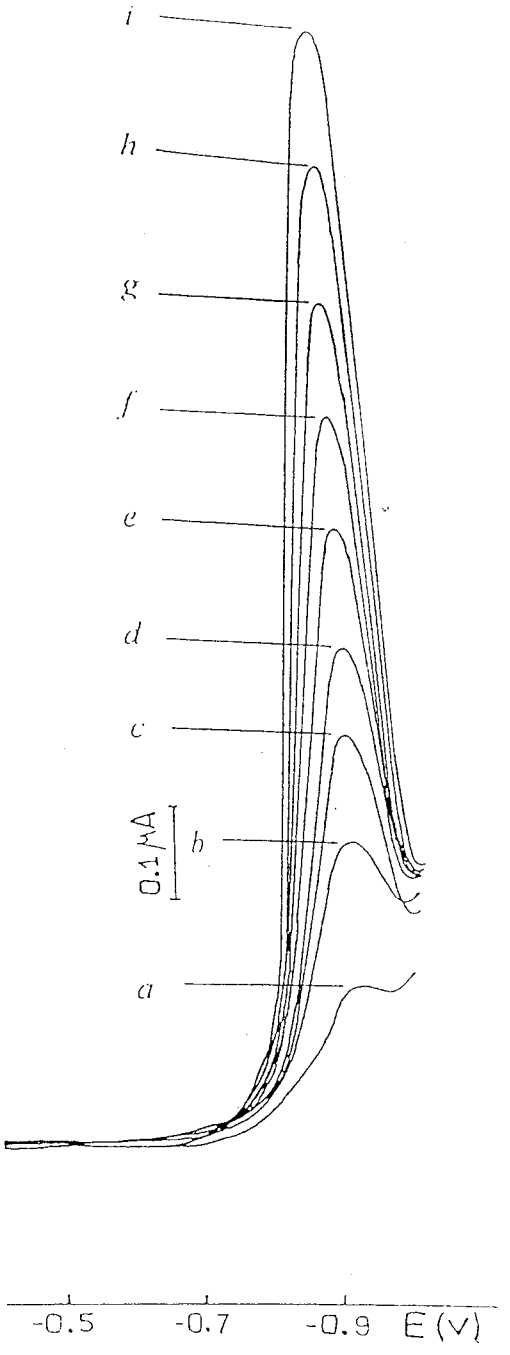

Fig. 8. Square wave voltammograms of real sample (a) and spiked samples with different concentrations: (b) 50 ng ml^{-1}; (c) 100 ng ml^{-1}; (d) 150 ng ml^{-1}; (e) 200 ng ml^{-1}; (f) 250 ng ml^{-1}; (g) 300 ng ml^{-1}; (h) 350 ng ml^{-1} and (i) 400 ng ml^{-1}.

This process was repeated four times, collecting a total volume of 20.3 ml at the outlet of the column.

Square wave voltammetry was used for the measurement under the same conditions as the calibration of the abscisic acid. In order to find the ABA concentration contained in the extract, we performed standard additions. The intensity of the peak increases linearly with the concentration of the added ABA, fitting the equation:

$$i_p = 0.0529 + 2.108C; \quad r = 0.999$$

where the peak intensity is expressed in μA and the concentration in μg ml^{-1} (Fig. 8).

Extrapolating from the straight line, we find a 0.025 μg ml^{-1} concentration of ABA in the measurement cell. Taking into account the successive dilutions of the sample, and the calculated extraction yield (78%), we can calculate that the amount of abscisic acid contained in the initial pear sample was 3.1 ± 0.1 μg per gram of pear. This is the average value obtained in 5 samples for which the same extraction process was carried out. This method has been used since the signal obtained for the ABA through HPLC determination with UV detection remains under its quantification limit. In the same way, with a direct electrochemical measure, the nature of the sample produces adsorptions in the electrode that make the signal of the ABA to disappear. So, in this work, a separation through HPLC is combined with a very sensitive electrochemical detection. Hence, in whatever the vegetal sample it was necessary to determine ABA, this proposed method can be applied.

Acknowledgements

The authors gratefully acknowledge financial support from the Dirección General de Investigación of Spain under project PB92/132 and for a scholarship to F. Patón.

References

[1] R.J. Weaver (Ed.), Reguladores del crecimiento de las plantas en la agricultura. Trillas, Mexico, 1985.

[2] Nobutaka Takanashi, Chemistry of plant hormones. Department of Agricultural Chemistry. Faculty of Agriculture. The University of Tokio, Bunkio-Ku, Tokio, Japan. CRC Press, Boca Raton, Florida, pp. 201–248.
[3] M.J. Chrispeels, J.E. Varner, Nature (London) 212 (1966) 1066.
[4] R.M.F. Van Stevenich, Nature (London) 183 (1959) 1246.
[5] C.J. Mittelheuser, R.F.M. Van Stevenich, Nature (London) 221 (1969) 281.
[6] E.W. Weiler, Planta 144 (1979) 225–263.
[7] A.G. Netting, B.V. Milborrow, A.M. Duffield, Phytochemistry 21 (1982) 385.
[8] B. Anderson, N. Haggstrom, K. Anderson, J. Chromatogr. 157 (1978) 303.
[9] M. Iwamoto, A. Webber, R.A. Osteryoung, Anal Chem. 56 (1984) 1202.
[10] A.J. Bard and L.R. Falkner, Electrochemical Methods. Wiley, New York, 1980, p. 224.
[11] R. Mallaby, G. Ryback, J. Chem. Soc. Perkin Trans. 2 (1972) 919.
[12] M. Lovric, S. Komorsky-Lovric, R.W. Murray, Electrochem. Acta 33 (6) (1988) 739–744.
[13] J.J. O'Dea, A. Ribes, J.G. Osteryoung, J. Electroanal. Chem. 345 (1993) 287–301.
[14] P. Husek, LC-GC international, The Magazine Separation Sci. 59 (1992) 43–49.

ELSEVIER

Talanta 44 (1997) 1793–1801

Talanta

Spectrophotometric determination of iron with ferrozine by flow-injection analysis

M.I. Pascual-Reguera *, I. Ortega-Carmona, A. Molina-Díaz

Department of Physical and Analytical Chemistry, Faculty of Experimental Sciences, University of Jaén, E-23071 Jaén, Spain

Received 14 August 1996; received in revised form 22 November 1996; accepted 10 February 1997

Abstract

Two methods for the determination of iron by normal FIA and reversed FIA were developed using sodium 3-(2-pyridyl)-5,6-diphenyl-1,2,4-triazine-4′,4″-disulphonate (ferrozine). The reagent formed a chelate with Fe(II) in hexamethylentetramine buffered medium at pH 5.5. In one previous reaction coil Fe(III) was reduced to Fe(II) by ascorbic acid and in the other reaction coil the complexation reaction was developed. The linear range of the determination was 0.5–6 and 0.1–5 μg ml^{-1} of iron for normal FIA and reversed FIA respectively. The proposed method was sensitive (detection limit 0.012 and 0.010 μg ml^{-1}), rapid and reproducible (RSD 0.3 and 0.28%). The method was satisfactorily applied to the determination of iron in waste water, toadstool tissue, potato leaves, human hair and bauxites at a sampling rate of 90 and 50 samples h^{-1} for normal FIA and reversed FIA respectively. © 1997 Elsevier Science B.V.

Keywords: Flow system; Spectrophotometry; Iron; Ferrozine

1. Introduction

The relative importance of iron for man can be assessed when compared with other common elements. So, accordind to Nelson [1], iron is seen to make up 1.5% of, and is the eighth most abundant element in, the lithosphere. A means of measuring the relative importance of different elements in pure chemistry is to compare the relative numbers of compounds they form. Such a comparison showed a few years ago that iron occurred in around 2.3% of all known compounds, the total number listed being around 8.5 millions [2]. The iron is one of the most important element involved in the living process, being indispensable to all members of the plants and animal kingdom.

Flow-injection analysis (FIA) is a well accepted analytical technique owing to its versatility, flexibility, ease of operation and high sample throughput [3].

The measurement of the absorbance of the complex formed between iron(II) and some typical chromogenic reagents is one of the methods most frequently used for the determination of iron in many kinds of samples. Before total iron can be determined, either oxidation of iron(II) to iron(III) or reduction of iron(III) to iron(II) is required [4–9].

* Corresponding author.

PII S00 9-9140(97)00050-7

This paper describes the development of two flow injection systems (normal and reversed) for the determination of total iron based on the use of ferrozine (sodium 3-(2-pyridyl)-5,6-diphenyl-1,2,4-triazine-4′,4″-disulphonate)(Fz), as a chelating agent for iron (II) after reduction of Fe(III) with ascorbic acid. Fz is a very sensitive and selective reagent for iron(II) giving a 1:3 (Fe:Fz) magenta chelate with a sharp absorption peak at 562 nm and a molar absorptivity of 27 900 l. mol^{-1} cm^{-1} [10]. This is an important advantage with respect to the popular method based on the iron(II)-1,10-phenantroline complex. Nevertheless, Fz is a more expensive reagent. For this reason, as is usual in FIA techniques when the reagent constitutes the major cost of the determination, a second method based on reversed FIA [11] (where the reagents are injected into a continuous stream of the sample) is also proposed in this paper besides normal FIA method. Reversed FIA mode increases the sensitivity in many applications providing a lower range of concentrations to be reached [3]. This is a very important feature in trace analysis when the volume of sample is not a limiting factor. The reverse FIA mode is here adequate, compensating the drawback of the higher consumption of sample volume.

2. Experimental

2.1. Reagents

All reagents were of analytical-reagent grade and bidistilled water was used throughout.

Standard iron(III) solution. Prepared by dissolving 0.0860 g of iron(III) ammonium sulphate (Panreac R.A.) in 0.1 M sulphuric acid, which was standardized by EDTA titration, to give 100 mg l^{-1} stock solution of iron(III). The stock solution was diluted to an appropriate concentration as required after adding 0.05 M sulphuric acid.

Sodium 3-(2-pyridyl)-5,6-diphenyl-1,2,4-triazine-4′,4″-disulphonate (ferrozine, Fz) (Fluka, R.A.). Solutions of various concentrations were prepared by dissolving Fz in water. These solutions were stored under refrigeration. In these conditions they went stable for at least 30 days.

Buffer solutions (pH 5.5.) were made by dissolving 4 g of hexamethylentetramine (HMTA) and 2 ml of hydrochloride acid 1 M in 200 ml of water.

Ascorbic acid solution 1%.

2.2. Apparatus

Ultraviolet and visible spectra and real-time data acquisition of flow injection peaks were obtained using a Lambda 2-UV-VIS Spectrophotometer (Perkin Elmer). The instrument was interfaced to an IBM PS/2 mod. 30-286 running Perkin-Elmer computerized spectroscopy software (PECSS V 4.1). The flow cell used (Hellma 178.011-OS) had a 80-μl internal volume and a 10-mm light pathlength. The pump used was a GILSON MINIPULLS three peristaltic pump. The pH measurements were made with a Crison Model 2002 pH-meter fitted with a glass-saturated calomel electrode assembly and a temperature probe.

2.3. Manifolds

The two manifolds used are shown in Fig. 1.

2.4. Treatment of samples

2.4.1. Water

Waste water was filtered through a 0.45-μm membrane filter (Millipore) and collected in a polyethylene container carefully cleaned with nitric acid. The sample was stored at 4°C until analysis. Analyses were performed with the least possible delay. The usual general precautions were taken to avoid contamination.

2.4.2. Toadstood tissue (Amanita muscaria)

Firstly all foreign matter, especially adhering soil, was removed from the sample by means of successive washings with distilled water, 0.1 M HCl and doubly distilled water (we avoided an excessive washing in order to prevent leaching). The sample was rapidly dried into a forced draft oven for 24 h at 70°C prevent decomposition or weight loss by respiration and ground in a hand-mill. A suitable quantity was weighed

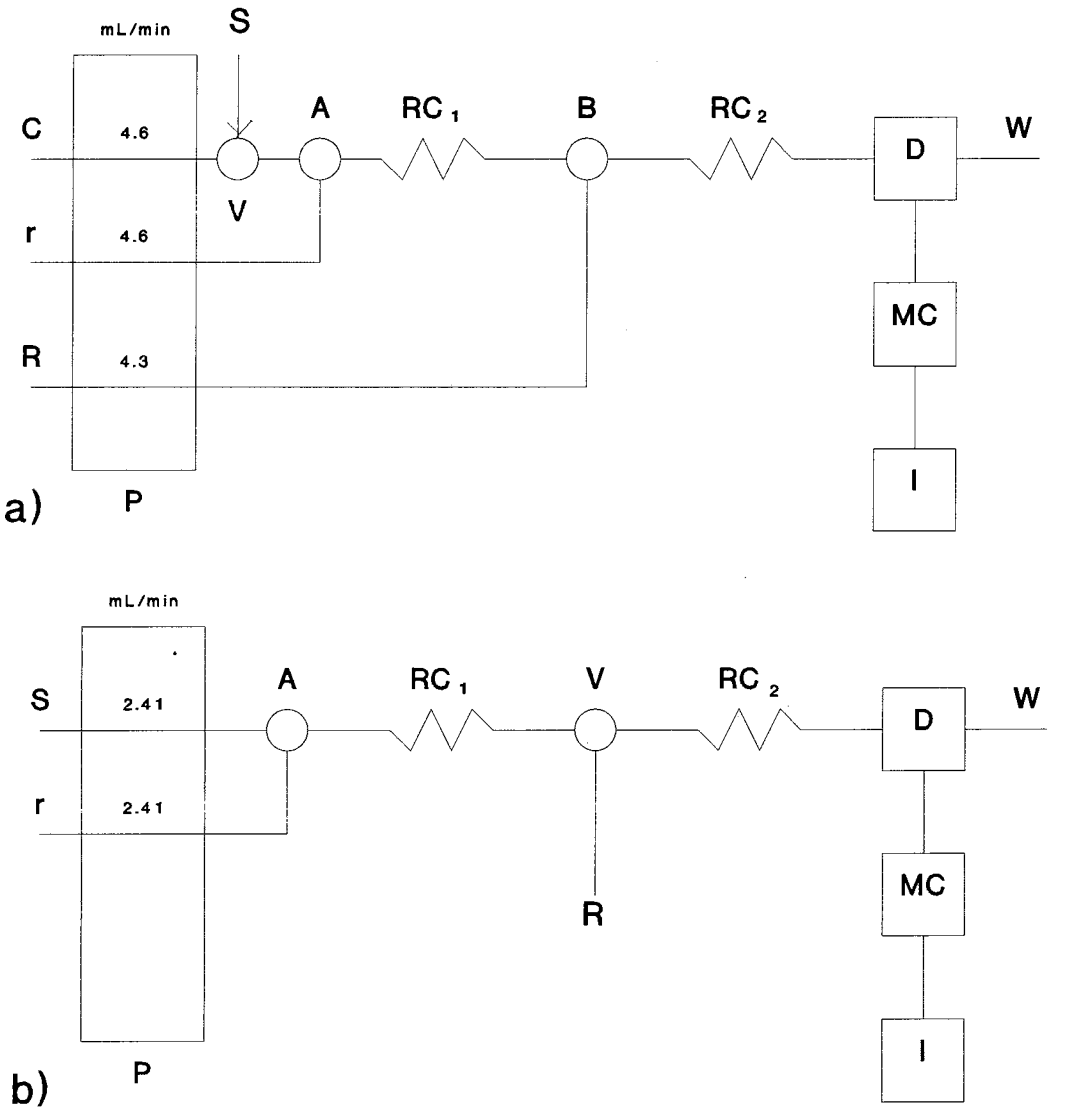

Fig. 1. Manifold configuration. (a) Normal FIA; (b) reversed FIA; S, sample; C, carrier solution (water); r, reducing agent solution (ascorbic acid 1%); R, buffered solution (pH = 5.5) of Fz (10^{-2} M); P, pump; V, 4-way rotary injection valve equipped with teflon tube loops of 600 μl (a) and 30 μl (b); A and B, confluence points; RC_1 reaction coil (0.8 mm i.d; 100 cm long); RC_2 reaction coil (0.8 mm i.d; 150 cm long); W, waste; D, detector equipped with flow cell; MC, microcomputer; I, impresor.

(1.0370 g dry material) into a quartz crucible and placed in a cool furnace; the mineralization was carried out as described by Pinta [12], heating slowly to 450°C for 2 h and holding at this temperature for 2 h. further. The sample was removed, cooled, the ashes were carefully wet with a fine stream doubly distilled water, and then 1 ml of 3 M HCl was added. The crucible was covered with a watch glass, cautiously heated on a hot plate until boiling point and finally let to stand for a few minutes. The solution was filtered through Whatman No. 42 paper over a 100-ml volumetric and diluted to volume. The iron content was determined on an aliquot, as described in the procedure.

2.4.3. Human hair

Firstly, the sample was washed with Mistol detergent and then, oven-dried with forced-draft for 24 h at 60°C. A suitable quantity was weighed (10 g) and treated successively with 30 ml of nitric acid and 3 ml of sulphuric acid until boiling. Finally, 25 ml of hydrogen peroxide were added little by little until the solution was colourless and then evaporated nearly to dryness. The final solution was transferred to a 25-ml volumetric flask, and diluted to volume.

2.4.4. Bauxites

The sample (≈ 0.1 g) was dissolved in a HF–HCl–H_2SO_4 mixture in a teflon crucible in the usual way and the solution obtained transferred to a 100-ml volumetric flask, and diluted to volume.

2.4.5. Potato leaves

The sample was oven-dried with forced-draft for 18 h at 65°C. Then, the sample was ground into fine pieces successively with a glass roller and a hand-mill and overnight dried at 70°C. A suitable quantity was weighed (5 g) into a quartz crucible and burned at 450°C as described above. The solution obtained was quantitatively transferred into a 25-ml volumetric flask.

3. Results and discussion

The iron reacts with Fz forming an only coloured (magenta) chelate compound whose absorption spectra measured against a reagent blank had a maximum absorption at 562 nm, as indicated in the literature [10].

4. Normal FIA

4.1. Flow injection procedure

The manifold of the normal flow injection system used is shown in Fig. 1a. A 3-line system was used for the determination of iron. The sample (600 μl) containing 0.5–6 μg Fe/ml at pH 2, is injected into the carrier (bidistilled water) stream by a 4-way injection valve Reodhyne to which a volume control loop is attached. In the first confluence point, the stream is mixed with the reductor (ascorbic acid) in the 100-cm reaction coil (RC_1). At this point the reduction of Fe(III) to Fe(II) is achieved. The 1×10^{-3} M ferrozine solution buffered at pH 5.5 with HMTA/HCl is pumped at 4.3 ml min^{-1} and mixed in the 150-cm reaction coil (RC_2) where the formation of coloured complex is carried out. The absorbance of the complex in the flow cell is measured at 562 mn. The PTFE tubing is of 0.8 mm i.d.

4.2. Optimization of flow system

4.2.1. Effect of pH on iron complex formation

The dependence on pH of the complex formation with ferrozine was studied in the range pH 1–11 (Fig. 2) using Fe(II) and without using buffer solution. The peak signals were maximum and constant between pH 4 and 8. These results agree with those found by other authors [10,13]. The manifold used was similar to the one described above but suppressing the line of the reducing agent and the raction-coil RC_1. The chosen value of pH was 5.5.

Buffer nature and concentration. Different buffer solutions (KH_2PO_4/NaOH, potassium phthalate/HCl, HOAc/NaOAc and HMTA/HCl) were tested. The latter buffer (pH 5.5) was found to yield the best results. The effect of the concentration of buffer solution was investigated from 0.07 to 0.25 M HMTA and no change in the absorbance values was found. As concentrations below 0.10 M are not recommended because the 'buffering capacity' is low, we propose a solution of 0.14 M HMTA. If we work with Fe(III), a previous step of reduction, which has to be made at low values of pH, is necessary. If the buffer is made to merge after mixing the reagent and the sample, the signal decreases owing to the dilution and dispersion. By buffered reagent merge with the reduced iron, the signal remains. This option was chosen for ulterior experiments.

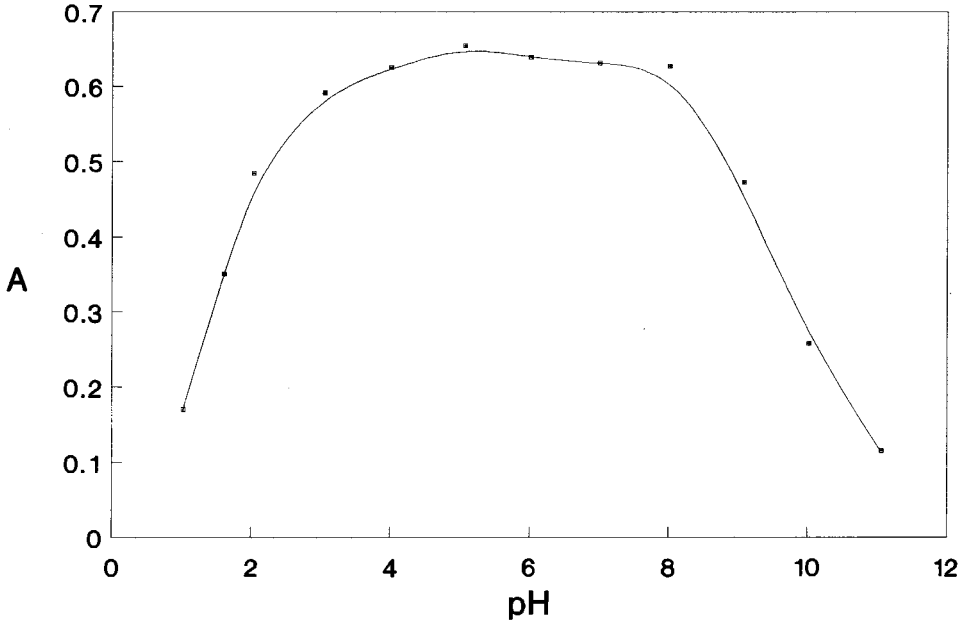

Fig. 2. Effect of pH on the iron complex formation. [Fe(II)] = 8.96×10^{-5} M; [Fz] = 3.60×10^{-4} M.

4.3. Sample volume

The influence of the sample volume on the absorbance was investigated by injecting volumes in the range 100–700 μl of 8.96×10^{-5} M iron standard solutions. A 600-μl volume was selected as optimun because the maximun signal of absorbance reached a constant value from 500 μl.

4.4. Reagent concentration

The influence of Fz concentration was studied in the range 1.0×10^{-4} to 1.0×10^{-2} M being the last selected.

4.5. Effect of reducing agent

For the determination of total iron, a reductant must be used. The effect of the nature of a few reducing agents was examined and the ascorbic acid (1%) was chosen.

4.6. Influence of pH of the sample

The influence of pH sample is shown in Fig. 3. The absorbance decreases drastically from pH 2.5 because the reduction of Fe(III) by ascorbic acid requires high acidity according to other authors [14].

The pH values above four give no detectable signals. A value pH 2 is recommended for the procedure. The decrease of the reducing efficiency of the ascorbic acid (AC) on Fe(III) has two reasons: (i) The reduction is due to the fully protonated form of the AC, that is why the shape of Fig. 3 resembles a titration curve. The dissociation constant of AC is $K_1 = 6.17 \times 10^{-5}$ and (ii) the formation of $Fe(OH)_3$ for pH$>$3 it is also possible by this concentration of Fe(III) in the working solutions, because the solubility of $Fe(OH)_3$ is very low ($K_{sp} = 6 \times 10^{-38}$).

4.7. Effect of the reaction coil lengths

The effect of the length of the reaction coils (RC_1 and RC_2 in Fig. 1) was examined. The results

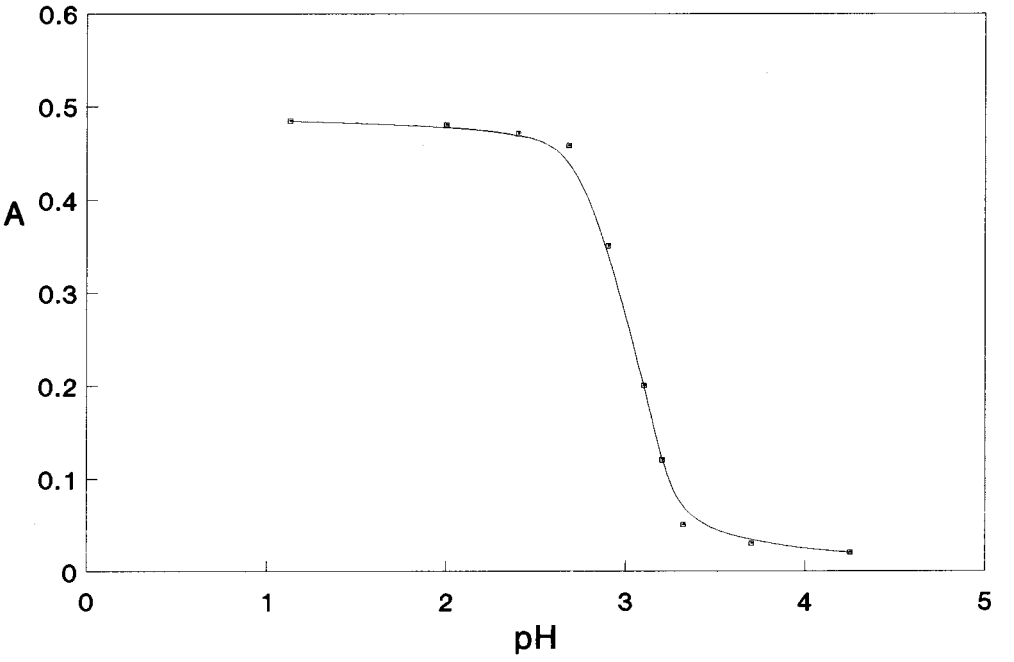

Fig. 3. Effect of sample acidity. [Fe(III)] = 8.96×10^{-5} M; [Fz] = 10^{-2} M; [Ascorbic acid] = 1%.

indicated that both reaction of reduction (RC_1) and formation of coloured chelate compound (RC_2) are fast because the influence of reaction coil lengths are not very significant. If the lenghts of both coils were shortened by 50%, the signal decreases only by 10%. The chosen values were 100 and 150 cm respectively.

4.8. Effect of flow-rate of the solutions

The effect of the flow-rate of the peristaltic pump was examined by varying the range from 2.63 to 5.25 ml min^{-1}. Since the absorbance value is constant from 30 rpm, the optimum value chosen was 4.6 ml min^{-1}.

4.9. Calibration graph

The calibration graph was linear in the range 0.5–6.0 μg ml^{-1} of iron(III). The analytical parameters are summarized in Table 1.

4.10. Interferences

The effect of various ions on the determination of 5 μg ml^{-1} of Fe(III) were investigated using the proposed manifold. The tolerance limit was taken as the amount which caused an error of ± 5% in each peak height. The tolerance limits for the ions studied are shown in Table 2. Of the ions tested, the only major interferences were from EDTA, PO_4^{3-} owing to the reaction with the

Table 1
Analytical parameters for the determination of iron

Parameters	n-FIA	r-FIA
Linear dynamic range (μg ml^{-1})	0.5–6.0	0.1–5.0
Intercept	0.011	0.018
Slope	0.158	0.177
Detection limit ($K = 3$) (μg ml^{-1})	0.012	0.010
Determination limit ($K = 10$) (μg ml^{-1})	0.040	0.033
RSD (%)	0.30	0.28

Table 2
Effect of foreign ions on the determination of 5 μg ml^{-1} of iron

Foreign ion	Tolerance (ng ml^{-1})
SO_4^{2-}, Cl^-, Na^+, NO_3^-, K^+, Zn(II), Mn(II), CO_3^{2-}, HCO_3^-, Ca(II), Mg(II), CN^-	>1000
NO_2^-	1000
Ni(II), F^-, As(III)	500
Al(III), Cr(III)	100
Co(II)	15
Cu(II)	4
PO_4^{3-}	1
EDTA	0.1

sample, and Cu(II) owing to the reaction with the reagent. 0.1 M semicarbazide removes the last interference. The method is very selective.

4.11. Applications

The method was applied successfully to the determination of total iron in waste water, toadstool tissue, potato leaves, human hair and bauxites.

4.12. Potato leaves

Two samples were analysed by the proposed procedure. The standard addition calibration graph method was applied owing to the matrix effect. This fact could be evaluated from the ratio of the slopes of the standard addition calibration graph to that of the standard calibration graphs. The ratios were 0.834 and 0.677 respectively. The results obtained (Table 3) by the proposed method were in good agreement with those obtained by atomic absorption spectrometry (AAS) because there was not significative difference ($P<0.05$) between the average values obtained by both methods (t-Student criterion).

4.13. Human hair, toadstool tissue ('Amanita Muscaria') and bauxites

The bauxites selected were *Bauxite (Dominican)* Ref. 697 and *Bauxite(Arkansas)* Ref. 69b provided by National Bureau of Standard. Since no matrix effect was found, the determination of iron in these samples was performed by applying the standard calibration graph method ($y = 0.011 + 0.158x$). As in the above samples, the results obtained were compared with those found by AAS or with the certified values and equally the concordance was excellent, by using the same criterion as above.

4.14. Waste water

The method was applied to the determination of iron in a waste water from 'Batán' (Jaén city), by standard calibration graph. The result obtained was 0.116 μg ml^{-1}. In order to check the accuracy of the proposed method, a recovery study was carried out. The results shown in Table 3 confirm the validity of the method proposed.

5. Reversed FIA

In this case, the manifold used is shown in Fig. 1(b). Now, the sample is used as carrier and it is reduced by ascorbic acid in reaction coil RC_1. Once this reduction takes place, buffered Fz is directly injected in the manifold, the colour being developed in the reaction coil RC_2. No significant influence on the signal was found when varying the length of RC_1 and RC_2. Therefore, the same length as for the manifold for normal FIA mode (Fig. 1(a)) was used. The flow-rate of the pump gave the highest signal at 2.41 ml min^{-1}. The influence of the concentration of the reagent and the acidity of the sample was also similar to that in normal FIA mode. The optimum sample injection volume was 30 μl.

Calibration graph was linear for the iron range 0.1–5 μg ml^{-1}, which means that reversed FIA allowed determinations over a wider range than normal FIA. Other figures of merit are shown in Table 1. As it is evident from the results the reversed FIA offers a some more high sensitivity and a lower detection limit than normal FIA mode. Nevertheless, the most remarkable advantage of reversed FIA versus normal FIA method is the lower consumption of a very expensive

Table 3
Analytical applications

Sample		Iron content found ($\mu g\ g^{-1}$)	Iron content found by AAS ($\mu g\ g^{-1}$)
Potato leaves[d]	Sample 1	223 ± 15[b]	
		225 ± 15[c]	224 ± 3
	Sample 2	296 ± 11[b]	
		294 ± 12[c]	289 ± 3
Human hair		4.2 ± 0.1[b]	
		4.3 ± 0.1[c]	4.3 ± 0.3
		Iron content found ($mg\ g^{-1}$)	Iron content found by AAS ($mg\ g^{-1}$)
Toadstool tissue (‘*Amanita Muscaria*’)		33.3 ± 0.1[b]	33.8 ± 0.6
		34.0 ± 0.1[c]	
Bauxites	Ref. 697	139 ± 2[b]	140[a]
		141 ± 2[c]	
	Ref. 69b	50 ± 1[b]	50[a]
		51 ± 1[c]	
	Iron added ($\mu g\ ml^{-1}$)	Iron found ($\mu g\ ml^{-1}$)	Recovery (%)
Waste water[e] (Batán)	—	0.166[b]	
	—	0.117[c]	
	0.5	0.61[b]	98.8
		0.60[c]	96.6
	1.0	1.10[b]	98.3
		1.12[c]	100.3
	1.5	1.60[b]	99.4
		1.59[c]	98.2

Data are average of three determinations.
[a] Certified values.
[b] Normal FIA.
[c] Reversed FIA.
[d] Standard addition calibration graph.
[e] Recovery study. Standard calibration graph.

reagent such as Ferrozine. Sampling rate was 50 samples h^{-1}.

5.1. Applications

Reversed FIA mode was also applied satisfactorily to the same samples as it is shown in Table 3.

References

[1] P.G. Nelson, Important Elements, J. Chem. Ed. 68 (1991) 732–737.
[2] J. Silver (Ed.), Chemistry of Iron, Blackie, Glasgow, 1993.
[3] J. Ruzicka and E. Hansen, Flow Injection Analysis, 2nd Edn., Wiley, New York, 1988.
[4] J. Mortatti, F.J. Krug, L.R.C. Pessenda, A.G. Zagatto, S.S. Jorgensen, Analyst 107 (1982) 659.
[5] S.W. Kang, T. Sakai, N. Ohno, F. Ida, Anal. Chim. Acta 261 (1992) 197.
[6] B.P. Bubnis, M.R. Straka, G.E. Pacey, Talanta 30 (1983) 841.
[7] A.T. Faizullah, A. Townshend, Anal. Chim. Acta 167 (1985) 225.
[8] V.V.S. Eswarw Dutt, D. Scheelen, H.A. Mottola, Anal. Acta 94 (1977) 289.
[9] H. Wada, G. Nakagawa, K. Oshita, Anal. Chim. Acta 153 (1983) 199.

[10] L.L. Stookey, Anal. Chem. 42 (1970) 779.
[11] K.S. Johnson, R.L. Petty, Anal. Chem. 54 (1982) 1185.
[12] M. Pinta, 'Méthodes de référence pour la determination des éléments minéraux dans les végétaux. Determination des éléments Ca, Mg, Fe, Mn, Zn et Cu par absorption atomique', C.I.I. 28 (2) (1973) 87.
[13] S.K. Kundra, M. Katyal, R.P. Singh, Anal. Chem. 46 (1974) 1605.
[14] Z. H. Kalowska, Anal. Chim. Acta 123 (1981) 279.

ELSEVIER

Talanta 44 (1997) 1803–1806

Talanta

Application of microemulsions in determination of chromium naphthenate in gasoline by flame atomic absorption spectroscopy

Bin Du [a,*], Qin Wei [a], Shuren Wang [b], Weile Yu [c]

[a] *Department of Applied Chemistry, Shandong Institute of Building Materials, Jinan 250022, People's Republic of China*
[b] *Environmental Science Center, Shandong University, Jinan, People's Republic of China*
[c] *Lanzhou Institute of Chemical Physics, Chinese Academy of Sciences, Lanzhou, People's Republic of China*

Received 4 November 1996; received in revised form 22 January 1997; accepted 23 January 1997

Abstract

A new method using microemulsified samples is presented. It is for the determination of chromium naphthenate in gasoline by flame absorption spectroscopy. The method has the advantage of simplicity, speed and the use of aqueous standards for calibration instead of organic standards. Coexistent elements do not disturb the determination. Results obtained by this method were better than those obtained by other methods for the same samples. © 1997 Elsevier Science B.V.

Keywords: Chromium Naphthenate; Gasoline; Microemulsion; Flame atomic absorption spectroscopy

1. Introduction

In order to apply gasoline to various uses, certain amounts of organometallic additives are often added to gasoline to improve its property. The most commonly encountered additive elements in gasoline are lead, manganese, calcium, magnesium, copper, cobalt, chromium, nickel, and zinc. For examples, alkyl lead compounds and methylcyclopentadienyl manganese tricarbonyl are added to gasoline as anti-knock agents. Chromium naphthenate and cobalt naphthenate are added to gasoline as anti-static agents. The control of the additive concentrations is important in the control of the physical and chemical properties of gasoline. Atomic absorption spectroscopy is a technique of particular utility in the determination of the additive element concentrations in gasoline. It combines the virtues of simplicity, sensitivity and relatively low cost. In recent years the flame is still by far the most popular and convenient atomization source employed in atomic absorption spectroscopy. The flame provides sufficient sensitivity for most organometallic additives' analysis requirements met in the petroleum industry.

The gasoline sample must be prepared for analysis prior to its presentation to the atomic absorp-

* Corresponding author.

PII S00 9-9140(97)00053-2

tion spectrometer. The choice of sample preparation is varied, each method having its own particular advantages and limitations. The conventional methods to prepare gasoline samples are: dry ashing, wet digestion, extraction and dilution with solvent. A major disadvantage of dry ashing is the possible loss of volatile elements or compounds. The wet digestion method and the extraction method involve intricate steps, are time-consuming and prone to causing deviation. The method of dilution with solvent may cause low nebulization efficiency, fuming flame and unstable absorption measurements when the gasoline samples have especially great viscosity and interfacial tension values. In addition, this method is inconvenient because the standards must be prepared with organometallic standard substances that are difficult to purify and prepare. We have solved above problems by adding surfactant, cosurfactant and water into gasoline to form microemulsion systems, then directly introducing the microemulsions into the flame of an atomic absorption spectrometer. This principle has been applied to the determination of ferrocene and cobalt naphthenate in gasoline samples [1,2].

2. Experimental

2.1. Apparatus and reagents

A Model GFU-202 atomic absorption spectrometer made by Beijing Analytical Instrument Factory, equipped with an air–acetylene flame burner and hollow-cathode lamp for chromium were used. All glassware and polythene bottles were acid washed with a solution containing 2.0 mol l^{-1} HNO_3 and 1.5 mol l^{-1} HCl and rinsed with redistilled water (18.0 MΩ cm^{-1}).

Standard chromium stock solutions of 1000 μg ml^{-1} was prepared by dissolving chromic chloride ($CrCl_3$) in redistilled water and diluted to needed concentration when being used.

The reagents including sodium dodecyl sulfate (SDS), sodium dodecyl sulfonate (AS), butanol, *n*-hyptane, octane and nonane were of analytical reagent grade, and water was redistilled.

2.2. Operating parameters for determination

Wavelength: 357.9 nm; lamp current: 2.5 mA; slit width: 0.2 mm; air flow: 7.5 l min^{-1}; acetylene flow: 1.75 l min^{-1}; burner height: 19.0; measurement time: 5 s.

2.3. Procedure

In a 25 ml volumetric flask, 1.00 ml oil to be analyzed was added accurately. Then, 5.4 ml butanol, 1.8 g sodium dodecyl sulfate were added. Finally, water was added to adjust the volume to 25 ml. After being vibrated for 1 min, the microemulsion system of the oil sample was obtained. Absorbance was then measured at selected operating parameters of the apparatus.

2.4. Method for preparing standard solution

In a 25 ml volumetric flask, 1.00 ml *n*-heptane was added accurately; 5.4 ml butanol and 1.8 g sodium dodecyl sulfate were added also. Then standard solution of chromium in needed volume was added, and water was added to adjust the volume to 25 ml. After being vibrated for 1 min, the standard microemulsion system of chromium was obtained.

3. Results and discussions

3.1. Properties of microemulsions

Microemulsions are transparent or translucent, low viscosity and homogeneous stable systems consisting of water, oil, surfactant and cosurfactant, spontaneously formed at appropriate ratio. According to their different compositions, microemulsion systems can be divided into three types: the O/W (oil in water) type, the W/O (water in oil) type and the B.C. (bicontinuous) type. Particle diameters of the disperse phase in microemulsion systems are between 0.01 and 0.1 μm, and the oil–water interfacial tensions are less than 10^{-5} N m^{-1}. Microemulsion systems have great stability, are mixable with oil, water certain concentration ranges. They have strong solubilization power to organic and inorganic substances [3–5].

Table 1
Concentration ranges of water in the microemulsion systems

Systems	Gasoline (ml)	SDS (g)	AS (g)	Butanol (ml)	Water (ml)*
A	0.5	3.3		4.2	10.7–>50
B	1.0	1.8		5.4	7.8–35
C	6.0	2.6		5.4	8.4–19.8
D	8.0	2.2		7.2	6.4–15.2
E	0.5		3.4	4.2	7.3–>50
F	3.0		6.7	8.4	5.5–21.5

*The lower limits are clear points, the upper limits are cloud points.

3.2. Selection of the concentration ranges of water in microemulsion

In the experiments, the amounts of gasoline, SDS, AS and butanol were decided respectively at first. Then water was slowly added into the systems. Volumes of water added into the systems, were recorded respectively at clear points and cloud points. Thus the concentration ranges of water in the microemulsion systems at experimental conditions were decided. The results are given in Table 1.

Different compositions were chosen for the respective determination of the samples according to the concentrations of chromium naphthenate in gasoline to be analyzed. In our previous experiments [1,2], we found that SDS, one of the most typical anionic surfactants, acts not only to enhance absorption but also to suppress interferences. Using the slope of the working curve as a measure of sensitivity, the optimum the concentration ranges of water in the microemulsion systems is system B. In subsequent experiment, the system B was chosen as the concentration ranges of water in microemulsion. No difference of ralative standard deviation (RSD) was observed between the system B microemulsion system and a nonideal microemulsion system.

3.3. Effects of existing forms of chromium in microemulsion systems on absorbance

Experimental results showed that the absorbances of microemulsion systems only had connection with concentrations of chromium, and the existing forms of chromium are not relevant to it. That is to say, both organic standards and inorganic standards were good.

3.4. Effects of coexistent elements on absorbance

In a 25 ml microemulsion system containing chromium of 1.0 μg/ml, 50 μg Ca^{2+}, 50 μg Mg^{2+}, 50 μg Hg^{2+}, 50 μg Pb^{2+}, 50 μg Zn^{2+}, 40 μg Al^{3+}, 40 μg V^{5+}, 30 μg Cu^{2+}, 30 μg Cd^{2+}, 30 μg Mn^{2+}, 30 μg Co^{2+}, 20 μg Fe^{3+} and 20 μg Ni^{2+} were added respectively, and absorbances were obtained according to the method stated above. The results showed that, compared with the microemulsion systems having no coexistent elements, the variations of absorbances were all less than 5.0%. So it could be concluded that the coexistent elements stated above did not disturb the determination of chromium naphthenate in gasoline.

3.5. Effects of variety of alkanes on absorbance

Gasoline is a kind of alkane mixture system mostly consisting of 7–9 carbons. In the experiments, microemulsion systems containing 1.0 μg ml^{-1} of chromium were prepared using *n*-heptane, octane, nonane as oil phases respectively. The results showed that the variations of absorbance were less than 5.0%. So in our experiments, *n*-heptane was chosen as oil phase in place of gasoline to prepare the standard microemulsion systems.

Table 2
Analytical results of gasoline samples and standard addition recovery experiments

Samples	Cr Found (μg/ml)	RSD (%)	Cr added (μg/ml)	Cr Recovered (μg/ml)	Recovery (%)
1	18.71	2.04	10.00	10.24	102.4
2	17.54	2.77	10.00	9.73	97.3
3	17.15	3.41	10.00	9.65	96.5
4	19.67	2.20	10.00	10.39	103.9
5	17.17	1.55	10.00	9.66	96.6

3.6. Working curve

The standard microemulsion systems containing chromium of 1.00, 2.00, 3.00, 4.00 and 5.00 μg ml^{-1} were prepared and their absorbances were determined. The corresponding regression equation and coefficient of correlation were calculated. The results were as follows:

$A = 0.0034 + 0.0571C$ (μg ml^{-1})

$r = 0.9962$

The standard addition curve of gasoline samples was also determined and graphed at the same time, and the two curves have almost the same slope ratio. That also showed that coexistent elements in gasoline samples did not disturb determination.

3.7. Determination of the samples

According to the experimental method stated previously, concentrations of chromium naphthenate in five gasoline samples were determined respectively. At the same time, standard addition recovery experiments were conducted. The results were given in Table 2.

4. Conclusions

When the method is applied to analysis of gasoline, the dry ashing and wet digestion steps to prepare the samples can be avoided. The analytical time is shorten. At the same time, because of the small interfacial tensions of microemulsion systems, the nebulization efficiency of the samples is high, the average diameter of gasoloid particles is small, the combustion of the flame is stable. Another advantage is that in the analytical process there is no need to substitute aqueous standards of chromium for organic standards.

References

[1] Q. Wei, B. Du, Z.H. Du, Fenxi Huaxue 22 (1994) 971.
[2] Q. Wei, B. Du, D.B. Hui, X. Shen, Fenxi Huaxue 22 (1994) 423.
[3] M.J. Schwuger, K. Stickdorn, R. Schmäcker, Chem. Rev. 95 (1995) 849.
[4] Q. Wei, B. Du, X. Shen, D.B. Hui, Fenxi Huaxue 22 (1994)
[5] B. Du, S.R. Wang, Q. Wei, S.J. Xu, Fenxi Huaxue 23 (1995) 662.

ELSEVIER

Talanta 44 (1997) 1807–1813

Talanta

Analysis of 2-ethylhexyl-*p*-methoxycinnamate in sunscreen products by HPLC and Raman spectroscopy

Jingcai Cheng [a], Ying-Sing Li [a,*], Richard L. Roberts [b], George Walker [b]

[a] *Department of Chemistry, The University of Memphis, Memphis, TN 38152, USA*
[b] *Schering-Plough Healthcare Products, Memphis, TN 38151, USA*

Received 25 October 1996; received in revised form 3 February 1997; accepted 3 February 1997

Abstract

The analyses of 2-ethylhexyl-*p*-methoxycinnamate (EHMC) using HPLC and Raman spectroscopy have been undertaken and compared. EHMC, which is one of the most widely used sunscreen agents in suncare products in the US, exhibits a strong Raman signal. This signal clearly appears in both ethanol solutions of EHMC as well as in commercial sunscreen lotions containing this sun screen agent. A method for the direct detection and analysis of EHMC has been developed using Raman spectroscopy. This was accomplished by correlating the Raman intensities with the HPLC assays for a series of prototype suncare formulations. Based upon this information, it would be possible to employ Raman spectroscopy as an in-process control method in the commercial production of suncare products containing EHMC. The possibility of applying surface-enhanced Raman scattering for trace analysis was discussed. © 1997 Elsevier Science B.V.

Keywords: Sunscreen lotion; HPLC; Raman spectra; Surface-enhanced Raman scattering; Fiber optic probe

1. Introduction

Because skin cancer and photoaging appear to be related to excessive sunlight exposure, and the layer of ozone above us (providing protection from UV) is reported as decreasing, sun screen product use is becoming more popular than ever [1]. It is well-known that the most dangerous UV light is UVB (290–320 nm) which has short wavelengths and thus relatively higher energy. It is important to protect human skin from damage which can be caused by UVB. Among the various UVB sunscreen agents approved for use in sun screen products, 2-ethylhexyl-*p*-methoxycinnamate (EHMC) is the one most widely used [2]. It is effective in absorbing UVB, is insoluble in water, has a good safety record and is relatively inexpensive. Being considered as drug products, sunscreen products must be analyzed for their sunscreen content. Consequently, it is important to have a simple, fast analytical method for the product quality control. Like most drug and cosmetic products, EHMC in sunscreen lotions is usually analyzed by HPLC using UV detection [3]. Compared to infrared, ultraviolet, nuclear magnetic resonance and mass spectrometry,

* Corresponding author. Fax: +1 901 6783447.

PII S00 9-9140(97)00054-4

HPLC not only makes the isolation of the many components in sunscreen products possible, but also provides qualitative and quantitative information. While these benefits are significant, the method is also rather time-consuming, fails to supply definite qualitative information from a simple experiment, and can not be used as an on-line detection method.

Like infrared spectroscopy, Raman spectroscopy can provide 'finger prints' for molecules and is useful for quantitative analysis and structural determination. Applying multichannel detection techniques has significantly reduced the Raman data collection time. Additionally, an optical fiber probe can be employed in conjunction with a Raman spectrophotometer to collect Raman spectra of samples in remote sites [4]. These would make it possible to develop an on-line analytical process, which is useful for more rigorous production control of sunscreen products. If surface enhanced Raman scattering (SERS) [5] is applied, a very high sensitivity of detection can be achieved [6].

2. Experiment

2.1. Instrumentation

The Raman spectroscopic system used in the present study has been described previously [7]. An argon ion laser (Lexel Laser, Model Excel 3000) line at 514.5 nm was used with the laser power adjusted to 100 mW at the laser head unless mentioned otherwise. Glass capillary tubes filled with solution samples were positioned by using a Spex 1438 sample holder. The resulting Raman scattering signals were collected with a 6:1 off-axis ellipsoidal mirror. Silica/silica optical fiber (200 μm cone diameter, 230 μm cladding diameter, NA 0.22) was used for sample excitation and Raman signal collection. The excitation fiber and the collection fiber (3M company) were arranged in a 1×6-fiber bundle configuration, and oriented normal to the sample surface. The optical probe was fabricated by Nanjing Institute of Glass Technology, China. An Eppendorf Model 5414 centrifuge was employed in the sample preparation.

HPLC assays used an octadecyl silica (ODS) column which was a 250×4.6-mm Supelcosil LC-18 (5 μm) and kept at ambient temperature during analysis. The guard column was a 20×4.6-mm cartridge column filled with a 5-μm Supelosil packing and was held on a reusable column holder. UV detection was at 308 nm and absorbance unit full scale was at 0.50. The mobile phase was composed of 85% methanol, 14.5% water and 0.5% acetic acid with a constant flow speed of 1.5 ml min^{-1}.

2.2. Chemicals

EHMC, 2-ethylhexyl-2-hydroxybenzoate (EHHB) and 3,3,5-trimethylcyclohexyl-2-hydroxybenzoate (THHB) were provided by Schering-Plough Healthcare Products and used without further treatment. Glacial acetic acid was ACS grade while isopropanol and methanol were HPLC grade. Ethanol was obtained from Aaper Alcohol and Chemical Co. and used as received. Different concentrations of a prototype suncare formulation were provided by Schering-Plough Healthcare Products. Water used throughout this work was deionized with Milli-Q™ Water System and subsequently distilled.

2.3. Procedure

All sunscreen active ingredients used in this study are soluble in ethanol. For Raman measurements, samples of the pure ingredients or their alcohol solutions were directly injected into glass capillary tubes through the open end and these open ends were immediately sealed using Critoseal. Ethanol was also used as a solvent to extract the active ingredient from the sunscreen lotion prior to Raman measurements. After mixing a defined weight of lotion with ethanol, the mixture was mixed ultrasonically at 50–60°C for 30 min, stirred at room temperature for 5 min, and then again ultrasonically treated at 50–60°C for another 30 min. The liquid fraction of the mixture was separated by centrifuging the sample for 30 min. The resulting liquid was then used for Raman However, when an optical fiber probe was used for Raman detection, no extraction and isolation was conducted.

SER experiments were carried out by adsorbing samples onto the surfaces of silver particles or silver films. The SERS-active substrates were prepared following the methods described previously [8,9].

For HPLC analyses, both standard and sample solutions were prepared using isopropanol as the solvent. The stock solution was prepared by dissolving 0.5 g EHMC into 250 ml of isopropanol. The working standard solution was then prepared by diluting 8.0 ml of the stock solution to 100 ml with isopropanol. The sample solution was obtained through 1:10 dilution of the extraction solution.

3. Results and discussion

3.1. Raman spectroscopy of EHMC, EHHB and THHB

Fig. 1 shows the Raman spectra of pure EHMC, EHHB and THHB. For EHMC (Fig. 1A), there are three very strong peaks located at 1176, 1608 and 1640 cm^{-1}. The bands around 3000 cm^{-1} are relatively weak. Raman spectra of EHHB and THHB (Fig. 1B and Fig. 1C, respectively) are distinctly different from that of EHMC. Additionally, the relative intensities of Raman signals of both EHHB and THHB are quite low when compared with the three intense peaks of EHMC (about 1:15).

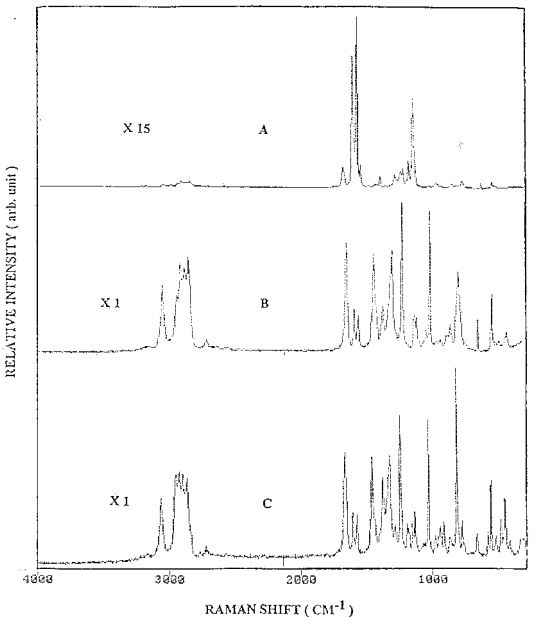

Fig. 1. Raman spectra of pure sun block agents: (A) EHMC; (B) EHHB; (C) THHB. The intensity of spectrum A has been reduced by a factor of 15.

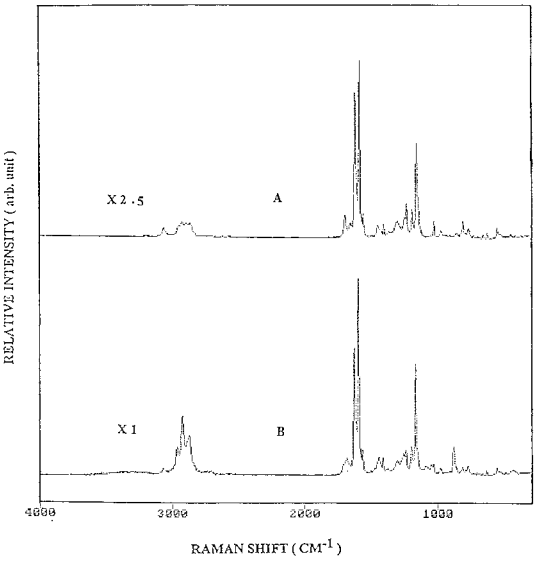

Fig. 2. Raman spectra of two different mixtures of EHMC, EHHB and THHB. Weight rates: (A) EHMC/EHHB/THHB = 1:1:1; (B) EHMC/EHHB/THHB = 7.5:5:8. The intensity of spectrum A has been reduced by a factor of 2.5.

3.2. Raman spectroscopy of mixtures of EHMC, EHHB and THHB

In this study, two different mixtures were prepared and their Raman spectra were recorded. The first one is composed of an equal proportions of each ingredient. The second mixture contained all these ingredients in the appropriate ratios similar to those employed in commercial sunscreen products. Fig. 2 displays the Raman spectra of the mixtures. Due to large Raman cross section of EHMC, the spectra of the mixtures primarily show EHMC features.

3.3. Calibration curve for EHMC

Because of the dominance of the EHMC Raman intensity in common mixtures, quantitative information of EHMC can be obtained from Raman spectroscopy without isolation or other pretreatment. In this study, the 1176-cm^{-1} band of EHMC was chosen for all measurements because of its high intensity, better resolution, and lack of interference from the other nearby bands. In the Raman spectral intensity measurements, two possible sources of deviation are the uneven background near the measured Raman peaks and the optical misalignment. One method to reduce the deviation and to improve the analytical precision is the use of an internal standard. In the Raman spectra of EHMC solutions, there are no overlapping major peaks between ethanol (solvent) and EHMC (see Fig. 3) that may reduce the accuracy of intensity measurements. Fig. 3 also clearly shows that the Raman spectral intensity of

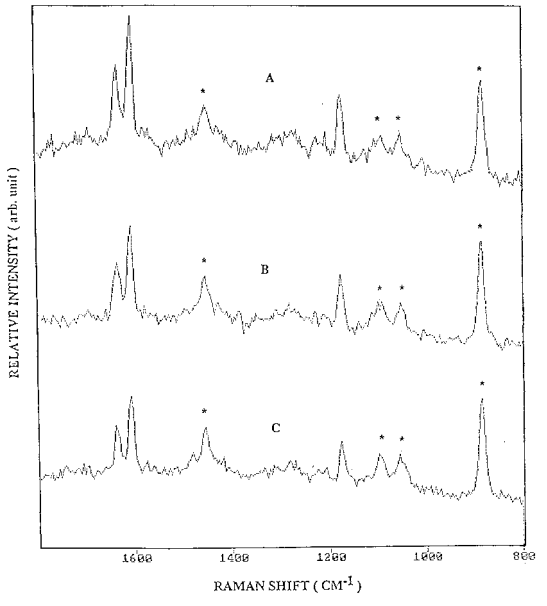

Fig. 3. Raman spectra of sun block lotions solutions obtained for ethanol extractions from different amounts of the lotion: (A) 30%; (B) 25%; (C) 20% by weight. Peaks marked with * are contributed by ethanol; unmarked peaks are due to EHMC. The composition of EHMC in the lotion is 7.5% by weight.

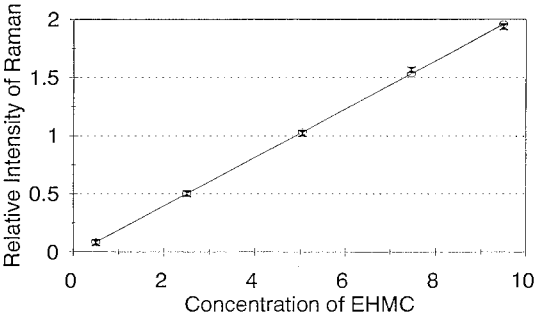

Fig. 4. Calibration curve of EHMC by Raman spectroscopic analysis. Linear regression equation: $Y = 0.2082X - 0.0202$.

EHMC increases with the weight percentage of EHMC in the ethanol extractions from the sunscreen lotion. It appeared that ethanol is a good internal reference because of the absence of overlapping of its 888-cm^{-1} band.

To reduce the effect of the uneven background of the Raman spectra, we measured the base-line at several different wavelengths and used them as background reference points for the intensity measurement of the 888 cm^{-1} band. Similarly, eight measurements of base-line were made as background reference points for correcting the measured intensity of the EHMC band at 1176 cm^{-1}. The final intensity was the average value of these measurements. Fig. 4 shows the calibration curve constructed for EHMC based on the intensity ratio of EHMC and ethanol in the concentration range of 0–10% by weight. This calibration curve demonstrates that a high degree of linearity exists between concentration and relative Raman intensity in the concentration range studied. A linear regression of the intensity data gave:

$$Y = 0.2082X - 0.0202$$

,where X is the concentration of EHMC in % (W/W), and Y is the relative Raman intensity. The correlation coefficient for the linear regression equation is 0.9993.

3.4. Analysis of EHMC in ethanol solution by Raman spectroscopy

Three different methods, Raman detection via capillary method, Raman detection via optical

Table 1
Measured concentrations[a] of EHMC in ethanol solution analyzed by Raman spectroscopy and HPLC methods

Concentration of EHMC	Raman capillary method		Raman optical fiber method		HPLC mean concentration[c]
	Mean value[b]	S.D.	Mean value[b]	S.D.	
1.25	1.14	0.048	1.35	0.168	1.20
2.51	2.56	0.043	2.44	0.094	2.27
3.17	3.23	0.067	3.16	0.112	2.94
5.05	5.02	0.107	5.07	0.545	4.89
6.20	6.25	0.292	6.27	0.427	5.90
7.46	7.59	0.052	7.27	0.315	6.90
8.85	8.71	0.363	9.17	0.459	8.60

[a] All concentrations are expressed as % (W/W).
[b] Each given value obtained by Raman spectroscopic method is an average of three measurements.
[c] HPLC concentrations are obtained from duplicate measurements.

fiber probe method, and HPLC, were used. In the capillary method, Raman scattering measurement was conducted for the sample filled into a capillary tube. In the fiber optical method, the optical fiber probe was either inserted into the sample solution or placed close to the solution/air or the solution/glass interface.

In the Raman spectroscopic analysis of sunscreen samples, the same conditions as those used in establishing the EHMC calibration curve were used. Seven different concentrations of solutions were prepared by mixing the weighed amounts of EHMC and ethanol. The concentrations of these samples were determined by measuring the relative Raman intensity of the solution along with the use of the calibration curve. For each sample, the spectral intensity measurement was repeated in triplicate with the use of an internal standard. The mean concentrations along with the standard deviations are listed in Table 1. No significant differences between the results obtained from these two Raman optical configurations are noticeable. The Raman signal-to-noise ratio obtained with the capillary method was better than that obtained by the fiber optical method. For this reason, the results obtained from the capillary method have smaller standard deviations than those obtained with the fiber optic probe.

3.5. Analysis of EHMC in ethanol solutions by HPLC

Also listed in Table 1 are the measured concentrations of EHMC using HPLC method. In each case, the listed concentration is an average of two HPLC measurements. It is seen from Table 1 that the accuracy of the results obtained by HPLC for the low concentration sample is better than that from the Raman spectroscopy methods. This probably arises from the low Raman spectral intensity resulting from the low concentration of sunscreen agent present in these sample solutions. However, there are no obvious differences among these three methods at higher concentrations.

3.6. Analysis of EHMC in sunscreen lotion

In the Raman spectroscopic analysis, only the capillary method was used to determine the concentration of EHMC in sunscreen lotion from the measured spectral intensity. In the experiments, each datum point was determined in triplicate. Listed in Table 2 are the measured concentration obtained by Raman spectroscopic method and by HPLC method. For the same reason given above, the experimental results obtained the low concentration of EHMC are more accurately determined by HPLC than by Raman spectroscopy.

Table 2
Measured concentrations[a] of EHMC in sunscreen lotion extracted with ethanol by Raman spectroscopy with capillary and HPLC methods

Concentration of EHMC	Raman capillary spectroscopy method		HPLC mean conc.[c]
	Mean conc.[b]	S.D.	
2.50	2.62	0.016	2.52
5.00	4.86	0.041	5.04
7.50	7.32	0.028	7.36
10.00	9.27	0.056	9.35

[a] All concentrations are expressed as % (W/W).
[b] Each measured value by Raman spectroscopic method is an average of three measurements.
[c] HPLC concentrations are obtained from duplicate measurements.

3.7. Summary and prospects in the future development of Raman spectroscopy analysis

Results obtained from the present study idicate that the quantitative analysis of EHMC in commercial sunscreen products can be achieved using Raman spectroscopy. It has also demonstrated the possibility of measuring the Raman spectrum of EHMC in sunscreen lotion using an optical fiber probe. These results, combined with those of recent studies on the fiber optical pathway configuration, and its Raman signal background [10–12] show that the technique may be developed into a useful method as an in-process monitoring in the commercial preparation of suncare product.

Experimental data reveal that the normal Raman intensity of EHMC is one order of magnitude more intense than those of EHHB and THHB. This make it feasible to detect EHMC than to detect EHHB and THHB in mixtures by Raman spectroscopy. The intense EHMC bands can interfere and overshadow the weak Raman spectra of EHHB and THHB. One potential method to lower the Raman spectroscopic detection limit of EHMC and to detect EHHB and THHB in mixtures is to measure the SER spectra by using different silver sols and silver plates as SERS-active substrates [13]. A basic requirement for developing a Raman spectroscopic method for the trace analysis of the active ingredients of suncare products is to make these components SERS-active.

In the present study, attempts to obtain the SER spectrum for any of the sunscreen ingredients in the water-based silver substrates failed which is probably due to the hydrophobic character of esters. Earlier studies [8,14–16] have demonstrated that the surface Raman enhancement of organic acids are active because the carboxylate group can easily be adsorbed onto the surfaces of silver particles. For this reason, we carried out a hydrolysis for EHMC under an alkaline condition and collected the SER spectrum of the hydrolysis products adsorbed in hydrogen peroxide silver sols [8]. Fig. 5 shows the SER spectrum of 1.0×10^{-4} M EHMC hydrolysis solution along with the SER spectrum of *p*-methoxycinnamic acid in ethanol. *p*-Methoxycinnamic acid is expected to be a hydrolysis product of EHMC. A comparison of these two spectra in Fig. 5A and Fig. 5B indicates that *p*-methoxycinnamic acid is the major contributor to the SER spectrum of the hydrolysis solution. No normal Raman spectrum could be detected for the same hydrolysis solution (see Fig. 5C)—an indication of the high sensitivity of SERS detection. The present SER experiment has increased the spectral intensity of EHMC by at least a factor of 1000. Expectively, the sensitivity of the Raman spectroscopic analysis for EHMC can be improved by the same factor.

Acknowledgements

The authors are grateful to Dr J. Ma for his assistance with the fiber optic experiments. This

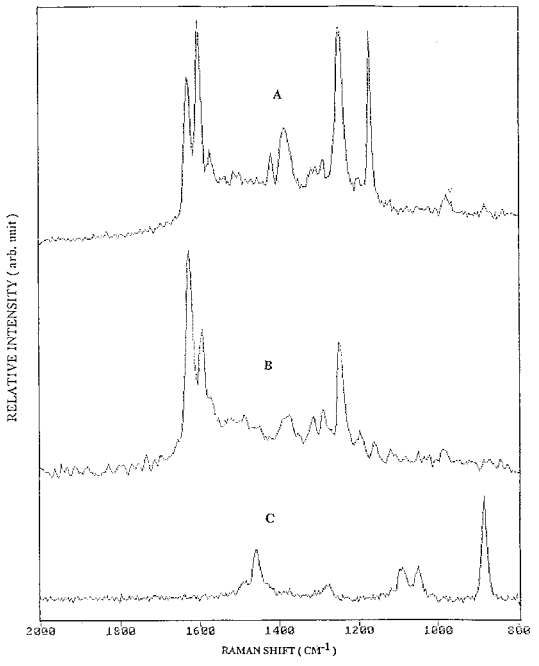

Fig. 5. (A) SER spectrum of the hydrolysis product solution of 1.0×10^{-4} M EHMC in ethanol; (B) SER spectrum of 1.0×10^{-4} M *p*-methoxycinnamic acid in ethanol/water (1:1) mixture; (C) normal Raman spectrum of the hydrolysis solutions of 10^{-4} M EHMC in ethanol, all the observed peaks are contributed by ethanol.

work was supported in part by the University of Memphis Faculty Research Grants.

References

[1] N.J. Lowe, Physician's Guide to Sunscreens, Marcel Dekker, New York, 1991.
[2] K. Klein, Cosmetics and Toiletries 107 (1992) 45.
[3] J. Meijer, M. Loden, J. Liq. Chrom. 18 (1995) 1821.
[4] R.L. McCreery, M. Fleischmann, P. Hendra, Anal. Chem. 55 (1983) 146.
[5] R.K. Chang and T.E. Furtak, Surface Enhanced Raman Sacttering, Plenum, New York, 1982.
[6] K. Kneipp, Y. Wang, R.R. Dasari, M.S. Feld, Appl. Spectrosc. 49 (1995) 780.
[7] Y.S. Li, A.S. Lee, Y. Wang, J. Raman Spectrosc. 22 (1991) 191.
[8] J. Cheng and Y.S. Li, XVth Int. Conf. Raman Spectrosc., Pittsburgh, PA, 1996, p. 644.
[9] Y.S. Li, Y. Wang, Appl. Spectrosc. 46 (1992) 142.
[10] J. Ma, Y.S. Li, Appl. Spectrosc. 48 (1994) 1529.
[11] J. Ma and Y.S. Li, XVth Int. Conf. Raman Spectrosc., Pittsburgh, PA, 1996, p. 1222.
[12] J. Ma, Y.S. Li, Appl. Opt. 35 (1996) 2527.
[13] J. Cheng, J. Ma, K. Wang and Y.S. Li, 109th AOAC Internat. Meeting and Expo, Nashville, TN, Sept. 1995.
[14] H. Seki, J. Ele. Spectrosc. Rel. Phenom. 39 (1986) 289.
[15] Y.S. Li, A.S. Lee, Spectrosc. 3 (1992) 115.
[16] A.S. Lee, Y.S. Li, Spectrochim. Acta 52A (1996) 173.

ELSEVIER

Talanta 44 (1997) 1815–1822

Talanta

Chemometric alternatives for resolution of classical analytical problems
Spectrophotometric determination of lanthanide mixtures

Patricio Peralta-Zamora *, Lorena Cornejo-Ponce, Noemi Nagata, Ronei J. Poppi

Universidade Estadual de Campinas, Instituto de Química, C.P. 6154, 13083-970, Campinas-SP, Brazil

Received 13 August 1996; received in revised form 12 November 1996; accepted 4 February 1997

Abstract

The simultaneous determination of lanthanide family elements is one of the greatest problems in analytical chemistry, due to the close similarity of their chemical properties. Spectrophotometric methods are generally of limited use, due to the various mutual spectral interferences involved. By using multivariate calibration methods (partial least-squares regression, PLSR), it was possible to obtain a model that adjusts itself perfectly to the values of the mixture concentrations used in the calibration. The model used absorption spectra in the 290–800 nm range for a set of 20 different mixtures of Ce, Pr, Nd and Sm, and made possible the determination of Ce, Pr and Nd concentrations of a commercial rare-earth product, with significantly greater precision than the conventional univariate calibration method. Determination of the Sm concentrations was not possible, since its concentration was below the concentrations used in the model definition. © 1997 Elsevier Science B.V.

Keywords: Lanthanides; Spectrophotometric determination; Multivariate calibration

1. Introduction

The technological and industrial development of the last decades has promoted a pronounced increase in the demand for elements from the rare-earth family. Due to their various and interesting applications, they are required in many different fields, such as in the glass and ceramic industries, metallurgy, nuclear chemistry, electronics, etc. [1,2]. This large demand has promoted the development of many studies intending to find new methods for the quantification of these species, which is extremely difficult due to the close similarity of their chemical properties [1,2], making it difficult to use conventional analytical methods [3,4].

Analytical methodologies that are relatively specific and sensitive are found only within the group of modern instrumental techniques, among which are plasma atomic emission spectroscopy [5], fluorescence spectroscopy in the optical and X-ray regions [6,7], radiochemical [8,9] and chromatographic techniques [10], etc. Classical and universally used techniques such as atomic ab-

* Corresponding author.

PII S00 9-9140(97)00055-6

sorption and emission flame spectroscopy are of very limited use since the elements under study characteristically present a tendency to form refractory oxides and to ionisation, which implies complex absorption spectra [11,12]. The unavailability of selective chromogenic reactants means that spectrophotometric techniques are only useful for the determination of the total quantity of the elements of this family. The selectivity is restricted, in the best cases, to the determination of a single element, from a mixture with two or three components [13–16].

Banks and Kingman in 1956 [17], and Stewart and Kato in 1958 [18], presented their results of exhaustive studies intended to verify the feasibility of determining mixtures of rare-earths through spectrophotometry. These works showed the great complexity of the absorption spectra from a mixture of this kind, presented calculations of interference factors that allow to correct some of the various spectral interferences, and finally, proposed a procedure that would allow the determination of mixtures of rare-earth elements. As described, these methodologies are of little use for analytical determination, due to factors such as:

The use of interference correction factors will work correctly only when it is possible to estimate previously the concentration of the interfering component. The determination of different species in the presence of a large number of congeners is practically impossible, due to the various interferences.

This methodology allows for the determination of mixtures with two or three components, all of them with concentration of the same order of magnitude, typically 10–100 g l^{-1}.

The determination involves various precipitation, dissolution and transference operations, which makes the process lengthy, tedious and subjected to many possible error sources.

In this work the possibility of implementing an analytical methodology for mixtures of rare-earth elements (cerium, praseodymium, neodymium and samarium) is investigated, applying the spectrophotometric technique proposed by Banks and Klingman [17], and Stewart and Kato [18], but with the use of multivariate calibration techniques (partial least-squares regression, PLSR). The utilisation of this statistical method to the resolution of chemically related problems was initiated by Wold and colaborators in the early 1980s [19]. After this, the number of works using this method has increased significantly, mostly in working out data for spectral, spectrographic and electrochemical analyses [20].

2. Experimental

2.1. Reactants and standard solutions

The cerium standard solution was prepared from $CeCl_3$. $7H_2O$ (98.5%, Merck), the praseodymium standard solution from Pr_2O_3 (99.5%, Koch-Light), the neodymium standard solution from a $Nd_2(CO_3)_3$ (reactant supplied by the brazilian Federal Fiscal Service, without purity specifications) and the standard solution of samarium from Sm_2O_3 (99.9%, Aldrich). All these solutions were prepared by direct dissolution of the reactants in 2.0 mol l^{-1} $HClO_4$ (assisted by heating in a water bath), and complexometrically standardised by the use of EDTA and xylenol orange [21].

2.2. Working sample

The sample utilised is commercially distributed by NUCLEMON (Nuclebrás de Monazita e Associados Ltd., Brazil) as 'rare-earth chloride', corresponding to a concentrate obtained by chemical treatment of 'Brazilian monazite'. The monazite is submitted to various physical and chemical processes for the separation of thorium, uranium, lead and other radioactive species. The resulting rare-earth chloride is then concentrated and packed as a final product, containing approximately 250 g of rare-earth oxides per liter of solution. The distribution of rare-earth elements in this product is presented in Table 1. The solution for analysis was obtained by precipitation of the hydroxides with an aqueous solution of NH_3 from a volume of 100 mL of the sample, with later dissolution in 100 ml of 2.0 mol l^{-1} $HClO_4$.

2.3. Instruments

Spectrophotometric measurements were made with a Hitachi spectrophotometer, model U-2000, using 1 cm quartz cells. Standard solution volumes were taken in a Metrohm microburette, using 0.5000 ml taps.

2.4. Analytical procedure

Known amounts of the standard solutions or working sample were placed in a 5-mL volumetric flask and completed to the final volume with 2.0 mol l^{-1} $HClO_4$. The final concentration of these solutions varied between 1.0 and 4.0 g l^{-1} of cerium, and 2.0 and 8.0 g l^{-1} of praseodymium, neodymium and samarium. The absorption spectra were taken in the 290–800 nm range.

2.5. Experimental design

The Calibration of the methodology under study was made with the conventional univariate method and a PLSR [19], using the recorded adsorbance values between 290 and 800 nm as the dependent variables, with intervals of 2 nm. The experimental planning used for the multivariate calibration of the method is presented in Table 2. The mathematical program MATLAB 4.0 was used for the absorbance data processing. The PLSR was performed by using the PLS-toolbox 1.5 [22], based on NIPALS algorithm.

Table 1
Composition of the working sample (rare-earth chloride)

Element	Concentration (gL^{-1})
Ce	96.68
La	46.90
Pr	11.38
Nd	39.65
Sm	5.40
Gd	3.25
Y	2.55
Dy	1.53
Eu	0.085
Other rare-earths	1.00
Total rare-earths	208.43
Total oxides	250.00

Data provide by NUCLEMON.

Table 2
Experimental design for multivariate calibration

Sample	Concentration (g l^{-1})			
	Cerium	Neodymium	Praseodymiun	Samarium
1	4.07	2.00	0.80	0.40
2	4.07	4.00	1.60	0.80
3	4.07	6.01	2.40	0.40
4	4.07	2.00	2.40	0.80
5	4.07	4.00	1.60	0.40
6	4.07	6.01	0.80	0.80
7	4.07	2.00	2.40	0.40
8	4.07	4.00	2.40	0.80
9	4.07	6.01	0.80	0.40
10	4.07	4.00	0.80	0.80
11	6.10	6.01	1.60	0.40
12	6.10	6.01	0.80	0.80
13	6.10	4.00	0.80	0.40
14	6.10	4.00	1.60	0.80
15	6.10	4.00	2.40	0.40
16	6.10	2.00	0.80	0.80
17	6.10	2.00	1.60	0.40
18	6.10	2.00	2.40	0.80
19	6.10	4.00	1.60	0.40
20	6.10	2.00	1.60	0.80

3. Results and discussion

3.1. Conventional calibration

The complexity of the spectra presented in Figs. 1 and 2 points to the difficulties that can been found in a determination of this kind, particularly due to the various spectral interferences that can be observed. Each of the studied elements, however, presents at least one absorption peak that is subjected to less interference and that can be used for analytical purposes. By the criterion of the lowest possible interference, the following spectral lines were chosen for the analysis:

Cerium: 295 nm; Neodymium: 793 nm; Praseodymi um: 442 nm; Samarium: 401 nm

Using these absorption lines and pure standard solutions, conventional calibration curves were made, whose equations and correlation indexes are presented in Table 3. By using these calibration curves, of excellent linearity, individual deter-

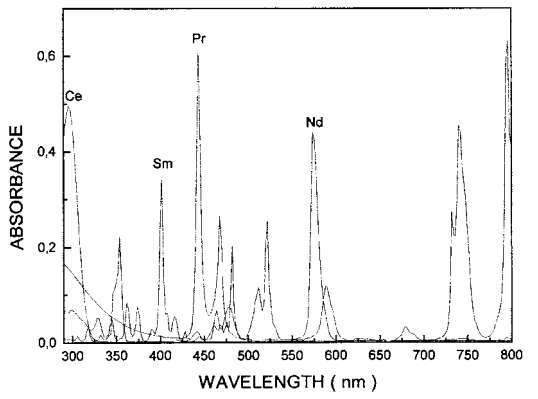

Fig. 1. UV-VIS spectrum of the lanthanides. Ce = 5.0 g l^{-1}; Nd = 10.0 g l^{-1}; Pr = 10.0 g l^{-1}; Sm = 20.0 g l^{-1}.

minations were performed for each of the species of interest, to which different quantities of the other elements were added. The results, presented in Table 4, confirm different degrees of interference in the determination of neodymium, cerium and samarium; this interference becomes more significant for increasing concentrations of the interfering elements, and becomes critical for cerium and samarium. In the case of praseodymium the interference is of little significance, not causing large errors in this case. These same curves were used for the determination of the elements of interest in the problem sample. Since this is a rare-earth concentrate, with larger concentrations cerium and neodymium and much smaller concentrations of praseodymium and samarium, different dilutions of the solution were analysed in such a way that the concentration of each of the monitored species would reach, is at least one of these solutions, the concentration range established for the calibration. The results obtained, as presented in Table 5, are useful to illustrate the difficulties of this determination. Even though the determination of synthetic mixtures indicated discrete interferences, the determination of the sample becomes much more difficult due to the diversity of species involved and the large differences in concentrations found. The percentile difference between the real and obtained values (20–40%) invalidates the determination of Pr, Sm and Ce by this classical univariate method.

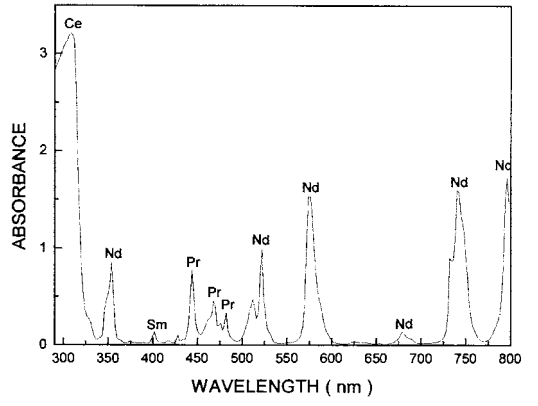

Fig. 2. UV-VIS spectrum of the working sample.

3.2. Multivariate calibration

By utilising the PLSR, and following the experimental design described in Table 2, a model for calibration was obtained that allowed determination of concentration of the components present in the calibration mixtures.To determine the optimal number of principal components to be used in the model, a full cross validation procedure can be used. In this procedure, the calibration is repeated N times, where N is the number of samples in calibration, each time treating one calibration sample as prediction object. At length all the calibration objects have been treated as prediction objects and the estimated prediction residual error sum of squares (PRESS) are used for determining the number of principal components necessary to establish the better model. Since full cross validation is based on repeated calibrations which may be some time-consuming for the computer, an important alternative is to perform cross validation by only splitting the calibration set into M ($M < N$) segments. In our case, the model was rebuilt and tested ten times, with 14 samples to build the model and six samples to validate it, in each time. The result of this cross validation procedure is presented in Fig. 3. Ideally, the predictive capacity of a model can only be assessed by testing on new objects. However, in many cases cross validation give sensible results with

Table 3
Conventional univariate calibration

Element	Detected[a] peaks (nm)	Molar absortivity (ϵ, 1 mol^{-1} cm^{-1})	ϵ[b]	Equation of the calibration curve	Correlation index (r)
Nd	354	2.88	5.20		
	521	3.60	4.41		
	575	6.35	6.93		
	740	6.71	7.20		
	793	***9.12***	***11.78***	$A = 5.965\times 10^{-5}C + 0.020$	***0.9999***
	867	3.36	3.10		
Pr	***445***	***7.75***	***10.49***	$A = 4.780\times 10^{-5}C + 0.012$	***0.9990***
	466	2.60	—		
	480	2.32	4.10		
	590	1.76	1.95		
Sm	***401***	***2.01***	***3.31***	$A = 1.400\times 10^{-5} + 0.008$	***0.9900***
Ce	***295***	***10.28***	***26.00***	$A = 9{,}770x10^{-5}C + 0.018$	***0.9999***

[a] Analytical peaks.
[b] Reported by Banks and Klingman [17], and Stewart and Kato [18].

high information about the predicting ability of the model [19]. From Fig. 3 it is possible to verify that after the sixth principal component no significant improvement in PRESS is obtained. Then was chosen 6 principal components to perform the calculations.

By working out the model in terms of these six principal components, and by the elaboration of a graphic of the residuals as function of the leverage (relative position of the observations of the independent variables) as shown in Fig. 4, it was possible to verify the presence of two anomalous samples (outliers).In this figure, it was drawn the relative position of the observations for all 4 analytes being determined simultaneously (appearing four times the same number for each sample). The large value of the leverage (a criterion used for anomalous sample detection) of the standard solutions 14 and 17 in the calibration stage shows that both are outliers. Therefore, these standard solutions were removed from the calibration stage, and the PLSR methodology was applied again. As this system is more robust than other analogous statistical tools [19], it was seen that the parameters from the previously obtained model did not change very much due to the removal of the two samples from the calibration.

The concentrations predicted by the model are very close to the real concentrations, as shown in Table 6 (mean percentile difference around 2–3%), which indicates the validity of the calibration set. Using the linear PLSR model developed here, different dilutions of the problem sample were analysed, with the results presented in Table 7.It was performed determinations directly on the working sample without dilution, and determinations after dilution of 1.7, 2.5, 5 and 10 times. It is possible to verify from Table 7 that the determinations for neodymium and praseodymium could be carried out even without any dilution. The results for diluted sample or not were very similar. This ability for extrapolation outside of the concentration calibration range is very important, since samples with large difference in concentrations of neodymium and praseodymium can be analysed. For cerium it was necessary a dilution of ten times to be possible its determination.

It can be observed from this set of results that the neodymium determination is perfectly feasible, as it was by conventional calibration, since the interferences are of little significance. For praseodymium and cerium the multivariate calibration model allows the reduction of the error by approximately 100%, making the determination of these elements also feasible. For samarium, on the other the determination was not possible, since its concentration was below the values used in the model definition.

Table 4
Determination of synthetic mixtures of lanthanides using conventional univariate calibration

Element (λ, nm)	Real concentration (g l^{-1})	Interferents (Conc., g l^{-1})	Found concentration (g l^{-1})	Error (%)
Nd (793)	4.00	Sm,Pr (2.0),Ce(1.0)	4.42	+10.6
	4.00	Sm,Pr (4.0),Ce(2.0)	4.56	+14.0
	8.00	Sm,Pr (2.0),Ce(1.0)	8.94	+11.7
	8.00	Sm,Pr (4.0),Ce(2.0)	8.43	+5.4
Pr (442)	4.00	Sm,Nd(2.0),Ce(1.0)	3.93	−1.7
	4.00	Sm,Nd(4.0),Ce(2.0)	4.33	+8.3
	8.00	Sm,Nd(2.0),Ce(1.0)	8.01	+0.2
	8.00	Sm,Nd(4.0),Ce(2.0)	8.03	+0.4
Sm (401)	4.00	Pr,Nd(2.0),Ce(1.0)	5.01	+25.2
	4.00	Pr,Nd(4.0),Ce(2.0)	6.32	+58.0
	8.00	Pr,Nd(2.0),Ce(1.0)	10.5	+31.2
	8.00	Pr,Nd(4.0),Ce(2.0)	14.8	+85.0
Ce (295)	2.00	Pr,Nd,Sm(2.0)	2.71	+35.6
	2.00	Pr,Nd,Sm(4.0)	3.47	+73.5
	4.00	Pr,Nd,Sm(2.0)	5.01	+25.1
	4.00	Pr,Nd,Sm(4.0)	5.49	+37.2

The error of about 10% on the praseodymium and cerium determination can be explain in terms of interferences by other species present in the working sample. On the other hand, the presence of impurities in various standard which contain significant amounts of each other is also a limiting factor for the analytical performance of the methodology. Neodymium oxide from Fluka, for example, contains about 0.1% of Pr_6O_{11} and Sm_2O_3, while praseodymium oxide contains 0.1% of CeO_2 and Nd_2O_3. Nevertheless, the reduction of the error in relation to determination by univariate ways is very significant, and demonstrate that the multivariate method is a powerful tool for difficult determinations like this.

The results obtained for neodymium and praseodymium in the working sample using univariate and multivariate methods (Tables 5 and 7)

Table 5
Lanthanide determination on the working sample using conventional univariate calibration

Element	Certified[a] conc. (g l^{-1})	Found concentration[b] (gL^{-1})					Average (error, %)[c]
		D0	D3	D5	D7	D9	
Nd RSD (%)	39.65	—	40.34	40.91	39.43	40.44	40.28
		—	2.1	1.6	1.9	2.3	(+1.6)
Pr RSD (%)	11.38	—	13.87	13.39	13.45	13.24	13.49
		—	3.2	2.6	2.8	3.0	(+18.4)
Sm RSD (%)	5.40	8.31	8.99	8.65	7.97	7.97	8.38
		5.1	4.5	4.2	3.2	3.5	(+55.2)
Ce RSD (%)	96.68	—	—	116.4	114.4	117.4	116.1
		—	—	1.3	1.7	1.2	(+20.1)

D0 corresponds to a determination carried out directly on the working sample.
D3, D5, D7 and D9, correspond to determinations carried out on dilutions of 3.0, 5.0, 7.0 and 9.0 times.
[a] Concentration provide by NUCLEMON.
[b] Mean of two
[c] Error relative to the certified concentration.

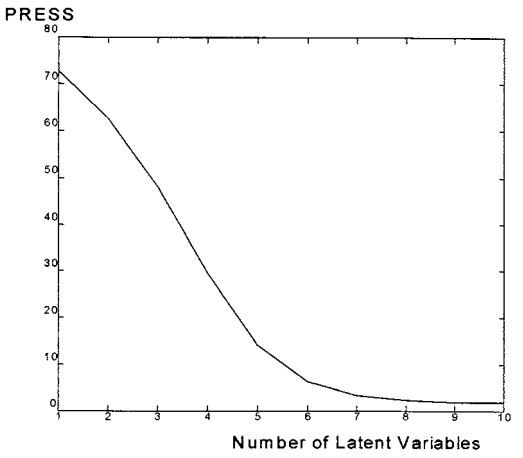

Fig. 3. Cumulative PRESS as a function of number of latent variables.

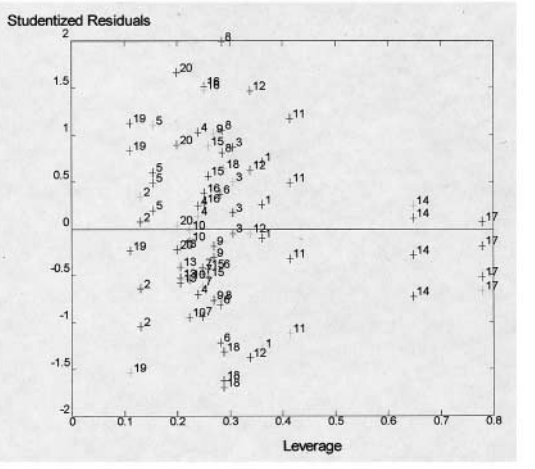

Fig. 4. Studentized residuals as a function of leverage.

can be statistically compared using Students' *t*-test. A significant difference between the average results for praseodymium, and no difference for neodymium, were found using a significance level of 5%. This results denote, one more time, the superior ability of the multivariate method in the praseodymium determination.

Table 6
Concentration obtained for the calibration mixtures by the PLS-linear model

Sample	Found concentration (g l^{-1}) (error, %)			
	Cerium	Neodimium	Praseodimium	Samarium
1	3.98 (−2.2)	1.97 (−1.5)	0.80 (0.0)	0.46 (+15)
2	3.99 (−1.9)	4.05 (+1.2)	1.63 (+1.9)	0.78 (−2.5)
3	3.99 (−1.9)	6.00 (−0.2)	2.37 (−1.2)	0.38 (−5.0)
4	4.05 (−0.5)	1.99 (−0.5)	2.36 (−1.7)	0.79 (−1.2)
5	3.95 (−2.9)	3.98 (−0.5)	1.59 (−0.6)	0.34 (−15)
6	3.97 (−2.4)	6.04 (+0.5)	0.85 (+6.2)	0.82 (+2.5)
7	4.07 (0.0)	2.02 (+1.0)	2.42 (+0.8)	0.43 (+7.5)
8	3.93 (−3.4)	3.91 (−2.2)	2.37 (−1.2)	0.84 (+5.0)
9	4.05 (−0.5)	6.01 (0.0)	0.81 (+1.2)	0.35 (−12)
10	4.04 (−0.7)	4.05 (+1.2)	0.81 (+1.2)	0.80 (0.0)
11	5.93 (−2.8)	5.98 (−0.5)	1.61 (+0.6)	0.45 (+12)
12	6.09 (−0.2)	5.97 (−0.7)	0.74 (−7.5)	0.80 (0.0)
13	6.04 (−1.0)	4.02 (+0.5)	0.82 (+2.5)	0.41 (+2.5)
14	6.01 (−1.5)	4.00 (0.0)	1.62 (+1.2)	0.79 (−1.2)
15	6.03 (−1.1)	4.02 (+0.5)	2.38 (−0.8)	0.36 (−10)
16	5.97 (−2.1)	1.99 (−0.5)	0.74 (−7.5)	0.73 (−8.8)
17	6.01 (−1.5)	2.01 (+0.5)	1.60 (0.0)	0.42 (+5.0)
18	6.09 (−0.2)	2.08 (+4.0)	2.46 (+2.5)	0.77 (−3.8)
19	5.91 (−3.1)	3.96 (−1.0)	1.61 (+0.6)	0.48 (+20)
20	5.88 (−3.6)	1.96 (−2.0)	1.61 (+0.6)	0.80 (0.0)

Table 7
Lanthanide determination on the working sample by multivariate calibration (PLS-linear)

Element	Certified[a] conc. (g l^{-1})	Found concentration[b] (g l^{-1})					Average (error, %)[c]
		D0	D1	D2	D3	D4	
Nd RSD (%)	39.65	39.19	39.79	40.87	41.06	39.67	40.12
		2.0	1.9	2.3	1.8	2.2	(+1.2)
Pr RSD (%)	11.38	10.66	10.00	9.66	9.87	11.16	10.27
		4.2	3.7	4.1	4.0	3.3	(−9.7)
Sm RSD (%)	5.40	ND	ND	ND	ND	ND	—
		—	—	—	—	—	—
Ce RSD (%)	96.68	[d]	[d]	[d]	[d]	88.50	88.50
		—	—	—	—	1.2	(−8.5)

D0 corresponds to determinations carried out directly on the working sample.
D1, D2, D3 and D4, correspond to determinations carried out on dilutions of 1.7, 2.5, 5.0 and 10.0 times.
ND = Concentration below the limits of the model.
[a] Concentration provide by NUCLEMON.
[b] Mean of two determinations.
[c] Error relative to the certified concentration.
[d] Absorbance above the limits of the model.

4. Conclusions

The spectrophotometric determination of Ce, Pr, Nd and Sm present many inconveniences, arising from the complexity of their absorption spectra. Using a conventional calibration and monitoring just the wavelengths of maximum absorption, the obtained results carry significant errors, arising from the multiple interferences mentioned above. By using a multivariate calibration, that allows to establish a calibration model through the use of the whole absorption spectrum, the results obtained have much smaller errors, basically because the monitoring of various wavelengths makes the contribution of the interference signals to significantly smaller.

References

[1] T. Moeller, The Chemistry of the Lanthanides, Pergamon Texts in Inorganic Chemistry 26 (1976) 1.
[2] Z. L Barbieri, Anais do VI Simpósio Anual da ACIESP 1 (1982) 110.
[3] V.A. Fassel, R.H. Curry, R.N. Kniseley, Spectrochim. Acta 18 (1962) 1127.
[4] R.C. Vickery, Analytica Chemistry of the Rare Earths, Pergamon Press, Oxford, 1961.
[5] L.H.J. Lajunen, G.R. Choppin, Rev. Anal. Chem. 9 (1989) 3.
[6] J. Gao, J. He, X. Wane, Z. Wane, E. Bai, Analyst 112 (1987) 1081.
[7] R.H. Heidel, V.A. Fassel, Anal. Chem. 30 (1958) 176.
[8] W.M. Jackson, G.I. Gleason, P.J. Hammons, Anal. Chem. 42 (1970) 1243.
[9] W.M. Jackson, G.I. Gleason, Anal. Chem. 45 (1973) 2125.
[10] K. Robards, S. Clarke, E. Patsalides, Analyst 113 (1988) 1757.
[11] A.P. D'Silva, R.N. Kniseley, V.A. Fassel, R.H. Curry, R.B. Myers, Anal. Chem. 36 (1964) 532.
[12] V.A. Fassel, R.H. Curry, R.N. Kniseley, Spectrochim. Acta 18 (1962) 1127.
[13] S. Bhattacharya, S. Lyle, R. Maghzian, R. Talanta 27 (1980) 59.
[14] S.J. Lyle, N.A. Zatar, Anal. Chim. Acta. 135 (1982) 327.
[15] N.S. Poluektov, M.A.J. Sandu, J. Anal. Chem. USSR 25 (1970) 1302.
[16] P.K. Spitsyn, V.S.J. Shvarev, J. Anal. Chem. USSR 25 (1970) 1297.
[17] C.V. Banks, D.W. Klisgman, Anal. Chim. Acta 15 (1956) 356.
[18] D.C. Stewart, D. Kato, Anal. Chem. 30 (1958) 164.
[19] H. Martens and T. Naes, Multivariate Calibration, Wiley, Chichester, 1993.
[20] F. Salinas, A. Espinosa-Mansilla, P.L. Lopez de Alba, Anal. Lett. 28 (1995) 193.
[21] S.J. Lyle, M. Rahman, Talanta 10 (1963) 1177.
[22] B.M. Wise and Gallagher, PLS – Toolbox for use with Matlab, version 1.5.1, 1995.

ELSEVIER

Talanta 44 (1997) 1823–1831

Talanta

Diagnosis of lung cancer based on metal contents in serum and hair using multivariate statistical methods

Yulin Ren [a], Zhuoyong Zhang [b,*], Yuqiu Ren [c], Wei Li [a], Mengcai Wang [d], Gang Xu [d]

[a] *Department of Chemistry, Jilin University, Changchun 130022, People's Republic of China*
[b] *Department of Chemistry, Northeast Normal University, Changchun 130024, People's Republic of China*
[c] *Baicheng Medical School, Baicheng 137000, People's Republic of China*
[d] *Norman Bethune University of Medical Sciences, Changchun 130021, People's Republic of China*

Received 10 October 1996; received in revised form 6 February 1997; accepted 12 February 1997

Abstract

The classification of normal and cancer groups with four multivariate methods according to metal contents in serum and hair samples has been discussed in the present paper. Results show that the four multivariate methods, stepwise discrimination analysis, principal components analysis, hierarchical cluster analysis, and stepwise cluster analysis can distinguish the two groups correctly. The independent samples of both normal and cancer groups were tested and can be distinguished correctly by the four methods. Therefore, these methods can be used as an aid for diagnosis of lung cancer according to the metal contents in serum and hair samples. © 1997 Elsevier Science B.V.

Keywords: Cancer; Classification; Hair; Inductively coupled plasma atomic emission spectrometry; Multivariate analysis; Serum

1. Introduction

With the development of industry, our bodies as well as our environment have been polluted by numerous pollutants which have been proved as a cause of cancer. The relationship between trace metal contents and cancer has attracted many researchers for some years. The reason is of two-fold. First, some trace elements are nutrients for human health. These elements play an important role in the biochemical process of human body. On the other hand, these elements must be kept below certain levels, otherwise, they become toxic. The correlation between metal contents in human body and cancer has been proved to be existent. Some researchers declared that the metal contents of copper in serum can be used to diagnose liver cancer [1,2], ovary cancer [3] and alimentary channel cancer [4]. The contents of zinc and copper in serum have been used to diagnose liver cancer and lung cancer [5–7]. The contents of manganese, copper, zinc, arsenic, nickel, chromium, cadmium, and iron, etc., in serum and blood have been used to diagnose lung cancer and gastric cancer [8–10].

* Corresponding author. Fax: +86 431 5684009.

PII S00 9-9140(97)00062-3

In recent years, metal contents in human body have been used as an aid for diagnosing various diseases including cancer in clinical medication. Wang et al. [11,12] have used chemometric methods to diagnose cancer patients according to metal contents obtained by inductively coupled plasma atomic emission spectrometry (ICP-AES). Even though the biochemical mechanism of these elements for the cause of cancer in human body is not very clear in the present stage, more research work has to be done to get a better understanding of the relationship and more clinical investigations should be given to make the correlation more useful and more reliable.

In the present paper, the metal contents in serum and hair samples obtained by inductively coupled plasma atomic emission spectrometry (ICP-AES) have been used for the classification of normal people and cancer patients. Four multivariate statistical methods, stepwise discrimination analysis, principal components analysis, hierarchical clustering, and stepwise clustering, were used for the classification. Independent prediction samples were tested and they were distinguished correctly by the four methods.

2. Experimental

2.1. Apparatus

A multichannel inductively coupled plasma atomic emission spectrometer (Mark-II type of Jarrell-Ash 800 series, manufactured by Fisher Scientific, Jarrell-Ash Division) was used for the present study. The operating conditions are given in Table 1.

Table 1
Operation conditions for the ICP spectrometer

Forward power	1.15 kW
Observation height	18 mm ALC
Plasma argon gas	17 l min^{-1}
Auxiliary argon gas	1.0 l min^{-1}
Carrier argon gas	0.5 l min^{-1}
Sample uptake rate	3.0 ml min^{-1}

An 80 486 personal computer was used for multivariate statistical computation. The program package for the multivariate analysis written with Quick BASIC was developed in the laboratory. The fundamentals and algorithms are not given here because they can be found elsewhere, for example, in [13,14].

2.2. Standards and reagents

The standard stock solutions of the elements studied in this work were prepared from high purity metals or oxides. High purity nitric acid, perchloric acid and distilled water were used for the sample digestion and the blank.

2.3. Sampling

Two groups of samples were used for the study, one for controlled (normal) group and the other for cancer group. The samples (serum and hair) of controlled group were taken from healthy persons. The samples of cancer group were taken from lung cancer patients in the clinical hospitals of Norman Bethune University of Medical Sciences, Changchun, People's Republic of China. The cancer patients were not committed by any radioactive or chemical treatment. The distributions of ages and sex were similar in the two groups.

2.4. Procedure

2.4.1. Serum

The blood samples of controlled and cancer groups were sampled from healthy people and lung cancer patients, respectively, between 5 and 8 am and were centrifugalized for 30 min by a $3500 \times g$ centrifugal machine. The serum were kept at -20°C for storage. The serum sample was digested with $HNO_3 - HClO_4$ (5.0:0.5 ml) mixture at the temperature of 120°C and then diluted to proper volume for determination.

2.4.2. Hair

The hair samples taken between 1–10 mm from root were washed by detergent first and then by distilled water until they were ensured being clean.

Table 2
Basic statistics for measurement of serum samples (μg ml^{-1})

Variable	Element	Normal group (n = 39)		Cancer group (n = 36)	
		Mean	S.D.	Mean	S.D.
x_1	Fe	1.988	0.913	2.168	0.938
x_2	Ca	93.78	6.851	75.62	11.14
x_3	Mg	24.58	2.655	20.16	3.77
x_4	Cu	0.929	0.232	1.392	0.278
x_5	Cr	0.111	0.164	1.706	1.326
x_6	P	116.1	32.76	103.7	17.60
x_7	Zn	0.033	0.014	0.029	0.012
x_8	Sr	0.762	0.253	0.753	0.209

The hair sample was digested with HNO_3-HClO_4 (5.0:0.5 ml) at the temperature of 120°C after pre-digestion with concentrated HNO_3 for over night.

3. Results and discussion

3.1. Basic statistics

The serum and hair samples of normal and cancer groups were analyzed by inductively coupled plasma atomic emission spectrometry (ICP-AES). The basic statistics for serum and hair samples are given in Table 2 and Table 3, respectively. For the serum, 39 samples for normal group and 36 samples for cancer group were used and eight elements were analyzed. For the hair, 21 samples were used for both normal and cancer groups and 19 elements were analyzed. It can be seen from the Table 2 and Table 3 that some significant differences of elemental concentrations exist between normal and cancer groups for both serum and hair samples. For example, the contents of aluminum are significantly different between the normal and cancer groups. It seems that the content of aluminum can be used as a simple criterion to discriminate the normal and cancer groups. However, to use this only one element may be dangerous for a diagnosis. In the results reported by Zhu et al. [12] for human hair samples, there was not a significant difference of aluminum content between normal and cancer groups, while the difference of zinc content between the two groups is quite big (266.7 μg g^{-1} for normal people and 179.7 μg g^{-1} for cancer patient). This means that except for the difference of metal contents from region to region, there may be some interactions between elements. To find out the relationship between cancer and elemental concentrations is not an easy task because the cancer is related with overall elemental concentrations rather than one by one, and there are also close relations between elements (variables). For this reason, conventional univariate approach for correlating the cancer and an elemental concentration failed to reach this goal. Multivariate statistical method is a good choice because it takes the overall elemental concentration and the interaction between elements into account to establish the relationship.

3.2. Stepwise discrimination

The stepwise discrimination analysis is a linear discrimination method based on F-test for the significance of the variables. In each step one variable will be selected on the basis of its significance. Nine samples were taken from the normal and cancer group, respectively, in a random manner, which were used as prediction set. Therefore, 57 samples, of which 30 are in normal group and 27 in cancer one, were used to get the discrimination functions. Five significant variables (elements) were extracted from the eight variables investigated after five steps for serum: x_2 (Ca),

Table 3
Basic statistics for measurement of hair samples (μg ml^{-1})

Variable	Element	Normal group ($n=21$)		Cancer group ($n=21$)	
		Mean	S.D.	Mean	S.D.
x_1	Al	12.82	4.104	1.879	2.405
x_2	Fe	16.18	4.619	23.10	13.55
x_3	Ca	1215	822.2	969.3	944.7
x_4	Mg	141.8	107.9	77.33	93.22
x_5	B	1.896	0.953	0.277	0.386
x_6	Ba	156.9	114.8	96.78	117.9
x_7	Cd	0.245	0.501	0.051	0.048
x_8	Co	0.057	0.047	0.033	0.036
x_9	Cu	11.54	1.237	9.827	1.526
x_{10}	Cr	0.814	0.401	—[a]	
x_{11}	La	0.728	0.372	0.369	0.381
x_{12}	Mn	1.130	1.714	2.523	1.898
x_{13}	Mo	0.132	0.075	0.158	0.221
x_{14}	Ni	0.454	0.907	0.117	0.168
x_{15}	P	203.1	44.16	176.8	38.91
x_{16}	Pb	4.476	7.295	2.364	2.302
x_{17}	Sr	4.894	3.889	3.037	2.663
x_{18}	Y	—[a]		0.010	0.033
x_{19}	Zn	171.1	41.16	151.38	37.16

[a] Not detected.

x_4 (Cu), x_5 (Cr.), x_6 (P), and x_7 (Zn). The discrimination function is given below and the discrimination and prediction results are given in Table 4.

$$y_1 = -72.24 + 1.36x_2 + 3.57x_4 + 0.59x_5 + 0.084x_6 + 67.34x_7$$

$$y_2 = -58.69 + 1.08x_2 + 16.03x_4 + 3.86x_5 + 0.053x_6 - 44.97x_7$$

For the classification and prediction using hair samples, five samples in each group were utilized for prediction. Samples, 32, of which 16 in normal and cancer groups, respectively, were used to obtain the discrimination functions. In a similar way, five significant variables (elements) were obtained from the initial 19 elements for hair samples after five iterations: x_1 (Al), x_5 (B), x_{10} (Cr), x_{15} (P), and x_{17} (Sr). The discrimination function is given below and the results are given in Table 5.

$$y_1 = -48.86 + 1.66x_1 + 8.25x_5 + 15.43x_{10} + 0.19x_{15} + 1.80x_{17}$$

$$y_2 = -12.47 + 0.58x_1 + 1.98x_5 + 2.29x_{10} + 0.12x_{15} - 0.88x_{17}$$

From the scores given in Table 4 and Table 5 for serum and hair samples, respectively, it can be seen that the classification can be made by comparing Y_1 and Y_2 values: regarding as normal when $Y_1 > Y_2$; regarding as cancer when $Y_1 < Y_2$. Table 4 and Table 5 also show that all the independent prediction samples are distinguished correctly for both serum and hair samples using the discrimination functions. This means that this criterion is valid for the prediction of normal and cancer groups based on the elemental contents in serum and hair samples.

3.3. Principal components analysis (PCA)

Principal components analysis (PCA) is a projection method that reduces the dimensionality in a data matrix retaining most significant information. PCA has been used for processing the trace elemental contents to extract principal

Table 4
Discrimination results for serum sqamples

No.	Score		Judge[a]	No.	Score		Judge[a]
	Y1	Y2			Y1	Y2	
1	79.54	63.18	n	40	50.22	60.27	c
2	62.57	52.42	n	41	38.40	46.84	c
3	90.68	68.74	n	42	15.79	29.83	c
4	66.72	61.27	n	43	52.08	63.01	c
5	82.26	72.53	n	44	28.07	37.51	c
6	72.23	66.37	n	45	46.27	54.41	c
7	62.89	55.74	n	46	31.58	39.99	c
8	70.48	63.99	n	47	59.42	67.86	c
9	69.04	62.69	n	48	34.35	49.81	c
10	61.91	56.84	n	49	56.36	63.58	c
11	65.59	58.08	n	50	67.63	81.95	c
12	70.82	61.21	n	51	65.45	78.44	c
13	81.43	71.70	n	52	45.56	55.16	c
14	70.80	62.76	n	53	40.86	50.40	c
15	91.59	75.99	n	54	63.83	67.55	c
16	77.47	71.98	n	55	57.85	61.17	c
17	64.98	60.22	n	56	87.49	96.56	c
18	85.30	74.48	n	57	45.63	48.72	c
19	84.91	80.49	n	58	56.65	60.74	c
20	67.52	60.50	n	59	52.94	62.03	c
21	58.53	57.12	n	60	54.15	58.75	c
22	81.72	73.98	n	61	54.68	56.85	c
23	59.52	55.85	n	62	60.05	65.70	c
24	81.13	72.07	n	63	43.32	56.07	c
25	73.44	64.21	n	64	56.21	62.18	c
26	59.34	51.92	n	65	55.90	59.17	c
27	62.71	55.80	n	66	46.45	50.14	c
28	79.85	70.23	n	67	24.16	44.56	c[b]
29	58.70	56.94	n	68	59.07	72.16	c[b]
30	73.57	66.24	n	69	32.71	45.02	c[b]
31	59.81	52.88	n[b]	70	79.13	86.14	c[b]
32	71.76	63.02	n[b]	71	37.26	45.27	c[b]
33	69.42	63.94	n[b]	72	37.47	46.38	c[b]
34	59.92	52.18	n[b]	73	19.57	31.74	c[b]
35	66.40	59.47	n[b]	74	12.81	25.07	c[b]
36	72.72	61.97	n[b]	75	37.84	49.56	c[b]
37	75.02	67.10	n[b]				
38	76.23	69.55	n[b]				
39	46.18	40.86	n[b]				

[a] 'n' refers to normal group and 'c' refers to cancer group.
[b] Prediction sample.

components (significant variables) and to establish the classification of cancer patients and normal persons. Unlike the stepwise discrimination method discussed in the previous section, the PCA is an unsupervised classification method. For serum, eight variables (elements) are reduced to two new variables. These are vectors PC1 and PC2 (first and second principal components). The new variables are also referred to as Factor 1 and Factor 2. According to the loading values of the stated components, it can be deduced that the variables (elements) x_2 (Ca), x_3 (Mg), x_4 (Cu),

Table 5
Discrimination results for hair samples

No.	Score		Judge[a]	No.	Score		Judge[a]
	Y1	Y2			Y1	Y2	
1	52.21	31.01	n	22	−7.83	9.30	c
2	40.84	27.16	n	23	−7.99	10.20	c
3	49.95	30.33	n	24	−10.29	9.47	c
4	61.11	31.30	n	25	−18.03	6.49	c
5	58.23	33.25	n	26	−9.15	13.27	c
6	64.48	34.57	n	27	−3.99	13.76	c
7	30.87	23.12	n	28	−19.61	5.50	c
8	31.26	15.27	n	29	−15.02	8.10	c
9	45.87	29.06	n	30	12.58	19.24	c
10	64.18	35.88	n	31	−9.40	12.35	c
11	59.37	34.12	n	32	−7.18	14.55	c
12	44.65	27.68	n	33	−5.11	14.26	c
13	43.20	32.74	n	34	−8.51	11.38	c
14	35.77	25.47	n	35	−7.03	12.96	c
15	50.78	38.57	n	36	5.73	18.21	c
16	49.06	30.41	n	37	8.44	20.49	c
17	48.98	20.45	n[b]	38	−3.20	9.57	c[b]
18	32.42	20.86	n[b]	39	0.08	10.57	c[b]
19	27.66	20.22	n[b]	40	−4.14	12.43	c[b]
20	39.60	24.85	n[b]	41	−5.82	10.99	c[b]
21	61.98	30.78	n[b]	42	9.33	18.21	c[b]

[a] 'n' refers to normal croup and 'c' refers to cancer group.
[b] Prediction sample.

x_5 (Cr), x_6 (P), x_7 (Zn), and x_8 (Sr) are the most significant factors in the classification. To display the points in two principal components dimensions, the first two principal components are chosen to represent the information. Firstly, 57 samples, the same as the training set used in the stepwise discrimination in last section, were processed by PCA and were presented in a two-dimensional graph. Then the 18 samples used as prediction set in the discussion of stepwise discrimination were added to the training set, and then all the samples were analyzed by PCA. The localization of 75 samples (39 for normal group and 36 for cancer group), according to their score values, on the plane defined by the new variables Factor 1 and Factor 2 are shown in Fig. 1. By comparing the two-dimensional presentation graphs of before and after adding the 18 prediction samples, it was found that the localization of the training set slightly changed and all the prediction samples fell into the right groups, respectively.

In a similar way, the 16 hair samples used as training set in the stepwise discrimination were analyzed by PCA first, then all the hair samples including training and prediction sets were processed by the method. The PCA reduces the initial 19 variables (elements) to two new variables. The localization of 42 samples (21 for normal and cancer groups, respectively) on the plane of Factor 1 and Factor 2 are shown in Fig. 2.

Most serum samples for normal people and cancer patients shown in Fig. 1 can be distinguished by a line, except for one for each group, resulting in the correct answers of over 97%. For the samples the normal and cancer groups can be clearly distinguished by a straight line (see Fig. 2).

3.4. Clustering analysis

Hierarchical clustering analysis (HCA) provides a visual means of estimating relationships among multidimensional points. Euclidean distance has been used to represent the similarity between samples. HCA is also an unsupervised recognition method and no a prior knowledge is needed. Prediction samples can be added to the samples with known classifications (working as training set) and then be analyzed by HCA. The classification of prediction samples can be distinguished from dendrograms or distances. The clustering diagram for serum and hair are given in Fig. 3 and Fig. 4, respectively. It can be seen that all the samples including training and prediction samples for both serum and hair have been correctly classified into normal and cancer groups.

Stepwise clustering analysis (SCA) is a dynamic clustering method. This method has also been used for the classification of normal and cancer groups for variables (elements) of serum and hair samples. The Euclidean distances from the centroids of two classes have been calculated for all

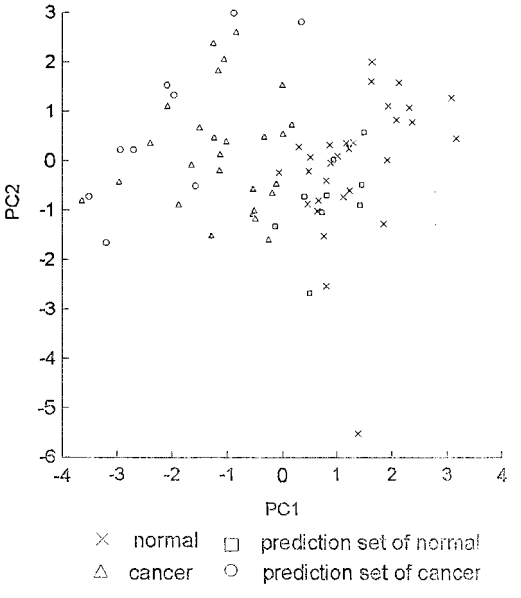

Fig. 1. Localization of 39 samples of group and 36 samples of cancer group for serum on the plane defined by two principal components.

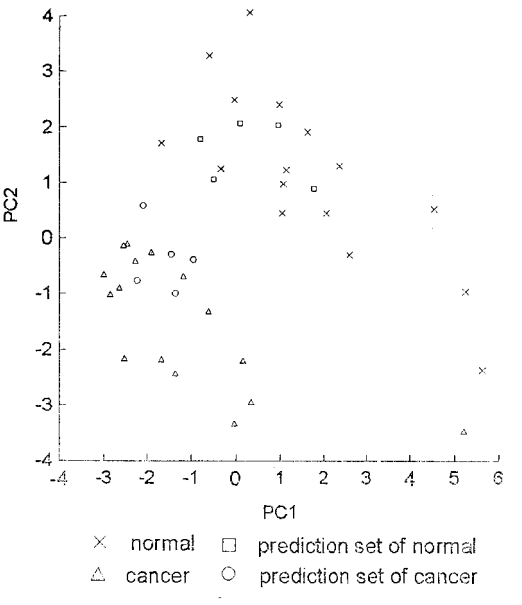

Fig. 2. Localization of 21 samples of both normal and cancer groups for hair on the plane defined by two principal components.

serum and hair samples, respectively. The stepwise clustering results for training and prediction samples based on the metal contents in serum and hair samples are given in Fig. 5 and Fig. 6, respectively. It can be seen that the normal and cancer groups for serum samples can be discriminated by a straight line. For the hair samples, the two groups can be classified correctly with an exception. One cancer sample was fallen in normal group. This sample needs further investigation.

4. Conclusions

1. The metal contents in serum and hair samples can be used to distinguish the normal people and cancer patients.
2. Multivariate statistical methods such as stepwise disaffirmation, principal components analysis, hierarchical clustering, and stepwise clustering analysis can be used as an aid for diagnosis of lung cancer according to the metal contents in serum and hair samples.

3. In some cases, exceptions may occur. However, the classification is statistically correct. The exception does not distort the significance of this method in aiding the diagnosis of lung cancer.

4. The main advantage of these multivariate methods is the fact that no a priori information on the classification is needed, and the significant information can be extracted during the statistical treatment.

5. The studies on diagnosis of cancer based on metal contents are now at the preliminary stage, so this kind of method is rather empirical at this stage. More work has to be done to establish the relationship between metal contents and cancer, even though the collection of samples is difficult and costly.

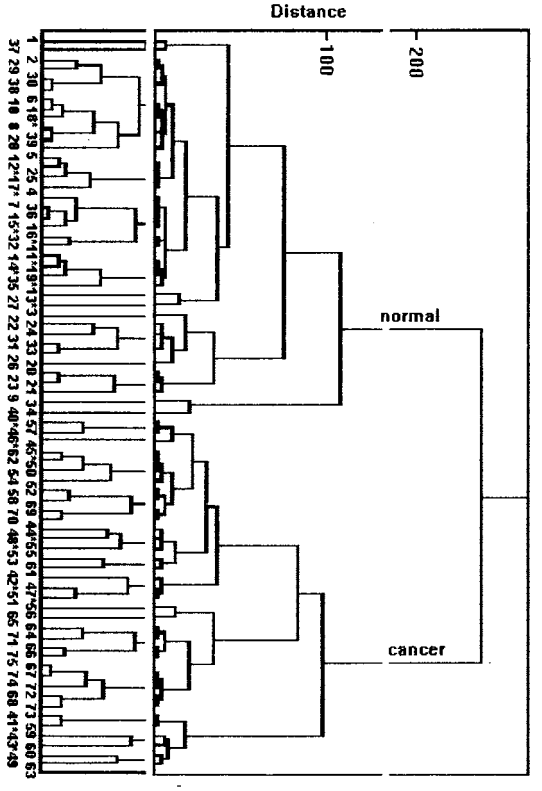

Fig. 3. Dendrogram (Ward method) of of normal and cancer groups for serum (predictions sample[a]).

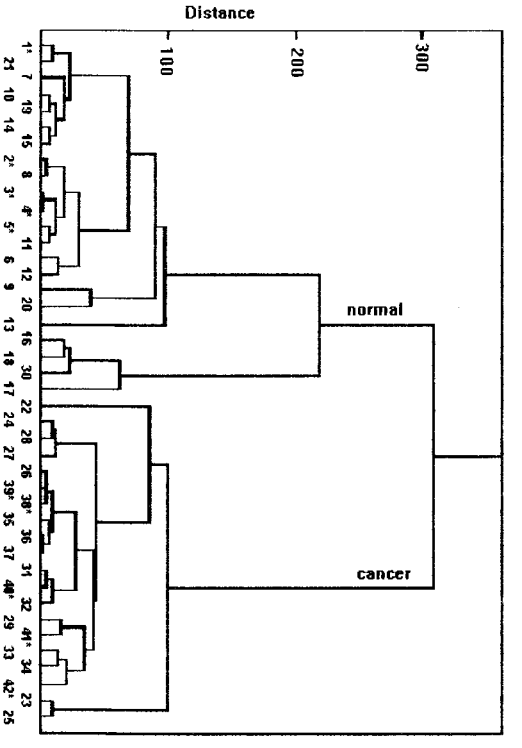

Fig. 4. Dendrogram (Ward method) of samples of normal and cancer groups for hair (prediction sample[a]).

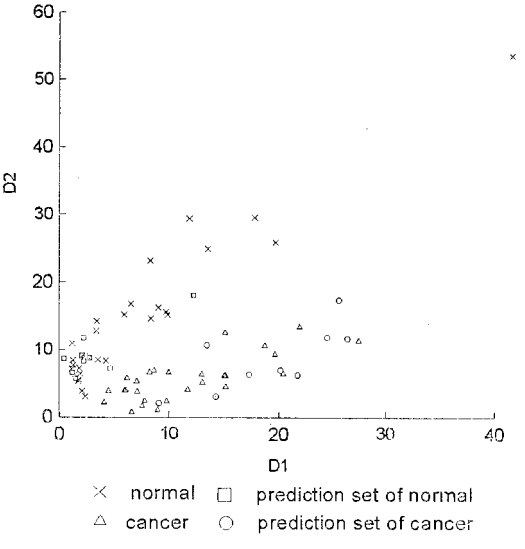

Fig. 5. Graphical presentation of samples of serum according to their Euclidean distances.

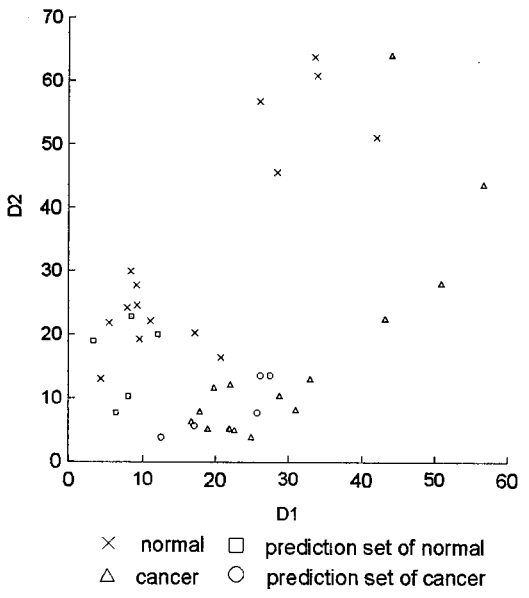

Fig. 6. Graphical presentation of samples of hair according to their Euclidean distances.

Acknowledgements

This was supported by the National Natural Science Foundation of China and the Foundation for Young Teachers, National Commission of Education, People's Republic of China.

References

[1] O. Miatto, M. Casaril, G.B. Gabriell, N. Nicoli, G. Bellisola, R. Corrocher, Cancer 55 (1985) 774.
[2] Li Guifen, J. Clin. Liver Gallbladder Dis. 7 (1991) 43.
[3] Chen Yihua, Pract. J. Cancer 1 (1993) 27.
[4] E.J. Margalloth, R. Udassin, J. Moor, J.G. Schenker, Cancer 56 (1985) 856.
[5] F.I. Brain, Cancer 47 (1978) 1845.
[6] M. Diez, F.J. Cerdan, M. Arroyo, J.L. Balibrea, Cancer 63 (1989) 726.
[7] Liu Xiuming, Zhao Qiren, Ye Zhangcheng, Zhang Dazhong, Chen Suqing, Chin. J. Tumor 7 (1985) 411.
[8] Xu Bihui, Trace Elements 4 (1990) 7.
[9] Liu Zhengxian, Liao Qiang, Chen Nianyi, Shi Kuixiong, Xu Lizhi, Chin J. Tumor 9 (1987) 173.
[10] Xu Guangwei, Chin. J. Tumor 12 (1990) 512.
[11] X. Wang, E. Zhu, X. Yan, P. Yang, B. Huang, Acta Chim. Sinica 51 (1993) 1094.
[12] E. Zhu, X. Wang, Z. Deng, P. Yang, B. Huang, Chem. J. Chin. Univ. 14 (1993) 621.
[13] D.L. Massart, B.G.M. Vandeginste, S.N. Deming, Y. Michotte, L. Kauffman, Chemometrics: a textbook, Elsvier, Amsterdam, 1988.
[14] D.L. Massart, L. Kauffman, The Interpretation of Analytical Chemical Data by the Use of Cluster Analysis, Wiley, New York, 1993.

ELSEVIER

Talanta 44 (1997) 1833–1838

Talanta

Spectrophotometric studies and application on the β-type complex of Y-CPApK

Yang Ru [a,*], Lu Yan [b], Wu Wenyan [b], Pan Jiaomai [c]

[a] *Department of Chemistry, Fudan University, Shanghai 200433, People's Republic of China*
[b] *Department of Applied Chemistry, Shandong Institute of Building Materials, Jinan, Shandong 250022, People's Republic of China*
[c] *Department of Chemistry, China East Normal University, Shanghai 200062, People's Republic of China*

Received 11 July 1996; received in revised form 6 February 1997; accepted 12 February 1997

Abstract

The β-type complex formed between yttrium and *p*-carboxychlorophosphonazo (CPApK) has been studied. It was found that Y-CPApK complex can give a maximum absorptivity in a buffer media of HAc–NaAc ranging from pH 3.5–4.3 and at a wavelength of 732 nm. Under the conditions employed, the molar absorptivity was found to be 7.72×10^4 l mol^{-1} cm^{-1} and the molar ratio of Y-CPApK was 1:2. The linear range was within 2–16 μg of yttrium in 25 ml solution. One of the characteristics of the complex was its high tolerance for calcium and hence a method of separation and enrichment of microamounts of yttrium by using calcium oxalate precipitate was developed and applied to measure yttrium in nickel-base alloys. The parameters which were related to the formation of the β-type complex of Y-CPApK were discussed and a comparison of existing β-type complexes between yttrium and the chlorophosphonazo reagents of chromotropic acid was made. © 1997 Elsevier Science B.V.

Keywords: β-type complex; *p*-carboxychlorophosphonazo; Spectrophotometric

1. Introduction

Due to their excellent analytical behavior, the bisazo reagents of chromotropic acid have been widely studied and applied in the field of spectrophotometry [1]. Some of these reagents can react with yttrium to form β-type complexes, such as *p*-chloro-chlorophosphonazo (CPApC) [2], *p*-methyl-chlorophosphonazo (CPApM) [3,4], *p*-nitro-chlorophosphonazo (CPApN) [5], *p*-ethoxycarbony-chlorophosphonazo (CPApE) [6]. These methods can differentiate the absorption spectra of yttrium complexes from those of rare-earth-element complexes so that yttrium can be measured in the presence of rare earths.

p-Carboxychlorophosphonazo (CPApK), synthesized in our laboratory, has the same characteristics as the reagent mentioned above, i.e., it can react with yttrium to form a sensitive β-type complex. In this paper, the optimum conditions for color development of the Y-CPApK complex are reported in detail. It was found that Y-CPApK complexes can give the maximum absorption in the buffer media of HAc–NaAc

* Corresponding author.

PII S00 9-9140(97)00063-5

ranging from pH 3.5–4.3 and at the wavelength of 732 nm. Under the conditions employed, the molar absorptivity was found to be 7.72×10^4 l mol^{-1} cm^{-1}. One of the characteristics of the complex is its high tolerance for calcium, so a method of separation and enrichment of microamounts of yttrium by using calcium oxalate precipitate was developed and applied for the determination of yttrium in nickel-base alloys satisfactorily.

2. Experimental

2.1. Apparatus

Absorbances were measured on a Shimadzu UV-3000 dual-wavelength/double-beam recording spectrophotometer with 1.0 cm cells. A model PHS-2 pH meter (Shanghai Second Analytical Instruments Factory) was used for pH measurement.

2.2. Reagents

A standard stock solution of yttrium (1 mg ml^{-1}) was prepared by dissolving 0.1270 g of Y_2O_3 (Spectrum pure) with 5 ml of 6 M hydrochloric acid and transferring the solution to a 100 ml flask, diluted to volume. The working solution (10 μg ml^{-1}) was prepared by dilution with distilled water. HAc–NaAc buffer (pH 3.9) was prepared by mixing 26.54 g of $NaAc \cdot 3H_2O$ and 77.3 ml of HAc and diluting to 500 ml. The pH 5.0 HAc–NaAc buffer was prepared by mixing 26.54 g of $NaAc \cdot 3H_2O$ and 6.0 ml of HAc and diluting to 500 ml with distilled water. CPApK was synthesized by coupling the diazotized 4-aminobenzoic acid, which was run by dropwise adding sodium nitrite solution in 4 M HCl at 0°C, and chlorophosphonazo I in a pH 9–10 solution which was adjusted with 10% lithium hydroxide. The details were described in a previous paper [7]. Purification of CPApK follows the procedure used commonly for the chlorophosphonazo reagents of chromotropic acid as discussed in [8]. The CPApK working solution (0.02%) was prepared by dissolving 0.02 g of CPApK in 100 ml of water. All the reagents used were of analytical reagent grade.

2.3. Procedure for the determination of yttrium

To an aliquot containing 2–26 μg of yttrium in a 25 ml flask, add 1.5 ml of pH 3.9 HAc–NaAc buffer solution, 1 ml of 0.02% CPApK and ect, stand for 15 min. Dilute to volume with water and mix well. The absorbance was measured at 732 nm in a 1 cm cell against a reagent blank.

3. Results and discussion

3.1. Absorption spectra

The absorption spectra of CPApK and its β-type complex of Y-CPApK are shown in Fig. 1. The absorption maximum of CPApK was at 560 nm, while the yttrium complex had a characteristic absorption peak at 732 nm wavelength, where the absorption of CPApK was negligible. In fact, water can also be used as a reference solution for the determination of Y-CPApK complex at the chosen wavelength of 732 nm.

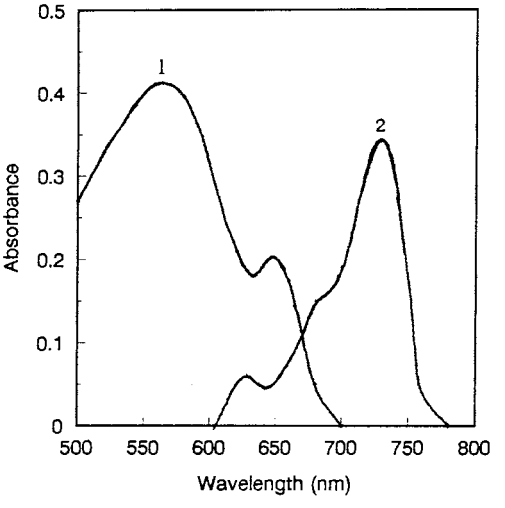

Fig. 1. Absorption spectra of CPApK and β-type complex of Y-CPApK. (1) CPApK against water blank. (2) Y-CPApK against blank reagent; Y, 10 μg; CPApK, 1.18×10^{-5} mol l^{-1}; pH 3.9 HAc–NaAc buffer, 1.5 ml; standing time in small volume, 15 min.

3.2. Effects of acidity and media

The pH value of the colored solution was adjusted by introducing HAc to the pH 5.0 HAc–NaAc buffer and the absorbance was recorded. The pH range of 3.5–4.3 is favorable to form the β-type complex of Y-CPApK and the absorbance is constant over this range. In the experiment, pH 3.9 is chosen. Various volumes of pH 3.9 HAc–NaAc buffer solution were introduced into the colored solution to test the effecting of amounts of HAc-NaAc. It was found that the complex can obtain its maximum and constant absorption within 1–2 ml of pH 3.9 buffer solution. So 1.5 ml of pH 3.9 HAc–NaAc solution was chosen. When the same pH value (pH 3.9) was buffered with hexamethylidine-tetramine(HMTA)–HCI or potassium hydrogen phthalate (KHP), the absorbances of the Y-CPApK complex at 732 nm were near to zero, i.e., the results suggested that no β-type complex formed in the two media.

3.3. Effect of amounts of CPApK

It was found that 0.8–1.5 ml of 0.02% CPApK was required to obtain the favorable absorbance for 10 μg of yttrium. Hence 1.0 ml of CPApK solution was used in all subsequent work.

3.4. Effect of surfactants

Generally speaking, introduction of surfactant can improve sensitivity and/or selectivity of the colored complexes between rare-earth elements and bisazo reagents of chromotropic acid by forming colloid bundles. Here, effect of surfactants was tested. An appropriate surfactant was not found to improve the analytical characteristics of the Y-CPApK complex. For instance, introducing animal glue can cause the solution turbid, adding cetylpyridy-bromide (CPB) resulted in precipitate and using Tween-80, TritonX-100 or ethylalcohol impeded the β-type complex to form.

3.5. Stability of the Y-CPApK complex

The prepared color solutions were kept in small volumes (not more than 10 ml) to stand for different time before dilution to 25 ml. Then dilute and record their absorbances (See Fig. 2). When the standing time was more than 10 min, full color was developed and kept constant at least 15 h. A standing time of 15 min was used in this work.

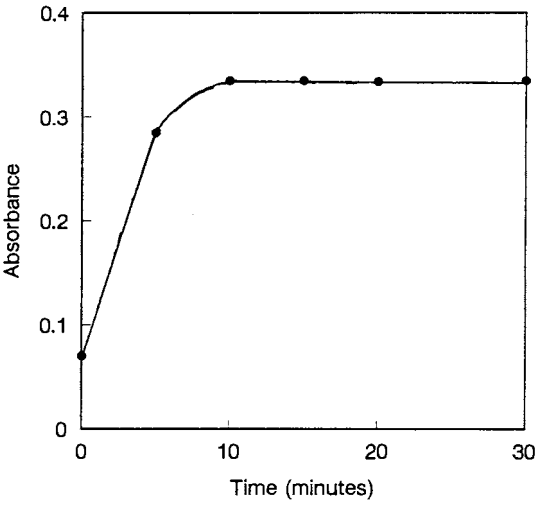

Fig. 2. Effect of standing time in small volume; Other conditions as in Fig. 1.

3.6. Calibration graph

Various amounts of yttrium were used to develop the color of the complex under the conditions employed and measure the absorbances. Plot the calibration graph of absorbance against amount of yttrium. The linear range was within 2–16 μg of yttrium in 25 ml solution and the molar absorptivity was found to be 7.72×10^4 l mol^{-1} cm^{-1}.

3.7. Effect of foreign ions

Colored solutions containing 10 μg of yttrium and various amounts of foreign ions were prepared and follow the determination procedure. If an error of 5% was considered tolerable, the tolerance limits of foreign ions were listed in Table 1. Among them, Bi^{3+}, Fe^{3+}, Ai^{3+}, Zn^{2+} and Cr^{3+} interfered, but Ca^{2+} had a higher tolerance limit. There were low tolerances (less

than 10 μg) for rare-earth elements. So a method of separation and enrichment of microamounts of yttrium was established by using the co-precipitate of yttrium and calcium oxalate.

4. Sample analysis

A sample of 0.5 g of nickel-base alloy was weighed into a 100 ml beaker, 16 ml of mixture of nitric acid and hydrochloric acid (1:3) was added to dissolve it and the mixture was heated to evaporate the solution to near dry. Distilled water, 20 ml, were added to the beaker and then 2 ml of 10% $H_2C_2O_4$. The pH value of the solution was adjusted to the range of 2.0–2.5 with 1:1 ammonia solution. After 2 ml of 10% calcium chloride was introduced, a small amount of calcium oxalate precipitate was formed. When the pH value of the solution continued to increase to 4, more precipitate formed in the solution. The solution was filtered and the precipitate washed with water. The precipitate was redissolved from the filter paper with 2 ml of 1:10 HCl and the filtrate collected in a 50 ml flask and diluted to the volume. Sample solution No.A-s-81, 2 ml, and 5 ml of No.A-s-82 sample solution were taken into 25 ml calibrated flask respectively, and follow the determination procedure. Yttrium in eight samples of A-s-81 and A-s-82 nickel-base alloys was determined, respectively. For A-s-81 sample, the percentage of mean yttrium content found in eight determinations was 0.0456, (standard value, 0.046) and relative standard deviation was 0.87. For A-s-82 sample, the percentage of mean yttrium content found was 0.0101, (standard value, 0.01) and relative standard deviation was 2.25. As the yttrium content in No.A-s-81 sample was beyond the linear range, less amounts of this sample had to be taken.

Table 1
Tolerance limits for foreign ions in the determination of 10 μg of yttium

Ion	Tolerance limit (μg)	Ion	Tolerance limit (μg)
K^+	10 000	Mn^{2+}	500
Na^+	10 000	Mg^{2+}	500
NH_4^+	10 000	Pb^{2+}	200
Cl^-	10 000	Cd^{2+}	100
NO_3^-	10 000	Ce^{2+}	100
SO_4^{2-}	10 000	Cr^{2+}	20
Ca^{2+}	2500	Zn^{2+}	13
Ni^{2+}	1000	Al^{3+}	10
Fe^{2+}	1000	Fe^{3+}	10
Co^{2+}	500	Bi^{3+}	8

5. Form change of Y-CPApK

H.C. Liu [9] has surveyed the β-type complexes formed between rare earth elements and bisazo reagents of chromotropic acid in detail. Generally speaking, the sort of reactions were closely related with such factors as medium, temperature, volume of color development, surfactant and organic reagent, etc. Here, the effects of the above factors were discussed on the formation of the β-type complex of Y-CPApK.

5.1. The change of absorption spectra of Y-CPApK from α-type to β-type

Usually, the change of the complexes (e.g., listed in Table 2) from α-type to β-type performed faster in a high-concentration solution than that in a dilute solution. The effect of standing times was tested. Absorption spectra were recorded at different standing times, (i.e., the newly prepared color solution was kept in a small volume and allowed to stand for different times before dilution), as shown in Fig. 3. Among them, curve 1 was recorded after the solution was prepared and diluted immediately (i.e., zero standing time), and curve 2 and curve 3 had a standing time of 5 and 10 min, respectively. Curve 1 had three peaks with the maximum absorption wavelength of 630, 680 and 732 nm. The two peaks with the wavelength less than 700 nm were called α-type and the third peak with the wavelength more than 700 nm was named β-type as defined in the references [10,11]. It was shown in Fig. 3 that the absorption of the peak at 732 nm increased and the peak at 680 nm decreased with the increase of standing time. When the standing

Table 2
Comparison of β-complex characteristics of yttrium

Reagent	Medium	λ (nm)	ϵ (1×10^4) (mol l^{-1} per cm)	Linear range (μg per 25 ml)	Molar ratio	Tolerance limit for Ca^{2+} (μg)	Ref.
CPApM	pH 5.0 HAc–NaAc	755	18.2	6–12	1:2	1000	[3,4]
CPApN	0.1 mol l^{-1} HCl	730	6.67	8–25	—	100	[5]
CPApE	pH 3.5 HAc–NaAc	726	4.48	6–14	—	300	[6]
CPApC	pH 4.5 HAc–NaAc	746	15.6	3–14	1:1	2000	[2]
CPApK	pH 3.9 HAc–NaAc	732	7.72	–16	1:2	2500	[a]

[a] This paper.

time was more than 10 min (curve 3), the β-type complex can reach its maximum absorption. Fig. 2 described that the maximum and constant absorbance of the β-type complex of Y-CPApK can be reached by employing standing time of 10–30 min. If the color solution was prepared and diluted to the mark immediately, the change of the complex from α-type to β-type needed more time to reach completion, i.e., needed much longer standing time in a normal solution volume.

5.2. Effect of medium

Conditions for the formation of β-type complexes were relatively rigid. For the complex of Y-CPApK, a complete change from α-type to β-type took place only in the medium of HAc–NaAc with the pH ranging from 3.5 to 4.3. When the pH value of the color solution was more than 4.3 or less than 3.5, the reaction did not go to completion. In the medium of hexamethylidine tetramine (HMTA)–HCl or potassium hydrogen phthalate (KHP) with the same pH value (pH 3.9), the absorption peak at 732 nm can not be observed. This result was coincident with those in Table 2, except that of CPApN. We can not conclude that the acetate system was critical, but at least favourable for the formation of the β-type complexes.

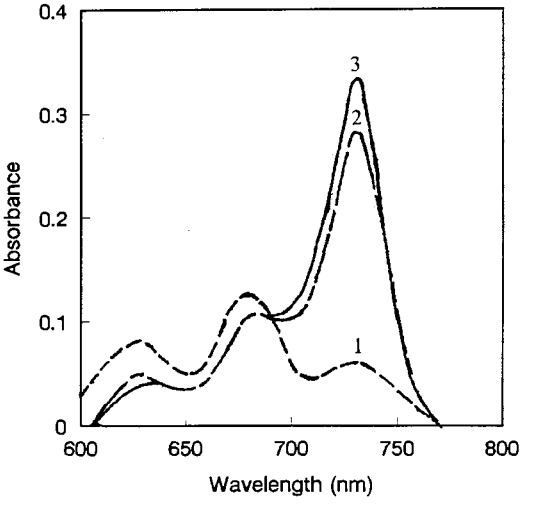

Fig. 3. Absorption spectra of Y-CPApK at different standing time in small volume. (1) 0 min, (2) 5 min, (3) 10 min; other conditions as in Fig. 1.

5.3. Effect of temperature

In the course of color development, the α-type complex of Y-CPApK formed first and then gradually changed to β-type. This reaction was affected greatly by temperature. Between 20–30°C, Y-CPApK reached its maximum absorption after 10 min. When a lower temperature was employed, the rate of reaction decreased. When temperature increased to 45°C, the reaction reached completion in not more than 10 min, but the absorbance at 732 nm was less than that at 25°C. Precipitation occurred in the solution when temperature was 60°C.

5.4. Composition of the complex

The molar composition of the Y-CPApK complex, formed under the condition employed, was ascertained by the molar-ratio method and Job's method of continuous variations. Both methods indicated that the ratio of metal to ligand was 1:2.

6. Comparison between the β-type complexes of yttrium

Several existing β-type complexes between yttrium and bisazo reagents of chromotropic acid presented in references were listed in Table 2. All the listed complexes had maximum absorption wavelength of more than 700 nm and most of them needed a weak HAc–NaAc buffer. On the other hand, the β-type complex of Y-CPApK had a much higher tolerance for calcium, which established the basis of separation and enrichment of microamounts of yttrium by using calcium oxalate precipitate.

References

[1] C. Wu, Q. Ying, Fenxi Huaxue 15 (1987) 175.
[2] W.R. Chen, J.M. Pan, Z. Wu, Huaxue Shiji 8 (1986) 238.
[3] C.G. Hsu, Y.X. Du, J.M. Pan, Huaxue Shiji 13 (1991) 273.
[4] Y.X. Du, C.G. Hsu, J.M. Pan, Chin. J. Chem. 9 (1991) 199.
[5] C.G. Hsu, J.M. Pan, Analyst 110 (1985) 1245.
[6] X. Lu, Z.P. Ou, C.L. Wang, Fenxi Huaxue 18 (1990).
[7] R. Yang, Y. Lu, G.L. Song, T. Wang, J.M. Pan, Anal. Chim. Acta 314 (1995) 95.
[8] R. Yang, Y. Lu, J.M. Pan, Fenxi Huaxue 24 (1) (1996) 119.
[9] H.C. Liu, Lihua Jianyan, 20 (2) (1984) 57; 20 (3) (1984) 59; 20 (4) (1984) 56.
[10] T. Taketatsu and N. Kono, Chem. Lett. (1974) 989.
[11] Taketatsu, Bull. Chem. Soc. Tpn 50 (1977) 1758.

ELSEVIER

Talanta 44 (1997) 1839–1846

Talanta

Thermodynamic parameters for the formation of dimeric hydrolytic species of copper(II) in aqueous $NaClO_4$ solution at different ionic strengths

Alessandro De Robertis *, Concetta De Stefano, Claudia Foti, Grazia Signorino

Dipartimento di Chimica Inorganica, Chimica Analitica e Chimica Fisica dell'Università, Salita Sperone 31, I-98 166 Messina (Vill. S. Agata), Italy

Received 12 November 1996; accepted 26 February 1997

Abstract

The hydrolysis of copper(II) has been studied in experimental conditions for which polynuclear species are formed prevalently. The study has been carried out by the pH-metric technique at different temperatures and ionic strengths in $NaClO_4$ aqueous solution. As previously reported in literature, the most important hydrolytic species is $Cu_2(OH)_2^{2+}$. For copper(II) concentrations greater than 75 mmol dm^{-3}, also the species $Cu_2(OH)^{3+}$ is formed in appreciable amount. The formation constants of these species have been determined, together with their dependence on ionic strength. The temperature coefficients of equilibrium constants allowed to obtain the relative formation enthalpies. © 1997 Elsevier Science B.V.

Keywords: Aquatic chemistry; Dependence on ionic strength; Hydrolysis of copper(II); Polynuclear hydroxo species

1. Introduction

The hydrolysis of copper(II) has been studied by several researchers, using different techniques [1–13]. Nevertheless remarkable discrepancies can be found among the different works, both as concern the type of hydrolytic species, and the values of the thermodynamic parameters associated to the formation of such species. A series of objective difficulties gives account of these discrepancies. (a) The study of the hydrolysis of copper(II) is before all hindered by the formation of precipitate at relatively low pH, and the percentage of hydrolized copper in solution is always quite low [1]. (b) The precipitates that are formed are gelatinous and of different stoichiometry [$Cu(OH)_2$, CuO, $Cu(OH)_{1.5}X_{0.5}$ ($X = Cl^-$, NO_3^-), $Cu(OH)_{1.714}(ClO_4)_{0.286}$] [1,14]. (c) For copper(II) concentrations greater than 1 mmol dm^{-3}, different polynuclear species are formed. (d) The formation of the gelatinous $Cu(OH)_2$ has been often interpreted as formation of the bis-complex, and this has led to the calculation, for this species, of an unreliable hydrolysis constant. (e) The pH-metric measurements (that are the most suitable

* Corresponding author. Fax: +39 90 392827; e-mail: derobertis@chem.unime.it

PII S00 9-9140(97)00075-1

for this type of study) are limited from the fact that fairly high metal ion concentrations must be used (greater than 0.1 mmol dm^{-3}), while for the scarce solubility of the hydrolytic products it would be convenient to work with more diluted solutions; on the other hand solubility and ISE-Cu measurements are strongly limited by other factors (gelatinous, active solids with high surface energy precipitates; adsorption of copper within the apparatus; kinetic influences on the response of ISE-Cu).

In the literature there is generic agreement only on the formation of the dimeric species $Cu_2(OH)_2^{2+}$ (also the reported hydrolysis constants are generally in fairly good agreement). The formation of monomeric species $Cu(OH)_j^{(2-j)+}$ ($j = 1,\ldots, 4$) has been hypothesized, but the relative reported hydrolysis constants must be considered critically. Moreover, the formation of many other polynuclear species has been proposed [$Cu_2(OH)^{3+}$, $Cu_3(OH)_4^{2+}$, $Cu_3(OH)_2^{4+}$, and 'core plus link' species $Cu_{n+1}(OH)_{2n}^{2+}$], however without agreement among the different authors both on the type of species and on their hydrolysis constants. Finally, there are no systematic researches on the ionic strength dependence, and on medium effects of hydrolysis constants.

Recently, we have undertaken a work on the complexation of copper(II) with ligands of different nature, in different ionic media, in order to obtain a picture, as realistic as possible, on the speciation of this cation in the natural fluids, in presence of low molecular weight ligands (also in relation with our interest to the effect of the ionic medium on the complexation). Therefore it is necessary (particularly in the study of complexes of ligands not very stable, with protonation constants in the neutral-acidic range, such as polycarboxylic acids) the exact knowledge of the hydrolysis constants of the copper(II), at different analytical concentrations, at different temperatures, and at different ionic strengths and media.

In this first paper, we report an investigation on the copper(II) hydrolysis at fairly high analytical concentrations, where it is expected the formation of polynuclear species only, at different temperatures (10, 25, 37, 45°C) and ionic strengths ($0 \leq I \leq 1$ mol dm^{-3}) in $NaClO_4$. This medium was chosen assuming that it is fully dissociated, and that ClO_4^- does not form ion pairs with copper(II).

2. Experimental

2.1. Materials

Solutions of $Cu(ClO_4)_2$ were prepared from Fluka puriss. reagent and standardized complexometrically. For $NaClO_4$ solutions, Fluka puriss. reagent was used, after purification according to Grenthe [15], and drying under vacuum. Standard $HClO_4$ solutions were prepared from the concentrated reagent (C.Erba r.p.) and standardized against sodium carbonate (C.Erba r.p.); standard NaOH solutions were prepared by diluting concentrated ampoules Fluka, and standardized against potassium biphthalate. All the solutions were prepared with bidistillated water, and grade A glassware.

2.2. Apparatus

The concentration of the free hydrogen ions was measured by means of different potentiometric systems. (a) Potentiometer Metrohm mod. 654 connected to a combination Ross type electrode Orion mod. 8102; (b) potentiometer Metrohm E605 coupled with a Metrohm glass electrode and an Ingold saturated calomel electrode; (c) potentiometer Amel mod. 337, connected to a combination Ross type electrode Orion mod. 8102. All potentiometric systems had minimum reading 0.1 mV and reproducibility ± 0.2 mV. The three equipments were connected to a Metrohm motorized burette Dosimat mod. 665 (minimum reading 0.001 ml), and to a PC that, with appropriate software, allows the fully computerized titrations. The measurement cells (50 ml) were thermostatted at 25 ± 0.1°C and the solutions were stirred magnetically. In order to eliminate O_2 and CO_2, pre humidified N_2 was bubbled into solutions.

2.3. Procedure

The solution (30 ml) containing copper(II) (50–125 mmol dm^{-3}), $NaClO_4$ and an excess of $HClO_4$ (2–5 mmol dm^{-3}) was titrated with standard NaOH up to the precipitation (about 60–70 experimental points), i.e., 5.4 (diluted solutions) $\leq pH_{max} \leq 4.9$ (concentrated solutions). $NaClO_4$ was added to the same solution, in order to reach the prefixed ionic strength value (max $\sim$ 1 mol dm^{-3}). $HClO_4$ was added in order to calculate the internal E^0_{int} value. By separate titration (as a check), we calculate E^0_{ext}, at the same temperature and ionic strength value; if $|E^0_{int} - E^0_{ext}| > 1.5$ mV, the titration was rejected and repeated. From these data also the liquid junction potential ($E_j = j_a[H^+]$) was calculated.

2.4. Calculations

The nonlinear least squares computer program ESAB2M [16] was used for the refinement of all parameters of an acid–base titration (E^0, K_W, coefficient of junction potential, (j_a), analytical concentration of reagents). For the calculation of complex formation constants (β_{pq}), together with the parameters for the dependence on ionic strength, BSTAC [17] and STACO [18] computer programs were used. β_{pq} values are referred to the reaction $pCu^{2+} + qH_2O = Cu_p(OH)_q^{(2p-q)+} + qH^+$. Statistical methods were used for the selection of species, as proposed by Vacca and Sabatini [19]. ES4ECl [17] program was used to draw the distribution diagrams.

2.5. Ionic strength dependence of formation constants

The general Debye–Hückel type Eq. (2.1) can be used to take into account the dependence on ionic strength of formation constants (β = generic equilibrium constant; $^T\beta$ = constant at infinite dilution)

$$\log \beta = \log^T \beta - g(I) + CI + DI^{3/2} + EI^2 \qquad (2.1)$$

were

$$g(I) = z^* I^{1/2} \times (2 + 3I^{1/2})^{-1}$$

$$z^* = \Sigma\,(\text{charges})^2_{\text{reactants}} - \Sigma\,(\text{charges})^2_{\text{products}}$$

C, D and E are empirical parameters, which can be obtained by fitting experimental data. Results of a series of investigations [20–22], showed that, when all the interactions occurring in the solution are considered (or they are negligible, i.e., $K < 0.1$ dm^3 mol^{-1}), in the range $0 \leq I \leq 1$ mol dm^{-3}, the above empirical parameters are dependent only on stechiometry of the formation reaction:

$$C = 0.10p^* + 0.23z^*; \qquad D = -0.10z^*;$$

$$E = 0$$

with

$$p^* = \Sigma\,(\text{moles})_{\text{reactants}} - \Sigma\,(\text{moles})_{\text{products}}$$

(the parameter E becomes relevant for $I > 1$ mol dm^{-3}). When considering hydrolysis reactions, the activity of water must be taken into account, too. For the electrolytes here considered, the simple relationship $\log a_w = -0.015\ I$ (with a mean error $\epsilon \sim 0.002\ I$) can be used. Therefore

$$C = 0.085p^* + 0.23z^*$$

If refined C (for data at $I \leq 1$ mol dm^{-3}), Eq. (2.1) reduces to

$$\log \beta = \log^T \beta - z^*[I^{1/2} \times (2 + 3I^{1/2})^{-1} + 0.1I^{3/2}] + CI \qquad (2.2)$$

3. Analysis of literature data

Some literature data on the hydrolysis of copper(II) are reported in Table 1. In this Table only thermodynamic parameters for the species $Cu_2(OH)_2^{2+}$ and $Cu_2(OH)^{3+}$ are reported. Other proposed polynuclear species are not, in our opinion, to be taken into consideration (see also hereafter). The mononuclear $Cu(OH)^+$ species is formed in very low percentages, and a rough estimate of its formation constant is sufficient for the study of the other more important species. By considering $\log \beta_{11}$ reported (in $NaClO_4$) and some ΔH^0 values, we were able to estimate the first hydrolysis constant of copper(II) in the ranges $5 \leq T \leq 50$°C and $0 < I \leq 3$ mol dm^{-3}:

$$\log \beta_{11} = \log^{T} \beta_{11} - g(I) + CI - 0.09I^2 \quad (3.1)$$

$$\log^{T} \beta_{11} = -7.5 + 0.020(T-25) \quad (3.2)$$

$$C = 0.47 - 0.003(T-25) \quad (3.3)$$

with a mean error ± 0.15 ($>95\%$ confidence interval).

4. Results and discussion

4.1. Selection of the species and determination of hydrolysis constants

Several calculations were performed, with both BSTAC and STACO computer programs [17,18], in order to select the best set of species formed in our experimental conditions. The possible formation of following species was taken into account: $Cu_2(OH)^{3+}$, $Cu_2(OH)_2^{2+}$, $Cu_2(OH)_3^{+}$, $Cu_3(OH)_4^{2+}$, (the hydrolysis constant of monomeric species $Cu(OH)^{+}$ was kept constant in the calculations, using the values of Eqs. (3.1), (3.2) and (3.3)). As expected, for all temperatures and ionic strengths, calculations showed that the more important species is $Cu_2(OH)_2^{2+}$; for $C_{Cu} \geq 75$ mmol dm^{-3}, the species $Cu_2(OH)^{3+}$ is formed in appreciable amount and cannot be neglected. At 25°C the ratio (BSTAC calculations) $s_1^2/s_0^2 \cong 2$ [s_1^2 = variance in e.m.f., considering the formation of $Cu_2(OH)_2^{2+}$; s_0^2 = idem, considering the formation of $Cu_2(OH)_2^{2+}$ and $Cu_2(OH)^{3+}$], which is highly significant (for 495 experimental points). Analogous calculations, for the other temperatures with both computer programs, gave also significant statistical parameters for the formation of two dimeric species. In Table 2, the hydrolysis constants are reported at different temperatures and ionic strengths, in both molar and molal scales. The dependence of hydrolysis constants on ionic strength and on temperature is shown in Fig. 1 and Fig. 2.

Table 1
Some literature data on the hydrolysis of copper(II), in aqueous solution

T(°C)	I(mol dm^{-3})	$\log \beta_{21}$	$\log \beta_{22}$	Ref.
18	0	−6.92	−10.89	[5]
20	0		−10.53	[6]
25	3 ($NaClO_4$)		−10.6	[8]
25	3 ($NaClO_4$)		−10.75	[9]
25	0		−10.57	[7]
25	3	−5.8	−10.6	[3]
25	3 ($NaClO_4$)	−5.75		[12]
25	3 ($LiClO_4$)	−6.22	−11.21	[4]
25	0		−10.36	[1]
25	0.1 ($NaClO_4$)		−10.75	[10]
25	3 ($NaClO_4$)	−6.02	−10.93	[11]
50	3 ($NaClO_4$)	−5.65	−9.81	[11]
		ΔH_{21}^0 / kJ mol^{-1}	ΔH_{22}^0 / kJ mol^{-1}	
25	3 ($NaClO_4$)		66.1	[13]
25	0.1 ($NaClO_4$)		78.0	[10]
15–42	0		73.2	[6]
25–50	3 ($NaClO_4$)	25	76.1	[11]

4.2. Dependence on ionic strength of hydrolysis constants

The dependence on ionic strength of hydrolysis constants (Fig. 1) was taken into account by using Eq. (2.2). The refined value of C (see Table 2) is in accordance with the one found for systems when no significant interactions between components and background salt occur. In fact, for the species $Cu_2(OH)_2^{2+}$, at 25°C, we found $C = 0.361$, and in a preceding work on the hydrolysis of $(CH_3)_2Sn^{2+}$ [23] it was found $C = 0.365$ in $NaNO_3$ and/or $NaClO_4$ solutions [23]; both values of this parameter agree with $C = 0.375$ found in a general analysis of the dependence on ionic strength of formation constants [22]. These C values agree also with several other ones obtained in previous investigation [20–22,24]. Analogous considerations can be made for the dependence on ionic strength of the species $Cu_2(OH)^{3+}$. The above results allow to consider the hydrolysis constants of copper(II) in $NaClO_4$ as the baseline for other studies in different media. Moreover, the temperature gradient of C for both dimeric species, through affect by a quite large error, is in accordance with previous findings [17,21].

Table 2
Equilibrium constants for the hydrolysis of copper(II) in aqueous $NaClO_4$ solutions

T(°C)	I[a]	Molar scale		I[b]	Molal scale	
		$\log \beta_{21}$	$\log \beta_{22}$		$\log \beta_{21}$	$\log \beta_{22}$
10	0	-6.86 ± 0.27[c]	-11.15 ± 0.05	0	−6.86	−11.15
	0.1	-6.67 ± 0.23	-11.33 ± 0.04	0.100	−6.67	−11.33
	0.25	-6.62 ± 0.19	-11.36 ± 0.03	0.253	−6.62	−11.35
	0.5	-6.59 ± 0.12	-11.36 ± 0.02	0.511	−6.59	−11.35
	0.75	-6.58 ± 0.11	-11.35 ± 0.03	0.774	−6.58	−11.33
	1	-6.56 ± 0.16	-11.33 ± 0.05	1.044	−6.56	−11.32
		(C = −0.304)[d]	(C = 0.418)			
25	0	-6.26 ± 0.17	-10.54 ± 0.06	0	−6.26	−10.54
	0.1	-6.08 ± 0.14	-10.72 ± 0.05	0.101	−6.08	−10.72
	0.25	-6.06 ± 0.11	-10.76 ± 0.04	0.254	−6.06	−10.75
	0.5	-6.07 ± 0.07	-10.77 ± 0.03	0.513	−6.07	−10.76
	0.75	-6.09 ± 0.06	-10.77 ± 0.02	0.778	−6.09	−10.76
	1	-6.11 ± 0.09	-10.78 ± 0.04	1.050	−6.11	−10.76
		(C = −0.456)	(C = 0.361)			
37	0.15	—	-10.24 ± 0.01	0.152	—	−10.23
45	0	-5.93 ± 0.12	-9.76 ± 0.03	0	−5.93	−9.76
	0.1	-5.76 ± 0.10	-9.95 ± 0.02	0.102	−5.76	−9.95
	0.25	-5.75 ± 0.08	-10.00 ± 0.02	0.256	−5.75	−9.99
	0.5	-5.77 ± 0.07	-10.02 ± 0.02	0.517	−5.77	−10.01
	0.75	-5.80 ± 0.09	-10.04 ± 0.03	0.786	−5.80	−10.02
	1	-5.84 ± 0.13	-10.06 ± 0.04	1.061	−5.84	−10.03
		(C = −0.505)	(C = 0.302)			

[a] Ionic strength in mol dm^{-3}.
[b] Ionic strength in mol kg^{-1}
[c] ± 3 (std. dev.).
[d] Empirical parameter of Eq. (2.1).

4.3. Dependence on temperature of hydrolysis constants

The dependence on temperature (see Fig. 2) shows, as expected, that hydrolytic reactions are endothermic. We found for the reaction (ΔH^0 in kJ mol^{-1}, ΔS^0 in J K^{-1} mol^{-1}; $T = 25$°C, $I = 0$ mol dm^{-3}; obtained from $\log \beta_{pq}$ molal values)

$$2Cu^{2+} + 2H_2O = Cu_2(OH)_2^{2+} + 2H^+,$$

$$\Delta H^0_{22} = 68.1(\pm 1.8),$$

$$\Delta S^0_{22} = 27 \pm 1$$

and for the reaction

$$2Cu^{2+} + H_2O = Cu_2(OH)^{3+} + H^+,$$

$$\Delta H^0_{21} = 46.1(\pm 2.7),$$

$$\Delta S^0_{21} = 35 \pm 2$$

By considering Eq. (3.2) and Eq. (3.3), we have, for the reaction

$$Cu^{2+} + H_2O = Cu(OH)^+ + H^+,$$

$$\Delta H^0_{11} = 34(\pm 5),$$

$$\Delta S^0_{11} = 30 \pm 3$$

Finally, for the dimerization reaction, we have

$$2Cu(OH)^+ = Cu_2(OH)_2^{2+},$$

$$\Delta H^0_d = 0 \pm 5,$$

$$\Delta S^0_d = 86 \pm 4$$

4.4. Relevance of the hydrolysis of copper(II)

In Fig. 3 we report some distribution (% species versus pH) in different analytical conditions. The pH range for the hydrolysis of cop-

Table 3
Smoothed values of equilibrium constants (molar scale) for the hydrolysis of copper(II) in $NaClO_4$ aqueous solution

T(°C)	I(mol dm^{-3})	log β_{11}	log β_{21}	log β_{22}
5	0	−7.9	−7.06	−11.30
5	0.1	−8.1	−6.87	−11.50
5	0.25	−8.1	−6.84	−11.55
5	0.5	−8.0	−6.84	−11.57
5	1	−7.9	−6.86	−11.57
5	2	−7.7	−6.85	−11.56
5	3	−7.6	−6.69	−11.59
15	0	−7.7	−6.61	−10.91
15	0.1	−7.9	−6.42	−11.11
15	0.25	−7.9	−6.39	−11.16
15	0.5	−7.8	−6.39	−11.18
15	1	−7.7	−6.42	−11.17
15	2	−7.5	−6.41	−11.14
15	3	−7.5	−6.26	−11.15
25	0	−7.5	−6.28	−10.53
25	0.1	−7.7	−6.10	−10.72
25	0.25	−7.7	−6.07	−10.77
25	0.5	−7.6	−6.07	−10.79
25	1	−7.5	−6.11	−10.77
25	2	−7.4	−6.11	−10.73
25	3	−7.4	−5.97	−10.73
35	0	−7.3	−6.07	−10.15
35	0.1	−7.5	−5.89	−10.34
35	0.25	−7.5	−5.86	−10.38
35	0.5	−7.5	−5.86	−10.40
35	1	−7.4	−5.90	−10.38
35	2	−7.2	−5.91	−10.32
35	3	−7.3	−5.78	−10.30
45	0	−7.1	−5.96	−9.77
45	0.1	−7.3	−5.77	−9.96
45	0.25	−7.3	−5.75	−10.00
45	0.5	−7.3	−5.76	−10.01
45	1	−7.2	−5.80	−9.99
45	2	−7.1	−5.82	−9.92
45	3	−7.2	−5.69	−9.88
50	0	−7.0	−5.93	−9.58
50	0.1	−7.2	−5.75	−9.78
50	0.25	−7.2	−5.72	−9.81
50	0.5	−7.2	−5.73	−9.82
50	1	−7.1	−5.78	−9.79
50	2	−7.1	−5.80	−9.72
50	3	−7.1	−5.68	−9.68

and Martell [3] give log $\beta_{22} = -10.6$ ($I = 0$ mol dm^{-3}, $T = 25$°C). Our value log $\beta_{22} = -10.54 \pm 0.06$ lies between the two above ones. Analogous considerations can be made for ΔH^0 values. As regards the species $Cu_2(OH)^{3+}$ only hydrolysis constants at $I = 3$ mol dm^{-3} can be found [3,4,11,12]. Smoothed values of log β_{11}, log β_{21} and log β_{22}, at different temperatures and ionic strengths (obtained using data from this work and from literature), are reported in Table 3.

4.6. Concluding remarks

Main conclusions of this work are as follows.

(i) Hydrolytic species of copper(II), in moderately concentrate solutions, are $Cu_2(OH)_2^{2+}$ and $Cu_2(OH)^{3+}$, with small amounts of $Cu(OH)^+$.

(ii) The dependence on ionic strength (in $NaClO_4$ solutions) (simply described by Eq. (2.2) with C values of Table 2) shows that reported log β_{pq} values can be used, in the ranges $0 < I \leq 1$ mol dm^{-3} and $10 \leq T$ (°C) ≤ 45, as baseline for further studies in other media (NaCl, synthetic sea water, etc.).

(iii) Smoothed values of Table 3, can be used as recommended values for the hydrolysis of copper(II).

Acknowledgements

We thank MURST and CNR for financial support and Professor Silvio Sammartano for helpful discussion.

References

[1] C.F. Baes Jr., R.E. Mesmer, The Hydrolysis of Cations, Wiley, New York, 1976; C.F. Baes Jr., R.E. Mesmer, Am. J. Sci. 281 (1981) 935.
[2] E. Högfeld, Stability Constants, Inorganic Ligands, Pergamon Press, Oxford, 1982.
[3] R.M. Smith, A.E. Martell, Critical Stability Constants: Inorganic Complexes, Plenum, New York, 1976, First supplement, 1982, Second supplement, 1989.
[4] H. Othaki, T. Kawai, Bull. Chem. Soc. Jpn. 45 (1972) 1735.
[5] K. Pedersen, Kgl. Dan. Vidensk, Selsk. Mat.-Fis. Medd. 20 (1943) 7.
[6] D.D. Perrin, J. Chem. Soc. 3189 (1960).
[7] F. Achenza, Ann. Chim. (Rome) 48 (1958) 565.
[8] C. Berecki-Biedermann, Ark. Kemi 9 (1956) 175.
[9] H. Kakihana, T. Amaga, M. Maeda, Bull. Chem. Soc. Jpn. 43 (1970) 3155.
[10] G. Arena, R. Cali, E. Rizzarelli, S. Sammartano, Thermochim. Acta 16 (1976) 315.

[11] K.A. Burkov, E.A. Bus'ko, L.S. Lilich, I.N. Ivanova, Russ. J. Inorg. Chem. 27 (1982) 819.
[12] E. Neher-Neumann, Acta Chem. Scand. A38 (1984) 517.
[13] R. Arnek, C.C. Patel, Acta Chem. Scand. 22 (1968) 1097.
[14] R. Näsänen, V. Tamminen, J. Am. Chem. Soc. 71 (1949) 1994.
[15] I. Grenthe, D.R. Williams, Acta Chem. Scand. 21 (1970) 341.
[16] C. De Stefano, P. Princi, C. Rigano, S. Sammartano, Ann. Chim. (Rome) 77 (1987) 643.
[17] C. De Stefano, P. Mineo, C. Rigano, S. Sammartano, Ann. Chim. (Rome) 83 (1993) 243.
[18] C. De Stefano, C. Foti, O. Giuffrè, P. Mineo, C. Rigano, S. Sammartano, Ann. Chim. (Rome) 86 (1996) 257.
[19] A. Vacca and A. Sabatini, How to select the most probable equilibrium model: a tentative strategy, in: A.J. Jenne, E. Rizzarelli, V. Romano, S. Sammartano (Eds.), Metal Complexes in Solution, Piccin, Padua, 1986.
[20] P.G. Daniele, A. De Robertis, C. De Stefano, S. Sammartano, C. Rigano, J. Chem. Soc., Dalton Trans. 2353 (1985).
[21] P.G. Daniele, A. De Robertis, C. De Stefano, S. Sammartano, in: S. Alegret, J.J. Azias, D. Barcelò, J. Casal, G. Rauter (Eds.), Miscellany of Scientific Papers Offered to Eric Casassas, Universitat Autonoma de Barcelona, Bellaterra, 1991.
[22] A. Casale, P.G. Daniele, C. De Stefano, S. Sammartano, Talanta 36 (1989) 903.
[23] C. De Stefano, C. Foti, A. Gianguzza, M. Martino, L. Pellerito, S. Sammartano, J. Chem. Eng. Data 41 (1996) 511.
[24] P.G. Daniele, C. S. Sammartano, V. Zelano, Talanta 41 (1994) 1577.

ELSEVIER

Talanta 44 (1997) 1847–1858

Talanta

Determination of ion-selective electrode characteristics by non-linear curve fitting

Paddy Kane, Dermot Diamond *

School of Chemical Sciences, Dublin City University, Dublin 9, Ireland

Received 11 September 1996; received in revised form 3 February 1997; accepted 7 February 1997

Abstract

A simple practical method of determining potentiometric selectivity coefficients of ion-selective electrodes (ISEs) is described in which electrode characteristics (slope, potentiometric selectivity coefficients and cell constant) can be determined by fitting the experimental data obtained using the fixed interference (FI) method to an appropriate model by non-linear least-squares regression. The proposed method is simple to implement practically, and data processing can be easily achieved through use of the optimisation add-on, Solver, bundled with Microsoft Excel. The flexibility of the method is demonstrated by modelling the response of a valinomycin potassium-selective electrode with the Nikolskii–Eisenman equation and a recently proposed alternative to the Nikolskii–Eisenman equation for cases where the ionic charges on the primary and interfering ions are unequal. © 1997 Elsevier Science B.V.

Keywords: Curve-fitting; Excel; Ion-selective electrode; Potassium; Potentiometric selectivity coefficients; Valinomycin

1. Introduction

The most widely used methods for determining potentiometric selectivity coefficients of ISEs have been the separate solution (SS) method [1], the fixed interference (FI) method [1] or what Umezawa et al. [2] refer to as the two-solution method. The fixed primary ion (FPI) method [1] has also been used but is less popular. The matched potential (MP) method, developed by Gadzekpo and Christian [3], has been recommended by Umezawa et al. [2] when the ionic charges of the primary and interfering ions are unequal or when the electrode response to either ion is non-Nernstian. In a variation of the SS method, Bakker [4] has described a method where the ISE is conditioned in a solution of interfering ion.

In practical terms, all of these methods involve the transfer of electrodes to different solutions and as such, are subject to 'carryover' error. The SS method and Bakker's variation on it [4], have the disadvantage that they are not realistic representations of the practical behaviour of the electrode since in practice, measurements are made in the presence of both primary and interfering ions, and competitive processes can have a significant effect on the electrode response. However, Bakker's approach is interesting in that the ISE, with a membrane containing the tetraphenylbo-

* Corresponding author.

rate salt of an interfering ion, is conditioned in an interfering ion solution. The difficulty that the interfering ion has in displacing the primary ion from the membrane when the ISE is conditioned in a primary ion solution and then transferred to an interfering solution, is thus avoided and a Nernstian response is expected from interfering ions, something which does not always occur when electrodes are conditioned in primary ion solutions. The potentiometric selectivity coefficients obtained are therefore more representative of the ion-exchange process. However, they are not representative of practical electrode behaviour, where the conditioning and calibration of the ISE in solutions of the primary ion, is standard practice.

The FI method, as traditionally used [1], involves the preparation of a range of solutions with different primary ion activities but with a constant activity of interfering ion and, as such, the method is tedious and open to operator error. Furthermore, analysis of the data obtained by this method usually involves manually finding the point of intersection of the extrapolated linear portions of a plot of the cell potential versus the log of the activity of the primary ion [1]. This has two disadvantages; firstly, a decision has to be made as to which points are part of the linear portions of the plot and this makes the method subjective. Secondly, as Moody and Thomas [5] point out, the potentials in the plateau region of this plot are subject to an unacceptable degree of irreproducibility and drift. Srinivasan and Rechnitz [6] derived two equations for high and low values of potentiometric selectivity coefficients, respectively, and these allow potentiometric selectivity coefficients to be determined from data relating to a range of activities. However, their methods require some a priori knowledge of selectivity before choosing the activities of the primary and interfering ions and the appropriate equation. Furthermore, their methods allow no 'at a glance idea' of selectivity, as provided by the traditional FI method.

In principle, the MP method requires just two experimental points to calculate the potentiometric selectivity coefficient (or the interference ratio since, as Maccà [7] points out, the quantity obtained by the MP method is by definition, different to the traditional potentiometric selectivity coefficient). In practice, however, this method requires measurements to be made in solutions of different concentrations of interfering ion and then sophisticated interpolation if it is to be accurate. As such, it is no less tedious or time consuming than the traditional FI method. Another disadvantage of the MP method is that for electrodes which are very selective, the level of interferent required to equalise the potentials may be so high as to make the method unrealistic since, in practice, such levels of interferents are unlikely to be encountered and extrapolation to lower interfering ion activity is not generally advisable. Furthermore, Maccà [7] claims that the interference ratio is more concentration dependent than the potentiometric selectivity coefficient.

Therefore, there is a need for an approach which is practically simple to implement, and which removes the subjectivity of the conventional FI method [1]. Previously, Yuliang et al. [8] used a non-linear regression approach with electrode measurements of halide ion mixtures. However, they have given no indication (either numerical or graphical) of the quality of the fit to Nikolskii–Eisenman equation. Furthermore, they give no details of how their approach was implemented, and therefore it is impossible to comment on the reliability of their results or how easy it is to process data with their method. In a variation on the FI method, Davey et al. [9] plotted the peak heights obtained using a flow-analysis approach versus the log of the primary ion activity at constant concentration of interfering ion. They then used values in the curved region of the plot to determine potentiometric selectivity coefficients using a data linearisation technique based on the Nikolskii–Eisenman equation. Unfortunately, their method did not yield a value for the Nernstian Slope Factor. Diamond and Forster [10,11] and Saez de Viteri and Diamond [12] have proposed very rigorous non-linear modelling approaches based on multivariate calibration and simplex optimisation which enabled potentiometric selectivity coefficients to be in mixed solutions containing up to four ions. However, these methods are not simple to implement, as

even with partial factorial design, 32 calibration solutions are required to characterise a four-electrode array.

There has been some discussion in the literature on alternatives to the Nikolskii–Eisenman equation. Morf et al. [13] proposed an equation for neutral carrier-based calcium-selective ISEs, relating to mixed-ion solutions where the interfering ion is singly-charged. Meyerhoff and coworkers [14] have developed a formalism for ISEs of three different carrier types, for mixed-ion solutions which is applicable to all combinations of primary and interfering ions of different charge.

In this paper, we describe a very simple procedure for obtaining experimental data, and subsequently fitting the data to a mathematical model in order to obtain estimations of the cell constant, the Nernstian Slope Factor and potentiometric selectivity coefficients. In the proposed method, the primary ion activity is varied by means of a series of small volume 'spikes', added to a single solution, with the electrodes continually in contact, and measuring the cell potential after each addition. Therefore, no transfer of electrodes between measurements is involved and the preparation of relatively few solutions is required. The entire response curve is then fitted to an appropriate model (for example, the Nikolskii–Eisenman equation or the Meyerhoff formalism [14]) to obtain the electrode parameters (Nernstian Slope Factor, cell constant and potentiometric selectivity coefficient for the interfering ion) which provide the best-fit to the experimental data through minimisation of the least-squares error. This non-linear analysis is carried out using the Solver optimisation add-on available in Microsoft Excel for Windows 95, version 7.0 which, with its graphical user interface, is very simple to use. As Excel is normally bundled with PCs these days, the user does not have to invest in any relatively expensive specialised mathematical or statistical packages to perform the calculations.

Despite the known limitations of the Nikolskii–Eisenman equation (the primary and interfering ions should have Nernstian slopes and the same ionic charge), we decided to use this model because of the large database of information on this model in existence in the literature. For the same reason, we chose a valinomycin-based potassium selective electrode because of the wealth of data available for this ISE to which we could compare our results.

2. Experimental

2.1. Materials

All metal chlorides used were of analytical reagent grade. High molecular weight poly(vinyl chloride) (PVC) lithium chloride, potassium chloride, valinomycin, tetrahydrofuran, bis(2-ethylhexyl)sebacate (DOS) and potassium tetrakis(4-chlorophenyl)borate (KTpClPB) were purchased from Fluka. Magnesium chloride, calcium chloride and barium chloride were purchased from BDH. Sodium chloride and ammonium chloride were purchased from Riedel de Haen. Milli-Q grade distilled water from Millipore was used throughout.

2.2. Apparatus

A potassium-selective electrode was prepared according to the procedure of Lu et al. [15] using valinomycin as the ionophore. The components and composition of the membrane used in the ion-selective electrode (ISE) are the same as that used by Knoll et al. [16] and are given in Table 1. Membrane resistance and potential measurements were made with a Hewlett Packard 34401 A multimeter and a standard calomel electrode (SCE) as a reference, obtained from EDT Instruments, Dover, Kent, UK.

2.3. Determination of potentiometric characteristics

The ISE and the SCE were placed in 25.0 cm^3 of a 0.1 mol dm^{-3} aqueous solution of an interfering chloride, for example, sodium chloride. Aliquots (2, 5, 20, 45, 70 and 100 μdm^3) of mixture 1 (0.01 mol dm^{-3} potassium chloride
0.1 mol dm^{-3} interfering chloride (aq.)) and

Table 1
Membrane composition (m/m%) for valinomycin ISEs

	Valinomycin	Other components[a]		
This report	2.0	KTpClPB, 0.5	DOS, 64.7	PVC, 32.8
Knoll et al. [16]	2.0	KTpClPB, 0.5	DOS, 64.7	PVC, 32.8
Cosofret et al. [26] (Membrane L)	1.0	KTpClPB, 0.5	DOS, 49.5	PVC[b], 49.0
Ammann et al. [27] (Membrane 23)	5.0	KTpClPB, 2.0	DBS, 68.0	2,3 DMNB, 25.0
Ammann et al. [27] (Membrane 8)	1.0	—	DOS, 66.0	PVC, 33.0
Anker et al. [28] (PVC/DOS)	1.0	—	DOS, 66.0	PVC, 33.0
Jenny et al. [29] (PVC/DOS)	1.0	—	DOS, 66.0	PVC, 33.0
Miyahara and Simon [30] (PVC/DOS)	1.0	—	DOS, 66.0	PVC, 33.0
Miyahara and Simon [30] (PVC/TOTM)	1.0	—	TOTM, 66.0	PVC, 33.0
Miyahara and Simon [30] (OH-PVC/DOS)	1.0	—	DOS, 66.0	OH-PVC, 33.0
Moody et al. [31]	0.9	—	NPOE, 67.3	PVC, 31.8
Anker et al. [28] (PVC/BBA)	1.3	—	BBA, 68.3	PVC, 30.4
Anker et al. [28] (Silopren K 1000)	2.5	—	Silopren K 1000, 83.0	Cross-linking agent K11, 14.5
Jenny et al. [29] (Silopren K 1000)	2.5	—	Kilopren K 1000, 83.0	Cross-linking agent K11, 14.5
Gadzekpo and Christian [3][c]				

[a] Abbreviations (those not listed in Table 2 are given in Section 2): DOS, dioctylsebacate; DBS, dibutylsebacate; 2,3 DMNB, 2,3-dimethyl-nitrobenzene; TOTM, tri-(2-ethylhexyl)trimellitate; NPOE, ortho-nitrophenyloctylether; BBA, bis(1-butylpentyl)adipate.
[b] Carboxylated.
[c] The valinomycin ISE used was obtained from Beckmann Instruments.

then mixture 2 (5, 15, 30, 100, 400 and 1000 μdm^3), (1.00 mol dm^{-3} potassium chloride (aq.), 0.1 mol dm^{-3} interfering chloride (aq.)) were added in the order given. These additions were made with micropipettes, keeping the tip of the micropipettes just above the surface of the solutions while making the addition. The solution was stirred magnetically throughout. After each addition, the potential of was recorded after 1 min. After all additions had been made, the entire procedure was repeated twice. In this manner, the primary ion (K^+) concentration was varied over a very wide range (8.0×10^{-7}–0.06 mol dm^{-3}) while the interfering ion concentration was kept constant without having to transfer the electrodes to new solutions.

This procedure was repeated for other interfering ions (Li^+, NH_4^+, Ca^{2+}, Mg^{2+} and Ba^{2+}).

Potentiometric selectivity coefficients were also determined by the SS method [1] (0.1 mol dm^{-3} solutions of metal chlorides) for comparison.

2.4. Treatment of results

The potential, E, of a potassium-selective electrode in the presence of both K^+ and an interfering ion, B^{z+}, is given by the Nikolskii–Eisenman equation:

$$E = E^0 + S \log(a_K + k_{KB}^{Pot} a_B^{1/z}) \quad (1)$$

where: E^0 is the cell constant; S is the Nernstian slope factor; k_{KB}^{Pot} is the potentiometric selectivity coefficient; a is the activity of the subscripted ion; z is the ionic charge on the interfering ion.

Single-ion activity coefficients, f, were calculated using the Davies equation:

$$\log f = -Az^2 \left(\frac{\sqrt{I}}{1+\sqrt{I}} - 0.2I \right) \quad (2)$$

where I is the ionic strength of the solution and A is the Debye–Hückel parameter which was determined using:

$$A = 1.82481 \times 10^{-6} (DT)^{-1.5} \text{ mol}^{1.5}\text{dm}^{-0.5} \quad (3)$$

where T is the absolute temperature and D is the dielectric constant of the solvent.

The values used for D for the solvent water were either the known value at 20°C [17] or calculated values based on the temperature of the experiment and empirical equations [18]. Corrections were made to experimental potentials using estimations of the liquid junction potentials, E_J, of the reference electrode, calculated according to the Henderson formula [19] using single-ion activities. A typical set of results are given in Table 2 for Na^+ as the interfering ion.

Non-linear curve fitting was carried out to fit the mean experimental values of the corrected cell potentials given in Table 2, to the Nikolskii–Eisenman model (Eq. (1)), using the optimisation add-in, Solver, available in Microsoft Excel for Windows 95 version 7.0 and the method of Walsh and Diamond [20]. The optimised model returned estimates for the model parameters k_{KB}^{Pot} (see Table 3, Study 1), E^0 and S (both given in Table 4). In the case of each interfering ion, the potential of the solution containing interfering chloride only was ignored in the analysis as the drift in this reading was far greater than that for any other reading (typically after 1 min, when the reading was taken, the drift was 0.1 mV s^{-1} for the solution containing interfering chloride only but for any other reading, it was approximately 0.2 mV min^{-1} after 1 min). It is worth noting that for a given set of measurements, optimisations with Solver produced the same set of values for E^0, S and k_{KB}^{Pot} regardless of the initial values of these parameters. Thus, we can be confident that the optimisations converged at the global minimum, and that the error space is relatively smooth. The experimental potentials and those obtained by Solver are plotted in Fig. 1(a)–(f).

Table 2
Potentials (E_{mean}) obtained in solutions containing a fixed background concentration of 0.1 mol dm^{-3} and variable K^+ concentration

a_K	a_{Na}	E_{mean} mV^{-1}	S.D.[a] mV^{-1}	E_J mV^{-1}
0	0.07726	−176.0[b]	3.8	0.052
6.18E-07	0.07726	−172.9	4.1	0.052
2.16E-06	0.07726	−168.8	3.8	0.052
8.34E-06	0.07726	−160.0	3.5	0.052
2.22E-05	0.07726	−149.2	3.2	0.052
4.37E-05	0.07726	−138.6	2.7	0.052
7.41E-05	0.07725[c]	−128.8	2.5	0.052
2.27E-04	0.07724[c]	−104.4	1.4	0.052
6.86E-04	0.07720	−77.6	1.3	0.052
0.001599	0.07713	−57.1	1.1	0.051
0.004618	0.07689	−31.4	0.5	0.050
0.016499	0.07600	0.5	1.5	0.045
0.043794	0.07433	25.3	0.8	0.037

The Na^+ activity remains relatively constant except for the most concentrated solution.
[a] S.D., standard deviation.
[b] This value was not used in the non-linear analysis as the drift in the reading was too great, as is explained in Section 2.4.
[c] The mean of these a_{Na} values were used to calculate the LOD (Eq. (7)).

An alternative to Eq. (1) for a mixture of a primary ion and an interfering ion with ionic charges of $+1$ and $+2$, respectively, has recently been proposed by Meyerhoff and co-workers [14]:

$$E = E^0 + \frac{RT}{F} \ln\left(\frac{a_K}{2} + \frac{\sqrt{{a_K}^2 + 4a_B(k_{KB}^{Pot})^2}}{2}\right) \quad (4)$$

Replacing the RT/F term with the Nernstian slope factor, S and using common logs, Eq. (4) becomes:

$$E = E^0 + S \log\left(\frac{a_K}{2} + \frac{\sqrt{{a_K}^2 + 4a_B(k_{KB}^{Pot})^2}}{2}\right) \quad (5)$$

Using the same experimental data, Eq. (5) was fitted to the mean values of the corrected cell potentials, in the cases of the doubly-charged interfering ions. See Fig. 2(a)–(c) for the response curves and Table 3, Study 2 and Table 4 for the electrode characteristics obtained using Eq. (5) as the model for the response curve.

The data obtained from calibration of the ISE (i.e., where measurements are made on solutions containing only the primary salt) can also be modeled with this Solver technique, simply by assuming that the sum of the $k_{KB}^{Pot}a_B^{1/z}$ terms in the extended version of Eq. (1) for several interfering ions is constant for each of the calibration solutions. However, Eq. (5) was not used to model the calibration results as it is applicable only for a mixture of a primary ion of charge $+1$ and one interfering ion of charge $+2$.

Table 3
Log of potentiometric selectivity coefficients, $\log K_{KB}^{Pot}$, for valinomycin ISEs

Study		Method	Interfering ion					
			Li^+	Na^+	NH_4^+	Mg^{2+}	Ca^{2+}	Ba^{2+}
1	This report	[a,b]	−4.16	−3.71	−1.94	−4.30	−4.08	−4.03
2	This report	[b,c]				−4.35	−4.13	−4.09
3	This report	[b,d]	−4.11	−3.60	−2.22	−4.17	−4.10	−3.87
4	This report	[b,e]				−4.04	−3.98	−3.73
5	This report	SS[b]	−4.39	−3.98	−1.85	−4.70	−4.01	−4.44
6	Knoll et al. [16]	MS[b]	−4.3	−4.2	—	—	—	—
7	Cosofret et al. [26] (Membrane L)	SS[b]	−3.98	−3.56	−1.81	—	−4.30	—
8	Ammann et al. [27] (Membrane 23)	SS[b]	−4.0	−3.5	—	−5.1	−4.4	−5.0
9	Ammann et al. [27] (Membrane 8)	SS[b]	−4.3	−4.1	−2.0	−4.9	−4.7	−4.6
10	Anker et al. [28] (PVC/DOS)		−4.3	−4.0	−2.0	−4.8	−4.6	−4.5
11	Jenny et al. [29] (PVC/DOS)	SS[a]	−4.28	−4.04	−2.01	−4.82	−4.59	−4.51
12	Miyahara and Simon [30] (PVC/DOS)	SS[a]	−4.47	−3.92	−1.87	−4.97	−4.50	—
13	Miyahara and Simon [30] (PVC/TOTM)	SS[a]	−4.80	−4.09	−2.04	−4.92	−4.82	—
14	Miyahara and Simon [30] (OH-PVC/DOS)	SS[a]	−3.53	−2.40	−1.82	−3.44	−3.98	—
15	Moody et al. [31]	SS[f]	−2.88	−3.02	—	−3.96	−3.80	—
16	Anker et al. [28] (PVC/BBA)		−4.7	−3.7	−1.9	−4.6	−4.8	−5.4
17	Anker et al. [28] (Silopren K 1000)		−4.3	−4.0	−1.8	−4.3	−4.2	−3.8
18	Jenny et al. [29] (Silopren K 1000)	SS[b]	−4.33	−4.00	−1.81	−4.31	−4.16	−3.77
19	Gadzekpo and Christian [3]	MS[g]	—	−3.54	—	—	—	—
20	Gadzekpo and Christian [3]	SS[h]	—	−2.15	—	−3.92	−3.74	—
21	Gadzekpo and Christian [3]	SS[i]	—	−3.17	—	−3.70	−3.68	—
22	Gadzekpo and Christian [3]	MP	—	−4.08	—	−3.68	−3.43	—

[a] Modified FI method combined with non-linear analysis based on Eq. (1).
[b] 0.1 mol dm^{-3} solutions of metal chloride.
[c] Modified FI method combined with non-linear analysis based on Eq. (5).
[d] Obtained using Eq. (7), with an LOD estimated using Eq. (1) as the model.
[e] Obtained using Eq. (7), with an LOD estimated using Eq. (5) as the model.
[f] 0.01 mol dm^{-3} solutions of metal chloride.
[g] 0.140 mol dm^{-3} solution of sodium chloride.
[h] Equal concentrations of primary and interfering ions.
[i] Unequal concentrations of primary and interfering ions.

The goodness of fit of the optimised model to the experimental data can be quantified by the standard deviation of the experimental values from best-fit curve, σ [21]:

$$\sigma = \sqrt{\frac{\Sigma (E^* - E)^2}{n - p}} \quad (6)$$

where: E^* is the predicted potential; E is the measured potential; n is number of measurements (12 in this case); p is the number of parameters to be varied to determine the curve of best fit (three in this case).

σ, unlike the correlation coefficient which can be used in linear regression only, is approximately equal to experimental error of the dependent variable and has the same unit of measurement.

For comparison, Table 3 also lists potentiometric selectivity coefficients, obtained using the SS method [1] (Study 1), and the FI method [1] (Study 3 and 4, in the case of the doubly charged interfering ions) using the same FI experimental data and Eq. (7) [22]. The limit of detection (LOD) used when applying Eq. (7) is estimated by determining the K^+ activity for which the linear and rising portion of the graph deviates by $2.303RT \log 2/F$ mV from the curved part as described the Nikolskii–Eisenman model (Study 3) or by Eq. (5) (Study 4). As the interfering ion

Table 4
Other ISE characteristics

Interfering ion	S mV^{-1} decade$^{-1a,b}$	E^0 mV$^{-1a,b}$	LOD ($\log a_K$)	Model equation
—	57.84 ± 0.24	100.65 ± 0.65	-5.70	Eq. (1)
Li^+	58.23 ± 0.06	101.28 ± 0.33	-5.22	Eq. (1)
Na^+	56.87 ± 0.49	101.83 ± 0.30	-4.72	Eq. (1)
NH_4^+	56.67 ± 0.50	99.44 ± 0.83	-3.17	Eq. (1)
Mg^{2+}	57.00 ± 0.13	96.27 ± 0.27	-4.97	Eq. (1)
Ca^{2+}	56.88 ± 0.04	96.98 ± 0.33	-4.90	Eq. (1)
Ba^{2+}	55.94 ± 0.68	96.09 ± 1.56	-4.67	Eq. (1)
Mg^{2+}	55.43 ± 0.20	92.82 ± 0.12	-4.84	Eq. (5)
Ca^{2+}	55.05 ± 0.11	93.14 ± 0.14	-4.78	Eq. (5)
Ba^{2+}	53.98 ± 0.81	91.95 ± 1.80	-4.53	Eq. (5)

[a] The S and E^0 values quoted were obtained by linear analysis on the mean of the corrected potentials.
[b] The errors quoted are the standard deviation of the values obtained from non-linear analysis of three replicate data sets for the interfering ion studies. In the case of pure K^+ solutions (first row), the errors are the standard error of the slope and intercept of the regression line calculated over the activity range 10^{-4}–0.1 M.

activity varies slightly (for example, see Table 2), the mean value of a_B^{1/z_B} in the region of the LOD was used to calculate the potentiometric selectivity coefficient when using Eq. (7).

$$k_{KB}^{Pot} = \mathrm{LOD}/a_B^{1/z_B} \quad (7)$$

The estimated limits of detection are given in Table 4.

3. Results and discussion

Before testing newly fabricated electrodes, the membrane integrity was checked by measuring the d.c. resistance. These were found to lie in the range 1.0–1.1 MΩ, which is typical for PVC-membrane ISEs [23].

Table 3 shows that the $\log k_{KB}^{Pot}$ values obtained using the data analysis method based on Nikolskii–Eisenman model (Study 1) are very similar to those obtained for similar membrane compositions using both the conventional FI method (Study 3) and the SS method (Study 5). Given the variety of experimental conditions, methods and conditions under which the measurements were made, the degree of agreement between the results of the various studies illustrated in Table 3 is very encouraging. In almost every case, the general trend is the same ($Li^+ < Na^+ < NH_4^+$ and $Mg^{2+} < Ca^{2+}$), and the values are within an order of magnitude of each other. One exception is the value for the Li^+ potentiometric selectivity coefficient reported by Moody et al. (Study 15) [31] which is significantly lower than all other studies. Gadzekpo and Christian [3] obtained very different $\log k_{KB}^{Pot}$ values (by four different methods) for a valinomycin-based potassium ISE (see value for Na^+ potentiometric selectivity coefficient for example, Studies 19–22). In the case of Ca^{2+} and Ba^{2+}, good selectivity is obtained by all three methods used in this research, although there are some slight differences in the values of the coefficients. However, this is to be expected in these types of measurements, and is reflected in the variations reported by other researchers (see Table 3). Metzger et al. [24] and Gadzekpo et al. [25] have also demonstrated with a number of ionophores that different values for potentiometric selectivity coefficients are obtained depending on whether the FI method or the MP method is used. We believe that our new method is to be preferred as it involves minimising the sum of the squares of the errors over the entire data set (covering a wide range in primary ion activity) rather than using selected portions of the response curve in a very subjective way.

Of results quoted from other researchers in Table 3, those from Knoll et al. [16] (Study 6) are

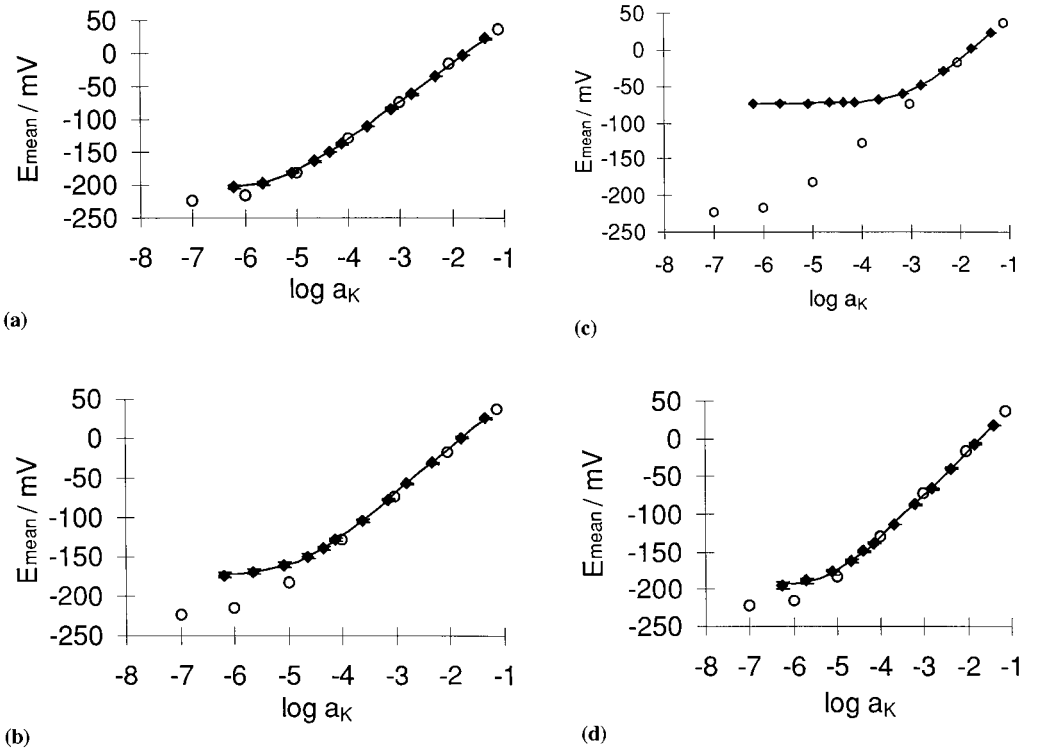

Fig. 1.

important as the membrane components and composition employed are identical to those used in this investigation, and they used the FI method [1] for determining potentiometric selectivity coefficients. Cosofret et al. [26] (with Membrane L in their paper) used membranes with similar components and composition to this investigation but estimated the potentiometric selectivity coefficients by means of the SS method (Study 7). In both cases, while the values are not an exact match with our data (Study 1), the variations are reasonable given the differences in experimental methods and design.

Table 3 also lists the $\log k_{KB}^{Pot}$ values obtained with the formalism (Eq. (5)) recently proposed by Meyerhoff and co-workers for situations where the primary ion charge is $+1$ and the interfering ion charge is $+2$ (Study 2). These values were calculated using the same experimental data used for the Nikolskii–Eisenman model (Study 1), but with the least squares error generated from Eq. (5). The trends in the $\log k_{KB}^{Pot}$ values using both models are the same ($Mg^{2+} < Ca^{2+} \approx Ba^{2+}$), but Eq. (5) generates slightly more negative values. With both models, the average relative standard deviation of the potentiometric selectivity coefficient for the three doubly charged interferents is 15–16% ($n = 3$). The trends in the $\log k_{KB}^{Pot}$ values obtained with the conventional FI method [1], using both the Nikolskii–Eisenman equation and Eq. (5) are also the same ($Mg^{2+} \approx Ca^{2+} < Ba^{2+}$, see the Study 3 and 4 results).

In the light of Bakker's work on ISEs conditioned in an interfering ion solution [4], it could be argued that the potentiometric selectivity coefficients obtained are merely an indication of the detection limit of the ISE. If our results were in fact a measure of the LOD of the electrode, then one expect that the effect of the interfering ion would be the same in each case. However, the

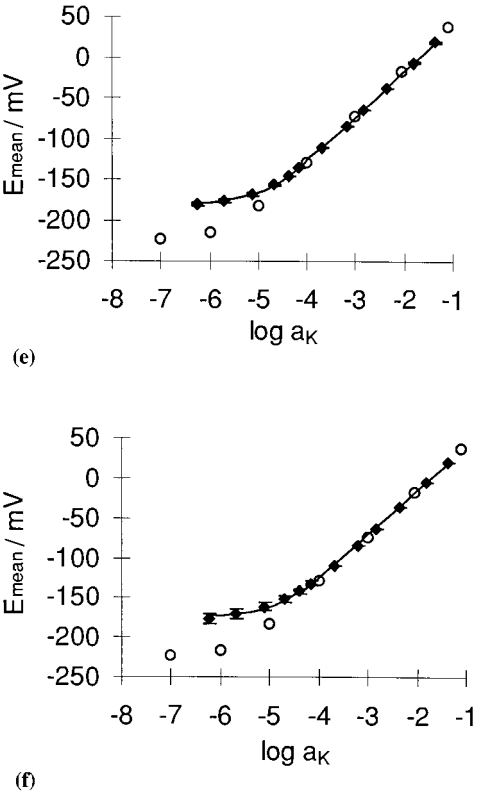

Fig. 1. (a)–(f) Plot of mean experimental potentials (◆) and predicted potentials (line) according to the optimised model based on Eq. (1), versus log a_K with standard deviations as error bars ($n = 3$). The interfering ions are Li^+ (a), Na^+ (b), NH_4^+ (c), Mg^{2+} (d), Ca^{2+} (e) and Ba^{2+} (f). The circular points are potentials obtained with pure potassium chloride solutions.

response curves in Fig. 1 invalidates this latter argument as the location of the plateau region of the graph is clearly dictated by the identity of the interfering ion. Clearly therefore, the log k_{KB}^{Pot} values obtained with our new method are a measure of practical selectivity.

The Nernstian Slope Factors, S, obtained using the Nikolskii–Eisenman model and Eq. (5) (given in Table 4), are all close to the ideal Nernstian values, as would be expected for a valinomycin ISE.

The cell constants, E^0, obtained with the Nikolskii–Eisenman model (Table 4), are similar for interfering ions of a given charge but are different for ions of different charge. One reason for this difference is that the E^0 values for the doubly-charged ions decreased by approximately 2 mV on correcting the experimental potentials for variation in the liquid junction potentials but this correction brought about negligible change in the E^0 values for the singly-charged ions (i.e., agreement was closer prior to correction). Similar values are obtained with Eq. (5) as the model as would be expected. Nernstian slope factors obtained in the presence of doubly-charged interfering ions are slightly higher (by ca. 0.6 mV) and the log (LOD) values are slightly more negative using Eq. (5) as the model. Overall, the differences in electrode parameters returned by the two models are small. Given the ease with which Excel can be set up to model either equation with the same data sets, it would be for other groups to compare electrode parameters obtained with both approaches. We have already obtained data show-

ing similar agreement for parameters calculated Meyerhoff's formalism and the Nikolskii-Eisenman equation from data obtained with the calcium selective electrode and several singly-charged interferents.

In any curve-fitting exercise, it is useful to compare the quality of the fits obtained with the experimental data. One approach is to use the standard deviations of the experimental values from the best-fit curves, σ (see Eq. (6)) [21].

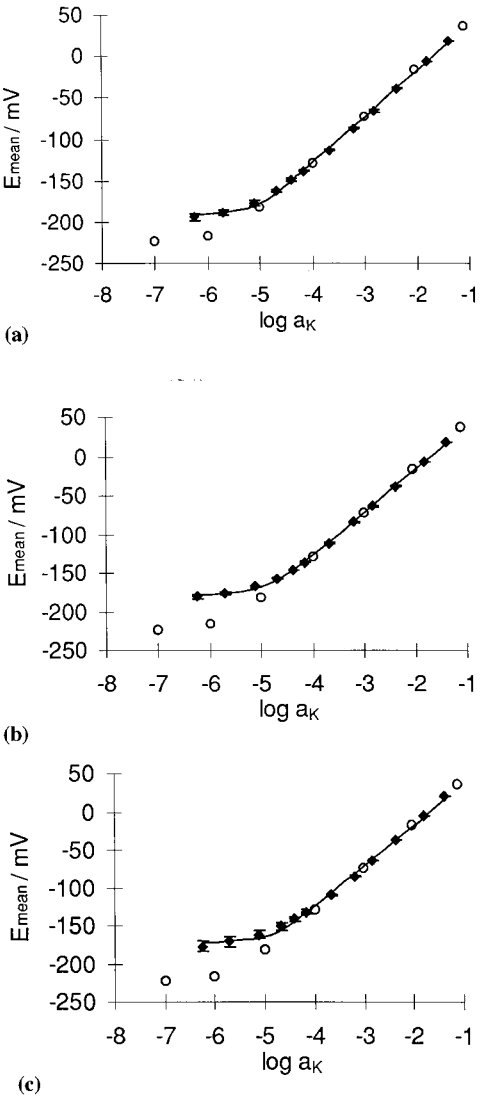

Fig. 2. (a)–(c) Plot of mean experimental potentials (◆) and predicted potentials (line) according to the optimised model based on Eq. (5), versus $\log a_K$ with standard deviations as error bars ($n = 3$). The interfering ions are Mg^{2+} (a), Ca^{2+} (b) and Ba^{2+} (c). The circular points are potentials obtained with pure potassium chloride solutions.

Table 5
Standard deviation of the experimental values from the curve of best fit, σ

Interfering ion	σ/mV$^{-1a,b}$	σ/mV$^{-1a,b}$
	Model: Eq. (1)	Model: Eq. (5)
Li^+	0.68 ± 0.02	
Na^+	0.86 ± 0.22	
NH_4^+	0.51 ± 0.04	
Mg^{2+}	0.96 ± 0.12	2.28 ± 0.18
Ca^{2+}	0.71 ± 0.02	2.03 ± 0.04
Ba^{2+}	2.07 ± 0.58	3.50 ± 0.35

[a] Obtained by non-linear analysis of the mean corrected potentials.
[b] The errors quoted are standard deviation of the values obtained from non-linear analysis of the individual potentials.

Table 5 lists the σ values obtained using Eq. (1) (and Eq. (5) for the doubly charged interfering ions) as the models. These values are low enough to suggest that the optimised model fits the experimental data very well for each interfering ion and that therefore, the values returned for the model parameters are accurate. For example, in the case of Na^+, the σ value of 0.86 mV is very low considering the large range in potentials covered (more than 200 mV), and the standard deviation in the experimental mean potentials which vary from 0.8 mV (at high K^+ activity) to 4.1 mV ($n = 3$). The utility of the σ parameter is well illustrated by comparing the values for the different ions. Clearly, Ba^{2+} gives by far the worst fit for both models, and this is confirmed by visually comparing the actual curves (see Fig. 1(f) in comparison with other curves in Fig. 1 and Fig. 2(c) in comparison to other curves in Fig. 2).

The σ values obtained when using Eq. (5) as the model for the doubly-charged interfering ions, are greater than that obtained when using the Nikolskii–Eisenman model. This would suggest, in the case of our data, that the –Eisenman model (Eq. (1)) gives a better overall fit to the experimental data than Eq. (5).

The residual plots resulting from the fits obtained by the two models are illustrated in Fig. 3(a)–(c). These plots confirm that the Nikolskii–Eisenman model gives better fits in all three cases to those obtained with Eq. (5). Our results therefore suggest that there is no major difference in the electrode parameters obtained with either model, but that the quality of the fit is superior with the Nikolskii–Eisenman model for these particular data.

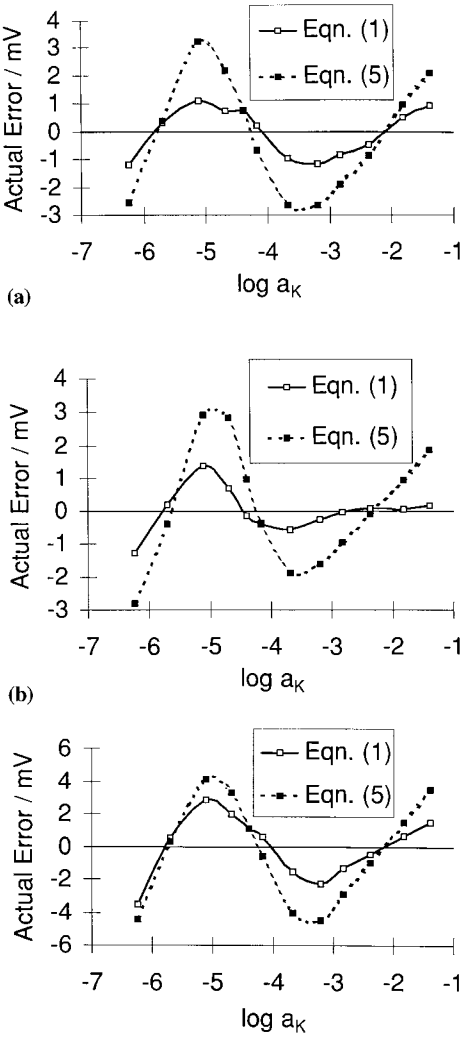

Fig. 3. Plot of residual error resulting from the fit of the Eq. (1) (solid line) and Eq. (5) (broken line) to the mean experimental potential versus log a_K. The interfering ions are Mg^{2+} (a), Ca^{2+} (b) and Ba^{2+} (c).

4. Summary

We believe that the method of determination of potentiometric selectivity coefficients described in this paper is superior to the conventional mixed solution and SS methods for the following reasons:

1. Conventional beaker-to-beaker measurements are prone to carry-over contamination between measurements; this cannot occur in the experimental procedure that we have developed as all measurements are performed in a single vessel.
2. Relatively few solutions need to be made up, and the experimental procedure is practically simple to implement. Hence it is easy to replicate data sets.
3. Transfer of electrodes between beakers results in the formation of an open circuit with associated large transient shifts in cell potential, which the cell may or may not fully recover from. This does not happen in the proposed method as the electrodes are in continuous contact with the sample, and no open circuit is generated at any time during an experimental run.
4. The use of a non-linear curve fitting approach means that all the experimental data are used to estimate the electrode parameters. Unlike the conventional FI method [1], there is no element of subjectivity, and the approach can easily cope with ions of differing charge.
5. The ease with which Excel spreadsheets can be modified allows the analyst to quickly investigate the usefulness of models other than the Nikolskii–Eisenman equation such as Eq. (5). A macro can be easily written (with the Record Macro option on the Tools menu) for modifying the Worksheet relating to one interfering ion and this macro is then executed for each of the other interfering ions.
6. The quality of the electrode parameters can be compared at a glance through the σ value in a single run. Furthermore, examination of the response curves in Fig. 1 and Fig. 2, or the residual error plots (Fig. 3) enable a very comprehensive picture of the data quality to be obtained.

7. Finally, Solver can change up to 200 parameters simultaneously and so, in principle, potentiometric selectivity coefficient measurements can be made for a primary ion in the presence of many interfering ions, should this be required.

In conclusion, we feel that this approach, if adopted by other investigators, would enable electrode parameters to be more rigorously measured, and would lead to much greater confidence in the applicability of these data.

Acknowledgements

The authors gratefully acknowledge grand aid from the Irish American Partnership, Forbairt and City Research for P.K.

References

[1] G.G. Guilbault, R.A. Durst, M.S. Frant, H. Freiser, E.H. Hansen, T.S. Light, E. Pungor, G. Rechnitz, N.M. Rice, T.J. Rohm, W. Simon, J.D.R. Thomas, Pure Appl. Chem. 48 (1976) 127.
[2] Y. Umezawa, K. Umezawa, H. Sato, Pure Appl. Chem. 67 (1994) 507.
[3] V.P.Y. Gadzekpo, G.D. Christian, Anal. Chim. Acta 164 (1984) 279.
[4] E. Bakker, J. Electrochem. Soc. 143 (1996) L83.
[5] G.J. Moody, J.D.R. Thomas, Selective Ion Sensitive Electrodes, Marrow, Watford, 1971.
[6] K. Srinivasan, G.A. Rechnitz, Anal. Chem. 41 (1969) 1203.
[7] C. Maccà, Anal. Chim. Acta 321 (1996) 1.
[8] W. Yuliang, Z. Zhiang, Z. Zhiyi, Fenxi Shiyanshi 13 (4) (1994) 56.
[9] D.E. Davey, D.E. Mulcahy, G.R. O'Connell, Electroanalysis (N.Y.) 8 (3) (1996) 274.
[10] R. Forster, D. Diamond, Anal. Chem. 64 (1992) 1721.
[11] D. Diamond, R.J. Forster, Anal. Chim. Acta 276 (1993) 75.
[12] F.J. Saez de Viteri, D. Diamond, Analyst 119 (1994) 749.
[13] W.E. Morf, D. Ammann, E. Pretsch, W. Simon, Pure Appl. Chem. 36 (1973) 421.
[14] E. Bakker, R.K. Mervura, E. Pretsch, M.E. Meyerhoff, Anal. Chem. 66 (1994) 3021.
[15] J. Lu, Q. Chen, D. Diamond, J. Wang, Analyst 118 (1993) 1131.
[16] M. Knoll, K. Cammann, C. Dumschat, M. Borchardt, G. Högg, Sens. Actuators B20 (1994) 1.
[17] D. Lide (Ed.), CRC Handbook of Chemistry and Physics, 76th ed., CRC Press, 1995, pp. 6–160.
[18] D. Lide (Ed.), CRC Handbook of Chemistry and Physics, 76th ed., CRC Press, 1995, pp. 6–193.
[19] P.C. Meier, D. Ammann, W.E. Morf, W. Simon, in: J. Koryta (Ed.), Medical and Biological Applications of Electrochemical Devices, Wiley, Chichester, 1980, p. 22.
[20] S. Walsh, D. Diamond, Talanta 43 (4) (1995) 561.
[21] J.H. Noggle, Practical Curve Fitting and Data Analysis, Ellis Horwood, 1993.
[22] A.K. Covington (Ed.), Ion Selective Electrode Methodology, vol. 1, CRC Press, Boca Raton, Florida, 1979.
[23] D. Diamond, F. Regan, Electroanalysis (N.Y.) 2 (2) (1990) 113.
[24] E. Metzger, D. Ammann, R. Asper, W. Simon, Anal. Chem. 58 (1986) 132.
[25] V.P.Y. Gadzekpo, J.M. Hungerford, A.M. Kadry, Y.A. Ibrahim, R.Y. Xie, G.D. Christian, Anal. Chem. 58 (1986) 1948.
[26] V.V. Cosofret, E. Erdösy, R.P. Buck, W.J. Kao, J.M. Anderson, E. Lindner, M.R. Neuman, Analyst 119 (1994) 2283.
[27] D. Ammann, W.E. Morf, P. Anker, P.C. Meier, E. Pretsch, W. Simon, Ion-selective Rev. 5 (1983) 38.
[28] P. Anker, H.-B. Jenny, U. Wuthier, R. Asper, D. Ammann, W. Simon, Clin. Chem. 29 (1983) 1447.
[29] H.-B. Jenny, C. Riess, D. Ammann, B. Magyar, R. Asper, W. Simon, Mikrochim Acta II (1980) 309.
[30] Y. Miyahara, W. Simon, Electroanalysis (N.Y.) 3 (1991) 287.
[31] Moody, B. Saad Bahruddin, J.D.R. Thomas, Analyst 114 (1989) 15.

ELSEVIER

Talanta 44 (1997) 1859–1863

Talanta

Differential pulse polarographic determination of dicrotophos, crotoxyphos and chlorfenvinphos in grains and soils

N.Y. Sreedhar *, P. Rajendra Kumar Reddy, G.V. Subba Reddy, S.J. Reddy

Department of Chemistry, Sri Venkateswara University, Tirupati 517 502, India

Received 25 November 1996; received in revised form 17 February 1997; accepted 18 February 1997

Abstract

A simple, sensitive and rapid differential pulse polarographic method has been developed for the quantitative determination of organophosphorus pesticides such as dicrotophos, crotoxyphos and chlorfenvinphos in agricultural formulations in universal buffers of a pH range 2.0–12.0. The sample is treated with ethanol to facilitate the dissolution of these pesticides. Both standard addition and calibration methods can be used for the analyses. The lower detection limits are 1.25×10^{-9}, 1.05×10^{-9} and 1.0×10^{-9} M, respectively. The method can be applied successfully to determination of these pesticides in grains and soil. © 1997 Elsevier Science B.V.

Keywords: Chlorfenvinphos; Crotoxyphos; Dicrotophos; Differential pulse polarography

1. Introduction

One of the most important classes of insecticides is organophosphorus compounds. Dicrotophos [I], crotoxyphos [II] and chlorfenvinphos [III] are systemic and general insecticides [1,2]. These are effective against a wide range of insects on fruits, vegetables, and commercial crops. Today these are widely used because of their low persistence and high effectiveness. Reliable analytical procedures are therefore needed for their determination.

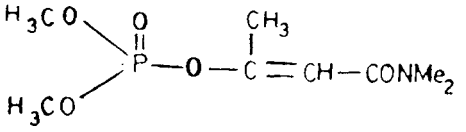

(I)

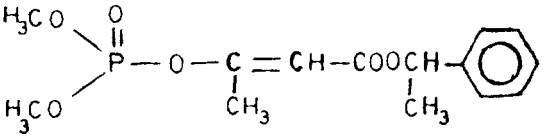

(II)

* Corresponding author.

PII S00 9-9140(97)00081-7

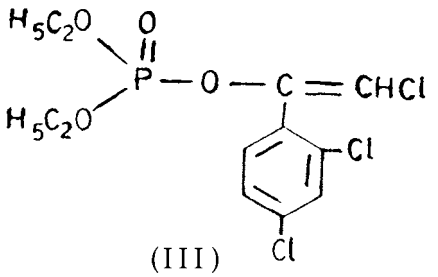

(III)

By reviewing literature of many studies [3–7] it is found that a number of organophosphorus pesticides have been determined by means of techniques such as gas chromatography, thin-layer chromatography, high performance liquid chromatography as well as spectrophotometry. A gas chromatographic method has been used for the determination of dicrotophos in foods [8], and fruits and vegetables [9]. Crotoxyphos has been determined by a gas chromatographic method [10] in industrial chemical residues and by HPLC [11]. Electrochemical techniques [12,13] have been widely used for the determination of $>C{=}C<$ containing pesticides. But no discussion has been given to understanding the differential pulse polarographic behavior of the title compounds and to the determination of these compounds by means of differential pulse polarography.

This article attempts to understand the pulse polarographic behavior of these pesticides and describes an electroanalytical procedure for the determination of these pesticides in formulations, grains and soil samples with the aid of differential pulse polarography.

2. Experimental

Differential pulse polarograms were obtained with a Metrohm E506 polarecord connected to a E616 VA Scanner. The three-electrode assembly consisted of a dropping mercury electrode (of area 0.0223 cm^2) as working electrode, a saturated Ag/AgCl(s), Cl^- reference electrode, and a platinum wire auxiliary electrode. All experiments were performed at 25 ± 1°C; pH measurements were carried out with a Elico digital pH meter. Dissolved air was removed from the solutions by degassing with oxygen-free nitrogen for 10 min.

The compounds were supplied by 'Promochem', West Germany. The purity of the compounds was tested by boiling point determination. Stock solutions were prepared by dissolution of the required amounts of compounds in ethanol. The Universal buffers of pH 2.0–12.0 are prepared from 0.2 M boric acid, 0.05 M citric acid and 0.1 M tri sodium orthophosphate [14]. All chemicals used were of AnalaR grade.

3. Results and discussions

The differential pulse polarographic behavior of dicrotophos, crotoxyphos and chlorfenvinphos was examined over the pH range 2.0–12.0. All these compounds were found to give a single well-defined peak in all the buffer systems studied. The single peak is attributed to reduction of the carbon-carbon double bond ($>C{=}C<$) in a two-electron process. Typical differential pulse polarograms for crotoxyphos and chlorfenvinphos are shown in Fig. 1.

The reduction process for these pesticides is diffusion controlled and adsorption free in all the buffer systems studied, as evidenced by the linear plots of i_m (i_m = maximum current observed in differential pulse polarography) versus $t^{2/3}$ (t = drop time) passing through the origin [15]. Variation of E_m (E_m = potential at maximum current in differential pulse polarography) values toward more negative potentials upon increasing the concentration of depolarizer [16,17] indicated the irreversibility of the electrode process. In the above compounds, E_m values depend on pH and shift towards more negative potentials with an increase in pH of the buffer solutions (Fig. 2).

It is observed from a comparison of the peak potentials of the three compounds that chlorfenvinphos is more easily reduced than dicrotophos and crotoxyphos. The presence of two electron-withdrawing chlorines in chlorfenvinphos makes reduction of the carbon-carbon bond easier in chlorfenvinphos than in dicrotophos and crotoxyphos. The order of reduction is as follows

(from the comparison of peak potentials): chlorfenvinphos > crotoxyphos > dicrotophos.

3.1. Analysis

In Fig. 2, the variation of peak current for reduction of dicrotophos as a function of pH is presented. It can be observed that the peak current shows a maximum at pH 4.0, since in this media proton involvement is high making > C=C < group protonated which in turn gets reduced more easily. But in basic media (pH 8.0–12.0), the reduction of > C=C < group is not easily facilitated owing to the less availability of protons. The polarographic peaks obtained at pH 4 and 6 for the title compounds were well-resolved and used for the analysis. For the quantitative estimation of the three compounds, both calibration and standard addition methods were used. Peak heights were found to be linear in the range 1.0×10^{-5}–1.9×10^{-9} M, 1.5×10^{-5}–4.0×10^{-9} M, and 1.25×10^{-5}–1.5×10^{-9} M for dicrotophos, crotoxyphos and chlorfenvinphos, respectively. The detection limits were found to be 1.25×10^{-9} M, 1.05×10^{-9} M, and 1.0×10^{-9} M for the respective compounds. The detection limit (dl) [18] was calculated using the expression dl = 3 S.D./m, where S.D. = standard deviation and m = slope of the calibration plot.

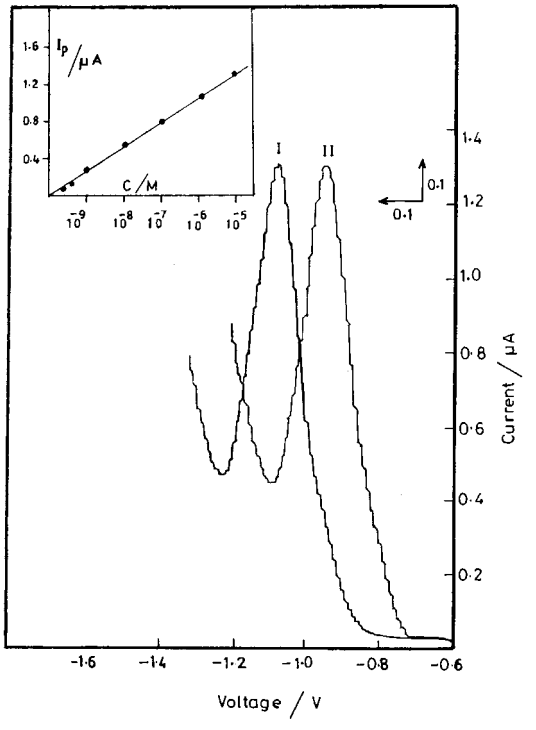

Fig. 1. Typical differential pulse polarograms of crotoxyphos (I) and chlorfenvinphos (II) in pH 4.0. Concentration = 1.0×10^{-5} M; Drop time = 2 s; Pulse amplitude = 50 mV. The linear plot of peak current versus concentration of crotoxyphos is shown in the inset.

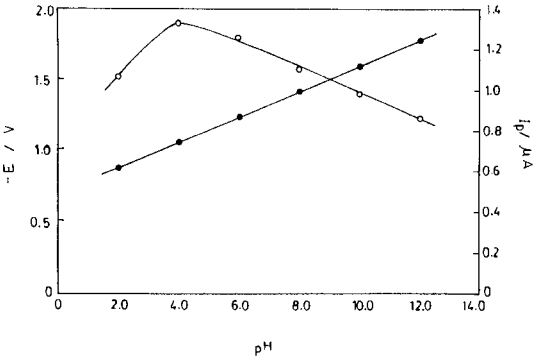

Fig. 2. Variation of peak current (○) and peak potential (●) for dicrotophos reduction as a function of pH. Concentration = 1.0×10^{-5} M; Drop time = 2 s; Pulse amplitude = 50 mV.

3.2. Recommended analytical procedure

A stock solution (1.0×10^{-5} M) is prepared by dissolution of the appropriate amount of the electroactive species in ethanol. Standard solution, 1 ml, is transferred into a polarographic cell and diluted with 9 ml of supporting electrolyte and then deoxygenated with nitrogen gas for 10 min. After the polarogram is recorded, small increments (0.2 ml) of standard solution are added and a polarogram is recorded after each addition under similar conditions. In present study, the best precision was obtained at pH 4.0, with a drop time of 2 s, a pulse amplitude of 50 mV, and an applied potential of −1.05 V, −1.12 V, and −0.95 V (vs. Ag/AgCl(s)), respectively, for the three compounds. The relative standard deviations and correlation coefficients were found to be 1.24 and 0.993%, 1.1 and 0.998%, and 1.29 and 0.996% for the respective compounds.

Table 1
Determination of dicrotophos, crotoxyphos and chlorfenvinphos in formulations by differential pulse polarography

Compound	pH of the supporting electrolyte	Labelled amount (mg)	Average amount found ± S.D. (mg)*	Average recovery (%)
Dicrotophos formulation				
Bidrin	4.0	5.0	4.98 ± 0.013	99.60
	4.0	3.0	2.95 ± 0.020	98.30
	6.0	5.0	4.85 ± 0.050	97.00
	6.0	3.0	2.91 ± 0.096	97.00
Carbicron	4.0	5.0	4.96 ± 0.020	99.20
	4.0	3.0	2.98 ± 0.010	99.33
	6.0	5.0	4.86 ± 0.073	97.20
	6.0	3.0	2.92 ± 0.032	97.33
Crotoxyphos formulation				
Ciodrin	4.0	5.0	4.95 ± 0.020	99.00
	4.0	3.0	2.97 ± 0.010	99.00
	6.0	5.0	4.90 ± 0.015	98.00
	6.0	3.0	2.89 ± 0.036	96.33
Cypona	4.0	5.0	4.97 ± 0.020	99.40
	4.0	3.0	2.96 ± 0.020	98.66
	6.0	5.0	4.86 ± 0.026	97.20
	6.0	3.0	2.91 ± 0.030	97.00
Chlorfenvinphos formulation				
Dermaton	4.0	3.0	2.99 ± 0.010	99.67
	4.0	5.0	4.92 ± 0.050	98.40
	6.0	3.0	2.92 ± 0.026	97.33
	6.0	5.0	4.87 ± 0.026	97.40
Birlane	4.0	3.0	2.95 ± 0.036	98.33
	4.0	5.0	4.93 ± 0.020	98.60
	6.0	3.0	2.90 ± 0.026	96.67
	6.0	5.0	4.89 ± 0.043	97.80

* Each value is an average of three determinations.

This procedure was successfully used for the determination of these compounds in their formulations at different pH values.

3.3. Analysis of formulations

The required quantity of formulation corresponding to a 1.0×10^{-3} M stock solution was accurately measured and transferred into a 100 ml volummetric flask containing 50 ml of ethanol. A solution of approximately 1.0×10^{-5} M was prepared by dilution of this stock solution with universal buffer. Assay results for dicrotophos, crotoxyphos, and chlorfenvinphos in formulations at pH 4.0 and 6.0 are given in Table 1.

3.4. Analysis of pesticides in grains or soil

Grain (rice or wheat) samples (50 g) or soil sample (25 g) were sprayed with known amounts of dicrotophos, crotoxyphos, or chlorfenvinphos and left for 2–4 h. The extracts were prepared by treatment of a crushed sample with 100 ml of acetone. The extract was evaporated to dryness. The residue of dicrotophos, crotoxyphos, or chlorfenvinphos was dissolved in ethanol and transferred to a 50 ml volummetric flask.

Results obtained for the determination of pesticides in grains and soil are presented in Table 2. Recoveries of dicrotophos, crotoxyphos, and chlorfenvinphos from 96.33 to 99.67%, which indicates the accuracy and reproducibility of the proposed differential pulse polarographic method.

Table 2
Recovery of dicrotophos, crotoxyphos and chlorfenvinphos added to grains and soil

Compound	Amount added (mg)	Average amount found* (mg)			Average recovery (%)		
		Wheat	Rice	Soil	Wheat	Rice	Soil
Dicrotophos	5.0	4.863	4.954	4.962	97.25	99.08	99.24
	10.0	9.895	9.845	9.825	98.95	98.45	98.25
	15.0	14.81	14.74	14.98	98.72	98.25	98.85
	20.0	19.84	19.89	19.81	99.18	99.45	99.05
Crotoxyphos	5.0	4.874	4.945	4.943	97.48	98.90	98.85
	10.0	9.810	9.915	9.855	98.00	98.65	98.55
	15.0	14.79	14.87	14.79	98.62	99.15	98.65
	20.0	19.42	19.86	19.79	97.08	99.32	98.95
Chlorfenvinphos	5.0	4.850	4.858	4.868	97.00	97.15	97.35
	10.0	9.850	9.890	9.780	98.50	98.90	97.80
	15.0	14.81	14.86	14.81	98.70	99.04	98.70
	20.0	19.52	19.65	19.78	97.60	98.25	98.90

* Each value is an average of three determinations.

The data incorporated in Tables 1 and 2 suggest that, in addition to dicrotophos, crotoxyphos, and chlorfenvinphos, other constituents present in grains and soil do not interfere in the proposed method. The proposed method is simple, rapid, reliable, and sensitive and hence can be used in insecticidal formulations. The method does not involve the elaborate clean-up procedures required with the other methods.

References

[1] W.J. Hayes (Ed.), Pesticides Studied in Man, Williams and Wilkins Publications, London, 1982.
[2] E.H.F. Donald (Ed.), Chemistry of the Pesticides, 3rd Edn., Van Nostrand, New York, 1955.
[3] E.R. Clark, I.A. Quazi, Analyst 105 (1990) 564.
[4] S. Derek Farrington, F.J. Lovett, P.V. Lynch, Analyst 108 (1983) 353.
[5] F.A. Gunther, Y. Iwater, B. Berck, G.V. Smith, Bull. Environ. Cont. Toxicology 24 (6) (1980) 903.
[6] S. Joseph, Anal. Chem. 63 (1991) 118R.
[7] S. Joseph, Anal. Chem. 67 (14) (1995) 1R.
[8] H.J. Stan, D. Mrowetz, J. High Resolut. Chromatogr. Commun. 6 (5) (1983) 255.
[9] W. Liao, T. Joe, W.G. Cusick, J. Assoc. Off. Anal. Chem. 74 (3) (1991) 554.
[10] N.V. Fehringer, S.M. Waltery, J. Assoc. Off. Anal. Chem. 67 (1) (1984) 91.
[11] L.G. Rice, J. Chromatogr. 317 (1984) 523.
[12] M. Subbalakshmamma, S.J. Reddy, Electroanalysis 6 (1994) 521.
[13] G. Madhavi, P.R.K. Reddy, S.J. Reddy, Bulletin Electrochem. 11 (10) (1995) 490.
[14] D.D. Perrin, D. Boyd (Eds.), Buffers for pH and Metal ion control Chapman and Hall, London 1974, p. 156.
[15] M.R. Smyth, J.G. Osteryoung, Anal. Chim. Acta 96 (1978) 335.
[16] M.A. Gomez Nieto, M.D. Luque De Castro, M. Valcarcel, Electrochim. Acta 28 (1983) 335.
[17] M.A. Gomez Nieto, M.D. Luque De Castro, M. Val- Electrochim. Acta 27 (1982) 435.
[18] C.S. Reddy, S.J. Reddy, Electroanalysis 4 (1992) 725.

ELSEVIER

Talanta 44 (1997) 1865–1871

Talanta

Extraction of uranium from aqueous solution by phosphonic acid-imbedded polyurethane foam

S. Katragadda, H.D. Gesser, A. Chow *

Department of Chemistry, University of Manitoba, Winnipeg, MB, R3T 2N2, Canada

Received 14 October 1996; received in revised form 25 February 1997; accepted 4 March 1997

Abstract

Phenylphosphonic acid was imbedded into the matrix of the polyurethane foam during the fabrication process of the polymer. The extraction of uranium by phosphonic acid-imbedded polyurethane foam and blank polyurethane (i.e., foam without phosphonic acid functional groups) was investigated. Phosphonic acid-imbedded foam showed superior extractability of uranium from solutions with $pH = 7.0 \pm 1.5$ over a wide range of temperature. © 1997 Elsevier Science B.V.

Keywords: Aqueous; Phosphonic; Polyurethane; Uranium

1. Introduction

Polyurethane foams have received considerable attention over the past two decades for their use in the separation and concentration of a wide variety of organic and inorganic compounds from aqueous solutions [1,2]. These foams have also been successfully used as inert supports for various extractants [3–9]. In this paper we describe a procedure for the preparation of a polyurethane foam using Hypol™ prepolymer and the incorporation of phosphonic acid groups into the polyurethane foam.

Polyurethane foams that are both elastomeric and hydrophilic, can be made by reacting Hypol™ prepolymer with active hydrogen-containing compounds (i.e., H_2O, ROH, etc.). Hypol™ prepolymers are a mixture of prepolymers derived from toluene diisocyanate. Polyurethane foams can be prepared by mixing equal weights of Hypol™ prepolymers and water. Additives may be introduced in either or both of the organic and aqueous layers [10,11].

A number of papers have been published describing the synthesis of sorbents containing phosphonic acid for the selective sorption of uranium from aqueous systems [12–16]. The synthesis of these sorbents is often tedious and difficult to undertake.

A relatively simple preparation of a phosphonic acid-imbedded polyurethane foam and the evaluation of its ability to extract uranium from aqueous solutions with a wide range of pH and temperatures will be discussed in this paper.

* Corresponding author. Fax: +1 204 2750905.

2. Experimental

2.1. Apparatus

Absorbance measurements for the determination of uranium were made with a Hewlett–Packard Model 8452A diode-array spectrophotometer. Sample solutions were pumped through a 0.5 cm pathlength, quartz flow cell using a Piper Pump™ Model P10T peristaltic pump.

The synthesized polyurethane foams were initially cut into small pieces and then placed in liquid nitrogen. The frozen foams were ground into a fine powder in a stainless steel container on a Waring™ blender. Sample solutions at 4 and 22°C were shaken with a Burrell Wrist-Action Shaker. Similarly at 40 and 70°C a Dubnoff Metabolic Shaking Incubator was used for shaking the samples. Measurements of pH were obtained using a Fisher Accumet™ Model 825MP pH meter.

2.2. Reagents

All chemicals were reagent grade and the water used was purified initially by reverse osmosis and then passed through a Barnstead Nanopure II™ system. Uranium solutions ranging from 1 to 10 ppm were prepared by successive dilution of a 2000 ppm uranium solution which was made from uranyl acetate (BDH, England).

Phenylphosphonic acid and the photometric reagent, Arsenazo III, were obtained from Aldrich (WI, USA). The prepolymer used for the production of the polyurethane foams was a sample of Hypol™ FHP2002 provided by W.R. Grace (MA, USA).

2.3. Analysis

The determination of uranium involved the use of Arsenazo III as the photometric reagent. Arsenazo III has been used as the preferred choice of chromogenic reagent for the spectrophotometric determination of uranium over the last three decades [17,18]. In moderately acidic media, uranium forms a 1:1 complex with Arsenazo III with a stability constant, $\log \beta_1 = 5.42$ [19,20]. The Arsenazo III concentration was always kept at levels slightly higher than that of uranium to ensure the complete formation of the complex while keeping the background as low as possible.

A continuous flow spectrophotometric method was employed for the determination of uranium [21]. Analysis by this method involves the simultaneous pumping of the photometric reagent (0.006% Arsenazo III in 0.12 *M* HCl) and the uranium solution into a flow mixing cell to form the uranium-Arsenazo III complex. This complex then enters the analytical flow cell where the absorbance measurements are recorded using the diode-array spectrophotometer.

The choice of dissolving Arsenazo III in 0.12 *M* HCl permitted the analysis of uranium solutions with a wide range of pH values. Acid concentrations greater than 0.12 *M* HCl produced larger errors with low pH uranium solutions due to changes in the uranium species present in highly acidic solutions. Concentrations lower than 0.12 *M* HCl resulted in larger errors with higher pH uranium solutions because this mixture resulted in neutral or basic solutions which affect the solution constituents.

Quantitative analysis of uranium was obtained by using the 'Quantitation' program which was part of the software menu for the Hewlett–Packard system. Internal referencing was used to improve the precision of the readings by reducing the impact on the baseline of any changes due to dust, air or variations in lamp intensity. The absorbance at 768 nm on the baseline was subtracted from the absorbance at the analytical wavelength of 650 nm. The difference in absorbance was used for both calibration and sample analysis. The calibration curve shown in Fig. 1 was obtained by using a second order curvefit for uranium standards ranging from 1 to 10 ppm. A 10 ppm uranium standard solution and a water blank were analysed ten times to determine the precision of the analytical technique. The averages found were 10.0 ± 0.03 and 0.0 ± 0.05 ppm uranium [21].

2.4. Procedure

Polyurethane foams can be made by mixing Hypol™ prepolymers with water and improvements to the foam can be attained by mixing in different additives. In a preliminary study [21], several experiments were performed to investigate the effects of changing the ratio of Hypol™ prepolymer to aqueous layer and the effect of phenylphosphonic acid as an additive in the aqueous layer.

The foams were prepared by mixing 10 ml of Hypol™ prepolymer with various amounts of water in a 150 ml glass beaker and stirring with a glass rod. Phenylphosphonic acid was added to the aqueous layer. Foams were prepared with the aqueous layer adjusted to pH values of 1, 7 and 13. A solution of pH 1 was obtained by simply dissolving phenylphosphonic acid; pH 7 and 13 solutions were prepared by the addition of 2 *M* NaOH.

When the ratio of the polymer to aqueous layer was 1:0.5, the result was a strong but hydrophobic foam. When the ratio was 1:2, the foam produced

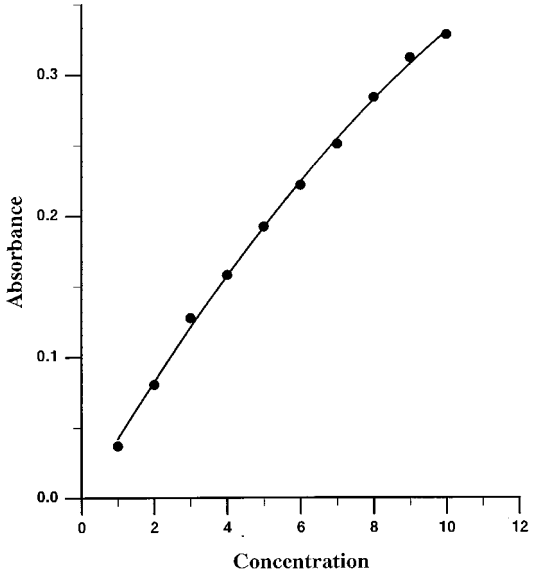

Fig. 1. Calibration graph for uranium standards between 1 and 10 ppm. A 5 mm Markson™ cell and 0.006%. Arsenazo III in 0.12*M* HCl were used.

was weak in mechanical strength but hydrophilic in nature. The optimal foam which is both hydrophilic and strong was obtained when the ratio of reagents was 1:1. Several other variations in polymer to aqueous layer ratios were studied. In some experiments a surfactant was added and/or a weak vacuum applied in an attempt to improve the formation of the foam. Among the various formulations attempted, only one produced a foam that was hydrophilic, elastomeric and capable of sorbing uranium from aqueous solution. This foam, called 'phosphonic acid foam', was used for all subsequent experiments. This phosphonic acid foam was obtained by mixing the prepolymer and water in a 1:1 ratio with 5% wt/wt phenylphosphonic acid in the aqueous layer with this layer at pH 1.0. The mixture was rapidly stirred for 15 s with the use of a glass rod. The mixing resulted in a cloudy emulsion followed by a slow increase in volume due to the release of carbon dioxide.

The resulting phosphonic acid foam became tack-free within 5 min and was air-dried in a fumehood for 8 h. The dried foam was cut into small pieces and immersed in liquid nitrogen. The frozen foam became brittle and was easily ground to a fine powder using a blender. Powdering the foam was necessary to reach equilibrium more quickly between the polymer and the uranium solution and to ensure more reproducible results. The powdered foams were initially soaked in water for 4 h and the resulting slurry was then filtered through a Whatman™ No. 541 filter paper using a Buchner funnel. The foam was recovered from the filter and the complete procedure, soaking and filtering, was repeated twice more. The foam was then cleaned in an identical manner with acetone. This procedure should remove all water or acetone soluble impurities from the foam. The clean, powdered foam was then vacuum dried for 4 h to remove traces of acetone from the foam. Blank polyurethane foam was prepared by a similar process without the addition of phenylphosphonic acid. The colour of the phosphonic acid foam was light brown in comparison to the blank foam which was white.

The capability of the foams to extract uranium was tested by adding 25 ml of 10 ppm uranium

solution to a 60 ml Nalgene™ polypropylene screwtop bottle together with 0.200 ± 0.003 g of the powdered foam. The capped bottles were shaken for 5 h using an automatic shaker. The solutions were filtered and then analyzed for uranium content. The Nalgene™ bottles with standard solutions were used to obtain a calibration curve and Fig. 1 shows that there was no sorption of uranium by the bottles.

2.5. Evaluation of the foam

Uranium solutions with pH values between 1.4 and 11.0 and at different temperatures between 4 and 70°C were used to evaluate the extraction characteristics of the phosphonic acid foam and the blank foam. The pH of the solutions was adjusted with 2 *M* HCl or 2 *M* NaOH using a pH meter. Uranium solutions were equilibrated to the required temperatures for several hours before adding them to the plastic bottles containing the foams. The uranium solutions were shaken at 4 and 22°C using a Burrell Wrist Action Shaker and at 40 and 0°C using a Dubnoff Metabolic Shaking Incubator with a variable temperature-controlled water bath. Temperature measurements were within ± 2°C during the shaking process.

The percentage extraction was calculated as

$$\%E = 100 \times \frac{(I - F)}{I}$$

where $\%E$ is the percent extraction, F is the concentration of uranium remaining in solution after extraction and I is the original concentration of uranium available for extraction. I is the concentration of uranium of a standard solution after treating it to the same filtration, pH and temperature conditions as the foam sample solutions with the exception of the foam.

The concentration of available uranium must be used rather than the calculated initial concentration to adjust for any loss of uranium during filtration due to precipitation of uranium. Uranium precipitation is known to occur at $pH > 2$ although this is not generally visible; Feldman et al. [22] observed the precipitation from uranyl nitrate solutions at $pH > 4.5$ by using centrifugation. Experiments were performed in triplicate at the same pH and temperature and the average values of I and F used to calculate $\%E$.

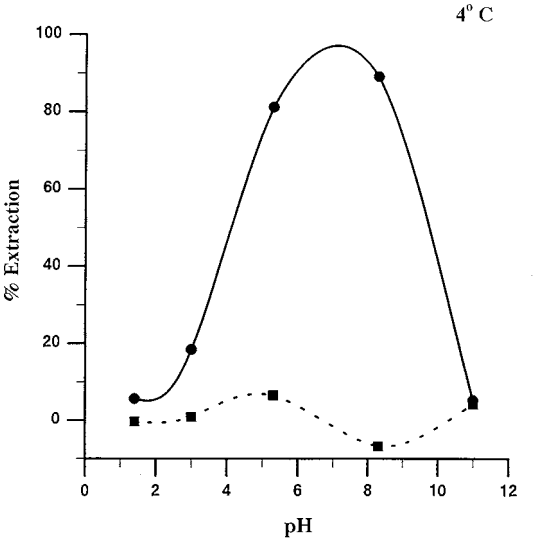

Fig. 2. Comparison of the extraction capability of urganium from aqueous solutions by phosphonic acid-imbedded polyurethane foam and blank foam at 4°C. – • – Phosphonic acid foam – ■ – blank foam.

3. Results and discussion

A study was done at 22°C using various times for the equilibration process. It was found that the extraction increased up to 2.5 h and then stabilized. In all subsequent experiments a time of 5 h was used to ensure equilibrium. Phosphonic acid foam exhibits good extraction capabilities for the sorption of uranium, which exists as various oxycation species of uranium (VI), between pH 5.3 and 8.2. The extraction capability decreases at either end of the pH range as shown in Figs. 2–5. The decrease in extraction is due to the presence of different proportions of several uranium species dependent on the pH of the solution. The species formed in aqueous HCl solutions below pH 3 and UO_2Cl_2 and UO_2Cl^+ [23] which do not seem to be extractable. In basic solutions above pH 10, other species which may not be extractable by the phosphonic acid foam, such as $UO_2(OH)_3^-$ are formed because of the hydrolysis of the uranyl ion [23].

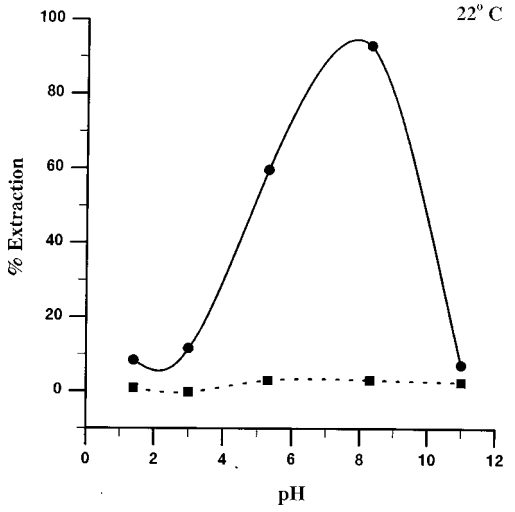

Fig. 3. Comparison of the extraction capability of uranium from aqueous solutions by phosphonic acid-imbedded polyurethane foam and blank foam at 22°C. – • – Phosphonic acid foam – ■ – Blank foam.

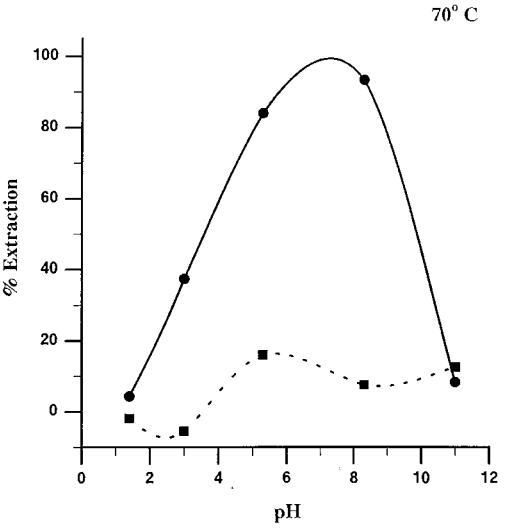

Fig. 5. Comparison of the extraction capability of uranium from aqueous solutions by phosphonic acid-imbedded polyurethane foam and blank foam at 70°C. – • – Phosphonic acid foam – ■ – Blank foam.

The extraction of uranium generally increases with an increase in temperature from 4 to 70°C between pH 3 and pH 8 as shown in Figs. 2–5. For this phosphonic acid foam, the best extraction is achieved at 70°C for aqueous uranium solutions at pH 3 to 8. At this temperature more extraction was observed over a broader pH range. It can be seen that the maximum extraction occurs at pH values close to 7.0 where approximately 95% extraction is obtained. This may be useful as natural waters are generally in the pH range 6–8. Although the discussion above is based partly on interpolated data, the general performance of the phosphonic acid foam can be observed for a wide range of temperatures and pH values. It was also visibly apparent in these studies that uranium is extracted more rapidly at higher temperatures. The decrease in extraction efficiency at either end of the pH range suggests that solutions with pH less than 1 or greater than 11 can be used as eluting agents to desorb uranium from the foam. Blank foams formed without the inclusion of phenylphosphonic acid, showed little capability to extract uranium from aqueous solutions in comparison to the phosphonic acid foam produced as shown in Table 1.

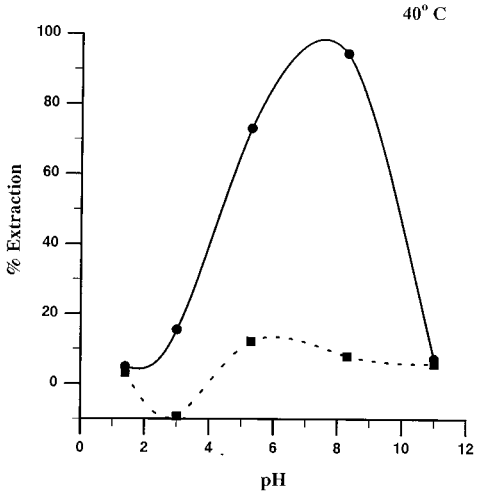

Fig. 4. Comparison of the extraction capability of uranium from aqueous solutions by phosphonic acid-imbedded polyurethane foam and blank foam at 40°C. – • – Phosphonic acid foam – ■ – Blank foam.

Phosphonic acid foam performs better than the β-diketone foam [11] at 4°C in its ability to extraction uranium at natural water pH (i.e., at pH about 7). The ideal temperature for maximum

Table 1
Comparison of the extraction capabilities of phosphonic acid foam with the blank foam for the extraction of uranium from aqueous solutions at various temperature and pH values

pH	Phosphonic foam % extraction	Blank foam % extraction	Temperature °C
1.4	5.6 ± 2.3	−0.33 ± 3.4	4
3.0	18.4 ± 21.3	0.82 ± 9.5	4
5.3	81.1 ± 1.1	6.5 ± 6.1	4
8.3	89.0 ± 0.5	−6.8 ± 4.1	4
11.0	5.2 ± 1.4	4.1 ± 5.8	4
1.4	8.4 ± 5.0	0.84 ± 3.2	22
3.0	11.6 ± 3.6	−0.28 ± 15.5	22
5.3	59.6 ± 4.4	3.0 ± 4.0	22
8.3	93.0 ± 0.6	−3.1 ± 5.1	22
11.0	7.2 ± 2.4	2.5 ± 3.0	22
1.4	4.9 ± 2.0	3.2 ± 3.1	40
3.0	15.5 ± 3.8	−9.3 ± 20.5	40
5.3	73.1 ± 1.3	12.2 ± 11.1	40
8.3	94.5 ± 0.4	7.9 ± 9.7	40
11.0	7.3 ± 3.0	5.8 ± 2.3	40
1.4	4.3 ± 5.3	−1.8 ± 6.8	70
3.0	37.4 ± 2.4	−5.5 ± 22.6	70
5.3	83.9 ± 2.3	16.1 ± 3.8	70
8.3	93.2 ± 0.5	7.5 ± 5.0	70
11.0	8.3 ± 5.7	12.6 ± 10.0	70

extraction using the β-diketone foam [11] was 40°C. The extraction ability decreased with increasing temperature which can be attributed to the instability of the β-diketone foam at these higher temperatures. The phosphonic acid foam material is more stable and extracts uranium effectively from 4 to 70°C.

Preliminary experiments showed that the phosphonic acid was capable of extracting uranium from an artificial seawater [21]. This seawater was prepared by dissolving 750 g of a synthetic salt mixture, 'Instant Ocean' in deionized water to make 20 l. The composition of 'Instant Ocean' is given in Table 2. Laboratory air was bubbled through the seawater solution to adjust the pH to the natural seawater level of 8.4. The resulting solution was spiked with a known amount of uranium and allowed to equilibrate for at least 5 h before use.

The selective extraction capability of phosphonic acid-imbedded foam was determined by equilibrating 25 ml of artificial seawater which was spiked to a level of 16.5 ppm uranium with 0.5 g of foam. The filtered solutions were analysed by direct current plasma emission spectroscopy which minimises any interferences from the salt matrix. The phosphonic acid foam showed 90% extraction of uranium while the blank foams showed no extraction under identical conditions [21].

The experiments in this study were done using a batch process in order to determine the equilibrium extraction results. It is expected that if the phosphonic acid foam material was used in separation columns, that quantitative extraction would be obtained at any temperature over a wide pH range. Column extractions in general would provide improved retention over batch extractions because new sorbent that has not achieved equilibrium is available throughout the length of the column.

4. Conclusions

Phenylphosphonic acid was imbedded the matrix of the polyurethane foam during the fabrication of the foam. The resulting phosphonic acid

foam is most capable of extracting uranium from aqueous solutions with pH between 5 and 8. Phosphonic acid foam is simple to prepare, relatively inexpensive, has high porosity and good chemical and mechanical stability. These qualities make the phosphonic acid foam a good sorbent for the preconcentration of uranium from solutions in the pH range is 6–8. This sorbent appears promising for a number of industrial applications including the nuclear industry and may be usable either as a foamed material or as a separation column for the clean-up of uranium spills or mine wastes. The ability to sorb uranium from solutions at temperature as low as 4°C would make this polymer material attractive for use with environmental water at any time of the year. Phosphonic acid-imbedded foam shows promising results from the selective sorption of uranium from seawater. Future work should investigate the extraction mechanism and obtain a more detailed extraction profile for this new sorbent material.

Acknowledgements

The authors acknowledge the financial assistance provided by the Natural Sciences and Engineering Research Council of Canada. Hypol™ FHP2002 prepolymer was a sample provided by W.R. Grace (MA, USA).

Table 2
Chemical composition of 'Instant Ocean' [24]

Component	% by Weight
NaCl	65.226
$MgSO_4 \cdot 7H_2O$	16.307
$MgCl_2 \cdot 6H_2O$	12.762
$CaCl_2$	3.261
KCl	1.737
$NaHCO_3$	0.4963
KBr	0.07206
H_3BO_3	0.06214
$SrCl_2 \cdot 6H_2O$	0.04689
$MnSO_4 \cdot H_2O$	0.009379
$Na_2HPO_4 \cdot 7H_2O$	0.009379
LiCl	0.002343
$Na_2MoO_4 \cdot 2H_2O$	0.002343
$Na_2S_2O_3 \cdot 5H_2O$	0.002343
$Ca(C_6H_{11}O_7)_2 \cdot H_2O$	0.001669
$Al_2(SO_4)_3 \cdot 18H_2O$	0.001202
RbCl	0.000405
$ZnSO_4 \cdot 7H_2O$	0.0002563
KI	0.0002403
EDTA · NaFe	0.0001936

References

[1] G.J. Moody, J.D.R. Thomas, Chromatographic Separation and Extraction with Foamed Plastics and Rubbers, Marcel Dekker, New York, 1982.
[2] T. Braun, J.D. Navratil, A.B. Farag, Polyurethane Foam Sorbents in Separation Science, CRC Press, FL, USA, 1985.
[3] M.A.J. Mazurski, A. Chow, H.D. Gesser, Anal. Chem. Acta 65 (1973) 99.
[4] A. Chow, D. Buksak, Can. J. Chem. 53 (1975) 1373.
[5] G.N. Lypka, H.D. Gesser, A. Chow, Anal. Chim. Acta 78 (1975) 367.
[6] T. Valente, H.J.M. Bowen, Anal. Chim. Acta 90 (1977) 315.
[7] K. Srikameswaran, H.D. Gesser, J. Environ. Sci. Health A15 (1978) 415.
[8] T. Braun, A.B. Farag, Anal. Chim. Acta 71 (1974) 133.
[9] H.D. Gesser, S. Ahmed, J. Radioanal. Nucl. Chem. 140 (1990) 395.
[10] Hypol Plus™ Laboratory Procedures and Foam Formulations, W.R. Grace, MA, USA, 1987.
[11] S. Katragadda, H.D. Gesser, A. Chow, Talanta 42 (1995) 725.
[12] C. Kantipuly, S. Katragadda, A. Chow, H.D. Gesser, Talanta 37 (1990) 491.
[13] S.D. Alexandratos, D.R. Quillen, M.E. Bates, Macromolecules 20 (1987) 1191.
[14] S.D. Alexandratos, D.R. Quillen, W.J. McDowell, Sep. Sci. Technol. 22 (1987) 983.
[15] M. Marhol, Z. Anal. Chem. 231 (1967) 265.
[16] M. Marhol, H. Beranova, K.L. Cheng, J. Radioanal. Chem. 21 (1974) 177.
[17] A. Bermejo-Barrera, M.C. Yebra-Biurrun, L.M. Fraga-Trillo, Anal. Chim. Acta 239 (1990) 321.
[18] J.A. Perez-Bustamante, F. Palomares-Delgado, Analyst 96 (1971) 407.
[19] K. Sekine, H. Onishi, Anal. Chim. Acta 62 (1972) 468.
[20] M. Suchanek, F. Sipek, L. Kabrt, V. Radil, J. Makovicka, Sb. Vys. Sk. Chem-Technol. Praze, Anal. Chem., H23 (1989) 65; Chem. Abstr. 111 (1989) 161 517z.
[21] S. Katragadda, Ph.D. Thesis, University of Manitoba, 1993.
[22] I. Feldman, W.F. Neuman, J.R. Havill, Report UR-85, 1949, in: E. Rabinowitch, R.L. Belford (Eds.), Spectroscopy and Photochemistry of Uranyl Compounds, Pergamon Press, New York, 1964.
[23] R. Djogic, L. Sipos, M. Branica, Limnol Oceanogr. 31 (1986) 1122.
[24] Instant Ocean Salt, Aquarium Systems, OH, USA, 1967.

ELSEVIER

Talanta 44 (1997) 1873–1881

Talanta

Application of HPLC capacity coefficients to characterize the sorption of polycyclic aromatic compounds to humic acid

Torben Nielsen [a,*], Christian Helweg [a], Katrin Siigur [a,b], Uuve Kirso [b]

[a] *Chemical Reactivity, Department of Environmental Science and Technology, MIL 313, Risø National Laboratory, P.O. Box 49, DK-4000, Roskilde, Denmark*

[b] *Institute of Chemical Physics and Biophysics, Akadeemia tee 23, EE-0026, Tallinn, Estonia*

Received 14 August 1996; received in revised form 24 February 1997; accepted 11 March 1997

Abstract

The sorption coefficients to humic acid of 46 PAC having a wide range in polarity were compared with the capacity coefficients of the PAC to a non-polar HPLC column material (ODS) and a polar one (Diol). It is shown that polar interactions contribute to the sorption of polar PAC in addition to the non-polar interactions. The results also suggest that humic acid may contain different hydrophilic adsorption sites. The non-polar column material was only the best model substrate, if the test materials were limited to the hydrophobic unsubstituted PAC, PAH + O,S-PAC. © 1997 Elsevier Science B.V.

Keywords: Polycyclic aromatic compounds; HPLC; Capacity coefficient; Humic acid; Sorption

1. Introduction

The transport, fate and bioavailability of organic pollutants in the aquatic and terrestrial environment is very dependent of the partitioning of these compounds between water, dissolved humic matter and soil or sediment humic matter [1,2]. Humic and fulvic acids have a very complex composition and show great variations in their composition and properties dependent of their origin and history [3–7].

The major concern in relation to pollution with polycyclic aromatic compounds (PAC) is that many are considered to be carcinogenic [8]. In addition acridine, a N-PAC, has recently been shown to be a strong phytotoxin towards terrestrial plants [9] and some photooxidation products of PAH have been shown to be toxic towards water plants [10]. The PAC cover a group of compounds having a great variation in polarity, water solubility and other physico-chemical properties [11–17]. A number of different PAC have been identified in the environment. The best known group is the hydrophobic, parent polycyclic aromatic hydrocarbons (PAH), but also N-, O-, S-PAC, a number of different derivatives, alkyl, nitro, cyano, chloro, bromo, methoxy, N-oxides and different oxygenated derivatives, phenols, quinones, ketones, aldehydes and carboxylic acid derivatives have been found [13,18–30]. The

* Corresponding author.

PII S00 9-9140(97)00083-0

ubiquitous PAC originates from a number of different sources. The most important ones are oil pollution, combustion processes and the manufacturing and application of creosote and coal tar [31–35]. Photochemical reactions during the transport in the atmosphere and in the aquatic environment [13,21,36–39] and microbiological oxidation in the aquatic and terrestrial system [40–42] contributes to the complexity of the composition of PAC in the environment.

Several studies have investigated the sorption of the hydrophobic PAH to organic matter in the environment, e.g., Refs [5,6,43]. A few studies have dealt with other PAC compounds, e.g., dibenzothiophene, some amino-PAH, anthracene-9-carboxylic acid, 1-naphthol and a few N-PAC compounds [44–48]. These studies show that the sorption is determined by nonpolar interactions between the PAC and the organic matter and increases with diminishing water solubility of the PAC [46] as well as with increasing content of carbon and especially aromatic carbon of the organic matter [5,6]. Some evidences suggest that hydrophobic adsorption rather than phase partitioning is the dominant mode of binding non-polar PAC compounds [49], while some suggest, that both partitioning and site-specific sorption occur both for polar and nonpolar organic compounds [50]. In reversed phase HPLC it appears that retention of non-polar compounds is governed by a partitioning process, rather than by adsorption [51]. Reversed phase HPLC capacity coefficients for a cyanoalkyl column have been shown to correlate with the humic acid K_{oc} values for aromatic hydrocarbons and pesticides [52,53]. This paper shows that the sorption of PAC to humic matter is affected by polar interactions, especially hydrogen bonds, but also ionic interactions and dipole-dipole interactions or charge transfer complexion, in addition to non-polar interactions. Our recent values of the sorption coefficients, K_{oc}, to humic acid of 46 PAC having a wide range in polarity [15] are compared with the capacity coefficients, k', using a HPLC column with a monomeric column material consisting of nonpolar octadecylsilyl groups, ODS, and a Diol-column (Diol, -$CH_2CH_2CH_2OCH_2$-CH(OH)CH_2OH) both applied in the reverse phase mode. It is shown that the HPLC capacity coefficients can be applied to interpret the humic acid sorption mechanism of PAC.

2. Experimental

2.1. Chemicals and materials

The test compounds, listed in Tables 1 and 2, were obtained from several sources as pure compounds. Their identity was confirmed by UV absorption spectra. The preparation of the bromopyrenes is described elsewhere [15,54]. The compounds were dissolved in methanol (Lichrosolv 99.8% or Lab Scan HPLC) with a typical concentration of 0.04 g l^{-1}.

2.2. HPLC method

The HPLC system used was a gradient low pressure Shimadzu LC-10HPLC system with PDA detector, thermostatted column oven and autoinjector. The Diol column (25.0 cm × 4.6 mm ID) was slurry packed with Nucleosil 7 OH from Macherey-Nagel. The ODS columns used were Phenomenex Prodigy ODS-2 columns (15.0 cm × 4.6 mm ID and 5.0 cm × 4.6 mm ID) with a particle size of 5 μm. The ODS columns were endcapped and experiments with *n*-hexane as eluent showed no difference in the retention times of benzene and nitrobenzene confirming a negligible amount of silanol groups. The eluents were mixed from laboratory grade ion exchanged water extra purified on a Millipore-Q water purification system and Lichrosolv methanol 99.8% from Merck or Lab Scan HPLC methanol. The eluent consisted of 35% methanol and 65% water applying the Diol column, and 65% methanol and 35% water applying a ODS column. Appropriate mixtures of the compounds were chromatographed and the retention time (v_r) of each compound was recorded. All measurements were repeated at least three times. The temperature was kept at 30°C for all measurements. The dead volume, v_0, of the system used for calculating the capacity coefficient, $k' = (v_r - v_0)v_0^{-1}$, was determined by chromatographing water (Diol) and $NaNO_3$ (ODS).

Table 1
Parent PAC: Humic acid sorption coefficient, log K_{oc} [15], HPLC capacity coefficients, k'(Diol) and k'(ODS), and size

Compound	No. of rings	Log K_{oc}	k' (ODS)	k' (Diol)
N-PAC				
Quinoline	2	2.88	0.86	0.40
Isoquinoline	2	3.09	0.90	0.41
4-azafluorene	3	3.63	1.41	0.70
Acridine	3	4.00	2.85	0.89
Benzo[f]quinoline	3	4.07	3.96	1.07
Benzo[h]quinoline	3	4.13	5.17	0.96
Phenanthridine	3	4.06	2.82	1.01
Benz[a]acridine	4	5.00	7.96	2.28
10-azabenzo[a]pyrene	5	5.86	24.51	5.85
Dibenz[a,c]acridine	5	6.17	74.19	6.59
Dibenz[a,h]acridine	5	6.05	73.46	6.02
Dibenz[a,j]acridine	5	5.86	24.12	5.55
Dibenz[c,h]acridine	5	6.26	154.72	9.19
Carbazole	3	4.74	4.02	0.86
PAH				
Naphthalene	2	3.74	5.29	0.42
Fluorene	3	4.68	14.33	0.76
Anthracene	3	4.65	18.50	1.38
Phenanthrene	3	4.65	17.46	1.37
Pyrene	4	5.14	26.40	2.86
Benz[a]anthracene	4	5.62	60.33	4.43
Benzo[a]pyrene	5	6.27	105.13	9.71
Dibenz[a,c]anthracene	5	6.54	165.88	14.86
Dibenz[a,h]anthracene	5	6.44	193.76	17.12
Dibenz[a,j]anthracene	5	6.58	193.18	14.13
O,S-PAC				
Dibenzofuran	3	4.15	10.98	0.75
Dibenzothiophene	3	4.59	15.93	1.19

2.3. Humic acid sorption coefficients, K_{oc}

The determination of log K_{oc} is described in details elsewhere [15] but in short, the sorption coefficients were achieved by means of the following correlation: log $K_{oc} = (1.50 \pm 0.15)$*log $k' + (4.16 \pm 0.12)$, $r = 0.99$, SE $= 0.27$, where k' is the capacity coefficient for a HPLC column having Aldrich humic acid chemically immobilized to the silica material. The coefficients of the correlation were attained by calibration with the following compounds, quinoline, naphthalene, anthracene, phenanthrene, benz[a]anthracene and benzo[a]pyrene, for which experimental K_{oc} values are known.

3. Results and discussions

3.1. Variation of the capacity coefficients

The capacity coefficients, k', of unsubstituted PAH and N-PAC increased with the molecular size for both types of columns (see Table 1). k' varied a factor of 37 from the bicyclic naphthalene to the pentacyclic dibenz[a,j]anthracene for the ODS column and a factor of 34 for the Diol column. Thus for both columns k' increases with decreasing water solubility of the PAH. The similarity in the PAH k' ratios for the columns suggest perhaps that the retention mechanism on the two columns has been the same. The

Table 2
Substituted PAC: Humic acid sorption coefficient, log K_{oc}[15], HPLC capacity coefficients, k'(Diol) and k'(ODS)

Compound	log K_{oc}	k' (ODS)	k' (Diol)
Substituted PAH			
9-acetylanthracene	4.21	5.37	0.92
9-anthracenecarboxamide	4.09	0.76	0.56
9-anthracenecarboxylic acid methylester	4.47	6.21	1.35
9-bromoanthracene	5.15	53.26	2.36
9-chloroanthracene	4.95	46.30	2.32
9-cyanoanthracene	4.70	8.02	1.30
9-formylanthracene	4.03	7.09	0.80
9-methoxyanthracene	4.43	14.78	1.23
9-methylanthracene	4.86	31.82	1.81
9-nitroanthracene	4.69	4.82	1.56
Anthraquinone	4.32	4.25	0.46
1-bromopyrene	5.67	77.24	5.01
2-bromopyrene	5.66	78.48	4.61
4-bromopyrene	5.71	79.23	5.16
1,3-dibromopyrene	6.20	293.24	9.62
1,6-dibromopyrene	6.04	237.41	8.74
1,8-dibromopyrene	6.18	246.33	9.29
Substituted N-PAC			
2-hydroxyquinoline	2.70	0.42	0.20
Quinoline-N-oxide	2.00	0.24	0.26
N-methylquinolinium iodide	3.10	0.22	0.01

Diol column material consists of a nonpolar part, a silanopropyl group, that joins the polar part, the diol moiety to the silica surface. For the retention of PAH, it appears that the silanopropyl group is the active part.

For the corresponding N-PAC, quinoline and dibenz[a,j]acridine k' varied a factor of 28 for the ODS column and 14 for the Diol-column. Dibenz[a,j]acridine was selected for the comparison, as it is the only one of the dibenzacridines, that do not have any steric shielding of the nitrogen atom [15,16]. The explanation of the minor variation of k' for N-PAC on the Diol-column appears to be that the ability of N-PAC to form hydrogen bonds with the diol surface diminishes with increasing size of the N-PAC, so that bi- and tricyclic N-PAC are bound more strongly than the pentacyclic N-PAC. Thus, the increased water solubility of, e.g. the pentacyclic N-PAC compared to PAH [12] causes the pentacyclic N-PAC to elute faster than the pentacyclic PAH, while the water solubility has only a minor influence on the retention of bicyclic N-PAC compared to that of naphthalene. Therefore, e.g., the ratio $(k'_{\text{quinoline}})/(k'_{\text{napthalene}}) = 0.95$ is larger than the ratio $(k'_{\text{dibenz[a,j]acridine}})/(k'_{\text{dibenz[a,j]anthracene}}) = 0.39$. In contrast to this, the effect of nitrogen for k'(ODS) is independent of the size of the PAH and N-PAC. Thus $k'_{(\text{N-PAC})}/k'_{(\text{PAH})} = 0.16 \pm 0.03$ for quinoline, isoquinoline, 4-azafluorene, acridine, benzo[f]quinoline, phenanthridine, 10-azabenzo[a]pyrene and dibenz[a,j]acridine and the analog PAH. The other N-PAC, e.g. dibenz[c,h]acridine (0.80), have higher ratios than 0.16, because the steric shielding of the nitrogen atom, which diminishes the basicity of the nitrogen atom and increases the hydrophobicity [15,16], affects k'(ODS) much more than it affects k'(Diol). Carbazole has a neutral nitrogen atom in contrast to the other N-PAC. This may be the reason that $k'_{(\text{carbazole})}/k'_{(\text{fluorene})}$ (0.28 for ODS and 1.13 for Diol) is higher than most of the other $k'_{(\text{N-PAC})}/k'_{(\text{PAH})}$ values for both types of columns.

The behavior of the two model compounds for O- and S-PAC, dibenzofuran and dibenzothiophene, on the two columns were similar to that PAH and not to that of N-PAC, although the analog tricyclic aromatics of the fluorene type had

some differences in their retention on the two columns, and the variations of k'(Diol) were much minor than those of k'(ODS). Thus, k'(ODS) decreased in the range dibenzothiophene (15.9) ~ fluorene (14.3) > dibenzofuran (11.0) > carbazole (4.0) > 4-azafluorene (1.4), and k'(Diol) decreased in the range dibenzothiophene (1.19) > carbazole (0.86) > fluorene (0.76) ~ dibenzofuran (0.75) ~ 4-azafluorene (0.70). The k'(ODS) gives a reasonable description of the variations of log K_{oc} for the three hydrophobic PAC, dibenzothiophene (log $K_{oc} = 4.59$, see Table 1), fluorene (4.68) and dibenzofuran (4.15), but the influence of hydrogen bonds between humic acid and N-PAC becomes evident, if carbazole (log $K_{oc} = 4.74$) and 4-azafluorene (3.63) also are taken into account. The k'(Diol) predicts the ranking of the five humic acid sorption coefficients better than k'(ODS) and especially that log K_{oc} of carbazole should be high compared to e.g., that of fluorene. The comparison also suggests that the sorption mechanism of carbazole to humic acid may differ from that of 4-azafluorene and the other N-PAC.

The capacity coefficients, k', of PAH increased with the addition of lipophilic substituents and decreased with the addition of polar substituents for both types of columns (see Table 2). Both column materials gave the same ranking as log K_{oc} of the lipophilic substituents, Br > Cl > CH_3. Previously, it has been shown [15] that the effect of Br substituents on log K_{oc} is additive. Comparing anthracene, 9-bromoanthracene, pyrene and the six bromopyrenes, it appeared log k'(ODS) increased with 0.480 ± 0.014 and log k'(Diol) increased with 0.242 ± 0.013 for each substituted bromo atom independent of the aromatic ring system.

k'(Diol) increased for the substituted polar anthracenes in the range quinone < $CONH_2$ < CHO < $COCH_3$ < OCH_3 ~ CN ~ $COOCH_3$ < NO_2, and k'(ODS) increased in the range $CONH_2$ < quinone < NO_2 < $COCH_3$ < $COOCH_3$ < CHO < CN < OCH_3. The largest difference between the two types of columns is that 9-nitroanthracene elutes relatively early on the ODS column compared to the Diol column. The corresponding ranking for log K_{oc} was CHO ~ $CONH_2$ < $COCH_3$ ~ quinone < OCH_3 ~ $COCH_3$ < NO_2 ~ CN. This ranking is reasonably predicted by means of k'(Diol). The log K_{oc} ranking of 9-formyl- and 9-nitroanthracene are poorly predicted by k'(ODS), and k'(ODS) indicate that 9-anthracenecarboxamide should have a much lower log K_{oc} compared to the other anthracenes than observed.

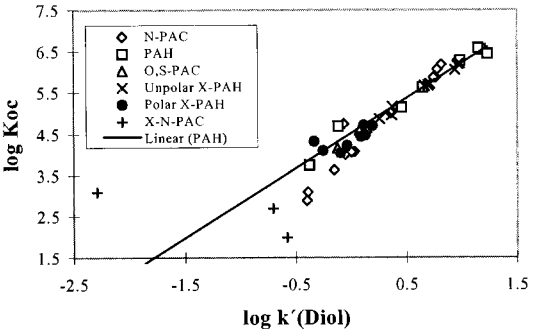

Fig. 1. The log to log correlation between the sorption coefficient (K_{oc}) to humic acid and the capacity coefficient (k') on the HPLC Diol stationary phase for 46 PAC (Table 1). The line showed is the best fit for the correlation of the hydrophobic PAH. All the regression lines are compared in Table 3.

3.2. Comparison of humic acid sorption coefficients and HPLC capacity coefficients

Fig. 1 compares the humic acid sorption coefficients with the Diol capacity coefficients for the 46 PAC, and Fig. 2 compares the sorption coefficients with the ODS capacity coefficients. The

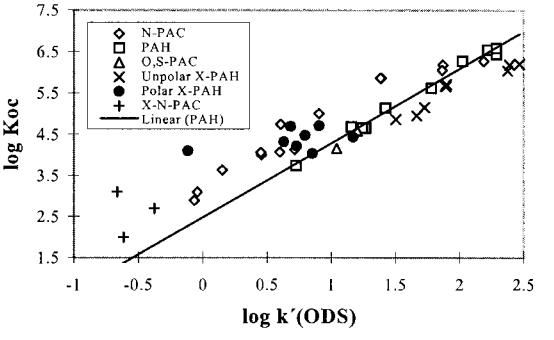

Fig. 2. The log to log correlation between the sorption coefficient (K_{oc}) to humic acid and the capacity coefficient (k') on the HPLC ODS stationary phase for 46 PAC (Table 1). The line showed is the best for the correlation of the hydrophobic PAH All the regression lines are compared in Table 3.

Table 3
Results from linear regression analyses between humic acid sorption coefficients and HPLC capacity coefficients for different PAC groups

Group of compounds	Column type	Factor to k'(Diol)	Factor to k'(ODS)	Intercept	Standard error of the log K_{oc} estimate	r
All PAC	**Both**	**1.39**	**0.47**	**3.90**	**0.265**	**0.972**
All PAC	Diol	2.06		4.26	0.298	0.963
All PAC	ODS		1.29	3.33	0.378	0.941
Polar PAC	**Both**	**1.34**	**0.67**	**3.81**	**0.313**	**0.963**
Polar PAC	Diol	2.31		4.21	0.350	0.951
Polar PAC	ODS		1.49	3.33	0.376	0.943
Hydrophobic PAC	**Both**	**1.56**	**0.17**	**4.27**	**0.127**	**0.989**
Hydrophobic PAC	Diol	1.73		4.47	0.125	0.989
Hydrophobic PAC	ODS		1.57	2.68	0.243	0.958
Unsubstituted PAC	**Both**	**1.28**	**0.61**	**3.80**	**0.223**	**0.981**
Unsubstituted PAC	Diol	2.05		4.27	0.280	0.969
Unsubstituted PAC	ODS		1.46	3.21	0.346	0.952
Substituted PAC	**Both**	**1.19**	**0.52**	**3.85**	**0.319**	**0.962**
Substituted PAC	Diol	2.09		4.25	0.338	0.955
Substituted PAC	ODS		1.15	3.39	0.354	0.950
N-PAC	**Both**	**1.64**	**0.50**	**3.86**	**0.250**	**0.981**
N-PAC	Diol	2.38		4.12	0.255	0.978
N-PAC	ODS		1.55	3.32	0.305	0.968
PAH	**Both**	**0.09**	**1.71**	**2.58**	**0.119**	**0.995**
PAH	Diol	1.69		4.51	0.174	0.986
PAH	ODS		1.80	2.48	0.111	0.994
Substituted PAH	**Both**	**1.56**	**0.10**	**4.35**	**0.170**	**0.977**
Substituted PAH	Diol	1.73		4.44	0.166	0.977
Substituted PAH	ODS		0.94	3.72	0.280	0.932
PAH+O,S-PAC	**Both**	**0.20**	**1.63**	**2.64**	**0.120**	**0.994**
PAH+O,S-PAC	Diol	1.72		4.48	0.162	0.988
PAH+O,S-PAC	ODS		1.84	2.40	0.115	0.994

The analyses includes the data in Tables 1 and 2 with the except of N-methylquinolinium iodide.

results of regression analyses (without N-methylquinolinium iodide) for both columns, separate and in combination, are shown in Table 3. The results are shown both for all PAC and for different subgroups (polar and hydrophobic PAC), (unsubstituted and substituted PAC) and (N-PAC, PAH + O,S-PAC, PAH and substituted PAH). The polar PAC includes N-PAC, substituted N-PAC and PAH with polar substituents. The hydrophobic PAC includes PAH, dibenzofuran, dibenzothiophene and PAH with lipophilic substituents (CH_3, Cl and Br). From Fig. 2 and Tables 1 and 2, it can be deduced that the sorption of polar PAC to humic acid are stronger than the sorption of PAH compared to their sorption to the hydrophobic ODS column material. Thus the sorption to humic acid of N-PAC, substituted N-PAC and PAH with polar substituents are affected not only by hydrophobic interactions, but also by polar interactions. From Fig. 1 and Tables 1 and 2, it can be deduced that the sorption to humic acid for PAC with more than two rings generally are reasonably characterized by means of the k'(Diol) values, no matter whether the

compounds belong to the hydrophobic PAH or contain polar atoms or groups. Therefore, the k'(Diol) values give a fair simulation of the hydrophobic interactions between humic acid and hydrophobic PAC, e.g., PAH. The pitfalls of the results applying the Diol column material indicate that some polar PAC are adsorbed to humic acid by another mechanism than the basic N-PAC. Thus it can be seen from Fig. 1 and Table 2 that anthraquinone and especially N-methylquinolinium iodide have relatively high K_{oc} values compared to their k'(Diol) values.

N-methylquinolinium iodide was excluded in the regression analyses in Table 3, as the behavior of the cation was totally different from that of the other polar PAC. The cation forms probably an ion bond to the negatively charged carboxylate groups in humic acid. This means that the sorption mechanisms of N-methylquinolinium iodide to humic acid and to the Diol column material is totally different. The best characterization of the sorption of all PAC to humic acid is achieved by applying a linear combination of k'(Diol) and k'(ODS). The standard error of the log K_{oc} estimate for the linear combination for all PAC was 0.27. It was higher, respectively, 0.30 and 0.38 applying either k'(Diol) or k'(ODS) separately. Table 3 also shows that for the two groups of unsubstituted hydrophobic PAC, PAH and PAH + O,S-PAC, the k'(ODS) standard error of the log K_{oc} estimate is not larger (0.11 and 0.12, respectively) than that of the combined model (both 0.12). However, by including polar and substituted PAC into the comparison the combined model becomes better suited to model the K_{oc} values than the model applying only k'(ODS). Thus, the difference between the standard error of the log K_{oc} estimate for both columns and that for the ODS column increases in the range PAH $(-0.01) \sim$ PAH + O,S-PAC $(0.00) <$ Substituted PAC $(0.04) \sim$ N-PAC $(0.05) \sim$ Polar PAC $(0.06) <$ Substituted PAH $(0.11) =$ All PAC $(0.11) \sim$ Hydrophobic PAC $(0.12) =$ Unsubstituted PAC (0.12). The Diol column is better to simulate the humic acid sorption of polar PAC, e.g. N-PAC and the polar substituted PAH. Thus, the difference between the standard error of the log K_{oc} estimate for both columns and that for the Diol column was below 0.02 for the groups, N-PAC, substituted PAH and substituted PAC. While, the difference increased to 0.04–0.06 for the two groups of unsubstituted hydrophobic PAC, PAH and PAH + O,S-PAC. The group of polar PAC includes N-PAC and the polar substituted PAC. The mixing of these two groups increased the difference to 0.04. The increase, although minor, is expected, as the polar PAC may be adsorbed to humic acid by means of different mechanisms. Thus hydrogen bonds between the nitrogen atom and HO groups of phenolic compartments and carbohydrate residues in humic acid may contribute to the sorption of basic N-PAC. Carbazole may form hydrogen bonds to the negatively charged carboxylate groups in humic acid. Dipole-dipole interactions or charge transfer complexes between, e.g., anthraquinone and phenolic compartments of humic acid appear also to be a possible mechanism. It is interesting that the Diol column appeared to be better to simulate the humic acid sorption than the ODS column, when the unsubstituted and substituted hydrophobic PAC were treated as one group (hydrophobic PAC).

Our findings are supported by the observations of others. Brown and Flagg [55] observed that polar organic compounds did not fit very well into an empirical K_{oc} and K_{ow} relationship for a series of hydrophobic PAH and chlorinated hydrocarbons. Vowles and Mantoura [52], Kördel et al. [53] and Szabó et al. [56] concluded that HPLC columns with semipolar stationary phases are very suitable to simulate the sorption properties of the organic matter content of soils. Our observations agree also with the complex composition of humic acids, as humic materials contain both hydrophobic and different hydrophilic compartments [4]. For PAH and O,S-PAC the most favorable sites appear to be the hydrophobic parts. The ODS column material can be considered to be a model substrate for these parts. The results also suggest that different kinds of humic matter having large variations in their composition will possess different abilities to adsorb different types of polar PAC [57]. Polar functional groups humic acid will be hydrated. Corresponding the Diol moiety will be embedded in the solvent molecules, mainly

the water molecules. The polar interactions can in both cases happen in two ways:

1. The polar PAC competes with the water molecules on the adsorption site.
2. The polar PAC is adsorbed to the adsorbed water cluster.

The pitfall of especially N-methylquinolinium ion, but also carbazole and anthraquinone, indicate that the former mechanism is operating, but probably both mechanisms contribute to the sorption both to the humic acid and to the Diol column.

4. Conclusions

The best simulation of the sorption to humic acid of 46 polycyclic aromatic compounds (PAC) having a wide range in polarity was achieved by applying a linear combination of the retention factors of PAC to a polar and a non-polar HPLC column material. The Diol column material gave generally a better simulation of the sorption of all PAC than the non-polar ODS column material. However, the non-polar column material was the best model substrate, if the test material was limited to the hydrophobic unsubstituted PAC, PAH + O,S-PAC. The comparison shows that polar interactions, e.g., hydrogen bonds, contribute to the sorption to humic acid of polar PAC in addition to the hydrophobic interactions. The results perhaps also indicate that the favorable adsorption sites for polar and unpolar PAC may be different, and that humic acid may contain different types of hydrophilic compartments.

Acknowledgements

Funding from the Center for Ecotoxicological Research under the Danish Environmental Research Program and the Danish Science Research Council is gratefully appreciated. Dr Walther Batsberg, Risø, is thanked for helpful suggestions to this work.

References

[1] R. Calvet, Environ. Hlth. Perspec. 83 (1989) 145.
[2] R.P. Schwarzenbach, P.M. Gschwend, D.M. Imboden, Environmental Organic Chemistry, Wiley, New York, 1993.
[3] R.L. Malcolm, P. MacCarthy, Environ. Sci. Technol. 20 (1986) 904.
[4] R.L. Wershaw, J. Contam. Hydrol. 1 (1986) 29.
[5] T.D. Gauthier, W.R. Seitz, C.L. Grant, Environ. Sci. Technol. 21 (1987) 243.
[6] J.F. McCarthy, L.E. Roberson, L.W. Burrus, Chemosphere 19 (1989) 1911.
[7] A.S. Mathuthu, J.A. Marinsky, J.H. Ephraim, Talanta 42 (1995) 441.
[8] IARC (International Agency for Research on Cancer) IARC Monographs on the Evaluation of the Carcinogenic Risks of Chemicals to Humans. Polynuclear Aromatic Compounds. Part I, Chemical Environmental and Experimental Data; IARC, WHO, Lyon, France, 1983.
[9] G. Gissel-Nielsen, T. Nielsen, Polycyclic Aromatic Comp. 8 (1996) 243.
[10] D. Warshawsky, T. Cody, M. Radike, R. Reilman, B. Schuman, K. LaDow, J. Schneider, J. Chem.-Biol. Interact. 97 (1995) 131.
[11] T. Nielsen, Analyt. Chem. 55 (1983) 286.
[12] R.S. Pearlman, S.H. Yalkowsky, S. Banerjee, J. Phys. Chem. Ref. Data 13 (1984) 555.
[13] B.J. Finlayson-Pitts, J.N. Pitts, Jr. Atmospheric Chemistry: Fundamentals and Experimental Techniques, Wiley, New York, 1986.
[14] R. Krasnoschekova, U. Kirso Perin, F. Perin, P. Jacquignon, Polycyclic Aromatic Comp. 3 (1994) 41.
[15] T. Nielsen, K. Siigur, C. Helweg, O. Jørgensen, P.E. Hansen, U. Kirso, Environ. Sci. Technol. 31 (1997) 1102.
[16] C. Helweg, T. Nielsen, P.E. Hansen, Chemosphere 34 (1997) 1693.
[17] C. Helweg, T. Nielsen, P.E. Hansen, Polycyc. Aromat. Comp. (1997) submitted for publication.
[18] W.W. Youngblood, M. Blumer, Geochim. Cosmochim Acta 44 (1975) 415.
[19] S. Krisknan, D.A. Kaden, W.G. Thilly, R.A. Hites, Environ. Sci. Technol. 13 (1979) 1532.
[20] D.R. Choudhury, B. Bush, Anal. Chem. 53 (1981) 1351.
[21] T. Nielsen, T. Ramdahl, A. Bjørseth, Environ. Health Perspec. 47 (1983) 103.
[22] T. Nielsen, B. Seitz, T. Ramdahl, Atmos. Environ. 18 (1984) 2159.
[23] T. Nielsen, P.A. Clausen, F.P. Jensen, Analyt. Chim. Acta 187 (1986) 223.
[24] P. Haglund, T. Alsberg, Å. Bergman, B. Jansson, Chemosphere 16 (1987) 2441.
[25] M.T. Galceran, E. Moyano, Talanta 40 (1993) 615.
[26] D. Domine, J. Devillers, P. Garrigues, H. Budzinski, M. Chastrette, W. Karcher, Sci. Tot. 155 (1994) 9.
[27] N. Sera, K. Fukuhara, N. Miyata, H. Tokiwa, Mutagenesis 9 (1994) 47.

[28] M.T. Tena, M.D.L. de Castro, M. Valcárcel, Chromatographia 38 (1994) 431.
[29] M. Murayama, P.K. Dasgupta, Analyt. Chem. 68 (1996) 1226.
[30] T. Nielsen, Atmos. Environ. 30 (1996) 3481.
[31] P.S. Pedersen, J. Ingwersen, T. Nielsen, E. Larsen, Environ. Sci. Technol. 14 (1980) 71.
[32] M.G. Fowler, P.W. Brooks, M. Northcott, M.W.G. King, J.F. Barker, L.R. Snowdon, Org. Geochem. 22 (1994) 641.
[33] K. Granby, N.H. Spliid, Mar. Poll. Bull. 30 (1995) 74.
[34] S.R. Wild, K.C. Jones, Environ. Pollut. 88 (1995) 91.
[35] O. Kiilerich, E. Arvin, Ground Water Monitoring Remediation 16 (1996) 112.
[36] R.M. Kamens, H. Karam, J. Guo, J.M. Perry, L. Stockburger, Environ. Sci. Technol. 23 (1989) 801.
[37] U. Kirso, L. Paalme, H. Uibopuu, N. Irha, E. Urbas, P.C. Jacquignon, Polycyclic Aromatic Compounds 3 Suppl. (1993) 103.
[38] P.S. Holder, E.L. Wehry, G. Mamantov, Polycyclic Aromatic Compounds 4 (1994) 135.
[39] J. Kochany, R.J. Maguire, Sci. Tot. Environ. 144 (1994) 17.
[40] W.E. Pereira, C.E. Rostad, D.M. Updegraff, J.L. Bennett, Environ. Toxicol. Chem. 6 (1987) 163.
[41] J.B. Sutherland, J.P. Freeman, A.J. Williams, C.E. Cerniglia, Exp. Mycol. 18 (1994) 271.
[42] J.V. Pothuluri, A. Selby, F.E. Evans, J.P. Freeman, C.E. Cerniglia, Can. J. Bot. 73 (1995) 1025.
[43] W.J.M. Hegeman, C.H. van der Weijden, J.P.G. Loch, Environ. Sci. Technol. 29 (1995) 363.
[44] J.J. Hassett, J.C. Means, W.L. Banwart, S.G. Wood, S. Ali, A. Khan, J. Environ. Qual. 9 (1980) 184.
[45] J.J. Hassett, J.C. Means, W.L. Banwart, S.G. Wood, Soil. Sci. Soc. Am. J. 45 (1980) 38.
[46] W.L. Banwart, J.J. Hassett, S.G. Wood, J.C. Means, Soil Sci. 133 (1982) 42.
[47] J.C. Means, S.G. Wood, J.J. Hassett, W.L. Banwart, Environ. Sci. Technol. 16 (1982) 93.
[48] G.R. Southworth, J.L. Keller, Bull. Environ. Contam. Toxicol. 32 (1984) 445.
[49] E.M. Murphy, J.M. Zachara, S.C. Smith, J.L. Phillips, T.W. Wietsma, Environ. Sci. Technol. 28 (1994) 1291.
[50] B.S. Xing, J.J. Pignatello, B. Gigliotti, Environ. Sci. Technol. 30 (1996) 2432.
[51] J.G. Dorsey, W.T. Cooper, Anal. Chem. 66 (1994) 857A.
[52] P.D. Vowles, R.F.C. Mantoura, Chemosphere 16 (1987) 109.
[53] W. Kördel, J. Stutte, G. Kotthoff, Sci. Total Environ. 162 (1995) 119.
[54] P.E. Hansen, A. Berg, Acta Chem. Scand. B35 (1981) 131.
[55] D.S. Brown, E.W. Flagg, J. Environ. Qual. 10 (1981) 382.
[56] G. Szabó, J. Guczi, R.A. Bulman, Chemosphere 30 (1995) 1717.
[57] K. Siigur, T. Nielsen, Grøn, C. Helweg, U. Kirso, O. Jørgensen, P.E. Hansen, J. Chromatogr. (1997) submitted.

ELSEVIER

Talanta 44 (1997) 1883–1889

Talanta

Simultaneous determination of ampicillin and tetracycline in milk by using a stopped-flow/T-format spectrofluorimeter

B. Gala *, A. Gómez-Hens, D. Pérez-Bendito

Department of Analytical Chemistry, Faculty of Sciences, University of Córdoba, E-14004 Córdoba, Spain

Received 10 October 1996; received in revised form 28 January 1997; accepted 4 March 1997

Abstract

A fast and simple fluorimetric method is described for the simultaneous determination of ampicillin and tetracycline in milk by combining the stopped-flow mixing technique with a T-format spectrofluorimeter. Ampicillin determination is based on its hydrolysis with penicillinase and reaction with mercuric chloride, while the intramolecular energy transfer from tetracycline to europium ions in the presence of thenoyltrifluoracetone is used for tetracycline determination. The similar excitation wavelengths of both systems and the separation between the corresponding emission wavelengths allow the direct determination of both analytes by measuring simultaneously the initial rate of the ampicillin system and the equilibrium signal of the tetracycline system. The relative standard deviations were lower than 2%. The proposed method was applied to the determination of these antibiotics in different milk samples with a recovery of 95.0–103.3% for ampicillin and 93.3–103.3% for tetracycline. © 1997 Elsevier Science B.V.

Keywords: Fluorimetry; Ampicillin; Tetracycline; Stopped-flow; Milk

1. Introduction

The availability of simple and automatic methods to control traces of antibiotics in milk is of great analytical interest as it is known that the continuous intake of these compounds, even at low doses, is a risk to human health. Hazards may include direct toxic effects, development of allergic reactions and production of antibiotic resistance in pathogenic organisms transmissible to man. Generally, the presence of antibiotics in milk arises from their use as part of therapy to treat animal diseases such as bovine mastitis and, sometimes, in low concentrations, as constituents of animal feed to increase feed utilization and thus to accelerate animal growth.

Although immunoassay [1,2] and electrophoretic [3] methods have been described for the determination of antibiotics in milk, liquid chromatography is the most used technique for this purpose [4–7]. A wide variety of clean-up procedures such as ultrafiltration, liquid-liquid extraction, solid-phase extraction, immunoaffinity and deproteination have been described for the sample pretreatment [5]. Because almost without exception these methods are long and time-consuming, the availability of alternative methods is always desirable, specially when the sample is not

* Corresponding author.

PII S00 9-9140(97)00084-2

very complex and only two or three analytes must be determined. This justifies the development of the fluorimetric method described in this paper.

As described elsewhere [8], the simultaneous determination of two analytes by using a T-format spectrofluorimeter with a single excitation monochromator requires that the reaction products of the analytes have similar excitation wavelengths and very different emission wavelengths in order to avoid spectral emission overlap. This allows to obtain independently quantitative data of each analyte from its corresponding emission channel in a very simple way, avoiding the use of mathematical methods. On the other hand, the experimental conditions such as pH and temperature must be compatible for the adequate development of the chemical systems involved and no interaction between the reactants must occur. Although these requirements limit the general use of this approach for multicomponent determinations, the high number of presently available fluorescence derivatization reactions facilitates its application.

This paper shows the usefulness of this instrumentation for simultaneous determination of two antibiotics, namely ampicillin and tetracycline, in milk. The determination of ampicillin is based on its transformation into α-aminobenzylpenicilloate and formation of a fluorescent product with mercuric chloride [9], while the reaction between tetracycline, thenoyltrifluoracetone (TTA) and europium (III) in the presence of Triton X-100 [10] has been chosen for tetracycline determination. Both systems fulfil the requirements above indicated, which allows to obtain separately the data concerning each analyte in the corresponding emission channel. In addition, the coupling of stopped-flow mixing technique to the T-format spectrofluorimeter allows to achieve the automation of the measurement step of the method. Owing to the different kinetic behaviour of the two chemical systems involved, kinetic and equilibrium measurements have been carried out to obtain quantitative data for penicillin and tetracycline, respectively.

2. Experimental

2.1. Instrumentation

An SLM-Aminco (Urbana IL) Model 8100 photon-counting spectrofluorimeter was used in a T-format configuration. The excitation wavelength was set at 342 nm via the excitation monochromator. The wavelength of one of the optical emission arms (channel A) was set at 410 nm through the emission monochromator and that of the other emission arm (channel B) was selected by placing a Schott OG-550 filter. The instrument was fitted with an SLM-Aminco Milliflow stopped-flow reactor which was furnished with an observation cell of 0.2 cm path length. This module was controlled by the associated electronics, the computer and a pneumatic syringe drive system. The solutions in the stopped-flow module were kept at a constant temperature of 30°C by circulating water from a thermostated tank.

2.2. Reagents

All chemicals used were of analytical reagent grade. Stock solutions (100 μg ml^{-1}) of ampicillin and tetracycline (Sigma) were prepared in distilled water. The following aqueous solutions were also prepared: 10^{-3} M europium (III) nitrate pentahydrate (Aldrich), 1.5×10^{-3} M mercuric chloride (Merck), 0.1% Triton X-100 (Serva) and 0.1 M Tris [tris(hydroxymethyl)-aminomethane] (Merck) buffer solution (pH 7.4). An 1 unit ml^{-1} solution of penicillinase (Sigma) was daily prepared in this Tris buffer. Finally, a 4.5×10^{-3} M solution of TTA (Aldrich) was made in 2% ethanol.

2.3. Procedure

Two solutions were prepared to fill the two 5-ml reservoir syringes of the stopped-flow module. One of the solutions contained ampicillin (0.01–15 μg ml^{-1}), tetracycline (0.04–10 μg ml^{-1}), Triton X-100 (0.01%) and Tris buffer (1.5×10^{-2} M). The other syringe was filled with an aqueous solution containing europium (III) (2×10^{-5} M), TTA (5.4×10^{-6} M), mercury (II)

(1.5×10^{-4} M), penicillinase (0.15 U ml^{-1}) and Tris buffer (1.5×10^{-2} M). After the two 2-ml drive syringes were filled, 0.04 ml of each solution was mixed at a flow-rate of 20 ml s^{-1} in the mixing chamber in each run. The excitation wavelength used was 342 nm. The variation of the fluorescence intensity with time throughout the ampicillin reaction was monitored on channel A at 410 nm. The initial rate method was applied to the values acquired from this detector, which were processed by the microcomputer, furnished with a linear regression program for application of this kinetic method. The initial rate of the ampicillin reaction was determined in about 5 s and the blank signal was found to be negligible. The equilibrium signal obtained in channel B, by using a 550-nm cut-off filter was related to the tetracycline concentration through the formation of the Eu (III)-tetracycline-TTA complex. In this case, the contribution of the blank signal was substracted from the equilibrium fluorescence intensity obtained for the sample. All measurements were carried out at 30°C and each sample was assayed in triplicate.

2.4. Determination of ampicillin and tetracycline in milk samples

A volume of 10 ml of milk was treated with 1 ml of 1.7 M acetic acid, 1 ml of 1 M sodium acetate and 75 ml of distilled water heated at 40°C and the solution was stirred for 5 min. Then, it was cooled to room temperature, carefully and quantitatively transferred into a 100-ml calibrated flask, diluted to the mark with distilled water and subsequently filtered. A volume of the filtrate (4 ml) was finally treated as described above. The concentrations of each antibiotic in the samples were determined by interpolation from the working curves prepared by adding 4 ml of a previously prepared antibiotic-free milk whey to each standard.

3. Results and discussion

As indicated above, a requirement to attempt the simultaneous determination of ampicillin and tetracycline by using the stopped-flow/T-format spectrofluorimeter combination is to achieve the experimental conditions which allow the adequate development of both chemical systems. The fluorimetric method for ampicillin based on its alkaline hydrolysis and reaction of the penicillonate formed with mercuric chloride [9] was improved by applying kinetic methodology [11] where the use of stopped-flow mixing technique and the addition of hydrogen peroxide allowed to obtain analytical data in only few seconds. However, the basic medium required cannot be used for the determination of tetracycline based on its reaction at pH 7.0–7.5, with europium (III) and TTA, which gives rise to an intramolecular energy-transfer process from the ligands to the lanthanide ion [10]. With the aim of using both chemical systems together, the alkaline hydrolysis of ampicillin was changed to the enzymatic hydrolysis using penicillinase, which takes place at pH close to 7.0. The excitation and emission spectra obtained for both systems under these conditions (Fig. 1) show the complete overlaping of the excitation bands and the resolution of the emission bands.

The study of the kinetic behaviour of both ampicillin and tetracycline systems together by using stopped-flow mixing technique, showed that

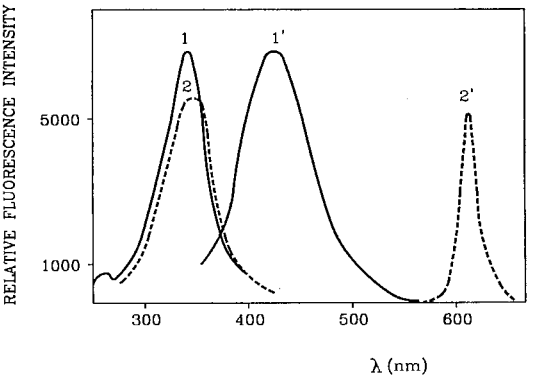

Fig. 1. Excitation (1, 2) and emission (1′,2′) spectra obtained for ampicillin and tetracycline systems. [ampicillin] = [tetracycline] = 0.05 μg ml^{-1}, [Hg (II)] = 1.5×10^{-4} M, [penicillinase] = 0.15 unit ml^{-1}, [Eu (III)] = 2×10^{-5} M, [TTA] = 5.4×10^{-6} M, [Triton X-100] = 0.01%, [Tris buffer] = 1.5×10^{-2} M.

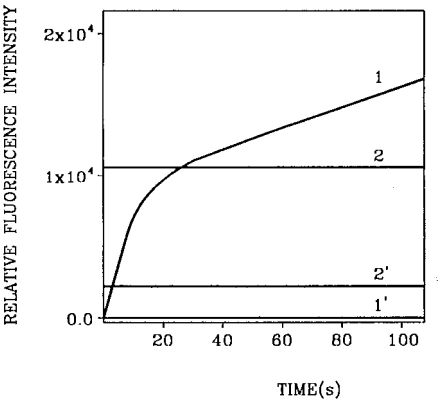

Fig. 2. Kinetic behaviour of the ampicillin (1) and tetracycline (2) systems in the presence of whey matrix. 1′ and 2′: blank of ampicillin and tetracycline systems, respectively. λ_{ex} 342 nm, λ_{em} 410 nm for ampicillin and 610 nm for tetracycline. [ampicillin] = [tetracycline] = 0.1 μg ml^{-1}, [Hg (II)] = 3×10^{-5} M, [penicillinase] = 0.15 unit ml^{-1}, [Eu (III)] = 2×10^{-5} M, [TTA] = 5.4×10^{-6} M, [Triton X-100] = 0.01%, [Tris buffer] = 1.5×10^{-2} M.

it is possible to obtain simultaneously the kinetic curves of both systems by selecting the corresponding emission wavelength in each emission channel. No chemical interaction between the reagents involved in both systems was found. However, as the aim of this study was to know the possible application of this approach to the determination of both antibiotics in milk, it was also carried out in the presence of this matrix, after removing casein. Under these conditions, the same kinetic behaviour was obtained for the ampicillin system but the initial rate of the tetracycline system was increased so that the equilibrium was instantaneously reached and it was impossible to obtain the kinetic curve. However, both chemical systems can be jointly used with analytical purposes by using kinetic measurements for ampicillin determination and equilibrium measurements for tetracycline determination. This is possible thanks to the availability of two emission channels where an adequate instrumental sensitivity can be used for each chemical system and the resolution achieved for both analytes does not depend on the relative values of the rate involved. Fig. 2 shows the kinetic curve obtained for the ampicillin system, where can be seen that the initial rate can be obtained in only 5 s and the blank signal is negligible. In addition, the kinetic curve obtained under these conditions does not show the short induction period found when the alkaline hydrolysis was used [11]. Unlike this system, the tetracycline system reaches instantaneously the equilibrium and the blank signal, which can be ascribed to the europium (III)-TTA reaction, must be substracted to obtain the net signal for tetracycline.

3.1. Optimization of variables

The variables affecting each system were optimized by the univariate method. All concentrations given are initial concentrations in the syringes (twice the actual concentrations in the reaction mixture at time zero after mixing). Each result was the mean of three measurements.

The study of the optimal experimental conditions for the development of the tetracycline system showed these are the same than those previously described [10] where the positive effect of TTA and Triton X-100 was widely discussed. Under these conditions, the detection limit obtained by using equilibrium measurements was lower than by kinetic measurements, although an advantage on the use of kinetic methodology lies in the negligible effect of the blank signal, unlike the equilibrium method where all measurements need to be corrected for the blank signal. However, as indicated above, only equilibrium measurements can be obtained for the tetracycline system in the presence of the whey matrix.

With regard to the ampicillin system, the requirements for working to a pH suitable for both ampicillin and tetracycline systems compelled to change the alkaline hydrolysis previously described [9,11] by the enzymatic hydrolysis by using penicillinase. Unlike the alkaline hydrolysis where hydrogen peroxide was used to increase the initial rate, it was not required in this case. Fig. 3 shows the effect of the penicillinase concentration on the kinetic behaviour of the ampicillin system at pH 7.4, where can be seen the initial rate is independent of this variable from a concentration of 0.15 unit ml^{-1}. The study of the effect of mercury (II) concentration showed that this vari-

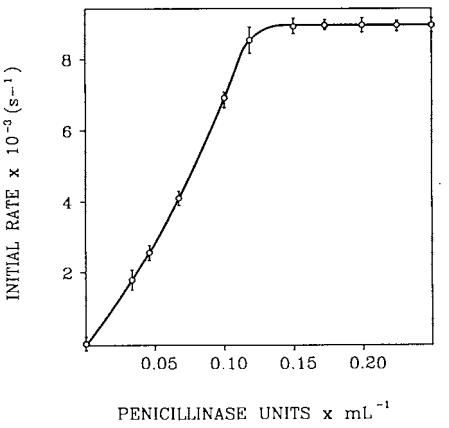

Fig. 3. Effect of penicillinase concentration on the initial rate obtained for the ampicillin system. [ampicillin] = 0.1 μg ml^{-1}, [Hg (II)] = 3×10^{-5} M, [Tris buffer] = 0.01 M.

able does not affect the initial rate when the concentration is larger than 10^{-4} M, which is ca. three times higher than when the alkaline hydrolysis is used [11].

Different assays were carried out for deproteination of the milk samples. Sodium tungstate and trichloracetic acid were unsuitable because the milk serum obtained in the first case was cloudy and the tetracycline reaction was inhibited in the presence of the second reagent. However, it was possible to use the conventional method for casein separation based on the insolubility of this protein in weakly-acidic media while whey proteins are soluble.

3.2. Analytical features

Under the optimum experimental condition described above, kinetic data corresponding to the ampicillin system were obtained from channel A with the emission monochromator set at 410 nm. These data were processed by the initial-rate method. Simultaneously, equilibrium data corresponding to the tetracycline system were obtained from channel B by placing a 550-nm cut-off filter. The excitation wavelength for both kinetic and equilibrium measurements was set at 342 nm via the excitation monochromator.

All ampicillin and tetracycline standards solutions used to obtain the calibration graphs were prepared in the presence of 4 ml of milk whey, in order to compensate the matrix effect on the samples. Under these conditions, the calibration graphs were linear over the ranges 0.01–15 μg ml^{-1} ampicillin and 0.04–10 μg ml^{-1} tetracycline. The wide linear ranges obtained required using three different instrumental sensitivities on each emission channel. Table 1 summarizes the figures of merit of the different calibration graphs. The detection limits obtained for ampicillin and tetracycline, in the presence of the milk whey volume indicated above and calculated according to IUPAC's recommendations [12], were 0.003 and 0.01 μg ml^{-1}, respectively, which corresponds to 0.04 and 0.125 μg ml^{-1}, respectively, in milk.

The separation between the emission wavelengths of both ampicillin and tetracycline systems and the lack of contribution of each analyte to the analytical signal of the other, allows the direct resolution of the mixture. The simultaneous

Table 1
Analytical figures of merit of the proposed method

Compound	Linear range (μg ml^{-1})	Slope ± SD[a]	Intercept ± SD	n	r	SEE
Ampicillin	0.01–1.5	$(1.2 \pm 0.2) \times 10^3$	-6.1 ± 0.2	9	0.999	19
	1.5–5.0	$(2.5 \pm 0.3) \times 10^2$	50 ± 4	7	0.998	21
	5.0–15.0	46 ± 5	189 ± 11	6	0.998	11
Tetracycline	0.04–1.5	(4.6 ± 0.3)x10^4	(-1.5 ± 0.2)x10^3	9	0.999	108
	1.5–5.0	$(9.3 \pm 0.4) \times 10^3$	$(5.1 \pm 0.5) \times 10^3$	7	0.998	69
	5.0–10.0	$(2.3 \pm 0.3) \times 10^3$	$(8.3 \pm 0.3) \times 10^3$	5	0.990	73

[a] Units: Kinetic method: s^{-1} μg^{-1} ml; Equilibrium method: 1 μg^{-1} ml (I = Relative fluorescence intensity); SEE = Standard error of the estimate.

Table 2
Recovery of ampicillin and tetracycline added to milk samples

Sample[a]	Ampicillin (μg ml^{-1})			Tetracycline (μg ml^{-1})		
	Added	Found*	Recovery (%)	Added	Found	Recovery (%)
1	0.2	0.19 ± 0.01	95.0	0.6	0.62 ± 0.02	103.3
	0.6	0.60 ± 0.01	100.0	1.2	1.21 ± 0.01	100.8
	1.0	1.01 ± 0.02	101.0	2.0	2.00 ± 0.05	100.0
2	0.2	0.20 ± 0.02	100.0	0.6	0.57 ± 0.03	95.0
	0.6	0.62 ± 0.06	103.3	1.2	1.18 ± 0.02	98.3
	1.0	1.00 ± 0.04	100.0	2.0	2.00 ± 0.05	100.0
3	0.2	0.19 ± 0.05	95.0	0.6	0.56 ± 0.01	93.3
	0.6	0.59 ± 0.02	98.3	1.2	1.14 ± 0.02	95.0
	1.0	1.02 ± 0.05	102.0	2.0	1.94 ± 0.02	97.0

[a] (1) Whole milk, (2) Skimmed milk, (3) Raw milk.
*Average of three determinations ± SD.

method can be applied to a wide range of concentrations of both analytes thanks to the lack of overlapping of the emission spectra and the independent behaviour of each chemical system. In addition, the fast development of both systems allows the instantaneous measurement of the equilibrium signal corresponding to tetracycline, while the measurement of the reaction rate of ampicillin takes only 5 s. Hence the method is a useful alternative to routine determination of these analytes.

The precision of the method was evaluated at two concentrations of each analyte by assaying replicates of milk samples, which were treated as described under Procedure, so that the final concentration of each analyte was 0.05 and 0.1 μg ml^{-1}. The relative standard deviation thus obtained was 1.1 and 0.5% for ampicillin and 1.9 and 1.0% for tetracycline.

In order to study the selectivity of the method and its possible general use for tetracyclines and penicillins determination in milk, several of these compounds were assayed. All the tetracyclines examined showed luminescence signal in the presence of europium (III) and TTA, giving tetracycline the highest signal (100), oxytetracycline (92), doxitetracycline (60) and chlortetracycline (49). However, among the different penicillins assayed (ampicillin, amoxicillin cloxacillin, dicloxacillin and oxacillin), only amoxycillin gave a slight initial rate with the ampicillin system, about 15-times lower than that obtained for ampicillin. Also, several cephalosporins (cephalexin, cephradine, cephaloridine, cephalozin) were assayed by using this system, but no reaction was observed with any of them. These results show that the kinetic determination of ampicillin based on enzymatic hydrolysis is more selective than the one based on alkaline hydrolysis [11] where other penicillins and cephalosporins such as cloxacillin and cephradine interfered with the ampicillin determination.

3.3. Analysis of milk samples

The proposed method was applied to the simultaneous determination of ampicillin and tetracycline in three spiked milk samples. For this purpose, different amounts of these antibiotics were added to each sample in order to carry out the recovery study. The treatment of the samples to obtain the milk whey is described in the Procedure. Table 2 summarizes the recoveries obtained which ranged from 95.0 to 103.3% (average 99.4%) for ampicillin and between 93.3 and 103.3% (average 98.1%) for tetracycline.

4. Conclusions

According to the results obtained, the joint use of stopped-flow mixing technique and a T-format

spectrofluorimeter provides a simple and fast approach for the simultaneous determination of mixtures. While the former allows the automation of the measurement step and the simple adaptation of the method to routine analysis, the availability of two emission channels allows to obtain analytical data from the chemical systems involved whichever is the kinetic behaviour of each one provided that mutual kinetic effects are absent. Thus, the proposed method is the first application of the combined use of kinetic and equilibrium measurements.

This method also shows that it is possible to obtain analytical results by mixing two relatively complex systems. Thus, the fluorescence of the ampicillin system is obtained after a multi-step process which involves the enzymatic hydrolysis of the antibiotic and the reaction of its mercapto group with mercuric chloride, while the tetracycline determination is based on the formation of the ternary complex with europium (III) and TTA in the presence of Triton X-100 and the intramolecular energy-transfer precess from the ligands to the lanthanide ion. However, the lack of interaction between the reagents of both systems allows the individual development of each system. The main limitation of the method is its application to the analysis of milk samples containing very low concentration levels of these antibiotics. In this case, a pre-concentration step such as solid phase extraction would be required.

The methods reported in the literature for the determination of antibiotics in milk involve in most cases the determination of several penicillins such as ampicillin, amoxicillin and cloxacillin [6,7,13,14], or several tetracyclines such as tetracycline, oxytetracycline and chlortetracycline [15–17], by using liquid chromatography. However, no methods for the simultaneous determination of a penicillin and a tetracycline have been described up to date. Generally, the chromatographic methods show lower LODs than those obtained in the proposed method, as they involve the pre-concentration of the analytes, but it is faster and is the first automatic method described for the simultaneous determination of these antibiotics in milk.

Acknowledgements

The authors acknowledge financial support from the Spanish CICyT (Grant No. PB91-0840).

References

[1] R. Jackman, S.J. Mitchell, S.D. Dyer, J. Chesham, Food Agric. Immunol. 3 (1991) 3.
[2] E. Märtlbauer, E. Usleber, E. Schneider, R. Dietrich, Analyst 119 (1994) 2543.
[3] J.H. Cutting, W.M. Kiessling, F.L. Bond, J.E. McCarron, K.S. Kruezer, J.A. Hurlbut, J.N. Sofos, J. AOAC Int. 78 (1995) 663.
[4] D.R. Bobbitt, K.W. Ng, J. Chromatogr. 624 (1992) 153.
[5] B. Shaikh, W.A. Moats, J. Chromatogr. 643 (1993) 369.
[6] W.A. Moats, R. Harik-Khan, J. AOAC Int. 78 (1995) 49.
[7] R. Harik-Khan, W.A. Moats, J. AOAC Int. 78 (1995) 978.
[8] B. Gala, A. Gómez-Hens, D. Pérez-Bendito, Anal. Chim. Acta 310 (1995) 453.
[9] K. Miyazaki, Chem. Pharm. Bull. 22 (1974) 1910.
[10] P. Izquierdo, A. Gómez-Hens, D. Pérez-Bendito, Anal. Chim. Acta 292 (1994) 133.
[11] P. Izquierdo, A. Gómez-Hens, D. Pérez-Bendito, Fresenius J. Anal. Chem. 342 (1992) 606.
[12] G.L. Long, J.D. Wineforner, Anal. Chem. 55 (1983) 712A.
[13] W.A. Moats, J. AOAC Int. 77 (1994) 41.
[14] R.F. Straub, R.D. Voyksner, J. Chromatogr. 647 (1993) 167.
[15] C.L. Chen, X.L. Gu, J. AOAC Int. 78 (1995) 1369.
[16] W.A. Moats, R. Harik-khan, J. Agric. Food Chem. 43 (1995)
[17] M.C. Carson, W. Breslyn, J. AOAC Int. 79 (1996) 29.

.

ELSEVIER

Talanta 44 (1997) 1891–1899

Talanta

Determination of formation constants of hydroxo and carbonate complexes of Pr^{3+} in 2 M NaCl at 303 K

H. López-González [a,b], M. Jiménez-Reyes [a,*], A. Rojas-Hernández [b], M. Solache-Ríos [a]

[a] *Instituto Nacional de Investigaciones Nucleares, Depto. de Química, Apdo. Postal 18-1027, 11801 Mexico, DF, Mexico*
[b] *Universidad Autónoma Metropolitana-Iztapalapa, Area de Electroquímica, Apdo. Postal 55-534, 09340 Mexico, DF, Mexico*

Received 6 December 1996; received in revised form 12 March 1997; accepted 14 March 1997

Abstract

The hydrolysis of praseodymium III in 2 M sodium chloride at 303 K was studied. Two methods were used: pH titration followed by a computational refinement and solvent extraction in the presence of a competitive ligand. The hydrolysis constants obtained by pH titration were: $\log \beta_{1,H} = -7.68 \pm 0.07$, $\log \beta_{1,2H} = -15.10 \pm 0.03$, and $\beta_{1,3H} = -23.80 \pm 0.04$. The stability constants of praseodymium carbonate complexes were determined by pH titration as well and were: $\log \beta_{1,CO_3^{2-}} = 5.94 \pm 0.08$ and $\log \beta_{1,2CO_3^{2-}} = 11.15 \pm 0.15$. Praseodymium carbonate species were taken into consideration for calculating the first hydrolysis constants by the solvent extraction method and the value obtained was: $\log \beta_{1,H} = -7.69 \pm 0.27$. The values for $\log \beta_{1,H}$ attained by both methods are the same. The species-distribution diagram was obtained from the stability constants of praseodymium carbonate complexes and hydrolysis products in the conditions of the present work. © 1997 Elsevier Science B.V.

Keywords: Carbonate complexes; Hydrolysis; Praseodymium

1. Introduction

It is observed in the lanthanide series, from the published data, that the values of the first hydrolysis constant for the same metal ion differ widely [1,2]. Further work in this field is highly desirable in view of the basic importance of the problem by itself, as well as for understanding the chemical behaviour of these metal ions in various natural and artificial environments [3,4]. The differences among the values can be attributed to the various experimental conditions used, such as the concentration of the element or the pH range, and probably to the contribution of the affinity of lanthanide and carbonate ions, which has been regarded as negligible.

The hydrolysis constants of praseodymium III have been determined mainly by pH titration (Table 1) [5–10]. The concentration of praseodymium III and the ionic strength ranges used in all these works are wide. However, little information is available regarding the behaviour of praseodymium in aqueous solution.

* Corresponding author.

PII S00 9-9140(97)00085-4

Table 1
Literature data of the first hydrolysis constant of praseodymium

Reference no.	Method, T (K)	Ionic strength (M)	$[Pr^{3+}]$	$\log \beta_{1,H}$
5	pH titration, 298	0.001–0.01 M, $Pr_2(SO_4)_3$	0.001–0.01 M, $Pr_2(SO_4)_3$	−9.0
6	pH titration, 298	0.3 M, $NaClO_4$+0.02 M $Ba(OH)_2$	0.004–0.009 M, $Pr(ClO_4)_3$	−9.45
7	Solvent exraction	0.1 M $LiClO_4$	1×10^{-7}M	-7.1 ± 0.15
8	pH titration, 298	3 M $NaClO_4$	0.2–0.8 M, $Pr(ClO_4)_3$	-9.56 ± 0.03
9	pH titration, 298	3 M $NaClO_4$	xM $Pr(ClO_4)_3$	-8.5 ± 0.4
10	pH titration, 333	3 m $LiClO_4$	0.03−1 m	-8.74 ± 0.01
Present work	pH titration, 303	2 M NaCl	1.7×10^{-4}M, $Pr(NO_3)_3$	-7.68 ± 0.07
Present work	Solvent extraction, 303	2 M NaCl	1.45×10^{-5} M, $Pr(NO_3)_3$	-7.69 ± 0.27

The aim of this paper was therefore to determine the hydrolysis constants of praseodymium III, in 2 M sodium chloride ionic strength, at 303 K. According to the suggestions of the IUPAC, in this work the first hydrolysis constant was determined by two methods, the solvent extraction in the presence of a competitive ligand and pH titration.

2. Theory

In general, the reaction for the formation of a hydrolysis product can be written as follows:

$$x\mathrm{M}^{z+} + y\mathrm{H_2O} \rightleftarrows \mathrm{M}_x(\mathrm{OH})_y^{zx-y} + y\mathrm{H}^+ \qquad \text{(a)}$$

where the equilibrium constant is $\beta_{x,y}$. In the present work the polynuclear species are neglected due to the low concentration values of praseodymium (1.45×10^{-5} M for the solvent extraction and up to 1.7×10^{-4} M for the pH titration). Therefore, only $\beta_{1,H}$, $\beta_{1,2H}$ and $\beta_{1,3H}$ have been considered, which correspond to the first, second and third hydrolysis global constants, respectively.

2.1. pH Titration

Potentiometric titration is a precise and direct technique that allows the experimental determination of the stability constants, through the analysis of the titration curves by graphic or numeric methods. If the indicator electrode is sensitive to pH, it is important to distinguish between the minus logarithm of the hydronium concentration (pC_H) and the experimental pH value measured in systems with high ionic strength.

The analysis of the titration curve can be performed with the aid of a computational program. SUPERQUAD is a program created by Gans et al. [11] that refines equilibrium constant values by a least-squares method from the cell potential (or pH) obtained during potentiometric titrations.

The Marquardt algorithm is applied in SUPERQUAD in order to achieve the minimum of the cell potential (E) quadratic residual sum of Eq. (1):

$$U = \sum(\Delta E)^2 = \sum(E_{\text{calculated}} - E_{\text{experimental}})^2 \qquad (1)$$

The cell potential for each added volume from the titrant solution is calculated by SUPERQUAD with the aid of: (a) experimental normal (or zero-pH) potentials and slopes of the electrodes used; and (b) metal cations, ligands and/or proton concentration values obtained from cations, ligands and charge balance equations for the system. In general, it is necessary to follow an iterative procedure in order to obtain precise solutions of the system of equations formulated.

The input file data that should be feed to SUPERQUAD includes the added volumes and the cell potentials (or pH) measured, as well as a chemical model that includes stoichiometry and the values of the formation constants of the species present during the titrations. The refined values the formation constants and a very complete statistical analysis of data are obtained in the output file.

2.2. Solvent extraction

The principle of the solvent extraction method, in the presence of a competitive ligand, has been described previously [12,13] Hence, only the main equations are included here, particularly those concerning the reactions of praseodymium with hydroxide and diglycolate ions, the latter being the competitive ligand in the extraction.

The extraction of praseodymium to an organic phase can be achieved with an extracting agent ($\overline{HX}$) and in many cases it can be considered that the extractant is only present in this phase. The extraction equilibrium of praseodymium can be represented by the following equation:

$$Pr^{3+} + 3\overline{HX} \rightleftarrows \overline{PrX_3} + 3H^+ \quad \text{(b)}$$

with:

$$K_{ext} = \frac{[\overline{PrX_3}][H^+]^3}{[Pr^{3+}][\overline{HX}]^3} \quad (2)$$

where $[\overline{PrX_3}]$, $[\overline{HX}]$, $[Pr^{3+}]$ and $[H^+]$ represent the total concentrations of praseodymium and the extractant in the organic phase, and the concentration of praseodymium and hydronium in the aqueous phase, respectively. The distribution coefficient is:

$$D_0 = \frac{[\overline{PrX_3}]}{[Pr^{3+}]} = \frac{K_{ext}[\overline{HX}]^3}{[H^+]^3} \quad (3)$$

When pC_H is low and a competitive ligand, such as a diglycolate ion (L^{2-}), is added, the distribution coefficient is modified. According to Grenthe and Tobiasson [14], PrL^+ is the most important species; then the equation for the distribution coefficient in the absence of hydrolysis products, D_1, is:

$$D_1 = \frac{[\overline{PrX_3}]}{[Pr^{3+}](1+\beta_{1,L}[L^{2-}])} = \frac{D_0}{1+\beta_{1,L}[L^{2-}]} \quad (4)$$

Therefore, a graph of $1/D_1$ versus $[L^{2-}]$ led us to calculate the stability constant of the praseodymium diglycolate complex ($Pr(DG)^+$), by means of the following equation:

$$\frac{1}{D_1} = \frac{1}{D_0} + \frac{\beta_{1,L}}{D_0}[L^{2-}] \quad (5)$$

The presence of the hydrolysis complexes also modifies the distribution coefficient (D_2). When Pr^{3+}, $Pr(OH)^{2+}$, and $Pr(DG)^+$ are present in the aqueous phase, Eq. (4) can be written as:

$$D_2 = \frac{[\overline{PrX_3}]}{[Pr^{3+}](1+\beta_{1,OH}[OH^-]+\beta_{1,L}[L^{2-}])} \quad (6)$$

In the absence of diglycolate ions, D_0' can be defined as follows:

$$D_0' = \frac{[\overline{PrX_3}]}{[Pr^{3+}](1+\beta_{1,OH}[OH^-])} \quad (7)$$

From Eqs. (6) and (7), it is found that:

$$\frac{1}{D_2} = \frac{1}{D_0'} + \frac{\beta_{1,L}'}{D_0'}[L^{2-}] \quad (8)$$

where $\beta_{1,L}'$ represents a conditional stability constant which is equal to

$$\beta_{1,L}' = \frac{\beta_{1,L}}{1+\beta_{1,OH}[OH^-]} \quad (9)$$

If pC_H is constant, the denominator of the previous equation is also constant.

The conditional stability constant ($\beta_{1,L}'$) can be evaluated from Eq. (8) and a graph of $1/D_2$ versus $[L^{2-}]$. Finally, according to the Eq. (9), $\beta_{1,OH}$ can be calculated as follows:

$$\beta_{1,OH} = \frac{(\beta_{1,L}/\beta_{1,L}')-1}{[OH^-]} \quad (10)$$

3. Experimental

3.1. Reagents

All reagents were analytical grade and deionized water was used to prepare the solutions. In all cases, the aqueous solutions were 2 M NaCl ionic strength. The extraction vials were treated as described elsewhere [15] in order to minimize adsorption of the tracers.

The praseodymium oxalate was prepared from the nitrate; it was calcined at 693 and then at 1063 K, according to the literature [16], to obtain Pr_6O_{11}, which was identified by X-ray diffraction. The oxide was treated with nitric acid and finally dissolved in 10^{-3} M nitric acid. ^{142}Pr was ob-

tained for solvent extraction experiments by irradiating the solution in a TRIGA MARK III nuclear reactor for 1 h at a thermal neutron flux of 1×10^{13} cm^{-2} s^{-1}. This isotope was identified [17] by its gamma radiation spectrum (1570 keV) using a GeH detector and no interfering radiation was observed. The half-life was also verified (19.2 h).

3.2. pH Titration

A high precision pH-meter (Taccussel-Radiometer, model LPH430T) equipped with a glass electrode, which has low interference coefficients for alkaline ions, and an AgCl/Ag reference electrode together with a digital burette (Brand II) were used for these experiments. Nitrogen was bubbled in the solutions and the nitrogen atmosphere was kept during measurements. The experiments were done at 303.0 ± 0.1 K and this was controlled by a constant temperature circulator (Cole Parmer, Polystat).

Solutions of 0.1, 0.01, and 0.001 M sodium hydroxide and hydrochloric acid were prepared in 2 M sodium chloride ionic strength. The pH values were measured in these solutions and the calibration lines were obtained by plotting $pC_H = -\log[H^+]$ against measured pH.

The pH titrations carried out were as follows:

(i) Determination of the appropriate concentration of Pr^{3+}. It was determined by titration of praseodymium nitrate solutions, 7.3×10^{-3}, 3.6×10^{-3} and 4.5×10^{-4} M, with sodium hydroxide solutions: 1×10^{-2} M for the first and the second and 1.25×10^{-3} M for the third. The precipitation of praseodymium hydroxide was observed for praseodymium nitrate concentration higher than 4.5×10^{-4} M. This fact was therefore taken into account, in order to avoid precipitation during the pH titrations.

(ii) Praseodymium nitrate solutions, 1.7×10^{-4} M, with sodium hydroxide solutions, 1.25×10^{-3} M.

(iii) A 7.3×10^{-5} M solution of praseodymium nitrate was left open to the air for 24 h and was then titrated with 1×10^{-3} M sodium hydroxide. In this case, nitrogen was not bubbled, and only the nitrogen atmosphere was kept over the solution.

(iv) Solutions of 0.05 M diglycolic acid (DGA) were titrated with 0.1 M sodium hydroxide.

The data obtained from the pH titrations were refined with the program SUPERQUAD to obtain the equilibrium constants and at least three experiments were done in the same conditions to analyze reproducibility.

3.3. Solvent extraction

The solvent extractions of praseodymium were done at the following pC_H values: 2.91, 3.52 and 7.64. The organic and aqueous solutions were pre-equilibrated between them until the pC_H did not change. The aqueous solutions for the experiments were composed as follows: 5 ml of the solution 2 M NaCl, 10 μl of the irradiated praseodymium solution and the required volume of diglycolic acid solution, for each concentration. The organic phases were 5 ml of a solution of dibenzoylmethane (DBM) and tri-*n*-octyl phosphyne oxide (TOPO) in benzene. The ratio [TOPO]/[DBM] and their concentrations were determined experimentally in order to get D_0 and D'_0 around 1 to enhance accuracy of measurements. The concentrations of DGA, DBM and TOPO used in each batch of experiments are shown in Table 2. The shaking time to attain the equilibrium in the phases was determined experimentally. The vials were then shaken for 20 h, in a thermostated bath (Cole Palmer, Polystat) at 303 K. The concentration of praseodymium in each experiment was 1.45×10^{-5} M. After shaking, the samples were centrifuged for 5 min and then 4 ml of each phase were taken out. The radioactivity of ^{142}Pr was measured in both phases by means of a NaI(Tl) well detector, coupled to a monochannel analyzer (Picker Spectroscaler). The value $1/D$ was calculated from the radioactivity in the aqueous phase divided by that in the organic phase. On the other hand, the total radioactivity was measured by means of 10 μl of the radioactive solution added to 4 ml of 1 M hydrochloric acid. A pH-meter (Orion) with a combined (glass AgCl/Ag) electrode was utilized for measurements in the aqueous phases.

4. Results and discussion

According to the X-ray diffraction, the prepared praseodymium oxide was $PrO_{1.83}$, which had a high crystallinity. This compound is a mixture of Pr^{3+} and Pr^{4+} oxides and it forms only Pr^{3+} in aqueous solution [10].

The equations obtained to correct the pH measurements to pC_H values were the following. In the solvent extraction method, it was:

$$pC_H = (1.019 \pm 0.005)pH + (0.314 \pm 0.047)$$
$$r = 0.999 \quad (11)$$

and the equation used for pH titration was:

$$pC_H = (1.005 \pm 0.012)pH + (0.276 \pm 0.060)$$
$$r = 0.999 \quad (12)$$

The slight difference between these empirical equations can be attributed to the equipment used for the determination of each one.

Ion product of water values ($\log K_w$) for 2 M NaCl ionic strength and 303 K were calculated using the literature value [1] for $I = 2$ M ($\log K_{w,288\,K} = -13.96 \pm 0.01$) and the Van't Hoff equation. The obtained value was $\log K_{w,303\,K} = -13.80$. This parameter was also calculated using values [2] for $I = 2.01$ and 3.00 m at 298 K by linear interpolation. The ionic strength of the NaCl solution was converted to the molal scale (2 M = 2.08 m), taking into account the density (1.077 g ml^{-1}) which was measured. The $\log K_{w,298\,K}$ value deduced was -13.85 and the corrected value at 303K was -13.69.

Table 2
Concentrations of the utilized solutions

Parameter	Batch number		
	1	2	3
2 M NaCl, pC_H	2.99	3.65	7.64[a]
[DGA] (M)	0.45	0.055	0.011
[DBM] (M)	0.003	0.002	0.002
[TOPO] (M)	0.029	0.023	0.004
$[OH^-]$ (M)	–	–	8.3×10^{-7}
$[CO_3^{2-}]$ (M)	–	–	2.5×10^{-6}
$\beta_{1,DG}$	61 855	74 355	–
$\beta'_{1,DG}$	–	–	10 797

DGA, aqueous solution of diglycolic acid; DBM and TOPO, solutions of dibenzoylmethane and tri-*n*-octyl phosphine oxide in benzene. Hydroxide and carbonate ion concentrations, $\beta_{1,DG}$ and $\beta'_{1,DG}$ obtained in each batch of solvent extraction experiments.

[a] A total of 0.01 m of *N*-Tris[hydroxymethyl]methyl-2-aminoethane sulfonic acid (TES) was added as buffer.

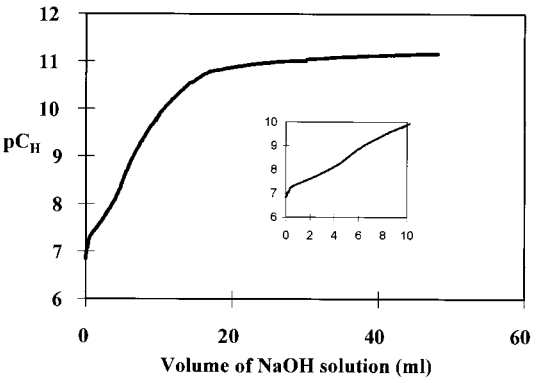

Fig. 1. Typical pC_H titration curve of 1.7×10^{-4} M praseodymium nitrate with 1.25×10^{-3} M sodium hydroxide in 2 M sodium chloride ionic strength at 303 K in the absence of carbonate ions.

4.1. Hydrolysis constants by pH titration

Fig. 1 shows a typical curve of praseodymium nitrate titration in the absence of carbonate ions. Precipitation was observed when the praseodymium concentration was between 7.3×10^{-3} and 3.6×10^{-3} M and it was not observed at or below 4.5×10^{-4} M. It was found that the successive hydrolysis constant values of the three complexes formed are closer than expected; however, the third inflection can be observed, as shown in the inset of Fig. 1. Analysis of data showed that three equivalents of NaOH are consumed per mole of praseodymium.

The three hydrolysis constants obtained from the pH titration data (Fig. 1) and the refinement

achieved with the program SUPERQUAD were: $\log \beta_{1,H} = -7.68 \pm 0.07$, $\log \beta_{1,2H} = -15.09 \pm 0.03$ and $\log \beta_{1,3H} = -23.80 \pm 0.40$. The $\log K_w$ could be well refined simultaneously (-13.68); for this refinement, $\sigma_{total\,(mV)} = 21.69$ and $\chi^2 = 17.96$. The $\log K_w$ value was in good agreement with the values calculated as described above and it was used for calculations. It is important to note that, to the best of our knowledge, values of $\beta_{1,2H}$, and $\beta_{1,3H}$ for praseodymium had not been reported before for any ionic strength. The distribution diagram of the species present through the titration, obtained from the three hydrolysis constants, is shown in Fig. 2. It is observed that the Pr^{3+} species is found at $pC_H < 9$, the $Pr(OH)^{2+}$ species between 5.5 and 9, the $Pr(OH)_2^+$ species between 6.5 and 11, and finally the $Pr(OH)_3$ from $pC_H \geqslant 7.5$. It is important to note that the $Pr(OH)^{2+}$ species is not a predominant species in this system.

4.2. First hydrolysis constant by solvent extraction

Fig. 3 shows the plots of $1/D$ against $[DG^{2-}]$ for all batches of experiments. The concentration of diglycolate ion in the solutions was calculated, taking into account the amount of diglycolic acid added to the aqueous phases, the pK values and the pC_H measured in the aqueous phases after the extractions, for each batch of experiments. Points in Fig. 3 represent the mean value from 6–10

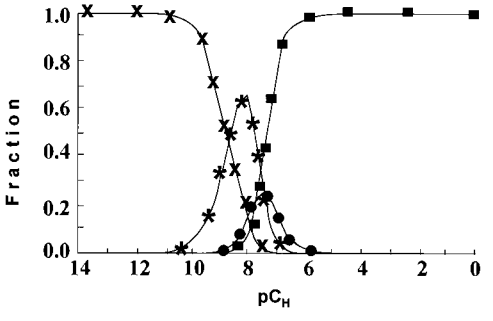

Fig. 2. Species-distribution diagram obtained from the stability constants of hydrolysis products of praseodymium. $[Pr^{3+}]_{TOT} = 0.17$ mM; (■) Pr^{3+}; (●) $Pr(OH)^{2+}$; (*) $Pr(OH)_2^+$;X) $Pr(OH)_3$.

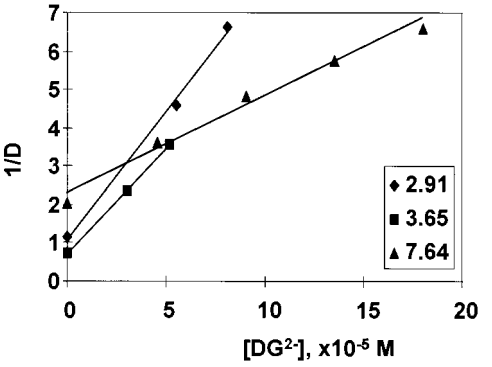

Fig. 3. $1/D$ vs. DG^{2-} concentration at different pC_H values.

independent experiments. The error bars of $1/D$ measurements, not indicated in the figure, were about 10% of the mean values for the experiments. Taking into account Eqs. (5) and (8), from the least-square regression analysis of data the following relations were obtained:

$$pC_H = 2.91{:}1/D_1 = 63\,441[DG^{2-}] + 1.12 \quad (r = 0.998) \tag{13}$$

$$pC_H = 3.52{:}1/D_1 = 54\,606[DG^{2-}] + 0.73 \quad (r = 0.9999) \tag{14}$$

$$pC_H = 7.64{:}1/D_2 = 24\,916[DG^{2-}] + 2.31 \quad (r = 0.991) \tag{15}$$

The value $\beta_{1,DG}$ was calculated from data of Eqs. (13) and (14) and $\beta'_{1,DG}$ was calculated from data of Eq. (15); the values are shown in Table 2. The $\log \beta_{1,OH}$ was calculated from $\beta_{1,DG}$, $\beta'_{1,DG}$ values and Eq. (10). It was 6.80 ± 0.05 and $\log \beta_{1,H} = -6.89 \pm 0.05$. This value is similar to the one obtained by Guillaumont et al. [7] ($\log \beta_{1,H} = -7.1 \pm 0.15$) by solvent extraction and at 0.1 M $LiClO_4$ ionic strength. However, it is different from the value obtained by pH titration in the present work. This difference was attributed to the presence of praseodymium carbonate complexes in the solvent extraction solutions.

The remaining radioactivity in the aqueous and organic solutions after the solvent extraction was between 90 and 98% of the original radioactivity. According to these values, the loss of praseodymium by adsorption on the vials was regarded as negligible.

4.3. Stability constants of carbonate complexes

A solution of praseodymium nitrate left open to the air was titrated as described above. Fig. 4 shows a typical pC_H titration obtained in these conditions. It is important to note that at the same concentration of Pr^{3+}, the pC_H values at the beginning of the titration are lower in the presence of CO_2. This effect is an evidence of the formation of praseodymium carbonate complexes.

Table 3 shows two models refined with SUPERQUAD from pC_H titration (Fig. 4), in the presence of carbonate ions. In the first case, the praseodymium carbonate complexes were neglected and in the second case, they were considered. The best model is the later, because the σ_{total} value is almost half of that found in the first model. This demonstrates the presence of the praseodymium carbonate complexes. It is observed that the log K_w was well refined and was in good agreement with the calculated values given above. This agreement supports the validity of the values obtained for the praseodymium carbonate complexes. The standard deviation for log $\beta_{1,2CO_3^{2-}}$ is high in comparison with the other refined values, and it should therefore be taken carefully.

Fig. 5 shows the species-distribution diagram obtained from the stability constants of praseodymium carbonate complexes and hydrolysis products. According to this diagram, at $pC_H = 7.64$, the working value for the solvent extraction experiments, the following species: $PrOH^{2+}$, $Pr(OH)_2^+$, $Pr(CO_3)^+$ and $Pr(CO_3)_2^-$, are present in the solutions. All these species have to be considered in Eq. (6) and therefore Eq. (10) becomes:

$$\beta_{1,OH} = ((\beta_{1,L}/\beta'_{1,L}) - 1 - \beta_{1,CO_3^{2-}}[CO_3^{2-}] - \beta_{1,2CO_3^{2-}}[CO_3^{2-}]^2 - \beta_{1,2OH}[OH^-]^2)/[OH^-] \quad (16)$$

The dissociation of carbonic acid were found in the literature [4] for 1 M $NaClO_4$

Table 3
Statistical refinement obtained by the program SUPERQUAD for pH titrations of 7.3×10^{-5} M $Pr(NO_3)_3$ in the presence of CO_2 with 1×10^{-3} M NaOH

Equilibrium	log β	σ
1st Model: praseodymium carbonate complexes were not considered		
$Pr^{3+} + H_2O \rightleftarrows PrOH^{2+} + H^+$	−7.68 (Fixed)	
$Pr^{3+} + 2H_2O \rightleftarrows Pr(OH)_2^+ + 2H^+$	−15.09 (Fixed)	
$Pr^{3+} + 3H_2O \rightleftarrows Pr(OH)_3 + 3H^+$	−23.80 (Fixed)	
$CO_3^{2-} + H^+ \rightleftarrows HCO^{3-}$	9.96	0.02
$CO_3^{2-} + 2H^+ \rightleftarrows CO_2 + H_2O$	16.96	0.02
$H_2O \rightleftarrows H^+ + OH^-$	−13.71	0.01
σ_{total} (mV) = 5.60 mV; $\chi^2 = 19.37$		
2nd Model: praseodymium carbonate complexes were considered		
$Pr^{3+} + H_2O \rightleftarrows PrOH^{2+} + H^+$	−7.68 (Fixed)	
$Pr^{3+} + 2H_2O \rightleftarrows Pr(OH)_2^+ + 2H^+$	−15.09 (Fixed)	
$Pr^{3+} + 3H_2O \rightleftarrows Pr(OH)_3 + 3H^+$	−23.80 (Fixed)	
$Pr^{3+} + CO_3^{2-} \rightleftarrows Pr(CO_3)^+$	5.94	0.08
$Pr^{3+} + 2CO_3^{2-} \rightleftarrows Pr(CO_3)_2^-$	11.15	0.15
$CO_3^{2-} + H^+ \rightleftarrows HCO_3^-$	9.90	0.02
$CO_3^{2-} + 2H^+ \rightleftarrows CO_2 + H_2O$	16.94	0.01
$H_2O \rightleftarrows H^+ + OH^-$	−13.72	0.01
σ_{total} (mV) = 3.95 mV; $\chi^2 = 15.03$		

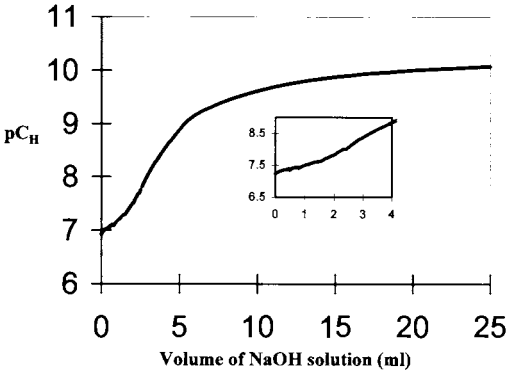

Fig. 4. Typical pC_H titration curve of 7.3×10^{-5} M praseodymium nitrate with 1×10^{-3} M sodium hydroxide in 2 M sodium chloride ionic strength at 303 K, in the presence of carbonate ions.

ionic strength and they were also adjusted by the SUPERQUAD program to our experimental conditions (see Table 3). The above mentioned program also let us to calculate the CO_2 concentration in the solutions (6.02×10^{-4} M). Dissociation constants of carbonic acid, CO_2 concentration and pC_H were used to calculate the carbonate ion concentration in the aqueous phases of the solvent extraction system. This last value, the stability constants of praseodymium carbonate complexes and the values obtained in the solvent extraction for $\log \beta_{1,DG}$ and $\log \beta'_{1,DG}$ (Table 2) were applied in Eq. (16). The $\log \beta_{1,OH}$ was 6.02 ± 0.27 and $\log \beta_{1,H}$ was -7.69 ± 0.27. This value is equal to the one obtained by pH titration in the present work.

4.4. Comparison with other works

In general, the $\log \beta_{1,H}$ value obtained in this work is lower than those values reported previously and this difference can be attributed to the following: the concentration of praseodymium plays an important role for the pH titrations. It was observed in this work that praseodymium hydroxide precipitates during pH titration in concentrations higher than 1.7×10^{-4} M and this effect may give erroneous values. The data found in the literature (Table 1) were obtained with praseodymium concentrations higher than the one used in this work, for pH titrations; however it was not indicated whether precipitation was observed.

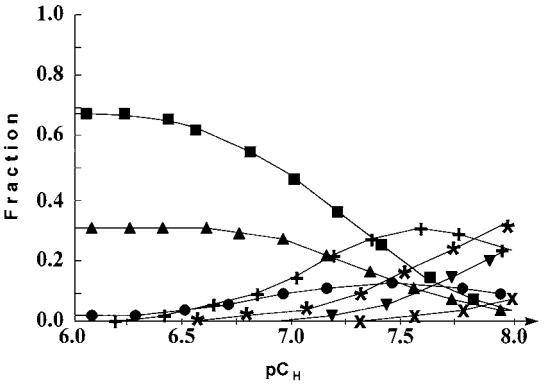

Fig. 5. Species-distribution diagram obtained from the stability constants of praseodymium carbonate complexes and hydrolysis products shown in Table 3. The diglycolate species is also included. $[CO_3^{2-}]_{TOT} = 0.60$ mM; $[Pr^{3+}]_{TOT} = 14.5$ μM; $[DGA^{2+}] = 11.00$ μM. (■) Pr^{3+}; (▲) $Pr(DGA)^+$; (●) $Pr(OH)^{2+}$; (+) $Pr(CO_3)^+$; (*) $Pr(OH)_2^+$; (▼) $Pr(CO_3)_2^-$;X) $Pr(OH)_3$.

Polynuclear complexes have been only considered by Burkov et al. [8] and Ciavatta et al. [10]. However, in most cases praseodymium concentrations used were high and polynuclear species were probably formed in the systems studied.

The value of $\log \beta_{1,H}$ found in the present work is higher than the one reported elsewhere at 333 K [10]. This difference could be attributed to the fact that the complexes are more stable at lower temperature.

The $\log \beta_{1,H}$ has been determined before by solvent extraction [7]; however, in that work carbonate complex formation was neglected. It is important to note that when this last effect was not considered in the present work, for the solvent extraction system, a value similar to that reported before [7] was obtained.

The values of the hydrolysis constant at different ionic strengths have been related to each other by an empirical relation [2]. According to this relation, $\log \beta_{1,H}$ for praseodymium should be -9.2, in 2 M NaCl ionic strength. However, our experimental results indicated, by both the solvent extraction and pH titration methods, that $\log \beta_{1,H}$ is higher, (-7.68). This value is similar to -8.1 reported for $I = 0$ [2]. These results are not surprising, considering that Lundqvist [4] obtained higher values for the hydrolysis constants than expected when working with europium and americium.

Lundqvist [4] suggested that the hydrolysis studies are generally complicated by simultaneously occurring disturbing processes like sorption, precipitation and/or formation of polynuclear and colloid species. In the present work, the sorption and precipitation did not affect the measured distribution values after the solvent extraction, since the loss of praseodymium by adsorption on the vials may be regarded as negligible. As mentioned above, more than 90% of praseodymium was found in solution after the solvent extractions. On the other hand, the concentration of praseodymium was decreased until

no precipitation was observed and the curve shape remained unchanged during the pH titrations. Furthermore, in the solvent extraction method, the concentration of praseodymium was even lower than for pH titrations, and precipitation and polynuclear species formation are therefore very unlikely to occur in the experiments. Colloidal formation has not been considered in any of the published works on the hydrolysis constant of praseodymium and it could be an important parameter to understand the behaviour of lanthanides in solutions.

Acknowledgements

The authors wish to express their sincere thanks to Dr A. Vacca for the copy of the SUPERQUAD program and to Mr V.H. Lara for the X-ray diffraction data.

References

[1] R.M. Smith, A.E. Martell, Critical Stability Constant, vol. 4, Plenum Press, New York, 1977.
[2] C.F. Baes Jr., R.E. Mesmer, The Hydrolysis of Cations, Wiley, New York, 1976.
[3] P.K. Mohapatra, P.K. Khopkar, Polyhedron 8 (1989) 2071.
[4] R. Lundqvist, Acta Chem. Scand. 36A (1982) 741.
[5] T. Moeller, in: C.F. Baes Jr., R.E. Mesmer, The Hydrolysis of Cations, Wiley, New York, 1976 (reprint from J. Phys. Chem. 50 (1946) 242).
[6] U.K. Frolova, V.N. Kumok, V.V. Serebrennikov, Izv. Vysshikh Uchebn. Zavedenii, Khim. i Khim. Tekhnol. 9 (1966) 176 (CA: 65, 9816c, 1966).
[7] R. Guillaumont, B. Désiré, M. Galin, Radiochem. Radioanal. Lett. 8 (1971) 189.
[8] K.A. Burkov, E.A. Bus'ko, I.V. Pichugina, Russ. J. Inorg. Chem. 27 (1982) 362.
[9] R.S. Tobias, A.B. Garrett, J. Am. Chem. Soc. 80 (1958) 3532.
[10] L. Ciavatta, R. Porto, E. Vasca, Polyhedron 8 (1989) 983.
[11] P. Gans, A. Sabatini, A. Vacca, J. Chem. Soc. Dalton Trans. (1985) 1195.
[12] M.S. Caceci, G.R. Choppin, Radiochim. Acta 33 (1983) 101.
[13] G.R. Choppin, J.N. Mathur, Radiochim. Acta 52–53 (1991) 25.
[14] I. Grenthe, I. Tobiasson, Acta Chem. Scand. 17 (1963) 2101.
[15] M.S. Caceci, G.R. Choppin, Radiochim. Acta 33 (1983) 113.
[16] O.A. Songina, Rare Metals, Israel Program for Scientific Translation, Jerusalem, 1970 (original work published: Izdatel'stvo. Metallurgiya, Moscow, 1964).
[17] C.M. Lederer, J.M. Hollander, I. Perlman, Tables of Isotopes, Wiley, 1968.

ELSEVIER

Talanta 44 (1997) 1901–1909

Talanta

Spectroscopic identification and quantitative analysis of binary mixtures using artificial neural networks

M.L. Ganadu [a,*], G. Lubinu [a], A. Tilocca [a], S.R. Amendolia [b]

[a] *Dipartimento di Chimica, Università di Sassari, Via Vienna 2, I-07100 Sassari, Italy*
[b] *Istituto di Matematica e Fisica, Università di Sassari, Via Vienna 2, I-07100 Sassari, Italy*

Received 1 August 1996; received in revised form 24 February 1997; accepted 27 February 1997

Abstract

This work deals with the application of artificial neural networks to two common problems in spectroscopy: the identification of distorted UV-visible spectra of a specific class of organic compounds, and the quantitative determination of single components in binary mixtures of these compounds. The examined species were six organic indicators, whose spectra are very similar to each other; the trained networks have proven to be very powerful in both applications. © 1997 Elsevier Science B.V.

Keywords: Mixtures; Networks; Neural; Spectra

1. Introduction

Artificial neural networks [1–4] have been proven to be a suitable tool for the automated interpretation of spectral data. Some previous applications included the identification of a wide range of functional groups from the infrared spectra of organic compounds [5–9], the verification of peak-shaped signals from IR spectral data [10], the identification of carbohydrates on the basis of their ^{1}H NMR spectra [11,12], the classification of mass spectra [13]. Neural networks have also been used to model quantitative measurements from ultraviolet-visible spectroscopic data [14–16].

The advantages of the neural network approach to the spectral interpretation are well-known: the network architecture is easily programmed, with the aid of some freely-available computational packages; the computational effort ends with the learning session, after which the response is immediate: then the trained network can operate in real-time, which is of great importance in many applications. Moreover, the correlations between spectral features and structural categories need not to be known in advance: the neural network can 'learn by example', i.e., no a priori assumptions need to be made on the behavior of the data. This leads to the ability to process input data containing some degree of uncertainty. Spectrophotometric data (e.g., in vivo and in vitro measurement) often contains a high degree of noise, either inherent in the measurement or in the variation of the spectral pattern itself; the difficulties in the interpretation of such distorted

* Corresponding author.

PII S00 9-9140(97)00088-X

spectra can lead to errors either in the identification and in the quantitative measurements. If used properly, the neural networks performances, compared with other approaches, are less influenced by subtle perturbations and noise in the input signals. If the only purpose is to obtain accurate classifications and/or quantitative predictions, the trained network can be used as a 'black box': the connection weights stored after the learning procedure represent the 'knowledge' acquired through the examples, which permits to give accurate evaluations on new data. It is important to note that the trained network can discriminate between 'objects' in some way connected to those from which it has learned, but when 'extraneous' objects are presented to it, its responses are no more reliable. In other words, the network has the ability to interpolate, not to extrapolate, between the training patterns. However, the network should be trained in such a way to classify an extraneous object as 'unknown', i.e., it must not be confused with one of the learned patterns.

From this perspective, this work aims at testing the performances of neural networks in two distinct problems: the identification of distorted UV-visible spectra of a specific class of organic compounds, and the quantitative determination of single components in binary mixtures of these compounds. In the latter case, from the complete set of 15 possible two-component combinations of six pure compounds, we chose to study in particular two binary mixtures, which well represent the full set. This simplification was done because our purpose was only to test the performances of a neural approach to these kind of problems; then, in our opinion, a full analysis of all the possible mixtures is not needed.

Three neural networks, each one with a different task, were constructed. The first can be used to identify a pure compound (out of a group of six) from its absorbance spectrum; we have verified that the recognition is reliable also in the eventual presence of an 'extraneous' pattern. The other two systems work on binary mixtures of known components: each network can predict the composition of a specific mixture.

2. Network description

A three-layered, full connected FF-network was used in both problems. Each neuron of the input layer is fully interconnected with all the neurons of the hidden layer, which in turn are interconnected with each neuron of the output layer. There are no connections between the neurons within a layer, nor any direct connections between those of the input and output layer. Each connection has a weight associated with it, representing the connection strength, which is adjusted during learning.

A sigmoidal activation function was used, with a bias associated to each unit; therefore the output of the j-th neuron (belonging to the hidden or to the output layer) is:

$$o_j = \frac{1}{1 + \exp\left(-\sum_i w_{ij} \cdot o_i - \vartheta_j \right)} \tag{1}$$

where w_{ij} is the weight of the connection between i and j units, o_i is the output of an i unit in the preceding layer, and θ_j is the bias of the j unit. The connection weights were initialized randomly in the $[-1, 1]$ range.

3. Learning

The standard back-propagation algorithm [1] was used to train the networks; the weights update rule reads as follows:

$$\Delta w_{ij}^{n} = \eta \cdot \delta_j^{n} \cdot o_i^{n-1} \tag{2}$$

where η is the learning rate (constant); the change of the weight $\Delta w_{ij}^{\mathrm{n}}$ of the connection between the neuron j (on the layer n) with the neuron i (on the preceding layer) will be proportional to the error δ_j^{n} produced on the neuron j, and to the signal $o_i^{\mathrm{n}-1}$ coming from neuron i. The problem of how to calculate the delta values for each layer is discussed in [2].

In supervised learning the training patterns are iteratively presented to the network together with the desired output vector (target or teaching output). The input is propagated forward in the until the output layer is reached; the errors (δ's)

on the output neurons are then calculated and propagated backward to the inner units, updating all the weights. One learning iteration (epoch) is defined as the input, the check, and the correction of weights in all layers of all training vectors. The iteration proceeds until the output error falls below an acceptable level; then the resulting connection weights matrix may be used to classify previously unseen patterns, i.e., patterns which have not been used to train the network. The learning rate η adopted in this work is 0.2: this value is little enough to avoid local minima in the training session, but leads however to a fast convergence (i.e., a low training mean square error, see below).

4. Input

The number of input neurons was varied between 90 and 450. The latter value corresponds to the whole spectrum with a resolution of 1 nm (the wavelength varies in the range 250–700 nm). In the trials with a lower number of input data, we selected a subset from the whole spectrum by sampling the required number of points at regular intervals.

5. Output

Usually the dimension of the output vector corresponds to the number of classes to be separated (six in our case). In the classification problem the target vector had only one non-zero element, corresponding to the class of the associated pattern: this element has value one. In this way, the first output neuron represents the first compound (red cresole), and so on. In the mixture case, the target vector has only two elements, whose values range between 0 and 1 (while in the classification problem the only possible values for each element of the target vector were 0 and 1), representing the fraction of component 1 and component 2 in the mixture.

6. Spectra

The source of the spectral data is [17]; it reports the parameters of the gaussian bands of six sulfonephtalein indicators, in acid and basic form. The basic forms of these indicators were chosen for the present study, and the relative abbreviations which will be used in the following are reported in Table 1. The complete spectra are shown in Fig. 1. The two mixtures studied were: 3′,3″,5′,5″-Tetraiodophenolsulfonephtalein (abbreviation, ind7B) mixed in various proportions with 3,4,5,6-Tetrabromophenolsulfonephtalein (ind2BrB), and ind2BrB mixed with Clorophenol red (ind4B). As stated above, these two mixtures should well represent the full set (from six pure compounds one can obtain 15 possible binary combinations); actually, the pure spectra are rather similar to each other, and the two selected mixtures represent two ‘extreme’ cases, in terms of overlapping: the peaks in the spectra of ind2BrB and ind4B considerably overlap, while the overlap is lower for the other mixture. In other words, the complete range of overlapping should be covered in this way.

We reconstructed the original spectra by linear combining the above-mentioned gaussian bands, and by renormalizing each single spectrum. Random noise, gaussian-distributed, was added to each spectrum, in such a way as to reproduce the experimental noise (see the Appendix A).

The training set for the classification problem was made of 60 samples of each spectrum, with different random noise added. Thus, the training set, in this case, is made of 360 patterns. Moreover, a test set of another 360 distorted spectra (60 patterns for each of the six compounds, as for

Table 1
Compounds and abbreviations

Abbreviation	Compound
ind1B	Cresol red
ind4B	Clorophenol red
ind7B	3′,3″,5′,5″-Tetraiodophenolsulfonephtalein
ind1CH_3B	Xylenol
ind2BrB	3,4,5,6-Tetrabromophenolsulfonephtalein
ind6BrB	Tetrabromophenol blue

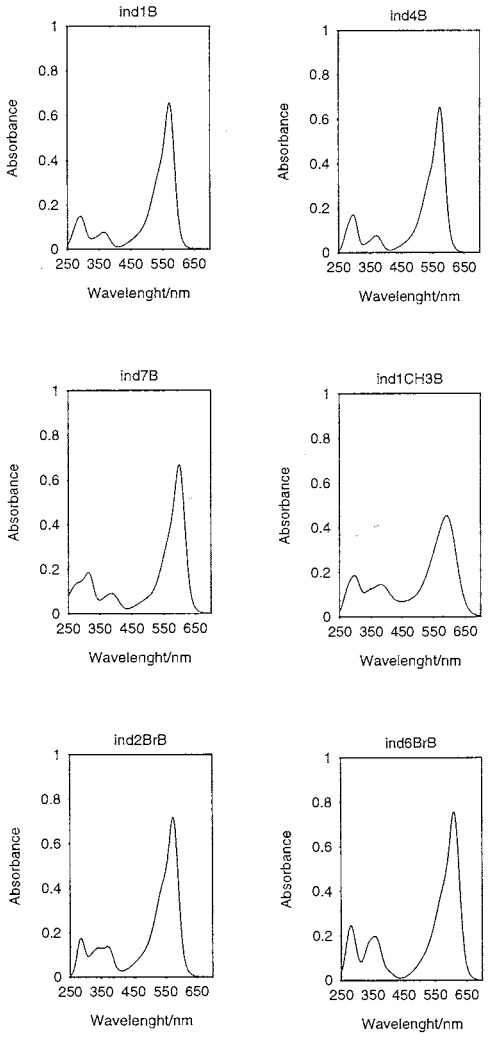

Fig. 1. Absorbance spectra of the six compounds studied (samples taken from the training set).

the training set) was generated. This set was used to test the generalization ability of the trained net, by presenting to it some samples which were not used in the training session. The distorted spectra can be divided in three groups: they are reported in Table 2, together with their relative abbreviations. Finally, a validation set made of 60 patterns generated in the same way as the '01' group of the test set, but with a different random noise compared it, was used, together with the training set, in the training session (see below). In Fig. 2 one of the '01' distorted spectra of ind7B is shown, to be compared with the non-distorted spectrum in Fig. 1.

Table 2
Test patterns and abbreviations

Patterns	Abbreviations
10×6 Spectra with added noise ten-fold greater than the experimental one	001
10×6 Spectra with added noise 50-fold greater than the experimental one	05
10×6 Spectra with added noise 100-fold greater than the experimental one	01
5×6 Spectra left-shifted one data point	L1
5×6 Spectra left-shifted four data points	L4
5×6 Spectra right-shifted one data point	R1
5×6 Spectra right-shifted four data points	R4
5×6 Spectra with intensities reduced by a factor of 1,5	S15
5×6 Spectra with intensities reduced by a factor of 2	S2

The training set for the mixture problem is slightly different: for each mixture, two spectra were rescaled and superimposed, in such a way to reproduce 11 different percentages of component 1 and component 2, i.e.,: 0–100, 10–90,..., 100–0. Then, random noise was added to the mixture spectrum, in order to obtain ten samples for each composition, resulting in a training set made of 110 patterns for each mixture. Fig. 3 shows the

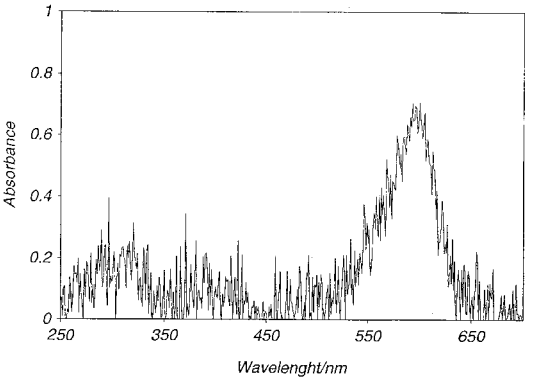

Fig. 2. Spectrum of ind7B with superimposed noise 100-fold greater than the experimental one.

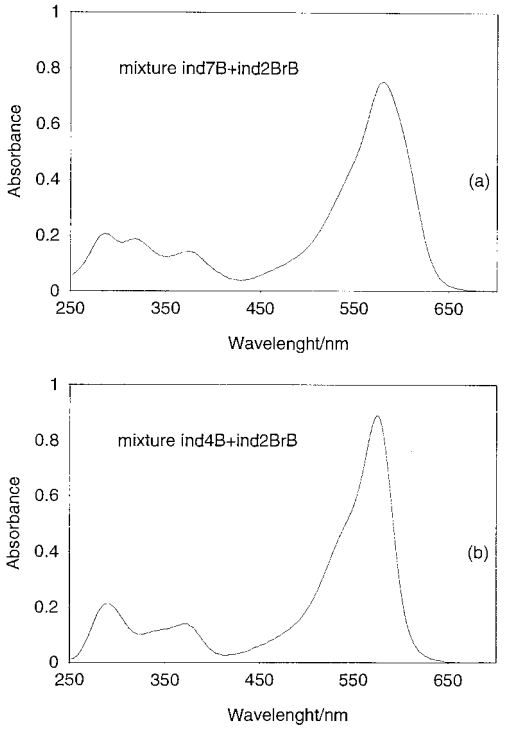

Fig. 3. (a) Absorbance spectrum of 1:1 mixture of ind7B and ind2BrB; (b) absorbance spectrum of 1:1 mixture of ind4B and ind2BrB.

spectra of 1:1 mixtures of the above-mentioned compounds. The test set, for both mixtures, was made of another 50 patterns: five samples for ten spectra, having different percentages with respect to the training set: 5–95, 15–85,..., 95–5. The validation set was generated in the same way as the test set, yet with a different random noise added.

To summarize, the used patterns were:

Classification problem:

Training set: 360 patterns (60 samples × 6 spectra)

Test set: 360 distorted patterns (60 samples × 6 spectra, see Table 2)

Validation set: 60 patterns (10 samples × 6 spectra)

Mixtures problem:

Training set: 220 patterns (10 samples × 11 compositions × 2 mixtures)

Test set: 100 patterns (5 samples × 10 compositions × 2 mixtures)

Validation set: 100 patterns (5 samples × 10 compositions × 2 mixtures).

7. Criteria adopted in the training session

During the training session the training patterns were presented in random order to the network, monitoring the mean square error (MSE), as defined by:

$$\mathrm{MSE} = \frac{1}{N_\mathrm{p}} \sum_{\mathrm{p}=1}^{N_\mathrm{P}} \sum_{i=1}^{N_0} (o_i - t_i)^2 \qquad (3)$$

where N_p is the total number of patterns, N_o is the number of output neurons, o_i is the output of the neuron i and t_i is the teaching output of the same neuron. The double sum (not divided by the total number of patterns) is the standard square error (SSE). The MSE done by the network on the training set was monitored together with the MSE on the corresponding validation set.

The training session ended when the MSE on the training set fell below 4×10^{-4} units; this choice was made because of the following observations: after a steep fall, the two error curves continue to decrease very slowly (Fig. 4). There is an increase in the validation SSE only after 20 000 or more epochs, so we can state that, for the particular problem studied, overfitting is absent if we stop the training before that time. Moreover, the performances of the network which satisfy the above-mentioned criterion are very similar to

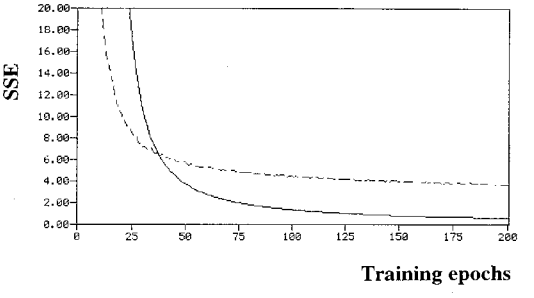

Fig. 4. Trend the standard square error on the training set (continuous curve) and on the validation set (dashed curve).

those of the network trained just before the overfitting (stopped-training method [18]); then the chosen criterion seems to be a good one, because it requires less training epochs and leads to similar results compared with the stopped-training method.

The calculation time required by the training sessions was 30–40 min for the classification problem, while the response of the trained network to the test patterns was immediate.

8. Criteria for output interpretation

The interpretation of the output values was made with the ANALYSE program, included in the SNNS package; by comparing the teaching output and the actual output, one could obtain three kinds of response, on the basis of two fixed threshold parameters, h and l:

right: the network classified correctly the test pattern if:

(a) the output of exactly one output unit is $\geq h$;

(b) the teaching output of this unit (target equal to 1) is the maximal teaching output for the pattern;

(c) the output of all other output units is $\leq l$;

wrong: the network identified a wrong compound if:

(a) the output of exactly one output unit is $\geq h$;

(b) the teaching output of this unit is NOT the maximal teaching output for the pattern;

(c) the output of all other output units is $\leq l$;

unknown: a test pattern is unclassified in all other cases.

There are no exact rules for determining the parameters h and l. Usually a trial procedure is adopted (as for the choice of the learning parameters): the best parameters are those which give the best results. In this case, we observed an improvement when passing from $h = 0.9$, $l = 0.1$, to $h = 0.8$, $l = 0.2$, to $h = 0.7$, $l = 0.3$, while using $h = 0.6$, $l = 0.4$ the percentages of correct classifications worsened again. Therefore, the thresholds adopted in this work were $h = 0.7$ and $l = 0.3$. With this criterion, the percentage of correct responses has been calculated. In the mixture case, as we stated before, the actual output was the fraction of the two components in the test spectrum, then the calculation of the error was easier: one has only to average the absolute residuals (differences between the real output and the 'wanted' output).

9. Results and discussion

9.1. Classification problem

We tried to reduce the number of input neurons in order to optimize the generalization ability of the network. In fact, every additional input neuron increases the size of the network by six connections, resulting in a larger amount of calculations to be made in the training session, which leads in turn to a poor generalization: the network is 'too well' fitted to the training data. On the other side, a sufficient amount of data points should be provided to the network in order to adequately represent the spectral details. We trained three networks with 450, 222 and 90 input neurons; the number of epochs needed was 750, 920 and 950, respectively. As stated above, the test set was made of 60 distorted patterns for each of the six compounds. The ability of the network in the recognition of each compound was first investigated, by separately observing the network responses to each group: in Table 3 the percentage of correct classifications for each compound (calculated over its 60 test patterns) is shown, together with the MSE on the test set. The best overall performances result from the network with 450 input nodes (over 91% of patterns are correctly classified, see Fig. 5). We also optimized the number of hidden nodes by training and testing three other networks with 4, 8 and 12 hidden neurons and 222 input neurons. The results are shown in Table 3: the best performances (in terms of percentage of right classifications) are those of the network with six hidden neurons: over 86% of responses are correct. We can then state that, among the tested architectures, the best network for the classification problem should have 450 input and six hidden neurons. have then investigated the accuracy of this architecture in the classification of each group of patterns, shown

Table 3
Performances of the trained networks (classification problem)

Network	1B	4B	7B	1CH3B	2BrB	6BrB	MSE
450-6-6	83.3	80	100	100	83.3	100	0.086
222-6-6	86.7	85	90	98.3	65	91.7	0.1
90-6-6	65	68.3	100	81.7	63.3	91.7	0.214
222-12-6	68.3	60	98.3	100	70	95	0.13
222-8-6	70	81.7	100	91.7	63.3	100	0.126
222-4-6	78.3	66.7	100	98.3	75	91.7	0.152

in Table 4. For comparison, the same data for the 222-6-6 architecture are shown. As expected, the ability of the network to correctly classify the test patterns decreases with the increase of the random noise. The one-point shifted spectra are all classified correctly, while when the four-points shifted spectra are presented as input, the errors increase considerably. The trained network recognizes all the spectra with intensities reduced by a factor of 1.5, while only 66.7% of the patterns with intensities reduced to a half is recognized. If we excluded from the test set the 01, L4, R4, S2 patterns, which are less common from an experimental point of view, we would obtain a percentage of right responses of 99.5% for the 450-6-6 network, and of 97.1% for the 222-6-6 architecture. Then the performances of both networks in the recognition of the less-distorted patterns are excellent.

The response of the net to an extraneous spectrum was tested with the spectrum shown in Fig. 6: it is the absorbance spectrum of the E100 candy dye, obtained from the Color Spectra Database (available via Internet at address ftp.lut.fi). The wavelength resolution of the spectrum is 2 nm, therefore we had to present it to the 222-6-6 network. The network classifies the spectrum as 'unknown', and the output vector is (0, 0, 0.905, 0.916, 0.967, 0). If we wanted six zero values as output vector, we should include in the training set also some 'negative' patterns, i.e., extraneous spectra with a (0, 0, 0, 0, 0, 0) teaching output vector. However, the 'unknown' response obtained is fully satisfactory to our aims.

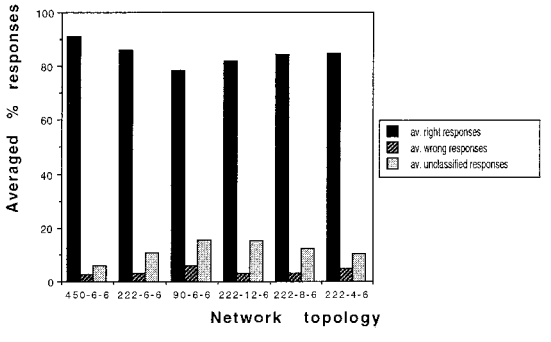

Fig. 5. Responses of the networks: for each topology, the three bars represent the percentages of right, wrong and unknown responses, respectively.

9.2. Mixtures problem

The training of the ind7B/ind2BrB mixture network was easier than that of the ind4B/ind2BrB mixture network; it could be explained by observing the spectra of the 50:50 mixtures (Fig. 3). In the first case, the two spectra show little overlapping in the low-wavelength region, while in the second case the two spectra considerably overlap in that region. Therefore the network encounters more difficulties to learn the mixed patterns of ind2BrB and ind4B; actually, it showed overfitting before the learning criterion adopted (training set MSE < 0.0004) was satisfied. In order to compare the performances of the two networks, we stopped the training sessions when the training set MSE fell below 0.0006 units, for both networks. The ind7B/ind2BrB network needed only 600 epochs to be trained, while the other one needed 3500 epochs. There are five samples of each test mixture, and for each sample the trained networks give the predicted amounts of the two components, whose averages are shown in Table 5,

Table 4
Percentage of correct responses for each test pattern group

Network	001	005	01	L1	R1	L4	R4	S15	S2
450-6-6	100	98.3	90	100	100	83.3	66.7	100	66.7
222-6-6	100	98.3	85	100	100	50	66.7	83.3	66.7

together with the exact amounts. The total average errors are 0.61% for the ind7B/ind2BrB network, and 0.72% for the ind4B/ind2BrB network. Both networks seem to make greater errors with the mixtures with one almost-pure component (see Fig. 7). The maximum absolute errors found are lower than 1.5%.

10. Technical notes

The simulation of the network was carried out with the SNNS (Stuttgart Neural Network Simulator) program, version 4.0, which is distributed by the University of Stuttgart (Institute for Parallel and Distributed High Performance Systems) as 'free software'. Information about it and the ANALYSE program included are available at the Internet address http://www.informatik.uni-stuttgart.de/ipvr/bv/projekte/snns/snns.html. The calculations were made on a IBM-RISC 6000 workstation with 32 Mbytes of memory, running AIX 3.2.5 and X-Windows.

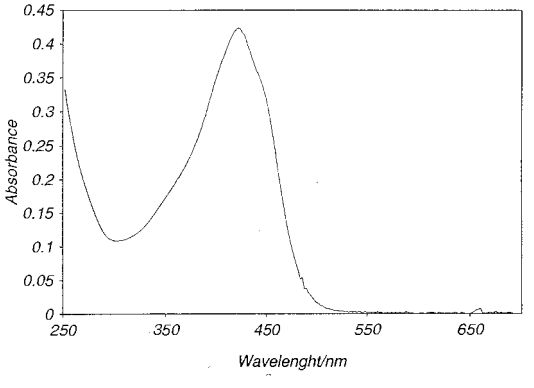

Fig. 6. Absorbance spectrum of E100 candy dye.

11. Conclusions

A multilayer network with a large number of input nodes has been shown to be capable to discriminate between spectra very similar and with few spectral details, as the UV-visible spectra in Fig. 1. In addition, the percentage of right recognitions is quite satisfactory also when highly distorted patterns are presented to the network. Moreover, we demonstrated that a specific network can be trained to give accurate estimates of the concentrations of two components in a binary mixture. It must be remarked that no preliminary transformation or reduction of data is needed: the input patterns are the absorbances at each wavelength in the spectral range chosen. Then the neural 'black box' as is could be useful in order to obtain a fast and accurate response in the identification and/or quantitative determination of real data.

Appendix A

The noise added to each point was given by $y = \tilde{A} + \mathrm{rnd} \cdot \sigma$, where rnd is a random number sampled from a normal gaussian distribution; using $\tilde{A} = 0.0015$ and $\sigma = 0.001$, the experimental noise is reproduced, as for the training spectra. The width of the gaussian is always constant in every group of spectra; the distorted spectra with greater noise have been generated simply with a greater σ value (e.g., $\sigma = 0.01$ for the spectra with added noise ten-fold than the experimental one).

Table 5
Averaged output of the trained networks (mixtures problem)

	Exact amounts	Network ind4B/ind2BrB	Network ind7B/ind2BrB
Test 1	0.05	$0.0604 \pm 0.28 \cdot 10^{-3}$	$0.056 \pm 0.15 \cdot 10^{-3}$
	0.95	$0.9406 \pm 0.29 \cdot 10^{-3}$	$0.9419 \pm 0.16 \cdot 10^{-3}$
Test 2	0.15	$0.1364 \pm 1.1 \cdot 10^{-3}$	$0.1354 \pm 0.63 \cdot 10^{-3}$
	0.85	$0.8639 \pm 1.1 \cdot 10^{-3}$	$0.8627 \pm 0.57 \cdot 10^{-3}$
Test 3	0.25	$0.245 \pm 1.7 \cdot 10^{-3}$	$0.249 \pm 0.37 \cdot 10^{-3}$
	0.75	$0.7539 \pm 1.7 \cdot 10^{-3}$	$0.7511 \pm 0.33 \cdot 10^{-3}$
Test 4	0.35	$0.3503 \pm 0.94 \cdot 10^{-3}$	$0.3566 \pm 0.39 \cdot 10^{-3}$
	0.65	$0.6479 \pm 0.92 \cdot 10^{-3}$	$0.6455 \pm 0.47 \cdot 10^{-3}$
Test 5	0.45	$0.4486 \pm 0.90 \cdot 10^{-3}$	$0.4544 \pm 0.63 \cdot 10^{-3}$
	0.55	$0.5504 \pm 0.86 \cdot 10^{-3}$	$0.5466 \pm 0.65 \cdot 10^{-3}$
Test 6	0.55	$0.5435 \pm 0.98 \cdot 10^{-3}$	$0.5484 \pm 0.27 \cdot 10^{-3}$
	0.45	$0.4569 \pm 0.92 \cdot 10^{-3}$	$0.4514 \pm 0.61 \cdot 10^{-3}$
Test 7	0.65	$0.6445 \pm 0.71 \cdot 10^{-3}$	$0.6436 \pm 0.33 \cdot 10^{-3}$
	0.35	$0.3568 \pm 0.77 \cdot 10^{-3}$	$0.3553 \pm 0.34 \cdot 10^{-3}$
Test 8	0.75	$0.7541 \pm 0.68 \cdot 10^{-3}$	$0.751 \pm 0.44 \cdot 10^{-3}$
	0.25	$0.247 \pm 0.72 \cdot 10^{-3}$	$0.2486 \pm 0.56 \cdot 10^{-3}$
Test 9	0.85	$0.8588 \pm 0.79 \cdot 10^{-3}$	$0.8643 \pm 0.45 \cdot 10^{-3}$
	0.15	$0.1408 \pm 0.83 \cdot 10^{-3}$	$0.136 \pm 0.42 \cdot 10^{-3}$
Test 10	0.95	$0.9356 \pm 0.70 \cdot 10^{-3}$	$0.9431 \pm 0.17 \cdot 10^{-3}$
	0.05	$0.0632 \pm 0.74 \cdot 10^{-3}$	$0.0573 \pm 0.14 \cdot 10^{-3}$

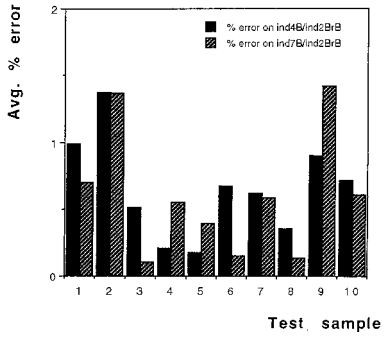

Fig. 7. Errors made by the networks trained in the mixtures quantitation; for each test sample, the two bars represent, respectively the average percent error on the ind4B/ind2BrB mixture and on the ind7B/ind2BrB mixture.

References

[1] D.E. Rumelhart, J.L. McClelland, in: Parallel Distributed Processing, vol. 1, MIT Press, Cambridge, MA, 1986.
[2] J. Zupan, J. Gasteiger, Anal. Chim. Acta 248 (1991) 1–30.
[3] G. Bologna, Il Nuovo Saggiatore 3 (4) (1995) 50–
[4] J. Hertz, A. Krogh, R. Palmer, Introduction to the Theory of Neural Computation, Addison-Wesley, Redwood City, CA, 1991.
[5] E.W. Robb, M.E. Munk, Mikrochim. Acta (Wien) 1 (1990) 131–155.
[6] M.E. Munk, M.S. Madison, E.W. Robb, Mikrochim. Acta [Wien] II (1991) 505–514.
[7] R.J. Fessenden, L.J. Gyorgyi, Chem. Soc. Perkin Trans. 2 (1991) 1755–1762.
[8] M. Meyer, T. Weigelt, Anal. Chim. Acta 265 (1992) 183–190.
[9] D. Ricard, C. Cachet, D. Cabrol-Bass, T.P.J. Forrest, Chem. Inf. Comput. Sci. 33 (1993) 202–210.
[10] B.J. Wythoff, S.P. Levine, S.A. Tomellini, Anal. Chem. 62 (1990) 2702–2709.
[11] J. Thomsen, B.J. Meyer, Magn. Res. 84 (1989) 212.
[12] B. Meyer, T. Hansen, D. Nute, P. Albersheim, A. Darvill, W. York, J. Sellers, Science 251 (1991) 542.
[13] B. Curry, D.E. Rumelhart, Tetrahedron Comput. Methodol. 3 (1990) 213–237.
[14] J.R. Long, V.G. Gregoriou, P.J. Gemperline, Anal. Chem. 62 (1990) 1791–1797.
[15] C. Lin, J.C. LaManna, Y. Takefuji, Biol. Cybern. 67 (1992) 303–308.
[16] N. Majcen, K. Rajer-Kanduc, M. Novic, J. Zupan, Anal. Chem. 67 (1995) 2154–2161.
[17] R. Casula, G. Crisponi, F. Cristiani, V. Nurchi, M. Casu, A. Lai, Talanta 12 (1993) 1781–1788.
[18] W.S. Sarle, in: Proceedings of the 27th Symposium on the Interface, 1995.

ELSEVIER

Talanta 44 (1997) 1911–1918

Talanta

Gas chromatographic determination of pollutants in the chlorination and caustic extraction stage effluent from the bleaching of a bamboo pulp

C. Sharma, S. Mahanty, S. Kumar *, N.J. Rao

Institute of Paper Technology (U.O.R.), Saharanpur, 247001 (U.P.), India

Received 28 August 1996; received in revised form 6 March 1997; accepted 12 March 1997

Abstract

The gas chromatographic detection and quantitative determination of various chlorophenolics as well as resin and fatty acids have been carried out in the chlorination and caustic extraction stage effluents generated in the laboratory by bleaching a bamboo pulp. A number of chlorinated phenols, catechols, guaiacols, syringaldehydes and resin acids as well as non-chlorinated saturated and unsaturated fatty acids together with resin acids have been detected. The concentration of various compounds detected have also been compared with the reported $^{96}LC_{50}$ values. © 1997 Elsevier Science B.V.

Keywords: Bamboo; Bleaching effluent; Chlorophenolics; Gas chromatography; Pollutants; Resin and fatty acids

1. Introduction

The dwindling forest cover and increasing demands of the paper, industry worldwide is increasingly requiring the use of hardwoods and nonwoods (agroresidues and grasses) for making paper. Bamboo (Bambusa), a grass, has been one of the most popular raw materials used by the Indian paper industry. It gives a long fibered pulp (comparable to softwoods) that forms a strong paper. With the diminishing forests in India bamboo has also, become scarce but is still used by a large number of paper mills, particularly in eastern and southern India.

The paper industry is a high pollution load industry. Among the various sections, bleaching often accounts for the largest fraction of toxicity. The pulp produced by digestion with chemicals is brownish in color and requires bleaching to produce pulps of acceptable brightness. In developing countries the use of chlorine and other chlorinated compounds such as calcium or sodium hypochlorite with an intermediate caustic extraction is common for nonwoody materials.

The compounds responsible for the toxicity of chlorination (C) and caustic extraction (E) stage effluents are chlorophenolics together with resin and fatty acids [1,2]. The chlorophenolics are formed during the C-stage of pulp bleaching and

* Corresponding author. Tel: +91 132 727062; fax: +91 132 727387.

PII S00 9-9140(97)00090-8

are solublized in the E-stage. The nature and amount of chlorophenolics formed will depend upon the nature of the lignin and the bleaching conditions [3,4]. The resin and fatty acids found in bleach plant effluent originate from the fibrous raw material. Their amount depends on the species and on the degree of washing of the unbleached pulp.

During the last two decades intense research efforts have been devoted to the identification of the various compounds [5–10] in bleach plant effluents and to the investigation of their possible biological effects [11–15]. These studies have been performed mostly on softwoods. Very little information is available on the nature and the quantities of various compounds present in bleach plant effluents formed from Indian varieties of hardwoods or agroresidues. In the present investigation we report the results of the detection and quantitative determination of various pollutants formed during the chlorination and extraction stages of the bleaching of bamboo pulp.

2. Experimental

The chlorophenols and fatty acids used were obtained from the Sigma Chemical Company (St. Louis, USA) and Aldrich Chemical Company (Milwaukee, USA). The chlorocatechols, chloroguaiacols, chlorovanillins, chlorosyringaldehydes, chlorosyringols, resin acids and chloro fatty acids were supplied by Helix Biotech. Corporation (Richmand, B.C. Canada). Solvents comprising *n*-hexane, acetone, diethyl ether and methyl tertiary butyl ether used were HPLC grade. Analytical grade acetic anhydride was used after redistillation. Other reagents used for detection studies were of analytical reagent grade. Standard solutions of chlorophenols were prepared in acetone/water (10:90), resin and fatty acids in methanol/diethyl ether (10:90) solution.

Unbleached washed (bamboo) kraft pulp was provided by Central Pulp and Paper Research Institute (CPPRI), Saharanpur. Tappi Test method T_{236} cm-85 was used to determine the residual lignin content (kappa number = 37.4) of the pulp.

Pulp bleaching was carried out in more than one bleaching stages. A fraction (70%) of the chlorine demand (0.25 × kappa number) was applied as elemental chlorine in chlorination stage. All chemicals were applied as %O.D. (oven dried) pulp.

Unbleached pulp (35 g O.D. basis) was bleached under the conditions shown in Table 1. The volumes of effluent generated in the C and E stage were 1.81 and 2.02 l, respectively. The effluents were characterized by pH, total dissolved solids, BOD_5 (biochemical oxygen demand), COD (chemical oxygen demand) [16] and color measured on a Shimadzu spectrophotometer model UV 2100/S.

Extraction of chlorophenols from the effluents was performed by simple modification of the procedure suggested by Lindstrom and Nordin [5]. The E-stage effluent (500 ml) or the C-stage effluent (1000 ml) was adjusted to pH 2 and extracted with 200 and 400 ml of 90:10 diethyl ether/acetone mixture for 48 h, respectively with intermittent shaking. Extraction of resin and fatty acids from effluents has been achieved as suggested by Voss and Rapsomatiotis [8]. The effluent (E-stage 50 ml or C-stage 100 ml) was adjusted to pH 9 and extracted with equal volume of methyl tertiarybutyl ether for 1 h.

Chlorophenols as acetyl derivatives [17], resin and fatty acids as methyl esters [18] were analysed using Shimadzu gas chromatograph (Model GC-9A). The GC conditions are given in Table 2. Retention times (RT) were determined using standard solutions of various chlorophenolic compounds, resin and fatty acids. In each case 1 ml sample was derivatized and 1 μl of the derivatized extract was injected into the column.

Table 1
Bleaching conditions

Parameters	C-stage	E-stage
Cl_2 applied (% (demand))	70	—
NaOH applied (% (OD pulp))	—	03
Consistency (%)	3.5	10
pH	1.8–2.0	11–12
Temperature (°C)	25	60
Time (min)	60	75

All chemicals charged as %O.D. (oven dried) pulp.

Table 2
GC conditions for the analysis of chlorophenolics and resin and fatty acids

Parameters	HR-1	OV-101
Detector	FID	FID
Detector range	10°	10°
Chart speed (cm min^{-1})	5	5
Sample size (μl)	0.5–1	0.5
Injection (min) (splitless)	2	2
Column dimensions	30 m × 0.32 mm	25 m × 0.32 mm
Film thickness	0.25 μm	0.27 μm
Injection and detector temp (°C)	275	300
Column temperature (°C)	80 for 3 min	190 for 4 min
	80–160 at 2°C min^{-1}	190–210 at 1°C min^{-1}
	160 for 5 min	210–230 at 2°C min^{-1}
	160–260 at 10°C min^{-1}	230–250 at 3°C min^{-1}
	260 for 15 min	250 for 15 min

3. Derivatization procedure

3.1. Chlorophenolics

To 4.5 ml of sample (or diluted sample) taken in teflon lined screw capped glass tube, 0.5 ml of 0.5 M Na_2HPO_4 and 0.05 ml of acetic anhydride were added. After adding 1 ml of *n*-hexane, the mixture was shaken for 3 min and 0.5–1.0 μl of the hexane extract was injected into the HR-1 column.

3.2. Resin and fatty acids

Resin and fatty acids were derivatized with dropwise addition of etheral solution of diazomethane to 1 ml of the sample till a yellow color persisted for some time. The excess diazomethane was destroyed by dropwise addition of glacial acetic acid. The resulting solution was evaporated to dryness with a current of nitrogen gas. The dried mass was dissolved in methanol/diethylether (10:90) solution and making the total volume 1 A 0.5 μl of this solution was injected into OV-101 column.

3.3. Extraction efficiency determination

3.3.1. Chlorophenolics

The standard solution of 0.1 mg chlorophenolics (1000 ml) was extracted and derivatized. Another solution of 0.1 mg chlorophenolics (1 ml of 100 mg l^{-1}) was derivatized without extraction. The extracted and nonextracted chlorophenolics derivatives were injected into HR-1 column (0.5 μl each) and the peak areas were determined in both the cases. The extraction efficiency (EF) was calculated from the equation:

$$\mathrm{EF}(\%) = \frac{\text{Peak area of extracted sample}}{\text{Peak area of nonextracted sample}} \times 100 \quad (1)$$

3.3.2. Resin and fatty acids

The standard solution of resin and fatty acids (50 ml of 0.1 mg l^{-1}) was extracted and derivatized. Another solution (1 ml of 5 mg l^{-1}) containing 5 μg of resin and fatty acid was derivatized without extraction. The extracted and nonextracted resin and fatty acid were injected into OV-101 column (0.5 μl each) and the peak areas were determined in both the cases. The extraction efficiency was calculated using the Eq. (1).

The various chlorophenolics, resin and fatty acids were detected by matching the retention time with those of pure standards within ± 0.1 min. For some compounds the value of RT were nearly the same. In these cases the average quantities were determined. For carrying out quantitative analysis, response factor (RF) and extraction efficiency (EF) of various compounds were determined.

4. Results

The characteristics of effluents generated in laboratory are shown in Table 3. The values of RT and concentration of various detected chlorophenolics, resin and fatty acids are given in Table 4 and Table 5, respectively. The values of RT show that most of the chlorophenolics and resin and fatty acids can be separated on Ulbon HR-1 glass

Table 3
Characteristics of effluents generated in the laboratory

Parameters	Effluent	
	C-stage	E-stage
pH	2.2	10.7
Dissolved solid (mg l^{-1})	1088.0	1288.0
BOD (mg l^{-1})	120.0	136.0
COD (mg l^{-1})	593.0	722.0
Colour (Pt. Co)	1134.0	3875.0

capillary and fused silica OV-101 capillary columns, respectively. The quantities of various categories of chlorophenolics, resin and fatty acids expressed as g per tonne of oven dried pulp (g odt^{-1}) are given in Table 6 and Table 7, respectively.

5. Discussion

5.1. Chlorophenols

Six categories of chlorophenolics are present in spent bleach liquor obtained from Indian variety of bamboo pulp. These are chlorophenols, chlorocatechols, chloroguaiacols, chlorosyringols, chlorosyringaldehydes and chlorovanillins. The retention times and concentration of various chlorophenolics observed in the bamboo spent bleach liquor are given in Table 4.

Table 4
Retention time and concentrations of various chlorophenolics in the effluent

Chlorophenolics	RT (min)	C-stage (g odt^{-1})	E-stage (g odt^{-1})
2-Chlorophenol	7.82	0.21	—
3-Chlorophenol	8.89	—	4.61
4-Chlorophenol	9.03	0.21	1.15
2,6-Dichlorophenol	12.96	0.51	—
2,5-Dichlorophenol[a]	13.97	1.81	9.52
2,4-Dichlorophenol[a]	14.05	1.81	9.52
2,3-Dichlorophenol	15.71	—	0.06
3,4-Dichlorophenol	17.51	0.36	—
6-Chloroguaiacol	17.94	—	0.11
2,4,6-Trichlorophenol	19.10	2.58	25.38
2,3,5-Trichlorophenol	22.30	0.51	0.23
2,4,5-Trichlorophenol	22.75	1.03	—
2,3,4-Trichlorophenol	24.61	0.26	—
4,6-Dichloroguaiacol	24.88	—	1.15
3,4-Dichloroguaiacol	25.44	—	1.15
4,5-Dichloroguaiacol	27.96	—	2.88
3,6-Dichlorocatechol	28.51	7.75	—
3,5-Dichlorocatechol	29.65	23.78	—
3,4,6-Trichloroguaiacol[a]	30.49	0.18	2.88
6-Chlorovanillin[a]	30.58	0.18	2.88
3,4,5-Trichloroguaiacol	34.01	0.36	6.35
3,4,6-Trichlorocatechol	36.29	1.55	—
2-Chlorosyringaldehyde	38.75	20.68	—
Pentachlorophenol	39.21	2.07	46.16
3,4,5-Trichlorocatechol	39.79	35.67	16.15
Tetrachloroguaiacol	40.58	0.51	3.46
Trichlorosyringol	41.70	0.26	2.30
Tetrachlorocatechol	45.96	17.06	6.34
2,6-Dich.syringaldehyde	46.38	7.24	46.16

odt, dried tonne pulp.
[a] Indicate single unresolved peak.

Table 5
Retention time and concentrations of various resin and fatty acids in the effluent

Acids	RT (min)	C-stage (g odt^{-1})	E-stage (g odt^{-1})
Palmitic[a]	4.92	49.11	154.00
Heptadecanoic[a]	6.55	0.36	3.05
Oleic[bf]	8.07	2.58	8.07
Linolenic[bf]	8.11	2.58	8.07
Stearic[a]	8.71	1.03	17.30
Pimaric[c]	11.30	0.31	0.29
Sandaracopimaric[c]	11.70	1.55	5.77
Isopimaric[c]	12.90	2.58	16.15
Dihydroisopimaric[c]	13.90	0.52	—
Arachidic[a]	15.00	0.41	3.46
Neoabietic[c]	17.90	1.55	1.15
Chlorodehydroabietic I[d]	21.60	1.03	8.07
Chlorodehydroabietic II[d]	23.00	3.62	3.46
Tricosanoic[a]	28.90	3.10	1.73
12,14-Dich.dehydroabietic[d]	30.40	1.03	1.15
Lignoceric[a]	33.30	5.17	17.30
9,10,12,13-Tetrach.stearic[e]	35.70	2.06	1.73

odt, Oven dried tonne pulp.
[a] Saturated fatty acid.
[b] Unsaturated fatty acid.
[c] Resin acid.
[d] Chloro resin acid.
[e] Chloro fatty acid.
[f] Indicate single unresolved peak.

The structure of lignin is very complex. It is a polymer formed by an enzyme initiated dehydroabietic polymerization of a mixture of three different *p*-hydroxy cinnamyl alcohols (*p*-coumeryl, coniferyl and sinapyl alcohols). Compared with wood lignin, the structure of grass lignin has been less studied. It varies significantly with source. Some grass lignins are thought to contain mainly *p*-coumaryl units but other grass lignins appear to approximate the hardwood lignin [19]. During pulp chlorination lignin is chlorinated and breaks down to simpler chlorophenolic compounds. The solubility of chlorophenolics is low in acidic condition (C-stage) and they are solubilized in alkaline condition (E-stage). The nature and concentration of different chlorophenolic compounds formed that ultimately end up in SBL depend upon quantity of lignin i.e., kappa number of pulp, nature of lignin, and bleaching conditions, i.e., chlorine charged, pH, temperature and consistency (expressed as g O.D. pulp per 100 g pulp suspension).

Among the various chlorophenolics found in C-stage effluent the maximum contribution came from 3,4,5-trichlorocatechol (35.67 g odt^{-1}). Other significant contribution came from 3,5-dichlorocatechol (23.78 g odt^{-1}), 2-chlorosyringaldehyde (20.68 g odt^{-1}), tetrachlorocatechol (17.06 g odt^{-1}). Small contributions were made by 2,6-dichlorosyringaldehyde (7.24 g odt^{-1}), 3,6-dichlorocatechol (7.75 g odt^{-1}). Minor quantities of 2,4/2,5-dichlorophenol (3.62 g odt^{-1}), 2,4,6-trichlorophenol (2.58 g odt^{-1}), pentachlorophenol (2.07 g odt^{-1}), 3,4,6-trichlorocatechol (1.55 g odt^{-1}), 2,4,5-trichlorophenol (1.03 g odt^{-1}) were also present. Other chlorophenolic compounds detected in the effluent had concentration about 0.5 g odt^{-1} or less.

In E-stage maximum contribution came from 2,6-dichlorosyringaldehyde (46.16 g odt^{-1}) and pentachlorophenol (46.16 g odt^{-1}). Significant contribution came from 2,4,6-trichlorophenol (25.38 g odt^{-1}), 2,5/2,4-dichlorophenol (19.04 g odt^{-1}), 3,4,5-trichlorocatechol (16.15 g odt^{-1}).

Table 6
Quantity of various categories of chlorophenolics in the bleaching effluent

Chlorophenolics	C-stage (g odt^{-1})	E-stage (g odt^{-1})	(C+E)	
			(g odt^{-1})	%
Chlorine substitution				
Monochlorophenols	21.28	8.75	30.03	9.53
Dichlorophenols	43.26	70.44	113.70	36.09
Trichlorophenols	42.40	53.29	95.69	30.38
Tetrachlorophenols	17.57	9.80	27.37	8.69
Pentachlorophenols	2.07	46.16	48.23	15.31
Reactive group				
Phenols	11.36	96.63	107.99	34.28
Catechols	85.81	22.49	108.30	34.38
Guaiacols	1.05	17.98	19.03	6.04
Other phenols	28.36	51.34	79.70	25.30
Total chlorinated phenolics	126.58	188.44	315.02	100.00

Minor quantities of tetrachlorocatechol (6.34 g odt^{-1}), 3,4,5-trichloroguaiacol (6.35 g odt^{-1}), 3,4,6-dichloroguaiacol/6-chlorovanillin (5.76 g odt^{-1}), 3-chlorophenol (4.61 g odt^{-1}), trichlorosyringol (2.3 g odt^{-1}), tetrachloroguaiacol (3.46 g odt^{-1}), 4,5-dichloroguaiacol (2.88 g odt^{-1}), 4-chlorophenol, 4,6-dichloroguaiacol and 3,4-dichloroguaiacol (1.15 g odt^{-1} each) were also present. Other chlorophenolic compounds detected in the effluent had concentrations about 0.5 g odt^{-1} or less.

The chlorophenolics can be categorized on the basis of chlorine substitution. The total quantities of mono, di, tri, tetra and penta chlorophenolic compounds (g odt^{-1}) in C-stage, E-stage and combined spent bleach liquor (C stage + E stage) are given in Table 6. Dichloro and trichloro compounds contribute 66% of the total detected chlorophenolic compounds in the combined SBL. Similarly the components can be categorized based on the reactive groups. Catechols, vanillins, syringaldehydes and syringols contribute 60% of the total chlorophenolics components in the combined SBL. The concentration of chlorinated guaiacols is higher in the E-stage liquor than in the C-stage liquor. The chlorinated catechols predominate in C-stage effluent. This behavior is similar to the behavior observed with effluents of wood pulps. This is presumably, due to the low solubility of chlorinated guaiacols at low pH and the sorption of these compounds on the fibers. Alternatively these chloroguaiacols may form only upon the alkaline hydrolysis of chlorinated lignin in the E-stage.

5.2. Resin and fatty acids

Table 5 gives various categories of resin and fatty acids detected in the effluent. These are saturated fatty acids, unsaturated fatty acids, resin acids chlorinated resin and fatty acids. The quantities of resin and fatty acids are higher in E-stage effluent than in C-stage effluent. This is due to the higher solubility of resin and fatty acids in alkaline media. The quantities of various chlorinated and non-chlorinated resin and fatty acids in C-stage, E-stage and combined spent bleach liquor (C stage + E stage) are given in Table 7. From the table we can conclude:

1. The quantities of fatty acids are much higher than resin acids.
2. The quantities of total saturated fatty acids are much higher than unsaturated fatty acids.
3. The quantities of chlorinated resin acids are much higher than chlorinated fatty acids.

The palmitic acid was the most significant saturated fatty acid (203 g odt^{-1}) of the detected resin and fatty acids. Other major saturated fatty acids

Table 7
Quantity of various categories of resin and fatty acids in the bleaching effluent

Acids	C-stage (g odt^{-1})	E-stage (g odt^{-1})	(C+E)	
			(g odt^{-1})	%
Non-chlorinated				
Saturated fatty acids	59.18	196.84	256.02	77.74
Unsaturated fatty acids	5.16	16.14	21.30	06.47
Resin acids	6.51	23.36	29.87	09.07
Chlorinated				
Chloro fatty acids	2.06	1.73	3.79	01.15
Chloro resin acids	5.68	12.68	18.36	05.57
Total resin and fatty acids (both chlorinated and non chlorinated)	78.59	250.75	329.34	100.00

were lignoceric (22.5 g odt^{-1}) and stearic acid (18.33 g odt^{-1}). Minor quantities of heptadecanoic, arachidic, tricosanoic acid (3.4–4.8 g odt^{-1}) were also detected. Among the various unsaturated fatty acids oleic/linolenic acids were found in significant amounts (about 21 g odt^{-1}).

Isopimaric was the major resin acid (18.73 g odt^{-1}) detected. Significant amount of sandaracopimaric acid (7.32 g odt^{-1}) was also detected. Minor quantities (0.5–2.7 g odt^{-1}) of pimaric, dihydroisopimaric and neoabietic acid were detected. Both the isomers of monochlorodehydroabetic acid contributed major share (16.18 g odt^{-1}) to the detected chloro resin acids. Minor quantities of 12,14-dichloroabetic acid (2.18 g odt^{-1}) and 9,10,12,13-tetrachlorostearic acid (3.79 g odt^{-1}) were also detected.

6. Toxicity

The toxicity of the effluent was evaluated by comparing the quantities of various chlorophenolics, resin acids and fatty acids detected in the effluent with the values reported in the literature [4,20,21]. $^{96}LC_{50}$ is the lethal concentration at which 50% of the test organisms will get killed when the test organism is exposed to the toxicant for a period of 96 h under standard test conditions. Reported $^{96}LC_{50}$ values indicate that chlorophenolics, resin acids, unsaturated fatty acids and chlorinated resin and fatty acids are toxic. Resin acids are more toxic than unsaturated fatty acids.

The concentrations of 2,4,6-trichlorophenol (0.44 mg l^{-1}) and pentachlorophenol (0.80 mg l^{-1}) in E-stage and dichlorocatechols (0.61 mg l^{-1}) in C stage were found to be higher than the reported respective $^{96}LC_{50}$ values. The concentrations of all other chlorophenolics, resin and fatty acids were less than the respective $^{96}LC_{50}$ values.

The $^{96}LC_{50}$ value indicates the toxic concentration of a particular compound when present alone. However, when a number of toxic compounds are present, interfering effect may be observed. Substantial evidence now exists which indicates that the threshold toxic concentration may be as low as 5–10% of $^{96}LC_{50}$ values [22].

Apparently concentrations of a large number of chlorophenolics, resin and fatty acids may exceed their respective threshold concentrations. So it can be inferred that the untreated spent bleach liquor of bamboo is of environmental concern.

Acknowledgements

Financial assistance for this provided by the Council of Scientific and Industrial Research (CSIR), New Delhi, India is gratefully acknowledged.

References

[1] J.M. Leach, A.N. Thakore, J. Fish Res. Board Canada 32 (1975) 1249–1257.
[2] J.M. Leach, A.N. Thakore, Prog. Water Technol. 9 (1977) 787–798.
[3] R.H. Voss, J.T. Wearing, A. Wong, Tappi 64 (3) (1981) 167–170.
[4] R.H. Voss, J.T. Wearing, R.D. Mortimer, T. Kovacs, A. Wong, Pap. Puu 62 (12) (1980) 809–814.
[5] K. Lindstrom, J. Nordin, J. Chromatogr. 128 (1976) 13–26.
[6] K.P. Kringstad, K. Lindstrom, Environ. Sci. Technol. 18 (8) (1984) 236A–248A.
[7] J. Knuutinen, J. Chromatogr. 248 (1982) 289–295.
[8] R.H. Voss, A. Rapsomatiotis, J. Chromatogr. 346 (1985) 205–214.
[9] B. Holmbom, K.J. Lehtinen, Pap. Puu 11 (1980) 673–684.
[10] T.M. Xie, Z.J. Lu, Nord. Pulp Pap. Res. J. 2 (1987) 56–60.
[11] C.C. Walden, T.E. Howard, Tappi 60 (1) (1977) 122–125.
[12] I.H. Rogers, J.C. Davis, G.M. Kruzynski, H.W. Mahood, J.A. Servizi, R.W. Gordon, Tappi 58 (7) (1975) 136–140.
[13] B. Holmbom, R.H. Voss, R.D. Mortimer, A. Wong, Environ. Sci. Technol. 18 (5) (1984) 333–337.
[14] D.W. Reeve, P.F. Earl, Pulp Pap. Can. 90 (4) (1989) 128–132.
[15] R. Crooks, J. Sikes, Appita 43 (1) (1990) 67–76.
[16] L.S. Clesceri, A.E. Greenberg, R.R. Trussell, Standard Methods, 17th ed., Pub. American Public Health Association, 1989, p. 2(74), 4(94), 5(2) and 5(12).
[17] K. Abrahamsson, T.M. Xie, J. Chromatogr. 279 (1983) 199–208.
[18] A.I. Vogel, A Text Book of Practical Organic Chemistry, 3rd ed., Pub. English Language Book Society, London, 1975, p. 292.
[19] J.M. Harkin, in: G.W. Butler, R.W. Bailey (Eds.), Chemistry and Biochemistry of Herbage, Academic Press, New York, 1973, vol. 1, Ch. 7.
[20] S.A. Heimburger, D.S. Blevins, J.H. Bostwick, G.P. Donnini, Tappi 71 (11) (1988) 69–77.
[21] H.B. Lee, T.E. Peart, J.M. Carron, J. Chromatogr. 498 (1990) 367–379.
[22] Environmental Management in the Pulp and Paper Industry, UNEP-Industry and Environment Manual Series, 1981, vol. pp. 1–59 and 1–64.

ELSEVIER

Talanta 44 (1997) 1919–1922

Talanta

Short communication

Investigation of performance enhancement of flame photometric signal using a cylindrical impactor in the spray chamber

Ladislau Kékedy-Nagy

Department of Analytical Chemistry, Babeş-Bolyai University, Str. Arany J. 11, RO 3400 Cluj-Napoca, Romania

Received 9 April 1996; received in revised form 11 February 1997; accepted 21 February 1997

Abstract

The effect of a cylindrical impactor in the spray chamber of a flame photometer on the characteristics of the aerosol formed, on the transport-efficiency of the nebulizer—spray chamber system, as well as on the analytical signal has been investigated. The variables were: the diameter Φ of the cylindrical impactor and its position, i.e., the distance d in front of the tip of pneumatic nebulizer capillary where the impactor was fixed. The performance characteristics of an 1 mm Φ impactor was fixed at $d = 5$ mm was superior to that of a conventional 8 mm Φ spherical bead. © 1997 Elsevier Science B.V.

Keywords: Flame photometry; Impactor; Pneumatic nebulization

1. Introduction

Pneumatic nebulization is the most frequently used technique to introduce the sample solution into the flame in flame photometric determinations. This is a decisive step of the analysis, because the concentration and the physical properties of the resulting aerosol essentially influences the resulting analytical signal and thus the sensitivity and reproducibility of the determinations. In order to obtain aerosols with small droplets in high concentrations, high performance nebulizers have been recently developed [1–5]. In the spray chamber, the fragmentation of the larger droplets is generally promoted by means of impact beads placed at some distance in front of the droplet forming capillary. Mostly the impactors used are spherical glass beads of 8 mm Φ placed at ~25 mm before the nebulizer capillary. During our experiments with such systems, it was observed that the stability of the analytical signal could be improved by using an impactor of adequate shape, placed at a certain distance from the nebulizer capillary in the spray chamber. In our preliminary experiments, the attention was directed towards cylindrical impactors, scarcely mentioned in the literature [6–8] and not used in commercial instruments.

PII S00 9-9140(97)00074-X

The aim of this work is to investigate the effect of a cylindrical impactor on the characteristic of the resulting aerosol, on the transport-efficiency of the nebulizer—spray chamber system and on the analytical signal, respectively, as a function of the diameter of the cylinder and the impactor distance from nebulizer capillary tip.

2. Experimental

As cylindrical impactors, pieces of enamelled copper wires of 20 mm length and of 0.6, 1, 2, 4 and 8 mm diameter, were used. They were properly mounted on the pneumatic nebulizer, in an AAS-1 (Karl Zeiss Jena) commercial flame spectrophotometer in place of the original spherical impactor. They could be moved vertically at several distances (d) in front of the tip of the capillary in steps of 1 ± 0.1 mm. The schematic diagram of the nebulizer-impactor assembly is shown in Fig. 1.

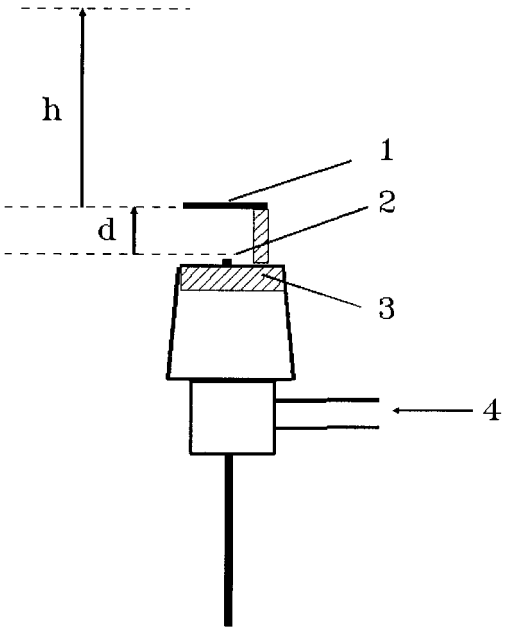

Fig. 1. schematic diagram of the nebulizer-impactor assembly: (1) impactor; (2) capillary tip; (3) holder; (4) air inlet.

The nebulizer was operated with an air stream of 500 l h^{-1}, triply distilled water being used as the sample solution. The primary and secondary aerosols formed were observed with the nebulizer removed from the spray chamber, the tertiary ones with the nebulizer in the spray chamber.

The concentration of the aerosols formed was determined by light scattering measurements. According to Mie scatter theory, the intensity of the scattered light is proportional to the total surface of the droplets, i.e., with the concentration of the aerosol [9]. For this purpose, the aerosol was illuminated with a 300 W mercury vapour lamp, the scattered light intensity of the Hg 453.5 nm line being measured at a right angle to the incidence light beam. Because of a lack of suitable aerosol standards, we only obtained information about the variation of the aerosol's concentration. The transport-efficiency of the nebulizer-spray chamber system was determined by weighing the mass of the empty system and after nebulization of 10 ml of water, respectively. The effect of the impactor on the flame emission signal was determined by measuring the emission of a 10 μg l^{-1} NaCl solution, at the 589.5 nm Na line, in a methane-air flame [10].

3. Results and discussion

The intensity of the scattered light was measured at several heights in the (secondary) aerosol (h) without impactor (I_0) and with impactors (I_d) of different diameters (Φ) being placed at various distances (d) from the tip of the nebulizer capillary. The relative intensity ($I_{rel} = I_d/I_0$) was then calculated for each Φ, d and h values. The data were processed further by using the MicroCal Origin Software package, version 3.0 (MicroCal Software, MA, USA) and plotted as 2D contour map (Fig. 2).

One can observe that the concentration of the aerosol depends both of d and h. At $h > 40$ mm, the aerosol is homogeneous, its final concentration being virtually constant. With the impactor of $\Phi = 0.6$ mm the concentration of the aerosol was maximal at $d = 4$ mm and $h = 11$ mm. The plots obtained with thicker impactors ($\Phi =$

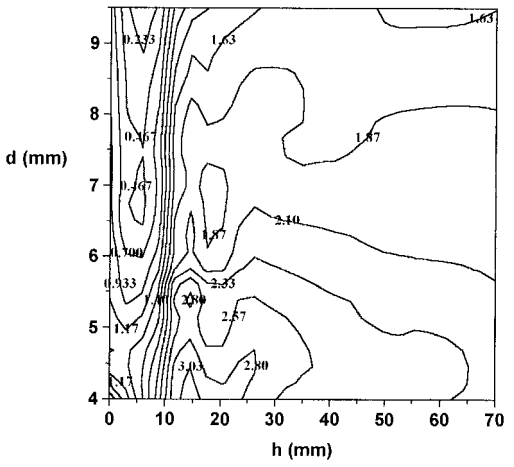

Fig. 2. The 2D contour map of the I_{rel} vs. h and d relation. Impactor $\Phi = 0.6$ mm. The data labels on the plot indicate the grid matrix values.

1, 2, 4, 8 mm) were similar to those represented in Fig. 2. The efficiency of impactors of different diameters was estimated by determining the I_{rel} values at $h = 55$ mm in the aerosol for different d values and plotted as 2D contour map (Fig. 3).

One can observe the different behaviour of impactors of different diameters. Each impactor is

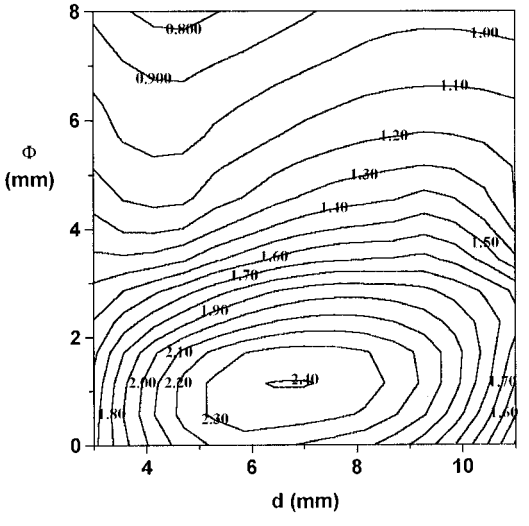

Fig. 3. The 2D contour map of the I_{rel} at $h = 55$ mm vs. Φ and d relation. The data labels on the plot indicate the grid matrix values.

the most efficient being placed at a given d distance from the nebulizer capillary. Impactors with small diameter ($\Phi = 0.6$, 1, 2 mm) were more efficient than the thicker ones ($\Phi = 4$, 8 mm). The maximal secondary aerosol concentration was obtained with the impactor of $\Phi = 1$ mm, being placed at $d = 5$ mm distance from the nebulizer capillary tip. If we assume that the $\Phi = 8$ mm diameter cylindrical impactor has the same effect as a spherical one of the same diameter, one can state that a smaller cylindrical impactor is more efficient than the 8 mm Φ spherical one. The plots obtained for the variations of the tertiary aerosol concentration with Φ and d, were similar to those represented in Fig. 3, the optimal Φ and d values being the same.

The impactor increased the transport-efficiency (TE) of the nebulizer-spray chamber system too. The maximal increase was obtained with an impactor of $\Phi = 4$ mm; at $d = 7.5$ mm. In this case, 21% of the nebulized liquid entered in the flame. For comparison, the TE of the system without the impactor was 7.5% with the commercial spherical one the TE was 9.8% and with a cylindrical one of the same diameter, the TE was 13%.

Finally the effect of impactors on the flame emission signal of Na was investigated. For this purpose, the emission signal was determined first without the impactor in the spray chamber (I_0) and then with impactors of different diameters placed at different d distances (I_d). Then it was calculated the $I_{rel,\,Na}$ and the data (average of four parallel determinations) were plotted as 2D contour map (Fig. 4).

The map shows that the impactor increased the emission signal too. The effect of the distance d is relatively small, but that of the impactor's diameter is considerable. The greatest increase was observed with thin impactors. Being placed at $d = 5$ mm, the 1 mm Φ cylindrical impactor increased the analytical signal by a factor 2.6; that of 8 mm by 1.1; and the usual spherical one by a factor of 1.4 against a spray chamber without impactor.

The precision (reproducibility) of the data is influenced by the exact centering of the impactor, in this aspect the thin impactors are more sensitive than the thicker ones. From the data ob-

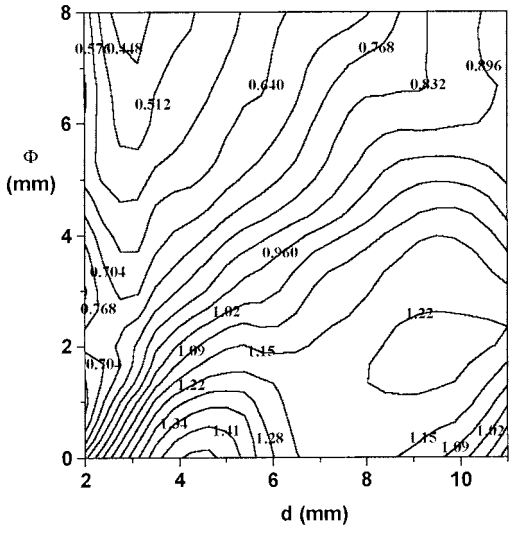

Fig. 4. The 2D contour map of the emission of 10 μg l^{-1} Na, $I_{rel, Na}$, vs. Φ and d relation. The data labels on the plot indicate the grid matrix values.

tained, the S/N ratios of the emission signals were computed too. The greatest value of S/N = 247.3 was obtained with the impactor of Φ = 1 mm placed at a distance of $d = 5$ mm. In comparison, the same S/N ratio without impactor was 108.7, and with the spherical one the S/N ratio was only 83.4. In this last case, the standard deviation more than double of that observed with the cylindrical impactor.

4. Conclusions

The results obtained proved the efficiency of a cylindrical impactor in the nebulizer spray chamber of an emission flame photometer. The cylindrical impactor increased both the analytical signal and its S/N ratio, decreasing the standard deviation. The best value (S/N = 247.3) was obtained with the cylindrical impactor of Φ = 1 mm, placed at $d = 5$ mm distance from the nebulizer tip. The same value for the usual 8 mm Φ spherical impactor was S/N = 83.4. Substitution of the spherical impactor in commercial apparatus with the cylindrical one will increase its performance characteristics.

References

[1] S.A. Pergantis, E.M. Heithmer, T.A. Hinners, Anal. Chem. 67 (1995) 4530.
[2] K.E. Lawrence, G.W. Rice, V.A. Fassel, Anal. Chem. 56 (1984) 289.
[3] D.R. Wilderin, R.S. Houk, Appl. Spectrosc. 45 (1991) 1408.
[4] J.W. Olesik, J.A. Kinzer, B. Harkleroad, Anal. Chem. 66 (1994) 2022.
[5] H. Liu, A. Monstaser, Anal. Chem. 66 (1994) 3233.
[6] I.L. Garcia, C.E. O'Grady, M.S. Cresser, J. Anal. At. Spectrom. 2 (1987) 221.
[7] F.J. Fernadez, B. Lumas, M.M. Beaty, At. Spectrosc. 1 (1980) 55.
[8] L.R. Layman, F.E. Lichte, Anal. Chem. 54 (1982) 638.
[9] G. Kortüm, Reflectance Spectroscopy, Springer-Verlag, Berlin, 1969, pp. 92.
[10] L. Kékedy-Nagy, Ph.d. Thesis, Babes-Bolyai University, Cluj-Napoca, 1984.

ELSEVIER

Talanta 44 (1997) 1923–1928

Talanta

Short communication

Simultaneous voltammetric determination of uric and ascorbic acids in urine

E.M Strochkova, Ya.I. Tur'yan, I. Kuselman *, A. Shenhar

The National Physical Laboratory of Israel, Danciger A Building, Givat Ram, Jerusalem 91 904, Israel

Received 25 October 1996; received in revised form 24 February 1997; accepted 27 February 1997

Abstract

Anodic voltammetric method for simultaneous determination of uric acid (UA) and ascorbic acid (AA) in urine has been developed with the use of a commercial working rotating glassy carbon electrode. UA may be determined in a sample diluted by the buffer supporting electrolyte ($HOAc + NH_4OH$; pH 5.1–5.2) $\approx$ 100 times, and AA-in a sample diluted $\approx$ 20 times. Before obtaining the analytical signal the electrode should be maintained in the diluted sample during 3 min at potential 0 V and the working electrode rotating 100 rpm, for achievement of the adsorption equilibrium of inhibitors from the urine matrix. For UA the electron transfer is close to reversible, for AA it is an irreversible one. Optimal voltammetric techniques are the square-wave for UA and the differential pulse for AA. Calibration curves, detection limits and recoveries for both determinations were evaluated as satisfactory. © 1997 Elsevier Science B.V.

Keywords: Anodic voltammetry; Ascorbic acid; Urine; Uric acid

1. Introduction

Determination of uric acid (UA) and ascorbic acid (AA) in urine by anodic voltammetry for UA [1–5] and polarography for AA [6] is an important biochemical analysis. These methods are more selective than colorimetric (spectrophotometric) ones [6–8] including the method using a spectrophotometric autoanalyzer [7]. Comparison of the voltammetric and HPLC methods [9] showed either close results, although the selectivity, naturally, in each case should be proved. On the other hand, the voltammetric methods are simpler, cheaper and less time-consuming.

In spite of separation of the UA and AA voltammetric anodic signals in urine on carbon-based working electrodes [3,5] a simultaneous voltammetric determination of UA and AA in urine was not carried out up today. For determination of UA in urine with low detection limit, the working electrode surface was specially activated by the anodic pretreatment in alkaline medium and voltammetric analysis in the same

* Corresponding author.

PII S00 9-9140(97)00087-8

solution has been carried out [3]. Modification of a glassy carbon surface by ruthenium catalyst was also used [5].

In our work a method for simultaneous anodic voltammetric determination of UA and AA was developed with the use of a commercial working rotating glassy carbon electrode (RGCE) without any special activation of the electrode surface.

2. Experimental

Anodic voltammetric measurements were performed with the use of commercial potentiostat-galvanostat 263 EG and G PAR (USA) with rotating disk electrode system model 616 and working RGCE having the diameter of 4 mm. A Pt wire was used as auxiliary electrode, while the reference electrode was Ag/AgCl, KCl 3 M. Three different voltammetric techniques were estimated: direct current (DCV), square-wave (SWV) and differential pulse (DPV). Conditions for DCV were the followings: scanning rate 40 mV s^{-1} in the range from -100 to 800 mV, scanning increment 2 mV; for SWV: scanning rate 100 mV s^{-1} in the range from -100 to 700 mV, scanning increment 2 mV, pulse height 5 mV, frequency 25 Hz; and for DPV: scanning rate 40 mV s^{-1} in the range from -100 to 700 mV, scanning increment 4 mV, pulse height 25 mV.

The cleaning of the working electrode by 3 M HNO_3 and then rinsing with water, polishing with aluminium oxide (1 and 0.05 μm) and again rinsing with water in an ultrasonic bath (Astrason, USA) were carried out before each analysis.

Water used in the experiments was deionized. AA and UA for biochemistry, and analytical grade reagents HNO_3, HCl, HOAc, NH_4OH, $NaNO_3$, NaOH were purchased from Merck (Darmstadt, Germany). Aluminium oxide was purchased from BDH (Poole, England).

Two types of buffer solutions for the supporting electrolyte were studied: the 0.2 M acetate buffer (HOAc + NaOH, pH = 3.6–6.3) and the analogous buffer where NaOH was replaced by NH_4OH in the same pH range. The electrolytes with lower pH values: 0.01 M HCl + 0.1 M $NaNO_3$ (pH ≈ 2) and 0.1 M HCl (pH ≈ 1) were studied too. The pH measurements were carried out with a pH/ion meter PH M95 (Radiometer; Copenhagen, Denmark).

Stock solutions of UA $5.0 \cdot 10^{-3}$ M were prepared by dissolving in 0.01 M KOH, and of AA $1.0 \cdot 10^{-2}$ M in water.

Samples of urine from laboratory personnel were filtered through triton-free 0.45 μm Millipore membrane filter (mixed esters of cellulose; Bedford, MA) and stored at 4°C [5].

All measurements were performed in the positive potentials range without removing of dissolved oxygen, at room temperature, in triplicates.

3. Results and discussion

Components of the urine matrix have a significant inhibiting influence on the analytical signal detected on the glassy carbon electrode (the peak current i_p in SWV and DPV or the limiting current i_l in DCV). The inhibition effect is observed even at large (1 + 499) dilution of the sample. Note, this effect was not observed on carbon paste electrodes [1,3] and glassy carbon electrodes modified by the ruthenium catalyst [5]. The working electrode rotation accelerates the achievement of a stable analytical signal. Therefore the inhibition effect is most likely caused by the adsorption of urine matrix components on the electrode surface. It is possible that at the same time simultaneous adsorption of UA and AA and their corresponding preconcentration take place, although earlier the adsorption of UA was detected on a carbon paste electrode at potential 0.15 V and was not detected on glassy carbon electrode [1]. The stable analytical signal was obtained at RGCE velocity 100 rpm and potential 0 V within 3 min. The increase of the velocity in SWV and DPV practically did not influence neither i_p nor resolution, which is depended, in the main, on $\Delta E_p = E_p(UA) - E_p(AA)$, where E_p is peak potential of UA or AA correspondingly. In DCV the resolution $\Delta E1/2$ was worsened, where $\Delta E_{1/2} = E_{1/2}(UA)\text{-}E_{1/2}(AA)$ and $E_{1/2}$ is the half-wave potential. So, the relatively low working electrode rotating rpm was used for beginning of the analysis and then was maintained during the analysis also.

The effect of urine matrix is significant especially for UA at SWV measurements (Table 1). The electrolytic oxidation of UA and AA is described by a two-electron process [10–12]. Since the chemical reactions follow the electron transfer step [10–12], i_l/C values (C is a concentration) in DCV are dependent only on diffusion rate. Therefore the i_l/C values for UA and AA are close at the same dilution of the sample (Table 1).

For UA the electron transfer step is close to the reversible one and its rate is independent from dilution of the sample. It follows from the closeness of the half-width of the peak $\Delta E_{p/2}$ to the 3.52 RT/2F in SWV [13] and DPV [14] (Table 1). Some increase of $\Delta E_{p/2}$ in the presence of the urine sample shows that the reversibility is not complete. The electron transfer for AA is irreversible (Table 1). The closeness to the reversibility for UA and the irreversibility for AA explains [13,14] the following relations: i_p/C_{UA} higher than i_p/C_{AA} in SWV and DPV, i_p/C_{UA} in SWV higher than in DPV for greatly diluted samples, and i_p/C_{AA} in DPV higher than in SWV. The decrease of i_l and i_p under the influence of the sample matrix can be explained by both the increase of the irreversibility of the electrons transfer and the decrease of the active surface of the working electrode because of the adsorption of matrix components.

As is seen from Fig. 1 sufficient resolution is observed for the analytical signals of UA and AA in all voltammograms obtained, but in SWV and DPV the resolution is better than in DCV. Therefore SWV for UA and DPV for AA should be preferred taking also into account the relations: i_p for UA in SWV higher than in DPV, and i_p for AA in DPV higher than in SWV.

The peak potential E_p in SWV and DPV, and the half-wave potential $E_{1/2}$ in DCV for the given acid and dilution of the sample are close. Decrease of the sample dilution displaces the values E_p and $E_{1/2}$ of AA to the positive direction because of the increase of irreversibility, but E_p and $E_{1/2}$ of UA remain almost unchanged. For example, for DPV at pH 5.1 ($HOAc + NH_4OH$) in the electrolyte without urine $E_p(UA) = 428$ mV and $E_p(AA) = 181$ mV, the same with urine diluted $1 + 204$: $E_p(UA) = 426$ mV and $E_p(AA) = 188$ mV, while if dilution is $1 + 19$, $E_p(UA) = 439$ mV and $E_p(AA) = 258$ mV.

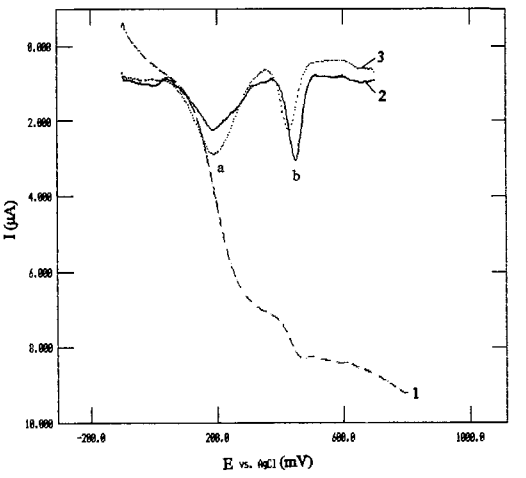

Fig. 1. Anodic voltammograms: 1. direct current; 2. square wave; and 3. differential pulse for fortified urine sample diluted 205 times. (a) AA, $C_{AA} = 28$ mg l^{-1}; b) UA, $C_{UA} = 4$ mg l^{-1}.

The $i_p(UA)$ value is decreased in electrolyte without urine, when pH is increased in the range 2.0–3.5 (Fig. 2), that corresponds to the data by Zen et al. [5]. In the presence of urine the dependence shown in Fig. 2 is opposite: increase of pH from 1–2 to 5–6 causes doubling of $i_p(UA)$. The resolution in the buffer $HOAc + NaOH$ is de-

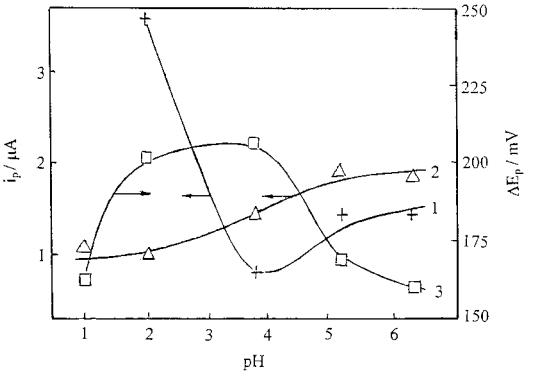

Fig. 2. Dependences $i_p(UA)$ and ΔE_p versus pH for DPV. 1. $i_p(UA)$ in the solution of UA 3 mg l^{-1} and AA 21 mg l^{-1} dissolved in $HOAc + NaOH$ buffer, without any urine; 2 and 3. $i_p(UA)$ and ΔE_p, correspondingly, in an urine sample diluted + 19 by $HOAc + NaOH$ buffer.

Table 1
Influence of the urine sample dilution by HOAc+NH_4OH buffer having pH 5.1 on the voltammetric parameters for uric and ascorbic acids

Dilution	Uric acid					Ascorbic acid			
	DCV	SWV		DPV		DCV	SWV	DPV	
	i_e/C, μA mM^{-1}	i_p/C, μA mM^{-1}	$\Delta E_p/2$, mV	i_p/C, μA mM^{-1}	$\Delta E_p/2$, mV	i_l/C, μA mM^{-1}	i_p/C, μA mM^{-1}	i_p/C, μA mM^{-1}	$\Delta E_p/2$, mV
1+∞[a]	43.5	140	39	98.0	39	36.6	8.7	9.7	124
1+199	26.9	84.6	44	65.4	46	28.7	8.4	—	145
1+49	21.0	19.7	44	—	—	22.5	4.5	—	—
1+19	19.3	20.6	51	21.9	47	22.1	—	6.8	130

[a] 0.0016 mM UA and 0.04 mM AA the buffer only (without any urine).

Table 2
Results of determinations of ascorbic and uric acids (DPV and SWV, correspondingly) in an urine sample diluted by HOAc + NH_4OH buffer having pH 5.1

Acid	Dilution	C ± S, mg l^{-1}
AA	1+18	57 ± 3
UA	1+99	554 ± 12
UA	1+199	550 ± 7
UA	1+499	543 ± 15

C ± S are mean concentration (of triplicates) and corresponding standard deviation of the replicate measurements.

creased with pH increasing to 5–6. In case of the buffer $HOAc + NH_4OH$ the resolution is sufficiently high also at pH 5–6 (≈ 200 mV). The influence of NH_4^+-ion on ΔE_p is caused by decreasing E_p(AA), i.e., by the acceleration of the electron transfer. Moreover, acceleration of AA oxidation by dissolved oxygen with pH increasing (>5) should be taken into consideration also. Therefore the buffer $HOAc + NH_4OH$ with pH 5.1–5.2 was chosen for the analysis.

Relatively low dilution of the sample (1 + 19) was used to obtain sufficiently high signal of AA. For UA the dilution of the sample was 1 + 99, by analogy with Ref. [5], because of limited solubility of UA. It was shown that higher dilution do not influence on the analysis results (Table 2).

Thus, the technique of the analysis described below was formulated.

3.1. Analytical procedure

The procedure consists of two steps. The first step is UA determination by SWV, the second one is AA determination by DPV in one and the same urine sample. In the first step the sample is diluted up to around 1 + 99 by 0.2 M supporting buffer electrolyte $HOAc + NH_4OH$ having pH = 5.1–5.2. The conditions of the analysis are: RGCE is maintained in the electrolyte during 3 min at potential 0 V, than the potential is scanned from 250 to 600 mV in SWV; the working electrode rotating is 100 rpm. In the second step (AA determination) a new portion of the sample is added into the voltammetric cell with the previous sample solution to increase the ratio between sample and electrolyte from 1 + 99 up to around 1 + 19. The analysis conditions in this step are: RGCE is maintained during 3 min at potential 0 V, than the potential is scanned from 0 to 400 mV in DPV; the working electrode rotating is maintained the same, as in first step (100 rpm). This succession of operations allows to minimize the change of the supporting electrolyte volume during analysis. The calibration 'peak current i_p versus acid concentration C_{ad} added to the sample' is based on the method of standard additions. Calibration curves for UA and AA (e.g., Fig. 3) are plotted by the regression analysis. According to standard addition method, the results of the analysis (C_{AA} and C_{UA}) are the absolute values of concentrations at the intersection points of the extrapolated calibration curves (dotted lines) with the abscissa.

3.2. Evaluation of the metrological characteristics

The regression calibration curves 'peak current versus acid concentration added to the sample' have squares of correlation coefficients higher than 0.999. The sensitivities i_p/C are shown in Table 1.

The repeatability (the standard deviations of the replicate measurements) shown in Table 2 satisfy the AOAC requirements [16].

The detection limit, calculated from the calibration curves [15] for UA is 3×10^{-8} M and for AA

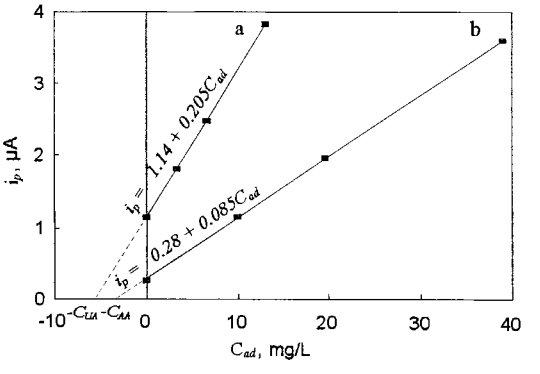

Fig. 3. Calibration curves for determinations of UA (a) and AA (b) in an urine sample by the standard additions method. The dilution's of the sample are: (a) 1 + 99; 1 + 18. Other conditions see in the analytical procedure (Section 3.1).

Table 3
Evaluation of the recovery for ascorbic and uric acids (DPV and SWV, correspondingly) in urine

Acid	Measured conc. in unfortified sample, %	Spike, %	Measured conc. in fortified sample, %	Recovery, %
AA	0	0.01	0.0085	85
AA	0	0.01	0.0092	92
AA	0	0.01	0.0088	88
AA	0	0.03	0.0283	94
AA	0	0.03	0.0280	93
AA	0	0.03	0.0288	96
AA	0	0.1	0.0939	94
AA	0	0.1	0.0983	98
AA	0	0.1	0.1007	101
UA	0.0549	0.0273	0.0833	106
UA	0.0549	0.0273	0.0834	104
UA	0.0549	0.0273	0.0839	106
UA	0.0549	0.0546	0.1107	102
UA	0.0549	0.0546	0.1038	104
UA	0.0549	0.0546	0.0994	99
UA	0.0549	0.0820	0.1406	105
UA	0.0549	0.0820	0.1406	105
UA	0.0549	0.0820	0.1360	99

is 3×10^{-6} M. Thus, the detection limit for UA obtained by us on a commercial glassy carbon electrode is lower than for glassy carbon electrode with ruthenium catalyst coating (1.1×10^{-7} M [5]). At the same time UA detection limit may be decreased up to 1×10^{-9} M due to the anodic pretreatment in alkaline medium [3]. However, it is noted above, the use of alkaline supporting electrolyte can accelerate the oxidation of AA by the dissolved oxygen.

The recovery, as an index of accuracy was estimated using spiked urine samples with certain amounts of AA and UA (the concentration of UA was fortified on 50, 100 and 150% from the initial one in the sample themselves). The recovery values for average of triplicates are given in Table 3. The results satisfy the AOAC requirements [16] too.

Acknowledgements

The authors would like to express their gratitude to Prof. E. Schoenberger for helpful discussion.

References

[1] J. Wang, B.A. Freiha, Bioelectrochem. Bioenerg. 12 (1984) 225.
[2] M. Moutet, R. Vallot, R. Buvet, Bioelectrochem. Bioenerg. 18 (1987) 137.
[3] X. Cai, K. Kalcher, C. Neuhold, B. Ogorevc, Talanta 41 (1994) 407.
[4] R.N. Goyal, A. Mittal, S. Sbarma, Electroanalysis 6 (1994) 609.
[5] Jyn-Myng Zen, Jen-Sen Tang, Anal. Chem. 67 (1995) 1892.
[6] J. Polak, D. Hartlova, J. Volke, Cesk. Hyg. 28 (1983) 113.
[7] G. Park, R.N. Adams, W.R. White, Anal. Lett. 5 (1972) 887.
[8] F.N. Keedy, P. Vadgama, Biosens. Bioelectron. 6 (1991) 491.
[9] R. Farre, A. Frigola, J.C. Popez, J.M. Romers, M. Ramirez, A. Gil, Food Chem. 52 (1995) 99.
[10] W.A. Struck, Ph.J. Elving, Biochemistry 4 (1965) 1343.
[11] G. Dryhurst, K.M. Kadish, F. Scheller, R. Renneberg, Ascorbic acid, in: Biological Electrochemistry, vol. 1, pp. 256–278, Academic Press, New York, 1982.
[12] Ya.I. Tur'yan, R. Kohen, Croat. Chem. Acta 70 (2) (1997).
[13] M. Geibler, C. Kuhnhardt, Square-Wave Polarographie, VEB Deutsher Verlag fur Grundstoffindustrie, Leipzig, 1970, p. 36.
[14] A.M. Bond, Modern Polarographic Methods in Analytical Chemistry, Khimiya, Moscow, 1983, p. 169.
[15] G.T. Wernimont, Use of Statistics to Develop and Evaluate Analytical AOAC, USA, 3rd ed., 1990.
[16] AOAC Peer-Verified Methods Program, AOAC International, Arlington, Virginia, USA, 1993.

ELSEVIER

Talanta 44 (1997) 1929–1934

Talanta

Sol–gel carbon composite electrode as an amperometric detector for liquid chromatography

Prasad V.A. Pamidi [a], Concepción Parrado [a], Stephen A. Kane [a], Joseph Wang [a,*], Malcolm R. Smyth [b], José Pingarrón [c]

[a] *Department of Chemistry and Biochemistry, New Mexico State University, Las Cruces, NM 8803, USA*
[b] *School of Chemical Sciences, Dublin City University, Dublin 9, Ireland*
[c] *Department of Analytical Chemistry, Faculty of Chemistry, Complutense University, 28040 Madrid, Spain*

Received 20 June 1996; received in revised form 22 July 1996; accepted 22 July 1996

Abstract

The performance characteristics of an electrochemical detector for liquid chromatography based on a sol–gel carbon composite working electrode in a wall-jet configuration are described. The new detector combines the versatility of sol–gel processes with several favorable characteristics, including fast electron-transfer kinetics, mechanical rigidity and renewability. Factors influencing the amperometric response are explored and optimized. Detection limits of 58–170 pg are reported for various neurotransmitters. Repetitive injections yield peak heights with relative standard deviations of 2.6–3.7%. The prospects of using sol–gel derived electrochemical detectors are discussed. © 1997 Elsevier Science B.V.

Keywords: Amperometry; HPLC detector; Sol–gel carbon; Electrode

1. Introduction

The coupling of liquid chromatography with electrochemical detection (LCEC) offers a highly sensitive and selective tool for the determination of a wide variety of electroactive compounds [1,2]. The success of the electrochemical detection scheme is strongly influenced by the working electrode material. The selection of such material depends mainly on the redox behavior of the target analytes and the background current (and associated noise) at the operating potential. Other considerations include the potential window, mechanical properties, chemical inertness, electrical conductivity and cost.

Carbon-based electrodes have typically served as working electrodes for the detection of oxidizable species in the anodic region. A variety of carbon electrode materials have been developed for LCEC, with glassy carbon and carbon paste being most popular. Yet, the development of new and improved electrode materials remains a very important need in LCEC [2].

In this report we describe the performance characteristics of a wall-jet amperometric detector employing a sol–gel derived carbon composite

* Corresponding author. Fax: +1 505 6462649.

PII S0039-9140(96)02051-6

working electrode. Sol–gel carbon composites represent a new class of carbon–based electrodes, that are composed of graphite powder homogeneously dispersed in modified silica ceramics [3]. Recent electroanalytical applications of these carbon ceramic electrodes include amperometric biosensing [4,5] and gas-phase monitoring [6]. As desired for LCEC, such sol–gel derived carbon electrodes display favorable electron-transfer kinetics and a wide potential window, are physically rigid, have renewable surface, are amenable to chemical or biological (bulk) modification, and are stable in various solvents. Such attractive features are combined with the versatility of sol–gel processes [7]. Sol–gel carbon materials thus, appear to be a viable alternative to other carbon-based working electrodes used in LCEC. The opportunities accrued from the development of LCEC detectors based on sol–gel carbon composite electrodes are explored in the following sections.

2. Experimental

2.1. Reagents

All the solutions were prepared in HPLC grade water. Catechol, epinephrine, arterenol (norepinephrine) and 3-hydroxytyramine (dopamine) were purchased from Sigma. Methyltrimethoxysilane (Fluka), ethanol (200 proof, Quantum Chemical Company) and graphite powder (grade # 38, Fisher Scientific) were used for the preparation of the sol–gel carbon composite electrodes. Chloroacetic acid (Aldrich), ethylenediaminetetraacetic acid (EDTA) disodium (Fisher Scientific) were used for the preparation of the mobile phase. Nylon membranes (0.2 μm pore size, 47 mm diameter, MF 5621) were used for filtering the mobile phase. Micro filters (MF 5500) and microfilter membranes (MF 5658) were used for filtering the samples. All were obtained from Bioanalytical Systems Inc. (BAS). Ultrahigh purity helium gas (Agile Welding Supply, Albuquerque, NM) was used as received for degassing the mobile phase and solutions.

2.2. High performance liquid chromatography

All experiments were performed on a reverse phase HPLC system (BAS, Model 480) in connection with a dual reciprocating pump (PM-80, BAS) and an amperometric detector (BAS, Model LC-4C) along with a homemade wall-jet electrode configuration. Injections were made through a Rheodyne valve with 20 μl loop onto a C_{18} column (ods-3, BAS, Model MF 6213, 3 μm, 3.2 × 100 mm). Chromatograms were recorded on an Ominiscribe strip-chart dual pen recorder (Houston Instruments). The sol–gel carbon working electrode, the Ag/AgCl (RE-1, BAS) reference electrode and the platinum wire counter electrode were joined through the holes in the Teflon cover of the wall-jet cell.

2.3. Electrode preparation

Sol–gel derived carbon electrodes were prepared by mixing 500 μl methytrimethoxysilane, 750 μl ethanol and 50 μl 11 M hydrochloric acid, sonicating the mixture for 1 min and adding 2.0 g of graphite powder. This mixture was sonicated, mixed thoroughly and filled into the cavities of 3 mm i.d. glass tubes. These composites were dried under ambient conditions for 24 h. Similar procedures were used for making more porous sol–gel electrodes, except for the fact that the initial mixture (before the addition of graphite) was sonicated for the longer times of 15 and 30 min. The sol–gel carbon electrodes were polished after drying on a 400 grade emery paper and polished again on weighing paper. The resulting electrode surfaces were shiny and smooth. Carbon-paste electrodes were prepared by thoroughly mixing graphite powder and mineral oil in the ratio of 70:30. This mixture was filled into the cavities of 3 mm i.d. glass tube. The connections were made by inserting a copper wire through the other end of the capillary in both sol–gel and carbon paste electrodes.

2.4. Procedure

All the measurements were carried out under ambient conditions. Amperometric measurements

were carried out after applying the appropriate potential to the electrode and allowing the transient signal to reach the steady-state value. The mobile phase used was 0.1 M chloroacetic acid solution containing 0.2 g of disodium EDTA adjusted to pH 3.5 with phosphoric acid. All analyte standard solutions were prepared in mobile phase. All mobile phase, standard solution, samples were filtered and degassed prior to use. Urine samples were obtained from healthy volunteers, filtered by passing through 10–15 μm glass filters, and diluted (1:50) with mobile phase solution.

3. Results and discussion

The sol–gel process involves a low-temperature production of ceramic materials through the hydrolysis and polycondensation of alkoxides [7]. By incorporating graphite powder in the initial sol–gel mixture, it is possible to obtain black rigid xerogels with percolating graphite powder in the silica backbone [3]. The preparation conditions (e.g. hydrolysis time, water/silica ratio) can be controlled to manipulate the physical characteristics (particularly the microporosity) of the resulting electrodes [8]. Because of the composite carbon character of these sol–gel derived electrodes, their performance is compared with that of common carbon-paste based detectors.

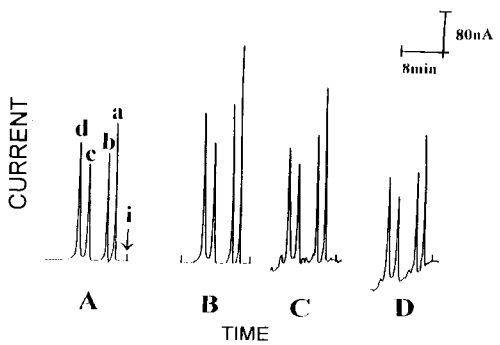

Fig. 1. Chromatograms of 100 μM norepinephrine (a), 100 μM epinephrine (b), 100 μM dopamine (c) and 100 μM catechol (d) at a carbon-paste electrode (A) or sol–gel carbon composite electrodes with 1 min (B) or 15 min (C) or 30 min (D) hydrolysis times. Applied potential: 0.75 V; flow rate: 0.5 ml min^{-1}; mobile phase: 0.15 M chloroacetic acid with 0.2 g EDTA.

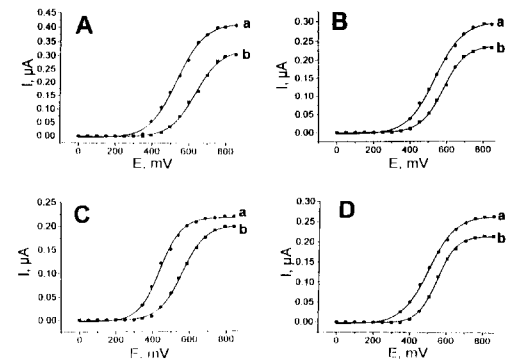

Fig. 2. Hydrodynamic voltammograms of 100 μM norepinephrine (A), 100 μM epinephrine (B), 100 μM dopamine (C) and 100 μM catechol (D) at sol–gel carbon composite electrodes with 1 min hydrolysis (a) and a carbon-paste electrode (b) in HPLC detection. Other conditions as in Fig. 1.

Fig. 1 compares chromatograms for a mixture of 0.1 mM norepinephrine, epinephrine, dopamine and catechol, obtained with a conventional carbon-paste electrode and using sol–gel carbon composite surfaces of different porosities. The well-defined peaks and low noise level of the nonporous sol–gel carbon composite compare favorably with those of the carbon–paste detector (compare B and A). In contrast, the porous composite electrodes display a large noise level and drifting baseline, and overall an inferior performance (associated with the penetration of mobile phase into the electrode interior). All subsesquent work was thus, carried out using the nonporous sol–gel carbon composite detector.

Fig. 2 shows hydrodynamic voltammograms at the sol–gel derived carbon and carbon-paste wall-jet detectors for norepinephrine, epinephrine, dopamine and catechol. The carbon–ceramic composite detector displays well-defined waves and potential-independent transport limited currents for all four compounds. The anodic wave starts at +0.25 V, and rises rapidly. A limiting-current plateau is reached at potentials higher than +0.65 V (C) and +0.7 V (A,B,D). The sol–gel carbon detector offers a substantial decrease in the potential of the voltammetric wave for all four compounds, compared with the carbon-paste surface ($\Delta E_{1/2}$ ranging from 67 mV (D) to 155 mV (A). In addition, an increase in the

mass-transport controlled response (up to 38% in the case of norepinephrine) is observed in comparison to the carbon-paste detector. In view of the use of the same graphite powder, the more favorable redox behavior observed at the sol–gel detector may be attributed to a catalytic action by the silicon oxide component. Enhanced electron-transfer kinetics by metal-oxide surface catalysts has been used previously to lower the operating potential of LCEC detectors [9]. While the sol–gel network is negatively charged, it does not appear that the cationic catecholamines interact with the surface under the chromatographic conditions employed in this study. (Note that the enhanced signal for the neutral catechol offered by the sol–gel carbon detector, vs. the carbon paste one, is similar to that observed for the cationic neurotransmitters.) Similarly, there is no indication of electrostatic repulsion of anionic compounds, in view of the similar data for ascorbic and uric acids (not shown). Based on the data of Fig. 2, a potential of +0.75 V was used throughout this study.

The dependence of the chromatographic peak currents upon the flow rate is shown in Fig. 3. The peak heights increase linearly with the flow rate at first (between 0.2 and 0.3 ml min^{-1}) and then more slowly up to 0.5 ml min^{-1}. The peaks decrease slightly between 0.5 and 0.8 ml min^{-1}, and then rise slightly. Such profiles reflect the combined flow rate effect upon the chromatographic peak (band) broadening and on the mass transport towards the detector surface. Unlike continuous wall-jet electrodes where the steady-state current is proportional to $U^{3/4}$, the composite character of the present sol–gel derived electrode reduces the influence of forced convection upon the response. A flow rate of 0.5 ml min^{-1} was chosen as optimum for all further studies.

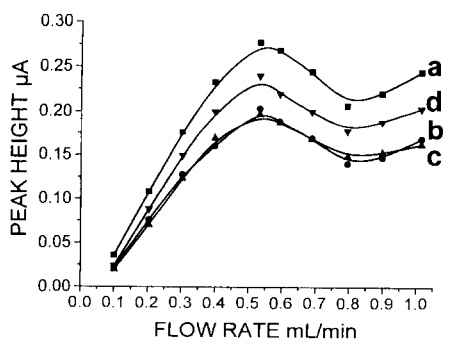

Fig. 3. Effect of flow rate on the amperometric peak current in the HPLC detection of 100 μM norepinephrine (a), 100 μM epinephrine (b), 100 μM dopamine (c) and 100 μM catechol (d) at a sol–gel carbon composite electrode. Other conditions as in Fig. 1.

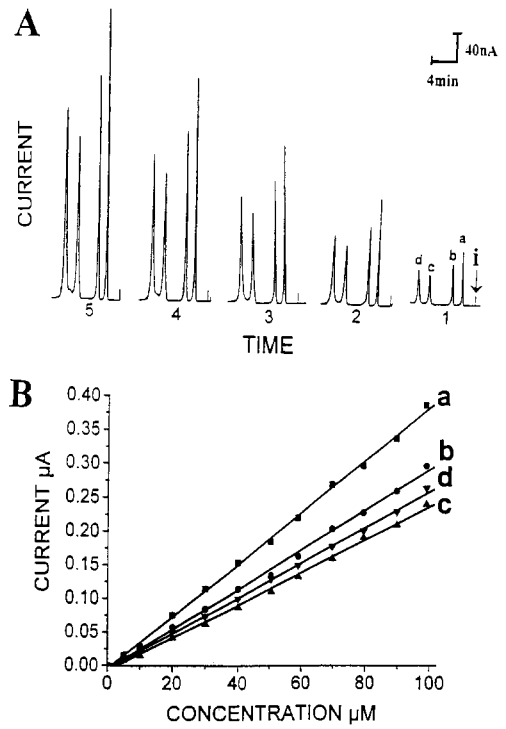

Fig. 4. Current–time recordings (A) and calibration plot (B) of norepinephrine (a), epinephrine (b), dopamine (c) and catechol (d) at a sol–gel carbon composite electrode for the successive additions of the analytes in HPLC detection. 1–5 represents the concentrations of 20–100 μM, respectively. Other conditions as in Fig. 1.

The sensitivity and linearity of the response were evaluated using 11 successive injections of mixtures containing increasing concentrations of various catecholamines (from 5 to 100 μM). Well-defined peaks were obtained at the micromolar level (Fig. 4A). The peak response increased linearly upon increasing the concentration of these analytes (Fig. 4B). The slopes of these calibration plots correspond to sensitivities of 3.84 (nore-

pinephrine), 2.95 (epinephrine), 2.43 (dopamine) and 2.62 (catechol) nA μM^{-1} (correlation coefficients, 0.999).

An injection of a 0.5 μM mixture of the catecholamines was used to estimate the minimum detectable quantities (Fig. 5A). Based on a signal-to-noise ratio of three, the detection limits were 25 (norepinephrine), 32 (epinephrine), 50 (dopamine) and 25 (catechol) nM. Such levels correspond to 85, 110, 170 and 55 pg, respectively, in the 20 μl injected volumes. Such extremely low detection limits are attributed to the composite character of the sol–gel derived carbon surface.

The suitability of the sol–gel detector for assays of body fluids is illustrated in Fig. 5B. The chromatogram for the diluted (1:50) urine sample displays defined ascorbic acid and uric acid peaks at retention times of 2.0 and 3.5 min, respectively.

The reproducibility was assessed from a series of 20 successive injections of a mixture containing 100 μM of the various catechol compounds during an unbroken 200 min period (conditions, as in Fig. 1). The mean peak currents found were 405 (norepinephrine), 288 (epinephrine), 218 (dopamine) and 256 (catechol) nA, with relative standard deviations of 2.6, 3.1, 3.2 and 3.7%, respectively.

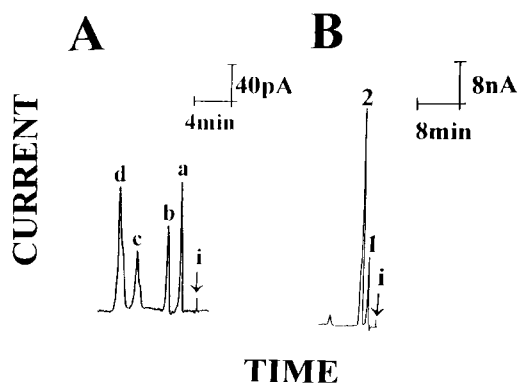

Fig. 5. Chromatograms for submicromolar concentrations of catecholamines (A) and a urine sample diluted (1.50) in mobile phase (B) at a sol–gel carbon composite electrode. 1 and 2 represents ascorbic acid and uric acid, respectively; a–d represent norepinephrine, epinephrine, dopamine and catechol, respectively, at 0.5 μM. Other conditions, as in Fig. 1.

In conclusion, the experiments described above clearly indicate that sol–gel carbon composites can provide versatile, easy-to-prepare, renewable LCEC detectors, possessing high sensitivity, selectivity and stability. While such features are presented in connection with a wall-jet detector, other detector configurations could benefit from the attractive properties of sol–gel carbon composites. The shape and form of the sol–gel derived electrodes can be controlled to suit the specific application. Application of this detector for monitoring other eleectroactive compounds in chromatographic effluents appear promising. Enzyme-based detectors (e.g. for phenols, amino acids or carbohydrates) could also benefit from the attractive, low-temperature encapsulation of biocomponents within sol–gel networks. Doping of the sol–gel carbon composite with an electrocatalyst (e.g. dispersed metal particles) could offer additional detection advantages.

Acknowledgements

Financial support from Sandia NL is gratefully acknowledged (DOE Contract DE-AC04-94AL85000). CP acknowledges a fellowship from the Direcion General de Investigacion Científica y Enseñanza Superior (DGICYES: PR95-310). SAK acknowledges a fellowship from the US Environmental Protection Agency in the National Network for Environmental Management Studies Program.

References

[1] J. Wang, in G. Patony (Ed.), HPLC Detection VCH, NY, 1992, p. 91.
[2] C. Lunte, in P. Kissinger and W. Heineman (Eds), Laboratory Techniques in Electroanalytical Chemistry, 2nd ed., Marcel Dekker, NY, 1996.
[3] M. Tsionsky, G. Gun, V. Glezer and O. Lev, Anal. Chem., 66 (1994) 1747.
[4] I. Prankratov and O. Lev, J. Electroanal. Chem., 393 (1995) 35.
[5] J. Wang, P.V.A. Pamidi and D.S. Park, Anal. Chem., 68 (1996) 2705.

[6] J. Jun, M. Tsionsky, L. Rabinovich, Y. Golan, I. Rubenstien and O. Lev, J. Electroanal. Chem., 395 (1995) 57.
[7] B. Dave, B. Dunn, J.S. Valentine and J. Zink, Anal. Chem., 66 (1994) 1120A.
[8] O. Lev, M. Tsionsky, L. Rabinovich, V. Glezer, S. Sampath, I. Pankratov and J. Gun. Anal. Chem., 67 (1995) 22A.
[9] J. Wang and B. Freiha, Anal. Chem., 56 (1984) 2266.

ELSEVIER

Talanta 44 (1997) 1935–1940

Talanta

Potentiometric determination of stability constants of Lanthanon(III) complexes with some Schiff bases and benzothiazolines

Perihan Gürkan *, Nurşen Sarı

Gazi Üniversitesi Fen Ed. Fakültesi, Kimya Bölümü Teknikokullar, 06500 Ankara, Turkey

Received 29 November 1995; received in revised form 3 July 1996; accepted 9 August 1996

Abstract

The protonation constants of five Schiff base and two benzothiazoline type ligands and stability constants of their complexes with six lanthanide ions were determined by potentiometrically in ethanol–water solution (1:1, v/v) at 25 ± 0.1°C. The Schiff base-type ligands were salicylidene 2-iminopyridine (SAPy), salicylidene-5-methyl-2-iminopyridine (SAPyMe), salicylidene-5-chloro-2-iminopyridine (SAPyCl), 2-(2-pyridylmethyleneamino) phenol (PyOH), 2-(2-quinolylmethyleneamino) phenol (QuOH) and the benzothiazoline-type ligands were pyridine-2-carbozaldehydebenzothiazoline (PyS) and quinoline-2-carboxaldehydebenzothiazoline (QuS). The order of stability constants was found to be for metal ions La(III) < Pr(III) < Nd(III) < Eu(III) < Ho(III) < Yb(III), and for ligands SAPyCl < SAPy < QuS < QuOH < PyS < PyOH < SAPyMe. The FORTRAN programs PKAS and BEST were used for the calculation of protonation constants and stability constants, respectively. © 1997 Elsevier Science B.V.

Keywords: Benzothiazolines; Lanthanon(III) complexes; Potentiometry; Protonation constants; Schiff bases; Stability constants

1. Introduction

Potentiometric studies on and the coordination chemistry of lanthanide cations with Schiff bases have been investigated and reviewed over the last few years [1–4]. The stability constants of 1:1 complexes of Pr(III), Nd(III), Sm(III) and Gd(III) with SAPy have been reported [5]. The characterization of cobalt, manganese, nickel and some lanthanide complexes of PyOH and QuOH [6–10] and silicon, niobium, manganese and lead complexes of PyS have also been reported [11–14], but a literature survey indicated that no work has been done on complex formation equilibria of

* Corresponding author.

PII S0039-9140(96)02058-9

these ligands. Such studies have now been undertaken and are reported in this paper. The structures of the ligands are shown below.

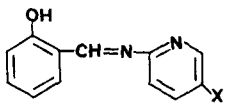

X=H SAPy
X=Cl SAPyCl
X=Me SAPyMe

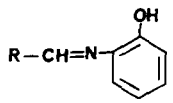

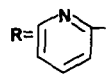

PyOH

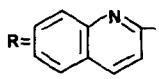

QuOH

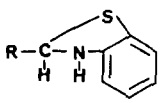

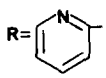

PyS

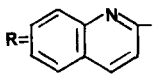

QuS

2. Experimental

2.1. Synthesis of ligands

SAPy, SAPyCl and SAPyMe were synthesized by condensing 1:1 molar amounts of salicylaldehyde with 2-aminopyridine, 2-amino-5-chloropyridine and 2-amino-5-methylpyridine, respectively in ethanol as reported earlier [15–17]. PyOH and QuOH were synthesized by condensing 2-hydroxaniline in 1:1 molar ratio with pyridine-2-carboxaldeyde and quinoline-2-carboxaldehyde, respectively, as reported earlier [6–10]. PyS and QuS were prepared by the condensation of 2-mercaptoaniline with pyridine-2-carboxaldehyde and quinoline-2-carboxaldehyde respectively in a 1:1 molar ratio in benzene [11–14].

The ligands were fully characterized by their melting points, elemental analysis (C, H, N) IR and NMR spectra.

2.2. Reagents and solutions

Ethanol–water (1:1, v/v) prepared from triply distilled water and absolute ethanol was used as a solvent. All metal ion solutions were prepared from their analytical-grade chlorides (Aldrich) and were standardized by EDTA titration [18]. Carbonate-free KOH solution was standardized with potassium hydrogen phthalate. KCl (Merck, extra pure) and concentrated HCl (Merck, extra pure) were used for the preparation of 1.00 M KCl and 0.017 M HCl solutions. The HCl solution was standardized with standard KOH.

2.3. Potentiometric measurements

Measurements were carried out using a Corning M-240 pH-meter equipped with a Corning semimicro combined glass electrode. The system was calibrated to read hydrogen ion concentration by titration of hydrochloric acid solution at 25 ± 0.1°C and 0.2 M KCl ionic strength with KOH solution according to Gran's method [19]. Small amounts of ($\Delta v = 0.05$ cm^3) titrant KOH solution were added with a microburette. The waiting period was 3 min. Sample solutions were titrated in a double-walled glass cell maintained at 25 ± 0.1°C by circulating water and were stirred magnetically under a continuous flow of nitrogen. Titration were performed over the pH range 2.0–12.0 using 25 ± 0.01 cm^3 samples in a medium of constant ionic strength (0.20 M KCl). There were no precipitation in the pH range in which the titration were performed. The concentration of the ligands was 5.0×10^{-4} M and the metal-to-ligand molar ratios was 1:4. Corrections for pH measurements in the aqueous–organic system were performed as described by van Uitert and Haas [20].

2.4. Calculations

The protonation constants of the ligands and stability constants of the complexes were computed form titration data using the FORTRAN programs PKAS and BEST, respectively [21]. The number of experimental (v, pH) points was more than 39 (maximum 62) for each titration. In

refining the overall constants, some experimental points, especially, around the equivalent points, were neglected. The error estimate for each constant was between 0.01 and 0.07 log units.

3. Results and discussion

3.1. Protonation constants of ligands

The protonation constants of the ligands and stability constants of the complexes are given in Table 1. For Schiff base ligands, the first constants refer to protonation of phenolate ions and the second constants to protonation of pyridine or quinoline nitrogens.

As can be seen from Table 1, the first protonation constants of PyOH and QuOH are higher than that of SAPy. This means that the electron densities of the phenolic oxygen atoms of PyOH and QuOH are higher than that of SAPy. This can be explained as follows. The lone pair on the nitrogen atom of the imino group participates in the resonance of the phenol (or quinolinol) ring and increases its electron density. The $\log K_2^H$ values of these ligands also support this observation, because the second protonation constant of SAPy is higher than those of PyOH and QuOH, contrary to the $\log K_1^H$ values of these ligands. For SAPy, SAPyCl and SAPyMe ligands, both of the protonation constants follow the order SAPyCl < SAPy < SAPyMe. Because of the inductive electron withdrawing effect of the chlorine atom, the basicity of the pyridine nitrogen in SAPyCl is lower than that of SAPy. On the other hand, the inductive electron-donating effect of the methyl group increases the basicity of the pyridine nitrogen in SAPyMe. The more basic the pyridine nitrogen is, the more stable is its proton–ligand complex.

As can be seen in Table 1, pyridine-2-carboxaldehyde benzothiazoline and quinoline-2-carboxaldehydebenzothiazoline ligands also have two protonation constants.

The potentiometric titration curve of PyS is given in Fig. 2. The high values of the first protonation constants (11.46 for PyS and 11.30 for QuS) indicate a very weak acidic proton in these molecules; it might be a methynic hydrogen atom in thiazoline ring. Since the methynic carbon is bonded to nitrogen and sulphur atoms in the thiazoline ring and to the pyridine (or quinoline) ring, the inductive electron-withdrawing effect of these three enhances the acidity of the methynic hydrogen atom to some extent.

The second protonation constants of PyS and QuS ligands (2.61 and 2.48, respectively) are lower than those of PyOH ad QuOH ligands. These lower values indicate that the second protonation occurs on either the nitrogen or sulphur atom of thiazoline ring, but not on the pyridine (or quinoline) nitrogen, although the pyridine (or quinoline) nitrogen is more basic than sulphur and nitrogen atoms of the thiazoline ring. No reasonable explanation can be given for this result.

3.2. Stability constants of complexes

First, the complex-forming reactions of Schiff base and benzothiazoline-type ligands with metal ions were investigated. For this purpose, 1:1 and 1:2 molar ratios of Pr^{3+} ion to PyOH Schiff base ligand and La^{3+} ion to PyS benzothiazoline ligand were titrated against 0.084 M KOH. The data are plotted in Fig. 1 and Fig. 2, respectively.

A break near $m = 2$ for all 1:1 systems can be explained by the release of two hydrogen ions from protonated form of the ligand molecules for each metal ion when complexes were formed. The 1:2 M:L systems contain four titratable protons per metal ion, and further there is a break in each of the curves near $m = 4$.

The complex-forming equilibria can be given as follows:

$$Ln^{3+} + H_2L^+ \rightleftharpoons LnL^{2+} + 2H^+$$

$$LnL^{2+} + H_2L^+ \rightleftharpoons LnL_2^+ + 2H^+$$

The stability constants of the Lanthanon(III) chelates of all ligands are given in Table 1. For the same ligand, the $\log K_1$ values were found to increase in the order La(III) < Pr(III) < Nd(III) < Eu(III) < Ho(III) < Yb(III), which is in accordance with the order of increasing acidity of the metal ions.

Table 1
Protonation constants of the ligands and stability constants of the complexes

Ion	Parameters	SAPyMe		SAPyCl		SAPy		PyOH	QuOH	PyS	Ous
		25 ± 01°C	50 ± 0.1°C	25 ± 0.1°C	50 ± 0.1°C	25 ± 0.1°C	50 ± 0.1°C	25 ± 0.1°C	25 ± 0.1°C	25 ± 0.1°C	25 ± 0.1°C
H^+	Log K_1^H	9.56	9.47	8.98	8.90	9.25	9.02	10.48	10.55	11.46	11.30
	Log K_2^H	7.09	6.54	4.16	3.69	6.41	6.30	4.55	4.35	2.61	2.48
	σ_{fit}	0.03	0.04	0.02	0.02	0.00	0.03	0.01	0.01	0.02	0.01
La^{3+}	Log K_1	6.37	5.85	3.76	3.45	4.69	4.31	6.47	5.89	6.05	5.61
	Log K_2	4.06	4.02	3.16	2.91	3.52	3.24	5.60	4.74	4.88	4.53
	Log K_3	4.03	3.73	—	—	2.65	2.40	—	—	—	—
	σ_{fit}	0.05	0.04	0.07	0.06	0.03	0.05	0.02	0.01	0.02	0.02
Pr^{3+}	Log K_1	7.14	6.57	4.26	3.92	5.15	4.74	6.56	6.21	6.32	5.97
	Log K_2	4.92	4.54	3.23	2.97	4.02	3.71	5.70	5.01	5.17	4.84
	Log K_3	4.40	4.06	—	—	2.97	2.74	—	—	—	—
	σ_{fit}	0.01	0.03	0.03	0.03	0.02	0.03	0.02	0.01	0.04	0.03
Nd^{3+}	Log K_1	7.22	6.65	4.42	4.07	5.32	4.90	6.63	6.34	6.50	6.09
	Log K_2	5.08	4.69	3.25	3.00	4.15	3.81	5.76	5.18	5.29	4.93
	Log K_3	4.51	4.16	—	—	3.08	2.84	—	—	—	—
	σ_{fit}	0.01	0.03	0.04	0.03	0.01	0.02	0.02	0.02	0.02	0.02
Eu^{3+}	Log K_1	7.57	7.00	4.95	4.58	6.15	5.69	7.05	6.58	6.89	6.35
	Log K_2	5.20	4.80	3.29	3.03	4.31	3.97	5.99	5.43	5.64	5.17
	Log K_3	4.72	4.35	—	—	3.21	2.97	—	—	—	—
	σ_{fit}	0.03	0.04	0.03	0.02	0.05	0.02	0.02	0.02	0.04	0.01
H_0^{3+}	Log K_1	7.82	7.24	5.28	4.89	6.25	5.79	7.30	6.81	7.02	6.51
	Log K_2	5.42	5.00	3.33	3.06	4.57	4.22	6.08	5.58	5.71	5.36
	Log K_3	4.81	4.44	—	—	3.31	3.05	—	—	—	—
	σ_{fit}	0.01	0.03	0.02	0.03	0.02	0.04	0.01	0.01	0.03	0.01
Yb^{3+}	Log K_1	8.03	7.44	5.35	4.96	6.52	6.04	7.41	6.90	7.19	6.68
	Log K_2	5.61	5.15	3.35	3.09	4.75	4.38	6.15	5.69	5.89	5.49
	Log K_3	4.94	4.54	—	—	3.57	3.29	—	—	—	—
	σ_{fit}	0.03	0.02	0.06	0.02	0.05	0.02	0.02	0.01	0.03	0.02

The stability constants of the complexes of three salicylidenpyridine ligands with the same metal ion also followed the same order as the proton ligand stability constants of the ligands, i.e. SAPyCl < SAPy < SAPyMe. This may be attributed to the different basicities of the donor atoms of the ligands caused by the inductive substituent effects as discussed earlier. The ML_3-type complexes of SAPyCl were not observed in the pH range in which the titration were performed, because of their low stabilities. The order of log K values of the other four ligands with the same metal ions expected is as PyOH < QuOH < PyS < QuS. Because the donor oxygen atom present in PyOH and QuOH ligands is a harder base than the donor sulphur atom present in PyS and QuS ligands, the lanthanon(III) ions, being hard acids should preferentially bond to oxygen donor ligands. Contrary to these expectations, the order of log K values of four ligands with the same metal ion was found to be PyOH < PyS < QuOH < QuS. This might be attributed to steric hindrance of quinoline ring.

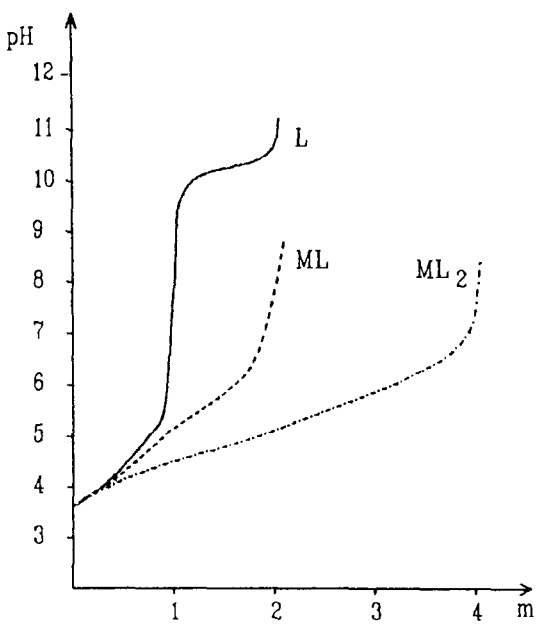

Fig. 1. Potentiometric titration curves for PyOH (L) and 1:1 and 1:2 stochiometries of Pr^{3+} to PyOH (ML and ML_2) as a function of added KOH. m = Moles of base added per mole of metal ion (or ligand) present.

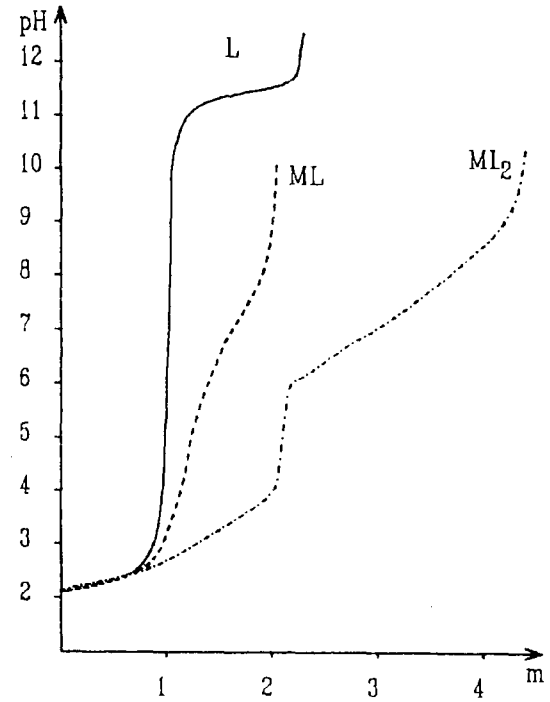

Fig. 2. Potentiometric titration curves for PyS (L) and 1:1 and 1:2 stochiometries of La^{3+} to PyS (ML and ML_2) as a function of added KOH. m = Moles of base added per mole of metal ion (or ligand) present.

The stability constants of the ML-type complexes of all ligands with the same metal ion except La(III) were found to increase in the order SAPyCl < SAPy < QuS < QuOH < PyS < PyOH < SAPyMe. The log K value of PyOH with La(III) ion was higher than that of SAPyMe.

3.3. Thermodynamic parameters

The stability constants of three salicylidenepyridine ligands with metal ions were also determined 50 ± 0.01°C and the thermodynamic parameters ΔG and ΔH for complexation reactions of their ML-type complexes were evaluated. The proton–ligand and metal–ligand stability constants decreased with increasing temperature, as expected. The thermodynamic parameters were calculated using the following relationships:

$$\Delta G = -RT \ln K$$

$$\mathrm{d} \ln K/\mathrm{d}(1/T) = -\Delta H/R$$

Table 2
Thermodynamic parameters of ML-type complexes of SAPy SAPyCl and SAPyMe with Lanthanon(III) ions at 25 ± 0.1°C and μ = 0.2 M KCl

Metal ion	Ligand	$-\Delta G$ (kJ mol^{-1})	$-\Delta H$ (kJ mol^{-1})
La^{3+}	SAPyMe	36.3 ± 0.3	36 ± 11
	SAPy	26.8 ± 0.2	28 ± 6
	SAPyCl	21.4 ± 0.4	23 ± 9
Pr^{3+}	SAPyMe	40.68 ± 0.05	42 ± 3
	SAPy	29.3 ± 0.1	30 ± 4
	SAPyCl	24.3 ± 0.2	25 ± 4
Nd^{3+}	SAPyMe	41.1 ± 0.05	42 ± 3
	SAPy	30.32 ± 0.05	31 ± 2
	SAPyCl	25.2 ± 0.02	26 ± 5
Eu^{3+}	SAPyMe	43.2 ± 0.2	42 ± 5
	SAPy	35.1 ± 0.3	34 ± 5
	SAPyCl	28.3 ± 0.2	27 ± 4
H_0^{3+}	SAPyMe	44.67 ± 0.05	43 ± 3
	SAPy	35.7 ± 0.1	34 ± 4
	SAPyCl	30.2 ± 0.1	29 ± 4
Yb^{3+}	SAPyMe	45.9 ± 0.2	43 ± 4
	SAPy	37.2 ± 0.3	35 ± 5
	SAPyCl	30.56 ± 0.3	29.6 ± 6

The overall free energy and enthalpy changes are reported in Table 2.

The negative free energy and enthalpy changes of all the complexes indicated a spontaneous and exothermic nature of complexation reactions.

Acknowledgements

We are grateful to Gazi University Research Fund for supporting this study.

References

[1] R.L. Dutta and B.R. Das, J. Sci. Ind. Res., 47 (1988) 547.
[2] P.A. Vigato and D.E. Fenton, Inorg. Chim. Acta, 139 (1987) 39.
[3] V. Chowdhary, M. Parihar and R.K. Mehta, Z. Phys. Chem., 271 (1990) 413.
[4] K.S. Siddiqui, R.I. Kureshy, N.H. Khan, S. Tabassum and S.A.A. Zaidi, Inorg. Chim. Acta, 151 (1988) 95.
[5] S. Goel, O.P. Pandey and S.K. Sengupta, Thermochim. Acta, 133 (1988) 359.
[6] N. Kaprivanac, Z. Grabaric, J. Meixner and K.J. Javonoivic, Michrochem. J., 46 (3) (1992) 36.
[7] Z. Grabaric, Z. Lazarevic and N. Kaprivanac, Anal. Lett, 26 (1993) 2455.
[8] Z. Grabaric, B.S. Grabaric, N. Kaprivanac and I. Eskinja, Chem. Pap., 47 (1993) 282.
[9] S. Papic, N. Kaprivanac, Z. Grabaric and P.D. Osterman, Dyes Pigments, 25 (1994) 229.
[10] W. Bo, Y. Shiyan and J. Doasen, Polyhedron 13 (1994) 2089.
[11] K. Singh, R.V. Singh and J.P. Tandon, Inorg, Chim. Acta 151, (1988) 179.
[12] K. Singh, R.V. Singh and J.P. Tandon, Inorg, Synth. React. Inorg. Met. Org. Chem, 17, (1987) 385.
[13] N. Kanoongo, R.V. Singh and J.P. Tandon, Synth. React. Inorg. Met. Org. Chem, 19, (1989) 113.
[14] K. Singh, R.V. Singh and J.P. Tandon, J. Prakt. Chem, 331 (1989) 525.
[15] R.K. Parashar, R.C. Sharma, A. Kumar and G. Mohan, Inorg. Chim. Acta, 151 (1988) 201.
[16] H. Ranganathan, T. Ramasami, D. Ramaswamy and M. Santappa, Indian J. Chem, 25A (1986) 127.
[17] P. Chatterjee, H.K. Duggal, B.V. Agarala and A.K. Dey, J. Indian Chem. Soc., 66 (1986) 550.
[18] J.V. Frank, The Analytical Uses of EDTA, Van Nostrand, New York 1965.
[19] G. Gran, Analyst, 77 (1952) 661.
[20] L.G. Van Uitert and C.G. Haas, J. Am. Chem. Soc., 75 (1953) 451.
[21] A.E. Martell and R.J. Motekaitis, Determination and Use of Stability Constants, VCH, New York, 1988.

ELSEVIER

Talanta 44 (1997) 1941–1947

Talanta

Investigation of arsine-generating reactions using deuterium-labeled reagents and mass spectrometry

Spiros A. Pergantis, Witold Winnik, Edward M. Heithmar *, William R. Cullen [1]

U.S. Environmental Protection Agency, National Exposure Research Laboratory, Characterization Research Division, P.O. Box 93478, Las Vegas, Nevada 89193-3478, USA

Received 1 April 1996; received in revised form 27 August 1996; accepted 27 August 1996

Abstract

Mass spectrometry was used to detect transfer of deuterium from labeled reagents to arsines following hydride-generation reactions. The arsine gases liberated from the reactions of arsenite, arsenate, methylarsonic acid, and dimethylarsinic acid with HCl and $NaBD_4$ in H_2O, or with DCl and $NaBH_4$ in D_2O, were examined. Differences in the mode of deuterium incorporation for the various arsines were detected. These results may help explain some of the observed variations in arsine-generation efficiency for various arsenic compounds present in environmental and biological samples. © 1997 Elsevier Science B.V.

Keywords: Arsenate; Arsines; Arsenic; Arsenite; Dimethylarsinic acid; Hydride generation; Mass spectrometry; Methylarsonic acid

1. Introduction

Hydride-generation (HG) methodology coupled to element-specific detectors has been used extensively for the trace determination of hydride-forming elements such as arsenic, bismuth, selenium, and antimony [1], germanium [2], tellurium and tin [3], and lead [4]. Such analyses are accomplished by first converting the metal or metalloid into its corresponding gaseous hydride followed by transfer to a spectrometric detector. HG coupled to atomic absorption spectrometry (AAS) or inductively coupled plasma mass spectrometry (ICPMS) has been used extensively for the determination of arsenic in a variety of sample types [5–10]. These methods allow the separation of analytes from the sample matrix, and provide high sensitivity and low limits of detection. For these reasons, HG techniques are widely used by the U.S. Environmental Protection Agency for the determination of the toxic elements arsenic and selenium. Hydride generation can also be interfaced with gas chromatography for the speciation of organometallics [11–13]. Because of the efficient analyte introduction into the detector afforded by HG, it may also improve the sensitivity of liquid chromatographic arsenic speciation techniques [14].

* Corresponding author.

[1] Address: Department of Chemistry, University of British Columbia, Vancouver, B.C., Canada V6T 1Z1.

PII S0039-9140(96)02079-6

Despite its many advantages, a number of problems are associated with the HG approach. Interferences caused by transition metals have been extensively reported [15–17]. Variations in the hydride-generation efficiency for different compounds of the same element have also been reported [17–21]. To compensate for these variations, digestions usually must be performed to convert all species of an element into the same form. Even though these effects are well documented, little effort has been made to elucidate their relationship to the mechanisms involved in hydride formation.

In this report, we describe experiments in which deuterium-labeled reagents and mass spectrometry were used to study the generation of arsines from aqueous solutions. The objective was to investigate differences in the reactions generating arsine, methylarsine, and dimethylarsine. Deuterium transfer from the reagents to the generated arsines was monitored by using a mass spectrometric detector.

2. Experimental

2.1. Instrumentation

A Finnigan-MAT TSQ 700 Gas Chromatograph (GC)/Mass Spectrometer (MS) system was used for most of the experiments in this study. The instrumental operating conditions were as follows: electron impact (EI) ionization mode, electron energy 70 eV, tuning and calibration with perfluorotributylamine (FC43). A Varian 3400 GC system was equipped with a fused-silica column 0.18-mm I.D. × 20-m Crossbond® phenylmethylpolysiloxane (Restek, USA) column. A GC ion-trap mass spectrometer (Finnigan-MAT Magnum™) was also used for some of the experiments.

2.2. Reagents

The following arsenic reagents were used: dimethylarsinic acid (Sigma Chemical, St. Louis, MO), disodium methylarsonate (Chemical Service, West Chester, PA), sodium m-arsenite (Sigma Chemical), and sodium arsenate (Sigma Chemical). Solutions of each of the arsenic compounds were made up in H_2O or D_2O, depending on the experiment.

Sodium borohydride (98 atom %deuterium), deuterium oxide (99.8 atom %D), and a deuterium chloride solution in D_2O (37% w/v) were purchased from Aldrich Chemical Company, (Milwaukee, WI, USA). Hydrochloric acid (double sub-boiling distilled in quartz) was obtained from Seastar Chemical (Sidney, B.C., Canada), and sodium borohydride was obtained from J.T. Baker Chemical (Philipsburg, N.J.).

2.3. Procedures

Reactions were carried out in 2 ml glass vials with rubber septa. Unless stated otherwise, reaction conditions were as follows: 50 μl of 100 ppm arsenic solution for each of the arsenic compounds investigated, along with 50 μl of HCl (20% w/v) were added initially to the reaction vial. The vial was flushed with argon and sealed prior to the injection of 70 μl of 2% w/v $NaBH_4$. Sampling of the headspace was accomplished by inserting a syringe needle through the cap septum and withdrawing a 2 μl gas sample. The sample was immediately injected, in the splitless mode, onto the GC/MS. The following GC temperature program was used: 0.5 min at 50°C, ramped up to 150°C in 3.5 min, and held at 150°C for 3 min.

3. Results and discussion

When arsenite was reacted with DCl and $NaBH_4$ in D_2O, most of the arsine detected was non-deuterated. The mass spectrum of the gaseous products of this reaction is presented in Fig. 1a. The ion at m/z 79 (8%) indicates the presence of a small amount of AsH_2D. An experiment was conducted to examine variations in product formation over time. Hydride-generating reactions were carried out in four separate vials. Hydrides were sampled and injected onto the GC/MS at 0, 8, 18 and 28 min. The spectra obtained were identical to the one presented in Fig. 1a. From the above data it can be proposed

that hydrogen is transferred from borohydride to the arsenic atom without any further reaction of the arsine with the deuterated acid present in D_2O. To confirm this assumption, arsenite was reacted with HCl and $NaBD_4$ in H_2O. The generated arsine was deuterated, as indicated by its mass spectrum presented in Fig. 1b. The ion at m/z 80 (6%) indicates a small amount of AsD_2H present in the gaseous products. Identical mass spectra were obtained when arsenate, instead of arsenite, was used for these reactions.

When methylarsonic acid (MAA) was reacted with DCl and $NaBH_4$ in D_2O, the resulting methylarsine was a mixture of $MeAsH_2$, $MeAsD_2$, and MeAsHD (Fig. 2). To confirm the presence of these arsine species, a time-series study was conducted. Four identical reactions were carried out in separate vials, which were sampled after 0.5, 7, 14 and 22 min, respectively. The mass spectrum

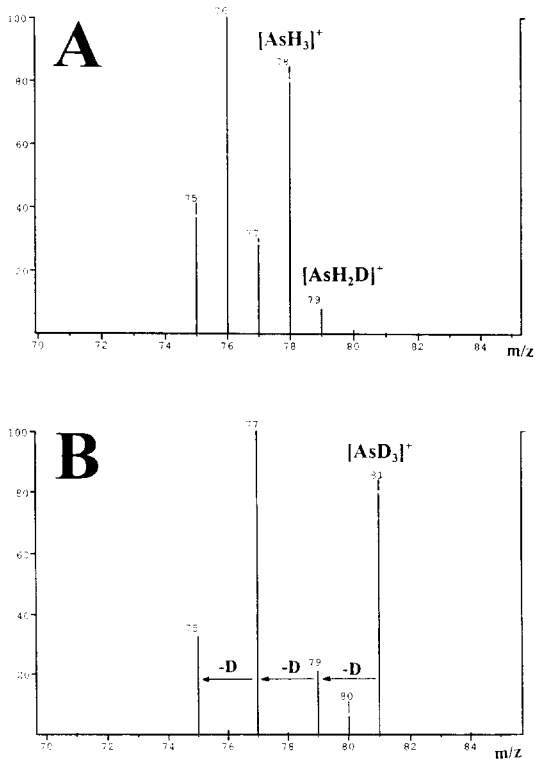

Fig. 1. A: mass spectrum of arsine generated from arsenite, DCl, and $NaBH_4$ in D_2O, B: mass spectrum of arsine generated from arsenite, HCl and $NaBD_4$ in H_2O.

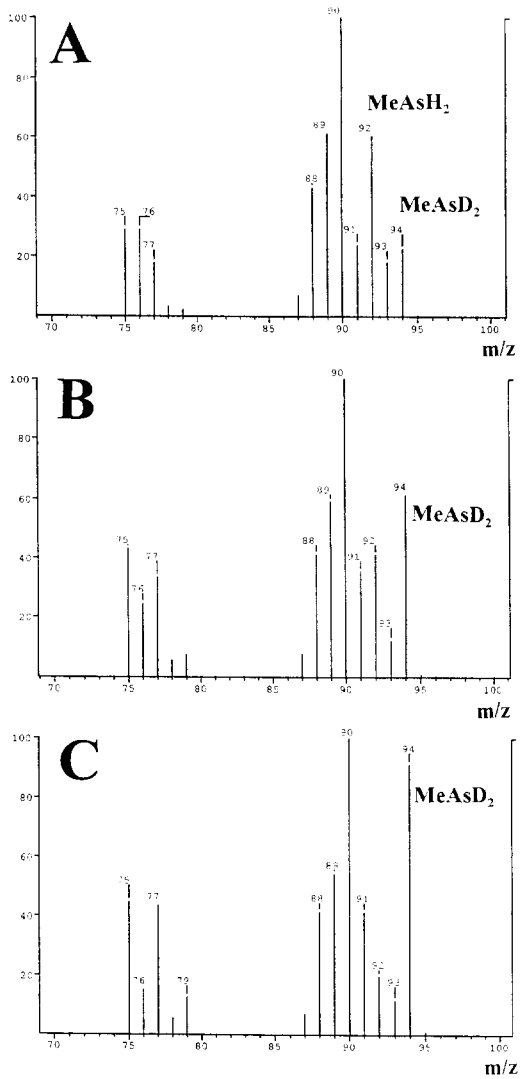

Fig. 2. Mass spectrum of methylarsine generated from methylarsonic acid, DCl, and $NaBH_4$ in D_2O, after reacting for; A: 0.5 min, B: 7 min and C: 14 min.

after 7 min is presented in Fig. 2b, and the mass spectrum after 14 min is shown in Fig. 2c. This time-series study clearly demonstrates the formation of $MeAsD_2$ (m/z 94) and the disappearance of $MeAsH_2$ (m/z 92) over time. The sample injected after 22 min did not produce a mass spectrum that matched those obtained for methylarsine. This may be due to extensive decomposition or adsorption of the methylarsine gas in the reaction vial.

Further evidence for the presence of the mixture of deuterated and non-deuterated methylarsines was extracted from the mass spectrum of $MeAsH_2$ generated from HCl and $NaBH_4$ in H_2O (Fig. 3a) and from the mass spectrum of $MeAsD_2$ generated from DCl and $NaBD_4$ in D_2O (Fig. 3b). The combination of these two mass spectra results in a mass spectrum containing ions of similar relative intensity to those shown in Fig. 2b. Similar observations were made when MAA was reacted with HCl and $NaBD_4$ in H_2O; initially $MeAsD_2$ was detected, along with a smaller amount of $MeAsH_2$. The ratio of non-deuterated to deuterated methylarsine increased with time. The gradual conversion of $MeAsH_2$ to $MeAsD_2$, and vice versa, indicates that arsines once generated may further react with acids present in the reaction mixture, thus, allowing for hydrogen-deuterium exchange.

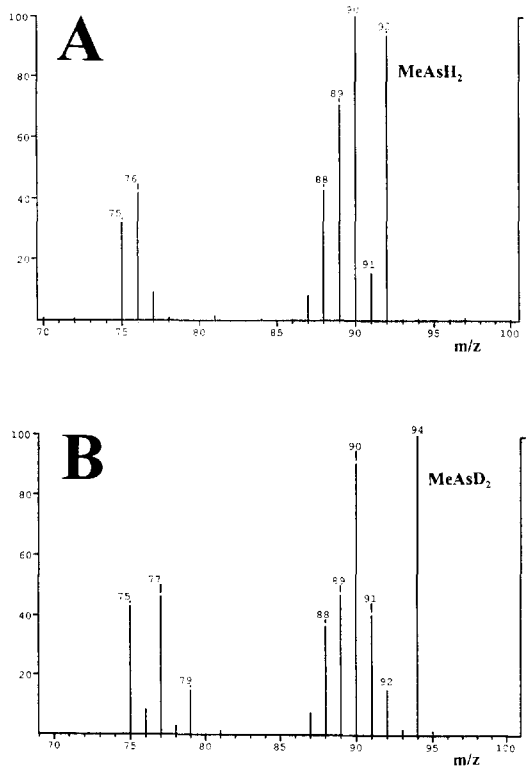

Fig. 3. Mass spectra of monomethylarsines generated from; A: HCl and $NaBH_4$ in H_2O, and B: DCl and $NaBD_4$ in D_2O.

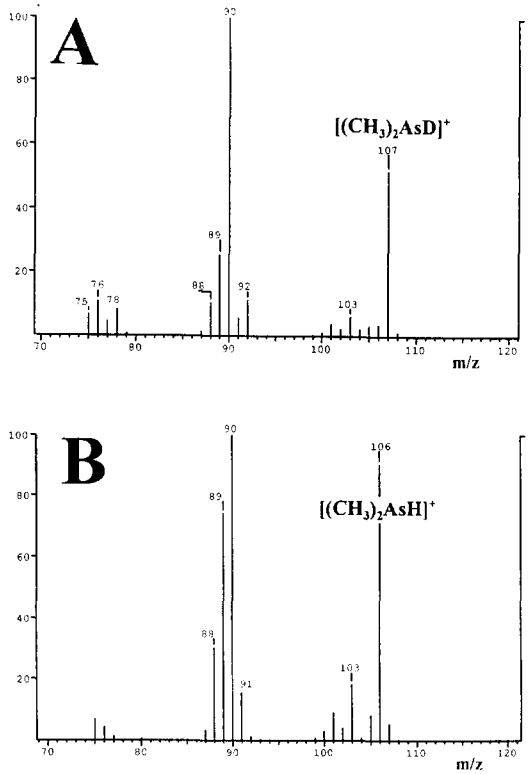

Fig. 4. A: mass spectrum of dimethylarsine generated from dimethylarsinic acid, DCl, and $NaBH_4$ in D_2O, and B: mass spectrum of dimethylarsine generated from methylarsinic acid, HCl, and $NaBD_4$ in H_2O.

When dimethylarsinic acid (DMAA) was reacted with DCl and $NaBH_4$ in D_2O, the resulting dimethylarsine was identified as Me_2AsD (Fig. 4a). When DMAA reacted with HCl and $NaBD_4$ in H_2O the resulting arsine was Me_2AsH (Fig. 4b). The products of these reactions formed rapidly and did not change over time, indicating that any hydrogen-deuterium exchange in these products is rapid. Table 1 contains a summary of the data obtained from these experiments. The reactions in Table 1 are based on data presented in this paper along with the reaction schemes proposed by others [5,22,23].

The relative rates of hydrogen-deuterium exchange for the arsines in these experiments varies in the same order as their basicity ($AsH_3 < MeAsH_2 < Me_2AsH$) [24]. Because Me_2AsH is the most basic of the three arsines, the following

protonation reaction would be expected to be the most favorable:

$$Me_2AsH + H^+ \rightleftarrows Me_2AsH_2^+ \quad (1)$$

To test the hypothesis that this protonation is involved in the observed hydrogen–deuterium exchange, an experiment was conducted in which Me_2AsD was generated in a sealed vial (vial A), and a 800-μl gas sample was then removed from vial A and bubbled through a 250-μl HCl/H_2O solution present in another sealed vial (vial B). A gas sample was immediately removed from vial B and injected onto the GC column. The resulting mass spectrum is presented in Fig. 5a. The molecular ion present at m/z 106 indicates that reaction Eq. (1) takes place rapidly, relative to the time-scale of the experiment. In a similar experiment, Me_2AsD was injected into the headspace of a vial

Table 1
Summary of arsine generating reactions carried out in this study

Arsenic compound	Proposed reactions[a]
$As(OH)_3$	**$As(OH)_3$ (aq) + BH_4^- (aq) + D^+ (aq) + D_2O** → $\underline{AsH_3\ (g)}$ + H_3BO_3/D_3BO_3 (aq) + H_2/D_2 (g)
$As(OH)_3$	**$As(OH)_3$ (aq) + BD_4^- (aq) + H^+ (aq) + H_2O** → $\underline{AsD_3\ (g)}$ + H_3BO_3/D_3BO_3 (aq) + H_2/D_2 (g)
H_3AsO_4	**H_3AsO_4 (aq) + BH_4^- (aq) + D^+ (aq) + D_2O** → $\underline{AsH_3\ (g)}$ + H_3BO_3/D_3BO_3 (aq) + H_2/D_2 (g)
H_3AsO_4	**H_3AsO_4 (aq) + BD_4^- (aq) + H^+ (aq) + H_2O** → $\underline{AsD_3\ (g)}$ + H_3BO_3/D_3BO_3 (aq) + H_2/D_2 (g)
$CH_3AsO(OH)_2$	**$CH_3AsO(OH)_2$ (aq) + BH_4^- (aq) + D^+ (aq) + D_2O** → $\underline{CH_3AsD_2(g)/CH_3AsH_2\ (g)}$ + H_3BO_3/D_3BO_3 (aq) + H_2/D_2 (g)
$CH_3AsO(OH)_2$	**$CH_3AsO(OH)_2$ (aq) + BD_4^- (aq) + H^+ (aq) + H_2O** → $\underline{CH_3AsD_2(g)/CH_3AsH_2\ (g)}$ + H_3BO_3/D_3BO_3 (aq) + H_2/D_2 (g)
$(CH_3)_2AsO(OH)$	**$(CH_3)_2AsO(OH)$ (aq) + BH_4^- (aq) + D^+ (aq) + D_2O** → $\underline{(CH_3)_2AsD\ (g)}$ + H_3BO_3/D_3BO_3 (aq) + H_2/D_2 (g)
$(CH_3)_2AsO(OH)$	**$(CH_3)_2AsO(OH)$ (aq) + BD_4^- (aq) + H^+ (aq) + H_2O** → $\underline{(CH_3)_2AsH\ (g)}$ + H_3BO_3/D_3BO_3 (aq) + H_2/D_2 (g)

[a] Boldface indicates reagents, underline indicates products identified by using mass spectrometry.

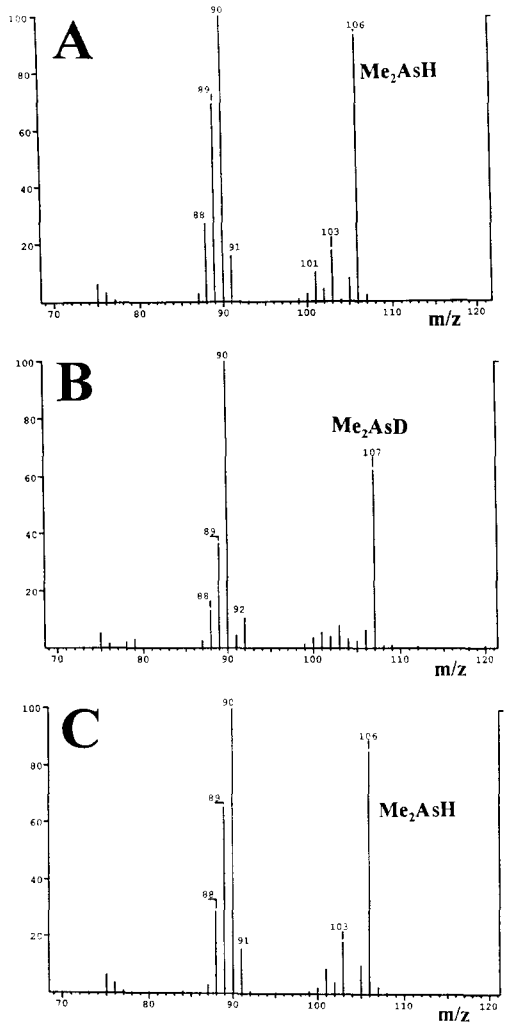

Fig. 5. Mass spectrum of gaseous products formed after bubbling; A: Me_2AsD through a HCl/H_2O solution, B: Me_2AsH through a DCl/D_2O solution, and C: Me_2AsH through a D_2O solution.

containing HCl/H_2O, rather than being bubbled through the solution. The mass spectrum obtained was identical to the one shown in Fig. 5a, thus, indicating that reaction Eq. (1) occurs even though the arsine is not bubbled through an acid containing solution. An additional series of experiments was conducted with Me_2AsH bubbled through a D_2O/DCl solution. As expected, the molecular ion appeared at m/z 107 (Fig. 5b). To further understand the acid effect on dimethy-

larsine, an experiment was conducted in which the Me_2AsH was bubbled through D_2O, in the absence of DCl. The resulting mass spectrum (Fig. 5c) did not show evidence of reaction Eq. (1) taking place because of the molecular ion present at m/z 106, not 107. These results clearly demonstrate that the protonation of dimethylarsine occurs only under acidic conditions. Also, to check if hydrogen-deuterium exchange occurs in the gas phase, a 250 μl sample of HCl/H_2O vapor was withdrawn, by using of a 500 μl gas-tight syringe, from a reaction vial containing 200 μl of HCl/H_2O. Subsequently, a 250 μl sample of Me_2AsD was withdrawn into the same syringe along with the HCl/H_2O vapor. A portion of this mixture was then analyzed by using GC/MS. The mass spectrum of dimethylarsine showed no Me_2AsH. Thus, hydrogen-deuterium exchange appears to occur only in the aqueous phase, further supporting exchange through reaction Eq. (1).

Reaction Eq. (1) can thus explain the formation of Me_2AsD when generated from DCl and $NaBH_4$, and the formation of Me_2AsH when generated from HCl and $NaBD_4$. Protonation of $MeAsH_2$ similar to that of Me_2AsH in reaction Eq. (1) would be expected to be less favored, due to the lower basicity of $MeAsH_2$. This hypothesis is supported by the more gradual hydrogen–deuterium exchange indicated by the mass spectra shown in Fig. 2. Apparently, protonation of AsH_3 does not occur to any appreciable degree. These conclusions can be further supported by the results obtained from the following experiment. A mixture of arsines (AsH_3, $MeAsH_2$, Me_2AsH) was generated in one vial, a sample of which was immediately injected onto the GC/MS. Subsequently, a 1 ml gas sample was removed from the vial and then injected into the headspace of a second vial containing 200 μl of HCl/H_2O. After 4 min, a gas sample was removed from the second vial and injected onto the GC/MS. The purpose of this experiment was to investigate any loss of arsines as a result of their dissolution in the HCl/H_2O solution. To a first approximation, if the protonation of the arsines varies in the order $Me_2AsH > MeAsH_2 > AsH_3$, then the solubility of the arsines in the aqueous acid should vary the same way. The results obtained from this experiment indicated a greater loss of Me_2AsH compared with $MeAsH_2$ and AsH_3. This was clearly observed when comparing the relative amounts of the arsines detected in the two chromatograms (Fig. 6) obtained from the arsine samples taken from the first and second vial. This experiment was conducted in triplicate, and a control was carried out in which the second vial only contained 200 μl of H_2O. The control experiment demonstrated that the arsine solubility variations observed in HCl/H_2O do not occur in H_2O.

Hinners [18] emphasized the critical effect of acid concentration on the hydride-generation responses from arsenite, arsenate, MAA, and DMAA. He was unable to find a compromise acid concentration at which the same response could be obtained for the four arsenic species. For HCl concentrations of 4–10 M, DMAA gave only 15% or less of the signal that was obtained from the same amount of arsenite. Other studies have clearly indicated that when using 5 M hydrochlo-

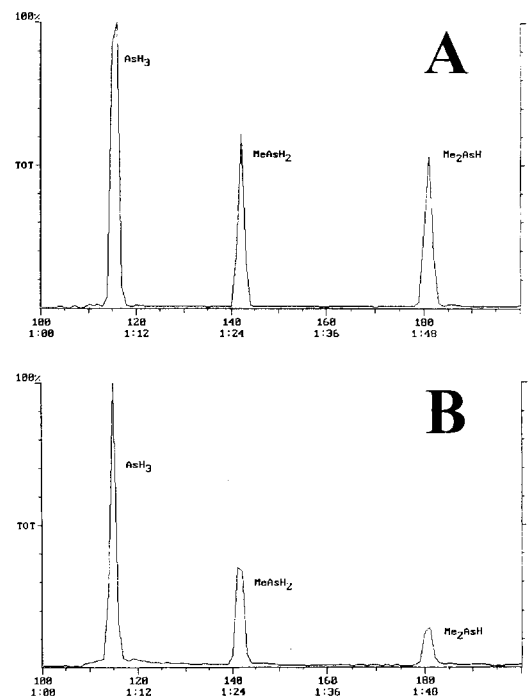

Fig. 6. GC/MS chromatograms of an arsine mixture; taken before (A) and after (B) injection of the arsine mixture into the headspace of a vial containing an HCl/H_2O solution.

ric acid, DMAA is underestimated [19]. A number of studies have demonstrated that each arsenic species has a different acid concentration for optimal efficiencies of hydride generation [14,19–21]. The results presented in this paper indicate that generated Me_2AsH further reacts with hydrochloric acid, producing a water-soluble dimethylarsonium species in equilibrium with gaseous dimethylarsine. This observation could help explain why the efficiency of generating Me_2AsH is reduced compared with the efficiency obtained when generating other, less basic, arsines.

Le et al. [7] demonstrated that by using 2% cysteine and 0.3–0.7 M HCl, maximum and identical results are obtained from all four arsenic species. It was proposed that arsenate, MAA, and DMAA, all in the As(V) state, are reduced to the As(III) state as organo-sulfur-arsenic(III) compounds through reaction between the arsenic species and thiol. These products, organosulfur derivatives of As(III), easily react with tetrahydroborate(III) under similar conditions to afford the arsines without interference from cysteine. It is our intention to further study the proposed mechanism of action of cysteine on hydride-generation of arsines, by using deuterium labeled reagents and mass spectrometric techniques.

4. Conclusion

In this study we have investigated differences governing the process of arsine generation for various arsenic compounds. The results obtained indicate that Me_2AsH reacts with hydrochloric acid forming water-soluble arsonium species. This is also expected to occur to some extent with $MeAsH_2$. However, this is not the case when arsines are generated from arsenite and arsenate. Furthermore, it was demonstrated that mass spectrometry can be a useful tool for investigating the mechanisms responsible for hydride generation.

Acknowledgements

The U.S. Environmental Protection Agency (EPA), through its Office of Research and Development (ORD), funded and collaborated in the research described here. It has been subjected to the Agency's peer review and has been approved as an EPA publication. The U.S. Government has a non-exclusive, royalty-free license in and to any copyright covering this article. Mention of trade names or commercial products does not constitute endorsement or recommendation of use. This work was performed while S.A. Pergantis and W. Winnik held National Research Council/CRD-LV Research Associateships.

References

[1] F.J. Schmidt and J.L. Royer, Anal. Lett., 6 (1973) 17.
[2] E.N. Pollock and S.J. West, At. Absorpt. Newsl., 12 (1973) 6.
[3] F.J. Fernandez, At. Absorpt. Newsl., 12 (1973) 93.
[4] K.C. Thompson and D.R. Thomerson, Analyst, 99 (1974) 595.
[5] J.W. Hershey and P.N. Keliher, Appl. Spectrosc. Rev., 25 (1990) 213.
[6] J.W. Jones, S.G. Capar and T.C. O'Haver, Analyst, 107 (1982) 353.
[7] X.-C. Le, W.R. Cullen and K.J. Reimer, Anal. Chim. Acta, 285 (1994) 277.
[8] M.L. Cervera, J.C. Lopez and R. Montoro, Microchem. J., 49 (1994) 20.
[9] H. Narasaki and M. Ikeda, Anal. Chem., 56 (1984) 2059.
[10] R.E. Sturgeon, S.N. Willie and S.S. Berman, J. Anal. At. Spectrom., 1 (1986) 115.
[11] W.R. Cullen, H. Li, S.A. Pergantis, G.K. Eigendorf and L.G. Harrison, Chemosphere, 28 (1994) 1009.
[12] M.O. Andreae, Anal. Chem., 49 (1977) 820.
[13] K.J. Reimer, Appl. Organomet. Chem., 3 (1989) 475.
[14] X.-C. Le, W.R. Cullen, K.J. Reimer and I.D. Brindle, Anal. Chim. Acta, 258 (1992) 307.
[15] X.-C. Le, W.R. Cullen and K.J. Reimer, Talanta, 40 (1993) 185.
[16] P. Barth, V. Krivan and R. Hausbeck, Anal. Chim. Acta, 263 (1992) 111.
[17] F.D. Pierce and H.R. Brown, Anal. Chem., 49 (1977) 1417.
[18] T.A. Hinners, Analyst, 105 (1980) 751.
[19] M.H. Arbab-Zavar and A.G. Howard, Analyst, 105 (1980) 744.
[20] F.D. Pierce, H.R. Lamoreaux, H.R. Brown and R.S. Fraser, Appl. Spectrosc., 30 (1976) 38.
[21] P. Seyler and J.M. Martin, Mar. Chem., 29 (1990) 277.
[22] W.B. Robbins and J.A. Caruso, Anal. Chem., 51 (1979) 889A.
[23] P.D. Wentzell, N.G. Sundin and C. Hogeboom, Analyst, 119 (1994) 1403.
[24] W.R. Cullen and D.C. Frost, Can. J. Chem., 40 (1962) 390.

ELSEVIER

Talanta 44 (1997) 1949–1958

Talanta

Spectrophotometric determination of trace water in organic solvents with a near infrared absorbing dye

Mingshu Li, Gilbert E. Pacey

Chemistry Department, Miami University, Oxford, OH 45056, USA

Received 26 April 1996; received in revised form 23 September 1996; accepted 23 September 1996

Abstract

A spectrophotometric method for the determination of trace water in organic solvents using a near infrared absorbing dye has been developed. This method is based on the effect that a minor change in polarity of the solvent caused by trace water content determines the extent of aggregation of a near-infrared dye monomer. This change can be detected spectrophotometrically. The calibration curves for methanol, ethanol, and isopropanol were determined. This method has the highest sensitivity (em = 16.73 unit) for water in isopropanol and the lowest sensitivity (em = 2.806 unit) for water in methanol. The correlation coefficient $(R)^2$ values for the regression lines ranges from 0.990–0.998. The linear range of the method for ethanol is 0.001–0.5%, for isopropanol is 0.001–0.1%, and for methanol is 0.001–1.0%. The limit of detection for ethanol, isopropanol, and methanol are 0.0001, 0.0001, and 0.005% water, respectively. The developed method is sensitive, simple and easy to operate, and the cost of analysis is low. © 1997 Elsevier Science B.V.

Keywords: Infrared absorbing dye; Organic solvents; Trace water

1. Introduction

The determination of water in organic solvents has been of interest to chemists for many years [1]. The majority of water determinations in organic solvents are performed by the Karl Fisher titration [2]. The Karl Fisher titration method requires special equipment and expertise to obtain good accuracy and precision [3]. The method exhibits interferences from oxidizing agents, unsaturated compounds, and sulfur compounds [4–6]. The Karl Fisher titration method is not considered a low level method [7]. In addition, there are safety concerns about the highly toxic reagent. Recent refinements in the Karl Fisher method have concentrated on improving accuracy and extension to other solvent systems [2,4,6,8]. The Karl fisher method has been automated using flow-injection analysis [9] where improved precision and accuracy were observed, but the detection limit was a disappointing 0.03%.

Other methods that are used include thermal conductivity detection gas chromatography [10]; electrochemical sensors based on thin-film perfluorosulfonate ionomer (PFSI) coated with cellulose triacetate; polyvinyl alcohol (PVA)-H_3PO_4; or PVA-PFSI-H_3PO_4 composite films operated in a pulsed voltammetric mode [1]; an organic phase

PII S0039-9140(96)02111-X

enzyme electrode [11] where the enzyme activity has been shown to be strongly dependent upon the water content; an FIA-spectroscopic method [12] based on the reaction between group IV and V metal halides and water; HPLC methods where the water peak was detected by either electric conductivity [5] or optical absorption [13]; Solvatochromic effect [3,14,15]; and a spectrofluorimetric method [7] based on formation of the exciplex of pyridoxal. More recently, FIA-NIR spectrophotometry [16] was used for the direct determination of water in organic solvents by using the O–H stretch absorbance bands. In most of these methods either the detection limits were too high or the method did not work in highly polar solvents.

During investigations of near infrared dyes in this laboratory, it was observed that these dyes appeared to be unstable in alcohol solvents at room temperature. However, this instability was not observed in extremely dry alcohols. Upon further investigation, it was discovered that the dye dimerized or polymerized in the alcohol solutions. The extent of polymerization depends on the solvent polarity, temperature, and the basicity. Trace amount of water in the solvent alters the polarity of the solvent and that the polymerization reaction was directly proportional to the water concentration in the alcohol. This paper discusses a new near infrared dye, spectrophotometric method for the determination of low level water in polar organic solvents.

2. Experimental

2.1. Chemicals

Methanol was purchased from Fisher Scientific (acetone free, absolute methanol with water concentration of 0.02%). This methanol was further purified as suggested by Lund and Bjerrum [17]. A 200 ml volume of methanol reacted with 24 g of magnesium turnings for 6 h (reaction is vigorous under heating). A 3 l amount of methanol was added and the mixture was refluxed for 5 h and then the methanol was distilled into 500 ml glass bottles containing 5 g of molecular sieves. The first 50 ml of collected methanol was discarded. This procedure produced about 2 l of dry methanol. Ethanol was obtained from Quantum Chemical Corporation (200 proof dehydrated alcohol with water concentration of 0.02%) and was further purified with the same method as used for methanol. Isopropanol was purchased from fisher Scientific (suitable for electronic use, water concentration was 0.04%) and was dried with molecular sieves for 2 weeks.

2.2. Synthesis of the near infrared dye

The near infrared dye, 2-[4′-chloro-7-(3″-ethyl-2″-benzothiazothiazolinylidene)-3′,5′-(1″,3″-propanediyl) - 1′3′5′ - heptatrien - 1′ - yl] - 3 - ethylbenzothiazolium iodide as shown in Fig. 1, was prepared as the bromide analog [18]: ethyl iodide and 2-methylbenzothiazole were refluxed in dimethlyformamide at 153°C overnight. The mixture was refrigerated for 2 h and then slowly added diethyl ether to initiate crystallization of the product. The crystals were filtered, washed with diethyl ether, and dried under reduced pressure. The dried product, 3-ethyl-2-methyl-benzothiazolium iodide, was refluxed with *N*-[(3-(anilinomethylene)-2-chloro-1-cyclohene-1-yl)-methylene]analene momohydrochloride in ethanol under the presence of anhydrous sodium hydrochloride for 1 h and kept in a refrigerator for 1 h. The crystals were filtered off, washed with distilled water, benzene, and ether and dried under a vacuum. The product was recrystallized in ethanol and dried under a vacuum at 50°C for 6 h. The nuclear magnetic resonance spectrometry (NMR) and matrix assisted laser desorption ionization mass spectrometry (MALDI-MS) spectra were presented in Fig. 2 and Fig. 3.

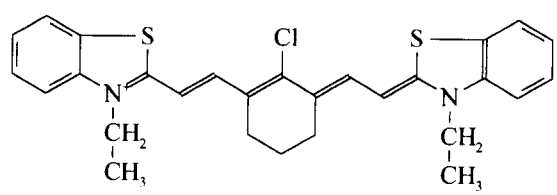

Fig. 1. Structure of dye 1.

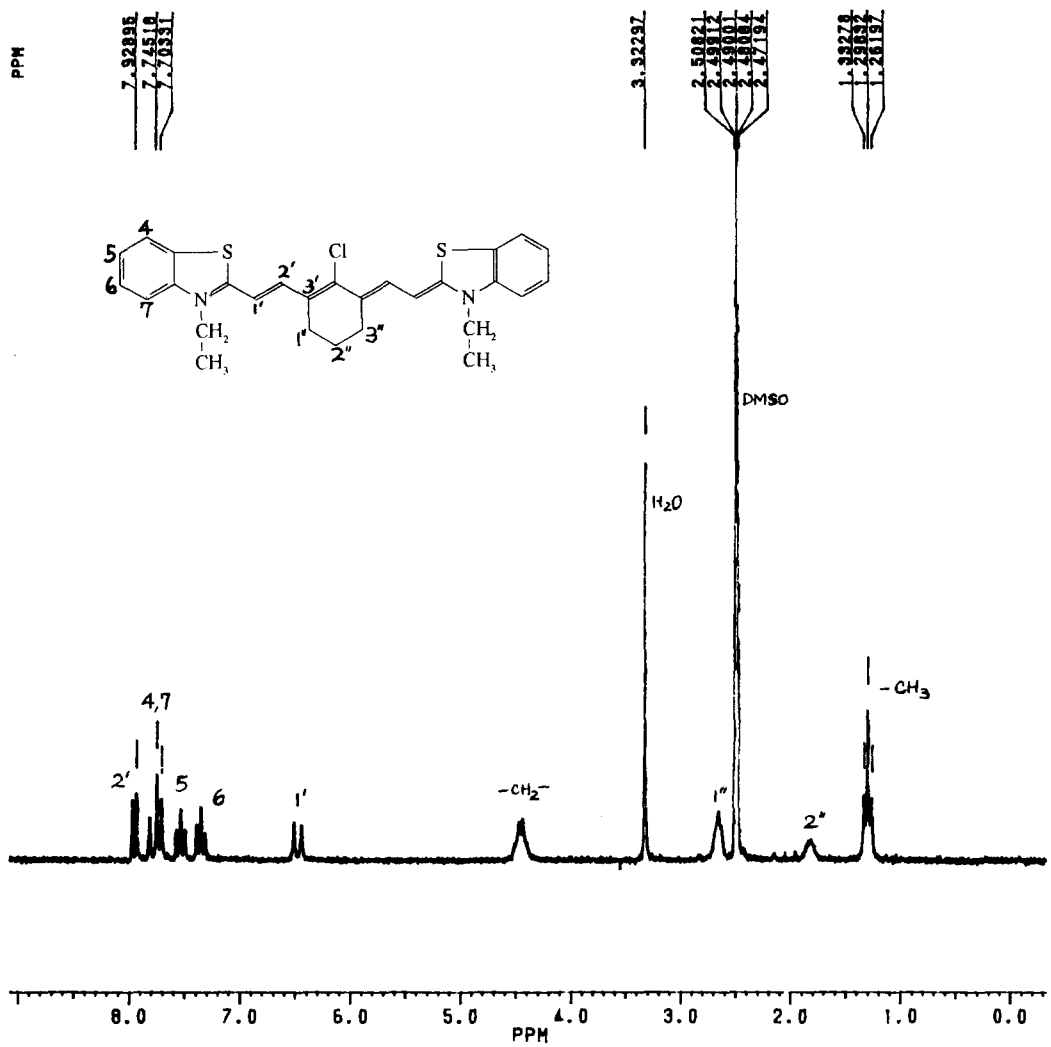

Fig. 2. NMR spectrum of dye 1. 200 MHZ NMR, DMSO as solvent.

2.3. Safety consideration

Methanol, ethanol, and isopropanol are highly flammable and toxic by inhalation, in contact with skin, and swallowed. Chloroform is volatile at room temperature and is highly toxic cancer suspect agent.

2.4. Apparatus

A Hewlett Packard 8452A Diode Array Spectrophotometer was used to scan the spectra and absorbance measurements. Tekmar utility bath was used for heating and temperature control. All glassware was cleaned with detergent, rinsed with distilled water, rinsed with acetone, dried in the oven at 100°C for 1 h and cooled in a dedicator before use. MALDI-MS spectra were obtained with the Bruker Reflex II TOF-MS mass spectrometer equipped with a Nd:YAG laser model Minilase-10. NMR spectra were acquired with Bruker AC-200 MHZ NMR spectrometer.

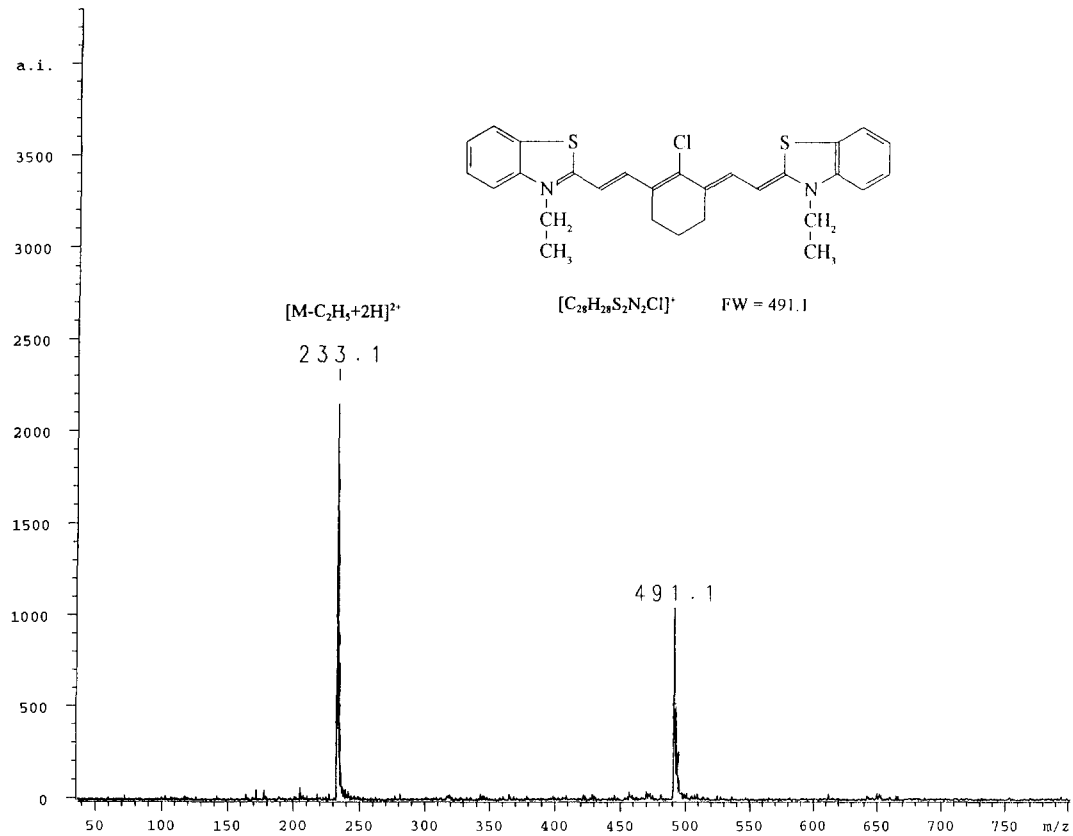

Fig. 3. MALDI-MS spectrum of dye 1. Nd:YAG laser (355 nm), matrix was α-cyano-4-hydroxy cinnamic acid, and CH_3CN as the solvent. Number of shots was 40.

2.5. Reagents

1.125×10^{-3} M dye solution was made in methanol–chloroform (50:50) solution and was kept in the refrigerator. Upon storage, aggregates of the dye were formed and the solution was no longer useful for the analysis. The solution can be dept up to 2 months in a refrigerator and 1 week at room temperature. A 1.0×10^{-3} M potassium hydroxide solution was prepared as follows: dissolve a certain amount of potassium hydroxide in dried ethanol, filter the solution, and dilute to the volume with ethanol. The standard stock solution of 1% water was made with dried solvents and deionized water.

2.6. Procedure

A 10 ml volumetric flask was filled about half full with the sample solution, add 0.2 ml of KOH solution and 0.2 ml of dye solution, and then dilute with the sample to the volume and mix well. The solution mixture was placed into a hot water bath with the cap on at 60–70°C for 10 min and cooled at room temperature for 15 min. The reduction of absorbance was measured at about 800 nm depending on the solvents. The water concentration in the solvents was derived from the calibration curve. The calibration curve was obtained by measuring the absorbance of 0, 50, 100, 200, 300, and 500 ppm (v/v) standard solutions.

These standard solutions were prepared in 10 ml volumetric flasks adding 0, 0.05, 0.10, 0.20, 0.30 and 0.50 ml water working solution (10 000 ppm) and following the same procedure of sample analysis described above.

3. Results and discussion

Near-infrared dyes absorb light between 600–1200 nm and exhibit large molar absorptivities ($\approx 200\,000$ Abs cm^{-1} M^{-1}), thereby enhancing their potential for low level detection. In addition, most NIR dyes are strongly fluorescent in solution [18–20]. When NIR dyes are used for analytical applications, detection can be carried out in the longer wavelength regions creating a reduced background and interferences from coexisting species. Despite these attributes and the large number of NIR dyes available, the use of NIR dyes has not gained much attention in analytical applications. Dye I has been used as a hydrophobicity probe for aliphatic alcohols and other water-miscible organic solvents [18] with water/organic solvent ratio ranged from 50–100 (pure water). This dye has a molar absorptivity of 1.83×10^5 [18] and absorbance maximum wavelength of 800 nm in ethanol. Absorption spectra of the dye changed significantly depending on the solvent hydrophobicity. With higher concentration (over 50%) methanol, the maximum absorption band of the dye solution was at 811 nm. When the methanol concentration was decreased from 50% to 0 (pure water), the absorption peak at 811 nm disappeared and a new peak at 698 nm appeared. It was suggested that the observed change in the NIR absorption spectra is a result of dye dimerization [18].

It is known that aqueous NIR dye solutions, especially at higher dye concentrations, exhibit an absorption band different from the absorption band that can be observed in less concentrated solutions or in less polar organic solvents. These spectral changes have long been attributed to dye molecule aggregation. The NIR dyes also display this type of behavior in water, where they tend to form dimmers ($\lambda = 698$ nm) or higher aggregates ($\lambda = 450 - 500$ nm) because of the strong dispersion forces associated with the high polarizability of the polymethane chain [21]. Experimental results in this lab revealed that dimerization conditions for the cyanine dyes depend on the following factors: dye concentration, water concentration, temperature, reaction time, exposer to light, and the basicity of the solution. The dependence of the dimer formation on the dye concentration and water content in the solution has been proven by West and Pearce [21] and Patonay et al. [18]. Dimmers usually do not form in pure organic solvents. The dimmersband and the higher-aggregate band were observed at 698 and 450 nm, respectively, in 1×10^{-5} M aqueous solutions. Fig. 4 presents the spectra obtained in this lab for the dye in 60% water/ethanol solution with increasing basicity and reaction time. Five peaks are observable in the wavelength range of 320–820 nm. The peak at 800 nm is the dye monomer, 692 nm is the dimer peak, and the rest are the peaks for higher aggregates of the dye. As the solution basicity increased, the 656 nm and 380 nm aggregate peaks were decreased and the 496 nm peak increased, the 692 nm dimer peak initially persisted and then started to decrease when the 656 nm peak disappeared. As the 656, 698, 380 nm aggregate peaks decreased, the 800 nm monomer peak increased until the dimer peak became a shoulder of the monomer peak and then decreased with increasing basicity.

These changes in the spectra indicate that dimers form in neutral solutions at high concentrations of water in aliphatic alcohols. When a small amount of base is added, the polymer at 656 nm and the dimer decompose to their monomer. When the basicity is further increased, polymerization to higher aggregates happens. Using the optimized conditions for the method, the 656 and 698 nm peaks did not exist (Fig. 5), instead, higher aggregates represented by the peak at 496 nm were formed.

There are at least three isosebestical points at 575, 405 and 363 nm. These points indicate that there are three equilibrium systems in the solution. In the solution without added basicity (spectrum 1 in Fig. 4(a)), dimers and the aggregates at 656 nm were formed and there is equilibrium between the aggregate of 656 nm and the monomer. With increasing basicity (spectra 2–5 in Fig. 4(a)), the dye is distributed between the dimers and the aggregates at 496 nm. When the

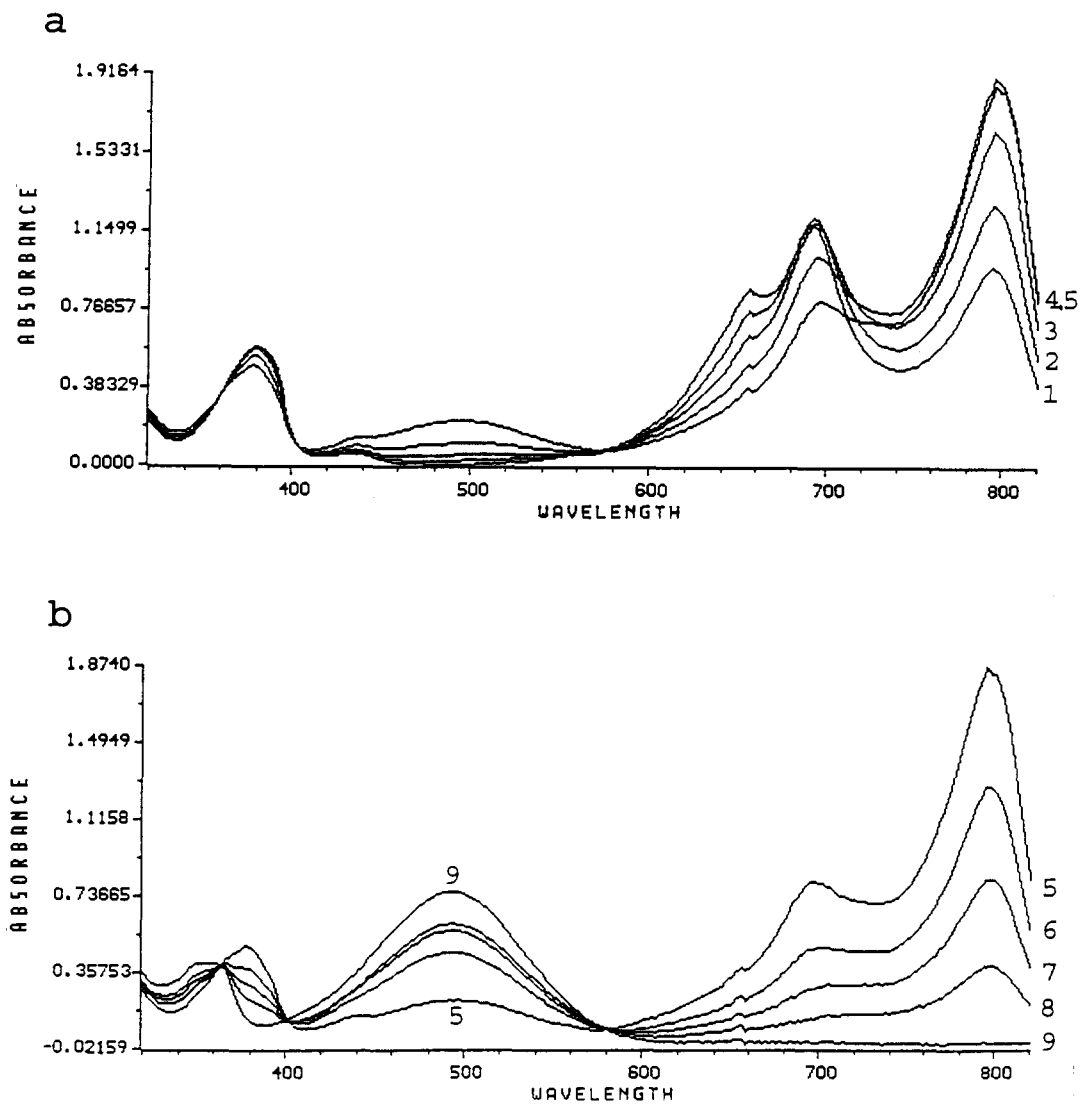

Fig. 4. Absorption spectra of the dye in 60% water/ethanol solution: (a) with different KOH concentration: 1-neutral solution; 2–2.8 × 10^{-4} M; 3–8.4 × 10^{-4} M; 4–1.4 × 10^{-3} M; 5–2.8 × 10^{-3} M; (b) under different reaction time: 5–5 min; 6–10 min; 7–20 min; 8–35 min. Spectrum 9 was obtained after heating the solution of 2.8 × 10^{-3} M in KOH 10 min at 70°C.

basicity of the solution was further increased or the basic solution sat for long time (spectra 6–8 in Fig. 4(b)), the equilibrium shifted toward the monomer and the polymer at 496 nm. The polymerization rate of the monomer to the aggregate at 496 nm is slow. It took 30 min to convert spectrum 5–8 in Fig. 4(b) at room temperature. But when the solution was heated for 10 min at 70°C, the conversion was completed almost immediately (spectrum 9 in Fig. 4(b)).

When the system was going through higher-aggregation and a reduction of the monomer peak was observed, the sensitivity was higher than the dimerized system. This was one of the reasons that the determination of trace amount of water in organic solvents is possible in this method. Representative absorption spectra of the dye in dry ethanol (spectrum 1) and in 0.05% water in ethanol solution (spectrum 2) are presented in Fig. 5. The peak reduction at 800 nm was used for

the quantitative analysis of trace water concentrations in organic solvents.

As it was mentioned earlier, besides the dye concentration and water content in the system, basicity of the solution is an important factor for the process being dimerization or higher-aggregate formation. It can be seen in Fig. 4(a) that dimers were formed in neutral ethanol solutions and with increasing basicity the dimer peaks would disappear. When the solution was basic and heated at a certain temperature for a period of time, even a little change in polarity by trace amounts of water in the solvent caused aggregation of the dye in the solution. The extent of aggregation was proportional to the water concentration in the solvent. Both monomer and *H*-aggregate peaks can be used for the measurement, but he monomer peak at 800 nm is the most sensitive.

Basicity of the solution was adjusted by adding different amount of KOH/ethanol solution. Reagent grade KOH was kept in a desiccator and the carbonate impurities were insoluble in alcohols and were removed by filtration. The result of the basicity experiment is shown in Fig. 6. With increasing KOH concentration from $0–8.0 \times 10^{-4}$ M, the net absorbance of 0.05% water/ethanol solution increased, reaching a maximum at 4×10^{-4} M of KOH. Therefore, the KOH concentration of 4×10^{-4} M was chosen.

It was pointed out [18] that formation of *H*-aggregates of the dye was observable in 1×10^{-4} M aqueous solution. If the concentration is lower

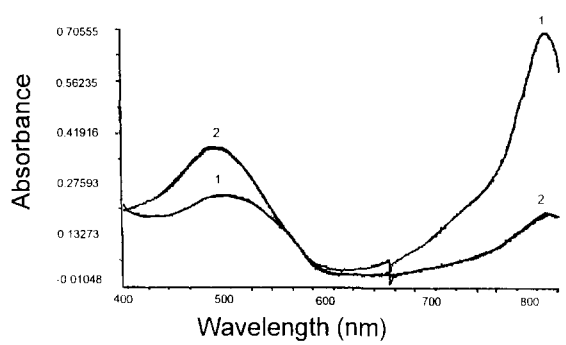

Fig. 5. Absorption spectra of the dye in dry ethanol [1] and in 0.05% water/ethanol solution [2].

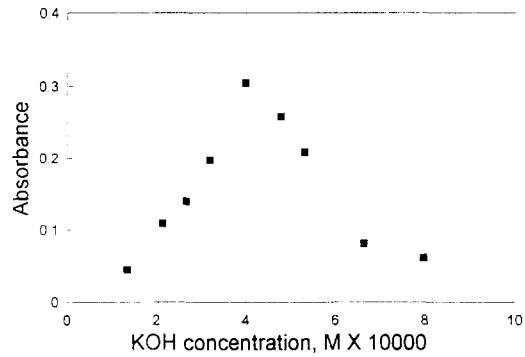

Fig. 6. Effect of KOH concentration on the absorbance of the dye in water/ethanol solution.

than 1.25×10^{-5} M, then the higher aggregate band diminished. In the range of dye concentration tested, no dimer peaks were seen. When the dye concentration increased from $0–1.3 \times 10^{-4}$ M, the absorbance for both blank and 0.2% water/ethanol solutions increased (Fig. 7(a)) and reached the maximum absorbance. The rates of absorbance increases were different. Blank absorbance was increasing faster than the water solution. The absorbance difference between blank and water solution was biggest at the dye concentration of 6.8×10^{-5} (Fig. 7(b)). Since at this concentration the absorbance of dry solvent was about three absorbance unit, accurate absorbance measurement is questionable. Therefore, a dye concentration of 4.5×10^{-5} M was selected.

Heating prevented dimer formation and catalyzed the higher aggregation process. Heating was also the main factor for the dye responding to trace water concentration. At room temperature, the lowest water concentration measurable was 1% in ethanol after 45 min. When the solution was heated, there were some changes in the spectral properties of the dye (Fig. 8). Both in dry ethanol and 0.05% water/ethanol solution, the peak at 800 nm shifted to 816 nm and the peak at 460 nm move to 495 nm when the temperature increased from 43.2–62.3°C. The peak reduction at 800 nm was much bigger in the water/ethanol solution than in dry ethanol. When the temperature of the solution was increased, the absorbance for both blank and 0.05% water/ethanol solution decreased (Fig. 9). After about 50°C, the blank

absorbance persisted and remained constant up to 85°C. The absorbance of 0.05% water solution was further decreased and kept constant between 60–85°C. The maximum absorbance difference occurred between 60–70°C. Therefore, heating at 60–70°C was utilized. The aggregation reaction under elevated temperature was a reversible process. Heating provided the energy for shifting the reaction equilibrium toward the formation of the aggregates. When the solution was cooled at room temperature, absorption peak of the monomer increased with decreasing temperature and was stable after 15 min at room temperature.

Formation of the aggregates at 496 nm from their monomers was a relatively slow process.

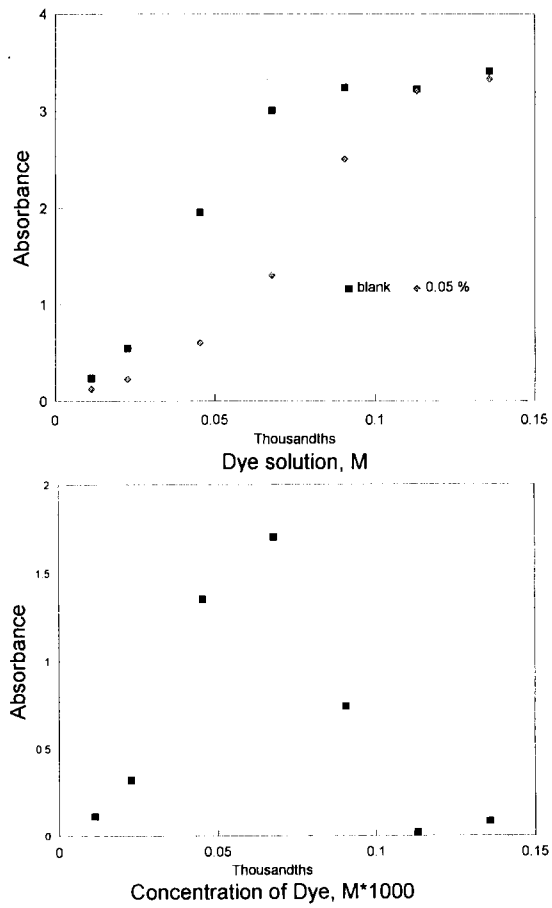

Fig. 7. Effect of the dye concentration. (a) Absorbance of the dye in dry ethanol and 0.05% water/ethanol solution. (b) Net absorbance of the 0.05% water solution.

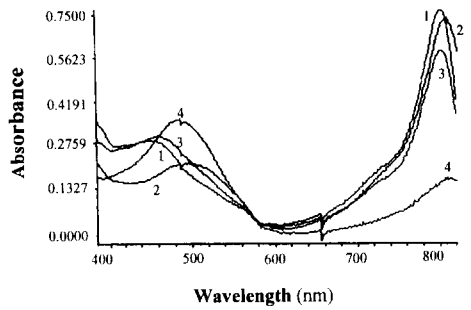

Fig. 8. Absorbance spectra of the dye at different temperature and water contents. Spectra 1 and 2 are for dye in dry ethanol at 43.2 and 62.3°C, respectively. Spectra 3 and 4 are for the dye in 0.05% water in ethanol solution at 43.2 and 62.3°C, respectively.

After 30 min at room temperature, the conversion process was still active (Fig. 4(b), spectrum 8). At higher temperature, aggregate formation immediately complete in higher concentration of water/ethanol solution. When water concentration is very low (0.1–0.001%), heating was needed to catalyze the aggregation process. Fig. 9 is the result of the experiment to determine the reaction time needed at 70°C. With increasing heating time from 0–30 min, the absorbance of the blank solution was decreased at almost a constant rate. But 0.05% water solution exhibited rapid reduction in absorbance between 0–10 min heating at 70°C was utilized, Fig. 10.

Calibration curves (Fig. 11) were obtained under the optimized conditions for methanol,

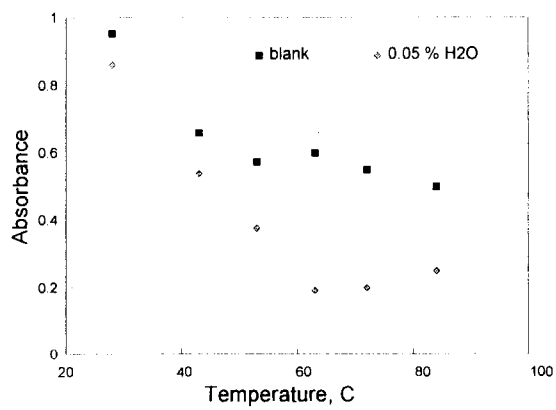

Fig. 9. Temperature effect of the dye in dry ethanol and 0.05% water/ethanol solution.

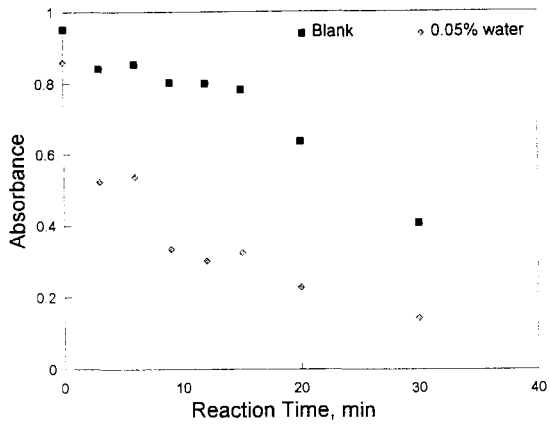

Fig. 10. Effect of heating time on the dye absorbance dry ethanol and 0.05% water/ethanol solution.

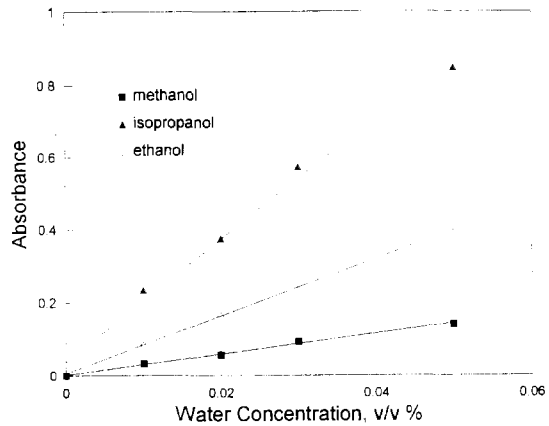

Fig. 11. Calibration curves.

ethanol, and isopropanol and the results of the curves are summarized in Table 1. This method has the highest sensitivity (em = 16.73 unit) for water in isopropanol and the lowest sensitivity (em = 2.806 unit) for water in methanol. The correlation coefficient $(R)^2$ values for the regression lines ranged from 0.990–0.998. The linear range of the method for ethanol is 0.001–0.5%, for isopropanol is 0.001–0.1%, and for methanol is 0.001–1.0%. The limit of detection for ethanol, isopropanol, and methanol are 0.0001, 0.0001 and 0.005% water with relative standard deviations of 2.62, 2.25 and 2.59% at 0.05% water concentration, respectively. The limits of detection depend mostly on the preparation of dry solvents.

4. Conclusions

In this study we demonstrated for the first time that trace amount of water in polar organic solvents can be determined by the fact that a minor change in polarity of the solvent caused by trace water content determines the extent of aggregation of a near-infrared dye monomer, which can be detected easily by measuring the absorbance reduction at 800 nm. By using a NIR dye, the detection was moved to longer wavelength where background interferences were minimized. Sensitivity of the method was very high, owing to the high molar absorptivity of the dye solution and formation of a higher aggregate in the system. The limits of detection were lower than that of most reported methods. The developed method is simple, easy to operate, and the cost of analysis is low. Current work in our laboratory concerns the possibility of applying this method to different organic solvents.

Table 1
Results of calibration curves

Solvent	Equation A = $a+b$ [C]	R^2	Linear range v/v, %	LOD v/v, %
Methanol	$a = 0.002649 \pm 0.004509$ $b = 2.806 \pm 0.117$	0.991	0.001–1.00	0.005
Ethanol	$a = 0.006375 \pm 0.006375$ $b = 7.825 \pm 0.153$	0.998	0.001–0.10	0.001
Isopropanol	$a = 0.03783 \pm 0.03462$ $b = 16.73 \pm 0.82$	0.995	0.001–0.50	0.001

References

[1] T. Mitchell Jr. and D.M. Smith, Aquametry, part III (The Karl Fisher Reagent), A Treatise on Methods for the Determination of Watter, A Wiley-Interscience Publication, Wiley, 1977.

[2] I. Nordin-Andersson and A. Cedergren, Anal. Chem., 57 (1985) 2571–2575.

[3] H. Langhals, Anal. Lett., 23(12) (1990) 2243–2258.

[4] A. Cedergren and C. Oradd, Anal. Chem., 66 (1994) 2010–2016.

[5] T.S. Stevens and K.M. Chritz, Anal. Chem., 59 (1987) 1716–1720.

[6] C. Oradd and A. Cedergren, Anal. Chem., 67 (1995) 999–1004.

[7] Y. Ci and X. Jia, Talanta, 31(7) (1984) 556–558.

[8] C. Oradd and A. Cedergren, Anal. Chem., 66 (1994) 2603–2607.

[9] C. Liang, P. Vacha and W.E. Van Der Linden, Talanta, 35(1) (1988) 59–61.

[10] T. Mitchell Jr. and D.M. Smith, Aquametry, part I, A Treatise on Methods for the Determination of Water, Wiley-Interscience Publication, Wiley, 1977.

[11] J. Wang and A. Reviejo, J. Anal. Chem. 65 (1993) 845–847.

[12] J. Rhee, P.K. Dasgupta and D. Olson, Anal. Chim. Acta, 220 (1989) 55–63.

[13] J.S. Fritz and J. Chen, Am. Lab., July (1991) 24J–24Q.

[14] S. Kumoi, H. Kobayashi and K. Ueno, Talanta, 19 (1972) 505–513.

[15] S. Kumoi, K. Oyama, T. Yano and H. Kobayashi, Talanta, 17 (1970) 319–327.

[16] S. Garrigues, M. Gallignani and M. Guardia, Anal. Chim. Acta, 281 (1993) 259–264.

[17] H. Lund and J. Bjerrum, Ber. Stsch. Chem. Ges., 64 (1931) 210.

[18] G. Patonay, M.D. Antoine, S. Devanathan and L. Strekowski, Appl. Spectro., 45(3) (1991) 457–461.

[19] G. Patony, Advances in near-infrared measurements, I (1993) 113–138.

[20] M. Matsuoka, Infrared Absorbing Dyes, Plenum Press, 1990.

[21] W. West and S. Pearce, J. Phys. Chem., 69(6) 1965 1894–1903.

ELSEVIER

Talanta 44 (1997) 1959–1965

Talanta

Simultaneous determination of mebendazole and pyrantel pamoate from tablets by high performance liquid chromatography–reverse phase (RP-HPLC)

A.P. Argekar *, S.V. Raj, S.U. Kapadia

Analytical Laboratory, Department of Chemistry, The Institute of Science, 15 Madam Cama Road, Mumbai 400 032, India

Received 3 June 1996; received in revised form 19 September 1996; accepted 27 September 1996

Abstract

A new, simple, precise, rapid and stability indicating RP-HPLC method has been developed for the simultaneous determination of mebendazole and pyrantel pamoate from tablets. Chromatography was carried out on a Shodex C8 column using a mixture of 0.05 M monobasic sodium phosphate: acetonitrile: triethylamine (60:40:1.5, v/v), adjusted to pH 6.8 with phosphoric acid. Detection was carried out at 290 nm using a UV detector. Retention times for pamoic acid, pyrantel base and mebendazole were 3.61, 6.41 and 12.81 min, respectively. Linearity was obtained in the concentration range of 20–160 μg and 30–240 μg for pyrantel pamoate and mebendazole, respectively. The method after its application for the assay of pyrantel pamoate and mebendazole from tablets, was statistically evaluated for its accuracy and precision. © 1997 Elsevier Science B.V.

Keywords: High performance liquid chromatography; Mebendazole; Pyrantel pamoate

1. Introduction

Mebendazole (MEB) chemically, methyl 5-benzoyl 1-H-benzimidazol-2-ylcarbamate,is an anthelmintic drug [1]. It is official in I.P. [2], B.P. [3], U.S.P. [4]. Various methods, such as spectrophotometry [5] and HPLC [6,7] are reported in the literature for its determination from formulations and biological fluids.

Pyrantel pamoate (PYP) chemically, 1,4,5,6-tetrahydro-1-methyl-2-[(E)-2-(2-thienyl)vinyl]-pyrimidine 4,4′-methylenebis (3-hydroxy-2-napthoate), is an anthelmintic drug [1]. It is official in U.S.P. [4]. Various methods, such as Ion selective electrode [8] and HPLC [9,10] are reported in the literature for its determination from formulations and biological fluids Fig. 1.

Fixed dose combinations containing MEB and PYP are widely available in the market, however there is no reported method for the simultaneous determination of these two drugs from formulations.

We report in this paper a new RP-HPLC method for the simultaneous determination of MEB and PYP from tablets, which is simple, precise, rapid and stability indicating.

* Corresponding author.

PII S0039-9140(96)02118-2

2. Experimental

2.1. Instrumentation

High pressure liquid chromatograph (HPLC) Tosho CCPE pump equipped with a universal injector and an integrator (Oracle-2) were used.

2.2. Solvents and chemicals

Reference standards of mebendazole and pyrantel pamoate procured from Tata Pharma, Patalganga, Maharashtra, India. These standards were tested as per U.S.P. Monographs, 23, and were found to be 98.93 and 99.07% pure, respectively. Tablet formulations were procured from the market. A.R. Grade diethylamine (DEA), triethylamine (TEA), phosphoric acid, monobasic sodium phosphate were used. Acetonitrile and methanol were of HPLC grade, supplied by S.D. Fine Chemicals, Thane, India.

2.3. Mobile phase

A mixture of 0.05 M monobasic sodium phosphate: acetonitrile: triethylamine (60:40:1.5, v/v), adjusted to pH 6.8 with dilute phosphoric acid was used as a mobile phase.

2.4. Stationary phase

C_8 Shodex column (3.9 mm × 25 cm) (5 μ).

2.5. Diluents

Acetonitrile: diethylamine: acetic acid (90:10:10, v/v).

2.6. Standard stock solution

Accurately weighed 50 mg of standard PYP and 75 mg of standard MEB were taken in a 50 ml volumetric flask. Glacial acetic acid, 15 ml, was added and kept in an ultra sonic bath for 30 min, then it was kept on a boiling water bath for 15 min. The solution was cooled,then 30 ml of diluent was added in a hood and kept in an ultra sonic bath for 10 min. Volume was made upto the mark with the diluent. Standard stock solution, 3 ml, was taken in a 50 ml standard volumetric flask, diluted upto the mark with the mobile phase and used as a working standard.

Pyrantel Pamoate

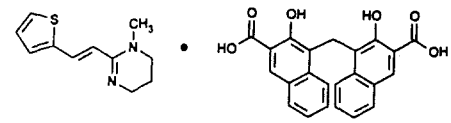

Mebendazole

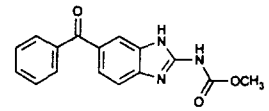

Fig. 1. Structure of pyrantel pamoate and mebendazole.

2.7. Sample solution

Tablets, 20, were weighed and finely powdered. An accurately weighed portion of the powder equivalent to 50 mg of PYP and 75 mg of MEB

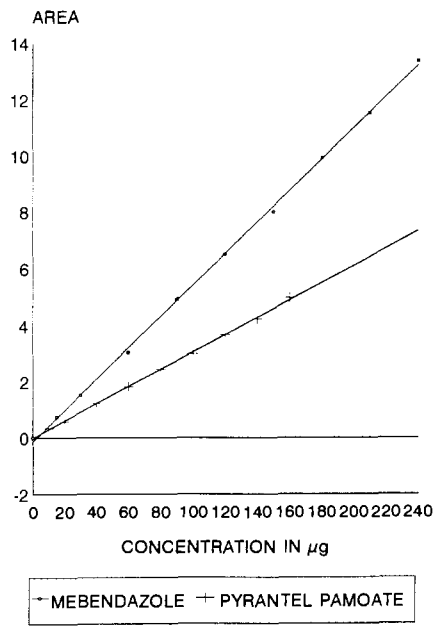

Fig. 2. Calibration curve of mebendazole and pyrantel pamoate.

Table 1
Parameters of system suitability

Sr. No.	Parameters	PYP	MEB
1.	Theoretical plates	5000	8000
2.	Resolution factors	1.64	2.28
3.	Tailing factor	1.3	1.1
4.a.	R.S.D.—Brand I (%)	1.23	0.95
4.b.	R.S.D.—Brand II (%)	0.97	0.89
5.	Relative retention time of pyrantel base to pamoic acid	—	1.0:0.53
6.	Limit of detection (μg)	10	15
7.	Limit of quantification (μg)	40	60

was taken in a 100 ml volumetric flask. About 25 ml of glacial acetic acid was added and kept in an ultrasonic bath for 30 min. It was then kept on a waterbath for 20 min, cooled and diluted with 65 ml of diluent A in a hood and then sonicated for 20 min. Volume was made upto the mark with the diluent and mixed—(Solution A). This solution was filtered through Whatman No. 42 filter paper. The filtrate solution, 6 ml aliquot, was taken in a 50 ml volumetric flask, diluted upto the mark with mobile phase and then used for the analysis.

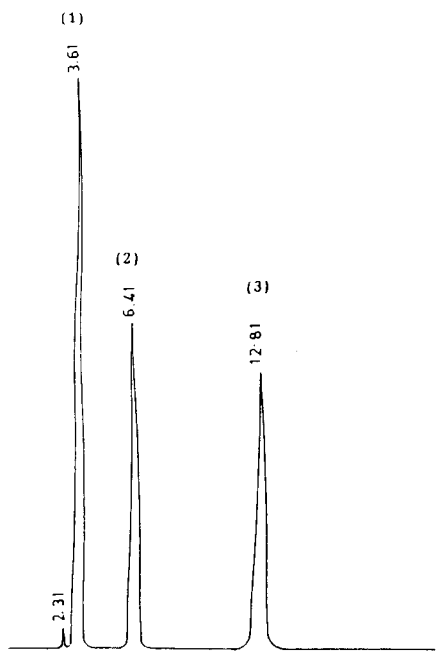

Fig. 3. Typical chromatogram of mebendazole and pyrantel pamoate.

2.8. Calibration

Aliquots of standard stock solution of MEB and PYP were taken in different 10 ml standard volumetric flasks and diluted upto the mark with mobile phase such that the final concentrations of MEB and PYP were in the range of 30–240 μg and 20–160 μg, respectively. Evaluation of both drugs were performed with a UV detector at 290 nm. Peak areas were recorded for all the peaks Fig. 2.

2.9. Assay

Each of the standard and the sample solutions were injected into the chromatographic HPLC system and peak areas were recorded as described in the calibration procedure.

From the peak area of MEB and PYP, the respective amounts were computed as,

$$\text{Amount of MEB and PYP*} = \frac{\text{Rspl} \times C \times D \times \text{Average wt.}}{\text{Rstd} \times W} \times \text{Factor*}$$

where,

Rspl = area of MEB or PYP in sample solution.

Rstd = area of MEB or PYP in standard solution.

Table 2
Results of HPLC assay from tablets

	Sr. No.	Pyrantel base (mg Tab^{-1}) (label claim: 100 mg Tab^{-1})	Mebendazole (mg Tab^{-1}) (label claim: 150 mg Tab^{-1})
Brand I	1	98.02	150.33
	2	98.58	151.93
	3	100.82	149.76
	4	98.88	148.47
	5	100.50	151.68
	Mean	99.36	150.43
	R.S.D	1.23%	0.95%
Brand II	1	98.82	151.38
	2	98.17	150.81
	3	98.75	150.47
	4	100.62	148.35
	5	98.45	148.72
	Mean	98.96	149.95
	R.S.D.	0.97%	0.89%

C = concentration of standard in mg ml^{-1}.
D = dilution factor.
W = weight of tablet in mg.
Factor = 0.347, conversion factor for PYP to PYRANTEL base.

3. Results and discussion

3.1. System suitability

According to U.S.P. 23, method (621), system suitability tests are an integral part of gas and liquid chromatographic methods. They are used to verify that the resolution and reproducibility of the chromatographic system are adequate for the analysis to be done. To ascertain its effectiveness system suitability tests were carried out on freshly prepared standard stock solution of MEB and PYP and the parameters obtained are shown in Table 1. The results are in concurrence with U.S.P. 23 requirements.

3.2. Chromatography

The mobile phase resolved the two drugs very efficiently into three distinct peaks of pamoic acid, pyrantel base and mebendazole as shown in Fig. 3. The retention times of pamoic acid, pyrantel base and mebendazole were about 3.61, 6.41 and 12.81 min, respectively. The relative retention times of pamoic acid and pyrantel base were about 0.55 and 1.0 min, respectively, which corresponds to relative retention times given for the same in U.S.P. monographs for PYP. A wavelength of 290 nm was selected for the detection purpose to match the sensitivities of these two drugs.

3.3. Linearity, limit of detection and determination

The plot of peak area, versus the respective concentrations of MEB and PYP were found to be linear in the range of 30–240 and 20–160 μg (Fig. 2). They were represented by linear regression equations:

$$Y_{MEB} = 50.56555 \times + 0.37205 \quad (r = 0.999)$$

$$Y_{PYP} = 30.33034 \times + 0.38508 \quad (r = 0.999)$$

The limit of detection (LOD) and the limit of quantification (LOQ) of MEB and PYP were calculated on the peak area using the following equations:

$$LOD = 3 \times N/B; \; LOQ = 10 \times N/B$$

Table 3
Results of recovery analysis from tablets

Brand	Drug	Amount of drug added (mg)	Amount found* (mg)	S.D. (±)	R.S.D. (%)
I	PYP	0	99.23	0.85	0.85
		20	118.28	1.31	1.11
		40	138.16	0.92	0.67
		60	158.22	1.28	0.81
% Recovery = 98.43%					
II	PYP	0	98.68	0.92	0.93
		20	118.62	1.09	0.92
		40	138.15	0.98	0.71
		60	158.33	0.97	0.61
% Recovery = 98.90%					
I	MEB	0	150.11	1.54	1.02
		30	179.18	1.46	0.81
		60	208.24	1.65	0.79
		90	237.26	1.64	0.69
% Recovery = 98.53%					
II	MEB	0	149.94	1.27	0.85
		30	177.84	1.59	0.89
		60	207.79	1.68	0.81
		90	237.89	1.55	0.65
% Recovery = 98.29%					

*Average of three experiments.

Where N, the noise estimate, is standard deviation of the peak areas (five injections) of the drugs, B is the slope of the corresponding calibration curve. The limit of detection/the limit of quantification for MEB and PYP were found to be 15 μg/60 μg and 10 μg/40 μg respectively.

3.4. Assay

The contents of MEB and PYP (equivalent to pyrantel base) per tablet for two commercial brands found by the proposed method were 150.43 mg Tab^{-1} (R.S.D. = 0.95%) and 99.36 mg Tab^{-1} (R.S.D. = 1.23%) for Brand I and 149.95 mg Tab^{-1} (R.S.D = 0.89%) and 98.96 mg Tab^{-1} (R.S.D. = 0.97%) for Brand II, respectively, as shown in Table 2. The low values of R.S.D. indicate that the method is precise and accurate.

Table 4
Stability indicating ability

Degradation with respect to	Labelled amount MEB (150 mg Tab^{-1})/ PYP (100 mg Tab^{-1})
Heat @100°C for 1 month	141.26 (mg Tab^{-1})/94.51 (mg Tab^{-1})
Sunlight for 1 h	149.83 (mg Tab^{-1})/92.67 (mg Tab^{-1})

3.5. Accuracy and precision

To study the accuracy and precision of the proposed method, recovery experiments were carried out by standard addition technique, by adding standards at four different levels to the preanalysed sample. Each level was repeated thrice.

A plot of the drug found in mg by the proposed method (Y-axis) against the amount of the standard drug added (X-axis) was drawn. Intercept on the Y-axis indicates the amount of the drug found in mg per tablet.

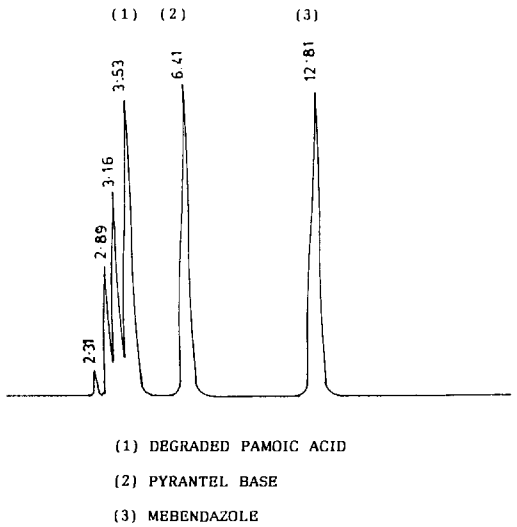

Fig. 4. Chromatogram of mebendazole and pyrantel pamoate on degradation with respect to sunlight.

From the amount of the drug found, % recovery was calculated using the formula:

$$\%\ \text{Recovery} = \frac{N(\Sigma XY) - (\Sigma X)(\Sigma Y)}{N(\Sigma X^2) - (\Sigma X)^2} \times 100$$

where,

X = amount of standard drug added.

Y = amount of drug found by the proposed method.

N = number of observation.

The recoveries of PYP and MEB obtained were 98.43 and 98.53% for Brand I and 98.90 and 98.29% for Brand II, respectively as shown in Table 3. This shows that there is no interference from the excipients present in the tablets.

3.6. Stability indicating ability

Stability indicating ability of the method was studied with two different parameters:

(a) Degradation with respect to heat.

(b) Degradation with respect to sunlight.

3.6.1. Degradation with respect to heat

Tablets were kept in an oven at 105°C for 1 month and analysed according to the proposed method. There was no secondary degraded peak, but the assay values were found to be less for MEB and PYP as reported in Table 4.

3.6.2. Degradation with respect to sunlight

The solution of the tablets used for assay preparation (Solution A) were prepared and before it was analysed by the proposed method was kept in sunlight for 1 h and the degradation profile was studied. Pyrantel pamoate is a salt of pamoic acid and pyrantel base as shown in Fig. 1. It was observed that pamoic acid degraded and showed degraded peaks as shown in Fig. 4. Pyrantel base did not show any degraded peaks but the assay values were low (92.67 mg Tab^{-1}), MEB remained unaffected on photodegradation.

4. Conclusion

The proposed RP-HPLC method is accurate, precise, rapid and stability indicating for the simultaneous determination of MEB and PYP in tablets. Hence it can be easily and conveniently adopted for routine quality control analysis.

Acknowledgements

The authors are grateful to M/s Merind Ltd, Bombay for providing HPLC facilities.

References

[1] Martindale The Extra Pharmacopoeia, 28th edn.
[2] I.P. 1985, p. 296.
[3] B.P. 1995, p. 1350.
[4] U.S.P. 23, pp. 934, 1342–1343.
[5] N.M. Sanghavi and V. Tandel, (Univ. Dept. Chem. Technology, Bombay-400019, India), Indian Drugs. Mar., 30 (3) (1993) 136–137.
[6] S. Ramnathan, N.K. Nair, S.M. Mansor and V. Navratnan, (Centre Drug Research; Univ. Sains Malaysia; Malaysia). J. Chromatogr. Biomed. Appl. 126 (1993) 303–307 (J. Chromatogr., 615).

[7] P. Betto, M. Gianbenedetti, F. Ponti, R. Ferreti, J.G. Settim, M. Gargiulo and R. Lorenzini, (Lab. Chim. Farmaco. 1st Superiore Sanita, 00161 Rome, Italy). J. Chromatogr, Biomed. Appl. 101 (1991) 115–123 (J. Chromatogr, 563).
[8] R. Aubeck and N. Hampp, (Inst. Phys. Chem. Ludwig-Maximalians-Univ; W-8000, Munich 2; Germany) Anal. Chim. Acta, 256 (2) (1992) 257–262.
[9] W.J. Allender, J. Chromatogr. Sci., 26 (9) (1988) 470–472.
[10] V.A. Thorpe, J. Chromatogr. Sci., 26 (11) (1988) 545–550.

ELSEVIER

Talanta 44 (1997) 1967–1971

Talanta

Complexant efficiency of 2′-hydroxy-4-R-chalcones for Aluminium (III) and substituent's effect

Nora B. Debattista *, Nora B. Pappano

Department of Chemistry, San Luis National University, Chacabuco 917, 5700 San Luis, Argentina

Received 30 May 1996; received in revised form 12 September 1996; accepted 26 September 1996

Abstract

The complexant efficiency with aluminium of 2′-hydroxy-4-R-chalcones, which depends on the nature and positions of the substituent was studied by a spectrophotometric method. The apparent formation constant was determined. The quantitative analysis of the substituent's influence on the complexation reaction equilibrium was made using the Hammett relation. The constant σ magnitudes of groups OH, OCH_3, Cl and F in the 4-position agree with values reported in the literature. © 1997 Elsevier Science B.V.

Keywords: Aluminium; 2′-hydroxy-4-R-chalcones; Spectrophotometric

1. Introduction

Chalcones and their analogues are well known for having variable bactericidal [1], fungicidal [2] and carcinogenic activity [3]. Moreover, 2′-hydroxychalcones have been employed as analytical reagents for some metal ions [4,5].

Considering their complexant efficiency, which depends on the substituent character and position, the 2′-hydroxychalcone—aluminium (III) systems were studied by a new spectrophotometric method. The combining ratio and kinetic behaviour were described, determining the apparent formation constants. The quantitative analysis of the substituents influence on the complexation reaction equilibria was made using the Hammett relation.

* Corresponding author. Fax: + 54 652 30224.

2. Experimental

2.1. Apparatus

All the absorption spectra were measured by a UV-160 spectrophotometer (Shimadzu, Japan) at constant temperature.

2.2. Reagents

The substances studied were the following:

I. 2′-hydroxychalcone,
II. 2′,4-dihydroxychalcone,
III. 2′-hydroxy-4-methoxychalcone,
IV. 2′-hydroxy-4-chlorochalcone,
V. 2′-hydroxy-4-fluorochalcone,

Their structures and the numbering system are shown in Fig. 1.

PII S0039-9140(96)02123-6

2′-hydroxy-4-R-chalcones were prepared by reaction of 2-hydroxyacetophenone with substituted benzaldehydes according to a method reported in the literature [6]. They were purified by LH 20 Sephadex column chromatography with methanol as eluent and identified according to physical, chromatographic and spectroscopic properties.

2′-hydroxychalcone: Rf(TLC): 0.38; mp 88–88.5°C; UV λ_{max}^{MeOH} nm 312, 350, 220; IR $\nu(CCl_4)$ cm^{-1}: 1639(C=O), 3480 (OH).

2′,4-dihydroxychalcone: Rf(TLC): 0.23; mp 158–159°C; UV λ_{max}^{MeOH} nm: 365, 240; IR $\nu(CCl_4)$ cm^{-1}: 1641 (C=O), 3600 (OH).

2′-hydroxy-4-methoxychalcone: Rf(TLC): 0.32; mp 90–91°C; UV λ_{max}^{MeOH} nm: 360, 240; IR $\nu(CCl_4)$ cm^{-1}: 1635(C=O), 3480 (OH).

2′-hydroxy-4-chlorochalcone: Rf(TLC): 0.28; mp 137–138°C; UV λ_{max}^{MeOH} nm: 318, 355 sh; MS m/z 258 M^+, 165, 147, 137, 120, 102.

2′-hydroxy-4-fluorochalcone: Rf(TLC): 0.38; mp 116–117°C; UV λ_{max}^{MeOH} nm: 316, 353 sh, 224; MS m/z 242 M^+, 149, 147, 121, 120, 102.

The complex solutions in methanol were prepared by mixing variable concentrations of aluminium (III) and 2′-hydroxy-4-R-chalcones (10^{-4} M–10^{-5} M). Ionic strength (0.01 M), temperature (32°C ± 0.1) and a metal:ligand ratio (3:1) were maintained constant. The equilibrium solution absorbances were measured at the maximum absorption wavelength of the complexes (λ_{max}).

3. Results and discussion

The molar composition for all the complexes was determined by a molar-ratio method [7] and a 1:1 (metal:ligand) stoichiometry was found (see Fig. 2).

Semiquantitative kinetic experiments allowed to establish more suitable reaction times (1–4 h) for each system.

The values of the apparent formation constants were determined by a new linear graphical method [8]. This method, applicable to mono and polynuclear complexes does not have the limitations of the other methods proposed [9,10]. It is easy and of extensive applicability. Its application only requires: analytical concentrations of reactants, ligand molar absorbtivity and absorbances for equilibrium solutions.

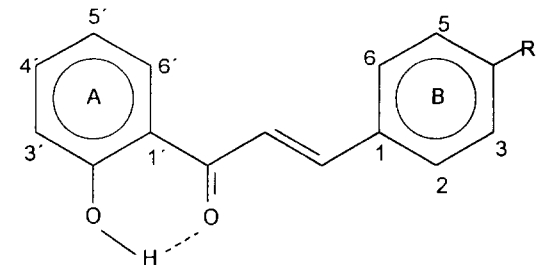

Fig. 1. Structure and numbering system of 2′-hydroxy-4-R-chalcones.

In a chemical reaction

$$n\,LH + M^{n+} \rightleftharpoons LnM + n\,H^+ \quad (1)$$

where LH is the complexant reagent, M^{n+} is the metallic ion and n is the stoichiometry coefficient, the equilibrium thermodynamic constant (K_a) is:

$$K_a = \frac{a_{H^+}^n \cdot a_{L_nM}}{a_{LH}^n \cdot a_{M^{n+}}} = K_c \cdot K_\gamma \quad (2)$$

where a, c and γ are the species activities, molar concentrations and activity coefficients, respectively [11].

In the considered system, at ionic strength and pH constant, the apparent formation constant (K'), is

$$K' = \frac{[L_nM]}{[LH]^n[M^{n+}]} = \frac{K_c}{[H^+]^n} \quad (3)$$

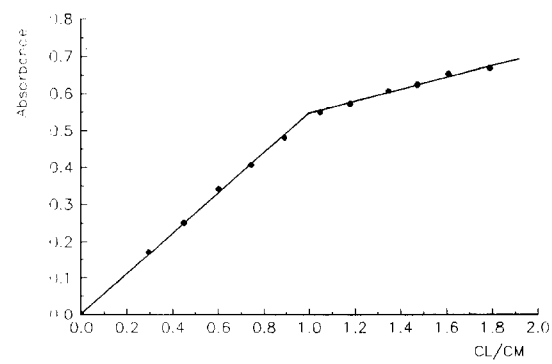

Fig. 2. Application of Yoe-Jones method to 2′-hydroxy-4-Cl-chalcone—Al(III) system.

where the brackets refer to the substance molar concentrations. If a and b are the ligand and metal molar analytic concentrations, respectively, and x is the complex equilibrium molar concentration, the apparent formation constant can be written as:

$$K' = \frac{x}{(a - \mathrm{n}x)(b - x)} \tag{4}$$

Considering the Newton binomial expansion [12]

$$(\alpha + \beta)^{\mathrm{m}} = \alpha^{\mathrm{m}} + \mathrm{n}\alpha^{\mathrm{m}-1}\beta + \frac{\mathrm{n}(\mathrm{n}-1)\alpha^{\mathrm{m}-2}\beta^2}{2!} + \frac{\mathrm{m}(\mathrm{m}-1)(m-2)\alpha^{\mathrm{m}-3}\beta^3}{3!} + \ldots \tag{5}$$

Starting from Eq. (4) the following polynomial is obtained

$$\frac{(\mathrm{n}-1)(\mathrm{n}-2)a^{\mathrm{n}-3}}{3!}(\mathrm{n}x)^4 - \frac{(\mathrm{n}-1)}{2}\left[\frac{b\mathrm{n}(\mathrm{n}-2)a^{\mathrm{n}-3}}{3} + a^{\mathrm{n}-2}\right](\mathrm{n}x)^3 + \left[a^{\mathrm{n}-1} + \frac{b\mathrm{n}(\mathrm{n}-1)a^{\mathrm{n}-2}}{2!}\right](\mathrm{n}x)^2 - [a^{\mathrm{n}} + b\mathrm{n}^2a^{\mathrm{n}-1} + K'']x + ba^{\mathrm{n}} = 0 \tag{6}$$

with $K'' = 1/K'$.

On the other hand, according to Beer's law, the reacting solution absorbance (A) can be expressed as

$$A = \epsilon_{\mathrm{L}}(a - \mathrm{n}x)l + \epsilon_{\mathrm{M}}(b - x)l + \epsilon_{\mathrm{C}}xl \tag{7}$$

where ϵ_{L}, ϵ_{M} and ϵ_{C} are the ligand, metal and complex molar absortivities, respectively, and l is the path length. If $\epsilon_{\mathrm{M}} = 0$ at the selected wavelength, then

$$x = \frac{A - A_{\mathrm{L}}}{l(\epsilon_{\mathrm{C}} - \mathrm{n}\epsilon_{\mathrm{L}})} \tag{8}$$

where, A_{L} (ligand absorbance) is

$$A_{\mathrm{L}} = \epsilon_{\mathrm{L}}al \tag{9}$$

From Eq. (8) it is evident that the complex concentration ratio (D) of two equilibrium solutions 'j' and 'r', is

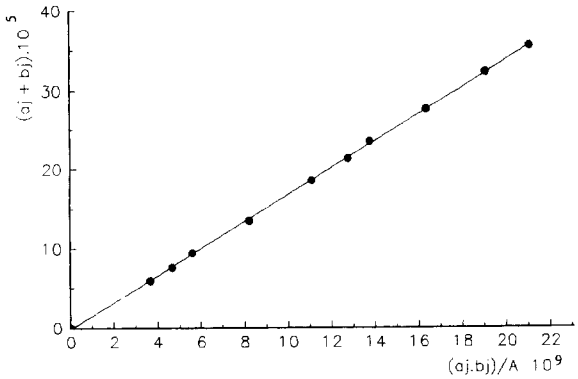

Fig. 3. Formation of 2'-hydroxy-4-F-chalcone—Al(III) in methanol at 32°C.

$$\mathrm{D} = \frac{x_j}{x_r} = \frac{(A - A_{\mathrm{L}})_j}{(A - A_{\mathrm{L}})_r} \tag{10}$$

Now,

1. applying the polynomial Eq. (6) to the 'j' and 'r' solutions;
2. expressing the 'j' polynomial solution in terms of x using Eq. (10);
3. confronting the two polynomials in x and formulating the equations that link equal degree terms;
4. combining and reordering the previous expressions, Eq. (11) is obtained

$$a_j^{\mathrm{n}} + \mathrm{n}^2b_ja_j^{\mathrm{n}-1} = \frac{(a_r^{\mathrm{n}} + \mathrm{n}^2b_ra_r^{\mathrm{n}-1} + K'')(A - A_{\mathrm{L}})_r}{a_r^{\mathrm{n}}b_r}\frac{a_j^{\mathrm{n}}b_j}{(A - A_{\mathrm{L}})_j} - \frac{1}{K'} \tag{11}$$

It is the general validity and for the particular cases is simplify. For example, the expression for complexes LM (n = 1) is

$$(a_j + b_j) = \frac{(a_r + b_r + K'')(A - A_{\mathrm{L}})_r}{a_rb_r}\frac{a_jb_j}{(A - A_{\mathrm{L}})_j} - \frac{1}{K'} \tag{12}$$

Fig. 3 shows the graphic representation of this equation for the system 2'-hydroxy-4-fluorochalcone-Aluminium(III). The values for apparent formation constants of different complexes studied are listed in Table 1.

Table 1
Apparent formation constants(K') of 2'-hydroxy-4-R-chalcones—Al(III) in methanol at 32°C

System	λ_{max}	Slope	Intercept $\times 10^6$	$K' \times 10^{-5}$
I-Al	424	16153	8.40	1.26[a]
II-Al	443	42372	3.70	2.69
III-Al	437	33807	4.80	2.09
IV-Al	355	21364	3.64	2.75
V-Al	427	16952	2.61	3.41

[a] Ref. [13].

The general expression of the Hammett equation, [14] applicable for aromatic compounds with the same reaction centre, is as follows:

$$\log K' = \log K'_0 + \rho\sigma \quad (13)$$

where K'_0 is the equilibrium constant of the standard compound, K' is the equilibrium constant of a particular derivative, σ is the substituent constant present in the derivative, ρ is the reaction constant. This constant ρ, which depends on the reaction characteristics and the external conditions, shows a negative value for a reaction that is hindered by electron withdrawal of the benzene ring. The complexation reactions of the 2'-hydroxy-4-R-chalcones with Al(III) present this behaviour. Substituents that withdraw ring B electrons hinder the complex formation by an electronic density decrease of the oxygen atoms that are involved in the chelate (carbonylic oxygen and hydroxylic oxygen bound to C'_2).

If Eq. (2) is applied to the systems studied, using the I-Al(III) complex as the standard reaction and $\rho = -1$ to the complexation reactions of 2'-hydroxy-4-R-chalcones, then:

Table 2
Constant σ values for 4-substituted 2'-hydroxychalcones

System	Experimental σ value	Reported σ value[a]
II-Al	−0.33	−0.37
III-Al	−0.22	−0.27
IV-Al	−0.34	−0.31
V-Al	−0.43	−0.48

[a] Refs. [15] and [16].

$$\sigma = \log \frac{K'_0}{K'} \quad (14)$$

from which the substituent constant was estimated for OH, OCH_3, Cl and F groups in the ring B 4-position of 2'-hydroxychalcones (see Table 2).

4. Conclusions

According to the above results, the following conclusions may be drawn:

Under the working conditions taken up, 2'-hydroxy-4-R-chalcones—Al(III) chelates are found to be stable for at least 48 h and to have a ligand:metal stoichiometric relation 1:1.

The original method used is suitable for the mono-nuclear (and polynuclear) complexes studied and only analytical concentrations of reactants, absorbances for equilibrium solutions and ligands molar absortivity are requested for its applications.

The constant magnitudes of groups OH, OCH3, Cl and F in the 4-position (2'-hydroxychalcones ring B), evaluated by application of the Hammett equation, agree with the values reported in the literature.

Acknowledgements

The present work was supported by the San Luis National University.

References

[1] N.B. Pappano, O.P. Centorbi and F.H. Ferretti, Rev. Microbiol. Sao Paulo, 25 (1994) 305.
[2] S.D. Lorimer and N.B. Perry, Planta Med., 60 (1994) 386.
[3] V.S. Parmar, R. Jain, S.K. Sharma, A. Vardhan, A. Jha, P. Taneja, S. Singh, B.M. Vyncke, M.E. Bracke and M.M. Marcel, J. Pharm. Sci., 83 (1994) 1217.
[4] W.E. Rudzinski and T.M. Aminabhavi, Inorg. Chim. Acta, 70 (1983) 175.
[5] T.S. Rao, K.L. Reddy and P. Lingaiah, Proc. Indian Acad. Sci., 100 (1988) 363.
[6] J.B. Harborne, T. Mabry and H. Mabry, The Flavonoids, Vol. 1, Academic Press, New York, 1975, p. 131.
[7] G.D. Christian and J.E. O'Reilly (Eds.), Instrumental Analysis, Allyn and Bacon, Boston, 1986, p. 186.

[8] N.B. Debattista, Doctoral Tesis 1990, N.B. Debattista and F.H. Ferretti, ALDEQ, 1992, II, 289.
[9] N.P. Komar, Tr. Inst. Khimi Khar 'Kovsk, 8 (1951) 51, from S.I. Gusev and E.N. Nikolaeva, Anal. Chem. U.S.S.R., 21 (1966) 281.
[10] F.H. Ferretti, R. Olsina and C. Marone, Anal. Asoc. Quim. Argent., 70 (1982) 501.
[11] S. Glasstone, Termodinámica para Químicos (Ed.) Aguilar, Madrid, 1977, p. 426.
[12] J.B. Dence, Técnicas Matemáticas Aplicadas a la Química (Ed.), Limusa, México, 1978, p. 204.
[13] N.B. Debattista, E.J. Borkowski, N.B. Pappano, J. Kavka and F.H. Ferretti, An. Asoc. Quim. Argent., 74 (1986) 179.
[14] J. March, Advanced Organic Chemistry, Wiley, New York, 1985, p. 242.
[15] D.H. McDaniel and H.C. Brown, J. Org. Chem., 23 (1958) 420.
[16] L.P. Hammett, Physical Organic Chemistry, McGraw-Hill Kogakusha, Tokyo, 1970, p. 384.

ELSEVIER

Talanta 44 (1997) 1973–1978

Talanta

Analytical properties of 5,5-dimetyl 1,3-cyclohexanedione dithiosemicarbazone monohydrochloride; spectrophotometric determination of chromium(VI) in alloy steels and industrial effluents

C.S. Devaragudi, K. Hussain Reddy *

Department of Chemistry, Sri Krishnadevaraya University, Anantapur 515 003, India

Received 6 May 1996; received in revised form 16 October 1996; accepted 18 October 1996

Abstract

The analytical properties of 5,5-dimethyl 1,3-cyclohexanedione dithiosemicarbazone monohydrochloride (5,5-DiMe-1,3-CHDT.HCl) are described. The reagent gives pink coloured solutions with chromium(VI) in acetic medium. The maximum colour intensity is observed in 0.5–2.5 pH range. This colour reaction (molar absorptivity, 1.63×10^4 l mol^{-1} cm^{-1} at 360 nm) has been used for the spectrophotometric determination of total chromium in alloy steels and industrial effluents. © 1997 Elsevier Science B.V.

Keywords: Alloy steels; Chromium(VI); Industrial effluents; Spectrophotometric

1. Introduction

Thiosemicarbazones are interesting analytical reagents [1–3]. Although monothiosemicarbazones have been widely used for the spectrophotometric determination of metal ions, dithiosemicarbazones are not exploited much possibly due to their lower solubilities in aqueous medium. However, 1,3-cyclohexanedione dithiosemicarbazone monohydrochloride (1,3-CHDT.HCl) has been extensively used for the spectrophotometric determination of Chromium(VI) [4], osmium(VIII) [5], palladium(II) [6] and nickel(II) [6]. In the light of good analytical potentialities of 1,3-CHDT.HCl, herein we report the synthesis, characterization and analytical properties of a derivative of 1,3-CHDT.HCl viz. 5,5-dimethyl 1,3-cyclohexanedione dithiosemicarbazone monohydrochloride (5,5-diMe-1,3-CHDT.HCl). The determination of chromium(VI) using this reagent is also included in this paper.

2. Experimental

2.1. Preparation of 5,5-diMe-1,3-CHDT.HCl

The reagent was prepared by simple condensa-

* Corresponding author.

PII S0039-9140(96)02138-8

tion of 1 mol of dimedone with 2 mol of thiosemicarbazide. In a 250 ml round bottom flask, a hot ethanolic solution of 5,5-dimethyl 1,3-Cyclohexanedione (dimedone) (0.031 mol) and aqueous solution of thiosemicarbazide (0.062 mol) were mixed. Then 6 ml of conc. HCl was added and heated to reflux for 1 h on water bath. On cooling and slow evaporation of the reaction mixture, a white product was separated out, collected by filtration, washed with cold methanol, yield 76%, m.p. 208°C.

2.2. Characterization of 5,5-diMe-1,3-CHDT.HCl

The purity of the product was found to be 99.5% by direct titration with 0.05 M NaOH using phenolphthalein indicator. Elemental analysis, found C, 39.48%, H, 5.35% and N, 25.53%. Calculated for $C_{16}H_{19}N_6S_2Cl$ C, 37.09%, H, 5.56% and N, 25.96%.

The pK_a values are determined by recording the UV–Visible spectra of μM (4×10^{-5} M) solutions of ligand at various pH values and by taking the arithmetic mean of the values obtained from the measurements at four different wavelengths. The values of the deprotantion of the ligand are 6.5 (pK_1) and 9.3 (pK_2).

The ^{1}H-NMR spectrum of the reagent was recorded in DMSO solvent. It shows signals corresponding to $-CH_3$ (gem), CH_2 (ring), NH and NH_2 protons at 1.96 (S, 6H); 2.43 (d, 6H, $J=4$); 5.57 (S, 2H) and 7.90 (d, 6H), respectively.

The reagent solution (0.01 M) was prepared by dissolving 325 mg of the compound in 100 ml of distilled water and it is stable for at least 12 h.

Hydrochloric acid (1 M)—sodium acetate (1 M) (pH 0.5–3.5); 0.2 M NaOAc–0.2 M AcOH (pH 4–6) and 2 M NH_4Cl–2M HN_4OH solutions were used. The standard chromium(VI) solution (1×10^{-2} M) was prepared using analytical reagent grade potassium dichromate (previously dried at 140°C). Solutions of diverse ions of suitable concentrations were prepared using AR grade chemicals.

2.3. Reactions with metal ions

The reactions of some important metal ions were tested at different pH values. The samples were prepared in 25 ml volumetric flasks by adding 10 ml of buffer, metal ion, 2.5 ml of dimethylformamide (DMF) and 1 ml of 0.01 M 5,5-diMe-1,3-CHDT HCl solution. The reaction mixture was diluted to the mark with distilled water. The absorbance was measured in 350–600 nm range against the reagent blank. The results are summarized in Table 1.

Table 1
Analytical characteristics of 5,5-dimethyl-1,3-cyclohexane dione dithiosemicarbazone monohydrochloride compounds

Metal ion	pH	nm	l mole^{-1} cm^{-1}
Fe(II)	10.0	400	1.50×10^4
Co(II)	8.0	400	2.59×10^4
Ni(II)	8.0	405	3.51×10^4
Cu(II)	6.0	445	6.22×10^4
Zn(II)	10.0	367	1.97×10^4
Cr(VI)	1.5	360	1.64×10^4
Pd(II)	8.0	380	3.46×10^4
Os(VIII)	10.0	432	3.77×10^4
Pb(II)	10.5	435	1.52×10^4
Cd(II)	10.5	435	2.50×10^4
Hg(II)	11.0	450	2.30×10^4

Table 2
Interferences of foreign ions in the determination of 0.85 μg ml^{-1} of chromium

Ion added	Tolerance limit (μg ml^{-1})
Tartrate, $EDTA^{2-}$	600
$S_2O_3^{2-}$, I^-, Cl^-, ClO_4^-	500
SO_4^{2-}, Br^-, SCN^-, $C_2O_4^{2-}$, F^-, Al(III)	320
Fe(III)*, NO_3^-	95
Citrate, Cr(III)	80
Mn(II), Fe(III), Ni(II), Mo(VI), Zr(IV), Zn(II), Co(II)	24
Hg(II), W(VI), V(V)	20
Cu(II), Pd(II), Pt(IV)	2

* In the presence of 285 μg ml^{-1} of fluoride.

2.4. Recommended procedure for the determination of chromium(VI)

An aliquot of the solution containing 0.15–1.5 μg ml^{-1} (or ppm) of chromium(VI), 10 ml of NaOAc–HCl (buffer) solution (pH, 1.5), 2.5 ml of DMF and 1 ml of 0.01 M 5,5-diMe-1,3-CHDT.HCl were combined in a 25 ml volumetric flask and the mixture was diluted to the mark with distilled water. The absorbance of this solution was read at 360 nm against reagent blank. The measured absorbance is used to compute the amount of chromium from the predetermined calibration curve.

2.5. Apparatus

Schimadzu 160A UV-visible spectrophotometer equipped with 1.0 cm quartz cells and an ELICO, model LI-120 pH meter were used in the present study.

3. Results and discussion

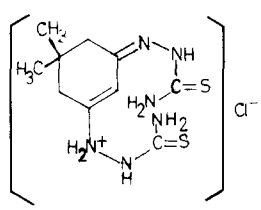

I

5,5-Dimethyl-1,3-cyclohexanedione dithiosemicarbazone monohydrochloride is as easily obtained as the ∞-dithiosemicarbazones [7], probably because it is stabilized as the hydrochloride(I). A 0.01 M solution of this reagent solution is stable for 12 h. The bathochromic shift of strong absorption band from 215 to 310 nm indicates that in solution on increasing the pH, the acid is neutralized and the >C=S group is enolized and dissociated [8].

The colour reactions of some important metal ions with 5,5-diMe-1,3-CHDT.HCl are summarized in Table 1. Two types of colour reactions are implicated. They are: 1. redox reactions; and 2. complex formation reactions. The former type of reactions take place with metal ions such as Cr(VI) and Os(VIII) as dithiosemicarbazones are easily oxidized. But this property is infrequently used for the determination of metal ions [4,9] in higher oxidation state. The redox reaction between Cr(VI) and the reagent may be written as

$$2Cr(VI) + 3(\text{reduced reagent}) \rightleftharpoons 2Cr(III) + 3(\text{oxidized reagent})$$

Two electrons are involved for each reagent molecule and the oxidation of the two >C=S groups give $>\dot{C}-S-S-\dot{C}<$. The oxidation products are formed by either intermolecular (II) or intranolecular (III) sulphur sulphur bonding.

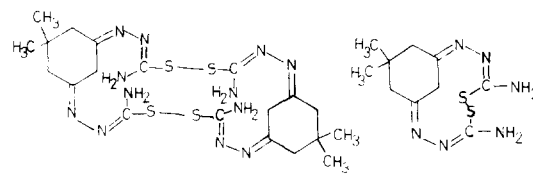

II III

The latter type of reactions occur with divalent metal ions such as Ni(II), Zn(II), Pb(II) and Cd(II) in basic medium to give intense coloured complexes. In basic medium, the ligand presumably exists in enolic form and coordinates the metal ion as dianion to give neutral complex [10,11].

3.1. Determination of chromium(VI)

Chromium(VI) reacts with 5,5-diMe-1,3-CHDT.HCl in acidic pHs to give pink coloured species. No colour reactions of the reagent with Cr(III) is observed. However, the colour reaction of Cr(VI) with the reagent is instantaneous even at room temperature (28 ± 2°C) in the pH range 1–5. The absorbance of the pink coloured species (λ_{max}, 360 nm) remains constant for 1 h. The maximum colour intensity is observed in the pH range 0.5–2.5.

A 20-fold molar excess of the reagent is adequate for full colour development. Addition of

Table 3
Analysis of chromium in alloy steels

Sample	Composition, %	Chromium certified value	Chromium content[b] by the present method, %
BCS 409	0.48 Mn; 3.14 Ni; 0.79 Mo; 0.23 Cu; 0.028 V; rest Fe[a]	1.22	1.22 ± 0.007
BCS 406	0.55 Mn; 1.04 Mo; 1.69 Ni; 0.32 Cu; 0.02 V; rest Fe[a]	2.10	2.10 ± 0.04
BCS 483	10.8 W; 1.94 Co; 0.54 V; 0.29 Mn; 0.17 MO; rest Fe[a]	3.21	3.21 ± 0.05

[a] Masked with 285 μg ml^{-1} of fluoride.
[b] Average ± S.D. of five determinations.

Table 4
Determination of chromium in industrial effluents

Name of Industry	Chromium found in	
	Present method mg l^{-1}	Diphenyl carbazide method mg l^{-1}
M/S. Vijaya Metal Finishes, Bangalore	1.86	1.72
M/S. Electrometals and chemicals, Bangalore	3.19	3.21
M/S. Electrochemical Metal Finishes, Bangalore	2.38	2.19

excess reagent has no adverse effect on the absorbance. The order of addition of metal ion, reagent and buffer solution has no effect on the absorbance, provided DMF is added prior to the reagent solution.

3.2. Analytical characteristics

The system obeys Beer's law over the concentration range 0.16–1.49 μg ml^{-1}. The optimum range for the determination of chromium(VI) from Ringbom's plot was found to be 0.30–1.40 μg ml^{-1}. The molar absorptivity and Sandell's sensitivity of the method were 1.63×10^4 l mol^{-1} cm^{-1} and 0.0031 μg cm^{-2}, respectively. The relative standard deviation for ten replicate analyses of a solution containing 0.83 μg ml^{-1} cobalt was 1.62%.

3.3. Nature of oxidation reaction

Job's and Molar ratio methods gave the composition of pink coloured species as 2:3 (metal:ligand). Hence 2 mol of chromium(VI) reacts with 3 mol of reagent. Accordingly and in analogy with previous observations [4,12] the redox reaction is proposed (Section 3).

3.4. Interferences

The effect of some of the ions which often accompany chromium has been studied by adding different amounts to 0.84 μg ml^{-1} of chromium in solution. The colour is developed as described in the standard procedure. An error of ±2% in the absorbance reading is considered tolerable. The results are given in Table 2. Higher amounts of iron(III) (95-fold molar excess) could be tolerated with fluoride.

3.5. Analysis of alloy steels

Alloy steel sample solutions were prepared by following the procedure given in the literature [13]. A sample containing 0.5 g of steel sample was dissolved in 30 ml of 1:4 sulphuric acid. A 5 ml volume of nitric acid was added to remove the carbaneous residue. The solution was boiled to

Table 5
Comparison of spectrophotometric methods for the determination of chromium

Reagent	λ_{max}, nm (ϵ, l mol^{-1} cm^{-1})	Tolerance limit of foriegn ions (Interfering ion: Cr(VI; wt/wt)					Ref.
		V(V)	Fe(III)	Co(II)	Ni(II)	Cu(II)	
8-Hydroxyquinoline[a]	410 (3×10^3)	[b]	5	5	5	5	[23]
1.3-Cyclohexanedione dithiosemicarbazone monohydrochloride	370 (1.2×10^4)	0.2	200	20	9	0.5	[4]
2-(5-Bromo)-2-pyridyl-azo-5-diethylamio phenol[c]	600 (7.9×10^4)	0.01	1	1	1	1	[24]
Tropolone[c]	400 (1.96×10^4)	[b]	[b]	150	150	[b]	[25]
2-Oximinodithiosemicarbazone	485 (5.6×10^3)	0.5	0.5	0.5	1	0.5	
5,5-Dimethyl-1,3-cyclohexanedione dithiosemicarbazone Monohydrochloride	360 (1.63×10^4)	23	110	28	28	2.3	Present method

[a] Extracted into molten naphthalene.
[b] Seriously interferes.
[c] Methods involving heating of the reaction mixture.

remove excess of nitric acid, cooled and diluted to 80 ml. A 2 ml volume of a 1.5% silver nitrate solution and 2 g of potassium persulphate were added and the solution was swirled for dissolution to occur and the reaction mixture heated at 80°C for 15 min. The purple colour of manganese was destroyed by the addition of a few drops of 1:1 hydrochloric acid. The solution was evaporated to almost dryness, cooled and diluted in order to obtain the required concentration of chromium in the stock solution.

To 10 ml of NaOAc–HCl solution of pH 1.5, 1.5 ml of 0.1 M sodium fluoride, steel sample solution (in the optimum concentration range), 2.5 ml of DMF and 1 ml 0.01 M reagent solution were added. The solution was diluted to volume (25 ml) with distilled water and the absorbance was measured at 360 nm against reagent blank. The results are presented in Table 3.

3.6. Analysis of effluents

Effluents samples were collected from three different electrometal (Chrome plating) and metal finishing industries located in Bangalore city, India. The sample (150 ml) was acidified with 2 ml of conc. HCl. Then 25 mg of ferric chloride was added and the pH was adjusted to 7.5 with borate buffer solution. The solution was allowed to stand overnight and filtered. Then 2 ml of 30% H_2O_2 was added and evaporated to dryness. The dried mass was dissolved in 1 ml 1:1 H_2SO_4 and diluted to 25 ml. Known aliquots of this sample was taken and colour was developed as described in the recommended procedure. The results are given in Table 4.

3.7. Conclusions

Most of the spectrophotometric methods [14,15] involve either heating of the reaction mixture [16–18] or extraction [19–22]. However, heating at a specific temperature and for a long time is laborious and time consuming. Also for some methods tolerance limit for associated ions is low. The present method compares (Table 5) favourably with come recently reported spectrophotometric methods [4,23–26] for the deter-

mination of chromium(VI), published in standard international journals. Further, the reagent is easy to synthesize using commercially available dimedone. The most favourable feature of 5,5-diMe-1,3-CHDT.HCl is its solubility in water. Moreover, the present method is simple, rapid, reasonably sensitive and selective without the need for heating or extraction.

Acknowledgements

One of the authors (C.S.D) is grateful to University Grants Commission, New Delhi for awarding Teacher Research Fellowship.

References

[1] R.R. Singh, B.S. Garg and R.P. Singh, Talanta, 25 (1978) 619.
[2] K. Hussain Reddy and D. Venkata Reddy, Q. Chem. Rev., 1 (1985) 47.
[3] B.S. Garg and V.K. Jain, Mikrochem J., 38 (1988) 144.
[4] K. Hussain Reddy and D. Venkata Reddy, Analyst, 108 (1983) 1247.
[5] K. Hussain Reddy and D. Venkata Reddy, Anal. Lett., 17 (1984) 1275.
[6] K. Hussain Reddy and D. Venkata Reddy, Indian J. Chem., 22 (1983) 723, 824.
[7] K. Butler, US Patent 3 382 266 (C1, 260–438.1) 07 (May, 1968), Appl. 28 October, 1964.
[8] B.A. Gringas, R.L. Somozjai and C.H. Bayley, Can. J. Chem., 39 (1961) 973.
[9] M. Guzman, D.P. Bendito and F. Pino, Anal. Chem. Acta., 83 (1976) 259.
[10] K. Hussain Reddy and D. Venkata Reddy, Indian J. Chem., 24 (1985) 154.
[11] A. Krishna, K. Hussain Reddy and D. Venkata Reddy, Inorg. Chim. Acta, 173 (1990) 13.
[12] R.S. Ramakrishna and H.M.N.H. Irving, Anal. Chim. Acta, 48 (1969) 251.
[13] B.H. Alden and J.A. Dean, Anal. Chem., 29 (1957) 1298.
[14] K. Hussain Reddy and D. Venkata Reddy, Chim. Acta Turc., 13 (1985) 441.
[15] F.D. Snell, Photometric and Fluorometric Methods of Analysis Part I, Wiley Interscience, New York, 1978, pp. 703–744.
[16] Y. Mamamoto, T. Murata and M. Veda, Bunseki Kagaku, 25 (1976) 851.
[17] B. Subramanyam and M.C. Eswar, Mikrochim. Acta, (1976) 579.
[18] M.H. Husmi, A. Rashid, H. Ahmed, A.A. Ayaz and F. Azam, Anal. Chem., 37 (1965) 1027.
[19] J.R. Johnston and W.T. Holland, Mikrochim. Acta, (1972) 321.
[20] S.V. Vartangyam and V.M. Tarayan, Arm. Khim. Zh., 29 (1976) 303.
[21] S. Kamatsu and K. Yakahashi, Nippon Kagaku Zasshi, 83 (1962) 879.
[22] J.P. McKaveney and H. Freiser, Anal. Chim. Acta, 30 (1958) 1965.
[23] B.K. Puri and M. Gautam, Talanta, 25 (1978) 484.
[24] W. Fusheng, Z. Yurui, Q. Pelhua and Y. Peng, Mikrochim. Acta, (1983) 21.
[25] G.H. Rizvi, Mikrochim. Acta, (1983) 21.
[26] F. Salinas, T.J. Sanchez and T.G. Diaz, Mikrochim Acta, (1985) 245.

ELSEVIER

Talanta 44 (1997) 1979–1986

Talanta

Direct determination of cadmium at parts-per-billion level in waters by derivative atomic absorption spectrometry using atom trapping technique

Hanwen Sun *, Lili Yang, Deqiang Zhang, Jianmin Sun

Department of Chemistry, Hebei University, Baoding, 071002, People's Republic of China

Received 24 July 1996; received in revised form 18 October 1996; accepted 29 October 1996

Abstract

A method has been described for the direct determinations of trace cadmium using derivative atom trapping flame atomic absorption spectrometry with an improved water-cooled stainless steel trapping equipment. The characteristic concentration (gave a derivative absorbance of 0.0044) and detection limit (3σ) of cadmium were 0.028 and 0.02 ng ml^{-1} when collecting for a 1 min, respectively, which were 992 and 145-fold better than those of the conventional flame atomic absorption spectrometry. The detection limit and sensitivity of the proposed method for a 2 min collection time were 1 and 2 orders of magnitude higher than those of conventional flame atomic absorption spectrometry. The present method was applied to the determinations of cadmium in water samples with a recovery range of 91 ~ 111% and a relative standard deviation of 4.7 ~ 5.6%. © 1997 Elsevier Science B.V.

Keywords: Derivative atomic absorption spectrometry; Atom trapping; Cadmium

1. Introduction

There is an increasing number of studies dealing with the determination and quantification of heavy metals in various waters, because even low concentrations of them can cause serious toxic effects to organisms. From a public health viewpoint, it is necessary to determine the heavy metal contents in various potable waters. Methods reported for the determinations of trace levels of cadmium in water samples include spectrophotometry [1–6], anodic stripping voltammetry (ASV) [7–9], electrothermal atomic absorption spectrometry (ETAAS) [10–16], flame atomic absorption spectrometry (FAAS) [17–23] and atom trapping flame atomic absorption spectrometry (ATFAAS) [24–30].

The atom trapping technique developed by Lau et al. is a method of preconcentrating the analyte atoms in the flame. This technique was applied to the determination of cadmium with a characteristic concentration of 0.4 ng ml^{-1} for a 2 min collection [24]. In another paper reported by Lau et al., cadmium was determined using ATAAS with a detection limit of 0.1 ng ml^{-1} and a relative standard deviation (RSD) of 7.4% at 10

* Corresponding author. Fax: +86 312 5016914.

PII S0039-9140(96)02157-1

ng ml^{-1} level of cadmium when collection for 2 min [25]. Khalighie et al. [26] studied the determination of Cd with atom-trapping technique, the characteristic concentration was found to be 1.3 ng ml^{-1} for 8 min collection. For the determination of Cd in soil, Fraser et al. [27] described the use of atom-trapping technique with a detection limit (2σ) of 0.0016 mg ml^{-1} and the RDS was found to be 11.8% at 0.007 mg ml^{-1} level of cadmium. Roberts and Kahokola [28] described the use of V_2O_3 as the coating material in atom-trapping, the best characteristic concentration of 0.26 ng ml^{-1} was obtained. Turner et al. [29] studied the determination cadmium with atom-trapping technique and the sensitivity was found to be 0.3579 ng ml^{-1}. In our previous paper, the use of water cooled stainless steel tube as an atom collector has been described for the direct determination of cadmium by FAAS, the sensitivity for a 2 min collection were nine-fold better than that of conventional FAAS [30]. Derivative flame atomic absorption spectrometry (D-FAAS) was found by combining the laboratory derivative measurement system with atomic absorption spectrometer. The sensitivity and detection limit of D-FAAS were enhanced 50 and 10 times compared with those of conventional FAAS, respectively [31]. The requirement for analysis at trace and ultra-trace concentration of cadmium has demanded increasingly lower detection capabilities from modern analytical methods.

The main purpose of this paper is to establish a sensitive, simple and reproducible method that affords low determination limit with low analytical costs. For this purpose, the laboratory derivative measurement system was used and the original atom trapping equipment [30,32,33] was improved. The method was applied successfully to the determinations of cadmium in water samples.

2. Experimental

2.1. Apparatus

A WYX-402 atomic absorption spectrometer (Shenyang Analytical Instrument Factory, Shenyang, China) was employed for the measurement of the absorbance. A spectral slit width of 0.2 nm was used to isolate the 228.8 nm resonance line.

The improved atom trapping equipment with a water-cooled stainless steel trap tube in an air-acetylene flame and the laboratory derivative measurement system were used throughout the experiments. The derivative measurement system consists of two parts, i.e., magnification and differential unit. Five sensitivity grades, expressed by 2, 5, 10, 20 and 50 mV min^{-1}, were designed in the derivative measurement system. Increase in the derivative signal intensity of the same cadmium solution is accompanied by a decrease in the number of the sensitivity grade. The derivative measurement system was connected between the atomic absorption spectrometer and the double-pen recorder. The derivative and conventional signals were recorded simultaneously by the recorder set at the 10 mV range.

2.2. Reagents

A cadmium stock solution, 1000 μg ml^{-1}, was prepared by dissolving 1.1423 g of cadmium oxide (analytical reagent grade) in 20 ml of 5 mol l^{-1} HCl and diluting to 1000 ml with sub-boiling distilled water. Working solutions were prepared daily by serial dilution of the stock solution with sub-boiling distilled water just before use.

All the other reagents were of analytical-reagent grade. Sub-boiling distilled water was used throughout.

2.3. Procedure

A stainless steel trap tube (5 mm o.d.) was positioned 7 mm above the burner and 2 mm under the light path. The cooled tap water at a flow rate of 2 l min^{-1} was passed through the tube during the collection cycle. Cadmium solutions were aspirated normally into the flame with an air flow of 6 l min^{-1} and acetylene flow of 1.5 l min^{-1} for an appropriate collection time. An appreciable proportion of the analyte condensed on the cool surface of the tube. After the collection cycle, the tap water was shut off, and then the coolant water flow out of the tube automati-

cally. Cadmium was released into the flame by rapidly heating of the trap tube. The signals of conventional and derivative atom-trapping atomic absorption spectrometry were recorded simultaneously by the double-pen recorder. Sensitivity grade, 20 mV min^{-1}, and 1 min collection time were used during the optimization of experimental conditions, unless otherwise stated. The recommended experimental conditions are summarized in Table 1.

3. Results and discussion

3.1. Characteristic of D-AT-FAAS signal

The laboratory derivative measurement system consists of magnification and differential unit. The input signal was magnified through the measurement system and there is a rigorous derivative relation between the output and input signal. The output signal of the system will keep in base-line when the variation of the input signal is zero, and when the variation of the input signal is not zero, the output signal is in direct proportion to the variation of the input signal. The absorption signals of conventional AT-FAAS and D-AT-FAAS recorded simultaneously by a double-pen recorder were shown in Fig. 1.

Fig. 1 (I) showed the absorption signal of cadmium obtained by conventional AT-FAAS during the collection, $A \rightarrow C$, followed by the aspiration of the blank solution $D \rightarrow E$ and the release $E \rightarrow G$. The derivative absorption signal consists of four peaks, i.e., *a*, *b*, *c* and *d* (Fig. 1 (II)). The peak *a* and *b* are corresponding to the cycle $A \rightarrow B$ and $C \rightarrow D$ of the conventional signal, respectively. The peak *c* and *d* correspond to the releasing cycle $E \rightarrow F \rightarrow G$. The peak-height measurement was used in the present work. The total height of peak *c* and *d*, which is in direct proportion to the concentration of cadmium according to our experimental results, was considered as the absorbance of D-AT-FAAS.

Table 1
Recommended experimental conditions

Wavelength (nm)	228.8	Coolant water (l min^{-1})	2
Lamp current (mA)	3	Recorder grade (mV)	10
Air flow rate (l min^{-1})	6	Trap position	
Acetylene flow rate (l min^{-1})	1.5	Above the burner (mm)	7
		Below the burner (mm)	2

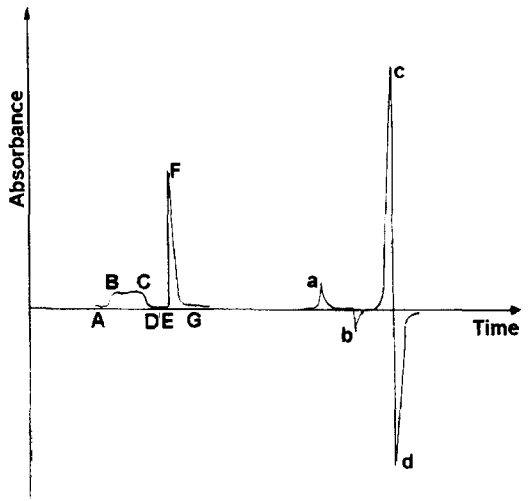

Fig. 1. The absorption signals of conventional AT-FAAS (I: left) and DAT-FAAS (II: right).

3.2. Modification of trapping equipment

Up to now, all of the atom trapping methods found in the literature required to flush the cooled water out of the trap tube rapidly by a blast of air via the control tap system during the releasing cycle. If the air blast was continuously passed or the cooled water was not flushed out of the tube completely and rapidly, the surface of the trap tube would not be heated up rapidly, which will influence the signal intensity of cadmium. Thus, it is important to keep the air flow high enough and optimum air-passing time in each operation. In order to simplify the trapping equipment and operation procedure, the original trapping equipment was improved in our work. The sketch of the improved equipment was shown in Fig. 2.

The coolant water was passed through the trap tube during the collection cycle. During the release cycle, the tap water was shut off by turning the three-way valve and the coolant water auto-

matically flow out of the trap tube through I and II without a blast of air. Under the same instrumental conditions, the sensitivity and precision for the determination of cadmium with the improved system were compared with those with the previous system. The signals of conventional AT-FAAS and D-AT-FAAS were recorded and the analytical results indicated that the precisions obtained with the improved equipment are consistent with that obtained from the original equipment without loss in sensitivity. Although the improved system does not give a higher sensitivity and a lower detection limit than the original one, the former simplified the analytical procedures in the release cycle. Thus, the improved trapping equipment was used in the sequent experiments.

3.3. Effect of trap position

The tube position was optimized with respect to both the light path and the flame. This is done by varying its distance from the burner or the light path, one at a time, and measuring the derivative signal from cadmium solution of 0.05 μg ml^{-1} in each position until the maximum derivative signal is obtained. Effect of the position of the trap tube between the light path and the burner on the peak height of the derivative absorption signal was shown in Fig. 3.

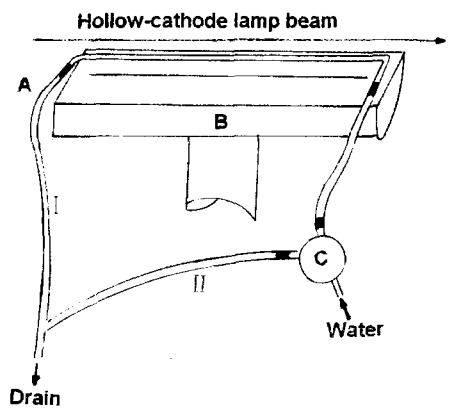

Fig. 2. The sketch of the improved trapping equipment: A, trapping tube; B, burner; and C, water control system.

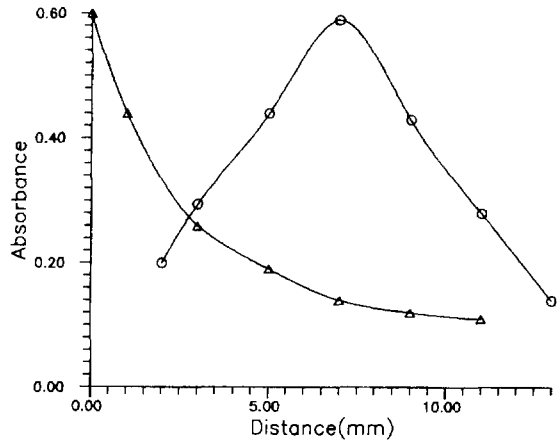

Fig. 3. Influence of the position of the tube trap on absorbance of cadmium: (△) absorbance versus distance of the trap from the lamp beam; (○) absorbance versus distance of the trap from the burner slot.

As shown in Fig. 3, the maximum derivative absorption signal was obtained by raising the trap tube until its intersection with the absorption beam caused about a 5% intensity loss, but it will be achieved with sacrifice in precision. The optimum position of the trap tube corresponded to the distance of 2 mm under the light path and 7 mm above the burner.

3.4. Effect of flame condition

The influence of flame condition on the sensitivity of cadmium with D-AT-FAAS was investigated by altering the acetylene flow rate with a fixed air flow rate of 6 l min^{-1}. The derivative signals obtained by aspirating 0.05 μg ml^{-1} cadmium standard solution varied over the range 0.48, 0.52, 0.58 and 0.57 for the acetylene flow rates of 0.5, 1.0, 1.5 and 2.0 l min^{-1}, respectively. The derivative absorbances of cadmium were not very different for collecting or releasing in a lean and full-rich flame. The sensitivity of D-AT-FAAS for cadmium appeared to be virtually independent of the flame condition. The acetylene flow rate of 1.5 l min^{-1} and air flow rate of 6 l min^{-1} were used for further experiments during the collection and release cycles.

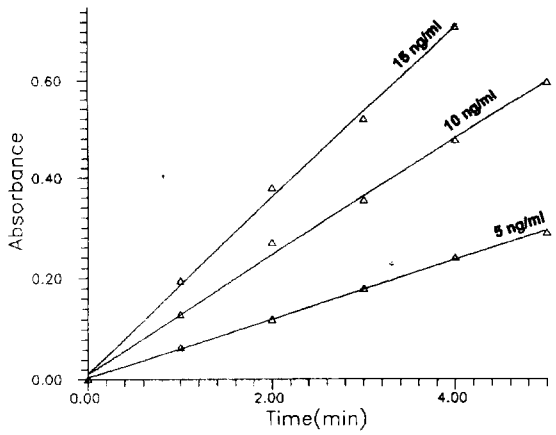

Fig. 4. Collection of cadmium as a function of time.

3.5. Effect of coolant water flow

Effect of coolant water flow on derivative absorbance was studied with cadmium solution of 0.05 μg ml^{-1}. The results showed that the temperature of the outlet water increase with the decrease of the flow rate when the temperatures of inlet water remain constant. At a temperature of 17°C of the inlet water, when the flow rate is of 2.5 and 0.3 l min^{-1}, the temperature of outlet water is 19°C and 31°C, respectively. No significant differences were found in the derivative absorbance when a coolant water flow rate of 0.3–2.5 l min^{-1} were used during the collection cycle of cadmium solution.

3.6. Effect of collection time

The deposition of cadmium on the trap tube surface is not a one-way process, but will eventually reach an equilibrium. To test the efficiency of collection from different dilution, aqueous solutions of cadmium were collected for different time. Fig. 4 shows the effect of collection time on the analytical growth curves for various concentration of cadmium standard solutions.

The plot (Fig. 4) illustrated that the derivative absorbance is linearly dependent on collection time for cadmium solution. For a 1 min collection time, the characteristic concentration of D-AT-FAAS was 0.37 ng ml^{-1}, which was improved 6.2 times compared with 2.3 ng ml^{-1} obtained by AT-FAAS. The sensitivity could be further enhanced when 2, 5 and 10 mV min^{-1} sensitivity grades were used.

3.7. Effect of derivative sensitivity grade

The derivative measurement system is an electric differential apparatus. The output signal of the atomic absorption spectrometer was magnified at first and then differentiated. The derivative measurement system has five sensitivity grades, 2, 5, 10, 20 and 50 mV min^{-1}. In order to examine the influence of the sensitivity grade on sensitivity of D-AT-FAAS, the derivative absorption signals were measured using different sensitivity grades with cadmium standard solutions. The results are given in Table 2.

As shown in Table 2, the smaller the number of derivative sensitivity grade, the bigger the derivative absorbance with the same cadmium solution.

Table 2
Effect of derivative sensitivity grade on the derivative absorbance

Sensitivity grade (mV min^{-1})	Absorbance			
	2 ng ml^{-1}	5 ng ml^{-1}	10 ng ml^{-1}	20 ng ml^{-1}
50		0.028	0.057	0.120
20	0.030	0.065	0.140	0.295
10	0.062	0.133	0.312	0.641
5	0.131	0.272	0.645	
2	0.340	0.668		

Table 3
Comparison of sensitivity (S) and detection limit (D.L.)

Method	Sensitivity grade (mV min^{-1})	Collection time (min)	S (ng ml^{-1})	D.L. (ng ml^{-1})	Improvement factor[a]	
					S	D.L.
FAAS			27.8	2.9		
AT-FAAS		1	2.3	0.8	12	3.6
	50	1	0.95	0.39	29	7
D-AT-FAAS	20	1	0.37	0.15	75	19
	10	1	0.17	0.11	163	26
	5	1	0.08	0.06	347	48
	2	1	0.028	0.02	992	145
		2	0.014		1985	
		3	0.01		2780	
		4	0.008		3475	
		5	0.006		4633	

[a]Compared with S and D.L. of FAAS.

The highest and lowest sensitivity were obtained by 2 and 50 mV min^{-1} sensitivity grades, respectively. The derivative sensitivity grade could be selected according to the amount of cadmium in real samples.

3.8. Analytical performance of D-AT-FAAS

For a 1 min collection of the cadmium solution, the linear regression equations of D-AT-FAAS obtained at the sensitivity grades of 50, 20, 10, 5 and 2 V min^{-1} were $A = 0.0046C + 0.001$, $A = 0.0119C-0.004$, $A = 0.0258C + 0.009$, $A = 0.0550C-0.010$ and $A = 0.1571C-0.051$ with the coefficients of 0.9935, 0.9945, 0.9947, 0.9989 and 0.9971, respectively, where the A = derivative absorbance and C = concentration of cadmium solution (ng ml^{-1}).

The concentration ranges were $0 \sim 180$, $0 \sim 70$, $0 \sim 34$, $0 \sim 17$ and $0 \sim 7$ ng ml^{-1} at 50, 20, 10, 5 and 2 mV min^{-1} sensitivity grade, respectively. The good linearity is the basis of quantitative analysis by D-AT-FAAS.

Under the optimal instrumental conditions, the sensitivities of D-AT-FAAS, AT-FAAS and FAAS were compared, where sensitivity is defined as the concentration of analyte that provides the peak absorbance of 0.0044. The detection limits of the three methods, based on the triple value of the standard deviation of the blank ($n = 11$), were determined, respectively. The results were shown in Table 3. At the sensitivity grades of 50, 20, 10, 5 and 2 mV min^{-1}, the sensitivities of D-AT-FAAS were 0.95, 0.37, 0.17, 0.08 and 0.028 ng ml^{-1} for a 1 min collection time, respectively, which were 29, 75, 163, 347 and 992-fold better than that of FAAS. The sensitivities of different sensitivity grades could be further enhanced with the extension of collection time. At 2 mV min^{-1} grade, the sensitivities of D-AT-FAAS was three orders of magnitude higher than that of FAAS for a 2 min collection time, the detection limit was improved for two orders of magnitude for 1 min collection.

For a 1 min collection of standard cadmium solution, the precisions (relative standard deviation) of D-AT-FAAS, AT-FAAS and FAAS were evaluated by seven replicate determinations, respectively. The results showed that the relative standard deviation (RSD) of D-AT-FAAS method is in the range of 2.6–4.5% at the cadmium concentration level of 50–2 ng ml^{-1}, that of AT-FAAS method is 2.5% at the cadmium concentration level of 100 ng ml^{-1} and that of FAAS method is 1.9% at the cadmium concentration level of 1000 ng ml^{-1}.

The above results indicated that D-AT-FAAS had better sensitivity, lower detection limit and

good reproducibility compared with those of AT-FAAS and FAAS.

3.9. Sample analysis

The proposed method was applied to the determinations of cadmium in several water samples. The recovery results of cadmium spiked to water samples are in the range of 90–111% which indicated that the proposed method is reliable.

The slope of the calibration graphs prepared with standard curve method for water samples was found to be almost identical with that of the standard additions plot. The standard curve method was used in the determinations of various samples.

The accuracy of the proposed method was checked by comparing the sample analysis results with those of ETAAS. The results of sample analysis are listed in Table 4.

The content of cadmium in samples given in Table 4 showed that the concentration of cadmium determined by D-AT-FAAS was in good agreement with that obtained by ETAAS. A 't' test has been done on the results listed in Table 4, which indicates that no significant difference was found at the confidence level of 95%. The precision of the method, when applied to real samples, was in the range of 4.7–5.6% expressed as RSD%. The results showed the applicability of the proposed method for the determinations of ng ml^{-1} level cadmium in water samples.

Table 4
Comparison of the results obtained with D-AT-FAAS and ETAAS for cadmium content in water samples[a]

Water sample	Content in sample (ng ml^{-1})	
	D-AT-FAAS	ETAAS
1	0.25 ± 0.13	0.23 ± 0.024
2	0.18 ± 0.010	0.20 ± 0.009
3	0.32 ± 0.015	0.31 ± 0.027
4	0.21 ± 0.012	0.23 ± 0.019
5	0.35 ± 0.018	0.35 ± 0.030

[a]2 mV min^{-1}, collecting for 5 min, average of seven determination and standard deviation.

4. Conclusions

The combination of AT-FAAS with the derivative technique significantly improved the sensitivity and detection limit compared with those obtained with AT-FAAS and FAAS for the determination of cadmium. The obtained results point to the feasibility of using D-AT-FAAS for the routine determinations of trace cadmium in water samples. The advantages of the present method include simplicity of the procedure, shorter time required for analysis, less risk of contamination and less analytical cost.

References

[1] S. Chakravarty, M.K. Deb and R.K. Mishra, J. AOAC Int., 76 (1993) 604.
[2] J. Hu, W. Qi and B. Pu, Mikrochim. Acta, 109 (1992) 295.
[3] L. Wang, P. Sun and N. Shen, Fenxi Huaxue, 20 (1992) 648.
[4] G. Huo, X. Cui and Y. Li, Lihua Jianyan, Huaxue Fence, 28 (1992) 161.
[5] X. Li and X. Zhang, Beijing Gongye Daxue Xuebao, 18 (1992) 54.
[6] X. Lin, J. Xiong and Z. Li, Fenxi Ceshi Tongbao, 11 (1992) 70.
[7] S. Daniele and G.A. Mazzocchin, Anal. Chim. Acta, 273 (1993) 3.
[8] Q. Si, S. Xu, J. Cai, R. Lu and Y. Zhu, Fenxi Huaxue, 20 (1992) 272.
[9] P. Sun, Henan Daxue Xuebao, 20 (1990) 65.
[10] E. Nakamura, H. Nimiki and N. Sakurabayashi, Kogyo Yosui, 401 (1992) 9.
[11] C.R. Lan, Analyst, 118 (1993) 189.
[12] J.Y. Cabon and A. Le Bihan, J. Anal. At. Spectrom., 7 (1992) 383.
[13] M. Hiraide, T. Usami and H. Kawaguchi, Anal. Sci., 8 (1992) 31.
[14] H. Chuang and S. Huang, Spectrochim. Acta, 49B (1994) 283.
[15] F. Sugimato, Y. Maeda and T. Azumi, Kankyo Gijutsu, 19 (1990) 763.
[16] F. Sugimato, Y. Maeda and T. Azumi, Nippon Kaisui Gakkaishi, 44 (1990) 124.
[17] A.K. Singh and S.K. Dhingra, Analyst, 117 (1992) 889.
[18] H. Ince, S. Akman and U. Koklu, Fresenius J. Anal. Chem., 342 (1992) 560.
[19] S. Akman, H. Ince and U. Koklu, J. Anal. At. Spectrom., 7 (1992) 187.
[20] M.C. Yebra-Biurrun, A. Bermejo-Barrera, M.P. Bermejo-Berrera and M.C. Barciela-Alonso, Anal. Chim. Acta, 303 (1995) 341.

[21] M.C. Yebra-Biurrun, A. Bermejo-Barrera and M.P. Bermejo-Berrera, Analyst, 116 (1991) 1033.
[22] D. Tsalev, C. Li and M. Ivanova, Colloq. Atomspektrom. Spurenanal., 5th (1989) 465.
[23] Z. Fang, T. Guo and B. Welz, Talanta, 38 (1991) 613.
[24] C.M. Lau, A.M. Ure and T.S. West, Anal. Proc., 20 (1983) 114.
[25] C.M. Lau, A.M. Ure and T.S. West, Anal. Chim. Acta, 146 (1983) 171.
[26] J. Khalighie, A.M. Ure and T.S. West, Anal. Chim. Acta, 131 (1981) 27.
[27] S.M. Fraser, A.M. Ure, M.C. Mitchell and T.S. West, J. Anal. At. Spectrom., 1 (1986) 19.
[28] D.J. Roberts and Kang.ombi V. Kahokola, J. Anal. At. Spectrom., 4 (1989) 185.
[29] A.D. Turner, D.J. Roberts and Y.L. Cor, J. Anal. At. Spectrom., 10 (1995) 721.
[30] H. Sun, J. Liang and S. Xie, Hebei Daxue Xuebao, 11 (1991) 24.
[31] H. Sun, W. Wang, D. Zhang and L. Yang, The Second International Symposium of Worldwide Chinese Scholar on Analytical Chemistry, Jinan University Press, Shenzhen, China, 1995.
[32] H. Sun, W. Kang, X. Yang and Z. Li, Fenxi Huaxue, 13 (1985) 703.
[33] H. Sun, L. Yang and D. Zhang, J. Anal. At. Spectrom., 1 (1996) 265.

ELSEVIER

Talanta 44 (1997) 1987–1993

Talanta

DC arc vaporization as a sample introduction technique for analysis of solids by ICP-OES

D.A. Rusak, R.L. Litteral, B.W. Smith, J.D. Winefordner *

Department of Chemistry, University of Florida, Gainesville, FL, 32611, USA

Received 8 August 1996; received in revised form 24 October 1996; accepted 25 October 1996

1. Introduction

In a continuing search to find the most advantageous method for the analysis of solid samples, many methods for the introduction of solids into an inductively coupled plasma (ICP) have been developed. These methods span from early techniques such as direct insertion [1,2] to the more recent approach of laser ablation [3–5], with nebulization [6], electrothermal vaporization (ETV) [7–9], arcs and sparks [10,11], and various types of slurry sampling [12,13] in between. The ideal method for the analysis of solid samples would eliminate sample dissolution, minimize sample preparation, and maximize transport into the ICP. These goals are yet to be realized with any of the introduction techniques currently used for the ICP.

The main complication that hinders the various nebulization techniques is the need for lengthy sample preparation involving digestion procedures. When preparing aqueous solutions of solid samples for these introduction methods, many problems can be encountered, such as incomplete dissolution, precipitation of insoluble analyte elements, loss of volatile analytes during heating and contamination of the sample [3]. In order to avoid these difficulties, slurry sample introduction techniques have been used. However, slurry nebulization, unlike nebulization of aqueous solutions, can result in an aerosol that is unrepresentative of the original sample. Because of irregular particle size distributions, larger particles are removed from the spray chamber. This is especially true for geological samples which contain minerals that are more resistant to grinding [12]. Nebulization also suffers from poor transport efficiency which can lead to memory effects if the sample is deposited in the transport tubing. This problem has been addressed by other ICP sample introduction techniques.

ETV, laser ablation, and arc and spark ablation rely on direct analysis of solid samples with minimal to no sample preparation. These methods were developed for sample vaporization and transport to the ICP and therefore separate species based on their volatility. ETV is superior to nebulization for analysis of most solids because it has low sample consumption and high transport efficiency [5]. However, ETV is hindered by spectral and nonspectral interferences that may occur when sample matrices reach the plasma and is limited by the kinds of samples that can be analyzed [9]. In contrast, laser ablation offers direct solid sampling for almost any sample and can also be used to determine spatial distribution of elements in a solid [1]. A disadvantage of laser

* Corresponding author. Fax: +1 352 3924651; e-mail: ;dwin@chem.ufl.edu

PII S0039-9140(96)02159-5

ablation is that it is difficult to know how much sample is being ablated or whether the ablated sample is representative of the entire solid [1]. Spark ablation may be used as an alternative to laser ablation, but requires that the sample be a conducting solid [10]. The direct current (DC) arc, historically used as an excitation source for optical emission experiments [14], is capable of vaporizing 7 mg of many solid samples in a short (10–20 s) period of time. If these vapors are collected and transported to an ICP, the DC arc then becomes a viable sample introduction technique.

This paper presents a method for determining magnesium in geological samples by DC arc-ICP optical emission spectroscopy (DC arc-ICP-OES). Minimal sample preparation is required and detection limits in the ppm range are obtainable. A method of standard additions is used in conjunction with internal standardization for the Mg determinations.

2. Experimental

2.1. Apparatus

Fig. 1 is a schematic of the experimental setup. The power supply (Cat. # 2001-30, Zeebac, Barea, OH.) is a constant current device capable of yielding a continuous range between 4 and 30 A at an open circuit voltage of 300 V. Ignition is automatic and a timer can be set to terminate the current at any time less than 120 s after ignition.

Because the vapors generated by the DC arc must be transported to the ICP, the design of the arc chamber has several unique requirements. First, it must be essentially air tight to prevent the escape of analyte. Second, it must have an inlet and an outlet through which argon can pass to carry the analyte vapors to the plasma. Third, it should have as small a volume as possible to minimize dilution of the analyte vapor and thus loss in sensitivity. Finally, the chamber must provide for easy sample manipulation and must also be constructed of a material which can withstand the heat produced by the arc but which does not produce any interferences when heated.

Several chamber designs constructed of water cooled glass or ceramic chambers with brass electrode holders were evaluated. Because of the inherent differences in the thermal expansion coefficients of these materials, it was difficult to maintain an air-tight enclosure. Vaporized analyte could not be effectively contained, and ambient air could enter the chamber and subsequently the plasma. The design used in the present experiments consisted of a glass dome, with an inlet and an outlet, which was sealed onto a ceramic disk. The ceramic disk had two holes in it which allowed connection of the power supply to the cathode and the anode. The total volume of the chamber was about 100 cm^3 and it was found that water cooling was not necessary. This design was air-tight, mechanically robust, and simple to use.

The power supply was connected to the arc chamber by a positive and negative lead, both of which connect to the bottom of the chamber. The

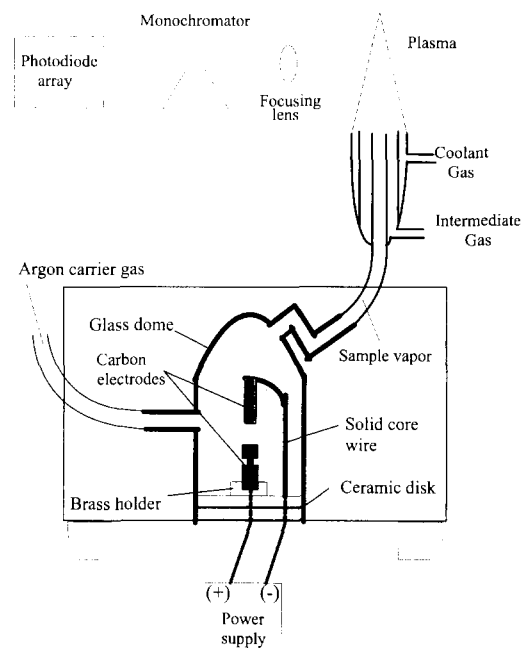

Fig. 1. Schematic of DC Arc Vaporization for ICP-AES. The two carbon electrodes are enclosed by the glass dome which forms an air-tight seal with a ceramic disk. Argon carrier gas flows through the glass dome and carries vaporized sample to the plasma torch. At the torch, intermediate and coolant gas (both argon) are introduced.

sample containing electrode (anode) fit into a holder and was secured with a set screw while the upper electrode (cathode) screwed into a holder supported by 4 ga. solid core wire. The anode was a crater electrode (Ultra Carbon, Bay City, MI) with an outer diameter of 0.185 in. and a sample capacity of 0.025 cm^3. The upper electrode was a post electrode (Ultra Carbon, Bay City, MI) which had been snapped off behind the taper so that it was a simple cylinder of uniform diameter 0.125 in. It was observed that this geometry minimized arc wandering on the sample electrode. The electrodes and electrode holders were enclosed by the glass dome which sealed to the ceramic base, allowing collection of vaporized sample and transport to the plasma by a sample gas flow.

The inductively coupled plasma (Thermo Jarrell Ash, Franklin, MA) was a 40 MHz argon plasma which operated at forward powers between 700–1500 W. The lower portion of the enclosure (just below the torch) was removed to allow for easy switching between sample introduction techniques.

The detector used was an intensified photodiode array (ST-120, Princeton Instruments, Trenton, NJ) which was fitted to a monochromator (82020 Scanning Monochromator, Thermo Jarrell Ash) containing a grating of 1180 lines mm^{-1} blazed at 250 nm. The plasma was imaged onto the entrance slit by a lens mounted in the plasma enclosure. The linear dispersion of the monochromator was 1.2 nm mm^{-1} and the 1024 diode array had a total length of 25 mm, so that a spectral window of about 30 nm could be viewed when the photodiode array was in the focal plane of the monochromator.

2.2. Technique

In early experiments, the arc chamber was connected to the plasma torch by a 20 cm length of 6 mm i.d. Tygon tubing. This length was intentionally kept short to minimize diffusion of analyte vapor during transfer. Integration of the emission signal from the ICP was initiated at the same time the arc was ignited and continued until approximately 2 s after the arc was terminated, a total of 12 s. In this way, the emission from an entire 2 mg sample of Mg in graphite was collected.

One problem with this technique which immediately became evident was that the argon plasma was noticeably unstable during the operation of the arc, which led to large fluctuations in the emission signal obtained at any given instant. Integration of the signal over the total time of 12 s gave relative standard deviations of $\sim 50\%$. The problem of plasma stability was solved by coupling the arc chamber to the plasma with a 2 m length of Tygon tubing. With this longer length of tubing, it was found that the analyte vapors did not arrive at the plasma until ~ 10 s after the arc was ignited. The vaporization of sample was complete by this time, so the arc was extinguished before the arrival of analyte at the plasma. The emission could then be collected from the much more stable plasma, and it was found that sample dilution was not significant as the signal still lasted a total of about 10 s, and was of roughly equal intensity to that with the shorter transfer tube.

Initial characterization of the experimental setup was performed on Mg standards prepared in graphite powder. Initially less than 0.2 g of $MgCl_2$ was weighed into a plastic vial and mixed with graphite powder (Ultra Carbon, Bay City, MI). Serial dilutions of the sample with graphite powder were carried out to achieve a range of Mg concentrations from 1 to 88 ppm. Different weights of the graphite matrix standards could be reproducibly loaded into the sample electrodes by use of a solids pipette (Drummond, Broomall, PA).

The current, electrode gap, and sample size were evaluated to find a combination of these three parameters which would provide total vaporization of the analyte with maximum reproducibility. The range of current available was 0–30 A and the electrode gap range (limited by the chamber) was 0–15 mm.

The voltage drop across the electrodes was measured for different electrode gaps. At a gap of 10 mm and a current of 10 A, the voltage between the electrodes was 25 V; the voltage decreased to 14 V at a gap of 5 mm. Temporal profiles of vaporized Mg in graphite powder for different gap and current settings showed that the time required to vaporize a given mass of sample was

more dependent on the gap length than the arc current. At a gap of 5 mm, a minimum current of 8 A was required to produce a smooth vaporization of a 2 mg sample of Mg in graphite. The Mg emission from the ICP was transient over a 10 s period. At a current of 10 A, the temporal profile remained largely unchanged but the emission intensity increased slightly. Further increases in current for the 5 mm arc gap produced little change in the signal observed. With the arc gap set to 10 mm, the signal from the vaporized analyte was considerably more intense but also more unstable. At an electrode gap of 10 mm, the arc tended to wander around the sample electrode causing discontinuous vaporization and erratic emission. The time required to vaporize a 2 mg sample could not be well-defined. For this reason, and because this larger gap greatly increased the heating of the chamber and reduced the life of the electrodes, it was decided that a gap of 5 mm would be used with a current of 10 A.

The intermediate gas flow rate had little effect on the signal intensity over the range in which a stable plasma could be formed, and a value of 1 l min^{-1} was used for all experiments. Similarly, the coolant gas flow rate affected the signal insignificantly, and was set to a value of 10 l min^{-1} which gave the most symmetrical plasma shape. The carrier gas flow rate, however, had a large effect on signal intensity. A minimum of 1 l min^{-1} was needed to puncture the plasma and form a sample channel; this flow rate provided the greatest signal level which dropped rapidly with increasing flow rates. In an effort to examine carrier gas flow rates of less than 1 l min^{-1}, an auxiliary flow was coupled to the flow through the chamber so that a sample channel could be maintained at flow rates of less than 1 l min^{-1} through the chamber. However, it was found that the signal intensity did not increase and so a carrier flow of 1 l min^{-1} was used with no auxiliary flow.

The effect of the forward power of the plasma on emission intensity was examined over the range 1000–1400 W and a value of 1250 W was chosen as much for plasma stability as for signal intensity. The image of the ICP was focused onto the entrance slit of the monochromator, and the effect of plasma viewing height on signal and background intensities was measured. Fig. 2 is a plot of background versus viewing height for the nebulizer and DC arc sample introduction. The background during nebulization falls sharply with increased viewing height while the background with DC arc introduction is fairly constant over the entire height of the ICP plasma. This phenomenon is probably due to the large amount of water introduced to the plasma with the nebulizer as compared with the DC arc. The result is that the optimum S/N ratio for DC arc sample introduction is found at a somewhat lower viewing height (14 versus 18 mm above the load coil) than for nebulization, although the maximum signal for both types of sample introduction is found at 14 mm. The width of the entrance slit was set at 50 μm giving a spectral resolution of 0.1 nm.

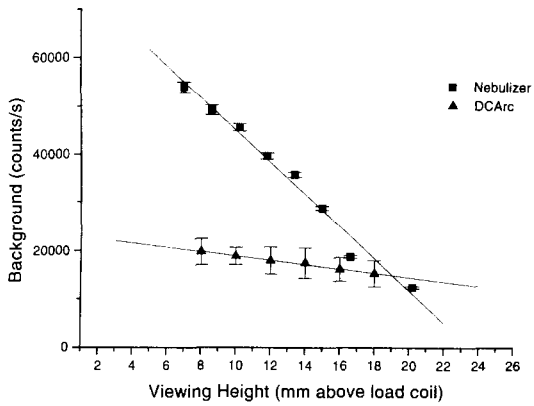

Fig. 2. Backround versus viewing height for nebulizer and Dc Arc. The background counts obtained at low plasma viewing heights are much higher for aqueous nebulization than for DC arc vaporization. As a result, the optimum viewing height is lower in DC arc vaporization than in nebulization.

The photodiode array was set to collect emission for a total of 10 s and to display a spectrum of average intensity over the 10 s integration. The Mg 279.6, 280.3, and 285.5 nm lines could all be viewed simultaneously in the window which extended from 260–290 nm. The 279.6 nm line was the strongest line observed for Mg emission in the UV/VIS region.

3. Results and discussion

Two different experiments were performed to test the feasibility of calibrating based on a total energy procedure in which emission is integrated for the entire sample [14]. First, different masses of sample of the same Mg concentration were vaporized, then equal masses of samples of different Mg concentrations. The plot of signal versus mass was linear over a mass range of 0.5–2.0 mg and the plot of signal versus concentration was linear over a concentration range of 1–100 ppm. The slope of the signal versus concentration shows that the arc is capable of determining analytes in solids with a sensitivity superior to that found in nebulization of liquids. However, large relative standard deviations indicated that this calibration technique was not sufficient to perform determinations with precision better than about 20%. The sensitivity of the DC arc technique is due to the high transport efficiency relative to nebulization. For comparison, a calibration curve was generated by nebulizing aqueous Mg standards. Table 1 is a comparison of the analytical figures of merit. A comparison of the sensitivities (counts ng^{-1}) for nebulization ICP-OES and DC Arc-ICP-OES can be done as follows.

With a nebulizer flow rate of 1 ml min^{-1}, 16 ng s^{-1} ppm^{-1} of Mg enter the nebulizer. Dividing the slope of the nebulization calibration curve by this factor gives (3175 counts s^{-1} ppm^{-1})/(16 ng s^{-1} ppm^{-1}) = 198 counts ng^{-1}. The nebulization ICP-OES gives 198 counts ng^{-1} of Mg consumed.

With a 2 mg sample of Mg in graphite powder in the DC arc, 2 ng ppm^{-1} of analyte are vaporized. Dividing the slope of the DC arc vaporization calibration curve by this factor gives (23272 counts ppm^{-1})/(2ng ppm^{-1}) = 11635 counts ng^{-1}. The DC arc gives 11635 counts ng^{-1} of Mg consumed.

Table 1
Comparison of analytical figures of merit for nebulization ICP-OES and DC Arc-ICP-OES

	Nebulization	DC arc vaporization
Sensitivity (slope)	3175 counts s^{-1} ppm^{-1}	23 272 counts ppm^{-1}
Precision (RSD)	4%	23%
Limit of detection	5×10^2 ppb	4×10^2 ppb

The DC arc system therefore produces 60 times as much emission ng^{-1} of Mg as the nebulizer system. If the transport efficiency of the nebulizer is assumed to be 1–2%, then the transport efficiency of the arc introduction is approaching unity. This high efficiency provides increased sensitivity.

A common technique for analysis of solids by ICP-OES is dissolution of the solid into an aqueous solution followed by nebulization of the solution. This technique inherently dilutes the analyte concentration usually by several orders of magnitude. Because the DC arc has a limit of detection roughly equal to that of the nebulizer but requires far less sample dilution (samples may be mixed with graphite powder to aid vaporization), it is a much more efficient sample introduction method for analyzing trace concentrations in solids, especially when only a small amount of sample is available.

For instance, a 10 mg solid sample containing 1 ppm of analyte could be analyzed five times by DC arc sample introduction of 2 mg samples containing 1 ppm of analyte. If the same 10 mg sample were to be analyzed by nebulization, it would first have to be dissolved in a minimum of 10 ml of solution which would then contain the analyte at a concentration of 1 ppb. Clearly, if both methods have equal limits of detection, the DC arc sample introduction is more desirable. The disadvantage is poor precision.

To improve the precision, an internal standard was used. Initial investigations were carried out with phosphate rock and coal fly ash as samples. The Si line at 288.1 nm was used as the internal standard because it corresponded to a fairly strong transition of a major element which could be viewed in the 30 nm window containing the Mg transition at 279.6 nm. It was found that when the intensity of the Mg 279.6 nm line was ratioed to the intensity of the Si 288.1 nm line, RSD's of less than 10% could be obtained for successive measurements on both types of samples.

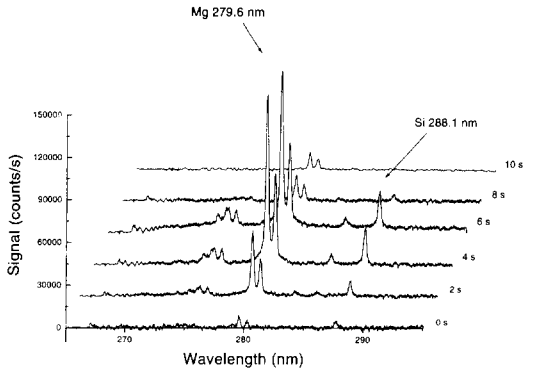

Fig. 3. Temporal profile of emission from NIST Coal 1632b. The signal is transient over about 10 s. The Mg 279.6 nm line intensity is ratioed to the Si 288.1 nm line intensity.

Because the amount of silicon varied from sample to sample, internal standardization did not aid calibration. However, because it reduced run to run deviation, it could improve precision if standard additions were used in the determination. This possibility was examined with two new NIST samples, coal and estuarine sediment, both mixed with graphite. These samples, like the coal fly ash and phosphate rock contained Si which could be used to standardize analyte emission. By spiking the prepared samples with a known amount of analyte, the original analyte concentration was found by plotting the Mg 279.6 nm/Si 288.1 nm intensity versus concentration in a standard addition plot.

The coal standard, NIST Coal 1632b, was mixed with an equal amount of graphite powder (1.00 g/1.00 g) and mixed in a ball mill to give a sample which was 50% by weight coal. The same standard was mixed with an equal amount of a 218 ppm Mg in graphite powder standard prepared from $MgCl_2$ (1.00 g/1.00 g). In this way, the second sample had a Mg concentration 109 ppm greater than the first.

The arc gap was set to 5 mm and the power supply was set to provide 12 A of current for a 10 s duration. At these settings, the signal produced from the vaporized coal was transient over about a 10 s period. The temporal profile was similar to that observed for the Mg standards. Fig. 3 shows spectra taken at 2 s intervals when a 2 mg sample of 50% coal was introduced by the arc. A 2 mg portion of the first sample was placed in the sample electrode by means of the solids pipette and the arc was ignited. The analyte vapors reached the plasma just as the arc was extinguished (as evident by the appearance of the Mg 279.6 nm line) and the signal integration was initiated. After 10 s, the emission had decayed almost to background and signal collection was terminated. The average emission intensity of the Mg 279.6 nm and Si 288.1 nm lines over the 10 s integration were recorded.

This procedure was repeated a total of five times for the first sample and then the spiked sample was run five times in an identical manner. The Mg/Si intensity ratio was determined for each of the runs. The certified value for the Mg concentration in the coal sample was 385 ppm. The value determined for the 50% coal sample by extrapolation of the standard addition plot was 175 ppm. When this value is doubled (to account for sample dilution with graphite powder), the Mg concentration determined is 350 ppm, an error of 9%. When a second point was added to the standard addition curve, by preparing a sample to be plotted at 55 ppm added, the intercept was at -200, giving a concentration in the coal of 400 ppm, with error of 4%.

NIST Estuarine Sediment 1646 was mixed with graphite powder to give a sample which was 10% sediment (0.20 g sediment/1.80 g graphite) and mixed with 280 ppm Mg (0.20 g sediment/1.80 g 280 ppm Mg) to give a spiked sample to be plotted at 252 ppm added. The analysis was carried out the same way as the coal analysis and the standard addition plot gave an intercept of -1005 ppm. Correction for the dilution factor of 10 gave a Mg concentration of 1.01% in the original sample. The certified value for Mg in the estuarine sediment was 1.08%, a 6% error.

4. Conclusions

The DC arc-ICP-OES method involving standard additions to an internally standardized sample allows quantitation of Mg with good accuracy and precision, as evidenced in the determination in two NIST standards. The disadvantages of

such a technique are that some sample preparation is required and some a priori knowledge of the analyte concentration is required in order to make appropriate additions. Furthermore, simultaneous determinations of more than one analyte would require additions of more than one element to the spiked samples. Nevertheless, the technique is capable of performing accurate determinations in solids without dissolution, and if the run to run variations in the transport efficiency can be reduced, simultaneous multi-element determinations should be possible in non-conductive solids with no sample preparation and no internal standardization.

Laser ablation has the potential to do similar determinations, but because the mass of material introduced to the plasma is small and varies greatly between matrices, detection limits are seldom below ppm (for emission experiments) and an internal standard must often be used.

In direct sample insertion techniques, the vaporization, atomization, and excitation all take place in the plasma, and independent optimization of any one of these parameters is impossible. Determinations at the sub-ppm level by emission can be done only in select matrices, and fractionation makes multi-element determinations extremely challenging.

Electrothermal vaporization is perhaps the technique most similar to DC arc introduction. Larger sample loadings can be introduced to the plasma, and detection limits for emission experiments are into the ppb range. Precision on the order of 5–15% is obtainable [9]. ETV sample introduction is very sensitive to matrix effects, however, and temperature programs must be optimized for each matrix to be analyzed.

It has been shown in this work that an inductively coupled plasma can tolerate 2 mg of solid vaporized by a DC arc over a period of 10 s. Determination of Mg in graphite powder by atomic emission gave a detection limit of 400 ppb, and determination of Mg in NIST Coal 1632b and Estuarine Sediment 1646 by standard additions using similar experimental parameters gave an average precision of 5%.

Future work will include the redesign of the arc chamber and possibly of the transfer tubing in an attempt to stabilize the transport efficiency. Use of fluxing agents (NaF, etc.) to act as carriers, and of additions of O_2 to the argon carrier gas, are being investigated at present for determinations in ceramics. Ultimately the arc may be connected to an ICP-MS for mass spectrometric detection of vaporized analytes.

Acknowledgements

The authors would like to acknowledge the financial support of the Engineering Research Center (ERC) for Particle Science and Technology at the University of Florida, The National Science Foundation (NSF) grant # EEC-94-02989, and the Industrial Partners of the ERC.

References

[1] W.T. Chan and G. Horlick, Appl. Spectrosc., 44 (1990) 380.
[2] M. Umemoto, K. Hayashi and H. Haraguchi, Anal. Chem., 64 (1992) 257.
[3] E.R. Denoyer, K.J. Fredeen and J.W. Hager, Anal. Chem., 63 (1991) 445.
[4] P. Richner, D. Evans, C. Wahrenberger and V. Dietrich, Fresenius J. Anal. Chem., 350 (1994) 235.
[5] R.E. Russo, Appl. Spectrosc., 49 (1995) 14.
[6] D.R. Wiederin, F.G. Smith and R.S. Houk, Anal. Chem., 63 (1991) 219.
[7] R.D. Edigerand and S.A. Beres, Spectrochim. Acta, 47B (1992) 907.
[8] J. Wang, J.M. Carey and J.A. Caruso, Spectrochim. Acta, 49B (1994) 193.
[9] L. Moens, P. Verrept, S. Boonen, F. Vanhaecke and R. Dams, Spectrochim. Acta, 50B (1995) 463.
[10] N. Jakubowski, I. Feldmann and D. Stuewer, Spectrochim. Acta, 50B (1995) 639.
[11] A.G. Coedo, M.T. Dorado and B. Fernandez, J. Anal. At. Spectrom., 10 (1995) 859.
[12] L. Halicz, I.B. Brenner and O. Yoffe, J. Anal. At. Spectrom., 8 (1993) 475.
[13] N.J. Miller-Ihli, Spectrochim. Acta, 50B (1995) 477.
[14] P.W.J.M. Boumans, Theory of Spectrochemical Excitation, Plenium Press, New York, 1966.

ELSEVIER

Talanta 44 (1997) 1995–2001

Talanta

The study for optimization of chromatographic condition by means of artificial neural networks

Weiqiang Guo [1,a,*], Ping Zhu[1, b], Horst Brodowsky [c]

[a] *Department of Chemistry, Hangzhou University, Hangzhou, 310028, People's Republic of China*
[b] *Department of Physics, Hangzhou University, Hangzhou, 310028, People's Republic of China*
[c] *Institute of Physical Chemistry, Kiel University, 24118, Kiel, Germany*

Received 31 May 1996; received in revised form 5 November 1996; accepted 13 November 1996

Abstract

In this paper, the optimization of gas chromatographic experimental parameters is investigated using a three layer feed-forward neural network with the back-propagating. The design, development, and testing of the neural network are described in detail. The chosen structure is 4-6-2 system with a learning rate η of 0.6 and a momentum constant μ of 0.4. The results of several simulations are very satisfactory. Network results are compared with the results obtained by the orthogonal method. © 1997 Elsevier Science B.V.

Keywords: Gas chromatographic; Neural network; Optimization

1. Introduction

Optimization of chromatographic operating conditions is a complicated process which requires much time and effort because many parameters must be taken into consideration. In general, the determination of optimal experimental conditions is based on either the orthogonal testing or the simplex optimization method. The orthogonal testing is a method using an 'Orthogonal Table' to arrange the multifactors testing, which can find the better analytical conditions with relatively few testing times. But, in general, it is only the self effects but the mutual cross effects of the factors are considered that it is not easy to reach the global optimization. The optimizing process of Simplex Optimization Method, in a sense, just likes 'a blind person climbing a mountain', to observe the much conditions, such as the best point, worst point, expansive point, reflective point and so on, before every experiment. So it is time-consuming and costly, especially if a large number of parameters is involved. Thus, there is a need for a new optimizing method to select the optimum experimental conditions.

Recently, much attention has been paid to the application of the novel method of artificial neural networks (ANN's) in chemistry and some satisfactory results have been achieved [1–4]. In analytical chemistry, ANN's have been used for calibration [5–8], parameter estimation [9–11],

* Corresponding author.
[1] Visiting scholar at Keil University, Germany.

PII S0039-9140(96)02171-6

Table 1
The experimental parameters

Testing No.	Column temperature (°C)	Carrier gas flow (ml min^{-1})	Thermal desorption temperature (°C)	Thermal desorption temperature (°C)
1	123	15	80	1
2	138	30	80	2
3	153	40	80	3
4	123	30	93	3
5	138	40	93	1
6	153	15	93	2
7	123	40	105	2
8	138	15	105	3
9	153	30	105	1

Table 2
The RMSE values of different number of hidden nodes system (trained 10 000 times)

Hidden nodes	3	4	5	6	8	10
$\eta = 0.5$ $\mu = 0.5$	0.04709	0.04346	0.03812	0.02405	0.04070	0.03504
$\eta = 0.6$ $\mu = 0.4$	0.02845	0.02092	0.02305	0.02531	0.02507	0.02968
$\eta = 0.4$ $\mu = 0.5$	0.08245	0.04348	0.05035	0.04320	0.02673	0.04359
$\eta = 0.4$ $\mu = 0.3$	0.09020	0.09132	0.09315	0.08482	0.09142	0.09094

prediction [12–15], spectrophotometric research [16–19], and optimization of analytical conditions [20,21].

ANN's utilize the weight matrices to perform the mathematical transformation of the input vector to the output vector. The feed-forward neural networks trained by back-propagation of errors have one obvious advantage: there is no need to know the exact form of the analytical function on which the model should be built. That is, neither the functional type (linear, polynomial, exponential, logarithmic etc.) nor the number and position of the parameters are required. Therefore, ANN's are suitable for experimental condition optimization since the relationship between evaluating indices and the experimental input parameters is complex, nonlinear, and often cannot be expressed with a certain mathematical formula.

In this paper, optimizing conditions of the thermal desorption-gas chromatography experiments were studied. The task consists of handling the information on three levels or layers: an input layer; an output layer; and a hidden layer. The input layer consists of four chromatographic experimental parameters, which are column temperature (T_c), carrier gas flow (F_c), and the temperature and time of thermal desorption (T_d and t_d). The output layer consists of the two output signals of peak height (H) and resolution (R). A third level with a certain number of nodes, the hidden layers, is inserted between the input and output layers. The number of nodes in the hidden layers is not fixed but is itself to be adjusted for optimal results, six in the case. As shown in Fig. 1, every node on a lower level sends a signal to every node on the next level above, constituting a feed-forward network. A so-called backward propagating algorithm was applied to arrive at specific result. For the purpose of mathematical treatment, the four input parameters and the two output signals are regarded as nodes. The optimizing results from the network having hidden layer nodes from 2 to 10 are compared. A 4-6-2 system was selected as the most suitable structure. The simulation of the experimental results was very satisfactory. The optimal ranges of values for the experiment obtained from the neural network were compared with that obtained by the orthogonal method.

Table 3
The RMSE with different η and μ (iterated 10 000 times)

η	1.2	1.2	1.0	1.0	0.7	0.7	0.7	0.6
μ	0.5	0.8	0.5	0.8	0.3	0.6	0.7	0.6
4-4-2	0.07187	0.04403	0.08311	0.03451	0.07436	0.04086	0.03359	0.03925
4-6-2	0.03820	0.03709	0.05486	0.04187	0.07250	0.03528	0.06502	0.07868

Table 4
The RMSE with different η' and μ' (iterated 10 000 times, $\eta = 0.6$ and $\mu = 0.4$)

η'	1.2	1.0	0.8	0.5	1.0	1.0
μ'	0	0	0	0	−0.1	0.1
4-6-2	0.06775	0.02531	0.04527	0.07951	0.08643	0.06586

2. Theory

The topological architecture of the three-layer feed-forward neural networks is shown in Fig. 1. The numbers of input layer and output layer, in the study, are four and two, which are referred to as the chromatographic experimental parameters and as the evaluating indices or output signals. The number of hidden layer nodes is discussed in Section 4.1.

For an input layer node, the output is equal to its input:

$$X_i = O_i \tag{1}$$

In Eq. (1), the subscript i indicates the ith input layer node. The output from the input layer are weighted and fed to the hidden nodes. The net input of jth hidden node is:

$$\text{net}_j = \sum_{i=0}^{m} O_i \times W_{ij} \tag{2}$$

where W_{ij} indicates the weight of the connection between the ith input node and the jth hidden node. The outputs of the hidden layer nodes (O_h) are given after transformation by the sigmoidal function:

$$O_{hj} = f(\text{net}_j) \qquad f(x) = \frac{1}{1+e^{-x}} \tag{3}$$

The subscript hj in Eq. (3) represents the jth hidden layer node. The output of the bias node in both input and hidden layer is a constant, 1.

The output of the last layer (output layer) nodes are given by the sum after weighted input from the hidden layer nodes and the transformation:

$$O_j = f\left(\sum_{j=0} O_j \times W_{ij}\right) \tag{4}$$

where W_{jl} is the weight connecting the jth hidden node to the lth output layer node. The relative error between the output value and the target value for the evaluation indices H and R is

$$E_l = \frac{Y_l - O_l}{Y_l} \tag{5}$$

where Y_l is the target value of lth index, i.e., the experimental value of H and R. The calculation repeated after moving to another experimental point.

After carrying out the procedure about for all combination of input signals, the root-mean-square error (RMSE) was given by Eq. (6).

$$\text{RMSE} = \sqrt{\sum_{s=1}^{n} \sum_{l=1}^{n_i} \frac{E_l^2}{n_i n}} \tag{6}$$

where n is the number of trained samples, and n_i is the number of output layer nodes.

The every weight, which initial value is given by the computer randomly and remained equal in all systems with different hidden nodes in order to compare them conveniently, is changed automatically via Eq. (7) and then the training's are re-

Table 5
Comparison between the experimental and the computational values

No.	Experimental		Calculation[a]		Absolute (relative)	Error
	H	R	H	R	H	R
1	632	2.10	636[b]	2.09[b]	4 (0.63)	4 (0.63)
			634[c]	2.08[c]	2 (0.32)	2 (0.32)
2	742	2.32	750[b]	2.34[b]	8 (1.10)	8 (1.10)
			740[c]	2.43[c]	−2 (−0.27)	−2 (−0.27)
3	799	2.95	793[b]	2.94[b]	−6 (−0.79)	−6 (−0.79)
			807[c]	2.83[c]	8 (1.00)	8 (1.00)
4	668	1.78	663[b]	1.74[b]	−5 (−0.74)	−5 (−0.74)
			666[c]	1.81[c]	−2 (−0.30)	−2 (−0.30)
5	876	2.52	879[b]	2.51[b]	3 (0.34)	3 (0.34)
			873[c]	2.56[c]	−3 (−0.34)	−3 (−0.34)
6	858	2.56	855[b]	2.57[b]	−3 (−0.36)	−3 (−0.36)
			853[c]	2.59[c]	−5 (−0.58)	−5 (−0.58)
7	664	1.73	669[b]	1.76[b]	5 (0.75)	5 (0.75)
			676[c]	1.76[c]	6 (0.90)	6 (0.90)
8	548	1.54	549[b]	1.55[b]	1 (0.16)	1 (0.16)
			553[c]	1.42[c]	5 (0.91)	5 (0.91)
9	570	1.84	569[b]	1.85[b]	−1 (−0.18)	−1 (−0.18)
			569[c]	1.87[c]	−1 (−0.18)	−1 (−0.18)

[a] After trained RMSE = 0.00194.
[b] The initial weights were different from c group.

peated until RMSE falls into a acceptable region, the trained network is obtained.

$$\Delta W_{ij}(t) = \eta \delta_j O_i + \mu \Delta W_{ij}(t-1) \quad (7)$$

In Eq. (7), t is the number of iterations of the neural computation. The proportionality constant η is the learning rate and determines how fast the changes $\Delta W_{ij}(t)$ should be implemented in the iteration cycles. The momentum constant μ prevents sudden changes in the direction in which corrections are made. The error δ can be expressed as:

$$\delta_l = E_l f'(\mathrm{net}_l) \quad (8)$$

for output layer lth node and:

$$\delta_j = \left(\sum_{l=0}^{n_l} \delta_l l_{lj} \right) f'(\mathrm{net}_{hj}) \quad (9)$$

for hidden layer jth node. Here $f'(\mathrm{net}_{hj})$ is the partial derivative with respect to W_{ij} of the transformation function.

We let trained network scan automatically and intensively near the range of experimental points, and give a series of vectors of calculation results, which must include optimal point(s).

3. Experiment

The thermal desorption-gas chromatography experiments were done on a 8701 model thermal desorber manufactured by Shanghai Fourth Analytical Instrument Factory, China and a GC-9002 model gas chromatograph with a 100 cm length of stainless steel column manufactured by Shanghai Xinhu Precision Analytical Instrument Factory, China. The chromatographic indices were recorded and calculated by Chromatopac C-R3A, a data processor for chromatographs, Shimadzu, Japan. The neural computation was run on a 486-PC micro-computer.

Nine group parameters were selected as gas chromatographic experimental conditions by means of the orthogonal method (see Table 1), taking $CHCl_3$ and another impurity in drugs as test sample. The experimental results were trans-

Table 6
The corrected reliability coefficient of the two methods

	The first group		The second group	
	H	R	H	R
Reliability coefficient	0.9994	0.9982	0.9997	0.9934

Table 7
The optimal regions obtained by neural network computation

No.	Optimal region				Range of peak height	Range of resolution
	a	b	c	d		
1	145 ~ 153	15	80 ~ 86	2 ~ 3	800 ~ 900	2.5 ~ 2.8
2	123 ~ 153	35 ~ 45	80 ~ 86	1 ~ 2	780 ~ 920	2.4 ~ 2.8
3	135 ~ 153	40 ~ 45	100 ~ 105	1	830 ~ 880	2.2 ~ 2.5
4	135 ~ 145	40 ~ 45	93	1 ~ 2	780 ~ 880	2.3 ~ 2.8

a Column temperature (°C).
b Carrier gas flow (ml min^{-1}).
c Thermal desorption temperature (°C).
d Thermal desorption time (min).

formed to the evaluating indices: peak height (H) and resolution (R). The experimental parameters and devaluating indices were used in the neural computational program as straining data. The optimized experimental parameters were selected from the output of the computational results.

4. Results and discussion

4.1. Selection of the number of hidden layer nodes

In order to obtain the best neural network structure, several ANN systems with different number of hidden nodes were tested in the study. The RMSE values after iterating ten thousand times are listed in Table 2. From the RMSE values the 4-4-2 and 4-6-2 systems are better than the others. In the two systems, the RMSE's of 4-6-2 system are all smaller than that of 4-4-2 systems except for the case $\eta = 0.6$ and $\mu = 0.4$. After iterating the two structure neural network ($\eta = 0.6$ $\mu = 0.4$) 30 000 times, the RMSE's of the two networks were further decreased from 0.02531 to 0.00861 (for 4-6-2 system) and from 0.02092 to 0.01038 (for 4-4-2 system), respectively.

For these reasons, we chose 4-6-2 structure as the optimized system.

4.2. Selection of the η and μ

The initial architecture of the neural network (the number of layers, neurons, and especially for weights) is only an initial guess, it must be modified after performing calculations. Since the feed-forward neural networks is a non-linear optimization system, there is the problem of local minimal, in other words, there is the possibility that the procedure may end in a local minimum, if the learning rate η and the momentum constant μ are not selected very carefully. The steepest way downhill dose not necessarily lead to the global minimum, and it is not possible in the back-propagation approach to justify the weights infinitesimally [22]. In training process, if the value of the learning rate and the momentum constant were too small (< 0.4), RMSE would show large fluctuation, and could not reach a global minimum quickly. The same would occur when the chosen values were too large (see Fig. 2).

The another phenomenon to be noted found from Fig. 2(b) and Table 2 and Table 3 is that RMSE was smaller when the values of η and μ are close to each other but not equal. If η was greater than μ, the RMSE's were oscillatory for a certain range in training. Good values for the learning rate η lie between $0.5 \sim 0.7$ in the study, the optimal momentum constant μ was slightly smaller.

Another problem for modifying weights was how to determine the η' and μ' when the RMSE$(t) >$ RMSE$(t-1)$. It cannot be assured that the RMSE decreases smoothly in the training process for all neural networks. If RMSE$(t) >$ RMSE$(t-1)$, the direction of the modifying weights value (ΔW_{ij}) must be changed, i.e., the η and μ (denoted as η' and μ') have to be changed. The test results are listed in Table 4, and the best value are $\eta' = 1.0$ and $\mu' = 0$.

4.3. Evaluation of the stability of the network

After settling the optimal values of $\eta = 0.6$ and $\mu = 0.4$, the network was trained 200 000 times, Table 5 showed the results obtained from chromatographic experiment and neural computation. It should be noted that the predicted results are satisfactory, and that the difference between experimented and calculated values is small: 8 (1.10%) for peak height and -0.12 (-6.49%) for resolution. If initial weights are chosen differently, the agreement between the experimental results and the computational values is very much the same.

Table 8
Comparison between the experimental and the computational values

No.	Optimal region				Calculation		Experimental	
	a	b	c	d	H	R	H	R
1	145	15	80	2	875	2.79	882	2.76
2	145	15	86	2	863	2.62	866	2.65
3	123	40	80	1	896	2.62	890	2.60
4	138	40	86	1	890	2.70	891	2.73
5	145	40	105	1	853	2.27	860	2.30
6	153	40	100	1	870	2.48	865	2.52
7	135	40	93	1	876	2.38	866	2.44
8	145	40	93	2	787	2.47	770	2.38

a Column temperature (°C).
b Carrier gas flow (ml min^{-1}).
c Thermal desorption temperature (°C).
d Thermal desorption time (min).

The corrected reliability coefficient [23] was calculated in order to test the reliability between the neural computation and the chromatographic experiment. The results are listed in Table 6, they show that the results of the neural network calculation have a high degree of reliability.

4.4. The determination of optimal experimental regions

Fig. 4 shows the relationship of peak height (H) and resolution (R) to the four chromatographic parameters in the orthogonal method. Though the resolution was influenced slightly by changes in thermal desorption time and column temperature, changes in thermal desorption temperature and carrier gas flow had larger effects on R. The peak height was influenced significantly by all four parameters. Additionally, the experiment showed that the column efficiency decreased if the carrier gas flow was greater than 45 ml min^{-1}.

From these observations, the optimal operating region selected was: column temperature: 148°C; carrier gas flow: 40 ml min^{-1}; thermal desorption temperature: 93°C; thermal desorption time: 2 min. Because the effects of the four parameters were considered independently and their mutual cross effects were overlooked, it cannot be guaranteed that the selected region is globally optimal.

As opposed to the orthogonal method, the neural network method scanned the whole range of experimental parameters intensively, i.e., it took the mutual influence of the four parameters into account. Therefore much more faith may be placed in the optimal region obtained by the neural network method.

Based on the neural computational data, there are four favorable regions with higher values of peak height and resolution (Table 7). Only one region was found by the orthogonal method, and it is second worst of the four found by the ANN. Additionally, the ANN revealed some general trends: (1) long thermal desorption times are

needed in combinative relatively low thermal desorption temperatures; (2) short thermal desorption times are needed in combinative relatively high thermal desorption temperatures; and (3) the peak height and the resolution will be much smaller ($H < 50$ and $R < 0.6$) if the thermal desorption temperature is higher than 130°C and the carrier gas flow is less than 30 ml min^{-1}.

After further experiments and researching, we found that the experimental results of H and R were nearly the same to the computational values (Table 8). It is proved that the ANN can be used to optimize the chromatographic conditions.

5. Conclusion

Based on the discussion above, it can be concluded that the neural network method is very suitable for optimizing chromatographic experimental conditions, especially for multi-parameter experiments. It provides a new, efficient, and optimal approach in analytical chemistry.

Acknowledgements

This research was supported by the University of Kiel, Germany. We would also like to thank Mr Christopher Bartlett, Kiel University.

References

[1] J. Zupan and J. Gasteiger, Anal. Chim. Acta, 148 (1991) 1.
[2] Z. Li, Z.N. Cheng, Xu Li and T.H. Li, Anal. Chem., 65 (1993) 393.
[3] J.M. Andrews and S.H. Lieberman, Anal. Chim. Acta, 285 (1994) 237.
[4] S. Ventura, M. Silva and D. Perez-Bendito, Anal. Chem., 67 (1995) 1521.
[5] B. Hitzmann and T. Kullick, Anal. Chim. Acta, 294 (1994) 243.
[6] P.J. Gemperline, J.R. Long and V.G. Gregorion, Anal Chem., 63 (1991) 2313.
[7] T.B. Blank and S.D. Brown, Anal. Chem., 65 (1993) 3081.
[8] T.B. Blank and S.D. Brown, Anal. Chim. Acta, 277 (1993) 273.
[9] L.S. Anker and P.C. Jurs, Anal. Chem., 64 (1992) 1157.
[10] M.D. Wessel and P.C. Jurs, Anal. Chem., 66 (1994) 2480.
[11] J. Han, R.R. Ruan and C.H. Park, Biotechnol. Tech., 9(9) (1995) 637.
[12] M.D. Wessel and P.C. Jurs, Anal. Chem., 66 (1994) 2480.
[13] K.L. Paterson, Anal. Chem., 64 (1992) 379.
[14] T.H. Fischer, W.P. Petersen and H.P. Luthi, J. Comput. Chem., 16 (8) (1995) 923.
[15] R. Keshavaray, R.W. Tock, R.S. Narayan and R.A. Bartsch, Ind. Eng. Chem., 34 (11) (1995) 3974.
[16] J.W. Ball and P.C. Jurs, Anal. Chem., 65 (1993) 505.
[17] J.W. Ball and P.C. Jurs, Anal. Chem., 65 (1993) 3615.
[18] C.R. Mittermayr, A.C.J.H. Drouen, M. Otto and M. Grasserbauer, Anal. Chim. Acta, 294 (1994) 227.
[19] R. Bro, J. Chemom., 9 (5) (1995) 423.
[20] H. Mo and B. Deng, Fenxi Huaxue, 23 (1995) 779.
[21] J. Zupan and J. Gasteiger, Neural Network for Chemists, VCH Weinheim, 1993, p. 197.
[22] J. Zupan and J. Gasteiger, Neural Network for Chemists, VCH Weinheim, 1993, p. 133.
[23] J.R. Thomas and J.K. Nelson, (Eds.) Introduction to Research, Human Kinetics Publishers, Illinois, 1993.

ELSEVIER

Talanta 44 (1997) 2003–2010

Talanta

Electrochemical biosensor for detecting DNA sequences from the pathogenic protozoan *Cryptosporidium parvum*

Joseph Wang *, Gustavo Rivas [1], Concepción Parrado [2], Xiaohua Cai, Mark N. Flair

Department of Chemistry and Biochemistry, New Mexico State University, Las Cruces, NM 88003, USA

Received 24 October 1996; received in revised form 26 November 1996; accepted 26 November 1996

Abstract

An electrochemical hybridization biosensor was developed for the detection of short DNA fragments specific to the deadly waterborne pathogen *Cryptosporidium*. The sensor relies on the immobilization of a 38-mer oligonucleotide unique to the *Cryptosporidium* DNA onto the carbon-paste transducer, and employs a highly sensitive chronopotentiometric transduction mode for monitoring the hybridization event. Variables of the probe-immobilization, hybridization and indicator-detection steps are optimized to offer convenient quantitation of ng ml^{-1} levels of the *Cryptosporidium* DNA target, in connection with short (3–15 min) hybridization times. The suitability for direct detection of the spiked *Cryptosporidium* DNA target in untreated drinking and river water samples is demonstrated. Similar performance characteristics are observed at DNA-coated microfabricated thick-film carbon strips. This and similar developments hold great promise for field screening of *Cryptosporidium* and other microorganisms in environmental samples. © 1997 Elsevier Science B.V.

Keywords: Carbon paste electrode; *Cryptosporidium*; DNA biosensor; Environmental monitoring; Hybridization; Screen printed electrode; Sequence-specific detection; Water quality

1. Introduction

Protozoans of the genus *Cryptosporidium* are obligate intracellular parasites which invade the gastrointestinal systems of their mammalian hosts [1]. Infection by *Cryptosporidium* can cause debilitating, and sometimes life-threatening gastroenteric and diarrheal illness. In humans, *Cryptosporidium* can spread from person to person through direct contact, as has been observed in hospitals [2] or, as has been subsequently recognized, through waterborne outbreaks [3]. A recent, highly-publicized example of the latter occurred in Milwaukee in 1993, in which *Cryptosporidium* caused illness in some 400 000 people, and out of which there were 104 deaths [4]. Five other waterborne outbreaks of *Cryptosporidium* were reported in N. America since 1985 [5].

* Corresponding author. Fax: +1 505 6466033; e-mail: joewang@nmsu.edu

[1] Permanent address: Department Físico Química, Universidad Nacional de Córdoba, 5016 Córdoba, Argentina.

[2] Permanent address: Department Química Analítica, Facultad de Ciencias Químicas, Universidad Complutense, E-28040, Madrid, Spain.

PII S0039-9140(96)02191-1

In particular, the species *Cryptosporidium parvum* has been recognized as a significant global health threat, one of several critical etiologic agents causing severe diarrheal illness, particularly in developing countries [6]. According to the World Health Organization, this debilitating syndrome, resulting in dehydration and malnutrition, is responsible for the deaths of 11 000 children each day and 5 million people a year worldwide, making it the second leading cause of death behind cardiovascular disease [7]. The EPA estimates that 155 million people in the United States are at risk of exposure to *Cryptosporidium* [4]. There currently exists no effective drug treatment for this infection [5], and routine chlorination treatment does not eradicate dormant *Cryptosporidium* organisms in drinking water [4].

Due to the environmental health threat posed by waterborne *Cryptosporidium parvum*, there is an urgent need for a routine test that reliably detects the presence of the pathogen in water supplies. Yet, despite these major concerns and increasing efforts by the EPA, no analytical method satisfactorily detects the *Cryptosporidium* microorganism. The current indirect fluorescence antibody (IFA) assay, prescribed by the EPA, often fails to detect oocysts in spiked samples [4,8]. A variety of other methods, ranging from flow cytometry to immuno-(ELISA or electrorotation) ones, have been proposed, but to date are still in early developmental stage [4,8]. Accordingly, nonspecific turbidity assays commonly serve as the best indicator for the presence of *Cryptosporidium*. A direct, fast and specific sensing scheme, with minimal sample manipulations, is desired for minimizing losses of the oocysts, and providing a rapid warning capability essential for a quick corrective/preventive action by water utilities.

The present article describes the characterization and optimization of a new DNA electrochemical biosensor for detecting *Cryptosporidium* DNA sequences. Genetic methods, relying on the high specificity of DNA hybridization/recognition reactions, hold great promise for environmental monitoring of microorganisms. A highly sensitive protocol for *Cryptosporidium*, based on the coupling of DNA PCR amplification, electrophoretic separation and chemiluminescent measurement, has been developed recently for detecting this protozoan in water samples [5]. Faster and simpler DNA sensing schemes are highly desired for effective wide-scale monitoring at drinking water facilities. Miniaturized hybridization electrochemical sensors, coupling the inherent specificity of DNA recognition reactions with the remarkable sensitivity and portability of electrochemical transducers [9], are particularly attractive for on-site detection of drinking-water pathogens. The new electrochemical biosensor relies on the immobilization, onto the carbon electrode transducer, of a 38-mer oligonucleotide probe, unique to *Cryptosporidium parvum* DNA [5,10] (taken from the gene which codes for the small (18S) subunit of rRNA). Highly sensitive constant-current chronopotentiometry [11,12], is used for transducing the hybridization event, along with the $Co(phen)_3^{3+}$ redox indicator. The use of the $Co(phen)_3^{3+}$ indicator and carbon paste transducers for sequence-selective electrochemical detection was illustrated by Mikkelsen's group [13].

2. Experimental

2.1. Materials

The 38-mer probe (5′-GGG GAT CGA AGA CGA TCA GAT ACC GTC GTA GTC TTA AC-3′, P-sequence) and 38-mer target (5′-GTT AAG ACT ACG ACG GTA TCT GAT CGT CTT CGA TCC CC-3′, T-sequence) were purchased from Life Technologies (Grand Island, New York, USA) as their ammonium salts.

Other oligonucleotides were also received from Life Technologies, and their sequences are given in the Table 1. Single-stranded calf thymus DNA (ssDNA, lyophilized powder, Catalog No. D8899) and double-stranded calf thymus DNA (dsDNA, activated and lyophilized, Catalog No. 4522) were purchased from Sigma (St. Louis, MO). Guanidine hydrochloride (Catalog No. G3272), sodium chloride (Catalog No. S3014), monosodium phosphate (Catalog No. S3139), sodium acetate buffer (3 M, pH 5.2 ± 0.1 at 25°C, Catalog No. S7899), Tris–HCl buffer (1.00 ± 0.05

M, pH 7.00 ± 0.05 at 25°C, Catalog No. T2413) and Tris–EDTA (TE) buffer (100 × concentrate, 1.0 M Tris–HCl, 0.1 M EDTA, pH 8.0, Catalog No. T9285) were also received from Sigma. The above reagents were free of DNase and RNase. Tris(1,10-phenanthroline) cobalt(III) perchlorate was synthesized at NMSU using the method of described by Dollimore and Gillard [14].

DNA stock solutions (nominally 1000 μg ml^{-1}) were prepared with the TE buffer (1 × concentrate, 10 mM Tris–HCl, 1 mM EDTA, pH 8). Sterile distilled water was used for preparing all the solutions. A diode array spectrophotometer (Model 8452A, Hewlett Packard) was employed to correct the concentration of nucleic acids by measuring optical density ($\lambda = 260$ nm).

All glassware, containers, pipette tips and the cell (with exception of the electrodes) were sterilized by autoclaving for 30 min. Sterilized water were used to rinse the electrodes prior to use.

A river water sample was taken from the Rio Grande River (Picacho Bridge, Las Cruces, NM); a tap water sample was collected in this laboratory; waste water samples were collected from the influent and effluent water of the waste water plant of Las Cruces, NM.

Table 1
Effect of various nucleic acids on the hybridization response

Nucleic acid[a]	Concentration (μg ml^{-1})	Signal change (%)
ssDNA	1	+7.7
dsDNA	1	+4.6
totalRNA	1	−4.0
42-mer DNA	1	−0.1
	2	−3.3
36-mer DNA	1	+0.2
	2	+4.1
27-mer DNA	1	+6.2
	2	+10.0
25-mer DNA[b]	1	+1.7
	2	+7.6
15-mer DNA	1	+6.2
	2	−13.2

The CPE with the immobilized 38-mer DNA (P-sequence) was immersed into the hybridization solution containing the complementary strand (1 μg ml^{-1} 38-mer DNA (T-sequence)) alone or its mixture with the interferent given in the table. After 5 min incubation, the electrode was rinsed and transferred into 0.1 mM Co(phen) indicator for 2 min, followed by the chronopotentiometric measurement. The enhancement of the chronopotentiometric signal due to the hybridization of the probe (P-sequence) with the complementary target (T-sequence) served as 100%. Other conditions as in Fig. 1.

[a] The sequence of the DNA oligomers are as below: 42-mer DNA 5′-ACT GCT AGA GAT TTT CCA CAC TGA CTA AAA GGG TCT GAG GGA-3′, 36-mer DNA 5′-CCA CAT GGC CTG TAC TTT AAA AGC TTC CGG ATG ACC-3′, 27-mer DNA 5′-GTC GTC AGA CTC AAA ACC ACG AGA GGG-3′, 25-mer DNA 5′-CAG GAT ATG TGG CGG ATG AGC GGC A-3′, 15-mer DNA 5′-TGT ACG TCA CAA CTA-3′.

[b] The sequence corresponds to a portion of *E. coli* DNA.

2.2. Electrode preparation

Carbon paste was prepared in the usual way by hand-mixing graphite powder (Catalog No. G67-500, Fisher Scientific, Pittsburgh, PA) and mineral oil (Catalog No. M5904, free of DNase, RNase and protease, Sigma) in a 70:30 ratio. The surface was polished to a smoothed finish before use. The body of the working electrode was a Teflon sleeve (3.5 mm, i.d.) tightly packed with the carbon paste. The electrical contact was made with a stainless steel screw.

Some experiments employed screen-printed carbon strip electrodes (SPEs), prepared using a semiautomatic screen printer (Model TF-100, MPM, Franklin, MA). Commercial carbon ink (Product No. C10903D14, Gwent Electric Materials, UK) was printed onto the alumina ceramic plate (33.5 × 101.5 mm, Coors Ceramic Company, Golden, CO) through a patterned stencil to give a group of ten printed carbon electrodes with each carbon strip consisting of a 1.5 × 30 mm area. The electrodes were subsequently cured for 1 h (at 180°C), and were allowed to cool. A layer of an insulator was then placed onto part of the printed carbon strip, leaving a nominal 1.5 × 5 mm working area.

2.3. Chronopotentiometry

Constant-current chronopotentiometric measurements were performed in a three-electrode electrochemical cell (2 ml, Kimble Glass, Vineland, NJ), using a TraceLab potentiometric stripping unit (PSU 20, Radiometer, Denmark) in

connection with an IBM PS/2 55SX computer. According to the TraceLab protocol, the potentials were sampled at a frequency of 30 kHz and the derivative signal (dt/dE) versus potential (E) was recorded following baseline fitting. The analytical signal was evaluated using the peak areas; the reported result is the peak area for the duplex DNA minus the peak area for the probe DNA alone (Δ PSA). The three-electrode system consisted of a carbon-paste working electrode, Ag/AgCl reference electrode (Model RE-1, BAS, W. Lafayette, IN), and a platinum wire auxiliary electrode. The three electrodes entered the cell through a Teflon cover.

2.4. Procedure

2.4.1. Probe immobilization

The 38-mer DNA probe was immobilized on a freshly smoothed CPE by applying a potential of +1.7 V (or +1.8 V in the case of the printed strip) for 1 min followed by 2 min at +0.5 V in a stirred acetate buffer solution (0.2 M, pH 5.2) containing 5 μg ml^{-1} of the DNA probe (P-sequence). The electrode was then rinsed with a solution containing 0.5 M NaCl and 0.02 M phosphate buffer (pH 7.0) for ca. 10 s.

2.4.2. Hybridization

For hybridization reactions, the probe-coated electrode was immersed into the stirred hybridization solution (1 M guanidine HCl, 0.5 M NaCl, 0.02 M phosphate buffer, pH 7.0; 1 or 2 ml) containing the DNA target for the desired time (depending on the target concentration), while holding the potential at +0.5 V. Then the electrode was rinsed with 0.02 M Tris–HCl buffer (pH 7.0) for 10 s.

2.4.3. Indicator binding

The $Co(phen)_3^{3+}$ was accumulated onto the surface hybrid by immersing the electrode into the stirred Tris–HCl buffer solution containing 0.1 mM $Co(phen)_3^{3+}$ for 2 min while holding the potential at +0.5 V. Then the electrode was rinsed with the Tris–HCl buffer for 10 s.

2.4.4. Chronopotentiometric transduction

The surface-accumulated $Co(phen)_3^{3+}$ was measured, after transfer to a blank Tris–HCl buffer solution, using constant-current chronopotentiometry with an initial potential of +0.5 V and a constant current of −6 μA (−3 μA for the screen-printed electrode).

Repetitive measurements were carried out by renewing the surface of the CPE, or by using a new carbon strip, and repeating the above procedure. All operations were carried out at room temperature (22.0 ± 0.5°C).

3. Results and discussion

The 38-mer *Cryptosporidium*-DNA specific probe displayed a strong adsorptive accumulation at the carbon (paste or strip) electrodes. Such interfacial accumulation was exploited for immobilizing the probe onto the surface. Conditions for attaining a full surface coverage and a stable probe layer were explored. Using a 5 μg ml^{-1} solution of the 38-mer probe (P-sequence), surface saturation was achieved following a 2 min accumulation while holding the electrode at +0.5 V. The surface-confined oligonucleotide layer was stable for at least 30 min upon immersing the electrode into the stirred hybridization solution, and maintains the conformation essential for efficient binding of its complementary target strand.

Fig. 1 displays chronopotentiograms for the $Co(phen)_3^{3+}$ at the 38-mer probe coated electrode after immersion in the 1 μg ml^{-1} *Cryptosporidium* target sequence solution for different periods (1–7 min, a–f). The longer the hybridization time, the more duplex is formed, and the more indicator is 'collected' at the surface, leading to larger chronopotentiometric signals. In contrast, no peak enhancement is observed upon repeating this time-dependent experiment in the absence of the *Cryptosporidium* target (dotted lines). Such target-independent blank response reflects the association of the indicator with the ss-probe. The increased peak area in the presence of the target thus serves as the hybridization signal. The resulting plot of the signal versus hybridization time is also shown in Fig. 1 (inset). The response in-

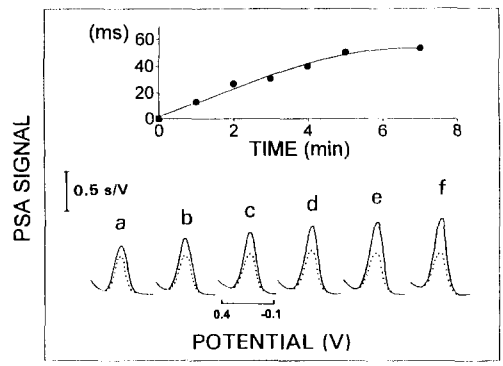

Fig. 1. Chronopotentiograms for $Co(phen)_3^{3+}$ at the probe 38-mer DNA (P-sequence)-modified CPEs towards the target 38-mer DNA (T-sequence) following increasing hybridization times: 1 (a), 2 (b), 3 (c), 4 (d), 5 (e) and 7 (f) min. Dotted traces denote the corresponding blank responses. Also shown (inset) is the resulting plot of chronopotentiometric (PSA) signal versus hybridization time. Probe immobilization: 1 min at +1.7 V followed by 2 min at +0.5 V in 0.2 M acetate buffer (pH 5.2) containing 5 μg ml^{-1} 38-mer (P-sequence); hybridization: 0–7 min at +0.5 V in 0.5 M NaCl, 1 M guanidine HCl, 0.02 M phosphate buffer solution (pH 7) containing 1 μg ml^{-1} 38-mer DNA (T-sequence); indicator binding: 1 min at +0.5 V in 0.02 M Tris–HCl buffer (pH 7) containing 0.1 mM $Co(phen)_3^{3+}$; PSA transduction: in the blank Tris–HCl buffer solution with a constant current of −6 μA and an initial potential of +0.5 V.

creases linearly with hybridization time at first (up to 4 min), and then more slowly. Overall, these data indicate that μg ml^{-1} levels of the *Cryptosporidium* DNA target can be readily quantified following short hybridization times.

Hybridization conditions (other than the time) have a profound effect upon the performance of the *Cryptosporidium* DNA biosensor. Fig. 2 displays the influence of hybridization solution conditions, such as the ionic strength (A) and accelerator level (B). The response rises slowly upon changing the sodium chloride concentration between 0 and 0.2 M and then more rapidly up to 0.5 M; a sharper decline is observed at higher salt levels. The hybridization signal also increases slowly upon raising the concentration of the guanidine accelerator between 0 and 1.0 M, and decreases gradually at higher levels. All subsequent work thus employed a 0.5 M sodium chloride solution containing 1.0 M guanidine. Other potential hybridization accelerators, including several polyethylene glycols (MW 1000–22 000) and dextran sulfate (MW 500 000), were also tested, but did not produce the expected signal enhancement effect. The operating potential also affects the hybridization response. The signal increases slowly from 28 to 47 ms upon changing the potential from 0.0 to +0.5 V, and decreased to 38 ms at +0.6 V (not shown; conditions, as in Fig. 1e). Electrostatic attraction of the negatively-charged target sequence, as well as improved retention of the probe, may account for this potential dependence. The decreased response at very positive hybridization potentials can be ascribed to the direct oxidation of the probe (guanine moiety).

The influence of the $Co(phen)_3^{3+}$-indicator concentration and its association time is shown in Fig. 3. The response increases gradually upon increasing the marker concentration up to 1×10^{-4} M, and decreases rapidly above 2.0×10^{-4} M (A). Very short indicator association times are sufficient for obtaining high sensitivity (B). The response increases rapidly with the association time up to 1 min, and decreases gradually above 2 min. The decreased hybridization signal at high indicator levels or for long indicator-association times is due to a larger indicator response at the

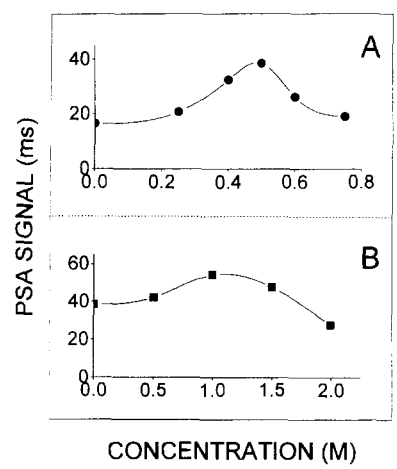

Fig. 2. Effect of sodium chloride (A) and guanidine HCl (B) in the hybridization solution on the response of the target 1 μg ml^{-1} 38-mer DNA (T-sequence) at the probe 38-mer DNA (P-sequence)-modified CPEs using $Co(phen)_3^{3+}$ as indicator. Hybridization time: 5 min; concentration of guanidine HCl: 0 (A) and 0–2 M (B); other conditions as in Fig. 1.

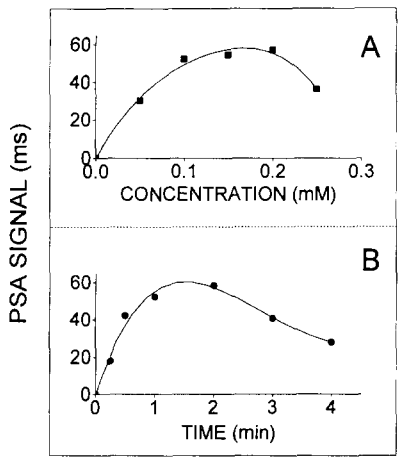

Fig. 3. Effect of $Co(phen)_3^{3+}$ concentration (A) and indicator-binding time (B) on the response of the target 1 μg ml^{-1} 38-mer DNA (T-sequence) at the probe 38-mer DNA (P-sequence)-modified CPEs. Hybridization time: 5 min; other conditions as in Fig. 1.

ss-probe modified electrode (and does not reflect a decrease of the absolute signal).

Fig. 4 displays calibration data for ng ml^{-1} and μg ml^{-1} concentrations of the target *Cryptosporidium* sequence following different hybridization times (1(a), 3(b) and 5(c) min). As expected for saturation of the probe binding sites, shorter hybridization times allow extension of the linear range. For example, while with a 5 min hybridization period linearity prevails up to 500 ng ml^{-1}, the linear range extends to 2.0 μg ml^{-1}

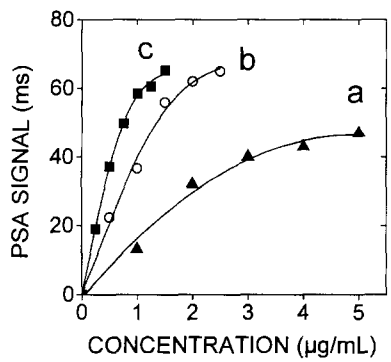

Fig. 4. Calibration plot for the target 38-mer DNA (T-sequence) at the probe 38-mer DNA (P-sequence) modified CPEs using $Co(phen)_3^{3+}$ as indicator. Hybridization time: 1 (a), 3 (b) and 5 (c) min; indicator-binding time, 2 min; other conditions as in Fig. 1.

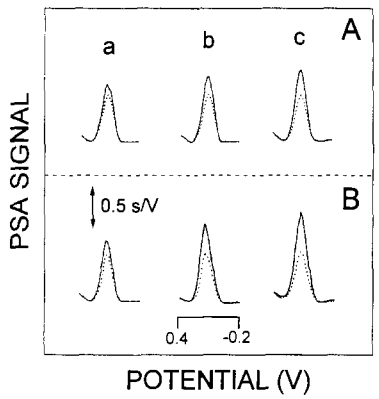

Fig. 5. Chronopotentiograms for the tap water (A) and river water (B) samples spiked with different concentrations of the target 38-mer DNA (T-sequence): 0.5 (a), 1.0 (b) and 1.5 (c) μg ml^{-1} at the probe 38-mer DNA (P-sequence) modified CPEs using $Co(phen)_3^{3+}$ as indicator. Dotted traces denote the corresponding responses of the unspiked solutions. Volume percentage of the water samples in the hybridization solution: 95%; hybridization time: 5 min; indicator binding time: 2 min; other conditions as in Fig. 1.

using a 1 min hybridization. The sensitivity (slope of the linear portions) corresponds to 13.9, 36.4 and 59.2 ms.ml $μg^{-1}$ for the 1, 3, and 5 min hybridization. The data of Fig. 4c indicates convenient measurements of the *Cryptosporidium* DNA target over the 250–1500 ng ml^{-1} range using a 5 min hybridization. Significantly lower levels of 100 and 50 ng ml^{-1} were readily detected using 15 and 30 min hybridization periods, respectively (not shown). Despite these extremely low detection limits, coupling of the sensor with a PCR amplification unit would be required for the detection of a few *Cryptosporidium* parasites in environmental samples.

Fig. 5 demonstrates the suitability of the DNA sensor for direct measurement of the *Cryptosporidium* sequence in untreated drinking-water (A) and river-water (B) samples. Small (500 ng ml^{-1}) increments in the target concentration yield a well-defined hybridization response in connection with a short (5 min) hybridization period. Such defined peaks are similar to those observed in 'synthetic' samples (e.g., Fig. 1c), indicating a lack of major interferences in these environmental samples. In contrast, large interferences were observed in the presence of waste-water matrices.

For example, adding a 12.5% (v/v) and 50% (v/v) sample of the waste water influent and effluent, respectively, to the hybridization solution resulted in 80- and 45% diminution of the hybridization response to the 1 μg ml^{-1} target (not shown; 5 min hybridization). Such severe interference is attributed to competitive adsorption by numerous surfactants present in large excess in waste water samples.

The sensor offers a very good discrimination against non-complementary nucleic acids (Table 1). These selectivity data were obtained by challenging the sensor with various noncomplementary oligomers of different lengths (ranging from 15 to 42 mer), including one corresponding to a portion of the *E. coli* DNA, as well as with chromosomal DNA. The response to the *Cryptosporidium* DNA target increases only slightly (7.7- and 4.6%) in the presence of ss- and dsDNA, respectively. The various oligomers also display a small effect upon the target sequence peak, with signal changes ranging from −3.3 to −13.2% in the presence of excess of the 42- and 15-mer oligomers, respectively. The small changes reported in Table 1 are also attributed to nonspecific adsorption (and its effect upon the attached probe), and not to base-pair recognition.

As desired for on-site environmental applications, we also examined the suitability of microfabricated carbon strips for transducing the recognition of the Cryptosporidium DNA target. Several performance characteristics of the screen-printed DNA biosensor are shown in Fig. 6. The response increases nearly linearly with the hybridization time up to 3 min, and decreases gradually above 4 min hybridization (A). The response also increases linearly with the target concentration up to 750 ng ml^{-1}, and then more slowly (B). While the sensitivity of the strip is lower compared with that of the carbon-paste based device (e.g., versus Fig. 4b), the microfabricated sensor offer extremely low (ng) detection limits. This is indicated from Fig. 6C that displays chronopotentiograms in the absence (a) and presence (b) of 50 ng ml^{-1} *Cryptosporidium* DNA target. Such detectability is similar to that reported above for the carbon paste electrode. The operation of these disposable *Cryptosporidium* sensors may be coupled with the hand-held chronopotentiometric analyzer [15] or microfabricated PCR units [16], for further facilitating their field operation.

In conclusion, we have described a new hybridization biosensor for electrochemical detection of sequences specific to *Cryptosporidium* DNA. Such effort addresses the urgent needs and analytical challenges of detecting *Cryptosporidium* in drinking-water and natural water samples. It should be pointed out, however, that the new device is still in the developmental stage, and additional work is required prior to adaptation for routine environmental testing. In addition to coupling with compact PCR units, attention should be given to the sample collection/treatment step, and to the minimization of nonspecific adsorption effects. Simple freeze-thaw lysis methods should be sufficient for releasing the target nucleic acid from the oocysts. New probes, based on the peptide nucleic acids (PNA) DNA mimics [17] should offer improved biosensor performance, including greater specificity. Work is in progress

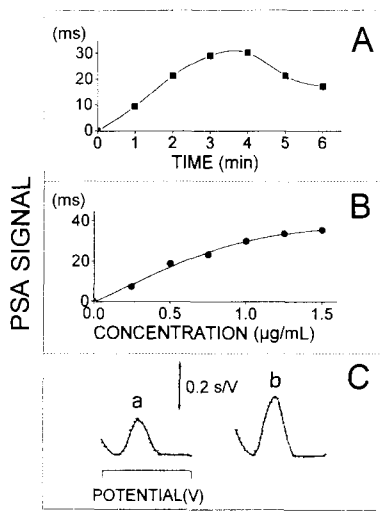

Fig. 6. Response of the microfabricated DNA biosensor: (A) Effect of hybridization time on the the response of the target 1 μg ml^{-1} 38-mer DNA (T-sequence) at the probe 38-mer DNA (P-sequence)-modified SPE using $Co(phen)_3^{3+}$ as indicator. (B) Calibration plot for 0–1.5 μg ml^{-1} 38-mer DNA (T-sequence) at the SPEs following a 3 min hybridization. (C) Chronopotentiograms for 0 (a) and 0.05 (b) μg ml^{-1} target 38-mer DNA (T-sequence) at the SPE following a 30 min hybridization; indicator binding time, 2 min; other conditions as in Fig. 1.

towards the development of similar devices for detecting *E. coli* DNA sequences. Ultimately, we wish to design high-density arrays of microelectrodes coated with probes specific for different bacterial and viral pathogens. This and similar developments should have a profound impact upon environmental monitoring of microorganisms. The miniaturized and nonradioactive nature of electrochemical devices, coupled with their low-power requirements, should further facilitate their adaptation for field-screening of waterborne pathogens. The procedure should also prove useful for clinical diagnostic testing for *Cryptosporidium*.

Acknowledgements

Financial support from the US DOE and DOE-WERC program is gratefully acknowledged. G.R. and C.P. acknowledge fellowships from CONICET (Argentina) and DGICYS: PR95-310 (Spain). Useful discussions with Dr K. Rogers (the US EPA, Las Vegas) are also gratefully acknowledged.

References

[1] J. Watkins, P. Kemp and K. Shepard, in Betts, W.B., et al, (Eds.), Protozoan Parasites and Water, The Royal Society of Chemistry, Oxford, UK, 115 (1995).
[2] K.L. Koch, D.J. Phillips, R.C. Aber and W.L. Current, Ann. Intern. Med., 102 (1985) 593.
[3] R.G. D'Antonio, R.E. Winn, J.P. Taylor, T.L. Gustafson, W.L. Current, M.M. Rhodes, G.W. Gary and R.A. Zajac, Ann. Intern. Med., 103 (1985) 886.
[4] A. Newman, Anal. Chem., 67 (1995) 731A.
[5] D.W. Johnson, N.J. Pieniazek, D.W. Griffin, L. Misener and J.B. Rose, Appl. Environ. Microbiol., 61 (1995) 3849.
[6] W.L. Current and L.S. Garcia, Clin. Microbiol. Rev., 4 (1991) 325–358.
[7] WHO Reports Decry Neglect of World Health Problems, ASM News, 56 (1990) 358.
[8] A. Newman, Environ. Sci. Tech., 29 (1995) 248A.
[9] S.R. Mikkelsen, Electroanalysis, 8 (1996) 15 and references therein.
[10] GenBank Accession Number L16997.
[11] J. Wang, X. Cai, G. Rivas and H. Shiraishi, Anal. Chim. Acta., 326 (1996) 141.
[12] J. Wang, X. Cai, G. Rivas, H. Shiraishi, P. A. Farias and N. Dontha, Anal. Chem., 68 (1996) 2629.
[13] , K.M. Millan, A. Saraullo and S.M. Mikkelsen, Anal. Chem., 66 (1994) 2943.
[14] L.S. Dollimore and R. Gillard, J. Chem. Soc. Dalton Trans., 933 (1973).
[15] J. Wang, Analyst, 119 (1994) 763.
[16] P. Wilding, M. Shoffiner and I. Kricka, Clin. Chem., 40 (1994) 1815.
[17] J. Wang, E. Palecek, P. Nielsen, G. Rivas, X. Cai, H. Shiraishi, N. Dontha, D. Lou and P. Farias, J. Am. Chem. Soc., 118 (1996) 7667.

ELSEVIER

Talanta 44 (1997) 2011–2018

Talanta

Investigation and comparison of the electrochemical behavior of some organic and biological molecules at various conducting polymer electrodes

Gamze Erdoğdu [a], A. Ersin Karagözler [b,*]

[a] *İnönü University, Faculty of Education, Department of Chemistry, 44069, Malatya, Turkey*
[b] *İnönü University, Faculty of Arts and Sciences, Department of Chemistry, 44069, Malatya, Turkey*

Received 3 October 1996; received in revised form 2 December 1996; accepted 3 December 1996

Abstract

Electrodes modified by the electrodepozition of conducting organic polymers such as poly(3-methylthiophene)(PMT), polypyrrole (PPY) and polyaniline (PAN) were used as chemical sensors for voltammetric analysis and flow injection detection of some organic and biological molecules. The electrochemical behaviors of catechol, ascorbic acid, hydroquinone, dopamine, epinephrine, acetaminophen and *p*-aminophenol were examined by differential pulse voltammetry. The electrochemical behavior of these molecules at different electrodes was compared and the effects on behavior of electrolyte type and its pH and the film thickness were systematically examined. The results showed that the proposed modified surface catalyzes the oxidation of these compounds. Electrocatalytic 'efficiency' decreases in order of poly-3-methylthiophene, polypyrrole and polyaniline. Voltammetric peak positions were affected by the nature of the electrolyte and its pH. Also, the effect of increasing film thickness was to observe increased peak heights. Polymer coated electrodes were also used in an amperometric detector for flow injection analysis of most of the these compounds. The responses of the polymer electrode were 5–15 times larger as compared with those of bare platinum. PMT showed improved performance as an amperometric detector for flow injection analysis systems over other types of polymer electrodes. Detection limits as low as 10^{-8}–10^{-9} M were achieved using the PMT, compared with 10^{-6}–10^{-8} M using platinum electrodes. In the flow injection analysis, with increasing molecular weight of analyte molecules was to observe decreased peak heights. © 1997 Elsevier Science B.V.

Keywords: Biological; Electrochemical; Organic; Polymer

1. Introduction

The electrode materials most commonly used in amperometric systems are glassy carbon [1], platinum and gold electrodes [2]. Mercury electrodes, namely; dropping, thin-film mercury and amalgam electrodes have a relatively wide potential range because of the high hydrogen overvoltage at their surfaces [3]. However, several limitations were reported in the application of mercury electrodes in flowing solutions such as their poor mechanical stability and the dissolution of mer-

* Corresponding author. Fax: +90 422 3410034.

PII S0039-9140(96)02196-0

cury at low potentials, which resulted in their inadequacy in the detection of organic and biological compounds. On the other hand, the performance of gold, platinum, glassy carbon and pyrolytic graphite electrodes depends mainly on the method and quality of surface polishing and pretreatment [4].

Recently, the concept of chemically modifying the electrode surface has gained extensive attention among analytical chemists and others. The properties of the modifying 'layer' coated onto the substrate are deliberately designed to alter the sensitivity and the selectivity of the measurement [5–10].

In the last two decades, the need for high sensitivity and selectivity for the analysis of biomolecules has been increasing [11]. Poly(3-methylthiophene) (PMT), Polypyrrole (PPY) and Polyaniline (PAN) are electronically conducting organic polymers which are easily deposited onto electrodes by the electrooxidation of their monomers. Their applications have been discussed and emphasized in terms of electrochromic effects and energy storage and conversion [12–14].

The use conducting polymers as electrode modification agents for voltammetric determination of some biologically important compounds has been demonstrated in a very limited number of works. PMT-coated electrodes were used by Wang and Li [15] to eliminate the passivation problems, in voltammetric measurements of phenolic compounds. They also observed significantly larger oxidation peaks for acetaminophen. In a different study Wang et al. [16] showed that conducting polymers could be used for controlling size exclusion selectivity.

However, these studies concerning the use of conducting polymers for non-mediated electron transfer were limited to a small number of compounds. Also, no observations were made regarding the effects of film thickness and electrolyte properties on the electrocatalytic ability of the conducting polymer electrodes.

Previous work by Atta and coworkers [17] examined the electrochemical behavior of a large number of biologically important compounds at a PMT electrode. The electrocatalytic property of the PMT was demonstrated as well as the effect of the nature and pH of the base electrolyte. Galal and coworkers [18] examined and compared the electrochemical behavior of some neurotransmitters and other organic compounds at different conducting polymer electrodes.

In this paper we examine the electrochemical behavior of a large number of biologically important compounds at PMT, PPY and PAN modified electrodes. Although limited, the effects of the nature and pH of the supporting electrolyte and film thickness were also studied. Electrocatalysis effects of polymer coated electrodes are clearly demonstrated and selective voltammetric determination of binary mixtures were shown to be possible. Additionally, the polymer coated electrodes were also used for sensitive determinations in a flow injection analysis amperometric detection regime. It is observed that the larger the molecular weight of the substance, the smaller the peak heights obtained.

2. Experimental

2.1. Chemicals

3-methylthiophene, pyrrole (Sigma), dopamine, ascorbic acid, epinephrine, *p*-aminophenol, catechol, acetaminophen, aniline, tetrabutylammonium tetrafluoroborate, acetonitrile, sodium sulphate, sodium chloride, sodium nitrate, sodium perchlorate, lithium chloride, calcium chloride, magnesium chloride, sodium phosphate and sodium fluoride (Merck) were used as received. Acetonitrile and H_2SO_4 were used as solvent for electrochemical polymerization. 3-methylthiophene and pyrrole freshly distilled before use. Flow injection analysis of mentioned compounds were performed using Sörensen buffer (pH = 6.9) as mobile phase.

2.2. Apparatus

Electropolymerization with bulk electrolysis (BE) mode was conducted with a BAS (Bioanalytical Systems) 100BW electrochemical analyzer, in

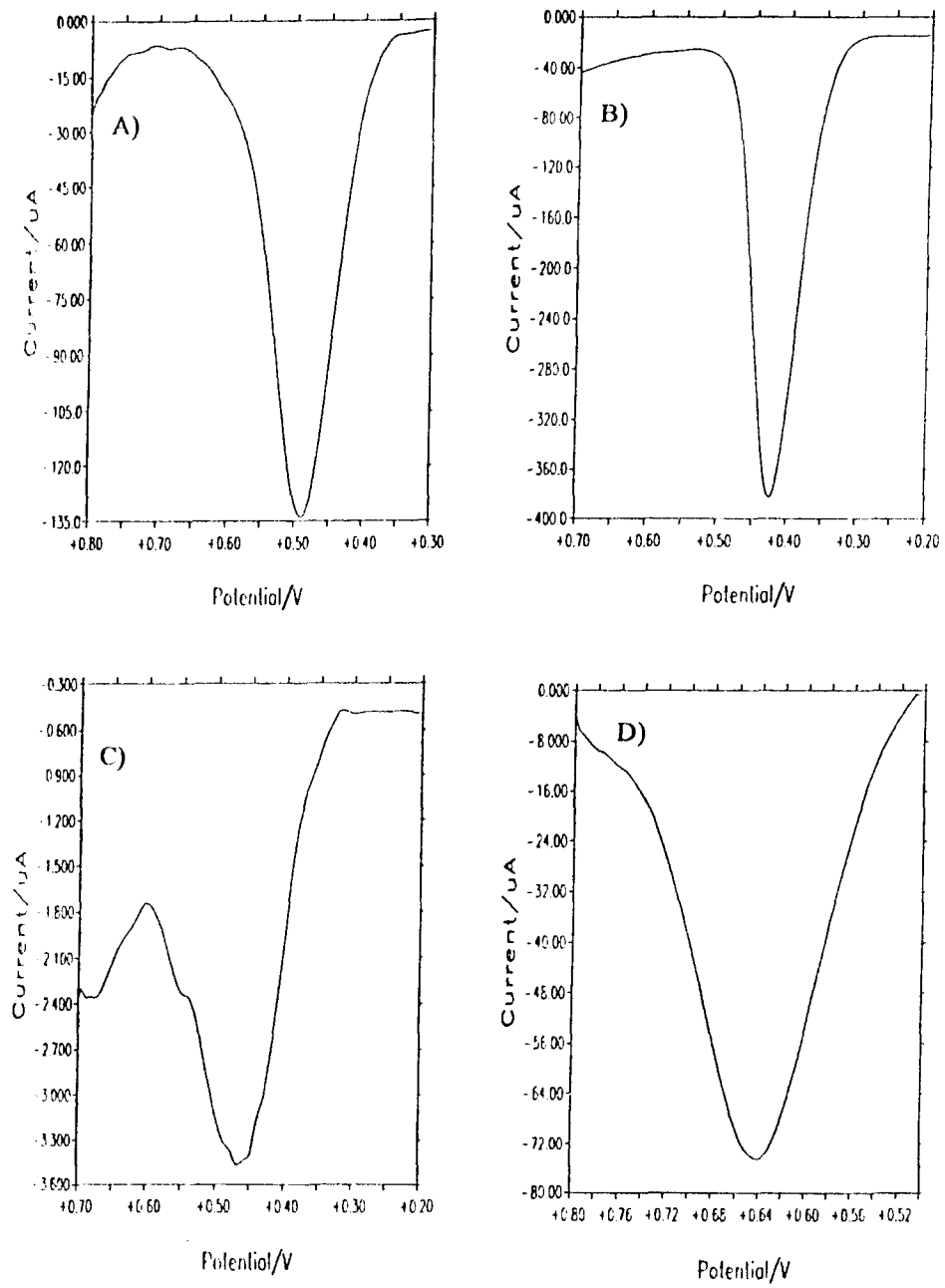

Fig. 1. Differential pulse voltammetry of 20 mM hydroquinone in 200 mM Na_2SO_4 (pH = 2) at PMT (A), PPY (B), PAN (C), and Au (D) electrodes. All films were prepared under similar conditions.

a three electrode cell with gold (BAS, MF-2013) and platinum disk (BAS, MF-1012) as working electrodes, Ag/AgCl (BAS, MF-2063) reference electrode and a Pt wire coil auxiliary electrode. The pH of the solution was measured with a Hanna HI 8314 pH-meter.

Table 1
Differential pulse voltammetric peak potentials for *p*-aminophenol at conducting polymer electrodes[a]

Electrolyte	pH	PMT/Au (mV)	PPY/Au (mV)	PAN/Au (mV)	Au (mV)
$CaCl_2$	2	408	548	520	676
$NaClO_4$	2	281	424	432	460
Na_2SO_4	5	424	392	372	448
NaCl	5	279	436	330	432
LiCl	5	400	470	456	472
NaF	8	184	342	324	348
$NaNO_3$	8	236	399	314	420

[a] *p*-aminophenol and electrolyte concentrations were 20 and 200 mM, respectively.

2.3. Preparation of polymer electrodes

The gold and platinum disk electrodes were cleaned according to standard procedure; namely, polished with successively finer grades of diamond polishing compounds and aqueous alumina slurry (Johnson Mathey Catolog, USA) down to 0.5 μm.

Electrochemical polymerization was carried out in a one compartment cell containing deaerated acetonitrile, 100 mM tetrabutylammonium tetrafluoroborate and 150 mM monomer (in case of 3-methylthiophene, pyrrole) and 0.1 M H_2SO_4 and 485 mM of aniline. The polymer films were grown on gold electrode by bulk electrolysis at a constant potential of 1650 mV versus Ag/AgCl for poly-3-methylthiophene, 950 mV versus Ag/AgCl for polypyrrole and 1700 mV versus Ag/AgCl for polyaniline. The polymer films were grown on platinum disk electrode by bulk electrolysis at a constant potential of 1700 mV versus Ag/AgCl for poly-3-methylthiophene and polyaniline, 1000 mV versus Ag/AgCl for polypyrrole. Electrolysis period was normally 10 s in each case.

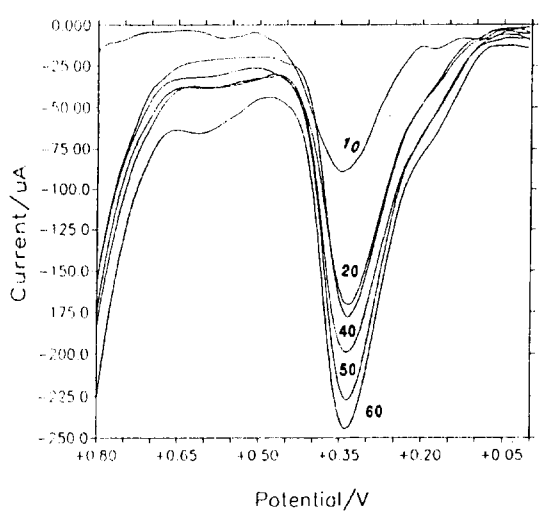

Fig. 2. Effect of film thickness on anodic peak potential for 20 mM catechol on PMT film. The period for film growth with bulk electrolysis is given on each voltammogram. Electrolyte, 200 mm Na_2SO_4 (pH = 2).

3. Results and discussion

3.1. The electrochemical behavior at different polymer electrodes

Fig. 1 shows the differential pulse voltammograms of hydroquinone in Na_2SO_4 at PMT, PPY, PAN and gold electrodes. As can be seen in Fig. 1, the anodic peak potential of hydroquinone at all the polymer electrodes was always much lower than those obtained at the bare gold electrode in the electrolyte chosen for this study (200 mM Na_2SO_4). The comparison of the oxidation peak potential E_{ox} depicted in Table 1, at these electrodes for 20 mM *p*-aminophenol showed two important facts: (i) all the polymer electrodes have relatively lower E_{ox} values as compared with that obtained at Au; and (ii) for the series of polymer electrodes studied, the E_{ox} values increase in the order of PMT < PAN < PPY < Au.

3.2. Effect of film thickness

The effect of film thickness on the anodic peak potential for catechol at conducting electrodes is

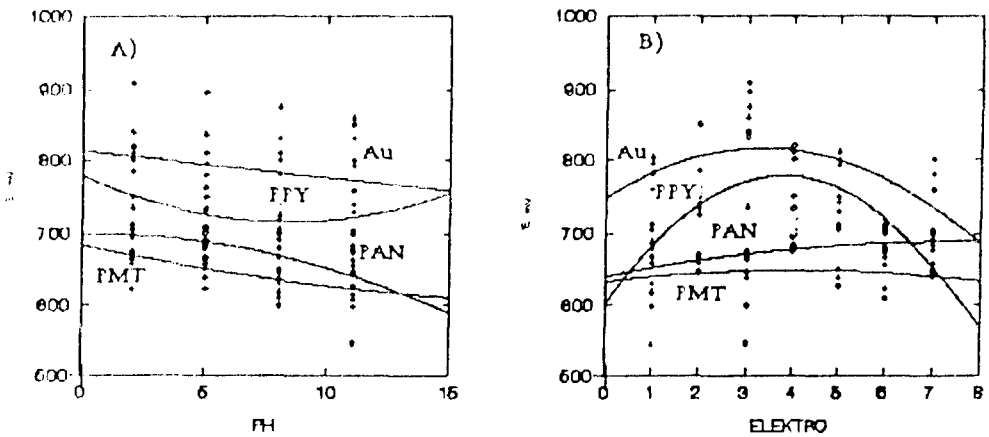

Fig. 3. Effect of (A) pH and (B) electrolyte type on the anodic peak potential of 20 mM epinephrine at different electrodes. Elektrolitler: 1 = NaF; 2 = NaCl, 3 = LiCl, 4 = $CaCl_2$; 5 = $NaNO_3$, 6 = $NaClO_4$ and 7 = Na_2SO_4.

given in Fig. 2. Film thickness had an effect, not only on the peak potentials, but also on the peak current magnitudes. This is expected as with the increasing film thickness surface area of the electrode increases almost regularly.

3.3. Effect of electrolyt type and it's pH

Earlier works involving the use of conducting polymer coated electrodes [19] employed only one type of base electrolyte with a defined pH value to examine the behavior of a certain class of compounds. Although extensive studies have been conducted on the effect of supporting electrolyte for the test substances examined in this work, electrolyte effect will be demonstrated for all these molecules.

Fig. 3 shows effects of pH and electrolyte type on the anodic peak potential of 20 mM epinephrine at different electrodes. As can be seen Fig. 1, the anodic peak potential of catechol at all the polymers electrodes was always much lower than those obtained at bare gold electrodes in all the electrolyte types.

The comparison of the oxidation peak potential E_{ox} at these electrodes for analytes in various electrolyte types showed two important facts: (i) at all the electrodes E_{ox} values shifted to more negative potentials with increasing pH; (ii) in general, with electrolytes containing perchlorate, nitrate and sulphate as anions peak positions for both analytes seem to have shifted to more positive potentials with respect to those electrolytes having fluoride or chloride.

3.4. Stability of the electrode response

The electrodes were prepared under similar conditions, the results showed that the three polymers studied exhibited improved electrocatalytic activity when compared with Au electrode. When the same polymer electrode was used for repetitive runs, stability of the PMT electrode was exceedingly superior over other polymers as depicted in previous work [20].

3.5. Amperometric detection/flow injection analysis of test substances

Amperometric measurements under flow injections or liquid chromatographic conditions are particularly beneficial since the fouling problems are not as severe as in batch experiments, because of small amount of product that is generated. This is especially true for works at low concentrations.

Flow injection analyses of catechol, ascorbic acid, dopamine, epinephrine, *p*-aminophenol, hydroquinone and acetaminophen were performed using Sörensen buffer as mobile phase, 20 μl of

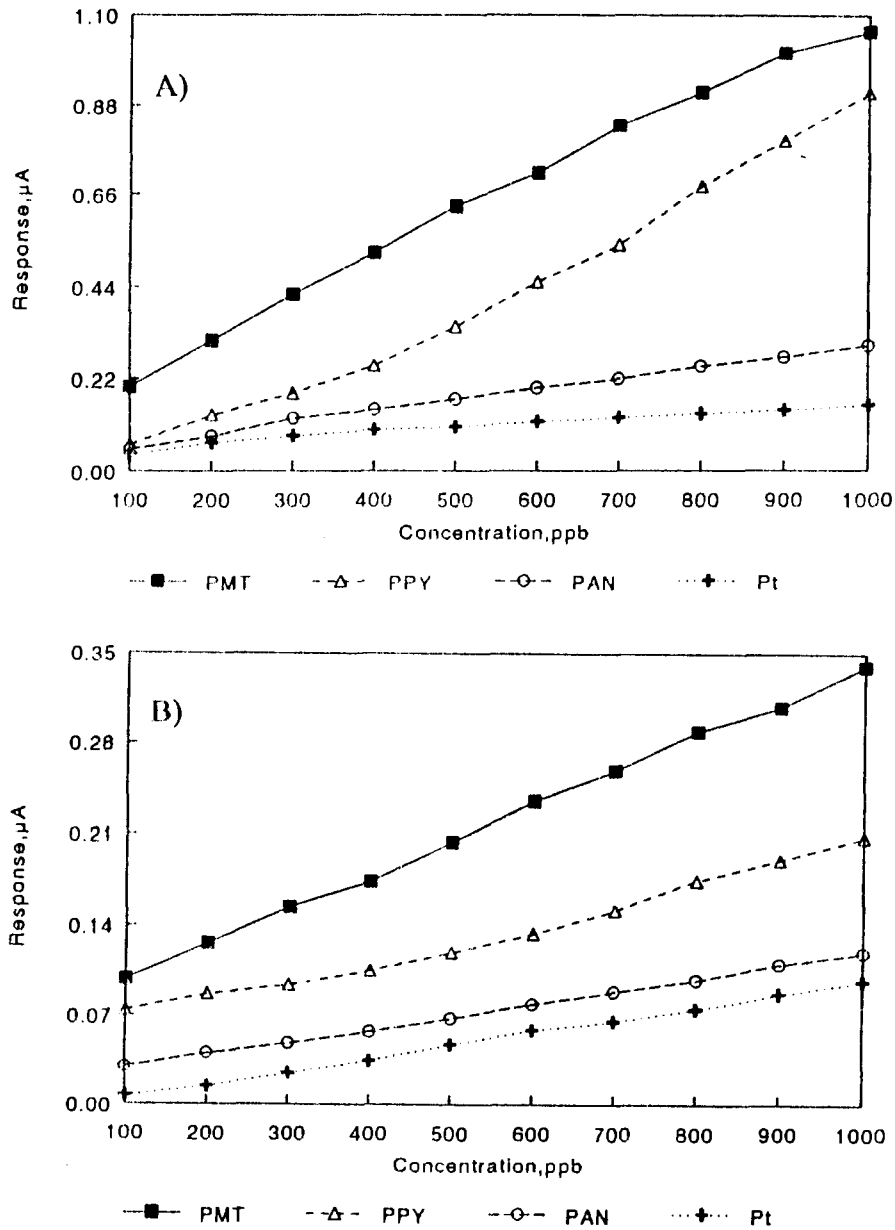

Fig. 4. Flow injection-amperometric detection calibration curves for hydroquinone (A) and ascorbic acid (B) at PMT (■), PPY (Δ), PAN (o) and Pt (+) electrodes. Sample size, 20 ml; mobile phase, Sörensen buffer (pH = 6.9); flow rate, 0.229 ml min^{-1}. Working electrode potential, 0.400 mV.

each test substance having concentration levels of 1–100 ppm with 10 ppm increments were injected and current signals were measured from the recorded peak heights. Working electrode potential for each substance was set at a value that was slightly above the anodic peak potentials of each compounds shown for the polymer electrodes in flow injection analysis responses.

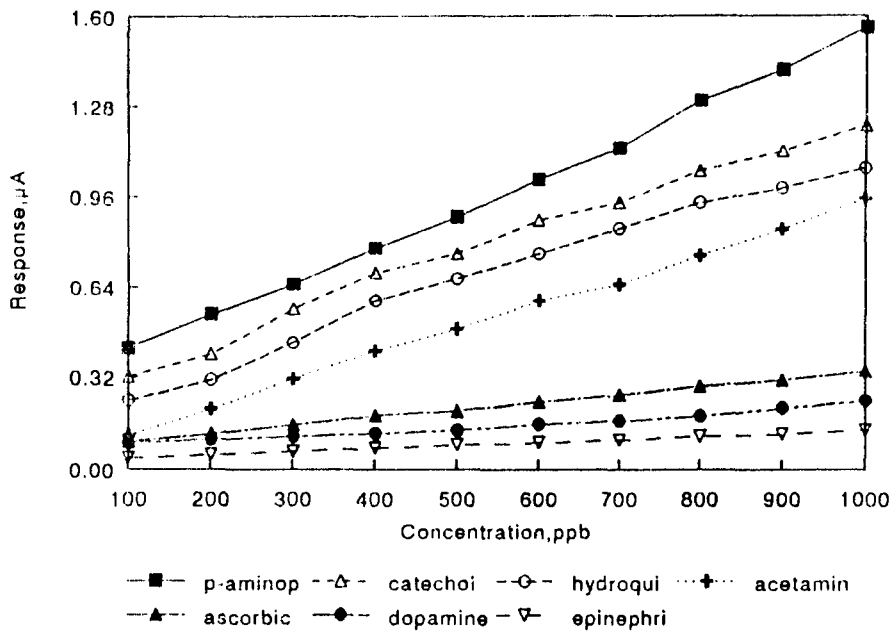

Fig. 5. Flow injection-amperometric detection at PMT electrode. ■: *p*-aminophenol, △: catechol, o: hydroquinone, +: acetaminophene, ▲ ascorbic acid, ●: dopamine and ▽: epinephrine. Sample size, 20 ml; mobile phase, Sörensen buffer (pH = 6.9); flow rate, 0.229 ml min^{-1}. Working electrode potential, 0.400 V.

Fig. 4 shows the calibration curves for hydroquinone and ascorbic acid obtained on polymer electrodes and platinum electrodes. Current responses at polymer electrodes were 5–15 times higher (depending on analyte type) than those obtained on platinum, and excellent linearity was observed for all of the substances for the concentration range studied. For the estimation of detection limits 1, 10 and 100 ppb solutions of respective test substances were injected and the concentration, which produced a current signal with a magnitude at least 2–5 times as high as the signal that is caused by the injection of buffer itself is accepted as a practical limit for detectability. Fig. 5 shows the calibration curves for these compounds on PMT. Detection limits estimated from the procedure described above were 10 ppb for catechol, hydroquinone, dopamine, epinephrine, *p*-aminophenol, ascorbic acid, 5 ppb for acetaminophen and 20 ppb for *p*-aminophenol.

4. Conclusions

In this work, we compared the electrochemical behavior of some organic and biological molecules at different conducting polymer electrodes. The electrodes were prepared under similar conditions, the results showed that the three polymers studied exhibited improved electrocatalytic activity when compared Au or Pt disk electrode.

In the flow injection analysis, with increasing molecular weight of analyte molecules was to observe decreased peak heights.

However, the PMT electrode showed better reversibilty and stability over the other polymers studied. The use of polymer electrodes in flow injection analysis proved to be superior the use of Pt. PMT electrode showed to be stable and more sensitive than Pt. The detection limits obtained using the PMT electrode were as low as 0.1–0.2 ng ml^{-1}. This polymer electrode showed promising results for the resistance surface active agents.

Acknowledgements

This work has been Supported by the Scientific and Technological Council of Turkey (Tübitak) through grant KTÇAG-DPT-6.

References

[1] T. Ishimitsu and S. Hirose, J. Chromatogr., 337 (1985) 239.
[2] K. Stulfk and V. Pacakova, J. Chromatogr., 208 (1981) 269.
[3] K. Stulfk and V. Pacakova, Chem. Listy., 73 (1979) 795.
[4] K. Stulfk and V. Pacakova, Chem. Listy., 68 (1979) 800.
[5] R.W. Murray, Acc. Chem. Rev., 13 (1980) 135.
[6] R.W. Murray, in 'Electroanalytical Chemistry', Vol. 13, A.J. Bard (Ed.), Dekker, New York, 1984, p. 192.
[7] R.W. Murray, A.G. Ewing and R.A. Durst, Anal. Chem., 59 (1987) 379A.
[8] J.G. Redepenning, Trac, 6 (1987) 18.
[9] R.W. Murray, Acc. Chem. Rev., 13 (1980) 315.
[10] R.W. Murray, in 'Electroanalytical Chemistry', Vol. 13, A.J. Bard (Ed.), Dekker, New York.
[11] G.A. Junter, in 'Electrochemical Detection Techniques in the Applied Biosciences' (Ed.), Ellis Horwood, Chichester, 1988.
[12] G. Tourillion, in ' Handbook of Conducting Polymers', Vol. 1, T.A. Skotheim (Ed.), Dekker, New York, 1986 pp. 293–350.
[13] G.K. Chandler and C. Pletcher, in 'The Electrochemistry of Conducting Polymers', 1986, 117.
[14] R.W. Murray, A.G. Ewing and R.A. Durst, Anal. Chem., 59 (5) (1987) 379.
[15] J. Wang and R. Li, Anal. Chem., 61 (1989) 2809.
[16] J. Wang, S.P. Chen and M.S. Lin, J. Electroanal. Chem., 273 (1989) 231.
[17] N.F. Atta, A. Galal, A.E. Karagözler, G.C. Russell, H. Zimmer and H.B. Mark Jr., Biosens. Bioelectron., 6 (1991) 333.
[18] A. Galal, N.F. Atta, J.F. Rubinson, H. Zimmer and H.B. Mark Jr, Anal. Lett., 26 (7) (1993) 1361.
[19] R.A. Saraceno, J.G. Pack and A.G. Ewing, J. Electroanal. Chem., 197 (1986) 265.
[20] G. Erdoğdu, H.B. Mark Jr. and A.E. Karagözler, Anal. Lett. 29 (2) (1996) 221.

ELSEVIER

Talanta 44 (1997) 2019–2025

Talanta

Extraction behavior of divalent first row transition metal ions with *N*,*N*′-bis(2-hydroxyphenylmethyl)-*N*,*N*′-bis(2-pyridylmethyl)-1,2-ethanediamine and its derivatives

Naoki Hirayama [a,*], Nobuya Ichitani [1,a], Koji Kubono [b], Yuka Matsuoka [c], Hisao Kokusen [c], Takaharu Honjo [a]

[a] *Department of Chemistry, Faculty of Science, Kanazawa University, Kakuma-machi, Kanazawa 920–11, Japan*
[b] *Division of Natural Science, Osaka Kyoiku University, Asahigaoka, Kashiwara 582, Japan*
[c] *Department of Chemistry, Faculty of Education, Tokyo Gakugei University, Nukui-Kita-machi, Koganei 184, Japan*

Received 10 September 1996; received in revised form 3 December 1996

Abstract

For the fundamental study on the development of novel extractants, extraction behavior of divalent first row transition metals such as manganese, nickel, copper and zinc was studied with using *N*,*N*′-bis(2-hydroxyphenylmethyl)-*N*,*N*′-bis(2-pyridylmethyl)-1,2-ethanediamine (H_2bbpen) and its derivatives as extractants. From the numerical analysis of the intricate extraction behavior of the metals, it was found that they were extracted into chloroform not only as uncharged chelate complexes but also as ion-pairs of charged complexes with a counter anion in aqueous solution. In other words, these ligands seemed to act not only as divalent hexadentate extractants but also as monovalent tri- or tetra dentate ligands, forming positively charged complexes. Furthermore, the order of the extractabilities between the metals did not coincide with the Irving-Williams series of stability because of the 'cavity size' in the ligands and the structural rigidity of them. © 1997 Elsevier Science B.V.

Keywords: Chelate extraction; Ion-pair extraction; *N*,*N*′-bis(2-hydroxyphenylmethyl)-*N*,*N*′-bis(2-pyridylmethyl)-1,2-ethanediamine; The first row transition metals

1. Introduction

Solvent extraction [1–4] is a very effective method for the separation of metal species in solutions and a lot of extraction systems have been developed for the separation, the concentration and the selective determination of many kinds of metal ions. As the method has operational convenience and needs no specific instrument, it is also very effective for analyzing some complexation reactions in aqueous solutions.

The compound *N*,*N*′-bis(2-hydroxyphenylmethyl)-*N*,*N*′-bis(2-pyridylmethyl)-1,2-ethanedi-

* Corresponding author. Fax: +81 762 645742.

[1] Present address: Department of Polar Science, The Graduate University for Advanced Studies, Kaga, Itabashi, Tokyo 173, Japan.

0039-9140/97/$17.00
PII S0039-9140(96)02200-X

amine (H_2bbpen) [5,6] is a divalent hexadentate ligand having amine nitrogen, pyridine nitrogen and phenolate oxygen donor atoms. This ligand has been reported as models for manganese- [6], vanadium- [5,7,8] and ruthenium-containing [9] metalloenzymes. Furthermore, the coordination structures of gallium(III) and indium(III) [10,11] complexes with the derivatives of the ligand have been studied. These researches, however, were performed without focusing the complexation reactions in solution.

In the previous study, we investigated extraction behavior of lanthanoids(III) with H_2bbpen and β-diketones and it was found that the structural rigidity of H_2bbpen leads to strict size recognition of lanthanoids [12]. However, the complexation reactions between divalent metals and these ligands have not been investigated in spite that the formation of neutral complexes is expected.

In this study, we investigated extraction behavior of divalent first row transition metals into chloroform with H_2bbpen and its derivatives, *N*,*N*′-bis(5-bromo-2-hydroxyphenylmethyl)-*N*,*N*′-bis(2-pyridylmethyl)-1,2-ethanediamine (H_2Brbbpen), *N*,*N*′-bis(5-chloro-2-hydroxyphenylmethyl)-*N*,*N*′-bis(2-pyridylmethyl)-1,2-ethanediamine (H_2Clbbpen) and *N*,*N*′-bis(3,5-dichloro-2-hydroxyphenylmethyl)-*N*,*N*′-bis(2-pyridylmethyl)-1,2-ethanediamine (H_2dClbbpen), as fundamental approach for the development of novel extractants. The structures of these ligands are shown in Fig. 1. As a result, it was found that, in the extraction system, these ligands act not only as divalent hexadentate extractants but also possibly as monovalent tri- or tetra-dentate ligands, forming positively charged complex. Furthermore, the rigid structure of them influenced the extraction behavior.

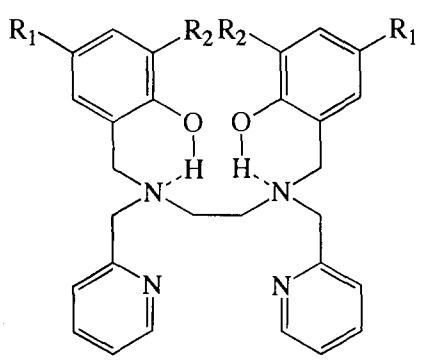

Fig. 1. Structure of the ligands used in this study. $R_1 = R_2 =$ H, H_2bbpen; $R_1 =$ Br and $R_2 =$ H, H_2Brbbpen; $R_1 =$ Cl and $R_2 =$ H, H_2Clbbpen; $R_1 = R_2 =$ Cl, H_2dClbbpen.

2. Experimental

2.1. Reagents

The syntheses of H_2bbpen, H_2Brbbpen, H_2Clbbpen and H_2dClbbpen were performed according to the methods of Neves et al. [6] and Wong et al. [10]. All other chemicals were reagent-grade materials and distilled deionized water was used throughout.

2.2. Distribution of the metals

The distribution of metal ions were studied as follows: in a 30 cm^3 centrifuge tube, an aliquot of chloroform (10 cm^3) containing 1×10^{-2} M of a ligand (H_2L) and equal volume of an aqueous phase containing 1×10^{-4} M of M^{2+} (M = Mn, Fe, Co, Ni, Cu and Zn), 1×10^{-1} M of sodium nitrate or perchlorate and 1×10^{-2} M of the buffer (chloroacetic acid ($2.0 < pH < 4.0$), acetic acid ($3.5 < pH < 6.0$), 2-(*N*-morpholino)ethane-sulfonic acid (MES, $5.5 < pH < 7.0$), *N*-(2-acetamido)-2-aminoethanesulfonic acid (ACES, $6.0 < pH < 7.5$), 3-(*N*-morpholino)propanesulfonic acid (MOPS, $6.5 < pH < 7.9$), 3-[4-(2-hydroxyethyl)-1-piperazinyl]propanesulfonic acid (EPPS, $7.5 < pH < 8.5$), *N*-tris(hydroxymethyl)methyl-3-aminopropanesulfonic acid (TAPS, $7.7 < pH < 9.1$), 2-(cyclohexylamino)ethanesulfonic acid (CHES, $8.6 < pH < 10.0$), or 3-(cyclohexylamino)propanesulfonic acid (CAPS, $9.5 < pH < 10.0$)) were shaken at 25 ± 1 °C for 12-72 h. After the two phases were separated by centrifugation, pH and the metal concentration in the aqueous phase were determined with a Hitachi-Horiba F-12 pH meter and a Shimadzu ICPS-1000 III inductively coupled argon plasma spectrometer. In addition, it was established that all of used buffers has no influence on the extraction judged from the obtained smooth extraction curves.

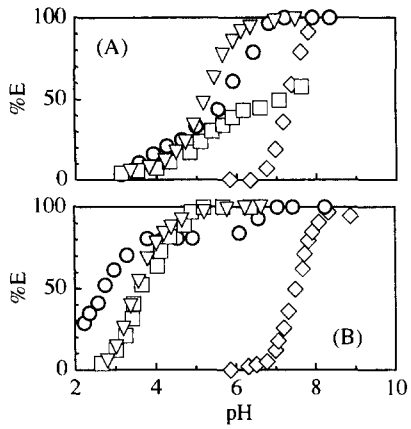

Fig. 2. Plots of the extracted percentages (%E) of some divalent transition metals as a function of the aqueous phase pH equilibrated with organic phase (chloroform) in H_2bbpen–$NaNO_3$ (A) and H_2bbpen–$NaClO_4$ (B) systems. Initial concentrations were 1×10^{-3} M for H_2bbpen in chloroform and 1×10^{-1} M for $NaNO_3$ or $NaClO_4$ in aqueous phase. ◇, Mn^{2+}; ○, Ni^{2+}; □, Cu^{2+}; ▽, Zn^{2+}.

Linear and non-linear least-squares fits to obtain the equilibrium constants were performed using an Apple model Power Macintosh 8100/80 personal computer system and a Delta Point model Delta Graph Pro Ver.3.5 data analysis software package.

3. Results and discussion

3.1. Extraction behavior of divalent first row transition metal ions

The extracted percentages (%E) of Mn^{2+}, Ni^{2+}, Cu^{2+} and Zn^{2+} in H_2bbpen–$NaNO_3$ and H_2bbpen–$NaClO_4$ systems were plotted as a function of the aqueous phase pH in Fig. 2. The %E became constant with shaking for more than 6 h for Mn^{2+} and Zn^{2+} and 60 h for Ni^{2+} and Cu^{2+} in all of H_2L–NaX (X$-$ = NO^{3-} or ClO_4^-) systems investigated. The relationship between %E and pH was not simple and the result suggested that plural kinds of the complexes were extracted. (The extraction behavior of Fe^{2+} and Co^{2+} was more complicated possibly because the extraction reaction was accompanied with the irreversible oxidation process of these metals to trivalent species. Therefore, further study concerning Fe^{2+} and Co^{2+} was not performed).

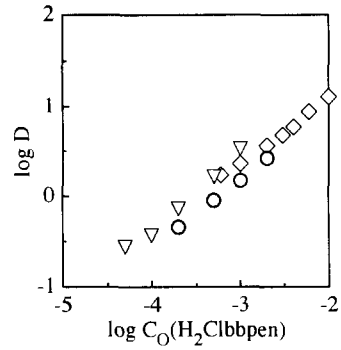

Fig. 3. Plots of the logarithmic distribution ratios (log D) of some divalent transition metals as a function of the concentration of H_2Clbbpen in H_2Clbbpen–$NaClO_4$ system at a fixed equilibrium pH. The value of [ClO_4^-] was 1×10^{-1} M. ◇, Mn^{2+} (pH 6.9); ○, Ni^{2+} (pH 2.1); ▽, Zn^{2+} (pH 3.7).

The extractability of these metals, except for Mn^{2+}, in H_2L–$NaClO_4$ system was higher than that in H_2L–$NaNO_3$ system at lower pH region. This phenomenon means the extracted species at the pH region is an ion-pair of a positively charged metal complex with X^-.

To analyze the composition of these extracted species, the values of the logarithmic distribution ratios (log D) of these metals were plotted as a function of the logarithmic equilibrated concentrations ($[H_2L]_o$) of H_2L in the organic phase, where subscript 'o' means organic phase, or the aqueous phase pH. (From very high hydrophobicity of H_2L [12], $[H_2L]_o$ can be regarded as equal to initial concentration of H_2L in organic phase.) Fig. 3 and Fig. 4 show the plots in H_2Clbbpen–$NaClO_4$ or H_2Clbbpen–$NaNO_3$ system as examples. As shown in Fig. 3, all of the plots of log D versus log$[H_2L]_o$ gave straight line with slope close to 1 (the obtained slopes ranged from 0.8 to 1.0), which means that the extracted species is obtained by the reaction between one M^{2+} cation and one H_2L molecule. To the contrary, as shown in Fig. 4, the plots of log D versus pH gave several kinds of curves. To put it concretely, the plots were grouped into the following four classes:

(i) straight line with slope $\simeq$ 1,
(ii) straight line with slope $\simeq$ 2,
(iii) curve with increasing slope from 1 to 2,

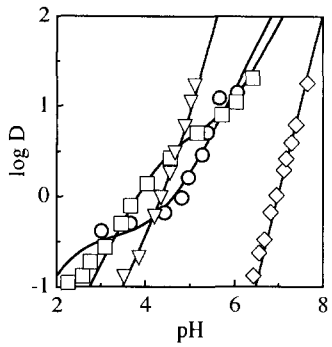

Fig. 4. Plots of the log D of some divalent transition metals as a function of the equilibrium pH in H_2Clbbpen–$NaNO_3$ system. The values of $[H_2Clbbpen]_o$ and $[NO^{3-}]$ were 1×10^{-3} M and 1×10^{-1} M, respectively. ◇, Mn^{2+}; ○, Ni^{2+}; □, Cu^{2+}; ▽, Zn^{2+}. Solid curves were obtained by a non-linear least-squares fit.

(iv) zigzag curve having two slope $\simeq 1$ regions.

For example, Mn^{2+}, Ni^{2+}, Cu^{2+} and Zn^{2+} in Fig. 4 were classified as (ii), (iv), (iv) and (iii), respectively. The overview of each plot is summarized in Table 1. From the results, it was considered that one or two protons are released by the extraction reactions. The extraction mechanism is detailed in the following section.

Table 1
Overview of the log$D$ versus pH plot in M^{2+}-H_2L-NaX extraction system

H_2L	H_2bbpen	H_2Brbbpen	H_2Clbbpen	H_2dClbbpen
$M^{2+} = Mn^{2+}$				
$X^- = NO_3^-$	(ii)	(ii)	(ii)	(ii)
$X^- = ClO_4^-$	(ii)	(ii)	(ii)	(ii)
$M^{2+} = Ni^{2+}$				
$X^- = NO_3^-$	(iv)	(iv)	(iv)	(iv)
$X^- = ClO_4^-$	(iv)	(iv)	(iv)	(iv)
$M^{2+} = Cu^{2+}$				
$X^- = NO_3^-$	(iv)	(iv)	(iv)	(iv)
$X^- = ClO_4^-$	(i)	(iv)	(i)	(iv)
$M^{2+} = Zn^{2+}$				
$X^- = NO_3^-$	(iii)	(iv)	(iii)	(iv)
$X^- = ClO_4^-$	(i)	(iv)	(i)	(iv)

(i), straight line with slope $\simeq 1$.
(ii), straight line with slope $\simeq 2$.
(iii), curve with increasing slope from 1 to 2.
(iv), zigzag curve having two slope $\simeq 1$ regions.

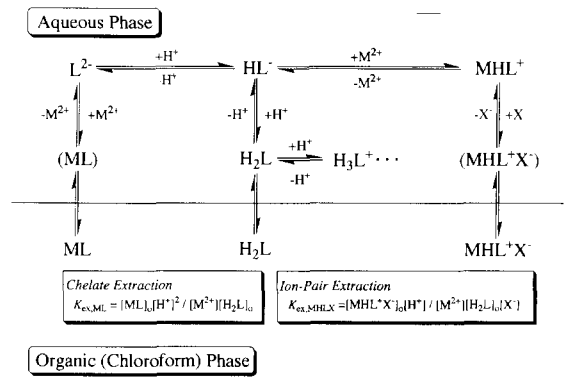

Fig. 5. Equilibria existing in the M^{2+}–H_2L–NaX extraction systems. The existence of ML and MHL^+X^- in aqueous phase was negligible in this study.

3.2. Determination of extraction constants

To interpret the intricate extraction behaviors mentioned above, we considered the chemical equilibria shown in Fig. 5. Since distribution behavior of H_2bbpen into $NaClO_4$ solution was the same as that into $NaNO_3$ solution, the extraction of an ion-pair of the protonated ligand with a counter anion, such as $H_3L^+X^-$ was negligible in the system.

In practice, the ligand H_2L acts as divalent hexadentate ligand (L^{2-}). However, as reported previously [12], the acid dissociation constants of H_2bbpen in aqueous solution, defined as

$$K_{ai} = [H^+][H_{6-i}\text{bbpen}^{(4-i)+}]/[H_{7-i}\text{bbpen}^{(5-i)+}] \quad (1 \le i \le 6) \qquad (1)$$

were determined as $pK_{a1} \ll 2$, $pK_{a2} \ll 2$, $pK_{a3} = 3.35$, $pK_{a4} = 6.08$ and $pK_{a5} + pK_{a6} = 24.4$ and the logarithmic distribution constant ($\log K_D$) between chloroform and aqueous phases were 5.12. (The other ligands seem to have similar pK_{ai} and $\log K_D$ values). Furthermore, Schwingel et al. [13] reported the pK_a values of H_2bbpen in 70% (v/v) ethanol as $pK_{a3} = 3.11$, $pK_{a4} = 5.99$, $pK_{a5} = 12.00$ and $pK_{a6} = 13.26$. These values show the high hydrophobicity of H_2L and the hard dissociability of phenolic proton in H_2L by the formation of six-membered ring including hydrogen bond. It was considered that, in relatively acidic condition, H_2L can act as monovalent tridentate (or tetra-

dentate) ligand (HL^-) and form the charged complex (MHL^+) with M^{2+}, having hydrophobicity enough to be extracted into chloroform as the ion-pair (MHL^+X^-). In this case, it is presumed that one phenolate-O, one amine-N and one (or two) pyridine-N atoms coordinate to M^{2+}.

On considering the equilibria shown in Fig. 5, D is expressed as follows:

$$D = ([MHL^+X^-]_o + [ML]_o)/([M^{2+}] + [MHL^+])$$
$$= (K_{ex,\,MHLX}[H_2L]_o[X^-]/[H^+] + K_{ex,\,ML}[H_2L]_o/[H^+]^2)/(1 + \beta'_{MHL}[H_2L]_o/[H^+]) \quad (2)$$

where K_{ex}, ML means the chelate extraction constant of the following reaction:

$$M^{2+} + H_2L_o \rightleftarrows ML_o + 2H^+ \quad (3)$$

$$K_{ex,ML} = [ML]_o[H^+]^2/[M^{2+}][H_2L]_o \quad (4)$$

$K_{ex,MHLX}$ means the ion-pair extraction constant of the following reaction:

$$M^{2+} + H_2L_o + X^- \rightleftarrows MHL^+X_o^- + H^+ \quad (5)$$

$$K_{ex,MHLX} = [MHL^+X^-]_o[H^+]/[M^{2+}][H_2L]_o[X^-] \quad (6)$$

and β'_{MHL} means the equilibrium constant of the following charged complex formation reaction:

$$M^{2+} + H_2L_o \rightleftarrows MHL^+ + H^+ \quad (7)$$

$$\beta'_{MHL} = [MHL^+][H^+]/[M^{2+}][H_2L]_o \quad (8)$$

Eq. (2) reproduces the (iv)-type log D versus pH plot with experimentally determined values of $K_{ex,ML}$, $K_{ex,MHLX}$ and β'_{MHL}.

In the case that $[MHL^+]$ is negligible, Eq. (2) can be transformed as

$$D = ([MHL^+X^-]_o + [ML]_o)/[M^{2+}]$$
$$= K_{ex,MHLX}[H_2L]_o[X^-]/[H^+] + K_{ex,ML}[H_2L]_o/[H^+]^2 \quad (9)$$

and the (iii)-type log D versus pH plot can be analyzed numerically by using Eq. (9). Furthermore, the (i) and (ii)-type log D versus pH plots can be interpreted by considering simple ion-pair extraction system shown in Eq. (5) and simple chelate extraction system in Eq. (3), respectively. In these cases, Eq. (2) can be transformed as

$$D = [MHL^+X^-]_o/[M^{2+}] = K_{ex,MHLX}[H_2L]_o[X^-]/[H^+] \quad (10)$$

and

$$D = [ML]_o/[M^{2+}] = K_{ex,ML}[H_2L]_o/[H^+]^2 \quad (11)$$

respectively.

The equilibrium constants of $K_{ex,ML}$, $K_{ex,MHLX}$ and β'_{MHL} values were obtained from log D versus pH plots by a non-linear least-squares fit using Eq. (2), Eq. (9), Eq. (10) or Eq. (11). These obtained values are listed in Table 2. Since the values of stability constants of $M(OH)^+$ are $10^{3.4}$, $10^{4.1}$, $10^{6.3}$ and $10^{5.0}$ for M = Mn, Ni, Cu and Zn, respectively [14], the hydrolysis of the M^{2+} was negligible at pH < 6 for Cu^{2+} and pH < 8 for the others.

The solid curves in Fig. 4 were obtained from the fits. All of the experimental data was reproduced accurately by the curves. (In all cases studied, correlation coefficients were more than 0.98). The results shows the extraction model mentioned above is suitable for the extraction system in this paper.

In the chelate extraction, the order of $K_{ex,ML}$ on a fixed H_2L was about Mn < Cu < Zn < Ni, which differs from the Irving-Williams series of stability, Mn < Ni < Cu > Zn. Previously, it was suggested that the 'cavity' formed by the two pyridylmethyl and the two hydroxyphenylmethyl groups in H_2L is suitable for metal ions having ionic radii of ~60–80 pm [10]. The six-coordinate ionic radii of Mn^{2+}, Ni^{2+}, Cu^{2+} and Zn^{2+} are 83.0, 69.0, 73.0 and 74.0 pm, respectively [15] and the above-mentioned order seems to show the size recognition effect of these ligands. The result shows one possibility that a polydentate ligand having structural rigidity acts as high-selective extractant originated from its size recognition ability similar to crown ethers or calixarenes. In addition, the order Cu < Zn is possibly caused by Jahn-Teller distortion of divalent six-coordinate Cu complex.

On the formation of charged complex MHL^+, the order of β'_{MHL} was Ni > Cu. When H_2L acts as monovalent tridentate (or tetradentate) ligand,

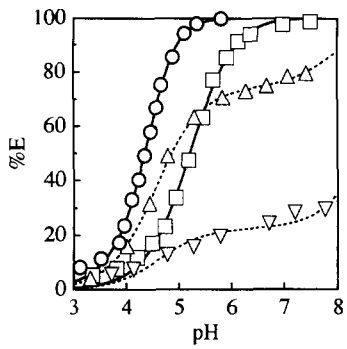

Fig. 6. Comparison between %E-pH plots for divalent zinc in several H_2L–$NaNO_3$ systems. Initial concentrations were 1×10^{-3} M for H_2L in chloroform and 1×10^{-1} M for $NaNO_3$ in aqueous phase. $H_2L = H_2$bbpen (□), H_2Brbbpen (△), H_2Clbbpen (○) and H_2dClbbpen (▽). Curves were obtained by a non-linear least-squares fit.

Table 2
Determined equilibrium constants (25°C, $I = 0.1$)

H_2L	H_2bbpen	H_2Brbbpen	H_2Clbbpen	H_2dClbbpen
$M^{2+} = Mn^{2+}$				
$\log K^{a}_{ex,ML}$	−11.77	−11.41	−10.65	−10.91
$M^{2+} = Ni^{2+}$				
$\log K^{a}_{ex,ML}$	−6.74	−9.34	−4.07	−7.18
$\log K_{ex,MHLX}$				
$X^- = NO_3^-$	−0.42	−0.50	1.32	0.14
$X^- = ClO_4^-$	1.42	1.32	2.34	0.47
$\log \beta^{a}_{MHL}$	−0.58	0.73	0.76	−0.28
$M^{2+} = Cu^{2+}$				
$\log K^{a}_{ex,ML}$	−10.01[b]	−8.37	−6.55[b]	−10.75
$\log K_{ex,MHLX}$				
$X^- = NO_3^-$	−1.34	−0.06	0.26	−1.15
$X^- = ClO_4^-$	0.22	0.90	1.63	−0.64
$\log \beta^{a}_{MHL}$	−2.32[b]	−0.96	−1.44[b]	−2.71
$M^{2+} = Zn^{2+}$				
$\log K^{a}_{ex,ML}$	−8.97[b]	−7.51	−6.26[b]	−10.21
$\log K_{ex,MHLX}$				
$X^- = NO_3^-$	−1.17	−0.64	−0.51	−0.97
$X^- = ClO_4^-$	0.33	0.69	0.42	−0.90
$\log \beta^{a}_{MHL}$	N.D.	−1.53	N.D.	−1.78

N.D., not determined.
[a] The mean of the values in M^{2+}–H_2L–$NaNO_3$ and M^{2+}–H_2L–$NaClO_4$ systems (the difference between them is less than 0.2.).
[b] The value in M^{2+}–H_2L–$NaNO_3$ system.

the coordination number of acceptor M^{2+} seems to be four. On forming square-planer complex of Cu^{2+} with HL^-, the complex is possibly instabilized by the steric distortion of the ligand for the formation of phenolate-O–amine-N–pyridine-N-M plane.

3.3. Effect of substituent on the extractability

Fig. 6 shows comparison between %E-pH plots for divalent zinc in several H_2L–$NaNO_3$ systems as an example. Whether X^- was NO_3^- or ClO_4^-, the order of extractability for a metal was about H_2bbpen–NaX < H_2Brbbpen–NaX < H_2Clbbpen–NaX > H_2dClbbpen–NaX. Also the orders of $K_{ex,ML}$, $K_{ex,MHLX}$ and β'_{MHL} shown in Table 2 were almost the same manner. The order H_2bbpen–NaX < H_2Brbbpen–NaX < H_2Clbbpen–NaX corresponded to that of the ability of the release of phenolic proton in H_2L, which is necessary step for the formation of ML. The relative low extractability in H_2dClbbpen–NaX system was possibly originated from the steric hindrance by o-Cl substituent on the phenolic group.

Acknowledgements

This study was financially supported in part by Grants-in-Aid for Scientific Research No. 06740556, No. 07854045 and No. 08740572 from the Ministry of Education, Science and Culture, Japan.

References

[1] S. Alegret, Developments in Solvent Extraction, Wiley, New York, 1988.
[2] T. Sekine and Y. Hasegawa, Solvent Extraction in Chemistry, Dekker, New York, 1977.
[3] J. Stary, The Solvent Extraction of Metal Chelates, Pergamon Press, Oxford, 1964.
[4] Y. Marcus and A.S. Kertes, Ion Exchange and Solvent Extraction of Metal Complexes, Wiley, London, 1969.
[5] A. Neves, A.S. Ceccato, S.M.D. Erthal and I. Vencato, Inorg. Chim. Acta, 187 (1991) 119.

[6] A. Neves, S.M.D. Erthal, I. Vencato, A.S. Ceccato, Y.P. Mascarenhas, O.R. Nascimento, M. Horner and A.A. Batista, Inorg. Chem., 31 (1992) 4749.
[7] A. Neves, A.S. Ceccato, I. Vencato, Y.P. Mascarenhas and C. Erasmus-Buhr, J. Chem. Soc. Chem. Commun., (1992) 652.
[8] A. Neves, A.S. Ceccato, C. Erasmus-Buhr, S. Gehring, W. Haase, H. Paulus, O.R. Nascimento and A.A. Batista, J. Chem. Soc. Chem. Commun., (1993) 1782.
[9] A. Neves, M.A. De Brito, G. Oliva, O.R. Nascimento, E.H. Panepucci, D.H.F. Souza and A.A. Batista, Polyhedron, 14 (1995) 1307.
[10] E. Wong, S. Liu, S. Rettig and C. Orvig, Inorg. Chem., 34 (1995) 3057.
[11] E. Wong, P. Caravan, S.J. Rettig and C. Orvig, Inorg. Chem., 35 (1996) 715.
[12] K. Kubono, N. Hirayama, Y. Matsuoka and H. Kokusen, Anal. Sci., 12 (1996) 133.
[13] E.W. Schwingel, K. Arend, J. Zarling, A. Neves and B. Szpoganicz, J. Braz. Chem. Soc., 7 (1996) 31.
[14] S. Kotrlý and L. Šůcha, Handbook of Chemical Equilibria in Analytical Chemistry, Ellis Horwood, Chichester, 1985.
[15] R.D. Shannon, Acta Crystallogr., A32 (1976) 751.

ELSEVIER

Talanta 44 (1997) 2027–2032

Talanta

Investigation of suitable digestion methods for the determination of total phosphorus in soils

Derya Kara [a,*], Cengiz Özsavaşçi [b], Mahir Alkan [c]

[a] *Department of Chemistry, Faculty of Art and Science, University of Balikesir, Balikesir, Turkey*
[b] *Department of Sciences, Gazi Education Faculty, University of Gazi, Ankara, Turkey*
[c] *Department of Chemistry, Necatibey Education Faculty, University of Balikesir, Balikesir, Turkey*

Received 12 April 1996; received in revised form 29 December 1996; accepted 29 December 1996

Abstract

Total phosphorus in five soils with different compositions which were obtained from different places were extracted by using Na_2CO_3 fusion, $HClO_4$ digestion, $HClO_4 + HNO_3$ digestion, $HF + HClO_4$ digestion or NaOBr oxidation methods. In order to test the suitability of the $HF + HClO_4$ digestion the results obtained by this method were compared with the others above, especially the Na_2CO_3 fusion which is accepted as a standard method. The phosphorus amount found with the $HF + HClO_4$ digestion method were almost the same as the phosphorus amount by the Na_2CO_3 fusion method, while the superiority in extracting phosphorus when compared to other methods were obvious. The methods used in the study were evaluated according to the recovery of total phosphorus, ease of application and rapidity with which they were performed. Orthophosphate in the soil extracts was determined by the molybdenum blue colour method. The relationships between methods are examined statistically. © 1997 Elsevier Science B.V.

Keywords: Phosphorus extraction; Soil analysis; Spectrophotometry; Total phosphorus

1. Introduction

The determination of total phosphorus in soils is very important for agricultural studies. It is important to know the phosphorus status of soil for predicting the need to apply phosphatic fertilizers. The determination of total phosphorus in soils involves extraction of solubilized inorganic phosphorus and mineralized organic phosphorus and subsequent determination of orthophosphate in the extracts of soils. The Na_2CO_3 fusion procedure is relatively lengthy and also requires considerable technical skill [1]. Perchloric acid digestion procedures are more amenable to routine estimation of total phosphorus in a large number of soil samples. However, these digestions are conducted commonly in either semimicro-Kjeldahl flasks [2] or tubes using the aluminum digestion block [1]. Of these, the Na_2CO_3 fusion and $HClO_4$ digestion methods as described in 'Methods of Soil Analysis' Part 2 are the recognized standards [3]. Dick and Tabatabai used an alkaline hypobromite

* Corresponding author.

PII S0039-9140(97)00014-3

(NaOBr) oxidation, thereby eliminating the potential for explosions with hot $HClO_4$ oxidations [4].

Orphanos studied the extraction of phosphorus from the five major types of Cyprus soils ranging in $CaCO_3$ content from 0 to 71% using the water and bicarbonate methods. Bicarbonate extracted more phosphorus from the highly calcareous soil and less phosphorus from the igneous soil relative to the water method [5]. A potassium persulfate–sulfuric acid autoclave digestion was used to determine phosphorus in 10–50 mg soil and sediment samples by Nelson [6]. This safe, convenient digestion method released a larger fraction of the phosphorus than that released by the hazardous $HClO_4$ digestion method. A rapid and precise extraction procedure was developed in which sequential additions of concentrated H_2SO_4, H_2O_2, and HF were made to soil samples [7]. Although this method is more quantitative than the $HClO_4$ method, it is not easily used with a large number of samples because of the need to use teflon beakers instead of the calibrated glass tubes used with block digestion. Digestion with $HClO_4$ has been shown to give low results unless the digestion mixture contains HF to ensure destruction of silicates containing phosphatic mineral inclusions [1,8].

Schoenau and Huang evaluated and compared the following available *P* indices as to their ability to predict *P* availability and suitability for routine testing: a novel anion-exchange membrane (AEM) technique, water extraction and 0.5 M $NaHCO_3$ (pH 8.5) extractable total and inorganic *P*. They found that these methods showed identical abilities of the tests to predict soil *P* availability in the range of soils examined and that in testing for *P* alone, AEM was considered superior to the other methods due to low cost, simplicity, independence of soil type and high correlation with plant uptake [9]. Cihacek and Lizotte studied the use of an Al digestion block for the alkaline oxidation method for routine analysis of large numbers of soils. They claimed that using an Al digestion block for NaOBr–NaOH oxidation of soils for total *P* determination allows for a simple, precise alternative to sand bath digestion and to potentially hazardous $HClO_4$ procedures [10].

In this work the results from the different methods used in the determination of total phosphorus in soils were examined. The $HF + HClO_4$ digestion method was not more rapid than other methods but extracted phosphorus amounts were found to be larger than others and there was not any significant difference in terms of precision accuracy.

2. Experimental

2.1. Reagents

All the following chemicals were made of Merck.

(1) Dissolved 15 g of ammonium molybdate in 300 ml of distilled water. Added to 290 ml concentrated H_2SO_4 and diluted to 1 l in a calibrated flask.

(2) Dissolved 17.5 g of stannous chloride in 125 ml glycerine and diluted to 250 ml in a calibrated flask.

(3) A 0.4393 g amount of potassium dihydrogen orthophosphate (KH_2PO_4) was dissolved in water and diluted to 1 l in a calibrated flask. Standard working solutions were prepared by diluting the above stock solutions.

(4) Dissolved 60 g of ascorbic acid, 100 mg ethylene diaminetetra acetate (Na_2EDTA) and 4 g of formic acid in distilled water and completed to 1 l with distilled water.

(5) Reducing agent: the reducing agent was prepared by mixing 5 ml of (4) 5 ml of (2) and 10 ml concentrated H_2SO_4.

(6) NaOBr solution: prepare this reagent immediately before use by adding 3 ml of bromine slowly (approximately 0.5 ml min^{-1}), and with constant stirring, to 100 ml of 2 M NaOH. The NaOBr solution must be prepared in a fume hood, because bromine is very toxic.

2.2. Procedure

Calibration: blank solutions were prepared for all the methods and 1 ml of which were added into 50 ml calibrated flasks. For the standard working solutions, dilute 25 ml of the standard *P*

stock solution to 1000 ml with distilled water and mix the solution thoroughly. Then pipette 0.0, 1.0, 2.0, 3.0, 4.0, 5.0, 6.0 ml aliquots of this standard working solution into 50 ml calibrated flasks. Then add 2 ml of reagent (1) and 35–40 ml of distilled water. Add 2–3 drops of (5) and diluted to 50 ml. The pH of these solutions are approximately 3. After 7 min the absorbance of each solution was measured by using a Hitachi Model 100-20 UV-VIS spectrophotometer with 1 cm cell at 660 nm against a reagent blank and a calibration curve (absorbance versus concentration) was plotted.

2.3. Preparation of sample solution

The Na_2CO_3 fusion method [11]: place 1 g of Na_2CO_3 in a platinum crucible and add 0.8–1.0 g of soil sample and then 4 g of Na_2CO_3 and cover the upper of the crucible content with 1 g of Na_2CO_3. The fusion was continued in an electrical furnace for 60 min. The remainder was dissolved with H_2SO_4 and evaporated to dryness. Then the remainder was dissolved with distilled water, filtrated and diluted to 250 ml.

The $HClO_4$ digestion method [11]: place 0.2 g of soil sample in a Kjeldahl flask and add 3 ml of 60%, d: 1.54 g ml^{-1} $HClO_4$. Place it in sand bath and digest the sample at 203°C for 75 min. The digest was cooled, filtrated and diluted to 100 ml in a calibrated flask. However this method is worked with the tubes in the aluminum block which contained holes in which test tubes and a termometer are placed.

The $HNO_3 + HClO_4$ digestion method: place 0.2 g of soil sample in a Kjeldahl flask and add 1 ml of 65%, d: 1.4 g ml^{-1} HNO_3. Place it in sand bath and heat the flask until its content was evaporated to dryness. Then add 3 ml of 60% d: 1.54 g ml^{-1} $HClO_4$ and digest the sample at 203°C for 60 min. The digest was cooled, filtrated and diluted to 100 ml in a calibrated flask. However this method was worked with the tubes in the aluminum block which contained holes in which test tubes and a termometer are placed.

The $HF + HClO_4$ digestion method: place 0.2 g of soil sample in a platinum crucible and add 1–2 ml of 45%, d: 1.14 g ml^{-1} HF and evaporate to dryness. Weight the crucible, again digest with HF until constant weight. Then add 3 ml of 60%, d: 1.54 g ml^{-1} $HClO_4$ and digest for 60 min. The digest was cooled, filtrated and diluted to 100 ml in a calibrated flask.

The NaOBr oxidation digestion method [4]: place 0.2 g of soil sample in a Kjeldahl flask and add 3 ml of the NaOBr solution. Place it in a sand bath and heat the flask until its content was evaporated to dryness and continue heating for an additional 30 min. Remove the flask from the sand bath, allow it to cool for about 5 min, add 4 ml of distilled water and 1 ml of formic acid, mix the contents and then add 25 ml of 1 N H_2SO_4. Filtrate the content and dilute to 100 ml. However, this method was worked with the tubes in the aluminum digestion block which contained holes in which test tubes and a termometer are placed.

Determination of orthophosphate in soil extracts: for the determination of phosphorus in samples solutions, add 1 ml of the sample into a calibrated flask. Add 2 ml of (1) and 10–15 ml of distilled water and bring the solution to pH 3 by checking with 2,4 dinitrophenol indicator. Add 2–3 drops of the reducing agent and dilute to 50 ml. The absorbance of the solution was measured.

3. Results and discussion

The results obtained from the methods used for five different soil samples are shown in Table 1. As seen total phosphorus values obtained by $HF + HClO_4$ digestion method were essentially a bit greater than those obtained by Na_2CO_3 fusion. The more phosphorus was recovered from soils digested by the Na_2CO_3 fusion method than by the conventional $HClO_4$ method [1,8,12]. This also was found to be the case in this study (Table 1). For the $HF + HClO_4$ method, efficiency in recovery was greatest for the sample II, which has the highest organic phosphorus content.

The comparison of the phosphorus contents of five soils samples obtained by different extracting methods were made by using t-test [13].

The test results shown in Table 2 indicate that there is a significant difference between the HF +

Table 1
Average total soil phosphorus and standard deviations obtained by different methods (all results were given as mg P 100 g^{-1} soil)

Sample No.	Na_2CO_3 fusion	$HClO_4$ digestion at tubes	$HClO_4$ digestion at flask	$HClO_4+HNO_3$ digestion at tubes	$HClO_4+HNO_3$ digestion at flask	$HF+HClO_4$ digestion	NaOBr oxidation at tubes	NaOBr oxidation at flask
I. Scotland	226 ± 2	222 ± 3	222 ± 2	225 ± 0.9	224 ± 0.7	226 ± 3	225 ± 2	225 ± 2
II. Scotland	170 ± 0.4	169 ± 2	165 ± 0.4	165 ± 3	164 ± 1	177 ± 3	168 ± 0.6	164 ± 3
III. Polatli	120 ± 3	117 ± 2	116 ± 2	115 ± 0.9	116 ± 2	121 ± 1	116 ± 3	115 ± 0.6
IV. Ankara	85 ± 0.4	84 ± 0.2	83 ± 4	85 ± 1	84 ± 3	86 ± 1	83 ± 2	83 ± 4
V. Sincan	70 ± 0.9	63 ± 1	65 ± 0.3	65 ± 2	65 ± 0.6	69 ± 2	64 ± 0.9	65 ± 2

Samples of 3, 4 and 5 are obtained from Turkey.

Table 2
Results of t-test between $HF+HClO_4$ digestion and other methods

Soil No.	Na$_2$CO3		$HClO_4$ at tubes		$HClO_4$ at flask		$HClO_4+HNO_3$ at tubes		$HClO_4+HNO_3$ at flask		NaOBr at tubes		NaOBr at tubes	
	X_1-X_2	$\mp ts\frac{\sqrt{N_1+N_2}}{N_1N_2}$	X_1-X_2	$\mp ts\frac{\sqrt{N_1+N_2}}{N_1N_2}$	X_1-X_2	$\mp ts\frac{\sqrt{N_1+N_2}}{N_1N_2}$	X_1-X_2	$\mp ts\frac{\sqrt{N_1+N_2}}{N_1N_2}$	X_1-X_2	$\mp ts\frac{\sqrt{N_1+N_2}}{N_1N_2}$	X_1-X_2	$\mp ts\frac{\sqrt{N_1+N_2}}{N_1N_2}$	X_1-X_2	$\mp ts\frac{\sqrt{N_1+N_2}}{N_1N_2}$
I	0	5.86	4.47	5.83	4.4	5.3	1.73	5.2	2.6	5.07	1.0	5.8	1.6	5.63
II	6.5	5.21	7.8	5.72	12.1	5.22	11.9	6.52	12.3	4.75	12.4	7.08	8.7	5.24
III	1.3	3.31	3.8	1.82	5.2	2.4	5.9	1.79	4.5	3.40	5.5	1.86	4.8	4.26
IV	1.14	1.79	1.31	2.28	3.46	4.49	1.31	2.28	2.13	5.78	3.56	5.97	2.76	2.92
V	−1.1	4.71	5.08	5.13	3.92	4.61	3.46	5.174	3.87	4.64	3.49	5.49	4.53	4.81

(If the experimental difference (X_1-X_2) is smaller than the computed value $[\pm ts\sqrt{N_1+N_2/N_1\times N_2}]$, no significant difference between the means has been accepted at the 95% confidence level).

Table 3
Selected chemical properties of tested soils

Soil No.	Sand %	Clay %	Silt %	Organic C %	pH	$CaCO_3$ %
I	80.5	6.2	3.9	5.77	6.48	0.2
II	18.1	72.6	9.7	12.13	7.50	8.0
III	44.8	36.0	19.2	—	7.87	—
IV	29.8	37.2	33.0	—	7.80	26.4
V	26.9	33.2	39.9	1.74	7.30	—

$HClO_4$ digestion and the Na_2CO_3 fusion methods for only sample II, while there are significant differences for sample II and III by comparing $HF + HClO_4$ digestion with other methods. There was no significant difference between the methods for other three samples. If we consider the high clay and organic content of the sample II, the fact that higher phosphorus values were extracted by the $HF + HClO_4$ methods shows that this extraction method may be more suitable for this kind of soils.

The equations of the straight lines obtained by plotting the total phosphorus amounts by the $HF + HClO_4$ digestion against that of by other methods and relevant correlation coefficients can be given as following.

$$P_{HF+HClO_4} = 1.014P_{Na_2CO_3} - 0.2914 \quad r = 0.9991$$

$$P_{HF+HClO_4} = 1.0096P_{HClO_4} - 3.5400 \text{ (in tube)} \quad r = 0.9995$$

$$P_{HF+HClO_4} = 1.0202P_{HClO_4} + 3.1866 \text{ (in flask)} \quad r = 0.9987$$

$$P_{HF+HClO_4} = 1.0109P_{HNO_3+HClO_4} + 3.4310 \text{ (in tube)} \quad r = 0.9978$$

$$P_{HF+HClO_4} = 1.0134P_{HNO_3+HClO_4} + 3.3946 \text{ (in flask)} \quad r = 0.9981$$

$$P_{HF+HClO_4} = 0.9976P_{NaOBr} + 4.7880 \text{ (in tube)} \quad r = 0.9991$$

$$P_{HF+HClO_4} = 1.0018P_{NaOBr} + 4.9575 \text{ (in flask)} \quad r = 0.9978$$

These equations give what amount of total phosphorus found by the $HF + HClO_4$ digestion method can be determined by other extraction methods. If two results by two methods had been equal, the slope of the line would have been equal to 1, the intersection 0 and $r = 1$. According to these equations the $HF + HClO_4$ digestion method is the best fitted method with the Na_2CO_3 fusion method, Table 3.

The interferences from silica was hindered by evaporating the silica in these two methods each of these methods gives higher total phosphorus amount than those obtained by the other methods. When worked in tubes and Kjeldahl flasks with $HClO_4$ digestion, $HNO_3 + HClO_4$ digestion and NaOBr oxidation methods, it was observed according to t-test that there was no significant difference between the methods, however the time required when worked in tubes were shorter than in Kjeldahl flasks.

The good precision of the method described is illustrated by Table 4, which gives the average results of three independent determinations, which were selected by Q-test [13] among a number of replicated analysis. The total phosphorus values of these samples ranged from 226.3 to 68.7 mg P 100 g^{-1} soil and the coefficient of variation ranged 0.84–3.1%.

The fact that higher phosphorus amounts can be extracted and that interference effects of silica can completely be prevented may be mentioned as advantages of the $HF + HClO_4$ digestion method and therefore this extraction procedure may be selected in quantitative studies.

Table 4
Precision of $HF+HClO_4$ digestion for total phosphorus in soils (results are the averages of three independent determinations)

Soil No.	Average (x) mg P 100 g^{-1} soil	Range (w) mg P 100 g^{-1} soil	Standard deviation P 100 g^{-1} soil	Coefficient of variation
I	226.30	223.8–229.8	3.12	1.38
II	176.60	174.8–180.3	3.24	1.84
III	120.80	119.7–121.7	1.02	0.84
IV	86.16	85.02–87.03	0.98	1.14
V	68.70	69.0–71.4	2.13	3.10

References

[1] L.W. Sommers and D.W. Nelson, Soil Sci. Soc. Am. Proc., 36 (1972) 902.
[2] H.L.S. Tandon, M.P. Cescas and E.H. Tyner, Soil Sci. Soc. Am. Proc., 32 (1968) 48.
[3] S.R. Olsen and L.E. Sommers, Agronomy, 9 (1982) 404.
[4] W.A. Dick and M.A. Tabatabai, Soil Sci. Soc. Am. J., 41 (1977) 511.
[5] P.I. Orphanos, Plant and Soil, 49 (1978) 417.
[6] N.S. Nelson, Commun. in Soil Soc. Plant Anal., 18 (4) (1987) 359.
[7] R.A. Bowman, Soil Sci. Soc. Am. J., 52 (1988) 1301.
[8] J.K. Syers, J.D.H. Williams, A.S. Campbell and T.W. Walker, N.Z. J. Agric. Res., 11 (1968) 757.
[9] J.J. Schoenau and W.Z. Huang, Commun. in Soil Sci. Plant Anal., 22 (5 and 6) (1991) 465–492.
[10] L.J. Cihacek and D.A. Lizotte, Commun. in Soil Sci. Plant Anal., 21 (19 and 20) (1990) 2361–2370.
[11] K. Burhan, Toprak Analizleri, Ankara University Faculty of Agricultural ed., ISBN 975-7717-04-5, 218–226.
[12] J.K. Seyers, J.D.H. Williams, A.S. Campbell and T.W. Walker, Soil Sci. Soc. Am. J., 31 (1967) 752–756.
[13] A.S. Douglas, M.W. Donald and F.J. Holler, Fundamentals of Analytical Chemistry 6th Ed., 1991.

ELSEVIER

Talanta 44 (1997) 2033–2039

Talanta

Identification of combustible material with piezoelectric crystal sensor array using pattern–recognition techniques

Xi-Wen He *, Wan-Li Xing, Yan-Hong Fang

Department of Chemistry, Nankai University, Tianjin 3000071, People's Republic of China

Received 29 April 1996; received in revised form 22 August 1996; accepted 30 December 1996

Abstract

A promising way of increasing the selectivity and sensitivity of gas sensors is to treat the signals from a number of different gas sensors with pattern recognition (PR) method. A gas sensor array with seven piezoelectric crystals each coated with a different partially selective coating material was constructed to identify four kinds of combustible materials which generate smoke containing different components. The signals from the sensors were analyzed with both conventional multivariate analysis, stepwise discriminant analysis (SDA), and artificial neural networks (ANN) models. The results show that the predictions were even better with ANN models. In our experiment, we have reported a new method for training data selection, 'training set stepwise expending method' to solve the problem that the network can not converge at the beginning of the training. We also discussed how the parameters of neural networks, learning rate η, momentum term α and few bad training data affect the performance of neural networks.

Keywords: Artificial neural networks (ANN); Piezoelectric crystal sensor array; Stepwise discriminant analysis (SDA)

1. Introduction

Potentially, piezoelectric detectors are very attractive sensors of gaseous species due to the wide availability of the principle quartz crystal component and the relatively simple electric instrumentation. The possibility of their application has been demonstrated for the detection of several inorganic species, such as sulfur dioxide [1], nitrogen dioxide [2], ammonia [3], hydrogen cyanide [4], hydrogen chloride [5], hydrogen sulfide [6]. But, the piezoelectric crystal sensor, as with most chemical sensors, is susceptible to interfering analytes, since the adsorptive coating employed is rarely totally selective for a single component. In real environment, it is impossible for only one kind of pure gas to exist. The combustible materials detected in our experiment are just the case. Being burned, the combustible materials decompose and produce various gases, e.g., plastic, which contain chlorine, may produce hydrogen chloride; grain, which contain nitrogen, may produce nitrogen dioxide, ammonia and hydrogen cyanide; wood, which contain sulfur, may produce sulfur dioxide, etc. Different material will produce gas mixture which has different gas com-

* Corresponding author.

PII S0039-9140(97)00020-9

ponents. So, an array of sensors was constructed by coating with a different partially selective material. The advantage of an array device of this kind is that the array's response for each analyte corresponds to a fingerprint response pattern with component identification analogous to spectrometry. In this experiment, we investigated the application of artificial neural networks (ANN) and conventional multivariate techniques to the classification of signals from sensor array to identify four kinds of combustible materials.

Artificial neural networks are a form of artificial intelligence that mathematically simulate biological nervous systems. They have been employed in a diverse range of applications in recent years [7] including signal processing of sensor array [8]. The ANN approach was selected because it possess several advantages over conventional methods in terms of adaptability (learning, self-organization, generation and training), noise tolerance, fault tolerance, distributed associated memory, inherent parallelism generating a high speed of operation subsequent to training [9]. The application of ANNs to signal classification problems requires far less restrictive assumptions about the input signal than traditional multivariate techniques. The results of our experiment show that the prediction ability of ANN is superior to stepwise discriminant analysis (SDA) for the four kinds of combustible materials. This method is hoped to be an effective measure for fire alarm.

2. Experimental

2.1. Instrument

The apparatus consisted of seven AT-cut piezoelectric quartz crystal with a fundamental frequency of 9 MHz, 12.0 mm in diameter, with gold or silver plated electrodes of 6.0 mm in diameter on both sides. The oscillator circuit was designed by our laboratory, and its power was supplied by a PL2002A d.c. voltage regulator. The frequency change of each sensor was monitored in sequence by a N3165-type frequency counter and collected by a data acquisition system made in our laboratory. The programs for data acquisition were written in Turbo C. The BP network of ANN in data analysis was also written in Turbo C. SDA program was obtained commercially from SPSS program package. All data were treated by a PC-DX486 computer.

2.2. Reagents

The coating material used for sensors are: polyvinylpyrrolidone (PVP); triethylamine; Vitamin B6 hydrochloride; L-glutamic acid hydrochloride; ascorbic acid; triacetin glycerol triacetate and polychlorobiphenyl. All the reagents are of analytical-reagent grade. The coating of the crystals was performed by preparing a 5% w/w solution of the coating material in a highly volatile solvent such as chloroform or ethanol. Each solution was brushed onto both sides of a crystal with a cotton swab until a frequency shift of approximately 2000–5000 Hz was obtained after evaporation of the solvent.

2.3. Measurement method

The scheme of the measuring system can be seen in Fig. 1. Smoke was generated from a certain amount (1.5 g) of different materials (paper, wood, plastic, grain, et al.) by electric heating in the first box (smoke generator). The sensor array was mounted in the second (measuring) box connected to the first one by pipes and prefilter. The prefilter consisted of calcium chloride and silica gel was set after the smoke generator to

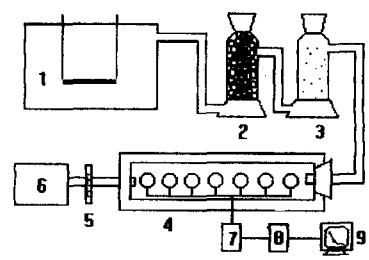

Fig. 1. Instrument diagram of piezoelectric crystal sensor array. (1) Smoke generator, 5600 cm^2; (2) solica gel; (3) calcium chloride; (4) Piezoelectric crystal sensor array; (5) flowmeter; (6) vacuum pump; (7) oscillators; (8) frequency counter; (9) computer.

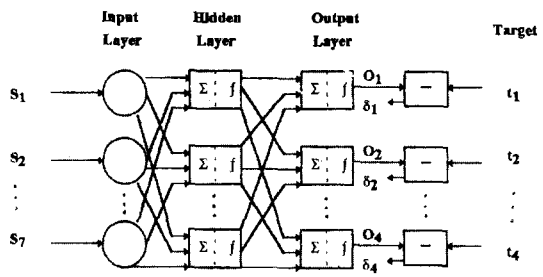

Fig. 2. Two-layer back-propagation model.

move water vapour produced during burning. Soot, liquid and other solid particle burning products were moved using defatting cotton and filter paper put inside the pipes. A small electromagnetic pump forced a continuous gas flow through the system (80 ml min^{-1}). Approximately 5 min after burning of the combustible material, the frequency of the sensors began to fall. The frequency response of each sensor was measured in sequence by a data acquisition system made in our laboratory. The sampling time for each sensor is 0.1 s. The frequency response difference between sample and blank (air) was calculated and displayed in real time on the computer screen and stored on disk for later analysis. After the frequency shift maximum was observed and became stable, the chamber was purged with clean air for 30–60 min. The largest frequency shift of each sensor was used as input for ANN and SDA. Every sample was measured in triplicate to estimate the precision of the sensor array.

2.4. Network design

Fig. 2 shows a generalized two-layer back-propagation network used in our experiment that has seven inputs (sensors) in the input layer, an arbitrary number of artificial neurons in the hidden layer (six, in this experiment) and four artificial neurons in the output layer (combustible materials). Each of the inputs ($O_{(l-1)i}$) is multiplied by an associated weight (w_{lji}), where l is the actual layer of the network, i is the neuron of the layer before, j is the neuron of the actual layer. Each weight has a value that reflects the strength if the synaptic link and thus the importance of a particular input (e.g., sensor). The output signal (y_{lj}) is further processed by a non-linear activation function that 'squashes' the data. In our study, we have used a sigmoid activation function so the neural output O_{lj} is given by

$$O_{lj} = 1/[1 + \exp(-y_{lj})] \qquad l = 1, 2 \tag{1}$$

and

$$y_{lj} = \sum_{i=1}^{n} w_{lij} O_{(l-1)i} \tag{2}$$

The back-propagation training algorithm uses a gradient search technique to minimize a cost function E equal to the mean square difference between the desired output t_j and the actual output vector O_{2j} (two layers).

$$E = 0.5(O_{2j} - t_j)^2 \tag{3}$$

The backward pass starts with the calculation of $\partial E/\partial O_{lj}$ (an example calculation for the two-layer network is given in parentheses):

$$\delta^*_{lj} = \partial E/\partial O_{lj} \qquad (\delta_{2j} = O_{2j} - t_j) \tag{4}$$

The next step is the estimation of $\partial E/\partial y_{lj}$:

$$\delta_{lj} = \partial E/\partial y_{lj} \qquad (\delta_{2j} = f'(O_{lj})\delta^*_{2j} = O_{2j}(1 - O_{2j})\delta^*_{2j} \tag{5}$$

The previous terms δ^*_{l-1} can be computed from δ_l:

$$\delta^*_{(l-1)i} = \sum_{j}^{k} w_{lji}\delta_{lj} \tag{6}$$

where k is the number of neurons in layer l.

Finally, $\partial E/\partial w_{lji}$ can be calculated:

$$\partial E/\partial w_{lji} = \delta_{lj} O_{(l-1)i} \tag{7}$$

So the weights can be adapted:

$$\Delta w_{lji}(m+1) = \eta\delta_{lj} O_{(l-1)i} + \alpha\, \Delta w_{lji}(m) \tag{8}$$

$$w_{lji}(m+1) = w_{lji}(m) + \Delta w_{lji}(m+1) \tag{9}$$

Where m means the number of training iterations. So the weights are adjusted by one term that is propagational to the error with a constant of the proportionality, called the learning rate (η). The second term is used to improve the stability of the learning process and is called the momentum term (α).

3. Results and discussion

3.1. Data selection method to avoid unconvergence at the beginning of networks training, 'training set stepwise expanding method'

For the performance of networks, the property of initial data is quite important. In the area of data selection and effects of bad data upon performance of networks, no system investigation has been studied. In our experiment, we discovered that, in the case where the identification problem was complicated or there was large similarity between the categories we wanted to identify and some difference or bad data existed among data in certain category, the effects of particular bad data on performance of networks were considerable, sometimes, the error of the network increased suddenly and it was quite difficult for the network to converge. These data are not sure to be bad ones to be deleted. It is possible that the difference of these data with other data in certain category is somewhat large. For this case, if we use all the samples of training set to train at the same time, the network can not converge. At this time, we can adopt 'training set stepwise expanding' method. The details are as following steps: firstly, we compared the response patterns of training samples, in each category, we selected one or two samples as initial training set whose difference with data of samples of other categories was relatively large. If the network could converge indeed, then after several hundred to thousand iterations, training set could be expanded by selecting again one or two samples which were relatively similar to the data in the forward training set of certain category, and the weights of last training should be used to train the network continuously. These steps were done until training set had included all the samples which were prepared to be as training set. Adopting this method, if the network still can not converge when using initial training set, conclusion may be drawn that the similarity among categories is too large to be discriminated by the networks. Measures should be taken to select more selective input variables. If the error increased suddenly and the network became difficult to converge due to a certain expanding, then there may be at least one bad data in this expanding data set. Check those data one by one, the bad data can be found and might be deleted. If we did not select the expanding sample according to the principle of similarity mentioned above, the data whose difference with the other data in certain category is relatively large may be deleted mistakenly. In fact, these data can make the network converge if we select them according to the above principle.

The data in our experiment is just the case as above. To guarantee the generalization of sampling, we made the data in certain category have somewhat difference. Additionally, the input layer only have seven neurons which makes the network difficult to converge. There are 52 samples in the training set, 13 samples in every category. The means of response of every category from sensor array are shown in Fig. 3. If we use them as training set altogether at the beginning to train the network, it did not converge at all, the error of the network was very large, though various data normalization methods had been tried. In contrast, it converged well when using the method mentioned above. The logarithm of the frequency shift was used as input, in order to accommodate the actual values, which spanned more than two orders of magnitude (from 20 to 5000 Hz). The prediction results are quite well as shown in Table 2. This method is suitable not only to the case where network can not converge at all at the beginning of training, but also to the case where the error of the network is relatively large or the network converge very slowly.

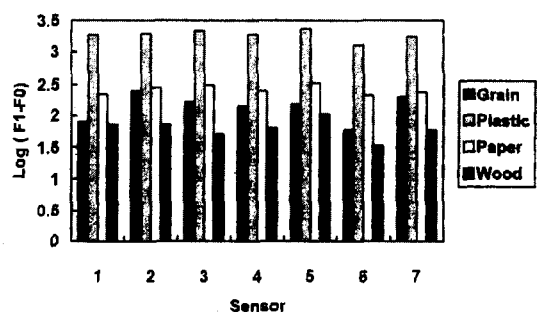

Fig. 3. Response patterns for means of every category of combustible material.

Table 1
Discriminant result of stepwise discriminant analysis (SDA)

Sample No.	Actual class	Predicted class	Sample No.	Actual class	Predicted class	Sample No.	Actual class	Predicted class
1	A	A	23	B	B	45	D	D
2	A	A	24	B	B	46	D	D
3	A	A	25	B	B	47	D	D
4	A	A	26	B	B	48	D	D
5	A	A	27	C	C	49	D	D
6	A	A	28	C	C	50	D	D
7	A	A	29	C	C	51	D	C[b]
8	A	A	30	C	C	52	D	D
9	A	A	31	C	C			
10	A	A	32	C	C	53[a]	A	A
11	A	A	33	C	C	54[a]	A	A
12	A	A	34	C	C	55[a]	A	A
13	A	A	35	C	C	56[a]	B	B
14	B	B	36	C	C	57[a]	B	B
15	B	B	37	C	C	58[a]	B	B
16	B	B	38	C	C	59[a]	C	C
17	B	B	39	C	C	60[a]	C	C
18	B	B	40	D	D	61[a]	C	B[b]
19	B	B	41	D	D	62[a]	D	D
20	B	B	42	D	D	63[a]	D	D
21	B	B	43	D	D	64[a]	D	D
22	B	B	44	D	D			

Note: A, grain; B, plastic; C, paper; and D, wood.
[a] Test sample.
[b] Discriminant mistake.

3.2. Prediction results for ANN and SDA

In order to avoid the dependence between independent variables leading to low precision of data computation and unstable discriminant functions, SDA was adopted. As can be seen in Table 1, the 64 samples were divided into calibration set, consisting of 52 samples, 13 samples in each category, and test set, consisting of 12 samples, three samples in each category. After processing with SDA, from the calibration set six discriminant variables which supplied more information were selected. The prediction correct rates were 98% for calibration set and 83% for test set. Fig. 4 shows the plot of discriminant Function 1 against 2.

It is customary to adopt an output element value of 0.9 to show reasonable convergence, however, a slightly lower level, 0.8, is also accepted for reasonable convergence from Gardner's experience [10]. Table 2 lists the prediction results for ANN, which used the same training set and test set as that used for SDA. It can be seen that outputs generated during testing were typically of the order of 0.8 or above compared with an ideal value of 1.0, and of the order of 0.2 or below compared with an ideal value of 0. These results show that the network discriminates well

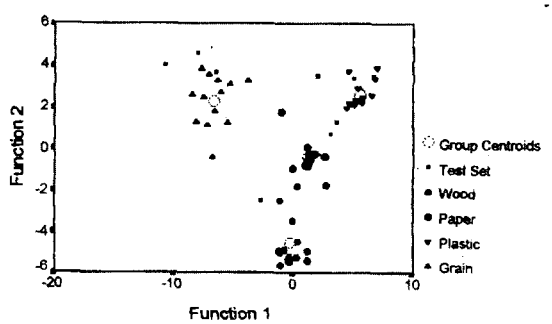

Fig. 4. Discriminant functions plot using SDA.

Table 2
Prediction result of artificial neural networks

Sample No.	Output 1		Output 2		Output 3		Output 4	
	actual	target	actual	target	actual	target	actual	target
1	0.8877	1	0.1625	0	0.0000	0	0.0003	0
2	0.9771	1	0.0006	0	0.0000	0	0.0007	0
3	0.9799	1	0.0000	0	0.0004	0	0.0002	0
4	0.0000	0	0.9995	1	0.0000	0	0.0012	0
5	0.0000	0	0.9998	1	0.0000	0	0.0003	0
6	0.0000	0	0.9968	1	0.0000	0	0.0004	0
7	0.0000	0	0.0000	0	0.9999	1	0.0002	0
8	0.0000	0	0.0000	0	0.7984	1	0.0059	0
9	0.0000	0	0.0000	0	0.9999	1	0.0001	0
10	0.0001	0	0.0000	0	0.0000	0	1.0000	1
11	0.0000	0	0.0000	0	0.0000	0	1.0000	1
12	0.0000	0	0.0000	0	0.0000	0	1.0000	1

between these chemical species and compare favorably with the result of SDA. In addition, because of adopting 'training set stepwise expanding' method mentioned above, training time which took only several minutes was far less than usual approaches.

3.3. Effects of learning rate and momentum term

Values of the learning rate η and momentum coefficient α affect the performance of a network. It is generally recommended that the ratio of these parameters is 1.5. Fig. 5 and Fig. 6 show the variation of the network performance with momentum coefficient ($\eta = 0.9$) and learning rate ($\alpha = 0.6$), after the training set has been expanded to contain all the initial data and training has process 400 iterations, where the performance of the network is presented by network error, ϵ, the sum of difference between ideal output and actual output of every neuron in the output layer of training set, and 10 000, 20 000, 30 000, 40 000 are training iterations. From Fig. 5 we can see that when momentum coefficient arrives 1.0, error of network arrives minimum and keep constant when momentum coefficient continue to increase. Fig. 6 shows that the minimum does not appear when learning rate arrives 1.4. We also have tested even larger learning rate up to 16 which are not shown in the figure, but minimum was still not found, though the decreasing rate of the error of network became slow gradually. The above phenomena are different with that in Gardner's work [10], (he found error minimums with learning rate $\eta = 0.9$ and momentum coefficient $\alpha = 0.7$, respectively), which may be attributed to the difference of data structure.

4. Conclusion

We have shown that ANN was able to identify the four combustible materials correctly from an array of seven piezoelectric sensors and superior to multivariate techniques, such as SDA. If we want to identify more combustible materials, we can select more sensors with more coating materials which have appropriate selectivity. The data

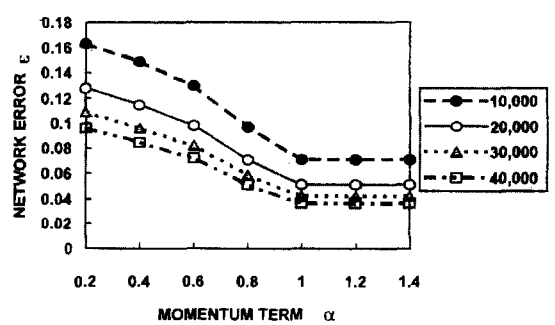

Fig. 5. Variation in network performance with momentum coefficient ($\eta = 0.6$).

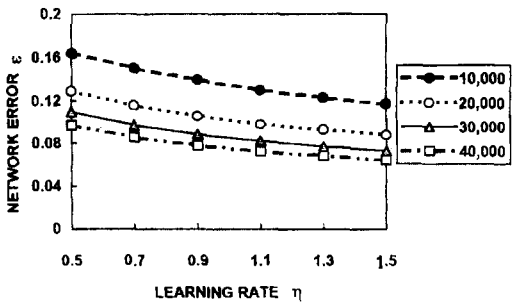

Fig. 6. Variation in network performance with learning rate ($a = 0.6$).

selection method 'training set stepwise expanding' has been put forward to improve convergence of the networks and increase training speed, which is believed to be an encouraging method for the applications of ANN.

Acknowledgements

This work was supported by the National Natural Science Foundation of People's Republic of China.

References

[1] K.H. Karmarkar and G.G. Guilbault, Anal. Chim. Acta, 71 (1974) 419.
[2] K.H. Karmarkar and G.G. Guilbault, Anal. Chim. Acta, 75 (1975) 111.
[3] J. Hlavay and G.G. Guilbault, Anal. Chem., 50 (1978) 1044.
[4] J.F. Aldar, A.E. Bentley and P.K.P. Drew, Anal. Chim. Acta, 182 (1986) 123.
[5] J. Hlavay and G.G. Guilbault, Anal. Chem., 50 (1978) 965.
[6] J.F. de Andrade, A.A. Suleiman and G.G. Guilbault, Anal. Chim. Acta, 217 (1989) 187.
[7] J.A. Burns and J.A. Whitesides, Chem. Rev., 93 (1993) 2583.
[8] J.W. Gardner, E.L. Hines and M. Wilkinson, Meas. Sci. Technol., 1 (1990) 446.
[9] D.E. Rumelhart and J.L. McClelland, Parallel Distributed Processing, MA: MIT Press, Cambridge, 1986, p. 318–362.
[10] J.W. Gardner, E.L. Hines and H.C. Tang, Sens. Actuator, B9 (1992) 9.

ELSEVIER

Talanta 44 (1997) 2041–2049

Talanta

Rapid automated in-situ monitoring of total dissolved iron and total dissolved manganese in underground water by reverse-flow injection with chemiluminescence detection during the process of water treatment

Yanxiu Zhou, Guoyi Zhu *

Changchun Institute of Applied Chemistry, Chinese Academy of Sciences, National Analytical Research Center of Electrochemistry and Spectroscopy, Changchun 130022, People's Republic of China

Received 27 August 1996; received in revised form 5 November 1996; accepted 20 January 1997

Abstract

Measurement of iron and manganese is very important in evaluating the quality of natural waters. We have constructed an automated Fe(II), total dissolved iron(TDI), Mn(II), and total dissolved manganese(TDM) analysis system for the quality control of underground drinking water by reverse flow injection analysis and chemiluminescence detection(rFIA-CL). The method is based on the measurement of the metal-catalyzed light emission from luminol oxidation by potassium periodate. The typical signal is a narrow peak, in which the height is proportional to light emitted and hence to the concentration of metal ions. The detection limits were 3×10^{-6} μg ml^{-1} for Fe(II) and the linear range extents up to 1.0×10^{-4} and 5×10^{-6} μg ml^{-1} for Mn(II) cover a linear range to 1.0×10^{-4} μg ml^{-1}. This method was used for automated in-situ monitoring of total dissolved iron and total dissolved manganese in underground water during water treatment. © 1997 Elsevier Science B.V.

Keywords: Dissolved iron; Manganese; Water

1. Introduction

Measurement of iron and manganese is very important in evaluating the quality of natural waters. It is well known that excessive intake of iron and manganese influences human health [1]. So a simple and rapid method is required for iron and manganese detection. Chemiluminescence (CL) methods are a means of enabling the rapid, simple and economical detection of various substances.

Several CL systems have been proposed for the sensitive determination of iron and manganese on the basis of CL reaction. The most famous CL system is the luminol reaction. The intrinsic sensitivity of the luminol system to small metal concentrations makes it very attractive for trace analysis. Fe(II) [2–4], Fe(III) [5–7], Mn [8–12] can be determined by its reported catalytic effect on the oxidation of luminol by oxidants, such as

* Corresponding author. Fax: +86 431 5685653.

PII S0039-9140(97)00029-5

dissolved oxygen [11–16], hydrogen peroxide [8,9,17–25] and potassium periodate [26,27]. One of the most extensively studied of this system is to determinate Fe(II), which has been developed as an analytical method for Fe(II) in many materials [28,14], but seldom application [28] to natural sample was reported. Kalinichenko [22,23] determined 0.05–5 ng of manganese using luminol, but many other transition metal interfered. Dubovenko and Tovmasyan [24] reported a similar system for determining 0.1–1 μg ml^{-1} manganese with photographic rather than photoelectric detection. Geng et al. [26] obtained a detection limit 8×10^{-6} μg ml^{-1} manganese using a luminol-KIO_4 system, but Co(II) and Cr(III) interfered. Ibusuki [29] discussed the interference of trace manganese(II) and Fe(III) in the luminol system. So selectivity is the most important thing in CL reaction for a technique to be used for analytical purpose.

Lucigenin can be used in place of luminol [30–32]. Photographic detection enables manganese at the 1–3 μg ml^{-1} level to be determined, but again, many metal ions interfere [30,31]. Fe(III), Cu(II), Tl(III) and Mn(II) can be simultaneously measured by its catalytic effect on the oxidation of lucigenin by hydrogen peroxide, but Cu(II) and Tl(III) are interferences in analytical methods for Fe(II) and Mn(II) [31]. So even this system can not be utilized to simultaneously determine Fe(III) and Mn(II) in practice.

The brilliant sulfoflavine(BSF) was used to determined Fe(II)/Fe(III), Cr(III) based on the Fenton or Fenton-like reaction, the reaction with hydrogen–peroxide [33]. Yamada [33] described the CL reaction resulting from the addition of Fe(II) to solution of H_2O_2 and alkaline BSF. Johnson [34] modified this system and used it to determine subnanomolar levels of iron(II) and total dissolved iron in seawater.

Yamada [35] demonstrated that 0.01–10 ng Mn(II) can be determined with high sensitivity by exploiting the Mn(II) catalyzed oxidation of 7,7,8,8-tetracyanoquinodimethane(TCNQ) by O_2. Johnson [36] adapted the method and applied it to the shipboard determination of manganese in seawater, but Fe(III) and Mg(II) interfered.

Babko et al. [37,38] determined 0.1–10 μg of manganese by oxidation to permanganate with peroxodisulphate and reaction of the permanganate with siloxene to produce chemiluminescence. Lin [39] determined Co(II) and manganese(II) simultaneously by CL oxidation of gallic acid and formaldehyde in the presence of thiourea by alkaline H_2O_2.

A CL method has not been proposed to simultaneously determinate Fe and Mn. Until now, separation or elimination of interfering species has been required prior to the determination of an analyte. Several pretreatment procedures have been reported: ion exchange [40], for example 8-hydroxy-quinoline resin was used to preconcentrate Fe [36] and then detected in TCBQ CL system and Mn [34] in BSF CL system. Nakayama [10] have developed a method based on the combination of selective electrolytic preconcentration and luminol CL system to determine Mn(II) in seawater. Addition of masking agents such as sodium citrate, quinolin-8-ol [27] for metal interferences to form inactive complexes and then detected in a luminol-KIO_4 system or using activator in luminol CL system, for example TETA(Fe(III) [4], Mn [10]), DETA(Fe(III)) [19,20], EDTA(Fe(II)) [16], TEA(Mn(II)) [26], phenanthrolin (Mn(II)) [22,23], TETA or TEPA(Fe(II), Fe(III) Cr(III)) [33] and sodium dodecylsulfonate [41].

This paper reports a simple and automatic method for specifically measuring trace concentration of TDI and TDM in the presence of other metal ions with the luminol-KIO_4 CL reaction by rFIA. Specificity for TDI is achieved by adding *o*-phenanthrolin(*o-p*) and taking advantage the Fe(*o-p*) complex formed as activator. In the same way, specificity for TDM is achieved by adding TEA and H_3PO_4 with most metal ions including iron ion being masked. The proposed method was applied to monitor TDI and TDM in underground water during the water treatment process for the quality control of drinking water.

2. Experimental

2.1. Apparatus

The rFIA system was illustrated in Fig. 1 and was constructed to realize automated Mn and Fe detection in underground drinking water in collaboration with the Daqing Water Supply. It employed a eight-channel peristaltic pump and a microprocessor-controlled Teflon rotary injection valve. All manifold tubing was Teflon (0.8 mm i.d.) except for the standard peristaltic pump tubing (poly(vinyl chloride)(PVC)). A transparent spiral tube with 12 cm length and 1.08 mm i.d. was employed as the CL flow cell in this system. Light intensities were measured with a R212UH photomultiplier operated at -729 volts. All the experiments were performed at room temperature at a flow rate of 2.1 ml min^{-1} for each pathway. The flow rate was determined from later studies. In this research, the experiments for optimization of the measuring conditions were performed during construction and adjustment of this system.

2.2. Procedure for CL measurements

The system was operated as follows. For Fe(II) the CL reagent I passes through a 30 μl sample loop and the excess is fed to a waste vessel. The sample and $NaHSO_3$ are mixed at mixing just prior to the injection valve and then mixed with the luminol CL reagent I. The reaction mixture reacts for 20 s in the mixing coil before being injected by the three way valve to the detection. The CL is measured in a transparent spiral tube by a neighboring photomultiplier. For determination of TDM the procedures with almost the same as above except the three-open valve was turned to position 2.

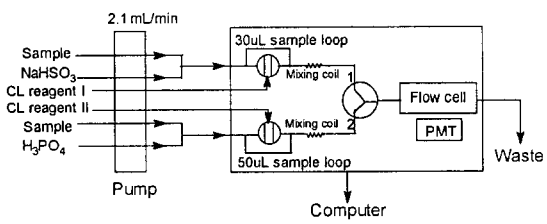

Fig. 1. Schematic diagram of the reaction manifold used for the rFIA-CL determination of iron and manganese.

Underground water samples were collected automatically and directly pumped into flow cell after water treatment. The samples were at natural pH and did not need to be acidified. No loss of TDI and TDM due to wall adsorption was observed.

2.3. Reagents

Luminol was purchased from Merck-Schuchardt. Potassium periodate from Beijing Center-union Chemical. Triethanolamine from Shanghai Chemical. *o*-phenanthrolin hydrochloric acid was from Merck Darmstadt and potassium hydroxide from Beijing Chemical. The other reagents were all A.R. grade. Reagent solutions were made with doubly distilled water from a quartz apparatus.

Stock solutions of luminol were prepared in 0.1 mol l^{-1} KOH solution, adjusted to 0.01 mol l^{-1} and stored at 4°C. A 0.1 mol l^{-1} H_3BO_3-KOH buffer was used to control the pH. CL reagent I (for determination of TDI) contained: 6×10^{-4} mol l^{-1} luminol, 2.5×10^{-4} mol l^{-1} *o*-phenanthrolin hydrochloric acid(*o*-*p*) and 10^{-4} mol l^{-1} KIO_4 in 0.1 mol l^{-1} H_3BO_3-KOH buffer(pH 10.0), and was left for at least one hour to stabilize. CL reagent II (for determination of TDM) contained: 2×10^{-3} mol l^{-1} luminol, 1.125% triethanolamine(TEA) and 2×10^{-3} mol l^{-1} KIO_4 in 0.125 mol l^{-1} NaOH and was also left for at least one hour to stabilize.

3. Results and discussion

3.1. Investigation of the measuring system

Initial investigation was performed with standard solution in distilled water using a reverse flow injection manifold.

3.1.1. Effect of length of mixing coil

To ensure the efficient reaction between CL reagent I or CL reagent II with the sample, a mixing coil with length from 16 to 90 cm was used

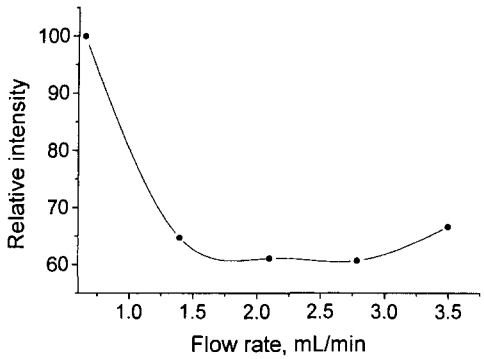

Fig. 2. Effect of flow rate on the CL intensity of 0.010 μg ml^{-1} Fe(II) in the presence of 6×10^{-4} mol l^{-1} luminol, 2.5×10^{-4} mol l^{-1} *o-p* and 1×10^{-4} mol l^{-1} KIO_4 in 0.1 mol l^{-1} H_3BO_3-KOH buffer solution, pH 10.0.

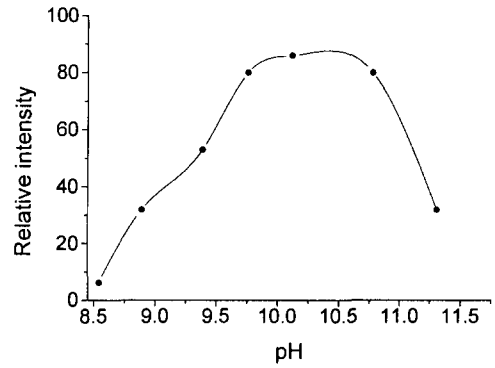

Fig. 3. Effect of pH on the CL intensity from 0.005 μg ml^{-1} Fe(II) in the presence of 6×10^{-4} mol l^{-1} luminol, 2.5×10^{-4} mol l^{-1} *o-p* and 1×10^{-4} mol l^{-1} KIO_4 in 0.1 mol l^{-1} H_3BO_3–KOH buffer solution, pH 10.0.

for comparison. It was found that a suitable length with a high CL intensity was 60 cm for both systems, shorter or longer than this length would cause the decrease of CL intensity because of the deficient reaction or a considerable dilution.

3.1.2. Effect of flow rate

We investigated the effect of flow rate for the Fe(II) system. The signal did not vary significantly from 1.75–2.8 ml min^{-1} as shown in Fig. 2. In addition, the pump can be adjust to only one flow rate for eight channels, so the 2.1 ml min^{-1} was chosen as the optimum flow rate for both systems.

4. TDI measurement

4.1. Effect of pH

Light emission did not vary significantly from 9.75–11.0 (Fig. 3). The optimal pH for CL reaction was pH 10.0 and the 0.1 mol l^{-1} H_3BO_3-KOH buffer was used to control the pH of CL reagent I solution. Since pH control is not critical, the buffered Fe(II)-KIO_4-luminol system may be characterized by using a calibration curve rather than the standard additions.

4.2. Optimization of reagents

The concentrations of luminol, KIO_4, *o-p* and potassium hydroxide were all optimized for the rFIA-CL system. The concentration of each reagent was varied independently.

4.2.1. Effect of luminol concentration

The intensity of light catalyzed by 0.01 μg ml^{-1} Fe(II) as a function of luminol concentration showed that the reaction is most efficient at $6 \times 10^{-4} \sim 7 \times 10^{-4}$ mol l^{-1} luminol, as shown in Fig. 4. The decrease of light at the highest luminol concentrations may be due to Fe(II) complexing with luminol or with the aminophthalate product of the luminol oxidation.

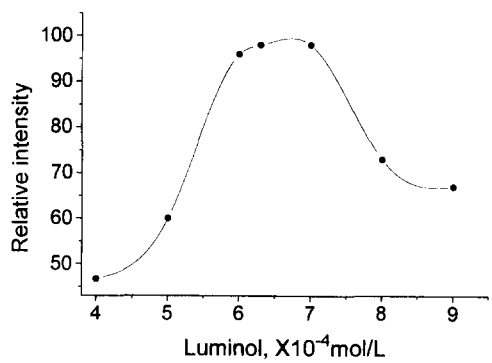

Fig. 4. Effect of luminol concentration on the CL intensity from 0.01 μg ml^{-1} Fe(II) in the presence of 2.5×10^{-4} mol l^{-1} *o-p* and 1×10^{-4} mol l^{-1} KIO_4 in 0.1 mol l^{-1} H_3BO_3–KOH buffer solution, pH 10.0.

Table 1
Interference of other metals to chemiluminescence for Fe(II)

Metal	Concn. μg ml^{-1}	Recovery(%)	Metal	Concn.	Recovery(%)
Mn(II)	0.1	100.6	Co(II)	0.1	147.9
Ni(II)	0.1	100.8	Cd(II)	0.1	100
Hg(II)	0.1	104.1	Fe(III)	3.0	104.3
Cr(III)	0.1	102.2	Cu(II)	0.2	100.4

Intensities are relative to the intensity of 0.01 μg ml^{-1} Fe(II).

4.2.2. Effect of potassium periodate concentration

The optimum potassium periodate concentration was 1×10^{-4} mol l^{-1}. Although hydrogen peroxide as an oxidant reagent instead of KIO_4 was tested, the result showed that it was easily bubbled in tubing and also the peak was too wide than that of KIO_4.

4.2.3. Effect of o-phenanthrolin hydrochloric acid concentration

o-p Itself did not give any CL signal. It must be an activator for the CL reaction of luminol with potassium periodate by Fe(II), after formation of Fe(II)-*o-p* complexes, *o-p* may be oxidized by KIO_4 and weak CL was produced as it is oxidized by H_2O_2 [17]. When the *o-p* concentration was $5 \times 10^{-5} - 2.5 \times 10^{-4}$ mol l^{-1}, the system had better selectivity than that of without *o-p* and good reproducibility for Fe(II).

4.3. Iron(III) reduction

Total dissolved iron can be determined by reducing Fe(III) to Fe(II) prior to analysis. The aqueous chemistry of iron is rather complex, since this metal enters into several protolysis and oxidation–reduction reactions [2,6,7]. When the groundwater comes to the surface, Fe(II) may be oxidize to Fe(III) by oxidants such as O_2 in the air and is subsequently precipitated as $Fe(OH)_3$. Sodium hydrogen sulfite was a suitable reagent due to its rapid and efficient reducing power [42,28]. The optimal concentration of sodium hydrogen sulfite for the reduction of Fe(III)–Fe(II) was dependent on the iron concentration. A 0.1% sodium hydrogen sulfite was chosen for 0.01 μg ml^{-1} Fe(III).

4.4. Interference studies

The ions which are thought interfere with luminol-KIO_4 CL of Fe(II) are Mn(II), Ni(II), Hg(II) and Cr(III), Fe(III), Cd(II), Cu(II). Table 1 shows the recovery of these elements at indicated concentration. Metal solutions for these studies were prepared from A.R. salts. Except for a substantial interference was observed when Co(II) was present at 0.1 μg ml^{-1}, none of the above elements significantly affected the iron signal when their concentrations equaled to or ten times higher than that of Fe(II).

4.5. CL kinetic property and analytical parameters

With all of the above established conditions, the CL intensity reached the maximum value in only 1–2 s, and the half peak width is 2.5 s when 0.005 μg ml^{-1} Fe(II) was injected.

Various concentrations of Fe ions were measured under these experimental conditions. The calibration curve was linear in the range $1 \times 10^{-4} - 0.6$ μg ml^{-1} of Fe(II): signal(relative intensity) = 455[Fe(II)] + 59.25 ($r = 0.998(n = 5)$). The relative standard deviation was 0.93% for 0.005 μg ml^{-1} ($N = 9$). Repeatability was measured with standard solutions. Since this system employed reverse flow injection analysis, the blank was zero, 3×10^{-6} μg ml^{-1} was the lower limit that can be detected.

5. TDM measurement

Manganese and iron have similar chemistry in water [43]. Mn(II) and Fe(II) both exist in an anaerobic environment. They can be oxidized by oxygen to MnO_2 and $Fe(OH)_3$ respectively, which exist as colloids and can be removed by filtration. If a sample to be analyzed for Fe(II) is filtered, then manganese in the form of Mn(II) will interfere with the Fe(II)-catalyzed CL. In the absence of dissolved oxygen and other oxidants, Mn(II) is the stable form in aquatic systems [44], so after filtering the concentration of Mn(II) is equivalent to TDM.

5.1. Effect of pH

The influence of the pH on CL intensity was investigated. The maximum and stable intensity of light for determination of Mn(II) was obtained when pH was 12.9, as shown in Fig. 5.

5.2. Optimization of reagents

5.2.1. Effect of luminol concentration

The intensity of light as a function of luminol concentration showed that the reaction is most efficient for luminol between 2×10^{-3} and 3×10^{-3} mol l^{-1} (Fig. 6).

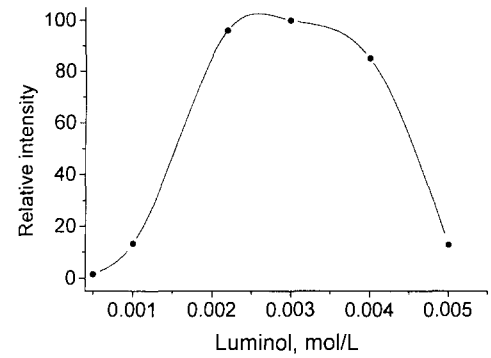

Fig. 6. Effect of luminol concentration on the CL intensity from 0.01 μg ml^{-1} Mn(II) in the presence of 1.125% mol l^{-1} TEA and 2×10^{-3} mol l^{-1} KIO_4 at pH 12.9.

5.2.2. Effect of potassium periodate concentration

The optimum potassium periodate concentration was more than 2×10^{-3} mol l^{-1}, as shown in Fig. 7.

5.2.3. Effect of TEA concentration

Various amines increase the CL observed from luminol-oxidant-Mn mixtures [33,5,10,19,29,22, 23], TEA was found the suitable activator for the CL system of luminol-KIO_4-Mn(II) [26]. TEA can also acts as masking reagent for a lot of metal ions, so it was chosen as an activator and masking reagent for determination of Mn(II). The optimum TEA concentration was 1.125% (Fig. 8).

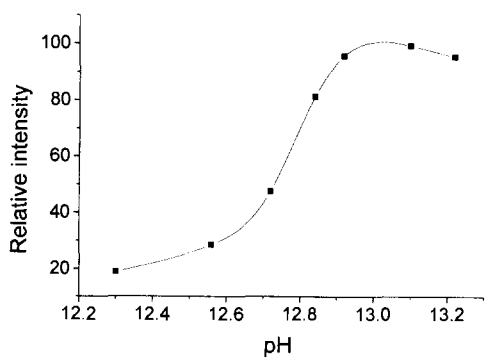

Fig. 5. Effect of pH on the CL intensity from 0.01 μg ml^{-1} Mn(II) in the presence of 2×10^{-3} mol l^{-1} luminol, 1.125% mol l^{-1} TEA and 2×10^{-3} mol l^{-1} KIO_4.

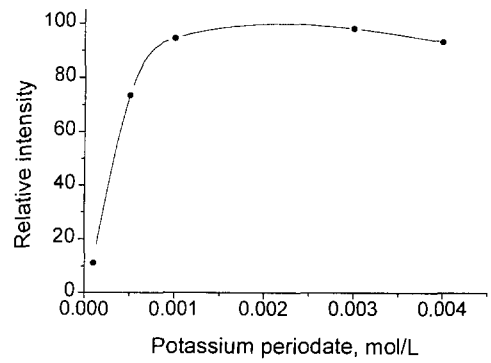

Fig. 7. Effect of KIO_4 concentration on the CL intensity from 0.01 μg ml^{-1} Mn(II) in the presence of 1.125% mol l^{-1} TEA and 2×10^{-3} mol l^{-1} luminol at pH 12.9.

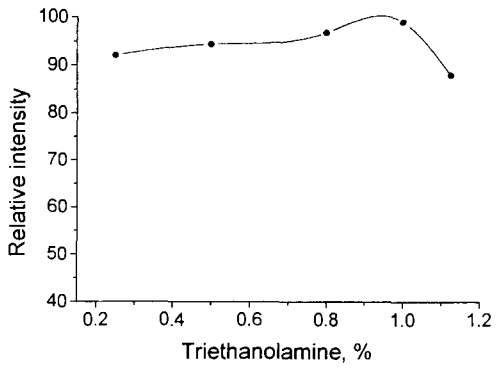

Fig. 8. Effect of TEA concentration on the CL intensity from 0.01 μg ml^{-1} Mn(II) in presence of 2×10^{-3} mol l^{-1} KIO_4 and 2×10^{-3} mol l^{-1} luminol at pH 12.9.

5.3. Interference studies

Besides Mn(II), several metal ions, such as Co(II), Fe(II), Fe(III), Ti(IV) and Mo(VI) catalyze the luminol-periodate CL reaction. Others, such as Cu(II), Pb(II), Ni(II), Cd(II), In(III) and Ce(IV), inhibit the CL [27]. In the presence of 1.125% TEA, commonly encountered ions, except Mn(II), can be masked (Table 2). In addition, 0.292 mol l^{-1} H_3PO_4 was chosen as a masking reagent on iron. So two kinds of masking reagent TEA and H_3PO_4 were used in this system.

5.4. CL kinetic property and analytical parameters

Using established conditions, the CL kinetic curve showed a CL signal reaching the maximum value in only 1–4 s, and the half peak width is 1.5 s for a 0.01 μg ml l^{-1} Mn(II) sample.

The system response for Mn(II) was linear in the range $1 \times 10^{-4} - 0.6$ μg ml^{-1} of Mn: $I = 702.714[Mn(II)] + 16.627$($r = 0.999$($n = 6$)). The relative standard deviations was 0.37% for 0.01 μg ml^{-1} ($n = 11$). The blank of this system was also zero. The lower limit that can be detected was 5×10^{-6} μg ml^{-1}.

6. Analysis

We have developed a CL system for the measurement of TDI and TDM in underground water. Table 3 gives the results obtained for different samples of underground fresh water. This method was used in monitoring the TDI and TDM in underground water during water treatment [45]. In practical use, as TDM concentration is more than 0.3 mg l^{-1} and TDM 0.1 mg l^{-1}, the system will give alarm in order to control the process of water treatment. We had been keeping watch on this system for one month. It performed very stable.

7. Conclusion

The proposed method is very sensitive and shows good reproducibility. The use of KIO_4, unlike hydrogen peroxide, prevents the formation of bubble in the tubing system. This method can be used to determine TDI and TDM at ng ml^{-1} level in water and also for water quality control in Daqing Water Supply, in China.

Table 2
Interference of other metals to chemiluminescence for Mn(II)

Metal	Conc. μg ml^{-1}	Recovery(%)	Metal	Conc. μg ml^{-1}	Recovery(%)
Co(II)	0.1	103.5	Cu(II)	20	98
Cr(III)	0.1	104.8	Pb(II)	20	95.8
Fe(II)	10	100.1	Ni(II)	20	99.7
Fe(III)	20	104.2	Cd(II)	20	99.2
Tl(III)	1	101	In(III)	20	96.9
Mo(VI)	0.2	100	Ce(IV)	12	95

Intensities are relative to the intensity of 0.01 μg ml^{-1} Mn(II).

Table 3
Results of the determination of TDI and TDM in different samples from underground water

Sample	Fe(II) in sample ($\times 10^{-3}$ μg ml^{-1})	Mn(II) in sample ($\times 10^{-3}$ μg ml^{-1})	Fe(II) added ($\times 10^{-3}$ μg ml^{-1})	Recovery (%)	Mn(II) added ($\times 10^{-3}$ μg ml^{-1})	Recovery (%)
1	1.7	0.325	5	97.0	1	100
2	2.0	0.325	5	102	1	103
3	3.8	0.351	5	98.5	1	99.2
4	0.36	4.56	3	102	3	104.0
5	1.02	3.12	5	102	3	99.7
6	0.44	2.36	3	104	3	97.5
7	6.34	1.54	5	105	3	97.6
8	10.67	0.67	10	103	3	103.8

Acknowledgements

The authors gratefully acknowledges the financial support of this work from the Daqing Water Supply.

References

[1] National Interim Primary Drinking Water Regulations, Federal Register, 40 (248) (1975) 59 566.
[2] B. Yan, P.J. Worsfold, Anal. Chim. Acta., 236 (1990) 287.
[3] X.H. Lu, Huanjing Kexue Yu Jishu, 2 (1989) 23.
[4] K. Robards, P.J. Worsfold, Anal. Chim. Acta, 266 (1992) 147.
[5] H. Obata, H. Karatani, E. Nakayama, Anal. Chem., 65 (1993) 1524.
[6] Z.B. Wang, Z.Z. Zhen, G.W. Wu, Xiamen Daxue Xuebao, 33 (3) (1994) 364.
[7] J.R. Lu, X.R. Zhang, G.F. Zhang, M. Li. Sanxi Shifan Daxue Xuebao, 20 (2) (1992) 35.
[8] X.H. Lu, M.G. Lu, Guangpuxue Yu Guangpu Fenxi, 12(5) (1992) 121.
[9] Z.Z. Zheng, Z.B. Wang. Fenxi Huaxue, 13 (7) (1985) 510.
[10] E. Nakayama, K. Isshiki, Y. Sohrin, H. Karatani, Anal. Chem., 61 (1989) 1392.
[11] W.R. Seitz, D.M. Hercules, Anal. Chem., 44 (13) (1972) 2143.
[12] J.Z. Lu, Z.J. Zhang, Gaodeng Xuexiao Huaxue Xuebao, 16 (7) (1995) 1034.
[13] L. Klopf, T.A. Nieman, Anal. Chem., 55 (1983) 1080.
[14] Z.H. Song, Z.J. Zhang, Henliang Fenxi, 1 (1986) 50.
[15] E.G. Sarantonis, A. Townshend, Anal. Chim. Acta, 184 (1986) 311.
[16] H.S. Zhang, X.C. Yang, L.P. Wu, Fenxi Huaxue, 24 (2) (1996) 220.
[17] S.Q. Li, X.Y. Zhang, Yankuang Ceshi, 24 (1987) 267.
[18] A.A. Alwarthan, A. Townshend, Anal. Chim. Acta, 196 (1987) 135.
[19] J.E. Klinichensko, O.M. Grishchenko, Ukr. Khim. Zh., 36 (6) (1970) 610.
[20] A.K. Babka, J.E. Kalinichenko, Ukr. Khim. Zh., 31 (1965) 948.
[21] A.A. Alwarthan, Talanta, 41 (10) (1994) 1683.
[22] I.E. Kalinichenko, Ukr. Khim. Zh. 34 (3) (1968) 307.
[23] I.E. Kalinichenko. Russ. Pat., Sept. 22 252 712, 1969.
[24] L.I. Dubovenko and A.P. Tovmasyan, Ukr. Khim. Zh., 37 (1971) 943.
[25] J.L. Burguera, A. Townshend, Talanta, 28 (1981) 731.
[26] Z. Geng, Z.Q. Zhang, L.J. Bian, Gaodeng Xuexiao Huaxue Xuebao, 9 (11) (1988) 1114.
[27] Q. Lin, A. Guiradm, R. Escobar, Anal. Chim. Acta, 283 (1993) 379.
[28] R.T. Powell, D.W. King, W.M. Landing, Mar. Chem., 50 (1–4) (1995) 13.
[29] T. Ibusuki, Taiki Osen Gakkaishi, 3 (1985) 215.
[30] L.I. Dubovenko, A.P. Tovmasyan, Zh. Analit. Khim., 25 (1970) 940.
[31] L.I. Dubovenko and A.P. Tovmasyan. Arm. Khim. Zh., 23 (1970) 690.
[32] A.P. Tovmasyan, Konf. Molodykh Uch. Spets., Acad. Nauk. Arm. SSR, 1972, pp. 188.
[33] M. Yamada, A. Sudo, S. Suzuki, Chem. Lett., 1985, pp. 801.
[34] V.A. Elrod, K.S. Johnson, K.H. Coale, Anal. Chem., 63 (1991) 893.
[35] M. Yamada, S. Kamiyama, S. Suzuki, Chem. Lett., 1985, pp. 1597.
[36] T.P. Chapin, K.S. Johnson, K.H. Coale, Anal. Chim. Acta, 249 (1991) 469.
[37] A.K. Babko, L.I. Dubovenko, L.S. Mikhailova, Sov. Prog. Chem., 32 (1966) 471.
[38] A.K. Babko, L.I. Dubovenko and L.S. Mikhailova, Ukr. Khim. Zh., 32 (1966) 614.
[39] S. Lin and Y. Liu, Gaodeng Xuexiao Huaxue Xuebao, 11 (1990) 1199.

[40] W.R. Seitz, D.M. Hercules, Intern. J. Env. Anal. Chem., 2 (1973) 273.
[41] X. Lu, M. Lu, Huaxue Shijie, 9 (1990) 409.
[42] F.J. Millero, M. Gonzalex-Davila, J.M. Santana-Casiano, J. Geophys. Res., [Atmos], 100 (D4) (1995) 7235.
[43] J.J. Morgan, W. Stumm, Proceeding of the Second International Water Pollution Research Conference, Tokyo, 1964.
[44] S.D. Faust, O.M. Aly, Chemistry of Water Treatment, Butterworth Publishers, 1983, p. 483.
[45] Y.X. Zhou and G.Y. Zhu, Fenxi Huaxue, in press.

ELSEVIER

Talanta 44 (1997) 2051–2058

Talanta

Spectrophotometric determination of enzymatically generated hydrogen peroxide using Sol-Gel immobilized horseradish peroxidase

Faida A. El-Essi [a], Ali Z. Abu Zuhri [a], Suleiman I. Al-Khalil [a], Monzir S. Abdel-Latif [b,*]

[a] *Chemistry Department, Faculty of Science, An-Najah National University, P.O. Box 707, Nablus, Palestine*
[b] *Chemistry Department, The Islamic University, P.O. Box 108, Gaza, Palestinian Authority, Israel*

Received 27 August 1996; received in revised form 6 January 1997; accepted 14 January 1997

Abstract

Peroxidase entrapment in different Sol-Gel matrices was successful. The enzyme did not show a decrease in activity for at least 2 months as well as storage at room temperature and dry condition for periods exceeding 3 weeks. It was evident that the enzymatic activity was a function in the type of the alkoxysilane precursor. In addition, the optimum temperature which resulted in maximum enzymatic activity was also dependent on the type of Sol-Gel matrix. Excellent results were obtained for the determination of glucose in serum samples using soluble glucose oxidase in conjunction with the Sol-Gel entrapped peroxidase. The enzymatically produced hydrogen peroxide is oxidized by the entrapped peroxidase yielding oxygen which oxidizes the faint blue variamine blue into the intensely violet colored species (the molar absorptivity is about 1.8×10^4 l mol^{-1} cm^{-1}). The characteristics of this chromogenic system as well as optimized conditions for its use in the spectrophotometric determination of enzymatically generated hydrogen peroxide were investigated. Excellent agreement between the results obtained by the proposed method and the widely used standard method, utilizing a commercial reagents kit, was always observed. © 1997 Elsevier Science B.V.

Keywords: Sol-Gel; Enzyme immobilization; Peroxidase; Variamine blue

1. Introduction

The high specificity of enzymes in catalyzing some chemical reactions is an important feature that has been utilized for the selective and accurate determination of many substrates. Analytes are usually selectively converted into other species which can be easily monitored. Many enzymatic reactions result in the generation of hydrogen peroxide as a by-product of the conversion of appropriate substrates. Therefore, there has been a great deal of emphasis on the development of sensitive and highly reliable methods for the quantitative determination of hydrogen peroxide concentration which is an indirect indication of analyte concentration [1–3]. Several electrochemi-

* Corresponding author.

PII S0039-9140(97)00032-5

cal, spectrophotometric, and luminescence methods were suggested and procedures based on these methods were optimized for such systems. However, enzymes are usually expensive and their use as homogeneous catalysts is, most of the time, costly. In addition, the disposal of these active catalysts can impose environmental problems in many situations. Therefore, it is justified that efforts be directed towards designing approaches to immobilize these biomolecules so that they can be reused as well as be confined to a specific matrix [4]. Several methods for the immobilization of enzymes were suggested using different approaches. Physical adsorption of enzymes to an activated solid support is an important method of enzyme immobilization. However, these preparations are usually unstable and enzymes tend to come off in solution. Covalent binding of enzymes to solid surfaces like membranes or other solid supports is one of the most widely used approaches. However, several steps for the preparation of an adequate functional group on the solid support are usually involved prior to the final crosslinking step. These procedures are usually complicated and require good experience in this field. In addition, the enzymatic activity decreases appreciably and the immobilized enzymes do not retain their activity over long periods, beside some other disadvantages [4]. Recently, some biomaterials were trapped into a silicate glass matrix under mild conditions [5–8]. This was accomplished by the Sol-Gel method where room temperature polymerization of an alkoxysilane, after partial hydrolysis of the alkoxy groups results in a silicate polymer gel. The thus obtained gel solidifies with time as the polymerization continues and ultimately a glass-like silicate solid matrix is obtained. When an enzyme or any biomaterial is added to the silane precursor after partial hydrolysis, these materials can be entrapped into the polymeric matrix after complete solidification. Fortunately, enzymes show considerable retention of their activity in such immobilization matrices. Small substrate molecules can diffuse into the pores of the polymeric matrix and reach the active site of the enzyme and thus be converted to other simpler species which can diffuse back into solution where it can be detected. The relatively large size of the enzyme assures minimum leaching from the solid matrix. The Sol-Gel process for enzyme immobilization seems very promising especially due to the mild conditions that are used for the immobilization process as well as the simplicity of the procedure involved. In addition, the immobilization matrix can be optimized so that transparent monoliths, thin films or fine particles are formed depending on the ultimate application of the preparation. Detailed description of the Sol-Gel process can be found in the many books and reviews on this topic [9–16].

Braun et al. [6] suggested that the encapsulation of glucose oxidase in conjunction with peroxidase and a chromogen in a tetramethoxysilane Sol-Gel matrix was good for the determination of glucose. However, no analytical data was presented. Yamanaka et al. [7] investigated the activity of glucose oxidase entrapped in a Sol-Gel matrix using a conventional photometric scheme for detection of the generated peroxide. The turnover number and the dissociation constant were reported to be similar and two-fold greater than the corresponding values for the native enzyme, respectively. Also, storage conditions were reported to have significant influence on the activity of the enzyme.

In this study, we present results on a new chromogenic system for the determination of hydrogen peroxide as well as results of peroxidase entrapment in different silicate glass matrices prepared by the Sol-Gel method. The system is optimized for the determination of enzymatically generated hydrogen peroxide produced from the bioconversion of glucose by glucose oxidase. Details of the system characterization as well as results of the determination of glucose in serum blood samples will be presented.

2. Experimental section

2.1. Instrumentation

Absorbance measurements were recorded using a double beam Perkin-Elmer Lambda 15 UV-Vis spectrophotometer. The instrument is microprocessor based with excellent performance char-

acteristics. Also, a Spectronic 20D spectrophotometer was occasionally used for absorbance measurements. The pH of the different solutions was adjusted using a Hanna digital pH meter. Temperature controlled studies were conducted using a conventional water bath.

2.2. Chemicals and reagents

3-[Trimethoxysilyl]-1-propanthiol (TMSP), triethoxypropylsilane (TEPS), 3-aminopropyltriethoxysilane (APES), 3-chloropropyltriethoxysilane (CPES), triethoxyvinylsilane (TEVS), horseradish peroxidase (180 U mg^{-1}), and glucose oxidase from *Aspergillus niger* (100 U mg^{-1}) were purchased from Merck Chemical Company, Germany. Disodium hydrogen phosphate, citric acid, sodium citrate, and succinic acid were obtained from Reidel de Haen, Germany. Variamine blue was obtained from UCB Chemicals, Belgium. Glucose standards and controls as well as commercial kits for glucose determination were purchased from Sigma Chemical Company, USA. Thymol-indophenol, thionine, methylviologen, phenosafranine, and 7,8-benzoflavone were from BDH, England. All chemicals and reagents used in this study were of the analytical grade and were used as received without further purification. Distilled, deionized water was used throughout this work.

3. Procedures

3.1. Preparation of a variamine blue working solution

Variamine blue is slightly soluble in water yielding a light bluish solution which darkens with time. The procedure for the preparation of a working solution of variamine blue involved the transfer of about 90 mg of the material into a beaker followed by the addition of about 40 ml of distilled water. The solution was heated with stirring to about 80°C. The solution was then filtered and the final volume was then adjusted to 50 ml by addition of distilled water. The thus prepared solution contains about 80 mg of variamine blue. This solution was kept for 1 week before use since it was observed that the absorbance of this solution increased with time for the first 5 days before stabilization. Therefore, we recommend the storage of the freshly prepared variamine blue for a period exceeding 5 days before actual use so that reproducible readings can be achieved.

3.2. Preparation of the Sol-Gel matrix

3.2.1. Sol stock solution

First, 2.25 ml of the appropriate alkoxysilane derivative was transferred into a small glass bottle followed by addition of 0.7 ml of distilled water and 50 μl of 0.1 M HCl. The bottle was firmly capped and the mixture was shaken for about 3 h. At this stage, partial hydrolysis of the alkoxysilane derivative was accomplished. The thus prepared partially hydrolyzed silane derivatives were kept in capped bottles at room temperature.

3.2.2. Peroxidase entrapment

The entrapment procedure involved the mixing of a 1:1 ratio of the previously prepared Sol stock solution and a buffered peroxidase solution (0.1 M phosphate buffer at pH 6). The solution was then shaken so as to obtain a homogeneous mixture which was allowed to solidify at room temperature. The formation of the Sol-Gel starts few minutes after mixing and complete solidification (constant weight) after about 5–10 days. The Sol-Gel immobilized peroxidase was kept at room temperature for at least 2 weeks before washing with successive solutions of 1.0 M NaCl, 0.1 M phosphate buffer at pH 6, and plenty of distilled water, respectively. This washing procedure is necessary to wash out any residual or surface adsorbed peroxidase.

3.3. Analytical procedure for peroxide determination

The general procedure for the quantitation of hydrogen peroxide involved the transfer of 2–4 ml of the buffer solution into a test tube containing the Sol-Gel entrapped peroxidase. An appropriate known amount of peroxide (or glucose and glucose oxidase) was then added and the enzy-

matic reaction was allowed to proceed for 10 min. Just before the absorbance measurements, a 100-μl portion of the variamine blue working solution was added. The absorbance of the oxidized variamine blue (violet color) was measured immediately at 550 nm against a blank.

4. Results and discussion

Initially, experimental conditions were optimized in order to obtain a sensitive chromogenic system for the determination of hydrogen peroxide using soluble peroxidase. Several redox systems were tried in an attempt to find a good system for such determinations. Variamine blue resulted in a very sensitive system for the determination of hydrogen peroxide while thymol-indophenol, thionine, methylviologen, phenosafranine, and 7,8-benzoflavone did not result in any appreciable signal. Therefore, all the following experiments were done using variamine blue.

4.1. Effect of pH on absorbance

Variamine blue is oxidized by hydrogen peroxide in presence of peroxidase. The resulting violet color was found to be highly dependent on the pH of the buffer solution. Fig. 1 shows the relationship between the absorbance signal and the pH of the buffer solution. It can be concluded from the figure that very little oxidation takes place at pH values above pH 7 and essentially no observable oxidation takes place at pH values above pH 8. Lower pH values result in more improved absorbance signals than measurements performed at higher pH values while optimum pH of the buffer solution occurs at about pH 5. Therefore, all subsequent studies were performed with buffer solutions at pH 5 even though this pH value does not match the optimum pH for maximum peroxidase activity. This could possibly be justified since the activity of peroxidase used at pH 5 is still very high although not highest possible.

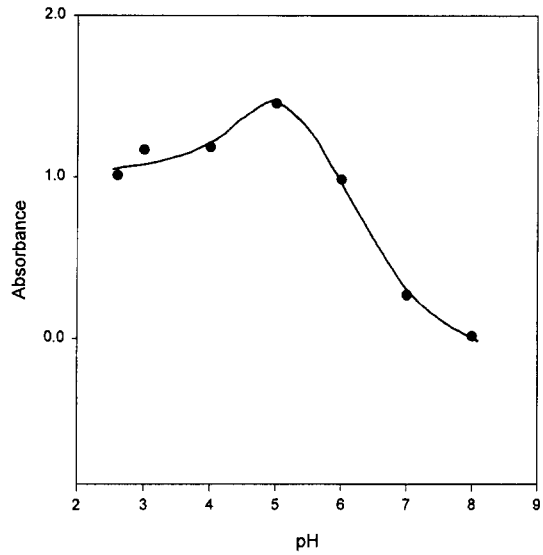

Fig. 1. Effect of the pH on the absorbance. Conditions: 0.1 M buffer solution, 5×10^{-5} M peroxide, 2.5 U peroxidase, and 3×10^{-4} M variamine blue. The absorbance signal was monitored at 550 nm.

4.2. Effect of buffer concentration

The concentration of the buffer solution used also affects the value of the absorbance signal as can be seen in Fig. 2. It can be shown from this figure that there was an increase in the ab-

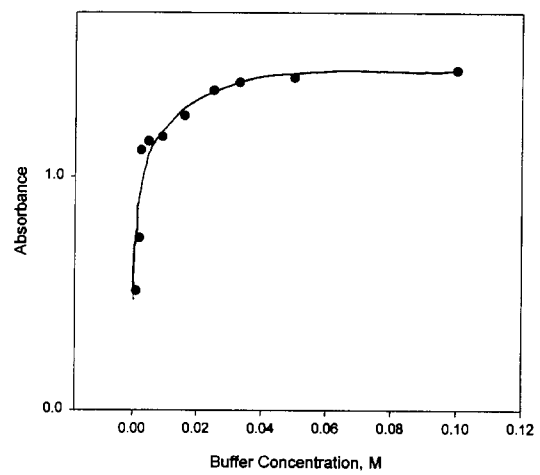

Fig. 2. Effect of buffer concentration on the absorbance signal. Conditions: buffer solutions at pH 5 but different concentrations. Other conditions are the same as in Fig. 1.

sorbance signal as the concentration of the buffer solution was increased at pH 5. However, the increase in the absorbance signal with concentration was not linear and absorbance increased only slightly at buffer concentrations greater than 3.3×10^{-2} M, and a plateau is essentially obtained at buffer concentrations exceeding 3.6×10^{-2} M. It is also clear from the figure that large increase in the absorbance signal was obtained as the buffer concentration was increased in the lower range of buffer concentration. Therefore, it seems advantageous to use higher buffer concentrations as low concentrations of buffer result in lower absorbance signals. A 0.1 M buffer concentration was judged suitable and was thus used in all further experiments.

It should also be indicated that buffer type was found to affect the absorbance signal where it was observed that buffers containing acetate or citrate resulted in improved absorbance signals while those containing succinate resulted in lower results.

4.3. Effect of variamine blue concentration

As expected, an increase in the variamine blue concentration resulted in an increase in the value of the absorbance signal. This is due to formation of more of the oxidized chromogen so that the equilibrium expression could be satisfied. Fig. 3 shows the dependence of the absorption signal on the variamine blue concentration. However, it is noteworthy to indicate that the background absorbance increased as the concentration of variamine blue was increased. Therefore, a variamine blue concentration of about 3×10^{-4} M was selected and was thus used in all subsequent experiments.

4.4. Effect of temperature

It is well established that temperature has pronounced effects on the activity of enzymes and thus the rate of enzymatic reactions. The temperature effects on peroxidase activity is depicted in Fig. 4. It can be shown from this figure that the optimum temperature for the determination of hydrogen peroxide, in presence of peroxidase and

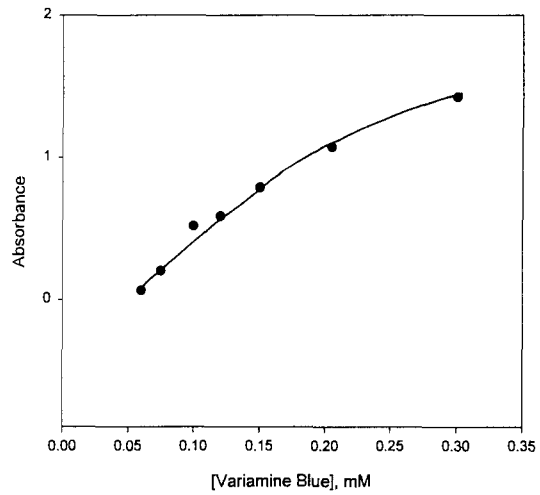

Fig. 3. Effect of the concentration of variamine blue on the absorbance signal. Conditions: 0.1 M buffer solution at pH 5. Other conditions are the same as in Fig. 1.

using variamine blue as the chromogenic material, is about 30°C. However, Fig. 4 also suggests a relatively small dependence of the absorbance signal on temperature at lower temperatures. Abrupt changes in the value of the absorbance signal was observed at temperatures exceeding about 33°C. Unless otherwise indicated, room temperature, 25°C was used throughout this work.

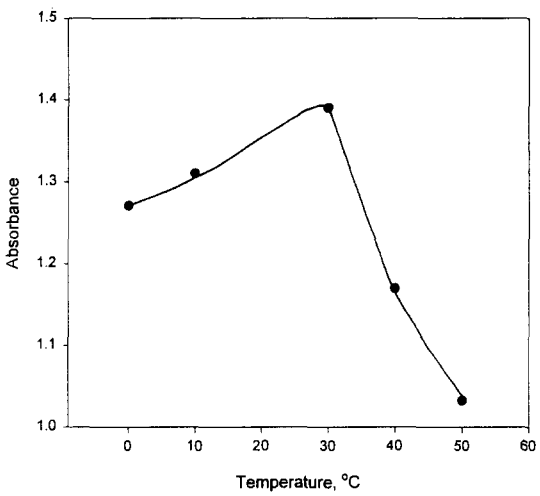

Fig. 4. Effect of temperature on the absorbance signal. Conditions: same as in Fig. 3.

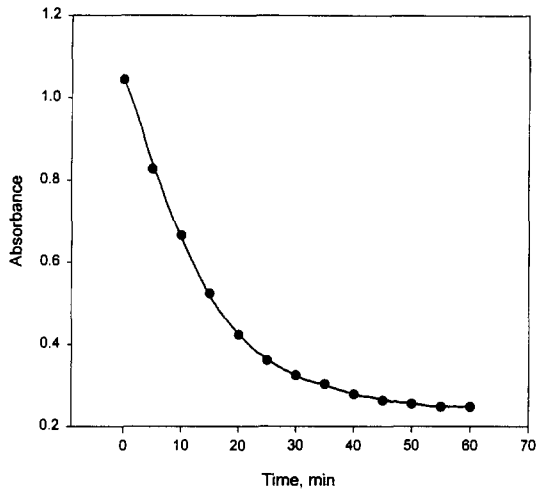

Fig. 5. Stability of the oxidized variamine blue with time. Conditions: same as in Fig. 4 except for the peroxide concentration (3.6×10^{-5} M).

4.5. Stability of the oxidized variamine blue

A very interesting behavior of oxidized variamine blue absorption with time can be seen in Fig. 5. It is clear from this figure that sensitive results can only be obtained when measurements are done immediately after the addition of the last reagent. This is because the absorbance signal starts to deteriorate with time. Initially, we suspected that the oxidized variamine blue was light sensitive. However, running a parallel experiment in a system completely isolated from light resulted in the same absorbance as that which was exposed to light. Therefore, this roles out the possibility of light instability of the oxidized chromogen. Unfortunately, the instability of the oxidized species can not be explained at this time. Throughout this study, absorbance measurements were done immediately after the addition of variamine blue, peroxidase, or hydrogen peroxide, depending on the experiment of interest.

4.6. Sensitivity of the variamine blue system

The variamine blue system showed a higher sensitivity for the determination of hydrogen peroxide, in presence of peroxidase, than the 4-aminophenazone system which is used, in a commercial kit, as the chromogen for hydrogen peroxide determination in presence of peroxidase. The molar absorptivity of the oxidized variamine blue (1.8×10^4 l mol^{-1} cm^{-1}) was about twice that of the 4-aminophenazone. Therefore, the optimized variamine blue system was subsequently used for the determination of enzymatically generated hydrogen peroxide using entrapped peroxidase.

4.7. Dependence of peroxidase activity on the entrapment matrix

Four different entrapment matrices were used to check whether peroxidase activity changes with the type of matrix in which it is immobilized. The composition of these matrices is detailed below:

Matrix I: 200 μl of the Sol containing 3-[trimethoxysilyl]-1-propanthiol was mixed with 300 μl of the Sol containing 3-chloropropyltriethoxysilane, 300 μl of peroxidase, and 200 μl of a papain solution (0.4 mg).

Matrix II: 500 μl of the Sol containing 3-chloropropyltriethoxysilane was mixed with 400 μl of peroxidase and 100 μl of papain (0.2 mg).

Matrix III: 300 μl of the Sol containing triethoxyvinylsilane was mixed with 200 μl of the Sol containing 3-chloropropyltriethoxysilane, 250 μl of peroxidase, and 250 μl of papain (0.25 mg).

Matrix IV: 400 μl of the Sol containing triethoxyvinylsilane was mixed with 100 μl of the Sol containing 3-chloropropyltriethoxysilane and 300 μl of peroxidase, but no papain.

All four matrices were left in a desiccator, at room temperature, for 20–23 days although full solidification occurred within 5–10 days. The weights of the samples after washing and drying were 0.168, 0.183, 0.096, and 0.201 g, respectively.

It is worth mentioning that the preparation of the Sol-Gel matrices was always reproducible under the specified conditions. Throughout this work, many different matrices were successfully and reproducibly prepared using the described procedures.

The procedure for the determination of hydrogen peroxide concentration involved soaking the appropriate solid matrix in 2.5 ml of buffer solution at pH 5 followed by addition of 30 μl of the

peroxide solution. The reaction was allowed to proceed for a specific period of time then a 100 μl portion of the variamine blue solution was added. The absorbance signal of oxidized variamine blue was immediately measured at 550 nm. Fig. 6 shows the relationship between the absorbance value and reaction time. It is clear from the figure that Matrix II shows highest absorbance value and lowest reaction time. This may suggest that hydrogen peroxide can easily diffuse through that matrix and reach the active site of the enzyme and thus be converted to oxygen which oxidizes the chromogenic material, resulting in the intense violet color. The three other matrices show approximate equilibration times but still the absorbance value varies for each one, where the absorbance measured using Matrix I was greater than that produced when Matrix III was used. The absorbance value was lowest when Matrix IV was used. It may be interesting to indicate that peroxide activity appears to be proportional to the amount of the 3-chloropropyltriethoxysilane precursor in the entrapment matrix. Therefore, it is clear that the entrapment matrix significantly affects the enzymatic activity and thus the value of the absorbance signal and the equilibration time as well.

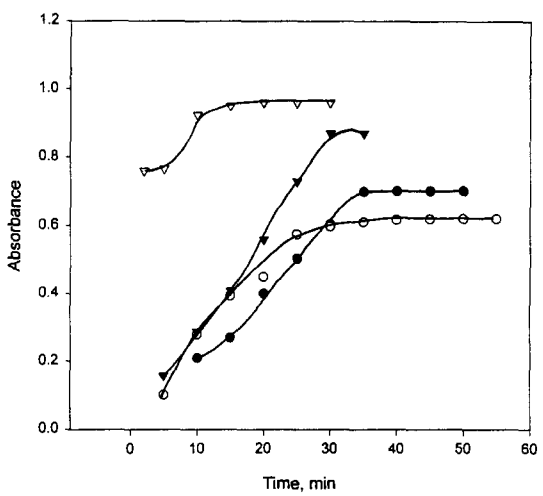

Fig. 6. Effect of the Sol-Gel matrix on the immobilized peroxidase activity. Matrix I (▼), Matrix II (△), Matrix III (●), and Matrix IV (○).

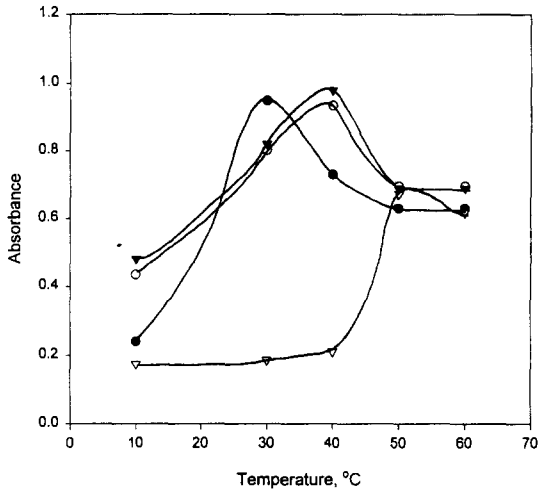

Fig. 7. Effect of temperature on the Sol-Gel entrapped peroxidase. Matrix I (●), Matrix II (▼), Matrix III (○), and Matrix IV (△).

4.8. *Effect of temperature on immobilized peroxidase*

Immobilized peroxidase in different matrices showed a rather interesting behavior at different temperatures as compared to the behavior of the enzyme in solution. The matrix composition seems to be very influential in the determination of the optimum temperature which results in maximum enzymatic activity. The optimum temperature for peroxidase was very similar to that of the soluble enzyme when the TMSP silane derivative was used. However, a significant shift in the optimum temperature of peroxidase (about 20°C) was observed when peroxidase was entrapped in a matrix which has TEVS as the predominant silane derivative but without papain as an additive (Fig. 7). Using comparable amounts of papain with the CPES or a mixture of TEVS and CPES silane derivatives resulted in a comparable shift in the optimum temperature of peroxidase that is about 10°C. Papain was used as an additive to the silane matrix hoping to improve the stability and enhance the activity of peroxidase in the Sol-Gel matrix. According to our experience and observations, proteins like papain or bovine serum albumin (BSA) improve the stability of some enzymes especially at solid surface matrices. We attribute

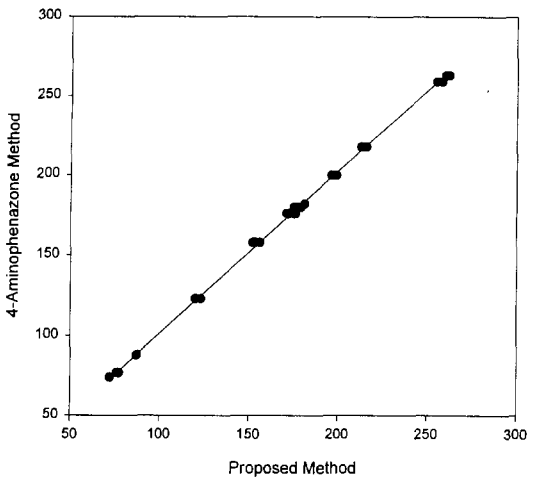

Fig. 8. Determination of serum glucose by the proposed method and the 4-aminophenazone method (34 experiments).

this to decreased interactions of the enzyme with the solid support due to competition between the enzyme and the additive for the very active surface of the solid support.

4.9. Determination of glucose in serum samples

The Sol-Gel immobilized peroxidase was used for the determination of glucose in serum. The blood samples were collected from a nearby clinic and were analyzed by both the standard method as well as our proposed method. The standard method uses a commercially supplied kit with 4-aminophenazone as the chromogenic material while the proposed method uses variamine blue in addition to Sol-Gel immobilized peroxidase. Excellent agreement between the two methods was always observed which is demonstrated in Fig. 8. The absolute difference between the results in the two methods was always less than 3% for any individual sample which can also be attributed to delay in doing the measurement by the proposed method due to time required to transfer the serum samples from the clinic to our laboratories.

4.10. Stability of the Sol-Gel immobilized peroxidase

After the formation of the solid matrix incorporating the enzyme, the Sol-Gel enzymatic matrix was kept in a desiccator, at room temperature, for 2 weeks. Then the different Sol-Gel preparations were used for the analysis of the peroxide/glucose samples for 35 days. No change in the performance characteristics of the Sol-Gel immobilized enzyme was observed. This may suggest excellent stability of the entrapped enzyme inside the Sol-Gel matrix. Although a long-term stability study was not performed, it is anticipated from initial results of about 2 month that these enzymatic preparations will be stable for longer periods. Even after the analysis of about 50 serum samples for glucose, consistent and reproducible results were always obtained. The relative standard deviation for repetitive determinations ($n = 10$) was less than 1% in all cases. It should also be indicated that the Sol-Gel enzymatic preparations were kept refrigerated at the end of each working day.

References

[1] S. Igarashi, W.L. Hinze, Anal. Chem. 60 (1988) 446.
[2] M.S. Abdel-Latif, G.G. Guilbault, Anal. Chem. 60 (1988) 2671.
[3] M.S. Abdel-Latif, A.A. Suleiman, G.G. Guilbault, Anal. Lett. 21 (1988) 943.
[4] R.F. Taylor, Protein Immobilization: Fundamentals and Applications, Marcel Dekker, New York, 1991.
[5] R. Zusman, C. Rottman, M. Ottolenghi, D.J. Avnir, J. Non-Cryst. Solids 122 (1990) 107.
[6] S. Braun, S. Shtelzer, S. Rappoport, D.J. Avnir, J. Non-Cryst. Solids 147 (1992) 739.
[7] S. Yamanaka, F. Nishida, L. Ellerby, C. Nishida, B. Dunn, J. Valentine, J. Zink, J. Chem. Mater. 4 (1992) 495.
[8] R. Wang, U. Narang, P. Prasad, F. Bright, Anal. Chem. 65 (1993) 2671.
[9] C.J. Brinker, G.W. Sherer, Sol-Gel Science, Academic Press, New York, 1989.
[10] M. Yamane, T.J. Kujima, J. Non-Cryst. Solids 44 (1981) 181.
[11] D.L. Wood, E.M.J. Rabinovich, J. Non-Cryst. Solids 107 (1989) 199.
[12] H.J. Shmidt, J. Non-Cryst. Solids 73 (1985) 681.
[13] R. Assink, B.J. Kay, J. Non-Cryst. Solids 99 (1988) 359.
[14] C.J. Brinker, J. Non-Cryst. Solids 100 (1988) 31.
[15] L. Hench, J. West, Chem. Rev. 90 (1990) 33.
[16] P. Wanadi, W. Davis, C.J. Cummins, J. Am. Chem. Soc. 117 (1995) 2110.

ELSEVIER

Talanta 44 (1997) 2059–2067

Talanta

Protonation and silver(I) complex-formation equilibria of some amino-alcohols

Silvia Canepari [b], Vincenzo Carunchio [a], Paola Castellano [a], Antonella Messina [a,*]

[a] *Department of Chemistry, University of Rome, La Sapienza, P.le Aldo Moro, 5-00185 Rome, Italy*
[b] *CIMS-Bioanalitical Chemistry Section, University of Rome, La Sapienza, P.le Aldo Moro, 5-00185 Rome, Italy*

Received 7 August 1996; received in revised form 21 January 1997; accepted 4 February 1997

Abstract

Formation constants of the silver(I) complexes with some amino-alcohols have been determined at 25°C in 0.5 M KNO_3 by means of two independent potentiometric measurements employing glass and silver electrode. The ligands considered are: sec-butylamine, 2-amino-1-propanol, 2-amino-1-methoxy-propane, 2-amino-2-methyl-1-propanol, 2-amino-1-butanol, 2-amino-1-pentanol, 2-amino-1-hexanol, 2-amino-1,3-propanediol, 2-amino-1,3-hexandiol, 2-amino-2-methyl-1,3-propanediol and Tris(hydroxymethyl)–aminomethane. Protonation constants of the selected ligands have also been determined. Calculations were made using HYPERQUAD computer program. The influence exerted by the introduction of hydroxy groups and by the presence of alkyl residuals in the ligand structure on the formation equilibria, is discussed. © 1997 Elsevier Science B.V.

Keywords: Amino-alcohols; Complex formation equilibria; Silver(I)

1. Introduction

The amino-alcohols represent a largely diffused class of biologically active substances. They characterise the moiety of several drugs and natural substances like ephedrine, adrenaline and noradrenaline and of some naturally occurring sphingoid like sphingosine and sphinganine. Due to the coordinating properties of amino and hydroxy groups, the study of formation equilibria of complex species with metal ions can help to clarify the biological role of these substances. The knowledge of complexing properties of amino-alcohols is not yet exhaustive and only a few data related to their complex equilibria are known [1–14]. In particular sphingosine and sphinganine in the last few years have received great attention because of their activity as inhibitors of tumoral cells growth [15–18]. Notwithstanding this, the mechanism of their biological activity has not yet been clarified and their pharmaceutics application is nowadays hampered by the cytotoxic effect shown at high concentration [19]. However, it is known that the antitumoral effect of these sphingoids depends on the structure of their polar head and in particular on the presence of an amino-group, positively charged, in position 2 [15,20], so that when the $-NH_2$ is chemically bonded, as an example by acylation, the inhibiting effect does not occur.

* Corresponding author.

PII S0039-9140(97)00044-1

Then, is presumable that a coordination bond involving the amino group also influences the pharmacological activity of these compounds. Furthermore, as the interaction with metal ions is usually reversible and rapid, the study of complex formation equilibria may allow an efficient regulation of active species concentration.

In this context, the present paper is concerned with the study of complexation equilibria of some amino-alcohols with Ag(I). The considered ligands are: sec-butylamine (L_I), 2-amino-1-propanol (L_{II}), 2-amino-1-methoxy-propane (L_{III}), 2-amino-2-methyl-1-propanol (L_{IV}), 2-amino-1-butanol (L_V), 2-amino-1-pentanol (L_{VI}), 2-amino-1-hexanol (L_{VII}), 2-amino-1,3-propanediol (L_{VIII}), 2-amino-1,3-hexandiol (L_{IX}), 2-amino-2-methyl-1,3-propanediol (L_X) and Tris(hydroxymethyl)-aminomethane (L_{XI}).

The ligands, which have a structure similar to the polar head of sphingosine and sphinganine, have been chosen in order to evidence the effect of the number of substituent hydroxy-groups and of the addition of alkyl residual on the coordinating properties of 2-amino-alcohol moiety.

The study has been extended to Tris(hydroxymethyl)-aminomethane (TRIS, THAM), whose complexing properties have been not sufficiently documented even if it is often added as a buffer to solutions prepared to investigate biochemical reaction involving transition metal ions [12–14,21–24].

Among the elements of the same periodic group, silver has been the least studied one, probably due to its extremely low presence in biological systems. However, our attention has been focused on silver(I) compounds, firstly because of the lack of thermodynamic data and secondly because, as already observed for other metal ions whose presence is not relevant in biological systems [25–27], their applicative importance can not be excluded.

2. Experimental

2.1. Materials

All the commercial products employed for the preparation of L_{III} and L_{IV}, were by Fluka.

Twice distilled and deionized water was used for preparing all solutions. All the reagents were obtained in high purity. Ultra pure KNO_3 (Suprapur grade, Merck) was used as ionic strength buffer.

Silver(I) nitrate (Carlo Erba) stock solutions were standardized by titration with standard reagent NaCl (Merck) and using K_2CrO_4 (Merck) as indicator following the Mohr's method [28].

Ligand stock solutions. As all the considered ligands are highly hygroscopic and uptake easily CO_2, the direct weighing was not possible and all the solutions had to be handled in strictly air-free conditions. Stock solutions were then prepared by taking a volumetric sample in a glove-box under an argon atmosphere and diluting with appropriate volumes of water. The titre was successively controlled from series of crossed acid–base titrations with a potentiometric end point detection.

2-Amino-1,3-propanediol has been supplied as oxalate salt. The quantitative precipitation of oxalate ion with calcium(II) was then performed before preparing stock solutions. The presence of a 0.5% excess of calcium(II) nitrate, needed in order to assure the quantitative precipitation of oxalate, has been checked by EDTA titration.

Potassium hydroxide 0.1 M (CO_2-free solution, Merck) was standardized by potentiometric titrations against a solution of potassium hydrogen phthalate (Merck pro analysis, dried at 120°C) using the Gran method [29] for the evaluation of the end point.

Nitric acid solution (0.1 M) was prepared by diluting the pure concentrated product (Merck) and standardized by potentiometric titrations against tris(hydroxymethyl)aminomethane (Merck), dried at 100°C for 24 h.

An independent check of the analytical procedure was also carried out by a direct titration of potassium hydroxide solution against the nitric acid.

2.1.1. Synthesis of 2-amino-1-hexanol and 2-amino-1,3-hexandiol

As 2-amino-1-hexanol and 2-amino-1,3-hexandiol are not commercially available, these products were prepared following the synthetic path summarized in Scheme 1 [30].

2.1.2. EMF measurements

Glass electrode. The alkalimetric titrations were carried out adding KOH to the test solution placed in a thermostatic vessel, under agitation and under a stream of purified argon presatured with a 0.5 M KNO_3 solution. The temperature control (25 ± 0.1°C) was achieved by means of water circulation in the jacketed vessel from a water thermocryostat (thermostat HAAKE DC3 and chryostat HAAKE K15). The initial volumes of the titrated solutions were 25 ml.

The KOH solution was delivered in the titration vessel by a Metrohm Dosimat 655 digital burette with a total volume of 5 ml. In order to have CO_2-free potassium hydroxide, the solution was preserved in a bottle stopped by a soda lime plug and kept under argon atmosphere. In these conditions the solution was stable up to 1 month.

Potentiometric titrations were carried out using a Metrohm mod. 665 pH/mVmeter, with a glass electrode (INGOLD) and a double junction Ag/AgCl electrode (INGOLD) as a reference. The outer solution of the reference electrode was 0.5 M KNO_3.

The potentiometric apparatus was made completely automatic by applying an IBM mod.30 personal computer with a parallel interface and using an appropriate software program. [31]

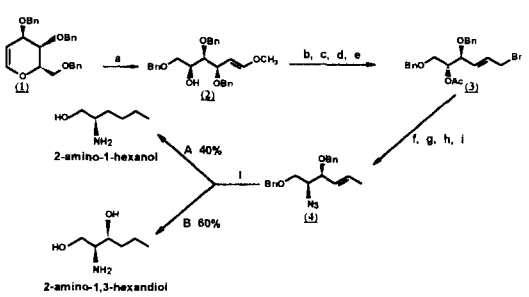

Scheme 1.

The electrode standard potentials E° were determined every day from the acid region of the titration of a 0.005 M HNO_3 solution (0.5 M ionic strength buffer) against 0.1 M KOH. Similarly the response of the glass electrode was checked every week evaluating the value of pK_W from the basic portion of the calibration curve. The linearity of E versus pH function was also checked; the slope of the straight line obtained was, within the experimental errors, coincident with the theoretical value.

For the evaluation of the protonation constants, solutions 0.5 M in KNO_3 containing different quantities of ligand and acidified with a known excess of HNO_3 were titrated with potassium hydroxide solution.

For the formation constant determination of Ag(I) complexes, solutions at various concentrations of Ag(I) nitrate and ligands were titrated with KOH. Before the titrations all the solutions were acidified with a known excess of nitric acid. The ionic strength was always adjusted to 0.5 M by adding solid potassium nitrate.

Ag electrode. All the measurements regarding Ag(I) complexation equilibria were repeated also by employing an Ag electrode (Metrohm) in order to have an independent measurement.

The calibration of the Ag electrode was performed by measuring the potential of five solutions at different Ag(I) concentration containing KNO_3 0.5 M as ionic strength buffer. E° and slope were determined by linear regression of data ($r^2 = 0.99$) and the obtained values were in good agreement with the theoretical ones (error < 1%).

The operative conditions employed for the determination of stability constants were the same as those related to glass electrode measurements.

All the calculations for the calibration of the glass electrode and for the determination of ligand protonation and complex formation constants were carried out by employing HYPERQUAD least squares computer program [32].

3. Results and discussion

Particular attention had then to be paid to the choice of concentration ranges, considering the

Table 1
Initial analytical concentrations (mM) of ligand (C_L) and acid (C_H) and $-\log[H^+]$ ranges for the determination of the protonation constant of 2-amino-1-hexanol at $I = 0.5$ M KNO_3 and $T = 25°C$

Ligand	Expt. no	C_L	C_H	$-\log[H^+]$ ranges
2-Amino-1-hexanol	1, 2, 3	1.8	3.0	3.08–10.61
	4	3.7	5.0	3.07–10.34
	5	6.7	10	3.08–10.43

method sensitivity and the best operative conditions for the calculation of the constants. Good results were obtained in all the examined systems when the ligand concentration was maintained lower than 7 mM.

In fact, by a preliminary examination of the experimental data, turns out that the ligand concentration influences the results. In particular, there is a progressive worsening of the fit on increasing the ligand concentration in the titration vessel.

3.1. Protonation equilibria

The calculation of the protonation constants has been performed by elaborating the data obtained by five titration runs for each system. In Table 1 the operative conditions are reported for 2-amino-1-hexanol as an example. Similar conditions have been employed for all the other ligands. As can be noted, one of the titrations has been repeated three times in order to check the reproducibility of the experimental measurements. Repeated runs also allowed a better control of the ligand concentrations, whose determination requires particular care (Section 2). In fact the amounts of ligands in the titration vessel (C_{0L}) have been refined by HYPERQUAD program and the resulting values were in a good agreement with the calculated ones (2% error).

In Table 2 the pK_a values obtained by the simultaneous elaboration of all the titration curves are reported. The error between brackets is the standard deviation provided by HYPERQUAD calculations. The statistical parameters are satisfactory also considering that, due to the basicity of ligands, E.F.M. measurements had to be performed in the basic region.

The pK_a values related to sec-butylamine [33], 2-amino-1-butanol [34] and THAM [12–14,21–24] are in a good agreement with literature data.

From the examination of the reported data, two main effects on the acidity of protonated ligands can be evidenced. Firstly, the insertion of hydroxy group causes a relevant lowering of pK_a values. This effect could be caused either by the intramolecular hydrogen bond formation [35], which is stronger in the deprotonated form than in the protonated one, or by an electron-withdrawing polar effect due to the hydroxy group. Comparing the pK_a values related to L_{II} and L_{III} it is evident that the second effect is prevalent. Furthermore, the methoxy group seems to be more effective than hydroxy group, in spite of the lower electronic-withdrawing capabilities of this group with respect to hydroxy one. This reversal, already observed for similar compounds [36] was ascribed to the modification of the true inductive effect of the hydroxy group by solvation.

Secondly, the addition of alkyl residuals in the ligand structure causes an increase of the pK_a values. The effect is mainly ascribable to a field effect of the alkyl group, which results in an increase in the electron density on the nitrogen atom [36]. Furthermore, from the results it can be

Table 2
Protonation constant values and related statistical parameters for the considered ligands at $I = 0.5$ M KNO_3 and $T = 25°C$

Ligands	pK_a	χ^2	σ
Sec-butylamine	10.599(3)	19.23	3.72
2-Amino-1-propanol	9.450(6)	13.54	2.01
2-Amino-1-methoxy-propane	9.424(2)	10.29	1.34
2-Amino-2-methyl-1-propanol	9.612(6)	14.37	2.98
2-Amino-1-butanol	9.554(5)	15.00	2.80
2-Amino-1-pentanol	9.766(3)	17.50	3.01
2-Amino-1-hexanol	9.90(6)	18.41	4.00
2-Amino-1,3-propanediol	8.786(1)	10.32	1.09
2-Amino-1,3-hexandiol	8.901(2)	11.73	3.21
2-Amino-2-methyl-1,3-propanediol	8.780(6)	15.68	2.90
Tris(hydroxymethyl)-aminomethan	8.156(1)	5.23	0.56

Table 3
Initial analytical concentrations (mM) of ligand (C_L), metal (C_M) and acid (C_H), C_L/C_M ratios and p[H] ranges employed in calculations of complexation constant of 2-amino-1-hexanol –Ag(I) at $I = 0.5$ M KNO_3 and $T = 25°C$

Expt. no	C_L	C_M	C_L/C_M	C_H	p[H] ranges
1	4.10	4.10	1	6.10	7.42–8.26
2	1.49	0.75	2	3.50	7.78–9.25
3	2.84	1.42	2	4.85	7.60–8.93
4	3.70	1.85	2	5.70	7.50–8.85
5	4.24	1.41	3	6.10	7.92–9.48
6	3.20	1.09	3	3.52	7.78–9.56
7	2.00	0.69	3	2.20	7.65–9.75
8	4.05	0.81	5	6.10	7.54–10.20

noted that the insertion of methyl group in position 2 in L_{IV} and L_X causes an increase of pK_a lower than the one expected on the basis of the field effect. This is in agreement both with the steric hindrance on the quaternary carbon, which could stabilize the intramolecular hydrogen bond with the consequent lowering in basicity and with the differential hydration [37] which is less effective when a $-CH_3$ group is added in position 2.

3.2. Complexation equilibria

In order to evidence both mononuclear and polynuclear species, the determination of complexation constants has been carried out for each considered system on a stock of eight solutions containing various C_L/C_M ratios and at different ligand and metal initial concentrations. In Table 3 are reported, as an example, the operative conditions for 2-amino-1-hexanol-Ag(I) system.

As can be noted, the $-\log[H^+]$ ranges are variable depending on experimental conditions and have been identified considering all the equilibria involved, in order to avoid precipitation equilibria.

All the experimental runs were firstly elaborated by HYPERQUAD one by one, afterwards an elaboration of each set obtained with glass or Ag electrode was performed. Finally all the titration curves were elaborated simultaneously. Different equilibrium models were examined. The species ML, ML_2 M_2L, M_2L_2, MLOH, ML_2OH and ML_3, were systematically considered in different combinations. These species were either rejected by HYPERQUAD or caused a worsening of the statistical parameters σ and χ^2 [38] or lead to not acceptable chemical models.

The absence of systematic errors was tested refining also the dangerous parameters as C_{0M}, C_{0L}, C_{0H} (total mmoles of metal, ligand and proton, respectively, in the reaction vessel). The deviation of calculated values from input ones can be considered within the experimental error (about 2%).

Hydrolysis constants [39] were considered in the calculation. However they do not influence the $\log \beta$ values, apart from a slight ($\sim 1\%$) effect on the results related to the titration curves with $C_L/C_M = 1$.

The calculations related to Ag electrode measurements give statistical parameters better than those obtained with glass electrode, probably due to the working pH range in which the alkaline error is not negligible. Anyway, the stability constants obtained with the two independent measurements are in good agreement as evident in Table 4 in which the results related to Ag and glass electrode measurements for Ag(I)-2-amino-1,3-propanediol system are reported.

In Table 5 the results of the overall elaboration obtained for all the considered systems, are summarized. Two different models, i.e., ML-ML_2 (model 1) and ML-ML_2-MLOH (model 2), are reported as the most significative ones. Is worth noting that is not possible from the potentiometric measurements, to deduce whether the species indicated as MLOH is a hydroxy complex or a complex where ligand acts as a chelate, with the deprotonation of the hydroxy groups. Due to steric reasons and considering $\log \beta$ values the first alternative seems to be more probable [21]. On the other hand, the enhancement of the affinity for OH-compared with the hydrated silver ion has been already observed from other authors in the presence of aromatic [40] or aliphatic [21,41] *N*-ligands.

From a critical view of the Table 5 it is evident that the model 2 is the most representative at least for the ligands L_{VIII}, L_{IX}, L_X and L_{XI}, in which two or three hydroxy groups are present. The

Table 4
Formation constants of complexes of 2-amino-1,3-propanediol with Ag(I), and related statistical parameters obtained at $I = 0.5$M KNO_3 and $T = 25$°C

	Ag electrode		Glass electrode		Total	
	Model 1	Model 2	Model 1	Model 2	Model 1	Model 2
$\log \beta_{1,1,0}$ ($\log K_1$)	3.39 (1)	3.407 (6)	3.40 (6)	3.39 (5)	3.38 (1)	3.39 (1)
$\log \beta_{2,1,0}$	6.72 (1)	6.64 (1)	6.79 (2)	6.69 (3)	6.76 (1)	6.65 (2)
$\log K_2$	3.33	3.23	3.39	3.30	3.38	3.26
$\log \beta_{1,1,-1}$	—	−6.24 (4)	—	−6.40 (7)	—	−6.34 (5)
$\log K_a(AgL^+)$	—	−9.6	—	−9.8	—	−9.7
χ^2	28.00	21.00	62.13	30.20	50.25	22.15
σ	3.85	1.58	5.18	2.60	4.31	2.19

presence of the MLOH species is evident in Fig. 1 in which the comparison between the two models for Ag(I)-THAM system is reported as a plot of experimental and calculated data. For all the other systems, the presence of ternary species MLOH is uncertain and its addition to the speciation model does not improve significantly the fitting. This may be due both to the reduction in acidity of the bonded water (see $\log K_a(AgL^+)$ values in Table 5) and to the formation constant values, so that the presence of ML_2 species is predominant in the examined experimental conditions (Fig. 2 and Fig. 3).

As far as the stability order of the complexes is concerned, the same trend as observed for pK_a values has been found. It is then evident that the coordination is due to the aminic nitrogen and that no chelate structures are formed. As found

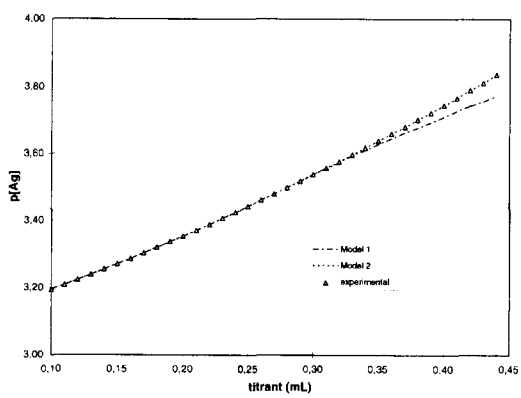

Fig. 1. Comparison between experimental and calculated curves related to either model 1 (ML, ML_2) or model 2 (ML, ML_2, MLOH) for the Ag(I)-THAM system with Ag electrode. $C_L = 3.2$ mM, $C_M = 1.1$ mM, $C_H = 3.5$ mM, I = 0.5 M KNO_3 and $T = 25$°C.

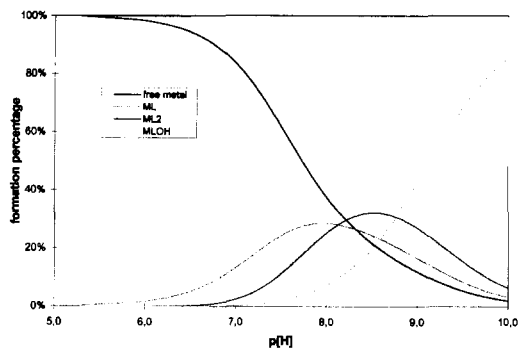

Fig. 2. Plots of formation percentages vs p[H] related to ML, ML_2 and MLOH species for Ag(I)-THAM. $C_L = 3.2$ mM, $C_M = 1.1$ mM, $C_H = 3.2$ mM. Formation constants as reported in Table 5 (model 2).

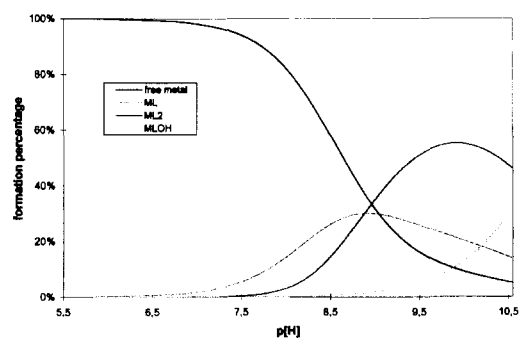

Fig. 3. Plots of formation percentages vs p[H] related to ML, ML_2 and MLOH species for Ag(I)-2-amino-1-propanol. $C_L = 3.2$ mM, $C_M = 1.1$ mM, $C_H = 3.2$ mM. Formation constants as reported in Table 5 (model 2).

Table 5
Formation constants of complexes formed between sec-butylamine (L_I), 2-amino-1-propanol (L_{II}), 2-amino-1-methoxy-propane (L_{III}), 2-amino-2-methyl-1-propanol (L_{IV}), 2-amino-1-butanol (L_V), 2-amino-1-pentanol (L_{VI}), 2-amino-1-hexanol (L_{VII}), 2-amino-1,3-propanediol (L_{VIII}), 2-amino-1,3-hexandiol (L_{IX}), 2-amino-2-methyl-1,3-propanediol (L_X) and Tris(hydroxymethyl)-aminomethane (L_{XI}) with silver(I) and related statistical parameters obtained by overall elaboration of Ag and glass electrode elaboration at $I = 0.5$ M KNO3 and $T = 25$°C

		L_I	L_{II}	L_{III}	L_{IV}	L_V	L_{VI}	L_{VII}	L_{VIII}	L_{IX}	L_X	L_{XI}
Model 1	$\log \beta_{1,1,0}$ ($\log K_1$)	3.70 (3)	3.43 (1)	3.456 (6)	3.41 (1)	3.53 (1)	3.56 (2)	3.53 (3)	3.38 (1)	3.37 (1)	3.297 (7)	3.121 (4)
	$\log \beta_{2,1,0}$	7.67 (1)	7.083 (8)	7.042 (9)	7.15 (1)	7.10 (1)	7.21 (2)	7.25 (2)	6.76 (1)	6.64 (1)	6.797 (6)	6.405 (5)
	$\log K_2$	3.97	3.65	3.59	3.74	3.57	3.65	3.72	3.38	3.27	3.50	3.28
	χ^2	24.59	12.89	23.39	17.71	29.82	32.45	29.80	50.25	25.12	39.89	23.21
	σ	3.93	2.91	2.38	3.97	3.35	4.01	3.11	4.31	3.89	4.73	2.78
Model 2	$\log \beta_{1,1,0}$ ($\log K_{11}$)	3.70 (3)	3.444 (8)	3.448 (5)	3.40 (2)	3.53 (1)	3.51 (2)	3.53 (3)	3.39 (1)	3.37 (1)	3.301 (6)	3.126 (4)
	$\log \beta_{2,1,0}$	7.67 (1)	6.98 (7)	6.97 (3)	7.08 (1)	7.10 (1)	7.16 (2)	7.25 (2)	6.65 (2)	6.54 (1)	6.78 (1)	6.310 (2)
	$\log K_2$	3.97	3.54	3.52	3.68	3.57	3.65	3.72	3.26	3.17	3.48	3.18
	$\log \beta_{1,1,-1}$	Rejected	−6.75 (6)	−6.52 (7)	−6.8 (1)	Rejected	−6.72 (9)	Rejected	−6.34 (5)	−6.43 (6)	−6.35 (3)	−5.47 (5)
	$\log K_a$ (AgL^+)	—	−10.2	−10.0	−10.2	—	−10.2	—	−9.7	−9.8	−9.7	−8.6
	χ^2	24.59	10.27	33.65	29.57	29.82	35.20	29.80	22.15	20.00	16.00	5.8
	σ	3.93	2.18	1.94	3.46	3.35	3.82	3.11	2.19	2.51	2.90	1.13

for other systems [6,42], $(\log K_1)/pK_a$ ratio is constant for all the considered ligands, the average value being 0.37 ± 0.02.

It is worth noting that in the systems containing L_{IV} and L_X as ligands, the stability of the ML species is lower than the one expected considering the pK_a values. These results can be ascribed to the steric hindrance which is more influent on the tetrahedral structure of ML species with respect to the linear one characteristic of ML_2 species in silver(I)-aliphatic amines systems.

Furthermore, it can be noted that $\log K_2$ values are higher than $\log K_1$ ones, with the exclusion of 2-amino-1,3-hexandiol and 2-amino-1,3-propane- diol. This different behaviour can be explained assuming that the K values, as suggested by Orgel [43] and interpreted in detail by Martin [44] in terms of cooperative effect, are made up of two parts which are in competition each other. The first is mainly due to a statistical-electronic effect and causes a fall off of stability from K_1 to K_n. The second part can be attributed to an energetic effect associated to the change of the complex structure from tetracoordinate to linear and determinates an increasing of stability. Depending on which is the prevalent effect, K_2 value will be lower or higher than K_1.

Acknowledgements

This work was supported financially by a National Project of Italian M.U.R.S.T., Rome, Italy.

References

[1] A. Braibanti, G. Mori, F. Dallavalle, L. Leporati, J. Chem. Soc. Dalton (1975) 1319.
[2] A. Braibanti, G. Mori, F. Dallavalle, J. Chem. Soc. Dalton (1976) 826.
[3] A. Braibanti, G. Mori, F. Dallavalle, J. Chem. Soc. Dalton (1979) 1050.
[4] C. Van Poucke, Z. Eeckhaut, Bull. Soc. Chim. Belges 81 (1972) 363.
[5] B.A. Timini, D.H. Everett, J. Chem. Soc (B) (1968) 1380.
[6] D.J. Alner, R.C. Lansbury, A.G. Smeeth, J. Chem. Soc (A) (1968) 417.
[7] J.J. Christensen, R.M. Izatt, D.P. Wrathall, L.D. Hansen, J. Chem. Soc (A) (1969) 1212.
[8] A.Y. Sychev, A.P. Gerbeleu, P.K. Migal, Russ. J. Inorg. Chem., 8 (1963) 1081.
[9] P.K. Migal, A.N. Pushnyak, Russ. J. Inorg. Chem. 4 (1959) 601.
[10] P.K. Migal, A.N. Pushnyak, Russ. J. Inorg. Chem. 5 (1960) 293.
[11] J.M. Antelo, F. Arce, J. Casado, M.C. Regal, A. Varela, J. Chem. Research(s) (1982) 144.
[12] L. Bologni, A. Sabatini, A. Vacca, Inorg. Chim. Acta 69 (1983) 71.
[13] K.S. Bai, E. Martell, J. Inorg. Nucl. Chem. 31 (1969) 1697.
[14] W. Forsling, Acta Chem. Scand. A 32 (1978) 57.
[15] Y.A. Hannun, R.M. Bell, Science 243 (1989) 500.
[16] A.H. Merrill Jr., M. Sereni, V.L. Stevens, Y.A. Hannun, R.M. Bell, J.M. Kinkade Jr., J. Biol. Chem. 261 (1986) 2610.
[17] M. Faucher, N. Girones, Y.A. Hannun, R.M. Bell, R.J. Davis, J. Biol. Chem. 263 (1988) 5319.
[18] L.A. Speizer, M.J. Watson, L. Brunton, Fed. Proc. 46 (1987) 2065.
[19] Y.A. Hannun, R. Bell, Science 235 (1987) 678.
[20] E. Wilson, M.C. Olcott, R.M. Bell, A.H. Merrill Jr., J.D. Lambeth, J. Biol. Chem. 261 (1986) 12616.
[21] I. Granberg, W. Forsling, S. Sjoberg, Acta Chem. Scand. 36 (1982) 819.
[22] K. Tanaka, R.G. Bates, Anal. Chem. 53 (1981) 1021.
[23] D. Masi, C. Mealli, M. Sabat, A. Sabatini, A. Vacca, F. Zanobini, Helv. Chim. Acta 67 (1984) 1818.
[24] J.L. Hall, J.A. Swisher, D.G. Brannon, T.M. Liden, Inorg. Chem. 1 (1962) 409.
[25] P. Kopf-Maier, H. Kopf, Chem Rev. 87 (1987) 1137.
[26] I. Haiduc, C. Silvestru, Coord. Chem. Rev. 99 (1990) 253.
[27] M. Zimmer, Chem Rev. 95 (1995) 2629.
[28] A.I. Vogel, A Text Book of Quantitative Inorganic Analysis, 3rd ed., Chap. 3, Longmans, London, 1961.
[29] G. Gran, Analyst 77 (1952) 661.
[30] P. Passacantilli, private communication.
[31] G. Arena, G. Maccarrone, private communication.
[32] P. Gans, A. Sabatini, A. Vacca, Coord. Chem. Rev. 120 (1992) 389.
[33] R.D. Hancock, J. Chem. Soc. Dalton Trans. 3 (1980) 416.
[34] L.C. Van Poucke, Z. Eekhaut, Bull. Soc. Chim. Belges 81 (1972) 363.
[35] M. Eckert-Maksic, in S. Patai (Ed.), The chemistry of functional groups-Supplement E2: The chemistry of hydroxyl, ether and peroxide groups, Wiley, New York, 1993, pp. 299.
[36] H.C. Brown, D.H. Mc Daniel, O. Hofliger, in E.A. Braude and F.C. Nachod (Eds.), Determination of organic structures and physical methods, Academic Press, New York, 1955, pp. 567.
[37] J. March, Advanced Organic Chemistry, 2nd ed., Mc Graw-Hill Book Company, New York, 1977, pp. 243.

[38] P. Gans, A. Sabatini, A. Vacca, J. Chem. Soc. Dalton Trans., 1985, pp. 1195
[39] R.M. Smith, A.E. Martell, Critical Stability Constants, vol. 4, Plenum Press, New York, 1976, pp. 8.
[40] I. Granberg, S. Sjoberg, Acta Chem Scand. 33 (1979) 531.
[41] H. Ohtaki, Y. Ito, J. Coord. Chem. 3 (1973) 131.
[42] R.J. Breuehlman, F.H. Verhoek, J. Am. Chem. Soc. 70 (1948) 1401.
[43] L.E. Orgel, An Introduction to Transition-Metal Chemistry-Ligand-Field Theory, 2nd ed., Chap. 5, Methuen and Co, London, 1966.
[44] R.B. Martin. Comments Inorg. Chem. 18 (1996) 249.

ELSEVIER

Talanta 44 (1997) 2069–2073

Talanta

In-situ FTIR spectroelectrochemical investigation of cobalt(II)-cyanoferrate polymeric film coated on a glassy carbon electrode

Hong-Qiang Zhang, Xiang-Qin Lin *

Laboratory of Electroanalytical Chemistry, Changchun Institute of Applied Chemistry, Changchun 130022, People's Republic of China

Received 25 July 1996; received in revised form 27 January 1997; accepted 4 February 1997

Abstract

Cobalt(II)-cyanoferrate polymeric film has been electrochemically deposited on a glassy carbon electrode and investigated by cyclic voltammetry and in-situ reflection FTIR spectroscopy. A reorientation of the terminal C≡N groups upon redox reactions was proposed. The stretching vibration mode of the terminal C≡N groups associated with Fe(III) was observed at 2122 cm^{-1}, however, the stretching vibration mode for terminal groups associated with Fe(II) did not appear. This process could result in a switch between lattice-closed and lattice-opened surface structure.

Keywords: Cobalt(II)-cyanoferrate; Glassy carbon electrode; Stretching vibration

1. Introduction

Cobalt hexacyanoferrate (CoHCF) is an important member of the family of mixed-valence transition metal hexacyanometallates. The CoHCF polymeric film has excellent properties in electrocatalysis, zeolitic towards specific cations, bichromic and chemical stability. All of these traits and low cost of such inorganic polymeric film coated electrode make it obvious candidate for electroanalytical applications such as electron transfer mediation, electrochromism devices and ion selective electrode [1]. Several electrochemical and spectroscopic techniques have been employed to characterize the CoHCF polymeric film and its analogues.These methods include cyclic voltammetry [1], in-situ UV-vis spectroscopy [2], in-situ Mossbauer Spectroscopy [3], AC Impedance [4], XPS [4], ex-situ IR Spectroscopy [1,5,6], etc. Ex-situ IR investigations can provide useful information, but it also leads to a question as to whether or not the observed spectra correspond to the actual electrochemical surface species. Unfortunately, no in-situ IR investigation has been reported for this problem in the literature. In-situ IR technique have attracted considerable atten-

* Corresponding author. Current address: Department of Chemistry, The University of Science and Technology of China, Hefei 230026, People's Republic of China. Fax: + 86 551 3631760; e-mail: xqlin@mail.ach.ustc.edu.cn

0039-9140/97/$17.00
PII S0039-9140(97)00052-0

tions of many research groups [7] since the pioneer work at the beginning of the 1980s [8]. Owing to the fact that it allows the electrochemical environment of the reactive centers to be preserved, in-situ IR method becomes a powerful tool in studies of film-coated electrodes.

The CoHCF film has 3-dimensional inorganic network which may contain coprecipitated or occluded ions, possibly hydrolyzed ferrocyanide and indefinite amounts of water. Such a complex materials may have variable stoichiometry and structural disorder. There are still interesting questions to be answered concerning the film structure, ion permeability and correlation of redox potential with supporting electrolyte cations.

The present work reports the by using in situ IR technique study the structure of the in-situ reflection FTIR spectroelectrochemical study of the CoHCF film on glassy carbon electrode and try to correlate the film structure to the property of the film-coated electrode.

2. Experimental

Analytical grade $K_3Fe(CN)_6$, $NaNO_3$ and NaCl were used without further purification. Solutions were prepared with doubly distilled water.

The CoHCF film was prepared on glass carbon (GC) electrode (8 mm diameter) by electrochemical deposition similar to that reported in literature [1]. Perio to film deposition, the GC electrode was polished to a mirror finish on an optical flat using 1.0, 0.3 and 0.05 mm alumina, then rinsed and ultrasonicated with 1:1 water-methanol mixture, and finally thoroughly rinsed with distilled water. The film was obtained by cycling the electrode potential between 1.0 and 0.0 V (vs SCE) at 100 mV s^{-1} for 5 min in 1.0 M $NaNO_3$ solution containing 1 mM $Co(NO_3)_2$ and 1 mM $K_3Fe(CN)_6$. Then the film-coated electrode was thoroughly rinsed with the supporting electrolyte solution for further experiments.

A home-made in-situ external reflection FTIR spectroelectrochemical cell was used [9]. A Nicolet 520 SX FTIR spectrometer with a DTGS detector, and a variable angle specular reflectance attachment (Spectra Tech Inc.) was used. The instrument was calibrated using a polystyrene film. The IR beam was aligned for 66° incidence angle at the electrode/solution interface. All spectra were collected by using potential modulation method [7]. Two hundred scans were averaged for a spectrum. Larger number of scan average times can be used for further reduction of noise level. However, longer acquisition time may cause significant baseline distortion.

A home-built cyclic voltammetric analyzer coupled with a series 60000 X-Y recorder (Liaoning Precision Instruments MFY, China) was used. All potentials were reported with respect to the saturated calomel electrode (SCE). $E^{0\prime}$ was estimated as $(E_{pc} + E_{pa})/2$, and ΔE_p was measured as $E_{pa} - E_{pc}$.

3. Results and discussion

3.1. Voltammetric measurements

Fig. 1 shows the typical cyclic voltammogram (CV) of the prepared CoHCF/GC electrode in 1M NaCl solution. As seen in Fig. 1, a couple of symmetric redox peaks appeared at $E^{0\prime}$ of 0.45 V (vs. SCE) with peak-to-peak separation ΔE_p of zero at 100 mV s^{-1}. The half width for both of

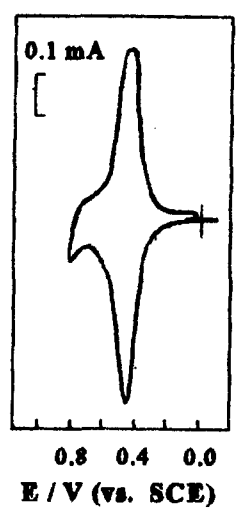

Fig. 1. Cyclic voltammograms at CoHCF/GC electrode in 1.0 M NaCl solution at scan rate of 100 mV s^{-1}.

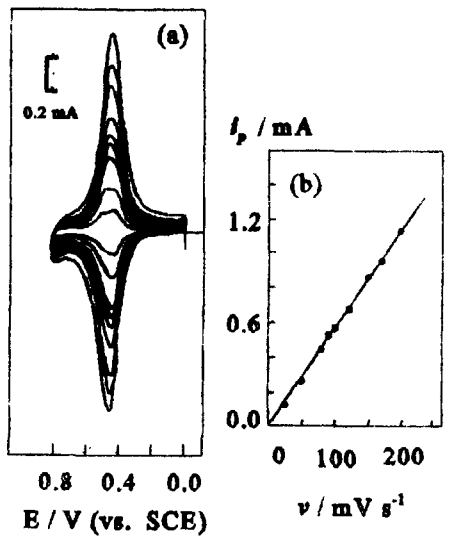

Fig. 2. (a) Cyclic voltammograms of CoHCF/GC electrode in 1.0 M NaCl solution at different potential scan rates (25, 50, 80, 90, 100, 120, 150, 170, 200 mV s^{-1}); (b) Scan rate dependence of the reduction peak current for CoHCF/GC electrode in 1.0 M NaCl solution.

the reduction and oxidation peaks was about 140 mV. It is known that the cobalt center is not electrochemically active in this potential region. The redox step at 0.45 V is attributed to the electron transfer processes of the Fe center [1].

The CVs upon variation of potential sweep rate are shown in Fig. 2(a). The peak current was linearly proportional to the sweep rate as shown in Fig. 2(b). These typical characteristics of surface wave are well expected for this system.

3.2. In-situ IR spectroscopic measurements

Fig. 3 shows the in-situ reflection-absorption difference spectra on the CoHCF/GC electrode. As shown in this figure, the IR band extending upwards at 2068 cm^{-1} indicates the disappearance of the stretching vibration mode of bridging C≡N ligand associated with Fe(II) and the downward peak at about 2098 cm^{-1} indicates the appearance of stretching vibration mode of bridging C≡N ligand associated with Fe(III) [1,10–12]. The transformation of these two vibration modes with the potential jumping from 0 to 0.50 V indicates the redox step of the Fe(II/III) in the CoHCF film. It is also seen in this figure that when the potential increased from 0.50 to 0.70 V, the downward band at 2090 cm^{-1} decreased and shifted to 2098 cm^{-1}. Meanwhile, a well defined downward peak appeared at 2122 cm^{-1}. The little shift of the 2090 cm^{-1} band may be resulted from the Stark effect, however, it is also consistent with the fact that the oxidation of Fe(II) to Fe(III) weakens the π back donation from metal d orbital to the cyanide π^* orbital and thus enhances the carbon–nitrogen bond strength and results in shifting toward higher wavenumber for the C≡N stretching frequency.

Of particularly interesting, the new band arising at 2122 cm^{-1} can be assigned to the characteristic band of terminal cyanide associated with Fe(III). Because the stretching frequency in free $Fe(CN)_6^{3-}$ anions is at 2114 cm^{-1} [13], only +8 cm^{-1} shift may be resulted from the fact that the

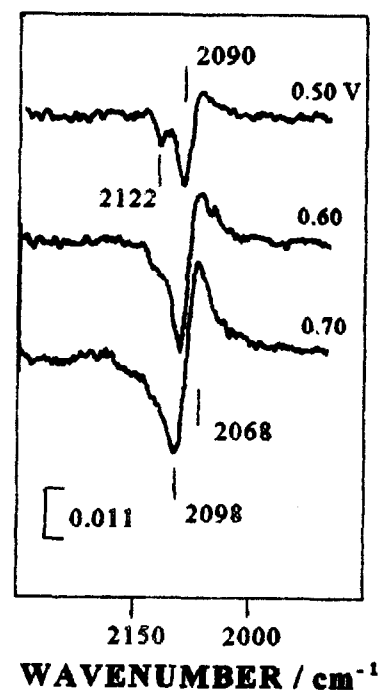

Fig. 3. FTIR potential difference reflection-absorption spectra obtained at CoHCF/GC electrode in 1.0 M NaCl solution. Reference potential: 0.0 V (vs. SCE). Sampling potential: as indicated, V (vs. SCE). 200 interferograms were averaged.

terminal cyanide is connected to the polymeric network of the CoHCF. When the potential increases positively, the electrode withdraws electrons from Fe center through the polymeric network. This weakens the π back donation from Fe to the cyanide π^* orbital and enhances the strength of C≡N bond.

The 2122 cm^{-1} band emerged at the potential of 0.50 V. It became less visible because of the increasing intensity of the wings of the broad band at 2098 cm^{-1} with potential increasing from 0.50 to 0.70 V. It is reasonable to observe an upward band for the disappearance of the stretching vibration mode for the terminal C≡N associated with Fe(II). This band can be expected to appear at about 2040 cm^{-1} [13]. However, no such an upward peak in this region was found, only a small upward spike can be seen at about 2050 cm^{-1} at 0.6 V spectrum.

This phenomenon probably arises from the effect of the surface selection rule [14]. Among the normal modes of a molecule, only the vibrational modes having a non-zero component of the dipole derivative perpendicular to the reflection surface, $(\delta R/\delta Q) \neq 0$, are able to interact with the IR radiation. Although, the Surface Selection Rule has been well established at metal surfaces, because of the excellent electric conductivity of the GC electrode, we may expect the same applicability. According to the face-centered cubic lattice structure of mixed-valance heavy-metal hexacyanometallates [1,15],the surface of CoHCF film adjacent to the solution can be described as shown in Fig. 4.

In the cubic lattice structure of CoHCF, cobalt and iron atoms alternate at the cubic corners. The bridging cyano groups located in such a way that all irons coordinated to carbon and all cobalt to nitrogen [1]. We consider that the terminal cyano groups should connect to the iron atoms and like whiskers growing on the surface of this film. However, when the electrode potential was lower and the film was in reduced state, the terminal cyano groups could be oriented on the surface forming a 'closed' lattice. Such an orientation in the surface selection rule is IR-inactive and led to the 'disappearance' of the stretching mode for the C≡N associated with Fe(II).

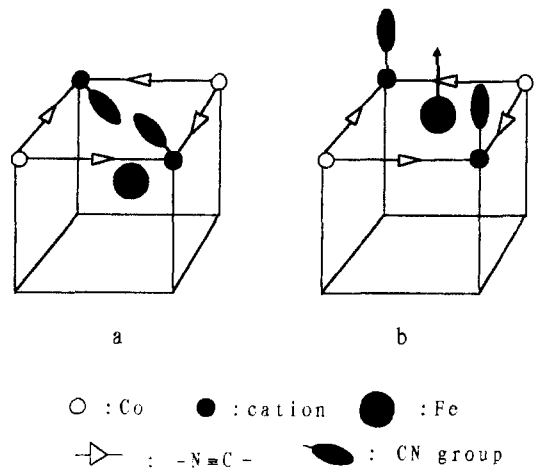

Fig. 4. Closed (a) and opened (b) lattice mode for the surface structure of CoHCF film adjacent to the solution

With the potential increasing positively, the orientation of these terminal cyano groups may become perpendicular to the cubic surface. This reorientation process could be related to the releasing dopant lattice cations. When the potential reached to 0.50 V, the oxidation process of the lattice was completed, the lattice became 'opened' with the terminal C≡N group vertical to the surface. This mechanism consists with the appearance of 2122 cm^{-1} band in Fig. 3.

The transition of orientations for the terminal C≡N groups could also be influenced by electric field of the double layer. Because the Fe(II) center prefers C-coordination, however, the Fe(III) center prefers N-coordination, it is possible that the oxidation of the CoHCF film results in a reoriented-coordination of the terminal C≡N. When the film was in the reduced state the partially negative charged free N-end of the terminal C≡N group could be forced down by the electrostatic field as shown in Fig. 5(a). However, when the electrode potential shifting positively, the oxidation of the Fe(II) to Fe(III) could release the partially positive charged C-end. The electrostatic field could force the C-end up forming the vertical orientation as shown in Fig. 5(b).

The redox potential of the surface film is significantly influenced by the property of electrolyte cations, however, the electrolyte anions have been

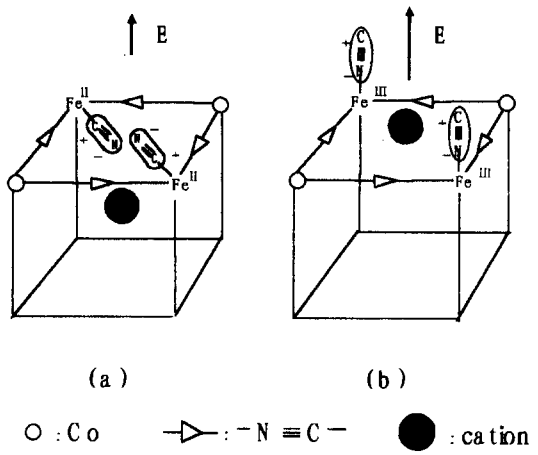

Fig. 5. Reorientation of terminal C≡N group in CoHCF film in (a) reduced and (b) oxidized state.

found to play scarcely role on CoHCF electrochemistry [1]. Besides the size effect, the existing of the whiskers-like terminal cyano groups on the lattice surface can be expected to play a subtle role on the ion channeling kinetics of the film.

4. Conclusion

In-situ IR spectra of the cobalt(II)-cyanoferrate polymeric film coated glassy carbon electrode revealed a transformation band at 2122 cm^{-1} for the terminal C≡N groups. It is expected that the orientation of the terminal C≡N groups on the lattice surface can be reoriented upon redox reaction of the Fe center and switched between on-surface state and whiskers-like state. This process may result in ion-channel closed or opened lattice. This switch-adjustment effect to the ion channeling process of the polymeric film may be interesting.

Acknowledgements

The authors gratefully acknowledge support from the National Natural Science Foundation of China and the laboratory of Electroanalytical Chemistry, Chinese Academy of Sciences.

References

[1] M. Jiang, X. Zhou, Z. Zhao, Ber. Bun. Phys. Chem. 95 (1991) 720.
[2] K. Itaya, H. Akahoshi, S. Toshima, J. Electrochem. Soc. 129 (1982) 1498.
[3] K. Itaya, T. Ataka, S. Toshima, T. Shinohara, J. Phys. Chem. 86 (1982) 2415.
[4] L.M. Siperko, T. Kuwana, J. Electrochem. Soc. 130 (1983) 396.
[5] J.A. Cox, B.K. Das, J. Electroanal. Chem. 233 (1987) 87.
[6] S. Dong, Z. Jin, J. Electroanal. Chem. 256 (1988) 193.
[7] K. Ashley, S. Pons, Chem. Rev. 88 (1988) 673.
[8] A. Bewick, K. Kunimatsu, S. Pons, Electrochim. Acta 25 (1980) 465.
[9] X.Q. Lin, H.Q. Zhang, Electrochim. Acta 41 (1996) 2019.
[10] D.A. Downs, A. Haim, W.K. Wilmarth, J. Inorg. Nucl. Chem. 21 (1961) 33.
[11] S.N. Ghosh, J. Inorg. Nucl. Chem. 36 (1974) 2465.
[12] D. Ellis, M. Eckhoff, V.D. Neff, J. Phys. Chem. 85 (1981) 1225.
[13] S. Pons, M. Datta, J.F. McAleer, A.S. Hinman, J. Electroanal. Chem. 160 (1984) 369.
[14] R.M. Hexter, M.C. Albrecht, Spectrochim. Acta A. 35 (1978) 233.
[15] H.J. Buser, D. Schwarzenback, W. Petter, A. Ludi, Inorg. Chem. 11 (1977) 1704.

ELSEVIER

Talanta 44 (1997) 2075–2079

Talanta

Fourier transform infrared spectroscopic determination of cypermethrin and deltamethrin in emulsifiable concentrate formulations

K.K. Sharma *, Suman Gupta, S.K. Handa

Division of Agricultural Chemicals, Indian Agricultural Research Institute, New Delhi 110 012, India

Received 1 July 1996; received in revised form 28 January 1997; accepted 6 February 1997

Abstract

Fourier tranform infrared (FT-IR) spectroscopic method has been developed for determination of cypermethrin and deltamethrin in emulsifiable concentrate formulations. The known concentration of formulation was subjected to preparative thin layer chromatography and the active ingradient zone was scrapped from the plate. Pyrethroids were eluted from the adsorbent with chloroform and estimated by measuring the ester carbonyl absorption band at 1749 cm^{-1} in cypermethrin and at 1743 cm^{-1} in deltamethrin using base line technique. Recoveries of cypermethrin and deltamethrin from commercial and laboratory prepared formulations were 90 to 97% in both the cases. The validity of FT-IR method was confirmed by comparing the results with standard HPLC method. © 1997 Elsevier Science B.V.

Keywords: Fourier tranform infrared spectroscopy; Cypermethrin; Deltamethrin

1. Introduction

Cypermethrin (RS)-α-cyano-3-phenoxybenzyl (1RS)-*cis*, *trans*-3-(2,2-dichlorovinyl)-2,2-dimethylcyclopropanecarboxylate and deltamethrin (S)-α-cyano-3-phenoxybenzyl (1R)-*cis*-(2,2-dibromovinyl)-2,2-dimethylcyclopropanecarboxylate are non-systemic stomach and contact synthetic pyrethroids effective against broad range of pests. These pyrethroids are commercially available as emulsifiable concentrate (EC), wettable powder (WP) and ready-for-use ultra low volume formulations (ULV).

The active ingradient in technical material and commercial formulations is determined by either high performance liquid chromatography (HPLC) or gas liquid chromatography (GLC) [1–4]. In the present Fourier transform infrared (FT-IR) spectroscopic method, the active ingredient was separated from commercial formulation by preparative thin layer chromatography (TLC) and the ester carbonyl absorption band was estimated by FT-IR. The method is simple, rapid and has been applied satisfactorily for the estimation of active ingradient of cypermethrin and deltamethrin in EC formulations.

* Corresponding author. Fax: +91 11 5766420.

PII S0039-9140(97)00056-8

Table 1
Rf values of cypermethrin and deltamethrin in different solvent systems

System number	Solvent system (v/v)	Cypermethrin Rf	Deltamethrin Rf
1	Benzene	0.50	0.61
2	Hexane–benzene (7+3)	0.41	0.43
3	Hexane–benzene (1+1)	0.47	0.44
4	Hexane–toluene (1+1)	0.55	0.55
5	Hexane–chloroform (9+1)	0.15	0.12
6	Hexane–chloroform (4+1)	0.46	0.44
7	Hexane–chloroform (1+1)	0.67	0.74
8	Hexane–diethyl ether (9+1)	0.41	0.50
9	Hexane–diethyl ether (4+1)	0.59	0.61
10	Hexane–acetone(9+1)	0.64	0.60
11	Hexane–acetone (4+1)	0.69	0.66
12	Hexane–ethyl acetate (19+1)	0.43	0.42
13	Hexane–ethyl acetate (9+1)	0.61	0.59
14	Benzene–ethyl acetate (19+1)	0.66	0.74
15	Benzene–ethyl acetate(9+1)	0.77	0.83
16	Carbon tetrachloride–acetone (9+1)	0.77	0.77
17	Hexane–chloroform–benzene (9+1+4)	0.55	0.54

2. Experimental

FT-IR spectrophotometer (Nicolet, Impact 400) matched liquid cells with NaCl window having optical path length of 0.05 mm. HPLC, Waters HPLC pump (501), Rheodyne injector (7125) equipped with 20 μl loop, variable wavelength tunable absorbance detector (Waters, 484), Stainless steel reverse phase column, RT 250-4; packed with 10 μM Lichrosorb RP-8 (Hiber); mobile phase, acetonitrile, flow 0.5 ml min^{-1}, detection wavelength 235 nm.

TLC equipment: variable thickness chromatofilm spreader, No. 20011 (Warner Chilott Laboratories, Instruments Division); Cypermethrin and deltamethrin, both analytical grade (99%) obtained from Institute of Organic Chemistry Warsaw, Poland; Cymbush (25 EC), cypermethrin formulation obtained from ICI (India) Ltd, Madras; Decis (2.8 EC), deltamethrin formulation obtained from Hoechst (India) Ltd, Bombay.

2.1. *o-Dinitrobenzene solution*

Prepared by dissolving 0.25 g of *o*-dinitrobenzene in 10 ml methyl cellosolve.

2.2. *p-Nitrobenzaldehyde solution*

Obtained by dissolving 0.30 g *p*-nitrobenzaldehyde in 10 ml methyl cellosolve.

2.3. *Preparation of laboratory prepared formulations*

Cypermethrin (25 EC) and deltamethrin (2.8 EC) were prepared by mixing 2.5 g of cypermethrin and 0.28 g of deltamethrin separately with 100 mg of Tween-80 and making upto 10 g with cyclohexanone.

Solvents acetone, chloroform, hexane, benzene, toluene, ethyl acetate, diethyl ether (all analytical grade), carbon tetrachloride (IR grade), acetonitrile (HPLC grade) were used.

Silica gel (G) for TLC (S.D. Fine Chemicals, Bombay).

Sodium hydroxide: 2N in methyl alcohol.

2.4. *Stock solutions*

Standard solution of cypermethrin and deltamethrin were separately prepared by dissolving 0.4 ± 0.01 g of sample in CCl_4 and volume made upto 10 ml and was further diluted to different concentrations.

2.5. Solution of cypermethrin formulation

Dissolve 0.8 ± 0.01 g sample of cypermethrin formulation (25 EC) in 10 ml of CCl_4 (~ 20 mg ml^{-1}) and dilutions were made accordingly.

2.6. Solution of deltamethrin formulation

Dissolve 7.14 ± 0.01 g sample of deltamethrin formulation (2.8 EC) in 10 ml of CCl_4 (25 mg ml^{-1}) and dilutions were made accordingly.

2.7. Preparation of TLC plate

Preparative TLC plates (200 × 200 mm) were prepared by coating with a slurry of silica gel G in distilled water (1 + 2) to a thickness of 0.75 mm. Plates were air dried for 1 h and activated by heating it at 110°C for about 1 h.

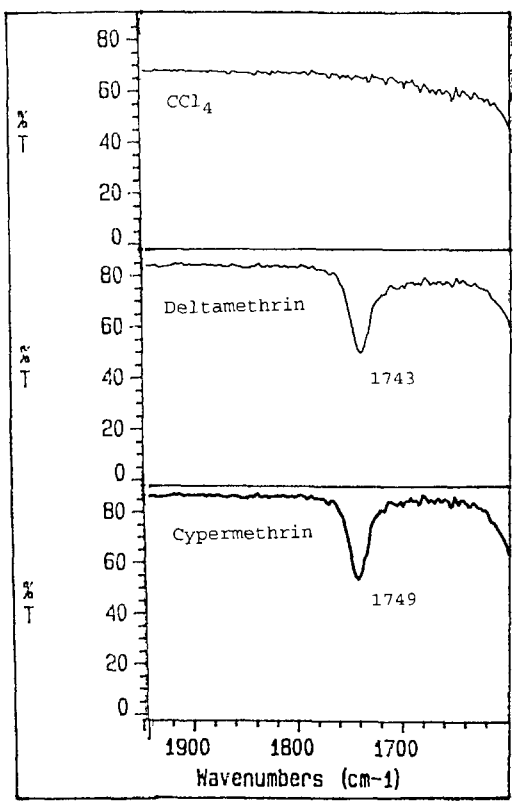

Fig. 1. FT-IR percentage transmittance of CCl_4, deltamethrin and cypermethrin in the ester carbonyl region.

Table 2
Analysis of commercial and laboratory prepared cypermethrin and deltamethrin formulations (%)

Serial no.	Commercial formulation (%)		Laboratory prepared (%)	
	FT-IR	HPLC	FT-IR	HPLC
Cypermethrin				
1	24.54	24.51	24.71	24.00
2	24.78	24.60	24.62	24.36
3	25.00	24.75	24.67	24.92
4	24.64	24.79	24.82	25.12
5	24.90	24.38	24.98	25.13
Average	24.77	24.61	24.76	24.71
S.D.	±0.19	±0.17	±0.14	±0.50
Deltamethrin				
1	2.70	2.87	2.73	2.89
2	2.79	2.80	2.81	2.82
3	2.89	2.77	2.83	2.74
4	2.74	2.80	2.76	2.82
5	2.77	2.74	2.91	2.71
Average	2.78	2.80	2.81	2.80
S.D.	±0.07	±0.05	±0.07	±0.07

2.8. Procedure

Standard solution of cypermethrin (20 mg ml^{-1}) in CCl_4 was spotted on the preparative TLC plate together with a marker spot (100 μg) of pure cypermethrin at the end of plate. Loaded plate was developed in a presaturated TLC chamber using hexane–acetone (4 + 1, v/v) as a solvent. After the solvent front had reached the distance of about 170 mm, the plate was removed from the chamber and dried in air. Developed plate was partially covered with another glass plate leaving the marker spot exposed. The marker spot was sprayed with NaOH solution (2N) followed by chromogenic reagent [5] consisting of *o*-dinitrobenzene and *p*-nitrobenzaldehyde which gave pink colour spot for the pyrethroids. The corresponding band of cypermethrin was scrapped off and eluted with chloroform. The solvent was evaporated in Kuderna Danish evaporator and diluted to 1 ml with CCl_4. The absorbance of the sample and the standard was measured against CCl_4 using base line technique.

Table 3
Recovery of cypermethrin and deltamethrin

Serial number	Added (mg)	Cypermethrin		Deltamethrin	
		Found (mg)	Recovery (%)	Found (mg)	Recovery (%)
1	20	18.75	93.75	17.82	89.12
2	20	18.91	94.55	18.16	90.82
3	20	19.24	96.20	17.87	89.33
4	20	19.14	95.70	18.08	90.41
5	20	19.17	95.85	18.41	92.03

In the present FT-IR method, the spectral resolution was 4 and 32 scans were recorded for each sample. The percentage of cypermethrin was calculated by the following formula [6]:

$$\% \text{ cypermethrin (by weight)} = \frac{A_f \times W_s}{A_s \times W_f} \times \% \text{ purity of standard}$$

where A_s and A_f are absorbances of standard and formulation respectively; W_s and W_f are weight in g per 100 ml of standard and formulation.

The same experimental procedure was repeated for the determination of % deltamethrin in its formulation. In the later case, hexane–diethyl ether (9 + 1, v/v) was used as a developing solvent for preparative TLC.

3. Results and discussion

The Rf value of cypermethrin and deltamethrin were recorded in different solvent systems (Table 1). For cypermethrin, hexane–acetone (9 + 1, v/v) with Rf 0.64 and for deltamethrin hexane–diethyl ether (9 + 1, v/v) with Rf 0.50 were found to be satisfactory solvent systems.

Scan of 20 mg cypermethrin and deltamethrin ml^{-1} in CCl_4 from 4000 to 400 cm^{-1} showed the presence of ester carbonyl band at 1749 and 1743 cm^{-1} respectively.

In the present study, the ester carbonyl band was selected for the quantitative determination of synthetic pyrethroids as this band is very strong and appears at transparent region of CCl_4 (Fig. 1). The base line of the absorption spectrum was established between 1770 and 1720 cm^{-1} in both the cases. The method is applicable to 1–40 mg of these synthetic pyrethroids in 1 ml of solution. Commercial cypermethrin (25 EC) and a laboratory prepared formulation (25 EC) were analysed with five determination of each sample (Table 2). Carbon tetrachloride from the samples was evaporated, residues were dissolved in acetonitrile and diluted to 200 ppm before analysing by reverse phase HPLC method. Similarly commercial deltamethrin (2.8 EC) and a laboratory prepared formulation (2.8 EC) were also analysed (Table 2).

The percentage recovery was checked by loading a known amount of analytical grade material (20 mg) on the preparative thin layer chromatographic plate and subjecting the plate to above described procedure. Recoveries in both the cases were in the range of 90 to 97% (Table 3) and by HPLC method, it was found to be 92–96%. The results of analysis of commercial and laboratory prepared formulation by FT-IR were compared with standard HPLC method (Table 2) and were found to be comparable. The method described for analysis of cypermethrin and deltamethrin emulsifiable concentrate formulations is simple, specific, rapid and precise.

References

[1] G. Zweig (Ed.), Analytical Methods for Pesticides and Plant Growth Regulators, Vol. XIII, Academic Press, New York, 1984, p. 36.
[2] CIPAC Handbook, 1C (1985) 2047.
[3] CIPAC Handbook, D (1988) 57.

[4] G. Zweig (Ed.), Analytical Methods for Pesticides and Plant Growth Regulators, Vol. XIII, Academic Press, New York, 1984, p. 53.
[5] R. Khazanchi, S.K. Handa, J. Assoc. Off. Anal. Chem. 72 (3) (1989) 512.
[6] G. Zweig (Ed.), Analytical Methods for Pesticides and Plant Growth Regulators, Vol. II, Academic Press, New York, 1964, p. 490.

ELSEVIER

Talanta 44 (1997) 2081–2086

Talanta

An automatic photometric method with high precision by gradually diluting a sample

Aimin Tan *, Cailin Xiao

Department of Chemistry, Central South University of Technology, Changsha 410083, People's Republic of China

Received 3 January 1997; accepted 12 February 1997

Abstract

An automatic photometric method to increase the precision of measurement is proposed, which is based on the injection of a very small volume of sample by rotary valve and the subsequent homogeneous mixing in a small reaction cell made of glass of the sample with a color-developing reagent gradually delivered by a syringe piston pump until the absorbance of the mixture approaches 0.434, where the lowest relative error in the concentration locates. This photometric method is characteristic of uniformly high precision, low sample and reagent consumption, and high sampling rate of 30 samples per h. The other advantages of this method include easy calibration with only one standard solution and no strict requirements on photometric components. While applied for the determination of cobalt ranging from 0.21 to 1.43 g l^{-1}, the relative standard deviations are all below 0.4%. © 1997 Elsevier Science B.V.

Keywords: Precision spectrophotometry; Differential spectrophotometry; Spectrophotometry; Micro-analysis; Flow analysis

1. Introduction

Absorption spectroscopy in the visible region is one of the most useful tools available to the chemist for quantitative analysis. Although it is mainly employed for the determination of the analytes with low concentrations, concentrated components may also be determined with one of the several precision spectrophotometric (differential spectrophotometric) methods [1].

Hiskey [2] proposed a precision spectrophotometric technique that involves comparing an unknown solution with a reference. The reference scale is set at zero using a solution of a highly colored (radiation-absorbing) species in place of a reagent blank. Concentrations of the unknown higher than the reference are then measured against this zero in the usual way. However, a standard solution with a higher concentration than the unknown may be used for the adjustment of 0% T, whereas the 100% T is adjusted as usual [1,3]. The latter method is less frequently used than the former, since the measured absorbance is not linearly related to the unknown's concentration, and repeated adjustments of 0 and 100% T are required.

* Corresponding author.

PII S0039-9140(97)00061-1

Reilley and Crawford [3] described a precision spectrophotometric method that involves the use of two standard solutions to set the 0 and 100% T readings of the photometer. By this means, the full scale can be used for a concentration range much narrower than usual, and precision is thus, increased. This method generally requires two standard solutions and several other standard solutions of intermediate concentration to construct a calibration curve, since the measured absorbance is often not a linear function of concentration. For the improvement of this method, Du zhikun [4] and Guan zongjie [5] introduced a new method, which employs a counter micro-current in place of the higher standard solution in Reilley and Crawford's method for the extension of transmittance scale in 0% T direction, with the adjustment of 100% T maintained unchanged. Some instruments based on the above principle have been developed [6], and many applications have been reported [1].

Common to all the above methods, linear relation between absorbances and concentrations is required, and several standard solutions are usually necessary for the construction of a calibration line. Furthermore, stricter restrictions on both the differences among different cuvettes and the intensity of radiation sources are generally required. A method described by Ramaley and Enke [7] replaces the two-standard and calibration-curve procedure with only one standard and isomation. This method involves a titration in which the absorbance of the unknown determines the endpoint. A known amount of the solvent is placed in an absorption cell. A standard solution of the sample substance is then added to the cell until the absorbance, and hence the concentration, is identical to that of the unknown solution. To obtain the maximum accuracy, the cell lengths are calibrated. This method has some good characteristics, however it is limited in applications because of the elaborate procedure and no corresponding instruments available for its automation. In addition to this, since the concentration of a sample is unknown, its absorbance may be large or small dependent upon its concentration, which results in ununiform errors in determining the endpoint for titration.

In this paper, a similar but different approach is proposed, which employs the instrument components in flow injection analysis [8] for the automation of solution handling and the reduction of reagent and sample consumption. Moreover, the titration with standard is substituted by gradually diluting a sample with a color-developing reagent, just like the automatic micro-titration method proposed by us previously [9], until the absorbance of the product formed by the analyte with the reagent approaches 0.434, where the highest precision for concentration measurement is located. The concentration of the analyte is calculated from the volume of the reagent added and the concentration of a standard solution corresponding to an absorbance of 0.434. Neither the calibration procedure with a series of standard solutions nor linearity between absorbances and concentrations in a wide range is necessary.

2. Experimental

2.1. Reagents and solutions

Cobalt chloride solution, containing 100 g l^{-1} of cobalt. The other standard solutions with lower concentrations are prepared by dilution.

Nitroso R salt solution, 0.2%

Sodium acetate-acetic acid buffer at pH 5.7 is prepared by dissolving 100 g of $NaCH_3COO \cdot 3 H_2O$ in distilled water containing 13 ml of acetic acid (6 mol l^{-1}), and diluted to 500 ml.

Reagent solution for the determination of cobalt is prepared by mixing nitroso R salt, the buffer, and distilled water at a ratio of 1:1:8.

All the reagents except otherwise stated are of analytical grade.

3. Apparatus

The automatic dilution system depicted in Fig. 1 were constructed from the following components: a 16-port rotary valve (Zhaofa Automatic Analysis Research Institute, Shenyang, China), a self-designed variable-speed,linear flow piston pump, equipped with 3 disposable plastic syringes

of 10 ml (diameter 17 mm); a self-constructed reaction cell; a photometer; a magnetic stirrer (Model GSP-80-04, Taixian Radio Factory, Jiangsu, China), and an intel 8031 based single-chip microcomputer system for pump, valve and magnetic stirrer control, data acquisition and processing. The valve is driven by a stepper motor (Model 45BF3/3A, Shanghai Instrument Motor Factory, China) through two gears with a diameter ratio of 1:4.5. Through the control of the microcomputer, the valve can be turned to either load or inject position. The piston pump, also driven by two stepper motors, can be controlled to a precision of 2 μl. Since syringes need to be refilled, the pump's movements should be in accordance with the valve's position. The piston's forward wavement requires the valve in inject position, while backward wavement needs the valve in load position. Each measurement always begins with the piston's backward movement for filling the syringes, and ends with the piston's forward movement to deliver reagent. The reaction cell, made of glass, has a volume about 12 ml and a inner diameter of 18 mm. In its outside, above the mixing rod are mounted a photo-

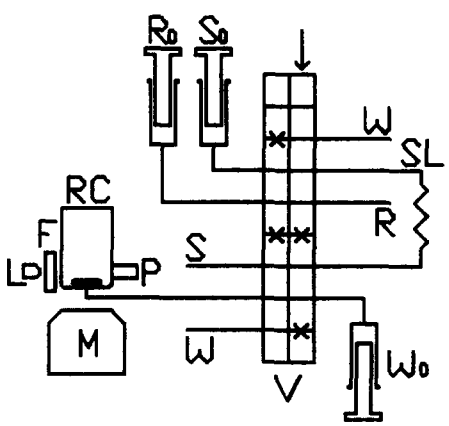

Fig. 1. The system configuration, R_0, S_0 and W_0 are the syringes for reagent (R), sample (S), and the drainage of the reaction cell (RC), respectively. V is the value, W is the waste. M is the magnetic stirrer. SL is the sample loop, L, F and P are the tungsten lamp, the filter, and the phototransistor, respectively.

transistor and a small tungsten lamp with a focusing head (6 V, 0.5 A). A light beam of 530 nm is selected from its irradiations by a filter for absorbance measurement, which falls onto the phototransistor after being absorbed by the solution in the reaction cell. The electric signal generated is then amplified and digitized by an A/D converter, AD574, whose output is sent to the microcomputer for further processing. The reaction cell together with the photometric components are put in a light-tight box to prevent the influence of ambient lights.

There are two distinct steps in the procedure, sample loading and reagent addition. During the first step, the valve turns to the load position, the syringes move backward, the reagent taken into the reagent syringe directly, while the sample flowing through the sample loop first and then to the sample syringe. The reaction cell is also drained by another syringe, which is driven by a separate stepper motor and should be operated a little bit longer than the reagent syringe to secure the complete drainage of the reaction cell. After sample loading step, the valve is turned to inject position, followed by the forward movement of the syringes. The reagent delivered by syringe R_0 propels the loaded sample into the reaction cell, where homogeneous mixing of the sample and the reagent is obtained magnetically. After 1 ml of reagent is added, the mixture in the reaction cell reaches the height of light beam, and the mixture's absorbance is then monitored quickly by the photometer. The absorbance will gradually decrease with the increased amount of reagent. Once the absorbance reaches 0.434, stop the addition of reagent and read out the volume of the reagent added.

All the absorbance measurements are made against the reagent blank, which is produced by the above procedure with distilled water in place of a sample.

A spectrophotometer (Model 721, Shanghai No. 3 analytical Instrument Factory, China) is also employed for absorbance measurements in some experiments.

4. Results and discussion

4.1. Calibration and dynamic range

Since both sample analysis and calibration are stopped at the same absorbance of 0.434, the analyte's concentrations in the reaction cell at endpoint are thus the same for all measurements if linearity between absorbance and concentration in the neighbourhood of 0.434 exists, i.e.,

$$V_oCs/(V_o + V_s) = V_oC_x/(V_o + V_x) \quad (1)$$

where V_o is the volume of the sample loop; C_o and C_x are the analyte's concentrations in the standard and sample solutions, respectively; V_o and V_x are the volumes of reagent delivered to obtain an absorbance of 0.434 in calibration and sample analysis.

To maintain the consistence of reagent concentration and pH for all measurements, both in calibration and sample analysis, the sample volume should be selected as small as possible while compared with the reagent volume, otherwise, some volume corrections should be made. In this experiments, a sample loop of 8 μl is constructed by the inner connection of the two corresponding ports on the rotary valve, whereas the reagent volume are above 1.5 ml. Therefore, the analyte's content in the sample may be readily determined by the following equation, without the necessity of constructing a calibration line with a series of standard solutions.

$$C_x = C_sV_x/V_s \quad (2)$$

Even though both the readout and the procedure are the same as a photometric titration, the principle is different because the reagent is not chemically equivalent to the analyte in this method.

Considering that the mixing rod will block light; a minimum of 1.5 ml reagent solution must be delivered before accurate absorbance measurement can be made. As the maximum reagent volume is 10 ml, the dynamic range in this method is from C_s $(1.5/V_s)$ to C_s $(10/V_s)$.

4.2. The carry-over effect

As the reaction cell and the tube connecting the reaction cell to the valve is drained, the carry-over effects in this method depend mainly on the volume of residual solution after drainage. To determine this volume approximately, a sample containing 100 g l^{-1} of cobalt is injected and diluted to 10 ml, the residual solution after drainage is then washed with distilled water and the resulting solution is transferred to a 25 ml calibrated flask. The cobalt content is determined by spectrophotometry with nitroso R salt [10], from which the volume of residual solution can be determined. The residual solution's volume, as the results of 11 measurements done this way determine, ranges from 0.01 to a maximum of 0.1 ml.

The relative error caused by the residual solution can be calculated by the following equation,

$$RE = (A1/A2 - 1)V_r/(V_r + V_x) \quad (3)$$

where V_r is the volume for the residual solution; A1 and A2 are the real absorbances at the endpoint for the two neighbouring samples. Because A1 and A2 are almost the same and V_x is at least 15 times larger than V_r, the carry-over effect will be negligible.

4.3. The precision

It is evident that the precision of this method is influenced by the dilution factor and endpoint determination. Since homogeneous mixing is achieved by magnetic stirring, the precision for dilution is dependent upon both the sample volume and the reagent added.

Since the sample loop's volume, albeit as small as a few μl, could be maintained as constant over a very long period, the precision is therefore only dependent on the volume of reagent added. To measure the precision for reagent delivery, the reaction cell is substituted by a small clean dry weighing bottle accurately weighted before use. After the addition of the required volume of reagent, the weighing bottle is weighted again, and the reagent added is calculated from the difference of the two weights. For the experiments done this way with increasing volumes of reagent

from 1 to 10 ml with 1.5 ml interval, the regression equation between the reagent volume (V, ml) and the steps (S) the motor takes is as following,

$$V = 1.9580 \times 10^{-3} S \quad (6)$$

whose regression coefficient is 0.99999. The linearity error in the whole range is below 0. 21%. The relative standard deviation for delivering a known volume of reagent is 0.033%, which is much better than the linearity is because of the small variations of inner diameter of the syringe, which, however, could be calibrated to increase the precision, if one wishes.

The precision for endpoint determination is related to absorbance measurement's precision near the absorbance of 0.434. Because samples are diluted differently to produce the same concentration, the result for a sample may be regarded as the product of its reagent volume by the analyte's concentration corresponding the absorbance of 0.434. In other words, the relative errors caused by endpoint determination for all samples should be identical to that in concentration measurement at the absorbance of 0.434, i.e., uniform precision is obtained for different samples. In this experiment, the precision for transmittance measurement is estimated as $\pm 0.1\%$, which corresponds to a relative error of 0.27% in the concentration measurement.

4.4. The influence of reagent concentration

In conventional photometric analysis, including precision spectrophotometric techniques, the reagent, particularly the chromogenic agent, should be in large excess so that the color development reactions go well to completion and linearity may be maintained. While in this method, lower chromogenic agent's concentration might be used and no evil influence on the determination will be produced so long as the linearity near the absorbance of 0.434 is maintained. As shown in Fig. 2, a steady state is recorded with lower reagent concentration, but the endpoint determination is not affected. However,if different product is formed with low reagent concentration, the reduction of reagent concentration should be avoided.

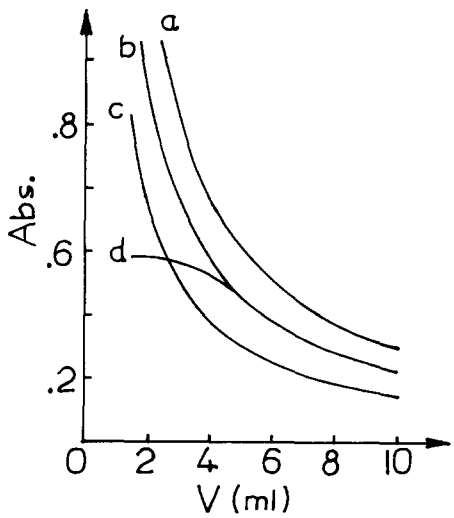

Fig. 2. Absorbance as the function of reagent volume. Curve a, b and c are recorded for the samples containing 1.0, 0.75 and 0.5 g l^{-1} of cobalt, respectively. Curve d is the same as curve c except for that the concentration of nitroso R salt is only one fifth of that in curve c.

4.5. The sampling frequency

A typical analysis cycle include sampling and reagent delivery. Among them, the sampling can be operated very quickly to increase sampling rate. the reagent delivery step is performed quickly at first, and then gradually slow down when the endpoint approaches in order to obtain better accuracy and enough reaction time. Since the flow rates could be easily adjusted with the microcomputer control, the above requirements might be readily met. In this method, 0.5 and 1.5 min are assigned for sampling and reagent delivery, respectively, with a sampling rate of 30 samples per h.

4.6. Sample analysis

Concentrated cobalt chloride in metallurgical samples in the production of cobalt are determined by this method, and the results obtained (Table 1) match well with those by complexometric titration method with EDTA. The relative standard deviations by this method is less than 0.4%.

Table 1
The results of sample analysis (g l^{-1})

Sample No.	EDTA method	This method					Average	RSD (%)
1	0.2531	0.2541	0.2533	0.2526	0.2540	0.2523	0.2533	0.32
2	0.4875	0.4885	0.4902	0.4888	0.4862	0.4858	0.4879	0.38
3	1.026	1.030	1.031	1.023	1.025	1.029	1.028	0.33
4	1.254	1.248	1.257	1.253	1.250	1.247	1.251	0.32

5. Conclusions

Uniformly high precision for photometric determinations is obtained by gradually diluting a sample with color-developing agent until the product formed by the analyte with the reagent produces an absorbance of 0.434, where the lowest relative error in concentration locates. To maintain the consistence of reagent concentrations in all measurements, the sample's volume should be much smaller than the volume of the reagent added. This new method is characteristic of high precision, easy calibration, low sample and reagent consumption, and no requirement for wide linear range. If higher precision and accuracy is required, precision spectrophotometry may be employed for more accurate determination of endpoint and the variations in syringe's diameter should be compensated.

References

[1] Q.R. Luo, Y.Z. Deng, Y.X. Cai, Y.E. Zeng, Spectrophotometric Anaylsis, Science Publisher, Beijing, 1992.
[2] C.F. Hiskey, Anal. Chem. 21 (1949) 1440.
[3] C.N. Reilley, C.M. Crawford, Anal. Chem. 27 (1955) 716.
[4] Z.K. Du, S.Q. Yang, Phys. Chem. Testing (Chemical Part) 4 (1980) 5.
[5] Z.J. Guan, Phys. Chem. Testing (Chemical Part) 4 (1983) 5.
[6] Z.J. Guan, Phys. Chem. Testing (Chemical Part) 1 (1985) 54.
[7] L. Ramaley, C.G. Enke, Anal. Chem. 37 (1965) 1073.
[8] J. Ruzicka, E.H. Hansen, Flow Injection Analysis, Wiley and Sons, New York, 1988.
[9] A.M. Tan, W.P. Ma, Y.C. Xu, A.Z. Mao, J.L. Huang, J.H. Xu, X.N. Zhao, Fenxi Huaxue (Chin. J. Anal. Chem.) 22 (1994) 482.
[10] S.Y. Shun, L.G. Shun, J.X. Ying, B. Fu, Handbook for the Analysis of Ores and Non-Ferrous Metals, Metallurgical Industry Press, Beijing, 1990.

ELSEVIER

Talanta 44 (1997) 2087–2094

Talanta

Accurate values of stability constant of Ca^{2+}-murexide complex

Tapan Kumar Khan, Pinaki Gupta-Bhaya *

Department of Chemistry, Indian Institute of Technology, Kanpur 208016 (UP), India

Received 9 October 1996; received in revised form 12 February 1997; accepted 24 February 1997

Abstract

In published reports, the values of stability constants of 1:1 complex of Ca^{2+} and the dye ammonium purpurate (murexide) were not determined under controlled conditions and were not properly corrected for the binding of Ca^{2+} with ions of buffer used to maintain pH and that of the background electrolyte used to maintain ionic strength. We report the molar absorptivities (ε) of murexide at pH 7.0, 7.5, 8.0, as well as the differential molar absorptivities ($\Delta\varepsilon$). Using these, we calculate the stability constants of the Ca-murexide complex at pH 5.0, 6.0, 6.5, 7.0, 7.5 and 8.0 at 15, 25 and 35°C and 0.100 M ionic strength using KCl as background electrolyte. No buffer was used and the complication arising from buffer binding is thus avoided. These values are compared with those determined in the presence of buffers that bind metal ions negligibly (Tris at pH 7.5 and 8.0) or whose binding constant to Ca^{2+} is reported and therefore can be corrected for (acetate at pH 5.0, Bistris at pH 6.5). Agreement is obtained within errors of measurement. The reported values are not true stability constants but can be used to calculate the concentration of free Ca^{2+} ion in a metal–ligand mixture with high precision and accuracy. The effect of K^+ binding to murexide is considered and is found not to alter the calculated value of free calcium concentration in a mixture. © 1997 Elsevier Science B.V.

Keywords: Calcium, determination of; Calcium, spectrophotometric estimation by murexide; Murexide

1. Introduction

Ammonium purpurate (murexide) has been extensively used as a colorimetric indicator of Ca^{2+} ion concentration in thermodynamic and kinetic studies of Ca^{+2} ion binding to macromolecular systems [1–6]. More recently, its rate of decomposition has been used as an indicator of proton activity in mixed solvents and microemulsions [7]. Other metallochromic indicators have also been used recently [8–14]. The dyes have different thermodynamic properties and spectral characteristics upon metal-complex formation. Each dye has its own advantages. Murexide is particularly suitable for the study of weak complex formation where a high metal concentration ($\approx 10^{-2}$ M) is needed to saturate the ligand. In our laboratory, we have found it useful for the study of Ca^{2+} ion binding to lipid vesicles in which mM concentration of free Ca^{2+} is needed in order to titrate to saturation. Other dyes used more recently, BAPTA and its brominated derivatives [12–14] and arsenazo III and antipyrylazo III [11], are less suitable for this purpose because they would saturate at the

* Corresponding author. Fax: +91 512 250260/250007.

PII S0039-9140(97)00078-7

Ca^{2+} concentration needed to obtain titration data over the whole range of ligand saturation. The need for precision and accuracy of K_{CaMu} is particularly important in those experiments where a small amount of bound Ca^{2+} ion is calculated as a difference of two comparable concentrations of Ca^{2+} ion, viz when the Ca^{2+}-ligand stability constant is small. The precision of reported data of K_{CaMu} determined under not very precisely controlled condition is however low, making the present study necessary. In earlier reports on the stability constant of the Ca^{2+}-murexide complex, a buffer was used to maintain pH but binding of buffer anions to Ca^{2+} was either not considered [15] or incorrectly taken into account [16]. The problems related to taking the buffer and the background electrolyte into account have been discussed in detail in a recent paper from our group on the stability constant of Eu^{3+}-murexide complex formation [17]. Shamsipur et al. [18] have reported values of the Ca^{2+}-murexide stability constant in non aqueous solvents. In this paper, we report the values of stability constant of Ca^{2+}-murexide complex at several values of temperature and pH. Different electrolytes (KCl, NaCl, $NaClO_4$) were used to maintain constant ionic strength in order to test if the chemical nature of background electrolyte influences the measured stability constant.

2. Experimental

2.1. Reagents

$CaCl_2$ was obtained from BDH. The purity of murexide (analytical grade, Koch-Light) was checked by C,H,N analysis. Ca^{2+} concentration was determined by weight titration against EDTA and the standardization error was about 0.5%. Other materials used were analytical grade. In all experiments, high precision was achieved by using mass to calculate the volumes of reagents dispensed, with careful adjustment to desired values by dispensing from calibrated μl pipettes with maximum error of ≈ 1 μl. The absorbance measurements were done in a Shimadzu Spectrophotometer calibrated using spectroscopic grade Cobaltammoniumsulphate solution (with absorbance at 470, 506 and 520 nm) as prescribed in the literature [19].

2.2. Buffer solutions and pH measurements

Buffer solutions of precisely known concentrations were prepared by weighing. Sodium acetate–acetic acid buffer was prepared by addition of acetic acid to sodium carbonate preheated to 230°C for 2 h.

2.3. ε values of murexide

Murexide solution was prepared in 0.100 M KCl with buffer (10.0 mM Tes ([*N*–tris (hydroxymethyl) methyl-2-aminoethane sulfonic acid] at pH 7.0; 10.0 mM Tris (Tris (hydroxymethyl) aminomethane) at pH 7.5 and 8.0). A weighed quantity of murexide was dissolved in 1000 ml of buffer and 0.100 M KCl. The absorbance was measured at 520 and 506 nm against the corresponding buffer blank. Two independent measurements agreed within $\approx 0.1\%$ (Table 1). The two reported pK_a values of proton dissociation for murexide are 9.2 and 10.5 at room temperature [15]. As expected, the ε of murexide reported here does not change in going from pH 7.0 to 8.0 and it is equal to its values at pH 5.0 and 6.5 within error [17]. At pH 8.0, $\approx 6\%$ of singly deprotonated murexide forms, but results in a negligible difference in ε.

Table 1
Molar absoptivity of murexide (ε)

pH	Temperature (°C)	$\varepsilon \times 10^4$ l mol^{-1} per cm	
		at $\lambda = 506$ nm	at $\lambda = 520$ nm
7.0	15	1.256 ± 0.002	1.362 ± 0.003
	25	1.241 ± 0.003	1.342 ± 0.001
	35	1.230 ± 0.002	1.326 ± 0.002
7.5	15	1.251 ± 0.003	1.361 ± 0.004
	25	1.239 ± 0.002	1.342 ± 0.002
	35	1.229 ± 0.003	1.326 ± 0.004
8.0	15	1.255 ± 0.002	1.355 ± 0.003
	25	1.238 ± 0.001	1.337 ± 0.002
	35	1.226 ± 0.004	1.320 ± 0.004

Table 2
Differential molar absorptivity ($\Delta\varepsilon$)

pH	Temperature (°C)	$\Delta\varepsilon \pm s^a$ (10^4 l mol^{-1} per cm)
5.0	15	1.211 ± 0.003
	25	1.201 ± 0.004
	35	1.183 ± 0.006
6.0	15	1.181 ± 0.008
	25	1.166 ± 0.007
	35	1.151 ± 0.008
6.5	15	1.150 ± 0.008
	25	1.133 ± 0.006
	35	1.114 ± 0.008
7.0	15	1.128 ± 0.005
	25	1.110 ± 0.009
	35	1.094 ± 0.006
7.5	15	1.094 ± 0.008
	25	1.071 ± 0.005
	35	1.050 ± 0.008
8.0	15	1.056 + 0.005
	25	1.033 ± 0.004
	35	1.010 ± 0.006

[a] Average of six independent measurements. Concentration of murexide being saturated is in the range 3.0×10^{-5}–9.0×10^{-5} M. The $\Delta\varepsilon$ values are independent of the absolute value of the concentration of murexide.

2.4. Determination of $\Delta\varepsilon$:

An identical volume of murexide solution in buffer (8.840 mM sodium acetate–acetic acid at pH 5.0, 18.210 mM and 6.860 mM Bistris ([bis (2-hydroxyethyl) imino-tris (hydroxy-methyl) methane]) at pH 6.0 and 6.5, respectively, 18.320 mM Tes at pH 7.0 and 12.135 mM Tris at pH 7.5 and 5.752 mM Tris at pH 8.0) and KCl solution were added to sample and reference cuvette to achieve an ionic strength of 0.100 M. A precalculated volume of 0.1 M $CaCl_2$ solution was added to the sample cuvette till murexide is fully saturated by $CaCl_2$. The absorbance of the sample solution (ΔA) was measured at 473 nm (the maximum of the difference spectrum) and divided by the total murexide concentration (which is equal to the concentration of Ca-Mu complex) to give $\Delta\varepsilon$. The value was checked by adding another 100 μl $CaCl_2$ solution to the sample and buffer/KCl solution and to the reference cell and redetermining ΔA. The differential molar absorptivity of calcium–murexide complex at three different temperature and a range of pH are given in Table 2. The presence of ≈0.100 M KCl does not affect measured $\Delta\varepsilon$ significantly. The concentrations of free murexide, $[Mu]_f$, and hence the K^+-murexide complex (KMu), differs between the sample and reference cells; however, this has negligible effect on $\Delta\varepsilon$, because at 473 nm, KMu and Mu_f absorb nearly equally. We have checked that 473 nm is at the tail end of the difference spectrum of murexide in the presence and in the absence of 100 mM KCl (the difference is ≈2%). The maximum in the difference spectrum is at 518 nm, where the difference is 8% [17]. The presence of buffer does not alter $\Delta\varepsilon$, since the Ca^{2+}-buffer complex, the free Ca^{2+} ion and the Ca^{2+}-Cl^- complex absorb negligibly at 473 nm. Values of $\Delta\varepsilon$ determined in the absence of buffer differ from those reported in Table 2 negligibly. Schwarzenbach and Gysling [15] reported $\Delta\varepsilon$ at $\lambda = 480$ nm, pH 8.53 and room temperature in veronal buffer to be 1.13×10^4 which is close to that reported here, 1.033×10^4 at $\lambda = 473$ nm, pH 8.0 and 25°C. Some difference is expected because of a change in pH from 8.0 to 8.53, a shift towards the pK_a of 9.2. The difference is consistent with the trend of decrease of $\Delta\varepsilon$ with increasing pH observed in Table 2. The pH dependence of $\Delta\varepsilon$ even at those values of pH where ε of murexide is not pH dependent arises from the presence of pH dependent equilibria involving the Ca^{2+} complex of murexide.

2.5. Metal-murexide stability constant

The determination of stability constants of Ca^{2+}-murexide complex in the absence of buffer were carried out using a method described by Jain and Gupta-Bhaya [17]. Briefly, identical volumes of murexide solution were added to the two cuvettes followed by the addition of metal ion solution to the sample cell and identical volume of KCl solution to the reference cuvettes. The pH of the solution in the sample cell was adjusted by addition of dilute sodium hydroxide solution (pH ≈9.0), the approximate volume of base needed having already been estimated in a separate experiment. The solution was mixed and the final pH checked with a microelectrode inserted into the cuvette. The pH was almost always within 0.05 of

the pH of the murexide solution in the reference cuvette. If it was slightly outside this range, a small measured volume (1–2 μl) of base or acid was added by μl pipette to bring the pH closer to the desired value. The liquid lost when the microelectrode is removed after the pH measurement, does not alter the concentration. In spite of a small difference in pH (≈ 0.05) between the two cuvettes the reproducibility is not affected. The absorbance of the test solution in the sample cell (ΔA) was measured against the murexide reference solution at the desired temperature at 473 nm.

Using

$$\Delta A = \Delta\varepsilon[\mathrm{CaMu}] \quad \text{(unit path length)} \tag{1}$$

$$[\mathrm{Mu}]_f = [\mathrm{Mu}]_t - [\mathrm{CaMu}] \quad \text{(t denotes total)} \tag{2}$$

$$[\mathrm{Ca}]_f = [\mathrm{CaMu}]/K_{\mathrm{CaMu}}[\mathrm{Mu}]_f \tag{3}$$

we calculate K_{CaMu} determined in the absence of buffer. The values at pH 5.0, 6.0, 6.5, 7.0, 7.5 and temperature 15, 25, 35°C are given in Table 3.

The determination of K_{CaMu} in the presence of buffers (5.752 mM Tris at pH 8.0, 12.135 mM Tris at pH 7.5, 18.210 mM Tes at pH 7.0, 6.860 mM Bistris at pH 6.5, and 8.840 mM Sodium acetate–acetic acid buffer at pH 5.0) whose binding to Ca^{2+} are weak and/or well characterized is done using essentially the same method, except that no adjustment of pH in the cells is necessary. Also, the sample murexide solution and the blank solution are buffered and as metal ion in buffer is added to the sample cell, buffer solution is added to the blank. The values of K_{CaMu} so determined have been corrected for metal–buffer binding (in cases where values of $K_{\mathrm{metal-buffer}}$ are known) as described later in this paper. The corrected values are given in Table 3.

Table 3
Stability constants K of Ca^{2+}-murexide association equilibria

pH	Temperature (°C)	$\log K \pm \sigma$ (buffer free expt.)	$\log K_{\mathrm{corr}}$
5.0	15	$2.454_1 \pm 0.008_4$	2.446 ± 0.011
	25	2.384 ± 0.011	2.361 ± 0.013
	35	$2.300_7 \pm 0.008_3$	2.176 ± 0.011
6.0	15	$2.521_7 \pm 0.004_4$	
	25	2.452 ± 0.012	
	35	2.371 ± 0.011	
6.5	15	2.642 ± 0.011	
	25	2.615 ± 0.011	2.601 ± 0.013
	35	2.534 ± 0.013	
7.0	15	$2.680_0 \pm 0.008_6$	
	25	$2.637_3 \pm 0.006_2$	
	35	2.590 ± 0.011	
7.5	15	2.732 ± 0.011	2.729 ± 0.011
	25	$2.666_6 \pm 0.004_3$	2.665 ± 0.002
	35	2.643 ± 0.010	2.643 ± 0.013
8.0	15		2.955 ± 0.013
	25		2.848 ± 0.011
	35		2.722 ± 0.013

All measurements are at $\mu = 0.100$ M.

2.6. Instability of murexide

Murexide in KCl solution, in the presence and in the absence of buffer decomposes very slowly. The deterioration is significantly more rapid at lower pH (5.0 compared with 6.5). At pH 5.0, in the absence of buffer and in the presence of acetate buffer $\approx 3\%$ of murexide decomposes in 1 h at 35°C. This value is $\approx 1\%$ at pH 6.5 in the absence of buffer. At pH > 5.0 in the presence of Bistris, Tes and Tris buffer used in this work, the decomposition is $\approx 2\%$ or less in 1 h at 35°C. These rates are significantly lower at 25 and 15°C. Our results are not significantly affected by this process, because we store freshly prepared murexide in ice bath and make spectral measurements on aliquots taken therefrom. Also, measurement times for both K and $\Delta\varepsilon$ are sufficiently short so that the results are not significantly affected by decomposition of murexide. However, this process of decomposition contributes to the error of measurement, particularly at lower pH (e.g., 5.0) and higher temperature (e.g., 35°C).

3. Results and discussion

3.1. Comparison with published values

The value of $\log K_{\mathrm{CaMu}}$ reported by Schwarzenbach and Gysling [15] at a pH 4.65 (0.1 M $CaCl_2$, unspecified temperature and 0.1 M acetate buffer) is 2.6. This differs from the value (2.367) reported

in this paper at 25°C, pH 5.0. But the value reported by them at pH 7.85 (in veronal buffer) is 2.8 and at pH 8.15 (same buffer) is 2.9 and these values are very close to that reported in this paper at pH 8.0 (Tris buffer, 25°C, 0.1 M KCl, $\log K =$ 2.848). Other values of K_{CaMu} reported by Schwarzenbach and Gysling [15] are in the higher pH range which we have not studied. The values reported by Balaji et al. [16] deviate appreciably from the values given above because the higher concentration of acetate and phosphate buffer used in these studies led to considerable metal–buffer binding, whose effect is not properly corrected for [17]. Schwarzenbach and Gysling [15] have not used KCl in the experiments for maintaining the ionic strength and the values are reported at unspecified temperature.

3.2. Estimate of precision

The maximum error of the volume measurements made by weighing was 5×10^{-5} ml (maximum weighing error 0.05 mg) and is negligible. The error in absorbance measurement was estimated from the fluctuation in the absorbance reading and the standard deviation (σ) is 0.3%. The calcium concentration has a σ of $\approx 0.5\%$, which is largely due to the end-point error. The EDTA concentration has a maximum error of $\approx 0.5\%$, arising from the purity of the EDTA used, weighing error and the error in making up the solution to standard volume. This error does not affect the precision since only one EDTA solution was made. The error in measuring the molar absorptivity depends on the absorbance value ($\sigma \approx 0.3\%$); error in murexide concentration (weighing error $\approx 0.2\%$ and dilution error $\approx$ 0.04%) is $\approx 0.3\%$, equivalent to a relative standard deviation of $\approx 0.1\%$. Using these values, we calculate the precision of K_{CaMu} by use of standard formulae [20] and find that the calculated values of σ are of the same order as the observed values given in Table 3. The experimentally observed σ is only slightly larger. The observed σ is expected to be slightly higher than that calculated, because error in calibration of the spectrophotometer and that due to slow decomposition of murexide (Section 2) are ignored in the calculation. From this analysis we conclude that the adjustment of pH done inside the cuvette does not lead to any additional error. This conclusion is further supported by the agreement between the values of K_{CaMu} determined in the presence and in the absence of buffer at pH 5.0, 6.5, 7.5. The buffers used at pH 5.0 (sodium acetate–acetic acid) and pH 6.5 (Bistris) bind Ca^{2+} significantly. K_{CaMU} determined in the presence of these two buffers when corrected (see below) gives good agreement with K_{CaMu} determined in the absence of buffer. The relative errors of K_{CaMu} values are comparable to those of K_{EuMu} values reported from our laboratory[17].The mean values of K_{EuMu} are orders of magnitude larger.

The data in Table 3 and Table 4 are quoted to one decimal place beyond the last significant digit to avoid the possibility of truncation errors on calculated $[Ca]_f^{2+}$. The precision of calculated $[Ca]_f^{2+}$ is only slightly less than that of K_{CaMu} reported here. The $\log K$ values in Table 3 are quoted to three places of decimal, but wherever the σ of $\log K$ is in the third decimal place, the fourth decimal place of both $\log K$ and σ are written as a subscript.

3.3. Correction of stability constants due to metal–buffer binding

Balaji et al. [16] pointed out that the stability constants determined in the presence of buffer should be corrected for metal–buffer binding. The corrected values (K_{corr}) can be obtained from the conditional values K_{app} calculated by ignoring metal binding by buffer using the relation,

$$K_{corr} = K_{app}(1 + \sum_i K_{MB}[B]^i) = K_{app}\gamma$$

where $\gamma = 1 + \Sigma_i K_{MB_i}[B]^i$ (B is the species that bind the metal ion in a 1:1 complex).

Using the relations:

$[B]_t = [B] + [BH] + [MB]$ and $[MB] = K_{MB}[M]_f[B]$,

(B: acetate ion, neutral Tes, Tris, Bistris; each can bind a proton; BH: protonated B, $[B]_t$: total concentration of buffer in both forms; MB: 1:1 metal-buffer complex, ($i = 1$); K_{BH} and K_{MB} are association constants of B and H^+, Ca^{2+} and B, respectively) one obtains $\gamma = 1 + K_{MB}[B]$, where

Table 4
Typical data to show correction of K due to binding of Ca^{2+} ion to buffer, (ionic strength = 0.100 M)

$[B]_t(\times 10^3)$	$[B](\times 10^3)$	$\gamma(=1+K_{MB}[B])$	K_{app}	K_{corr}	$K_{corr} \pm \sigma$	$K \pm \sigma$(buffer free expt.)
Bistris buffer of pH 6.5 at 25°C						
6.3597	2.819	1.502	271.5	407.8		
6.0552	2.613	1.465	263.7	386.3	398.9 ± 8.6	411.8 ± 9.5
5.7922	2.430	1.432	277.6	397.5		
5.5625	2.280	1.405	282.5	396.9		
5.4118	2.177	1.387	292.7	406.0		
Acetate buffer of pH 5.0 at 25°C						
8.840	7.085	1.027	221.2	227.2		
8.349	6.689	1.025	222.5	228.1	229.4 ± 2.8	242.1 ± 8.1
7.859	6.290	1.024	223.4	228.8		
7.009	5.603	1.021	228.6	233.4		

Ca^{2+}-Bistris: log $K = 2.25$ (25°C, $\mu = 0.1$); Bistris-H^+: log $K = 6.56$ (25°C, $\mu = 0.1$)[21].
Ca^{2+}-Acetate: log $K = 1.24$ (25°C, $\mu = 0$), $\Delta H° = 0.91$ K Cal per mol[22].
Corrected values used in our calculation: K_c at $\mu = 0.100$ and 15, 25 and 35°C: 3.288, 3.759, 4.253, respectively. The value 3.759 agrees very well with log $K = 0.57$ reported in the literature under identical conditions ($\mu = 0.1$)[23].
Acetate-H^+: log $K = 4.55$ (20°C, $\mu = 0.1$) log $K = 4.64$ (25°C, $\mu = 0.2$)[22].
Corrected values used in our calculation: log K_c at $\mu = 0.100$ and 15, 25, 35°C: 4.442, 4.389, 4.102, respectively.

$$[B] = \frac{[B]_t}{1 + K_{BH}[H^+] + K_{MB}[MMu]/K_{MMu}[Mu]_f}$$

The values of K_{corr} so obtained are given in Table 3. The experimental values of K_{app} are found in each case, as expected, to be less than K determined in absence of buffer. Agreement between calculated values of K_{corr} (in those cases, where γ could be calculated) and K of buffer free experiments is good.

Table 4 gives examples of calculation of K_{corr} from K_{app} using actual experimental data at pH 6.5 and 5.0 in the presence of Bistris and acetate buffer, respectively. The values of K_{BH}, K_{MB} are obtained from the literature [21,22] and corrected to our experimental conditions wherever necessary. The corrected value of Ca^{2+}-acetate stability constant at 25°C agrees very well with the experimentally determined value reported in the literature [23] under identical conditions. This agreement verifies the validity of the corrected values. The details are given in Table 4. We could calculate K_{corr} for Bistris only at 25°C, because K_{MB} and K_{BH} are reported only at this temperature. The agreement of the values of K determined in the absence of buffer and K_{corr} is good. For Bistris, the two agree within error. Log K of Ca^{2+}–Tris association is ≤ 0.7 [21]. Using this, we obtain, γ at pH 7.5 and 8.0 to be ≈ 1.0. In agreement with this, K determined in the absence of buffer and that in its presence at pH 7.5 are equal within error of measurement. K of Ca^{2+}-Tes association is not reported. Therefore, the agreement between K_{corr} and K determined in buffer-free experiments could not be verified at pH 7.0; it is however observed, as expected, that K_{app} is less than K determined in buffer free experiments. An estimate of binding constant of Ca^{2+} and Tes (deprotonated neutral form) can be made from the values of K_{CaMu} determined in the presence and in the absence of buffer and is found to be ≈ 18 at 25°C, a reasonable value. The corresponding quantity for Eu^{3+}, determined using murexide as an indicator of free Eu^{3+} concentration is ≈ 110, which is consistent with that for Ca^{2+}-Tes system.

3.4. Effect of binding of potassium by murexide

Potassium chloride of 0.100 M concentration was used to maintain ionic strength constant. Though the affinity of murexide for potassium is less than that for Ca^{2+}, it cannot be ignored. The difference $[Mu]_t - [MMu] = [Mu]'_f$ is not the true value of free murexide $[MU]'_f$, but is related to it

by $[Mu]_f = [Mu]_f + [KMu]$. $[KMu]$ is given by $K_{KMu}[K^+]_f[Mu]_f$. Since $[K^+] \approx 10^4[Mu]$, $[K^+]_f \approx [K^+]_t$ and $[Mu]_f = [Mu]_f'/\alpha_{Mu(K^+)}$, where $\alpha_{Mu(K^+)} = 1 + K_{KMu}[K^+]_t$. Thus, K_{CaMu} calculated by ignoring the presence of KMu is $\alpha_{M(K^+)}$ times that corrected for its presence. In the absence of published values of K_{KMu}, it is not possible to calculate $\alpha_{Mu(K^+)}$. The corrected value of K_{CaMu} therefore cannot be calculated. We now show that in spite of this, the calculated values of $[M]_f$ in a mixture ($[M]_f = [MMu]/K_{CaMu}[Mu]_f$) using the values of K_{CaMu} reported in this paper are correct. Even though K_{CaMu} and $[Mu]_f$ both acquire a correction factor because of the presence of KCl, their product remains unchanged. In addition, the relation $\Delta A = \Delta\varepsilon[MMu]$ holds even when KCl is present. The expression of $\Delta\varepsilon$ however is $\varepsilon_{CaMu} - \{\varepsilon_{KMu}/\alpha + \varepsilon_{KMu}(1 - 1/\alpha)\}$. The quantity $[Mu]_f' = [Mu]$-$[MMu]$ is now partitioned into true $[Mu]_f$ and $[KMu]$. The relative proportion is $(1/\alpha)/(1 - 1/\alpha)$, where α is a constant for a given total concentration of KCl. Thus [MMu] calculated as $\Delta A/\Delta\varepsilon$ in the presence of KCl as background electrolyte is correct.

3.5. Effect of replacing K^+ by Na^+

The buffers contribute Na^+ ions to different extents which replace K^+ ions of the background electrolyte. In order to verify, that this replacement does not alter the results, we have conducted experiments with NaCl and $NaClO_4$ in place of KCl as background electrolyte and find that within errors of measurements the results indeed do not change.

3.6. Nature of the stability constants

The values of K_{CaMu} reported in this paper are conditional constants, because: (a) they are not corrected for the presence of KMu; and (b) the concentrations $[Mu]_f$ and [MMu] are sums of concentrations of different ionised forms of $[Mu]_f$ and their metal complex.

3.7. Need for precise values of K_{CaMu}:

At 25°C, pH 8.0, $\mu = 0.100$ we report $\log K = 2.848$, in contrast to its value reported in [15], namely $\log K = 2.8$ at an unspecified room temperature and pH 7.85. The need for this additional precision is clear from the following example based on experiments performed in our laboratory. The mean value of Ca^{2+} concentration bound to a suspension of lipid vesicles (cardiolipin, lipid concentration = 0.748 mM, concentration of vesicle spheres = 2.0×10^{12} vesicles ml^{-1} solution, total Ca^{2+} ion concentration = 2.2 mM) calculated by using K reported here and that reported in [15] differ by 11%. At lower pH, the difference is larger. We report $\log K = 2.367$ at 25°C, pH = 5.0, $\mu = 0.100$ whereas Schwarzenbach and Gysling [15] report $\log K = 2.6$ at pH = 4.65 and at an unspecified room temperature. The difference between the two calculated mean Ca^{2+} concentration in the same experiment is 72%.

3.8. Potential use of K_{CaMu}:

In addition to their purely analytical use for detection of metal ions, the stability constants of metal-dyestuff complexes are useful for the determination of stability constants and rate constants of metal-ligand systems. In our laboratory we are studying calcium ion induced fusion of phospholipid vesicles. The threshold concentration needed for fusion of vesicle is ≈ 10 mM [24]. For 90% saturation of the metallochromic indicators murexide, ArsenazoIII, AntipyrylazoIII, Quin2 and 5,5′-Br_2BAPTA, the concentration of Ca^{2+} needed are 20.746, 2.1375, 0.3375, 7.5×10^{-4} and 1.43×10^{-2} mM, respectively. So, murexide turns out to be the only choice for the measurement of free Ca^{2+} ion concentration in experiments on calcium ion induced fusion of phospholipid vesicles.

In contrast to Ca^{2+} sensitive electrodes [25], the spectrophotometric method using murexide is free from interference from K^+, Na^+, Tris, Mg^{2+}, chemicals of common occurrence in biochemical experiments. At low pH (< 4), murexide is unstable and the electrode also gives error.

References

[1] L. Mela, B. Chance, Biochemistry 7 (1968) 4059.
[2] A. Scarpa, Methods Enzymol. 24 (1972) 343.
[3] T. Ohnishi, E.J. Masaro, H.A. Bertrand, B.P. Yu, Biophys. J. 12 (1972) 1251.
[4] H. Rottenberg, A. Scarpa, Biochemistry 13 (1974) 4811.
[5] R.H. Kretsinger, D.J. Nelson, Coordination Chem. Rev. 18 (1976) 29.
[6] S.T. Ohnishi, Anal. Biochem. 85 (1978) 165.
[7] S. Barrabass, K. Stickdorn, W. Knoche, J. Chem. Soc. Faraday Trans. 91 (1995) 637.
[8] A. Scarpa, F.J. Brinley Jr, G. Dubyak, Biochem. 17 (1978) 1378.
[9] S.T. Ohnishi, Biochim. Biophys. Acta 586 (1979) 217.
[10] R.Y. Tsien, Biochemistry 19 (1980) 2396.
[11] E. Rios, M.F. Schneider, Biophys. J. 36 (1981) 607.
[12] G.W. Feigenson, Biochemistry 25 (1986) 5819.
[13] G.W. Feigenson, Biochemistry 28 (1989) 1270.
[14] B. Svensson, B. Jonssön, M. Fushiki, S. Linse, J. Phys. Chem. 96 (1992) 3135.
[15] G. Schwarzenbach, H. Gysling, Helv. Chimica. Acta 32 (1949) 1314.
[16] K.S. Balaji, S.D. Kumar, P. Gupta-Bhaya, Anal. Chem. 50 (1978) 1972.
[17] S. Jain, P. Gupta-Bhaya, Talanta 39 (1992) 1647.
[18] M. Shamsipur, S. Madaeni, S. Kashanian, Talanta 36 (1989) 773.
[19] C. Burgess, A. Knowles (eds.), Standards in Absorption Spectrometry, vol. I, chapter 4, Chapman and Hall, London, 1981.
[20] F.K. Harris, Electrical Measurement, chapter 1, Wiley, New York, 1952.
[21] K.H. Scheller, T.H.J. Abel, P.E. Polanyi, P.K. Wenk, B.E. Fischer, H. Sigel, Eur. J. Biochem 107 (1980) 455.
[22] A.E. Martell, Stability Constants of Metal-Ion Complexes, The Chemical Society, Burlington House, 1971, p. 251.
[23] A.E. Martell, P.M. Smith (Eds.), Critical Stability Constants, Vol. 6, Plenum Press, 1974.
[24] S. Nir, in: J. Wilschut, D. Hockstra (Eds.), Membrane Fusion, Ch. 5, Marcel Dekker, New York, 1991.
[25] Orion Research Incorporated, Instruction Manual, Calcium-ion electrode, Model 93-20, Cambridge, Mass, U.S.A., 1979.

ELSEVIER

Talanta 44 (1997) 2095–2102

Talanta

Recovery of plutonium and americium from laboratory acidic waste solutions using tri-*n*-octylamine and octylphenyl-*N*-*N*-diisobutylcarbamoylmethylphosphine oxide

K.M. Michael [a], G.H. Rizvi [b], J.N. Mathur [b,*], S.C. Kapoor [a], A. Ramanujam [a], R.H. Iyer [b]

[a] *Fuel Reprocessing Division, Bhabha Atomic Research Centre, Bombay 400085, India*
[b] *Radiochemistry Division, Bhabha Atomic Research Centre, Bombay 400085, India*

Received 16 September 1996; received in revised form 12 February 1997; accepted 24 February 1997

Abstract

Plutonium from acidic waste solutions has been recovered quantitatively using tri-*n*-octylamine (TnOA) in xylene and americium using a mixture of octylphenyl-*N*-*N*- diisobutylcarbamoylmethylphosphine oxide (CMPO) and TBP in dodecane by extraction and extraction chromatographic methods. The Pu(IV)/TnOA species extracted into the organic phase from higher nitric acid concentrations has been confirmed as $(R_3NH)_2Pu(NO_3)_6$ (where R_3N = TnOA) by employing slope analysis as well as spectrophotometric studies. © 1997 Elsevier Science B.V.

Keywords: Recovery; Plutonium; Americium; Tri-*n*-octylamine; Octylphenyl-*N*-*N*-diisobutylcabamoylmethylphosphine oxide; Solvent extraction; Extraction chromatography; Laboratory waste solutions

1. Introduction

During the processing of plutonium, several types of acidic liquid wastes are generated through different routes, of which two main routes are (i) anion exchange waste and (ii) Whatman No.1 paper wipings ignited and dissolved in nitric acid. The first one contains Pu and Am in the ranges of 10–40 and 0.2–0.5 mg l^{-1} respectively in 7.5 M nitric acid. In the second stream Pu and Am could be in the ranges of 300–600 and 0.2–0.3 mg l^{-1} respectively in nitric acid concentrations varying between 6 and 12 M. The objective of the present study was to develop a procedure for the recovery of Pu and Am from such highly acidic laboratory waste solutions and to understand the nature of Pu species extracted into the TnOA phase.

Amines are reported to be one of the highly selective extractants for the recovery of actinides [1–6]. Among the various amines, TnOA is reported to extract Pu(IV) from 1–12 M nitric acid [6]. CMPO is a versatile reagent for the extraction of tri-, tetra- and hexavalent actinides and trivalent lanthanides from acidic solutions [7–17]. In an earlier publication by Mathur et al. [17] it was

* Corresponding author.

PII S0039-9140(97)00079-9

shown that three contacts with a mixture of 0.2 M CMPO and 1.2 M TBP in dodecane could extract ~98% of Pu and Am from 7.5 M HNO_3. While stripping, the combined stripped Am fractions contained ~26% Pu. In order to separate Pu and Am in radiochemically pure form from such acidic waste solutions without recourse to any feed adjustments, it was decided to utilize a two step solvent extraction procedure comprising of extraction of Pu(IV) with TnOA–xylene followed by extraction of Am by a mixture of CMPO + TBP.

The extraction chromatographic technique has been utilized for the recovery of actinides and lanthanindes [18–21] and also column separations are easily amenable for purification of nuclides at very high α, β or γ doses. It was, therefore, thought worthwhile to use TnOA adsorbed on chromosorb-102 (TnOAC) and CMPO adsorbed on chromosorb-102 (CAC) for the recovery of Pu and Am respectively in a pure form.

2. Experimental

TnOA supplied by K&K Labs, USA, was used as such. CMPO, solvent extraction grade was synthesised and purified in this lab [14].

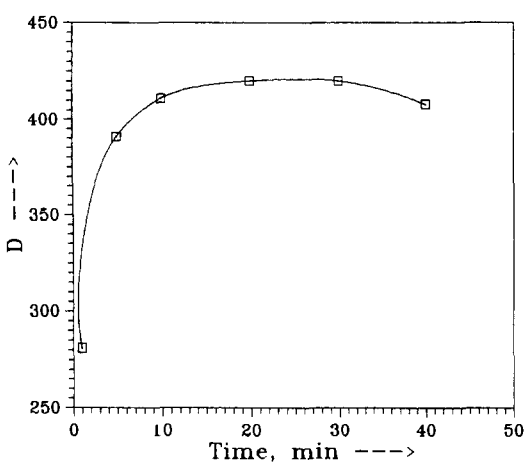

Fig. 1. Extraction of Pu(IV) with 20% TnOA–xylene at different time intervals.

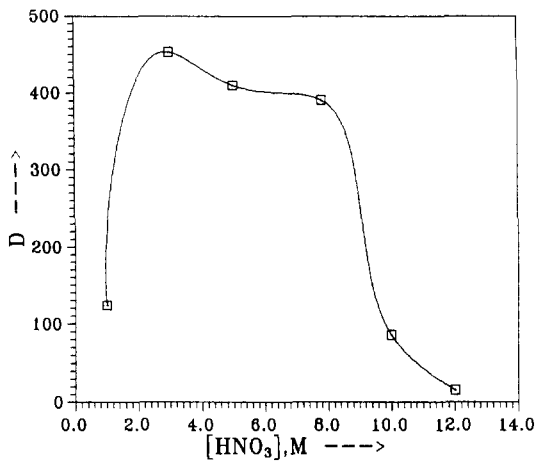

Fig. 2. Extraction of Pu(IV) with 20% TnOA–xylene at various acidities; [Pu] = 33.4 mg l^{-1}.

Chromosorb-102 (100–120 mesh size, styrene-divinylbenzene polymer) was obtained from Johns Manville, USA. Xylene was obtained from BDH, India, and dodecane was obtained from Transware Chemica Handelsgeselschaft, Hamburg, Germany. All other chemicals used were of Analytical Reagent grade. TnOAC and CAC were prepared by contacting the three phase system of TnOA or CMPO, chromosorb-102 (1:1, w/w) with methyl alcohol–water (50:50) for 12 h as reported elsewhere [21]. Throughout this work Pu nitrate solution was conditioned with sodium nitrite and ammonium *meta* vanadate to maintain it in the tetravalent state except for the actual samples where only sodium nitrite was used.

Table 1
Extraction of Pu by 20% TnOA–xylene; [HNO_3] = 7.5 M; organic to aqueous phase ratio = 1

[Pu] (mg l^{-1})	D	Extraction (%)
16.7	368.7	99.73
33.4	390.6	99.74
50.1	384.5	99.74
83.5	396.3	99.75
100.2	425.9	99.77
150.3	458.3	99.78

Table 2
Loading of Pu on 20% TnOA–xylene at various organic to aqueous phase ratios
[Pu] = 33.4 mg l^{-1}; [HNO_3] = 7.5 M

Phase ratio (o:a)	Extraction (%)
1:1	99.74
1:3	99.72
1:5	99.73
1:7.5	99.72
1:10	99.73

2.1. Procedures employed in solvent extraction

Extraction studies were carried out between 0.5 and 15 min to establish the time period required for attaining the equilibrium. All the solutions were subsequently equilibrated for 15 min in all the extraction studies.

Extraction of Pu(IV) into 20% TnOA–xylene was done at various acidities keeping the Pu concentration fixed and also at varying Pu concentrations at 7.5 M HNO_3. 0.5 ml Pu solutions were contacted with 0.5 ml TnOA solution at 25 ± 0.1°C. Also the Pu solution was contacted with 20% TnOA–xylene in various organic to aqueous phase ratios (1:1–1:10). After settling the phases were centrifuged and samples taken for radioassay by using a liquid scintillation counter.

To ascertain the nature of the species extracted in the TnOA phase, experiments were done by varying the TnOA concentrations while keeping the HNO_3 and Pu concentrations constant.

Pu(IV) spectra were recorded in 3.0, 7.5 and 12 M HNO_3 solutions and also those of the solutions extracted into 20% TnOA–xylene from such acidic solutions.

Table 3
Extraction of Pu with varying TnOA concentration
[HNO_3] = 7.5 M; [Pu] = 33.4 mg l^{-1}; organic to aqueous phase ratio = 1

[TnOA] (%)	D	Extraction (%)
5	53.0	98.15
7.5	200.9	99.50
10	220.0	99.54
12.5	252.7	99.61
15	287.0	99.65
20	390.7	99.74

Table 4
Stripping of Pu from loaded TnOA phase by various strippants

No. of strip	Pu stripped (%)		
	Nitric acid	Acetic acid	Ascorbic acid
1	2	96.98	99.87
2	12	2.52	0.11
3	10	0.17	0.01
4	11	-	-
5	11	-	-
Total	46	99.99	99.67

Total Pu in organic phase: 33.4 mg l^{-1}.

In extraction studies with Am solution, 0.5 ml Am solutions of varying concentrations, were extracted by contacting with 0.5 ml 0.2 M CMPO + 1.2 M TBP in dodecane for 15 min at 25 ± 0.1°C. The phases were centrifuged, separated and assayed for Am by γ counting using a NaI (Tl) detector.

Five ml of the actual laboratory waste solution containing 541 mg l^{-1} Pu and 0.3 mg l^{-1} Am in 7.5 M HNO_3 was first contacted with 20% TnOA–xylene at a 1:1 ratio. The organic phase was removed and the raffinate was contacted once again with 1.5 ml of 20% TnOA–xylene. The raffinate thus obtained contained only Am and was contacted twice with 5 ml portions of 0.2 M CMPO + 1.6 M TBP in dodecane.

In the Pu stripping experiments, 5 ml each of the loaded organic phase was contacted separately with equal volumes of 0.5 M HNO_3, 0.5 M acetic

Table 5
Extraction of varying amounts of Am by 0.2 M CMPO + 1.2 M TBP in dodecane
[HNO_3]) = 7.5 M; organic to aqueous phase ratio = 1

[Am] (mg l^{-1})	D
0.1	10.4
0.2	10.5
0.3	10.7
0.4	10.7
0.5	10.4
0.6	10.8

Table 6

A. Uptake of Pu on TnOAC, varying HNO_3 concentrations ([Pu] = 33.4 mg l^{-1})

$[HNO_3]$ (M)	1.0	2.0	3.0	5.0	7.5	10.0	12.0
D	3870.4	4473.3	7505.1	7529.8	4101.8	1185.0	199.5

B. Uptake of Pu on TnOAC, varying Pu concentrations ($[HNO_3]$ = 7.5 M)

[Pu] (mg l^{-1})	22.05	33.07	44.10	55.12	66.15
D	6543.3	4080	2292.3	1707.4	1394.9

acid or 0.2 M ascorbic acid in 0.3 M HNO_3 for 15 min. While in the case of Am, 5 ml of the extracted CMPO phase was contacted with equal volume of 0.008 M nitric acid for 15 min.

2.2. Procedures employed in extraction chromatography

In the extraction chromatographic experiments 5 mg of TnOAC–CAC was equilibrated with 1 ml Pu–Am solutions at different acidities and also varying concentrations of Pu–Am at 7.5 M HNO_3. After centrifuging, aliquots were taken for radioassay. The D values in the batch experiments were evaluated as:

$$D = \frac{A_i - A_f}{A_f} \times \frac{V}{M}$$

where A_i and A_f are the initial and final activities of the solutions, V and M are solution volume and weight of TnOAC or CAC.

In a separate experiment 100 mg TnOAC was taken in a column (4 mm × 450 mm) and the actual waste solution containing 541 mg l^{-1} Pu and 0.28 mg l^{-1} Am was passed through it at a rate of ~2 ml h^{-1}. Periodic assay of the effluent was done for Pu and Am. 10.0 ml Of the solution was passed. The raffinate which did not contain any Pu was passed through another column (4 mm × 450 mm) containing 425 mg of CAC at a rate of ~2 ml h^{-1}. The effluent was periodically analysed for the presence of Am.

TnOAC column loaded with Pu was eluted at the rate of ~2 ml h^{-1} with freshly prepared 0.2 M ascorbic acid solution. The CAC column loaded with Am was eluted at the rate of ~2 ml h^{-1} with 0.008 M nitric acid. The purity of the products (Pu and Am) was checked by α and γ spectrometry. Other cationic impurities were analysed by ICP-AES.

3. Results and discussions

3.1. Extraction and stripping of Pu

Fig. 1 gives the distrbution ratios (D) for Pu (33.4 mg l^{-1}) in 7.5 M HNO_3, equilibrated with 20% TnOA–xylene at various intervals of time. The D values were calculated as:

$$D = \frac{[\text{Pu}] \text{ in organic phase}}{[\text{Pu}] \text{ in aqueous phase}}$$

Even after 1 min the D value was very high but the equilibrium was attained in about 10 min. Fig. 2 gives the plot of D of Pu at varying concentrations of HNO_3. The D increases to 3 M, then it decreases slowly to 7.5 M and then sharply at higher concentrations. It could be explained on the basis that at 3 M HNO_3 the less extractable or inextractable species like $HPu(NO_3)_6^-$ and $H_2Pu(NO_3)_6$ are not formed which results to the maximum D value. The lower D value at 1 M HNO_3 is due to the less availability of nitrate ions for the formation of even the neutral species $Pu(NO_3)_4$, whereas the decrease in the D values between 7.5 and 12 M is due to the formation of species like $HPu(NO_3)_6^-$ and $H_2Pu(NO_3)_6$.

The D values of Pu (Table 1) at its varying concentrations in 7.5 M nitric acid, were almost

Table 7

A. Uptake of Am on CAC, varying HNO_3 concentrations ([Am] = 0.54 mg l^{-1})

$[HNO_3]$ (M)	1.0	3.0	5.0	7.5	10.0
D	1506.9	1786.3	1746.1	1167.2	899.7

B. Uptake of Am on CAC, varying Am concentrations ($[HNO_3]$ = 7.5 M)

[Am] (mg l^{-1})	0.109	0.217	0.326	0.435	0.652
D	941.1	1051.9	999.7	1124.6	1296.0

constant and high indicating nearly 99.8% extraction of Pu under these conditions. Table 2 gives the data for loading of Pu (in 7.5 M HNO_3) in 20% TnOA–xylene at various organic to aqueous phase ratios (1:1–1:10). Very high extraction ($\sim$ 99.7%) even at the ratio of 1:10 was achieved. These results suggest that at such Pu concentrations TnOA does not get loaded to any significant extent such that the percentage extraction may get decreased.

Table 3 gives the D values of Pu with varying concentration of TnOA (5–20%), keeping Pu concentration at 33.4 mg l^{-1}. It can be seen that the D value increased with increasing concentration of TnOA but even at 5% TnOA, the extraction of Pu is $\sim$ 98%. Thus, for near complete recovery of Pu from such solutions of about 10% TnOA–xylene could ideally be used.

It can be seen from Table 4 that while stripping with 0.5 M HNO_3 even after five contacts only about 46% Pu could be stripped. This is understandable since the D values of Pu even at low HNO_3 concentration of 1 M is found to be about 100. With acetic acid in three contacts almost the entire Pu comes to the aqueous phase. Ascorbic acid was found to be the best stripping agent since 99.9% Pu gets stripped just in one contact. Ascorbic acid stripping has an added advantage since Pu gets reduced to the trivalent state during this process which is the ideal valency state for its precipitation as oxalate [22].

3.2. Extraction and stripping of Am

It has been reported that the D values of Am in 0.2 M CMPO + 1.2 M TBP in dodecane increase with increasing acidity to about 2 M and then it remains almost constant ($\sim$ 25) to 6 M HNO_3 [14]. However, at 7.5 M HNO_3, the D decreases to about 10 [17]. In the present study, the D values for Am in 7.5 M HNO_3 was determined at varying Am concentration (0.1–0.6 mg l^{-1}). It can be seen from Table 5 that the D value remains almost constant at all the concentrations of Am studied. The stripping of Am was done with 0.008 M HNO_3 and in three contacts the recovery was quantitative. This is in accordance with the very low D value of Am of nearly 0.01 at such low acidities ($\sim$ 0.01 M) [7,8,14].

3.3. Extraction and stripping of Pu and Am from actual laboratory waste solution

When the actual waste solution (Pu, 541 mg l^{-1} and Am, 0.3 mg l^{-1}) was contacted with 20% TnOA–xylene, $\sim$ 99.8% Pu was extracted into the organic phase in the first contact. A second contact with a small volume of TnOA–xylene was given to ensure complete removal of Pu. The raffinate was subsequently contacted with 0.2 M CMPO + 1.2 M TBP in dodecane which showed the formation of a third phase. However, when the TBP concentration was raised to 1.6 M, keeping the CMPO concentration at 0.2 M, no third phase formation was noticed. The TnOA raffinate was contacted twice with equal volumes of 0.2 M CMPO + 1.6 M TBP in dodecane and the loaded CMPO phase was collected together.

Stripping Pu from the TnOA phase was done with an equal volume of 0.2 M ascorbic acid in 0.3 M HNO_3. Two contacts with the strippant gave nearly complete recovery of Pu (99.99%).

Table 8
Purity of Pu and Am product—spectroscopic result

Element	Detection limit (μg ml^{-1})	Feed (μg ml^{-1})	Pu product (μg ml^{-1})	Am product (μg ml^{-1})	Last effluent (μg ml^{-1})
Al	<0.005	875	54.0	2.34	650
B	<0.025	8	—	—	10.5
Ca	<0.01	725	65.0	6.21	700.0
Cr	<0.01	133	—	0.41	95.0
Cu	<0.005	50	—	0.81	33.0
Fe	<0.005	2300	95.0	440.00	1000.0
Mg	<0.005	220	44.0	1.41	200.0
Mn	<0.005	65	7.5	5.00	45.0
Mo	<0.005	—	27.5	0.92	31.0
Ni	<0.005	160	—	1.70	100.0
Pb	<0.01	45	20.0	2.80	12.0
Si	<0.02	75	5.0	0.60	72.0
Zn	<0.02	750	40.0	19.00	685.0

Combined CMPO phase was given three contacts with equal volumes of 0.008 M HNO_3. Am recovered in the aqeous phase was 99.9%.

4. Extraction chromatographic studies

4.1. Uptake of Pu on TnOAC

Table 6a gives the D values for the uptake of Pu at various acidities between 1 and 12 M HNO_3. The D values are high and they increases to about 5 M HNO_3 and then start decreasing.

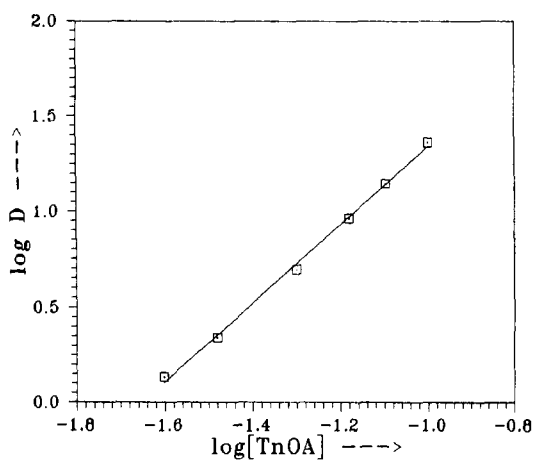

Fig. 3. Plot of log D vs. log[TnOA] for Pu(IV) at 7.5 M HNO_3.

Experiments were also carried out for the uptake of Pu in the range 30–150 mg l^{-1} in 7.5 M HNO_3 on TnOAC and it was found that the D value decreases with increasing Pu concentration (Table 6b).

4.2. Uptake of Am on CAC

Uptake of Am at various acidities by CAC (Table 7a) showed a gradual increase in D value to 3 M, remained almost same at 5 M and then it decreased at higher acidities. Also, experiments were carried out at varying concentrations of Am in the range 0.1–0.6 mg l^{-1} at 7.5 M HNO_3. The D value (Table 7b) at all the Am concentrations was found to be almost constant.

4.3. Column loading and elution

Ten ml of the actual waste solution was passed through the TnOAC column with a breakthrough of 0.009 mg l^{-1}. Thus 5.4 mg Pu was loaded on the TnOAC column. This could be quantitatively eluted in 10 ml 0.2 M ascorbic acid. 9.5 ml Of the raffinate (which did not contain any Pu) was passed through the CAC column and 2.8 μg Am was loaded without any breakthrough. This could be eluted in 8 ml of 0.008 M HNO_3.

The purity of the products was checked by α and γ spectrometry and also by analysing the

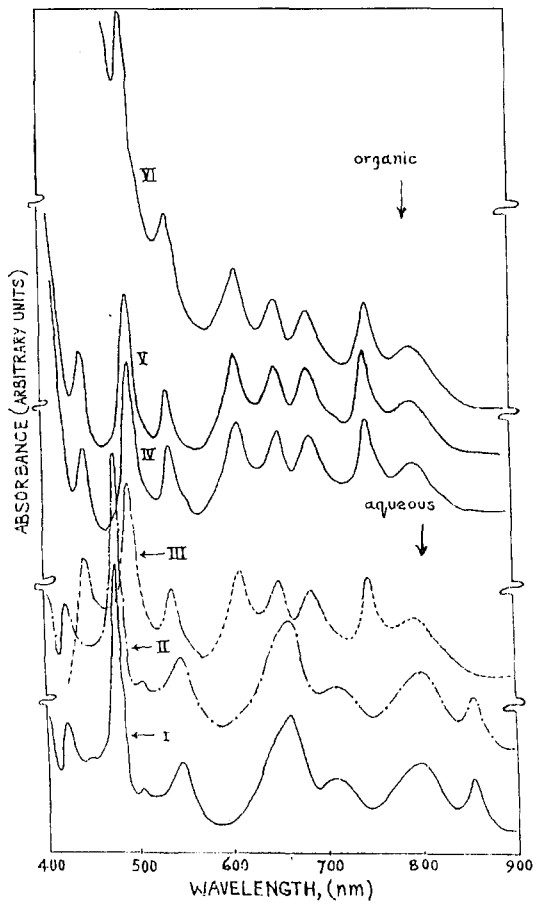

Fig. 4. Absorption spectra of Pu(IV): I. 3 M HNO_3, II. 7.5 M HNO_3, III. 12 M HNO_3 extracted in 20% TnOA–xylene from: IV. 3 M HNO_3, V. 7.5 M HNO_3, VI. 12 M HNO_3.

solutions for metallic impurities using ICP-AES. It was observed that the product, Pu and Am were radiochemically pure and also free from the common metallic impurities (Table 8).

4.4. Slope analysis and spectrophotometric studies of Pu(IV)–TnOA system

The plot of log D versus log[TnOA] (Fig. 3) at a fixed Pu and HNO_3 concentrations gave a straight line with a slope of 2 which suggests that each Pu ion is attached with two molecules of TnOA.

To get a better understanding of the Pu species extracted, visible spectra of Pu in 3, 7.5 and 12 M HNO_3 (using corresponding acid blanks) and Pu extracted from these solutions in 20% TnOA (using corresponding acid treated TnOA as blank) were recorded on a Beckmann DU-7 spectrophotometer using a 1 cm quartz cell. It can be seen from the spectra (Fig. 4) that Pu species in 12 M HNO_3 (absorption peaks at wavelengths 785, 744, 683, 648, 608, 535 and 492 nm) are different than those formed in 3.0 M. At 7.5 M nitric acid the peak positions are nearly the same as those in 3 M HNO_3 but the peak at 659 nm gets broadened and further at 12 M HNO_3 it splits into a triplet. Ryan [23] has reported that the peaks at 608 and 744 nm are due to the formation of hexanitrato complex of Pu(IV). In the case of the species extracted into the TnOA phase from all the three acidities, the nature of spectra was similar to that observed in the case of aqueous Pu in 12 M nitric acid. This suggests that the species extracted from all the acidities (between 3 and 12 M) are the same and similar to that formed in the aqueous 12 M HNO_3. At 12 M HNO_3 considerable amounts of the acidic species $H_2Pu(NO_3)_6$ and $HPu(NO_3)_6^-$ will be present [23,24] and when extracted with TnOA it seems that $Pu(NO_3)_6^{2-}$ is converted to the form $(R_3NH)_2Pu(NO_3)_6$. Thus from the slope analysis as well as Pu spectral studies it could be concluded that the species extracted into the organic phase is only $(R_3NH)_2Pu(NO_3)_6$.

5. Conclusions

Plutonium and americium from high acid laboratory waste solutions could be recovered quantitatively by employing a two stage solvent extraction procedure using TnOA in xylene for Pu and then 0.2 M CMPO + 1.6 M TBP in dodecane for Am. The loaded Pu from the TnOA phase could be stripped quantitatively either by 0.5 M acetic acid or 0.2 M ascorbic acid. Am from the CMPO phase could easily be stripped by 0.008 M HNO_3.

To avoid the problems encountered during the handling of organic solutions inside glove-boxes extraction chromatographic technique using

TnOAC for Pu and CAC for Am can be used for near complete recovery of Pu and Am from high acidic waste solutions. This can further be modified for remote operations while handling large volumes of such waste solutions. The Pu(IV)/TnOA species extracted into the organic phase has been confirmed as $(R_3NH)_2Pu(NO_3)_6$ by slope analysis as well as by spectrophotometric studies.

References

[1] A.S. Wilson, in: Proceedings of second United Nations International Conference on the peaceful uses of Atomic Energy, Vol. 17, United Nations, Geneva, 1958, pp. 348–351.

[2] W. Kraak, R. Bac, in: Solvent extraction chemistry of metals, Eds., H.A.C. Mckay, T.V. Healy, I.L. Jenkins, A. Naylor, Chemical Rubber Co. Press, Cleaveland, 1967, pp. 267–274.

[3] L.P. Bupp, USAEC report H.W. 53299C, No. 8, 1957.

[4] J.C. Shepperd, USAEC report H.W. 51958, August, 1957.

[5] U. Bertocci, British reports, AERE-R-2933, May, 1959.

[6] W.E. Keder, J.C. Sheppard, A.S. Wilson, J. Inorg. Nucl. Chem. 20 (1961) 131.

[7] D.G. Kalina, E.P. Horwitz, L. Kaplan, A.C. Muscatello, Sep. Sci. Technol. 16 (1981) 1127.

[8] E.P. Horwitz, D.G. Kalina, L. Kaplan, W.G. Mason, H. Diamond, ibid 17 (1982) 1261.

[9] E.P. Horwitz, H. Diamond, D.G. Kalina, Symposium Series 216, Plutonium Chemistry in: W.T. Carnall, G.R. Choppin (Eds.), 1983, 433 p.

[10] E.P. Horwitz, D.G. Kalina, Solvent Extr. Ion Exch. 2 (1984) 179.

[11] E.P. Horwitz, K.A. Martin, H. Diamond, R. Kaplan, ibid 4 (1986) 449.

[12] Z.J. Kolarik, E.P. Horwitz, ibid 6 (1988) 247.

[13] B.J. Mincher, ibid 7 (1989) 645.

[14] J.N. Mathur, M.S. Murali, P.R. Natarajan, L.P. Badheka, A. Banerji, Talanta 39 (1992) 493.

[15] J.N. Mathur, M.S. Murali, P.R. Natarajan, L.P. Badheka, A. Banerji, A. Ramanujam, P.S. Dhami, V. Gopalkrishnan, R.K. Dhumwad, M.K.Rao, Report BARC/1992/E/009, 1992.

[16] J.N. Mathur, M.S. Murali, P.R. Natarajan, L.P. Badheka, A. Banerji, A. Ramanujam, P.S. Dhami, V. Gopalkrishnan, R.K. Dhumwad, M.K. Rao, Waste Management 13 (1993) 317.

[17] J.N. Mathur, M.S. Murali, P.R. Natarajan, L.P. Badheka, A. Banerji, K.M. Michael, S.C. Kapoor, R.K. Dhumwad, J. Radioanal. Nucl. Chem., Letters 165 (1992) 219.

[18] R.E. Louis, G. Duyckaerts, J. Radioanal. Nucl. Chem. Articles 90 (1985) 105.

[19] A. Akatsu, T. Kumura, J. Radioanal. Nucl. Chem. Articles 140 (1990) 195.

[20] E.P. Horwitz, M.L. Dietz, R. Chiarzia, J. Radioanal. Nucl. Chem. Articles 161 (1992) 575.

[21] J.N. Mathur, M.S. Murali, P.R. Natarajan, J. Radioanal. Nucl. Chem. Articles 162 (1992) 171.

[22] J.M. Cleaveland, The Chemistry of Plutonium, Gordon and Breach Science Publishers, 1970, p. 398.

[23] J.L. Ryan, J. Phys. Chem. 64 (1960) 1375.

[24] R.W. Durham, R. Mills, Canadian report, CEI- 62 (Rev) October, 1961.

ELSEVIER

Talanta 44 (1997) 2103–2108

Talanta

The determination of wear metals in used lubricating oils by flame atomic absorption spectrometry using sulphanilic acid as ashing agent

E.J. Ekanem *, J.A. Lori, S.A. Thomas

Department of Chemistry, Ahmadu Bello University, Zaria, Nigeria

Received 5 November 1996; received in revised form 24 February 1997; accepted 27 February 1997

Abstract

A simple and reliable ashing procedure is proposed for the preparation of used lubricating oil samples for the determination of calcium, magnesium, zinc, iron, chromium and nickel by flame atomic absorption spectrometry. Sulphanilic acid was added to oil samples and the mixture coked and the coke ashed at 550°C. The solutions of the ash were analysed by flame AAS for the metals. The release of calcium, zinc, iron and chromium was improved by the addition of sulphanilic acid to samples. The relative standard deviations of metal concentration results in the initial oil samples were 1.5% for Ca (1500 mg l^{-1} level), 0.3% for Mg (100 mg l^{-1} level), 3.1% for Zn (1500 mg l^{-1} level), 0.7% for Fe (500 mg l^{-1} level), 0.02% for Cr (50 mg l^{-1} level) and 0.002% for Ni (10 mg l^{-1} level). The optimum sample size for efficient metal release was 20 g while the optimum sulphanilic acid to oil ratio was 0.05 g per gram of oil for Zn and Cr and 0.10 g for Ca and Fe. Results obtained by this procedure were highly reproducible and comparable with those obtained for the same samples using standard procedures. © 1997 Elsevier Science B.V.

Keywords: Aided-ashing; Lubricant; Metal determination

1. Introduction

The performance characteristics of lubricating oils are usually improved by the additives incorporated to improve the colour, pour point, viscosity, antiwear, antifrictional, antifoaming, oxidation and corrosion inhibition properties. These additives contain various metals in varying amounts. In use, a lot more of some of these metals are added to the lubricating oils from friction and wear [1,2]. A simple, rapid and accurate analytical procedure is needed for routine determination of these elements in order to provide an indication of the degree of wear of the oil wetted parts within an engine. A specific application is in the analysis of used lubricating oils to indicate potential failure in internal combustion engines as well as the metal pollution potentials of such oils if they are disposed directly into surface water or on land.

Although wear metal particles are not uniformly distributed in oils, they are generally deter-

* Corresponding author.

PII S0039-9140(97)00086-6

mined by using techniques traditionally applicable to the determination of metals in homogeneous solutions [3]. Various methods have been reported for the preparation of samples prior to instrumental analysis [3–7]. The possible loss of certain naturally occurring volatile constituents during unaided ashing of petroleum or its products has been reported [8–10]. Hence, the determination of trace metals in petroleum oils has relied on ashing procedures that aim at preventing metal losses by volatilization [11,12] during ashing.

Benzenesulphonic acid has been applied as ashing agent for the determination of Ni and V in petroleum distillates [11,13] while *p*-xylenesulphonic acid has been used for ashing petroleum distillates [12] and crude petroleum [14] for the determination of trace metals. Unlike these reagents which are hygroscopic and difficult to handle and store [15], sulphanilic acid has a very long shelf life and was investigated as ashing reagent in this work. The purpose of the present work was to establish the optimum conditions for the ashing of used lubricating oils applying sulphanilic acid to contain any volatilization losses.

2. Experimental

2.1. Reagents, apparatus and samples

All reagents used in this work were of analytical grade. Sulphanilic acid was obtained from BDH. Doubly distilled water was used in preparing all aqueous solutions. The muffle furnace used was a Carbolite (Sheffield, UK) capable of maintaining constant temperatures in the range 20–1200°C. The Perkin Elmer 290 B atomic absorption spectrophotometer, equipped with a premix chamber and a single slot burner head operated on air-acetylene flame, with automatic background correction and mono-element hollow cathode lamps was used for solution analysis. The parameters selected on the spectrophotometer for the determination of the test metals conform with those recommended by Perkin Elmer for this spectrometer. The oil samples analysed were collected from private vehicles and automechanic workshops in Zaria, Nigeria.

2.2. Working standard solutions

$CaCO_3$, $MgCl_2 \cdot 6H_2O$, ZnO, $(NH_4)_2SO_4 \cdot FeSO_4 \cdot 6H_2O$, $Ni(NO_3)_2 \cdot 6H_2O$ and chromium powder were dissolved appropriately and diluted with water to obtain 1000 mg l^{-1} stock solutions of Ca, Mg, Zn, Fe, Ni [16] and Cr [17]. Working standard solutions were obtained from the respective stock solutions by appropriately diluting them with water introducing 5% (m/v) lanthanum as the nitrate in the case of Ca and Mg to control the interferences of ions like phosphate, aluminate and silicate.

2.3. Recommended procedure

A mixture of 10.0 g used lubricating oil and 1.0 g sulphanilic acid in a 250 cm^3 pyrex beaker was heated in a heating mantle in the fume cupboard. The smoke issuing from the beaker was ignited and the set-up left until the flame was extinguished. The coke formed was muffled at 550°C until the ash was free of carbon particles; this required 45 min. The ash was allowed to cool before it was dissolved in 20 cm^3 of 6M HCl and digested in a boiling water bath to obtain a clear solution. This solution was made up to 50 cm^3 with distilled water in a volumetric flask, introducing 5% (m/v) La and analysed by FAAS for Ca, Mg, Zn, Fe, Cr and Ni against a blank solution prepared by digesting 20.0 cm^3 of the 6M HCl in the boiling water bath in the same way as the sample digests and making up to 50 cm^3 with distilled water as done for the sample solution.

3. Results and discussion

3.1. Optimization of ashing conditions

3.1.1. Temperature and time

Optimization of parameters was based on 10 g replicates [18] of samples. Temperatures were observed in the range 400–650°C for durations of 15–120 min. The progress and completeness of ashing was visually determined.

The lowest muffling temperature that yielded carbon-free ash was 550°C and this was achieved

Table 1
Effect of ignition

Sample treatment	Coking time (min)	Metal concentration (mg l^{-1})					
		Ca	Mg	Zn	Fe	Cr	Ni
Without ignition	20	1470	88	1350	387	32.5	9.5
With ignition	18	1470	88	1390	426	35.6	9.6

in the shortest time of 45 min. Though a higher muffling temperature could be selected for a more rapid ashing, 550°C was regularly applied in this work to avoid the disfiguration of the pyrex beakers that may occur at higher temperatures [19]. The oxides of the metals determined are known to be stable even above 1000°C [20], hence volatilization of the metals would be prevented by rendering them as oxides in the ash at 550°C. This ashing temperature has been recommended by the Institute of Petroleum [21] in a procedure that does not specify coking and muffling times and includes an overnight delay and a filtration step. The present procedure has eliminated the need for ash solution filtration and the attendant delay by achieving carbon-free ash in a short time. The chances of error arising from contamination during the filtration are removed in this procedure.

3.1.2. Ignition of samples

Coking time was the duration up to the cessation of smoke when the smoke issuing from the samples was not ignited. In the cases where the smoke was ignited as it issued from the sample, coking time was the time taken for the smoke to finish burning and the flame to be extinguished.

Satisfactory coking was achieved in 20 min without ignition and in 18 min when the smoke was ignited. Ignition did not, however, alter muffling time because the coke derived with and without ignition both yielded good ash in 45 min of muffling.

The ashes obtained were completely soluble in 20 cm^3 of hydrochloric acid and a clear solution was obtained after 2 min of digestion. Therefore, there was no need to filter the solution as recommended by the direct ignition method for the determination of additive metals in unused lubricating oils [21]. The results presented in Table 1 for the determination of the test metals in sample number 1 were typical of those obtained for all samples in this work and show that there was increased metal retention in the ignited sample particularly for Zn, Fe and Cr. For these metals, the ignition allows metal complexes that would have escaped in the smoke to burn and return their metal constituents to the coke as metal oxides. The differences in the determinant levels of ignited and unignited samples give an indication of which determinants are more prone to volatilization losses in lubricating oils. Though there was no change in the levels of some of the test metals, the enhancement in the levels of even a few of the test metals advised the adoption of ignition of lubricating oils for determining trace metals. A similar advantage of sample ignition while coking has been reported for petroleum crudes [14] and petroleum distillates [22].

3.2. Sulphanilic acid as ashing reagent

Various levels of sulphanilic acid were added to 10 g replicates of oil analysed by the recommended procedure and yielded results as detailed in Table 2. The addition of sulphanilic acid to the samples did not alter the ashing efficiency of the samples: it did not alter either the ignition time or the muffling time and the ash produced in the presence of it was still completely soluble in 20.0 cm^3 of 6M HCl. The muffling of 1.0 g of sulphanilic acid alone at 550°C under similar conditions to those applied for ashing oil samples left no residue at the end of 45 min. This implies that SA did not contribute to the ash. The digest of 2.0 g of sulphanilic acid in 6 M HCl yielded blank levels of all the metals determined. The sulphanilic

Table 2
Sulphanilic acid (SA) as ashing reagent

Mass of SA added (g)	Metal concentration (mg l^{-1})					
	Ca	Mg	Zn	Fe	Cr	Ni
0	1470	88	1390	426	35.2	9.6
0.1	1472	88	1390	428	35.7	9.6
0.2	1475	87	1393	428	36.1	9.6
0.3	1485	88	1395	434	36.3	9.7
0.4	1498	88	1397	455	36.7	9.7
0.5	1500	88	1400	456	37.3	9.7
0.6	1500	89	1400	457	37.3	9.7
0.8	1501	89	1400	458	37.0	9.7
1.0	1502	89	1400	468	37.0	9.7
1.5	1500	89	1400	468	37.3	9.7
2.0	1501	89	1400	468	37.3	9.7

acid was therefore shown to be free from the determinants.

The results presented in Table 2 for 10.0 g of oil sample 1 show that there was an improvement in metal release especially for Ca, Zn, Fe and Cr as the sulphanilic acid to oil ratio increased until peak values were obtained at 0.05 g of SA for Zn and Cr and 0.1 g for Ca and Fe per gram of oil. Once obtained, the peak determinant levels persisted when higher ratios of sulphanilic acid were applied, up to 0.2 g of SA per gram of oil. The same trend was observed also for samples other than sample number 1. That peak metal release is achieved at different ratios of releasing agent for different determinants reflects the differences in stabilities of the metal complexes in which the determinant species are encaged in the oil samples [23]. These results suggest that the zinc and chromium metallocomplexes are less thermodynamically stable than the calcium and iron ones. Similar differences in the stabilities of porphyrins and metallocomplexes of metals occurring in crude oil have been reported [14]. The addition of 0.1 g of sulphanilic acid per gram of oil to samples was adopted in this work and is recommended for the ashing of used lubricating oils for the determination of trace metals by FAAS. Its stability and long shelf life make it preferable to other similar reagents like benzene-sulphonic and *p*-xylenesulphonic acids, which are hygroscopic and require special handling [14].

3.3. Evaluation of the procedure

When the same oil was ashed in six replicates and the ash analysed for the test metals in the replicates, the results showed that the recommended procedure is highly reproducible with relative standard deviations (% rsd) of 1.5, 0.3, 3.1, 0.7, 0.02 and 0.002 for Ca, Mg, Zn, Fe, Cr and Ni, respectively at the respective concentration levels 1500, 100, 1500, 500, 50 and 10 mg l^{-1}.

All five samples were analysed in triplicates by this procedure, the direct ignition procedure [22] and the Universal Oil Product (UOP) method 800-79 [24] and the average results are compared in Table 3. From observation, the results indicate that the values obtained by the direct ignition procedure are generally lower than those obtained by either the recommended or UOP method 800-79 procedures; the values obtained by the recommended procedure are generally closer to those obtained by the UOP procedure. A regression analysis of the results reveals a closer fit between the recommended procedure and the standard UOP procedure than between the direct ignition and the UOP procedures. The respective regression lines are

$$y = 1.004x^{r} - 1.884 \qquad r = 0.9993$$

and

$$y = 1.017x^{i} + 5.356 \qquad r = 0.9982$$

Table 3
Comparison of sample results obtained by three ashing procedures

Sample No.	Determinant	Measured levels (mg l^{-1})		
		Recommended procedure	Direct ignition procedure	UOP method 800-79
1	Ca	1508.4	1503.4	1513.4
	Mg	90.0	87.7	90.7
	Zn	1411.8	1372.6	1401.9
	Fe	472.2	346.8	460.3
	Cr	36.0	36.0	35.0
	Ni	9.7	9.3	10.3
2	Ca	1739.9	1706.1	1756.8
	Mg	93.6	92.6	94.9
	Zn	1475.5	1446.1	1446.1
	Fe	440.5	428.6	452.4
	Cr	28.0	26.0	28.0
	Ni	9.3	9.3	9.3
3	Ca	1638.5	1621.6	1706.1
	Mg	85.0	82.0	88.7
	Zn	1441.2	1446.1	1446.1
	Fe	412.7	412.7	420.6
	Cr	22.0	22.0	21.0
	Ni	9.3	9.3	9.3
4	Ca	878.4	810.8	844.6
	Mg	32.1	30.5	31.1
	Zn	1034.3	1029.4	1012.8
	Fe	281.8	264.8	281.8
	Cr	64.0	63.0	64.0
	Ni	11.3	10.3	11.3
5	Ca	641.9	608.1	641.9
	Mg	28.5	29.8	29.5
	Zn	872.6	853.0	857.9
	Fe	388.9	388.9	388.9
	Cr	67.0	66.0	69.0
	Ni	11.7	11.3	11.7

where y represents UOP values, x^r represents values from the recommended procedure, x^i represents values from the direct ignition procedure and r is the correlation coefficient.

The application of Student's t-test to the data of Table 3 reveals that the results obtained by the direct ignition procedure are significantly different from those obtained by the UOP method 800-79 while there is no significant difference between the results obtained by the recommended and the UOP procedures.

These statistics support the argument that while the UOP method 800-79 and the recommended procedures realise maximum release of metals, the direct ignition procedure fails to achieve maximum metal release, hence the generally low values obtained by the latter procedure and the significant difference between it and the former two procedures. The advantage of sulphanilic acid causing enhanced metal release as indicated in Table 2 is reflected in the results of these statistical analyses. The recommended procedure has an additional advantage in being faster than the UOP method 800-79.

4. Conclusion

Used lubricating oil may be conveniently coked and ashed at 550°C in 45 min for determining

wear and other metals by flame atomic absorption spectrometry. Sulphanilic acid applied as ashing agent improves the release of metals and the accuracy of the analytical results. The procedure reported is simple, rapid and precise.

References

[1] O.I. Milner, Analysis of Petroleum for Trace Elements, International Series of Monographs on Analytical Chemistry, vol. 14, Pergamon Press, Oxford, 1963.
[2] C.R. Hodgkins, J. Hansen, Anal. Chem. 26 (1954) 1759.
[3] J. Hernandez-Mendez, L. Polo-Diez, A. Bernal-Melchor, Anal. Chim. Acta 108 (1979) 39.
[4] C.S. Saba, W.E. Rhine, K.J. Eisentraut, Anal. Chem. 53 (1981) 1099.
[5] C.M. De la Gaurdia, C.A. Salvalor, N.V. Berenguer, Analusis 8 (1980) 448.
[6] J.L. Fabec, M.L. Ruschak, Anal. Chem. 57 (1985) 1853.
[7] C.S. Saba, K.J. Eisentraut, Anal. Chem. 49 (1977) 454.
[8] J.H. Karchmer, E.L. Gunn, Anal. Chem. 24 (1952) 1733.
[9] O.I. Milner, J.R. Glass Jr., J.P. Kirchner, A.N. Yurich, Anal. Chem. 24 (1952) 1728.
[10] L.W. Gamble, W.H. Jones, Anal. Chem. 27 (1955) 1456.
[11] J.E. Shott Jr., T.J. Garland, R.O. Clark, Anal. Chem. 33 (1961) 506.
[12] W.A. Row, K.P. Yates, Anal. Chem. 36 (1963) 368.
[13] Institute of Petroleum, Method IP 286/77(a), Standards for Petroleum and its Products, Part 1, Methods for Analysis and Testing, vol. 2, 1985, pp. 286.
[14] A.P. Udoh, S.A. Thomas, E.J. Ekanem, Talanta 39 (1992) 1591.
[15] A.P. Udoh, Ph.D. Thesis, Ahmadu Bello University, Zaria, 1989.
[16] P.J. Whitehead, Pye Unicam Atomic Absorption Data Book, Pye Unicam, Cambridge, 1975.
[17] A.I. Vogel, A Textbook of Quantitative Inorganic Analysis, 3rd ed., ELBS-Longmans, London, 1961.
[18] ASTM method D-811-82, Annual Book of ASTM Standards, vol. 5.01, 1984, pp. 341.
[19] A.P. Udoh, S.A. Thomas, E.J. Ekanem, Bull. Chem. Soc. Ethiop. 4 (1990) 13.
[20] R.C. Weast (Ed.), Handbook of Chemistry and Physics, 55th Edition, CRC Press, Ohio, 1974, pp. B. 63.
[21] Institute of Petroleum, Methods IP 110/82 (a), IP 111/82 (b) and IP 117/82 (c), Standards for Petroleum and its Products, Part 1, Methods for Analysis and Testing, 45th ed., vol. 1, 1985, pp. 110.1 (a), 111.I (b) and 117.I (c).
[22] A.P. Udoh, S.A. Thomas, E.J. Ekanem, AJST (B) 5 (2) (1991) 8.
[23] R.H. Filby, in: T.F. Yen (Ed.), The Role of Trace Metals in Petroleum, Ann Arbor Science Publishers, Ann Arbor, Michigan, 1975, pp. 31.
[24] Universal Oil Products, UOP method 800-79, Laboratory Test Methods for Petroleum and its Products, vol. 2, UOP Process Division, 1979, pp. 1–12.

ELSEVIER

Talanta 44 (1997) 2109–2119

Talanta

Coordination properties of cefadroxil antibiotic: synthesis and equilibrium studies of the binary and ternary complexes involving amino acids and DNA units

Mohamed M. Shoukry *, Wafaa M. Hosny, A. Abd Razik, Ramadan A. Mohamed

Department of Chemistry, Faculty of Science, Cairo University, Giza, Egypt

Received 4 November 1996; received in revised form 10 March 1997; accepted 11 March 1997

Abstract

The formation equilibria for the binary complexes of Cu^{II}, Ni^{II}, Co^{II}, Zn^{II}, Mn^{II}, Hg^{II}, Cd^{II}, Ca^{II}, and Mg^{II} with cefadroxil (Cef) and for the ternary complexes Cu(Cef)(L), where L refers to amino acid or DNA, were investigated. The protonation constants of cefadroxil and formation constants of the formed complexes were determined at 25°C and $\mu = 0.1$ M $NaNO_3$. Copper(II) and cobalt(II) complexes of cefadroxil were isolated in solid state and characterized by elemental analysis, infrared and electronic spectral, conductivity and magnetic measurement. © 1997 Elsevier Science B.V.

Keywords: Amino acid complexes; Binary and ternary complexes; Cefadroxil complexes; DNA complexes; Stability constants

1. Introduction

Much interest has been shown in the chemistry of β-lactam antibiotics in relation to their useful biological activities in recent years [1–4]. β-Lactam antibiotics, such as penicillins, cephalosporins and oxacephalosporins, represent the most important class of drugs against infectious diseases caused by bacteria. Following the recent evidence of the important roles of calcium and magnesium in the transport of these drugs in blood plasma [5], it is suggested that copper can act as a cofactor of their antibiotic activity: first, the structural flexibility of copper binary complexes is expected to favour mixed-ligand coordination with bacterial nucleic acids; then, through the formation of such ternary complexes, copper may induce the attack of free radicals known to damage these nucleic acids [6].

In continuation of our previous studies of the metal complexes of antibiotics [7–10], the present investigation reports equilibrium studies of the binary and ternary complexes of some metal ions with cefadroxil and amino acids or DNA units (see Scheme 1). Copper(II) and cobalt(II) complexes with cefadroxil were synthesized and characterized.

* Corresponding author.

PII S0039-9140(97)00089-1

2. Experimental

2.1. Materials and reagents

The metal salts, in the form of nitrates, were provided by BDH. Concentrations of stock solutions of metal ions were determined by conventional analytical methods [11]. Cefadroxil monohydrate (Bristol Standard 99%) was supplied by Bristol–Myers–Squib, Egypt. According to its elemental analysis, it was sufficiently pure and, therefore, used without further purification. Due to the instability of antibiotics in aqueous media [12], fresh solutions were prepared immediately before use by dissolving it in aqueous equimolar nitric acid solution. The amino acids and DNA units used were: glycine, alanine, proline, valine, β-phenylalanine, *S*-methylcysteine, iso-leucine, threonine, methionine, serine, 2-amino-*n*-butyric acid, histidine·HCl, histamine·2HCl, aspartic acid, ornithine·HCl, imidazole, inosine, uracil, uridine, cytosine, cytidine, thymine, thymidine and adenine. These materials were from Sigma Chemical. Imidazole, cytosine, cytidine and adenine were prepared in the protonated form by dissolution in nitric acid. All solutions were prepared in deionized water.

2.2. Apparatus

Potentiometric titrations were performed by means of a Metrohm 686 titroprocessor equipped with a 665 dosimat (Switzerland-Heriaue). The titroprocessor was calibrated using standard buffer solutions prepared according to NBS specifications [13]. All pH–metric titrations were carried out at 25.0 ± 0.1°C in a purified nitrogen atmosphere using a titration vessel described previously [14]. Conductance of solutions were measured on a WTW LBR conductivity bridge (Germany). Infrared absorption spectra were taken by a Perkin–Elmer 1430 spectrophotometer using a KBr disc. Electronic spectra were scanned on Shimadzu UV-160 A recording spectrophotometer. Magnetic susceptibility of the solid complexes were determined by using Gouy's powder technique.

2.3. Procedure and techniques

The protonation constants of the ligands, in the protonated form, were determined by titrating 40 ml of aqueous ligand solution (2.5×10^{-3} M) and $NaNO_3$ (0.1 M). The conditions of measurements for the determination of the stability constant of the binary complexes were the same as for the protonation constants, but a part of $NaNO_3$ was replaced by M^{II} ion with the concentration ratio 1:1 and 1:2 (M:Cef) for Cef (where $M = Cu^{II}$, Ni^{II}, Co^{II}, Zn^{II}, Mn^{II}, Hg^{II}, Cd^{II}, Ca^{II} and Mg^{II}, and 1:2 for Cu^{II}–amino acids complexes. The conditions of measurements for the titration of the ternary complexes were the same as for the

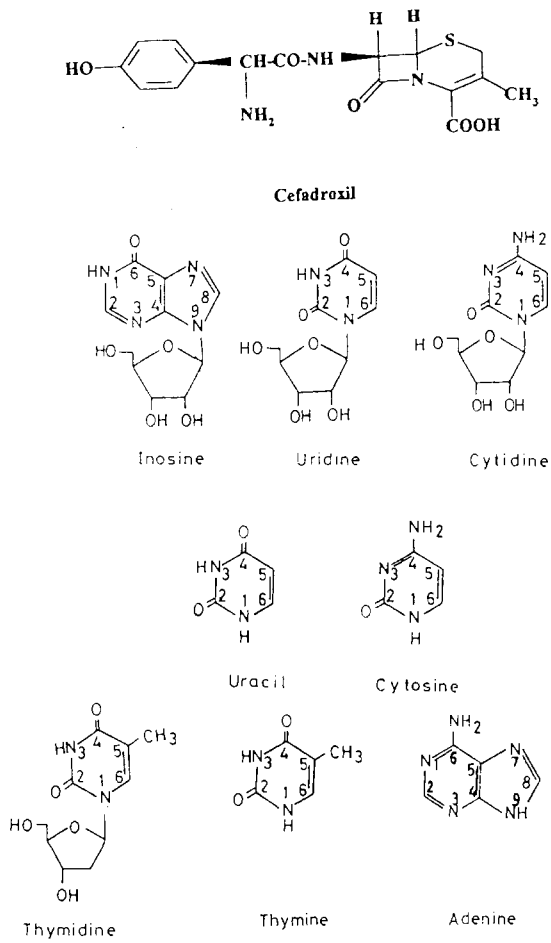

Scheme 1. Structural formulae of the investigated ligands.

binary ones, but the solutions contained equivalent amounts of Cef, Cu^{2+} and the other ligand (L).

The calculations were performed using the computer program MINIQUAD-75 [15] loaded on an IBM 486 computer. The stoichiometries and stability constants of the complexes formed were determined by trying various possible composition models for the system studied. The calculations were restricted to data obtained in a pH range where no precipitation occurred. The model selected was that which gave the best statistical fit to and which was chemically consistent with the titration data, without giving any systematic bias in residuals, as described elsewhere [15]. Tables 1–3 list the formation constants together with their standard deviations and the sum of the square of residual as obtained from the program MINIQUAD-75. The concentration distribution diagrams were obtained with the program SPECIES [16] under the experimental conditions used.

2.4. Metal chelates of cefadroxil (Cef)

The metal chelates of cefadroxil (Cef) with copper(II) and cobalt(II) were prepared in the ratio 1:1 (metal:ligand). The metal carbonate (1 mmol) is mixed with the antibiotic (1 mmol) in the least amount of water. The resulting mixture was refluxed for 1–2 h. The solid complexes were precipitated, filtered, washed with water, ethanol and finally with ether.

3. Results and discussion

3.1. Proton–cefadroxil equilibrium

A maximum number of three protons can be released from the cefadroxil in the fully protonated form ($Cef = H_3L^+$) on titration with a strong base. The titration data indicates the presence solely of simple HL^-, H_2L, H_3L^+ complexes. The differential log protonation constants were found to be 1.70, 7.07 and 9.14. In considering the nature of the donor groups involved in the successive protonation reactions, it is helpful to invoke the protonation constants of amoxycillin (2.41, 7.19 and 9.38) [9] analogue, where the protonation centres are the carboxylic, amino, phenolic groups. In acid medium, cefadroxil is protonated to give a cationic species H_3L^+. Addition of base produces, in the first stage, the deprotonation of the carboxylic group ($pK_{a1} = 1.70$) yielding the zwitter ion species $H_2L^{\pm}$, existing in the pH range 4–6. When the pH is increased, the deprotonation of the amino group $-NH_3^+$ ($pK_{a2} = 7.07$), followed by that of the phenolate group ($pK_{a3} = 9.14$).

3.2. Metal ion–cefardoxil complexes

Potentiometric titration curves of cefadroxil and its copper(II) complexes, taken as being representative, are shown in Fig. 1. In the metal complex curve, there is a significant lowering from that of the free cefadroxil, indicating formation of metal complexes by release of protons. Different equilibrium models have been tried to fit the experimental potentiometric data for the M^{II}–(cefadroxil). The model that best fits the potentiometric data is found to consist of $[MHL]^+$ and [ML] species. The validity of the same is proven where an excellent fit can be observed between the experimental data points from the titration of metal ion–cefadroxil complex, and the theoretical curve calculated from the values of the protonation constants of cefadroxil and the formation constants of the corresponding complexes.

The acid dissociation constant of the protonated complex, [MHL] is given by Eq. (1) [17]:

$$pK^{(H)}_{M(L)(H)} = \log K^{M}_{M(L)(H)} - \log K^{M}_{M(L)} \quad (1)$$

The value of pK_H of the protonated complexes is in the range 4.78–8.73. This value may compare with the protonation constant of the phenolic group. Coordination to the amino group lowers the pK_a of the phenolic group. A lowering of up to 2 units was reported for the coordination of DNA units to a series of divalent earth alkali and transition metal ions [18].

The protonation constants of amino acids and DNA units and the formation constant of the copper(II) complexes with amino acids were determined under conditions identical to those for ternary systems, i.e., at 25°C and ionic strength of

Table 1
Formation constants of binary complexes

System	l	p	q[a]	log β[b]	S[c]
Cef	0	1	1	9.14 (0.09)	
	0	1	2	16.21 (0.02)	7.9×10^{-8}
	0	1	3	17.91 (0.07)	
Cu(II)–Cef	1	1	0	8.11 (0.01)	2.4×10^{-7}
	1	1	1	12.89 (0.11)	
Ni(II)–Cef	1	1	0	3.72 (0.03)	2.2×10^{-7}
	1	1	1	11.62 (0.05)	
Co(II)–Cef	1	1	0	3.12 (0.03)	1.3×10^{-7}
	1	1	1	10.87 (0.14)	
Cd(II)–Cef	1	1	0	3.85 (0.04)	4.6×10^{-7}
	1	1	1	11.58 (0.09)	
Ca(II)–Cef	1	1	0	2.61 (0.05)	9.9×10^{-8}
	1	1	1	11.18 (0.09)	
Ba(II)–Cef	1	1	0	3.10 (0.05)	2.2×10^{-7}
	1	1	1	11.75 (0.07)	
Mn(II)–Cef	1	1	0	3.78 (0.07)	1.5×10^{-6}
	1	1	1	11.73 (0.12)	
Mg(II)–Cef	1	1	0	1.93 (0.09)	8.7×10^{-8}
	1	1	1	10.66 (0.17)	
Hg(II)–Cef	1	1	0	6.96 (0.04)	1.0×10^{-6}
	1	1	1	13.14 (0.07)	
Cu(II)–glycine	0	1	1	9.61 (0.01)	1.5×10^{-7}
	0	1	2	11.23 (0.02)	
	1	1	0	8.16 (0.01)	2.2×10^{-8}
	1	2	0	15.07 (0.02)	
Cu(II)–alanine	0	1	1	9.69 (0.01)	9.3×10^{-8}
	0	1	2	11.89 (0.02)	
	1	1	0	8.00 (0.03)	6.0×10^{-8}
	1	2	0	14.86 (0.04)	
Cu(II)–proline	0	1	1	10.52 (0.01)	4.4×10^{-8}
	0	1	2	12.03 (0.04)	
	1	1	0	8.74 (0.03)	5.7×10^{-8}
	1	2	0	16.08 (0.05)	
Cu(II)–valine	0	1	1	9.57 (0.01)	10.0×10^{-8}
	0	1	2	11.71 (0.02)	
	1	1	0	8.02 (0.02)	2.7×10^{-8}
	1	2	0	14.98 (0.02)	
Cu(II)–β-phenyl alanine	0	1	1	9.12 (0.01)	8.0×10^{-8}
	0	1	2	11.01 (0.03)	
	1	1	0	7.72 (0.02)	4.2×10^{-8}
	1	2	0	14.81 (0.03)	
Cu(II)–*S*-methyl cysteine	0	1	1	9.01 (0.02)	3.4×10^{-7}
	0	1	2	11.39 (0.04)	
	1	1	0	7.71 (0.03)	1.5×10^{-7}
	1	2	0	13.57 (0.09)	
Cu(II)–iso-leucine	0	1	1	9.76 (0.01)	3.5×10^{-8}
	0	1	2	12.22 (0.01)	
	1	1	0	8.46 (0.04)	1.7×10^{-7}
	1	2	0	15.54 (0.07)	
Cu(II)–2-amino-*n*-butyric acid	0	1	1	9.60 (0.03)	8.1×10^{-8}
	0	1	2	12.45 (0.07)	
	1	1	0	8.22 (0.05)	5.2×10^{-8}
	1	2	0	12.85 (0.07)	

Table 1 (continued)

System	l	p	q[a]	$\log \beta$[b]	S[c]
Cu(II)–threonine	0	1	1	9.06 (0.01)	8.0×10^{-8}
	0	1	2	11.03 (0.02)	
	1	1	0	8.04 (0.01)	5.1×10^{-8}
	1	2	0	14.81 (0.03)	
Cu(II)–methionine	0	1	1	9.10 (0.01)	9.0×10^{-8}
	0	1	2	11.09 (0.03)	
	1	1	0	7.86 (0.01)	3.6×10^{-9}
	1	2	0	14.60 (0.01)	
Cu(II)–hydroxy proline	0	1	1	8.97 (0.01)	1.5×10^{-7}
	0	1	2	11.18 (0.03)	
	1	1	0	8.35 (0.01)	3.0×10^{-7}
	1	2	0	15.88 (0.01)	
Cu(II)–imidazole	0	1	1	7.04 (0.01)	2.6×10^{-9}
	1	1	0	4.15 (0.05)	6.9×10^{-8}
	1	2	0	7.62 (0.04)	
	1	3	0	10.35 (0.05)	
Cu(II)–serine	0	1	1	9.14 (0.01)	1.7×10^{-8}
	0	1	2	11.40 (0.01)	
	1	1	0	8.03 (0.02)	6.0×10^{-8}
	1	2	0	14.65 (0.04)	
Cu(II)–histidine	0	1	1	9.53 (0.01)	1.8×10^{-7}
	0	1	2	15.81 (0.02)	
	0	1	3	17.81 (0.06)	
	1	1	0	10.66 (0.03)	2.3×10^{-8}
	1	2	0	18.96 (0.03)	
	1	1	1	14.86 (0.02)	
Cu(II)–histamine	0	1	1	9.88 (0.01)	2.4×10^{-8}
	0	1	2	15.97 (0.01)	
	1	1	0	9.55 (0.01)	1.9×10^{-10}
	1	2	0	16.10 (0.02)	
	1	1	1	12.70 (0.09)	
Cu(II)–ornithine	0	1	1	10.58 (0.00)	1.0×10^{-8}
	0	1	2	19.44 (0.01)	
	0	1	3	21.39 (0.02)	
	1	1	0	12.25 (0.06)	8.9×10^{-8}
	1	2	0	15.62 (0.08)	
	1	1	1	18.04 (0.04)	
Cu(II)–aspartic acid	0	1	1	9.68 (0.01)	3.9×10^{-8}
	0	1	2	13.35 (0.01)	
	1	1	0	8.84 (0.01)	3.9×10^{-8}
	1	2	0	15.90 (0.03)	
	1	1	1	12.13 (0.07)	
Cu(II)–inosine	0	1	1	8.55 (0.01)	1.2×10^{-8}
	1	1	0	4.00[d]	
Cu(II)–thymidine	0	1	1	9.47 (0.01)	4.2×10^{-8}
	1	1	0	4.7[e]	
Cu(II)–uracil	0	1	1	8.80 (0.01)	1.1×10^{-7}
	1	1	0	4.55[f]	
Cu(II)–uridine	0	1	1	8.76 (0.01)	8.9×10^{-8}
	1	1	0	4.03[g]	
Cu(II)–adenine	0	1	1	9.40 (0.01)	5.1×10^{-7}
	0	1	2	13.69 (0.02)	
	1	1	0	6.77[h]	

Table 1 (continued)

System	l	p	q[a]	$\log \beta$[b]	S[c]
Cu(II)–cytosine	0	1	1	4.38 (0.03)	5.0×10^{-7}
Cu(II)–cytidine	0	1	1	3.67 (0.03)	5.0×10^{-7}
Cu(II)–thymine	0	1	1	9.67 (0.06)	2.5×10^{-7}

[a] The values l, p and q are the stoichiometric coefficients corresponding to metal(II), amino acids and H^+, respectively.
[b] Standard deviations are given in parentheses.
[c] Sum of square of residuals.
[d,e,f,g,h] Taken from Refs. [30–34].

0.1 M (KNO_3). The results (Table 1) are in good agreement with the literature data [19], after allowing for changes in experimental conditions and calculation methods.

3.3. Ternary complex formation equilibria

The general four-component equilibrium can be written as follows (charges are omitted for simplicity):

$$l\mathrm{Cu} + p(\mathrm{Cef}) + q(\mathrm{A}) + r\mathrm{H} \rightleftarrows \mathrm{Cu}_l(\mathrm{Cef})_p(\mathrm{A})_q(\mathrm{H})_r \quad (2)$$

where l, p, q and r are the stoichiometric coefficients corresponding to the copper(II), cefadroxil, amino acid and H^+, respectively.

The overall formation constants are defined as:

$$\beta_{lpqr} = \frac{[\mathrm{Cu}_l(\mathrm{Cef})_p(\mathrm{A})_q(\mathrm{H})_r]}{[\mathrm{Cu}]^l[\mathrm{Cef}]^p[\mathrm{A}]^q[\mathrm{H}]^r} \quad (3)$$

The ternary complex formation may proceed through step-wise or simultaneous mechanism, depending on the chelating potentiality of cefadroxil and amino acid or DNA unit. The formation constants of the 1:1 copper(II) complexes with cefadroxil and amino acids are of the same order (Table 1). Consequently the ligation of the antibiotic and amino acid will occurs simultaneously. The titration data of the mixed-ligand complexes with amino acids and cefadroxil fit satisfactorily on the basis of the complexes Cu(Cef)(A) and Cu(Cef)-(A)(H). The formation constants obtained for the mixed ligand complexes are given in Table 2.

The relative stability of the ternary complexes formed through a simultaneous mechanism, as compared to those of the corresponding binary complexes, is expressed in terms of $\Delta \log K$ as defined by Eqs. (4) and (5).

$$\mathrm{Cu(Cef)} + \mathrm{Cu(A)} \rightleftarrows \mathrm{Cu(Cef)(A)} + \mathrm{Cu} \quad (4)$$

$$\Delta \log K = \log K^{\mathrm{Cu}}_{\mathrm{Cu(Cef)(A)}} - [\log K^{\mathrm{Cu}}_{\mathrm{Cu(Cef)}} + \log K^{\mathrm{Cu}}_{\mathrm{Cu(A)}}] \quad (5)$$

Since more coordination sites are available for bonding of the first ligand to a metal ion than for the second ligand, $\Delta \log K$ should in general be negative. With Cu^{II} usually having a coordination number of four, the expected value for $\Delta \log K$ would be -0.6 [20,21]. The reported $\Delta \log K$ values for most Cu–cefadroxil–amino acids complexes are of the same order.

The potentiometric titration curve of the ternary system Cu^{II}–cefadroxil–inosine (as a representative of DNA) coincides with the 1:1 Cu^{II}–Cef curve in the region $0 < a < 2$ (a = number of moles of base added per mole of ligand), Fig. 2. In this region, the Cu^{II}–Cef–complex is formed firstly due to its high stability compared to that of the Cu^{II}–DNA complex (Table 1). Beyond $a = 2$, the formation of a ternary complex was ascertained by comparison of the mixed-ligand titration curve with the composite curve obtained by graphical addition of inosine titration data to that of the Cu^{II}–Cef titration curve. The mixed-ligand system was found to deviate considerably from the resultant composite curve, indicating the formation of a ternary complex. Thus, formation of ternary complex can be described by the following equilibria (charges are omitted for simplicity) [6,7]:

$$\mathrm{Cu} + \mathrm{Cef} \rightleftharpoons \mathrm{Cu(Cef)} \quad (6)$$

$$\mathrm{Cu(Cef)} + \mathrm{Ino} \rightleftharpoons \mathit{Cu(Cef)(Ino)} \quad (7)$$

The relative stability of the ternary complexes formed through a step-wise mechanism, as com-

Table 2
Formation constants of Cu–Cef–amino acid complexes

System	l	p	q	r[a]	log β[b]	S[c]	Δlog K
Cu–Cef–glycine	1	1	1	0	15.38 (0.04)	1.43×10^{-6}	−0.89
Cu–Cef–alanine	1	1	1	0	15.01 (0.055)	2.25×10^{-6}	−1.10
Cu–Cef–proline	1	1	1	0	15.84 (0.03)	1.2×10^{-7}	−1.01
Cu–Cef–valine	1	1	1	0	16.12 (0.08)	1.77×10^{-6}	−0.01
Cu–Cef–β-phenylalanine	1	1	1	0	14.83 (0.07)	3.19×10^{-6}	−1.00
Cu–Cef–*S*-methylcysteine	1	1	1	0	14.89 (0.07)	5.8×10^{-6}	−0.93
Cu–Cef–isoleucine	1	1	1	0	14.85 (0.13)	7.09×10^{-6}	−1.72
Cu–Cef–2-amino-*n*-butyric acid	1	1	1	0	15.07 (0.02)	4.24×10^{-7}	−1.26
Cu–Cef–threonine	1	1	1	0	16.34 (0.11)	8.4×10^{-6}	+0.19
Cu–Cef–methionine	1	1	1	0	14.75 (0.075)	3.99×10^{-6}	−1.22
Cu–Cef–hydroxyproline	1	1	1	0	15.08 (0.12)	7.59×10^{-6}	−1.38
Cu–Cef–imidazole	1	1	1	0	11.96 (0.09)	7.5×10^{-6}	−0.30
Cu–Cef–serine	1	1	1	0	15.77 (0.05)	7.18×10^{-7}	−0.37
Cu–Cef–histidine	1	1	1	0	16.34 (0.06)	1.97×10^{-6}	−2.43
Cu–Cef–histamine	1	1	1	0	15.38 (0.09)	1.95×10^{-6}	−2.28
Cu–Cef–ornithine	1	1	1	0	16.28 (0.07)	1.04×10^{-6}	−4.08
	1	1	1	1	24.93 (0.06)		
Cu–Cef–aspartic acid	1	1	1	0	15.58 (0.06)	3.3×10^{-6}	−1.37

[a] The values l, p, q and r are the stoichiometric coefficients corresponding to Cu(II), amino acids, cefadroxil and H^+, respectively.
[b] Standard deviations are given in parentheses.
[c] Sum of square of residuals.

pared to those of the corresponding binary complexes, is expressed in terms of Δlog K as defined by Eq. (8).

$$\Delta\log K = \log K^{Cu(Cef)}_{Cu(Cef)(D)} - \log K^{Cu}_{Cu(D)} \quad (8)$$

The Δlog K values given in Table 3 are invariably negative. This means that the DNA units form more stable complex with the free copper(II) ion than with the Cu(Cef) complex.

Inosine has two donor sites, N_1 and N_7. In the acidic pH range, N_1 remains protonated, while the metal ion is attached to N_7. The gradual change from N_7-binding to N_1-binding with increasing pH has been rather extensively documented by nuclear magnetic resonance (NMR) [22] and electron paramagnetic resonance (EPR) [23] spectroscopic measurements. The proposed structure for the mixed ligand complex studied in the pH range 7–9 involves N_1-binding.

The protonation constant of uridine, uracil, thymine and thymidine is that of the [N(3)–C(4)O] group. The values obtained from this study have been compared with those of the protonation of the analogous [N(1)–C(6)O] grouping in inosine. The purinic derivatives are slightly more acidic than the pyrimidinic ones, a property which can be related to the existence in the anion of the purinic derivatives of a higher number of resonance forms in equilibrium because of the presence of two condensed rings in this ligand. Based on the existing data, uracil, uridine, thymine and thymidine ligate in the deprotonated form, through N_3. The thymine and thymidine complexes are more stable than those of uracil and uridine, most probably due to the higher basicity of the N_3 site of thymine and thymidine resulting from the inductive effect of the extra electron-donating methyl group.

Acid–base equilibria of adenine in the protonated form (H_2D^+) involve deprotonation from N(1) and N(9) sites. The accepted model for the mixed-ligand titration of adenine consists of Cu(Cef)(D) species. The question of the point or points of attachment of adenine to a metal centre has been discussed by a number of workers, notably by Hodgson [24] and Marzilli [25]. They discussed both solution and solid complex studies which have indicated that N(9) is the ligating site.

Table 3
Formation constants of Cu–Cef–DNA units complexes

System	l	p	q[a]	$\log \beta$[b]	S[c]	$\Delta \log K$
Inosine	1	1	0	4.49 (0.06)	1.9×10^{-6}	+0.49
Thymidine	1	1	0	5.55 (0.07)	6.2×10^{-7}	+0.85
Uracil	1	1	0	4.86 (0.06)	8.4×10^{-7}	+0.31
Uridine	1	1	0	4.93 (0.06)	3.8×10^{-7}	+0.90
Adenine	1	1	0	6.99 (0.16)	4.4×10^{-6}	+0.22
Thymine	1	1	0	5.50 (0.05)	1.5×10^{-6}	

[a] The values l, p and q are the stoichiometric coefficients corresponding to Cu(II)–Cef complex, DNA units and H^+, respectively.
[b] Standard deviations are given in parentheses.
[c] Sum of square of residuals.

From the potentiometric titration curves for Cu(Cef)–cytosine or –cytidine, the horizontal addition procedures showed the absence of any significant interaction between the Cu–Cef complex and cytosine or cytidine. Similar behaviour was found for the system M–EDTA–cytosine or –cytidine [26].

Estimation of equilibrium concentrations of various complex species as a function of pH provides a useful picture of metal ion binding in the biological fluids. The species distribution patterns

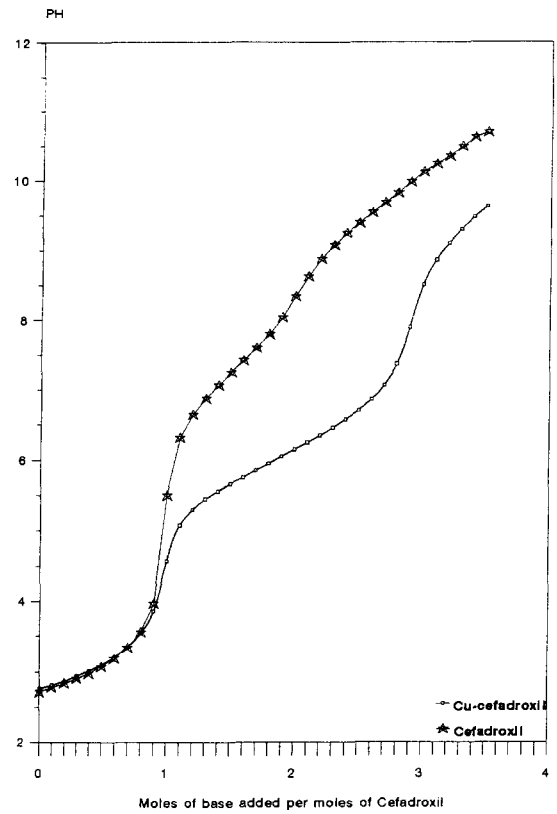

Fig. 1. Potentiometric titration curves of Cu(II)–Cefadroxil system.

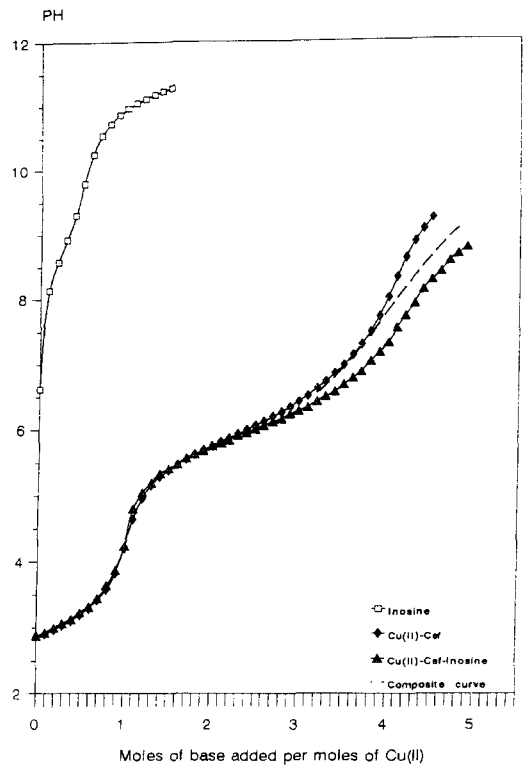

Fig. 2. Potentiometric titration curves of Cu(II)–Cef–inosine system.

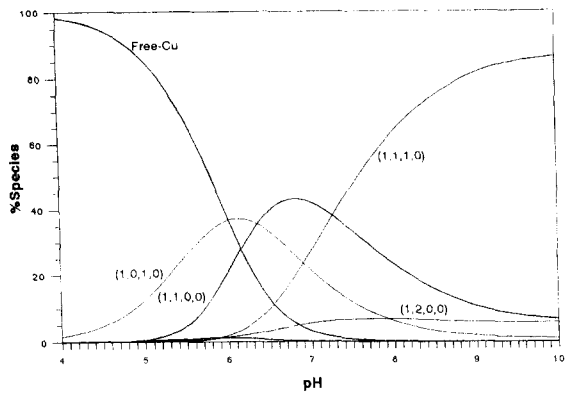

Fig. 3. Concentration distribution of various species as a function of pH in the Cu(II)–Cef–proline system.

for the Cu–Cef–proline, taken as a representative of amino acids and given in Fig. 3, indicate that the mixed-ligand complex starts to form at pH ≈ 6 and reaches a maximum concentration (60%) at pH = 9. Mixed-ligand complexes formed with DNA units are less favoured; they reach the maximum concentration of approximately 50% at pH = 11. Thus, the amino acid will compete with the DNA for the reaction with the Cu–Cef complex.

3.4. Composition and structure of solid complexes

Elemental analysis data of the investigated metal complexes obtained in the solid state (Table 4) indicate that cefadroxil acts as a dibasic ligand. The proposed general chemical formulae of the complexes may be represented by $ML \cdot xH_2O$, where L is the deprotonated form of the ligand and M is Cu^{II} and Co^{II}. The molar conductance values of 0.001 M DMF complex solutions are in the range 9–12 $cm^2\ (\Omega \cdot mol)^{-1}$, which indicates their non-electrolytic nature.

The infrared spectrum of cefadroxil exhibits bands at 2585, 1759 and 1686 cm^{-1}, assigned to $-NH_3^+$, β-lactam carbonyl and amide carbonyl groups [27]. In the spectra of the complexes, the NH_3^+-band disappeared and the two carbonyl bands were significantly shifted to lower wave numbers, a behaviour which provides a convincing evidence for coordination through the amino and the two carbonyl groups. The OH band oc-

Table 4
Analytical data and physical properties of the metal complexes of cefadroxil (Cef)

Complex	Colour	Yield (%)	Dec. point (°C)	Found (calc.) (%)					Λ (mhos·cm²·mol⁻¹)	μ_{eff} (BM)
				C	H	N	S	M		
$CuL \cdot 2H_2O$ $[C_{16}H_{19}N_3O_7SCu]$	Grey	80	> 290	41.9 (41.7)	4.3 (4.1)	9.2 (9.1)	7.0 (6.9)	13.6 (13.8)	12	1.95
$CoL \cdot 4H_2O$ $[C_{16}H_{23}N_3O_9SCo]$	Dark brown	90	> 270	39.0 (39.0)	4.6 (4.7)	8.5 (8.5)	6.6 (6.5)	12.0 (12.0)	9	4.50

curring at 3506 cm^{-1} in the spectrum of the cefadroxil disappeared upon complexation. This indicates that the hydrogen ion of the cefadroxil OH group is released to neutralize the positive charge of the metal ion, forming a neutral complex.

The electronic absorption spectrum of the copper(II) complex consists of a broad band in the region 14 400–14 900 cm^{-1}, which is assigned to $^2B_{1g} \leftarrow {}^2A_{1g}$ transitions as well as a shoulder in the range 21 600–22 200 cm^{-1}, characteristic of a square planar geometry for the copper(II) complex [28]. The complex has a magnetic moment that amounts to (1.95) BM, which justified the square planar configuration.

The electronic spectrum of the cobalt(II) complex exhibits three bands at 8058, 16 000 and 19 048 cm^{-1}, which are assigned to ν_1: $^2T_{2g} \leftarrow {}^4T_{1g}$, ν_2: $^4A_{2g} \leftarrow {}^4T_{1g}$ and ν_3: $^4T_{1g}(p) \leftarrow {}^4T_{1g}$ transitions, respectively, indicating an octahedral configuration around the Co(II) ion [29]. The octahedral geometry of the Co^{II} complex is further confirmed by the value of the magnetic moment (4.5 BM).

Further investigation to provide more convincing evidence for the structure of these complexes requires further studies including, e.g., X-ray diffraction studies and other structural investigations.

4. Conclusion

The present investigation may have important biological implications. The structural flexibility of bioactive cefadroxil as well as its capacity to coordinate copper(II) via three different donor sites may favour the formation of ternary complexes with various ligands occurring in vivo. In particular, such mixed-ligand coordination is likely to occur with bacterial nucleic acids.

References

[1] W. Drurckheimer, J. Blumbach, R. Lattrell, K.H. Sheunemann, Angew. Chem., International Edition in English 24 (1985) 180.
[2] M.I. Pag, Acc. Chemical Research 17 (1984) 144.
[3] E.H. Flynn, Cephalosporins and Penicillins: Chemistry and Biology, Academic Press, Indianapolis, IN, 1972, p. 662.
[4] F.A. Jung, W.R. Pilgrim, J.P. Poyser, P.J. Siret, Topics in Antibiotic Chemistry 1 (1980) 4.
[5] M.J. Jung, W.R. Pilgrim, J. P Poyser, P.J. Siret, Topics in Antibiotic Chemistry 4 (1980) 1.
[6] G.J. Bojczuk, L. Lambs, H. Kozlowski, G. Berthon, Inorganic Chemistry 32 (1993) 428.
[7] M.M. Shoukry, E.M. Shoukry, S.M. El-Medani, Monatsh für Chem. 126 (1995) 909.
[8] M.M. Shoukry, Ann. Chim. (Rome) 83 (1993) 147.
[9] M.M. Shoukry, Talanta 39 (1992) 1625.
[10] M.M. Shoukry, A.K. Abdel-Hadi, Croat. Chimica Acta 62 (1989) 67.
[11] F.J. Welcher, The Analytical Uses of Ethylenediamine–tetraacetic Acid, Van Nostrand, Princeton, NJ, 1965.
[12] S.T. Day, W.G. Grauthamel, L.C. Martinelli, J.K.H. Ma, Journal of the American Chemistry Society 67 (1978) 1518.
[13] R.G. Bates, Determination of pH—Theory and Practice, 2nd edition, Wiley Interscience, New York, 1975.
[14] M.M. Shoukry, W.M. Hosny, M.M. Khalil, Transition Metal Chemistry 20 (1995) 252.
[15] P. Gans, A. Sabatini, A. Vacca, Inorg. Chimica Acta 18 (1976) 237.
[16] L. Pettit, personal communication, University of Leeds, UK, 1984.
[17] M.M. Shoukry, Bull. Soc. Chem. Fr. 130 (1993) 117.
[18] H. Sigel, S.S. Massoud, N.A. Corfu, Journal of the American Chemistry Society 116 (1994) 2958.
[19] D.D. Perrin, Stability Constants of Metal Ion Complexes: Part B, Organic Ligands, Pergamon Press, Oxford, 1979.
[20] L. Ji, N.A. Corfu, H. Sigel, Inorg. Chimica Acta 206 (1993) 215.
[21] H. Sigel, N.A. Corfu, R.B. Martin, Comments on Inorganic Chemistry 13 (1992) 35.
[22] K. Maskos, Acta Biochimica Polonica 28 (1981) 318.
[23] K. Maskos, Journal of Inorganic Biochemistry 25 (1985) 1.
[24] D.J. Hodgson, Progress in Inorganic Chemistry 23 (1977) 211.
[25] L.G. Marzilli, Progress in Inorganic Chemistry 23 (1977) 255.
[26] K. Ramalingan, C.R. Krishnamoorthy, Inorg. Chimica Acta 67 (1982) 167.
[27] L.J. Bellamy, The Infrared Spectra of Complex Molecules, Wiley, New York, 1966.
[28] K.N. Timmaiah, G.T. Chandrappa, W.D. Lloyd, C. Parkanyi, Inorg. Chimica Acta 107 (1985) 1.

[29] G.A. Kolawole, A.O. Adeyemo, J. Coord. Chem. 22 (1991) 299.
[30] S.H. Kim, R.B. Martin, Inorg. Chimica Acta 91 (1984) 19.
[31] A.M. Fiskin, M. Beer, Biochemistry 4 (1965) 1289.
[32] E. Casassas, A. Izquierdo-Ridorsa, R. Tauler, Journal of Inorganic Biochemistry 39 (1990) 327.
[33] B. Taqui Khan, M.R. Raja, S.M. Zokeeruddin, Journal of Coord. Chemistry 16 (1987) 237.
[34] R. Ghose, K. Dey, Acta Chimica Acad. Sci. Hung. 108 (1981) 9.

ELSEVIER

Talanta 44 (1997) 2121–2128

Talanta

Determination of ammonium in Kjeldahl digests by gas-diffusion flow-injection analysis with a bulk acoustic wave-impedance sensor

Xiao-Li Su, Li-Hua Nie, Shou-Zhuo Yao *

College of Chemistry and Chemical Engineering, Hunan University, Changsha 410082, People's Republic of China

Received 4 November 1996; received in revised form 11 March 1997; accepted 12 March 1997

Abstract

A novel flow-injection analysis (FIA) system has been developed for the rapid and direct determination of ammonium in Kjeldahl digests. The method is based on diffusion of ammonia across a PTFE gas-permeable membrane from an alkaline (NaOH/EDTA) stream into a stream of diluted boric acid. The trapped ammonium in the acceptor is determined on line by a bulk acoustic wave (BAW)-impedance sensor and the signal is proportional to the ammonium concentration present in the digests. The proposed system exhibits a favorable frequency response to 5.0×10^{-6}–4.0×10^{-3} mol l^{-1} ammonium with a detection limit of 1.0×10^{-6} mol l^{-1}, and the precision was better than 1% (RSD) for 0.025–1.0 mM ammonium at a through-put of 45–50 samples h^{-1}. Results obtained for nitrogen determination in amino acids and for proteins determination in blood products are in good agreement with those obtained by the conventional distillation/titration method, respectively. The effects of composition of acceptor stream, cell constant of conductivity electrode, sample volume, flow rates and potential interferents on the FIA signals were discussed in detail. © 1997 Elsevier Science B.V.

Keywords: Ammonium determination; Bulk acoustic wave sensor; Gas-diffusion flow-injection analysis; Kjeldahl digestion

1. Introduction

Developed in 1883, the Kjeldahl procedure remains one of the most accurate and widely used methods for determining nitrogen. By this procedure, almost all organic nitrogen-containing substances are converted to ammonium. The ammonium is often quantified by distillation in alkaline medium followed by titration or colorimetry, or by means of micro-diffusion method [1]. All these methods, however, are time-consuming and suffer from inadequate sensitivity and reproducibility. Direct spectrophotometric determination of ammonium in the digest is possible and is implemented in some automatic analyzers. But this direct determination may suffer from changes in acid concentration, presence of metal ions and sample turbidity [2].

* Corresponding author.

PII S0039-9140(97)00091-X

Flow injection analysis based on gas-diffusion separation (GD-FIA), characterized by its high selectivity, promising sensitivity, excellent precision and rapidity, has proven useful in determining ammonium in complex matrices including Kjeldahl digests [3–7]. In this technique, the sample is injected into, or merged with an alkaline solution, and the ammonium formed diffuses across a gas-permeable membrane into a recipient stream. The trapped ammonium has been determined spectrophotometrically with an acid–base indicator, potentiometrically with an ammonium-selective electrode, or conductometrically. The conductometric method has some important advantages over the others without the sacrifice of sensitivity, selectivity and precision, the equipment as well as the reagent required is simpler and less expensive. A drawback, however, is that the high background conductivity of the recipient stream can cause an unacceptable noise level [4]. Hence, distilled water is the most often used acceptor, and sometimes it is designed to flow through a small column of mixed-bed ion exchanger for final purification before it enters the gas-diffusion cell [3], which makes the FIA system more complicated and expensive.

The bulk acoustic wave (BAW)-impedance sensor, as described previously [8], is constructed by connecting an AT-cut piezoelectric quartz crystal and a conductivity electrode in series, and has particular advantages over the classical conductometry, e.g., it can detect a slight change in solution conductivity in the presence of an excess of a foreign electrolyte, and the sensitivity and accuracy are better than those obtained in the absence of the foreign electrolyte. Moreover, it possesses the same sensitivity to the conductivity and permittivity of the solution as the normal piezoelectric sensor, in which the quartz crystal is in direct contact with the solution, and a better frequency stability, lower frequency-temperature coefficient and much lower frequency dependence on the density and viscosity of the solution because only the electrode is immersed in the liquid and the crystal is out of contact with the solution. Thus, it is not surprising that BAW-impedance sensor has been used so widely, e.g., for end-point determination in titration [9], for determination of microorganism [10], and for biochemical and physiological study of blood [11,12]. To the best of our knowledge, there has been no publication that combines FIA with piezoelectric detection except a feasibility study of the combination of FIA with the thickness-shear mode acoustic wave sensor [13]. This paper is a preliminary report describing the development of a novel FIA system based on the conjunction of BAW-impedance sensor with GD-FIA technique, and its practical application for the rapid and direct determination of ammonium in Kjeldahl digests obtained from amino acids and blood products.

2. Experimental

2.1. Apparatus

Schematic diagram of the FIA manifold is illustrated in Fig. 1(a), it is composed of a peristaltic pump (Xiangshan Dingshan Instrument Factory,

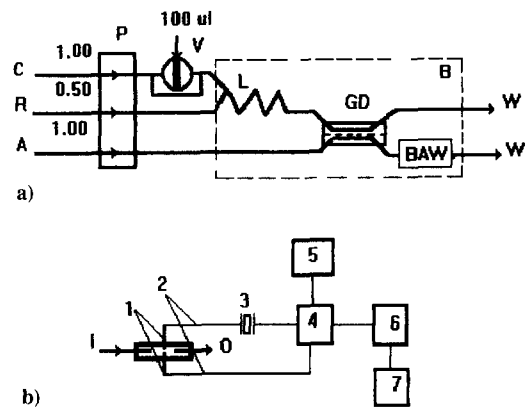

Fig. 1. (a) Schematic diagram of FIA manifold for determination of ammonium in Kjeldahl digests. P, peristaltic pump; V, injection valve; L, mixing tube (40 cm × 0.6 mm i.d.); GD, gas-diffusion cell; W, waste; B, water bath; C, carrier: H_2O; R, reagent: 2 mol l^{-1} NaOH + 1% EDTA; A, acceptor: 0.01 mol l^{-1} boric acid. Flow rates are given in ml min^{-1}. (b) Schematic diagram of BAW-impedance sensing system. I, inlet for fluid from gas-diffusion cell; O, outlet for waste solution; 1, stainless-steel needles; 2, leading wires; 3, piezoelectric quartz crystal; 4, IC-TTL oscillator; 5, d.c power supply; 6, frequency counter; 7, computer.

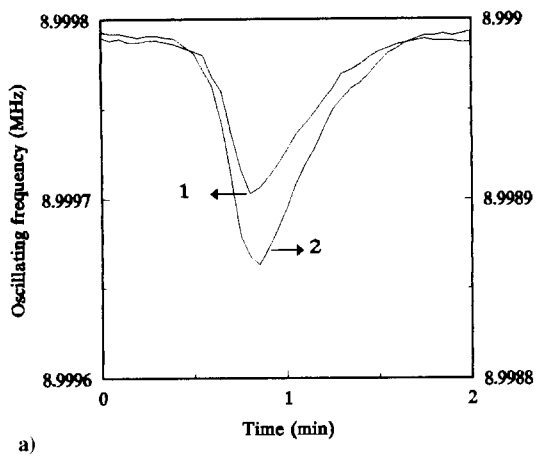

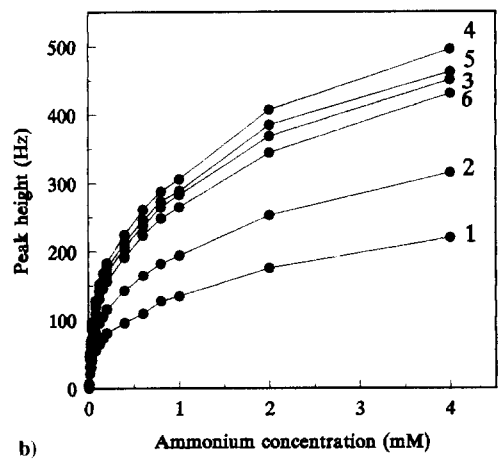

Fig. 2. (a) FIA profiles obtained with various acceptor streams. Numbers 1 and 2 refer to acceptor of H_2O and 0.02 mol l^{-1} boric acid respectively. Donor flow rate, 1.50 ml min^{-1}; acceptor flow rate, 1.50 ml min^{-1}; ammonium concentration, 10^{-4} mol l^{-1}; injection volume, 200 μl. (b) Influence of acceptor stream on the sensitivity. Numbers 1–6 refer to concentrations of boric acid of 0, 0.001, 0.005, 0.01, 0.02 and 0.05 mol l^{-1}, respectively. Other conditions as given in Fig. 2(a).

Zhejiang, China), a flow manifold of PTFE tubes (0.8 mm i.d.), a home-made PTFE rotatory valve with variable injection volume, a gas-diffusion unit with two channels of 125 mm length, 3 mm width and 0.1 mm depth which are separated by a PTFE gas-permeable membrane (pore size 0.02 μm, purchased from Jiangsu Electroanal. In-

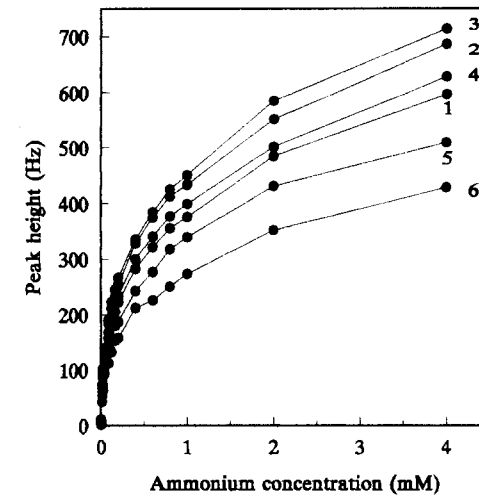

Fig. 3. Influence of cell constant of the conductivity electrode on the sensitivity. Numbers 1–6 refer to cell constant of 0.4, 0.67, 1.05, 1.67, 2.5 and 4.0 cm, respectively. Injection volume, 100 μl; donor flow rate, 1.00 ml min^{-1}; acceptor flow rate, 0.50 ml min^{-1}.

strumt. Factory, China), and a BAW-impedance sensor shown in Fig. 1(b). The sensor was constructed by connecting an AT-cut 9 MHz piezoelectric quartz crystal with a conductivity electrode in series to make up the feedback circuit of the IC-TTL oscillator. The oscillator was supplied with 5 V by a d.c. voltage regulator, a universal frequency counter (Model SC-72001,

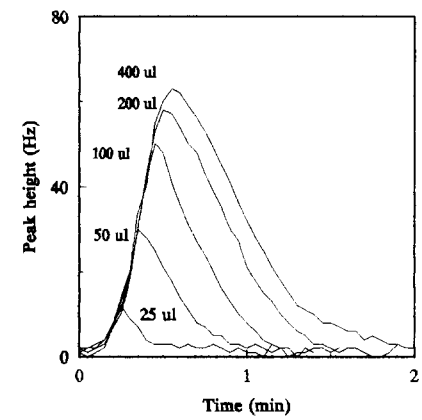

Fig. 4. FIA profiles obtained with various sample volume. Donor flow rate, 1.50 ml min^{-1}; acceptor flow rate, 1.00 ml min^{-1}; ammonium concentration, 10^{-5} mol l^{-1}.

Table 1
Dependence of peak height on the flow rates of the donor and acceptor streams[a]

V_D	Peak height (maximum frequency decrease, Hz) for different V_A					
	0.15	0.25	0.50	1.00	1.50	2.00
0.15	192	152	98	77	66	57
0.25	178	145	93	74	61	53
0.50	125	103	85	65	53	39
1.00	94	87	72	57	48	32
1.50	87	71	63	49	40	28
2.00	79	61	54	40	28	23

[a] V_A, acceptor flow rate (ml min^{-1}); V_D, donor flow rate (ml min^{-1}); injection volume, 100 μl; standard concentration, 10^{-5} mol l^{-1} ammonium.

Iwatsu, Japan) was used to record its oscillating frequency, and a computer (Model 4192 A, Hewlett-Packard) was used for data analysis. The conductivity electrode was made from two stainless-steel needles (diameter 1 mm) inserted parallely and oppositely in a 15 μl-flow-through cell (5 mm × 2 mm i.d.). Design of the oscillator was given in a previous paper [8]. Temperature control (25 ± 0.1°C) was achieved with a constant temperature water bath.

2.2. Reagents

Amino acids were of biochemical-reagent grade (Shanghai Biochemical-reagent Factory). Albumin and *r*-globulin were of pharmaceuticals. All other chemicals were of analytical-reagent grade or better quality. Doubly distilled/deionized water was used throughout. Standard ammonium solutions were made by serial dilution of a 0.1 mol l^{-1} ammonium chloride stock solution. The carrier stream was water, the alkaline reagent stream was 0.1 mol l^{-1} NaOH for optimization tests and 2 mol l^{-1} NaOH containing 1% EDTA for real samples, respectively, for composition of the acceptor streams, see Section 3.

2.3. Procedure

To a given quantity of amino acids or a given volume of blood products water was added to produce a solution equivalent to 0.2–1.0 mg ml^{-1} nitrogen. To 1 ml of the resulted solution 3 ml of concentrated sulfuric acid and 0.3 g of a mixture of potassium sulphate and cupric sulphate (3:1) was added, mixed and heated until a clear solution was obtained. After cooling, the mixture was diluted to 100 ml. A blank for blood products was prepared by precipitating the proteins therein with trichloroacetic acid, the clear supernatant thus obtained underwent digestion as described above. The concentration of ammonium was calculated from a calibration graph based on its peak height (the maximum frequency decrease). Then the nitrogen content in amino acids and the protein content in blood products were obtained (each mmol of ammonium is equivalent to 14.01 mg of nitrogen or 87.56 mg protein).

3. Results and discussion

3.1. Theoretical considerations

The proposed method described here is based on diffusion of ammonia across a PTFE gas-permeable membrane from an alkaline stream (pH > 11), which causes conversion of ammonium to ammonia and creates a medium where ammonia is only slightly soluble, it is trapped into a stream of diluted boric acid, and the trapped ammonium in the acceptor is determined on line by a BAW-impedance sensor.

The oscillating frequency (F) of the BAW-impedance sensor can be expressed as [8]

$$F = F_0\left[1 + \frac{\pi F_0 C_q(2\pi F_0 C_s - YG)}{G^2 + 4\pi^2 F_0^2 C_s(C_0 + C_s) - 2\pi F_0 C_0 YG} - \pi F_0 C_q R_q Y\right] \quad (1)$$

where F_0, C_q, C_0, and R_q are the resonant frequency, motional capacitance, static capacitance and motional resistance of the piezoelectric quartz crystal, respectively. $G = k\chi$ and $C_s = k\epsilon + C_p$ are the conductivity and capacitance of the solution, k the cell constant of the conductivity electrode, χ the specific conductivity and ϵ the solution permittivity, C_p the parasitic capacitance between the

Table 2
Interference in determination of ammonium

Interferent	Interferent concentration (μM)	Ammonium concentration (μM)	
		Added	Measured
Methylamine	10	100	106.4
Dimethylamine	15	100	108.5
Diethylamine	20	100	110.8
n-Butylamine	50	100	109.6
Cyclohexylamine	100	100	110.3

leading wires of the electrode, and Y a parameter related to phase shift of the oscillator. For a diluted electrolyte solution, the change of F is chiefly dependent upon solution conductivity because the change in permittivity is negligible and other above-mentioned parameters were always kept unchanged. The sensitivity of BAW-impedance sensor to conductivity, i.e., the slope of the plot of oscillating frequency F versus conductivity χ, can be calculated by differentiating Eq. (1) F with respect to χ

$$\frac{\partial F}{\partial \chi} = \frac{\pi k F_0^2 C_q (4\pi^2 F_0^2 C_s^2 Y + 4\pi F_0 C_s G - YG^2)}{[4\pi^2 F_0^2 C_s (C_0 + C_s) - 2\pi F_0 C_0 YG + G^2]^2} \quad (2)$$

From this equation, it can be deduced that the sensitivity is determined by the solution conductivity G and the cell constant k. In the proposed GD-FIA system, conductivity of the solution flowing through the flow-cell is directly related to composition of the acceptor and concentration of the ammonium trapped in it. Obviously, the latter is determined by the mass transfer of the ammonia formed across the membrane and the recipient volume, i.e., that part of the acceptor stream passing the cell during diffusive sample transport across the membrane. The mass transfer (m) is given by the equation $m = Jt$, where t is the residence time (s) in the donor channel. J is the diffusive flux (mol s^{-1}), it can be derived from Fick's law, based on a simple diffusion model, leading to the equation

$$J = kD(A/L)\Delta c \quad (3)$$

where A is the contact area (m^2) between donor and acceptor stream, L the membrane thickness (m), D the diffusion coefficient (m^2 s^{-1}) of ammonia in air, Δc the concentration difference (mol m^{-3}) and k a lump constant including gas transport in the aqueous phase, and partition of ammonia between aqueous and gaseous phase [4]. At high donor flow rates, the diffusive flux is high but the ammonia transfer efficiency is low. Thus, in FIA, where sample volumes are commonly small, sufficiently low flow rates of the donor stream are appropriate and should guarantee high transfer efficiency. Besides, the sample injected undergoes dispersion resulting in a peak-shaped concentration profile, the intensity and shape of which are influenced by a number of parameters of the FIA manifold.

3.2. Operational parameters

With regard to the above-discussed aspects, the effect of several parameters on the performance of the proposed FIA systems were studied.

Fig. 2(a) shows FIA profiles of the proposed BAW-impedance sensor system obtained with the same manifold except the acceptor being water and diluted boric acid, respectively. In both cases, the injection of ammonium results in a decrease in the oscillating frequencies, which is attributed to the increase in conductivity of the acceptor solution due to the dissociation of the ammonia diffused from the donor stream. However, the acceptor of boric acid gives a stabler baseline and larger frequency shift. Further optimization of the composition of the acceptor resulted in a 0.01 mol l^{-1} boric acid (Fig. 2(b)). When the concentration of boric acid (C_{BA}) is lower than 0.01 mol l^{-1}, the sensitivity of the proposed method increases with the increasing C_{BA}, when $C_{BA} > 0.01$ mol l^{-1},

however, the sensitivity decreases with the increasing C_{BA}.

Influence of cell constant of the electrode, k, was investigated under the same FIA condition while the cell constant varied from 0.4 to 4.0 cm. Various values of k result in a marked difference in the sensitivity to the conductivity (χ), and alter the solution capacitance (C_s). When k increases, the sensitivity to the conductivity increases ($G = k\chi$); meanwhile, the solution capacitance also increases ($C_s = k\epsilon + C_p$) which reduces the sensitivity of the frequency response of the sensor to solution conductance. The sensitivity of the sensor is determined by these two opposing factors. As can be seen in Fig. 3, the sensitivity of the proposed method increases with increasing cell constant at first, then begins to decrease. The maximum sensitivity was obtained with the cell constant 1.05 cm.

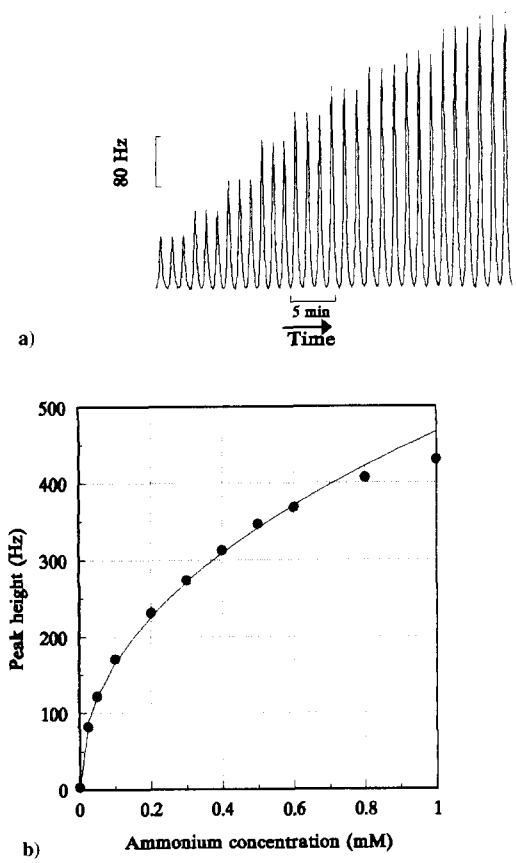

Fig. 5. (a) Calibration run for ammonium standards. From left to right: triplicate signals for 0.025, 0.05, 0.10, 0.20, 0.30, 0.40, 0.50, 0.60, 0.80 and 1.00 mM ammonium, respectively. Conditions as given in Fig. 1(a). (b) Calibration graph for the determination of ammonium in Kjeldahl digests.

As shown in Fig. 2(b) and Fig. 3, the proposed system exhibits a favorable response to 5.0×10^{-6}–4.0×10^{-3} mol l^{-1} ammonium, with a detection limit of 1.0×10^{-6} mol l^{-1}. All calibration graphs obtained demonstrate the same features even with different manifold parameters, e.g., the graphs are not linear, and the sensitivity is higher at the lower ammonium concentration.

The influences of sample volume and flow rates are illustrated in Fig. 4 and Table 1, respectively. In Fig. 4, the frequency decrease is plotted as a positive signal to yield a conventional FIA profile, and it is shown that increasing injection volume increased the intensity of the signal, but also increased the time necessary for the signal to return to baseline. As shown in Table 1, the sensitivity is inversely proportional to both of the acceptor flow rate and the donor flow rate, and a significant enhancement of sensitivity can be achieved especially by decreasing the acceptor flow rate. But the sampling rate had to be reduced, for example, when the acceptor flow rate was decreased from 2.0 to 0.15 ml min^{-1} with the same donor flow rate 1.5 ml min^{-1}, a seven-fold enhancement in the signal intensity was achieved, but the analysis time for per sample increased from 1 to 5 min. Additionally, the baseline stability as well as the signal reproducibility became worse. Further experiments lead to the final design of the FIA manifold illustrated in Fig. 1(a), which offered the adequate sensitivity, excellent reproducibility and required throughput for real samples.

3.3. Potential interference

The interference arises from the presence of those substance that can pass through the membrane and then cause change in conductivity of the acceptor solution. It has been established previously that PTFE membranes used in the FIA gas-diffusion studies are effective barriers for ionic species [14,15]. In the described method,

Table 3
Results for nitrogen and protein determination[a]

Sample	Nitrogen (%)		Protein (%, g ml^{-1})	
	Proposed method	Conventional method[b]	Proposed method	Conventional method[b]
Glycine	18.90 ± 0.16	19.21 ± 0.28		
DL-aspartic acid	10.73 ± 0.09	10.87 ± 0.15		
L-glutamic acid	9.72 ± 0.07	9.54 ± 0.19		
Albumin injection			19.45 ± 0.19	19.81 ± 0.34
γ-Globulin injection			10.37 ± 0.10	10.28 ± 0.26

[a] All measured results are average values with standard deviations from five determinations of the same digest.
[b] Distillation/titration method.

with the use of alkaline reagent, the interference from volatile acids is negligible, and with addition of the complexing agent EDTA into the alkaline reagent, interference from the metal ions, which can form hydroxide precipitates with the alkaline reagent, can be prevented [3,6]. A test of interference from some volatile amines is given in Table 2, the thresholds were obtained at an interference level (relative error > 5%) considering the precision of the proposed method is within 1% RSD (described below). It is shown that the interference from methyl-, dimethyl-, and diethylamine had to be considered if these volatile amines present at levels of 10–20% of ammonium, and *n*-butylamine and cyclohexylamine interfere if present at 50–100% of ammonium.

3.4. Analysis of samples

The described method was applied to the determination of ammonium in Kjeldahl digests obtained from amino acids and blood products. As the volatility of ammonia depends on its solubility and partial pressure which in turn are influenced by temperature, pressure and ionic strength, a constant temperature bath was used, and standards as well as blanks for these determinations were prepared to contain sulfuric acid, potassium sulfate and cupric sulfate at concentrations similar to those of the samples. A typical output for standards in the range 0.025–1.0 mM is shown in Fig. 5(a). The calibration graph is not linear (Fig. 5(b)), it fits the following equation:

$$y = 461.3x^{0.45}$$

where y is the height of the FIA profile (the maximum frequency decrease in Hz) and x the ammonium concentration in mM. Table 3 shows that results for nitrogen determination in amino acids and for proteins determination in blood products are in good agreement with those obtained by the conventional and distillation/titration method, respectively, and the average precision of the proposed method is within 1% (RSD), better than that of the titration method.

4. Conclusion

For an overall evaluation of the GD-FIA/BAW-impedance sensor system for the ammonium determination, a comparison of the proposed method and other methods is given in Table 4. GD-FIA provides a selective, precise and rapid determination of ammonium in Kjeldahl digests. In combination with BAW-impedance sensor, the method proposed here has some advantages over other detection modes, e.g., the reagents and equipment required are simpler and cheaper than that required by spectrophotometric method, the background conductivity of the acceptor stream can improve the detection sensitivity while it may cause an unacceptable noise level in the conductometric method, and the stability of the analytical signals is better than that of the signals obtained by the conductometric method or potentiometric method. The advantages of the new method, GD-FIA/BAW-impedance sensor system, should make it an attractive alternative to

Table 4
Comparison of the proposed method and other methods

Method	Response range (mol l^{-1})	Detection limit (mol l^{-1})	RSD (%, $n = 100$)	Ref.
GD-FIA/BAW (proposed)	5.0×10^{-6}–4.0×10^{-3}	1.0×10^{-6}	0.95	This paper
GD-FIA/conductometry	5.9×10^{-6}–4.1×10^{-3}	1.2×10^{-6}	<2	[6]
	5.9×10^{-5}–3.5×10^{-3}	1.8×10^{-6}		[7]
GD-FIA/potentiometry	10^{-7}–10^{-2}	3×10^{-8}	<2	[6]
	10^{-7}–10^{-4}	$<10^{-7}$		[4]
[a]GD-FIA/spectrophotometry				
A	5.9×10^{-5}–3.5×10^{-3}	5.9×10^{-5}	1.5	[7]
B	1.2×10^{-4}–3.5×10^{-3}	5.9×10^{-5}	0.92	[7]

[a] A, based on Berthelot reaction; B, based on acid–base indicator method.

the methods currently in use especially to the conductometric method.

Acknowledgements

The authors are grateful to the Natural Science Foundation and Education Commission Foundation of China for supporting this work.

References

[1] E.J. Conway, Microdiffiusion Analysis and Volumetric Error, 5th ed., Crosby Lockwood, London 1962, pp. 134.
[2] P.L. Searle, Analyst 109 (1984) 549.
[3] C. Pasquini, L.C. de Faria, Anal. Chim. Acta 193 (1987) 19.
[4] G. Schulze, C.Y. Liu, M. Brodowski, O. Elsholz, W. Frenzel, J. Möller, Anal. Chim. Acta 214 (1988) 121.
[5] S.W. Gibb, R.F.C. Mantoura, P.S. Liss, Anal. Chim. Acta 316 (1995) 291.
[6] W. Frenzel, C.Y. Liu, Fresenius J. Anal. Chem. 342 (1992) 276.
[7] A. Cerda, M.T. Oms, R. Forteza, V. Cerda, Anal. Chim. Acta 311 (1995) 165.
[8] D.Z. Shen, W.H. Zhu, L.H. Nie, S.Z. Yao, Anal. Chim. Acta 276 (1993) 87.
[9] D.Z. Shen, Z.Y. Li, L.H. Nie, S.Z. Yao, Anal. Chim. Acta 280 (1993) 209.
[10] F.J. He, W.H. Zhu, Q. Geng, L.H. Nie, S.Z. Yao, Anal. Lett. 27 (1994) 555.
[11] S.H. Si, D.Z. Shen, L.H. Nie, S.Z. Yao, Bioelectrochem. Bioenerg. 36 (1995) 161.
[12] S.H. Si, Y.J. Xu, L.H. Nie, S.Z. Yao, J. Biochem. Biophys. Methods 31 (1996) 135.
[13] M.S. Yang, M. Thompson, Anal. Chim. Acta 269 (1992) 167.
[14] W.E. van der Linden, Anal. Chim. Acta 151 (1983) 359.
[15] D.A. Hollowell, G.E. Pacey, G. Gordon, Anal. Chem. 57 (1985) 2851.

ELSEVIER

Talanta 44 (1997) 2129–2136

Talanta

Enhanced spectrophotometric determination of chromium (VI) with diphenylcarbazide using internal standard and derivative spectrophotometry

Katarzyna Wróbel *, Kazimierz Wróbel, Pedro Luis López-de-Alba, Leticia López-Martínez

Instituto de Investigaciones Científicas, Universidad de Guanajuato, 36000 Guanajuato, Mexico

Received 4 December 1996; received in revised form 11 March 1997; accepted 12 March 1997

Abstract

In the present work, erioglaucine A was applied as internal standard to enhanced spectrophotometric determination of chromium (VI) with diphenylcarbazide. The following procedure was used: (1) addition of internal standard and formation of ion pairs of Cr (VI) with benzyltributylammonium bromide (BTAB) (sample volume 100 ml), (2) extraction to 10 ml of methylene chloride, (3) evaporation in nitrogen stream, and (4) redissolution in a micro-volume with addition of diphenylcarbazide for color development (final volume 200 μl). The preconcentration factor achieved was about 400 and it was shown that, using internal standard, the analytical errors due to sample treatment were reduced. The analytical signals for chromium and internal standard were obtained at 591.30 and 653.50 nm from first derivative spectra, normalized against $^{1}D_{653.50nm}$. The analytical characteristics evaluated were: detection limit = 0.06 μg l^{-1}, quantification limit = 0.19 μg l^{-1}, precision for 1 μg l^{-1} 14.2%, and for 10 μg l^{-1} 3.2%, correlation coefficient of linear regression was 0.9985. The proposed procedure was applied to determination of chromium (VI) in tap water. Total chromium was determined by electrothermal atomic absorption spectrometry, the recovery of hexavalent chromium added was then evaluated and compared with the results of the proposed procedure. In this experiment, good agreement was obtained between results obtained by the two methods. © 1997 Elsevier Science B.V.

Keywords: Chromium (VI); Derivative spectrophotometry; Internal standard; Natural waters

1. Introduction

Speciation of chromium in environmental and biomedical materials has extensively been studied. The need for such analyses has increased after reports on different biological role of chromium (III) and chromium (VI) species in plants, animals and humans [1–5]. Trivalent chromium is considered as the essential nutrient, because of its specific action in metabolism of carbohydrates [6,7]. On the other hand, strong evidence exists on chromium (VI) toxicity. The mechanism of this toxicity is often related with the formation of free

* Corresponding author. Fax: +52 473 26252; e-mail: katarzyn@quijote.ugto.mx

PII S0039-9140(97)00092-1

radicals during the reduction of Cr (VI) occurring inside the cells [6,8]. Thus, for reliable evaluation of environment contamination with chromium, the selective and sensitive analytical tools are needed for discrimination and quantification of different chromium species. Great majority of the procedures reported for chromium speciation in natural waters include preconcentration and/or separation step prior to detection. Extraction [5,9–11], high performance liquid chromatography (HPLC) [2–4,12], sorption on membranes [13,14] or in microcolumns [1,15–18] in flow system were used for separation, and detection was carried out by spectrophotometry or atomic spectroscopy techniques. Spectrophotometric detector has some advantages over the atomic spectrometry. It is more available, easy to automation and to on-line interface with separation system. Although the detection limit for direct spectrophotometric determination of hexavalent chromium with diphenylcarbazide is relatively poor (10 μg l^{-1} [12]), this reagent has been frequently applied in speciation studies. Thus, post column derivatization was used for spectrophotometric detection of chromium (VI) in ion chromatography [19,20], and in flow analysis [1,13,14,18].

On the other hand, the extraction-spectrophotometric procedures were reported for hexavalent chromium, based on the ion pair formation with some surfactants [21–23]. Recently, we have shown that addition of internal standard (IS) at the beginning of such complicated, many-steps spectrophotometric procedure had improved the analytical performance [24]. In the cited work, analytical errors due to sample manipulation were reduced by taking the ratio of analyte to internal standard signals. First derivative spectral data were obtained to assure better resolution of absorption signals corresponding to analyte and internal standard.

In the present work application of internal standard is proposed for extraction-spectrophotometric determination of hexavalent chromium at ppb level. The preconcentration was carried out by extraction of ion pairs (Cr (VI)-benzyltributylammonium bromide) to organic phase, evaporation, and redissolution in the micro-volume. Diphenylcarbazide was used for spectrophotometric detection.

2. Experimental

2.1. Apparatus

A Spectronic 3000 Diode Array Milton Roy spectrophotometer was used (resolution 0.35 nm), coupled to a 486 PC. User Data version 2.01 (Milton Roy Inst. Co.) software was used for acquisition, storage and manipulation of spectral data. All data treatment operations was carried out using a Hewlett-Packard Vectra 486/66 VL microcomputer equipped with the GRAMS/386 TM software package, version 3.01A (Galactic Ind. Co., Salem, MA).

A model 3110 Perkin-Elmer atomic absorption spectrometer with HGA 600 and autosampler AS60 was used.

2.2. Reagents

Chromium (VI) stock solution, 1000 mg l^{-1}, was prepared by dissolving 2.8287 g of $K_2Cr_2O_7$ in deionized water and diluting to a final volume of 1 l. Working solutions were prepared daily by appropriate dilution.

A stock diphenylcarbazide solution, 0.25% in acetone, was prepared daily from Merck reagent.

Hexadecyltrimethylammonium bromide (CTAB) was from Sigma and benzyltributylammonium bromide (BTAB) was from Aldrich. Stock solutions, 2%, were prepared of the two surfactants.

Phosphate buffer solution (1 mol l^{-1}, pH 4) was prepared from the respective sodium phosphate salts (Sigma) with addition of CTAB or BTAB (final concentration 1.0%).

Sulphuric acid solution (2 mol l^{-1}) was prepared by diluting the concentrated acid (Aldrich) in deionized water.

Erioglaucine (A) solution, 0.1%, was prepared from analytical grade reagent (J.T. Baker Chemicals) by dissolution in deionized water. Working solution contained 2.5 10^{-4}% of erioglaucine (A) and was prepared daily.

Methylene chloride, acetone, methanol, formamide, butanol, chromium (III) chloride, copper sulphate, mercury (II) sulphate, sodium molybdate, sodium sulphate and sodium chloride were from J.T. Baker Chemicals.

Deionized water (Labconco) was used throughout.

2.3. Procedures

For calibration, a series of solutions containing different chromium concentrations was prepared in separatory funnels by adding 0, 10, 20, 50, 100, 150 and 200 μl of intermediate Cr (VI) standard (10 mg l^{-1}) to 100 ml of deionized water. Then, exactly 200 μl of working erioglaucine (A) solution (IS), about 4 ml of phosphate buffer solution (containing BTAB or CTAB) and about 1 ml of butanol (to improve phases separation) were added to each funnel. Extraction was carried out with 10 ml of methylene chloride. After separation of phases, the organic phase was collected in test tubes, which were then placed in water bath (40°C). A glass capillary was introduced to each tube, through which the nitrogen stream was passed to evaporate organic solvent. Then 500 μl of acetone was added and evaporated (to eliminate traces of methylene chloride). The dry residue was redissolved in 80 μl of acetone and color was developed by adding 100 μl of diphenylcarbazide solution and 20 μl of sulphuric acid. The absorption spectra were recorded in the wavelength range 450–700 nm against acetone with diphenylcarbazide as a blank. The obtained spectra were smoothed through 21 experimental points and first derivative spectra were calculated ($\Delta\lambda = 9$ nm) using the Savitzky-Golay procedure [25]. The derivative spectra were normalized against the derivative absorbance at 653.50 nm (IS) and the analytical signals of chromium were obtained as the difference between derivative absorbances taken from normalized spectrum of calibration sample and from normalized spectrum of IS at 591.30 nm.

Tap water was spiked with hexavalent chromium (2, 4 and 8 μg l^{-1}) and analyzed using the same procedure (five repetitions).

These same samples of tap water were analyzed for total chromium by electrothermal atomic absorption spectrometry (conditions given in Table 1). Recovery of hexavalent chromium added (2, 4 and 8 μg l^{-1}) was evaluated.

3. Results and discussion

Diphenylcarbazide is commonly used for spectrophotometric determination of hexavalent chromium. However, the determination at ppb levels requires many fold preconcentration of the analyte. In several papers, the separation/preconcentration of Cr (VI) was achieved by extraction of ion pairs formed between chromium (VI) and different cationic surfactants [21–23,26]. In the present work two quaternary ammines: hexadecyltrimethylammonium bromide (CTAB) and benzyltributylammonium bromide (BTAB) were used for such purpose. Chromium preconcentration was carried out in two steps:

1. extraction to organic phase
2. evaporation of organic solvent and dissolution of the residue in the micro-volume.

3.1. Simultaneous measurement of chromium (VI) with diphenylcarbazide and of internal standard by derivative spectrophotometry

In this work erioglaucine (A) was tested as internal standard and, in Fig. 1, first derivative spectrum of chromium with diphenylcarbazide and first derivative spectrum of erioglaucine (A) are shown. Quite good spectral resolution of the two compounds can be observed in this figure: analyte derivative spectrum has a minimum at 591.30 nm and derivative spectrum of erioglaucine

Table 1
Electrothermal atomic absorption determination of chromium

Wavelength	357.9nm
Background correction	Off
Atomization technique	Wall atomization
Atomization surface	Pyrocoated tube
Modifier	No
Temperature programme	

Step	Temp., °C	Ramp, s	Hold, s
1	120	15	15
2	1100	15	15
3	20	1	15
4*	2300	0	4 (Gas stop)
5	2600	1	3

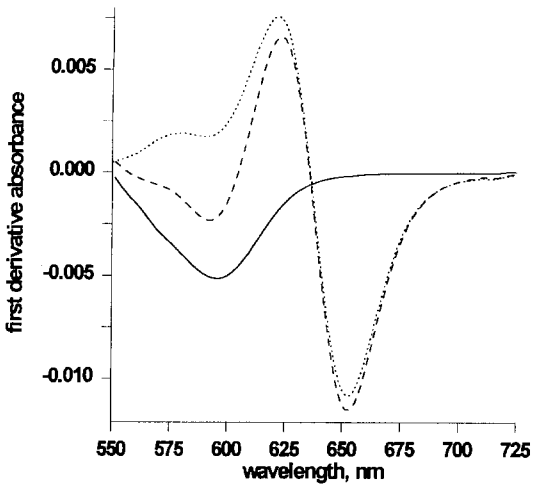

Fig. 1. First derivative spectra of preconcentrated samples: (—) 10 μg·l^{-1} chromium with diphenylcarbazide, (• • •) 5·10^{-7}% IS (erioglaucine (A)), (- - -) 10 μg·l^{-1} chromium with diphenylcarbazide + IS.

(A) has a minimum at 653.50 nm. Zero-crossing conditions exist for IS at 653.50 nm (spectral contribution of the analyte at this wavelength is zero). However, taking analytical signal of chromium at 591.30 nm (spectral minimum), some spectral contribution of erioglaucine (A) can be observed. So, the signal obtained for IS at this wavelength should be rested from the signal obtained for sample containing chromium (VI) and IS. First derivative spectra of IS and of samples containing chromium and IS were normalized against first derivative absorbance at 653.50 nm (Fig. 2). Chromium analytical signal was evaluated as a difference between $^1D_{Cr+IS}$ (first derivative absorbance taken from the normalized derivative spectrum of sample containing chromium (VI) and IS internal standard at 591.30 nm after color development with diphenylcarbazide) and $^1D_{IS}$ (first derivative absorbance taken from the normalized derivative spectrum of IS). The value of $^1D_{IS}$ at 591.30 nm was 0.1541 ± 0.0007 (calculated for 10 repetitions). Under such measurement conditions erioglaucine (A) was used as internal standard in further studies. It was observed that spectrum of erioglaucine (A) was not affected in the presence of: Cr (VI), Cr (III), quaternary amines studied, humic acid, alkaline and alkaline earth metal ions, using their concentrations up to 5000 times higher than that of erioglaucine (A). Moreover, erioglaucine (A) is not a natural component of tap water.

3.2. Preconcentration by extraction

At first, effect of contra-ion on the extraction of hexavalent chromium and erioglaucine (A) was studied. Extraction yields of chromium (VI) and of erioglaucine (A) are presented in Fig. 3, as a function of BTAB or CTAB concentrations. It can be observed that, with increasing concentration of contra-ion in aqueous phase, the extraction yield of chromium increased up to 60% for 0.04% CTAB and up to 82% for 0.04% BTAB. It can also be observed in Fig. 3, that extraction yield of erioglaucine (A) increased in the presence of BTAB and CTAB. It seems possible that sulfonic groups in the molecule of erioglaucine (A) could contribute in formation of ion pairs with cationic contra-ions. Increasing concentration of BTAB had very similar effect on extraction of erioglaucine (A) and chromium (VI) (Fig. 3a) and this effect was more pronounced than effect observed in the presence of CTAB (Fig. 3b). The

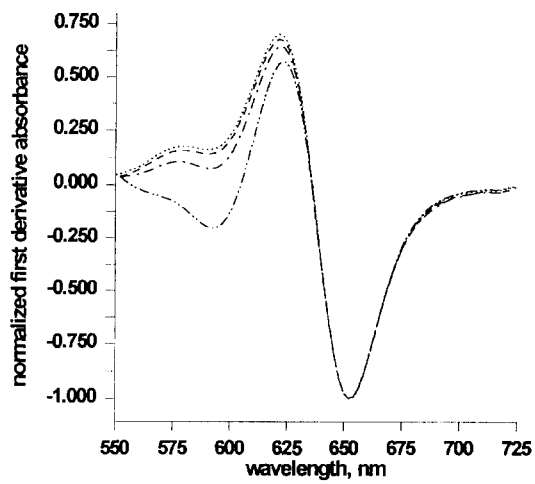

Fig. 2. First derivative spectra of preconcentrated samples, normalized against $^1D_{653.50nm}$. (• • •) 5·10^{-7}% IS (erioglaucine (A)), (- - -) 1 μg·l^{-1} chromium with diphenylcarbazide + IS; (– • –) 2 μg·l^{-1} chromium with diphenylcarbazide + IS; (– •• –) 10 μg·l^{-1} chromium with diphenylcarbazide + IS.

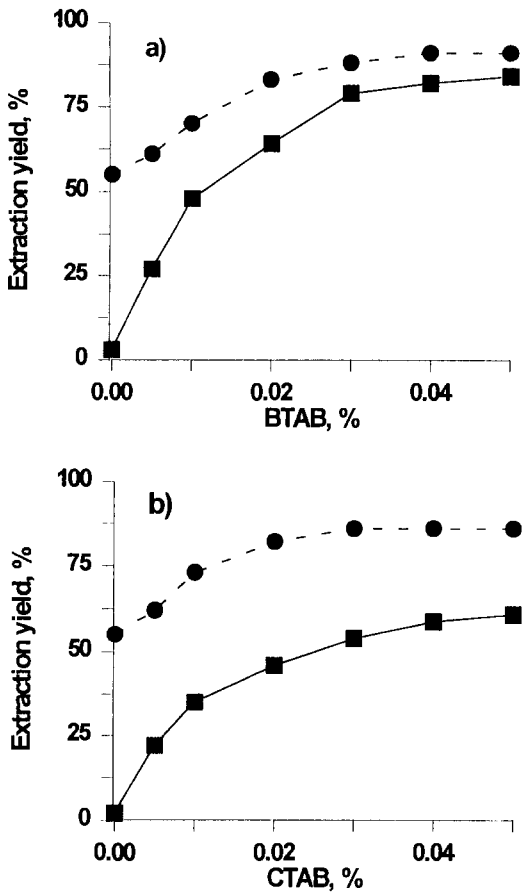

Fig. 3. Extraction yields of: (-■-) hexavalent chromium (0.1 $mg \cdot l^{-1}$) and (-●-) erioglaucine (A) ($5 \cdot 10^{-5}$%) in the presence of: (a) BTAB and (b) CTAB. Aqueos phase: 100 ml, pH 4; Organic phase: 5 ml methylene chloride.

obtained results indicate that using BTAB, the possible extraction errors should be eliminated if relating the analytical signal of chromium to that of IS.

Effect of pH on extraction of chromium and IS in the presence of CTAB and BTAB was also studied. For extraction of chromium (VI), the maximum pH was selected, for which the extraction yield was still about 60% in the presence of CTAB and about 82% in the presence of BTAB (pH 4). Although redox potential of chromium is pH dependent, natural speciation of Cr (VI)/Cr (III) at pH 4 should not be altered, as reported by Sperling et al. [27]. In the range of pH 2 to 7, the extraction yield of erioglaucine (A) was not afected in the presence of the two surfactants (about 80% with BTAB and about 70% with CTAB). This means that, using erioglaucine (A) as IS, possible changes in extraction yield of chromium due to lack of precise pH control would not be compensate (extraction yield of IS does not depend on pH) and, in the proposed procedure, pH must be exactly adjusted.

For further studies 0.04% of BTAB was selected and extraction was carried out at pH 4. Again, it should be stressed out that using erioglaucine (A) as IS there was no need to control the extraction yield, however pH had to be precisely controlled.

3.3. Preconcentration by evaporation and redissolution

After extraction, the organic phase containing chromium (VI), erioglaucine (A) and excess of BTAB, was introduced to test tube and further preconcentration was carried out by evaporation in nitrogen stream. It was observed that methylene chloride hindered color reaction of chromium (VI) with diphenylcarbazide. In order to remove possible residues of this solvent, 500 μl of acetone was added to the residue in each tube and evaporated. Solid residue was then dissolved in micro-volume of acetone with addition of diphenylcarbazide for color development (final volume 200 μl). Analytical errors due to analyte losses, imprecise dilution, etc., expected in this stage of the procedure, should be compensate by the use of IS method [24].

The final solutions obtained were turbid, probably due to excessive amount of BTAB. Such turbidity problems can be partly eliminated by using derivative spectrophotometry [28], however, studies were carried out to select the most adequate solvent. Turbidity of solutions and sensitivities of chromium determination with diphenylcarbazide in the presence of BTAB (2%) were compared using the following solvents: water, acetone, methanol and formamide. In Table 2 the equations of linear regression calibration of chromium (0–2.0 $mg\ l^{-1}$) obtained in these four solvents are presented. The best solubility of BTAB was ob-

Table 2
Effect of solvent on quantification of chromium with diphenylcarbazide in the presence of 2% BTAB

Solvent	Linear regression equation	Correlation coefficient
Water	$A_{542} = 0.6294c_{Cr} - 0.0302$	0.9996
Acetone	$A_{542} = 0.6314c_{Cr} - 0.0174$	0.9998
Methanol	$A_{542} = 0.4302c_{Cr} - 0.0190$	0.9968
Formamide	$A_{542} = 0.5253c_{Cr} - 0.0187$	0.9987

served in acetone and, as can be seen in Table 2, this solvent enabled the best sensitivity of calibration.

The experimental conditions for the second step of chromium (VI) preconcentration are given in Section 2.3: the residue was dissolved in 80 μl of acetone, 20 μl of sulphuric acid (2 mol l^{-1}) and 100 μl of diphenylcarbazide (0.25%) were added.

Using the described two-step procedure the preconcentration factor of about 400 was achieved.

3.4. Analytical performance of the proposed procedure

As described in Section 2.3 and in Section 3.1, the absorption spectra of final solutions were obtained and processed to calculate analytical signal of chromium (related to IS signal by normalizing spectra against first derivative absorbance at 653.50). The analytical performance of the proposed method was evaluated as recommended by IUPAC [29] and, detection limit, quantification limit, linear range and precision at two chromium concentrations are presented in Table 3. If not using IS the correlation coefficient of linear regression did not exceeded 0.9 and

Table 3
Analytical characteristics evaluated for the proposed procedure

r for linear regression ($P<0.05$)	0.9985
Detection limit	0.06 $\mu g \cdot l^{-1}$
Quantification limit	0.19 $\mu g \cdot l^{-1}$
Linear range	0.2–30 $\mu g \cdot l^{-1}$
Precision for 1 $\mu g \cdot l^{-1}$ of Cr(VI)	14.2%
Precision for 10 $\mu g \cdot l^{-1}$ of Cr(VI)	3.2%

precision for 10 μg l^{-1} of Cr (VI) was about 70%. These results clearly confirm that application of erioglaucine (A) improved analytical performance.

3.5. Interference studies

Effect of foreign ions, possible interfering in chromium (VI) determination in natural waters by the proposed procedure, was studied. To do so, solutions (100 ml, 0.04% BTAB, $5 \cdot 10^{-7}$% IS, pH 4) containing 10 μgl^{-1} of hexavalent chromium and increasing concentrations of: chromium (III), copper (II), mercury (II), iron (III), molybdenum (VI), phosphate, sulphate and chloride ions [1,6] were prepared and the described procedure was carried out. Analytical signals of chromium (VI) were evaluated in the absence and in the presence of the foreign ions: the interference was considered significant if the observed change of chromium signal was higher that 5%. The concentration range of interferents was 20 μg l^{-1}–10 mg$\cdot l^{-1}$ and studies were carried out starting from the highest interferent concentration. The obtained results are presented in Table 4. As can be observed in this Table 4, chromium (III), iron (III), copper (II) and mercury (II) did not interfere significantly up to their concentration of 10 mg l^{-1}. Under experimental conditions selected, the selective extraction of anionic species was achieved (formation of ion pairs with BTAB), thus eliminating possible interferences of cations in reaction of chromium (VI) with diphenylcarbazide. It should be noted that, using alumina for preconcentration of chromium (VI), significant interferences were reported for iron (III) [6], while using our preconcentration system such problem can be partly overcome. However, in our procedure we observed important interferences in the presence of anionic species.

3.6. Analytical results

The proposed procedure was applied to analysis of tap water samples. The average chromium (VI) concentration obtained was 0.3 ± 0.1 μg l^{-1} (5 repetitions). These same samples were also analyzed by atomic absorption spectrometry with

Table 4
Relative signals obtained for 20 $\mu g \cdot l^{-1}$ of chromium (VI) in the presence of foreign ions using the proposed extraction-spectrophotometric procedure

Foreign ions	Concentration of foreign ions, $mg \cdot l^{-1}$							
	0.02	0.05	0.1	0.2	0.5	1.0	5.0	10.0
Cr (III)								1.00
Fe (III)							0.97	0.92
Cu (II)								1.01
Hg (II)							0.96	0.99
Mo (VI)		0.98	0.93	0.82	0.78	0.72	0.65	0.52
SO_4^{2-}				0.97	0.90	0.75	0.70	0.62
PO_4^{3-}				0.98	0.94	0.83	0.79	0.66
NO_3^-						0.97	0.93	0.89
Cl^-						0.95	0.90	0.87

electrothermal atomization and total chromium concentration found was 1.2 ± 0.1 $\mu g\ l^{-1}$. Then, these samples were spiked with chromium (VI) (always 5 repetitions) and recovery experiments were carried out using the proposed procedure and ETA-AAS. The obtained recovery results are given in Table 5: satisfactory recoveries and the good agreement with ETA-AAS results can be observed for the proposed procedure. However, the precision of the proposed method is clearly worse as compared with ETA-AAS.

4. Conclusions

In this work erioglaucine (A) is proposed as internal standard for enhanced spectrophotometric determination of chromium (VI) at ppb levels. About 400-fold preconcentration of the analyte was achieved in two steps:

Table 5
Recovery results of chromium (VI) in tap water using the proposed method and ETA-AAS ($n = 5$)

	Mean recovery ± SD (%)	
Cr(VI) added, $\mu g \cdot l^{-1}$	Proposed method	ETA-AAS
2	110 ± 12	108.3 ± 3.4
4	108 ± 5	105.0 ± 4.2
8	96 ± 5	103.8 ± 2.1

1. extraction of chromium (VI) in the presence of BTAB to methylene chloride
2. evaporation of organic solvent, redissolution in micro-volume of acetone and color reaction with diphenylcarbazide.

It was shown that using IS, the expected analytical errors in such complicated procedure can be reduced. Interferences due to cationic species were partly eliminated, however serious interferences occurred in the presence of anionic species. Quite good analytical performance of the proposed method was obtained (see Table 3) and method was successfully applied for the analysis of tap water.

Acknowledgements

Financial support from the CONACyT (Mexico), project 0463P-A9506 is gratefully acknowledged.

References

[1] M.C. Pannain, R.E. Santelli, Talanta 42 (1995) 1609.
[2] R. Milacic, L. Stupar, Analyst 119 (1994) 627.
[3] F.A. Byrdy, L.K. Olson, N.P. Vela, J.A. Caruso, J. Chromatogr. A 712 (1995) 311.
[4] J.F. Jen, G.L. Ou-Yang, C.S. Chen, S.M. Yang, Analyst 118 (1993) 1281.
[5] S. Dyg, R. Cornelis, B. Griepnik, P. Quevauviller, Anal. Chim. Acta 286 (1994) 297.

[6] S.A. Katz, H. Salem, The Biological and Environmental Chemistry of Chromium, VCH, New York, 1994.
[7] B.W. Morris, S. MacNeil, T.A. Stanley, T. A Gray, R. Fraser, J. Endocrinol. 139 (1993) 339.
[8] E.J. O'Fleherty, Toxicol. Lett. 68 (1983) 145.
[9] J.L. Manzoori, F. Shemirani, J. Anal. At. Spectrom. 10 (1995) 881.
[10] A. Golwelker, K.S. Patel, R.K. Mishra, Bull. Chem. Soc. Jpn. 63 (1990) 605.
[11] D.T. Burns, M.D. Dunford, Anal. Chim. Acta 319 (1996) 205.
[12] R. Milacic, J. Stupar, N. Kozuch, J. Korosin, Analyst 117 (1992) 125.
[13] S.B. Savvin, L.M. Trutneva, O.P. Shvoeva, Zh. Anal. Khim. 48 (1993) 502.
[14] L.Q. Li, C.D. Wu, H.G. Zheng, Y.D. Li, Fenxi Huaxe 22 (1994) 159.
[15] A.M. Naghmush, K. Pyrzynska, M. Trojanowicz, Anal. Chim. Acta 288 (1994) 247.
[16] J.L. Manzoori, M.H. Sorouraddin, F. Shemirani, Talanta 42 (1995) 1151.
[17] C.A. Johnson, Anal. Chim. Acta 238 (1990) 273.
[18] C.R.M. Peixoto, Y. Gushikem, N. Baccan, Analyst 117 (1992) 1029.
[19] H. De-Beer, P.P. Coetzee, S. Afr. J. Chem. 44 (1991) 105.
[20] E.J. Arar, J.D. Pfaff, J. Chromatogr. 546 (1991) 335.
[21] K. Tanaka, A. Ishimaru, Bunseki Kagaku 31 (1982) 191.
[22] D.T. Burns, D. Chimpalee, P.F. Hagan, Anal. Chim. Acta 198 (1987) 293.
[23] K. Ohashi, K. Shikina, H. Nagatsu, I. Ito, K. Yamamoto, Talanta 31 (1984) 1031.
[24] K. Wróbel-Zasada, K. Wróbel-Kaczmarczyk, P.L. López-de-Alba, L. López-Martínez, M.A. García-López, Talanta 43 (1996) 1055.
[25] A. Savitzky, M.J.E. Golay, Anal. Chem. 36 (1964) 1627.
[26] D.T. Burns, M. Harriot, S.A. Barakat, Anal. Chim. Acta 259 (1992) 33.
[27] M. Sperling, S. Xu, B. Welz, Anal. Chem. 64 (1992) 3101.
[28] K.M. Wollin, F.F.E. Randow, Jena Rev. 35 (1990) 33.
[29] Analytical Methods Commitee, Royal Society of Chemistry (UK), Analyst 112 (1987) 199.

ELSEVIER

Talanta 44 (1997) 2137–2143

Talanta

Microextraction of volatile organic compounds using the inside needle capillary adsorption trap (INCAT) device

Mark E. McComb, Richard D. Oleschuk, Eugene Giller, Hyman D. Gesser *

Department of Chemistry, University of Manitoba, Winnipeg, MB R3T 2N2, Canada

Received 19 December 1996; received in revised form 6 March 1997; accepted 12 March 1997

Abstract

A novel method of solventless extraction has been developed based on a combination of solid phase micro extraction and purge and trap methods. In this technique, a hollow needle with either a short length of GC capillary column placed inside it, or an internal coating of carbon, is used as the preconcentration device. Sampling may be performed on ambient air, on solution, or the solution headspace, by passing the gas or liquid through the device either actively with a syringe, or passively via diffusion. The VOC are sorbed and concentrated onto either the carbon layer, or the liquid stationary phase of the capillary column, within the needle. Placing the needle into a heated GC injection port thermally desorbs the organic compounds directly into the GC without the need for solvent extraction. Results suggest that this procedure provides a rapid and sensitive alternative method to those currently available.

Keywords: INCAT; Microextraction; Organic compounds; Volatile

1. Introduction

Volatile organic compounds (VOC) are found as contaminants in both air and water, at concentrations ranging from 1 ppbv–1000 ppmv (part per billion/million by volume) [1,2]. The presence of these compounds in air has been linked to various health problems [3,4] making the analysis and monitoring of these compounds necessary.

Several methods exist for the analysis of VOC [5]. These methods include solid phase micro extraction (SPME) [6], purge and trap, activated carbon cloth (ACC), [7,8] as well as commercial active and passive samplers manufactured by Perkin-Elmer, SKC and 3 M. Each of these methods is based on the sorption of the VOC by a solid or liquid sorbent followed by either solvent extraction, or thermal desorption prior to analysis by gas chromatography (GC).

Here we introduce a novel method for the sorption and solventless extraction of VOC followed by GC analysis. Inside needle capillary absorption trap (INCAT) is a technique that uses a hollow needle with either a short length of GC capillary column placed inside it, or an internal coating of carbon, as the preconcentration medium. Sampling may be performed on ambient air, on solution, or on the solution headspace, by

* Corresponding author. Fax: + 1 204 2750905.

0039-9140/97/$17.00
PII S0039-9140(97)00093-3

passing the gas or liquid through the device actively with a syringe, or passively via diffusion. Organic compounds present in the sample are sorbed onto the deposited carbon sorbent, or the liquid stationary phase of the capillary, within the needle. The INCAT device with the sorbed organic compounds is placed into the injection port of a GC. The rapid heating of the metal needle induces the desorption of the organic compounds. This eliminates the need for a solvent extraction step prior to analysis.

In this paper we introduce the INCAT technique for the analysis of VOC including BTEX compounds (benzene, toluene, ethylbenzene, and xylenes). The use of the INCAT device in either an active or passive sampling mode is demonstrated.

2. Experimental

All reagents used in the preparation of solutions were analytical grade. Water used was purified with a Barnstead NanoPure™ water filtration system using a reverse osmosis-treated feedstock.

Gas chromatography was performed on a Varian Aerograph 2100 GC equipped with a flame ionization detector (FID) and a 30 m × 0.25 mm Supelcowax capillary column (Supelco). Analysis of the BTEX compounds was performed on a Hewlett Packard 5710A GC equipped with a FID. Separation was performed using a 2 m × 3 mm packed column; 5% bentone, 5% isodecylphthalate on Chromosorb W. Stainless steel capillary tubing used in the INCAT devices was purchased from Small Parts (Miami Lakes, Fl).

2.1. Preparation of the INCAT device

The INCAT devices were prepared using tubing with inside diameters of 0.250 and 0.406 mm. A 75 mm length of steel capillary tubing was cut from stock material and the ends sanded smooth. The cut length of tubing was then pressed into the end of a common Luer-Lok™ fitting. The junction was sealed with two part epoxy cement. Within the needle, a 2.5 cm length of GC capillary column (DB-5™) was inserted, and held in place by crimping the circumference of the needle. The short length of capillary column with its internal coating of liquid stationary phase provides the media for the preconcentration of sampled VOC.

As alternate methods, coatings of carbon were deposited within the needle to provide a media for the preconcentration of VOC. Two methods of carbon coating were investigated. In the first, colloidal graphite paint (SPI Supplies, West Chester, PA) was drawn within the needle using a syringe and allowed to dry. The needle was then baked at 175°C for 7 min under a flow of nitrogen to remove any traces of solvent from the paint. In the second method a layer of thermally deposited carbon was applied. Deposition of carbon was effected by passing CH_2Cl_2 through the needle via an aspirator while heating the end of the needle with a torch. A diagram of INCAT devices with the two types of preconcentration media is given in Fig. 1.

2.2. Sampling protocol

Two types of samples were investigated in this work; ambient air and the headspace over an aqueous solution. With the INCAT device, sampling may be carried out either passively or actively. Passive sampling is performed simply by

Fig. 1

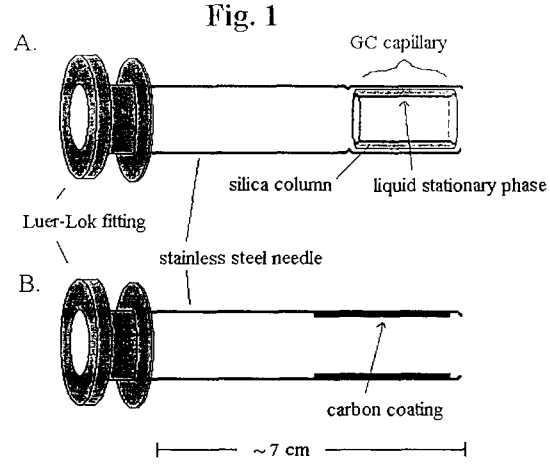

Fig. 1. Diagram of INCAT devices with A; 2.5 cm length of GC column, and B; carbon.

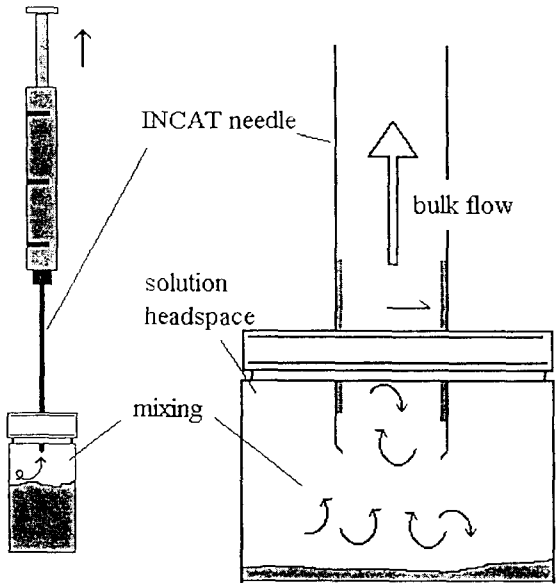

Fig. 2. Diagram showing the active mode of sampling using the INCAT device over the headspace of a solution.

exposing the end of the INCAT device to the sample allowing the sample to diffuse into the needle and onto the sorbent within. Active sampling (Fig. 2) is performed by drawing the sample through the device with either a syringe or pump. In both cases, the VOC are sorbed and concentrated onto the inner surface of the device. Chromatographic analysis of sorbed VOC is performed by clamping a piece of GC septum within the end of the INCAT device at the Luer-Lok™ fitting and then placing the needle into the heated injection port of a GC. Thermal desorption of the VOC then occurs directly within the injection port allowing chromatographic analysis. A desorption temperature of 175°C was used with the time of desorption fixed at 15 s. A cleaning step involving heating the INCAT device to temperatures greater than 175°C between injections eliminated the possibility of sample carryover.

3. Results and discussion

3.1. Headspace sampling of benzene in water

The INCAT technique is based upon the premise that if one could expose a short length of a GC capillary column to a sample of interest and re-connect the column to the GC for analysis, then a very easy and sensitive means of analysis may be obtained. INCAT devices were thus constructed with 2.5 cm lengths of GC capillary columns and tested. Preliminary results indicated that the devices performed well. A chromatogram obtained from the headspace sampling over a saturated solution of benzene in water is given in Fig. 3. The chromatogram shows only the peak for benzene (Rt = 5.4 min) and no peak due to the presence of water in the sample injected. A large degree of peak tailing was observed with the

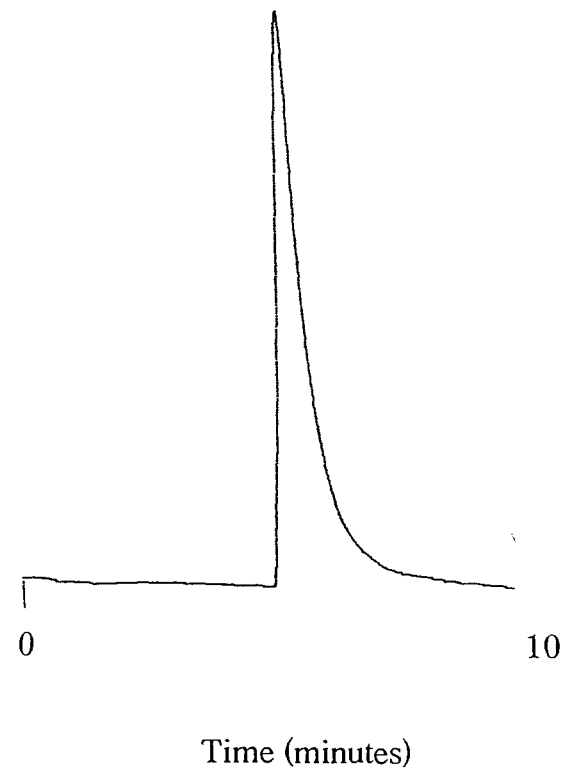

Fig. 3. Chromatogram from the headspace sampled over a saturated solution of benzene in water. Conditions: passive sampling of headspace for 7 min.

initial INCAT devices. This indicated that the transfer of heat from the injection port of the GC to the capillary within the INCAT device was a relatively long process. Initial experiments performed indicated that the time and temperature of desorption were optimized at 15 s and 175°C. Desorption temperatures lower than 175°C and desorption times of less than 15 s resulted in peak tailing due to insufficient heating of the INCAT device within the injection port. Desorption temperatures greater than 175°C or desorption times longer than 15 s did not result in any significant improvement. This resulted in less than a 5% carryover during replicate sampling with the same INCAT device. A cleaning step which involved flushing the INCAT device with N_2 at 175°C for 60 s eliminated the 5% sample carryover between injections.

3.2. Passive and active sampling

Passive diffusive sampling was investigated as it has the same accuracy in analysis as active sampling but does not require the use of a syringe or pump [9]. The analyte is allowed to passively diffuse into the needle and concentrate onto the sorbent within. The limiting step in this case is the diffusion of the analyte from the sample through the end of the needle, a process which may be used to calibrate the passive monitoring of VOC in ambient air [10].

The precision of replicate sampling with a single INCAT device was examined for the passive sampling of the headspace over a saturated solution of benzene in water. The results are presented in Table 1 for sampling times of 3 min. The error involved, ~7% RSD, was attributed primarily to differences in the manual sampling technique in replicate injections which could be improved with automation. However, this precision is sufficient to allow the application of the INCAT device for the passive monitoring of VOC in ambient air [11].

The headspace of a saturated solution of benzene in water was sampled passively for increasing periods of exposure up to 45 min. The amount of benzene sorbed was found to be dependent on the time of exposure. The results are presented in Fig. 4. Initially, a linear correlation is observed with the concentration of benzene in solution, up to ~5 min of exposure ($R^2 = 0.998$). Overall, the sorption profile indicates that after 45 min, saturation or equilibrium has not been reached. This suggests that long exposure times may be possible in an environmental setting without the problems associated with saturation.

Table 1
Reproducibility in replicate measurements using the INCAT device

Trial No.	Peak area
1	254 234
2	287 986
3	309 464
4	266 401
Mean area	276 897
S.D.	19 583
RSD	7.1%

Headspace sampling of a saturated solution of benzene in water. Conditions: passive sampling, 3 min exposure.

With active sampling the analyte is drawn through the INCAT device with a syringe at a fixed rate as indicated in Fig. 2. This results in the active transfer of the analyte from the sample through the INCAT device and effectively eliminates the time required for the analyte to diffuse

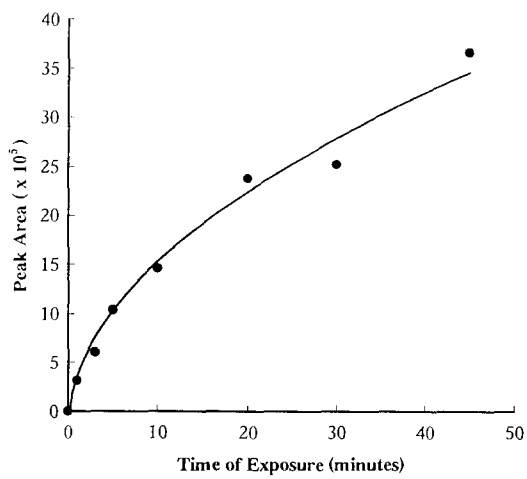

Fig. 4. Sorption characteristics with respect to the time of sampling over a saturated solution of benzene in water. Conditions: passive sampling of headspace.

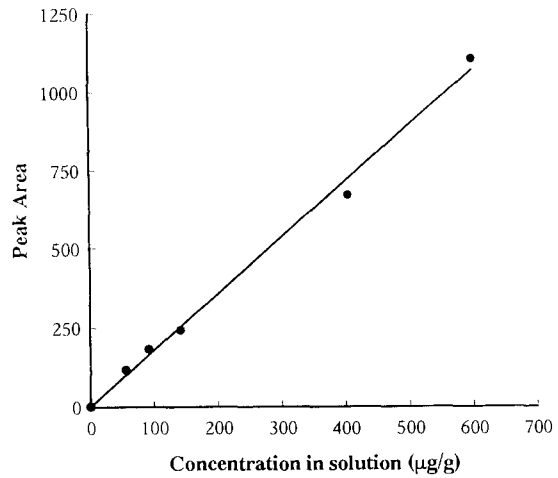

Fig. 5. Concentration dependence on sampling of 1,1,1-trichloroethane. Conditions: active sampling, 50 ml of headspace withdrawn during 60 s.

from the sample to the preconcentration media. Active sampling increases the speed of analysis considerably compared with passive diffusion sampling in which the rate limiting step in sampling is the diffusion of the analyte to the surface of the sorbent.

The dependence of sampling on the concentration of an analyte in solution was investigated. Active sampling of the headspace over solutions containing increasing amounts of 1,1,1-trichloroethane in water was performed. Approximately 50 ml of the headspace was passed through the INCAT device over a 60 s interval using a gas-tight syringe. The 50 ml sample and the 60 s time interval were chosen to ensure that enough sample passed through the INCAT device for analysis. Other sample sizes and times were not investigated at this time. A linear correlation was observed with respect to the initial concentration in solution, $R^2 = 0.998$ (Fig. 5). These results indicate that quantitative analysis is possible with the INCAT device in an active sampling mode.

The active mode of sampling was found to be superior to the passive sampling mode in the case of headspace sampling. This was due to the shorter time required to take up a sufficient amount of sample for analysis by GC in the active mode. In passive sampling the rate of diffusion of the analyte through the end of the needle is slow relative to the rate of analyte transfer within the needle itself during active sampling. This slow rate of sampling in the passive mode is advantages for the determination of long term average concentrations of VOC in air.

3.3. Carbon coated INCAT devices

Use of carbon as the extraction media was investigated as an alternative to the internal piece of GC capillary column. The choice of a carbon sorbent was based upon a number of criteria, foremost of which was the experience in our laboratory with carbon-based passive monitors for VOC in air [7,8]. As well, carbon as a sorbent has several advantages over that of a liquid stationary phase. Carbon fibres exhibit a high level of saturation (> 20% weight of fibre) [12,13] which is greater than the liquid stationary phase available with a short length of gc column. Activated carbon monitors have been found to be essentially independent of temperature and pressure fluctuations during sampling [14–16]. Carbon based coatings have been used previously with SPME for the analysis of environmental air samples [17]. Use of the carbon coating resulted in an improvement in the desorption of VOC from within the INCAT device. This was attributed to an increase in thermal conductivity of the thin carbon film in comparison with the relatively thick fused silica layer and liquid stationary phase of the capillary column.

A colloidal graphite-coated INCAT device was compared with an uncoated INCAT device for the analysis of the headspace over a saturated solution of BTEX compounds. Sampling was performed actively by passing ~ 5 ml of headspace over a 60 s interval using a gas-tight syringe. A 1.0 ml direct injection of the aqueous sample was also performed for comparison. The results in Fig. 6 illustrate that the coated INCAT device performed well in comparison with the uncoated device and the direct injection. The uncoated INCAT device was essentially used as a blank, demonstrating the effectiveness of the graphite-coated INCAT device. The peak due to the presence of water in the direct injection (Rt = 2.5 min)

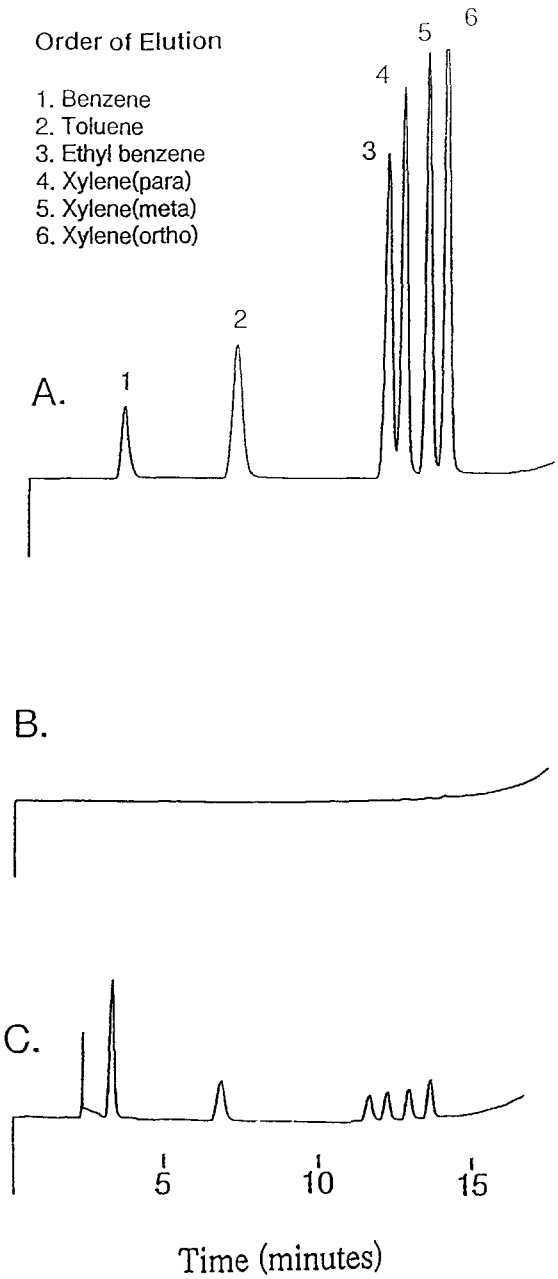

Fig. 6. Comparison between A; colloidal graphite coated INCAT device, B; blank needle and, C; 1.0 μl direct injection of BTEX compounds. Conditions for A and B: active sampling, 5 ml headspace withdrawn through the needle over 60 s; saturated solution of BTEX compounds in water; equivalent GC parameters.

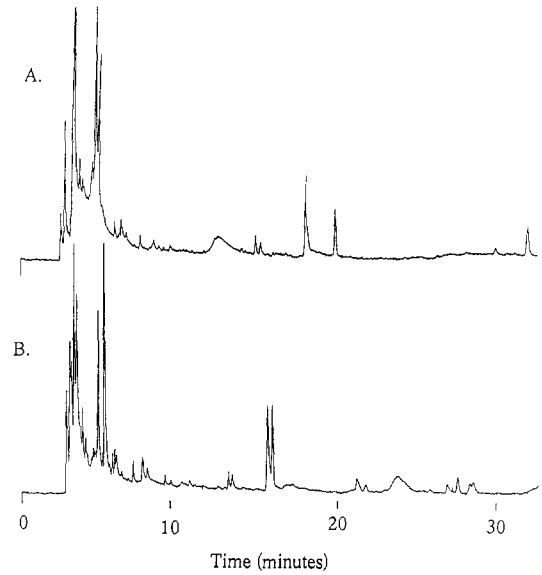

Fig. 7. Chromatograms from a thermally deposited carbon coated INCAT device exposed to ambient air. Sampling locations were: A; the laboratory and B; solvent storage cabinet. Conditions: passive sampling for 24 and 2 h, respectively.

is absent in the chromatograms of both the INCAT injections indicating that water is not taken up by the INCAT device in an observable amount.

The possibility of using the INCAT device as a passive monitor for VOC in air was examined using a needle with thermally deposited carbon. An INCAT device was left exposed to ambient air at various locations within our laboratory and then analysed by GC. Sampling was performed passively with the duration of exposure fixed at 24 h. The chromatogram is given in Fig. 7(a). Several similar chromatograms were obtained at different sampling locations within the laboratory. A chromatogram derived from exposing one of the INCAT devices to the inside of a solvent storage cabinet for 2 h is given in Fig. 7(b). These results indicate that a number of compounds may be taken up by the device in sufficient quantities for analysis by GC. These results demonstrate the feasibility of using the INCAT device as a method for the passive monitoring of VOC in air. Passive sampling of ambient air was attempted using a graphitized carbon without success. This was pre-

sumably due to the lower surface area of the colloidal graphite as compared with the thermally deposited carbon.

4. Conclusions

It is noted that these results are still preliminary. However, some of the possible advantages of such a device are given here. The INCAT device is mechanically simple with no moving parts and inexpensive to produce. The use of solventless extraction ensures maximum sensitivity in analysis. The active mode of sampling with its short diffusion path length may provide for more rapid analysis times in the laboratory as compared with passive diffusive sampling. The passive mode of sampling with a 7% error in replicate measurements would allow for the passive monitoring of VOC in the environment.

Results suggest that the INCAT device may provide for a rapid and sensitive alternate method for the analysis of VOC in both air and water samples in either an active or passive sampling mode. We are currently investigating the physical characteristics and possible applications of this device.

Acknowledgements

The authors would like to thank H. Perreault, A. Chow and G.R.B. Webster for their advice and assistance with this work. We also thank NSERC and CMHC for financial support.

References

[1] S. Coffel, K. Feiden, Indoor Pollution, Fawcett Columbine, New York, 1990.
[2] J.D. Splender, K. Sexton, Science 221 (1983) 9.
[3] H.N. MacFarland, Am. Ind. Hyg. Assoc. 47 (1986) 704.
[4] M. Tancrede, R. Nilson, L. Zeise, E.A. Crouch, Atmos. Environ. 21 (1987) 2187.
[5] R.E. Clement, C.J. Koester, Anal. Chem. 65 (1993) 85R.
[6] C.L. Arthur, J. Pawliszyn, Anal. Chem. 62 (1990) 2145.
[7] E. Giller, M.Sc. Thesis, University of Manitoba, 1994.
[8] H.D. Gesser, E. Giller, Environ. Int. 6 (1995) 839.
[9] C. Xu-Liang, H.C. Nicholas, Environ. Technol. 12 (1991) 1055.
[10] A. Berlin, R.H. Brown, K.J. Saunders, CEC Publication # 10555EN, Commission of European Communities, 1987, Brussels-Luxembourg.
[11] M.B. Colella, S. Siggia, R.M. Barnes, Anal. Chem. 52 (1980) 2347.
[12] K.L. Foster, R.G. Fuerman, J. Economy, S.M. Larson, M.J. Rood, Chem. Mater. 4 (1992) 1068.
[13] J. Economy, K.L. Foster, A. Andreopoulus, H. Jung, Chem. Tech. 10 (1992) 597.
[14] A. Baily, P.A. Hollingdale-Smith, Ann. Occup. Hyg. 20 (1977) 345.
[15] P.L. Braun, J.A. Trine, US Pat. # 3950980, 1976.
[16] L.H. Nelms, K.D. Reszner, P.W. West, Anal. Chem. 49 (1977) 944.
[17] M. Chai, J. Pawliszyn, Environ. Sci. Technol. 29 (1995) 693–701.

ELSEVIER

Talanta 44 (1997) 2145–2150

Talanta

Liquid–liquid distribution of ion associates of tetrabromoindate(III) with quaternary ammonium counter ions

Koichi Yamamoto *, Akiko Matsumoto

Department of Materials Science, Yonago National College of Technology 4448, Hikona-cho, Yonago-shi, Tottori 683, Japan

Received 17 January 1997; received in revised form 18 March 1997; accepted 19 March 1997

Abstract

The solvent extraction of an ion associate of tetrabromoindate(III) ion, $InBr_4^-$, with quaternary ammonium cations (Q^+) has been studied. The extraction constant (K_{ex}) were determined for the ion associates of $InBr_4^-$ with Q^+ between an aqueous phase and several organic phases (chloroform, chlorobenzene, benzene and toluene). A linear relationship was found between log K_{ex} and the total number of carbon atoms in Q^+; from the slope of the lines, the contribution of a methylene group to log K_{ex} was calculated to be 0.91 for the chloroform extraction system and 0.52 for the other extraction systems. The extractability with alkyltrimethylammonium cations was larger than that with symmetrical tetraalkylammonium cations and the mean difference in log K_{ex} for two cations (one of each type) with the same number of carbon atoms was about 1.3. From the extraction constant obtained, the extractability of $InBr_4^-$ among metal-halogeno complex anions was in the order $TlBr_4^- > BiI_4^- > AuBr_4^- > AuCl_4^- > TlCl_4^- > InBr_4^- > CuCl_2^-$. © 1997 Elsevier Science B.V.

Keywords: Solvent extraction; Tetrabromoindate(III); Quaternary ammonium ion; Ion association

1. Introduction

An extraction of indium from an aqueous halide medium into an organic solvent has been frequently used for the spectrophotometric determination of indium. Suzuki et al. reported on the extraction of indium from hydrobromic acid solutions [1] or potassium iodide-sulfuric acid solutions [2] with xylene solution of a high molecular weight amine and its determination. Light-absorbing cationic dyes, such as Malachite Green [3], Victoria Blue [4,5], Pyronine G [6,7], Rhodamine B [8], Ethylrhodamine B [9] and Butylrhodamine B [8,10] have been used as a counter ion of indium bromo complex anions, thus providing sensitive extraction-spectrophotometric methods for indium. However, the extraction behaviour of indium bromo complex anion has not yet been examined in quantitative form.

In the present work, the extraction constants for the ion-associates of tetrabromoindate(III) anion with various quaternary ammonium counter-ions distributed between aqueous and four organic phases (toluene, benzene, chlorobenzene and chloroform) were determined and correlated with the number of carbon atoms in the counter

* Corresponding author.

PII S0039-9140(97)00094-5

Table 1
Salts of quaternary ammonium cations examined

Salt (abbreviation)	Formula	Supplier	Purity (%)
Tetraalkylammonium salts			
Tetrapropylammonium chloride (TPA)	$(C_3H_7)_4$ NCl	B	>90
Tetrabutylammonium chloride (TBA)	$(C_4H_9)_4$ NCl	A	>98
Tetraamylammonium chloride (TAA)	$(C_5H_{11})_4$ NCl	B	>95
Alkyltrimethylammonium salts			
Octyltrimethyl ammonium chloride (OTMA)	$C_8H_{17}N(CH_3)_3$ Cl	A	>98
Decyltrimethyl ammonium chloride (DTMA)	$C_{10}H_{21}N(CH_3)_3$ Cl	A	>95
Dodecyltrimethyl ammonium chloride (DDTMA)	$C_{12}H_{25}N(CH_3)_3$ Cl	A	
Tetradecyltrimethyl ammonium chloride (TDTMA)	$C_{14}H_{29}N(CH_3)_3$ Cl	A	>98
Cetyltrimethyl ammonium chloride (CTMA)	$C_{16}H_{33}N(CH_3)_3$ Cl	A	>95

A, Tokyo Kasei; B, Wako Pure.

ions. Extractability of tetrabromoindate(III) was compared with that of other metal-halogeno complex anions. The information concerning the extraction constants and the extractability for tetrabromoindate(III) are useful for designing the novel extraction systems for the separation and determination of indium.

2. Experimental

2.1. Apparatus

A JASCO Uvidec-430 spectrophotometer was used for recording spectra and absorbance measurements in quartz cells of 10 mm light-path length. The pH values were measured with a Hitachi-Horiba (Model F-8 dp) pH-meter. An Iwaki (Model V-SX type KM) shaker was used for horizontal shaking of the 25 ml stoppered test-tubes for extraction.

2.2. Reagents

A standard indium(III) solution (8.71×10^{-4} M) was prepared by diluting 10 ml of a 1000 ppm standard indium(III) solution (8.71×10^{-3} M indium in a 0.5 N nitric acid, Wako Pure Chem.) to 100 ml with distilled water. Hydrobromic acid was used for the formation of a indium(III)-bromo complex. Quaternary ammonium ion (Q^+) solutions were prepared from the salts listed in Table 1, after drying under reduced pressure. Accurately weighed amounts of the dried salts were dissolved in distilled water to give stock standard solutions, which were diluted before use. 1-(2-Pyridylazo)-2-naphthol (PAN) solution (0.1 wt./vol%) was prepared by dissolving 0.1 g of PAN in 100 ml of ethanol. Commercially available toluene, benzene, chlorobenzene and chloroform were used without further purification, and were saturated with distilled water before use. All of the reagents were of analytical-reagent grade and were used as received.

2.3. Procedure

One ml of a 8.71×10^{-4} M indium(III) solution was transferred to a 25 ml stoppered test tube. To it, 3 ml of a concentrated hydrobromic acid solution (8.59 M) was added. The volume of the solution was brought to 5 ml by adding an appropriate amount of aqueous quaternary ammonium salt solution. The aqueous solution was mechanically shaken with 5 ml of an extracting solvent for 20 min at 25°C. After phase separation, the aqueous phase was used for the determination of indium by the extraction-spectrophotometric method with PAN.

Transfer 2 ml of the aqueous solution into a 50 ml beaker and add 18 ml of distilled water and 1 ml of 0.1 wt./vol% PAN solution. Adjust the pH range of the solution to about 5.5–5.9 with sodium hydroxide and acetate buffer solutions.

Transfer this solution into a 50 ml separatory funnel and stand for 5 min. Shake this mixture with 10 ml of chloroform. After phase separation, measure the absorbance of the organic phase at 560 nm against chloroform and calculate the concentration of indium in the original aqueous phase by means of a calibration graph.

2.4. Calculation of extraction constants

In the aqueous phase, indium(III) reacts with bromide to form $InBr_n^{(3-n)}$. The stability constants [11] of the indium(III)-bromo complexes $InBr^{2+}$, $InBr_2^+$, $InBr_3$ and $InBr_4^-$ are $\log \beta_{1,1} = 2.08$, $\log \beta_{1,2} = 3.4$, $\log \beta_{1,3} = 4.0$ and $\log \beta_{1,4} = 4.8$, respectively. These complexes are distributed between the aqueous and organic phases:

$$InBr_3 \rightleftharpoons (InBr_3)_o;$$

$$K_D(InBr_3) = [InBr_3]_o/[InBr_3] \quad (1)$$

$$InBr_4^- + Q^+ \rightleftharpoons (Q^+ \cdot InBr_4^-)_o;$$

$$K_{ex}(InBr_4^-) = [Q^+ \cdot InBr_4^-]_o/[Q^+][InBr_4^-] \quad (2)$$

where K_{ex} is the extraction constant; the subscript o refers to the organic phase and the absence of a subscript indicates the aqueous phase.

The distribution ratio of indium between the aqueous and organic phases (D_{In}) is given by

$$D_{In} = \frac{[InBr_3]_o + [Q^+ \cdot InBr_4^-]_o}{[In^{3+}] + [InBr^{2+}] + [InBr_2^+] + [InBr_3] + [InBr_4^-]} \quad (3)$$

The side-reaction coefficient of the complexes of indium(III) with bromide in the aqueous phase, $\alpha In^{3+}(Br^-)$, is given by

$$\alpha In^{3+}(Br^-) = \frac{[In^{3+}] + [InBr^{2+}] + [InBr_2^+] + [InBr_3] + [InBr_4^-]}{[In^{3+}]}$$

$$= 1 + \beta_{1,1}[Br^-] + \beta_{1,2}[Br^-]^2 + \beta_{1,3}[Br^-]^3 + \beta_{1,4}[Br^-]^4 \quad (4)$$

When the total concentration of bromide in the aqueous phase is 5.15 M, the fifth term on the right-hand side of Eq. (4) has the greatest contribution to $\alpha In^{3+}(Br^-)$ by the calculation with the stability constants. Hence it is reasonable to consider that in the aqueous phase almost all the indium(III) is present as $InBr_4^-$, and Eq. (3) can be written as

$$D_{In} = \frac{[Q^+ \cdot InBr_4^-]_o}{[InBr_4^-]} = \frac{[In^{3+}]_i - [InBr_4^-]}{[InBr_4^-]} \quad (5)$$

where $[In^{3+}]_i$ is the initial concentration in the aqueous phase. In the extraction of tetrabromoindate(III), the concentration of indium in the aqueous phase after extraction was determined based on the extraction-spectrophotometric method with PAN and the concentration of indium in the organic phase after extraction was determined by subtracting the concentration of indium in the aqueous phase after extraction from the initial concentration of indium in the aqueous phase. The distribution ratios of indium at different concentrations of the quaternary ammonium ions were calculated from Eq. (5).

Hence, the following Eq. (6) can be derived from Eqs. (2) and (5).

$$D_{In} = K_{ex}(InBr_4^-) \cdot [Q^+] \quad (6)$$

where

$$\log D_{In} = \log K_{ex} + \log[Q^+] \quad (7)$$

The side-reaction coefficient for the quaternary ammonium ion $\alpha Q^+(Br^-)$ is given by

$$\alpha Q^+(Br^-) = \frac{[Q^+]'}{[Q^+]} = \frac{[Q^+] + [Q^+ \cdot Br^-]_o}{[Q^+]} = 1 + K_{ex}(Q^+ \cdot Br^-) \cdot [Br^-] \quad (8)$$

where $[Q^+]'$ is the total concentration of the quaternary ammonium ion that is not bound in ion associates with tetrabromoindate(III) and $K_{ex}(Q^+ \cdot Br^-)$ is the extraction constant of a quaternary ammonium ion with a bromide ion. $[Q^+]$ can be calculated by

$$[Q^+] = [Q^+]'/\alpha Q^+(Br^-) \quad (9)$$

$[Q^+]'$ is evaluated by the following equation:

$$[Q^+]' = C_T(Q^+) - [Q^+ \cdot InBr_4^-]_o \quad (10)$$

where $C_T(Q^+)$ is the total concentration of the quaternary ammonium ion. $[Q^+]$ can be calculated using Eqs. (8)–(10).

3. Results and discussion

3.1. Effect of the concentration of bromide ion

TBA and chloroform were used as a counter ion of an indium(III)- bromo complex and an extracting solvent, respectively. The effect of the concentration of bromide ion on the formation of the indium(III)-bromo complex was examined by determining indium in the aqueous phase after extraction based on the extraction-spectrophotometric method with PAN. The concentration of indium in the aqueous phase first decreased along with an increase in the bromide concentration, and then became constant. Constant absorbances were obtained at 4.29–6.01 M bromide concentration range. Therefore, 5.15 M bromide was used for the formation of the indium(III)-bromo complex and $InBr_4^-$ was the predominant indium species in the aqueous phase.

3.2. Determination of extraction constants

In a low-polarity solvent (its dielectric constant is less than about 10), the extraction equilibrium is simple and is given by Eq. (2) because the dissociation of the ion associate in the organic phase is negligibly small. Toluene, benzene, chlorobenzene and chloroform were used as a low-polarity extraction solvent. In the extraction of tetrabromoindate(III), the distribution ratios of indium at different concentrations of the quaternary ammonium ions were determined. The values of log D_{In} were plotted against log$[Q^+]$; the results for $Q^+ \cdot InBr_4^-$ extraction systems are shown in Fig. 1 (chloroform and chlorobenzene) and Fig. 2 (benzene and toluene). As expected from Eq. (7), straight lines with a slope of 1 were obtained for all of the extraction systems. This means that the extraction equilibrium of Eq. (2) holds, and that the extracted species is $Q^+ \cdot InBr_4^-$. The extraction constants calculated from Eq. (7) are summarized in Table 2; the standard deviation is small.

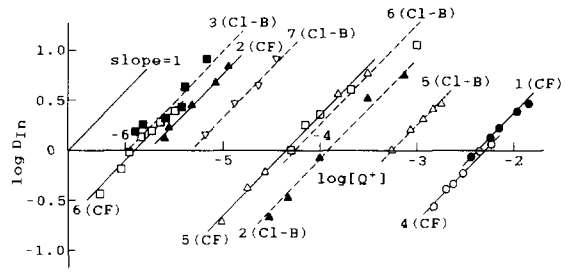

Fig. 1. Plots of log D_{In} vs. log$[Q^+]$. Extracting solvent: chloroform (CF), chlorobenzene (Cl-B); Q^+: (1) TPA, (2) TBA, (3) TAA, (4) OTMA, (5) DTMA, (6) DDTMA, (7) TDTMA.

3.3. Relationship between the extraction constant and the number of carbon atoms in the quaternary ammonium ion

The values of the extraction constants (log K_{ex}) were plotted against the number of carbon atoms in the quaternary ammonium ion (N_c). The results are shown in Fig. 3. For the same carbon number, the extractability (log K_{ex}) with long-chain alkyltrimethylammonium cations (group I) is larger than that with symmetrical tetraalkylammonium cations (group II), and the mean difference in log K_{ex} values between these two groups was about 1.3. The ion association reaction in a low-polar solvent extraction process is based on a hydrophobic interaction and an electrostatic interaction: the effect of the former on the ion association is larger than that of the latter, which contributes to an increase in log K_{ex} value with increasing N_c. However, the differences in log K_{ex}

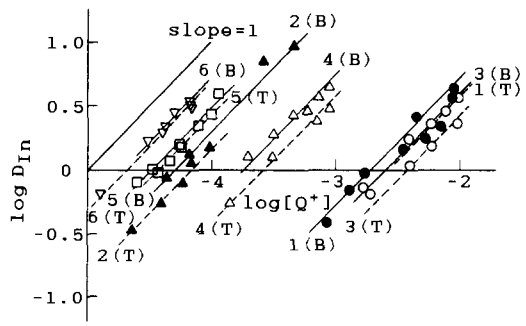

Fig. 2. Plots of log D_{In} vs log$[Q^+]$. Extracting solvent: benzene (B), toluene (T); Q^+: (1) TBA, (2) TAA, (3) DTMA, (4) DDTMA, (5) TDTMA, (6) CTMA.

Table 2
Extraction constants ($\log K_{ex}$) obtained between aqueous and organic phases

Q^+	Extracting solvent[a]	$\log K_{ex}$	
		$InBr_4^-$ [b]	Br^- [c]
TBA	T	2.56 ± 0.05 (4)	−5.35
TAA	T	4.18 ± 0.03 (5)	−2.99
DTMA	T	2.43 ± 0.05 (4)	−5.92
DDTMA	T	3.58 ± 0.03 (4)	−4.74
TDTMA	T	4.41 ± 0.01 (4)	−3.56
CTMA	T	4.70 ± 0.03 (4)	−2.38
TBA	B	2.71 ± 0.04 (5)	−4.55
TAA	B	4.29 ± 0.06 (4)	−2.19
DTMA	B	2.59 ± 0.03 (5)	−5.12
DDTMA	B	3.75 ± 0.04 (6)	−3.94
TDTMA	B	4.52 ± 0.04 (5)	−2.76
CTMA	B	4.73 ± 0.03 (4)	−1.58
TBA	Cl-B	3.94 ± 0.06 (5)	−2.25
TAA	Cl-B	5.98 ± 0.09 (6)	0.11
DTMA	Cl-B	3.25 ± 0.02 (5)	−2.82
DDTMA	Cl-B	4.24 ± 0.08 (5)	−1.64
TDTMA	Cl-B	5.12 ± 0.01 (4)	−0.46
TPA	CF	2.35 ± 0.05 (5)	−1.01
TBA	CF	5.73 ± 0.03 (5)	1.35
OTMA	CF	2.31 ± 0.02 (6)	−0.40
DTMA	CF	4.39 ± 0.07 (5)	0.78
DDTMA	CF	5.90 ± 0.04 (7)	1.96

[a] Solvent: T, toluene; B, benzene; Cl-B, chlorobenzene; CF, chloroform.
[b] Mean value ± S.D. The figures in parentheses are the number of measurements.
[c] Ref. [12].

values between these two quaternary ammonium ions for the same carbon number indicates that the electrostatic attraction of the cations in group I for the anionic complex is larger than that of the cations in group II, which can be explained by an effect of a flexibility of a quaternary ammonium ion: the flexibility of the alkyltrimethylammonium ion decreases the distance between the cation and the anion. In the $\log K_{ex}$–N_c plots for the benzene extraction systems, the points for the alkyltrimethylammonium ions having more than 17 carbon atoms (group I–II) deviate from the straight line for those up to 17 carbon atoms (group I–I). In the $\log K_{ex}$-N_c plot for the toluene extraction system, the points for the alkyltrimethylammonium ions having more than 15 carbon atoms (group I–II) deviate from the straight line for those upto 15 carbon atoms (group I–I). These may be because the increment in spread of the hydrophobic alkyl chain of the cations in group I–II is smaller than that of the cations in group I–I. The slopes of the two lines for groups I and II were identical for each extraction system, and from them the contribution of a methylene group to $\log K_{ex}$ ($\Delta \log K_{ex}/-CH_2-$) was found to be about 0.91 for the chloroform extraction system and about 0.52 for the chlorobenzene, benzene and toluene extraction systems on average. The value of $\Delta \log K_{ex}/-CH_2-$ for the chloroform extraction system is larger than those for the other three extraction systems. This may be caused by the effect of the solvation of chloroform on tetrabromoindate(III): tetrabromoindate(III) ion is more solvated by chloroform than by the other extracting solvents, and tetrabromoindate(III) is more easily extracted into chloroform. The values of $\Delta \log K_{ex}/-CH_2-$ for chlorobenzene, benzene, toluene extraction systems are in good agreement with the previously reported values [13–21].

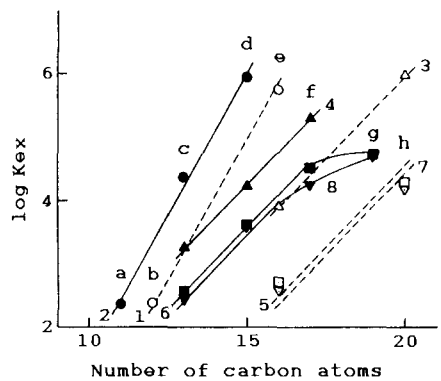

Fig. 3. Relation between $\log K_{ex}$ and the number of carbon atoms in the quaternary ammonium ion. Extracting solvent: (1) and (2) chloroform, (3) and (4) chlorobenzene, (5) and (6) benzene, (7) and (8) toluene; Q^+: (1), (3), (5) and (7) tetraalkylammonium ion (b) TPA, (e) TBA, (h) TAA, (2), (4), (6) and (8) alkyltrimethylammonium ion (a) OTMA, (c) DTMA, (d) DDTMA, (f) TDTMA, (g) CTMA.

Table 3
Extraction constants of ion associates of various metal-halogeno complex anions with octyltrimethylammonium cation in chloroform-extraction

X^-	Metal-halogeno complex	log K_{ex}	Δ log K_{ex}
Cl^-	$CuCl_2^-$	1.57[a]	2.09
	$TlCl_4^-$	3.66[b]	
	$AuCl_4^-$	4.23[c]	0.57
Br^-	$InBr_4^-$	2.31	2.66
	$AuBr_4^-$	4.97[c]	
	$TlBr_4^-$	5.33[b]	0.36
I^-	BiI_4^-	5.31[d]	

[a] Ref. [17].
[b] Ref. [18].
[c] Ref. [19].
[d] Ref. [20].

3.4. Extractability of tetrabromoindate(III)

The extraction constants (log K_{ex}) for the 1:1 ion associates of metal-halogeno complex anions with $OTMA^+$ into the chloroform extraction are listed in Table 3. From these values, it was found that the extractability of metal-halogeno complex anions was in the order $TlBr_4^- > BiI_4^- > AuBr_4^- > AuCl_4^- > TlCl_4^- > InBr_4^- > CuCl_2^-$; the differences in log K_{ex} between two metal-halogeno complex anions in this order were 0.02, 0.34, 0.74, 0.57, 1.35 and 0.74.

In the design of new sensitive and selective extraction-spectrophotometric methods for indium utilizing the ion association, the use of the extraction constants and the extractability for tetrabromoindate(III) described above has the advantages of saving of time, low cost and less labour in the experiment, e.g. from the extraction constants obtained, the contribution of some factors to the extraction constants and the extractabilities of cations, anions and extracting solvents, possible extraction systems for a spectrophotometry for indium may be predicted.

References

[1] T. Suzuki, T. Sotobayashi, Bunseki Kagaku 12 (1963) 910.
[2] T. Suzuki, T. Sotobayashi, Bunseki Kagaku 14 (1965) 420.
[3] T. Matsuo, S. Funada, H. Koide, M. Suzuki, Bunseki Kagaku 13 (1964) 763.
[4] G. Popa, C. Patroescu, T. Nascutiu, Chim. Anal. (Bucharest) 1 (1971) 144; Chem. Abstr. 76 (1972) 107533.
[5] C. Constantinescu, L. Antonescu, Rev. Roum. Chim., 20 (1975) 985; Chem. Abstr. 83 (1975) 157430.
[6] C. Patroescu, Rev. Chim. (Bucharest) 21 (1970) 409; Chem. Abstr. 73 (1970) 126629.
[7] G. Popa, C. Patroescu, C. Rev, Chim. (Bucharest) 21 (1970) 770; Chem. Abstr. 74 (1971) 134630.
[8] A. Garcic, L. Sommer, Collect. Czech. Chem. Commun. 35 (1970) 1047.
[9] I.A. Bochkareva, I.A. Blyum, Zh. Anal. Khim. 30 (1975) 874.
[10] L. Sommer, A. Garcic, Proc. Anal. Chem. Conf., 3 (1) (1970) 135; Chem. Abstr. 74 (1971) 38025.
[11] R.M. Smith, A.E. Martell, Critical Stability Constants: Inorganic Complexes, vol. 4, Plenum Press, New York, 1976.
[12] S. Motomizu, Dojin News 38 (1987) 3.
[13] S. Motomizu, S. Hamada, K. Toei, Bunseki Kagaku 32 (1983) 648.
[14] R. Modin, G. Schill, Acta Pharm. Suecica 7 (1970) 585.
[15] G. Schill, Acta Pharm. Suecica 2 (1965) 13.
[16] K. Yamamoto, T. Fujibayashi, S. Motomizu, Solvent Extr. Ion Exch. 10 (1992) 459.
[17] K. Yamamoto, S. Motomizu, Talanta 36 (1989) 561.
[18] K. Yamamoto, M. Endo, Anal. Sci. 12 (1996) 739.
[19] K. Yamamoto, S. Inada, Anal. Sci. 11 (1995) 643.
[20] K. Yamamoto, M. Endo, Anal. Sci. 10 (1994) 755.
[21] K. Yamamoto, S. Katoh, Talanta 43 (1996) 61.

ELSEVIER

Talanta 44 (1997) 2151–2159

Talanta

Amperometric detection of uric acid and hypoxanthine with Xanthine oxidase immobilized and carbon based screen-printed electrode. Application for fish freshness determination

M-A. Carsol [a], G. Volpe [b], M. Mascini [a,*]

[a] *Dipartimento di Sanità Pubblica, Epidemiologia e Chimica Analitica Ambientale, Sezione di Chimica Analitica, Via Gino Capponi 9, 50121 Firenze, Italy*

[b] *Laboratorio Alimenti ISS, Viale Regina Elena 299, 00161 Roma, Italy*

Received 16 December 1996; received in revised form 14 March 1997; accepted 25 March 1997

Abstract

Carbon-based screen-printed electrodes are suitable for uric acid detection. Xanthine oxidase (XO) was immobilized either directly on the surface of the electrode or in a reactor with CPG aminopropylsilane in a FIA assembly. Higher reproducibility and lifetime was obtained with the reactor. Optimum conditions were found for the determination of Hypoxanthine (Hx), Inosine (HxR) and Inosine monophosphate (IMP). Calibration curves for IMP, HxR and Hx are linear up to 50 μM with detection limit of 1 μM for 50 μl injection. One assay is completed within 30 s. The reproducibility of 20 μM of Hx was obtained with CV 2%. © 1997 Elsevier Science B.V.

Keywords: Screen-printed electrodes; Uric acid detection; Xanthine oxidase; Hypoxanthine detection; Fish freshness

1. Introduction

Rapid non destructive methods would be useful in monitoring fish meat quality during processing, transportation and marketing.

Freshness has been determined on the basis of indicators such as ATP-related compounds which normally don't exist in the living tissues of fish. Adenosine triphosphate (ATP) is decomposed in fish meat, adenosine diphosphate (ADP), adenosine monophosphate (AMP) and related compounds are formed by autolysis and/or microbial actions following the death of fish. ATP is then degraded to uric acid (AU) through the following pathway:

$$ATP \rightarrow ADP \rightarrow AMP \rightarrow IMP \rightarrow HxR \rightarrow Hx \rightarrow X \rightarrow AU$$

Hypoxanthine (Hx) and inosine (HxR) concentrations depend upon the species of fish. Inosine monophosphate (IMP) is one of the major contributing factors to the pleasant flavour of fresh fish. The accumulation of Hx and/or xanthine (X) during the storage results in an 'off-taste'. The concentration of Hx, one of the intermediates of

* Corresponding author. Tel: +39-55-2757274; fax: +39-55-2476972; e-mail: mascini@cesit1.unifi.it

PII S0039-9140(97)00098-2

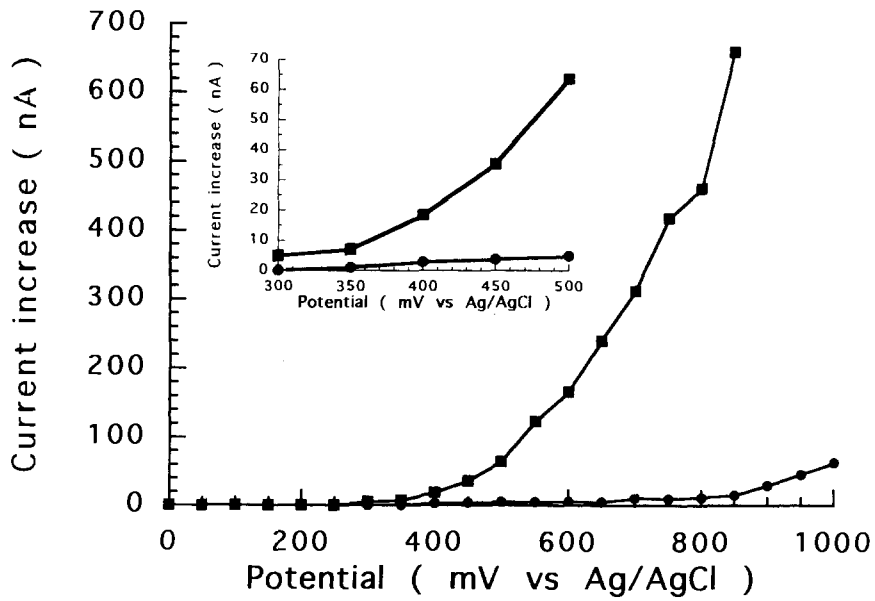

Fig. 1. Hydrodynamic voltammogram of (■) uric acid, 29 μM, and (●) hydrogen peroxide, 3 mM.

these reactions increases with prolonged storage and thus can be used as an indicator of fish meat freshness [1].

Simultaneous determination of these compounds is also necessary for a rapid estimation of freshness.

IMP, HxR and Hx determinations are based on the following enzyme reactions:

$$IMP \xrightarrow{N_T \text{ (or AlP)}} HxR$$

$$HxR + P_i \xrightarrow{N_P} Hx + \text{Ribose} - 1 \text{ Phosphate}$$

$$Hx + 2O_2 \xrightarrow{XO} AU + 2H_2O_2$$

where N_T is 5′-nucleotidase, AlP alkaline phosphatase, N_P nucleoside phosphorylase and XO xanthine oxidase. XO is a flavoprotein which possesses the flavine adenine dinucleotide (FAD) as a cofactor at the active site.

Time consuming, expensive and complex methods such as paper chromatography, anion-exchange chromatography, precipitation, spectrophotometry [2,3] are described for the determination of Hx, X and AU in fish tissue extract.

Electrochemical methods have attracted considerable attention for the determination of Hx and X using an immobilized enzyme-modified oxygen electrode [1,4–12]. Oxygen electrode coupled with bacteria was exploited for evaluation of fish meat quality [13]. These procedures are all based upon the amount of oxygen consumed near the surface of the sensor. A voltammetric procedure for the simultaneous determination of Hx, X and AU has been also reported using a pyrolytic graphite electrode and standard solutions [14]. IMP, HxR and Hx concentrations have been also determined by measuring the hydrogen peroxide formation using a Clark hydrogen peroxide probe [15,16].

An amperometric sensor for Hx and X based on the detection of uric acid with XO adsorbed on a carbon paste electrode has been proposed [17].

Flow Injection Analysis (FIA) has been used combining a reactor with an alkaline phosphatase (AlP) immobilized and a second reactor with a purine nucleoside phosphorylase-xanthine oxidase (N_P–XO) coimmobilized for the determination of purine nucleotides (ATP, ADP, AMP) with a flow through glassy carbon electrode measuring the uric acid produced [18].

A system with double enzyme reactors (XO–N_P and N_T–N_P–XO) coupled with oxygen electrode and FIA apparatus was developed for the determination of fish freshness [19].

An oxygen electrode coupled with three enzymes: 5′-N_T, XO and N_P was introduced in a FIA system at 30°C, pH 7.8 (1.4 ml min^{-1}) for determination of IMP. Calibration curves are linear in the range 1–5 mM for a 50-µl injection [8].

In this paper we report the use in a FIA assembly of a carbon based screen-printed electrode. This sensor is very sensitive and selective for uric acid detection; hydrogen peroxide is not detected by such electrode at the potential of 450 mV (Fig. 1).

The coupling of this disposable sensor with XO enzyme has been realized immobilizing directly the enzyme on the carbon or by use of a glass bead reactor where the enzyme was immobilized. Hx therefore is quantitatively analysed and, by

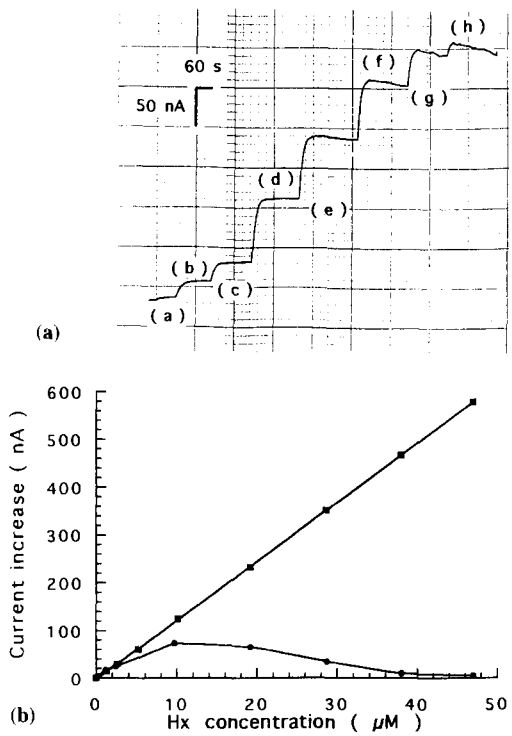

Fig. 2. (a) Amperometric detection with immobilized XO screen-printed electrode: Response of the XO sensor to Hx (a) 0.2 µM, (b) 1 µM, (c) 2 µM, (d) 5 µM, (e) 10 µM, (f) 19 µm, (g) 29 µM and (h) 38 µM. (b) Hx calibration curves of the XO-screen-printed electrode by (●) successive additions of the standard solution or by (■) washing the electrode before each addition.

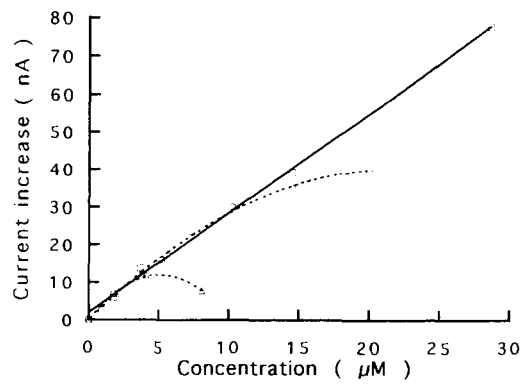

Fig. 3. Amperometric detection with immobilized Xanthine oxidase (XO) screen-printed electrode: Calibration curves for determinations of (□) Hx, (○) HxR and (△) IMP.

using the other enzymes in solution (N_P and N_T or AlP), the related compounds, IMP and HxR, could be also evaluated.

Use of real samples indicates that the reactor gave higher reproducible results and with an easy procedure quantitative determination of AU, Hx, HxR and IMP in real samples in few minutes is obtained.

2. Experimental

2.1. Chemicals

Xanthine oxidase (XO) (EC 1. 1. 3. 22; from buttermilk; 0.4 U mg^{-1}; Fluka), 5′-nucleotidase (EC 3. 1. 3. 5; from Crotalus Adamanteus; 110 U mg^{-1}; Fluka), nucleoside phosphorylase (EC 2. 4. 2. 1; bacterial; 9,7 U mg^{-1}; Fluka), hypoxanthine, xanthine, inosine, inosine monophosphate, uric acid, phosphate potassium dihydrogenphosphate, imidazole and BSA were purchased from Sigma Chemical Co., St Louis, MO (USA). Glutaraldehyde (25% aqueous solution) and L-hydrochloride lysine were obtained from Merck.

2.2. Screen-printed electrode

Screen-printing is a simple and fast technique for mass production of disposable electrochemical sensors. These electrodes, single-use, have several

advantages like avoidance of contamination between samples, constant sensitivity and high reproducibility of the different printed sensors. The sensor coupled with enzyme avoided the denaturation effect due to multiple samples.

With this technique, the ink used to print electrodes can be varied easily and therefore different properties of the final sensor can be achieved. Many different inks are commercially available and some of them are based on noble metals. Carbon can also be mixed with different compounds (mediators, enzymes, metal catalytic particles...) and therefore modified sensors and biosensors can be easily mass produced.

The inks can be printed on several kind of supports like glass, ceramic and plastic sheet. In our opinion, the most interesting material for printing electrochemical sensors are the carbon-based inks as they can be printed on plastic sheets at very low firing temperature (from room temperature to 120°C).

Screen-printing technology consists in depositing different inks on a substrate in a film of controlled pattern and thickness. The inks consisted of finely divided particles of different materials in a blend of thermoplastic resins. The printed ink must be heated to polymerize the ink and then it is ready for an ensuing printing step. After every printing step electrodes were heated at 110°C for 10 min.

The screen-printed electrodes were used in a 3-electrode configuration with a Ag/AgCl as reference electrode and a silver electrode as counter. They were realized by several steps corresponding to the deposition of different layers:

- a first layer of silver ink for the conductive pad,
- a carbon pad positioned over a part of the silver track for the working electrode
- a silver/silver chloride over the silver track for the reference electrode
- and finally an insulating layer with openings to allow electrical contact on a polyester flexible film [20].

2.3. Preparation of a XO immobilized electrode

Before enzyme immobilization, the electrode was poised at 1.7 V vs Ag/AgCl for 20 s in order to oxidize the carbon surface. This treatment was found very important for the reproducibility of the biosensor behaviour:

- 3 μl of a solution prepared by mixing
- 20 μl of phosphate buffer 0.05 M pH 7.8 containing 0.023 U XO, 0.015 mg BSA
- and 2 μl of 0.025% glutaraldehyde,

were placed on the carbon surface (geometrical area = 4 mm^2). The membrane was air-dried for about 2 h then washed for 20 min in 0.05 M phosphate buffer pH 7.8 with 0.5 M lysine to remove the excess of glutaraldehyde. The enzyme electrode was stored at 4°C until use. All experiments were performed in 0.05 M Imidazole buffer pH 7.8 containing 50 mM phosphate and 0.1 M KCl.

2.4. Preparation of the XO immobilized reactor

The Xanthine oxidase is immobilized by glutaraldehyde to activated controlled pore glass beads (aminopropyl glass, average pore size 700 Å, particle size 80–120 mesh obtained from Sigma). To a suspension of 50 mg of activated pore glass in 300 μl of buffer, 500 μl of 2.5% glutaraldehyde solution is added. This mixture is gently stirred at room temperature for 1 h, then washed with water. We add 1.2 mg of XO (0.5 U) to the mixture and this is stirred at 4°C for 24 h.

The activated glass (about 20 mg) is packed in Tygon™ tube of 0.60 mm internal diameter and 20 mm long.

The working buffer for the procedure is 0.05 M Imidazole containing 0.1 M KCl and 50 mM KH_2PO_4 at pH 7.8. The reactor is stored at about 4°C in the working buffer when not in use.

2.5. Flow systems and procedure

The system consisted of a pump (Minipuls 3 Peristaltic Pump Gilson), an injector (Rheodyne 5701). An amperometric biosensor detector (Universal Sensors, Inc) was used as potentiostat and connected with an Amel model 868 recorder.

The screen-printed 3 electrode was placed in a suitable flow cell. The working buffer solution is continuously transferred to the flow cell at a constant rate by a peristaltic pump. When the

current reaches a stable value (drift less than 1% in 10 min), a known volume (50 μl) of sample solution is injected through the sampling valve.

2.6. Amperometric determinations

Hypoxanthine and related compounds determination were based on uric acid detection at a potential of 450 mV vs Ag/AgCl with carbon-based screen-printed electrode.

IMP, HxR, Hx and AU standard solutions were prepared by dissolving reagent in Imidazole buffer 0.05 M containing 0.1 M KCl-50 mM KH_2PO_4 and were diluted with the buffer solution. Suitable amount of N_T (or AlP) and N_P enzymes added for the detection of IMP and HxR were optimized according to literature [16].

The 3 electrode system was used in beaker and in the flow cell.

In the beaker, the 3 electrode with immobilized XO was immersed in buffer and standard solution of AU and Hx were added. In the flow system, the 3 electrode was loaded into the flow cell and the standard solutions were injected.

Calibration curves were therefore obtained with the two procedures. Standard solutions of HxR and IMP were added with N_P and N_P-N_T enzymes and after few minutes (5–10) could be employed for calibrations. In the case of IMP we found that the conversion rate was increased at 30°C.

2.7. Preparation of samples for fish freshness determination

Several authors proposed a treatment of fish sample according to Ehira's methods [2]. A simpler method has been used. Exudate of fish muscle (10 μl) obtained by press treatment were diluted with 5 ml of buffer Imidazole 0.05 M pH 7.8 containing 0.1 M KCl and 50 mM KH_2PO_4 and used immediately as the sample.

Samples for the determination of fish freshness were prepared from the specie gilthead bream. AU concentration is determined using the FIA system without the XO reactor.

3. Results and discussion

3.1. Uric acid amperometric response

The carbon electrode gave a very fast and reproducible response to uric acid. The calibration curve obtained with standard solutions added to buffer was perfectly linear in the range 1–50 μM with a standard deviation of 5% and a limit detection of 0.2 μM. This was the basic finding and we tried to exploit such linear behaviour for hypoxanthine determination and then for freshness evaluation.

3.2. Hypoxanthine detection with XO immobilized

Enzyme immobilized on carbon sensor allows a rapid signal when hypoxanthine standard solution was added to the buffer.

However, the signal decreases very soon and the enzyme becomes poisoned just after the addition (Fig. 2a). If we add a second addition, the enzyme results inhibited.

However, if we change the buffer solution and we add a new aliquot of hypoxanthine standard solution, we could obtain a current value proportional to the addition. Therefore we could obtain a linear calibration curve by changing the buffer solution before the addition of hypoxanthine and by monitoring the maximum value of current (Fig. 2b).

The calibration curve obtained with such procedure is linear up to 50 μM and is stable and reproducible for more than 50 assays in this range. Then, the response of the sensor decreases slowly.

The calibration curve with HxR and IMP standard solutions treated respectively with N_P and N_P–N_T enzymes showed a linear range more narrow. Fig. 3 reports the comparison of the calibration obtained from Hx, HxR and IMP.

From these experiments we learned that XO is inhibited by the enzyme product, probably adsorbed by the carbon matrix and only the extensive washing of the electrode allows a new determination. Moreover the presence of the other enzymes N_P or N_P-N_T in the solution inhibits more the XO enzymatic reaction, decreasing the linear portion of the calibration curve.

3.3. Flow injection system with XO immobilized screen-printed electrode

Previous results led to the conclusion that only a FIA procedure could be useful to exploit the linearity of the uric acid probe.

The best flow rate and the sample loop were found 0.5 ml min^{-1} and 50 μl (dispersion coefficient was 1.05).

Fig. 4a reports the calibration curve obtained with hypoxanthine and uric acid standard solutions. We can observe the linearity of the calibration curve and that XO converts hypoxanthine completely up to almost 100 μM. However, Fig. 4b reveals how after 2 h (40 additions) the curve is linear only up to 50 μM. The detection limit is 5 μM.

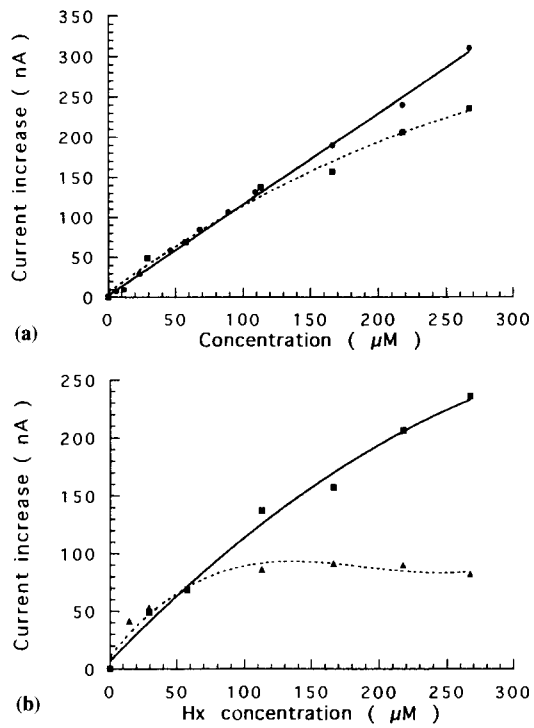

Fig. 4. (a) Amperometric detection with immobilized Xanthine oxidase (XO) screen-printed electrode using Flow Injection Analysis: Calibration curves for determination of (●) AU and (■) Hx. pH 7.8; T, 20°C; flow rate, 0.5 ml min^{-1}; sample volume, 50 μl. (b) Influence of time on output current of the Hx sensor (■: zero time; ▲: after 2 h). Sample volume, pH and flow rate were 50 μl, 7.8 and 0.5 ml min^{-1}, respectively.

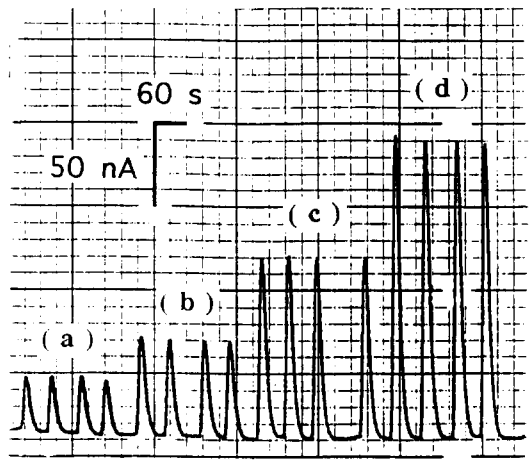

Fig. 5. Amperometric detection utilizing immobilized Xanthine oxidase (XO) reactor and screen-printed electrode: Typical signals for 50 μl injections of standard solution Hx, (a) 8 μM; (b) 16 μM; (c) 32 μM and (d) 62 μM). Carrier solution (0.05 M Imidazole buffer at pH 7.8 containing 0.1 M KCl and 0.05M KH_2PO_4) was pumped at a flow rate of 0.5 ml min^{-1}.

The experiments reveal how the enzyme was still poisoned if high concentration of Hx were flowed.

3.4. FIA with XO reactor and screen-printed electrode

A reactor loaded with XO was introduced into the FIA assembly and results obtained (Fig. 5)

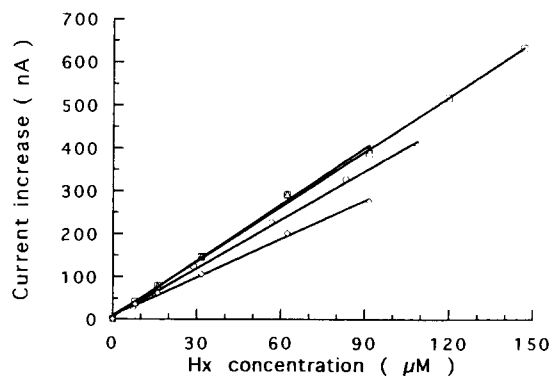

Fig. 6. Hx calibration curve: Effect of the storage time ((□) 0 h, (○) 24 h, (△) 48 h and (◇) 72 h). pH 7.8; T, 20°C; flow rate, 0.5 ml min^{-1}; sample volume, 50 μl.

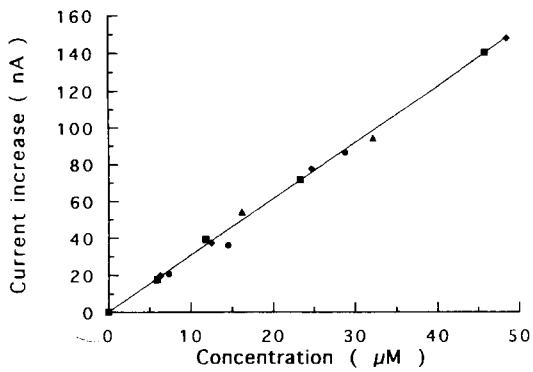

Fig. 7. Amperometric detection utilizing immobilized Xanthine oxidase (XO) reactor and screen-printed electrode: Calibration curves for determination of (■) AU, (●) Hx, (▲) HxR and (◆) IMP. Flow rate, temperature, pH and sample volumes were 0.5 ml min^{-1}, 20°C, 7.8 and 50 μl, respectively.

showed high linearity, high reproducibility and fast recovery. The sampling rate is about 100 samples h^{-1}.

The relative standard deviations for 4 replicate injections were 2% for a concentration of 20 μM.

The XO immobilized enzyme reactor was used repeatedly to evaluate the lifetime (Fig. 6). The system shows linear response after repetitive use even after 2–3 months with standard solutions

The response curves to IMP, HxR and Hx were compared. After the output current reached a steady state, an aliquot of each compound was injected into the sensor system.

Any appreciable difference was observed in the response times for IMP, HxR, Hx and AU.

In Fig. 7 the calibration curves for IMP, HxR, Hx and AU are reported in the range 1–50 μM indicating a total conversion of IMP, HxR and Hx to AU. The responses are linear in this range and the detection limit is 1 μM.

3.5. Real samples

Exudates from fishes are generally diluted, filtered through 0.45 μm pore filters and injected without any pretreatment into the sampling valve.

Preliminary experiments showed a drastic effect on the current obtained after repetite sample injections.

Fig. 8(a) and Fig. 8(b) report the drastic reduction (around 80%) obtained with standard solutions of uric acid and hypoxanthine before and after 100 injections of fish samples diluted 50 times with the buffer.

The decrease is related to the electrode fouling which appears as a reduction of the active area. The calibration curve is still linear for both uric acid and hypoxanthine but much decreased. Therefore it appears that the enzyme reactor is still converting all hypoxanthine in uric acid but it is the electrode which is unable to oxidise uric acid.

Moreover additions of standard solutions of uric acid or hypoxanthine to the samples indicate a nonlinear behaviour of the current obtained.

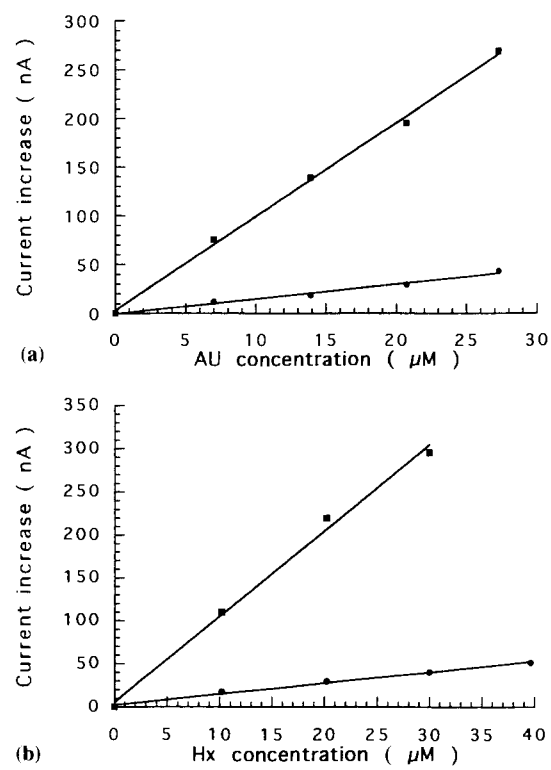

Fig. 8. (a and b) Amperometric detection utilizing immobilized Xanthine oxidase (XO) reactor and screen-printed electrode: Calibration curves for determination of AU and Hx (■) before and (●) after 100 injections of fish samples diluted 50 times with buffer. Flow rate, temperature, pH and sample volumes were 0.5 ml min^{-1}, 20°C, 7.8 and 50 μl, respectively.

Table 1
Results obtained with real samples (Gilthead bream) stored in different conditions

Storage method	Time from death	[AU] (mM)	[Hx] (mM)	[HxR] (mM)	[IMP] (mM)	K (%)
4°C	48	0	1.85	0.5	11.8	17
	72	0.5	2.65	0.3	12.05	22
	96	0.1	1.1	0.1	4	24
	120	-	0.4	0.2	5.45	26
	168	0	0.6	0.45	2.7	28
	192	0.1	2.35	0.25	5.3	34
4°C with ice	48	0	1.25	1.25	20.15	11
	72	0	1.05	0.2	5.7	18
	96	0.15	0.05	0.3	1.9	21
	120	0	0.6	0.35	2.6	27
	168	0	0.5	1	3.95	27.5
	192	0.05	1.05	1.05	6.35	25
	216	0.25	0.25	0.95	3.5	29
	240	0.8	1.15	2.75	9.05	34

However, if the exudates are diluted 500 times or more with the buffer, linear behaviour in the final range 0–10 μM is obtained with a detection limit of 0.2 μM. Therefore a detection limit of 0.1 mM in the exudate can be obtained. Uric acid and hypoxanthine gave the same calibration curve and it was estimated that 40 assays can be realized with a single sensor. After this number of real samples the sensor has to be discarded and substituted with a new one. Therefore a disposable sensor is necessary for such kind of measurement.

Additions of N_P and N_T (or AlP) enzymes to the diluted exudates allow the detection of HxR and IMP in the sample as reported in the experimental section.

The hypoxanthine oxidase reactor showed a good operational stability during 2–3 months for at least 200–300 assays. The CV was around ± 3% for a sample containing 1.20 mM of Hx or HxR and IMP.

Moreover the proposed procedure allows the determination of uric acid in the exudate (by excluding the reactor) and this information could be useful to assess quality studies.

In Table 1 we report a study on the determination of AU, Hx, HxR and IMP of real samples (gilthead bream) stocked in different conditions. Therefore the sensor appeared promising for routine determination of fish freshness.

K value, indicator of fish freshness, based on the degradation of ATP in fish meat is defined as

$$K = 100\,(HxR + Hx)/(IMP + HxR + Hx) \quad (1)$$

as ATP, ADP and AMP disappear around 24 h after the death of the fish.

Species showed a K value of about 11–17%, 48 h after the death. During storage at 4°C, the K value increased to 34% after 192 h while the fish kept at 4°C with ice reached this value after 240 h. These results showed that the degradation is higher at 4°C without ice than with ice.

These preliminary datas were confirmed with an amperometric procedure based on platinum electrode and hydrogen peroxide detection [16].

4. Conclusion

An amperometric detection based on FIA procedure using Xanthine oxidase reactor and a carbon based screen-printed electrode is proposed for freshness detection. Exudates of fish can be only diluted and injected into the system, therefore any preparation step is avoided.

Screen-printed carbon-based electrode can be used for 30–40 assays without further calibration. An oxidase reactor can be exploited for 2–3 months or at least 200–300 samples.

To determine HxR and IMP, relative enzymes converting to Hx should be added in suitable amounts according to a proposed procedure and the sample is then directly injected into the FIA system. AU can be also quantitatively determined without the oxidase reactor.

Therefore AU, Hx, HxR and IMP values can be obtained in 30 s with CV of 2–3% if the concentration is around 1–5 mM in the original sample; quality studies on fish samples can be easily performed.

References

[1] E. Watanabe, K. Ando, I. Karube, H. Matsuoka, S. Suzuki, J. Food Sci. 48 (1983) 496.

[2] S. Ehira, H. Uchiyama, F. Uda, H. Matsumiya, Nippon Suisan Gakkaishi 36 (1970) 491.

[3] E.H. Lee, T. Oshima, C. Koizumi, Nippon Suisan Gakkaishi 48 (1982) 255.

[4] E. Watanabe, T. Ogura, K. Toyama, Enzyme Microb. Technol. 6 (1984) 207.

[5] E. Watanabe, K. Toyama, I. Karube, H. Matsuoka, S. Suzuki, J. Food Sci. 49 (1984) 114.

[6] E. Watanabe, K. Toyama, I. Karube, H. Matsuoka, S. Suzuki, Appl. Microbiol. Biotechnol. 19 (1984) 18.

[7] E. Watanabe, H. Endo, T. Hayashi, K. Toyama, Biosensors 2 (1986) 235.

[8] E. Watanabe, H. Endo, K. Toyama, Appl. Microbiol. Biotechnol. 29 (1988) 341.

[9] I. Karube, H. Matsuoka, S. Suzuki, E. Watanabe, K. Toyama, J. Agric. Food Chem. 32 (2) (1984) 314.

[10] J.M. Kim, R.D. Schmid, In: R.D. Schmid, F. Scheller (Eds.), Biosensors Applications in Medicine, Environmental Protection and Process Control, 1989, p. 13.

[11] M. Suzuki, H. Suzuki, I. Karube, R.D. Schmid, In: R.D. Schmid, F. Scheller (Eds.), Biosensors Applications in Medicine, Environmental Protection and Process Control GBF monographs, 1989, p. 13.

[12] Y. Hasebe, A. Gokan, S. Uchiyama, Anal. Chim. Acta 302 (1995) 21.

[13] M. Hoshi, Y. Sasamoto, M. Nonaka, K. Toyama, E. Watanabe, Biosensors and Bioelectronics 6 (1991) 15.

[14] R.N. Goyal, A. Mittal, S. Sharma, Electroanalysis 6 (1994) 609.

[15] A. Mulchandani, J.H.T. Luong, K.B. Male, Anal. Chim. Acta 221 (1989) 215.

[16] G. Volpe, M. Mascini, Talanta 43 (1996) 283–289.

[17] E. Gonzalez, F. Pariente, E. Lorenzo, L. Hernandez, Anal. Chim. Acta 242 (1992) 267.

[18] T. Yao, K. Tsureyama, Electroanalysis 6 (1994) 165.

[19] H. Okuma, H. Takahashi, S. Yazawa, S. Sekimukai, Anal. Chim. Acta 260 (1992) 93.

[20] A. Cagnini, I. Palchetti, I. Lionti, M. Mascini, A.P.F. Turner, Sensors and Actuators B 24–25 (1995) 85–89.

ELSEVIER

Talanta 44 (1997) 2161–2163

Talanta

Announcements

The quantity 'pH'

The growing awareness amongst analytical chemists of the need for expressing the traceability and uncertainty of results has brought new pressure to reconsider the difficult situation of the realisation of the quantity 'pH', IUPAC Commission V. 5, responsible for pH matters [1], is proposing new works towards a unified pH scale. The adoption of a scientifically sounder assumption for activity coefficients in mixed electrolytes, the Pitzer treatment [2], to replace the Bates-Guggenheim Convention, will lead to the best possible definition of pH, the closest to the 'true', unattainable, pa_H value. By this means known standard buffers, with or without background electrolyte, can be assigned calculated pH values on the unified pH scale.

Before this unified pH scale can be formulated, an extensive further programme of experimental work on pH standard buffers is required. It is the intention to enlist the co-operation of some dozen suitably equipped laboratories world-wide to make extensive new e.m.f. measurements of Harned cells with buffer substance components over a wide temperature range to derive the necessary information. A subsequently formed working party will then reconsider the current IUPAC (1985) Recommendations [1]. A number of laboratories have already offered support. Requests for further details, offers of help, and comments on this proposal and on the existing IUPAC Recommendations should be sent to:

Prof. Arthur K. Covington,
Department of Chemistry,
University of Newcastle upon Tyne. NE1 7RU,
UK.
Fax: +44 191 2226929,
e-mail: a.k.covington@newcastle.ac.uk

References

[1] A.K. Covington, R.G. Bates and R.A. Durst, Pure Appl. Chem., 57 (1985) 531.
[2] A.K. Covington and M.I.A. Ferra, J. Solution Chem., 23 (1994) 1.

PII S0039-9140(96)02185-6

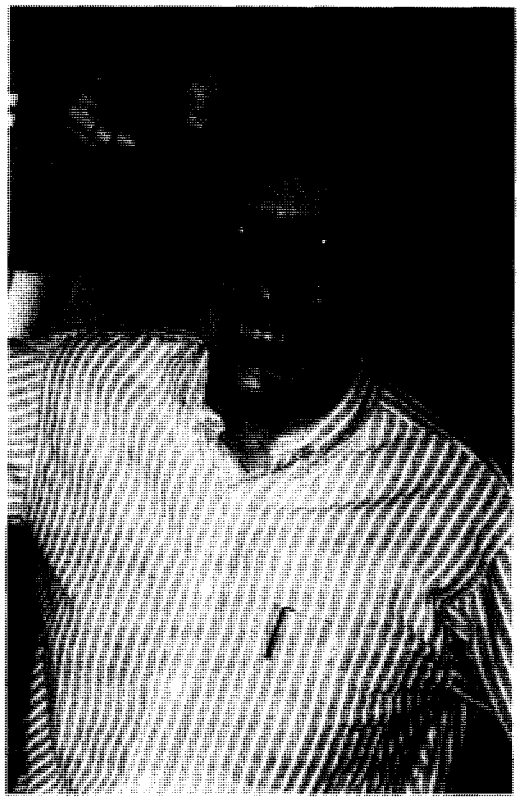

The Benedetti-Pichler Award

The American Microchemical Society is pleased to announce that it has chosen Professor John G. Dorsey, from Florida State University, as the 1997 A.A. Benedetti-Pichler Awardee. In general, Professor Dorsey has made outstanding contributions to analytical chemistry and to an understanding of chromatographic retention mechanisms. In particular, he has made seminal contributions to flow analysis, and to the estimation of biological and environmental partitioning processes. The Foley-Dorsey equation is now the recognized standard for calculation of the number of theoretical plates that measure the resolving power of a separation. The paper in which this equation was published, Anal. Chem. 55, 730–737 (1983) has been cited 239 times through June of 1996.

The Award will be presented at the Eastern Analytical Symposium and Exposition 1997, Somerset, New Jersey, USA on Thursday Nov. 20th, 1997 at a symposium in Prof. Dorsey's honor.

8th Symposium on Handling of Environmental and Biological Samples in Chromatography
26th Scientific Meeting of the Group of Chromatography and related Techniques of the Spanish Royal Society of Chemistry

Almería, Spain
October 26–29, 1997

Organized by:
International Association of Environmental Analytical Chemistry Group of Chromatography and Related Techniques of the Spanish Royal Society of Chemistry, Faculty of Sciences, University of Almería, Spain.

This meeting intends to cover new developments and reviews established handling and preparation techniques (such as liquid–liquid, solid phase extraction and supercritical fluid extraction) as well as more recent techniques. These include specific methods utilizing enzymes, immuno interactions and tailor made reagents and membrane techniques. GC, LC, SFC, CE, hyphenated techniques, MS techniques and automation will also be considered. A separate session will be devoted to water monitoring, international regulations and quality assurance principles of pesticide analysis. Subtopics will be introduced by plenary and invited research lectures followed by brief research posters. The symposium language will be English with no translation.

The program will consist of Plenary and Keynote Lectures. An equally important means for exchange of information will be via Poster Sessions. The posters will be selected to complement the series of lectures so that all factors affecting development of new analytical techniques, instrumentation and procedures for environmental and biological studies will be presented.

For further details contact:
Mrs M. Frei-Häusler, IAEAC Secretariat, Postfach 46, CH-4123 Allschwil 2, Switzerland. Tel.: +41 61 4812789; fax: +41 61 4820805; e-mail: iaeacmfrei@access.ch

1998 Winter Conference on Plasma Spectrochemistry

Scottsdale (Arizona)
January 5–10 1998

Developments in plasma spectrochemistry by: ICP, DCP, MIP and GDL, HCL sources.

For further information please contact:
1998 Winter Conference on Plasma Spectrochemistry,
%ICP Information Newsletter,
Department of Chemistry,
Lederle GRC Towers,
University of Massachusetts,
Box 34 510,
Amherst, MA 01003-4510,
USA
Attn: Dr. Ramon Barnes, Conference Chairman
Tel: + 1 413 5452294;
Fax: + 1 413 5453757;
e-mail: winterconf@chem.umass.edu.

Schedule of activities

Call for papers, abstracts due	July 1, 1997
Exhibitor registration	September 8, 1997
Conference pre-registration	October 10, 1997
Hotel pre-res ervation	October 10, 1997
Late pre-registration deadline	December 5, 1997
1998 Winter conference short courses	January 2–4, 1998
1998 Winter conference on plasma spectrochemistry	January 5–10, 1998

8th International Symposium on Luminescence Spectrometry in Biomedical and Environmental Analysis—Detection Techniques and Applications in Chromatography and Capillary Electrophoresis
Las Palmas de Gran Canaria (Canary Islands), Spain
26–29 May 1998

Organized by the University of Las Palmas de G.C. (Spain) in collaboration with the University of Ghent (Belgium), the University of Tokyo (Japan) and the Complutense University of Madrid (Spain).

For further information please contact:
Professor Dr José Juan Santana Rodríguez, Symposium Chairman, Department of Chemistry, Faculty of Marine Sciences, University of Las Palmas de G.C., 35017 Las Palmas de G.C., Spain. Fax: + 34 9 28452922; Tel.: + 34 9 28452915/452900; e-mail: josejuan.santana@quimica.ulpgc.es

ELSEVIER

Talanta 44 (1997) 2165

Talanta

Erratum

Erratum to 'Kinetic determination of organic vapor mixtures with single piezoelectric quartz crystal sensor using artifical neural networks' [Talanta 44 (1997) 959][1]

Wan-Li Xing, Xi-Wen He *

Department of Chemistry, Nankai University, Tianjin 300071, People's Republic of China

The publisher regrets that some words were ommitted from p. 961, 2nd column. The sentence beginning on line 12, should read:

From the initial reaction time, the frequency values (f(t)) at every 10 s were recorded. Of particular interest were the 10 min period after injection of the samples and 15 min after purging the detection cell.

* Corresponding author.

[1] PII of original article: S0039-9140(96)02142-X

PII S0039-9140(97)00222-1

ELSEVIER

Talanta 44 (1997) 2167–2184

Talanta

A review of the main factors influencing the FT-IR-PLS abilities exemplified with petrochemical qualimetric applications[1]

J.M. Andrade *, M.V. Garcia, P. Lopez-Mahia, D. Prada

Department of Analytical Chemistry, University of A Coruña, Campus A Zapateira, s/n E-15071, A Coruña, Spain

Received 5 June 1996; received in revised form 11 September 1996; accepted 1 October 1996

Abstract

Quality control usually involves monitoring several variables directly related with industrial necessities using univariate tests. One powerful alternative is to link multivariate analytical techniques and multivariate chemometrics. In this way, Fourier Transform Infrared spectroscopy and Partial Least Squares regression are used to discuss and review several advantages and drawbacks encountered in using such combination in industrial facilities. Typical drawbacks are selection of data pretreatment, errors in reference methods, selection of calibration and validation sets and model-aging. This review is exemplified with petrochemical applications although other fields are also considered (mainly when dealing with data pretreatment). © 1997 Elsevier Science B.V.

Keywords: Infrared; PLS; Qualimetrics; FT-IR; Review

1. Introduction

Qualimetrics is a novel term [1] which can be defined as a subfield of chemometrics concerned with using chemometric methods to improve quality control and quality assurance. Quality control, in turns, usually involves measuring chemically-related properties using some univariate, time-consuming, training-demanding, specific tests.

Qualimetrics, without doubt, is strongly related to Process Analytical Chemistry (PAC) [2–4] being the only shade that not all the PAC methods are statistical but of chemical engineering, too. Qualimetrics and PAC works have been explicity considered at the 4th International Chemometrics Conference (Czech Republic, July 3–7, 1995), the Euroanalysis IX (Italy, September 1–7, 1996) and it was considered as one of the cores of the 4th Symposium on Analytical Sciences (Brussels, June 3–5, 1996), EUCHEM—Conference on Chemometrics (Göteborg, Sweden, June 3–6, 1996) and one of the main focus of the VI International Conference in Chemometrics in Analytical Chemistry (Spain, June 25–29, 1996), just to mention several recent international meetings.

* Corresponding author.

[1] Part of this work was previously presented as an Invited Lecture (JMA) at the 4th Symposium on Analytical Sciences, Brussels, June 3–5, 1996.

PII S0039-9140(97)00034-9

Qualimetrics comprises a new way of thinking in industry-applied analytical chemistry. This term, to some extent, raise to the traditional univariate, time-consuming tests, though most of them can not be avoided due to contractual agreements. Alternatives should combine well-known multivariate (or state-of-the-art) analytical techniques with some predictive, statistical technique. Such combinations are of great power and useful not only to simultaneously control several parameters but to achieve excellent results as well as indirect benefits (lower delay times, lower workloads, better precision figures, etc.).

This paper deals with combining Fourier Transform Medium-Infrared spectroscopy (FT-MIR) and Partial Least Squares regression (PLS). Such topic is not absolutely recent so the main intention is to bring the industrial point of view our group has been involved with; exposing, briefly, benefits and drawbacks. Examples related with petrochemical properties measured using liquid samples are to be presented since this was our main concern during several years. No problem should exist to broadly extend the discussions to other fields. It should be underlined that the main intention is not to perform a detailed review of all the published works comprising qualimetrics and/or FTIR-PLS applications, instead it was pretended to rely on a half-way between a primer and a typical review. Two recent reviews focused on combining IR spectroscopy and chemometrics [5,6]. Another two reviews will be of interest though they are centered onto spectroscopic applications [7,8].

2. The problem

In the petrochemical arena, some standard tests are time-consuming (e.g. flash point test by the manual method [9]; thermal stability of kerosene [10]; knock indexes of gasolines [11,12], etc.), some are difficult to perform (e.g. % of aromatics and olefins [13]) and, even, others are highly subjective (e.g. freezing point of kerosene [14,15]). One result of these remarks is that precision figures (repeatability and reproducibility) are too broad when compared with current wishes from process control people giving excesive stress on analytical laboratories.

Additionaly, several tests need high amounts of reagents, from which several are harmful (e.g. benzene, toluene, aniline etc.). Standard apparatus are expensive and particular training is needed. The most typical example of a little desirable method is the measurement of the knock characteristics of automotive gasolines. Table 1, partially extracted from [16], resumes the most unsatisfactory characteristics of these two standard methods [11,12] and shows the chemometric method is an interesting alternative. Similar considerations could be determined for other test methods. Indirect costs appear when considering delay time, repeating analysis because a lack of confidence, higher workloads, staff demoralization etc.

3. Overcoming the problem

Assuming that the chemical composition measured by the IR spectroscopy determines, in some way, the physico-chemical parameters, spectral data can be used to calibrate and, then, predict fuel properties. The basic chemical background is the Lambert-Beer's law.

From Table 1, it can be followed that almost all the problems posed above could be avoided in routinary analyses using the FT-IR-PLS approach. Whether this multivariate approach can be used as accepted test method for certifying final products or not is a question of mutual agreement and confidence in quality control. At present, they are not accepted but we have little doubts on their promising future.

Benefits are quite obvious. What about drawbacks? In the following, the main problems found on applying the chemometric approach to daily production activities are to be briefly presented.

4. Spectral pretreatment methods

Two notes have to be posed now, the first one because the following classification is not sharply defined and, so, some techniques could be simul-

Table 1
ASTM methods vs. the FT-IR-PLS method: advantages and disadvantages

Item	ASTM methods	Chemometric method
Initial cost	High (~US$ 180 000)	Medium (~US$ 32 000)
Maintenance/repairs	Frequent/expensive	Infrequent/not expensive
Robustness	Not	Yes
Staff	Highly skilled	Not skilled
Precision	Repeatability, ~0.3 Reproducibility, ~0.9	Repeatability, ~0.1 Reproducibity, ~0.3
Automation	Very difficult	Simple
Connection to LIMS network	Level I (manual)	Level II (automated)
Sample	1 l	20 ml
Reagents	~500 ml blends of isoctane, *n*-heptane, toluene	None
Noise	Quite high	None
Vapours (fumes)	From reagents, from motor performance, from samples	Only from gasoline samples (few amounts)
Delay time to get one characteristic (considering one sample)	35 min	5 min
Residues	Fumes, isooctane, *n*-heptane, toluene, gasoline samples (about 200 ml of useless blends)	Only 10 ml of gasoline per sample. They can be used to clean heavy products from glassware (e.g. fuel, vacuum residues, etc.)
Indirect costs	High	Low

taneously classified in several items. The second warning is that the pretreatment review will not only concentrate on petrochemical applications (mostly made on liquid samples) but will also be extended to other different techniques in an attempt to get a broadest view. In this way, those who are interested in more details are encouraged to refer to the references.

The first decission to be taken is to select the spectral units to work with; i.e. absorption, transmittance, some of their derivatives or any other data transform. Generally speaking, there is not universal criterium in the literature; in fact, it greatly depends on the particular type of IR technique being used. The final objective of every data pretreatment is to simplify the mathematical model, thereby trying to improve the ultimate performance of the method. Some few examples can be considered.

4.1. Fourier Transform

The first step when dealing with Fourier Transform (FT) spectroscopy is the mathematical transformation from the time domain to the wavenumber/wavelength domain. This step can be considered as the first pretreatment of the analytical signal and it has been considered in several works. Brereton [17] reviewed the basics, usefulness and advantages of Fourier methods when used to get the spectroscopic data. Another review comprising FT in UV, VIS and NIR spectroscopy can be found on Williams [18].

Before those two works, Giancaspro and Comisarow [19] had presented a paper taking into account the problems associated to different FT spectra interpolation procedures as a function of both the number of zero-fillings and the ratio of the acquisition time to the relaxation time of the time domain signal. Nowadays, the Fourier Transform is automatically performed and such kind of problems (including, e.g. the sampling interval, resolution, etc.) are minimized.

4.2. Background correction

The simplest background correction is to record a 'blank' spectrum, store it in the computer and

substract it from each recorded spectrum. This is the most common situation since most FT-IR spectrophotometers make use of only one radiation beam. As a practical approach, the blank should consider the cell windows, the optical pathlength, and the background environment, i.e. air-filled or solvent-filled (even solvent mixtures) etc. A new background record should be made each time a change in the environmental conditions is suspected (solvents, room environment etc.).

In spite of this broadly used, simple application, background correction can be much more complicated. Several examples will illustrate this assessment. Karstang and Kvalheim [20] compared three techniques for background correction in quantitative analysis. Using as starting point a principal component analysis (PCA), the PCA model is them combined with a function describing the spectrum of the background constituents. The background methods comprised curve fitting, iterative target transformation factor analysis and local curve fitting.

We think the main objection it could be posed to such work is to find a function defining the background spectrum and that all the matrix constituents are not always known (e.g. when considering very complex mixtures as gasolines, kerosenes etc.). In this way, Gemperline et al. [21] selected a more simple approach. They used principal component regression in order to correct for background absorption. Thus, spectra of the pure background components are not needed. The main idea, of course, is to use only the first factors explaining most of the information in the data and discard the final ones where (hopefully) most random/background/noise will be present. This idea is discussed in more detail by Gillette and Koenig [22].

Kvalheim participated also in another work [23] where background correction was studied in hyphenated chromatographic/spectroscopic data. They also take into account baseline drift.

Karstang and Henriksen [24] included background correction techniques to get a quantitative prediction of additives in high-density polyethylene. They used the same three methods as in [20] and found that spectral substraction did not satisfactory worked due to interferences between all the additives in the prediction step.

4.3. Spectral units

With regard to the petrochemical field, the pioneering work from Honigs et al. [25] was made on absorption values as well as those from Martens et al. [26], Kelly et al. [27], Descales et al. [28], Parisi et al. [29], Blanco et al. [30], Garrigues et al. [31] or Andrade et al. [16]. Far from the refineries, some other applications were also made considering absorbance units as e.g. Zen and Patonay [32] did when preparing a NIR probe for pH-determination or Robert et al. [33] when analysing milk.

On the contrary, Kisner et al. [34] take transmittance (%) for determining triglycerides, phospholipids and cholesteryl ester by IR spectra. Bye [35] found that three silica modifications of quartz, cristobalite and amorphous silica can be quantitatively predicted using the KBr disc procedure, MIR-%T data and PLS regression.

Derivatives (generally, first- and second-order derivatives) were broadly used to correct spectral artifacts. They allow a sharp definition of each maximum possition but their main disadvantage is that noise is also increased, which can be determinant for some applications (e.g. when dealing with weak signals). Hruschka explains [36] that higher-order derivatives are occasionally valuable for increasing peak resolutions although they are rarely used due to difficulty in interpretation (analysis of pharmaceuticals were considered).

Kelly and Callis [37] considered the absorption units and the first and second order derivatives on SW-NIR and LW-NIR; they found no great differences excepting for the second derivative in LW-NIR which was attributed to a problem of sample-positioning in the instrumental (on-line) cell holder.

Evans et al. [38] studied classification rates for discriminant analysis of orange juice applying no transformation, first and second derivatives, multiplicative scatter correction and standard normal variate transformation (see Section 4.4). They found no differences being the 'no transformation' results as good as or better than any other combination; they also pointed out that one rea-

son for this could be the inherent smoothing of the NIR spectrophotometer.

Bertran [39] and Gonzalez [40] concentrated on studying which of the absorption, transmittance, or the first and second order absorption derivatives was the most adequated one to develop PLS and/or PCR models. Their results are not definitive since in some problems they selected the absorption units and in other different situations the first derivative was slightly better.

The following applications clearly reinforce the idea that no recipe can be used for data pretreatment and that each particular situation has to be considered. Esbensen and Martens [41] used PLS for predicting permeability, porosity and other petrophysical core parameters directly from wireline logs in oil wells using discrete variables (in this work IR was not used). According with their kwnowledge and previous studies, they found that one of the variables had to be $\log_{10}$ transformed, two of them, $\log_2$ transformed and another one was recomputed as $x^{1/3}$, where x represents the original values. The main reason to do so was that these variables showed a marked skewness.

Almost as a contrast to the previous application, Bak and Larsen [42] managed a problem where absorbance vs. concentration of CO was found to be highly nonlinear. A linearization step was applied to the spectroscopic data prior to computing the calibration model. It was found that the integrated absorbance areas, rather than the absorbance values, were more useful for modeling. The result was an improved calibration model with increased concentration prediction accuracy over the wide concentrations of CO.

A similar approach was selected by Kueustner et al. [43] when measuring hemoglobin in unlysed blood by NIR. They had to use the 1740/1346 nm ratio of the second derivative spectrum to get a successful calibration vs concentration.

Up to this point, one conclusion can be drawn inmediately, i.e. absorption units were mainly selected to perform multivariate predictions in liquid samples, at least in the petrochemical arena-. Broadly speaking, the first derivative is often used to correct for baseline shifts and the second derivative is used to handling scatter effects [44].

4.4. Baseline correction

In the most common situation, the baseline effects can be attributed to the sample matrix influence and consequently, it is desirable to skip such effect. Closely related to background correction, baseline correction can be made using first- and second-order derivatives (see Section 4.2). One of the disadvantages of using the second derivative is the spectral shape that it is obtained. Without doubt, another more intuitive approach could be desirable to eliminate the matrix effect. Unfortunately, this is far from easy (see e.g. Section 4.6) although Mamantou et al. [45] reviewed a set of analytical applications of matrix isolation in FTIR spectroscopy. They presented practical techniques for obtaining analytically useful results.

Liu and Koenig [46] developed a baseline correction algorith using a least-squares procedure. Linear or quadratic types of baselines are obtained through succesive fitting. After the entire spectrum or a subsection is fitted, the standard error of estimate is utilized as a criterium to determining if the fluctuation of each data point about the line can be thought of as the baseline function.

Lipkus [47] proposed a method for eliminating baseline variation for use on biological FTIR spectra. The expanded espectra in terms of a set of orthonormal polynomials derived from the Legendre polynomials and leading terms of the expansion, which contain most of the baseline variation, are removed.

In a relatively recent work, Dobrowolski et al. [48] made use of the intensian method to account for baselines. In the authors' words, 'the intensian concept leads to simple formulas which can be perceived as a generalization of the Beer-Lambert law'. This method can be extended to chromatography and other similar techniques, as well. The method was explained to be a continuation of the Morton and Stubbs' three point approach, from 1946. Dobrowolski et al. cited more baseline treatments including Gaussian and Lorentzian functions, ultra-low-frequency filtering in the frequency domain, and correction of second harmonic of spectra by fitted baseline.

One typical example of the baseline effect can be encountered in the IR films analysis. Many times polymers are cut in a thin slide (film). Due to errors in such preparation the thickness will vary and, so, originate a baseline shift. Karstang and Henriksen [24] proposed a normalization scheme comparing three normalization/scaling techniques, namely normalization based on selective regions, multiplicative signal correction and optimized scaling. Best results were achieved using the first and the latter options.

Jamroz and Dobrowolski developed the so-called autostandard method [49] which can be complementary of the ratio method (also known, method of the internal standard). The ratio method needs an analytical band that originates from one, and only one, substance in the system; the autostandard method needs a band common to all components into the system. The autostandard method can be applied where the layer thickness is difficult or impossible to measure.

4.5. Smoothing

Smoothing is often used to improve the signal-to-noise ratio of the spectral data. It is effective against noise that it is not correlated between adjacent wavelengths. The first, simplest approach is to average several spectra since noise tend to cancel or, at least, to greatly diminish. Alternatively to this simple way, a lot of options exist.

Among them, one of the simplest ones is to smooth data by a moving average. In this procedure (Moving Average or Boxcar), one chooses a window of a fixed odd number of points and calculates the average of all data points inside the window. The mean value of all points inside the window is recalculated and replaces the central point [50]. Its main disadvantage is that a band widening is obtained. Closely related, exponential averaging is obtained by calculating the weighted average of the points in a moving window of m points. The last point in the window (the point to be smoothed) is given the greatest weight and each preceding point is attributted a lower weight determined by the shape of the exponential function [$\exp(-j/T)$; T = the smoothing constant]. Because of the asymmetry of this smoothing function, a unidirectional distortion is introduced into the smoothed data, producing a lowering and shift of the peak maximum.

One of the broadest used filtering algorithm is that from Savitzky and Golay [7,51]. Despite its usefulness, this kind of filters should be used with care, particularly when severe or repetitive smoothing is required, as it was studied by Madden [7]. This filter works according with the following simplified scheme: consider a window of 9 points, the central one, the 5th, is the datum to be smoothed. The Savitzky-Golay filter (polynomial filter) consists of fitting a polynomial model through all the points in the window (excepting the central one) in the least-squares sense. Predict the value of the central datum using the adjusted polynomial and substitute the value of the central point by this predicted (smoothed) one. The process is repeated until filtering all the spectrum. Computational simplifications can be applied (see [50]). The application of polynomial smoothing has many disadvantages, among them is that for interpolation (smoothing) of physical data the behaviour in a particular interval may differ significantly from the behaviour in adjoining intervals [52]. One of the typical problems of the Savitzky-Golay filters is the non-filtering (truncation) of the end sections of the spectra. Very recently, Hui and Gratzl [53] estudied one of the proposals for addressing truncation. The 1990 Gorry's algorithm was modified to make it able to cope with several undesirable effects. Therefore, for purposes of interpolation and approximation it is more convenient to select locally defined functions that can be connected at the end-point. These functions are called splines, being the B-spline, a base spline with some particular mathematical properties [51].

Gans and Gill [54,55] explained in much more detail the B-splines and compared their performance with that from the Savitzky-Golay technique. Another interesting use of the B-splines can be seen in Section 4.8.

Bussian and Härdle [56] realized that filtering polynomials using the least-squares approach impelled to take care of the existance of outliers. They developed a robust smoothing procedure which rejects the huge noise spikes. The algorithm

has to be tunned with two parameters: the signal-to-noise ratio and the halfwidth of the spectral bands. Several IR-Raman examples are used.

Jones and Shimokoshi [57] studied the most appropriate domain to perform the filtering step: in the wavenumber or in its Fourier transform domain. Depending on the choice of the filter, one may achieve reduction in random noise, reduction of systematic instrumental errors and/or resolution enhancement.

Kawata and Minami [58] proposed an adaptive smoothing method based on a least-squares estimation. The mean and variance of the observed spectrum at a individual sampled point are calculated point by point from its local mean and variance. The resultant spectrum possesses a maximized signal-to-noise ratio at any local section of the entire spectrum. They also found different advantages when compared with conventional smoothing methods based on polynomial curve fitting. Bialkowski [59] used another kind of adaptive data smoothing filter (based on the Gaussian function) to study and correct the instrumental shot noise. Barak [60] worked, also, in one adaptive-degree polynomial filter trying to handle the different spectral characteristics that could be present in different regions of any spectrum.

Fourier Transform can be used as a smoothing technique. Thus, Cameron and Moffatt [61] used Fourier transforms in order to get smoothed even-order derivative spectra.

A digital Fourier filter is used by Hazen et al. [62] in combination with PLS regression to provide a calibration model that is insensitive to temperature when measuring glucose in aqueous solution. Baseline deviations are handled even when they are orders of magnitude greater than the glucose absorption bands. Very recently, Chung et al. [63] followed a similar approach for measure glucose, glutamine, ammonia, lactate and glutamate by NIR. They used both Fourier filtered absorbance spectra and raw data. Prediction abilities are found to be almost equal excepting a reduction in the number of PLS factors when Fourier filtering was used, which is consistent with removal of nonanalyte spectral variations by the filter.

4.6. Infrared reflectance

Reflectance spectroscopy is used for samples that are difficult to analyze by transmission. The samples can usually be analysed without modification. Reflectance measurements are divided into two categories: internal reflectance measurements are made by using an ATR (Attenuated Total Reflectance) element in contact with the sample. Alternatively, external reflectance measurements are made using an infrared beam reflected directly from the sample surface (Diffuse Reflectance, DR). In the former case, the ATR crystal is designed to enable total internal reflection which creates an evanescent wave at the crystal surface. This wave extends into a sample held in intimate contact with the crystal and absorption spectra can be recorded as a result. In DR, incident radiation is focused onto the sample and two forms of reflection occur: diffuse and specular. On a rough surface (e.g. powder) specularly reflected light is a minor contributor to the overall signal.

Some papers will be mentioned regarding ATR, the first one from Huang and Urban [64] because they made an evaluation and analysis of Attenuated Total Reflectance FTIR spectra using Kramers-Kronig transforms. In this work, a comparison is made between different algorithms to handle ATR-FTIR data: (1) the original Bertie's algorithm (suitable for weak bands) and the Dignan's one (more suitable for strong ATR bands); (2) Kramers-Kronig transformation; (3) they refine both algoritms by applying the McLaurin method to the Kramers-Kronig transform.

In the petrochemical field, Fodor [65,66] selected ATR spectra in order to predict two quite conflictive gasoline properties: the MON and RON antiknock indexes.

Depuy et al. [67] measured latex in paper coatings using ATR, as well. Recorded spectra were not modified excepting that first- and second-order derivatives were obtained. In order to avoid a decrease in the signal-to-noise ratio during differentiations, a seven-point moving average smoothing was performed on the profiles. Both treatments, differentiation and smoothing, were simultaneously made using a Savitzky-Golay filter.

4.7. Diffuse reflectance (DRIFTS)

In spite of the application of Shawn and Kratochvil [68] where absorption units were enough to determine bitumen contents in oil and sand, diffuse reflectance needs a wider, detailed exposition. More details have been considered in the specific review from Martin [8] and interested readers are encouraged to gain benefits from his work. In the present paper, we will only consider some topics related to the PLS application and previous steps.

The relationship between diffuse reflectance and concentration is more complex than the Beer-Lambert's law for transmission. DR depends on scatter for remission of the incident energy. More efficient scattering results in less penetration of energy into the sample and, therefore, less absorption. The pathlength is, accordingly, related inversely to the scattering coefficient. Such relation is defined by the theory of Kubelka and Munk being the Fuller and Griffiths' paper one of the first ones [69]. However, the Kubelka-Munk function is valid only for diffuse illumination and over a limited concentration range. From this point, a lot of work has been done trying to solve such problem. Nevertheless, the Kubelka-Munk function is almost universally used to theoretically describe the diffuse-reflectance measurements [8].

Good examples could be those from Cueller et al. [70] and McKenzie et al. [71] combining DRIFTS and the Kubelka-Munk algorithms to directly characterize glass fiber and polymer films and coatings.

Christy et al. [72] determined coal maturity by DRIFTS spectra in a Kubelka-Munk format and PLS as an alternative to the classical vitrinite reflectance method which presents poor precision values.

Birth [73] evaluated the application of the Kubelka-Munk theory to the light- scattering of foods and found significant deviations. Hecht [74] compared the Kubelka-Munk, Rozemberg and Pitts-Giovanelli methods of analysis of diffuse reflectance for several systems. He found that the latter two algorithms are useful alternatives that may be applied to diffusely reflecting samples that fail to conform the Kubelka-Munk theory.

Boroumand et al. [75] presented an adaptation of the Kubelka's general model to nonideal scattering samples. It was applied to quantitative FTIR spectroscopy of nondiluted surface-derivatized silica powders. Corrections were also present in order to take into account two common problems that often prevent a truly quantitative application of DRIFTS, namely background absorption and specular reflection on the surface.

Mandelis and Grossman [76] considered the Kubelka-Munk problem applied to nonhomogeneus optical media with arbitrary depth-dependent absorption and scattering coefficients.

Loyalka and Riggs [77] studied the accuracy of the Kubelka-Munk equations and proposed a new set of equations based on considerations from the radiation transport theory.

Ohta and Ishida [78] compared several numerical integration methods in order to seach for the most effective one for the Kramers-Kronig transformation, being the Kramers-Kronig transform a way to obtain 'constant' spectra from the substancies. Their methods involved the use of (1) MacLaurin's formula, (2) trapezium formula, (3) Simpson's formula, and (4) succesive double Fourier transform methods.

As it can be seen, scatter correction and baseline shifts are important points to deal with when considering diffuse reflectance. More on these subjects can be found onto the next works:

Devaux et al. [79] studied the effects of particle size on the DRIFTS spectra of wheat and Rape Seed Meal mixtures. Applying principal component analysis the first PC described the scattering effect; the second PC, the proportions at the sample surface and the third PC was necessary to make up for the overestimations of the smallest particles.

Downey et al. [80] followed a normalization strategy in order to minimize particle size effects by reducing the area under each spectrum. The same idea was used by Bertrand and Scotter [81] when analyzing gelatinized starch by NIR spectroscopy.

Multiplicative Scatter Correction (MSC) was proposed by Geladi et al. [82,83] as a way for scattering correction. MSC is based on the fact that if the reflectance values of each sample are

plotted against those of the mean for each wavelength the data fall on an approximately straight line. The intercept and slope of this line can be estimated for each spectrum by linear regression and then used to correct each sample spectrum to the intercept and slope values of the mean spectrum. The intercept, or additive effect, was found to be primarily due to specular reflectance effects, while the slope representing the multiplicative effect, was found to be due to sample homogeneity.

MSC is typically applied to linearize $\log(1/R)$ spectra (R = reflectance). Isaksson and Naes [84] have described the advantages of using MSC, indicating that prediction results are improved through better fit to a multivariate linear model and less irregularity in the scatter-corrected data. An advantage over the second derivative method is that the MSC-corrected data maintain the appearance of the original $\log(1/R)$ data.

A similar transform was proposed by Murray and Hall, more details can be found on Martin [8].

MSC was quickly adopted by researchers and some examples will cover quite different areas. Thus, Martens and Martens [85] used DRIFTS and MSC to predict sensory variables (hardness, juiciness and sweetness) of peas. Isaksson and Naes [84] studied the effect of MSC in linearity improvement in NIR. PCR regression was used after MSC correction and it was found that not only spectral interpretation was better but also that prediction was optimized. Three main reasons were argued: (1) MSC removes irrelevant information; (2) MSC increases linearity; and (3) MSC gives a regular and compact distribution of sample scores.

Ilari et al. [86] focused on light scattering effects as a way to determine the mean particle size in powders. The reflectance spectra are MSC-corrected and used for PLS regression. Up to 99% of the particle size variance was explained by the regression.

Vigerust et al. [87] made quantitative analysis of additives in low-density polyethylene using infrared spectroscopy, transforming to absorbance units and correcting with MSC prior to MLR and PLS regressions. The same approach (MSC-corrected spectra) was used by Dahlberg et al. [88] prior to discriminant-PLS and SIMCA classification techniques when classifying vegetable oils.

Blanco et al. [89] compared the performance of several preprocessing methods (absorbance, 1st and 2nd derivatives, normalization and MSC). They found not great differences in the prediction abilities of the different models, which it was ascribed to the weak scatter effect present on the samples.

Isaksson and Kowalski [90] modified the MSC algorithm to a new Piece-wise Multiplicative Scatter Correction (PMSC) one. This new method offers an advantage over the MSC method by correcting for nonlinear additive and multiplicative scatter effects. The PMSC offers linear regression fits to local wavelength regions of the spectra using a moving window of wavelengths.

A sort of spectrum autostandardization called Standard Normal Variate transformation—SNV—was proposed by Barnes et al. [91]. SNV has proved useful for the extraction of nonspecific scatter and particle size effects thanks to its scaling effect. In this way, SNV could be really useful to unify spectra from software libraries. The other dominant factor in NIR diffuse reflectance is the increasing level of the $\log(1/R)$ reflectance values over the 1100–2500 nm.To account for this baseline effect, application of a second-degree polynomial was also proposed being called De-trending (previous SNV transform can or can not be applied). An interesting feature of SNV is that it renders spectral shapes quite similar to the $\log(1/R)$ ones and, hence, interpretability is simplified. Although different in time, the end objectives of this work and that from Isaksson and Kowalski [90] are closely related.

SNV was also used by Blanco et al. [89] encountering that no important advantages are achieved over other simpler data treatments whether weak scatter effects are present.

Remember that Downey et al. [80] and Bertrand and Scatter [81], cited above, proposed a different kind of normalization intented to minimize particle size effects.

4.8. Data reduction

The main objective of data reduction is to diminish the total number of data to be handled by the analyst and computers and, thus, avoiding the usage of huge data matrices.

One of the simplest approaches could be to drawn attention only to that spectral regions where saturation is not achieved and 'good' peaks/bands are observed, discarding all the resting data. This approach needs some knowledge about the system under study to avoid possible pitfalls. This way was taken, e.g. quite recently by Dahlberg et al. [88], to classify vegetable oils.

More objective criteria can be found in literature, for example, Brown [92], Lindgren et al. [93,94] and Xu and Schechter [95] presented different criteria for wavelength selection. Jouan-Rimbaud et al. [96] selected a new, growing tool called genetic algorithms for choosing wavelength sets.

In a previous study, Honigs et al. [97] had described a quantitative criteria for choosing the minimum number of samples and wavelengths to develop a near infrared regression method.

If multivariate methods are considered, factor analysis, singular value decomposition and others constitute one possible solution to data reduction. We will briefly consider this point.

Wang et al. [98] utilized characteristic vector regression analysis (principal component analysis) combined with multiple regression. The key idea is that all the spectra in a data set show relatively restricted variation in form and that there exists a high correlation among them. Under the assumption that the spectra represent the structure of the matter, it is reasonable to break down the measured spectra into several representative spectra to reveal those responsible for the pure structure of the matter and for the measurement conditions. This approach suggests that we could, first, divide the spectra in the database into several representative spectra; second, find the correlation coefficientes between the spectra and the representative spectra; and third, save the representative spectra and correlation coefficients instead of all the spectra. Due to the small number of representative spectra and correlation coefficients, less memory is required for saving both sets than is needed for saving all the spectra.

The maximum entropy reduction method was proposed by Full et al. [99] and it was used by Christy et al. [72] to determine coal maturity and Karstang and Eastgate [100] in order to develop a multivariate calibration of an X-ray diffractormeter using PLS. The main idea of the maximum entropy approach (taken from Full et al., see [100]) is to preserve maximum information about the independent variables (spectra) by creating new 'maximum entropy' spectra with equal total information content (IR-data) in each variable and, so, subjective variable selection is avoided.

The wavelet method is gaining an important role in signal processing. Bos and Hoogendam [101] apply wavelets to evaluate peak intensities in flow-injection analysis and Bos and Vrielink [102] as a preprocessing tool for infrared spectra for the identification of mono- and di-substituted benzenes. In this latter work, the authors demonstrated that the wavelet method reduced IR spectra more than 20-fold with a significant improvement in the classification process. The wavelet theory takes a similar idea to the one posed by Wang et al. [98] since it involves the decomposition of a signal function or vector (i.e. spectrum) into simpler, fixed building blocks at different scales and positions. Like Fourier Transform, wavelet operates on a signal and transforms it linearly from its domain, which is the wavelength, to a different domain. However, unlike FT, whose frequency domain is one dimension only, wavelet generates two-dimensional domains with two parameters: the scale parameter and the position parameter. This property is an improvement of wavelet over FT and provides only the average information of the signal at assigned frequencies along the wavelenght domain. Much more details can be found on two recent books from Chui [103] and the CRC collection [104].

Chau et al. [105] developed a modified algorith named fast wavelet transform. They also studied the side-lobe problems and proposed two algorithms for minimizing them. Examples (UV-VIS spectra) are presented to study the performance of the algorithms. Walczak et al. [106] applied wavelets to NIR spectra and gave

Table 2
Prediction abilities when different measurement units are considered into the PLS-models in order to predict the motor octane number (MON)

	%T	Abs	%T		Abs	
			1st Derivative	2nd Derivative	1st Derivative	2nd Derivative
PLS-1 (SEP, $n = 156$)	0.18	0.25	0.15	0.17	0.18	0.17
PLS-1 (SEC, $n = 30$)	0.19	0.19	0.19	0.19	0.20	0.21

SEP, standard error of prediction; for comparisons, standard errors of calibrations—SEC—are given.

basic ideas in the Section 1 and 'Theory' parts of the paper. Schulz et al. [107] did not use wavelets although they divided the spectra in intervals, the relative entropy of information in the set of intervals is calculated and finally, each information is coded. Algorithms are presented for each step.

Different ways of data compression (reduction) exist, among them those proposed by Alsberg and Kvalheim [108,109], using B-splines (they also compared B-splines and the maximum entropy method) and that from Devaux et al. [110] where fast Fourier Transform is applied as a data compression method before principal component analysis. None of them found essential loss of information using such methods.

As mentioned at the begining of this chapter, the petrochemical applications have been mostly made on liquid samples. In one attempt to select the best choice for our particular problems, we made an extensive survey of the prediction capabilities of several models where absorption, transmittance and different derivatives were considered [111]. Again, results were not definitive though it could be deduced derivatives do not improve prediction values of uncorrelated samples. We have found not important differences between absorption or transmittance units excepting slightly better results if transmittance is used (see Table 2, studies made on untreated gasoline samples taken from production units and predicting antiknock values-broadly known as octane rating numbers). One reason could be, perhaps, the highly satisfactory performance of most nowadays IR spectrophotometers, even more when considering the Fourier Transform techniques. Our samples did not present baseline effects or scatter (we always used clean liquids). In this way, baseline or scatter effects are minimized or negligible, which could not be the same when considering, e.g. meat [112] or other complex matrices.

Of course, an alternative to data pretreatment is not to make data pretreatment at all. But this calls for a totally different approach in the regression step. Thus, Oman et al. [113] proposed to make no data pretreatment and instead, use a non-linear calibration model. This topic is a bit far from our objectives and no more emphasis will be made on it (related topics could be genetic algorithms, neural networks, nonlinear calibrations, and so on).

5. Errors in standard methods

Current regression techniques based on classical least squares assume there is negligible error associated with the predictable values obtained using the reference methods. Unfortunately, this is not always true and 'standard values' could present quite large confidence intervals. Independently of other statistical problems, one of the main consequences is that such uncertainties will contaminate the resulting parameters in the calibration model and, therein, the prediction capabilities. Thought this assumption is not true for PLS since it performs an inverse least squares step, such uncertainties will affect the prediction capabilities. This is nicely covered by Martens and Naes [114] when talking about what beginners should not expect from the PLS-prediction capabilities. The problem is really important in some particular predictions; good examples are two ASTM standard methods for determining both the octane rating and the percentage of aromatics [11–13,16,37,115].

We have to be guarded against this drawback because there is a trend, currently experienced in factories, to demand excellence from the FT-IR-PLS approach. The real fact is there is like a 'background' error difficult to reduce in our predictions. Such value can be grossly (under)-estimated as $SEP >> \sigma_{ref}/\sqrt{n}$ [114], where SEP = Standard Error of Prediction, substitutes the RMSEP from the reference, n = number of samples into the calibration set, and σ_{ref} = precision level of the reference method. Considering the ASTM standard reproducibility values for octane rating ($n = 20$) and % aromatics ($n = 17$), SEP values would be at the very least 0.05 and 0.33, respectively; without doubt, real SEP values can be expected to be bigger which do not necessarily means a bad performance of the chemometric methodology.

This latter rather subjective assessment we had experienced several times was systematically studied by DiFoggio [116] who stated two important corrections for their corresponding misconceptions (another third statement will not apply in the present paper because of its relationship with calibration transferability): (1) IR prediction can be better than the reference method; (2) regression models that only use terms that are linear can account for nonlinear effects, indeed. Briefly (readers are suggested to read DiFoggio's paper), examples are given where the apparent SEC (Standard Error of Calibration) grossly understimatethe real prediction capabilities of the IR-chemometric regression model. The main reason for this advantageous performance of the method itself is that the regression process itself is averaging out most of the random noise in the reference values and yielding an equation whose predictions are more accurate than the noisy data used for calibration.

The second important point is that the usual linear regression methods can cope with nonlinearities since the resultant correlation will account for nonlinear interaction effects and not just for a correlation to spectrometer nonlinearities at high absorbances (an example where up to ca. 3.2 units of absorbance were handled was presented). This paper is an important pillar to objectively justify several satisfactory performance characteristics we have experienced in our petrochemical applications. Generally, we had attributed the good prediction capabilities of the models to the inherent extraction of useful information that PLS is able to get. Now, more reasons can be used.

Aastveit and Marum [117] took into account several mathematical considerations from which better standard deviations for the predicted values than for the reference ones could be expected (when the reference values are obtained using a nonsatisfactory standard method). This fact was confirmed using NIR-reflectance spectroscopy on forage breeding.

A positive fact is the FT-IR-PLS approach offers excellent values either in repeatability and reproducibility [31,65], which is highly advantageous for industrial control. Our experience shows SEP values are generally lower than the standard reproducibility ones showing that predicted values are included into the standard confidence intervals. Exceptions occur when the reference methods are 'excellent' or when they define the property by themselves. Two such situations are the manual standard methods for determining gravity and viscosity in hydrocarbons [118,119]. Both methods are manually performed following exactly the definitions of gravity and viscosity; glassware is well known and calibrations are directly traceable to reference materials; additionally, tests are easy to perform. Under these circumstances, we obtained repeatability and reproducibility values for FT-IR-PLS lower that the manual ones but we have not been able to get SEP values lower than the standard reproducibility values [31] (neither Fodor et al. did, [65]), even with prediction errors of $\sim 0.25\%$ for gravity. One reason could be the validation set was not too broad although ongoing studies considering more samples do not drastically improve our figures. Another reason could lies in the loosening of lighter hydrocarbons from the sample fuels although this should be not important since our spectra were performed almost simultaneously to the ASTM ones and samples were always refrigerated.

In such cases, a good decision could be not to change the analytical approach since classical methods are simple to perform, with simple traceability and simple labware.

Table 3
SEP values found using several models, validation set (n = number of samples)

Gasoline type	PLS-1		PLS-2	
	RON	MON	RON	MON
FCC[a]	0.4 (44)	0.38 (132)	0.39 (50)	0.4 (50)
Platforming A[b]	0.37 (15)	0.33 (61)	0.43 (15)	0.32 (15)
Platforming B[b]	0.42 (36)	0.31 (112)	0.51 (34)	0.45 (35)

Tests for RON are less frequent than MON.
MON, motor octane number; RON, research octane number.
[a] Fluid catalytic cracking (FCC) processes.
[b] A and B are two different types of gasoline samples from Platforming processes, being the A-type quite infrequent.

6. Model validation and running

Calibration is the first step where sample collection is made to get the calibration (learning) set; trivial? We are aiming for a good prediction model so samples have to be selected covering the broadest possible range of production events were acceptable product is obtained in each particular factory. This usually needs time-expanded collections and, of course, the more samples, the better; what could be not easy due to software/production constraints.

Once models were developed (which it is not addressed here), it is time to assess if any of the models work. In D. Steele's words, 'the proof of the pudding is in the eating' [120]. The unique way to verify that your pre-selected model works well is to take new samples and predict them. Esbensen et al. [44] covered several ways of validation including leverage correction, cross-validation using small data sets, leave-one-out cross-validation and testing new samples.

After collecting the initial data set, samples have to be distributed in one calibration and one validation set. This could present one main drawback since in our experience it is rather easy to get 'excellent' models if you collect, say, 50 samples and from them you pick out say, 30, for calibrating and use the resting ones for validation. Since you are modeling what you are predicting, models are good. Problems, surely, will arise when using your model to predict samples after, say, one month.

Consequently, another different approach was used trying to get models having a good predictive ability, but also being robust against small changes. Firstly, calibration and model development using the leave-one-out validation scheme; second, selection of the two or three most promising models; third, testing each model using newly-collected samples (at least, one week after the calibration ones); forth, selection of the best model; fifth, intensive control/maintenance of the model running it with daily samples. Without doubt, this approach has three main drawbacks:

(i) More samples are needed, which could not be easy in some circumstances

(ii) More time is required to get a model. Note that it is assumed that all the samples taken from step 1 to step 4 will cover the habitual production characteristics (which is quite true for our particular situation and, surely, not very difficult to get in other situations). If any sample is strongly different (due to, e.g. an abnormal situation) it is presumed that it will be discovered in the calibration or testing studies. Of course, the models will not be robust to any change

(iii) More work has to be done since more models are discarded and new ones assayed

But, this is the best way to obtain reliable models. Thereby, 46 FCC gasoline samples were used to select the best model for octane rating prediction (stages 3rd and 4th) and 50 new ones for a final test [16]; also, 68 reformed naphthas were used for calibration and 118 ones for testing another similar model [121]. SEP values are presented on Table 3. It also shows that the PLS

Table 4
Prediction capabilities for octane rating models using different analytical techniques

Technique	Reported prediction capabilities	Reference
High resolution gas chromatography	Maximum difference between ASTM and predicted values <0.8 O.N.	[122]
Gas chromatography	SEP(RON) = 0.48 SEP(MON) = 0.32	[123]
NIR	SEP(RON) = 0.29 SEP(MON) = 0.34	[29]
NIR (660–1215 nm) (selecting specific wavelenths)	Using PLS: SEP(RON + MON/2) = 0.30	[27]
	Using MLR: SEP(RON + MON/2) = 0.32	
NIR	SEP(RON) ~ 0.3; SEP(MON) ~ 0.35	[28]
MIR (selecting wavelenths)	SEP(RON) = 1.57	[124]
MIR-GC	SEP(RON) ~ ± 1 O.N.	[125]
MIR (ATR system)	SEP(RON) = 0.50 SEP(MON) = 0.31	[61]

2-block could be suitable for FCC gasolines predictions but PLS 1-block should be selected for predicting Platforming naphthas.

There is another reason to gain confidence in each particular work. As it was noted, and due to several reasons, the MIR region was used to perform these studies. Most of previous works that can be found in the literature (some examples were covered here) refer to the NIR region. Doubts could arise on which IR region (MIR vs NIR) is best suited for developing prediction models. Of course, each one has its advantages and disadvantages, at this point we are not interested on them; but, rather in deciding if our approach could be comparable to the ones using NIR or, even, to other analytical techniques. In this paper one comparison for octane rating predictions is presented because more works have been published on it (see Table 4).

Comparison of Tables 3 and 4 reveal that our approach is good. It should be taken into account that pretty more samples have been considered into the testing sets and they are collected three or four months after development of the calibration models. So, the FT-MIR-PLS way appears to be highly satisfactory for use in off-line or near-line measurements. Besides, MIR advances are occurring quite fast and we can get now fiber optics of several meters with satisfactory performance [126,127].

We would like to pose a final problem that could be defined as model-aging.

When validating the model using daily samples during several months, it can be found that at the long time, the regression model suffers from a lack of fit respecting the standard method values. This is evidenced by, e.g. the absolute difference between figures obtained using the two methods but, also, for a broadening in the calculated confidence intervals. In our opinion, such problem was not too broadly discussed despite of its importance. One reason for this lack of fit in the long term is that factory production is not stable in time, at least, considering medium/long time. It is well known by chemists working in production units that product quality change (little but continuously) with time and corrective actions have to be taken. Such changes modify, to some extent, composition and/or chemical properties. Sometimes, the standard method is not so sensitive to detect these minor variations but the IR spectroscopy does, indeed. It appears as, in some sense, our spectral-chemometric approach could be too sensitive. Our experience in this respect is linked to the octane rating methods and some other fuel properties.

The problem is that calibration has to be limited on time and, therefore, the unique solution to what we called 'model aging' is recalibration. One particular, empirical solution is to be exposed though more efforts are needed. Recalibration was briefly considered also by Gemperline and Salt [128]. Recalibratiion (updating) was also studied by Helland et al. [129]. We have found

that our main problem when updating is the increase in the calibration matrix dimensions. This question was the main focus of the Helland's paper. They proposed a new algorithm for PLS regression (recursive-PLS) designed to keep the size of the matrices entering the PLS algorithm after new samples are added. The main drawback is that the typical autoscaling step is not easy to maintain along the updating steps due to the mathematical treatment and, therefore, centering is not recommended. This will result in one extra factor in the regression models. This paper is an interesting step forward towards simplification of parameter monitoring by PLS models.

When no particular events occured onto the production units, our models usually began to fail during the third or forth month. Failure was detected analyzing both the absolute errors for predicted values (FT-IR-PLS predicted values minus the standard method ones) as well as confidence intervals for several new samples. Once the problems were detected, several new samples were introduced into the learning set, calibration was repeated and ran again. Generally, satisfactory results were obtained for new samples from this point. Unfortunately, a fixed recalibration frequency is not easy to stablish; considering the octane rating prediction and our particular models, recalibration is advisable during the third month of model use, although it depends on many factors, among them on production stability.

Since our examples are not general, it was pretended to open discussions and to get conscientiousness on exercising care to develop industry-focused, statistical models for property prediction. This calls for one analytical chemist, with a chemometric background, working interdisciplinary on both the analytical laboratory and the production units.

7. Conclusion

Several current problems regarding multivariate statistical models for property prediction in quality control have been discussed. Among them, there are four important ones: (i) data pretreatment; (ii) errors in standard methods; (iii) model validation; and (iv) updating the regression model to cope with slightly changes in product composition-recalibration.

Acknowledgements

The Spanish Ministry of Education is acknowledged for a grant (MVG) partially supporting this work. Authors wish to honestly thank the suggestions made by two anonymous referees which greatly improved this work.

References

[1] S.D. Brown, T.B. Blank, S.T. Sum, L.G. Weyer, Anal. Chem. 66 (1994) 315R–359R.
[2] F. McLennan, Process Analytical Chemistry in perspective, in F. McLennan and B.R. Kowalski (eds.), Process Analytical Chemistry, Chapman and Hall, London, 1995.
[3] J.B. Callis, D.L. Illman, B.R. Kowalski, Anal. Chem. 59 (1987) 624A–635A.
[4] M.T. Riebe, D.J. Eustace, Anal. Chem. 62 (1990) 65A–71A.
[5] J.J. Workman, P.R. Mobley, B.R. Kowalski, R Bro, Appl. Spectrosc. Rev. 31 (1 and 2) (1996) 73–124.
[6] J.D. Kirsch, J.K. Drennen, Appl. Spectrosc. Rev. 30 (3) (1995) 139–174.
[7] E. Stark, K. Luchter, M. Margoshes, Appl. Spectrosc. Rev. 22 (4) (1986) 335–399.
[8] K.A. Martin, Appl. Spectrosc. Rev. 27 (4) (1992) 325–383.
[9] IP 170, Flash Point by the Abel Closed Cup, British Institute of Petroleum, 1995.
[10] ASTM D3241, Test Method for Thermal Oxidation Stability of Aviation Turbine Fuels (JFTOT Procedure), Annual Book of ASTM Standards, Vol. 05.03, 1995.
[11] ASTM D2699, Standard Test Method of Knock Characteristics of Motor Fuels by the Research Method, Annual Book of ASTM Standards, Vol 05.03, 1995.
[12] ASTM D2700, Standard Test Method of Knock Characteristics of Motor and Aviation Fuels by the Motor Method, Annual Book of ASTM Standards, Vol 05.03, 1995.
[13] ASTM D1319, Standard Test Method for Hydrocarbon Types in Liquid Petroleum Products by Fluorescent Indicator Adsorption, Annual Book of ASTM Standards, Vol 05.01, 1995.

[14] ASTM D2386, Test Method for Freezing Point of Aviation Turbine Fuels, Annual Book of ASTM Standards, Vol 05.02, 1995.
[15] J.M. Andrade, D. Prada, S. Muniategui, B. Gómez, M. Pan, Quimica Analitica 11 (3) (1992) 181–193.
[16] J.M. Andrade, S. Muniategui, P. López, D. Prada, Analyst 120 (1994) 249–253.
[17] R.G. Brereton, Chemom. Intell. Lab. Sys. 1 (1986) 17–31.
[18] R. Williams, Appl. Spectrosc. Rev. 25 (1) (1989) 63–79.
[19] C. Giancaspro, M.B. Comisarow, Appl. Spectrosc. 37 (2) (1983) 153–166.
[20] T.V. Karstang, O.M. Kvalheim, Chemom. Intell. Lab. Sys. 12 (1991) 147–154.
[21] P.J. Gemperline, S.E. Boyelte, K. Tyndall, Appl. Spectrosc. 41 (3) (1987) 454–459.
[22] P.C. Gillette, J.L. Koenig, Appl. Spectrosc. 36 (5) (1982) 535–539.
[23] Y.Z. Liang, O.M. Kvalheim, A. Rahmani, R.G. Brereton, Chemom. Intell. Lab. Sys. 18 (1993) 265–279.
[24] T.V. Karstang, A. Henriksen, Chemom. Intell. Lab. Sys. 14 (1992) 331–339.
[25] D.E. Honigs, T.B. Hirschfeld, G.M. Hieftje, Anal. Chem. 57 (1985) 443–445.
[26] H. Martens, T. Karstang, T. Naes, J. Chemometrics 1 (1987) 201–219.
[27] J.J. Kelly, C.H. Barlow, T.M. Jinguji, J.B. Callis, Anal. Chem. 61 (1989) 313–320.
[28] B. Descales, D. Lambert, A. Martens, Pétrole et Techniques 349 (1989) 2–8.
[29] A.F. Parisi, L. Nogueiras, H. Prieto, Anal. Chim. Acta 238 (1990) 95–100.
[30] M. Blanco, J. Coello, F. González, H Iturriaga, S Maspoch, X Tomas, J. Pharm. Biomed. Anal. 12 (4) (1994) 509–514.
[31] S. Garrigues, J.M. Andrade, M. De la Guardia, D. Prada, Anal. Chim. Acta 317 (1995) 95–105.
[32] J. Zen, G. Patonay, Anal. Chem. 63 (1991) 2934–2938.
[33] P. Robert, D. Bertrand, M.F. Devaux, R. Grappin, Anal. Chem. 59 (1987) 2187–2191.
[34] H.J. Kisner, C.W. Brown, G.J. Kavarnos, Anal. Chem. 54 (1982) 1479–1485.
[35] E. Bye, Chemom. Intell. Lab. Sys. 14 (1992) 413–417.
[36] W.R. Hruschka, Data analysis: wavelength selection methods, in: P. Williams and K. Norris (Eds.), Near-Infrared Technology in the Agricultural and Food Industries, American Association of Cereal Chemists, 1987.
[37] J.J. Kelly, J.B. Callis, Anal. Chem. 62 (1990) 1444–1451.
[38] D.G. Evans, C.N.G. Scotter, L.Z. Day, M.N. Hall, J. Near Infrared Spectrosc. 1 (1993) 33–44.
[39] E. Bertran-Gimferrer, Doctoral Thesis, Universitat Autónoma de Barcelona, Spain, 1995.
[40] F. González-Dou, Doctoral Thesis, Universitat Autónoma de Barcelona, Spain, 1991.
[41] K.H. Esbensen, H. Martens, Chemom. Intell. Lab. Sys. 2 (1987) 221–232.
[42] J. Bak, A. Larsen, Appl. Spectrosc. 49 (4) (1995) 437–443.
[43] J.T. Kueustner, K.H. Norris, W.F. McCarthy, Appl. Spectrosc. 48 (4) (1994) 484–488.
[44] K. Esbensen, T. Midtgaard, S. Schönkoft, in: A.S. Camo (Ed.), Multivariate Analysis in Practice, Norway, 1994
[45] G. Mamantou, A.A. Garrison, E.L. Wehry, Appl. Spectrosc. 36 (4) (1982) 339–347.
[46] J. Liu, J.L. Koenig, Appl. Spectrosc. 41 (3) (1987) 447–449.
[47] A.H. Lipkus, Appl. Spectrosc. 42 (3) (1988) 395–400.
[48] J.C. Dobrowolski, G.J. Strzemecki, M.H. Jamroz, Chemom. Intell. Lab. Sys. 15 (1992) 39–50.
[49] M.H. Jamroz, J.C. Dobrowolski, Appl. Spectrosc. 47 (8) (1993) 1209–1213.
[50] D.L. Massart, B.G.M. Vadeginste, S.N. Deming, Y. Michotte, L. Kaufman, Chemometrics: A Textbook, Elsevier, Amsterdam, 1988.
[51] A. Savitzky, M.J.E. Golay, Anal. Chem. 36 (1964) 1627–1639.
[52] M. Meloun, J. Militky, M. Forina, Chemometrics for Analytical Chemistry, PC-Aided Regression and Related Methods, Vol. 2, Ellis Horwood, Chichester, 1994.
[53] K.Y. Hui, M. Gratzl, Anal. Chem. 68 (1996) 1054–1057.
[54] P. Gans, J.B. Gill, Appl. Spectrosc. 37 (6) (1983) 515–520.
[55] P. Gans, J.B. Gill, Appl. Spectrosc. 38 (3) (1984) 370–376.
[56] B.M. Bussian, W. Härdle, Appl. Spectrosc. 38 (3) (1984) 309–313.
[57] R.N. Jones, K. Shimokoshi, Appl. Spectrosc. 37 (1) (1983) 59–67.
[58] S. Kawata, S. Minami, Appl. Spectrosc. 38 (1) (1984) 49–58.
[59] S.E. Bialkowski, J. Chemom. 4 (1990) 271–289.
[60] P. Barak, Anal. Chem. 67 (1995) 2758–2762.
[61] D.G. Cameron, D.J. Moffatt, Appl. Spectrosc. 41 (4) (1987) 539–544.
[62] K.H. Hazen, M.A. Arnold, G.W. Small, Appl. Spectrosc. 48 (4) (1994) 477–483.
[63] H. Chung, M.A. Arnold, M. Rhiel, D.W. Murhammer, Appl. Spectrosc. 50 (2) (1996) 270–276.
[64] J.B. Huang, M.W. Urban, Appl. Spectrosc. 46 (11) (1992) 1666–1672.
[65] G.E. Fodor, K.B. Kohl, R.L. Mason, Anal. Chem. 68 (1996) 23–30.
[66] G.E. Fodor, Analysis of Petroleum Products by Midband Infrared Spectroscopy, SAE Technical Paper. 1994.
[67] N. Dupuy, L. Duponchel, B. Amram, J.P. Huvenne, P Legrand, J. Chemom. 8 (1994) 333–347.
[68] R.C. Shawn, B. Kratochvil, Anal. Chem. 62 (1990) 167–174.
[69] M.P. Fuller, P.R. Griffiths, Appl. Spectrosc. 34 (1980) 533–539.

[70] S.R. Cueller, M.T. McKenzie, L.J. Fina, H. Ishida, J.L. Koenig, Appl. Spectrosc. 38 (6) (1984) 791–795.
[71] M.T. McKenzie, S.R. Cueller, J.L. Koenig, Appl. Spectrosc. 38 (6) (1984) 786–790.
[72] A.A. Christy, R.A. Velapoldi, T.V. Karstang, O.M. Kvalheim, E. Sletten, N. Telnaes, Chemom. Intell. Lab. Sys. 2 (1987) 199–207.
[73] G.S. Birth, Appl. Spectrosc. 36 (1982) 675–682.
[74] H.G. Hecht, Appl. Spectrosc. 37 (4) (1983) 348–354.
[75] F. Boroumand, J.E. Moser, H. van der Bergh, Appl. Spectrosc. 46 (12) (1992) 1874–1886.
[76] A. Mandelis, J.P. Grossman, Appl. Spectrosc. 46 (5) (1992) 737–745.
[77] S.K. Loyalka, C.A. Riggs, Appl. Spectrosc. 49 (8) (1995) 1107–1110.
[78] K. Ohta, H. Ishida, Appl. Spectrosc. 42 (6) (1988) 952–957.
[79] M.F. Devaux, N. Nathier-Dufour, P. Robert, D. Bertrand, Appl. Spectrosc. 49 (1) (1995) 84–91.
[80] G. Downey, P. Robert, D. Bertrand, P.M. Kelly, Appl. Spectrosc. 44 (1) (1990) 150–155.
[81] D. Bertrand, C.N.G. Scotter, Appl. Spectrosc. 46 (9) (1992) 1420–1425.
[82] P. Geladi, M. MacDougall, H. Martens, Appl. Spectrosc. 39 (1985) 491–500.
[83] H. Martens, S.A. Jensen, P. Geladi, in: Proc. Nordic Symposium Applied Statistics, Stokkand Forlag, Stavanger, Norway, June 1983.
[84] T. Isaksson, T. Naes, Appl. Spectrosc. 42 (7) (1988) 1273–1284.
[85] M. Martens, H. Martens, Appl. Spectrosc. 40 (3) (1986) 303–310.
[86] J.L. Ilari, H. Martens, T. Isaksson, Appl. Spectrosc. 42 (5) (1988) 722–728.
[87] B. Vigerust, K. Kolset, S. Nordensen, A. Henriksen, K. Kleveland, Appl. Spectrosc. 45 (2) (1991) 173–177.
[88] D.B. Dahlberg, S.M. Lee, S.J. Wenger, J.A. Vargo, D.C.S. Guyot, Communication presented at the VI CAC, Int. Conf. Chemometrics in Analytical Chemistry, Tarragona (Spain), June 25–29, 1996.
[89] M. Blanco, J. Coello, S. Maspoch, C. de la Pezuela, Communication presented at the VI CAC, Int. Conf. Chemometrics in Analytical Chemistry, Tarragona (Spain), June 25–29, 1996.
[90] T. Isaksson, B.R. Kowalsi, Appl. Spectrosc. 47 (5) (1993) 702–709.
[91] R.J. Barnes, M.S. Dhanoa, S.J. Lister, Appl. Spectrosc. 43 (5) (1989) 772–777.
[92] P.J. Brown, J. Chemom. 6 (1992) 151–161.
[93] F. Lindgren, P. Geladi, S. Rännar, S. Wold, J. Chemom. 8 (1994) 349–363.
[94] F. Lindgren, P. Geladi, A. Berglund, M. Sjöström, S. Wold, J. Chemom. 9 (1995) 331–342.
[95] L. Xu, I. Schechter, Anal. Chem. 68 (1996) 2392–2400.
[96] D. Jouan-Rimbaud, D.L. Massart, R. Leardi, O.E. De Noord, Anal. Chem. 67 (1995) 4295–4301.
[97] D.E. Honigs, G.M. Hieftje, T. Hirschfeld, Appl. Spectrosc. 38 (6) (1984) 844–847.
[98] H. Wang, Y. Zhu, L. Zhang, Z. Wang, Appl. Spectrosc. 45 (9) (1991) 1504–1507.
[99] W.E. Full, R. Ehrlich, S.K. Kennedy, J. Sediment. Petrol. 54 (1984) 117–126.
[100] T.V. Karstang, R.J. Eastgate, Chemom. Intell. Lab. Sys. 2 (1987) 209–219.
[101] M. Bos, E. Hoogendam, Anal. Chim. Acta 267 (1992) 73–80.
[102] M. Bos, J.A.M. Vrielink, Chemom. Intell. Lab. Sys. 23 (1994) 115–122.
[103] C.K. Chui, An Introduction to Wavelets, Academic Press, 1992.
[104] J.J. Benedetto, M.W. Frazier (eds.), Wavelets: Mathematics and Applications, CRC, Boca Raton, FL, 1994.
[105] F.T. Chau, T.M. Shih, J.B. Gao, C.K. Chan, Appl. Spectrosc. 50 (3) (1996) 339–348.
[106] B. Walczak, B. van den Bogoert, D.L. Massart, Anal. Chem. 68 (1996) 1742–1747.
[107] H. Schulz, K. Tetzlaff, L. Vogel, J. Chemom. 9 (1995) 143–168.
[108] B.K. Alsberg, O.M. Kvalheim, J. Chemom. 7 (1993) 61–73.
[109] B.K. Alsberg, E. Nodland, O.M. Kvalheim, J. Chemom. 8 (1994) 127–145.
[110] M.F. Devaux, D. Bertrand, P. Robert, J.L. Morat, J. Chemom. 1 (1987) 103–110.
[111] M.V. Garcia, J.M. Andrade, P. Lopez-Mahia, D. Prada, E. Fernandez, Communication presented at the Euroanalysis IX, Bologna (Italy), September 1–7, 1996.
[112] J. Workman, H. Andren, Int. Lab. April (1993) 26–32.
[113] S.D. Oman, T. Naes, A. Zube, J. Chemom. 7 (1993) 195–212.
[114] H. Martens, T. Naes, Multivariate Calibration, Wiley, New York, 1989.
[115] T.A. Norris, M.G. Rawdon, Anal. Chem. 56 (1984) 1767–1769.
[116] R. DiFoggio, Appl. Spectrosc. 49 (1) (1995) 67–75.
[117] A.H. Aastveit, P. Marum, Appl. Spectrosc. 45 (1) (1991) 109–115.
[118] ASTM D1298, Test Method for Density, Relative Density (Specific Gravity) or API Gravity of Crude Petroleum and Liquid Petroleum Products by Hydrometer Method, Annual Book of ASTM Standards, Vol. 05.01, 1995.
[119] ASTM D445, Test Method for Kinematic Viscosity of Transparent and Opaque Liquids (and Calculation of Dynamic Viscosity), Annual Book of ASTM Standards, Vol. 05.01, 1995.
[120] D. Steel, Spectrosc. Eur. 8 (1) (1996) 34–36.
[121] D. Prada, J.M. Andrade, S. Muniategui, E. Fernández, Communication presented at the 4th Int. Chemometrics Conf., Pardubice (Czech Republic), July 3–7, 1995.
[122] G. Protic-Lovasic, N. Jambree, D. Deur-Siftar, M.V. Prostenik, Fuel 69 (1990) 525–528.

[123] N.R. Crawford, W.W. Hellmuth, Fuel 69 (1990) 443–447.
[124] H.A. Rashid, S.B. Dekran, N.A. Fakhri, H.J. Aziz, Fuel Sci. Technol. Int. 7 (3) (1989) 237–250.
[125] H. Ichikawa, N. Nonaka, I. Takada, S. Ishimori, Appl. Spectrosc. 46 (6) (1992) 966–971.
[126] M.J. Smith, T.E. May, Int. Lab. May (1992) 18–24.
[127] H. Sadeghi-Jorabchi, W.M.E. Wood, F. Jeffery, A. Bruster-Davies, N. Loh, D. Coombs, Spectrosc. Eur. 6 (2) (1994) 16–21.
[128] P.J. Gemperline, A. Salt, J. Chemom. 3 (1989) 343–357.
[129] K. Helland, H.E. Berntsen, O.S. Borgen, H. Martens, Chemom. Intell. Lab. Sys. 14 (1991) 129–137.

ELSEVIER

Talanta 44 (1997) 2185–2192

Talanta

Determination and fractionation of sulphur in a contaminated dredged sediment[1]

F.M. Tack *, F. Lapauw, M.G. Verloo

Laboratory of Analytical Chemistry and Applied Ecochemistry, University of Ghent, Coupure Links 653, 9000 Gent, Belgium

Received 5 June 1996; received in revised form 9 October 1996; accepted 14 October 1996

Abstract

Conversion of sulphur compounds in reduced, contaminated sediments that are brought in upland conditions may largely affect the potential mobility of heavy metal contaminants. We applied selected methods for the determination of total sulphur and sulphur fractions in a contaminated sediment in the reduced state and after gradual drying and oxidation during 1 month. Dry ashing, followed by ion chromatographic detection, was reliable for the determination of total sulphur. Good recoveries were obtained in both reference samples and spiked samples. Total sulphur was 14.5 ± 0.6 g kg^{-1} relative to dry sediment. Wet chemical methods that involve the determination of acid-volatile, Zn–HCl-reducible, chromium-reducible, acetone-soluble and HI-reducible sulphur were used to estimate specific sulphur forms. Results for acetone-soluble sulphur were to high and not consistent with results for other fractions. Major part of sulphur in the sediment (90%) was inorganic. Sulphides were converted partially to sulphate and to intermediary oxidised sulphur compounds upon oxidation of the sediment. The results suggested that the intermediary oxidised sulphur pool in the reduced sediment (2.5 g kg^{-1}) mainly consisted of pyrite, that was not converted during drying and oxidation. No significant changes in organic sulphur were detected. © 1997 Elsevier Science B.V.

Keywords: Extraction; Oxidation/reduction; Sulphur compounds

1. Introduction

Contaminated dredged materials that are disposed on the land may be subjected to oxidation. As a result, the mobility of contained metals may change [1–3]. In that context, conversions of sulphur compounds may play an important role. Iron and metals are released when their sulphides are moved into oxidising environments where they are unstable. [1] The oxidation of metal sulphides may also result in acidification in soils that are drained and aerated [4].

Various sulphur compounds occur in soils and sediments. Inorganic sulphur forms include sulphates (SO_4^{2-}), elementary sulphur (S), metal sulphides (e.g., FeS) and pyrite (FeS_2). In between the sulphates (oxidation state VI) and the sulphides, several intermediary oxidised sulphur species can exist or be formed, e.g., bisulphide (S_2^{2-}, oxidation state – I), polysulphide (Sn^{2-}, $-II/n$),

* Corresponding author.

[1] Presented at the Symposium on Analytical Sciences (SAS) IV, Belgium, 3–5 June, 1996.

PII S0039-9140(97)00035-0

disulphuroxide (S_2O (g), + I), sulphur monoxide (SO (g), + II), thiosulphate ($S_2O_3^{2-}$, + II), dithionite ($S_2O_4^{2-}$, + III), sulphur dioxide (SO_2 (g), + IV), sulphite (SO_3^{2-}, + IV) and sulphur trioxide (SO_3 (g), + VI) [5]. Organic sulphur forms are generally divided into the ester sulphate group and the carbon-bonded sulphur compounds [6–8]. In well drained, well-aerated soils, most of the inorganic sulphur normally occurs as sulphate. Under anaerobic conditions, the main form of inorganic sulphur in soils and sediments is sulphide and often elemental S [7].

Sulphur contents in soils generally are between 0.1 and 0.5 g kg^{-1} [7]. Polluted sediments may contain more than 5 g kg^{-1}. Inorganic sulphur compounds tend to dominate in polluted sediments while organic sulphur compounds normally make up the largest fraction in unpolluted sediments [8,9].

In determination of total sulphur in soils and sediments, the various sulphur forms are converted by oxidation, most often to sulphate. This is achieved by digestion with concentrated acids, ashing with Ag_2O and $NaHCO_3$, [10] oxidation with $NaOBr_7$ or alkaline fusion [11]. For the determination of sulphur in the extract, ion chromatography compared favourably with the methylene blue method [10,12]. Indirect atomic absorption [13] and ICP [14,15] may also be used to quantify sulphate in the extract. The use of X-ray fluorescence for determination of total sulphur in soils gave satisfactory results [16,17]. Elemental analysers are being developed to determine total sulphur in soils and sediments. Their advantage lies in simplicity, speed and convenience. They appear, however, unsatisfactory for research requiring accurate and precise determination of total sulphur in soils or sediments [7,18].

The classical procedures for the determination of reduced and intermediary oxidised sulphur compounds in soils and sediments involve their reduction to H_2S and trapping the evolved H_2S in Zn–acetate solutions. Trapped sulphide is classically determined by colorimetry with methylene blue or by iodometric titration [7]. Instrumental techniques such as high resolution X-ray spectrometry [17], reflectance analysis [19] or a combination of thermogravimetric techniques [20] are being developed to directly determine specific sulphur compounds in the solid sample, but as yet are not largely applied in environmental sulphur analysis.

Accurate determination of the reduced forms of inorganic sulphur is difficult, partly because of the ease with which they can be oxidised on exposure to air, but mainly because of the limitations of current analytical methods [7]. We applied wet chemical methods for the determination of acid-volatile sulphur (AVS), Zn–HCl-reducible sulphur (Zn–HCl S), chromium–reducible sulphur (Cr^{2+}–reducible S), acetone-soluble sulphur and hydroiodic-acid–reducible sulphur (HI–reducible S) on a reduced, contaminated sediment, which was subjected to gradual drying and oxidation such as occurs upon land disposal. The analytical results allow to estimate resulting changes in sulphur compounds that may occur upon land disposal of contaminated dredged materials and are critically evaluated. This may contribute to a better understanding and interpretation of analytical results from sulphur compound analysis and to an improved understanding of the factors that govern the fate and behaviour of pollutants in contaminated dredged materials.

2. Experimental

2.1. Sampling

Sediment was sampled from the confined upland disposal site Geuzenhoek, situated on the left bank of the Gent-Terneuzen canal, Belgium. The canal crosses an industrial area (steel production, thermal power plant, chemical and food industry). The sediment was dredged and disposed 1 year before our sampling. It was characterised by a high carbonate content (15.2%) and a pH (1:5 in H_2O) of 8, and was polluted with heavy metals and organics [21]. It was strongly reduced (− 200 mV versus the standard hydrogen electrode). Organic matter content was 9.5%.

At the time of sampling, 20–50 cm of water covered the sediments. Sediment grab samples were taken in October 1992 and collected in 10 l polyethylene containers. Care was taken to min-

imise the contact time with the air. The sediment was stored covered with canal water.

2.2. Experiment

To assess sulphur fractions affected by gradual drying and oxidation of this reduced sediment, an 8 cm layer of the sediment (dry matter content: 44%) was brought in a rectangular container (50 cm length, 30 cm width and 10 cm height) and kept in the air at an ambient temperature of 20–22°C. No water was allowed to drain: removal of water occurred by evaporation only. Every 2 days, the sediment was stirred using a rinsed polyethylene tube, and 5–10 g were sampled in a plastic bag. The bag was purged with N_2 and sealed, and the sediment was homogenised by kneading. After about 2 weeks, the sediment had dried to the extent (dry matter content: 60%) that aggregates remained upon mixing. These were broken to a diameter size of at most 2 cm.

Total sulphur and various sediment characteristics were determined at the start of the experiment. Calcium carbonate content, organic matter content and sulphur fractions were determined at the start and after 16 and 30 days. Acid-volatile sulphur, extractable sulphate and chromium–reducible sulphur were determined every 2 days.

2.3. Chemical analysis

Organic matter was estimated by ashing during 3 h at 450°C [22]. Carbonate content was determined by back titrating an excess of 0.5 mol l^{-1} HCl added to an amount of sample containing 1 g dry matter with 0.5 mol l^{-1} NaOH [23]. The pH of the sediment was measured potentiometrically in a 1:5 solid:liquid suspension of the sediment in distilled water. Redox potentials were measured by inserting a platinum electrode and a saturated calomel electrode in the sediment paste and waiting for a stable reading. During the experiments, redox measurements were performed in a 1:5 solid:liquid suspension. The values obtained therefore are not actual redox potentials in the undisturbed sediment, but should be considered merely as relative indicators for the progress of oxidation.

2.4. Sulphur determinations

2.4.1. Total sulphur

Total sulphur was determined by dry ashing [7] and sulphate detection using ion-chromatography [24]. Air dry sediment (0.5 g) was ashed with 2.5 g $NaHCO_3$ and 0.1 g Ag_2O during 3 h at 550°C. The ashed residue was boiled in 50 ml of carbonate/bicarbonate buffer (2.6 mmol l^{-1} Na_2CO_3 – 2.4 mmol l^{-1} $NaHCO_3$) during 3 h under reflux to extract sulphates, that were analysed in the filtrate by ion chromatography (Dionex 2000i/SP). Aqueous standard solutions of sulphate (5 and 10 mg l^{-1}), freshly prepared using reagent grade anhydrous sodium sulphate (UCB, Brussels), were used for calibration.

2.4.2. Extractable sulphate

An amount of wet sediment, equivalent to approx. 0.5 g dry matter, was extracted in 50 ml carbonate/bicarbonate buffer (2.6 mmol l^{-1} Na_2CO_3 + 2.4 mmol l^{-1} $NaHCO_3$) in a 250 ml polyethylene centrifuge tube. The extracting solution was previously flushed with N_2-gas. The centrifuge tube was sealed using laboratory film after flushing the head space with N_2-gas. The suspension was mechanically shaken during 1 h [25], centrifuged (1500 × g during 20 min), and the supernatant liquid was analysed for sulphate by ion-chromatography.

2.4.3. Acid-volatile sulphur (AVS)

The following procedures for quantifying sulphur fractions involved the reduction of sulphur to H_2S in an Johnson-Nishita apparatus [26] and trapping the evolved H_2S in Zn–acetate solutions. Acid-volatile, Zn–HCl-reducible, chromium-reducible, acetone-soluble and hydriodic-acid–reducible sulphur were determined as described by Wieder et al. [27] The sample (50 mg for the hydriodic-acid–reducible sulphur and 500 mg for the other fractions) was added to the reaction flask and the system was purged with N_2 at a bubbling rate in the Zn–acetate traps of 1–2 bubbles per s for 10 min before the introduction of reagents.

AVS was determined by introducing 8 ml of 12 mol l^{-1} HCl into the reaction flask. After 10 min,

the suspension was brought to boiling and after 45 min the traps were removed and the sulphides titrated.

2.4.4. Zn–HCl–reducible sulphur (Zn–HCl S)

The procedure for the determination of Zn–HCl S was similar to that for AVS, except that 3 g Zn-metal were added at the same time as the acid. The material was boiled during 1 h before removal of the traps and titration.

2.4.5. Chromium–reducible sulphur (Cr^{2+}–reducible S)

Cr^{2+}–reducible S was determined by percolating a 1 mol l^{-1} solution of $CrCl_3$. $6H_2O$ in 0.5 mol l^{-1} HCl through a Jones reductor column containing Zn amalgamated with Hg [28]. Of the reduced chromium solution, 16 ml were introduced into the reaction flask. After 10 min, heat was applied and the material treated as for Zn–HCl S.

2.4.6. Acetone-soluble sulphur (acetone-soluble S)

To determine acetone-soluble S, 0.5 g sediment were extracted during 16 h with 20 ml of analytical grade acetone. The extraction flask was covered with Parafilm and placed on a horizontal shaker. The mixture was filtered and diluted to 25 ml. The entire filtrate volume was introduced into the reaction flask and subjected to Cr^{2+} – reduction as described above.

2.4.7. Hydriodic-acid–reducible sulphur (HI–reducible S)

For the determination of HI–reducible S, a solution of 50% hypophosphorous acid, 90% formic acid and 57% hydriodic acid in a proportion of 4:2:1 was prepared daily. Instead of 8 ml [27] of that solution, 20 ml were brought in the reaction flasks. After 10 min, the suspension was heated to boil during 90 min.

2.4.8. Sulphide determination

After each of the extraction/distillation procedures, trapped sulphide was determined by iodometric titration [28]. To the sequential wash bottles, 1 mol l^{-1} KIO_3 (8 ml to the first and 2 ml to the second bottle), 1.5 g KI and 4 ml of concentrated HCl (37%) were added. The contents of the wash bottles were pooled in a 500 ml erlenmeyer and titrated with 0.01 mol l^{-1} $Na_2S_2O_3$ using starch as an indicator.

3. Results and discussion

3.1. Total sulphur

Analysis of total sulphur in reference plant material (spruce needles, CRM 101, Community Bureau of Reference, Commission of the European Communities, Brussels) agreed closely with the certified value (Table 1). For the sediment reference sample (CRM 277), we obtained higher results. Sulphur in the sediment reference material, however, was not certified, but indicative only. Reproducibility was excellent for the plant sample, but lower for the sediment samples. During ashing of sediments, as opposed to plant material, the large mineral matrix remaining may be responsible for the lower reproducibility. The higher variability in the analysis of the Geuzenhoek sample as compared with the reference sediment may result from additional random error related with the handling of wet sediments, i.e., increased possibility of sample heterogeneity and more uncertainty about the exact dry weight of the sample.

Table 1
Analysis of total sulphur in reference samples, the Geuzenhoek sediment and spiked sediment samples (g kg^{-1} dry sediment)

	Determined	Reference value
Spruce needles (CRM 101)	1.67 ± 0.05 ($n = 10$)	1.70 ± 0.10[a]
Estuarine sediment (CRM 277)	6.06 ± 0.25 ($n = 10$)	5.17 ± 0.18[b]
Addition		
Geuzenhoek	14.5 ± 0.6 ($n = 15$)	
K_2SO_4	21.2 ± 0.2 ($n = 5$)	21.3 ± 0.6
Sulphanylamide	19.3 ± 0.3 ($n = 5$)	19.9 ± 0.6

[a] Certified value.
[b] Indicative value.

Table 2
Determination of sulphur fractions (g kg^{-1} dry sediment)

	Reduced sediment	Oxidised sediment[a]
Total S	14.5 ± 0.6[b]	
AVS	10.4 ± 0.3[c]	0.0
Zn–HCl S	11.6 ± 0.2[c]	2.3
Cr2+–reducible S	12.9 ± 0.2[c]	5.5
Acetone-soluble S	6.9 ± 1.2[c]	—
HI–reducible S	13.9 ± 0.1[c]	14.1
Extractable sulphate	0.08 ± 0.01[c]	6.2

[a] No replicate measurements performed. Estimates on reproducibility may be obtained from replicate determinations on the reduced sediment.
[b] $n = 15$.
[c] $n = 3$.

Spikes of inorganic (potassium sulphate) and organic sulphur (sulphanylamide) were recovered well. Sulphur contents determined were not significantly different from the expected value (*t*-test at the 0.05 level of significance), although the recovery of organic sulphur tended to be somewhat lower. Total sulphur analysis was therefore accurate and reproducible.

3.2. Sulphur fractions

Different sulphur fractions are thought to consist of specific sulphur forms. Sulphur contents in both the reduced and oxidised sediments were determined using various determination procedures (Table 2). The contents of specific sulphur forms may be estimated from the various sulphur determination procedures (Table 3).

Acid-volatile sulphur (AVS) is mostly sulphide S [27,29]. In the reduced sediment, 70% of total sulphur was sulphide S. AVS was quantitatively converted during drying and oxidation of the sediment (Table 2). The formation and accumulation of inorganic sulphur fractions is typical for polluted sediments and is related to a large influx of sulphur compounds, protons and metals [8].

3.3. Zn–HCl sulphur

It has been assumed that Zn–HCl S represents all inorganic sulphur except sulphate [30]. Landers et al. [25] used the Zn–HCl distillation procedure for the determination of inorganic non-sulphate sulphur but warned for incomplete recovery of pyrite when present in reduced soils or sediments. Wieder et al. [27] found the procedure of questionable value because sulphur from S^0, FeS_2 and SO_4^{2-} was only partially recovered.

Zn–HCl S was significantly higher than AVS (Table 2). As extractable sulphates were negligible in the reduced sediment, the difference (1.2 g S^{-1} kg sediment) must be attributed to the presence of FeS_2–S or S^0–S.

In the oxidised sediment, the difference between Zn–HCl S and AVS was 2.3 g as compared with 1.2 g in the reduced sediment. This may result from sulphates in the oxidised sediments, that are partially determined as well. [27]

Wieder et al. [27] determined extraction/distillation efficiencies by analysing pure sulphur compounds with the different methods. They found that 15.5–24.0% of the added sulphate was determined as Zn–HCl S. Assuming a recovery of 20%, then 1.24 g of Zn–HCl S should have originated from sulphates present in the oxidised sediment (6.2 g). The remaining sulphur (1.06 g) agreed with the difference between Zn–HCl S and AVS in the reduced sediment (1.2 g). This may

Table 3
Estimation of sulphur fractions (g kg^{-1} dry sediment)

	Reduced sediment	Oxidised sediment
Total S	14.5 ± 0.6	14.5[a]
Organic S	1.5 ± 2.5	2.8
Carbon-bonded S	0.6 ± 2.0	0.2
Ester sulphate S	0.9 ± 0.6	2.6
Inorganic S	12.9 ± 0.8	11.7
Sulphide	10.4 ± 0.3	0.0
Intermediary oxidised	2.5 ± 0.5	5.5
Sulphate	0.08 ± 0.01	6.2

[a] Estimated from the total content determined at the start of the experiment.

suggest either that the intermediary oxidised sulphur compounds were not affected in the dried, oxidised sediment, or that intermediary oxidised sulphur formed during oxidation was balanced by removal.

3.4. Chromium–reducible sulphur

Chromium–reducible sulphur represents all inorganic reduced and intermediary oxidised sulphur, i.e., iron monosulphides, pyrite (FeS_2) and elemental S [27,31]. The difference between Cr^{2+}–reducible S and AVS was therefore listed as intermediary oxidised sulphur in Table 3.

Intermediary oxidised sulphur was estimated to be 2.5 g kg^{-1} in the reduced sediments. If this was S^0, then 0.25 g kg^{-1} should be extracted in the Zn–HCl-fraction, assuming 10% recovery [27]. If instead it was all FeS_2, then 45% or 1.13 g kg^{-1} should be found in that fraction. The latter value agrees with the observed difference between Zn–HCl S and AVS (1.2 g kg^{-1}) and therefore suggests that intermediary oxidised sulphur in the reduced sediment largely was FeS_2–S.

In the oxidised sediment, 1.06 g out of 2.3 g Zn–HCl S was assumed to originate from intermediary oxidised sulphur (see before). Applying the percent recovery values for FeS_2 in the Zn–HCl and Cr^{2+}-reducible extractions determined by Wieder et al., [27] one can estimate the recovery of this intermediary oxidised sulphur as $1.06 \div 46\% \times 93\% = 2.14$ g S, assuming that it is all FeS_2–S. Otherwise, if this intermediary oxidised sulphur were S^0–S, $1.06 \div 12\% \times 94\% = 8.3$ g sulphur should be extracted in the Cr^{2+}-reducible fraction. The latter value is far in excess of the experimentally found Cr^{2+}-reducible sulphur in the oxidised sediment (5.5 g), while the former value corresponds with the intermediary oxidised sulphur in the reduced sediment (FeS_2–S). It is therefore suggested that FeS_2 was not largely affected during drying and oxidation of the sediment. Other Cr^{2+}–reducible S in the oxidised sediment may include S^0 and perhaps $S_2O_4^{2-}$ and $S_2O_3^{2-}$, formed by oxidation of sulphide S.

It is not likely that new FeS_2 would have been formed during oxidation of the sediment. The formation of pyrite in nature generally is a very slow process, taking months, years, or decades as amorphous iron monosulphides (FeS) react with elemental sulphur (S^0) [32]. It has been shown that pyrite may also form rapidly without iron monosulphides as intermediates, provided soluble sulphides are present and iron monosulphides are undersaturated [32]. These conditions are not likely to have occurred in the sediment studied, as large amounts of FeS were present.

3.5. Acetone-soluble sulphur

The method to determine acetone-soluble S is believed to be specific for S^0 [27]. We found it difficult to obtain reproducible results for acetone-soluble sulphur. Visual detection of the endpoint of the titration was hindered by the presence of a turbidity in the wash bottles. The reproducibility was much lower than for the other sulphur fractions and the results obtained, moreover, were inconsistent with the other fractions.

Acetone-soluble S (6.9 g S kg^{-1} dry sediment) was much higher than intermediary oxidised sulphur, estimated as the difference between Cr^{2+}–reducible S and AVS (2.3 g S kg^{-1} dry sediment). Moreover, the sum of AVS and acetone-soluble S was higher than the total sulphur. It is therefore not possible to obtain an estimate for elemental sulphur from acetone-soluble S. It could be concluded from these high values that intermediary oxidised sulphur largely consisted of elemental sulphur in this sediment, but this is in contradiction with the results obtained for Zn–HCl S and Cr^{2-}–reducible S, as illustrated before.

3.6. HI–reducible sulphur

HI-reduction is commonly used to measure organic ester sulphate S, with the attendant assumption that the procedure liberates sulphur from all inorganic sulphur compounds as well [27]. Ester sulphate S may thus be estimated by the difference between HI–reducible S and the sum of Cr^{2+}–reducible S and sulphate S. Carbon-bonded sulphur is estimated as the difference between total S, inorganic S and ester sulphate S.

The estimation by difference was uncertain because of the large inorganic sulphur pool com-

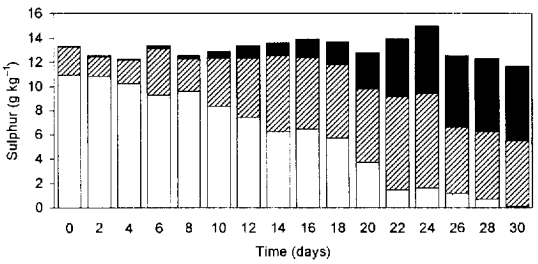

Fig. 1. Sum of chromium-reducible sulphur and sulphate sulphur as a function of time. Sulphide forms were plotted as a fraction of chromium-reducible sulphur.

pared with organic sulphur in our sediment. For comparison, Wieder et al. [27] estimated sulphur fractions in peat soils, containing approx. 0.9 g ester sulphate S and only 0.6 g inorganic S kg^{-1} dry sediment.

3.7. Changes in inorganic sulphur fractions with time

Changes in inorganic sulphur fractions with time are shown in Fig. 1. Sulphides steadily decreased to zero within 30 days. The decrease proceeded faster at day 16 and coincided with the sediment starting to form aggregates upon mixing. A better contact with the air was thus established, resulting in a faster drying and a faster increase in redox potential (Table 4).

The significant decrease in carbonate content shows that a substantial amount of acidity was produced upon oxidation of the sediment. The oxidation of metal sulphides is a major cause of acidification in soils that are drained and aerated [4]. Because of the high carbonate content, the sediment was efficiently buffered, as illustrated by the pH values. Gambrell et al. [33] reported on a carbonate free sediment for which the pH dropped from neutral (7.0) to strongly acidic (3.0) after stirring under air for 8 days.

4. Conclusions

The determination of total sulphur by dry ashing, followed by ion chromatographic detection of sulphate, was reliable. Application of a fractionation scheme allowed to estimate sulphur fractions, but because of the possibility of large relative errors, the estimation of minor fractions may be difficult. Our determination of S^0 by acetone extractable sulphur suffered from a low reproducibility. Values obtained were too high and were

Table 4
Evolution in sediment characteristics during drying and oxidation of the sediment

Day	DM %	EC mS cm^{-1}	pH	ORP mV	$CaCO_3$ %	OM %
0	44	0.45	8.9	−200	14 ± 1	9.3 ± 0.2
2	45	0.60	8.0	−5		
4	47	0.82	8.0	−5		
6	48	0.75	8.2	5		
8	50	0.80	8.1	10		
10	51	1.07	7.9	20		
12	54	1.13	7.9	30		
14	56	1.28	7.6	45		
16	59	1.43	7.6	45	12 ± 2	9.2 ± 0.2
18	65	1.79	7.6	60		
20	69	2.01	7.5	100		
22	74	1.93	7.6	170		
24	85	1.92	7.7	280		
26	90	1.91	7.6	290		
28	92	1.92	7.6	280		
30	94	1.93	7.6	290	10 ± 0.8	9.2 ± 0.2

DM, dry matter content; EC, specific electrical conductivity; and ORP, oxido-reduction potential.

not consistent with results obtained for the other fractions.

Major part of sulphur in the sediment was inorganic. Sulphides were converted partially to sulphate and to intermediary oxidised sulphur compounds upon oxidation of the sediment. The results suggested that an intermediary oxidised sulphur pool in the reduced sediment consisted of pyrite, that was practically not affected within 1 month. No significant changes in organic sulphur were detected.

References

[1] J.N. Moore, W.H. Ficklin and C. Johns, Environ. Sci. Technol., 22 (1988) 432.
[2] R.P. Gambrell, J. Environ. Qual., 23 (1994) 883.
[3] U. Förstner, Int. J. Environ. Anal. Chem., 51 (1993) 5.
[4] S. Satawathananont, W.H. Jr. Patrick and P.A. Jr. Moore, Plant Soil, 133 (1991) 281–290.
[5] L.W. Lindsay, Chemical Equilibria in Soils, Wiley, New York, 1979.
[6] D.J. Casagrande, K. Siefert, C. Berschinski and N. Sutton, Geochim. Cosmochim. Act., 41 (1977) 161.
[7] M.A. Tabatabai, in C.A. Black et al. (Ed.), Methods of Soil Analysis, Part 2, Chemical and microbiological properties, 2nd ed., ASA, Madison, Wisconsin, 1982, pp. 501.
[8] J.O. Nriagu and Y.K. Soon, Geochim. Cosmochim. Acta, 49, (1985) 823.
[9] M.J. Mitchell, D.H. Landers, F.B. Brodowski, G.B. Lawrence and B. David, Water Air Soil Pollut., 21 (1984) 231.
[10] M.A. Tabatabai, N.T. Basta and H.J. Pirela, Commun. Soil Sci. Plant Anal., 19 (1988) 1701.
[11] E.A. Stallings, L.M. Candelaria and E.S. Gladney, Anal. Chem., 60 (1988) 1246.
[12] W.A. Dick and M.A. Tabatabai, Soil Sci. Soc. Am. J., 43 (1979) 899.
[13] M.C. Du Toit and C.C. Du Preez, Commun. Soil Sci. Plant Anal., 26 (1995) 69.
[14] M.W. Pritchard and J. Lee, Anal. Chim. Acta, 157 (1984) 313.
[15] P.F. Vendrell, K. Frank and J. Denning, Commun. Soil Sci. Plant Anal., 21 (1990) 1695.
[16] M.A. Tabatabai and J.M. Bremner, Soil Sci. Soc. Am. Proc., 34 (1970) 417.
[17] Q.G. Wang, Z.H. Huang, Q. Zhang, Environ. Chem., 11 (1992) 55.
[18] J.F. Artiola, Int. J. Environ. Anal. Chem., 41 (1990) 159.
[19] J.I. Wilcox and R.D. del Delumyea, Anal. Lett., 27 (1994) 2805.
[20] F. Paulic and M. Arnold, J. Thermal Anal., 39 (1993) 1079.
[21] F.M. Tack, O.W.J.J. Callewaert and M.G. Verloo, Environ. Pollut., 91 (1996) 199.
[22] E.R. Rhodes, P.Y. Kamara and P.M. Sutton, Soil Sci. Soc. Am. J., 45 (1981) 1132.
[23] L.E. Allison and C.D. Moodie, in C.A. Black et al. (Ed.), Methods of Soil Analysis, Part 2, Chemical and microbiological properties, 2nd edn., ASA, Madison, Wisconsin, 1965, pp. 1379.
[24] J.W.M. Rudd, C.A. Kelly, A. Furutani, Limnol. Oceanogr., 31 (1986) 1281.
[25] D.H. Landers, M.B. David, M.J. Mitchell, Intern. J. Environ. Anal. Chem., 14 (1983) 245.
[26] C.M. Johnson and H. Nishita, Anal. Chem, 24 (1952) 736.
[27] R.K. Wieder, G.E. Lang and V.A. Granus, Limnol. Oceanogr., 30 (1985) 1109.
[28] A.I. Vogel, Vogels's Textbook of Quantitative Inorganic Analysis, 5th edn., Longman, London, 1989.
[29] A.E. Giblin, G.E. Likens, D. White and R.W. Howarth, Limnol. Oceanogr., 35 (1990) 852.
[30] M.B. David, M.J. Mitchell and J.P. Nakas, Soil Sci. Soc. Am. J., 46 (1982) 847–852.
[31] R.W. Howarth and S. Merkel, Limnol. Oceanogr., 29 (1984) 598.
[32] R.W. Howarth, Science, 203 (1978) 49.
[33] R.P. Gambrell, R.D. DeLaune, W.H. Jr. Patrick, in M.B. Jackson, D.D. Davies and H. Lambers (Eds.), Plant life under oxygen deprivation, SPB Academic, The Hague, 1991, pp. 101.

ELSEVIER

Talanta 44 (1997) 2193–2199

Talanta

Fluorimetric properties of a 2-hydroxypropyl-β-cyclodextrin: 9-methyl-benzo[a]phenothiazine inclusion complex in aqueous media. Analytical usefulness[1]

Mounir Maafi [a], Maria Carmen Mahedero [b], Jean-Jacques Aaron [a,*]

[a] *Institut de Topologie et de Dynamique des Systèmes de l'Université de Paris 7, Denis Diderot, associé au CNRS, URA-34, 1, rue Guy de la Brosse, 75005 Paris, France*

[b] *Department of Analytical Chemistry, Faculty of Sciences, University of Extremadura, 06071 Badajoz, Spain*

Received 25 June 1996; received in revised form 11 October 1996; accepted 14 October 1996

Abstract

The formation of an inclusion complex between 9-methyl-12*H*-benzo[*a*]phenothiazine (MeBPHT) and 2-hydroxypropyl-β-cyclodextrin (HP-β-CD) was investigated in aqueous medium. A 12-fold fluorescence emission intensity enhancement was found for the complexed relative to the free analyte. MeBPHT forms a 1:1 stoichiometry complex with HP-β-CD. A formation constant of 460 ($\pm$ 100) M^{-1} was calculated using the Benesi-Hildebrand method and fluorimetric data. The limit of detection was 7 ng ml^{-1} for MeBPHT in the presence of HP-β-CD instead of 60 ng ml^{-1} in the absence of HP-β-CD. © 1997 Elsevier Science B.V.

Keywords: Inclusion complex; Benzophenothiazines; Cyclodextrin; Fluorescence properties

1. Introduction

The most important property of phenothiazines (PHT) is their antidepressant activity [1]. Thereby, they enter in a variety of tranquilizing drug formulations. Also, they possess photochemotherapeutic abilities against carcinoma and they can be used as insecticides [2,3]. Recently, new benzophenothiazines (BPHT) have been synthesized, and their medical and physico-chemical properties have been investigated [4–11]. BPHT are potential anthelmintics and they are endowed with antiviral activity which inhibits multiplication of encephalomyocarditis in tissue culture [4]. The differentiation of three human myelogenous leukemic cell lines into maturing monocytes/macrophage was induced by unsubstituted BPHT and its 5-oxo derivative [3,5,6]. Motohashi et al. [7,8] established a correlation between the π electron density and the antitumoral activity of several BPHT derivatives and found the existence of substituent effects on the T antigen expression of adenovirus infected cells. Among BPHT derivatives, 9-methyl-benzo[*a*]phenothiazine (MeBPHT) (Fig. 1) presents the most potent anticancer activ-

* Corresponding author.

[1] Presented at the Symposium on Analytical Sciences (SAS) IV, Belgium, 3–5 June, 1996.

PII S0039-9140(97)00038-6

ity and possesses the highest electronic density on the nitrogen atom [7,8]. On the other hand, the pronounced coloration of BPHT derivatives allows them to be applied in polymer area as polycyclic dyes and pigments [9].

Several analytical methods, including thin layer chromatography (TLC), [12] high performance liquid chromatography (HPLC), [13] flow injection analysis (FIA), [14] and spectrofluorimetry, [15] have been reported for the determination of phenothiazines. Also, in our laboratory, photoinduced fluorescence was used to improve the PHT derivatives detection [16–18]. However, with the exception of Azure A:β-cyclodextrin (CD) complex [19], for which the limit of detection was approximately three times lower than that of the uncomplexed species, the fluorimetric determination of cyclodextrin-complexed PHT or BPHT derivatives has hiterto not been exploited.

In fact, the presence of CD and correctly-sized organic molecule in aqueous solutions results generally in the formation of inclusion complexes [20–22]. It is well documented that even a partial binding to the CD cavity is accompanied by noticeable changes in the photophysical properties of the guest compound. Among other interesting features, fluorescence intensity enhancement [23] and chiral activity induction [24] are obtained upon addition of CD. Accordingly, better enantiometric separations by HPLC, [25,26] TLC [27] or capillary zone electrophoresis, [28] have been reported for various compounds. Also, the spectrofluorimetric determination of procaine [29] and nalidixic acid [30] was improved by the preparation of host:guest complexes.

This paper describes the effect of HP-β-CD on the fluorescence intensity of MeBPHT, and the stoichiometric and thermodynamic characteristics of the inclusion complex. The fluorescence signal enhancement is used to develop a novel cyclodextrin-induced spectrofluorimetric method for the determination of MeBPHT. The possibility of applying this analytical approach to other biomedically-important, structurally-related benzophenothiazines is discussed.

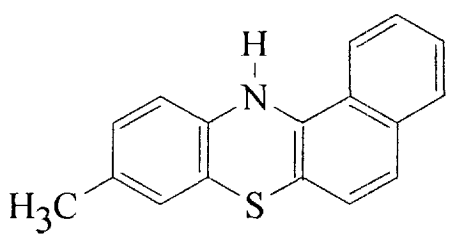

Fig. 1. 9-Methyl-12*H*-benzo[*a*]phenothiazine (MeBPHT) structure.

2. Experimental

2.1. Reagents

9 - Methyl - 12*H* - benzo[*a*]phenothiazine (Me - BPHT) was a kind gift of Professor N. Motohashi (Meiji College of Pharmacy, Tokyo, Japan). 2-Hydroxypropyl-β-cyclodextrin (HP-β-CD) was purchased from Aldrich Co., and used without further purification. HP-β-CD was selected for the following reasons: larger solubility in aqueous media (162 g/100 ml in ethanol/H_2O, 50:50, v/v) [20] relative to that of unsubstituted β-CD (1.3 g/100 ml in ethanol/H_2O, 50:50, v/v); [20] convenient size of its cavity for housing MeBPHT, and inexpensive cost relative to other CDs. Solvents used were purified, liquid chromatographic grade water and ethanol (Merck, analytical-grade reagent).

2.2. Apparatus

Fluorescence spectra were recorded on a Perkin-Elmer model LS 50 luminescence spectrometer equipped with a 20 W pulsed xenon lamp, with impulsions of a 8 μs duration. The instrument was connected via an RS-232 interface to an IBM PS\2 80386-SX microcomputer. Data acquisition and analysis were performed with the Perkin-Elmer fluorescence data manager software, version 2.70. Fluorescence spectra were obtained using 15 nm bandwidth excitation and emission slits. The monochromator scan rate was maintained at 240 nm/min. Fluorescence measurements were done at 20°C, using a thermostatically-controlled cell holder and a Selecta Model 382 thermostatically-controlled water bath.

2.3. Procedure

First, 10^{-3} M MeBPHT stock solutions were freshly prepared in ethanol, and kept in the dark to avoid photooxidation and degradation of the analyte. These solutions were used for preparing 10^{-5} M diluted samples for analytical purposes. Also, 0.1 M HP-β-CD aqueous stock solutions were utilized. The general procedure consisted to add a suitable volume of HP-β-CD solution to 0.1 ml of a 10^{-3} M MeBPHT ethanolic solution, and to dilute to the mark in a 10 ml calibrated flask with water. The mixture ratio was 99:1 (water/ethanol, v/v) for all working solutions. At such MeBPHT concentration (10^{-5} M) and solvent composition, the solutions were homogeneous, showing that MeBPHT becomes soluble in this predominantly aqueous medium in the presence of HP-β-CD.

The calculation of the complex formation constant as well as the statistical treatment of analytical data were performed using a software Origin, version 3.5 program.

3. Results and discussion

3.1. Effect of the medium composition

The effects of solvent and of HP-β-CD on the fluorescence spectral properties of MeBPHT were investigated. Fig. 2 shows the excitation and emission fluorescence spectra of MeBPHT in various media: ethanol (curve 1), water/ethanol (99:1, v/v) (WE) mixture (curve 2), and WE mixture with 0.1 M HP-β-CD (WECD) (curve 3). The excitation maxima are located in the 320–340 nm region, and are slightly red shifted ($\Delta\lambda_{exc} \cong 15$ nm) in ethanol and WECD media relative to WE mixture; while one broad emission band occurs at 515 nm and 513 nm in WE and WECD solutions, respectively. The latter value corresponds to a 8 nm red-shift relative to the emission maximum in pure ethanol. This radiative process can be attributed to the π^*, π deactivation transitions belonging to the naphthalene moiety, as previously reported [10,31].

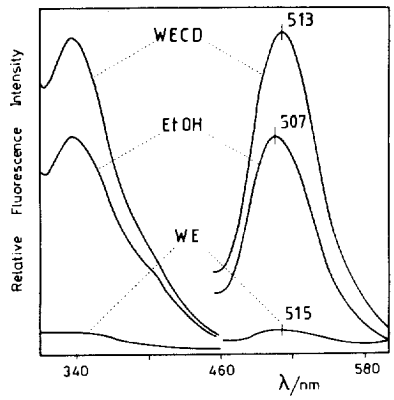

Fig. 2. Excitation and emission fluorescence spectra of 9-methyl-benzo[*a*]phenothiazine (10^{-5} M) in (WE) water/ethanol 1:99 (v/v) mixture; (EtOH) ethanol; (WECD) water/ethanol mixture in the presence of 0.1 M HP-β-CD.

A significant increase of the MeBPHT fluorescence intensity occurs in the presence of HP-β-CD (Fig. 3). Indeed, the emission spectrum of MeBPHT, presents a fluorescence intensity 12 times higher in WECD than in WE. Moreover, the fluorescence signal is approximately 1.5 times higher in HP-β-CD than in an ethanolic solution.

All these spectral features are in agreement with other literature data showing spectrofluorimetric evidence of the complexation with CDs [19,20,30]. Indeed, encapsulation of organic fluorophores in

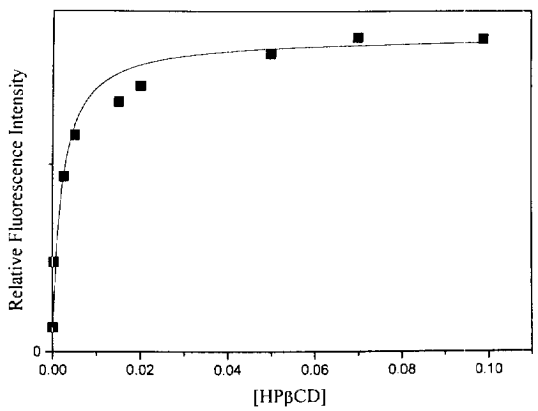

Fig. 3. Influence of HP-β-CD concentration on the fluorescence intensity of a 10^{-5} M MeBPHT solution. The solid line was calculated through the use of Eq. (4), assuming a 1:1 stoichiometry and F_∞ and K_f values obtained by non-linear regression analysis.

cyclodextrins, has generally a minor effect on the ground and excited electronic states energy levels, but it modifies significantly the radiative and radiationless transition rates. This behaviour can be attributed to the restricted mobility of the analyte within the CD cavity, and/or to the shielding of the radiative singlet excited-state from quenching processes by solvent molecules. Also, the hydrophobic effect allows interaction between the apolar CD interior and MeBPHT, which contributes to stabilize the analyte and dissolve it in water. The mechanism of inclusion of MeBPHT in HP-β-CD might be attributed to various hydrophobic/lipophilic processes, as suggested recently [22].

3.2. Effect of HP-β-CD concentration

The HP-β-CD effect was studied quantitatively by adding increasing concentrations of HP-β-CD (from 0 to 0.09 M), to MeBPHT (5×10^{-5} M) solutions, in WE medium. As can be seen in Fig. 3, the increase of HP-β-CD concentration, produces an important enhancement of the complex fluorescence intensity. Indeed, for a HP-β-CD concentration of about 0.02 M, the fluorescence emission intensity reaches a value which is about 12 times that in the absence of HP-β-CD. Higher HP-β-CD concentrations produce only small intensity variations, as shown by the plateau region observed between 0.03 to 0.09 M. This phenomenon can be attributed to completion of the complexation. It is possible to evaluate the molar fraction (f) of complexed MeBPHT, using Eq. (1) proposed by Flamigni [32].

$$f = 1 - \frac{1}{1 + [\mathrm{HP} - \beta - \mathrm{CD}] \cdot K_f} \tag{1}$$

We found f values higher than 0.93, indicating that a majority of the BPHT molecules are complexed by the HP-β-CD host reagents at a concentration of 0.03 M. In Eq. (1), K_f is the formation constant of the inclusion complex. K_f was calculated using the relative fluorescence intensity enhancement data correlated with the HP-β-CD concentrations, as described in the following section.

3.3. Stoichiometry and thermodynamic properties of the inclusion complex

The stoichiometry and the formation constant (K_f) of the HP-β-CD:MeBPHT, host-guest inclusion complexes were determined as previously [19,23]. Assuming a 1:1 stoichiometry ratio, the complex formation constant K_f of the equilibrium (Eq. (2)):

$$[\mathrm{HP} - \beta - \mathrm{CD}] + [\mathrm{MeBPHT}] \rightleftharpoons [\mathrm{HP} - \beta - \mathrm{CD{:}MeBPHT}] \tag{2}$$

will be given by:

$$K_f = \frac{[\mathrm{HP} - \beta - \mathrm{CD{:}MeBPHT}]}{[\mathrm{HP} - \beta - \mathrm{CD}] \cdot [\mathrm{MeBPHT}]} \tag{3}$$

Based on Eq. (1) and Eq. (2), and using the Benesi-Hildebrand method, [33,19] it is possible to express the relation between the fluorescence increment and the HP-β-CD concentration by the following equation:

$$F = F_0 + \frac{(F_\infty - F_0) \cdot K_f \cdot [\mathrm{HP} - \beta - \mathrm{CD}]}{1 + K_f \cdot [\mathrm{HP} - \beta - \mathrm{CD}]} \tag{4}$$

where F_0 and F_∞ denote the fluorescence intensity of MeBPHT, respectively, in the absence and in the presence of 0.1 M HP-β-CD, and F is the observed fluorescence at each HP-β-CD concentration tested.

The data of the above equation, can be represented using either a Scatchard plot, [33] or more conveniently the double-reciprocal plot given by:

$$\frac{1}{F - F_0} = \frac{1}{(F_\infty - F_0) \cdot K_f \cdot [\mathrm{HP} - \beta - \mathrm{CD}]} + \frac{1}{F_\infty - F_0} \tag{5}$$

If the stoichiometry of the complex is supposed to be 2:1, Eq. (6) becomes applicable:

$$\frac{1}{F - F_0} = \frac{1}{(F_\infty - F_0) \cdot K_f \cdot [\mathrm{HP} - \beta - \mathrm{CD}]^2} + \frac{1}{F_\infty - F_0} \tag{6}$$

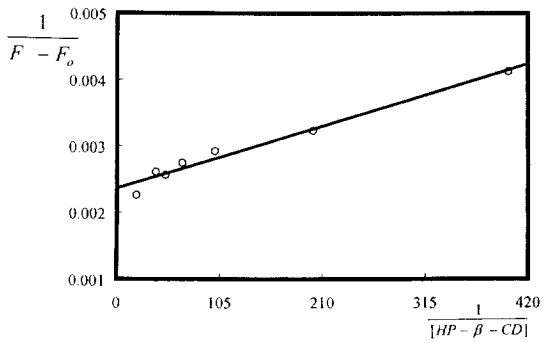

Fig. 4. Double reciprocal plot. A linear relationship is obtained when the data are plotted assuming a 1:1 HP-β-CD:MeBPHT stoichiometry.

Our experimental fluorimetric data fit the mathematical model of Eq. (4), suggesting a stoichiometry 1:1 for the MeBPHT:HP-β-CD complex (Fig. 3). This result is confirmed by the use of the double-reciprocal plot. In Fig. 4, a linear relationship is obtained when $1/F - F_0$ is plotted against $1/[\text{HP-}\beta\text{-CD}]_0$ according to Eq. (5). In contrast, a downward concave curvature is obtained when the data are used according to Eq. (6) (Fig. 5).

The formation constant of the inclusion complex was directly determined by the iterative process of the non-linear least-squares regression analysis, using our data and Eq. (4). The initial parameters needed for the iteration were obtained from the linear plot [33]. The calculated association constant for the MeBPHT:HP-β-CD complex has a value of $460 \pm 100\ M^{-1}$.

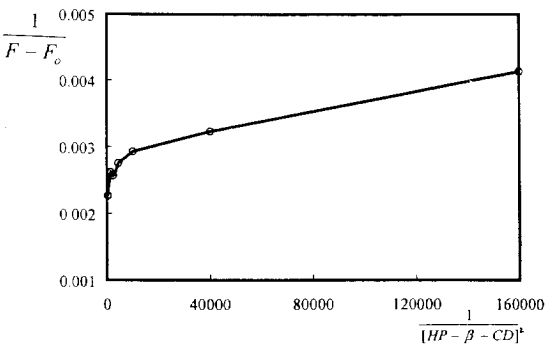

Fig. 5. Double reciprocal plot. Downward concave curvature relationship of $(F - F_0)^{-1}$ vs. $[\text{HP-}\beta\text{-CD}]^{-2}$, using Eq. (6) and assuming a 1:2 $(\text{HP-}\beta\text{-CD})_2$:MeBPHT stoichiometry.

This K_f value is significantly higher than that obtained, under the same conditions, for the complex of unsubstituted benzo[*a*]phenothiazine with HP-β-CD ($K_f = 100 \pm 22\ M^{-1}$) [23]. The formation constant of the Azure A photoproduct:β-CD complex [19] was also $110 \pm 40\ M^{-1}$. Therefore, based on these results, the MeBPHT:HP-β-CD complex seems to be slightly more stable than the others. Our K_f value compares to those of inclusion complexes formed between 2-substituted naphthalene derivatives and β-CD ($560\ M^{-1}$) [34].

3.4. Analytical usefulness

In order to demonstrate the analytical usefulness of the complexation of MeBPHT by HP-β-CD, we compared the analytical figures of merit obtained in the different media under study (Table 1). Linear calibration plots are established over about one order of magnitude, with satisfactory precision, as shown by the correlation coefficient values close to unity. The linear dynamic range is larger in WECD than in ethanol and WE. The slope of the regression equation is more than ten times greater in WECD than in WE, indicating a higher sensitivity of the spectrofluorimetric method in the presence of HP-β-CD. The limit of detection (LOD) of MeBPHT is greatly improved by the formation of the inclusion complex in water solutions. Indeed, the LOD values lay in the low ng/mL range, and are significantly lower for the complexed MeBPHT than in ethanol or WE. A 10-fold decrease is observed for the MeBPHT LOD value in the presence of HP-β-CD relative to WE mixture.

By taking advantage of this HP-β-CD-induced fluorescence enhancement and of the water-solubility improvement, it would be possible to use also this method in combination with an HPLC and/or a FIA technique for increasing the sensitivity and, possibly, the specificity of analysis of other benzophenothiazines. To apply our method to the analysis of BPHT derivatives in biological liquids or in drugs, a separation (or a prepurification) step may be needed to avoid interferences in these complex matrixes.

Table 1
Analytical data for the determination of MeBPHT in various media

Medium	$\lambda_{ex.}$ (nm)	$\lambda_{em.}$ (nm)	Linear dynamic range (μg ml^{-1})	Regression equation	Correlation coefficient	LOD[a] (ng ml^{-1})	R.S.D.[b] (%)
Organic medium							
Ethanol	335	507	0.1–1.7	$294.5C+2.6$	0.999	11	4.5
Aqueous medium							
WE[c]	320	515	0.2–1.4	$29.7C-0.5$	0.998	60	6
WECD[d]	336	513	0.07–1.9	$465C-2.8$	0.998	7	4

[a] LOD, limit of detection, defined as the amount of analyte giving a signal-to-noise ratio of 3.
[b] R.S.D., relative standard deviation for MeBPHT concentrations ranging between 0.5 and 1 μg ml^{-1} ($n = 7$).
[c] WE, H_2O/EtOH (99:1, v/v) mixture.
[d] WECD, H_2O/EtOH (99:1, v/v) mixture in the presence of 0.1 M HP-β-CD.

4. Conclusion

We have shown that the important increase of the fluorescence intensity of MeBPHT in the presence of HP-β-CD aqueous solution can be attributed to the formation of an inclusion complex of a 1:1 stoichiometry. Its association constant value of 460 ± 100 M^{-1} was calculated using the Benesi-Hildebrand method. The enhancement of the analytical signal allows to develop a sensitive cyclodextrin-induced spectrofluorimetric method for the determination of MeBPHT. Moreover, this approach permits to lower by about 10 times its detection limit in water.

This HP-β-CD-induced fluorescence technique is presently under investigation for analytical application to other biomedically-important BPHT derivatives.

References

[1] (a) S.G. Dahl, in E. Udsin, S.G. Dahl, L.F. Gram (Eds.), Clinical Pharmacology Psychiatry: Neuroleptic Antidepressant Research, MacMillan, London, 1981, p. 125–137; (b) S.M. Curry, Drug Psychiatry, 3 (1985) 79.
[2] G.J.S. Foncer, R.J. Reej, R. Devonshire, J. Photochem. Photobiol. 52 (1990) 489.
[3] (a) C.O. Okafor, Dyes Pigm. 1986, 7, 249; (b) R.R. Gupta (Ed.), Phenothiazines and 1,4-Benzothiazines, Chemical and Biological Aspects, Elsevier, Amsterdam, 1988.
[4] (a) V.K. Pandley, Indian J. Chem. 26B (12) (1987) 1280; (b) V.K. Pandley, D. Misra, M.N. Joshi, K. Chandra, Pharmacol. Res. Commun. 20 (1988) 153.
[5] N. Motohashi, Y. Sasaki, Y.-I. Wakabayashi, H. Sakagami, J. Molinár, T. Kurihara, Anticancer Res. 12 (1992) 1423.
[6] J. Molnár, H. Sakagami, N. Motohashi, Anticancer Res. 13 (1993) 1019.
[7] N. Motohashi, H. Sakagami, K. Kamata, Y. Yamamoto, Anticancer Res. 11 (1991) 1933.
[8] R. Putzai, N. Motohashi, C. Párkányi, J.J. Aaron, B.K. Rao, J. Molnár, Anticancer Res. 16 (1996) 2961.
[9] (a) M. Matsuoka, S.H. Kim, Y. Kubo, T.Kitao, J. Soc. Dyers Colour 102 (1986) 232; (b) T.Kitao, M. Matsuoka, K. Takagi, Jpn. Kokai Tokkyo Koho, JP. 61, 204, 273 [86, 204, 273]; Chem. Abstr., 106 (1987) 68710d.
[10] J.J. Aaron, M. Maafi, C. Kersebet, C. Párkányi, M.S. Antonious, N. Motohashi, Spectrosc. Lett. 28 (1995) 1111.
[11] K. Kubo, K. Yoshida, K. Jpn.Kokai Tokkyo Koho, JP. 01, 228, 976 [89, 228, 976]; Chem. Abstr. 112 (1990) 189089f.
[12] O. Fridan, A.G. Davidson, J. Chromatogr. 442 (1988) 363.
[13] S. Li, W.S. Purdy, J. Pharm. Biomed. Anal. 9 (1991) 409.
[14] J. Martinez Calatayud, C. Gomez Benito, Anal. Chim. Acta 256 (1992) 105.
[15] M.C. Guttierez, A. Gomez-Henz, D. Perez-Bendito, Anal. Lett. 20 (1987) 1847.
[16] B. Laassis, J.J. Aaron, M.C. Mahedero, Anal. Chim. Acta 290 (1994) 27.
[17] M.C. Mahedero, J.J. Aaron, Anal. Chim. Acta 269 (1992) 193.
[18] B. Laassis, J.J. Aaron, M.C. Mahedero, Talanta 41 (1994) 1985.
[19] M. Maafi, B. Laassis, J.J. Aaron, M.C. Mahedero, A. Muñoz de la Peña, F. Salinas, J. Incl. Phenom. 22 (1995) 235.
[20] K.H. Frömming, J. Szejtli, in: J.E. Davis (Ed.), Topics in Inclusion Science: Cyclodextrin in Pharmacy, Kluwer, Dordrecht, 1994.
[21] G. Wenz, Angew. Chem. Int. Ed. Engl. 33 (1994) 803.
[22] H.J. Schneider, Angew. Chem. Int. Ed. Engl. 30 (1991) 1417.
[23] M. Maafi, J.J. Aaron, M.C. Mahedero, F. Salinas, J. Fluorescence 7 (1997) 11.

[24] A.Y. Will, J.M. Schuette-Parson, R.A. Agbaria, I.M. Warner, Appl. Spectrosc. 49 (1995) 1762.
[25] A.M. Stalcup, K.H. Gahm, Anal. Chem. 68 (1996) 1369.
[26] D.W. Armstrong, S.M. Han, Y.L. Han, Anal. Biochem. 167 (1987) 261.
[27] D.W. Armstrong, F.-Y. He, S.M. Han, J. Chromatogr. 448 (1988) 345.
[28] T.J. Ward, Anal. Chem. 66 (1994) 632A.
[29] F. Garcia Sanchez, A.L. Ramos Rubio, C. Cruces Blanco, M. Hernandez Lopez, J.C. Marquez Gomez, C. Carnero, Anal. Chim. Acta 205 (1988) 139.
[30] I. Duran-Meras, A. Muñoz de la Peña, F. Salinas, I. Rodriguez Caceres, Analyst 119 (1994) 1215.
[31] (a) J.J. Aaron, M. Maafi, C. Kersebet, C. Párkányi, M.S. Antonious, N. Motohashi, J. Photobiol. Photochem. A. Chem., in press; (b) C. Párkányi, C. Boniface, J.J. Aaron, M. Maafi, Spectrochim. Acta, 49A (1993) 1715.
[32] L. Flamigni, J. Phys. Chem. 97 (1993) 9566.
[33] K.A. Connors, in: Binding Constants, The Measurements of Molecular Complex Stability, Wiley, New York, 1987.
[34] A. Muñoz de la Peña, F. Salinas, N.J. Gomez, M.I. Acedo, M. Sanchez Peña, J. Incl. Phenom. 15 (1993) 131.

ELSEVIER

Talanta 44 (1997) 2201–2208

Talanta

Multielemental speciation of As, Se, Sb and Te by HPLC-ICP-MS[1]

T. Guerin [a], M. Astruc [a,*], A. Batel [b], M. Borsier [b]

[a] *Université de PAU et des Pays de l'Adour, Laboratoire de Chimie Analytique, Avenue de l'Université, 64000 Pau, France*
[b] *BRGM, Département Analyse, Avenue de Concyr, BP 6009, 45060 Orléans cedex 2, France*

Received 5 June 1996; received in revised form 26 November 1996; accepted 6 December 1996

Abstract

An anion exchange HPLC-ICP-MS procedure allowing the simultaneous multielemental speciation analysis of arsenic, selenium, antimony and tellurium has been developed. Four arsenic species (As^{III}, As^{V}, monomethylarsonic acid and dimethylarsinic acid), two selenium species (Se^{IV} and Se^{VI}) may be determined in a single run as well as one antimony (Sb^{V}) and one tellurium species (Te^{VI}). Alternatively Sb and/or Te may be used as internal standards for As and Se speciation studies. Optimisation of ICP-MS conditions led to satisfactory relative (0.01 (Sb^{V}) to 1.8 (Se^{VI}) ng ml^{-1}) and absolute detection limits (1–180 pg). Reproducibility ranged from 3.1 to 5.6% and the linearity was verified in the 0–200 ng ml^{-1} range. © 1997 Elsevier Science B.V.

Keywords: Multielemental speciation; Arsenic; Selenium; HPLC-ICP-MS

1. Introduction

It is now well known that the toxicological and biological properties of most metals depend upon their chemical form. Chemical speciation analysis aims to determine the nature and concentration of the compounds of an element present in a given material. Knowledge of speciation is especially necessary for As, Se, Sb and Te compounds for which oxydated inorganic species are among the most toxic forms, whereas methylated forms such as monomethylarsonic acid (MMA) or dimethylarsinic acid (DMA) are much less toxic. Arsenic is a very common pollutant deserving special attention. Selenium is of particular interest because of its dual role as an essential ultratrace nutrient on one hand and as a toxic when ingested at higher levels on the other hand. Antimony and tellurium have been the object of very few environmental studies.

Several instrumental techniques have been developed that allow selective detection of different species at very low levels. Inductively Coupled Plasma Mass Spectrometry (ICP-MS) is a relatively new technique allowing the total concentration determination of many elements with the

* Corresponding author.

[1] Presented at the Symposium on Analytical Sciences (SAS) IV, Belgium, 3–5 June, 1996.

PII S0039-9140(97)00036-2

high sensitivity of mass spectrometry. ICP-MS is well suited as a detector for inorganic and organometallic species separated by High Performance Liquid Chromatography (HPLC) [1], comparing favourably with other atomic spectrometric techniques particularly when an aqueous mobile phase is used. Moreover sample pretreatment may be minimized when ICP-MS is used restricting eventual changes in the relative concentration of individual species.

As early as 1986 [2] HPLC-ICP-MS has been applied to As speciation studies. In 1992, a review by McLaren et al. [3] referred four studies about HPLC-ICP-MS arsenic speciation in biological matrices. Some more papers in this field appeared in recent years [4–10] as well as others dealing respectively with sediments [7,11] or natural waters [12,13]. We found few papers dealing with Se speciation using HPLC-ICP-MS [14–16] or HPLC-ICP-AES [17] and only one about Sb [18] to our knowledge. Simultaneous speciation of As and Se compounds has been realised using only emission spectrometry detection [19], eventually preceded by hydridization [20].

The use of ICP-MS as HPLC detector leads to some constraints on the choice of chromatographic conditions concerning the nature and concentration of buffer salts in the chromatographic mobile phase and the presence of organic solvents. Therefore, ion exchange, size exclusion or reversed phase chromatographies are generally preferred and isocratic separations are advisable.

In this work we used an anion exchange PRP-X100 column and a phosphate buffer eluent known from previous optimisation to allow a good separation of four arsenic species (arsenite (As^{III}), arsenate (As^{V}), DMA, MMA), two selenium species (selenite (Se^{IV}) and selenate (Se^{VI})), tellurate (Te^{VI}) and antimonate (Sb^{V}) [21].

The aim of the present study was to optimize the ICP-MS detection in order to develop a fast, sensitive and accurate analytical procedure for the simultaneous speciation of arsenic, selenium, tellurium and antimony. The final objective is the speciation of these elements in soil extracts.

2. Experimental

2.1. Reagents and solutions

Di-arsenic trioxide (As_2O_3, p.a.), di-sodium selenate (Na_2SeO_4, suprapur) and di-sodium selenite (Na_2SeO_3, suprapur) were purchased from Merck. Ammonium hydrogen phosphate ($(NH_4)_2HPO_4$), ammonium hydroxide (NH_4OH), all RPE qualities, methanol (CH_3OH) and acetonitrile (CH_3CN), both HPLC grade, and monomethylarsonic acid (MMA) di-sodium salt (purum) were purchased from Carlo Erba. Dimethylarsinic acid sodium salt trihydrate (DMA, purum), potassium hexahydroxyantimonate(V) (H_6KO_6Sb, analytical reagent), telluric acid ($Te(OH)_6$, analytical reagent) and standard solution (1000 mg As l^{-1}) of arsenate (H_3AsO_4, spectrosol) were obtained from Fluka, Prolabo, Aldrich and BDH, respectively.

Arsenite (As^{III}) standard solution (1000 mg As l^{-1}) was prepared by dissolution of As_2O_3 in 0.2% NaOH solution leading to the formation of sodium arsenite. Other 1000 mg l^{-1} (as element) stock solutions were prepared in deionized water (Milli-RO/Milli-Q system from Millipore, 18 mW). These standards were used without any further purification. All standards (1000 mg l^{-1}) were stored at 4°C in the dark; stability over several months has been confirmed excepted for selenium compounds (1 month). Working standards (10, 1 or 0.1 mg l^{-1}) were obtained daily by dilution in the chromatographic eluent just before use and stored in the dark. Phosphate buffer (12.5 mmol l^{-1}) was prepared by dissolving di-ammonium hydrogen phosphate in deionized water (Millipore) and pH adjustment was obtained by dropwise addition of 30% ammonia. The mobile phase was filtered (0.45 mm) and degassed before use.

2.2. Apparatus

The HPLC system consisted of a Varian 9001 isocratic solvent delivery unit fitted out with a PRP-X100 anion exchange column (Hamilton, Reno, Nevada) (25 cm × 4.1 mm I.D.; spherical 10 μm particles of a styrene–divinylbenzene co-

polymer with trimethylammonium exchange sites; stable between pH 1 and 13; exchange capacity 0.19 meq g^{-1}). In this work a 100 µl loop (Peek, Interchim) was selected in conjunction with a Rheodyne six-port injection valve.

A VG PQ3 ICP-MS (VG Elemental, Winsford, Cheshire, U.K.) was used to detect the compounds in the column effluent. The ICP mass spectrometer was equipped with a Fassel Torch, a Meinhard-type concentric glass nebulizer (Glass Expansion, Pty, Australia) and a doubled pass Scott-type spray chamber with liquid coolant, the temperature of which was maintained at 1°C by a recirculating refrigeration-heating system.

2.3. Method optimization

ICP-MS sensitivity was optimised by varying one instrumental setting at a time during the analysis of standard solutions of the various species studied. A peristaltic pump was used for conventional sample introduction of the analyte solution at 1.5 ml min^{-1} in order to optimize detection conditions or to evaluate either the relative sensitivities of the various analytes or signal enhancement by addition of organic solvents to the mobile phase. Both scanning and peak jumping modes were used. Instrument setting adjusted were the physical positioning of the mass spectrometer relative to the plasma, ion lens voltages, aerosol carrier argon gas flow and R.f. power input to the argon plasma. The optimal conditions were found as differing somewhat from one element to the other. However for multielemental speciation studies only one set of conditions must be chosen. Arsenic being the main centre of interest in this study the instrument settings optimized for this element were retained in all experiments.

Coupling between HPLC column outlet and ICP-MS nebulizer was reduced to a short length (5 cm) of Teflon capillary tubing (0.5 mm I.D.) in order to minimize dead volume and improve peak shape. Isocratic elution was carried out with a 1.5 ml min^{-1} flow rate compatible with the normal sample uptake rate of the ICP- MS device.

Optimised ICP-MS and HPLC settings are summarized in Table 1.

The mass spectrometer was set to sample ion intensities using Time Resolved Acquisition mode (TRA) following mass to charge ratios (m/z) ($^{75}As^+$), ($^{82}Se^+$), ($^{126}Te^+$) and ($^{121}Sb^+$) during the coupling measurements. Those analyte masses were selected taking in account possible interferences caused either by isotopes of other elements or by polyatomic species with the same m/z value as the analyte that are now well known in ICP-MS detection [22]. The problem is relatively simple for As and Sb because of the existence of a single ^{75}As and of only two ^{121}Sb and ^{123}Sb iso-

Table 1
Operating conditions

ICP-MS	VG Plasma Quad 3
R.f. power	1350 W
Nebulizer	Meinhard type K
Spray chamber	Doubled-pass Scott type, cooled at 1°C
Ion sampling	
Sampler cone	Platinum: 1 mm orifice
Skimmer cone	Nickel: 0.75 mm orifice
Argon flow rates	
Outer	14 l min^{-1}
Intermediate	1.00 l min^{-1}
Aerosol carrier	0.92 l min^{-1} (Variable)
Pressures	
Expansion	1.87 mbar
Quadrupole chamber	6.5 E^{-7} mbar
Detector voltage (P.C.)	−3281 V
Time Resolved Acquisition parameters	
Dwell time per mass	50 ms
Points across peak	3
Data acquisition mode	Graphics (signal intensity versus time)
Chromatography	
Anion-exchange column	PRP-X 100 (250 × 4.1 mm I.D.)
Mobile phase	12.5 mmol l^{-1} $(NH_4)_2HPO_4$ in water with 3 % v/v MeOH
pH	8.5 with NH_4OH
Flow rate	1.5 ml min^{-1}
Injected volume	100 µl

Table 2
Effect of mobile phase composition

Matrix	As^{III}	DMA	MMA	As^{V}	Se^{IV}	Se^{VI}	Sb^{V}	Te^{VI}
Water								
S (counts s^{-1})	34 635	35 712	39 316	38 301	3 878	4 700	161 971	25 825
R (%)	(88)	(91)	(100)	(97)	(83)	(100)	—	—
S/N ratio	222	229	252	245	136	164	3 050	929
Mobile phase								
S (counts s^{-1})	36 101	37 110	42 973	36 974	4 292	3 746	17 0210	24 083
R (%)	(84)	(86)	(100)	(86)	(100)	(87)	—	—
S/N ratio	18.6	19.1	22.2	19.1	4.4	3.9	412	6.2

S, intensity obtained for a 10 ng (as element) ml^{-1} species concentration after direct aspiration in ICP-MS (mean of 3 replicates).
R, ratio of species intensity to the most sensitive one.
N, base-line noise standard deviation for 10 blank replicates.
Mobile phase, $(NH_4)_2HPO_4$ 12.5 mmol l^{-1} + NH_3 to pH 8.5.

topes. ^{121}Sb was retained because it is not subjected to major interferences and is the most abundant. Despite of its lesser abundance ^{82}Se was chosen as free from $Ar–Ar^+$ polyatomic interference and ^{126}Te being not disturbed by the $^{130}Xe^+$ monoatomic interference.

Signal intensities obtained depend on the degree of corrosion of the sampler and skimmer cones in use. Throughout this work, a sampler cone made of platinum was used in order to avoid a rapid degradation by phosphorus ions of the mobile phase.

3. Results and discussion

3.1. Effect of mobile phase composition

Comparison of ICP-MS signal intensities obtained for each species prepared either in water or in the chromatographic eluent without methanol, was made using conventional aspiration at 1.5 ml min^{-1} (Table 2). Ammonium salts are classically used as the counter cation in anion exchange HPLC-ICP-MS studies in order to avoid non-spectroscopic interferences in the presence of alkaline cations such as Na^+ [23]. A phosphate buffer was chosen from previous investigations [21] on a series of buffer solutions tested, it contained 12.5 mmol l^{-1} $(NH_4)_2HPO_4$ adjusted to pH 8.5 by ammonia addition.

Signal intensities obtained for the various species of a single element in a single matrix varied somewhat (Table 2). This was previously noted by Larsen and Stürup [24] in water. Moreover these authors obtained a different order of relative sensitivities for the four arsenic species. Inter-species signal intensities variations reported in this study ($\leq \pm 8\%$ for As or Se species) are quite low compared to those quoted in the literature. It seems that ionization processes differ somewhat from one ICP-MS instrument to the other. Signal intensities obtained for the various species are approximately equivalent in water or mobile phase matrice with only slight signal variations in the presence of the chromatographic eluent (-20 to $+10\%$ at most for all species studied).

However, base-line noise (N) was amplified by a factor of 10 at least by the mobile phase, inducing an equivalent decrease of the signal intensity to noise ratio (S/N). For example we found a 12.8 S/N ratio decrease factor for As^V between water and phosphate buffer. Using a carbonate buffer (0.1 mol l^{-1} $(NH_4)_2CO_3$ at pH 10.3) Larsen and Stürup [24] observed a 1.3 S/N ratio decrease factor only. The difference cannot be explained by the different salt concentrations of the buffers with 1.6 g l^{-1} (this work) and 8.4 g l^{-1} [24]. It appears therefore that the nature of buffer salts may have a significant influence on the HPLC-ICP-MS responses by modifying either plasma chemistry or ionic interactions in the plasma-mass spectrometer interface.

The ICP-MS sensitivity variations depending on species analysed evidence a major problem for the choice of standard solutions in classical ICP-MS total element determination, problem already underlined by Larsen and Stürup [24] for As determination.

3.2. Influence of solvent additions

We have studied the effect of the addition of organic carbon (as methanol or acetonitrile) to the mobile phase on some species signal intensities during direct aspiration at 1.5 ml min^{-1} in ICP-MS. Examples of the ICP-MS responses in a range of 0–7% solvent addition are given in Fig. 1.

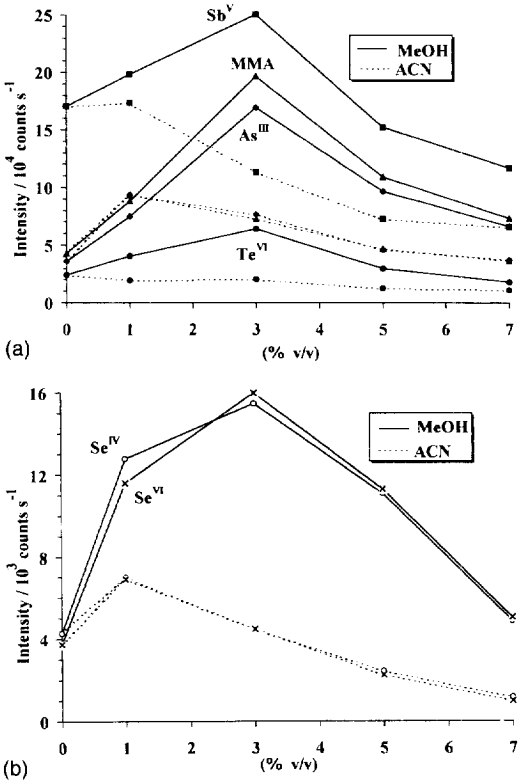

Fig. 1. ICP-MS signal intensities for (a) two arsenic species, one antimony and one tellurium compounds, and (b) two selenium species versus % of methanol or acetonitrile in the mobile phase. Signal intensities are given as count s^{-1} for 10 ng ml^{-1} of each compound.

Table 3
Effects on sensitivity and base-line noise of 3% v/v MeOH addition to phosphate buffer solution

Species	S_r	N_r	S_r/N_r
As^{III}	4.7	2.2	2.2
DMA	4.8	2.2	2.2
MMA	4.6	2.2	2.1
As^{V}	5.1	2.2	2.4
Se^{IV}	3.6	1.8	2.0
Se^{VI}	4.3	1.8	2.4
Sb^{V}	1.5	0.9	1.6
Te^{VI}	2.7	3.3	0.8

S_r, ratio of signal intensities obtained with or without addition of 3% v/v MeOH.
N_r, ratio of base-line noise obtained with or without addition of 3% v/v MeOH.

The loading of organic solvent in the plasma results in energy removal due to pyrolysis and the maximum signal intensity enhancement was obtained for all species of all elements with a 3% v/v addition of methanol. Signal improvements due to the addition of 3% methanol to the phosphate buffer (Table 3) are similar for various species of a same element but differ widely between elements. Similar conclusions were reached by other authors [4,7,12] but with variable optimal percentages of methanol (1–5%) probably due to differences in plasma torch operation conditions. Simultaneously, background level and base line noise amplitude increased more or less depending on the species studied. The signal to noise ratio (S/N) was improved in the presence of 3% methanol for most species (Table 3) but not all. Larsen and Stürup [24] noted already similar effects of methanol addition.

As regards acetonitrile, a 1% v/v addition to the mobile phase led to a maximum signal enhancement. Signal intensities were enhanced by a factor of about 2.2 for As species, 1.5 for selenium species, 1.0 for Te and Sb when base-line noise increased by a factor of 16 for As, slightly for Se (1.5), Sb (1.1) and decrease for Te (0.8), resulting in a slight S/N ratio improvement for Te (1.3), an equivalent S/N ratio for Se and Sb or a degradation of the S/N ratio for all arsenic species. It is difficult to compare in details these results to those of previous studies as either the mobile

phase, direct aspiration flow or plasma conditions differed somewhat [7,12,24]. The general output appears nevertheless clearly in favour of an addition of 3% methanol to the mobile phase for HPLC-ICP-MS studies of these four elements.

3.3. Performances of the coupled HPLC-ICP-MS device

If only As and Se species are present in samples then both Te and Sb could be used as internal standards in order to improve accuracy and reduce analysis time. Sb^{V} as potassium hexahydroxyantimonate was found most convenient for this use. A typical chromatogram of a mixture of all arsenic, tellurium and selenium species together with the internal standard Sb is shown in Fig. 2. Run time was ≈ 17 min. For six replicate injections, the maximum standard deviation (S.D.) obtained for the retention time of any compound was less than 4 s (Table 4). The presence of 3% v/v methanol in the mobile phase caused a slight but significant increase in the retention time (4–50 s) of each species, compared to those obtained without addition of methanol [21]. The increase differs depending on the species considered, effect which may be ascribed to the reduced ionic dissociating power in presence of organic solvent. The elution capacity of the mobile phase is therefore slightly reduced as the more retained species (As^{V}, Se^{VI}) would suffer a larger increase of retention time.

Reproducibility of peak heights was determined from six replicate injections of 5 ng of As and Te species, 20 ng of Se and 1 ng of Sb species (Table 5). Even without using internal standard, the relative standard deviations (R.S.D.) never exceeded 7%. Reproducibility was slightly better when using peak heights rather than peak areas. The linearity of calibration curves plotted with both peak heights and peak areas was satisfactory for all species in the range of concentrations studied (0–200 ng ml^{-1}) (Table 5). Correlation coefficients obtained by using peak height and peak area measurements are excellent and almost identical.

Detection limits (L.O.D.) defined according to IUPAC standard [25] are presented in Table 5. As expected, the limits of detection of Se, Te and Sb species have been improved with about the same factors (S/N ratio) which were obtained by addition of 3% v/v of methanol in the previous signal enhancement study (Table 3). However, detection limits obtained for As species were practically the same as those obtained in a previous study [21] with the same chromatographic conditions but without addition of organic solvent. This could probably be explained by a larger enhancement of the base line noise (N) than expected in the previous signal enhancement study. Anyway L.O.D.

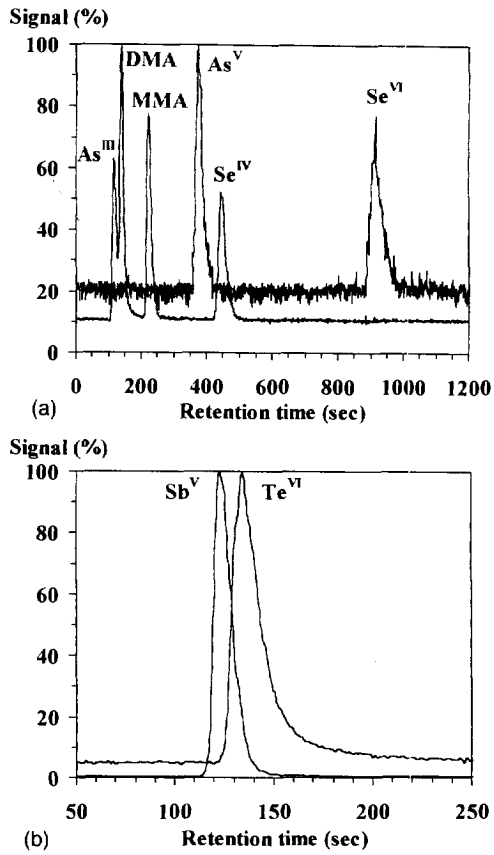

Fig. 2. Typical HPLC-ICP-MS chromatogram of a mixture of 25 ng (as element) ml^{-1} (A) arsenic (As^{III}, DMA, MMA, As^{V}), selenium (Se^{IV}, Se^{VI}), and (B) tellurium (Te^{VI}) species, with antimony (Sb^{V}) 5 ng ml^{-1} as internal standard in a 12.5 mmol l^{-1} phosphate buffer at pH 8.5 with 3% v/v methanol addition. Signal intensities are given as a ratio (%) of species intensity to the most sensitive one for each element. Flow rate: 1.5 ml min^{-1}.

Table 4
HPLC-ICP-MS retention times

Compound	Retention time[a] (± S.D., s)
As^{III}	116 ± 2
DMA	139 ± 2
MMA	222 ± 2
As^{V}	445 ± 2
Se^{IV}	375 ± 2
Se^{VI}	913 ± 4
Sb^{V}	123 ± 2
Te^{VI}	134 ± 2

[a] Mean of six determinations for each compound.

values for As species obtained in this work (ranging from 10 to 23 pg) still compare well with those reported by Demesmay et al. [7] (10–30 pg), Larsen et al. [4] (80–150 pg) or Thomas and Sniatecki [12] (45–150 pg) who did not use IUPAC definition of L.O.D. however.

3.4. Monitoring the argon chloride interference

Spectral and non-spectral interferences in ICP-MS have been recently considered by Dams et al. [22]. The formation of the polyatomic ion $^{40}Ar^{35}Cl^{+}$ which interferes with the detection of arsenic at m/z 75 has been proved to occur in chloride rich samples such as urine [4,6] or sea water, and the authors have suggested to avoid the formation of the $ArCl^{+}$ ion by addition of a few percent of nitrogen to the argon plasma [6]. Another approach consisted in separating chemically arsenic species from the interfering chloride by formation of volatile arsines [26]. Other studies have shown that chloride present in samples can be chromatographically separated from arsenic species [5,11,27]. The latter approach was tested in the present study and investigated by injecting a 0.9 g l^{-1} sodium chloride solution spiked with arsenic species into the anion exchange HPLC-ICP-MS device and the elution of the chloride ion (monitored as the $^{35}Cl^{16}O^{+}$ ion at m/z 51) occurred as a small peak with a 299-s retention time, completely separated from those of MMA (220 s) and As^{V} (442 s) as shown in Fig. 3.

The formation of $ArCl^{+}$ from the eluting chloride does not consequently interfere in the on line HPLC-ICP-MS analysis of the arsenic containing analytes.

4. Conclusion

The HPLC-ICP-MS method presented allow the simultaneous speciation analysis of four elements (As, Se, Sb, Te). Sensitivity variations between species of a single element and under changes of experimental ICP-MS conditions have been noted and daily individual calibration appear necessary; the use of one of these elements as internal standard may be useful.

Table 5
Performances of the anion exchange HPLC-ICP/MS method with addition of 3% v/v of MeOH

Species	R.S.D. (%)[a]	Calibration curves		Detection limits[d]	
		Slope[b] (CPS ng ml^{-1})	r^2	Relative[c] (ng ml^{-1})	Absolute (pg as element)
As^{III}	3.5	5 418	0.9995	0.17	17
DMA	4.3	8 347	0.9999	0.10	10
MMA	3.1	6 554	0.9994	0.13	13
As^{V}	4.8	3 839	0.9999	0.23	23
Se^{IV}	4.4	330	0.9995	0.94	94
Se^{VI}	5.6	175	0.9964	1.77	177
Sb^{V}	3.8	12 262	0.9996	0.01	1.0
Te^{VI}	3.4	1 667	0.9993	0.35	35

[a] Peak height reproducibility (6 replicates).
[b] Mean for 6 replicate experiments (peak height).
[c] Injection loop: 100 μl.
[d] Defined as 3 × standard deviation of 20 blanks/slope of calibration curve (IUPAC, $k = 3$).

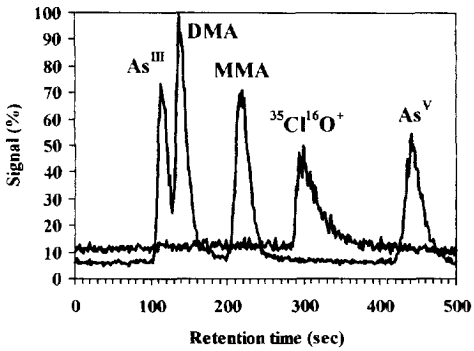

Fig. 3. Separation of chloride ion ($^{35}Cl^{16}O^{-}$) from arsenic species by HPLC-ICP-MS. Same chromatographic conditions as in Fig. 2. Signal intensities are given as a ratio (%) of species intensity to the most sensitive one and are multiplied by ten for ClO^{+} ion.

Further work is in progress to apply this method to the analysis of environmental samples (polluted soils, sediments and sludges).

Acknowledgements

The authors would like to grateful to Dr A. Astruc, University of Pau, and R. Cottier, BRGM (Orléans), for their useful technical assistance during the liquid chromatographic and ICP-MS studies, respectively.

References

[1] G. Lespes, M. Potin-Gautier, A. Astruc, Environ. Technol. 13 (1992) 207.
[2] J.J. Thompson, R.S. Houk, Anal. Chem. 58 (1986) 2541.
[3] J.W. McLaren, K.W. Siu, S.S. Berman, Instrumentation for Trace Organic Monitoring, Lewis, Chelsea, 1992.
[4] E.H. Larsen, G. Pritzl, S.H. Hansen, J. Anal. Atom. Spectrom. 8 (1993) 557.
[5] B.S. Sheppard, J.A. Caruso, D.T. Heitkemper, K.A. Wolnik, Analyst 117 (1992) 971.
[6] S. Branch, L. Ebdon, P. O'Neill, J. Anal. Atom. Spectrom. 9 (1994) 33.
[7] C. Demesmay, M. Olle, M. Porthault, Fresenius J. Anal. Chem. 348 (1994) 205.
[8] K. Kawabata, Y. Inoue, H. Takahashi, G. Endo, Appl. Organomet. Chem. 8 (1994) 245.
[9] X.C. Le, W.R. Cullen, K.J. Reimer, Talanta 41 (1994) 495.
[10] H. Ding, J. Wang, J.G. Dorsey, J.A. Caruso, J. Chromatogr. 694 (1995) 425.
[11] S.H. Hansen, E.H. Larsen, G. Pritzl, C. Cornett, J. Anal. Atom. Spectrom. 7 (1992) 629.
[12] P. Thomas, K. Sniatecki, J. Anal. Atom. Spectrom. 10 (1995) 615.
[13] C. Hwang, S. Jiang, Anal. Chim. Acta 289 (1994) 205.
[14] S.C. Shum, R.S. Houk, Anal. Chem. 65 (1993) 2972.
[15] K.T. Suzuki, M. Itoh, M. Ohmichi, J. Chromatogr. 666 (1995) 13.
[16] Y. Cai, M. Cabañas, J.L. Fernàndez-Turiel, M. Abalos, J.M. Bayona, Anal. Chem. Acta 314 (1995) 183.
[17] A. Hagege, S. Niemczyk, M.J.F. Leroy, Analysis 23 (1995) 476.
[18] P. Smichowski, Y. Madrid, C. Cámara, Química Analítica 14 (1995) 210.
[19] J.P. McCarthy, J.A. Caruso, F.L. Fricke, J. Chromatogr. Sci. 21 (1983) 389.
[20] D. Schlegel, J. Mattush, K. Dittrich, J. Chromatogr. 683 (1994) 261.
[21] T. Guérin, A. Astruc, M. Astruc, A. Batel, M. Borsier, J. Chromatogr. Sci., Accepted for publication.
[22] R.F.J. Dams, J. Goossens, L. Moens, Mikrochim. Acta 119 (1995) 277.
[23] A. Gray, A.R. Date, Analyst 108 (1983) 1033.
[24] E.H. Larsen, S. Stürup, J. Anal. Atom. Spectrom. 9 (1994) 1099.
[25] International Union of Pure and Applied Chemistry, Nomenclature, symbols, units and their usage in spectrochemical analysis—II. Data interpretation. Spectrochim. Acta Part B, 33 (1975) 241.
[26] W.C. Story, J. Caruso, D.T. Heitkemper, L. Perkins, J. Chromatogr. Sci. 30 (1992) 427.
[27] J. Goossens, L. Moens, R.F.J. Dams, J. Anal. Atom. Spectrom. 8 (1993) 921.

ELSEVIER

Talanta 44 (1997) 2209–2215

Talanta

Improvement of poly(amphiphilic pyrrole) enzyme electrodes via the incorporation of synthetic laponite-clay-nanoparticles[1]

J.-L. Besombes, S. Cosnier*, P. Labbé *

Laboratoire d'Electrochimie Organique et de Photochimie Rédox, UMR CNRS 5630, Université Joseph Fourier Grenoble 1, BP 53, 301 rue de la Chimie, 38041 Grenoble Cedex 9, France

Received 2 August 1996; received in revised form 5 November 1996; accepted 9 December 1996

Abstract

The electropolymerization of an enzyme-amphiphilic pyrrole ammonium-laponite nanoparticles mixture preadsorbed on the electrode surface provides the simultaneous immobilization of the enzyme and the hydrophilic laponite-clay-nanoparticles in a functionalized polypyrrole film. The presence of incorporated laponite particles within the electrogenerated polymer induces a strong improvement of the analytical performances (I_{max} and sensitivity) of amperometric biosensors based on polyphenol oxidase. These beneficial effects have been attributed to a marked enhancement of the apparent specific activity of the immobilized enzyme (from 0.21 to 0.85% of the specific activity of the free enzyme), the permeability of the host polymer being unchanged. This strategy of biosensor performance improvement was tested with cholesterol oxidase as an enzyme model. The presence of laponite additive in the poly(amphiphilic pyrrole) host matrix induces a similar enhancement of sensitivity and I_{max} for cholesterol biosensing as well as a large improvement of the storage stability of the polypyrrole-cholesterol oxidase electrode. © 1997 Elsevier Science B.V.

Keywords: Biosensor; Enzyme electrode; Laponite nanoparticles; Additive; Polypyrrole; Polyphenol oxidase; Cholesterol oxidase

1. Introduction

Enzyme immobilization technology has attracted much attention in connection with the design, fabrication and applications of amperometric biosensors [1–3]. The main conventional approaches for enzyme immobilization on electrodes surfaces include adsorption, cross-linking with glutaralaldehyde, covalent attachment using carbodiimine chemistry and entrapment in polymeric gels or carbon paste. Among these various techniques, the electrochemical polymerization appears as a simple and attractive avenue for fabricating biosensors [4]. This method is based on the enzyme entrapment during the growth of conductive polymers generated by electrochemical oxidation of a suitable monomer from a solution containing enzyme. In particular, the incorpora-

* Corresponding authors. Tel.: +33 4 76 514998; fax: +33 4 76514267.

[1] Presented at the Symposium on Analytical Sciences (SAS) IV, Belgium, 3–5 June, 1996.

PII S0039-9140(97)00039-8

tion of enzymes in active polypyrrole matrices has been widely used [5] since the first example reported by Foulds et al. in 1986 [6]. Such one-step immobilization procedure allows the facile functionalization of microelectrode surfaces [7], the electrochemical control of the amount of deposited polymeric material [8,9] as well as the electrical wiring of immobilized enzymes [10–12]. However, the electrochemical entrapment of enzymes in polypyrrolic films induces always a strong decrease in the specific activity of the immobilized enzymes [13].

This phenomenon could be due to some internal diffusional limitations of substrates and products but also to the hydrophobic character of these organic matrices [14–16]. A possibility to preserve the activity of entrapped enzymes could be the modification of the enzyme microenvironment by incorporation of hydrophilic additives within the polypyrrole host matrices. Recently Lutz et al. [17] have described the beneficial effect of a number of solid and chemical additives such as sugars, sugar alcohols and cationic polymers on the sensitivity and operationnal stability of tyrosinase carbon paste electrodes. In addition, it has been reported that the incorporation of fumed silica within carbon paste matrices greatly enhanced the sensitivity and the stability of dehydrogenase and glucose oxidase based biosensors [18,19]. Moreover, it has been demonstrated that enzymes and additives such as flavin coenzymes [20] or phospholipidic vesicles [21] can be simultaneously incorporated in polypyrrole films. This coimmobilization induces a marked improvement of the biosensors performances.

With this aim in view, we report here a novel and efficient approach to improve the sensitivity and lifetime of biosensors based on conductive polymers. This procedure is based on the simultaneous adsorption of amphiphilic pyrrole (**1**), enzyme and hydrophilic laponite nanoparticles [22,23] on an electrode surface followed by the electrochemical polymerization of the adsorbed pyrrole derivatives [24]. This induces the entrapment of enzyme and additives within the resulting polypyrrole film.

1 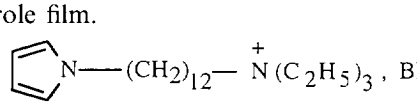

Thus, the beneficial effect of laponite clay nanoparticles on the analytical performances of the biosensor has been investigated for a polyphenol oxidase (PPO) electrode. In particular, the use of the catechol-PPO electroenzymatic system [25,26] has allowed to distinguish the influence of the synthetic clay additives on the immobilized enzyme activity and on the biomaterial permeability.

2. Experimental

2.1. Instrumentation

The electrochemical instrument consisted of a PAR model 362 potentiostat in conjunction with a Tracelab BD 90 recorder. All electrochemical experiments were carried out using an undivided thermostated three-electrode cell. The working electrode was a glassy carbon disk or a platinum disk (diameter 5 mm) polished with diamond paste. An Ag/AgCl (saturated KCl) reference electrode and a platinum counter electrode were also used. All measurements were carried out at 30°C with PPO or 37°C with cholesterol oxidase (CO).

Spectrophotometric measurements were performed with a Shimazu UV-Vis 2101 PC spectrophotometer.

2.2. Reagents

Polyphenol oxidase (EC 1.14.18.1, from mushroom, 1700 U mg^{-1}) cholesterol oxidase (EC 1.13.6., from *Streptomyces*, 25 U mg^{-1}) and cholesterol were purchased from Sigma. Catechol and phenol were obtained from Fluka and Prolabo respectively. Triton X-100 (TX 100) was purchased from Merck. The amphiphilic pyrrole derivative **1** ((12-pyrrol-1-yldodecyl)triethylammonium tetrafluoroborate) was synthetized as previously reported [27] and laponite is obtained from Laporte Industries.

Supporting electrolytes were 0.1 M $LiClO_4$ (from Janssen) and 0.1 M phosphate buffer (pH 6.5 or pH 7) prepared by mixing $NaH_2PO_4 \cdot 2H_2O$ and $Na_2HPO_4 \cdot 2H_2O$ from Fluka in desionised water.

2.3. Preparation of enzyme electrodes

The poly **1**-PPO electrode and the poly **1**-PPO-laponite electrode were prepared according to the method similar to that previously reported [24]. An aqueous colloidal suspension (5 g l^{-1}) was prepared by dispersing overnight laponite in pure water. Aqueous dispersion of monomer **1** (6 mM) and laponite colloidal suspension were mixed in water to produce a 3 mM aqueous dispersion of **1** containing 0.5 g l^{-1} laponite. Then, 0.3 mg of PPO was dissolved in 30 ml of this latter dispersion. The mixture deposited at the surface of a glassy carbon electrode was dried under vacuum. The polymerization of the dry adsorbed monomer **1**-laponite-enzyme coating was carried out by controlled potential electrolysis for 30 min at 0.78 V in deaerated aqueous 0.1 M $LiClO_4$ solution. Before electrochemical experiments, the electrodes were potentiostated at −0.17 V or 0.7 V for 30 min allowing the background current to decay to a steady state value.

The poly **1**-CO and poly **1**-CO-laponite electrodes were prepared following the same process with a platinum disk electrode. The functioning principle of the cholesterol sensor was based on the amperometric detection of hydrogen peroxide. The amperometric response of the poly **1**-CO and the poly **1**-CO-laponite electrodes have been investigated in 0.1 M phosphate buffer (pH 7) containing Triton X-100 (0.05% v/v) by setting the platinum enzyme electrode at 0.53 V vs. Ag/AgCl.

2.4. Determination of amount and activity of entrapped enzyme

In order to determine the amount of PPO really entrapped in the poly **1** or poly **1**-laponite film, we used a spectrophotometric assay based on the enzymatic oxidation of L-tyrosine by PPO. First the activity of 0.3 mg of free PPO was correlated with our assay: 1 ml of electrolyte containing 0.3 mg of PPO was added to 1 ml of 50 mM phosphate buffer (pH 6.5) and 1 ml of L-tyrosine aqueous solution (1 mM). The L-tyrosine oxidation was monitored at 280 nm by measuring the increase in adsorbance vs. time. The slope of the rectilinear part of the adsorbance versus time dependence was further used as a reference corresponding to 0.3 mg of PPO. The amount of enzyme lost during the electropolymerization step of biosensor construction was evaluated from the enzymatic activity of the electrolyte solution measured following the same procedure. Comparison with the activity of 0.3 mg free enzyme allowed to determine the weight of released enzyme, and then by difference with the amount initially adsorbed, to estimate the amount of PPO really entrapped.

The apparent specific activity of the immobilized PPO was estimated as previously reported [14]. The enzyme electrode was immersed in a 3 ml of stirred phosphate buffer containing 0.3 mM catechol. The increase in concentration of 1,2-benzoquinone enzymatically produced was monitored at 380 nm by measuring the increase of the adsorbance at 1 min intervals. Then, the enzymatic activity is obtained from the slope of the linear part of the adsorbance vs. time dependence. Knowledge of the weight of immobilized PPO (as previously described) allowed to obtain the apparent specific activity of PPO molecules entrapped in the polymer.

3. Results and discussion

Laponite is a synthetic hectorite whose structure and properties have been extensively presented in previous papers [22,23]. Isomorphic substitution of monovalent cation for bivalent cations within the crystalline network is the source of the permanent negative charge of the laponite layers. This excess negative charge is compensated by adsorption of exchangeable cations, Na^+ in laponite. Consequently the laponite cation exchange capacity (cec) is 7.3×10^{-4} mol g^{-1}. When suspended in deionized water, at a concentration less than 10 g l^{-1} a complete delamination process of the elementary laponite layers stacked together occurs leading to a colloidal suspension of negatively charged elementary platelets measuring in size 40 nm × 10 nm × 1 nm on average [28].

On the other hand, the cationic amphiphilic monomer **1** having a very low solubility in water can be ultrasonically dispersed in pure water [27].

These properties allow to prepare a mixed dispersion containing 3 mM of **1** and 0.5 g l^{-1} laponite nanoparticles. Then, the enzyme electrodes are obtained by dissolving PPO into this latter dispersion and the resulting mixture is coated on a glassy carbon electrode surface. The electropolymerization of the adsorbed biological layer yields poly **1**-PPO-laponite electrode or poly **1**-PPO electrode in the absence of laponite in the dispersion.

As previously reported [14], the leakage of PPO during the polymerization step is determined from the enzymatic activity of the electrolyte solution. Thus the quantity of PPO really entrapped in the poly **1** film and the poly **1**-laponite film were evaluated, respectively, as 50% and 40% of the initially adsorbed amount. This slight decrease could be the consequence of electrostatic repulsion between the negatively charged laponite particles and the PPO protein which carries a net negative charge at pH 6.5.

Polyphenol oxidase catalyzes the oxidation of several monohydroxy and *o*-dihydroxybenzene derivatives to *o*-quinones involving molecular oxygen. So, PPO when used in a biosensor configuration, allows to determine a whole group of substrates or inhibitors [14,24,29–31], owing to the electrochemical reduction of the enzymically formed *o*-quinone. As reported previously, the analytical capabilities of the poly **1**-PPO electrode and the poly **1**-PPO-laponite electrode have been investigated in air saturated 0.1 M phosphate buffer by potentiostating the electrodes at −0.17 V. Fig. 1 shows the calibration curve of the poly **1**-PPO electrode and the poly **1**-PPO-laponite electrode obtained with phenol as substrate. The beneficial influence of the incorporated laponite particles is illustrated by the enhancement of the biosensor sensitivity since its value (determined as the slope of the linear range) increases from 36 mA M^{-1} cm^{-2} to 159 mA M^{-1} cm^{-2} in the absence and in the presence of the solid additive in the polypyrrolic matrix. In addition, calibration curves also display a higher maximal current under saturating phenol conditions recorded with the poly **1**-PPO-laponite configuration (I_{max} = 20.4 mA cm^{-2} with laponite and I_{max} = 5.9 mA cm^{-2} without laponite).

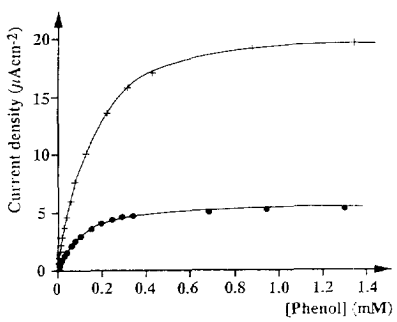

Fig. 1. Calibration curves for phenol obtained at the poly **1**-PPO electrode (●) and at the poly **1**-PPO-laponite electrode (+). Applied potential −0.17 V vs. Ag/AgCl (saturated aqueous KCl), air saturated 0.1 M phosphate buffer (pH 6.5) kept under vigourous stirring at 30°C.

The poly **1**-PPO electrode provides also better limit of detection (based on a signal-to-noise ratio of 3) for phenol, namely 0.1 mM as compared to the 0.6 mM recorded with a poly **1**-PPO electrode. Furthermore, the laponite particles incorporation leads to a slight increase of the electrode response time, since it was of order of 50 s whereas its value reaches 30 s without laponite. These different results could arise from the modification of two parameters induced by the presence of the additive: the activity of the immobilized enzyme, and the biomaterial permeability. In order to estimate the influence of each of these factors, an electrochemical study involving the catechol-PPO system [25,26] has been realized and completed with the determination of the enzymatic activity for the poly **1**-PPO-laponite electrodes.

Indeed, with an amperometric PPO-based electrode, catechol can be detected, on the one hand via the enzymically generated *o*-quinone (Fig. 2B) and on the other hand, via its electrooxidation at 0.7 V whatever the enzyme reactive state, active or inactive (Fig. 2A). Owing to this feature, the various functioning configuration of the PPO-catechol system give informations about the biomaterial permeability as well as the immobilized enzyme activity [25,26]. Fig. 3 shows the calibration curves for catechol obtained at 0.7 V in stirred phosphate buffer with the two kinds of modified electrode after the thermal denaturation of the immobilized PPO. By this way, the current density is connected with the catechol diffusion through the inactivated biomaterial. The response

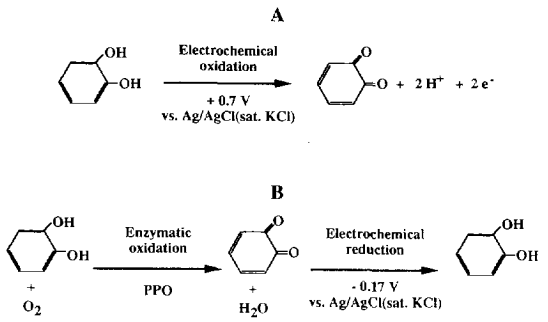

Fig. 2. Schematic description of the catechol electrochemical detection with a PPO electrode. A, bioelectrode potentiostated at 0.7 V, PPO being inactivated; B, bioelectrode potentiostated at −0.17 V.

of a bare glassy carbon electrode has also been reported under the same experimental conditions. In the substrate concentration range investigated, a linear relationship is observed. As expected, the modified electrodes exhibit lower sensitivities than the one obtained on a bare electrode. This behavior simply arises from the presence of the polypyrrolic film which gives additional diffusion barrier where the catechol diffusion coefficient is lower than in the bulk electrolyte. Surprisingly, the curves do not show a marked difference between the poly **1**-PPO and the poly **1**-PPO-laponite electrodes since sensitivities are 486 mA M^{-1} cm^{-2} and 444 mA M^{-1} cm^{-2}, respectively. Consequently, the incorporated laponite particles

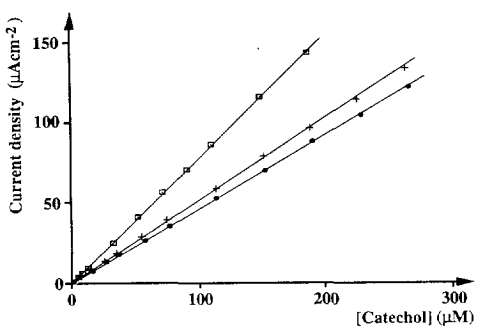

Fig. 3. Calibration curves for catechol obtained at (□) the bare glassy carbon electrode, (+) the poly **1**-PPO electrode, and (●) the poly **1**-PPO-laponite electrode. Immobilized PPO has been previously denaturated and the applied potential was 0.7 V vs. Ag/AgCl (saturated aqueous KCl). Other experimental conditions as in Fig. 1.

lead to only a slight decrease of the biomaterial permeability.

In contrast and as expected, the biosensor sensitivity towards catechol at −0.17 V is greatly enhanced in the presence of laponite. Indeed, in the dynamic range of the biosensors, the amperometric response of the poly **1**-PPO-laponite electrode is nearly two times higher since its value reaches 893 mA M^{-1} cm^{-2} as compared to 539 mAM^{-1} cm^{-2} recorded with the poly **1**-PPO electrode. Since the laponite particles have a slight negative effect onto the biomaterial permeability, the improvement of the biosensor sensitivity could be attributed to a better activity of the immobilized enzyme. Owing to their surface structure characterized by silanol groups and the presence of hydrated sodium counterions [22], the laponite particles can counterbalance the hydrophobic character of the polypyrrole matrix providing a less denaturating microenvironment for the immobilized enzymes. As reported previously for carbon paste matrices [17,32] and poly(amphiphilic pyrroles) matrices [31], the biosensor performances depend on the amount of bound water to PPO. Consequently, the hydration layer of enzymes, necessary for their activity, can be more important and stabilized with the incorporation of the hydrophilic clay particles within the polymeric matrices.

On the other hand, the laponite particles effect on the biosensor response is higher for phenol as a substrate than for catechol: sensitivity is increased by a factor of 4.4 with phenol, wheras this factor is only 1.7 with catechol. Indeed, it is well known that the enzymatic oxidation of phenol requires two successive steps. First the hydroxylation from phenol to catechol followed by its oxidation to *o*-quinone. It has been reported that the first step is preceded by a lag-phase [17,33] slowing down the enzymatic conversion of phenol. Consequently, our results seem to indicate that the laponite-PPO coimmobilization in the poly **1** allows at the one and the same time an higher enzymatic activity and the decrease of the lag-phase. A similar effect has already been reported for chemical additives incorporated within carbon paste matrices [17].

In order to confirm these results, the activity of each PPO electrode has been determined by spectrophotometric measurements (Section 2). Since our method of enzyme immobilization allows us to determine the quantity of PPO really entrapped in the poly **1** film, we were able from these measurements to estimate the apparent specific activity of the immobilized PPO. These apparent specific activities were evaluated in absence and presence of laponite additives, respectively, as 0.21% and 0.85% of the free enzyme. These low values can be explained by the fact that immobilization procedures usually lead to an important lowering of the specific activity because of interactions between the immobilized enzymes and the matrix and subsequent denaturation. In addition, because of diffusion constraints within the biomaterial and development of substrate and cosubstrate concentration gradients, only an apparent specific activity lower than the specific activity can be determined. Nevertheless, it is interesting to notice that the amount of immobilized PPO is practically the same in absence and presence of laponite particles. In contrast, the apparent specific activity is four times higher in the presence of laponite. Taking in mind that the presence of laponite induces a slight decrease of the biomaterial permeability toward catechol, these activity measurements demonstrate that laponite allows to keep a higher specific activity for immobilized PPO. The presence of hydrophilic laponite should confer a favourable microenvironment to PPO by reducing hydrophobic interactions with the long hydrocarbon tails of poly **1** and subsequent denaturation resulting from the protein unfolding [34]. These activity measurements are in good agreement with the improvement of the biosensor performances (higher sensitivity and I_{max}) in the presence of laponite additive.

This interesting strategy can be extended, following our immobilization procedure, to a wide range of enzymes. Thus, we have verified this behavior with cholesterol oxidase (CO), choosen as a model of an important class of enzyme: the oxidases whose substrate molecular recognition is followed by production of hydrogen peroxide. Fig. 4 compares the calibration curves for cholesterol obtained with a poly **1**-CO and a poly **1**-CO-laponite electrode. As previously observed with PPO, a similar enhancement of sensitivity and I_{max} is observed for cholesterol biosensing in the presence of laponite additive. More interestingly we observed that laponite additive markedly enhanced the enzyme electrode stability. Indeed, under the best storage conditions, the poly **1**-CO-laponite electrode retained 74% and 50% of its initial sensitivity after 4 and 20 days, respectively, while the biosensor being totally inactive after 17 days in the absence of laponite. This strong increase of the storage stability confirms again the benefic modification of the enzyme microenvironment induced by the presence of hydrophilic laponite nanoparticles.

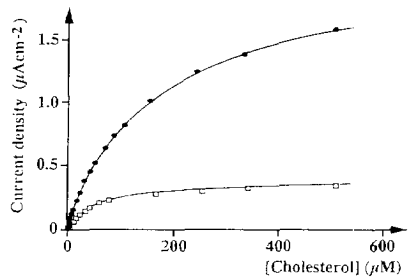

Fig. 4. Calibration curves for cholesterol obtained at the poly **1**-CO electrode (□) and at the poly **1**-CO-laponite electrode (●). Applied potential +0.53 V vs. Ag/AgCl (saturated aqueous KCl), air saturated 0.1 M phosphate buffer (pH 7) containing 0.05% (v/v) Triton X-100 kept under vigorous stirring at 37°C.

In conclusion, this strategy is interesting since by tuning the hydrophilic/hydrophobic character of electrogenerated polymer films, it is possible to counterbalance the negative effect of the hydrophobic microenvironment of the immobilized enzyme and thus to improve its biocompatibility. Following this way the developement of new hydrophilic electropolymerizable organic additives is in progress and comparison with solid additives will be realized.

Acknowledgements

The authors thank Dr A. Deronzier for his interest in this work.

References

[1] A.P.F. Turner, I. Karube, G.S. Wilson (Eds), Biosensors: Fundamentals and Applications, Oxford University Press, New York, 1987.
[2] J. Wang, Anal. Chem. 63 (1991) 235R.
[3] G.G. Guilbault, M. Mascini (Eds.) Use of Immobilized Biological Compounds, NATO ASI Series, Kluwer, Dordrecht, Vol. 252, 1993.
[4] P.N. Bartlett, J.M. Cooper, J. Electroanal. Chem. 362 (1993) 1.
[5] W. Schumann, Mikrochim. Acta 121 (1995) 1, and references therein.
[6] N.C. Foulds, C.R. Lowe, J. Chem. Soc. Faraday Trans. 82 (1996) 1259.
[7] W. Schumann, C. Kranz, J. Auber, H. Wohlschläger, Synth. Met. 61 (1993) 31.
[8] M. Umana, J. Waller, Anal. Chem. 58 (1986) 2979.
[9] P.N. Bartlett, R.G. Whitaker, J. Electroanal. Chem. 224 (1987) 27.
[10] S. Yabuki, H. Shinohara, M. Aizawa, J. Chem. Soc. Chem. Commun. 7 (1989) 945.
[11] T. Tatsuma, M. Gondaira, T. Watanabe, Anal. Chem. 64 (1992) 1183.
[12] T. Tatsuma, M. Gondaira, T. Watanabe, J. Electroanal. Chem. 356 (1993) 245.
[13] L. Coche Guérente, S. Cosnier, C. Innocent, P. Mailley, J.-C. Moutet, R. M. Morelis, B. Leca, P. R. Coulet, Electroanalysis 5 (1993) 647, and references therein.
[14] S. Cosnier, C. Innocent, Bioelectrochem. Bioenerg. 31 (1993) 147.
[15] S. Cosnier, C. Innocent, Anal. Lett. 27 (1994) 3198.
[16] L. Coche Guérente, S. Cosnier, C. Innocent, P. Mailley, Anal. Chim. Acta 311 (1995) 23.
[17] M. Lutz, E. Burestedt, J. Emnéus, H. Lidén, S. Gobhadi, L. Gorton, G. Marko-Varga, Anal. Chim. Acta 305 (1995) 8.
[18] J. Wang, J. Liu, Anal. Chim. Acta 284 (1993) 385.
[19] J. Wang, N. Naser, Electroanalysis 6 (1994) 571.
[20] A. Kitani, N. Kasyu, K. Sasaki, Electrochim. Acta 39 (1994) 7.
[21] B. Leca, R.M. Morelis, P.R. Coulet, Talanta 41 (1994) 925.
[22] P. Labbé, G. Reverdy, Langmuir 4 (1988) 419.
[23] B. Brahimi, P. Labbé, G. Reverdy, Langmuir 8 (1992) 1908.
[24] S. Cosnier, C. Innocent, J. Electroanal. Chem. 328 (1992) 361.
[25] J.-L. Besombes, S. Cosnier, P. Labbé, Talanta (in press).
[26] V. Desprez, P. Labbé, J. Electroanal. Chem. (in press).
[27] L. Coche-Guérente, A. Deronzier, B. Galland, P. Labbé, J.-C. Moutet, G. Reverdy, J. Chem. Soc. Chem. Commun. 9 (1991) 386.
[28] R.G. Avery, J.D.F. Ramsay, J. Colloid Interface Sci. 109 (1986) 448.
[29] J.-L. Besombes, S. Cosnier, P. Labbé, G. Reverdy, Anal. Lett. 28 (1995) 405.
[30] J.-L. Besombes, S. Cosnier, P. Labbé, G. Reverdy, Anal. Chim. Acta 311 (1995) 256.
[31] L. Coche Guérente, S. Cosnier, C. Innocent, Anal. Lett. 28 (1995) 1005, and references therein.
[32] F. Ortega, E. Dominguez, E. Burestedt, J. Emneus, L. Gorton, G. Marko-Varga, J. Chromatogr. 675 (1994) 65.
[33] E. Valero, R. Varon, F. Garcia-Carmona, J. Food Sci. 53 (1988) 1482.
[34] C. Bourdillon, M. Majda, J. Am. Chem. Soc. 112 (1990) 1799.

ELSEVIER

Talanta 44 (1997) 2217–2224

Talanta

Analysis of volatiles emitted by potato plants by means of a Colorado beetle electroantennographic detector[1]

Bernhard Weißbecker *, Stefan Schütz, Anita Klein, Hans E. Hummel

Justus Liebig University Gießen, Institute for Phytopathology and Applied Zoology, Division of Biological and Biotechnical Plant Protection, Ludwigstr. 21b, D-35390 Gießen, Germany

Received 5 June 1996; received in revised form 9 September 1996; accepted 10 January 1997

Abstract

An electroantennographic detector based on the antenna of the Colorado potato beetle (*Leptinotarsa decemlineata* Say, 1824) was used to investigate volatile organic compounds emitted by injured potato plants (*Solanum tuberosum* L., 1753). Samples were collected on charcoal traps using the CLSA method. Analyses were performed with a GC-EAD-FID setup as well as a GC-MS system. The experiments revealed that several groups of compounds are perceptible to the Colorado potato beetle. The ability of the Colorado potato beetle to detect green leaf odours (e.g. (*Z*)-3-hexen-1-ol and (*E*)-2-hexenal), linalool and some terpenes has been noticed before [Visser et al., J. Chem. Ecol. 5 (1979) 13]. In this work the presence of (*Z*)-3-hexen-1-ol, (*E*)-2-hexenal and linalool in the potato odour could be confirmed. Moreover, β-myrcene, benzeneethanol, and several sesquiterpenes (e.g. caryophyllene and germacrene-D) were identified. The GC-EAD experiments reveal that apart from the green leaf odours and linalool prominent reactions of the Colorado bettle antenna are induced by benzeneethanol and the sesquiterpene fraction. © 1997 Elsevier Science B.V.

Keywords: Electroantennographic detection; Colorado potato beetle; Plant volatiles; Plant-insect interaction

1. Introduction

Electrical potentials in the hemolymph of insect antennae are influenced by surrounding olfactory receptor cells. The depolarisation of many adjacent receptor cells leads to a slow change in the hemolymph potential called electroantennogram or EAG [2]. The EAG represents a summation of reactions of many receptors with different specificity thus providing unspecific information on the insect's olfactory perception. Yet, when stimulated with an isolated compound the amplitude of the EAG-signal correlates with the strength of the stimulus. Single cell recordings (SSR) of olfactory sensillae [3] may reveal more specific information as compared to EAG but suffer from higher apparative expense and difficulties in quantitative interpretation.

The high sensitivity and selectivity of insect olfactory receptors in combination with a chro-

* Corresponding author.

[1] Presented at the Symposium on Analytical Sciences (SAS) IV, Belgium, 3–5 June, 1996.

PII S0039-9140(97)00037-4

matographic separation offers a powerful analytical technique [4]. The connection between GC and EAG can be made *indirectly* by collecting fractions of the GC-effluent with subsequent analysis of these samples in an EAG-setup [5]. The *direct* employment of an EAG-setup as a detector in gas chromatography ('electroantennographic detector', EAD) offers extended analytical capacities. However, the coupling of GC with EAG is not as straightforward as physicochemical detectors linked in tandem since the GC-effluent may be very hot and possibly will damage the antenna used as a biological detector. Therefore an interface has to be used which mixes the GC-effluent with cool humidified air. First experiments using an electroantennographic detector in combination with a GC equipped with a packed column were published by Moorhouse [6]. Adaptation and loss of sensitivity of the insect antenna during long-lasting GC-peaks suggested the use of capillary columns. This technique was first published by Arn et al. [7]. A coupling of a device for single-sensillum recordings with a GC was reported by Wadhams [8] as well as Van Der Pers and Löfstedt [9].

The use of GC-EAD-systems is well established in the analysis of pheromones (e.g. [10–14]) but so far has rarely been used for detection of food odours [15–22] of insects. The aim of this report is the employment of a GC-EAD system based on the antenna of the Colorado potato beetle for the analysis of volatiles emitted by the potato plant.

The Colorado potato beetle is able to recognize its host plant by olfactory cues and is attracted by the odour of the potato and other solanaceous plants [23–25]. Visser et al. [1] as well as Mitchell and McCashin [26] examined the volatiles emitted by potato plants and identified several saturated and unsaturated alcohols and aldehydes with 6 carbon atoms. These compounds are found in most green plants and therefore are referred to as green leaf odour (GLO). Moreover, Visser et al. [1] observed linalool and some unidentified terpenes.

The sensitivity of the olfactory receptors of the Colorado potato beetle for GLOs is very high [27] so that it consequently should be able to perceive all green plants emitting these compounds. Visser and Avé [28] hypothesized that the ability to discriminate between host plants and non-host plants is based upon the relative intensities of the GLOs emitted by the plants. The importance of non-GLO substances for the host plant recognition of the Colorado potato beetle so far has not been evaluated.

One possible application of the GC-EAD system is the elucidation of the mechanisms involved in host plant recognition of the potato beetle. Samples for GC-EAD are obtained by closed-loop stripping analysis (CLSA) of plant volatiles. Along with GC-EAD analysis the samples are analysed with a GC-MS system in order to allow identification of the volatiles emitted by the potato plant.

2. Experimental

2.1. Plants and beetles

Experiments were performed with potato plants *Solanum tuberosum* var. Granola, grown in a greenhouse with 16 h light/8 h dark and temperatures ranging from 15 to 25°C.

Colorado potato beetles are reared in a laboratory stock culture under artificial light (16 h light/8 h dark) and temperatures ranging from 20 to 25°C. Beetles are fed with potato plants grown under conditions as described above.

For the experiments female beetles at an age ranging from 7 to 14 days after emerging from pupae were used exclusively. Beetles assigned for experiments are taken from the rearing cages and kept in plastic boxes for 1–2 h without food. In blowflies (*Phormia regina*), an increasing chemoreceptor activity of gustatory receptors was observed after sustained starving [29]. We could not confirm this effect for the olfactory chemoreceptors of the Colorado beetle. Nonetheless, a period of starvation was maintained, allowing the beetles to empty their guts and thus enhancing cleanliness of the preparation. The air in the plastic box is humidified by a filter paper soaked with water in order to prevent desiccation of the beetles. A beetle is fixed with parafilm and dentist's wax before one of it's antennae is cut off

with a pair of microscissors. The time needed for the preparation of an antenna amounts to 15 min. After removal from the body of the beetle the antenna remains operational for 1–2 h.

2.2. Sampling of volatiles

In order to investigate the volatile emissions of potato plants injured by chewing insects, 20 g (fresh weight) of potato leaves were placed in a 500 ml round-bottom flask together with 20 Colorado potato beetles. This procedure provides a continuous source of fresh injuries on the leaves leading to an elevated emission of leaf volatiles. The volatiles were collected on a charcoal trap (CLSA-Filter, Kollbrunn, Switzerland) using the closed-loop stripping technique [30,31]. Air is circulated through the trap by a miniature pump (Fürgut, Aichstetten, Germany) at a flow of 0.8 l min^{-1}. All surfaces getting in touch with the volatiles (pump, capillaries) are either PTFE or stainless steel. The sampling time was varied from 1 to 24 h in order to examine time dependence of the emissions. Adsorbed volatiles are eluted with 50 µl of dichloromethane/methanol (2:1). The solvents used are of analytical quality (Merck, Darmstadt, Germany). The mixture of dichloromethane and methanol provides a solvent capable of eluting the volatiles from the charcoal moistened by the transpiration of the plants. On the other hand, the content of dichloromethane allows dissolving of volatiles with low polarity. After elution, samples are stored in a refrigerator at −25°C. Nonetheless samples were analysed within 24 h after elution.

2.3. GC-MS

A GC-MS system was used to analyse composition of the volatiles collected with the CLSA setup. The system consists of a gas chromatograph HP 5890 Series II and a quadrupole mass spectrometer HP 5989 A (both Hewlett Packard, Palo Alto, USA). The GC is equipped with a capillary column (25 m × 0.2 mm I.D., HP-1) and a KAS-2 cold injection system (Gerstel, Mülheim, Germany). Helium was used as carrier gas at a pressure of 100 kPa (gas flow 0.5 ml min^{-1}, gas vector 28 cm s^{-1} at 70°C). The following temperature programs were employed: GC: start at 70°C, hold for 3 min, rate 10°C min^{-1}, end temperature 250°C, hold for 4 min. KAS: start at 50°C, hold for 1 min, rate 10°C s^{-1}, end temperature 250°C, hold for 3 min.

Within the first min after injection a purge valve prevents excess solvent from entering the column. The loss of substances with high volatility (GLO) in this period was tolerable since the main interest of this work is the identification of compounds with low volatility.

The MS was connected to the GC by a direct coupling interface heated to a temperature of 250°C. The ion source was operated in the EI-mode at an electron energy of 70 eV. The instrument was tuned using the Autotune option of the chemstation-software (HP59944B, ver. B.04.03). Measurements were performed in the scan mode, detecting a mass range from 35 to 250 amu. The operating parameters of the GC and the MS were chosen in order to analyse the compounds of the green leaf odour (molecular weight ~ 100, boiling point ~ 155°C) as well as sesquiterpene hydrocarbons ($C_{15}H_{24}$, mw. 204, bp. ~ 270°C).

2.4. GC-EAD

Experiments were performed with a GC-EAD system consisting of a gas chromatograph (Vega 6300-01, Carlo Erba, Rodano, Italy), an EAD-interface (Syntech, Hilversum, Netherlands), and an EAG-amplifier (Dr. Koch, University of Kaiserslautern). The GC is equipped with a capillary column (30 m × 0.32 mm I.D., DB-1), a flame ionisation detector (FID) and a split-splitless injector. The injector is operated in the splitless-mode. Nitrogen was used as carrier gas at a pressure of 100 kPa (gas flow 2.5 ml min^{-1}, gas vector 50 cm s^{-1} at 50°C).The following temperature program was employed: start at 70°C, rate 10°C min^{-1}, end temperature 200°C.

A split connection at the end of the capillary column allows division of the GC-effluent into two capillaries leading to the FID (length 35 cm, 0.2 mm I.D.) and the EAD (length 45 cm, 0.32 mm I.D.), respectively. This provides a split ratio of 1:5 (FID/EAD). The EAD-interface (Fig. 1) is

under thermostat control and guides the capillary column through the wall of the GC-oven thus preventing condensation of the sample in the cooler segments of the column. The end of the column projects into a small chamber where the effluent is mixed with cold humidified air (400 ml min^{-1}). A PTFE-clad flow tube leads the airflow to the detector cell. The flow tube is provided with an injection port for manual calibration pulses. A PTFE tube guides the tip of an injection needle into the centre of the flow tube. 'Side-port' injection needles (Supelco, Deisenhofen, Germany) allow injection parallel to the air flow. Solutions of (*Z*)-3-hexen-1-ol in paraffin oil (both Merck, Darmstadt, Germany) are used as calibration standard. The calibration syringe contains a filter paper soaked with 50 µl of a standard solution, typically a 10^{-3} dilution of (*Z*)-3-hexen-1-ol in paraffin. The air contained in the syringe thus has a concentration of ca. 4.5 ng (*Z*)-3-hexen-1-ol ml^{-1} of air.

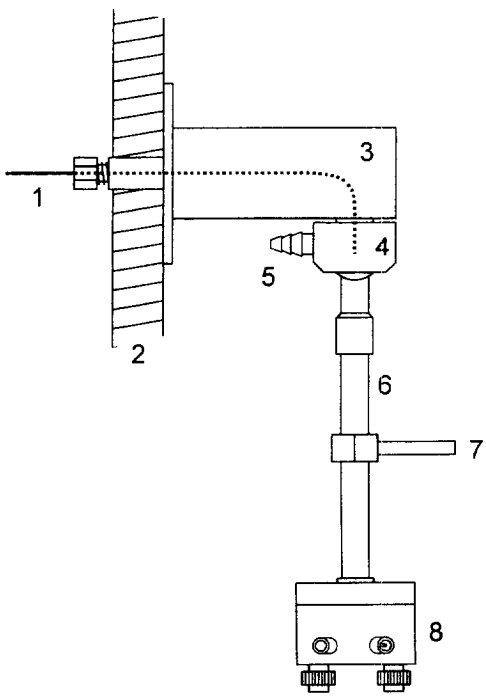

Fig. 1. EAD-interface (schematic). 1, capillary column; 2, wall of GC oven; 3, heated column-guide; 4, mixing chamber; 5, inlet for humidified air; 6, flow tube; 7, inlet for calibration pulses; 8, detector cell

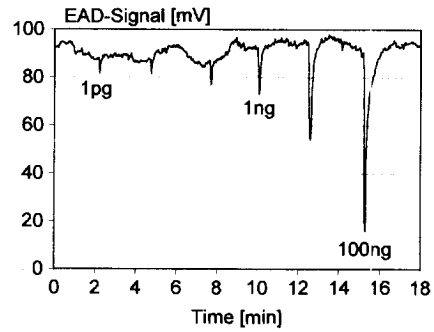

Fig. 2. GC-EAD measurement of a dilution series of (*Z*)-3-hexen-1-ol injected successively in the GC, operated at a constant temperature of 80°C.

The antenna of a Colorado potato beetle is housed in a detector cell designed by Koch [32]. Both ends of the antenna are contacted to Ag/AgCl electrodes via hemolymph Ringer solutions. The Ringer solutions are composed according to Kaissling and Thorson [33]. EAG-potentials of the antenna are amplified by a factor of 100 and recorded with a Chromstar® data acquisition system (Bruker, Bremen, Germany).

3. Results and discussion

3.1. Performance test with standard solutions

In order to evaluate the detection threshold of the GC-EAD system for substances of the green leaf odour measurements were performed with standard solutions of (*Z*)-3-hexen-1-ol in methanol. The GC was operated at a constant column temperature of 80°C. Test solutions containing (*Z*)-3-hexen-1-ol in amounts from 1 to 100 ng were injected successively in 2.5 min intervals. The result of this performance test is depicted in Fig. 2. The solvent methanol leads to broad fluctuations in the EAD signal starting about 1 min before the sharp peaks induced by (*Z*)-3-hexen-1-ol. Apart from the structures caused by methanol the noise of the baseline amounts to approximately 2 mV. One pg of (*Z*)-3-hexen-1-ol elicits an EAD signal of 6.5 mV and thus can be regarded as limit of detection.

The high sensitivity of the Colorado potato beetle for (*Z*)-3-hexen-1-ol and (*E*)-2-hexen-1-ol with detection limits around 20 fg was already noticed by Visser [1]. It was expected that the detection limit in EAD experiments could not match the results obtained from EAG experiments since the compound does not reach the antenna in a short pulse (< 0.5 s in EAG) but is rather stretched over some seconds in the GC column.

The relationship between the EAD signal and the stimulus concentration is depicted in Fig. 3. The EAD signal of an insect antenna may last for some seconds even if the stimulus is very short. If the stimulus lasts for a longer time, the sensitivity of the antenna may decrease during the stimulus (adaptation). With respect to these facts the peak amplitude was chosen as a measure for the EAD response instead of the peak area.

The relationship between the EAD amplitude and the concentration of the sample is not linear. However, it was not possible to describe the obtained data by the model predicted by Beidler [34].

The results observed in the calibration demonstrate that the employed EAD setup is able to detect (*Z*)-3-hexen-1-ol in amounts down to 1 pg. The observed detection limit is comparable to the sensitivity of other selective detectors used in gas chromatography, for example electron capture detectors (detection limit 100 fg for halogen compounds) or the nitrogen-phosphorus-sensitive detector (detection limit ~ 1 pg for compounds containing N or P atoms).

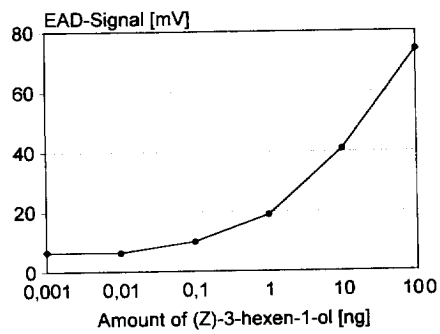

Fig. 3. Dose-response curve for stimulation of an antenna of the Colorado potato beetle with (*Z*)-3-hexen-1-ol in amounts ranging from 1 to 100 ng. The electroantennographic signal is amplified by a factor of 100.

The capability of the EAD of detecting GLOs in high concentrations is limited by saturation of the chemoreceptors and a possible adaptation to the stimulating compound. Saturation only leads to an uncertainty in the quantification of the actually detected compound but adaptation may cause the antenna to overlook compounds eluting from the column shortly after an intense peak. (*Z*)-3-hexen-1-ol in an amount of 1 μg already leads to a strong broadening of the peak so 100 ng are regarded as upper limit for the applicability of the EAD based on the antenna of the Colorado potato beetle. Thus the dynamic range of the used EAD setup covers a range from 10 pg to 100 ng for (*Z*)-3-hexen-1-ol.

Another remarkable feature of the EAD system is the very low sensitivity for methanol and other solvents. In the first measurements immediately after preparation of the antenna usually an olfactory reaction to the solvent methanol is observed. After some injections of methanol, however, no more reaction of the chemoreceptors occurs. This may indicate a selective adaptation of one class of chemoreceptors while the receptors responsible for the detection of green leaf odours are still operational.

Usually an exponential decrease of the sensitivity is observed after the antenna is removed from the head of the beetle. During the first 10–15 min after the preparation the sensitivity is very high but the baseline is quite unstable. After this period a performance test should be undertaken. The amplified EAD signal measured after injection of 3 ml air from a syringe containing a 10^{-3} dilution of (*Z*)-3-hexen-1-ol should amount to 50–100 mV. If this signal is lower than 50 mV the antenna should be rejected. The performance test is repeated before each new GC run.

A drawback of the EAD method is the limited quantitative reproducibility of the signals obtained during the lifetime of one antenna or signals from different antenna preparations. Therefore, an internal calibration should be used in order to test the momentary performance of the antenna employed in the GC-EAD system. Alternatively, calibration can be done by injections in the calibration port.

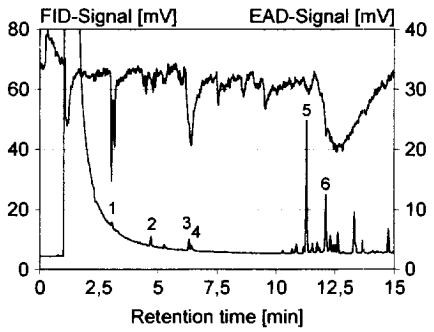

Fig. 4. GC-EAD-FID chromatograms of volatiles sampled 12 h from potato leaves injured by feeding of Colorado potato beetles. The upper line represents the EAD signal, the lower line depicts the FID signal. Peak assignations: 1, green leaf odour ((*E*)-2-hexenal, (*Z*)-3-hexen-1-ol); 2, β-myrcene; 3, linalool; 4, benzeneethanol; 5, caryophyllene; 6, germacrene-D.

3.2. Analysis of volatiles emitted by potato plants

Samples diluted from the charcoal trap after 1, 12 and 24 h sampling time were analysed by GC-MS and GC-EAD. (*Z*)-3-hexen-1-ol and (*E*)-2-hexen-1-ol were found in very low concentrations hardly exceeding the detection threshold of the MS in consideration of the employed mode of operation. Further substances identified in the sample are β-myrcene, linalool, benzeneethanol, caryophyllene, germacrene-D, γ-cadinene, δ-cadinene and some other sesquiterpenes.

The variety and abundance of the emissions reached its maximum in the sample taken after 12 h of exposition to the plant volatiles. The same sample analysed with the GC-EAD setup resulted in the chromatogram depicted in Fig. 4. In order to compensate for the unstable baseline of the EAD, a 2nd order polynomial regression curve was subtracted from the original data.

The solvent (dichloromethane/methanol) elicits a moderate deflection in the EAD signal. The green leaf odours leaving the GC column at retention times (t_R) around 3 min are hardly detectable with the FID whereas the EAD signal reveals a strong reaction of the olfactory receptor cells of the Colorado potato beetle. At retention times between 4 and 5 min several small peaks are visible in the EAD signal probably indicating an olfactory reaction induced by β-myrcene and other terpenes.

Around $t_R = 6$ min the FID is able to detect two peaks corresponding to linalool and benzeneethanol. The olfactory reaction induced by these compounds leads to one broad peak that is not resolved in the EAD signal. The ability of the Colorado potato beetle to perceive linalool and its presence in the odour of the potato plant was already noticed by Visser [1,27]. Experiments with standard solutions revealed that the sensitivity of the Colorado potato beetle for benzeneethanol is about 10–100 times higher as compared to linalool.

An olfactory reaction observed at $t_R = 9.5$ min might be of special interest. The compound inducing this EAD signal was identified as a branched alkane, possibly 5-ethyl-undecane or 6-ethyl-2-methyl-decane. This is not a typical plant volatile and thus could be a hint on a pheromone of the Colorado potato beetle.

At retention times between 10 and 15 min strong peaks are observed both in the EAD and FID signal. The most abundant peak in the FID signal ($t_R = 11.3$ min) corresponds to caryophyllene but its match in the EAD signal is rather small. Instead, a broad peak in the EAD signal starting at $t_R = 12$ min is observed. Using standard solutions containing caryophyllene and germacrene-D it was confirmed that the peak width induced by these compounds amounts to about 1 min. Apparently, the broad structure in the EAD signal is a reaction of the antenna induced by too much of different sesquiterpenes eluting from the GC column in too short intervals.

These results demonstrate that the time resolution of the EAD system is excellent in case of small retention times. The EAD is able to resolve the peaks of (*Z*)-3-hexen-1-ol and (*E*)-2-hexen-1-ol which are only 8 s apart. At higher retention times the peaks in the EAD signal are broadening and the multitude of peaks that is visible in the FID signal cannot be resolved.

3.3. Host plant recognition of the Colorado potato beetle

The sense of smell is of particular importance in host plant recognition of monophagous and oligophagous insects. The first interaction be-

tween the Colorado potato beetle and a potential host plant is mediated by olfactory cues. Only if the odour of a plant is acceptable to the beetle it will approach the plant and proceed with a tactile and gustatory examination. In this respect a detailed knowledge of the olfactory interaction between the Colorado potato beetle and its host plants might be useful for development of new measures in plant protection.

So far it is not fully known which constituents of the potato odour are essential for the host plant recognition of the Colorado potato beetle. Experiments of Visser and Avé [28] indicated that the Colorado potato beetle perceives relative intensities of different compounds and thus can distinguish the potato plant from other plants emitting the same compounds but in other concentrations.

The EAD chromatogram depicted in Fig. 4 indicates that the importance of terpenes and sesquiterpenes in host plant recognition of the Colorado potato beetle might be comparable to that of green leaf odours. Preliminary experiments revealed that the attractivity of potato plants to the Colorado potato beetle is enhanced when they are treated with green leaf odours, linalool or caryophyllene in concentrations simulating the emissions of injured plants. Further experiments are in progress and will be published elsewhere [35].

Acknowledgements

Support by Dr. U. Koch (University of Kaiserslautern, Germany) who provided the detector cell, some holding devices, and a lot of good advice is gratefully acknowledged. We thank Nikola Bitsch for assisting in the first tests of the GC-EAD interface. Professor Dr. W. Boland (University of Karlsruhe, Germany) helped us getting started with the CLSA-technique. We thank Dr. H. Surburg (Haarmann and Reimer GmbH, Holzminden, Germany) for support in identification of the sesquiterpenes emitted by the potato plant. The authors are indebted to the generosity of both the Federal Ministry of Science and Technology, Bonn, and the Ministry of Arts and Sciences of the State of Hesse, Wiesbaden, who jointly provided the generous funds for the quadrupole mass spectrometer used in this study.

References

[1] J.H. Visser, S. van Straten, H. Maarse, J. Chem. Ecol. 5 (1979) 13.
[2] D. Schneider, Z. Vergl. Physiol. 40 (1957) 8.
[3] J. Boeckh, Z. Vergl. Physiol. 46 (1972) 212.
[4] D.L. Struble, H. Arn, in: H.E. Hummel, T.A. Miller (Eds.), Techniques in Pheromone Research, Springer, New York, 1984, pp. 161.
[5] W.L. Roelofs, in: H.E. Hummel, T.A. Miller (Eds.), Techniques in Pheromone Research, Springer, New York, 1984, pp. 131.
[6] J.E. Moorhouse, R. Yeadon, P.S. Beevor, B.F. Nesbitt, Nature 223 (1969) 1174.
[7] H. Arn, E. Städler, S. Rauscher, Z. Naturforsch. C 30 (1975) 722.
[8] L.J. Wadhams, Z. Naturforsch. C 37 (1982) 947.
[9] J.N.C. Van Der Pers, C. Löfstedt, Physiol. Entomol. 8 (1983) 203.
[10] G. Gries, R. Gries, A.L. Perez, A.C. Oehlschlager, L.M. Gonzales, H.D. Pierce Jr., M. Zebeyou, B. Kouame, Z. Naturforsch. C 49 (1994) 363.
[11] W.S. Leal, M. Hasegawa, M. Sawada, M. Ono, Y. Ueda, J. Chem. Ecol. 20 (1994) 1643.
[12] M. Tóth, H.R. Buser, P.M. Guerin, H. Arn, F. Schmidt, W. Francke, G. Szöcs, J. Chem. Ecol. 18 (1992) 13.
[13] D. Obeng-Ofori, B. Torto, P.G.N. Njagi, A. Hassanali, H. Amiani, J. Chem. Ecol. 20 (1994) 2077.
[14] C. Löfstedt, B.S. Hansson, E. Petersson, P. Valeur, A. Richards, J. Chem. Ecol. 20 (1994) 153.
[15] P.M. Guerin, E. Städler, H.R. Buser, J. Chem. Ecol. 9 (1983) 843.
[16] D. Thiery, J.M. Bluet, M.H. Pham-Delègue, P. Etiévant, C. Masson, J. Chem. Ecol. 16 (1990) 701.
[17] B.V. Burger, W.G.B. Petersen, Z. Naturforsch. C 46 (1991) 1073.
[18] B. Gabel, D. Thiery, V. Suchy, F. Marion-Poll, P. Hradsky, P. Farkas, J. Chem. Ecol. 18 (1992) 693.
[19] R. Baur, P. Feeny, E. Städler, J. Chem. Ecol. 19 (1993) 919.
[20] L.J. Wadhams, M.M. Blight, V. Kerguelen, M. Le Metayer, F. Marion-Poll, C. Masson, M.H. Pham-Delègue, C.M. Woodcock, J. Chem. Ecol. 20 (1994) 3221.
[21] A.A. Cossé, J.L. Todd, J.G. Millar, L.A. Martinez, T.C. Baker, J. Chem. Ecol. 21 (1995) 1823.
[22] M.M. Blight, J.A. Pickett, L.J. Wadhams, C.M. Woodcock, J. Chem. Ecol. 21 (1995) 1649.
[23] N.E. McIndoo, Proc. Entomol. Soc. Wash. 37 (1935) 36.
[24] J. de Wilde, Symp. Biol. Hung. 16 (1976) 291.
[25] J.H. Visser, J.K. Nielsen, Entomol. Exp. Appl. 21 (1977) 14.

[26] B.K. Mitchell, B.G. McCashin, J. Chem. Ecol. 20 (1994) 753.
[27] J.H. Visser, Entomol. Exp. Appl. 25 (1979) 86.
[28] J.H. Visser, D.A. Avé, Entomol. Exp. Appl. 24 (1978) 738.
[29] E. Omand, J. Zabara, Comp. Biochem. Physiol. 70A (1981) 469.
[30] K. Grob, F. Zürcher, J. Chromatogr. 117 (1976) 285.
[31] W. Boland, P. Ney, L. Jaenicke, G. Gassmann, in: P. Schreier (Ed.), Analysis of Volatiles, Walter de Gruyter, Berlin, 1984, pp. 371.
[32] A.E. Sauer, G. Karg, U.T. Koch, J.J. de Kramer, R. Milli, Chemical Senses 17 (1992) 543.
[33] K.-E. Kaissling and J. Thorson, in: D.B. Satelle, L.M. Hall, J.G. Hildebrand (Eds.), Receptors for Neurotransmitters, Hormones and Pheromones in Insects, Elsevier/North-Holland, Amsterdam, 1980, pp. 261.
[34] L.M. Beidler, Prog. Biophys. Biophys. Chem. 12 (1962) 107.
[35] S. Schütz, B. Weißbecker, A. Klein, H.E. Hummel, Naturwissenschaften 84 (1997) in press.

ELSEVIER

Talanta 44 (1997) 2225–2230

Talanta

Newly designed flow field-flow fractionation channel for macromolecules and particles in the submicrometer and micrometer range[1]

R.A. Zahoransky [a,*], H. Dummin [b], E. Laile [b], T. Schauer [c]

[a] *Fachhochschule Offenburg, Badstr. 24, D-77652 Offenburg, Germany*
[b] *Wizard Zahoransky KG, Schwarzwaldstr. 3, D-79674 Todtnau, Germany*
[c] *Forschungsinstitut f. Pigmente u. Lacke e.V., Allmandring 37, D-70569 Stuttgart, Germany*

Received 5 June 1996; received in revised form 14 February 1997; accepted 25 March 1997

Abstract

The flow field-flow fractionation (FIFFF) technique is a promising method for separating and analysing particles and large size macromolecules from a few nanometers to approximately 50 μm. A new fractionation channel is described featuring well defined flow conditions even for low channel heights with convenient assembling and operations features. The application of the new flow field-flow fractionation channel is proved by the analysis of pigments and other small particles of technical interest in the submicrometer range. The experimental results including multimodal size distributions are presented and discussed. © 1997 Elsevier Science B.V.

Keywords: Particle separation; Flow fractionation

1. Introduction

The separation of particles and macromolecules in a flow field at low Reynolds numbers and under a cross flow field is principally known since the late 1960s [1]. But only in recent years, has this technique received wider attention as an analytical tool for analysing small particles in the submicrometer and micrometer range.

The flow field-flow fractionation (FIFFF) is a complementary technique to the SEC, capillary electrophoresis, capillary injection and centrifuge methods. FIFFF has advantages in the cases where a high selectivity and resolution, gentle, shear free conditions and a broad measurement range from nanometer to over 50 μm is necessary [2,3]. Furthermore, FIFFF allows physical separation of the size fractions of the particle mixture. The technique was recently used for the separation of proteins [4,5], antibody aggregates [6], polymers [7], biological material [8] and calibration particles [9]. For industrial purposes, FIFFF has been applied successfully to analyse pigments and paints [10,11].

This paper describes the newly designed channel and the experimental results gained with selected test particles of technical interest.

* Corresponding author.

[1] Presented at the Symposium on Analytical Sciences (SAS) IV, Belgium, 3–5 June, 1996.

PII S0039-9140(97)00220-8

2. Basics

In Fig. 1 the FIFFF channel is schematically shown. An appropriate force field is perpendicularly applied to the particle loaden flow field. In the case of FIFFF, the force field is realised by a cross flow over the whole channel length. The width and length of the channel lie typically between 75 and 300 μm and 30 cm, respectively. The measuring set-up of FIFFF is shown schematically in Fig. 2 and Fig. 3 is a photographic representation of the measuring assembly.

2.1. Normal mode

The investigated particle sample is injected at the tip of the channel. Relaxation occurs, which is carried out according to the stop-flow procedure. During the relaxation, the axial flow is deactivated and one to two channel volumes of the carrier fluid are pumped across the channel. Due to the cross flow, the particles are driven toward the membrane covering the bottom frit. However, the diffusion of particles acts in the opposite direction. In consequence, each particle fraction reaches its equilibrium position in the channel, depending on the particular diffusion coefficient. After relaxation is completed, the axial flow is activated and the particle fractions are driven to the channel outlet.

Thus, the parabolic flow velocity profile and the diffusion coefficient related positioning of particles in the channel cause a fractionation of the sample. Applying the Einstein–Stokes equation which couples diameter and diffusion coefficient for small spherical particles, a relationship Eq. (1) for the retention time t_r and the particle diameter d can be derived:

$$t_r = \frac{t^0}{R} = \frac{d\pi\eta w^2 V_c}{2kTV} \quad (1)$$

where t_r is the retention time, t^0 the void time, $R = t^0/t_r$ the retention ratio, d the hydrodynamic particle diameter, η the viscosity of the fluid, w the channel height, k the Boltzmann constant, T the temperature, V_c the volume flow of cross flow, and V the volume flow of channel flow. If the molecular weight M of macromolecules is of interest, the following relation between molecular weight and diameter is generally applied:

$$d = A'M^b \quad (2)$$

where A' and b are constants.

Eq. (1) describes the normal mode of operation. In this mode, small particles are located towards the channel center and bigger ones are closer to the membrane. The channel flow with its parabolic velocity profile, therefore moves the smaller particles faster so the detector at the channel end is passed first. When the FIFFF is operating in the normal mode, it is an absolute method for measuring diffusion coefficients and particle size under certain conditions. Therefore, calibration is not necessary. Where diffusion forces are dominant, particles with small diameters (≤ 1 μm), can be fractionated in this normal mode.

2.2. Steric mode

For particles with $d > 1$ μm, the diffusion motion can generally be neglected. At this point it is solely the particle size that is of importance for the elusion and fractionation. Compared with the normal mode it is the outflow sequence of the particles that reverses and the large particles are detected first. The duration for the analysis is much shorter and instead of Eq. (1) the Eq. (3) applies:

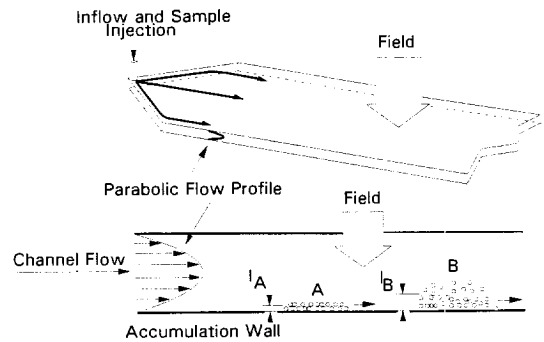

Fig. 1. Principle of field-flow fractionation. A, B, different particle fractions; l_A, l_B, specific distance from the accumulation wall for both fractions.

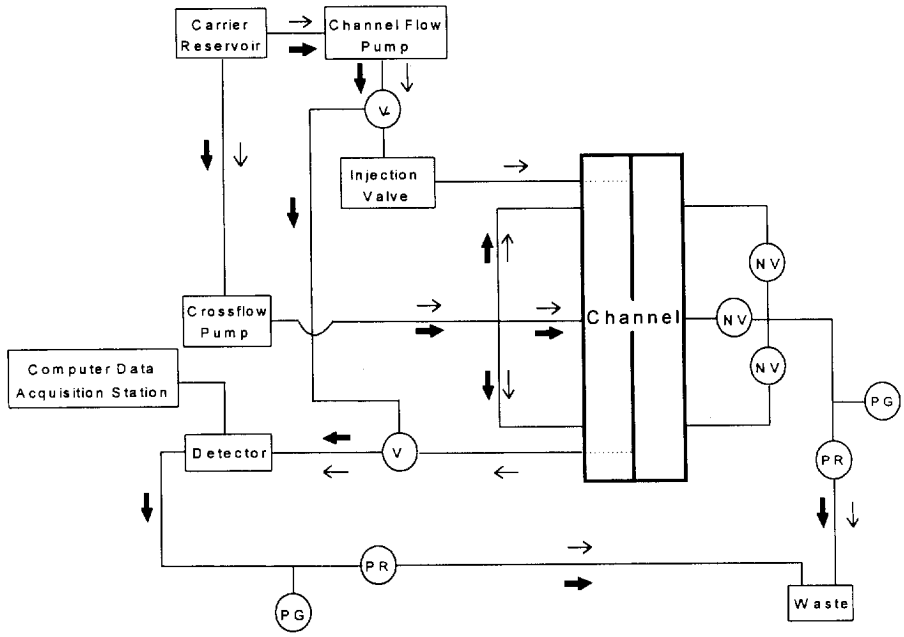

Fig. 2. Schematic diagram of FIFFF setup: V, valve; PR, pressure regulator; PG, pressure gauge; NV, needle valve; full and empty arrows represent the relaxation and elution period, respectively.

$$t_r = \frac{wt^0}{3\gamma d} \tag{3}$$

where γ correction factor $1 \leq \gamma < 2$. Previous calibration using a suspension with known size distribution is mandatory to find the applicable correction factor γ.

2.3. Hyperlayer mode

In the hyperlayer mode, the initial fractionation of large particles is due to the hydraulic lifting force. Again, the larger particles are preferentially driven towards the channel center. Consequently, these particles are detected first. The analysis time is short, whereas Eq. (3) is also used with a correction factor $\gamma \geq 2$. Calibration is mandatory to gain the numerical value of γ for the individual flow conditions.

It is advantageous for routine analysis to work in the steric or hyperlayer mode as the measurement time is short. However, this requires the proper adjustment of the channel height and flow conditions.

2.4. Determination of flow mode

Fig. 4 illustrates schematically the different flow modes, depending on the particle size and its position in the channel.

It is not known a priori which operating mode is applicable for a given sample. In practice, the optimal mode can be found by experiments with latex standards of different sizes. Fig. 5 shows the results gained at specific flow conditions with a channel height of 100 μm [11].

The minimum in the retention ratio versus the diameter separates the modes. Small particles which are diffusion driven follow the normal mode whereas larger ones undergo the hyperlayer or steric mode fractionation. The limit of the modes for the conditions of Fig. 5 lies at a particle diameter of approximately 0.6 μm. This limit depends on the channel height and selected flow conditions and can be to some extend changed.

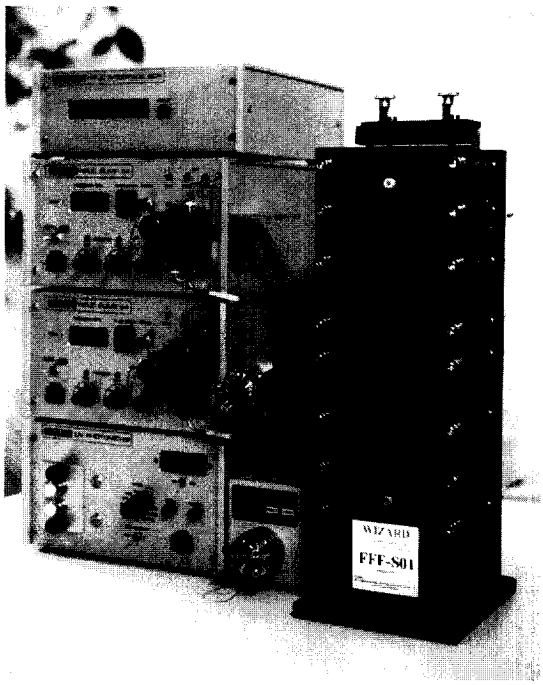

Fig. 3. Photography of the channel setup.

3. Channel design

The channel dimensions like width b, height w and length l are in principle freely selectable. The aspect ratio b/l must be sufficiently low to fulfil the assumption of an indefinitely long channel.

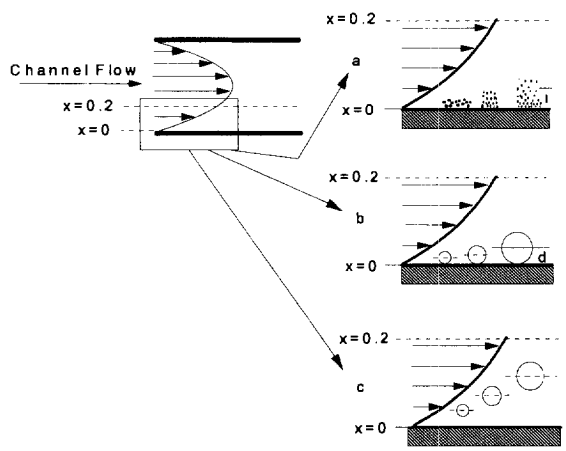

Fig. 4. Illustration of normal (a), steric (b) and hyperlayer (c) mode of operation.

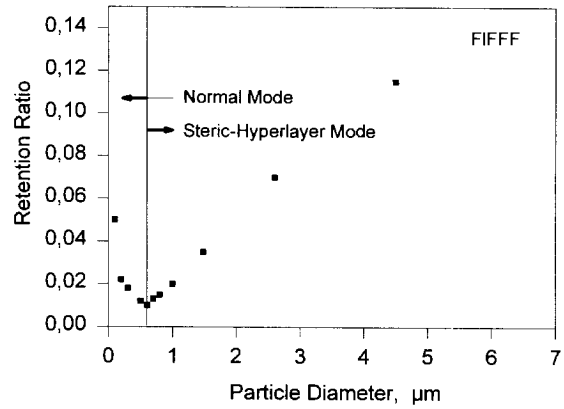

Fig. 5. Determination of flow mode.

The length and height affect via the ratio V_c/V of Eq. (1) the retention time, the flow mode and the separation output. The FIFFF channel under consideration has a length of 300 mm and a width of 20 mm. The channel height was varied between 100 and 250 µm to optimise the resolution and the retention time.

A major feature of the new channel is the division of the hollow compartment under the frit into three separate chambers with an independent pressure control to eliminate pressure drop differences along the channel and to assure a uniform cross flow in the whole channel. As evidenced in [12], the cross flow uniformity in the channel can be adversely influenced by a membrane. Fig. 6 gives an internal view of the separate chambers under the frit.

The handling of the new channel is most simple. Attention is given to a comfort assembling and dissembling of the channel. The change of the spacer or membrane can be done within a short time. The secure replacement and stretching of the delicate membrane is solved by special spring loaded clamping devices [13].

4. Experimental results

The samples were injected into the channel using a 20 µl loop and the stop-flow relaxation was conducted (two void volumes were pumped across the channel by deactivated axial channel

flow). After the relaxation of approximately 30 s, the channel flow was switched on and the fractionated samples were detected with a UV detector.

As submicrometer particles were of interest, only the normal mode was used for the presented data. Because of the simple linear relation between the elution time and the particle diameter in Eq. (1) for the normal mode, the time abscissa can be readily recalculated to the diameter scale. A system peak is typically generated at the UV detector when the valve for the channel flow is activated.

Several test particle samples were investigated. A systematic analysis on the particle shape influence was not made so far. The obtained diameter can be considered as a hydrodynamic one.

Fig. 7 shows a raw data record of intensity versus time for a red iron oxide pigment water suspension. The experimental settings were $V = 1.5$ ml min^{-1}, $V_c = 0.55$ ml min^{-1}, $w = 250$ μm.

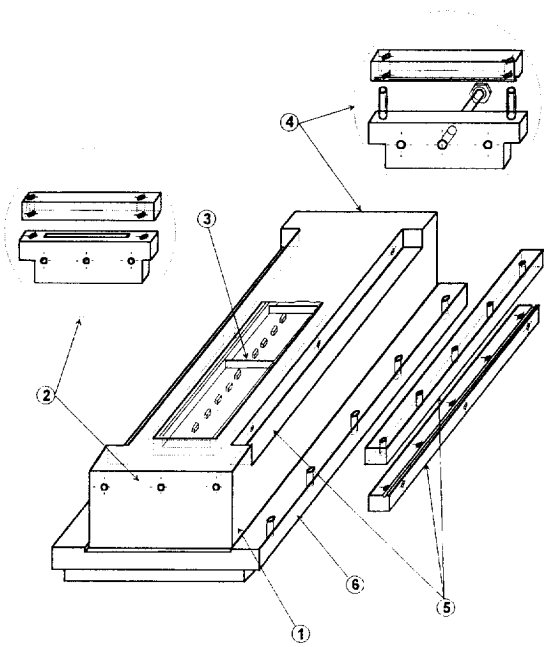

Fig. 6. View of the separated chambers under the frit of the fractionation channel, 1—plexiglass block; 2, 4 and 5—membrane clamping and tensioning device; 3—camber separator; 6—supporting plate.

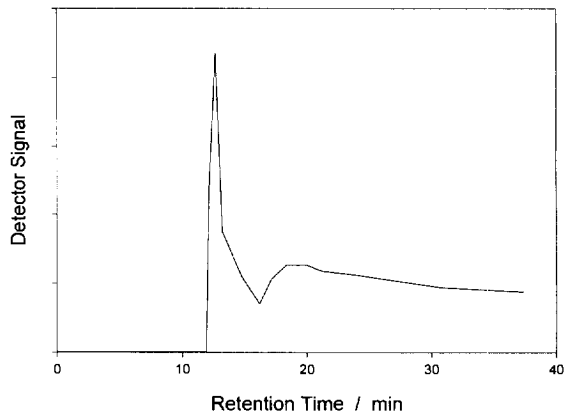

Fig. 7. Printout of the UV detector signal for the iron oxide pigment; flow conditions: $V = 5.5$ ml min^{-1}, $V_c = 0.8$ ml min^{-1}, $w = 210$ μm.

The size distribution has its broad maximum at approximately 20 min which corresponds approximately to a size of 0.1 μm. The broad size distribution is typical for an industrial pigment. The large peak at 12 min is the system peak which is normally equivalent to the void peak and arises when the head of the initiated channel flow arrives at the detector which is approximately the void time (Eqs. (1) and (2)). The system peak, which does not contribute to the measurement results, is omitted in the following data graphs. It can easily be distinguished from the sample and be eliminated by the data acquisition and presentation software. This is a standard procedure.

Fig. 8 represents a detector signal for a bimodal size distribution of a mixture of TiO_2 pigment (Kronos 2057, Kronos) and an acrylic emulsion (Mowilith DM-772, Hoechst AG). Despite that the sizes of both species are rather close together, it was possible to resolve both distributions with the maxima at 0.265 and 0.691 μm. The experimental settings were $V = 5.5$ ml min^{-1}, $V_c = 0.8$ ml min^{-1} and $w = 210$ μm.

Fig. 9 shows again the high resolution of FIFFF. The SiO_2 sample of a narrow distribution was clearly detected with a mean size of 0.496 μm which corresponds within 10% with the manufacturers analysis.

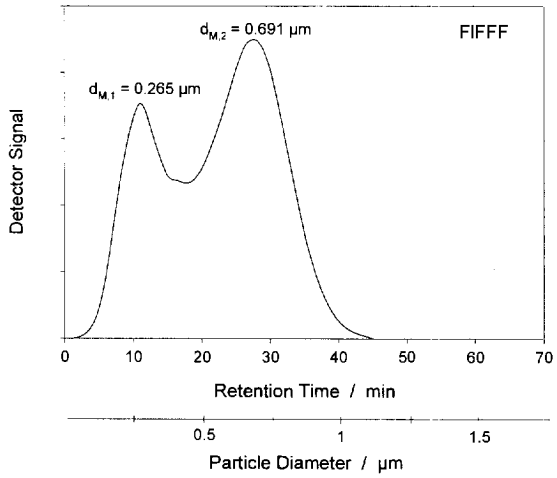

Fig. 8. FIFFF spectrum for a two component sample, consisting of TiO_2 (33 wt.%) and acrylic emulsion (67 wt.%); flow conditions: $V = 5.5$ ml min^{-1}, $V_c = 0.8$ ml min^{-1}, $w = 210$ µm.

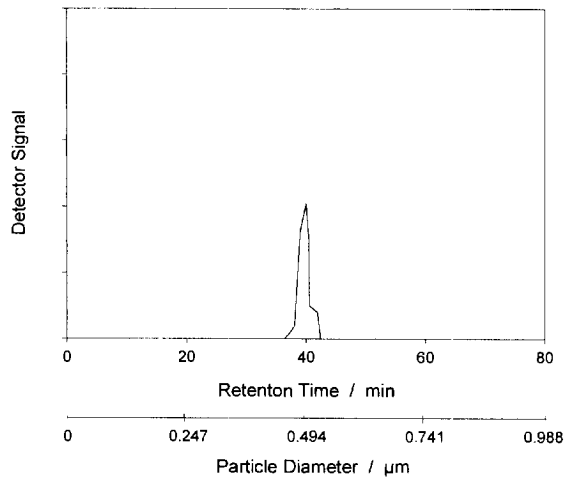

Fig. 9. FIFFF spectrum for SiO_2 sample; flow conditions: $V = 1$ ml min^{-1}, $V_c = 0.2$ ml min^{-1}, $w = 250$ µm.

5. Summary

FIFFF offers an interesting alternative for the fractionation and separation of small particles and the measurement of the molecular weight of macromolecules. Particularly, the broad measuring range from approximately 1 nm to over 50 µm must be mentioned. Of advantage is the possibility to function in different operating modes, i.e. normal, steric and hyperlayer mode. For the two latter modes, the measurement times are remarkably short.

The new FIFFF channel proved its capability to investigate small particles. The design makes the handling easy and fast so that it can be used for standard laboratory applications.

References

[1] J.C. Giddings, Separation Sci. 1 (1966) 123.
[2] S.K. Ratanathanawong, J.C. Giddings, ACS Symp. Ser. 521 (1993) 13.
[3] K.D. Caldwell, in: H.G. Barth, J.W. Mays (Eds.), Modern Methods of Polymer Characterization, Wiley, New York, 1991, p. 113.
[4] A. Litzen, M.B. Garn, H.M. Widmer, J. Biotechnol. 37 (1994) 291.
[5] M.-K. Liu, P. Li, J.C. Giddings, Protein Sci. 2 (1993) 1520.
[6] A. Litzen, J.K. Walter, H. Krischollek, K.-G. Wahlund, Anal. Biochem. 212 (1993) 469.
[7] M.E. Miller, H. Lee, X. Li, R. Szetirmay, J.C. Giddings, Polym. Prepr. (ACS Div. Polym. Chem.) 35 (1994) 764.
[8] B.N.J. Barman, Colloid Interface Sci. 167 (1994) 467.
[9] H. Thielking, D. Roessner, W.-M. Kulicke, Anal. Chem. 67 (1995) 3229.
[10] T. Schauer, GIT Fachz. Lab. 10 (1995) 922.
[11] T. Schauer, Part. Part. Syst. Charact. 12 (1995) 284.
[12] J. Granger, J. Dodds, N. Midoux, Chem. Eng. J. 42 (1989) 193.
[13] German Patent Application P4414826.7-43 from 28.04.94.

ELSEVIER

Talanta 44 (1997) 2231–2235

Talanta

Multicomponent analysis in luminescence spectroscopy[1]

M. Dalibart

LSMC URA 124, Universite Bordeaux I, 351 Cours de la Liberation, 33405 Talence Cedex, France

Received 13 June 1996; received in revised form 2 May 1997; accepted 15 May 1997

Abstract

Multicomponent analysis of absorption spectra (infrared or electronic spectra) by factor analysis is a suitable method to use. The algorithm of factor analysis is now available for luminescence spectroscopy. The first possibility, as in absorption spectroscopy, is to determine pure components emission spectra for a unique set of spectra of mixtures in overdetermined conditions. On the other hand, it is also possible to extract pure components emission and excitation spectra of the only data corresponding to the 3D fluorescent spectrum of a single mixture. The results are evaluated in respect to noise level and concentrations ratio on both simulated and real spectra. © 1997 Elsevier Science B.V.

Keywords: Factor analysis; Simulated spectra; Luminescence; 3D-spectrum

1. Introduction

Multicomponent quantitative analysis allows correlations between the spectra and the concentrations of the calibration set. Numerous methods of least-squares analysis: classical least squares (CLS), inverse least squares (ILS) or bilinear analysis: principal components regression (PCR), partial least squares (PLS) are suitable and can be found in the monograph by Martens and Naes [1]. All these methods require a calibration set of solutions.

On the other hand, factor analysis [2] attempts to predict concentration without the calibration step and can be used when the components are not clearly identified or are not available. In this way, factor analysis appears as a self-calibration method that can be applied to problems concerning mixtures of an unknown number of unknown components.

2. Experimental

The emission, excitation and 3D-spectra were recorded on a SFM25 instrument from KONTRON and processed on a PC computer.

Numerous simulated spectra of mixtures were generated by using experimental spectra of pure components (anthracene and perylene) and adding noise to various level (0–20%).

Our factor analysis programmes were performed on a PC computer for the first method

[1] Presented at the Symposium on Analytical Sciences (SAS) IV, Belgium, 3–5 June, 1996.

PII S0039-9140(97)00221-X

and on a RISC IBM 6000 station for the diagonalisation of the 3D matrix.

3. Theory

The mathematical techniques of factor analysis have been well described in the excellent monographs by Malinowsky [3] and are well covered in the literature [4–12] and we shall restrict our presentation to an abstract.

In absorption spectroscopy the formalism is based on Beer's law:

$$|A| = |K| \cdot |C|$$

where $|A|$ $(p \cdot m)$ is the absorbance matrix; $|K|$ $(p \cdot n)$ represents the product of the absorptivity by the path length; and $|C|$ $(n \cdot m)$ is the concentration matrix $(n \cdot m)$; using n components, a set of m solutions and a set of p absorption wavelengths ($n < m$ and $n < p$).

The first step is to build the covariance matrix:

$$|Z| = |A|^T \cdot |A|$$

where $|Z|$ is a $(m \cdot m)$ small triangular matrix; and $|A|^T$ is the transpose absorbance matrix.

The $|Z|$ matrix is then diagonalised and the number of principal factors is determined, using criteria such the IND indicator [2]. A set of abstract mathematical meaning eigenvector matrices $|R_a|$ and $|C_a|$, but devoid of real physical or chemical meaning, is computed:

$$|A| = |K_a| \cdot |C_a|$$

where $|K_a|$ represents the abstract pure components spectra; and $|C_a|$ is the abstract concentration matrix.

Previously self-modelling method [6–8] or rank annilation method [9–12] were used to convert, in some particular cases, these factors into physically significant matrices.

We have written a more general iterative algorithm to convert these factors using rotation, for two or three factors, and target testing for general cases. In contrast to previous methods, the only assumption is that the computed spectra matrix must only contains positive values [13–15].

Using these computational methods the real spectra $|K_r|$ is obtained. The concentration $|C_r|$ matrix is finally computed by using the CLS method [1]. During these last steps, the extracted matrices $|K_r|$ and $|C_r|$ must be normalised [13–15].

4. Emission spectroscopy

For dilute solutions, the fluorescence intensity is linear versus concentrations and thus the law can be written:

$$|I| = |K| \cdot |C|$$

where $|I|$ is the intensity matrix; $|K|$ represents the product of the absorption coefficient by the path length and by the fluorescence efficiency; and $|C|$ is the concentration matrix; that is to say stickly the formalism used in absorption.

Thus, using a set of emission spectra of mixtures, it is possible to compute both pure components spectra ($|K|$ matrix) and concentration values ($|C|$ matrix).

Fig. 1 presents the comparison of the pure components spectra and the computed spectra of simulated mixtures. The computed spectra are good for reasonable noise level. Factor analysis was performed with noise level from 0 to 20%, the relative error on calculated concentration varies from 0.5 to 1.5% and the quadratic error on computed spectra was estimated (Table 1).

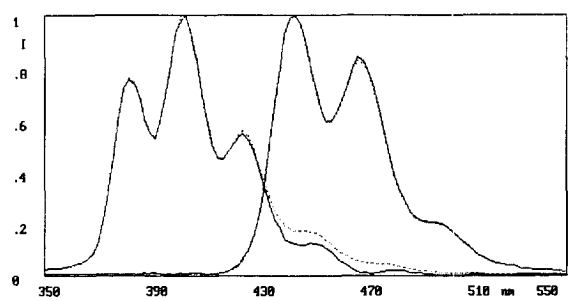

Fig. 1. Comparison of the emission spectra of simulated mixtures of anthracene and perylene. ··· pure components spectra; —— computed spectra.

Table 1
Computation errors on concentrations and spectra vs. noise level for simulated mixtures of anthracene and perylene

% Noise level	% Concentrations error	Quadratic errors on computed emission spectra
0	0.53	0.00002
1	0.55	0.00002
2	0.59	0.00003
5	0.72	0.00004
10	1.50	0.00022
20	1.52	0.00070

5. D-fluorescence data

A 3D-fluorescence spectrum is a set of emission spectra, that is to say intensity versus emission wavelengths, recorded with various excitation wavelengths. A |I| matrix is obtained. The rows represent the emission spectra of the mixture and the columns are the excitation spectra of the mixture [9–12]:

$$|I| = |F| \cdot |E|$$

where |I| $(p \cdot m)$ is the 3D-spectrum; |F| $(p \cdot n)$ represents the emission spectra of the pure components; and |E| $(n \cdot m)$ is the excitation spectra of the pure components; and |E| $(n \cdot m)$ is the excitation spectra of the pure components; using n components, a set of m excitation wavelengths and a set of p emission wavelengths.

The computational methods used for by previous authors [9–12] require wavelengths where only one component emits.

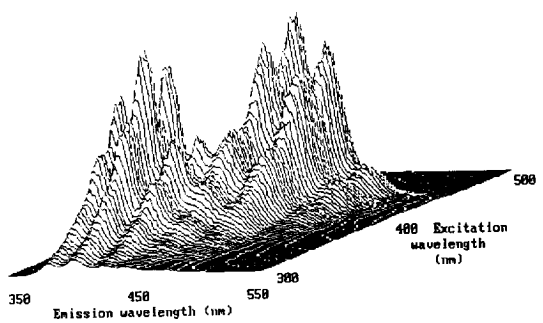

Fig. 2. Simulated 3D-spectrum (anthracene/perylene mixture with 5% noise level).

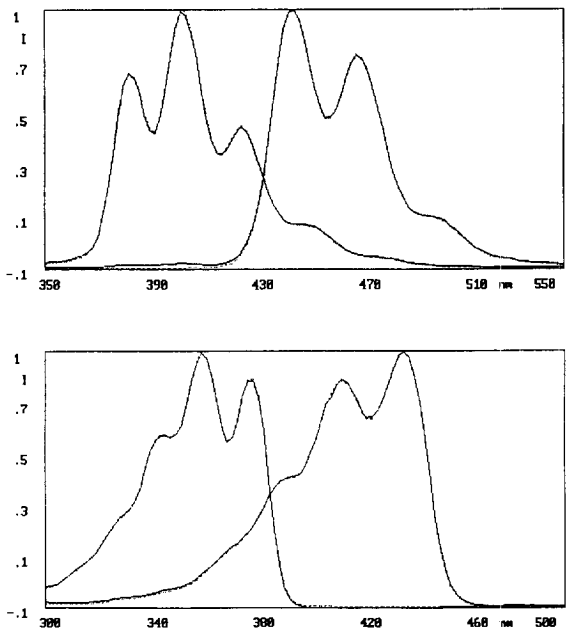

Fig. 3. Emission (a) and excitation (b) spectra computed from a simulated 3D-spectrum (see Fig. 2). ··· pure components spectra; —— computed spectra.

To recover physical meaning, we have used our algorithm described before. The covariance matrix, |Z| is then a $p \cdot p$ matrix, that is to say, for our data, a 101.101 matrix. The diagonalisation is the time consuming step and thus was performed on a RISC station.

Fig. 2 presents a typical 3D-simulated spectrum (anthracene/perylene 1/1). The emission and excitation spectra are displayed on Fig. 3(a, b). The

Table 2
Quadratic errors for computed emission and excitation spectra vs. noise level for 3D simulated spectra (anthracene/perylene)

% Noise level	Quadratic errors on computed spectra	
	Emission	Excitation
0	0.00005	0.00003
1	0.00004	0.00003
2	0.00003	0.00005
5	0.00004	0.00003
10	0.00016	0.00012
20	0.00031	0.00022

Table 3
Quadratic errors for computed emission and excittion spectra vs. concentrations ratio for 3D simulated spectra (anthracene/perylene)

Concentrations ratio A/P	Quadratic errors on computed spectra			
	Emission		Excitation	
	P	A	P	A
1/1	0.00006	0.00002	0.00002	0.00004
1/2	0.00003	0.00003	0.00002	0.00004
1/3	0.00003	0.00007	0.00002	0.00009
1/4	0.00001	0.00043	0.00002	0.00007
1/5	0.00005	0.00055	0.00003	0.00018
1/10	0.00003	0.01150	0.00009	0.00095
1/20	0.00002	0.2650	0.00005	0.00218

accuracy of the prediction is very good although the 3D-spectrum was somewhat noisy. This result shows the great efficacity of the data compression step to extract components spectra from noise. Quadratic errors are of the same order of magnitude for emission and excitation (see Table 2).

Table 3 shows the influence of the relative concentration of the two emitting species, the results are quite good for relative abundances varying from 1/1 to 1/5. Of course, the results are better for the predominant species. But, the table shows also that the results are better for computed excitation spectra than for emission spectra. This result clearly demonstrates that the CLS computation steps are not the main errors source because excitation spectra are computed from emission spectra.

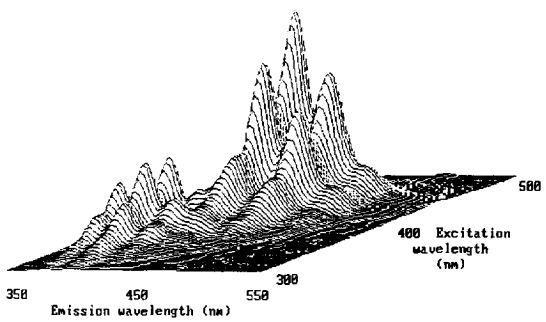

Fig. 4. Experimental 3D-spectrum (anthracene/perylene mixture).

Real experimental results are displayed on Fig. 4 and Fig. 5. The spectra are in very good agreement with those obtained with simulated data, except some inner filter problems, due to concentrations.

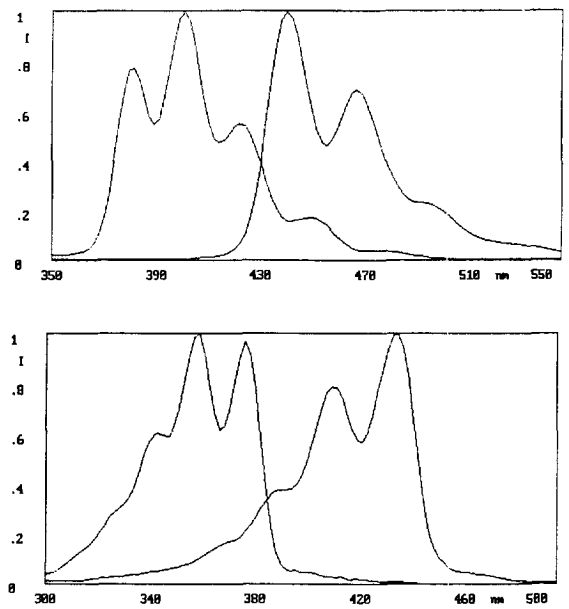

Fig. 5. Emission (a) and excitation (b) spectra computed from an experimental 3D-spectrum (anthracene/perylene mixture).

6. Conclusion

This work demonstrates that factor analysis can now be used to solve multicomponent problems in luminescence spectroscopy, without any assumptions on the pure components spectra.

If a set of mixtures are available, both the pure component spectra and the concentration matrix can be extract from the data by factor analysis.

If the only data is a 3D-spectrum of a unique mixture, the pure emission and excitation spectra are computed, but the concentrations cannot be estimate.

References

[1] H. Martens, T. Naes, Multivariate Calibration, Wiley, Chichester, 1989.
[2] E.R. Malinowsky, D.G. Howery, Factor Analysis in Chemistry, 1st ed., Wiley, New York, 1980.
[3] E.R. Malinowsky, Factor Analysis in Chemistry, 2nd edition, Wiley, New York, 1991.
[4] P.M. Fredericks, J.B. Lee, P.R. Osborn, dom A.J. Swinkels, Appl. Spectrosc., 39 (1985) 303.
[5] P.M. Fredericks, J.B. Lee, P.R. Osborn, dom A.J. Swinkels, Appl. Spectrosc., 39 (1985) 311.
[6] V.H. Lawton, E.A. Silvestre, Technometrics, 13 (1971) 617.
[7] N. Ohta, Anal. Chem., 45 (1973) 553.
[8] C.H. Lin, S.C. Liu, J. Chim. Chem. Soc., 25 (1978) 167.
[9] I.M. Warner, G.D. Christian, E.R. Davidson, J.B. Callis, Anal. Chem., 49 (1977) 56.
[10] G. Cruciani, A. Spalletti, G. Bartocci, Z. Phys. Chem., 172 (1991) 227.
[11] A. Spalletti, G. Bartocci, F. Masetti, U. Mazzucato, G. Cruciani, Chem. Phys., 160 (192) 131.
[12] G. Bartocci, A. Spalletti, F. Masetti, G. Cruciani, J. Mol. Struct., 298 (1993) 165.
[13] M. Dalibart, Spectra 2000, 116 (1986) 69.
[14] M. Dalibart, J. Derouault, Z. Phys. D-Atoms, Molecules, Clusters, 2 (1989) 489.
[15] M. Dalibart, J. Derouault, Z. Phys. D-Atoms, Molecules Clusters, 19 (1991) 211.

ELSEVIER

Talanta 44 (1997) 2237–2245

Talanta

Application of an artificial neural network (ANN) and piezoelectric chemical sensor array for identification of volatile organic compounds[1]

György Barkó, József Hlavay *

Department of Earth and Environmental Science, University of Veszprém, P.O. Box. 158, 8201 Veszprém, Hungary

Received 24 July 1996; received in revised form 26 May 1997; accepted 27 May 1997

Abstract

A piezoelectric chemical sensor array was developed using four quartz crystals. Gas chromatographic stationary phases were used as sensing materials and the array was connected to an artificial neural network (ANN). The application of the ANN method proved to be particularly advantageous if the measured property (mass, concentration, etc.) should not be connected exactly to the signal of the transducers of the piezoelectric sensor. The optimum structure of neural network was determined by a trial and error method. Different structures were tried with several neurons in the hidden layer and the total error was calculated. The optimum values of primary weight factors, learning rate ($\eta = 0.15$), momentum term ($\mu = 0.9$), and the sigmoid parameter ($\beta = 1$) were determined. Finally, three hidden neurons and 900 training cycles were applied. After the teaching process the network was used for identification of taught analytes (acetone, benzene, chloroform, pentane). Mixtures of organic compounds were also analysed and the ANN method proved to be a reliable way of differentiating the sensing materials and identifying the volatile compounds. © 1997 Elsevier Science B.V.

Keywords: Piezoelectric sensor array; Artificial neural network; Identification of organic compounds

1. Introduction

Chemical sensor systems and detector arrays are widely applied for determination of organic vapors, gases and odors in the atmosphere. A piezoelectric quartz crystal can be used as a chemical sensor that is able to measure the chemical concentration reversibly. There are two fundamental methods to develop a chemical sensor from quartz crystal; the crystal can be used for preparing either surface acoustic wave (SAW) or piezoelectric quartz microbalance (PQM) sensors. Due to Sauerbrey's fundamental equation (Eq. (1)), the change of frequency is proportional to the change of loaded mass [1].

$$\Delta F = -2.3 \times 10^6 \times F^2 \times \frac{\Delta M}{A} \quad (1)$$

* Corresponding author.

[1] Presented at the Symposium on Analytical Sciences (SAS) IV, Belgium, 3–5 June, 1996.

PII S0039-9140(97)00168-9

where ΔF is the change of frequency (Hz); F is the basic frequency of the quartz crystal (MHz); ΔM is the change of mass (g); A is area coated (cm^2).

From this simple mass balance a sensitive and selective chemical sensor can be developed by coating the surface with different organic and/or inorganic compounds as sensing materials. The fundamental experiments with the first PQM sensor were carried out by King [2]. The quartz crystal was coated by stationary phases used in gas chromatography and the trace amount of organic compounds could be determined. This simple sensor device was not able to differentiate and could not be used directly to measure the concentration of analytes, it showed a low selectivity on the organic compounds.

The requirements for a reliable piezoelectric chemical sensor are the sensitivity, selectivity and reversibility towards the analyte to be determined. However, to find an entirely selective material for only one analyte is almost unrealizable. On the other hand, application of the chemical sensor in the environmental analysis is hampered by the fact that several compounds are in the matrix and generally only one has to be detected. Mathematical algorithms have to be developed for the data processing, and chemometric methods are necessary to explain the behavior of non-selective chemical sensors. Principal component analysis (PCA), cluster analysis, pattern recognition (PARC) and artificial neural network (ANN) methods can be applied to perform the data evaluation. The artificial neural network approach based upon the biological neuron model is an up-to-date tool for extraction of the main information from the signals. Although, the human nervous system contains about 10^{10} biological neurons, the common back propagation algorithms are computed by only 10^1 to 10^4 artificial neurons [3,4]. The biological odor sensors—like the olfactory neurons—have excellent sensitivity (ppm or ppb, depending upon the analytes), but does not have any specificity.

In the food and drug industry, several metal-oxide semiconductors, piezoelectric, surface acoustic, amperometric, optical and thermal detectors were applied for identification and determination of the gases and odors. Smells of coffee, wine, beans, whisky, beer, meat, fish and perfumes were analysed using an 'artificial nose' [5]. Fraser et al. [6] made a sensor system for detection of ammonia and other inorganic air pollutants. A chemical sensor with five piezoelectric quartz crystals was developed by Klinkhachorn et al. [7] and inorganic compounds were measured in nanogram levels. Signal processing based upon the pattern recognition algorithm was applied for data handling. Schmautz [8] has built a piezoelectric sensor system for determination of anesthetic gas mixtures. Quartz crystals were coated by different sensitive layers and pattern recognition was used for investigation of the mixing ratio. Chang et al. [9] developed an odor recognition device using quartz crystals coated by lipids for measurements of odor components. A few common odors (i.e. fragrance of rose, wine) were investigated and different adsorption coefficients were found on the lipids. A computer program based upon the artificial neural network was developed. A sensor system with nine piezoelectric chemical detectors has been developed by Carey et al. [10] for determination mixtures of analytes using partial least-squares and multiple linear regression methods. As an industrial application, discrimination of liquor aromas was achieved by Aishima [11] using gas sensor array and chemometric methods. The complex aroma materials were discriminated and the beverages were classified. Principal component analysis and cluster analysis were successfully applied.

2. ANN based on the back propagation method

The back propagation method is part of the parallel distributed processing system [12]. One-layer networks like Hopfield and Kohonen structure, and multilayer systems like counter propagation and back propagation of errors, can be used for chemical applications. In these cases the processing unit is a so-called *neuron*. Two neurons are linked by a connection. Every connection has a weight factor (W), the input values $I_j(t)$ correcting by the weight factor are summarized (see Eq. (2)). The i and j neurons are connected by $W(i,j)$.

$$I_j(t) = \sum_i W_{i,j}(t) O_i(t) \quad (2)$$

First, the system has to be taught. The output values ($O(t)$) go through the connections between the neurons. The neuron unit (N) has an activity level (A) in every time step t. The output value (O) depends on the activity A of the neuron, this is an output function (see Eq. (3)).

$$O(t) = f(A(t)) \quad (3)$$

The status of the active neuron can be written with an activity function (F):

$$A(t) = F(A,I)(t) \quad (4)$$

During the learning process the weights are changed time by time with a ΔW value. The change of the weight among the t and $t+1$ time steps depends upon the difference between the measured and taught values. F is used to determine the activity level (A) of a neuron. The activity level may be a discrete or continuous value. For example, if the input of the neuron is smaller than the threshold limit, $A = 0$. If the input is higher than the threshold, the activity may even be a value between 0 and 1, or equal to 1. Below the threshold value the neuron has no output, while above the threshold limit the neuron has an answer proportional to the activity. The strength of the effect of a neuron on the other neuron depends on the weight of the connections between the two neurons. The higher weights cause a higher effect of input data on the receiver neuron. If $W < 0$, the effect is similar to the inhibition, if $W = 0$, the connection has no role in the network.

In multilayered neural networks, the neurons are arranged in layers. During the teaching process, the strengths of the connections are changed. In most cases Hebb's law of selection is used for computing the modification of the weight factors. The rule can simply be written (Eq. (5)), where $O(t)$ is the output signal of the i-th neuron (see Eq. (3)) and η is the learning rate. Generally, the higher the learning rate the faster the adaptation of the model.

$$\Delta W_{i,j}(t) = \eta \cdot A_j(t) \cdot O_i(t) \quad (5)$$

Other form is the delta-rule or generalized perception rule, where $T(t)$ is the teaching level of the neuron:

$$\Delta W_{i,j}(t) = \eta \cdot (T_j(t) - A_j(t)) \cdot O_i(t) \quad (6)$$

The detailed processes can be applied in different computational methods, not only in chemical data handling. Before the artificial neural networks had been developed, the simple pattern recognition method was utilized. It can be used for classification of species by generating patterns, if the groups of the analytes have characteristic features. The neural network with back propagation of error method is an advanced development for data processing. The delta rule (Eq. (6)) can be composed as a square error function to determine the accurate error of the determination ($E^{(p)}$). During the teaching, the aim of the computing is to minimize the difference between the O_j^p output values and T_j^p taught values.

$$E^{(p)} = \tfrac{1}{2} \sum_j (T_j^{(p)} - O_j^{(p)})^2 \quad (7)$$

The rule says if there are two active neurons and the first unit sends data to the second one, the connection will be more powerful, proportional to the activity of the processing neurons [13].

In this work the identification of volatile organic compounds (i.e. acetone, benzene, chloroform, pentane) is carried out by a non-selective and differently sensitive piezoelectric gas sensor array using the ANN method.

3. Experimental

3.1. The sensor system

Four AT-cut quartz crystals with 9 MHz fundamental frequencies were used (Gamma Co., Hungary). The crystals were arranged in an array and coated by gas chromatographic stationary phases like OV1 (poly-dimethyl siloxane, Supelco), OV275 (poly-cyanoakryl organosilane, Supelco), ASI50 (poly-methyl-phenyl siloxane, Applied Science Laboratories Inc.), and polyphenyl-ether (Carlo Erba), respectively. The appropriate stationary phases were found using

experimental and theoretical means based upon a principal component analysis [14]. The thin film of the coating was formed by solvent evaporation. The coated surface was 0.2 cm^2 and the frequency of the quartz crystals decreased usually by about 8 kHz. Nitrogen (T 45, Messer Griesheim, Hungary) was used as carrier gas and 20 l h^{-1} mass flow was maintained by a GFM17 $3\frac{1}{2}$ digit flow controller (AALBORG). The nitrogen contained 30 ppm water vapor and it was dried by a CRS 202268 packed GC column (Chromatography Research Supplies, USA) to remove the traces of water. The analyte was injected by a syringe. A NAFION drying unit (DM-060-24, Perma Pure Inc., USA) was set into the carrier line for declining the interference of the trace amount of moisture. A data handling card was built and a computer program was developed to measure the frequency changes. The computer program compared the measured frequency to that of the clock of the computer. The detailed set-up of the system was published in Ref.[15].

3.2. The connection of the neural network to the sensor array

The ANN model based on the back propagation of error method can be used to handle the frequency signals of the piezoelectric quartz crystal sensors. All neurons are active in any time, so the activity function has not been applied. There are no threshold limits for the neurons. During the teaching period only the weights of the connections are changed. The second (hidden) and the third (output) layers are linked by connections to the layer above the current one. The layers are fully connected, since every neuron in the current layer is connected to all neurons in the previous layer.

The detector array has four crystals and there are three layers in the neural network. The first (input) layer consists of four neurons, equal to the number of chemical sensors (Fig. 1). This first layer is used only to share the information. The input data are the four lowest output frequencies (X_{pm}) of the four detectors measured during one teaching experiment. The ratio of the measured frequencies was characteristic, and can be used to discriminate the analytes. The effect of the unstable concentration of the compounds was investigated, and frequency signal normalization was applied (see details in Ref. [15]). The same frequency ratio was found in the 100–700 vppm range. Only a limited effect was observed on the repeatability of the analyte's pattern in the mentioned concentration range [15]. However, the teaching experiments were carried out at 600 vppm in all cases because qualitative measurements were performed. Quantitative determination could also be established by ANN [16], but it was not the aim of the current development.

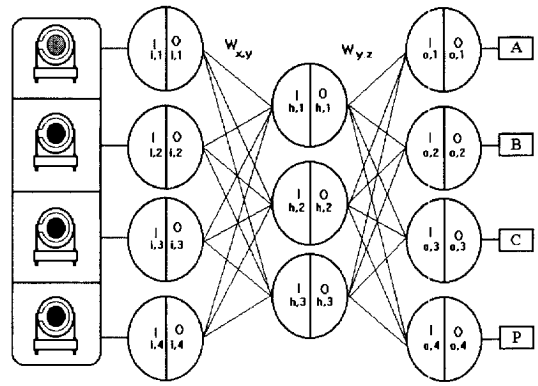

Fig. 1. The sensor system and the artificial neural network.

When an experiment was performed, the four frequency values were read by the computer program and were used as input $I(1)$–$I(4)$ (see Table 1 and Fig. 1). The amount of the analytes was

Table 1
The frequency values in the first 10 training sets of acetone (Hz)

Training set	$I(1)$	$I(2)$	$I(3)$	$I(4)$
1	−250	−110	−260	−390
2	−252	−112	−262	−392
3	−250	−110	−260	−392
4	−253	−110	−260	−391
5	−252	−111	−262	−390
6	−252	−113	−263	−390
7	−250	−110	−261	−391
8	−252	−111	−260	−392
9	−250	−113	−263	−390
10	−250	−110	−260	−393

generated by a vapor generator device and the reproducibility of the generation was determined. The generator performance was validated by gas chromatography [17]. The number of the teaching experiments—and the data sets as well—is p. Every data set consists of four frequency values, extracted from the curves of the measured analytes. One training set is formed by the lowest frequencies of the curves of benzene, acetone, pentane and chloroform. The signals which correspond to the four analytes will be arranged in four columns. To perform the $I(1)$–$I(4)$ input data from the measured signals, X_{pm} training set values are extracted as X_{p1} is the lowest frequency value which has been measured on the quartz crystal coated by OV1, X_{p2} is that coated by ASI50, X_{p3} is that coated by OV275, and finally, X_{p4} is that coated by polyphenyl-ether, respectively, in the p-th sample set. The input layer has four neurons ($m = 4$) with a simple identical output function:

$$O_{i,x}(t) \equiv X_{i,x}(t) \tag{8}$$

The qualitative information can be transformed into real numbers. The simplest way is to use a teaching value 0 for the output neurons where the current analyte answers are not expected, and 1 where the analyte is predicted. In our experiments, 0.9 as a target value of the analyte and 0.1 as a target value of the unexpected answer were used for computing of the back propagation of error algorithm. The taught values are added to the output layer during the teaching process. T_{pn} is the taught sample set and it consists of four values between of 0.05 and 0.95. These values are fed on the output neurons during the teaching process in every time step t. The output layer has four neurons ($n = 4$) connected to the four taught analytes. T_{p1} is the value between 0.8 and 0.95 on the first neuron in the output layer of the p-th sample set. If in our experiment the taught compound is benzene, T_{p2}, T_{p3} and T_{p4} are in the range of 0.05 and 0.2. In Fig. 1 the benzene is assigned to the answer box B. If T_{p2} is between 0.8 and 0.95 on the second neuron in the output layer, the taught compound is acetone, and T_{p1}, T_{p3}, T_{p4} are in the range of 0.05 and 0.2 (Fig. 1, A). T_{p3} is the value between 0.8 and 0.95 on the third neuron in the output layer and this refers to the chloroform. T_{p1}, T_{p2} and T_{p4} are also in the range of 0.05 and 0.2 (Fig. 1, C). If T_{p4} is between 0.8 and 0.95 on the fourth neuron in the output layer, the taught compound is pentane (Fig. 1, P), and T_{p1}, T_{p2}, T_{p3} are in the range of 0.05 and 0.2.

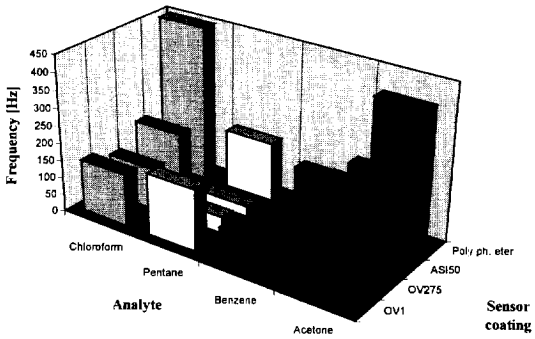

Fig. 2. The frequencies of the chemical sensors for pure analytes.

There are two phases of the application of the ANN. First, the system has to be taught. This means that the compounds are directly introduced into the sensor-array and the output values of the network are calculated. The analytical information is transformed to mathematical values. The four most characteristic frequency values of the four sensing compounds are transferred into the input layer. The frequencies measured on the four sensors are used as the input neurons (Fig. 2). The 600 ppm of organic compounds injected was always kept constant to avoid disturbance of the different concentrations. For example, using acetone as an analyte, signals of the sensor were measured, the output values of the neurons were calculated, and sent to the next layer via connections. Depending upon the weight factors of the connections, the values had more or less effect on the neurons in the layer above the current one.

The frequency values are given to the input layer (Eq. (8)). The output values are computed from layer to layer; first in the input layer, then in the hidden one, and at last in the output layer (Fig. 1). Depending on the weight of connections, the input of the hidden neurons (Eq. (9)), the output of the hidden neurons (Eq. (10)), the input of the output neurons (Eq. (11)) and the output of the output neurons (Eq. (12)) can be calculated:

$$I_{h,y}(t) = \sum_{x=1}^{4} W_{x,y}(t) \cdot O_{i,x}(t) \quad y = 1..3 \tag{9}$$

$$O_{h,y}(t) = \frac{1}{1 + e^{-\beta \cdot I_{h,y}(t)}} \quad y = 1..3 \tag{10}$$

$$I_{o,z}(t) = \sum_{y=1}^{3} W_{y,z}(t) \cdot O_{h,y}(t) \quad z = 1..4 \tag{11}$$

$$O_{o,z}(t) = \frac{1}{1 + e^{-\beta \cdot I_{o,z}(t)}} \quad z = 1..4, k = 0.6 \tag{12}$$

After computing, four output values are available for the correction of the weight factors of the neural network. The difference between the calculated and taught data set is decreased using the delta rule. The teaching process means that the weights of the connections are changed according to the difference between the calculated output of the network (O) and the taught values (T). First, the weights between the output and hidden layers, then that of between the hidden and input layers are calculated (Eq. (13)).

$$W_{y,z}(t+1) = W_{y,z}(t) + \delta_p \cdot \eta \cdot O_{o,z}(t) \tag{13}$$

The proper learning rate, h can be determined by a trial and error method. The error pointer of the p-th training data set $\delta_{p,z}$ is calculated by different way in the two weight matrices. One training set ($T_{p,z}$) is used to determine the δ error pointer between the output and hidden layer (Eq. (14)).

$$\delta_{p,z} = n \cdot O_{o,z}(t) \cdot [1 - O_{o,z}(t)] \cdot [T_{p,z} - O_{o,z}(t)] \tag{14}$$

where n is the number of the neurons in the output layer ($n = 4$).

The error pointer of these weight factors (Eq. (14)) is used to compute the error between the hidden and input layers (Eq. (15)).

$$\delta_{p,y} = n \cdot O_{h,y}(t) \cdot [1 - O_{h,y}(t)] \cdot \sum_{n=1}^{4} \delta_{p,z} \cdot W_{y,z}(t+1) \tag{15}$$

A new training experiment should be performed after computing the weight changes until the error pointer (Eq. (7)) has been decreased to an appropriate level. Considering this theory, new weights were first computed between the last and the middle layers, and then between the middle and the first layers. During the calculation the error was calculated back to the network layer by layer. Experiments should be carried out until the proper learning level has been reached, and the error of recognition would be the lowest value.

4. Results and discussion

Since the number of the input neurons was equal to the number of sensors, and the number of the output neurons was equal to the number of the analytes (Fig. 1), the estimation of the optimum number of hidden neurons was necessary. The optimum structure of the neural network can be determined by a trial and error method. Four different structures were tried with 3, 4, 6, and 8 neurons in the hidden layer. The error ($E_{(p)}$) was calculated and primary parameters of η, μ and β, respectively, suggested by Zupan and Gasteiger [18] were used. It was found that, with increasing number of the neurons in the middle layer, the error of the estimation did not decrease considerably. Instead of further declining the error, calculation of the best computing parameters (η, μ and β) proved to be a better technique to reach the optimal computing performance.

Depending upon the proper primary weight values, the speed of adaptation during the teaching process can be increased. However, local interruption of the computing might also be caused by unsuitable primary weight factors and an inappreciable answer for the network can be achieved after the teaching process. The optimum primary weight factors can be determined by experiments. First, the weight matrices were filled with randomly generated values between -1 and $+1$. The minimum of the total error could be calculated by the algorithm, hence, the trapping of the calculation in a local minimum has to be avoided. The speed of the convergence depends not only upon the structure but the number of the iteration, as well.

The speed of the changing of weight was determined by the learning rate (η). This factor was applied to control the effect of the new weight factor. However, the momentum term (μ) was utilized to determine the interference of the previous weight factor on the new weight value. Theoretically, the error will be decreased during the

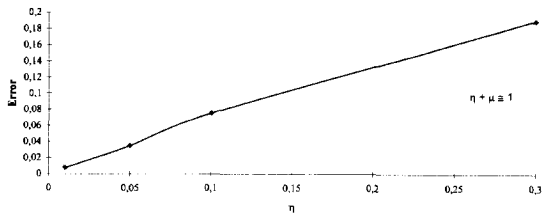

Fig. 3. The effect of learning rate on the total error.

analysis. Naturally, sometimes disturbances of the algorithm could be accomplished and oscillation of the error could occur. The sum of the learning rate and the momentum term was generally 1 [18]. The neural network with 3 hidden neurons was applied, and the optimum η and μ values were searched (Fig. 3). The higher the learning rate, the shorter the time of teaching. However, irrelevantly high η and μ values make the computing almost impossible. The optimum learning rate ($\eta = 0.15$) and the momentum term ($\mu = 0.9$) were successfully determined by experiments. Not only the optimum values of primary weight factors, learning rate, and momentum term, but the sigmoid parameter (β) could also be determined by experiments. It was found that using $\beta = 1$ the total error of the calculation was at a minimum. The value $\beta = 1$ was also suggested from other findings [12,13,18].

To avoid overtraining of the network, the optimum number of teaching experiments has to be estimated using the back propagation method [13,18]. Several teaching experiments were performed, and a decrease of error was expected. The effect of overtraining was observed after about 1000 iteration steps (Fig. 4), while the error slowly increased. Masters [19] suggested that using too

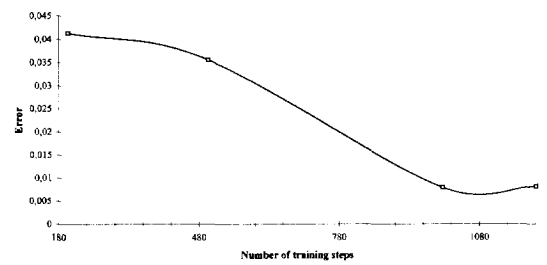

Fig. 4. The effect of overtraining on the total error.

many hidden neurons, the overfitting effect could easily be observed. So, a new network structure was tried. With increasing number of the neurons in the hidden layer, the error will not decrease to any measure and the possibility of overfitting will also be higher. Finally, in our experiments, 3 hidden neurons and 900 training cycles were applied.

4.1. Identification of pure analytes and mixtures

After the teaching process had been completed, the ANN has been able to give a response on the output layer for the taught analytes. Of course, the analytes, that had not been taught yet, could also be investigated, but all of the output neurons gave almost the same value. Only the previously investigated and taught analytes were determined by the ANN successfully. The unknown analyte has not been classified by the network, since the discrimination can be carried out by the existing training set. For example, if a taught analyte was injected—depending upon the compound—only one output neuron gave a value of 0.9, and all of the other output neurons produced a value of 0.1. If an unknown analyte was injected, every neuron in the output layer showed a value between 0.20 and 0.24.

The performance of the identification can be characterized by the number of hits of the taught analyte. For example, with the trained network, 100 analyses were performed. The analyte was correctly found in 99 cases, but in one case a wrong analyte was assigned to the output neuron. Thus, the error of the estimation proved to be 1%. The error calculated by Eq. (7) is often used to estimate the quality of the identification. After 900 teaching steps, it was found that the four investigated compounds could be identified. The differences between the taught and calculated values are summarized in Table 2. As can be seen, the identification has been completed for all analytes investigated. The unknown analyte was also injected and an output value of 0.2333 was obtained.

Three kinds of two-component mixtures with a 1:1 mixing ratio in 150 ppm was also taught (Fig. 5). The aim of this research was to discriminate

Table 2
The predicted values (O_j) for the pure compounds after 900 training steps

	Output				Error (see Eq. (3))
	Neuron 1	Neuron 2	Neuron 3	Neuron 4	
Benzene	0.8967	0.1188	0.1189	0.1214	0.0006
Pentane	0.1214	0.8970	0.1188	0.1188	0.0006
Acetone	0.1188	0.1214	0.8967	0.1190	0.0006
Chloroform	0.1189	0.1188	0.1214	0.8968	0.0006
Taught value of the target neuron (T_j)	0.9000	0.9000	0.9000	0.9000	
Absolute error ($T_j - O_j$)	0.0033	0.0030	0.0033	0.0032	

the mixtures from each other, and the selection of the components in one mixture has not been performed yet. On the other hand, the piezoelectric sensor coated by sensing materials as gas chromatographic stationary phases is not an additive sensor in the applied concentration range. For classification of the compounds in mixtures the system should be retrained. This simple model has been applied to test the sensor-array and to try the classification ability of the ANN. In the food industry, several examples could be found for discrimination of similar alcoholic beverages (e.g. Ref. [11]).

In this examination, different analytes were selected to perform a set of experiments with the mixtures. Considerable differences in frequency values of the sensing compounds were observed. The ANN was used for data evaluation similar to the identification of the pure analytes. All mixtures were successfully differentiated. The error of the identification was slightly higher than that of pure compounds (Fig. 6). Further experiments are needed for the investigation of the effect of different concentration ranges and mixture ratios on the pattern.

The performance of the developed method was compared to the previously used PARC without ANN [15] and PCA [14] methods, and the accomplishment of other similar systems described in the literature [20–23]. The former PARC method could be used for classification of compounds using the stored patterns of the analytes with 80% probability. The new ANN technique was successfully applied for identification of organic compounds with higher efficiency. The error of the identification was insignificant (Table 2), and after 15 determinations had been made no error was observed. These findings are similar to the results described in Ref. [20], and even superior to the recognition probability in Refs. [21,22]. Ema et al. [22] reported that the recognition probability was found to be 67–73% depending upon the structure and the training of the network. The results

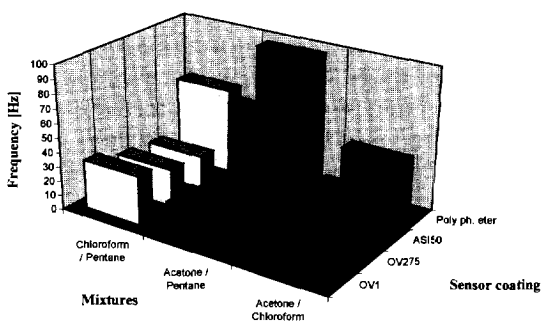

Fig. 5. The frequencies of sensors for different mixtures of volatile organic compounds.

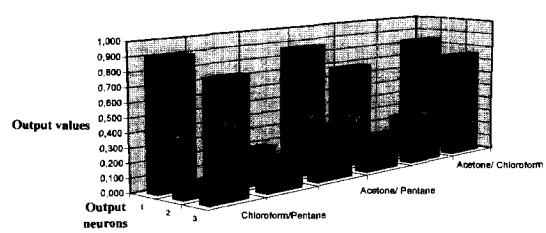

Fig. 6. Identification of the mixtures using the values of output neurons.

were compared to discrimination analysis (DA). The comparison has shown the advantages of the ANN: the recognition probability was 67% (ANN with 6 hidden neurons), 73% (ANN with 8 hidden neurons), and 64% (DA). Chang et al. [21] reported a 70% probability only. The application of the improved sensor arrays and software tools proved to be better than the earlier systems. After 5000 training steps, 14 entirely successful analyses were made by Nanto et al. [20]. Comparison of the developed ANN and pattern recognition methods using supervised (i.e. principal component analysis, discrimination analysis, template matching/partial least-squares, back propagation/artificial neural network, learning vector quantization) and unsupervised (i.e. Euclidean and other cluster analysis, Kohonen network) can be found in Ref. [23].

5. Conclusions

The application of the ANN method proved to be remarkably advantageous if the measured property (mass, concentration, etc.) should not be connected exactly to the signal of the transducers of a chemical sensor. The frequency values of the compounds were taught by a computer program. The optimum structure of neural network was determined by a trial and error method. Four different structures were tried with several neurons in the hidden layer, and the total error was calculated. It was found that the calculation of the best computing parameters (η, μ and β) proved to be an appropriate technique to reach the optimal computing performance. The optimum values of primary weight factors, learning rate ($\eta = 0.15$), momentum term ($\mu = 0.9$), and the sigmoid parameter ($\beta = 1$) were determined by experiment. Three hidden neurons and 900 training cycles were applied. Mixtures of organic compounds were also analysed and the ANN method proved to be a reliable way to differentiate the sensing materials and to identify the volatile compounds.

Acknowledgements

The financial support of the Hungarian National Science Foundation (OTKA 16315) is greatly appreciated.

References

[1] G.Z. Sauerbrey, Zt. Physik 155 (1959) 206.
[2] W.H. King Jr., Anal. Chem. 36 (1964) 1735.
[3] B.J. Wythoff, Chemometrics Intell. Lab. Systems 18 (1993) 115.
[4] G. Kateman, Chemometrics Intell. Lab. Systems 19 (1993) 135.
[5] J.W. Gardner, P.N. Bartlett, Sensors Actuators B 18–19 (1994) 211.
[6] S.M. Fraser, T.E. Edmonds, T.S. West, Analyst 111 (1986) 1183.
[7] P. Klinkhachorn, B. Huner, E.B. Overton, H.P. Dharmasena, D.A. Gustowski, IEEE Trans. Inst. Meas. 39 (1990) 264.
[8] A. Schmautz, Sensors Actuators B 6 (1992) 38.
[9] S.M. Chang, Y. Iwasaki, M. Suzuki, E. Tamiya, I. Karube, H. Muramatsu, Anal. Chim. Acta 249 (1991) 323.
[10] W.P. Carey, K.R. Beebe, B.R. Kowalski, Anal. Chem. 59 (1987) 1529.
[11] T. Aishima, Anal. Chim. Acta 243 (1991) 293.
[12] D.E. Rumelhart, J.L. McClelland, Parallel Distributed Processing, MIT Press, USA, 1986.
[13] R. Beale, T. Jackson, Neural Computing: An Introduction, IOP Publishing Ltd., Bristol, England, 1990.
[14] G. Barkó, J. Hlavay, Submitted to Sensors and Actuators B.
[15] G. Barkó, B. Papp, J. Hlavay, Talanta 42 (1995) 475.
[16] G. Barkó, J. Hlavay, Fresenius' J. Anal. Chem. (in press).
[17] V. Sommer, P. Tobias, D. Kohl, H. Sundgren, I. Lundström, Sensors Actuators B 28 (1995) 217.
[18] J. Zupan, J. Gasteiger, Neural Networks for Chemists, VCH, Germany 1993.
[19] T. Masters, Practical Neural Network Recipes in C++, Academic Press, Inc., Boston, USA, 1993.
[20] H. Nanto, S. Tsubakino, M. Ikeda, F. Endo, Sensors Actuators B 24–25 (1995) 794.
[21] S.M. Chang, Y. Iwasaki, M. Suzuki, E. Tamiya, I. Karube, Anal. Chim. Acta 249 (1991) 323.
[22] K. Ema, M. Yokohama, T. Nakamoto, T. Moriizumi, Sensors Actuators B 18 (1989) 291.
[23] J.W. Gardner, P.N. Bartlett, Sensors Actuators B 18–19 (1994) 211.

LIST OF CONTENTS

January

October

November

December

Papers presented at the 4th Symposium on Analytical Sciences, Brussels, June 3–5, 1996

Talanta

The International Journal of Pure and Applied Analytical Chemistry

Volume 44 (1997)

ELSEVIER

Amsterdam–Lausanne–New York–Oxford–Shannon–Tokyo

ELSEVIER

Talanta 44 (1997) vii

Talanta

Editorial

It was a pleasure for the Editors of Talanta to arrange this special issue, proposed by Professor Vasile Cosofret, honoring Professor George Baiulescu on the occasion of his 65th birthday. The great diversity of the research fields presented in this issue actually reflects the broad activity of Professor Baiulescu covered during his career in Analytical Chemistry. Professor Baiulescu has significantly contributed in separation sciences, spectroscopy and electrochemistry by the quality of his publications. We are particularly thankful to Professor V. Cosofret for having solicited numerous experts and friends of Professor Baiulescu for contributing to this issue.

Jean-Michel Kauffmann
Gary Christian

AUTHOR INDEX

SUBJECT INDEX